TECHNOLOGY:
ENABLING A SAFER TOMORROW

INTRODUCTION

The Enhanced Safety of Vehicles (ESV) program originated in 1970 under the North Atlantic Treaty Organization (NATO) Committee on the Challenges of Modern Society, and was implemented through memorandums of understanding between the Governments of the United States, France, Germany, Italy, the United Kingdom, Japan, and Sweden. The participating nations agreed to develop experimental safety vehicles to advance the state-of- the-art technology in automotive safety engineering and to meet periodically to exchange information on their progress. Since its inception the number of international partners has grown to include the Governments of Canada, Australia, The Netherlands, Hungary, Poland, Republic of Korea, and two international organizations the European Enhanced Vehicle-safety Committee, and the European Commission. A representative from each country/organization serves as a Government Focal Point in support of the ESV program.

In the interest of information exchange, The U.S. Department of Transportation, National Highway Traffic Safety Administration (NHTSA), distributes the Proceedings of the 26th International Technical Conference on the Enhanced Safety of Vehicles. The technical papers in this publication detail safety research efforts underway worldwide, and share the common interest of reducing motor vehicle related fatalities and injuries.

The opinions, findings, and conclusions expressed in the publications are the original written work of the author(s) and not necessarily those of the U.S. Department of Transportation, National Highway Traffic Safety Administration. Traditional papers are accepted after the corresponding abstracts undergo technical review. To enhance the scientific content, several papers were accepted for peer-review and published in a special edition of ***Traffic Injury Prevention*** by Taylor and Francis Group. These papers are available to the public via https://www-esv.nhtsa.dot.gov/

On behalf of the Conference Organizing Committees we thank our international participants for their dedication and support of the 26th ESV Conference and look forward to your future participation.

ESV 2019 Organizing Committee

Technical Organization
U.S. Department of Transportation
National Highway Traffic Safety Administration (NHTSA)

ESV Government Focal Point Chairman

Tim Johnson
Acting Associate Administrator for Vehicle Safety Research
Email: Tim.Johnson@dot.gov

NHTSA Organization Committee

Cem Hatipoglu
Acting Associate Administrator for National
National Center for Statistics and Analysis
Email: Cem.Hatipoglu@dot.gov

Stephen Summers
Division Chief
Structural and Restraints Research
ESV Technical Program Lead
Email: Stephen.Summers@dot.gov

Dee Williams
Deputy Associate Administrator
Vehicle Safety Research
ESV Operations Manager and U.S. Government Awards Coordinator
Email: Dee.Williams@dot.gov

Matthew Craig
Division Chief
Human Injury Research
Email: Matthew.Craig@dot.gov

Kevin Moorhouse
Division Chief
Applied Biomechanics
Email: Kevin.Moorhouse@dot.gov

Chris Monk
Division Chief
Human Factors/Engineering Integration
Email: Chris.Monk@dot.gov

Robert Kreeb
Division Chief
Intelligent Technologies Research
Email: Robert.Kreeb@dot.gov

Don Wilke
Division Chief
Applied Crashworthiness and Defects Analysis
Vehicle Research & Test Center
Email: Don.Wilke@dot.gov

Frank Barickman
Applied Crash Avoidance
Vehicle Research & Test Center
Email: Frank.Barickman@dot.gov

Deanna Barbour
Office of Communications & Consumer Information
Email: Deanna.Barbour@dot.gov

Carla Young
Vehicle Safety Research
Email: Carla.Young@dot.gov

Arthur Carter
Student Safety Technology Design Competition Coordinator
Vehicle Safety Research
Email: Arthur.Carter@dot.gov

Lisa Floyd
Vehicle Safety Research
Email: Lisa.Floyd@dot.gov

Yvonne Clarke
Vehicle Safety Research
Email: Yvonne.Clarke@dot.gov

Debbie Sweet
Vehicle Safety Research
Email: Debbie.Sweet@dot.gov

GFP MEMBERS

UNITED STATES OF AMERICA | **Tim Johnson**
Acting Associate Administrator for Vehicle Safety Research
National Highway Traffic Safety Administration
Email: Tim.Johnson@dot.gov

AUSTRALIA | **Sharon Nyakuengama**
General Manager
Vehicle Safety Standards
Email: Sharon.Nyakuengama@infrastructure.gov.au

CANADA | **Peter Burns**
Chief, Ergonomics & Crash Avoidance
Transport Canada
Email: peter.burns@tc.gc.ca

EUROPEAN COMMISSION | **Gwenole Cozigou**
Acting Director
European Commission
Email: gwenole.cozigou@ec.europa.eu

FRANCE | **Daniel Kopaczewski**
Department Head
Vehicle Security and Emissions, Ministry of Ecology, Sustainable Development and Energy
Email: pierre.bazzucchi@developpement-durable.gouv.fr

GERMANY | **Stefan Strick**
President and Professor 3
Federal Highway Research Institute (BASt)
Email: praesident@bast.de

HUNGARY | **János Déak**
Head of the Technical Co-ordination Centre for EU and UN-ECE Activities on Road Vehicles
KTI/Institute for Transport Sciences
Email: deak.janos@kti.hu

ITALY | **Antonio Erario**
Head of Division I, International Regulation Affairs
Ministry of Infrastructure and Transport, Department for Transport
Email: antonio.erario@mit.gov.it

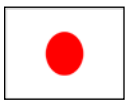

JAPAN | **Hiroyuki Inomata**
Director for Technical Planning Office
Road Transport Bureau Ministry of Land
E-mail: inomata-h2hv@mlit.go.jp

POLAND |
ESV Member Country

REPUBLIC OF KOREA | **Kirim Elisabeth Lee**
Deputy Director, Motor Vehicles Management Division
Ministry of Land, Infrastructure and Transport (MOLIT)
Email: guht@korea.kr

SWEDEN | **Matteo Rizzi**
Analyst, PhD.
Road Safety Department
Swedish Transport Administration
Email: matteo.rizzi@trafikverket.se

THE NETHERLANDS | **Peter Striekwold**
Manager, Vehicle Standards Development
RDW
Email: pstriekwold@rdw.nl

UNITED KINGDOM | **Jim Hand**
Head of Safety Systems and Consumer Incentives
International Vehicle Standards Division
Department for Transport
Email: Jim.hand@dft.gov.uk

26th ESV TECHNICAL SESSION CHAIRS & CO- CHAIRS

Technical Session	Session Chair (Country)	Session Co-Chair (Country)
Protection of Vulnerable Road Users	Rikard Fredriksson (Sweden)	Yasuhiro Matsui (Japan)
Safety Performance in Frontal and Rear Crashes	Youghan Youn (Republic of Korea)	Stephen Summers (US)
Crash Avoidance: Driving Automation Systems Level 0, 1, and 2. Product Evolution; Evaluation; and Real-World Deployment Challenges	Dr. Jost Gail (Germany)	Eric Traube (US)
Biomechanics: Advances in Experimental and Mathematical Biomechanics and Injury Research	Matthew Craig (US)	Rainer Hoffmann (Germany)
Safety Performance in Side Impact and Rollover Crashes	Thomas Belcher (Australia)	Suzanne Tylko (Canada)
Crash Avoidance: Automated Driving Systems Levels 3, 4 and 5: Product Evolution; Evaluation; and Real-World Deployment Challenges	Riender Happee (Netherlands)	Professor Kyongsu Yi (Republic of Korea)
Biomechanics: Advances in Crash Test Dummies, Instrumentation and Data Analysis	Philippe Vezin (France)	Dr. Kevin Moorhouse (US)
Restraint System Design and Performance Challenges: Addressing the Needs of Diverse Populations (Age, Gender, Stature)	Riske Meijer (Netherlands)	Lotta Jakobsson (Sweden)
Crash Avoidance: Human-Machine Interface Design and Driver Monitoring Technologies in Vehicles	Peter Burns (Canada)	Dr. Chris Monk (US)
Consumer-Focused Approaches in Vehicle Safety to Drive the Automotive Market on a Global Scale	Andre Seeck (Germany)	Michiel van Ratingen (Netherlands)
Crash Avoidance: Continuation Session	Eric Traube (US)	Tetsuya Niikuni (Japan)
Adapting Safety Evaluation Approaches for Vehicles with Automated Driving Systems	Jim Hand (UK)	Nicole van Nes (Netherlands)
Automated and Integrated Crash Safety	Jac Wismans (Netherlands)	Marcus Wisch (Germany)
Assessment of New and Improved Field Data Collection, Analysis and Benefits Assessment Methods	Chip Chidester (US)	Rob Eenink (Netherlands)

U.S. GOVERNMENT AWARD RECIPIENTS
Presented at the 26th ESV Conference, Eindhoven, Netherlands

U.S. Government Special Awards of Appreciation

In recognition of and appreciation for outstanding leadership and special contributions in the field of motor vehicle safety

Bernd Lorenz	Germany
Adam McNeill	Germany
Hans Ammerlaan	Netherlands
Dr. Nils Lubbe	Sweden
Martin Magnusson	Sweden
Bernie Frost	United Kingdom
Daniel Smith	United States
David Zuby	United States

U.S. Government Awards for Safety Engineering Excellence

In recognition of and appreciation for exceptional scientific contributions in the field of motor vehicle safety engineering and for distinguished service to the motoring public

Yasuhiro Matsui	Japan
Kyongsu Yi	Korea
Anders Kullgren	Sweden
Dr. Mikael Ljung Aust	Sweden
Tom Hollowell	United States
Sue Bai	United States

26th ESV INTERNATIONAL STUDENT SAFETY TECHNOLOGY DESIGN COMPETITION FINALISTS

ASIA PACIFIC

REGIONAL COORDINATOR: MASASHI YUKAWA, JSAE, JAPAN

School	Nihon University Biomechanics Team, Japan
Project Title	Development of New Lumbar-Abdominal Dummy for Vehicle Occupants
Advisor	Tetsuya Nishimoto

REGIONAL COORDINATOR: YOUNGHAN YOUN, KOREA

School	School of Mechanical and Aerospace Engineering, Seoul National University, Korea
Project Title	Health Monitoring and Emergency Braking Algorithm for Automated Driving Vehicle Fail-Safe System
Advisor	Kyongsu Yi

NORTH AMERICA

REGIONAL COORDINATOR: ART CARTER, NATIONAL HIGHWAY TRAFFIC SAFETY ADMINISTRATION (NHTSA), UNITED STATES

School	California Polytechnic State University, San Luis Obispo, CA
Project Title	Autonomous Collision Avoidance System for Collaborative Vehicle Platooning
Advisors	Dr. Charles Birdsong (Overall Advisor) Bruce Edward DeBaruhl (Computer Engineering Team Advisor)

School	Oregon State
Project Title:	Automatic Vehicle Damage and Passenger Injury Assessment
Advisor	Dr. David Hurwitz

School	Virginia Tech Transportation Institute (VTTI)
Project Title	Pre-Rear End Positioning and Risk Extenuation System (PREPARES)
Advisor	Dr. Zachary Doerzaph

A TEST SYSTEM OF AUTOMATED DRIVING SYSTEMS

Chung-Jen Hsu Ph.D.
Bowhead Logistics Solutions
USA

Paper Number 19-0002

ABSTRACT
Automated Driving Systems (ADS) use sensors (e.g., cameras, lidars, and radars) to detect vehicles, pedestrians, traffic signs and signals, lane markings, and other relevant objects. ADS use the information from these sensors to perceive driving environments, inform decisions they make, and assist in executing vehicular maneuvers. ADS also use machine learning algorithms to enhance the performance of perception and driving capabilities. The research objective of this paper is to identify a test system that uses objective test procedures to evaluate the performance of ADS. The test system would be used to verify perception accuracy and to validate the decision-making choices of ADS. The ADS test system consists of hardware and software components used to implement test procedures, and consists of three subsystems: (1) data collection; (2) data communication interface; (3) and performance evaluation. The data collection vehicle travels the planned route with all sensors activated, collecting Operational Design Domain (ODD) data. The data are then processed and stored in the ODD and Object and Event Detection and Response (OEDR) libraries (databases). With sufficient testable cases in the database, the test team can select the desired test cases from the database and send them to the ADS vehicle Under Test (AUT). It is assumed that an AUT can switch into the test mode and all the sensor data it retrieves from the data communication interface would be treated as real-time data from its own sensors. The AUT can perceive ODDs and react by sending speeds, acceleration/deceleration, and yaw rates to the backend computer for evaluating the performance with the comparison of safe driving OEDR and AUT trajectories. This paper explores a potential framework of an ADS test system and potential test procedures using the framework. The test system may evaluate ADS in selected ODDs without implementing field tests. When conducting field tests, the desired ODDs and traffic conditions may not always be available. The test system concept developed in this study has the potential to address issues associated with driving exposure and repeatability of desired test conditions. If the test system implements test procedures, it should be able to evaluate ADS objectively and repeatedly.

INTRODUCTION

An Automated Driving System (ADS) uses sensors like cameras, lidars, and radars to detect vehicles, pedestrians, traffic signs and signals, lane markings, and relevant objects to perceive the driving environment and choose vehicular maneuvers. ADS vehicles also utilize machine learning algorithms to enhance the performance of perception and driving capabilities. The public will expect ADS vehicles to drive safely at different levels of automation (levels three to five [13]), and their safety needs to be identified. The objective of this research is to identify a test system that uses a variety of testing procedures for analyzing the level of ADS performance, in the hopes of someday building a metric that could evaluate ADS safety. The test system is expected to verify the perception correctness and validate the decision-making results of an ADS vehicle Under Test (AUT). The performance level that an AUT can achieve depends on its perceptive and decision-making. Fundamental safety responsibilities of an AUT are that it can perceive and track vehicles, pedestrian, and other objects timely and correctly in the proximity of its moving path, and evaluate potential risks of crash to make decisions of safe maneuvering correctly.

Two types of ADS testing have been commonly used by manufacturers to validate the systems of AUTs at the vehicle level. One is functionality-based [8] and the other is scenario-based. Functionality-based tests are designed to test driving tasks in three parts — sensing/perception, decision, and actions that are analogous to the behavior of human drivers. Functionality-based tests can evaluate the level of safety for ADS vehicles quantitatively, however; they may lack testing of all aspects of certain scenarios. Scenario-based tests [3] can provide the required scenarios or events for testing overall capabilities of AUTs, but the evaluation and analysis of perception, decision, and maneuver tasks at a more granular level are omitted. The availability of testing scenarios may be limited due to resources, driving environments, and other reasons. Additionally, creating the same scenario repeatedly for testing AUTs objectively can be a challenge under any circumstances. A test system of ADS capable of implementing functionality- and scenario-based tests that are both objective and repeatable is needed for ensuring the safety of ADS and other vehicles in the proximity.

This study identifies a new ADS testing framework capable of generating desired test functionalities and scenarios. This framework collects ADS data including the of ADS vehicles' maneuvering and sensor data. Based on the applicable Operational Design Domain (ODD [14]), a data collection vehicle can collect sensor and vehicle maneuver data on the planned route. An ODD describes the specific operating domain(s) including physical infrastructure, operational constraints, objects, connectivity, environmental conditions, and zones in which an ADS vehicle is designed to function [16]. Collected data will be categorized based on the ODDs and all the tasks of Object and Event Detection and Response (OEDR). An OEDR consists of tasks of dynamic driving including recognizing the driving environment and executing appropriate maneuvers to perceived objects and events. A test team may select the desired testable case(s) for testing an AUT by sending the test data to the AUT via an interface device. This interface device may also retrieve the responses from the AUT and send them back to the backend for evaluating the performance. The AUT would start driving from the start to end points with the provision of Global Positioning System (GPS) data and sensor data with ODD elements in the proximity. The speed of data injection should be synchronized with the AUT's trajectories determined by the speed, heading direction, yaw rate, and acceleration/deceleration rate. This synchronization is analogous to the driving simulator operation that the driver's view is determined by the operations of throttle, brake and steering wheel.

The test system is expected to perform functionality- and scenarios-based tests simultaneously. Essentially, the idea of this test system comes from the integration of a vehicular emission test box and a driving simulator. Instead of a human driver sitting in a driving simulator facing big screens playing videos of ODDs, the test system feeds sensor data into the AUT via a test interface dongle like an emission test box.

METHODS

The concept of ADS test framework is shown in Figure 1. The test team could have a list of desired ODDs and scenarios or events. The test team may seek and find actual locations and roadways where the desired ODDs exist in terms of physical infrastructure, operational constraints, objects, connectivity, environmental conditions, and zones. A trip can be planned for collecting all the required data for testing AUTs. A data collection vehicle equipped with all types of sensors travels a planned route and collects ODD data. After completion of data collection, all data are processed and stored in the ODD and OEDR libraries (databases). The driver of the data collection vehicle is supposed to drive safely without any crashes and the collected data will be tagged as crash free (the baseline scenario) in the database. If a crash occurs in the process of data collection, then the collected data will be tagged as

a crash event (this is not supposed to happen). Several data collection trips can be made for collecting multiple sets of ODD and OEDR data. With feasible testable cases in the database, the test team can select the desired test cases from the database and send them to an AUT in a test. The AUT is assumed to enter the test mode when it receives test data from the test data interface dongle. When the AUT is under the test mode, all the sensor data would be treated as real-time data from its own sensors. With the provision of sensors and GPS data, the AUT should be able to perceive ODDs and react by sending kinematic data of speed, acceleration/deceleration, and yaw rates to the test data interface dongle. These kinematic data can be transmitted to the backend computer for evaluating the AUT's performance by comparing its trajectories with that of the data collection vehicle (without crashes). The AUT's relative speeds and distances to all vehicles and objects in the proximity can also be used to evaluate the probability of potential crashes.

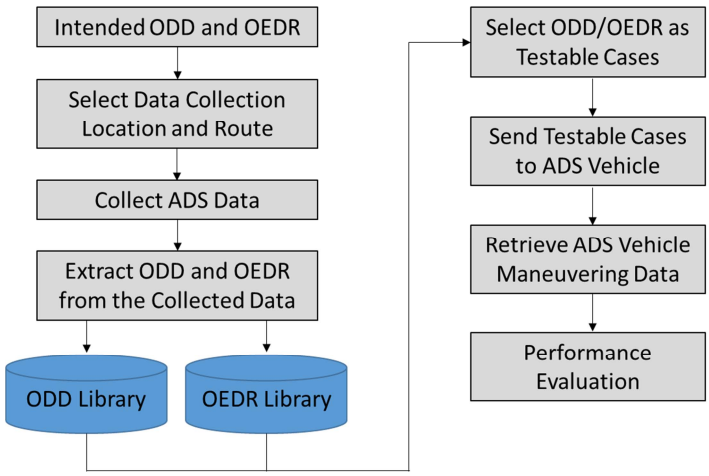

Figure 1 The Test System Framework of ADS.

The test system's dataflow is shown in Figure 2. The sensor data from the data collection vehicle can be stored in the backend and sent to the test data interface dongle for injecting into the AUT (red dash lines). Also, the AUT's kinematic maneuvering data can be retrieved by the test data interface dongle and sent back to the backend for evaluating the performance (blue lines). Details of system operations are addressed in the following sections.

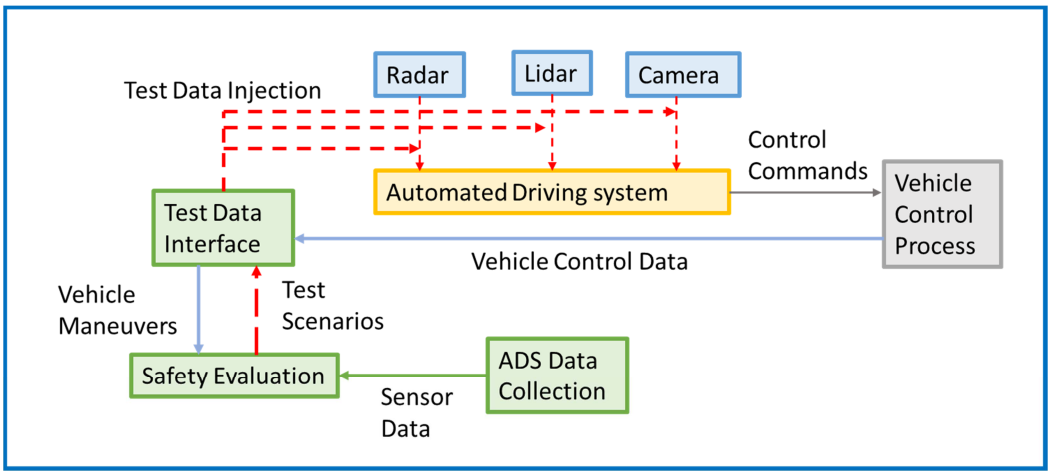

Figure 2 The Dataflow of Test System.

ADS TEST SYSTEM

The test system of ADS tests AUTs at the vehicle level, meaning that the interim results of ADS operations such as perception results of vehicles and pedestrians will not be verified or validated. Instead, only the results of decision

making in vehicular maneuvers (likely made in response to perception data) are evaluated in terms of level of safety. Many ADS vehicles are expected to operate in different ODDs that define the background environment including area (urban/rural), roadway (freeway/arterial/intersection), weather, traffic, signs/signals, lane markings, etc. Some specific ODDs may not be available during the data collection period, and thus would not be a part of the testing. For example, a scenario consisting of snowing in the evening with peak hour traffic at a signalized intersection may not be available for the test team to conduct the field test in July. In addition, searching and identifying the appropriate intersection with the desired traffic and geometric design conditions is a task that needs to be completed before implementing the test. Moreover, waiting for a snow day with the desired intensity or accumulation is another challenge that the test team needs to face. If a data collection system can be established to collect all desired ODD data using cameras, lidars, and radars, then the ODD data can be injected into the AUT anytime as needed. All the collected ODD data can be stored and compiled as a library in a way that users can select the desired ODD to conduct the test.

The test system of ADS may provide various ODDs and OEDRs that can be used to test AUTs under the specific conditions of traffic, environment, and event occurrence without a field test of the AUT itself. To achieve this objective, three subsystems — ADS data collection, ADS test data interface, and ADS performance evaluation are identified as shown in Figure 3. The ADS data collection subsystem gleans sensors, vehicle control, and ground truth data and transfers them to the performance evaluation subsystem. When the ADS test data interface subsystem connects with the AUT, it starts to retrieve test data and inject them into the AUT. The AUT goes into the test mode when it receives the test commands and reacts to the injected sensors and GPS data.

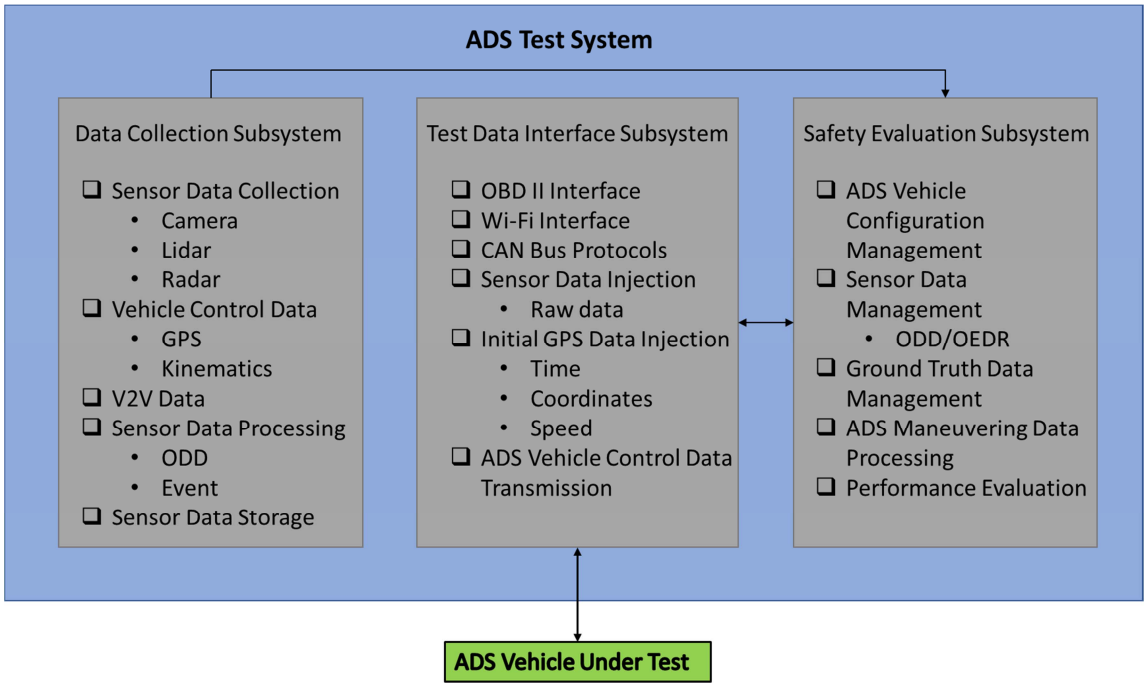

Figure 3 Functional Architecture of Test System.

ADS Data Collection Subsystem

The ADS data collection subsystem collects all the ODD and OEDR data for testing AUTs. The data collection vehicle should be able to travel to all locations under all required ODD conditions. Figure 4 shows the three components of this subsystem. The sensor data recorder saves the raw data of radar, lidar, and camera. The ground truth recorder uses a centimeter level GPS receiver to record the ground truth of trajectories along the planned route including GPS times and coordinates, speeds, headings, yaw rates, and acceleration/deceleration rates. The ODD and OEDR recorder consists of object detection and recognition software to classify and discern ODD elements, and the collected data are saved in the backend database. All the sensor data should be timestamped based on the ground truth GPS times. Also, the data bus of the data collection subsystem should have a sufficient bandwidth to accommodate high data rates to minimize the lag of data timestamping.

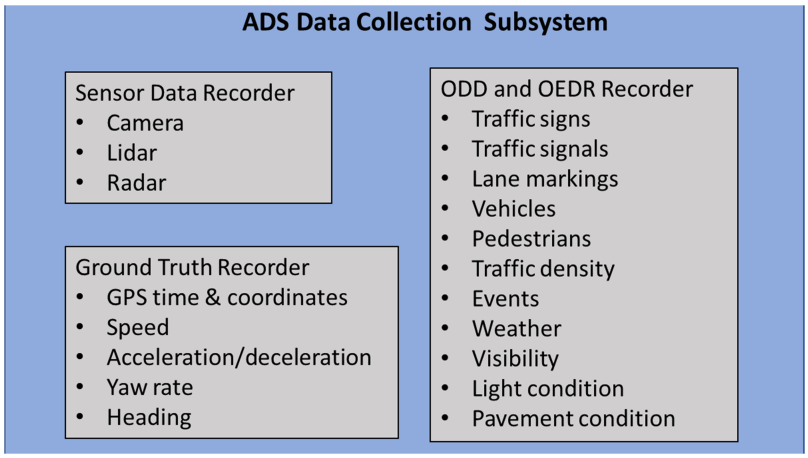

Figure 4 ADS Data Collection Subsystem.

The data collection subsystem may collect data from the same route in different ODDs. For example, the data collection vehicle can travel through the same route at the same time in fair weather and other weather conditions such as rain, fog, and snow. The data collected in a fair day are saved as the base scenario, and other data collected in bad weather days are stored as contrast scenarios that can be used as fault injections [12].

Sensor Data Recorder Radar, lidar, and camera are the most common sensors used on ADS vehicles [9]. These sensors provide different detection ranges, coverages, and capabilities for ADS vehicles to perceive vehicles, pedestrians and other objects that may cause potential risks to dynamic driving tasks.

Radar
Radars emit millimeter-waves to detect distances between an ADS vehicle and other objects in the range. Radar sensing has a narrower detection field horizontally and vertically as compared to lidars. Radars have been widely used in adaptive cruise control systems that measure distances to the preceding vehicle continuously. Different types of radars can be installed on the data collection vehicle for gathering distance data of objects in the detection ranges.

Lidar
Lidars emit invisible laser waves to detect distances to objects by receiving the backscattered energy. Lidar sensing scans a scene at 10–15 Hz using occupancy grid methods to segment objects of interest from the background [15]. Segmented objects can be identified as vehicles, pedestrian, traffic signs, and other objects of interest, an ADS vehicle can track multiple moving objects simultaneously to avoid a crash. A 360-degree lidar can be installed on the roof of the data collection vehicle for gathering data at detail resolutions. The sampling rate of lidar should be set to the highest for recording the maximum amount of data.

Camera
Cameras are vision-based sensing to detect objects in the visible range using image processing technologies. Unlike radar or lidar emitting waves to detect objects, cameras perceive light pixels and process disparities of pixel arrays to classify and identify objects as vehicles, pedestrians, and other objects of interest. Cameras with different viewing ranges can be installed on several locations of the data collection vehicle to obtain a panoramic view and various viewing depths.

Ground Truth Recorder A ground truth recorder can record high precision data that can be used as the ground truth data. The ground truth data including GPS times and coordinates, speeds, yaw rates, and headings that can be used as the baseline and background information for labeling ODD and characterizing OEDR scenarios. In addition, the recorder can keep track of vehicular maneuver data under all circumstances. The ground truth recorder needs to be calibrated and tuned constantly to maintain its high fidelity and precision.

ODD and OEDR Recorder The data of desired ODDs can be obtained when the data collection vehicle travels through the designated routes where the weather, light, and pavement conditions are recorded. OEDR data can also be obtained if the data collection vehicle encounters any events or scenarios. Special events can be arranged to occur on test tracks because these events (e.g., a crash or hard braking event) may be unlikely to encounter in the traveled route. All the collected data will be saved on the data collection vehicle and transferred to the backend computer for further processing.

ADS Test Data Interfaces Subsystem

For injecting ODD test data into the AUT, a test data interface needs to be established for converting raw sensor data into the format that most ADS manufacturers may be able to process. ADS software may reside on various operation systems (e.g., embedded systems, Windows, or Linux, etc.) using different hardware interfaces, so the data interface should act as a device that is compatible with most file systems. ADS vehicle manufacturers may use different software interfaces to retrieve sensor data internally; nonetheless, a common hardware interface is needed externally for receiving injected test data. Based on the current applications of vehicular communication interfaces, the test data interface may be OBD II (On-Board Diagnostic) or Universal Serial Bus (USB), either is able to carry out data transfers at different data rates.

An OBD II or USB port can host a test data interface dongle to transfer test data. The dongle can receive test data from the ODD library via a wireless interface (e.g. Wi-Fi) and inject test data into the AUT. When an AUT receives the test data injection command it switches into the test mode. Under the test mode the AUT may receive sensors and GPS data and make decisions of maneuvers without shifting gears and moving literally. The ADS's control and maneuver commands should not be sent to Electronic Control Units (ECU) that control the steering wheel, throttle, and brake under the test mode. Also, the test interface dongle should have color lights to display the progress of data communications, including receiving data from the backend computer, transferring data to the AUT, completion of data transfer, and receiving AUT's maneuver data. Figure 5 shows the functionalities of ADS test data interface subsystem.

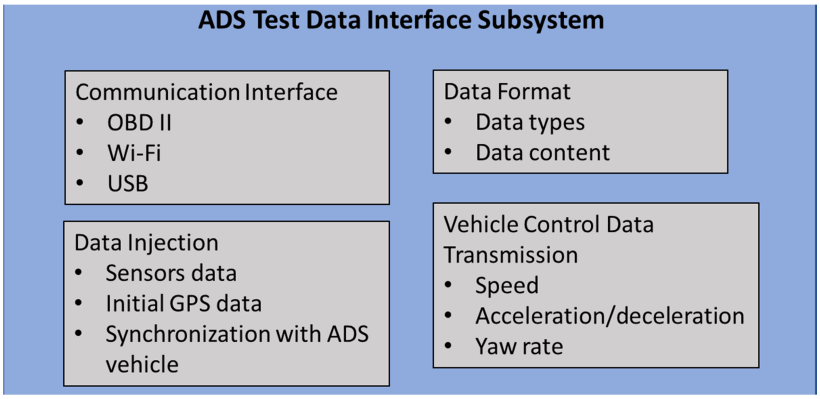

Figure 5 ADS Test Data Interface Subsystem.

Communication Interface The communication interface consisting of two components, one is transmitting and receiving data to and from the backend computer, and the other is injecting and retrieving data to and from the vehicular communication interface (e.g., USB). Depending on the availability of onboard communication ports, either OBD II (connected with Controller Area Network, CAN bus) or USB can be used to connect with the test data interface subsystem. The test data injection can be completed in two steps. First, the sensor data files are transferred from the test data interface to the AUT's storage. Second, the AUT opens the data files and reads data into the memory for further processing. A conservative estimate the demand of sensor data rate is implemented for evaluating the appropriateness of two data communication interfaces.

For example, a 10-minutes (600 seconds) video has a frame size of 640x480 pixels at a color depth of 24-bits, and a frame rate of 8 frames per second. This video has 307,200 (640 * 480) pixels per frame, 7.03 (307,200 * 24 /2^{20}) Mbit per frame, 56.25 (7.03 * 8 fps) Mbit/s data rate, and 4.12 (56.3 Mbit/s * 600 s / 8 / 2^{10}) Gbyte file size. Likewise, lidar data can be estimated as 80,000 points per scan, distance and intensity of 3 bytes per point, 240,000

(80,000 * 3) bytes per scan, 2,400,000 (240,000 * 10) bytes per second (10 Hz scan frequency), 18.31 (2,400,000 * 8 / 2^{20}) Mbit/s data rate, and 1.34 (18.3 Mbit/s * 600s / 8 / 2^{10}) Gbyte file size. Based on the above calculations, the demand of data rate is on the level of tens of Mbit/s at least (e.g., the Velodyne lidar [18] provides 100 Mbit/s Fast Ethernet as the communication interface).

OBD II is an automotive standard for all light vehicles and it supports data communications with ECUs through CAN bus. ADS may use CAN bus to send commands to ECUs for controlling vehicular maneuvers; however, ADS should not do so under the test mode. Vehicular data bus systems such as High-Speed CAN (1 Mbit/s bandwidth) and CAN-FD (Flexible Data Rate, 12 Mbit/s bandwidth) may cause delays in data communications due to their insufficient bandwidths. ADS may encounter more delays when it receives massive sensor data from the CAN bus. The next-generation automotive Ethernet with Gbit/s bandwidth may be sufficient for transferring data from sensors to ADS without excessive delays.

The bandwidth of USB 3.0 can reach 5 Gbit/s that may provide faster data transfers as compared to OBD II. The USB 3.1 and 3.2 standards (USB 3.x [17]) provide even higher bandwidths for data transfers. In operation, when an AUT detects its USB port is activated, it should perform security checks first to ensure the interface device is legitimate and then start transferring sensor data files. Wi-Fi can be used as the data communication interface between the backend computer and test data interface dongle. Newer Wi-Fi devices support the 802.11 ac standard may reach a data rate of 1.3 Gbit/s, this bandwidth may provide less delays when transferring massive sensors data files.

Data Format Each lidar data packet contains header, flag, azimuth (3D coordinate), distance, intensity, and timestamp data. Each scan point has a data packet and all data packets can be saved in a binary file. Video data are commonly saved in different file coding formats. The file extensions show the format names such as .avi, .mov, .wmv, .mp4, etc. The video decoder or player can open and read (decode) the stored pixel data according to the coded format. The frame resolution, color bits, and number of frames per second should be specified for the AUT to open and decode image data correctly. Radar data elements are the distance, speed, and angle to the detected object, one data record can be saved in each scan cycle. The file format of radar data can be binary or others (e.g., .csv) depending the system design.

Data Injection The data injection process consists of sensor data transferring and processing. When an AUT's engine is turned on and the transmission gear stays in park position, it is ready to enter the test mode. The AUT switches to the test mode when it detects an ADS test data interface dongle is plugged into the USB or OBD II port. The AUT starts to verify the dongle's identity and after verifying as a valid and safe connected device, it has the authorization to access all sensor data files. The AUT can open data files in the dongle's folder, or copy them into its local storage. In general, the AUT can copy sensor data files into its local storage to avoid lagging of data transfers. The AUT reads sensor data into its memory for processing as if they are from the real installed sensors. The AUT can identify objects based on the provided radar, lidar and video data and make the decisions of vehicular maneuvers by sending out ECU control commands to the USB/OBD II port.

An AUT needs to synchronize sensors and GPS data with its current speeds and coordinates that is like synchronizing the front view video speed based on the driving speeds in a driving simulator. Corresponding sensor data are retrieved and processed based on the AUT's locations, the AUT calculates its current location based on heading, acceleration, deceleration and yaw rates. The ODD test data also contains the test route information including start and end coordinates of each link. Essentially, the AUT perceives the driving environment provided by the sensor data and maneuvers based on its own ADS capabilities.

Vehicle Control Data Transmission All AUT's maneuver data including speed, acceleration (engine's RPM and gear position), deceleration (braking), yaw rate (turning angle of steering wheel), and calculated coordinates can be sent to the test data interface dongle. The performance data evaluation subsystem can translate these maneuver data into trajectories of AUT. The ADS performance data evaluation subsystem can evaluate the AUT's performance based on the received trajectories.

ADS Performance Data Evaluation Subsystem

The ADS performance data evaluation subsystem is a backend software suite including AUT configuration management, sensor data management, ground truth data management, AUT maneuvering data processing, and

performance data evaluation as shown in Figure 6.

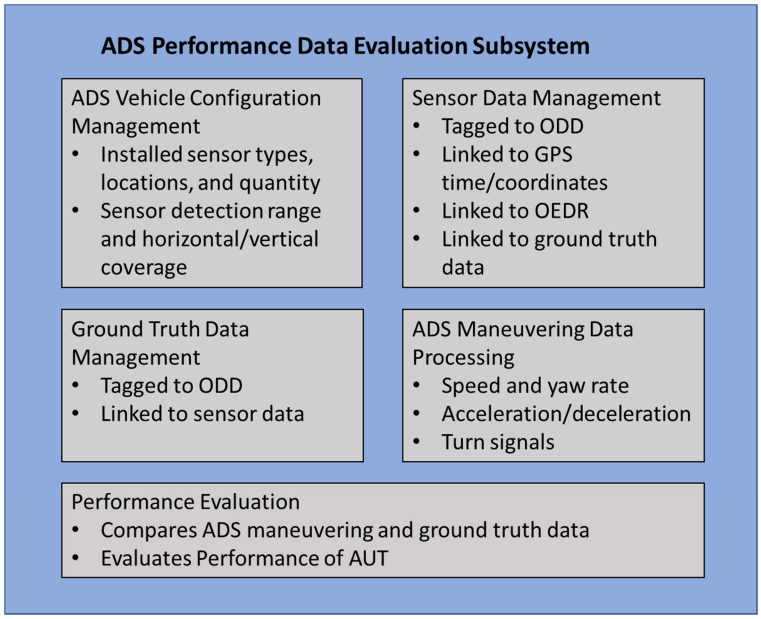

Figure 6 ADS Performance Data Evaluation Subsystem.

ADS Vehicle Configuration Management Each AUT may have different numbers and types of sensors installed on specific positions. The functionalities of ADS vehicle configuration management are to configure the parameters of each sensor installed on potential AUTs. A graphical interface would be convenient for users to configure each sensor. Operational parameters of lidar, radar, and camera can be selected or entered from the user interface. The data collection subsystem can provide the corresponding data of sensors based on the parameter selections.

Sensor Data Management Each record of sensor data needs to be tagged with GPS time and coordinates from the ground truth device. In addition, if the data is related to an OEDR event then they should also be linked with vehicular maneuver data. The temporal and spatial boundaries of an ODD or OEDR event can be identified manually by viewing the data collection videos. The start and end of each phase in an event or crash related to a specified ODD and OEDR need to be identified and saved in the database. When a user requests data of interest, the corresponding datasets can be selected from the database and sent to the ADS test data interface subsystem. Fault injections can also be implemented by selecting the desired test scenarios from the database.

Ground Truth Data Management The ground truth data device provides a higher granularity of GPS time and coordinates along with the vehicular maneuver data including speed, acceleration, deceleration, and yaw rates. As mentioned above, the sensor data at 10 Hz or 8 fps (8 Hz) can be tagged with the ground truth time and coordinates (at 100 Hz) in association with an ODD or OEDR. Essentially, this is a sampling process that selects the closest timestamp from the ground truth to link with the sensor data. A database tool can be utilized to develop this functionality.

Collected ODD data can be processed to extract information of interest automatically. For example, traffic signs, signals and other objects can be recognized from lidar and camera data [6] [11] using algorithms. Likewise, synthesizing radar and lidar data (data fusion) can be used to detect and classify vehicles and pedestrians in the proximity [4] of data collection vehicle. GPS and camera data can be used to locate in which lane the data collection vehicle is traveling [5] using map matching algorithms [1]. Automatic object recognition and classification can accelerate the process of ODD and OEDR identifications without excessive labor involvement; however, human verifications are still needed to ensure the correctness of identification. For improving the accuracy of weather data, weather station data along the data collection routes may be used to verify weather and visibility data.

ADS Maneuvering Data Processing AUT's maneuvering data are saved in the database for further processing. Acceleration, deceleration, heading, speeds, and yaw rates are received with timestamps from the test data dongle. The AUT's trajectories can be calculated based on the ground truth GPS coordinates and maneuvering data.

Performance Data Evaluation By means of integrating and matching the AUT's trajectories with the designated scenario/event's ground truth data, test results can be obtained by evaluating the risk of crash occurrence. If no crash was observed in the test results, then an evaluation metric is needed to distinguish levels of safety. A potential metric is time to collision [2]. A longer time to collision means a higher level of safety; on the contrary, a shorter time to collision represents a lower level of safety. The analysis of performance data considers the AUT's trajectories related to trajectories of potential colliding vehicles. Level of performance of an ODD scenario/event can be evaluated based on the timing and reaction of an AUT including the perception of objects (vehicles, pedestrians, signals, signs, etc.), detection of an event, and maneuvers of maintaining safety. Each ODD and scenario/event may present a different level of driving difficulty for various AUTs, as different AUTs may use differentiated sensor technologies and decision-making algorithms. An objective test system should be able to discern the performance among various AUTs based on the same test data set.

DEVELOPMENT OF POTENTIAL TEST PROCEDURES

Test procedures can be configured to test AUTs objectively and repeatedly when the ADS test system is established. A typical test procedure is developed in the following and similar test procedures can be developed in the same manner as well. The steps of the test procedure are listed in Table 1.

Table 1.
Steps of Test Procedures

Steps	**Actions**
Select and verify the AUT's sensors	Verify sensors' types, numbers, positions, and data generation frequencies. If no exact match can be found in the database, then the closest configuration can be selected and a new configuration can be established.
Select an ODD and/or an Event(s)	Select the desired ODD and/or event for testing the AUT. After completing the selection process, the user can download the sensor data to the test data interface subsystem.
Receive AUT's trajectory data	Verify test data interface subsystem has connected with the AUT, and the data download has completed. When the AUT starts to react to the test ODD and/or event, verify maneuver data are received by checking the status of communication lights on the dongle.
Compare AUT's trajectories to selected OEDR	Generate the AUT's trajectories and verify they cover all links in the test route. Any error occurs during the test may cause abnormal AUT trajectories or a missing AUT. Verify the AUT can avoid a crash or maneuver correctly to pass the test, or it may fail the test with a crash or incorrect maneuvers.
Evaluate data	The test team can also evaluate the data of each AUT and refer to the visual verifications to make the final decision based on testing results.

An example of test procedures is presented with a test scenario consisting of AUT, ODD, event, and OEDR as listed in Table 2. The test scenario is that the AUT approaches a crosswalk where a pedestrian is crossing the road at night with ambient lighting.

Table 2.
An Example of Test Procedures

Steps	**Actions**
Select and verify the AUT's sensors	Start the AUT and plug the test data interface dongle into a USB/OBD II port. Verify the sensors' specifications as: Lidar: 360° field of view, 0.09 angular resolution (azimuth), 26.8° up and 24.8° down vertical field of view with 64 equally spaced angular

	subdivisions, 10 Hz scan rate, and 120 m scan range. Installed on the center point of rooftop. Camera: Three 2-Megapixel (1600×1200) cameras with five positioned in a horizontal row and positioned on the front windshield facing forward at 0°, +45°, and -45°. The field of view of each camera is 50° for 50 m, and 8 fps in raw format (uncompressed). Radar: a mid-range radar is installed in the center of front bumper for detecting objects up to 160 m.
Select an ODD and an Event(s)	An ODD is selected as: urban signalized 4-way intersection, asphalt wet surface, 2 straight lanes with clear lane and crosswalk markings, 35 mph speed limit, light traffic, raining, street lights on, sun is down, low-beam headlights on. An event scenario is selected as: a pedestrian is crossing the intersection at 3 mph with dark clothes. The AUT is 30 m from the pedestrian when he/she is leaving the curbside. The AUT is approaching the intersection at 35mph and the traffic signal is green, the pedestrian is crossing on red pedestrian signal without noticing the AUT.
Receive AUT's trajectory data	Verify the test data interface dongle has been plugged into the AUT, and the data download has completed. When the AUT starts to react to the test ODD and event, verify the maneuver data are received by checking the status of communication lights on the dongle.
Compare AUT's trajectories to selected OEDR	Generate the AUT's trajectories and verify the test procedures are all completed correctly. Observe the AUT's speed while approaching the intersection and the visibility condition of the pedestrian before entering the crosswalk. Identify the time when the AUT starts to slow down and verify whether it stops to avoid hitting the pedestrian.
Evaluate Performance	Check the speed, heading and acceleration/deceleration data of the AUT, and verify the variation of time to collision for determining the level of safety.

CONCLUSIONS

A potential test system of ADS consisting of data collection, data interface, and data evaluation subsystems has been identified for testing AUTs objectively and repeatedly. The functionalities and interfaces of each subsystems are specified considering the current level of technological maturity and operational efficiency. The test system may implement various test procedures with differentiated AUTs, ODDs, events and OEDRs. An example of a typical test procedure is also elucidated for enhancing the applicability of the system by providing details of test steps and actions.

The potential test system of ADS can also generate training data sets to train ADS at the stage of system research and development. In addition, sensor failure tests [7] can be conducted and implemented by using this test system. It is expected that the test system can grow and become versatile by increasing the scenarios of ODDs, events, and OEDRs in the database. Moreover, the problems of edge cases that fall outside the boundary of ODD or sensor capabilities may be explored and tackled by utilizing this test system.

REFERENCES

[1] Atia M. M., Hilal A. R., Stellings C., Hartwell E., Toonstra J., Miners W. B., and Basir O. A. A Low-Cost Lane-Determination System Using GNSS/IMU Fusion and HMM-Based Multistage Map Matching. IEEE Transactions on Intelligent Transportation Systems. 2018; 19 (4): 1773 – 1795.

[2] Bila C., Sivrikaya F., Khan M. A., and Albayrak S. Vehicles of the Future: A Survey of Research on Safety Issues. IEEE Transactions on Intelligent Transportation Systems. 2017; 18 (5): 1046 – 1065.

[3] Broggi A., Buzzoni M., Debattisti S., Grisleri P., Laghi M. C., Medici P., and Versari P. Extensive Tests of Autonomous Driving Technologies. IEEE Transactions on Intelligent Transportation Systems. 2013; 14 (3): 1403 – 1415.

[4] Chavez-Garcia R. O. and Aycard O. Multiple Sensor Fusion and Classification for Moving Object Detection and Tracking. IEEE Transactions on Intelligent Transportation Systems. 2016; 17 (2): 525 – 534.

[5] Chen L-W, Shih H-W, Tsai M-F, and Deng D-J. Finding Lane Positions of Vehicles — Infrastructure-Less

Cooperative Lane Positioning Based on Vehicular Sensor Networks. IEEE Intelligent Transport Systems Magazine. 2015; 70 – 80.
[6] Gargoum S., El-Basyouny K., Sabbagh J. and Froese K. Automated Highway Sign Extraction Using Lidar Data. Transportation Research Record, 2017; 2643: 1–8.
[7] Koopman P. and Wagner M. Autonomous Vehicle Safety: An Interdisciplinary Challenge. IEEE Intelligent Transport Systems Magazine. 2017; 91 – 96.
[8] Li L., Huang W-L, Liu Y., Zheng N-N, and Wang F-Y. Intelligence Testing for Autonomous Vehicles: A New Approach. IEEE Transactions on Intelligent Vehicles. 2016; 1 (2): 158 – 166.
[9] Mukhtar A., Xia L., and Tang T. B. Vehicle Detection Techniques for Collision Avoidance Systems: A Review. IEEE Transactions on Intelligent Transportation Systems. 2015; 16 (5): 2318 – 2338.
[10] Pandey G., McBride J.R., and Rustice R.M. Ford Campus Vision and Lidar Data Set. International Journal of Robotics Research. 2011; 30 (13): 1543 – 1552.
[11] Rozsa Z. and Sziranyi T. Obstacle Prediction for Automated Guided Vehicles Based on Point Clouds Measured by a Tilted LIDAR Sensor. IEEE Transactions on Intelligent Transportation Systems. 2018; 19 (4): 1773 – 1795.
[12] Rubaiyat A.H.M., Qin Y., and Alemzadeh H. Experimental Resilience Assessment of An Open-Source Driving Agent. CoRR, abs/1807.06172, 2018.
[13] SAE International. Guidelines for safe on-road testing of SAE Level 3, 4, and 5 prototype Automated Driving Systems (ADS), SAE J3018; 2015.
[14] SAE International. Taxonomy and Definitions for Terms Related to Driving Automation Systems for On-road Motor Vehicles, SAE J3016; 2018.
[15] Sivaraman S., and Trivedi M. M. Looking at Vehicles on the Road: A Survey of Vision-Based Vehicle Detection, Tracking, and Behavior Analysis. IEEE Transactions on Intelligent Transportation Systems. 2013; 14 (4): 1773 – 1795.
[16] Thorn E. and Kimmel S. Testable Cases and Scenarios for Automated Driving Systems – Final Report. Washington, DC: National Highway Traffic Safety Administration, US Department of Transportation; 2018. DTNH22-14-D-000328L/003.
[17] USB 3.x data rates. Accessed on 6/19/2018. https://en.wikipedia.org/wiki/usb#usb_3.x.
[18] Velodyne Lidar Datasheet. Accessed on 6/15/2018. http://velodynelidar.com/lidar/products/brochure/hdl-64e%20s2%20datasheet.pdf

BENEFITS OF INTUITIVE AUDITORY CUES FOR BLIND SPOT IN SUPPORTING PERSONALIZATION

Toshihiro Hashimoto
Honda R&D Co. Ltd.
Japan

Alessia Knauss
Tobias Aderum
Ola Bostrom
Veoneer
Sweden

Tetsuya Matsushita
Autoliv
Japan

Da Wang
Autoliv
Sweden

Elaine KY Chung
Veoneer
Japan

Toshiya Hirose
Shibaura Institute of Technology
Japan

Paper Number 19-0006

ABSTRACT
Supporting drivers with auditory cues has been shown beneficial, but is also known to reach a certain level of annoyance. To fully understand the benefits of intuitive auditory cues as an HMI element, further research is needed.

This paper investigates the benefits of increasing input to aid in the reduction of hazard risks caused by blind spot using intuitive auditory cues. Intuitive auditory support is a naturalistic sound of an object using volume to indicate the distance of the side object (including blind spot area). The experiment involved twenty participants (2 women, 18 men) between 21 and 24 years of age. The experiment was conducted in a 360-degree view simulator with a car body on a turntable with a six-axis control. Using lane change scenarios, participant-perceived benefits of enhanced awareness of hazards, feelings of increased security, and annoyance caused by intuitive auditory support, were compared to a USNCAP target blind spot warning system (with buzzer), and unsupported as baseline systems. For this, subjective measures (i.e., survey analysis), as well as galvanic skin response data to measure participants' physiological responses, were used. The results indicate that intuitive auditory cues support enhanced hazard awareness, increase the participants feeling of security, and are perceived to be less annoying for rare drivers compared to blind spot warning, while for frequent drivers a blind sport warning seems to better support these variables.

Our results indicate that auditory support provides a suitable basis for supporting

those who drive only rarely in lane change maneuvers (supporting maneuverability, providing a feeling of security, and decreasing annoyance levels compared to BSW). Research thus far shows that auditory support could irritate drivers. However, our results do not confirm this. Intuitive auditory support appears less annoying than existing BSW technology. Furthermore, ASIS seems to decrease drivers' stress levels compared with no support.

We suggest that personalization could improve blind spot warning systems, by integrating auditory cues for drivers who drive rarely and keeping BSW technology for the remaining groups.

KEYWORDS
Auditory support; Personalization; Blind Spot Warning;

1. INTRODUCTION

Supporting drivers by means of auditory cues has been shown to provide numerous benefits. Human beings have the innate ability to respond quickly to hazards when exposed to a certain triggering sound. However, inappropriate sound levels may increase annoyance. The sound system design should therefore consider both the annoyance factor and effectiveness in conveying necessary information to the driver. Intuitive sound has been shown to facilitate a more rapid and accurate driver's response with greater user satisfaction [4]. However, whether it is helpful in complex driving tasks was not addressed. Previous research has tested an advisory 3D auditory cue (earcon) for blind spot information showing an effect on improving driver performance and situation awareness [9]. Although participants generally rated the system as useful, they did not find it satisfying. Therefore, it is necessary to further investigate the benefits of using auditory cues considering the HMI elements in supporting real driving contexts.

This paper investigates the benefits of intuitive auditory support for blind spot, targeting the research question:
Do intuitive auditory cues for blind spot increase the perception of improved driving?

We broke down our research question into three detailed questions focusing on enhanced hazard awareness, feelings of security, and annoyance levels:

- Is the use of intuitive auditory cues perceived as increasing awareness of hazards?
- Does the use of intuitive auditory cues support a greater feeling of security?
- Is the use of intuitive auditory cues perceived as annoying?

We investigated these research questions for the scenario of using intuitive auditory cues with naturalistic sounds of side objects (including the blind spot area), using volume change, increasing as the side object comes closer, arguing that for an auditory support to be intuitive, it must use volume to indicate extraneous vehicle movement. Intuitive auditory support is compared to blind spot warning (BSW) systems and no support.

Subjective ratings (e.g., user surveys) were documented to compare results. Furthermore, galvanic skin response (GSR) measures were used to investigate the physical response of participants during lane change activity.

The experiment involved 20 participants (2 women, 18 men) between 21 and 24 years of age. They had normal or corrected-to-normal eyesight, and had their driving licenses from less than one to over 3 years (i.e., one participant less than one year, ten from one to three years, and nine more than three years) and a mix of rare to frequent drivers (i.e., seven rare, seven occasional, six frequent drivers).

Our results indicate that

- ASIS supports an increase in enhanced awareness of hazards for rare drivers (ease of driving), while for frequent drivers it seems to be the case with BSW,
- ASIS increased a feeling of security for rare drivers, while frequent drivers showed a tendency towards an ease in driving using BSW,
- Rare drivers seemed less annoyed using ASIS than BSW, while frequent drivers think the opposite,
- In general, all groups felt ASIS was less annoying than BSW,
- All drivers had decreased GSR levels, which indicates less stress with ASIS.

From these results we conclude that ASIS seems to be generally less annoying for users than BSW while decreasing GSR values, indicating lower stress levels using ASIS compared to no support. Furthermore, when it comes to personalization, ASIS seems highly supportive to rare drivers in lane-changing activities, as our results suggest that this group feels a heightened awareness of hazards, a greater feeling of security, and less annoyance than using BSW support.

While we have not shown significant results for all these measures for the other two groups, it appears that frequent drivers show a tendency to prefer BSW. However, more research is needed to further investigate whether ASIS or BSW would be the system of choice.

2. EXPERIMENTAL DESIGN

2.1. Participants

The experiment involved 20 participants (18 men, 2 women), whose ages ranged from 21 to 24 and had normal or corrected-to-normal eyesight. Prior to the start of the experiment, all participants received an explanation of the contents and the risk of the experiment, their rights, and voluntarily signed a participation agreement. This study was approved by the Ethical Committee of Shibaura Institute of Technology and by the Honda Motor Co., Ltd., respectively.

Participants held a driver license from less than 1 year to over 3 years (i.e., one participant less than one year, ten from one to three years, and nine more than three years). Their driving frequency varied (from driving once yearly to daily).

The literature indicates that driving experience has an impact on driver perception and awareness. For example, experienced drivers are more skilled and have a shorter response time the detection of potential hazards [7, 2]. Gazing behavior studies also indicated a difference in visual search strategies and characteristics depending on driving experience [3]. In addition, the cognitive workload level was significantly different between experienced and inexperienced drivers in traffic conditions of varying complexities [6].

Hence, for the purpose of investigating our hypothesis, we have allotted participants to three groups, based on their driving experience. We define participants that drive as:

Rare (7 participants): Driving once a year to once a month.
Occasional (7 participants): Driving once a month to 4 times a week.
Frequent (6 participants): Driving equal to or more than 5 times a week.

2.2. Simulator Setup

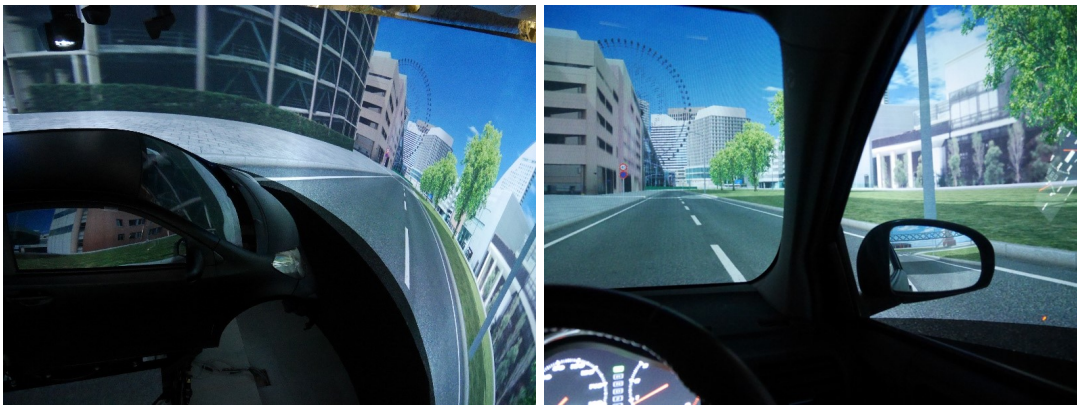

Figure 1. Simulator provides a seamless 360-degree view and a six-axis control turntable

The simulator of Shibaura Institute of Technology was used for this experiment. It contains an actual car body, has seamless 360-degree screen integration and a six-axis control with a turntable to simulate a natural driving experience. Participants drove in a simulator; the scenario was a sudden lane change. Participants drove on a two-lane street in a city zone (no motorway, no pedestrians or cyclists were involved). The side-objects involved in the scenario consisted of two-wheelers (motorcycles) and four-wheelers (passenger vehicles, some buses and trucks): the composed ratio was 2:8, respectively. Participants were instructed to adjust their speed to synchronize with the surrounding vehicles' speed. The speed of all surrounding vehicles was set at 40km/h to avoid unnecessary distraction from watching the speedometer to control speed accurately. Hence, both lanes had vehicles driving at the same speed. They were then instructed to stay in the same lane except when the occasion required a lane change. The lane change was initiated by having the vehicle in front of the ego vehicle decelerating/stopping. Examples of such occasions were vehicles that would decelerate at a bus stop behind a slowing bus, a vehicle turning to park by a shop or restaurant, a vehicle stopping to react to fallen objects, and so on.

Each participant performed 18 driving iterations in the simulator consisting of four lane changes. For the 18 iterations, the test conditions were altered both by support system (ASIS vs. BSW vs. NS) and environmental conditions. The environment was switched between suburban and city with different levels of congestion. In the city the time headway between vehicles in the same lane was 3.2 seconds, and for suburban it was 3.5 seconds. To achieve variation in the tests the operator changed the relative position of the vehicles in the two lanes. While each participant started the first test iteration with NS, other test conditions were randomized. For each of the three systems, six iterations were performed, three iterations for city and three iterations for suburban conditions. After participants completed the three test iterations for one specific system for one specific condition, they received the survey to complete.

Three lane changes did not have a system trigger and was therefore removed, so the analyzed data set consisted of 1337 lane changes.

2.3. Stimuli

Based on the above simulator setup and lane change scenario, three systems are compared, one baseline and two systems that inform the existence of an approaching vehicle in the blind spot area. A blind spot area is defined as the area the driver cannot confirm with mirrors (illustrated in Figure 2).

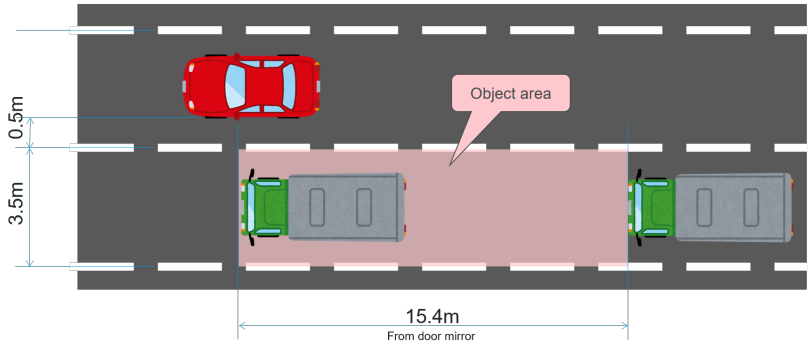

Figure 2. The blind spot area is 15.4m long. The ASIS area for side object identification has been extended to 37m to be able to use increasing volume as a way of creating an intuitive auditory support.

The systems used in this experiment are explained as follows:

ASIS (Intuitive Auditory Surround Information System): This is the main system of evaluation in this study. This information system has been designed for this study and has not yet been introduced to the market. ASIS uses auditory cues based on information from the blind spot area, extending the considered area to 37 m to integrate an intuitive auditory support system by increase their volume. Reflecting moving object signals (distance, velocity etc.) a sound relative to the ego vehicle was used. Natural sounds (i.e., vehicle and motorcycle motor sounds for the two types of objects (2- and 4-wheelers) were transferred to the driver through headphones when an object reached the blind spot. Thus, subjects could expect information of an approaching vehicle, approximate distance and speed by 3D sound control, which is not just on or off but also sounding more intuitive. The volume was changed based on the distance of the object to the ego vehicle (e.g., sound turns louder as the object comes closer to the ego vehicle) linearly reflecting its relative distance/speed. However, the relationship between sound volume and distance or speed could be affected by the subject's own experiences and interpretations.

BSW (Blind Spot Warning): This system is used in the evaluation and represents an existing system, well known to consumers. The driver receives support through a blind spot warning. In this experiment, we used a BSW vehicle algorithm (USNCAP target) and indication method illustrated in Figure 3.

The amber BSW symbol is illuminated when a moving object enters the designated blind spot area and switches off when the object moves out of the area. Even if some objects remain in the blind spot when a driver turns the steering wheel to initiate a lane change, a buzzer is provided and continues while the steering wheel is turned. The buzzer's sound is similar to a normal beep with intervals.

NS (No Support): This is used as a baseline in the experiment and represents current or older vehicles unequipped with systems to inform the driver of surrounding

Figure 3. BSW indication method used (USNCAP target).

situations, but where the driver needs to recognize and judge it through their own eyes and physical mirrors with no technical machinery support.

2.4. Measurements

To understand the benefits of intuitive auditory cues for blind spot to support personalization this experiment included questionnaires to collect participants' views and evaluations. Furthermore, this data was enriched by including physiological measures.

Subjective Measures: Subjective measures were collected four times from each participant throughout the experiment. After each test of a specific support system (i.e., BSW city, BSW suburban, ASIS city, ASIS suburban) was completed, participants were requested to respond to the following questions:

- Did you feel it was easier to drive with the support system?
- Did you feel an increased level of security using the support system?
- Did you find the support system annoying?
- Please add any other opinions about the support system.

For the rating, a five-level Likert scale was used, ranging from 1 (absolutely disagree), 2 (slightly disagree), 3 (neither agree nor disagree), 4 (slightly agree), to 5 (definitely agree).

Physiological Measures: To include physiological reactions from the drivers on each of the system supports used, Galvanic skin response data was collected using an electrodermal activity unit (AP-U030, Miyuki Giken Co.) with electrodes placed on the soles of the feet to measure skin sweat gland (e.g. eccrine gland) activity in microSiemens (μS). Skin glands are responsive primarily to emotional (e.g. stress and arousal) and psychological stimuli. GSR was used as an indicator of stress level during real world driving tasks [5, 8]. Data was then processed using Ledalab (version 3.4.9) to extract the phasic and tonic components of a discrete response triggered by lane change maneuvers. The sum of amplitudes of all significant reconvolved GSR functions within the onset time window were compared by using a two-way ANOVA analysis.

3. RESULTS

3.1. Ease of Driving

Figure 4 depicts the answers from the participants on the first question of easier driving from the questionnaires, representing subjective data. It can be observed that

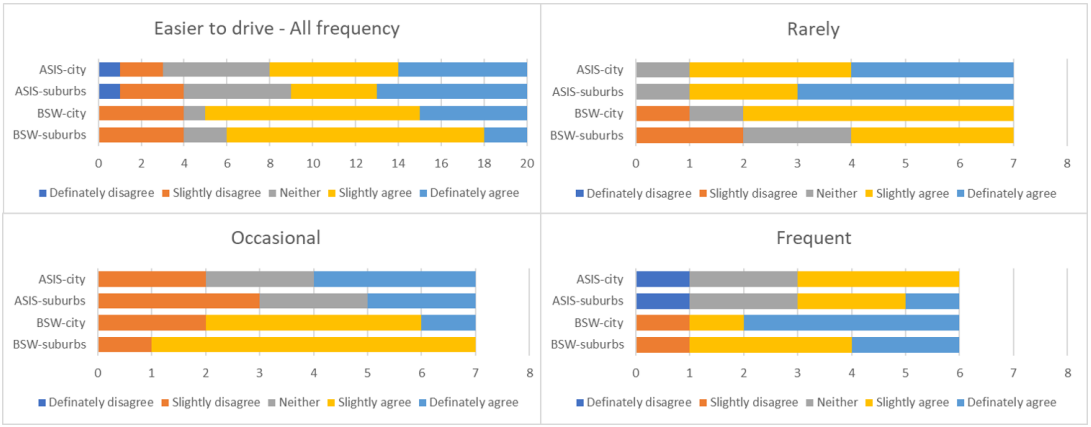

Figure 4. Overview of participant answers for easier to drive.

for both systems, BSW and ASIS, more participants agreed than disagreed that the system made driving easier. When analyzing driving frequency separately, it showed that drivers who rarely drive rank the ASIS system highest, with similar results for both environments, city and suburban roads. However, from the frequent driver group more participants agree (definitely) that BSW enables easier driving. The ratings for occasional drivers are spread between "slightly disagree" and "slightly agree" for BSW and between slightly disagree to definitely agree for ASIS.

Table 1 presents the overall descriptive statistics. The median was used as an indication of the general tendency of participant's feeling on the system. The results suggest that rare drivers felt an increase in ease of driving compared to the BSW group. On the other hand, frequent and occasional drivers felt an increase in ease of driving with BSW. A preliminary test on this data for statistical significance confirmed that for rare drivers ASIS is ranked significantly higher, while for the combined group of frequent and occasional drivers BSW ranked significantly higher than ASIS.

Table 1. Overview of median and standard deviation for ease of driving.

	BSW median	**ASIS median**	**BSW S.D.**	**ASIS S.D.**
Rare	4	4.5	0.842	0.745
Occasional	4	3	0.929	1.336
Frequent	4.5	3.5	1.115	1.215
All	4	4	0.992	1.207

3.2. Feeling of Security

The descriptive statistics for the feeling of security score are depicted in Table 2. The results indicate that for the rare driver group ASIS provided an increase of secure feeling (for details of secure feeling all responses from the participants are depicted in Figure 5). For frequent drivers, we see a tendency towards BSW for an increase of a secure feeling.

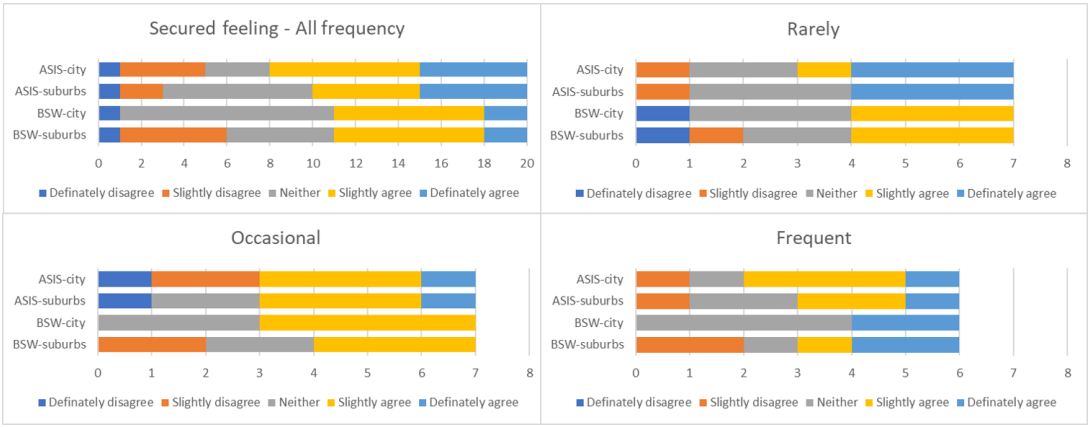

Figure 5. Overview of participant answers for a feeling of security.

Applying preliminary statistical testing, it seems that ASIS can contribute to a significantly increased secure feeling for the rare driving group as well as the combined group of rare and occasional drivers.

Table 2. Overview of median and standard deviation for secure feeling.

	BSW median	ASIS median	BSW S.D.	ASIS S.D.
Rare	3	4	0.726	0.699
Occasional	3	3	1.072	1.151
Frequent	3.5	3	1.155	1.348
All	3	4	0.997	1.176

3.2.1. Objective results measured by Galvanic Skin Response.

The electrodermal activity data was processed by standard deconvolution analysis (nonnegative deconvolution), resulting in full decomposition of tonic and phasic components of GSR [1]. The sum of amplitudes of all significant reconvolved GSR for corresponding phasic driver-peaks (μS), with onset in the response window of each lane change maneuver, was then calculated. Data was tested and proved to be significant for multivariate normality with Kolmogorov-Smirnov goodness of fit test.

The results of the two-way ANOVA tests on the effects of 'frequency' and 'system', and their interaction on GSR are depicted in Table 3. Both 'frequency' and 'system' have a significant effect on GSR (p-value $\leq$0.05). Fig. 6 shows the comparison of the marginal means of GSR sum of amplitudes (μS), indicating that the frequent group (left) and ASIS group (right) had less GSR response than the corresponding groups.

3.3. Annoyance

All answers from the participants on the measure of annoyance are depicted in Figure 7. The descriptive statistics are shown in Table 4. As the question for annoyance is phrased in a negative way (i.e., did you find the support system annoying?), the results

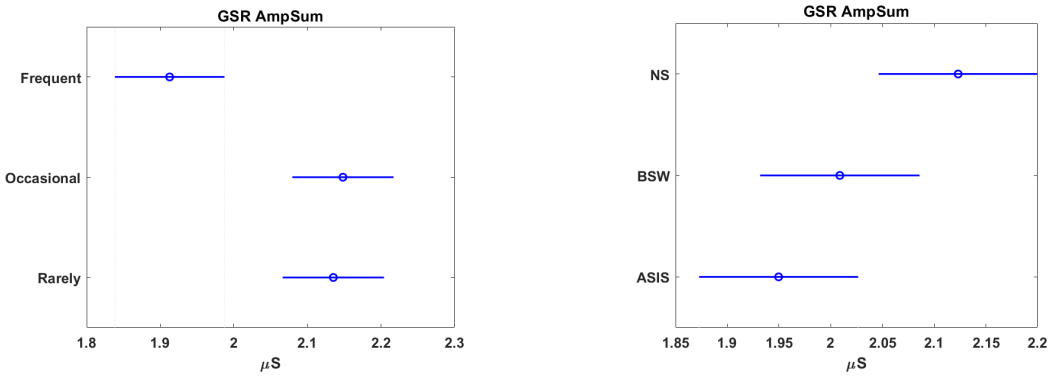

Figure 6. Multiple comparison of the mean of GSR AmpSum in microSiemens (μS) of groups: Frequency (left); System (right).

Table 3. 2-way ANOVA for the Sum of Amplitudes of Galvanic Skin Response.

	SS	DOF	MS	F	p_value
Frequency	15.85	2	7.9273	9.15	0.0001
System	7.72	2	3.8612	4.46	0.0118
Interaction (Frequency & System)	3.44	4	0.8607	0.99	0.4098
Error	1239.97	1428	0.8662		
Total	1264.14	1436			

need to be interpreted the other way around as the two measures above. Hence, a 2 is a supportive measure, while a 4 is a rather negative response (i.e., slightly agree that the support system was annoying).

The results indicate that ASIS was less annoying for rare drivers compared with BSW, while for frequent drivers there was indication that BSW was less annoying compared to ASIS. A first statistical analysis seems to confirm that the results for the group of rare drivers are statistically significant.

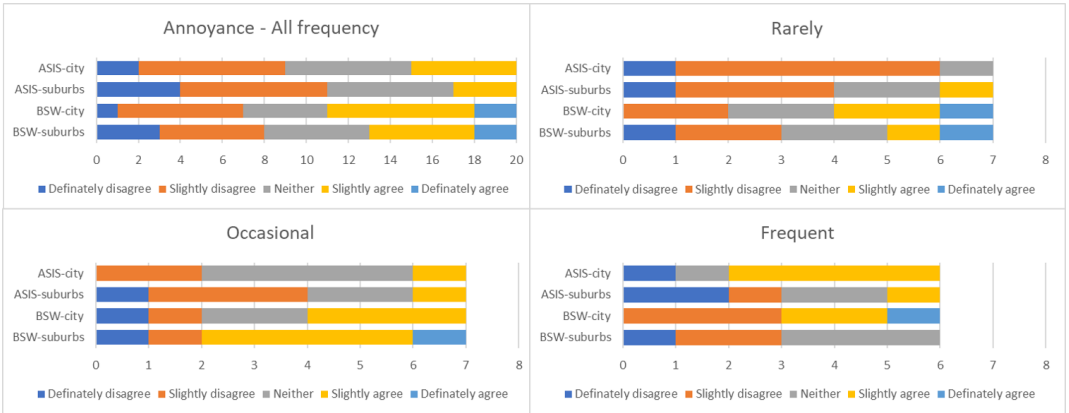

Figure 7. Overview of participant answers for annoyance.

Table 4. Overview of median and standard deviation for annoyance.

	BSW median	ASIS median	BSW S.D.	ASIS S.D.
Rare	3	2	0.877	0.616
Occasional	3	3	1.267	1.122
Frequent	2.5	3	1.422	1.030
All	3	2.5	1.187	0.986

4. DISCUSSION

We found that rare drivers feel it is easier to drive with ASIS support. We assume that rare drivers did not become accustomed to driving. Switching lanes is a difficult driving maneuver. Hence, ASIS seems to help drivers to perceive objects in the blind spot area by means of hearing naturalistic sound from the ASIS system. While ASIS uses a natural sound from the object, it also uses volume to indicate its distance. Furthermore, the distance at which support is activated is extended with ASIS, compared to BSW (37m instead of 15.4m). Hence, ASIS is not only providing support in the blind spot area, but also in an extended area. Extending this area and providing information about side objects earlier than BSW might have been the cause of such positive results for rare drivers. Occasional drivers, and frequent drivers in particular, might not need this extra time to get a full overview of the surroundings for changing lanes.

To support our assumption, participant' free comments corroborate them. For example, a rare driver (participant 9) commented, "It is easy to estimate the distance to the car behind in the next lane with ASIS than with BSW. I can concentrate on driving by looking ahead." Another rare driver (participant 13) commented: "The sound made driving easier. Because of the sound, the position of the car was estimated by hearing it."

For the rare drivers group, we found an increase in the feeling of security. ASIS does not only provide information on the existence of obstacles in the blind spot, but also relates the object's position and speed through an increase in volume, while BSW only indicates the existence of obstacles by lighting. These modality and informational differences might affect drivers' sense of security. Using ASIS, participants could constantly perceive blind spot information by hearing if an object was approaching. On the other hand, participants must "intentionally" check if the blind spot is safe or not. These differences might be due to the fact that rare drivers lack the resources to intentionally check the blind spots visually, while feeling more secure by passively receiving audio signals.

Our assumptions were corroborated by participants' free comments. For example, a rare driver (participant 12) commented that: "I felt that hearing was more appealing to the senses than seeing. I felt the sound indicator made driving easier", and another rare driver (participant 17) commented that, "It was good to know that the car was coming faster so that I knew I had to accelerate [to keep safer distance]."

The GSR level is lower for frequent drivers, which could explain our results. Because of this, they seem to have a better grasp of the surrounding and hence, probably need no additional support during lane change. For the rare and occasional drivers, the GSR level is significantly higher, which might explain why they felt better supported

(have an increased feeling of security) through ASIS, and rare drivers felt it is easier to drive.

5. CONCLUSION

This study investigated the benefits of intuitive auditory support on the awareness of hazards, a feeling of security, and its impact on feeling annoyed compared to blind spot warning and no support for blind spot. Our results indicate that, especially for rare drivers, intuitive auditory support is the system of choice and should be considered for personalization. ASIS supports an enhanced awareness of hazards so that participants feel it is easier to drive, increases the feeling of security, and seemed to be less annoying for rare drivers compared to BSW. Research so far shows that auditory support has the risk of being annoying. However, our results do not confirm this assumption. Our results indicate that ASIS is less annoying and reduces the GSR level for all drivers.

We found indications that frequent drivers prefer BSW to ASIS. However, more research is needed to fully understand the effect ASIS has on occasional and frequent drivers, as our results have shown no statistical significance compared to BSW.

Acknowledgements

We wish to thank Tomiji Sugimoto for discussions on this topic. Christian Svensson, Arun Muthumani, and Nils Lubbe for their feedback on the study. Furthermore, we thank the members of Shibaura University for running our simulator study, especially Yasunori Tanikawa for preparing the scenario, programming, and the simulator operations.

References

[1] Benedek, M. and Kaernbach, C. (2010). Decomposition of skin conductance data by means of nonnegative deconvolution. *Psychophysiology*, 47(4):647–58.

[2] Borowsky, A. and Oron-Gilad, T. (2013). Exploring the effects of driving experience on hazard awareness and risk perception via real-time hazard identification, hazard classification, and rating tasks. *Accident Analysis and Prevention*, 59:548–565.

[3] Crundall, D., Underwood, G., and Chapman, P. (1999). Driving Experience and the Functional Field of View. *Perception*, 28(9):1075–1087.

[4] Fagerlnn, J. and Alm, H. (2010). Auditory signs to support traffic awareness. *IET Intelligent Transport Systems*, 4(4):262–269.

[5] Healey, J. and Picard, R. (2005). Detecting Stress During Real-World Driving Tasks Using Physiological Sensors. *IEEE Transactions on Intelligent Transportation Systems*, 6(2):156–166.

[6] Patten, C. J., Kircher, A., stlund, J., Nilsson, L., and Svenson, O. (2006). Driver experience and cognitive workload in different traffic environments. *Accident Analysis and Prevention*, 38(5):887–894.

[7] Scialfa, C. T., Borkenhagen, D., Lyon, J., Deschnes, M., Horswill, M., and Wetton, M. (2012). The effects of driving experience on responses to a static hazard perception test. *Accident Analysis and Prevention*, 45:547–553.

[8] Singh, R. R., Conjeti, S., and Banerjee, R. (2012). Bio-signal based On-road Stress

Monitoring for Automotive Drivers. In *Proceedings of the National Conference on Communications*, pages 1–5, Kharagpur, India. IEEE.

[9] Wang, M., Lyckvi, S. L., Chen, C., Dahlstedt, P., and Chen, F. (2017). Using Advisory 3D Sound Cues to Improve Drivers' Performance and Situation Awareness. In *Proceedings of the CHI Conference on Human Factors in Computing Systems*, pages 2814–2825, Denver, Colorado, USA. ACM Press.

DEVELOPMENT OF PROPOSED DYNAMIC CRASH TESTS AND PERFORMANCE CRITERIA FOR THE AUSTRALIAN CONCESSION GO-KARTS STANDARD

Raphael Grzebieta,
George Rechnitzer,
Keith Simmons,
David Hicks,
Transport and Road Safety (TARS) Research Centre, University of New South Wales (UNSW), Sydney Australia

Ross Dal Nevo,
Drew Sherry,
Roads and Maritime Service, Crashlab, NSW,
Australia

Paper Number 17-0157

ABSTRACT

Go-karting is a popular recreational motor sport in Australia and many other countries. Go-karts are small, motorised vehicles that are capable of relatively high speeds. Because of their small size, go-karts present unique crashworthiness challenges to their designers (not unlike micro automobiles and quadricycles). The small distances involved result in limited opportunity for ride-down decelerations of crash forces in frontal and other crash involvements. The international commercial and racing go-karting industry continues to recommend the rider be unbelted, so they can eject from the go-kart during a crash. Hence, the European Commission's EN 16230 standard specifying go-kart into go-kart crashworthiness tests only requires an effective velocity change (delta V) of 7 km/h claiming higher test speeds are impractical.

This study demonstrates that a crashworthy go-kart for higher impact speeds with the rider restrained with a 3-point belt is possible. A practical dynamic crashworthiness performance functional test for commercial hire go-karts and associated track barrier and other infrastructure systems was developed. The results of this research are being considered as a crashworthiness test requirement in a revision of the Australian Standard for concession go-karting and associated track infrastructure safety.

The crash test described in this paper were developed based on results from reconstructions of two fatal go-kart crashes reported elsewhere. For each fatality, a MADYMO model was developed to represent the driver, go-kart and barrier system. Alternative barrier designs and seat belt configurations were then modelled. Based on results of those fatal crash reconstructions and modelling of different barrier and restraint scenarios, it was demonstrated that requiring riders to wear seat belts and carrying out crash tests at higher speeds was practical and would improve go-kart crashworthiness. Subsequently, a series of crash tests were devised in conjunction with industry representatives, that would be demonstrative of typical crash scenarios in a concession based go-kart environment. Go-kart into go-kart impacts were conducted in frontal and nose-tail at 50 km/h based on European test configurations at the New South Wales state government Crashlab facility near Sydney in Australia. Tests were also conducted on a range of barrier designs. Two impact configurations were tested: one at 25 km/h at a 90 degree impact angle and one at 50 km/h at 25 degree impact angle.

The results of modelling of fatal crashes as well as crash testing into different barrier configurations and vehicle to vehicle testing has proven high energy crashes (crashes at the track design top speed) involving go-karts on concession tracks can be made survivable with the use of appropriate restraint systems in the vehicle and effective barriers designed for likely impacts. The study outcomes have revealed that the European Commission (2016) EN 16230 standard frontal impact test should be set at a much higher impact speed, encouraging improvements to be made to occupant protection and crash barriers systems for go-karts used in that jurisdiction.

INTRODUCTION

Go-karting is a popular recreational motor sport in Australia and many other countries (Commission Internationale de Karting, 2017). Go-karts are small, motorised vehicles that are capable of relatively high speeds. Because of their small size, go-karts present unique crashworthiness challenges to their designers (not unlike micro automobiles and quadricycles). The small distances involved result in limited opportunity for ride-down decelerations of crash forces in frontal and other

crash involvements such as into barriers or infrastructure hard points.
Investigation of Australian fatality and injury data between 2000 – 2007 (Grzebieta, Mitchell and Zou, 2014) identified there had been around 10 go-kart related deaths in Australia in that period, or more than one per year. Half of these (5) occurred at commercial race tracks and four at off-site locations. One death was subject to a Coroner's Inquest at the time (Grzebieta et al, 2014). Grzebieta et al (2014) also found there were around 37 hospital admissions across Australia each year for the period 2002/03 to 2009/10. A US study (Collins et al, 2007) showed go-kart injuries constituted approximately 13.7% of around 1.2 million non-automobile motorised vehicle related injuries that presented at emergency departments (ED) between 1990 – 2003.

The international commercial and racing go-karting industry continues to recommend the rider be unbelted, so they can eject from the go-kart during a crash. Hence, the European Commission (2016) EN 16230 standard that specifies go-kart into go-kart crashworthiness tests only requires an effective velocity change (delta V or ΔV) of 7 km/h claiming higher test speeds are impractical. The standard does not specify any tests into barriers that redirect the go-kart.

This position, recommending the rider be unbelted, is contrary to the principles of vehicle occupant protection first espoused in the widely acclaimed work *Accident Survival – Airplane and Passenger Automobiles* by De Haven in 1952. De Haven related occupant protection in vehicles to the packaging principles used in the transport industry. In simple terms, De Haven's four principles are:

(a) The vehicle occupant compartment should contain its occupants (no ejection) and should not collapse under reasonable or expected conditions of force.

(b) The materials that surround and shield the occupant compartment should be capable of resisting crash forces by yielding and absorbing energy.

(c) Vehicle occupants should be restrained within the occupant compartment to prevent the second collision (injurious impact with the interior of the occupant compartment).

(d) Padding must be provided for parts of the occupant compartment that the occupant might strike.

De Haven's principles remain as directly relevant to vehicle safety today as they were in 1952 and apply equally to go-karts as for any other vehicle types.
The objectives of this study were to demonstrate that a crashworthy go-kart rated at a higher delta V impact speed with the rider restrained with a 3-point belt is possible, and to develop practical functional dynamic crashworthiness performance tests for commercial hire go-karts and associated track barriers and other infrastructure systems trackside.

The results of this research are being considered in the current revision of the Australian Standard AS 3533.4.4-2011 (Standards Australia, 2011) as a possible crashworthiness performance requirement for go-karts and track barrier safety.

METHODS AND DATA SOURCES

Two fatal go-kart crashes were reconstructed by Grzebieta et al. (2013, 2014). The first involved a crash that occurred at an organised street racing event called the Wollongong City Kart Prix in Australia (Grzebieta et al., 2013). The go-kart track was lined with empty plastic barriers that would otherwise be filled with water for ballast in order to redirect an errant vehicle in traffic conditions at roadworks. After crossing the finish line, the go-kart impacted the barriers at a speed estimated to be in excess of 100 km/h. The driver was flung from the kart head first into the barrier and received fatal spinal and other injuries. The fatality was reconstructed using computer simulation. A MADYMO model was developed to represent the driver, go-kart and barrier system. A second model was constructed where the driver was properly restrained and the barrier was redesigned to have a smooth interface and heavier than the empty KI 1000 barriers. The smooth barrier was capable of safely redirecting the go-kart such that it travelled parallel to the barrier after impact and the seat belts restrained the rider from being thrown forward. The rider would have likely survived the crash.

A reconstruction of a second fatal crash involving a helmeted and four-point harness seat belted small female rider who suffered a basilar skull fracture was also undertaken (Grzebieta, et al., 2014). The fatal crash occurred at a speed of 25 km/h and an impact angle of 90 degrees into the concrete barrier of a hire go-kart track that was lined with a single row of unconnected car tyres. The reconstruction again included use of MADYMO computer simulation models to determine how a four-point harnessed occupant could receive the fatal injury.

Investigation of the effectiveness of a single tyre against a concrete wall barrier for crash energy absorption was undertaken. A Baldwin universal compression-testing machine was used to determine the load deformation characteristics of the tyre compressed across its diameter. This load deformation curve produced was then used to simulate the interaction between the go-kart and the barrier.

Two different barrier scenarios were then modelled. The first scenario employed tyres joined together laterally and placed 0.5 metres in front of the concrete wall. The second scenario employed two tyres placed in series in front of the wall. A fourth scenario was modelled, adding a crotch strap fifth point of attachment to the safety harness to stop harness "ride up".

Based on results of the crash reconstructions and modelling of different scenarios, a series of crash tests were developed, in conjunction with industry partner committee members helping revise the Australian Standard AS 3533.4.4-2011 for go-karts and associated track infrastructure safety. Both go-kart into go-kart tests and go-kart into barrier tests were devised that would be representative of typical higher energy crash scenarios and test configurations that the EN 16230 standard requires in a concession based go-kart environment. The objective of the tests was a proof of concept that crash tests could be carried out, that practical results could be obtained and that the crashworthiness of go-karts and barriers could be improved at these higher ΔV values. These dynamic tests were undertaken at the New South Wales (NSW) State Government Roads and Maritime Services Agency's Crashlab test facility.

A survey of Australian kart operators identified a common maximum speed for indoor karts at 45 km/h and outdoor karts at 70 km/h. Hence, a design speed for concession tracks was chosen as 50 km/h. The striking (bullet) go-kart travelling at 50 km/h impacting the stationary target go-kart of the same model and mass, results in a ΔV = 25 km/h. For barrier impacts, angled impacts (25 degrees) were conducted at 50 km/h. This is equivalent to a striking impact velocity of 21 km/h perpendicular into the barrier. For this reason, the impact speed for perpendicular impacts (90 degrees) was set at 25 km/h.

The test vehicle used for all crash tests was a RiMO EVO6 go-kart supplied by RiMO Australia being representative of the current generation of go-kart fleets in Australia. Kingston Park Raceway supplied all the barriers.

The Crashlab tow system was used to propel the striking go-kart up to the either required impact test speeds of 25 km/r and 50 km/h. The tow cable was released just prior to impact. Instruments to measure three axis of linear and rotational acceleration were fitted at the go-kart's centre of gravity. A data acquisition system, emergency remote control braking system and a power supply (battery) were also fitted to the kart. To maintain the original in-service vehicle mass and weight distribution it was necessary to remove the engine in the strike vehicle to accommodate the Crashlab test equipment. The impacted (target) go-kart was the same go-kart with no alterations and same mass.

All vehicles used in testing had a 50th percentile Hybrid III Anthropomorphic Test Device (ATD) with a nominal mass of 78kg fitted. The 50th percentile Hybrid III represents the average sized adult male and is the most widely used and commonly available crash test dummy in the Hybrid III ATD family. The advantage of using the Hybrid III 50th ATD in providing the required occupant ballast is that it also simulates the occupant's likely kinematic response (dynamic movement) in a real world crash during impact.

The first set of tests carried out were the go-kart into go-kart tests. Test 1 is a head on collision set up as shown in Figure 1 based on the European test configuration (European Commission, 2016). The striking go-kart travels at 50 km/h and impacts the stationary go-kart nose to nose such that the two longitudinal axes of the go-karts are aligned. Because the two go-karts have the same mass the change in velocity experienced by the ATD in either go-kart will be half the striking go-kart's speed, i.e. ΔV = 25 km/h.

A second go-kart into go-kart test was also carried out albeit the configuration was such that the striking go-kart hits the rear of the stationary go-kart that was again the same make and mass as the striking go-kart as shown in Figure 2. Again, the test configuration was based on the European test (European Commission, 2016) the change in velocity both ATDs experienced was 25 km/h.

As mentioned earlier, tests were also conducted on a range of barrier design options at 25 km/h at 90 degree impact angle and 50 km/h at 25 degree impact angle. The test matrix for the barrier test sequence is shown at Table 2.

A video recording at 500 frames per second 50 ms just prior to impact and until the end of the crash event was taken. An overhead and side view that clearly showed the striking vehicle and object struck through the whole crash event and until the

striking vehicle and objects struck (either go-kart or barrier) came to rest, was recorded.

Photographs of the test configurations that include images of the respective vehicles and barriers from overhead, side, forward and rear views before and after testing were also recorded and documented.

The deceleration in the longitudinal and lateral directions within the go-kart's horizontal plane was measured and recorded. The accelerometers were attached to an appropriate fixture that was located on the go-kart's longitudinal centreline as close as practicable to the go-kart's centre of gravity in the test configuration, i.e. vehicle combined with instrumentation and ATD. The accelerometers mounting fixture are directly fixed to the go-kart's main chassis frame in such a manner so as to ensure that any decelerations measured were of the frame and not of any other part that moves relative to the frame during the crash test.

For each crash test configuration specified, deceleration of the striking go-kart and acceleration of the struck go-kart was sampled at a frequency of 10 kHz and processed using a CFC180 filter. The velocity of the go-kart was also recorded just before impact.

EVALUATION CRITERIA

The evaluation of the go-kart into go-kart tests and each barrier's crash test performance included observations and assessment of the risk to the go-kart rider, and in the case of the barrier tests the barrier's structural adequacy, and the trajectory of the vehicle. The criteria commonly used to assess road safety barriers in the United States (US) Recommended Procedures for the Safety Performance Evaluation of Highway Features (Ross et al., 1993) based on the Flail Space model (Tan et al., 2017) was adapted to both the go-kart into go-kart tests and the go-kart into barrier tests. This is described in more detail as:

Structural Adequacy
Detached elements, fragments or other debris during impact from either the go-kart or the safety barrier should not present an undue hazard to the driver, to other go-kart drivers or track personnel operating the facility.

Occupant Risk.
The two measures of occupant injury based on acceptable Occupant Impact Velocity and Ride-down Acceleration as shown in Table 2 and Table 3 respectively.

Table 1.
Occupant Impact Velocity for barrier testing

Occupant Impact Velocity	Preferred (m/sec)	Max. (m/sec)
Longitudinal (V_x)	9	12
Lateral (V_y)	+/-9	+/-12

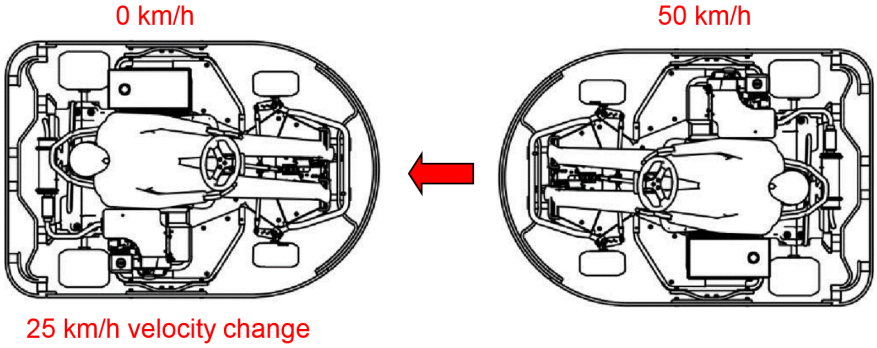

Figure 1. Test 1: Head-on impact conducted at 50 km/h into a stationary target vehicle

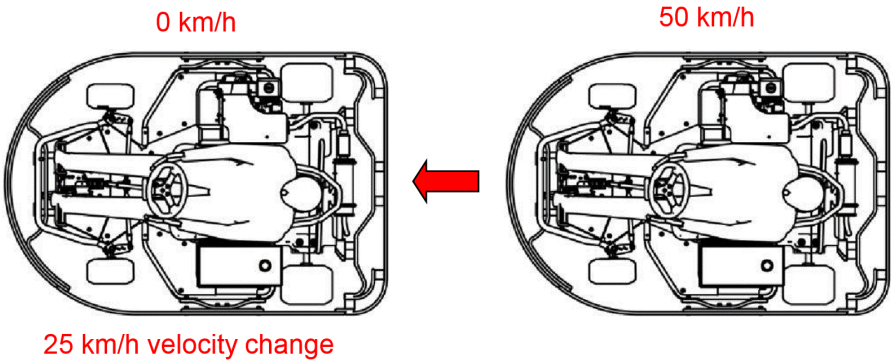

Figure 2. Test 2: Rear impact Rear impact test conducted at 50 km/h into stationary target vehicle

Table 2.
Barrier Test Matrix

Run #	Vel Km/h	Impact Angle (0°)	Barrier Configuration	Description
B14012	25	90	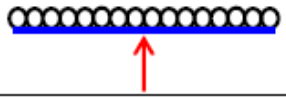	Tyre wall 16 tyres long, 2 tyres high, bolted together, with a conveyor belt bolted on front face.
B14013	25	90	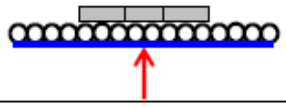	Same as test B14012, with bolted tyre wall (16 x 2) with conveyor belt front, back against concrete jersey barriers.
B14014	25	90	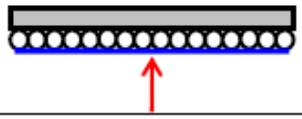	Repeat of B14013, with bolted tyre wall (16 x 2) with conveyor belt front, back against a rigid concrete wall.
B14015	25	90	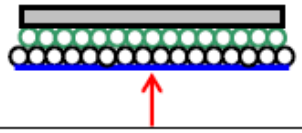	Tyre wall 16 tyres long, 2 tyres high, with convey belt front separated from rigid concrete wall by row of double height loose tyres.
B14016	25	90	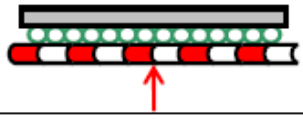	Plastic barrier, 10 segments long connected together with 35 kg of water ballast in each. Separated from rigid concrete wall by row of double height loose tyres.
B14017	25	90	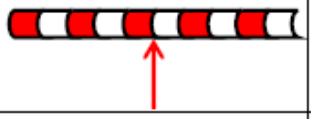	Plastic barrier wall, 10 segments long connected together with 35 kg of water ballast in each. Perpendicular impact at connection of barriers in centre of wall.
B14018	50	25	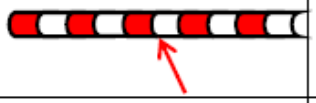	Plastic barriers, 10 segments long connected with 35 kg of water ballast in each. Angled impact on barrier connection at centre of wall.
B14019	50	25		Tyre wall 16 tyres long, 2 tyres high, bolted together with a conveyor belt on front face. Angled impact at centre of wall between junction of tyres.
B14020	50	25	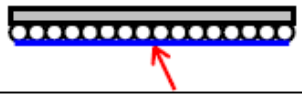	Same as B14020, with tyre barrier against concrete wall.
B14021	50	25	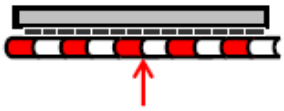	Plastic Barriers, as per B14017, with barrier separated from concrete wall by single row of loose standing tyres.
B14022	50	25	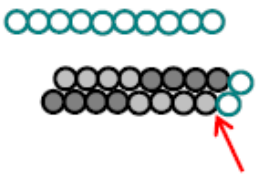	Bolted tyre segments, 4 tyres long and 2 tyres high. Double depth wall formed by overlapping 4 segments (not connected). Row of loose single tyres placed 2M behind and parallel to barrier. Angled impact at leading edge of non-connected segments.

.

Table 3:
Acceptable Occupant Ride-down Accelerations for barrier testing

Ride-down Acceleration	Preferred (g's)	Max. (g's)

Longitudinal (G_x)	-15	-20
Lateral (G_y)	+/-15	+/-20

The Occupant Impact Velocity is the velocity at which a hypothetical, unrestrained occupant would impact a hypothetical vehicle interior surface. Ride-down acceleration is determined as the 10 millisecond average deceleration a hypothetical, unrestrained occupant would experience when impacting a hypothetical vehicle interior surface, i.e. flailing and striking the steering wheel in the case of a go-kart.

Go-kart Into Go-Kart Performance Criteria
For the go-kart into go-kart crash tests the following criteria were established:

- In accordance with Table 2, the driver impact velocity must be less than 12 m/s (43 km/h) but preferably 9 m/s (32 km/h) or less;
- In accordance with Table 2, the average ride down deceleration must be less than 20 g's but preferably 15 g's or less;
- Driver's head in both the striking and the struck go-kart should not contact the steering wheel.
- The go-kart should remain upright during and after collision although moderate roll, pitching and yawing are acceptable;
- The go-kart should not penetrate into, under-ride, or over-ride the struck go-kart such that it presents a hazard to the rider of the striking vehicle or the struck vehicle;
- Controlled deformation of either go-kart's bumper system is acceptable so long as any deformation or fracture does not present a hazard to either driver or track personnel operating the facility;
- Detached elements, fragments or other debris during impact from either go-kart should not present an undue hazard to either driver or track personnel operating the facility;

Go-kart Into Barrier Performance Criteria

For the go-kart into barrier crash tests the following criteria were established:

- In accordance with Table 2, the driver impact velocity must be less than 12 m/s (43 km/h) but preferably 9 m/s (32 km/h) or less;
- In accordance with Table 2, the average ride down deceleration must be less than 20 g's but preferably 15 g's or less;
- The striking go-kart's exit angle from the safety barrier preferably should be less than 15 degrees, measured at time of the go-kart's loss of contact with the safety barrier;
- The go-kart should not penetrate through, under-ride, or override the safety barrier although controlled lateral deflection (working width) of the safety barrier is acceptable.
- The go-kart preferably should not snag or be pocketed in the case of an angled 25 degree impact by the barrier during impact;
- The go-kart should remain upright during and after collision although moderate roll, pitching and yawing are acceptable;

RESULTS
The head on impact (B14007) and the rear impact (B14008) test results are respectively shown in Appendix A. For both head-on and rear impact tests the Occupant Impact Velocity and the Ride-down Acceleration were within limits of the injury criteria based on the flail space model. However, for the head-on impact in both the striking (bullet) go-kart and struck (target) go-kart the helmet on the ATD contacted the steering wheel. On closer observation of the high speed videos, it was clear that excessive real out of the sash part of the belt in combined with the deflection of the go-kart's roll bar to which the sash guide was attached, led to the helmet contacting the steering wheel. It was proposed that stiffening the roll bar and using webbing clamps to reduce belt real out would help prevent this contact.

The test results B14012 to B14022 for the go-kart into barrier crash tests are also respectively shown in Appendix A. For all barrier tests, the Occupant Impact Velocity and the Ride-down Acceleration were also within limits of the injury criteria based on the flail space model. However, in tests B14013, B14014, B14015, B14016, B14019 and B14020 the ATD's helmet made contact with the steering wheel. There was no damage to the vehicle or barrier in tests B14012, B14013, B14014, B14015, B14016, and B14017.

However, of particular concern with the go-kart into barrier tests was test B14019. The go-kart was not redirected by the barrier but instead continued forward and under-rode the barrier. This resulted in the barrier impacting the ATD in the chest and head. The steering wheel was bent backwards by

the force. This impact would have been particularly hazardous for a rider.

A similar under-ride situation was observed is Test B14020. The go-kart commenced to under-run the barrier on impact without any redirection until it pocketed and then began to rotate in a clockwise direction. The steering wheel was forced to turn hard right and was struck by the Hybrid III's helmeted head.

DISCUSSION AND LIMITATIONS

The results of modelling of fatal crashes as well as crash testing go-kart into go-kart impacts and go-kart into different barrier configurations has proven higher energy crashes than those adopted in the EN 16230 standard (European Commission, 2016) involving go-karts on concession tracks are practical and offer increased crashworthiness with the use of appropriate restraint systems in the vehicle and effective barriers designed for likely impacts. Had the go-karts and barriers undergone such testing in the case of the two fatalities investigated by Grzebieta et al. (2013, 2014) both deceased riders would have survived the crash, highly likely without serious injury.

Ride down accelerations have been demonstrated to be able to be kept below injurious levels (less than 9 m/s) and occupant injury values less than 15 g through use of a 3 point seat belt and appropriate barrier design.

Go-kart Into Go-kart Tests.

The results of the go-kart into go-kart impact crash testing showed Occupant Impact Velocity and Ride-down Accelerations were within tolerable limits, but head strike against an unpadded steel steering wheel remained problematic. Use of a helmet complying with Australian and New Zealand Standard 1698: *Protective Helmets for Vehicle Users*, as well as using a deformable steering wheel rim and padded steering hub can assist with mitigating this injury risk. However, use of a 3 point belt with a webbing clamp and a stiffened roll bar where the sash is either anchored or guided, would sufficiently restrain the rider's torso so that head strike does not occur. Alternatively, improved seat belt configuration (correctly adjusted 5 point restraint with a crotch strap) was shown by modelling to minimise the risk of head strike in crashes (Grzebieta et al., 2014).

Go-kart into Barrier Tests:

The results of go-kart into barrier crash testing showed Occupant Impact Velocity and Ride-down Accelerations were also within tolerable limits, but head strike against an unpadded steering wheel was also problematic in a number of those impacts. In two cases the go-kart under-rode the barrier.
Key issues detected among the go-kart into various barrier tests conducted were:

- Two storey tyre configurations tended to allow under-ride of the barrier, even with a conveyor belt front piece fitted. Continuous smooth facia plastic barriers should be used to control and redirect an errant go-kart;

- Sufficient dynamic working width distance (movement during impact) behind the barrier is required to allow the barriers to effectively absorb crash energy through control movement without under-ride; and

- Tyre barriers fitted against a solid concrete wall resulted in head strike against the steering wheel. The implication here is where available track design space does not permit a large dynamic working width distance for the barrier to operate, then go-karts fitted with 3 point restraint systems need to have webbing clamps with a properly stiffened roll bar through which the sash part of the belt is fed. Alternative, a 5 point seat belt harness can be fitted but these belts must be correctly adjusted to a snug fit to minimise occupant movement relative to the vehicle.

General Comments

The study outcomes have revealed that the EN 16230 standard frontal and rear impact test (European Commission, 2016) should be set at a much higher delta V, encouraging improvements to be made to occupant protection systems for go-karts used in that jurisdiction. The EN 16230 standard should also include go-kart into barrier crash tests.

The results of this research are being considered for possible inclusion into the revised Australian Standard for go-kart and associated track infrastructure safety (Australian Standard 3533.4.4 *Amusement Rides and Devices - Go Karts*).

The data and results contained in this paper relate only to the specific vehicle and safety barriers tested. The vehicle tested was a used vehicle supplied as being suitable for the purpose of conducting go-kart barrier tests. The method by which safety barriers and components are assembled and the conditions under which they are installed may vary the performance results.

CONCLUSIONS

Simulations and crash tests revealed that it is possible to reduce injury risk for much higher

impact speeds involving go-karts than is currently considered appropriate by the international commercial and racing go-karting industry. This study also proves it is possible to develop a practical and realistic dynamic crashworthiness performance test for commercially manufactured go-karts.

This paper has focussed on the research related to the safety performance of a go-kart that is subject to the same deceleration distance challenges as the micro and sub-compact cars, in terms of restraint and crashworthiness in a frontal crash with a special emphasis of restraint design pertaining to the rider. Wider application of these results may be possible for example in the go-kart racing environment with additional research.

ACKNOWLEDGEMENTS

The Authors would like to thank the technical staff at the NSW Roads and Maritime Services Crashlab facility for preparing and carrying out the crash tests. The Authors would also like to thank Mr. Terry Skene and staff at the Kingston Park Raceway in Queensland, Australia for assisting with preparation and supply of the barriers funded by their organisation and for providing advice and feedback from go-kart track owners. The support of the Chair of the Australian Standards Committee revising the Australian Standard for go-karts Ms Anthea Hammond from Scenic World, Katoomba in NSW, Australia, is also gratefully acknowledged.

Funding is always critical to the success of any safety related project. The bulk of the funding for testing was provided by The Australian Amusement, Leisure and Recreation Association Inc. (AALARA) with contributions from other track owners interested in the test results, for which the Authors are most grateful. RiMO Rental Karts Australia are also gratefully acknowledged for supplying the go-karts for testing.

REFERENCES:

[1] American Association of State Highway and Transportation Officils (AASHTO), (2016). Manual for Assessing Safety Hardware (MASH), 2nd Edition.

[2] Collins C., Smith G., and Comstock R., (2007). “Children plus non-automobile motorized vehicles (not just all terrain vehicles) equals injuries”, *Paediatrics*: Vol 120 (1) pp 134-141.

[3] Commission Internationale de Karting, (2017). Federation Internationale de l'Automobile. *Commission Internationale de Karting, Federation Internationale de l'Automobile*. 18 March 2017. <http://www.cikfia.com/home.html>.

[4] De Haven H., (1952). “Accident Survival – Airplane and Passenger Automobiles.”, SAE Technical Paper 520016, doi:10.4271/520016.

[5] European Commission, (2016) EN 16230-1:2013+A1:2014 Leisure karts - Part 1: Safety requirements and test methods for karts, https://www.nlfnorm.cz/en/ehn/5182

[6] Grzebieta R.H., Mitchell R., Zou R., Rechnitzer G., (2013). “Go-kart related injuries and fatalities in Australia”, *International Journal of Crashworthiness*, Vol 18, No. 4, pp 397-404.

[7] Grzebieta R., Rechnitzer G. and Mitchell R., (2014). “Reconstruction of a go-karting fatality”, *International Journal of Forensic Engineering*, Vol 2, No1, pp 71–86.

[8] Grzebieta R., Zou R. and Rechnitzer G., (2004). “Go-Karts - Can they be Crashworthy?”, Proc. 4th Int. Crashworthiness Conf. ICRASH2004, ed. Chirwa E.C. and F. Bandak, Bolton Institute U.K., San Francisco, July.

[9] Ross H.E., Sicking D.L., Zimmer R.A. and Michie J.D., (1993). Recommended Procedures for the Safety Performance Evaluation of Highway Features, National Cooperative Highway Research Program (NCHRP), Report 350, Transportation Research Board, National Research Council, National Academy Press, Washington D.C., ISBN 0-309-04873-7.

[10] Standards Australia, (2011). AS 3533.4.4-2011 Amusement rides and devices Specific requirements - Concession go-karts, Sydney, Australia.

[11] Tan T.C., Grzebieta R.H. & McIntosh A.S., (2017) Review of flail-space's lateral impact velocity criterion for thoracic impacts, Journal of Transportation Safety & Security, 9:2, 239-258, DOI: 10.1080/19439962.2016.1181690

APPENDIX

The following results have been extracted from the NSW Roads and Maritime Services Crashlab TEST Report No BR2014/012 Go Kart Crash Barrier Tests, Project No: S/07509 authored by Dal Nevo R. and Lai A. for the client TARS UNSW.

Crashlab Test Number: B14007 Summary of Results Test Date: 6 March, 2014

50 km/h 0 km/h

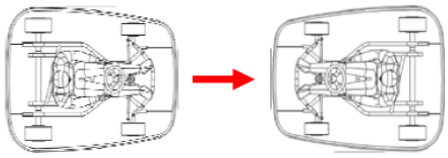

= 25 km/h velocity change

Bullet vehicle damage:

- Front RHS bumper bracket (steel) bent & fractured.
- Rear bumper guide tube displaced.
- Helmet contact with steering wheel at top of visor opening.
- Visor opened and detached during impact.

Target vehicle damage:

- Front RHS & LHS bumper brackets bent.
- Helmet contact with steering wheel at top of visor opening.
- Visor detached during impact.

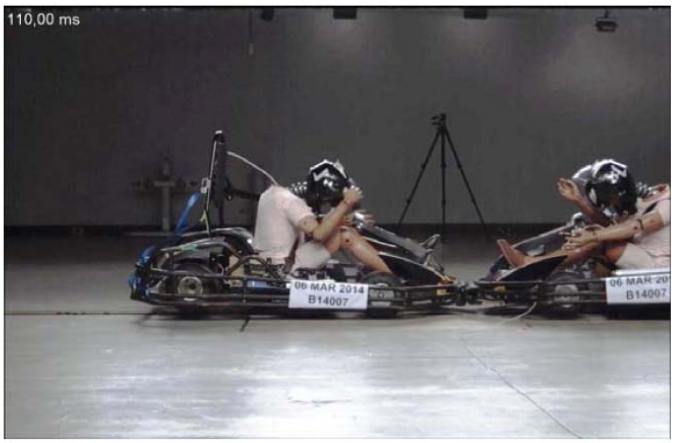

Test Vehicle	Bullet	Target		
Vehicle model	Rimo EVO 6	Rimo EVO 68		
Designation	#8 ID: 071312724	#68 ID: 061312731		
Test mass (incl. ATD)	233.5kg	230.0kg		
Impact speed	50.0km/h	0 km/h		
Occupant Impact Velocity			*Preferred*	*Maximum*
Longitudinal (Vx)	**8.3**	**7.9**	*9*	*12*
Lateral (Vy)	**-0.1**	**0.3**	*+/-9*	*+/-12*
'Occupant impact' time	0.093s	0.100s		
Ridedown Acceleration			*Preferred*	*Maximum*
Longitudinal (Gx)	**-3.0**	**-1.7**	*-15*	*-20*
Lateral (Gy)	**-4.2**	**-2.6**	*+/-15*	*+/-20*
Maximum Cof Gx (g)	-34.6g @ 19.8ms	-32.6g @ 29.3ms		
Maximum Cof Gy (g)	-8.8g @ 112.9ms	-13.2g @ 58.6ms		
Maximum Cof Gz (g)	-34.4g @ 110.0ms	-27.1g @ 61.1ms		
Maximum roll angle	-2.1deg @ 334.9ms	deg @ ms		
Maximum pitch angle	-6.4deg @ 214.8ms	10.2deg @ 226.3ms		
Maximum yaw angle	-0.7deg @ 62.2ms	1.0deg @ 49.4ms		

Crashlab Test Number: B14008 **Summary of Results** **Test Date: 6 March, 2014**

50 km/h 0 km/h

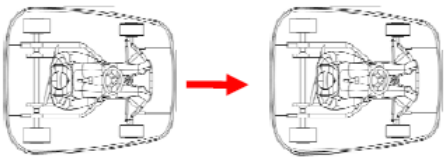

= 25 km/h velocity change

Bullet vehicle damage:

- Front RHS bumper bracket (steel) bent & (aluminium) fractured.
- Front LHS bumper bracket (steel) bent.
- Both rear bumper guide tubes dislodged.
- Helmet contacted steering wheel at top of visor opening and chin bar at steering wheel rim and hub.

Target vehicle damage:

- Rear bumper bent 20mm and both mounting brackets bent.
- No helmet contact with steering.

Test Vehicle	Bullet	Target		
Vehicle model	Rimo EVO 6	Rimo EVO 68		
Designation	#8 ID: 071312724	#68 ID: 061312731		
Test mass (incl. ATD)	233.5kg	230.0kg		
Impact speed	50.0km/h	0 km/h		
Occupant Impact Velocity			*Preferred*	*Maximum*
Longitudinal (Vx)	**8.2**	**-8.7**	*9*	*12*
Lateral (Vy)	**0.0**	**-0.8**	*+/-9*	*+/-12*
'Occupant impact' time	0.092s	0.439s		
Ridedown Acceleration			*Preferred*	*Maximum*
Longitudinal (Gx)	**-2.7**	**2.5**	*-15*	*-20*
Lateral (Gy)	**-3.6**	**6.2**	*+/-15*	*+/-20*
Maximum Cof Gx (g)	-39.9g @ 19.0ms	40.8g @ 16.9ms		
Maximum Cof Gy (g)	-14.8g @ 36.1ms	8.1g @ 69.3ms		
Maximum Cof Gz (g)	-31.1g @ 28.1ms	19.2g @ 66.4ms		
Maximum roll angle	3.1deg @ 160.0ms	-1.6deg @ 107.8ms		
Maximum pitch angle	-7.2deg @ 236.8ms	-17.7deg @ 299.1ms		
Maximum yaw angle	0.4deg @ 722.7ms	deg @ ms		

Crashlab Test Number: B14012 **Summary of Results** **Test Date: 24 March, 2014**

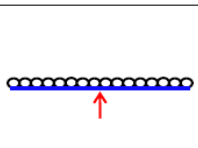

Test article	Bolted tyre wall, 16 long x 2 high, with conveyor belt front face.
Installation length	10.1 m
Height of barrier	Nominal 420 mm (400mm to 440mm)
Material	Passenger car tyres, nom. 205 x 65R x 15"
Weight of barrier	378 Kg (32 x9kg/tyre + 90kg conveyor)
Installation	Free standing on painted steel and concrete floor φ = 0.4
Test vehicle	Rimo EVO 6 Go Kart
Designation	#8 ID: 071312724
Test mass (incl. ATD)	225.5kg
Impact speed	25.2 km/h
Impact angle	90 degrees
Exit speed	
Exit angle	

Occupant Impact Velocity	Actual	*Preferred*	*Maximum*
Longitudinal (Vx)	**3.3**	*9*	*12*
Lateral (Vy)	**0.0**	*+/-9*	*+/-12*
'Occupant impact' time	0.259 s		
Ridedown Acceleration	Actual	*Preferred*	*Maximum*
Longitudinal (Gx)	**-0.9**	*-15*	*-20*
Lateral (Gy)	**-0.2**	*+/-15*	*+/-20*
Permanent barrier deflection	x-direction	2.735m	
Maximum Cof Gx (g)	-6.9g @ 28.1ms		
Maximum Cof Gy (g)	0.8g @ 59.4ms		
Maximum Cof Gz (g)	2.7g @ 9.8ms		
Maximum roll angle	0.1deg @ 166.9ms		
Maximum pitch angle	-0.4deg @ 50.7ms		
Maximum yaw angle	-0.6deg @ 399.4ms		

Observations:
No damage to vehicle or barrier. Vehicle pocketed at point of impact and penetrated into barrier 2.735 meters with no rebound.

Crashlab Test Number: B14013 **Summary of Results** **Test Date: 24 March, 2014**

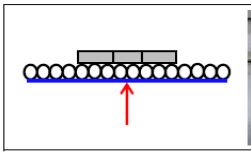

Test article	Bolted tyre wall, 16 long x 2 high, conveyor belt front, back against concrete barriers.
Installation length	10.1 m
Height of barrier	Nominal 420 mm (400mm to 440mm)
Material	Passenger car tyres, nom. 205 x 65R x 15"
Weight of barrier	378 Kg plus concrete barriers
Installation	Free standing on painted steel and concrete floor φ = 0.4
Test vehicle	Rimo EVO 6 Go Kart
Designation	#8 ID: 071312724
Test mass (incl. ATD)	225.5kg
Impact speed	25.2 km/h
Impact angle	90 degrees
Exit speed	
Exit angle	

Occupant Impact Velocity	Actual	*Preferred*	*Maximum*
Longitudinal (Vx)	**7.5**	*9*	*12*
Lateral (Vy)	**-0.1**	*+/-9*	*+/-12*
'Occupant impact' time	0.147 s		
Ridedown Acceleration	Actual	*Preferred*	*Maximum*
Longitudinal (Gx)	**-2.7**	*-15*	*-20*
Lateral (Gy)	**-1.0**	*+/-15*	*+/-20*
Permanent barrier deflection	x-direction	0.23m *(0.29m concrete)*	
Maximum Cof Gx (g)	-7.9g @ 83.6ms		
Maximum Cof Gy (g)	1.6g @ 71.4ms		
Maximum Cof Gz (g)	-6.9g @ 400.4ms		
Maximum roll angle	0.7deg @ 176.4ms		
Maximum pitch angle	-4.7deg @ 244.9ms		
Maximum yaw angle	-0.4deg @ 65.2ms		

Observations:
No damage to vehicle or tyre barrier. Dynamic penetration greater than residual deflection of 230mm. Concrete barrier displaced 290mm. Rear tyres of kart became airborne during rebound. Helmet visor opened and contacted steering wheel during impact.

Crashlab Test Number: B14014 **Summary of Results** **Test Date: 25 March, 2014**

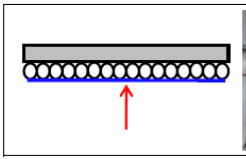

Test article	Bolted tyre wall, 16 long x 2 high, conveyor
	belt front, against rigid concrete wall.
Installation length	10.1 m
Height of barrier	Nominal 420 mm (400mm to 440mm)
Material	Passenger car tyres, nom. 205 x 65R x 15"
Weight of barrier	378 Kg plus concrete wall
Installation	Free standing on painted steel and
	concrete floor φ = 0.4
Test vehicle	Rimo EVO 6 Go Kart
Designation	#8 ID: 071312724
Test mass (incl. ATD)	225.5kg
Impact speed	25.3 km/h
Impact angle	90 degrees
Exit speed	
Exit angle	

Occupant Impact Velocity	Actual	*Preferred*	*Maximum*
Longitudinal (Vx)	**8.2**	*9*	*12*
Lateral (Vy)	**-0.0**	*+/-9*	*+/-12*
'Occupant impact' time	0.147 s		
Ridedown Acceleration	Actual	*Preferred*	*Maximum*
Longitudinal (Gx)	**-2.7**	*-15*	*-20*
Lateral (Gy)	**-1.5**	*+/-15*	*+/-20*
Permanent barrier deflection	x-direction	-0.02m	
Maximum Cof Gx (g)	-8.9g @ 98.3ms		
Maximum Cof Gy (g)	2.5g @ 455.7ms		
Maximum Cof Gz (g)	-6.9g @ 445.1ms		
Maximum roll angle	-1.3deg @ 302.3ms		
Maximum pitch angle	-5.8deg @ 270.4ms		
Maximum yaw angle	-2.8deg @ 491.7ms		

Observations:
No damage to vehicle or barrier. Front face of barrier rebounded off wall by 20mm. Helmet visor opened and then detached after helmet made contact with steering wheel. Rear tyres of the kart became significantly airborne during rebound off the barrier.

Crashlab Test Number: B14015 **Summary of Results** **Test Date: 25 March, 2014**

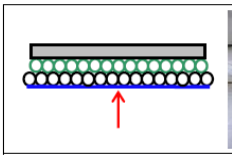

Test article	Bolted tyre wall (16 x 2), conveyor front,
	back to double height loose tyres & wall.
Installation length	10.1 m
Height of barrier	Nominal 420 mm (400mm to 440mm)
Material	Passenger car tyres, nom. 205 x 65R x 15"
Weight of barrier	378 Kg plus concrete wall
Installation	Free standing on painted steel and
	concrete floor φ = 0.4
Test vehicle	Rimo EVO 6 Go Kart
Designation	#8 ID: 071312724
Test mass (incl. ATD)	225.5kg
Impact speed	25.2 km/h
Impact angle	90 degrees
Exit speed	
Exit angle	

Occupant Impact Velocity	Actual	*Preferred*	*Maximum*
Longitudinal (Vx)	**7.0**	*9*	*12*
Lateral (Vy)	**-0.1**	*+/-9*	*+/-12*
'Occupant impact' time	0.168 s		
Ridedown Acceleration	Actual	*Preferred*	*Maximum*
Longitudinal (Gx)	**-3.0**	*-15*	*-20*
Lateral (Gy)	**0.6**	*+/-15*	*+/-20*
Permanent barrier deflection	x-direction	-0.10m	
Maximum Cof Gx (g)	-6.9g @ 29.9ms		
Maximum Cof Gy (g)	1.1g @ 47.1ms		
Maximum Cof Gz (g)	-2.6g @ 373.1ms		
Maximum roll angle	-0.7deg @ 261.8ms		
Maximum pitch angle	-2.2deg @ 247.4ms		
Maximum yaw angle	-2.4deg @ 543.0ms		

Observations:
No damage to vehicle or barrier. Front face of barrier rebounded off tyres and wall by 100mmon centreline and by 180mm and 220mm on the left and right ends respectively. The helmet visor opened and made light contact with steering wheel but remained attached to the helmet. Rear tyres of the kart became significantly airborne during rebound off the barrier.

Crashlab Test Number: B14016 **Summary of Results** **Test Date: 25 March, 2014**

Test article	10 linked plastic barriers, 35kg water in each
	against double height loose tyres & wall.
Installation length	10.1 m
Height of barrier	Nominal 575mm
Material	Moulded plastic designed to hold water
Weight of barrier	550Kg (10 x 20kg barrier +10 x 35kg water)
Installation	Free standing on painted steel and
	concrete floor φ = 0.4
Test vehicle	Rimo EVO 6 Go Kart
Designation	#8 ID: 071312724
Test mass (incl. ATD)	225.5kg
Impact speed	25.3 km/h
Impact angle	90 degrees
Exit speed	
Exit angle	

Occupant Impact Velocity	Actual	*Preferred*	*Maximum*
Longitudinal (Vx)	**7.4**	*9*	*12*
Lateral (Vy)	**-0.0**	*+/-9*	*+/-12*
'Occupant impact' time	0.147 s		
Ridedown Acceleration	Actual	*Preferred*	*Maximum*
Longitudinal (Gx)	**-2.8**	*-15*	*-20*
Lateral (Gy)	**1.2**	*+/-15*	*+/-20*
Permanent barrier deflection	x-direction	-0.10m	
Maximum Cof Gx (g)	-12.4g @ 17.4ms		
Maximum Cof Gy (g)	-3.3g @ 60.8ms		
Maximum Cof Gz (g)	5.7g @ 14.4ms		
Maximum roll angle	0.8deg @ 197.8ms		
Maximum pitch angle	-2.1deg @ 224.7ms		
Maximum yaw angle	-0.2deg @ 25.6ms		

Observations:
No damage to vehicle or barrier. The plastic barrier rebounded off the loose tyres. The barrier rebounded 100mm along the centreline of the impact and 250mm and 225mm at the next connection points to the left and right respectively. The helmet visor opened and the top edge of the helmet opening contacted the steering wheel before the visor was dislodged. Rear tyres of kart became moderately airborne on rebound off barrier.

Crashlab Test Number: B14017 **Summary of Results** **Test Date: 25 March, 2014**

Test article	10 linked plastic barriers, 35kg water in each
	free standing on floor.
Installation length	10.1 m
Height of barrier	Nominal 575mm
Material	Moulded plastic designed to hold water
Weight of barrier	550Kg (10 x 20kg barrier +10 x 35kg water)
Installation	Free standing on painted steel and
	concrete floor φ = 0.4
Test vehicle	Rimo EVO 6 Go Kart
Designation	#8 ID: 071312724
Test mass (incl. ATD)	225.5kg
Impact speed	25.2 km/h
Impact angle	90 degrees
Exit speed	
Exit angle	

Occupant Impact Velocity	Actual	*Preferred*	*Maximum*
Longitudinal (Vx)	**3.4**	*9*	*12*
Lateral (Vy)	**0**	*+/-9*	*+/-12*
'Occupant impact' time	0.241s		
Ridedown Acceleration	Actual	*Preferred*	*Maximum*
Longitudinal (Gx)	**-0.6**	*-15*	*-20*
Lateral (Gy)	**0.6**	*+/-15*	*+/-20*
Permanent barrier deflection	x-direction	4.00m	
Maximum Cof Gx (g)	-11.4g @ 19.1ms		
Maximum Cof Gy (g)	2.7g @ 81.1ms		
Maximum Cof Gz (g)	-4.5g @ 28.6ms		
Maximum roll angle	0.3deg @ 180.1ms		
Maximum pitch angle	-0.7deg @ 159.9ms		
Maximum yaw angle	0.6deg @ 296.4ms		

Observations:
No damage to vehicle or barrier. Vehicle pocketed at point of impact and penetrated into barrier 4.00 meters with no rebound.

Crashlab Test Number: B14018 **Summary of Results** **Test Date: 25 March, 2014**

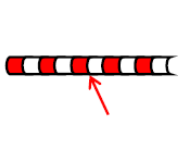

Test article	10 linked plastic barriers, 35kg water in each
	Free standing on floor.
Installation length	10.1 m
Height of barrier	Nominal 575mm
Material	Moulded plastic designed to hold water
Weight of barrier	550Kg (10 x 20kg barrier +10 x 35kg water)
Installation	Free standing on painted steel and
	concrete floor φ = 0.4
Test vehicle	Rimo EVO 6 Go Kart
Designation	#8 ID: 071312724
Test mass (incl. ATD)	225.5kg
Impact speed	50.1 km/h
Impact angle	25 degrees
Exit speed	
Exit angle	> approach

Occupant Impact Velocity	Actual	*Preferred*	*Maximum*
Longitudinal (Vx)	**4.5**	*9*	*12*
Lateral (Vy)	**3.7**	*+/-9*	*+/-12*
'Occupant impact' time	0.136 s		
Ridedown Acceleration	Actual	*Preferred*	*Maximum*
Longitudinal (Gx)	**-11.8**	*-15*	*-20*
Lateral (Gy)	**-11.2**	*+/-15*	*+/-20*
Permanent barrier deflection	x-direction		
Maximum Cof Gx (g)	-17.2g @ 105.4ms		
Maximum Cof Gy (g)	-13.9g @ 103.1ms		
Maximum Cof Gz (g)	-18.8g @ 380.6ms		
Maximum roll angle	3.0deg @ 270.8ms		
Maximum pitch angle	1.2deg @ 63.2ms		
Maximum yaw angle	-196.7deg @ 1,386.7ms		

Observations: No vehicle damage. Impact was at junction of 5th and 6th barrier in the 10 barrier assembly. Barrier 6, on the down stream side of the impact sustained a long fracture to the lower ridge line and leaked water. The kart rotated counter clockwise by more than 90 degrees as a result of the subsequent impacts with 5 barrier segments. The barrier assembly was displaced up to 6.3 meters longitudinally and 8m laterally. The Hybrid III right hand and lower forearm made heavy contact with two barriers during the impact.

Crashlab Test Number: B14019 **Summary of Results** **Test Date: 26 March, 2014**

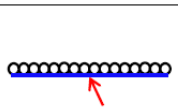

Test article	Bolted tyre wall, 16 long x 2 high, with
	conveyor belt front face.
Installation length	10.1 m
Height of barrier	Nominal 420 mm (400mm to 440mm)
Material	Passenger car tyres, nom. 205 x 65R x 15"
Weight of barrier	378 Kg (32 x 9kg/tyre + 90kg conveyor)
Installation	Free standing on painted steel and
	concrete floor φ = 0.4
Test vehicle	Rimo EVO 6 Go Kart
Designation	#8 ID: 071312724
Test mass (incl. ATD)	225.5kg
Impact speed	50.0 km/h
Impact angle	25 degrees
Exit speed	
Exit angle	None

Occupant Impact Velocity	Actual	*Preferred*	*Maximum*
Longitudinal (Vx)	**4.4**	*9*	*12*
Lateral (Vy)	**0.9**	*+/-9*	*+/-12*
'Occupant impact' time	0.225 s		
Ridedown Acceleration	Actual	*Preferred*	*Maximum*
Longitudinal (Gx)	**-1.8**	*-15*	*-20*
Lateral (Gy)	**3.8**	*+/-15*	*+/-20*
Permanent barrier deflection	x-direction		
Maximum Cof Gx (g)	-4.3g @ 16.5ms		
Maximum Cof Gy (g)	4.6g @ 369.0ms		
Maximum Cof Gz (g)	8.4g @ 529.2ms		
Maximum roll angle	2.0deg @ 376.2ms		
Maximum pitch angle	-2.2deg @ 232.7ms		
Maximum yaw angle	58.6deg @ 2,781.3ms		

Observations: The kart was not redirected by the barrier but continued in its forward direction lifting the convey belt and under-riding the barrier towards the down stream end. The kart's momentum drag the barrier forward before rotating clockwise. The longitudinal displacement of the barrier was up to 4.9m with a lateral displacement at the downstream end of almost 5m. The Hybrid III's right arm and helmeted head were impacted by the barrier which also bent the steering wheel backwards. The plastic fairing at the front of the kart was also cracked.

Crashlab Test Number: B14020 **Summary of Results** **Test Date: 26 March, 2014**

Test article	Bolted tyre wall, 16 long x 2 high, conveyor
	belt front, against rigid concrete wall.
Installation length	10.1 m
Height of barrier	Nominal 420 mm (400mm to 440mm)
Material	Passenger car tyres, nom. 205 x 65R x 15"
Weight of barrier	378 Kg plus concrete wall
Installation	Free standing on painted steel and
	concrete floor φ = 0.4
Test vehicle	Rimo EVO 6 Go Kart
Designation	#8 ID: 071312724
Test mass (incl. ATD)	225.5kg
Impact speed	50.0 km/h
Impact angle	25 degrees
Exit speed	
Exit angle	> approach

Occupant Impact Velocity	Actual	*Preferred*	*Maximum*
Longitudinal (Vx)	**8.0**	*9*	*12*
Lateral (Vy)	**2.0**	*+/-9*	*+/-12*
'Occupant impact' time	0.136 s		
Ridedown Acceleration	Actual	*Preferred*	*Maximum*
Longitudinal (Gx)	**-6.6**	*-15*	*-20*
Lateral (Gy)	**--2.8**	*+/-15*	*+/-20*
Permanent barrier deflection	x-direction	-0.53m	
Maximum Cof Gx (g)	-9.2g @ 157.0ms		
Maximum Cof Gy (g)	-5.8g @ 73.8ms		
Maximum Cof Gz (g)	9.8g @ 178.7ms		
Maximum roll angle	6.7deg @ 639.4ms		
Maximum pitch angle	-4.0deg @ 248.6ms		
Maximum yaw angle	127.0deg @1,455.5ms		

Observations: The kart commenced to under-run the barrier on impact without any redirection, until it pocketed and began rotating in a clockwise direction. The steering wheel was forced to turn hard right and was struck by the Hybrid III's helmeted head. The barrier rebounded off the concrete wall by up to 530mm. The back of the Hybrid III's right hand impacted the barrier during under-ride. There was no structural damage to the kart only some superficial scuffing on the front fairing.

Crashlab Test Number: B14021 **Summary of Results** **Test Date: 26 March, 2014**

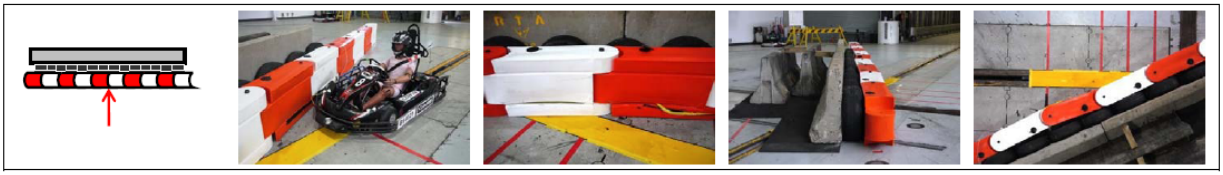

Test article	10 linked plastic barriers, 35kg water each,
	against row of standing loose tyres & wall.
Installation length	10.1 m
Height of barrier	Nominal 575mm
Material	Moulded plastic designed to hold water
Weight of barrier	550Kg (10 x 20kg barrier +10 x 35kg water)
Installation	Free standing on painted steel and
	concrete floor φ = 0.4
Test vehicle	Rimo EVO 6 Go Kart
Designation	#8 ID: 071312724
Test mass (incl. ATD)	225.5kg
Impact speed	50.0 km/h
Impact angle	25 degrees
Exit speed	Still to be calculated
Exit angle	< 15 degrees. (still to be checked)

Occupant Impact Velocity	Actual	*Preferred*	*Maximum*
Longitudinal (Vx)	**4.0**	*9*	*12*
Lateral (Vy)	**5.3**	*+/-9*	*+/-12*
'Occupant impact' time	0.136 s		
Ridedown Acceleration	Actual	*Preferred*	*Maximum*
Longitudinal (Gx)	**-6.9**	*-15*	*-20*
Lateral (Gy)	**--7.0**	*+/-15*	*+/-20*
Permanent barrier deflection	x-direction	0.03m	
Maximum Cof Gx (g)	-12.7g @ 44.2ms		
Maximum Cof Gy (g)	-13.9g @ 43.5ms		
Maximum Cof Gz (g)	7.7g @ 134.4ms		
Maximum roll angle	-1.9deg @ 476.9ms		
Maximum pitch angle	-1.1deg @ 210.9ms		
Maximum yaw angle	-54.8deg @1,000.0ms		

Observations: The kart was successfully redirected by the barrier with no pocketing and exit angle appearing to be within the allowable 15 degrees.. The two barriers that were impacted split at the lower ridge line with some loss of water. The filler cap was also forced off the first barrier impacted with some loss of water. The Hybrid III's right hand contacted the barrier during impact and the helmet head come close to contacting the top edge of the barriers. The maximum rebound of the barriers off the tyres and wall was no more than 30mm.

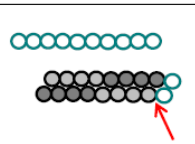

Test article	Tyre segments (4x2), double row overlapped
	With row of single loose tyres behind.
Installation length	5.6 m
Height of barrier	Nominal 420 mm (400mm to 440mm)
Material	Passenger car tyres, nom. 205 x 65R x 15"
Weight of barrier	324kg = 4 x 72kg (groups) +4 x 9kg (loose)
Installation	Free standing on painted steel and
	concrete floor φ = 0.4
Test vehicle	Rimo EVO 6 Go Kart
Designation	#8 ID: 071312724
Test mass (incl. ATD)	225.5kg
Impact speed	50.0 km/h
Impact angle	25 degrees
Exit speed	
Exit angle	

Occupant Impact Velocity	Actual	*Preferred*	*Maximum*
Longitudinal (Vx)	**5.9**	*9*	*12*
Lateral (Vy)	**-0.4**	*+/-9*	*+/-12*
'Occupant impact' time	0.136 s		
Ridedown Acceleration	Actual	*Preferred*	*Maximum*
Longitudinal (Gx)	**-2.3**	*-15*	*-20*
Lateral (Gy)	**3.0**	*+/-15*	*+/-20*
Permanent barrier deflection	x-direction		
Maximum Cof Gx (g)	-7.6g @ 42.1ms		
Maximum Cof Gy (g)	3.4g @89.2ms		
Maximum Cof Gz (g)	-4.8g @ 271.4ms		
Maximum roll angle	3.0deg @ 1.277ms		
Maximum pitch angle	-0.5deg @ 207.7ms		
Maximum yaw angle	157.4deg @2.099ms		

Observations: The kart was not redirected at all but rather immediately pocketed and commenced to rotate in a clockwise direction scattering the tyre bundles with it. The kart penetrated approximately 5.0m into the barrier arrangement and rotated 180 degrees from its original direction of travel.

TOWARDS A QUANTITATIVE "SAFETY" METRIC FOR AUTONOMOUS VEHICLES

Arturo Tejada, Michel J. E. Legius
TNO, Integrated Vehicle Safety Department
5700 AT Helmond The Netherlands

Paper Number 19-0012

ABSTRACT

Future mobility systems are expected to incorporate a broad range of transport modalities (passenger cars, truck platoons, etc.) at different automation levels (SAE Levels 3/4/5). During operation, automated vehicles will have to independently take safety-critical decisions (e.g., when to brake or change lanes) and estimate the impact of their behavior on the surrounding traffic, thus balancing individual and group safety. To achieve this, automated vehicles will require a quantitative metric of safety to guide their actions.

This article proposes one such metric, suitable for decision-making and autonomous navigation. The metric is meant to provide a quantification of the risk a vehicle incurs during operation by taking into account three main aspects of its operation: the probability of a hazard occurring (e.g., a rear-end collision), the potential impact of the driving conditions on the health of the vehicle's passengers were the hazard to occur, and the capability of the vehicle to avoid the hazard. The article focuses on introducing the conceptual aspects of the metric first and then presents the initial results on estimating and collision probabilities. The other two aspects will be addressed elsewhere.

INTRODUCTION

Automated vehicles (car, buses, trucks) are widely considered to be a promising solution to the road safety and congestion problems. On the one hand, such vehicles would not be subject to distractions or lapses of judgement that currently lead to the majority of road accident involving human drivers [1], thus improving road safety. On the other hand, their shorter reaction times and ability to communicate with road infrastructure would allow them to drive more efficiently on the roads, increasing road utilization and capacity, while improving traffic flow.

To realize the aforementioned benefits, automated vehicles would have to drive according to a notion of *correct behavior*[1], which presumably would maximize (or at least maintain) the safety level of all traffic participants. Trained (and experienced) human drivers are able to judge the safety of their situations and act accordingly (most of the time). This is generally done unconsciously based on implicitly learned behaviors and models of the world. Automated vehicles, on the other hand, must make explicit judgements about their safety in order to take decisions regarding their behaviors[2]. Such decisions may include when to activate automated emergency braking systems, which trajectory to follow while driving, which route to use to reach a particular location, when to allow a human driver to regain vehicle control, etc. Thus, reasoning about safety would be needed at several layers of an automated vehicle's architecture [2, 3].

Much as the notion of correct behavior (see Footnote 1), safety is also a difficult concept to define precisely, and it varies with the stake holder considering it. As summarized in the next section, safety has been addressed from at least three perspectives: traffic system safety, vehicle hazard (collision) avoidance, and vehicle certification (functional safety). Briefly, from the traffic system perspective, safety is related to understanding (and preventing) the factors that contribute to traffic crashes and injuries (e.g., vehicle technologies, infrastructure design, etc. [4,5]); safety from the hazard avoidance perspective is related to determining thresholds on proximity metrics to trigger warning and/or collision avoidance systems (see, among

[1] *Correct behavior* is a societally-agreed concept that encompass not only normative or engineering-like goals (e.g., "follow the traffic rules") but also elements such as "use an acceptable driving style", which vary widely by country, age group, etc.

[2] Arguably, an automated vehicle could be completely controlled by machine-learning-based algorithms trained to mimic human driving behavior without explicitly reasoning about safety. Not all automated vehicles, however, would be so controlled.

many examples, [6, 7]; while safety from the certification perspective is related to developing the vehicular electronics and software at the necessary automotive safety integrity levels (ASILs) [8]. Unfortunately, none of these approaches directly provide a definition of safety that could be operationalized to reason safety as needed for autonomous vehicle operation.

This article, introduces a framework to compute one such metric. It can be thought of as an extension of existing techniques on estimation of probability of collision [9, 10] to incorporate measures of both the consequences of a potential collision and the ability of the vehicle to avoid such collision. The framework is modelled after the concepts used in the ISO 262622 standard to assigned ASIL levels, and the resulting metric can be considered as a measure of interaction severity, when applied to interactions of two vehicles.

The rest of this article is organized as follows: The framework of estimating safety is introduced next, after a brief summary of available literature on safety definitions. This is followed by a description of our initial work on estimating the probability of collision in two dimensions, one of the main three elements on our framework (the other two elements are outlined but described in detail elsewhere). Finally, the paper ends with out conclusions.

FRAMEWORK FOR SAFETY ESTIMATION

As mentioned in the introduction, the framework for safety estimation proposed here draws from concepts of safety defined by other researchers and stakeholders. To avoid confusion between the use of "safety" in the vernacular, and "safety" as a subject of study, the latter will be italicized in the sequel. Several concepts of *safety* are summarized next.

A Brief Overview of Safety in the Literature

Perhaps the most frequently recognized concept of *safety* comes from the field of traffic safety: it is the absence of road accidents that may lead to severe injury, deaths, and or property damages (see, e.g., [11]). From this perspective, *safety* cannot be directly measured[3]. The *lack of safety*, however, can be described via accident statistics, and it is know to have a large impact in terms of loss of life, livelihood, and economic output [13]. This is why its minimization is of great interest for governments and regulators. Minimizing (or, hopefully, eliminating) the *lack of safety*, however, depends not only on the actions of individual vehicles in traffic, but also on the right combination of vehicle technologies, infrastructure design, and traffic policies. Thus, the aim of traffic safety research is not to measure *safety* in order to allow vehicle automation, but rather to show whether or not the introduction of new technologies or traffic policies lead to demonstrable reductions of severe road accident statistics (see [14, 15] and the references therein).

The aim of minimizing the *lack of safety* as defined above, gave raise to a number of technologies that help vehicles avoid or minimize the effect of severe traffic conflicts, which in turn can lead to severe collisions [14]. Severe traffic conflicts can be defined as traffic interactions where two or more participants are in collision course and "too close" either in space or time [16]. Collision courses are determined using simplifying assumptions on the vehicles' behavior (e.g., constant acceleration), while proximity is measured using any number of indicators, most commonly, time to collision. Appropriate thresholds over these indicators allow for the automatic activation of a vehicle's warning and/or collision avoidance systems [6, 7]. Vehicles equipped with such technologies are assumed to be safer because they minimize the chance of occurrence and/of the effects of accidents, which is usually confirmed via testing (see, e.g., [17]). Note, however, that *safety* does not need to be (and it is not) directly defined/measured in these approaches.

A different perspective altogether on automotive safety is that of *functional safety*. This concepts, presented in detail in the ISO26262 standard [8] is related to minimizing the risk of occurrence of particular hazards due to technological failures (e.g., rear-end collision due to braking failure). To accomplish this, a vehicle's hardware (i.e., electronics) and software are developed in a way that they attain specific automotive safety integrity levels (ASILs). These, in turn, are derived by analyzing the time and possibility of the vehicle

[3]From this perspective, *safety* (i.e., the absence of loss of life under all traffic circumstances) cannot be formally proven. This is, however, a very compelling and important goal to pursue, as stated by the Vision Zero philosophy [12]

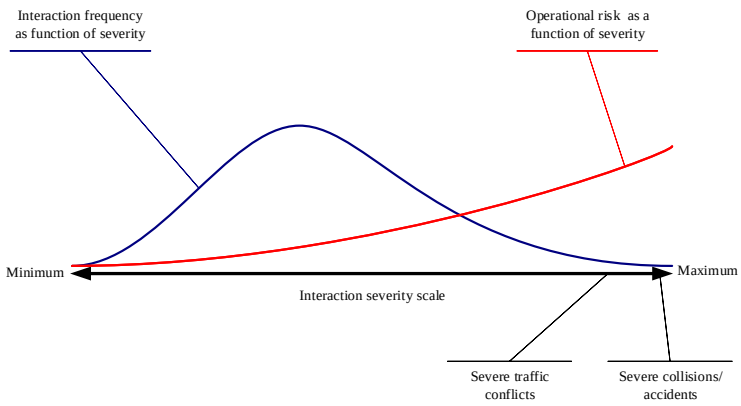

Figure 1: Severity scale for traffic interactions and associated risk (adapted from [4])

being exposed to the said hazards, the gravity of injuries that might be caused were the hazards to occur, and the likelihood that the injuries could be prevented by the actions of a typical driver. A vehicular system so designed is said to be functionally safe. Though functional safety is precisely defined in the ISO26262 standard, it cannot be directly quantified.

Finally, it is important to point out that there are several metrics in the literature that are used to allow vehicle automation [15, 18, 19]. Such metrics have been used for, among other applications, collision avoidance and path planning [6, 7, 20]). To the best of our knowledge, such metrics are application specific and do not always take into account the consequence of potential collisions on the drivers involved. The framework proposed next aims to address both these issues.

On Safety Estimation

A well-known concept from traffic safety literature is that all traffic interactions can be placed along a continuous "severity" scale [4, 14] (see Figure 1). On one end of the scale lie the least severe interactions, which lead to accidents with very low probability (e.g., a vehicle driving alone in a road). Towards the middle of the scale lie the mid-severe interactions. They are the most frequent interactions and, generally speaking, lead to accidents with low probability. On the other end of the scale one finds the most severe and rare interactions (i.e., the severe traffic conflicts) that lead to severe accidents with (presumably) high probability. This suggests that one could reason about the degree of *safety* of a given vehicle in traffic, by quantifying the severity of the traffic interactions affecting it at a given time.

Unfortunately, there seems not to be yet a consensus in the literature on how to quantify interaction severity, although it is expected that multiple indicators should be combined to produce such quantification (see, e.g., [14, 19, 21]). Here, we propose an approach motivated by the method ISO 26262 standard to assign ASILs. That is, each traffic interaction involving a vehicle of interest (called *host*) is treated as a potential hazard and assigned a severity value equal to the operational risk it imposes on the host. Clearly, the higher the severity of the interaction, the higher the risk for the host (see Figure 1).

To assign a risk value, we consider the potential hazard's likelihood, hazardousness, and avoidability[4]. The relationship among these factors are illustrated in Fogire 2: the (blue) host vehicle keeps a constant distance with the (yellow) vehicle in front of it. During this interaction, another (green) vehicle begins a cut-in maneuver between them. This maneuver creates a potential collision hazard. The risk induced by this hazard depends on the likelihood of the collision (usually estimated from prediction models). Intuitively, the higher the collision likelihood, the higher the host's risk. Further, a mild collision presents a lower risk to the passengers involved than a severe collision , as the latter has a higher chance to produce severe injuries. Thus,

[4]These concepts mirror exposure, severity and controllability in ASIL assignment [8].

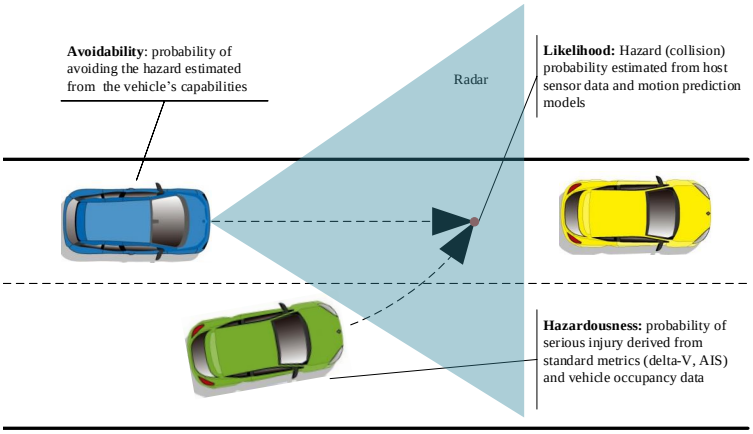

Figure 2: Example scenario showing the factors contributing to operational risk.

the hazardousness of the potential collision has also a strong bearing on the host's risk. Finally, depending on its capabilities, the host may be able to ameliorate the hazard's consequences or to avoid it all together. Thus, the hazard's avoidability also plays an important role on understanding the host's operational risk.

Formally, let $S : \mathbb{R}^+ \to [0, 1]$ and $R : \mathbb{R}^+ \to [0, 1]$ denote the host's (degree of) safety and operational risk functions respectively ($\mathbb{R}^+$ denotes the non-negative real numbers). Then, the host's (degree of) safety in the next $T \in \mathbb{R}^+$ seconds is given by

$$S(T) = 1 - R(T) \triangleq \mathrm{P}\{\mathcal{H}\}(1 - \mathrm{P}\{\mathcal{A}\})\mathrm{P}\{\mathcal{I}|\mathcal{H}\}, \tag{1}$$

where $\mathrm{P}\{\mathcal{H}\}$ denotes the probability that "a hazard occurs in the next T seconds" and $\mathrm{P}\{\mathcal{I}|\mathcal{H}\}$ denotes the probability that "severe injury or death occur if the hazard occurs in the next T seconds" and $\mathrm{P}\{\mathcal{A}\}$ denotes the probability that the vehicle "can perform an action to avoid the hazard in the next T seconds". These three probabilities denote, respectively, the likelihood, hazardousness and avoidability of hazard $\mathcal{H}$.

Remark 1. That a hazard occurs in a given period depends, among other factors, on the actions of the host and other traffic participants during that period. An automated vehicle can only *estimate* these future actions based on past and present sensor data and behavior prediction models. The greater the period T, the more uncertain the estimations become. This uncertainty is captured by $\mathrm{P}\{\mathcal{H}\}$. ♦

Remark 2. $\mathrm{P}\{\mathcal{A}\}$ estimates the capability of the host to perform a hazard avoidance action on time to prevent the hazard from occurring. In (1), as a first approximation, it is assumed that $\{\mathcal{H}\}$ and $\{\mathcal{A}\}$ are independent events. However, it is clear that the more capable the host is of avoiding a hazard, the lower the latter's likelihood. Nevertheless, note that even when $\mathrm{P}\{\mathcal{A}\} = 1$, $\mathrm{P}\{\mathcal{H}\} > 0$ since the hazard likelihood does not depend solely on the hosts actions. ♦

Finally, if the host faces more than one hazard simultaneously (see Figure 2), (1) can be extended as follows

$$S(T) = 1 - R(T) \triangleq \sum_i \mathrm{P}\{\mathcal{H}_i\}(1 - \mathrm{P}\{\mathcal{A}_i\})\mathrm{P}\{\mathcal{I}_i|\mathcal{H}_i\}, \tag{2}$$

where each $\mathcal{H}_\rangle$, $i = 1, 2, \cdots$, denotes a separate independent hazard (under the assumption that hazards can be treated independently).

The rest of the document will focus only on collision hazards and will present a method to estimate $P\{\mathcal{H}\}$. Details on how to estimate the probability of injury given specific collision conditions can be found in [22]. Methods to estimate collision avoidance capabilities are currently under investigation and will be presented elsewhere.

ON PROBABILITY OF COLLISION

As mentioned in the previous section, $\mathrm{P}\{\mathcal{H}\}$ represents the host's uncertainty in determining whether a collision will occur in a give timeframe. It arises due to: 1) imprecisions in the host's sensor measurements and 2) the uncertainty associated with predicting the *future* behavior of other traffic participants (called *targets*) relative to the host.

The general approach used to estimate $\mathrm{P}\{\mathcal{H}\}$ is as follows:

- The host's perception system measure or derives kinematic quantities like host/target positions, headings, lengths and widths, etc.
- These quantities, together with behavioral assumptions on both the host and target, are used to infer the relative positions of the host and target in the future T seconds[5].
- Determine if the target and host overlap.

Typical behavioral assumptions used to estimate future host/target behavior are that they either move with constant speed or with constant acceleration (see [9]). This allows one estimate both their future relative positions and their associated probability density functions. From this information one can infer the probability density function of the host/target overlap. Determining whether two vehicles overlap is akin to determining whether two convex polygons intersect. This is discussed next.

On Intersections of Convex Polygons

The main tool used to analyze whether two convex sets intersect is called the Separating Hyperplane Theorem (SHT, see [23]).

Theorem 1 (SHT)**.** *Suppose C and D are nonempty disjoint convex sets, i.e., $C \cap D = \phi$. Then, there exists $a \neq 0$ and b such that $a^T x \leq b$ for all $x \in C$ and $a^T x \geq b$ for all $x \in D$.*

The proof of this theorem is constructive (see [23, p. 46]) and can be used to extend the theorem in several ways by adding additional conditions to the sets C and D as shown next (see [24, 25]):

Lemma 2. *Suppose $C, D \in \mathbb{R}^n$ are nonempty, closed, convex sets, at least one of which is bounded, and are such that $C \cap D = \phi$. Then, there exists $a \neq 0$ and b such that $a^T x < b$ for all $x \in C$ and $a^T x > b$ for all $x \in D$.*

The converse of these theorems seems to be true for finite dimensional spaces (like $\mathbb{R}^n$), though no formal proof has been found. In the finite dimensional case, using the additional concept of "separating axis" (i.e., a line perpendicular to a separating hyperplane) the following corollary of the Separating Hyperplane Theorem can be stated:

Lemma 3 (Separating Axis Theorem (SAT))**.** *Let $C, D \in \mathbb{R}^n$ be nonempty, closed, convex sets. If there exists a line L for which the projections of C and D, respectively $P_L(C)$ and $P_L(D)$, onto it do not intersect, then the $C \cap D = \phi$.*

SAT is stated without proof by most authors (although a proof is reportedly available in [26]). This corollary does not show how to find L so one presumably would have to identify it by inspection or by trial and error. Fortunately, in the case of convex polygons, the search space for L can be narrowed significantly. To do this, let L be defined as follows:

$$L \triangleq \{x \in \mathbb{R}^2 | x = a + t\hat{v}, \quad t \in (-\infty, \infty)\},$$

[5] More precisely, one should estimate the positions of the host and the target at time $\min\{TTC, T\}$, where TTC denotes the time to collision [15]

where a is a point in $\mathbb{R}^2$ and $\hat{v}$ is a unitary vector in the desired direction of L. Further, let the operator P_L be defined as follows:

$$\begin{aligned} P_L : \mathbb{R}^2 &\to \mathbb{R}^2 \\ x &\mapsto a + \langle x - a, \hat{v} \rangle \hat{v}, \end{aligned}$$

where $\langle ., . \rangle$ denotes the standard inner product. $P_L(x)$ returns the location of the orthogonal projection of x on L. This concept can be extended to a set $C \subset \mathbb{R}^2$, with a slight abuse of notation, as follows:

$$P_L(C) \triangleq \{y \in R^2 | y = P_L(x), x \in C\}$$

The next result then follows (see [27, sec. 7.7.2]).

Corollary 4 (SAT for Convex Polygons)**.** *Let $C, D \in \mathbb{R}^n$ be $n-$ and $m-$sided convex polygons, respectively, and let S be a set of lines, each normal to a different edge of C and D. If there exist $L \in S$ such that $P_L(C) \cap P_L(D) = \phi$ then $C \cap D = \phi$.*

Note that S is not unique, since the translation of a separating axis is also a separating axis. Hence, it is sufficient for S to contains lines that cross the origin (i.e., for which $a = 0$). Also note that $P_L(C)$ and $P_L(D)$ are, by construction, line segments.

Detection of Vehicle Collision

To apply the results of the previous subsection to determining whether two vehicle overlap (i.e., have collided), consider the setup in Figure 3, which shows a host and a target. All coordinates in this figure are measured with respect to an arbitrary, fixed, ground coordinate system $\{G\}$. The figure's nomenclature is given in Table 1.

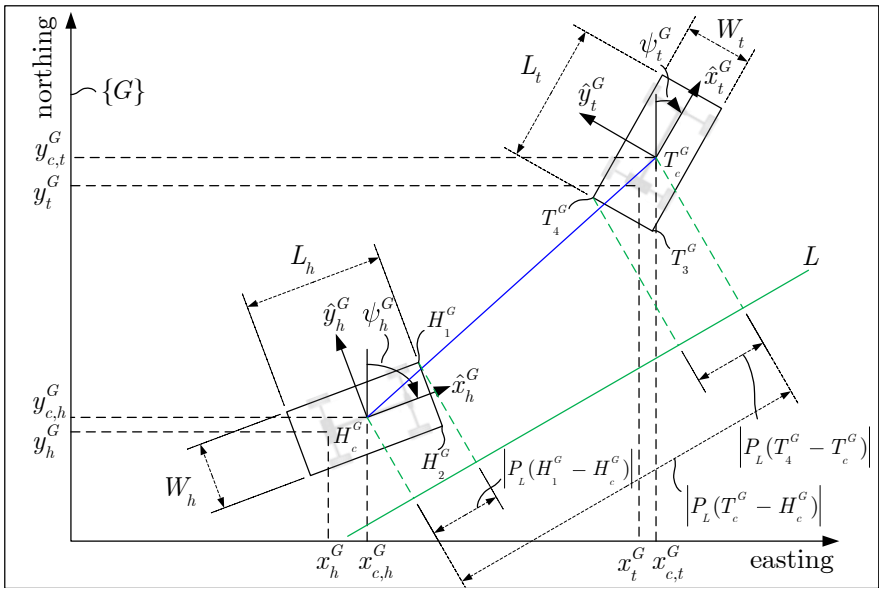

Figure 3: Coordinate framework for collision detection showing a host and a target vehicle.

To determine whether the host and target overlap, one can apply the SAT for convex polygons. Thus, assume that in Figure 3 the line L is a separating axis. Theorem 1 and Lemma 3 imply that

$$P_L(\text{Host}) \cap P_L(\text{Target}) = \phi \iff |P_L(T^G_c - H^G_c)| > 1/2|P_L(\text{Host})| + 1/2|P_L(\text{Target})|. \tag{3}$$

That is, the host and the target *do not collide* if the right hand side on the expression above holds[6]. The latter can be expanded as follows:

$$|P_L(T_c^G - H_c^G)| > \max\{|P_L(H_1^G - H_c^G)|, |P_L(H_2^G - H_c^G)|\} + \max\{|P_L(T_4^G - T_c^G)|, |P_L(T_3^G - T_c^G)|\}. \quad (4)$$

This inequality can be expressed in term of the variables shown in Figure 3 by noticing that

$$|P_L(H_1^G - H_c^G)| = |\langle H_1^G - H_c^G, \hat{v}\rangle \hat{v}| = |\langle L_h/2\hat{x}^H + W_h/2\hat{y}^H, \hat{v}\rangle|,$$

and that

$$\begin{aligned} |P_L(H_2^G - H_c^G)| &= |\langle L_h/2\hat{x}^H - W_h/2\hat{y}^H, \hat{v}\rangle|, \\ |P_L(T_4^G - T_c^G)| &= |\langle -L_t/2\hat{x}^T + W_t/2\hat{y}^T, \hat{v}\rangle|, \\ |P_L(T_3^G - T_c^G)| &= |\langle -L_t/2\hat{x}^T - W_t/2\hat{y}^T, \hat{v}\rangle|. \end{aligned}$$

Thus, condition (4) is equivalent to

$$\begin{aligned} |P_L(T_c^G - H_c^G)| > \max\{|\langle L_h/2\hat{x}^H + W_h/2\hat{y}^H, \hat{v}\rangle|, |\langle L_h/2\hat{x}^H - W_h/2\hat{y}^H, \hat{v}\rangle|\} \\ + \max\{|\langle L_t/2\hat{x}^T + W_t/2\hat{y}^T, \hat{v}\rangle|, |\langle L_t/2\hat{x}^T - W_t/2\hat{y}^T, \hat{v}\rangle|\}. \quad (5) \end{aligned}$$

According to Corollary 4, it is sufficient to limit the search for a line L that would fulfill (5) to those parallel to the sides of the host and target vehicles. If no one if these lines satisfies (5), then the host and target vehicles overlap. This leads to the following result.

Corollary 5. *The host and target vehicles shown in Figure 3* do not *collide if and only if* any *the following four conditions holds:*

$$\begin{aligned} |\langle T_c^G - H_c^G, \hat{x}_h^G\rangle| &> L_h/2 + \max\{|\langle L_t/2\hat{x}_t^G + W_t/2\hat{y}_t^G, \hat{x}_h^G\rangle|, |\langle L_t/2\hat{x}_t^G - W_t/2\hat{y}_t^G, \hat{x}_h^G\rangle|\}, \\ |\langle T_c^G - H_c^G, \hat{y}_h^G\rangle| &> W_h/2 + \max\{|\langle L_t/2\hat{x}_t^G + W_t/2\hat{y}_t^G, \hat{y}_h^G\rangle|, |\langle L_t/2\hat{x}_t^G - W_t/2\hat{y}_t^G, \hat{y}_h^G\rangle|\}, \\ |\langle T_c^G - H_c^G, \hat{x}_t^G\rangle| &> L_t/2 + \max\{|\langle L_h/2\hat{x}_h^G + W_h/2\hat{y}_h^G, \hat{x}_t^G\rangle|, |\langle L_h/2\hat{x}_h^G - W_h/2\hat{y}_h^G, \hat{x}_t^G\rangle|\}, \\ |\langle T_c^G - H_c^G, \hat{y}_t^G\rangle| &> W_t/2 + \max\{|\langle L_h/2\hat{x}_h^G + W_h/2\hat{y}_h^G, \hat{y}_t^G\rangle|, |\langle L_h/2\hat{x}_h^G - W_h/2\hat{y}_h^G, \hat{y}_t^G\rangle|\}. \end{aligned}$$

Proof : This result follows directly from Theorem 1 and Corollary 4. ∎

The inequalities in Corollary 5 can be simplified by using a more conservative definition of "non-collision" conditions as follows.

Corollary 6. *The host and target vehicles shown in Figure 3* do not *collide if* any *the following four conditions holds:*

$$|\langle T_c^G - H_c^G, \hat{x}_h^G\rangle| > \left(L_h + \sqrt{(L_t)^2 + (W_t)^2}\right)/2, \quad (6)$$

$$|\langle T_c^G - H_c^G, \hat{y}_h^G\rangle| > \left(W_h + \sqrt{(L_t)^2 + (W_t)^2}\right)/2, \quad (7)$$

$$|\langle T_c^G - H_c^G, \hat{x}_t^G\rangle| > \left(L_t + \sqrt{(L_h)^2 + (W_h)^2}\right)/2, \quad (8)$$

$$|\langle T_c^G - H_c^G, \hat{y}_t^G\rangle| > \left(W_t + \sqrt{(L_h)^2 + (W_h)^2}\right)/2. \quad (9)$$

Although simpler, conditions (6)-(9) are more conservative. That is, a host and a target may not satisfy these condition and still not be in collision. As it will be seen next, these leads to an over estimation of the probability of collision.

[6]The inequality in (3) is often stated as a "greater or equal" inequality, to allow for the fact that the vehicles may share common edge (i.e., just touch). Here, a "more than" inequality is used to guarantee full separation between vehicles.

[1]The world currently outputs the position of the center of a vehicle's back axel (host or target). Here it is assumed that, in the future, the world model will also output the length, L, and width, W, every target vehicle.

Table 1: Figure 3 nomenclature.

	Signal	Explanation	Unit
Target	$T_c^G = (x_{c,t}^G, y_{c,t}^G)$	Target geometric center position w.r.t. $\{G\}$	m,m
	$x_{c,t}^G$	Target geometrical center[1] easting position	m
	$y_{c,t}^G$	Target geometrical center northing position	m
	x_t^G	Target rear axle center easting position	m
	y_t^G	Target rear axle center northing position	m
	ψ_t^G	Target rear axle heading (clockwise positive)	rad
	$\hat{x}_t^G$	Unitary vector parallel to the Target's heading in $\{G\}$ coordinates	
	$\hat{y}_t^G$	Unitary vector perpendicular to the Target's heading in $\{G\}$ coordinates	
	L_t	Target vehicle's length	m
	W_t	Target vehicle's width	m
	T_3^G (T_4^G)	Target vehicle's back right (left) corner position w.r.t. $\{G\}$	m,m
Host	$H_c^G = (x_{c,h}^G, y_{c,h}^G)$	Host geometric center position w.r.t. $\{G\}$	m,m
	$x_{c,h}^G$	Host geometrical center[1] easting position	m
	$y_{c,h}^G$	Host geometrical center northing position	m
	x_h^G	Host rear axle center easting position	m
	y_h^G	Host rear axle center northing position	m
	ψ_h^G	Host rear axle heading (clockwise positive)	rad
	$\hat{x}_h^G$	Unitary vector parallel to the Host's heading in $\{G\}$ coordinates	
	$\hat{y}_h^G$	Unitary vector perpendicular to the Host's heading in $\{G\}$ coordinates	
	L_h	Host vehicle's length	m
	W_h	Host vehicle's width	m
	H_1^G (H_2^G)	Host vehicle's front right (left) corner position w.r.t. $\{G\}$	m,m
Projections	L	Separating axis candidate	
	$\lvert P_L(T_c^G - H_c^G)\rvert$	Projection magnitude of vector $T_c^G - H_c^G$ over L	m
	$\lvert P_L(H_1^G - H_c^G)\rvert$	Projection magnitude of vector $H_1^G - H_c^G$ over L	m
	$\lvert P_L(T_4^G - T_c^G)\rvert$	Projection magnitude of vector $T_4^G - T_c^G$ over L	m

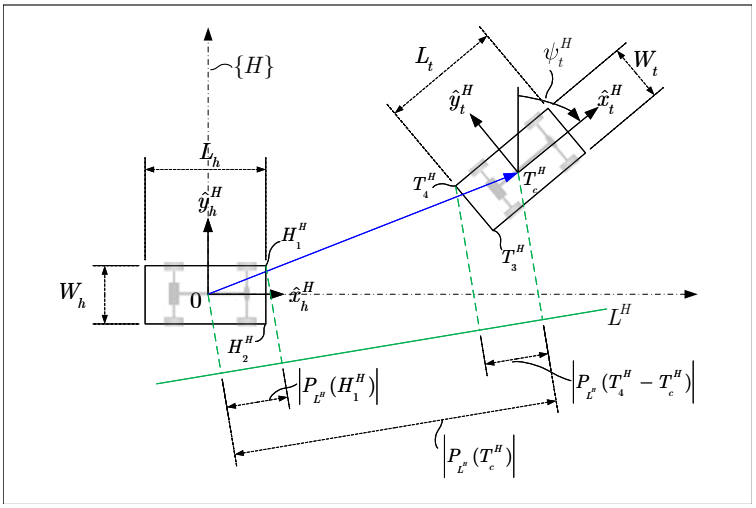

Figure 4: Host coordinate framework for collision detection showing a host and a target vehicle. The variables are defined as in Table 1, replacing the superscript ^{G} with ^{H}.

Estimation of Probability of Collision

The estimation of probability of collision is performed by the host vehicle based on measurements provided by its perception system. These measurements include the target position w.r.t. the host, T_c^H, and the target's heading w.r.t., ψ_t^H, and assume the frame of reference shown in Figure 4 (a rotated version of Figure 3). It follows from this figure that:

$$H_c^H = 0, \quad \hat{x}_h^H = (1,0), \quad \hat{y}_h^H = (0,1), \quad \hat{x}_t^H = (\sin(\phi_t^H), \cos(\phi_t^H)), \quad \hat{y}_t^H = (-\cos(\phi_t^H), \sin(\phi_t^H)).$$

As mentioned before, the uncertainty associated with the host vehicle sensor measurements and the predictions of future host/target behavior is what makes checking (6)-(9) non-deterministic. The uncertain sensor measurements can be treated as random variables with associated Probability Density Functions (PDFs). These variables will be denoted in the sequel in boldface fonts. The primary sensor measures, upon which any other quantities are derived, are listed next.

Assumption 1. *The following (primary) quantities are assumed to be independent random variables defined over the probability space* $(\Omega, \mathscr{F}, \mathrm{P})$. *They are shown with their associated PDFs.*

$$\boldsymbol{T}_c^H = (\boldsymbol{x}_{c,t}^H, \boldsymbol{y}_{c,t}^H) \sim f_{T_c} = f_{x_{c,t}} f_{y_{c,t}}, \quad \text{where} \quad \boldsymbol{x}_{c,t}^H \sim f_{x_{c,t}} \quad \text{and} \quad \boldsymbol{y}_{c,t}^H \sim f_{y_{c,t}}$$
$$\boldsymbol{\psi}_t^H \sim f_{\psi_t}, \quad \boldsymbol{L}_t \sim f_{L_t}, \quad \boldsymbol{W}_t \sim f_{W_t}.$$

Since current automated vehicle not in general have the ability of directly estimating W_t or L_t from sensor measurements, the following assumption will be accepted as true in the sequel.

Assumption 2. *The target's size is communicated via vehicle-to-vehicle communication to the host.*

These assumptions and conditions (6)-(9) can be used to derive an over-estimate of the probability of collision as follows: Let $C_1, C_2, C_3, C_4 \subset \Omega$ be the following events

$$C_1 \triangleq \{\omega \in \Omega \mid |\boldsymbol{x}_{c,t}^H| > \left(L_h + \sqrt{(L_t)^2 + (W_t)^2}\right)/2\},$$
$$C_2 \triangleq \{\omega \in \Omega \mid |\boldsymbol{y}_{c,t}^H| > \left(W_h + \sqrt{(L_t)^2 + (W_t)^2}\right)/2\},$$
$$C_3 \triangleq \{\omega \in \Omega \mid |\boldsymbol{x}_{c,t}^H \sin(\boldsymbol{\psi}_t^h) + \boldsymbol{y}_{c,t}^H \cos(\boldsymbol{\psi}_t^h)| > \left(L_t + \sqrt{(L_h)^2 + (W_h)^2}\right)/2\},$$
$$C_4 \triangleq \{\omega \in \Omega \mid |\boldsymbol{x}_{c,t}^H \cos(\boldsymbol{\psi}_t^h) - \boldsymbol{y}_{c,t}^H \sin(\boldsymbol{\psi}_t^h)| > \left(W_t + \sqrt{(L_h)^2 + (W_h)^2}\right)/2\}.$$

Further, let $A \subset \Omega$ be the event "host and target do not collide" defined according to Corollary 6. That is, $A \triangleq \left\{\omega \in \Omega \,|\, \omega \in \bigcup_{i=1}^{4} C_i\right\}$. It follows from this definition and from De Morgan's laws that $\bar{A} \triangleq \Omega - A$, the "host and target collide" event, is given by:$\bar{A} \triangleq \left\{\omega \in \Omega | \omega \in \bigcap_{i=1}^{4} \bar{C}_i\right\}$, where $\bar{C}_i = \Omega - C_i$, $i = 1, \cdots, 4$. This lead to the following result

Theorem 7. *Consider the host and target vehicle in Figure 4. Under Assumptions 1 and 2, the probability of collision between the host and target,* $\mathrm{P}\{\mathcal{H}\}$ *can be* overestimated *as follows:*

$$\mathrm{P}\{\mathcal{H}\} = \mathrm{P}\{\text{"Host-Target Collide"}\} \leq \mathrm{P}\{\omega \in \Omega \,|\, \omega \in \bar{A}\} = \mathrm{P}\{(\boldsymbol{x}_{c,t}^H, \boldsymbol{y}_{c,t}^H, \boldsymbol{\psi}_t^H) \in R_1 \cap R_2(\boldsymbol{\psi}_t^H) \times [0, 2\pi)\},$$

where $R_1, R_2(\boldsymbol{\psi}_t^H) \subset \mathbb{R}^2$ *are rectangular regions in* $\mathbb{R}^2$ *given, respectively, by:*

$$R_1 \triangleq \{(x,y) \in \mathbb{R}^2 \,|\, |x| \leq 0.5(L_h + \sqrt{(L_t)^2 + (W_t)^2}), |y| \leq 0.5(W_h + \sqrt{(L_t)^2 + (W_t)^2})\},$$

and

$$R_2(\boldsymbol{\psi}_t^H) \triangleq \left\{(x,y) \in \mathbb{R}^2 \,|\, (x,y) = r \begin{bmatrix} \sin(\boldsymbol{\psi}_t^H) \\ \cos(\boldsymbol{\psi}_t^H) \end{bmatrix} + s \begin{bmatrix} \cos(\boldsymbol{\psi}_t^H) \\ -\sin(\boldsymbol{\psi}_t^H) \end{bmatrix}; \right.$$
$$\left. |r| \leq 0.5(L_t + \sqrt{(L_h)^2 + (W_h)^2}), |s| \leq 0.5(W_t + \sqrt{(L_h)^2 + (W_h)^2}) \right\}.$$

Proof: Recall that A is defined based on conditions (6)-(9). Since these are conservative, it follows that A is a subset of the event "Host and Target do not Collide". This in turn implies that $\mathrm{P}\{\text{"Host-Target Collide"}\} \leq \mathrm{P}\{\omega \in \Omega \,|\, \omega \in \bar{A}\}$. Next, observe from the definition of A that

$$\bar{A} = \left\{\omega \in \Omega | \omega \in (\bar{C}_1 \cap \bar{C}_2) \cap (\bar{C}_3 \cap \bar{C}_4) \cap \Omega\right\}. \tag{10}$$

The three terms in the RHS of the expression above can be further developed.

$$\begin{aligned} \bar{C}_1 \cap \bar{C}_2 &= \left\{\omega \in \Omega \,|\, |\boldsymbol{x}_{c,t}^H| \leq \left(L_h + \sqrt{(L_t)^2 + (W_t)^2}\right)/2\right\} \\ &\qquad \bigcap \left\{\omega \in \Omega \,|\, |\boldsymbol{y}_{c,t}^H| \leq \left(W_h + \sqrt{(L_t)^2 + (W_t)^2}\right)/2\right\} \\ &= \left\{\omega \in \Omega \,|\, |\boldsymbol{x}_{c,t}^H| \leq \left(L_h + \sqrt{(L_t)^2 + (W_t)^2}\right)/2, |\boldsymbol{y}_{c,t}^H| \leq \left(W_h + \sqrt{(L_t)^2 + (W_t)^2}\right)/2\right\} \\ &= \left\{\omega \in \Omega \,|\, (\boldsymbol{x}_{c,t}^H, \boldsymbol{y}_{c,t}^H) \in R_1\right\}. \end{aligned} \tag{11}$$

Similarly:

$$(\bar{C}_3 \cap \bar{C}_4) \cap \Omega = (\bar{C}_3 \cap \bar{C}_4) \cap \{\omega \in \Omega \,|\, \boldsymbol{\psi}_t^H \in [0, 2\pi)\}$$

and

$$(\bar{C}_3 \cap \bar{C}_4) = \{\omega \in \Omega \,|\, |\boldsymbol{x}_{c,t}^H \sin(\boldsymbol{\psi}_t^h) + \boldsymbol{y}_{c,t}^H \cos(\boldsymbol{\psi}_t^h)| \leq \left(L_t + \sqrt{(L_h)^2 + (W_h)^2}\right)/2,$$
$$|\boldsymbol{x}_{c,t}^H \cos(\boldsymbol{\psi}_t^h) - \boldsymbol{y}_{c,t}^H \sin(\boldsymbol{\psi}_t^h)| \leq \left(W_t + \sqrt{(L_h)^2 + (W_h)^2}\right)/2\}.$$

The above expression can be further developed by letting $\boldsymbol{r} = \boldsymbol{x}_{c,t}^H \sin(\boldsymbol{\psi}_t^h) + \boldsymbol{y}_{c,t}^H \cos(\boldsymbol{\psi}_t^h)$ and $\boldsymbol{s} = \boldsymbol{x}_{c,t}^H \cos(\boldsymbol{\psi}_t^h) - \boldsymbol{y}_{c,t}^H \sin(\boldsymbol{\psi}_t^h)$, and observing that

$$\begin{bmatrix} \boldsymbol{r} \\ \boldsymbol{s} \end{bmatrix} = \begin{bmatrix} \sin(\boldsymbol{\psi}_t^h) & \cos(\boldsymbol{\psi}_t^h) \\ \cos(\boldsymbol{\psi}_t^h) & -\sin(\boldsymbol{\psi}_t^h) \end{bmatrix} \begin{bmatrix} \boldsymbol{x}_{c,t}^H \\ \boldsymbol{y}_{c,t}^H \end{bmatrix},$$

so

$$\begin{bmatrix} \boldsymbol{x}_{c,t}^H \\ \boldsymbol{y}_{c,t}^H \end{bmatrix} = \begin{bmatrix} \sin(\boldsymbol{\psi}_t^h) & \cos(\boldsymbol{\psi}_t^h) \\ \cos(\boldsymbol{\psi}_t^h) & -\sin(\boldsymbol{\psi}_t^h) \end{bmatrix} \begin{bmatrix} \boldsymbol{r} \\ \boldsymbol{s} \end{bmatrix} = \boldsymbol{r} \begin{bmatrix} \sin(\boldsymbol{\psi}_t^h) \\ \cos(\boldsymbol{\psi}_t^h) \end{bmatrix} + \boldsymbol{s} \begin{bmatrix} \cos(\boldsymbol{\psi}_t^h) \\ -\sin(\boldsymbol{\psi}_t^h) \end{bmatrix}.$$

This implies that

$$(\bar{C}_3 \cap \bar{C}_4) \cap \Omega = \Big\{ \omega \in \Omega \mid \begin{bmatrix} \boldsymbol{x}_{c,t}^H \\ \boldsymbol{y}_{c,t}^H \end{bmatrix} = \boldsymbol{r} \begin{bmatrix} \sin(\boldsymbol{\psi}_t^h) \\ \cos(\boldsymbol{\psi}_t^h) \end{bmatrix} + \boldsymbol{s} \begin{bmatrix} \cos(\boldsymbol{\psi}_t^h) \\ -\sin(\boldsymbol{\psi}_t^h) \end{bmatrix}, \\ |\boldsymbol{r}| \leq 0.5(L_t + \sqrt{(L_h)^2 + (W_h)^2}), |\boldsymbol{s}| \leq 0.5(W_t + \sqrt{(L_h)^2 + (W_h)^2}); \boldsymbol{\psi}_t^H \in [0, 2\pi) \Big\}$$

or, equivalently, that

$$(\bar{C}_3 \cap \bar{C}_4) \cap \Omega = \Big\{ \omega \in \Omega \mid (\boldsymbol{x}_{c,t}^H, \boldsymbol{y}_{c,t}^H) \in R_2(\boldsymbol{\psi}_t^H); \psi_t^H \in [0, 2\pi) \Big\}. \tag{12}$$

Replacing (11)-(12) into (10) yields

$$\begin{aligned} A &= \Big\{ \omega \in \Omega \mid (\boldsymbol{x}_{c,t}^H, \boldsymbol{y}_{c,t}^H) \in R_1 \cap R_2(\boldsymbol{\psi}_t^H); \psi_t^H \in [0, 2\pi) \Big\} \\ &= \Big\{ \omega \in \Omega \mid (\boldsymbol{x}_{c,t}^H, \boldsymbol{y}_{c,t}^H, \boldsymbol{\psi}_t^H) \in R_1 \cap R_2(\boldsymbol{\psi}_t^H) \times [0, 2\pi) \Big\}, \end{aligned}$$

which proves the Theorem. ∎

To end this section, we provide a numerical implementation of the results in Theorem 7.

A Numerical Implementation

The goal here is to compute $\mathrm{P}\{(\boldsymbol{x}_{c,t}^H, \boldsymbol{y}_{c,t}^H) \in R_1 \cap R_2(\boldsymbol{\psi}_t^H); \boldsymbol{\psi}_t^H \in [0, 2\pi)\}$. Formally,

$$\mathrm{P}\{(\boldsymbol{x}_{c,t}^H, \boldsymbol{y}_{c,t}^H) \in R_1 \cap R_2(\boldsymbol{\psi}_t^H); \boldsymbol{\psi}_t^H \in [0, 2\pi)\} \\ = \iiint 1_{\{(x,y,\psi) \in R_1 \cap R_2(\boldsymbol{\psi}_t^H) \times \in [0,2\pi)\}} f_{x_{c,t}, y_{c,t}, \psi_t} \mathrm{d}x \mathrm{d}y \mathrm{d}\psi.$$

Under Assumption 1, the above expression can be further simplified as follows:

$$\mathrm{P}\{(\boldsymbol{x}_{c,t}^H, \boldsymbol{y}_{c,t}^H) \in R_1 \cap R_2(\boldsymbol{\psi}_t^H); \boldsymbol{\psi}_t^H \in [0, 2\pi)\} \\ = \int 1_{\{\psi \in [0,2\pi)\}} \left(\iint 1_{\{(x,y,\psi) \in R_1 \cap R_2(\boldsymbol{\psi}_t^H)\}} f_{x_{c,t}, y_{c,t}} \mathrm{d}x \mathrm{d}y \right) f_{\psi_t} \mathrm{d}\psi. \tag{13}$$

To further simplify the expression above, knowledge of the specific type of distributions for each random variable would be needed. In the absence of emperical information, the following assumption will be made:

Assumption 3. *$\boldsymbol{x}_{c,t}^H$, $\boldsymbol{y}_{c,t}^H$, and $\boldsymbol{\psi}_t^H$ are uniformly distributed random variables.*

Since the world model provides estimates of the mean, μ, and variance, σ^2, for each measured variable, the probability density functions associated with $\boldsymbol{x}_{c,t}^H$, $\boldsymbol{y}_{c,t}^H$, and $\boldsymbol{\psi}_t^H \boldsymbol{x}_{c,t}^H$, $\boldsymbol{y}_{c,t}^H$, and $\boldsymbol{\psi}_t^H$ are given by:

$$f_{x_{c,t}} = \frac{1}{\sqrt{12}\sigma_{x_{c,t}^H}} 1_{\{x \in [\mu_{x_{c,t}^H} - \sqrt{3}\sigma_{x_{c,t}^H}, \mu_{x_{c,t}^H} + \sqrt{3}\sigma_{x_{c,t}^H}]\}},$$
$$f_{y_{c,t}} = \frac{1}{\sqrt{12}\sigma_{y_{c,t}^H}} 1_{\{y \in [\mu_{y_{c,t}^H} - \sqrt{3}\sigma_{y_{c,t}^H}, \mu_{y_{c,t}^H} + \sqrt{3}\sigma_{y_{c,t}^H}]\}},$$

and

$$f_{\psi_t} = \frac{1}{\sqrt{12}\sigma_{\psi_t^H}} 1_{\{\psi \in [\mu_{\psi_t^H} - \sqrt{3}\sigma_{\psi_t^H}, \mu_{\psi_t^H} + \sqrt{3}\sigma_{\psi_t^H}]\}}.$$

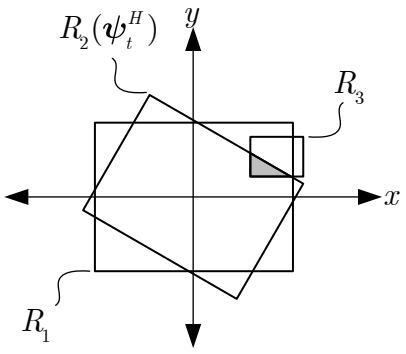

Figure 5: The gray area shows the region of integration associated with (14).

Replacing the above functions in (13) yields, after a few manipulations, the following:

$$\mathrm{P}\{(\boldsymbol{x}_{c,t}^H, \boldsymbol{y}_{c,t}^H) \in R_1 \cap R_2(\boldsymbol{\psi}_t^H)\boldsymbol{\psi}_t^H \in [0, 2\pi)\}$$
$$= \frac{1}{12\sqrt{12}\sigma_{x_{c,t}^H}\sigma_{y_{c,t}^H}\sigma_{\psi_t^H}} \int_{\mu_{\psi_t^H}-\sqrt{3}\sigma_{\psi_t^H}}^{\mu_{\psi_t^H}+\sqrt{3}\sigma_{\psi_t^H}} \left(\iint 1_{\{(x,y,\psi)\in R_1\cap R_2(\psi)\cap R_3\}} \mathrm{d}x\mathrm{d}y \right) \mathrm{d}\psi, \quad (14)$$

where $R_3 \subset \mathbb{R}^2$ is the rectangular subset of $\mathbb{R}^2$ given by:

$$R_3 \triangleq \{(x,y) \in \mathbb{R}^2 \mid x \in [\mu_{x_{c,t}^H} - \sqrt{3}\sigma_{x_{c,t}^H}, \mu_{x_{c,t}^H} + \sqrt{3}\sigma_{x_{c,t}^H}], y \in [\mu_{y_{c,t}^H} - \sqrt{3}\sigma_{y_{c,t}^H}, \mu_{y_{c,t}^H} + \sqrt{3}\sigma_{y_{c,t}^H}]\}.$$

Note that the expression between parenthesis in (14) is the area of the polygon created by intersecting R_1, $R_2(\psi)$, and R_3 (the intesection could also be empty). An example of this intersection is shown in Figure 5. Let $m(R_1 \cap R_2(\psi) \cap R_3)$ denote this area and observe that it is a function of the angle ψ. Although a formula could be derived to compute this area as a function of ψ, such an expression would not provide more insights or lead to simplifications. Hence, a numerical approach is better suited to compute (14).

To this end, let $1 \leq n \in \mathbb{Z}^+$ and set $\psi_i = \mu_{\psi_t^H} + \sqrt{3}\sigma_{\psi_t^H}\left(\frac{2i}{n} - 1\right)$, $i = 0, \ldots, n-1$. The right hand side of (14) can now be approximated as follows:

$$\mathrm{P}\{(\boldsymbol{x}_{c,t}^H, \boldsymbol{y}_{c,t}^H) \in R_1 \cap R_2(\boldsymbol{\psi}_t^H)\boldsymbol{\psi}_t^H \in [0, 2\pi)\} \approx \frac{1}{12n\sigma_{x_{c,t}^H}\sigma_{y_{c,t}^H}} \sum_{i=0}^{n-1} m(R_1 \cap R_2(\psi_i) \cap R_3) \quad (15)$$

where, for every ψ_i, $m(R_1 \cap R_2(\psi_i) \cap R_3)$ can be computed using standard functions for polygon intersection (see, e.g., Sutherland-Hodgman Polynomial Clipping Algorithm in [28]) and polygon area [29]. The calculation of (15) can be performed numerically by implementing Algorithm 1.

CONCLUSIONS

This article proposed a methodology to compute the "safety" of a vehicle quantitatively, so it can be used by automated vehicle for decision making and control. The methodology treats each interaction a vehicle has with other road user and road interactions as potential hazards and assigns each value of risk. The risk a hazard imposes on the vehicle in derived from the hazard's likelihood, hazardousness, and from the capability of the vehicle to avoid it. The article also offered a theoretical method to estimate the likelihood of two-dimensional collision hazards (an extension of the work in [9]) and recommendations on how to estimate hazard hazardousness.

Algorithm 1 InSTProbColEstimator: Instantaneous, Single Target, Host-Target Probability of Collision Estimator

Require: $W_h > 0, L_h > 0, W_t > 0, L_t > 0$ {host & target dimensions}

Require: $x^H_{c,t}, y^H_{c,t}, \sigma_{x^H_{c,t}} \geq 0, \sigma_{y^H_{c,t}} \geq 0$ {mean and variance of the target position w.r.t. the host}

Require: $\psi^H_t, \sigma_{\psi^H_t} \geq 0$ {mean and variance of the target's heading w.r.t. the host's vertical axis}

Require: $n \geq 1$ {number of discretization points for the range of $\boldsymbol{\psi}^H_t$ }

Ensure: $PCol =$ Probability of Collision

$PCol \leftarrow 0$ {$PCol$ is zero by default}

$$R_1 \leftarrow \begin{bmatrix} -0.5(L_h+\sqrt{(L_t)^2+(W_t)^2}) & -0.5(W_h+\sqrt{(L_t)^2+(W_t)^2}) \\ 0.5(L_h+\sqrt{(L_t)^2+(W_t)^2}) & -0.5(W_h+\sqrt{(L_t)^2+(W_t)^2}) \\ 0.5(L_h+\sqrt{(L_t)^2+(W_t)^2}) & 0.5(W_h+\sqrt{(L_t)^2+(W_t)^2}) \\ -0.5(L_h+\sqrt{(L_t)^2+(W_t)^2}) & 0.5(W_h+\sqrt{(L_t)^2+(W_t)^2}) \end{bmatrix} \{R_1 \text{ vertices, counterclockwise (CCW)}\}$$

$$R_3 \leftarrow \begin{bmatrix} x^H_{c,t}-\sqrt{3}\sigma_{x^H_{c,t}} & y^H_{c,t}-\sqrt{3}\sigma_{y^H_{c,t}} \\ x^H_{c,t}+\sqrt{3}\sigma_{x^H_{c,t}} & y^H_{c,t}-\sqrt{3}\sigma_{y^H_{c,t}} \\ x^H_{c,t}+\sqrt{3}\sigma_{x^H_{c,t}} & y^H_{c,t}+\sqrt{3}\sigma_{y^H_{c,t}} \\ x^H_{c,t}-\sqrt{3}\sigma_{x^H_{c,t}} & y^H_{c,t}+\sqrt{3}\sigma_{y^H_{c,t}} \end{bmatrix} \{R_3 \text{ vertices, CCW}\}$$

$[RisEmpty, R] \leftarrow PolyIntersect(R_1, R_3)$ {R: $R_1 \cap R_3$ CCW vertices. If empty, $RisEmpty = 1$}

if $\neg RisEmpty$ **then**

  for $i = 0$ to $n-1$ **do**

    $\psi \leftarrow \psi^H_t + \sqrt{3}\sigma_{\psi^H_t}\left(\frac{2i}{n} - 1\right)$

$$R_2 \leftarrow \begin{bmatrix} -0.5(L_t+\sqrt{(L_h)^2+(W_h)^2}) & 0.5(W_t+\sqrt{(L_h)^2+(W_h)^2}) \\ -0.5(L_t+\sqrt{(L_h)^2+(W_h)^2}) & -0.5(W_t+\sqrt{(L_h)^2+(W_h)^2}) \\ 0.5(L_t+\sqrt{(L_h)^2+(W_h)^2}) & -0.5(W_t+\sqrt{(L_h)^2+(W_h)^2}) \\ 0.5(L_t+\sqrt{(L_h)^2+(W_h)^2}) & 0.5(W_t+\sqrt{(L_h)^2+(W_h)^2}) \end{bmatrix} \begin{bmatrix} \sin(\psi) & \cos(\psi) \\ -\cos(\psi) & \sin(\psi) \end{bmatrix} \{R_2(\psi_i) \text{ CCW vertices}\}$$

    $[R_aEmpty, R_a] \leftarrow PolyIntersect(R, R_2)$ {R_a:$R_1 \cap R_3 \cap R_2(\psi)$ CCW vertices. If empty, $R_aEmpty = 1$}

    if $\neg R_aEmpty$ **then**

      $PCol \leftarrow PCol + PolyArea(R_a)$

    end if

  end for

  $PCol \leftarrow PCol/(12n\sigma_{x^H_{c,t}}\sigma_{y^H_{c,t}})$

end if

Further work is required to link the likelihood estimator with motion predictor models, and to validated the complete methodology first by detailed simulations and they by experimentation.

Acknowledgements
The authors would like to thank Stefanie Hair-Buijssen (TNO), Richard van der Horst, Aliaksei Laureshyn (Lund University), Erwin de Gelder (TNO), Jan-Pieter Paardekooper (TNO), Ron Snijders (TNO), and Jeroen Manders (TNO) for important information and discussions that sharpened the ideas in this article.

References

[1] NHTSA. (2017) 2016 fatal motor vehicle crashes: Overview. Accessed on March 07, 2019. [Online]. Available: https://www.nhtsa.gov/press-releases/usdot-releases-2016-fatal-traffic-crash-data

[2] S. Behere and M. Törngren, "A functional reference architecture for autonomous driving," *Information and Software Technology*, vol. 73, pp. 136 – 150, 2016.

[3] Y. Luo, A. K. Saberi, T. Bijlsma, J. J. Lukkien, and M. van den Brand, "An architecture pattern for safety critical automated driving applications: Design and analysis," in *2017 Annual IEEE International Systems Conference (SysCon)*, April 2017, pp. 1–7.

[4] A. Svensson and C. Hydén, "Estimating the severity of safety related behavior," *Accid Anal Prev*, vol. 38, no. 2, pp. 379 – 385, 2006.

[5] L. Zheng, K. Ismail, and X. Meng, "Traffic conflict techniques for road safety analysis: open questions and some insights," *Canadian Journal of Civil Engineering*, vol. 41, no. 7, pp. 633–641, 2014.

[6] F. Diederichs, T. Schüttke, and D. Spath, "Driver intention algorithm for pedestrian protection and automated emergency braking systems," in *2015 IEEE 18th International Conference on Intelligent Transportation Systems*, Sep. 2015, pp. 1049–1054.

[7] E. Dagan, O. Mano, G. P. Stein, and A. Shashua, "Forward collision warning with a single camera," in *IEEE Intelligent Vehicles Symposium, 2004*, June 2004, pp. 37–42.

[8] ISO 26262-1:2018, road vehicles – functional safety – part 1: Vocabulary. ISO. [Online]. Available: https://www.iso.org/standard/68383.html

[9] T. van den Broek and J. Ploeg, "Collision warning system based on probability density functions,," in *WIT 2010 - 7th International Workshop on Intelligent Transportation*, March 2010, pp. 141–148.

[10] E. van Nunen, T. van den Broek, M. Kwakkernaat, and D. Kotiadis, "Implementation of probabilistic risk estimation for VRU safety," in *WIT 2011 - 8th International Workshop on Intelligent Transportation*, March 2011, pp. 149–155.

[11] D. Lord and S. Washington, *Chapter 1. Introduction*, 2018, ch. Chapter 1, pp. 1–10.

[12] M. Belin, R. Johansson, J. Lindberg, and C. Tingvall, "The vision zero and its consequences1," in *4th International Conference on Safety and the Environment in the 21st Century*, Nov. 1997, pp. 1–14.

[13] W. Wijnen, W. Weijermars, W. Vanden Berghe, A. Schoeters, R. Bauer, L. Carnis, R. Elvik, A. Theofilatos, A. Filtness, S. Reed, C. Perez, and H. Martensen, "Crash cost estimates for european countries," Eindhoven University of Technology, Deliverable 3.2 of the H2020 project SafetyCube, 2017, http://www.safetycube-project.eu/publications/.

[14] A. Laureshyn, T. De Ceunynck, C. Karlsson, A. Svensson, and S. Daniels, "In search of the severity dimension of traffic events: Extended Delta-V as a traffic conflict indicator," *Accid Anal Prev*, vol. 98, pp. 46–56, Jan 2017.

[15] A. P. Tarko, *Chapter 17. Surrogate Measures of Safety*, 2018, ch. Chapter 17, pp. 383–405.

[16] A. Laureshyn, A. Svensson, and C. Hydén, "Evaluation of traffic safety, based on micro-level behavioural data: Theoretical framework and first implementation," *Accident Analysis & Prevention*, vol. 42, no. 6, pp. 1637 – 1646, 2010.

[17] O. op den Camp, S. van Montfort, J. Uittenbogaard, and J. Welten, "Cyclist target and test setup for evaluation of cyclist-autonomous emergency braking," *International Journal of Automotive Technology*, vol. 18, no. 6, pp. 1085–1097, Dec 2017.

[18] S. S. Mahmud, L. Ferreira, M. S. Hoque, and A. Tavassoli, "Application of proximal surrogate indicators for safety evaluation: A review of recent developments and research needs," *IATSS Research*, vol. 41, no. 4, pp. 153 – 163, 2017.

[19] A. Laureshyn, "Application of automated video analysis to road user behaviour," Ph.D. dissertation, Lund University, 2010.

[20] F. A. Mullakkal-Babu, M. Wang, H. Farah, B. van Arem, and R. Happee, "Comparative assessment of safety indicators for vehicle trajectories on highways," *Transportation Research Record*, vol. 2659, no. 1, pp. 127–136, 2017.

[21] K. Ismail, T. Sayed, and N. Saunier, "Methodologies for aggregating indicators of traffic conflict," *Transportation Research Record*, vol. 2237, no. 1, pp. 10–19, 2011.

[22] S. Yoshida, T. Hasegawa, S. Tominaga, and T. Nishimoto, "Development of injury prediction models for advanced automatic collision notification based on japanese accident data," *International Journal of Crashworthiness*, vol. 21, no. 2, pp. 112–119, 2016.

[23] S. Boyd and L. Vandenberghe, *Convex Optimization*. Cambridge: Cambridge University Press, 2009.

[24] V. L. Klee, Jr, "Strict separation of convex sets," *Proc. American Mathematical Society*, vol. 7, no. 4, pp. 735–737, August 1956.

[25] A. A. Ahmadi. (2016) Convex and conic optimization, lecture notes 5. Accessed on March, 2018. [Online]. Available: https://goo.gl/d4qTCY

[26] S. Gottschalk, "Separating axis theorem," Department of Computer Science, UNC Chappel Hill, Tech. Rep. TR96-024, 1996.

[27] P. J. Schneider and D. H. Eberly, *Geometric Tools for Computer Graphics*. Boston: Elsevier Science, 2003.

[28] J. D. Foley, A. van Dam, S. K. Feiner, and J. F. Hughes, *Computer Graphics: Principles and Practice*. Addison-Wesley Publishing Company, 1996.

[29] P. Bourke. (1988) Calculating the area and centroid of a polygon. Accessed on April 26, 2018. [Online]. Available: http://paulbourke.net/geometry/polygonmesh

DEVELOPMENT AND EVALUATION OF A THORAX INJURY PREDICTION TOOL (TIPT) AND POSSIBILITIES FOR INCORPORATION WITHIN IMPROVED TEST AND ASSESSMENT PROCEDURES – RESULTS FROM SENIORS

Oliver Zander
Marcus Wisch
Julian Ott
Federal Highway Research Institute (BASt)
Germany

Mark Burleigh
Humanetics Innovative Solutions
Germany

Alba Fornells
Applus IDIADA
Spain

Christer Lundgren
Autoliv
Sweden

Paper Number 19-0014

ABSTRACT

Test and assessment procedures for passive pedestrian protection of passenger cars are in place for many years within world-wide regulations as well as consumer test programmes. Nevertheless, recent accident investigations show a stagnation of pedestrian fatality numbers on European roads alongside increasing injury severities for older road users. The EU-funded SENIORS (Safety ENhancing Innovations for Older Road userS) project developed and evaluated a thorax injury prediction tool (TIPT) for later incorporation within test and assessment procedures.

Accident data indicates an increasing portion of AIS2 and AIS3+ thoracic injuries of older pedestrians and cyclists which are currently not assessed in any test procedure for vulnerable road users. Therefore, SENIORS focused on the development of a test tool predicting the risk of rib fractures of vulnerable road users (VRU). While injury risk functions were reanalyzed, human body model (HBM) simulations against categorized generic vehicle frontends served as input for the definition of test setups and corresponding impact parameters. TIPT component tests against a generic frontend and an actual vehicle were used for the evaluation of the technical feasibility.

The TIPT component tests shows the general feasibility of a test procedure for the assessment of thoracic injuries, with good repeatability and reproducibility of kinematics and results. Impact parameters such as the inclination angles of the thorax, angles of the velocity vector and impact speeds well replicate the parameters gained from the HBM simulations. The proposed markup and assessment scheme offers the possibility of a homogeneous evaluation of the protection potential of vehicle frontends while maintaining justifiable testing efforts. During evaluation testing, the proposed requirements were entirely met.

The developed prototype of TIPT and launching system offer impact angles and speeds as suggested by HBM simulations. However, since thorax impacts during pedestrian accidents do not occur perpendicularly to the vehicle surface in most cases, the TIPT built-in linear potentiometers do not acquire the true resultant intrusions on the ribcage and thus, TIPT rib deflections do not reflect the actual human injury risk. However; for the impact forward to the bonnet leading edge, the TIPT seems applicable without further modifications.

The test and assessment procedures using the TIPT offer for the first time the possibility of replicating the kinematics of a pedestrian thorax with a component test. The developed assessment scheme gives a first indication

on how the risk for thoracic injuries could be implemented within the Euro NCAP Box 3 assessment. Future development of the TIPT may focus on implementing a rib cage that can deflect in all axes in a humanlike way.

INTRODUCTION

Test and assessment procedures for passive pedestrian protection which are based on developments by the European Enhanced Vehicle-safety Committee (EEVC, 2002) have been introduced more than a decade ago within and harmonized to a large extent between world-wide regulations such as UN-GTR9 (2009) and consumer test programmes like Euro NCAP (2018). Despite continued improvements to passive vehicle safety of passenger cars, latest accident investigations resulted in a stagnation of pedestrian fatality numbers on European roads (European Commission, 2017), facing the risk of not meeting the European Union's goal of halving the number of road fatalities by the year 2020. The EC-funded research project SENIORS under the HORIZON 2020 framework programme developed modified pedestrian test and assessment procedures and impactors with the aim to improve passive pedestrian safety. In-depth accident studies investigated the injury severity of the mostly affected body regions of vulnerable road users (VRU) to figure out relevant fields of action. Current pedestrian impactors were analyzed regarding their ability to address recent accident scenarios and remaining open gaps were closed describing new impactor concepts. Paired simulations with human body models (HBM) and impactor models against generic test rigs were performed to generate correlations that could be used for thoracic injury criteria. Finally, a test tool for predicting thoracic injuries was prototyped and tested according to modified test and assessment procedures.

ACCIDENT STUDIES AND INJURY PATTERNS

A recent in-depth investigation of road accidents in Germany showed the injury severity of different VRU body regions subsequent to collisions with passenger cars. Besides the consistent relevance of severe pedestrian head and leg injuries in collisions with passenger cars registered between 1995 and 2005 and between 2006 and 2013 respectively, i.e. before and after implementation of pedestrian safety legislation, two body regions were in the focus of interest in accidents with type-approved passenger cars. The first was the pelvis area with 14.9 percent of all AIS2+ injuries and 23.3 percent of all AIS3+ injuries. The second body region, with an increased percentage of severe injuries was the thorax, having 17.2 percent of all AIS2+ injuries and 26.7 percent of all AIS3+ injuries. Therefore, in terms of AIS3+ pedestrian injuries, the thorax was the most relevant body region followed by the head, pelvis and lower extremities (Zander et al., 2015). A similar trend could be observed for bicyclists. Here, the relevance of head and leg injuries was nearly unchanged in terms of AIS2+ injuries. For AIS3+ injuries, a slight decrease was observed. Similar to the pedestrians, the thorax area demonstrated an increased relevance regarding AIS2+ as well as AIS3+ injuries. Altogether, focusing on AIS3+ injuries, lower extremities were the most relevant body region (34.1 percent), followed by the thorax (31.7 percent) and the head (17.1 percent). Also for AIS2+ injuries, these body regions remained the mostly affected ones.
SENIORS aimed to consider the safety needs in particular of older road users. Based on German and Swedish collision data from GIDAS and STRADA as reported by Wisch et al. (2017), the percentages of AIS1, AIS2, and AIS3+ injuries to the different body regions of the age groups 25-64 and 65+ are displayed in Figure 1 exemplarily for pedestrians in collisions with passenger cars:

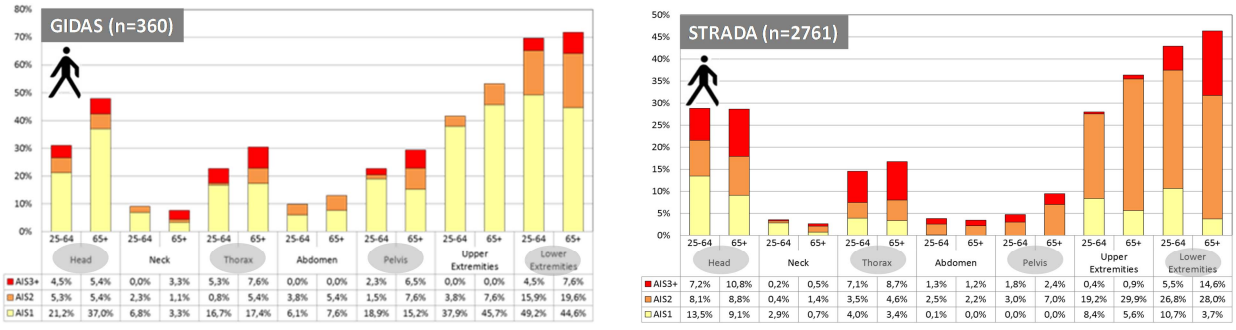

Figure 1. Percentages of injury severities for the different pedestrian body regions within GIDAS and STRADA. Each column adds up to 100 percent by adding all percentages from AIS0 to AIS9. (Wisch et al., 2017).

Both databases agree regarding the mostly affected body regions for pedestrians and cyclists and their particular relevance for the elderly. Regarding the pedestrian injury levels, head, thorax, pelvis and lower extremities are the most relevant body regions with the highest portions of AIS2 and AIS3+ injuries, with the elderly suffering more frequently from severe injuries than younger pedestrians.
Also injuries to bicyclists show the highest injury levels for the head, the thorax and the lower extremities being the key affected body regions for both age groups.
The data shows the thorax currently representing a higher percentage of severe injuries for both groups of vulnerable road users. Meanwhile, the importance of head and lower extremity injuries remains in most cases at the same level as before. Furthermore, injury severities of the elderly especially in the described body regions are higher than for the age group 25-64 years. It thus can be concluded, that the main focus in the revision and further development of impactors and test procedures needs to be settled to the head, the thorax and the lower extremities.

METHODOLOGY

At this point in time, no component test procedures related to the assessment of thoracic injuries of VRU are in use. Fredriksson et al. (2007) reported about sled tests with the EUROSID 2 (ES2) dummy as external surrogate concluding good measurement capabilities for the chest and abdomen area. Based on these findings, the torso of the ES2 model was uncoupled for subsequent use as an injury prediction tool during pedestrian component tests. In a next step, simulations with the uncoupled ES2 torso, named thorax injury prediction tool (TIPT), were performed according to impact conditions previously defined by HBM simulations. Finally, tool revision and fine tuning were done towards improving the correlation between TIPT and HBM kinematics and loadings. For validation, physical component tests were carried out under various test setups with a prototyped TIPT against a generic vehicle frontend as well as an actual vehicle model.

The general workflow for the development of the TIPT is illustrated in Figure 2:

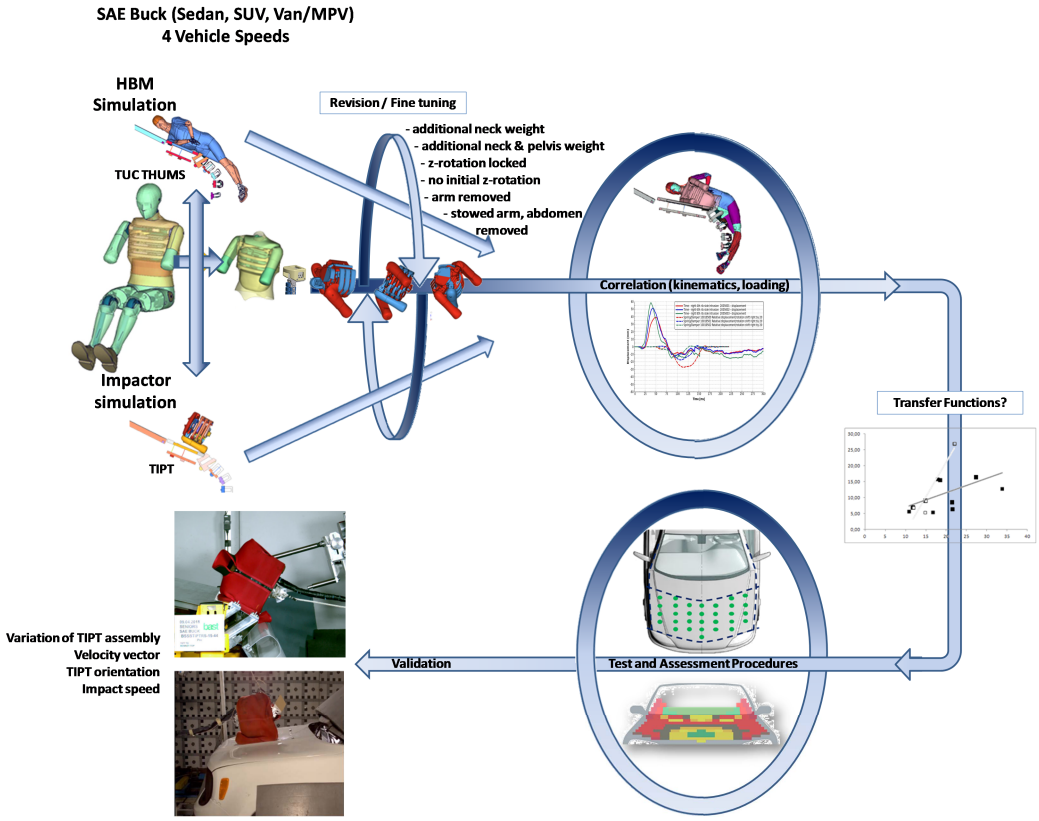

Figure 2. Workflow describing the development of TIPT and its test and assessment procedures.

HUMAN BODY MODEL SIMULATIONS

First input for correlation studies to be carried out were HBM simulations with the Total HUman Model for Safety of the THUMS User Community (THUMS TUC) against a vehicle buck of the Society of Automotive Engineers (SAE Buck – Pipkorn et al., 2012) and two derivatives, SUV and MPV, at vehicle speeds of 20km/h, 30km/h, 40km/h and 50km/h, see Figure 3:

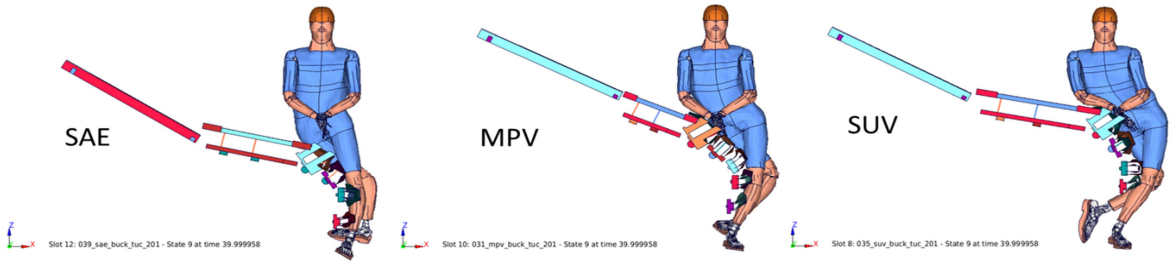

Figure 3. THUMS TUC simulations against SAE, MPV and SUV buck.

THUMS TUC V2.01 was positioned in the stance according to SAE (2010) and impacted on its right side, i.e. rear leg impacted first. HBM tracking points that were recorded during simulations were head centre of gravity (CoG), neck (C1 and C7), thorax (T1 and T12), and pelvis. Rib 4, 6 and 8 lateral deflections were also recorded with implemented spring elements.
The present study was focusing on the thorax loadings, only. The thorax impact velocity relative to the car depended on both, Buck velocity and geometry. The SAE Buck impacted THUMS lower on the legs compared to the remaining two Buck geometries and gave the highest thorax rotational velocity. In all 30km/h load cases the left arm got trapped between the thorax and the bonnet, causing higher rib deflections. The highest deflection on the impact side was measured for the 30km/h MPV load case. On the non-impact side (left) the deflection increased with the impact velocity and seemed not to be affected by the impact location.
Subsequent simulations with TIPT used the thorax orientations and speeds of THUMS for each load case.

FE IMPACTOR SIMULATIONS

Finite element (FE) simulations with TIPT were carried out against identical setups and load cases, i.e. using the thorax orientations and speeds of THUMS for each load case, compare Figure 4.

Setup and Evaluation Method

The TIPT readings used for comparison with the HBM results were rib deflection, spine acceleration and tracking points. To match HBM with TIPT anatomy for the tracking points, T1 and T12 were used, as illustrated in Figure 5.

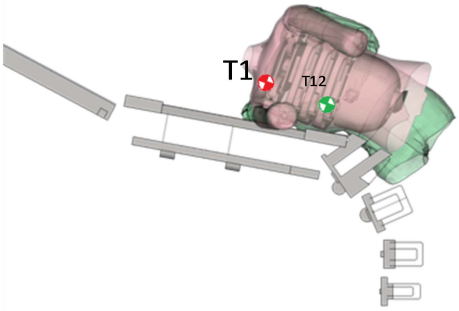

Figure 4. Comparative simulations with THUMS and TIPT.

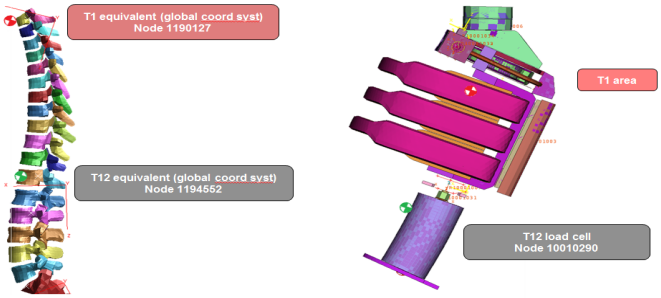

Figure 5. HBM and TIPT points used for tracking and speed matching.

For comparable results between HBM and TIPT simulations the impactor was propelled at angles, speeds and arm positions identical to those of the HBM at the time of head impact. While the HBM simulations were carried out with the Buck impacting the stationary HBM, the TIPT FE model was propelled against the stationary Buck.

HBM vs. TIPT Correlation

Altogether, seven test setups within five simulation loops with TIPT against the SAE Buck and its derivatives SUV and Van/MPV at impact speeds between 20 and 50km/h were carried out, see Table 1:

Table 1.
Overview of simulations with TIPT

Loop	Description	Generic Frontends	Vehicle Speed
1	Baseline	Sedan, SUV, Van/MPV	20/30/40/50 km/h
2a	additional neck weight	Sedan, SUV, Van/MPV	20/30/40/50 km/h
2b	as loop2a but with additional pelvis weight	Sedan, SUV, Van/MPV	20/30/40/50 km/h
3	z-rotation locked	Sedan, SUV, Van/MPV	20/30/40/50 km/h
3r1	no initial z-rotation	Sedan, SUV, Van/MPV	20/30/40/50 km/h
4	w/o interaction arm vs. vehicle	Sedan, SUV, Van/MPV	20/30/40/50 km/h
5	as loop3r1 but with stowed arm w/o abdomen	SUV, Van/MPV	30/40 km/h

TIPT baseline simulations using the conditions derived from THUMS TUC simulations (loop1) showed the very low sensitivity of all three ribs of the ES2 ribset during low speed tests, while simulations at higher impact speeds resulted in higher deflections. These observations were underlined looking at the ribwise maximum TIPT displacement vs. the maximum THUMS rib intrusion. The best maximum correlation over all impact speeds and vehicle shapes was found for the 4th rib. On the other hand, when focusing on higher impact speeds (≥ 40km/h) and under consideration of the maximum rib displacement over all ribs as injury assessment criterion, the coefficient of determination could be improved, compare Figure 8.
The impact condition of TIPT was assumed as the major reason for the altogether low correlation of maximum output values. Using the test setup of the baseline loop, the TIPT simulations were therefore amongst other things replicated neglecting the initial impactor rotation around the local z-axis (loop3r1). Here, at initial position, the TIPT was kept in a yz-plane parallel to the xz-plane of the impacted vehicle, being the plane in which rib displacement is measured with the ES2 dummy. While the correlation of readings was good to acceptable for lower impact speeds, the TIPT overpredicted the rib deflections at higher speeds in most cases. One of the reasons could be due to the different impact locations of THUMS ribs compared to those of TIPT, as demonstrated in Figure 6 and Figure 7.

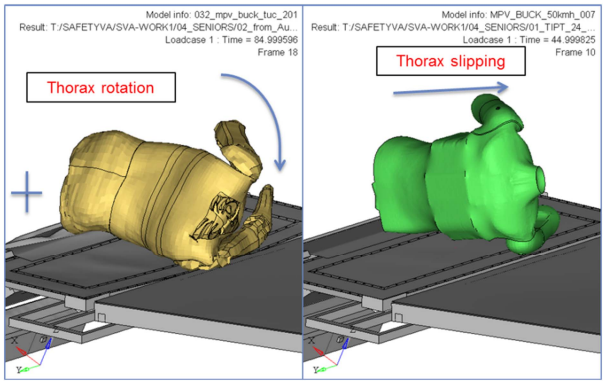

Figure 6. THUMS vs. TIPT kinematics on MPV SAE Buck 50 km/h simulation – rotation vs. translation.

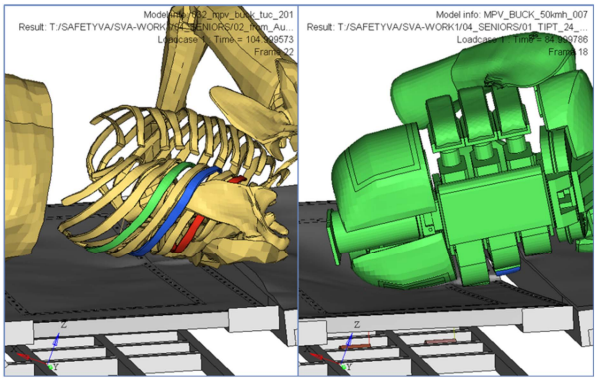

Figure 7. THUMS vs. TIPT impact point on MPV SAE Buck 50 km/h simulation – different impact locations.

During simulations at 50km/h with the Van/MPV Buck, a remarkably different thorax kinematics in the impact event (rotation with THUMS and translational sliding with TIPT) was found as the main cause of the different impact locations of the ribs. In this load case, the upper and middle TIPT rib deflection were influenced by the lower part of the windshield while the ribs didn't get in contact at all with the windshield during the THUMS simulation. Altogether, the global coefficient of determination for TIPT maximum rib deflection with THUMS maximum rib intrusion remained almost unchanged.
A fourth simulation loop was carried out, starting from the TIPT position neglecting the initial rotation around the z-axis and excluding the arm of the impactor from contact with SAE buck models. Intention was to determine the effect of arm interaction on peak rib deflection, showing a general overestimation of the peak loadings with TIPT. In some cases the interaction between TIPT ribs and SAE buck models were characterized by a high load on the ribs in the 'neck-pelvis' direction. The fourth simulation loop didn't show any considerable improvement. An increment of TIPT rib sensitivity at lower velocities was confirmed. There was however no further improvement of the coefficient of determination neither under consideration of the maximum deflection over all the ribs nor accounting for each rib separately.
A final simulation loop5 was carried out, using a revised TIPT FE model with stowed arm on the struck side and without abdomen, pelvis and without arm on the non-struck side, reducing the TIPT mass from 32.85kg to 22.15kg. These modifications aimed at increased feasibility and higher repeatability for subsequent physical testing. Using this TIPT configuration, the load cases at 30 and 40km/h on SUV and Van/MPV Buck models were replicated. Impactor positions and velocities were identical to those used in loop3r1.
Compared to loop3r1, loop5 showed lower rib deflections and a more uniform distribution of the peak rib deflections. The time histories for THUMS TUC and TIPT rib deflection were however hardly comparable. A correlation study using loop 5 simulations resulted in a reasonable coefficient of determination with THUMS, especially for the 4th rib, with a good linear correlation, see Figure 9:

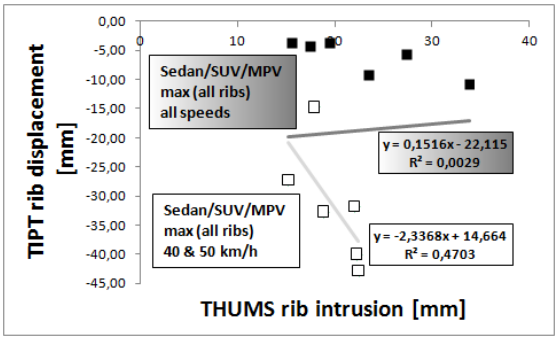

Figure 8. Correlation of THUMS maximum rib intrusion vs. TIPT maximum rib deflection at all and at higher impact speeds, loop 1.

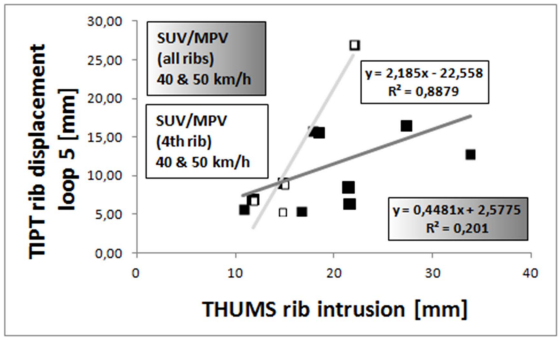

Figure 9. Correlation of THUMS maximum rib intrusion vs. TIPT maximum rib deflection for all and for the uppermost rib at higher impact speeds, loop 5.

In an effectiveness study of side airbags, Hayashi et al. (2006) investigated the responses between THUMS and ES2. While THUMS showed higher rib deflections in the lower parts, ES2 showed considerable deflections in the upper segments.
Altogether, the predominant discrepancy between THUMS and TIPT besides the different TIPT impact kinematics is represented by a rib extension phase of the HBM before the thorax impact against SAE Buck models, during all simulations. It was not possible to catch this phenomenon with the TIPT; thus the conditions of THUMS and TIPT ribs, immediately before the impact against all SAE Buck derivatives were very different in high velocity load cases.

FE Simulations on actual Vehicle

Subsequent to the finalization of the TIPT model and test setup, further simulations were carried out on an actual SUV representative. Four simulations using loop5 setup were performed with TIPT impact points located in different areas of the bonnet. Three additional simulations were conducted against the grille area of the vehicle in order to replicate a possible impact between a high front-end vehicle and a small stature pedestrian.
The impact locations were positioned on the intersections of four different wrap around distance lines (WAD) with the longitudinal vertical vehicle centreplane and with two longitudinal vertical planes at a distance of 133.5mm (half

of the impactor width) inwards the side reference lines (SRL - contact line of a 700 mm straight edge inclined by 45° inwards on both sides of the car). The impact locations were aimed at with the TIPT reference point, defined by the intersection of the middle rib plane with the yz-plane passing through the shoulder reference point and the centre rib. The TIPT was then rotated and aligned on the WAD along the direction of the velocity vector.
The simulations against the SUV bonnet resulted in very low levels of rib deflection (≤ 11mm) and spine acceleration (< 10g). During the simulations against the grille, the perpendicular orientation and different kinematics of TIPT led to significantly higher rib deflections (17.8-55.3mm) and spine accelerations (29.5–54.4g).

TIPT DESIGN AND PROTOTYPING

As test tool, the ribcage of the ES2 was used as standalone TIPT. Simulations concluded to add the ES2 arm in stowed position on the impact side. This was realized using a TIPT suit with fixed sleeve, compare Figure 10. A pusher device was designed for attachment to the pedestrian test stand, with the possibility of adjustment of the impact angle within the launcher to the values defined according to the test procedures, see Figure 11:

Figure 10. Final TIPT prototype.

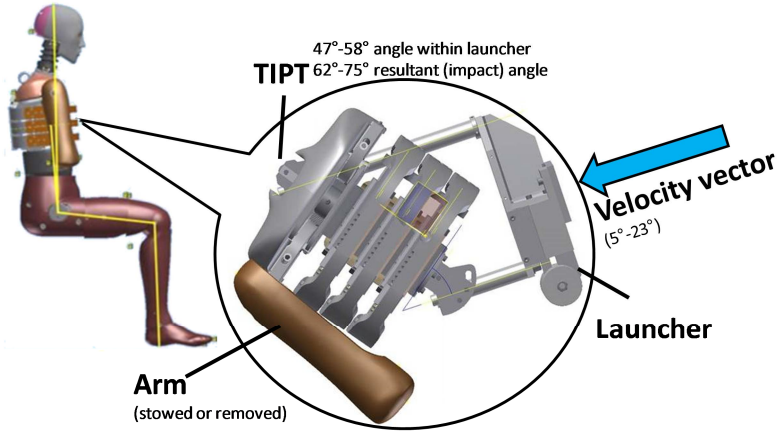

Figure 11. TIPT setup and launching device.

TEST PROCEDURES

Anthropometric Data

For an assessment of the VRU protection potential of passenger cars related to thoracic injuries, information on the human and dummy anthropometry as well as the kinematics of impact is needed.
In principle, the entire vehicle front can contain potentially injury causing parts affecting the human thorax during an accident. The test and assessment area for the thorax however further depends on the vehicle height, human anthropometry and the dimensions of the impactor to be used. Figure 12 summarises the most relevant human data for the 5th female, the 50th male, the 95th male (DIN, 2005) and the thorax-related proportions derived from the human body models THUMSv4 and the family of MAthemtical DYnamic MOdels (MADYMO). Based on anthropometric data, the test area should be described by WADs coinciding with the height of the lowermost rib of the six year old child (6YO) and the height of the uppermost rib of the 95th adult male. Under consideration of THUMS 50th, the area would then be described by WAD 1192 and WAD1485. Taking into account the MADYMO family (6YO–95th), the test area would be limited by WAD770 and WAD1540.
Since the TIPT is derived from the ribcage of the ES2 (between WAD1156 and 1316), the test area needs to be verified against all locations on the vehicle front that can potentially be impacted by the ES2. Figure 13 shows the dimensions including the theoretical standing height of the ES2 dummy. From these measurements, the potential impact area of the ES2 ribcage can be approximated between WAD 1156 and 1316. The entire ribcage is thus covered by the impact area described by the anthropometric data as shown in Figure 12.

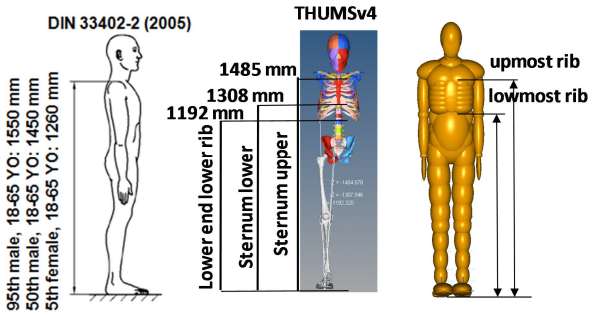

Figure 12. Anthropometric data: human, THUMSv4 (50th) and MADYMO.

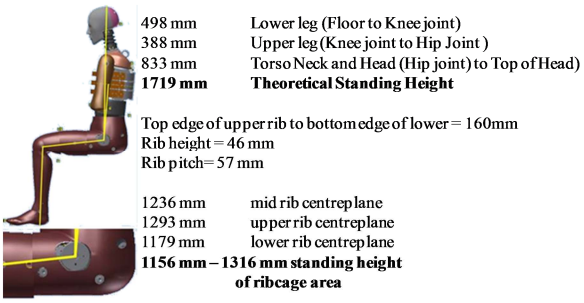

Figure 13. Dimensions and theoretical standing height of ribcage area of ES2 dummy.

Vehicle Markup

The test area for TIPT that needs to cover the aforementioned aspects is thus defined by:
- WAD770 (height of lowermost rib of 6YO)
- WAD1540 (height of uppermost rib of 95th)
- SRLs.

All impact points are aimed at with the intersection of the TIPT mid rib and vertical rib centreplanes (see Figure 14). Furthermore, all impact points are located within the test area and
- 80mm rearward of WAD770 (=WAD850)
- 80mm forward of WAD1540 (=WAD1460)
- 133.5mm laterally inwards the SRLs.

A grid with a resolution of 133.5mm*80mm derived from the dimensions of the ES2 ribcage (compare Figure 14) is marked on the vehicle, starting with the intersection of y0 with WAD850, marking a grid point every 80mm in rearward wrap around direction until WAD1460. Starting from each y0 intersection with the particular WAD, it is moved laterally rightwards (leftwards) and a grid point is marked every 133.5mm until 133.5mm laterally inwards the SRL, see Figure 15:

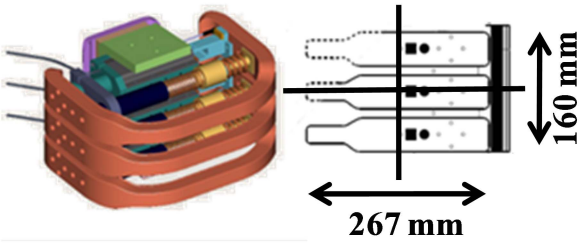

Figure 14. ES2 ribcage dimensions.

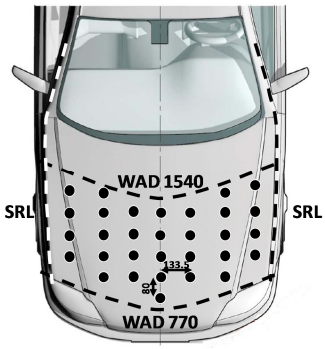

Figure 15. TIPT test area and vehicle markup.

Test Parameters

TIPT impact speeds and angles have been determined during the FE simulations of THUMS TUC against the SAE Buck and its derivatives. It has been found that thorax speed and impact angle mainly depend on the geometry of the vehicle front. Thus, the TIPT speeds and angles derived from the HBM simulations mainly depend on the vehicle to be tested. The categorization of vehicles should in principle follow the method developed by the International Harmonized Research Activity Pedestrian Safety Working Group IHRA (Mizuno, 2005).

Subsequent, the TIPT impact speeds, impact angles and angles of the velocity vectors derived from the corresponding parameters of the thorax during THUMS TUC simulations were defined as outlined in Table 2 and illustrated in Figure 16:

Table 2.
Impact parameters for TIPT component tests

	Vehicle category	Sedan	SUV	Van / MPV
Rwd of BLE-RL*	TIPT impact angle	15 ° (75°)	20° (70°)	28 ° (62°)
	Angle of velocity	19°	23°	5°
	TIPT impact speed	27 km/h	15 km/h	21 km/h
Fwd to BLE-RL*	TIPT impact angle	90° (0°)		
	Angle of velocity	0°		
	TIPT impact speed	40 km/h		

*: Bonnet Leading Edge Reference Line

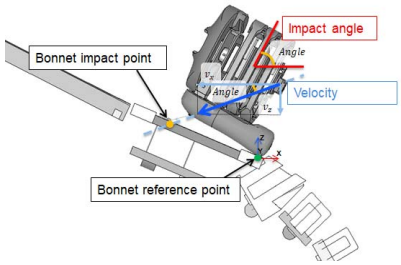

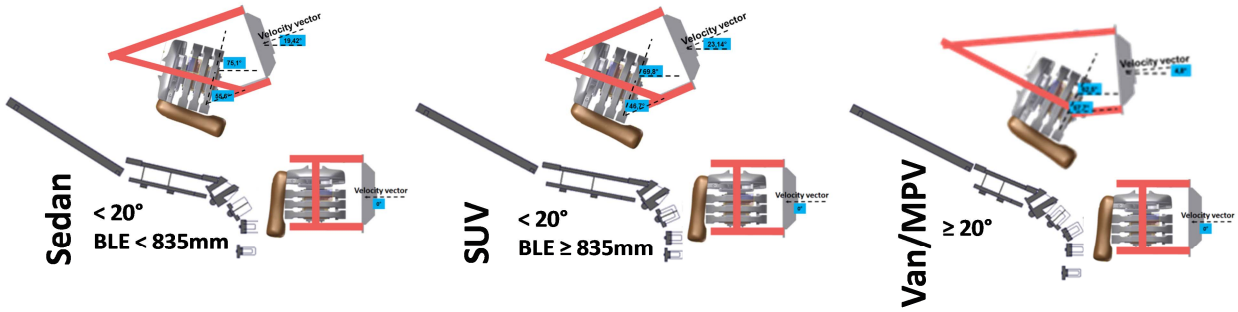

Figure 16. Illustration of impact parameters for TIPT component tests.

These angles, due to the kinematics of the human thorax during the impact, differ from each other, i.e. that also the angle of the velocity vector in the component test is not perpendicular to the TIPT.

ASSESSMENT

Derivation of Impactor Thresholds

Until 2014, the ES2 dummy was used as a car occupant surrogate in the Euro NCAP lateral impact tests. Limits for the lateral chest compression were used as assessment indicator for 45YO and 67YO car occupants suffering AIS3 injuries. While the upper performance limit for maximum rib deflection in both crash modes was set to a value of 28mm, representing a 5% AIS3 injury risk for the 67YO, the lower performance limit and, in terms of the side impact with the mobile deformable barrier, the capping limit, were defined at 50mm, indicating a 30% AIS3 injury risk for the 45YO. The capping limit for the pole side impact was defined at 55mm, representing a 50% risk of the 45YO for suffering AIS3 injuries (Euro NCAP, 2014).
Lowne et al. (n.d.) developed risk curves for suffering AIS2+, AIS3+ and AIS4+ thoracic injuries as functions of peak rib deflections out of PMHS tests and normalized the results to a 45YO and to the production prototype EuroSID injury parameters. The presented injury risk functions were based on four series of PMHS tests performed in the 1970's and 1980's, using AIS injury coding. The same injury risk functions still form the basis of the UN Regulation 95 (UNECE, 2014) thorax performance requirement and thus were used in the SENIORS project.
In accordance with findings from the accident data analysis, SENIORS focused on AIS3+ injuries. Following the 5 color scheme being applied in the Euro NCAP VRU assessment (Euro NCAP, 2018-2), the TIPT total score is calculated from threshold values for maximum rib deflection.

Test Synthesis

Prior to testing, a prediction of grid point results is to be given by the vehicle manufacturer for the performance in terms of maximum rib deflection, to be indicated with the colors green – yellow – orange – brown – red, compare Table 3:

Table 3.
TIPT thresholds (maximum rib deflection)

Colour (points)	Maximum rib deflection	Covering (human injury risk)
Green (1)	< 28mm	5% AIS3 (67 YO)
Yellow (0.75)	28mm… 35mm	20% AIS3+ (45 YO)
Orange (0.5)	35mm… 40 mm	30% AIS3+ (45 YO)
Brown (0.25)	40mm… 44mm	40% AIS3+ (45 YO)
Red (0)	≥ 44mm	50% AIS3+ (45 YO)

Random test point selection is to be done according to the headform test procedure of Euro NCAP (2018).
Following the approach for the upper legform impactor assessment, the maximum rib deflection for each TIPT impact location is taken into account. As for the headform test, a grid approach is also followed for the TIPT impact procedure. For consistency with the current assessment procedures, the total amount of points is calculated by scaling the total grid point score to the maximum number of achievable points for this subsystem test. Visualisation of results is done likewise to the headform procedure. The flowchart of TIPT testing and assessment is illustrated in Figure 17:

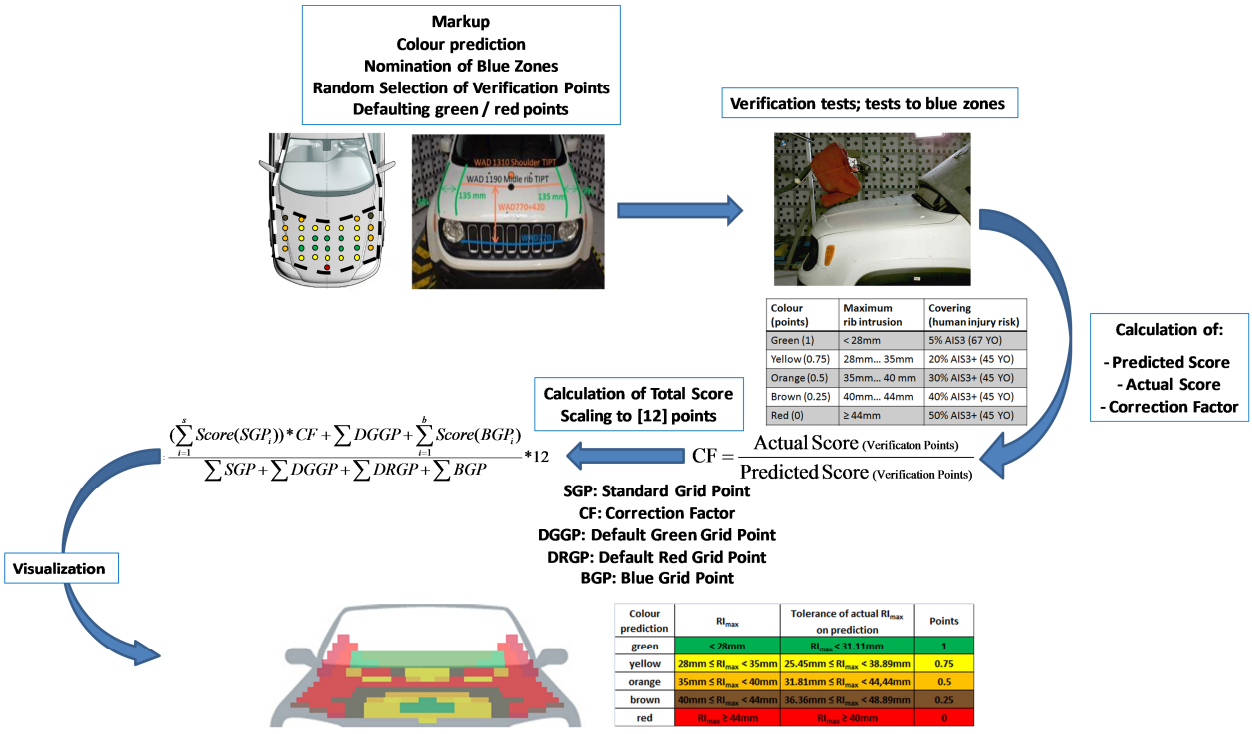

Figure 17. TIPT testing and assessment flowchart.

Scenario for Euro NCAP Box 3 Rating

The Euro NCAP Pedestrian Test and Assessment Procedures currently include the child and adult headform, the upper legform and the FlexPLI with a weighting of 66 ⅔ vs. 16 ⅔ vs. 16 ⅔ percent (Euro NCAP, 2018-2). Recent studies of injuries suffered by pedestrians and bicyclists for all age groups and focused on the elderly (65+) during collisions with passenger cars in Germany confirm a change in injury patterns in the last years. Here, depending on where the focus is set, different scenarios for balancing the nowadays most relevant body regions head, thorax and lower extremities (including femur, knee and tibia) are possible. In light of a considerable number of AIS3+ injuries to the mentioned body regions within the GIDAS database it is suggested to equally balance the three body regions in a first step, allocating a maximum of 12 points to each the head, the thorax and the lower extremities (introducing the FlexPLI with upper body mass) within Euro NCAP Box 3. This, in the end, would result in scaling the thorax test synthesis to the maximum of 12 points.
Altogether, if the weighting for AEB Pedestrian and Cyclist systems remained unchanged after 2019, the Box 3 rating scheme would result in a point distribution as summarised in Table 4:

Table 4.
Possible scenario for Box 3 weighting, in-Box balancing and overall balancing of pedestrian safety performance in Euro NCAP after introduction of the TIPT test procedures

Test Procedure / Year	Score	2016-2017		2018-2019		2022		Score	Test Procedure / Year
Headform	24	24	57,1%	24	50,0%	12	25,0%	12	**Headform**
Upper Legform	6	6	14,3%	6	12,5%	12	25,0%	12	**TIPT**
Lower Legform	6	6	14,3%	6	12,5%	12	25,0%	12	**FlexPLI-UBM**
AEB Pedestrian	6	6	14,3%	6	12,5%	6	12,5%	6	**AEB Pedestrian**
AEB Cyclists	6			6	12,5%	6	12,5%	6	**AEB Cyclists**
Total		42	100,0%	48	100,0%	48	100,0%		**Total**
Total passive		36	85,7%	36	75,0%	36	75,0%		**Total passive**
5 star threshold (Balancing)		25,2	60%	28,8	60%	28,8	60%		**5 star threshold (Balancing)**
4 star threshold (Balancing)		21	50%	24	50%	24	50%		**4 star threshold (Balancing)**
Min. passive for AEB inclusion		22	61,1%	22	61,1%	22	61,1%		**Min. passive for AEB inclusion**

TIPT TESTING

Taking into account all HBM and TIPT simulations, loops3r1 and 5 were considered as reflecting the most realistic as well as most feasible impact conditions for physical testing. Therefore, it was decided to initially use these setups and TIPT geometries for the experimental test programme.
Several tests were performed against the SAE Buck and its derivatives and against one actual SUV front-end. For comparison, two tests were carried out as full scale tests with the Sedan Buck against the ES2 pedestrian dummy with first impact at vehicle centerline. All further tests were performed as pedestrian component tests, using TIPT. The major goal was to check the applicability of the defined draft test procedures alongside the sensitivity of the test tool, to investigate the correlation between FE simulation and physical testing and to study the impactor behaviour at the lateral borderlines of the test area.
An overview of all tests with TIPT is given in Table 5. Altogether, 24 tests with the TIPT were performed. For each of the vehicle categories represented by the SAE Buck, baseline TIPT tests were carried out, following the standard test configuration used in the TIPT simulations. At a later stage, several parameters were changed to investigate the test tool performance and sensitivity. Moreover, TIPT tests following the defined test protocol were performed against an actual SUV representative.

Table 5.
Test matrix for experimental tests with the TIPT

Surrogate/ Vehicle	TIPT			
SAE Buck (Sedan)	y0 according to draft test procedure	Full scale test configuration repeat (2)		impact angle variation; steeper angle of the velocity vector
SAE Buck (Sedan)	y0 vs. bonnet according to draft test procedure	y0 vs. bonnet variation of TIPT assembly, aiming point, velocity vector, TIPT angle, impact speed (6)		y0 vs. BLE variation of aiming point (2)
SAE Buck (SUV)	y0 according to draft test procedure	y0 sensitivity / bottoming out		y0 sensitivity / light bottoming out with reinforced structure
SAE Buck (Van/MPV)	y0 according to draft test procedure	y0 increased impact speed		
Actual SUV	y0 – WAD 1190 (3)	+SRL - 133.5 WAD 1330	y0 – WAD 1330	y0 – WAD 1010

The impact speed, angle of the velocity vector and TIPT inclination angle were determined according to Table 2. Impact points on the actual SUV were the aiming points of the TIPT velocity vector intersecting the shoulder reference point.

Sedan Buck

The peak rib deflections during simulations with HBM and TIPT and experimental tests with ES2 pedestrian dummy and TIPT against the Sedan Buck are depicted in Figure 18 and Figure 19:

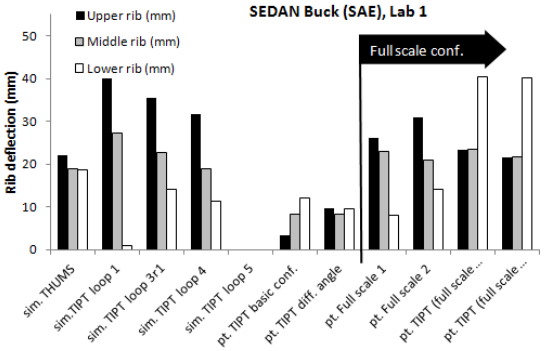

Figure 18. Peak rib deflections during simulations (sim.) with HBM and TIPT and experimental tests (pt.) with ES2 pedestrian dummy and TIPT – Sedan Buck, Lab 1.

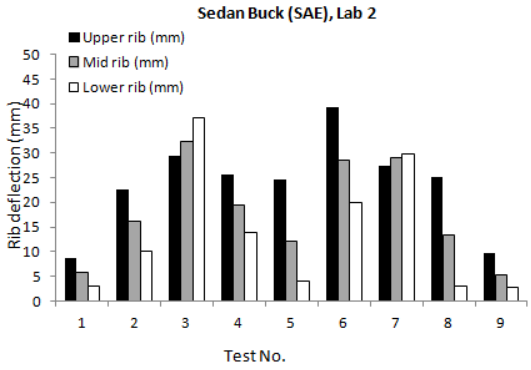

Figure 19. Peak rib deflections during experimental tests (pt.) with TIPT – Sedan Buck, Lab 2.

Lab 1 While TIPT tests according to the test specifications and with modified impact angle showed very low peak deflections, those replicating the ES2 full scale test configuration resulted in higher loadings, in particular for the lower rib. This is contrary to the ES2 tests where the highest deflections were obtained by the upper rib. Altogether, neither the simulations nor the full scale dummy tests could be properly reflected by the tests with TIPT. Also the full scale pedestrian dummy test results were not comparable to the HBM simulations with THUMS TUC.

Lab 2 Subsequent to a repetition of the baseline test with TIPT against the centre of the bonnet of the Sedan Buck, several modifications to the TIPT and the test and impact parameters were done in order to study the influence on the test results and vehicle safety performance.

All tests following the baseline test were carried out without the arm to more directly load the TIPT ribcage. Additionally, a rubber layer between ribcage and jacket was added to more equally distribute the loading on the entire ribcage. As from test 3 onwards the shoulder was removed from the TIPT to avoid interaction during the impact, once again bringing more severe loadings into the ribcage. Most tests were carried out against the center of the bonnet; only during two tests (no. 3 and no. 7) the TIPT impacted the centre of the bonnet leading edge (BLE). For all except the first two tests against the bonnet, a structure was installed underneath the bonnet at different distances, causing bottoming out of TIPT. Regarding the impact parameters, six tests followed the draft test procedure (see Figure ***20***), thereof one with reduced impact speed (no. 9). During the tests against the BLE (compare **Error! Reference source not found.**), a most possible upright position of TIPT in the launcher was chosen to follow a more realistic impact scenario in that area.

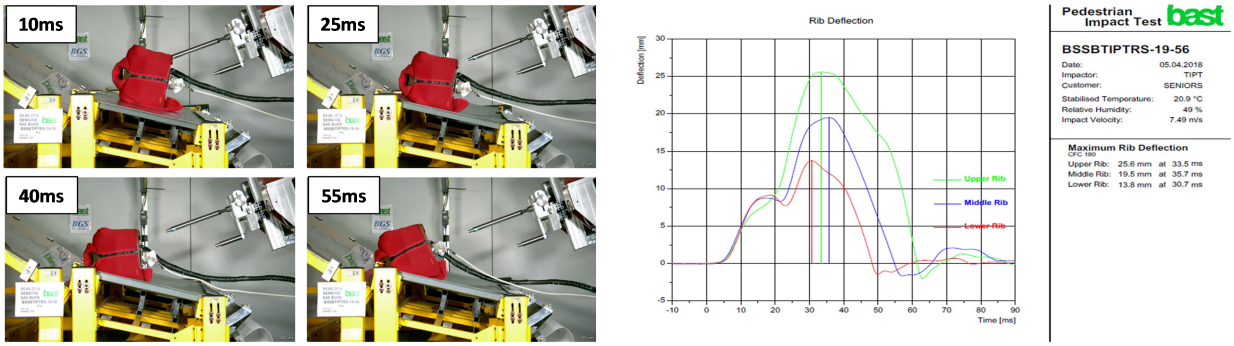

Figure 20. TIPT to bonnet test.

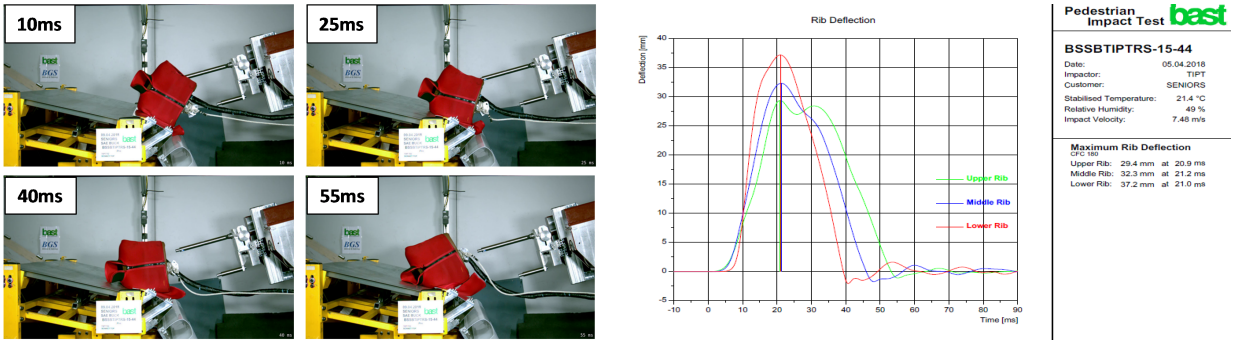

Figure 21. TIPT to BLE test.

In another test (no. 6), the steepest possible velocity vector was chosen to achieve the highest possible lateral loadings to the ribs, taking into account the limitations of ES2. Test 5 was a repetition of test 4.

Altogether, comparatively low rib deflections (all below 40mm) were measured during all tests against the Sedan Buck, thereof the majority below the tentative upper performance limit to a green assessment (28mm). As expected, the highest rib deflections were achieved during the test against the center of the bonnet with the steepest possible velocity vector, and during the two tests against the centre of the BLE. The mentioned impact configurations resulted in highest possible lateral loadings, following the properties of the ES2 ribcage where potentiometers allow for a proper acquisition of deflections in a linear direction, only.

The repeatability of test results was not satisfactory in particular for the mid rib with a range of 7.3mm and the lower rib with a range of 9.8mm.

Interestingly, lab-to-lab variability was extraordinary high for the baseline test. While in lab 1 the deflection of the lower rib was highest and the deflection of the upper rib lowest, the opposite tendency was observed in lab 2; however, all measured rib deflections in those two tests were far below the borderline to green assessment according to the draft assessment procedures.

In the vast majority of tests, regardless of the rib location aiming at the impact point, rib deflections were highest for the upper rib and lowest for the lower rib. Only the tests against the BLE resulted in maximum deflections in the lower rib and minimum deflections in the upper rib.

The application of the rubber layer between ribcage and jacket did not result in a more equal distribution of rib deflections. On the other hand, significantly higher rib deflections were observed in all tests subsequent to the removal of the impacting arm.
Testing without the arm contributed to a reduced TIPT rotation around the z-axis.

SUV Buck and actual SUV

The peak rib deflections during simulations with THUMS TUC and TIPT (both against the SUV Buck only) and experimental tests with TIPT against the SUV Buck and the actual SUV are shown in Figure 22.
Both, TIPT tests against the SUV Buck as well as the actual SUV resulted in rib deflections significantly below the proposed threshold values. The loadings obtained during THUMS TUC as well as TIPT simulations could not be replicated during physical testing. TIPT results cannot be directly related to real life injury risk of a pedestrian during a vehicle accident.

Van/MPV Buck

The same observation was made during simulations with HBM and TIPT and experimental tests with TIPT against the Van/MPV Buck, as illustrated in Figure 23. Peak rib deflections during the tests were very low and not comparable to the loadings measured during the simulations.

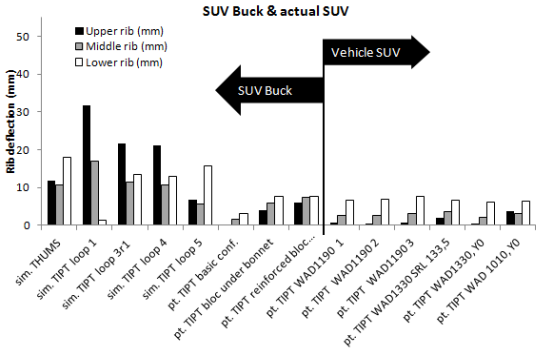

Figure 22. Peak rib deflections during simulations (sim.) with HBM and TIPT (SUV Buck) and experimental tests (pt.) with TIPT (SUV Buck, actual SUV).

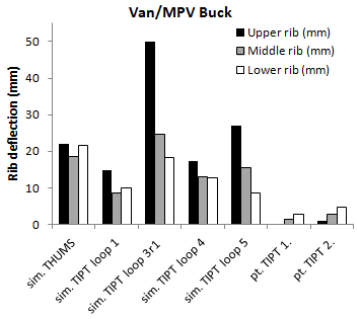

Figure 23. Peak rib deflections during simulations (sim.) with HBM and TIPT and experimental tests (pt.) with TIPT – Van/MPV Buck.

DISCUSSION

The reported simulations related to the assessment of thoracic injuries show the basically good approach of using the isolated ribcage of the ES2 dummy during component tests. However, several limitations need to be considered. First, the ES2 dummy was designed as vehicle occupant for the assessment of lateral impacts. HBM simulations show the kinematics of the human thorax in many cases differing from this load case, with oblique thorax angle and the velocity vector not perpendicular to the thorax. The capacity of capturing oblique loadings with the available instrumentation is limited. THUMS rib extension before the impact, rotational elements in THUMS kinematics and translational movement of the TIPT furthermore result in different impact locations and loadings. Thus, besides the diverging time histories of THUMS intrusions and TIPT rib deflections, also the quantitative correlations are unsatisfactory in most cases. When using a TIPT based on the ES2 ribcage, establishing impactor limits should rather be based on injury criteria for the ES2.

CONCLUSIONS

Collision investigations stress the change in injury patterns for pedestrians and cyclists with respect to all age groups. These converted safety requirements underline the need for revised test and assessment procedures towards a further improved VRU protection of passenger cars. From the reported changes, new requirements for external

road users were derived. Regarding the thorax area, a new test tool and new test procedures address, in principle, these requirements.
Based on a review and evaluation of the current test and assessment procedures, updates, incorporating the new test tool TIPT, were proposed together with the corresponding biomechanical limits.
Tests with the TIPT showed the feasibility of the assessment of thoracic injury risks of vulnerable road users, using for the first time a component test procedure, with acceptable repeatability and reproducibility of kinematics and test results. It needs however to be taken into account that the impact conditions such as thorax inclination angle and angle of the velocity vector differ from those in the lateral impact with ES2 dummy where the TIPT is derived from. The linear potentiometers of the ribcage do not acquire the actual rib deflections unless perpendicularly loaded.
Modifications of the load transducers would thus be needed for the TIPT component test rearward of the BLE. Future development of the TIPT may need to focus on developing a rib cage that can deflect in all axes in a humanlike way, and on developing an injury metric that takes account of these multi-axes deflections. By way of comparison, the THOR frontal impact ATD displays large y- and z-axis deflections, even though the primary loading is in the x-axis. Current THOR injury criteria also make use of the resultant deflection, not just the x-axis deflection, and it is likely that similar improvements in biofidelity and injury criteria would be of benefit for future development of the TIPT. For the impact forward to the BLE however the TIPT seems applicable without further modifications.
A straight launcher was designed and manufactured to test the TIPT at the end of the project when the need to launch directly in line with the deflection sensors was identified. The fixture was designed so that the effect of the linear rib sensors could be assessed. This is because the TIPT tested in the project was launched at simulated angles that did not directly load the sensors in their direction of measurement. This was considered the main reason for the lower than expected deflections seen in physical testing. FE analysis had shown higher deflections so it could have been a friction problem with the hardware not seeing expected results. Therefore, further testing with the TIPT will help to establish the sensitivity of the sensors and to better understand the requirements for an improved test tool.
A set of new test and assessment procedures for the thorax led to a draft rating scheme for Box 3 of Euro NCAP. Impactor thresholds were derived from studies of impact biomechanics alongside correlation studies between impactor and HBM simulations. A synthesis of the particular assessment was proposed as an example of VRU overall rating within Euro NCAP. However, despite of first promising results, several significant modifications will be necessary prior to implementation within consumer or regulatory test procedures.

ACKNOWLEDGEMENTS

The research leading to the results of this work has received funding from the European Union's Horizon 2020 research and innovation programme under grant agreement No 636136.

REFERENCES

Deutsches Institut für Normung (DIN). 2005. „Ergonomie – Körpermaße des Menschen – Teil 2: Werte“ Deutsche Norm DIN 33402-2, 2005.

European Commission. 2017. “Traffic Safety Basic Facts on Pedestrians.” European Commission, Directorate General for Transport, June 2017.

European Enhanced Vehicle-safety Committee. 2002. “EEVC Working Group 17 Report Improved test methods to evaluate pedestrian protection afforded by passenger cars.” December 1998 with September 2002 updates. www.eevc.net.

European New Car Assessment Programme. 2014. “Assessment protocol – Adult occupant protection.” Version 7.0.1, July 2014. www.euroncap.com.

European New Car Assessment Programme. 2018. “Pedestrian Testing Protocol Version 8.5” Euro NCAP, October 2018. www.euroncap.com.

European New Car Assessment Programme. 2018-2. “Assessment Protocol – Pedestrian Protection Version 9.0.4” Euro NCAP, September 2018. www.euroncap.com.

Fredriksson R., Flink E., Boström O., Backman K. 2007. “Injury mitigation in SUV-to-pedestrian impacts.” Paper no. 07-0308 of 20th ESV conference proceedings. Lyon, 2007.

Hayashi S., Yasuki T., Kitagawa Y. 2008. “Occupant kinematics and estimated effectiveness of side airbags in pole side impacts using a human FE model with internal organs.” Stapp Car Crash J. 2008 Nov;52:363-77.

Lowne R., Janssen E. n.d. “Thorax injury probability estimation using production prototype EUROSID.” ISO/TC22/SC12/WG6 document N302.

Mizuno Y. on behalf of the IHRA Pedestrian Safety Working Group. 2005. “Summary of IHRA Pedestrian Safety Working Group activities (2005) – proposed test methods to evaluate pedestrian protection afforded by passenger cars.” Paper no. 05-0138 of 19th ESV conference proceedings. Washington (USA), 2005.

Pipkorn B., Fredriksson R., Oda S., Takahashi Y., Suzuki S., Ericsson M. 2012. “Development and Validation of a Generic Universal Vehicle Front Buck and a Demonstration of its Use to Evaluate a Hood Leading Edge Bag for Pedestrian Protection.” Paper no. IRC-12-25 of IRCOBI 2012 conference proceedings. Dublin (Ireland), 2012.

Society of Automotive Engineers, Human Biomechanics and Simulations Standards Steering Committee. 2010. “Performance Specifications for a Midsize Male Pedestrian Research Dummy.” Surface Vehicle Information Report J2782. Warrendale, PA: SAE International.

United Nations Economic Commission for Europe. 2009. “Addendum to global registry, created on 18 November 2004, pursuant to Article 6 of the agreement concerning the establishing of global technical regulations for wheeled vehicles, equipment and parts which can be fitted and/or be used on wheeled vehicles (ECE/TRANS/132 and Corr.1). Done at Geneva on 25 June 1988: Global technical regulation No. 9 Pedestrian Safety (Established in the Global Registry on 12 November 2008).”

United Nations Economic Commission for Europe. 2014. “Addendum 94 to the agreement concerning the adoption of uniform technical prescriptions for wheeled vehicles, equipment and parts which can be fitted and/or be used on wheeled vehicles and the conditions for reciprocal recognition of approvals granted on the basis of these prescriptions: Regulation No. 95 Revision 2 - Uniform provisions concerning the approval of vehicles with regard to the protection of the occupants in the event of a lateral collision.” UNECE, 2014.

Wisch M., Vukovic E., Schäfer R., Hynd D., Barrow A., Khatry R., Fiorentino A., Fornells A., Puthan P., Lübbe N. 2017. "Road traffic accidents involving the elderly and obese people in Europe incl. investigation of the risk of injury and disabilities.” SENIORS Deliverable D 1.2.

Wisch M., Zander O., Vukovic E., Schäfer R., Hynd D., Fiorentino A., Fornells A. 2017. „Road traffic crashes in Europe involving older car occupants, older pedestrians or cyclists in crashes with passenger cars – results from SENIORS.” Paper no. 17-0398 of 25nd ESV conference proceedings. Detroit, 2017.

Zander O., Wisch M. 2015. “Kausal-zusammenhänge bei Radfahrer-Pkw-Unfällen, Verletzungsmuster von Radaufsassen und Maßnahmen von Gesetzgebung und Verbraucherschutz zur Minderung der Verletzungsschwere.“ Annual Report 2013-2014 of the Federal Highway Research Institute (BASt). 2015.

Zander O., Ott J., Wisch M., Fornells A., Fuchs T., Hynd D., Lemmen P., Burleigh M., Lopez-Valdes F., Luera A., Lundgren C. 2017. „Safety-enhanced innovations for older road users (SENIORS): Further development of test and assessment procedures towards an improved passive protection of pedestrians and cyclists.” Paper no. 17-0268 of 25nd ESV conference proceedings. Detroit, 2017.

A PRELIMINARY COST EFFECTIVENESS ANALYSIS FOR PEDESTRIAN AND BICYCLIST PROTECTION ON SINGLE UNIT TRUCKS AND SEMITRAILERS IN THE UNITED STATES

Shashi Kuppa
Robert Mazurowski
National Highway Traffic Safety Administration
USA

Paper Number 19-0015

ABSTRACT

As part of Vision Zero initiatives, a few cities in the United States (U.S.) are requiring side guards on city-owned or city-contracted single unit trucks (SUTs) to mitigate pedestrian and bicyclist fatalities. In light of these initiatives, the National Highway Traffic Safety Administration (NHTSA) conducted a preliminary analysis to examine the cost effectiveness of equipping side guards on all new SUTs and truck-trailers/semitrailers (semitrailers) for pedestrian and bicyclist protection.

The target population of pedestrian and bicyclist fatalities and injuries in crashes with SUTs and semitrailers was obtained from the Fatality Analysis Reporting System (FARS) and the National Automotive Sampling System – General Estimates System (NASS-GES) for the five-year period 2010 to 2014. The benefits were derived from published effectiveness estimates of side guards on trucks in the United Kingdom (U.K.). Costs of side guards were obtained from a vendor of side guards for trucks.

The preliminary analysis indicates that equipping side guards on all new SUTs would cost $857.2 million annually and would prevent approximately three to eight pedestrian and bicyclist fatalities annually. Preliminary estimates indicate that equipping side guards on all new semitrailers would cost $895.9 million annually and would prevent about six to ten pedestrian and bicyclist fatalities annually. The preliminary estimates of the cost per equivalent life saved of equipping side guards on new SUTs is $100.9 million to $295.6 million, and that for new semitrailers is $94.3 million to $144.5 million. This preliminary analysis indicates that equipping side guards on all new SUTs and semitrailers for pedestrian and bicyclist protection is not cost effective.

INTRODUCTION

Lateral protection devices or side guards have been required for SUTs and trailers in Europe since 1989 per the Economic Commission for Europe Regulation No. 73 (ECE R.73), "Uniform provisions concerning the approval of lateral protection devices," [1] for mitigating injuries to pedestrians and bicyclists in collisions with these vehicles. The geometric and strength requirements for side guards in the current ECE R.73 include a maximum ground clearance (distance of the bottom of the guard from ground level) of 550 mm and a capability of withstanding a horizontal static load of 1,000 Newtons applied perpendicular to the surface of the guard with no more than 150 mm guard deflection. In 2005, a study conducted by the Transportation Research Laboratory (TRL) [2] found the fatality rate in the U.K. for bicyclists and pedestrians colliding with the side of a truck moving straight ahead decreased by 61% and by 20%, respectively, after a requirement for side guards on trucks was implemented.

In the past five years, a few cities in the U.S., under Vision Zero initiatives [3], are requiring side guards on city-owned and city-contracted SUTs and semitrailers to mitigate pedestrian and bicyclist fatalities. In 2014, Epstein et al. [4] published a report on implementing side guards on city owned vehicles in New York City. Epstein et al. further recommended that side guards installed on trucks have a ground clearance no greater than 350 mm, which is significantly lower than the maximum allowable ground clearance of 550 mm for side guards specified in European standards. Epstein claimed that the lower ground clearance of 350 mm would provide greater protection for vulnerable road users but did not provide data to support this claim. The side guards installed on single unit trucks used in the Vision Zero programs in Boston, Cambridge, and other cities were in accordance with the recommendations by Epstein et al.

In its 2005 study, TRL analyzed the STATS19 road accident dataset [5] for the years 1980-1982 (before the original introduction of side guards) and 1990-1992 (10 years later when side guards were standard in the U.K. truck fleet). In bicyclist impacts into the side of trucks, where the truck and the bicyclist were traveling straight in the same direction, there was a 61% reduction in fatalities (based on a sample size of 34 fatalities for the combined six years of analysis (1980-1982 and 1990-1992)), 13% reduction in serious injuries (sample size = 101 for the six years), and 25% increase in minor injuries (sample size = 209 for the combined 6 years) after the implementation of side guards. However, in bicyclist crashes into the side of trucks in other pre-crash vehicle maneuvers, such as the vehicle turning right or left, the proportion of killed or seriously injured cyclists was similar before and after side guards were introduced. TRL noted that this suggests side guards are only effective in crashes where the bicyclist and truck are traveling straight in the same direction before the crash. TRL also found that in crashes involving pedestrians colliding with the side of a truck that was moving straight ahead, there was a 20% reduction in the proportion of pedestrian fatalities after side guards were required but no reduction in serious or minor injuries. The STAT19 data also showed that there was no reduction in pedestrian fatalities in other pre-crash vehicle maneuvers (vehicle turning left or right).

TRL also conducted an in-depth study which suggested that crashes between cyclists and trucks turning left (a left turn in U.K. is equivalent to a right turn in the U.S.) often involve a collision toward the front of the vehicle which knocks the cyclist to the ground [3]. As the truck progresses with its turn, the rear of the vehicle cuts into the corner, and the sideguard passes over the top of the prone cyclist who then gets run-over by the rear wheels of the truck.

A follow up study by TRL [6] in 2010 comparing STATS19 accident data of crashes where the truck and the bicyclist were traveling straight in the same direction for the years 2006-2008 and 1980-1982 showed that after side guards became a standard feature in the U.K. truck fleet, bicyclist fatalities decreased by 56% (sample size = 31), serious injuries increased by 3% (sample size = 90), and minor injuries increased by 17.5% (sample size = 158) in impacts to the side of trucks when both the truck and cyclist were traveling straight in the same direction. However, the STATS19 accident data also showed that side guards had no effectiveness in preventing bicyclist fatalities and injuries for other pre-crash vehicle maneuvers such as when the truck is turning left or right. TRL suggested that a lower ground clearance than the required 550 mm could improve the effectiveness of side guards in left turn crashes but noted that further technical evaluations are needed.

In March 2010, the National Research Council (NRC) in Canada published a study to better understand how side guards would affect Canadian heavy vehicle operators, vulnerable road users (pedestrians and bicyclists), and the environment [7]. The NRC stated that while data from Europe indicates a reduction in death and serious injuries to

vulnerable road users because of the introduction of side guards on trucks, it is not clear if this reduction is entirely related to side guards or if side guards are just one of the contributing factors.

In light of the Vision Zero initiatives in various cities, NHTSA undertook a preliminary cost effectiveness analysis for equipping side guards on new SUTs and semitrailers for protecting pedestrians and bicyclists in crashes with these vehicles.

REAL-WORLD CRASH DATA

To better understand pedestrian and bicyclist fatalities and injuries in the U.S., NHTSA analyzed the FARS [8] and NASS-GES [9] data for the five-year period 2010 to 2014. FARS is a census of fatal motor vehicle crashes in the U.S., and NASS-GES is a nationally representative probability sample of police reported crashes. The FARS data were analyzed for determining pedestrian and bicyclist fatalities, and the NASS-GES data were analyzed for determining pedestrian and bicyclist injuries.

FARS and NASS-GES data were queried for single-vehicle crashes involving SUTs or semitrailers with a GVWR greater than 4,536 kg where the first harmful event in the crash was a collision with a pedestrian or bicyclist. The factors considered in the analysis were the pre-crash maneuver of the truck and the initial impact point on the truck/trailer with the pedestrian or bicyclist. Average annual fatalities and injuries were determined by averaging the five-year data from 2010 to 2014. The summary of the FARS and NASS-GES data analysis is discussed in the following sections.

Summary of the Analysis of 2010-2014 FARS and NASS-GES Data

Pedestrian Data

Police-Reported Crashes

- On average, there were an estimated 872 pedestrians struck by SUTs or semitrailers with a GVWR greater than 4,536 kg annually.
    - 701 (80.3%) were struck by SUTs, and 171 (19.7%) were struck by semitrailers.
    - 168 (24.0%) of pedestrians struck by SUTs sustained incapacitating or fatal injuries.
    - 100 (58.5%) of pedestrians struck by semitrailers sustained incapacitating or fatal injuries.

Fatalities

- On average, there were 232 pedestrian fatalities in crashes with heavy trucks annually.
    - 97 (41.8%) were struck by SUTs, and 135 (58.2%) were struck by semitrailers.
- Among the 97 pedestrian fatalities in crashes with SUTs,
    - Initial impact
        - **67.0% were initial impacts to the front of the vehicle,**
        - 5.8% were to the right, and
        - 3.9% to the left of the vehicle.
    - Pre-crash vehicle movement
        - **57.0% were when the SUT was going straight,**
        - 8.5% when the SUT was turning right, and
        - 10.3% when the SUT was turning left.
- Among the 135 pedestrian fatalities in crashes with semitrailers,
    - Initial impact
        - **71.8% were initial impacts to the front of the vehicle,**
        - 10.8% to the right, and
        - 3.7% to the left of the vehicle.
    - Pre-crash vehicle movement
        - **73.5% were when the semitrailer was going straight,**
        - 7.4% when the semitrailer was turning right, and
        - 2.5% when the semitrailer was turning left.
- **Annually in the U.S., there were 9.4 pedestrian fatalities in crashes with SUTs and 19.6 pedestrian fatalities in crashes with semitrailers where the initial impact was to the left or right side of the vehicle.**

Bicyclist Data

Police-Reported Crashes

- On average, there were an estimated 664 bicyclists annually struck by heavy trucks or semitrailers (with a GVWR greater than 4,536 kg),
    - 477 (71.8%) were struck by SUTs, and 187 (28.2%) were struck by semitrailers.
    - 198 (41.5%) bicyclists struck by SUTs sustained incapacitating or fatal injuries.
    - 64 (34.2%) bicyclists struck by semitrailers sustained incapacitating or fatal injuries.

Fatalities

- On average, there were 62.5 bicyclist fatalities annually in crashes with heavy trucks.
    - 32 were in crashes with SUTs and 30.5 were in crashes with semitrailers.
- Among the 32 bicyclist fatalities in crashes with SUTs,
    - Initial Impact
        - **57.9% were initial impacts to the front of the vehicle,**
        - 26.4% were to the right, and
        - 3.8% to the left of the vehicle.
    - Pre-crash vehicle movement
        - **49.7% were when the SUT was going straight,**
        - 29.5% when the SUT was turning right, and
        - 9.4% when the SUT was turning left.
- Among the 31 bicyclist fatalities in crashes with semitrailers,
    - Initial Impact
        - **42.5% were initial impacts to the front of the vehicle,**
        - 24.2% to the right, and
        - 5.9% to the left of the vehicle.
    - Pre-crash movement
        - **59.5% were when the semitrailer was going straight,**
        - 25.5% when the semitrailer was turning right, and
        - 5.2% when the semitrailer was turning left.
- **Annually in the U.S., there were 9.6 bicyclist fatalities in crashes with SUTs and 9.2 bicyclist fatalities in crashes with semitrailers where the initial impact was to the left or right side of the vehicle.**

These results are slightly different from the pedestrian and bicyclist fatalities in crashes with SUTs with GVWR greater than 4,536 kg reported by the National Transportation Safety Board (NTSB) using the Trucks in Fatal Accidents (TIFA) data for the five-year period from 2005 to 2009 [10]. For the years 2005 to 2009, NTSB found an annual average of 122.6 pedestrians and 38.6 bicyclists killed in impacts with SUTs and 151.8 pedestrians and 36.2 bicyclists killed in impacts with semitrailers. NTSB noted in the report that in 25% of pedestrian fatalities and 44% of bicyclist fatalities in impacts with SUTs, the initial impact was to the left or right side of the vehicle. Additionally, NTSB noted that in 29% of pedestrian fatalities and 55% of bicyclist fatalities in collisions with trailers, the initial impact was to the left or right side of the vehicle [11]. Differences in the results by NTSB and NHTSA could partly be attributed to the different years of data used in the analysis; NHTSA analyzed FARS data for the years 2010 to 2014 while NTSB analyzed data for the years 2005 to 2009.

PRELIMINARY COST EFFECTIVENESS ANALYSIS OF SIDE GUARDS ON SUTS

This section presents a preliminary cost effectiveness evaluation for equipping side guards on new SUTs with a GVWR greater than 4,536 kg.

Target Population

Table 1 and Table 2 present the annual pedestrian and bicyclist fatalities in the U.S. in single-vehicle crashes with SUTs when the first harmful event was collision with the pedestrian or bicyclist by initial point of impact on the vehicle and pre-event movement of the vehicle (FARS 2010-2014).

Table 1.

Annual pedestrian fatalities in the U.S. in single-vehicle crashes with SUTs when the first harmful event was collision with the pedestrian by initial point of impact on the vehicle and pre-event movement of the vehicle (FARS 2010-2014)

Initial Point of Impact on Vehicle	Pre-Event Movement of Vehicle							Total
	Going Straight	Turning Right	Turning Left	Overtaking Another Vehicle	Changing Lanes	Making a U-Turn	All Others	
Front	44.4	4.6	8.4	0.4	0.8	0	6.2	64.8
Right	3.6	1	0.2	0	0	0.2	0.6	**5.6**
Left	2.6	0.2	0.6	0	0	0	0.4	**3.8**
Back	0.2	0.4	0	0	0	0	10.2	10.8
Other	4.2	2	0.8	0	0	0	4.6	11.6
Total	55.0	8.2	10.0	0.4	0.8	0.2	22.0	96.6

Table 2.

Annual bicyclist fatalities in the U.S. in single-vehicle crashes with SUTs when the first harmful event was collision with the bicyclist by initial point of impact on the vehicle and pre-event movement of the vehicle (FARS 2010-2014)

Initial Point of Impact on Vehicle	Pre-Event Movement of Vehicle					
	Going Straight	Turning Right	Turning Left	Overtaking Another Vehicle	All Others	Total
Front	11.4	3	1.6	0.2	2.2	18.4
Right	2.0	5.2	0.8	0.2	0.2	**8.4**
Left	0.8	0	0.4	0	0	**1.2**
Back	0.4	0.4	0.2	0	0.4	1.4
Other	1.2	0.8	0	0.2	0.2	2.4
Total	15.8	9.4	3.0	0.6	3.0	31.8

On average in the U.S., 9.4 (= 5.6 + 3.8) pedestrians and 9.6 (= 8.4 + 1.2) bicyclists are killed annually in crashes with SUTs with GVWR greater than 4,536 kg where the initial impact is to the left or right side of the vehicle. Among these fatalities, 6.2 (= 3.6 + 2.6) pedestrians and 2.8 (= 2 + 0.8) bicyclist fatalities are when the vehicle is moving straight ahead before the impact.

Effectiveness and Benefits Estimates of Side Guards on SUTs

TRL [2] estimated a 20% effectiveness of side guards in preventing pedestrian fatalities and a 61% effectiveness in preventing bicyclist fatalities when initial impact is to the sides of the vehicle and the vehicle is moving straight ahead. The TRL report also noted that side guards had no effectiveness in preventing pedestrian or bicyclist fatalities when the truck was turning left or right. Using these effectiveness estimates for side guards on SUTs would result in saving 1.2 pedestrian and 1.7 bicyclist lives annually (calculations are shown in Table 3). Because the TRL studies [2, 6] indicated that side guards had little to no effect in preventing serious and minor injuries, injuries were not considered in this analysis.

Table 3.

Estimation of Annual Pedestrian and Bicyclist Lives Saved by Installing Side Guards on All New SUTs

Pedestrian	
Pedestrian Fatalities with First Impact on Side of Vehicle when vehicle is Going Straight (a)	6.2
Effectiveness of Side Guards for Pedestrians (b)	20%

Pedestrian Lives Saved = (a) x (b)	1.2
Bicyclist	
Bicyclist Fatalities with First Impact on Side of Vehicle when Vehicle is Going Straight (c)	2.8
Effectiveness of Side Guards for Bicyclists (d)	61%
Bicyclist Lives Saved = (c) x (d)	1.7

Since Epstein et al. [4] claimed side guards with lower ground clearance than those installed in the U.K. would provide greater protection to vulnerable road users, NHTSA evaluated side guards meeting the Epstein et al. specifications ("improved" side guards) by making certain assumptions. Since no effectiveness estimates are available for these "improved" side guards, NHTSA first assumed that these "improved" side guards would also be effective in preventing fatalities in all pre-crash maneuvers of the truck (going straight, right turn, left turn, overtaking another vehicle, changing lanes, making a U-turn, and others). Second, NHTSA assumed that the effectiveness of "improved" side guards on SUTs in preventing fatalities to pedestrians and bicyclists in all pre-crash vehicle maneuvers is 20% and 61%, respectively. These two assumptions would likely result in an upper bound of the population of pedestrian and bicyclist fatalities addressable by "improved" side guards and an upper bound of the overall effectiveness of "improved" side guards and therefore result in an upper bound of the estimated benefits for side guards. Based on these two assumptions, the "improved" side guards (guards designed and installed per Epstein et al. specifications) would save 1.9 pedestrian lives and 5.9 bicyclists lives annually (calculations are shown in Table 4).

Table 4.

Estimation of Annual Pedestrian and Bicyclist Lives Saved by Installing "Improved" Side Guards on All New SUTs

Pedestrian	
Pedestrian Fatalities with First Impact on Side of Vehicle (a)	9.4
Effectiveness of Side Guards for Pedestrians (b)	20%
Pedestrian Lives Saved = (a) x (b)	1.9
Bicyclist	
Bicyclist Fatalities with First Impact on Side of Vehicle (c)	9.6
Effectiveness of Side Guards for Bicyclists (d)	61%
Bicyclist Lives Saved = (c) x (d)	5.9

Cost and Weight of Side Guards on SUTs

Based on a review of implementation of side guards in various cities in the U.S. and a survey of vendors of side guards, Epstein et al. estimated that the cost of fitting a SUT with side guards ranges from $600 to $2,500 per vehicle [4]. The large range in the cost is likely related to the length of the side guards, type of materials used (steel, aluminum, fiberglass, and others), and the type of guards (rails or panels). The length of a guard fitted on a SUT is not only dependent on the length of the SUT but also on any equipment on the side of the SUT, which would exclude installing a guard at that location.

Airflow Deflector, [12] a vendor of side guards on trucks and trailers, indicated the cost of side guards for pedestrian protection range between $308 per meter to $473 per meter depending on the material and type (2-rails, 3-rails, or panel) of guard. The rail guards, which cost less than the panel guards, are available in lengths of 2.4 or 3 meters. Assuming that on average both sides of SUTs are installed with 2.4-meter guards at a cost of $308 per meter, the average cost of installing side guards on a SUT is $1,478 (= 2 sides x 2.4-meter guard x $308 per meter). Based on this data, NHTSA estimated that the average cost of installing side guards on SUTs with a GVWR greater than 4,536 kg is about $1,478. There are about 580,000 SUTs with a GVWR greater than 4,536 kg sold annually in the U.S. [13]. The annual cost of equipping side guards on new SUTs with GVWR greater than 4,536 kg would be $857.2 million (= $1,478 x 580,000).

Installing side guards on SUTs adds weight to the truck, which would reduce its fuel economy and payload capacity. According to AirFlow Deflector, a 1.5-meter fiberglass panel used to mitigate pedestrian and bicyclist fatalities weighs less than 15.9 kg. The cheaper 2.4-meter rail guard weighs about 25.5 kg and a similar 3-meter rail guard weighs 32 kg. Depending on the length of the panels or rails installed as side guards on SUTs, we estimate that the installation of these guards on SUTs with a GVWR greater than 4,536 kg would increase the weight of the vehicle by 31.8 kg (2x15.9 kg for 1.5-meter fiberglass panels) to 64 kg (2x32 kg for 3-meter rail guards).

Cost/Benefit Analysis for Side Guards on SUTs

As shown in Table 3, 2.9 lives (= 1.2 + 1.7) could potentially be saved annually by installing side guards on all new SUTs. Since the 2005 TRL report indicated that the side guards had little effect on serious and minor injuries to bicyclists and pedestrians, the number of lives saved is the same as the number of equivalent lives saved (because the equivalent lives saved from preventing serious and minor injuries is near zero). The annual cost of equipping side guards on new SUTs with a GVWR greater than 4,536 kg is estimated to be $857.2 million. Therefore, the cost per equivalent lives saved = $295.6 million (= $857.2M / 2.9).

Under the assumption that "improved" side guards with lower ground clearance would be 20% and 61% effective in preventing pedestrian and bicyclist fatalities, respectively, regardless of pre-impact vehicle maneuver, 7.8 lives (= 1.9 + 5.9) would be saved annually (Table 4). The cost per equivalent lives saved (undiscounted) in this case would be approximately $109.9 million (= $857.2M / 7.8).

Note: The estimated cost of side guards does not include the additional lifetime fuel costs because of increased weight of the vehicle, the additional cost because of reduced payload, and the higher lifetime cost of maintaining a vehicle with side guards. Including these three cost factors would increase the estimated cost per lives saved. Additionally, the number of lives saved were not discounted to present value; discounting the lives saved would further increase the cost per equivalent lives saved.

PRELIMINARY COST EFFECTIVENESS ANALYSIS OF SIDE GUARDS ON SEMITRAILERS

This section presents a preliminary cost effectiveness evaluation for equipping side guards on new semitrailers with a GVWR greater than 4,536 kg. The analysis follows the same methodology as that for SUTs presented in the previous sections.

Target Population

Table 5 and Table 6 present the annual pedestrian and bicyclist fatalities in the U.S. in single-vehicle crashes with semitrailers when the first harmful event was collision with the pedestrian or bicyclist by initial point of impact on the vehicle and pre-event movement of the vehicle (FARS 2010-2014).

Table 5.

Annual Pedestrian Fatalities in The U.S. in Single-Vehicle Crashes with Semitrailers when the First Harmful Event was Collision with the Pedestrian by Initial Point of Impact on the Vehicle and Pre-Event Movement of the Vehicle (FARS 2010-2014)

Initial Point of Impact on Vehicle	Pre-Event Movement of Vehicle							Total
	Going Straight	Turning Right	Turning Left	Overtaking Another Vehicle	Changing Lanes	Making a U-Turn	All Others	
Front	78.4	4.8	1.8	0	1.6	0	10.6	97.2
Right	**9.0**	2.2	0.2	0.2	0.4	0	2.6	**14.6**
Left	**3.6**	0.4	0.2	0	0	0	0.8	**5.0**
Back	2.0	1.4	0.6	0	0	0	1.6	5.6
Other	6.6	1.2	0.6	0.2	0.2	0	4.2	13
Total	99.6	10.0	3.4	0.4	2.2	0	19.8	135.4

Table 6.

Annual bicyclist fatalities in the U.S. in single vehicle crashes with semitrailers when the first harmful event was collision with the bicyclist by initial point of impact on the vehicle and pre-event movement of the vehicle (FARS 2010-2014)

Initial Point of Impact on Vehicle	Pre-Event Movement of Vehicle					
	Going Straight	Turning Right	Turning Left	Overtaking Another Vehicle	All Others	Total
Front	7.4	3.4	1.0	0	1.2	13.0
Right	**4.6**	2.0	0	0.2	0.6	**7.4**
Left	**1.4**	0.2	0	0	0.2	**1.8**
Back	1.8	0.6	0.4	0	0.4	3.2
Other	3.0	1.6	0.2	0	0.4	5.2
Total	18.2	7.8	1.6	0.2	2.8	30.6

On average in the U.S., 19.6 (= 14.6 + 5.0) pedestrians and 9.2 (7.4 + 1.8) bicyclists are killed annually in crashes with semitrailers with initial impact to the left or right side of the vehicle. Among these fatalities, 12.6 (= 9.0 + 3.6) pedestrians and 6.0 (= 4.6 + 1.4) bicyclist fatalities are when the vehicle is moving straight ahead before the impact.

Effectiveness and Benefits Estimates of Side Guards on Semitrailers

TRL [2] estimated side guards on trucks and trailers are 20% effective in preventing pedestrian fatalities and 61% effective in preventing bicyclist fatalities when initial impact is to the side of the vehicle and the vehicle is traveling straight ahead. The TRL report also noted that side guards had no effectiveness in preventing pedestrian/bicyclist fatalities when the truck was turning left or right. Using these effectiveness estimates for side guards on semitrailers would result in saving 2.5 pedestrian and 3.7 bicyclist lives annually (calculations are shown in Table 7). Because the TRL studies indicated that side guards had little to no effect in preventing serious and minor injuries, injuries were not considered in this analysis.

Table 7.

Calculation of Annual Pedestrian and Bicyclist Lives Saved by Equipping Side Guards on New Semitrailers

Pedestrian	
Pedestrian Fatalities with First Impact on Side of Vehicle when vehicle is Going Straight (a)	12.6
Effectiveness of Side Guards for Pedestrians (b)	20%
Pedestrian Lives Saved = (a) x (b)	2.5
Bicyclist	
Bicyclist Fatalities with First Impact on Side of Vehicle when Vehicle is Going Straight (c)	6.0
Effectiveness of Side Guards for Bicyclists (d)	61%
Bicyclist Lives Saved = (c) x (d)	3.7

As in the analysis for side guards on SUTs, NHTSA assumed that "improved" side guards on semitrailers (side guards designed and installed according to Epstein et al. specifications) would be 20% and 61% effective in preventing pedestrian and bicyclist fatalities in impacts to the sides of trailers, respectively, for all pre-impact vehicle maneuvers. As stated above, these assumptions result in an upper bound of the population of pedestrian and bicyclist fatalities addressable by "improved" side guards and an upper bound of the effectiveness of "improved" side guards and therefore result in an upper bound of the estimated benefits for side guards. Under these

assumptions, NHTSA estimates that "improved" side guards on semitrailers would save 3.9 pedestrian lives and 5.6 bicyclists lives annually (calculations are shown in Table 8).

Table 8.
Calculation of Annual Pedestrian and Bicyclist Lives Saved by Equipping "Improved" Side Guards on New Semitrailers

Pedestrian	
Pedestrian Fatalities with First Impact on Side of Vehicle (a)	19.6
Effectiveness of Side Guards for Pedestrians (b)	20%
Pedestrian Lives Saved = (a) x (b)	3.9
Bicyclist	
Bicyclist Fatalities with First Impact on Side of Vehicle (c)	9.2
Effectiveness of Side Guards for Bicyclists (d)	61%
Bicyclist Lives Saved = (c) x (d)	5.6

Cost and Weight of Side Guards on Semitrailers

In May 2018, NHTSA published a report [14] on research conducted by the Texas A&M Transportation Institute on the design, cost, and weight of side trailer guards to mitigate passenger compartment intrusion of passenger cars in sideswipe crashes with trailers. The Texas A&M study estimated a guard length of 6 meters would be needed for the typical semitrailer to provide protection from just behind the trailer landing gear to the front of the tire of the rear bogie.

ECE R.73 requires lateral protection devices (side impact guards) on trailers that echoes the dimensions estimated in the Texas A&M study equating to approximately 6 meters for a typical 16-meter semitrailer. AirFlow Deflector offers single, double, and triple beam guards as well as fiberglass panels designed for pedestrian/cyclist protection. The cost/weight information from Airflow Deflector (provided on its website) for pedestrian/cyclist side guard protection on SUTs is used here by extrapolation to estimate the cost of adding similar side impact protection to semitrailers.

AirFlow Deflector offers SUT pedestrian/cyclist side underride kits up to 3 meters in length. Two 3-meter length sections on each side would be required for a complete application to a semitrailer. AirFlow Deflector provides costs for double rail side guard systems with either aluminum or steel rails designed specifically to meet the recommended side guard design by Epstein et al. [4]. However, because of the increased frame height of a semitrailer a triple rail guard system would most likely be needed to provide protection with the minimum ground clearance recommended by Epstein et al. AirFlow Deflector offers additional 3-meter length single guard rails for $106 each but does not specify the material (steel or aluminum) of these additional pieces.

For a 3-meter double aluminum rail system covering both sides of an SUT, AirFlow Deflector quotes a cost of $1,875. This would need to be doubled for a 6-meter application on a semitrailer. Additionally, a third guard rail would need to be added to each double rail section for a total estimated cost of $4,174 per semitrailer (= 2 x $1,875 for the double side guard kits + 4 x $106 for the additional third guard rail pieces).

For a 3-meter double steel rail system covering both sides of an SUT, AirFlow Deflector quotes a cost of $2,016. This would need to be doubled for a 6-meter application on a semitrailer. Additionally, a third guard rail would need to be added to each section for a total estimated cost of $4,456 (= 2 x $2,016 for the double side guard kits + 4 x $106 for the additional guard rail sections = $4,456).

Therefore, a reasonable cost estimate of side guards for pedestrian/cyclist protection on a semitrailer would start at $4,174 per trailer for the aluminum application. There are about 214,634 semitrailers with GVWR greater than 4,536 kg sold annually in the U.S. [13]. The total cost of equipping side guards on all new semitrailers would be about $895.9 million (=$4,174 per trailer x 214,634 semitrailers).

As with SUTs, installing side guards on semitrailers adds weight which would reduce fuel economy and the payload capacity of the semitrailer. AirFlow Deflector quoted a weight of 32 kg for each 3-meter section of side guard. Material or number of guard rails in each was not specified. Therefore, applying four 3-meter SUT kits to a semitrailer would probably result in approximately a 128 kg (=4 x 32 kg) increase in trailer weight.

Cost/Benefit Analysis for Side Guards on Semitrailers

As shown in Table 7, 6.2 lives (= 2.5 + 3.7) could potentially be saved annually by equipping side guards on all semitrailers. Since the 2005 TRL report indicated that the side guards had little effect on serious and minor injuries to bicyclists and pedestrians, the number of lives saved is the same as the number of equivalent lives saved (since the equivalent lives saved from preventing serious and minor injuries is near zero). The annual cost of equipping side guards on all new semitrailers with GVWR greater than 4,536 kg would be about $896 million. Therefore, the cost per equivalent lives saved (undiscounted) is approximately $144.5 million ($895.9M / 6.2 = $144.5M).

Under the assumption that "improved" side guards with lower ground clearance would be 20% and 61% effective in preventing pedestrian and bicyclist fatalities, respectively, regardless of pre-impact maneuver, 9.5 lives (= 3.9 + 5.6) would be saved annually (Table 8). The cost per equivalent lives saved (undiscounted) in this case would be about $94.3 million (= $895.9M / 9.5).

Note: the estimated cost of side guards does not include the additional lifetime fuel costs because of increased weight of the vehicle, the additional cost because of reduced payload, and the higher lifetime cost of maintaining a vehicle with side guards. Including these three cost factors would increase the estimated cost per lives saved. Additionally, the number of lives saved were not discounted to present value; discounting the lives saved would further increase the cost per equivalent lives saved.

DISCUSSION

Data on the real-world effectiveness of sideguards in the U.S. is not available because there are currently very few SUTs with side guards in the U.S. therefore, the effectiveness analysis is based on data collected in the U.K. Additionally, because there are virtually no semitrailers with side guards for pedestrian and bicyclist protection on U.S. roads today, the cost estimates were derived from the cost data for SUTs.

The preliminary cost effectiveness analysis indicated that the cost per equivalent lives saved for a mandate for side impact guards to protect pedestrians and bicyclists is about $109.9 million to $295.6 million for SUTs and $94.3 million to $144.5 million for truck-trailers and semi-trailers. This is significantly greater than the $9.6 million current value of a statistical life used by the U.S. Department of Transportation [15]. Therefore, side guards on all new SUTs and semitrailers with GVWR greater than 4,536 kg for pedestrian/bicyclist protection is not a cost-effective countermeasure. In this preliminary analysis, the fatalities were not discounted to present value, and the additional lifetime fuel costs due to the increase in vehicle weight, possible higher cost of maintaining a vehicle with side guards, and the additional cost of reduced payload were not taken into consideration. Including these effects would further increase the cost per equivalent lives saved.

This preliminary analysis indicates that equipping side guards on all new SUTs and semitrailers for pedestrian and bicyclist protection is not cost effective. Crash avoidance technologies such as cameras and mirrors to improve driver visibility, detection and warning systems, and automatic emergency braking systems may be more effective in mitigating truck impacts with pedestrians and bicyclists. In addition, changes to infrastructure, such as adding bike lanes and sidewalks and improving intersection designs, may further reduce pedestrian and bicyclist crashes.

REFERENCES

[1] UNECE Regulation No.73, "Lateral protection devices." http://www.unece.org/trans/main/wp29/wp29regs61-80.html.
[2] Knight, I., Dodd, M., Bowes, D., Donaldson W. et al, Integrated safety guards and spray suppression – final summary report, 2005. http://www.trl.co.uk/reports-publications/report/?reportid=5450
[3] Vision Zero Network, https://visionzeronetwork.org/about/vision-zero-network/.

[4] Epstein, A.K., Price, S., Breck, A., Cooper, C., Segev, E., "Truck sideguards for Vision Zero - review and technical recommendations for Safe Fleet Transition Plan pilot deployment," DOT-VNTSC-DCAS-14-01, December 2014, https://rosap.ntl.bts.gov/view/dot/12164.
[5] The STATS19 road accident dataset consists of road accidents on the public highway in Great Britain, reported to the police and which involve human injury or death. http://www.adls.ac.uk/department-for-transport/stats19-road-accident-dataset/?detail#top.
[6] Cookson, R. Knight, I., "Side Guards on Heavy Goods Vehicles: Assessing the effects on pedal cyclists injured by trucks overtaking or turning left." Transportation Research Laboratory (TRL) Report PPR514, June 2010.
[7] National Research Council Canada, "Side guards for trucks and trailers, Phase 1: Background information," March 2010.
[8] Fatality Analysis Reporting System, https://www.nhtsa.gov/research-data/fatality-analysis-reporting-system-fars.
[9] National Automotive Sampling System-General Estimates System https://www.nhtsa.gov/national-automotive-sampling-system-nass/nass-general-estimates-system.
[10] Crashes Involving Single-Unit Trucks that Resulted in Injuries and Deaths, Safety Study, NTSB/SS-13/01, PB2013-106637, National Transportation Safety Board. http://www.ntsb.gov/safety/safety-studies/Pages/SS1301.aspx.
[11] NTSB Safety Recommendations H-14-001 through -007. https://www.ntsb.gov/safety/safety-recs/recletters/H-14-001-007.pdf.
[12] https://airflowdeflector.com.
[13] Ward's Automotive group, ISBN Number 978-0-910589-31-4, Southfield, MI 2013. http://wardsauto.com/.
[14] Bligh, R. P., Dobrovolny, C.S., Sheikh, N., Abu-Odeh, A., Kovar, J., "Computer Modeling and Evaluation of Side Underride Protective Device Designs," April, 2018, DOT HS 812 522, https://www.nhtsa.gov/document/computer-modeling-and-evaluation-side-underride-protective-device-designs.
[15] Guidance on the treatment of the economic value of a statistical life (VSL) in U.S. Department of Transportation analyses – 2016 Adjustment, August 8, 2016, https://www.transportation.gov/sites/dot.gov/files/docs/2016%20Revised%20Value%20of%20a%20Statistical%20Life%20Guidance.pdf.

INTENTION OF MANOEUVRE AND MOTION PREDICTION OF OTHER ROAD USERS: A HYBRID APPROACH

Irene Cara
Jeroen Uittenbogaard

TNO Helmond
The Netherlands

Paper Number 19-0023

ABSTRACT

Automated driving is gaining more and more interest in the recent years. In order to drive safely, automated vehicles reconstruct the environment using mainly the information coming from the in-car sensors. By using this reconstruction a prediction of the future states of the surrounding vehicles can be computed, which in turn is used to decide which manoeuvre and accompanying path to accomplish. This problem is known as motion prediction. Whilst physics-based models perform well on a short horizon, machine learning has the potential to predict a more accurate motion on a longer horizon, especially if the manoeuvre of the other road user is known in advance (manoeuvre-based prediction).

In this paper a hybrid approach is proposed that consists of an intention of manoeuvre predictor, a physics-based motion predictor and a manoeuvre-based motion predictor.

The vehicles around the host vehicle are continuously tracked. The intention of manoeuvre predictor, based on Support vector machines (SVM), computes the probability for each surrounding vehicle of changing lane or of staying in lane. In addition, a kinematical model which assumes a constant turn rate and velocity (CTRV) is used to predict the trajectories. Once the intention of manoeuvre is known, the manoeuvre-based motion model, based on machine learning algorithms as Gaussian Processes and SVR, predicts the lane change or lane following trajectories. The models are trained using a collection of cut-ins manoeuvres from 60 hours of naturalistic driving. In the end, the physics-based and the manoeuvre-based motion predictions are merged together by a weighting function.

The models were validated with cross-validation and the performance and the integration between sub-modules was tested in a Hardware In the Loop (HIL) environment. The models are capable of detecting the intention of a surrounding vehicle of changing lane with a positive predictive value of 82% 1.2 second before it crosses the lane marker. The combination of SVR and CTRV is capable of predicting well for shorter and longer horizons, keeping the advantages of both methods. The combined model predicts the longitudinal distance and the lateral distance with an error that is 50% lower than the one using the physics-based model, after 4s and an even better performance on shorter horizons in comparison with SVR.

The presented approach is capable of predicting the motion of the other road users in a standard situation. In order to handle more sophisticated scenarios, the road information should be used for training. The training set needs to be extended for better results and the models need to be validated on safety-critical scenarios.

A hybrid approach for predicting the motion of vehicles from a host vehicle perspective is presented in this work. A combination of machine learning and physics-based models is used to enhance the accuracy of the prediction in shorter and longer horizons. The information coming from the prediction module can be used path planning of (partly) automated vehicles.

The results and the integration in the HIL environment show great potential to allow autonomous driving to go to higher levels of automation.

INTRODUCTION

Automated driving is gaining more and more interest in the recent years. In order to ensure more safety on the road, higher levels of automation are needed. The automated vehicle must be able to reconstruct the environment using the information coming from the in-car sensor. The current state of the environment and traffic around is not enough to make safe decisions on which path to follow: prediction of the future states of road participants around the automated vehicle is required.

Another important use case in which the prediction of other road users is needed is truck platooning, when two or three trucks drive with short inter-vehicle distance to reduce fuel consumption and improve traffic efficiency [1]. Early prediction of the behaviour of the car performing the cut-in will help to increase operational safety, because the controllers can use this additional information to anticipate the behaviour of the car, which is especially important in case the Vehicle-To-Vehicle communication fails.

The prediction of road participants can be separated in two phases: intention of manoeuvre and motion prediction. The intention of manoeuvre prediction gives as output the most likely manoeuvre that the road participant will accomplish, before the manoeuvre has clearly started. Typical manoeuvres are lane change, lane following, accelerating, braking, turning. The intention can be predicted using e.g. logistic regression [5] or Support Vector Machine [6].

The motion prediction gives as output the most likely trajectory that the road participant will follow in the future. Machine learning is broadly used to accomplish this task, for example using Gaussian Processes [7], Gaussian Mixture Models [8], Bayesian Networks [9], Neural Networks [6], Support Vector regression [4].

Based on [3], there are 3 main families of motion prediction algorithms:

1. Physics-based models: kinematics or vehicle dynamics is used to predict the motion in the future.

2. Manoeuvre-based models: the intended manoeuvre is known and based on this, the motion is predicted.

3. Interaction-aware models: the motion is modelled taking into account the interaction with the other road users

Interaction-aware models will be not considered in this paper, because they require a big amount of data in order to be trained. The focus of this work is predicting the intention and the motion of other road users on the highway, where the complexity is still limited and interactions can be ignored up to a certain extent. In this case, manoeuvre-based approaches can achieve a good performance ([10], [12]), if the intention of manoeuvre is known in advance.

Whilst physics-based models perform well on a short horizon, machine learning has the potential to predict a more accurate motion on a longer horizon, especially if trained on a manoeuvre-specific training set. In order to get the best out of both methods, physics-based prediction and machine learning can be combined. For example in [11] Dynamic Bayesian Network and Constant Turn Rate and Acceleration (CTRA) are used to predict lane change motion.

In this paper a hybrid approach is proposed that consists of an intention of manoeuvre prediction, a physics-based motion predictor and a manoeuvre-based motion predictor.

The models are then integrated in a Hardware In the Loop (HIL) environment and are suitable for online deployment in an automated vehicle.

METHOD

The objective is to increase safety of automated vehicle by making predictions of the future states of road users on the highway, catching the intention before the manoeuvre actually started, from the point of view of the instrumented vehicle (host vehicle).

In order to predict the motion of other road users, we segmented our solution into the following modules:

- Intention of manoeuvre predictor
- Physics-based motion predictor
- Manoeuvre-based motion predictor
- Combination of the physics-based and manoeuvre-based models

The general architecture of the abovementioned modules is depicted in Figure 1. The intention of manoeuvre predictor computes the probability for each surrounding vehicle of cutting in or of staying in lane. In addition, a kinematical model is used to predict the trajectories (short term). Once the intention of manoeuvre is known, a manoeuvre-based motion model, predicts the cut-in trajectories (long term). In the end, the physics-based and the manoeuvre-based motion predictions are merged together by a weighting function.

In the next subsections, the different modules will be explained in detail.

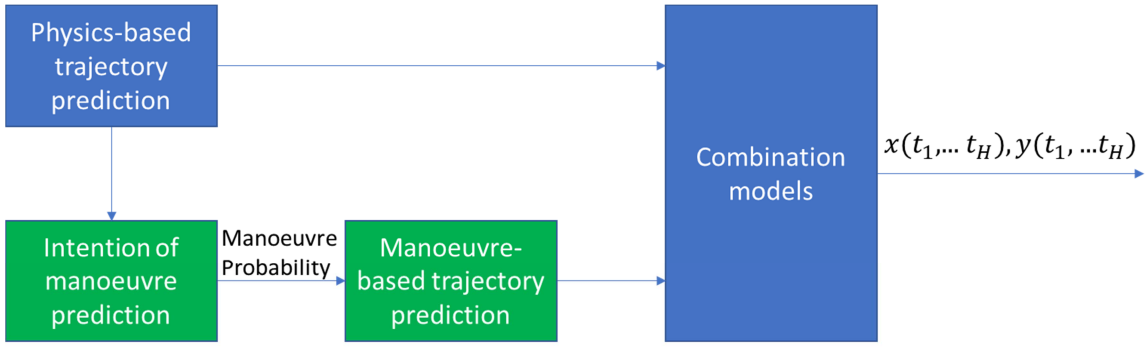

Figure 1 High-level architecture of the prediction models. The green modules are data-driven, based on machine learning. The blue modules are based on physical laws and rules.

Intention of manoeuvre prediction

The manoeuvre intention predictor, based on Support vector machines (SVM), computes the probability for each surrounding vehicle of cutting in or of staying in lane. The vehicles around the host vehicle are continuously tracked. To achieve the most accurate input for the cut in manoeuvre intention prediction algorithm, tests are performed with a high accuracy measurement system (OxTS) together with the vehicle sensors (radar and MobilEye camera). In total 80 cut-ins are performed in a highway setting. The data of all these cut-ins are synchronized at the moment of lane crossing. The start of the cut-in is defined as the last time when it a velocity towards the lane marker (looking back from the moment of lane crossing). As a control, lane keeping data is gathered from naturalistic driving. From all this data relevant parameters are extracted:

- Lateral distance/velocity and acceleration (to vehicle and lane)
- Longitudinal distance, velocity
- Yaw angle, rate and acceleration

These parameters are used in a SVM machine learning algorithm to classify an upcoming cut-in. The final chosen parameters are based on a performance check based on cross validation and a sequential forward selection method where additional parameters need to contribute at least 5% to the performance score to be included. Furthermore a simple computation provides the time it will take to this cut-in to provide an indication of the algorithms usefulness. Finally a validation is performed on said naturalistic driving data to provide an insight in the algorithms accuracy. In this validation a cut-in is predicted when the probability is higher than 0.95 for at least 0.1s to prevent unstable predictions.

Kinematic motion prediction model
For the kinematic model a constant turn rate (w) and velocity (v) algorithm is used (CTRV) [2]. This algorithm computes the longitudinal (x) and lateral (y) position and yaw angle(α) over a certain prediction horizon vector (T) as shown in the equation below:

$$x(T) = \frac{v}{w}\ sin(wT)$$

$$y(T) = \frac{v}{w}\ [cos(wT) + 1]$$

$$\alpha(T) = wT$$

where $T = [t_1, t_2 .. t_H]$.

Manoeuvre-based motion prediction model
Once the intention of manoeuvre is known, the manoeuvre-based motion model, based on machine learning algorithms, predicts the cut-in trajectories.

The machine learning models used are Gaussian Processes and Support Vector Regression. In general Support vector Machines and Gaussian Processes are capable of predicting only one value in the future. To make them predict a complete trajectory, an architecture called Direct Recurrent was used, as explained in our previous work [7]. This allows to avoid the propagation of error typical of recurrent architectures but to keep the relationship between consequent timesteps. The two models will be called DR-SVR and DR-GPR from now on.

The resulting predicted trajectory will be a couple of positions over time, with a horizon t_H up to 4 seconds:

$$(x(T), y(T)) = ((x(t_1), y(t_1)), (x(t_2), y(t_2)), \dots (x(t_H), y(t_H))$$

with $t_H = 4s$.

The prediction algorithms were developed by training on vehicle-kinematics data of cut-ins. The selected features are:

- Host vehicle: speed and acceleration.
- Other road user (to be predicted): longitudinal speed and acceleration, longitudinal and lateral distance with respect to host vehicle.

The training set was extracted from naturalistic driving data, that is part of the TNO Streetwise scenario database [13]. The vehicle used was the a passenger car with a radar and Mobileye system for lane detection**.**

Combination-hybrid model
Based on the crossvalidation results, a weighting function was designed to combine the outputs of the two models (see Figure 2). The physics-based model is used for a horizon up to 1.6s, afterwards only the manoeuvre-based is used. In the first interval of time a combination of the two is output, starting with 100% of physics-based output going to 100% of manoeuvre-based output after 1.6s. The cut-off value 1.6s is the horizon at which the manoeuvre-based model starts to perform better than the physics-based one when predicting the longitudinal distance, as it will be presented later in the Result section.

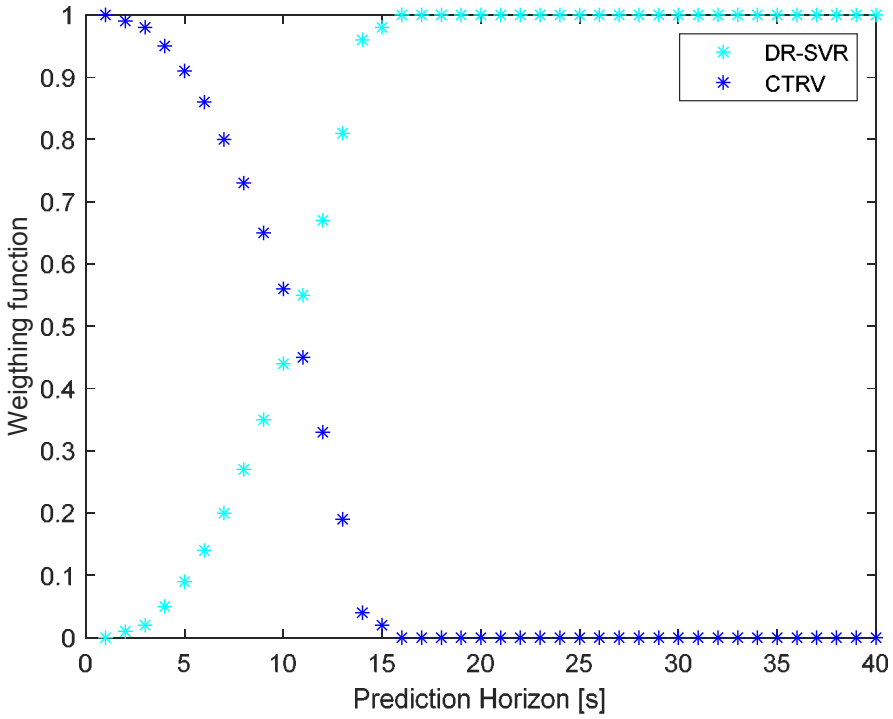

Figure 2 Weighting function used to combine the physics-based model (CTRV), in blue, and the manoeuvre-based model (DR-SVR).

RESULTS

Intention of manoeuvre prediction

For the intention of manoeuvre prediction algorithm the distance to the lane marker had the highest predictive score. Adding the velocity towards the lane made the prediction even better. Adding the best parameter in the third round (longitudinal distance) only added ~2% in prediction score. For that reason this and all following parameters are not included. Figure 3 shows the data used for the cut-in prediction with the cut-in (blue) and going straight events (black) with respect to the selected parameters. It can be seen that cut-ins can be identified by a small distance and substantial negative velocity to the lane marker. The outcome of the SVM machine learning algorithm can be seen in Figure 4. From this result a probability of an cut-in can be computed by using the current values of the 2 selected parameters.

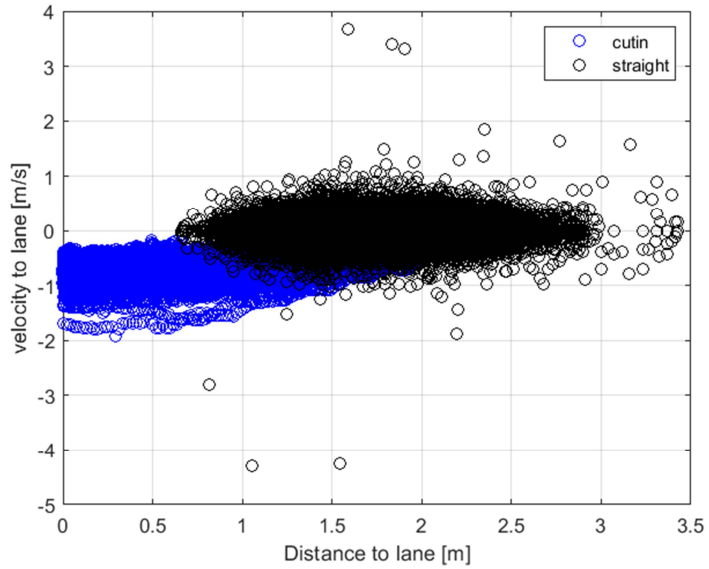

Figure 3 Data used to make the prediction algorihm with the selected parameters on the x- and y axis. Blue is cutin data and black is lane keeping data.

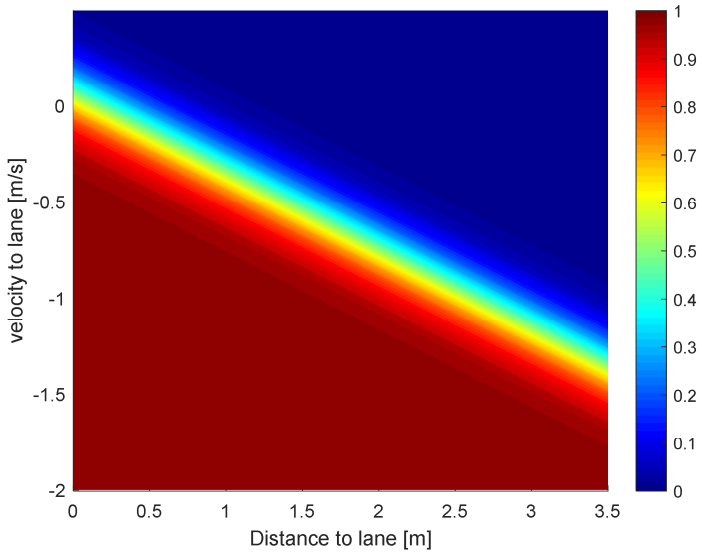

Figure 4 The cut-in prediction algorithm based on distance and velocity to the lane marker. Red area is high chance on a cut-in, while blue are is low chance

The validation showed a positive predictive value of 82%, meaning that 82% of a positive detection are cut-ins. At the moment of detection the average time to lane crossing for these cut-ins is 1.18s (0.27 STD).

Manoeuvre-based prediction

For the manoeuvre-based prediction, two models were considered: DR-SVR and DR-GPR models, as explained in the section Method. The models were validated with cross-validation and the root mean square error for the longitudinal distance and lateral distance are depicted in Figure 5 and Figure 6 respectively. For DR-GPR, the lateral distance RMSE does not exceed 0.5m, while the longitudinal distance RMSE is within the 1.6m limit after 4s. After 1s, 2s, 3s, 4s, DR-SVR has a RMSE of:

- 0.08m, 0.28m, 0,64m and 1,15m for the longitudinal distance

- 0.22m, 0.28m, 0.30m and 0.30m for the lateral distance.

DR-SVR suffers less from the small size of the training set, showing lower errors for both distances. For this reason, we will use this as baseline for the combination with the physics-based prediction result, described in next subsection.

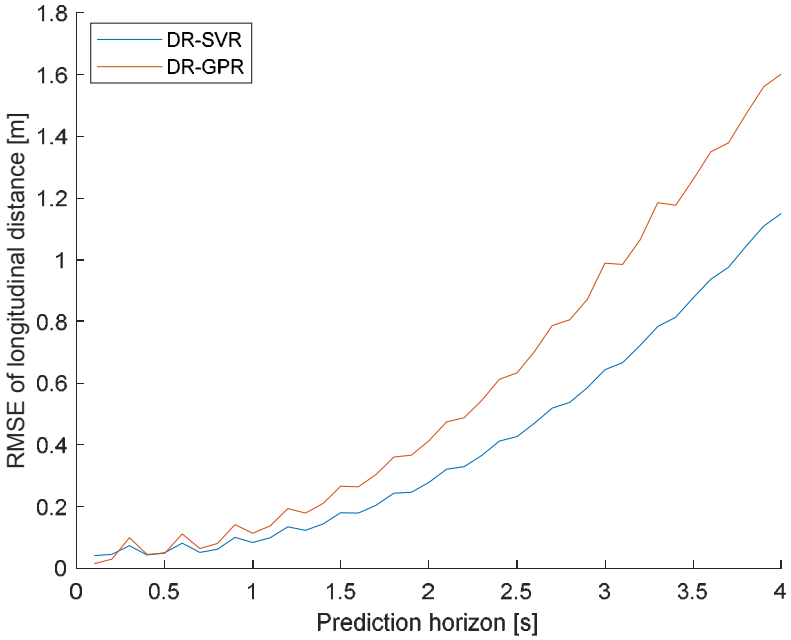

Figure 5 RMSE over time of longitudinal distance: the blue line and red line correspond respectively to DR-SVR and DR-GPR.

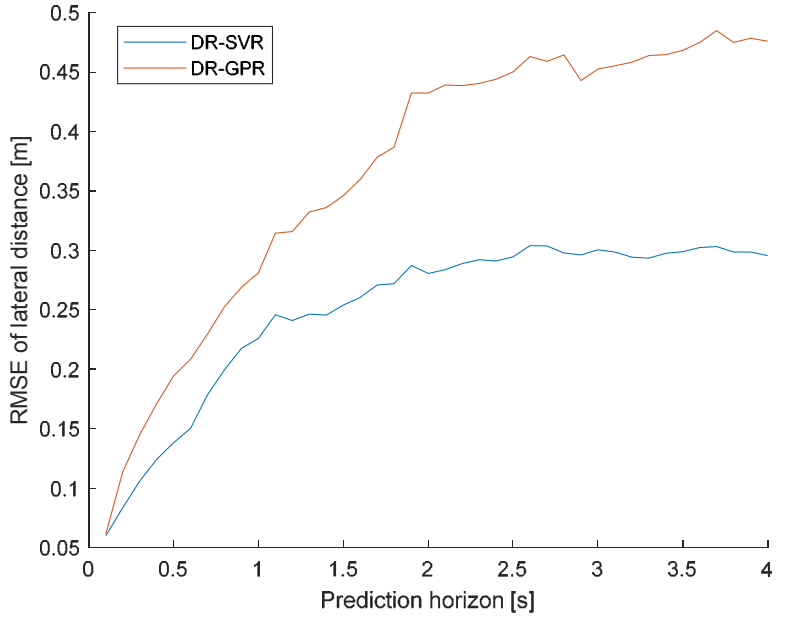

Figure 6 RMSE over time of lateral distance: the blue line and red line correspond respectively to DR-SVR and DR-GPR.

Comparison of physics-based and manoeuvre-based trajectory prediction

The manoeuvre based models (DR-SVR and DR-GPR) were compared with the physics-based (CTVR). Based on the results, the combination of DR-SVR and CTVR was based on the weighting function depicted in Figure 2.

As the CTRV requires more input signals than DR-SVR and DR-GPR in order to perform well, a new validation set was chosen to compare the performance of the different models. We selected the same set used for training the maneuver intention predictor, as explained in Method section. In Figure 10, the profiles of lateral distances of cut-ins are depicted; as it can be seen, both right and left cut-ins are included in the set.

In Figure 8 and Figure 9, the RMSE of the longitudinal distance and the lateral distance are showed. The physics-based model, CTRV, outperforms the manoeuvre based models up to $1.6s$ for the longitudinal distance and $2s$ for the lateral distance. The results show that the manoeuvre-based approach outperforms the physics-based approach for longer horizons, especially DR-SVR for longitudinal distance and DR-GPR for lateral distance. The combination of DR-SVR and CTRV is capable of predicting well for shorter and longer horizons, keeping the advantages of both methods. The combined model predicts the longitudinal distance and the lateral distance with an error that is 50% lower than the one using the physics-based model, after 4s. Looking at short horizons, the combined model is characterized by a RMSE that is one sixth of the RMSE of DR-SVR after 0.5s for the longitudinal distance and a RMSE 62% lower than DR-SVR for the lateral distance. Some examples of prediction are depicted in Figure 7.

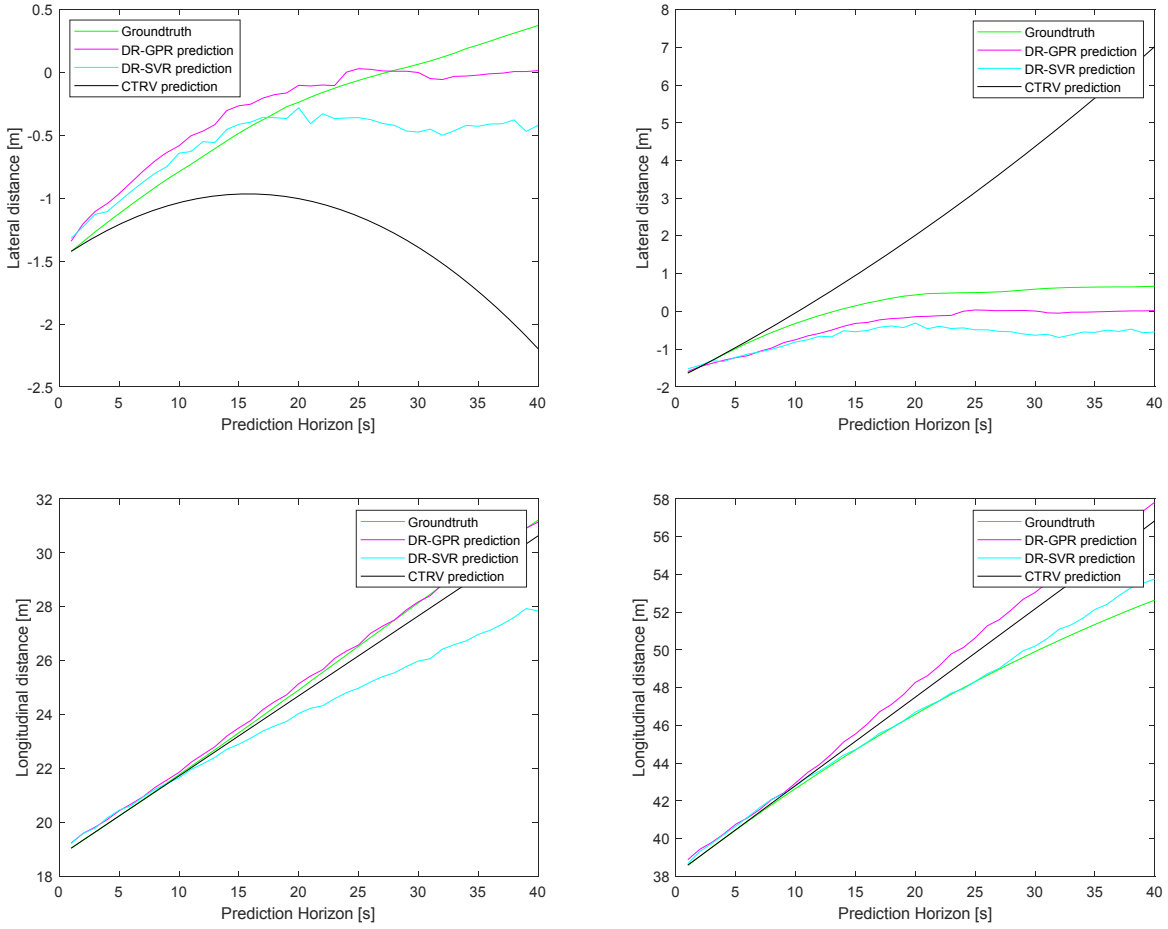

Figure 7 Examples of predictions using the different models. The groundtruth is represented in green, DR-GPR in magenta, DR-SVR in cyan and the CTRV in blue.

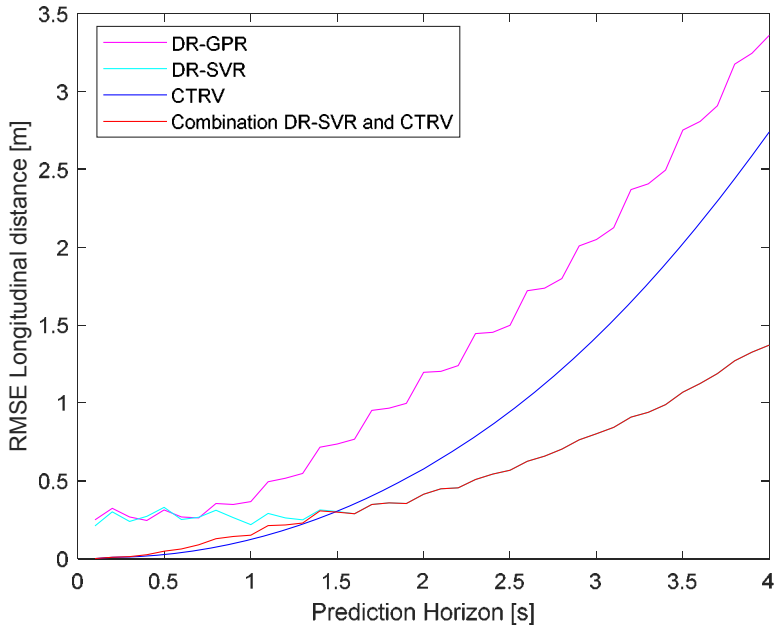

Figure 8 RMSE of longitudinal distance, based on the validation set, for the following models: DR-GPR (magenta), DR-SVR (cyan), CTRV (blue) and the combination of DR-SVR and CTRV (red).

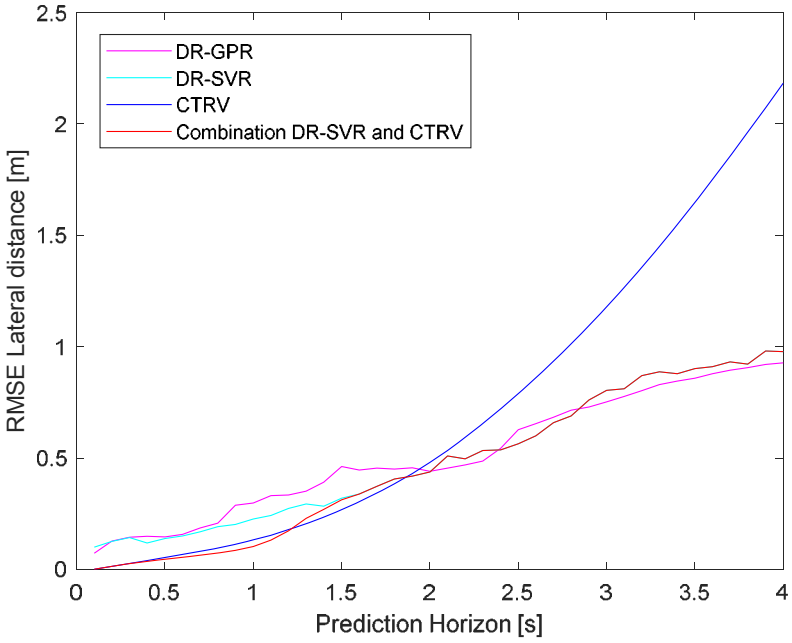

Figure 9 RMSE of lateral distance, based on the validation set, for the following models: DR-GPR (magenta), DR-SVR (cyan), CTRV (blue) and the combination of DR-SVR and CTRV (red).

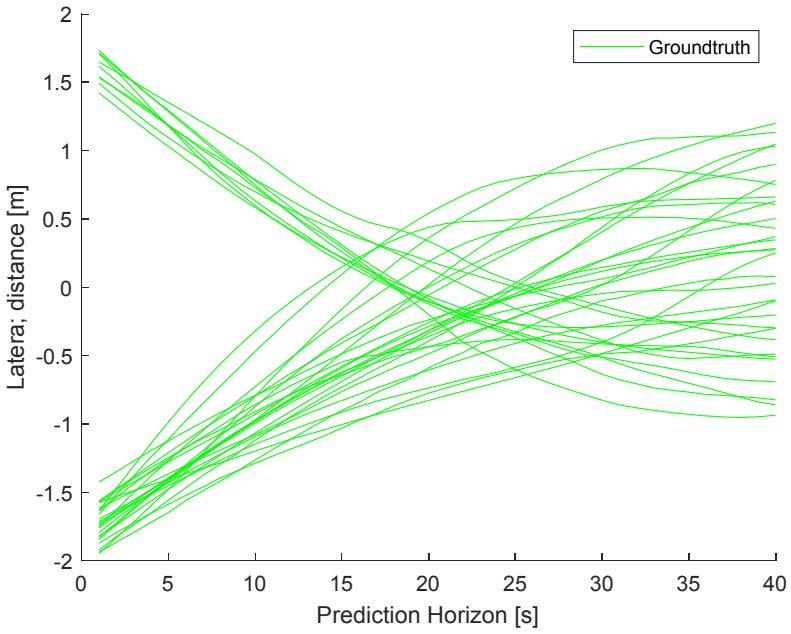

Figure 10 Validation set: the lateral distance over time of all cut-ins used for validation.

HIL setup

The prediction models are meant to be used to enhance automated driving functions. Knowing the future states of dynamic objects, as other vehicles, enables highly automated driving and increases safety. These models are often tested only via Software simulations, which can assess the accuracy of the models but doesn't ensure that these models can be integrated with the controllers and that they can infer in real-time using the data perceived by sensors such as radars or cameras. The Hardware-in-the-loop environment allows to test the functionality of the abovementioned model as if they were integrated in a real automated vehicle, testing the integration of them software and controllers with actual hardware components usually present in an automated vehicle, to give more realistic feedback. The models run in real-time and work correctly with the other components. The interfaces were facilitated by creating a ROS node of our model.

In Figure 11, three important moments from a demo video are depicted. The blue vehicle is the host vehicle, which is instrumented and it is going to predict the trajectory of the red vehicle. In the first moment, the red vehicle is not in the field of view of the blue vehicle yet. For this reason, the probability of cut-in and the time to cut-in are not measured yet. In the second snapshot, the cut-in is predicted with a probability of 98% and with a predicted time to lane crossing of 1.16s. The red continuous line is the physics-based prediction, based on CTVR. The third moment shows that the cut-in is already happening, therefore also the manoeuvre-based mode can be used, and it is the magenta line in the figure. As it can be seen, the manoeuvre-based prediction is far more accurate than the physics-based prediction.

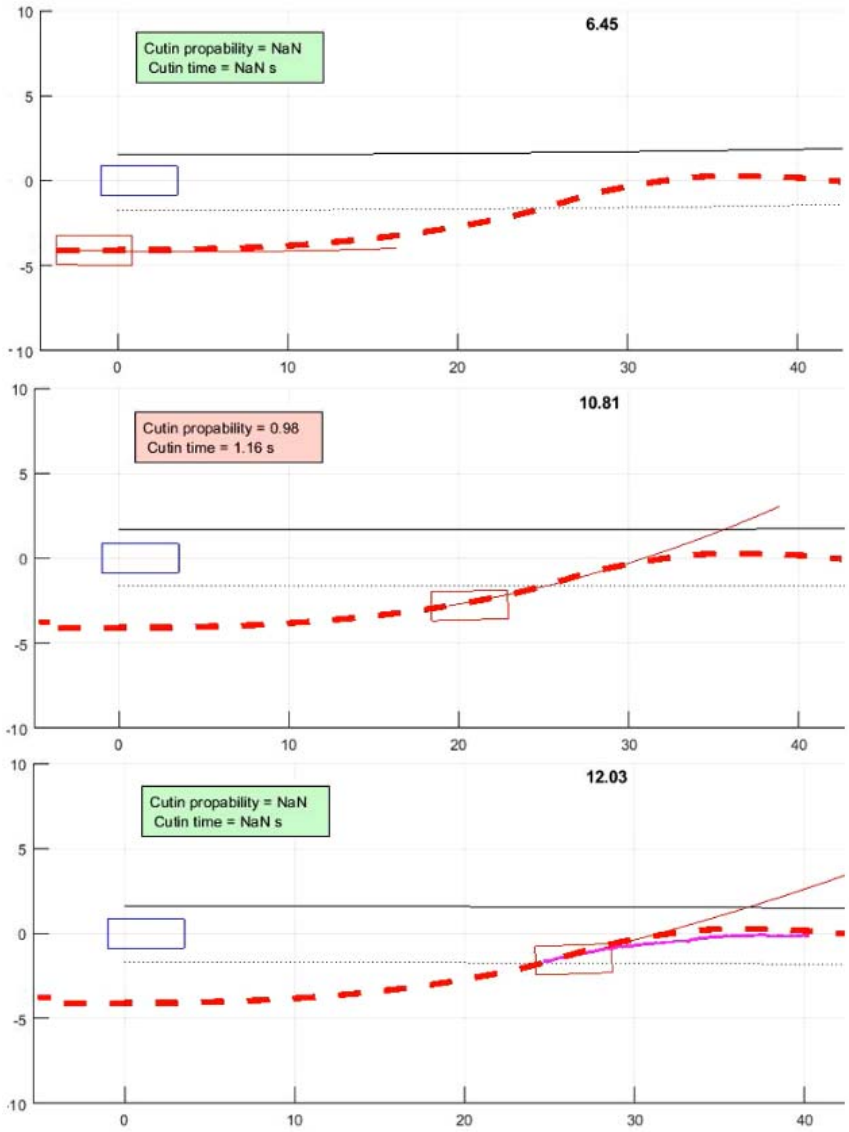

Figure 11 Three snapshots from a video where the models are functioning at the same time. The blue vehicle is the automated vehicle, which is instrumented and it is going to predict the trajectory of the red vehicle.

DISCUSSION

Validation of the cut-in prediction algorithm showed that the algorithm had problems with merging scenarios. This makes sense since the lane marker seen by the MobilEye is not the lane marker relevant for the target vehicle in merging situations. This induces large velocities towards the lane marker providing false positives. When removing these scenarios (which can be done online with the use of GPS and map data). the positive predictive value of 82% can become substantially higher when the lane detection on the Mobileye is improved. In almost all of the false positives, it is the erratic detection of the lane that triggers the cut-in prediction. For the computation of the average time to lane crossing a small portion of the detections is omitted. In this small portions the detections occur immediately when the object comes into view of the sensors, which induces a unrepresentative small time to lane crossing. In this research the Constant Turn Rate and Velocity (CTRV) kinematic model is chosen to be used for short prediction. There are other models, e.g. Constant Turn Rate and Acceleration (CTRA), Constant Steering

Angle and Velocity (CSAV) or Constant Curvature and Acceleration (CCA), which may or may not provide better results in the presented cut-in scenario.

The manoeuvre-based models have been trained also for predicting lane following trajectories and for predicting the orientation α over time. In both cases the models were not successful: the lane following set was too small to train appropriately the models, showing overfitting and therefore it was decided to use CTRV that shows quite good results for this kind of linear behaviour. Future work will focus on training machine learning models capable of predicting trajectories for lane following as well. The orientation is very difficult to predict, as it can't be accurately measured by current sensor sets and therefore the available training sets are not good enough to ensure a valid training of the models.

In the results, the Gaussian Processes model (DR-GPR) underperform compared to the support vector regression (DR-SVR), because DR-GPR suffers more of the incompleteness in the range of the feature space. However, we will keep investigating DR-GPR because of its potential. For example, it can also output the confidence of the predicted trajectory. This information is very valuable, as in case the prediction is not reliable, the automated vehicle might decide to ignore it and assume (for example) the worst case in order to ensure safety, or a set of prediction models can be used and the one with the highest confidence can be selected while driving on the road. In addition to this, gaussian processes are very good with handling noisy data, which is exactly the case for data sensed by current automotive sensor sets.

The presented approach is capable of predicting the motion of the other road users in a standard situation. In order to handle more sophisticated scenarios, the road information should be used for training. The training set needs to be extended for better results, and the validity of the models needs to be checked for safety critical scenarios. This can be done in the HIL, where critical scenarios can be simulated and therefore the models can be tested on them.

CONCLUSIONS

A hybrid approach for predicting the motion of vehicles from a host vehicle perspective is presented in this work. A combination of manoeuvre-based and physics-based models is used to enhance the accuracy of the prediction in shorter and longer horizons. The combined model predicts the longitudinal distance and the lateral distance with an error that is 50% lower than the one using the physics-based model. In addition to this, the combined model is characterized by a RMSE that is one sixth of the RMSE of SVR after 0.5s for the longitudinal distance and a RMSE 62% lower than SVR for the lateral distance. The information coming from the prediction module can be used path planning of (partly) automated vehicles. The integration in the HIL environment shows great potential to allow autonomous driving to go to higher levels of automation. Future work will focus on a broader use of machine learning for prediction and on the validation on safety-critical scenarios using the HIL environment.

REFERENCES

[1] Janssen, R. and Zwijnenberg, H. and Blankers, I. and de Kruijff, J. 2015. "Truck platooning driving the future of transportation."

[2] Robin Schubert, Eric Richter, Gerd Wanielik , 2008, Comparison and Evaluation of Advanced Motion Models for Vehicle Tracking

[3] Lefèvre, S., Vasquez, D., & Laugier, C. (2014). A survey on motion prediction and risk assessment for intelligent vehicles. ROBOMECH journal, 1(1), 1.

[4] Cara, I., Paardekooper, J. P., & Helmond, T. N. O. (2017). The Potential of Applying Machine Learning for Predicting Cut-In Behaviour of Surrounding Traffic for Truck-Platooning Safety. In 25th International Technical Conference on the Enhanced Safety of Vehicles (ESV) National Highway Traffic Safety Administration.

[5] Klingelschmitt, S., Platho, M., Groß, H. M., Willert, V., & Eggert, J. (2014, June). Combining behavior and situation information for reliably estimating multiple intentions. In 2014 IEEE Intelligent Vehicles Symposium Proceedings (pp. 388-393). IEEE.

[6] Izquierdo, R., Parra, I., Muñoz-Bulnes, J., Fernández-Llorca, D., & Sotelo, M. A. (2017, October). Vehicle trajectory and lane change prediction using ANN and SVM classifiers. In 2017 IEEE 20th International Conference on Intelligent Transportation Systems (ITSC) (pp. 1-6). IEEE.

[7] Georgiou, T., & Demiris, Y. (2015, June). Predicting car states through learned models of vehicle dynamics and user behaviours. In 2015 IEEE Intelligent Vehicles Symposium (IV) (pp. 1240-1245). IEEE.

[8] Wiest, J., Höffken, M., Kreßel, U., & Dietmayer, K. (2012, June). Probabilistic trajectory prediction with Gaussian mixture models. In 2012 IEEE Intelligent Vehicles Symposium (pp. 141-146). IEEE.

[9] Moser, D., Reiter, M., & del Re, L. (2017). Stochastic prediction of lane change trajectories for adaptive cruise control. IFAC-PapersOnLine, 50(1), 8907-8912.

[10] Klingelschmitt, S., & Eggert, J. (2015, September). Using context information and probabilistic classification for making extended long-term trajectory predictions. In 2015 IEEE 18th International Conference on Intelligent Transportation Systems (pp. 705-711). IEEE.

[11] Xie, G., Gao, H., Qian, L., Huang, B., Li, K., & Wang, J. (2018). Vehicle trajectory prediction by integrating physics-and maneuver-based approaches using interactive multiple models. IEEE Transactions on Industrial Electronics, 65(7), 5999-6008.

[12] Houenou, A., Bonnifait, P., Cherfaoui, V., & Yao, W. (2013, November). Vehicle trajectory prediction based on motion model and maneuver recognition. In 2013 IEEE/RSJ International Conference on Intelligent Robots and Systems (pp. 4363-4369). IEEE.

[13] Elrofai, H., Paardekooper, J. P., Gelder, E. D., Kalisvaart, S., & Op den Camp, O. (2018). StreetWise: scenario-based safety validation of connected automated driving. TNO

AN OPTIMIZATION-BASED METHOD TO IDENTIFY RELEVANT SCENARIOS FOR TYPE APPROVAL OF AUTOMATED VEHICLES

Thomas Ponn
Frank Diermeyer
Technical University of Munich
Germany

Christian Gnandt
TÜV SÜD Auto Service GmbH
Germany

Paper Number 19-0024

ABSTRACT

The objective of this paper is to propose a novel approach for an intelligent selection of relevant scenarios for the certification of automated vehicles. During this process, two main challenges occur. Firstly, since the number of possible traffic situations is unlimited, a selection of a manageable number of representative situations to be tested must be applied during the certification of automated vehicles. Secondly, nowadays a limited number of standardized test cases are used for the type approval of vehicles. This can lead to so-called gaming of tests, which means that the manufacturer optimizes the system's performance in the predefined test cases. A prominent example are the current discussions about the large differences between the emissions of vehicles in the driving cycle (e.g., WLTP) and in everyday use in road traffic. This paper addresses both stated challenges and exemplifies a method for the system-specific selection of test cases for the certification of automated vehicles, which are not known to the manufacturer in advance. Based on a system analysis and an objective driving behavior characterization, weak spots of the system under test are identified and connected to complex scenarios to be tested. This approach allows an economic and meaningful certification process for automated vehicles.

INTRODUCTION

In recent years, intensive work has been carried out on the implementation of highly automated and autonomous vehicles (Level 3 and higher according to the SAE classification [1]). Many manufacturers already have prototypes of these vehicles, which are increasingly being tested in real traffic, especially in the USA. A high level of safety is indispensable for social acceptance - especially due to the danger posed to uninvolved parties in the event of system faults.

It is difficult to prove the safety of automated vehicles in an economically feasible manner, due to the open parameter space. For the type approval of vehicles, in particular, only a very limited scope can be tested. Therefore, an intelligent and manufacturer-unknown selection of the scenarios to be tested is necessary in order to avoid the so-called gaming of tests and to prove a sufficient safety performance. In addition, regulations and laws for the certification of automated vehicles are still missing.

In general, due to the infinite number of possible traffic situations, there is a need for an economically feasible method of performing safety assessments on automated vehicles. A promising approach is scenario-based testing. Based on the assumption that a large part of traffic situations is irrelevant and uncritical, scenario-based testing is limited to meaningful events (scenarios). The framework for this approach is being developed, for example, in the German funding project PEGASUS [2]. The challenge of selecting and finding all relevant scenarios remains with this approach. Since only an extremely limited number of tests can be carried out during certification, it is particularly important for this application to conduct an intelligent selection of scenarios. This contribution, therefore, presents a novel approach for a system-specific selection of relevant scenarios for the certification of automated vehicles. Furthermore, with this approach, the manufacturer can no longer perform so-called gaming of tests.

The article is structured as follows: First, an overview of existing literature is given, and the research objective is derived. Subsequently, the procedure developed is described in detail in the METHODOLOGY section. An exemplary derivation of results using the method presented is explained in the RESULTS section. Then, the approach will be critically discussed, and its limitations demonstrated. The paper concludes with a summary and an outlook on future work.

LITERATURE REVIEW AND RESEARCH OBJECTIVE

This section addresses in detail the challenges already raised in the introduction regarding the certification of automated vehicles. Finally, the state of the art is critically evaluated, and the main research question of this paper is derived.

Unlimited number of possible traffic situations

Due to the infinite number of possible traffic situations, the safety assessment of automated vehicles can no longer be carried out economically in road tests [3]. With the scenario-based approach, the level of effort required can be reduced considerably if possible traffic situations are restricted to relevant events. Irrelevant situations, such as driving in a straight line with no action taken by drivers in surrounding traffic are left out. Nevertheless, the challenging task of finding all relevant scenarios remains with this approach. Before we examine existing methods for the selection of these scenarios in detail, important terms are defined.

Definition of vocabulary

Object and Event Detection and Response (OEDR): Different factors influence the safety of automated vehicles. These are, for example, the human machine interface (HMI) as well as the functional safety and cyber security of the vehicle. In our approach, we focus on Object and Event Detection and Response (OEDR) according to NHTSA [4, p. 7]. OEDR includes the detection of objects, their classification, the planning of a suitable response to the detected object and the execution of the planned action.

Operational Design Domain (ODD): According to SAE [1], the ODD is defined by the area for which the automated vehicle was developed. The ODD can be restricted, for example, by road classes (e.g., highway or city center) or environmental conditions (e.g., weather conditions).

System Under Test (SUT): The automated vehicle to be tested and certified is denoted as system under test.

Traffic Participant (TP): All kinds of movable objects within a traffic situation are called traffic participants. Among others, this includes pedestrians, cyclists, motorcycles, passenger cars and trucks.

Scenario: ULBRICH [5] defines a scenario as:

> *[…] the temporal development between several scenes in a sequence of scenes. Every scenario starts with an initial scene. Actions & events as well as goals & values may be specified to characterize this temporal development in a scenario. Other than a scene, a scenario spans a certain amount of time.*

Where a scene is defined as:

> *[…] a snapshot of the environment including the scenery and dynamic elements, as well as all actors' and observers' self-representations, and the relationships among those entities. Only a scene representation in a simulated world can be all-encompassing (objective scene, ground truth). In the real world it is incomplete, incorrect, uncertain, and from one or several observers' points of view (subjective scene).*

Furthermore, MENZEL [6] distinguishes between three types of scenario – functional, logical and concrete scenarios. Functional scenarios represent a linguistic description of the scenario on a semantic level. The information content of this description is low. For logical scenarios, the parameters required to describe the scenario, such as the initial speed of the SUT or the lane widths, as well as their ranges are included. Concrete scenarios have the most information content. Starting from a logical scenario, a specific value is defined for each parameter in the concrete scenarios and is thus unambiguous. It should also be noted that the term test case is used here as a synonym for a concrete scenario, although in [7] the test case also includes pass-fail criteria. In the present use case, pass-fail criteria can be regarded as prescribed by future regulations for the type approval of automated vehicles.

Relevant scenarios: All scenarios that contribute to the type approval of automated vehicles are considered relevant. Relevant scenarios can also be very simple, such as the beginning of a speed limit. This is relevant for certification because an automated vehicle must comply with existing traffic regulations. This type of scenario is taken into account in the method developed when driving behavior is characterized. A subset of the relevant scenarios are critical and complex scenarios (Figure 1). These two subsets are defined below.

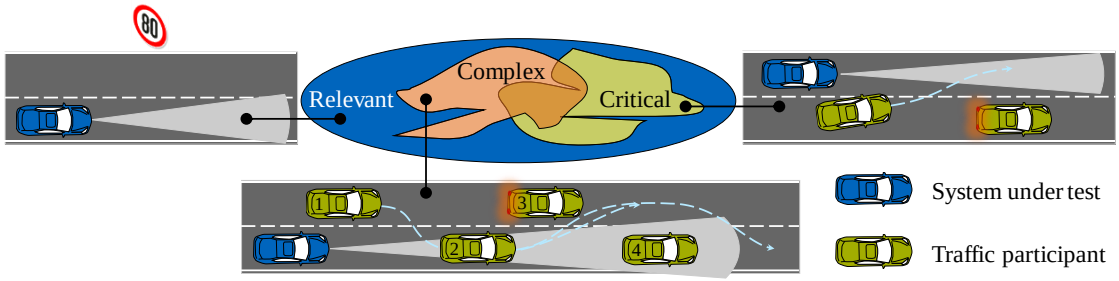

Figure 1. Definition of relevant, complex and critical scenarios

Complex scenarios: Complex scenarios are scenarios that present a challenge for the planning algorithm of the SUT. This is achieved by the presence and movement of other TPs. Complexity can thus be understood as how difficult it is for the planning algorithm to plan a safe trajectory under consideration of other TPs. Other influences such as the width of the road or the need to maneuver are not explicitly taken into account in this method.

Critical scenarios: Criticality is defined in this paper as the closeness to an accident. To measure criticality, indicators such as Time-To-Collision (TTC) [8] can be used. The smaller the value of this indicator, the more critical the scenario is. Critical scenarios can have two different causes. On the one hand, they can arise due to high differential speeds and small distances. This means that a logical scenario is not inherently critical. However, a critical concrete scenario can very easily be derived from any logical scenario if the distances between the objects and their velocities are adjusted accordingly. Thus, a cut-in situation is not automatically critical. But if a slow-moving TP changes into the SUT's lane at a short distance before it, it

is very critical. These types of critical scenarios can be defined without extensive analysis and will not, therefore, be considered further in this publication. On the other hand, critical situations can arise due to errors of the SUT. These can be errors and inaccuracies in perception and errors in the planning algorithm. The former is considered in the developed methodology in the analysis of the sensor setup, while the latter is addressed in the complexity of the traffic situations. It is assumed that increasing complexity increases the probability of an error in the planning algorithm. An example of a critical scenario due to an error in the SUT is a (complex) traffic situation in which the SUT incorrectly predicts the trajectory of a TP, resulting in an accident in the further progress of the scenario. Since this type of criticality is taken into account in the methodology by the analysis of the sensor setup used and also by the addition of complexity, the identification of critical scenarios is no longer explicitly discussed in the following.

In summary, it can be concluded that relevant scenarios may be very simple (e.g., speed limitation). In addition, critical scenarios are not automatically complex (e.g., accident involving an autonomous prototype in the USA [9]) and, on the other hand, not all complex scenarios are automatically critical (e.g., if the algorithm masters the scenario correctly). Nevertheless, all types of scenarios mentioned are relevant for the type approval of automated vehicles.

Five-layer model: To define the required parameters for the scenarios in a systematic manner, SCHULDT [10] introduces a four-layer model, which BAGSCHIK [11] extends to a five-layer model. This allows all relevant parameters for the following five layers to be defined:

- Road-level (L1)
- Traffic infrastructure (L2)
- Temporary manipulation of L1 and L2 (L3)
- Objects (L4)
- Environment (L5)

The five layers also contain continuous parameters. These include, for example, the speed of other objects. More specifically, this may be the speed of a traffic participant cutting in front of the SUT. Through the theoretically infinitely fine discretization of continuous parameters, an infinite number of concrete scenarios can be defined. In addition, each concrete value of a parameter can be combined with any other value of the remaining parameters, which corresponds to the so-called N-wise testing. Consequently, the scenario-based approach also requires a methodology that identifies relevant test cases. For this reason, an outline of existing procedures in the literature for selecting and reducing concrete scenarios is given below.

Scenario selection and reduction methods

Instead of combining all values of one parameter with every other parameter (N-wise testing), an intelligent selection of parameter combinations is chosen during the Design of Experiments (DoE). According to KUHN [12], DoE-approaches can be used for complex software systems, because only the combination of a few parameters is sufficient to cause a faulty behavior of the system, which is expressed by the failure triggering fault interaction (FTFI) number. At NASA, for example, the combination of only six parameters covers almost 100 % of the errors occurring [12]. Further information on various methods of DoE, such as covering arrays, as well as the application in the field of automated driving, can be found in [13–16].

+ Good parameter space coverage
– The selection of important parameters is difficult in advance
– No selection of test cases based on relevance

SAATY [17] provides the basis for an approach to detect important parameters and their connection using the Analytic Hierarchy Process (AHP). XIA [18, 19] takes this as a basis and uses the AHP, in combination with an expert knowledge-based analysis of key influencing factors. The scenarios generated are evaluated using a complexity index.

+ Analytical method for the determination of relevant parameters
+ Creation of complex scenarios
– Requires expert knowledge
– Does not consider presumably simple scenarios that nevertheless lead to faulty behavior

An approach that relies entirely on expert knowledge is the creation of scenarios with the help of ontologies [11, 20, 21]. Ontologies are a formal representation of knowledge and its relations, which have their origin in the Semantic Web. Starting from the definition of knowledge, for which the five-layer model by BAGSCHIK [11] described above

can be used as a basis, scenes are automatically derived to safeguard the automated driving function. Scenarios can be created by sequencing individual scenes. Furthermore, knowledge-based approaches ensure that elements from the knowledge base can also be found in the scenes and scenarios created. For example, if a pedestrian is defined in the knowledge base, it can be ensured that there are also test scenarios that contain a pedestrian.

+ Elements defined in the knowledge base are also part of the test catalog
– Solely based on expert knowledge
– No evidence of the relevance of the defined scenarios for the proof of safety

Instead of using expert knowledge, test scenarios for automated driving can also be based on real and simulated traffic situations with a high level of criticality. All extracted scenarios can be stored in a database. This approach, with a database filled with scenarios as the central element of the validation procedure, is used in the German-funded project PEGASUS [22, 23]. In addition to the data sources already mentioned, in principle all possible sources of scenarios can be taken into account. For example, these can also be scenarios from a knowledge-based approach.

+ Inclusion of scenarios of various origins possible
– High storage requirements with nearly identical scenarios
– If the number of stored scenarios exceeds a manageable number, a method for selecting relevant scenarios is required again

Existing accident databases can also be used to select relevant scenarios [24]. Accident scenarios are reconstructed in simulation and examinations are performed to establish whether the accident could have been prevented or mitigated by the automated driving function to be tested. The prerequisite for this is detailed accident data that contains information about the pre-crash trajectories of the vehicles involved in the accident scenario. These currently only exist for driver assistance systems. Consequently, the significance of the safety level of automated vehicles based on these accidents is extremely limited. This can be improved by further varying the parameters, such as the ego speed.

+ Shows accident avoidance potential of the automated vehicle
– Detailed accident data required
– Provides only limited information on new risks and accidents introduced by the automated vehicle

Another method based on real driving data from human drivers is the accelerated evaluation of automated vehicles [25–28]. Based on the real driving data of a maneuver (e.g., cut-in), frequency distributions of the parameters involved (e.g., relative speed) are determined. These parameter distributions are adapted in such a way that more severe situations arise that can be used for the accelerated evaluation of the SUT. The importance sampling theory is used to ensure that the accelerated result is valid, and that the acceleration factor can be calculated. Thus, a factor of up to 10^5 can be achieved, which means that each simulated kilometer corresponds to a real distance of 10^5 kilometers.

+ Conversion from simulated to real life traffic kilometers
+ Straightforward comparability with human performance through, for example, kilometers per accident
– Frequency distributions of all relevant parameters necessary → time-consuming and cost-intensive data collection
– Number of necessary involved parameters unknown

The aim of [29–32] is to adapt existing logical scenarios in such a way that relevant, and as critical as possible, concrete scenarios can be created based on them. Starting from a baseline scenario, the trajectories of road users are adapted in such a way that the planning of a safe trajectory for the automated vehicle becomes particularly challenging. Starting with the start scene, the possible trajectories of the road users are predicted into the future. The Reachable Sets, for example, can be used here. All areas in which no other road users can be located in the future are considered safe. Minimizing these safe areas results in particularly important situations for the trajectory planning module of the SUT.

+ Also suitable for online evaluation of the selected ego trajectory
– Trajectory planning is more the focus of the tests than the overall system

While all previously explained procedures evaluate scenarios before they are executed, and optimize them with regard to criticality, critical scenarios can also be derived with the help of simulation executions [14, 33]. A concrete scenario is chosen as the starting point, executed in simulation and evaluated using a criticality metric. Subsequently, specific parameters of the scenario are varied and the change in criticality is evaluated. To maximize criticality during optimization, classical optimization methods [14] as well as machine learning approaches [33] can be used. Theoretically, this approach is also possible in real experiments, but due to the high number of experiments, this is not feasible.

+ Criticality optimization during test execution ensures that critical scenarios are discovered
– Numerous simulations of concrete scenarios required → Particularly time and cost-intensive when high-fidelity simulation models for vehicle dynamics, sensors and environment are used

One approach to reducing the number of relevant scenarios that can be used in parallel to the methods mentioned above is functional decomposition. Based on the decomposition of the human driving task into five layers by GRAAB [34], AMERSBACH [35, 36] adapted this division to fit automated vehicles, using a six layer model. This division can be seen as a further subdivision of the well-known sense-plan-act principle. The aim is to reduce the number of relevant scenarios by considering the individual functional levels separately. For example, to test layer three (situation understanding), all parameters that have no influence on this layer can be omitted.

+ Approach can be used in parallel with other scenario selection methods
– Tests at overall system level are still necessary
– Reduction of the number of scenarios in the overall assessment not yet conclusively clarified

As a final method for the reduction and selection of relevant scenarios for the safety verification of automated vehicles, the formal methods will be introduced [37–39]. The aim of this approach is a mathematical proof of the safety of the SUT. If this proof is successful, then the formal methods are the most effective reduction method, because all tests, whether in simulation or in real tests, become obsolete. This currently fails because of assumptions that must be made but that do not correspond to reality. For example, the authors of [39] assume that the automated vehicle can always precisely determine the current coefficient of friction. However, the exact online determination of the coefficient of friction has been an unsolved problem for years.

+ If formal proof is provided, no tests need to be carried out
– Assumptions must be made that do not accurately reflect reality
– Whether or not driving behavior according to the formal methods leads to unreasonably defensive behavior has not yet been conclusively determined
– It must be demonstrated that an automated vehicle is implemented according to formal methods

Gaming of tests during type approval

As already mentioned in the INTRODUCTION, type approval of automated vehicles is the central application of this publication. In this context, gaming of tests is referred to as a performance optimization towards the standardized test cases. For type approval, the regulations of the UNECE[1] are relevant for the European area. These regulations must be tested by a technical service and confirmed to be complied with so that a new vehicle model can be introduced onto the market in the countries of the contracting parties. To this day, the UNECE regulations for the type approval of vehicles have made significant effort to ensure comparability and reproducibility. For this reason, the test execution, environmental conditions and evaluation of the tests are defined precisely in the regulations. This offers vehicle manufacturers the advantage of knowing in advance which tests are to be carried out, and of optimizing the performance of their systems within these test cases. A reliable statement about the system's behavior in real traffic conditions is, therefore, only possible to a limited extent, as the problems in the emission tests starting in September 2015 [40] clearly revealed.

With regard to vehicle emissions, UNECE Regulation 83 Revision 5 [41] is relevant for vehicle approval. In addition, the UNECE Global Technical Regulation 15 [42], which applies to a larger number of contracting parties (e.g., including the USA), specifies the Worldwide Harmonized Light Vehicle Test Procedure (WLTP). These two regulations stipulate the exact procedure for carrying out the tests and the ambient conditions to be satisfied. On October 10th, 2017, the UNECE clarified in Amendment 5 to Regulation 83 Revision 5 that the Contracting Parties using this Regulation in combination with Global Technical Regulation 15 (WLTP) no longer have to accept type approval on the basis of these Regulations as an alternative to their national/regional laws. The UNECE is currently revising the regulations within the Working Party on Pollution and Energy (GRPE), so that they reflect the actual emissions in real traffic more accurately [43][44, p. 2] and the results thus correspond better to actual driving behavior. By 2020, new regulations shall be adopted on the basis of test procedures already developed by other organizations (e.g., the European Union) [43]. The European Union already introduced its own methods and approval regulations in September 2017, which determine Real Driving Emissions (RDE) in a test procedure under real driving conditions [45]. The 100-percent reproducibility is thereby limited at the expense of better transferability to real traffic events.

[1] https://www.unece.org/info/ece-homepage.html

Initial tendencies exist not only in the area of emissions, but also in assisted driving, to reduce the exact reproducibility for a higher significance under real traffic conditions. In assisted and, especially, automated driving, the behavior of the system in real driving conditions is very important because these are safety-relevant systems. Therefore, it is important to prioritize the prevention of gaming of tests in this area. UNECE Regulation 79 Revision 4 [46] makes a first step in this direction by defining, among other things, the test cases for the Lane Keeping Assist (LKA). However, not all concrete test scenarios are explicitly defined. The logical scenario is defined in which the vehicle approaches a curve, where the lane shall have a clearly visible lane marking line on both sides. The test is passed if the vehicle does not cross a marking line during the test. In addition, paragraph 3.2.1.3 of Annex 8 [46] states: "the vehicle manufacturer shall demonstrate to the satisfaction of the Technical Service that the requirements for the whole lateral acceleration and speed range are fulfilled." This means that the technical service can define and test any combination of lateral acceleration and speed as a concrete scenario. It is not only within UNECE that the definition of exclusively standardized tests is avoided. In its Federal Automated Vehicles Policy [47, p. 77], the NHTSA also clearly opposes the exclusive use of standardized tests.

While today the UNECE Regulation 79 specifies a variation of two parameters (lateral acceleration and speed) for the LKA, the number of parameters to be varied will continue to increase with higher degrees of automation. It is conceivable, for example, that legislation (e. g., UNECE Regulation) will only define logical scenarios (e. g., cut-in) for the type approval of automated vehicles. During the certification process of the automated vehicle, the manufacturer and technical service have to find all relevant concrete scenarios of the predefined logical scenario by varying all possible parameters from the five-layer model introduced in the previous section. This gives the technical service the chance to adapt the concrete test cases towards the system's individual weaknesses. Additionally, this prevents performance optimization towards standardized tests, the so-called gaming of tests.

Research objective

The last sections revealed that it is important but difficult to reduce the number of test cases for the safety assessment and certification of automated vehicles. To achieve this, a system-specific derivation of relevant test scenarios is advantageous. None of the approaches stated above explicitly include system-specific properties, and therefore this kind of approach is lacking from the current state of the art. In addition, the method developed is intended to prevent the so-called gaming of tests in the certification process, ensuring the safety of automated vehicles even under real traffic conditions.

The aim of this paper is to propose a novel method of including system-specific characteristics for an efficient and individual scenario selection during the certification process of automated vehicles conducted by a technical service.

METHODOLOGY

This section describes in detail the overall procedure used, from the required input, to the method to the generated output. An overview can be found in Figure 2.

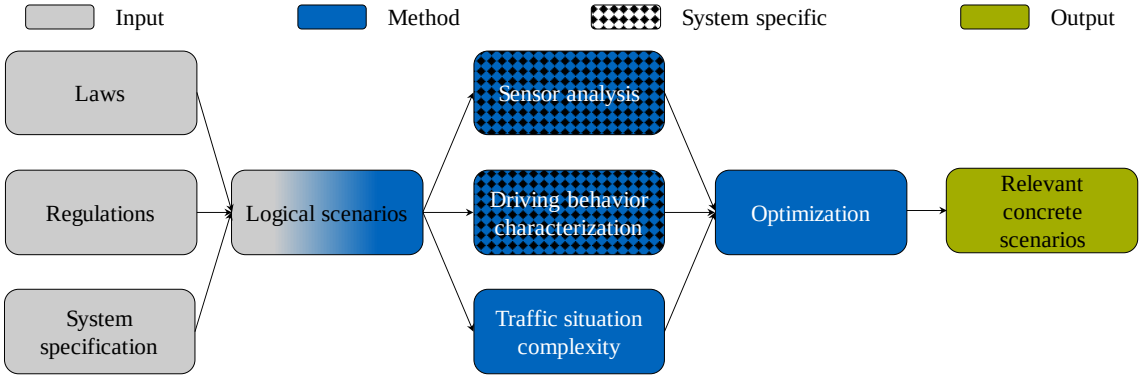

Figure 2. Overview of the procedure developed. Logical scenarios are assigned both to the input and to the method, because these are partly specified in regulations and in these cases, they serve as input.

Summary of presented approach

The starting point of the methodology developed is logical scenarios defined in laws and regulations. From each predefined logical scenario, an infinite number of concrete scenarios can be generated by a theoretically infinitely fine

discretization of the parameters. The aim of the method is to restrict the parameters of the logical scenarios in such a way that a technical service can efficiently identify the most relevant test cases for the certification of the automated vehicle. This results in two special requirements for the procedure. On the one hand, it should be system-specific so that different versions of various manufacturers can be addressed efficiently. On the other hand, it should be able to work without using the driving function to be tested as far as possible, because the technical service will not usually have access to the software. What will be available to the technical service is a system specification of the SUT. The information contained therein is used in the further course of the approach.

The parameters of the logical scenarios are determined by optimization, based on the three main elements of the concept. These elements are the analysis of the sensors, consideration of the driving behavior and integration of complexity. The first two elements are specially adapted to the identified weak spots of the SUT, and thus enable a system-specific definition of relevant scenarios. The predefined logical scenarios contain only a simple description of a scenario that is suitable for demonstrating certain basic skills. For example, in a cut-in scenario, only one vehicle is defined that performs a lane change into the lane of the SUT during the course of the scenario. In order to give the scenario a certain degree of difficulty, system-independent complexity is integrated in the scenario in the final step by defining further TPs. In the optimization, all three elements must be considered in parallel. The result will be relevant concrete scenarios that are adopted towards the SUT weaknesses, which are used by the technical service for the certification process. Below, each step of the method is explained in detail.

Input

Laws, regulations and a system specification are required as input for the approach developed and will be explained in more detail below.

Laws If an automated vehicle performs the driving task, the system also takes responsibility for the actions performed. Consequently, the actions of the automated vehicle must comply with the applicable laws. In Germany, for example, these may be the Road Traffic Act (in German: Straßenverkehrsgesetz (StVG)) or the Road Traffic Regulations (in German: Straßenverkehrs-Ordnung (StVO)), which define, for example, the minimum safety distance from the vehicle in front, or maximum speeds on certain types of road. The applicable laws can be explicitly tested in a scenario, or at least considered in the evaluation of the tests carried out.

Regulations Referring back to the LITERATURE REVIEW AND RESEARCH OBJECTIVE section, certain regulations must be complied with for type approval. For the European market, these are the UNECE regulations, which represent the central aspect in the considered use case of the approach developed. Like already discussed, the UNECE regulations no longer define all tests in detail, but provide a certain framework for the tests to be carried out, which may also implicitly mean logical scenarios. Furthermore, the system manufacturer and the technical service are assigned an increasingly higher responsibility, because they have to verify that the defined requirements are met over the entire operating range. This, in turn, gives the technical service the opportunity to define all scenarios that it considers relevant for the system to be tested as definite test cases during the certification process.

System specification In the future, the number of automated systems with different functional capabilities will continue to increase. For example, there will be a wide variety of systems for the highway domain. These will differ in terms of whether special situations, such as construction sites, ramps and exits etc., can be handled by the automated driving function. In order for the selection of the logical scenarios to be tested to be as effective as possible, a system specification with the definition of the system boundaries must be available to the technical service. The system boundaries can also be used to generate test cases where the system boundaries are exceeded. The SUT also has to achieve a safe state in these scenarios. In addition, the technical service must be informed of both the sensors used and their installation position. All in all, the type and level of detail of the information provided by the manufacturer in the system specification must be such that, on the one hand, the technical service has sufficient information available for the relevant scenarios to be selected reliably and, on the other hand, the manufacturer does not have to reveal too much manufacturer-specific data in order to protect internal know-how.

Logical scenarios If logical scenarios are already defined in applicable regulations, these can be used as input for the developed approach. It may also be possible that further logical scenarios are required for the method, for example to test system functions or compliance with road traffic laws, which are required in the regulation but for which no logical scenarios are defined. An example could be that the UNECE specifies that speed limits must be observed by the system but does not specify a framework in which the tests are to be carried out. For the reasons described, the

logical scenarios in Figure 2 are assigned to both the input and the method. Requirements can also be specified in the regulation without a logical scenario being defined for the verification of these requirements. This may require the technical service to define further logical scenarios during the type approval process. It is also conceivable that a scenario is only described in linguistic terms and is therefore, by definition, a functional scenario. In this case, the corresponding logical scenario must also be defined by the technical service.

Output
The output of the presented approach is represented by relevant concrete scenarios for the type approval of automated vehicles. All scenarios required to prove compliance with the requirements (e.g., by UNECE) are considered relevant for testing. The unique selling point of the developed procedure is a system-specific adaptation of the relevant scenarios to accommodate possible weak points of the system to be certified.

Method
The following explanations of the methodology blocks shown in blue in Figure 2 outline how the output described here is generated from the input described above.

Sensor analysis The perception sensors of an automated vehicle have the objective of collecting information about the environment of the vehicle, which is an important part of the driving task. Only if sufficient information about the environment is available, a safe planning of appropriate actions of the automated vehicle is possible. Not only sufficient information needs to be available, but it must also correspond to reality. Currently, in the automotive sector, the perception sensors mainly used are Radar, Lidar, camera and ultrasonic. Each of these sensor types has its own advantages and drawbacks. In order to enable the driving task to be performed safely, the various sensor types are therefore combined, and the information obtained from them is fused. For the sake of simplicity, perception sensors are simply referred to as sensors in the following.

The resulting sensor costs have a major influence on the choice of the number and type of sensors installed, especially in mass production vehicles. Furthermore, there may be restrictions due to the package. Consequently, every vehicle manufacturer will use an individual sensor setup. The goal of this section is to formulate a method for a structured analysis of the sensor setup used and to identify its weaknesses. This is particularly relevant for technical services in type approval, because they have to efficiently test vehicles from different vehicle manufacturers with different sensor configurations. In addition to the ODD (e.g., motorway or urban area) of the vehicle under consideration, the type and number, as well as its installation position and pose, also play a critical role. In the following section, the most important influencing variables of the sensors are examined in more detail. All this data must be specified by the manufacturer in the system specification for each sensor.

1) **Field of view:** The field of view describes the visual area of a sensor and is influenced by the following properties:
    a. **Range**: The different sensor types have widely-varying ranges. Ranges vary from a few meters with ultrasonic to several hundred meters with radar sensors. Different ranges also occur within the same sensor type, for example with camera sensors. While the range only has a secondary role in inner-city operation, it is a decisive factor in the use case of the highway pilot, due to the high speeds.
    b. **Opening angles:** One can differentiate between the horizontal and vertical opening angle. Both the horizontal and vertical opening angles are particularly important for detecting the vehicle's immediate surroundings. Large opening angles can reduce or even eliminate blind spots between the mounting positions of the sensors, and improve the detection of low-lying objects. As the distance from the vehicle increases, the importance of the vertical opening angle decreases, because only a relatively narrow area of the environment is relevant in the vertical direction. Only with Lidar sensors, which usually have a small vertical opening angle, does this have to be taken into account at higher distances. For example, when braking strongly, a pitch angle can occur that shortens the range of the Lidar sensor.
    c. **Mounting position:** The mounting position influences the field of view of the sensor. In general, high mounting positions are advantageous, because, in particular, objects at great distances can be detected better. In addition, sensors with high mounting positions are better protected against damage. These can be, for example, contamination by whirled-up dust and dirt, parking bumpers and similar.
    d. **Orientation:** In addition to the mounting position, the orientation of the sensors is also relevant for the field of view. Sensors pointing slightly downwards can be used primarily to cover the immediate

surroundings, whereas sensors for the more distant surroundings tend to be oriented almost horizontally.

2) **Quality of data:** The quality of the recorded data is not always the same and varies depending on the following factors:
    a. **Type**: As already mentioned, camera, Radar, Lidar and ultrasonic sensors are mainly used in the automotive industry. These sensor types have different strengths and weaknesses due to their physical principle.
    b. **Performance attributes:** The performance attributes of the sensors used must be evaluated in detail. These attributes include, for example, the cycle times of the measurement data acquisition, which can provide information about the minimum reaction time of the system. In addition, sensor type-specific information, such as the transmitted power of the Radar or the number of pixels of the camera used, may be of interest. The latter, for example, provides information about the achievable depth of detail of the recorded sensor data.

Considering the interaction of all the factors shown, the sensor setup used can be examined. In the first step, the ideal sensor coverage of the system is investigated. This requires influencing factor 1), which is explained above. "Ideal" in this context means that all objects within the field of view of the sensor are correctly detected. This makes it possible to conclude not only whether and where the sensor setup shows blind spots, but also which areas are covered by several sensors or even several sensor types. From blind spots to multiple sensors to multiple sensor types, the probability of correct detection and classification of objects generally increases.

In the second step, phenomenological sensor models based on influencing factors 1) and 2) are used to study sensor coverage at greater distances from the SUT. These extend the ideal sensor models used previously by modeling individual phenomena, such as attenuation due to weather influences or the decrease of the signal received with increasing distance from the object. Phenomenological models, therefore, have a higher information content, but also require more computing resources. For completeness, reference is also made to physical sensor models that simulate the physical effects of the sensor and, thus, best represent reality. One example is so-called ray-tracing methods, which do, however, require enormous computing capacities and are therefore not practicable for the desired purpose. Phenomenological models, on the other hand, represent a good compromise between information content and required computing capacity.

With the phenomenological sensor models used, it is possible to investigate whether there are not only areas in the far field of the SUT that are not within the detection range of the sensors, but also areas in which the detection probability is poor. It is also possible to investigate whether any prevailing weather conditions are particularly critical for the sensor setup to be investigated. Road topology may also have an influence on the probability of an object being detected. Depending on the characteristics of the sensor setup under consideration, other curve radii, longitudinal slopes, or hilltops and valleys may pose special challenges for the SUT.

This investigation is particularly interesting for systems where the highway is part of the ODD. With the procedure described, environmental conditions, such as critical curve radii or weather conditions, can be identified, thus reducing the number of relevant scenarios. A further reduction of the number of scenarios is the adaptation of the trajectories of the other traffic participants. The trajectories can be optimized in such a way that the traffic participants approach the SUT in areas where the detection probability is as low as possible.

An extension of the sensor analysis is the inclusion of the sensor data processing, which allows the entire module of the perception to be considered. A detailed insight into the data processing software will not be available to the technical service, but it is still possible to include known state-of-the-art weaknesses in the adaptation of the tests. According to DIETMAYER [48], errors that can occur in the perception are assigned to the following three categories:

1) **State uncertainty:** Deviations between the measured state variables (such as position or speed) and those that are correct.
2) **Class uncertainty:** The classification of the detected object is incorrect. One example is the classification of a motorcycle as a cyclist.
3) **Existence uncertainty:** An existing object is not detected, or a non-existent object is incorrectly detected as an object (ghost object).

The technical service cannot accurately predict the occurrence of these errors, but the current state of the art can be used to identify situations in which the probability of one of the three error types occurring increases. For example, it is known that Radar sensors have problems in detecting stationary objects. This information can be taken into account when creating concrete scenarios.

In summary, the objective of analyzing the sensor setup used is for the technical service to adapt the given logical scenarios. This enables concrete test cases that address the identified weaknesses of the SUT's sensor setup to be selected efficiently for certification.

Objective characterization of driving behavior The aim of the objective characterization of the driving behavior of the automated vehicle is to identify systematic weak points in the driving behavior, so that the scenarios used for type approval can be adapted accordingly. This should be possible by means of a limited number of functionality-based tests carried out in advance in special scenarios, so-called characteristic situations. An example of this is the curve driving behavior of the system, which can be investigated beforehand. There may be systems that tend to drive on the inside of curves and others that have a more outside tendency. This information can be used, for example, to adapt cut-in situations in curves specifically to the side where the automated system is more likely to drive. If it drives on the inside of a turn, a vehicle cutting in from the inside direction is more relevant for this vehicle, because the lateral distance between the vehicles tends to be smaller.

A structured approach is required to ensure that all the necessary information can be obtained efficiently. Figure 3 gives an overview of the procedure used. Information sources are displayed in gray, the generated situation catalog in blue and the further utilization in green. Most of the information sources used are state-of-the-art and are already known, at least for manually controlled vehicles. The novelty of this approach is the transfer to automated vehicles and the further use of the information acquired for their safety assessment.

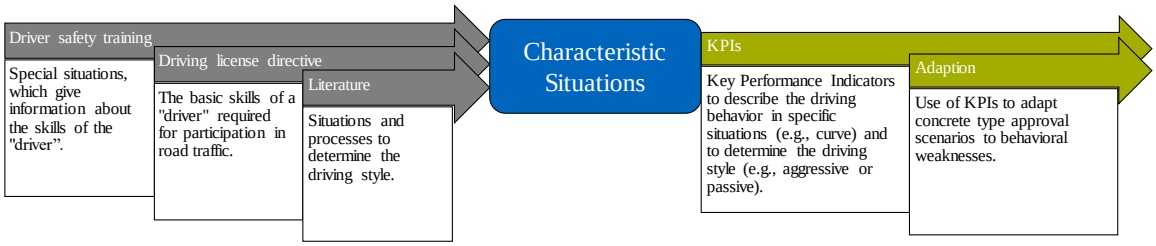

Figure 3. Developed approach for an objective characterization of SUT's driving behavior

In driver safety training courses, the driving skills of human drivers are tested in particularly difficult situations, some of which do not appear or occur extremely rarely in real road traffic. Nevertheless, some tests of driving safety trainings can be used to make a statement about the "capabilities" of automated vehicles. For example, the behavior of the automated vehicle at low coefficients of friction can be investigated.

In Germany, the Driving License Directive defines the minimum requirements that a person must meet in order to be allowed to actively drive a vehicle in road traffic. Not all requirements (e.g., correct adjustment of the side mirrors before driving) can be transferred to an automated vehicle. However, the practical driving test does include some requirements for behavior that can also be applied or transferred to an automated vehicle. These are applicable if the driving examiner drives the automated vehicle in real road traffic and can, at some effort, be transferred if they are carried out in simulation and the requirements of the driving examiners have to be objectified and automated. In addition, the theoretical exam contains a category of questions on how to behave in certain sample situations. These are currently being shifted into theory because the probability of these situations occurring is relatively low. When automated vehicles are tested, these types of tests can be transferred to simulation, and the correct behavior of the vehicles can be tested. From this, it can be concluded that, in addition to the accident-free handling of the type approval tests, the "functional" requirements of the Driving License Directive must also be considered and continuously checked. These types of scenario represent relevant scenarios that do not necessarily have to be critical or complex.

Existing literature can be used to determine the driving style. Studies have already been carried out to determine the driving style of both human drivers [49] and for automated vehicles. Comparisons have also been made between manual and automated driving, such as in [50]. Abnormal behavior (whether aggressive or defensive) can lead to

increased risk in the interaction between human drivers and automated vehicles. Hazards occur when the behavior of an automated vehicle does not match the response expected from human drivers, which may be due to inadequate communication between the driver and the automated vehicle. In order to identify this type of risk and integrate it into the further course of the type approval process, it is advisable to use the Systems-Theoretic Process Analysis (STPA) [51] risk analysis method. This method is particularly suitable because it examines the interaction between complex systems as the cause of errors. The individual systems themselves can operate error-free. Applied to our use case, this means that neither the automated vehicle nor the human driver behaves incorrectly, but their interaction nevertheless leads to risks.

Combining the knowledge from the three information sources shown, a catalog with characteristic situations can be created. If these are carried out in a real test or simulation, key performance indicators can be evaluated that reflect the driving style and weaknesses in driving behavior. This information can then be used for the further type approval process by adapting all future test scenarios to suit the weaknesses identified in the vehicle's driving behavior. For this part of the method, the driving function is required for a limited number of tests. If this is not available, the overall method is still applicable - however, the efficiency in selecting the test cases decreases.

Complexity The aim of this section is to design the concrete scenarios for the type approval of automated vehicles as complex as possible. For a better understanding of the distinction between complex and critical scenarios, we refer once again to the 'Definition of vocabulary' subsection. In future regulations (e.g., UNECE), logical scenarios will be defined that confirm that functional requirements for the system to be tested are fulfilled correctly. One example of this could be the possible logical scenario "object in the SUT's lane", in which the automated vehicle must react appropriately to an object in its lane. In [52], the functional requirement for this logical scenario is that the vehicle must be able to avoid the object by means of braking, steering or a combination of both. Analogous to the currently applicable UNECE R79, which requires proof that the Lane Keeping Assist can be transferred to general situations, this will also be required here. Adding complexity to traffic situations represents an essential component in the transfer to general situations in which an object is located in one's own lane.

The procedure described here should, therefore, be used to introduce a general system-independent difficulty to the given, simple logical scenarios. This is accomplished by adding complexity to the given logical scenario. In general, complexity can be caused by components of all five layers, according to BAGSCHIK [11]. For example, a change in the sign of the lateral slope of the roadway (roadway twisting), which is assigned to layer one of the five-layer model, can represent a particular complexity for the lateral guidance of the vehicle. Consequently, all five layers must be examined separately. This paper limits itself to layer four (objects). Objects are used here as an overarching term for obstacles and other road users of all kinds. Objects can, therefore, be stationary or movable. Due to the limitation to layer four, complexity is understood in this publication as the difficulty faced by the planning algorithm in planning a safe trajectory resulting from the movement or presence of objects.

According to BACH [53], no abstract definition of complex situations for automated vehicles has yet been determined. One approach is offered by SCHAUB [54], who has defined eight criteria for complex situations in which people have difficulty making decisions. In his work, SCHULDT [55] examined how these criteria can be transferred to the complexity of traffic situations for automated vehicles in theory, and concludes that they are also adaptable to this application. The complexity criteria defined by SCHAUB [54] and confirmed by SCHULDT [55] for automated vehicles are as follows:

- Number of elements
- Number of states per element
- Interdependency
- Self-dynamics
- Intransparency
- Multiple conflicting goals
- Openness of the target situation
- Novelty

For a detailed description of the meaning of each criterion in relation to complex traffic situations for automated vehicles, see Chapter 2 in SCHULDT [55]. It is not possible to use these characteristics directly to create complex scenarios, because they only exist in verbal form so far. In addition, the characteristics are used to evaluate existing scenarios and not to generate new ones. A further aspect that impedes direct use is the fact that the evaluation has so

far only been carried out subjectively. This is not sufficient for the procedure developed here, because an automated optimization of the scenarios is conducted in the next step.

In order to apply the criteria for describing complexity that exists in literature, four main points need to be analyzed. The procedure is summarized in Figure 4. First of all, it is necessary to ascertain whether further criteria are required to generate the scenarios carried out here. This can be accomplished by defining a list of requirements and comparing the extent to which the existing criteria meet all of them. Secondly, an evaluation must be performed to determine whether the characteristics have a certain upper limit. The number of the involved elements (objects) is theoretically not limited, but due to the physical allocation only a limited number of objects are important for executing the driving task. The number of objects to be considered must be examined in order to apply the presented method efficiently. Thirdly, the criteria that were previously only defined verbally must be described mathematically in order to be usable for the subsequent optimization. Finally, the objectified attributes must be validated using simulations and real driving data. Since complex scenarios do not necessarily have to lead to a critical outcome of the scenario, special key performance indicators are necessary for validation. A parameter that could be used for the validation is, for example, whether the automated vehicle changes its decision about the actions to be performed during the scenario. If the vehicle starts to dodge an object on the left and then decides to dodge it on the right, this is an indication of a complex scenario, even if the outcome of the scenario is not critical.

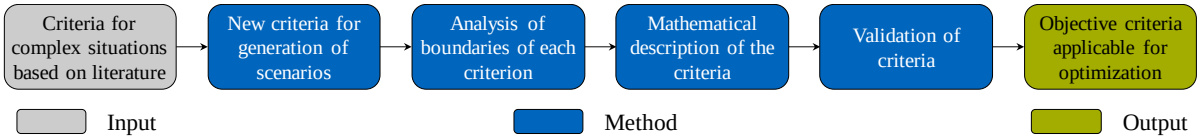

Figure 4. Approach for the definition of an objective complexity metric.

Optimization In the last step of the developed methodology, the individual components previously described are integrated. For this step, the driving function to be tested does not have to be available. The starting point is an arbitrary logical scenario, which is prescribed in the regulation under consideration. The aim is to adapt or select parameters of the logical scenarios that BAGSCHIK [11] defines in a five-layer model in such a way that relevant concrete scenarios are derived from the given logical scenario. Each of the three methods described in detail above contributes to the determination of specific parameter values within the five layers, which is described below and summarized in Table 1. The temporary manipulation of L1 and L2 (L3) represents unusual traffic situations, such as a changed lane routing marked by pylons within a temporary construction site. These special situations are not the focus of this work and will not, therefore, be considered further.

Table 1. Considered influence of the individual aspects on the determination of the parameters of the five-layer model according to BAGSCHIK [11].

	L1	L2	L3	L4	L5
Sensor analysis	✓	✓	✗	✓	✓
Driving behavior	(✓)	(✓)	✗	✓	(✓)
Complexity	✗	✗	✗	✓	✗

Influence: ✓ high (✓) weak ✗ none ✗ neglected

Sensor analysis: The sensor analysis can be used to determine parameters from all four considered layers of the five-layer model. For optimization, the relationship between the individual layers must be taken into account. If, for example, obstructions are taken into account, the position of objects (L4) can have an influence on infrastructure elements such as traffic signs (L2). In addition, connections also exist between complexity and sensor analysis. Sensor analysis identifies areas in which the probability of detection is low. In the subsequent optimization of the complexity, the trajectories of the objects are calculated in such a way that the scenario is as complex as possible, and the potential conflict partner is located, as far as is possible, in the previously-identified areas with weak sensor coverage. A potential conflict partner is the object that forces the SUT to act. Thus, an object in its own lane can be the potential conflict partner forcing the SUT to avoid or brake.

Driving behavior: The influence of the identified driving behavior on the optimization of the parameters is evaluated as weak for most layers. Thus, in Road-level (L1), the analysis of driving behavior cannot determine which exact curve radius is of particular importance for the system, but it can conclude whether the system tends to drive through curves more on the inside or outside. This information can then be used to adjust the position of the potential conflict partner from layer four (objects) within curves.

Complexity: The parameters of the fourth layer (objects) can be determined by systematically introducing complexity. As mentioned before, other layers can also contribute to increasing complexity, which is neglected in this paper. The definition of complexity is defined here as the complexity of the motion and presence of objects. Here, the connection to both other aspects is given by calculating the trajectories of the objects in such a way that they address not only the complexity but also the sensor deficiencies, as well as the identified driving behavior. While the two previous steps are mainly limited to the trajectory of the conflict partner, the optimization of complexity also focuses on defining further objects and their optimal trajectory.

All in all, this results in a two-stage procedure in which the parameters of layer one, two and five are first optimized by sensor analysis and consideration of driving behavior. In addition, the trajectory of the potential conflict partner (L4) is determined. In the second step, further objects are defined by considering complexity and their trajectories are optimized. Therefore, two consecutive optimizations are carried out, each with a suitable algorithm. Especially in the second optimization step, a multi-objective optimization (Pareto optimization) can be of significant importance due to the competition of multiple factors of complexity.

The definite cost function for the first optimization step will vary from system to system, because these two aspects have the very objective of finding system-specific weaknesses. Since the result influences the second optimization step, these results will also be dependent on the SUT. In addition, when optimizing the parameters and, in particular, when optimizing the trajectories of the objects, it must be ensured that certain constraints are met. For example, there must be enough space for the SUT that it is physically able to cope with the scenario without causing an accident, meaning that so-called dilemma situations are not considered. In addition, the trajectories of the objects or the other TP must be physically possible. Depending on the type of TP, approximations such as a simple point mass model, the circle of forces or a single-track model can be used.

The optimization method presented results in more than one relevant concrete scenario from the given logical scenario, due to the applied multi-objective optimization. To execute these scenarios efficiently, simulation is suitable, in which the required parameters - in contrast to test site tests - can also be set without major expense.

RESULTS

This chapter shows an exemplary elaboration of the concept using a driving function designed for the ODD highway. The individual blocks of the approach shown in Figure 2 and the resulting concrete scenario for the example function are explained.

The input of the exemplary results shown here is a fictive system description including the used sensors and a draft of a regulation[2] for the certification of automated vehicles. Within this fictitious regularity, the logical scenario "avoidance of a stationary obstacle" is defined, which represents the starting point for the individual steps of the method. The purpose of the predefined logical scenario is to show that the SUT has the principal functionality needed to avoid a stationary obstacle. A schematic sequence of the scenario in its simplest form is shown in Figure 5 on the left-hand side. The SUT drives in the right lane of a two-lane highway and detects a stationary object with its sensors. Detection takes place at an early stage due to the unrestricted view. Since the adjacent lane is not occupied, the SUT can change lanes and drive past the stationary object with sufficient side clearance. The successful handling of this scenario can be understood as the fulfilment of the functional requirements mentioned above. If, analogous to the existing UNECE R79, the technical service, in cooperation with the manufacturer, is required to prove that this capability can be transferred to general situations (here: general evasive situations of a stationary obstacle), the methodology developed can be used to define system-relevant concrete scenarios that are not previously known to the manufacturer.

[2] Proposal in UNECE ‘Working Party on Automated/Autonomous and Connected Vehicles (GRVA)’ informal working group ‘UN Task Force on Automated Vehicle Testing (AutoVeh)’ [52]

The following paragraph explains how the optimized relevant scenario (right-hand side of Figure 5) can be identified systematically using the method presented. In the optimized scenario, the SUT's view of the stationary object is restricted by a curve on the one hand, and by another TP on the other. Since the object was detected at a late stage, it is no longer possible to brake to a standstill in front of the object. The SUT must switch to the left lane to prevent an accident. This lane is blocked by other vehicles moving at slightly higher speeds than the SUT. The SUT must brake to avoid colliding with the object, but cannot brake too much, in order to avoid a risk to TP 3 when it changes lanes into the gap between TP 2 and TP 3.

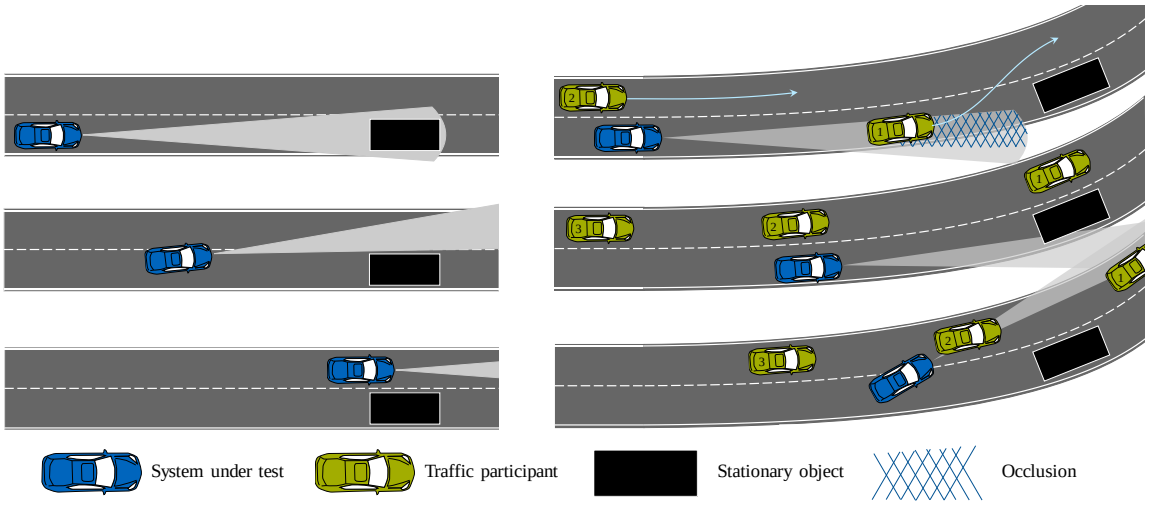

Figure 5. Logical scenario "avoidance of a stationary obstacle" in its basic version (to the left) and in an optimized version (to the right).

Sensor analysis: Using the system specification, disadvantageous Road-level (L1) parameters for the sensor setup used can be determined. In the example shown here, this is a curve with a certain radius, which means that the sensors used can hardly see the course of the road. In addition, the sensor analysis defines another TP (L4), which increases the occlusion of the stationary object. The distance between the SUT and the TP is defined on the basis of the opening angles of the sensors used, so that optimum occlusion of the stationary object is achieved during cornering. In addition, the environmental conditions (L5) can be selected in the scenario (no environmental conditions are shown in Figure 5, with the result that the operational weak points of the sensors used are taken into account. In a system that mainly uses cameras, this can be direct sunlight from the front.

Driving behavior: Characteristic tests carried out in advance show that the SUT tends to use the outer side of curves for orientation. Therefore, in the scenario under consideration, a left-hand curve is chosen because the lateral distance of the SUT to a safe position is then maximized. Instead of testing both left-hand and right-hand curves, this method allows a well-founded selection of this parameter.

Complexity: In the last step, system-independent complexity is added to the scenario on the basis of the criteria of SCHAUB [54] and SCHULDT [55]. For example, the number of elements is increased (definition of further TPs). The trajectories of this TP are adapted in such a way that they increase the number of actions required by the SUT to achieve a safe state, for example by representing restrictions on action. In the specific example, in order to successfully pass this scenario, the SUT has to brake in a controlled manner and reeve into a gap between two vehicles traveling at different speeds, because braking to a complete standstill is no longer possible without colliding with the stationary object. As already explained in the subsection ‘Definition of vocabulary’, the speed of the TP and the starting speed of the SUT are also increased, and distances between the TPs are reduced in order to increase criticality. In addition, a connection to the sensor analysis is made so that the other TPs stay as long as possible in areas with low sensor coverage or even in blind spots that are not visible to any sensor.

From the technical service's point of view, this scenario is relevant for the SUT to be tested and should, therefore, be taken into account when the SUT is certified. This can support the required proof of transferability of the capabilities to general situations in which an object must be evaded in its own lane. At the same time, it is difficult for the

manufacturer to prepare for the tests, due to the individual adaptation of the scenarios, and thus so-called gaming of tests is prevented, and the safety level achieved during certification can be transferred more effectively to real driving conditions.

For simplicity's sake, this example does not discuss all parameters that can be determined by the optimization. For example, further parameters of the road geometry can be adapted to the weak points of the SUT sensors. Even if not all parameters are explained, the example shows very clearly which results are achieved with the developed method.

DISCUSSION AND LIMITATIONS

This section critically discusses the developed approach. This concept has been specially developed for the type approval process of automated vehicles. As indicated in the section LITERATURE REVIEW AND RESEARCH OBJECTIVE, the focus is on Object and Event Detection and Response (OEDR), and therefore not all tests required for type approval are addressed. One of the basic assumptions of this paper is the specification of logical scenarios for type approval by legislation. This assumption is justified because UNECE already has existing regulations for ADAS according to this principle, and UNECE working groups already have initial proposals [52] for automated vehicles that also work with the definition of logical scenarios. In addition, large research projects, such as PEGASUS (highway) [2] and CETRAN (urban) [56], also work with the definition of logical scenarios.

With the method presented, it is not possible to determine all parameters of the five layers model precisely, because it is not entirely possible to determine the relevance of a parameter for a scenario. For instance, even after the methodology has been applied, it is unclear whether the type and shape of the central lane marking in the scenario in Figure 5 has an effect on the outcome of the scenario. Consequently, a parameter variation must still be performed in simulation. However, the extent of this variation is significantly reduced by the parameters that have already been defined. Despite constantly increasing computing power, it is important to keep the number of necessary tests in simulation low, because high-precision simulation models with considerable computing costs must be used for a meaningful simulation-based test of the overall system. The presented method thus has an advantage compared to the exclusive criticality optimization through simulation execution, because no additional prior knowledge is included in the latter. Using this prior knowledge, edge cases can be identified more efficiently with the novel method presented. In addition, the procedure presented here can largely be carried out without the actual driving function, which is of great importance for a technical service. The actual driving function is only necessary for a limited number of tests in order to determine the driving behavior. As stated in the subsection ‘Objective characterization of driving behavior’, if the driving function is not available, the overall method is still applicable - however, the efficiency with which test cases are selected decreases.

As with all methods for selecting and reducing scenarios described in the subsection ‘Scenario selection and reduction methods’, the method developed does not cover the entire parameter space. Therefore, there is no guarantee that all errors of the SUT will be detected. Finding as many faults as possible is of great importance for the system manufacturer in terms of product liability. The situation is different for a technical service when it comes to system certification. The main purpose of the type approval is to test relevant scenarios under given framework conditions by regulations. The technical service must ensure, with minimum effort, that no relevant error cases remain undetected and that the SUT conforms to the applicable regulations, which is achieved with the developed approach.

It is also possible to combine the method with existing methodologies for scenario selection. For example, it can be combined with the use of critical accident scenarios from a database. An accident stored in the database can be considered as a logical scenario to which the developed methodology can be applied. Thus, it is possible to show whether the SUT can prevent existing accidents even under disadvantageous conditions.

CONCLUSION AND FUTURE WORK

This paper presents a novel and advanced method for defining relevant test cases for the future type approval of automated vehicles. The method is specifically adapted to the requirements of a technical service performing type approval. Based on regulations currently under development, such as UNECE and other laws to be complied with, scenarios relevant to the system under test are identified. As with existing UNECE regulations (e.g., for the Lane Keeping Assist), it can be assumed that not all tests are specified in detail in the regulations, but only in the form of logical scenarios. This enables the technical service to carry out scenarios that are relevant from its perspective, thus preventing so-called gaming of tests, and at the same time perform an efficient evaluation of the vehicle to be tested.

The methodology presented is essentially based on three pillars: analysis of the sensor setup used, inclusion of driving behavior and consideration of complex traffic situations. In the first two steps, system-specific weaknesses of the system to be tested are identified. In the third step, the logical scenario given by the regulation is extended to include a complex traffic situation in order to challenge the planning algorithm of the vehicle. After a final optimization, in which the three mentioned sub-methods are combined, the concrete scenarios relevant for type approval are obtained.

The methodology for the analysis of the sensors is partly available and will be continuously improved in further work. A comprehensive analysis is currently being carried out for the characterization of driving behavior to determine what information on driving behavior can be included in the future type approval process for automated vehicles. In the future, the methodology for integrating complexity into the tests to be performed will be developed. To achieve this, linguistic definitions of complexity from existing literature will be analyzed and transformed into a mathematical form. Subsequently, a validation of the complexity will be carried out by means of simulations and real driving data. Finally, the complexity can be included in the optimization. If all three components described are available, the optimization can be carried out in a final work and the total method can be applied to a real system as well as being validated.

ACKNOWLEDGEMENT AND CONTRIBUTIONS

The work for this paper was funded and supported by TÜV SÜD Auto Service GmbH. Thomas Ponn (corresponding author) initiated and developed the main parts of this paper. Christian Gnandt provided essential scientific background information regarding the safety assessment of Advanced Driver Assistance Systems and Automated Driving. Frank Diermeyer contributed to the conception of the research project and revised the paper critically for important intellectual content. He gave final approval of the version to be published and agrees to all aspects of the work. As a guarantor, he accepts responsibility for the overall integrity of the paper. The author would also like to thank Alexander Schwab for the critical and productive discussions on how to characterize the driving behavior of automated vehicles objectively.

REFERENCES

[1] *Taxonomy and Definitions for Terms Related to On-Road Motor Vehicle Automated Driving Systems*, J3016_201609, 2016.

[2] Deutsches Zentrum für Luft- und Raumfahrt e. V. (DLR), *PEGASUS-Projekt.* [Online] Available: http://www.pegasus-projekt.info/de/. Accessed on: Feb. 18 2019.

[3] W. Wachenfeld and H. Winner, "The Release of Autonomous Vehicles," in *Autonomous Driving: Technical, Legal and Social Aspects*, M. Maurer, J. C. Gerdes, B. Lenz, and H. Winner, Eds., Berlin, Heidelberg: Springer Berlin Heidelberg, 2016, pp. 425–449.

[4] NHTSA, *Automated Driving Systems 2.0: A Vision for Safety*. September 2017. [Online] Available: https://www.nhtsa.gov/sites/nhtsa.dot.gov/files/documents/13069a-ads2.0_090617_v9a_tag.pdf. Accessed on: Feb. 18 2019.

[5] S. Ulbrich, T. Menzel, A. Reschka, F. Schuldt, and M. Maurer, "Defining and Substantiating the Terms Scene, Situation, and Scenario for Automated Driving," in *2015 IEEE 18th International Conference on Intelligent Transportation Systems*, 2015, pp. 982–988.

[6] T. Menzel, G. Bagschik, and M. Maurer, "Scenarios for Development, Test and Validation of Automated Vehicles," in *2018 IEEE Intelligent Vehicles Symposium (IV)*, 2018, pp. 1821–1827.

[7] *Road vehicles — Safety of the intended functionality*, ISO/PAS 21448, 2019.

[8] J. C. Hayward, "Near-Miss Determination Through Use of a Scale of Danger," *Highway Research Record*, no. 384, 1972.

[9] National Transportation Safety Board, *Preliminary Report Released for Crash Involving Pedestrian, Uber Technologies, Inc., Test Vehicle.* [Online] Available: https://www.ntsb.gov/news/press-releases/pages/nr20180524.aspx. Accessed on: Feb. 18 2019.

[10] F. Schuldt, F. Saust, B. Lichte, M. Maurer, and S. Scholz, "Effiziente systematische Testgenerierung für Fahrerassistenzsysteme in virtuellen Umgebungen," https://publikationsserver.tu-braunschweig.de/receive/dbbs_mods_00052570.

[11] G. Bagschik, T. Menzel, and M. Maurer, "Ontology based Scene Creation for the Development of Automated Vehicles," in *2018 IEEE Intelligent Vehicles Symposium (IV)*, 2018, pp. 1813–1820.

[12] D. R. Kuhn, D. R. Wallace, and A. M. Gallo, "Software fault interactions and implications for software testing," *IEEE Transactions on Software Engineering*, vol. 30, no. 6, pp. 418–421, 2004.

[13] B. S. Ahmed and K. Z. Zamli, "A review of covering arrays and their application to software testing," *Journal of Computer Science*, vol. 7, no. 9, p. 1375, 2011.
[14] M. Tatar, "Chasing Critical Situations in Large Parameter Spaces," in *Autonomous Vehicle Test & Development Symposium*, Stuttgart, 2018.
[15] F. Schuldt, A. Reschka, and M. Maurer, "A Method for an Efficient, Systematic Test Case Generation for Advanced Driver Assistance Systems in Virtual Environments," in *Automotive Systems Engineering II*, H. Winner, G. Prokop, and M. Maurer, Eds., Cham: Springer International Publishing, 2018, pp. 147–175.
[16] M. Grindal, J. Offutt, and S. F. Andler, "Combination testing strategies: a survey," *Software Testing, Verification and Reliability*, vol. 15, no. 3, pp. 167–199, 2005.
[17] T. L. Saaty, *The Analytic Hierarchy Process: Planning, Priority Setting, Resource Allocation*, 1st ed. New York: McGraw-Hill, 1980.
[18] Q. Xia, J. Duan, F. Gao, T. Chen, and C. Yang, "Automatic Generation Method of Test Scenario for ADAS Based on Complexity," in *SAE Technical Paper*, 2017.
[19] Q. Xia, J. Duan, F. Gao, Q. Hu, and Y. He, "Test Scenario Design for Intelligent Driving System Ensuring Coverage and Effectiveness," *International Journal of Automotive Technology*, vol. 19, no. 4, pp. 751–758, 2018.
[20] W. Chen and L. Kloul, "An Ontology-based Approach to Generate the Advanced Driver Assistance Use Cases of Highway Traffic," in *10th International Joint Conference on Knowledge Discovery, Knowledge Engineering and Knowledge Management*, 2018.
[21] M. Huelsen, *Knowledge-Based Driver Assistance Systems*. Wiesbaden: Springer Fachmedien Wiesbaden, 2014.
[22] A. Pütz, A. Zlocki, J. Küfen, J. Bock, and L. Eckstein, "Database Approach for the Sign-Off Process of Highly Automated Vehicles," in *25th International Technical Conference on the Enhanced Safety of Vehicles (ESV) National Highway Traffic Safety Administration*, 2017.
[23] A. Pütz, A. Zlocki, J. Bock, and L. Eckstein, "System validation of highly automated vehicles with a database of relevant traffic scenarios," in *12th ITS European Congress*, Strasbourg, 2017.
[24] L. Wang, F. Fahrenkrog, T. Vogt, O. Jung, and R. Kates, "Prospective safety assessment of highly automated driving functions using stochastic traffic simulation," in *25th International Technical Conference on the Enhanced Safety of Vehicles (ESV) National Highway Traffic Safety Administration, Detroit*, 2017.
[25] D. Zhao, X. Huang, H. Peng, H. Lam, and D. J. LeBlanc, "Accelerated Evaluation of Automated Vehicles in Car-Following Maneuvers," *IEEE Transactions on Intelligent Transportation Systems*, vol. 19, no. 3, pp. 733–744, 2018.
[26] Z. Huang, D. Zhao, H. Lam, D. J. LeBlanc, and H. Peng, "Evaluation of Automated Vehicles in the Frontal Cut-in Scenario - an Enhanced Approach using Piecewise Mixture Models," *CoRR*, vol. abs/1610.09450, 2016.
[27] Z. Huang, H. Lam, and D. Zhao, "Towards affordable on-track testing for autonomous vehicle — A Kriging-based statistical approach," in *2017 IEEE 20th International Conference on Intelligent Transportation Systems (ITSC)*, 2017, pp. 1–6.
[28] Z. Huang, H. Lam, and D. Zhao, "Sequential experimentation to efficiently test automated vehicles," in *2017 Winter Simulation Conference (WSC)*, 2017, pp. 3078–3089.
[29] M. Althoff and J. M. Dolan, "Online Verification of Automated Road Vehicles Using Reachability Analysis," *IEEE Transactions on Robotics*, vol. 30, no. 4, pp. 903–918, 2014.
[30] M. Althoff and S. Lutz, "Automatic Generation of Safety-Critical Test Scenarios for Collision Avoidance of Road Vehicles," in *Proc. of the IEEE Intelligent Vehicles Symposium*, 2018, pp. 1326–1333.
[31] S. Manzinger, M. Leibold, and M. Althoff, "Kooperative Bewegungsplanung autonomer Fahrzeuge unter Verwendung von Manöver-Templates," in *AAET-Automatisiertes und vernetztes Fahren*, 2017.
[32] F. Gruber and M. Althoff, "Anytime Safety Verification of Autonomous Vehicles," in *2018 21st International Conference on Intelligent Transportation Systems (ITSC)*, 2018, pp. 1708–1714.
[33] M. Koren, S. Alsaif, R. Lee, and M. J. Kochenderfer, "Adaptive Stress Testing for Autonomous Vehicles," in *2018 IEEE Intelligent Vehicles Symposium (IV)*, 2018, pp. 1–7.
[34] B. Graab, E. Donner, U. Chiellino, and M. Hoppe, "Analyse von Verkehrsunfällen hinsichtlich unterschiedlicher Fahrerpopulationen und daraus ableitbarer Ergebnisse für die Entwicklung adaptiver Fahrerassistenzsysteme," in *3. Tagung Aktive Sicherheit durch Fahrerassistenz*, 2008.
[35] C. Amersbach and H. Winner, "Functional Decomposition: An Approach to Reduce the Approval Effort for Highly Automated Driving," in *8. Tagung Fahrerassistenz*, 2017.

[36] C. Amersbach and H. Winner, "Funktionale Dekomposition - Ein Beitrag zur Überwindung der Parameterraumexplosion bei der Validation von höher automatisiertem Fahren," in *12. Workshop Fahrerassistenzsysteme*, Walting, 2018.
[37] D. Heß, J. Oehlerking, M. Woehrle, and J. S. Cubillo, "The UnCoVerCPS Verification Approach to Automated Driving," in *20th International Forum on Advanced Microsystems for Automotive Applications*, 2016.
[38] M. Kamali, L. A. Dennis, O. McAree, M. Fisher, and S. M. Veres, "Formal verification of autonomous vehicle platooning," *Science of Computer Programming*, vol. 148, pp. 88–106, http://www.sciencedirect.com/science/article/pii/S0167642317301168, 2017.
[39] S. Shalev-Shwartz, S. Shammah, and A. Shashua, "On a Formal Model of Safe and Scalable Self-driving Cars," *CoRR*, vol. abs/1708.06374, http://arxiv.org/abs/1708.06374, 2017.
[40] European Commission, *New and improved car emissions tests become mandatory on 1 September.* [Online] Available: http://europa.eu/rapid/press-release_IP-17-2822_en.htm. Accessed on: Feb. 19 2019.
[41] UNECE, *Regulation No. 83 Revision 5: Uniform provisions concerning the approval of vehicles with regard to the emission of pollutants according to engine fuel requirements.* [Online] Available: https://www.unece.org/fileadmin/DAM/trans/main/wp29/wp29regs/R083r5e.pdf. Accessed on: Feb. 19 2019.
[42] UNECE, *Global Technical Regulation No. 15: Worldwide harmonized Light vehicles Test Procedure.* [Online] Available: https://www.unece.org/trans/main/wp29/wp29wgs/wp29gen/wp29glob_registry.html. Accessed on: Feb. 19 2019.
[43] UNECE, *UNECE works on global methodology to measure on-road car emissions.* [Online] Available: http://www.unece.org/?id=48872. Accessed on: Feb. 19 2019.
[44] Working Party on Pollution and Energy, *Proposal for Amendment 5 to global technical regulation No.15 (Worldwide harmonized Light vehicles Test procedures (WLTP)).* [Online] Available: https://www.unece.org/fileadmin/DAM/trans/doc/2019/wp29grpe/ECE-TRANS-WP29-GRPE-2019-02e.pdf. Accessed on: Feb. 19 2019.
[45] European Commission, *Emissions in the automotive sector: Emissions from light-duty vehicles.* [Online] Available: https://ec.europa.eu/growth/sectors/automotive/environment-protection/emissions_en. Accessed on: Feb. 19 2019.
[46] UNECE, *Regulation No. 79 Revision 4: Uniform provisions concerning the approval of vehicles with regard to steering equipment.* [Online] Available: https://www.unece.org/fileadmin/DAM/trans/main/wp29/wp29regs/2018/R079r4e.pdf. Accessed on: Feb. 19 2019.
[47] NHTSA, *Federal Automated Vehicles Policy: Accelerating the Next Revolution In Roadway Safety*. September 2016. [Online] Available: https://www.transportation.gov/sites/dot.gov/files/docs/AV%20policy%20guidance%20PDF.pdf. Accessed on: Feb. 18 2019.
[48] K. Dietmayer, "Predicting of Machine Perception for Automated Driving," in *Autonomous Driving: Technical, Legal and Social Aspects*, M. Maurer, J. C. Gerdes, B. Lenz, and H. Winner, Eds., Berlin, Heidelberg: Springer Berlin Heidelberg, 2016, pp. 407–424.
[49] W. Han, W. Wang, X. Li, and J. Xi, "Statistical-based approach for driving style recognition using Bayesian probability with kernel density estimation," *IET Intelligent Transport Systems*, vol. 13, no. 1, pp. 22–30, 2019.
[50] Björn Filzek, "Abstandsverhalten auf Autobahnen – Fahrer und ACC im Vergleich," Dissertation, Technische Universität Darmstadt, Darmstadt, 2002.
[51] N. G. Leveson and J. P. Thomas, *STPA Handbook.* [Online] Available: http://psas.scripts.mit.edu/home/get_file.php?name=STPA_handbook.pdf. Accessed on: Feb. 19 2019.
[52] UNECE, *Guideline for Intelligent & Connected Vehicle Autonomous Driving Functionality Test.* [Online] Available: https://wiki.unece.org/download/attachments/63309804/SG1-03-11%20China.docx?api=v2. Accessed on: Feb. 19 2019.
[53] J. Bach, S. Otten, and E. Sax, "Model based scenario specification for development and test of automated driving functions," in *2016 IEEE Intelligent Vehicles Symposium (IV)*, 2016, pp. 1149–1155.
[54] H. Schaub, "Exception error: über Fehler und deren Ursachen beim Handeln in Unbestimmtheit und Komplexität," *gdi impuls*, vol. 4, no. 96, pp. 1–12, 1996.
[55] F. Schuldt, "Ein Beitrag für den methodischen Test von automatisierten Fahrfunktionen mit Hilfe von virtuellen Umgebungen," Dissertation, Technische Universität Braunschweig, Braunschweig, 2017.
[56] Nanyang Technological University, *NTU, LTA and JTC unveil Singapore's first autonomous vehicle test centre.* [Online] Available: http://media.ntu.edu.sg/NewsReleases/Pages/newsdetail.aspx?news=39308c90-536c-4c3a-be6d-b9c07041a442. Accessed on: Feb. 19 2019.

THE ANALYSIS AND EXPERIMENTAL DEVELOPMENT OF ASPIRATED AIRBAGS FOR CONVENTIONAL AND AUTONOMOUS VEHICLES

David Breed
Automotive Technologies International, Inc.
USA

Nina Yurchenko,
Pavlo Vynogradskyy,
Konstantin Kuzmenko
Institute of Hydromechanics, National Academy of Sciences of Ukraine
Ukraine

Shawe Zhang,
Bobby Li
Shanghai East Joy Long Motor Airbag Co., Ltd., #219 Qingda Rd., Pudong New Area, Shanghai 2011201, China

Paper Number 19-0025

ABSTRACT

As a part of the Automated Driving Systems (ADS) strategy, the developed aspirated inflation system is applicable for conventional and autonomous motor vehicles where larger airbags are required and the location of vehicle occupants is less precise. It is built to provide for the air entrainment into an airbag from the car passenger compartment. The objective is set to inflate a 50 L airbag within 30 ms with an aspiration ratio, $A \geq 4$. Advantageous features of the offered system are a much smaller (less than 1/3) gas generator and stopped airbag deployment on contact with an occupant that eliminates out-of-position occupant injuries.
Regarding engineering, the aspirated inflator is a supersonic pulse ejector designed on the basis of Prandtl-Meyer effect realization. The modeling includes numerical flow simulation combined with subsequent engineering design, fabrication, and experimental testing of models. The results are presented for the "cold-gas" inflator testing where the gas generator operation is imitated by a jet generation from a compressed-air tank using a specially designed high-speed valve. Such an approach enables the verification of the numerical procedure and calculation results obtained for "cold" and "hot-gas" cases. The experimentally found "cold-gas" aspiration ratio is in a good agreement with the numerical prediction varying within A=3.1 – 2.1 depending on a particular design and the operational motive pressure. For the gas generator case, the aspiration ratio values are calculated to be ≥4.
Several different designs of the supersonic pulse aspirator are modeled, designed, manufactured, and tested including outer and inner circumferential slit nozzle and multi-nozzle systems. To meet the engineering requirements, multi-stage multivariate studies of measured pressure fields and airbag inflation process are performed.

INTRODUCTION

Figure 1. Safety is our goal

According to NHTSA, the Automated Driving Systems (ADS) must handle the whole task of safe driving by ~2025. The automation is successively provided by technology development both in hardware and software areas starting from cruise control and seat belts within 1995-2000 to lane departure warning, blind spot detection, automated emergency braking, traffic jam assist, self-parking, adaptive cruise control, and many other systems showing features of partially automated safety.
In this connection, the herein offered system of airbag aspirated inflation can significantly contribute to the further development of safety systems up to fully autonomous vehicles with arbitrarily located occupants.
The initial goal is to develop a supersonic pulse ejector for an airbag inflation system to cause air aspiration from a car compartment into the 50-60 L airbag to inflate it within 30 ms with the aspiration ratio above 4. This technology should have an application potential for larger airbags such as passenger side airbags, side curtain airbags, side-impact airbags and airbags for autonomous vehicles.

The main advantages of the offered aspirated inflator are as follows [1-5],

- the airbag stops deploying on contact with an occupant;
- the required gas generator is less than 1/3 the size of conventional gas generators (see e.g. [6]);
- most of the gas to inflate the airbag comes from the passenger compartment that prevents sudden pressure jump within a vehicle compartment (Figure 2);
- injuries to out-of-position occupants are eliminated;
- the need for staged airbag deployments is eliminated;
- the need for satellite crash sensors for frontal impact sensing is eliminated;
- occupant weight and position sensors are not required.

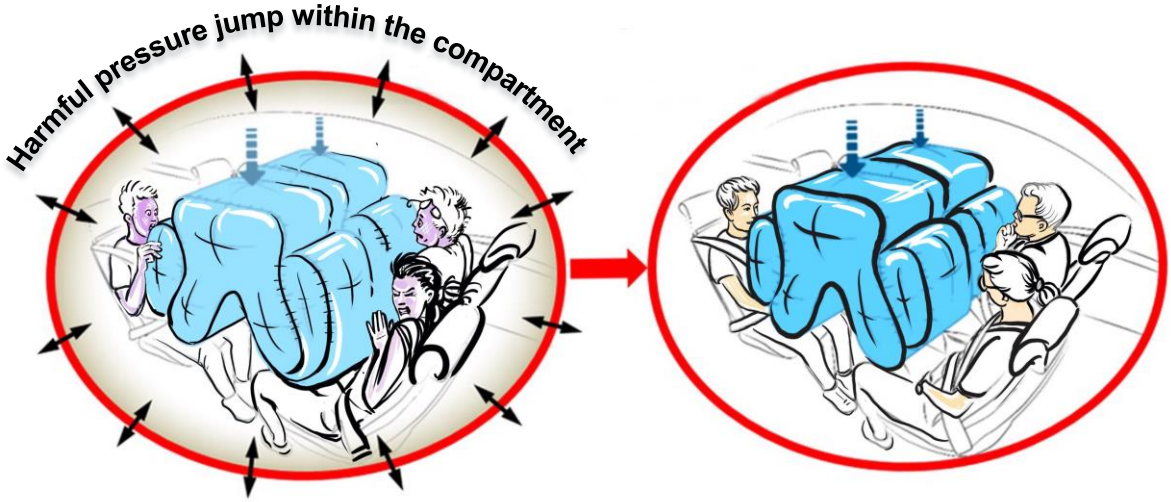

Figure 2. Illustrated impact of big deployed airbags: operation with conventional (left) and aspirated inflator systems (right)

The driver side system development comprises numerical modeling and laboratory experiments including the engineering aspirator design and its operation testing in a range of motive pressure values causing air entrainment. Achievement of high performance characterized by the aspiration (entrainment) ratio was realized through a search of an optimal geometry combined with an optimal operational mode.

Numerical simulation provides initial guidance on the aspirator geometry and flow parameters for two temperature regimes. The "cold-gas" regime strictly corresponds to experiments in the compressed-air facility equipped with a high-speed valve which are performed in the Laboratory for Advanced Aerodynamics & Interdisciplinary Research, National Academy of Sciences of Ukraine. Experimental results enable to verify the numerical procedure and calculation results as well as to distinguish flow features overlooked in the numerical studies. The "hot-gas" regime models the aspirator operation with a gas generator; it is tested experimentally using the commercial airbag gas generator technology in the laboratory of the Shanghai East Joy Long Motor Company.

METHOD OF INVESTIGATIONS AND INSTRUMENTATION

The research approach consists in matched and feedback-connected numerical and experimental investigations. As guidance to build a supersonic ejector, the Prandtl-Meier flow is considered [3, 5]. A supersonic jet-flow generated by a small gas generator should change its direction over the blunt angle coupling between a nozzle and a mixing chamber which causes a suction wave similar to that of Prandtl-Meyer flow. It is the proper pressure distribution in this area which motivates ejection of the atmospheric air into the mixing chamber.

Thus, the basic task of numerical simulation is to roughly determine the device geometry with its particular linear and angular dimensions which would create the required pressure fields in the inflator. To determine optimal operational parameters for the given geometry, instantaneous and integral gas-dynamic parameters are found for viscous incompressible gas using nonstationary Reynolds equations. To validate the numerical

problem formulation and used assumptions, 2 cases of "cold air" and "hot air" inflator operation are considered numerically. The first one imitates the laboratory conditions of the inflator operation using the compressed air tanks as a high-pressure source. The second one, models the situation of the inflator operation using a small pyrotechnic gas generator as the motive pressure source.

Obtained recommendations on slit, nozzle, mixing chamber parameters for a range of high motive pressure are taken as a basis for the engineering design which resulted in the detailed technological drawings and precision manufacture of the model.

The experimental task is to provide, thorough measurements of pressure fields in the aspirator system, a description of the jet behavior and, consequently, the air entrainment process. In addition to the measured values of aspiration ratio for different models and their operation conditions, this is visualized with the video recordings of airbag deployments using a high-speed camera.

Experiment arrangement. Test models.

The "cold air" system operation is realized experimentally due to the specially designed universal high-speed valve (UHSV-1). Its basic parameters are given in the Table 1.

Table 1.

Basic operating parameters of the UHSV-1 high-speed valve

Opening time	**≤ 0.004 s**
Closing time	≤ 0.005 s
Pressure range	0.6-6 MPa
Temperature range	+5 ºC ÷ +65 ºC
Supply voltage	80±6 V
Material	Steel 14X17H2
Dimensions	79 mm x 125 mm x 141mm
Weight	3 kg

These parameters enable to form a motive pulse jet from the nozzle to initiate the ambient air entrainment into the inflator mixing chamber as it is shown in Figure 3.

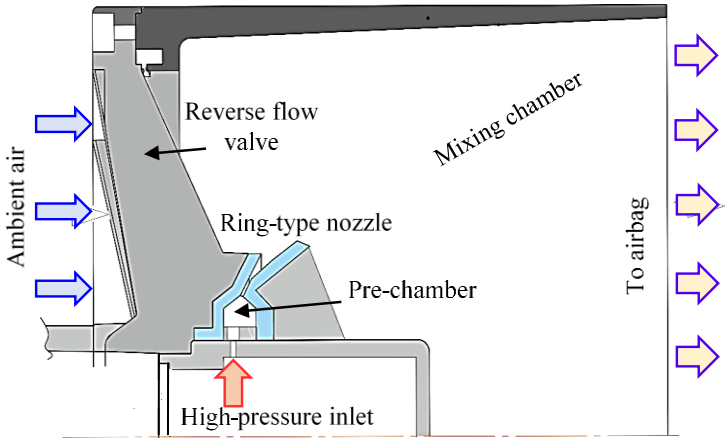

Figure 3. Sketch of an axisymmetric design of the aspirated inflator according to the numerically outlined geometry

A nozzle for the supersonic flow is designed to match the output pressure in the jet with the pressure in the mixing chamber. Consecutive investigation stages covered a range of varying angles of the slit and nozzle opening, slit width, geometry and sizes of pre-chamber and mixing chamber to determine an optimal set of design parameters.

Several aspirator models were designed, manufactured and tested as is partly described in [2-4]. They are axisymmetric following an overall design of the system to be located in the steering wheel. An essential feature of the first set is an external slit relative to the mixing chamber, i.e. the motive ring-type nozzle was located close to the internal wall of a mixing chamber. The second type combines aspirators with an internal slit ejecting the ring jet closer to the aspirator axis. The second type is considered here with its design illustrated by Figures 4 and 5.

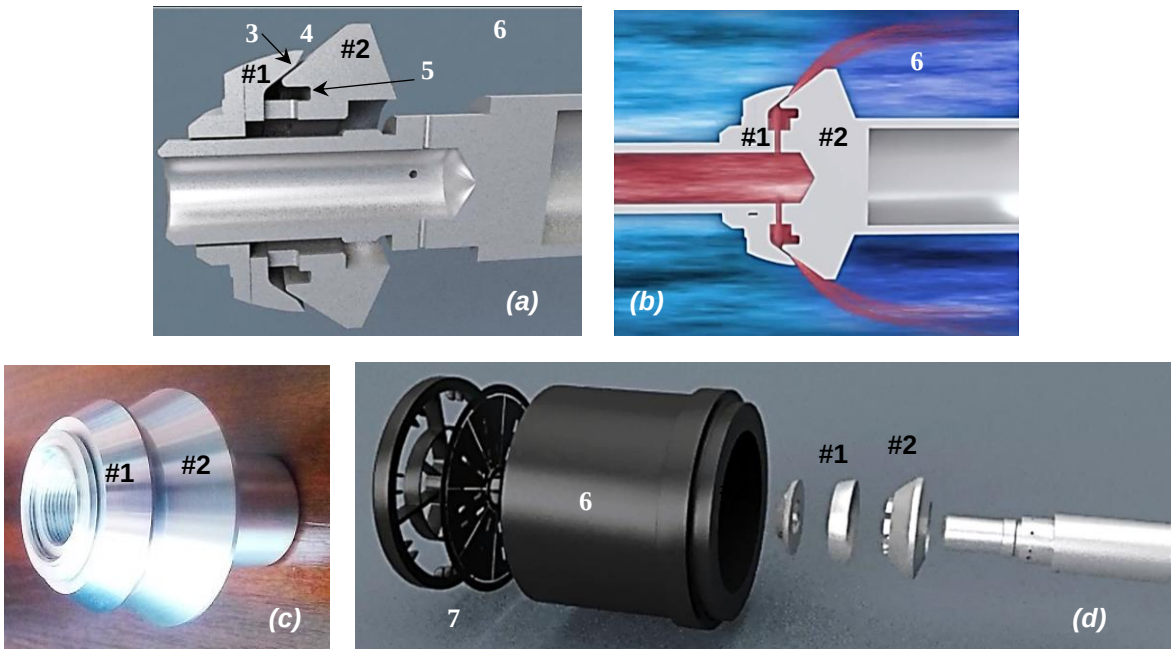

Figure 4. Internal-slit aspirated inflator: 3D model (a); aspirator operation (b); fabricated test model (c); aspirator assembly (d).
#1, #2 – two metal disks forming a relevant nozzle geometry for a supersonic jet injection,
3 – slit,
4 – nozzle,
5 – pre-chamber,
6 – plastic mixing chamber/housing,
7 – reverse flow valve

The sharp bent edge of one of the metal disks #1 or #2 is designed to realize the Prandtl-Meyer flow conditions. The whole design of the supersonic pulse ejector is to be substantially different from known ejectors made for operation in stationary flow conditions. Two basic design modifications of the internal-slit aspirator are shown in Figure 5. Other tested modifications embrace combinations of varied linear and angular dimensions of the basic aspirator elements like a slit, nozzle, pre-chamber, location of a motive pressure outlet in the pre-chamber, and mixing chamber including its shape, cylindrical or conical.

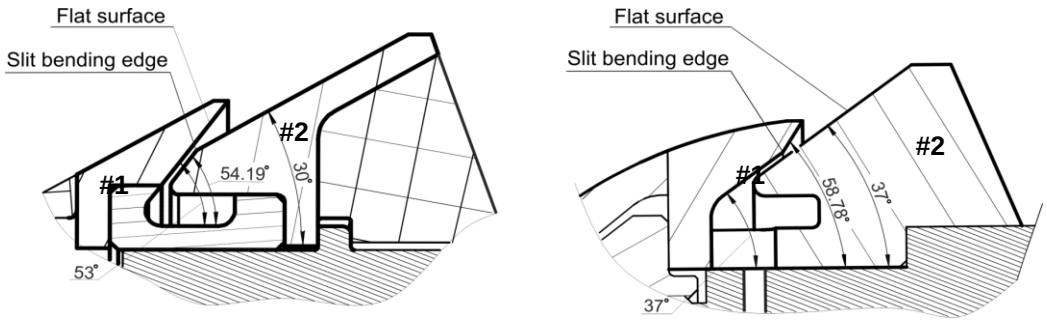

Figure 5. Geometry of the slit initiating aspiration in the internal-slit aspirator design, 2 versions: (a) aspirator #1; (b) aspirator #2

Overall dimensions were maintained the same according to the engineering requirements, i.e. the aspirator length is no more than 117 mm, its diameter is 120 mm.

Finally, an attempt was made to stabilize the supersonic jet with streamwise grooves over the #2 disk with the circumferentially regular spacing (Figure 6, a) for several values of a filling factor, F=c/C=6.7%, 13.3%, 26.7%, 53.3%, 100% (Figure 6, b) [see 7-9]. Effective slit width was calculated to vary within d=0.35mm—0.45mm.

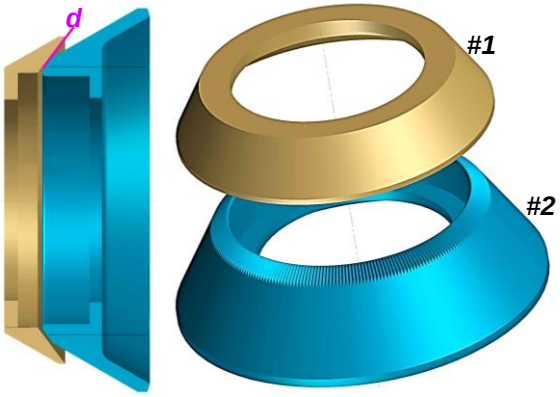

Figure 6, a. Grooved disk #2 modified to stabilize behavior of the supersonic jet

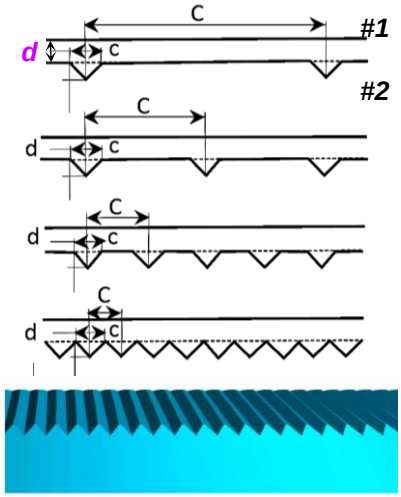

Figure 6, b. Grooved surface with various filling factors

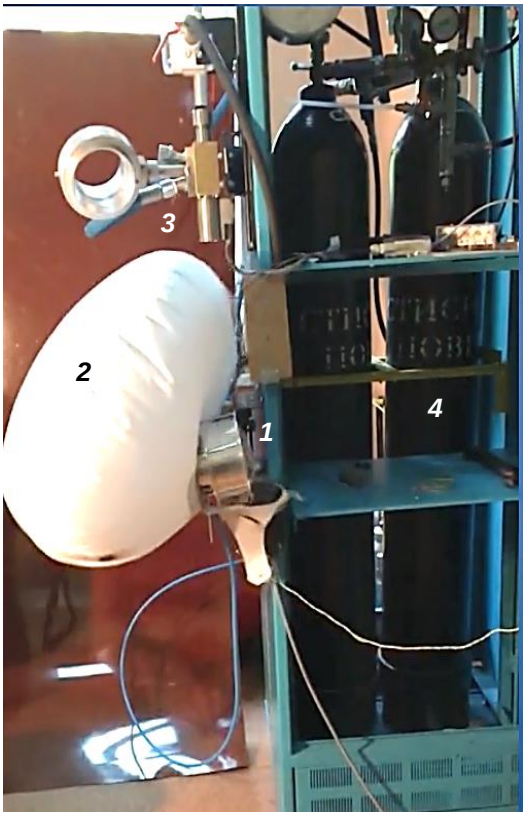

Figure 7. Experimental facility [2, 4, 10]:
1 – aspirated inflator model;
2 – airbag;
3 – high-speed valves;
4 – compressed air tanks, 0-100 bar

Experimental facility

The stage of experimental testing of the inflator operability started from the design and manufacturing of the compressed-air facility (Figure 7) and a number of appliances including the automated data acquisition and processing system, pressure-probe rakes, the aspiration ratio stand, etc.

During testing, the air is pumped into the 40-L high-pressure 250 bar tank by the high-pressure PE-100W compressor up to 100 bar. From this tank, air goes to the 40-L receiver of 150 bar through a reduction valve. The reduction valve is adjusted according to the range of motive pressure values, P_m, required in experiments. The UHSV-1 electronically controlled and the alternative commercial KB-20 pneumatically controlled high-speed valves are switched in the pneumatic tract. High-pressure sensors for 1-70 bars are mounted after each valve to measure pressure losses. Due to very short opening and closing time, high-speed valves form a jet flow within 20-40 ms similar to gas generators to initiate the ambient air entrainment as it is shown in Figure 4, b. Excessive pressure in the airbag is 0.2 bar that stops the inflation process.

The measurement program aims at the determination of the supersonic jet location and behavior inside a mixing chamber to find conditions for stable air entrainment. For that, corresponding to the particular inflator design, the pressure-probe rake (Figure 8, a) is fabricated to measure dynamic pressure at the mixing chamber outlet (2-10 locations shown in Figure 8, b). A number of other pressure probes are mounted so as to measure static pressure values along the mixing chamber wall (11-15 locations) and in the pre-chamber (probe location 1).

Other series of experiments were conducted under the same conditions with an airbag mounted to the inflator outlet. The process of airbag deployment is recorded using a high-speed 1000 f/s camera. It enables the analysis of the visualized inflation process together with corresponding measured pressure distributions.

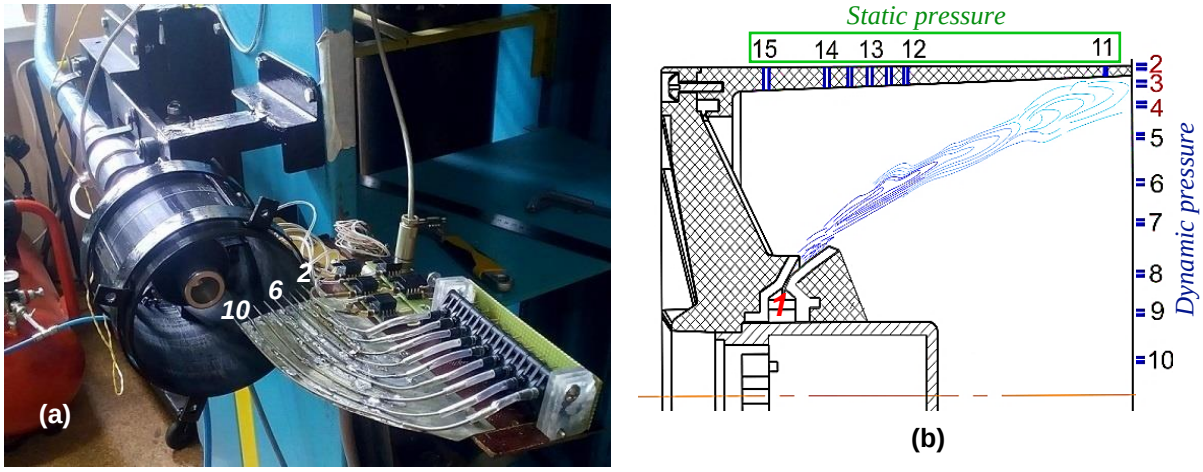

Figure 8. Pressure probe rake (a) and numbering of pressure probes (b)

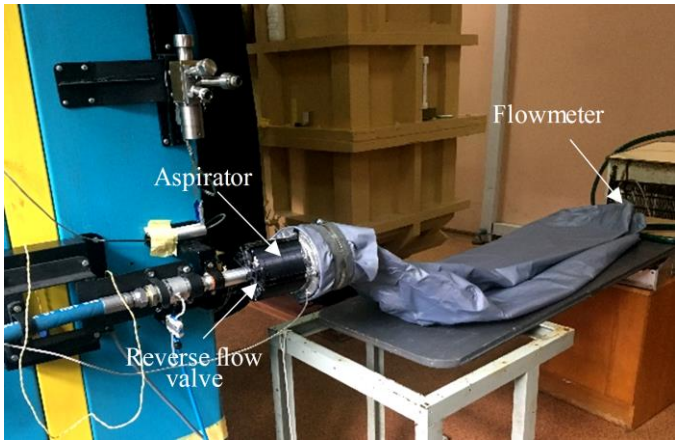

Figure 9. Stand for aspiration ratio measurements

The series of experimental tests is completed with measurements of the aspiration ratio values depending on motive pressure for every tested inflator design. Figure 9 shows the stand for aspiration ratio, A, measurements. It uses a 200 L bag mounted to the inflator outlet and to the flowmeter to measure the air volumes with and without the operating aspirated inflator:

$$A = \frac{V_{bag\ with\ aspiration}}{V_{bag\ without\ aspiration}}$$

Automated remote control of experimental runs and simultaneous data processing is illustrated in Figure 10.

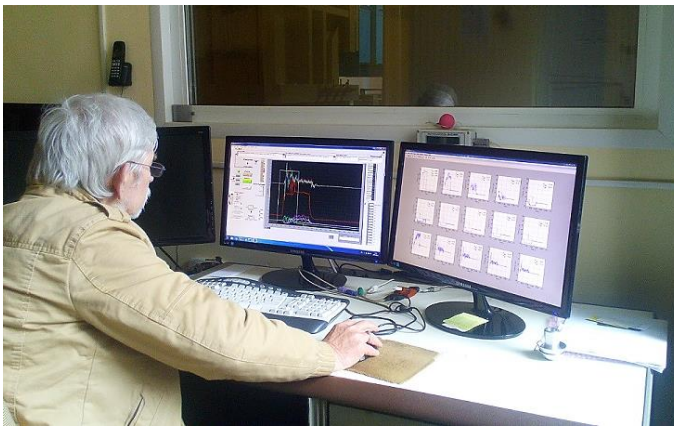

Figure 10. Automated remote experiment control

RESULTS AND DISCUSSION

The key feature of the formulated multivariate problem is a certain compromise between an optimal aspirator geometry with its specified dimensions and optimal parameters of its operation. This compromise is the only solution to satisfy the given engineering requirements. Thus, it is important to determine experimentally the ranges of acceptable operational parameters for an outlined aspirator design such as motive pressure P_m as well as a dominant jet direction and intensity within the aspirator housing (mixing chamber) which would result in the best air entrainment.

Pressure measurements

Pressure fields are measured in a process of air aspiration using 15 pressure probes distributed around the mixing chamber interior and in the inflator nozzle (Figure 8). #1 probe measures pressure in the nozzle, ##2-10 probes register the dynamic pressure at the exit from the mixing chamber, ##11-15probes show the static pressure along the mixing chamber wall. The obtained patterns of the type shown in Figure 11 enable the reconstruction of the jet behavior (intensity, shape and location) to determine its optimal location for best aspiration for a given aspirator model depending on the operational motive pressure P_m. The latter is correlated with a video-recorded airbag inflation process as well as with the measured values of aspiration ratio. For instance, jet instability can result in a significantly decreased entrainment of ambient air despite growing P_m.

The ejecting slit width, d, is a key parameter varied in experiments stepwise as 0.25, 0.35, 0.40, 0.45 mm within a pressure range of P_m=18-60 bar. Sets of measurements are made for P_m growing with a step of P=1-3 bar.

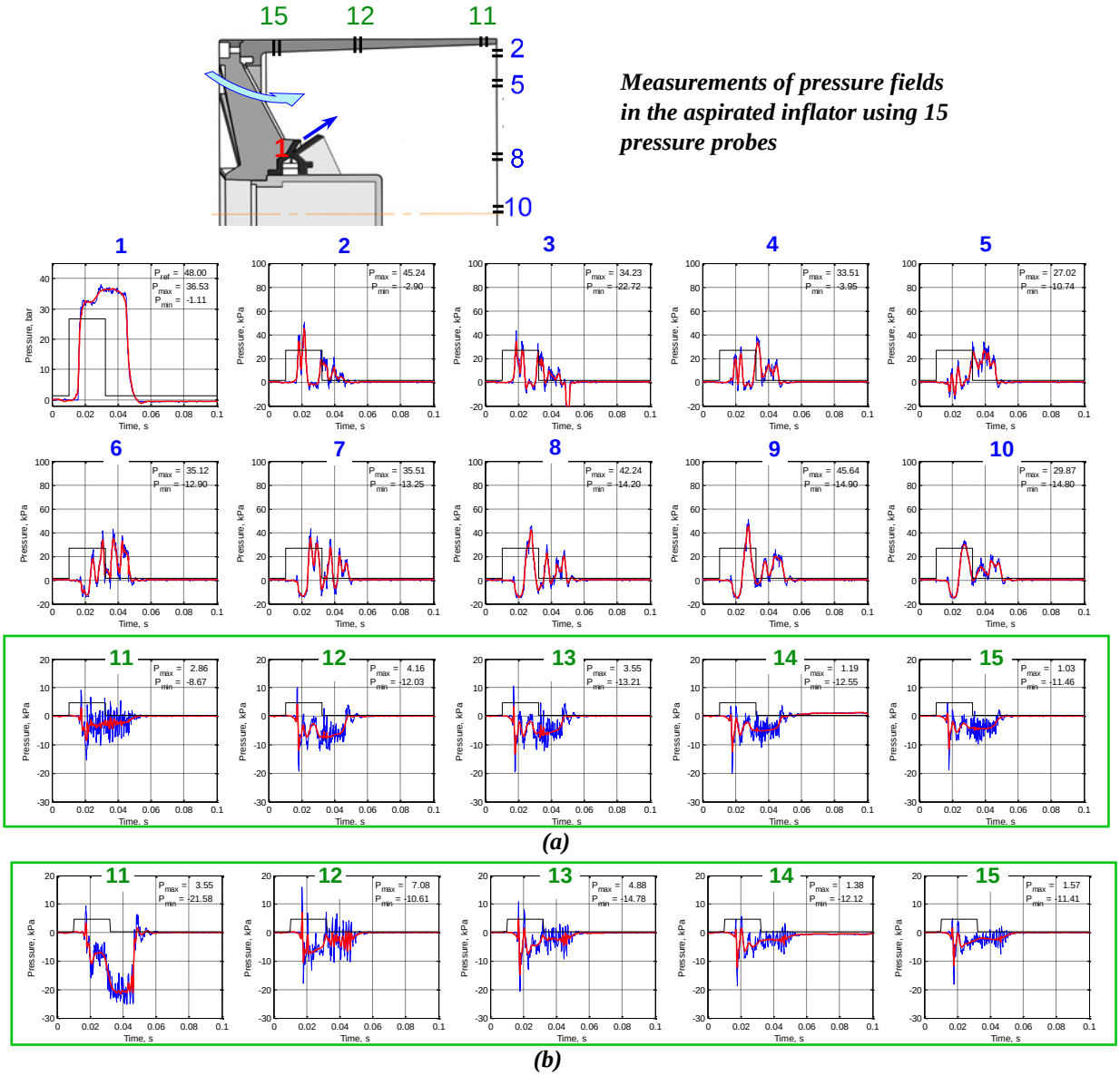

(a)

(b)

Figure 11. Measured dynamic pressure, 1-10, and static pressure, 11-15; d=0.4 mm; P_m = 48 bar (a); measured static pressure, 11-15 probes; d=0.4 mm; P_m = 51 bar (b)

Figure 11 shows a pretty wide jet flow with a moderate intensity distinguished by probes 2-10. Vacuum static pressure provides the air suction from the aspirator inlet with a reverse flow valve. P_m increased from 48 to 51 bar shows an area in the axial part (6-10 probes) with a formed reverse flow though maintained suction along the aspirator wall (Figure 11, b). A possibility to eliminate this flow instability was investigated on the basis of

earlier fundamental flow control studies [7-9]. Here, it was implemented using a modified disk surface shown in Figures 6 and 12. Formed circumferential flow regularity resulted in a much more intense flow in the aspirator mixing chamber especially near its peripheral part registered by ##2-5 probes. Simultaneously, it noticeably reduced the axial reverse flow.

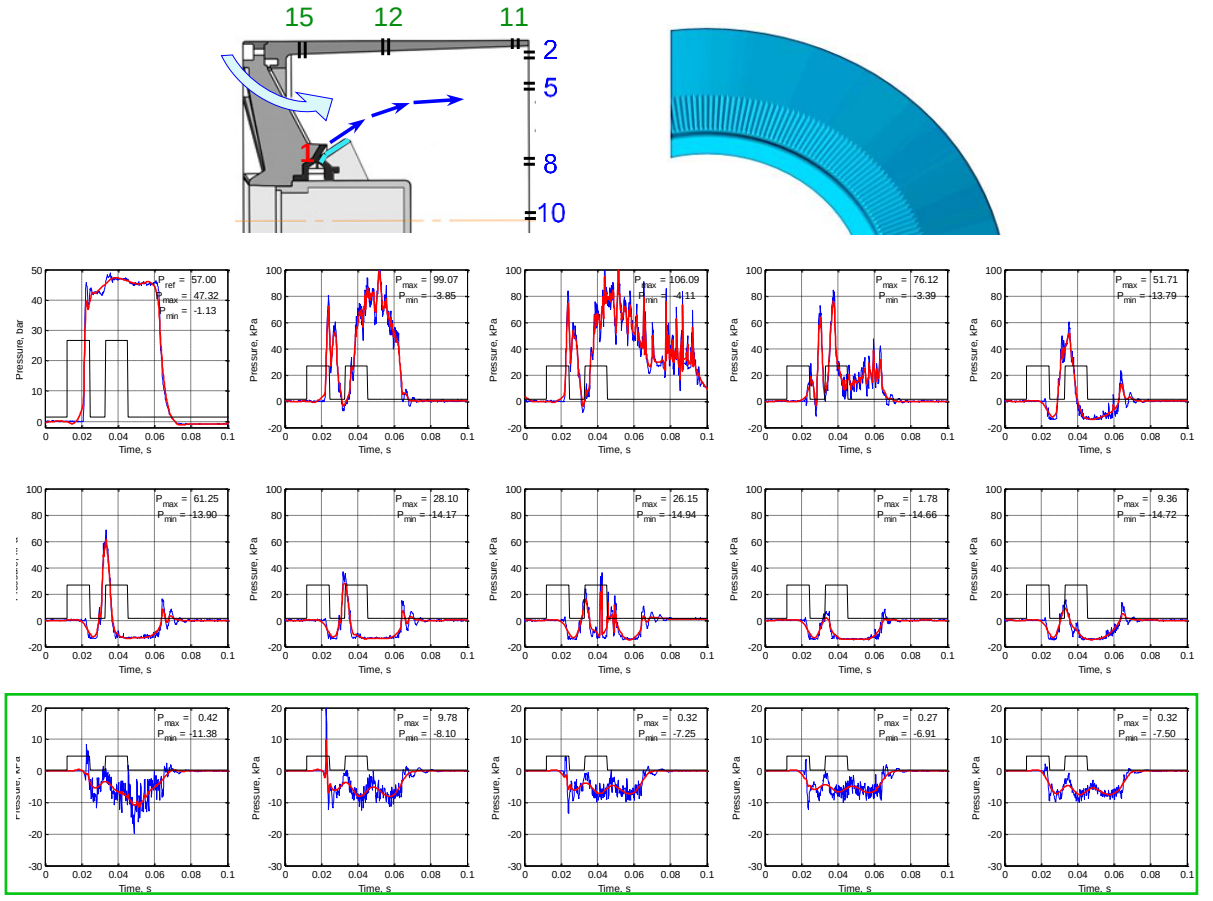

(a)

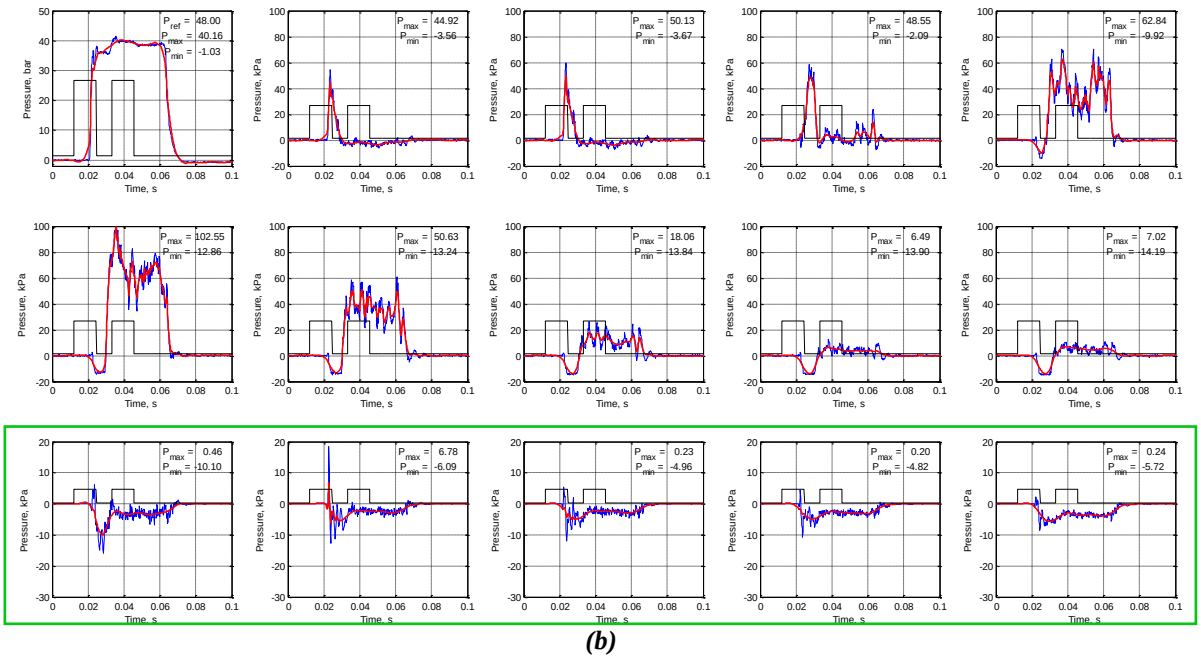

(b)

Figure 12. Measured pressure fields in the aspirated inflator with a grooved surface of #2 disk, filling factor F=53, 3% (see Figure 6, b); d_{eff}=0.4 mm; P_m = 57 bar (a) and P_m = 48 bar (b).

The modified design with F=53.3 % resulted in the slightly enlarged slit width from 0.35 to 0.4 mm and demonstrated its operability in a wider range of motive pressure. Results of Figures 12, a, b obtained for P_m =57 bar and 48 bar as well as for the values beyond this range do not differ as drastically as in the case of a smooth disk surface, while the values of suction pressure are more uniform along the aspirator mixing chamber.

Airbag inflation

A high-speed camera was used for video-recording of the airbag inflation within 30, 35, 40 ms, the inflation time having been regulated by a high-speed valve. Aspirators with a varying slit width were tested in a pressure range of 24-60 bar with a step of 3 bar. Figure 13 shows a sequence of pictures characterizing the airbag process inflation using optimized operation parameters for the aspirator design of Figure 5, a. P_m increased to 50 and 55 bar also showed good airbag inflation.

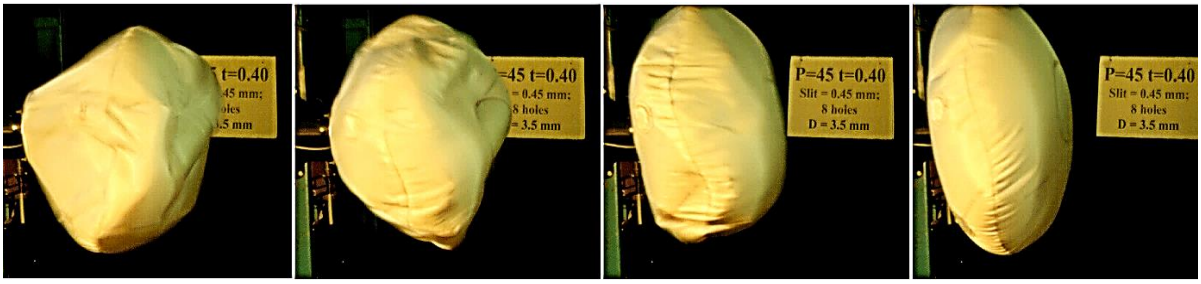

Figure 13. Successive stages of the airbag inflation process: d=0.35 mm; P_m = 45 bar.

Thus, the video-recorded inflation process of an airbag supplemented results of pressure measurements and enabled to recommend optimal sets of parameters for a given inflator design. These recommendations were also confirmed by aspiration ratios measured for various experimental conditions.

Measurements of the aspiration ratio

Values of aspiration ratio were measured both for the smooth model design of Figure 5, a and the grooved disk #2 surface of Figures 6 and 12. A 200-liter bag was connected to the aspirated inflator and to the flowmeter to enable the air easy filling with further volume measurement. Statistically obtained A values for every case of design and flow parameters are shown in Figure 14 where numerically obtained curves are placed for comparison, the red curve having described the "cold-gas case" comparable with experiments.

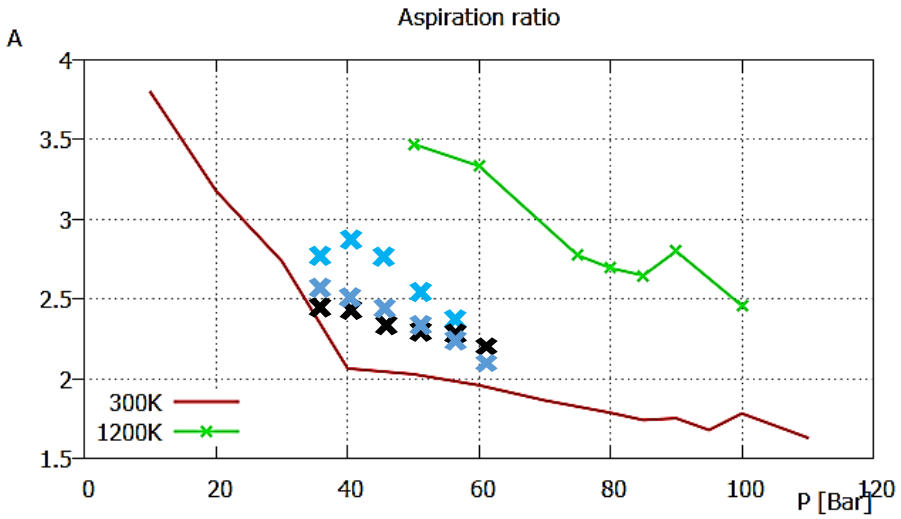

Figure 14. Aspiration ratio for cold (red curve) and hot (green curve) gas found numerically;
- ***- experiment, baseline smooth disk surfaces;***
- ***- experiment, grooved surface, F=6.7%;***
- ***- experiment, grooved surface, F=53.3%***

All of the experimental aspiration ratio values are higher of the numerical values. Therefore, taking into account 1.5-2 times higher hot gas volume aspiration, one can expect to satisfy the engineering requirement of A≥4 in case of the aspirated inflator initiated with a pyrotechnic gas generator. The combination of design and operation parameters play a significant role in the inflator operation which can be optimized using a proper choice of these parameters.

CONCLUSIONS

The aspirated inflation system is developed for a 50 L driver's airbag with an aspiration ratio, $A \geq 4$ which can be applicable for airbags of larger sizes. It provides the air entrainment into an airbag from the car passenger compartment due to the realized Prandtl-Meyer supersonic jet flow over a bent nozzle wall. The jet motivating the air entrainment is generated by a small gas generator; its operation is imitated in experiments by a system of high-pressure tanks controlled by a high-speed valve. One of the features built into the design is the 0.2 bar overpressure in the airbag which discontinues the air entrainment that stops airbag deployment on contact with an occupant and thus eliminates out-of-position occupant injuries.

The experimental investigation of the system operation is a multivariate problem where optimal combinations of design geometry and operation parameters are sought. The built experimental facility, appliances, automated measurement complex, and several manufactured and tested models enabled the validation of the numerical approach and results and to show the potential of the developed aspirated inflator.

Various modifications of the design including the circumferential surface regularity over one ring wall of the nozzle can result in noticeable variation of the motive jet behavior. As such, it can be stabilized providing a wider range of acceptable parameters for optimal inflator operation. In its turn, it can be very important in terms of less severe requirements to flatness of pressure curve produced by a pyrotechnic gas generator and thus to the motive gas generator itself.

REFERENCES

[1] Breed, David S. (2014), "Steering Wheel Mounted Aspirated Airbag System", United States Patent No. US20140361522A1, Pub. date: Dec. 11, 2014.

[2] Kuzmenko, K., Yurchenko, N., Vynogradskyy, P., Paramonov, Y. Optimization of ejector design and operation. EPJ Web of Conferences Volume 114, 2016, 02063-p.1-4

[3] D. Breed, G. Voropaiev, N. Yurchenko, Yu. Paramonov, A. Koshil. Airbag inflators including aspirators, *Internat. Patent Application Number PCT/US2018/013088, Int. Publication # WO 2018/132420 A1, published 19 July 2018.*

[4] David Breed, *Nina F. Yurchenko, Pavlo M.Vynogradskyy, Konstantin Kuzmenko, Yuriy Paramonov, Novel inflation system for airbags, *Proc. AASEM18/Structures18 Symposium Proceedings, Incheon, Korea, 2018, 27-31 Aug*., http://www.i-asem.org/publication_conf/structures18/12.ICAAE18/XH3A.1.AE1761_4762F3.pdf ,.

[5] D. Breed, S. Zhang, N. Yurchenko, G. Voropaiev, Development of an aspirated inflator for preventing out-of-position occupant injuries. *Proc. 14th Int. Symp. on Sophisticated Car Safety Systems, Mannheim, Germany, 2018, Nov. 26-28, 17 pp.*

[6] Kyoung-Su Im, Zeng-Chan Zhang, Grant. O. Cook Jr. Airbag Inflator Models in LS-DYNA. Proc. 14th Int. LS-DYNA Users Conf., June 2016.

[7] Yurchenko, N. A method of active boundary-layer control over bodies of complex geometry, 2009, "*Patent of Ukraine № 45240 (registered in Ukr. Patenting Office 26.10.2009)*

[8] Yurchenko, N.F. Energy-efficient flow control around blunt bodies, *Intl. J. of Advances in Aircraft and Spacecraft Science*, DOI: http://dx.doi.org/10.12989/aas. 2013.1.1.000. *V. 1, No. 1, pp. 15-25.*

[9] N. Yurchenko. Smart flow control based on generated spanwise flow regularity. *Lecture, 4 Dec. **2018**, Dep of Chemical/Applied Sciences, Delft University of Technology, Netherlands*.

[10] Aerodynamic Complex for Interdisciplinary Research with an integrated system for data acquisition and processing. N. Yurchenko, P. Vynogradskyy, Yu. Paramonov, V. Tsymbal, A. Koshil, K. Kuzmenko, R. Pavlovsky, A. Zhdanov, 2012, *Proc. World Congress "Aviation in the XXI-st Century", Kyiv, Ukraine (in Russian).*

DEVELOPMENT AND APPLICATION OF AN EXPERT ASSESSMENT METHOD FOR EVALUATING THE USABILITY OF SAE LEVEL 3 ADS HMIS

Naujoks, Frederik
Hergeth, Sebastian
Keinath, Andreas
BMW Group
Germany

Wiedemann, Katharina
Schömig, Nadja
Wuerzburg Insitute for Traffic Sciences (WIVW)
Germany

Paper Number 19-0026

ABSTRACT

With the Federal Automated Vehicles Policy, the U.S. National Highway Traffic Safety Administration (NHTSA) has provided an outline that can be used to guide the development and validation of Automated Driving Systems (ADS). Acknowledging that the Human-Machine-Interface (HMI) – identified as one of the 12 priority safety design elements in this voluntary guidance – will be crucial for the success of ADSs, we developed a two-step iterative test procedure that serves to evaluate the conformity of SAE level 3 ADS HMIs with the requirements outlined in NHTSA's Auomated Vehicles policy. The aim of this assessment is to evaluate whether minimum HMI requirements are met that facilitate a safe and efficient use of AVs. The present contribution describes the development of an expert-based checklist, how it was compiled from existing literature, how its content and application were refined in simulator and real-word studies, and how it can be employed as a complimentary or stand-alone tool to assess the conformity of SAE Level 3 ADS HMIs with NHTSA's AV policy. It also discusses boundary conditions for the application of the method and the generalization of findings. The described method can be employed in a variety of settings to evaluate SAE Level 3 ADS HMIs, therefore making it a valuable tool for both researchers and practitioners alike.

INTRODUCTION

Conditionally automated driving (SAE L3; [1]) will change how vehicles are used. Depending on the Operational Design Domain (ODD), user of ADS may no longer be required to monitor the driving situation continuously when the system is engaged in automated mode. However, the driver still needs to take back control over the vehicle as soon as a Request to intervene (RtI, also called take-over request) is issued. Therefore, the Human-Machine Interface is of crucial importance to enable a safe and efficient use of the ADS. The ADS has to inform the user through HMI indicators about the current system mode and support the user's awareness about their responsibilities corresponding with the respective mode. Therefore, the NHTSA has proposed that an AV HMI at minimum shall inform the user that the system is (NHTSA, [2]):

(1) Functioning properly
(2) Engaged in automated driving mode
(3) Currently 'unavailable' for use
(4) Experiencing a malfunction and/or
(5) Requesting a control transition from ADS to the operator

A suitable design of mode indicators should effectively support the driver in using an ADS and prevent a false understanding of the current driving mode. This is especially important when considering that a given vehicle may be equipped with different driver assistance systems as well that may be confused with ADSs. As this may produce undesired consequences, there is an urgent need to establish test and evaluation methods that can be applied during product development to ensure that these basic HMI requirements are met.

We developed a heuristic evaluation method that can be used by Human Factor and Usability experts to evaluate and document whether an HMI [3] meets the above-mentioned minimum requirements. In Usability Engineering, such heuristic assessment methods are commonly applied during the product development cycle [4] and can be used as a quick and efficient tool to identify and correct potential usability issues associated with the HMI. The heuristic assessment method consists of a set of AV HMI guidelines together with a checklist that can be used as a systematic HMI inspection and a problem reporting sheet. This paper describes the background and application of the checklist.

METHOD DESCRIPTION

Evaluators

The method should be conducted by a pair of HMI experts. Experts should have received formal training in Human Factors and Usability Engineering and have demonstrable practical experience in HMI assessment and evaluation.

Procedure

The HMI inspection is conducted in an on-road assessment of a production vehicle or a high-fidelity prototype. The aim of the assessment is to evaluate whether a set of pre-defined HMI principles (the "heuristics") are met. Therefore, each of the two evaluators completes a set of fixed use-cases, observes the visual, auditory and haptic HMI output and records potential usability issues arising from non-compliance with the HMI heuristics that have been compiled into a checklist (see [3] for a detailed description of the checklist). The use-case set depends on the specific design of the ADS with respect to the available levels of automation (e.g., whether only manual or conditional automation are available, or if driver assistance is also available within the same vehicle). For an extensive assessment, the use-case set presented in Table 1 should be completed (for a detailed description, see [5]). The aim of the heuristic assessment is twofold:

(1) For the minimum HMI requirements to be fulfilled, each of the use-cases presented in Table 1 should be reflected in a mode indicator or the change of a mode indicator that must be present in the in-vehicle HMI. The mode indicator can be presented visually, auditory and/or tactile.
(2) The design of the respective mode indicator should be in accordance with common HMI standards and best practices that are the basis of the checklist (see Table 2; an extended version of the checklist with corresponding examples and background literature can be found in [3]).

Reporting and documentation

Checklist compliance and identified usability issues should be initially documented independently by each of the raters. Each of the checklist items should be answered using the following rating categories:

- ''*major concerns*": non-compliance with guideline
- ''*minor concerns*": partial fulfillment of guideline, but some aspects of the HMI are non-compliant
- ''*no concerns*": compliance of all HMI aspects with guideline
- ''*measurement necessary*": no definite conclusion can be given on the basis of the checklist and empirical testing is needed; this may be the case when very innovative designs are used that are not covered by current standards and best practices.

Reasons for "major" and "minor" concerns should be documented. A problem reporting sheet can be found in [3]. After the individual assessment, the results should discussed between the evaluators to come to a joint assessment that should also be documented. Figure 1 summarizes the rating procedure.

Table 1: Use-Case set (adapted from Naujoks et al., 2018). Note that some use cases might not be applicable if a vehicle is not equipped with a respective system.

Minimum HMI requirement	Use Case	Description
Functioning properly	L3	Steady driving in L3 mode
Engaged in AD mode	L3 → L2	Driver voluntarily switches from L3 to L2
	L2 → L3	Driver voluntarily switches from L2 to L3
	L2	Steady driving in L2
Currently unavailable for use	$L3_{unavailable}$	Driving outside the system's ODD, L3 is not available; this use case applies to all lower levels of automation (i.e., L0, L1, L2)
Experiencing a malfunction	$L3_{degraded}$	Driving in or outside the ODD, L3 is not available because of a malfunction such as a sensor degradation; this applies to all lower levels of automation (i.e., L0, L1, L2)
Requesting a control transition from ADS to operator	L3 → L2	System initiated transition to L2
	L3 → L1	System initiated transition to L1 (either longitudinal or lateral assistance)
	L3 → L0	System initiated transition to L0

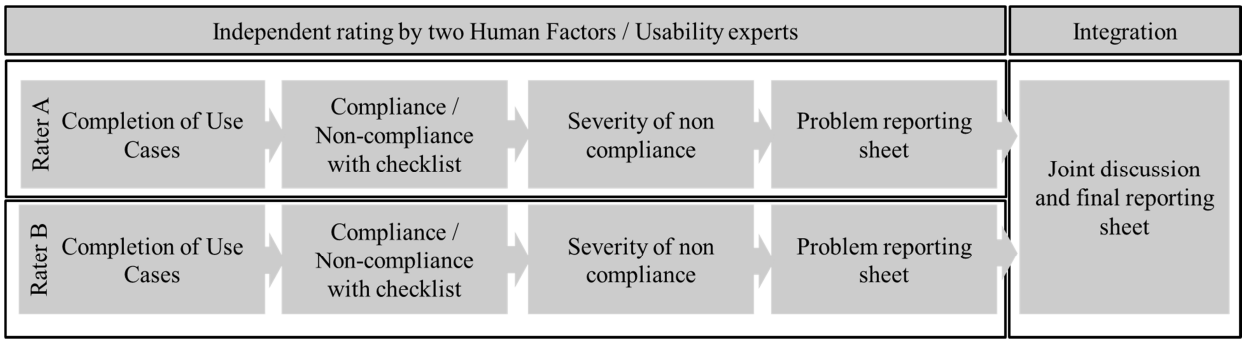

Figure 1: Rating procedure.

Table 2: Checklist items (adapted from [3]).

#	Item
1	Unintentional activation and deactivation should be prevented.
2	The system mode should be displayed continuously.
3	System state changes should be effectively communicated.
4	Visual interfaces used to communicate system states should be mounted to a suitable position and distance. High-priority information should be presented close to the driver's expected line of sight.
5	HMI elements should be grouped together according to their function to support the perception of mode indicators.
6	Time-critical interactions with the system should not afford continuous attention.
7	The visual interface should have a sufficient contrast in luminance and/or colour between foreground and background.
8	Texts (e.g., font types and size of characters) and symbols should be easily readable from the permitted seating position.
9	Commonly accepted or standardized symbols should be used to communicate the automation mode. Use of non-standard symbols should be supplemented by additional text explanations or vocal phrase/s.
10	The semantic of a message should be in accordance with its urgency.
11	Messages should be conveyed using the language of the users (e.g., national language, avoidance of technical language, use of common syntax).
12	Text messages should be as short as possible.
13	Not more than five colours should be consistently used to code system states (excluding white and black).
14	The colours used to communicate system states should be in accordance with common conventions and stereotypes.
15	Design for colour-blindness by redundant coding and avoidance of red/green and blue/yellow combinations.
16	Auditory output should raise the attention of the driver without startling her/him or causing pain.
17	Auditory and vibrotactile output should be adapted to the urgency of the message.
18	High-priority messages should be multimodal.
19	Warning messages should orient the user towards the source of danger.
20	In case of sensor failures, their consequences and required operator steps should be displayed.

METHOD EVALUATION

The method has been evaluated and refined with various approaches. The use of expert assessments may be practical and efficient, but it also comes with limitations. Expert raters might differ in their assessment, resulting in an unreliable outcome of the assessment. Furthermore, the validity of the assessment depends on the capability of the checklist items to predict the usability issues that would arise from non-compliance with them. Therefore, a series of validation experiments were conducted by the authoring team.

Study I: Inter-rater agreement [6]

The aim of the first evaluation study was to assess the *reliability* of the rating outcome in a realistic setting. Demonstrating inter-rater agreement is crucial to the generality of the findings generated from the heuristic assessment, as it is inherently influenced by the raters' subjective experiences and opinions. Therefore, it should be ensured that the ratings were not merely based on idiosyncratic judgements, but that different evaluators

would arrive at similar conclusions when using the method. Three teams of raters (i.e., six individual raters in total) conducted the heuristic assessment in an on-road setting. The employed checklist included two additional items[1]. As L3 systems are not yet available to consumers, a L2 system was used to validate the checklist instead. Each of the evaluators drove a section of a German motorway while switching between different automation levels (A70/A71 Schweinfurt/Bamberg; 2 lane-motorway with mainly unrestricted speed limit, including sections with partially missing lane markings and a tunnel). The heuristic evaluation including the final discussion took about six hours per rater pair. All evaluators were employees of the Wuerzburg Institute for Traffic Sciences (WIVW GmbH). They hold a university degree in Psychology or Computer Science and had several years of experience in Human Factors and Usability research.

Table 3: Use cases driven in the on-road evaluation study. $L1_{Long}$ = ACC, $L1_{Lat}$ = Steering Assistance. The use-cases were adapted to the available automation levels in the test vehicle.

Category	Use Case
Activation (driver initiated)	L0 → $L1_{long}$ → L2 L0 → $L1_{Lat}$ → L2 L0 → L2
Deactivation/ transition to lower level (driver- or system initiated)	L2 → $L1_{Long}$ → L0 L2 → $L1_{Lat}$ → L0 L2 → L0
Driving steady in a system state	L0, $L1_{long}$, $L1_{Lat}$, L2
Higher level not available (e.g., sensor failure)	L0 , $L1_{long}$, $L1_{Lat}$
Re-activation of passive system state (system-initiated)	L0 → $L1_{Lat}$ $L1_{long}$ → L2

During and after the test drives, the evaluators recorded their individual assessment before discussing with the other rater. After the team discussion, a final rating was given by every rating team. The main interest of the study was to assess the inter-rater agreement between the individual raters and rater pairs before and after the joint discussion of the rating outcome. Brennan & Prediger`s Kappa κ was used to evaluate the reliability of the ratings ([7]; for more details on differences to Cohen's Kappa κ, see [8]).

Table 4: Inter-rater agreement with an evaluation of the quality of the rating according to [9]. Rater pairs were Rater 1/2,Rater 3/4 and Rater 5/6.

	Brennan's κ	R1	R2	R3	R4	R5	R6
Pre	R1	-	0.29	0.36	0.08	0.14	0.13
	R2		-	0.55	0.37	0.48	0.42
	R3	"fair"* = κ > 0.21		-	0.21	0.37	0.48
	R4	"moderate" = κ > 0.41			-	0.45	0.12
	R5	"good" = κ > 0.61				-	0.48
	R6	"very good" = κ > 0.81					-
		R1	R2	R3	R4	R5	R6
Post	R1	-	0.79	0.48	0.48	0.40	0.40
	R2		-	0.40	0.40	0.48	0.48
	R3	"fair"		-	0.86	0.38	0.50
	R4	"moderate"			-	0.36	0.36
	R5	"good"				-	1
	R6	"very good"					-

As can be seen in Table 4, the inter-rater agreement was not sufficiently high on an individual level before the joint discussion. However, after the discussion among the rater pairs, agreement levels within each rater pair and between different rater pairs increased. This finding demonstrates that different rater pairs come to comparable

[1] The checklist used included two more items in addition to the initial item-set: "Instructions and information of the user manual facilitate the interaction with the HMI" (item #21) and "Interaction with the system is easy" (item#22). Note that these items do not directly pertain to the minimum HMI requirements as proposed by NHTSA.

conclusions using the heuristic evaluation approach, showing that it is a reliable tool to assess the HMI of AVs. However, the findings also highlight that the heuristic evaluation should always adhere to a four-eyes principle to ensure the quality of its outcome.

Study II: Predictive validity [10]

The usefulness of the heuristic HMI assessment not only depends on the reliability of the method, but also on its ability to *predict* usability problems that arise when the heuristics are violated. To test the predictive validity of the heuristics, we constructed two HMIs that are either compliant or non-compliant ("high-compliance" and "low-compliance" HMI) with several checklist items and ran a simulator study with N = 57 participants in the BMW Group's simulator facilities. A fixed-based driving simulator was used. A detailed description of the study is provided in [10].

The simulated ADS had four modes: (1) manual driving, L3 unavailable for use, (2) manual driving, L3 available for use, (3) L3 engaged, (4) system-initiated take-over request in L3 mode due to system limits. The mode indicators were presented in the instrument cluster. The high compliance HMI (see Figure 2, left) communicated information redundantly by means of pictograms and a textbox. Textual information was displayed in German language. During the approach of the system limits, the HMI announced system limitations through a take-over cascade in form of an announcement, a cautionary take-over request (*"cautionary TOR"*) and an imminent take-over request ("*imminent TOR*"). The request to intervene was shown by animated hands grasping a steering wheel in both HMI variants.

The low-compliance HMI differed from the high-compliance HMI in various aspects (see Figure 2 and Table 5) of non-compliant colour coding, symbol size and labelling. Use-cases included driver initiated activations and deactivations of L3 mode, steady driving in L3 mode and two take-over requests resulting in a transition from L3 to manual driving. The ADS under investigation did not contain L2 or L1 driving assistance. One drive lasted approximately 15 minutes. The study results support the predictive validity of the heuristics in several ways:

- *Perceived usability*: Participants rated the usability of the low-compliance HMI to be statistically significantly lower than the high compliance HMI on the System Usability Scale (SUS, [11]).
- *Observer usability ratings*: Trained observers rated the frequency and severity of usability problems during interactions with the ADS from video footage on a five-point scale ranging from "no problems" to "help from experimenter needed". Observed usability problems were significantly higher with the low compliance HMI.
- *Take-over time*: Participants reacted significantly slower to RtIs in the low compliance condition compared with the high compliance condition.

Study III: Predictive validity [12]

The predictive validity of the heuristics was further tested in another simulator study at the facilities of the WIVW GmbH. Again, two HMIs were designed that were either compliant or non-compliant with some of the checklist items (e.g., with regard to prominence of task responsibility in L2 assisted driving mode (item #2), color contrast coding (item #7 and item #14), readability of icons and text (item #8), additional explaining text (item #9), usage of understandable language (item #11), multimodality of urgent warnings/take-over requests (item #18) and button labeling consistent to functionality ("additional" item #22)). The HMI variant was varied as a between-subject factor. Twelve drivers completed a simulator drive either with the low- or high-compliant HMI. The participants experienced the HMI in a 30-minutes-driving course containing several use-cases, including driving in each available automation mode (L0 vs. L2 vs. L3), driver initiated-upwards and system-initiated downwards transitions between these levels. The results revealed that the classification of the HMI variants as low vs. highly compliant based on the heuristic evaluation was also reflected in participants' behavior and subjective ratings of the system and the HMI. The results further support the predictive validity of the heuristics. Differences between the two HMI variants were observed in the following measures:

- *Take-over reaction times*: Participants of the low compliance condition reacted significantly slower to a RtI (hands-on times and take-over times)
- *Usability problems in activating either L2 or L3 system*: participants in the low-compliance condition required more frequent support by the experimenter to successfully activate/reactivate the L3 system
- *Number of handsoff-warnings*: the number of participants experiencing at least one hands-off warning during L2 driving was higher in the low compliance condition
- *Perceived understandability and difficulty in system usage*: Participants in the low-compliance condition reported worse system understanding and perceived it as more difficult to activate the L3 system, to react to a take-over requests in L3 and to react to a system-initiated transition from L3 to L2

- *Global evaluation of the HMI*: Global ratings of the acceptability of the HMI by participants into three categories (very good, acceptable or not acceptable) showed a higher percentage of non-acceptable ratings for the low compliant condition after experiencing the HMI in the driving scenarios.

Mode	High-compliance HMI	Low-compliance HMI
L3 ADS active		
Cautionary TOR		
Imminent TOR		
L3 ADS not available for use		

Figure 2: HMI for high-compliance (left) and low-compliance (right) during normal functioning (top) cautionary TOR (2nd row), imminent TOR (3rd row) and L3 ADS not available (bottom). Figure adapted from [10].

Table 5: Variations for low compliance HMI for the two components with respective criterion and reference to heuristics; adapted from [10].

Variation of low-compliance HMI	**Guideline violation**
Activation and deactivation through long-press (i.e., 0.8 seconds)	System state changes should be effectively communicated.
Pictograms are 60% of the original size	Texts (e.g., font types and size of characters) and symbols should be easily readable from the permitted seating position.
No text information except for L3 ADS availability	The system mode should be displayed continuously System state changes should be effectively communicated. Commonly accepted or standardized symbols should be used to communicate the automation mode. Use of non-standard symbols should be supplemented by additional text explanations or vocal phrase/s.
No color coding for cautionary and imminent TOR	System state changes should be effectively communicated. The visual interface should have a sufficient contrast in luminance and/or colour between foreground and background. The colours used to communicate system states should be in accordance with common conventions and stereotypes.
No blue color coding for active L3 ADS	System state changes should be effectively communicated. The visual interface should have a sufficient contrast in luminance and/or colour between foreground and background. The colours used to communicate system states should be in accordance with common conventions and stereotypes.

Mode	High-compliance HMI	Low-compliance HMI
L3, ADS active	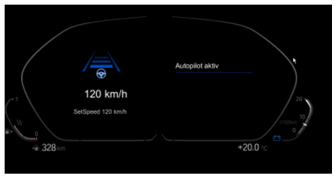	
L2 assisted driving active		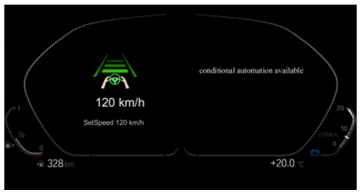
L2 Handsoff-warning	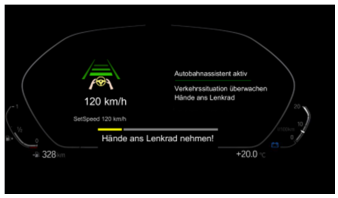	
Take-over request in L3	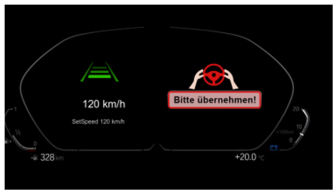	

Figure 3: HMI for high compliance (left) and low compliance (right) in selected system modes. Figure adapted from [12].

SUMMARY

This paper presented a heuristic method for the assessment of in-vehicle HMIs for automated vehicles. The aim of the heuristic assessment is to provide a quick but reliable and valid tool that can be used during the product development cycle. It was developed to include common standards and practices and apply them to the in-vehicle interface of AVs [3]. In a series of studies, the reliability and predictive validity of the heuristic assessment was investigated and demonstrated. In view of the minimum HMI requirements proposed in NHTSA's automated vehicle's policy, the method can be used to verify compliance on an analytical level.

It should be noted, however that the method should be applied with care and thought. A thorough application of the method requires (1) the selection and adequate training of HMI evaluators and (2) quality control by periodically checking the agreement between rater pairs as demonstrated in this paper. Otherwise, the outcome of the heuristic assessment might suffer from subjectivity of evaluations and resulting low reliability. It must also be emphasized that the heuristic assessment should be combined with empirical test methods such as simulator or test track studies involving potential users of AVs. The combination of expert evaluations and empirical user tests has a long and successful history in the general Human Factors and Usability context, but has not seen wide-spread application to the domain of AV HMIs in the scientific and technical literature so far.

REFERENCES

[1] Society of Automotive Engineers International J3016 (2018). Taxonomy and definitions for terms related to on-road motor vehicle automated driving systems. Warrendale, PA: SAE International.

[2] National Highway Traffic Safety Administration (2016). Automated Driving Systems 2.0: A Vision for Safety. Washigton, DC: NHTSA.

[3] Naujoks, F., Wiedemann, K., Schömig, N., Hergeth, S., & Keinath, A. (2019). Towards guidelines and verification methods for automated vehicle HMIs. Transportation research part F: traffic psychology and behaviour, 60, 121-136.

[4] Nielsen, J. (1994). Usability inspection methods. In Conference companion on Human factors in computing systems (pp. 413–414). ACM.

[5] Naujoks, F., Hergeth, S., Wiedemann, K., Schömig, N., & Keinath, A. (2018, September). Use Cases for Assessing, Testing, and Validating the Human Machine Interface of Automated Driving Systems. In Proceedings of the Human Factors and Ergonomics Society Annual Meeting (Vol. 62, No. 1, pp. 1873-1877). Sage CA: Los Angeles, CA: SAGE Publications.

[6] Wiedemann K., Schömig N., Naujoks F., Hergeth S., Neukum A. & Keinath, A (2018). Expert evaluation of automated driving HMI – does a checklist-based method work? Paper presented at: HFES Europe Chapter Annual Meeting. Berlin, Germany.

[7] Brennan, R. L. & Prediger, D. J. (1981). Coefficient λ: Some Uses, Misuses, and Alternatives. Educational and Psychological Measurement, 41, pp. 687-699.

[8] Umesh, U. N., Peterson, R.A., & Sauber M. H. (1989). Interjudge agreement and the maximum value of kappa. Educational and Psychological Measurement, 49, pp. 835-850.

[9] Landis, J.R. & Koch, G.G. (1977). The measurement of observer agreement for categorical data. Biometrics, 33 (1), pp. 159-174.

[10] Forster Y., Hergeth S., Naujoks F., Krems J.F. & Keinath A. (2019). Empirical Validation of a Checklist for Heuristic Evaluation of Automated Vehicle HMIs. In: International Conference on Applied Human Factors and Ergonomics. Cham: Springer.

[11] Brooke, J. (1996). SUS-A quick and dirty usability scale. Usability evaluation in industry, 189(194), 4-7.

[12] Schömig N., Wiedemann, K., Naujoks, F., Hergeth, S. & Keinath, A. (in preparation). The heuristic evaluation of HMI requirements for Automated Driving Systems – a validation study.

HEARING LOSS ANALYSIS IN FULL SCALE ACCIDENT RECONSTRUCTION

Johannes Holtz, Technische Universität Berlin, johannes.holtz@tu-berlin.de, Chair of Naturalistic Driving Observation for Energetic Optimisation and Accident Avoidance, Gustav-Meyer-Allee 25, 13355 Berlin

Gerd Müller, Technische Universität Berlin, gerd.mueller@tu-berlin.de, Chair of Automotive Engineering, Gustav-Meyer-Allee 25, 13355 Berlin

Heiko Johannsen, Johannsen.Heiko@mh-hannover.de, Medizinische Hochschule Hannover, Accident Research Unit, Carl-Neuberg-Str. 1, 30625 Hannover

Andreas Büchner, Buechner.Andreas@mh-hannover.de, Medizinische Hochschule Hannover, German Hearing Centre Hanover, Karl-Wiechert-Allee 3, 30625 Hannover

Marcus Wisch, wisch@bast.de, Federal Highway Research Institute (BASt), Referat F2, Brüderstraße 53, 51427 Bergisch Gladbach

Daniel Huster, huster@bast.de, Federal Highway Research Institute (BASt), Referat F2, Brüderstraße 53, 51427 Bergisch Gladbach

Paper Number 19-0028

ABSTRACT

Airbags are, together with the three-point belt, the most effective passive safety equipment of vehicles. However, literature shows that sound pressure levels of up to 170 dB can occur during airbag deployment. A literature review revealed no systematic experimental data on possible hearing loss by airbag deployment, that also takes any other crash accompanied noise into account, such as deformation and impact noise. Also the rising number of airbags per vehicle resulting in a higher number of deployed airbags in an accident was not addressed with respect to hearing loss. Thus, an extensive test matrix of noise measurements during airbag deployments was conducted including onboard measuring during crashes and static measurements. Dynamic and static experiments with single and multiple airbag deployments were conducted. The results of this study show, that in the analyzed crash constellations the acoustic emission of the collision as well as the car deformation can trigger the stapedius reflex before the airbag deployment. The stapedius reflex protects the inner ear at least partially in case of dangerous sound levels. However, it seems that multiple airbag deployments in a short sequence pose a considerable risk for hearing impairments despite the fully contracted stapedius muscle. Further and in line with Price et al. (2013) it was found that the risk of hearing loss is lower with closed windows. The analysis of patient and accident data showed no link between airbag deployment and hearing loss. This might be caused by low case numbers of reported hearing loss problems up to now.

In conclusion the results show that a singular analysis of the sound pressure of airbag deployments without crash accompanied noises is not sufficient as the protective effect of the stapedius reflex is neglected. Still, successive airbag deployments in a short timeframe raise the risk of hearing loss. Further investigation on hearing impairment due to airbag deployment and triggering of the stapedius reflex is needed and the data acquisition of accidents and patients should consider hearing loss aspects.

KEY WORDS

Airbag, hearing loss, accident reconstruction, stapedius reflex

INTRODUCTION

Casuistics show that hearing loss due to airbag deployment in passenger vehicles can be found in medical records of patients (Saunders et al., 1998). Allen et al. (1971) reported sound pressure levels of airbags of up to 170 dB, which is comparable to a gunshot, these sound pressure levels were verified for example by Price et al (1996) for further airbag generations. An exposure to such high sound pressure levels can induce steady hearing loss, which can lead to social isolation. Yaremchuk et al. (2001) analysed 71 patients with otologic symptoms after airbag deployment and showed that the hearing loss that occurred may have affected one or more frequencies. Based on the pure sound pressure level of airbag deployments, Saunders et al. (1998) estimated a 7000 to 28 000 hearing loss injuries due to airbag deployment between 1988 and 1998, but these number of cases were not reflected in clinical data bases or literature (Saunders et al., 1998).

Therefore, we screened accident and patient data to analyze how many cases can be identified based on actual data acquisition and to see if the problem of linking hearing loss statistically to airbag deployment in accidents can be addressed. Despite the low number of hearing loss due to airbag deployment reported by literature, experiments were conducted to address the high sound pressure levels reported in the literature. Previous studies have often neglected the link between the measured sound pressure levels caused by the airbag and noises accompanying a crash such as structural vehicle deformation and impact noises. For example in Rouhana et al. (1994), Price et al. (1996), Rouhana et al. (1998) and Banglmaier et al. (2003) experiments with deploying airbags were conducted with standing vehicle. Therefore, this study aimed to calculate the risk of hearing loss due to airbag deployment in combination with crash accompanied noise. Several aspects were addressed in these experiments. The influence of single or multiple airbag deployments concerning hearing loss was analyzed to address the increasing number of airbags per vehicle resulting in a higher number of airbag deployments in accidents. A comparison between risk of hearing loss caused by airbag deployment in vehicles with opened and closed windows was conducted, because it is not proven yet if a closed compartment lower the load on the inner ear.

METHODS

Patient and accident data

Within this study in-depth accident data from the German In-Depth Accident Study (GIDAS) (Johannsen et al., 2017) were analyzed using accident data with passenger vehicles with production start in 2001 or later. 2 053 driver and 533 passengers were considered for frontal collisions with another passenger vehicle, heavy goods vehicle or an object. 1 454 near-side occupants and 1 392 far-side occupants were considered for side collisions. These cases were analyzed with respect to hearing related injuries based on the Abbreviated Injury Scale (AIS 2005 Update 2008) wherein a tinnitus is the only codable hearing injury in GIDAS. Patient data was analysed based on expert reports of the German Hearing Centre Hanover that address hearing loss linked to accidents with airbag deployment. Another approach to gain patient data was a direct query of all patients of the German Hearing Centre Hanover between May 2016 and April 2017, if their hearing problem is linked to an airbag deployment.

Accident reconstructions and static airbag deployment experiments

In this study several experiments were conducted to address sound pressure emission of airbags. Two experimental accident reconstructions were conducted twice with different airbag triggering strategies. The first case was a frontal pole impact of a 2008 Seat Leon with 50 km/h colliding speed against a tree with 400 mm diameter and with 95 mm offset. Only the driver airbag was triggered in the experiment by the control unit of the vehicle at 43 ms (the passenger airbag was disconnected). In a variant of this accident reconstruction, the trigger time was set to 20 ms to address the poor chest deflection, all other parameters were set stable. Sound pressure was recorded with two different devices. The NTI Audio Analyzer XL2 with the microphone M4216 was used as an onboard device. This microphone was aligned to the steering wheel centre and attached to the camera stand replacing the passenger seat. The distance between steering wheel centre and microphone was 600 mm. The second sound pressure recorder was a Brüel & Kjaer 2250 with microphone 4189. This external recorder was aligned rectangular to the t_0-position of the steering wheel centre at the left side of the vehicle with distance 3 500 mm and height of 1 130 mm, serving as a backup device and for verification purposes. The SAE J247 was not used, because this standard includes only static measurement of acoustic impulses and no acoustical measurements during crash tests.

The second accident reconstruction was a full width rear end collision without offset, where a Fiat 500 (2008) collided with 35 km/h with a standing (hand brake activated) Skoda Fabia (2009) in an under ride situation. The under ride situation was addressed by suspension manipulation so that the lower side of the rear end crossbeam of the Skoda had a ground clearance of 525 mm. The suspension of the Fiat was not manipulated due to minimal ground clearance required by the crash facility of the Technical University of Berlin. The impact speed of 35 km/h was overestimated to ensure an airbag deployment triggered by the control unit of the vehicle. The impact speed of the accident was calculated between 15 and 30 km/h. In a variant of this accident reconstruction the airbag deployment was suppressed, because only marginal airbag interaction was seen for the driver and no airbag interaction was seen for the passenger. The same sound pressure recorders were used similar to the first accident reconstruction. The NTI Audio Analyzer XL2 with microphone M4216 was used as an onboard device. Due to the presence of two dummies in the vehicle the audio analyzer was attached to a mount, that was welded to the outer side of the driver door. The microphone was aligned to the steering wheel centre with a distance of 440 mm. The second sound pressure recorder was a Brüel & Kjaer 2250 with microphone 4189 and positioned similar to the previous accident reconstruction. The two accident cases were chosen based on an analysis of dummy readings addressing suboptimal trigger time in cases with poor structural interaction and unnecessary airbag deployment in accidents with low accident severity to address other work packages of the underlying project. The additional sound pressure measurements were performed parallel.

In order to validate the sound pressure recordings of the accident reconstructions, static analyses of airbag deployments were performed using the same vehicles with the same sound pressure recordings. Additionally, another Brüel & Kjaer sound pressure recorder with five high pressure microphones was used to double the previous microphone positions as a reference and to add other interesting positions inside the vehicle such as headrest of the driver and rear centre seat with direct view to the driver airbag. All microphone positions are shown in Figure 1. The test matrix of the static sound pressure analysis of deploying airbags included experiments to compare the static experiments with the measurements from the accident reconstructions (Seat Leon: driver airbag, Fiat 500: driver airbag, passenger airbag and driver's knee airbag) in order to assess the

influence of the crash accompanied noises such as deformation and impact noises. The driver, passenger, side and curtain airbag of the Seat Leon and the side and curtain airbag of the Fiat 500 were additionally analyzed to address their sound pressure separately and to investigate, if the risk of a hearing impairment is higher for a vehicle with closed or open windows.

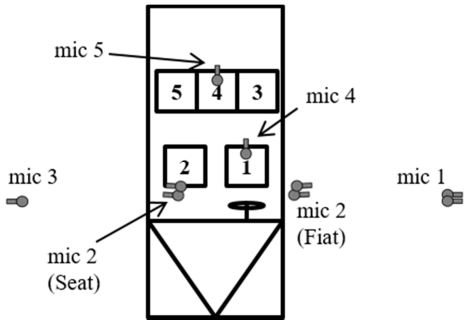

Figure 1: Microphone positions for all experiments, doubled microphones only used for the accident reconstructions

The recorded data were analyzed using the Auditory Hazard Assessment Algorithm for Humans (AHAAH) model that indicates the risk of a Compound Threshold Shift (CTS). A CTS is a reduction in hearing sensitivity due to the combined influence of temporary threshold shift (TTS) and permanent threshold shift (PTS). While a temporary shift recovers over time, the PTS remains as a chronic hearing loss. The AHAAH model was developed in the 80s by Price et al. (1986) and the recordings were analyzed using the version 2.1 from 2013 (Price et al., 2013). The model calculates the risk of a CTS due to blast events such as gunshots or airbag deployments. The AHAAH algorithm models the propagation of sound and blast waves in a free field situation and the transmission in the middle and inner ear. The high nonlinear behavior of the middle ear at high sound pressure levels is implemented in the model. In the analysis of sound pressure levels above 130 dB this nonlinear behavior needs to be considered to avoid overestimation (Price et al., 2013). The AHAAH model also includes the frequency dependent behavior of the 23 segments of the basilar membrane resulting in a calculated segmental deflection of the basilar membrane named Auditory Risk Unit (ARU). A higher deflection leads to a higher risk of damaging the basilar membrane. Experiments with cats, chinchillas and data from voluntary test persons from the 60s and 70s showed a correlation of 0.94 between the CTS and the ARU value following the empiric equation 1 (Price et al., 2013).

$$CTS = 26.6 * \ln(ARU) - 140.1 \quad \text{(Eq. 1)}$$

Price et al. (1986) determined a threshold value of 25 dB CTS measured directly after the blast event to expect PTS in humans. This careful assumption corresponds to clinical observations, but due to lack of sufficient data and highly individual behavior the relationship between CTS and PTS could not yet be statistically captured. For example, Liberman et al. (1982) showed in animal studies that a CTS of up to a maximum of 40 dB can fully recover in selected cases, demonstrating the absolute upper limit for a full recovery of hearing thresholds. Regarding the 25 dB CTS by Price et al. (1986) an ARU value of 500 and for the 40 dB CTS by Liberman et al. (1982), an ARU value of 868 is calculated as a limit for obtaining a PTS. In essence, it can be assumed that an ARU value higher than 500 indicates a possible PTS and an ARU value of 868 indicates a definite occurrence of a PTS. A complete risk curve for PTS in dependency of CTS would be highly desirable, but due to the lack of sufficient data and highly individual behavior this is not possible at the current stage. For the analysis of potential hearing loss in our experiments, we will use an ARU value of 500 as the threshold.

The AHAAH model considers two conditions of a test person: warned and unwarned ear condition. Price et al. (2013) elaborated that the risk of hearing loss due to a blast might be affected by the awareness of this upcoming blast event. This effect can be caused by the conditional triggering of the stapedius reflex. While the triggering of the stapedius reflex at sound pressure levels of 90 dB (pure tones) and 80 dB (broadband noise) is non-controversial, the conditional triggering of the stapedius reflex has not yet been proven conclusively. Nevertheless, both conditions are provided by the AHAAH model and will be both applied on our recorded data.

RESULTS

Patient and accident data

The analysis of GIDAS showed that in eight cases with frontal impact and in seven cases with side impact a tinnitus was coded. In a database query on all patients of the German Hearing Centre Hanover between May 2016 and April 2017, two patients linked their hearing problem to an airbag deployment. The analysis of 103 medical reports of the German Hearing Centre at MHH that investigated a potential causality between a hearing loss and an accident with airbag deployment did only reveal a single case where a link between airbag deployment and hearing loss could be demonstrated. These low occurrences correspond to other studies that also found a low number of clinical cases with airbag indicated hearing loss, e.g. Saunders et al. (1998), Traynor (2012) and McFeely et al. (1999).

Accident reconstructions and static airbag deployment experiments

In the first accident reconstruction sound pressure levels up to 134 dB of deformation noise at 18 ms after t_0 were measured which made triggering of the stapedius reflex possible. At 43 ms the airbag deployed and the sound pressure level reaches 160 dB, this maximum value happens in the rising phase of the stapedius muscle, which needs approximately 35 ms to take effect. Nevertheless an ARU value of 276.0 was calculated with the AHAAH in the unwarned condition. In warned condition an ARU value of 256.9 was calculated. In the same accident reconstruction with earlier airbag trigger time (20 ms) an ARU value in the unwarned condition of 452.6 and in the warned condition of 364.0 were calculated. Based on this recording the crash accompanied noises before the airbag deployment were eliminated in the sound file to address a trigger time of 3 ms of the airbag. An ARU value of 615.0 was calculated for this manipulated recording. This shows that the earlier the airbag deploys in the rising phase of the stapedius reflex the higher is the calculated ARU value. As the ARU values with crash accompanied noises were below 500 and therefore of low risk for PTS, the isolated airbag deployment noise indicates a possibility of a PTS. In the second accident reconstruction three airbags deployed: Driver, passenger and driver's knee airbag. The deformation noises lead to sound pressure levels up to 134 dB at 12 ms after t_0 so that the stapedius reflex could be triggered. The first airbag deploys at 67 ms, so that the stapedius reflex is fully developed, however in both conditions an ARU value of 714.4 were calculated for this accident reconstruction. For comparable results the passenger and knee airbag were removed from the audio file and an ARU value of 366.1 was calculated. This shows that the short sequence of airbag deployments (three airbags within 10 ms) can cause a PTS despite the triggered stapedius reflex. In the variant of this accident reconstruction without any airbag deployments an ARU value of 5.3 was calculated, so that the risk of a PTS is very low. With the results of this accident reconstruction with the Fiat, a telephone interview with the driver of the accident vehicle was conducted. The driver confirmed that a tinnitus occurred for one month after the accident, but the tinnitus was not reported to GIDAS and therefore not coded in the GIDAS data. An ear screening to proof if a PTS occurred

was not performed, but it could be assumed that a C5-dip appeared, which does not affect the subjective hearing of the patient, but speeds up presbycusia.

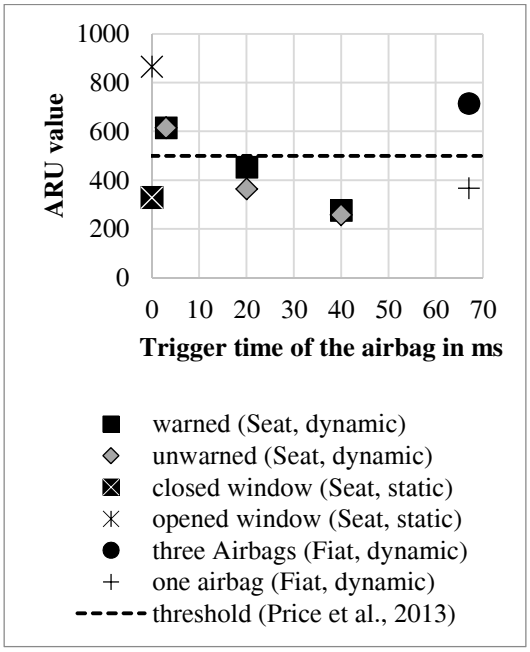

Figure 2: ARU values of the analyzed accident reconstructions (dynamic) and static experiments (airbag deployment in standing vehicle) with respect to the recommended threshold by Price et al. (2013) of 500 ARU

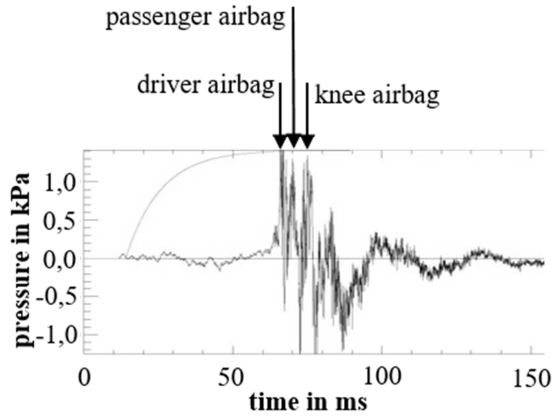

Figure 3: sound pressure graph for the accident reconstruction with Fiat 500, the three airbag deployment events are highlighted resulting in an ARU value of 714.4

The results of the static experiments are based on the recordings of the NTI XL2. The other recordings confirmed the measurements relative to the driver's ear. For example for the deployment of the driver airbag of the Seat Leon a sound pressure of 160 dB was calculated for the driver's ear based on the NTI XL2. The microphone 5 (Figure 1) measured 148 dB in a distance of 1 660 mm, so that both values can be calculated into each other with a failure of 0.36 dB based on the distance law, which describes a drop of 6 dB of sound pressure level per doubling distance. These measurements show that the use of the distance law inside the vehicle is applicable, but direct view between sender and receiver is required. For the driver airbag of the Seat Leon an ARU value of 865.2 was calculated showing a high risk of a PTS, while in the corresponding accident reconstruction an ARU value of 452.6 was calculated in the worst case with a low risk of a PTS. This shows that the stapedius reflex with its protective effect to prevent hearing loss can be triggered by crash accompanied

noises such as deformation noises. A singular analysis of the sound pressure of an airbag addressing the risk of a PTS is not recommended and the crash accompanied noises should be considered.
Comparing the sound pressure from the driver airbag of the Seat Leon with open and closed window, the ARU values for the opened window of 865.2 and 328.8 for the closed window were calculated. The lower value for the closed window is probably based on the static air pressure increase in the vehicle compartment. This forced the eardrum in a position of strong tension and the sound transmission to the inner ear is restricted, comparable to the function of the stapedius reflex.

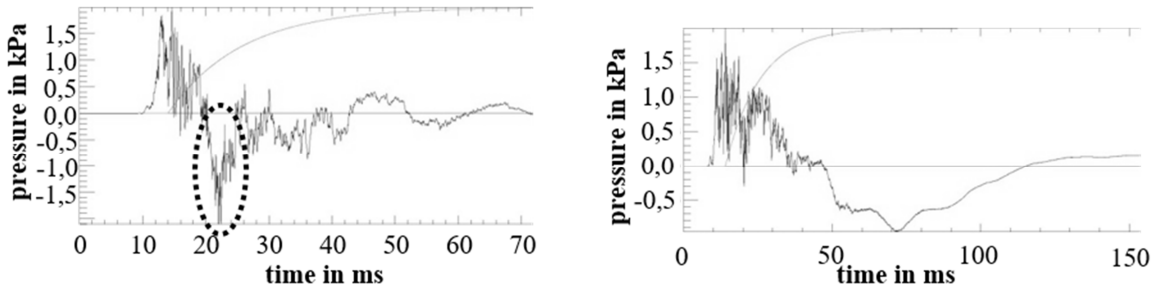

Figure 4: sound pressure graphs for experiment with open (left) and closed (right) window. The negative excursion is highlighted and occur only for open windows

DISCUSSION

The analysis of patient and accident data showed only a low number of cases. It needs to be investigated whether this is actually based on a low number of cases or if hearing loss is not sufficiently covered by data collections. Several aspects affect the data collection of hearing loss. For example, the patient does not notice a hearing loss immediatly because only higher frequencies are affected, that can only be seen in a frequency band. Secondly a hearing loss injury steps in the background of the patient, because other injuries are more obvious or relevant to the patient or thirdly a patient recognizes a hearing loss but did not link it to an airbag deployment. The third point can be addressed by awareness, but the first two points needs to be addressed with audiometry. With more extensive data collections the link between airbag deployment and hearing loss can be assessed statistically.

The accident reconstructions and static experiments were conducted with a limited number of experiments, vehicles and airbags. Continuative accident reconstructions of other constellations needs to be conducted to support the findings of this study for example full width impact or side collisions. Especially side impacts seem to be interesting, because of the short period of deformation noise before the airbag deployment interferes with the rising phase of the stapedius reflex. Also the selection of vehicles needs to be extended to suspend that the measurements are artefacts of the analyzed vehicles and their acoustical behavior. A continuous on-board recording of sound pressure should be applied to crash tests to collect data for different vehicles and impact conditions. The findings of the comparison of closed and opened windows neglect the accompanied crash noises. Considering the crash noise the ARU value decreases from 865.2 (static experiment with open window) to 452.6 for the case with open window and airbag deployment 20 ms after t_0 (dynamic experiment).

A limitation of this study is that hearing is an individual sense organ that reacts different in every human. So that a complete risk curve for PTS in dependency of CTS is not available at the current stage. For example, there exist so called vulnerable ears that are more sensitive to noise exposure. Ernst et al. (1997) report that 5 to 10 % of the population could be affected by such sensitive hearing. This corresponds to findings by Pfander (1975).

Also the stapedius reflex cannot be triggered in every human. Due to neurologic or anatomical abnormality the stapedius reflex cannot be triggered and the inner ear is unprotected against high levels of sound pressure.

Main limitation of this study is the use of the AHAAH model, which is well-established in analysis of gunshots and also in use for automotive analysis since 2003 (Price et al. 2013), but the interpretation of the ARU values and their correlation to PTS and CTS is limited. Only for two values (500 by Price et al. (1986) and 868 by Liberman et al. (1982)) the indication of a PTS is classified, so that the assessment of results close to the two values and in between both values is limited. An approach using injury risk curves for PTS should be a part for future scientific research.

CONCLUSION

In conclusion it was shown that cases with hearing loss after airbag deployment occur in a few cases of patient and accident data. In order to link airbag deployment and hearing loss statistically an extensive data acquisition concerning hearing loss in accidents is needed. The conducted accident reconstructions and the analysis of the sound pressure levels with an on-board microphone showed that sound pressure levels up to 160 dB can occur calculated for the driver's ear. Due to the protective effect of the stapedius reflex, which can be triggered by deformation and impact noise, the risk of a PTS is low for a single airbag deployment. In multiple airbag deployments it was shown that the risk of a PTS is higher due to short sequence of blast events. Due to the increase of the number of airbags per vehicle and higher number of airbag deployments in accidents the number of hearing loss needs to be monitored carefully. Further it was shown, that the risk of a PTS is lower if the windows of the vehicle are closed, due to the air pressure increase inside the vehicle.

For further investigations it should be noticed that measuring the sound pressure of airbags with respect to a risk of a PTS the crash accompanied noises should be considered in the analysis to address the influence of the stapedius reflex. In case of direct view between sender and receiver the distance law is applicable. As recommendation, the sound pressure of airbags should be lowered and unnecessary airbag deployment needs to be avoided. Additionally, the collection of injury data of accidents should address hearing loss to link such injuries to airbag deployment events.

ACKNOWLEDGEMENTS

All data were collected in the project "Accident injuries in vehicles equipped with airbags" (FE 82 0576 2012) funded by the Federal Highway Research Institute (BASt) and conducted by Technical University of Berlin and Hanover Medical School.

REFERENCES

Allen, C.H., Bruce, R.D., Dietrich, C.W., Pearsons, K.S., (1971): „Noise and inflatable restraint systems: final report", Cambridge, Massachusetts: Bolt, Beranek, and Newman

Banglmaier, R.F., Rouhana, S.W. (2003): "Investigation into the noise associated with air bag deployment: Part III – Sound pressure level and auditory risk as function of inflatable device", 47th annual proceedings of association for the advancement of automotive medicine

Ernst, A., Lenarz, T., (1997): "Otoacoustic emissions in predicting noise induced hearing loss in vulnerable inner ears", European commission concerted action – protection against noise. University College London

Johannsen, H., Krettek, C., Hannawald, L., Schaser, K.D. (2017): “Consideration of Accident Avoidance Technology within GIDAS”. 25th ESV Conference, Detroit, 2017

Liberman, M.C., Mulroy, M.J., (1982). ”Acute and chronic effects of acoustic trauma: Cochlear pathology and auditory nerve patho-physiology.” In: New Perspectives on Noise-Induced Hearing Loss, pp. 105-135. New York.

McFeely, W.J. Jr, Bojrab, D.I., Davis, K.G., Hegyi, D.F., (1999): „Otologic injuries caused by airbag deployment”, Otolaryngology – Head and Neck Surgery, 121(4): 367-73

Pfander, F., (1975): „Das Knalltrauma“, Heidelberg, Springer Verlag, 1975

Price, G.R., Kalb, J.T., (1986): „Mathematical model of the effect of limited stapes displacement on hazard from intense sounds”, J. Acoustical Society of America, Supplement 1, Vol. 80

Price, G.R., Rouhana , S.W., Kalb, J.T., (1996): “Hearing hazard from the noise of air bag deployment” The Journal of the Acoustical Society of America 99, 2464 (1996)

Price, G.R., Kalb, J.T., (2013): „Using the Auditory Hazard Assessment Algorithm (AHAAH)”, http://www.arl.army.mil/ARL-Directorates/HRED/AHAAH

Rouhana, S.W., Webb, S.R., Wooley R.G., McCleary, J.D., Wood, F.D., Salva, D.B. (1994): “Investigation into the noise associated with air bag deployment: Part I – Measurement technique and parameter study” SAE Transactions, Vol. 103, Section 6: JOURNAL OF PASSENGER CARS (1994), pp. 1752-1773

Rouhana, S.W., Webb, S.R., Dunn, V.C. (1998): “Investigation into the noise associated with air bag deployment: Part II – Injury risk study using a mathematical model of the human ear” 42nd Stapp Car Crash Conference Proceedings, Tempe, Arizona, November 2-4, 1998

Saunders J.E., Slattery, W.H., Lux-Ford, W.M., (1998): “Automobile airbag impulse noise: otologic symptoms in six patients”, Otolaryngology – Head and Neck Surgery, 118(2):228-34

Traynor, R., (2012): “The Effect of Automobile Air Bag Deployment on Hearing”, http://hearinghealthmatters.org/hearinginternational/2012/the-international-threat-of-air-bags/, accessed September 28, 2018

Yaremchuk, K., Dobie, R.A. (2001): “Otologic Injuries from Airbag Deployment” Otolaryngology – Head and Neck Surgery, 125(3):130-34

ANALYSIS OF KINEMATCIS AND HEAD INJURY MECHANNISMS IN CAR TO CHILD CYCLSIT COLLISION SIMULATION USING HUMAN FINITE ELEMENT MODEL

Tadasuke Katsuhara
Yasuo Yamamae
Tsuyoshi Yasuki
Toyota Motor Corporation
Japan

Hiroyuki Umetani
Toyota Systems
Japan

Paper Number 19-0030

ABSTRACT

According to the traffic accident data in Japan [1], the third largest number of fatalities is due to collision between car and cyclist. Head injuries are the most frequent cause of cyclist fatalities. Head injury risk depends on the stiffness of the head collision location of the vehicles. The collision location of a child's head is different from that of an adult's head in a traffic accident. Therefore, there is benefit of examining the injury mechanism of child cyclists for safety equipment.
In this study, a total of 400 cases of car-to-cyclist collision were simulated by varying car speed, bicycle speed and initial position of collision using child and adult human Finite Element (FE) models and the head injury mechanisms were analyzed by investigating the kinematics and the kinetics of child and adult cyclists. The THUMS Version 4 Ten Years Old (10YO) model was used for the child cyclist and the THUMS Version 4 American Mail 50%tile (AM50) model for the adult cyclist. The bicycle FE model of a city cycle was established bicycle. The occurrence risk of skull fracture and Diffuse Axonal Injury (DAI) was investigated in 10YO and AM50 cyclists. In 10YO, approximately 90 % of the head contact points were distributed on the car body and 10 % was distributed on the ground. In AM50, the head contact points on the ground accounted for approximately 30 %, 70 % were distributed on the car body.
It was found that the skull fracture and DAI occurrence were predicted in the 10YO when the head contacted the car hood in the car speed of 30 km/h or more. The impact velocity of the upper body was increased by contacting between the pelvis and the front edge of the car hood. As a result, head impact velocity and rotational velocity became high after the shoulder contacted the hood. In the AM50 whose pelvis rode on the hood, the upper body fell down toward the hood gradually. As a result, the skull fracture occurred when the head contacted the A-pillar in the car speed of 40 km/h or more, which was lower than that in the 10YO. In the case which bicyclists head contacted a ground after car collision, the skull fracture was predicted even in the car speed of 10km/h. The DAI occurrence was not predicted.

INTRODUCTION

According to the data collected by the Ministry of Internal Affair and Communications Statistics Bureau [2], 30 % of traffic accident fatalities involving children 14 years old and under. According to the statistical data of the National Police Agency in Japan [1], traffic accident fatalities of child cyclists under 15 years old is the third highest, preceded by pedestrians and car occupants. The authors have already studied the injury mechanisms of both child pedestrians [3] and child occupants [4]. In this study, the authors investigated injury mechanisms on child cyclists.
Recently cars which are equipped with the Automatic Emergency Brake (AEB) have been sold in Japan. When all cars are equipped with AEB, it is expected that the collision speed will reduce and the risk of cyclist injury will decrease during the cars collide to cyclists. However, the fatality risk will remain if the cyclists collides with the ground after a car-to-cyclist collision. In this study, not only head-to-car contact but also head-to-ground contact after car collision will be analyzed.
To analyze cyclist collision kinematics and injuries, physical tests using Anthropomorphic Test Devices (ATD) [5], [6] and simulation using MADYMO [7], [8] and human Finite Element (FE) models [9], [10] were

conducted. Maki et al. [7] studied traffic accident statistics and clarified the cyclist's kinematics after car collision using MADYMO. Omoda et al. [8] simulated ground contact of cyclists after car collision using MADYMO and indicated that the head injury risk of cyclist's head to ground was higher than that of head to car. Mizuno et al. [10] studied the difference of the kinematics after collision between pedestrians and cyclists using human FE models. Moreover, A-pillar to cyclist head with helmet collisions were simulated and the effect of the helmet was clarified. The brain injury such as Diffuse Axonal Injury (DAI) cannot be directly simulated using ATD and MADYMO, while human FE model with detail brain model is available to analyze DAI.

To simulate a real traffic accident, various collision conditions need to be considered. In this study, a total of 200 cases of car-to-child cyclist collisions based on the real traffic accident were simulated by using the human FE model representing a child cyclist in order to clarify the mechanisms of skull fracture and DAI for head to car and head to ground contact. For comparison, the car-to-adult cyclist collisions also were simulated in the same conditions as the child cyclist.

METHOD

Car and Ground Models

The FE car model was the same as used in a previous study [11] as shown in Figure 1. A sedan was selected as the car type. Rigid materials were assumed for the engine and deformable material was assumed for the other parts. The tires and the steering could rotate. The ground was assumed to be a rigid plane.

Figure 1.Car and ground FE models

Cyclist Model

The age of the cyclist was chosen to be 10 years old. The THUMS Version 4 10YO occupant model was used for the child cyclist (Figure 2). Bicycle type was a city cycle. A twenty two inches tire size bicycle was used for the child cyclist. The height of bicycle saddle was 0.7 m from the ground. The head height of the seated child cyclist was 1.35 m and his weight was 34.0 kg. The THUMS Version 4 AM50 occupant model was used for the adult cyclist. A twenty six inches tire size bicycle was used for the adult cyclist. The height of bicycle saddle was 0.9 m from the ground. The head height of the seated adult cyclist was 1.70 m and his weight was 77.0 kg. The friction coefficient between cyclists and the car was 0.3, for the ground was 0.7.

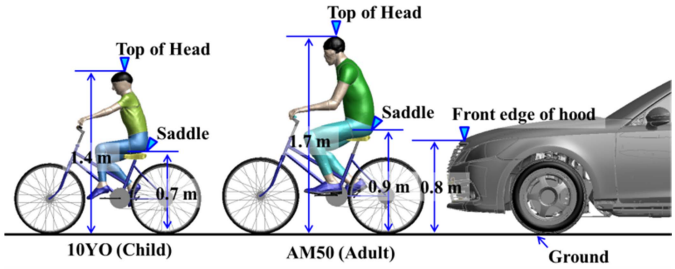

Figure 2. 10YO (Child) and AM50 (Adult) cyclist FE models

INJURY INDICIES AND CRITERIA

In this study, risk of the skull fracture and DAI were evaluated. HIC_{15} was used as an index of skull fracture in order to facilitate comparison with other studies. It was postulated that skull fracture (AIS3+, 30% probability) occurred when HIC_{15} exceeded 700 [12]. DAI was estimated using the cumulative strain damage measure (CSDM) proposed by Takhounts et al. [13]. CSDM is an index used to assess the occurrence of DAI based on the volume ratio of distortion areas in the brain exceeding a threshold value (25 %) with respect to the volume of the whole brain. According to the brain injury risk curve derived by Takhounts et al. [14], a CSDM value of 49 % was equivalent to a 50 % probability of DAI (AIS4+).

SIMULATION CONDITION

The simulation condition was shown in Table 1. The parameters were car speeds, bicycle speeds and initial impact positions. The car speed was changed from 10 km/h to 50 km/h at an interval of 10 km/h. The bicycle speed was changed from 5 km/h to 25 km/h at an interval of 5 km/h. The initial impact position of cyclist was changed from 1000 mm to - 400 mm based on cyclist head center of gravity at an interval of 200 mm as shown in Figure 3. A total of 400 cases were simulated in each 10YO and AM50. A number of 10YO cases were 200 cases (from Case 1 to Case 200). A number of AM50 cases also 200 cases (from Case 201 to Case 400).

Table 1. Simulation Conditions

Parameter	Variation							
Cyclist	THUMS Version 4 10YO (Child)				THUMS Version 4 AM50 (Adult)			
Bicycle tire size [inches]	22				26			
Car type	Sedan							
Car speed [km/h]	10	20	30	40	50			
Bicycle speed [km/h]	5	10	15	20	25			
Initial impact position [mm]	1000	800	600	400	200	0	-200	-400
Total Case	400 Cases							

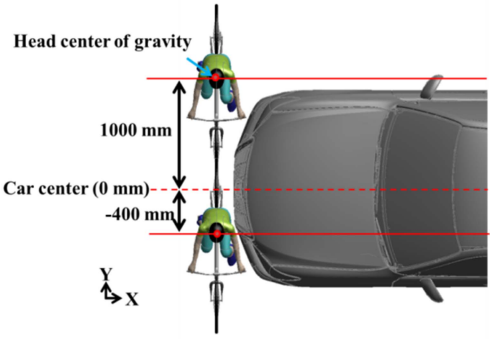

Figure 3. Definition of initial impact position

RESULTS

Distribution of HIC_{15} and CSDM

The distributions of HIC_{15} and CSDM are shown in Figure 4. Blue areas show the case which cyclist head contacted the car body. Red areas show the case which cyclist head contacted the ground. Based on the criterion of both HIC_{15} (700) and CSDM (49 %), all results were divided into three categories as follows (A, B, C). Category A are cases in which both HIC_{15} and CSDM are equal to and over their criteria (HIC_{15} 700, CSDM 49%). Category B are cases that only HIC_{15} is equal to and over the criterion. Category C are cases in which both HIC_{15} and CSDM are less than the criteria. For the 10YO cases, Category A for head car contact and head ground contact were 18 % and 0.5 % respectively. Category B for head car contact and head ground contact were 35 % and 9 % respectively. For the AM50 cases, Category A did not occur both head car and head ground contact cases. Category B in head car contact case was 12% and 18 % for head ground contact case.

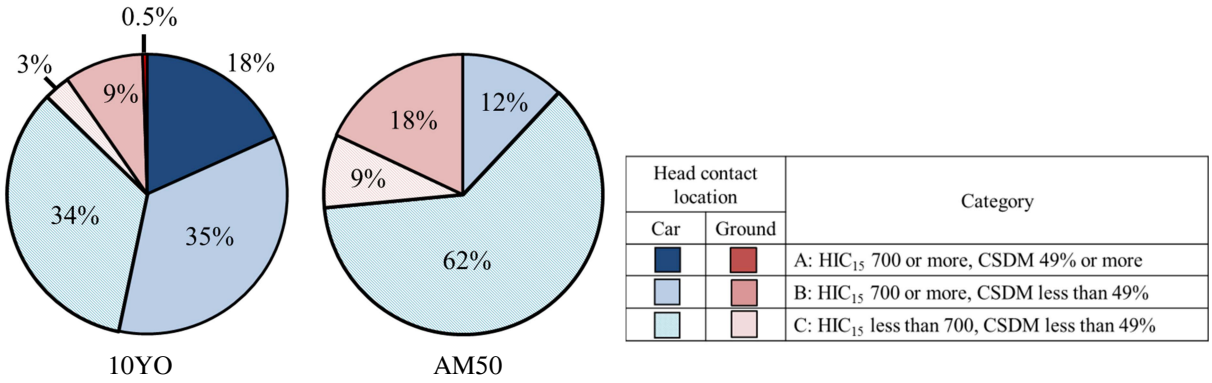

Figure 4. Distribution of HIC_{15} and CSDM of 10YO and AM50 cyclists

Relationship between head contact points and HIC_{15} is investigated as shown in Figure 5. Solid circles show the head contact points. Their color indicates the HIC_{15} level; red is $HIC_{15} \geq 700$ (skull fracture probability 30 %), yellow is $700 > HIC_{15} \geq 500$, green is $500 > HIC_{15} \geq 300$ and blue is $300 > HIC_{15}$. In 10YO of head car contact case, red solid circles ($HIC_{15} \geq 700$) distributed on the car rearward of the hood and the A-pillar while the blue solid circles distributed on the car front side of the hood. In 10YO of head ground contact case, most of head contact points show red color.

In AM50 of head contact case, red solid circles distributed on the A-pillar. The contact points of both hood and windshield show blue or green color. In also AM50 of head ground contact case, most of head contact points show red color.

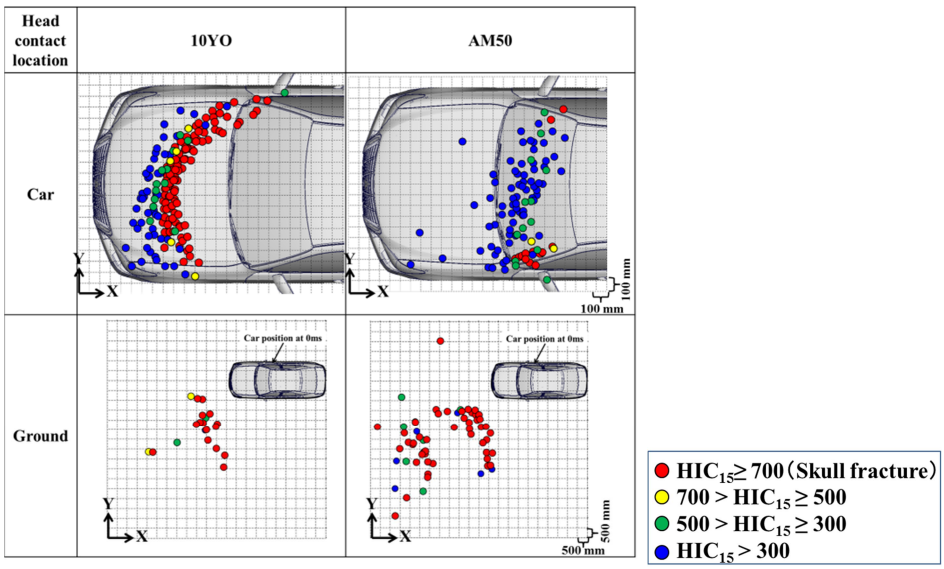

Figure 5. Distribution of head contact points with HIC_{15} levels

Relationship between head contact points and CSDM is investigated as shown in Figure 6. Solid circles show the head contact points. Their color indicates the CSDM revel; red is CSDM ≥ 49 % (DAI probability 50%), yellow is 49 % > CSDM ≥ 30 %, green is 30 % > CSDM ≥ 10 % and blue is 10 % > CSDM. In 10YO of head car contact case, red and yellow solid circles, which indicated high risk of DAI, were shown in the car rearward of the hood and A-pillar while green and blue solid circles distributed on the car front side of the hood. In 10YO of head ground contact case, red and yellow solid circles were shown in the furthermore from the car. In AM50 of head car contact case, there was no case which was over 30 % of CSDM. Most of cases were less than 10% of CSDM. In also AM50 of head ground contact case, there was no case which exceeded 49 % of CSDM.

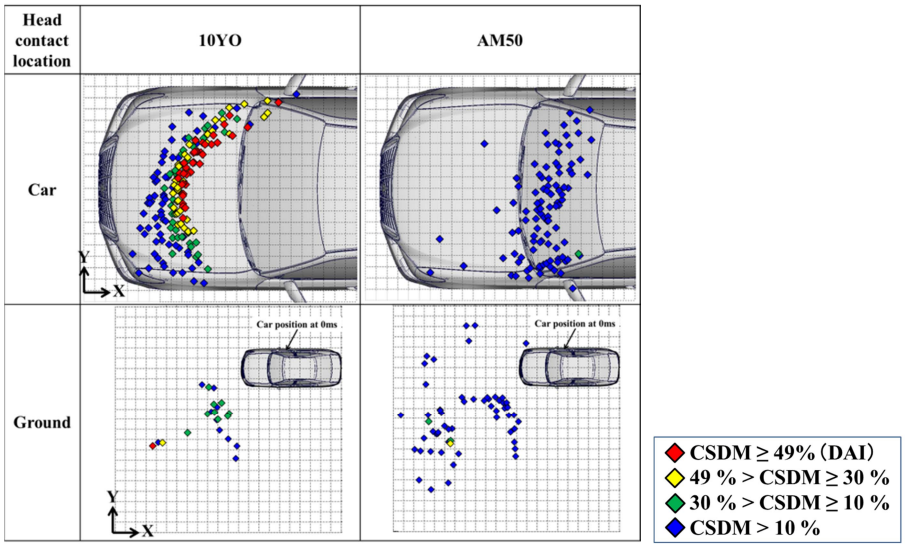

Figure 6. Distribution of head contact points with CSDM levels

Relationship between Car Speeds and Head Injury Indices (HIC_{15}, CSDM)

The relationship between car speeds and HIC_{15} is shown in Figure 7. In head car contact cases of both 10YO and AM50 cyclist, higher the car speeds were, the higher $HIC_{15}$was. At the car speed of 30 km/h, half of 10YO cases were over the criteria. On the other hand, only one case was over the criteria in AM50 cases. In head ground contact cases of both 10YO and AM50 cyclists , HIC_{15} in low car speed cases (10, 20, 30 km/h) were higher than that in high car speed cases (40, 50 km/h).

The relationship between car speed and CSDM was shown in Figure 8. In head car contact cases of both 10YO and AM50 cyclists, CSDM also was high with increasing car speed. In the 10YO, CSDM exceeded the criterion in car speed of 30 km/h or more. In the AM50, CSDM was lower than 10 %. In head ground contact cases, a correlation between CSDM and car speed was not found in either the 10YO and AM50 cases.

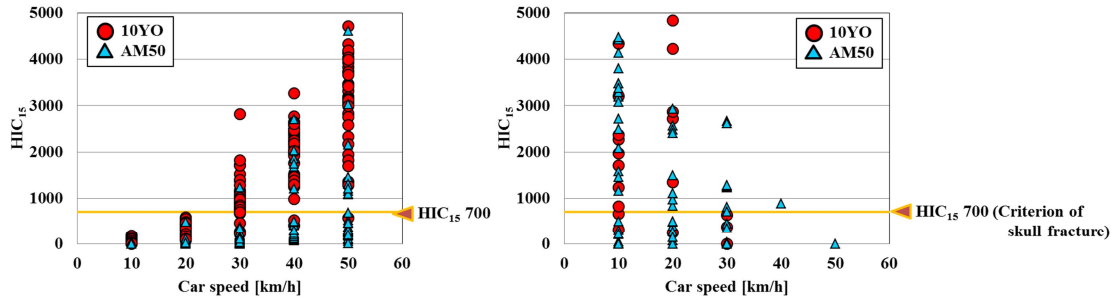

Car contact Ground contact

Figure 7. Relationship between car speed and HIC_{15} of 10YO and AM50 cyclists

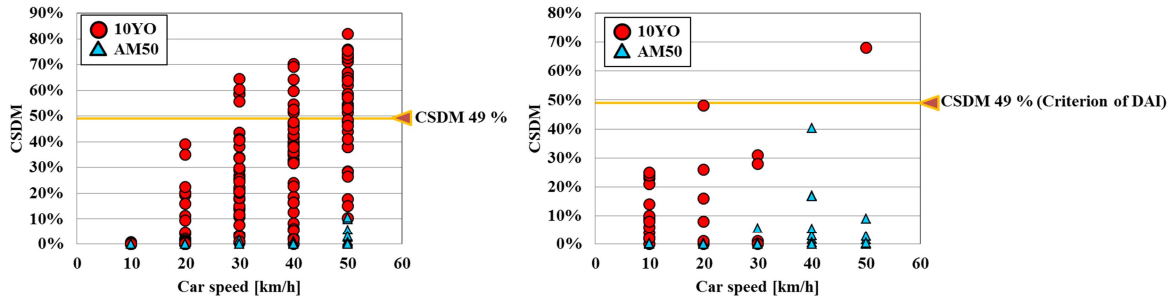

Car contact Ground contact

Figure 8. Relationship between car speed and CSDM of 10YO and AM50 cyclists

Relationship between Head Impact Velocities and HIC_{15}

The relationship between head impact velocity and HIC_{15} was shown in Figure 9. In head car contact cases, HIC_{15} became high in proportion to head impact velocities. Head impact velocities in AM50 cases trended to be lower than those of the 10YO cases. In head ground contact cases, HIC_{15} tended to be high in both 10YO and AM50 cases even though head impact velocity was low (between 5 m/s and 8 m/s).

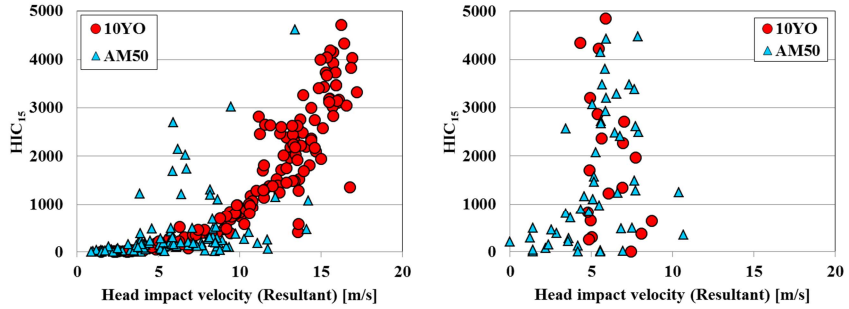

Car contact Ground contact

Figure 9. Relationship between head impact velocities and HIC_{15} of 10YO and AM50 cyclists

Relationship between Head Rotational Velocities, Accelerations and CSDM

The relationship between head rotational velocity and CSDM was shown in Figure 10. In head car contact cases of 10Y cyclist, CSDM became high in proportion to head rotational velocities. In AM50 cyclist, CSDM was low in all head rotational velocities. Regarding head ground contact cases of 10YO and AM50 cyclists, CSDM was similar to zero between head rotational velocity of 0 and 50 rad/s. From head rotational velocity 50 rad/s, CSDM increased up to 50%. The relationship between head rotational accelerations and CSDM was shown in Figure 11. In head car contact case of 10YO, head rotational acceleration was higher than that in AM50 cases. CSDM in 10YO also was higher than that in AM50.

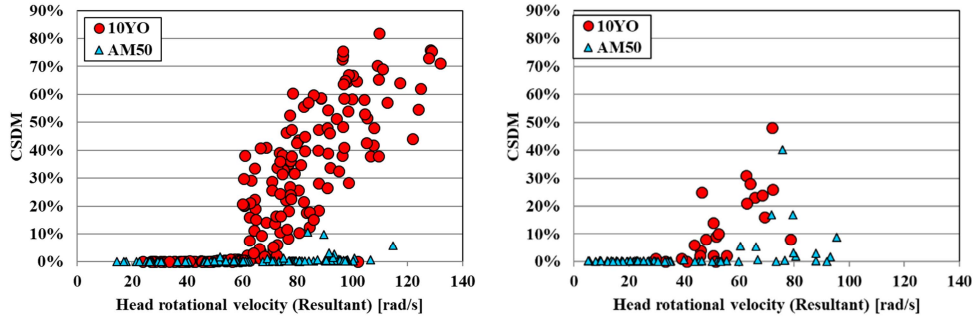

Car Contact Ground Contact

Figure 10. Relationship between head rotational velocities and CSDM of 10YO and AM50 cyclists

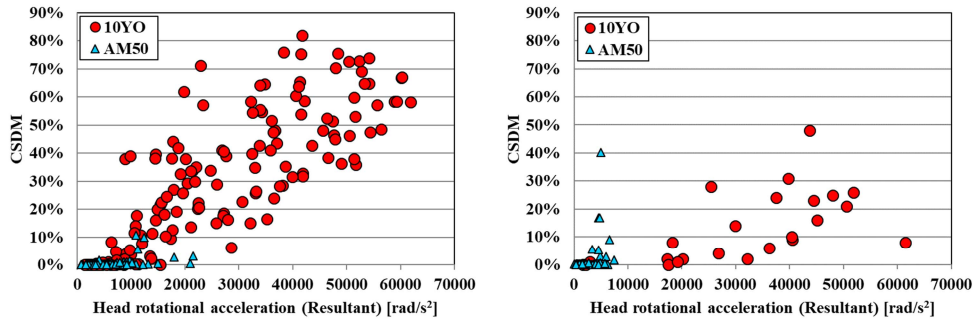

Figure 11. Relationship between head rotational accelerations and CSDM of 10YO and AM50 cyclists

Kinematics of a Car Contact Case

As an example of the case which cyclist head contacted the car body, the results of Case 119 (10YO) and Case 319 (AM50) were shown in Table 3. The collision conditions of both cases were car speed: 40 km/h, bicycle speed: 10 km/h and initial impact position: 200 mm. HIC_{15} was 2261 and CSDM was 55.5 % in Case 119 when 10YO head contacted the hood. HIC_{15} was 2034 and CSDM was 0.5 % in Case 319 when AM50 head contacted the A-pillar. The kinematics of 10YO and AM50 were shown in Figure 12 and 13. In the upper view, 10YO obliquely moved toward the car rearward and his head collided to the hood. On the other hand, AM50 obliquely moved to car rearward on the car hood and his head contacted to A-pillar. In the lateral view, 10YO lower leg and the thigh contacted the gill at 10 ms. At 20 ms, the pelvis contacted the front edge of the hood. At 30 ms, the upper body started to fall down toward the hood. At 60 ms, the shoulder contacted the hood. Finally, the head contacted the hood at 80 ms. In AM50 case, the lower leg contacted the grill at 10 ms and AM50 thigh contacted the hood at 20 ms. At 30 ms, his pelvis ridded on the hood and his upper body moved toward the car rearward. His upper body fell down toward the hood and his head contacted the lower parts of A-pillar at 170 ms.

Table 3. Head injury results in head car contact cases

Case No.	Bicyclist	Collision condition			Head impact location	HIC_{15}	CSDM
		Car speed	Bicycle speed	Impact position			
Case 119	10YO	40 km/h	10 km/h	200 mm	Hood	2216	55.5 %
Case 319	AM50				A-Pillar	2034	0.5 %

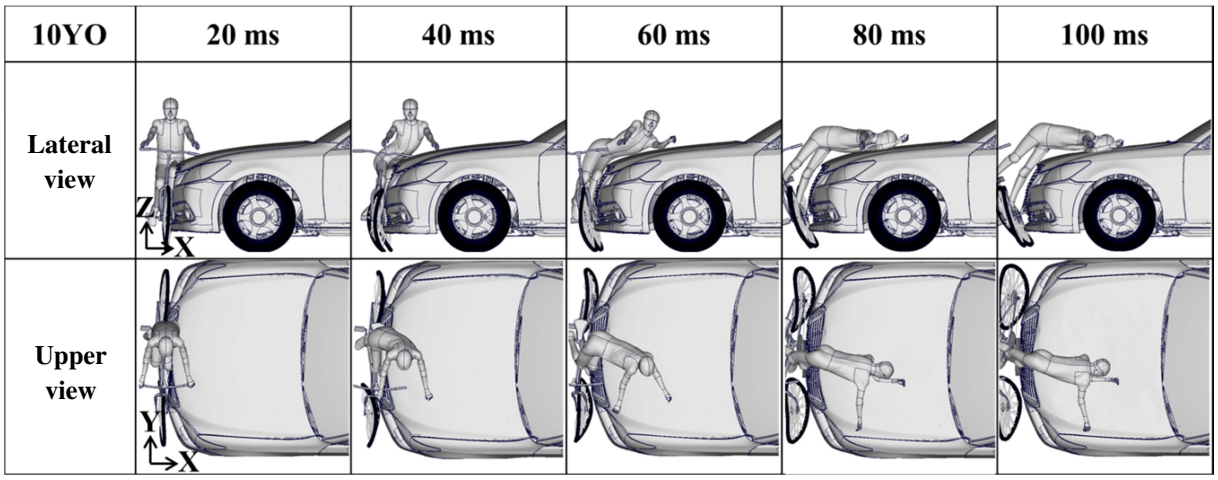

Figure 12. Kinematics of 10YO (Case 119) cyclist during impact

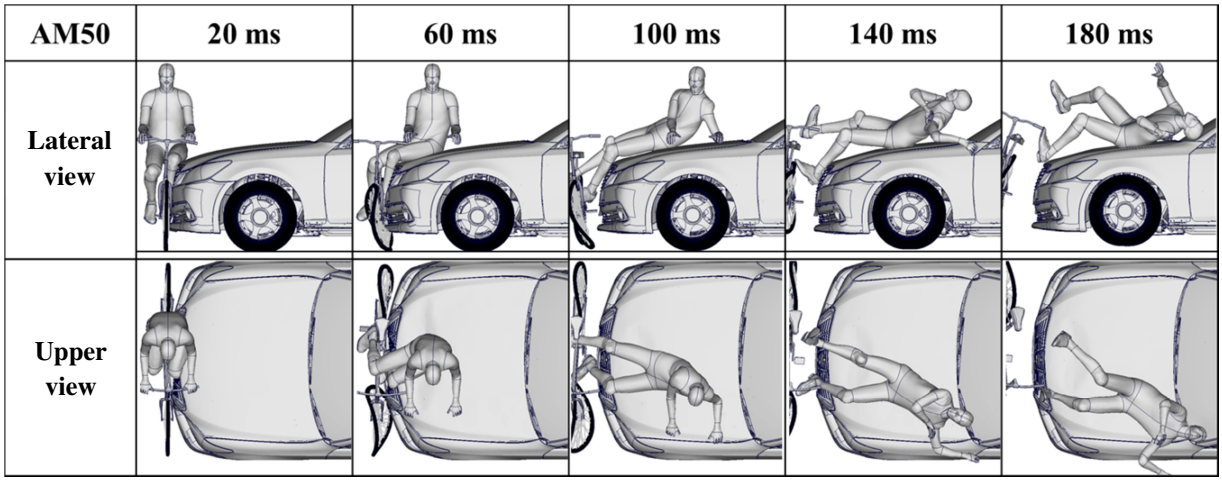

Figure 13. Kinematics of AM50 (Case 319) cyclist during collision

Kinematics and Kinetics of a Ground Contact Case

As an example of the case which cyclist head contacted the ground, the results of Case 149 (10YO) and Case 349 (AM50) were shown in Table 4. The collision conditions of Case 149 and Case 349 were car speed: 10km/h, bicycle speed: 25 km/h and initial impact position: 0mm (Car center). In Case 149 (10YO), HIC_{15} indicated 2268 and CSDM was 0.0 %. In Case 349 (AM50), HIC_{15} was 4606 and CSDM was 0.1%. As shown in Figure 14 and 15, the kinematics of Case 149 (10YO) was similar to that of Case 349 (AM50). Upper body of cyclist fell down toward the ground after car-to-bicycle collision. At first, lower legs contacted the ground and cyclists fell down toward the ground from their head. As a result, Z direction of head impact velocity in both cases decreased gradually and their head impacted at 6 m/s of head impact velocity (Figure 16). Head rotational velocity was approximately 10 rad/s before head contacted the ground (Figure 17). After head contacted the ground, head rotational velocity increased gradually to 60 rad/s. As a result, head rotational acceleration increased to 5500 rad/s^2.

Table 4. Head injury results in head ground contact cases

Case No.	Bicyclist	Collision condition			Head impact location	HIC_{15}	CSDM
		Car speed	Bicycle speed	Impact position			
Case 149	10YO	10 km/h	25 km/h	0 mm	Ground	2268	0.0 %
Case 349	AM50				Ground	4606	0.1 %

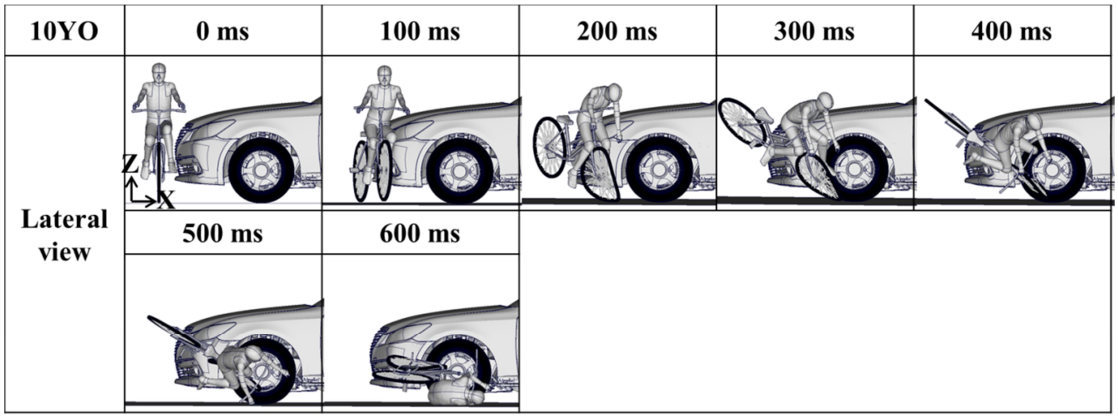

Figure 14. Kinematics of 10YO (Case 149) cyclist during collision

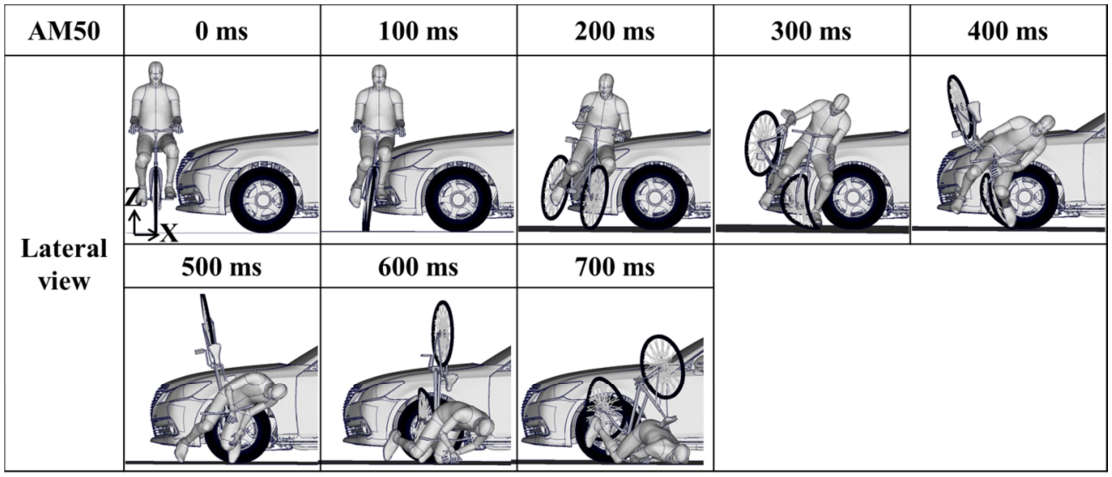

Figure 15. Kinematics of AM50 (Case 349) cyclist during collision

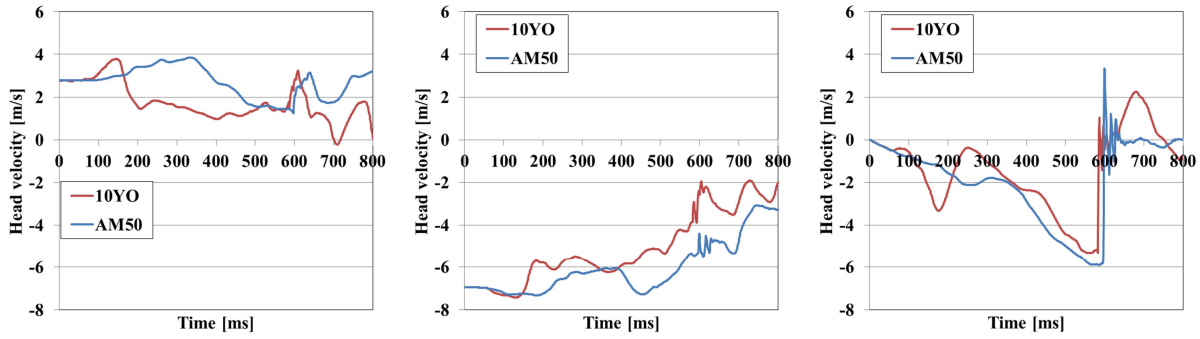

X direction Y direction Z direction

Figure 16. Head impact velocity of 10YO and AM50 cyclists

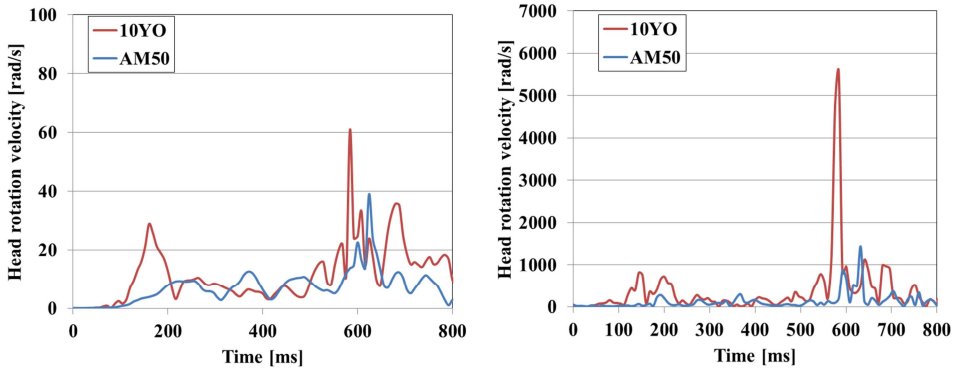

Rotational velocity Rotatonal acceleration

Figure 17. Head rotational velocity and rotational acceleration of 10YO and AM50 cyclists

DISCUSSION

A total of 400 cases of car-to-cyclist collision were simulated by using THUMS Version 4 10YO and AM50 models and the relationship between car speed and head injury (skull fracture, DAI) risk was investigated in 10YO and AM50 cyclists. In AM50 cyclist, the skull fracture was predicted when the head contacted the A-pillar in the car speed 40 km/h or more. On the other hand, the skull fracture and DAI were predicted in 10YO cyclist when head contacted the hood or A-pillar in the car speed 30 km/h or more. In the case which head contacted the ground, the skull fracture mostly occurred in both 10YO and AM50 cyclists even in the car speed 10 km/h while DAI was not predicted.

Relationship between Car Speed and HIC_{15}/CSDM

Both HIC_{15} and CSDM in 10YO cyclist exceeded their criteria when cyclist head contacted the hood or A-pillar at the car speed 30 km/h or more. Head impact velocity, rotational velocity and kinematics in 10YO cyclist were compared between car speed of 20 km/h and 30km/h as shown in Table 5. At the car speed 30 km/h (Case 68), head impact velocity was 11.4 m/s while head impact velocity was 8.3 m/s at the car speed 20 km/h (Case 67). As shown in Figure 9, high HIC_{15} values at the car speed 30 km/h were seemingly caused by high head impact velocity. The kinematics between the car speed 20 km/h (Case 67) and 30 km/h (Case 68) were compared as shown in Figure 18. The cyclist kinematics of car speed 30 km/h was similar to that of 20 km/h. Cyclist pelvis contacted the front edge of the car hood and cyclist head contacted the hood after shoulder contact. However, the contact timing of car speed 30 km/h case was higher than that of 20 km/h case. It was seemingly due to the difference of pelvis contact force. In car speed of 30 km/h case, cyclist pelvis was forcibly pushed away. As a result, cyclist upper body fell down and head rotated around shoulder rapidly. As a result, head translational velocity became high. Head rotational velocity also became high and high head rotational acceleration was generated when cyclist head contacted the hood. As a result, brain strain increased and exceeded 25 %. As shown in Figure 19, the higher pelvis contact forces were the higher head contact forces were in 10YO cyclist cases. On the other hand, the pelvis contact force in AM50 was not in proportion to the head contact force. It was due to AM50 pelvis riding on the hood.

Table 5.Comparison 10YO results between car speed of 20 km/h and 30km/h

Case No.	Bicyclist	Collision condition			Head impact location	Head impact velocity	Maximum head rotational acceleration	HIC_{15}	CSDM
		Car speed	Bicycle speed	Impact position					
Case 67	10YO	20 km/h	20 km/h	600 mm	Hood	8.3 m/s	7000 rad/s²	486	22 %
Case 68		30 km/h	20 km/h	600 mm	Hood	11.4 m/s	13000 rad/s²	1703	60 %

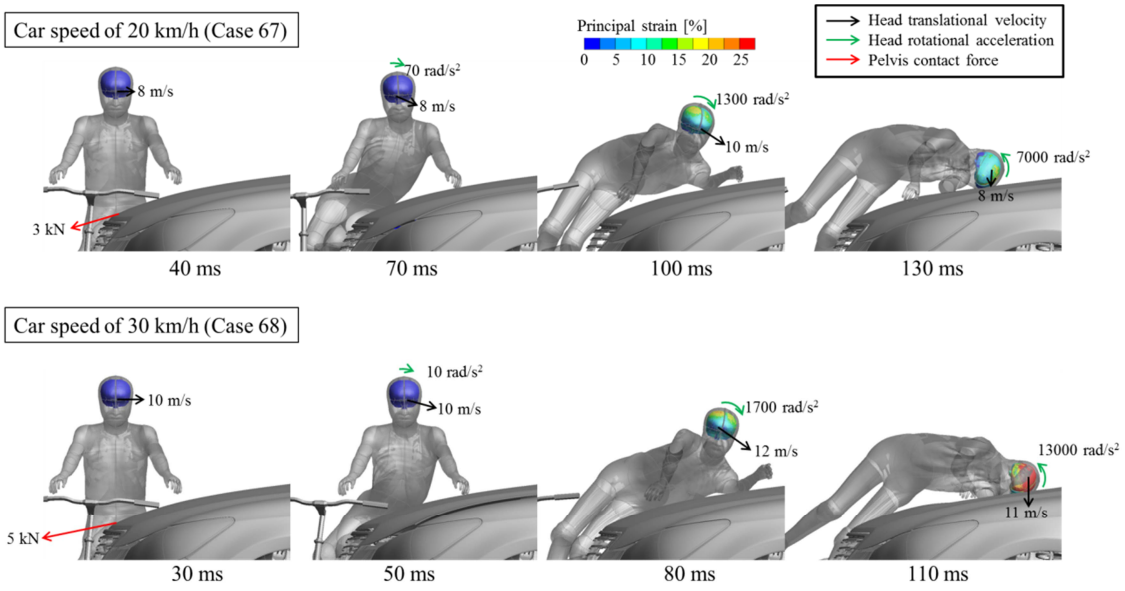

Figure 18. Comparison of kinematics, brain strains, head velocities and pelvis contact forces in 10YO bicyclist between car speed 20 km/h and 30 km/h

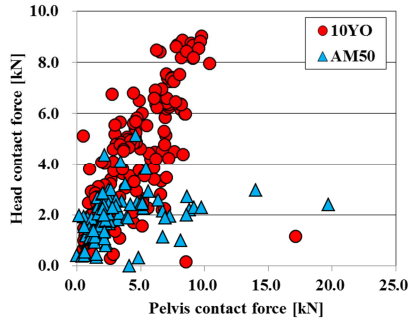

Figure 19. Relationship between head contact force and pelvis contact force

Head Injury Risk in Ground Contact Cases

In the case which head contacted the ground, the risk of skull fracture was high in 10YO and AM50 cyclists at the low car speed. As shown in Figure 16, Z direction of head impact velocity in both 10YO and AM50 monotonically decreased and head impacted the ground at approximately 6 m/s. As a result, HIC_{15} indicated 2268 in 10YO and 4606 in AM50. Matsui et al. [15] reported that HIC_{15} indicated 6525when an head impactor fell down toward a concrete ground from 1.5 m height (Head impact velocity: 5.4 m/s). HIC_{15} exceeded the criterion of skull fracture (700) in the results of both our study and Matsui's study.

CSDM in both 10YO and AM50 cyclists indicated the low value (under 49%). Low CSDM was seemingly attributed to the small head rotation. As an example of the case which head contacted the ground, AM50 cyclist case (Case 349) was shown in Figure 18. The large head rotation did not occurred when head contacted the ground. As a result, brain strain did not exceed 25 % at 670 ms.

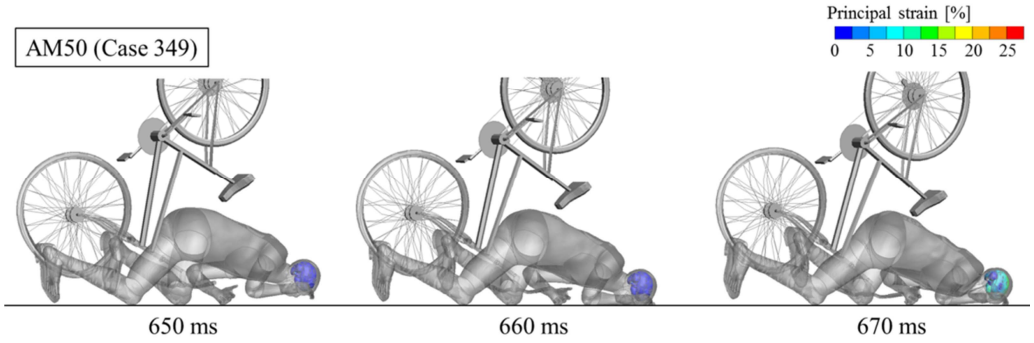

Figure 20. Kinematics and brain strain of cyclist in head ground contact case

LIMITATION

In this study, assumptions for car-to-child cyclist collision was used. In an actual car-to-cyclist accident, various collision directions, car types, bicycle types, cyclist ages are involved. The results of this research are not intended to represent all cyclist accident. Countermeasure development based on this research may not match intention when the car or bicycle types are different than those in this study. In the future, more research which takes these differences into account will be necessary.

CONCLUSIONS

A total of 400 cases of car-to-cyclist collision were simulated by using THUMS Version 4 10YO and AM50 FE models, and the relationship between car speed and skull fracture/DAI was investigated. It was found that the risk of skull fracture and DAI in the AM50 cyclist was reduced if the car speed was restrained to 30km/h. On the other hand, the car speed which reduced the skull fracture and DAI risk in 10YO cyclist was 20 km/h or more.

It was found that HIC_{15} in both 10YO and AM50 cyclists exceeded the criterion even in the car speed of 10 km/h when the cyclists fell down toward the ground from his head.

ACKNOWLEDEMENT

The study used computational resources of the K computer provided by the RIKEN Advanced Institute for Computational Science through the HPCI System Research project as a part of the Japan Automotive Manufacture Association, Inc.'s research activities (Project ID: hp170150). The authors would like to appreciate the RIKEN Advanced Institute for Computational Science and the Fujitsu Limited.

REFERENCES

[1] National Police Agency in Japan, 2018.
[2] Vital Statistics in Japan, Ministry of Internal Affair and Communications Statistics Bureau, 2016.
[3] Ito, K., Tokuyama, M., Miyazaki, H., Hayashi, S., Kitagawa, Y., Yasuki, T. 2017. "Development of Child Finite Element (FE) Models and Vehicle-To-Pedestrian collision Simulations." 25th ESV, 17-0279.
[4] Takahashi, T., Fukushima, S., Kitagawa, Y., Yasuki, T. 2015."Injury Simulation of Rear Seat Child Occupant in Offset Deformable Barrier Frontal Impact." 24th ESV, 15-0048.
[5] Hamacher, M., Kuhn, M., Hummel, T., Eckstein, Lutz. 2017."Effectiveness of Pedestrian Safety Measures at the Vehicle Front with Regard to Cyclists." 25th ESV, 17-0177.
[6] Zander, O., Hamacher, M., 2017."Revison of Passive Pedestrian Test and Assessment Procedures to Implement Head Protection of Cyclists." 25th ESV, 17-0376.
[7] Maki, T., Kajzer, J., Mizuno, K., Sekine, Y. 2003. "Comparison of Vehicle-Bicycle and Vehicle-Pedestrian Accidents in Japan." Accident Analysis and Prevention, 35, 927-940.
[8] Omoda, Y., Konosu, A. 2016."Analysis of Bicyclists' Head Protection Methods during Head Impacts to a Car and the Ground in Bicyclist and Car Traffic Accidents, Using a Computer Simulation Analysis Method." JSAE, 47, 2, 20164189 (Japanese).
[9] Fahlstedt, M., Halldin, P., Alvarez, V.S., Kleiven, S. 2016. "Influence of the Body and Neck on Head Kinematics and Brain Injury Risk in Bicycle Accident Situations." IRCOBI Conference, IRC-16-64.
[10] Ito, D., Yamada, H., Oida, K., Mizuno, K. 2014. "Finite Element Analysis of Kinematics Behavior of Cyclist and Performance of Cyclist Helmet for Human Head Injury in Vehicle-to-Cyclist Collision." IRCOBI Conference, IRC-14-21.
[11] Katsuhara, T., Miyazaki, H., Kitagawa, Y., Yasuki, T. 2014. " Impact Kinematics of Cyclist and Head Injury Mechanism in Car-to-Bicycle Collision," IRCOBI Conference, IRC-14-76.
[12] Mertz, H.J., Prasad, P., Nusholtz, G. 1996. "Head Injury Risk Assessment for Forehead Impacts." SAE 960099, 26-46.
[13] Takhounts, E.G., Eppinger, R.H., Campbell, J.Q., Tannous, R.E., Power, E.D., Shook, L.S. 2003. "On the Development of the SIMon Finite Element Head Model." Stapp Car Crash Journal, 47, 107-133.
[14] Takounts, E.G., Craig, M.J., Moorhouse, K., McFadden, J., Hasija, V. 2013. "Development of Brain Injury Criteria (BrIC)." Stapp Car Crash Journal, 57, 243-266.
[15] Matsui, Y., Oikawa, S. 2015. "Feature of Fatal Cyclist Injury in Vehicle-Versus-Cyclist Accident in Japan." SAE, 2015-01-1415.

PREDICTION OF PEDESTRIAN PROTECTION PERFORMANCE USING MACHINE LEARNING

Osamu, Ito
Jun, Shiraishi
Kazuo, Imura
Honda R&D Co., Ltd. Automobile R&D Center
Japan

Takeshi, Yamatoda
Yasuhiro, Kumatani
IDAJ Co., Ltd.
Japan

Paper Number 19-0031

ABSTRACT

According to WHO's report, there are over 270,000 people who are involved in traffic fatal accidents. This figure accounts for 22% of traffic fatalities in the world in 2013. To reduce those pedestrian accidents, many countries apply the pedestrian protection tests for the regulation and the third-party evaluation. For that reason, a method to design the pedestrian protection performance efficiently is required for many cars sold all over the world by automobile manufacturers. In recent years, there are some cases to assist or automate the development using the artificial intelligence acquired by the machine learning. The authors investigated whether it is possible to predict pedestrian head protection performance without using tests or CAE (Computer Aided Engineering) in this research.

The authors used the bonnet hood structures compatible with pedestrian protection and head injury value obtained from CAE for the training data. As for the hood structure, the data obtained by converting 3D geometry into a 2D image was used as the input data. Head injury value was examined by both classification and regression as output information. For the learning model, LeNet-5 of CNN (Convolutional Neural Network) was used, and the layer structure of the model was modified to be suitable for learning of pedestrian protection.

Using the learned model and validated it with some unknown hood images, the model predicted the pedestrian NCAP (New Car Assessment Program) score with an error less than 5% compared with CAE results. Also the predicted head injury criteria map agreed with accuracy more than 75%. In addition, LeNet-5 showed shorter computation time and higher accuracy when comparing the other algorithms.

Although the model was able to reasonably predict the head injury value in the center area t of hood, the accuracy of the perimeter area tended to be lower. Since the data around the perimeter area used for learning was small amount, it is considered that the accuracy is low. In future study, it is necessary to add such data or to device a method to improve accuracy even with the small amount of data.

INTRODUCTION

According to the traffic accident data, it is well known that pedestrian fatal accident is caused by head injury (See Figure 1). Based on this accident data, the third-party assessment organization define WAD (Wrap Around Distance) and validate pedestrian protection performance using a head impactor (See Figure 2). Because mostly test area is on the bonnet hood, it is important to design hood construction to improve head protection performance. As the hood construction depends on styling, it is one of the difficult parts to divert the structure developed in the past. Therefore, it takes a long time to design so that the structure can satisfy the pedestrian safety and other performance. In order to solve this issue, the authors studied the method to design efficiently using optimization techniques in past study [1]. However, the conventional method is required to define the design variables when the styling is changed. For that reason, we could not establish the design method such as to investigate the structure in a short time by using the response surface like.

On the other hand, research in machine learning has advanced in recent years, and cases of utilization are also being reported in design development of manufacturing industry [2]. Since deep learning especially has property to extract attribute by itself [3], the outcomes have been reported for cases where setting attribute and the prediction were difficult [4]. So the authors decided to research the method to investigate the structure satisfied the pedestrian performance in a short time by deep learning.

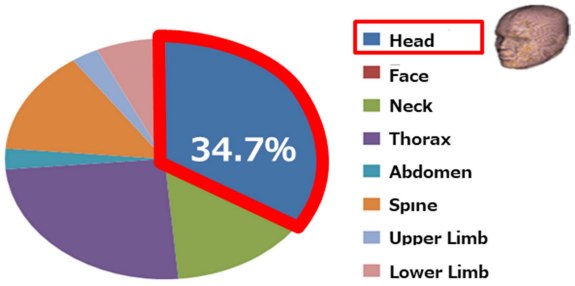

Figure 1. Fatality rate by injury site in pedestrian accident (PCDS 1994-1998)

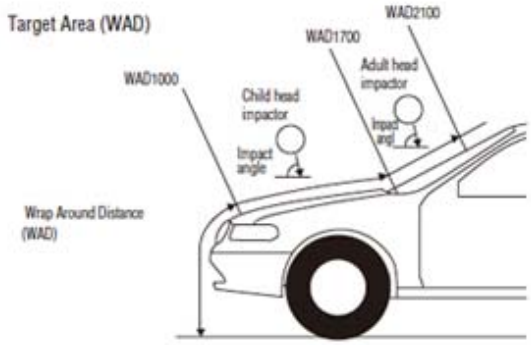

Figure 2. Wrap Around Distance (http://www.nasva.go.jp)

METHODOLOGY

Application process of machine learning

In general, the part design process follows the flow of Figure 3. A target value is set first, then a structure plan that satisfies the target is created and validated by CAE. In many cases, CAE is often performed multiple times with optimization CAE or the like so as to satisfy required characteristics. In this study, we used the surrogate model by machine learning between the structure design and the CAE as Figure 4. By doing this, we estimated the

approximate performance of the structure without using CAE, and decided to reduce the number of investigation by CAE.

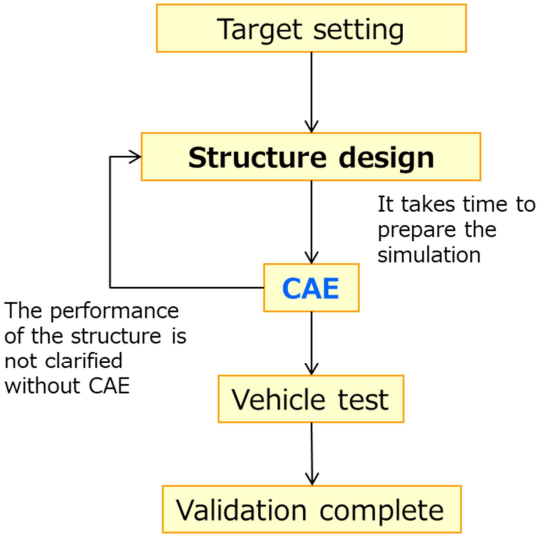

Figure 3. General process of component design

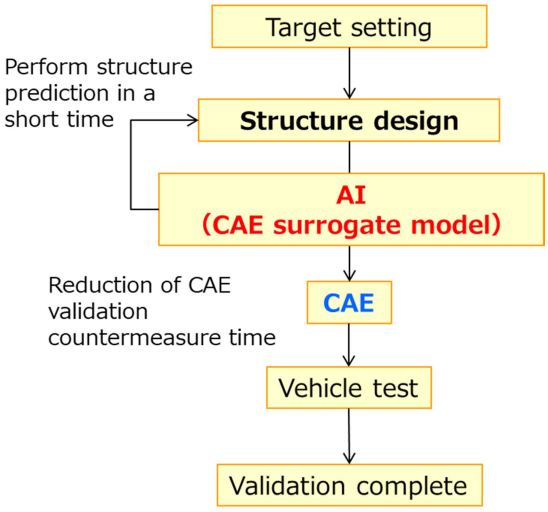

Figure 4. Process using surrogate model

Learning and validation data

The 29 vehicles which were developed for pedestrian protection were used for the learning. The 2D image of each different vehicle's hood data were prepared separately for hood skin, hood frame and others from CAD data. 3D information was represented by displaying the image depth. Furthermore, the difference images of skin and frame were prepared. Finally, a total of 4 images was taken as input data (See Figure 5). As each image was processed with the median filter, the tiny holes and fine shapes were simplified. Also, the input data were divided by 800mm square (48*48 pixel) for each head impactor crash point (See Figure 6). HIC

（Head Injury Criteria） of the CAE result was used for the training data. And the relationship between HIC and hood images near the crash point was learned. In order to validate the learned model, we prepared the 3 vehicles apart from learning data. These vehicles were selected from the category of Mini-van, SUV and Sedan respectively to be able to validate the different hood sizes.

The material and thickness of the hoods used for the learning and the validation were all same property. The ratio of the data used for the learning and validation was 1977: 269. However, 10% of the learning data was also used for checking the degree of learning. TensorFlow [5] was used for the model implementation. The learned model was based on LeNet-5 of CNN [6] but the input image was changed to 4 channels configuration. In addition, the output was set to regression in consideration of convenience. Figure 7 and Table 1 show this model architecture. In the following, this model is written as Modified LeNet-5.

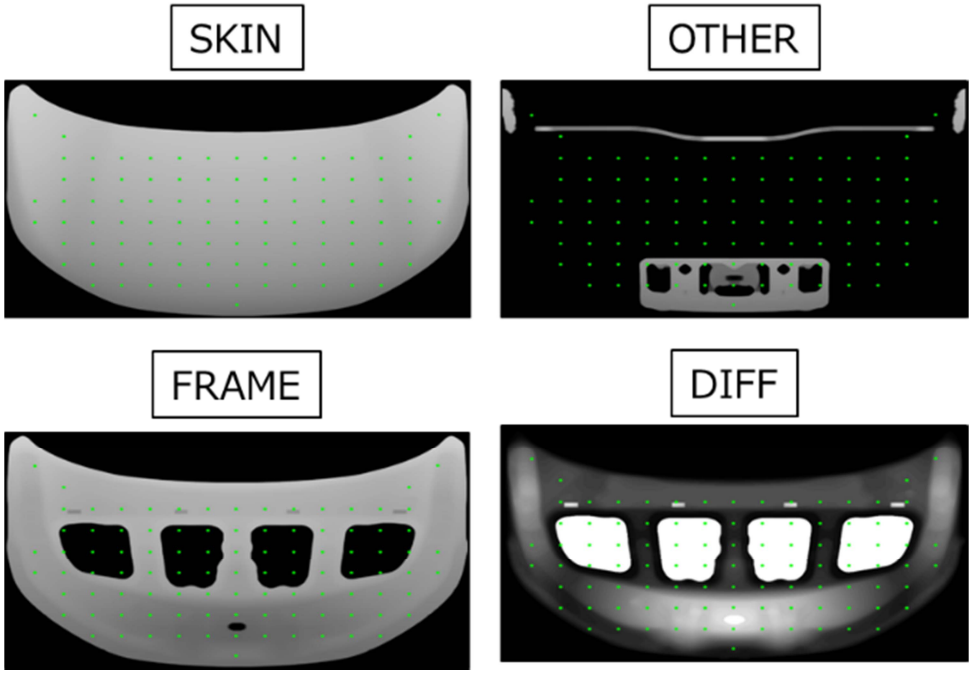

Figure 5. Input data for learning

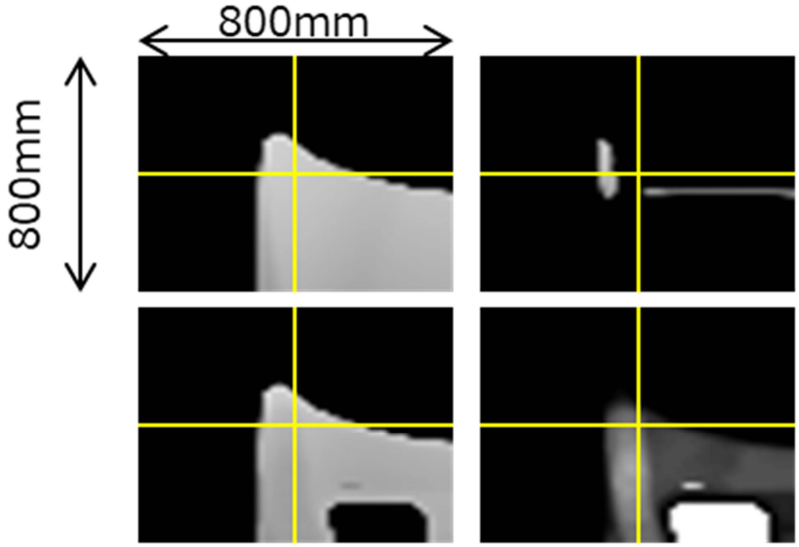

Figure 6. Image data for each crash point

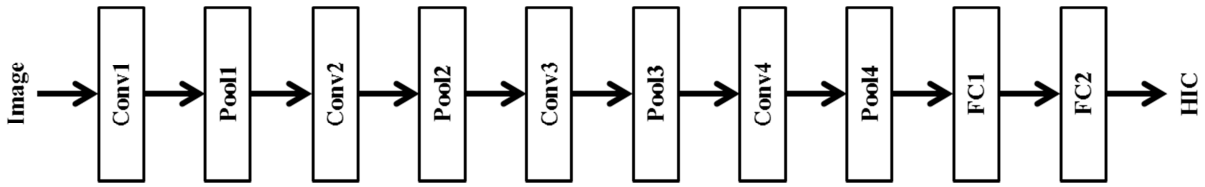

Figure 7. Network Architecture Diagram of our CNN model

Table.1
Network Topology of our CNN model

Network	**Input Size**	**Kernel Size**	**Stride Size**	**Channel Size**	**Output Size**	**Padding**	**Activation Function**
Conv1	48 x 48	5 x 5	1 x 1	16	44 x 44	VALID	Leaky ReLU
Pool1	44 x 44	2 x 2	2 x 2	16	22 x 22	VALID	-
Conv2	22 x 22	3 x 3	1 x 1	32	20 x 20	VALID	Leaky ReLU
Pool2	20 x 20	2 x 2	2 x 2	32	10 x 10	VALID	-
Conv3	10 x 10	3 x 3	1 x 1	64	8 x 8	VALID	Leaky ReLU
Pool3	8 x 8	2 x 2	2 x 2	64	4 x 4	VALID	-
Conv4	4 x 4	3 x 3	1 x 1	128	2 x 2	VALID	Leaky ReLU
Pool4	2 x 2	2 x 2	2 x 2	128	1 x 1	VALID	-
FC1	128	-	-	-	128	-	ReLU
FC2	128	-	-	-	1	-	-

RESULTS

GPU (NVIDIA Tesla GP100) was used for the learning. The mini batch size was set to 300 and the epoch number was set to 5000. MSE (Mean Square Error) was used for the loss function. The calculation time taken for the learning was 140 seconds. The history of loss function shows Figure 8. It indicates that the learning result was valid. Then we confirmed the pedestrian protection performance by using the learned model. The pedestrian protection performance was validated by a NCAP score and a degree of injury value map coincidence. The validation result of each vehicle shows Figure 9. The model predicted the pedestrian NCAP score with an error less than 5% compared with CAE results. The predicted head injury value map agreed with CAE results with accuracy more than 75%. Furthermore, creating an injury value map of each vehicle by CAE took about 40 hours, but the prediction time from the learned model was about 10 seconds. It was confirmed that the learned model can predict the CAE result with sufficient accuracy in a short time.

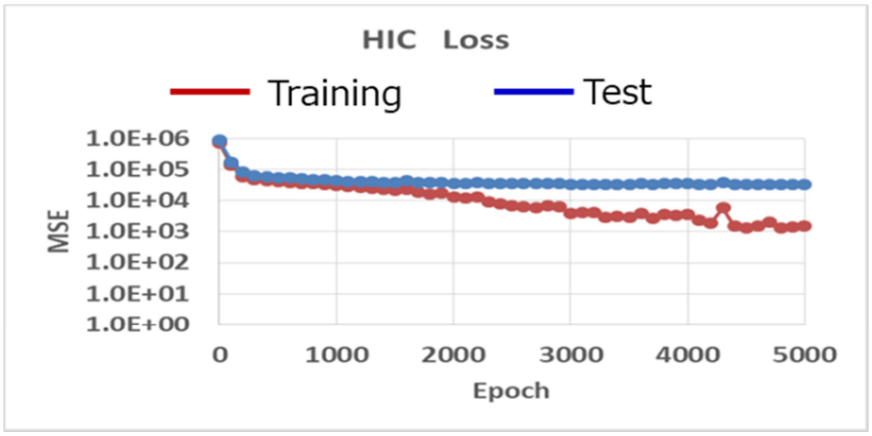

Figure 8. History of loss function

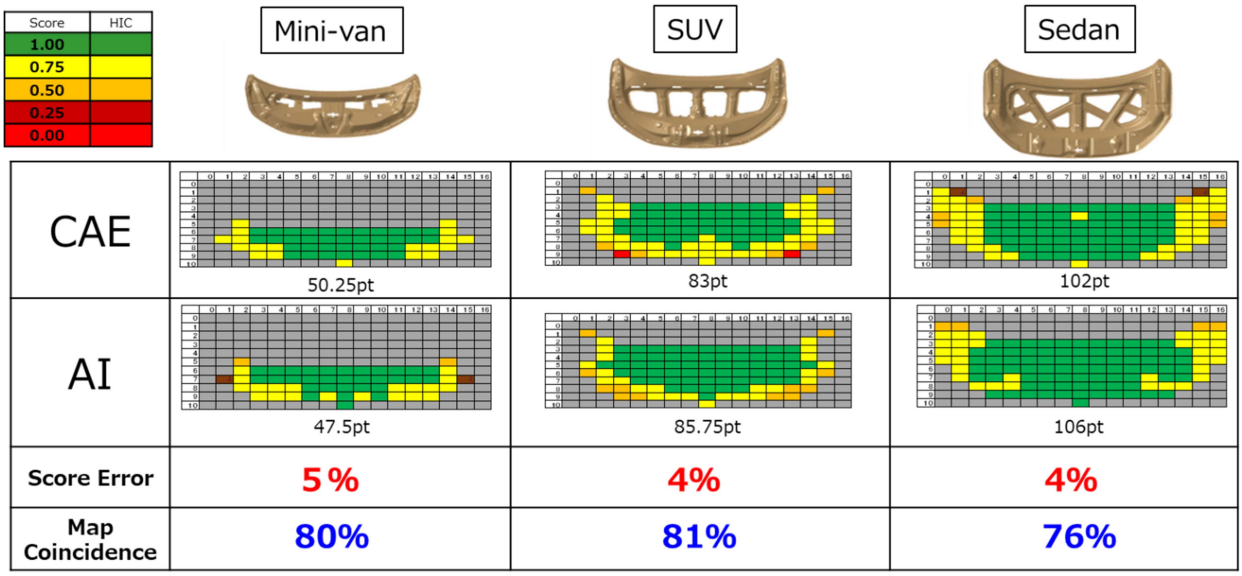

Figure 9. Validation result

DISCUSSION AND LIMITATION

There is room to improve of accuracy in the degree of map coincidence compared with the score error from the validation results. Therefore, the authors decided to further study to improve the accuracy of the map coincidence. Then we implemented the VGG16 [7] and InceptionV3 [8] which are the successor model of LeNet-5 and we compared the results and LeNet-5 result. As for VGG16, the input configuration was changed to 4 channels from the specification for ImageNet. Inception V3 was also set to 4 channels for the input. However, the image size was enlarged to 139*139 pixel due to the model restriction. Since VGG16 and InceptionV3 have a large model capacity, there is a possibility that the calculation does not converge when learning is performed by regression. In this study, the learning was performed by classification for these models considering the calculation stability. The mini batch size was set to 300 and the epoch number was set to 6000. Cross entropy was used for the loss function. The data used for the learning was the same as that used for Modified LeNet-5.

Figure 10 and 11 show the history of loss function for each model. Figure 12 and 13 show the accuracy of each model. Although VGG16 has certain accuracy, InceptionV3 has a low accuracy from these figures. In

addition, Table 2 shows the comparison of the map coincidence accuracy for each model. VGG16 accuracy was almost the same as Modified LeNet-5 but this model took more calculation time than Modified LeNet-5. Inception V3 resulted in quite low accuracy. This is considered that the model capacity is too large for this study with a small number of data. As shown in Figure 14, not only the hood but also the fender and the headlight affect the head impactor. Since the data used for the learning is only the hood images, it can be considered that the attribute of these parts could not be extracted. In addition, all data used in this study is at the completion of pedestrian protection development. Therefore, the data on high HIC was taken countermeasure, so there were few data available (See Figure 14). In order to improve the accuracy of the outer area of a hood, it is necessary to enhance such data.

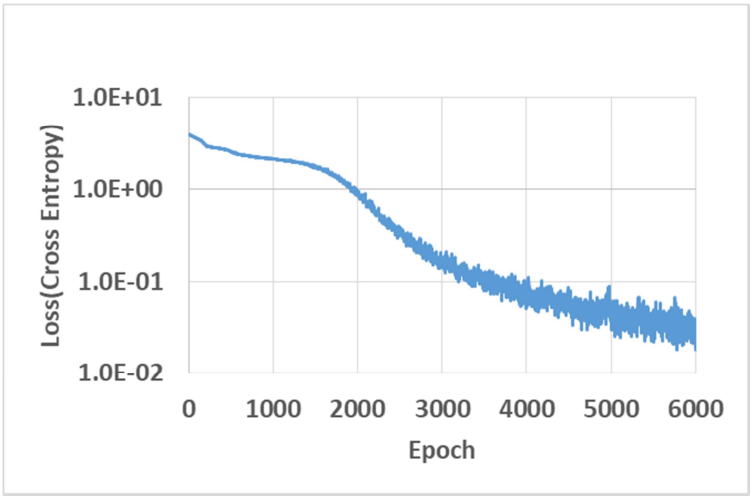

Figure 10. History of VGG16 loss function

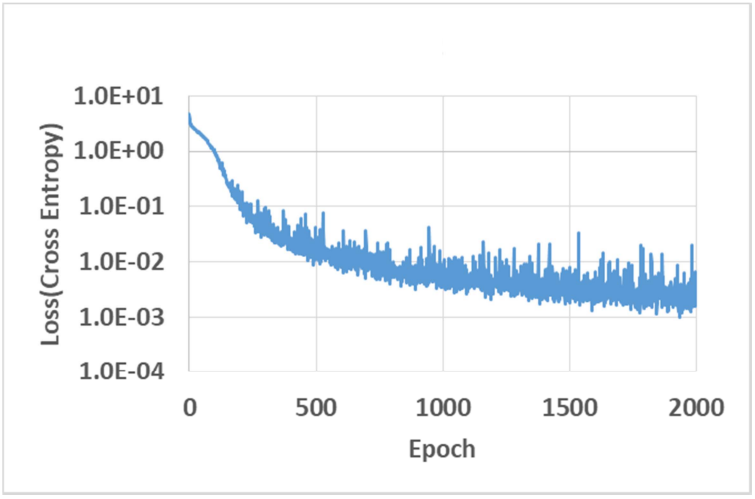

Figure 11. History of InceptionV3 loss function

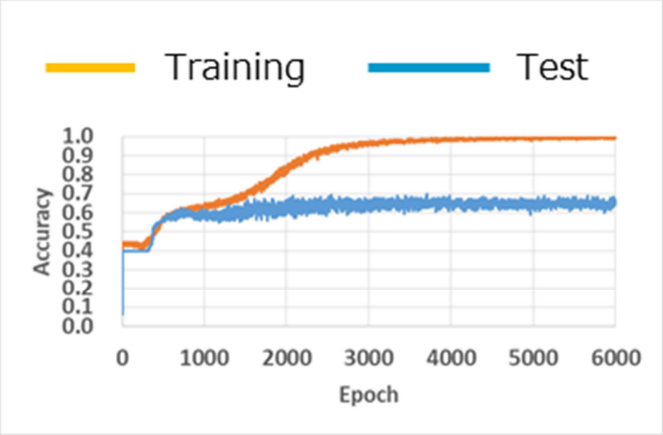

Figure 12. Accuracy of VGG16

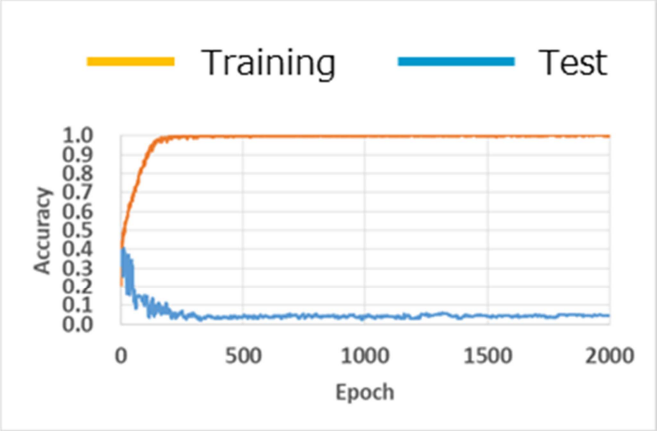

Figure 13. Accuracy of InceptionV3

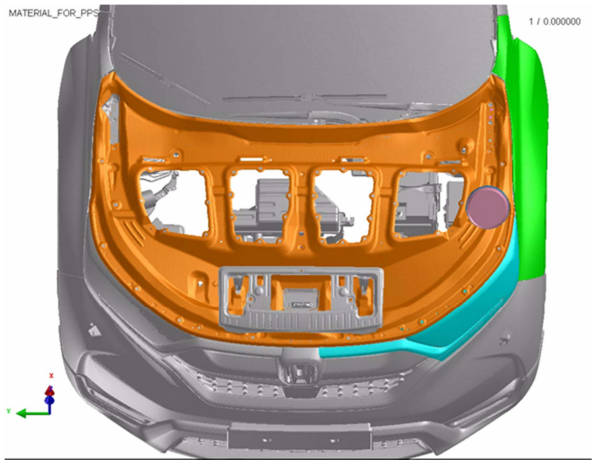

Figure 14. Effect of other parts in outer hood portion

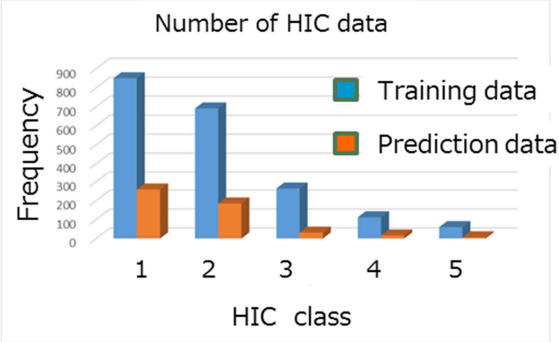

	HIC	Class
Green	HIC < 650	1
Yellow	650 ≦ HIC < 1000	2
Orange	1000 ≦ HIC < 1350	3
Brown	1350 ≦ HIC < 1700	4
Red	1700 ≦ HIC	5

Figure 15. Distribution of data by HIC

Table 2.
Comparison of accuracy of each model

		Modified LeNet-5 (Our method)	**VGG16**	**InceptionV3**
Convergence time		140 sec	1 hour	1.4 hours
Map coincidence	Mini-van	80%	81%	0%
	SUV	81%	64%	0%
	Sedan	76%	72%	2%

CONCLUSIONS

The authors studied whether it is possible to predict pedestrian head protection performance by deep learning without CAE.

Modified LeNet-5 was able to predict the score with an error less than 5% for the CAE result. The predicted color map by Modified LeNet-5 matched at 75% or more compared with CAE result.

The accuracy was mostly equivalent between VGG16 and Modified LeNet-5 but Modified LeNet-5 was more suitable considering the learning time.

The data that can be used for learning and validation was only 31 vehicles (2246 crash points), but the learned model could predict the pedestrian protection performance with sufficient accuracy.

For further improvement of accuracy, it is necessary to add or high HIC data or data obtained by increasing the attribute of the outer of hood area.

REFERENCES

[1] Osamu Ito et_al., 2017, RESEARCH OF ALUMINUM HOOD CONSTRUCTION FOR PEDESTRIAN PROTECTION BY OPTIMIZATION CAE, 25th ESV, Paper No 17-46

[2] Moojoon Shin et_al., 2016, CNN Based Lithography Hotspot Detection, International Journal of Fuzzy Logic and Intelligent Systems, Vol. 16, No. 3, pp. 208-215

[3] Ian Goodfellow et_al., Deep Learning, ISBN-13: 978-0262035613

[4] Quoc V. Le et_al., 2012, Building High-level Features Using Large Scale Unsupervised Learning, Proceedings of the 29th International Conference on Machine Learning

[5] https://www.tensorflow.org/

[6] Y. LeCun et_al., 1998, Gradient-based Learning applied to document recognition, Proceedings of the IEEE, 86(11) pp. 2278–2324

[7] Karen Simonyan et_al., 2014, Very Deep Convolutional Networks for Large-scale Image Recognition, ICLR 2015

[8] Christian Szegedy et_al., 2016, Rethinking the Inception Architecture for Computer Vision, Conference on Computer Vision and Pattern Recognition, pp. 2818-2826

Investigating Accidents Involving Highly Automated Vehicles: Concept of a Data Trustee and Data Model for Future Homologation

Dipl.-Ing. (FH) Melanie Kreutner, Dr. Christoph Lauterwasser, Dr. Johann Gwehenberger,

AZT Automotive GmbH - Allianz Center for Technology

Germany

Paper Number 19-0035

ABSTRACT

According to statements by the EU Commission, 95% of all traffic accidents involve human error, and in 76% of accidents, humans are solely to blame [1]. A similar picture also emerges in the settlement of damages by Allianz Versicherungs-AG, and in detailed analyses of the accident research by Allianz Center for Technology.

At the same time, human drivers set high standards with regard to road traffic safety. Based on market figures over the past few years, in Germany, a passenger car causes material damage only every 250.000 km, and personal injury every 2.3 million km. Since the 1960s, the number of liability claims per passenger car has decreased to a third of the previous figure, and today the claims frequency is at around 60 claims per 1.000 insured units per year [2].

Above the level of high vehicle automation [3] from which the driver is no longer responsible for continuously monitoring the vehicle and the driving task, however, completely new issues will arise in the road traffic accident statistics. In the case of highly automated driving, extremely high requirements must be placed on vehicle safety and on protecting functions in order to not only keep road traffic safety at the current level, but actually improve it significantly. Unfortunately, accidents in the USA with vehicle prototypes in highly automated driving mode show that some accidents cannot be prevented with the current state of technology. Coupled with this is the question as to how cases can be investigated should an accident or criminal misconduct involving a highly automated vehicle occur after the legal authorization of highly automated driving functions and their introduction into the market in the EU.

As explained elsewhere [4], the German liability and insurance system is well suited to covering the risks that exist in the operation of highly automated vehicles. However, the selective operation of the vehicle by the driver and by a highly automated driving function raises fundamental questions concerning the investigation of cases in the event of accidents or traffic offenses.

Early on, Allianz already supported creating conditions so that accidents involving automated vehicles can be reconstructed in the future in order that victim protection, clarification of liability, and regress and product liability claims can still be ensured in a non-discriminatory manner. This is because, in the course of the motor vehicle insurer investigating a case and settling claims, particular importance is attached principally to the driving mode (highly automated driving/transfer phase/driver in control) in which the vehicle was moving at the time of the accident or the traffic offense. On the one hand, a driving error by the driver could be the cause of damage, on the other hand, errors by sensors, inadequate algorithms, deficient software quality or interoperability of systems cannot be ruled out as the cause of an accident. The driver's statement that a collision or non-compliance with traffic regulations occurred after handing over control to the vehicle cannot be verified or disproved without a sufficient set of relevant data.

DRIVING MODE RECORDER / DSSAD

Whereas standards for the data logged in vehicle event data memories have been established in the USA for several years (NHTSA DOT rule 49 CFR Part 563 [5]), outside the USA, there are no such standards to date. In the current stock of vehicles in the EU, reading accident data remains primarily a privilege afforded to the vehicle manufacturer. For external parties, for example experts, reading data is possible only – if at all – with high technical expertise, suitable reading devices, and still limited to some vehicle models.

This problem has been recognized by both the EU and the German government. Thus, in the course of amending the regulation UN ECE-R79 Steering systems, the "World Forum for Harmonization of Vehicle Regulations (WP.29)" develops continuous driving mode storage. The "Data Storage System for Automated Driving", or DSSAD for short, is intended to store data relating to [5]:

- GPS location and time
- Activation of the AD System (Automated Driving Function)
- Transition demands
- Activation of a "minimal risk maneuver"
- Takeover of the driving task by driver
- System error

These data elements are also required in § 63a StVG [7] of the German Road Traffic Act, amended in 2017, in the case a vehicle is equipped with a highly or fully automated function.

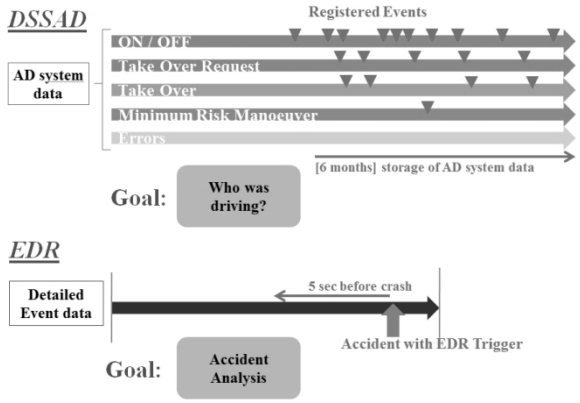

Figure 1: Difference between DSSAD and EDR

Figure 1 shows the difference between DSSAD and EDR. The DSSAD can clarify the question as to whether the vehicle or the driver is in control at a given time. But there is no trigger for data storage in an incident. Besides, it has not yet been determined how authorized persons or parties can access this data and in what location, internally in the vehicle or externally, said data have to be stored. Authorized persons or parties should have easy, tamper-proof, fair and non-discriminatory access to the relevant data elements. These requirements cannot be met when the data is solely stored in the vehicle. A brief example should illustrate this:
A person drives on the freeway in highly automated driving mode and, after this journey, receives a penalty notice as a result of having exceeded the maximum permitted speed by 20 km/h. If the data is stored only in the vehicle, the person in question would have to drive to a workshop or to an expert so that the data can be read in order to prove their innocence.
In the digital age, in which vehicles drive in a highly automated or even autonomous mode, this investment of money and time cannot be considered appropriate. Therefore, the data should be stored externally and should be accessible online, or available on request.

CONCEPT OF THE DATA TRUSTEE

Regulated external data storage and management could be ensured in practice by the concept of an independent data trustee. The data trustee must treat the encrypted raw data transmitted online impartially and check authorized access by interested parties. Figure 2 shows the advantages of double storage, i.e. in the vehicle and with an independent data trustee. Vehicle data that can be attributed to the occurrence of an accident or a criminal offense must not be made available exclusively to the driver, the insurer, the public prosecutors or the vehicle manufacturer. Independent data management by a trustee would ensure that the regulated dataset is accessible to all authorized persons or parties [2].

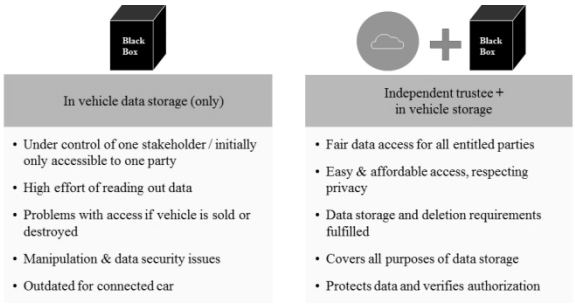

Figure 2: in vehicle storage versus data trustee and in vehicle storage

Example I:
In the case of a notification of a claim where responsibilities are to be clarified, the vehicle owner requests a clarification of the cause from the insurance company. On the basis of the owner's request and authorization and a specific loss event, the insurance company requests the data from the data trustee. In turn, the data trustee distributes the re-encrypted data to the insurance company via a secure channel for further analysis and, if necessary, to the OEM e.g. for product improvement (see Figure 3).
Since the request to the data trustee is ideally made only via a vehicle ID that is generated at the beginning of the authorization, it is not possible for the data trustee to establish a connection between the owner and the vehicle data.

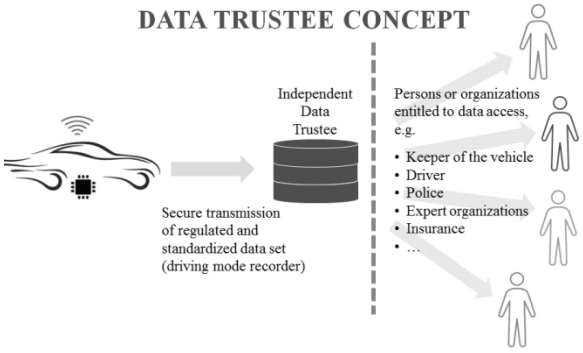

Figure 3: Data Trustee Concept

Example II:
If an owner wishes to view their data independently of the insurance company, e.g. to check for possible self-incrimination, they could make their request directly to the data trustee themselves or via the "Central Vehicle Register", via their attorneys or via an expert. As an alternative to personal requests, anonymous requests could also be answered in this way.
When data is transmitted to the data trustee, said trustee does not require any knowledge about the natural person with which a vehicle/driving mode memory is associated. From the perspective of the data trustee, the data is anonymous or under a pseudonym.
The data trustee should not have any direct contractual relationship with the data owner. Likewise, the data trustee should be independent and, in the relationship between the vehicle manufacturer, the vehicle owner, the driver, the other party involved in an accident (if applicable), and the insurance company, should represent a neutral party without own interests.

The data trustee guarantees the authenticity of the data (i.e. its origin and that it is unchanged) to the aforementioned parties and ensures that the (decrypted) data is provided

a) only to authorized parties,
b) only in authorized situations and
c) only in the regulated scope.

The trustee is also responsible for the security of the stored data against tampering, theft, etc.
Since the dataset as well as the access to data is defined by law, there is no need for the vehicle owner to sign a declaration of consent to storage. A data trustee would be able to provide the data to fulfill statutory require-

ments (e.g. a court order) without the permission of the data owner and, in standard circumstances, without access to the vehicle.
Technically, the requirements on data transmission can be met analogously, that is to say that the data transmission between the vehicle or the driving mode recorder and the trustee is carried out in a tamper-proof and tap-proof manner under any circumstances.
In this case, protecting the transmission via TLS (Transport Layer Security) is obvious, since this is an established protocol which, in addition to the encryption, also ensures that the vehicle's communication partner is also actually the chosen trustee. Additionally, a conventional asymmetric and symmetric encryption method could be used. Handling the data in this manner appears to be modern, convenient and fair.

NEED FOR ADDITIONAL DATA

As shown above some vehicle data have been subject to regulation, however the majority of vehicle data is not regulated in the EU. Figure 4 shows an overview of regulated and unregulated datasets in the EU. From the perspective of accident reconstruction, further standardization of the datasets would be desirable in order to clarify, in addition to the driving mode, the actual cause of the accident and additional questions of liability. An event data recorder is a prerequisite for:

- the ability of the driver and the vehicle owner to exonerate themselves where necessary and to assert product defects or service errors (e.g. in the case of updates and patches)
- protecting vehicle manufacturers and suppliers against unjustified claims
- a fair basis in any product liability cases/regress claims between the vehicle owner or the insurance company and the vehicle manufacturer or supplier

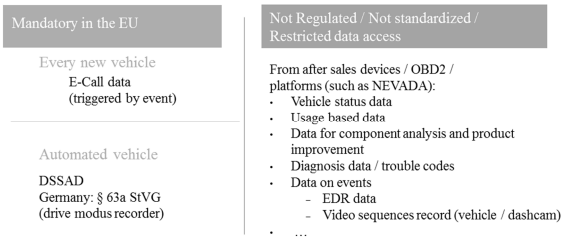

Figure 4: Overview of data handling in the EU

With a view to international harmonization of standards, the profile of requirements in NHTSA DOT rule 49 CFR Part 563 could be a starting point for standardized data logging. However, in the EU project VERONICA II [8] from 2007 to 2009, it has already been shown that this regulation also has its weaknesses in the triggering of an event and the correct interpretation of the data that is read. This also corresponds to the experiences in AZT [9]. In AZT crash tests, multiple tested vehicles from several manufacturers demonstrated good correlations with respect to the crash data when comparing external laboratory measuring equipment with the EDR data logged by the vehicle. The tests also show that it has to be provided that the limitations in data generation in the vehicle are recognized and taken into account.
The analysis of EDR protocols from real road traffic accidents shows that in particular the pre-collision speed data cannot always be interpreted unambiguously, and data elements (such as the turn signal) often are not available for inferring liability.

Regarding triggering an event, it should additionally be noted that the US regulation is not specifically adapted for the requirements of automated driving, but is rather focused on restraint systems being triggered by a change in speed of above approximately 8 km/h within 150 ms as a result of an impact. In the variety of collisions and accident types that are settled by vehicle insurers, from a present-day perspective in accordance with evaluations by Allianz Center for Technology, an airbag is triggered only in a very low percentage of less than 3% of the settled claims. Even fatal accidents involving vulnerable road users exceed the described trigger thresholds on urban road only in very few cases. However, based on 2016 data, in Germany, 27.8% of accidents with fatalities, 33.2% of accidents with severe injuries and 27.8% of accidents with minor injuries in road traffic were attributable to accidents involving cyclists and pedestrians [10]. In addition, a research initiative by Allianz, Continental and Munich University of Applied Sciences showed that approximately 40% of all passenger car accidents with material damage are parking and maneuvering accidents [11]. In these collisions as well, the change in speed of the passenger car as a result of an impact is generally below the trigger threshold of the US regulation.
With a view to protecting victims and clarifying questions of liability, in the future, a much higher percentage of accidents should be able to be captured and stored by an event data recorder in highly automated cars.

OUTLOOK FOR AHEAD DATA MODEL

Automated Driving requires a highly sophisticated degree of vehicle, event and accident information well above US-EDR standard for data capturing, period, recording, storage, retrieval and safety. The work group "AHEAD" (Aggregated Homologation-Proposal for Event-Recorder-Data for Automated Driving), established in 2017, a cooperation by Allianz, AXA, CARISSMA/TH Ingolstadt, Continental and DEKRA, has therefore committed to drafting detailed requirements for an event data recorder for vehicles with automated functions of level 3 and above. The aim is to develop a data model that allows transparent, non-discriminatory and tamper-proof accident reconstruction and is compatible with current data protection laws. Storing crucial vehicle data shall be limited to a short timeframe before, during and after a triggering an event with the goal of obtaining accurate, in-depth accident data. The technical level of EDR as defined in the VERONICA II Project (2007-09) and as referred to in the "European Parliament resolution of 27 September 2011 on European road safety 2011-2020 (2010/2235(INI))" is a good starting point. But with regard to Automated Driving it is not sufficient any more. AHEAD has set out to update the requirements. Building on the results from the EU project VERONICA II and taking into consideration the automated driving functions, AHEAD describes data elements and organizes them into four standardized categories. According to the AHEAD White Paper [**Error! Reference source not found.**] the AHEAD Data Model includes but is not limited to the following data:

- Driving Data
  - Vehicle Status, Operation Mode (e.g. manual, autonomous, remotely controlled), Speed, Yaw Angle, Control interventions of the assistance system, Takeover request
  - Diagnostic data of safety relevant systems and components (condition, status, system failures/ technical malfunction)…
- Driver Activity
  - Video feeds from cabin cameras, Steering, Seat Position, Pedal Positions, Driver Alertness…
- Surroundings- and Object Recognition
  - Video feeds from front and rear-facing cameras, Sensor Data, Classified Objects, Object Position, Object Direction, Object Speed, Calculated Movement…
- Crash
  - Date, Timestamp, Location, Acceleration, Collision Speed, Seat Belt Status, Airbag, Restraint System…
  - Sensor technology, e.g. advanced and sensitive trigger which recognizes accidents with low acceleration in order to detect and measure accidents with vulnerable road users involved, or parking/maneuvering accidents

Whereas the required driving data, the data elements relating to driver activity and the crash data can be described by individual signals, the data related to environment and object recognition consist of elements that may have already been merged, calculated and assessed, which make it possible to compare the generated model of the vehicle environment with the reality and to check the plausibility of the control commands of the vehicle. The process of generating a virtual world and moving in a real world provides a high potential for errors. A highly automated vehicle must therefore provide data relating to this process. Since the calculation algorithms of manufacturers' systems relating to sensor fusion, environmental model calculation and path planning of the highly automated ego-vehicle are strictly confidential, storing the raw sensor data is insufficient in this case.

The vehicle sensors, the vehicle cameras and other networking or communication channels of the highly automated and connected vehicle must be able to keep track of the entire vehicle environment. In practice, this means multiple overlapping and redundant "sensor cocoons" [13]. The detected sensor signals must be checked for plausibility, classified, provided with a time stamp, prioritized and annotated a thousand times per second. Lastly, in the generated environmental model, the location of the ego-vehicle relative to its environment must be determined in a repeatable manner and to within a centimeter. This processing of the signals can no longer take place by means of the bus systems used up to now, but rather must be processed by means of software blocks, which contain corresponding algorithms, on sensor platforms. The situational awareness of the highly automated vehicle which is calculated on said platforms part of the basis for the standardized data storage according to AHEAD.
The raw data supplied by the sensors (camera, laser scanner, radar, ultra sound) is prepared and evaluated by a number of different algorithms. The environment with the objects located in it must be classified and located by different methods. Thus the actual state of the vehicle environment is determined on the basis of a model, taking into consideration weather and visibility conditions. By means of GPS data, HD card data, the inertial sensor, the cameras, the laser scanner, the radar and ultrasound sensors, the ego-vehicle can locate itself in said environment. So that the ego-vehicle can also move in this environmental model, the future must also be calculated. For this purpose, numerous assumptions about the movements of other objects must be made. If the system has decided on path planning at a certain speed, this can ultimately be implemented in the form of control commands to the longitudinal and lateral control.
One of the greatest challenges for AHEAD will be getting this variety of data to a suitable level and an enforceable standard. This must also be done in accordance with the following AHEAD Guiding Principles for access to vehicle data:

- Consent
- Fair and undistorted competition
- Data privacy and data protection
- Tamper proof access and liability
- Data economy
- Standardized interface
- Crash resistance of data storage system in vehicle
- Event Data Storage for limited period of time before and after an incident (~ 30 sec)

Therefore the individual data elements required are continuously validated on the basis of real accidents and crash tests and evaluated and publicly discussed in various discussion groups. The AHEAD members invite stakeholders involved in setting the rules and requirements for Automated Driving (Parliament, Commission, Member States and others) to enter into dialogue.

CONCLUSIONS

An EU wide regulation with respect to a driving mode recorder, access to the data via a data trustee in combination with the introduction of an event data recorder for highly automated driving functions would have considerable advantages for the parties involved:

- The main focus would be on the public interest in integrity and victim protection.
- The ability of the driver and the vehicle owner to exonerate themselves where necessary and to assert product defects.
- Protecting vehicle manufacturers and suppliers against unjustified claims.
- Access to data would be politically endorsed and legitimized.
- Fairness for all parties.

In order for highly and fully automated driving to be widely accepted by society, the driver must only be able to be prosecuted for his own misconduct. It must therefore always be possible to clarify who is responsible (if the system has failed or if the person has failed). This driving mode data must be available for investigation through storage in order to clarify whether the vehicle was controlled by the automated system at the time of the incident or by the driver or was in the handover phase between the human driver and the automated system.
The necessary data must be in the hands of a neutral, independent third party (data trustee) in order to allow all authorized persons access to the data under the same legal conditions. In addition to storing the data in the vehicle itself, transmission to an independent third party is therefore mandatory. In the event of a vehicle being sold or after the vehicle has been destroyed in an accident, the data trustee is the only source of clarification in the interest of all parties involved.

Moreover, for highly automated vehicles (Level 3 and higher), a standardized event data set from the vehicle in the event of an incident is required. Only in this way will it be possible in future to clarify accidents or legally punishable events involving automated vehicles in a proper and transparent manner. The AHEAD working group develops parameters for such a data set. The data model includes elements on the vehicle status, driving environment, driving situation and driver activity which are defined for accident clarification. In addition trigger thresholds are defined with the goal of storing crucial vehicle data limited to a short timeframe before, during and after relevant events.

REFERENCES

1. European Commission. Digital Single Market, Mobility. Available at: https://ec.europa.eu/digital-single-market/en/mobility, accessed Mai 14, 2018

2. Hüttinger M.; Lauterwasser C.; Trinitis J., Standardized data recorders in highly automated vehicles [Standardisierter Datenschreiber bei hochautomatisierten Fahrzeugen] Insurance industry requirements and the data trustee model [Anforderungen der Versicherungswirtschaft und Modell eines Datentreuhänders], Haus der Technik, Developing methods for active safety and automated driving [Methodenentwicklung für aktive Sicherheit und Automatisiertes Fahren], 2nd Expert Dialog on Effectiveness – Controllability – Protection [2. Expertendialog zu Wirksamkeit – Beherrschbarkeit - Absicherung], expert verlag, Renningen 2017

3. Federal Highway Research Institute. Research Compact 11/12. Gasser T. et al. Legal consequences of an increase in vehicle automation. [Rechtsfolgen zunehmender Fahrzeugautomatisierung, Bundesanstalt für Straßenwesen, Forschung kompakt 11/12]. Available at: https://www.bast.de/BASt_2017/DE/Publikationen/Foko/Downloads/2012-11.html, accessed Mai 14, 2018

4. Stadler M. Civil law issues relating to automated driving. Paper presented at: 56th German Traffic Court Conference. Work Group II [56. Deutscher Verkehrsgerichtstag. Arbeitskreis II. Zivilrechtliche Fragen des Automatisierten Fahrens]. Goslar 2018

5. NHTSA National Highway Traffic Safety Administration. Rule 49 CFR Part 563. Event Data Recorders. Available at: https://one.nhtsa.gov/Laws-&-Regulations/Vehicles, accessed Mai 14, 2018

6. World Forum for Harmonization of Vehicle Regulations WP.29. ACSF-06-28 Secretary Consolidated document after 6th session. Available at: https://wiki.unece.org/display/trans/ACSF+6th+session. Accessed Mai 14, 2018

7. Dejure.org. Rechtsinformationssysteme GmbH. § 63a – 63b German Road Traffic Act [StVG]. Available at: https://dejure.org/gesetze/StVG/63a.html, Accessed Mai 14, 2018

8. Schmidt-Cotta R., EU Project VERONICA-II Final Report. Available at: http://www.veronica-project.net/. Accessed Mai 14, 2018

9. Dürnberger S.; Kreutner M. EDR data now and in the future [EDR-Daten heute und in Zukunft]. VKU Road Accidents and Vehicle Technology [Verkehrsunfall und Fahrzeugtechnik] 10/17. 55th Volume. October 2017

10. Federal Statistical Office of Germany. [Statistisches Bundesamt]. Road Accident. Fachserie 8 Reihe 7. Available at: https://www.destatis.de/DE/Publikationen/Thematisch/TransportVerkehr/Verkehrsunfaelle/VerkehrsunfaelleJ2080700167004.pdf?__blob=publicationFile. Accessed Mai 14, 2018

11. AZT Automotive GmbH, Continental, Munich University of Applied Sciences. A sudden bang when parking, Research Initiative on Parking and Maneuvering Accidents 2015. Press release [AZT Automotive GmbH, Continental, Hochschule für angewandte Wissenschaften München, Es kracht beim Ausparken,

Forschungsinitiative zu Park-und Rangierunfällen 2015, Pressemeldung]. Available at: https://www.allianzdeutschland.de/es-kracht-beim-ausparken/id_73896418/index. Accessed Mai 14, 2018

12. Forster, A. AHEAD Positions on EDR. EDR is active legal certainty and data privacy. Paper presented at: EU parliament. October 18, 2018, Brussels
13. Schrepfer J., Mathes J., Picron V., Barth H. Automated Driving and its Sensors under Test, ATZ Automotive Technology Magazine [Automatisiertes Fahren und seine Sensorik im Test, ATZ-Automobiltechnische Zeitschrift], 01/2018 Edition, Springer Professional, Wiesbaden, 2018

STATUS OF NHTSA'S EJECTION MITIGATION RESEARCH

Aloke Prasad
National Highway Traffic Safety Administration
United States of America

Corinn Pruitt
Transportation Research Center Inc.
United States of America

Paper Number 19-0036

ABSTRACT

The objective of this paper is to present an update on the research conducted by the National Highway Traffic Safety Administration (NHTSA) to assess the performance of roof glazing in production vehicles and certain countermeasure designs in preventing occupant ejections.

Federal Motor Vehicle Safety Standard (FMVSS) No. 226 "Ejection mitigation" set requirements for ejection mitigation systems to reduce the likelihood of complete and partial ejections of vehicle occupants through side windows during rollovers or side impact events.

In the preamble of the final rule establishing the standard (Jan 2011), the agency stated "NHTSA is interested in learning more about roof ejections and would like to explore this area further..." It also stated that while sun/moon roof ejection could be potentially cost effective to mitigate, the agency was not in a position to extend coverage to roof glazing in the final rule because the agency wanted to research a viable performance test procedure.

The assessment of ejection protection offered by sunroofs was made using a guided impactor (18 kg) directed toward roof glazing (pre-broken) from inside the vehicle, based on the procedures developed in the FMVSS No. 226 regulation[2], with test speeds of 14, 16, and 20 kilometers per hour.

Tests were conducted on production and countermeasure sunroof designs for the 2016 Ford F-150, production sunroofs for 2012 Toyota Prius, and production sunroofs provided by the Aisin Technical Center of America.

For sunroofs with both a fixed and a moving panel (F-150, Aisin), the movable panels presented more challenges to contain the headform than fixed panels. For the moving panels, the sunroof attachment structure separated at the inserts (into the rails). Fixed panels had higher excursions at unsupported transverse edges or edges without any metal encapsulation frames. The F-150 fixed rear panel had front and rear transverse unsupported edges, while the Aisin had longitudinal edges without metal frames. Laminated glazing panes with thicker polyvinyl butyral (PVB) inner layer in and polyethylene terephthalate (PET) film with tempered panes used as countermeasures for the F-150 sunroof reduced glazing stretch (and ram excursions). However, this transferred more forces to the edges and presented a greater challenge for movable panel containment at rail attachments.

The fixed polycarbonate panel used in the Prius had low ram excursions but high ram decelerations.

Meeting some excursion limit will require designs that have strong attachments to the vehicle roof or rails. Deformation of the glazing and encapsulation frame should be limited when impacted at the center of the panel. Any tear/rip of the plastic layer would add to the excursion of the ram.

The number of vehicle designs tested was limited by the availability of laminated glazing used in production or countermeasure designs.

This paper details performance of selected production and countermeasure sunroof designs in limiting headform excursions. Some of the fixed sunroof designs had excursions of less than 100 millimeters. The movable sunroof designs tested will require additional countermeasures to perform at this level.

INTRODUCTION

The National Highway Traffic Safety Administration (NHTSA) is continuing its exploration of roof ejection mitigation which commenced following NHTSA's issuance of FMVSS No. 226. FMVSS No. 226 sets requirements for ejection mitigation systems to reduce the likelihood of complete and partial ejections of vehicle occupants through side windows during rollovers or side impact events.

The final rule (Jan 2011) preamble said, "NHTSA is interested in learning more about roof ejections and would like to explore this area further...".[1] It also stated that while sun/moon roof ejection could be potentially cost effective to mitigate, the agency was not in a position to extend coverage to roof glazing in the final rule because the agency wanted to research a viable performance test procedure.

This paper addresses testing on production and prototype countermeasure sunroof designs to evaluate performance in preventing occupant ejections. In addition, a modified test setup with updated headform orientation and test speeds was evaluated. Additional production sunroof and countermeasure tests were completed with the new test setup.

TEST PROCEDURE AND EQUIPMENT

This study involved impacting three different production sunroofs and potential countermeasures aimed at improving occupant protection. Sunroofs and countermeasures were selected to represent a variety of constructions currently available in the market. The test method (equipment, initial selection of speeds) was adapted from the procedure used for FMVSS No. 226 and involved impacting the sunroofs with a featureless headform at different velocities.[2] The performance of each sunroof was evaluated by analyzing ram excursion, edge excursion using photogrammetry, observations of failures, and high-speed video.

Vehicle and Buck Descriptions

2016 Ford F-150 Construction The 2016 Ford F-150 (gross vehicle weight rating of 2767 kg to 3198 kg) was selected as it had large panels and was one of the widest sunroofs available at the time (Figure 1). It had a tilt slide sunroof with the front moveable panel sliding underneath the rear fixed panel. The sunroof module was bolted to the roof at twenty locations indicated by red arrows in Figure 2. The sunroof module consisted of a fixed panel and a movable panel (Figure 3). Both panels were assembled to the sunroof module using screws along the left and right sides, leaving the transverse sides unsupported (Figure 4). The production panels were made of laminated glass (2.1 – 0.76 – 2.1 mm; annealed glass – PVB – annealed glass) and were used as a baseline condition for the vehicle. Two countermeasure sunroof designs were tested. The first countermeasure increased the thickness of the PVB interlayer (2.1 – 1.52 – 2.1 mm; annealed glass – PVB – annealed glass). The second countermeasure investigated the performance of a polyethylene terephthalate (PET) protective film (Protec® II) applied to tempered glass (Protec® II film on inner surface; 5.0 mm tempered glass). The two countermeasure glass panels were attached to the sunroof assembly in the same manner as the production panels.

---

[1] 76 FR 3262, January 19, 2011

[2] 49 C.F.R. § 571.226, S5. Test Procedures

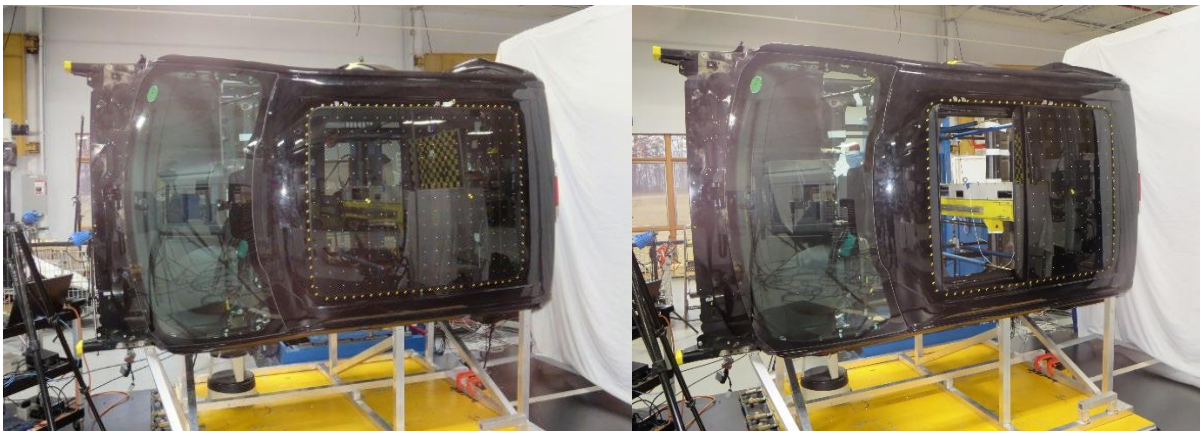

Figure 1. View of F-150 sunroof panel in both closed (left) and open (right) positions from outside. The F-150 had one of the largest sunroofs available at the time.

Figure 2. Red arrows indicate where sunroof module was bolted to the roof of the vehicle.

Figure 3. F-150 sunroof panels – left: front moveable panel, right: rear fixed panel.

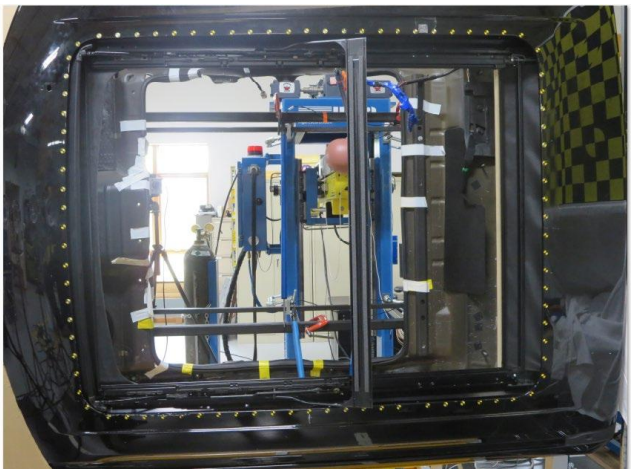

Figure 4. Front and rear panels assembled to module using screws along longitudinal edges.

2012 Toyota Prius V The 2012 Toyota Prius V had a large polycarbonate sunroof composed of one fixed panel with two daylight openings (Figure 5). The overall size of the panel was approximately one meter wide by one meter long. The test area of the daylight openings was approximately 0.29 meter^2. The panel was glued with polyurethane to the roof of the vehicle (Figure 6).

Figure 5. Toyota Prius V large polycarbonate sunroof with two daylight openings.

Figure 6. Sunroof panel glued to roof of vehicle with polyurethane.

Aisin Sunroofs Aisin Technical Center of America (Aisin) provided panoramic moveable sunroofs to be used for testing. The glazing composition of these sunroofs were 2.0-millimeter annealed glass (outside) – 0.76-millimeter PVB – 1.8-millimeter glass (inside). They were outer slider type sunroofs where the moveable front panel slides outside of the fixed rear panel (Figure 7). The sunroof module was attached to a custom-made test fixture at the same locations that it would be attached to the vehicle roof (Figure 8). The panels were attached to the sunroof module along the left and right longitudinal sides using a combination of plastic brackets and glue, while the transverse sides were unsupported (Figure 9).

Figure 7. Aisin outer slider sunroof – front slides outside of rear panel.

Figure 8. Sunroof module attached to custom-made frame at same locations as vehicle roof.

Figure 9. Panels attached to module using plastic brackets and glue along longitudinal edges.

Test Set-Up Description

The F-150 and Prius had the floor and other non-integral components removed, then were turned 90 degrees and mounted sideways to a rigid frame to allow the impactor to be aimed at the roof structure. The Aisin sunroof module was attached to a frame of the same geometry and attachment locations as the vehicle roof. To simulate damage experienced in a rollover crash, glass was pre-broken on both sides in a 75-millimeter offset pattern following the FMVSS No. 226 procedure,[3] except for the Protec® II film which was only punched on one (glass) side. The method used a 75-millimeter offset pattern, with a 75-millimeter by 75-millimeter pattern on the outside surface and the same pattern offset by 37.5 millimeters on the inside surface. Glass was broken using a spring loaded centerpunch. Prior to testing, the daylight opening was established, and an offset line 25 millimeters inside of the daylight opening was marked on the glass.

The ejection impactor used in this project meets FMVSS No. 226 specifications. It was a guided impactor that used a featureless headform (176.8 x 226.1 mm) attached to a shaft (Figure 10). The impactor had a mass of 18 kilograms. Impact velocities used in this project were 14, 16, and 20 kilometers per hour. Both 16 and 20 kilometers per hour are standard speeds used in FMVSS No. 226.

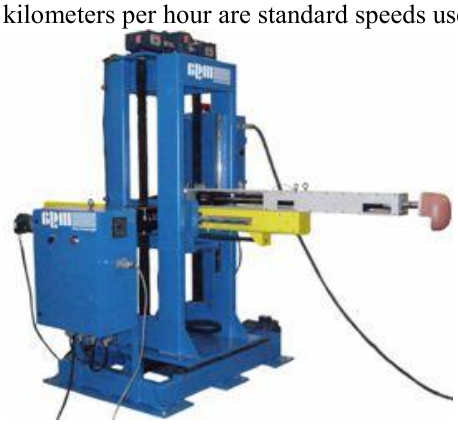

Figure 10. Ejection guided impactor with 18 kg featureless headform.

Measurements were recorded with a variety of transducers, which are summarized in Table 1.

Table 1.

Summary of Transducers Used.

Measurement	**Transducer Details**
Ram Velocity	LVDT (differentiated)
Ram Excursion	LVDT
Dynamic edge excursion	High speed video with targets (analyzed with photogrammetry)

Photographs were taken to document the test setup and post-test observations. High-speed video was used to capture the impact during each test.

Initial Baseline and Countermeasure Tests for the Ford F-150

The 2016 Ford F-150 production sunroof and countermeasures were initially evaluated using the test setup from previous rounds of testing (center and corner impact locations) with additional locations added. Additional locations were selected based on engineering judgement to greater evaluate loading on the glass and loading on panel attachments. These locations were believed more likely to have poor performance. To select these locations, it was assumed that the left and right sides of the panels were identical but the front and rear sides were not. Test locations used are shown in Figure 11. The headform was aligned so that its longitudinal axis was parallel to the vehicle's longitudinal axis. Test speeds were 16 and 20 kilometers per hour. The sunroof panels were replaced after each impact. The entire sunroof module was replaced after each panel was tested once.

---

[3] FMVSS No. 226, S5.4.1, Window glazing pre-breaking procedure

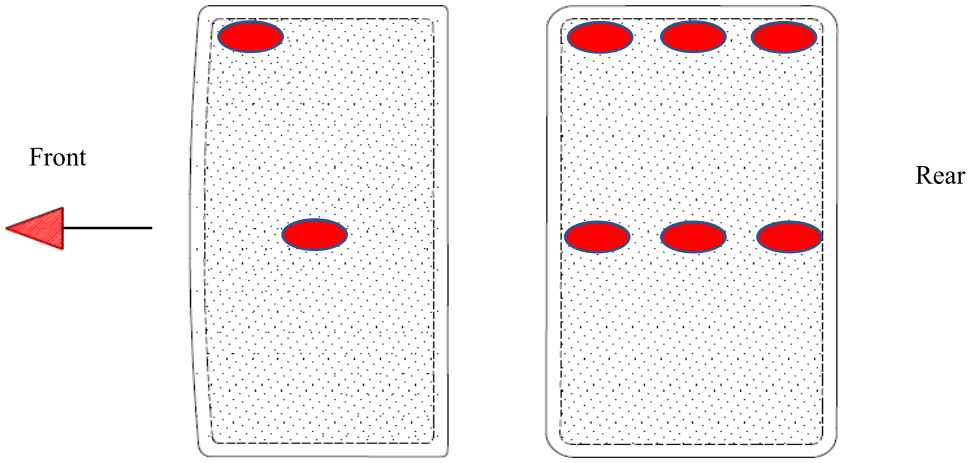

Figure 11. Initial test locations and headform orientation (F-150).

Countermeasures tested were the thicker PVB interlayer and the Protec® II glazing. Countermeasures were only tested at the center and front corner locations. Production glass was tested at the additional locations shown above. The test was setup following the procedure outlined in the section above for each of the tests. The only exception was test 74 where the Protec® II glazing was punched on both sides.

Initial Countermeasure Results

Countermeasures were compared to production glass and results are shown in the figures below. The top and bottom values represent ram excursion at 16 and 20 kilometers per hour respectively, at each location. Any asterisk (*) represents a rail mount failure (separation of the moving panel frame from the rail) at that speed and location. Excursion values exceeding 100 millimeters are shown in red color.[4] For the countermeasure tests, the percent change from the baseline production glass is also shown in parenthesis for instances without detachment at the rails. Full results (ram and edge excursions) can be found in Appendix A (Table A.1).

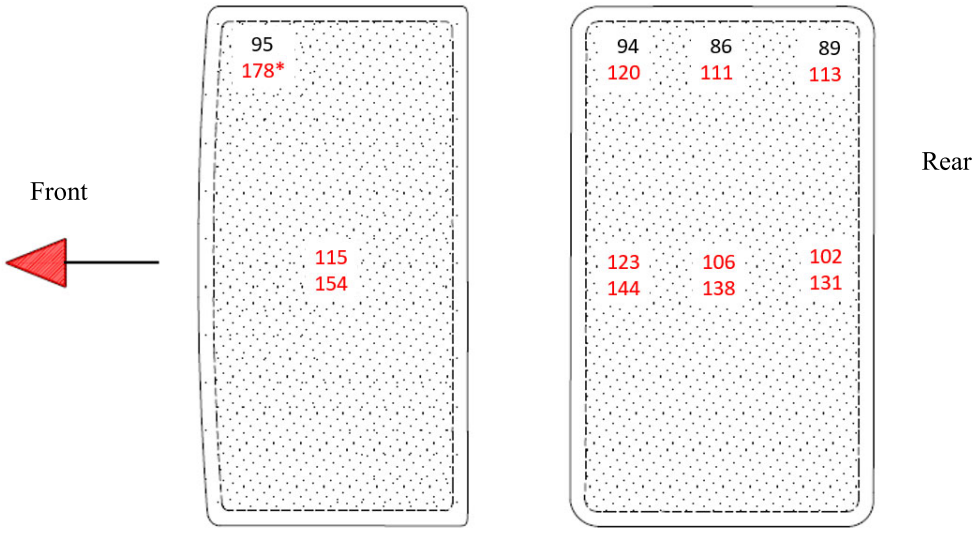

Figure 12. Production Glass (baseline) Results.

---

[4] FMVSS No. 226, S4.2.1 limits the headform displacement to 100 millimeters after impact with the glazing pane surface.

For production glass, on the front movable panel, hits at the center had PVB stretch and transverse frame bending. At the corner of the front panel there was rail failure using the higher impact speed and therefore a large ram excursion. On the rear fixed panel, there was no edge failure for any location. At 16 kilometers per hour, ram excursions were below or just over 100 millimeters, except for at the forward transverse edge which is thinner and weaker and therefore had a higher excursion.

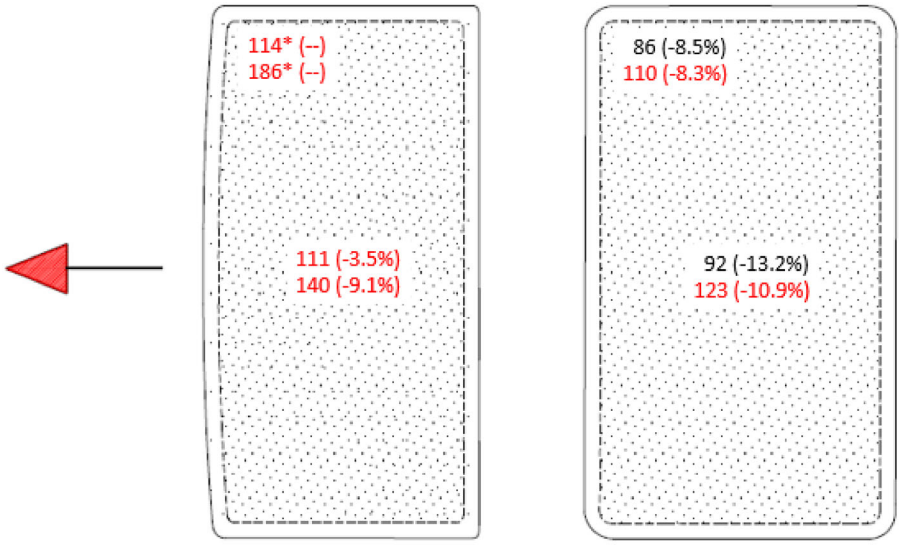

Figure 13. Thicker PVB Results.

For the thicker PVB panels, on the front movable panel, hits at the center showed less stretch but more transverse frame bending than the baseline panels. At the corners, catastrophic edge failure (complete detachment of the panel frame from the rail) was seen. On the rear panel, the thicker PVB reduced excursions by approximately 10 percent.

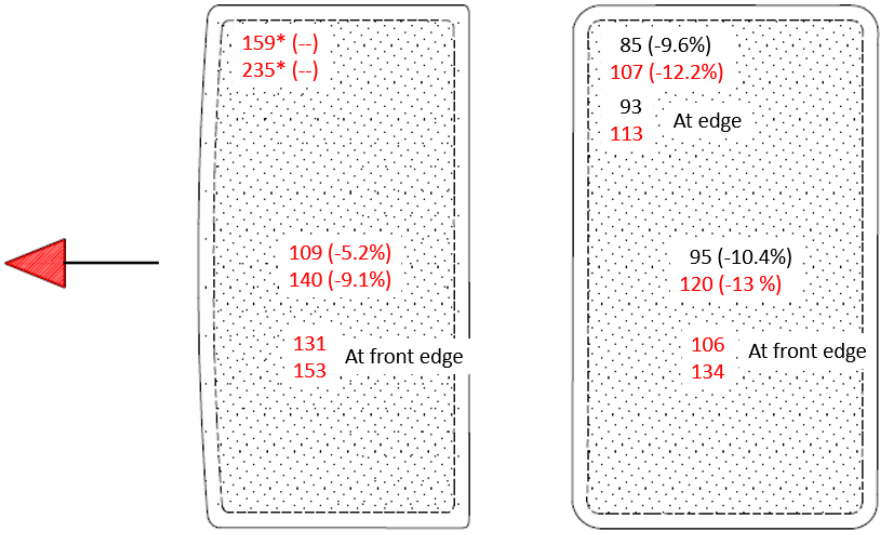

Figure 14. Protec® II Results.

For the Protec® II panels, hits on the front movable panel, at the center, had less film stretch but much more transverse frame bending than the baseline panels. At the corner, there was catastrophic edge failure at both speeds. On the fixed rear panel, there was approximately a 12 percent reduction in excursions. Like the thicker PVB, the reduced film stretching of the Protec® II led to increased loads on the edges.

Movable panels presented more challenges for containing the headform than fixed panels, for both the production panels and countermeasure panels. The thicker PVB and Protec® II panels did not tear and had reduced stretch, however this lead to more forces being transferred to the edges. Overall, baseline production panels showed feasibility at 16 kilometers per hour. Countermeasures showed they can improve the feasibility of meeting a 100-millimeter excursion limit; however, results can change for different panel designs.

Modified Test Conditions

Based on results from initial F-150 testing, impact locations and speeds were modified for future evaluations. The new test setup was based on the wording of FMVSS No. 226, as adapted for ejections through roof portals. Test locations included the corners, center, midpoint of transverse edges, and two-thirds of the longitudinal edge as shown in the figure below. Head orientation was changed so that the longitudinal axis of the headform was perpendicular to the longitudinal axis of the vehicle (Figure 15).

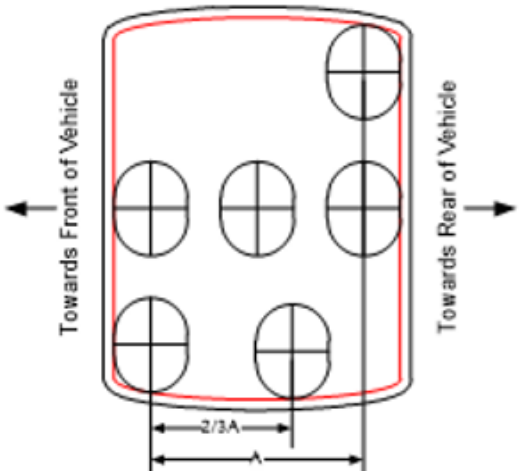

Figure 15. New Test Setup.

A test speed of 14 kilometers per hour was added. Each location was first hit at 16 kilometers per hour. If the ram excursion was greater than 100 millimeters, that location was then impacted at 14 kilometers. If the ram excursion was less than 100 millimeters at 16 kilometers per hour, then it was impacted at 20 kilometers per hour.

The test was setup following the procedure described in the section titled “Test Set-Up Description.”

Photographs were taken to document the test setup and post-test observations. High-speed video was used to capture the impact during each test. This video was also used for photogrammetry analysis to determine edge excursion.

EJECTION TEST RESULTS

Ford F-150 Results

The top, middle, and bottom values in Figure 16 represent the ram excursions (in millimeters) at speeds of 14, 16, and 20 kilometers per hour, respectively. An asterisk (*) indicates a rail mount failure. Green represents ram excursion values less than 100 millimeters and red represents excursion values greater than 100 millimeters. Six tests with thicker PVB (3 front panel and 3 rear panel) and one test with Protec® II were done. Tests with thicker PVB are shown in yellow and the test with Protec® II is shown in purple. Full results (ram and edge excursions) can be found in Appendix A (Table A.2).

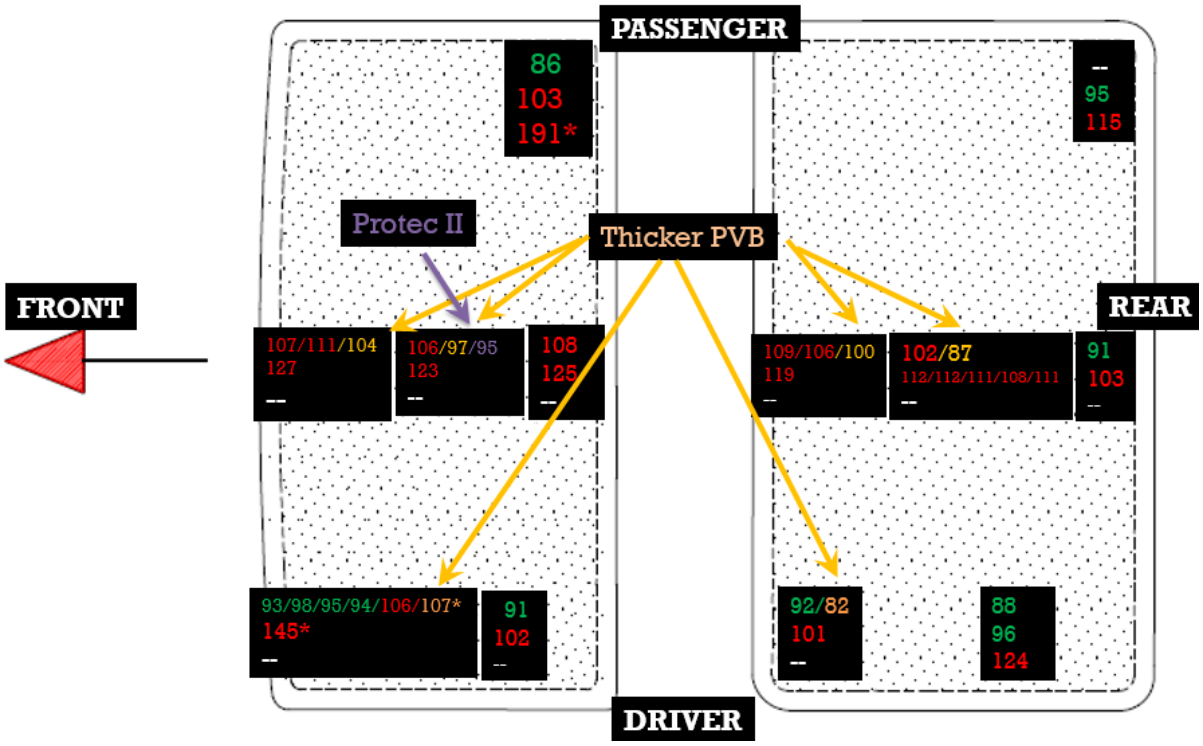

Figure 16. Ford F-150 Results.

As seen in previous testing, the movable panels presented more challenges in containing the headform than fixed panels. Failure at the inserts into the rails occurred on the moving panel. The fixed panel had higher excursions at the unsupported edges (front and rear edges of rear panel).

The plastic layer of the countermeasures (thicker PVB and Protec® II) did not tear in any test. Both countermeasures reduced plastic layer stretch and ram excursions compared to baseline. However, since more forces were transferred to the edges, larger openings were sometimes produced at the edges (i.e. edge excursions, highlighted in yellow in Tables A.1 and A.2).

Toyota Prius V Results

The polycarbonate panel on the Toyota Prius V was replaced after the first nine tests by a professional glass installer using the original glue sourced from Japan. There was no separation at the panel-roof glue interface during the entire test series for the Prius V roof. Ram excursions (in millimeters) can be seen in Figure 17 below. The top, middle, and bottom values represent excursions at speeds of 14, 16, and 20 kilometers per hour, respectively. Three tests were conducted on the rear panel at the two-thirds longitudinal edge locations and at 20 kilometers per hour, to assess the effect of repeated impacts. All three tests produced a ram excursion of 50 millimeters. The test with the * cracked the front windshield of the test vehicle. The windshield was replaced after this test. The test with ** caused the nearby roof structure to deform, however, this was a small static deformation of the structure. The roof structure was pushed back into its pre-impact shape and reinforcement was added. Full results (ram and edge excursions) can be found in Appendix A (Table A.3).

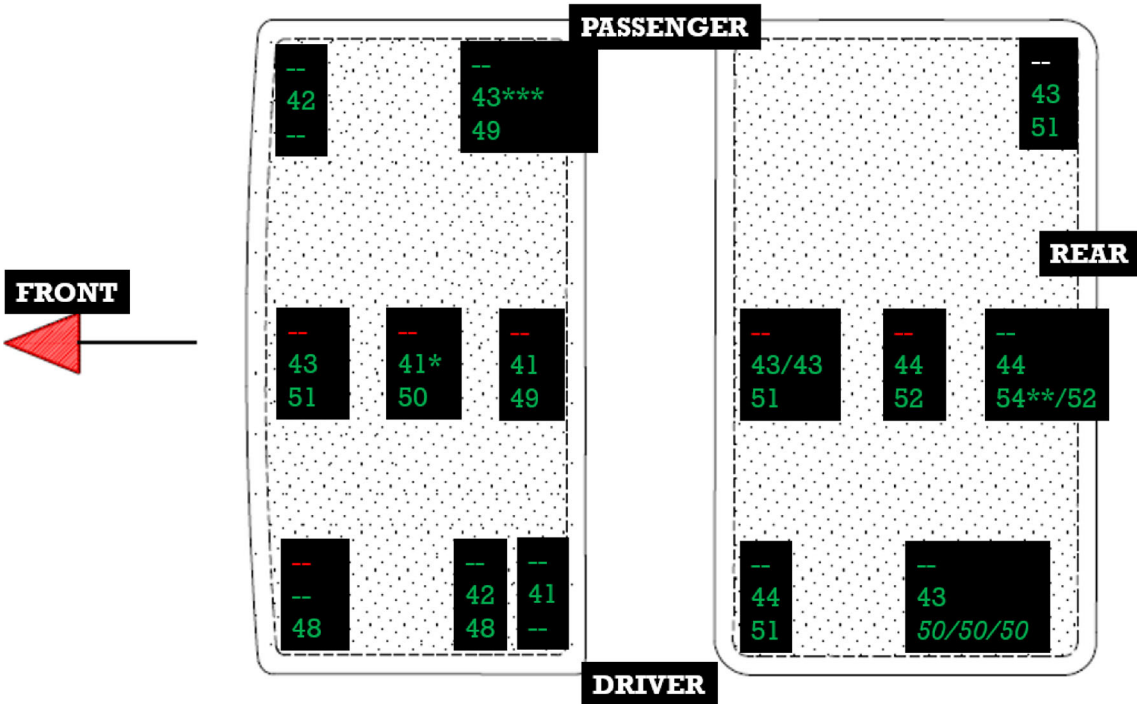

Figure 17. Toyota Prius V Results.

All Prius impacts had less than 100 millimeters excursions, generally around 50 millimeters. No separation at the glue interface was seen. Additionally, no failure of the polycarbonate or glue interface was seen even for multiple impacts at 20 kilometers per hour at the same location. Overall there were low ram displacements, however, due to less flexion of the sunroof panel there were high head deceleration values and therefore high forces on the headform. For example, when comparing an impact in the center of the Ford F-150 fixed panel at 16 kilometers per hour to an impact in the center of the Toyota Prius panel at 16 kilometers per hour, the forces on the headform were 2282 and 8663 Newtons, respectively. This is shown in Figure 18 below, with the F-150 in red and the Prius in blue.

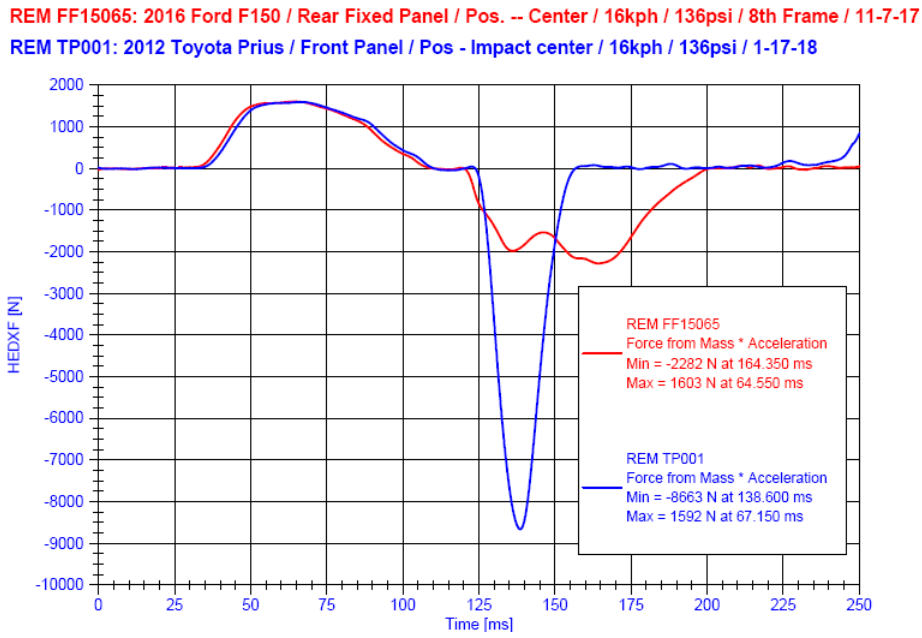

Figure 18. Comparison of forces on headform of F-150 (red) and Prius (blue).

Aisin Sunroof Results

Ram excursions (in millimeters) are shown in Figure 19 below. The top, middle, and bottom values represent excursions at speeds of 14, 16, and 20 kilometers per hour, respectively. An asterisk (*) means a rail insert failure occurred, double asterisks (**) mean an attachment bracket failure, triple asterisks (***) mean attachment glue-to-glass adhesion failure, and a # means a PVB failure, usually a rip in the PVB. Green values indicate excursions less than 100 millimeters and red indicate excursions greater than 100 millimeters. The four yellow values represent tests on the front movable panel where the panel was partially open so that the pin was in the metal rail. The panel was positioned so that for each of these four tests, the front edge of the window trim was 265 millimeters from a target on the front supporting frame. Full results (ram and edge excursions) can be found in Appendix A (Table A.4).

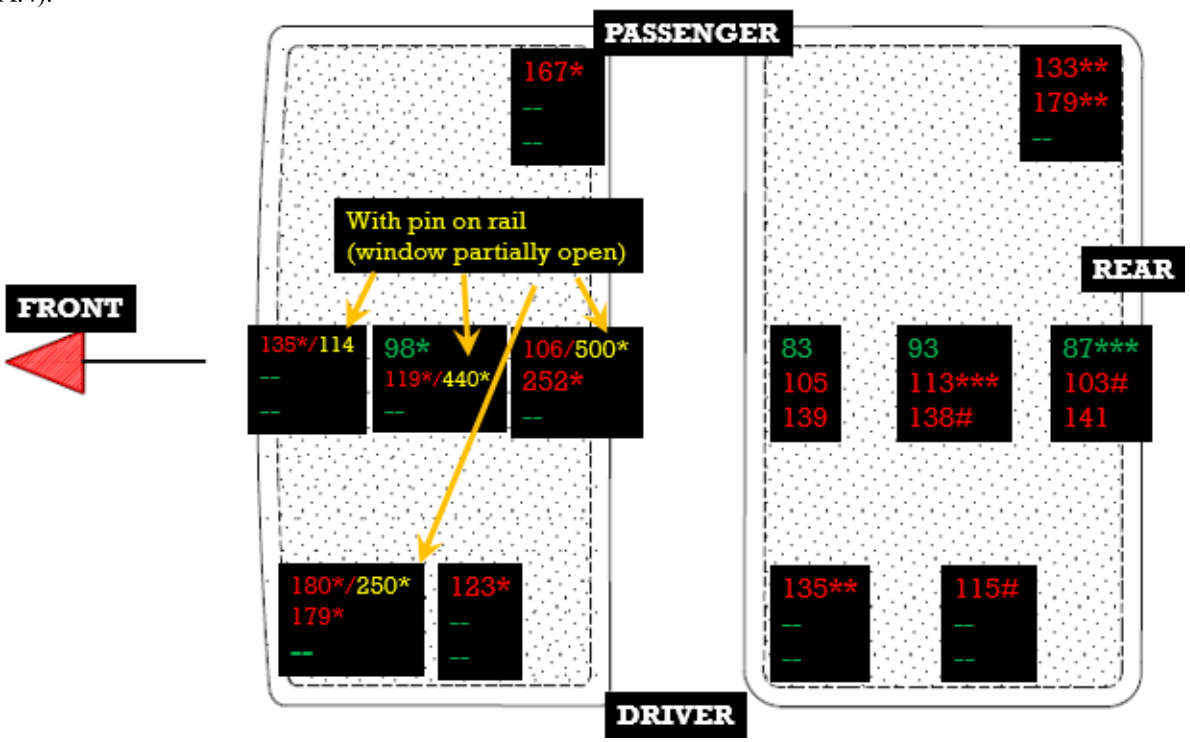

Figure 19. Aisin Sunroof Results.

The Aisin sunroof had many failure modes. Some examples of these failure modes are shown in Table 2 below.

Table 2.
Failure modes of Aisin sunroof.

		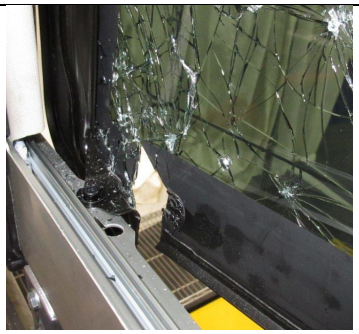
Rear panel - attachment bracket	Rear panel bracket – glue attachment	Rear panel – PVB tear at attachment
Glass PVB tear	Front panel corner pin -rail insert	Front panel corner pin and rear attachment

The headform did not push through the PVB layer for any of the tests. In some tests, where the frame inserts didn't fail, the PVB layers had tears in it. On the front movable, panel brittle fracture of the plastic cam, which is used to raise the front edge when sliding the panel to open, occurred in some tests. In tests where the panel was moved to a partially open configuration there were also rail insert failures. The rail inserts had weakness at all locations impacted on the front panel. The rear fixed panel had weakness at the attachment brackets. Failures occurred at the bracket to glass glue adhesion as well as at the bracket attachment bolt. Bending of the encapsulation frame was also observed for many tests.

CONCLUSIONS

This paper details performance of selected production and countermeasure sunroof designs in limiting headform excursions. Additionally, it describes a new test setup that was developed for roof ejection tests adapted from the wording of FMVSS No. 226. Test locations include the corners, center, midpoint of transverse edges, and two-thirds of the longitudinal edge. Head orientation was changed so that the longitudinal axis of the headform was perpendicular to the longitudinal axis of the vehicle. These locations tested attachment, frame, and glazing performance. On movable panels, failure of rail inserts happened when impacted near the rail attachments, and unsupported transverse edges bent when the panel was hit at the center or near the transverse edges. Stronger glazing transferred more load to the attachments.

Some of the fixed sunroof designs had excursions of less than 100 millimeters. The movable sunroof designs tested will require additional countermeasures to perform at this level. The research findings suggest that meeting some excursion limit similar to the 100-millimeter requirement of FMVSS No. 226 will require designs that have limited deformation of the glazing and encapsulation frame when impacted at the center of the panel, strong attachments, with no separation at the attachments. Tears or rips in the plastic layer may lead to additional impactor excursion. Impacts in close proximity to attachments frequently caused failure at the attachments. PVB elasticity also affects the excursions, particularly for center impacts. Any glued plastic sun roofs with low excursions, such as that of the Prius, can cause higher forces on the impactor than those produced from impacts to glass sunroofs. No comparison was made to forces produced from impacts with roofs that do not have a sunroof. The relationship between this loading and potential occupant injury was not assessed.

APPENDIX A: RESULTS TABLES

Table A1: 2016 Ford F-150 - Initial Tests

	Production																	
	Front Movable Panel						Rear Fixed Panel											
	Center		Forward Edge - Corner		Forward Edge - Mid		Center		Forward Edge - Corner		Forward Edge - Mid		Top Edge - Mid		Rear Edge - Mid		Rear Edge - Top Corner	
	Ram	*Edge*	*Ram*	*Edge*	*Ram*	*Edge*	*Ram*	*Edge*	*Ram*	*Edge*	*Ram*	*Edge*	*Ram*	*Edge*	*Ram*	*Edge*	*Ram*	*Edge*
16 Km/h	115 mm	86 mm	95 mm	75 mm	---	---	106 mm	80 mm	94 mm	70 mm	123 mm	89 mm	86 mm	56 mm	102 mm	64 mm	89 mm	43 mm
20 Km/h	154 mm	106 mm	178 mm	233 mm	---	---	138 mm	101 mm	120 mm	84 mm	144 mm	132 mm	111 mm	67 mm	131 mm	71 mm	113 mm	56 mm

	Double PVB											
	Front Movable Panel						Rear Fixed Panel					
	Center		Forward Edge - Corner		Forward Edge - Mid		Center		Forward Edge - Corner		Forward Edge - Mid	
	Ram	*Edge*	*Ram*	*Edge*	*Ram*	*Edge*	*Ram*	*Edge*	*Ram*	*Edge*	*Ram*	*Edge*
16 Km/h	111 mm (-3.5%)	95 mm	114 mm (--%)	174 mm	---	---	92 mm (-13.2%)	94 mm	86 mm (-8.5%)	54 mm	---	---
20 Km/h	140 mm (-9.1%)	137 mm	186 mm (--%)	241 mm	---	---	123 mm (-10.9%	113 mm	110 mm (-8.3%)	98 mm	---	---

	Protec II											
	Front Movable Panel						Rear Fixed Panel					
	Center		Forward Edge - Corner		Forward Edge - Mid		Center		Forward Edge - Corner		Center (punch both sides)	
	Ram	*Edge*	*Ram*	*Edge*	*Ram*	*Edge*	*Ram*	*Edge*	*Ram*	*Edge*	*Ram*	*Edge*
16 Km/h	109 mm (-5.2%)	131 mm	159 mm (--%)	235 mm	---	---	95 mm (-10.4%)	106 mm	85 mm (-9.6%)	93 mm	96 mm	109 mm
20 Km/h	140 mm (-9.1%)	153 mm	235 mm (--%)	363 mm	---	---	120 mm (-13%)	134 mm	107 mm (-12.2%	113 mm	---	---

Rail mechanism failure

Edge excursion greatear than ram excursion

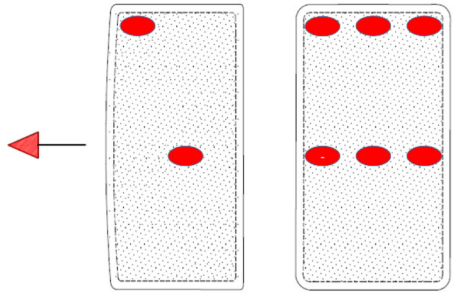

Table A2: 2016 Ford F-150 – New Test Setup

	Production											
	Front Movable Panel											
	Forward Edge - Corner		**Forward Edge - Mid**		**Center**		**Side Edge - 2/3 A**		**Rear Edge - Corner**		**Rear Edge - Mid**	
	Ram	*Edge*	*Ram*	*Edge*	*Ram*	*Edge*	*Ram*	*Edge*	*Ram*	*Edge*	*Ram*	*Edge*
14 Km/h	93/98/95/94/106	ND/120/114/104/127	*111/107*	*96/99*	*106*	*63*	*91*	*No video*	*86*	---	*108*	*91*
16 Km/h	145	194	127	121	123	81	102	*66*	103	76	125	106
20 Km/h	---	---	---	---	---	---	---	---	*191*	208	---	---

	Production											
	Rear Fixed Panel											
	Forward Edge - Corner		**Forward Edge - Mid**		**Center**		**Side Edge - 2/3 A**		**Rear Edge - Corner**		**Rear Edge - Mid**	
	Ram	*Edge*	*Ram*	*Edge*	*Ram*	*Edge*	*Ram*	*Edge*	*Ram*	*Edge*	*Ram*	*Edge*
14 Km/h	*92*	*67*	*109/106*	*87/87*	*102*	*69.3*	88	*42*	---	---	*91*	*47*
16 Km/h	101	120	119	99	112/112/111/108/111	78/84/84/90/86	96	50	95	37	103	58
20 Km/h	---	---	---	---	---	---	124	56	115	58	---	---

	Double PVB											
	Front Movable Panel						Rear Fixed Panel					
	Forward Edge - Corner		Forward Edge - Mid		Center		Forward Edge - Corner		Forward Edge - Mid		Center	
	Ram	*Edge*	*Ram*	*Edge*	*Ram*	*Edge*	*Ram*	*Edge*	*Ram*	*Edge*	*Ram*	*Edge*
14 Km/h	*107 mm*	*147 mm*	104 mm	*No Data*	97 mm	86 mm	*82 mm*	*74*	100 mm	95 mm	87 mm	78 mm

	Protec II											
	Front Movable Panel						Rear Fixed Panel					
	Forward Edge - Corner		Forward Edge - Mid		Center		Forward Edge - Corner		Center (punch both sides)		Center	
	Ram	*Edge*	*Ram*	*Edge*	*Ram*	*Edge*	*Ram*	*Edge*	*Ram*	*Edge*	*Ram*	*Edge*
14 Km/h	---	---	---	---	95 mm	93 mm	---	---	---	---	---	---

Rail mechanism failure

Edge excursion greatear than ram excursion

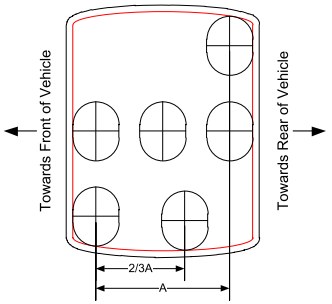

Table A3: 2012 Toyota Prius V

	Production											
	Front fixed Panel											
	Forward Edge - Corner		**Forward Edge - Mid**		**Center**		**Side Edge - 2/3 A**		**Rear Edge - Corner**		**Rear Edge - Mid**	
	Ram	*Edge*	*Ram*	*Edge*	*Ram*	*Edge*	*Ram*	*Edge*	*Ram*	*Edge*	*Ram*	*Edge*
14 Km/h												
16 Km/h	42	34	43	37	41	23	42	16	41/43	15/9	41	22
20 Km/h	48	10	51	21	50	10	48	7	49	10	49	9

	Production											
	Rear Fixed Panel											
	Forward Edge - Corner		**Forward Edge - Mid**		**Center**		**Side Edge - 2/3 A**		**Rear Edge - Corner**		**Rear Edge - Mid**	
	Ram	Edge	Ram	Edge	Ram	Edge	Ram	Edge	Ram	Edge	Ram	Edge
14 Km/h												
16 Km/h	44	26	43/43	32/7	44	7	43	6	43	8	44	9
20 Km/h	51	7	51	9	52	9	50/50/50	ND	51	10	54/52	69/19

Edge excursion greatear than ram excursion

Tests on original sunroof

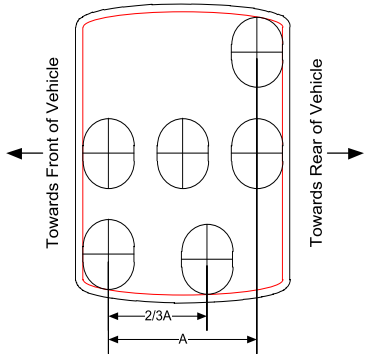

Table A4: Aisin Sunroof

	Production											
	Front moving Panel											
	Forward Edge - Corner		**Forward Edge - Mid**		**Center**		**Side Edge - 2/3 A**		**Rear Edge - Corner**		**Rear Edge - Mid**	
	Ram	*Edge*	*Ram*	*Edge*	*Ram*	*Edge*	*Ram*	*Edge*	*Ram*	*Edge*	*Ram*	*Edge*
14 Km/h	180/250*	197/500*	135/114*	143/272*	98	84	123	103	167	155	106/500*	96/500*
16 Km/h	179	212			119/440*	189/586*					252	315
20 Km/h												

	Production											
	Rear Fixed Panel											
	Forward Edge - Corner		**Forward Edge - Mid**		**Center**		**Side Edge - 2/3 A**		**Rear Edge - Corner**		**Rear Edge - Mid**	
	Ram	*Edge*	*Ram*	*Edge*	*Ram*	*Edge*	*Ram*	*Edge*	*Ram*	*Edge*	*Ram*	*Edge*
14 Km/h	135	107	83	39	93	45	115	108	133	93	87	ND
16 Km/h			105	82	113	93			179	197	103	38
20 Km/h			139	105	138	109					141	85

Rail mechanism failure (Front Panel)

Attachment failure (Rear Panel)

PVB failure (Rear Panel)

Edge excursion greatear than ram excursion

* Pin on aluminum rail

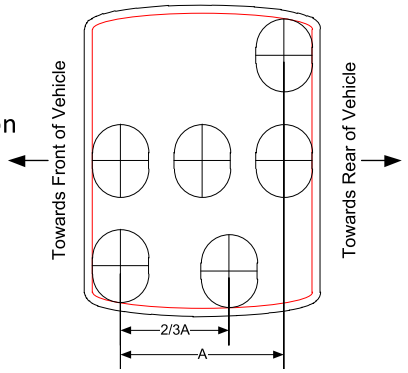

Research of Minimize Steering Grasping to Take over Driver from System in Advance Safety System

Shotaro Odate
Naohiro Sakamoto
Honda R&D Co., Ltd Automobile R&D Center

Paper Number 19-0039

ABSTRACT

Advances being made today in electronic technology are evolving the processes that make vehicles more intelligent, in addition to realizing safer and more comfortable driving. Lane departure prevention systems are also becoming practical due to millimeter-wave radar and onboard forward observation cameras. The U.S. Department of Transportation has implemented a National Automotive Sampling System Crashworthiness Data System (NASS/CDS) for North America that found 10,743 accidents in 2016 involved departure from the road. There were 12,043 fatalities in these accidents. Lane departure prevention systems are expected to make a major contribution to reducing accidents of this kind. Advances are also being made in the development of systems that will enable autonomous driving, and the system to ensure safe and comfortable vehicle operation is being developed.
These systems embody great potential for reducing the number of accidents caused by road departure. However, the validity of the systems is largely dependent on the level of acceptance by drivers. System validity will be determined by when they provide driving assistance, how much relaxation will be permissible on the driver's side, given that the driver needs to maintain contact with the steering wheel, and the extent of assistance provided by the system.
This paper will discuss research on the minimum necessary contact and contact strength with the steering wheel on the part of the driver when the autonomous system is in operation. Using a six-axis driving simulator employing an actual vehicle, the research conducted tests involving 22 test subjects, and studied the relationship between the status of the driver's contact in terms of steering angle speed and steering angular velocity and vehicle behavior when the system failed. The authors analyzed the influence on avoidance behaviors depending on the state in which the steering is held or not grasped when a person performs avoidance behavior.
When the steering torque activates, such as in a curve, the reaction will be faster if drivers touch the hand. In the case of a straight road with no steering torque activating, the result of the difference in reaction time depending on whether they are gazing at the front, regardless of grasping or non-grasping, has been clarified from this research.

INTRODUCTION

The advances being made in electronic technology today are causing evolution in the processes of making vehicles more intelligent. This is realizing greater safety and comfort in driving. In addition, millimeter-wave radar and forward-mounted cameras for observing the area around the vehicle are making lane departure prevention systems feasible. The US Department of Transportation has implemented a National Automotive Sampling System Crashworthiness Data System (NASS/CDS) that found 10,743 accidents in 2016 involving departure from the road [1]. These accidents involved 12,043 fatalities. It is expected that lane departure prevention and autonomous traveling system recognizing the lane's white line by the camera and performing autonomous operation will greatly contribute to this type of accident reduction (Figure A). Advances are also being made in the development of systems that will enable further automated autonomous driving, and the system to ensure safe and comfortable vehicle operation is being developed [2]. The evolution of this kind of advanced safety system, however, is raising concerns that drivers may feel excessively confident in the safety systems so that they take their hands off the steering wheel and stop paying attention while the systems are providing driving assistance [3]. Furthermore, In the event of a malfunction in a part of the safety system, it is necessary to immediately return the responsibility of the vehicle to the driver, but there is a possibility that the driver may not be able to respond adequately. For this reason, sensors to detect steering wheel operation by the driver are becoming increasingly important. The authors employed a six-axis driving simulator located at the Automobile R&D Center of Honda R&D Co., Ltd., to investigate the situation when an advanced safety system experiences a failure during operation so that responsibility is passed from the system to the driver. The extent of driver hand contact with the steering wheel that is needed in order to enable the driver to operate the vehicle correctly after such circumstances have occurred was clarified, and the least amount of grasp needed on the steering wheel was investigated.

System features

Figure B shows the layout and configuration of the steering wheel system developed for this research. The static capacitance sensor is used to determine whether or not the driver is grasping the steering wheel. Human hands have capacitance like that of a capacitor. By detecting this capacitance, the system can determine whether or not the driver has a hand or hands on the steering wheel (Figure B).

Methods

As far as the authors have ascertained, the driver modeling literature indicates that there are numerous factors involved in driving but sufficient attention in computer simulation [4,5]. There are almost no examples of simulations using complete models, but the existing models are able to be modified by incorporating insights from psychophysical and physiological research. In addition, the advancements that have been realized up to the present are in sensor technologies. Therefore onboard electronics make it possible to develop workable models [6,7].

Test subject

Twenty-two people who have driving licenses participated in the simulation tests. The test subjects ranged in age from their 20s to their 60s. In order to enable investigation of the question of whether there is a relationship between contact of the driver's hand with the steering wheel and the driver's grip strength, each driver's grip strength was measured (Table 1). The data acquired also included vehicle speed, steering angle, amount of braking, amount of acceleration, yaw rate, and steering torque (Figure E).

Data weighting

In order to eliminate the deviation of the measured data, we assumed that the reaction time would be earlier if the grip strength of the subject was high, and weighted the measured data using the normal distribution of Japanese grip strength.

Table 2. Normal distribution of Japanese grip strength [8].

N=72,157

	Grip strength (kg)			
	Male		Female	
Age	Average	Standard deviation	Average	Standard deviation
20-24	48.92	6.83	29.09	4.67
25-29	49.17	6.95	29.51	4.74
30-34	50.33	6.83	30.23	4.56
35-39	50.01	6.64	30.58	4.49
40-44	49.21	6.33	30.47	4.65
45-49	48.07	6.26	29.74	4.74
50-54	46.72	6.05	28.21	4.38
55-59	44.72	6.23	27.12	4.18
60-64	42.24	6.14	25.65	4.14
65-69	38.44	5.84	24.04	4.46
70-74	36.2	5.67	22.8	4.3
75-79	33.53	6.14	21.22	4.32

Assuming that the distribution is a normal distribution in table 2, weighting the individual's grip strength from the grip strength data of the whole country and add it to the result. As a calculation example, calculate with subject No. 6 as an example in the table 1.
Where, W is the weighting data, f is the function of normal distribution.
These are then substituted in the defined equation:

$$W = f(Ave, Nomal\ deviation, Grip\ strength)$$
$$= f(50.01, 6.64, 40.2)$$
$$= 0.022$$

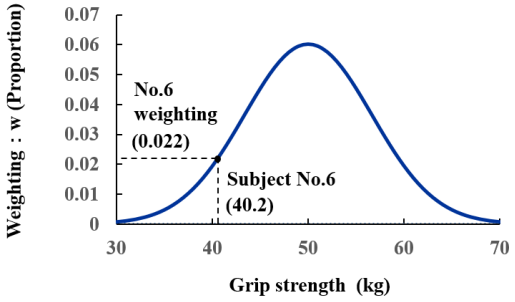

Where, i is the subject, n is the number of subjects, gi is the grip strength of the subjects, W(gi) is the weighting, RTi is the reaction time. RT is the result.

$$RT = \frac{\sum_i^n \big(W(gi)\big) \times RTi}{\sum_i^n W(gi)}$$

Simulation apparatus

Data was collected using a full motion simulator located at Honda's Tochigi Automobile R&D Center, an apparatus capable of conducting advanced simulations. This simulator surrounds an actual vehicle with a dome-shaped screen, and allows measurements to be conducted while a projector reproduces video images around the vehicle. In order to realize an environment in which the driver can believe that they are actually operating the vehicle, the system is able to move on six axes to reproduce vehicle behavior. The vehicle employed in the measurements was a 2013 model

year Honda legend (powertrain : Hybrid). Test subjects' manual contact with the steering wheel, the steering angle, and steering torque were measured (Figure F). The measured data was obtained using the vehicle's CAN. The vehicle's meters were modified, and warnings were provided to drivers via a liquid crystal panel, to help ensure that they were easy to understand (Figure G). These modified meters alerted drivers with takeover warnings in visual and audio form (Figure H).

Procedure

After having their grip strength measured, test subjects were provided with preliminary explanations and a discussion of informed consent, followed by a presentation explaining test procedure. The test subjects completed a five-minute practice drive on was a high-speed road used for test driving consisting of a straight section, a junction, and a curve. A light volume of traffic was also present on the road in order to allow the test subjects to get used to the simulator environment, but no events involving the safety system occurred during the practice drives. Following the practice drive, the test subjects ran through the test course using five patterns of manual contact with the steering wheel (contact with one finger, two fingers, three fingers, one hand, and no hands), and measurements were conducted of the extent to which the test subjects were able to operate the steering wheel when the request to take over operation came from the system. Although the method of holding the steering wheel is designated, even at the time of one finger, since the evasive behavior after that is avoided in a manner easy for the subject to perform, it is considered that there is no influence. In order to simulate distracted driving, the same tests were conducted with the navigation system in operation. Considering the possibility that drivers would become used to the requests to take over vehicle operation if they always came at the same time, measurements were conducted with requests made randomly, with and without any event having occurred. Each drive continued for approximately 30 minutes. The requests to take over control of the steering wheel are randomised in time with no reference to any external events. Test subjects were instructed to drive normally, observing the speed limits (Figure 8). The vehicle is traveling on a Highway at 100 (km/h), and enters a junction in order to take a new route. The vehicle reduces its speed to 60 (km/h) in order to negotiate the curve. As the vehicle is rounding the curve, automated driving systems suddenly fail and steering control is lost. the driver performs an emergency avoidance maneuver (Figure I).The vehicle is following a preceding vehicle at 100 (km/h) on a highway. The speed of the preceding vehicle suddenly drops, and the distance between the vehicles is reduced. At the same time, automated driving systems suddenly fail, and accelerator and brake control are lost. The driver conducts an emergency avoidance maneuver. In order to regulate the method used to avoid danger, the drivers were instructed in advance to use the steering wheel for this maneuver (Figure J). Even when the operating the navigation system, the same test cases were carried out as in the case of straight running and curved driving (Figure K).

Result

- When driving behind a vehicle ahead, delays were not observed in the reaction time from the termination of autonomous driving until avoidance was initiated, even when the driver's hands were off the wheel, except when the driver was operating the navigation system. Other than that, no differences were seen, including when the hands were not grasping the wheel when driver's hands were in the lap (Figure 1).
- When driving behind a vehicle ahead, the steering angle velocity in steering wheel operation following the termination of autonomous driving tended to be greater when the driver's hands were off the steering wheel than when the hands were touching the steering wheel. When the hands were off the steering wheel, whether they were in the driver's lap or operating the navigation system did not affect the result. In either case, the steering angle velocity grew greater in the same way. When the driver's hands were in contact with the steering wheel, the steering angle velocity exhibited the same tendency regardless of whether the driver was grasping the steering wheel, pinching the wheel with the fingers, or touching the wheel (Figure B).
- The reaction time from termination of autonomous driving until avoidance was initiated when driving through a curve was faster when the driver was touching the steering wheel than when the driver's hands were off the steering wheel. The reaction time grew even faster when the grasp was in the form of pinching the wheel with three fingers or grasping the wheel with one hand (Figure 3).
- When grasping the wheel with one hand or having one finger in contact with the wheel, the reaction curve described a small circle and avoidance was accomplished with minimal steering wheel operation. When the driver was not grasping the steering wheel, that circle grew larger and the driver would operate the steering wheel more than needed for avoidance (Figure 4,5,6).

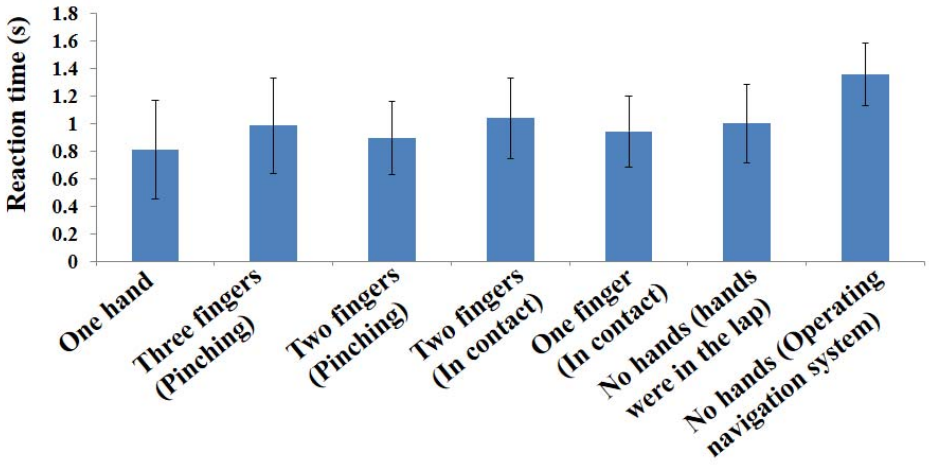

Figure 1. Reaction time from completion of automatic operation to avoidance start

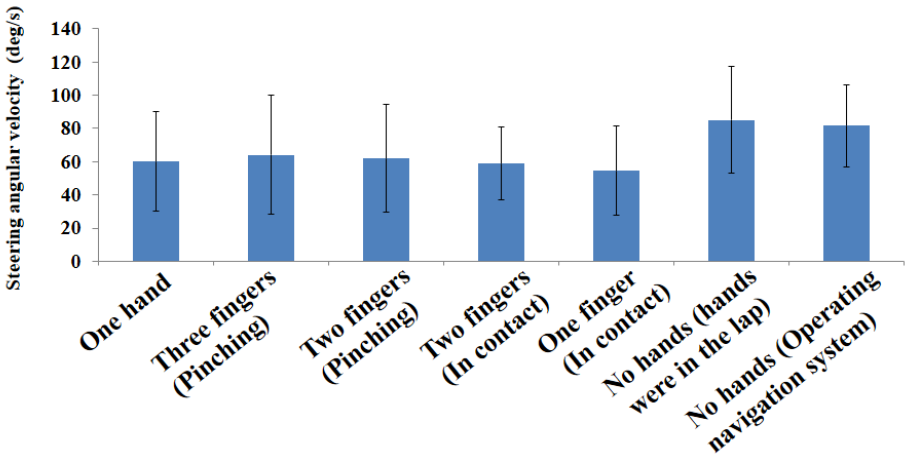

Figure 2. Steering operation during follow-up driving

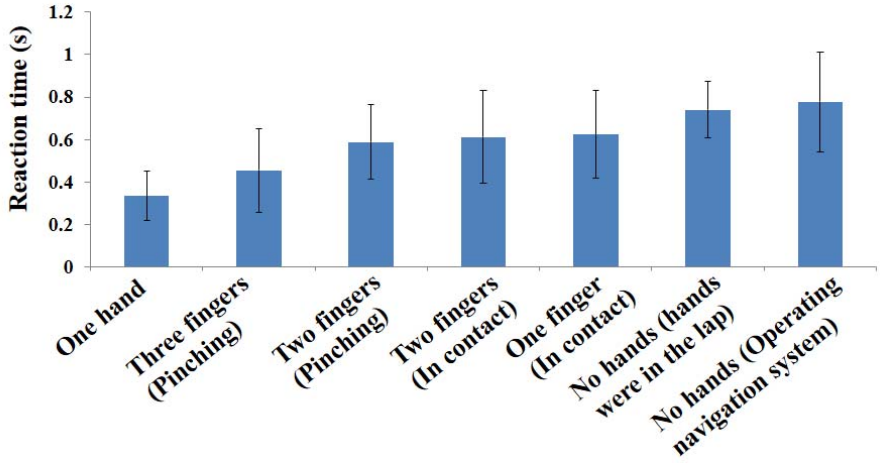

Figure 3. Time from completion of automatic operation in curves to start of avoidance

In order to judge the steering operation amount of the driver, the relation between the steering angle and the steering angular velocity was measured. When the reaction time is early, since the steering operation amount is accurately performed quickly, both the steering angle and the steering angular velocity become small, and the curve also draws a small circle. Also, when the reaction time is slow, the steering operation amount increases and the steering angle and the steering angular velocity show large values, so the curve becomes large.

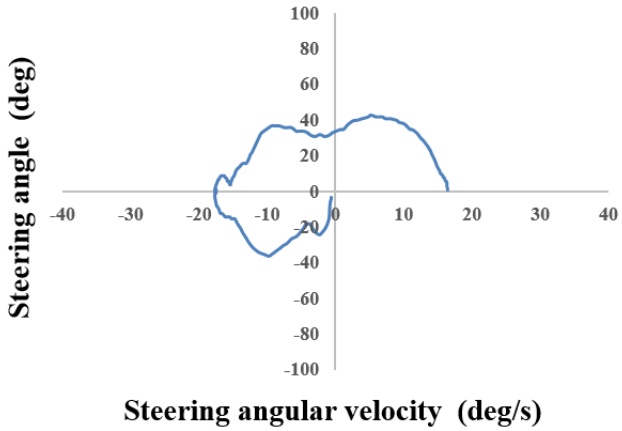

Figure 4. Steering operation when holding with one hand

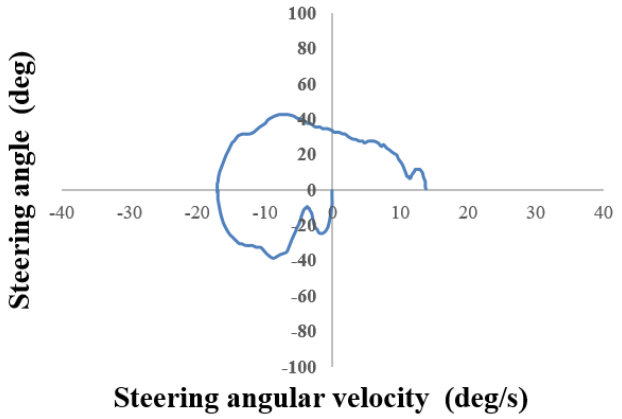

Figure 5. Steering operation at one finger

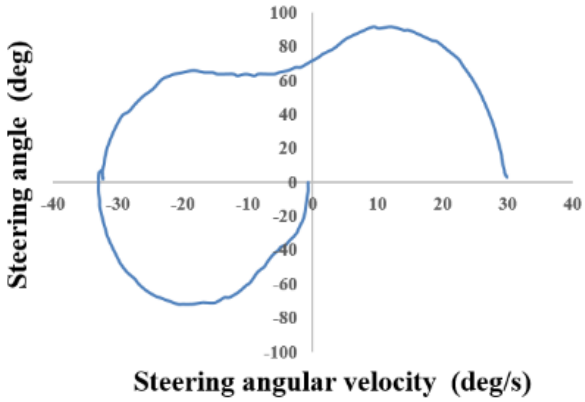

Figure 6. Non-gripping (state where hands are placed on knees)

Discussion

- The reaction time following the termination of autonomous driving when driving through a curve is thought to be faster when the driver's hand is in contact with the steering wheel because the steering wheel reaction force that occurs when autonomous driving cuts out can be felt by the tactile sense, and this enabled faster reaction than to sound or light.
- When driving behind a vehicle ahead, the reaction time from termination of autonomous driving until avoidance was initiated was the same whether the driver's hands were off the steering wheel or simply resting on the driver's lap with the driver looking to the front, and when the driver was in contact with the steering wheel and similarly looking to the front. However, when the driver was operating the navigation system, not only was the driver's hand touching it, but the driver's gaze was also directed toward the navigation system or control panel. This is thought to be the cause of the delay in reaction to the vehicle ahead.
- When driving behind a vehicle ahead and the status of steering wheel operation was suddenly changed from having the driver's hands off the steering wheel to operating the steering wheel, there was a visible tendency for steering wheel operation to become rough or uneven (the steering speed became faster). If the driver had even just a single finger in contact with the steering wheel, then the steering wheel was operated in the same way as when grasping the steering wheel with one hand. This suggested that having even slight contact with the steering wheel means that there is some readiness in the driver's consciousness to engage in operation.
- When the driver's hands were off the steering wheel, resumption of steering for avoidance sometimes involved sudden operation of the wheel. Therefore it appears advisable to provide a period of several seconds for the driver to have contact with the steering wheel before autonomous driving is terminated. However, the testing reported here did not include testing of how many seconds in advance would be desirable or what kind of human machine interface (HMI) should be used to notify the driver. The authors hope to pursue research from that perspective in the future.

Conclusion

Simulation tests were conducted in order to study the effect of the drivers' manual contact with the steering wheel. The following results were obtained ;

(1) The reaction time from termination of autonomous driving until avoidance was initiated when driving through a curve tended to be faster when the driver was in contact with the steering wheel than when the driver was not grasping it. Also, a trend toward even faster reaction times was observed when the driver was grasping the steering wheel by pinching the wheel with three fingers or grasping the wheel with one hand.

(2) The reaction time from termination of autonomous driving until avoidance was initiated when driving behind a vehicle ahead showed delays only when operating the navigation system, even when the driver's hands were off the steering wheel. Otherwise no difference was observed, including when the driver was not grasping the steering wheel (hands resting in the driver's lap).

(3) Steering wheel operation from termination of autonomous driving until avoidance was initiated when driving behind a vehicle ahead tended toward greater steering angle velocity when the driver's hands were off the steering wheel than when they were in contact with the steering wheel. When the driver's hands were off the steering wheel, the result was not affected whether the hands were in the driver's lap or operating the navigation system. In either case, the steering angle velocity grew greater in the same way. Also, when the driver was touching the steering wheel, the steering angle velocity tended to exhibit the same tendency whether the driver was grasping the steering wheel, pinching it with the fingers, or in contact with it.

References

[1] https://crashstats.nhtsa.dot.gov

[2] Young, R., "Revised Odds Ratio Estimates of Secondary Tasks: A Re-Analysis of the 100-Car Naturalistic Driving Study Data," SAE Technical Paper 2015-01-1387, 2015, doi:10.4271/2015-01-1387

[3] Gaspar, J., Brown, T., Schwarz, C., Chrysler, S. et al., "Driver Behavior in Forward Collision and Lane Departure Scenarios," SAE Technical Paper 2016-01-1455, 2016, doi:10.4271/2016-01-1455.

[4] Kamiji, K. and Akaba, H., "RESEARCH OF AN ADVANCED SEAT BELT SYSTEM," ESV 2003 Paper No. 480

[5] Ito, D., Ejima, S., Sukegawa, Y., Antona, J., Ito, H. and Komeno, F., "ASSESSMENT OF A PRE-CRASH SEATBELT TECHNOLOGY IN FRONTAL IMPACTS BY USING A NEW CRASH TEST SLED SYSTEM WITH CONTROLLABLE PRE-IMPACT BRAKING," ESV 2013 Paper Number 13-0274
[6] Rooij, L., Pauwelussen, J., Camp, O. and Jansse, R.,"DRIVER HEAD DISPLACEMENT DURING (AUTOMATIC) VEHICLE BRAKING TESTS WITH VARYING LEVELS OF DISTRACTION," ESV 2013 Paper Number 13-0403
[7] Infantes, E., Schaub, S., Kramer, S., Langner, T., Eggers, A., Caspar, M.E., Unselt, T. and Lemmen, P./ "EVALUATION OF OCCUPANT PROTECTION DURING THE CRASH PHASE CONSIDERING PRE-CRASH SAFETY SYSTEMS – RESULTS FROM THE EC-FUNDED PROJECT ASSESS," ESV 2013 Paper number 13-0419
[8] Physical fitness and exercise capacity investigation, Japanese Ministry of education in 2000 year

APPENDIX: TABLES AND FIGURES

Table 1. Subject details

No.	Age	Gender	Grip strength (Right) : kgf	Grip strength (Left) : kgf	No.	Age	Gender	Grip strength (Right) : kgf	Grip strength (Left) : kgf
1	Late 30s	Male	52	54.1	12	Late 20s	Male	45.9	52.1
2	Early 30s	Male	49	49	13	Early 30s	Male	47.4	43.8
3	Early 20s	Male	47.2	53.1	14	Early 30s	Male	48.1	44.1
4	Late 20s	Male	52.3	44	15	Early 60s	Male	35.6	29.3
5	Early 30s	Male	42	36	16	Early 30s	Male	48.2	40.6
6	Late 30s	Male	40.2	35.5	17	Late 30s	Female	26.9	27
7	Late 30s	Male	43.9	38.7	18	Early 30s	Male	48.7	42.6
8	Early 50s	Male	51.2	41.7	19	Early 30s	Male	59	52.8
9	Late 30s	Male	37.9	38.1	20	Late 50s	Male	48.6	54.9
10	Late 20s	Male	36.5	32.8	21	Late 20s	Male	37.5	33.9
11	Early 30s	Male	34.3	35.4	22	Early 30s	Female	33.6	32

Figure A. Image of the advanced safety system recognizes the white line on the road

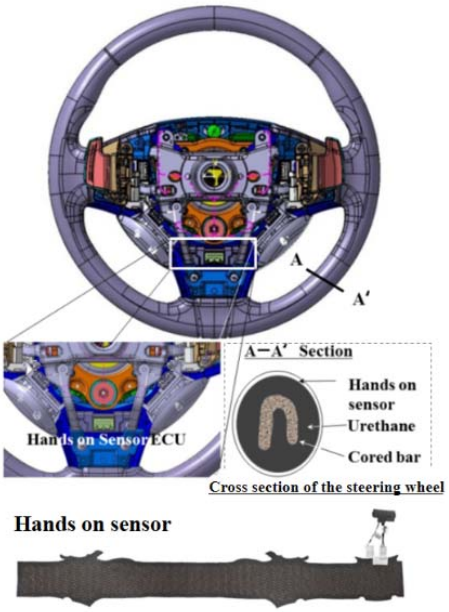

Figure B. Layout of Hands on sensor ECU

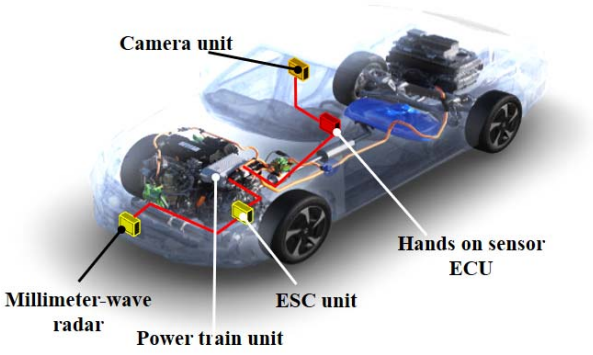

Figure C. Concept diagram of the system operation

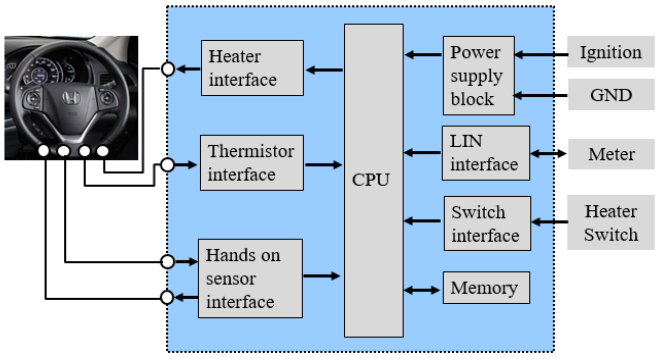

Figure D. System configuration diagram of hands-on sensor

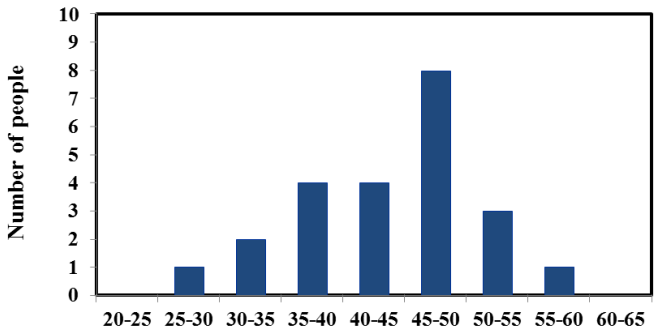

Figure E. Subject distributions

Figure F. Simulation equipment for this study

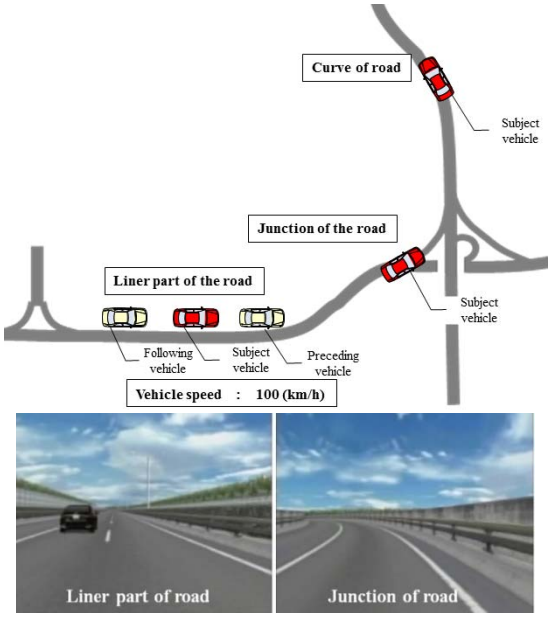

Figure G. Course of simulation

Figure H. Status of assumed steering grasping (The environmental conditions are measured at a temperature of 25 ° C and a humidity of 50%).

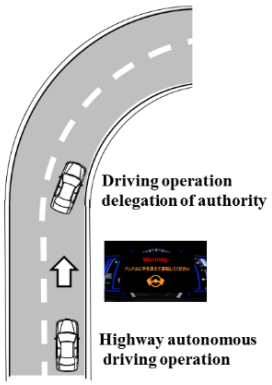

Figure I. Simulation with curve

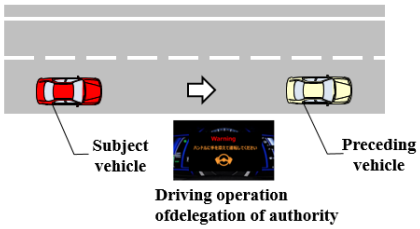

Figure J. Simulation on straight road

Figure K. The driver is manipulating the navigation

ESF 2019 – EXPERIMENTAL SAFETY VEHICLE MEETS AUTOMATED DRIVING MODE

Prof. Dr. Rodolfo Schöneburg
Dr. Martin Hart
Jochen Feese
Dr. Stephan Mücke
Dr. Julien Richert
Mercedes-Benz Cars, Daimler AG
Germany

Paper Number 19-0042

ABSTRACT

Since the early beginning of the Enhanced Safety Vehicle Program in 1969, Mercedes-Benz has created over 30 ESF cars, and thus played a key role in the development of modern automotive safety.

After more than 30 years Mercedes-Benz presented in 2009 a new ESF based on the very latest safety features, such as Advanced Driver Assistance Systems, Adaptive Restraint Systems, and Integrated Safety Systems (PRE-SAFE®)

Nowadays, the automotive industry is facing one of its most challenging paradigm shifts. In the coming years, connectivity, automated driving, shared services and electric cars will fundamentally change the usage of cars. After ten years Mercedes-Benz will show again a research car: the ESF 2019. Mercedes-Benz, as a worldwide leader in automotive safety, will demonstrate its vision and ideas for safety for this new vehicle generation: a vision of safety that goes beyond just the passenger and includes the vehicle's surroundings.

With all its innovations, the Mercedes-Benz Experimental Safety Vehicle 2019 represents a further milestone in automotive safety.

HISTORY ESF@Mercedes-Benz:

The genesis of Passive Safety

Passive Safety has a very long tradition at Mercedes-Benz, already before the foundation of the ESV program. One of the very first milestone of Passive Safety is surely the 23rd of January 1951, where Daimler-Benz AG registered a patent for the passenger car body with a passenger safety cell. This invention by Béla Barényi was granted Patent No. 845 157 with the title "Motor vehicle, specifically for personal transport". This was a trailblazing innovation, as it is still seen as the fundamental feature of passive automotive safety to this day. In 1959 the safety body with its rigid passenger cell entered series production for the first time in the Mercedes-Benz W 111 series (model 220b).

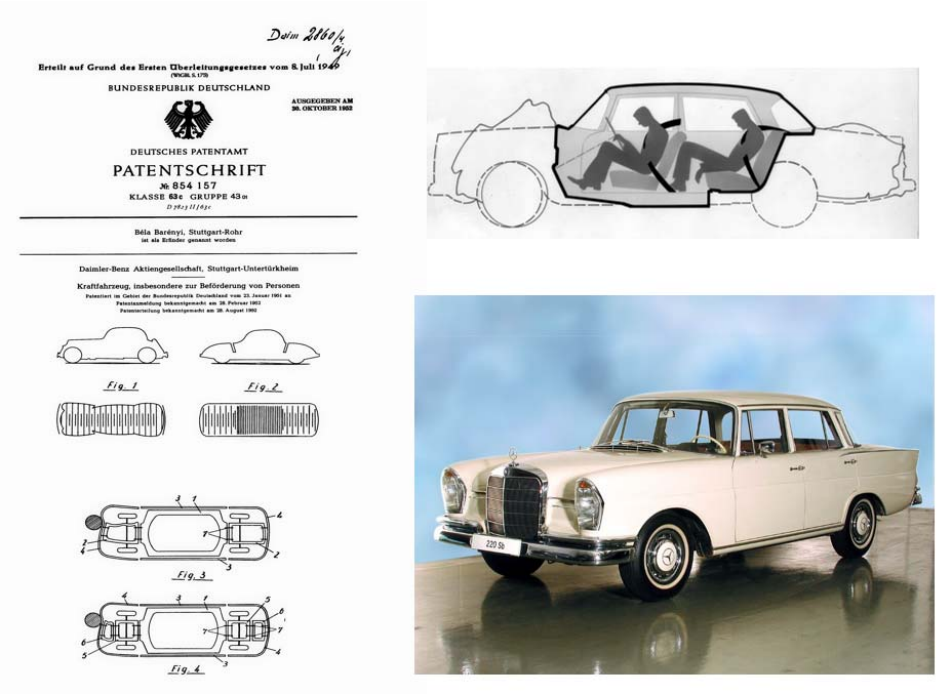

Fig. 1: Patent No. DBP 854 157, life-saver of thousands - the crumple-zone - Mercedes-Benz W111

Mercedes-Benz Experimental Safety Vehicles

In the 1960s it became impossible to ignore a negative aspect of mass motorisation: more and more people were being killed on the roads. In 1968 the US Department of Transport therefore started a programme for the development of Experimental Safety Vehicles (ESVs), and initiated the international "Technical Conference on the Enhanced Safety of Vehicles". Two years later the specifications to be met by the ESVs were defined. The American government also issued an invitation to foreign countries to take part in this safety research. In 1970 this gave rise to the still active European Enhanced Vehicle Safety Commitee (EEVC).

At Mercedes-Benz the challenge of designing vehicles with even more safety was taken up with great enthusiasm. After all, the company was already able to look back on more than 20 years of continual safety research at the time. MB has built a total of 35 ESF from the beginning of the program until today. Some major innovations were later introduced into production vehicles and have already been standard for years. Examples are ABS, belt tensioners and belt force limiters, airbag and side impact protection.

Mercedes-Benz presented the following four ESFs to the public, always as an input to the ESV conferences:

Fig.2: ESF 5: developed on the basis of the W 114 ("Strich Acht") series and presented at the 2nd International ESV Conference from 26 to 29 October 1971 in Sindelfingen

Fig.3: ESF 13: Stylistically revised variant of the ESF 5, presented at the 3rd International ESV Conference from 30 May to 2 June1972 in Washington (USA)

Fig.4: ESF 22: Based on the W 116 series (1971 S-Class) and presented at the 4th International ESV Conference from 13 to 16 March 1973 in Kyoto (Japan)

Fig.5: ESF 24: Modified S-Class (W 116) presented at the 5th International ESV Conference from 4 to 7 June 1974 in London (Great Britain)

Detailed specifications from the Mercedes-Benz ESVs can be found in [1]. The foundations for the current safety level of cars bearing the Mercedes star have therefore been laid. Extract from the summary test report (1975): "The ESF 24 can be regarded as the completion of the project, as this vehicle represents the best possible compromise between the original ESV requirements and our current series production cars."

At Mercedes-Benz safety was included in the development specifications for new cars as a matter of course decades before the ESV programme, and in rapid succession the ideas first realised as part of the ESF project entered series production as well. The milestones included:

- 1978: premiere of the ABS as an option for the S-Class
- 1980: driver airbag and belt tensioner available in the S-Class
- 1995: belt force limiters and sidebags enter series production of the E-Class

The ESV program was the starting point of modern safety. Over the years many additional safety features like passenger airbag or ESP were developed by Mercedes-Benz keeping alive the pioneering spirit of the ESV program.

After 35 years finally another ESV: ESF 2009

The ESF 2009 is the first Experimental Safety Vehicle Mercedes-Benz has built since 1974. Like its historic predecessors, it attractively combines trailblazing innovations in the field of safety and makes the progress achieved visible. The ESF 2009 was presented within the frame of the 21st ESV Conference from the 15 to 18 July 2009 in Stuttgart [2].

Fig.6: The ESF 2009: Son and heir of a successful family

The ESF 2009 aimed at demonstrating the safety benefit of the Integral Safety approach of Mercedes-Benz. This approach unites Active and Passive Safety and constitutes the foundation of the safety development for production cars. The Mercedes-Benz typical exemplary safety level is achieved when each of the 4 pillars of the integral safety approach reaches a high level. The following four phases describe the holistic safety approach:

- Safe driving: Provide safe driving environment with Intelligent Drive

- In detested critical driving situations: Assist with Intelligent Drive and prepare for a possible crash with PRE-SAFE®
- During a crash: Protect with sophisticated vehicle structures and adaptive restraint systems
- After a crash: Warn other road users and call for professional assistance if needed.

Fig.7: The Integral Safety Strategy of Mercedes-Benz

Core of the ESF 2009 are 13 safety innovations, which cover all the 4 pillars of the Integral Safety. One example for a system that addresses phase one is a new lighting system, the "Partial Main Beam" that allows the driver to leave the high beam constantly switched on while the oncoming or proceeding vehicle can be cut out. The 100 individually activated LED implemented in the headlight also enable the so-called spotlight function which allows potential hazard to be highlighted. Using a 360° sensor covering of the car surroundings, the ESF 2009 shows many new driver assistance systems such as Lane Keeping Assist, Blind Spot Assist and PRE-SAFE® Brake. The advanced radar sensors of the ESF 2009 allows the creation of very new preventive Safety Systems like PRE-SAFE® Pulse, PRE-SAFE® Structure and the Braking Bag. Braking Bag describes a special exterior airbag installed between the front axle carrier and the underbody paneling. If the sensor system concludes that an impact is inevitable, the Braking Bag is deployed just before the crash, supporting the car against the road surface by means of a friction coating. Activating this auxiliary brake in the vehicle floor improves both deceleration and compatibility with the other vehicle involved in the accident.

Fig.8: Left: Headlight and Radar Sensors of the ESF 2009- Right: Braking Bag

Even with this advanced sensor system, a collision still may be unavoidable. Therefore, the protection of the car passenger during a crash was also in focus of the car. Several Innovations like Beltbag, Size-Adaptive Airbag, Child Protect, Interseat Protection, … provide the appropriate safety countermeasure for different collision scenarios.

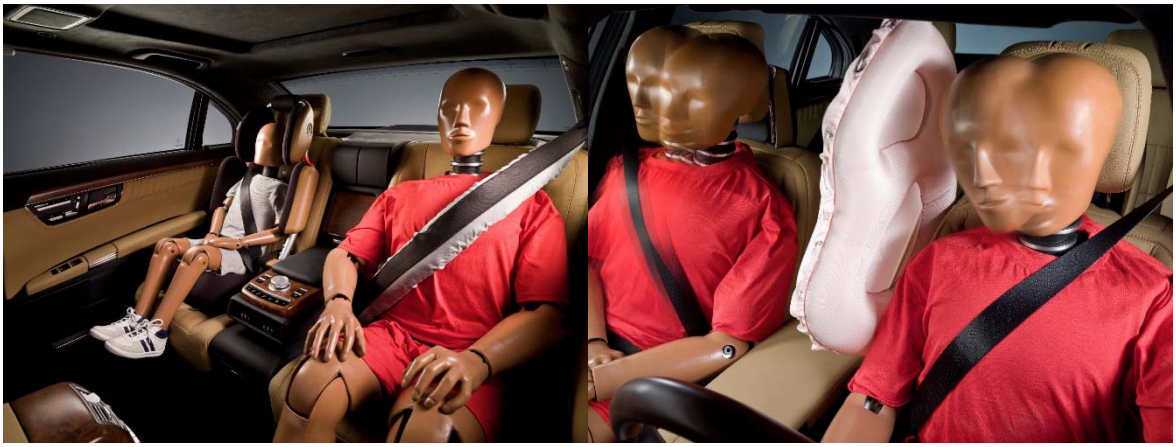

Fig.9: Some innovations of the ESF 2009: Child Protect, Beltbag and Interseat Protection

Like for its predecessors, many innovations shown in the ESF 2009 already find their way into series production cars:

- 2012: Beltbag (S-Class W222)
- 2014: MULTIBEAM LED headlamps (CLS-Class C218)
- 2016: PRE-SAFE® Impulse Side in (E-Class W213)

As the name already suggests, the Beltbag is a combination of a seat belt and airbag. When the crash sensors detect a serious frontal impact, the airbag control unit activates the Beltbag along with the pyrotechnical pretentioner. This leads to the inflation of the double-layered belt that practically doubles its width within fractions of a second. This increase in the width of the belt spreads the load over a wider area, thereby reducing the risk of injury.

The innovation “partial main beam” from the ESF 2009 hit the market a few years later under the name MULTIBEAM LED headlamps. The LED-based adaptive main beam system enables the driver to leave the main beams switched on constantly. As soon as the system detects oncoming traffic with the help of a camera, it automatically adjusts the light distribution accordingly. The MULTIBEAM LED headlamps use a very fast responding and high performing precision LED module as a matrix light source, which features 84 individual, high-performance LED moduls. Each of these LED chips can be actuated electronically and independently, depending on the information supplied by a camera on the windscreen.

PRE-SAFE® Impulse Side uses a 360-degree sensor system, which permanently senses the car surroundings, to anticipate an unavoidable collision. When an unavoidable side collision with another vehicle is detected, the pre-impacting restraint system PRE-SAFE® Impulse Side transfers a defined energy to the occupant, thus sets him in motion towards the middle of the car already before the collision occurs [3]. Using numerical simulation as well as sled and vehicle testing, certain relevant occupant loads have been shown to be reduced by up to 30 percent on average with the use of PRE-SAFE® Impulse Side [4].

Fig.10: The ESF 2009 and its "guarding angels"

Another important mission of the ESF 2009 was to communicate about safety. That is the reason why the car also presented most of the modern safety systems that were already available in series production cars at that time. The ESF aim's also at showing all the expertise of the safety engineers to the customers so that they can understand how Mercedes-Benz cars are reaching their high safety level. In order to explain the technical features of the car in a comprehensive way, the "guarding angels" communication concept was achieved. Beginning with the 2009 International Motor Show in Frankfurt (IAA), the car had been shown to the public all over the world during many years.

Even if the ESF 2009 still remains to some extends very forward-thinking, the on-coming changes in the society and in the way future cars will be used raised new questions for the automotive industry and for the safety domain in particular.

PURPOSE OF THE ESF 2019

The automotive industry will face major challenges over the coming years. The way coming vehicles will be used in the future will change dramatically compared to the way they have been used for the past 100 years.

This time, the occasion was the realization that the technical development and the expectations of automated driving change the requirements for safety technology in the car. Just like the first wave of ESV-vehicles was a reaction to mass motorization in the 1960s and its rising accident numbers, the new ESF reflects the mobility of the future and shows new approaches related to automated driving. At the same time, an ESF is always a technological figurehead for research and development in terms of safety. Not only does the ESF 2019 present innovations in Mercedes-Benz safety technology that go far into the future, but also it shows developments that are currently being prepared for introduction to series production.

What are the requirements for a safety system for an autonomous vehicle that operates in mixed traffic with changing infrastructure and differently equipped other road users? For a safety system that rides sometimes automated and sometimes controlled by the driver? Which of the classic passive security systems remain indispensable or need to be adapted? What additional new possibilities for avoiding accidents and reducing the consequences of accidents can be found in the technology developed in connection with autonomous driving?

Thus, the ESF 2019 is in some aspects a preview of what is coming, in others a vision, in others a contribution to the discussion and a tool to work on further improvements in road safety in the great tradition of Mercedes-Benz.

CONCLUSION

The ESF 2019 successfully ties in with the long-standing tradition of Experimental Safety Vehicles from Mercedes-Benz. Like its predecessors, it shows trailblazing innovations to further improve future vehicle safety.

REFERENCES

[1] Die Geschichte der Experimental-Sicherheits-Fahrzeuge (ESF) bei Mercedes-Benz: Meilensteine der Sicherheits-entwicklung, 2009 Press Release - Daimler Communications, 70546 Stuttgart, Germany -

[2] Ulrich Mellinghoff, Prof. Dr. Thomas Breitling, Prof. Dr. Rodolfo Schöneburg, Hans-Georg Metzler – The Mercedes-Benz Experimental Safety Vehicle 2009 – ESV Conference 2009, Stuttgart, DE, July 2009, Paper Number 09-0165

[3] Dr. J. Richert, R. Bogenrieder, U. Merz, Prof. Dr. R. Schöneburg – PRE-SAFE® Impulse Side Pre-impacting restraint system in case of imminent side impact – opportunity for occupant protection, challenge for environmental sensors - Daimler AG - 10th VDI Congress on Vehicle Safety, Berlin, Germany, 24 and 25 Nov. 2015

[4] Prof. Dr. Rodolfo Schöneburg, Michael Fehring, Dr. Julien Richert, Mario Glashagel, Jochen Ruf, Matthias Walz, Ralf Bogenrieder - "FROM A PREVENTIVE TO A PRE-IMPACTING RESTRAINT SYSTEM" - Daimler AG - ESV Conference 2017, Detroit, USA , June 2015, Paper Number 17-0252

THE L3PILOT COMMON DATA FORMAT – ENABLING EFFICIENT AUTOMATED DRIVING DATA ANALYSIS

Johannes Hiller
Institute for Automotive Engineering, RWTH Aachen University
Germany

Erik Svanberg
SAFER Vehicle and Traffic Safety Center at Chalmers University of Technology
Sweden

Sami Koskinen
VTT
Finland

Francesco Bellotti, Nisrine Osman
DITEN – University of Genoa
Italy

Paper Number 19-0043

ABSTRACT

Analyzing road-test data is important for developing automated vehicles. L3Pilot is a European pilot project on level 3 automation, including 34 partners among manufacturers, suppliers and research institutions. Targeting around 100 cars and 1000 test subjects, the project will generate large amounts of data. We present a data format, allowing efficient data collection, handling and analysis by multiple organizations.
A project of the scope of L3Pilot involves various challenges. Data come from a multitude of heterogeneous sources and are processed by a variety of tools. Recorded data span all data types generated in various vehicular sensors/systems and are enriched with external data sources. Videos supplement time-series data as external files. Derived measures and performance indicators – required to answer research questions about effectiveness of automated driving – are processed by analysis partners and included for each test session.
As a file format, we chose HDF5, which offers a data model and software libraries for storing and managing data. HDF5 is designed for flexible and efficient I/O and for high volume and complex data. The usage of different computing environments for specific tasks is facilitated by the portability that comes with the format. Portability is also important for exploiting the rising potential within artificial intelligence (e.g. automatic scene detection and video annotation).
Based on lessons learned from past field tests, we defined a general frame for the common data format that is aligned with the data processing steps of FESTA "V" evaluation methodology. The definitions include representation of the source signals and a hierarchical structure for including multiple datasets that are gradually supplemented (post-processed or annotated) during the various analysis steps. By using the HDF5 format, analysis partners have the freedom to exploit their familiar tools: MATLAB, Java, Python, R, etc. First comparisons between time-series data in previous projects (e.g. AdaptIVe) and the proposed data format show a reduction in storage size of around 80 %, without losses in performance. Much of that is due to efficient internal compression and structuring of data. Considering the amount of objective data involved in automated driving, this leads to a great benefit, in terms of usability.
This paper presents a compact, portable, and extensible format aimed at handling extremely large amounts of field test data collected in automated driving pilots. As a harmonized format between tens of organizations performing tests in the L3Pilot project, the proposed format has the potential to promote data sharing as well as development of common tools and gain popularity for use in other projects. The format is designed to allow efficient storing of data and its iterative processing with analysis and evaluation tools. The format also considers the requirements of AI tools supporting neural network training and use.

INTRODUCTION

Automated Driving (AD) technology has matured to a level motivating large-scale road tests which can answer key open questions before market introduction. These newly-attained levels of maturity will ensure an appropriate assessment of the impact of AD. Of interest is what is happening both inside and outside of the vehicles. Also ensuring vehicle safety is of utmost importance as well as evaluating societal impacts. As a further point, the evaluation of emerging business models is of interest.
A point that has proven to be the crux in many previous projects is the data exchange between partners, as well as the evaluation. This led to devising a data format common to the whole project, thereby easing the exchange of data and the further development of evaluation processes and tools based on the data.
First, we will present the organization of data in previous projects and present the current project, L3Pilot [1]. After that, we will show how the process for deriving the requirements for the data format came together, followed by a few formats shortlisted for storage of the data. We will then describe the format itself and afterwards discuss it and its limitations.

PREVIOUS PROJECTS AND EFFORTS

Over the years, numerous projects have paved the way for advanced driver assistance systems (ADAS) and AD. Each of those projects had a slightly different approach to data acquisition, handling and evaluation. This section shortly picks out a few of these projects and gives some details on the used methods.
In 2008, a big European project was started with euroFOT [2]. It identified and coordinated an in-the-field testing of new intelligent vehicle systems with the potential for improving the quality of European road traffic. During the project, the effectiveness of various lateral and longitudinal control functions and active safety functions on public roads was assessed. Data collection and analysis was organized from test sites. Each test site was using similar (Matlab based), but still with differences, data formats and individual analysis tools [3].
With AdaptIVe [4] in 2014, the focus moved from ADAS to AD. In the three and a half years of the project, AD functions for scenarios such as parking and motorway driving were developed and demonstrated. Raw data for the evaluation was delivered by the vehicle owners. At the evaluation partner, the needed signals (cf. [5], Annex 3) were extracted and converted to an internal evaluation format, a mixture of CSV and MATLAB.
From past EU Field Operational Test (FOT) projects, at least TeleFOT [6] and DRIVE C2X [7] used fixed formats when gathering data from several test sites to a central data storage. These projects assessed, in respective order, in-vehicle navigation systems and short-range vehicle communication prototypes.
In 2017, the L3Pilot project was kicked off. L3Pilot will test automated driving functions (ADFs) in 100 cars with 1,000 test subjects across 10 different countries in Europe. The tested functions will be mainly of SAE automation level 3, some of them of level 4 [8]. Together, European automotive industry, suppliers and researchers will pave the way for large-scale field operational tests on public roads creating a harmonized Europe-wide testing environment. The overall objective of L3Pilot is to test and study the viability of AD as a safe and efficient means of transportation, explore and promote new service concepts to provide inclusive mobility.

SIGNAL DERIVATION / METHOD / REQUIREMENTS

L3Pilot follows the FESTA V-process methodology [9] of setting up and implementing tests with the four main pillars and adapting the methodology to suit L3Pilot needs (cf. Figure 1). The four pillars in L3Pilot are: Prepare, Drive, Evaluate and address legal and cyber-security aspects.
This paper focuses on the Prepare pillar with additional focus on the early phase of the Evaluate pillar. The Drive pillar is handled by the vehicle owners. As can be seen in the figure, the first step in L3Pilot is the definition of automation functions and use cases, with a major attention on motorways. In a further step, the research questions for this project are derived from the specified use cases. Accompanying the research questions are various hypotheses that this project will investigate. In order to do this, different data are needed. One part will be subjective data, i.e. data that originate from questionnaires and user evaluation. Particularly interesting from a data processing point of view, and therefore for a data format, are the data recorded in the vehicles. To specify what data to record, performance indicators and derived measures are defined, which are used to answer the research questions and confirm the hypotheses. Derived measures, in this context, are quantities that are directly calculated from source signal time-series data. These can be vehicular signals or information about the environment delivered by car sensors. Performance indicators, on the other hand, are no longer time-series data. They take different forms depending on the indicators. They can be single values giving a certain value or the average in a recording or in a specific scenario. However, they can also be histograms over some value in multiple occurrences of a driving scenario. The set of signals needed for the calculation of these measures results in a list of required signals, that are to be recorded during each session in the pilot vehicles. The full process following the FESTA-V up to the data can be found in [10].

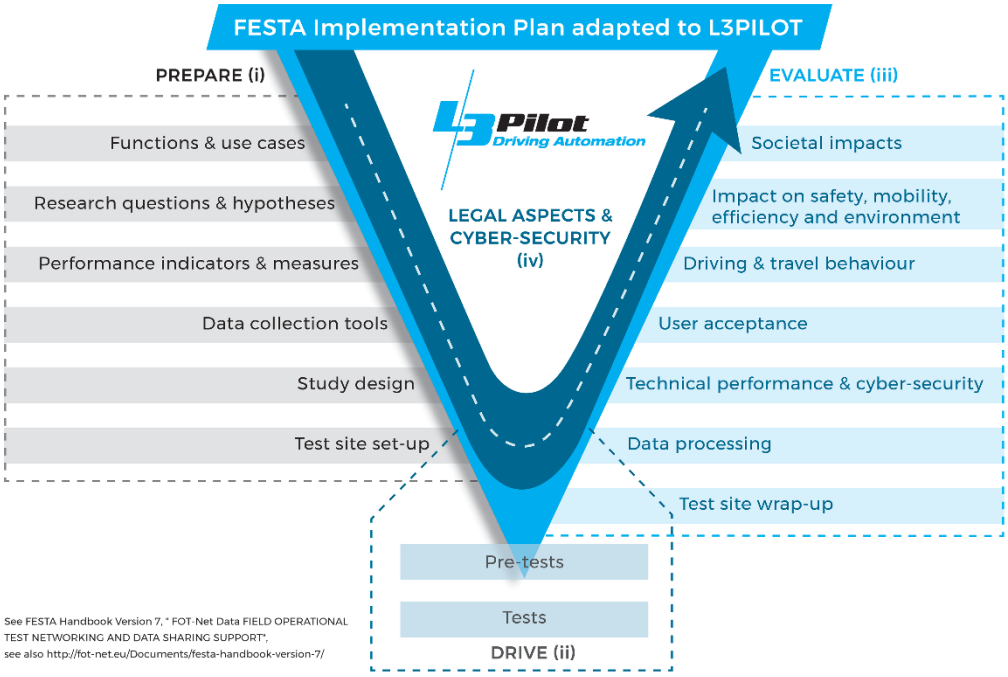

Figure 1. The FESTA implementation Plan adapted to L3Pilot

With the needed signals defined, the focus shifts towards the actual data. As stated before, different data are aggregated during the project. The three main sources are subjective data, objective data and video feeds. The data important for the L3Pilot Common Data Format (CDF) are the objective data. These include original vehicle signals and derived measures calculated from the source signals. In a project of the size of L3Pilot, there is not one platform running all the pilot vehicles and systems. One can think of platforms such as ADTF [11] or ROS [12] to just name two. Therefore, a simple export of the data collected in the car is not a viable option, since the export files of the different platforms are seldom compatible.
After the successful conversion, the Evaluate pillar starts with the data processing at the evaluation partner. Complementing the vehicle data will be data that originate from other, external, sources such as weather or map providers. Another factor is that multiple partners will be doing different analysis on the data, using different tools. One of the main programs used for post-processing and data analysis by the partners in this field is MATLAB. Additionally, in the previous years, Machine Learning has proven to be an important factor for the automatic detection of scenarios and video annotation. Therefore, a support of Python by the data format is of utmost importance. Considering statistical analysis of factors, some partners will also rely on R, SPSS or others. This leads to a requirement for a wide support of tools, platforms and programming languages.
Considering the aim of 1000 drivers in 100 cars, the amount of data recorded and transferred between vehicle owners and evaluation partners in terms of actual file sizes is another factor that should not be neglected. This leads to another criterion, the portability of files and results. For portability, memory efficiency is of course important.
Considering all these requirements, the common data format task force decided that a single file-based data format should be used in L3Pilot, to support an easy exchange of data between different partners. In order to reduce the amount of data that is transferred, compression was noted as another key feature to improve the process.
Within the L3Pilot project, it is agreed upon, that vehicle owners convert their datasets into the presented CDF. This enables the evaluation partners to use common tools to analyze the data, no matter which vehicle owner they work with.

CONSIDERED FILE FORMATS

As stated in the previous section, the decision upon a file-based format was taken quite early in the project. Therefore, going forward in the decision process, only file-based formats were considered. Solutions for big data storage were not further considered, although they can play an important role in the data management within an institution. As a first step towards the CDF, various file formats were evaluated and discussed. In various previous projects, that are partially listed in the section above, many different file formats were used. All of them have their own advantages and disadvantages. These differ strongly depending on the intended use of the formats. During the decision process for the CDF, many of them were evaluated and the pros and cons were compared. The

following formats were the ones taken into closer account during the decision process, as the task force already had experience with them, or they were deemed as promising.
A format that is commonly used among researchers in this field is the MATLAB file format [13]. The newest iteration is v7.3 that was introduced with MATLAB R2006b, however, the default version for files is v7. In it, data is stored in a binary format. It is a proprietary format, that is supported by MATLAB across all platforms that MATLAB supports. All datatypes included in MATLAB are supported and can be loaded and saved, while also supporting compression of data. One limitation is its strong link to MATLAB, however, for many research projects this was not an issue, since MATLAB is commonly used. This offers the opportunity to re-use existing tools from other or previous projects. The MATLAB file format was used in euroFOT [3] and internally during the evaluation in AdaptIVe [5].
A commonly used file format for exchange of numerical data is Comma-Separated Values (CSV). In it, values are simply stored as text, separated by commas (or any other type of delimiter), thus the name. Time-series are represented by new lines for each element. It is easy to use, doesn't need any updates and can be read and written by almost any program. However, there are also drawbacks to this format. CSV doesn't support the use of metadata. Therefore, value formats and e.g. minimum and maximum values of a column must be defined in a separate supporting document. One of the main advantages of CSV, the textual basis, is also one of its disadvantages, because it doesn't directly provide any compression and therefore takes up a lot of memory for long recordings. CSV was partially used for data transfers during the AdaptIVe project.
The Hierarchical Data Format (HDF) [14] exists in different versions. The current version is HDF5 revision 1.10.4 (as of January 2019). HDF was developed with portability in mind. It is supported by various languages such as C/C++, Fortran, Java, MATLAB and Python. Due to its support by a wide selection of programming languages, it can be used in the various available operating systems. It can therefore be easily implemented into different scripts and programs. HDF supports the storing of a wide array of datatypes including doubles, integers and strings. Additional datatypes can easily be added. To support portability, HDF has features for data compression. Different compression algorithms can be applied in order to save storage space. Metadata is stored in attributes in HDF files. This supports portability and simplifies the management of many files. Starting from version 7.3, the MATLAB file standard is based upon HDF5, thereby becoming compatible with HDF5 tools. As a disadvantage, for readability, HDF5 uses a binary format. An easy peek into the data without using the access libraries is therefore not possible. However, several data viewers exist. Editing the data can be another issue, depending on the viewers' capabilities. Another disadvantage is, that there is one inner core module on which almost all implementations of HDF5 rely upon. An error in this module would be devastating.
During L3Pilot, the main drawback of HDF5 was the somewhat limited documentation of programming examples. Another shortcoming and even a related bug were later found in Java libraries, as the main data viewer provided by HDF Group, HDFView, could not, at that time, display an array of compound datatypes used in the L3Pilot CDF. This was fixed by the HDF Group upon a report by the team.

L3PILOT COMMON DATA FORMAT

Considering the previously stated requirements, a file format was selected. The selection came upon HDF5. This allows us to define different datasets for the needed signals.
Since HDF5 supports a wide array of programming languages, the vehicle owners can use their preferred language and platform to convert their data recorded in their proprietary format. On the evaluation side, the corresponding partner should be able to use existing or preferred tools with small modifications. This allows for an efficient use of resources, as more time can be committed to developing and implementing new features.
HDF5 offers two ways of organizing data: datasets and groups [15]. Groups can contain zero or more HDF5 objects and can be accessed together using the group name. They can be hierarchically organized and have circular references. Datasets are where the data is stored. They are a collection of data elements, or raw data, and metadata that stores a description of the data elements, data layout, and all other information necessary to read, write and interpret the stored data. These data values can be of various datatypes. Already defined are datatypes such as double, integer, etc. However, the library also offers the opportunity to define new datatypes, if needed. Included in the datasets as well are the metadata, which include attributes. These attributes can be used to describe the contained data, thus allowing a verbal description of the data and, e.g., providing the unit of a logged signal. These attributes are independent and can be read and written without loading the complete HDF file. Datasets can be on the root level or belong to one or more groups. One advantage of datasets and groups is that each of them can be loaded individually without loading the complete file.
Derived through various iterations from the use cases and research questions, various logged signals are available on vehicle owner side. In order to allow for an efficient and quick access to the data, the signals are coarsely grouped according to their origin. For this purpose, datasets and groups are used by the CDF. All vehicle signals are organized in datasets on the top level of the file ("/") (cf. Table 1). The "egoVehicle" dataset contains all signals originating directly from the ego vehicle itself. This would be signals such as the ABS status or the speed

of the vehicle. All information about the lane markings, e.g. the distance to the lane markings and their type, is contained in the "laneLines" dataset. Dynamic objects and their properties such as speed and distance are saved in the "objects" dataset. Information from a global navigation satellite system (GNSS), e.g. GPS or Galileo, is stored in the "positioning" dataset. The previously discussed derived measures and performance indicators are calculated at the evaluation partners, and then stored in the "derivedMeasures" and "performanceIndicators" datasets.

In order to gain more information about the recorded trips, external data can be useful. Two important external data sources that were identified for the L3Pilot project are weather and map information. Weather information can be provided by various weather services and contains information about temperature, precipitation and cloud coverage. Map data provides information about the number of lanes, speed limits or intersections. These data are saved in the datasets "map" and "weather". These are located hierarchically under the "/externalData" group.

Some data cannot, or only with major difficulties, be derived from vehicle signals. One of these signals is, for example the secondary task performed by the driver during different situations. These kinds of signals are added by annotations through human experts, or students supervised by experts, watching the time-synced video feed of the recording. These annotations are normally added at the evaluation partner and not supplied by the vehicle owner. Annotations are located hierarchically under the "/annotations" group. For each annotation a subgroup is added with the name of the annotation. In this example it is "/sceondaryTask". It includes two datasets "comments" and "enum". In "comments" all comments that are additionally made by the annotator are stored, i.e. if there is an extraordinary reason for this annotation. The dataset "enum" contains the annotation as numerical value so that it can easily be reused in subsequent scripts and calculations. For the example of the secondary task, this would contain the annotated secondary task masked as an enum and the file time referencing it to the recording. Groups are used here, in order to have the possibility to flexibly extend the annotations.

Table 1.
All datasets according to the L3Pilot Common Data Format and the associated groups.

Group	*Dataset*	*Description*
/	egoVehicle	Signals directly concerning the ego vehicle
	laneLines	Information on the lane markings
	objects	A list of (dynamic) objects
	positioning	Information from the positioning system (local or GNSS)
	derivedMeasures	Contains all the derived measures
	performanceIndicators	Contains all the performance indicators
/externalData	weather	Contains information about the weather
	map	Contains map information
/annotation	-	Group containing various annotations
/annotation/secondaryTask	comments	Comments on the annotation by the annotator
	enum	The annotation values

Considering the memory usage and a memory efficient storage of the recorded data, the datatypes of all signals are carefully selected. For this purpose, the desired and expected precision of all signals is reviewed. Many signals such as vehicle speeds or accelerations come in high precisions, with many digits to the right of the decimal point. For these signals, the "double" datatype is used, which allows for a high precision. Other signals such as the ID of an object, the speed limit or the number of lanes are not needed with high precision. Therefore, these values are saved as integers. Another common signal in recorded data is the status of a system. In general, it takes very few distinct values that are known beforehand. These status signals are saved as "enums" in the CDF. HDF5 allows the definition of arbitrary enums. For the CDF, they are based upon "uint8" and take few distinct values. Table 2 summarizes the commonly used datatypes.

Table 2.
Different used datatypes in the Common Data Format, their sizes and examples

Datatype	*Size in byte*	*Exemplary value*	*Exemplary N/A value*
Double	8	3.14159265359…	NaN
int64	8	1545572564000	-1
int32	4	42	-1
enum (uint8)	1	ON (1)	N/A (-1)

In a project of the size of L3Pilot and with the wide variety of vehicle owners and sensor setups, not all the signals will always be available or will fit the same format. For the CDF this means, that some signals will not be available in some recordings. For missing values, "N/A" values are defined, i.e. values that are used when the signal is not provided. This makes it easier for programs and scripts to run on the data anyway. For floating point numbers, "not a numer" (NaN) [16] is used. Since NaN is not defined for integer types, values that are not expected to appear are used here, e.g. "-1".
All signals in the CDF are synchronized between the datasets. In order to achieve this, a frequency of 10 Hz was selected for the project. For reference, each dataset contains two different time signals. The first is the "FileTime" which simply counts up in discrete 10 Hz steps from the beginning of the recording. This can be used for easy reference in the file itself. The second time signal is the "posix" time in milliseconds, named "UTCTime" in the file. This allows references to external data sources such as weather or traffic services. The posix time is the time in seconds, milliseconds or nanoseconds (depending on the application) since 00:00:00 on 1 January 1970 in UTC. It doesn't include any leap seconds and therefore differs from the atomic time used in GNSS systems by currently 37 seconds (as of January 2019) [17].
Since not all signals are always recorded with the requested frequency of 10 Hz, interpolation methods are defined per signal. For continuously available signals, a simple linear interpolation is defined for most cases. However, since a linear interpolation is not applicable for status signals with few distinct values, a zero-order-hold (ZOH) interpolation is defined for these signals. Thereby each signal is held for one sample interval and then changes. In addition, a maximum time of loss is defined per signal. This is to prevent unreasonable behavior in signals when data loss was too long. For high precision variables this might be very close to zero seconds, for other signals (e.g. GNSS) this could be up to 10 seconds.
Another step towards memory efficient storage is the utilization of the HDF5 built-in compression. One common algorithm here is the "DEFLATE" compression [18]. This algorithm is not restricted by patents. Many different implementations for almost all common programing languages are available. The algorithm works especially well on data that does not change often. In that case, it will only save the value for the first occurrence and save the next value only if it changes. This saves a lot of memory especially for Boolean values and other mostly static variables.
In order to support faster I/O and memory efficient computing, HDF has a feature called chunking. Here, data is not saved in one continuous block in the file, but in so called chunks. These chunks are specified when creating the file according to the data that is to be stored. When reading the file, only one chunk at a time is loaded into the memory. This is especially useful, when handling large amounts of data. For the implementations in the L3Pilot project, the chunk size is selected in a way to get chunks of about 1 MB. Chunks are applied to the respective datasets. Since the size of a single timestep is known due to the mandated format and signals, the chunk size can be set accordingly.

DISCUSSION

For a preliminary assessment, memory consumption was measured for data coming from 32 hours of motorway data recorded in a previous project. The mean duration of one trip from this project is roughly 52 minutes. For that purpose, the raw data size was calculated from the known sizes of the datatypes and the length of the recordings. This is given in Table 3 as "Raw data, calculated" and taken as the reference for all other file sizes. This would lead to an average data file size of 84.54 MB for a recording length of 52 minutes. Using HDF5 for storing the data and activating the compression. the average reduction in file size is around 89 %. This results in an average file size of 9.63 MB. In terms of absolute memory, we can now save the recordings with only around 395 MB instead of the ~3.5 GB that would have been needed without the compression.

Table 3.
Comparison of file sizes for a selection of different file formats.

Format	*Mean file size*	*Relative*
Raw data, calculated	84.54 MB	100 %
HDF5, compression, DEFLATE	9.63 MB	11.17 %
csv	54.91 MB	64.94 %
mat file, v7	8.86 MB	10.48 %
mat file, v7.3	9.29 MB	10.98 %

For benchmarking, a few comparisons to other formats are done. The first one is CSV. All data that is written to the HDF5 files is taken and written to a csv file using the MATLAB function *dlmwrite*. This simply writes a matrix to a csv file. This results in an average file size of 54.91 MB. Compared to the raw calculated data size, this is only ~65 %, which can be explained by the fact, that data is written as ASCII characters, which only uses

one byte per character. Even though some numbers take up multiple characters, the overall number is still smaller than having double datatypes with eight bytes.
As another comparison, the MATALB mat file format is considered. Here the commonly used version 7 is compared as well as the newer version 7.3 which is however not enabled by default. v7.3 is built upon HDF5 and can therefore also be read using HDF5 tools. As can be seen from the table, v7 offers the best compression in the sense of the smallest average file size. With v7.3, the file size slightly increases which MATLAB also notes in its documentation, which can happen due to overhead in the description of the file contents.
Overall it can be seen, that the proposed format offers a good performance in terms of memory. It does not quite reach the memory efficiency of the long-matured MATLAB mat file format; however, it is not dependent on a proprietary program and can be accessed using multiple languages and programs.
The binary nature of the format, which is one of its advantages, because it allows compression, is also one of its disadvantages. The binary format leads to the restriction that the data can only be accessed using the appropriate tools and programming APIs. This also hides the structure of the data from peeks and from an easy overview of contained signals without using additional tools. This is however not seen as a drawback in the L3Pilot project, since the structure of the data is known beforehand by all partners.

CONCLUSIONS

In this paper we present the CDF approach we decided to implement to manage the heterogeneous data sources in the L3Pilot project. The intention of the format is to make the process of data exchange and evaluation more flexible and efficient. The paper showed the methodology used to define the signals needed for the evaluation in the project and presented the considerations that went into the decisions on the file format.
A preliminary test showed that the L3Pilot CDF using HDF5 is more efficient than some previously used formats, such as csv. On the other hand, it performs almost as well in terms of memory efficiency as the MATLAB proprietary format, while being independent of the software used. The portability is already by now exemplified by various tools built using the format but in different environments: Windows or Linux, and using Python, R or Matlab.
In the next months, the format will be extensively used and tested in the piloting phase of the L3Pilot project and will constantly evolve and mature, leading to a proven format that could be applied to many other projects of similar scale and type. Various analysis tools will be developed and adapted to support the format.

ACKNOWLEDGEMENT

This project has received funding from the European Commission Horizon 2020 program under the project L3Pilot, grant agreement number 723051. Responsibility for the information and views set out in this publication lies entirely with the authors. The authors would like to thank all partners within L3Pilot for their cooperation and valuable contribution.

REFERENCES

[1] "L3Pilot," 2017-2021. [Online]. Available: https://l3pilot.eu/index.php. [Accessed 20. December 2018].

[2] euroFOT, 2008-2012.

[3] S. Selpi, S. Borgen, J. Bärgman, E. Svanberg, M. Dozza, R. Nisslert, C. Norell, J. Kovaceva, D. Sanchez, M. Saez, C. Val, J. Küfen, M. Benmimoun and B. M, "D3.3 Data Management in euroFOT," euroFOT, Aachen, 2011.

[4] "AdaptIVe," 2014-2017. [Online]. Available: https://adaptive-ip.eu/. [Accessed 20. December 2018].

[5] C. Rodarius, J. Duflis, F. Fahrenkrog, C. Rösener, A. Várhelyi, R. Fernandez, L. Wang, P. Seiniger, D. Willemsen and L. V. Rooij, "Deliverable D7.1 Test and Evaluation Plan," AdaptIVe, 2015.

[6] P. Mononen and e. al., "TeleFOT Final Report, D1.15," 2012.

[7] M. Schulze, T. Mäkinen, T. Kessel, S. Metzner and H. Stoyanov, "DRIVE C2X Final Report, D11.6," 2014.

[8] SAE International, "Taxonomy and Definitions for Terms Related to Driving Automation Systems for On-Road Motor Vehicles," Society of Automotive Engineers, 2018.

[9] Y. Barnard, H. Chan, S. Koskinen, S. Imnamaa, H. Gellerman, E. Svanberg, A. Zlocki, C. Val, K. Quintero and D. Brizzolara, D5.4 Updated Version of the FESTA Handbook, FOT-Net Data, 2017.

[10] D. Hibberd, T. Louw, E. Aittoniemi, R. Brouwer, M. Dotzauer, F. Fahrenkrog, S. Innamaa, S. Kuisma, N. Merat, B. Metz, N. Neila, M. Penttinen, P. P. G. C. Rösener, A. Silla and A. Zerbe, "D3.1 From Research Questions to Logging Requirements," L3Pilot, 2018.

[11] Elektrobit, "EB Assist ADTF," [Online]. Available: https://www.elektrobit.com/products/automated-driving/eb-assist/adtf/. [Accessed 10 January 2019].

[12] M. Quigley, K. Conley, B. P. Gerkey, J. Faust, T. Foote, J. Leibs, R. Wheeler and A. Y. Ng, "ROS: an open source Robot Operating System," in *ICRA Workshop on Open Source Software*, 2009.

[13] The MathWorks, Inc., "MATLAB MAT-File Format," Natick, MA, 1999-2018.

[14] The HDF Group, Hierarchical Data Format, version 5, 1997 - 2019.

[15] The HDF Group, "Introduction to HDF5," 08. Februar 2018. [Online]. Available: https://portal.hdfgroup.org/display/HDF5/Introduction+to+HDF5. [Accessed 18. December 2018].

[16] IEEE, "IEEE Standard for Floating-Point Arithmetic," *IEEE Std 754-2008*, pp. 1-70, 2008.

[17] C. Bizouard, O. Becker, J.-Y. Richard, D. Gambis, S. Lambert, T. Carlucci and P. Baudoin, "INFORMATION ON UTC - TAI," 7 January 2019. [Online]. Available: ftp://hpiers.obspm.fr/iers/bul/bulc/bulletinc.dat. [Accessed 10 January 2019].

[18] L. P. Deutsch, "DEFLATE Compressed Data Format Specification version 1.3," 1996. [Online]. Available: https://tools.ietf.org/html/rfc1951. [Accessed 18. December 2018].

DEVELOPMENT OF ADAPTIVE SUPPLEMENTAL RESTRAINT SYSTEM

Yefim Kriger

Fairfield University, CT

USA

Paper Number 19-0051

ABSTRACT

The article relates to methods of mitigating results of improper value of force applied to the occupant's body at a time of an imminent front vehicle collision and preventing fatalities as well as injuries that may be caused. More particularly, the present article relates to a new method of accurately weighing vehicle occupants that eliminates obstacles to improve their safety in the event of a collision.

The statistics show that the number of victims is indirectly proportional to their weight. It means that to significantly improve safety of the vehicle occupants, it is necessary to put stress on controlling the forces applied to the occupants' bodies by more accurately measuring their weights. It is noted in [1] that the weight of an occupant measured by an air bag system is not the entire weight of the occupant since some of the occupant's weight will be supported by feet which are resting on the floor or pedals. As result, there is overlapping of weight classes in the Passenger Classification System that creates malfunction of the air bag and decreases the number of properly working weight classes to 3 instead of 5. This is a problem that does not allow to accurately weigh a vehicle occupant in a supplemental restraint system to provide the possibility of an accurate control of the air bag inflation force depending on the real value of the occupant's weight (mass) and eliminate extra force applied to the occupant's body at the time of collision. NHTSA, Department of Transportation, published in August 2004 requirements of the final rule of Section §571.208 Standard No. 208; "Occupant crash protection" [2] to improve the security of the air bags for children and light women. An object of the article is to find ways to improve the accuracy of the safety system for differentiating the weight of older children from the weight of the light women passengers and support the documents provided by NHTSA that say the modern safety systems should provide improved protection for occupants of different sizes.

The method described in the present article provides the possibility to extend the current Passenger Classification System by accurately measuring occupant's weight and more accurately controlling the force applied to lighter weighing people and youngsters in case of accident. The article provides a method of accurately weighing occupants of different weights by employing an ADaptive MUlti-force Safety (ADMUS) system that improves the Passenger Classification System for minimizing the risk of injury or death from a possible improper extra force applied to them by air bags in case of accident especially for light adults in contemporary and self-driving or autonomous vehicles

The ADMUS system, with its accurate innovative occupant weight measuring KEF method [3, 4], provides higher protection to occupant bodies of different weights by keeping an extra force from them in case of accident. The weighing error of a vehicle occupant weight measuring drastically decreased in applications [5, 6] by employing the occupant weighing innovative KEF method and using this weighing method and technology based on it to eliminate the weighing error.

Research Question/Objective.

Practically all American cars are equipped by safety systems such as Supplemental Restraint System (SRS) comprising an air bag. When the vehicle includes an occupant safety restraint device arranged to protect the occupant during a crash involving the vehicle, it is connected to the weight measuring system and arranged to provide a variable deployment depending on the determined weight of the occupant. During a crash event, the vehicle's crash sensor and other sensors provide crucial information to the air bag Electronic Computing and Control Unit (ECU), including weight and position of an occupant, usage of the seat belt, severity of impact, etc. Using this information, the air bag ECU's crash algorithm determines if the crash event meets the criteria for air bag deployment and triggers various firing circuits to deploy one or more air bag modules within the vehicle.

THE WAYS TO IMPROVE AIR BAG TECHNOLOGY

To improve safety of passengers in case of a possible crash, adaptive and advanced duel-depth air bag systems and, according to them, the Passenger Classification Systems were designed. Adaptive air bag systems may utilize multi-stage air bags to adjust the pressure within the air bag. Information regarding the occupants and the severity of the crash are used by the air bag control unit, to determine whether air bags should be suppressed or deployed, and if so, at various calculated output levels**.** In the advanced duel-depth air bag, the first and second chambers of the air bag are selectively pressurized with a gaseous fluid. The design of the advanced duel-depth air bag system shows that the car manufacturers try to improve the vehicle occupant safety employing the Passenger Classification System [7] by multiplying the number of stages of an air bag.

STATISTIC OF CASUALTIES.

The present article relates to a problem of mitigating results of improper value of force applied to the occupant's body at a time of an imminent vehicle collision on the road by preventing fatalities as well as injuries that may be caused. More particularly, the present article relates to a new method of accurately weighing vehicle occupants that provides elimination of obstacles to improve their safety in the event of a collision. The problem of vehicle occupant safety has now become a nation-wide problem for the USA and other countries. The air bag by itself may cause injuries if it doesn't work properly. From 1990 to 2000, the United States National Highway Traffic Safety Administration (NHTSA) identified 175 fatalities caused by air bags. Most of these (104) have been children, while the rest were adults. 262 deaths from1990 to 2006 reportedly have been caused by air bags inflating in low severity crashes, most of them in older model vehicles. These deaths include 87 drivers, 13 adult passengers, 138 children, and 24 infants. In 2016 alone, 37,461 people died in motor vehicle crashes. In 2016 publication [8], NHTSA provided overall crash population for a period of 2010-2013. Today's cars and trucks come with driver assistance technologies. The driver assistance technologies that include sensors, radars, cameras, GPS will help support Automated Driving Systems (ADS), more commonly referred to as "self-driving" [9] (SDV) or autonomous vehicles. These 2 types of vehicles in contrast to the contemporary vehicles might be able to take over all aspects of driving and may predict imminent crashes on the road and reduce vehicle crashes and resulting fatalities and injuries. The Table 1 was generated by this data.

Table 1.
Crashes in 2010 - 2013 and their results

	2010 - 2013 Annually				2010 - 2013 total costs	
	Crashes	Fatalities	1-5 Injuries	Property damage	Costs for society	Total costs
1	Registered crashes for all vehicles					
	5.5 M	33,020	2.7 M	6.3 M	$195 B	$721 B
2	Related to the V2V technology (2 cars crashes - 69%)					
	3.8 M	13,329	2.1 M	5.2 M		
3	For LV2LV vehicles only (62% of all crashes) - that a new technology may save					
	3.4 M	7,325	1.8 M	4.7 M	$109 B	$319 B
4	Crashes and their results that will be not covered by the V2V technology					
	2.1 M	25,695	0.9 M	1.6 M	$86 B	$402 B

In the row 1 of the Table 1, is given the data published by NHTSA. Based on 2010-2013 General Estimates System (GES) and Fatality Analysis Reporting System (FARS), of the 5.5 million annually crashes, which would translate to 33,020 fatalities, 2.7 million Maximum Abbreviated Injury Scale (MAIS) 1-5 injuries, and 6.3 million property damage only vehicles (PDOVs). NHTSA estimated that safety applications enabled by self-driving technology could eliminate or mitigate the severity of up to 80 percent of crashes, including crashes at intersections or while changing lanes. Most of the automobile companies, technology companies, component makers, and organizations have begun developing or forming partnerships around self-driving technology to decrease the number of crashes, fatalities, and injuries on the roads.

The Tesla's hardware [10] for self-driving model S electrical car employed in the SDV to make driving vehicles safer . The V2V (vehicle-to-vehicle) communication technology described by NHTSA. Detailed information about DSRC-based V2V vehicle communication system see in [8]. As the statistics show, the number of the victims is indirectly proportional to their weight. The sensors have to measure weight of a vehicle occupant but not the size of the occupant because the energy accumulated by the occupant's body in the moving vehicle and which a restraint system has compensate during the crash, is proportional to the mass but not to the size of the body. In the contemporary Passenger Classification Systems, the force applied by an air bag to the adult occupant, especially to the driver, in the air bag system is the same as applied to the person whose weight is 102 Lb and applied to the person whose weight is even 215 Lb or higher. A light occupant in such situation may be injured and a heavy occupant may be not protected enough. This is the reason that it is necessary to provide more classes in the Passenger Classification System to differentiate the forces applied to children and adult occupants in case of collision according to their weight**.**

Methods and data sources

OCCUPANT WEIGHING ERROR

As was mentioned before, the weight of an occupant measured by an air bag system is not the entire weight of the occupant since some of the occupant's weight will be supported by his or her feet which are resting on the floor or pedals. Contribution of the lost weight of the foot part of the body to a total weight of a person during measurement may be evaluated very easily, and it is about 15 -30%% or more of the whole body weight. This is a problem that does not allow to accurately weigh a vehicle occupant in supplemental restraint system to provide the possibility of an accurate control of the air bag inflation force depending on the real value of the occupant’s weight (mass) and eliminate extra force applied to the occupant’s body at the time of collision. So, to accurately weigh a vehicle occupant, it is necessary to weigh the whole body of a vehicle occupant including the weight of a foot part of his/her body. NHTSA published in [2] requirements of the final rule of Section § 571.208 Standard No. 208; "Occupant crash protection" to improve the security of the air bags for children and light passengers. It is not made in the on-board vehicle safety system yet. It is a goal of the methods of the present article to improve the occupant safety system by more extensive preparations for overcoming an imminent vehicle collision on the road and preventing fatality as well as injuries of the occupants that may be caused by an unsafe force applied to their bodies by the restraint system in the event of a collision. A principal object of the present article is to improve the accuracy of the safety system for differentiating the weight of older children from the weight of the light women passengers and support the documents provided by NHTSA that say the modern safety systems should provide improved protection for occupants of different sizes. So, it is the object of the present article to provide a safety system for controlling the force applied to the occupant's body measuring not the size, but with the accurately measured weight of the occupant. An object of the present article is to provide an accurate measuring weight of the vehicle occupants in a safety system of the contemporary, self-driving and autonomous vehicles by an accurate occupant weighing technology because the statistics show that the number of the accident victims depends on their weight. This provides the possibility to extend also the current Passenger Classification System and more accurately control the force applied to lighter weighing people and youngsters in case of accident.

ADMUS SYSTEM

This article provides a safety method for protection of the different weight occupants of the self-driving or autonomous vehicle by applying different forces to their bodies at the moment of an accident that are more accurately controlled through the control signals depending on their weights that are modified depending on the morphological data and factors of the car trip in the current situation that influence the force applied to the occupant's body. The article provides method of accurately weighing occupants of different weights by employing an ADaptive MUlti-force Safety (ADMUS) system that improves the Passenger Classification System for minimizing the risk of injury or death from a possible improper extra force applied to them by air bags in case of accident especially for children and light adults in contemporary and self-driving or autonomous vehicles. The ADMUS system, with its accurate innovative occupant weight measuring KEF method [3, 4], provides higher protection to occupant bodies of different weights from applying an extra force to them in case of accident by more extensive preparations for overcoming possible negative consequences of an imminent vehicle collision on the road and preventing fatal accidents as well as injuries of the occupants that may be caused by an unsafe force applied to their bodies by the restraint system.

KEF METHOD

The weighing error of a vehicle occupant weight measurement may be drastically decreased by employing the occupant weighing innovative KEF method and using this weighing method and technology based on it to eliminate all the weighing error. In this case, the energy generated by the occupant's body at the time of collision may be accurately measured before the collision and used for safety purposes in the vehicle air bag system. Using the KEF method is important to provide effectiveness and accuracy for occupant weighing. It is based on a horwest (horizontal weighing stability) effect that states: the value of a weight measurement of an object located in a closed system on a weighing unit doesn't change while this object provides a bi-directional force in a horizontal direction of a predetermined value to a vertical surface of another object, which is a predetermined distance away [see 3,4]. The horwest effect can be used to implement the simplified weighing apparatus for accurate vehicle occupant weighing. Moreover, the innovative KEF method can provide a simplified and accurate occupant's weight measurement in a car or a motor vehicle, especially a passenger vehicle such as an automobile, a van, a self-driving car, a corporate vehicle, a limousine, or a truck equipped with an occupant safety device such as air bag Supplemental Restraint System (SRS) by employing a weighing unit (weight sensors) connected to the seat of the vehicle occupant, whose output is connected to the computing and control unit of the SRS, by pushing horizontally a switch of the weighing moderator, located above the waist of the occupant on a substantially vertical surface of the vehicle (for example, on a steering wheel, an instrument panel, or a dash board) at the beginning of the trip, and simultaneously, conveniently lifting feet above the floor and keeping them up during the weight measurement, measuring occupant's weight by the weighing unit. Subsequent processing of the collected weight of the vehicle's occupant by the computing and control unit while receiving the signal from the switch of the weighing moderator, modifying this original weight measurement of the vehicle occupant by the current values of the morphological data and factors of the car trip situation and transmitting this processed value of the vehicle occupant's weight to the air bag control unit to apply, in case of a collision, an appropriate force to the occupant's body, whose value will be calculated according to the modified and accurately measured occupant's original weight.

SOURCES

The accuracy of weighing a vehicle's occupant and, accordingly, providing an accurate value of the force applied to the different weights of the occupants' bodies may be improved up to 20-30% by employing KEF method. It is further noted that the priority documents of the current article, namely U.S. Pat. No. 9,566,877 [3], issued on Feb. 14, 2017, **allowed** U.S. Divisional patent application Ser. No. 15/430,219 [4] filed on Feb. 10, 2017, U.S. Pat. No. 10,131,308 [6] issued on Nov. 20 , 2018 and U.S. Provisional Application No. 61/956,059 [11] filed on May 30, 2013, can provide a more detailed description of the novel horwest effect and KEF method. The present article provides a method for a contemporary or a self-driving or autonomous vehicle having an air bag safety system to communicate with an innovative weighing KEF technology for use in the accurate weighing of an occupant based on a weighing moderator to prevent extra force applied to the occupant’s body in case of collision. The present article provides modification of the occupant's original weight accurately measured by the innovative weighing technology in a contemporary or a self-driving or autonomous vehicle before the beginning of a trip in accordance with the values of such parameters as the severity of the crash, position of the occupant, using a seat belt.

Results

As was noted above, the measured weight of an occupant is not the entire original weight of the occupant since some of the occupant's weight will be supported by his or her feet which are resting on the floor or pedals. This effect creates a weighing error. The value of this error in a total original weight of a person may be evaluated very easily, and it is about 15-30% or more of the whole body weight. In [12] this loss of the occupant's weight was given as 20%. Some data for the weighing error provided in the current article have been received in experiments and shown in Tables 2 , 3, and 4. The whole picture of the weight lost by a vehicle occupant during measuring his/her weight while one is sitting in the car seat and the feet are resting on floor or pedals and supporting the body, may be clear after receiving a statistical data. The weighing error is a problem that does not allow to accurately weigh a vehicle occupant in on-board vehicle safety restraint system to provide the possibility of an accurate control of the air bag inflation force depending on the real original value of the occupant's weight (mass). The weighing error does not allow also to eliminate improper force applied to the occupant's body at the time of collision by improving the Passenger Classification System and providing an improved accuracy of the safety system for differentiating occupants by weight, especially children from the light women. The weight measurements of occupants of different groups age, sex, positions were made by the author and provided in Table 2.

Table 2.

The occupant's weighing error

	Date	Weight (Lb)					
		Original weight, sex, age	Horizontal distance D (cm) from feet on the floor to the torso on the scale	Feet position (torso on the scale)			Percentage of the occupant's weighing error
				Hands are on the groins	Hands down in the air	Hands on the knees	
1	3.29.2018	151 Man, 82	70 max	128	126	115	15.2-23.8 %
			55 mid	121	114	112	19.9-25.8 %
			40 min	114	109	107	24.5-29.1 %
2	3.30.2018	182 Female, 77	60 max	155	154	150	14.8-17.6 %
			50 mid	150	149	147	17.6-19.2 %
			40 min	143	140	138	21.4-24.2 %
3	3.29.2013	148, Man, 77	D min			109	25.8-26.4 %
4	7.25.2014	151 Man, 78	D min			110	27.2%
5	9.24.2016	144, Man, 80	D min			120	16.7%
6	7.14.2018	221 Man, 45	D max	197	193	188	10.9 - 14.9 %
			D mid	189	178	173	14.5 - 19.5 %
			D min	173	166	160	21.7 - 27.6 %
7	11.10.2018	134 F 15	D min			93	30.6%
8	11.10.2018	91 F 11	D min			65	28.6 %

As we may see from Table 2, the value of an error of measuring weight of an occupant sitting in a seat of the contemporary on-board vehicle SRS air bag safety system may reach around 30% of original occupant's weight. For example, in the Table 2 in the range from 144 to 221 Lb of the original weights of occupants, the value of the mistake of occupant weight measurement reaches 29.1%. This means that some two classes in the Occupant Classification System SRS may be overlapped. In the Fig.1,a is given the Table S7.1.4 "Weights and dimensions of the vehicle occupants referred to in Standard § 571.208: Occupant crash protection"[2].

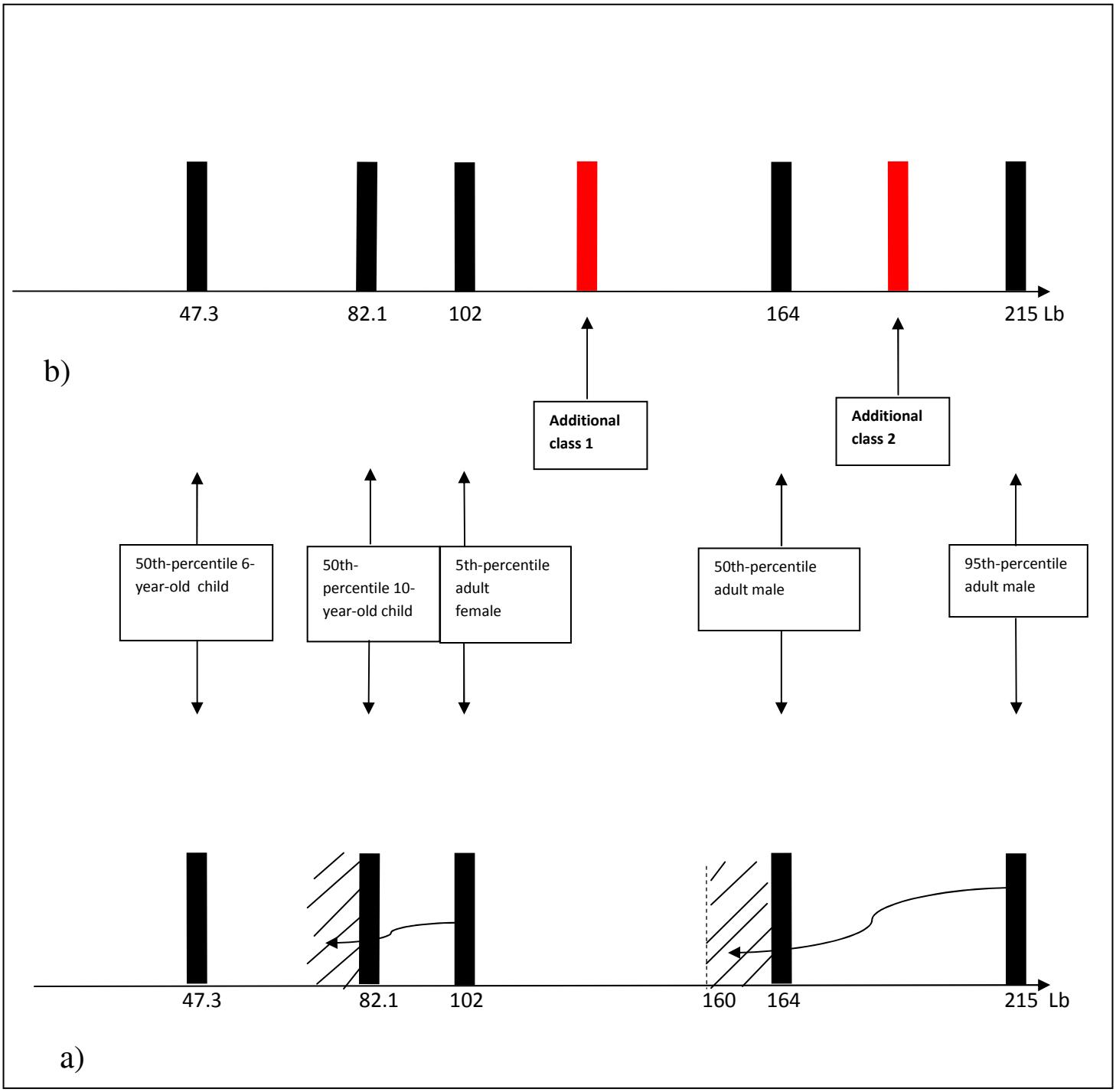

Fig.1. b) KEF method based Passenger Classification System

Fig.1. a) Overlapping in the Standard 208 Passenger Classification System

OVERLAPPING IN THE STANDARD §571 208

There are 5 classes of occupants in the Table S7.1.4 "Weights and dimensions of the vehicle occupants referred to in Standard § 571.208" [2] showed as 5 black bars in FIG.1,a:

50th-percentile 6-year-old child (47.3 Lb), 50th-percentile 10-year-old child (82.1 Lb), 5th-percentile adult female (102 Lb), 50th-percentile adult male (164 Lb), and 95th-percentile adult male (215 Lb). As we see from Table 2, in case of the 95th-percentile adult male whose original weight 221 Lb (that is close to the range 215 Lb) and its maximum variable weighing error value is 27.6%, 50th-percentile adult male class will be overlapped by the measured weight of the 95th-percentile adult male class**,** and the SRS air bag safety system will not recognize whom it is necessary to treat: 50th-percentile or 95th-percentile adult male, although the force applied to the bodies of these two different weight occupants should be different. For now it seems the worst case of overlapping is on the border of 50th-percentile 10-year-old child and 5th-percentile adult female. As in the previous example, in case of the 5th-percentile adult female whose original weight around 102 Lb (according to the Table S7.1.4 "Weights and dimensions of the vehicle occupants referred to in Standard § 571.208") and if its maximum variable weighing error value is more than 20%, the 50th-percentile 10-year-old child class will be overlapped by the measured weight of the 5th-percentile adult female class (see FIG 1, a). In this case, the air bag safety system will malfunction. It will suppress the air bag when it should be deployed because the 5th-percentile adult female is in the seat.

OVERLAPPING BY THE MEASURED DATA

Malfunction case was found in Table 3 when a group of adult people was checked for their value of weighing error. The weight measurement of this group of six adult women was provided by "ResCare" Adult Day Care Community Center, Hamden, CT. As we may see from Table 3, women ##5 and 6 may be related to the 5th-percentile adult females. Woman #5 has original weight of 113 Lb, and her measured weight in the simulator of the vehicle seat while her feet are on the floor, is 84 Lb. Her calculated weighing error is 25.7%. In case of the vehicle collision, the air bag system will recognize her as adult (84 Lb >82.1 Lb) and her air bag will be deployed. Woman #6 has original weight of 108 Lb, and her measured weight in the simulator of the vehicle seat while her feet on the floor, is 78 Lb. Her calculated weighing error is 27.8%. In case of her vehicle collision, the air bag system will malfunction by recognizing her as the 50th-percentile 10-year-old child (78 Lb <82.1 Lb), and her air bag will not be deployed.

Table 3.

The adult occupant's weighing error

No.	Date	Name	age	sex	Weight (Lb)			Percentage of the occupant's weighing error
					Original weight	Hands on the knees	Difference	
1	10.30.2018	Maya	82	F	154	110	44	28.6%
2	10.30.2018	Galina	79	F	148	101	47	31.8%
3	10.30.2018	Bella	81	F	135	103	32	23.7%
4	10.30.2018	Sophia	81	F	140	109	31	22.1%
5	10.30.2018	Angela	95	F	113	84	29	25.7%
6	10.30.2018	Inness	85	F	108	78	30	27.8%

The third such malfunction case was found in Table 4 when a group of 5th-percentile adult females was checked for their value of weighing error. The weight measurements in the Table 4 were provided by National Music Teachers Association (New Haven Chapter), a music studio in Woodbridge, CT.

As we may see from Table 4, women ##7 and 9 may be related by weight to the 5th-percentile adult females. Woman #7 has original weight of 105 Lb, and her measured weight in the simulator of the vehicle seat while her feet are on the floor, is 74 Lb. Her calculated weighing error is 29.5%. In case of her vehicle collision, the air bag system will malfunction by recognizing her as the 50th-percentile 10-year-old child (74 Lb <82.1 Lb) and her air bag will not be deployed.

Table 4.

The 5th-percentile adult females weighing error

No.	Date	Name	age	sex	Weight (Lb)			Percentage of the occupant's weighing error
					Original weight	Hands on the knees	Difference	
1	10.22.2018	Libby	12	F	77	54	23	29.8%
2	10.22.2018	Nell	13	F	83	59	24	28.9%
3	10.22.2018	Sienna	15	F	138	98	40	28.98%
4	10.22.2018	Mei	16	F	118	97	21	17.8%
5	10.23.2018	Sofia	15	F	158	108	50	31.6%
6	10.24.2018	Veronica	16	F	149	111	38	25.5%
7	10.24.2018	Sophia	13	F	105	74	31	29.5%
8	10.24.2018	Leila	14	F	158	105	53	33.54%
9	10.25.2018	Devin	12	F	102	74	28	27.45%
10	10.26.2018	Sophia	13	F	80	55	25	31.25%

Woman #9 in Table 4 has original weight of 102 Lb, and her measured weight in the simulator of the vehicle seat with her feet on the floor, is 74 Lb. Her calculated weighing error is 27.45%. In case of her vehicle's collision, the air bag system will malfunction because it will recognize her as 50th-percentile 10-year-old child (74 Lb <82.1 Lb), and her air bag will not be deployed.

The variable weighing error may be used to predict, find, and eliminate by KEF method a malfunction of an air bag safety system (especially for 5th-percentile adult females) in a contemporary, self-driving, and autonomous vehicle where an accurate weight measuring KEF technology of an occupant will be employed.

As we may see from FIG. 1,a and Tables 2-4, to mitigate the negative consequences of a crash on a road for a 5th - percentile woman sitting in the contemporary, self-driving, or autonomous vehicle, it is necessary to know in advance or measure it at the beginning of the trip by KEF method an accurate original weight of this occupant and her measured weight when she/he is sitting in the seat. This last weight will be less than original weight because the feet are resting on the floor or pedals. If this weight overlaps a closest child weight

range, it is necessary to eliminate the possible suppression of the air bag of the 5th -percentile woman before the vehicle's imminent crash during a trip. The time interval for regular weighing error measuring has to be established for contemporary, self-driving, and autonomous vehicles where the KEF weight measuring technology of an occupant is available.

FIG.1,b shows additional occupant's weight classes proposed in this ADMUS adaptive safety SRS system employing the accurate KEF occupant weighing technology. In the FIG.1,b seven weight classes proposed referred to ADMUS safety SRS system. Among these classes, there are all 5 classes (including children) that exist in the Table S7.1.4 "Weights and dimensions of the vehicle occupants referred to in Standard § 571.208: Occupant crash protection"[2]. The accuracy of KEF method and elimination of the weighing error, protects weight classes of Admus system from an overlapping that in turn provides room for at least 2 additional weight classes (red bars in the FIG.1,b).

The two additional classes may be used for the same purposes of applying different forces to the bodies of different (for example 125 and 190 Lb) weight occupants at the moment of an accident that are controlled through the control signals depending on their accurately measured weights and factors of the car trip in the current situation.

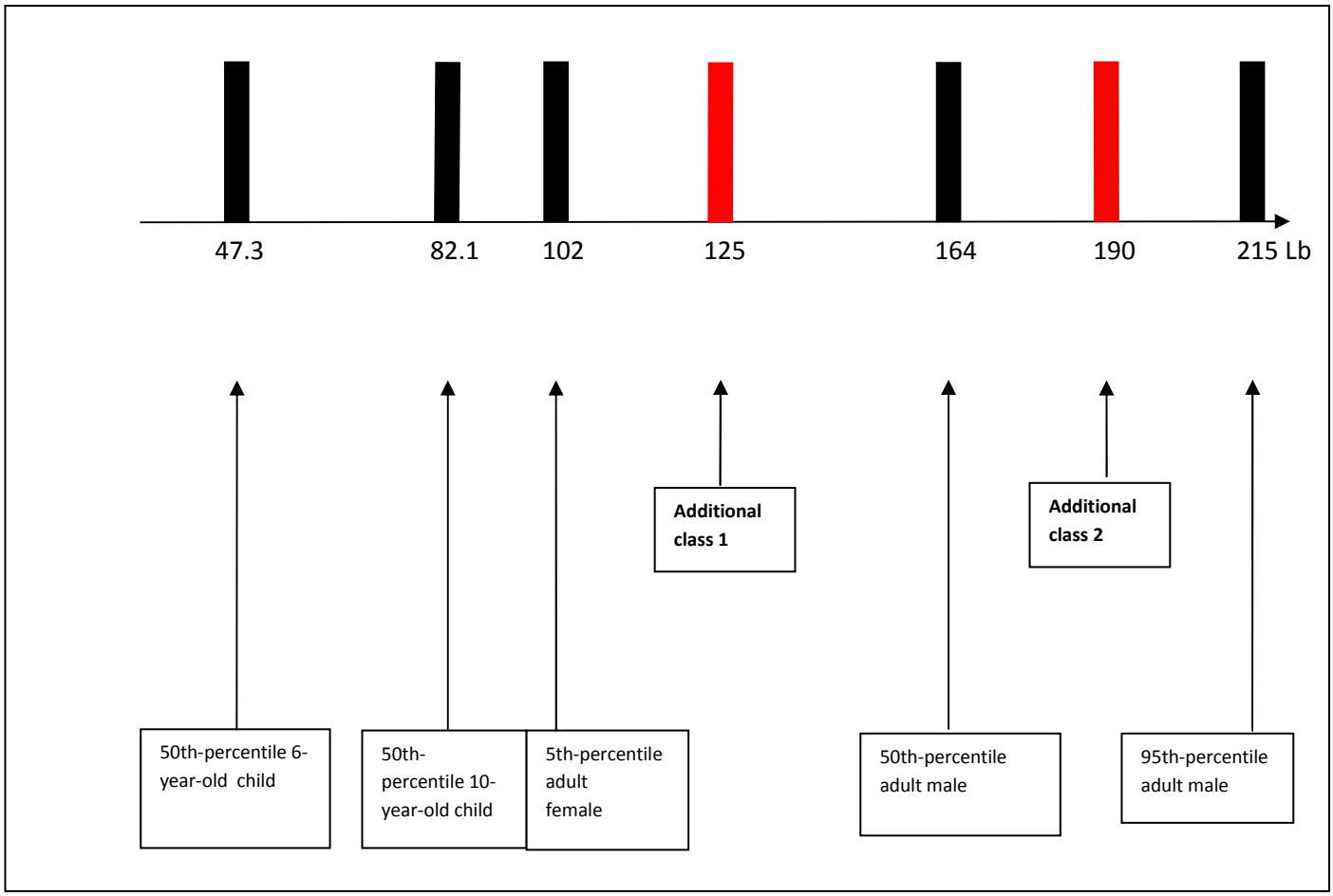

Fig.2. ADMUS Passenger Classification System

FIG.2 represents the proposed Passenger Classification System (PCS) based on accurate occupant's weight measuring KEF method and based in turn on this method the KEF technology that provide more accurate differentiation of different weight occupants and a safer restraint system. In Table 2 of [13], the number of passenger vehicles occupants that have been killed in crashes in 2016 is provided by age groups and restraint devices use. The ratio of the number of restrained passengers to the number of unrestrained passengers killed in the younger age groups such as <4 years old and 4-7 years old, and in the older aged groups 65 -74 and 75 + years old passengers, is 2-3 times higher than in other age groups despite that the percentage of known restrained was higher than the percentage of known unrestrained people killed in 2016. So, it seems that younger children group needs a more gentle restraint support during a crash, and proposed KEF method may help in this case also by extend the PCS.

Discussion and Limitations

Due to the of existence of the described above problem of overlapping and weighing error high value up to 30%, the number of properly functioning weight classes in the vehicles for adults in the Table S7.1.4 "Weights and dimensions of the vehicle occupants referred to in Standard § 571.208"[2] may really not be more than 3 classes that drastically decreases the accuracy of weighing occupants of a vehicle and their safety. This means it is necessary to provide a safety system for protection of the different weight occupants of the contemporary and self-driving or autonomous vehicles by applying different forces to their bodies that are more accurately controlled at the moment of an accident. The accuracy of the KEF technology of an occupant weighing improves safety system for differentiating the weight of older children from the weight of the light women passengers and supports the documents provided by NHTSA. The additional occupant's weight classes proposed in this ADMUS adaptive safety SRS system employing the accurate KEF occupant weighing technology that enhances safety (7 accurate weighing classes instead of 5) of the vehicle. These additional classes help to solve a problem of applying different forces to the bodies of different weight occupants by measuring weight of occupants accurately at a beginning of a trip and using these measurements at the moment of an accident to control the forces applied to the occupants' bodies depending on occupants' weights that are in the aftermath modified depending on the morphological data and factors in the current car trip.

.

Conclusions and Relevance to Session Submitted

Experimental data provided in the article clearly testifies that a weighing error of a vehicle occupants significantly reduces their safety by not restraining them by an accurate forces applied to their bodies. Additionally, weighing error, as shown in the article, leads to malfunction of the air bag for the 5th percentile of light women and for light old men. A simple KEF method of accurately weighing vehicle occupants provided in the article may help to avoid the weighing error in frontal and other types of crashes and enhance safety of vehicles. It is necessary to add that horrific numbers of child mortality provided in [13] forces us to make progress in this direction.

References.

1. U.S. Pat. No. 7,330,784. Johnson .W. et al. Weight measuring systems and methods for vehicles. February 12, 2008.
2. Final rule of Section § 571.208 Standard No. 208; Occupant crash protection. NHTSA. August 2004.
3. U.S. Pat. No. 9,566,877. Kriger Y. Technology and methods of on-board vehicle occupant accurate weighing by a simplified weighing apparatus based on weighing moderator and its applications in on-board occupant weighing systems, February 14, 2017.
4. U.S. Allowed Patent Application No.15/430219. Kriger Y. Technology and methods of on-board vehicle occupant accurate weighing by a simplified weighing apparatus based on weighing moderator and its applications in on-board occupant weighing systems, June 1, 2017
5. U.S. Pat. No. 10,017,078. Kriger Y. Relocatable/replaceable pad for accurate vehicle occupant weight measurement. July 10, 2018
6. U.S. Pat. No. 10,131,308. Kriger Y. Safety on-board vehicle multi-force restraint system employing a weighing moderator. November 20, 2018
7. U.S. Pat. No. 5,564,743. Marchant; Brent R. Multiple stage air bag inflator system. October 15, 1996.
8. Notice of Proposed Rulemaking. DOT of transportation NHTSA. 49 CFR Part 571 [Docket No. NHTSA-2016-0126] RIN 2127-AL55 Federal Motor Vehicle Safety Standards; V2V Communications.
9. NHTSA, " Driver assistance technologies". January 2018.
10. Tesla's Autopilot: The smart person's guide. By Hope Reese, TechRepublic, August 4, 2017.
11. U.S. Provisional Application No. 61/956,059. Kriger Y. filed on May 30, 2013
12. Development of occupant classification system. Tsutomu Takano, Nissan Motor Co., LTD 18 International ESV conference, Nagoya, May, 2003. Paper Number 206.
13. Traffic safety facts. 2016 data. DOT HS 812494. February 2018. NHTSA.

DEVELOPMENT OF A HUMAN FE MODEL FOR ELDERLY FEMALE OCCUPANTS IN SIDE CRASHES

Hisaki Sugaya, Yukou Takahashi, Yasuaki Gunji, Yasuhiro Dokko
Honda R&D Co., Ltd. Automobile R&D Center
Japan

Murthy Ayyagari, Bryant Whitcomb, Craig Markusic
Honda R&D Americas, Inc.
United States

Amanda Agnew, Yun-Seok Kang, John Bolte IV
Injury Biomechanics Research Center (IBRC), The Ohio State University
United States

Paper Number 19-0052

ABSTRACT

A high fatality rate of the elderly in traffic crashes is an important issue to consider when facing an aging society in the future. Left side impacts have been found to be the most frequent when considering severe crashes involving elderly people that resulted in Abbreviated Injury Scale (AIS) 4+ injuries in the United States. Additionally, the frequency of rib fractures in female occupants is significantly higher than males in those over sixty years in a side impact. Therefore, there is a need to reduce rib fractures in elderly females in side impacts, which should significantly decrease the number of fatalities in these types of crashes. Currently there are no evaluation tools for elderly female occupants with increased fragility. The objective of this study was to develop a Human Body Model (HBM) of an elderly female with increased fragility to use in simulations which focus on side impacts.

The material properties of rib cortical bone were determined using average data from published literatures. A rib bending simulation was conducted to compare force-deflection response with published experimental data. The rib cortex model included thirty-two sections of a rib, in which the thickness of each section was determined by comparing to published precise cross-sectional data. The evaluated rib model was then applied to the full-body HBM of an elderly male which was developed in a past study. Using the full body model geometrically scaled to elderly female, published side impact sled tests at 28 km/h of delta-V with post mortem human subjects were simulated to compare kinematics, rib fracture locations, and thoracic deflection obtained from chest band data. Comparison of the force-deflection response of the rib in bending showed that the simulation result fell within the overall experimental range. In the side impact sled simulations, the predicted trajectories of T1, T12, and the pelvis were found to be similar to those from the experiment. The number of rib fractures, fracture timing, fracture locations and overall thoracic deflection in the simulation exhibited a similar trend to the experimental data.

The HBM developed by applying rib material properties and geometrical scaling for an elderly female well represented upper body kinematics, rib fractures and thoracic deflection in a side impact when compared to published PMHS experiments.

INTRODUCTION

The National Highway Traffic Safety Administration (NHTSA) reported the elderly population, age 65 or older, in the U.S. reached 47.8 million in 2015; this is nearly 15 percent of the total U.S. population [1]. Also, the number of licensed elderly drivers increased by 33% from 2006 to 2015, reaching 40.1 million. Furthermore, Ortman et al. [2] predicted that the elderly population will expand to 83.7 million by the year 2050. NHTSA also reported the number of elderly fatalities increased by 3% from 2006 to 2015, even though the overall number of fatalities decreased by 19%. [1] Therefore, it is possible that the number of fatalities of elderly people in traffic crashes will further increase due to an aging society. As a result, protection for the elderly in traffic crashes is critical.

A previous study done by NHTSA analyzed the National Automotive Sampling System Crashworthiness Data System (NASS-CDS) and found that the percentage of drivers sustaining Maximum Abbreviated Injury Scale (MAIS) 4+ injuries relative to the number of drivers involved in crashes is significantly larger for the elderly population (greater than 65 years old) compared to occupants between 25 and 44 years old, 1.85% compared to 0.76%, respectively [3]. Specifically, for left-side impacts without rollover the percentage of elderly occupants becomes even larger and is the largest percentage of all crash modes. This suggests that the protection of elderly drivers involved in left-side impacts is important.

One of the factors that likely contributes to the high probability of severe and fatal injuries to elderly occupants is the increased fragility of their bones. For example, Agnew et al. [4] showed that in whole rib bending tests, the tensile failure strain in the rib significantly decreases with age. This group also showed that body height had a positive relationship with both peak force and total fracture energy. [5] Therefore, shorter occupants, such as small elderly females, may have a higher probability of severe and fatal injuries. Ramachandra et al. [6] revealed that the probability of AIS3+ injury in side impact crashes also depends on sex. According to the study, in near-side impacts, the probability of injury to the thorax and the ribs were significantly higher for females than for males within the elderly population, (over 60 years of age). All of these studies suggest that small, older female drivers in near-side impacts are more susceptible to thoracic injuries, particularly rib fractures.

Despite the growing importance to better understand how to protect elderly females in near-side impacts, few studies have investigated this impact configuration. A recent study by Shurtz et al. [7] conducted side impact sled tests using two small elderly female post-mortem human subjects (PMHS). These sled tests included realistic boundary conditions of a typical near-side impact including: seat-belt with a pretensioner, side airbag and intruding car door. In addition, there has only been one validated Human Body Model (HBM) representing an elderly female published to date [8]. This elderly female HBM was validated against a side sled test with rigid wall, which is not a realistic boundary condition. Unfortunately, at this time there is not a validated small elderly female HBM that could be used to test safety systems in near side impact scenarios. Therefore, the objective of this study was to develop a HBM of a small elderly female occupant under realistic boundary conditions in the near side.

METHOD

A two-phase approach, model creation and model validation, was taken to achieve our goal as shown in Figure 1. During the model creation phase, a three-step approach was taken including: (1) scale a whole body model from a 50th male (AM50) to a 5th female (AF5), (2) create a single rib model to match previous rib experimental testing, and (3) create an average elderly female rib model using literatures. The modeled fragile female ribs were then used in the creation of the AF5 model and validated. Validation was accomplished in terms of prediction of rib fractures and thoracic injury severity using three different experiments: (1) single rib experimental bending test, (2) a whole-body thoracic impact test series and (3) whole-body PMHS side sled test using realistic boundary conditions.

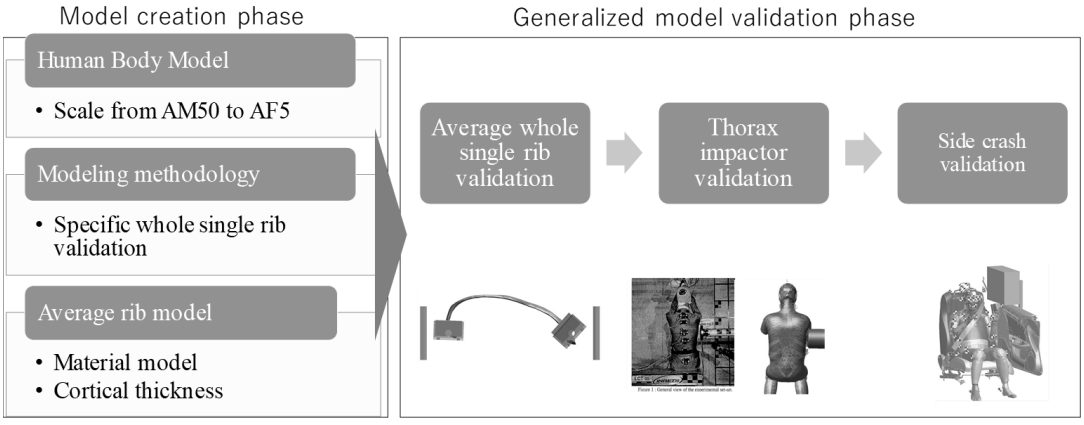

Figure 1. Scheme of development of HBM for elderly female

Model Creation Phase (Whole Human Body Model)
The Human Body Model (HBM) AM50 was evaluated as an elderly occupant by Dokko et al.[9]. This model served as the baseline model that was then adapted with finite element capable software, LS-DYNA (version R7.1 LSTC, Livermore, CA, USA) to convert it into the AF5 model. The thorax of the AM50 model had been developed based on a CT of a single elderly male with average body size, 175 cm in height and a mass of 77kg. The material properties used to represent the cortical bone located in the ribs were determined using tensile test results reported by Kemper et al. [10][11]. The AM50 elderly model was validated against thoracic impact tests documented in ISO-TR9790 (1997) [12] along with side and frontal sled tests conducted by Lessley et al. [13] and Shaw et al. [14]. The biofidelity score for these validation tests ranged from 0.23 - 1.18 based on the assessment scheme proposed by Rhule et al. [15].

The AM50 HBM was scaled to that of a small female body size (AF5). The model was scaled to 0.86 times relative to the x, y, and z axes equally to accomplish a stature of 151 cm. In addition, the densities of the internal organs were adjusted to match the target total body mass which was 47 kg based on a dataset published by Robbins et al. [16]. The skeletal model of the thorax of the AF5 was then compared with a statistical small female model published by Wang et al. [17]. It was found to be close to the statistical rib-cage geometry as shown in Figure 2. The AF5 thorax was approximately7% larger in width and 0.5% larger in depth.

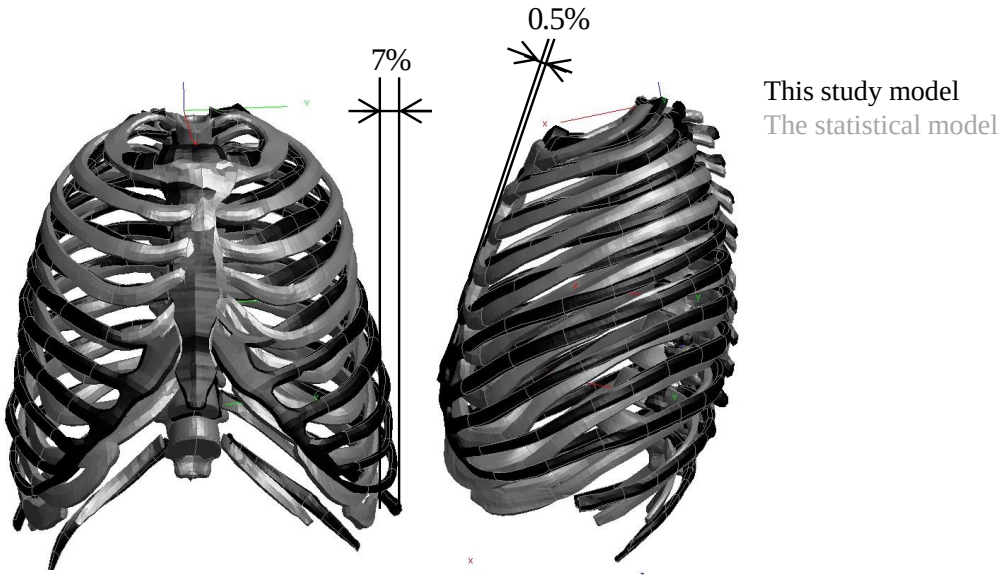

Figure 2. Comparison between thoracic skeletal morphology in the simulation and in the statistical model for the small elderly female

Model Creation Phase (Determination of modeling methodology for whole single rib – Parametric study)
As stated one of the validation parameters for the AF5 model is intended to be the number and location of rib fractures. Therefore, it was critical to model the correct material property for rib cortical bone and validate a whole single rib against published experimental testing. Whole single rib tests were simulated to determine the most appropriate rib modeling methodology; variables investigated included: number of sections along the length of the rib, cortical thickness of each section and the best material properties to use for cortical bone. Experimental bending tests using a whole 6th rib published by Agnew et al. [4] were simulated and the results were compared with the experimental results to determine the best modeling methodology.

Two ribs from two different female subjects used in the published whole bone experimental tests were selected to model and simulate. The two selected experimental ribs, subject 1 and subject 2, were scanned using both a FARO laser scanner, as well as computed tomography (CT). The images were used to create computer-aided design (CAD)

models of the surface of the ribs using Mimics (Ver. 12.0, Materialise, Leuven, Belgium). Cortical bone models were then developed with shell mesh and filled in with solid mesh to reproduce the trabecular bone from the CAD models. Cortical thicknesses of each rib was measured using both CT data and histological rib cross-section data. Each rib was sectioned into 8 cross-sections equally divided along the length of the rib. For each of the 8 cross-sections, four thicknesses were calculated: cutaneous, pleural, superior and inferior. The cortical thicknesses were measured for all 8 cross-sections from the CT images. However only one cross section of each rib, located 67% along the length of the rib, underwent histological analysis. The CT scan had an in-plane resolution of 0.146 mm, while the histological analysis had a resolution of 1,446 pix/mm (0.000692 mm/pix) as published by Agnew et al. [4]

The test set-up of the whole-rib simulation tests matched the experimental tests. The vertebral and sternal ends of the rib model were constrained in pots which were oriented perpendicular to the rib as it entered the pot. The pots on both ends were allowed to rotate about the z-axis. In addition, the sternal end could be moved posteriorly along the x-axis, representing a frontal crash. The reaction force was measured at the vertebral end of the rib in the experimental tests by Agnew et al. [4] and also in the simulation along with the displacement of the sternal end of the rib for a direct comparison to calibrate the model. As mentioned, a parametric study was conducted using this simulation changing three key parameters: number of sections along the length of the rib, cortical thickness of each section and the best material properties to use for cortical bone. The parametric study matrix is shown in Table 1.

Table 1.
Parametric study matrix of bending simulation and results

Case ID		Model 1	Model 2	Model 3	Model 4
Parameter	Number of total divisions in the rib	16	32	32	32
	Thickness source	CT	CT	Function between microscope and CT	Function between microscope and CT
	Material properties	MAT24 Tension	MAT24 Tension	MAT24 Tension	MAT124 Tension & Compression

Parameter 1 – Number of divisions in the rib: As stated earlier, the two modeled ribs were portioned into 8 sections longitudinally along the length of the rib. For each longitudinal section, the cortical bone was then broken into 4 sections circumferentially. The first variable the parametric study evaluated was how many divisions of cortical bone were needed to adequately model the experimental ribs. A comparison between a simplified model with 16 cortical bone divisions (Model 1) and a more detailed model of 32 cortical bone divisions (Model 2, Model 3 & Model 4) as shown in Figure 4. The simplified model only looked at using 4 of the longitudinal cross-sections versus all 8.

Parameter 2 – Cortical bone thickness source: Two types of cortical bone thickness values were applied. As mentioned previously, thickness values came from both the CT scans, in all 8 longitudinal cross-sections, and a histological measurement, at a single cross-section. On the cross-section that had both a CT measurement and a histological measurement, a correlation between the two measurement techniques was calculated. The relationship between the measured histological cortical thickness, which is considered the gold standard for measuring cortical bone thickness, and the CT thicknesses was calculated as shown in Table 2, Equation 1 and Figure 3. The relationship as defined in equation (1) had a R square value of 0.83 certifying good correlation between the data when using a linear approximation based on a least-squares fit. Model 1 and Model 2 used cortical bone thicknesses as measured using the CT scans only, while Model 3 and Model 4 used the function as defined in Equation 1 to calculate the thickness of each cortical bone segment.

$$D_{mod} = 1.2253 * D_{ct} - 0.6302 \quad \text{(Equation 1)}$$

Table 2.
Cortical thickness measurement between CT and Histological measurement

	Thickness source	CT (mm)	Histological measurement (mm)
Subject 1	Superior cortex	0.77	0.21
	Cutaneous cortex	0.86	0.25
	Inferior cortex	0.74	0.14
	Pleural cortex	1.00	0.63
Subject 2	Superior cortex	0.49	0.19
	Cutaneous cortex	1.17	0.81
	Inferior cortex	0.66	0.47
	Pleural cortex	1.24	0.97

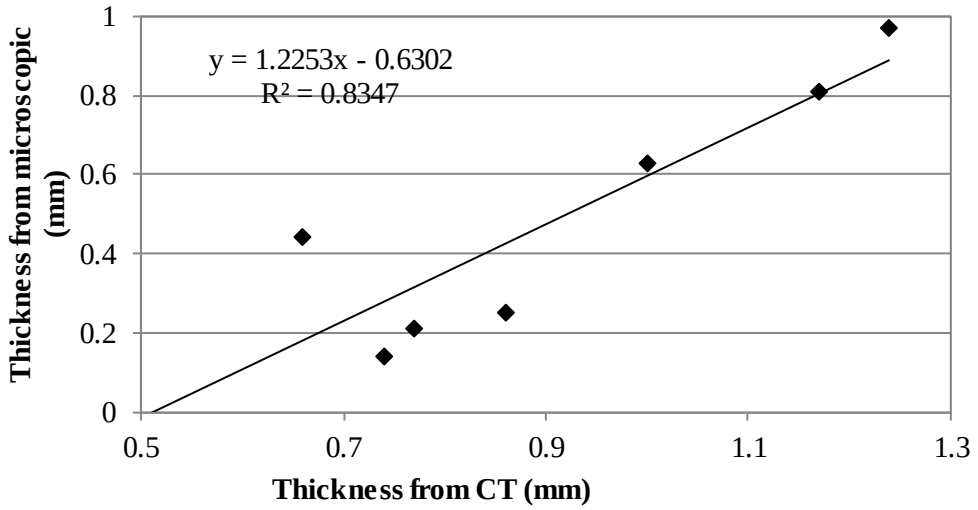

Figure 3. Relationship between measurements scanned from CT and from microscope

Parameter 3 – Cortical bone material property: The material properties of the two tested experimental ribs were calculated from experimental coupon tests conducted by Albert et al. [18]. After the ribs were tested in the whole-rib experimental set-up, the ribs were taken to Virginia Tech University where the coupon tests were completed. The material property of the trabecular bone was applied using the same value from Dokko et al. [9]. In addition, the strain rate of cortical bone and trabecular bone was applied according to a previous study by Takahashi et al. [19] The material properties for each subject was obtained from the coupon testing published by Albert et al. [18]. Compression property was determined as 1.2 times tension property from Kemper et al. [11] For Model 1, Model 2 and Model 3, these values were all the same as shown in Table 1 as MAT24 PIECEWISE_LINEAR_PLASTICITY specifying only tension. However, in Model 4, MAT124 PLASTICITY_COMPRESSION_TENSION were applied specifying tension and compression, respectively.

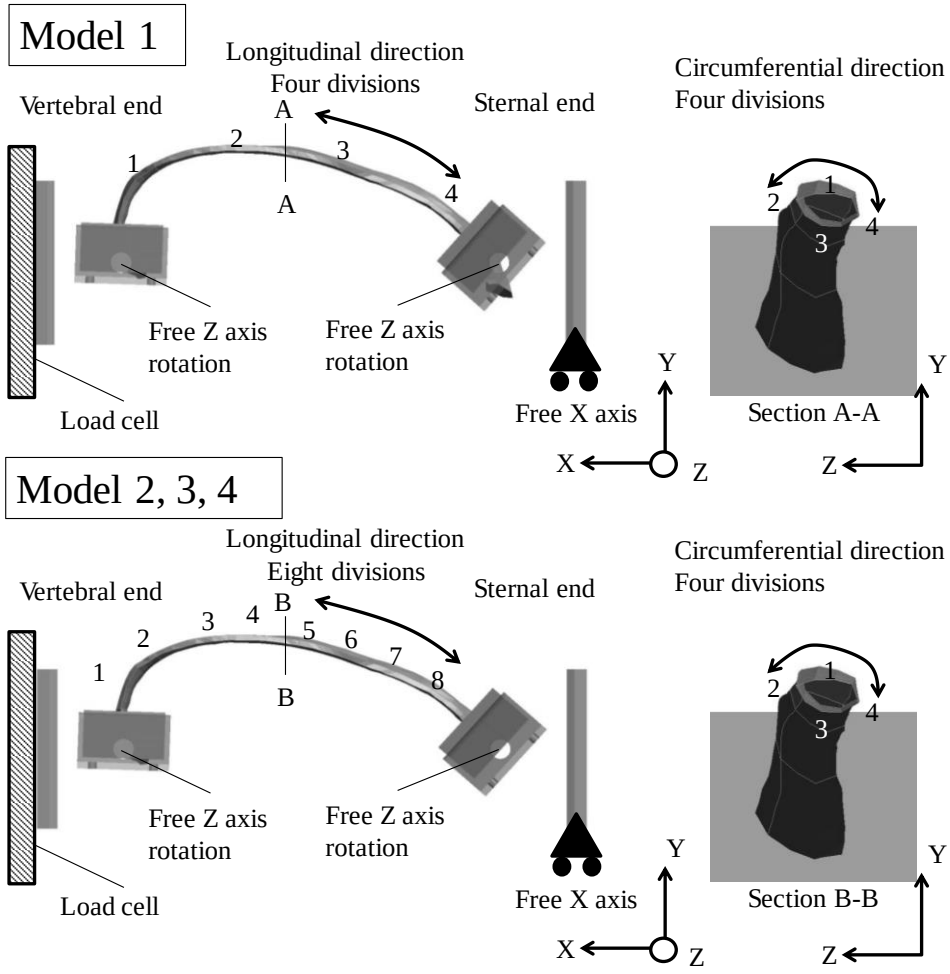

Figure 4. Bending test equivalent

Parametric Study – Method used to select the best model; As mentioned, the simulated reaction force time histories at the vertebral end of the rib were compared to the experimental data from Agnew et al [4]. The 4 versions of the model were evaluated both in terms of fracture reproducibility and force-displacement correspondence to determine the best method to model the whole-rib impact tests. The total energy, which was the total area under the force-displacement curve up to the time of fracture, was calculated and compared between each of the four parametric models and the experiment, and was used to evaluate the fracture accuracy. Also, the ratio of maximum force between simulation and experiment was used to evaluate the reaction force accuracy. Finally, the best modeling methodology was determined by averaging these two ratios. The average ratio closest to 1.0 indicated a good correlation between the simulation and the experiment.

Model Creation Phase (Determination of average material properties and cortical thicknesses for elderly female)

The representative material properties of the rib cortical bone for elderly female were determined using literatures. There are two human models for elderly female developed by Kalra et al. [20] and Iwamoto et al. [21] et al. They used the material properties for cortical thickness of rib as shown in Table 1A in Appendix. Our study used average material properties of two model. Young's modulus, Yield stress, Ultimate strain, and Ultimate stress were set by 11.1 GPa, 78.0 MPa and 0.022, respectively. The average cortical thickness was applied to median thickness value between two subjects of the bending test. Cortical thicknesses were used with average cortical thicknesses of two subjects as shown in Table.2A in Appendix. Average whole single rib were developed. Then, the average HBM were validated in next phase.

Model Validation Phase (Validation of whole rib bending test)

A whole-rib simulation test was validated using the rib bending test published by Agnew et al. [4] as detailed in the parametric methods section. The reaction force of the simulation was compared with the range of reaction forces documented in the experimental results. Simulation results were evaluated using the acronym of CORelation and Analysis (CORA) system. [22] The CORA rating is a method to evaluate the time-history signals, the reference curve (experimental result) and the predicted response (simulation result). CORA uses two methods to calculate the signals correlation: the corridor method calculates the deviation of the signal between two curves automatically created by the CORA software, while the cross-correlation method evaluates the characteristics of the signal such as phase shift, size, shape and progression. The total CORA score sums up the results of both metrics by using individual weighting factors from 0 to 1 for each metric. According to the rating stipulated in ISO/TR 18571 the resultants of the CORA score are classified into four categories: values above 0.94 are considered excellent, values between 0.94 and 0.8 are good, values between 08 and 0.58 are considered as a fair correlation and values below 0.58 are treated as a poor correlation.

Model Validation Phase (Validation of the HBM thorax in a side impact component test)

The evaluated whole-rib model was then applied to the full-body HBM for an elderly female. To validate the full-body HBM in a component level test, a lateral chest impact conducted by Talankinte et al. [23] was adopted to compare the thoracic impactor reaction force time histories. The thorax of the HBM was impacted in a lateral direction with a 150 mm diameter impactor, weighing 16 kg at a speed of approximately 6 m/s, matching the experimental conditions defined by Talankinte et al. [23] Only two female subjects (LCT02, LCT03) over 53 years old were tested in these experimental conditions. The geometric and inertial scaling method proposed by Mertz et al.[24] was performed on both subjects in order to better compare their results with the simulation. Force and time normalizing factors were calculated by Equations (2) and (5).

$$\mathrm{Rf} = (\mathrm{Rm}\ \mathrm{Rk})^{1/2} \qquad \text{(Equation 2)}$$

$$\mathrm{Rt} = (\mathrm{Rm})^{1/2}(\mathrm{Rk})^{1/2} \qquad \text{(Equation 3)}$$

where

$$\mathrm{Rm} = \mathrm{Ms}\ \mathrm{Mi}^{-1} \qquad \text{(Equation 4)}$$

$$\mathrm{Rk} = 308/L \qquad \text{(Equation 5)}$$

The mass ratio (Rm) was calculated using the total mass of the HBM (Ms), which was 47kg and the total mass of each experimental subject (Mi) as shown in equation 4. The stiffness ratio (Rk) uses a characteristic length ratio, in this scenario it is defined using chest width. Equation 8 defines RK to be the chest width of the 5th percentile elderly female HBM (308 mm) divided by chest width of each subject (L). Simulation results were then evaluated versus the experimental thoracic impacts using CORA as described in the validation of the whole-rib model.

Model Validation Phase (Validation of the HBM in a side impact sled test with realistic boundary conditions)
The published side impact sled tests with post mortem human subjects (PMHS) at an impact velocity of 28 km/h using a side airbag and simulating door intrusion (Shurtz et al.) [7] were simulated using the defined 5th percentile HBM. Comparisons between the simulation and the PMHS experiments were then conducted considering all of the following: spinal and pelvis kinematics, number of rib fractures and thoracic deflection from chest bands. The initial position of the HBM was set to match the experimental position data of each body segment and/or landmark including: head, sternal notch, olecranon and greater trochanter as shown in Figure. 5. The two PMHS responses were normalized to compare to the simulation responses using a length scale factor λz (seated height of the subjects) and a mass scale factor λm (total body mass). This normalization technique assumes equal density throughout each PMHS, so that the lateral displacement scale factor is defined by equation (6) proposed by Mertz et al.[25]

$$\lambda_y = Rm^{1/2}/\lambda z^{1/2} \qquad \text{(Equation 6)}$$

As with the whole-rib test and the thorax component test, the PMHS sled test simulation was evaluated using CORA. In addition, both the timing and location of the rib fractures predicted in the simulation were compared with those from the experimental results, when the fracture times were available in the PMHS tests.

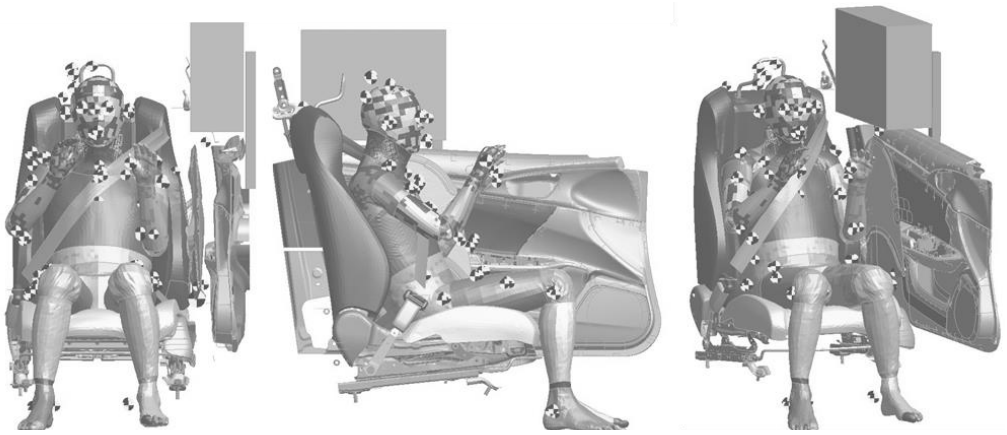

Figure 5. Comparison of seating position in the simulation with the experimental FARO data. Target mark indicates the experimental FARO data

RESULTS

Results of Parametric Study – Model Calibration
The parametric study parameters and evaluation results such as total energy ratio and max force ratio are shown in Table 4. The reaction force at the vertebral end of the rib is compared with the experimental data and shown in Figure 6. Based on the results, Model 4 appeared to be best represent the rib bending test given it has the values closest to 1.0 for both the total energy ratio and the max force ratio in this parametric study. Therefore, the modeling methodology for Model 4 was determined to be used for the validation phase of the models moving forward.

Table 4.
Parametric study matrix of bending simulation and results

		Case ID	Model 1	Model 2	Model 3	Model 4
Parameter		Number of divisions in the rib	16	32	32	32
		Thickness source	CT	CT	Function between Microscope and CT	Function between Microscope and CT
		Material properties	MAT24 Tension	MAT24 Tension	MAT24 Tension	MAT124 Tension & Compression
Evaluation	Subject1	Max force ratio	1.18	1.02	0.66	0.77
		Energy ratio	1.86	1.54	1.05	1.09
		Average ratio	1.52	1.28	0.86	0.93
	Subject2	Max force ratio	1.01	0.94	0.75	0.89
		Energy ratio	2.06	1.89	0.97	1.09
		Average ratio	1.54	1.42	0.86	0.99

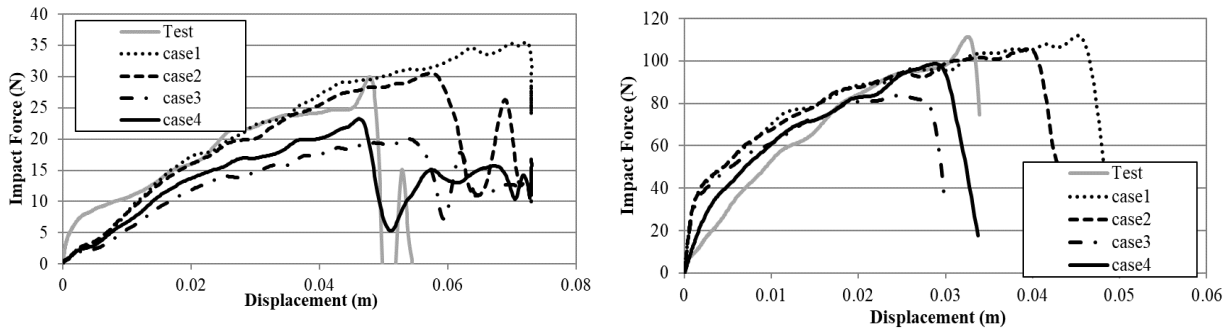

(A) (B)

Figure 6. Comparison of impactor force time history in parametric study ((A) subject1 results, (B) subject2 results)

Validation of Whole-Rib Model in Single Rib Bending Test

Figure 7 shows the comparison of the resulting force at the vertebral end of the whole rib and the total rib displacement between both experimental subject tests and the simulation with average material properties model. Peak force, which was 63 N was within the experiment results range of subject1 and subject2.

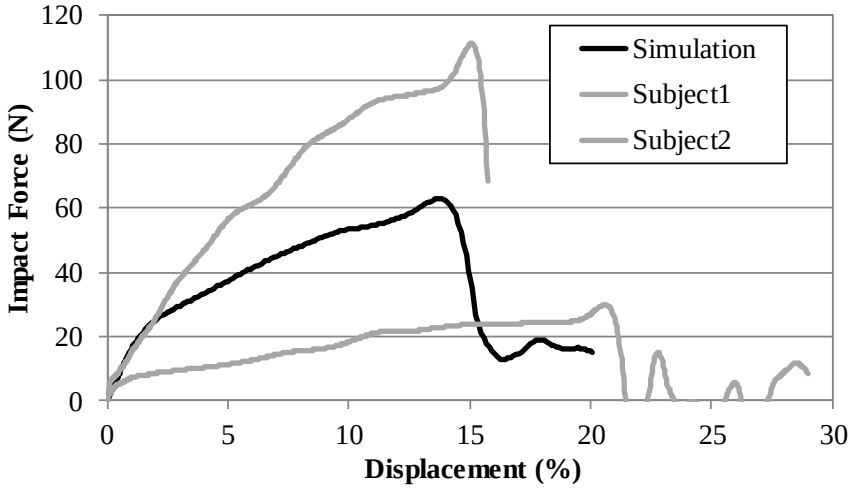

Figure 7. Comparison of bending impactor force displacement history in average rib model

Validation of Chest Side Impact Test

The modeling methodology for Model 4 was then applied to the thorax model of the HBM. Figure 8 shows the comparison of the chest impact force time history between the normalized experimental tests and simulation results. A standard deviation was calculated from the results of the normalized experiment results using two subjects. A CORA score of 0.885 is ranked "Good".

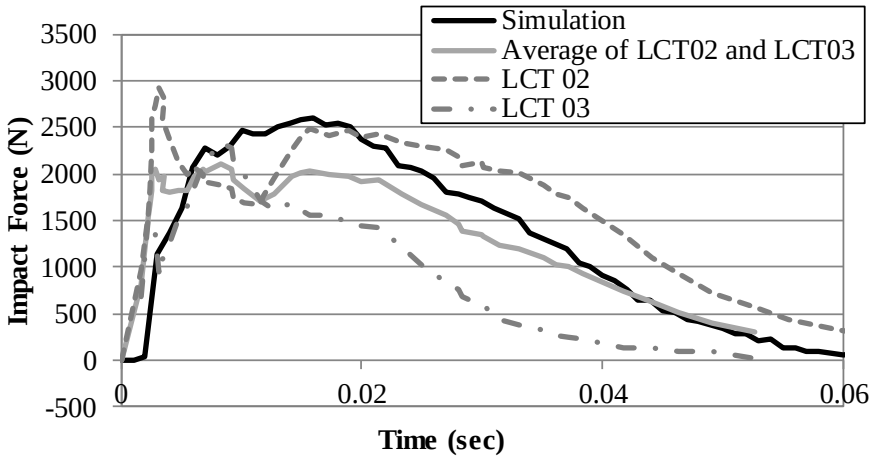

Figure 8. Comparison of impact force time history in simulation with the chest impact experiment

Validation of Side Impact Sled with Airbag

The seating position of the representative HBM showed good agreement with the experiential position point dataset as shown in Figure 5. Table 4 shows a summary of the CORA score regarding lateral displacement time histories of T1, T4, T12 and pelvis in the global coordinate system. The CORA score for lateral displacement indicates Excellent or Good, due to the range of CORA scores between 0.87-0.98. The lateral displacement time histories in the global coordinate system for each body region are also presented in Figures 9.

Table 4.
CORA Score and evaluation of lateral displacement at measurement points in sled test

Lateral displacement of body region	Corridor method	Correlation method	Total score
T1	0.99	0.89	0.95
T4	1.00	0.95	0.97
T12	1.00	0.97	0.98
Pelvis	0.86	0.87	0.87

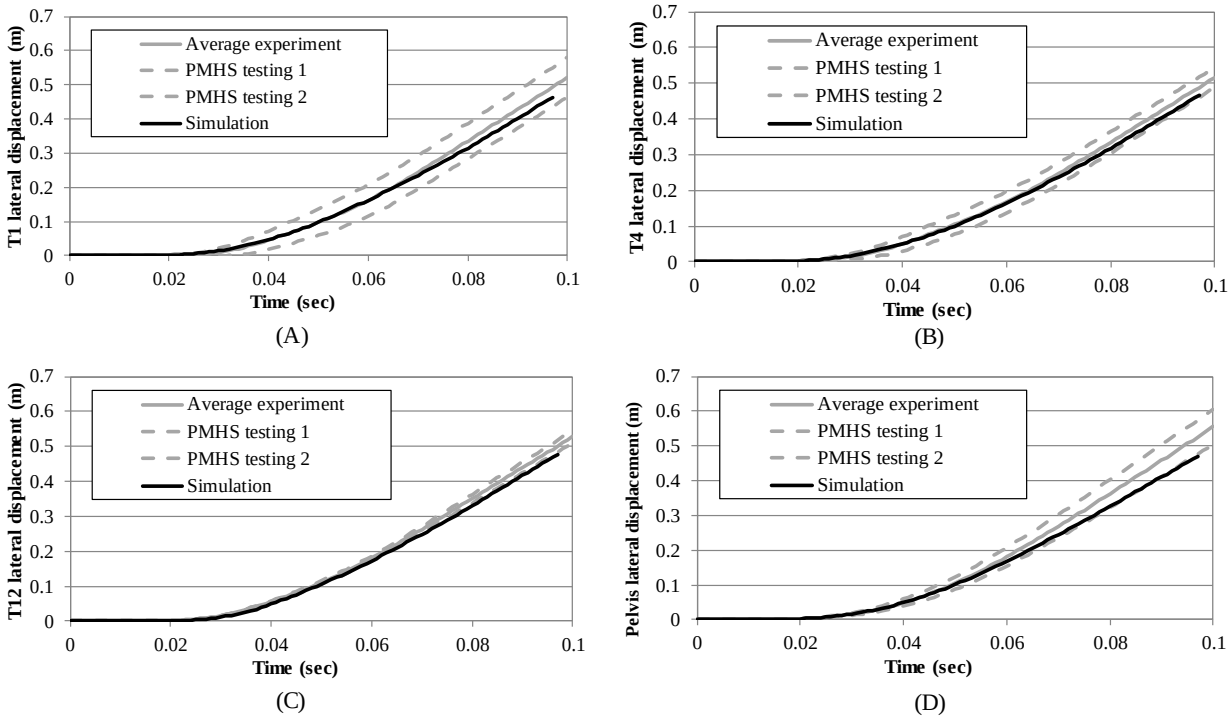

Figure 9. Comparison of lateral displacement of T1, T4, T12, and Pelvis between simulation and experiment ((A) T1 displacement, (B) T4 displacement, (C) T12 displacement, (D) Pelvis displacement)

Table. 5 shows the comparison between the fracture locations in the experiment with the simulation. In the simulation, shells of rib cortical bone were considered fractured when they reached 0.022 strain as defined by literatures. Fractures on the struck side occurred across the whole thorax, while fractures on the non-struck side occurred only in the upper and mid- thorax for both cases. The timing of rib fractures is also presented in Table 5. The first fracture occurred to the 7th anterior rib on the struck side of PMHS2 at 20 msec in both the experiment and

the simulation. Fractures on the non-struck side occurred later than fractures on the struck side. Thoracic deflection at the level of the axilla measured by the chestband were compared with the simulation results in both lateral and anterior-posterior (A/P) direction as shown in Figure 10. Maximum lateral thoracic deflection in the simulation and experiment were 14% and 15%, and both occurred at approximately 36 msec. Maximum anterior-posterior deflections were 5% and 6%, with both occurring approximately 19 msec.

Table 5.
Fractured rib location and timing in the sled test

Rib #	**PMHS1**		**PMHS2**		**Simulation**	
Fracture side	Struck	Non struck	Struck	Non struck	Struck	Non struck
Rib1						
Rib2	Fx:Ant(N/A)				Fx:Ant(28)	
Rib3	Fx:Ant(N/A)		Fx:Ant(26)	Fx:Ant(26)	Fx:Ant(23)	Fx:Ant(44)
Rib4	Fx:Ant(N/A)	Fx:Ant(47)	Fx:Ant,Post(27)	Fx:Ant(31)	Fx:Ant(28)	
Rib5			Fx:Ant.Post(21)	Fx:Ant(38)	Fx:Ant(44)	Fx:Ant(46)
Rib6	Fx:Ant(39)		Fx:Ant,Post(20)	Fx:Ant(39)	Fx:Ant(22)	
Rib7			Fx:Ant,Post(19)	Fx:Ant(N/A)	Fx:Ant(20)	
Rib8			Fx:Post(29)		Fx:Ant(28)	
Rib9					Fx:Ant(22)	
Rib10					Fx:Ant(20)	
Total number of fractured ribs	4	1	6	5	9	2

Fx=fracture, Ant=anterior, Post=posterior, ( ) = time of fracture msec, N/A= unknown

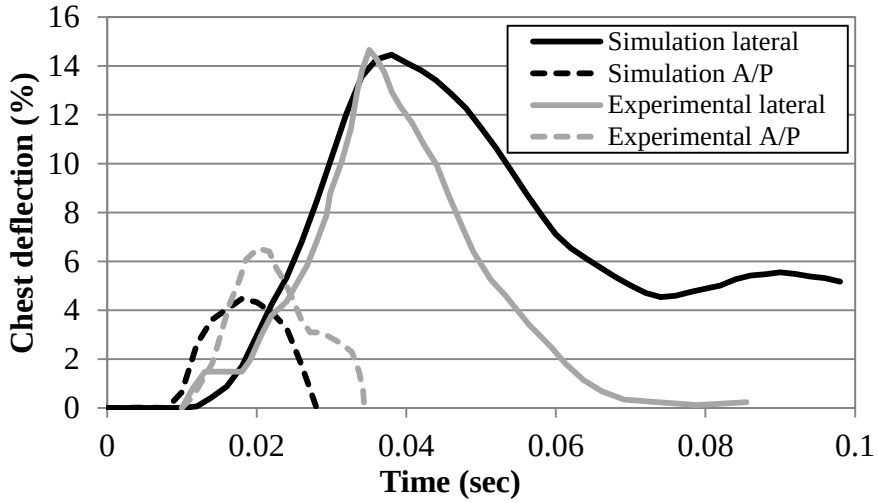

Figure 10. Comparison of thoracic deflection at the level of the axilla in side impact sled tests

DISCUSSION

In the parametric study, model 4 was more accurate than the other models for both subjects. It was found that number of rib divisions, thickness and material properties were significant parameters to predict rib fracture. Maximum force ratios were not effected in the parametric study. On the other hand, energy ratios were significantly effected in this parametric study. Therefore, these parameters were crucial to predict rib fractures, which means strain distribution of the rib were changed. As shown in Figure 11, increasing the number of rib divisions (Model 2) leads to more accurate energy ratios compared to in Model1. Similarly, Li et al. [26] found that use of variable cortical thickness distribution slightly decreased the failure displacement compared to the mode with constant cortical thickness. A more realistic cortical thickness distribution was crucial to predict the rib strain distribution.

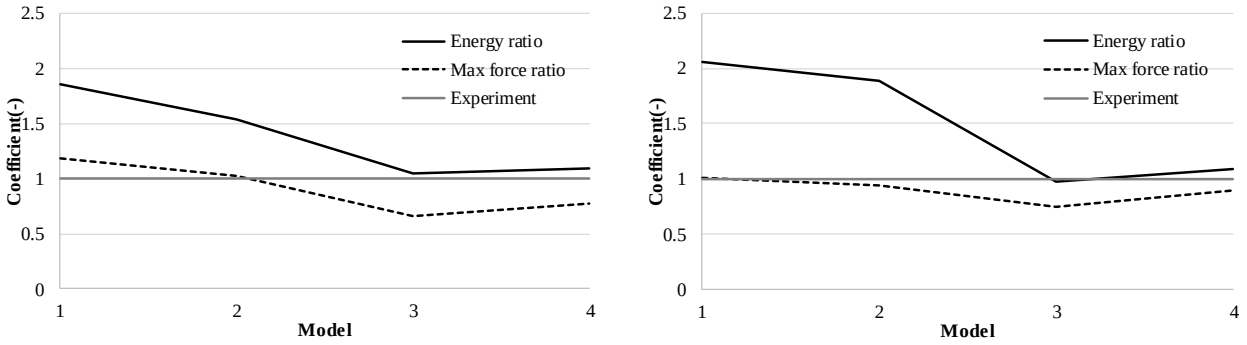

Figure 11. Comparison of max force ratio and energy ratio in parametric study ((A) subject1 results, (B) subject2 results)

Cortical thickness from the function between CT and histological measurement (Model 3) was more precise than both Model 1 and 2 in terms of energy ratio as shown in Figure 12. Actually, cortical thickness from histological measurement had a range of 0.14mm - 0.97mm. Because thresholding was used to reconstruct CT scans, cortical thickness from CT may overestimate the rib cortical thickness as can be seen in Table 2. Then rib strain may decrease so that the energy ratio was greater than the experiment. In a previous study, Perz et al. [27] found that utilizing CT images to result in greater than 100% error in cortical thickness. That difference of thickness affected mechanical response under antero-posterior loading to a single whole rib. In addition, Li et al also suggested that using for cortical thickness from a high-resolution CT data such as a micro CT would improve predicted fracture location. [26] Therefore, the resolution of the image based on cortical thickness is significant parameter for predicting rib fractures.

Considering compression (Model 4) helps to be more accuracy in this study. Kemper et al. found that cortical bone in the tibia has tension/compression asymmetry when looking at the stress-strain properties [11]. Fertschej et al. got more accuracy considering not only tension, but also additional properties (compression and shear, etc.) in the 3 point bending test using thermoplastics. [28] Shell strains-time history on the superior and inferior aspects of a middle of the rib in model 4 of parametric study were compared with those in model 3 as shown in Figure 12. Shell strain on the superior aspect of the rib in Model 4 was increasing earlier than in Model 3. Considering material asymmetry (Model 4), tensile strain distribution on the superior shell is higher than the symmetry material (Model 3) due to less the compression strain. Therefore, it is assumed strain distribution of the rib was changed when considering the compression property. It leads to be more accuracy.

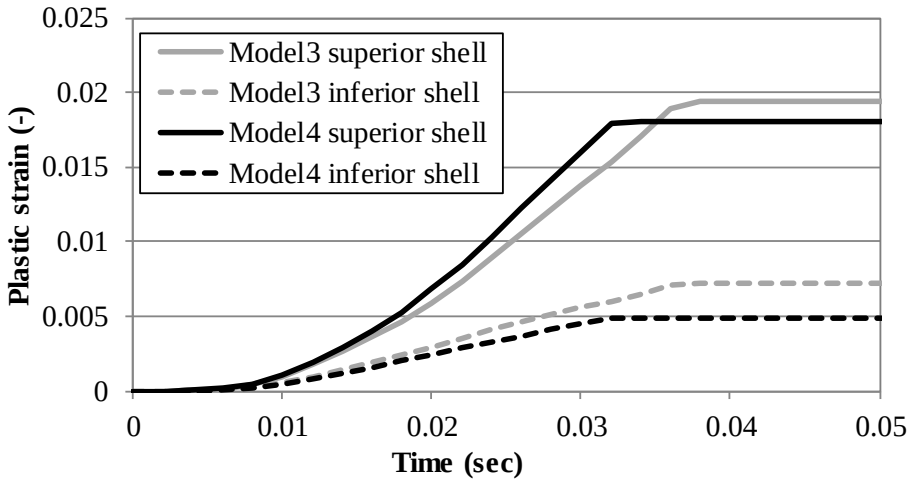

Figure 12. Comparison of plastic strain of the rib during the bending test (superior portion; inferior portion)

Regarding the whole-rib simulation validation results, the results were compared with the literature published by Agnew et al. [4] The experimental study showed peak force and peak displacement % were predicted using the following equations:

Peak force for female: FPeak = 133.58 - 0.950*Age (Equation 7)

Peak displacement for female: δPeak = 42.26 - 0.2724*Age (Equation 8)

If we assume an age of 75 years old was used for the simulation, the resulting Fpeak and δPeak would be 62.3 N and 21.3% respectively. The Average simulation results shows 68.5 N and 14% respectively, which reveal this rib model could be representative of a 75 years old of female.

This HBM showed fairly good agreement with the experiment results. A CORA score of kinematic response in the HBM is approximately 1.0, ranking Excellent. In addition, the location and timing of the fractured ribs in the simulation were compared with the experimental results. Fractures in both struck and non-struck side occurred in both simulation and in the experiments. Therefore, the simulation predicted not only the number of fractures, but also the fracture location using the deterministic method. However, humans have individual differences such as body type and varying material properties, so it should be further investigated to predict rib fractures using the probabilistic method.

CONCLUSION

The improved model for rib cortical bone was developed using thirty-two divisions of each rib, a cortical bone thickness value estimated from histological data, and material properties considering tension and compression.

The HBM developed by applying rib material properties along with geometrical scaling for an elderly female well represented the upper body kinematics, rib fractures and thoracic deflection in a side impact sled test from a published PMHS experiment.

ACKNOWLEDGEMENTS

Authors would like to grateful acknowledgement Dr. Jingwen Hu from University of Michigan Transportation Research Institute Department of Mechanical Engineering, University of Michigan (UMTRI), and Dr. Andrew Kemper from Virginia Tech-Wake Forest University for supporting their data through this study.

REFERENCES

[1] NHTSA-National Highway Traffic Safety Administration., 2017. “Traffic Safety Facts 2015.” DOT HS 812 372: 1-5

[2] Ortman, M., Jennife, R., Velkoff, V., Hongan, H., 2014. “An Aging Nation: The Older Population in the United States. Current Population Reports.”: 25-1140

[3] NHTSA-National Highway Traffic Safety Administration., 2005. “Characteristics of Crash Injuries Among Young, Middle-Aged, and Older Drivers.” DOT HS 810 857: 44-45

[4] Agnew, A., Murach, M., Dominguez, V., Sreedhar, A., Misicka, E., Harden, A., Bolte, J., Kang, Y., Stammen, J., Moorhouse, K., 2018.” Sources of Variability in Structural Bending Response of Pediatric and Adult Human Ribs in Dynamic Frontal Impacts.” Stapp Car Crash Journal, Vol.62, November: 119-192.

[5] Agnew, A., Murach, M., Misscka, E., Moorhouse, K., Bolte, J., Kang, Y., 2017. “The Effect of Body Size on Adult Human Rib Structural Properties.” In Proceedings of the IRCOBI Conference (Antwerp, Belgium, Sep. 11-13)

[6] Ramachandra, R., Kashikar, T., Bolte, J., 2017. “Injury Pattern of Elderly Occupants Involved in Side Crashes.” In Proceedings of the IRCOBI Conference (Antwerp, Belgium, Sep. 11-13)

[7] Shurtz, B., Agnew, A., Kang, Y., Bolte, J., 2018. “Application of Scaled Deflection Injury Criteria to Two Small, Fragile Female in Side Impact Motor Vehicle Crashes.” SAE International Technical Paper, April: 2018-01-0542

[8] Jin, X., Kalra, A., Hammad, A., Khandelwal, P., Porwal, V., Shen, M., Yang, K., 2018. “Development and Validation of Whole-Body Finite Element Occupant and Pedestrian Models of a 70-Year-Old Female” In Proceedings of the IRCOBI Conference (Athens, Greece, Sep. 12-14)

[9] Dokko, Y., Yanaoka, T., Ohashi, K., 2013. “Validation of Age-Specific Human FE Models for Lateral Impact.“ SAE International Technical Paper: 2013-01-1242.

[10] Kemper, A., McNally, C., Kennedy, E., Manoogian, S., Rath, A., Ng, T., Stitzel, J., Smith, E., Duma, S., Matsuoka, F., 2005. “Material Properties of Human Rib Cortical Bone from Dynamic Tension Coupon Testing.” Stapp Car Crash Journal, Vol.49, November: 199-230.

[11] Kemper, A., McNally, C., Kennedy, E., Manoogian, S., Duma, S., 2007. “The Material Properties Of Human Tibia Cortical Bone In Tension And Compression: Implacations For The Tibia Index.” In proceeding of International Technical Conference on the Enhanced Safety of Vehicles Conference (ESV) (Lyon, France, June. 18-21)

[12] ISO/TC22/SC12/WG5., 1997. “Road Vehicles - Anthropomorphic Side Impact Dummy – Lateral Impact Response Requirements to Assess the Biofidelity of the Dummy.” Document N455-Revision 4

[13] Lessley, D., Shaw, G., Parent, D., Arregui-Dalmases, C., Kindig, M., Riley, P., et al. 2010. “Whole-Body Response to Pure Lateral Impact.” Stapp Car Crash Journal, Vol.54: 289-336

[14] Shaw, G., Parent, D., Purtsezov, S., Kerrigan, J., Shin, J., Crandall, J., Zama, Y., Ejima, S., Kamiji, K., Yasuki, T., 2009. “Frontal Impact PMHS Sled Tests for FE Torso Model Development.” In Proceedings of IRCOBI Conference (York, United Kingdom, Sep. 9-11)

[15] Rhule, H., Maltese, M., Donnelly, B., Eppinger, R., Brunner, J., Bolte, J., 2002. “Development of a New Biofidelity Ranking System for Anthropomorphic Test Devices.” Stapp Car Crash Journal. Vol 46: 477-512

[16] Robbin, D., 1983. “Anthropometric Specifications For Small Female And Large Male Dummy, Volume3.” FINAL REPORT Oct: UMTRI-83-53-3

[17] Wang, Y., Cao, L., Bai, Z., Reed, M. Rupp, J., Hoff, C., Hu, J., 2016. "A Parametric Ribcage Geometry Model Accounting for Variations Among the Adult Population." Journal of Biomechanics. Vol 49: 2791-2798

[18] Albert, D., Kang, Y., Agnew, A., Kemper, A., 2017. "A Comparison of Rib Structural and Material Properties from Matched Whole Rib Bending and Tension Coupon Tests." In Proceedings of the 2017 IRCOBI Conference (Antwerp, Belgium, Sep. 11-13)

[19] Takahashi, Y., Kikuchi, Y., Konosu, A., Ishikawa, H., 2000. "Development and Validation of the Finite Element Model for the Human Lower Limb of Pedestrians." Stapp Car Crash Journal. Vol 44: 2000-01-SC22

[20] Kalra, A., 2017 "Development of an Elderly Female Torso Finite Element Model for Restraint System Research and Development Applications." Doctoral thesis. Wayne State University.

[21] Iwamoto, M., Nakahira, Y., Kimpara, H., Min, K., 2013. "Development of a Finite Element Model of 5th Percentile Female with Multiple Muscles and Its Application to Investigation on Impact Responses of Elderly Females." In Proceeding of the 23rd International Technical Conference on the Enhanced Safety of Vehicles (ESV) (Seoul, Republic of Korea, May 27-30)

[22] Gehre, C., Gades, H., Wernicke, P., 2009. "Objective Rating of Signals Using Test and Simulation Responses." In Proceedings of the 21st International Technical Conference on the Enhanced Safety of Vehicles Conference (ESV) (Stuttgart, Germany, June. 15-18)

[23] Talantikite, Y., Bouquet, R., Ramet, M., Guillemot, H., Robin, S., Voiglio, E., 1998. "Human Thorax Behaviour for Side Impact: Influence of Impact Masses and Velocities." In Proceedings of International Technical Conference on the Enhanced Safety of Vehicles Conference (ESV) (Ontario, Canada, May31-June 4)

[24] Mertz, H., 1984. "A Procedure for Normalizing Impact Response Data." In Proceedings of SAE International Congress and Exposition.: 840884

[25] Mertz, H., Irwin, A., Melvin, J., Stalnaker, R., Beebe, M., 1989. "Size, Weight and Biomechanical Impact Response Requirements for Adult Size Small Female and Large Male Dummies in Automotive Frontal Impacts." SAE, Warrendale, PA, : 133-144

[26] Li, Z., Kindig, M., Subit, D., Kent, R., 2010. "Influence of Mesh Density, Cortical Thickness and Material Properties on Human Rib Fracture Prediction." Medical Engineering & Physics, Vol 32, November: 998–1008

[27] Perz, R., Toczyski, J., Subit, D., 2015. "Variation in the Human Ribs Geometrical Properties and Mechanical Response Based on X-ray Computed Tomography Images Resolution." Journal of the Mechanical Behavior of Biomedical Materials. Volume 41, January: 292-301

[28] Reithofer, P., Fertschej, A., Hirschmann, B., Jilka, B., Rollant M., 2018. "Material Models for Thermoplastics in LS-DYNA from Deformation to Failure." In Proceedings of International LS-DYNA User Conference (Michigan, United states, June 11-12)

APPENDIX

Table 1A.
Average rib cortical material properties for elderly female

Data source	Young Modulus [GPa]	Yield Stress [MPa]	Ultimate Strain [-]
This study (Average)	11.1	78.0	0.022
Kalra et al.	7.3	54.0	-
Kimpara et al.	14.8	101.9	0.022

Table 2A.
Cortical thickness measurement calculated to histological measurement from CT

	Thickness source	5%	13%	25%	38%	50%	67%	75%	88%
Subject 1	Superior cortex (mm)	2.18	1.44	1.80	0.56	0.44	0.24	0.49	0.41
	Outer cortex (mm)	1.94	1.49	0.90	0.49	0.29	0.36	0.46	0.44
	Inferior cortex (mm)	2.55	1.47	1.23	1.78	0.75	0.20	0.49	0.51
	Inner cortex (mm)	0.87	0.94	1.44	1.10	0.99	0.60	0.41	0.39
Subject 2	Superior cortex (mm)	0.41	1.59	0.92	1.35	1.15	0.14	0.54	0.39
	Outer cortex (mm)	1.28	0.28	1.46	1.35	0.61	0.14	0.38	0.49
	Inferior cortex (mm)	1.86	1.39	1.63	1.77	1.30	0.92	1.20	0.39
	Inner cortex (mm)	1.28	0.28	1.46	1.35	0.61	0.14	0.38	0.49
Average	Superior cortex (mm)	1.29	1.52	1.36	0.95	0.80	0.19	0.52	0.40
	Outer cortex (mm)	1.90	1.44	1.26	1.13	0.80	0.64	0.83	0.42
	Inferior cortex (mm)	1.91	0.88	1.34	1.57	0.68	0.17	0.43	0.50
	Inner cortex (mm)	1.26	1.26	1.87	1.74	1.32	0.87	0.88	0.44

RESPONSES OF A 6-YEAR-OLD ATD RESTRAINED IN A BOOSTER CHILD SEAT ON THE FMVSS 213 TEST BENCH, PROPOSED UPGRADED TEST BENCH AND A VEHICLE SEAT IN SIMULATED FRONTAL IMPACTS

Jalaj Maheshwari, Nhat Duong, Shreyas Sarfare, Aditya Belwadi

Children's Hospital of Philadelphia
USA

19-0055

ABSTRACT

The National Highway Traffic Safety Administration (NHTSA) is considering upgrades to the FMVSS No. 213 standard seat assembly and test parameters that better represent current vehicle conditions. A preliminary prototype for the test bench was released with upgraded seat cushion stiffness, geometry, seatbelt assembly, and anchorage locations. The objective of this study was to compare the responses of the Q6 ATD (Humanetics Inc., MI) restrained in booster child seats (CRS) on the current and proposed upgrade of the FMVSS 213 test bench, and a vehicle seat in frontal impacts.

Three child seating conditions were evaluated: no-CRS, lowback booster (LBB), and a highback booster (HBB) installed on validated finite element (FE) models of the current FMVSS 213 bench, upgraded bench, and a 2012 Toyota Camry vehicle seat. Simulations (N=9) were carried out using LS-DYNA ver.971 (LSTC, CA) on a 16-node double precision cluster. Kinematics and kinetic data were extracted and processed as per SAEJ211 metrics.

Head resultant accelerations (Hr) across conditions were comparable, however, for LBB the current bench over predicted Hr by 26G (72.1G) as compared to the upgraded bench (46.1G). For HBB, there was a difference of 13.5G in Hr between the upgraded bench (60.1G) and vehicle seat (46.6G). Similarly, chest resultant accelerations (Cr) showed a difference of 23.2G (No-CRS), 14.8G (LBB), and 22.5G (HBB) between the 213 bench [no-CRS (72.9G); LBB (62.5G); HBB (56.3G)] and upgraded bench [no-CRS (49.7G); LBB (47.7G); HBB (78.8G)]. HBB showed a difference of 19.2G in Cr between the upgraded bench (78.8G) and vehicle seat (59.6G).

HIC36 values for the no-CRS and HBB conditions were lower by 53.4 and 115.4 respectively for the 213 bench [no-CRS (258.7); HBB (443.2)] compared to the upgraded bench [no-CRS (312.1); HBB (558.6)]. Similarly, these values were lower for no-CRS and HBB conditions by 74.3 and 163.6 respectively for the vehicle seat [no-CRS (237.8); HBB (395.0)] compared to the upgraded bench. Chest displacements were higher on the 213 bench [no-CRS (16.6mm); LBB (24.2mm); HBB (29.2mm)] and vehicle seat [no-CRS (18.3mm); LBB (22.6mm); HBB (25.5mm)] as compared to the upgraded bench [no-CRS (6.6mm); LBB (14.8mm); HBB (17.3mm)]. Neck Forces (Fz) were higher for the LBB on the 213 bench (2637.3N) than on the upgraded bench (1982.3N).

All injury and excursion values were within IARV limits for all simulations. However, CRSs installed on the 213 bench have larger rotations (sagittal plane) [LBB (-10.2º); HBB (-12.9º)] as compared to the upgraded bench [LBB (1.5º); HBB (-3.6º)] and the vehicle seat [LBB (4.8º); HBB (-3.6º)]. The child seats on the 213 bench, first compress the foam and then rotate over the edge of the foam [Foam thickness (Ft) = 6 inches (4+2)] due to its inherent overhang from the edge of the base structure causing higher rotations as compared to the upgraded bench (Ft= 4 inches) or the vehicle seat, which are similar in construction.

Overall, the responses of the upgraded bench matched the vehicle seat more closely than the current bench and is a step towards emulating a real vehicle seat environment.

INTRODUCTION

Booster seats provide child occupants the appropriate belt fit that a traditional vehicle seat cannot offer due to the occupant being too small. There is ample evidence from real world crashes that belt-positioning booster seats reduce injury risk. The estimated odds of injury after adjusting for child, crash, driver and vehicle characteristics were 59%

lower (Durbin et. al. 2003) for 4 to 7-year-old children in belt-positioning boosters as compared to standard three-point lap-shoulder seat belts. Further, child-restraint systems reduced fatality risk by 28% for children 2 to 6-years old as compared to standard seat belts (Elliot et. al. 2007).

There are primarily two types of booster seats used extensively by parents, namely highback (HBB), lowback or backless boosters (LBB. A typical booster seat raises a child relative to the vehicle seat, by about 100mm (Reed et. al. 2006). This improves the belt angle, making it more vertical, thus, making it less likely for the belt to slide off the pelvis and onto the abdomen during a crash. It also reduces the likelihood of the shoulder belt interacting uncomfortably with the neck, a situation that can lead to a child leaning away from the belt or tucking the belt under an arm or behind the back. Booster seats include features like belt routing guides which improve the routing of the belt around the child (Reed et. al. 2006; 2009).

The Federal Motor Vehicle Safety Standard (FMVSS) No. 213 test is a baseline test to assess the safety of child seats. The FMVSS No. 213 test bench represents a vehicle rear seat. The effective length and undeflected seat contour are representative of the rear seat in vehicles (Reed 2011). The last time the FMVSS 213 test bench was upgraded was in 2003, where anthropomorphic test devices (ATDs) were used and design changes were made to better represent a vehicle rear seat (Aram et al. 2012). However, no modifications were made to the seat cushion, which was found to be thicker and softer as compared to rear seats in vehicles at the time. Since then, there have been studies highlighting the discrepancy between the FMVSS 213 test bench and vehicle rear seats (Maltese et al. 2014).

The National Highway Traffic Safety Administration (NHTSA) released a preliminary prototype for the new 213-test bench with upgraded seat cushion stiffness, geometry, seatbelt assembly, and anchorage locations (Wietholter et. al. 2017). The new bench has a much stiffer foam and is supposed to represent a vehicle rear seat more accurately as compared to the current FMVSS 213 test bench (Wietholter et. al. 2016). Moreover, the new bench has a 2 inch thinner foam as compared to the current bench, which is 6 inches thick (4+2 inches, different foam stiffnesses).

The dynamic performance of the FMVSS 213 test bench as compared to a vehicle rear seat needs to be evaluated and quantified. Thus, this study aims to quantify responses of a 6-year-old ATD on the FMVSS 213 test bench, proposed upgraded prototype, and a vehicle seat in frontal crashes.

METHODS

A Q6 ATD (Humanetics Innovative Solutions, MI) child occupant finite element (FE) model was used for this study. The ATD was restrained in two types of booster seats on the FMVSS 213 test bench, the proposed upgraded bench, and a vehicle seat. Additionally, a no-CRS condition was also modeled.

FMVSS 213 Test Bench and Vehicle Seat Model

The CAD data for the FMVSS 213-test bench and the proposed upgraded bench was obtained from the National Highway Traffic Safety Administration (NHTSA) archives. Thereafter, an FE model for the bench was created using LS-DYNA v. 971. Foam load curves and properties were obtained from previous studies on the FMVSS 213 test bench (Wietholter et. al. 2016). The vehicle rear seat was extracted from a 2012 Toyota Camry model obtained from the National Crash Analysis Center (NCAC) archives.

Development of Booster Seat Models

Two booster child restraint seats available in the US market were used, namely a lowback or backless booster (LBB), and a highback booster (HBB). The CAD data for the booster seats were developed by scanning the seats using an Xbox Kinect Sensor (Belwadi et al. 2015) following which an FE model was developed.

FE Assembly Setup and Validation

The CRS and the Q6 ATD were gravity settled on the FMVSS 213 test bench, proposed upgrade, and vehicle seat after getting them into position. The seat belt was then routed around the child and the CRS. A full frontal, 0-degree, crash impact was simulated by applying the FMVSS No. 213 crash test pulse (24 G over 120 milliseconds) to the system. In order to validate the FE model, the resultant head and chest acceleration measured at the center of gravity of the head and at the chest potentiometer (Infra-Red Telescoping Rod for the Assessment of Chest

Compression - IRTRACC) respectively were compared with the physical sled test data for proposed upgrade test condition (Belwadi et al. 2017). The values were within ± 8% of maximum values.

Nine simulations were set up (three seating conditions, three benches) using Hypermesh v17.0 (Altair Inc., MI) as the pre-processor. The simulations were run and post-processed using LS-DYNA v. 971 and LS-PrePost v. 4.5 (LSTC, CA) respectively. Models were solved on a 4-node computing cluster on a double-precision explicit solver. HIC36, head and chest acceleration, chest and IR-TRACC displacement were extracted. Maximum head excursion, Nij and head trajectories were calculated. All simulations were carried out and data filtered as per SAEJ211 sign convention and filtering classes respectively.

RESULTS

Table 1.
Injury metrics across simulations

No.	Seat	Booster Condition	HIC36	Hr	Cr	Pr	IR-TRACC Chest Displacement	Neck Force Fz	Neck Moment My	Maximum Head Excursion	CRS Max Delta Angle
				(G)	(G)	(G)	(mm)	(N)	(N.m)	(mm)	(degrees)
1	Upgraded FMVSS 213 Test Bench	No CRS	312.1	49.4	49.7	47.7	6.6	1722.4	30.0	211.5	---
2		LBB	334.7	46.1	47.7	44.1	14.8	1982.3	34.2	298.2	1.5
3		HBB	558.6	60.1	78.8	52.7	17.3	2545.1	36.1	317.3	-3.6
4	Current FMVSS 213 Test Bench	No CRS	258.7	50.6	72.9	45.5	16.6	1866.0	32.0	237.0	---
5		LBB	352.6	72.1	62.5	45.7	24.2	2637.3	31.1	321.1	-10.2
6		HBB	443.2	57.5	56.3	49.1	29.2	2855.6	34.9	314.9	-12.9
7	Vehicle Seat	No CRS	237.8	50.9	49.1	51.1	18.3	2021.9	28.8	240.1	---
8		LBB	313.3	45.6	46.6	41.5	22.6	2014.9	35.8	280.1	4.8
9		HBB	395.0	46.6	59.6	53.5	25.5	1711.5	34.5	321.9	-3.6

Table 1 lists all the injury metrics across the nine simulations. Head resultant acceleration (Hr) values were mostly comparable across the benches and vehicle seat. However, compared to the upgraded bench, the child on LBB showed a 56.3% higher Hr on the current bench [LBB-Hr: Current (72.1G); Upgrade (46.1G); Vehicle (45.6G)]. Consequently, the Q6 on HBB showed a 22.4% lower Hr on the vehicle seat compared to the proposed upgrade [HBB-Hr: Current (57.5G); Upgrade (60.1G); Vehicle (46.6G)]. HIC36 values were 17.1% and 23.8% lower for the current bench and vehicle seat respectively for the no-CRS condition as compared to the upgrade bench [no-CRS-HIC36: Current (258.7); Upgrade (312.1); Vehicle (237.8)]. Similarly, HIC36 values were 20.7% and 29.3% lower for the current bench and vehicle seat respectively for the child on HBB as compared to the upgrade bench [HBB-HIC36: Current (443.2); Upgrade (558.6); Vehicle (395.0)]. Figure 1 shows the variation in HIC36 across the simulations. Figure 2 shows variation in head, chest, and pelvis acceleration across all simulated cases.

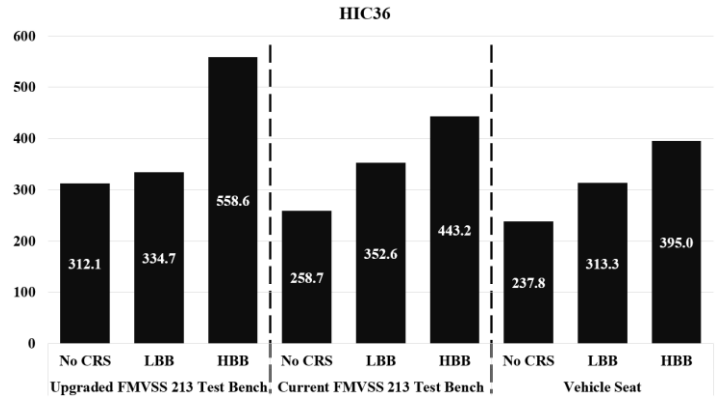

Figure 1: Variation in HIC36 across simulations

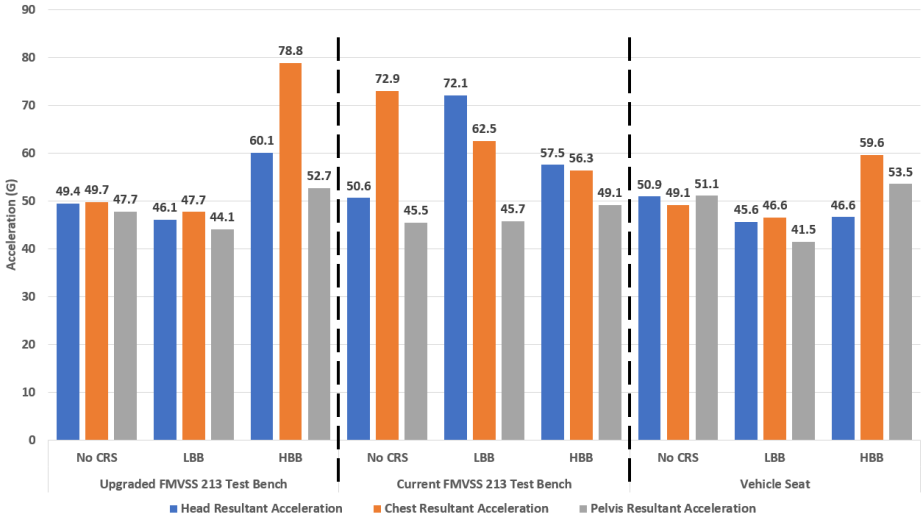

Figure 2: Variation in head, chest, and pelvis acceleration across simulations

Chest resultant acceleration (Cr) values showed greater variation in the current bench as compared to the upgraded bench, with values being 46.6% and 31.0% higher for no-CRS and LBB conditions, and 28.5% lower for HBB condition. Although the Q6 on the vehicle seat showed similar chest resultant acceleration values, for the child on the HBB, Cr was 24.4% lower on the vehicle seat as compared to the upgraded bench.

Chest displacements were consistently higher on the current bench and the vehicle seat as compared to the upgraded bench. The Q6 on the current bench showed 150.9%, 63.7%, and 68.9% higher chest displacements for the no-CRS, LBB, and HBB conditions respectively. Similarly, the Q6 on the vehicle seat showed 177.1%, 53.0%, and 47.6% higher chest displacements for the no-CRS, LBB, and HBB conditions.

Pelvis resultant accelerations (Pr) were within ± 7% for the current bench and vehicle seat as compared to the upgraded bench. Pr was 4.7% and 6.8% lower on the current bench for no-CRS and HBB, and was 3.6% higher for LBB. Contrarily, Pr was 7% and 1.6% higher on the vehicle seat for no-CRS and HBB, and was 5.9% lower for LBB.

The Q6 ATD showed a 33.0% higher neck force (Fz) on the current bench as compared to the upgraded bench for the LBB case. However, it showed a 32.8% lower Fz on the vehicle seat for the HBB case. Neck moment (My) was within ± 9% for the current bench, and ± 4.7% for the vehicle seat as compared to the upgraded bench.

The ATD experienced a 12.0% and 13.5% higher head excursion for the current bench and vehicle seat respectively for the no-CRS condition. Head excursion was 7.7% higher and 6.0% lower for the current bench and vehicle seat

respectively for the LBB condition. Minimal variation in head excursion was seen for the HBB case, with 0.8% lower, and 1.5% higher values for the current bench and vehicle seat respectively.

DISCUSSION

All injury metrics were within injury assessment reference value (IARV) limits for all simulated cases. To further evaluate the differences between the current FMVSS 213 test bench, the upgraded bench, and the vehicle seat, the change in CRS angle was calculated in the sagittal plane. The maximum change in CRS angle for the upgraded bench [LBB: 1.5deg; HBB: -3.6deg], current bench [LBB: -10.2deg; HBB: -12.9deg], and vehicle seat [LBB: 4.8deg; HBB: -3.6deg] were calculated from the CRSs initial position.

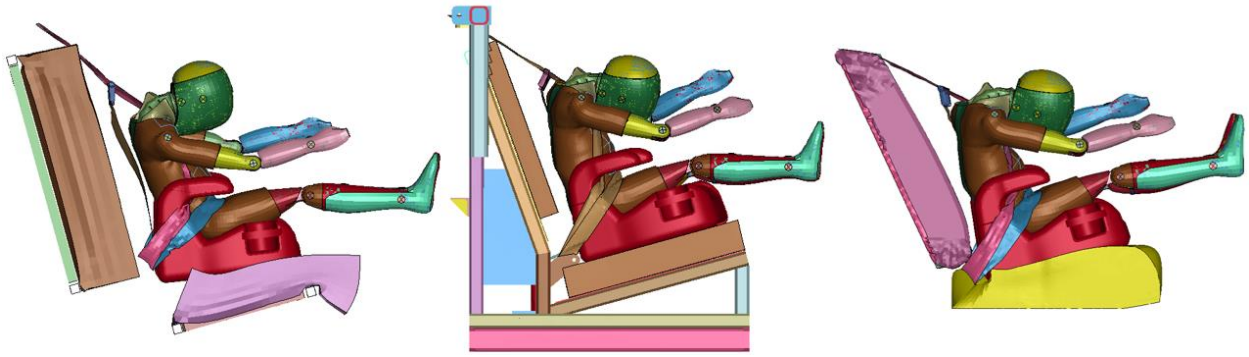

Figure 3: Foam compression in current FMVSS 213 test bench, upgraded bench, and vehicle seat

The large negative CRS angles represent the fact that the CRS pushes down on the seat cushion. Figure 3 depicts the behavior of the foams across the seating conditions for the current FMVSS 213 test bench, upgraded bench, and vehicle seat. Due to the softer foam and the inherent overhang on the current FMVSS 213 test bench, the CRSs rotate extensively by compressing the foam, and then rotating about the overhang. However, this situation is not represented in the upgraded bench and the vehicle seat, where the CRS behavior is similar. The LBB shows a positive CRS rotation for the upgraded bench and vehicle seat, while the HBB shows a slight negative rotation of the seat. This could also be due to the inertia of the HBB and slightly higher center of mass as compared to the LBB.

Limitations

There are a few important limitations to the study. The study only accounts for one make and model of a LBB and HBB. There could be variation due to the design of the CRS which could affect the ATDs kinematics and performance across these different seating structures. Further, the Q6 ATD is a mechanical device, thereby resulting in stiffer responses as opposed to an actual human being in the same crash condition. To evaluate the efficacy of the FMVSS 213 test bench, human body models can be used to provide a complete estimate into the limitations and possible upgrades to the test bench. Moreover, newer vehicle makes and models have rear seats equipped with retractors and pre-tensioners. The dynamic response of a pediatric occupant due to the presence and absence of a retractor and pre-tensioner could be a useful analysis into upgrading the current FMVSS protocols.

CONCLUSIONS

The upgrade to the current FMVSS 213 test bench better represents a vehicle rear seat under dynamic crash scenarios for a frontal impact. Due to the absence of the overhang and a much stiffer foam, ATDs in CRSs on the upgraded bench perform similar to vehicle seats.

REFERENCES

[1] Aram, M.L., Rockwell, T., “Vehicle Rear Seat Study,” July 2012. Docket No. NHTSA-2014-0012.

[2] Belwadi, A., Hanna, R., Eagle, A., Martinez, D., Kleinert, J., "Development of a Small Rear Facing Child Restraint System Virtual Surrogate to Evaluate CRS-to-Vehicle Interaction and Fitment," SAE 2015-01-1457, 2015.

[3] Belwadi, A., Duong, N., Maheshwari, J., Seth, F., Arbogast, K., "Effect of seat belt routing schemes on ATD kinetics and kinematics – a sled evaluation study", In press, Traffic Injury Prevention, 2017.

[4] Durbin, D.R., Elliott, M.R., Winston, F.K., "Belt-Positioning Booster Seats and Reduction in Risk of Injury Among Children in Vehicle Crashes," *JAMA.* 2003;289(21):2835–2840.

[5] Elliott, M.R., Kallan, M.J., Durbin, D.R., Winston, F.K., "Effectiveness of Child Safety Seats vs Seat Belts in Reducing Risk for Death in Children in Passenger Vehicle Crashes," *Arch Pediatr Adolesc Med.* 2006;160(6):617–621.

[6] Maltese, M.R., Tylko, S., Belwadi, A., Locey, C., Arbogast, K., "Comparative Performance of Forward-Facing Child Restraint Systems on the C/FMVSS 213 Bench and Vehicle Seats," Traffic Injury Prevention 15.sup1, 2014: S103–S110. Web.

[7] Reed, M.P., Ebert-Hamilton, S.M., Manary, M.A., Klinich, K.D., and Schneider, L.W., "Improved positioning procedures for 6YO and 10YO ATDs based on child occupant postures," Stapp Car Crash Journal, 2006, 50: 337-388.

[8] Reed, M.P., Sheila M. Ebert, Christopher P. Sherwood, Kathleen D. Klinich, Miriam A. Manary, "Evaluation of the static belt fit provided by belt-positioning booster seats", *Accident Analysis & Prevention*, Volume 41, Issue 3, 2009, Pages 598-607.

[9] Reed, M.P., "Measurement of the Contour and Deflection of Vehicle Seats for Comparison with the FMVSS 213 Dynamic Test Bench." SAE mobilus, 2011.

[10] Wietholter, K., Louden, A., Sullivan, L., & Burton, R. "Evaluation of Seat Foams for the FMVSS No. 213 Test Bench". June 2016. Washington, DC: National Highway Traffic Safety Administration. Docket No. NHTSA-2013-0055, Item No. 0013.

A PARAMETRIC STUDY OF AN ADAPTIVE LOAD-LIMITING RESTRAINT SYSTEM WITH WEIGHT SENSING CONSIDERATIONS

Jon van Poppel, M.Sc., P.E.
Amber Rath Stern, Ph.D., P.E.
David Fortenbaugh, Ph.D.
Grant Wilcox
Engineering Systems Inc.
United States

Paper Number 19-0057

ABSTRACT

The subject study provides an overview of several rear seat restraint configurations, with a focus on the restraint performance of a real-time adaptive (RTA) retractor system. The simulated RTA system assumes the integration of the TCJ Technology into the retractor. The near real-time response and high torque generation capabilities of the TCJ technology are briefly discussed and physical test data are shown in support. Simulations of both a conventional retractor and a 3kN LL retractor are carried out as well. The conventional retractor system is void of any specific energy management, other than the seatbelt stretch itself. Both the 3kN LL and the RTA systems are equipped with energy management functionalities. Simulations of the three restraint configurations are conducted in the MADYMO software with five different ATD models and six different crash pulses. The ATD models range from the HIII 6YO to the HIII 95th percentile male. The vehicle crash pulses originate from the NHTSA database for barrier impacts, with five pulses at the 35-mph severity level and one pulse at the 25-mph severity level. The MADYMO Control System modeling capabilities are relied upon to develop and implement the feedback control system for the RTA model. Seatbelt pay-out amounts and seatbelt pay-out rates are monitored during the simulated crash events. The sensor data are fed real-time into the RTA control system and real-time adaptive retractor seatbelt forces are thus generated. The research initially assumes direct occupant weight sensing is absent and later assesses that the RTA system can indeed function without this third input. A recommended load-limiting performance envelope for the RTA system is specified based on the simulation results. Data interpretation highlights the benefits of an RTA-type system for the full spectrum of modeled occupant sizes and weights, with an understanding that the smaller and more vulnerable occupants (elderly) tend to benefit most when restraint systems are more compliant, and yet able to prevent excessive seatbelt pay-outs for heavier occupants, without any significant detriment in injury numbers across the board. The noted improvements in the 25-mph simulation further bolster the broader benefit aspect, as a greater majority of occupant exposures occur at less than the 35-mph severity.

INTRODUCTION

The present research adds to recent reports and studies [1-5] that have investigated rear seat occupant safety systems. Contrary to front-seated locations, seatbelt systems are almost solely relied upon in rear-seated locations (for frontal impacts) because rear-seat locations cannot easily or very practically accommodate frontal airbag systems. Compared to front seat occupants, rear-seated passengers are also often of lighter weight (children). Further, the range of occupant sizes tends to be greater in rear-seated locations. Thus, rear seatbelt systems with different stiffness characteristics than those found in the current fleet might be desirable. Significant changes to rear seatbelt systems, however, cannot be easily realized under current regulations such as Federal Motor Vehicle Safety Standard (FMVSS) 209. Despite the FMVSS 209 requirements, the National Highway Traffic Safety Administration (NHTSA) recently sponsored a research project [6] that focused on broader rear restraint design possibilities, some of which edged on or went beyond FMVSS 209. A large segment of the NHTSA study included physical testing, but simulation results based on analyses with the MADYMO software were relied upon as well.

As in the NHTSA study, the work presented herein focused on tailoring the rear seat restraints performance envelope to a wider span of occupant weights, sizes, and types. The subject study also utilized the MADYMO software for baseline runs and alternative restraints design simulations. One of the alternative restraint designs was a real-time adaptive (RTA) seatbelt retractor system. The RTA system bases its performance characteristics on TCJ (Tailored Control Joint) technology, which has a fast response and high force generation capability [Appendix E]. As modeled, the RTA system represents a retractor in which the belt load adapts real-time to the dynamics of the

restraining event. Specifically, the RTA system is able to react to different occupant weights and sizes via a set of sensors and a control system whose definition is part of the work presented herein. The RTA control system ultimately operates based on the understanding that a heavy occupant will tend to yield a high seatbelt pay-out rate early in the crash pulse if the seatbelt force is too low, and the RTA system then drives the seatbelt force at the retractor to rise in such a case. Conversely, the seatbelt pay-out rate will typically be very low or zero for a lightweight occupant if the initial seatbelt force is too high, and the RTA system then drives the seatbelt force at the retractor to diminish in such a case, and thus increase the amount of seatbelt pay-out (increase of the light occupant ride-down distance).

Objectives of this study include addressing questions that relate to the investigation of real-world rear-seat restraints improvement opportunities, where frontal airbags are typically unavailable. Can an RTA system that responds as described above really be achieved without an occupant weight sensor signal from within the seat? What is an effective load range capability for the RTA retractor? Are the calculated injury values from the RTA model indeed tangibly lower across the collection of simulated ATD's? And also, how robust would such a system be, considering the unknown real-time nature of real-world crash pulses as they happen.

The RTA system is simulated together with other restraints configurations under a number of load conditions. Load conditions vary with combinations of different crash pulses ranging in severity from 25-mph to 35-mph and different anthropomorphic test devices (ATDs) ranging from the HIII 6YO to the HIII 95th percentile male. Results from the MADYMO simulations are then presented in the form of seatbelt performance data and injury metrics from the collection of ATDs.

BACKGROUND

The current research refers to some of the past work on rear seat restraints research, modeling and seatbelt system optimizations. Some of these studies have relied on the MADYMO or LS-Dyna simulation capabilities to investigate advanced and progressive rear seat restraints configurations, while others have relied on testing or a mix of the two approaches.

In a study conducted by Kawaguchi *et al.* [10], the proposed belt load controller was optimized with assistance of MADYMO modeling and concluded that a load limit value of 3.5 kN resulted in reduced injury values for all four of the modeled dummies. However, the overall results of the study suggested that lower load limits for small occupants and higher load limits for larger occupants would provide the best injury reduction potential when coupled with a pretensioner. A belt load limit of 2 kN and maximum pay-out length of 200 mm resulted in significantly reduced 6YO HIC and chest acceleration values when compared with the standard seatbelt model.

Hu *et al.* [11] used MADYMO, sled testing, and design optimization to examine whether a rear seating area designed for a 6-12 YO child would offer appropriate protection to other demographics including adults. Tradeoffs in occupant protection levels were observed with this approach. A design change that benefited one group sometimes reduced protection for another group. Hu *et al.* concluded the enhancement of rear seat occupant protection across all age groups for a single design required the use of adaptive or adjustable restraint systems.

Ravichandran [9] presented an optimization study conducted in the LS-Dyna explicit code environment with child dummies seated in rear positions. Seatbelt systems in the study were equipped with load-limiting levels ranging from 2 kN to 5 kN, stopper positions that varied from 0.8 to 1.5 torsion bar turns, and different pretensioner fire times. The study highlighted that the presented optimization method was an effective tool to identify an optimal restraint system to better protect second-row occupants.

A publication presented by Hong *et al.* [12] based several of their findings on 28 New Car Assessment Program (NCAP) tests in which a 10 YO child dummy was positioned in various rear seating positions. Nearly all 28 vehicles tested scored at least 4-stars for front seated occupants, while only a third of those vehicles maintained at least 4-stars for the rear seated occupants. The study also reported applicable belt loads and injury results curves.

Research on restraint system optimizations has also been conducted for first row seated locations [30 - 32]. Optimized systems typically owe their increased performance and injury reduction enhancements to appropriate

sensing technology, proper classification of the vehicle occupants, and/or ideal restraint systems modeling (systems that are not necessarily physical).

The current study operates similarly and proposes enhanced sensing technologies within the retractor, with active load-limiting functionalities based on a mechatronic system known as the TCJ technology. A TCJ-equipped system is characterized by a very fast response and a high force modulation capability – two features of significant importance to an RTA-type of retractor. The TCJ technology can generate an electrically controlled rotational friction force (effectively a torque) about the axis of rotation of a seatbelt retractor spool. Data from independent testing conducted at Intertek suggest a 15-millisecond response capability for multi-kN load changes, and minimal load variability either from the friction or from temperature variations (+/- 5% range of the target value). Belt loads from a TCJ-equipped retractor would typically vary around a pre-determined mid-point nominal load level (zero electrical input) from which the load can either increase or decrease, as needed. The mid-point load level for an initial exploration TCJ range of 1.5 kN to 6.0 kN, would be 3.75 kN, which is what was assumed in the current research (TCJ dimensions of approx. Ø65mm x L60 mm). A typical TCJ-retractor would have to be part of a control loop for the variation in the loads to be commanded (via a voltage input that is directly proportional to the generated restraint load). Appendix E provides reference information on the TCJ technology.

METHODOLOGY

The subject study investigated the performance of three seatbelt system configurations: a conventional belt (CB) system, a 3kN load-limited (3kN LL) belt system, and a real-time adaptive (RTA) restraint system. Both the 3kN LL and RTA systems incorporate what is known as an energy management (EM) system. Basic physics dictates that the dissipation of kinetic energy is directly dependent on a force time-history that is multiplied by a corresponding energy absorption distance (EAD) time-history. The objective of lowering the forces and maximizing the overall EAD of an occupant is then desirable, when possible, and EM systems are typically developed based on this strategy. For seatbelt cases, increased EADs come about by allowing seatbelt webbing to pay-out from the retractor via some form of tailored force that acts within the retractor as the seatbelt webbing spools out under the inertial loading of the occupant.

A wide variety of EM restraints technologies have been developed and produced over time, with most vehicles now equipped with some form of EM in their frontal restraint systems. There are currently limited possibilities for occupant-specific optimization of rear seat EM systems. The baseline CB case that was modeled herein is the most common implementation that meet FMVSS 209 guidelines [35], but it is void of any EM (aside from belt stretch properties). There are vehicles offering 6 kN LL-type belt systems at their rear-seated locations, and these systems also meet FMVSS 209. Such systems offer some EM benefits, but their performance is like CB systems for most occupants since lighter and mid-weight occupants will typically not generate the force needed to trigger the LL part of a 6kN LL system. To explore the patterns of LL effects for more occupant sizes, the present research incorporated the modeling of a 3kN LL EM system instead. A 3kN LL system represents a baseline technology to which the more complex RTA configuration can be compared. For the sake of reference, the RTA configuration, as modeled herein, operates both above and below the 3kN levels (with an initial 1.5 kN to 6.0 kN RTA load range capability).

The three retractor configurations in the current study were all subjected to the complete set of load case combinations stemming from the five different ATDs and six different crash pulses that were modeled. All six crash pulses originated from the NHTSA database. Table 1 offers a summary overview of the pulses, and Appendix A displays the pulse curves. The crash pulses were pulled from a small (B-segment) sedan, a C-segment sedan, a D-segment sedan, two medium SUVs, and an electric vehicle. All the crash pulses were 35-mph pulses, except for Pulse B, which was a 25-mph pulse.

Table 1.
Information on the selected NHTSA pulses.

Pulse Reference	Vehicle Type	NHTSA Test Impact Speed [mph]	Crash Type
A	Medium SUV	35	Fixed Barrier
B	Passenger Car (C-segment)	25	Fixed Barrier
C	Passenger Car (D-segment)	35	Fixed Barrier
D	Medium SUV	35	Fixed Barrier
E	Passenger Car (B-segment)	35	Fixed Barrier
F	Electric Vehicle (SUV-type)	35	Fixed Barrier

The five modeled ATDs consisted of the HIII 6YO, the Q10, the HIII 5th, the HIII 50th, and the HIII 95th. The parametric combination of six pulses, five ATDs, and three hardware configurations yielded a total of 90 MADYMO simulations.

Prior to generating restraint performance data and results from all the planned simulations, it was necessary to conduct a system identification process for the RTA system. The process started from the understanding that the RTA system could operate within an EM band that would range from 1.5 kN to 6.0 kN at the retractor, meaning that the RTA system would allow belt pay-out as soon as a 1.5 kN belt load was reached for some cases (light occupants or light pulse), but it could also "choose" to hold back any pay-out up to the 6.0 kN level (if needed, for heavier occupants), at which point pay-out would need to occur no matter what the energy profile of the crash event was. The system identification process continued as an iterative and non-automated process that considered the described EM load range for the RTA system (1.5 kN to 6.0 kN), the input for the assumed RTA sensor data sources, and the different load cases. An RTA system in which the belt load adapted real-time to the dynamics of the restraining event was thereby identified (i.e., the system adapts to the inertia of the occupant and to the severity of the crash pulse while maintaining favorable performance results).

Various simulation results from the RTA system in the subject study were analyzed and compared. RTA hardware results were first compared against the 3kN LL system to gauge the performance in terms of seatbelt pay-out amounts primarily. Shoulder belt load levels from the RTA system were also inspected and cross-compared in detail against the other systems. A review of injury numbers was conducted as well to evaluate the overall performance of the RTA system when compared against the most commonly implemented CB system. Reported injury metrics as generated from each of the modeled ATDs for all the simulated load cases included chest compression, chest acceleration, Head Injury Criterion (HIC), and Neck Injury Criterion (Nij) values. A brief sensitivity study was also carried out to evaluate the sensitivity of RTA injury results to variations in one of the key RTA modeling parameters.

MADYMO MODEL DESCRIPTION

The MADYMO software [37] is well-known for its ability to model automotive crash events incorporating ATDs, seatbelt systems, airbag systems, and the occupant environment itself. The software also offers Control Systems modeling capabilities, which were utilized herein as well. The build-up of the MADYMO simulations in the current study started from a simple and straightforward vehicle model that incorporated two front seats and a full rear seat bench. The right rear-seated location was the primary location of interest throughout this study. A three-point belt system was implemented at this location with one of three seatbelt retractor configurations:

1. the conventional belt (or CB) system, which is void of any EM beyond that of the belt stretch itself.
2. the previously described 3kN LL retractor system, with a static EM capability set at the 3kN force level.
3. the previously described RTA retractor system, equipped with an adaptive force generation system.

The modeling of the CB and 3kN LL retractor configurations was fairly straight forward. The RTA retractor modeling was more involved. It relied on real-time sensor signals to provide feedback about the retractor seatbelt pay-out and pay-out rate versus time. A MADYMO control system was thus implemented to collect these signals, process them, and command the seatbelt force level to the RTA retractor. Shown in Appendix D is a condensed view of the MADYMO syntax that was implemented for the RTA configuration, with each of the shown keyword lines having further syntax calls embedded within them. The formulations in MADYMO for the RTA system, and for the CB and 3kN LL systems, remained unmodified throughout the study, regardless of which ATD or pulse to which they were subjected.

MADYMO's pre-processor (XMADgic) was utilized to position a finite element model seatbelt around each modeled ATD. The HIII 6YO was positioned within a high back booster seat, whereas all the other ATDs were seated in a nominal position. In some simulations, ATDs occasionally interacted with the right front seatback via their extremities (light contacts, primarily with the hands and feet). In the modeled vehicle interior, there was enough space in all pulse cases to prevent the knees, even those of the HIII 95th percentile, from interacting with the seatback. Knee-to-seatback contacts might be likely in real-world situations, but it was preferred to initially isolate out this contact interaction in the subject simulations. Figure 1 shows schematic views of the RTA seatbelt system (a) prior to the crash, and (b) during the crash event. In more detail, Figure 1(b) illustrates the activated retractor, the seatbelt tension force, and the occupant belt loading which effects a Z(t) pay-out amount out of the retractor. The views shown in Figure 2 represent each of the five modeled ATDs, first shown at rest and then shown at the point where the maximum pay-out occurred out of the RTA retractor.

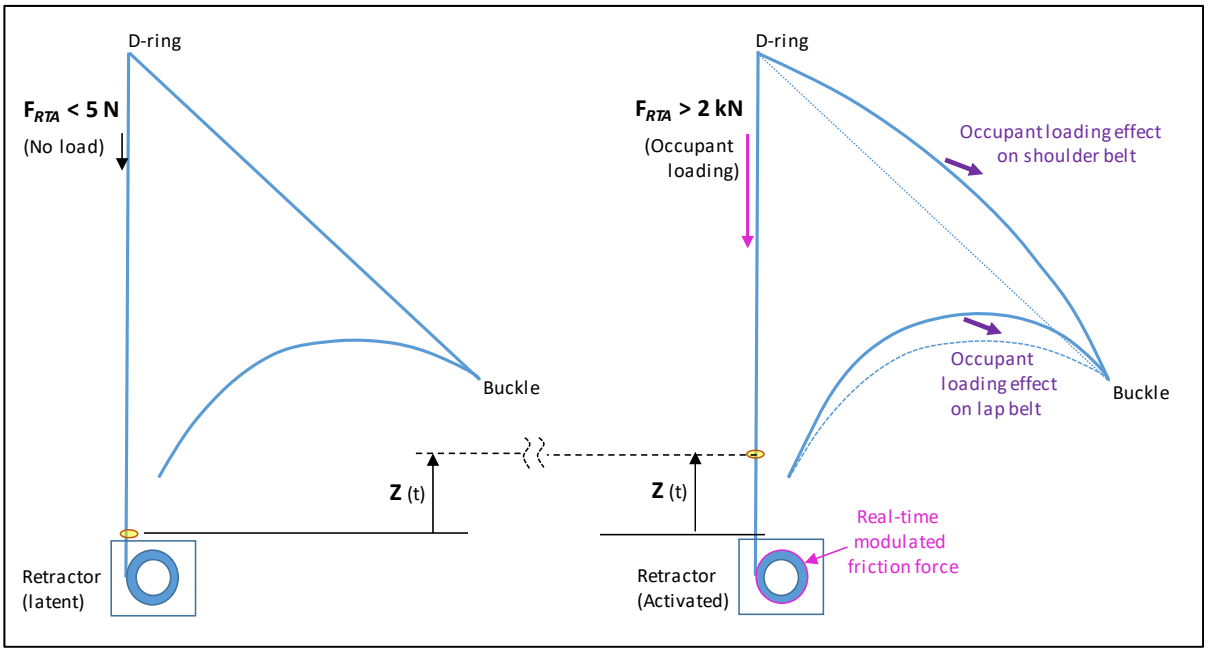

Pre-crash state of belt system ***(a)***

Snap-shot during a typical crash event ***(b)***

Figure 1. Diagrams of the RTA equipped 3-pt belt system.

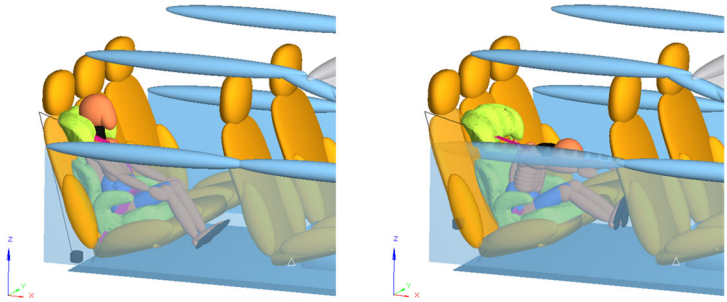

(a) HIII 6YO in high back booster seat

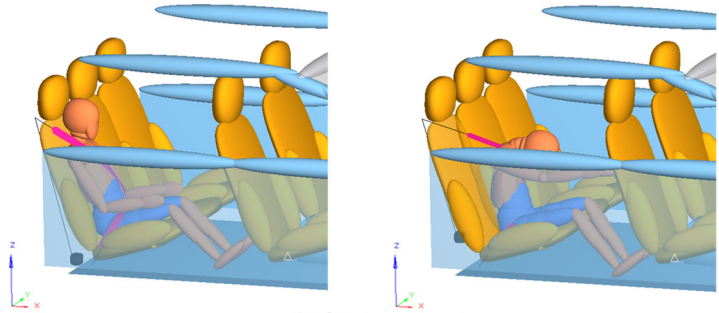

(b) Q10 in rear seat

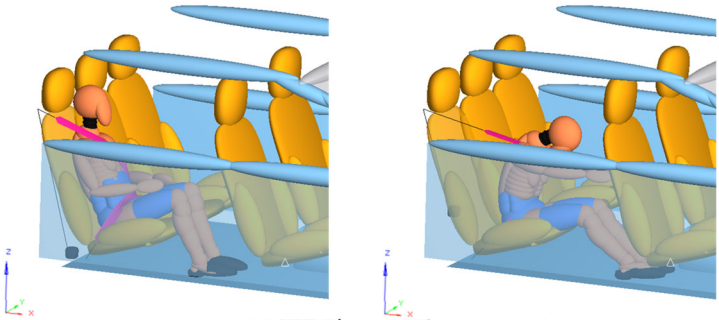

(c) HIII 5th percentile in rear seat

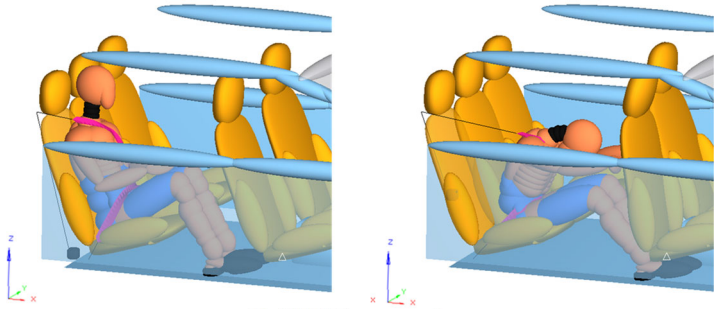

(d) HIII 50th percentile in rear seat

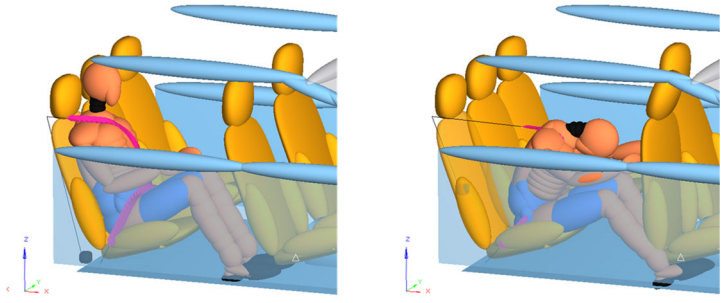

(e) HIII 95th percentile in rear seat

Figure 2. Sample Images from MADYMO simulations.

RESULTS

As discussed above, the simulations were carried out with three different seatbelt retractor configurations. Each hardware configuration yielded different seatbelt pay-out amounts and different seatbelt tension force time histories. An initial consideration of the retractor-specific data helps gauge their influence on the injury metrics. Recorded injury values from the different ATDs and crash pulses are reported in the Injury Metrics section provided below. The hardware results are reviewed first.

Hardware Results

Figures 3 and 4 provided below illustrate a sampling of the complete set of hardware simulation results. Both figures show only select curves from the HIII 50th percentile load case, for the purpose of identifying the trends.

Figure 3 displays retractor pay-out traces versus time for the 3kN LL and RTA configurations (there was no retractor pay-out for the CB case, and belt stretch effects were not accounted for in any of the pay-out data). The general trend was that for less forceful cases such as Pulse C (as marked in Figure 3), the RTA system tended to yield increased pay-out amounts over the 3kN LL case and vice versa for the more forceful cases, such as Pulse E (as marked in Figure 3 as well), in which the RTA system tended to withhold pay-out amounts over the 3kN LL case. Refer to Appendix B for the full collection of belt pay-out graphs for all ATDs and load cases.

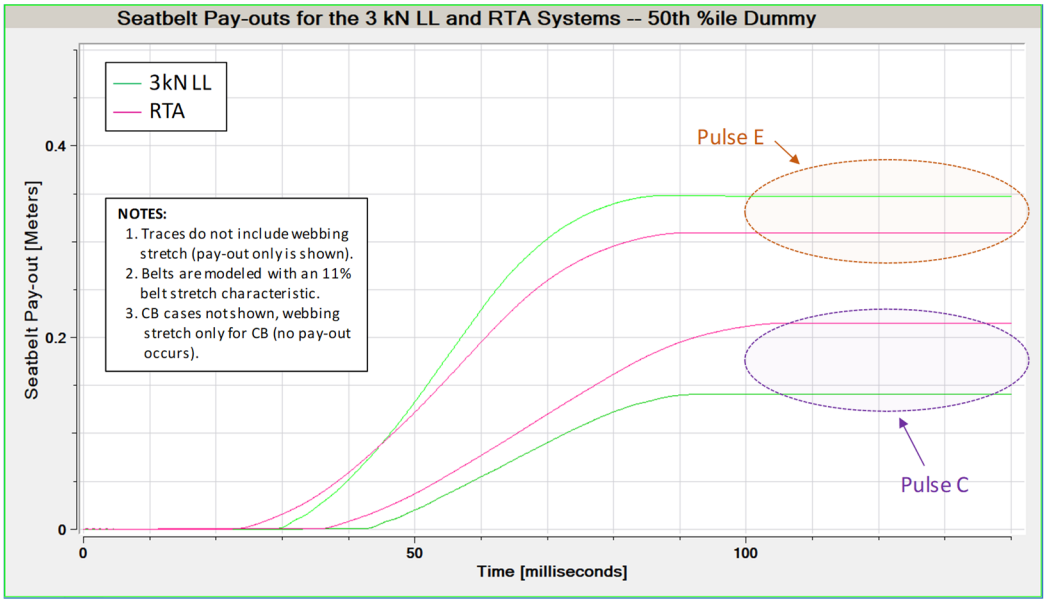

Figure 3. Webbing pay-outs out of retractor (sample results) – HIII 50th %ile ATD simulations.

Figure 4 is a sample graph of the shoulder belt load versus time traces, again for the HIII 50th percentile ATD only. As with Figure 3, shoulder belt load traces are shown only for two sample pulses (Pulses C and E). The contrast in Figure 4 is between result traces for the CB and RTA configurations primarily, since the 3kN LL hardware configuration always peaked out at approximately the same shoulder belt load level (being a 3kN LL configuration at the retractor, it peaked and remained steady at approximately 4 kN after belt passage over the D-ring for all cases). The CB simulations peaked at approximately 7 kN and 11 kN (Pulses C and E, respectively), and the RTA system peaked at approximately 3.6 kN and 6.2 kN for the same two Pulses C and E, respectively. Refer to Appendix C for a collection of shoulder belt load graphs for several ATD and load cases (lower severity Pulses B and C are omitted in the graphs in Appendix C only for the purpose of readability – Pulse C in Figure 4 provides a sense of the pattern for a lower severity pulse).

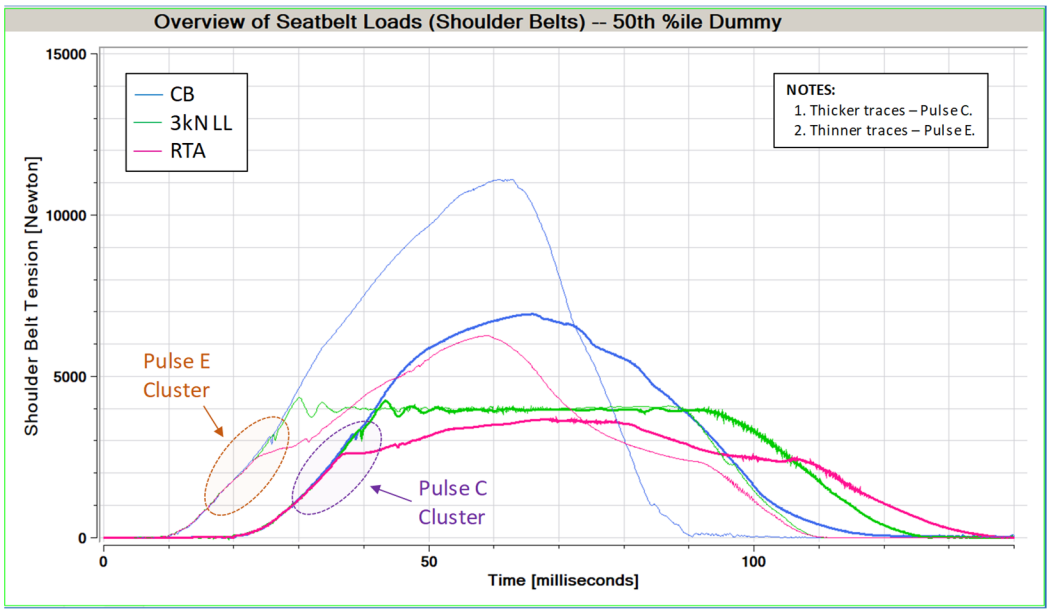

Figure 4. Seatbelt load traces (sample results) – HIII 50th %ile ATD simulations.

Injury Metrics Results

Injury metric results for the five dummies that were simulated in each of the parametric restraint and pulse conditions were analyzed. Four figures are provided below, each consisting of five histogram graphs (one per ATD -- see Figures 5 to 8). Six clusters of data appear within each histogram – one cluster per crash pulse. The data clusters are graphed in order of reducing crash pulse severity (from left to right). Detailed crash pulse information appears in Table 1 and traces are shown in Appendix A. Pulse E was the most severe of the collection of modeled pulses. Injury data are shown first in the form of chest compression values in Figure 5. Shown adjacent to the chest compression results are the chest acceleration results in Figure 6. Next, shown in Figures 7 and 8, are the HIC_{15} and N_{ij} values, respectively.

Results from the sensitivity study on RTA modeling parameters are presented as well, but they appear further below in the Discussion section. The sensitivity study is itself dependent on some of the findings brought forth in the Discussion section, and results for the sensitivity study are discussed then.

DISCUSSION

As mentioned previously, one objective of the subject study was to evaluate the likelihood of success, or feasibility, of an RTA system that is initially blind to the inertia of the occupant. As modeled herein, the RTA system thus relied on data originating only from two (admittedly assumed) sensors that measured the real-time seatbelt pay-out, $Z(t)$, and pay-out rate, $\dot{Z}(t)$, versus time. The RTA system was void of a seat-integrated weight sensor of any type. Upon examining Figures 5 through 8 and comparing the RTA data to the CB data, it transpires that RTA injury results improved in most instances, and often by a notable step, over CB results. Nij values did increase for the HIII 95th, but they remained below 1.0, while all the recorded high HIC values in the CB case for the HIII 95th were brought down to below 700 in all cases for the RTA configuration. Based on an overall review of injury numbers, it appears feasible therefore for an RTA system, as configured herein, to be successful.

Improved injury numbers as observed for the RTA system over results from the CB simulations should not, however, come at the expense of excessive seatbelt pay-out amounts. The more energetic simulations (HIII 95th percentile) for the 3kN LL case occasionally generated pay-out amounts that went beyond 400 mm. By contrast, the HIII 95th percentile pay-out results for the RTA system remained below 400 mm (maximum values of approximately 350 to 370 mm). Therefore, as it was configured herein, the RTA system appeared to capture the spirit of FMVSS 209, which allows up to 508 mm to be added to the belt system under high loading conditions (including belt stretch). As mentioned previously, belt stretch was not included in any of the reported seatbelt pay-out amounts in the subject study, and simulations were run with an 11% belt stretch characteristic.

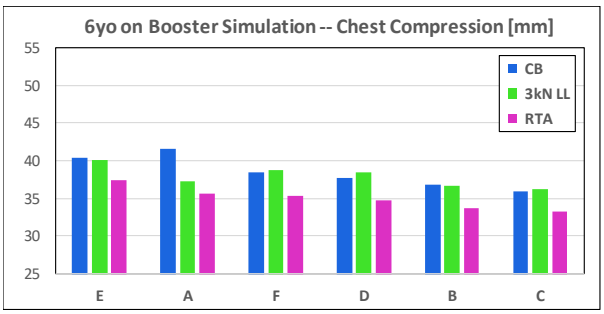

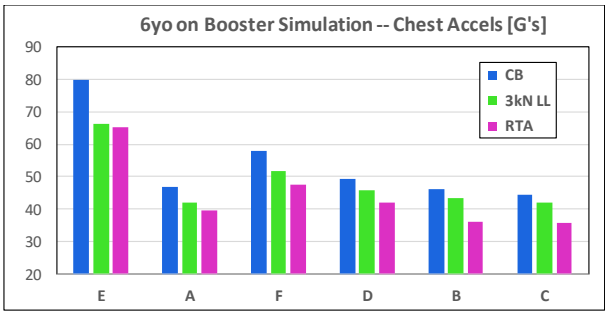

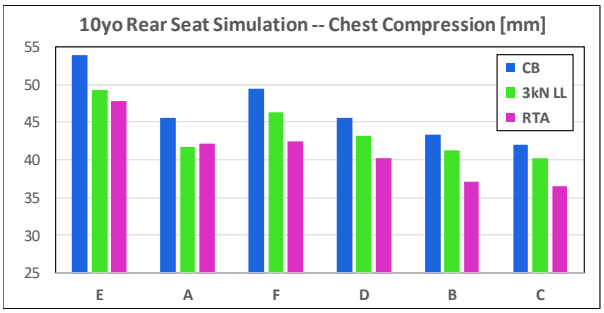

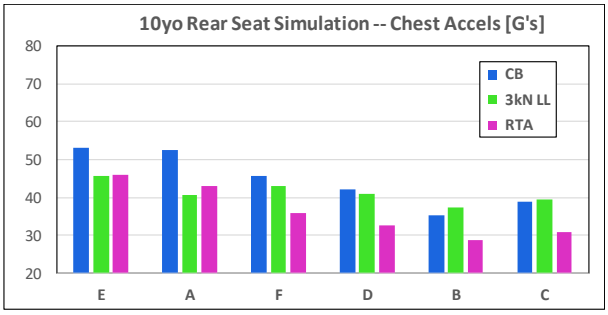

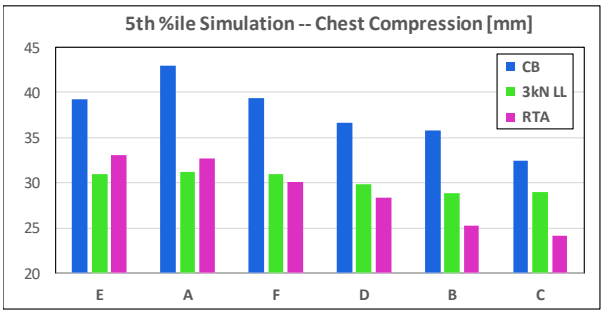

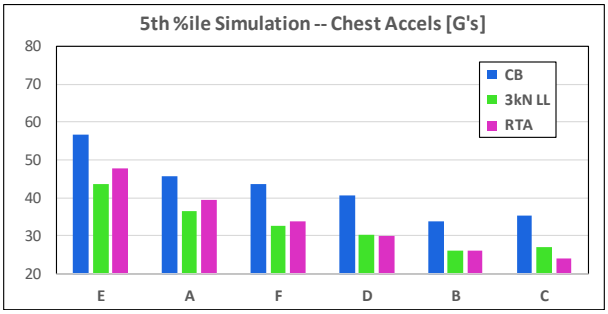

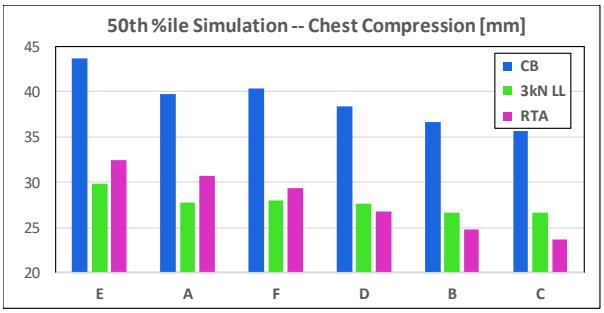

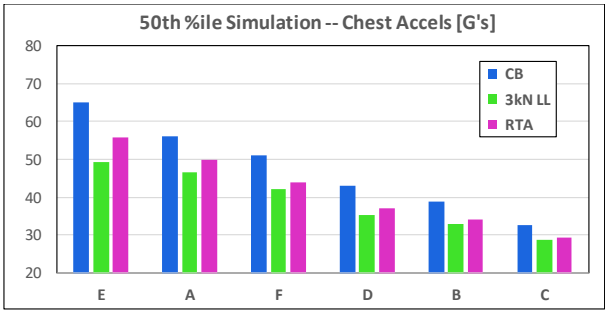

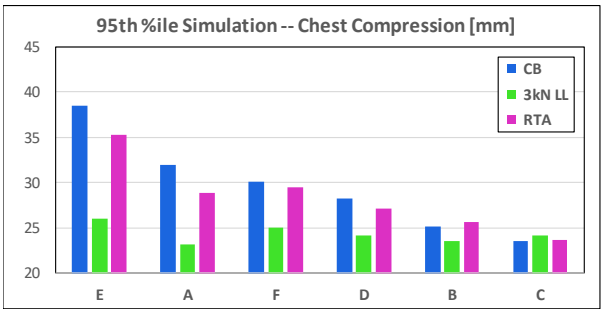

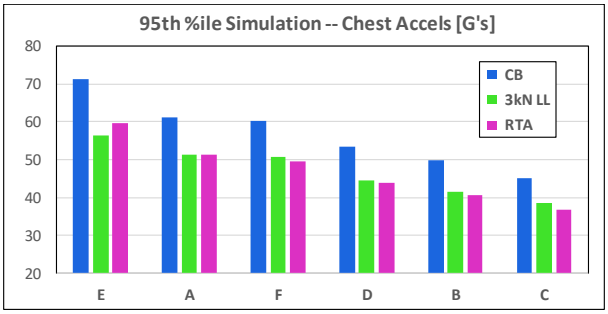

Figure 5. Chest Compressions – All load cases.

Figure 6. Chest Accelerations – All load cases.

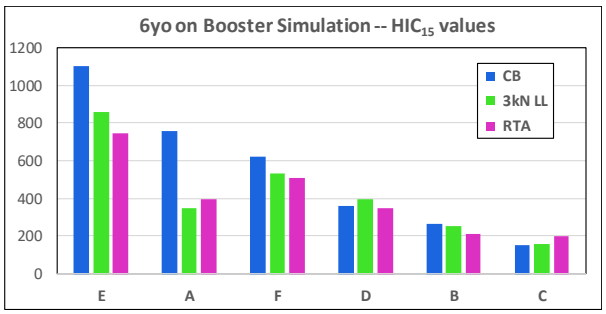

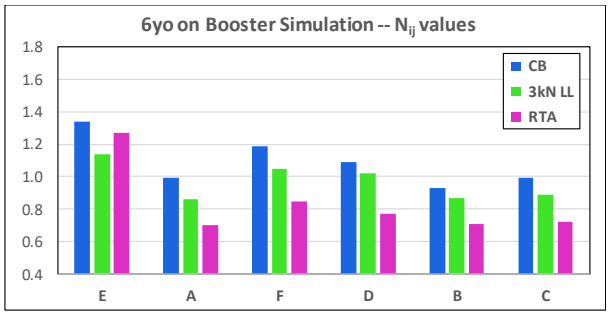

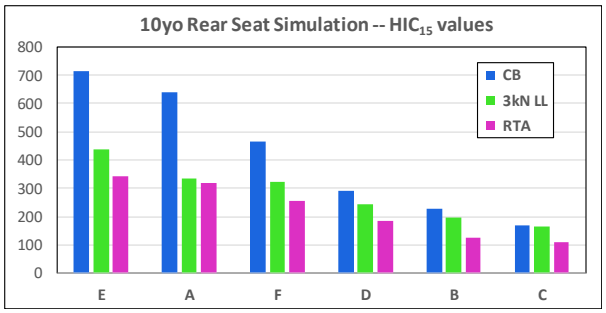

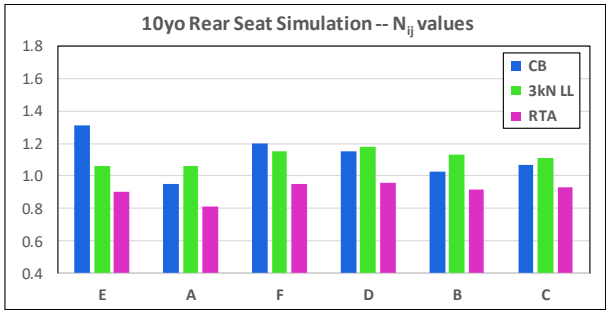

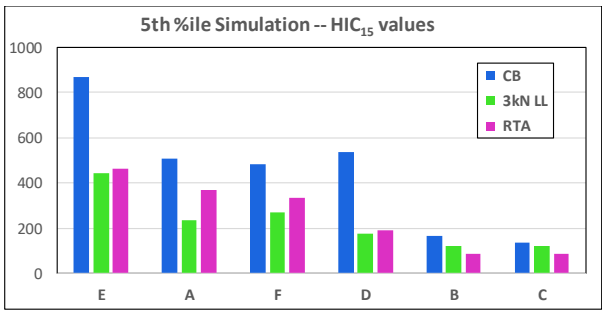

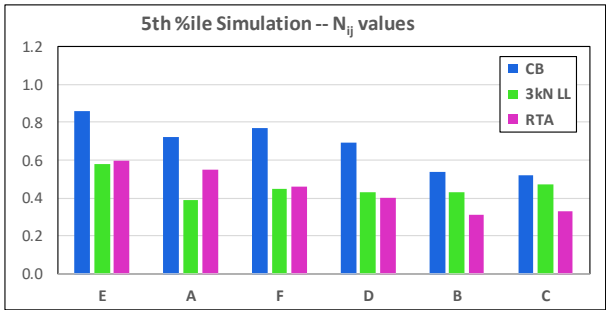

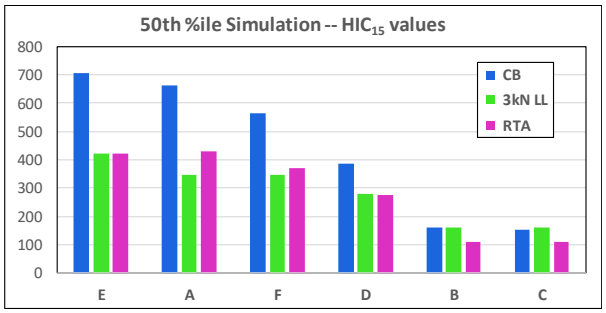

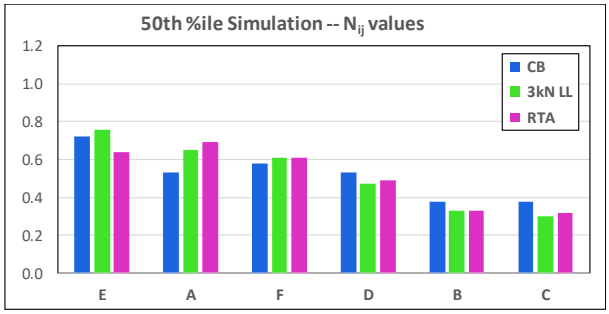

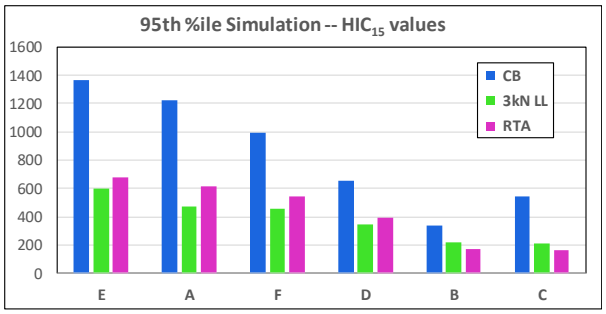

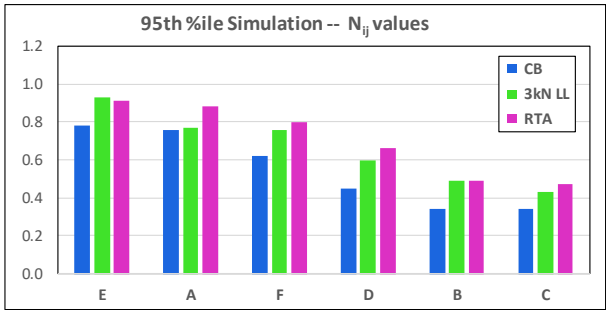

Figure 7. HIC_{15} Values – All load cases.

Figure 8. N_{ij} Values – All load cases.

Injury result trends and seatbelt performance data for the less energetic 25-mph crash severity (Pulse B) are of note as well. All four injury categories showed improvements in the RTA case for all the lower inertia ATDs. The significance of this observation is about the potential benefits for a wider segment of the population, with a focus on children and other more vulnerable occupants (elderly). While nominally tested ATDs already scored well with the CB system (5th and 50th ATD results are well below injury assessment reference values) in the 25-mph simulation, the RTA system continues to improve on those results. The potential real-world benefits associated with these improved responses are two-fold. First, a greater majority of crashes that occur on the roadways are indeed of delta-V's well below 35 mph [36]. Notable improvements in injury numbers for any crash severity lower than 35 mph apply then to a much greater number of real-world cases. This then increases the occupant exposures to improvements in real-world crashes. Secondly, the category of occupants that includes vulnerable populations such as the elderly and lighter weight individuals will benefit from the improved and adaptive performance of an RTA-type of system, while there was no appreciable adverse effects noted on the overall for the larger vehicle occupants.

As far as the system identification process is concerned, the understanding is that the RTA control system assimilates both the $Z(t)$ and $\dot{Z}(t)$ real-time information, and it then generates the adequate amount of retractor tension force, $F_{RTA}(t)$, that is required to manage the real-time dynamics of the restraining event. The system identification finding here is that the function, shown below in Equation (2), is one that in fact relates the two measured $Z(t)$ and $\dot{Z}(t)$ values to the retractor tension force, $F_{RTA}(t)$:

$$F_{RTA}(t) = f\left(Z(t),\ \dot{Z}(t)\right) \qquad \text{(Equation 1)}$$

$$= 2000 + k_1 * Z(t) * \dot{Z}(t) - k_2 * \left[\ 1 - k_3 * \dot{Z}(t)^{\,2}\ \right] + k_4 \qquad \text{(Equation 2)}$$

Equation (2) is a function derived from iterative MADYMO simulations in which one control module after another was added into the complete sequence of control system modules. The stack of modules, when all combined after satisfactory results were generated, eventually distilled down to the formulation shown above in Equation (2).

The constant "2000" in Equation (2) has a physical meaning in that it is reflective of the lower end load-limited operation range of the RTA retractor (2.0 kN). The shoulder belt data from the complete set of RTA simulations (Appendix C) indicated a "step" (a visible transition) in the data traces at approximately 2.6 kN. The difference between the 2.0 kN value (at the retractor) and 2.6 kN (shoulder belt load) was due to the modeled friction at the D-ring. The 2.6 kN level in the shoulder belt was the point at which the traces either ceased to increase rapidly for lightweight occupants, or it was the point where the traces continued to rise, albeit at a visibly different rate, for larger occupants and/or more aggressive pulses.

A sensitivity analysis was also conducted on the first constant parameter in Equation (2). The finding was that lowering the "2000" (or 2.0 kN) that is currently assigned resulted in undesirable trade-offs. On the basis of injury values provided in Figure 9(a) for the low-end inertia HIII 6YO and in Figure 9(b) for the high-end inertia HIII 95th ATDs, dialing the constant in Equation (2) back to "1500" yielded non-negligible increases (for higher severity pulses) in both the HIC and N_{ij} values of the HIII 6 YO, and no discernable improvements in chest compression and chest accelerations for the same HIII 6YOA were noted. A similar comparison is shown in Figure 10 for seatbelt pay-out amounts, where the "1500" setting was shown to generate excessive pay-out amounts for the higher inertia HIII 95th percentile ATD, with pay-out values either exceeding or coming close to 400 mm in many of the simulations. Thus, the overall preference was to retain a value of "2000" (or 2.0 kN for the lower LL threshold in the RTA system) for the first constant term in Equation (2).

The latter finding bolsters the outcome for the lower RTA range setting to remain at 2.0 kN. On the high-end of the range, despite an original set limit of 6.0 kN for the RTA system, none of the RTA simulations truly approached that value – the maximum observed was 5.3 kN (or 6.9 kN at the shoulder belt). A working RTA load range at the retractor of 2.0 kN to 5.3 kN appears reasonable then, for the collection of load cases reviewed herein. The 2.0 kN to 5.3 kN is a much narrower band than the initially specified 1.5 kN to 6.0 kN. The finding of a narrower band is a favorable outcome in that it diminishes the complexity and functional design requirements of an RTA-type of system, which then likely reduces development and further downstream costs. The updated range of 2.0 kN to 5.3 kN thus became the working range for the RTA simulations that generated all the results shown in Figures 3 through 8 (and Appendices B and C).

(a) *(b)*

Figure 9. Sensitivity analysis -- Injury values between two RTA settings.

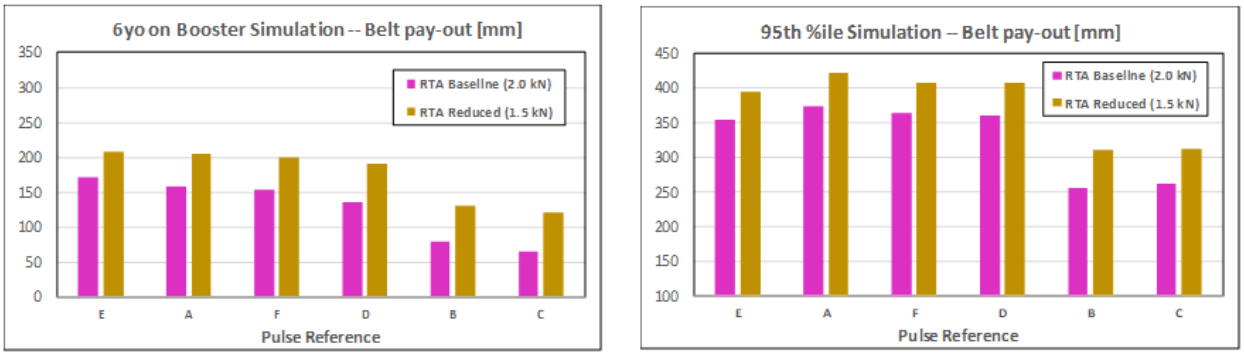

(a) *(b)*

Figure 10. Sensitivity analysis -- seatbelt pay-outs between two RTA settings and the 6YO(a) and HIII 95th(b).

CONCLUSIONS

Upon engaging into the subject research effort on adaptive restraints, it was unknown if an RTA retractor with the intended and ambitious functionalities could even be modeled successfully. An initial finding from this study is that the MADYMO software is able to model such an RTA-type of retractor, even with its native and somewhat limited MADYMO Control Systems commands (the coupling of MADYMO with MATLAB for more complex applications was not a necessary option herein). Also emerging as a finding from the subject research is that an overall and satisfactory restraint performance appears to be achievable with an RTA system that operates within a load-limited range spanning from 2.0 kN to 5.3 kN at the retractor. The overall RTA restraint performance was deemed satisfactory based on collected injury numbers from numerous simulation load cases, and on the basis that excessive seatbelt pay-out amounts were not observed, even for the higher inertia HIII 95th percentile ATD.

The RTA system was successfully simulated without relying on a weight sensing feature in the occupant seat. The RTA configuration instead assumed feedback for its control loop from both a seatbelt pay-out sensor and a pay-out rate sensor. The occupant inertia was therefore estimated from the instantaneous dynamics of the restraints event, and the RTA system reacted adequately thanks to the reversible and continuously variable capabilities of the TCJ technology, which the simulated RTA system was essentially representing.

The subject research is ultimately a feasibility study. Future work would be to focus on the details of the control system itself, such as sensor resolution characteristics, sensor response times, electronic actuation response times, and other possible component-specific dynamics. It remains to be seen, as such, how much effective lag time the RTA system could withstand and yet remain successful and useful. Also, the influence of the presence of a pretensioner remains to be investigated. Additional analyses related to specific injury potential, passenger interaction with the front seats of smaller vehicles, and crash pulses that are not primarily frontal in nature are areas of future focus as well. Despite the work that remains on several fronts, the subject research provided an initial concept validation for a physically realizable advanced restraint system that would likely benefit the more vulnerable vehicle occupants, such as children and elderly individuals, without generating any significant adverse effects for the typical adult weights and sizes upon which conventional restraint systems designs are usually based.

REFERENCES

[1] Vasilash, G. S. (2014, May 30) *Safety in the rear seat*. Automotive Design & Production. Retrieved from www.adandp.cm.

[2] Sahraei, E., Digges, K. and Marzougui, D. (2010). *Reduced Protection for Belted Occupants in Rear Seats Relative to Front Seats of New Model Year Vehicles*. In: 54th Annual Scientific Conference. Las Vegas, Nevada: Association for the Advancement of Automotive Medicine, pp.149-158.

[3] Sahraei, E., Soudbakhsh, D., and Digges, K. (2009) *Protection of Rear Seat Occupants in Frontal Crashes, Controlling for Occupant and Crash Characteristics*. Stapp Car Crash Journal*,* 53, pp. 75-91. Paper No. 2009-22-0003.

[4] Hu, J. (2016) *Surviving a Crash in Rear Seats: Addressing the Needs from a Diverse Population*. UMTRI, Transportation Research Institute University of Michigan, MADYMO User Meeting 2016.

[5] Dinh-Zarr, T. B. (2016, April 26) *Workshop: Rear Seat Safety in Passenger Vehicles*., National Transportation Safety Board, Washington, D.C.

[6] Hu, J., Rupp, J., Reed, M. P., Fischer, K., Lange, P., & Adler, A. (2016, March). *Rear seat restraint optimization considering the needs from a diverse population* (Report No. DOT HS 812 248). Washington, DC: National Highway Traffic Safety Administration.

[7] Hu, J., Reed, M., Rupp, J., Fischer, K., Lange, P. and Adler, A. (2017). *Optimizing Seat Belt and Airbag Designs for Rear Seat Occupant Protection in Frontal Crashes*. SAE International, SAE Technical Papers, 61st SAE Stapp Car Crash Conference, November 13-15, 2017, 61, 67-100.

[8] Wang, Y., Bai, Z., Cao, L., Reed, M., Fischer, K., Adler, A. and Hu, J. (2015). *A Simulation Study on the Efficacy of Advanced Belt Restraints to Mitigate the Effects of Obesity for Rear-Seat Occupant Protection in Frontal Crashes*. Traffic Injury Prevention, 16, S75–S83. DOI: 10.1080/15389588.2015.1010722.

[9] Ravichandran, V. (2018). *Multi-Objective Optimization for Vehicle Second Row Restraint System Considering Various Occupant Sizes and NCAP Requirements*. FISITA, 37th FISITA World Automotive Congress, October 2-5, 2018.

[10] Kawaguchi, K., Kaneko, N., Iwamoto, T., Fukushima, M., Abe, A., and Ogawa, S. (2003). *Optimized Restraint Systems for Various-Sized Rear Seat Occupants in Frontal Crash*. SAE International, SAE Technical Papers, SAE World Congress, March 3-6, 2003.

[11] Hu, J., Wu, J., Klinich, K., Reed, M., Rupp, J., and Cao. J. (2013). *Optimizing the Rear Seat Environment for Older Children, Adults and Infants*. Traffic Injury Prevention, 14: sup1, S13-S22, DOI: 10.1080/15389588.2013.796043.

[12] Hong, S. W., Park, C., Morgan, R., and Kan, C. (2008). *A Study of the Rear Seat Occupant Safety using a 10-Year-Old Child Dummy in the New Car Assessment Program*. SAE International, SAE Technical papers, Paper No. 2008-01-0511.

[13] Kent, R., Forman, J., Parent, D., and Kuppa, S. (2007). *Rear Seat Occupant Protection in Frontal Crashes and its Feasibility*. Enhanced Safety of Vehicles, 20th International Conference on the Enhanced Safety of Vehicles, Lyon, France, June 18-21, 2007.

[14] El-Jawahri, R. E., Kim A., Jaradi, D., Ruthinowski, R., Siasoco, K., Stancato, C. and Weerappuli, P. (2017). *Responses of Rear Seat ATDs in Frontal Impact Sled Tests: Evaluation of Two Seat Belt Configurations*. SAE International, SAE Technical Papers, 2SAE World Congress Experience, April 4-6, 2017.

[15] Forman, J., Michaelson, J., Kent, R., Kuppa, S., and Bostrom, O. (2008). *Occupant Restraint in the Rear Seat: ATD Responses to Standard and Pre-tensioning, Force-Limiting Belt Restraints*. Association for the Advancement of Automotive Medicine, Annals of Advances in Automotive Medicine: 52nd AAAM Annual Conference, October 2008.

[16] Hong, L., Yuhao, P., and Hongtao, X. (2018). *Research on the Safety of Rear Seat Female Occupant in the 50km/h Frontal Collision*. Institute of Physics Publishing, Journal of Physics: Conference Series, 1st

International Conference on Advanced Algorithms and Control Engineering, v 1087, n 5, ICAACE 2018, August 10-12, 2018.

[17] Hong, L. and Wu, Y. (2012). *Research on the Safety of Rear Seat Occupants in the Frontal Collision*. Trans Tech Publications, Advanced Materials Research, 569, 795-799.

[18] Hong, L., Ge, R., and Wu, Y. (2013). *Analysis and Optimization of Rear Occupant Safety in Car Head-On Collision*. Trans Tech Publications Ltd, Applied Mechanics and Materials, 328, 292-296.

[19] Tylko, S., and Bussieres, A. (2012). *Responses of the Hybrid III 5th Female and 10-year-old ATD Seated in the Rear Seats of Passenger Vehicles in Frontal Crash Tests*. International Research Council on the Biomechanics of Injury, 2012 IRCOBI Conference Proceedings, September 12-14, Paper No. IRC-12-65.

[20] Prasad, A. K. (2010). *Rear Seat Study*. SAE, Vehicle Research and Test Center NHTSA.

[21] Jakobsson, L., et al. (2019). *Rear Seat Safety in Frontal to Side Impacts – Focusing on Occupants from 3 Years to Small Adults.* Paper No. 11-0257.

[22] Hu, J., Fischer, K., Lange, P., and Adler, A. (2015). *Effects of Crash Pulse, Impact Angle, Occupant Size, Front Seat Location, and Restraint System on Rear Seat Occupant Protection*. SAE International, SAE Technical Papers, SAE 2015 World Congress and Exhibition, April 21-23, 2015.

[23] Tavakoli, M., and Brelin-Fornari, J. (2015). *Effects of Pretensioners and Load Limiters on 50th Male and 5th Female Seated in Rear Seat During a Frontal Collision*. SAE International, SAE Technical Papers, SAE 2015 World Congress and Exhibition, April 21-23, 2015.

[24] Forman, J., Lopez-Valdes, F., Lessley, D., Kindig, M., Kent, R., Ridella, S., and Bostrom, O. (2009). *Rear Seat Occupant Safety: An Investigation of a Progressive Force-Limiting, Pre-tensioning 3-Point Belt System Using Adult PMHS in Frontal Sled Tests.* SAE International, SAE Technical Papers, 2009-November, 53rd Stapp Car Crash Conference, November 2-4, 2009.

[25] Forman, J., Michaelson, J., Kent, R., Kuppa, S., and Bolstrom, O. (2008). *Occupant Restraint in the Rear Seat: ATD Responses to Standard and Pre-tensioning, Force-Limiting Belt Restraints*. Association for the Advancement of Automotive Medicine, Annals of Advances in Automotive Medicine: 52nd Annual Scientific Conference, October 6-8, 2008, 52, 141-153.

[26] Kent, R., Forman, J. Parent, D., and Kuppa, S. (2007). *The Feasibility and Effectiveness of Belt Pre-tensioning and Load Limiting for Adults in the Rear Seat*. Inderscience Enterprises Ltd, International Journal of Vehicle Safety, 2(4), 378-403.

[27] Michaelson, J., Forman, J. Kent, R. and Kuppa, S. (2008). *Rear Seat Occupant Safety: Kinematics and Injury of PMHS Restrained by a Standard 3-Point Belt in Frontal Crashes*. SAE International, SAE Technical Papers, 52nd Stapp Car Crash Conference, November 3-5, 2008.

[28] Bilston, L. E., Du, W., and Brown, J. (2010, November) *A Matched-Cohort Analysis of Belted Front and Rear Seat Occupants in Newer and Older Model Vehicles Shows That Gains in Front Occupant Safety Have Outpaced Gains for Rear Seat Occupants*. Elsevier Ltd, Accident Analysis and Prevention, 42(6), 1974-1977.

[29] Forman, J., Lopez-Valdes, F., Dennis, N., Kent, R., Tanji, H. and Higuchi, K. (2010). *An Inflatable Belt System in the Rear Seat Occupant Environment: Investigating Feasibility and Benefit in Frontal Impact Sled Tests with 50th Percentile Male ATD.* Association for the Advancement of Automotive Medicine, Annals of Advancement in Automotive Medicine: 54th Annual Scientific Conference, Las Vegas, Nevada, October 17-20, 2010, 111-125.

[30] Hesseling, R. J., Steinbuch, M. Veldpaus, F. E. and Klisch, T. (2002). *Control Design of a Safety Restraint System.* ASCC, The 4th Asian Control Conference, Singapore, September 25-27, 2002, 244-249.

[31] Gierczycka-Zbrozek, D. (2011). *Adaptive Restraints: Suggested Parameters for Occupant Classification System*. International Research Council on the Biomechanics of Injury, 2011 IRCOBI Conference Proceedings, 311-314. Paper No. IRC-11-74.

[32] Holding, P. N., Chinn, B. P., Happian-Smith, J. (2001). *An Evaluation of the Benefits of Active Restraint Systems in Frontal Impacts Through Computer Modeling and Dynamic Testing*. TRL Limited, Paper 328.

[33] Untaroiu, C. D. and Adam, T. (2012). *Occupant Classification for an Adaptive Restraint System: The Methodology and Benefits in Terms of Injury Reduction*. International Research Council on the Biomechanics of Injury, 2012 IRCOBI Conference Proceedings, September 12-14, 2012, 205-216. Paper No. IRC-12-28.

[34] Mroz, K., Pipkorn, B., Sunnevang, C., Eggers, A. and Brase, D. (2018). *Evaluation of Adaptive Belt Restraint Systems for the Protection of Elderly Occupants in Frontal Impacts*. International Research Council on the Biomechanics of Injury, 2018 IRCOBI Conference Proceedings, 60-75. Paper No. IRC-18-15.

[35] United States Code of Federal Regulations, Title 49, Subtitle B, Chapter V, §571.209, Federal Motor Vehicle Safety Standard No. 209; Seat belt assemblies.

[36] Goertz, A., Yaek, J., Compton, C. (2010). *Accident Statistical Distributions from NASS CDS.* Society of Automotive Engineers, Publication 2010-01-0139.

[37] MADYMO Software, Version 7.6, Release date : 14:01:49 Aug 31 2015, Copyright 2015, TASS International, Rijswijk, The Netherlands.

APPENDIX A – Vehicle crash pulses

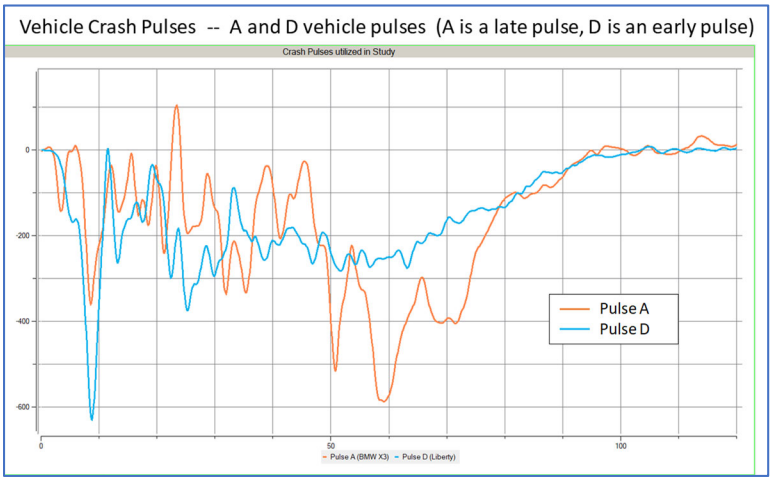

(a)

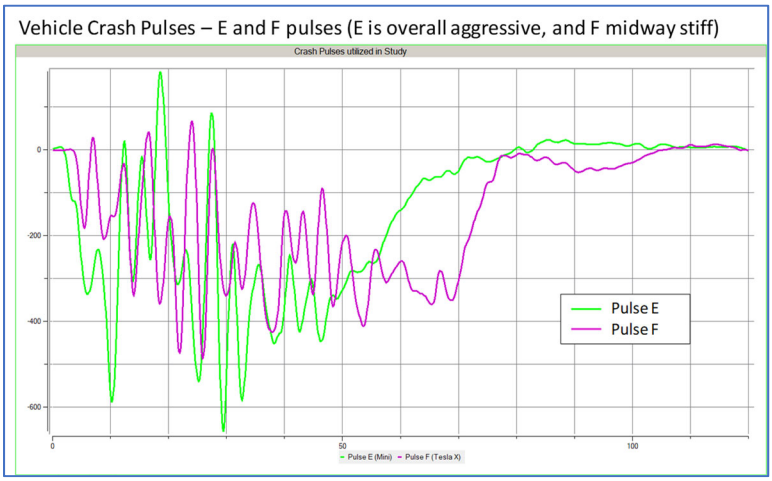

(b)

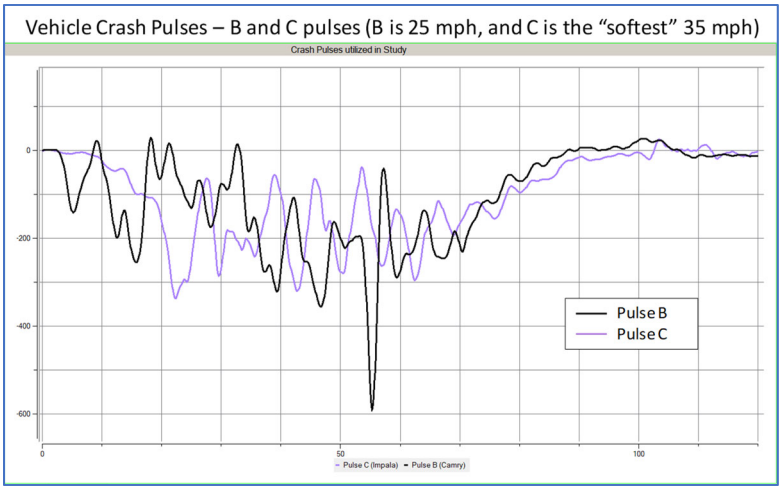

(c)

Figure A1. Overlays of the six simulation crash pulses (2 per graph).

APPENDIX B – Belt Pay-out amounts clustered per restraint technology

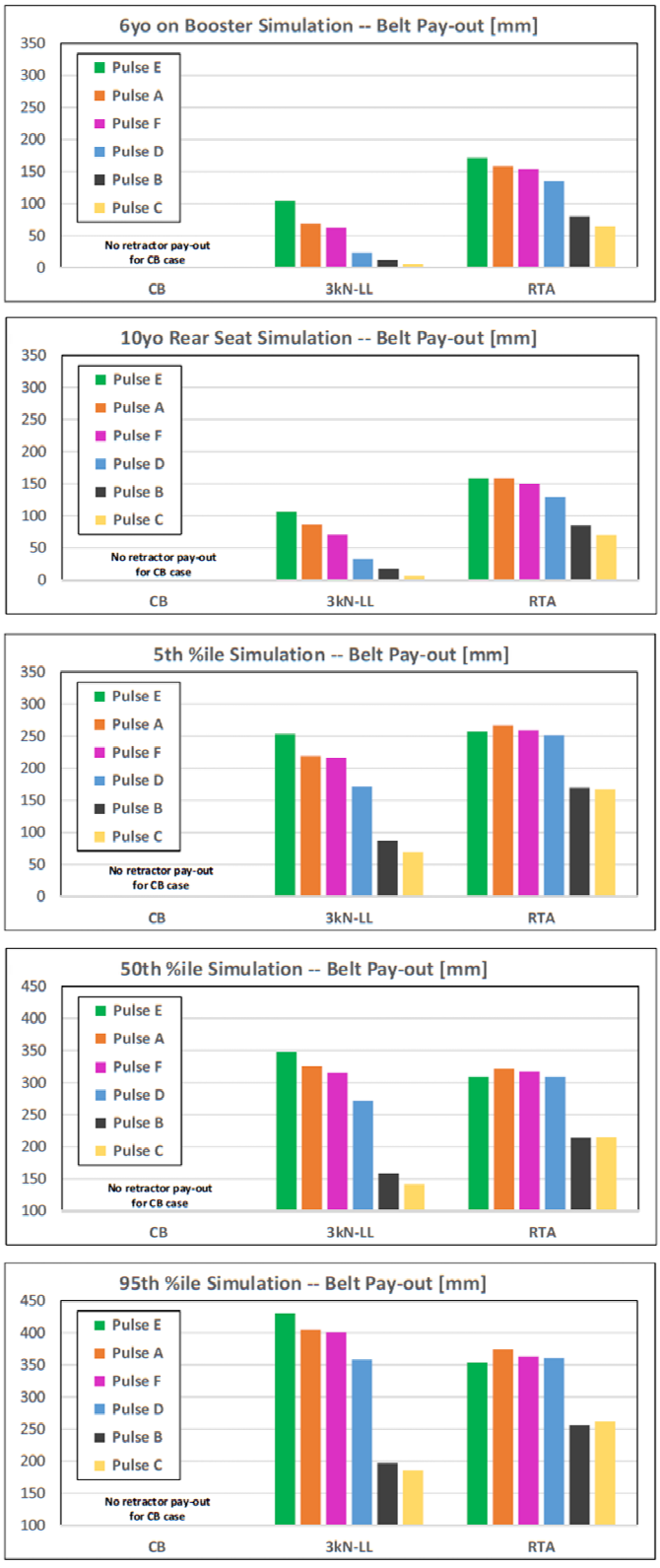

Figure B1. Simulation results – seatbelt pay-out amounts.

APPENDIX C – Shoulder belt seatbelt loads

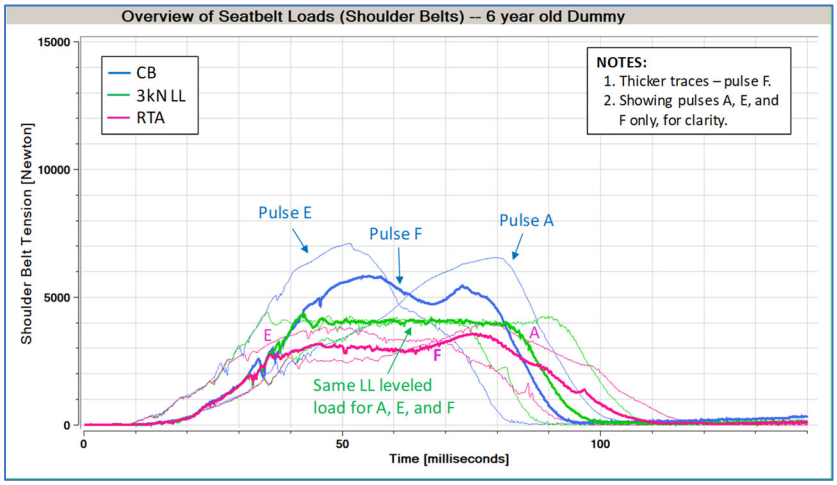

(a) HIII 6YO shoulder belt results.

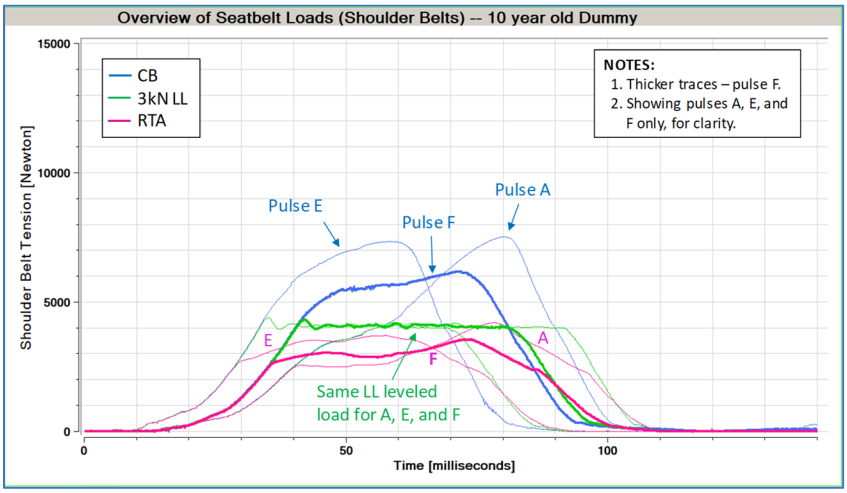

(b) Q10 shoulder belt results.

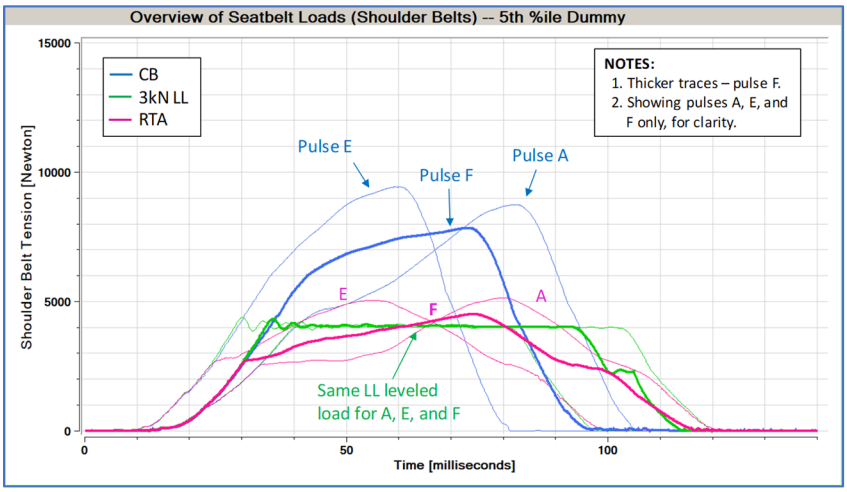

(c) HIII 5th percentile shoulder belt results.

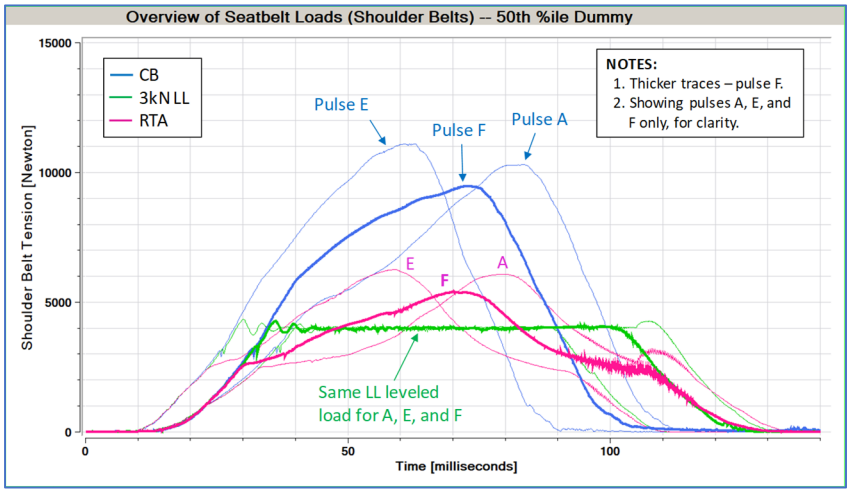

(d) HIII 50th percentile shoulder belt results.

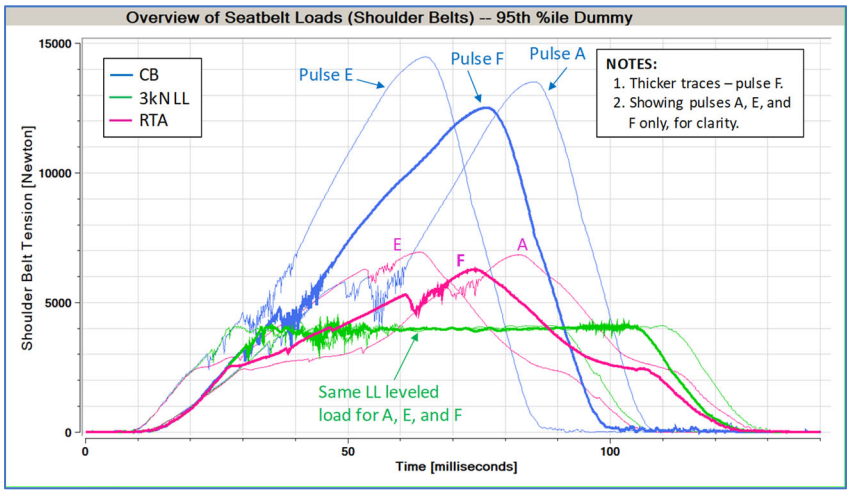

(e) HIII 95th percentile shoulder belt results.

Figure C1. Simulation results – shoulder belt loads.

APPENDIX D – Sample MADYMO Control System syntax

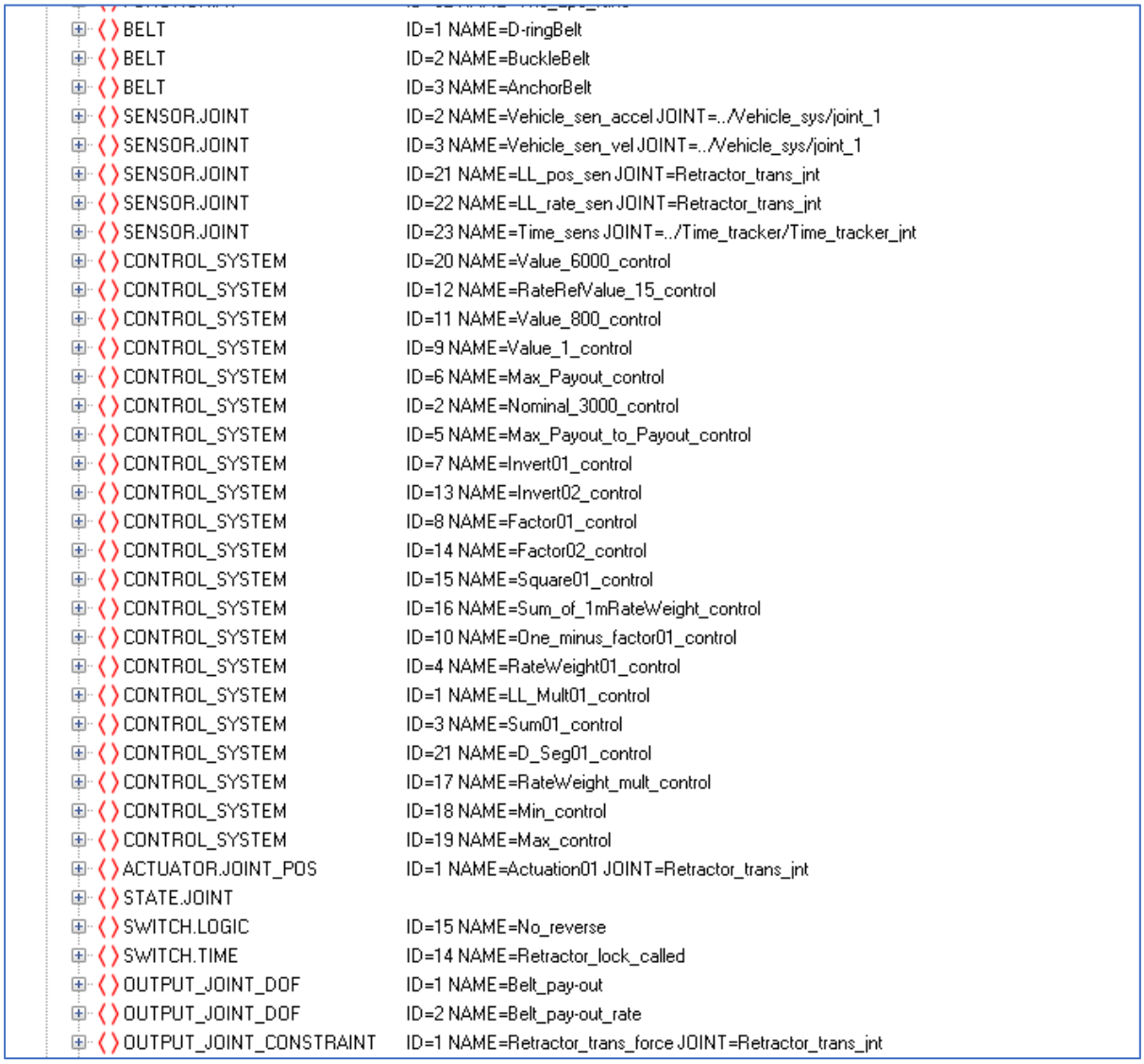

Figure D1. Sample MADYMO Control System syntax for RTA model.

APPENDIX E – TCJ Technology Reference Information

The Tailored Control Joint (or TCJ) Technology is a mechatronic system designed specifically for adaptive load control applications in the translational or rotational modes, and for clutch applications. Development and prototyping efforts currently occur at BGM Engineering, Shelby Township, MI, USA. Established patent rights (US Patent #6,384,518) and Patent Pending rights apply.

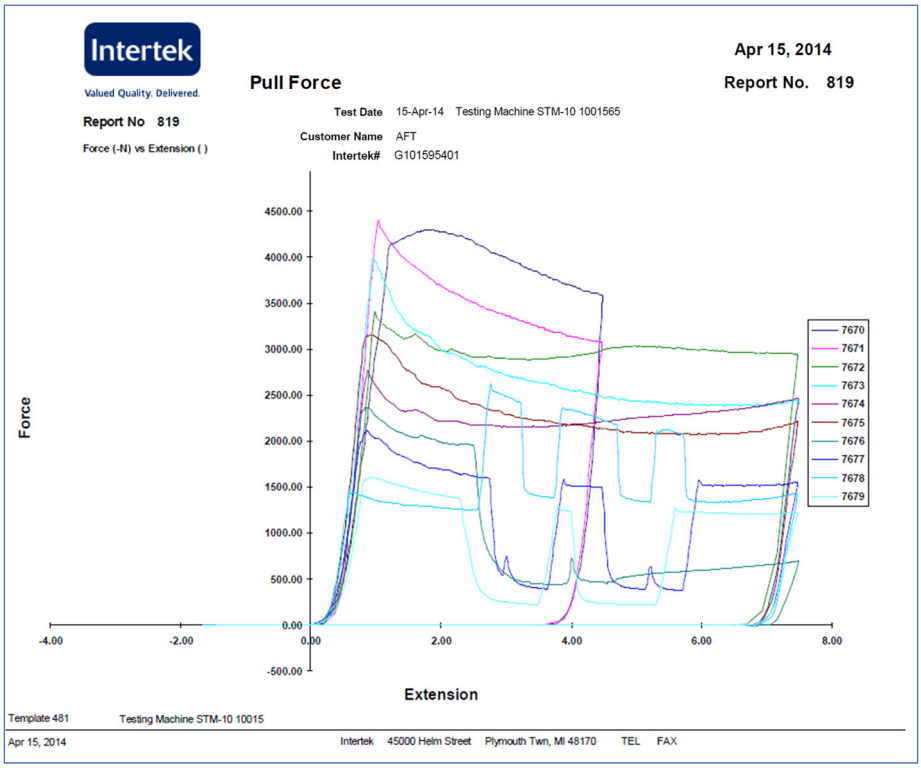

Figure E1. Sample TCJ technology test data conducted at Intertek, Plymouth, MI, USA.

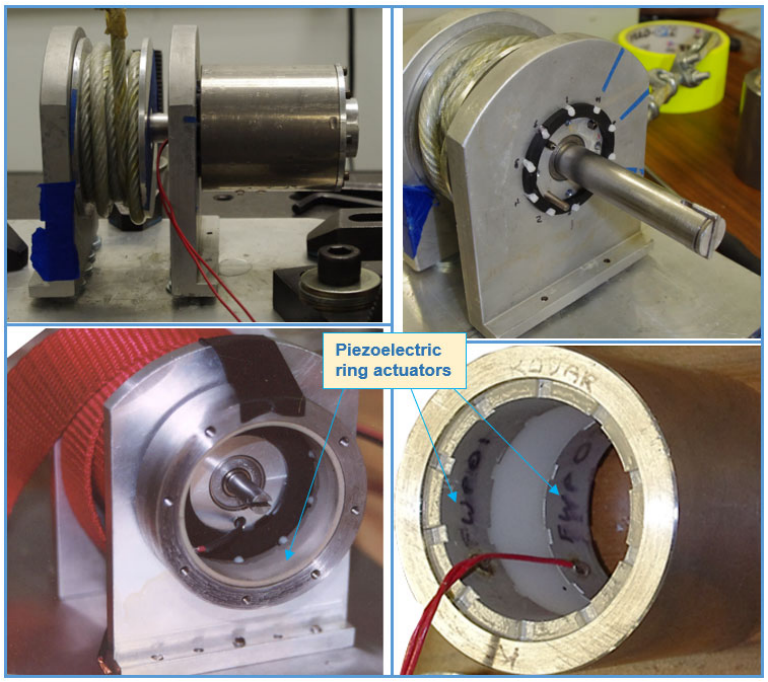

Figure E2. Sample TCJ technology prototypes and components.

CONTRAST BETWEEN ROAD AND ROADSIDE MATERIALS FOR ROAD EDGE DETECTION IN VEHICLE ROAD DEPARTURE MITIGATION SYSTEMS

Qiang Yi
Stanley Chien
Yaobin Chen
Transportation Active Safety Institute, Indiana University-Purdue University, Indianapolis
USA

Rini Sherony
Collaborative Safety Research Center, Toyota Motor North America
USA

Paper Number 19-0058

ABSTRACT

Vehicle roadway departure crashes results in a large number of fatalities in the U.S. Road departure mitigation (RDM) systems rely on the road edge and road boundary identification. Cameras are widely used in RDMS for identifying road edges. The contrast between road and road boundary objects is one of the key image features used by the camera to detect road edges. This paper analyzes and compares the contrasts between various road surfaces and road edges.

INTRODUCTION

Road departure (RD) crashes are frequently severe and account for a large number of fatalities in the United States. According to the report from Federal Highway Administration (FHWA), an annual average of 19,233 fatalities resulted from roadway departure from 2015 to 2017, which is 52 percent of all the traffic fatalities in the United States [1].

A road departure crash is defined as “a non-intersection crash which occurs after a vehicle crosses a road edge line or a center line, or otherwise leaves the traveled way” [2]. To effectively prevent RD crashes, the Federal Highway Administration (FHWA) has developed several strategic approaches and plans, which focus on three objectives: 1) Keep Vehicles on Roadway, 2) Provide for Safe Recovery, and 3) Reduce Crash Severity [1]. While these countermeasures implemented by FHWA are all infrastructures related, the new generation vehicles equipped with road departure mitigation (RDM) systems have been developed and introduced into the market in recent years. Vehicle RDM systems rely on sensors to detect the road edge or roadside objects [3, 4]. Three key sensors are used to detect the road edges, including camera, radar, and LIDAR. For the low-profile roadside objects, including grass, curbs, and gravel, the cameras are widely used in RDM systems. In general, camera sensors use multiple features for object recognition. The contrast between road and road boundary objects is one of the key image features, which could significantly affect the detection of the road edges [5, 6].

To support the evaluation of the RDM systems and help to improve the performance of RDM systems, a set of roadside surrogate objects have been developed by the Transportation Active Safety Institute (TASI) at Indiana University-Purdue University Indianapolis (IUPUI) [7-9]. The requirements for these objects are that they should have the same characteristics of the real U.S. roadside objects from the viewpoint of automotive sensors. This paper analyzes and compares the contrasts between various road surfaces and the low-profile roadside objects, including green grass, yellow grass, curbs, and gravels.

Google street view is used to gather the samples of the road and roadside objects in the United States. 24,762 randomly sampled road locations with street view images were used in this study. The road surface and road edge types of all these 24, 762 locations were identified. Considering only the images in which the roads do not have

clear road edge marking, 2,295 samples with green grass, 927 samples with yellow grass, 3,965 samples with curbs, and 771 samples with gravel were examined.

The contrast is defined as a function of gray levels of the road surface (new asphalt, old asphalt, concrete, and others) and roadside object (gravel, green grass, yellow grass, curb). A larger absolute contrast number means a higher contrast. Negative contrast number means that the road is brighter than the roadside; positive contrast number means that roadside is brighter than the road. Histograms are used to describe the sample distribution with respect to the contrast for each combination of the road surface and roadside.

THE ROADSIDE OBJECTS DATASET

Google Street View is used to gather the road/roadside object images in the U.S. The whole processing is shown in Fig. 1. 824,957 road locations in the U.S. were randomly sampled (including Hawaii and Alaska). Since these locations have significantly biased distributions such as concentration in small roads in the large rural areas, a stratified sub-sampling was conducted with the balancing consideration of road levels, geographic locations, and population densities. As a result, 44,000 stratified locations were generated. In our research, the high-resolution satellite top-view images and street-view images of these 44,000 road locations were purchased. Since the top-view images cannot provide sufficient resolution to determine roadside objects and analyze the contrast between roads and roadside objects, the street-view images at these locations were searched. However, only 24,762 out of 44,000 locations have street-view images, which are used in this study [8, 9].

Unlike the lane departure warning (LDW) system that uses the road marking to detect the road or lane markings, RDM systems detect the road edges without road markings or with obscure road markings. Thus, only the locations without road marking or with unclear road marking were considered in this study. As a result, a total 7,958 out of 24,762 locations have the low-profile roadside objects and do not have road makings or have unclear road markings. Among them, 2,295 samples have green grass roadside, 927 samples have yellow grass roadside, 3,965 samples have curbs, and 771 samples have gravel roadside. It should be noted that high profile roadside objects such as metal guardrails, concrete dividers, and traffic barrels are not studied in this paper.

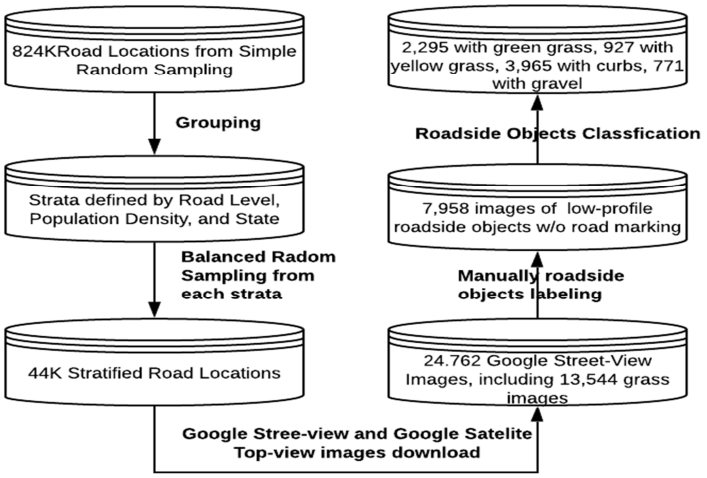

Fig. 1. The process of generating the data set of roadside objects.

THE DEFINITION OF CONTRAST

Contrast study is conducted in grayscale space. It is defined as a function of gray levels of the road surface (e.g., new asphalt, old asphalt, concrete, and others) and roadside object (e.g., gravel, green grass, yellow grass, curb). The calculation is shown in equation (1).

$$Contrast = \begin{cases} \frac{grayValue_{object}}{grayValue_{road}} - 1, & if\ \frac{grayValue_{object}}{grayValue_{road}} \geq 1 \\ -\frac{grayValue_{road}}{grayValue_{object}} + 1, & if\ \frac{grayValue_{object}}{grayValue_{road}} < 1 \end{cases} \quad (1)$$

This definition gives a continuous real number value. A larger absolute contrast number means higher contrast. If the contrast value is 0, it means that the brightness of the road boundary and road are the same (no contrast). If the contrast value is greater than 0, the roadside is brighter than the road. If the contrast value is less than 0, the road is brighter than the roadside.

To determine the contrast between the road and road boundary objects on an image, the representative samples on the road and roadside need to be gathered. A graphical user interface (GUI) was developed (shown in Fig. 2) to support manual marking on the road edges and to pick the representative sampling points on the image.

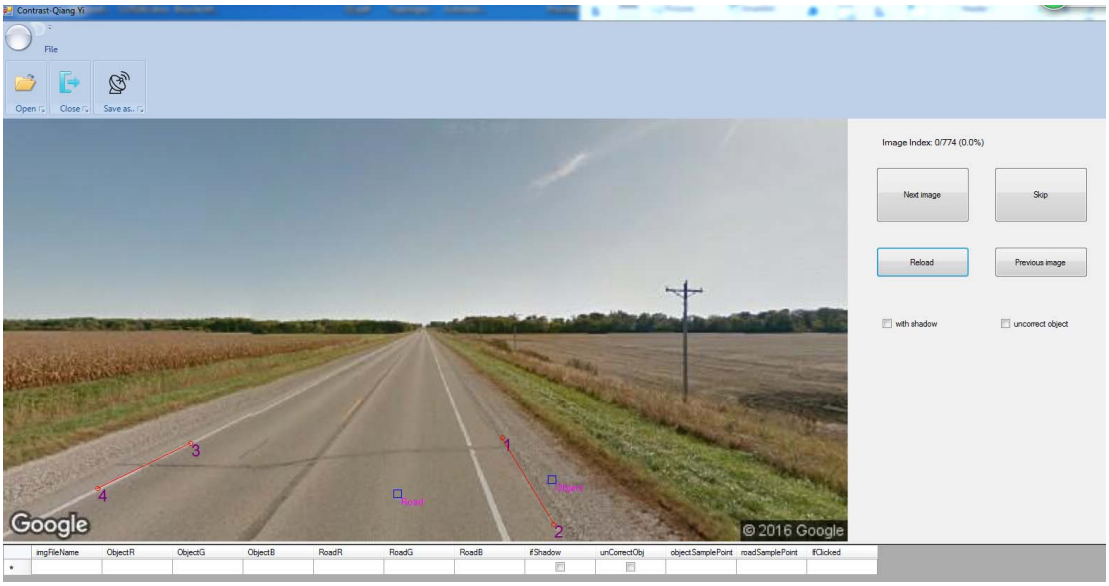

Fig. 2. The GUI for road edges marking and sample point selection.

THE RESULTS AND DISCUSSION

The contrast between roads and the road boundary with green grass

2,295 sample images of roadside green grass, which cover different road levels in the U.S. were used to obtain the contrast between the green grass and the road. Among these 2,295 sample images, 1,969 images have asphalt road, 98 images have a concrete road, and 228 have other types of road. Other types of the road include dirt, gravel, snow-covered road and wet road. It should be noted that the green grass and yellow grass was separately discussed because of their obvious visual differences. The definition of green and yellow grass could be found in [9].

Fig. 3 shows the overall distribution of contrasts of all road samples with the green grass road boundary. The horizontal axis is the contrast value; the vertical axis is the sample count. As shown in this Fig. 3, the contrast varies significantly, spreading from -5.13 to 1.23. The maximum distribution falls in the range of -0.3 to -0.2. Fig. 4 to Fig. 6 show the contrast distributions of the green grass boundary with different road types including asphalt, concrete, and others. The contrast distribution with asphalt road is similar to that of the overall roads. It spreads from -5.13 to 1.23. The range with -0.3 to -0.2 has the highest distribution. Different from that of the asphalt roads, contrasts between concrete roads and green grass roadside concentrate on the range of -0.65 to -0.25. They cover 62.2% of the concrete roads. The distribution of contrasts between green grass roadside with other types of roads including dirt,

gravel, snow-covered road and wet road shows a similar tendency with the overall distribution, but it is more concentrated. About 62.7% of the other types of road fall in the range of -0.6 to -0.2.

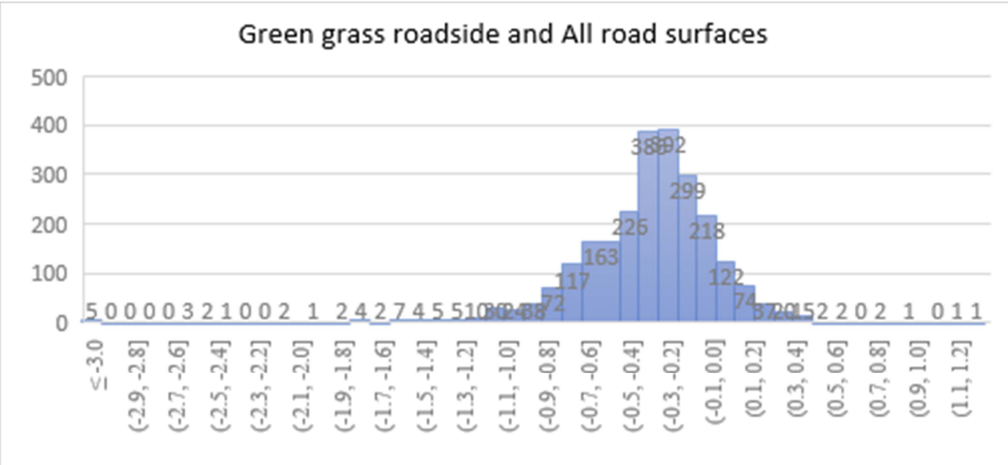

Fig. 3. The distribution of contrasts between all roads and green grass road boundaries.

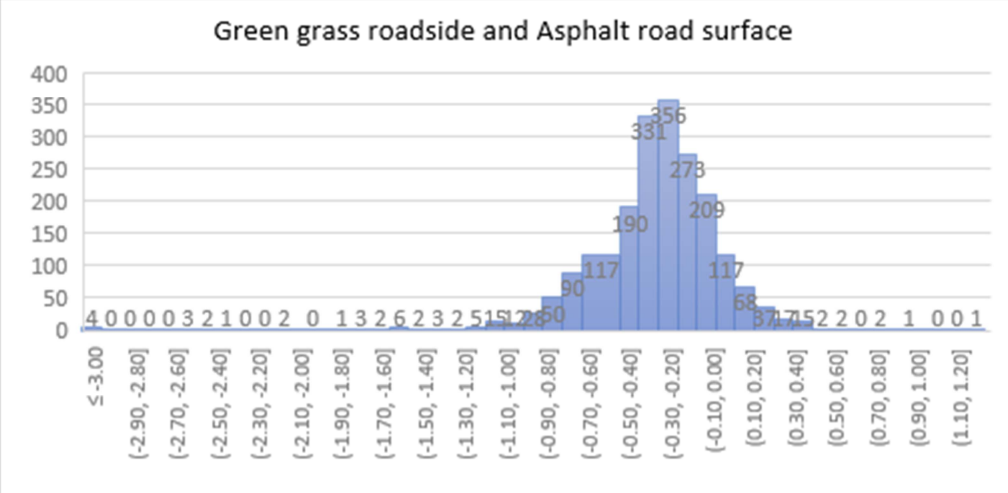

Fig. 4. The distribution of contrast between asphalt roads and green grass road boundaries.

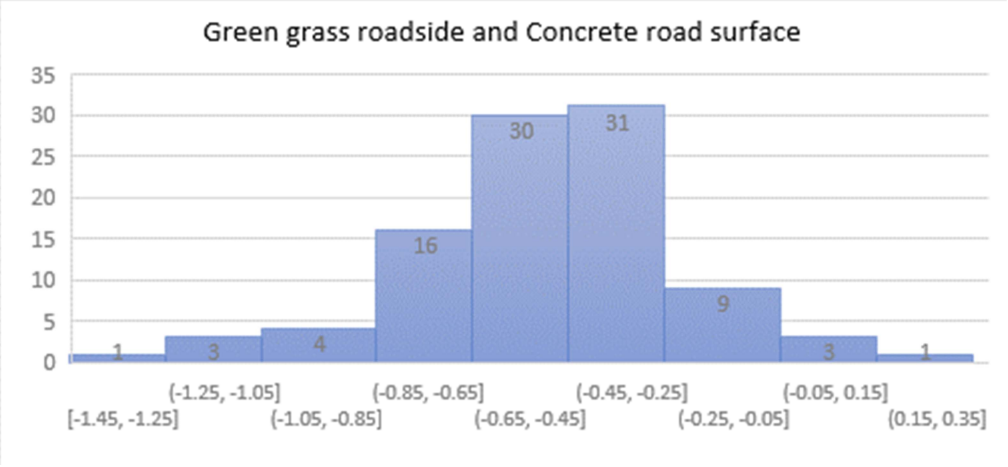

Fig. 5. The distribution of contrasts between concrete roads and green grass road boundaries.

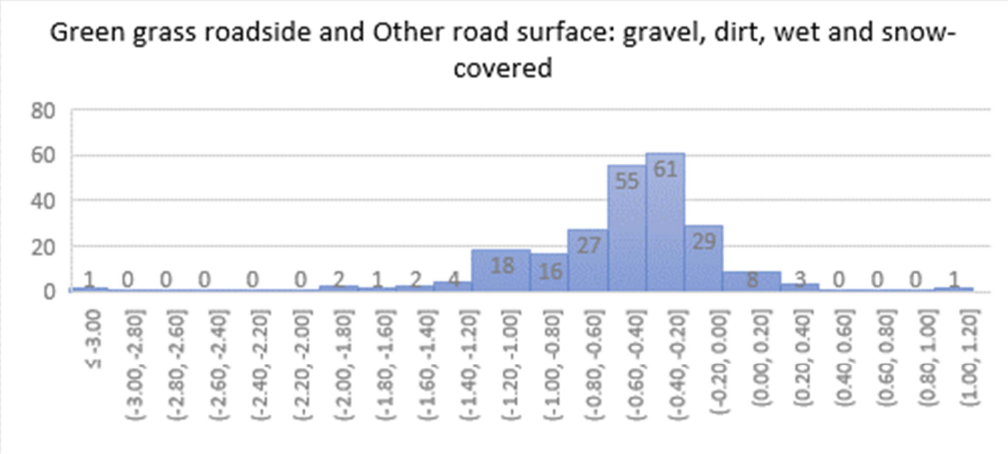

Fig. 6. The distribution of contrasts between other road types (including dirt, gravel and wet) and green grass road boundaries.

The contrast between all roads and the road boundary with yellow grass

927 sample images with yellow grass roadside were used to obtain their contrast. Among them, 827 images are with asphalt road, 14 images are with concrete road, and 86 with other types of road, including dirt, gravel, and wet road.

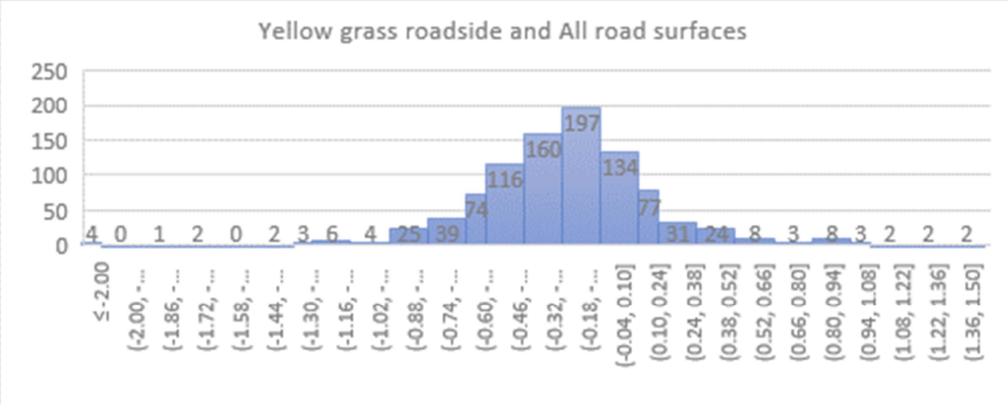

Fig. 7. The distribution of contrasts between all roads and yellow grass road boundaries.

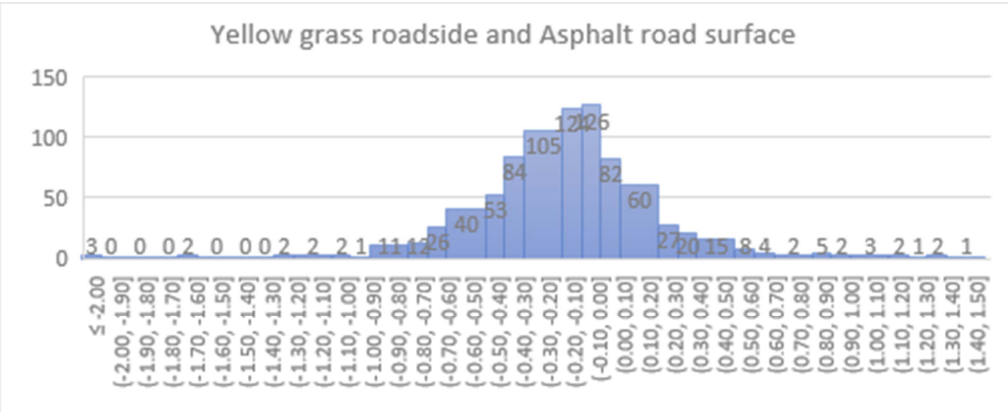

Fig. 8. The distribution of contrasts between asphalt roads and yellow grass road boundaries.

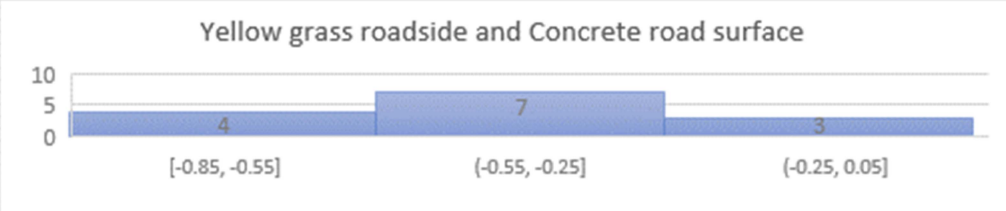

Fig. 9. The distribution of contrasts between concrete roads and yellow grass road boundaries.

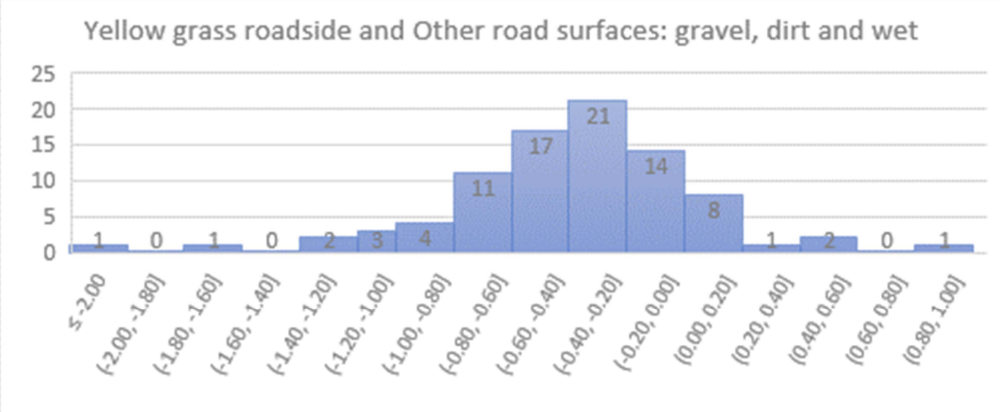

Fig. 10. The distribution of contrasts between other road types and yellow grass road boundaries.

The overall contrast distribution is shown in Fig. 7. It is similar to green grass, but the range is much narrower and more concentrated. The range varies from -2.27 to 1.47. The maximum distribution falls in the range of -0.18 to -0.04. Fig. 8 to Fig. 10 show the contrast distribution of different road types with yellow grass roadside. For the asphalt, the range -0.3 to 0 covers 42.9% of the asphalt roads. For the concrete road, only 14 samples are found. The contract varies from -0.85 to -0.04. For other types of road, the highest frequency is in the range of -0.4 to -0.2.

The contrast between roads and curbs

Curb is the most common road edge in the U.S. without considering road edge marking. 3,965 images were used to obtain the contrast between the roads and curb. Among them, 3,673 images have asphalt roads, 248 images have concrete roads, and 44 images have other types of roads (including dirt, gravel, and wet road). Fig. 11 shows the distribution of contrast in all 3,965 samples. The range spreads from -3.81 to 2.66. The highest portion is in the range of 0.1 to 0.2. The asphalt road has the same distribution with the maximum distribution in the range of 0.1 to 0.2 (shown in Fig. 12). The contrast between curbs and concrete roads is low, and the highest portion goes to 0 to 0.1 (shown in Fig. 13). For other road types, the range of -0.1 to 0.3 covers 52.3 % of samples (see Fig. 14).

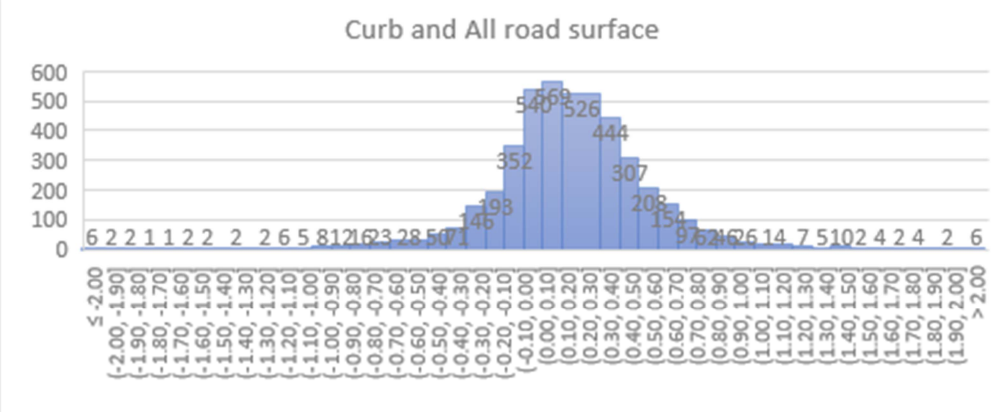

Fig. 11. The distribution of the contrast between all roads and curb road boundaries.

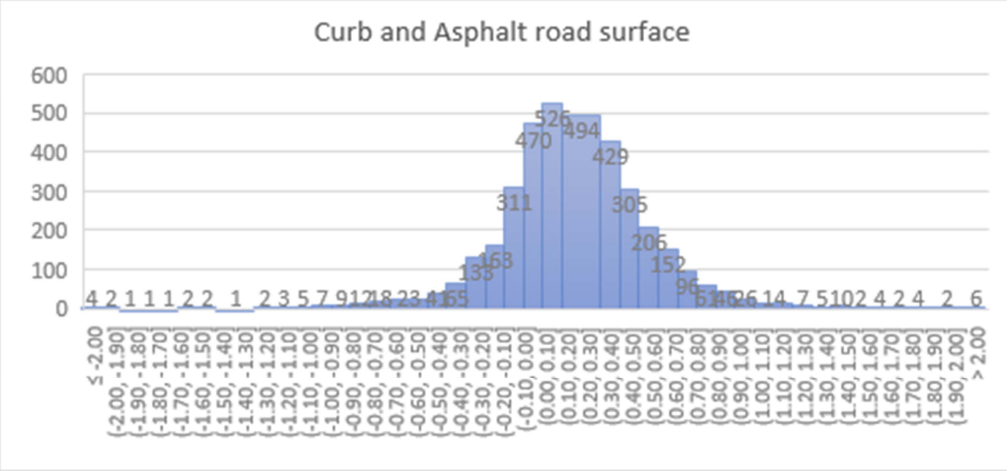

Fig. 12. The distribution of contrasts between asphalt roads and curb road boundaries.

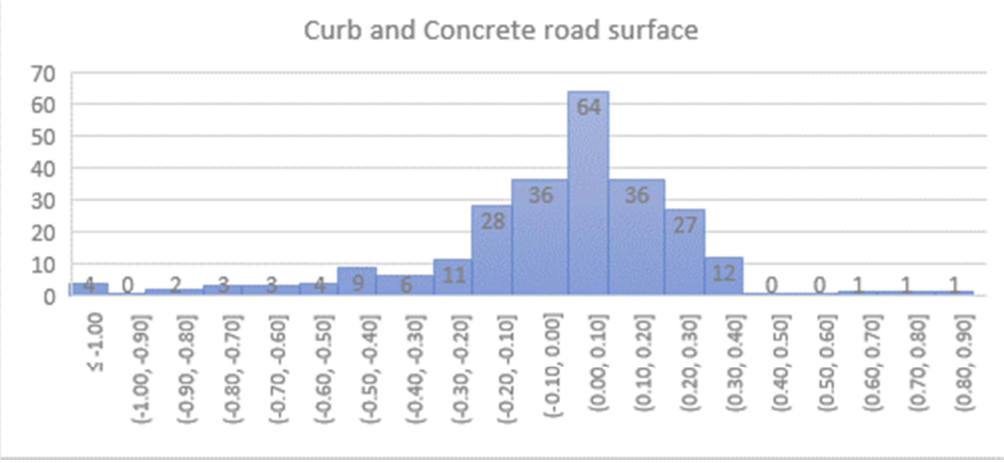

Fig. 13. The distribution of contrasts between concrete roads and curb road boundaries.

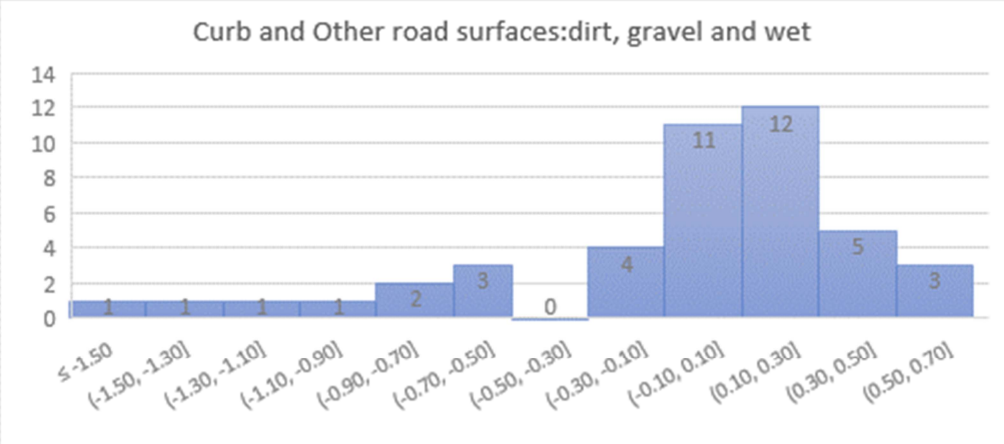

Fig. 14. The distribution of contrasts between other road types and curb road boundaries.

The contrast between the road and the gravel road boundary

771 sampled images with gravel road boundary were used to obtain the contrast. Among them, 698 images have asphalt road, 60 images have concrete roads, and 13 have other types of roads (including dirt, gravel, and wet road). Fig. 15 shows the overall contrast distribution. Comparing with other road boundaries, the contrast between all roads and gravel roadside is relatively low. The range varies from -1.73 to 2.02. The maximum distribution is in the range of -0.1 to 0. Fig. 16 to Fig. 18 show the contrast distribution of curb with asphalt, concrete, and other road types, respectively. The highest distributions are 0.1-0.2, -0.13-0.07 and 0.27-0.23, respectively.

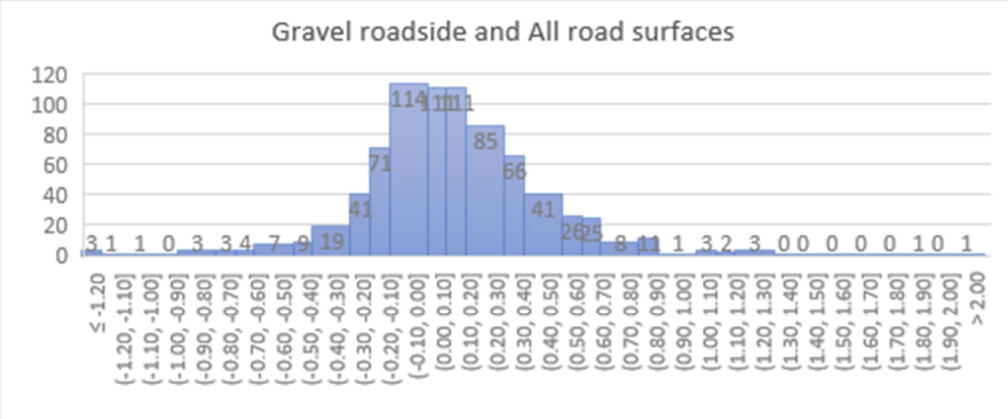

Fig. 15. The overall distribution of contrasts between roads and gravel road boundaries.

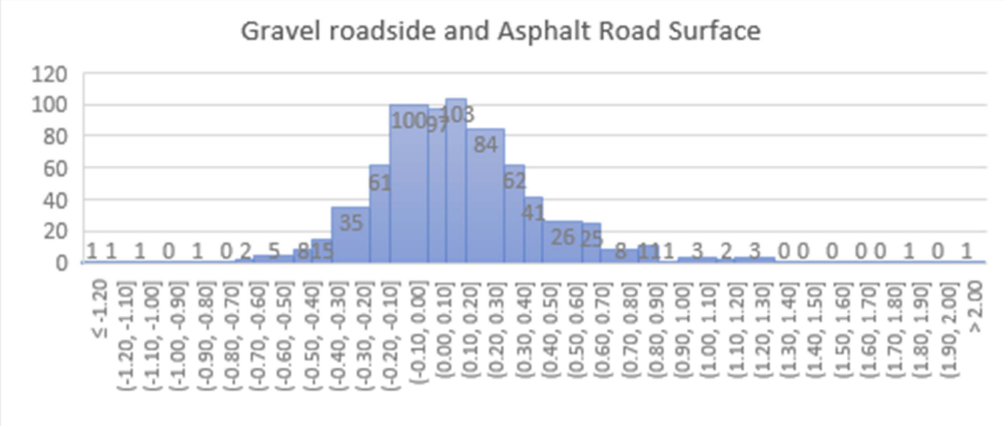

Fig. 16. The distribution of contrasts between asphalt roads and gravel road boundaries.

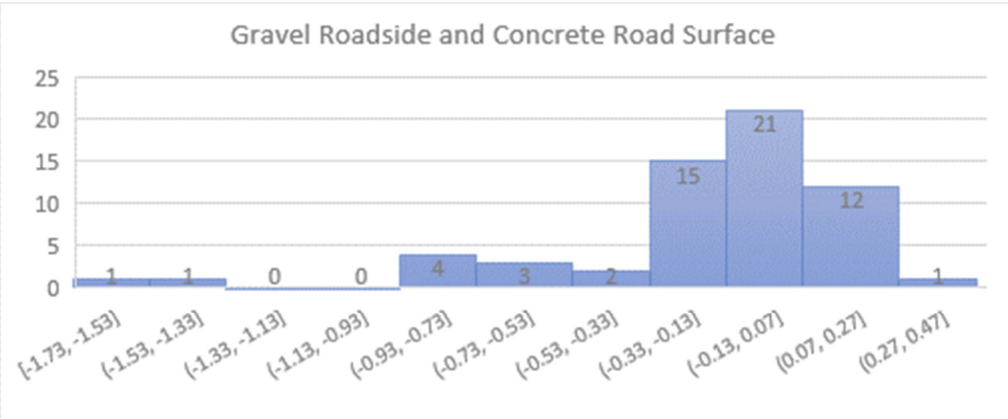

Fig. 17. The distribution of contrasts between concrete roads and gravel road boundaries.

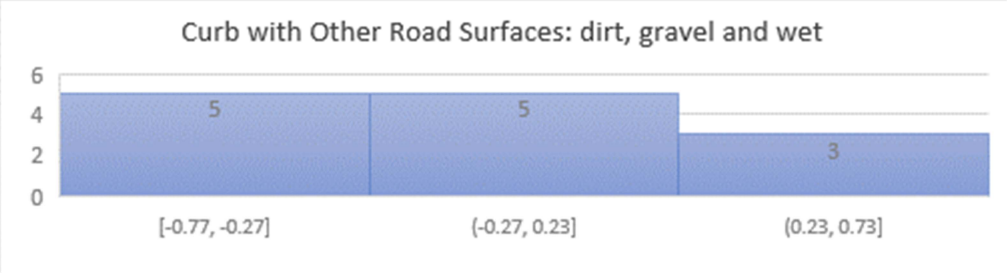

Fig. 18. The distribution of contrasts between other road types and gravel road boundaries.

CONCLUSIONS

This paper provides a contrast definition for analyzing the contrast between various road surfaces and the commonly seen low-profile roadside objects. Contrast values were surveyed based on randomly sampled 7,958 Google street-view images. The range and distribution pattern of contrast between the combination of the road surfaces and roadside were obtained and discussed.

The contrast of asphalt roads and green grass roadsides spreads from -5.13 to 1.23, but most frequently seen contrast is between -0.3 and -0.2. The contrast of concrete roads and green grass roadside spread from -0.45 to 0.15 with 62.2% concentrates between -0.65 and -0.25. The contrast between the concrete road and the curb is from -1 to 0.4 with the majority between -0.2 and 0.2, that means small or no contrast. The most frequently seen contrast of old asphalt road and yellow grass is in the range of -0.1 to 0. Table 1 is a summary of contrast range between different road surfaces and roadside object types, which covers the highest percentage of the samples in descending order. A positive value means that the roadside is brighter than the road. A negative value means that the road is brighter than the roadside.

Table 1.
Summary of the contrasts between road surfaces and roadsides

	Asphalt road	**Concrete road**	**Other roads**	**Note**
Green grass	[-0.3, -0.2]	[-0.45, -0.25]	[-0.4, -0.2]	Road is brighter
Yellow grass	[-0.1, 0]	[-0.55, -0.25]	[-0.4, -0.2]	Road is brighter
Gravel	[0.1, 0.2]	[-0.13, 0.07]	[-0.77, 0.27]	Similar to road
Curb	[0.1, 0.2]	[0, 0.1]	[0.1, 0.3]	Curb is brighter

ACKNOWLEDGMENT

This research was sponsored by the Toyota Collaborative Safety Research Center.

REFERENCES

[1] “Roadway Departure Safety.” https://safety.fhwa.dot.gov/roadway_dept/. March 2019.
[2] “Roadway Departure Countermeasures,” https://safety.fhwa.dot.gov/roadway_dept/rdctrm.cfm. March 2019.
[3] Katzourakis, D.I., de Winter, J.C., Alirezaei, M., Corno, M. and Happee, R., "Road-departure prevention in an emergency obstacle avoidance situation." IEEE transactions on systems, man, and cybernetics: systems 44, no. 5 (2014): 621-629.
[4] Gray, A., Ali, M., Gao, Y., Hedrick, J. and Borrelli, F., "Semi-autonomous vehicle control for road departure and obstacle avoidance." IFAC control of transportation systems (2012): 1-6.
[5] Charbonnier, P., Nicolle, P., Guillard, Y. and Charmer, J., 1998, September. "Road boundaries detection using color saturation." 9th European Signal Processing Conference (EUSIPCO), pp. 1-4. IEEE, 1998.
[6] Kong, H., Audibert, J.Y. and Ponce, J., 2010. "General road detection from a single image." IEEE Transactions on Image Processing 19, no. 8 (2010): 2211-2220.
[7] Qiang Yi, Dan Shen, Jun Lin, Stanley Chien, and Rini Sherony, "The Color Specification of Surrogate Roadside Objects for the Performance Evaluation of Roadway Departure Mitigation Systems," SAE Technical Paper 2018-01-0506, 2018, doi: 10.4271/2018-01-0506.

[8] Dan Shen, Jun Lin, Qiang Yi, Renran Tian, Stanley Chien, Rini Sherony, "Roadside Boundaries and Objects for the Development of Vehicle Road Keeping Assistance System," SAE Technical Paper 2018-01-0508, 2018, doi: 10.4271/2018-01-0508.

[9] Qiang Yi, Dan Shen, Jun Lin, Stanley Chien, Lingxi Li, Yaobin Chen, Rini Sherony, “Color and Height Characteristic of Surrogate Grass for the Evaluation of Vehicle Road Departure Mitigation System,” 2019 SAE World Congress, Detroit Michigan, April 2019, SAE Technical Paper 2019-01-1026 .

DETERMINE CHARACTERISTICS REQUIREMENT FOR THE SURROGATE ROAD EDGE OBJECTS FOR ROAD DEPARTURE MITIGATION TESTING

Stanley Chien
Qiang Yi
Jun Lin
Abir Saha
Lin Li
Yaobin Chen
Indiana University-Purdue University Indianapolis
USA

Chi-Chih Chen
Ohio State University
USA

Rini Sherony
Collaborative Safety Research Center, Toyota Motor North America
USA

Paper Number 19-0059

ABSTRACT

Road departure mitigation system (RDMS), a vehicle active safety feature, uses road edge objects to determine potential road departure. In the U.S., 45%, 16%, and 15% of car-mile (traffic flow * miles) roads have grass, metal guardrail, and concrete divider as road edge, respectively. It is difficult to test RDMS with real roadside objects. Lightweight and crashable surrogate roadside objects that have representative radar, LIDAR and camera characteristics of real objects have been developed for testing. This paper describes the identification of automotive radar, LIDAR, and visual characteristics of metal guardrail, concrete divider, and grass. These characteristics will be referenced for designing and fabricating the representative surrogate objects for RDMS testing. Colors and types of the roadside objects were identified from 24,735 randomly sampled locations in the US using Google street view images. The radar and LIDAR parameters were measured using 24GHz/77GHz radar and 350-2500nm IR spectrometer.

Metal guardrail: The peak 24GHz RCS (Radar Cross Section) of W-beam and I-beam of guardrail are 10dB and 13dB. The peak 77GHz RCS for W and I-beam are 15dB and 20dB. When the radar beam direction is not perpendicular to the metal guardrail surface, the reflectivity decreases significantly. As the illumination/measurement angle increases from 0 to 70°, the IR reflectance of metal guardrail decreases from 1.3 to 0.1, and the variation among samples decreases from 1.5 to 0.05. The age of the metal guardrail does not affect the RCS if steel rust is not present.

Concrete divider: Both 24GHz and 77GHz radar reflectivity are -7.3dB. The age of the concrete divider does not affect the radar reflectivity, but the surface smoothness and material affect the reflectivity. As the illumination/measurement angle increases from 0 to 70°, the IR (Infrared) reflectance of concrete divider increases by only 0.1.

Grass: The peak 77GHz RCS is -18dB at 10° depression angle. Different kinds of grass (wild vs. maintained, short vs. long, even vs. uneven) have similar RCS value when measured under the same conditions (same radar type, same polarization, and same pitch angle. Same grass field will produce different RCS during different seasons or after rain where the moisture content of grass produces different reflectivity. As the illumination/measurement angle increases from 0 to 70°, the IR reflectance of grass increases from 0.1 to 1 and the variation among samples increases from 0.2 to 1. The most representative grass road-edge is uneven yellow/green mixed short grass followed by even green and short grass. 18 most occurring grass color patterns were selected.

INTRODUCTION

According to the U.S Department of Transportation Federal Highway Administration, over half of the fatal vehicle crashes were related to road departure [1]. A vehicle road-departure crash is defined as when the vehicle moves from the road to the roadside and consequently leads to a crash [2, 3]. Road departure warning (RDW) and road keeping assistance (RKA) [4-12] are the new technology for reducing road departure crashes [13, 14]. The road departure detection can be based on the recognition of road edge markings. However, many US roads do not have road edge marking or clear road edge marking. Therefore, road edge detection needs to rely on the detection of roadside objects, such as grass, concrete divider, metal guardrail, etc. As RDW and RKA technologies are based on the detection of a roadside object, their performances need to be tested with the roadside objects. The performance testing of the RDW and RKA cannot be on the road with real roadside objects. Testing the RKA on the road with a real concrete divider or real metal guardrail is quite difficult. Testing the RDA on the road with grass road edge is also difficult. The test track may not have a proper grass road edge for RKA tests. To support the performance testing of RDW and RKA, surrogate roadside objects need to be developed so that the test can be performed on the test track repeatedly. Transportation Active Safety Institute (TASI) of Indiana University–Purdue University Indianapolis (IUPUI) studied the development of surrogate roadside objects for RDW and RKA testing with the support of Toyota Collaborate Safety Research Center (CSRC). This paper summarizes the representative shape, color, radar, LIDAR characteristic of the commonly seen roadside objects, such as concrete divider, metal guardrail, and grass. These characteristics can be used as the characteristics requirements for designing and fabricating the object surrogates. The design and fabrication of object surrogates are not in the scope of this paper and will be described in other papers.

MOST COMMON ROADSIDE OBJECTS

In our previous study [15], we sampled 24,762 Google Street view locations all over the United States. Based on location counts, we found that 55% locations have grass edge, 16% locations have concrete curbs, 8.68% locations have a metal guardrail, and 4.17% locations have the concrete divider as the road boundary. If we consider the traffic density on these locations (based on car-miles), we found that 44.6% locations have grass edge, 9.9% locations have concrete curbs, 16.1% locations have metal guardrails, and 15.3% locations have concrete dividers as the road boundary. Since concrete curb is mostly on the city roads with low-speed limits and RDW and RKA are mainly designed for roads with higher speed limits, metal guardrail, concrete divider, and grass road edges are the most common road edges detected by RDW and RKA. Since camera, 24 GHz and 77GHz radar, and automotive 800-1100 nm LIDAR are the most common sensors used for object detection in vehicle active safety, the scope of this paper is to present the representative characteristics of metal guardrail, concrete divider, and grass in the view of the camera, 24 GHz and 77GHz radar, and automotive 800-1100 nm LIDAR.

SPECIFICATIONS OF SURROGATE METAL GUARDRAIL

Physical Shape of the Representative Metal Guardrail

In aforementioned 24,735 randomly sampled road locations in the US, 2150 locations have various types of metal guardrails on the roadside. 81% of these 2,150 metal guardrails has horizontal W-beam with I-beam support (Fig. 1). The representative shape specifications of W-beam and I-Beam in the US can be found in [16]. The representative RGB color of the metal guardrail is (138,139,139) [17]. The physical shape specification of metal guardrail in other countries may be different.

RGB	Range (10% brightness)	
138, 139, 139	168, 168, 168	112, 113, 112

Fig. 1. Representative metal guardrail W-beam (left), and color (right).

Radar Characteristics Specifications of Representative Metal Guardrail

Since the metal guardrail surrogate is composed of the W-beam surrogate and the I-beam surrogate, the 24GHz and 77GHz RCS of five W-beams and I-beams were measured. The objects were placed on a rotating table, and their RCS at various angles were measured. The representative RCS of these objects are plotted in Fig. 2 to Fig. 5. Arrows in these figures and orientation of these objects show the viewing angles of the W-beams (blue) or I-beams (gray). The important RCS values that show the characteristics of the objects with respect to the viewing angles are circled. A variation of ±2dB for each circled value is observed with different samples. It was found that the age of the guardrail has little effect on their RCS values (assume the guardrail is not rusted).

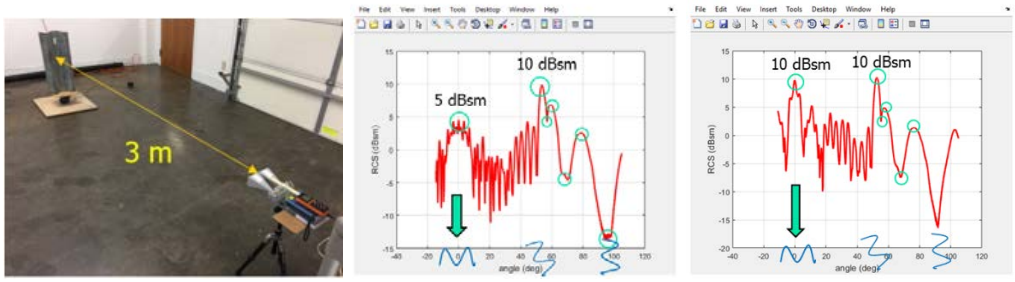

Fig. 2. 24GHz RCS of W-beam. Measurement (left), vertical polarization (middle) horizontal polarization (right).

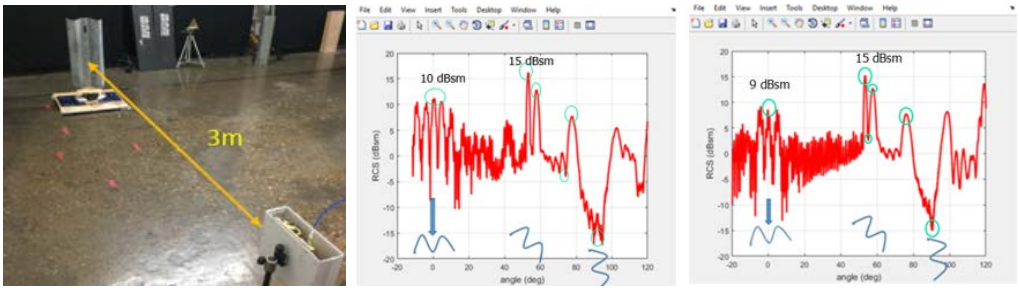

Fig. 3. 77GHz RCS of W-beam. Measurement (left), vertical polarization (middle) horizontal polarization (right).

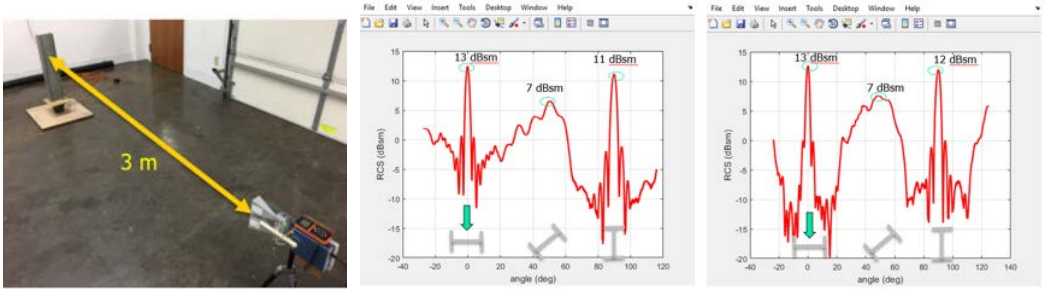

Fig. 4. 24GHz RCS of an I-beam. Measurement (left), vertical polarization (middle), horizontal polarization (right).

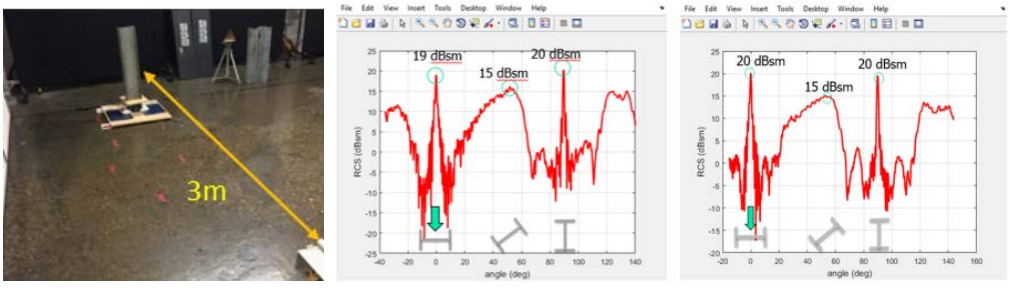

Fig. 5. 77 GHz RCS of an I-beam. Measurement (left), vertical polarization (middle), horizontal polarization (right).

LIDAR Characteristics of Representative Metal Guardrail

There is not a standard laser wavelength for the automotive LIDAR. Common automotive Lidar's wavelengths are in the range of 800-1100nm. We used a spectrometer to measure the diffusive reflectivity of 4 galvanized metal surface samples at various viewing angles. The light source and the measurement probe were put as close as possible to mimic the LIDAR operation. Multiple points on each sample surface were measured. Fig. 6 shows the upper and lower boundaries of the representative IR reflectivity of metal guardrail surface in various laser wavelengths at various measurement angles. 0 degree means that the LIDAR beam is perpendicular to the surface being measured. Since the IR reflectivity variation is small and we do not have a large sample set, the upper bound is the measured maximum reflectivity value plus 0.02, and the lower bound is the measured minimum reflectivity value minus 0.02. It can be seen that the IR reflectivity of the metal guardrail decreases as the viewing angle is getting away from the perpendicular direction to the measured surface. The diffusion reflectively is only applicable for diffusion surface and should be less than 1 in concept. However, the metal guardrail shows the specular reflection property when measured in low angles (0 to 15 degrees) and shows the diffusion reflection property when measuring in high angles (20 degrees and up).

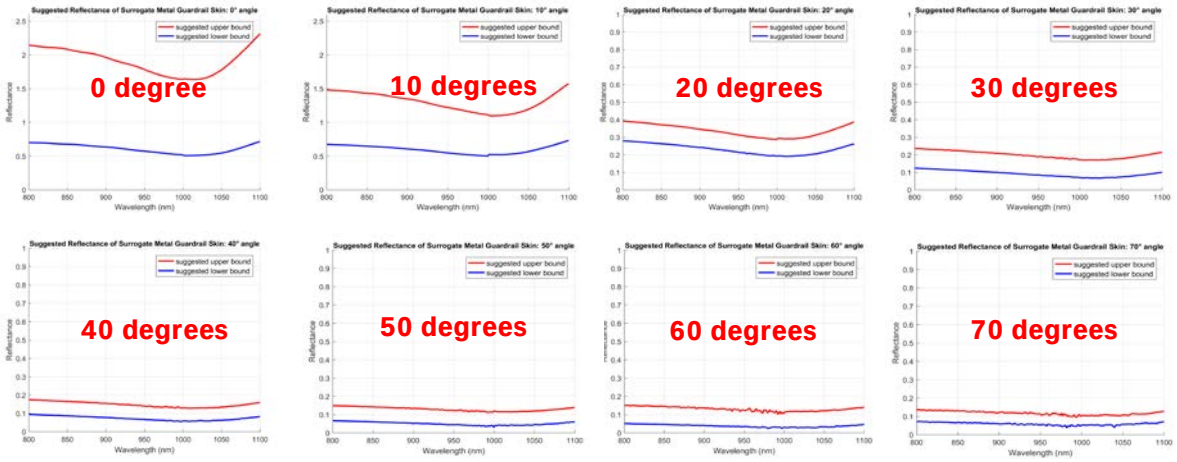

Fig. 6. Suggested IR reflectance range of metal guardrail surface from various viewing angles.

SPECIFICATIONS OF CONCRETE DIVIDER AND CURB SURROGATES

Physical Shape of the Representative Divider and Curb

Concrete curb has many different shapes. In aforementioned 24,735 randomly sampled road locations obtained from Google Street View images, 66% of the 856 concrete dividers observed are in F shape, New Jersey, and single slop shapes. We selected F-shape as the representative shape of the concrete divider. The representative shape specifications of F-shape concrete divider and curb in the US are shown in Fig. 7 [15]. The representative RGB color of concrete divider and curb in the US is (168, 161, 149) [17]. The representative shape and color of the concrete divider in other countries may be different.

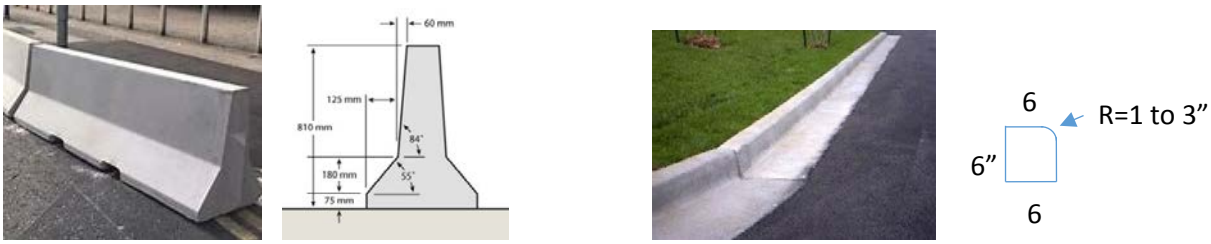

Fig. 7. Standard dimensions F-shaped concrete divider (left) curb (right).

Radar Characteristics of Representative Concrete Divider and Curb

Since the concrete divider has a large flat surface, its radar characteristics cannot be described by RCS. Therefore, we use the radar reflectivity to describe the radar property of the concrete divider surface. The proper surface reflectivity property and the correct shape of the surrogate will make it have the correct radar property of a real concrete divider. According to the 24GHz and 77GHz radar reflectivity measurements, forward-looking radar cannot detect concrete divider from a depression angle greater than 15 degrees. So all reflectivity measurement is measured with the radar beam perpendicular to the concrete surface. The measurement results of 7 concrete dividers and curbs suggested that both the representative 24GHz and 77GHz radar reflectivity of common smooth concrete divider surface are -7.3±1 dB under dry condition. The average reflectivity of concrete dividers with smooth surfaces are similar. As the surface is damaged with scratches, the reflectivity varies significantly. The radar reflectivity of the concrete surface increases with the increase in humidity. The color, protective coating, and age of the concrete dividers do not affect their radar reflectivity.

LIDAR Characteristics of Representative Metal Guardrail

A spectrometer that covers a large range of laser wavelength was used to measure the diffusive reflectivity of 7 concrete dividers and curbs of various ages at a range of viewing angles. The light source and the measurement probe were put as close as possible to mimic the LIDAR operation. Multiple points in each sample were measured. Fig. 8 shows the upper and lower boundaries of all measurements at various angles, where 0 degree means that the LIDAR beam is perpendicular to the surface being measured. The upper bound is the measured maximum reflectivity value plus 0.05, and the lower bound is the measured minimum reflectivity value minus 0.05. It can be seen that the IR reflectivity of the concrete surface increases as the viewing angle is getting further away from the perpendicular direction to the concrete surface. The concrete surface is diffusive in all viewing angles.

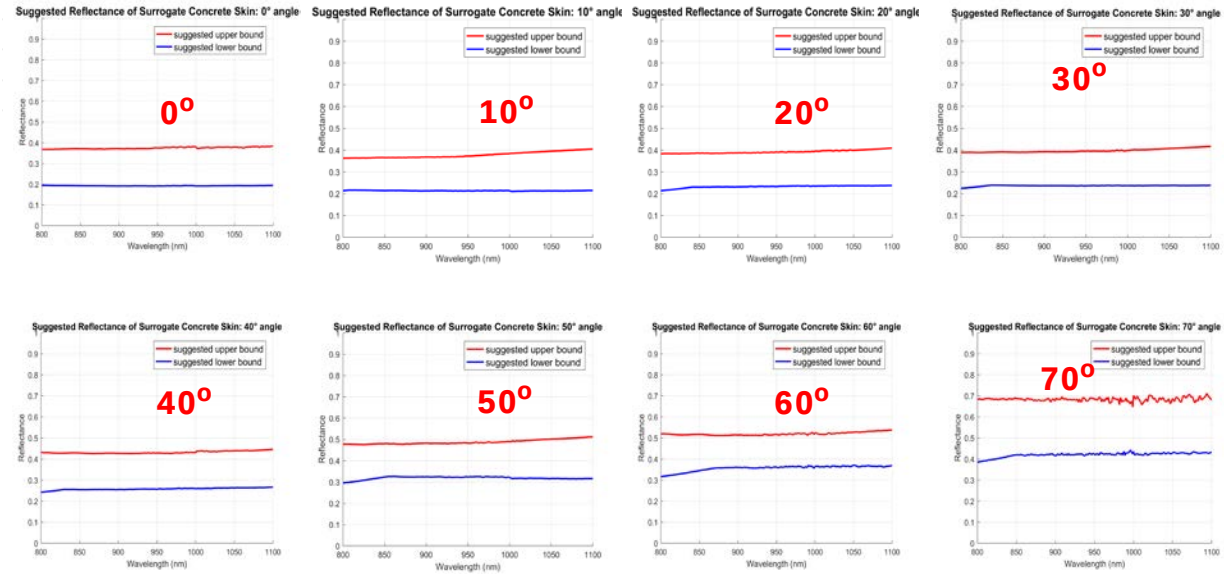

Fig. 8. Representative IR reflectance range of concrete surface from various viewing angles.

SPECIFICATIONS OF GRASS SURROGATES

Height and Color of Representative Grass

In the aforementioned 24,762 Google Street View images, the RGB color of 901 grass images in good weather and not under the shade were studied. The heights of grass in the images were estimated based on over 70 reference road images with known grass height of the grass road edge. The conclusion was that the height of over 80% roadside grass was short (2-4”) or medium (5-10”), about 46% of the roadside grass were mixed green and yellow, about 30% grass was green, and rest was brown/yellow. The color of the grass samples was clustered into 6 groups with the representative color as shown in Table 1. Since the grass color patterns have vast variations, we clustered the 901 grass samples and generated 18 color patterns (see

Fig. 9). For each color pattern, the left is an example image, and the right is the actual color pattern. Each color pattern can be a mix of several colors identified in Table 1.

Table 1.
Representative color components of grass.

Color	**Yellow**			**Green**		
R,G,B	111, 95, 65	146, 130, 96	170, 162, 135	99, 100, 55	105, 110, 44	139, 141, 87

Pattern 1

Pattern 2

Pattern 3

Pattern 4

Pattern 5

Pattern 6

Pattern 7

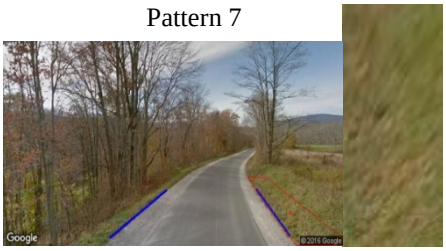

Pattern 8

Pattern 9

Pattern 10

Pattern 11

Pattern 12

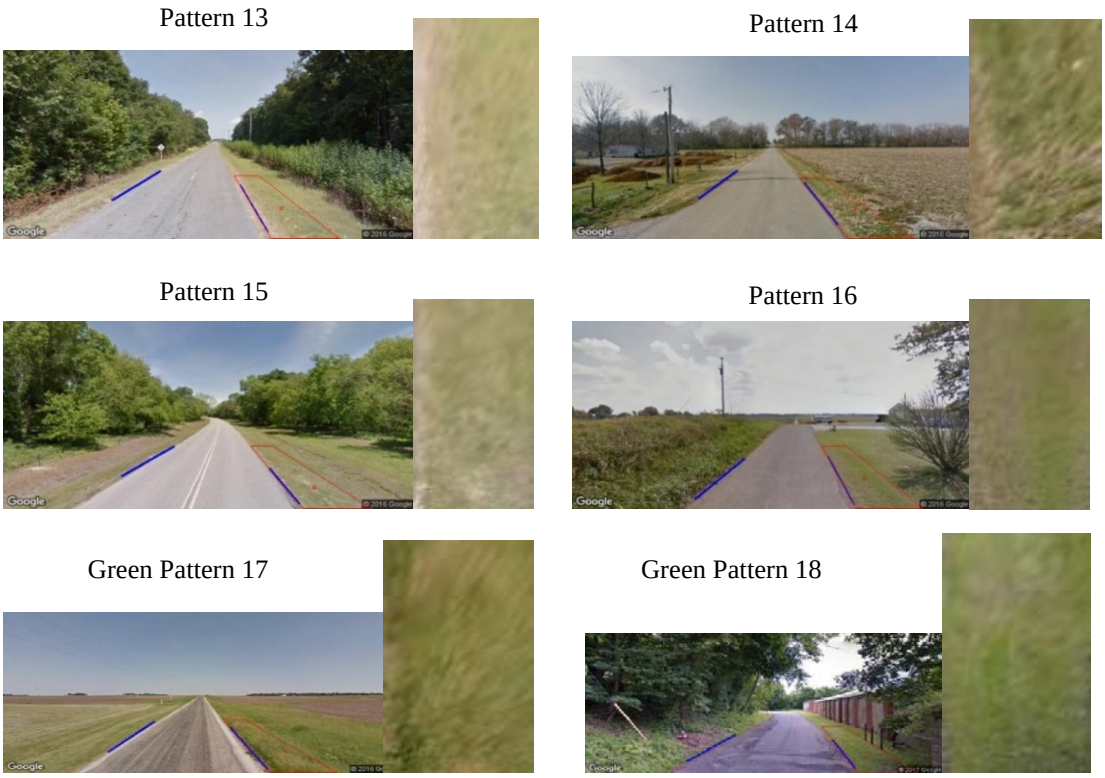

Fig. 9. Grass color patterns.

Radar Characteristics of Representative Grass

24GHz RCS and 77GHz RCS were measured on three grass samples. The physical appearance of these grass samples is shown in Table 2. The radar set up is illustrated in Fig. 10. The maximum, minimum, average and mean 77GHz RCS measurement result of these grass samples are in Fig. 11. The maximum, minimum, average and mean 24GHz RCS measurement result of these grass samples are in Fig. 12. The x-axis of the plot is the distance of the grass to the radar. The Y-axis is the RCS value. The blue vertical line indicates the location of the reference corner reflector. The RCS on the left of the vertical blue line is heavily influenced by antenna coupling and is not useful. The RCS on the right side of the dashed box is too weak and can be considered as background noise. The slop of the RCS plot in the region covered by the dashed box illustrates the RCS characteristics of the grass.

Table 2.
Grass samples used to measure 77GHz RCS.

Grass	**Height**	**Color**	**Surface Condition**	**Type**
1	Short (2-4 inches)	Green and Yellow	Somewhat even	Wild
2	Medium (8-10 inches)	Green and Yellow	Uneven	Wild
3	Short (2-4 inches)	Green	Very even	Well maintained

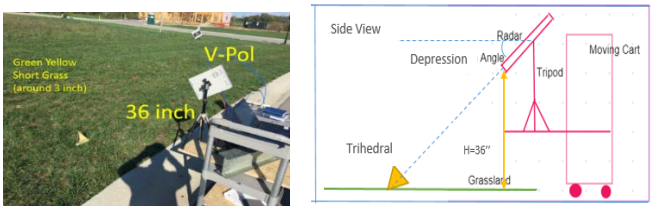

Fig. 10. Grass 77GHz RCS measurement.

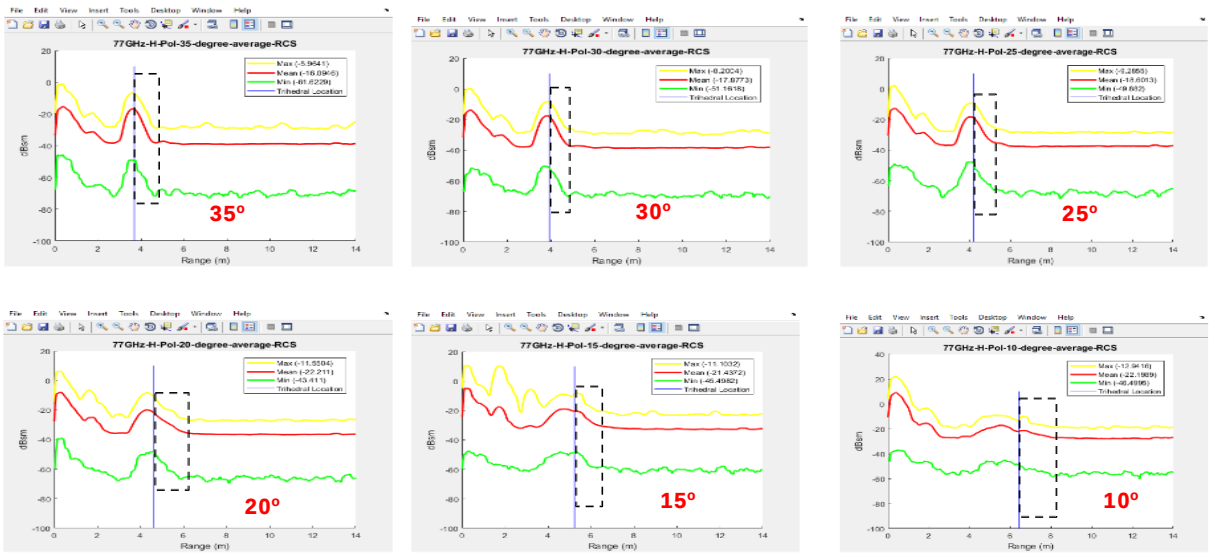

Fig. 11. Grass RCS Recommendation (77GHz Horizontal Polarization).

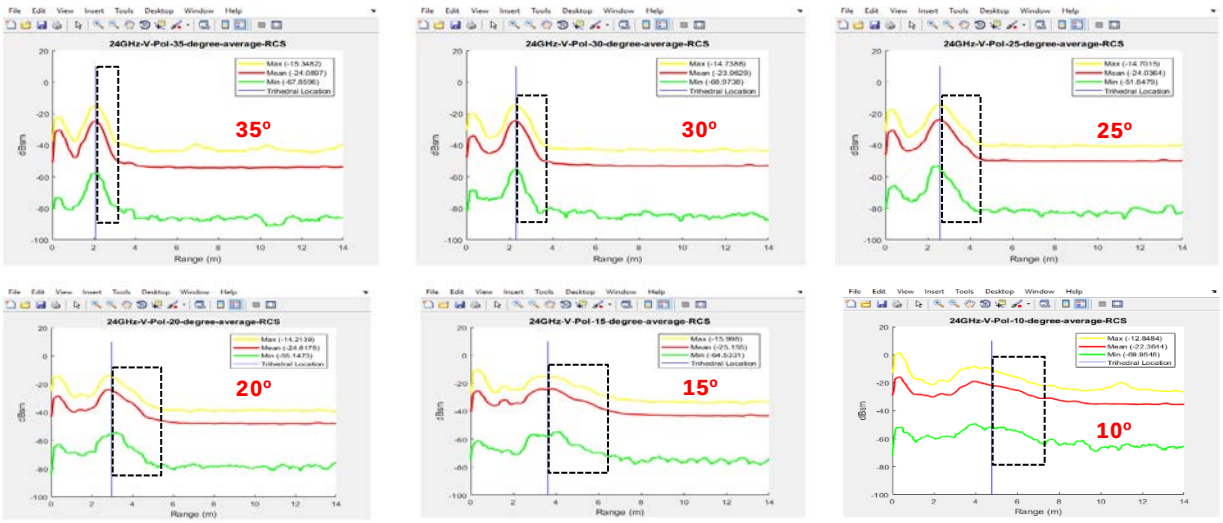

Fig. 12. Grass RCS Recommendation (24GHz Horizontal Polarization).

LIDAR Characteristics of Representative Grass

A spectrometer that covers a large range of light wavelengths was used to measure the diffusive reflectivity of 6 grass samples in indoor and outdoor at a range of viewing angles. The light source and the

measurement probe were placed as close as possible and aimed in the same direction to mimic the LIDAR operation. Multiple points were measured on each sample. Fig. 13 shows the upper and lower boundaries of all measurements at various angles, where 0 degree means that the LIDAR beam is perpendicular to the surface being measured. The upper bound is the measured maximum IR reflectivity value plus 0.05 and the lower bound is the measured minimum IR reflectivity value minus 0.05. It can be seen that the IR reflectivity of the grass increases as the viewing angle is getting further away from the perpendicular direction. The grass starts to show specular reflectivity when the measurement angle is above 50 degrees. The IR reflectivity also increases as the infrared wavelength increases in the 800-1100nm range.

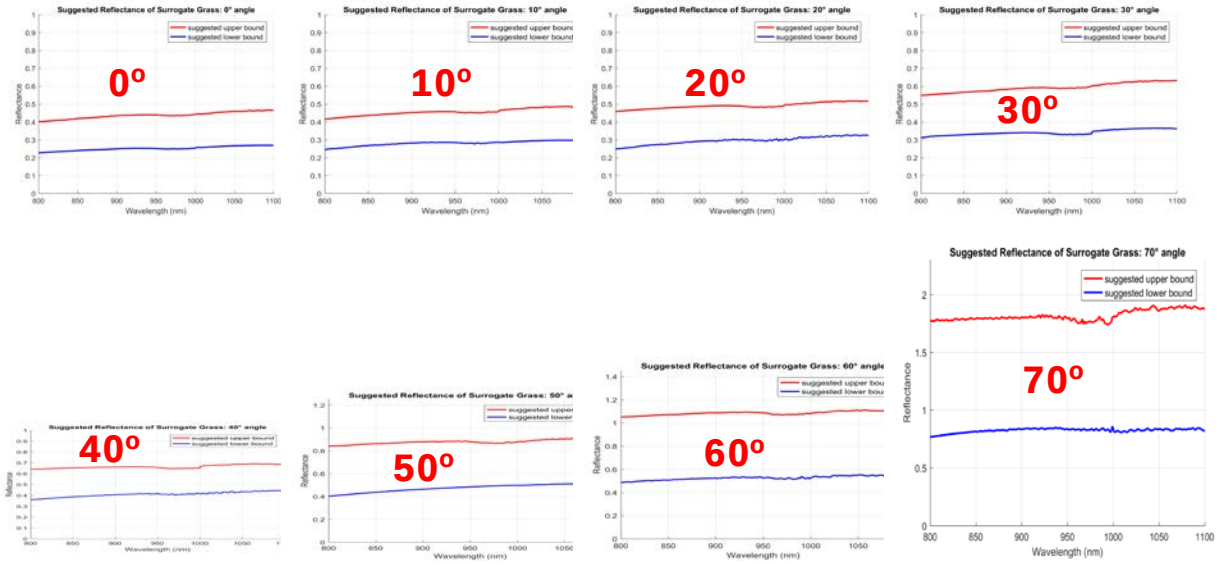

Fig. 13. The IR reflectance of grass fields at various measurement angles.

CONCLUSIONS

This paper summarized the 77GHz and 24GHz radar, LIDAR, and camera characteristics of grass, metal guardrail, and concrete divider. This information can be used for the development of grass, concrete divider, and the metal guardrail surrogates, which is essential for the standard evaluation of the Road Departure Warning and Road Keep Assistant systems. Based on this information, we have already developed surrogate grass, guardrail and concrete divider for testing. The design and testing of the surrogates will be described in future publications.

ACKNOWLEDGMENT

This research was sponsored by the Toyota Collaborative Safety Research Center.

REFERENCES

[1] "Roadway Departure Safety," U.S. Department of Transportation Federal Highway Administration. https://safety.fhwa.dot.gov/roadway_dept/ .

[2] Arora, Prashant, David Corbin, and Sean N. Brennan. "Variable-sensitivity road departure warning system based on static, mapped, near-road threats." In Intelligent Vehicles Symposium (IV), 2016 IEEE, pp. 1217-1223. IEEE, 2016.

[3] Lattke, Benedikt, Alfred Eckert, Harald Feifel, Dominik Fröhlich, J. Mcciain, Ganesh Adireddy, Florian Janda, and Erich Fuchs. "Road departure protection-a means for increasing driving safety beyond road limits." In 24th International Technical Conference on the Enhanced Safety of Vehicles (ESV), no. 15-0212. 2015.

[4] Harry W. Taylor, "Preventing Roadway Departures," US Department of Transportation Federal Highway Administration. https://www.fhwa.dot.gov/publications/publicroads/05jul/03.cfm.

[5] Charles F. McDevitt, “Basics of Concrete Barriers,” *Public Roads Magazine*, https://www.fhwa.dot.gov/publications/publicroads/00marapr/concrete.cfm.
[6] Sparbert, Jan, Klaus Dietmayer, and Daniel Streller. "Lane detection and street type classification using laser range images." In Intelligent Transportation Systems, 2001. Proceedings. 2001 IEEE, pp. 454-459. IEEE, 2001.
[7] Kirchner, Alexander, and Th Heinrich. "Model-based detection of road boundaries with a laser scanner." (1998).
[8] Cramer, Heiko, and Gerd Wanielik. "Road border detection and tracking in non-cooperative areas with a laser radar system." In Proceedings of German Radar Symposium, pp. 24-29. Bonn, Germany, 2002.
[9] Fardi, Basel, Ullrich Scheunert, Heiko Cramer, and Gerd Wanielik. "Multi-modal detection and parameter-based tracking of road borders with a laser scanner." In Intelligent Vehicles Symposium, 2003. Proceedings. IEEE, pp. 95-99. IEEE, 2003.
[10] Lakshmanan, Sridhar, and David Grimmer. "A deformable template approach to detecting straight edges in radar images." IEEE Transactions on Pattern Analysis and Machine Intelligence 18, no. 4 (1996): 438-443.
[11] Kaliyaperumal, Kesav, Sridhar Lakshmanan, and Karl Kluge. "An algorithm for detecting roads and obstacles in radar images." IEEE Transactions on Vehicular Technology 50, no. 1 (2001): 170-182.
[12] Ma, Bing, Sridhar Lakshmanan, and Alfred O. Hero. "Simultaneous detection of lane and pavement boundaries using model-based multisensor fusion." IEEE Transactions on Intelligent Transportation Systems 1, no. 3 (2000): 135-147.
[13] Katzourakis, Diomidis I., Joost CF de Winter, Mohsen Alirezaei, Matteo Corno, and Reinder Happee, "Road-departure prevention in an emergency obstacle avoidance situation." IEEE Transactions on Systems, Man, and Cybernetics: systems 44, no. 5 (2014): 621-629.
[14] Gupta, Rakesh, Ananth Ranganathan, and Jongwoo Lim, "Road departure warning system," U.S. Patent 9,077,958, issued July 7, 2015.
[15] Dan Shen, Jun Lin, Stanley Chien, Qiang Yi, Renran Tian, Rini Sherony, “Important Roadside Features for the Development of Vehicle Road Keeping Assistance System,” 2018 SAE World Congress, Detroit Michigan, April 2018.
[16] FLH Standard Drawings, https://flh.fhwa.dot.gov/resources/standard/Std617-11.pdf,
[17] Qiang Yi, Dan Shen, Jun Lin, Stanley Chien, Rini Sherony, “The color specification of surrogate roadside objects for the performance evaluation of roadway departure mitigation systems,” 2018 SAE World Congress, Detroit Michigan, April 2018.

DEVELOPMENT AND IMPLEMENTATION OF SAFETY EVALUATION SCENARIOS FOR AUTOMATED DRIVING VEHICLES ON TEST BED

Heungseok Chae
Seonwook Kim
Kyongsu Yi
School of Mechanical and Aerospace Engineering, Seoul National University
Korea

Myungsu Lee
Kyongchan Min
Korea Automobile Testing & Research Institute, Korea Transportation Safety Authority
Korea

Paper Number 19-0061

ABSTRACT

Regulation for the testing and operation of automated driving vehicles on public roadways has been recently developed all over the world. For example, the licensing standards and the evaluation technology for automated driving vehicles have been proposed in California, Nevada and EU. Like M-city, the test bed has been developed worldwide to evaluate automated driving vehicles and K-city has been developed as the test bed in Korea. The K-city has a variety of facilities such as merge, ramp, tollgate, tunnel, intersection and so on according to five road conditions: motorway, suburban road, urban road, community road and valet parking zone. Therefore, it is necessary to have automated driving evaluation scenarios that would actually be implemented in K-city. For scenario implementation as vehicle tests, automated driving vehicles are needed. The safety evaluation scenarios and criteria for level 3 and level 4 automated driving vehicles were developed in consideration of the actual driving conditions, the real road driving data, and the existed automated driving evaluation methods (ISO, NHTHA, and so on). Then, the safety evaluation scenarios were determined by considering whether the test bed could be realized, repeatable, and safety performance could be well assessed. In order to evaluate automated driving on actual test bed, vehicles as well as evaluation scenarios are needed. First of all, it needs an automated driving vehicle that is evaluated. The evaluated vehicle is called as a subject vehicle. Besides the subject vehicle, vehicles that can help evaluation are also needed and are referred to as target vehicles. Target vehicles have the ability to driving autonomously in accordance with the scenario, maintaining safety performance with the surrounding vehicles, and recognizing subject vehicle to measure safety criteria. For example, the target vehicles are used to produce a variety of situations, such as cutting in front of the subject vehicle, decelerating in front of the subject vehicle, or driving on the main road when subject vehicle is on the merge road. In the study, a subject vehicle and four target vehicles have been developed and utilized. To verify the developed evaluation scenarios, vehicle tests were conducted using subject vehicle and target vehicles. The subject vehicle has level 3 and level 4 of automated driving that have diverse functions such as lane keeping and lane change. In accordance with the scenarios, all vehicles were self-driving and the subject vehicle was checked whether it meets the evaluation criteria. Through vehicle tests, the developed evaluation scenario was verified to be feasible on the test bed and to evaluate the performance of subject vehicle well. In this paper, the vehicle test result of merge scenario is presented among various motorway scenarios.

INTRODUCTION

Evaluation technology of the automated driving is actively developed in accordance with the rapid development of automated driving system around the world [1, 2]. In the case of the advanced driver assistance system (ADAS), which is the basic technology of automated driving system, standards and evaluation techniques have been developed by organizations such as ISO, NCAP, and NHTHA [3, 4, 5]. About automated driving, research and collaboration have been conducted to create standards and evaluation criteria worldwide, including the EU and the United Nations [6, 7].

Since the automated driving system must be evaluated while driving, the driving environment is very important. For the autonomous driving, a system such as a temporary driving license for automated driving system was institutionalized [8, 9]. Initially, it was started on Nevada and California in the United States of America, and now the temporary driving license is being institutionalized in several countries around the world, including Korea. The temporary driving license system can be helpful for developing autonomous driving technology because it can travel with various vehicles on actual roads. However, it is difficult to reproduce the desired and repeated situation. Therefore, there is a great need for a test bed as well as an actual road for autonomous driving technology. M-city in the United States was built as a test bed specialized in automated driving evaluation [10]. Following M-city, many test beds specially developed for automated driving are being developed around the world, and K-city have been developed in Korea [11]. K-city simulates several driving environments such as motorway, suburban roads, urban roads, community roads and valet parking zone. In addition, facilities that can have an influence on autonomous driving are prepared such as such as V2X infra, GPS block tunnel and sensor barricade.

In this study, automated driving evaluation scenarios and criteria that can be implemented by K-city have been developed. Since the automated driving is an integrated and developed system of the existing ADAS, the existing ADAS evaluation technology was applied to the development of the automated driving evaluation technology. In addition, various evaluation criteria were developed considering actual driving data and physical characteristics of vehicles. The evaluation criteria consist of the states of the ego vehicle and the interactive states of the surrounding vehicles. To represent the interactive states of the surrounding vehicles, a variety of indices already exist such as clearance, time gap (TG), time to collision (TTC) and so on [12]. In this study, the lane keeping safety distance and lane changing safety distance are devised newly. Although various driving environments exist in K-city, only motorway scenarios are developed in this study since motorway is the closest environment to fully automated driving being realized. In the scenario verification, an automated vehicle to be evaluated and surrounding vehicles to assist in evaluation are needed. The basic automated driving function is need to the surrounding vehicles, because the vehicles is driven in accordance with the actual scenario. Using these vehicles, the evaluation scenario has been implemented and verified in K-city. In this paper, the vehicle test result of merge scenario is presented among various motorway scenarios. 3

THE CURRENT STATUS OF SAFETY EVALUATION OF ADV

Safety Evaluation Scenario and Criteria of ADAS

The automated vehicles generally is an integrated system of individual ADAS element technologies which are ACC, AEB, and LKAS. In order to evaluate the performance of the autonomous vehicle system, it is examined the evaluation scenarios and criteria of existing element systems. The test procedures are based on ISO, NHTHA and NCAP which focus the evaluation of vehicle safety system

ACC The ACC performance evaluation specified by ISO consists of straight-lane recognition performance, preceding vehicle identification performance, and preceding vehicle identification performance on curve lane. In straight-lane recognition performance test, the maximum recognition distance within 2 seconds is evaluated. In the identification performance test of the preceding vehicle, it is evaluated whether each front vehicle existing in the in-lane and the side lane in the straight road is recognized and identified. This is a test for verifying whether the ego vehicle follows the preceding vehicle on in-lane, without misrecognizing the vehicles on other lane. In the identification performance test of the preceding vehicle on curve lane, it is evaluated whether the ego vehicle can perceive and identify the preceding vehicle on curve lane. In addition, when the preceding vehicle is decelerated from the curved road, the behavior of the ego vehicle is also evaluated [3].

AEB The AEB performance assessment as defined by Euro NCAP is divided into two cases: City and Inter-Urban. For the City scenario, the AEB performance evaluation for stop targets is addressed for ego vehicle velocities of 10 to 50km/h. For the Inter-Urban scenario, the AEB performance evaluation is conducted for stop, moving, and deceleration targets for the ego vehicle velocity range of 30 to 80km/h. ISO AEB performance evaluation is based on two test scenarios . One is the case where the velocity of the preceding vehicle is 0km/h, the initial velocity of the ego vehicle is 80km/h, and the initial distance between the preceding vehicle and the ego vehicle is 120m. Second, the velocity of the preceding vehicle is 30km/h, the initial velocity of the ego vehicle is 80km/h, and the initial distance between the preceding vehicle and the ego

vehicle is 120m. The criteria to be evaluated in the test scenario are as follows. It is evaluated whether the ego vehicle provides one or more warnings before 1.4seconds of automatic emergency braking, provides two or more warnings before 0.8seconds, reduces velocity of more than 10 km/h at the point of impact, and operates no emergency braking before TTC 3seconds [4].

LKAS The ISO LKAS performance test evaluates the acceleration, the operated velocity range and so on. The test is conducted within the speed range of 72km/h to 108km/h in a curved section of 800 m radius. In the scenarios defined by NHTSA, progress is made at 72km/h. Performance test is performed from a lateral speed of more 0.6m/s to a maximum speed at which the lane departure prevention performance is maintained [5].

Safety Evaluation Scenario and Criteria of automated driving system

In accordance with the rapid development of automated driving, evaluation scenarios and criteria for the automated driving system are being actively developed around the world. In this paper, large projects in the EU and UN have dealt with.

Adaptive After 2014, the EU began developing the Adaptive Self Assessment Technology project. Adaptive takes account of the reflection on legal factors and human factors. In addition, evaluation scenarios are classified into proximity scenarios such as parking lots, urban scenarios, and highway road scenarios. In evaluation, framework and methodology are focused. Assessment is done from various perspectives like technical, user related and in-traffic assessments. Also, impact analysis have also been conducted. Lastly, deployment perspective for automated driving have been presented. The project lasted about three years [6].

WP29 WP 29 means the UNECE world forum for harmonization of vehicle regulations which is a unique worldwide regulatory forum within the institutional framework of the UNECE Inland Transport Committee. UN Regulations contain provisions related to safety and environmental aspects. They include performance-oriented test requirements, as well as administrative procedures. With the development of the automated driving system world widely, WP 29 focuses on automated driving systems. WP 29 contain globally harmonized performance-related requirements and test procedures. WP 29 also provide a predictable regulatory framework for the global automotive industry, consumers and their associations. Overall, the regulatory framework developed by the World Forum WP.29 allows the market introduction of innovative vehicle technologies, while continuously improving global vehicle safety. WP 29 have two principle operating groups. One is WP29 Informal Group to provide strategic direction for automated technology. This group focuses intelligent transport systems and automated driving (ITS/AD). Another is a group which have developed the UN regulation concerning vehicle steering systems to permit certain levels of autonomy. This group is called as GRRF and the GRRF Informal Working Group. WP 29 categories automated functions as six classification [7].

ENVIROMENTS OF ADV TEST BED

For test operation of automated driving vehicles, diverse methods has been recently developed all over the world. For example, the licensing standards for automated driving vehicles have been proposed in California, Nevada and EU. Although licensing has the advantage of driving on a real road, it is necessary to use a test bed because it is difficult to repeatedly test various situations. M-city is a test bed specialized in a typical automated driving system. Like M-city, the test bed has been developed worldwide to evaluate automated driving vehicles and K-city has been developed as the test bed in Korea. The Korea Automobile Safety Institute under the Ministry of Land, Infrastructure and Transport developed a test bed for safety evaluation of automated vehicles. The test bed is called as K-city and constructed various road environments in 360,000 square meter space. K-city can be divided into five major areas. There are urban roads, community roads, motorways, suburban roads, and valet parking facilities. K-city has implemented roads, transportation and communication environments similar to actual roads consisting of signal / non-signal intersections, rotary intersections, building facades, parking facilities and child protection areas for these five roads and facilities.

Motorway

Motorway environment reproduces the exclusive road traffic environment capable of high-speed movement. This environment is composed diverse constructions which are merge, split, main road, tollgate, guardrail and

tunnel. In this environment, driving test is available with wide velocity range. Functions, lane keeping, lane change and safety control with surrounding vehicles, can be tested in motorway.

Suburban Road
Suburban road environment recreates rural roads with insufficient infrastructure. This environment consists of rotary, a tree-lined street.

Urban Road
Urban road environment reproduces the road traffic environment of the city. This environment is composed diverse constructions which are signalized intersection, a bus-only lane, a bus stop and a temporary building.

Community Road
Community road environment reproduces the road traffic environment centered on pedestrians. This environment is composed diverse constructions which are a school zone, sidewalk and bicycle road.

Valet Parking Zone
Valet parking environment reproduce the parking environment where autonomous valet parking is possible. This environment consists of various shape parking spaces. Parallel, horizontal and oblique parking spaces are constructed.

Figure1. K-City Test Bed for Automated Driving System.

CRITERIA OF PERFORMANCE EVALUATION OF AUTOMATED VEHICLES

In this chapter, criteria for evaluating automated vehicles are presented. The criteria are calculated by taking into account the safety standards used in the existing ADAS, the actual road data, and the physical behavior of the vehicle. It is important to basically evaluate the state of the ego vehicle and evaluate interactive state with surrounding vehicles. Indices of safety with surrounding vehicles are clearance, time gap (TG), time to collision (TTC) and so on. In this paper, safety distance is devised as representing safety performance. In this study, since only the motorway environment is focused on, the driving situation can be largely divided into lane keeping and lane change. Different safety distances are suggested depending on the two situations.

States of Automated Vehicle

The states of the ego vehicle must be evaluated to confirm the abnormal behavior of the vehicle. Considering the existing ADAS evaluation criteria, the following state of charge is evaluated. First, it is necessary to evaluate whether the velocity of ego vehicle exceed or not in desired velocity by the scenario. And of course,
In the lane-keeping scenario, It should be evaluated whether the ego vehicle are driving inside the lane. It is important to evaluate longitudinal and lateral accelerations, which are related to abnormal behavior and ride quality. The permitted range of accelerations depends on the scenario. For example, a large area longitudinal acceleration is allowed in an emergency scenario where a front vehicle cuts in abruptly. On the other hand, a small area longitudinal acceleration is allowed in a normal driving scenario. As another example, the allowable

lateral acceleration in the lane-keeping scenario and the lane-changing scenario is different. The criteria for the states are different according to each scenario. The criterian is decided based on the existing ADAS evaluation criteria and the human driving data. The values of the specific states are given in the scenario description below.

Safety Distance in Lane Keeping Situation

Based on WP29, the safety distance in the lane keeping situation means the distance that the autonomous vehicle must proceed the safety distance control when the front vehicle is within the safety distance. For example, if the front vehicle cuts in at a distance within the safety distance, the automated vehicle must perform the safety distance control to maintain the distance over the safety distance. Safety distances are discussed internationally as in Eq. (1). The velocity of automated vehicle is multiplied by Time Gap, which means that the higher the speed, the higher the safety distance is required. The issue of how to set the time gap internationally remains an issue. In this study, the safety distance equation is presented considering the physical braking distance and actual driver driving data.

$$C_{LK} = \tau_{LK} \times V_{AV} \qquad \textbf{(1)}$$

where, τ_{LK} is time gap in lane keeping safety distance and V_{AV} is velocity of automated vehicle.

The physical braking distance can be calculated by the following parameters in consideration of the characteristics of automated vehicles that are currently being developed globally.

$$d_{brake} = (t_{sys} - {V_{AV}}/{2a_{\max,AV}}) \times V_{AV} \qquad \textbf{(2)}$$

where, τ_{LK} is system delay which sets 0.3 second and $a_{\max,AV}$ is maximum decelearion of automated vehicle which sets -9 m/s^2.

The actual driving data analyzed the distances when drivers were following the preceding vehicle in steady state [13]. The data were collected for 125 drivers of various age and sex. The following distance of this data is as follows.

$$c_{following} = c_0 + \tau_{following} \times V_x \qquad \textbf{(3)}$$

where, c_0 is the zero-speed clearance which sets 2m, $\tau_{following}$ is the linear coefficient, and V_x is the ego vehicle velocity.

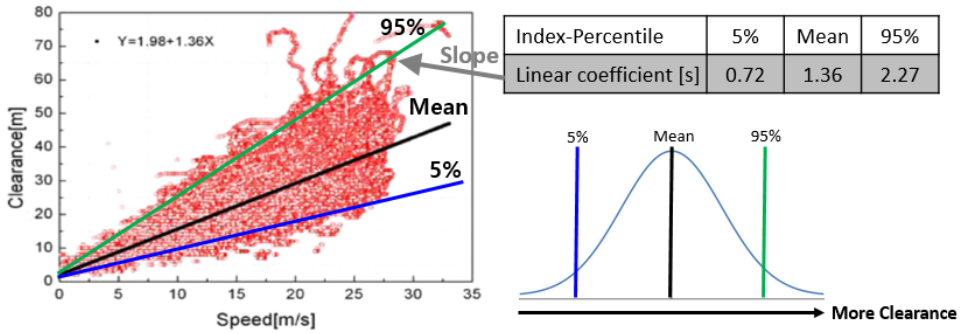

Figure2. Clearance driving data with a preceding vehicle in steady state following situation.

In pile-up accidents, the velocity of the preceding vehicle can become zero immediately without deceleration. Therefore, it need to be considered to calculate the safety distance over the braking distance in all velocity ranges. If setting the constant time gap to be discussed in WP29, time gap 2.3 second is needed to cover the braking distance of all velocity regions. This is too large in comparison with the actual driving data. And because too much safety distance is required in the low speed range, excessive and frequntely deceleration can occur. Therefore, the constant time gap is not proepr. If the time gap varies according to the velocity as Eq. (1), the safety distance is larger than the braking distance of all the velocity regions and does not largely differ from the driving data. Therefore, the safety distance in the lane keeping situation is proposed based on braking distance and driving data as Eq. (4).

$$C_{LK,proposed} = \tau_{LK,proposed}(V_{AV}) \times V_{AV} + c_0 \quad \textbf{(4)}$$

$$\tau_{LK,proposed} = 0.8 + (1.6 \times V_{AV} / 36.1) \quad \textbf{(5)}$$

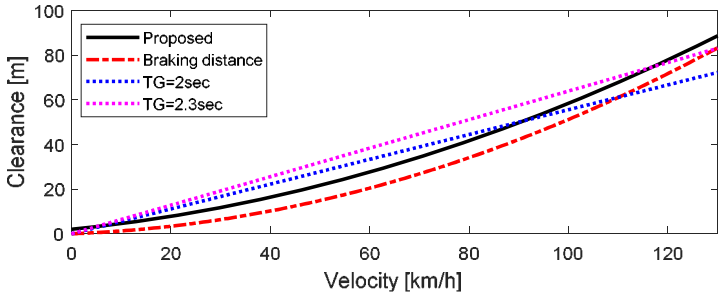

Figure3. Proposed safety distance in lane keeping.

Safety Distance in Lane Change Situation

Unlike lane keeping situation, which are important only for a preceding vehicle, all surrounding vehicles are important in lane change situation. Therefore, the lane change safety distance can be shown in Fig. 1. This distance indicates that a lane change is possible when no vehicle is present in this area. The vertical length of the area equals the lane width and the horizontal length consists of three distances which are a side, a rear and a front. The side distance is equal to the width of the ego vehicle.

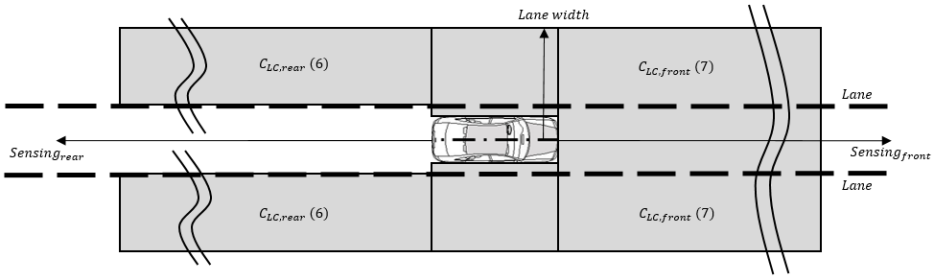

Figure4. Area by safety distance in lane change situation.

Eq. (6) indicates the rear distance which is calculated as a distance at which one second time gap is secured with a normal deceleration amount of the side-rear vehicle.

$$C_{LC,rear} = \begin{cases} (V_{rear} - V_{AV}) \times t_B + (V_{rear} - V_{AV})^2 / (2a_{rear}) + V_{rear} \times t_G & If\ V_{rear} \geq V_{AV} \\ V_{rear} \times t_G & else \end{cases} \quad \textbf{(6)}$$

where, V_{rear} is the velocity of the rear vehicle on target lane, t_B is time delay to reach target deceleration which sets 0.3second, a_{rear} is normal deceleration of the rear vehicle which sets -3 m/s^2 and t_G is time remaining between vehicles after the approaching vehicle decelerates which sets 1second.

If a front distance is applied to a rear distance, the safety distance is too large. In this case, since lane change is possible only when the vehicle does not exist in an area that is too large, it is difficult to perform lane change in practice. Therefore, the front distance is calculated by changing the parameters in consideration that the vehicle to be decelerated is an ego vehicle. Eq. (7) indicates the front distance

$$C_{LC,front} = \begin{cases} V_{AV} \times t_G & If\ V_{front} \geq V_{AV} \\ (V_{AV} - V_{front}) \times t_B + (V_{AV} - V_{front})^2 / (2a_{AV}) + V_{AV} \times t_G & else \end{cases} \quad \textbf{(7)}$$

where, V_{front} is the velocity of the front vehicle on target lane and a_{AV} is maximum decelearion of the ego vehicle which sets -9 m/s^2.

AUTOMATED DRIVING SYSTEM TEST SCENARIO

As described above, the K-city environment consists of motorway, suburban road, urban road, community road, and valet parking. In this paper, only motorway scenario is developed because the commercialization of fully autonomous driving is the closest in motorway. In the motorway, the driving function is largely divided into lane keeping and lane change, and scenarios are developed in consideration with situations that can occur according to each function. Table 1 shows test scenarios for the automated driving vehicle.

Table1.
Test scenarios for the automated driving vehicle.

Environment	Main Function	Specifics	Test No.
Motorway (+Suburban Road)	Lane Keeping	Solo Driving	M-1-1
		Preceding Vehicle	M-1-2
		Cut-in Vehicle	M-1-3
		Cut-out Vehicle	M-1-4
	Lane Change	Overtaking	M-2-1
		Merge	M-2-2
		Split	M-2-3

Motorway Lane Keeping Test (M-1)

Scenario the automated driving system should be able to keep the lane in solo driving (M-1-1). Lane keeping performance should be evaluated while varying the various velocity ranges and various curvatures within the road regulation. In addition, evaluation need to be conducted with surrounding vehicles in the vicinity. The automated driving system should be able to keep the lane as maintaining safety with a preceding vehicle (M-1-2). Along with lane keeping performance, it is necessary to evaluate whether the safety is maintained for various behaviors such as constant velocity, acceleration and deceleration of the preceding vehicle. The automated vehicle should be able to keep the lane as responding about sudden change of traffic condition such as cut-in case (M-1-3). It is necessary to evaluate the lane keeping and safety maintenance performance against the various behavior of the vehicle which performs cut-in maneuver from the adjacent lane to the in-lane. The automated vehicle should also keep the lane as responding about sudden change of traffic condition such as cut-out case (M-1-4). When a preceding vehicle is slower than the desired velocity of the automated vehicle, the automated vehicle need to follow the velocity of the preceding vehicle. It is necessary to assess whether the automated vehicle will recover the desired velocity when the preceding vehicle perform cut-out maneuver from the original lane to the adjacent lane.

Performance evaluation First, the lane keeping performance should be evaluated at various curvature and velocity conditions. And, when the surrounding vehicle exists, the maintenance of the safety with the surrounding vehicle must be evaluated. It should be assessed whether clearance with a preceding vehicle stay above a lane keeping safety distance. About the velocity, the desired velocity or the velocity of the preceding vehicle or the desired velocity recovery should be assessed depending on the scenario. Finally, in order to evaluate ride comfort and abnormal behavior, it is necessary to evaluate whether the longitudinal and lateral accelerations of the automated vehicle are maintained within a certain value.

Table2.
Performance evaluation of lane keeping situation.

Performance Index	Criteria
Lateral Position	Lane Keeping
Velocity	Desired Velocity / Velocity of Preceding vehicle
Longitudinal Acceleration (Normal Case)	$-3 \leq a_x \leq 2$

Longitudinal Acceleration (Severe Case)	$-9 \leq a_x \leq 2$
Lateral Acceleration	$-1 \leq a_y \leq 1$
Safety with a preceding vehicle	By lane keeping safety distance (4)

Motorway Lane Change Test (M-2)

Scenario Lane change can be classified as two cases. First, a case where a lane change is made by an influence of nearby vehicles on a normal road is referred to as a discretionary lane change (DLC). The most representative situation for DLC is overtaking situation (M-2-1). Therefore, when a preceding vehicle is slow or stopped, it should be evaluated whether the lane change is proceeding while maintaining the safety of the surrounding vehicles. Scenarios can be implemented by varying the velocity, the number and the location of the preceding vehicle and the side lane vehicles. Unlike DLC, a case where a lane change should be completed by road conditions is called a mandatory lane change (MLC). Representative situations of MLC are merge (M-2-2) and split (M-2-3). In order to perform DLC, the automated driving system should operate with the MAP. The automated vehicle must be to determine if it is located at merge or split. Then, the lane change need to be completed in limited distance and time constraints. In the merge scenario, various merge situations can be implemented by changing the position, the velocity and number of the vehicle in the target lane. In the split scenario, it is possible to implement various split situations by changing the preceding vehicle go to split lane or the preceding vehicle go straight in original lane.

Performance evaluation In a lane change scenario, the first thing to evaluate is the success of the lane change. In the case of an overtaking scenario, it is possible to perform a lane change while maintaining the safety of the surrounding vehicles, but it is also possible to maintain safety with a preceding vehicle by decelerating. In the case of merge or split scenario, the lane change must be successful while maintaining the safety of the surrounding vehicles. The lane keeping safety distance and the lane change safety distance are used for evaluation of safety with surrounding vehicles. Finally, it is necessary to evaluate whether the longitudinal and lateral accelerations of the subject vehicle are maintained within a certain area.

Table3.
Performance evaluation of lane keeping situation.

Performance Index	Criteria
Longitudinal Acceleration	$-3 \leq a_x \leq 2$
Lateral Acceleration	$-3 \leq a_y \leq 3$
Safety with surrounding vehicles	By lane change safety distance (6), (7)

IMPLEMENTATION OF EVALUATION SCENARIO UTILIZING AUTOMATED VEHICLES

In order to evaluate automated driving on actual test bed, vehicles as well as evaluation scenarios are needed. First of all, it needs an automated driving vehicle that is evaluated. The evaluated vehicle is called as a subject vehicle. Besides the subject vehicle, vehicles that can help evaluation are also needed and are referred to as target vehicles. Target vehicles have the ability to driving autonomously in accordance with the scenario, maintaining safety performance with the surrounding vehicles, and recognizing subject vehicle to measure safety criteria. For example, the target vehicles are used to produce a variety of situations, such as cutting in front of the subject vehicle, decelerating in front of the subject vehicle, or driving on the main road when subject vehicle is on the merge road. In the study, a subject vehicle and four target vehicles have been developed and utilized.

Subject vehicle

The subject vehicle must be capable of level 3 and 4 automated driving. The automated driving system is normally consist of localization, perception, motion planning and control functions. Localization function is achieved based on RTK GPS. In perception function, surrounding vehicles, obstacles and pedestrians are

detected using six IBEO LiDARs. Lane also is detected by AVM camera and a front vision system. In motion planning function, proper motion is planned considering both a safety and a task. Safety means that automated vehicle can maintain safety with surrounding vehicles, obstacles and pedestrians. Diverse tasks, which are lane keeping, lane change and intersection driving, exist and the task is decided by the road environment. Control function determines the control input to track the planned motion. Model predictive control based automated driving algorithm is applied to merge situation, which is the vehicle test environment of this paper [14].

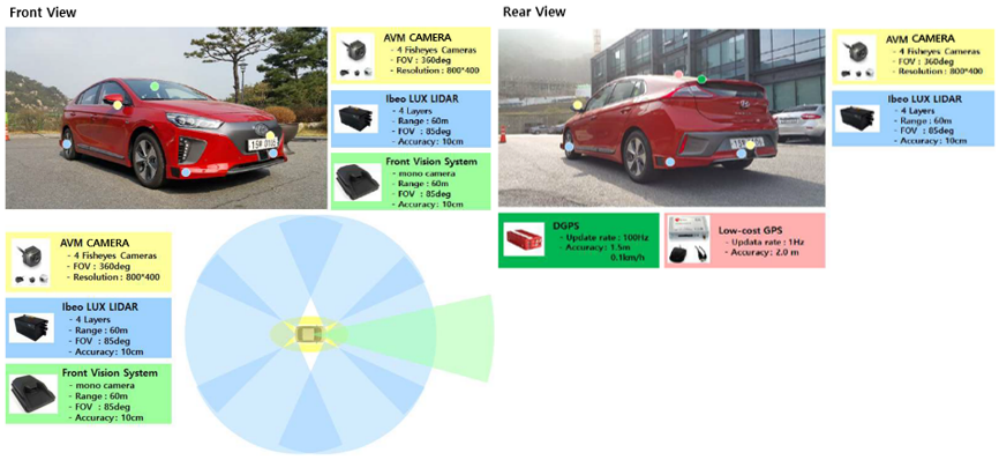

Figure5. Configuration and detection range of subject vehicle.

Target vehicle

Target vehicles have the ability to driving autonomously in accordance with the scenario, maintaining safety performance with the surrounding vehicles, and recognizing subject vehicle to measure safety criteria. Therefore, target vehicles also basic automated driving. As the subject vehicle, RTK GPS based localization function is equipped. LiDAR, Radar and Front Vision System based all-around vehicle detection can be possible to maintain safety performance with the surrounding vehicles, and to measure safety criteria of the subject vehicle. Target vehicle need to drive autonomously in accordance with a predefined scenario. For this purpose, target vehicle has a localization function using high performance RTK GPS. It also has path-generation algorithm which create a path as a predefined scenario. To decide desired steering torque as final lateral control input, path-tracking algorithm are implemented for tracking desired path [15]. Because target vehicle need to detect all-around vehicles for maintaining safety performance with the surrounding vehicles and measuring safety criteria of the subject vehicle, all-around vehicle detection module has been composed using LiDAR, radar and front vision system. For longitudinal control, two modules are considered. As first module, human driving data based ACC and AEB algorithms are equipped for safety control with surrounding vehicles [13]. As second module, scenario based velocity control algorithm is equipped. As final longitudinal control input, longitudinal acceleration is decided considering both modules. According to the above description, Fig. 6 represents algorithm structure of target vehicle. In addition, Fig. 7 shows configuration and sensor range of target vehicle.

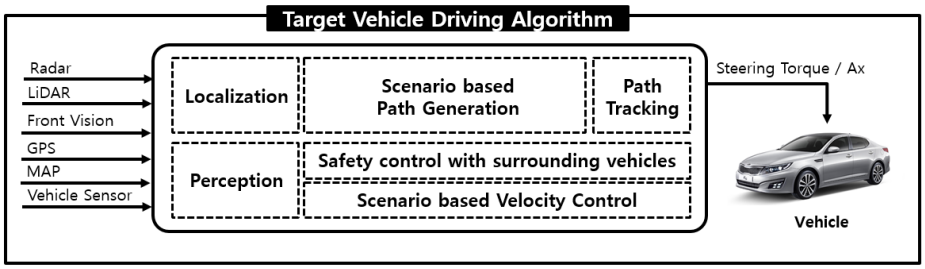

Figure6. Algorithm structure of target vehicle.

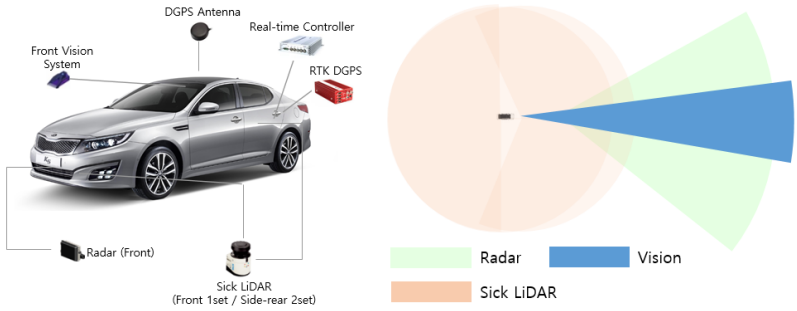

Figure7. Configuration and detection range of target vehicle.

VEHICLE TEST FOR VALIDATION OF EVAULATION SCENARIO

The actual vehicle test in K-city is carried out using the subject automated vehicle and the target vehicles which helps evaluation as mentioned earlier. Since all the scenarios cannot be shown, we present only merge scenario is presented. The merge situation is the most difficult scenario among motorway scenarios.

Test Case: Merge on Motorway

The merge scenario is shown in Fig. 8. The subject vehicle travels in merging lane, and the target vehicle which supports the evaluation travels on the target lane. Since the length of the merge lane is short as 100m in the K-city, vehicle test proceeds at a speed of 30km/h. In order to interfere with the merge of the subject vehicle, the target vehicle drives on side of the subject vehicle. Since the vehicle starts from a standstill, it must drive from the rear to meet the scenario situation. Fig. 9 represents the merge map and trajectory from the stationary state of two vehicles for the scenario situation.

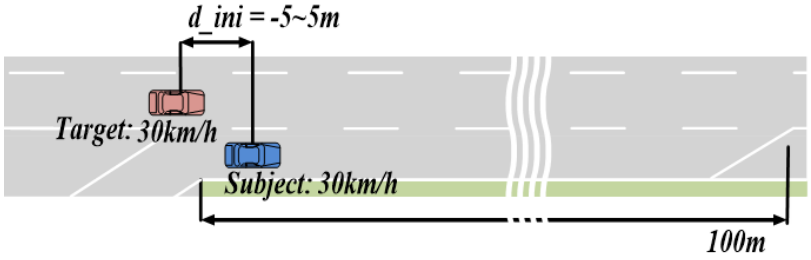

Figure8. Vehicle test condition in merge scenario.

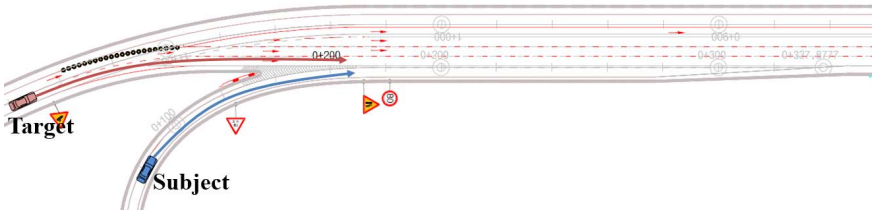

Figure9. Merge map and initial Trajectory for merge scenario condition.

The results and sanpshots of the vehicle test are presented in Fig. 10 and 11 respectively. At 3sconds, the subject vehicle that has reached the start point of merge lane tries to make a lane change to the left, but the lane change is not possible because the target vehicle occupies on target lane. The subject vehicle judges whether to go ahead or rear of the target vehicle in consideration of the remaining distance of the merge lane and the state of the target vehicle. The subject vehicle decelerates since it decides that going rear of target vehicle is better. After the distance between the subject vehicle and the target vehicle is enough to perform lane change, the subject vehicle proceeds lane change to target lane at 14.9seconds. After the lane change is

completed at 25seconds, the subject vehicle keeps a certain distance from the preceding vehicle in the lane keeping mode.

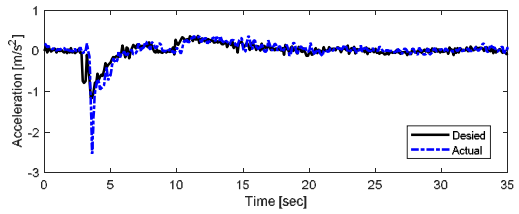

(a) Acceleration

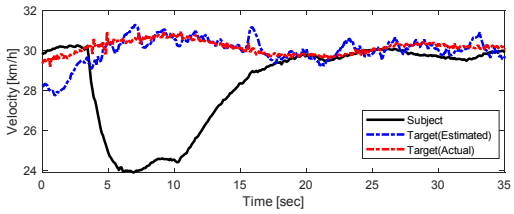

(b) Velocity of Each Vehicle

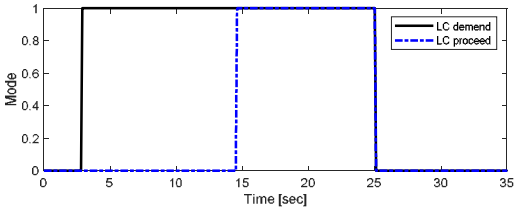

(c) Lane Change Mode

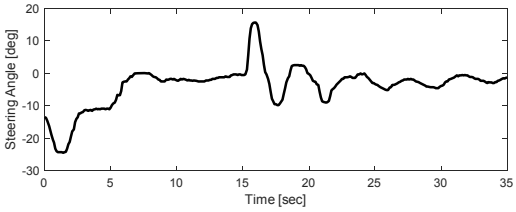

(d) Steering Angle

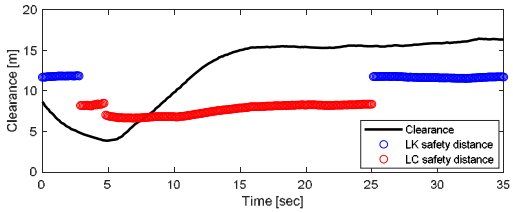

(e) Clearance

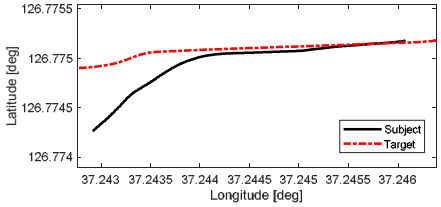

(f) Trajectory of Each Vehicle

Figure10. Vehicle test result of merge scenario.

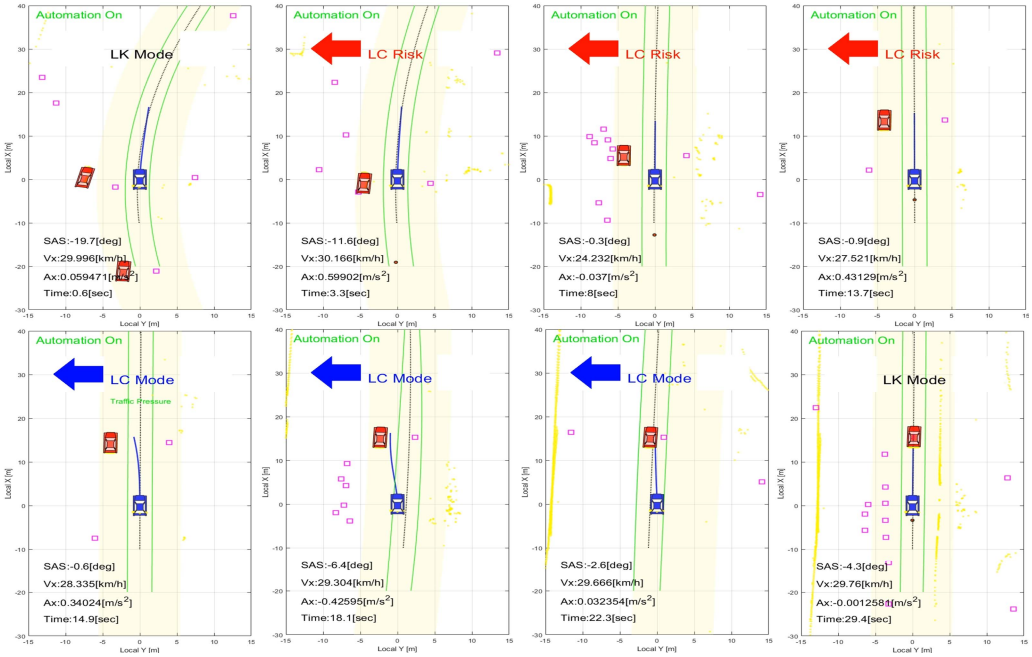

Figure11. Vehicle test snapshot of merge scenario.

CONCLUSIONS

According to the global demand for the development of evaluation technology of the automated driving system, the test bed has been developed worldwide to evaluate automated driving vehicles and K-city has been developed as the test bed in Korea. K-city simulates several driving environments such as motorway, suburban roads, urban roads, community roads and valet parking zone. In addition, facilities that can have an influence on autonomous driving are prepared such as such as V2X infra, GPS block tunnel and sensor barricade. In this study, automated driving evaluation scenarios and criteria that can be implemented by K-city have been developed. The evaluation criteria is developed considering existing ADAS evaluation criteria, driving data, and vehicle physics characteristics. The evaluation criteria consist of the states of the ego vehicle and the interactive states of the surrounding vehicles. To represent the interactive states of the surrounding vehicles, the lane keeping safety distance and lane changing safety distance are devised newly. The evaluation scenarios are developed taking into account repeatability, feasibility, and representative for driving situations. In the scenario verification, an automated vehicle to be evaluated and surrounding vehicles to assist in evaluation are needed. The basic automated driving function is need to the surrounding vehicles, because the vehicles is driven in accordance with the actual scenario. Using these vehicles, the evaluation scenario has been implemented and verified in K-city. In this paper, the vehicle test result of merge scenario is presented among various motorway scenarios. Future work requires development of evaluation scenarios and criteria for K-city remaining environments that are suburban road, urban road, community road and valet parking zone. In addition, verification would be conducted using one subject vehicle and four target vehicles.

* This research was supported by the Korea Ministry of Land, Infrastructure and Transport and the Korea Agency for Infrastructure Technology Advancement(Project No.: 18TLRP-B117133-03). This research was also supported by the Technology Innovation Program (10079730, Development and Evaluation of Automated Driving Systems for Motorway and City Road and driving environment) funded By the Ministry of Trade, Industry & Energy(MOTIE, Korea). This research was also supported by National Research Foundation of Korea(NRF) grant funded by the Ministry of Science, ICT & Future Planning (NRF-2016R1E1A1A01943543).

REFERENCES

[1] Carsten, O. M. J., and L. Nilsson. "Safety assessment of driver assistance systems." European Journal of Transport and Infrastructure Research 1.3 (2001): 225-243.
[2] Felix Fahrenkrog.,“Evaluation of automated driving functions”, ITS Europe, 2014.
[3] ISO, ISO 15622 Intelligent transport systems – adaptive cruise systems – performance requirements and test procedures, 2010.
[4] Euro NCAP, Euro NCAP AEB Test Protocol, 2013.
[5] ISO, ISO 11270 Intelligent transport systems – lane keeping assistance systems – performance requirements and test procedures, 2014.
[6] Etemad, Aria. "AdaptIVe: Automated Driving Applications and Technologies for Intelligent Vehicles." Automated Driving. Springer, Cham, 2017. 535-540.
[7] Automated Driving – UNECE International Harmonization
Bernie Frost, Chairman of UNECE/WP29/GRRF, 2016\
[8] California Department of Motor Vehicles, Adopted Regulations for Testing of Autonomous Vehicles by Manufacturers, 2014.
[9] Nevada Department of Motor Vehicles, Autonomous Vehicle Testing License, 2013.
[10] Mcity ABC Test: A Concept to Assess the Safety Performance of Highly Automated Vehicles, 2019.
[11] Kim, Tschangho John. "Automated Autonomous Vehicles: Prospects and Impacts on Society." Journal of Transportation Technologies 8.03 (2018): 137.
[12] Kim, Taewoo, et al. "Safety assessment procedure for advanced emergency braking system." 24th International Technical Conference on the Enhanced Safety of Vehicles (ESV). 2015.
[13] Moon, S. and K. Yi, Human driving data-based design of a vehicle adaptive cruise control algorithm. Vehicle System Dynamics, 2008. 46(8): p. 661-690.

[14] Chae, Heungseok, Kyong Chan Min, and Kyongsu Yi. Model Predictive Control based Automated Driving Lane Change Control Algorithm for Merge Situation on Highway Intersection. No. 2017-01-1441. SAE Technical Paper, 2017.
[15] Chanhee Jung. Design of adaptive steering controller for application to automated driving vehicle. Diss. Seoul National University Graduate School, 2015.

THE INFLUENCE OF RECLINED SEATING POSITIONS ON LUMBAR SPINE KINEMATICS AND LOADING IN FRONTAL IMPACT SCENARIOS

Dustin Draper
BMW AG, Ludwig-Maximilians-Universität, Germany
Andreas Huf
BMW AG, Germany
Philipp Wernicke
BMW AG, Germany
Steffen Peldschus
Ludwig-Maximilians-Universität, Germany

Paper Number 19-0062

ABSTRACT

With the advent of alternative seating positions in Highly Automated Vehicles, vehicle manufactures must take care to ensure the safety of new seating positions. The use of Human Body Models (HBMs) can aid in the use of analyzing these new concepts, as they closely represent a human being. HBMs are constructed with Finite Element (FE) modelled bones, muscles, and organs; whereas crash test dummies are made of foams, rubbers, and metallic structures. Due to these differences. HBMs show a different response compared to traditional crash test dummies. A sensitivity study on spinal posture using the THUMS v5 was performed using a BMW prototype reclined concept seat. By changing the initial of the posture of the lumbar spine, changes in spinal kinematics as well as varying force responses were observed during a frontal load case. This type of study could not be conducted with a crash test dummy as the spine of standard front crash dummies does not easily allow for postural changes. These variations suggest that initial spinal posture plays a role in the overall spinal kinematic response as well as the amount of force seen transmitted through the spine.

INTRODUCTION

As driver assistance systems become more advanced, the possibility that the occupants of vehicles will be able to focus on other tasks besides driving also is becoming more probable. Studies have shown that in cars with higher levels of automation passengers expect to be offered non-traditional seating arrangements [1]. In their *A Vision for Safety 2.0* document, NHSTA has stated that care should be taken to ensure that new non-traditional seating positions are safe for vehicle occupants, and that this evaluation might be made using simulation tools such as HBMs, in addition to the hardware tests which are the current standard [2]. In hardware tests all vehicles are tested according to a predefined protocol; in new seating positions this might not be possible. It is also likely that occupant kinematics in new seating positions will be sufficiently different to traditional seating positions that it would approach the limits of hardware dummy validity. Simulations using HBMs are a good candidate for this type of evaluation because their flexibility allows them to be used in many different configurations.

Traditional automotive safety standards have been adopted in accordance with what has been observed in the field, with the emphasis that predefined crash tests will cover a number of real world accident scenarios. This has been possible through the use of accident analysis which shows which kinds of crashes have a higher risk of injury and are the most prevalent [3].

Based on previous simulation studies of various future seating concepts a series of hardware tests were carried out at BMW to closer investigate a seat in a so called Zero-G reclined position [4]. From this study it was observed that the dummies exhibit a different kinematic chain in the reclined position than they do in the traditional upright position, which can be seen in Figure 1. Other studies have also shown non-standard kinematics in non-standard seating positions [5].

Figure 1: Dummy kinematics comparison: conventional seating configuration, above, and the prototype reclined configuration below, from [4].

The difference in kinematics was especially seen to have a large influence on the forces experienced by the lumbar spine sensors in the dummies. This is an indication that the lumbar spine should be more closely investigated. An investigation with a human body model was undertaken in an attempt to get the most realistic assessment of what happens to the spine during a frontal reclined crash, as the HBM spine more closely resembles that of an actual occupant than the spine of a crash test dummy, as seen in Figure 2.

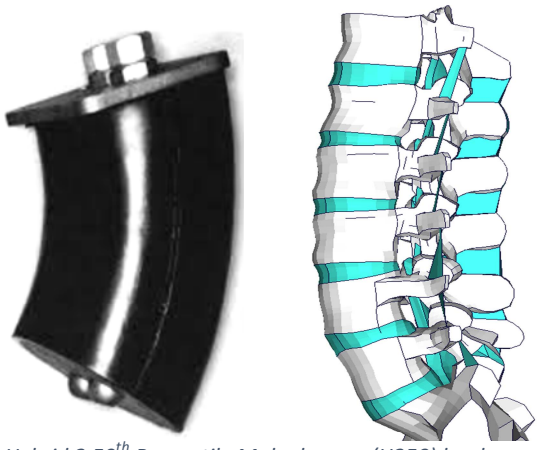

Figure 2: Comparison between a Hybrid 3 50th Percentile Male dummy (H350) lumbar spine [11] (left) and a HBM lumbar spine (right).

METHOD

The human body model chosen for this study was the THUMS v5 50th percentile Male. A preliminary simulation series was run in order to validate the simulation model of the seat with the hardware prototype seat using a H350 dummy.

The THUMS model was positioned first in a comparable manner to the H350 dummy which was used for the seat validation, but this position was ultimately found to be inadequate, because the H350 was not designed to be reclined. It is too stiff in some key areas relating to positioning, most notably resulting in a large gap between the head and the headrest. A second position was therefore derived combining two separate data sources. The first source of data is a set of anatomical landmarks found by probing a 50th percentile male occupant sitting in the seat using a Faro Arm. The second source was an Upright Magnetic Resonance Imaging (MRI) dataset from a different 50th

percentile male used to estimate the angles associated with the lumbar spine in a reclined seat. These two sets of data complement one another: one for the superficial surface and one for the internal spinal geometry. A comparison between the MRI data and the positioned human body model can be seen in Figure 3.

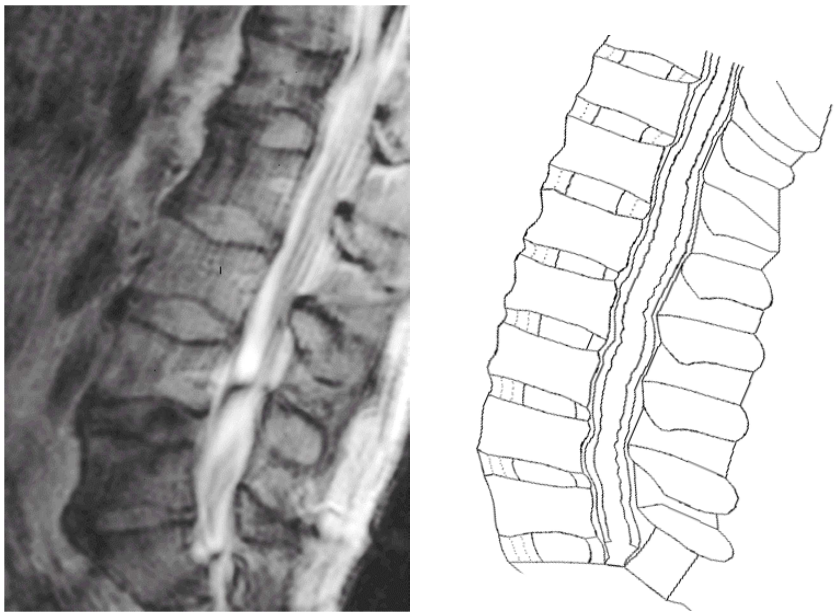

Figure 3: Lumbar spine position as measured using an Upright MRI, and the positioned THUMS 5 lumbar spine.

After the H350-based position was compared with the MRI based position it was found that there was a difference in peak lumbar spine forces, and that the models exhibited differing spinal and global kinematics, as well as different lumbar spine force responses. The differences between the H350-based and the MRI-based models can be seen in Figure 4.

A sensitivity study was then performed using the model with the MRI based seating position as a baseline. For the sensitivity study the pelvis angle and the lumbar spine curvature were varied to see how small changes in the lumbar spine posture affect the kinematics and force response in a frontal crash scenario. This positioning was performed using the Piper positioning tool [6]. Spinal rotation centers were defined in all of the intervertebral disks between the sacrum and T12. The pre-positioning module was then used to vary the spinal position with all bones being held fixed except for the pelvis, sacrum, and the lumbar spine. Then, a prescribed angle was given to all of the rotation centers and the lumbar spine was made to bend. After positioning in the pre-positioner module, the nodes were exported to a standard pre-processor, and smoothing operations were performed. The original position and the modified positions can be seen in Figure 4. Two positions were investigated, one where rotations were prescribed to make the initial geometry more lordodic, extended to be more like an s-curve, and one where the initial position was more kyphotic, or flexed like a c-curve. The more kyphotic state does not exhibit a pure kyphosis, but more so than the baseline position. This type of investigation could only be performed using a HBM: changing the spinal position of a dummy would either not be physically possible (i.e. H350 has no movable lumbar spine joints) or would result in a global change of position, with no possibility to isolate only the spine.

The new models were then run under the same boundary conditions as the MRI-based position model, with the same pulse, and the same restraint system.

RESULTS

Positioning

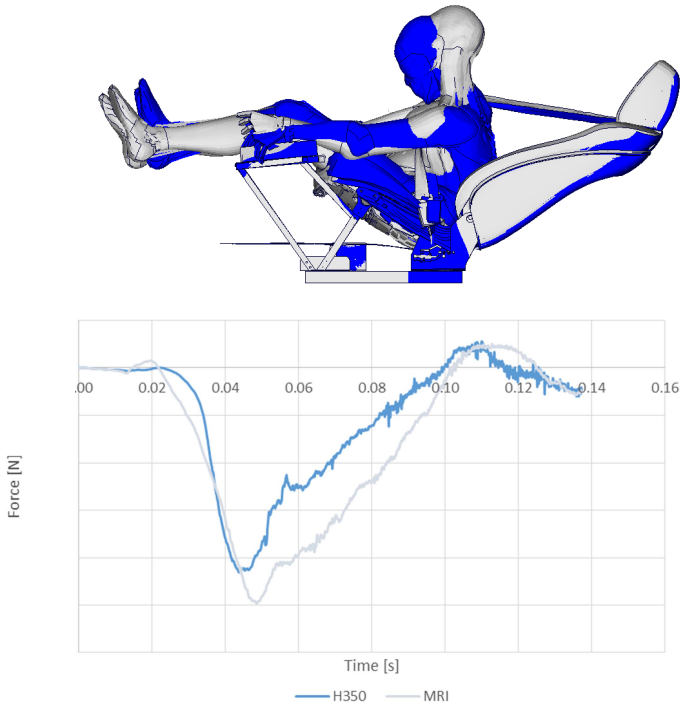

Figure 4: Differences between the H350-like positioned model, in blue, and the MRI-based positioned model, in grey. Forces are measured in the L5 vertebrae.

In Figure 4 large kinematic differences can be seen between the two original HBM positions, as well as a large difference in the peak force observed and the force development profile.

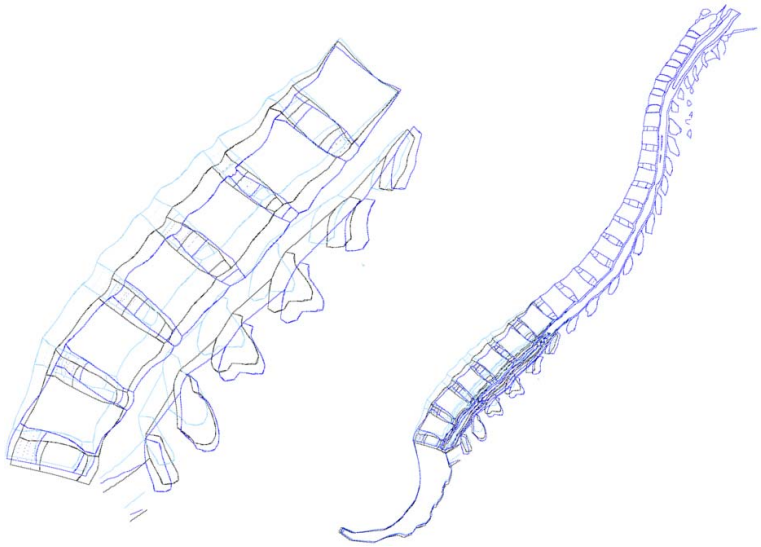

Figure 5: Model orientation after postural positioning, black is the original MRI based position, dark blue is the more kyphotic position, and light blue is the more lordotic position. Left is the lumbar spine where model differences can be easily identified. On the right hand side it can be seen that all the models have the same positioning in the cervical and thoracic spine.

After the postural positioning the two models had only minor differences. In Figure 5 one can see that the light blue and black colorations of the lordotic and baseline models, respectively, are only visible in the lumbar spine and

surrounding soft tissue, in the upper body and lower extremities the models exhibit no visible differences, as the dark blue of the kyphotic position is overlaid on the topmost layer in the graphic.

Force Response

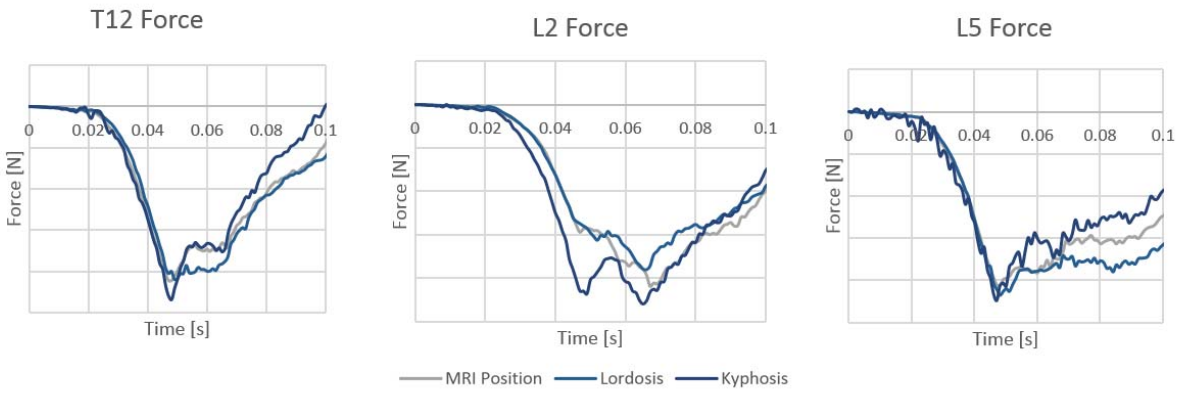

Figure 4: Force histories in selected thoracolumbar vertebra. MRI initial position seen in grey, the more lordodic position in light blue and the more kyphotic position in dark blue. Loading of the T12 and L5 vertebra are consistent across all configurations, whereas no trends hold true for unloading for of the states.

The first thing to note is that the peak force measured in the HBM is much lower than that measured in the dummy. In the HBM H350-like position, the forces are less than 60% of the peak force seen in the hardware tests. In the force time histories of the various postures as seen in Figure 6, one can see differences in the peak force values as well as in the general curve development, though the differences are not consistent across the spinal levels. In general the kyphotic case has the highest peak force, the lordotic case the lowest peak force, and the MRI-based position, a force level somewhere in between.

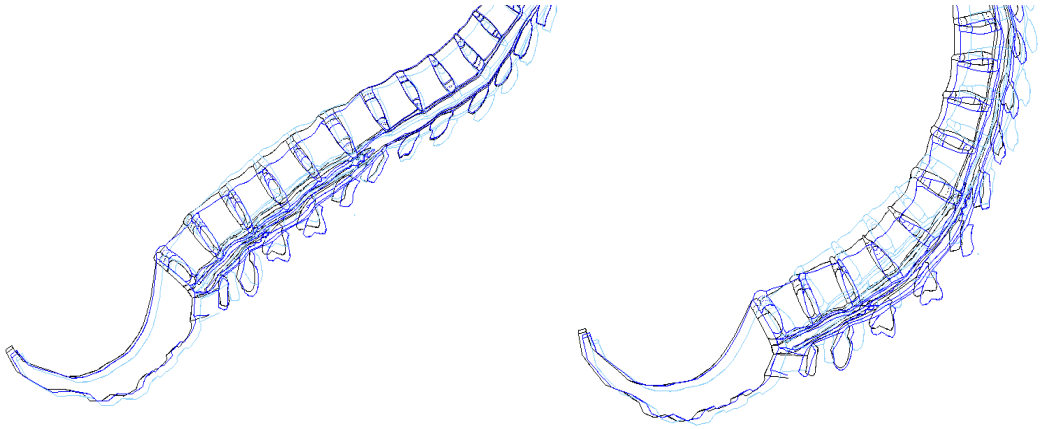

Figure 7: Spinal position at 50ms after the onset of the pulse left and 100ms after the onset of the pulse, right. Black is the original MRI based position, dark blue is the more lordotic initial position and light blue is the more kyphotic initial position.

Kinematics

The kinematics of the lumbar spine remain relatively consistent between the MRI-based and the more lordotic positions, but the kinematics of the more kyphotic position does not follow the same chain. The locations of the pelvis in each position are also quite divergent, and the position of the thoracic spine also shows a large disparity

between the positions especially for the more kyphotic position. All of these differences can be seen in Figure 7. Head kinematics appear to be relatively stable between positions, as seen in Figure 9.

DISCUSSION

Positioning

During the initial positioning using the Upright MRI and Faro arm data, a discrepancy between the model lumbar spine and the lumbar spine which was used to generate the MRI data was observed. It would have been impossible to position the model into alignment with all aspects seen from the MRI: either the positions of the vertebral bodies could be aligned by changing the pelvis rotation, or the observed disk angles could be made the same with the pelvis rotation being kept in the initial state. This is because the subject of the MRI has a different spinal geometry than that which is found in the THUMS HBM. The second approach was the one which was chosen: the pelvis was held fixed and the relative vertebral body angles were used as targets. In the MRI scan, the position was achieved using rigid foam blocks which were very dissimilar to the actual prototype seat. The Faro arm data on the other hand was taken using the prototype seat itself. Due to this it was decided that the pelvic angle should be used from the data were there was a higher confidence in its accuracy in the context of a real world setting. The MRI data was then incorporated in the form of the disk relative angles, starting from the sacrum. Another challenge associated with this position is that the MRI images, and what was measured in the ergonomics lab were two different subjects, whose spines are presumably different. But there is no way to know how different, as the MRI data was gathered as part of a different and separate study by the Ludwig-Maximilians-University in Munich. The study used a seating geometry designed to mimic a reclined position, but this geometry was different than the protype seat currently being studied, which means there are differences in the positioning. Any differences in positioning are also only part of the difference: differences in material properties, and age can also play a role, one which cannot be easily investigated with the present tools and methods.

The spinal rotation is achieved using the Piper positioning tool [6], using kinematic rotation centers defined at the disk center. The Piper approach is used because it allows for changes in the disk shape without causing any bulging that might result from a simulation based positioning process. Another added benefit of the Piper framework is that because the postural changes were localized, the soft tissue changes were also only seen the lumbar region, making the subsequent simulation more stable. The positioning resulted two separate initial postures, each chosen to be on either side of the baseline position. For the lordosis case the lumbar lordosis angle as measured from the top of L1 to the bottom of L5 as defined by Sato [7] was increased by 10°. The Pelvic angle as measured from the vertical to the line between the ASIS and the pubic symphysis [8] was decreased by 1.5°. Both of these changes fall within the range of normal physiological variation according to studies performed by Izumiyama [9], although the authors note that subjects fell into groups of spinal posture and so it can be assumed that the transfer from one posture to the other is likely not physiologically feasible. The kyphotic position saw a change in the lumbar lordosis of -15°, which is a large amount of variation, but yields a position, which is close to the mean values reported by Izumiyama [9]. The pelvic angle for the more kyphotic posture is almost the same as that of the lordodic posture: and both are lower than the pelvic angle of the baseline. This is likely an artifact of the positioning process, where artificial forces are applied to move the spine which resists with an artificial stiffness. It is likely that the kyphotic spine generated enough force to overcompensate the motion of the pelvis, pulling it the opposite way of what was prescribed.

Force Response

It was noted that the in HBM H350-like position, the forces are less than 60% of the peak force seen in the hardware tests. This is in part due to the positioning used to bring the HBM to match some of the H350 landmarks, does not match the reality of how an occupant would sit in the reclined seat. With the head lifted off of the headrest less axial forces are generated in the spine from the inertia of the head moving forward. This difference of position accounts for less than 10% of the difference in the peak force: the MRI based force response as seen in Figure 4 has a higher peak force than the H350-like position, but is still substantially lower to the forces seen in the dummies. Comparing forces measured in the dummies to forces measured in the HBM should also be done cautiously. The models have different geometries, so forces cannot be measured at exactly the same locations across models. These differences in geometry, as well as the use of materials with different stiffness moduli across models, also has an effect on the magnitude of these forces.

Comparing the forces across postures for the same HBM, as seen in Figure 6, the maximum force occurs when the pelvis is fully coupled with the seat. All configurations are seen to have a similar response for forces measured in the

T12 and L5 vertebrae. The kyphotic configuration for the force measured in the L2 vertebra shows a different response than the others with a faster ramp up to peak force, a higher peak force overall, and a double peaked curve behavior. The kinematics in the thoracic spine, as seen by comparing Figures 5 & 7, no longer have any overlap, which holds for all positions. The initial differences in pelvic position propagate, and causes similar changes in displacement and rotation then goes up the kinematic chain into the lumbar spine and the thoracic spine. Head position remains fairly consistent, as seen in Figure 9, likely due to inertial effects and the low relative stiffness in the cervical spine.

It can be seen for all of the various levels in Figure 6, that the peak force is influenced by the initial posture. At the L2, which experienced the largest influence due to the positions; the more lordotic posture had an 8% smaller peak force as compared to the MRI positioned posture, and the more kyphotic posture had a 9% larger peak force. Also at the L2 level, but not for the other levels plotted, the loading curve is significantly different for the more kyphotic posture: it experiences a double peak. The MRI position and more lordotic position both also have a small quasi peak at the same time, but they are more of a slight plateauing than a fully defined peak. At the time of the first peak the pelvis experiences maximum forward excursion before it begins to rotate. The more kyphotic posture experiences a larger force at this point because it has almost no curvature and can therefore maintain its position without deforming. The MRI position and the more lordotic position both have some curvature at this time, so they deform more easily, which doesn't allow the force peak to develop. Given this spread in forces, it is conceivable that there is a posture which exhibits the highest force for a given seating configuration. If future injury criteria are based on the force transmitted, then this posture should be the one which is always evaluated.

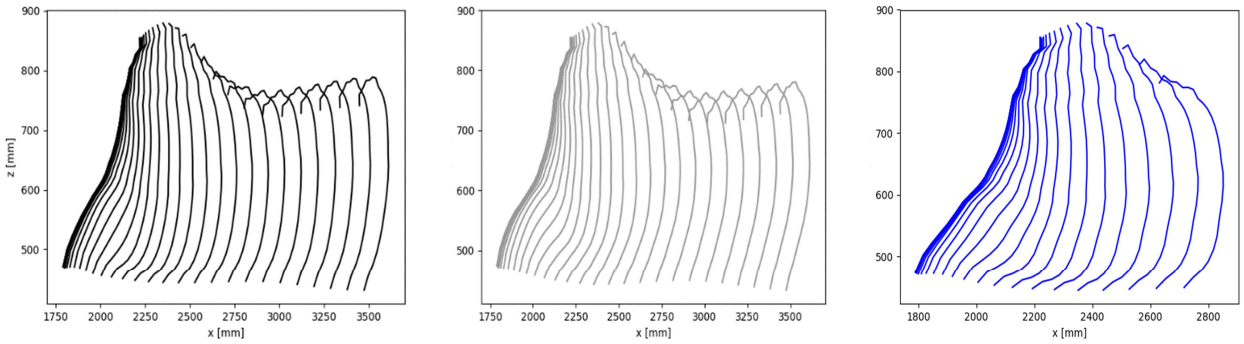

Figure 7: Global spinal kinematic time histories, black is the MRI position, grey is the more lordotic position, and blue is the more kyphotic position.

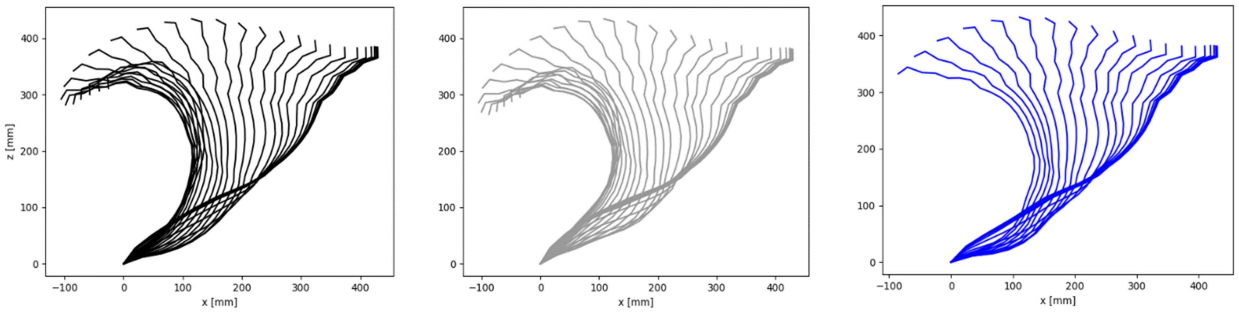

Figure 8: Relative spinal kinematics with the view fixed about the sacrum, black is MRI position, grey is the more lordotic position and blue is the more kyphotic position.

Kinematics

During the loading phase initial posture effects can be seen in the kinematic development of spinal motion. The MRI based position shows an initial instability during the early phase of the crash where the spine goes quickly into flexion around the L3 level. This can be seen in Figure 7, where the black plot can be seen to develop a curvature in the lower left corner. The lordodic initial position on the other hand, shown in grey in Figure 7, exhibits no such instabilities. In Figure 8 this can be seen in the location of inflection in the lower right of the respective subfigures: for the lordotic case the inflection is milder and occurs higher up the spine than is the case for the baseline. This instability immunity is because the lordotic case has more room to deform before it reaches the bifurcation point. One might think of this as a pendulum, where the MRI case is closer to the middle of the pendulum, and ends of crossing to the other side, and the lordosis case is further from the middle, and so never reaches the other side.

The more kyphotic case shows a different response. Towards the bottom of the blue subplot in Figure 8 one can see that the curves run almost horizontally. This leads eventually to an inflection point which is further left than the MRI position shown in black. This tighter, further forward inflection might be due to straighter spinal alignment, which is also seen in the higher force response and steeper ramp up that the kyphotic variant has in the L2 plot in Figure 6.

Also of note is that this local instability has very little effect on the global behavior. This can be seen in the overlay plot in Figure 9: all three models are visible, meaning there is some difference, but the composite result still looks like a coherent model, showing the differences to be small. This means that the head and other global kinematics are insulated from lumbar spine effects. One cannot speculate if this will hold for more pronounced lumbar spine positions, and this should be further investigated.

What can also be seen in Figure 9 is the differences realized between a traditional dummy and the HBM in the reclined seating position. The dummy sits much more upright at the point of maximum excursion as its spine does not allow for bending in the thoracolumbar region. This can be clearly seen in the dummy's very straight back as seen in the figure. Also related to the HBM's more flexible spine changes in the lateral position of the HBM, but not in the dummy. Being less flexible means that the dummy torso bends forward as a complete unit, whereas the HBM wraps around the belt causing a difference between the left and right sides of its torso.

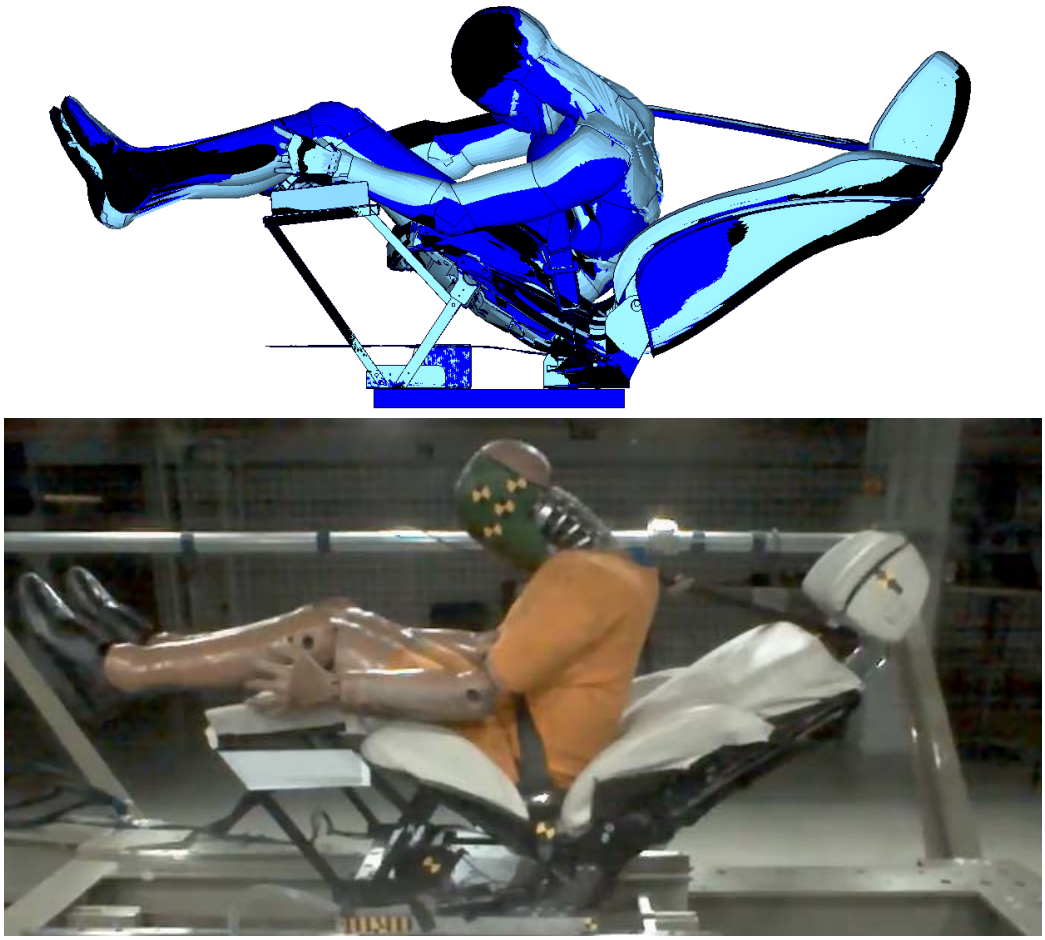

Figure 9: Comparison of global kinematics 100ms after the onset of the pulse. In the upper image are the FE simulations, with the MRI positioned model in black, the more lordotic model in dark blue and the more kyphotic model in light blue. In the lower image is the hardware test of a H350 dummy at 100ms after the onset of the pulse from [4].

Validity

These various results beg the question, what happens in actual humans who have varying spinal geometries? This is a difficult question to answer. The validity of human body models have been improving, but there are still large gaps of validity. One such gap has to do with the spine. As of now, no published studies exist with which to explicitly validate human body models in a reclined seating configuration, with respect to their spines. The spine is difficult to validate as tracking it is difficult. It is also difficult to measure the forces transmitted through the spine. In this simulation series the disks were compressed beyond the physiological levels observed in non-injurious tests [10], but there is a lack of data to say where the level of injury starts. The human body models themselves are also not validated in these regions and in these modes of excitement. Even with newly defined allowable safe levels of force, experiments are still needed to see if what the models predict matches the reality fot actual occupants. This study also shows that posture has an influence in HBM simulations, but the actual range of postures in a reclined seating concepts is currently unknown, and there is no best practice for measuring the spinal position to the accuracy needed to validate HBM simulations. There is a similar story for any sort of safety criteria. More research is required from governing bodies and original equipment manufacturers in order to define and harmonize safety standards.

CONCLUSIONS

The kinematic response of the Human Body Model simulation is very different to the response of the dummies in the reclined position. The HBM kinematic looks more realistic than the crash test dummies, as can be seen in how its spinal curvature develops in the HBM, as opposed to the permanently straight-backed dummy. However, there is no way to objectively evaluate how realistic current HBMs are in this kind of positions. The HBMs also experienced notably smaller forces in the lumbar than the dummies, of which only a small part can be attributed to difference in position. By making small changes to the initial spinal posture of an HBM sitting in a reclined seating configuration, changes of up to 9% were observed in the subsequent spinal kinematics and peak force response. As these changes were small, it is possible that larger changes will have larger effects. These postural changes have no analog in dummy testing, due to how dummies are constructed, and as such can only be investigated using HBMs.

Further work

The next steps to be undertaken should involve looking into larger changes in posture, as larger changes could result in still further divergent kinematics as to what has already been observed. Another area of exploration would be to investigate if one posture or group of postures experiences higher forces, or divergent kinematics, which might require special attention, i.e. the definition of a worst case scenario posture. As changes in posture were shown to have effects on kinematics and force response, validation experiments in the future should also consider and, if at all possible, measure and document initial spinal posture. In order to establish how accurate the HBM models are, more validation experiments are needed. The overall validity of HBMs in reclined positions should also be more closely investigated, which would require that more experiments designed to improve HBM validity in these new seating positions.

1. Sofia Jorlöv, et al. 2017. "Seating Positions and Activities in Highly Automated Cars– A Qualitative Study of Future Automated Driving Scenarios." Proceedings of IRCOBI

2. National Highway Traffic Safety Administration. 2017 "Automated Driving Systems 2.0: A Vision for Safety."

   <https://www.nhtsa.gov/sites/nhtsa.dot.gov/files/documents/13069a-ads2.0_090617_v9a_tag.pdf>

3. Sherwood, C. et al. 2009. “Characteristics of Small Overlap Crashes” Proceedings of the 21st ESV Conference,

4. Huf, A. et al. 2018. “Development of Occupant Restraint Systems for Future Seating Positions in Fully of Semi Autonomous Vehicles.” Proceedings of Airbag Conference

5. Östling, M. et al. 2018. “Driver Behaviour in Automated Vehicles and Effects on Safety – A Swedish and Chinese Perspective: How do we Save More Lives in the Future?” Proceedings of VDI Safety Systems

6. Beillas, Philippe, et al. 2015. "Specifications of a Software Framework to Position and Personalise Human Body Models." Proceedings of IRCOBI

7. Sato, F. et al. 2015. “Analysis of the alignment of whole spine in automotive seated and supine posture using an upright open MRI system.” Proceedings of JSAE Annual Congress

8. Kyo, T. et al. 2013. “Factors predicting change in pelvic posterior tilt after THA.” Orthopedics

9. Izumiyama, T. et al. 2018. “The Analysis of an Individual Difference in Human Skeletal Alignment in in Seated Posture and Occupant Behavior Using HBMs ” Proceedings of IRCOBI

10. Newell, Nicolas, et al. 2017. "Strain Rate Dependence of Internal Pressure and External Bulge in Human Intervertebral Discs during Axial Compression." Proceedings of IRCOBI

11. Foster, J. et al. 1977. "Hybrid III—A Biomechanically-based Crash Test Dummy." SAE Transactions,

COUPLING DEVICE FOR CHILD RESTRAINT SYSTEM (CRS) FOR INFANTS AFFECTED WITH OSTEOGENESIS IMPERFECTA: DESIGN AND NUMERICAL ASSESSMENT

Miguel Ángel, Martínez Miranda, Christopher René, Torres-San Miguel, Juan Alejandro, Flores Campos

Instituto Politécnico Nacional, Escuela Superior de Ingeniería Mecánica y Eléctrica, Sección de Estudios de Posgrado e Investigación, Unidad Profesional "Adolfo López Mateos" Zacatenco Edificio 5, 2° Piso Col. Lindavista C.P. 07738, México.

México.

Luis, Martínez-Sáez

Universidad Politécnica de Madrid

Spain
19-0063

ABSTRACT

The second death reason in children since 5 until 14 years is related with injures produced during traffic incidents mainly due to vehicle's passive safety systems, which are not designed to safeguard their lives. Thus, current traffic norms impose the usage of Child Restraint Systems (CRS).

Notwithstanding, CRS for children with different ailments as bone-degenerative ones do not exist. For instance, around half a million persons suffering Osteogenesis Imperfecta (OI) are estimated to exist. At the best knowledge of the authors, currently, there is no CRS specially development for children with OI.

This work in progress aims to provide a solution for car mobility of infants with OI based on a CRS designed to dissipate a part of kinetic energy during vehicular impacts.

The proposed mechanism consists on a Cartesian mechanism system with linear displacements in axis X, featuring springs and dampers, which is aimed to dissipate kinetic energy in order to reduce the decelerations reaches for the child during a frontal crash. The system is designed in CAD software and is then analyzed numerically, through a 2D dynamical Software simulation.

In order to obtain a cheap and adaptable CRS, it was established a methodology based on the research, recovery, and analysis of information. The mechanics has been development to the new European standard R129 (I-SIZE).

This appliance can dissipate kinetic energy in critical amounts, which could cause damage to OI minors. Numerical analyses show the appropriateness of the design for the purpose of safeguarding OI bones from fractures during front impacts.

Critical deceleration can be present during this kind of impacts. Nevertheless, numerical results validate them obtaining lower decelerations using the proposed system than using ones of the typical CRS.

Despite 2D dynamical recreation, manufacture of the prototype and its further test in a sled platform to confirm that the design accomplishes its goal for different age groups according to R129 is required. Further research on optimizing the CRS is required so to improve these features.

It is important to remark that even the new European standard R129 (introduced completely) in 2018, as well as traffic regulations around the world (up to the best the knowledge of the authors), do not require the usage of any specialized CRS for infants with OI or for any other bone-degenerative diseases. Thus, this research sets an important precedent for the development of this type of specific systems as well as for corresponding regulations to protect OI child population of high risk in vehicular accidents.

INTRODUCTION

Osteogenesis Imperfecta (OI), also known as brittle bone disease, is a genetic disorder. According to data from the European Federation of OI (OIFE), in the world, about 0.008% of the world population is affected by this disease [1]. Depending on the characteristics of the pathology and its severity, there are 4 types of OI [2]. The classification of this disorder directly concerns the type of gene in which the mutation occurred [3]. The elastic modulus of the bones of people who suffer from OI also depends on the classification of their disease.

The bone system of a healthy person has an elastic modulus of 90 ± 19 MPa, while an affected person with type III OI is 40 ± 10 MPa [4-5]. So is easier who they suffer fractures, mainly in the long bones, femurs, tibias, and ribs [6].

On the other hand, there are four anthropometric and mechanical parameters for the evaluation of the safety offered by a vehicle to an OI affected [7]. The first one is for people at higher risk of fractures, limiting their mobility, risk that decreases during puberty. The second type is the riskiest because the affected presents prematurity and low weight. The third one includes those affected with various and intense symptoms having progressive malformations. Finally, the fourth, very similar to type one, is differentiated by having moderate symptoms [8].

Previous research in the Department of Spanish Traffic (DSE), shows results of biomechanical response of sick with OI using three modified CRS and from different manufacturers. For the research, dummies of the series Q3, Q6 and Q10 were adapted to the anthropometric properties of affected with OI. The tests were development down the R129 standard in a Sled platform with a velocity of 50 km/h in a frontal crash. The results were favorable but, the protection offered by these systems was not adequate for the affected population [9].

The different fields of research related to OI have not been fully explored due to the low incidence of this genetic disorder. In the field of engineering, they have taken on the task of developing new technologies with the aim of increasing the quality of life of those affected. Nowadays, in the area of passive vehicle safety, most of them have only been designed CRS for people who do not suffer any kind of suffering. Therefore, people with OI travel in CRS that are not suitable for their anthropometric and biomechanical needs.

The design and function of the anchoring systems (ISOFIX, LACHT) and retention (safety belt and pretension systems) established in the CRS manufacturing, design and commercialization standards; they do not meet the needs of restraint and retention of OI affected. Although its function is to avoid the displacements of the CRS and the excursion of its occupant, in many cases the response of these systems is usually sub-damped or over-damped. In previous studies conducted in dummies of the Q3 series at a speed of 50km / h during a frontal impact, when a seatbelt stops a person's excursion, chest pressures of up to 4500 N are reached [10]. Exposing the physical integrity of a passenger to high risk and even more when he suffers from OI.

Emerging the need to design a retention device that allows the control of the displacements that a CRS experiment during at least one frontal collision, as they are the most frequent. Also, while the displacements happen, a damping system would work. By the performance of the damping system and with a suiting CRS as possible for the OI affected, the pressure exerted by the restraint systems will be less, decreasing the risks of fractures and injuries. The above because the excursion and displacements of affect's body will be less.

As already mentioned, the OI sick travel in CRS made by relatives of them, further reducing the safety and comfort of the passenger [11]. And, in addition, exposing them to a greater risk at the time of moving in vehicles and especially in case of a vehicular accident. If a device with the characteristics stablished before, the safety of the occupants would be increased.

Nowadays, in the category of "special needs", including R44 and R129 [12], there are no guidelines in which the needs of the population with OI are established. Therefore, the main objective of this research is to develop a device that be able to reduce the risk of injuries affected by OI in the event of a vehicular frontal impact accident. This research is organized as next; In the materials and methods section, the established guidelines for the design and evolution of the damping device for CRS are shown. The methodology is based on the search, collect and analysis of information. In order to identify the principal requirements then recognize the possible solutions and finally chose the best one according with the researcher's experience. Subsequently, the design was modelled. Detected the solution, the simulations were carried out to evaluate the system proposed. Within this same section, the conditions under which the system would work were established. In the results section, the graphs corresponding to the response of the damping mechanism, the sizing of the active components of the system and the response of the passenger's body. Finally, in the conclusions section, the achievements reached throughout the development of this research are presented. Also, compared with the peaks, the acceleration will be achieved through experimental and numerical analysis.
Versus the maximum peaks of accelerations with the use of the system develop. The experimental research with which the results are compared was worked out in a sled platform tested at $50\ km\ /\ h$ using a dummy of the Q3 series modified according to the anthropometric characteristics of a person suffering from OI [13].

The numerical research used in the comparation also developed for a vehicle frontal crash at $50\ km/h$ with a dummy of series Q3.

MATERIALS AND METHOD

The methodology proposed is based on the collection, recovery, and analysis of information. Through which the design criteria will be obtained, for this it is necessary to have knowledge of certain characteristics of OI. For example, knowing the elastic modulus of the osseous system of an affected OI and the malformations it undergoes [14-15]. In addition, it is necessary to study the current international norms of vehicular mobility of infants, as well as the manufacture and commercialization of CRS according to the Economic Commission of the United Nations of Europe (CEPE) [16].

The protocol where anthropometric information provided by the "Volume II: Biomechanics Test" of the National Highway Traffic Safety Administration (NHTSA) [17] was retaken and analysed. Similarly, the report of "Anthropometry of babies, children and young people up to 18 years for the design of safety products", from the University of Michigan [18]. Which has been coupled to the needs of people with OI, by the Polytechnic University of Madrid [19]. It was also required to collect and analyse information about the nature of a frontal vehicular impact, according to the science of road accidents and general forensic studies [20]. And of the biomechanics of the behaviour of an occupant of SRI during a frontal crash [21].

After the search and analysis of the information within the literature of free access, and in accordance with the experience of the researchers, it has been possible to establish the main characteristics of the design proposed. As a first instance, the device must be designed according to the current standards. Therefore, it must have the ability to change the orientation of the anchor ISOFIX, according to the age of the child. The design should allow for adaptability and the assembly with any model of automobile.

The proposed solution should allow control of the displacements and accelerations experienced by the occupant of the CRS. By means of the reduction of the accelerations suffered by the occupant, the pressures that the safety belts would exert will be lower. Also decreasing the possibility of collision with objects that are in front of the passenger. To reduce the cost, the design of the solution has been adapted to work as universal support adaptable to any type of CRS manufactured according to current standards. The solution will be established in an adaptable clamping and anchoring device for CRS. The proposed methodology is summarized in Figure 1.

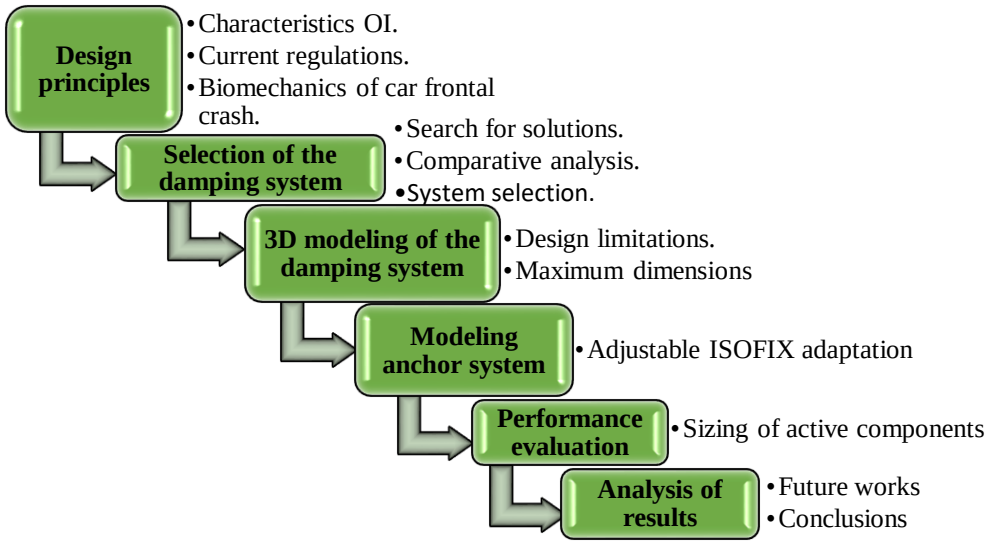

Figure 1: Design methodology of the damping adaptive device for CRS.

For the selection of the damping system, the analysis of the functions to be performed based on the inputs and outputs of the device is performed. The inputs are: the average accelerations ($G's[t]$) that a CRS experiences and the user when an accident occurs, as well as the force ($F[t]$) it receives and the mass (m) of both.

On the other hand, the displacement ($x[t]$), the velocity ($\dot{x}[t]$) and the accelerations ($\ddot{x}[t]$) of the CRS and the occupant are presented in the outputs.

It was determinate that the damping system should allow position, velocity and acceleration control ($x[t], \dot{x}[t], \ddot{x}[t]$) of the CRS and its occupant. In addition, based on the experience of the researchers, it was proposed to perform the analysis of two control systems, the first open loop and fully mechanical and the second a feedback electromechanical system. For the first case, a Cartesian mechanism was chosen that would have a set of springs and dampers as actuators. For the second option, a position control by reaction wheels with electric motors was selected. In Figure 2, you can see a block diagram of the first proposal.

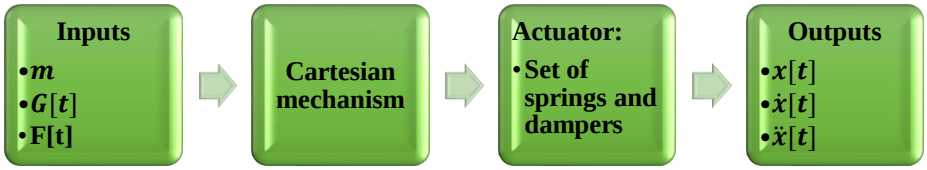

Figure 2: Diagram of inputs and outputs of Cartesian mechanism.

Figure 3 shows a block diagram of a position control system by reaction wheel type, where it should be noted that there are two additional inputs: electric power ($v[t]$) and the error input ($e(t)$).

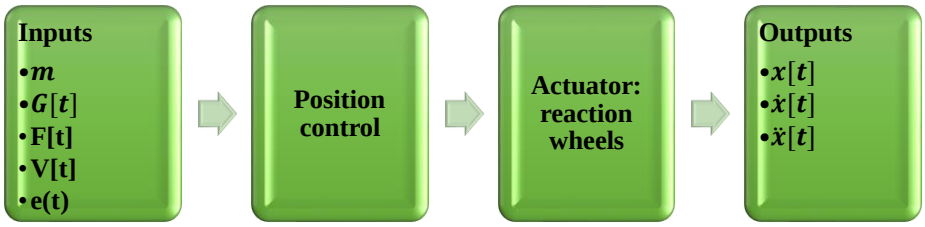

Figure 3: Block diagram of the inputs and outputs of a position control system by reaction wheels.

Determinate the possible solutions, they were thoroughly analysed, determining the advantages and disadvantages of each one based on the experience of the researchers. The main disadvantage of the Cartesian mechanism is that there is no feedback. Without feedback within the mechanism, no control strategy can be implemented, although it is possible to study its behaviour before certain inputs and thus size the system. In other hand the system has great advantages, the most important is that it does not require an external source of energy to function, also its easy implementation, and it is a robust system, characteristics that reduce the possibility of failures.

In contrast, the main advantage of the reaction wheel system is the existence of feedback. Establishing the possibility of use control strategies. But the main disadvantage of this system is that it requires an external power source of electrical energy ($V(t)$), Figure 3. Also, the implementation requires numerous electronic systems, increasing its cost and complexity.

After the above conditions, the set of reaction wheels is put at a disadvantage with respect to the first proposed. So, the Cartesian mechanism was selected with a set of springs and dampers as actuators. Although the response of the Cartesian system does not have feedback, the chances of failure are less, since it does not depend on an external source of energy. And the response speed of this system meets the established needs.

Modelling of adaptive support for CRS used by OI affected

Once the Cartesian mechanism was selected, it has been adapted a damping system. A proposal of the components and its dimensions has been presented. It was determined that it should be a system that allows linear displacements along the X axis.

Also, in order to dissipate the kinetic energy were add a pair of dampers and springs. The array of springs and dampers allows the displacements in a controlled oscillate way. In the end, two mass concentrators were attaching the system in order to make the behaviour of the system as a vibration absorber.

Cartesian mechanism, in Figure 4, you can see the diagram of the proposed mechanism. Which has a linear bearing (B1) arranged on the rails (X1, X2). It can also be observed that there are eight springs (RX1, RX2, RX3, RX4, RX5, RX6, RX7, and RX8) placed concentrically on the rails. The spring anchors, RX1, RX2, RX7, RX8, have a fixed point and a moving point. While the anchors of springs RX3, RX4, RX5, RX6 are all mobile and move according to the displacements of the concentrators of mass and the slide. Likewise, the dampers (A1, A2, A3, A4) can be observed, which have a fixed point and a moving point, anchored to the bearing (B1). It is important to mention that the mass concentrators (M1 and M2), are fundamental pieces when it comes to reducing the accelerations reached by the passenger when the crash happens.

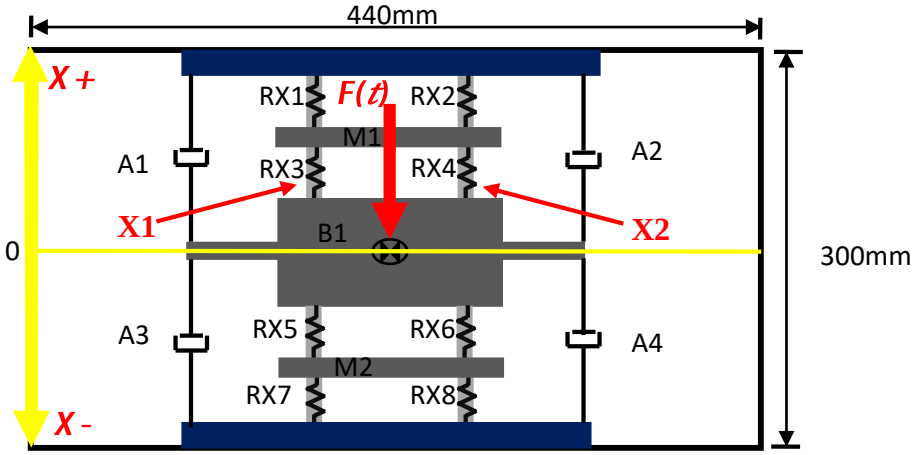

Figure 4: Diagram of the Cartesian mechanism.

Once the components of the Cartesian mechanism were established, as well as the arrangement and the maximum dimensions of the system, the three-dimensional model was generated. A computer program of Computer Aided Design (CAD), *SolidWorks ®* 2017 and high-performance computing equipment were used. In Figure 5, the proposed design of the Cartesian mechanism modelled in three dimensions can be observed.

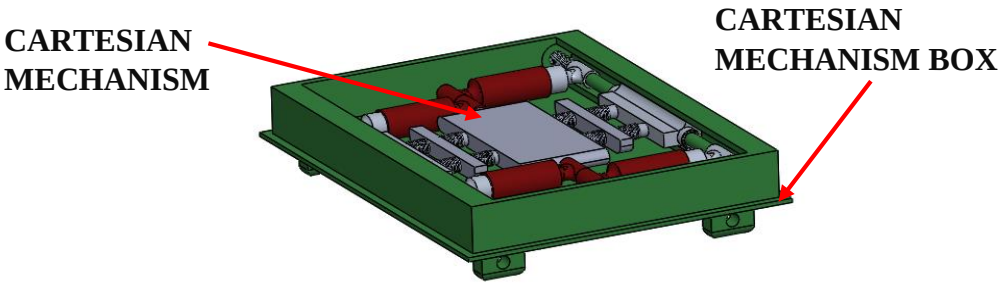

Figure 5: 3D model of the Cartesian mechanism.

With the Cartesian mechanism 3D model, the design of the support was carried out in conjunction with the anchoring system. As mentioned above, the adaptive support design was develop based on current standards. So, the system must have ISOFIX, according to the R129 standard. In the same way, it is necessary to establish a system in such a way that its orientation can be modified. Therefore, it has a set of insurance and rods that allow changing the orientation of the anchors, when necessary.

Anchoring of the adaptable support see Figure 6, the system consists of 3 rods, of which two are placed in the same direction and one in the opposite direction. The locks are designed in such a way that the rod presses into the lock. In addition, this one has an "L" shape, where the longest part is the one that penetrates the CRS, and the shortest one is with the locks.

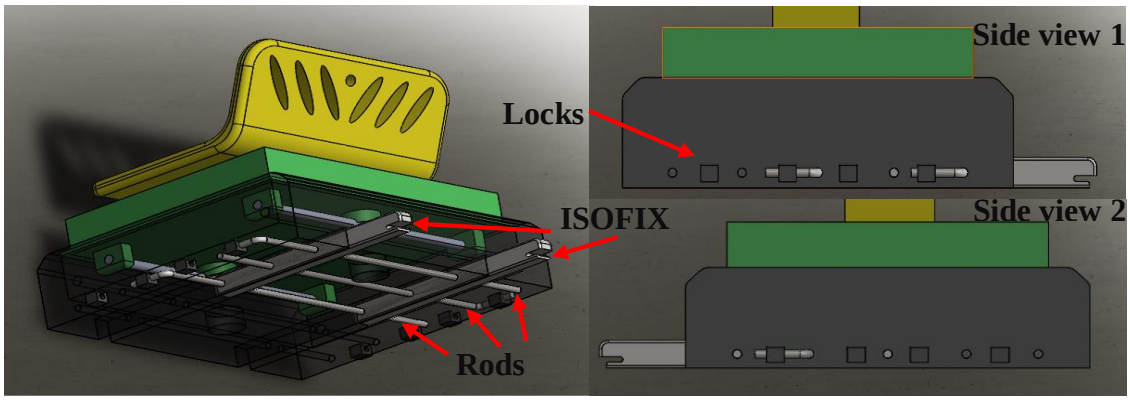

Figure 6: Anchoring of the adaptable support

As stipulated in the beginning, this research will develop an adaptive support for CRS, but not the retention system as such. Once the design of the anchoring system for the adaptable support has been established, it is only necessary to design a system that allows the correct CRS clamping.

CRS anchor, the main function is to keep the CRS fixed, in the adaptive support. See Figure 7, you can see the anchoring system of the CRS, which consists of a piece moulded to match the external part of the backrest and the base of a CRS. Also, in the lower part of the piece, there is the block that will be fixed to the slide B1, of the Cartesian mechanism; thus, joining the CRS with the adaptive support.

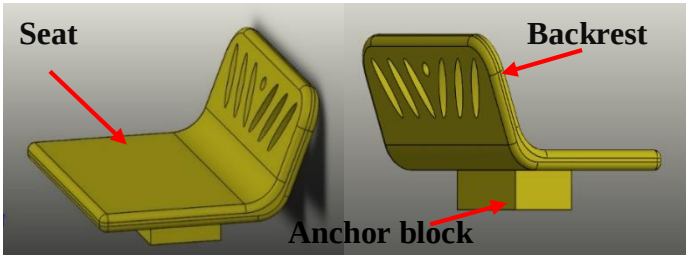

Figure 7: Anchoring system for the CRS.

The last design of the resulting adaptive support can be observed in Figure 8, where the car seat, the adaptive support and the CRS are presented.

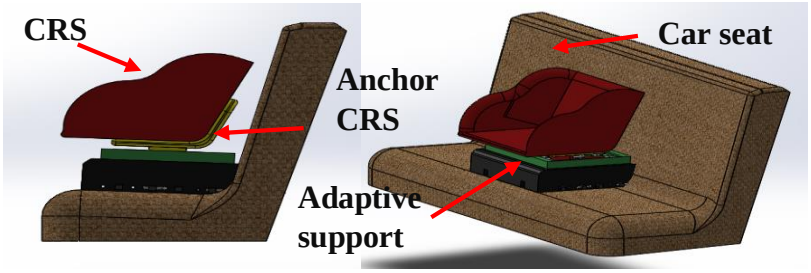

Figure 8: Final design of the adaptive shock absorber support with a CRS installed and arranged in an automotive seat.

Dynamic simulation in two dimensions

The modelling of the system was carried out, by means of a two-dimensional movement simulation computer program for dynamic designs. Through these simulations, it is possible to know the answer to external stimuli ($F(t)$). So, it was necessary to draw the Cartesian mechanism. The dimensions of the model made in the two-dimensional simulator should be the same as those of the CAD model in three dimensions.

In order to know the biomechanical response of the occupant, modelling of a dummy was made in 2D based on the anthropometric parameters of weight and length of the parts of the body of an affected one with OI obtained by means of statistical data collection [22]. It was also necessary to model a CRS, which was anchored using the ISOFIX system and where the dummy was placed. To simulate the retention of the safety belts, springs and dampers were placed strategically.

As well to study the biomechanical response of the occupant, a CRS was modelled that was placed on the designed damping device. As above, the dummy was set, and the damper spring systems were installed that emulate the behaviour of the safety belts. Once both models were finished, they were subjected to the accelerations that they would experience during a frontal impact.

To perform the dynamic simulations, it was necessary to know the impulses of force with which the operation of the system will be tested. It is required to know the average acceleration experienced by a child with an approximate weight of 15kg during a vehicular frontal collision at 50 km / h. The input pulses for the system will be collected from previous investigations developed under the guidelines of the R129 standard.

Cartesian Mechanism, the dynamic simulation of system behaviour, aims to know the linear displacements ($x(t)$), velocities ($\dot{x}(t)$) and accelerations ($\ddot{x}(t)$), in front a force ($F(t)$) perpendicular to the Y axis. As mentioned, the mechanism consists of a bearing (B1) anchored to the rails (X1 and X2), allowing the displacement along the length of the x axis. In addition, two mass concentrators (M1 and M2) are included, with an approximate weight of 2.5 Kg each, turn up Figure 1, you can see the diagram of the Cartesian mechanism, which must be modelled in the computation program for dynamic simulations in two dimensions, see Figure 9.

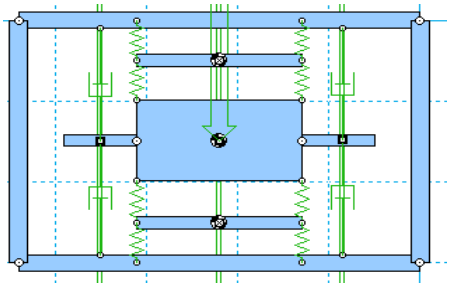

Figure 9: Dynamic simulation of behaviour on the X axis.

Development of the dummy and the CRS, for the modelling of the two-dimensional dummy, took advice previous researches, in which information was collected on the anthropometric parameters of weight and length of specific parts of the body of those affected. In Table 1, relevant information about the approximate weight and its distribution in the body of an affected by OI is observed [23].

Table 1:
Estimated mass distribution for an affected OI [23].

Part	Estimated mass (kg)
Head	3.94
Neck	0.25
Clavicle	0.29
Torso	5.59
Right arm	0.77
Left arm	0.77
Right Femur	1.22
Left Femur	1.19
Left tibia	0.84
Right tibia	0.90
Total mass	15.76

Known the approximate mass distribution of an affected OI, the weight parameters that would be used for modelling the dummy in 2D were established. Table 2 shows the amount of weight that was assigned to each part of the body of the proposed model. It is important to mention that the approximate weight of the clavicle and the arms were assigned to the torso, also being a model in two dimensions, the weight of both femurs and tibias was assigned to only one, see Figure 10.

Table 2:
Weights established for 2D dummy modelling

Part	Estimated mass(kg)
Head	3.94
Neck	0.25
Torso	7.42
Femur	2.41
Tibia	1.74
Total mass	15.76

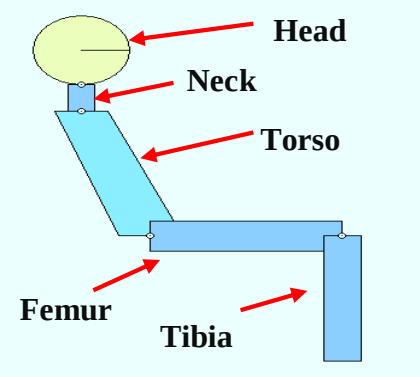

Figure 10: Dummy modelling for simulations

After the dummy modelling was completed, the design of two CRS was carried out, the first of them; using conventional anchoring systems (ISOFIX), see Figure 11 a). Then, the modelling of a CRS was performed, but using the buffer device proposed in this investigation, see Figure 11 b). And the dummy was placed on both CRS. With both models finalized, restrictions of linear displacement were established on the x axis, and the force ($F(t)$) was applied to which both bodies would be subjected (dummy and CRS); in the centre of mass, in case of vehicular frontal impact, see Figure 12. It is important to mention that the approximate weigh of each CRS established was about 5 Kg.

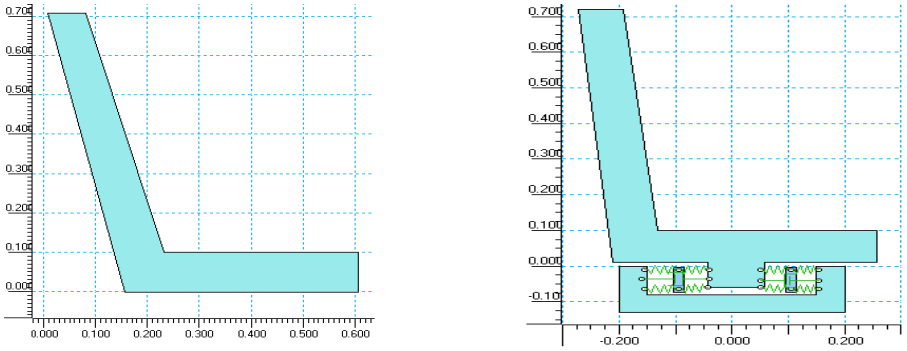

a) **b)**

Figure 11: a) Conventional CRS b) CRS modelled using the proposed damping device.

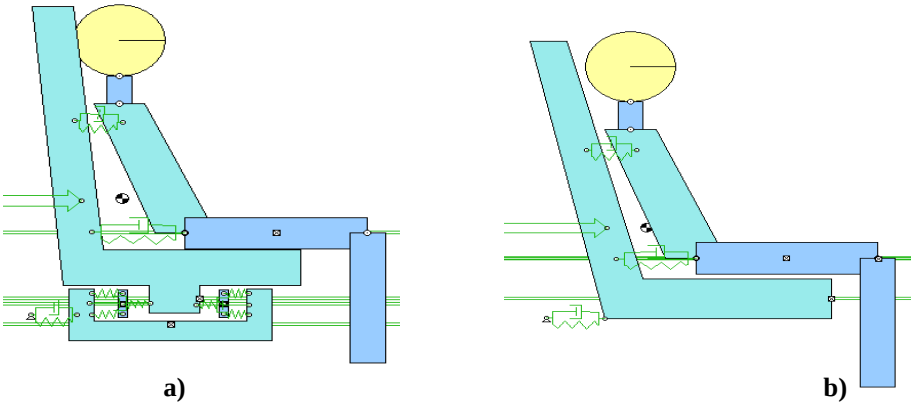

Figure 12: a) conventional CRS and dummy, b) CRS and dummy using the proposed damping device

Pulses of forces used for the numerical simulation, like the damping device is integrated by several springs and dampers with the function of control the displacements, velocities and accelerations ($x(t), \dot{x}(t)\ and\ \ddot{x}(t)$, respectively) which experiences a CRS and its occupant during a frontal collision. The response of the active components of the system (springs and dampers) must be studied. This test is done by applying the force pulse ($F(t)$) that a CRS and its occupant would receive during the impact. It is important to mention that these pulses of force must be obtained through tests carried out under the guidelines established by the R 129 standard for frontal impact tests at $50\ km/h$. Finally, the mass of the occupant with whom the study was conducted should be approximately $15kg$, since according to statistics it is the average weight of an affected OI [24].

To test the operation of the system in the event of a frontal impact, the data obtained from previous research was retaken. The study was to determine the average accelerations experienced by the body of a child under 36 months of age (dummy series Q3), weighing approximately $15\ kg$, and his CRS (weight approximately $5\ kg$) during a frontal impact at $50\ km/h$ under the guidelines of standard R129 [25]. Obtaining the graph of Figure 15, from which it can be highlighted that the maximum peak of the average accelerations that are experienced ($\ddot{x}(t)$) is approximately $100\ G's$ at around $38ms$ the curve obtained in this study was made with the help of a program of computation of numerical simulations using a finite element.

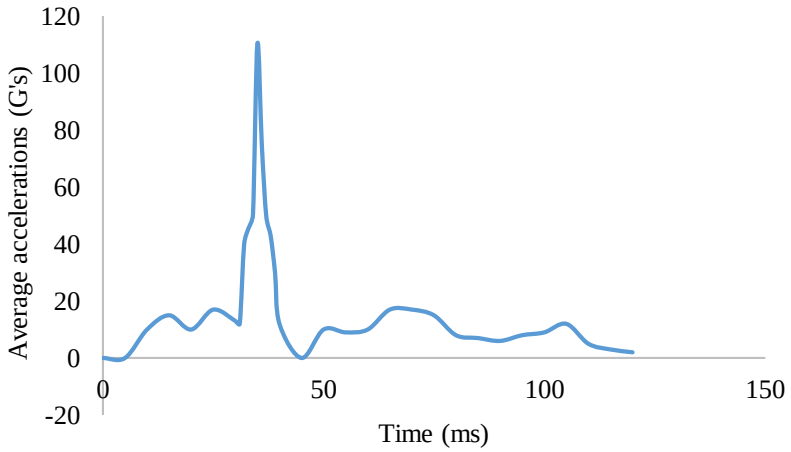

Figure 15: Average acceleration experienced by a minor during a frontal vehicular impact.

From the graph of Figure 11, it is also worth noting that the critical period in which the vehicle accident occurs is less than 120ms. In addition, it has a behaviour like that of a pulse function or Dirac Delta ($\delta(t)$). An algorithm was made to interpolate by the Lagrange method a polynomial as a function of time (Equation I) that describes the behaviour of the accelerations experienced by a CRS and its occupant from the acceleration curve of Figure 11.

$$\ddot{x}[t] = 7.807t - 1.885t^2 + 0.178t^3 - 0.007t^4 + 0.0001 - 0.000002t^6 + 1.582 \times 10^{-8}t^7 - 6.351 \times 10^{-11}t^8 + 1.067 \times 10^{-13}t^9 \quad \text{(Equation I)}$$

Figure 16 shows the graph of the polynomial as a function of time (Equation I), which describes the average accelerations $x(\ddot{t})$ experienced by the minor, during 120ms.

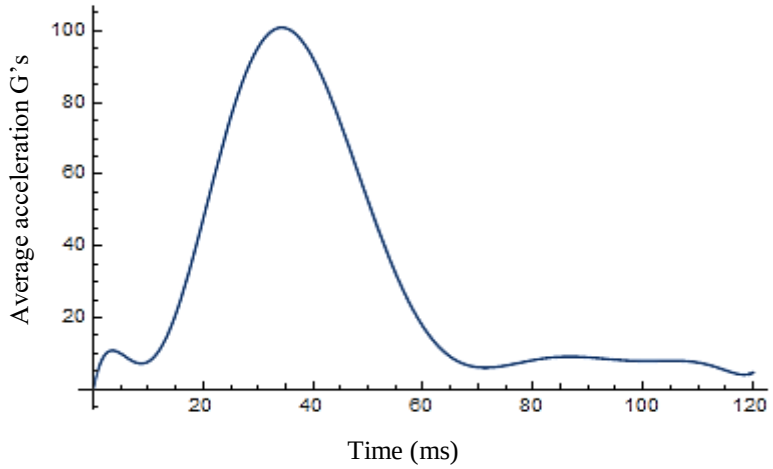

Figure 16: Graph corresponding to Equation I.

By Equation I, it is possible to obtain the force as a function of time($F(t)$), which will experience the child and its CRS during vehicular impact. The above is possible by Equation II. Where m, is the mass of child (approximately$15\ kg$) plus the mass of the SRI (approximately $5\ kg$), $\ddot{x}(t)$, is Equation I and $F(t)$, it will be the input force impulse used for the simulation dynamic. Applied for the first simulation in the centre of mass of the slide (B1) and in the second in de centre of mass of dummy an its CRS both during a time of$120ms$.

$$Fx(t) = m\,\ddot{x}(t) \quad \text{(Equation II)}$$

RESULTS

This stage of the research was divided into three parts, the first consisted of the sizing of the active components based on the experience of the researchers and the availability of the components in the current market. The second part was based on obtaining the displacement graphs ($x(t)$), and acceleration ($x(\ddot{t})$) of the bearing B1 of the Cartesian mechanism, the total weight (CRS and child), was assigned to bearing B1. The final stage consists of the average acceleration graphs experienced by the occupant's body using the three established proposals

Sizing of springs and dampers of the Cartesian mechanism.

The function played by these devices is important, through them it is possible to reduce the accelerations that could damage to the OI affected during frontal impact vehicle. Decreasing the possibility of injury or reduce the severity of them. Therefore, the sizing of the dampers and springs must be done as best as possible. The coefficients depend to a great extent on the mass of the CRS and its occupant. As mentioned, this study was carried out considering that the mass of the minor is approximately 15 kg and that of the CRS around 5 kg.

Table 3, you can see the proposals for the springs and dampers constants of the mechanism. In the first proposal, value A, a very high value was established for the spring's coefficient, while the value of the dampers is small. For option B, the coefficients were proposed, according to the experience of the researchers. Finally, the values of option C were proposed based on a catalogue of compression springs [26] and a catalogue of dampers [27], both commercial.

Table 3:
Constants of springs and dampers belonging to the Cartesian mechanism

Device	ID	A	B	C	Length
Dampers $(N\frac{m}{s})$	A1	1	15	12	15
	A2	1	15	12	15
	A3	1	6	12	15
	A4	1	6	12	15
Springs $(\frac{N}{m})$	RX1	50	10	10	5
	RX2	50	10	5	5
	RX3	50	5	5	5
	RX4	50	5	5	5
	RX5	50	10	5	5
	RX6	50	10	5	5
	RX7	50	10	5	5
	RX8	50	10	5	5

Graphs of displacement $x(t)$ and acceleration $\ddot{x}(t)$.
Knowledge of behaviour of the Cartesian mechanism face the force input ($F(t)$) of Equation II, during a time of $120ms$ applied at the centre of mass of the bearing (B1) is important. The displacement graphs allow us to know if the bearing (B1) stops before reaching the limit switches of the mechanism. The accelerations allow the evaluation of the response of the damping device before previously established injury criteria. At last, the comparison between the maximum peaks of the accelerations experienced when a conventional CRS is used, versus the use of system proposed. See Figure 17, the graphs resulting from acceleration are showed and the displacements in Figure 18, when the values proposed in Option A, B and C of Table 3 are used.

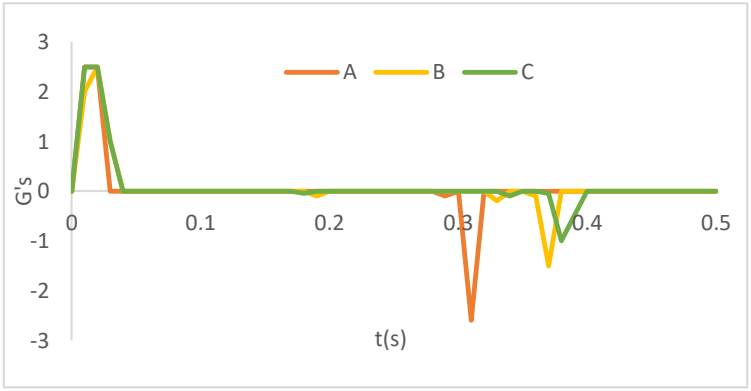

Figure 17: Response of the accelerations ($\ddot{x}(t)$) of the Cartesian mechanism face a force (F (t)) input.

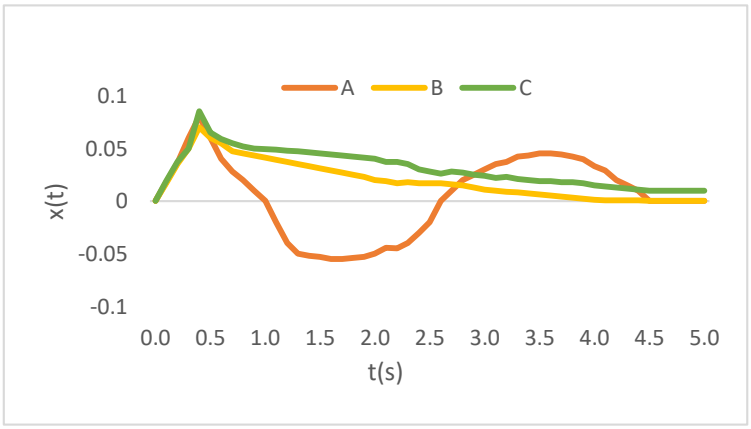

Figure 18: Response of the displacements ($x(t)$) of the Cartesian mechanism face a force (F (t)) input.

In Option A of Figure 17, the acceleration responses ($\ddot{x}(t)$) of the Cartesian mechanism are observed, where the maximum acceleration peak was of approximately $2.5G's$; also, at 0.3 s an acceleration is experienced in the opposite direction that reaches around $2.5G's$. The acceleration curve, from Option B, the maximum acceleration peak reached a value of about $2.5G's$.. Also is the presence of an acceleration in the opposite direction, approximately $1.5G's$ at around the$0.38s$. Finally, in Option C, the maximum acceleration peak reached a value of around $2.5G's$. Similarly, the presence of an acceleration in opposite direction of approximately $0.5G's$ at of around the $0.38s$.
In Figure 18, the displacement curve of Option A is seen; where a maximum peak of $0.08m$, is recorded, decreasing with each cycle that occurs and presenting oscillations. As for the curve of Option B, a maximum displacement peak of approximately $0.08m$ is recorded, then it begins to decrease logarithmically, until reaching the position of origin after $5s$. Finally, for the curve of Option C, a maximum displacement peak of approximately $0.08m$ is obtained and then logarithmically decremented, until reaching the origin position after $5s$.

Average accelerations experienced by the occupant of the CRS using the damping device.
Knowledge of the average acceleration experienced by the occupant is important, in order to validate the functionality of the damper system. As higher the accelerations experienced by the user are, the excursion of the head, neck, and thorax (whiplash) will also be higher. With a high excursion of the body, the pressure exerted by the safety belts on the body of the infant to stop the excursion and displacements increases. On the other hand, the possibilities of collision with the possible objects that are in front of the passenger increase.
Next, in Table 5, the average deceleration curves experienced by the occupant's body are shown. Using the damping device with the different coefficients of the options in Table 3. And the excursion suffered by the passenger when the frontal impact occurs.

Table 5:
Average accelerations and excursions experienced by the body.

ID	Average body deceleration curve	Excursion.
A	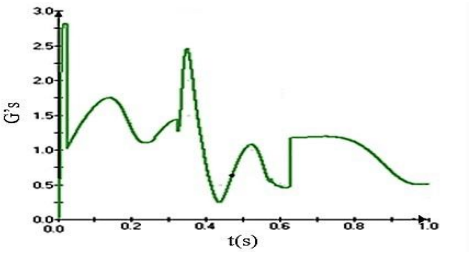	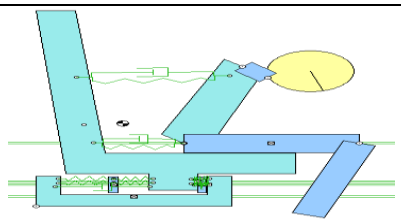
B	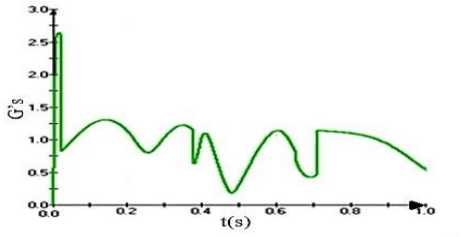	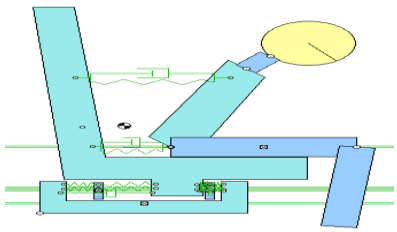
C	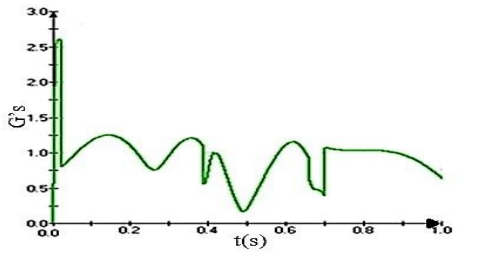	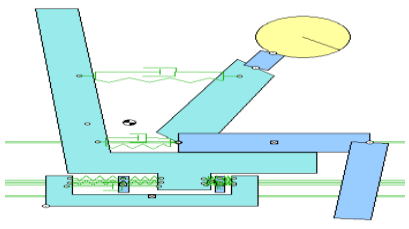

In the answer of the option, A, the maximum peak of the average decelerations experienced by the minor's body is approximately 2.8 G's. Subsequently, decelerations begin to decrease while oscillate, the second peak of approximately 2.5 G's is registered at 0.4 s. The behaviour in general of the decelerations experienced by the child are oscillating, but these do not reach large values. On the other hand, the excursion and displacements experienced by the child's body is reduced, as seen in Table 5, although the head jerks too much. For option B, in the deceleration curve, the maximum peak of the average decelerations experienced by the infant's body is approximately 2.6 G's, being the only peak registered. Subsequently, the decelerations begin to decrease while oscillate. The decelerations experienced by the minor are oscillating, but these do not reach high values. The excursion and displacements experienced by the infant's body is reduced and the head does not jerk a lot. At last option C the behaviour is like B answers. The maximum and only peak recorded was approximately 2.6 G's and the accelerations decreased oscillating. While the excursion of the body was also like B answer.

CONCLUSIONS

This research has allowed deepening the knowledge to increase passive safety in people affected by OI, by designing a damping device for CRS. Among the main conclusions that can be reached once this research has finished, are the following.

- It is possible to recreate a physical model in 2D (dummy), which represents those affected with OI, from the physical parameters. Obtained from data bases collected using statistical data on the anthropometric parameters of people suffering from OI.
- The recreation of a dummy in 2D with the physical characteristics of a OI patient, allows an application for future research allied to this condition and passive vehicle safety.
- Although the representative dummy modelling of the community with OI worked to study the behaviour of the damping device for CRS, it is necessary to create a 3D model in order to obtain results closer to reality as possible.
- It is possible to approximate a polynomial as a function of time ($\ddot{x}(t)$) to a deceleration curve obtained in previous studies, using interpolation techniques, which can describe the behaviour of the accelerations experienced by a child user of a CRS, during a vehicular frontal impact.
- With the polynomial ($\ddot{x}(t)$) and the mass of the passenger (m), it is possible to obtain a polynomial as a function of time that roughly describes the force ($F(t)$), which a passenger experiences during a vehicular impact.
- It is possible to implement a damping system using a Cartesian mechanism and a set of dampers, springs and mass concentrators.
- The addition of two mass concentrators in the Cartesian mechanism allows the system to behave as a vibration absorber.
- It is possible to study the response of the Cartesian mechanism face a force input as a function of time, by modelling the proposed damper device in dynamic simulation software and the polynomial F (t),
- From the dynamical simulations of the Cartesian mechanism, is concluded that the best behaviour is obtained when the elastic coefficients of the springs are small and those of the dampers are almost equal to twice the first.
- By the above configuration, the system response with few oscillations that allows the positive displacement of the main slide (B1). While the return to its origin is with a logarithmic and soften performance, as can be seen in the graph of Figure 18.
- When the coefficients of the springs are too high and those of the small dampers the system has a response, it presents oscillations with large peaks.
- Through the model of Cartesian mechanism, a CRS, a dummy representative of the community that suffers OI and the polynomial F (t), it is possible to know by 2D numerical simulations the behaviour of the occupant's body during a frontal impact.
- After analysing the response of the body and the accelerations experienced during a frontal vehicular accident, it is possible to estimate the level of protection provided by the damper system to the user.
- According to previous research, numerical [28] and experimental [29], the accelerations experienced by an infant occupant of a conventional CRS and using a seatbelt, peaks of up to 100 G's have been recorded in some parts of the body. See the graphs below, in Figures 19 and 20.

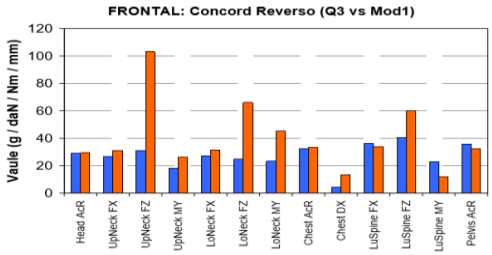

Figure 20: Maximum peaks of acceleration present in some parts of child's body during a frontal vehicular impact at 50km / h under the guidelines of the R129 standard. Develop by an experimental test on a Sled platform with a modified dummy according the physical characteristics of one affected with OI and a conventional CRS [28].

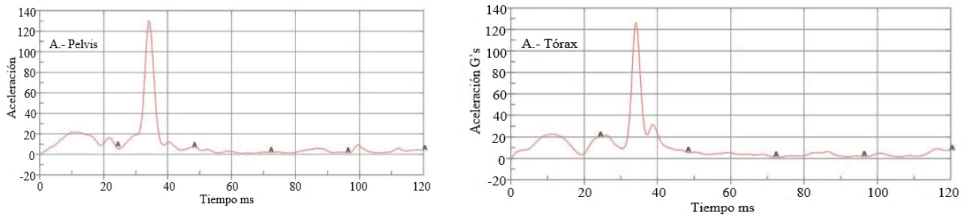

a) *b)*

Figure 20: Acceleration curves in a) Pelvis and b) Thorax, present in the body of a minor during a frontal vehicular impact at 50km / h under the guidelines of the R129 standard, obtained by the finite element method and a conventional CRS [29].

In addition, the behaviour of the average accelerations of the modelled dummy when a normal CRS is used, was studied, as well as the excursion of the body, yielding results like the last researches.

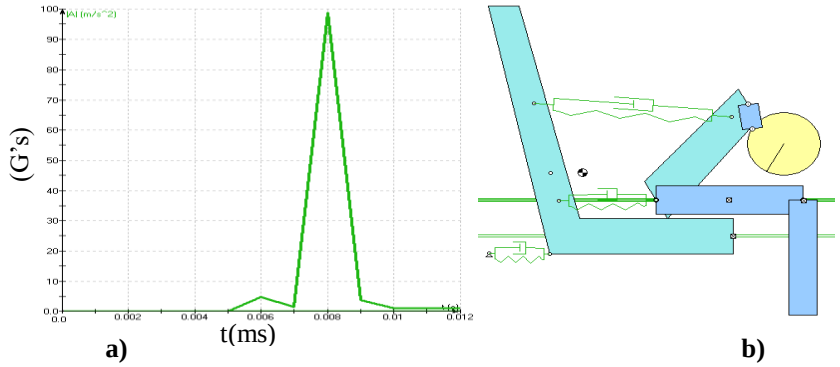

a) **b)**

Figure 21: a) Average acceleration curves, b) Excursion, in the body of a minor during a frontal vehicular impact at 50km / h under the guidelines of the R129 standard, obtained by 2D dynamical simulation using conventional CRS.

- Proceeding the simulation and with a comparison between the graphs shown in Table 5, it can be concluded that it is possible to reduce the accelerations experienced by the body of an OI affected during a frontal vehicular accident allowing the controlled displacement of the CRS by means of a damping device.
- The coefficients of the springs of the damping system must be small, while those of the dampers must be at least twice, otherwise, the system oscillates and the child's head jerks too much.
- It is necessary to design a restraint system for the occupant's head.
- The decrease in decelerations experienced by the body of the child reduces the excursion and displacement of the thorax.
- It is necessary to establish in the guidelines stipulated in the R129 standard for "Special needs", the considerations for the design of an SRI for OI patients.

- Despite the favourable results obtained in this work, it is necessary to manufacture the device in order to carry out experimental tests in a sled platform. In the same line is needed research using the Finite elements method.

Acknowledgment
The authors acknowledge the financial support for the realization of this work to the Government of Mexico by the National Council of Science and Technology (CONACYT), the Instituto Politécnico Nacional, also acknowledge partial support by Projects 20196710 and 1931, as well as EDI grant, all provided by SIP/IPN. And the participation of the biomechanics group of INSIA through the research project "SIRIMOI. Sistema de retención infantil mejorado. Aplicado a la Osteogénesis imperfecta." incorporated to the Universidad Politécnica de Madrid, from Spain.

REFERENCES

[1] Europe, O. I. F. (n.d.). OIFE Statistics. Retrieved October 04, 2018, from http://www.oife.org/index.php/EN/sub-the-oife/oife statistics
[2] Sillence, D., Senn, A., & Danks, D. M. (1979). Genetic heterogeneity in osteogenesis imperfecta. *Journal of medical genetics*, *16*(2), 101-116.
[3] Tipo, I. I. (2002). Tratamiento de la osteogénesis imperfecta. *Anales Españoles de Pediatría*, *56*(SUPLEMENTO 4), 73.
[4] Albert, C., Jameson, J., Smith, P., & Harris, G. (2014). Reduced diaphyseal strength associated with high intracortical vascular porosity within long bones of children with osteogenesis imperfecta. *Bone*, *66*, 121-130.
[5] Imbert, L., Aurégan, J. C., Pernelle, K., & Hoc, T. (2015). Microstructure and compressive mechanical properties of cortical bone in children with osteogenesis imperfecta treated with bisphosphonates compared with healthy children. *Journal of the mechanical behavior of biomedical materials*, *46*, 261-270.
[6] Rauch, F., & Glorieux, F. H. (2004). Osteogenesis imperfecta. *The Lancet*, *363*(9418), 1377-1385.
[7] Sáez, L. M., García, M. D. L. O., Álvarez, A. G., Ruiz, M. E., Torres, C. R., & Miguel, S. (2016, November). Parámetros antropométricos y mecánicos de los afectados por la osteogénesis imperfecta para evaluar su seguridad en vehículos. In *XXI Congreso Nacional de Ingeniería Mecánica: Libro de Artículos* (p. 82). Universidad Miguel Hernández.
[8] Martínez, L., de Loma-Ossorio, M., Pérez, R., Espantaleón, M., Ramírez, V., & Torres, C. R. Injury criteria for children affected by Osteogenesis Imperfecta.
[9] L. M., A. G., M. E., J. M., M. D., & C. T. (2015, December). Research to Increase Passive Safety of Affected by Osteogenesis Imperfecta. Retrieved January 09, 2019, from https://www.researchgate.net/publication/307922380_Research_to_Increase_Passive_Safety_of_Affected_by_Osteogenesis_Imperfecta.
[10] Calle Pinos, M. J., & Luna Jácome, R. F. (2016). Análisis del comportamiento de los cinturones de seguridad en base a la edad de los pasajeros de furgonetas de transporte escolar de la zona urbana del cantón de Cuenca (Bachelor's thesis).
[11] B. (n.d.). Manual del usuario ECE R44 04. Retrieved November 18, 2018, from https://www.besafe.com/wp-content/uploads/2015/10/BeSafe-iZi-Combi-X3-ISOfix-ES.pdf
[12] EUR-Lex Access to European Union law. (n.d.). Retrieved January 10, 2019, from https://eur- lex.europa.eu/legal-content/ES/TXT/?uri=CELEX:42011X0909(01)
[13] Sáez, L. M., García, M. D., Ruiz, M. E., & San Miguel, C. T. (2015). Estudio antropométrico en sujetos con Osteogénesis Imperfecta para la definición de propiedades de los maniquíes antropomorfos de impacto. V Reunión Del Capítulo Español De La Sociedad Europea De Biomecánica (ESB), 20. Retrieved January 30, 2019, from https://www.researchgate.net/publication/304988518.
[14] Hansen, B., & Jemec, G. B. (2002). The mechanical properties of skin in osteogenesis imperfecta. *Archives of dermatology*, *138*(7), 909-911.
[15] Fan, Z. F., Smith, P., Rauch, F., & Harris, G. F. (2007). Nanoindentation as a means for distinguishing clinical type of osteogenesis imperfecta. *Composites Part B: Engineering*, *38*(3), 411-415.
[16] Sáez, L. M., García, M. D., Ruiz, M. E., & San Miguel, C. T. (2015). Estudio antropométrico en sujetos con Osteogénesis Imperfecta para la definición de propiedades de los maniquíes antropomorfos de impacto. V Reunión Del Capítulo Español De La Sociedad Europea De Biomecánica (ESB), 20. Retrieved January 30, 2019, from https://www.researchgate.net/publication/304988518.

[17] L. B., R. C., & Ramos, N. L. (n.d.). Accidentología vial: Elementos de estudio forense. Cuadernos de Medicina Forense Argentina
[18] Sáez, L. M., Álvarez, A. G., Ruiz, M. E., & San Miguel, C. T. (2014). Diseño y validación de un sistema de retención infantil. Revista Facultad De Ingeniería Universidad De Antioquía, 70, 54-65. Retrieved January 30, 2019, from https://www.redalyc.org/articulo.oa?id=43030033005.
[19] Rey, R. E., Duart-Clemente, J., de la Llana, O. M., & Gúrpide, J. B. (2014). Osteogenesis imperfecta: Treatment and results of a case series. *Revista Española de Cirugía Ortopédica y Traumatología (English Edition)*, *58*(2), 114-119.
[20] L.S. (2007). Resortes de compresión. Retrieved March 01, 2019, from https://www.leespring.com/mx_compression_spec.asp?springType=C&forWhat=Search
[21] Lee Spring. (2015, April). Resortes Lee Spring, hechos a la medida y en stock. Retrieved January 26, 2019, from http://www.metalmecanica.com/temas/Resortes-Lee-Spring,-hechos-a-la-medida-y-en-stock 103765.
[22] D. (n.d.). Amortiguadores de impacto. Retrieved December 18, 2018, from https://dictator.es/herrajes -y- accionamientos/amortiguadores-hidraulicos/amortiguadores-de-impacto/amortiguadores-de-impacto
[23] Chang, P. C., Lin, S. Y., & Hsu, K. H. (2007). The craniofacial characteristics of osteogenesis imperfect patients. The European Journal of Orthodontics, 29(3), 232-237.
[24] Montpetit, R. J. D. O. D., & Fassier, K. R. F. F. F. (2011). Duval femoral roddingin children with osteogenesis imperfecta receiving bisphosphonates: functional outcomes at one year. *J Child Orthop*, *5*, 217-224.
[25] Brussels, European Commission. (2016). *Annexes to the proposal for a regulation of the european parliament and of the council on the approval and market surveillance of motor vehicles and their trailers, and of systems, components and separate technical units intended for such vehicles* (Vol. 31, pp. 110-300). Brussels: European Commission.
[26] L. S. (2007). Resortes de compresión. Retrieved March 01, 2019, from https://www.leespring.com/mx_compression_spec.asp?springType=C&forWhat=Search
[27] Los amortiguadores de impacto puertas correderas. (n.d.). Retrieved February 11, 2019, from https://es.dictator.de/productos/amortiguadores-hidraulicos/amortiguadores-de-impacto/
[28] Wismans, J., Waagmeester, K., Lemmen, P., Burleigh, M., Carroll, J., Visvikis, C., ... & Martinez, L. (2015). Q10 dummy Report: Advanced Child Dummies and Injury Criteria for Frontal Impact.
[29] Johannsen, H., Trosseille, X., Lesire, P., & Beillas, P. (2012, September). Estimating Q-dummy injury criteria using the CASPER project results and scaling adult reference values. In *Proceedings of IRCOBI Conference, Dublin, Ireland*.

HERTZ CONTACT MODEL TO ESTIMATE PEDIATRIC HEAD IMPACT RESPONSE VARIABLES

Nagarajan, Rangarajan
USA

19-0064

ABSTRACT

This paper describes a study to develop and validate methodology for simulating human infant head impact using the Hertz contact model. The study had two objectives. The first was to simulate Aprica 2.4 dummy head -rigid plate impact using the Hertz contact model to estimate head response variables. Model estimates were then compared with corresponding test variables. The second objective based on success of the first, was to evaluate the feasibility of using Hertz contact model to simulate human pediatric head – rigid plate impact at contact velocities ranging from 1.7 m/s to 6.26 m/s.

During objective 1 of this study, known geometric and material properties of the Aprica dummy head and steel plate were used as the Hertz model parameters. Model estimates of peak acceleration, peak head compression, pulse width, and time to peak displacement were compared with corresponding test data for contact velocity of 2.3 m/s. Percentage differences in response variables were: peak acceleration – 2.5*;* peak head compression – 1.3; pulse width – 6.1; and time to peak compression - 2.2.

During objective 2 of this study, human head impacts were divided into 4 age groups – neonate (under 1-month), 5-months, 9-months and 11-months. Objective 2 was divided into 2 stages – Model building and Model validation. In the Model Building stage, a method was developed to estimate Hertz contact model parameters using human 30 cm drop test data. In the Model Validation stage, the model was used to estimate head response variables for 15 cm, 30 cm and 2 m drops for all four age groups and compared with human test data. Model estimates for peak head acceleration of neonates in 15 cm and 30 cm drop tests differed from average test peak head acceleration by 11%, and 13% respectively. Neonate estimated pulse widths for the same drop heights differed from test average by 0% and 1%. Maximum and minimum differences for 5-, 9-, and 11-month infant model estimates from average test values in 15 cm and 30 cm drops were: 13.47% and 0.44% for peak acceleration and 6.68% and 0.03% for pulse width. Simulation results of 2 m drops of 5-month, 9-month, and 11-month old heads indicated that estimated head Jerk (rate of change of acceleration) was very close to human test results. Since the pediatric heads sustained fractures, it was not possible to compare peak accelerations.

The model reproduced, very closely, the static force-deformation curve for 5-month old but provided poor estimates for some neonates. Model reproduced finite element model results for 30 cm drop test for 5-month old head on to concrete and hard foam. The proposed model and methodology provide a simple procedure to estimate pediatric head acceleration, head deformation and pulse width for contact velocities ranging from quasi-static to 6.3 m/s onto rigid and soft surfaces.

INTRODUCTION

Availability of head impact models greatly facilitate understanding of head injury causation, determination of injury tolerance values, and design of dummy heads and head protective gear. Typically, models are based on results of several well-designed cadaver head impact tests. However, ethical and societal concerns prevent researchers from conducting requisite number of tests with pediatric heads to evaluate their material properties and to estimate their impact response. Limited isolated pediatric cadaver head testing has been conducted by Prange (2003) and Loyd (2011). They dropped isolated pediatric cadaver heads onto a rigid plate. Weber, et al. (1984, 1985) conducted full body child cadaver drop tests. They dropped un-instrumented cadavers onto rigid, and padded surfaces. However, these tests do not cover the full age and size range of the pediatric population.

Researchers have attempted to reconstruct free falls attempting to fill the information gap in pediatric head impact response. Snyder et al (1963, 1977) documented falls from heights up to 11m in their attempt to estimate the relationship between injury severity, fall height, and type of contact surface. They used a combination of detailed

medical documentation, scene investigation, and lumped mass modeling to relate fall heights and injury for free falls on to surfaces of varying stiffness.

Other researchers, Li, et al, (2015), Li, et al, (2013), Coats (2007), Ibrahim (2012), Roth (2008 and 2010) among others, have developed detailed finite element models of infant and child skull and brain. Some of these models have been validated against human impact data. Brooks, et al (2018) have provided a review of pediatric finite element models.

Engineers have idealized impact tests such as head drop tests as Sphere – Half-space impact using the Hertz contact model. This kind of modeling is used in a variety of fields such as evaluation of delamination propensity of composite wings due to small runway objects hitting the wings (Olsson, 2003), impact of biological cells (Biersack, 2010), flow of pharmaceutical powders (Antypov and Elliott, 2011). Abrate (2001) provides an overview of this class of problems and solution methods.

This study attempts to further fill the gaps in pediatric head impact data by evaluating use of the Hertz contact model to simulate human infant head – rigid surface impact. A successful attempt would provide designers with an easy to use tool to explore effects of impact in the pediatric population not covered by cadaver tests.

METHODS

The following topics will be discussed in this Section:

1. Assumptions used in this study.
2. Methodology for simulation of Aprica dummy head – rigid plate impact using the Hertz contact model.
    a. Simulation model development methodology
    b. Parameter sensitivity study methodology.
    c. Methodology used to reduce dummy drop test data.
3. Simulation of pediatric head – rigid plate impact.
    a. Model Building: This sub-section will provide details of methodology used to estimate Young's modulus of pediatric heads. The Hertz model parameters are; radii, Young's moduli, and Poisson's ratios of the two contacting partners and contact velocity. The value of material and geometric variables for the rigid (Aluminum) plate are well known. Pediatric head radius was calculated from its circumference. Head Poisson's ratio was estimated from literature sources. However, pediatric heads are composed of many deformable features such as cartilaginous bones, sutures, fontanels, etc. So, there was no obvious method to calculate the Young's modulus of this structure under impact. Young's modulus was therefore estimated using infant experimental data in this stage.
    b. Model Validation: Methodology used to validate the model developed above will be discussed in this sub-section.

1. Study assumptions

The following assumptions were made in this study:

- The head was modeled as a sphere whose radius was calculated from individual head circumferences listed in Loyd (2011).
- The plate was flat and rigid, and only the head deformed during impact.
- Air resistance was neglected in calculating contact velocity from drop heights.

2. Simulation of Aprica dummy head – rigid plate impact

The design of the Aprica 2.4 dummy has been described in Rangarajan, et al (2002), and head drop test methodology and results have been described in Rangarajan, et al. (2017). Methodology adopted to simulate dummy head drop tests will be described below.

2.a. Simulation model development

Hertz contact model equation governing impact of a sphere against a large, rigid plate where all the deformation is restricted to the area of contact, can be written as:

$$m\ddot{x} = -kx^{3/2} \qquad \text{(Equation 1)}$$

With initial conditions, x(0) = 0 and $\dot{x}(0) = \sqrt{2gh}$, the velocity at initial contact.

The term "k" which is the Contact Stiffness is defined as:

$$k = \frac{4}{3} E_{contact}\, R_{contact}^{1/2} \qquad \text{(Equation 2)}$$

And Contact modulus ($E_{contact}$) and Contact Radius ($R_{contact}$) are defined as:

$$\frac{1}{E_{contact}} = \frac{1-\nu_{plate}^2}{E_{plate}} + \frac{1-\nu_{sphere}^2}{E_{Sphere}} \qquad \text{(Equation 2a)}$$

$$\frac{1}{R_{contact}} = \frac{1}{R_{plate}} + \frac{1}{R_{Sphere}} \qquad \text{(Equation 2b)}$$

Where ν = Poisson's ratio.

Equation (1) was solved for the Aprica 2.4 dummy head drop test. Dummy head mass (0.85 kg) and circumference (0.34 m) were obtained from Rangarajan, et al. (2002). Young's modulus for the Shore 50A head was calculated using:

$$\log E = (0.0235*(S))-0.6493, \text{ where S = Shore A value (50)} \qquad \text{(Equation 3)}$$

Young's modulus was calculated to be 3.42 MPa. Contact velocity was computed from known drop height, neglecting air friction using the formula-

$$v = \sqrt{2gh}. \qquad \text{(Equation 4)}$$

Euler's method was used to solve equation (1) with a time step of 0.000001s. Solution was implemented in a spreadsheet. Time step was varied by an order of magnitude to confirm convergence. Time-wise plots of estimated head acceleration were output by the model. Acceleration was integrated to estimate variation of velocity and displacement with time. Since the plate was rigid, it was assumed that displacement of the head after contact represented its compression. Table 1 lists base simulation model parameters.

Table 1
Model Parameters for Base Simulation

Parameter	Plate	Head
Young's modulus Steel	210 GPa,	3.42 MPa
Radius	∞	0.0541m
Poisson's Ratio	0.2	0.48

2.b. Parameter sensitivity study

Hertz's model requires contact velocity, radius, and material properties of the plate and striking object. Of these, contact velocity is calculable with a degree of certainty. Material properties of the plate and its radius are known to a high degree of certainty. Dummy head was molded from 2-part Urethane as a prototype. Under these circumstances, the Shore hardness can vary + / - 4 around the base value of Shore A 50. This variation would cause approximately 25% change in modulus. I assumed that head circumference measurement by hand calipers could also vary by a maximum of 25%. Therefore, a parametric sensitivity was conducted first holding all other parameters constant and varying E_{head} by +/- 25% over its base value. R_{head} was also varied by +/- 25% while holding all other parameters at base value. Results of these sensitivity studies are shown in RESULTS section.

2.c. Reduction of dummy head drop test data

A tri-axial accelerometer cluster was used to measure dummy head acceleration at 10 kHz and filtered according SAE J-211. Head accelerations are shown in Rangarajan, et al (2017). Mean head acceleration from four isolated head drop tests was calculated. Mean acceleration was integrated to estimate head displacement and velocity. Time-wise variation of test head acceleration, velocity and displacement were compared with corresponding model estimated variables.

3. Simulation of pediatric head – rigid plate impact.

Simulation was divided into 2 stages as discussed below.

3.a. Model building – Development of contact model for infant – rigid plate impact

As discussed previously, it was necessary to estimate modulus of the infant head, a parameter required in the Hertz model (see Equation 2a). Pediatric drop test data from Loyd (2011) was used to build the model. The process was:

- Obtain average pulse width and average peak acceleration for 30 cm drop tests for four age groups - neonates (<1m old), 5-, 9- and 11- month old pediatric heads. For each age group, pulse width and peak acceleration in all drop directions (vertex, occipital, forehead, left parietal, right parietal) were included in the calculation of average.
- Use calculated average pulse width, average head mass, average head circumference of each pediatric age group, and, known pulse width, head circumference, head mass, and modulus of the Aprica dummy head to calculate Contact Stiffness as shown in the Appendix. The calculation is based on the formula for Pulse width in Hertz contact model which is (Abrate, 2001):

$$\tau = 3.2145\left(\frac{m^2}{Vk^2}\right)^{1/5} \qquad \text{(Equation 4)}$$

The rigid surface in these simulations was modelled as an Aluminum plate with modulus of 73.6 GPa and Poisson's ratio of 0.35. This completed Model Building.

3.b. Model Validation – Compare model estimates with infant head drop and static loading test data

To my knowledge, this is the first time the Hertz contact model has been validated against human pediatric test data. Therefore, I have attempted to validate the model extensively. Validation runs were made to evaluate accuracy of estimates across a range of infant ages and contact velocities. Simulation were run to evaluate accuracy of model estimates in quasi-static tests. The accuracy of model estimates was also evaluated for contacts against rigid Aluminum and steel plates, concrete, and against softer foam surface. Pediatric model estimates were compared with neonate infant head drop test and static compression data from Loyd (2011) to validate the model.

Results of these simulations will be discussed in the next section.

RESULTS

Results of the following validation tests will be discussed in this Section.

1. Model of the Aprica dummy head drop test was exercised and model estimates were compared to dummy test head response variables (Table 2).
    a) Base simulation results (Table 2)
    b) Parameter sensitivity simulation results (Tables 3 and 4)
2. Results of pediatric model building.
3. Validation of the pediatric Hertz contact model:
    a) Exercise neonate model developed in the Model building phase to simulate 15- and 30- cm drops and compare head response variables with neonate test data (Tables 5 and 6).
    b) Exercise 5-, 9- and 11- month child head model for 15- and 30- cm (Tables 7 and 8) and compare with test data.
    c) Compare model estimates of 2 m drops for 5-, 9- and 11-month old subjects with corresponding test data (Table 9, and Figures 4, 5 and 6)
    d) Compare estimated contact force, head deformation and time to peak deformation for neonate P03 with head drop test results (Table 10).
    e) Use estimated Contact Stiffness to calculate contact force for defined head deformation in quasi-static tests. Compare the resulting force – deflection data with corresponding human pediatric data (Figures 7 and 8).
    f) Model of 5-month old head was exercised to simulate various height drops onto hard foam and concrete Model estimates were compared with finite element model estimates (Li, et al. 2013). This comparison is presented in Figure 9, and Table 11.
4. Effects of idealizing the pediatric head as a sphere on estimated head accelerations is discussed (Table 12, 13, 14 and 15).

1. Comparison of test and model results for Aprica dummy isolated head impact

Model estimates (acceleration, head compression and velocity) from isolated head drop tests were compared with corresponding Aprica dummy isolated head drop tests. This was done to establish the applicability of Hertz contact model for non-elastic sphere in a Sphere – Half-space impact. The sphere's material and geometric properties were in the range of human pediatric subjects making this comparison meaningful to the objectives of this paper. Results of these simulations will be discussed first followed by simulation results of human head drop tests.

1.a. Base Aprica dummy head simulation results

Isolated head of the Aprica 2.4 dummy was dropped from a height of 0.376 m onto a steel plate such that the forehead contacted the plate. Drop test methodology and data collection techniques were discussed in Rangarajan, et al. (2017). Isolated dummy head drop tests were similar to infant drop tests. Dummy drops were simple tests where material and geometric properties of the contacting partners were known with a high level of certainty and so these could be used as control tests to investigate applicability of Hertz model to pediatric head impacts. Results of these tests are discussed in this Section.

Comparison between test and model estimated acceleration, velocity and compression are shown in Figs. 1, 2 and 3 respectively.

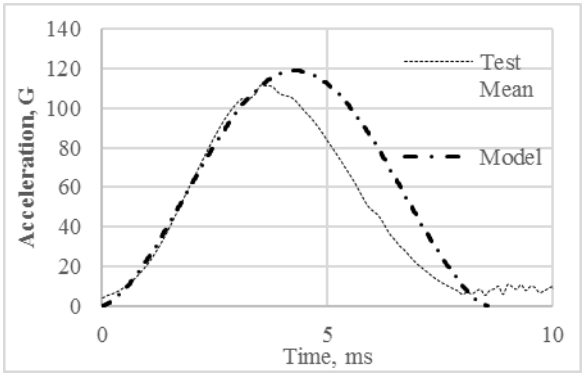

Figure 1: Comparison of test mean head resultant acceleration and model acceleration

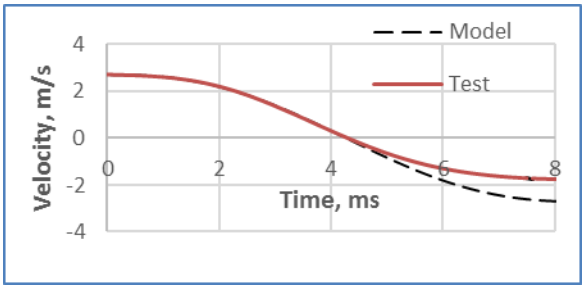

Figure 2: Comparison of test and estimated head velocity

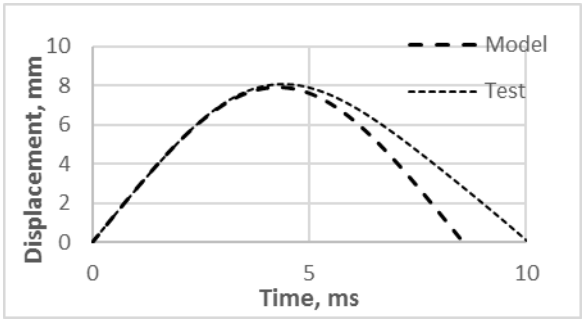

Figure 3: Comparison of test and model head compression

It is seen in Fig. 1 that test and model acceleration are coincident for the majority of deformation phase when the head velocity is being brought to zero from the initial contact velocity. The model acceleration is symmetric about the time velocity reaches zero as Hertz model assumes an elastic collision.

Figure 2 shows that model rebound velocity is equal to contact velocity because Hertzian contact is assumed to be purely elastic. However, the rebound velocity of the elastomeric head is lower than contact velocity leading to a coefficient of restitution of approximately 0.75. This shows that the Hertz contact model provides a good estimate of peak acceleration, peak deformation and pulse width for non-elastic impacts also during the crush phase.

Figure 3 shows that model head deformation follows test data until a maximum is reached. The model head deformation curve is symmetric about the time of maximum deformation whereas the test Aprica head regains it shape later.

Test and model estimated response variables for base simulation are summarized in Table 2.

Table 2
Comparison of test and model estimated head response variable values

Variable	Test Value	Model estimate	Difference [%]
Pulse Width [ms]	8.1	8.6	6.1
Hd Pk Accel [g]	115	119	2.5
Max Comp	8.0	7.9	1.3

1.b. Parameter sensitivity simulation results

Results of parameter sensitivity study are shown in Tables 3 and 4. Column 3 of Table 3 shows that if modulus of the head is increased by 25% over the base value, pulse width is lowered 9%, head peak acceleration is increased by 9% and peak head compression is increased by 8.5%, all increases over their respective base values. Column 4 shows results when head modulus is decreased by 25% over its base value.

Table 3
Variation in simulation estimates with ± 25% change in E_{head}

Variable	Base Value, E_{head}	E + 0.25 E_{head}	E - 0.25 E_{head}
Pulse Width [ms]	8.6	7.82 (9%)	9.6 (12%)
Head Pk Accel [g]	119	130 (9%)	105 (12%)
Max Compression [mm]	7.9	7.23 (8.5%)	8.9 (13%)

Column 3 of Table 4 shows that a 25% increase in R_{head} would cause a 5% reduction in pulse width, 4% increase in head peak acceleration and 10% decrease in peak compression. Column 4 provides figures when R_{head} is decreased by 25% over the base value.

Table 4
Variation in simulation estimates with ± 25% change in R_{head}

Variable	Base Value, R_{head}	E + 0.25 R_{head}	E - 0.25 R_{head}
Pulse Width [ms]	8.6	8.2 (5%)	9.1 (6%)
Head Pk Accel [g]	119	124 (4%)	112 (6%)
Max Compression [mm]	7.9	7.6 (4%)	8.4 (6%)

Reasonable estimates for head response variables for the Aprica dummy non-elastic head provided the momentum to apply Hertz contact model to pediatric head drops. Results of pediatric model simulation are provided in the next few sections.

2. Results of pediatric head model building

Model building procedure is described in the Appendix. Average head mass, and circumference of the 6 neonates (P03M, P05F, P06M, P07M, P08M and P13F in Loyd, 2011) were 0.534 kg and 0.323 m respectively. Average pulse width for 30 cm drop tests for these neonates was 16.38 ms. Aprica dummy head mass and circumference were 0.85kg and 0.34 m respectively and pulse width was 8.6 ms. Young's modulus and Poisson's ratio of Steel were 2.1GPa and 0.2 respectively and those for the elastomer which was used to mold the head were 3.42 MPa and 0.48 respectively.

The Appendix shows how these values were used to Contact Stiffness (k) and Young's modulus for neonates which were estimated to be $0.129*10^6$ N / $m^{3/2}$ and 0.464 MPa respectively. Contact Stiffness (k) for 5-month, 9-month

and 11-month child respectively were $0.624*10^6$ N / $m^{3/2}$, $0.949*10^6$ N / $m^{3/2}$, and $2.15*10^6$ N / $m^{3/2}$. Young's modulus for these infant heads were estimated to be 1.43 MPa, 2.01 MPa and 4.67 MPa respectively.

3. Validation of Hertz model for pediatric subjects

This Section will present comparison between estimated head response variables and corresponding test data for 15 cm, 30 cm for all age groups, and 2 m drop tests for 5-, 9- and 11-month old heads. In addition, quasi-static plate loading Force – Deflection test data will be compared with corresponding estimates.

3.a. Comparison of estimated and test variables for neonates

Table 5 and 6 present a comparison between test and model estimates of response variables for 6 neonates in the 15 cm and 30 cm drop test respectively. Value of Young's modulus [0.464 MPa] for the average infant was used in these simulations. The model estimates for peak acceleration and pulse width correlated well with average test acceleration and average test pulse width with estimate errors of 11% for peak acceleration and 0% for pulse width. Data shown in Table 6 indicate that errors of approximately the same magnitude are seen in 30 cm drop test estimates. Neonate average head acceleration and pulse width estimates in 30 cm drop tests differ from test values by 13% and 1% respectively.

Table 5
Comparison of estimated neonate response variables for 15 cm drop test with test variable

Subject	Neonate Average	P03M	P05F	P06M	P07M	P08M	P13F
Age, m		0.1	0.03	0.36	-1.58	-0.56	-1.35
Avg Test Accel, G	39.29 ± 9.62	49.8	33.64	33.16	43.7	28.72	46.72
Estimate Accel, G	35.13	38.38	33.76	33.03	38.11	32.66	37.06
Difference in Accel, %	10.59	22.93	-0.36	0.39	12.79	-13.72	20.68
Avg Test pulse width, ms	18.2 ± 5.04	13.06	23.04	22.34	15.42	23.12	12.1
Estimate pulse width, ms	18.29	16.74	19.03	19.45	16.86	17.68	17.34
Difference in pulse width, %	0	-28.18	17.4	12.54	-9.34	23.53	-43.31

Table 6
Comparison of estimated neonate response variables for 30 cm drop test with test variable

Subject	Neonate Average	P03M	P05F	P06M	P07M	P08M	P13F
Age, m		0.1	0.03	0.36	-1.58	-0.56	-1.35
Avg Test Accel, G	61.52 ± 16.79	81.22	51.76	52.94	74.94	47.96	60.3
Estimate Accel, G	53.25	58.17	51.17	54.59	62.88	53.87	61.14
Difference in Accel, %	13.44	28.28	1.14	-3.12	16.09	12.32	-1.30
Avg Test pulse width, ms	16.38 ± 3.88	12.28	19.78	19.28	12.94	20.5	13.5
Estimate pulse width, ms	17.07	15.62	17.76	18.15	16.73	18.36	16.18
Difference in pulse width, %	0.74	10.21	5.86	-29.29	10.44	-19.85	0.74

However, when peak acceleration and pulse width are estimated for individual infants, keeping the Young's modulus constant at value derived previously, i.e., 0.464 MPa, maximum error in estimates is 23% for acceleration of P03M, and 43% for pulse width for P13F in 15 cm drop simulations as seen in Table 5. The same trend is seen in Table 6 which indicates that peak acceleration for neonate P03M differs from test value by 29%. Estimated pulse width for neonate P06M differs from test value by 29%.

3.b. Comparison of estimated and test variables for 5-, 9- and 11-month old heads

Tables 7 and 8 show results of 15 cm and 30 cm drop simulations respectively for the 6-, 9- and 11-month old infants. Errors in estimates for both acceleration and pulse width trend lower for these infants compared to neonates which might be the result of a single head at each age being tested.

Table 7
Comparison of child drop test variables with simulation results for 15 cm drops

Subject	P12M	P14M	P15F
Age, m	6	9	11
Avg Test Accel, G	41.84 ± 3.15	35.48 ± 2.42	60.78 ± 14.93
Estimate Accel, G	46.62	40.26	62.8
Difference in Accel, %	-11.42	-13.47	-3.32
Avg Test pulse width, ms	12.96 ± 1.92	14.96 ± 0.2	10.33 ± 2.37
Estimate pulse width, ms	13.78	15.96	10.23
Difference in pulse width, %	-6.33	-6.68	1.37

Table 8
Comparison of child drop test variables with simulation results for 30 cm drops

Subject	P12M	P14M	P15F
Age, m	6	9	11
Avg Test Accel, G	70.98 ± 8.48	63.08 ± 9.69	87.76 ± 16.73
Estimate Accel, G	70.67	61.03	95.18
Difference in Accel, %	0.44	3.25	-8.45
Avg Test pulse width, ms	12.66 ± 0.99	13.64 ± 0.69	9.22 ± 1.84
Estimate pulse width, ms	12.86	14.89	9.55
Difference in pulse width, %	-0.03	-9.16	-3.58

3.c. Comparison of estimated and test accelerations in 2m drop tests

Test and estimated head acceleration for P12M, P14m and P15F heads are summarized in Table 9 and plotted in Figs. 4, 5, and 6 respectively. Figures 4 and 5 indicate that the model estimate for Jerk is very similar to test values in the loading or crush part of the acceleration pulse. Since all three heads fractured during 2m drop tests, it is not possible to compare peak accelerations. In Figures 4, 5 and 6, I have tried to retain salient points of the response plots from Loyd (2011) but test responses plots are not likely to be true through their extant.

Table 9
Comparison of test and estimated accelerations in 2m drop tests

Subject	P12M	P14M	P15F
Age, m	6	9	11
Test Peak acceleration, g	158	155	147
Test Peak force, N	1492	2630	2032
Estimated Peak Acceleration, g	223	207	309
Estimated Peak Force, N	2007	3569	4478

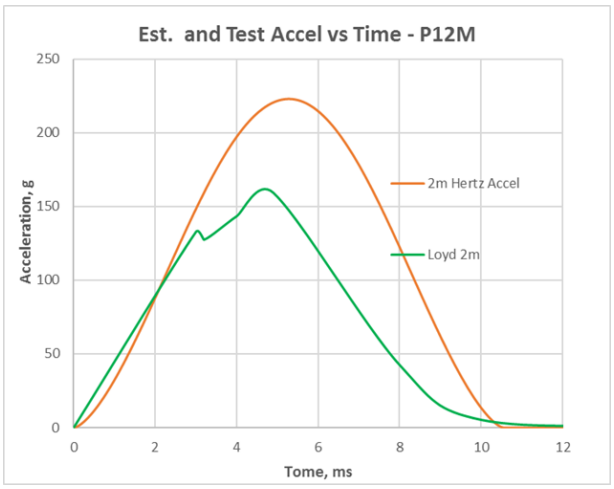

Figure 4: Test and estimated acceleration for P12M in 2m drop – Head fractured

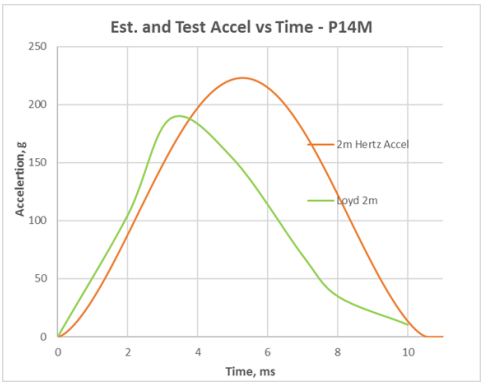

Figure 5: Test and estimated acceleration for P14M in 2m drop test – Head fractured

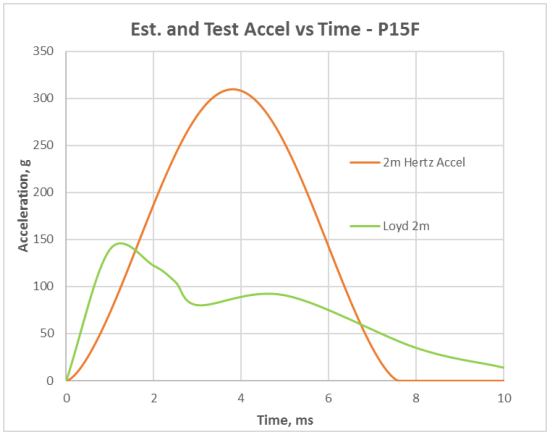

Figure 6: Test and estimated acceleration for P15F in 2m drop test – Head fractured

Figures 4 and 5 show that estimated acceleration vs time curve very closely follows the test data for P12M and P14M up to the point where head fractures. Correlation for P15F is shown in Figure 6 indicating that estimates are

worse than those for other two heads. Only one test each was conducted with 5-, 9- and 11-month old heads and more information is needed before model estimates can be meaningfully compared with human head responses.

3.d. Comparison of dynamic head compression in neonate tests

Loyd (2011) plotted head deformation and contact forces for 30 cm drop test on P05F head. Table 10 provides a comparison of response variables for this infant head at contact velocity of 2.43 m/s.

Table 10
Comparison of response variables for P05F head in 30 cm drop test

Mode	Peak Accel, g	Peak Compression, mm	Peak contact force, N	Time to Peak accel, ms
Test	51.76	~15	~305	~8
Simulation	51.17	14.7	301	~8.8

3.e. Comparison of response in quasi-static head compression tests

Loyd (2011) conducted quasi-static head compression tests in which the head was held between the platens of MTS machine. Figure 7 shows A-P compression data at 0.3/s loading rate compared with estimated force calculated using Equation (1). Model generated F-D curve is quite similar to test data. Comparison for P03M head was not as good and is shown in Fig. 8. This poor fit between estimated and test data caused errors in estimated acceleration and pulse width in drop tests seen in Tables 5 and 6.

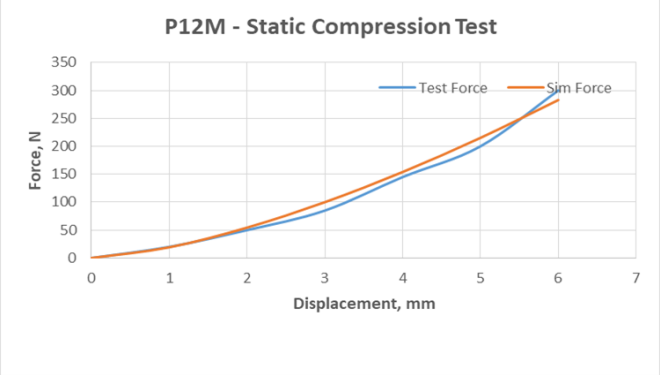

Figure 7: Comparison of quasi-static test and estimated compression for P12M

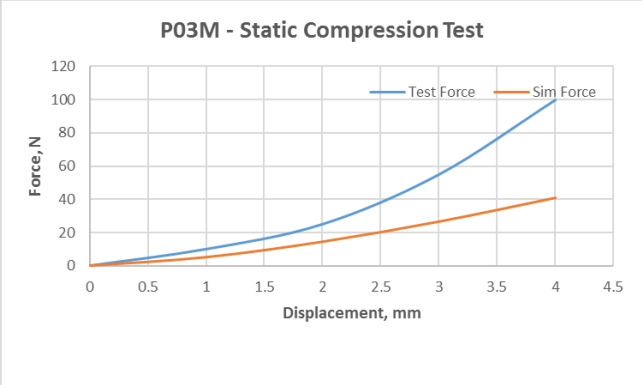

Figure 8: Comparison of quasi-static test and estimated compression for P03M

3.f. Comparison of 5-month old FE model and Hertz estimates for impact with soft surfaces

In order to complete the suite of verifications, this study replicated Li, et al. (2013) FE simulations of 6-month old infant head impact against soft foam and concrete. These simulations were conducted to suitability of the pediatric model to simulate head impact against non-rigid surface. Like Li, et al. (2013), Hertz contact model simulations were run for P13M [5-month old]. Results are tabulated in Table 11 and plotted in Fig. 9.

In these simulations, modulus and Poisson's ratio for Concrete were obtained from Li, et al. (2013) and were set in Hertz model as 30 GPa, and 0.15 respectively. Modulus for hard foam was obtained from a plot in the same paper and set at 1.6 MPa in the simulation model. Tabulated data and Fig. 9 indicate that the current model can provide reasonable estimates for peak acceleration when the head contacts a soft surface such as foam whose modulus is approximately 5 orders of magnitude softer than concrete.

Table 11
P13M fall onto concrete and hard foam – comparison of Hertz estimates with FE model

Drop Height, cm	Li Acceleration hard foam	Hertz estimated. hard foam	Li. Acceleration Concrete	Hertz Acceleration concrete
20	~30	41	~50	56
30	~40	53	~75	71
40	~55	63	~85	84
60	!75	81	~120	108

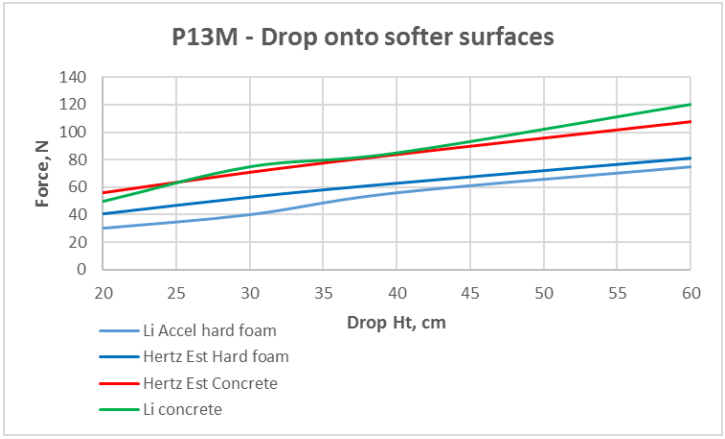

Figure 9: P13M head impact onto to concrete and hard foam

4. Effect of idealizing head as a sphere

Pediatric head has been idealized as a sphere in this study. However, Loyd (2011) has observed that peak head acceleration varies with impact direction. Vertex impacts generally generated the highest acceleration for any head in tests. A sphere will not show the effect of impact direction on head acceleration. Tables 12, 13, 14 and 15 show model estimated acceleration and average acceleration for each neonate impact direction. 5-month old, 9-month old, and 11-month old heads respectively. Neonate head accelerations for each impact direction for each drop height were averaged over 6 subjects.

Table 12 compares estimated accelerations and average test accelerations for each impact direction for neonates. It is seen that estimated accelerations are quite close (approximately 10% difference) to test accelerations for all impact directions except Vertex.

Table 12
Effect of idealizing neonate head as a sphere

Direction	Est. Accel, g	Neonate, avg. accel, g
15 cm Vertex	35.13	46.8 ± 10.5
15 cm Occiput	35.13	37.1 ± 6.76
15 cm Forehead	35.13	38.5 ± 11.5
15 cm Rt. Parietal	35.13	37.1 ± 6.5
15 cm Lt, Parietal	35.13	36.9± 6.8
30 cm Vertex	53.3	75.9 ± 19.9
30 cm Occiput	53.3	57.4 ± 9.7
30 cm Forehead	53.3	59.3 ± 19.4
30 cm Rt. Parietal	53.3	58.2 ± 12.6
30 cm Lt, Parietal	53.3	58.8 ± 11.2

Similar comparison is presented for 5-, 9- and 11-month heads in Tables 13, 14, and 15. It is not valid to draw meaningful conclusions from these data as only one subject has been tested in each age group. However, it is interesting that peak accelerations of P14M, a 9-month head in all impact directions are very close to those of neonates for both 15 and 30 cm drop tests even though both the modulus and CS of this head is nearly double that of the average neonate. This is because the increased head mass modulates the accelerations which is substantiated by model estimates which too are close to neonate estimates.

Table 13
Effect of idealizing 5-month head as a sphere

Direction	Est. Accel, g	Neonate, avg. accel, g
15 cm Vertex	46.6	44.9
15 cm Occiput	46.6	43.7
15 cm Forehead	46.6	44.5
15 cm Rt. Parietal	46.6	37.3
15 cm Lt, Parietal	46.6	38.8
30 cm Vertex	70.7	71.6
30 cm Occiput	70.7	81.0
30 cm Forehead	70.7	57.6
30 cm Rt. Parietal	70.7	78.5
30 cm Lt, Parietal	70.7	66.2

Table 14
Effect of idealizing 9-month head as a sphere

Direction	Est. Accel, g	Neonate, avg. accel, g
15 cm Vertex	40.3	35.4
15 cm Occiput	40.3	37.6
15 cm Forehead	40.3	38.0
15 cm Rt. Parietal	40.3	31.2
15 cm Lt, Parietal	40.3	35.2
30 cm Vertex	61.0	76.9
30 cm Occiput	61.0	71.6
30 cm Forehead	61.0	60.7
30 cm Rt. Parietal	61.0	52.3
30 cm Lt, Parietal	61.0	53.9

Table 15
Effect of idealizing 11-month head as a sphere

Direction	Est. Accel, g	Neonate, avg. accel, g
15 cm Vertex	62.8	39.6
15 cm Occiput	62.8	69.4
15 cm Forehead	62.8	62.1
15 cm Rt. Parietal	62.8	49.4
15 cm Lt, Parietal	62.8	63.1
30 cm Vertex	96.2	67.6
30 cm Occiput	96.2	104.8
30 cm Forehead	96.2	109.9
30 cm Rt. Parietal	96.2	82.3
30 cm Lt. Parietal	96.2	74.3

DISCUSSION

This work provides an unusual view of the material properties of the pediatric head. Unusual in the sense that average Young's modulus estimated from experimental data for neonates is approximately 0.5 MPa. It rises to approximately 5 MPa at age 11-months as shown in Figure 10. This is in stark contrast with Young's moduli of various structural elements that together make up the head l such as scalp, skull, suture and membranes in FE models. FE models of pediatric heads have defined the modulus of these parts to be 17 MPa [scalp], 500 – 1500 MPa [skull]. 8 MPa [sutures] and 32 MPa [membranes]. The modulus estimated by this model is several orders of magnitude lower than those used in current FE models.

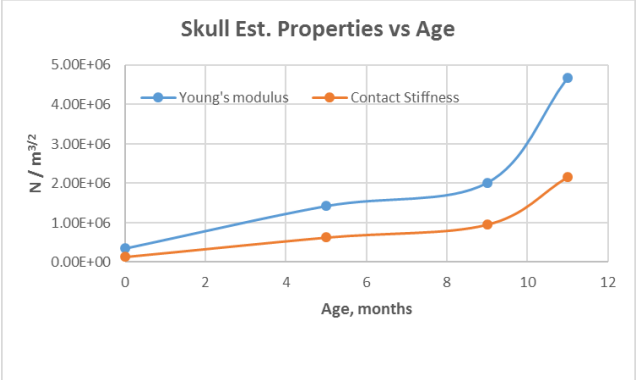

Figure 10: Contact stiffness and Young's modulus vs pediatric age.

My first inclination was to assume that the reasonableness of estimates with such a simple model was serendipitous. However, the model returns very reasonable estimates for all impact response variables including peak head deformation even when the model is extrapolated to estimate results of a 6.3 m/s impact. It also seems to return reasonable estimates when the head impacts foam whose modulus is several orders of magnitude lower than that of Steel.

Melvin (1995) might provide one explanation for the low value of modulus. Based on work by McPherson and Kriewall (1980), Melvin estimated that bone modulus scale factor for newborns as compared to adults was 0.243. Unpublished work by the author at GESAC, Inc established that Hybrid – III male 50th percentile head flesh had a Shore A hardness of 47 equivalent to 2.9 MPa. Based on Melvin's estimates, newborn modulus can be calculated to be 0.7 MPa and was recommended for the CRABI-6month dummy. In this study, modulus for neonates and 5-month old have been estimated to be 0.464 MPa and 1.43 MPa respectively. Therefore, Melvin's estimate fits well within the estimated developed in this study for the neonate – 6-month old age group. However, it would be very nice indeed to be able to estimate the composite modulus and structural stiffness of the neonate head directly from literature values of components.

Figure 10 shows estimated Contact Stiffness [CS] plotted against pediatric age. Data points were connected by a straight line. This is in keeping with Melvin, 1995 who observed that skull mechanical properties vary linearly with age from birth to 4.5 years. In any case, it is probably reasonable to assume that CS and modulus vary linearly in the small age range plotted in the figure.

Contact Stiffness [CS] is plotted in addition to estimated Young's modulus as CS includes Young's modulus and radius, a measure of child head geometry. Thus, CS can be different for the same Young's modulus depending on radius of the head.

Robustness and utility of a model is judged by its ability to provide interpolated and extrapolated estimates. Results of this study indicate that the model yields reasonable estimates for range of contact velocities from quasi-static compression to 6.3 m/s. Model estimates of peak acceleration when the head impacts softer surfaces are comparable to estimates of FE models in literature. So, it is possible to conclude that the Hertz contact model provides a robust, utile simulation tool for pediatric head impacts.

It has been noted previously in the RESULTS Section that model estimates away from the mean tend to differ significantly from experimental data. This is caused by the model producing single point estimates around mean experimental values. However, the model can be exercised to generate a range of estimates which will cover the extremes of experimental data. For example, the model currently uses mean pulse width to generate a single value of Young's modulus. The model can be used to generate a range of Young's moduli by using mean test pulse width ± SD as input. If these moduli are used, the model will provide good estimates of impact response variables. For example, if the E_{mean} + SD is used to calculate response in 15 cm drop tests for P03M head, the model returns acceleration of 47g as opposed to 38g listed in Table 5. Obviously, this new estimate quite close to the experimental

value of 49g. This procedure does not cure all problems with estimated values of variables. Analysts can use this procedure to generate a range of impact response variable values thus increasing the confidence in estimates.

CONCLUSION

- A method has been developed to estimate Young's modulus and Contact Stiffness of pediatric heads in conjunction with Hertz Contact model for head – rigid surface impacts.
- Study results indicate that the methodology and Hertz contact model yield reasonable estimates of head impact response variables.
- Proposed Model building methodology seems to yield reasonable estimates for a reasonably large pediatric age group ranging from <1-month to 11-month old. However, there is only 1 test specimen each for ages 5-, 8- and 11-months.
- There is a nearly 10-fold increase in the estimated modulus of the head in this age group.
- The reasonableness of impact response variables under various loading conditions indicates that Hertz model is appropriate to simulate pediatric head impact and is quite robust.
- This study indicates that modulus of the head to be much lower than the moduli of the components that constitute the pediatric head.
- The model seems capable of returning reasonable estimates for impact response variables for impacts against softer surfaces such as hard foam. The modulus of foam is several orders of magnitude lower than modulus of Steel and Aluminum which were used in infant cadaver and dummy head drop tests.
- Simulation results suggest that infant dummy heads can be molded out of 2-part elastomers which will lead to a head which is deformable, and very importantly has human-like moments of inertia about all axes. Such heads are also likely to be easy and inexpensive to manufacture and can be used to design head protection gear and vehicle components that might contact pediatric heads.

ACKNOWLEDGEMENTS

Many thanks are due to Aprica, Inc. Japan, which funded development of the Aprica dummy. Thanks to Mr. T. Fukuda and Mr. H. Morishima who conducted dummy drop and head calibration tests. Thanks also to C. Spade, and J. Poland and other GESAC, Inc staff who designed, and manufactured the dummy.

REFERENCES

[1] Abrate, S. "Modeling of impacts on composite structures". Composite structures 15. 2001.

[2] Antypov, D, Elliott, JA. "On an analytical solution for the damped Hertzian spring". EPI. 94B. 2001-50005. Doi:10.1209/0295-5075/94/50004.

[3] Biersack, F. "Simulation supported Hertzian theory calculations on living cell samples". Masterarbeit, Hochschule Muenchen, Fakultaet 06, Mikro- und Nanotechnolgie. 2010.

[4] Brooks, T, et al. "Finite element models and material data for analysis of infant head impact". Heliyon 4(201* e01010. Doi: 10.1016/j.Heliyon.2018.e01010. 2018.

[5] Coats, B. "Mechanics of head impacts in infants". PhD Thesis, University of Pennsylvania. 2007.

[6] Ibrahim, N.G. et al. "Influence of age and fall type on head injuries in infants and toddlers". Int. J. Dev Neurosci. May: 30(3): 201-6. 2012.

[7] Li, Z, Liu, W, Zhang, J, Hu, J. "Prediction of skull fracture injury risk for children 0-9 months old through validated parametric finite element model and cadaver test reconstruction". Int J Legal Med. Sep;129 (5):1055-66. 2015.

[8] Li, Z, et al. "Development / global validation of a 6-month old pediatric head finite element model and application investigation of drop-induced infant head injury". Comput. Methods Progr. Biomed. 112(3). 2013.

[9] Loyd, AM. "Studies of the Human Head from Neonate to Adult: An Inertial, Geometrical and Structural Analysis with Comparisons to the ATD Head". PhD Thesis. Duke University. 2011.

[10] McPherson, GK, and Kriewall, TJ. "The Elastic Modulus of Fetal Cranial Bone: A First Step Towards an Understanding of the Biomechanics of Fetal Head Molding". J. Biomechanics, Vol. 13, pp 9-16. 1980.

[11] Melvin, J.W. "Injury Assessment Reference Values for the CRABI 6-month Infant Dummy in a Rear-Facing Infant Restraint with Airbag Deployment". SAE International Congress and Exhibition, Detroit, Michigan. Paper 950872.

[12] Olsson, R. "Closed form prediction of peak load and delamination onset under small mass impact". Composite Structure 59. 2003.

[13] Prange, MT, Luck, JF, Dibb, A, Van Ee, CA, Nightingale, RW, Myers, BS. "Mechanical properties and anthropometry of the human infant head". Stapp Car Crash J. Nov;48:279-99. 2004

[14] Rangarajan, N, DeRosia, J, Humm, J, Tomas, D, Cox,J. "An improved method to calculate pediatric skull fracture threshold". Enhanced Safety Vehicle Conference Proceedings, Seoul, South Korea. 2013.

[15] Rangarajan, N, Shams, T, Jenny, C, and Fukuda, T. "Probability of pediatric skull fracture at various contact velocities". Enhanced Safety Vehicle Conference Proceedings, Detroit. 2017.

[16] Roth, et al. "Finite element analysis of impact and shaking inflicted to child". Int. J. Leg Med 121(3). 2007.

[17] Roth, et al. "Finite element modeling of pediatric head impact: global validation against experimental data". Comput. Meth. Progr. Biomed. 99(1). 2010.

[18] Snyder, R. G. 1963. "Human Survivability of Extreme Impacts in Free-Fall". Report, Civil Aeromedical Institute, Oklahoma City. 1963.

[19] Snyder, RG, Fousts, DR, and Bowman, BM. 1977. "Study of Impact Tolerance Through Free-Fall Investigations". Report UM-HSRI-77-8, University of Michigan. 1977.

[20] Weber, W. "Experimental studies of skull fractures in infants". Z Rechtsmed. 92(2):87-94. 1984 (Ger).

[21] Weber, W. "Biomechanical fragility of the infant skull". Z Rechtsmed. ;94(2):93-10. 1985 (Ger).

APPENDIX

Pulse width in Hertz contact model for a sphere [Head] – Half space [Flat Plate] impact is given by (Abrate, 2001):

$$\tau = 3.2145 * \frac{M^{0.4}}{k^{0.4} * V^{0.2}} \qquad \text{(Equation A- 1)}$$

Where:

$\tau = Pulse\ width$

$V = Contact\ velocity$

$k = Contact\ stiffness = \frac{4}{3}\ E_* * {R_h}^{0.5}$ (Equation A-2)

Where

$\frac{1}{E_*} = Contact\ Young's\ modulus\ of\ the\ plate\ and\ head = \frac{1-\nu_p^2}{E_p} + \frac{1-\nu_h^2}{E_h}$ (Equation A-3)

And

$$\frac{1}{R} = \frac{1}{R_p} + \frac{1}{R_h} \qquad \text{(Equation A-4)}$$

$R = Radius\ and\ subscripts$ "p" and "h" refer to rigid plate and head respectively

Procedure for calculating Young's modulus of Infant head

The procedure starts by recognizing that both infant head and dummy drop pulse widths are almost invariable with drop height [Rangarajan, et al, 2017(a, b)]. This information and known Young's modulus, mass and head radius of Aprica 2.5 dummy, and average mass and average radius of infant heads can be used to calculate Young's modulus of the infant head for the same contact velocity using Eq. A-1.

Thus, for the same contact velocity,

$$\frac{\tau_i}{\tau_d} = \frac{\frac{{M_i}^{0.4}}{{k_i}^{0.4}}}{\frac{{M_d}^{0.4}}{{k_d}^{0.4}}} \qquad \text{(Equation A-5)}$$

Or

$$\frac{\tau_i}{\tau_d} = \left[\frac{M_i * k_d}{M_d * k_i}\right]^{0.4} \qquad \text{(Equation A-5a)}$$

Subscripts "*I*" and "*d"* in Equation 2 and 2a refer to infant and Aprica 2.5 dummy respectively. Loyd, 2011 30 cm drop tests provide an estimated average infant head drop test pulse width of16.38 ms. Pulse width of the Aprica dummy 0.376 m drop tests is 8.6 ms. Thus, the of pulse widths ratio in Equation 2a above is 16.38 / 8.6 = 1.90

Table A.1 below lists values of variables in Equation 5a.

Table A- 1
Value of variables

Variable Name	Value	Units
Average infant head mass M_i	0.534	kg
Dummy head mass M_d	0.85	kg
Average infant head circumference	0.0323	m
Dummy head circumference	0.0340	m
Average infant head radius R_i	0.0514	m
Dummy head radius R_d	0.0542	m
Young's modulus infant E_i	TBD	MPa
Young's modulus Dummy E_d	3.42	MPa
Poisson's ratio infant head ν_i	0.46	
Poisson's ratio dummy head ν_d	0.46	

Data in Table A.1 can be used together with Equations A-1 through A-5a, to calculate Young's modulus for infant head. The calculated value is $4.64 * 10^5$ Pa. This value of Young's modulus is roughly equivalent to Shore A hardness of 13 and can be used in the Hertz contact model to estimate impact response variables. Estimated values of these variables are compared with experimental values for infant heads in the main text of this paper

EVALUATION OF THORACIC DEFLECTION CRITERIA IN FRONTAL COLLISION USING THORACIC IMPACTOR SIMULATION WITH HUMAN BODY FE MODEL

Takayuki Kawabuchi, Yasuhiro Dokko
Honda R&D Co., Ltd. Automobile R&D Center
Japan

Paper Number 19-0068

ABSTRACT

When involved in vehicle accidents, the fatality rate of thoracic injury is high, following head injury, and the major causality is a rise of organ injury rates due to an increase in the Number of Fractured Ribs (NFR). Previous studies suggested a high correlation between thoracic deflection and NFR. However, the correlation was evaluated primarily using test data in frontal collisions with restraint systems such as seatbelts or airbags. Thus, it was not evaluated by local loading. The objective of this paper is to evaluate the correlation between the thoracic deflection criteria and NFR under local loading conditions by thoracic impactor loading.

In order to evaluate the relationship between thoracic deflection criteria and NFR by localized loading, thoracic impact is more proper than sled impact, in which loading location and direction depend on restraint systems. Impact simulations were conducted on 19 points to cover the whole right side of the thorax. The simulations were conducted with the Global Human Body Model Consortium (GHBMC) 50th percentile male model for LS-DYNA. Deflection of each rib was measured at its anterior tip and Rmax was calculated using the deflections on the 4th rib and the 7th rib to represent Anthropometric Test Dummy (ATD) measurement points. In addition, Average Deflection of All Ribs (ADAR) and Weighted Average Deflection of All Ribs (WADAR) were calculated as proposed criteria. Then the correlation between NFR and each of those criteria was evaluated using the correlation coefficient.

The results showed that some specific impact points lower the correlation between NFR and Rmax. Impacts around 1st through 3rd ribs incur rib fractures without deflection on the representative points because the sternum and costal cartilage do not transmit the force and deflection to other ribs. On the other hand, ADAR showed a higher correlation with NFR than Rmax, and WADAR further improved correlation with NFR.

The results showed that WADAR needs to be taken into account to improve correlation between NFR and thoracic deflection. It suggests that deflection of all ribs modified by homogeneity of each rib deflection need to be considered in order to properly evaluate rib fractures caused by localized loadings.

The thoracic deflection criterion using weighted average deflection of all ribs showed the highest correlation with NFR and it allows evaluating rib fractures even under localized loading conditions.

INTRODUCTION

Thoracic fatal injuries sustained by seatbelt-restrained occupants in frontal crashes appeared to be as equally frequent as, or following, head fatal injuries [1]. Kent et al. described that the percentages of drivers who died with Maximum Abbreviated Injury Score (MAIS) related to rib fractures increased with aging and suggested that rib fracture was associated with the significantly increasing fatality rate of thoracic injuries, especially on elderly drivers [2]. In addition, approximately 47% of elderly drivers died due to fatal thoracic injuries, while 24% of younger drivers did [2]. Furthermore, it is estimated that the population of adults over 65 years old would increase up to 83.7 million by the year 2050 in the United States [3] and it would result in increasing number of drivers sustaining severe injury on the thorax in traffic accidents. Hence, the necessity of consideration for thoracic protection is growing more than ever.

Kent et al. suggested that the risk of rib fractures increased with the level of thoracic compression and that thoracic injury risk was often described by the antero-posterior deflection of the thorax [4]. Most of the correlation between thoracic deflection criteria and thoracic injury risk was evaluated primarily using test data by Anthropometric Test

Dummy (ATD) and Post Mortem Human Subjects (PMHS) in frontal collisions with restraint systems such as seatbelt and/or airbag. However, rib fractures may often be likely to occur not only by restraint systems but also by contact with interior components. Small overlap or oblique collisions cause oblique motion to occupants and the thorax has contact with deformed interior components [5] [6]. Such a loading condition differs from the loadings by restraint systems and it may rather be similar to some localized loading than a broad loading.

The objective of this study was to evaluate the correlation between the thoracic deflection criteria and the number of fractured ribs (NFR) under localized loading using thoracic impact simulations with various impact locations and directions using a human body model.

METHOD

Human Body Model

Global Human Body Models Consortium's 50th percentile male occupant model (GHBMC M50-O) v4.5 for LS-DYNA was adopted as a baseline model and was modified to have a thorax with elderly features for evaluation of thoracic deflection criteria. Rib fracture was predicted by elements exceeding the failure strain threshold, thus it was needed to validate the relationship between loading and strain on rib cortical bones. Single rib and rib cage of GHBMC M50-O was validated against the relationship between rib fracture and deformation under various boundary conditions [7]. As a validation for single rib, the relationship between rib deflection and strain of each rib was validated by an anterior to posterior bending test. [8] And as a validation for rib cage deformation, thoracic response against localized loading was validated by the point loading at various locations [9]. Based on those validations, the GHBMC M50-O model was considered to be able to evaluate rib fractures caused by localized loadings at various points.

The representative age for the elderly was set at 75 years old based on Ito et al [10]. The material properties of rib cortical bone for the baseline model was modeled with piecewise linear plasticity material model with Young's modulus, yield stress, and a failure strain. The Young's modulus of the rib cortical bone was set at 11.5 MPa and yield stress was set at 88 MPa based on Li et al [11]. Failure strain was determined by the sum of yield strain and ultimate plastic strain. Yield strain was 0.0077, which was calculated by Young's modulus and yield stress. The ultimate plastic strain of the cortical bone had correlation with age as given in Equation 1 [12] and set at 0.0088. Thus, the failure total strain as a rib fracture threshold resulted in 1.65% and shell elements constituting rib cortical bone model were judged as a fracture when the strain on an element exceeds the threshold.

$$\text{Ultimate plastic strain [unitless]} = \frac{-383age[years] + 37514}{10^6} \qquad \text{(Equation 1)}$$

Rib cortical bone thickness was decreased from the baseline model based on the aging function of linear relationship between age and rib cortical bone thickness described by Ito et al [10]. Since the base age of GHBMC M50-O was not explicitly defined, it was assumed average, and the cortical bone thickness at 75 years old was presumed. Rib cortical bone thickness of GHBMC M50-O v4.5 was distributed on every shell element of the rib derived from CT scan data and its average thickness was 0.67 mm [8]. Thereby base age was assumed as roughly 60 years old and was decreased based on the aging function. The Young's modulus of the costal cartilage was set at 19.7 MPa based on Yamada [13]. Kent et al. showed upward geometrical change by aging and described those changes on rib cage influences on increasing stiffness of rib cage [14]. On the other hand, Ito et al compared the contribution of thorax characteristic change by aging and showed that the influence of the geometrical change of rib cage was smaller than change of cortical bone thickness or failure strain [15]. In addition, the aim of this study was to evaluate the relationship between rib cage deformation and NFR on same subject. Therefore, the authors decided that the rib cage geometry was not to be modified in this study. The model with those modifications was validated against frontal thorax impact tests and belted full body frontal sled tests [16].

Thoracic impact simulation

Thoracic impactor loading was conducted in order to represent localized loading and reconstruct thoracic deformation due to a localized loading by interior components such as door trims. Besides, the thoracic impactor was presumed to be able to comprehensively evaluate the relationship between thoracic deflection criteria and NFR since the impactor did not depend on the character of restraint systems.

A rigid impactor model with a small diameter was employed in order to generate localized loading on the thorax. The impactor was a cylindrical shape with a 75 mm diameter and its mass was 22 kg. The initial velocity was set at high and low velocity along the axis direction of the impactor, 6.7 m/s and 4.7 m/s respectively as boundary conditions. Low velocity was determined to be a half of the kinetic energy of high velocity in order to evaluate velocity dependence of the relationship between rib fracture and thorax deflection. Centers of impactor contact locations were set at 19 points on the whole right half of the thorax. The impact region was focused on the single side based on the assumption that the rib cage was symmetrical. A base contact point was set to match the center of the impactor on a point on the sternum 70 mm superior to the tip of the xiphoid. The point was approximately the same height as the 4th rib. The impact direction was determined to be perpendicular to the plane on the thoracic surface, which was defined as 63.5 degrees to the horizontal plane and depicted as Figure 1. The other 18 contact points were set on each place with each direction described in Table 1 and Figure 1. Each contact point was set at a point on position Y and Z defined as lateral and vertical coordinates from the base contact point. The impact direction seen from the impactor side view was same as that of base contact point. The Z angle shown in Figure 1, which defines an angle of the impactor around vertical axis, was set to be perpendicular to the thoracic surface and angles at each point were shown in Table 1.

Table 1.
Impactor contact positions

Point No.	Position Z [mm]	Position Y [mm]	Angle Z [deg]
1	0	0	0
2	125	0	0
3	125	75	30
4	125	125	50
5	75	0	0
6	75	75	20
7	75	125	50
8	75	150	60
9	0	75	20
10	0	125	40
11	0	150	65
12	-75	0	0
13	-75	75	20
14	-75	125	40
15	-75	150	60
16	-150	0	0
17	-150	75	20
18	-150	125	40
19	-150	150	60

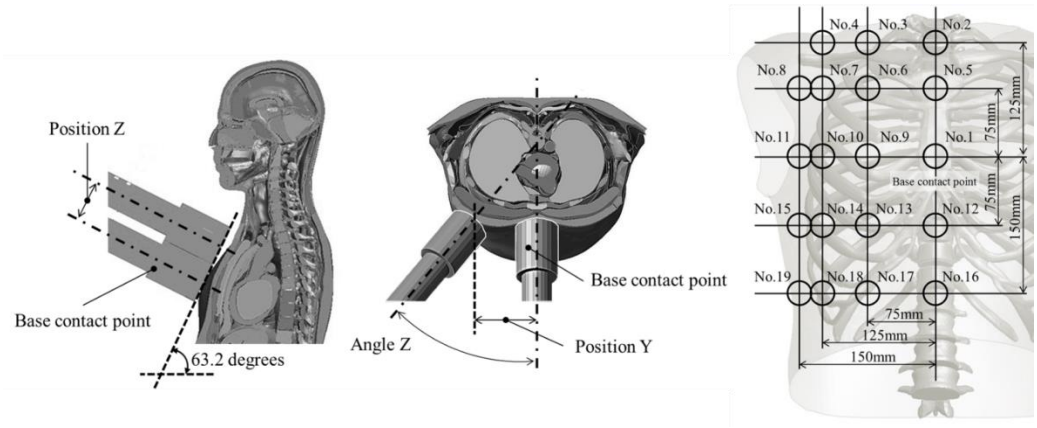

Figure 1. The definition of parameters and impact positions

Rib Deflection Measurement

Rib deflection in X, Y, and Z (XYZ) directions was measured at each rib anterior tip. The local coordinate system was defined at the costovertebral joint of each rib. The local x axis pointed anterior direction of the thorax, the local y axis pointed right-hand direction and the local z axis pointed upward. Since rib deformation caused by oblique loading was largely related to y deflection, resultant deflection was applied to criteria. Measurement results were processed and defined as a criterion and the correlation between the criteria and NFR were evaluated by the correlation coefficient defined as the R-squared values (R^2), which were calculated by linearization.

Rib deflection evaluation criterion

Two types of criteria were defined for rib deflection evaluation. One type was using a value of the largest deflection between all ribs and the other type was using an average value of normalized all rib deflections.

A. **Criterion using the largest rib deflection:** The criterion defined the larger one of maximum XYZ resultant deflections of the 4th Rib and the 7th Rib as a representative point. The representative ribs were determined to be similar to the measurement points of Infra-Red Telescoping Rod for the Assessment of Chest Compression (IR-TRACC) applied to Test device for Human Occupant Restraint (THOR) ATD. This criterion was defined as Rmax.

Furthermore, the largest one between the maximum XYZ resultant deflections of the 12 ribs was defined as a criterion. This was defined as Maximum Deflection of All Ribs (MDAR).

B. Criterion using average value of normalized all rib deflections: For a comparison with the criteria using maximum value, average value of the maximum XYZ resultant deflection of the 12 ribs was defined as a criterion. The amount of deflection to fracture is different among every rib since they have different shapes and lengths. Those differences should be taken into account to evaluate NFR by an average deflection of the 12 ribs. In order to remove the influences of that, each XYZ resultant deflection was normalized by initial length between a measurement point and the coordination origin of each rib. The definition of initial length and length of each rib were depicted in Figure 2 and Table 2, respectively. The criterion was defined as Average Deflection of All Ribs (ADAR) and given in Equation 2.

$$\mathrm{ADAR} = \frac{\sum_{i=1}^{n}(d_i/L_i)}{n} \qquad \text{(Equation 2)}$$

Where, di = normalized deflection of each rib

Li = rib initial length

n = Number of ribs. Here this is 12.

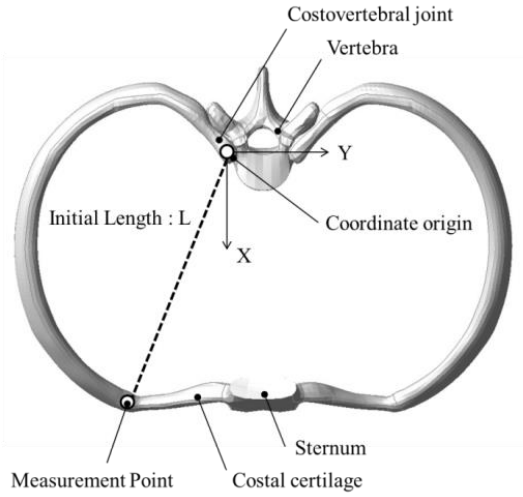

Figure 2. Rib measurement point and detail of the location

Table 2.
Initial length of each rib

Rib No.	Initial Length L [mm]
1	73.7
2	108.6
3	145.0
4	173.0
5	189.4
6	199.7
7	204.1
8	208.9
9	198.2
10	176.8
11	151.4
12	94.6

RESULTS

All results of evaluation criteria and NFR of each impact point were listed on Table A1 and Table A2.

The relationships between Rmax, MDAR, and NFR were shown in Figure 3(a) and 3(b). R^2 of Rmax was lower than that of MDAR. This is assumed because NFR were varied from 0 to 6 between Rmax 20 mm and 30 mm, while such a variance did not happen for MDAR. The relationship between ADAR and NFR was shown in Figure 3(c). The R^2 was higher than Rmax or MDAR and the scatter became smaller.

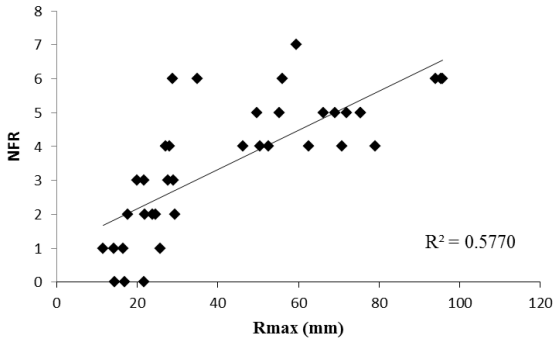

(a) Rmax vs NFR

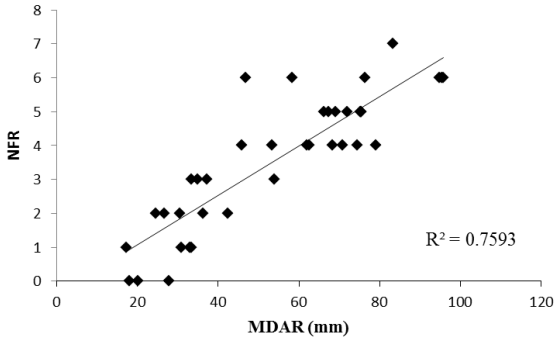

(b) MDAR vs NFR

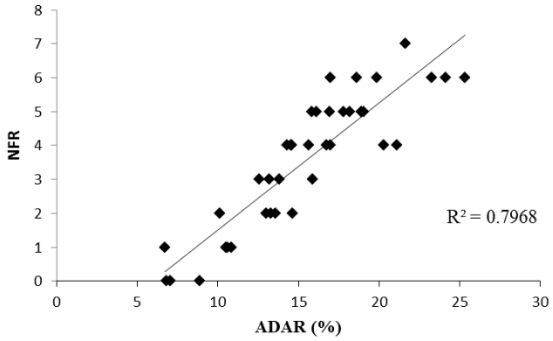

(c) ADAR vs NFR

Figure 3. Correlations between rib deflection criteria and NFR

However, some deformation patterns, which were provided in Figure 4(a) and 4(b), showed large different NFR even under the same ADAR. The impact point at No.6 incurred 4 fractured ribs while No.14 incurred 7 fractured ribs. It found that the difference of deformation shape affected NFR.

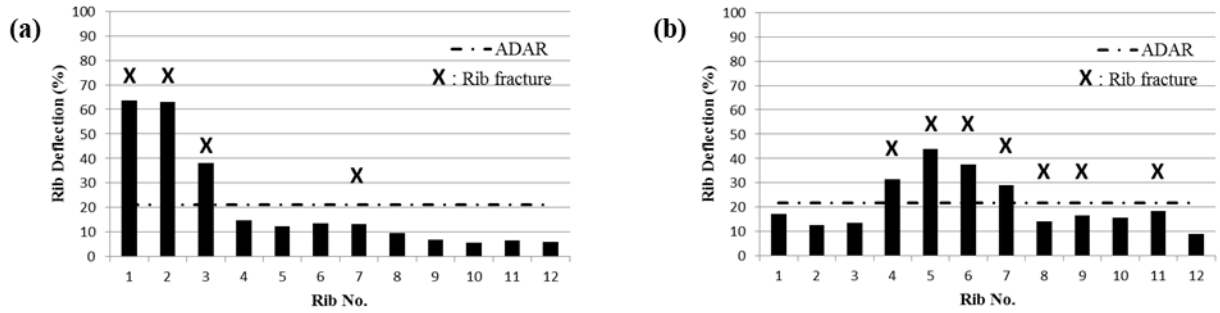

Figure 4. Each rib deflection: (a) at impact point No.6 and (b) at impact point No.14

Thus, a weighting factor was applied to ADAR in order to distinguish the deformation shape due to effects of impact point differences. Edwards et al suggested evaluating a degree of deformation of deformable barrier by homogeneity of deformation [17]. Based on this evaluation method, homogeneity of thoracic deformation shape was applied to a criterion adopting a weighting factor. The criterion was defined as Weighted Average Deflection of All Ribs (WADAR) as described in Equation 3. The weighting factor is the parentheses in the equation. The second term of the weighting factor, which indicates inhomogeneity, becomes large when the local deformation occurs largely on the thorax. In other words, the degree of local deformation, which has large ADAR and small NFR, is larger and WADAR becomes smaller. This weighting factor adjusts the inconsistency between ADAR and NFR as described above.

$$\mathrm{WADAR} = \left(0.2 - \frac{\sqrt{\sum_{i=1}^{n}(ADAR - d_i)^2}}{n}\right) \times ADAR \qquad \text{(Equation 3)}$$

Where, di = normalized deflection of each rib

n = number of ribs. Here, this is 12.

Further, the first term, 0.2, was empirically determined to make a correlation coefficient higher.

Figure 5 shows the relationships between WADAR and NFR. R^2 of WADAR is higher than that of ADAR. WADAR of No.6 and No.14 were 2.97% and 3.66%, respectively and they showed the differences although their ADAR was almost the same.

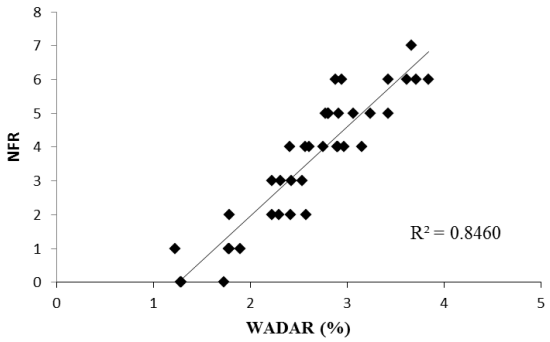

Figure 5. Correlation between WADAR and NFR

DISCUSSION

As mentioned above, WADAR indicated the highest R^2 between four criteria. Considering the fracture mechanisms, impact energy generated by a thorax impactor incurs thoracic deformation and rib fracture occurs when it becomes beyond the critical value. When larger energy is applied, NFR will increase. Since WADAR is based on ADAR, using the sum of all rib deflections as shown in Equation 2, it had a better correlation with NFR than those of criteria using maximum deflections as a representation. Impact on the upper region of the thorax concentrates the energy on one or a few neighboring ribs and incurs rib fractures around that limited region. Under such a condition, NFR increased without deformation at the representative point when remote region from representative points, such as around clavicle or upper part of rib cage, were impacted. Costal cartilage around the sternum deforms largely and just transmits little rib deformation to the 4th rib or the 7th rib, which was defined as a representative point for THOR's IR-TRACC. These results may suggest that the criterion using the deformation of representative points possibly has low sensitivity to evaluate rib fracture injury under localized loading conditions.

As indicated in Figure 4, large localized deformation of the thorax increases the average of rib deflection without NFR increase and results in overestimation of ADAR with R^2 reduction. This result indicates the necessity to distinguish deformation shape for NFR prediction. WADAR is possible to modify such overestimated ADAR by distinguishing such localized deformation from uniform deformation by a weighting factor. A weighting factor evaluates homogeneity of rib cage deformation shape. The weighting factors of the impact points at No.6 and No.14 were 0.141 and 0.169, respectively. As such, the value of the weighting factor is small for local deformation. The weighting factor modified overestimated ADAR, which shows large value although the NFR is small. Those modifications for distinguishing deformation patterns represented improvement of a correlation between the criterion and NFR.

This study proposed the criterion indicating high correlation with NFR. As future work, the accuracy and robustness should be improved in order for evaluation under same conditions as actual accidents with interior component and restraint systems, such as seatbelts and/or airbags. The criterion is currently based on the results under impact on a single side, thus, it should be improved to evaluate including the non-impacted side. Since this study did not show the physical meaning of coefficient in WADAR, the meaning of value should be considered in a future work.

In addition, the criterion was applied to only the human body, while the manner to apply to ATD should be considered. The THOR dummy is limited in evaluation for frontal collision mode and the thoracic deformation measurement device is currently only four IR-TRACCs. The alternative methods for these limitations should be considered to apply WADAR to the THOR dummy.

CONCLUSIONS

The thoracic deflection criterion using weighted average deflection of all ribs showed the highest correlation with NFR and it allows evaluating rib fractures even under localized loading conditions. Distinguishing deformation patterns improved the prediction of NFR by rib deflections. That suggested that the criterion using the deformation of representative points has possibly low sensitivity to evaluate rib fracture injury under localized loading conditions.

It is not possible to evaluate deflections of all ribs with the current ATD, thus a method to measure all rib deflections, or another alternative, is needed.

REFERENCES

[1] Kent, R.W., Henary, B., Matsuoka, F., 2005. "On the fatal crash experience of older drivers." Annu Proc Assoc Adv Automot Med. 49: 371–391.

[2] Kent, R.W., Woods, W., Bostrom, O., 2008. "Fatality risk and the presence of rib fractures." Ann Adv Automot Med. 52: 73–84.

[3] National Highway Traffic Safety Administration. 2017. "Traffic Safety Facts 2015." DOT HS 812 372, 1-5, Available at https://crashstats.nhtsa.dot.gov/#/DocumentTypeList/12. Accessed November 22, 2018

[4] Kent, R.W., Patrie, J., Poteau, F., 2003. "Development of an age-dependent thoracic injury criterion for frontal impact restrain loading." Proc. Int. Tech. Conf. Enhanced Safety Vehicles 2003; 12

[5] Iraeus, J., Lindquist, M., 2013. "Evaluation of chest injury mechanisms in nearside oblique frontal impacts." Ann Adv Automot Med. Sep; 57: 183–196.

[6] Brumbelow, M.L., Farmer, C.M., 2013. "Real-world injury patterns associated with hybrid III sternal deflections in frontal crash tests." Traffic Injury Prevention, vol. 14, issue 8

[7] Global Human Body Models Consortium, Available at http://www.ghbmc.com/publication/

[8] Li, Z., Subit, D., Kindig, M., Kent, R., 2010, "Development of a Finite Element Ribcage Model of the 50th percentile Male with Variable Rib Cortical Thickness." 38th International Workshop on Human Subjects for Biomechanical Research, National Highway Traffic Safety Administration, U.S. D.O.T.

[9] Poulard, D., Subit, D., 2015. "Unveiling the Structural Response of the Ribcage: Contribution of the Intercostal Muscles to the Thoracic Mechanical Response." Proc. Int. Tech. Conf. Enhanced Safety Vehicles 2015

[10] Ito, O., Dokko, Y., Ohashi, K., 2009. "Development of adult and elderly FE thorax skeletal models." SAE Technical Paper 2009-01-0381

[11] Li, Z., Kindig, M.W., Kerrigan, J.R., Untaroiu, C.D., Subit, D., Crandall, J.R., Kent, R.W., 2010. "Rib fractures under anterior–posterior dynamic loads: Experimental and finite-element study." Journal of Biomechanics, vol. 43, issue 2, 228 - 234

[12] Schoell, S.L., Weaver, A.A., Vavalle, N.A., Stitzel, J.D., 2015, "Age- and sex-specific thorax finite element model Development and Simulation." Traffic Injury Prevention, vol. 16, issue sup1

[13] Yamada, H., 1970. "Strength of biological materials." Williams & Wilkins

[14] Kent, R.W., Lee, S., Darvish, K., Wang, S., Poster, C.S., Lange, A.W., Brede, C., Lange, D., Matsuoka, F., 2005. “Structural and Material Changes in the Aging Thorax and Their Role in Crash Protection for Older Occupants.” Stapp Car Crash Journal, vol.49, 231-249

[15] Ito, O., Ito, Y., Dokko, Y., Mori, F., Ohhashi, K., 2010. “Successive development of adult and elderly FE thorax models (Japanese).” Paper presented at: Society of Automotive Engineers of Japan (JSAE), paper #20105713

[16] Kawabuchi, T., Takahashi, Y., 2018. “Verification of rib fracture prediction in frontal collision.” Paper presented at: International Research Council on Biomechanics of Injury (IRCOBI); September 12-14, 2018; Athens, Greece

[17] Edwards, M., Davis, H., Hobbs, A., Thompson, A., 2003. “Development of test procedures and performance criteria to improve compatibility in car frontal collisions.” Proceedings of the Institution of Mechanical Engineers Part D Journal of Automobile Engineering, 2003

APPENDIX A

Table A1.

Table of value of criteria at impactor speed 6.7m/s

Impact point No.	NFR	Rmax [mm]	MDAR [mm]	ADAR [%]	WADAR [%]
1	2	29.3	36.3	13.6	2.42
2	1	14.3	17.4	6.7	1.22
3	2	21.8	42.4	14.6	2.30
4	2	24.6	30.5	13.0	2.23
5	3	19.9	37.3	13.8	2.31
6	4	27.0	68.3	21.1	2.97
7	6	28.9	58.3	18.6	2.94
8	6	34.9	46.8	17.0	2.88
9	6	95.8	95.8	25.3	3.84
10	6	95.4	95.4	24.1	3.71
11	6	94.1	94.8	23.3	3.62
12	3	29.0	35.0	13.2	2.54
13	5	55.4	75.3	18.9	3.24
14	7	59.5	83.3	21.6	3.66
15	6	56.1	76.4	19.9	3.42
16	2	23.9	26.7	13.3	2.57
17	5	69.1	69.1	19.1	3.42
18	5	75.4	75.4	17.8	3.07
19	4	70.8	70.8	16.7	2.90

Table A2.

Table of value of criteria at impactor speed 4.7m/s

Impact point No.	NFR	Rmax [mm]	MDAR [mm]	ADAR [%]	WADAR [%]
1	1	25.7	31.0	10.6	2.42
2	0	14.5	18.1	7.1	1.22
3	1	16.5	33.1	10.8	2.30
4	2	17.7	24.5	10.1	2.23
5	1	11.5	33.5	10.5	2.31
6	3	21.7	54.0	15.9	2.97
7	4	28.0	45.8	14.6	2.94
8	3	27.7	33.5	12.6	2.88
9	4	79.1	79.1	20.3	3.84
10	5	75.4	75.4	18.2	3.71
11	5	71.9	71.9	16.9	3.62
12	0	21.8	27.9	6.8	2.54
13	4	46.3	62.0	15.7	3.24
14	4	50.6	74.5	17.0	3.66
15	5	49.8	67.4	16.1	3.42
16	0	16.9	20.2	8.9	2.57
17	4	52.6	53.3	14.3	3.42
18	5	66.2	66.2	15.8	3.07
19	4	62.6	62.6	14.5	2.90

INVESTIGATION OF STRAIN-INDUCED BRAIN INJURY MECHANISM IN SIMULATED CAR ACCIDENTS

Toshiyuki, Yanaoka Yukou, Takahashi Hisaki, Sugaya Takayuki, Kawabuchi
Honda R&D Co., Ltd. Automobile R&D Center
Japan

Paper Number 19-0070

ABSTRACT

Further reduction of brain injuries is crucial to diminish traffic fatalities. Past studies suggest that strain of incompressible brain tissue is generated mainly due to head rotation. Accident statistics show a higher rate of pedestrian fatalities resulting from strain-induced brain injuries in accidents with AIS 2+ brain injuries than that of car occupants. One factor for this difference would be larger translation and rotation of an unrestrained pedestrian body than those of a restrained car occupant. This study aimed to clarify the influence of whole body kinematics on the brain strain in pedestrians and occupants.

Time histories of the head translational and rotational accelerations were taken from the NHTSA crash test database for full frontal and MDB side impacts. Pedestrian crash simulations were conducted for frontal and side impacts using a human, small-sedan and SUV FE models to obtain head acceleration time histories. These time histories were applied to the skull of the GHBMC head/brain model. The time histories of the maximum principal strain from the GHBMC model were compared between occupants and pedestrians in the same impact direction. The body kinematics and the rotational velocity of the head were also compared to identify factors for the difference in the time history patterns of the maximum principal strain. In addition, these time histories were compared to that of the CIBIC (Convolution of Impulse response for Brain Injury Criterion) criterion developed in a previous study under each of the four conditions.

Peaks of brain strain were identified in both head pre-impact and impact phase for pedestrian while that was identified only in head impact phase for occupant, regardless of the impact direction. The flip of the rotational direction of the head in the head pre-impact phase was found only in pedestrian, likely resulting in the peak of brain strain prior to the head impact. This trend applied regardless of the direction of impact. The time history of the CIBIC criterion provided waveform patterns similar to the maximum principal strain time history in all impact conditions.

Peaks of brain strain in both head pre-impact and impact phase in pedestrian identified in this study would require reduction of peaks in both phases. A criterion predicting time history of brain strain, such as CIBIC, was found to be an effective tool to address reduction of peaks in multiple phases seen in pedestrian. These findings would lead to novel pedestrian safety technologies that control pedestrian kinematics to reduce the primary peak.

INTRODUCTION

According to the data from National Automotive Sampling System (NASS) Crashworthiness Data System (CDS) from 2010 to 2015 and Pedestrian Crash Data Study (PCDS) from 1994 to 1998, among fatal accidents, the most frequent injuries that sustain the Maximum Abbreviated Injury Scale (MAIS) are head injuries (33% for car occupants, 46% for pedestrians). Of those head injuries, the percentage of fatalities due to brain injuries is 78% for car occupants and 81% for pedestrians. These data indicate that reduction of brain injuries is crucial to reducing traffic fatalities.

Although brain injuries involve numerous injury patterns, they can be broadly classified into the three types; 1) focal injuries due to pressure and/or skull fracture (contusion and epidural hematoma), 2) injuries due to relative displacement of the brain and the skull (subdural hematoma), and 3) strain-induced brain injuries (subarachnoid hemorrhage, intracranial hemorrhage and diffuse axonal injury). The data from NASS CDS from 2010 to 2015 and PCDS from 1994 to 1998 show strain-induced brain injuries account for the largest percentage of fatalities due to

brain injuries, at 81% of car occupants and 73% of pedestrians. In addition, the percentage of fatalities due to strain-induced brain injuries in cases of AIS 2+ brain injuries is 17% for pedestrians and 8% for car occupants. Previous research (Holbourn et al.[1]) suggested that since the brain is incompressible, brain strain occurs mainly due to rotational inputs. One reason for this high rate of fatality caused by strain-induced brain injuries in pedestrian accidents may be the much larger movement and rotation of a pedestrian's head in a crash compared to that of a car occupant. Therefore, it is important to clarify the influence of difference in whole-body kinematics between pedestrians and car occupants on the brain strain.

Most previous research focusing on strain-induced brain injuries investigated criteria for predicting the maximum value of brain strain by applying the rigid body kinematics of the head to human head/brain FE models [2-6]. There are few known studies that focused on the time histories of brain strain needed to clarify the relationship between whole-body kinematics and brain strain. Takahashi et al. [7] and Gabler et al. [8] developed a criterion capable of simulating not only the maximum value but also the time history of brain strain, by representing the complex brain response characteristics with a simple physical model. However, these studies did not investigate characteristics of the time histories of their criteria for pedestrians and car occupants with respect to whole-body kinematics.

This study aimed to clarify the influence of whole-body kinematics on the brain strain in pedestrians and car occupants. The time history of brain strain was obtained by applying the rigid-body head kinematics obtained from representative load cases for car occupants and pedestrians to a human head/brain FE model. The relationship between whole-body kinematics and time history of brain strain was investigated. In addition, the effectiveness of an existing prediction method for time histories of brain strain to capture their characteristics was validated by comparing against brain strain time histories obtained from a human head/brain FE model.

METHOD

Relationship between Brain Strain and Kinematics

The relationship between whole-body kinematics and time history of brain strain was investigated in representative load cases of car occupants and pedestrians. Frontal and side impacts to the body were investigated for both car occupants and pedestrians to clarify the influence of the impact direction.

Time history of head acceleration: For occupant, head translational and rotational acceleration data of the drivers and video of car occupant kinematics were obtained from the National Highway Traffic Safety Administration (NHTSA) Vehicle Crash Test Database. Full frontal impact tests at 56 km/h and moving deformable barrier (MDB) side impact tests at 62 km/h performed by NHTSA for the United States New Car Assessment Program (US NCAP) were selected for the load cases for frontal and side impact to the body, respectively. In order to confirm the influence at various levels of brain strain, two cases approximating the maximum and minimum rotational acceleration were selected for each impact configuration (full frontal impact and MDB side impact) from among the data in the NHTSA Vehicle Crash Test Database. Cases where video of car occupant kinematics is not available and cases involving head impact with components other than airbags were excluded. The selected cases are shown in Table 1.

Table 1
Selected cases for occupant

Case ID	Crash Mode	NHTSA Test ID
OF1	Full frontal 56km/h	8156
OF2	Full frontal 56km/h	8314
OS1	MDB side impact 62km/h	7981
OS2	MDB side impact 62km/h	7984

For pedestrian, time histories of the head translational and rotational accelerations and video of pedestrian kinematics were obtained from the impact simulation to the front and side of a pedestrian at 40 km/h using a human

and a car FE model. In order to compare the kinematics between car occupants and pedestrians, the human FE model representing the size of average American male (AM50) developed by Takahashi et al. [9] was used to match the size of the occupant dummies used in US NCAP. This model has been validated at the component level for each of the neck, chest, pelvis, thigh, knee, and leg, and also for whole-body kinematics. A mid-gait stance was used to represent a lower limb posture with the limbs apart, as the limbs are not aligned in most of the time in a gait cycle. Since car shape strongly influences whole-body kinematics of a pedestrian, two production car FE models representing a small sedan (Car1) and an SUV (Car2) were used. The vehicle models were composed of the components needed to investigate the whole-body kinematics and head acceleration time histories, including body frame, bumper, hood, fenders, cowl top panel and windshield. The components not needed in this study were modeled as a rigid-body which consisted of a node located at the center of gravity of the car and the nodes located at the rear end of body frame. The total mass of the car model was adjusted to match the mass of the car with two occupants on board by adding the mass to the node located at the center of gravity of car. The initial velocity of the car model was set to 40km/h to simulate car-to-pedestrian impact. The car-to-pedestrian impact simulations were conducted until the end of head contact to the car. The time histories of translational and rotational acceleration of the head, and video data which shows the whole-body kinematics were obtained from the pedestrian impact simulations. Figure 1 shows the side view of car FE models used in this study and Table 2 shows dimensions of bonnet leading edge (BLE), rear end of hood at lateral center of the car and windshield angle. The combination of car FE models and impact directions for impact simulations are shown in Table 3.

Figure 1. Side view of car FE models

Table 2
Dimensions of BLE, rear end of hood at lateral center of the car and windshield angle

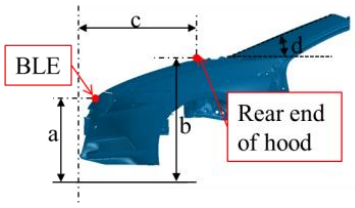

ID	Description	Car1	Car2
a	Height of BLE from ground [mm]	602	907
b	Height of rear end of hood from ground [mm]	904	1053
c	Longitudinal distance from car front end to rear end of hood [mm]	874	930
d	Windshield angle relative to ground[deg]	22	31

Table 3
Pedestrian impact configurations

CaseID	Impact Direction	Car Model
PF1	Frontal	Car1
PF2	Frontal	Car2
PS1	Side	Car1
PS2	Side	Car2

Time history of brain strain: The Global Human Body Models Consortium (GHBMC) head/brain FE model developed by Mao et al. [10] was used in this study. This model reproduces the brain structure in detail, and displacement and pressure response has been validated against the results of dynamic loading test using PMHSs.

Figure 4 shows the mid-sagittal section of the model. Although deformable material was used for flesh, facial bones and skull in the original model, these components were changed from deformable to rigid-body to investigate time histories of brain strain with respect to whole-body kinematics. Time histories of maximum principal strain (MPS) of all of the brain elements were obtained by applying time history data of head translational and rotational accelerations for car occupants and pedestrians to the rigid-body skull of the GHBMC head/brain FE model. The time history of MPS in the brain (hereafter called MPS_{brain}) was calculated from the maximum of MPS value among the all of the brain elements in each time step. In addition, in order to represent the direction of head rotational motion, time histories of head rotational velocity were obtained from the simulation results for both car occupants and pedestrians.

Figure 2. Mid-sagittal section of GHBMC head/brain FE model

Comparison of Kinematics with MPS_{brain}: In order to investigate factors producing differences in the time history patterns of MPS_{brain}, time history of the rotational velocity of the head and kinematics of head and upper body were compared between car occupant and pedestrian. Since head contact timing from barrier or pedestrian contact timing was significantly different between car occupants and pedestrians, factors were investigated by dividing the time from the start of barrier or pedestrian contact to the end of head contact into following two time domains; 1) from the start of barrier or pedestrian contact to the start of head contact (hereafter called pre-impact phase) and 2) from the start of head contact to the end of head contact (hereafter called impact phase). The start and end of head contact was identified from the time history of the head acceleration. In order to compare the difference of kinematics between car occupants and pedestrians, same local coordinate system shown in Figure 3 was used for both car occupants and pedestrians.

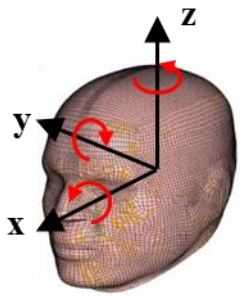

Figure 3. Local coordinate system used in this study

Comparison of Time Histories between CIBIC and MPS_{brain}

The time history of MPS_{brain} obtained from the GHBMC head/brain FE model was compared with that of an existing prediction method to validate the effectiveness for time histories of MPS_{brain} to capture their characteristics.

Existing motion-based brain injury criterion (CIBIC): By assuming that the strain response obtained from the GHBMC head/brain FE model can be reproduced by a simple one-dimensional linear viscoelastic model (Kelvin model) shown in Figure 4, Takahashi et al. [7] developed an injury criterion named CIBIC (Convolution of Impulse response for Brain Injury Criterion) that predicts the time histories of MPS_{brain}. CIBIC is expressed by the analytical solution of impulse response of the simple one-dimensional Kelvin model (Equations 1 and 2).

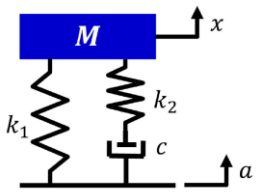

Figure 4. Linear viscoelastic model (Kelvin model) used for development of CIBIC (Takahashi et al. [7])

$$\mathbf{x}(t) = d_1 e^{-a_1 t} - e^{-a_2 t}\{d_1 cos(bt) + d_2 sin(bt)\}$$ (Equation 1, Takahashi et al. [7])

where a_1, a_2, d_1, d_2 and b is the coefficients identified from M, k_1, k_2 and c in Figure 4 to represent rotational response of the GHBMC head/brain FE model when step function with a 1ms duration was applied to the model.

$$\mathbf{CIBIC} = \sqrt{\sum_{i=1}^{3}\left\{\int_0^t x_i(t-\tau)\,\alpha_i(t)d\tau\right\}^2}$$ (Equation 2, Takahashi et al. [7])

where i=1,2,3 represent the x, y and z axis and α_i is rotational acceleration.

CIBIC is a criterion that enables prediction of brain strain time histories, as expressed by Equation 2. Time histories of CIBIC were calculated by using the time histories of the head rotational acceleration in car occupant and pedestrian, and compared with the time histories of MPS_{brain} obtained from the GHBMC head/brain model.

RESULTS

Relationship between Brain Strain and Kinematics

Figures 5 and 6 show the comparison of the time history of MPS_{brain} between occupant and pedestrian for frontal and side impact cases, respectively. Comparison of time histories of rotational velocity between occupant and pedestrian for frontal and side impact are shown in Figures 7 and 8, respectively. Kinematics from video in occupant and pedestrian are compared in Figures 9 and 10 for frontal and side impact cases, respectively. All graphs are plotted from the start of barrier or pedestrian contact to the end of head contact, and values are normalized by the peak. The start time of head contact which divide time domain into pre-impact phase and impact phase is also plotted.

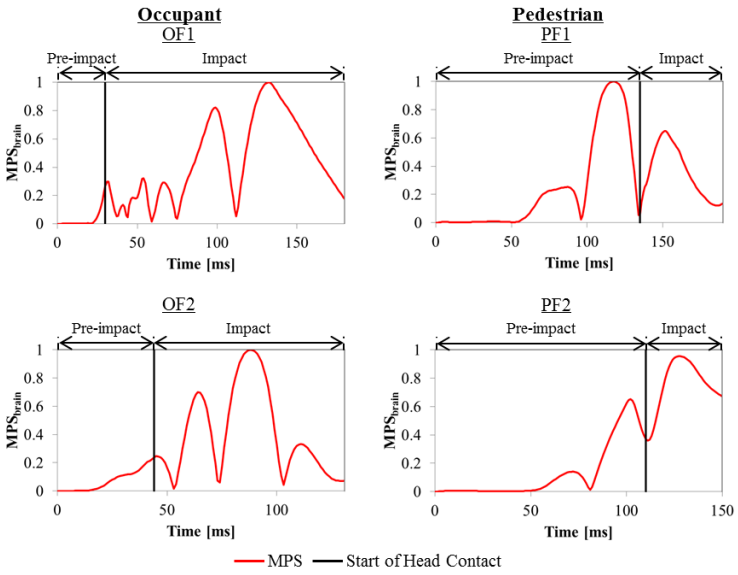

Figure 5. Comparison of time history of MPS_{brain} between car occupant and pedestrian in frontal impact

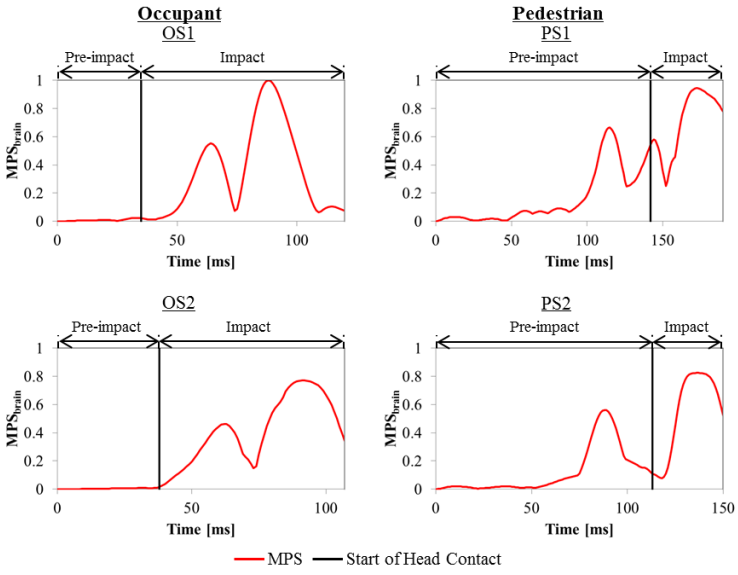

Figure 6. Comparison of time history of MPS_{brain} between car occupant and pedestrian in side impact

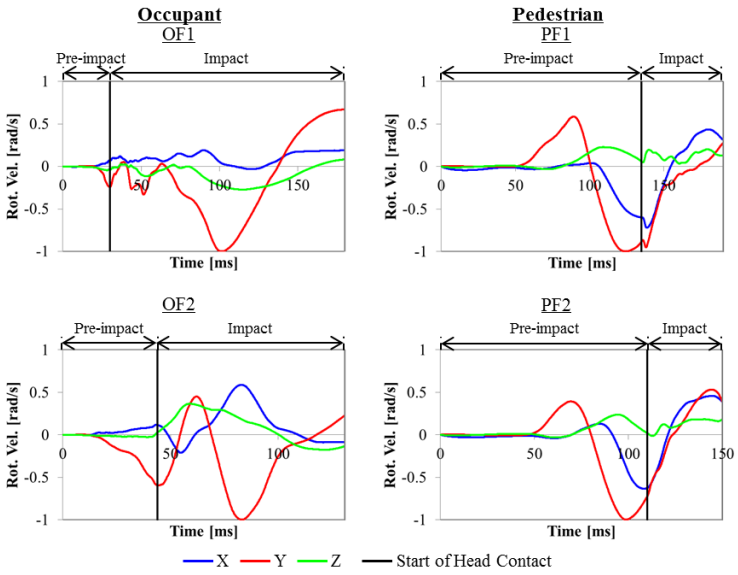

Figure 7. Comparison of time history of rotational velocity between car occupant and pedestrian in frontal impact cases

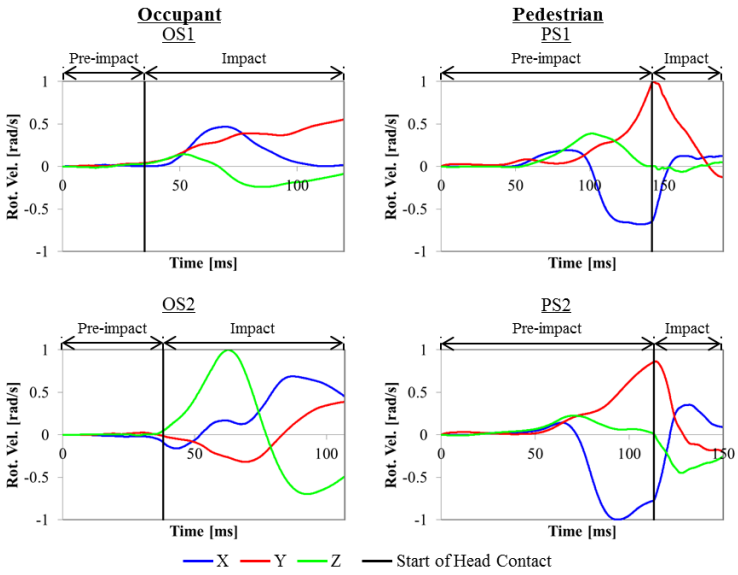

Figure 8. Comparison of time history of rotational velocity between car occupant and pedestrian in side impact

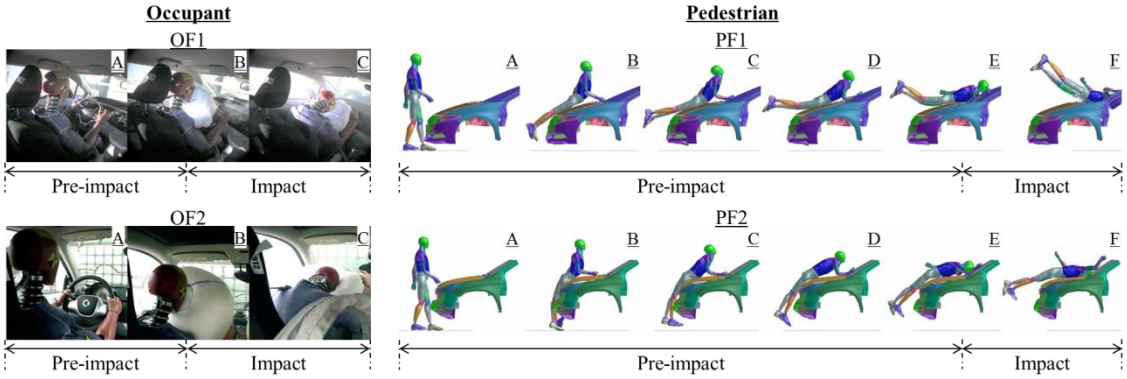

Figure 9. Comparison of kinematics between occupant and pedestrian in frontal impact (For car occupant, A: initial state, B: start of head contact and C: end of head contact. For pedestrian, A: initial state, B: head rotation in opposite direction of the car surface, C: flip timing of head rotation, D: head rotation toward the car surface, E: start of head contact and F: end of head contact)

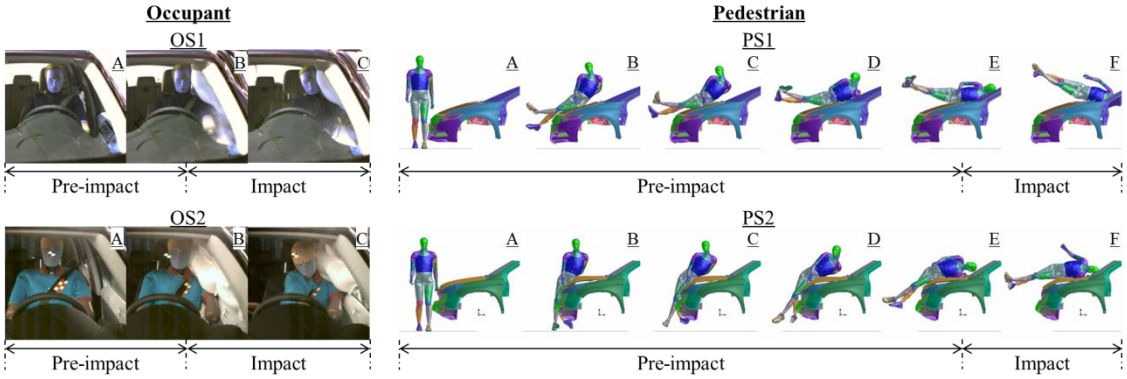

Figure 10. Comparison of kinematics between occupant and pedestrian in side impact cases (For car occupant, A: initial state, B: start of head contact and C: end of head contact. For pedestrian, A: initial state, B: head rotation in opposite direction of the car surface, C: flip timing of head rotation, D: head rotation toward the car surface, E: start of head contact and F: end of head contact)

Comparison of Time Histories between CIBIC and MPS_{brain}

Figures 11 through 14 compare the time histories of MPS_{brain} obtained from the GHBMC model and the time histories of CIBIC in full frontal impact, MDB side impact, pedestrian frontal impact and pedestrian side impact. All graphs are plotted from the start of barrier or pedestrian contact to the end of head contact, and values are normalized by the maximum value. The start time of head contact which divide time domain into pre-impact phase and impact phase is also plotted.

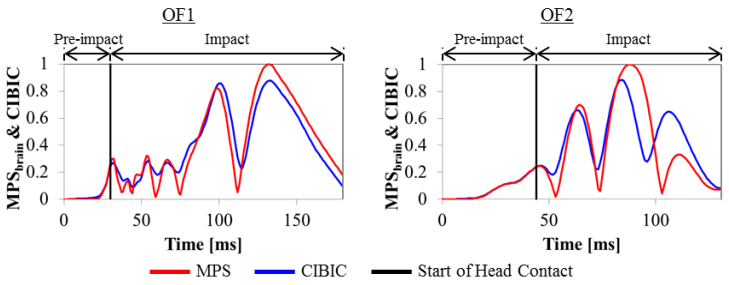

Figure 11. Comparison of time history of CIBIC with that of MPS_{brain} in full frontal impact

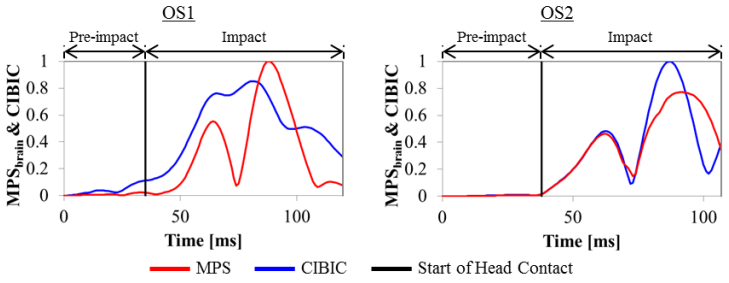

Figure 12. Comparison of time history of CIBIC with that of MPS_{brain} in MDB side impact

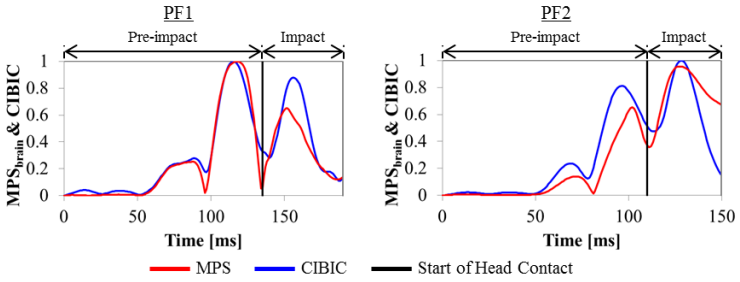

Figure 13. Comparison of time history of CIBIC with that of MPS_{brain} in pedestrian frontal impact

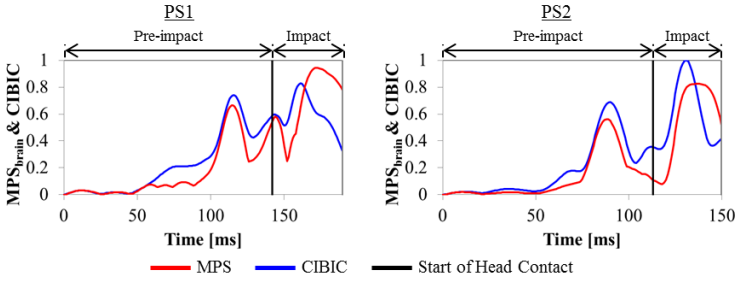

Figure 14. Comparison of time history of CIBIC with that of MPS_{brain} in pedestrian side impact

DISCUSSION

Figures 5 and 6 show that, regardless of the impact direction, peaks of MPS_{brain} occur in both the pre-impact phase and the impact phase in the pedestrian impact cases while peaks of MPS_{brain} occur only in the impact phase for the car occupant impact cases. In addition, Figures 7 and 8show that the sign of rotational velocity of dominant axis (Y

axis for frontal impact and X axis for side impact) flips in the pre-impact phase in the pedestrian impact cases, while this sign flip is not found in the car occupant impact cases. As shown in Figures 9 and 10, this tendency is also confirmed in the comparison of kinematics between car occupants and pedestrians. In addition, Figure 9 and 10 also show that, regardless of the impact direction, the rotation of upper body in the pre-impact phase in the pedestrian impact cases is significantly larger than that in the car occupant impact cases.

Since the head and upper body are connected by the flexible neck with a bending stiffness, the head rotates in the opposite direction relative to the upper body rotation due to the inertia of the head when the upper body inclines toward the car surface. Then, the rotational direction of the head flips by the reaction moment in the neck. Since brain has the inertia and softer material properties compared to the skull, peak of brain strain occurs with some delay relative to the flip timing of the rotational direction of the head (the zero-crossing time of the rotational velocity of the skull). As shown in Figures 9 and 10, since the rotation of upper body in the pre-impact phase in the pedestrian impact cases is significantly larger than that in the car occupant impact cases, these steps can occur during the pre-impact phase in the pedestrian impact cases. In addition, it is presumed that the change in the rotational velocity by the flip of the rotational direction of the head increases with the inclination of upper body. These are thought to be the reason why the pedestrian impact cases, which have flip of the rotational direction of the head due to large upper body inclination in the pre-impact phase, exhibit a large MPS_{brain} peak in this phase that does not occur for the car occupant impact cases. These results suggest that reduction of the probability of strain-induced brain injuries in pedestrians requires reduction of the peak MPS_{brain} in the pre-impact phase in addition to mitigating the impact force from the car body to the head in the impact phase. It is also suggested that pedestrian whole-body kinematics would need to be controlled to reduce the peak in pre-impact phase.

As shown in Figures 11 to 14, CIBIC accurately reproduces the MPS_{brain} response. Furthermore, as shown in Figures 12 and 13, CIBIC can reproduce the peak timing and value in the pre-impact phase of MPS_{brain} response which is typical response in the pedestrian impact. Since CIBIC is a criterion for predicting brain strain response using a simple physical model, it would be a criterion suitable for evaluating probability of injury with multiple peaks of brain strain.

It should be noted that the results of the current study depends on the validity of the FE models and crash test dummies. Further validation needs to be done once such simulation tools are improved in future studies.

CONCLUSION

It was demonstrated that, unlike car occupants, the peak value of MPS in the brain occurs during both the pre-impact and impact phases regardless of the impact direction. The strain-induced brain injury criterion, CIBIC, was found to accurately reproduce the time history of MPS in the brain predicted by an FE head/brain model under full frontal impact, MDB side impact and pedestrian frontal and side impact conditions, showing applicability of CIBIC in evaluating strain in the brain with multiple peaks.

REFERENCES

[1] Holbourn, A.H.S. 1943. “Mechanics of head injuries.” Lancet 2. October 9: 438.41

[2] Kimpara, H., Nakahira, Y., Iwamoto, M., Rowson, S., Duma, S. 2011. "Head injury prediction method based on 6 degree of freedom head acceleration measurements during impact." Internatinal Journal of Automotive Engineering, 20114490

[3] Kimpara, H. and Iwamoto, M. 2012. “Mild traumatic brain injury predictors based on angular accelerations during impacts.” Ann Biomed Eng., 40(1):114-26

[4] Newman, J.A., Shewchenko, N., Welbourne, E. 2000. “A proposed new biomechanical head injury assessment function - the maximum power index.” Stapp Car Crash J., 44: 215-47

[5] Takhounts, E.G., Craig, M.J., Moorhouse, K., McFadden, J., Hasija, V.2013. “ Development of brain injury criteria (BrIC).” Stapp Car Crash J., 57: 243-66

[6] Yanaoka, T., Dokko, Y., Takahashi, Y. 2015. “Investigation on an injury criterion related to traumatic brain injury primarily induced by head rotation.” SAE International Technical Paper, 2015-.01-1439

[7] Gabler, L.F., Joodaki, H., Crandall, J.R., Panzer, M.B. 2018. "Development of a single-degree-of-freedom mechanical model for predicting strain-based brain injury response." Journal of Biomechanical Engineering, Vol.140, 031002

[8] Takahashi, Y., Yanaoka, T. 2017. "A study of injury criteria for brain injuries in traffic accidents." Paper presented at: 25th ESV conference, Paper Number: 17-0040.

[9] Takahashi Y., Asanuma H., Yanaoka T. 2015 "Development of a Full‐Body Human FE Model for Pedestrian Crash Reconstructions." Paper presented at: IRCOBI Conference; 2015.

[10] Mao H., Zhang L., Jiang B., Genthikatti V.V., Jin X., Zhu F., Makwana R., Gill A., Jandir G., Singh A., Yang K.H. 2013. "Development of a finite element human head model partially validated with thirty five experimental cases." J Biomech Eng., 2013 Nov;135(11):111002.

SAFETY EVALUATION OF AUTOMATED VEHICLES THROUGH ACTUAL VEHICLE TESTS IN CUT-IN AND OFFSET CUT-IN SITUATIONS.

Seohang Lee
Jayil Jeong
Kookmin University
Republic of Korea

Yunseog Hong
Jaekon Shin
Inseong Choi
Korea Automotive Testing & Research Institute(KATRI)
Republic of Korea

Paper Number 19-0078

ABSTRACT

This paper describes the safety assessment results of level 2 automated vehicles in cut-in and overlap cut-in collision situations. The test results were compared with typical rear-end and 50% overlap rear-end collisions. From analysis of NASS CDS data, cut-in rear-end accidents occur at a rate of 25% out of rear-end accidents. The cut-in and 50% overlap cut-in situation were tested for the evaluation of level-2 automated vehicles. Main parameters of the cut-in scenario are speed of vehicles, TTC(Time to collision) and TLC(Time to lane changing). The speed of vehicles for scenario composition was selected from NASS CDS data analysis. The speed of the vehicle target was selected at 20km/h. The speed of the VUT(Vehicle Under Test) consisted of 5 types: 30, 40, 50,60 and 70 km/h.

Cut-in scenarios were designed with TTC 4 seconds and the target vehicle changes the lane to the front of the test vehicle at each TTC. The target vehicle's TLC was set to 2 seconds at all scenarios. For comparison, rear-end collision and 50%-offset rear-end collision scenarios suggested by EuroNCAP 2018 were also tested. A low platform robot vehicle target was utilized for all test scenarios. The low platform robot vehicle and a balloon dummy were used to imitating the causative vehicle in the accident and reproduce the accident situation. The robot vehicle target and the VUT were communicated with their position, speed, and acceleration data from GPS INS data. The data were recorded for further analysis.

OVERVIEW

The driver had to take risks such as personal and financial damages while driving the car.Various legal, institutional, and technical measures have been put in place to reduce the risk, and now it is possible to use safe and convenient vehicles based on the development and dissemination of autonomous vehicles.

In particular, the development and emergence of autonomous vehicles and assistive technologies are expected to prevent or reduce the risk of automotive crashes occurring at present. As a result, the demand for the development and distribution of safer autonomous vehicles is getting lighter, and the interest of the users is increasing. In response to this trend, the New Car Assessment Program (NCAP) urged developers of autonomous vehicles to upgrade their safety in accident situations.

However, the current NCAP standards are not a standard for dealing with various accidents that may occur on the current roads. In particular, among the functions of the autonomous vehicle, the evaluation criteria of AEB, which plays the most role in avoiding accidents in sudden accident situations, has a limitation that can be confirmed only for simple rearward collision situations. As the function of the autonomous vehicle increases, it is expected that the users will use the technologies more actively. Therefore, more rigorous safety of the autonomous vehicle is required and safety verification in various accident situations is required.

This paper identifies some of the AEB protocols provided by the NCAP, and develops real-world test scenarios for interrupt situations as a result of classifying dangerous accident situations that often occur on the roads. The AEB performance of the autonomous vehicle is conducted the actual vehicle experiment for the safety evaluation safety.

METHODS

Building of Scenario

Accident data analysising: NASS CDS data was analyzed for five years from 2100 to 2015. 2,633 cases in 2015, 2,896 cases in 2014, 3,385 cases in 2013, 3,581 cases in 2012, and 4,278 cases in 2011. The data were classified and analyzed according to the type of accident. More than 40 types of accidents type was classified by NASS CDS. It was classified into single vehicle accident, rear-end collision, cut-in rear-end collision, frontal collision and side collision..... As a result, shown in the Fig.1, the ratio of single vehicle accident was the highest at 36%, side collision was the second at 31%, rear-end collision and head on collision occupied at the third and fourth, with 5% of ratio.

Especially, when the type of accident was classified as rear-end collision, cut-in collision accounted for about 22% of the total rear collision. As a result of checking the ratio of AIS injuries according to the accident situation, the ratio of injury severity of simple collision accident to intervention collision was similar.

Through the results of the accident DB analysis, it can be seen that the rear-end collision is the most important accident type, which is the type of accident that is already evaluated through the NCAP protocol. However, the NASS CDS DB analysis shows that the rate of interruption in the collision is about 1/4, and the degree of injury in the case of interruption shows a similar tendency to the general collision.

Therefore, it is necessary to confirm the AEB performance not only in a simple rear-end collision situation but also in a cut-in rear-end collision situation. Considering the AEB test Protocol proposed by 2018 Euro NCAP, the cut-in collision scenario and 50% offset cut-in collision scenario were constructed according to the following procedure.

Set parameters for scenario configuration: Main parameters of the cut-in scenario are speed of vehicles, TTC(Time to collision) and TLC(Time to lane change). The parameters were determined by analyzing the results when an accident occurred. The speed of each vehicle was selected by referring to the results of NASS CDS accident database. TTC and TLC were selected by analyzing images acquired from dashboard camera image.

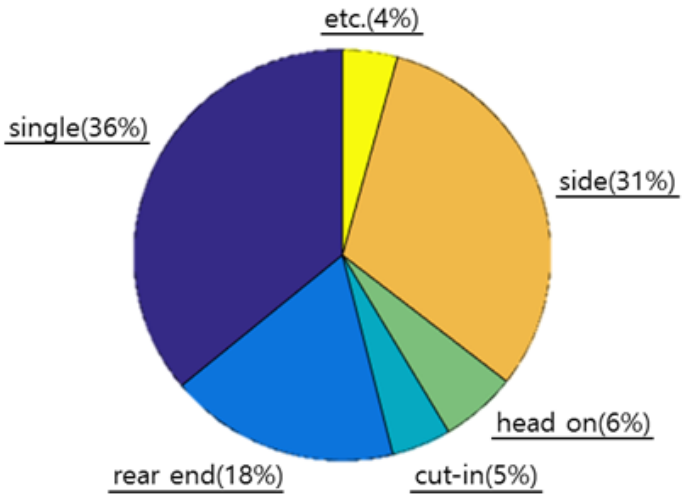

Figure 1. The frequency by accident type.

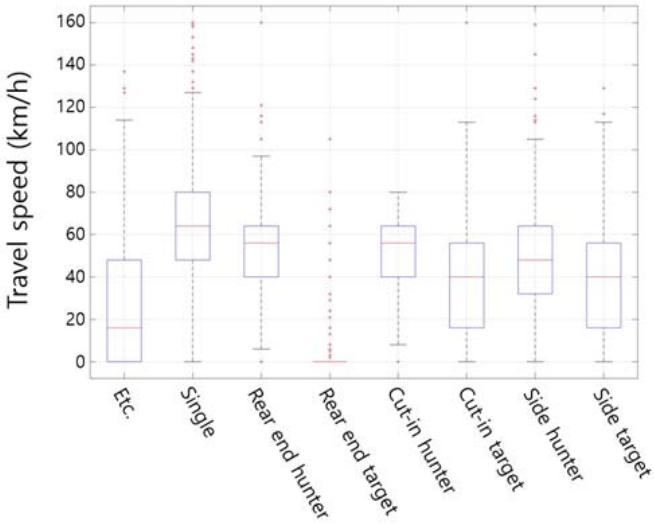

Figure 2. Velocity distribution by accident type (Public roads:Speed limit less than 80 km/h)

In the case of the target vehicle, 50% of the vehicles are present in the range of 20 to 50 km/h and the median value is 40 km / h. The speed of the target vehicles are present in the range of 20 to 40 km/h and the median value is 40km/h. TLC is selected by dashboard camera images in Korean intervention situation. In a total of 63 dashboard camera image data, it was confirmed that the average TLC in an accident situation was 1.85 seconds. It is difficult to determine when to start a cut-in from the black box images or accident DB analysis results. Therefore, the time to start cut-in was arbitrarily selected. Based on the results of the pre-test in one vehicle, the time to start cut-in was selected as TTC 4 seconds. That is, according to the constructed scenario, the time remains 2 seconds for the VUT to collide with the target vehicle when the cut-in complete. Based on these analyzed parameters, the following scenario table is constructed.

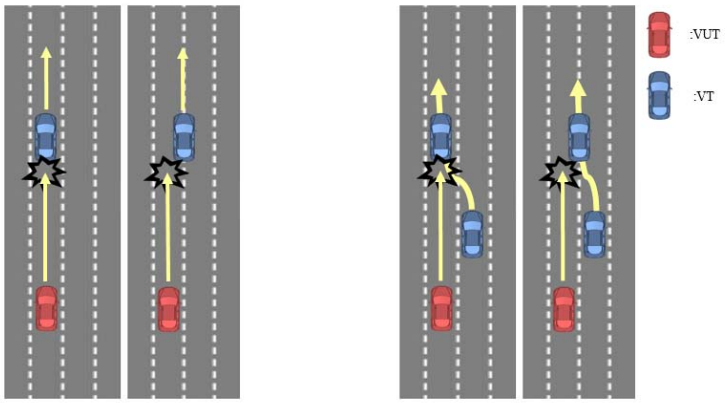

Rear-end & 50% offset Rear-end Collision test Scenario	
Vehicle Target	Vehicle Under Test
20km/h	30km/h
	40km/h
	50km/h
	60km/h
	70km/h

Cut-in Rear-end & 50% offset Cut-in Rear-end Collision test Scenario	
Vehicle Target	Vehicle Under Test
20km/h TLC 2s at TTC 4s	30km/h
	40km/h
	50km/h
	60km/h
	70km/h

Figure 3. Scenario Table for AEB collision test

Development of Testbed

Low-platform robot vehicle target: In the Euro NCAP protocol, the EVT(Euro NCAP Vehicle Target) used for the AEB test is a pile that shapes the rear-end collision of the vehicle, and serves as a forward vehicle in test such as rear-end collision. In case of EVT, it is not suitable for scenario that requires path following function because it is mounted on a rail or connected with a preceding vehicle. Therefore, a robot vehicle target capable of performing in various scenarios was designed.

In the case of robot vehicle target, it is necessary to be able to perform not only the rear collision test used in the existing NCAP test but also the forementioned cut-in scenario. In addition, in order to be able to repeat the experiment, the robot vehicle was designed so that the equipment, the VUT, and the experimenter would not be damaged or injured in the event of a collision due to the VUT not responding to the accident situation.

RVT (Low-Platform Robot Vehicle Target) was designed as a robot vehicle target. From the developed scenario, the maximum relative speed of VUT and RVT is 50km / h. It should be designed so that the test system is not damaged even if it collides at this speed. The height of the lower part of the vehicle differs by vehicle type, but the legal minimum ground height in Korea is 110mm. As a result, the height of the RVT is limited to 90 mm.
In order to carry out the scenario, The RVT equipped with a dummy model is designed to be able to travel at a maximum speed of 40 km/h and change lanes 3.5m within 2 seconds. The RVT and the VUT had configured communication systems to accurately measure each position and transmit data to each other. The type of data to be transmitted is the position, speed, and acceleration information of the vehicle. These data are also the main analytical elements obtained from the experimental results.It is confirmed that the vehicle and RVT were not damaged even when the vehicle stepped over at a speed of 60 km/h, and the RVT travel at a maximum speed of 60 km/h equipped with a dummy model.

3D ballon dummy: The VUT does not recognize the RVT as a vehicle.Therefore, a ballon dummy model should be mounted on the RVT. In the case of such a dummy model, The VUT must be able to recognize the dummy as a real vehicle when sensing the vehicle ahead with a radar or a camera. It should also not damage the VUT in the event of a collision.

As shown in the Figure 4 below, a 3D dummy model was created to have the shape of the actual vehicle using a balloon to minimize the impact quantity when colliding. The 3D balloon dummy was verified using a radar system. The radar used in the verification uses radio waves in the 24 GHz band. The verification method was evaluated by comparing the radar reflectance of the actual vehicle with the radar reflectance of the balloon target pile. Also, we confirmed that the target dummy was recognized as a vehicle by using the vehicle equipped with the actual AEBS.

The AEBS vehicle ran at more than 30 km/h with the balloon target pile up and checked whether there was a warning in the vehicle. The test results confirm that the head-up display gives a vehicle crash warning as shown in the Figure 5. This result shows that AEBS is recognized as a vehicle and can be used for testing.

Figure 4. Shape of Balloon dummy car

Figure 5. AEBS warning test of 3D balloon dummy car

ACTUAL VEHICLE TEST

An actual vehicle test was conducted on the scenarios developed using a real vehicle equipped with an AEB. Each of the scenarios was tested three times and the AEB operation and collision were observed. In case of collision, the velocity at the time of collision was observed. In case that a collision did not occur the minimum approach distance was observed. In addition, the deceleration of the vehicle caused by the AEB was also analyzed.

Scenario Test Results

Test Results: The AEB collision test scenarios shown in Figure 3 was repeated twice for each scenario. The results of the actual vehicle tests are summarized in Table 1. Based on the experimental speed of VT and VUT, it is classified into the items according to the scenario. The classified scenarios are Rear-end, Cut-in, 50% Offset Rear-end, and 50% offset cut-n. If there is no collision, 'no collision' is indicated and the minimum distance is indicated at the bottom. In case of collision, 'collision' is indicated and the speed of collision is indicated at the bottom.
In case that a collision did not occur in the actual vehicle experiment, the relative distance when the VUT was closest to the VT was measured. When a collision occurs, the relative velocity of the VUT and VT at the moment of collision is measured.

In the 10 tests with five rear-end collision scenarios, AEB was operating normally and did not crash. VT was very close to the VUT, but it was observed to avoid collision with a maximum of 3.11m margin. Therefore, in the simple rear-end collision situation proposed by the Euro NCAP, the present AEB function shows good performance.

In the 50% offset rear-end collision scenario, one collision occurred when the VUT speed was 70 km/h, but in all cases the AEB was operating normally. As the speed increases, the AEB fails to avoid one collision to the increased difficulty level, but still shows good performance. Also, It has been confirmed that if the AEB of the VUT is operating normally, it will defend the collision situation.

As a result of the general cut-in collision test scenario, five collisions occurred in 10 tests. The AEB response was delayed in all five crashes, which is the main reason for not recognizing the vehicle that changed the lane in the next lane. Likewise, it has been confirmed that the detection performance of the vehicle coming in the next lane is considerably deteriorated in the collision situation in which the AEB must respond.

Table 1. Scenario test results of vehicle test

VT	VUT	Rear-end		Cut-in	
		No Collision (Minimum relative distance) Collision occurred (Relative impact speed)			
20km/h	30km/h	No Collision 2.12	No Collision 2.58m	Collision 11.26km/h	Collision 11.29km/h
	40km/h	No Collision 3.11m	No Collision 2.96m	No Collision 6.02m	No Collision 9.95m
	50km/h	No Collision 1.06m	No Collision 0.58m	No Collision 0.06m	No Collision 12.99m
	60km/h	No Collision 1.44m	No Collision 2.06m	Collision 38.52km/h	Collision 39.20km/h
	70km/h	No Collision 0.15m	No Collision 0.06m	No Collision 0.78m	Collision 42.56km/h
VT	VUT	50% offset rear-end		50% offset Cut-in	
20km/h	30km/h	No Collision 3.14m	No Collision 1.31m	Collision 10.8km/h	Collision 7.19km/h
	40km/h	No Collision 1.58m	No Collision 1.45m	No Collision 0.70m	Collision 8.84km/h
	50km/h	No Collision 1.12m	No Collision 1.41m	Collision 2.49km/h	Collision 8.52km/h
	60km/h	No Collision 1.13m	No Collision 1.44m	Collision 18.3km/h	Collision 17.8km/h
	70km/h	Collision 9.83km/h	No Collision 1.14m	Collision 21.1km/h	Collision 19.7km/h

CONCLUSIONS

Experimental results show that level 2 automated vehicles have a lack of ability to avoid a crash in cut-in collision situations. 2018 Euro NCAP's proposed AEB test protocol scenarios did not have good response capabilities in a barrage situation, even for vehicles with good performance.

In some cases, the VUT did not detect the vehicle target so it strikes target without any deceleration. The sensor seems to detect only the same lane of the vehicle not for its side lanes.

In view of the injury analysis results, the current AEB performance alone does not seem to prevent any serious injury to the driver in the event of interruption.

The cut-in and 50% offset cut-in experimental scenarios were constructed from the actual accident. Four types of vehicle tests were conducted and test results were analyzed. In each scenario, relative speed and deceleration were analyzed. The safety performance for an automotive vehicle in cut-in rear collision situations was evaluated. Further studies on safety assessments in various test scenarios are needed in order to validate the safety performance of automated vehicles.

This research was supported by the Korea Ministry of Land, Infrastructure and Transport. It was also supported by the Korea Agency for Infrastructure Technology Advancement (Project No.: 17TLRP-B117133-02)

REFERENCES

[1] P. Ioannou, 1988, Development and Experimental Evaluatioin of Atuonomous Vehicles for Roadway /Vehicle Cooperative Driving, UCB-ITSPRR-09-0

[2] EuroNCAP, 2018, “EuroNCAP AEB Test Protocol.”

[3] ISO, 2010, “ISO 15622 Intelligent Transport Systems − Adaptive Cruse Systems − Performance Requirements and Test Procedures.”

[4] ASSESS, 2008, “Assessment of Integrated Vehicle Safety Systems for improved vehicle safety.”

[5] Gass, S.I. 1978. “Computer Model Documentation.” In Proceedings of the 1978 Winter Simulation Conference (Miami Beach, FL, Dec. 4-6). IEEE, Piscataway, NJ, 281-287

HEAVY TRUCK CRASHES INVOLVING PEDESTRIANS IN COMPARISON TO BICYCLISTS

Axel Malczyk, Jenö Bende
German Insurers Accident Research, GDV German Insurance Assoc.
Germany

Paper Number 19-0080

ABSTRACT

Although crashes with vulnerable road users account for a small proportion of all heavy truck accidents they cause particularly severe injuries. In Germany, collisions with bicyclists and pedestrians accounted for only 9% and 4%, respectively, of all injury crashes between a truck over 12,000 kg gross vehicle weight and another road user in 2015. However, vulnerable road users represented 26% of fatalities in these kinds of crashes. While collisions between trucks and bicyclists, particularly in right-turn situations, have recently gained attention in Europe, little research has been dedicated to crashes involving pedestrians. This study describes the circumstances and injury outcomes of severe crashes between heavy trucks and pedestrians in comparison to those involving bicyclists. The German Insurers Accident Database (UDB) provided data on accidents involving heavy trucks, defined as goods vehicles over 11,900 kg GVW: 39 crashes with 43 pedestrians, altogether, and 62 crashes with one bicyclist, each.

The majority of crashes occurred in built-up areas and during daylight, both for pedestrians and bicyclists. While most accidents involving pedestrians took place on a stretch of road (49%) the majority of accidents involving bicyclists occurred at junctions (77%). Females accounted for 58%, each, of the casualties among both groups of VRU's. Pedestrians averaged 57.8 years of age (median: 61 yrs.), and were approximately six years older than bicyclists with an average of 51.6 years (median: 52.5 yrs.). The collision situations for pedestrians and for bicyclist differed considerably. The truck was going straight in the large majority of cases where a pedestrian was struck. Often, the truck was initially stationary and then moved off and collided with the person walking or standing near the vehicle. Crashes between a heavy truck and a bicyclist, on the other hand, were clearly dominated by turning manoeuvres, mostly when the truck made a right-turn at a junction and hit a bicyclist who was travelling alongside on the right of the truck and intending to go straight. 40% of pedestrians were run over, five of them with fatal consequences. Bicyclists were run over in 52% of cases, resulting in nine fatalities. Despite different collision scenarios among pedestrians and bicyclists in crashes with trucks, their injury patterns and severities were very similar. MAIS3+ cases accounted for approximately two thirds among all casualties in both groups. The highest proportion of AIS3+ injuries for pedestrians was found in the thorax region (31%) and for bicyclists in the lower extremities region (40%).

The present work confirms previous studies related to accidents between trucks and vulnerable road users that noted the prevalence of older persons among the VRU's. It adds to the body of research by providing detail data on the different collision scenarios typical of truck accidents with pedestrians and with bicyclists and their injury patterns. Truck driver assistance systems hold a large potential to avoid or mitigate crashes with both VRU groups. While monitoring the right side of the vehicle is necessary to avoid crashes with bicyclists, pedestrian detection needs to focus on the area in front of the truck.

INTRODUCTION

Vulnerable road users (VRU) have been in the focus of accident research for a long time. However, pedestrians have been addressed primarily regarding collisions with passenger cars and bicyclist have gained increasing attention only during the last couple of years due to the popularity of cycling and the resulting stagnation – and in some countries even the increase – in the number of bicyclist casualties. For instance, the number of killed bicyclists in Germany did not decline in 2017 in relation to 2010 whereas the overall number of killed road users dropped by 13% [1]. While accidents between heavy vehicles and bicyclists are relatively rare, they have been of recent interest both for the public and research because they tend to result in very severe or even fatal outcome for the VRU despite the fact that these accidents typically happen at low speed. Several studies have looked at the causes of these crashes and the role of "blind spots" around trucks and truck-trailer combinations [2, 3]. They found that conflicts between

right-turning trucks and bicyclists riding alongside on their right side and continuing straight present a particularly dangerous situation due to the high risk that the bicyclist gets run over by the truck's wheels [2, 4]. In this context, the potentials of technical measures to enhance the direct and indirect view from the truck cab as well as the introduction of electronic turn-assistance for truck drivers to warn of VRU's in the immediate vicinity of the vehicle have been discussed [4, 5].

Research on crashes between heavy trucks and pedestrians is scarce, though. Recent data available from Belgium and Germany [3, 6], for instance, suggests that these kinds of accidents may be less frequent than those between heavy trucks and bicyclists, but may pose a similar risk for severe or fatal injury to the pedestrian. An analysis of the Rhône Road Trauma Registry in France [7], however, yielded much more pedestrians than bicyclists who collided with a truck.

The present study intends to shed more light on the similarities and differences of accidents between heavy trucks and pedestrians and bicyclists, based on in-depth data obtained from German motor liability insurers. While collisions between heavy trucks and bicyclists and their injuries were the subject of an earlier study [4], this evaluation adds data concerning pedestrians, but maintains the previous methodology. Thus, comparison of the results for the two groups in crashes with heavy vehicles should be facilitated, at least for the situation in Germany.

METHOD

Crash and injury data came from the German Insurers Accident Database (UDB). This database contains data from samples obtained retrospectively from claim files of German motor liability insurers. Cases recruited for the present study involving heavy trucks were required to have estimated initial claim costs of at least EUR 30,000, covering both personal and property damage, irrespective of the actual payments during claim processing and whether the truck driver or the vulnerable road user was at fault. Since crashes with pedestrians and bicyclists tend to result in higher bodily than material damage, these accidents present rather severe outcomes in terms of injury.

Heavy trucks were defined as goods and service vehicles with a gross vehicle weight (GVW) of 11,900 kg and over and their trailers where present. According to EU definition, goods transport vehicles over 12,000 kg fall into the N3, or N3G category, respectively. They include most tractors for semi-trailers, trucks for long distance transport, either as rigid units or in combination with drawbar trailers, and heavy-duty trucks used in the construction and the waste management industry. Trucks with a GVW of just below 12,000 kg, often registered with a weight of 11,990 kg, are popular particularly for regional distribution services. These trucks belong to the N2 or N2G category, respectively, and were included in the study as well. Buses, farm tractors and special equipment like mobile cranes, etc., were not considered.

Users of bicycles were categorised as "bicyclists" if they had mounted their bicycle at the time of collision. E-bikes and tricycles based on the design of conventional bicycles were taken into account, too, though rarely involved.

Bicyclists walking their bike were categorised as pedestrians as their characteristics resemble rather those of other persons walking when moving in traffic. This is in line with the coding rules for the German police when reporting road traffic accidents. The group of "pedestrians" included also users of devices like kick-boards as well as any person walking or standing on or near the road at the time of the accident. This comprised drivers of motor-vehicles who had just left their vehicle, or were about to enter it. Furthermore, road maintenance workers and the like were counted as pedestrians, although they are defined as a separate group of road users in German national statistics. Two cases of persons intending to commit suicide by running in front of an approaching truck, and being seriously injured, were considered for the analysis as well.

Vulnerable road users who were injured in the course of the accident, but not directly as a result of contact with the heavy truck, were excluded from the analysis. This, for instance, pertained to a car driver who was standing between his vehicle and a van, when a truck rear-ended the van, pushed it forward and wedged the driver between the front of the van and the trunk of his car.

The documentation of crashes usually comprised police reports, witness statements, hospital discharge information and sometimes accident reconstructions and post-mortem reports. Several variables were used to characterise the location of the crash and the actual event as well as the immediate phase preceding the collision.

Injury severity was categorised according to the definition used in the national statistics (killed, seriously injured, slightly injured) and according to AIS 2005, Update 2008 [8], where injury documentation provided enough detail. Furthermore, the Maximum AIS (MAIS) to characterise the overall injury severity, and the highest AIS values were determined for the following body regions: Head/face (including skull and brain), thorax, upper extremities (including shoulder and hands), abdomen, lower extremities (including pelvic bones and feet) and spine (cervical, thoracic and lumbar spine). For clarity, AIS injury severities were grouped into three categories: AIS0-1 for no or only minor injury, AIS2 for moderate injury, and AIS3+ for serious to maximum injury severity.

Run-over may be of particular importance with regard to the injury mechanism in vulnerable road users. For the purpose of this study, run-over is defined as one or more wheels of the vehicle rolling over a portion of the victim's body or at least wedging a body part between a wheel and the ground with resulting injury. Cases where the VRU got under the vehicle and possibly contacted the underbody, but not the wheels, were not counted as run-overs.

The analysis was carried out based on data sets of individuals, i.e., for each injured pedestrian or bicyclist and his or her circumstances of the accident. Thus, in cases of two vulnerable road users being injured in the same event, data pertaining to the infrastructure, the heavy truck and the surrounding conditions are counted twice. Depending on the detail and reliability of data, some of the cases had to be excluded from certain analyses. Therefore, percentage values from the data analysis relate to the number of valid cases.

Differences of values based on continuous variables were tested for significance using the t-test, for dichotomous variables the Chi-square test was applied. Statistical significance was assumed at a p-level of 0.05, otherwise the difference was considered non-significant (n. s.).

RESULTS

The German Insurers Accident Database (UDB) provided 39 crashes between heavy trucks (GVW of 11,900 kg and over) and pedestrians and 62 crashes between heavy trucks and bicyclists that occurred in Germany between 2007 and 2012, the majority of them (63 cases altogether) in 2012 due to a larger sample of truck accidents drawn for this year. In four accidents involving pedestrians, two persons, each, were injured by the same truck and thus the circumstances of such crashes enter the database twice. Therefore, the material contains 43 pedestrians and 62 bicyclists and the related circumstances of their accidents.

Road Infrastructure and Environmental Conditions

The large majority of crashes for both groups of VRU's occurred in built-up areas (pedestrians: n = 35; 81%; bicyclists: n = 57; 92%) (n.s.). Of the seven crashes with pedestrians outside of built-up areas, three occurred on a motorway, injuring four persons. While accidents involving pedestrians took place on a stretch of road in nearly half of the cases (n = 21; 49%), most accidents involving bicyclists were located at or in the immediate vicinity of junctions like crossings or T-junctions (n = 48; 77%). This difference in accident site characteristics between pedestrian and bicyclist crashes was statistically significant ($p < 0.01$). With eleven cases (26%), traffic was significantly less frequently controlled by traffic lights at junctions or crosswalks in pedestrian accidents than in bicyclist accidents (n = 33; 53%) ($p < 0.01$).

The large majority of cases were found for weekdays from Monday to Friday. Only three accidents with pedestrians and one with a bicyclist on a weekend were reported. The times of the accidents were almost entirely in the morning hours (6 AM to 12 AM) and the afternoon and early evening hours (12 AM to 6 PM) (pedestrians: n = 39; 91%; bicyclists: n = 58; 94%). Accordingly, the large majority of collisions took place during daylight both for pedestrians (n = 38; 88%) and bicyclists (n = 51; 82%) (n.s.). Road surfaces were rarely wet among both groups, but such conditions were significantly more frequent in crashes with pedestrians (n = 10; 23%) than in bicyclist crashes (n = 5; 8%) ($p < 0.05$).

Truck Characteristics, Truck Driver and VRU Demography

The general vehicle type could be determined for all heavy trucks colliding with pedestrians and those colliding with bicyclists. Among crash opponents for pedestrians, 18 (42%) were semi-tractors with trailers, four (9%) were truck-drawbar-trailer combinations and 21 (49%) were single rigid units. Trucks colliding with bicyclists were composed of 25 (40%) semi-trailers, 15 (24%) truck-drawbar-trailer combinations and 22 (35%) rigid trucks. The larger share of rigid trucks in crashes with pedestrians was not significant (n.s.). While only one bicyclist collided with a garbage truck, five trucks of this type were involved in pedestrian accidents, one of them with two pedestrians at the same time, thus appearing twice in the count.

Except for seven trucks, vehicle age at the time of the accident could be determined. It ranged from practically new vehicles to 20 years of age, averaging 5.2 years (median: 4 yrs.) of service for trucks colliding with pedestrians and 5.5 years (median: 5 yrs.) for those colliding with bicyclists.

With one exception, all truck drivers were males, their age ranging between 22 and 65 years (average: 45.4 yrs.; median: 46 yrs.) for those involved in pedestrian crashes and between 21 and 69 years (average: 44.6 yrs.; median: 45.5 yrs.) for those involved in bicyclist crashes (n.s.). Age was unknown for four drivers.

Females accounted for 58%, each, of the casualties among both groups of VRU's: 25 of the 43 pedestrians and 36 of the 62 bicyclists were women (Figure 1). Pedestrians averaged 57.8 years of age (median: 61 yrs.), and were approximately six years older than bicyclists with an average of 51.6 years (median: 52.5 yrs.). Although the VRU's ages appear relatively far from a normal distribution, a t-test was performed, but showed no significant difference between the groups (n.s.).

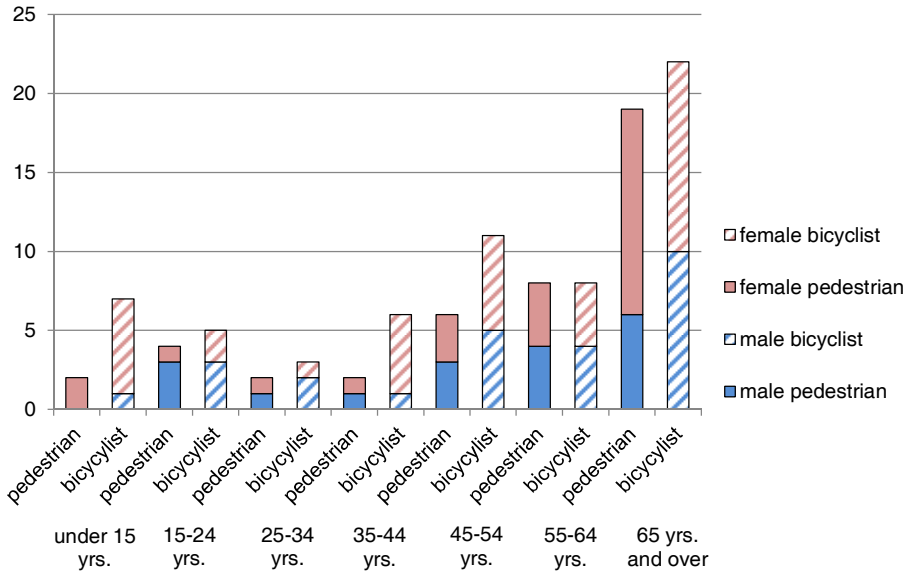

Figure 1. Pedestrian and bicyclist gender and age distribution

Females among pedestrians were approximately five years older than their male counterparts (females: average 60.0 yrs., median 67 yrs.; males: average 54.7 yrs., median 56 yrs.), whereas female bicyclists were four years younger than male cyclists (females: average 49.7 yrs., median 50.5 yrs.; males: average 54.2 yrs., median 56 yrs.). For both VRU groups, the difference in age between females and males was not significant (n.s.). Interestingly, five of the pedestrians, aged between 54 and 74 years, were walking their bicycle when they collided with a heavy truck.

Influence of alcohol was reported by the police for none of the truck drivers and only for two pedestrians and two bicyclists.

Collision Scenarios

The collision situations for crashes of heavy trucks with pedestrians and with bicyclists differed considerably. With regards to the motion of the truck and the motion or position of the vulnerable road user immediately before of the crash, the scenarios can be broken down into matrices as shown in Table 1 for crashes with pedestrians and in Table 2 for crashes with bicyclists.

The truck was going straight in the large majority of the 43 cases where a pedestrian was struck (Table 1). In most of these situations, the pedestrian was approaching from the right (n = 10; 23%), usually in an attempt to cross the road. In five cases (12%), the pedestrian was moving in the same direction as the truck. Apart from trucks travelling at regular speed, "going straight" includes also situations where a truck was initially stationary, e.g., waiting at a red light, and then moved off and collided with a person walking or standing close to the vehicle. Usually then, the pedestrian was walking slowly or standing right in front of the truck and the driver overlooked him or her when moving off at low speed. The five cases (12%) with a scenario "going in opposite direction" included also persons standing in the path of a continuously moving truck. In a number of cases, the truck side-swept the pedestrian either because the driver made an evasive manoeuvre to avoid the crossing pedestrian or the vehicle passed by a person too closely who was standing by the side of the road or driveway. Accidents with pedestrians were relatively rarely caused by turning trucks. In two cases, a reversing truck hit a pedestrian behind the vehicle.

With 35 cases (56%), crashes between a heavy truck and a bicyclist, on the other hand, were clearly dominated by turning manoeuvres (Table 2), mostly when the truck made a right-turn at a junction or into a driveway and hit a bicyclist who was travelling alongside on the right of the truck, intending to go straight. Situations with the truck going straight were comparably few and included both crashes with a crossing bicyclist and collisions with the truck side-sweeping a bicyclist during an overtaking manoeuvre by the truck driver. In one case, the truck reversed and collided with a bicyclist approaching from behind and in two incidents the truck was parked at nighttime and the bicyclist hit the rear of the trailer.

As a result of the collision, 17 pedestrians (40%) were run over on at least a part of their body by one or more wheels of the truck, in five cases with fatal consequences. Accordingly, 26 pedestrians (60%) were struck by the truck, but not run over in the sense of the above definition, and four of them died. Nevertheless, a number of pedestrians who were knocked down by the truck front face ended up under the vehicle without contact with the wheels. Bicyclists were run over in 33 cases (52%), resulting in nine fatalities. Of the remaining 29 bicyclists without run-over (48%), two were fatally injured. The smaller share of run-over among pedestrians compared to bicyclists was not significant (n.s.).

Table 1.
Absolute and relative frequency of accident scenarios between heavy truck and pedestrian

	Pedestrian motion / interaction with truck						
Heavy truck motion	going in same direction	going in opposite direction	coming from left	coming from right	swept by left side of truck	swept by right side of truck	moving/ standing behind truck
going straight	5 (12%)	5 (12%)	5 (12%)	10 (23%)	2 (5%)	7 (16%)	-
turning left	-	1 (2%)	-	-	-	2 (5%)	-
turning right	4 (9%)	-	-	-	-	-	-
reversing	-	-	-	-	-	-	2 (5%)

Table 2.
Absolute und relative frequency of accident scenarios between heavy truck and bicyclist

	Bicyclist motion / interaction with truck						
Heavy truck motion	going in same direction	going in opposite direction	coming from left	coming from right	swept by left side of truck	swept by right side of truck	moving/ standing behind truck
going straight	1 (2%)	-	-	5 (8%)	2 (3%)	5 (8%)	-
turning left	2 (3%)	4 (6%)	1 (2%)	1 (2%)	-	-	-
turning right	35 (56%)	-	1 (2%)	1 (2%)	-	1 (2%)	-
reversing	1 (2%)	-	-	-	-	-	-
stationary	2 (3%)	-	-	-	-	-	-

VRU Injury Patterns and Severities

Due to the selection criteria for the cases, all involved vulnerable road users sustained injuries, often being quite severe. Nine of the total of 43 pedestrians were killed (21%) and 34 were seriously injured (79%) according to the definition used in German national statistics. Of the 62 bicyclists, eleven were fatally (18%), 47 were seriously (76%) and four were slightly injured (6%). For five pedestrians and four bicyclists, the complete injury pattern could not be established. Even then, it was possible to derive the injury severity for the most severely affected body region and to determine the MAIS value for most of them. Figures 2–8 provide an overview of the injury patterns and severities.

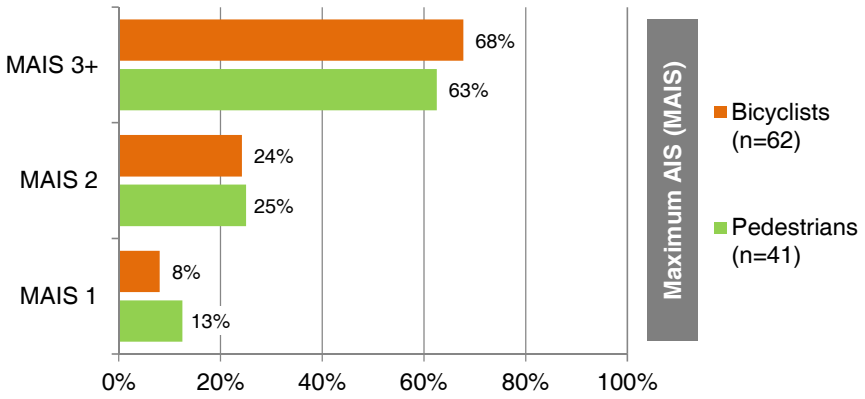

Figure 2. Distribution of MAIS1, MAIS2 and MAIS3+ for pedestrians and bicyclists

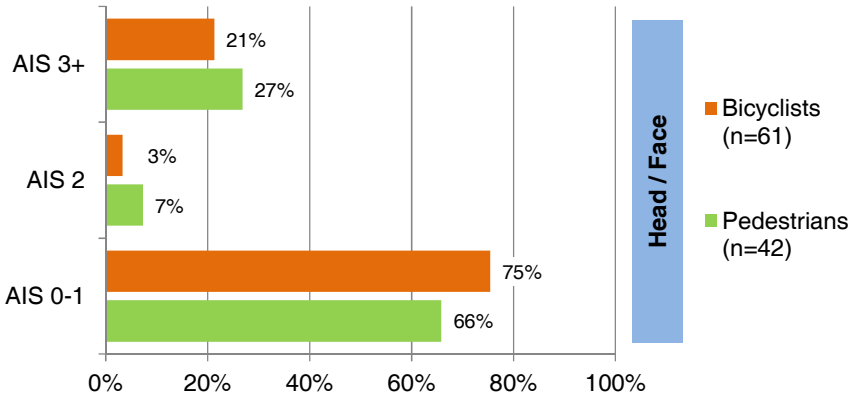

Figure 3. Distribution of head/face AIS0-1, AIS2 and AIS3+ for pedestrians and bicyclists

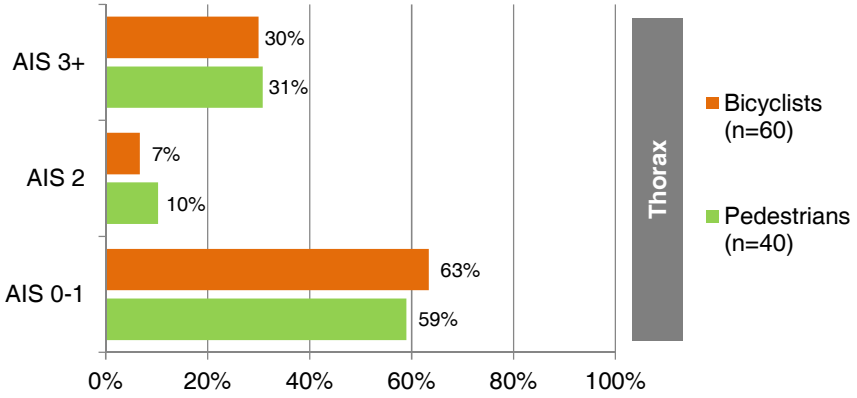

Figure 4. Distribution of thorax AIS0-1, AIS2 and AIS3+ for pedestrians and bicyclists

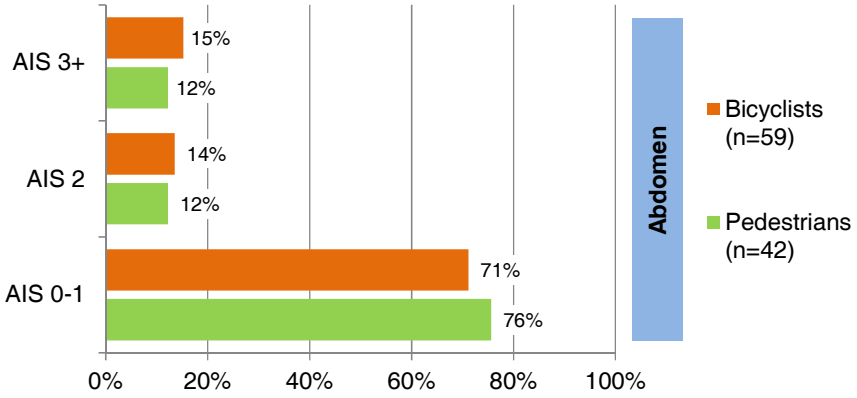

Figure 5. Distribution of abdomen AIS0-1, AIS2 and AIS3+ for pedestrians and bicyclists

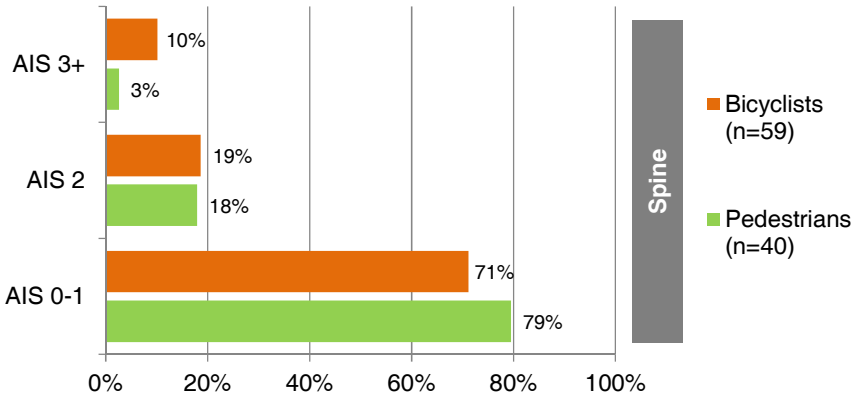

Figure 6. Distribution of spine AIS0-1, AIS2 and AIS3+ for pedestrians and bicyclists

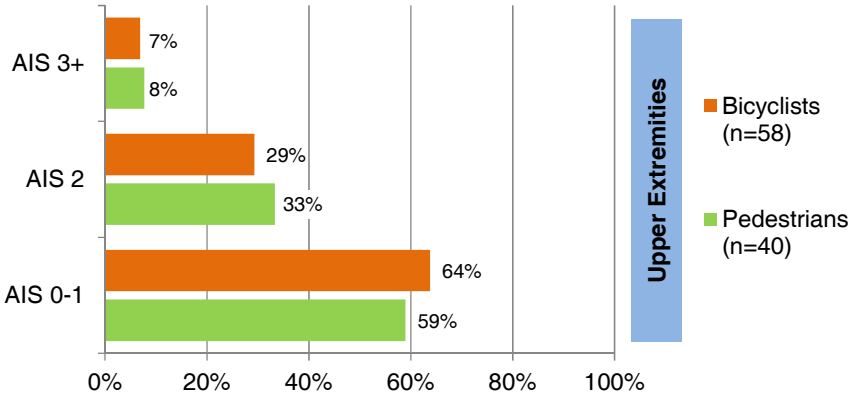

Figure 7. Distribution of upper extremities AIS0-1, AIS2 and AIS3+ for pedestrians and bicyclists

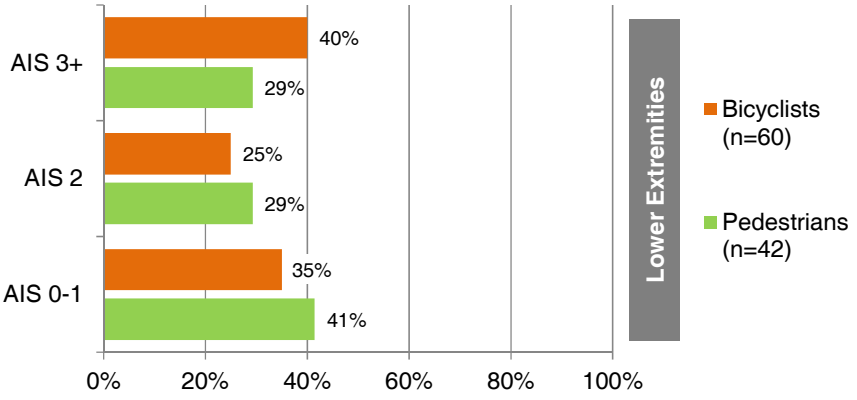

Figure 8. Distribution of lower extremities AIS0-1, AIS2 and AIS3+ for pedestrians and bicyclists

MAIS3+ cases accounted for approximately two thirds among all pedestrian and bicyclist casualties (n = 25; 63% and n = 42; 68%, respectively), including fatalities, whereas only five injured, each, (13% and 8%, respectively) were MAIS1. The highest proportion of serious to critical injuries (AIS3+) for pedestrians was found in the thorax region (31% among 40 pedestrians with respective injury data) and for bicyclists in the lower extremities region (40% among 60 bicyclists with respective injury data). Nevertheless, thorax and lower extremity trauma was frequent in both groups. AIS3+ injuries in the latter body region included fractures of the femur and the pelvic bones as well as open fractures of the lower leg. Often, lesions reaching into deep layers of the skin and decollement, both rated as AIS2, were present either as the only injury to the leg or foot or in combination with fractures. These types of injuries can be attributed mostly to a run-over mechanism of the respective body region. AIS3+ thorax injuries consisted primarily of rib series fractures and lung lacerations. AIS3+ abdominal injuries were mostly associated with run-over, too. Serious to critical head/face injuries (AIS3+) occurred in 27% of the pedestrians and 21% of bicyclists with known injury data. While in three bicyclists, AIS6 head injury was found in the form of head crush or brain stem laceration, no such injury mechanism was present in pedestrians. Still, five of them sustained AIS4 and AIS5 intracranial injuries due of severe impact by the truck front face. On the whole, pedestrians and bicyclists presented very similar injury patterns and severities in collisions with heavy trucks.

DISCUSSION

The present study compares circumstances and consequences of accidents that involved a heavy truck, defined as a goods and service vehicle with a gross vehicle weight of 11,900 kg and over, and either a pedestrian or a bicyclist. The underlying data and methodology have both strengths and limitations.

While past research work often addressed accidents between VRU's and heavy vehicles, in general, the present focus is on trucks of the N3 category. This limits the number of cases available for evaluation, but at the same time makes the results probably more dependable for the class of vehicles under scrutiny. With the chosen relatively high threshold of claim costs as a criterion for case inclusion, the evaluated sample likely reflects accidents with more severe outcome which can be inferred also from the fact that the entire material contained only four cases of VRU's who received merely out-patient care. By including, e.g., road maintenance workers and other persons that may not fit the "classic" image of a pedestrian, our study applied a wider definition of "pedestrians", resulting in a higher rate of injured pedestrians in relation to injured bicyclists (1:1.4 ratio). Nevertheless, the crash and injury mechanisms in collisions with trucks apply also for these casualties. Panwinkler, who did a special analysis of N3 truck accidents in Germany for 2015 [6], reported 318 pedestrian and 739 bicyclist casualties, i.e., a ratio of 1:2.3, but with 49 fatalities, each, in both groups. De Ceunynck et al. [3] quote the Belgian statistics according to which 8% of killed victims were pedestrians and 16% were bicyclists in crashes with heavy goods vehicles in Belgium. The data for the French Rhône region [7] shows the opposite numerical relationship with 73% pedestrians and 27% bicyclists in crashes with trucks. While our sample may reflect the German situation quite well, the ratio of pedestrians to bicyclists in collisions with trucks probably varies considerably in different countries and different regions, possibly owing to the local share of bicycle use.

Regardless of the case numbers for pedestrians and bicyclists, the results from our study underline findings from previous studies that crashes with involvement of heavy trucks are particularly severe. Run-over, at least of one part of the victim's body, was present in 40% of the pedestrians and 52% of the bicyclists. In an analysis of the Renault Trucks VRU database which included only fatal cases, Beillas et al. [7] reported an even higher rate of run-over with 75% among killed pedestrians and 79% among killed bicyclists.

A major factor that appears common to all studies related to accidents between heavy vehicles and vulnerable road users is the prevalence of older persons among the VRU's. With a growing share of seniors in the population in many western countries, the importance of this age group increases among road traffic casualties. 50.7% of all killed pedestrians and 58.6% of all killed bicyclists in Germany in 2017 were persons age 65 and over [1]. Seniors aged 65 years and over represented 44% among pedestrian and 35% among bicyclist casualties in our study. De Ceunynck et al. [3] in their analysis of blind spot accidents involving trucks in the Antwerp area also noted a high percentage of seniors: 80% of pedestrians and 37% of bicyclists were 60 years or older. Beillas et al. [7] reported a 50% share of VRU's over 61 years among fatalities in crashes with trucks. While the increased vulnerability of older victims may

play a role, too, their slower reaction to the unexpected conflict with a truck appears to be a crucial factor. A possible misunderstanding by older bicyclists of the truck's intention when negotiating around street corners was hypothesised by the authors in the previous study on these types of crashes [4]. For several cases of older pedestrians, the data and case descriptions in our material suggest that the seniors were not aware of the risk that the truck driver might not notice them when they passed by the vehicle, often at its front and in close proximity. This is not to say that the pedestrian was automatically at fault when the accident happened, though. In several incidents, the truck driver apparently did not look carefully or did not utilise the available mirrors when moving off from a stop.

CONCLUSIONS

Previous studies, so far, have come to the conclusion that driver assistance systems, particularly electronic turn-assistance, have a large theoretical potential to avoid or at least mitigate crashes between heavy vehicles and bicyclists [4, 5]. Similarly, pedestrians will likely benefit from driver assistance systems in conflicts with trucks. However, such systems need to be geared to the specific accident scenarios involving pedestrians. Unlike monitoring the right side of the vehicle which is necessary for turn-assistance to avoid accidents with bicyclists, pedestrian protection needs to focus on the area in front of the truck. Since many of these accidents occur when the truck is moving very slowly or is initially being stationary detection of VRU's in the immediate front area should be feasible with state-of-the-art sensory devices. At least one truck manufacturer has not only introduced turn-assistance as an option for its vehicles, but has also upgraded its forward collision alert by including the detection of pedestrians in front of the truck cab at lower speeds [9]. A considerable proportion of the evaluated accidents was apparently caused largely by either a misunderstanding of the present hazard on the part of the vulnerable road user or by negligence on the part of the truck driver. Trainings and campaigns to increase awareness should therefore be tailored to the specific population at risk.

REFERENCES

[1] Destatis, Statistisches Bundesamt 2018. "Unfallentwicklung auf deutschen Straßen 2017 – Begleitmaterial zur Pressekonferenz am 12. Juli 2018 in Berlin" Press conference of the German Federal Statistical Office, Berlin, Germany, July 12, 2018

[2] Thomas, P. et al. 2015. "Fatal Urban Cyclist Collisions with Lorries: An In-Depth Study of Causation Factors and Countermeasures Using a System-based Approach" In Proceedings of the 24th ESV Conference on the Enhanced Safety of Vehicles (Gothenburg, Sweden, June 8-11, 2015)

[3] De Ceunynck, T. et al. 2018. "Blind Spot Crashes between Vulnerable Road Users and Heavy Goods Vehicles in Belgium" In Proceedings of the 7th International Cycling Safety Conference ICSC 2018 (Barcelona, Spain, Oct. 10-11, 2018)

[4] Malczyk, A. and Bende, J. 2017. "Crashes between Heavy Vehicles and Bicyclists: Characteristics, Injury Patterns and Potentials for Driver Assistance Systems" In Proceedings of the 2017 IRCOBI Conference (International Research Council on Biomechanics of Injury) (Antwerp, Belgium, Sept. 13-15, 2017)

[5] Kalaiyarasan, A. et al. 2018. "Assessment of Improved Direct and Indirect Vision Measures for Heavy Goods Vehicles on Cyclist Casualties" In Proceedings of the 7th International Cycling Safety Conference ICSC 2018 (Barcelona, Spain, Oct. 10-11, 2018)

[6] Panwinkler, T. 2018. "Unfallgeschehen schwerer Güterkraftfahrzeuge" Berichte der Bundesanstalt für Straßenwesen, Heft M 277 (Reports of the German Highway Research Institute, Report M 277), Bergisch Gladbach, Germany

[7] Beillas, P. et al. 2011. "Accidents between Pedestrians and Industrial Vehicles: From Injury Patterns to Dummy and Truck Prototypes" In Proceedings of the 22th ESV Conference on the Enhanced Safety of Vehicles (Washington D.C., June 13-16, 2011)

[8] Association for the Advancement of Automotive Medicine, 2011. “Course Training Manual, A specialized Course on: Injury Scaling: Uses and Techniques, Introducing The Abbreviated Injury Scale - 2005 Update 2008, Version January 2011” Barrington, Illinois

[9] Daimler Global Media Site, “Mercedes-Benz Lkw: Sicherheit: Neue Assistenzsysteme: Notbremsassistent Active Brake: Assist 4 mit Fußgängererkennung und Abbiege-Assistent“, http://media.daimler.com/marsMediaSite/de/instance/ko/Mercedes-Benz-Lkw-Sicherheit-Neue-Assistenzsysteme-Notbremsassistent-Active-Brake-Assist-4-mit-Fussgaengererkennung-und-Abbiege-Assistent.xhtml?oid=12367326. [28 Mar. 2017]

ESTIMATING EXPECTED LEVELS OF MUTUAL INTERFERENCE IN AUTOMOTIVE RADAR AND SIMULATING SYSTEM IMPACTS

William Buller, Joseph Garbarino, Brian Wilson, Jack Kelly

Michigan Tech Research Institue, Michigan Technological University, USA

Paper Number 19-0081

ABSTRACT

The primary goal of this paper is estimate the power, due to other radar transmitters, expected to be incident on the receiving antenna of a given automotive radar, and secondly, simulate the impact this may have on the performance of an example radar system. The approach uses stochastic geometric methods to weigh the spatial, temporal, and spectral overlap, for realistic scenarios with multiple radars operating in proximity. The results show that a given radar receiving antenna may face more interference power (10 to 50 dB) than what is expected from the reference target used to specify system performance. Under these conditions, a radar system, without interference mitigation strategies, will likely suffer significant degradation in performance.

INTRODUCTION

The automotive industry is undergoing a fundamental transformation, made possible by a multitude of advancements in electronic, communication, and remote sensing technologies. Automobiles are being developed with varied levels of autonomy to increase efficiency, reduce congestion, improve safety, and provide reliable transportation to communities that formerly would be dependent on others for assistance.

This paper provides simplified expressions to estimate the environment in which automotive radars must operate, as market penetration of radar-equipped vehicles grows. Systems that operate well in environments with few other radars may suffer significant degradation of performance in radar congested environments. The results show that levels of interference based on operation of current systems in congested environments will be significant. In scenarios with many vehicles operating radars in the 76-81 GHz band, the power from other radars will likely exceed the power of echoes from targets needed for specified performance by several orders of magnitude, based on the model in this paper.

The modeling and simulation work focus on two questions:

- How much power does a given radar receive from other radar transmitters?
- How may this impact the performance of a collision warning system?

The first question is addressed by developing a model for nominal automotive radars and computing the amount of power overlapping in space, time, and spectrum. This work is done theoretically, assuming free space propagation of RF waves.

The second question is addressed by introducing the power computed for the interference, as noise, into a system simulation. This approach is common in past studies, and assumes the waveforms of the interfering radar are substantially different, so that their mutual energy does not correlate. This approach is taken here, in part, because it requires a minimum of assumptions about the signal processing chain behind the receiving radar's front end. To quantify possible system impacts, the processing functions are based on a generic model developed in cooperation with industry professionals and simulated in MATLAB's Automated Driving System (ADS) Toolbox. For this reason, the approach here does not capture the system impacts which depend on the multitude of interactions possible with different waveforms.

While radar interference is a well understood phenomena and studied for many decades, the concern of when and how this will impact the development of advanced driver assist systems and autonomous vehicles is relatively new. The European funding project MOre Safety for All by Radar Interference Mitigation (MOSARIM) began in January 2010 with the main objectives:

- Investigate possible automotive radar interference mechanisms
- Assess possible countermeasure and mitigation techniques

The MOSARIM study focused on simulation and empirical measurements to identify interference levels, evaluate mitigation strategies.

As well as the MOSARIM study, many other researchers have made contributions to the study of this problem, and were consulted for this study [1]-[6]. The novelty of this research is that it represents an end-to-end estimation of mean interference power for realistic traffic scenarios, and a modification of the MATLAB ADS Toolbox to simulate the system impact.

RADAR MODEL

In order to compute the interference level for a radar, we must create a model for the system under test, as well as the interfering systems. The model must be of sufficient fidelity to estimate the amount of power incident on the receiving aperture. For the purposes of modeling and simulation, parameters for a generic long range automotive radar were established, based on values selected from radar specifications.

The power arriving at a receiving antenna, P_{Rx}, from a transmitter at a range R, is a function of the power of the transmitter, P_{Tx}, gain of the transmitting antenna, G_{Tx} the wavelength of the transmission, λ, and the gain of the receiving antenna, G_{Rx}. This is the Friis formula [7], expressed in (Equation 1).

$$P_{Rx} = \frac{P_{Tx} G_{Tx} G_{Rx} \lambda^2}{(4\pi R)^2} \qquad \text{(Equation 1)}$$

The monostatic radar range equation computes the power received by a radar co-located with a transmitter, observing energy returned by a target with radar cross section, σ. This is written out in (Equation 2).

$$P_{Rx} = P_{Tx} G_{Tx} G_{Rx} \left(\frac{\lambda}{4\pi R}\right)^2 \frac{\sigma}{4\pi R^2} \quad \text{(Equation 2)}$$

The radar range equation shows the R^4 path-loss for radar returns, as opposed to the R^2 path-loss for transmission loss from another radar..

A long range radar for automotive radar applications is typically expected to detect and track vehicles more than 100 meters ahead. Typically, the radar performance is specified against a reference target with radar cross section of 0 dBm^2 at 100 meters.

The system noise for the radar is the product of the noise factor, f_N, and the thermal noise, which is the product of the operating temperature, T, the bandwidth of the receiver, B, and Boltzmann constant, k, expressed in (Equation 3)

$$N = f_N kTB \quad \text{(Equation 3)}$$

The values used for this paper are shown in Table I. Based on the radar range equation and the values in Table 1, the SNR, expressed in (Equation 4) for the reference target per pulse is 14.1 dB. The SNR value is before pulse compression. Following pulse compression, the signal power is elevated by the time-bandwidth product. This is accounted for in our simulation by condensing the signal power into the target range bin and uniformly distributing the noise power across the range bins.

$$SNR = P_{RX}/N \quad \text{(Equation 4)}$$

Table 1.
Parameters used for a generic long range radar to model interference level

	Value	**Units**
Mean Power	1	Watts
Reference Range	100	Meters
Reference RCS	0	Decibel Meters Squared
Bandwidth	200	Mega Hertz
Range res.	0.75	Meters
Range bins	200	Unitless
Comp. Gain	23	Decibel
Carrier Frequency	76-77	Giga Hertz
Noise Factor	10	Ratio (Unitless)
Duty Factor	0.5	Ratio (Unitless)
FOV Az.	20	Degree
FOV El.	5	Degree
Antenna Gain	27	Decibel
Az. Resolution	5	Degree
Range rate limits	[-100 100]	Meters Per Second

INTERFERENCE MODEL

This section details our approach to answer "How much power does a given radar receive from other radar transmitters?"

The expected interference experienced by a given receiver requires an estimate of the probability of intercepting (POI) other vehicles' radar transmissions in spectrum, time, and space.

Assumptions must be made about how the radar carrier frequency and pulse scheduling are selected. For this paper, the probability of intercept, POI, is based on the assumption that the choice of center frequency is selected randomly, uniformly distributed, in band, and there is no synchronization between systems on other cars.

The spectral POI for a pair of radars is based on the amount of the available band they occupy, or channel fraction. That is, a 200 MHz system, operating in the 76 to 77 GHz band, has a channel fraction of 0.2. For many operational systems, the channel fraction could be an order of magnitude smaller because the instantaneous bandwidth is chosen to be relatively narrow. For a population of K radars, the spectral POI for each of the radars is, ξ_K, is shown below in (Equation 5)

$$\omega_K = 1 - \prod_{k=1}^{K-1}(1 - CF_k) \qquad \text{(Equation 5)}$$

The temporal POI for a population of K radars follows a similar derivation, but the governing parameter is the duty factor for the interfering pair, DF_1 and DF_2. . For a population of K radars, the temporal POI, τ_K, is shown below in (Equation 6).

$$\tau_K = 1 - \prod_{k=1}^{K-1}(1 - DF_k) \qquad \text{(Equation 6)}$$

The temporal spectral overlap is then simply the product of the two, as shown in (Equation 7).

$$\xi_K = \omega_K \tau_K \qquad \text{(Equation 7)}$$

Mutual interference involves multiple radars. The radar under consideration is identified as the Ego radar. To compute the interference power at the Ego radar, I_1, we follow the approach of [6], shown in (Equation 8), which requires specification of the mean interferer density, λ, the transmitter power, P_0, the temporal-spectral overlap factor for pairs of radars, ξ_2, the minimum distance away from the Ego radar, on a road with lane spacing L, which an interferer with FOV θ must be to illuminate the Ego receiver, is $\delta = L/\tan(\theta/2)$, and the frequency dependent gain term, $\gamma_1 = {G_t}^2(c/4\pi f)^2$.

$$I_1 = \xi_2 \lambda P_0 \gamma_1 (\pi - 2\ \arctan(\delta/L))/2L \qquad \text{(Equation 8)}$$

In this stochastic geometric approach, the expected interference level is integrated over the interfering radars, so the temporal-spectral overlap is taken pair-wise. An example is computed in the Results section.

SYSTEM MODEL

To estimate the impact of interference on a collision warning system, the study introduces the interference power, calculated in the interference model (8), and introduces the interfering transmissions as uncorrelated noise. This approach is common in past studies and assumes the waveforms of the interfering radar are substantially different, so that their mutual energy does not correlate. This requires a minimum of assumptions about the signal processing chain behind the receiving radar's front end. While the approach neglects the possible impacts of interfering signals, which generate false tracks (ghost targets), the impact of elevated noise is less dependent on hardware architecture.

To quantify possible system impacts, the processing functions are based on a generic model developed in cooperation with industry professionals and simulated in MATLAB's ADS Toolbox. The approach can be adapted for higher fidelity models, with the specific signal processing chain for a particular brand and model of radar. However, in this study, the system model is intended to demonstrate the impact on a generic, but reasonable, radar system that can be reproduced by other researchers with access to the ADS Toolbox.

To model a vehicle with advanced driver assist sensors, it is necessary to be able to instantiate, manipulate, and support interactions between the various components within the scenario. This framework described here incorporates:

- Roadway definitions
- Scene actors, including pedestrians and vehicles
- Motion of actors within the scene
- Definition and placement of sensors on the vehicle(s)

- Sensor detection model
- Support for combining detections into tracks

The model must have the ability to extract per-time-step information relating to vehicle positions, detection and track information, and modify on a per-time-step basis the detector responses based on changing scene conditions.

For our simulations, we implemented the processing flow shown in Fig. 1.

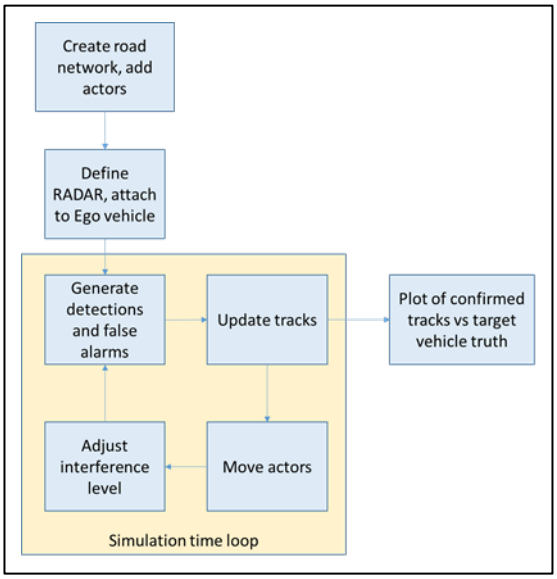

Fig. 1. Simulation Processing Flow

To implement our simulations, we chose to use the MATLAB platform (from MathWorks), with the add-on ADS Toobox. Introduced in 2017, the ADS Toolbox provided most of the capability we needed. In those instances, where it did not provide the desired interface, the implementation of the necessary extensions proved straight forward.

Generating Roadways and Vehicles

The ADS Toolbox provides methods for defining roadways, actors (vehicles and pedestrians), and motion profiles for those actors. The roadways are constructed from two-lane road segments, defined by a set of center-points in Cartesian coordinates (x, y, z) along the segment. The center-points are connected by piecewise clothoid curves.

Three classes of vehicles are referred to in this paper:

1. The Ego vehicle is the subject of interference.
2. The Target vehicles is the object, against which, the Ego vehicle's track performance is evaluated.
3. Interfering vehicles are other vehicles in the scenario with active radars.

Vehicles are added to the roadway by specifying a set of waypoints and velocities. The waypoints, like the road centers, are Cartesian coordinates. Examples of these displays are shown in Fig. 2. In this case, the Ego vehicle is blue, and the Interferers are yellow.

Sensor Definition and Placement

Sensors are attached to vehicles. Once a sensor is attached, it moves with the vehicle as it traverses the roadway. Each sensor has an update rate, which controls the number of detections the sensor generates, and may be different than the update rate of the scenario (i.e. movement of the vehicles).

The values of these parameters used in our simulations are shown in Table 1. An example display of an Ego vehicle radar azimuth field of view is shown in Fig. 3.

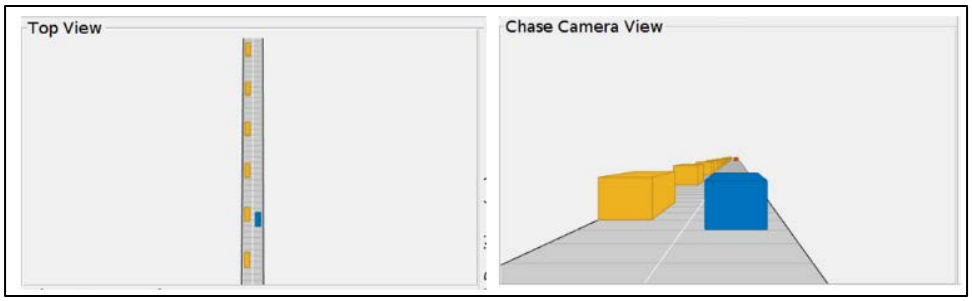

Fig. 2. Generated roadway with vehicles, where the Ego vehicle appears blue, and interferers are yellow.

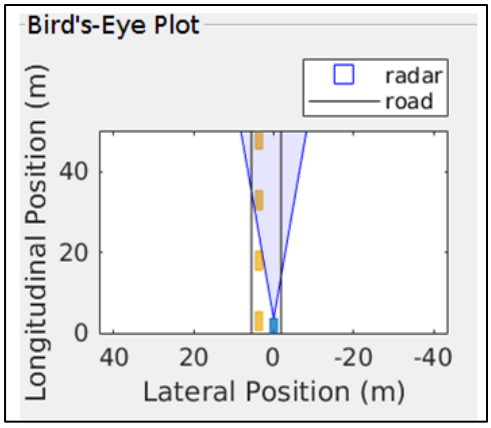

Fig. 3. Overhead view showing radar beam indicating azimuth field of view.

Modelling Detections

Detectability of targets is governed by three inter-related parameters: Probability of false alarm (PFA), probability of detection (PD), and signal-to-noise ratio (SNR). Probability of false alarm relates to the number of false detections that are allowed to occur. To insure that detections of real targets are generated, some amount of false alarms must be allowed. For our simulations, the PFA was set to 1e-6, meaning that a false alarm will occur every 1,000,000 detections. This PFA was selected to be on the low end of PFA values that are valid for Albersheim's equation (1e-7 < PFA < 1e-3), based on industry practices of limiting false alarms. The expectation is that some false alarms will be eliminated via the tracking system, since unlike true detections from vehicles, the false alarms may not correlate with a reasonable trajectory.

Once an acceptable level of false alarms has been set, the relationship between the PD and SNR is defined via a Receiver Operating Characteristic (ROC) curve. The ROC is derived from well understood radar reflection phenomenology. In the ADS Toolbox, radar reflections are assumed to be from non-fluctuating targets, with non-coherent pulse integration, generated via Albersheim's detection equation [8]. While this model for reflections is adequate for many uses, with more time and effort, this equation could be replaced with a richer model from Snidman's equations [8], based on Swerling models that provide for fluctuating responses generated from collections of potentially non-homogeneous scattering mechanisms of targets.

Detections are generated on a per-time-step basis. First, actors within the scenario are moved to their current position. Next, point targets are generated for the scene. The region-of-interest (ROI) is defined by the orientation and field-of-view of the radar. This ROI is sub-divided based on the minimum spacing defined by the azimuth and range resolutions as demonstrated in Figure 5, (in these simulations, elevation resolution is infinity, i.e. responses cannot be separated by height). Actors are represented as 6-sided cuboids. At most three sides of an actor are visible to the radar at any time. Point targets are generated wherever the side of an actor occupies one of the sub-divisions of the ROI.

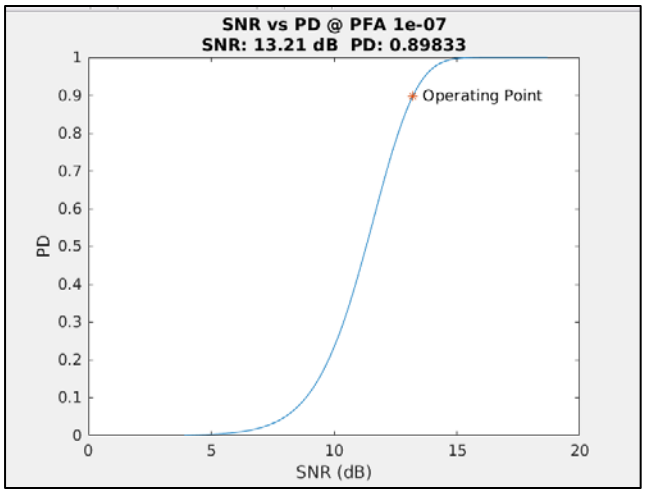

Fig. 4. Example ROC curve relating SNR and PD given desired PFA

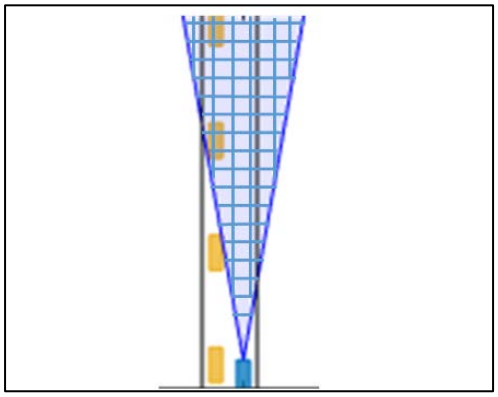

Fig. 5. Example of subdividing radar beam to identify point target responses

Each point target is assigned a radar cross section (RCS) value. This is the idealized response of the target at the given angle, without accounting for distance between the sensor and the target. Each actor is assigned a set of RCS values, which can differ with illumination angle. These set of RCS values are interpolated to get the point target response given the per-time-step illumination angle of the target. For our simulations, all vehicles are assigned an RCS value of 10 dBsm for all angles, which has been found in previous work [8] to be a good estimate of vehicle cross-section.

Point targets are then eliminated based on range rate. Range rate is a measure of the radar's ability to discern changes in relative range between the Ego and target vehicles. The limit on this ability comes from the rate at which the radar can transmit pulses, driven by an engineering tradeoff between expected maximum vehicle velocities, maximum range extent, and cost of the radar system. Point targets outside the minimum/maximum range rate are considered spurious and ignored.

Since the RCS of the target does not account for the distance between the sensor and point target, this number must be converted into the SNR at the point target. The SNR for each point target, SNR_T, is adjusted by the product of two ratios, the target RCS to reference RCS, and the two-way propagation loss (R^{-4}), at the target's range relative to the reference range, shown in (Equation 9).

$$SNR_T = SNR_R(RCS_T/RCS_R)(Rng_T/Rng_R)^{-4} \quad \text{(Equation 9)}$$

The total number of false alarms generated are chosen by calculating the total number of resolution cells for one sweep of the radar and multiplying that number by the false alarm rate. If false alarms are generated, the range and azimuth locations of the false alarms are chosen at random from a uniform distribution. False alarms are assumed to be marginal detections, therefore the SNR of each false alarm is set by applying Albersheim's equation, from [8], at the detection threshold level. Finally, the false alarms are grouped together with the target detections into one set of radar detections.

The radar detections are then fed into a tracking algorithm in order to attempt to group the current detections with previous detections and tracks. Any current detections that cannot be assigned to previous tracks are used to create new tracks. Previous tracks that are assigned new detections are updated and confirmed. Any tracks that did not get a new detection are initially coasted and, if they continue to fail to obtain detections in the future, are eventually deleted. The default tracker used in the ADS Toolbox, and in this paper, is a constant velocity linear Kalman filter.

The main metric used in determining the ability of the radar to detect a target in the presence of interference and noise is the terminal track range. This is the maximum range of a continuous track of the target. In other words, this is how far out the radar was able to initially detect the target and maintain that track through the completion of the simulation.

EXAMPLE SCENARIO

Consider a two lane highway with interference caused by forward looking radars on cars travelling opposite directions, as shown in Figure 6, below. The interference is measured at the Ego vehicle, shown in blue. The source of the interference is the radars on the yellow cars, *interfering vehicles*, travelling in the opposite direction. The impact of the interference on the system will be evaluated by how well the Ego vehicle can detect and track the green car, the Target vehicle.

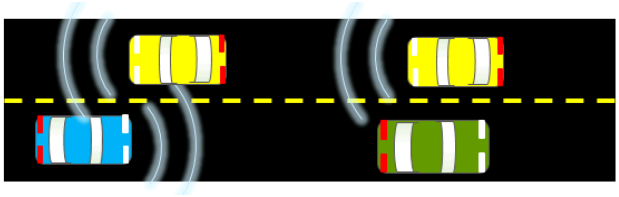

Fig. 6. Example scenario is represented schematically above. The Ego vehicle, in blue, operates a forward looking radar, following a target vehicle, in green. The Ego vehicle suffers from the interference of radars on the yellow cars travelling in the opposite direction.

The Ego vehicle is travelling at 80 kilometers per hour, and the Target vehicle is 200 meters ahead, travelling at a speed of 20 kilometers per hour. The two vehicles will collide after 12 seconds. The Interfering vehicles are Poisson distributed in the opposing lane with mean separation of 15 meters. The lane spacing is set at 3.7 meters, which is a nominal center to center spacing of US road ways.

RESULTS

The interference can be computed as a function of the density of the opposing traffic, by substituting in the values for all the other parameters determined by the lane spacing and radar parameters. Replacing the variables in (4) with the values that follow: $\xi_2 = 0.1$, $P_0 = 1\,W$, $\gamma_1 = 2.794 \times 10^{-2}\,m^2$, $\delta = 20.98\,m$, and $L = 3.7\,m$, we have an expression for the interference power at the Ego radar, I_1, as a function of the mean spacing of interfering vehicles, $\bar{x}$, in the opposing lane, in (Equation 10).

$$I_1(\bar{x} = \lambda^{-1}) = 1.32 \times 10^{-4}\ (W\,m)/\bar{x} \qquad \text{(Equation 10)}$$

For this situation the interference power is inversely related to the spacing of the interfering vehicles. If the mean spacing between the vehicles in the opposing lane is 15 meters, the interference power in (5) is estimated to be -51 dBW. For convenience, we assume the radar pair use significantly different waveforms, and following pulse compression, the power is uniformly spread over the 200 range bins. Thus, each range bin suffers approximately -73 dBW of interference power. The reference target is a 0 dBsm target at 100 meters, which using the same radar parameters has a return power of -107 dBW in the range bin at 100 meters.

The impact on performance is shown graphically, for the simulated system, by observing the distance from the target at which a *terminal* track is formed. A terminal track implies that the same track is maintained until the time of collision. Without interference, a terminal track is formed for the Target vehicle at a range of 196 meters, plotted in Fig.7. With interference, a terminal track with the Target vehicle does not exist beyond 21 meters, plotted in Fig.8. In both cases, additional tracks form as the Target vehicle becomes resolved in azimuth.

The implication is, without significant interference mitigation, the example automotive radar system, will suffer significant loss of performance for ADAS applications, as the range to the target is only 11% of the reference target specification. However, it should be stressed that this example is intended to high-light the approach on a generic radar model.

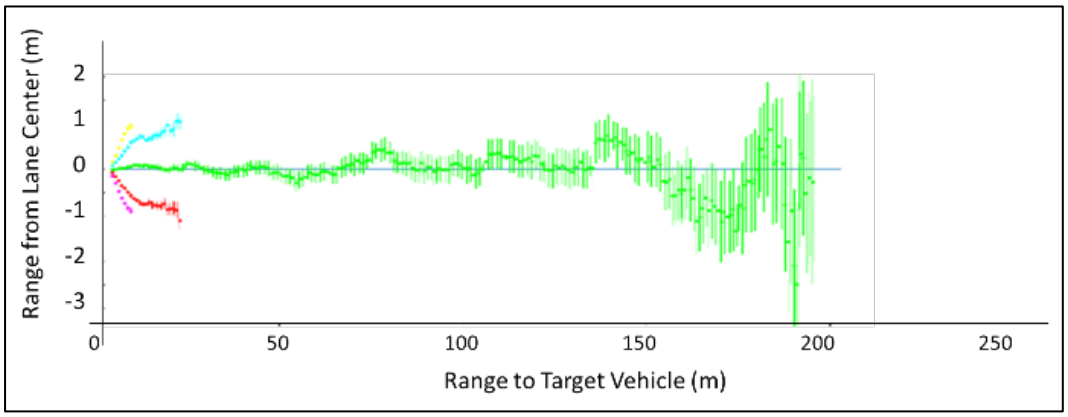

Fig. 7. Plot of terminal target tracks from example scenario, long-range radar with no interference. The plot shows the track position and uncertainty plotted as range from the Ego vehicle to the Target vehicle.

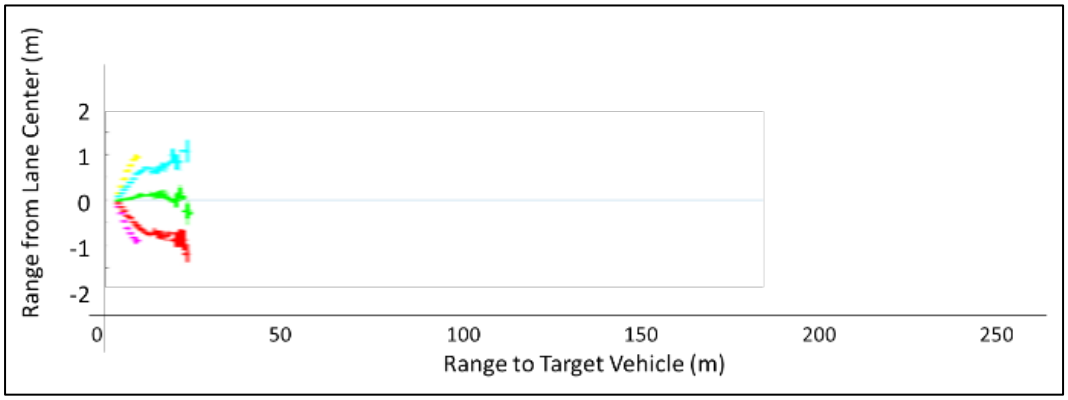

Fig. 8. Plot of persistent target tracks from Scenario 1, long-range radar, with interference, for the case of 76-77 GHz band. The plot shows the track position and uncertainty plotted as range from the Ego vehicle to the Target vehicle.

REFERENCES

[1] M. Kunert, “MOre Safet for All by Radar Interference Mitigation: Project Final Report”, Publishable Summary, 2012.

[2] Heuel, Steffen. Automotive Radar Sensors Must Address Interference Issues. Microwave Journal; Volume 59, Issue 12, 2016 pp 22-36.

[3] Brooker, G. M.. "Mutual Interference of Millimeter-Wave Radar Systems." IEEE Transactions on Electromagnetic Compatibility 49, 2007 pp 170-181.

[4] Daley, D. J. and D. Vere-Jones. "An Introduction to the Theory of Point Processes: Volume I: Elementary Theory and Methods, Second Edition." 2003.

[5] Haenggi, M. and Ganti, R.K.,. Interference in large wireless networks. Foundations and Trends in Networking, 3(2), 2009 pp.127-248.

[6] Al-Hourani, A., Evans, R. J., Kandeepan, S., Moran, B., & Eltom, H. . Stochastic Geometry Methods for Modeling Automotive Radar Interference. IEEE Transactions on Intelligent Transportation Systems. 2017.

[7] Friis, H. T. (1946). A note on a simple transmission formula. Proceedings of the IRE, 34(5), 254-256.

[8] Richards, Mark A. Fundamentals of radar signal processing. Tata McGraw-Hill Education, 2005

[9] W. T. Buller and D. J. LeBlanc, "Radar characterization of automobiles and surrogate test-targets for evaluating automotive pre-collision systems," IEEE International Symposium on Antennas and Propagation, Chicago, IL, 2012.

OCCUPANT ACTIVITIES AND SITTING POSITIONS IN AUTOMATED VEHICLES IN CHINA AND SWEDEN

Martin Östling
Autoliv Research
Sweden

Annika Larsson
Veoneer Research
Sweden

Paper Number 19-0083

ABSTRACT

To save lives in future traffic crashes, we need to understand what people will be doing in fully automated vehicles during various types of trips, and shape the restraint systems to protect for the resulting postures. This paper describes how participants of our study in China wished to sit and what they wanted to do as occupants during different trip scenarios, and how they compare to participants in a previous study in Sweden.

Both studies used the "Setting the stage" method to explore these future situations. The "stage" consisted of a space with four chairs, designated as a vehicle. This minimalistic setup has been claimed to stimulate the imagination to a greater extent than more developed designs, because it allowed participants to play a more dynamic role when designing and expressing their expectations of a fully automated vehicle, within the constraints of the trip scenarios posed to them.

The fully automated vehicle was described as a car that doesn't need to be driven at all; upon entering, the occupant only has to dial in a destination. Three trip scenarios were presented to the participants in China. After each presentation, participants were encouraged to discuss among themselves what they imagined they would do during such a trip, and how they would like to be seated. Participants could redesign the "vehicle" interior as they wished by manipulating the position of the chairs as they were speaking. An observer took notes and photos as participants were discussing.

For a short trip, to or from school or work, participants in China saw themselves seated in a traditional forward-facing, upright position. For weekend rides or longer trips with family, the traditional seating position and a living-room style position with participants facing each other were most commonly mentioned. Participants also suggested a 45- or 90-degree rotated version of the living room position and being able to sleep in a horizontal position. Activities mentioned include relaxing, watching movies and working.

Participants in both China and Sweden expected fully automated vehicles to allow for more varied sitting and more comfortable seats. Reclined seats were frequently mentioned, as were swivel seats. Both groups expected the fully automated vehicle, more than vehicles today, to support activities normally not done when driving. Participants in China also wished to lie down during longer trips. The requests for new sitting positions will require novel restraint systems—for example, new seatbelt concepts (such as belt-in-seat) and new types of airbags—as well as new tools to assess the systems' safety.

INTRODUCTION

To keep occupants safe in the future as well as today, we need to understand what people are doing during various types of trips. Factors such as the length of the journey, the vehicle interior, and who will be in the vehicle are likely to have an impact on occupants' behaviours and desires. For a fully automated vehicle, seating configurations will be influenced by the operational design domain (ODD) it is designed for. The ODD will very likely be different for different types of trips, as a commute may be different than visiting family or going on holiday. These trips are likely to involve different speeds as well as different road layouts and traffic environments; thus the likelihood of various types of crashes changes. Fully automated vehicles allow vehicle occupants to interact more, as there is no need for one person to focus on driving. The passenger car industry is adapting, trying to understand and predict how occupants in such vehicles will behave. This has been expressed in different types of concept vehicles [1-3].

To understand how occupants may wish to be seated in the future, we performed two studies: one in a small town in Sweden and one in a mega-city in China. The first study took place in Vårgårda, Sweden, a town with 5000 residents where the traffic environment consists mainly of rural traffic for daily commutes and highway driving in the countryside for longer weekend journeys. The study in Sweden was conducted in 2016 and described by Jorlöv in 2017 [4]. The second study was performed in 2017 in Shanghai, China, a city of roughly 24 million residents with mega-city daily-commuter traffic during the week and highway traffic for longer weekend journeys. This paper presents results from the participatory observation study conducted in Shanghai, China describing how people expect to be seated during trips of varying lengths in fully automated vehicles and discusses these results in relation to the previous participatory observation in Vårgårda, Sweden.

METHOD

The study used the "Setting the stage" method [5], allowing participants to play a dynamic role, using their imaginations when designing and expressing their expectations for a fully automated vehicle within the constraints of the trip scenarios posed to them. "The method's ambition is to move the participants into a tomorrow, different from today, but importantly still situated in their own life" [6]. The "stage" consisted of a space with four chairs, set up as a contemporary vehicle (Fig.1). The minimalist setup has been claimed to stimulate the imagination to a greater extent than more developed designs [6]. Two stages were set up at a shopping mall in Shanghai, similar to the setup used at the local fair in Vårgårda [4]. A convenience sample was selected by randomly choosing participants from visitors at the mall. The inclusion criterion for participants was an age between 10 and 65 years, to include drivers of the future as well as the older driving population, who may have different needs and preferences. Participants entered the study alone, in pairs, or in larger groups of up to four people (Fig.2). The duration of each test session was 10-20 minutes. Participants were informed that participation was voluntary and that they could abort at any time without stating a reason. For their participation, they were given a coffee voucher.

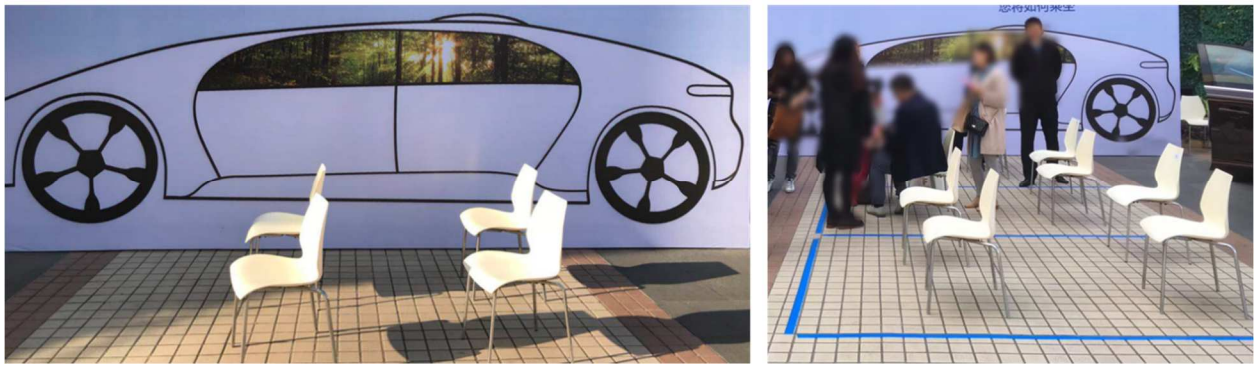

Figure 1. **Photos from the minimalist setup of a vehicle interior**

Figure 2. **Photos from participant interviews**

Procedure
In accordance with Pettersson and Karlsson [5] and the study in Sweden [4], the study in China was conducted in three parts, starting with a background questionnaire with structured questions about gender, age, habits related to car travel, and possession of a driving license. Participants were then given a description of the vehicle automation level targeted in the study and were presented with three trip scenarios, one at a time. Finally, the participants were asked about the use of extra restraints.

The fully automated vehicle was described as a car that doesn't need to be driven at all; upon entering, the occupant only has to dial in a destination—Level 5 automation, according to the Society of Automotive Engineers (SAE) [7].

In total, three trip scenarios were presented to the participants in China: riding to work or school, a weekend trip with family, and a longer vacation trip with family. In Sweden, two trip scenarios were presented, corresponding to scenario one: a shorter journey to work alone, and scenario three: a longer vacation journey with family [4]. After each presentation, the participants were encouraged to discuss among themselves using the "vehicle" interior what they would imagine they would do during such a trip, and how they would like to be seated. Participants could redesign the "vehicle" interior as they wished and manipulate the position of the chairs as they were speaking. By this procedure, both body and mind of the participants were involved in the reflective process.

In the end of the session, after the third trip scenario, the participants were asked two questions to explore their attitudes toward use of additional restraints in fully automated vehicles. The questions were formulated as:

1. If you were allowed to have a resting/sleeping position, would you mind fasten you in any additional way beyond the ordinary seat belt?

2. If you were allowed to rotate the seat, would you mind using an extra seat belt?

Data collection and analysis
Two observers per participant group collected data by taking notes and photos as participants discussed among themselves for all three scenarios. The data were analysed by conventional qualitative content analysis [8], which supports the question formulations and establishes the themes during data categorization and grouping. For ease of use, the observers' notes consisted of both free-form entries and a set of illustrated seating configurations based on the study in Sweden [4].

Participants
In China, 100 participants took part in all three trip scenarios used in the study. In Sweden, 18 participants were part of the study for the shorter trip scenario, and 31 participants for the longer trip scenario [4].

RESULTS

We present participant information, suggested seating positions, preferred activities, and further comments—and finally, participant attitudes toward additional restraints.

Participant information
Of the 100 participants in China, 51 were men and 49 were women; 77% were holders of a driving license. The ages varied from 10 to 59 years; 6% were younger than 18, 34% were between 18 and 30, 52% were between 30 and 50, and 8% were more than 50 years old. The majority of the participants, 67%, travelled daily by car, 18% travelled two to three times per week, and 15% travelled only two to three times per month. In general, the participants were optimistic about introduction of fully automated vehicles in China with 80% believing that it would happen before 2030.

Participants' suggested seating positions are reported per trip scenario:

<u>Trip scenario 1 – Ride to work or school</u>
In the trip scenario 1: Ride to work or school, most participants (56%) preferred the traditional forward-facing seating configuration A) (Fig.3) while 16% selected the "Face-to-Face" seating configuration B), also called the living room position. Another 5% selected C), with the front seats rotated slightly inboard. Variants of B) were suggested by 4% (four participants), with all seats rotated toward the centre, configuration D), or all seats rotated 90 degrees inboard. Another 4% wanted to be able to merge two seats into a bed, E). The remaining 15% proposed different layouts, with

variations in the number of seats, which seats were rotated (and how), or simply having all seats rotatable to any angle. One such proposal was rotating the seats outward to better see out of the windows.

Trip scenario 2 – Weekend ride with the family

In the trip scenario 2: Weekend ride with the family, 32% of the participants elected to sit in the traditional forward-facing seat configuration A). A similar number, 27%, chose the "Face-to-Face" seating configuration B) while 8% opted to rotate the front seats slightly inboard, like configuration C). Another 15% suggested variants of B): either all seats rotated toward the centre, as in D), or all seats rotated 90- degrees inboard. Two participants (2%) wanted to be able to merge two seats into a bed, E). The remaining 16% proposed other seat configurations with variations in the number of seats, which seats were rotated (and how), or simply having all seats rotatable to any angle. One example was simply rotating the front passenger seat 180 degrees.

Trip scenario 3 – Longer trip, going on vacation with family

For Trip scenario 3: Longer trip - going on vacation with family, 29 % of the participants selected the traditional forward-facing seat configuration A), and 30% the "Face-to-Face" seating configuration B). Three participants (3%) suggested rotating the front seats inboard, configuration C), and 20% selected to have all seats rotated toward the centre as a variant of B), either as D) or with all seats rotated 90 degrees inboard. For this longer trip, 8% wanted to be able to merge two seats into a bed, E). The remaining 10% suggested some other type of configuration, with variations in the number of seats, which seats were rotated (and how), or simply having all seats rotatable to any angle.

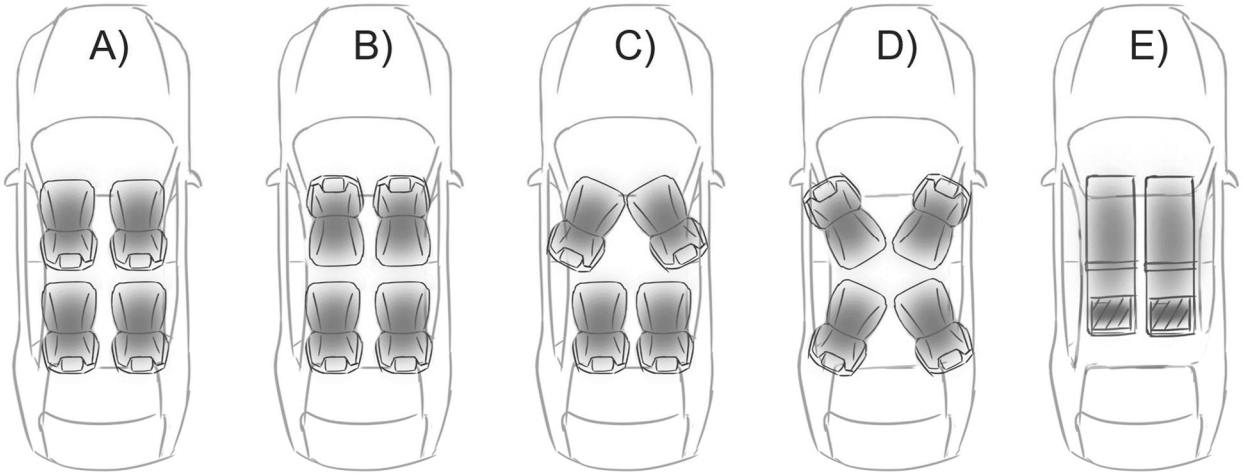

Figure 3. **Variants of seat configuration: A) represents the traditional forward-facing seat configuration, B) the "Face-to-Face" living room position, C) inboard rotated front seats, D) all seats rotated toward the centre, and E) front and rear seats merged into two beds.**

Activities

For Trip scenario 1, a short trip to work or school, the activities mentioned most often were relaxing (35%), playing on their phone (35%), watching a movie (22%), or working (20%). For Trip scenario 2, a weekend trip with family, chatting (30%), relaxing (28%), watching movies (25%), eating (22%), or playing on their phone (19%) were the preferred activities. For the third trip scenario, a longer vacation trip with family, activities such as relaxing (52%), watching movies (40%), eating (28%), and sightseeing (19%), were mentioned most often.

Other activities stated less often in the various trip scenarios were doing yoga, listening to music, taking phone calls, and playing board games or cards.

Interior design
Participants imagined that the interior design had features such as screens, a table, comfortable seats with the possibility of reclining, panoramic windows, and glass-transparency adjustment. Other suggestions included interior mood lighting, a conferencing system, rotatable seats, beds, a TV, an air purifier, a freezer, a coffee maker, and a karaoke machine.

Attitudes to additional restraints
When asked about the use of additional restraints, 63% of the participants were positive about using an extra seatbelt for a rotating seat, with the argument that safety is very important. Some of the participants pointed out that they would always use the extra seatbelt and that it was especially needed when they were resting, but it had to be comfortable. Other participants, on the other hand, pointed out that the extra belt (and even the traditional seatbelt) would hinder them from doing what they wanted to do. Most participants who did not want to wear an extra seatbelt considered it unnecessary and uncomfortable. Notably, the comfort aspect of the extra belt was indicated as important in both the positive and the negative responses. Two of the participants requested that the extra seatbelt have an automatic unlocking function, since an additional seatbelt could make it harder to escape from the car in the case of an accident.

DISCUSSION

A qualitative study was carried out to identify future seating positions and potential activities in fully automated vehicles. In both Shanghai, China and Vårgårda, Sweden, participants were placed in a minimalist setting, conceived to spark their imaginations regarding the design of fully automated vehicles and to direct their thinking as little as possible. Participants were asked to visualize three scenarios with different trip lengths. The test leaders encouraged participants to explain what activities they imagined themselves doing, and how they would prefer to sit, during each trip scenario.

The results from the study in China are first summarised, before a comparison to the study in Sweden is made.

Results from the study in China:
The results from the study in China are from a larger group than the results from the study in Sweden, which from a qualitative standpoint does not mean they are more or less valuable. Generally, qualitative results tend to converge after seven participants from one user group [9].

Seating positions and activities
For the trip scenario with shorter traveling time, more than half of the participants wanted to be seated traditionally forward-facing. For the longer traveling time this was reduced to one third with the living room layout being as common. If all versions of "face-to-face" layout were summaries for the longer traveling time, B) and D), those summarised to almost half of the participants.

Activities that came up for all three trip scenarios were either the socializing kind (chatting, playing cards or boardgames, taking phone calls), or the relaxing kind (playing games on their phones, reading, watching movies, listening to music or just doing nothing). Other activities mentioned were working, eating, sightseeing, and yoga.

Interior design
Participants envisioned the fully automated vehicles as having a setup more like an airplane than a conventional vehicle, with a functional chair and a table for other activities. The desired functions of the chair include reclining, providing massage, and being able to flatten out horizontally. Vehicle width would be affected by the occupants' desire to have chairs that can be rotated. The features desired are fairly luxurious, with a focus on comfort and privacy (such as extra soft or ergonomic seats and the ability to adjust window transparency). Other desired services are more common in homes than in vehicles—like screens, coffee makers, air purifiers, freezers, and karaoke machines.

Results from the study in China compared to results from the study in Sweden

The preferred seating positions were similar for Shanghai and Vårgårda, despite the differences in traffic and community size.

Seating positions and activities

The authors of the study in Sweden [4] suggested that people in mega-cities may wish to work in their cars more than people in small rural communities. The results of the study in China do not support this hypothesis. Working does come up as an activity in the shorter commute to work, but relaxing or playing on one's phone are far more commonly mentioned. Participants' occupations were not recorded, so it is difficult to know whether this preference is attributable to occupational requirements or personal preference.

Participants in both studies mention relaxing or sleeping as preferred activities for all trips, but for longer trips the participants in Sweden did not mention this as frequently. Instead, at least for the longer trips, their most frequently-mentioned activities were watching movies and TV series.

Phones or screens are important for in-vehicle activities in both China and Sweden, both as part of the longer, more social trip and the shorter, more individual one.

The ability to recline seats, even fully horizontal, was important for participants in both China and Sweden.

Interior design

The participants in both countries envision fully automated vehicles as luxurious, with features that cannot be found in public transport vehicles or mass-market cars. In Sweden, participants even mentioned a limousine feeling, whereas in China participants focussed on a multitude of comfort features. At the same time, both sets of participants appeared to see their daily commutes as similar to those of today, with seats in their traditional forward-facing position. During longer trips, however, the socializing part of travel may become more prominent, with participants in both studies wishing to face their co-passengers.

Safety implications and need of novel restraints in fully automated vehicles

It has been claimed that fully automated vehicles have the potential to reduce the number of crashes [10], but avoiding all crashes in mixed traffic with human drivers is impossible for several reasons: hardware failure, software failure, sensing mistake from the fully automated vehicle, or irrational human behaviour with too little time for the fully automated vehicle to react [11]. Occupant restraints (i.e. belts and airbags) and crash-safety evaluation therefore remain important. Actually, crash-safety evaluation might be even more challenging in the future than it is today, due to the new sitting positions and interior designs that are expected. The voluntary guide from NHTSA [12] encourages the crash-safety evaluation of any alternative planned seating configuration. However, current restraint systems are only tested in the traditional sitting position in homologation and consumer testing, in either pure frontal or pure side crashes. Improved restraints would most likely be needed to provide equal protection for occupants in any future alternative seating or interior configurations.

Restraints—and their evaluation methods—need to evolve in a world of fully automated vehicles. If the seats are allowed to rotate, translate, or recline more than they do today, we foresee the need for a new type of restraint, adapted to the seat position (e.g., seat-integrated belts and airbags). If, for example, the seat back is reclined, the risk that the lap belt will slip over the iliac wing and submarine into the abdomen increases [13]. Improved pre-tensioning of the lap belt, in combination with an inflatable seat pan structure, has been proposed to reduce the risk of submarining in reclined positions up to 45 degrees [13]. To improve the restraint function of the belt even further, an additional shoulder belt running across the opposite shoulder (criss-cross belt) can be beneficial, as the load from the seatbelt is more widely distributed than it is with a standard 3-point belt [14-15]. If the seat is rotated, the extra belt would also help keep the occupant from sliding out of the belt, which might happen with a standard 3-point belt [16]. Both the study in China and the study in Sweden showed positive attitudes towards an extra belt and encourage further efforts towards fleet-wide implementation. Another example of the possible evolution of the 3-point belt is the inflatable belt, proposed to protect the occupant from sliding out of the seat belt in a 45 degree angled impact [17]. An example of how the airbag could evolve is described in [18]; an airbag in the seatback which has the potential to protect the occupant in any seating position. As a further challenge, the restraint system also might need to protect the occupant from free-flying objects such as laptops and tablets in seating configurations B) and D) (Fig.3) as in those seating configurations such object might become free-flying with the risk to hit the persons sitting in the opposite position.

Protection is needed for all occupants, whatever their characteristics (stature, sex, age, etc; a diverse population). Therefore, we encourage the use of human body models (HBM) that could be morphed to better represent the full diversity of the human population than current crash test dummies, which are currently limited to three sizes: the 5th percentile female, 50th percentile male and 95th percentile male. Additionally, current crash test dummies are only validated for pure frontal or pure side impact in defined sitting positions. Since passengers of fully automated vehicles are likely to sit in rotated and/or reclined seats, assessment tools that are designed and valid for omnidirectional loading will be required. Further refinement of HBMs is necessary to accurately represent kinematics and predict injuries in new sitting positions with oblique loading.

Motion sickness

Motion sickness can occur when humans are exposed to motion that they seldom experience. The symptoms (sweating, pallor, flatulence, burping, salivation, apathy, etc.) vary between people in the order of occurrence and in their magnitude [19]. When travelling in a moving vehicle, a person can develop motion sickness if there is a conflict between visually perceived movement and the vestibular sense of body movement. Typically, this can happen when a person in a moving vehicle does not watch the road ahead [20]. The problem normally increases if the person does not control the motion; vehicle passengers experience motion sickness more frequently than drivers do [21]. In fully automated vehicles, everyone will become a passenger, which will lead to an increased risk of motion sickness [19]. Further, travelling facing backwards was found to lead to a significant increase in motion sickness symptoms [22].

In summary, although positions other than forward-facing and activities not focussing on the road are more likely to induce motion sickness [19-20, 22], the participants in the two studies did not always want to face forward. Moreover, they expect to be able to read, watch movies, play games and perform similar activities which divert the gaze from the road. Providing a solution to motion sickness in fully automated vehicles will be necessary to fulfil their expectations.

Limitations

The study in China was performed one year after the study in Sweden, and research on vehicle automation has evolved and new systems have been released during that time. This time lapse may have influenced the results, as participants' views may have shifted. However, the activities imagined by participants in China and Sweden were slightly (but not very) different; we can assume that participants primarily extrapolated from their current activities, which are unlikely to have shifted much in a year.

The trip scenarios in the two studies were somewhat different. This discrepancy makes it somewhat difficult to compare the trip scenarios between countries. The reason for providing different trip scenarios was to allow participants to consider a wide range of activities.

The "Setting the stage" method [5-6] has its own limitations (which are, at the same time, its strengths). The method provides a way for participants to visualize the future of mobility for themselves, without the constraints of a life-sized set on their imaginations. Further, since the study is conducted in a static setting, the limitations imposed by a moving vehicle, possibly on bumpy roads, and the risk for motion sickness, were not considered. Performing a study in a more realistic setting, such as on the road, may provide more information, but at the same time such a study would be difficult to perform from a safety perspective.

CONCLUSIONS

We have presented a study of future seating positions in fully automated vehicles using the "Setting the stage" method [5-6] with participants in Shanghai, China, and compared these results with previous results from Vårgårda, Sweden [4]. This comparison demonstrates that user expectations are similar, they expect fully automated vehicles to allow reclined sitting, versions of a living room setup, and more comfortable seats with screens and tables for various activities. New sitting positions will require the development of novel restraints for in-crash protection. Seatbelts and airbags need to adapt to new interiors; we have discussed some promising solutions such as seat integrated belt, additional shoulder belt, inflatable belt and seat integrated airbags.

ACKNOWLEDGEMENTS

The work was partly carried out at SAFER, the Vehicle and Traffic Safety Centre, at Chalmers, Sweden. We thank Vinnova, the Swedish Energy Agency, the Swedish Transport Administration, and the Swedish vehicle industry for

funding parts of this work through the strategic vehicle research and innovation (FFI) program for the project 2017-01945: Assessment of Passenger Safety in Future Cars.

Further we would like to thank Katarina Bohman at Volvo Cars and Haoran Wu, Shengqi Zhou, Chengkai Ding, Jingxiang Weng, Jin Wang, and Bo Sui, who were all at Autoliv China when the investigation was performed; without their help the study could not have been carried out. We also want to thank Arun Muthumani, Autoliv Research Sweden, for his help with insights into the area of motion sickness and for the silhouette sketch of the seating position variations. Finally, we would like to thank Kristina Mayberry for language revision.

REFERENCES

[1] The Mercedes-Benz F 015 Luxury in Motion. https://www.mercedes-benz.com/en/mercedes-benz/innovation/research-vehicle-f-015-luxury-in-motion

[2] Volvo Cars 360c. 2018. https://www.volvocars.com/intl/cars/concepts/360c

[3] Volkswagen Group, Concept Sedric 2018. https://www.volkswagenag.com/en/news/2017/03/Autonomous_driving.html

[4] Jorlöv, S., Bohman, K., and Larsson, A. 2017. "Seating Positions and Activities in Highly Automated Cars–A Qualitative Study of Future Automated Driving Scenarios." In Proceedings of IRCOBI conference. Antwerp, Belgium.

[5] Pettersson, I. and Karlsson, M. 2015. "Setting the stage for autonomous cars: a pilot study of future autonomous driving experiences." IET Intelligent Transport Systems, Volume: 9, Issue: 7.

[6] Pettersson, I. 2017. "Travelling from fascination to new meanings: Understanding user expectations through a case study of autonomous cars." International Journal of Design, 11.

[7] Society of Automotive Engineers International. 2016."Taxonomy and Definitions for Terms Related to On-Road Motor Vehicle Automated Driving Systems." J3016-SEP2016. https://www.sae.org/standards/content/j3016_201609/preview/

[8] Hsieh, H.F. and Shannon, S.E. 2005. "Three approaches to qualitative content analysis." Qualitative Health Research Vol 15, Issue 9.

[9] Faulkner, L. 2003. "Beyond the five-user assumption: Benefits of increased sample sizes in usability testing. Behavior Research Methods." Instruments, & Computers, 35(3), 379–383

[10] Lubbe, L., Jeppsson, H., Ranjbar, A., Fredriksson, J., Bärgman, J. and Östling, M. 2018. "Predicted road traffic fatalities in Germany: The potential and limitations of vehicle safety technologies from passive safety to highly automated driving." In Proceedings of IRCOBI conference. Athena, Greece.

[11] Shalev-Shwartz, S., Shammah, S. and Shashua, A. 2017. "On a Formal Model of Safe and Scalable Self-driving Cars." Mobileye, 2017

[12] The U.S. Department of Transportation's: Automated driving systems 2.0 a vision for safety, September 2017. https://www.nhtsa.gov/sites/nhtsa.dot.gov/files/documents/13069a-ads2.0_090617_v9a_tag.pdf

[13] Östling, M. Sunnevång, C. Svensson, C. and Kock, H.O. 2017. "Potential future seating positions and the impact on injury risks in a Learning Intelligent Vehicle." 11. VDI-Tagung Fahrzeugsicherheit, 29th of November 2017, Berlin, Germany.

[14] Östling, M., Saito, H., Vishwanatha, A., Ding, C., Pipkorn, B. and Sunnevång, C. 2017. "Potential Benefit of a 3+2 Criss Cross Seat Belt System in Frontal and Oblique Crashes." Proceedings of IRCOBI Conference, 2017. Antwerp, Belgium

[15] Mroz, K., Pipkorn, B., Sunnevång, C., Eggers, A. and Bråse D. 2018. "Evaluation of Adaptive Belt Restraint Systems for the Protection of Elderly Occupants in Frontal Impacts." In Proceedings of IRCOBI conference. Athena, Greece.

[16] Sengottu Velavan, S. and Huf, A. 2018. “Development of occupant restraint systems for future seating positions in fully or semi autonomous vehicles.” Proceedings of FISITA World Automotive Congress, Chennai, India.

[17] Edwards, M.A. and Nash, C.E. 2017. “Inflatable Shoulder Belts and Inboard Upper Anchor Shoulder-belt Geometry in Far-side Oblique Impacts.” In Proceedings of IRCOBI conference. Antwerp, Belgium.

[18] Matsushita, T, Saito, H. and Vishwanatha, A. 2019. “Evaluation of the protective performance of a novel restraint system for highly automated vehicles.” Proceedings of 26th International Technical Conference on the Enhanced Safety of Vehicles (ESV), Eindhoven, Netherlands.

[19] Diels, C. and Bos, J.E. 2016. ”Self-driving carsickness.” Applied Ergonomics Volume 53, Part B, March 2016, Pages 374-382

[20] Sivak, M and Schoettle, B. 2015. “Motion Sickness in Self-Driving Vehicles” UMTRI-2015-12. https://deepblue.lib.umich.edu/bitstream/handle/2027.42/111747/103189.pdf?sequence=1&isAllowed=y

[21] Reason, J.T., and Brand, J.J. 1975. Motion sickness. London: Academic Press.

[22] Salter, S., Diels, C., Herriotts, P., Kanarachos, S. and Thake, D. 2018. ”Motion sickness in automated vehicles with forward and rearward facing seating orientations.” Applied Ergonomics 70 (2019) 54-61.

FUTURE POTENTIAL OF AUTOMATIC EMERGENCY BRAKING SYSTEMS FOR HEAVY TRUCKS

Daniel Schmidt, Thomas Lich, Andreas Georgi
BOSCH Accident Research, Corporate Sector Research and Advance Engineering, Robert Bosch GmbH,
70465 Stuttgart
Germany

Paper Number 19-0088

ABSTRACT

The European Union requires an Automatic Emergency Braking System (AEBS) for all new heavy trucks (N3) since 2015. In case of an anticipated rear-end collision, the AEBS in accordance with EU regulation 347 – 2012 has to provide an adequate two-fold warning cascade and a subsequent emergency braking. After becoming a mandatory system, a strong increase of market penetration of AEBS has been established. However, first analyses in 2017 on German highways showed only minor impact of AEBS in the field [Petersen, E., "Wirksamkeit von Sicherheitssystemen im Straßengüterverkehr", Zukunftskongress Nutzfahrzeuge, Berlin, 08. Nov. 2017]. Identified reasons for the minor impact are, amongst others, overruling of the AEBS by braking / accelerating, a probable system deactivation by the driver, and limited implications of an EU conform AEBS. Concerning the requirements, the EU conform system demands in its current level (effective November 2018), for instance, a deceleration of 20 km/h during an emergency braking on a highway approaching with 80 km/h a standing opponent at the end of a traffic jam– the collision may still occur with up to 60 km/h. Being aware of the limitations of AEBS requirements, BOSCH established top level requirements for a high-performance AEBS assumed to not only mitigate but to prevent most rear-end collisions of trucks.

The present study evaluates the benefit of Automatic Emergency Braking Systems exemplarily for German roads. It comprises of a thorough analysis of rear-end collisions involving N3-trucks, followed by stochastic simulations of a truck assumed to be equipped with either of the systems: the current EU-conform AEBS or a generic high-performance Automatic Emergency Braking System. In the first part of the study, the German in-depth accident study (GIDAS) was used to identify a potential field of effect for AEBS. In the second part, a simulation frame work specifically designed for the stochastic approach was established. It includes a sensor system, various road conditions from on-spot measured data and a simplified truck driver model accounting for driver reaction times and the specific kind of driver reaction.

About 2 300 N3-truck rear-end collisions with casualties per year in Germany can be positively influenced by an AEBS (field of effect for truck AEBS). In the second part of the study, after 2.5 mio stochastic simulations, avoidance potentials of at least 7% for the EU-conform minimum system and up to 84% for the high-performance AEBS were identified (assuming full AEBS penetration in N3 vehicles). These avoidance potentials could scale up to 1 900 collisions with casualties in Germany per year, if each truck would be equipped with the high-performance AEBS. For the remaining accidents the collision velocity would be significantly reduced, too.

In summary, this study reveals that an AEBS applied to and accounting for real-world accident situations can increase the effectivity of an Automatic Emergency Braking System preventing rear-end collisions of trucks

INTRODUCTION

One of the most feared situations for many car drivers is imagining an accident situations on motorways where a heavy truck crashes with almost no speed reduction into a standing car at the end of a traffic jam. This type of accident often results in severe or fatal injuries for the car occupants. At the same time, the car occupants, despite having identified the severity of the situation in advance, have to await their fate helplessly. Severe accidents involving heavy trucks in a front-to-rear-end situation are neither common nor occur often. However, if there is an accident of that type, damages might become catastrophic as well as the medial attention is huge. Furthermore, the motorway is often closed for several hours for rescuing and cleaning the road leading to long traffic jams and thereby to possibly additional economic impact.

To reduce such front-to-rear-end collisions, the European Union requires trucks to be equipped with an Automatic Emergency Braking System (AEBS) [1]. The EU regulation 347 – 2012 is mandatory for middle and heavy trucks (typically >3.5 t, for semi-trailers >8 t) with registration dates after November 2015 (1st level). Three years later, in November 2018, the 2nd level of the regulation became effective. In general, the AEBS should initiate an emergency braking protocol in case of an anticipated collision with a slower or standing vehicle in front of the truck to mitigate or even avoid the collision at all. While the regulation in detail specifies requirements for AEB systems admitted to the European market, the key requirements with respect to physical effectivity of such systems are the ones given in the following. Specifically, the AEBS has to be fully equipped to be able to prevent collisions of constantly moving opponents with velocities larger than 32 km/h (1st level) and 12 km/h (2nd level) being in an in-line constellation. Furthermore, anticipating a collision with a standing opponent, the AEBS has to reduce the truck velocity by at least 10 km/h and 20 km/h for 1st and 2nd level, respectively.

As commercial vehicles such as heavy trucks have small turn-over cycles, the hope was to reach a state where severe accidents caused by heavy trucks on motorways will significantly reduce. Now, some years later, the share of trucks on motorways equipped with an AEBS should have reached a reasonable level, and first impact of the legislation should be visible. Yet, the situation, especially on German motorways seems to be the contrary [2,3].

Here in this study, we will review the typical accident prior to the AEBS legislation and estimate the impact of a system as demanded by EU regulations, especially for the current 2nd level requirements. In our simulations, we will fully implement a generic three-fold warning cascade with acoustic warning first, followed by partial braking and, in its final stage, an automatic emergency braking. Additionally, we will introduce a generic AEBS based on a high performance system and estimate the maximum in avoidance and mitigation potentials. Based on a comparison with the current status, we will provide insights into how future automatic emergency braking systems could be designed to not only achieve the ambitious aim of EU legislations but also to come close to the maximum with respect to avoidance and mitigation potential of a future AEBS.

STATUS: HEAVY TRUCKS REAR-END COLLISIONS IN GERMANY

For 2017, the Federal Statistical Office of Germany (Destatis) presented in the annual German national accident report a total number of 302 656 accidents with casualties on German roads [4]. In 29 170 accidents of the same year (almost 10%), at least one truck was involved with a total of 32 234 participating trucks [5]. While the official report separates into light trucks (≤3.5t), middle and heavy trucks (>3.5t) and semi-trailers, an individual reporting for heavy trucks (>12t) is not available. However, a trucks with mass >3.5t (middle and heavy trucks as well as semi-trailers) engaged in 15 805 accidents which serves as an upper bound for heavy trucks. Estimating the number of heavy trucks (>12t; N3) being involved in accidents with casualties on German roads will be a first step to assess the field of effect for a heavy truck AEBS.

Evaluating the effect of an AEBS for heavy trucks (>12t) requires a thorough analysis of the present status of the field of effect. For that purpose, the current study is based on in-depth accident data. A more than suitable database is the German in-depth accident study (GIDAS) recording detailed on-spot information about the accident, location and weather conditions, as well as all involved parties in more than 2 000 parameters per accident [6]. GIDAS is by now recording accidents for more than two decades. After recording the accidents, the course of events of each accident is reconstructed. Overall, GIDAS is a database with about 30 000 recorded and reconstructed accidents. By

weighting the distributions of accidents, locations and severity to the annual German national accident report, analysis of the GIDAS database is made representative for German roads. By construction, the GIDAS database records accidents with at least one injured occupant – consequently property-damages only incidents are not included in this study.

For the present study, we use a subsample of the GIDAS database containing the years 2005 to 2018 with a total of 28 225 accidents (Fig. 1). Thereof 933 accidents involved a heavy truck (>12t). Refining to an AEBS relevant scenario, defined by a collision of the truck's front with the opponent's rear-end in an in-line constellation, the GIDAS database provides 162 cases. Weighting these cases to German roads, a heavy truck is involved in about 12 500 accidents while the field of effect for an AEBS consists of a total of about 2 300 accidents in Germany.

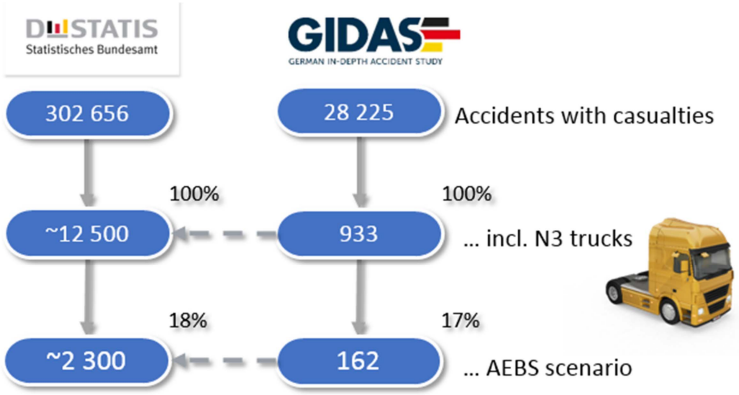

Figure 1: Case selection and basis for the present study, weighted for Germany 2017

In the following paragraphs, we present a thorough analysis of the 162 GIDAS cases – weighted to German roads. As a first result, the location of AEBS relevant crashes for heavy trucks is identified. Every second accident (48%) is found on a motorway, every fourth accident (21%) in rural areas and every third accident (31%) is found in urban areas (Fig 2a). Thereby, the typical road for front-to-rear-end collisions is a straight road – a relevant curve radius <500 m applies in only a marginal 2% of all cases.

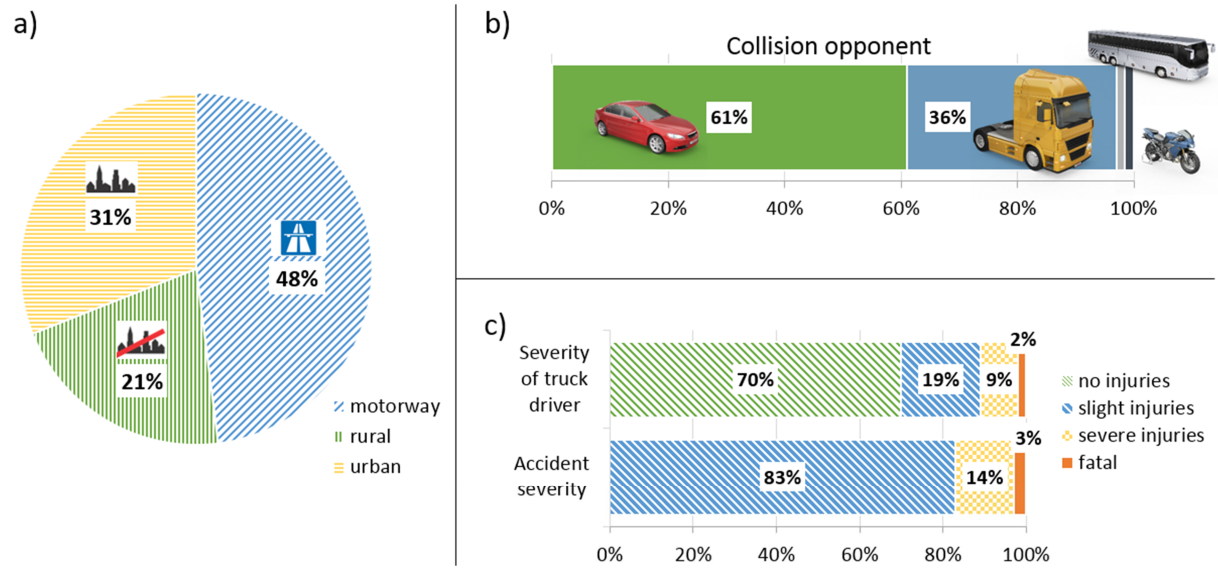

Figure 2: a) Share of collisions on motorways, in rural or urban environments. b) Type of collision opponent. c) Severity of truck driver in comparison to the accident severity. Please note: by construction of GIDAS the accident severity is at least "slight injuries".

Next, collision participants and severity are characterized. In a vast majority of all cases, the collision opponent is a car (61%) or a truck (36%). In the remaining cases, the opponent was a motorcycle or a bus (Fig 2b). The age of the truck at the time of the collision follows approximately the age distribution of trucks in Germany with 80% being younger than nine years. Due to the huge momentum of a heavy truck and a seating position of the truck driver in a height of two and more meters above the road surface, for more than two of three cases (70%) the truck driver was not injured, while the opponent was at least slightly injured (Fig 2c). The truck driver was identified with light and severe injuries in 19% and 9% of all accidents, respectively. Despite the advantages of height and momentum, in 2% of the accidents, the truck driver died. However, one possible reason for the truck driver severity could be the fact that about every 10th truck driver was not belted. For the opponent, the accident severity is typically increased compared to the truck. Accordingly, the accident severity of all AEBS relevant accidents with casualties involving a heavy truck is categorized as "slight" in 83%, "severe" in 14% and "fatal" in 3%.

A closer look on typical velocities reflects the dynamics of a typical AEBS relevant heavy truck collision. The reconstructed initial velocity of the truck before the collision has an average of 61 ± 24 km/h (mean ± one standard deviation, see Fig 3a). The initial state of the opponent was standing for 41% of all accidents (Fig 3b). In the other cases, the opponent was driving with an average of 45 ± 28 km/h, either moving with constant velocity (10%) or moving and braking before the collision (49%). The truck driver behavior prior to the front-to-rear-end collision concerning intensity of braking (with respect to the road condition) was in two of three cases classified as partial braking (66%). In only 10%, the truck driver was decelerating with full braking, while in 20% of all relevant accidents, the truck driver did not show any signs of braking (Fig 3a). The remaining cases (4%) are comprised of an accelerating truck, typically accelerating at traffic lights faster and/or earlier than the collision opponent in front of it.

The distribution of driver reactions prior to the collision reveals the true potential of an AEBS. A warning and subsequent automatic emergency braking could alert the 20% of drivers not braking and could support the 66% of drivers that were only partially braking. Moreover, the 10% of drivers that were fully braking could benefit from an early warning, too: applying the full brake load earlier could further reduce the collision velocity or possible avoid the anticipated collision at all.

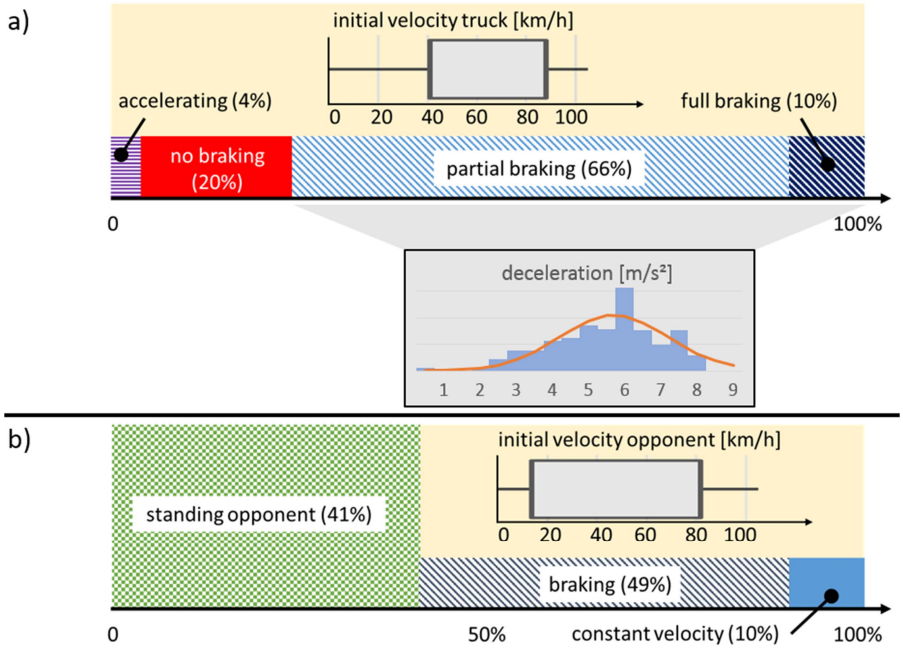

Figure 3: a) Initial truck velocities in a box plot (box equals to mean ± one standard deviation) and type of driver reaction. Inset: reconstructed decelerations for a braking driver as distribution (blue bars) and its Gaussian approximation (orange line). b) Share of standing, constantly moving and braking opponents. The box plot depicts the initial velocity of the opponent.

As reported in the previous section, the GIDAS analysis shows that about 10% of all opponents move with a constant velocity. As an AEBS according to the EU regulation is required to avoid collisions only with constantly moving opponents, the minimal avoidance rates of all EU conform AEB systems is given by the share of accidents with a constantly moving opponent and an initial velocity above the given thresholds of 32 km/h and 12 km/h for 1st and 2nd level, respectively. However, only about 3% of all opponents move with constant velocity and are faster than 32 km/h, while for the 12 km/h threshold the share increases to 7% (data not shown).

In conclusion, our analysis of the status of front-to-rear-end collisions of heavy trucks shows three major results. First, for a vast majority of collisions, the collision opponent is a car or truck and is prior to the collision in an in-line constellation. Thus, detecting and classifying the anticipated collision becomes possible for most cases. Second, an AEBS could warn 20% of truck drivers not braking prior to the collision and support about 2 out of 3 drivers by applying the maximal brake force. Third, a current EU-conform AEBS avoids only at least 7% of all AEBS relevant collisions involving a heavy truck. Here, even at this stage of the study, a possible benefit of a system beyond EU regulations becomes obvious.

SIMULATION STUDY

Simulation layout

The overall simulation study aims to unravel three main questions:

- What is the avoidance potential of a warning only system in comparison to a high performance AEBS?
- Which share of accidents is mitigated and what is the benefit in reduced collision velocity?
- What is the main advantage of a high performance system compared to a minimal system?

The simulation is designed to fully image the pre-crash trajectory of both main participants in the front-to-rear-end collision. Out of 162 cases in GIDAS identified as AEBS relevant front-to-rear-end collisions involving a heavy truck, a total of 127 cases provide all information necessary to reconstruct the pre-crash trajectories. At the initial state, both participants approach the scene with their respective reconstructed initial velocities. Here, the initial state is assumed to be at least five seconds before the original collision. If applicable, the opponent starts braking as it was reconstructed from the original case. Thereby, we assure to challenge the generic AEBS in the simulations with an opponent behavior as close as possible to the original case. The original truck driver commands are removed and it is assumed the truck driver will only react to AEBS warnings. With these assumptions, the benefit of an AEBS to a cautious truck driver stays beyond the scope of this study. However, the main purpose of the present study is the assessment of the effectivity of an AEBS conform to current EU regulations (2nd level) and the differences between this minimal AEBS and a high performance system.

For each of the 127 GIDAS cases and both types of AEBS specifications, the simulation is performed in three scenarios: first, there is no AEBS present, second, the system generates only an acoustic warning with the truck driver braking and, third, the full AEBS procedure (with acoustic warning, partial braking and in the final step an emergency braking) is applied. The simulation itself is set up as a stochastic simulation with variations in the reaction of the truck driver. In contrast, the reactions of the AEBS are deterministically parametrized as described below. To maintain a statistically stable simulation, a total of 10 000 simulations per GIDAS case are performed. Consequently, for each system involving truck driver reactions, warning only system and full AEBS, a total of 127 x 10 000 = 1.27 mio. runs is performed. The first system (re-simulating the original case without AEBS) is fully deterministic lacking the stochasticity of the other systems and, thereby, assures a proper foundation for a statistical analysis of the simulations.

The technical, yet generic design of the AEBS involves a threefold warning cascade. Upon detection of an AEBS relevant situation, an acoustic signal alerts the driver, followed by initiating a partial braking and finally establishing the emergency braking (see Fig. 4).

Figure 4: Schematic view of AEBS phases

The threefold warning cascade meets the EU regulations if the acoustic warning and the partial braking start at least 1.4 s and 0.8 s, respectively, before the emergency braking phase. While the acoustic warning in the simulation just alerts the truck driver to react and apply the brakes by himself, the partial braking follows a protocol simplified by three steps: (i) system reaction time (no braking), (ii) linear ramp up of the brake force up to the desired deceleration and (iii) holding the maximal constant deceleration of the partial braking phase. Typically, the partial braking phase reduces the velocity of the truck by only a few kilometers per hour and is subsequently followed by an emergency braking phase. After reaching the trigger level for the emergency braking phase, a brake protocol applies again with system reaction time, ramp up of brake force and constant deceleration – up until standstill if necessary. While following the same functional protocol, the individual parametrization is different for both phases. The overall AEBS system parameters are chosen as displayed in table 1, meeting a typical – yet generic – high performance parametrization specific to heavy trucks.

Table 1: Generic AEBS parameter specifications

Category	Value
Start warning phase before emergency braking	1.4 s
Start partial braking phase before emergency braking	0.8 s
System reaction time partial braking	0.4 s
Ramp up gradient partial braking	12.8 m/s³
Maximal deceleration partial braking	3.5 m/s²
System reaction time emergency braking	0.15 s
Ramp up gradient emergency braking	10.0 m/s³
Maximal deceleration emergency braking	8.0 m/s²

The AEBS reacts to an opponent, if a collision is anticipated. To detect the position and velocity of the opponent, the truck is equipped with a sensor module. In the case of AEBS relevant front-to-rear-end collisions, the opponent is typically in a straight line in front of the truck. Thus, the sensor consists of a list of ranges up to which opponents are detected depending on a generalized radar cross section for motorcycles, cars and trucks. The ranges were chosen to mimic a current state-of-the-art frontal long-range radar, independent of the manufacturer, ranging up to 200m.

For a simulation study of a driver assistance system, supporting the driver in his reactions, a truck driver model is needed. As a matter of fact, no released model for a truck driver is currently available. Thus, a generic model was set up. For the present comparative study, the truck driver is not initiating the emergency braking by himself but reacts only to an acoustic warning of the AEBS. The generic driver is modelled by a probability to react to the acoustic warning, a reaction time and a maximal deceleration. For this study the parameters were chosen as described in table 2 with reaction time and maximal deceleration being modelled as normal distributions with mean and standard deviation. Here, the probability to react to the acoustic signal is in accordance with recent finding [7] and mean and standard deviation for reaction time follow acknowledged data of the field [7-9]. In contrast, the maximal deceleration is motivated by the findings of the GIDAS analysis itself as presented in Fig. 3 a.

Table 2: Truck driver parameter specifications

Category	Value
Probability to react to acoustic warning	80%
Reaction time – mean	1.4 s
Reaction time – standard deviation	0.5 s
Maximal deceleration – mean (according to GIDAS)	5.7 m/s²
Maximal deceleration – standard deviation (according to GIDAS)	1.5 m/s²

In total, the simulation setup is well defined and allows for a stochastic simulation study of real-world accident data. Again, the driver assistance system AEBS is fully deterministic, while the truck driver is modelled by probability distributions for the main characteristic and, thereby, a stochastic approach is suitable.

Simulation results

An obvious parameter for an AEBS being of enormous interest is the avoidance potential. However, the simulation provides more than just the avoidance potential. First, the distances to the opponent at the time of initiating the emergency braking is analyzed. Second, avoidance potentials of the warning only and the full AEBS are highlighted. Here, an avoidance potential of an AEBS fulfilling the minimal EU requirements is estimated, too. Finally, the share of mitigated collisions and corresponding collision velocities as well as the velocity difference at the time of the collision is evaluated.

Analyzing the start of the emergency braking phase is most straight forward: given the AEBS parameters, as well as the position and velocities of both participants, the start of the emergency braking phase is calculated by the distance needed for braking the truck's velocity to the opponent's velocity. Here, the AEBS is neither triggered nor limited by thresholds of the variable "time to collision". In contrast, the chosen procedure to determine the start of emergency braking allows for a target braking. At the start of the emergency braking phase, the truck has a distance of 20.0 ± 12.8 m (mean ± standard deviation) to its opponent with larger distances in cases of a standing opponent. These distances correspond to times of 1.8 ± 1.1 s before the collision (for a detailed distribution see Fig 5a). For acoustic warning and partial braking, the respective phase is initiated 1.4 s and 0.8 s earlier, as required by EU regulation 347 – 2012.

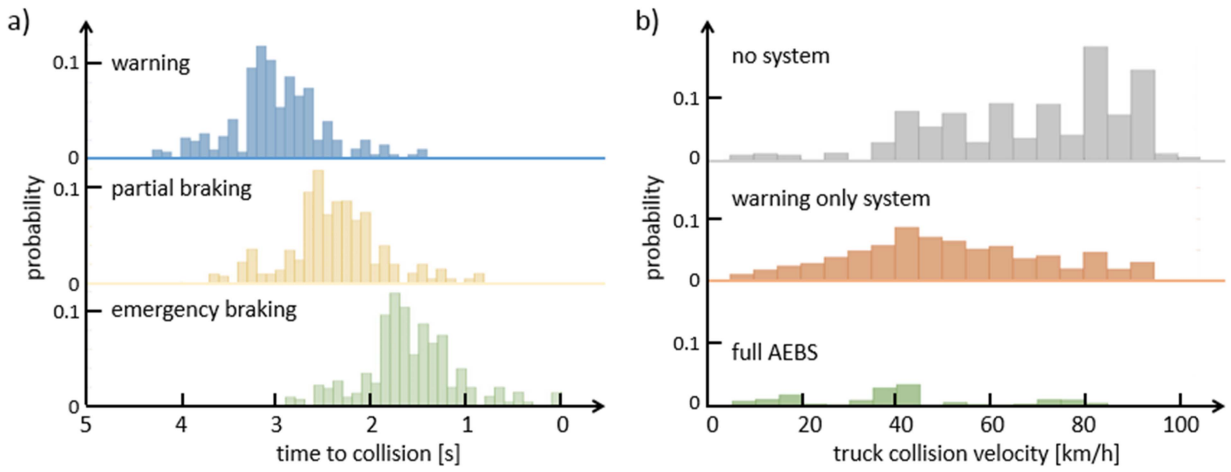

Figure 5: Simulation results: a) start of warning phase (top), partial braking phase (middle) and emergency braking phase (bottom) b) Truck collision velocities.

The most desired effect of an AEBS is its ability to avoid collisions. Given by the EU regulations effective since November 2018, an AEBS has to avoid a collision with an opponent moving with a constant velocity above 12 km/h. Thus, the minimal avoidance potential for any AEBS operating within the EU is given by the 7% of cases where the opponent fulfills the given requirement. However, there are three additional categories of opponent behavior: (i) standing opponent (41%), (ii) constantly moving opponent with v<12 km/h (3%), and (iii) moving but braking opponent (49%). While an advanced high performance AEBS would avoid collisions with any standing or constantly moving opponent (together 51% within the field of effect), a braking opponent is challenging as the opponent is actively decreasing the remaining distance between truck and opponent. In cases where a truck equipped with a high performance AEBS is approaching a braking opponent, two out of three collisions could be avoided (66%). Given the large share of 49% of all cases involving a braking opponent, the maximal share of avoided collisions for a high performance AEBS sums up to 41%+10%+66%x49% = 84% for a standing, a constantly moving and a braking opponent, respectively (Figure 6). In contrast, the minimal avoidance potential for a minimal AEBS is estimated by the share of accidents with a constantly moving opponent with velocity above 12 km/h, i.e.,

7%. Under the assumption, the minimal AEBS is performing equal or worse than the high performance system if the opponent is braking, the upper bound for the avoidance potential of a minimal AEBS is set by 7%+66%x49% = 40%. Compared to the maximal avoidance potential of 84% of a high performance system, a substantial increase in avoidance potential is still possible.

After analyzing the benefit of a full AEBS system, the avoidance potential of a warning only system is addressed. Here, the simulations show an avoidance potential of about 23%. However, the avoidance potential for this system is strongly dependent on the particular truck driver parametrization and large deviations become possible by changing the driver parametrization. For a rough estimate, we identify about one out of four collisions avoided by a warning only system, while more than four out of five collisions could be avoided by an advanced high performance system.

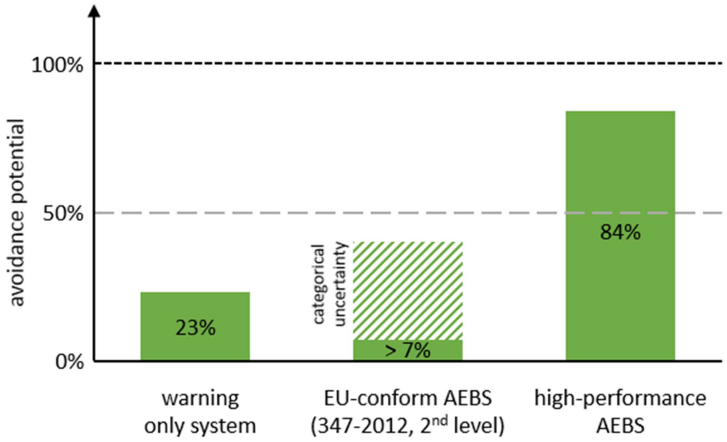

Figure 6: Simulation results: avoidance potentials for a warning only system vs EU-conform AEBS vs high-performance AEBS

In cases where avoidance stays out of reach, the collision velocity and the difference in velocities at the time of collision become important. Here, we compare three systems as described earlier: (i) cases without any intervention, (ii) warning only system and (iii) full AEBS. A weighted distribution of the truck collision velocities for the respective system is shown in Fig. 5b. Obviously, braking reduces the collision velocity drastically. In terms of means and standard deviations, for a warning only system the collision velocity is about 52 ± 22 km/h, while for the full system the mean becomes 43 ± 22 km/h. However, especially for the full AEBS, most cases are avoided and the reported mean and standard deviations of collision velocities are comprised of only few cases.

While for the EU conform AEBS (2nd level) the minimal avoidance rate is at least 7% for the collision velocity an upper bound is found: for all standing opponents, the collision velocity is reduced by at least 20 km/h. This results in a weighted mean collision velocity of maximal 53 km/h. Due to a further reduction of velocity of individual systems prior to a collision with a standing opponent or reducing the collision velocity with a braking opponent, the mean collision velocity of a current EU conform system is assumed to be reasonably smaller than 53 km/h.

Whether limitations of the sensor restrict the avoidance potential is another question that was addressed by the simulations. Here, we analyzed additional to the finite sensor ranges discussed above the avoidance potential of a system with a sensor of infinite range. However, the improvement of avoidance potentials by an infinite sensor is virtually not present: the avoidance potential with an infinite sensor is at the same rate as with the finite sensor. The reason is mainly that a combination of the generic sensor set with ranges up to 200 m with the restricted velocities of a truck is sufficient to not restrict avoidance potentials of an AEBS.

CONCLUSIONS

The present study reveals various insights of front-to-rear-end collisions in an in-line constellation for heavy trucks. First, an AEBS could address up to annually 2 300 accidents on German roads. More than every second collision was found on a motorway with typical opponents being other trucks or cars. Due to the large share of motorway incidents, the initial velocity of trucks is rather large with 61 ± 24 km/h. Additionally, due to heavy masses of large trucks and often very demanding conditions for truck drivers, 3% of all AEBS relevant accidents were fatal, and in an additional 18% the accident was classified as severe. Consequently, to avoid collisions with standing opponents, a large reduction in velocity is necessary which – in turn – demands highest requirements for such a system. On the other hand, the analysis showed the true potential of advanced automatic emergency braking systems: in two out of three reconstructed collisions, the truck driver was only partially braking before the collision. Here, an AEBS could support the driver and further reduce the collision velocity.

Our stochastic simulations estimated minimal and maximal benefits of AEB systems. For an AEBS conform to current EU regulation 347 – 2012 (2nd level) the benefit was estimated to:

- minimal avoidance rate of at least 7%
- reduced collision velocity for all mitigated collisions smaller than 53 km/h

For a high performance, yet generic AEBS the benefit could become:

- maximal avoidance rate up to 84%
- reduced collision velocity for the few remaining mitigated collisions 43 ± 22 km/h

The main limitations of the EU conform AEBS are given by requiring only for avoidance with constantly moving opponents faster than 12 km/h. For standing opponents, a speed reduction of at least 20 km/h is requested. Including full avoidance of all constantly moving as well as all standing opponents could boost the effectivity of truck AEBS with respect to avoidance from at least 7% up to 51% and more. Yet, improving sensor quality to secure a reliable detection of standing opponents is a key challenge for further improving future automatic emergency braking systems.

Given the enormous avoidance potentials of up to 84% within the field of effect, a strong decline in front-to-rear collisions of heavy trucks should be visible soon – even with only few systems on the street. However, recent studies on German motorways were yet not able to detect any decline in accident numbers at all [2,3]. Mostly a combination of AEBS penetration rates in truck stock and low avoidance rates required by the EU regulation could explain why a study of 2017 was not able to detect any impact of AEBS. On the other hand, the expected decline in accident numbers could result from small datasets and statistical outliers: with a hypothetical assumption of a market penetration of 50% only a little more than one year after AEBS became mandatory, an AEBS would address little above 500 accidents with casualties on German motorways (field of effect: 2 300 accidents with casualties in Germany; hypothetical market penetration: 50%, share of all accidents on motorways: 48%). Assuming the minimal avoidance potential (7%) for the 2nd level of EU regulation the system would avoid only less than 50 accidents with casualties on German motorways. Thus, from a statistical point of view, it is very challenging to detect effects due to AEBS. Nevertheless, often attributed and partially speculated reasons [2,3], e.g., truck drivers manually overriding the AEBS, could still play a role for explaining not-declining front-to-rear accident numbers involving heavy trucks and casualties.

REFERENCES

[1] European Commission (editor), “Commission Regulation (EU) No 347/2012”, (2012)

[2] Petersen, E.; Scholze, C.; Böhnke, R. „Notbremsassistenzsysteme im Lkw – Eine Analyse niedersächsischer Autobahnunfälle des Jahres 2017 und Einfluss aktueller Systeme“ *Z. f. Verkehrssicherheit* 64, (2018) Nr. 5, S. 336

[3] Petersen, E.; Simon, N.; Krupitzer, U. “Lkw-Unfälle mit schweren Personenschäden auf niedersächsischen Autobahnen und deren Relevanz sowie Vermeidbarkeit durch aktuelle Notbremsassistenzsysteme“ *Z. f. Verkehrssicherheit* 62, (2016) Nr. , S. 273

[4] Federal Statistical Office of Germany (editor) “Verkehrsunfälle 2017”, Fachserie 8 Reihe 7, (2018)

[5] Federal Statistical Office of Germany (editor) “Unfälle von Güterkraftfahrzeugen im Straßenverkehr 2017”, (2018)

[6] Liers, H.; „Traffic accident research in Germany and the German in-depth accident study (GIDAS)“, *SIAM Conference*, (2018)

[7] TANGO project, “Fahrerbeanspruchung bei unterschiedlichen Nebentätigkeiten und Automatisierungsstufen”, https://projekt-tango-trucks.com/ (2018)

[8] Taoka, G. T. “ Brake Reaction Times of unalerted drivers”, *ITE Journal*, 19, (1989)

[9] McGehee, D. V.; Mazzae, E. N.; Scott Baldwin, G. H. “Driver Reaction Time in Crash Avoidance Research: Validation of a Driving Simulator Study on a Test Track”, *Hum. Fac. Erg. Soc. P.*, 44, (2000)

PASSENGER CAR SAFETY BEYOND ADAS: DEFINING REMAINING ACCIDENT CONFIGURATIONS AS FUTURE PRIORITIES

Martin Östling
Nils Lubbe
Hanna Jeppsson
Autoliv Research
Sweden

Pradeep Puthan
Autoliv India
India

Paper Number 19-0091

ABSTRACT

New vehicles are increasingly equipped with a variety of Advanced Driver Assistance Systems (ADASs). As these systems have the potential to prevent accidents, accidents of the future will differ from those of today. Predicting the type and characteristics of these future accidents is therefore essential to current research and development in the occupant restraint and new ADAS fields.

In this study, accident avoidance of 15 ADASs was modelled using simple deterministic rules for each, creating both a conservative and an optimistic ruleset to account for current limitations and future possibilities. The rulesets were applied to the US National Automotive Sampling System Crashworthiness Data System data from 1995-2015 and verified through the literature. The residual passenger vehicle to passenger vehicle accidents were analysed, treating all accidents and accidents with at least moderate injuries in modern passenger vehicles (model year 2007 and later) separately.

Many accidents were found to be avoided through such systems, and their combined effectiveness ranged from 51% to 97% depending on ruleset. Electronic Stability Control (ESC), Lane Keep Assist (LKA), and Crossing and Rear End Automated Emergency Braking (AEB) were highly effective, individually preventing over 25% of accidents in the optimistic calculation. Importantly, remaining accidents will have a different distribution across accident types compared to today: rear end collisions will reduce, leaving turning and crossing scenarios to dominate future accidents.

For passenger vehicle to passenger vehicle accidents with at least moderate injuries in modern vehicles, four accident types alone were found to account for 93% of all remaining accidents in the optimistic estimate: Head On, Turn Across Path, Turn Into Path Opposite Direction and Straight Crossing Paths; the latter three are intersection-related and together represent three quarters of all remaining accidents.

The intersection accidents are analysed further for deformation pattern, impact direction, 90% cumulative delta velocity and injured occupant position in order to identify possible new impact conditions to be used when evaluating occupant restraints. The well-established frontal and side impacts will still generate many AIS2+ injuries, while new more oblique impact conditions will also be needed to represent the variety of intersection accidents remaining.

The description of future accidents and impact conditions presented here can serve as a basis for the research and design of future ADASs and occupant restraints. We propose virtual assessment methods with Human Body Models (HBM) based on these impact conditions.

INTRODUCTION

More than six million police-reported motor vehicle accidents occurred in the United States in 2016; of the 37 461 fatalities, 23 714 (63%) were occupants of passenger vehicles [1]. Over recent years, many Advanced Driver Assistance Systems (ADASs) have been introduced to the market, including Automated Emergency Braking (AEB) for rear end collisions and pedestrian impacts and Lane Keeping Assist (LKA), which are estimated to reduce the number of accidents significantly [2-8]. To reduce this number further, additional ADASs, such as AEB for intersections and Evasive Steering Assist (ESA), are under development as a stepwise progression to fully autonomous driving. Society of Automotive Engineers (SAE) describes these steps at five levels [9], where level 0 means no

driving automation and level 5 means full driving automation. Most ADASs today are designed for level 2, partial automation, which means that the driver needs to be fully engaged but the vehicle has automated emergency functions like braking and steering. Through monitoring the driver, driving environment and surrounding traffic, these functions intervene to prevent traffic accidents and support safe driving.

With the number of ADASs in the vehicle fleet increasing, the frequency distribution of accident types will change over time. It is of importance to be able to predict which accident types will remain and which will predominate; this is needed not only to guide the development of new or improved driver assistance systems, but also to guide the development of occupant restraints. However, the real-world effect of new ADASs is difficult to determine since they are not yet widely deployed to the market. Attempts to evaluate this may broadly be categorized as either retrospective or prospective, as follows.

Retrospective analyses tell what has happened. This is done by direct comparison of vehicles with and without the ADAS in question. Several researchers have reported on the number of accidents that could be prevented by various ADASs [3, 5, 10-14] using such an approach; however, newer ADASs like ESA, Driver Monitoring Systems (DMS), Traffic Jam Assist (TJA) and Highway Assist (HA) have not yet been evaluated as these have a rather low installation rate, making a retrospective investigation hard to execute. Retrospective analysis is also hard to execute if vehicles are equipped with several ADASs because any of the systems present may have prevented the accident and thus attributing the benefit to a specific ADAS is not clear-cut.

Prospective analyses tell what will happen. Alvarez et al. (2017) define four levels of prospective analyses from level 0, “Use of expert opinion to estimate the potentially addressed situations”, to level 3, “Use of simulation to generate reference situations (RS) and modified situations (MS) from the understanding and characterization of processes” [15]. Prospective analyses take in-depth accident data from accident scenes and then apply an intervention to assess its potential benefit. Such predictions are either made by detailed simulations or by some type of estimation. Simulation is used when a detailed understanding is needed, in which case a thorough set up of the accident boundary conditions is made. The ADAS is then applied to the situation to evaluate whether it prevents the accident or not. When simulating, it is also possible to vary the situation boundaries to evaluate situations that could have happened or to vary the magnitude of the intervention [16-18]. This method is by nature limited to the detailed data available and is time consuming since it requires the creation and validation of a simulation model as well as at least two simulation runs per accident, one reference and one modified with the ADAS. In contrast to this, the use of estimates for given situations gives an overall understanding of the potential of an ADAS [2, 19-21]. Assuming that a range of safety systems will be able to intervene in the future — for example, through the implementation of ADASs — one can model each of these interventions in low detail, apply this to historical crash data, and get estimations regarding future crashes which can be used to prioritize interventions and plan for subsequent ones [22]. This method has been validated for a 10-year time horizon using Swedish fatality data [23]. Although the result is not as detailed as for a simulation, it is nonetheless a significantly faster process.

The objective of this study is to investigate which passenger vehicle to passenger vehicle accident types will remain, and how the impacted vehicles are deformed, in a future when today’s known Level 2 ADASs have been implemented. New impact conditions, guiding the evaluations of occupant restraints, are defined based on these deformations. A prospective approach is taken using estimates to examine the effectiveness of 15 ADASs in avoiding accidents.

METHOD

The method used in this study contains five steps: data collection; definition of ADAS rulesets; verification of ADAS rulesets; accident description; and analysis of the deformation pattern of the remaining impacted vehicles (Fig. 1). First, data regarding passenger vehicle to passenger vehicle accidents and single passenger vehicle accidents were extracted from the National Automotive Sampling System Crashworthiness Data System (NASS CDS). In the second step, two deterministic rulesets, one optimistic and one conservative, were created for today’s known ADASs, 15 in total. The rulesets were then applied to the data to calculate the effectiveness in avoiding accidents of each ADAS alone and in combination. The third step verified the rulesets by comparing the computed effectiveness to the literature for accident avoidance, irrespective of injury severity. In the fourth step, the accidents were analysed in terms of accident scenario and general area of deformation. This analysis was only done for passenger vehicle to passenger vehicle accidents where at least one occupant sustained a moderate injury, i.e. a number equal or higher than two on the Abbreviated Injury Scale (AIS). In the fifth and final step, the accidents still remaining after the optimistic ruleset

had been applied were analysed in terms of accident type, delta velocities, corresponding Collision Deformation Classification (CDC) codes and the position of injured occupants.

Definition of terms

Accident scenario: Accident scenarios describe the overall kinematics before and during an impact of both vehicles involved. Accident scenarios are taken as the combination of two NASS CDS variables: crash category and crash configuration [24]. Examples are Same Direction – Rear End, Intersection Path – Straight Path and Vehicle Turning – Turn Across Path.

Accident type: Accident scenarios are divided into specific accident types (crash types in NASS CDS, in which 99 different crash types are described) with each vehicle involved being allocated a type. Examples of accident types are Drive Off Road, Turn Into Opposite Directions and Striking from the Right. An accident having two vehicles is described by a combination: for example, one vehicle is described as "Striking from the Right" and the other by "Struck on the Right".

Deformation pattern: Deformation patterns describe each vehicle's General Area of Damage (GAD), Principal Direction of Force (PDOF), and the Specific Longitudinal or Lateral Location of Deformation [25].

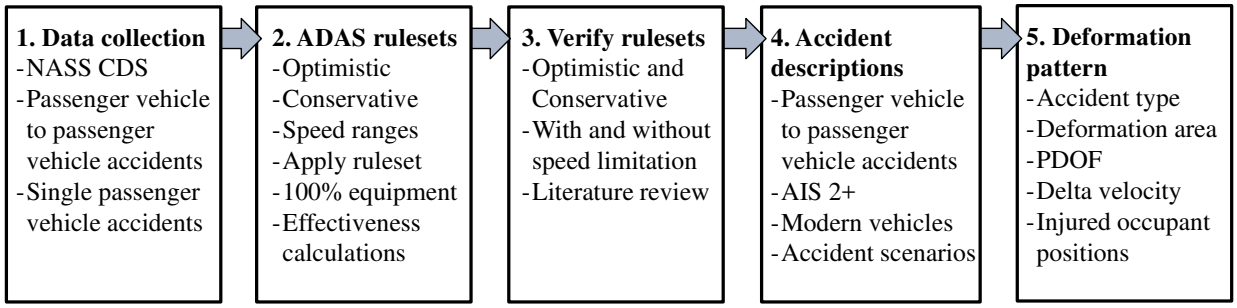

Figure 1. **Description of the five steps used in the study**

1. Data collection

Data regarding passenger vehicle to passenger vehicle accidents and single passenger vehicle accidents were collected from the NASS CDS database, a US nationwide accident data-collection program sponsored by the U.S. Department of Transportation. NASS CDS includes police reported accidents in which at least one involved vehicle is towed away due to damage. Details of around 5 000 accidents are collected every year and consist of accident scene reconstructions, interviews with police and vehicle occupants, medical charts, and detailed information about the vehicles involved. Data are collected on a representative stratified sample of minor, serious, and fatal accidents involving passenger vehicles (passenger cars, pickup trucks, and vans), large trucks, motorcycles, bicyclists, and pedestrians [26].

The data from 1995 to 2015 were extracted on accident level and weighted according to weighting factors provided in the NASS CDS (RATWGT) to compensate for sampling bias. Very heavily weighted accidents (greater than 5000) were removed from the dataset since such cases could influence the results in a disproportionate way [27]. This gave in total 83 038 unweighted and 33 022 646 weighted accidents, of which passenger vehicle to passenger vehicle accidents accounted for 52 462 (63.2%) unweighted and 22 308 978 (67.6%) weighted accidents. Passenger vehicle – Object/Run off/Rollover accounted for 30 576 (36.8%) unweighted and 10 713 668 (32.4%) weighted accidents.

2. ADAS rulesets

Today's known ADASs, 15 in total, were modelled to address a broad range of accident scenarios. Functions were grouped where possible. As an example, Forward Collisions Warning (FCW) and Brake Assist System (BAS) were assumed to be included in the AEB Rear End, and Lane Departure Warning (LDW) included in LKA. A conservative and an optimistic ruleset were created for each ADAS to take into account its limitations and its potentially improved future performance [28]. The conservative ruleset contained limitations which, if present in the accident scenario, would prevent an ADAS from avoiding an accident. These limitations include harsh weather, poor road conditions, including snow and ice on the road, missing lane markings, and unstable vehicle dynamics from skidding or speeding. Each ruleset also has a specific speed range within which the ADAS intervenes. If all the conditions in the rulesets

were met, the accident was removed from the dataset, i.e. the ADAS prevented the accident. If the accident scene included a limitation, that specific accident was not avoided in the conservative estimate.

It was assumed that all passenger vehicles in the dataset were equipped with all the ADASs; the rules did not take into account manual overriding. When calculating the effectiveness of all ADASs together, i.e. the combined effectiveness, an accident was only removed once. For example, a lane change related accident can hypothetically be avoided by both Lane Change Assist (LCA) and Blind Spot Detection (BSD), but it will only be counted once. For combined effectiveness, four groups were created, optimistic and conservative with and without speed limitation. The purpose was to identify what limited the effectiveness of the ADASs, i.e. the speed range or the conservative limitations.

Input for speed range and limitations was derived from Euro NCAP assessment procedures [29-30], Euro NCAP test results [31], driver manuals [32-34] and web pages [35-37]. Each ADAS is listed in Table 1 with a brief description of which accident scenario it addresses. A concise description of how the ADAS rulesets were created using NASS CDS variables [25, 38] can be found in Appendix A and B.

3. Ruleset verification and ADAS effectiveness in avoiding passenger vehicle accidents

Rulesets were verified using reference values obtained from literature based on US data only. This was done to keep the conditions as similar as possible to those in the dataset and to minimize noise factors that could affect the result, such as differences in traffic environment or vehicle fleet. Both retrospective and prospective references were used in the verification process to get a range that could be compared to the conservative and optimistic rulesets. Retrospective studies normally give lower effectiveness estimates because they by design include all ADASs limitations. Table 1 lists the 15 ADASs with descriptions and estimates of their effectiveness in avoiding single passenger vehicle and passenger vehicle to passenger vehicle accidents.

4. Accident description

In this step all passenger vehicle to passenger vehicle AIS2+ accidents were selected from the dataset and described by their accident scenario and general area of deformation, where each accident could either be:

- Front–Front, both vehicles had damage to their fronts, coded blue.
- Front–Rear, one of the vehicles had a damage to the front and the other had a damage to the rear, coded green.
- Front–Side, one of the vehicles had a damage to the front and the other had a side damage to left or right side, coded red.
- Other, the accident could be a Side–Side or Rear–Side impact, or be missing such data, coded brown.

Accident scenario and general area of deformation were then combined to give an overview of the accidents (see Fig 3). This was done for this for four groups A–D:

A. All passenger vehicle to passenger vehicle AIS2+ accidents, N = 14 351 accidents, weighted to 2 005 362 accidents.

B. All passenger vehicle to passenger vehicle AIS2+ accidents with model year 2007 and later, N = 1 391 accidents, weighted to 215 184 accidents.

C. The residual of the conservative ruleset with speed limitation of group B, N = 761 accidents, weighted to 117 463 accidents.

D. The residual of the optimistic ruleset with speed limitation of group B, N = 251 accidents, weighted to 42 407 accidents.

5. Analysis of accident type and deformation pattern of the remaining impacted vehicles

To study the optimistic safety potential of the 15 ADASs, the accidents in group D were analysed by accident type to determine the most frequent ones. For the most frequent accident types, the vehicles with an AIS2+ injured occupant were then described in terms of the deformation pattern, 90% cumulative delta velocity, and injured occupant position.

Table 1.
Investigated ADAS, description and its effectiveness

ADAS	**ADAS description**	**Effectiveness from literature**
Lane Keep Assist (LKA)	Detects if the vehicle is about to drift beyond the edge of the road or into oncoming or overtaking traffic in the adjacent lane and automatically steers back.	1 - 3 % [2, 4-6]
Lane Change Assist (LCA)	Detects when a is car entering the blind spot while the driver is switching lanes.	Not found
Blind Spot Detection (BSD)	Detects vehicles diagonally behind and to the side of the car, typically when the car is being overtaken by other vehicles.	3% - 7% [2, 10]
Advanced Front Lighting System (AFLS)	Includes special auxiliary optical systems within the vehicle's headlamp housings and measures steering angle and vehicle speed and swivels the headlamps accordingly.	2% [2]
Electronic Stability Control (ESC)	Detects loss of steering control and automatically applies the brakes to help "steer" the vehicle where the driver intends to go. This ruleset was only applied to vehicles with model year earlier than 2010 since newer cars are equipped with ESC due to regulation.	7% - 8% [12, 14]
AEB Rear End	Detects stationary vehicles or vehicles being approached while driving ahead in the same lane. The driver is warned and if does not react, braking is activated.	16% - 21% [2-4]
AEB Reversing	Detects the presence of vehicles or obstructions behind and automatically initiates braking or prevents acceleration while reversing.	0.7% - 2% [11,13]
AEB Crossing	Detects crossing vehicles at an intersection. The driver is warned and if does not react, braking is activated.	2% - 8% [17-18]
Emergency Steering (ES)	Steering assistance upon risk of head-on accident: detects oncoming traffic and intervenes by steering and/or braking within the lane to prevent narrow overlap head-on accidents.	Not found
Driver initiated Evasive Steering Assist (ESA)	Detects oncoming traffic and provides assistance by adding steering torque to support the movement of the steering wheel, swerve or evasive action by driver.	Not found
Driver Monitoring System (DMS	Detects impaired and distracted driving and gives appropriate warning and takes effective action.	Not found
Intelligent speed adaption (ISA)	Detects if the vehicle speed exceeds a safe or legally enforced speed.	Not found
Traffic Jam Assist (TJA)	Detects the vehicle in front of your own vehicle and paces it to automatically maintain a steady following distance. In combination with that it also steers to stay within the lane.	Not found
Highway Assist (HA)	Longitudinal and lateral control on divided roads.	Not found
Alcohol interlock	Prevents the driver from driving when affected by alcohol.	Not found

RESULTS

The results were obtained in a three-step approach corresponding to steps three to five outlined in the method. The first step presents the single and combined effectiveness of each ADAS, with and without limitations, to the full dataset, i.e. to all single passenger vehicle and passenger vehicle to passenger vehicle accidents. It also includes a comparison with the effectiveness found in the literature. In the second step, groups A-D are described regarding accident scenario and impact direction. In the third step, group D accidents are analysed regarding deformation pattern, 90% cumulative delta velocity, and injured occupant position.

Ruleset verification and ADAS effectiveness in avoiding passenger vehicle accidents

Effectiveness in avoiding single passenger vehicle and passenger vehicle to passenger vehicle accidents was calculated for each ADAS (Fig. 2) and, additionally, the combined ADAS effectiveness for the four combinations, the optimistic and conservative rulesets each with and without speed limitation, was assessed. For the optimistic ruleset without speed limitation the combined ADAS effectiveness was 97%. The ADASs with the greatest potential to avoid accidents are AEB crossing (38%), Rear End AEB (24%), Electronic Stability Control (27%) and Lane Keep Assist (27%) (see Fig. 2). However, it was found that the NASS CDS variables that were queried in the ruleset for the ESA and DMS systems included many cases with missing information about the steering before the crash and driver state before the crash, 35% and more than 50%, respectively, which rendered the defined rules inapplicable. This might lead to underestimating effectiveness of these two ADASs in our study.

When the speed limitation was applied to the optimistic rulesets, the combined effectiveness was reduced to 88%. The ADASs most affected by the speed limitation were LKA, AEB reversing and TJA, which saw their effectiveness reduced by 40% to 70% (Fig. 2). Speed limitation was not applied to AFLS, ESC, DMS and Alcohol interlock.

The combined effectiveness for the conservative ruleset without speed limitation was 72%, a reduction of 26% compared to the optimistic ruleset without speed limitation. However, the effectiveness of many of the ADASs was reduced by between 40% and 70%. One exception was ISA whose effectiveness was reduced by 95%, dropping from 8% to less than 1% (Fig. 2). The reason for this substantial reduction was that skidding often occurs in combination with speeding, and as the conservative rule includes the limitation to not prevent the accident if skidding occurs, these accidents are no longer avoided.

Finally, for the conservative ruleset with speed limitations, the combined effectiveness decreased to 51%. The ADASs that were most impacted by this were the same as for the optimistic ruleset, i.e. LKA, AEB reversing and TJA, and, in addition, AEB crossing, LCA and ESA also decreased. The effectiveness of these ADASs was reduced by between 40% and 70% (Fig. 2).

Compared to the reference literature, the optimistic effectiveness truly is an optimistic representation. The ADASs whose effectiveness in the literature reaches these levels were BSD and AEB Rear End. On the other hand, the conservative values were truly conservative, underpredicting effectiveness for BSD, AFLS and AEB Rear End. The effectiveness of LKA, ESC and AEB crossing was overpredicted even with the conservative ruleset. For AEB reversing, the values were in line with the literature. For LCA, Emergency steering, Evasive steering assist, DMS, ISA, TJA, HA and Alco interlock, no reference values were found in the literature.

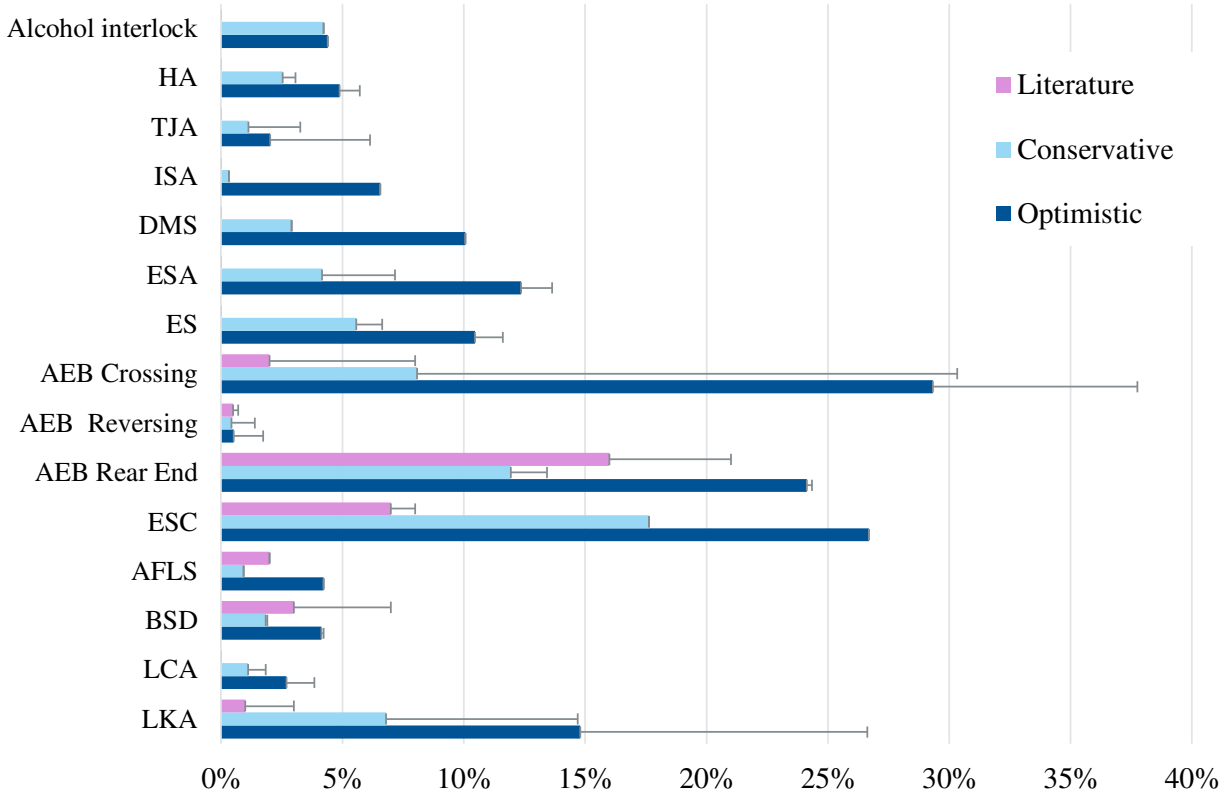

***Figure 2*. ADAS effectiveness and reference values from the literature. For conservative and optimistic rulesets, the error bars represent the effectiveness values without speed limitation. For the Literature the error bars represent the upper and lower values found.**

Accident description

Fig. 3 A) illustrates the breakdown of accident scenarios for group A, all passenger vehicle to passenger vehicle AIS2+. The top four accident scenarios are: Vehicles Turning – Turn Across Path, representing 25%; Intersection Path – Straight Path, 21%; Vehicle turning – Turn into path, 17%; and Same Direction – Rear End, 14%.

Fig. 3 B) illustrates this for group B, which is the same as group A but restricted to modern cars, model year (MY) 2007 or later. The same top four accident scenarios remain but with a small variation in percentage and order: as an example, Same Direction – Rear End increases to 20% and Vehicles Turning – Turn Across Path decreases to 20%.

Fig. 3 C) illustrates this for group C, the remaining modern passenger vehicle to passenger vehicle AIS2+ accidents with the conservative ruleset with speed limitations. The top four accident scenarios remain the same but Same Direction – Rear End accidents were reduced to 14% and Intersection Paths – Straight Path and Vehicle Turning – Turn Across Path increased to 27% and 26%, respectively.

Fig. 3 D) illustrates this for group D, which is as group C but with the optimistic ruleset with speed limitations. Same Direction – Rear End accidents are almost eliminated, and Vehicle Turning – Turn Across Path dominate the data. The new top four scenarios are Vehicle Turning – Turn Across Path, Vehicle Turning – Turn Into Path, Intersection Paths – Straight Paths and Opposite Direction Head. Together, these four accident scenarios represent 93% of all remaining accidents, with Vehicle Turning – Turn Across Path accounting for almost half.

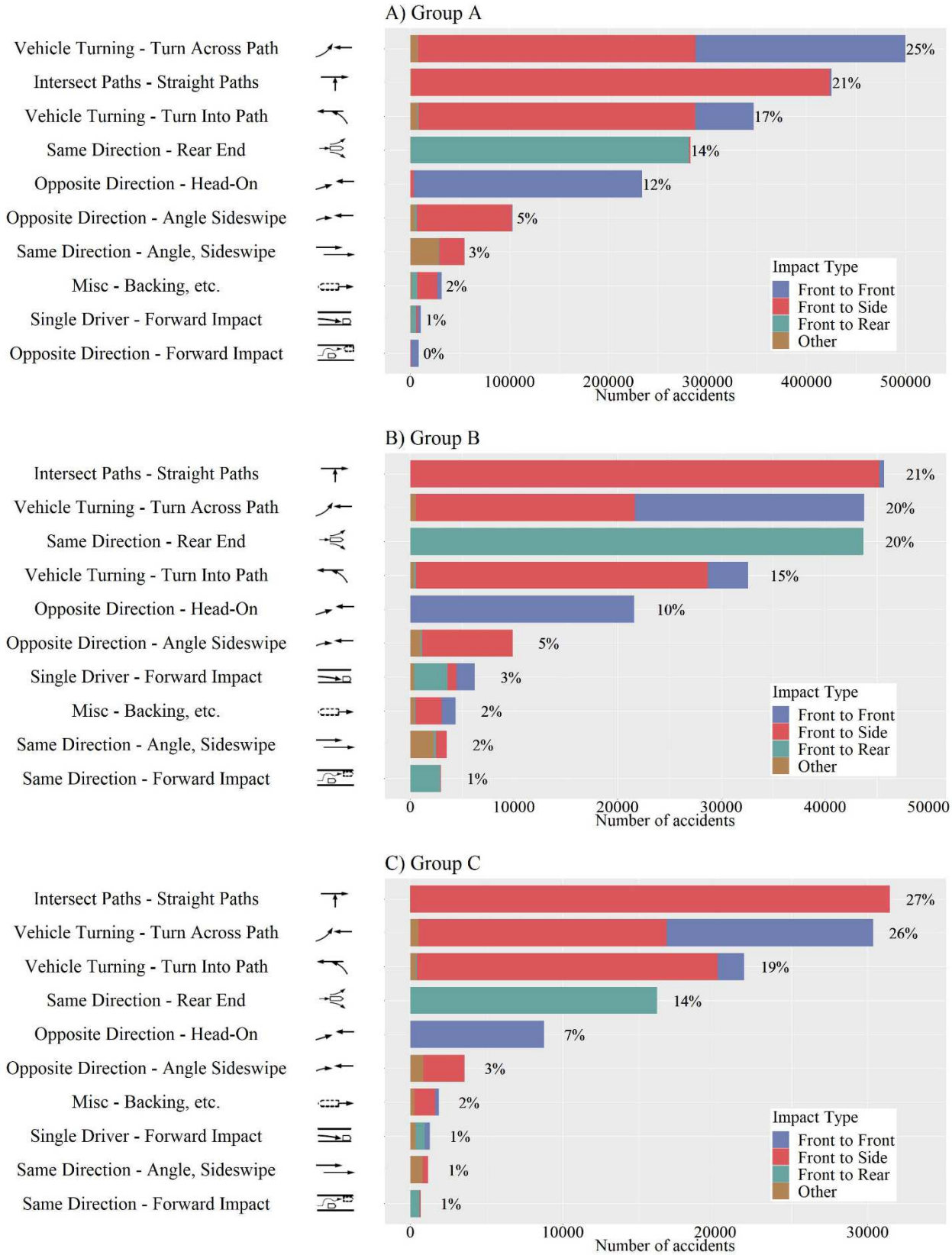
A) Group A
Vehicle Turning - Turn Across Path
Intersect Paths - Straight Paths
Vehicle Turning - Turn Into Path
Same Direction - Rear End
Opposite Direction - Head-On
Opposite Direction - Angle Sideswipe
Same Direction - Angle, Sideswipe
Misc - Backing, etc.
Single Driver - Forward Impact
Opposite Direction - Forward Impact
25%
21%
17%
14%
12%
5%
3%
2%
1%
0%
Impact Type
Front to Front
Front to Side
Front to Rear
Other
0
100000
200000
300000
400000
500000
Number of accidents
B) Group B
Intersect Paths - Straight Paths
Vehicle Turning - Turn Across Path
Same Direction - Rear End
Vehicle Turning - Turn Into Path
Opposite Direction - Head-On
Opposite Direction - Angle Sideswipe
Single Driver - Forward Impact
Misc - Backing, etc.
Same Direction - Angle, Sideswipe
Same Direction - Forward Impact
21%
20%
20%
15%
10%
5%
3%
2%
2%
1%
Impact Type
Front to Front
Front to Side
Front to Rear
Other
0
10000
20000
30000
40000
50000
Number of accidents
C) Group C
Intersect Paths - Straight Paths
Vehicle Turning - Turn Across Path
Vehicle Turning - Turn Into Path
Same Direction - Rear End
Opposite Direction - Head-On
Opposite Direction - Angle Sideswipe
Misc - Backing, etc.
Single Driver - Forward Impact
Same Direction - Angle, Sideswipe
Same Direction - Forward Impact
27%
26%
19%
14%
7%
3%
2%
1%
1%
1%
Impact Type
Front to Front
Front to Side
Front to Rear
Other
0
10000
20000
30000
Number of accidents

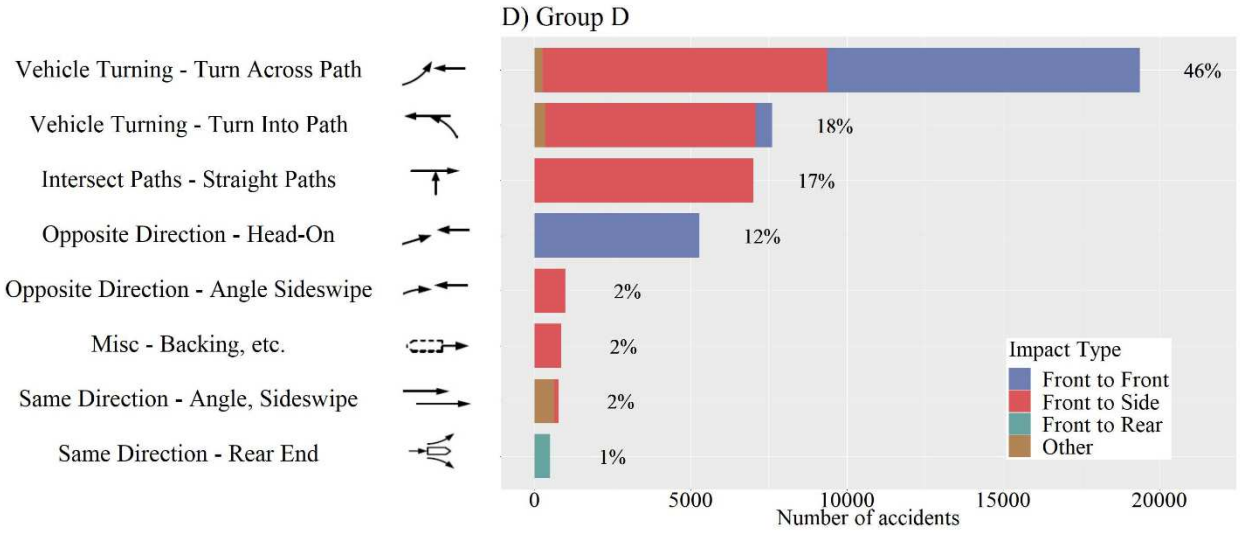

Figure 3. **Top 10 Accident scenarios for AIS2+ passenger vehicle to passenger vehicle accidents with colour code: Blue = Front to Front, Red = Front to Side, Green = Front to Rear, Brown = Other. A) Group A: All passenger vehicle to passenger vehicle AIS2+ accidents, initial population, no ADAS applied, N=2 005 362. B) Group B: All modern passenger vehicle to passenger vehicle AIS2+ accidents, no ADAS applied, N=215 184. C) Group C: Conservative residual with speed limitation of all modern passenger vehicle to passenger vehicle AIS2+ accidents, N=117 463. D) Group D: Optimistic residual with speed limitation of all modern passenger vehicle to passenger vehicle AIS2+ accidents, N=42 407.**

Analysis of accident type and deformation pattern of the remaining impacted vehicles

Accident scenarios are groups of accident types (see above) and breaking down Group D (remaining accidents from the optimistic rule set) further into accident types reveals that four predominate: Head On (12%), Turn Across Path (45%), Turn Into Path Opposite Direction (15%) and Straight Crossing Path (14%). Together these four accident types cover almost 90% of the group D accidents, almost three-quarters of which are intersection accidents.

Even though the intersection accidents are defined by accident type, how the vehicles actually impact each other will vary. To understand the deformation pattern for vehicles that had an AIS2+ injured occupant and were involved in an intersection accident, their CDC code was analysed and, based on their general area of deformation, they were divided into having frontal, left or right impacts. It was found that 54% sustained frontal impacts, 25% left impacts, and 19% right (Fig. 4), while 2% of these accidents were missing this type of information. The frontal, left and right cases were further investigated in four regards: the distribution of longitudinal or lateral location of the deformation; principal direction of force (PDOF); 90% cumulative delta velocity; and position of the injured occupant (Fig. 4).

All vehicles with frontal impacts had a distributed deformation involving 75% or more of the front with PDOF of between 11 and 1 o'clock, with the main part, 60%, at 12 o'clock. The 90% cumulative delta velocity is 39 km/h. 76% of the injured occupants are drivers and 23% are front seat passengers (see Fig. 4, left).

For the vehicles with left-side deformation, all vehicles sustained deformation to the part in front of the occupant compartment, i.e. the left wing, with 19% sustaining deformation to this part only. Just above half of the impacts have a PDOF that is perpendicular to the vehicle with the remainder being at 10 and 11 o'clock. The 90% cumulative delta velocity for the left-side impact is 45 km/h. 87% of the injured occupants are drivers and 5% are front seat passengers (see Fig. 4, mid).

Lastly, of the vehicles with right-side impacts, almost all (97%) had an impact that involved the occupant compartment. Most impacts have a PDOF of 2 o'clock. The 90% cumulative delta velocity for the right-side impact is 33 km/h. Of the injured occupants, 92% are drivers and 6% are front seat passengers (see Fig. 4, right).

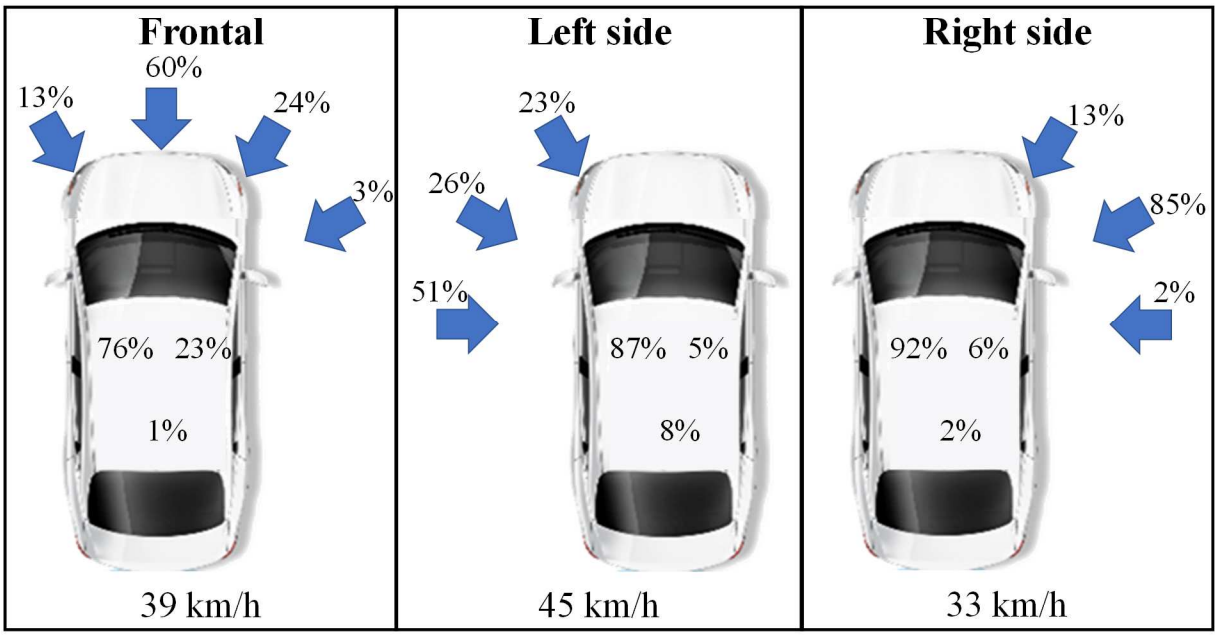

Figure 4. **Longitudinal and lateral deformation area, PDOF, 90% cumulative delta velocity and position of the injured occupant. Left: Frontal impacts. Mid: Left-side impacts. Right: Right-side impacts.**

DISCUSSION

We have presented estimates of the potential for accident reduction of current ADASs, and have included conservative estimates as well as future, optimistic estimates. The use of deterministic rules to create estimates for the effectiveness of an ADAS has a number of limitations but is straight forward, and data from the literature indicate that the calculated values are reasonable and sufficiently accurate for the purpose.

Applying the ADAS rulesets to the AIS2+ passenger vehicle to passenger vehicle accidents shows that to achieve a major change in the accident scenarios, the optimistic ruleset needs to be applied (Fig. 3). With the conservative ruleset, 55% of the accidents would still have occurred, compared to only 20% for the optimistic ruleset, and there is no clear change in the distribution of accident scenarios.

Factors that limit effectiveness

One way to analyse the ADAS effectiveness findings is to figure out what the limiting factor is: the speed range limitation, or the conservative ruleset, in which the limitations stem from either technical limitations of the sensors or vehicle dynamics. It was shown that both factors have a large effect on the total number of accidents avoided, and even more on individual ADAS effectiveness. This indicates that using more generous speed ranges can open the way for improvements in effectiveness, even without technical sensor improvements.

Single ADAS effectiveness and verification of the ADAS rulesets

The four ADASs that address most accidents are ESC, LKA, AEB crossing and Rear End AEB, each having an effectiveness of 25% or above in the most optimistic calculations. ESC has been mandatory in the US since 2010 in passenger vehicles [39] and when comparing accidents involving passenger vehicles older than MY 2010 to those involving newer passenger vehicles, 25% of the older passenger vehicles are coded as skidding prior to the accident compared to 5% of the newer passenger vehicles. This confirms that ESC has a positive effect in reducing accidents. LKA in this study shows an effectiveness of between 7% and 27%. This is much higher than that reported in other studies, which find an effectiveness of 1% to 3% [2, 4-6]. The NASS CDS variable queried here was PREEVENT equals to 10, 11, 12 and 13, which states whether the initial critical pre-crash event was that the passenger vehicle crossed a line (road lane marking) or ran off the road. This seems to be too optimistic a way to simulate LKA, given the findings from previous research, or, alternatively, could be seen as indicating potential for improvement. AEB crossing also gives very optimistic results unless the conservative ruleset with speed limitation is applied, which reduces its effectiveness to a level comparable with findings from the literature. This indicates potential in allowing

higher speeds for the AEB crossing. The Rear End AEB gave a result that is directly comparable with the literature with an effectiveness of between 12% and 24%. However, for many of the ADASs there were no references found in the literature and it is therefore hard to evaluate whether a method with a deterministic ruleset is sufficiently accurate.

Need for a new assessment crash test?
When looking at the remaining intersection accidents, and comparing the observed deformation patterns with regulation and consumer ratings [40-41], we see that the full frontal and side impact conditions are well covered by existing crash tests. It is also noteworthy that angled right-side impacts with the driver getting injured represent 17% of the remaining cases, which is a similar impact condition to that of the upcoming Euro NCAP far side crash test [42].

However, it is important to note that both front and side impacts occur at speeds well below the current regulatory and rating speeds yet still generate AIS2+ injuries in the remaining accidents. This indicates that human variations and sensibility to loadings are not fully covered by the current crash dummies, injury criteria and injury thresholds. The remaining injuries are further analysed in terms of occupant characteristics, accident type and injured body region in [43].

We also see oblique front and side impacts remaining which are not covered in current regulation and consumer crash tests. Evaluating these types of impacts would require vehicle dynamics that are hard to replicate in current crash test labs. It is also likely that current crash dummies (developed for pure frontal or side impact) will not respond in a biofidelic way when the load direction is not purely frontal or from the side. New ways of evaluating crashes are therefore required; an alternative might be to use virtual methods and human body models (HBMs). HBMs are by design more valid for omnidirectional loading than current crash dummies. To take this step would require the development of a new virtual assessment method as proposed by [44-46]. Applying these types of impact conditions would most likely also demonstrate a need for new and improved occupant restraints to protect the occupants. Such improved restraint systems are likely to include both pre-crash and in-crash activated components. For example, motorised belts have the potential to keep occupants in position during lateral pre-crash manoeuvres [47] and inflatable shoulder belts have the potential to avoid the shoulder slipping out of the belt, preventing the head and thorax from impacting various components of the vehicle interior [48].

Limitations
The estimations were based on the NASS CDS database which contains data from accidents occurring in the United States. Accident distributions may therefore not be representative of other areas where the driving environment and vehicle fleet differ. In addition, the database may include some degree of misclassification of the key variables used, or omit pertinent data, or may not include sufficient details to determine the true conditions. One such variable is vehicle speed, which is often not reported. In this study, the speed limit of the location was used if the vehicle speed was not reported. This could be one reason for the relatively low level of effectiveness obtained for Intelligent Speed Adaptation (ISA) as the speed may, in the real event, have been higher.

Using deterministic rulesets has some inherent limitations. In our implementation, an accident can only be prevented or not. In reality, accidents that are not prevented can still be mitigated. When analysing accidents with AIS2+ injuries, this is important because reducing the impact speed might also reduce the injury severity. This cannot be captured in this study.

Another example of an inherent limitation is that an ADAS can intervene in driving through braking or steering, thereby affecting the trajectory of the vehicle, and in consequence may not only avoid accidents but also cause new types of accident or modify deformation distributions; again, this cannot be accounted for in this study.

For some of the level 2 ADASs, drivers need to accept and use the information given by the system and respond appropriately. Drivers may, in fact, switch the system off, not trust it or, in a critical situation, be overwhelmed by the information and not take appropriate action, thus reducing the effectiveness of the ADAS from its potential [49-50]. This can also be seen in the literature, with retrospective analyses often giving a more conservative response than prospective studies. The method used here does not take into account inappropriate driver action.

Implementation rate
This study has assumed that all passenger vehicles in the vehicle fleet are equipped with all ADASs. In reality, it takes a long time for high implementation rates of a given ADAS to be attained [51]. However, the implementation rates of new systems might speed up in the near future through software updates during a vehicle's lifetime. This can be done

if a vehicle is equipped with sensors that recognise the driving conditions and driving environment and has the computing power to take the sensor data and make decisions [52].

CONCLUSIONS

The benefit of ADASs in reducing the number of passenger vehicle accidents is impressive. Still, even with a 100% implementation in passenger vehicles of the systems in use or under development today, accidents will occur. Occupant restraints, therefore, will still be needed to mitigate occupant's injuries into the future.

After applying today's known ADASs, 15 in total, to modern passenger vehicle accidents with severe injury outcome, almost 90% of the remaining accidents were found to fall into four accident types: Head On, Turn Across Path, Turn Into Path Opposite Direction and Straight Crossing Paths. The latter three are intersection accidents and represent as much as three quarters of all remaining accidents.

The detailed analysis of these remaining intersection accidents presented here indicates a need for new oblique impact conditions targeting lower impact speeds. These oblique impacts are a necessary complement to the existing and still relevant frontal and side crash tests to reduce the number of AIS2+ injuries. The impact conditions may be evaluated in virtual assessments with HBM and can guide the development of tomorrow's occupant restraint systems.

ACKNOWLEDGEMENTS

The work was partly carried out at SAFER, the Vehicle and Traffic Safety Centre, at Chalmers, Sweden. We thank Vinnova, the Swedish Energy Agency, the Swedish Transport Administration and the Swedish vehicle industry for funding parts of this work through the strategic vehicle research and innovation (FFI) program for the project 2017-01945 Assessment of Passenger Safety in Future Cars. We also thank Dr Helen East for her help with language revisions.

REFERENCES

[1] Traffic Safety Facts DOT HS 812 494, NHTSA 2018. https://crashstats.nhtsa.dot.gov/Api/Public/ViewPublication/812494

[2] Jermakian, J. 2011. "Crash avoidance potential of four passenger vehicle technologies." Accident Analysis and Prevention 43, 732–740

[3] Cicchino, J.B. 2017. "Effectiveness of forward collision warning and autonomous emergency braking systems in reducing front-to-rear crash rates." Accident Analysis and Prevention 99, 142–152

[4] Kusano, K. and Gabler, H.C. 2015. "Comparison of Expected Crash and Injury Reduction from Production Forward Collision and Lane Departure Warning Systems." Traffic Injury Prevention 16, S109–S114

[5] Cicchino, J.B. 2017. "Effects of lane departure warning on police-reported crash rates." Insurance Institute for Highway Safety

[6] Kusano, K. and Gabler, H.C. 2014. "Potential Occupant Injury Reduction in the U.S. Vehicle Fleet for Lane Departure Warning–Equipped Vehicles in Single-Vehicle Crashes." Traffic Injury Prevention 15, S157–S164

[7] Edwards, M., Nathanson, A. and Wisch, M. 2014. "Estimate of potential benefit for Europe of fitting Autonomous Emergency Braking (AEB) systems for pedestrian protection to passenger cars." Traffic injury prevention 15, pp.S173-82

[8] Rosén, E. 2013. "Autonomous Emergency Braking for Vulnerable Road Users." In Proceedings of IRCOBI conference. Gothenburg, Sweden, pp. 618–627.

[9] Society of Automotive Engineers International. 2016. "Taxonomy and Definitions for Terms Related to On-Road Motor Vehicle Automated Driving Systems." J3016-SEP2016, https://www.sae.org/standards/content/j3016_201609/preview/

[10] Cicchino, J.B. 2017. "Effects of blind spot monitoring systems on police-reported lane-change crashes." Insurance Institute for Highway Safety

[11] Cicchino, J.B. 2017. “Effects of rearview cameras and rear parking sensors on police-reported backing crashes.” Traffic Injury Prevention 18:8, 859-865.

[12] Dang, J.N. 2007. “Statistical Analysis of the Effectiveness of Electronic Stability Control (ESC) Systems.” Evaluation Division; National Center for Statistics and Analysis National Highway Traffic Safety Administration Washington, DC 20590. DOT HS 810 794.

[13] Flannagan, C.A., Kiefer, R.J., Bao, S., LeBlanc, D. J. and Geisler, S.P. 2014. “Reduction of Backing Crashes by Production Rear Vision Camera Systems.” Journal of ergonomics S3:8

[14] Farmer, C.M. 2004. “Effect of electronic stability control on automobile crash risk.” Traffic Injury Prevention 5(4):317–325, doi:10.1080/15389580490896951.

[15] Alvarez, S., Page, Y., Sander, U., Fahrenkrog, F., Helmer, T., Jung, O., Hermitte, T., Düring, M., Döring, S. and op den Camp, O. 2017. ”Prospective Effectiveness Assessment of Adas and Active Safety Systems Via Virtual Simulation: A Review of the Current Practices.” Proceedings of 25th International Technical Conference on the Enhanced Safety of Vehicles (ESV), Detroit, USA.

[16] Sander, U. 2017. “Opportunities and limitations for intersection collision intervention—A study of real world ‘left turn across path’ accidents.” Accident Analysis and Prevention 99, 342–355.

[17] Scanlon, J.M., Sherony, R. and Gabler, H.C. 2017. “Injury mitigation estimates for an intersection driver assistance system in straight crossing path crashes in the United States.” Traffic Injury Prevention 18:S1, 9–17

[18] Scanlon, J. M., Sherony, R. and Gabler, H.C. 2017. “Preliminary Effectiveness Estimates for Intersection Driver Assistance Systems in LTAP/OD Crashes.” Proceedings of Fourth International Symposium on Future Active Safety Technology: Toward zero traffic accidents (FAST-zero), Nara, Japan.

[19] Bahouth, G.T., Murakhovsky, D., Zuhurudeen, M., Asada, H., Fukaya, T., Maeda, M., Liers, H. and Wagner, M. 2017. “Potential Safety Benefit of ADAS Technologies In the US and Germany.” Proceedings of Fourth International Symposium on Future Active Safety Technology: Toward zero traffic accidents (FAST-zero), Nara, Japan.

[20] Puthan, P., Östling, M., Jeppsson, H. and Lubbe, N. 2018. ”Passive Safety Needs for Future Cars: Predicted Car Occupant Fatalities in the USA.” Proceedings of FISITA World Automotive Congress, Chennai, India

[21] Lubbe, L., Jeppsson, H., Ranjbar, A., Fredriksson, J., Bärgman, J. and Östling, M. 2018. ”Predicted road traffic fatalities in Germany: The potential and limitations of vehicle safety technologies from passive safety to highly automated driving.” In Proceedings of IRCOBI conference. Athena, Greece.

[22] Strandroth, J., Sternlund, S., Tingvall, C., Johansson, R. Rizzi, M. and Kullgren, A. 2012. ”A new method to evaluate future impact of vehicle safety technology in Sweden” Stapp Car Crash Journal, Vol. 56, October, pp. 497-509

[23] Strandroth, J. 2015. “Validation of a method to evaluate future impact of road safety interventions, a comparison between fatal passenger car crashes in Sweden 2000 and 2010.” Accident Analysis and Prevention 76. 133–140

[24] U.S. Department of Transportation National Highway Traffic Safety Administration. 2015. “National Automotive Sampling System — Crashworthiness Data System 2014 Coding and Editing Manual.” DOT HS 812 195

[25] SAE J224: Collision Deformation Classification. 2011. SAE International, reaffirmed 2011-05-18, Detroit USA.

[26] National Center for Statistics and Analysis National Highway Traffic Safety Administration. 2012. National Automotive Sampling System (NASS), Washington

[27] Kononen, D.W., Flannagan, C.A.C., and Wang, S.C. 2011. “Identification and validation of a logistic regression model for predicting serious injuries associated with motor vehicle crashes.” Accident Analysis and Prevention 43(1):112–122, doi:10.1016/j.aap.2010.07.018.

[28] Depth-sensing imaging system can peer through fog http://news.mit.edu/2018/depth-sensing-imaging-system-can-peer-through-fog-0321

[29] European New Car Assessment Program (Euro NCAP) Test Protocol – Lane Support Systems Version 2.0.1 November 2017, https://www.euroncap.com/en/for-engineers/protocols/safety-assist/

[30] European New Car Assessment Program (Euro NCAP) Test Protocol – AEB systems Version 2.0.1 November 2017, https://www.euroncap.com/en/for-engineers/protocols/safety-assist/

[31] Test result published at https://www.euroncap.com/en

[32] Mercedes-Benz USA. 2016. "S-Class Operator's Manual." Stuttgart, Germany: Daimler AG

[33] Volvo Car Corporation. 2017. "Volvo XC60 Owner's Manual." Gothenburg, Sweden

[34] Audi. 2016. "Audi Q7 Owner's Manual." Germany

[35] http://www.lexus.com/models/LS/safety

[36] https://www.nissan-global.com/EN/TECHNOLOGY/OVERVIEW/propilot.html

[37] https://www.audi-technology-portal.de/en/electrics-electronics/driver-assistant-systems/audi-q7-turn-assist

[38] Radja, A.G. 2016. "National Automotive Sampling System – Crashworthiness Data System, 2015 Analytical User's Manual." DOT HS 812 321

[39] FMVSS No. 126 Electronic Stability Control Systems

[40] European New Car Assessment Program (Euro NCAP) Assessment protocol – Adult Occupant Protection, Version 8.0.3, October 2018. https://cdn.euroncap.com/media/41746/euro-ncap-assessment-protocol-aop-v803.201811061520101516.pdf

[41] National Highway Traffic Safety Administration. 2012. "Laboratory Test Procedure For New Car Assessment Program Frontal Impact Testing. "

[42] European New Car Assessment Program (Euro NCAP) Far Side Occupant Test and & Assessment Procedure Version 1.1, November 2018. https://cdn.euroncap.com/media/41765/euro-ncap-far-side-test-and-assessment-protocol-v11.201811091249031149.pdf

[43] Östling, M., Puthan, P., Jeppsson, H., Lubbe, N. and Sunnevång, C. 2018. "Future passive safety needs: Predicted injury patterns and possible countermeasures." International Symposium on Sophisticated Car Safety Systems - airbag 2018, Mannheim, 26-28 November 2018

[44] http://osccarproject.eu/

[45] https://projectvirtual.eu/

[46] Ratingen, v. M. 2016. "Saving Lives with Safer Cars: The Past, Present and Future of Consumer Safety Ratings." In Proceedings of IRCOBI conference. Malaga Spanin.

[47] Holt, C., Douglas, E., Graci, V., Seacrist, T., Kerrigan, J., Kent, R., Balasubramanian, S. and Arbogast, K. 2018. "Effect of Countermeasures on Adult Kinematics during Pre-Crash Evasive Swerving." In Proceedings of IRCOBI conference. Athena, Greece.

[48] Edwards, M.A. and Nash, C.E. 2017. "Inflatable Shoulder Belts and Inboard Upper Anchor Shoulder-belt Geometry in Far-side Oblique Impacts." In Proceedings of IRCOBI conference. Antwerp, Belgium.

[49] Kidd, D.G., Cicchino, J.B., Reagan, I.J., and Kerfoot, L.B. 2017. " Driver trust in five driver assistance technologies following real-world use in four production vehicles". Traffic Injury Prevention, 18:sup1, S44-S50, DOI: 10.1080/15389588.2017.1297532

[50] Reagan, I.J. and McCartt, A.T. 2016. "Observed activation status of lane departure warning and forward collision warning of Honda vehicles at dealership service centers." Traffic injury prevention, 17, No 8, 827-832

[51] Highway Loss Data Institute. 2017. "Predicted availability and fitment of safety features on registered vehicles." IIHS Bulletin Vol. 34, No. 28, September

[52] Automotiv World January 2018. Special report:ADAS - a stepping stone to autonomous driving? https://www.automotiveworld.com/?s=ADAS+-+a+stepping+stone+to+autonomous+driving%3F

APPENDIX A

Table 2.
ADAS accident prevention conservative rulesets

ADAS	Ruleset using NASS CDS variables	Ruleset in text
LKA, Lane Keep Assist Typical accident scenarios that can be avoided are running off the road, drifting into oncoming vehicle and side swipes.	BODYTYPE == ("Cars","SUV","Van","Pickup_Truck") PREEVENT == (10,11,12,13) LANES != 99999 WEATHER == 0 or CLIMATE == (16,18,19) PREISTAB == 1 SURCOND != (3,4) PREEVENT !=5 PREEVENT != 6 TRAVELSP>= 60	Passenger vehicle Initial critical pre-crash event No missing lane marks No precipitation No skidding prior to accident No ice or snow on the road Good road condition No speeding Speed > 60 km/h
LCA, Lane Change Assist Typical accident scenarios that can be avoided are side swipes and rear end accidents when changing lane.	BODYTYPE == ("Cars","SUV","Van","Pickup_Truck") PREMOVE == 15 LANES != 99999 WEATHER == 0 or CLIMATE == (16,18,19) PREISTAB == 1 SURCOND != (3,4) PREEVENT !=5 PREEVENT ! =6 speeding TRAVELSP >= 60)	Passenger vehicle Pre-event movement: Changing lane No missing lane marks No precipitation No skidding prior to accident No ice or snow on the road Good road condition No speeding Speed > 60 km/h
BSD, Blind Spot Detection Typical accident scenarios that can be avoided are side swipes and rear end accidents when changing lanes or merging.	BODYTYPE == ("Cars","SUV","Van","Pickup_Truck") PREMOVE == (15,16) WEATHER == 0 or CLIMATE == (16,18,19) PREISTAB = 1 SURCOND != (3,4) PREEVENT != 5 TRAVELSP >= 10	Passenger vehicle Pre-event movement: Changing lane or merging accident No precipitation No skidding prior to accident No ice or snow on the road Good road condition Speed > 10 km/h
AFLS, Advanced Front Lighting System Typical accident scenarios that can be avoided are running off roads in dark conditions	BODYTYPE == ("Cars","SUV","Van","Pickup_Truck") LGTCOND == 2 ALIGNMNT == (2,3) WEATHER == 0 or CLIMATE == (16,18,19) PREISTAB == 1 PREEVENT != 6	Passenger vehicles Light condition equal to dark Curve to right or left No precipitation No skidding prior to accident No speeding
ESC, Electronic Stability Control Typical accident scenarios that can be avoided are skidding accidents.	BODYTYPE == ("Cars","SUV","Van","Pickup_Truck") PREISTAB == (2,3,4) MY =< 2010 SURCOND ! = (3,4) PREEVENT != 5 PREEVENT != 6.	Passenger vehicles Skidding prior to accident Model year earlier than 2010 No ice or snow on the road Good road condition No speeding
AEB Rear End, Autonomous Emergency Braking Rear End	BODYTYPE == ("Cars","SUV","Van","Pickup_Truck") GADEV1 == "R"	Passenger vehicles General Area of Damage equal to rear

Typical accident scenarios that can be avoided are impacts to rear end of vehicle in same lane.	GADEV2 == "F" WEATHER == 0 or CLIMATE == (16,18,19) SURCOND != (3,4) PREEVENT != 5 PREISTAB == 1 (TRAVELSP-TRAVELSP_OPP) <= 70	General Area of Damage equal to front No precipitation No ice or snow on the road Good road condition No skidding prior to accident Relative speed < 70 km/h
AEB reversing, Autonomous Emergency Braking Reversing Typical accident scenarios that can be avoided are impacts to another vehicle when reversing.	BODYTYPE == ("Cars","SUV","Van","Pickup_Truck") ACCTYPE == (92, 93, 98, 99) WEATHER == 0 or CLIMATE == (16,18,19) TRAVELSP<= 30	Passenger vehicles Backing accidents No precipitation Speed < 30 km/h
AEB Crossing, Autonomous Emergency Braking Crossing Typical accident scenarios that can be avoided are crossing and turning at intersections.	BODYTYPE == ("Cars","SUV","Van","Pickup_Truck") PREEVENT == (15,16,17,65,66,67,68) WEATHER == 0 or CLIMATE == (16,18,19) SURCOND != (3,4) PREEVENT !=5 PREISTAB == 1 TRAVELSP <= 30.	Passenger vehicles Initial critical pre-accident event crossing scenarios No precipitation No ice or snow on the road Good road condition No skidding prior to accident Speed < 30 km/h
Emergency Steering (ES) upon risk of head-on accident Typical accident scenarios that can be avoided are head on scenarios where the driver is not performing any maneuverer.	BODYTYPE == ("Cars","SUV","Van","Pickup_Truck") GADEV1 == "F" ? SHL == (“L”,”R”) MANEUVER != (6-9,11,12) WEATHER == 0 or CLIMATE == (16,18,19) SURCOND != (3,4) PREEVENT != 5 PREISTAB == 1 TRAVELSP <= 100 & TRAVELSP >= 40	Passenger vehicles General Area of Damage equal to front Specific longitudinal or lateral deformation location equals to left or right Driver is not initiating a maneuverer No precipitation No ice or snow on the road Good road condition Not skidding prior to accident 40km/h < Speed < 100 km/h
Driver initiated Evasive steering assist Typical accident scenarios that can be avoided are head on scenarios where the driver is not steering enough to avoid the accident.	BODYTYPE == ("Cars","SUV","Van","Pickup_Truck") GADEV1 == "F" MANEUVER == (6-9,11,12 WEATHER == 0 or CLIMATE == (16,18,19) SURCOND != (3,4) PREEVENT != 5 PREISTAB == 1 TRAVELSP <= 70 & TRAVELSP >= 20	Passenger vehicles General Area of Damage first vehicle equal to front Driver is initiating a manoeuvre No precipitation No ice or snow on the road Good road condition No skidding prior to accident 20km/h < Speed < 70 km/h
DMS, Driver drowsiness/distraction monitoring	BODYTYPE == ("Cars","SUV","Van","Pickup_Truck") DRIVDIST == 11 PREEVENT ! = 6	Passenger vehicles Driver sleepy No speeding

All types of accidents where driver is distracted can be addressed.		
ISA, Intelligent Speed Adaptation Accidents where the cause is speeding can be addressed	BODYTYPE == ("Cars","SUV","Van","Pickup_Truck") PREEVENT == 6 WEATHER == 0 or CLIMATE == (16,18,19) SURCOND != (3,4) PREEVENT !=5 PREISTAB == 1	Passenger vehicles Speeding accident No precipitation No ice or snow on the road Good road condition No skidding prior to accident
TJA, Traffic jam assist Typical accident scenarios that can be avoided are low speed side swipes and rear end impacts.	BODYTYPE == ("Cars","SUV","Van","Pickup_Truck") GADEV1 == ("F", "L", "R") TRAFFLOW == (1, 2, 3) RELINTER == (0, 3) WEATHER == 0 or CLIMATE == (16,18,19) SURCOND != (3,4) PREEVENT != 5 PREISTAB == 1 TRAVELSP <= 65	Passenger vehicles General Area of Damage first vehicle equal to front, left or right Divided road with and without barrier Traffic way not related to junction No precipitation No ice or snow on the road Good road condition No skidding prior to accident Speed < 65 km/h
HA, Highway Assist Typical accident scenarios that can be avoided are high speed side swipes and rear end impacts on highways.	BODYTYPE == ("Cars","SUV","Van","Pickup_Truck") GADEV1 == ("F", "L", "R") SPLIMIT > 50mph (80km/h) RELINTER == (0, 3) TRAFFLOW== (1,2,3) WEATHER == 0 or CLIMATE == (16,18,19) SURCOND != (3,4) PREEVENT !=5 PREISTAB == 1 PREEVENT != 6 TRAVELSP >= 80	Passenger vehicles General Area of Damage first vehicle equal to front, left or right Speed limit > 50 mph Traffic way not related to junction Divided road with or without barrier No precipitation No ice or snow on the road Good road condition No skidding prior to accident No speeding Speed > 80 km/h
Alcohol interlock Prevents the driver from driving when affected by alcohol.	BODYTYPE == ("Cars","SUV","Van","Pickup_Truck") DRINKING == 1 ALCTEST > 8 & ALCTEST< 200	Passenger vehicles Police reported alcohol presence Alcohol test result

APPENDIX B

Table 3.
ADAS accident prevention optimistic rulesets

ADAS	Ruleset using NASS CDS variables	Ruleset in text
LKA, Lane Keep Assist Typical accident scenarios that can be avoided are running off the road, drifting into oncoming vehicle and side swipes.	BODYTYPE == ("Cars","SUV","Van","Pickup_Truck") PREEVENT == (10,11,12,13) TRAVELSP>= 60	Passenger vehicle Initial critical pre-crash event Speed > 60 km/h
LCA, Lane Change Assist Typical accident scenarios that can be avoided are side swipes and rear end accidents when changing lane.	BODYTYPE == ("Cars","SUV","Van","Pickup_Truck") PREMOVE == 15 TRAVELSP >= 60)	Passenger vehicle Pre-event movement Changing lane Speed > 60 km/h
BSD, Blind Spot Detection Typical accident scenarios that can be avoided are side swipes and rear end accidents when changing lanes or merging.	BODYTYPE == ("Cars","SUV","Van","Pickup_Truck") PREMOVE == (15,16) TRAVELSP >= 10	Passenger vehicle Pre-event movement Changing lane change or merging accident Speed > 10 km/h
AFLS, Advanced Front Lighting System Typical accident scenarios that can be avoided are running off roads in dark conditions	BODYTYPE == ("Cars","SUV","Van","Pickup_Truck") LGTCOND == 2 ALIGNMNT == (2,3)	Passenger vehicles Light condition equal to dark Curve to right or left
ESC, Electronic Stability Control Typical accident scenarios that can be avoided are skidding accidents.	BODYTYPE == ("Cars","SUV","Van","Pickup_Truck") PREISTAB == (2,3,4) MY =< 2010	Passenger vehicles Skidding prior to accident Model year earlier than 2010
AEB Rear End, Autonomous Emergency Braking Rear End	BODYTYPE == ("Cars","SUV","Van","Pickup_Truck") GADEV1 == "R" GADEV2 == "F"	Passenger vehicles General Area of Damage equal to rear

Typical accident scenarios that can be avoided are impacts to rear end of vehicle in same lane.	(TRAVELSP-TRAVELSP_OPP) <= 100	General Area of Damage equal to front Relative speed < 100 km/h
AEB reversing, Autonomous Emergency Braking Reversing Typical accident scenarios that can be avoided are impacts to another vehicle when reversing.	BODYTYPE == ("Cars","SUV","Van","Pickup_Truck") ACCTYPE == (92, 93, 98, 99) TRAVELSP<= 30	Passenger vehicles Backing accidents Speed < 30 km/h
AEB Crossing, Autonomous Emergency Braking Crossing Typical accident scenarios that can be avoided are crossing and turning at intersections.	BODYTYPE == ("Cars","SUV","Van","Pickup_Truck") PREEVENT == (15,16,17,65,66,67,68) TRAVELSP <= 60	Passenger vehicles Initial critical pre-accident event crossing scenarios Speed < 60 km/h
Emergency Steering (ES) upon risk of head-on accident Typical accident scenarios that can be avoided are head on scenarios where the driver is not performing any maneuverer.	BODYTYPE == ("Cars","SUV","Van","Pickup_Truck") GADEV1 == "F" ? SHL == (“L”,”R”) MANEUVER != (6-9,11,12) TRAVELSP <= 140 & TRAVELSP >= 40	Passenger vehicles General Area of Damage equal to front Specific longitudinal or lateral deformation location equals to left or right Driver is not initiating a manoeuvre 40km/h < Speed < 140 km/h
Driver initiated Evasive steering assist Typical accident scenarios that can be avoided are head on scenarios where the driver is not steering enough to avoid the accident.	BODYTYPE == ("Cars","SUV","Van","Pickup_Truck") GADEV1 == "F" MANEUVER == (6-9,11,12 TRAVELSP <= 100 & TRAVELSP >= 20	Passenger vehicles General Area of Damage first vehicle equal to front Driver is initiating a manoeuvre 20km/h < Speed < 100 km/h
DMS, Driver drowsiness/distraction monitoring All types of accidents where driver is distracted can be addressed.	BODYTYPE == ("Cars","SUV","Van","Pickup_Truck") DRIVDIST == 3-8,11,12,13	Passenger vehicles Driver distraction

ISA, Intelligent Speed Adaptation Accidents where the cause is speeding can be addressed	BODYTYPE == ("Cars","SUV","Van","Pickup_Truck") PREEVENT == 6	Passenger vehicles Speeding accident
TJA, Traffic jam assist Typical accident scenarios that can be avoided are low speed side swipes and rear end impacts.	BODYTYPE == ("Cars","SUV","Van","Pickup_Truck") GADEV1 == ("F", "L", "R") TRAFFLOW == (1, 2, 3) RELINTER == (0, 3) TRAVELSP <= 65	Passenger vehicles General Area of Damage first vehicle equal to front, left or right Divided road with and without barrier Traffic way not related to junction Speed < 65 km/h
HA, Highway Assist Typical accident scenarios that can be avoided are high speed side swipes and rear end impacts on highways.	BODYTYPE == ("Cars","SUV","Van","Pickup_Truck") GADEV1 == ("F", "L", "R") SPLIMIT > 50mph (80km/h) RELINTER == (0, 3) TRAFFLOW== (1,2,3) TRAVELSP >= 80	Passenger vehicles General Area of Damage first vehicle equal to front, left or right Speed limit > 50 mph Traffic way not related to junction Divided road with or without barrier Speed > 80 km/h
Alcohol interlock Prevents the driver from driving when affected by alcohol.	BODYTYPE == ("Cars","SUV","Van","Pickup_Truck") DRINKING == 1 ALCTEST > 8 & ALCTEST< 200	Passenger vehicles Police reported alcohol presence Alcohol test result

A NEW METHODOLOGY TO MODEL DRIVER BEHAVIOUR ACCOUNTNG FOR THE VARIATION IN DRIVING MANNER USING NATURALISTIC DRIVING DATA

Niels, Ferson
Edoardo, Pizzigoni
Florent, Garnier-Follet
Toyota Motor Europe NV/SA
Belgium

Clément, Val
Centre Européen d'Etudes sur la Sécurité et l'Analyse des Risques (CEESAR)
France

Paper Number 19-0092

ABSTRACT

Our aim is to develop Advanced Driving Assistance Systems (ADAS) which are suitable for all customers in all driving conditions. To achieve this goal, a new methodology was developed to characterize driving manner in each scenario by a mathematical model based on Naturalistic Driving Study (NDS) data. To represent the variety of driving manners, a new parameter named "aggressiveness" is introduced. By adjusting "aggressiveness", the ADAS' behaviour can be modified, matching natural driving behaviour in a wide range of operating conditions. This methodology is applied to model when drivers start to brake when approaching another vehicle that's driving in the same lane. This model can be used to detect when a driver is not assessing a threat correctly by comparing his instantaneous driving behaviour with his normal driving behaviour.

INTRODUCTION

Background

Driver behaviour models can be grouped in 2 types of models: "continuous" and "psychophysical" models. Continuous models [1, 2, 3] are effective in representing a realistic general motion of a vehicle. This makes them suitable for microscopic simulations of traffic. Unfortunately these models cannot represent a different driving style other than the one used to fit them. Psychophysical models [1, 4, 5] are based on the biological sensory perception of humans. They assume humans will react when the sensory input is above their perceptual threshold. These thresholds vary strongly among drivers and among driving conditions. None of the existing psychophysical models takes into account the influence of the driving conditions and the variation in driving behaviour between drivers. The Risk Perception (RP) [10] model is an example of a psychophysical model. It is a model for the relative distance when drivers start to brake when approaching a vehicle. The RP model estimates the influence of the driving conditions. However it doesn't take into consideration the variation of driving manners.

Target & concept

The target of this study is to develop a methodology to create driver behaviour models taking into consideration the influence of the driving conditions (e.g. driving speed) on the driving behaviour (e.g. relative distance at brake start) and the variation in driving manner. The driving manner is assumed to be the variation in driving behaviour that is not caused by the driving conditions. First the parameters representing the driving conditions and the driving behaviour are extracted from NDS data. Next the correlations between the driving conditions and the driving behaviour are identified. Finally the influence of the driving manner on the correlations between the driving conditions and the driving behaviour is modelled.

METHODOLOGY AND MODEL DESCRIPTION

The below described methodology can be applied to all driving scenes. In this paper we explain how this method was applied to model when drivers start to brake when they approach a slower driving vehicle.

Driving scene extraction from naturalistic driving study data

The data collected in France within EUROFOT FP7 EU project [6] was used to create this driving behaviour model. EUROFOT was a Naturalistic Driving Study (NDS): ordinary drivers' own vehicles were instrumented,

and their behaviour continuously recorded during their usual trips. The French dataset was recorded between April 2010 and May 2012. It consists of 581 000 km / 13 400 hours of data. 35 private vehicles (14 Renault Clio III and 21 Renault Laguna III) were instrumented with a CAN / GPS data logger (CTAG data logger 2) and a millimeter wave long range radar (TRW AC20). Their owners lived in the West-Paris area. 5 additional vehicles (2 Renault Clio III and 3 Renault Laguna III) were instrumented with a 4-channel video logger, a Mobileye smart camera, and a Smarteye driver monitoring system. Each participant drove one of those vehicles during 3 two-weeks periods, which amounts to 15% of the dataset collected with this higher instrumentation level. The ego vehicle speed and brake activation were collected on the vehicles' CAN network, while the radar allowed measuring the relative speed, the longitudinal distance and lateral overlap to a target vehicle (Figure 1Figure 1).

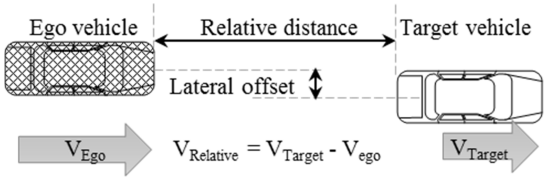

Figure 1. Recorded parameters.

To limit the events only to approaching another vehicle scenario, events with a lateral offset and a relative speed not exceeding a certain criteria, a positive target vehicle speed and a relative distance below 80m at the start of braking were selected. Lateral offset was calculated by compensating road curvature (estimated from yaw rate measurement). With these criteria more than 1 brake event per 3 kilometers of collected data was detected with a distribution as shown in Figure 2. Due to limitations of the allowed data to be extracted from the database, not all detected braking scenes could be extracted.

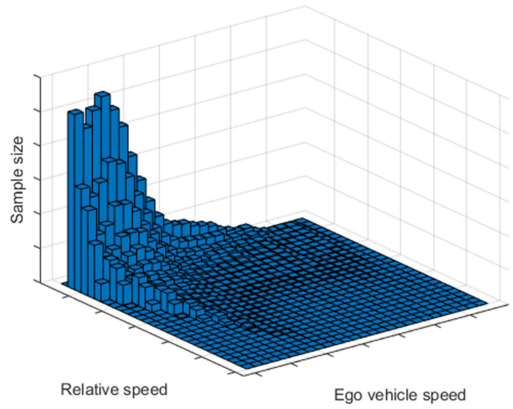

Figure 2. Distribution of the detected braking scenes in EuroFOT database.

For the conditions where a very high amount of brake events are detected, a limited amount of samples was randomly selected for extraction. For conditions with a limited amount of detected brake events, all detected samples were selected for extraction. This resulted in a total of more than 80 000 selected brake events with a distribution as shown in Figure 3.

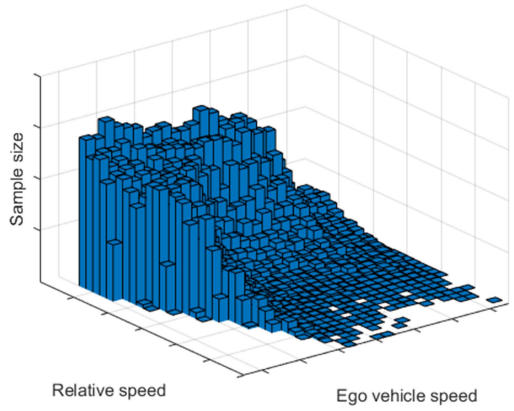

Figure 3. Distribution of the selected braking scenes.

Correlations between driving conditions, driving behaviour and driving manners.

First the correlations between the driving conditions and the driving behaviour are identified. The relative speed and the ego vehicle speed at the start of braking are selected as driving condition parameters because they showed the highest correlation. The relative distance at brake start is selected as the primary parameter representing the driver behaviour. The driving manner is the variation in relative distance when drivers start to brake for constant driving conditions. To visualise the correlations between the driving conditions and the driving behaviour, all brake applications are grouped in bins with a similar driving condition (relative speed and ego vehicle speed). For each bin the distribution of the percentiles of the relative distance at brake start is calculated. The results of the 50th percentile can be seen in Figure 4.

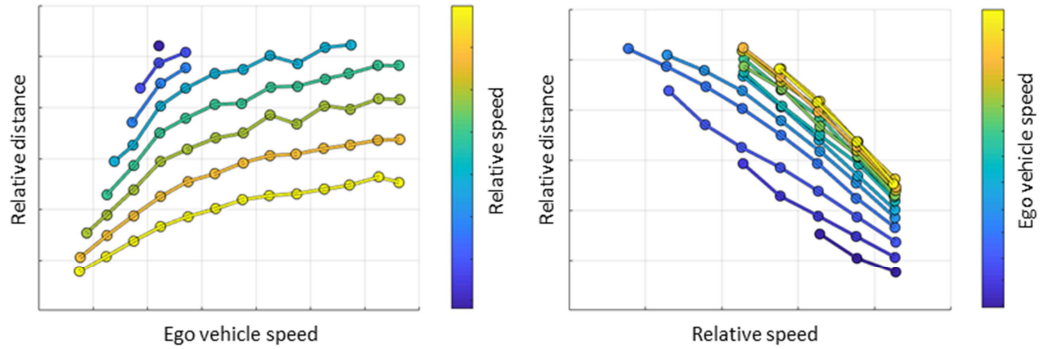

Figure 4. Relative distance at brake start in function of the relative speed and ego vehicle speed at brake start.

For each percentile there is a linear influence of the relative speed and a quadratic influence of the ego vehicle speed on the relative distance. The model for the relative distance when drivers start to brake can therefore be written in as a bi-variable polynomial of second order in function of the relative speed and ego vehicle speed as described in Equation 1.

$$\boldsymbol{D_{rel} = p_{00} + p_{01} \times V_{rel} + p_{10} \times V_{ego} + p_{11} \times V_{ego} \times V_{rel} + p_{20} \times V_{ego}^2} \quad \textit{(Equation 1)}$$

p_{00}, p_{01}, p_{10}, p_{11} and p_{20} are fitting parameters that vary in function of the driving manner. Equation 1 can be written as the product of 2 matrices with all fitting parameters combined in one matrix (Equation 2).

$$\boldsymbol{D_{rel} = [p_{00} \quad p_{01} \quad p_{10} \quad p_{11} \quad p_{20}\,] \times \left[1 \quad V_{rel} \quad V_{Ego} \quad V_{Rel} \times V_{Ego} \quad V_{ego}^2\right]' = P \times V'} \quad \textit{(Equation 2)}$$

In Figure 5 the surface is the relative distance calculated according to Equation 2 with the parameter matrix P optimised to fit the 50th percentile of the relative distance at brake start extracted from EuroFOT. The points are the 50th percentile of the relative distance at brake start extracted from EuroFOT.

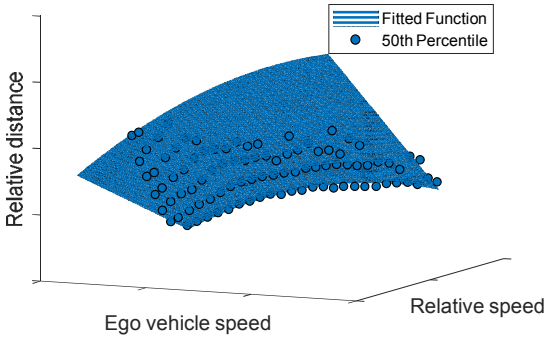

Figure 5. Comparison of 50th percentile relative distance at brake start from equation 2 and from NDS data.

To include the influence of the driving manner, the fitting parameters are calculated for every percentile of relative distance from the 5th until the 80th percentile. This range of percentiles was selected because the fitting accuracy reduces significantly when going outside of this range. To simplify the driver behaviour model it was assumed that the fitting parameters can be estimated in function of the distance percentile by 1st order linear regression (Figure 6).

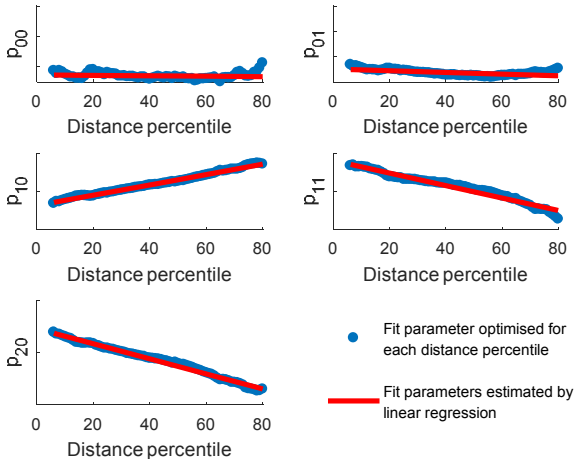

Figure 6. Fitting parameters for the range of 5th to 80th percentile of the relative distance.

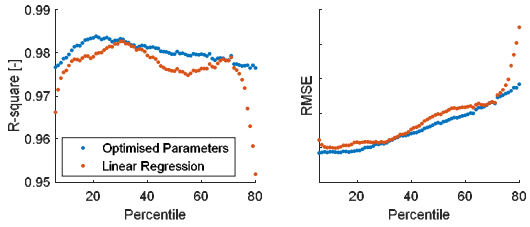

Figure 7. Fitting accuracy for the range of 5th to 80th percentile of the relative distance.

The fitting accuracy of the parameters estimated by linear regression is comparable to the accuracy of the optimised parameters for each percentile (Figure 7), therefore the assumption may be judged as reasonable. The model for the relative distance can be updated (Equation 3).

$$\boldsymbol{D_{rel} = (P_a \times Distance\ Percentile + P_b) \times V'} \quad \textit{(Equation 3)}$$

The distance percentile can be calculated by Equation 4.

$$\boldsymbol{Distance\ Percentile = \frac{D_{rel} - P_b \times V'}{P_a \times V'}} \quad \textit{(Equation 4)}$$

Quantifying driving manner

The distance percentile is calculated for all brake events extracted from the EuroFOT database with Equation 4. The probability density distribution and the cumulative probability distribution of the distance percentiles are shown in Figure 8. The calculated distance percentiles have values outside the range of zero to one hundred. Two reasons can be identified for this: the first one is that the fitting by Equation 2 is not 100% accurate (Figure 7). The second reason is the error caused by estimating the fitting parameters by linear regression in function of the distance percentile.

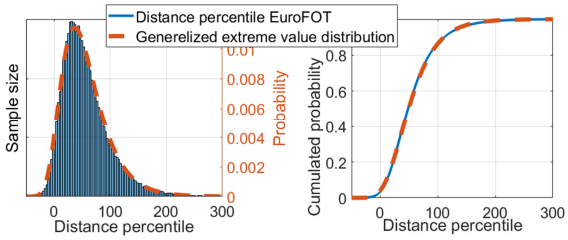

Figure 8. Distribution and cumulated probability of the distance percentile of all brake events.

A new parameter named *"Aggressiveness"* is introduced to quantify driver manner. Aggressiveness is defined as one minus the cumulated probability of the distance percentile when drivers start to brake. E.g. a brake application with aggressiveness 60%, is a brake application that starts at a relative distance that is the 40th percentile of the relative distance of all brake applications with similar driving conditions.

The distribution of the calculated distance percentiles is a generalized extreme value distribution (Figure 8). The aggressiveness can be calculated using the formula for the cumulated probability of the generalized extreme value distribution (Equation 5). The parameters k, μ and σ are calculated for the aggressiveness values calculated from EuroFOT data.

$$Aggressiveness = 1 - e^{-\left[1+k\times\frac{Distance\ Percentile-\mu}{\sigma}\right]^{-1/k}} \qquad \textit{(Equation 5)}$$

VALIDATION OF THE DRIVER BEHAVIOUR MODEL

Validation by EuroFOT data

The purpose of the driver behaviour model is to estimate the driver aggressiveness in function of the driving conditions and driving manner. If the influence of the driving conditions is correctly estimated, the distribution of the aggressiveness will be constant in function of the driving conditions. The distribution of the aggressiveness in function of the driving conditions for the brake scenes extracted from the EuroFOT database is shown in Figure 9. It can be noticed that the distribution of the aggressiveness is constant in function of the deceleration of the target vehicle although the deceleration of the target vehicle is not used as an input parameter to calculate the aggressiveness; we can therefore conclude that the target vehicle acceleration doesn't influence the relative distance at which drivers start to brake.

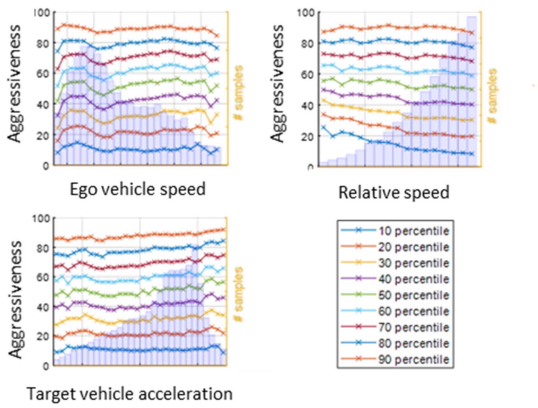

Figure 9. Distribution of aggressiveness in function of the driving conditions for all brake events extracted

from EuroFOT database.

Validation by UDRIVE data

The driver behaviour model for brake start timing was also validated using the UDRIVE [9] passenger cars database. This database was constituted during the UDRIVE FP7 EU project which also followed the Naturalistic Driving methodology. Passenger cars data was collected in France, Netherlands, Germany, Poland and UK. This dataset consists of 1 994 000 km / 43300 hours of data collected by 122 vehicles (Renault Clio III, IV and Renault Megane III) / 196 drivers. One significant difference between UDRIVE and EuroFOT is the sensor used to measure relative speed and distance to the target vehicle (Mobile Eye Q2 camera for UDRIVE; TRW AC20 radar for EuroFOT). The same method used for the EuroFOT dataset was implemented to extract 691,053 brake events from UDRIVE database The aggressiveness of each brake application is calculated using Equation 4 and 5, with all parameters optimised for EuroFOT data. For UDRIVE the distribution of the aggressiveness in function of the driving conditions is slightly less constant as for EuroFOT (Figure 10). There is a small influence of the relative speed and the target vehicle acceleration on the aggressiveness. Despite of this we can conclude that the driver behaviour model created by EuroFOT data is valid for UDRIVE.

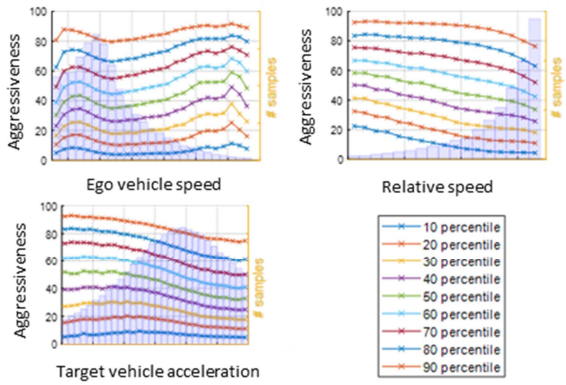

Figure 10. Distribution of aggressiveness in function of the driving conditions for all brake events extracted from UDRIVE database.

RESULTS

Comparison with other models for brake start timing

The same method was used to validate the accuracy of three main models for brake start timing; Time to Collision (TTC), Time Head-Way (THW) and RP (Figure 11). For each percentile of THW and TTC there is a significant influence of the ego speed and relative speed. The RP model can best estimate the influence of the driving conditions around its 50th percentile, however for other percentiles the RP model is less constant in function of the driving conditions. This demonstrates that among these models the aggressiveness model most accurately estimates the influence of the driving conditions on the driving behaviour for the complete range of driving manners.

$$TTC = -\frac{D_{rel}}{V_{rel}} \qquad THW = \frac{D_{rel}}{V_{Ego}} \qquad RP = \frac{V_{ego} - 4 \times V_{rel}}{D_{rel}}$$

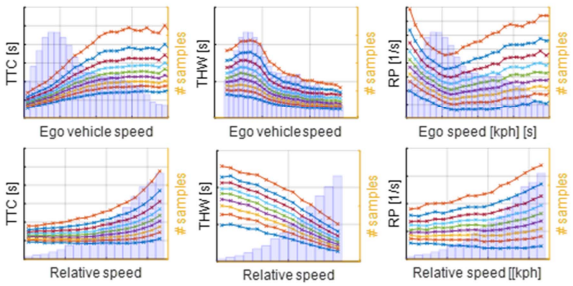

Figure 11. 10 to 90th percentile distribution of TTC. THW and RP in function of the driving conditions.

Understanding the brake start timing model

The relative distance and the TTC at brake start are plotted for an aggressiveness value of 50 in Figure 12 which shows two trends. The first one is that TTC at brake start increases when the ego vehicle speed increases. This indicates that drivers prefer to take less risk when the driving speed increases. Similar behaviour has been reported by Kusano et al. in 2014 [10]. The second trend is that the TTC at brake start reduces when the relative speed to the target vehicle increases. This is confirming that the drivers are perceiving relative speed by visual looming cues [5, 8].

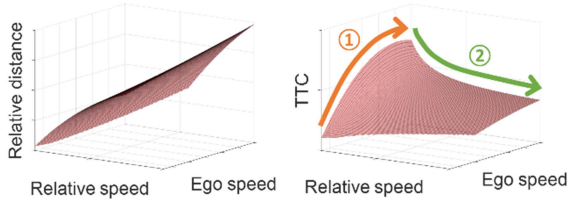

Figure 12. 50th percentile of relative distance and TTC at brake start.

CONCLUSION AND APPLICATIONS

Conclusion

A new methodology is proposed to create driver behaviour models from NDS taking into consideration the influence of the driving conditions on the driving behaviour for all variations of driving manners. A new parameter named “aggressiveness” is introduced to quantify driving manner.

Applications

The brake start timing model can be implemented in a driver monitoring system. It can be used to detect when a driver is not recognizing a threat correctly by comparing his instantaneous driving behaviour with his average behaviour. When the driver’s instantaneous aggressiveness is significantly higher than his average aggressiveness and he didn’t react to reduce the criticality, it is likely the driver didn’t correctly assess the criticality of the scenario. When used to adapt the activation timing of a forward collision warning (FCW) system, two benefits are expected compared to an FCW with constant activation timing. The first benefit is that for more aggressive drivers the frequency of unnecessary FCW activation will reduce and thereby increase customers’ trust and acceptance of the FCW. This is assumed to result in a more efficient reaction of the drivers to the forward collision warning and therefore increase the accident reduction performance. A second benefit is that for less aggressive drivers the FCW can activate earlier compared to the standard timing without increasing the unnecessary activation rate. This will allow the driver more time to react to the warning and thus result in an increase of the accident reduction performance.

REFERENCES

[1] Brackstone, Mark, and Mike McDonald. "Car-following: a historical review." *Transportation Research Part F: Traffic Psychology and Behaviour* 2.4 (1999): 181-196.

[2] Helly, Walter. "Simulation of bottlenecks in single-lane traffic flow." (1959).

[3] Treiber, Martin, Ansgar Hennecke, and Dirk Helbing. "Congested traffic states in empirical observations and microscopic simulations." *Physical review E* 62.2 (2000): 1805.

[4] Fancher, Paul, and Zevi Bareket. "Evolving model for studying driver-vehicle system performance in longitudinal control of headway." *Transportation Research Record: Journal of the Transportation Research Board* 1631 (1998): 13-19.

[5] Hoffmann, Errol R., and Rudolf G. Mortimer. "Scaling of relative velocity between vehicles." *Accident Analysis & Prevention* 28.4 (1996): 415-421.

[6] http://www.eurofot-ip.eu/download/final_event_PDFs/eurofot_session_63_reakka_krishnakumar_v5.pdf, Extracted on 19/04/2018

[7] Kusano KD, Montgomery J, Gabler HC, Age and Gender Differences in Time to Collision at Braking From the 100-Car Naturalistic Driving Study, Traffic Injury Prevention, 2014

[8] Markkula G, Engstrom J, Lodin J, Bargman J, Victor T, A farewell to brake reaction times? Kinematics-dependent brake response in naturalistic rear-end emergencies, Accident analysis & prevention volume 95, part A, October 2016, pages 209-226

[9] http://www.udrive.eu/index.php/about-udrive, Extracted on 19/04/2018
[10] Kondoh, T., et al. 2008. “Identification of Visual Cues and Quantification of Drivers' Perception of Proximity Risk to the Lead Vehicle in Car-Following Situations.” J. Mech. Sys. Transportation and Logistics 1, No. 2, 170-180

DRIVER AIRBAG DESIGN TO MITIGATE NECK AND CHEST INJURIES FOR US-NCAP AND OPTIMIZATION METHODS WITH A DYNAMIC META MODEL

Wonsuk Park
General Motors
USA

Paper Number 19-0094

ABSTRACT

The frontal airbag in a vehicle is considered supplemental to the safety belt restraint system and is important in lowering measured injury assessment values for Anthropomorphic Test Devices (ATD) during vehicle crash testing. The probability of neck and chest injuries is an important factor for a vehicle's performance rating under the United States-New Car Assessment Program (US-NCAP) protocol. A shorter lower tether was incorporated into the driver frontal airbag (DAB) to mitigate chest deformation injury, however higher neck injuries were observed with this change.
The purpose of this study is to identify the main factors influencing neck injury assessment values through the use of Design Of Experiments (DOE) techniques and find an optimum airbag design which mitigates neck and chest injury assessment values by using optimization techniques. Four different airbag designs were used in the first stage of the DOE, and one DAB design was chosen for the best performance in US-NCAP.
Traditional meta model based optimization of the chosen DAB design followed.
The direct optimization method requires a great deal of computational resource, whereas meta model based optimization methods use comparatively little computational resource once there are sufficient sample data from the DOE. Dynamic meta model based optimization methods were introduced with combined CAE runs to reduce computing resource in this study. CAE runs were periodically sampled to update the meta model and provide improved accuracy. Two different optimization methods with dynamic meta models were demonstrated and compared with traditional meta model based optimization.

INTRODUCTION

Since the current US-NCAP rating protocol was introduced in 2006 [3], neck and chest deformation injuries became more important for both the frontal driver and passenger injury matrix than in the previous US-NCAP rating system. The seat belt restraint system is one of the main countermeasures for US-NCAP occupant injury performance, and a low level of Single Load Limiter (SLL) and Dynamic Locking Tongue (DLT) were successfully proven to lower chest deformation injury. The frontal airbag is considered a supplemental restraint to the safety belt restraint system and is still important in lowering measured injury assessment values for Anthropomorphic Test Devices (ATD).
The purpose of this study is to find an optimum asymmetric airbag design which mitigates neck and chest injuries assessment values. A sled CAE model was built, and validation work was performed using physical tests. The base lower tether of the DAB was replaced by a shorter lower tether to mitigate chest deformation injury. Four DAB designs, differing according to the location of an upper tether attachment on the front panel of the DAB, were built and used as design factors in the DOE study. The relationship between the upper tether design and neck injuries was investigated, and the DAB design was chosen through a DOE study and meta model based optimization. A new asymmetric DAB was incorporated into the sled CAE model for the next airbag tether optimization process.
Meta models have been frequently used in place of time-consuming detailed CAE models. Usually, multiple CAE iterations are done before an optimization, and then a meta model is built and used for evaluation in optimization. Many researchers employed a dynamic learning approach utilizing a meta model [1], [4], [10], [11].
In this study, an initial DAB design was chosen from the first DOE, and another DOE was performed, which was then used to fit the meta model that is used for the following optimization. Meta model based optimization methods were used with an Elliptical Basis Function network algorithm (EBF) to reduce computing resource required. These meta models represented a dynamic learning approach that was periodically updated considering results from CAE iterations. Two approaches were demonstrated for airbag tether optimization work to improve US-NCAP

performance.

CAE MODELING AND VALIDATION

An occupant sled CAE model was built from a full vehicle structure model. Vehicle pulse, pitching and z-drop motion were extracted from barrier test results and validation work was performed.

Occupant sled CAE model

A sled CAE model, which has a rigid body-in-white (BIW), for use with prescribed motion was built. Some benefits of this approach are that it is easy to apply a vehicle pulse extracted from full-scale hardware tests, and this requires relatively lower computing resources than a full vehicle occupant model would. One weak point of this approach is that it is difficult to mimic instrument panel (I/P) intrusion. In most instances, a small amount of I/P intrusion was observed for full frontal rigid barrier loading conditions. Figure 1 shows an occupant sled model with belted driver ATD for US-NCAP.

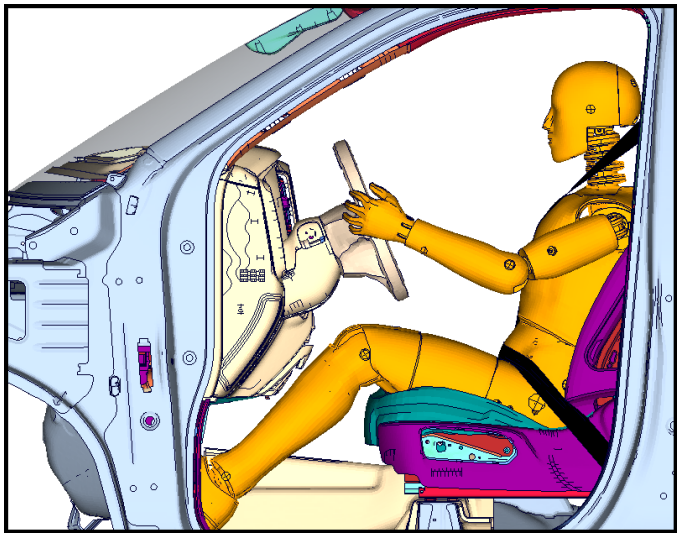

Figure 1. Occupant sled CAE model for frontal driver sides

Driver airbag model

Barrier tests were performed using an airbag design proposed by the airbag supplier. This airbag has an upper and a lower tether, and the tether length is 250mm for upper tether, and 220mm for lower tether. Typical tether length is 254mm (10") with traditional methods, such as 5"-30ms criterion [8], with the proposed target time to fire (TTF). One of the benefits of these upper and lower tether designs is easily controllable cushion depth for a vehicle crash test which has large pitching and vehicle z-drop motion. Tethers stretch during airbag deployment, because of the internal pressure of the airbag and airbag fabric material properties, and the magnitude of stretch depends on the characteristics of the selected airbag cushion fabric material and the number of fabric layers. Fabric materials have orthotropic characteristics [6] and usually have three axis loading component data, for instance, warp, weft and 45°. This airbag supplier uses a tether design which has a 45° direction and one layer fabric tether. This tether design showed greater stretched tether length compared to a warp or weft direction tether design from another airbag supplier. Figure 2 shows statically deployed airbags. Figure 3 shows expected tether stretch from CAE results.

Asymmetric or smiley DAB designs, which have a shorter lower tether than the upper tether are frequently used in order to mitigate chest deformation injury assessment values. Asymmetric or smiley DAB designs were considered for this work to improve US-NCAP performance for the next DOE study.

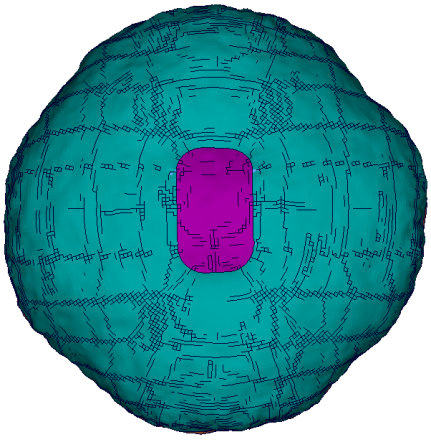

Figure 2.Static deployment of baseline airbag

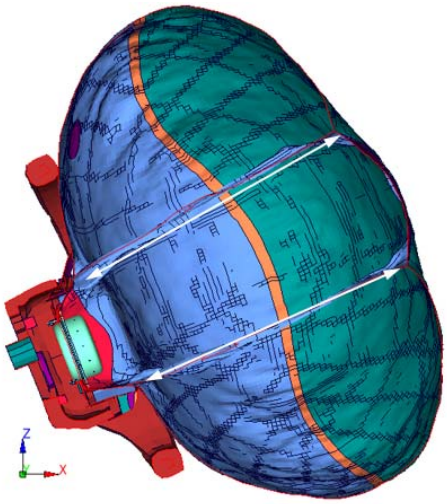

Figure 3. Tether stretch during deployment

Barrier test and validation work
It is important to verify the sled CAE model for subsequent optimization work. Validation work was performed with a belted 50th ATD in the 56kph full frontal loading condition, considering available data from a full-scale vehicle test. Figure A-1 and figure A-2 show the comparison between barrier test and the validated CAE model.

DOE STUDY

Asymmetric or smiley DAB designs, which have a shorter lower tether than the upper tether are frequently used in order to mitigate chest deformation injury assessment values. Airbag supplier proposed a smiley DAB for other vehicle program in past times and this asymmetric or smiley DAB design had been tried to mitigate chest deformation injury matrix, but these smiley DAB designs didn't lower chest deformation injury matrix significantly. It was hypothized that the attachment location on front panel of DAB for lower shorter tether was not appropriate, therefore smiley DAB had not lowered the chest deformation injury. Figure 4 shows proposed smiley (asymmetric) DAB by airbag supplier for other vehicle program in past time. Figure 5 shows interaction between smiley DAB and ATD from sled test, and figure 6 shows ATD's chest displacement transducer contact area on front panel of

smiley DAB, it suggests that tether attachment location for lower tether didn't match to ATD's chest displacement transducer contact area in previous work. The neck injuries were changed with smiley DAB, but it was not clear upper or shorter tether changed the neck injuries.
Asymmetric or smiley DAB designs were considered for this work again. DOE technique [12] was used to identify the significant design factors on neck injuries.
A parameter CAE study was performed to find the recommended location for the lower tether attachment on the front panel of the airbag, which can lead to decrease chest deformation injury assessment values. Several new asymmetric airbag designs were proposed and used as design variables for the DOE study to identify the effect of upper tether location (design) on neck injuries. The main design factors, affecting injuries assessment values, especially neck injuries assessment values, were identified in this DOE study. Additionally, meta model based optimization was performed with these DOE sample data, and an asymmetric airbag design was chosen for subsequent airbag tether optimization work.

Figure 4. Smiley (asymmetric) DAB which was proposed by supplier

Figure 5. Interaction between asymmetric DAB and ATD chest

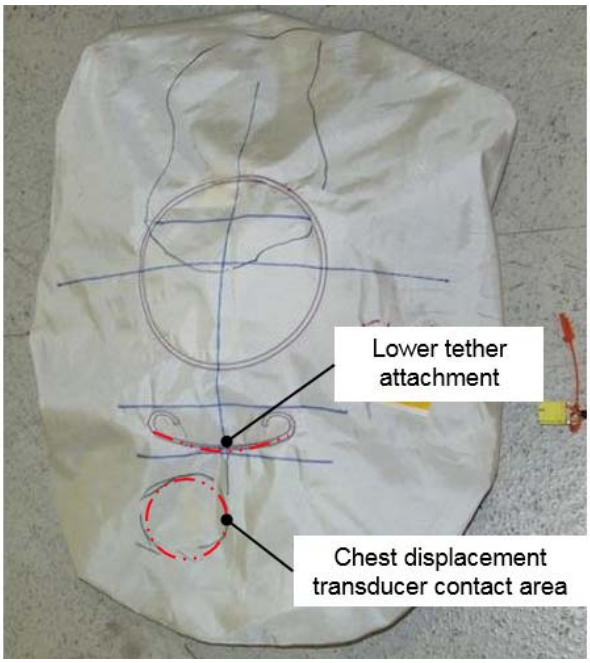

Figure 6. Lower tether attachment vs. chest potentiometer contact area with asymmetric DAB

New asymmetric airbag model

The results of several barrier tests showed higher neck and chest deformation injury assessment values than expected given the pulse severity. Therefore, the performance of the proposed occupant restraint systems resulted in a 4 star US-NCAP rating score. The motivation of this study was to find a better airbag design with the goal of improving US-NCAP performance rating without changing other restraint system components, such as the seat belt system.

Chest deformation can be lowered by removing pressure on the ATD chest, whereas chest acceleration injury can be lowered by using the ride down effect offered by the restraint systems [8]. One countermeasure to lower chest deformation is an asymmetric DAB design, which has a quite shorter lower tether length than upper tether length. A shorter lower tether length, 100mm, was incorporated into the baseline airbag by replacing the lower tether only. The internal airbag pressure may be high enough to tear this 45° angle fabric tether, so a warp or weft fabric direction tether with two or three layers of material was recommended. Proper location of the lower tether attachment on the front panel of the airbag was achieved by performing a parameter study. Figure 7 and figure 8 show the interaction between the airbag and ATD chest for the baseline DAB and asymmetric DAB, respectively.

The parameter study with 100mm lower tether length showed that chest deformation was significantly lowered, but neck assessment values, such as, Nij were increased contrarily. It was assumed that upper tether length and the location of the upper attachment on the front panel of the airbag might play a role in neck performance. Therefore, four different DAB designs were built by changing the location of the upper tether attachment on the front panel of the airbag with 250mm upper tether length. Figure 9 shows the proposed asymmetric DAB configurations, which were used as design variables in the DOE study (DAB #1, DAB #2, DAB #3, DAB #4).

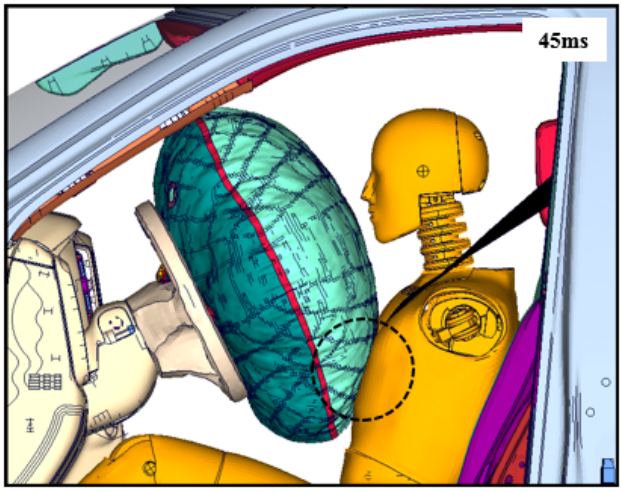

Figure 7. Interaction between baseline DAB and ATD chest

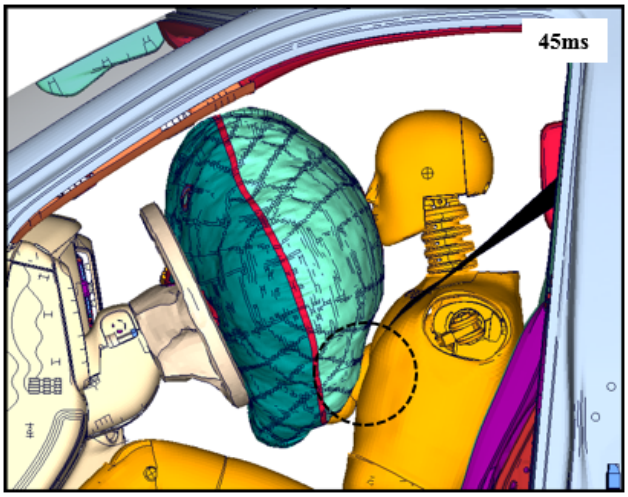

Figure 8. Interaction between asymmetric DAB and ATD chest

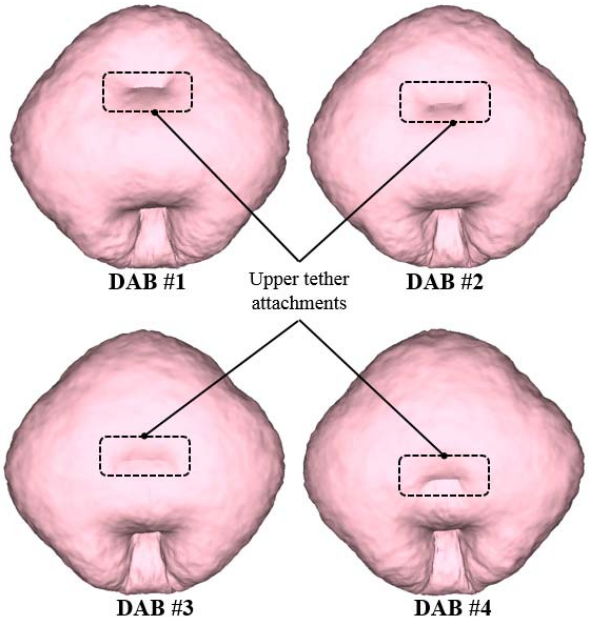

Figure 9. Asymmetric DAB, which were used as design variable in DOE

Design variables and DOE matrix

The purpose of this DOE work is to identify the main factors contributing to neck assessment values and to find the best DAB design through meta model based optimization. Four discrete design variables were defined. Vent size was one of the variables, because airbag internal pressure has a strong relationship with ATD measured assessment values. The variable name 'DAB' in the study represents different DAB designs according to the location of upper tether attachment. Upper tether length was also considered as one of the design variables in order to find the relationship between neck performance and upper tether length. An L27 orthogonal matrix was used for DOE sampling. Table-1 shows the variables and Table-2 shows the L27 orthogonal DOE matrix. A polynomial-base meta model [5] was built with L27 DOE sample data.

Table 1. Loading condition and design variables of DOE matrix

Loading condition and DOE matrix		
Matrix		L27 Orthogonal matrix
Loading condition	Speed	56kphFF US-NCAP
	Occupant	Driver 50th
	Belt condition	Belted
Design variables	Vent (2 x ϕmm)	35, 40
	DAB (UT attch location)	1, 2, 3, 4
	S/Column load (kN)	2.0, 3.0, 4.0
	Upper tether length (mm)	150, 200, 250

Table 2. L27 orthogonal DOE matrix

	Vent	DAB	SColumn	UTether
1	1	1	1	1
2	1	2	1	1
3	1	3	1	1
4	1	4	2	2
5	1	1	2	2
6	1	4	2	2
7	1	3	3	3
8	1	2	3	3
9	1	1	3	3
10	2	1	2	3
11	2	2	2	3
12	2	3	2	3
13	2	4	3	1
14	2	1	3	1
15	2	4	3	1
16	2	3	1	2
17	2	2	1	2
18	2	1	1	2
19	1	1	3	2
20	1	2	3	2
21	1	3	3	2
22	1	4	1	3
23	1	1	1	3
24	1	4	1	3
25	1	3	2	1
26	1	2	2	1
27	1	1	2	1

Sensitivity analysis and main design factors

The US-NCAP rating score consists of probability of head (Phead), neck (Pneck), chest (Pchest), and femur injuries (Pfemur) for the frontal impact loading conditions, and all of these four injury components are combined as "joint probability of injury (Pjoint)" [3]. Figure 10 shows that barrier test results suggest the following.

- The probability of neck injuries is the most important factor on NCAP
- The second most influential factor is the probability of chest injury

Neck assessment values, such as Nij [3], are calculated from upper neck moment and axial force. Figure A-1 and figure A-2 (in the Appendix) show that neck tension flexion moment (Ntf) is the major factor influencing the probability of neck injury for this specific vehicle. Figure 11 and figure 12 show that the main factors for Ntf are upper tether length (UTether) and the location of the upper tether attachment on the front panel of the airbag (DAB). Also, neck tension force was highly dependent on the location of the upper tether attachment, whereas neck flexion moment was highly dependent on the upper tether's length. Main effect plots suggests that DAB #4 design showed the best performance.

There were interaction effects between upper tether length (UTether) and the location of the upper tether attachment (DAB) on head, neck tension force, and neck flexion moment values. This suggests that a conventional DOE approach using a first order polynomial response surface model (RSM) would not work well to identify the best design configuration. Figure 13 shows interaction plots for head, neck tension force and neck flexion moment.

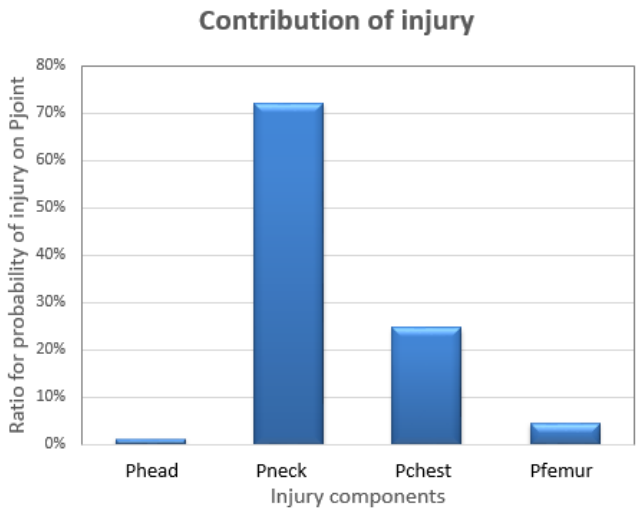

Figure 10. Comparisons for probability of injury on NCAP rating score (Pjoint)

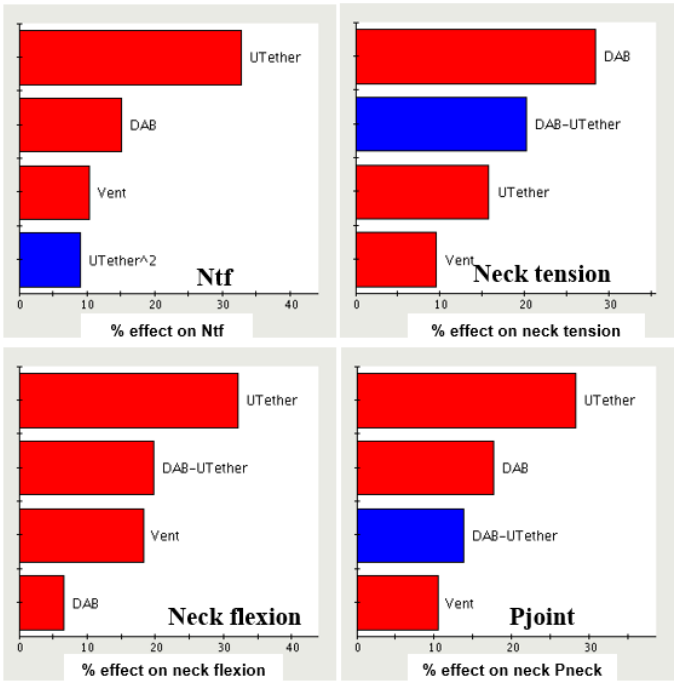

Figure 11. Pareto graph for neck assessment values and Pjoint

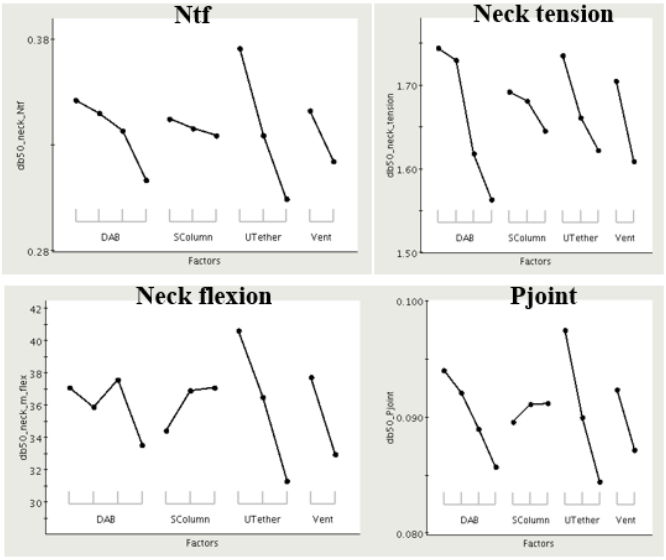

Figure 12. Main effect plots for neck assessment values and Pjoint

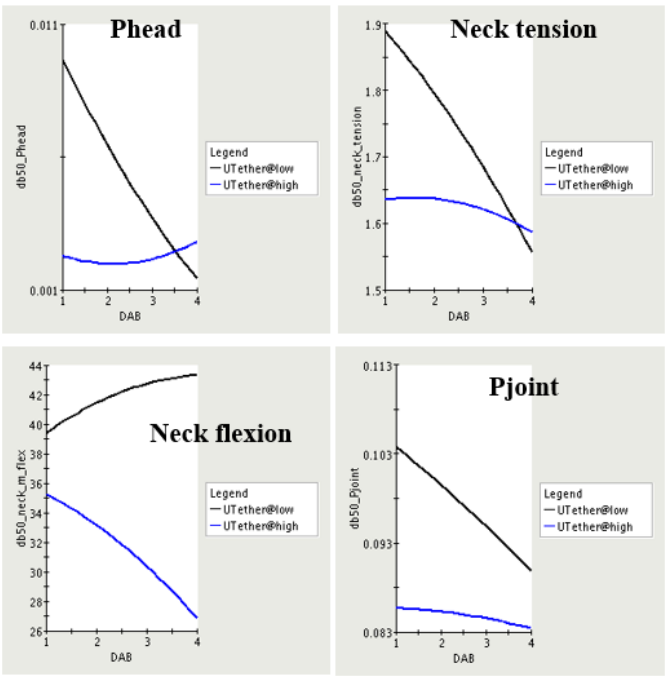

Figure 13. Interaction plots for Phead, neck tension force, neck flexion moment and Pjoint

Optimization by polynomial meta model

A polynomial 3rd order meta model was built with L27 DOE sample data. A Root Mean Square Error (RMSE) was used with leave-one-out cross validation analysis. Figure 14 shows errors are less than 15% for neck and chest deformation performance, but error for femur injury matrix is high, 36%, because there was not significant contact loading by knee-bolster, the femur loads were mainly caused by floor interaction to feet. A Genetic Algorithm (GA), such as NSGA-II algorithm [2], [5] was used for meta model based optimization [13], because occupant analyses have non-linearity. The predicted joint probability of injury (Pjoint) is

0.0823 based on meta model based optimization, and the corresponding confirmation CAE run showed 0.0820 of Pjoint. Table-3 shows the injury comparison between baseline DAB and the new asymmetric DAB design. Figure 15 shows a bar chart comparison of US-NCAP performance.

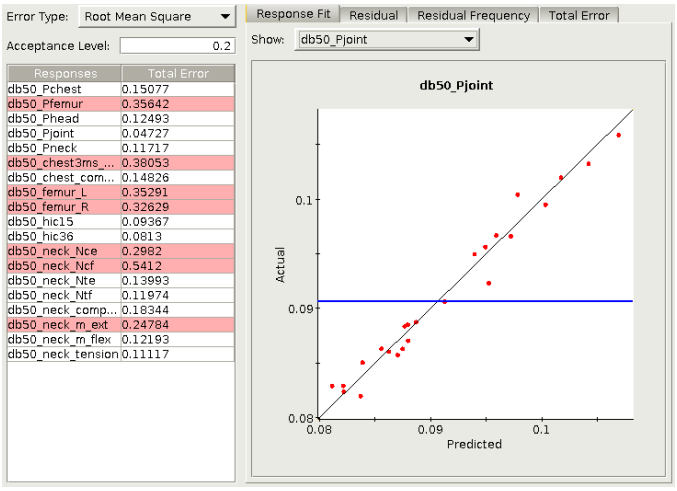

Figure 14. Error analysis for polynomial 3rd order meta model

Table 3. Injury comparison between baseline DAB and asymmetric DAB

56kph FF US-NCAP		
	Base DAB	Asymmetric DAB
DAB	Std.	DAB #4
Upper tether length	250 mm	246 mm
Lower tether length	218 mm	100 mm
Vent	2 x ϕ 35 mm	2 x ϕ 40 mm
S/Column	2.0 kN	3.8 kN
Phead	0.0010	0.0010
Pneck	0.0690	0.0660
Pchest	0.0240	0.0120
Pfemur	0.0040	0.0040
Pjoint	0.0960	0.0820

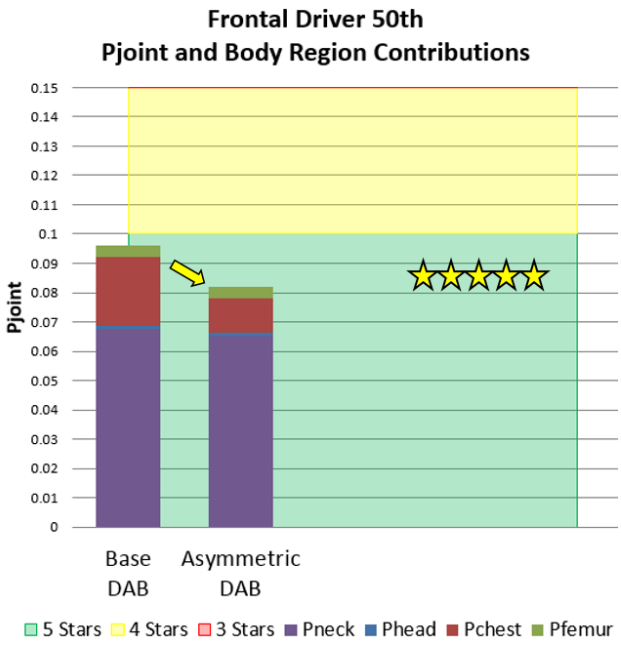

Figure 15. Bar chart comparison of US-NCAP performance

DYNAMIC META MODEL BASED OPTIMIZATION

Optimization was performed again with the goal of optimizing an upper and a lower tether length with new asymmetric airbag design, which was chosen from the DOE study section. Meta model based optimization was chosen with consideration of high computational cost. Traditionally, a meta model is built over the design space, and it is used in optimization. A dynamic learning approach was proposed with artificial neural network algorithms for time consuming water resource simulation models [10]. A Dynamic Kriging method was demonstrated to improve the accuracy of the meta model by dynamically selecting the optimal set of the basis function of the universal Kriging meta model [1], [11]. An adaptive meta model using a neural network algorithm was demonstrated. The meta model was initially built with the Latin Hypercube sampling method. Sequential designs using an adaptive error-based sampler were used to train the meta model [4].
In this study, meta model based optimization was combined with the dynamically trained meta model. Two approaches were compared and demonstrated.

Design variables and sampling method

Two continuous variables for the length of an upper and a lower tether were defined as design variables, and two discrete design variables for vent size and steering column collapse load were defined. Optimal Latin Hypercube [5] was used as the sampling method. The sampling number is twelve (3 times of the number of design variables). Table-4 shows the loading condition and continuous and discrete design variables.

Table 4. Loading condition and design variables for DOE sampling run

Loading condition and DOE matrix			
Matrix		Optimal Latin Hypercube 12	
Loading condition	Speed	56kphFF US-NCAP	
	Occupant	Driver 50th	
	Belt condition	Belted	
Design variables	Vent (2 x ϕmm)	30, 35, 40	
	S/Column load (kN)	2.0, 2.5, 3.0, 3.5, 4.0	
	Upper tether length (mm)	200 <	< 300
	Lower tether length (mm)	75 <	< 125

Meta model

Radial Basis Function network (RBF) is a kind of neural network algorithm which can be trained [9]. Mak, et al proposed the Elliptical Basis Function network (EBF) by replacing the base function of RBF and compared it to the original RBF [7]. In this study, EBF meta model was used after a comparison of accuracy between RBF and EBF with same sample data. Figure 16 shows the error analysis for an EBF meta model with 12 CAE data samples. The target of RMSE is less than 20%, but the error for Pneck is high, 20.72%, and exceeding 20% at initial EBF meta model output.

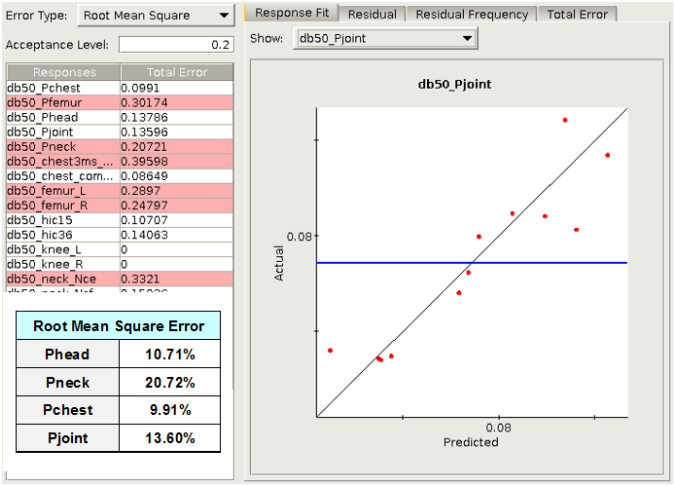

Figure 16. Error analysis for EBF Meta model with 12 CAE sample data

Optimization by dynamic meta model

The NSGA-II (Non-Dominated Sorting Genetic Algorithm) [2], [5] was used with the EBF meta model. The size of population = 12, the number of generations = 10, crossover probability = 0.9, crossover distribution index = 10, mutation distribution index =20. Two optimization methods were demonstrated. Method #1; perform optimization with meta model only; confirmation CAE run with optimized design, and update samples and meta model. Loop this process nine times. Method #2; 75% of populations were evaluated with the meta model and 25% of populations were evaluated by CAE runs, updating samples and meta model for each generation in order to get improved accuracy. Figure 17 shows work flow of optimization method #1, and Figure 18 shows work flow of optimization method #2.

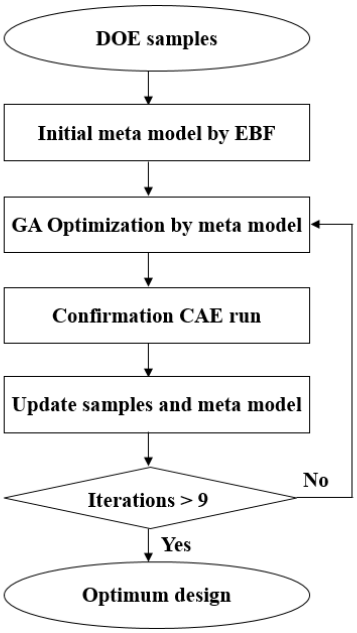

Figure 17. Work flow of optimization method #1

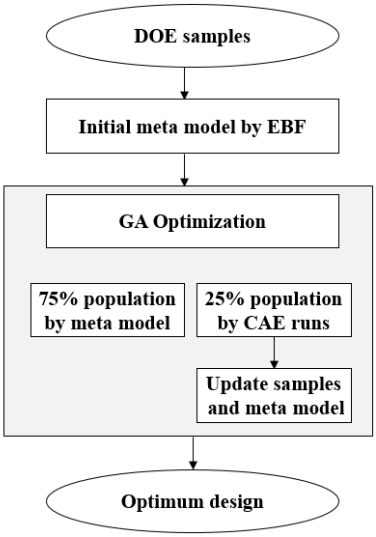

Figure 18. Work flow of optimization method #2

RESULTS

The accuracy of the EBF meta model was improved for both method #1 and method #2. Joint probability of injury was successfully lowered for both optimization methods. The accuracy of the meta model was better for method #2 with more sample data than method #1. The predicted joint probability of injury (Pjoint) by meta model is 0.0765 from method #2, and the corresponding confirmation CAE run showed Pjoint of 0.0770. Table-5 shows the comparison for the accuracy of the meta model between initial meta model and final meta models from method #1 and method #2. Table-6 shows the optimized design configuration and probability of injuries comparison, and figure 19 shows bar chart comparison of US-NCAP performance.

Table 5. Comparison of meta model accuracy: RMSE with leave-one-out cross validation

Root Mean Square Error			
Probability of injuries	Initial 12 samples	Method #1 12 + additional 8 samples	Method #2 12 + additional 28 samples
Phead	10.71%	9.11%	7.93%
Pneck	20.72%	13.73%	10.79%
Pchest	9.91%	7.98%	7.74%
Pjoint	13.60%	10.35%	7.76%

Table 6. Optimized design variable with dynamic meta model method

56kph FF US-NCAP				
	Base DAB	Asymmetric DAB	Optimization method #1	Optimization method #2
DAB	Std.	DAB #4	DAB #4	DAB #4
Upper tether length	250mm	246 mm	290 mm	296 mm
Lower tether length	218mm	100 mm	125 mm	78 mm
Vent	2 x ϕ 35 mm	2 x ϕ 40 mm	2 x ϕ 40 mm	2 x ϕ 40 mm
S/Column	2.0 kN	3.8 kN	2.5 kN	2.0 kN
Phead	0.0010	0.0010	0.0004	0.0005
Pneck	0.0690	0.0660	0.0631	0.0637
Pchest	0.0240	0.0120	0.0134	0.0093
Pfemur	0.0040	0.0040	0.0044	0.0045
Pjoint	0.0960	0.0820	0.0800	0.0770

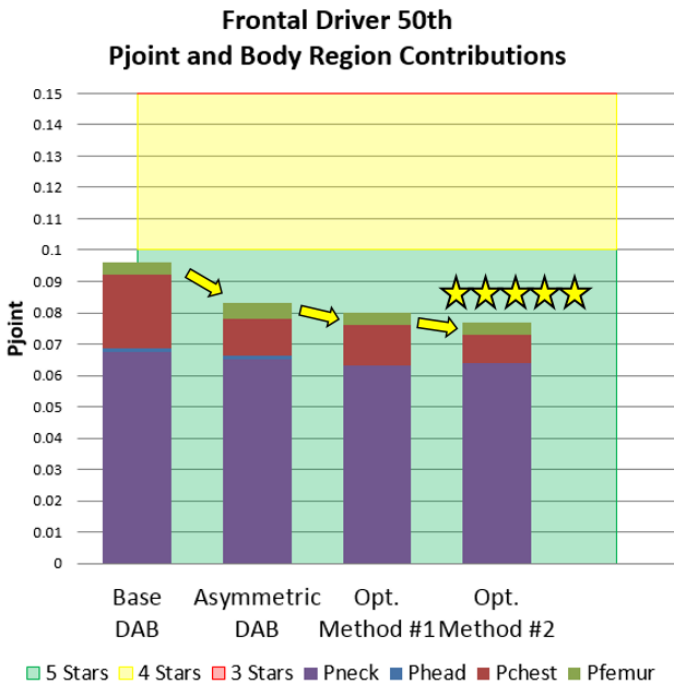

Figure 19. Bar chart comparison of US-NCAP performance

SUMMARY AND CONCLUSIONS

In this paper, an asymmetric airbag design was proposed with the goal of mitigating chest deformation and improving US-NCAP performance. The DOE technique was used to identify the main design factors for neck assessment values, and meta model optimization was performed to choose the location of an upper tether attachment on the front panel of the DAB. The DOE study shows; axial neck tension force was highly dependent on the location of upper tether attachment on the front panel of the DAB, whereas neck flexion moment was highly dependent on an upper tether's length. Meta model based optimization was performed to optimize tether length again, because a DOE study suggested that tether length has a role in neck flexion injuries. An initial EBF meta model was built with 12 data samples, and used for the evaluations. During the optimization, sample data and meta models were updated. Two methods using dynamic meta model were demonstrated, showed the accuracy of meta models were improved, and successfully found solutions. Method #2 shows better performance than method #1 with more sample data. For the future work, this asymmetric or smiley DAB needs to be verified for other loading conditions, for example, 40kph full frontal unbelted 5th and 50th. And low risk deployment performance also needs to be confirmed by actual hardware tests. There were arguments about performance with this asymmetric or smiley DAB in field condition, because the steering wheel can be rotated at real world field conditions and can show different performance.

REFERENCES

[1] Choi, K., Lee, I., Zhao, L., Noh, Y., Lamb, D., "Sampling-based RBDO using stochastic sensitivity and dynamic Kriging for broader army applications". NDIA ground vehicle systems engineering and technology symposium 2011.

[2] Deb, K., Agrawal, S., Pratap, A., Meyarivan, T. "A fast elitist non-dominated sorting genetic algorithm for multi-objective optimization: NSGA-II". IEEE Transactions of evolutionary computation, Vol. 6, No. 2, 2002.

[3] Docket no. NHTSA-2006-26555, www.regulations.gov

[4] Gorissen, D., Hendrickx, W., Dhaene, T., "Adaptive Global Metamodeling with Neural Networks". ESANN' 2007 proceedings – European Symposium on Artificial Neural Networks.

[5] Isight user's manual, version 5.9

[6] LS-DYNA user's manual volume 2, 262-273, version 7.1

[7] Mak, M., Li, C., "Elliptical Basis Function Networks and Radial Basis Function Networks for Speaker Verification: A Comparative Study". Neural Networks, IJCNN '99. International Joint Conference, 1999.

[8] Hwang, M., 2002 "Vehicle crash mechanics" 33-38, 74-77, CRC Press LLC

[9] Orr, M., "Introduction to Radial Basis Function Networks". https://www.cc.gatech.edu/~isbell/tutorials/rbf-intor.pdf, accessed Aug. 2017.

[10] Yan, S., Minsker, B., "Optimal groundwater remediation design using an Adaptive Neural Network Genetic Algorithm". Water resources research, Vol 42, W05407, doi:10.1029/2005WR004303, 2006.

[11] Zhao, L., Choi, K., Lee, I., "Metamodeling Method Using Dynamic Kriging for Design Optimization". AIAA Journal Vol. 49, No.9, September 2011.

[12] Park, G., 2007 "Analytic Methods for Design Practice", 312-317, 327-340, 360-367, Springer-Verlag London.

[13] Ryberg. A., 2013 "Metamodel-Based Design Optimization", 11-12, LiU-Tryck, Linkoping, Sweden ISBN 978-91-7519-721-0 ISSN0280-7971.

APPENDICES

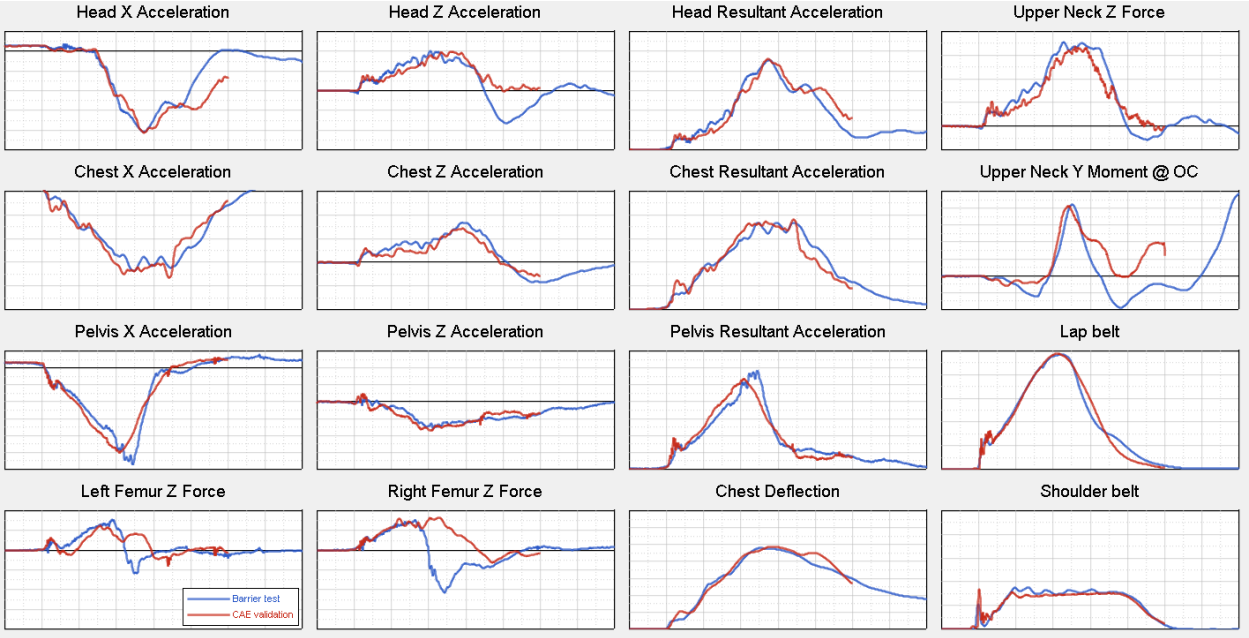

Figure A-1. Comparison between barrier test and validated CAE model for US-NCAP (blue: test, red: CAE)

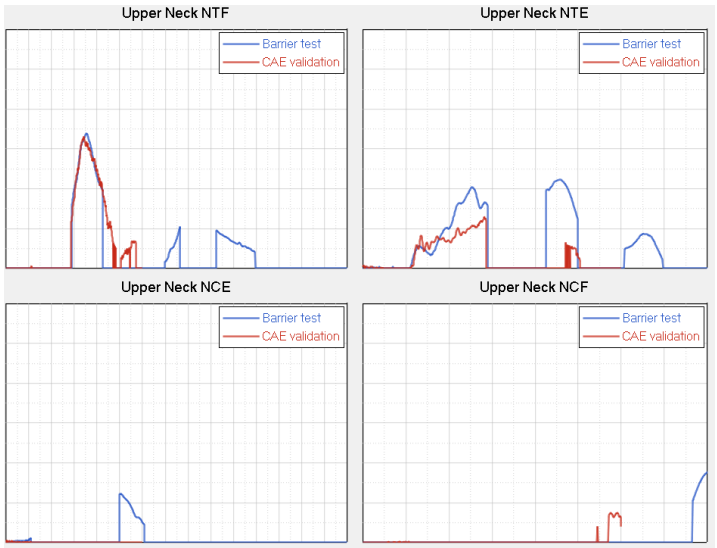

Figure A-2. Comparison between barrier test and validated CAE model for US-NCAP (blue: test, red: CAE)

Passenger Vehicle-Powered Two Wheeler Pre-Crash Trajectory Reconstruction and Conflict Analysis Results for Real-World Crashes in the EU and US and its Application to Advanced Crash Avoidance Technologies

R. Michael Van Auken
Dynamic Research Inc.
United States of America

John Lenkeit
Dynamic Research Inc.
United States of America

Terry Smith
Dynamic Research Inc.
United States of America

Scott Kebschull
Dynamic Research Inc.
United States of America

Paper Number 19-0096

ABSTRACT

Research Question / Objective: Advanced Driver Assistance Systems (ADASs) such as Forward Collision Warning have been developed for light passenger vehicles (LPVs) to avoid and mitigate collisions with other road users and objects. These technologies may have contributed to a reduction in LPV traffic fatalities in the EU and US. However the number of powered two wheeler (PTW) fatalities has remained relatively constant in the US. To fully realize the potential safety benefits across all vehicle categories, LPV crash avoidance technologies also need to be effective in avoiding collisions with PTWs. To accomplish this, knowledge of the pre-crash LPV-PTW vehicle trajectories and conflicts is needed to guide the development and testing of effective crash countermeasures for both LPVs and PTWs.

Methods and Data Sources: Crash scenario database development tools previously developed to evaluate LPV-LPV crash countermeasure effectiveness have been extended to LPV-PTW crash scenarios. This involved using information for a large sample of LPV-PTW crashes from the EU Motorcycle Accidents In-Depth Study (MAIDS) and US Motorcycle Crash Causation Study (MCCS) databases, which are based on in-depth crash investigations and the Organisation for Economic Co-operation and Development (OECD) Common Methodology. The vehicle pre-crash trajectories were estimated based on the coded data and digitized information from the scaled pre-crash scene diagrams. The pre-crash conflict state was then analyzed based on these trajectories.

Results: The estimated pre-crash trajectories using this method indicate that LPV-PTW pre-crash trajectories and conflicts in France, Germany, Italy, and the US have many similarities, but there are some differences as well. These results indicate that conflicts in several types of pre-crash scenarios, such as the LPV turning across the PTW path in the same direction or opposite direction, begin less than 1.5 sec before impact, which may not be sufficient time for some crash countermeasures based on conflict detection and driver warnings to be effective.

Discussions and Limitations: The accuracy of the results is based on a number of assumptions, approximations, and limitations in the data and methods used. These include the accuracy and representativeness of the data based on in-depth crash investigations, as well as the domain-of-validity and accuracy of the vehicle directional control models used.

Conclusion and relevance to session submitted: Analysis of real world accident data is critical to the development and evaluation of ADAS and automated driving systems. This analysis has shown that LPV-PTW crash countermeasures need to function with shorter pre-crash conflict epochs, or in the pre-conflict phase, in order

to be effective in preventing collisions. This information may help to define requirements for LPV-PTW crash countermeasures (e.g., C-ITS V2V and Blind Spot Detection), evaluate their effectiveness, and inform the development of performance confirmation tests (e.g., New Car Assessment Programs).

INTRODUCTION

Advanced Driver Assistance Systems (ADASs) such as Forward Collision Warning (FCW), Automatic Emergency Braking (AEB), and Blind Spot Warning (BSW) have been developed for Light Passenger Vehicles (LPVs) to avoid and mitigate collisions with other road users and objects. These crash avoidance and mitigation countermeasures may have contributed to the 41% reduction in the overall number fatalities in the EU from 43,151 in 2007 to 25,651 in 2016 [1], and a 9% reduction in the overall number of traffic fatalities in the US from 41,259 to 37,461 in the same time period [2]. A main component of these overall reductions were a 42% reduction in LPV occupant fatalities in the EU from 20,744 to 11,990, and an 18% reduction in the US from 29,072 to 23,714. Powered two wheeler (PTW) fatalities, comprising mopeds and motorcycles,[1] also decreased by 42% from 7,522 in 2007 to 4,334 in 2016 in the EU, but increased by 2% in the US over the same period. In an effort to explain the differences in the PTW versus LPV fatality trends in the US, one question is whether or not LPV ADASs are as effective in avoiding collisions with PTWs compared to other road users.

Lenkeit and Smith [4] evaluated the ability of eight 2016 model year LPVs equipped with FCW to detect an exemplar motorcycle and passenger car using two tests in the US National Highway Traffic Safety Administration (NHTSA) FCW confirmation test procedures. The results of this preliminary evaluation indicated that only two of the eight LPVs tested were able to pass the NHTSA test procedure scenario with a stationary motorcycle as the principal other vehicle (POV), compared to all LPVs passing the test with a stationary passenger car as the POV. Therefore these preliminary results tend to indicate that FCW systems may not be as effective in avoiding or mitigating collisions with a motorcycle as they are with a passenger car.

Van Auken et al. ([5],[6],[7]) then estimated the pre-crash trajectories and conflicts for 101 crashes in the US and 266 crashes in the EU involving one LPV and one PTW. This analysis was based on the European Motorcycle Accidents In-Depth Study (MAIDS) database [8] and the US Federal Highway Administration's (FHWAs) Motorcycle Crash Causation Study (MCCS) database [9]. Both of these databases were developed based on in-depth accident investigations using methodology based on the Organisation for Economic Co-operation and Development (OECD) Common Methodology [10].

Analysis of these estimated pre-crash trajectories indicated that the conflicts begin later, and therefore with smaller Time to Collision (TTC) values, compared to results for some LPV-LPV crashes. Therefore there may be less time for a driver or crash avoidance technology to avoid or mitigate a LPV-PTW crash after a conflict has been detected, compared to a LPV-LPV crash. As a result such systems may be less effective in avoiding LPV-PTW crashes.

Background

Dynamic Research, Inc. (DRI) has been developing and applying safety impact analysis methods for many years (e.g., [11]). This included the development of a comprehensive Safety Impact Methodology (SIM) in two Honda-DRI Advanced Crash Avoidance Technology (ACAT) programs for the US NHTSA. The comprehensive and general structure of this methodology and accompanying tools are well suited for the potential evaluation of LPV ADAS (e.g., FCW, AEB, and BSW) effectiveness in avoiding and/or mitigating collisions with PTWs with the extensions originally outlined in [12], as well as other applications such as pre-crash conflict analysis, the development of system requirements, and testing.

In-Depth LPV-PTW Crash Databases

Two databases that have sufficient suitable information to be integrated into this SIM methodology are from the European MAIDS study and the US MCCS study. Both of these studies had coded accident data and crash scene diagrams based on in-depth investigations.

[1] Powered Two Wheelers comprise L1 and L3 vehicles as defined in [3]. L1 vehicles are commonly known as mopeds. L3 vehicles are commonly known as motorcycles. See the Definitions/Abbreviations Section.

The MAIDS study was conducted from 1998 through 2002 by the European Association of Motorcycle Manufacturers (ACEM) with co-funding by the European Commission. It was developed using the OECD Common Methodology [10]. All of the cases are from France, Germany, Italy, Netherlands, and Spain. Most of the MAIDS cases are from the 1999 to 2001 calendar year time period.

The MCCS study was conducted by a team from Oklahoma State University, Westat, and Dynamic Sciences, Inc. and sponsored by the Federal Highway Administration (FHWA). It was also developed based the OECD Common Methodology with adaptions to the US motorcycling conditions. All of the cases are from Orange County, California. All of the MCCS cases are from the 2011 to 2015 calendar year time period.

Project Aims

The objective of this project was to extend the SIM tools and data to include the MAIDS and MCCS data in order to better understand the pre-crash conflicts of LPV-PTW crashes, to guide the development of LPV ADASs in avoiding and mitigating collisions with a PTW, and to evaluate their effectiveness and benefits.

SAFETY AREA TO BE ADDRESSED BY THE ADVANCED TECHNOLOGIES

The objective of the ACAT SIM with the PTW extensions is to evaluate the effectiveness and benefits of LPV ADASs (e.g., FCW, AEB and BSW) in avoiding or mitigating LPV-PTW crashes. It is assumed that these technologies could address crashes where the LPV driver inattention is a contributing factor, but may also be applicable to safety-relevant cooperative ITS (C-ITS) and other technologies as well.

The size of the problem to be addressed

One of the first steps in the development and evaluation a crash avoidance technology is to determine the size of the traffic safety problem in terms of broadly defined non-technology specific crash types. The estimated numbers of fatalities that represent the size of the problem for the entire EU and US motor vehicle fleets in the 2016 calendar year by the crash category and type of vehicle involved are listed in Table 1. Some of these crashes are not expected to be addressable by specific LPV technologies such as AEB due to either the vehicle application (e.g., not an LPV), the vehicle role (e.g., struck vehicle), or other technology relevant factors. For example, the results in Table 1 indicate there were 997 PTW fatalities in the EU involving only one vehicle (i.e., did not involve an LPV). These results also indicate that there were 3,337 PTW fatalities in the EU involving one or more other vehicles, which account for 13% of all traffic fatalities in the EU. There were also 3,273 PTW fatalities in the US involving one or more other vehicles, which account for 9% of all US traffic fatalities in the US. A large portion of these cases involve an LPV, which could be potentially addressed by an LPV ADAS.

Table 1. Estimated crash problem size for the entire EU and US motor vehicle fleets in the 2016 calendar year

(A)	(B)	(C)	(D)	(E)	(F)	(G)
Crash Category	**Number of EU Fatalities[a]**			**Number of US Traffic Fatalities[b]**		
	PTW	Other =(D)-(B)	Total	PTW	Other =(G)-(E)	Total
1 Vehicle	997[c]	6,658	7,655[d]	2,065	18,415	20,480
2+ Vehicle	3,337[e]	14,659	17,996[e]	3,273	14,053	17,326
Total	4,334[f]	21,317	25,651[g]	5,338	32,468	37,806

Sources:

[a] Based on EU Community database on road accidents (CARE) data.

[b] Based on US Fatality Analysis Reporting System (FARS, [13]) data (2018-05-18) query.

[c] Assumed equal to 23% of all PTW fatalities based on [14], p 10, Table 5. It is assumed that none of the single vehicle crashes are pedal cycles.

[d] [14], p 10, Table 5.

[e] =Total- Single Vehicle

[f] [1], p 19, Table 6 (677 moped fatalities) and p 20, Table 7 (3,657 motorcycle fatalities).

[g] [1], p 10, Table 2.

METHODS

The analytical approach involved refining and applying the methods developed in [5],[6],[7] for the EU MAIDS and US MCCS databases. The MAIDS and MCCS databases were developed using similar, but not identical, in-depth crash investigation methods. The MAIDS database was developed according the OECD common methodology. The MCCS database was developed using a methodology incorporating both the OECD and NHTSA methods.

Overview of the Crash Scenario Database Development Tools

A conceptual block diagram of the crash scenario database tools is given in Figure 1. These tools are collectedly referred to as "Module 1" in the Honda/DRI ACAT SIM. These Module 1 tools construct a harmonized crash scenario database for use in the development and evaluation of ADASs (e.g., requirements, simulation, and testing). The inputs are archival accident data such as the MAIDS and MCCS data as indicated at the top of the figure. The resulting crash scenario database comprises text summaries (to the extent available), harmonized coded data, scene diagrams, crash geometry and pre-crash time histories as depicted by the shaded database in Figure 1. These tools are organized into three sub-modules as follows:

- Submodule 1.1 assembles a crash scenario database with a representative sample of LPVs involved in real-world crashes. Ideally the crash scenario database would include all types of crashes and severities, which could be weighted to represent all crashes involving a LPV. This sub-module extracts cases from various coded accident databases such the MAIDS and MCCS data [8],[9].
- Submodule 1.2 is a tool to download or extract crash scene diagrams for each case in the crash scenario database if available.
- Submodule 1.3 is an Automated Accident Reconstruction Tool (AART) to reconstruct the pre-crash and crash position versus time trajectories of the LPVs for each case in the crash scenario file, provided there is sufficient information available and the case is within the domain-of-validity of the AART (e.g., there is a crash scene diagram, vehicle velocity, and contact information). The resulting reconstructions can be used for simulation and testing. These results can also be used for other analyzes, such as the identification of pre-crash conflicts described in [6].

The extensions of these tools for the US MCCS and EU MAIDS data were described in [5],[6],[7].

The results described herein are based on 367 cases from the US, France, Germany, and Italy that were reconstructed using this tool. The distribution of these cases is depicted in Figure 2. Each of these cases had sufficient information in the coded data, crash scene diagram, and supporting documentation to reconstruct the case. This excluded cases where a suitable scene diagram not available or did not have sufficient information about the locations of the vehicles prior to the impact and at the point of impact.

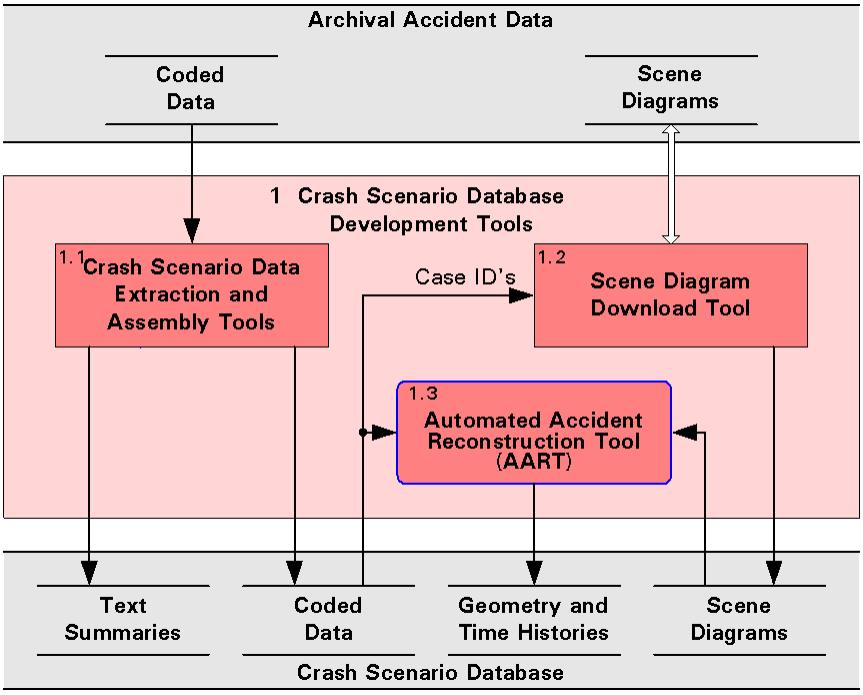

Figure 1. Crash Scenario Database Development Tools (e.g., [11]).

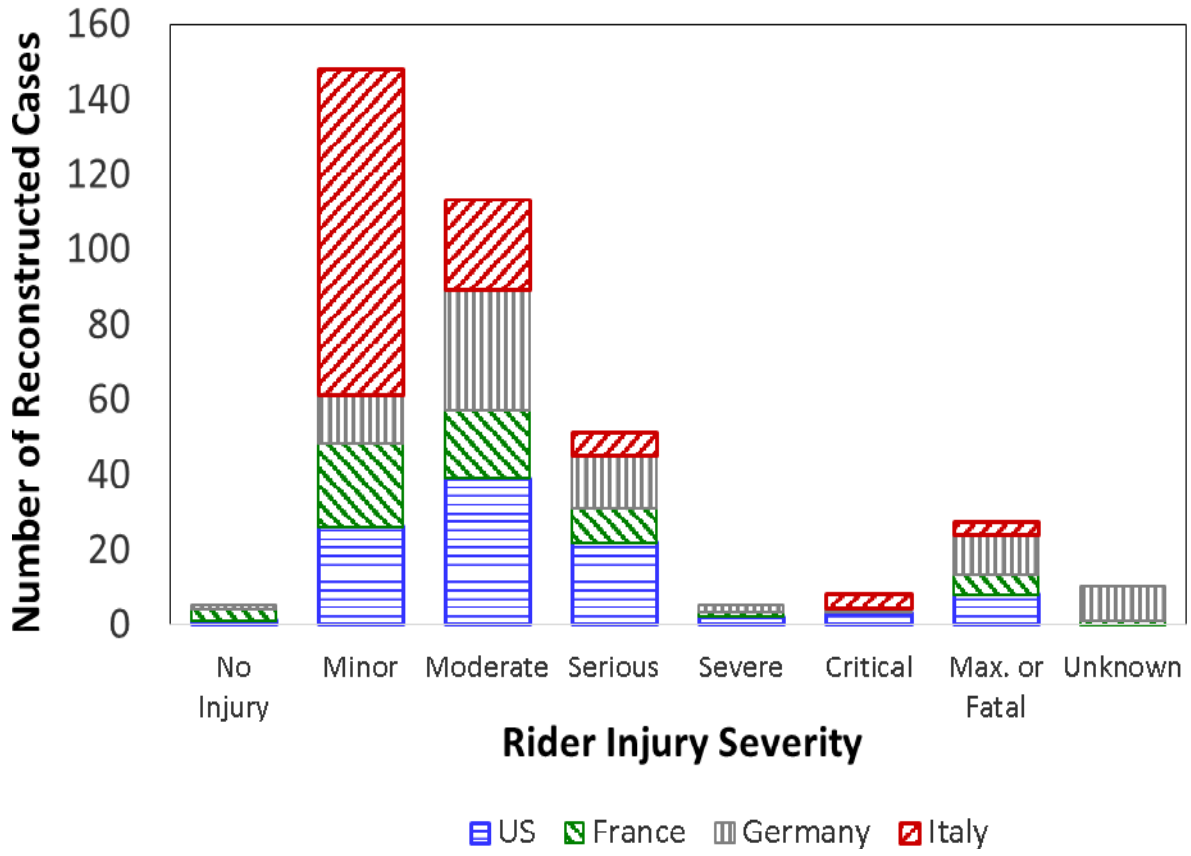

Figure 2. Number of reconstructed Cases by rider injury severity and country.

Extensions for the Current Results

The results presented herein are based on the following further refinements of the data and methods:

- Module 1.1
  - The NASS Accident Type described in Appendix A was coded for both vehicles in each of the reconstructed cases. The coded variables are VATYPE for the LPV and PATYPE for the PTW according to the conventions used in Appendix F of [11]. Reconstructed cases with similar crash types were then classified into the 24 different crash configuration groups listed in Table 2.
  - Data indicating if "*view obstructions* [were] *present and contributed to accident causation*," were extracted from the MAIDS and MCCS databases for both the LPV driver and PTW rider in order to further classify the reconstructed cases.
- Module 1.3 (Motorcycle Automated Accident Reconstruction Tool – M-AART)
  - The assumed pre-crash vehicle speeds in cases where the coded travel speed was missing or unknown to take into account coded data indicating the vehicle was traveling at a constant speed or accelerating.
  - Numerous refinements to the trajectory estimation algorithms to improve the accuracy of the estimated trajectories based on the available data. This includes new "reference trajectory" types with constant steer input rates or rider lean angle rates, which are consistent with the white process noise inputs assumed by the Kalman Filter-Smoother, provided there a are sufficient number of digitized pre-crash vehicle positions. The reference trajectories are initial solutions to the vehicle equations of motion that are used to determine locally linearized equations for the Kalman Filter-Smoother (e.g., [5]). It was also required that the PTW speed was either always less than or always greater than the critical speed of the Weir-Zellner model [16].[2] This avoids a singularity in the quasi-steady reference trajectory solution at the critical speed.

Table 2. Crash Configuration Groups based on NASS Accident Types

Crash Configuration Group based on NASS Accident Types		NASS Accident Types
Mnemonic	**Description**	**VATYPE/PATYPE**
HO/ODSS	Head-on or opposite direction side swipe	50/51, 51/50, 65/64
LPV LTAP/LD	LPV left turn across PTW path/lateral direction	82/83
LPV LTAP/OD	LPV left turn across PTW path/opposite direction	68/69
LPV LTAP/SD	LPV left turn across PTW path/same direction	72/73
LPV LTIP	LPV left turn into PTW path/same direction	76/77
LPV RE	LPV rear-end PTW	20/21, 24/25, 24/26, 28/29
LPV RTAP/SD	LPV right turn across PTW path/same direction	70/71
LPV RTIP/SD	LPV right turn into PTW path/same direction	78/79
LPV UT	LPV U-turn across PTW path	940/941…944
PTW LTAP/LD	PTW left turn across LPV path/lateral direction	83/82
PTW LTAP/OD	PTW left turn across LPV path/opposite direction	69/68
PTW LTAP/SD	PTW left turn across LPV path/same direction	73/72
PTW LTIP	PTW left turn into LPV path	77/76
PTW RE	PTW rear-end LPV	21/20, 25/24, 26/24, 29/28, 30/28
PTW RTAP/SD	PTW right turn across LPV path/same direction	71/70
PTW RTIP/OD	PTW right turn into LPV path/opposite direction	81/80
PTW RTIP/SD	PTW right turn into LPV path/same direction	79/78
SCP/L	Straight crossing path, PTW on left side of LPV	86/87, 89/88
SCP/R	Straight crossing path, PTW on right side of LPV	87/86, 88/89
SDSS/L	Same direction side swipe, PTW on the left of LPV	47/45
SDSS/R	Same direction side swipe, PTW on the right of LPV	46/45
T2/OD	Both vehicles turning/opposite direction	68/82
T2/SD	Both vehicles turning/same direction	76/78, 78/76
Other	Other	74/74, 98/98

[2] The "Norton 850" parameter values in [16] were assumed for motorcycles and the "Moped B" parameter values in [17] were assumed for mopeds.

Pre-Crash Conflict State Estimation

As previously described in [6], the state of conflict between the LPV and PTW can be estimated as a function of time before the impact based on the estimated vehicle trajectories. For the purpose of this analysis the conflict state C at time t was defined for $t \le t_{\text{impact}}$ as follows: $C(t) \triangleq \text{true}$ if the vehicles will contact each other at time t_{contact} if their linear and angular velocities remain constant between time t and t_{contact}; otherwise $C(t) \triangleq \text{false}$ if the vehicles will never contact.[3] For practical considerations the contact evaluation time interval was limited to up to 1 sec after the reconstructed impact time (i.e., $t \le t_{contact} \le t_{impact} + 1\text{sec}$). This definition can include momentary benign conflicts that may occur several sec before impact in addition to the final conflict, as illustrated by the example in Figure 4 and Figure 5. Of interest is the when the final conflict begins.[4]

RESULTS

The results in this section describe the estimated trajectories and conflicts for two example cases, followed by a summary for all of the cases.

Example pre-crash trajectories and state of conflict

Example Head-On Case

An example pre-crash trajectory reconstruction of a Head-On case is illustrated in Figure 3, Figure 4, and Figure 5. This case involves a moped overtaking two other PTWs and then impacting a LPV that was exiting a parking area and turning to the right onto the roadway. The coded data indicates that there were rider "*view obstructions present that contributed to accident causation*." Presumably these view obstructions were the other motorcycles. Figure 3 shows the pre-crash vehicle speeds that were assumed based on coded data. Figure 5 shows the estimated vehicle directional control inputs versus time. Figure 4 shows the resulting vehicle trajectories overlaid on the crash scene diagram. The vehicle trajectories were fit to the locations of the LPV and moped shown on the scene diagram. The estimated vehicle positions and orientations are depicted at 1 sec intervals and the movement of the cg positions are depicted by continuous curves. The control inputs and vehicle positions when $C(t) = \text{true}$ are shown highlighted in yellow. The LPV and PTW vehicle level NASS accident types illustrated in Appendix A that best describe this case were VATYPE=51 and PATYPE=50 respectively, and therefore the HO/ODSS crash configuration group according to Table 2.

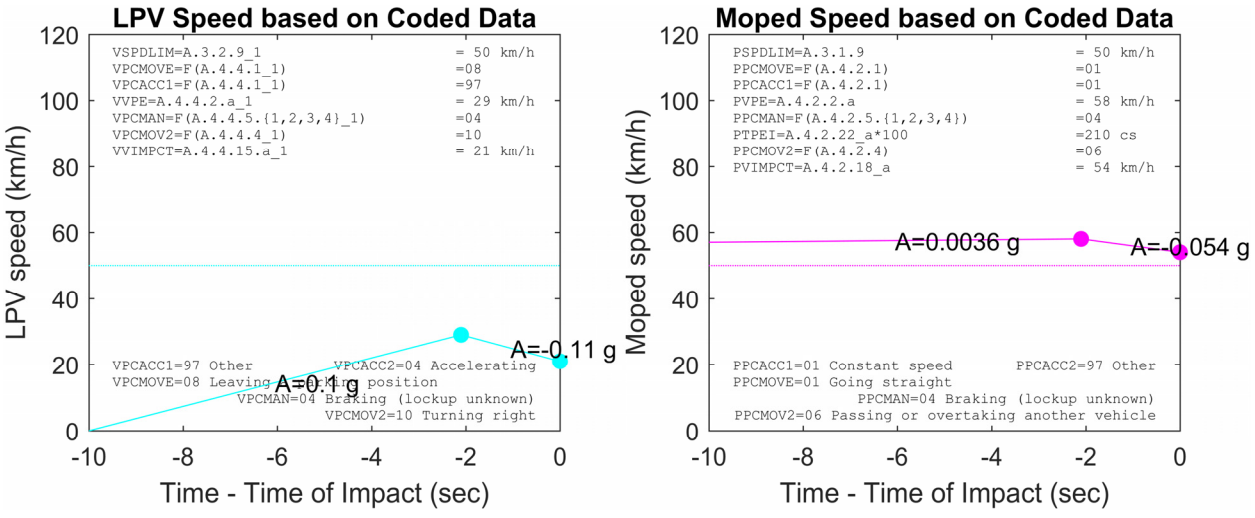

Figure 3. Assumed pre-crash speeds versus time for the exemplar head-on case based on coded data.

[3] The PTW handlebars were included in the potential contact with the LPV. It was assumed that the handlebars were 0.89 m wide for the purpose of this conflict analysis.

[4] See footnote 9 in [6] for addition background and rationale for this conflict definition.

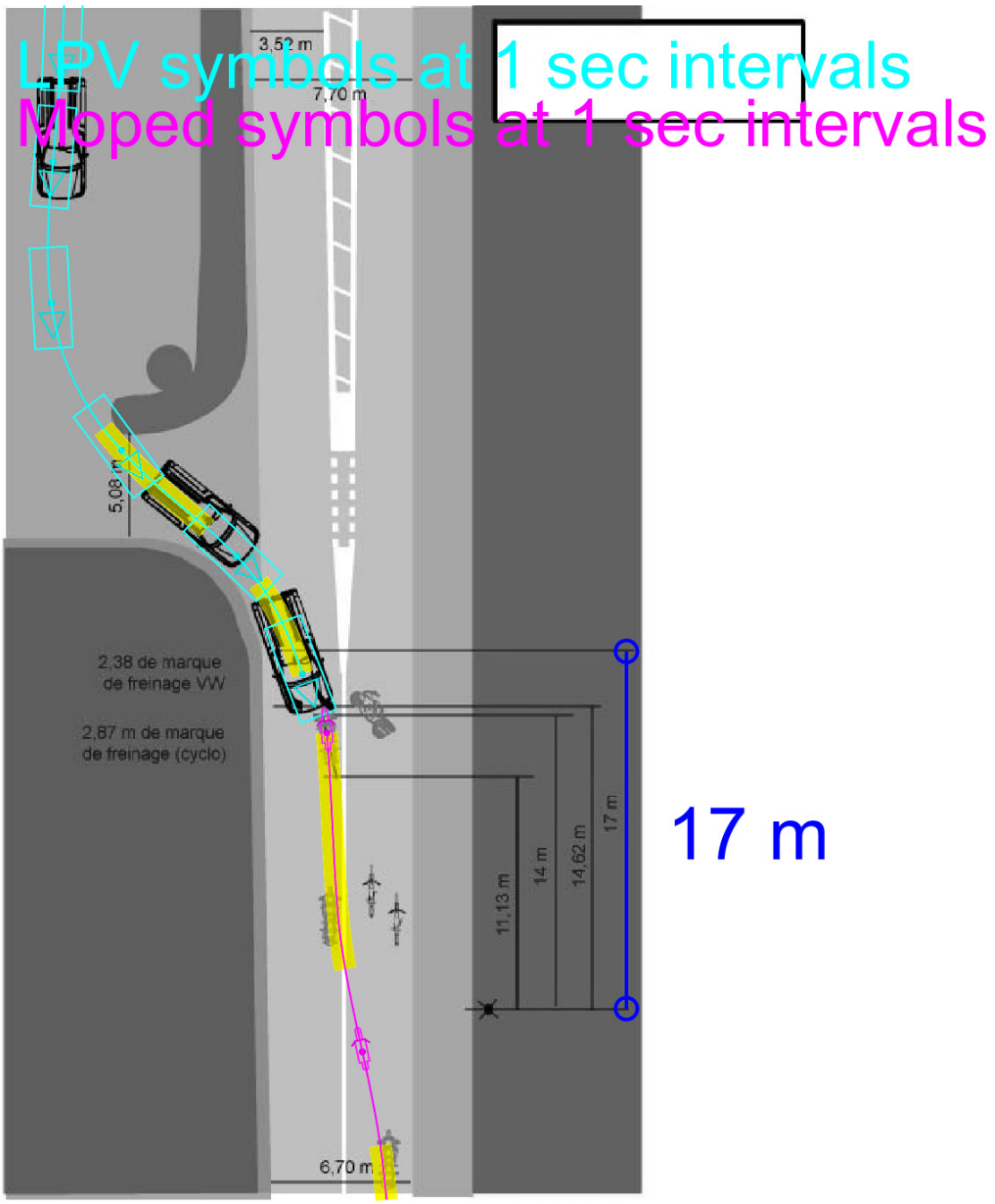

Figure 4. Estimated pre-crash trajectories for the examplar head-on case.

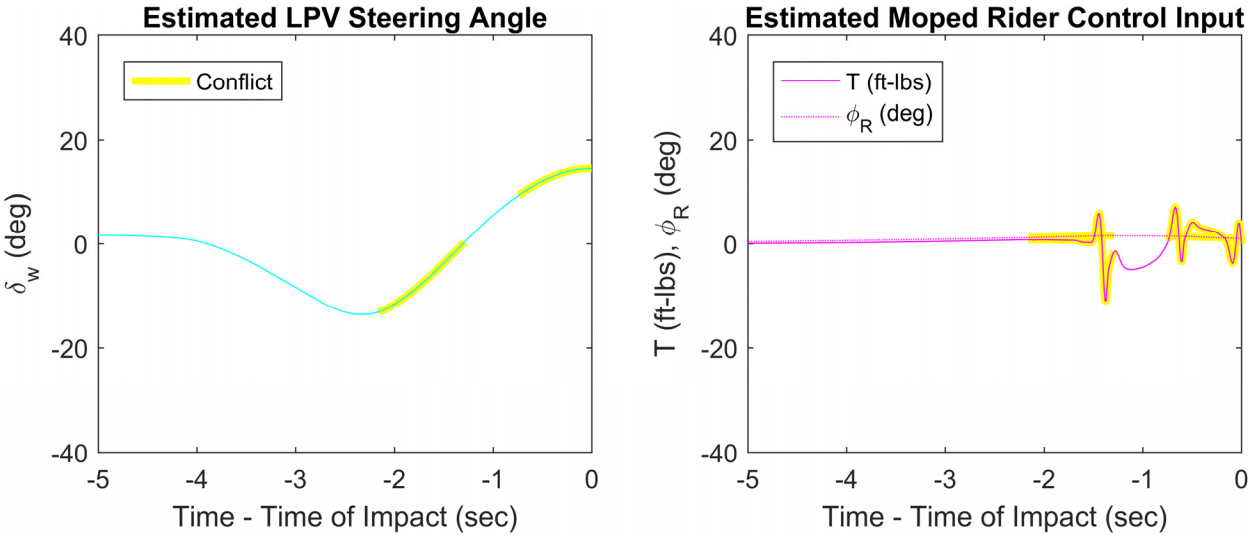

Figure 5. Directional control inputs versus time for the exemplar head-on case.

This example case illustrates the directional responses of the LPV and PTW to the vehicle control inputs. It was assumed for this case that the moped was traveling at approximately 7 km/h above the posted speed limit of 50 km/h 10 sec prior to impact.[5] At the same time a LPV was leaving a parked position. The M-AART estimated that the driver turned to the left (negative steer angle) to approach the roadway, then turned to the right (positive steer angle) to merge onto the roadway going in the opposite direction to the PTW. At the time of the coded precipitating event, 2.1 sec before impact, the coded data indicates the PTW was traveling at a constant speed of 58 km/h, and the LPV had accelerated to 29 km/h, as indicated in Figure 3. The rider then passed to the left of two other PTWs traveling in the same direction. The estimated rider passing maneuver involved first applying positive steer torque to turn to the left, then negative steer torque to turn to the right, then positive torque to recover as depicted in Figure 5. The coded data indicates both vehicles braked and the coded impact speeds were 21 km/h and 54 km/h respectively. Figure 4 shows the close agreement between the estimated vehicle trajectories and the available information. The maximum differences between the digitized LPV and PTW positions and the corresponding estimated trajectories are 0.7 m and 0.5 m respectively.

This example also illustrates both a momentary conflict which is benign and the final conflict which resulted in impact. The benign conflict occurs between t=-2.2 sec and t=-1.3 sec. This is when the LPV is headed towards the roadway and the vehicle velocity vectors intersect. The risk of collision will be small if the LPV turns to merge onto the roadway and the both vehicles stay within their respective lanes. This benign conflict ends as expected when the LPV turns to merge onto the roadway. The final conflict then begins 0.7 sec before impact. This is after the PTW crosses the lane boundary into the PTWs path. The coded data for this cases also indicates that the moped operator's view of the LPV was obstructed.

Example case with both vehicles turning

Another example pre-crash trajectory reconstruction is illustrated in Figure 6. This case involves a motorcycle turning left across the LPV path while the LPV is also turning left to follow the main roadway. Therefore both vehicles are turning left. The maximum differences between the digitized LPV and PTW positions and the corresponding estimated trajectories are 0.6 m and 0.2 m respectively. The estimated trajectories are in a state of conflict beginning 1.6 sec prior to impact. The coded data indicates that that there were LPV driver and PTW rider "*view obstructions present that contributed to accident causation*." Therefore the conflict may not have been detected because of visual obstructions. The LPV and PTW vehicle level NASS accident types illustrated in Appendix A that best describe this case were VATYPE=68 and PATYPE=82 respectively, and therefore the "T2/OD" crash configuration group according to Table 2.

[5] The coded data for this case indicate that the moped had enhanced motor power and a modified exhaust.

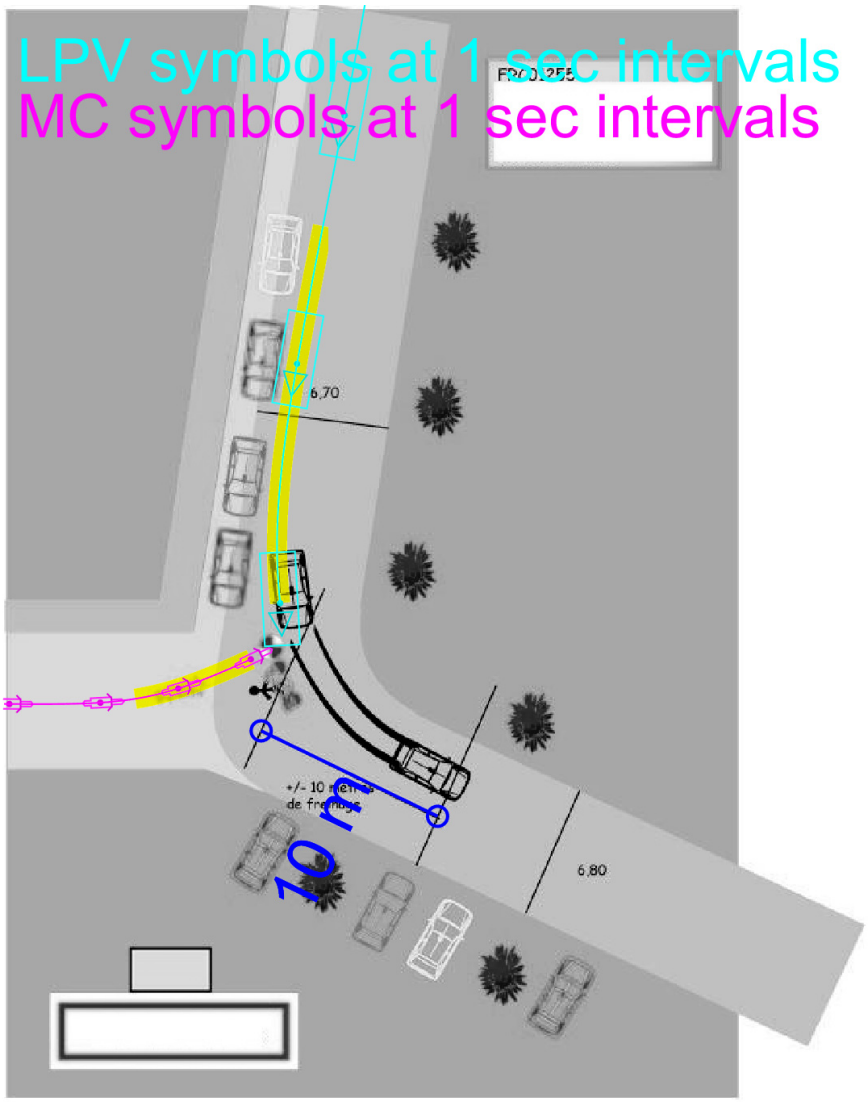

Figure 6. Estimated pre-crash trajectories and conflict for an exemplar case with both vehicles turning.

Pre-crash LPV-PTW trajectories

The estimated trajectories for the 367 reconstructed cases are summarized in Figure 7 through Figure 12. Figure 7 and Figure 8 show the results for the 266 EU MAIDS cases and 101 US MCCS data side by side. Figure 9 and Figure 10 show the results for the 242 cases involving a motorcycle and 125 cases involving a moped side by side. Figure 11 and Figure 12 show the results without and with a coded visual obstruction that contributed to the accident causation. Figure 7, Figure 9, and Figure 11 show the estimated PTW trajectories relative to the LPV in the LPV reference frame. The dotted lines show the relative positions of the PTW cg at 0.1 sec time intervals for the 3 sec prior to impact. Therefore pre-crash trajectories with higher velocities have larger spacing between the dots compared to trajectories with lower velocities. Likewise Figure 8, Figure 10, and Figure 12 show the estimated LPV trajectories relative to the PTW in the PTW reference frame. The relative vehicle positions when the conflict state $C(t) = \text{true}$ are highlighted in yellow.

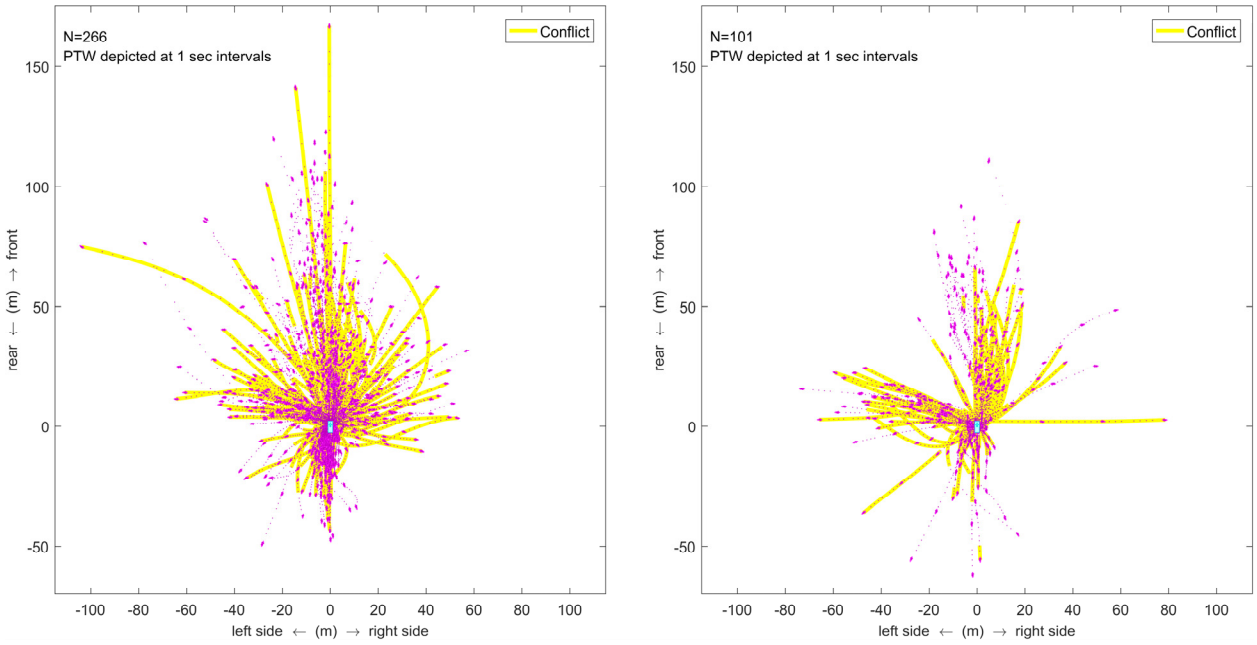

Figure 7. Estimated PTW trajectories and conflicts relative to the LPV for the 3 sec prior to impact by region (266 EU MAIDS cases on the left versus 101 US MCCS cases on the right).

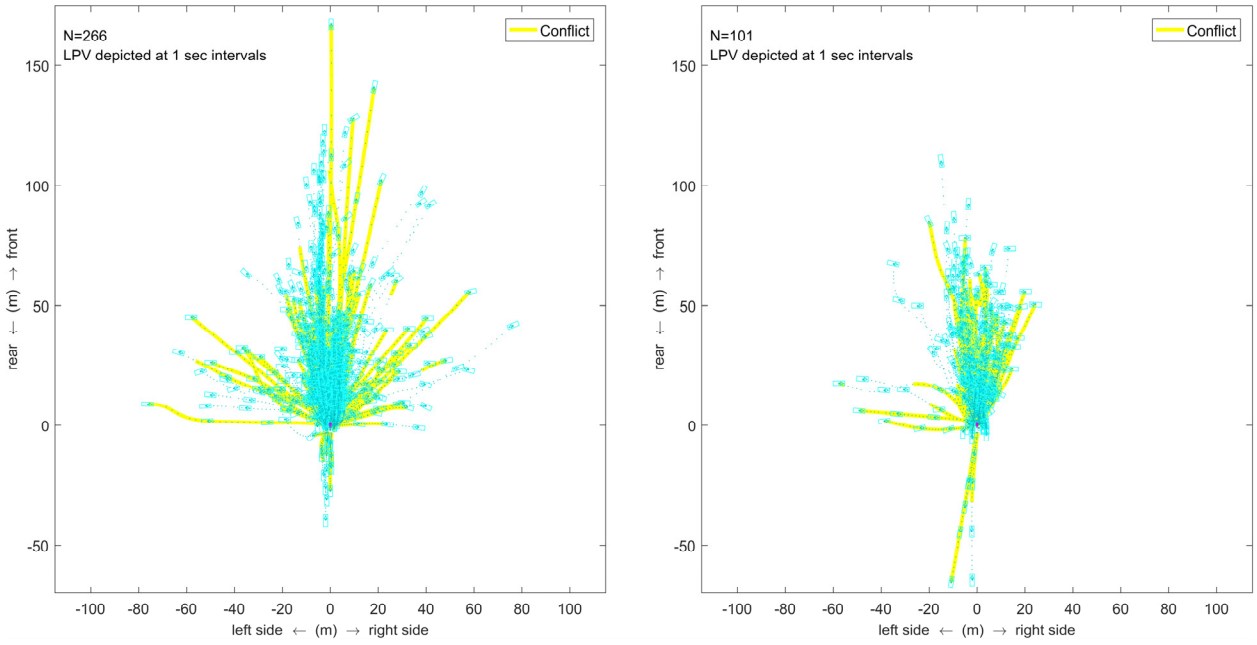

Figure 8. Estimated LPV trajectories and conflicts relative to the PTW for the 3 sec prior to impact by region (266 EU MAIDS cases on the left versus 101 US MCCS cases on the right).

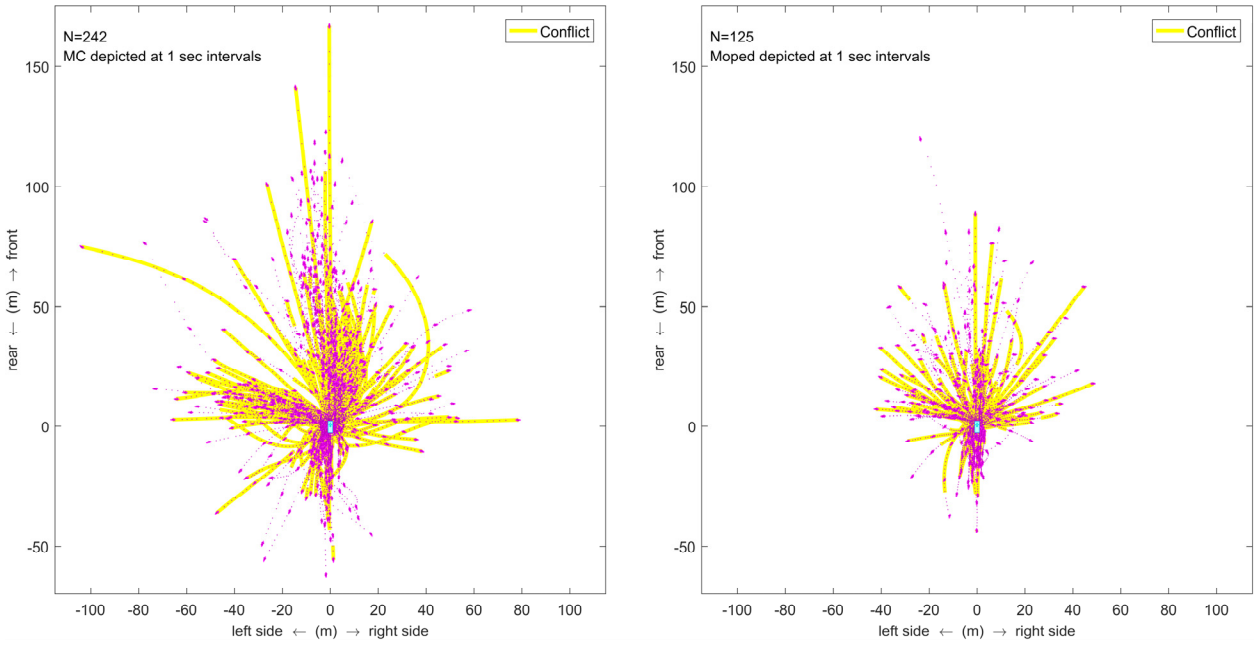

Figure 9. Estimated PTW trajectories and conflicts relative to the LPV for the 3 sec prior to impact by PTW type (242 motorcycle cases on the left versus 125 moped cases on the right).

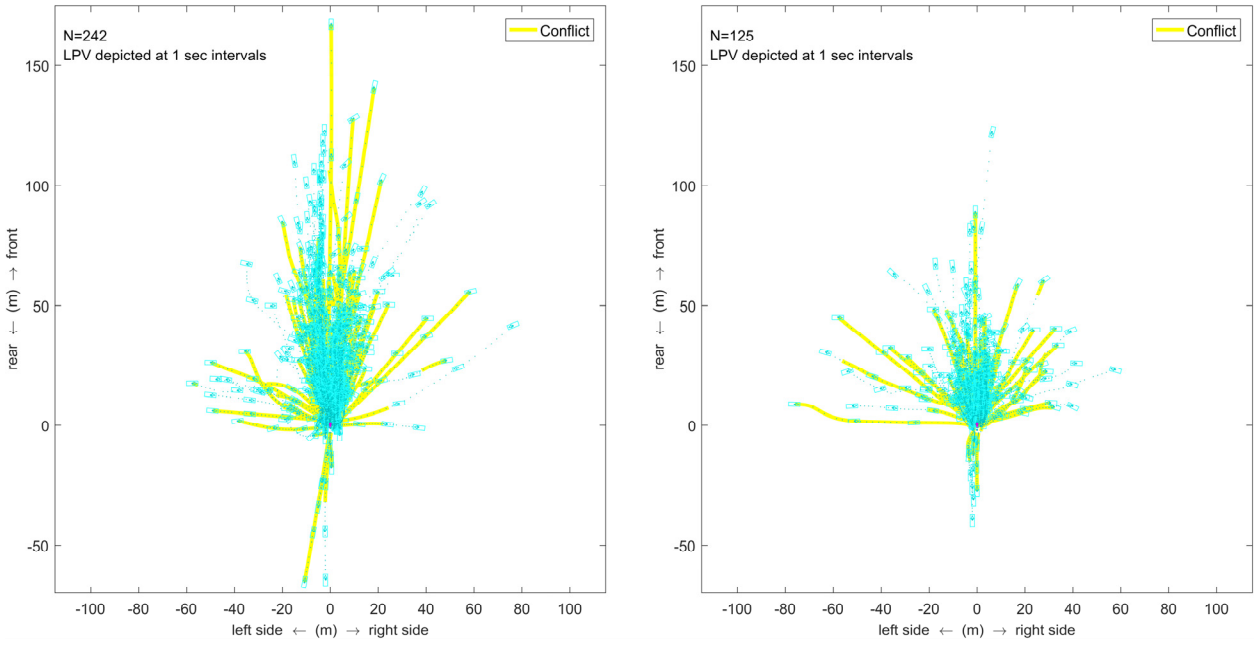

Figure 10. Estimated LPV trajectories and conflicts relative to the PTW for the 3 sec prior to impact by PTW type (242 motorcycle cases on the left versus 125 moped cases on the right).

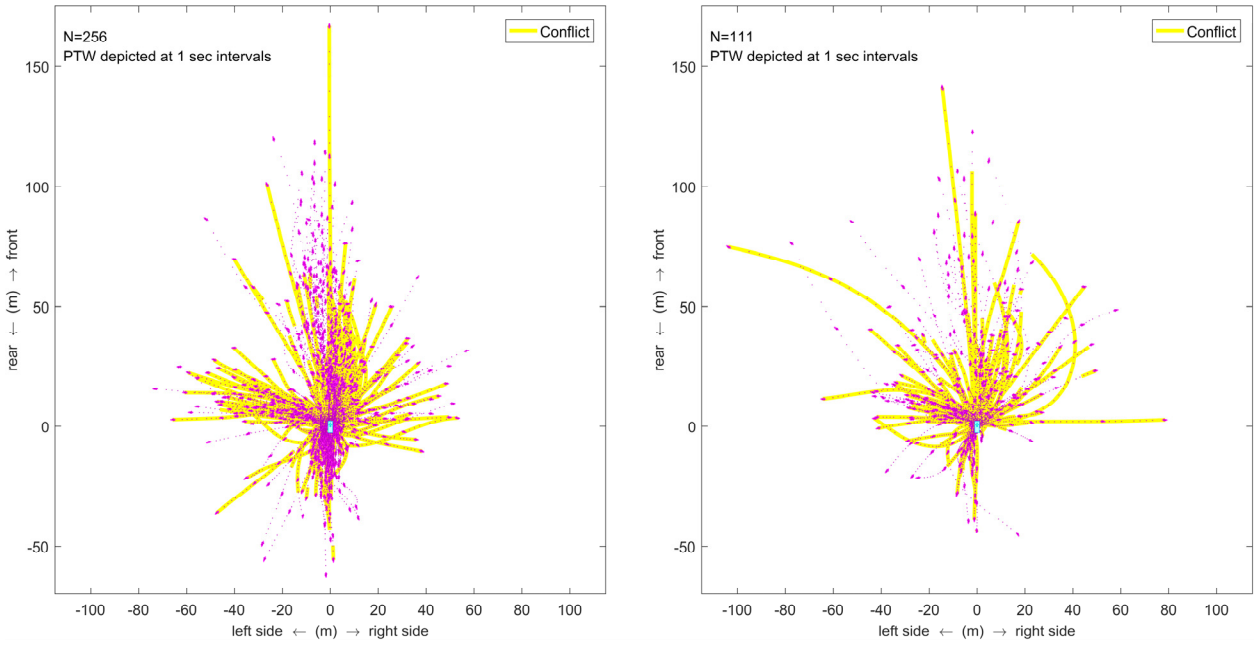

Figure 11. Estimated PTW trajectories and conflicts relative to the LPV for the 3 sec prior to impact by visual obstruction (256 cases without visual obstruction on the left versus 111 cases with visual obstruction on the right).

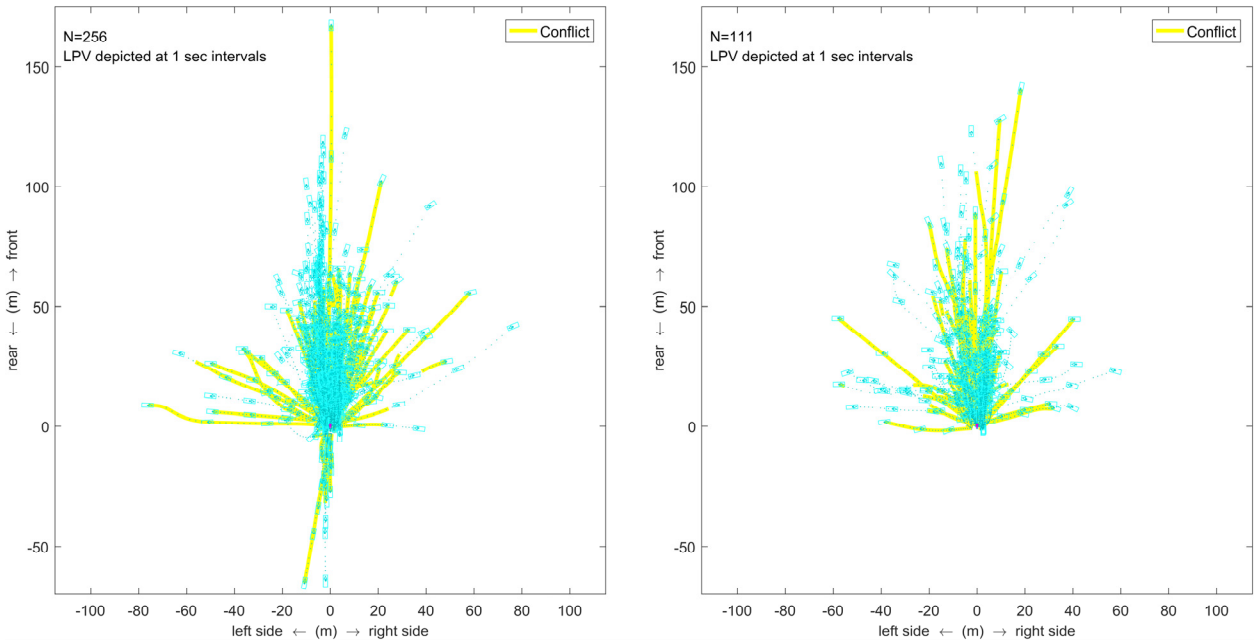

Figure 12. Estimated LPV trajectories and conflicts relative to the PTW for the 3 sec prior to impact by visual obstruction (256 cases without visual obstruction on the left versus 111 cases with visual obstruction on the right).

The results in Figure 7 and Figure 8 compare the 266 EU MAIDS cases and the 101 US MCCS cases. These results indicate that the some of the EU cases have higher relative pre-crash closing velocities than the US cases. These results also indicate that the EU cases are more broadly distributed in relative approach angle than the US cases. The

smaller distribution of US cases compared to the EU cases may be partially attributed to the smaller US sample size. The US cases are primarily from a suburban sampling region with very few cases on rural roads or limited access divided highways. The EU cases were also sampled ten years before the US cases.

The results in Figure 9 and Figure 10 compare the 242 cases involving a MC to the 125 cases involving a moped. All but one of the moped cases are from the MAIDS database. These results indicate that the LPV-MC cases tend to have higher relative closing velocities than the LPV-moped cases, which is consistent with moped speed restrictions in the EU. The differences are most apparent in the longitudinal direction in the PTW reference frame. Both the MC and moped cases have a wide distribution of relative approach angles.

The results in Figure 11 and Figure 12 compare the 111 cases that had a coded visual obstruction that contributed to the conflict to the 256 cases that did not. The most noticeable difference is that none of the PTW rear-end LPV cases had a visual obstruction. This suggests that these PTW rear-end LPV cases may involve rider distraction or other factors.

Pre-crash LPV-PTW conflicts

The highlighted conflict state results in Figure 9 to Figure 12 indicate that many of the conflicts begin less than 3 sec before impact. The median start time for the MAIDS and MCCS data are 1.4 sec and 1.6 sec before impact respectively, and approximately 1.4 sec before impact overall.

The distributions of the conflict start times by crash configuration group and PTW type are illustrated in Figure 13. The crash configuration groups on the horizontal axis of this graph are defined in terms of the NASS accident type according to Table 2. The pre-crash trajectories and conflicts for each of these crash configuration groups are depicted in Appendix B. The vertical axis of this graph is the estimated conflict start time relative to the time of impact, which is a negative value. The vertical range of each box in this figure represents the 25th and 75th percentile values for the conflict start time, and the horizontal line in each box represents the median value. The number of cases for each crash configuration group are indicated by the numerical value shown above the median in each box. The graph is limited to the 5 sec epoch before impact because earlier conflict times are increasingly sensitive to the assumed vehicle speeds and estimated vehicle trajectories (many of which were extrapolated backwards in time before the digitized vehicle positions in the scene diagrams). The last 1.5 sec before impact are indicated by a light red shaded background. This shading represents the epoch where there may be insufficient time for the driver or rider to react to an ADAS warning in order to mitigate or avoid the crash, and therefore the countermeasures involving simple conflict detection and driver warning may not be effective.[6]

The results in Figure 13 indicate 10 of 21 crash configuration groups with median conflict times that began less than 1.5 sec before impact. The six largest of these groups are the LPV LTAP/OD (90 cases), LPV LTAP/SD (29), LPV UT (22), PTW RE (22), HO/ODSS (20), and LPV RTAP/SD (19), which combined represent 55% (202/367) of the reconstructed cases. The 15 cases in the other four crash configuration groups all involve the PTW turning.

[6] According to Neale and Dingus, "[w]hen a driver is looking forward, driver reaction time averages about 1.5 seconds and may be as high as 2.5 or 3.0 seconds in all but the most extreme cases" [15].

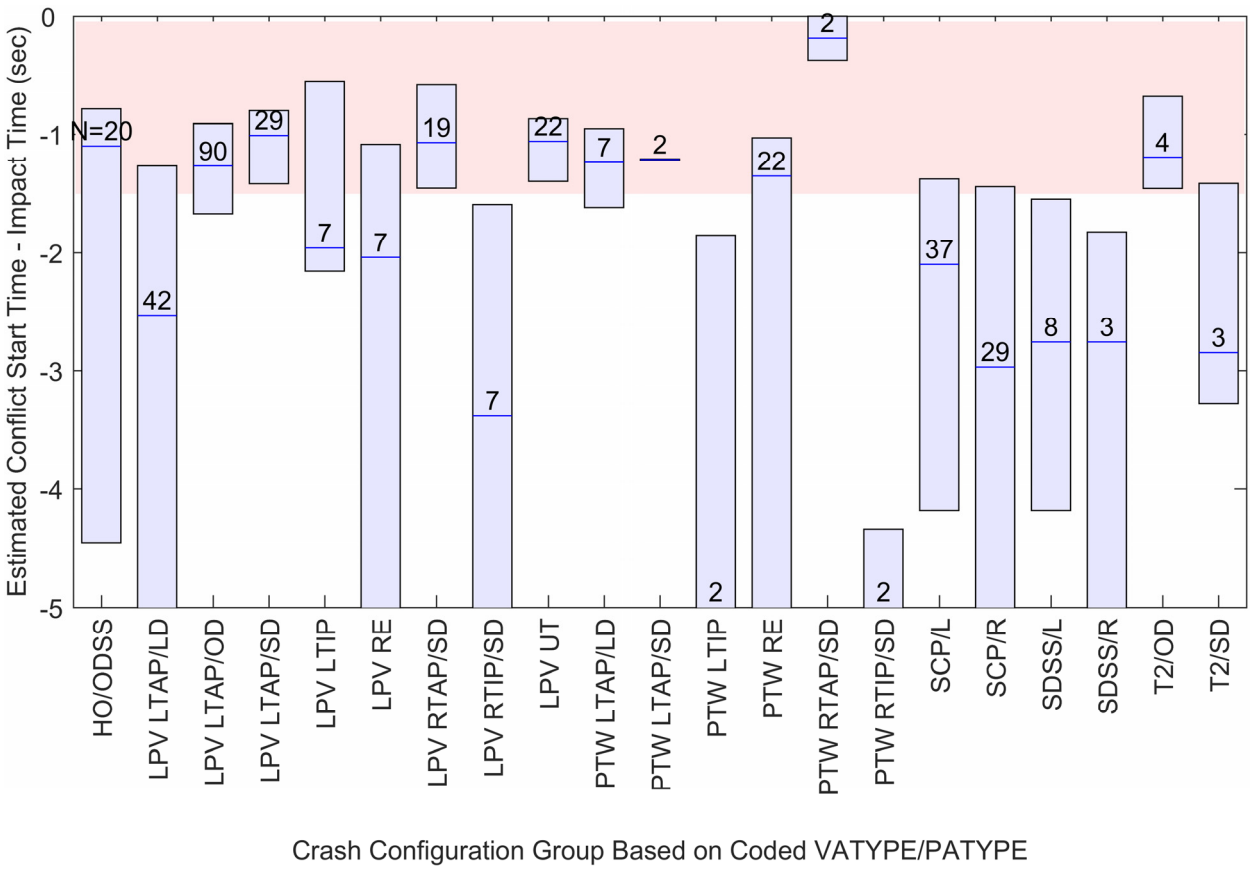

Figure 13. Distributions of estimated LPV-PTW conflict start times by crash configuration group.

Comparison of EU MAIDS and US MCCS cases

The estimated conflict start times are compared in further detail by data source in Figure 14. The format of Figure 14 is similar to Figure 13, but each crash configuration bar is split into pairs. The results for the EU MAIDS cases are depicted by the cyan colored boxes on the left, and the results for the US MCCS cases are depicted by the magenta colored boxes on the right.

The relative frequency of the MAIDS and MCCS cases were compared using a Pearson chi-square test. The resulting p-value=0.06 suggests that the relative frequencies of the MAIDS and MCCS cases are different, but the difference is not statistically significant at the 0.05 level.

The mean conflict start times for each pair were also compared using two-sample t-tests. The t-tests assumed that the start times in each sample are normally distributed with homogenous variance. Therefore only crash configuration groups with four or more cases were tested (i.e., two or more statistical degrees-of-freedom). The only crash configuration group with a statistically significant difference in the mean conflict start time is the LPV LTAP/OD group (p-value<0.01). This statistically significant difference is attributed to the large number of cases (90).

These results indicate that there are some differences between the two data sets, but that these differences are primarily related to the differences in the numbers of cases in each crash type rather than differences within each group. In other words, the conflict times within each crash configuration group are similar because they relative trajectories within each group are similar, as depicted in Appendix B. For example, there are more than 10 MAIDS and 10 MCCS cases in each of the LPV LTAP/LD, LPV LTAP/OD, and SCP/L groups, and the MAIDS and MCCS results for these groups are similar. Therefore we assumed that the two datasets can be combined without substantially changing the conclusions regarding conflict start times by crash configuration group.

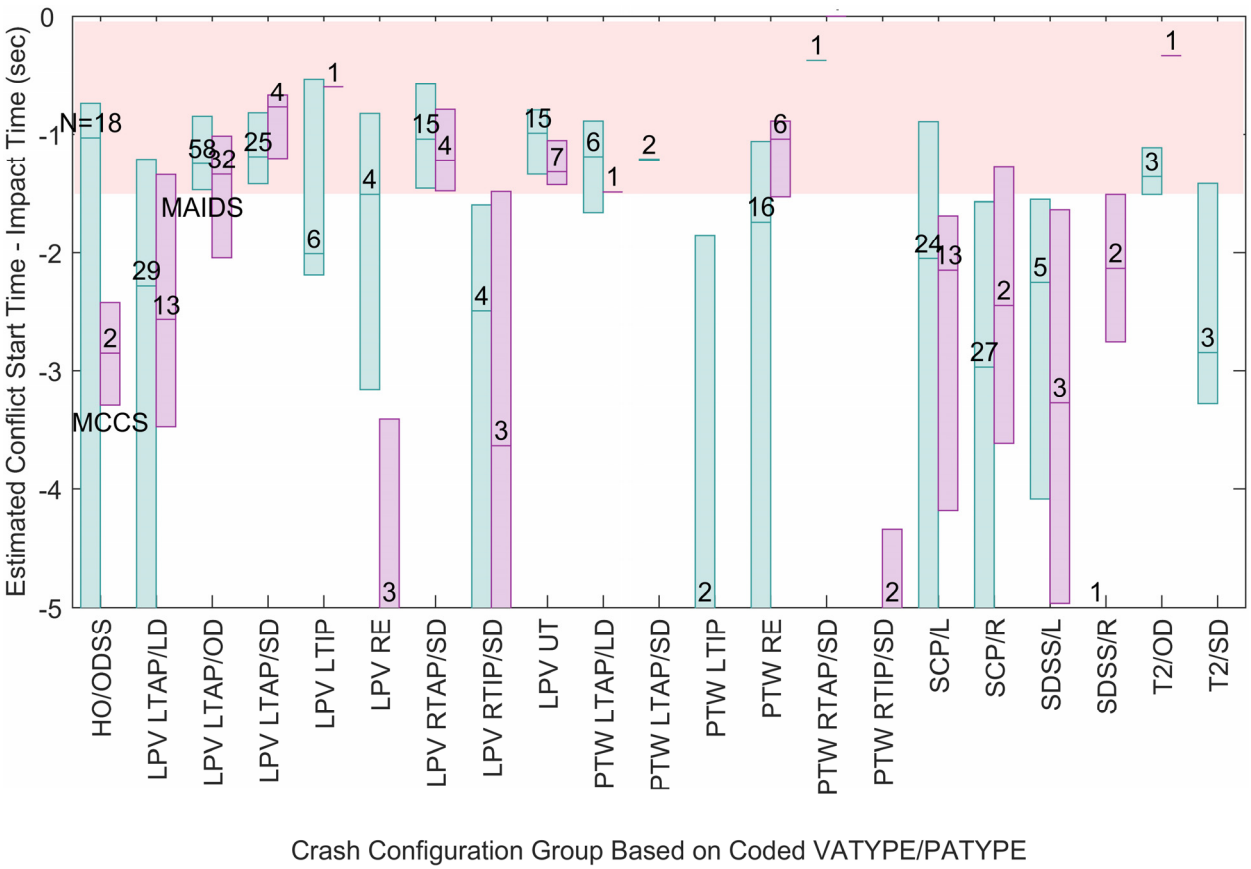

Figure 14. Estimated LPV-PTW conflict start times by crash configuration group and data source.

Comparison by PTW Type

Likewise the results in Figure 15 compare the estimated conflict start time results by PTW type. The format of Figure 15 is similar to Figure 14 but the paired bars are different. The results for motorcycles are depicted by cyan boxes on the left, and the results for mopeds are depicted by magenta boxes on the right.

The relative frequency of the MC and moped cases were also compared using a Pearson chi-square test. The resulting p-value=0.03 indicates that the relative frequencies of the MC and moped cases are statistically significantly different at the 0.05 level. However if the US MCCS cases are excluded, the resulting p-value is 0.37, which is not statistically significant.

The mean conflict start times for the MC and moped in each crash configuration group were also compared using t-tests. None of the groups had a statistically significant differences between the mean MC and moped conflict start times.

These results also indicate that the main differences between the MC and moped crash configurations are due to relative differences in sampling frequency, which may be attributed to difference in the US and EU, but the conflict start times are similar. There are more than 10 MC and 10 moped cases in each of the five LPV LTAP and SCP groups, and the MC and moped results in four of these groups are similar. Therefore we assumed that the two PTW types can be combined without substantially changing the conclusions about the conflict start time results for each crash configuration group.

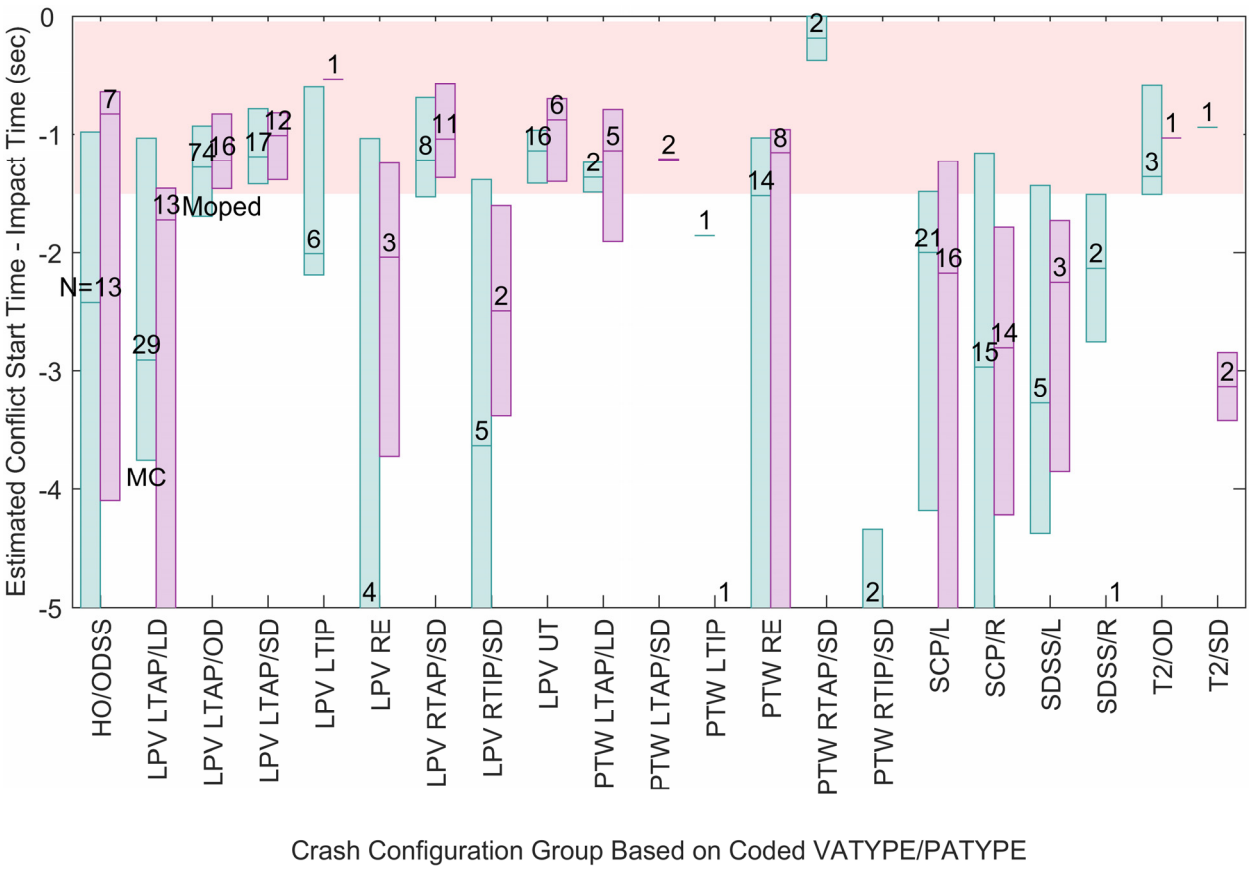

Figure 15. Estimated LPV-PTW conflict start times by crash configuration group and PTW type.

Comparison by Visual Obstruction

The results in Figure 16 compare the estimated conflict start time results by whether or not the coded data indicated that "*view obstructions were present and contributed to accident causation.*" The results in the cyan boxes on the left are without any visual obstruction, and the results in the magenta boxes on the right are with a view obstruction for either the LPV driver, PTW rider, or both. None of the crash configuration groups had a statistically significant difference in the mean conflict start times by visual obstruction, but the differences in the relative number of cases were statistically significantly different (p-value<0.01).

Most (86) of the 111 cases involving a visual obstruction were in the six HO/ODSS, LPV LTAP, and SCP crash configuration groups. There were 247 cases in these six groups combined, and 35% had a coded visual obstruction.

Nearly all (74) of the 79 cases in the LPV LTIP (6), rear end (7+20), RTAP/SD (18+2), and U-turn (21) groups did not have a coded visual obstruction. Therefore other factors such as operator distraction or error may be contributing to these types of crashes. It is unknown how many of the 22 U-turns were legal or not. The HO/ODSS, LPV LTAP/OD and LPV LTAP/SD groups had short conflict epochs regardless of whether or not there was a visual obstruction.

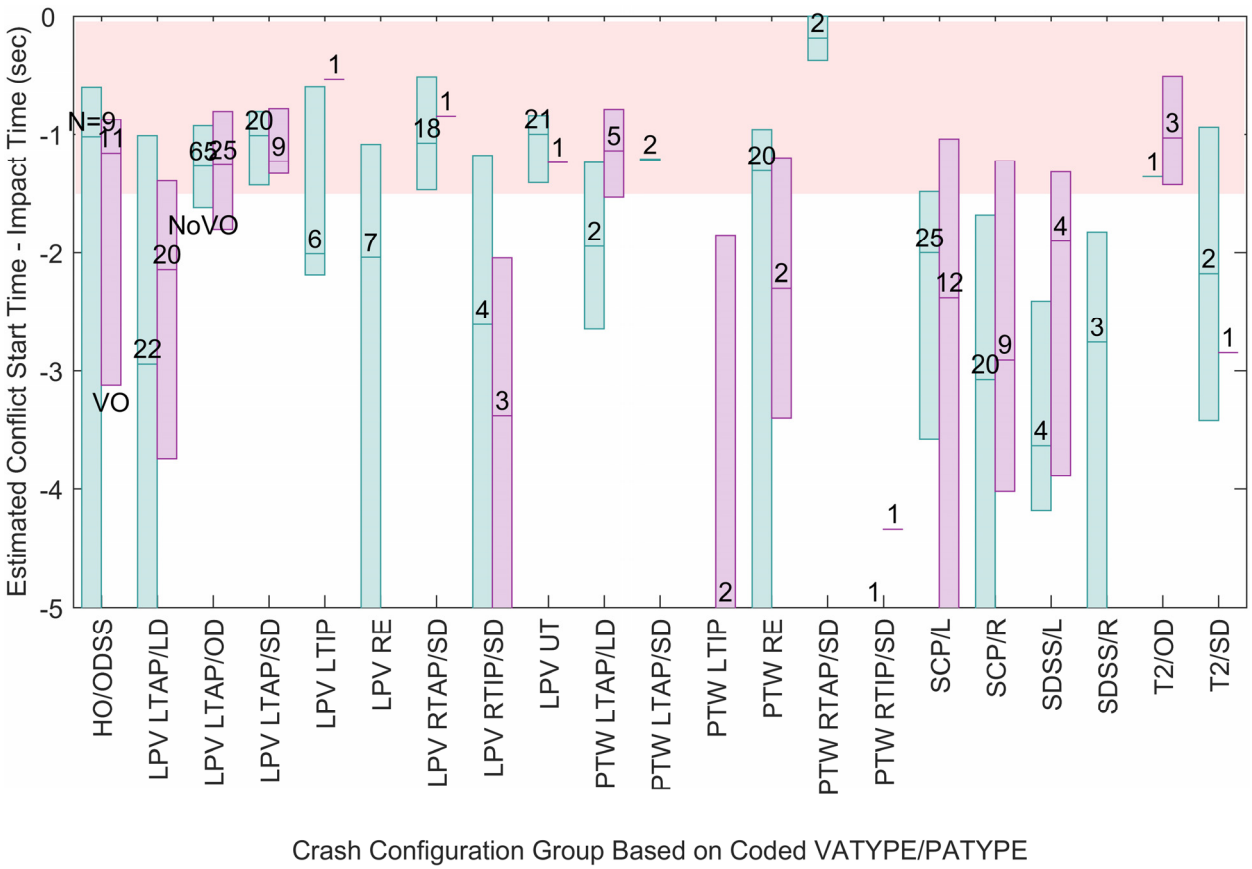

Figure 16. Estimated LPV-PTW conflict start times by crash configuration group and visual obstruction.

DISCUSSION

The effectiveness of potential conflict and crash countermeasures may depend on how soon the conflict is detected before impact. For comparison, the results in Figure 17 illustrate the distribution of conflict start times and collision effectiveness (CE) results for different technology relevant crash types (TRCTs) from a previous ADAS evaluation reported in [18]. The results for the "Primary" TRCT for which the crash avoidance countermeasure was intended to address, and three "secondary" TRCTs in which the technology designer thought the system might also be effective. A CE value of 0 indicates the technology is not effective in avoiding any of the crashes, which is undesirable. A CS value of 1 indicates the technology completely eliminates all of the crashes with the crash type, which is desirable. These results indicate that the crash avoidance countermeasure tends to be more effective for TRCTs with earlier conflict start times. Similar effectiveness results were observed in [11],[19].[7]

[7] The collision effectiveness results in Figure 17 are based on simulated cases that have been weighted to represent the US fleet in the 2009 calendar year. The conflict start times are based on the unweighted unique cases in the simulation sample. Results for the other secondary TRCTs are not shown due to insufficient numbers of reconstructable cases for the evaluation reported in [18].

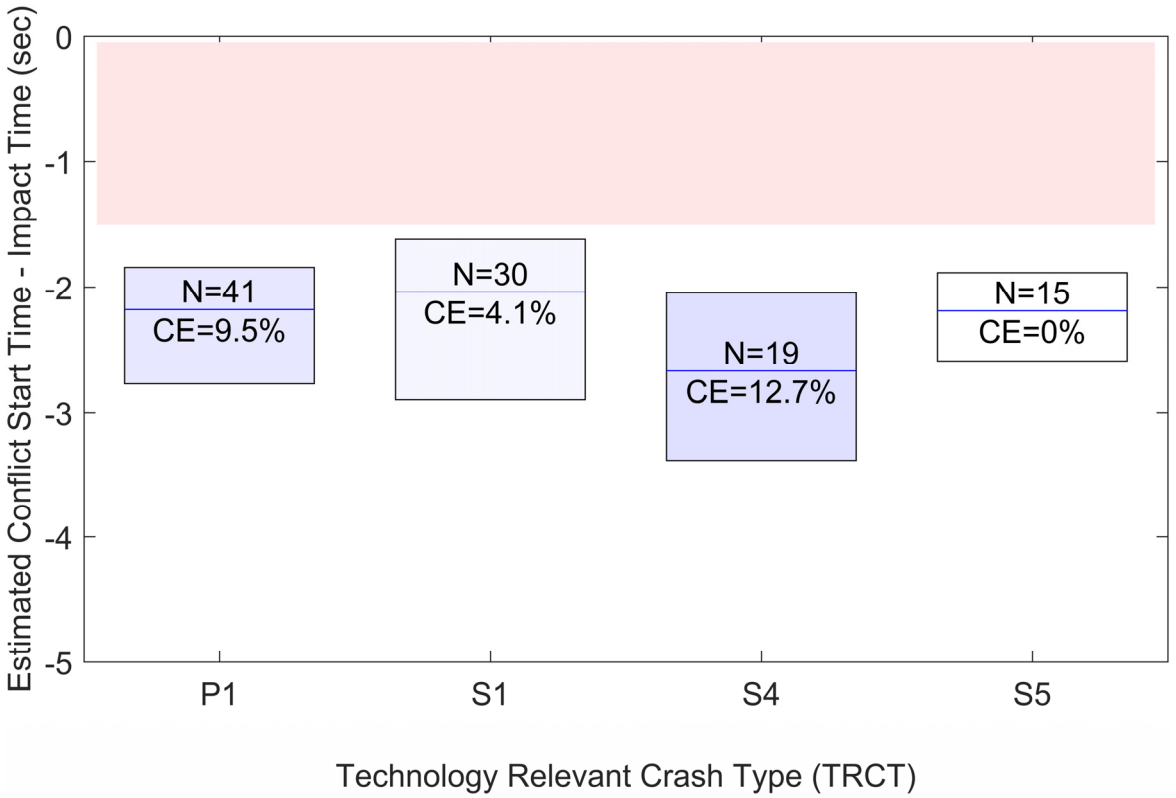

Figure 17. Boxplot distributions of estimated LPV-LPV conflict start times for a pre-production crash avoidance technology.

As previously described, the results in Figure 13 indicate several crash configuration groups with short pre-crash conflict times. The quartile and median times for the 90 LPV LTAP/OD cases were 0.9, 1.3, and 1.7 sec before impact respectively. The results in Figure B3 indicate that the cases from the front left tended to have short conflict times, and there would have been insufficient time to detect and warn the driver before a collision

The quartile and median times for the 29 LPV LTAP/SD cases were 0.8, 1.0, and 1.4 sec before impact respectively. The results in Figure B4 indicate many cases where the PTW may have been in the LPV blind spot during the conflict. However a BSW system might not have been able to detect a conflict and warn the driver with sufficient time to avoid a collision.

Other potential countermeasures could be ADASs such as AEB that are not affected by the driver response time, or by detecting and warning the driver about the impending conflict sooner. The conflict could be detected sooner by changing the vehicle "contact" criteria to include close encounters or use more advanced sensors and algorithms. However this could also result in false alarms, which is undesirable.

Impending conflicts could also be detected sooner and avoided or mitigated if the vehicle operators can see each other and properly communicate their intended paths before the conflict starts. One way to achieve this is by maximizing visual scanning strategies and vehicle conspicuity, and proper use and detection of turn signals. This could also be enhanced by safety-relevant cooperative C-ITS V2V communications systems such as Motorcycle Approach Indication (MAI) and Motorcycle Approach Warning (MAW)[20].

C-ITS also has the potential to address conflicts that cannot be detected early due to visual obstructions (e.g., the exemplar cases). The results in Figure 16 indicate that many HO/ODSS, LPV LTAP, and SCP crashes involved a visual obstruction, but there were also other crash configuration groups that did not.

LIMITATIONS

The accuracy of the results are based on a number of assumptions, approximations, and limitations in the data and methods used, many of which are described in [5], [6], [7], [11]. These include the accuracy and representativeness of the MAIDS and MCCS data, as well as the accuracy of the vehicle directional control models used.

SUMMARY/CONCLUSIONS

Pre-crash trajectories have been estimated for 367 crashes involving a light passenger vehicle (LPV) and a motorcycle or moped for the purposes of evaluating the effectiveness and benefits of crash avoidance technologies in avoiding or mitigating these types of crashes. This was accomplished by extending methods and tools to address LPV-PTW crashes. Pre-crash trajectories of 266 cases in the MAIDS database from France, Germany, and Italy and 101 cases in the US MCCS database were reconstructed using a new Motorcycle Automated Accident Reconstruction Tool (M-AART). The resulting pre-crash trajectories of the PTW as viewed from the LPV were broadly distributed in approach angle, with a possible gap from the right rear quadrant (i.e., between the 3 and 6 o'clock directions). The US MCCS data also exhibited a gap between the 10 and 11 o'clock directions. There were relatively few cases where the LPV approached the PTW from the rear (e.g., rear-end).

Further analysis of these estimated pre-crash trajectories indicate that the conflicts begin later, and therefore with smaller TTC values, compared to LPV-LPV crashes that were reconstructed for previous ADAS evaluations. This may be partially due to the smaller length and width of PTWs compared to LPVs, in which LPV-PTW close encounters do not result in a collision, but the same LPV-LPV trajectory would. Therefore LPV-PTW countermeasures may need to address the pre-conflict phase in order to be effective.

It was also observed that 30% of the cases involved a visual obstruction as reported in the crash databases. Many of the cases with a visual obstruction were in the HO/ODSS, LPV LTAP, or SCP crash configuration groups. These cases could potentially be addressed by C-ITS countermeasures such as MAI and MAW.

Only five of the 79 cases in the LPV LTIP, rear end, RTAP/SD, and U-turn crash configuration groups had a coded visual obstruction that contributed to the crash causation. Therefore other factors such as operator distraction and error may be contributing to these types of crashes.

This information can be used to guide further LPV-PTW crash avoidance research, including collecting and analyzing additional on-scene in-depth pre-crash and crash data, field operational experiments, driving simulator experiments, modeling and simulation. The results of this research can potentially help to define requirements for LPV-PTW conflict and crash countermeasures (e.g., BSW, C-ITS) and the development of performance confirmation tests (e.g., New Car Assessment Program (NCAP)). These pre-crash scenarios can also be integrated into the ACAT SIM Crash Sequence Simulation Module in order to estimate the safety benefits and effectiveness of potential countermeasures.

REFERENCES

[1] "Annual Accident Report 2018," European Commission, Directorate General for Transport, June 2018 (https://ec.europa.eu/transport/road_safety/sites/roadsafety/files/pdf/statistics/dacota/asr2018.pdf, accessed 2019-01-18).

[2] "Traffic Safety Facts 2016," DOT HS 812 554, National Highway Traffic Safety Administration, Washington, DC, May 2018 (https://crashstats.nhtsa.dot.gov/Api/Public/ViewPublication/812554, accessed 2018-07-29).

[3] UN ECE, "Consolidated Resolution on the Construction of Vehicles," ECE/TRANS/WP.29/78/Rev.2, United Nations Economic and Social Council, 2011.

[4] Lenkeit, J. F. and Smith, T., "Preliminary Study of the Response of Forward Collision Warning Systems to Motorcycles," Proc. 11th International Motorcycle Conference, Cologne, Germany, October 2016.

[5] Van Auken, R.M., Lenkeit, J., and Smith, T., "Passenger Vehicle-Motorcycle Pre-Crash Trajectory Reconstruction Results based on an Extended Application of the NHTSA-Honda-DRI ACAT Safety Impact Methodology," Paper No. 18-04891, Transportation Research Board Annual Meeting, Washington, DC, January 7-11, 2018.

[6] Van Auken, R.M., Lenkeit, J., and Smith, T., "Passenger Vehicle-Motorcycle Pre-Crash Trajectory Reconstruction and Conflict Analysis Results Based On an Extended Application of the Honda-DRI ACAT Safety Impact Methodology," SAE Technical Paper 2018-01-0510, 2018, doi:10.4271/2018-01-0510.

[7] Van Auken, R.M., Lenkeit, J., and Smith, T., and Kebschull, S, "Passenger Vehicle-Powered Two Wheeler Pre-Crash Trajectory Reconstruction and Conflict Analysis Results for Real-World Crashes in France, Germany, and Italy," Proc. 12th International Motorcycle Conference, Cologne, Germany, October 2018.

[8] MAIDS, "In-Depth Investigations of Accidents Involving Powered Two Wheelers, Final Report 2.0" ACEM, 2009 (http://www.maids-study.eu/pdf/MAIDS2.pdf, accessed 2017-11-13).

[9] Anon., "Motorcycle Crash Causation Study," accomplished by Oklahoma State University, Westat and Dynamic Sciences, Inc. for the FHWA, Turner Fairbank Highway Research Center, McLean, VA, 2016.

[10] OECD, "Motorcycles: Common international methodology for in-depth accident investigations," Organisation for Economic and Community Development, Paris, France, 2008.

[11] Van Auken, R.M., Zellner, J.W., Chiang, D.P., Kelly, J. et al., "Advanced Crash Avoidance Technologies (ACAT) Program – Final Report of the Honda-DRI Team," DOT HS 811 454, National Highway Traffic Safety Administration, Washington, DC, June 2011.

[12] Van Auken, R.M., Lenkeit, J., and Smith, T., "Potential Application of the NHTSA-Honda-DRI ACAT "Safety Impact Methodology" (SIM) to the Evaluation of Automatic Emergency Braking System Effectiveness in Avoiding and Mitigating Collisions with Motorcycles," Paper Number 17-0179, Proc. 25th International Technical Conference on the Enhanced Safety of Vehicles (ESV), Detroit, June 5-8, 2017.

[13] "Fatality Analysis Reporting System (FARS) Analytical User's Manual 1975-2016," DOT HS 812 447, National Highway Traffic Safety Administration, Washington, DC, October 2017.

[14] "Traffic Safety Basic Facts 2018 – Single Vehicle Accidents," European Road Safety Observatory, European Commission, 2018 (https://ec.europa.eu/transport/road_safety/sites/roadsafety/files/pdf/statistics/dacota/bfs2018_single_vehicle_accident.pdf, accessed 2018-06-25).

[15] Neale, V.L. and Dingus, T.A., "Motor Vehicle Warnings," in "Handbook of Warnings," (Mahwah, NY, Lawrence Erlbaum Associates, 2006), 687-700, doi: 10.1177/106480460701500307.

[16] Weir, D.H., Zellner, J.W., and Teper, G.L., "Motorcycle Handling, Volume II: Technical Report," Publication DOT HS 804 191, NHTSA, U.S. Department of Transportation, 1978.

[17] Zellner, J.W. and Weir, D.H., "Moped Directional Dynamics and Handling Qualities," SAE Technical Paper 790260, 1979, https://doi.org/10.4271/790260.

[18] Zellner, J.W., Van Auken, R.M., Silberling, J.Y., Kelly, J., Hagoski, B.K., Sugimoto, Y., and Urai, Y., "Evaluation of a Pre-Production Head-on Crash Avoidance Assist System using an Extended Safety Impact Methodology (SIM)," Paper Number 15-0176, Proc. 24th ESV, Gothenburg, June 2015.

[19] Scanlon, J.M., Sherony, R., Gabler, H.C., "Injury mitigation estimates for an intersection driver assistance system in straight crossing path crashes in the United States," Traffic Injury Prevention, 18:sup1, S9-S17, 2017, DOI: 10.1080/15389588.2017.1300257.

[20] Fischer, H., Kohlinger, O., and Purschwitz, A, "Motorcycles in connected traffic – a contribution to safety", 11th International Motorcycle Conference, Cologne, Germany, October 3, 2016.

CONTACT INFORMATION

R. Michael Van Auken
355 Van Ness Avenue, Suite 200
Torrance, California 90501
United States
RMV@DynRes.com
+1-310-212-5211.

ACKNOWLEDGMENTS

The European Association of Motorcycle Manufacturers (ACEM) provided the MAIDS database. Gratitude is expressed to Antonio Perlot, Veneta Vassileva, and John Paul Peters for their assistance.

Thanks to DRI staff member Paul Satrom for his assistance digitizing the scene diagrams for the M-AART reconstructions.

DEFINITIONS/ABBREVIATIONS

AART	Automated Accident Reconstruction Tool (Honda-DRI ACAT SIM Module 1.3).
ACAT	Advanced Crash Avoidance Technology.
ACEM	European Association of Motorcycle Manufacturers (https://www.acem.eu/).
ADAS	Advanced Driver Assistance Systems.
AEB	Automatic Emergency Braking.
BSW	Blind Spot Warning.
$C(t)$	The estimated state of conflict at time t based on the vehicle positions and velocities at time t. $C(t)$ is true if and only if the vehicles will eventually contact if their velocities remain constant.
CE	Collision Effectiveness – a measure of the ability to avoid a crash.
cg	Center of gravity
C-ITS	Cooperative Intelligent Transportation System.
DRI	Dynamic Research, Inc. (http://www.dynres.com/).
FCW	Forward Collision Warning.
FHWA	US Department of Transportation Federal Highway Administration (https://www.fhwa.dot.gov/).
L1	"A two-wheeled vehicle with an engine cylinder capacity in the case of a thermic engine not exceeding 50 cm^3 and whatever the means of propulsion a maximum design speed not exceeding 50 km/h" as defined in UN/ECE/TRANS/WP.29/78 Rev 2. (i.e., a moped).
L3	"A two-wheeled vehicle with an engine cylinder capacity in the case of a thermic engine exceeding 50 cm^3 or whatever the means of propulsion a maximum design speed exceeding 50 km/h" as defined in UN/ECE/TRANS/WP.29/78 Rev 2. (i.e., a motorcycle).
LPV	Light passenger vehicle, comprising passenger cars, light trucks and vans.
M-AART	A specialized version of the ACAT SIM AART for LPV-PTW crashes.
MAI	Motorcycle Approach Indication, a C-ITS V2V technology.
MAIDS	Motorcycle Accidents In-Depth Study [8] (http://www.maids-study.eu/).
MAW	Motorcycle Approach Warning, a C-ITS V2V technology
MC	Motorcycle (L3 vehicle).
MCCS	Motorcycle Crash Causation Study [9].
NASS	National Automotive Sampling System (https://www.nhtsa.gov/research-data/national-automotive-sampling-system-nass).
NCAP	New Car Assessment Program (e.g., EuroNCAP)
NHTSA	US Department of Transportation National Highway Traffic Safety Administration (https://www.nhtsa.gov/).
OECD	Organisation for Economic Co-operation and Development (https://www.oecd.org/).

POV	Principal other vehicle.
PTW	Powered two wheeler, comprising L1 and L3 vehicles.
SIM	Safety Impact Methodology.
TRCT	Technology Relevant Crash Type.
TTC	Time-to-Collision.
V2V	Vehicle-to-Vehicle [Communications].

APPENDIX A – NASS ACCIDENT TYPES FOR TWO-VEHICLE COLLISIONS

VATYPE and PATYPE Accident Type Codes

Category	Configuration	ACCIDENT TYPES (Includes Intent)		
II. Same Trafficway Same Direction	D. Rear-End	20 → 22, 21, 23 STOPPED 21, 22, 23 ; 24 → 26, 25, 27 SLOWER 25, 26, 27 ; 28 → 30, 29, 31 DECELERATING 29, 30, 31	(EACH - 32) SPECIFICS OTHER	(EACH - 33) SPECIFICS UNKNOWN
	E. Forward Impact	34→35 CONTROL/ TRACTION LOSS ; 36→37 CONTROL/ TRACTION LOSS ; 38→39 AVOID COLLISION WITH VEHICLE ; 40→41 AVOID COLLISION WITH OBJECT	(EACH - 42) SPECIFICS OTHER	(EACH - 43) SPECIFICS UNKNOWN
	F. Sideswipe Angle	44→46 ; 45→45 ; 47	(EACH - 48) SPECIFICS OTHER	(EACH - 49) SPECIFICS UNKNOWN
III. Same Trafficway Opposite Direction	G. Head-On	50→51 LATERAL MOVE	(EACH - 52) SPECIFICS OTHER	(EACH - 53) SPECIFICS UNKNOWN
	H. Forward Impact	54→55 CONTROL/ TRACTION LOSS ; 56→57 CONTROL/ TRACTION LOSS ; 58→59 AVOID COLLISION WITH VEHICLE ; 60→61 AVOID COLLISION WITH OBJECT	(EACH - 62) SPECIFICS OTHER	(EACH - 63) SPECIFICS UNKNOWN
	I. Sideswipe/ Angle	64→65 LATERAL MOVE	(EACH - 66) SPECIFICS OTHER	(EACH - 67) SPECIFICS UNKNOWN
IV. Change Trafficway Vehicle Turning	J. Turn Across Path	68→69 INITIAL OPPOSITE DIRECTIONS ; 70→71, 72→73 INITIAL SAME DIRECTION	(EACH - 74) SPECIFICS OTHER	(EACH - 75) SPECIFICS UNKNOWN
	K. Turn Into Path	77→76, 79→78 TURN INTO SAME DIRECTION ; 80→81, 82→83 TURN INTO OPPOSITE DIRECTIONS	(EACH - 84) SPECIFICS OTHER	(EACH - 85) SPECIFICS UNKNOWN
V. Intersecting Paths (Vehicle Damage)	L. Straight Paths	87→86 ; 88→89	(EACH - 90) SPECIFICS OTHER	(EACH - 91) SPECIFICS UNKNOWN
VI. Miscellaneous	M. Backing Etc.	92→93 OTHER VEHICLE OR OBJECT BACKING VEHICLE	98 OTHER ACCIDENT TYPE 99 UNKNOWN ACCIDENT TYPE 00 NO IMPACT	

Source: NASS GES Analytical User's Manual, 1998-2000.

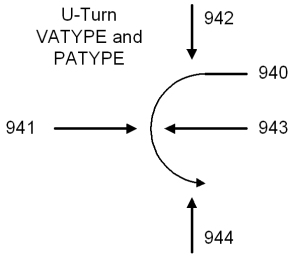

APPENDIX B – PRECRASH TRAJECTORIES AND CONFLICTS BY CRASH CONFIGURATION GROUP

The estimated pre-crash trajectories and conflicts for the 3 sec prior to impact are illustrated in Figures A1 through A24 for the 24 crash configuration groups defined in Table 2. The graph on the left side of each figure depicts the position of the PTW relative the LPV in the LPV frame, and is a subset of the cases depicted in Figure 7. The graph on the right side of each figure depicts the position of the LPV relative to the PTW in the PTW frame, and is a subset of the cases depicted in Figure 8. The yellow highlighting indicates the positions that are in a state of conflict defined herein as $C(t) = \text{true}$.

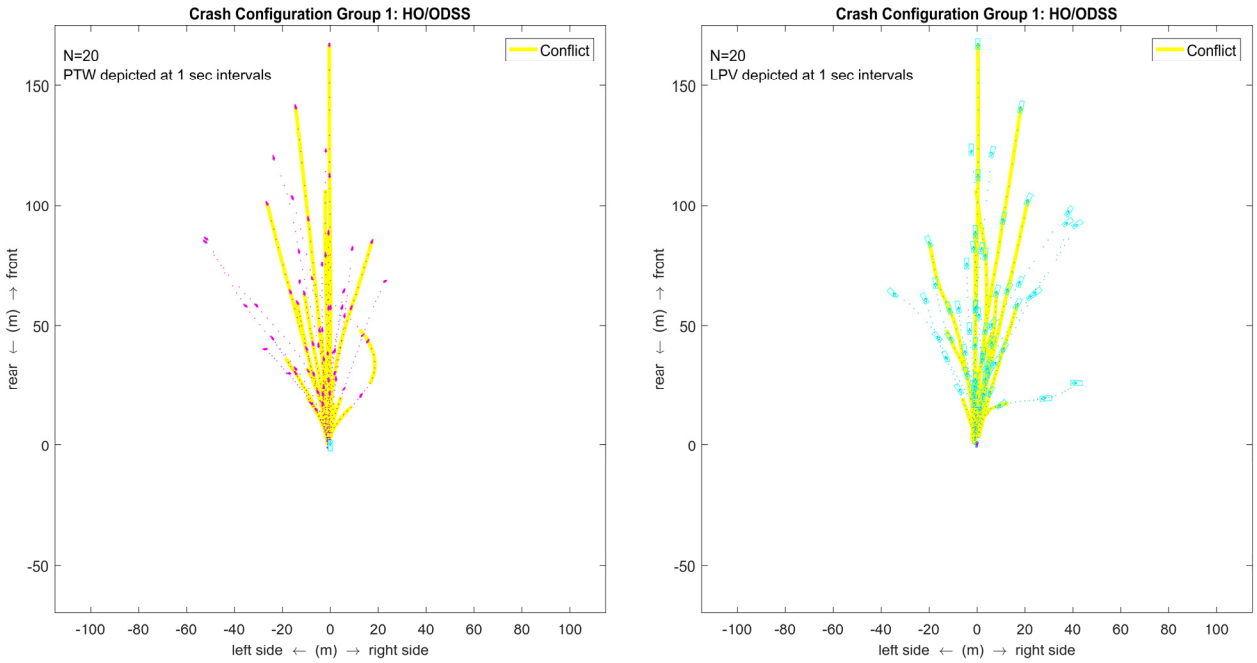

Figure B1. Head-on or opposite direction side swipe

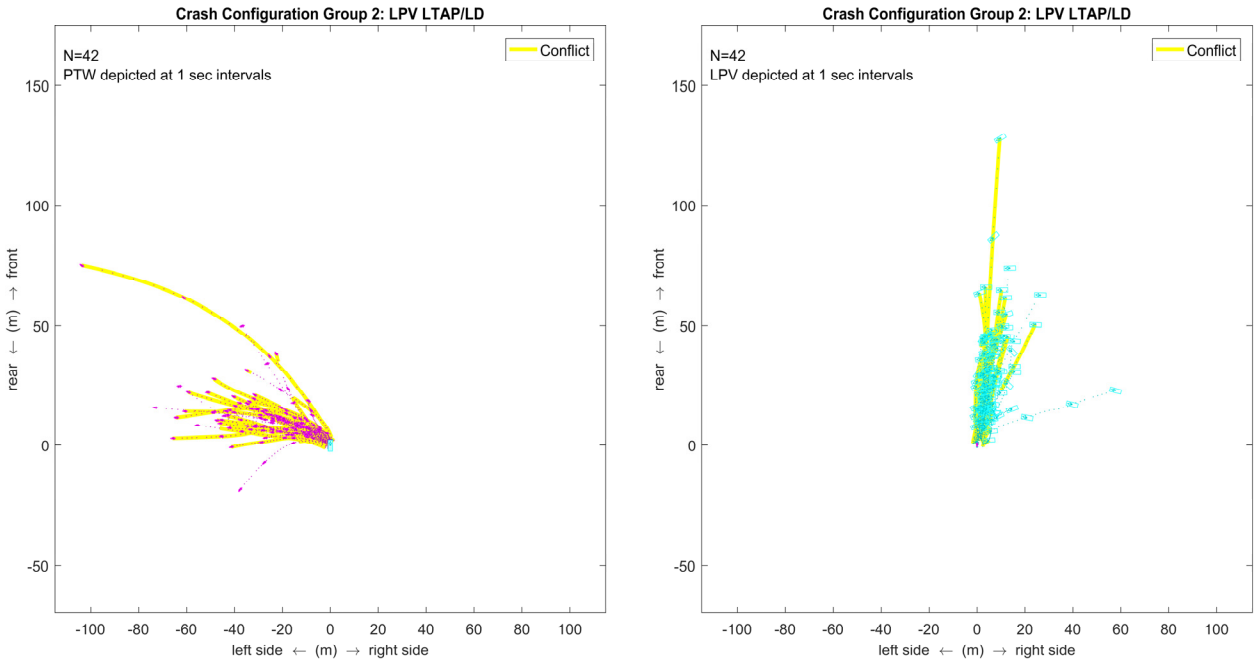

Figure B2. LPV left turn across PTW path/lateral direction

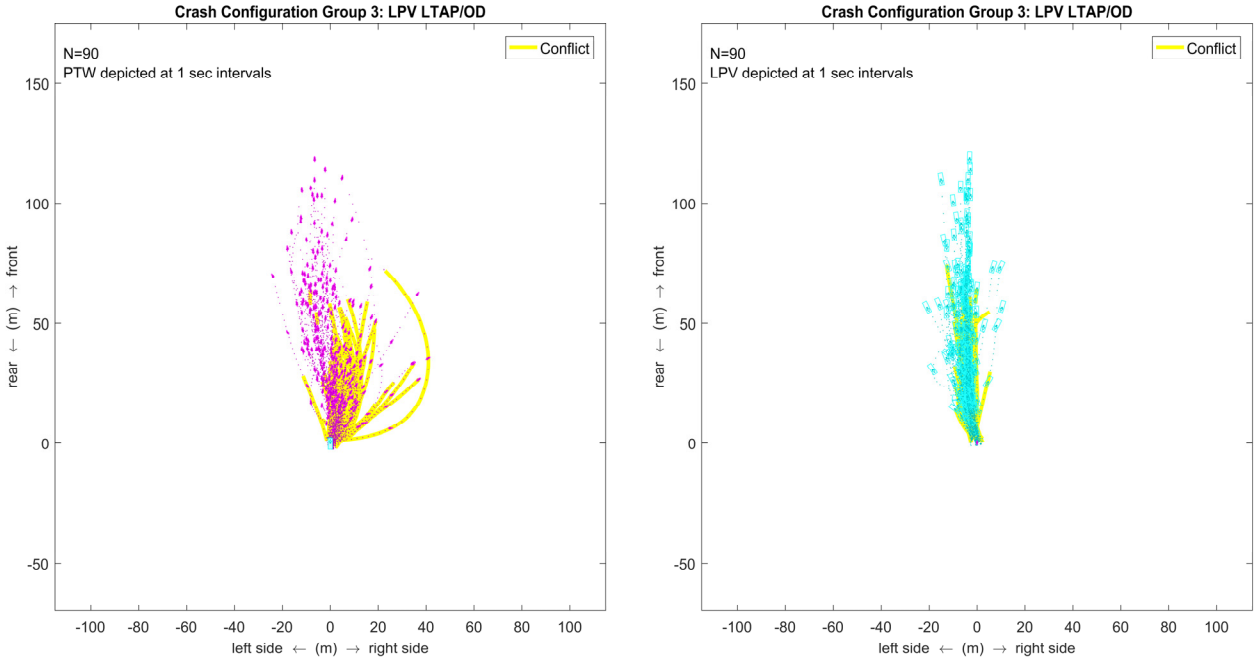

Figure B3. LPV left turn across PTW path/opposite direction

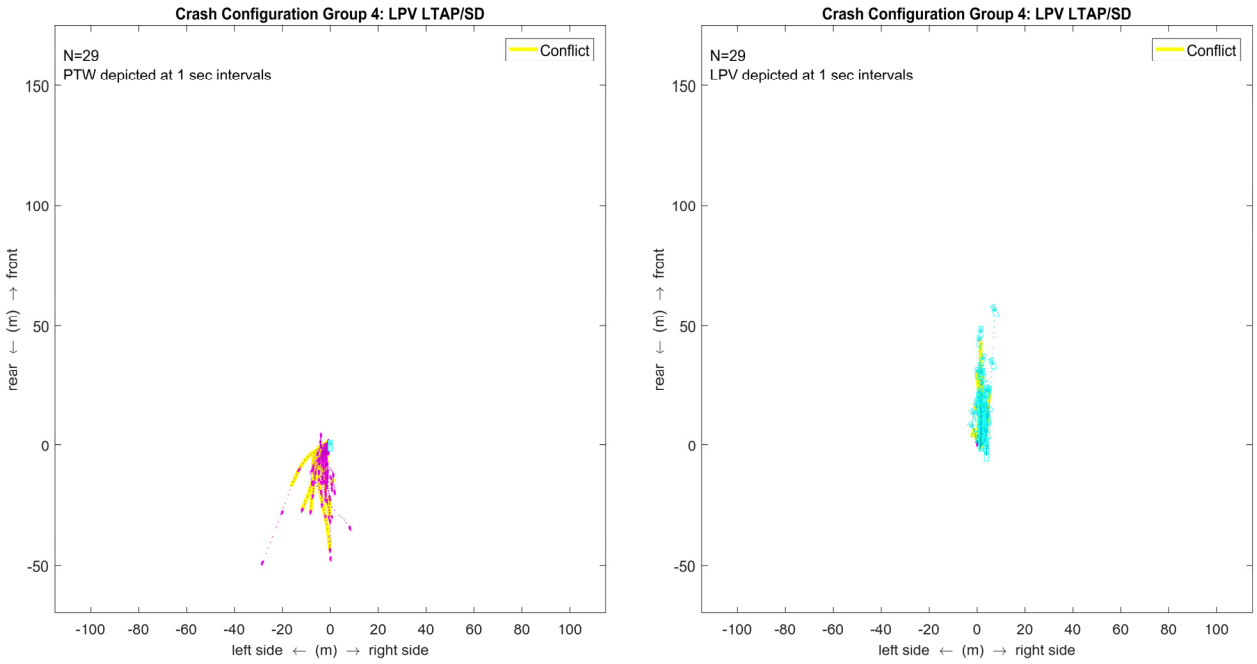

Figure B4. LPV left turn across PTW path/same direction

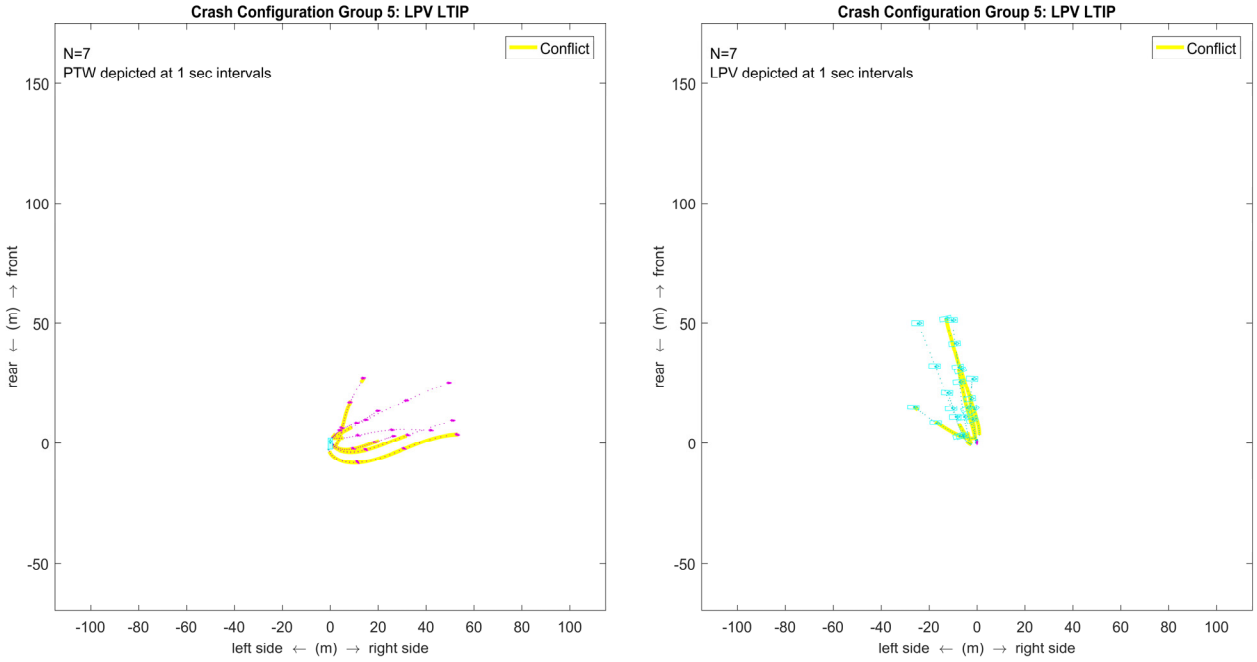

Figure B5. LPV left turn into PTW path

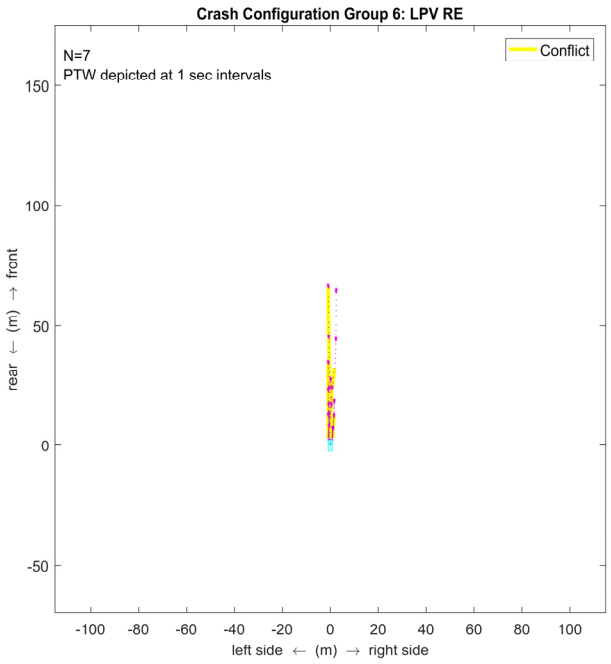

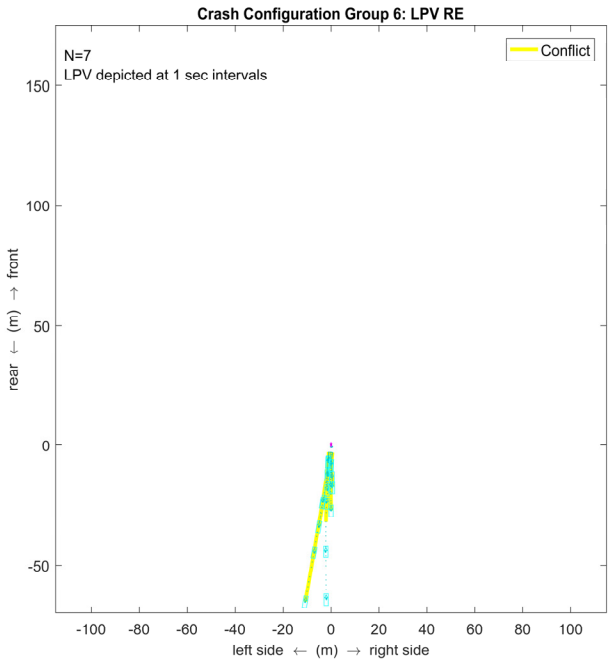

Figure B6. LPV rear-end PTW

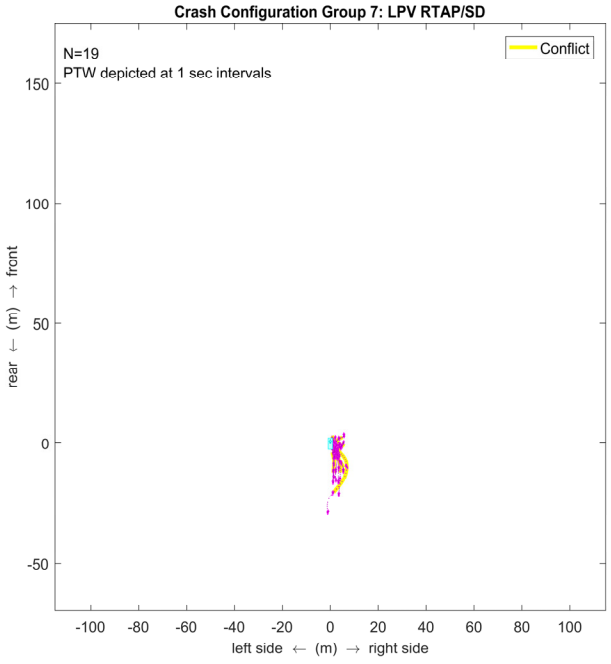

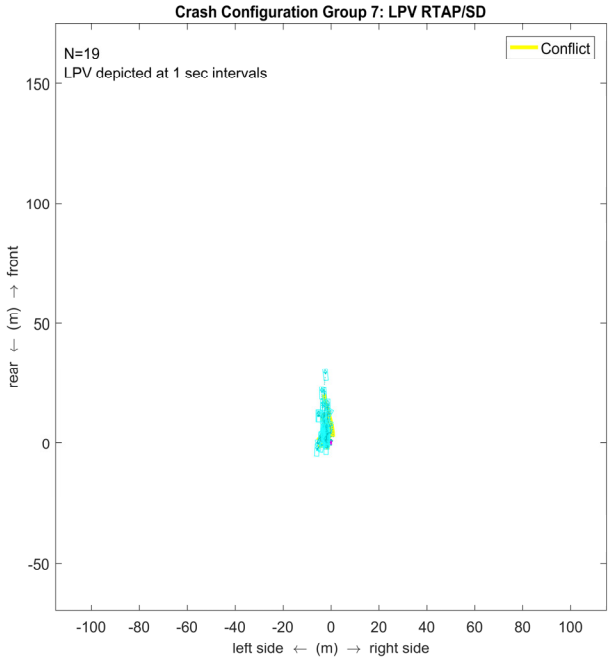

Figure B7. LPV right turn across path/same direction

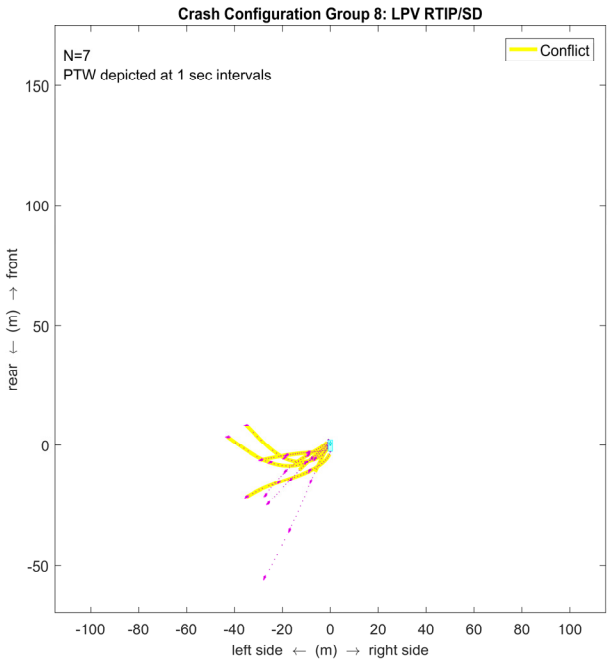

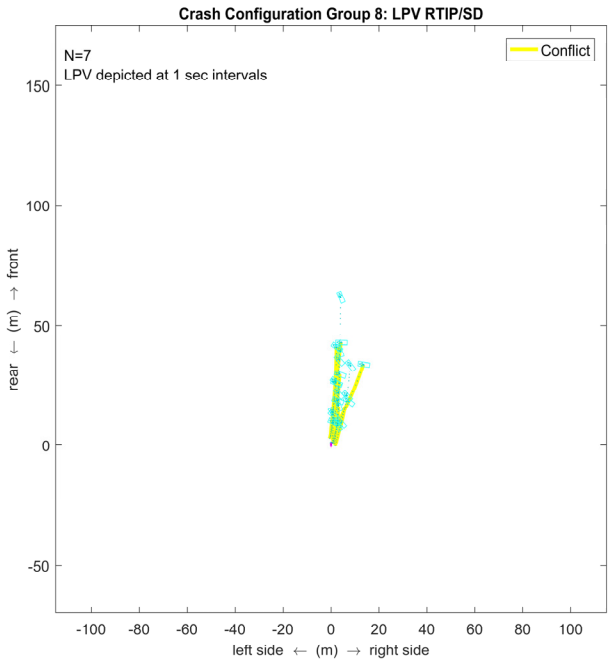

Figure B8. LPV right turn into path/same direction

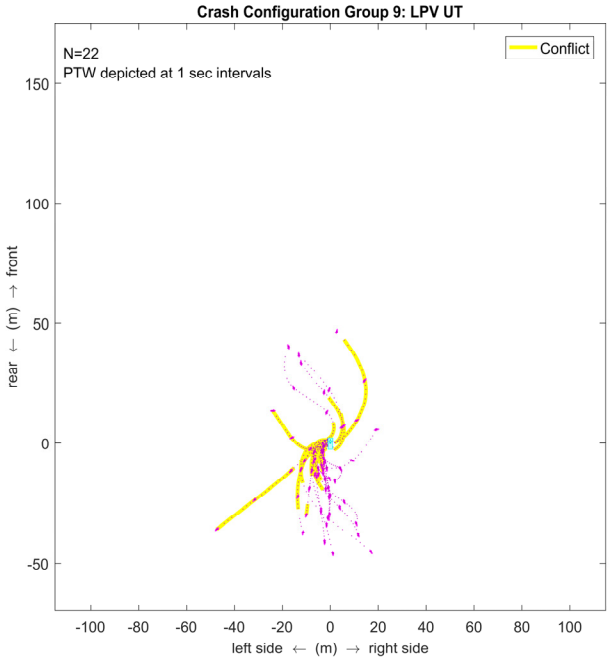

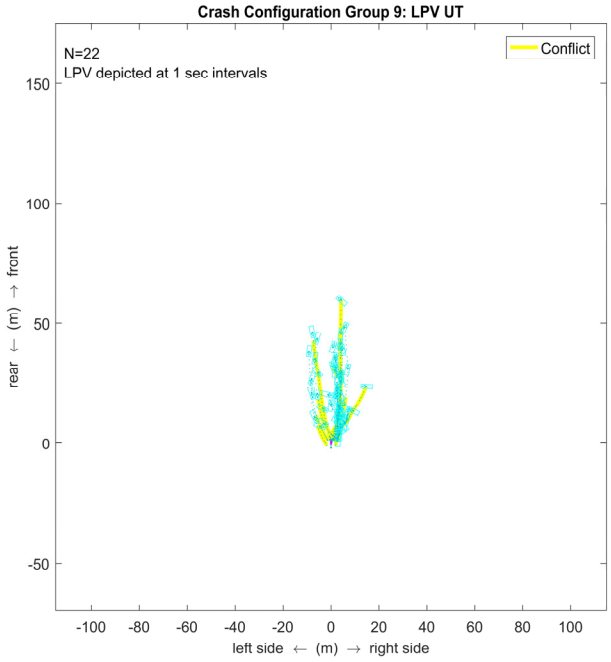

Figure B9. LPV U-turn across PTW path

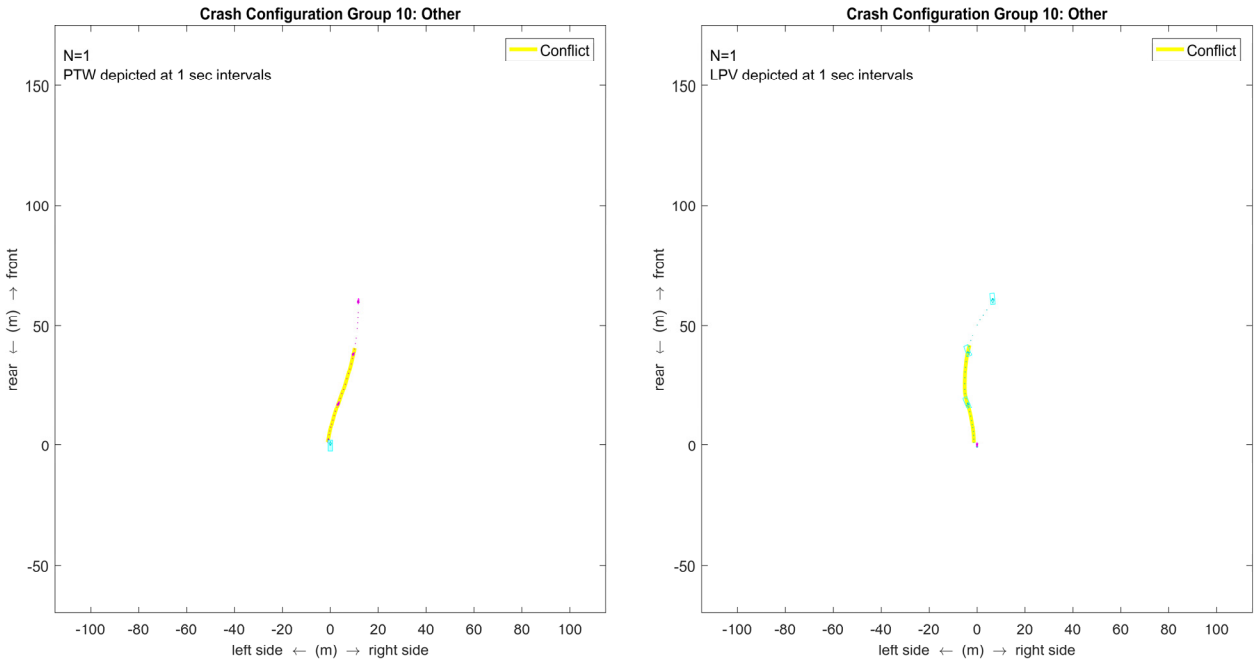

Figure B10. Other crash type

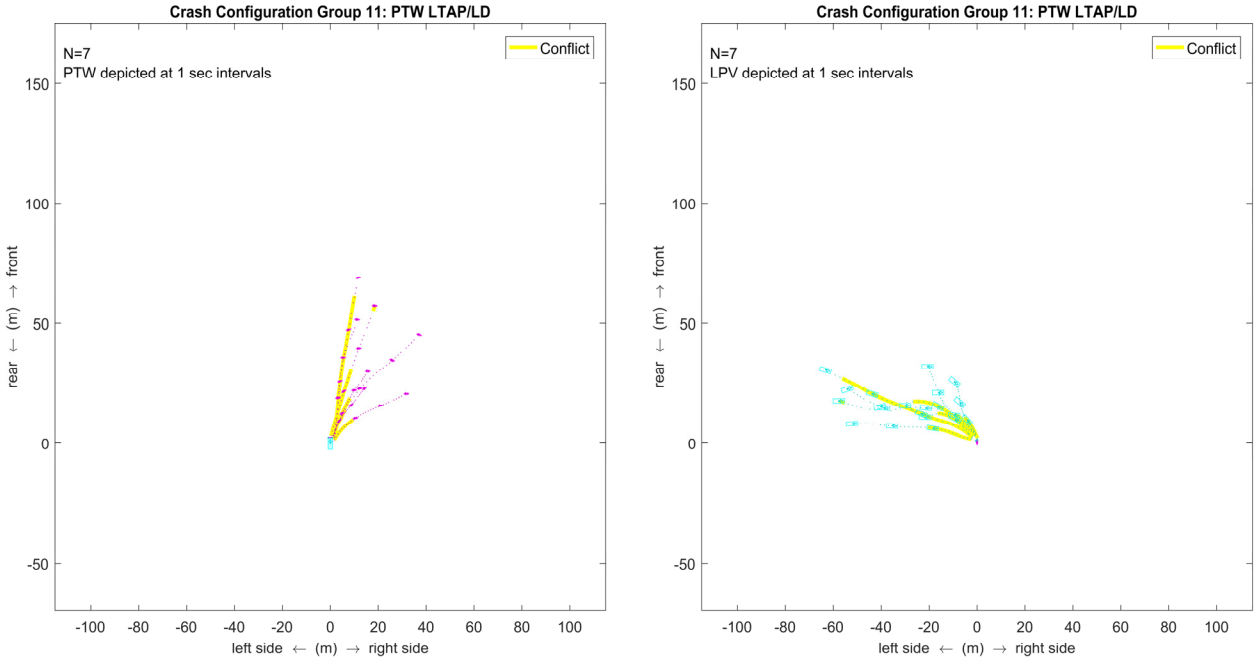

Figure B11. PTW left turn across LPV path/lateral direction

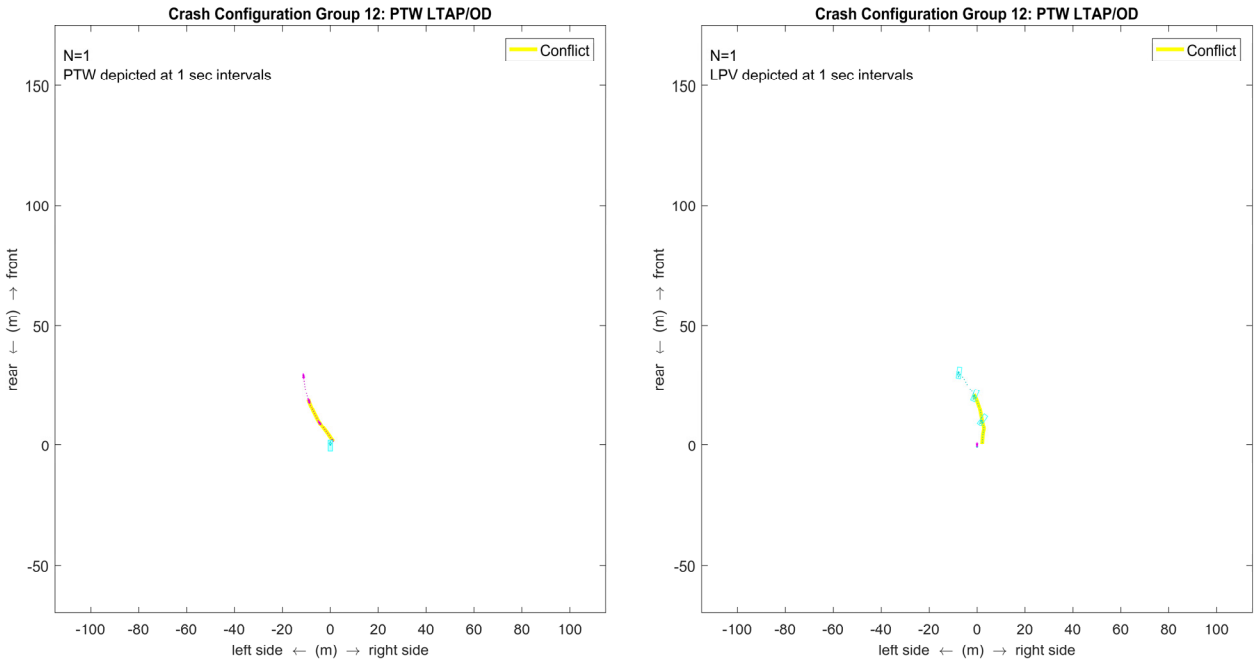

Figure B12. PTW left turn across LPV path/opposite direction

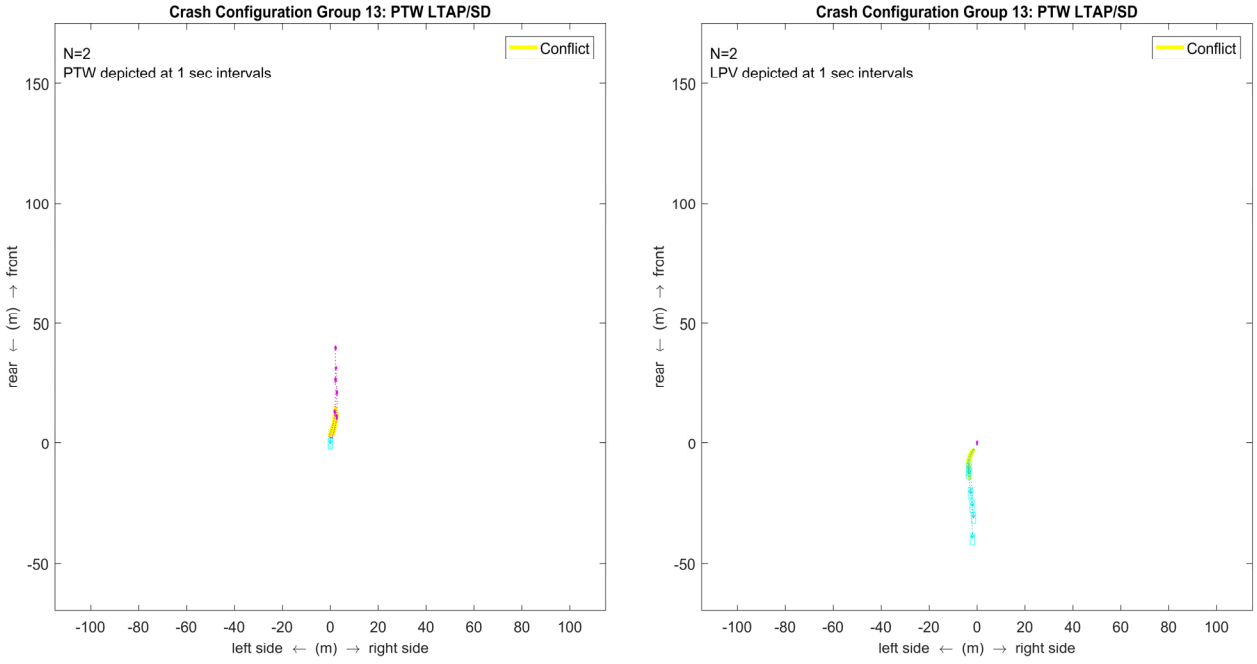

Figure B13. PTW left turn across LPV path/same direction

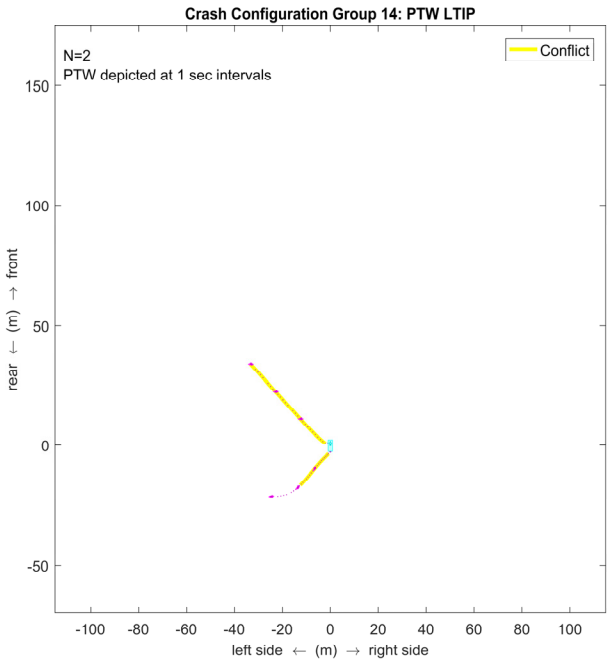

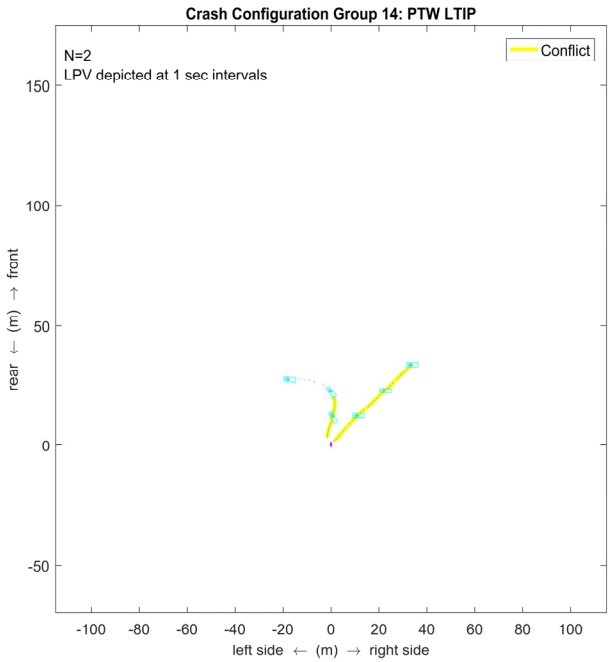

Figure B14. PTW left turn into LPV path

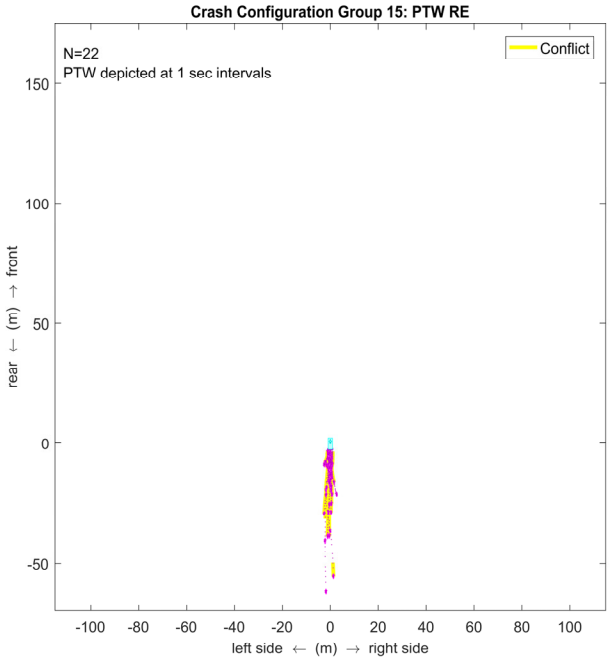

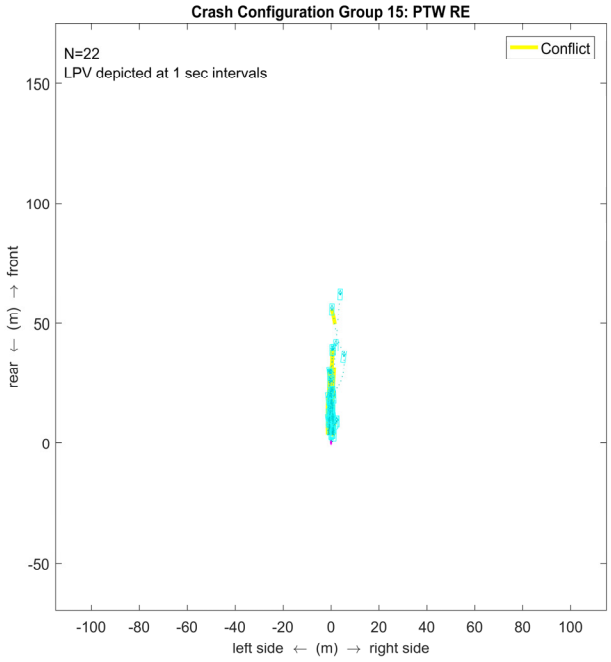

Figure B15. PTW rear-end LPV

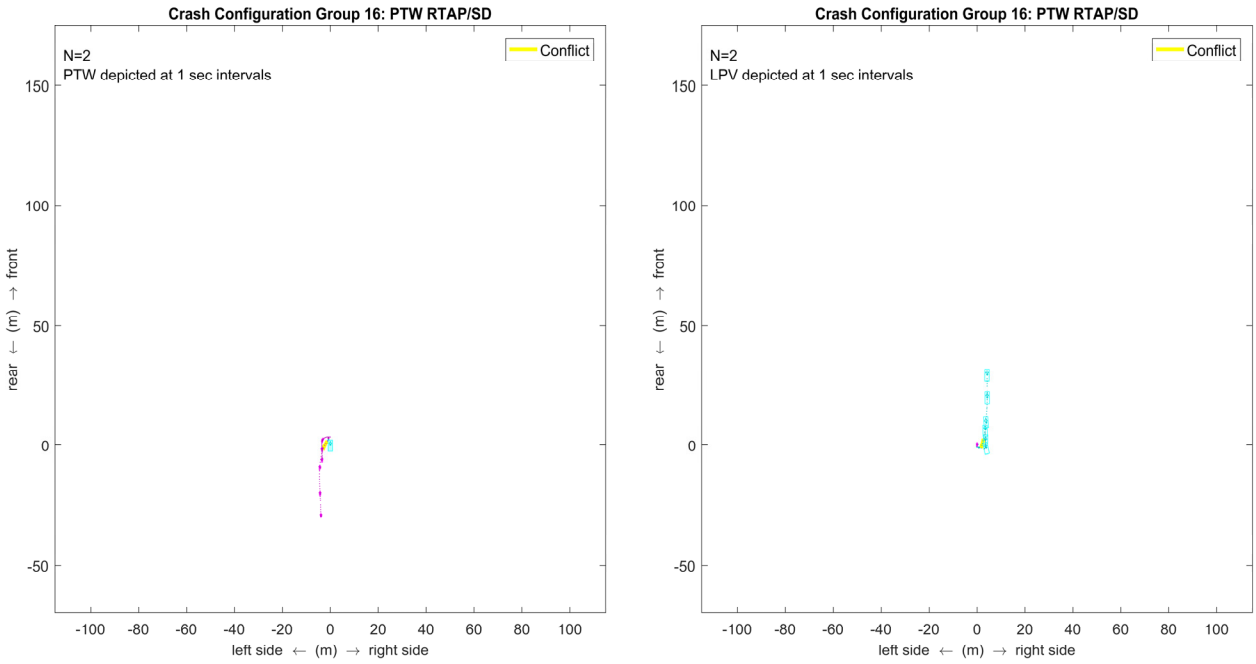

Figure B16. PTW right turn across LPV path/same direction

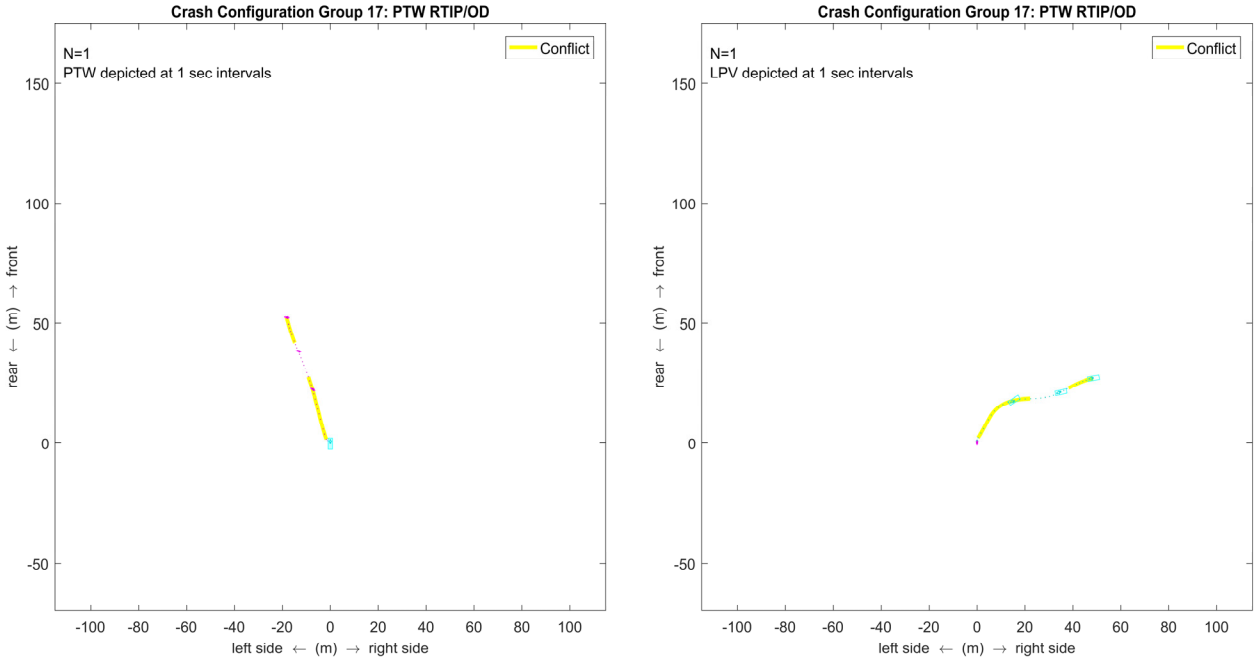

Figure B17. PTW right turn into LPV path/opposite direction

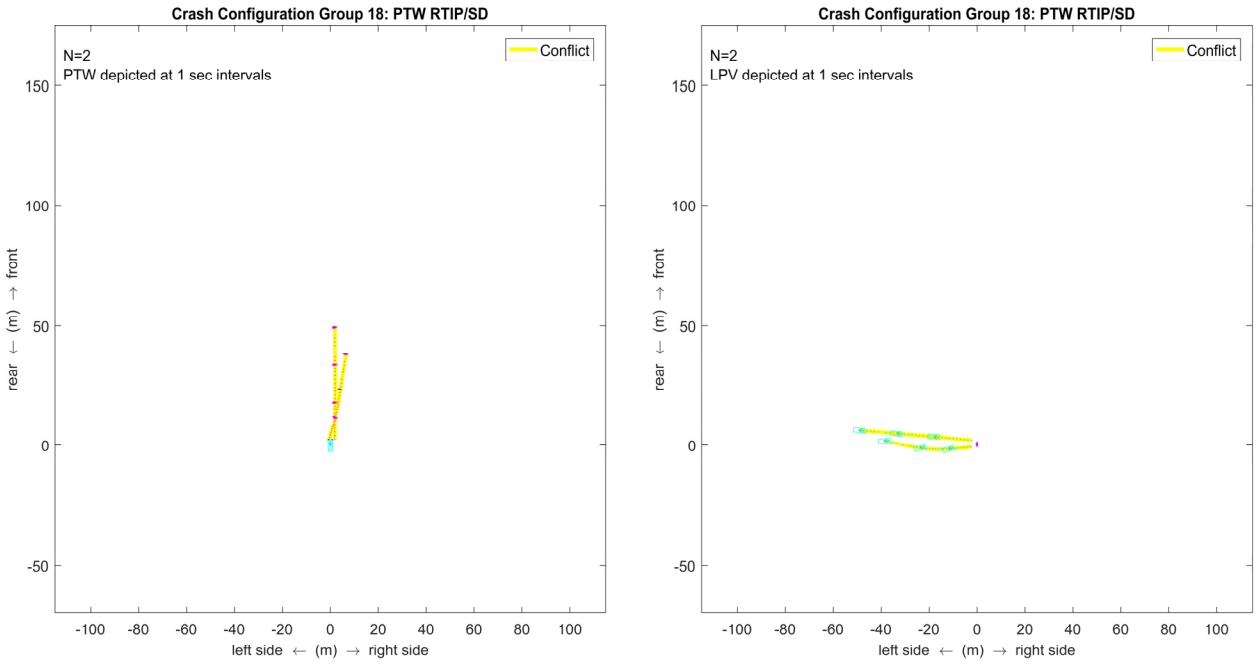

Figure B18. PTW right turn into LPV path/same direction

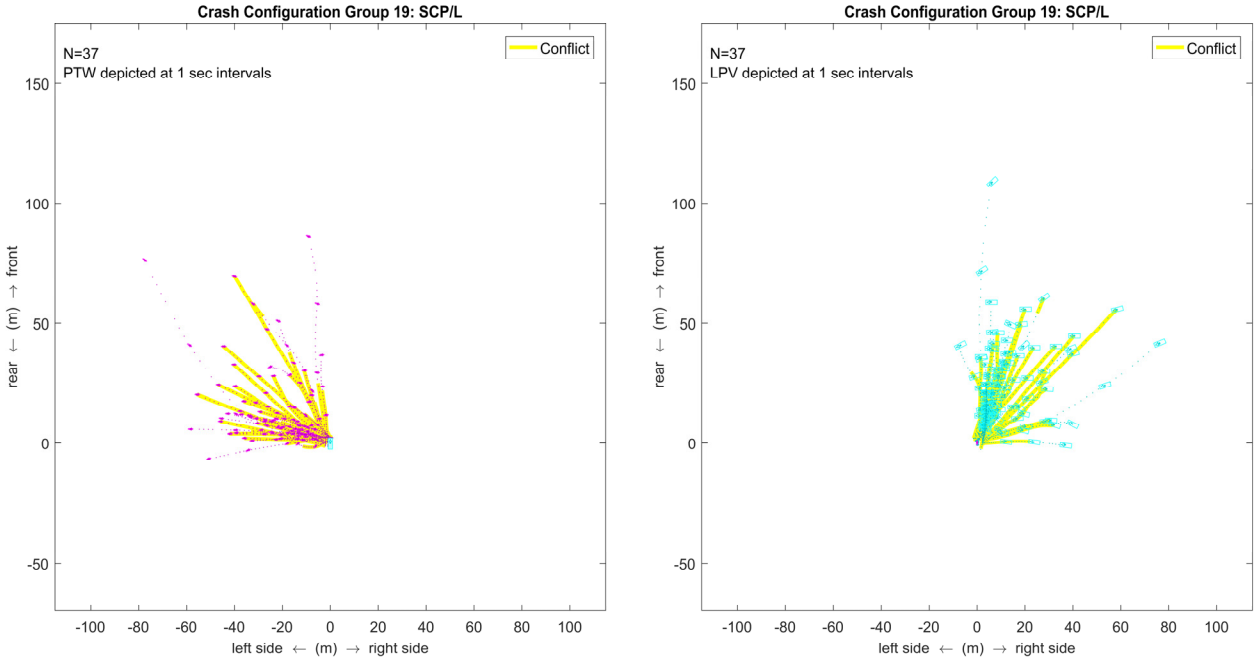

Figure B19. Straight crossing path/PTW on left side of LPV

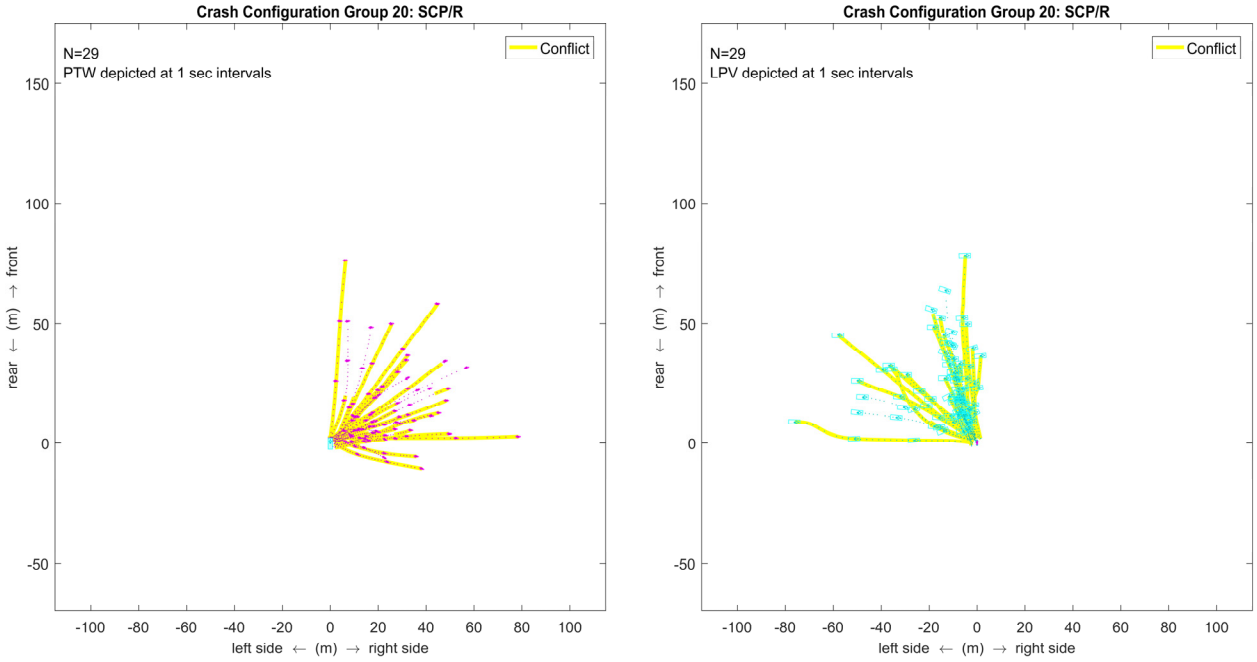

Figure B20. Straight crossing path/PTW on right side of LPV

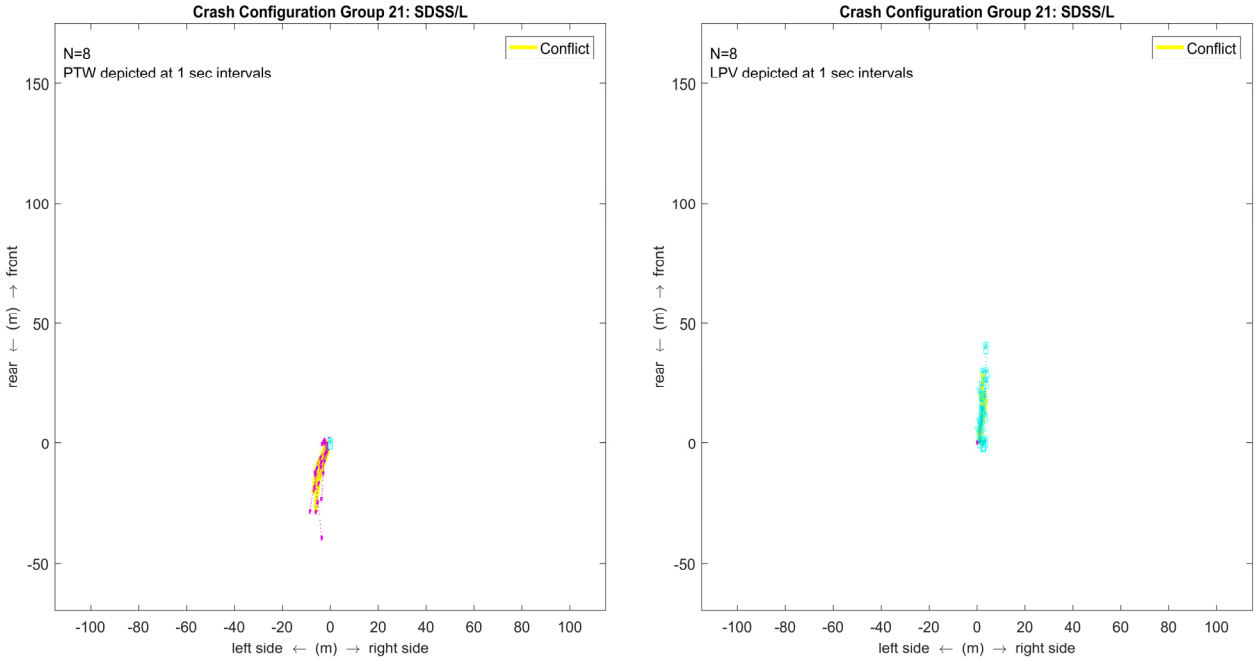

Figure B21. Same direction side swipe/PTW on the left side of LPV

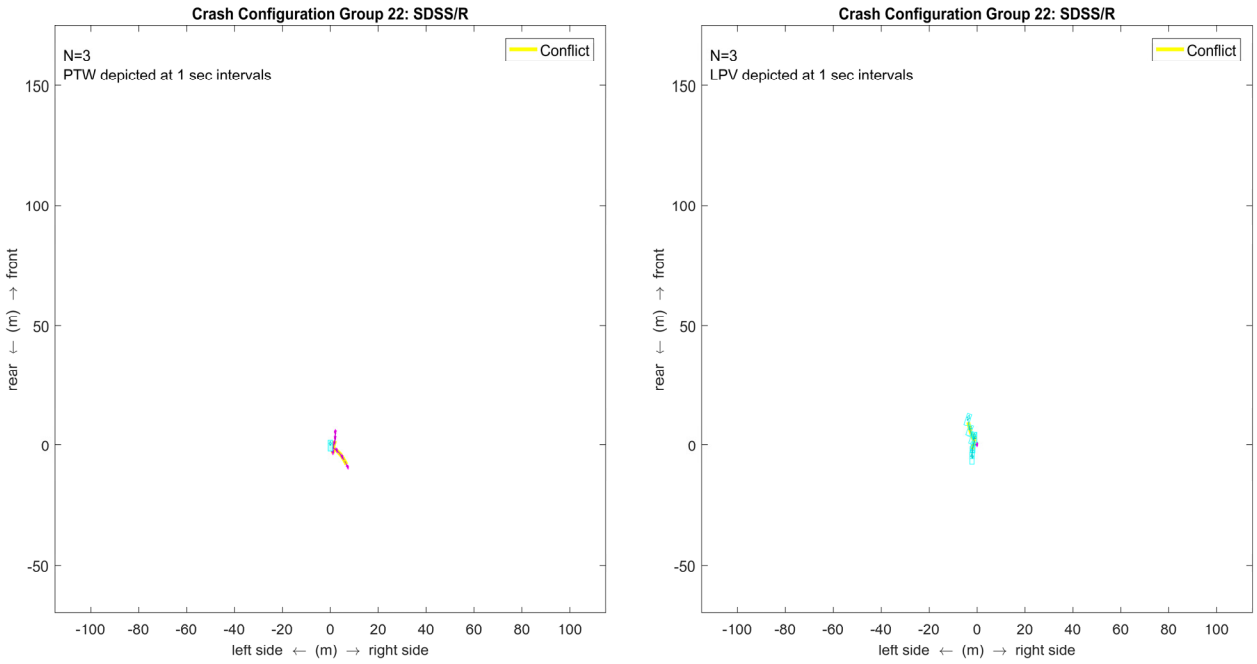

Figure B22. Same direction side swipe/PTW on the right side of LPV

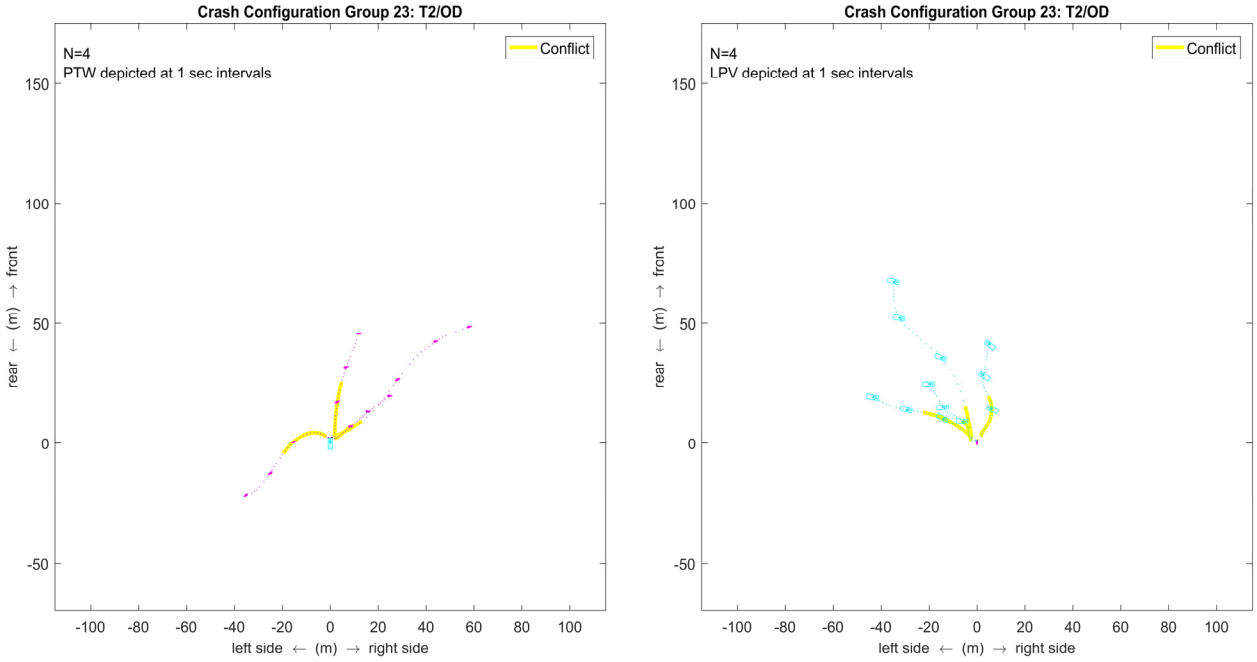

Figure B23. Both vehicles turning/opposite direction

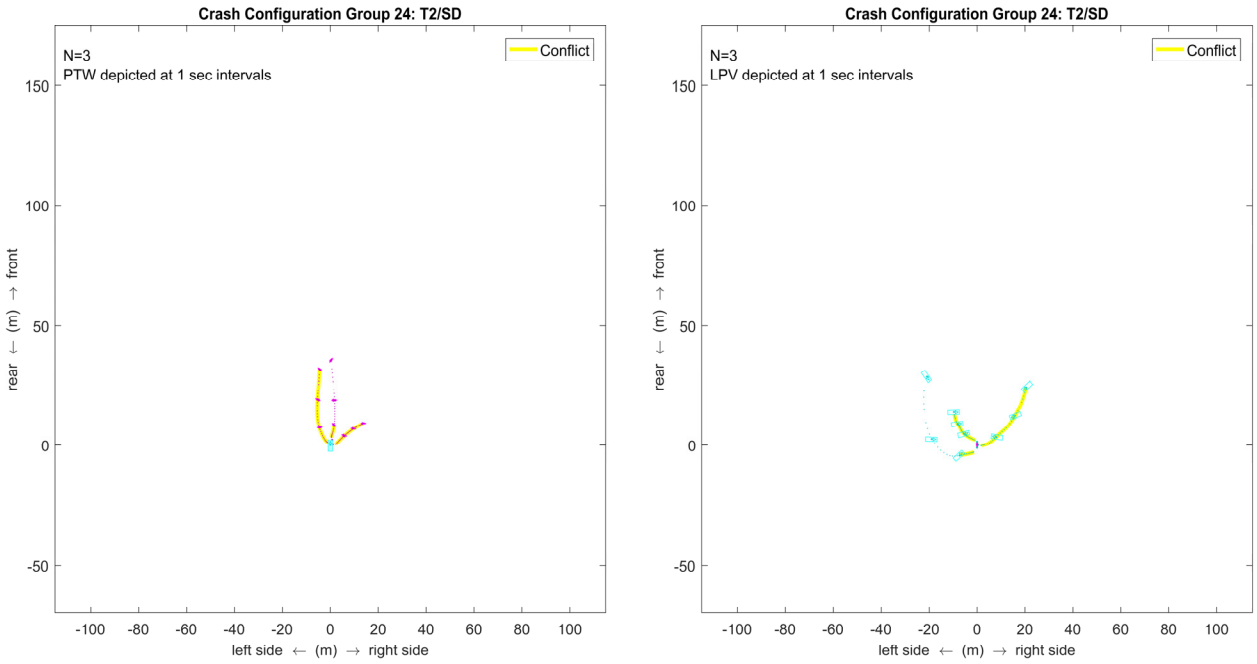

Figure B24. Both vehicles turning/same direction

SPEEDING IN CRASHES IN THE UNITED STATES OF AMERICA: A PILOT STUDY USING EVENT DATA RECORDER INFORMATION FROM NASS-CDS

Sam, Doecke
Craig, Kloeden
Centre for Automotive Safety Research, University of Adelaide
Australia

Michael Paine
Vehicle Design and Research
Australia

Paper Number 19-0097

ABSTRACT

The prevalence of speeding in crashes is only currently reported for fatal crashes in the United States of America (USA) using police reports, and the prevalence reported (27%) is well below that found in a national study that measured travel speeds (65%). The aim of this study was to explore how event data recorder (EDR) data from the National Automotive Sampling System – Crashworthiness Data System (NASS-CDS) database could be used to estimate the prevalence of speeding in crashes in the USA. EDR files collected as part of the NASS-CDS in 2015 were examined to determine the presence and extent of speeding, provided they met certain criteria. AIS coded injury data was also extracted when available to examine speeding by injury severity. 335 EDR files were identified as meeting the criteria. 188 of these had complete AIS coded injury information. From this sample, it was found 61% were speeding, but this reduced to 44% if NASS-CDS weightings were applied. Speeding by more than 10 mph was found in 26% of crashes (16% weighted). Speeding was found to increase with increasing injury severity: 76% of MAIS 3+ crashes involved speeding, and 52% involved speeding by more than 10 mph. EDR data was found to be a useful source of travel speed data that may be used to examine speeding in the USA. It indicates that speeding is a larger problem in crashes than suggested by the current method that uses police reports. Expanding the sample size by using more years of data and calculating the change in impact speed and associated change in injury severity would allow for more robust estimates of the prevalence of speeding and its contribution to road trauma in the USA.

INTRODUCTION

Speed is considered to be a major factor in the frequency and severity of road crashes [1,2]. Speed limits are set with the intention of controlling the maximum speed at which vehicles travel. However, drivers may still travel above the speed limit, termed speeding. A recent large-scale speed survey conducted in the United States of America (USA) by the National Highway Traffic Safety Administration (NHTSA) showed that 64.8% of vehicles were speeding, 40% speeding by more than 5 mph and 18.3% were speeding by more than 10 mph [3].

In the USA the prevalence of speeding in crashes is currently only estimated for fatal crashes. NHTSA defines a crash as speeding related if “any driver in the crash was charged with a speeding-related offense or if a police officer indicated that racing, driving too fast for conditions, or exceeding the posted speed limit was a contributing factor in the crash” [4]. This definition includes what might be termed “inappropriate speed for the conditions” as well as traveling above the speed limit. Even so, the estimate produced by this definition is only 27%, far lower than the percentage of drivers that are speeding or travelling at more than 5 mph above the speed limit in the speed survey [3].

The presence of speeding by a vehicle involved in a crash is often difficult to determine. Determining the travel speed of a vehicle prior to a crash is a specialised discipline known as crash reconstruction which is beyond the scope of most crash reports prepared by police, perhaps with the exception of some fatal crashes. Traditional crash

reconstruction methods rely on pre-impact tyre marks to calculate speed loss prior to impact and often produce an underestimate of travel speed as they cannot determine speed loss prior to the start of the tyre mark. This issue is further exacerbated by the advent of highly effective anti-lock braking systems on vehicles.

The advent of event data recorders (EDRs) provides a new opportunity to accurately ascertain the travel speed of vehicles involved in crashes and provide more accurate estimates of the prevalence of speeding in crashes of all severities. EDRs store a range of data from a vehicle's sensors in the event of a crash. In many cases this includes pre-crash travel speed for 2.5 to 5 seconds prior to the crash, typically recorded at 2 Hz. This data has been shown to be highly accurate for travel speed [5].

This paper details a pilot study that examined how EDR data from the National Automotive Sampling System – Crashworthiness Data System (NASS-CDS) database could be used to estimate the prevalence of speeding in crashes.

METHOD

As part of a separate study, the EDR files collected in NASS-CDS from vehicles crashed in the USA in 2015 were examined to identify EDR files that fulfilled the following criteria;

- From a striking vehicle
- From a vehicle that was not maneuvering (e.g turning)
- Injury severity for at least one vehicle was known
- Crash did not involve a heavy vehicle or motorcycle
- Crash was not a side-swipe or animal only impact
- EDR file had recorded crash data
- EDR file contained pre-impact speed
- Speed limit known

Each EDR file was individually checked to match the crash event data stored in the EDR file to the crash sampled in NASS-CDS by a person trained and experienced in interpreting EDR files. The travel speed was defined as the highest speed that the vehicle was recorded to be traveling in the pre-crash time period recorded on the EDR file. This travel speed was compared against the posted speed limit for that vehicle stated in the NASS-CDS database to determine speeding. Information on injury severity according to the maximum abbreviated injury score (MAIS) was also extracted from the NASS-CDS database, when available (injury information is only available for cars less than ten years old)

NASS-CDS sampling has a stratified, multiphase, unequal selection probability design that deliberately oversamples crashes with a higher injury severity. The NASS-CDS database provides case weights that can be used to account for the unequal selection probability. The weights of the sample crashes varied from 4.6 to 15,112. This high degree of variation in the weights means that, when considering small groups of crashes, some care must be taken to ensure that the result is not simply an artefact of the weighting. For example, the crash with the highest weight accounted for 36% of the total moderate injury weights, and 31% of the total serious injury weights, as opposed to 7% of the total sample. No consensus has been reached on how best to deal with this issue. The method suggested by Samaha, Prasad and Nix [6] of attenuating the weights to the 95% percentile value within an injury severity category was applied the data for this study. Weighted, weighted with attenuation, and unweighted results are shown for comparison.

RESULTS

1077 EDR files were collected from 970 crashes as part of NASS-CDS in 2015 and a total of 335 crashes met the criteria. A detailed breakdown of cases excluded is shown in Table 1.

Table 1.
Cases excluded by criterion

Criterion	Number excluded
Non-striking vehicle	244
Vehicle maneuvering	30
Injury severity unknown	210
Heavy vehicle or motorcycle involved	45
Sideswipe or animal strike	56
EDR file contained no data	20
EDR file did not contain speed data	27
Speed limit unknown	3
Total cases excluded	635

Table 2 shows the percentage of vehicles speeding in the 335 crashes. The percentage reduces when the data is weighted according to the weights provided in the NASS-CDS database. Attenuating the weights to the 95th percentile increase the percentages, but they remain closer to the weighted values than the unweighted.

Table 2.
Prevalence of speeding by level of speeding and weighting from 2015 NASS-CDS data

Speeding level	Unweighted		Weighted		Weighted - Attenuated	
	Number	Percentage	Number	Percentage	Number	Percentage
Total cases	335	-	219,124	-	177,243	-
Speeding	205	61.2	95,516	43.6	92,712	52.3
Speeding >8km/h (5mph)	131	39.1	51,333	23.4	50,159	28.3
Speeding >16km/h (10mph)	85	25.4	34,132	15.6	32,958	18.6

The percentage of vehicles speeding by crash injury severity is shown in Table 3. Only 188 of the 335 crashes had injury information available for all vehicles involved in the crash. When considering the unweighted results, the percentage of crashes involving speeding increases with increasing injury severity across all levels of speeding. However, the weighted results (with weighting attenuated) show a decrease in percentage of vehicles speeding for MAIS 2 crashes. The difference in percentage of crashes involving speeding between crash injury severity levels appears to increase at higher levels of speeding.

Table 3.
Prevalence of speeding by level of speeding and weighting from 2015 NASS-CDS data

Speeding level	MAIS 0,1				MAIS 2				MAIS 3+			
	Unweighted		Att. Weight		Unweighted		Att. Weight		Unweighted		Att. Weight	
	No.	%	No.	%	No.	%	No.	%	No.	%	No.	%
Total	128	-	68,185	-	35	-	8,741	-	25	-	1,697	
Speeding	77	60.2	40,220	59.0	24	68.6	2,745	31.4	19	76.0	1,068	62.9
Speeding >8km/h	52	40.6	26,145	38.3	17	48.6	2,083	23.8	16	64.0	845	49.8
Speeding >16km/h	33	25.8	17,589	25.8	12	34.3	1,418	16.2	13	52.0	736	43.3

DISCUSSION

The unweighted results for speeding (61%) are similar to the levels of speeding found in the US national speed survey conducted by NHTSA but are well above the current estimate of speeding in fatal crashes (27%). Once the results are weighted the percentage of speeding is less than found in the US national speed survey, but still well above the estimated level of speeding in fatal crashes. The exception to this finding is the results for speeding by 10 mph are closer to the NHTSA speeding survey result when they are weighted.

It would be expected that speeding would be more prevalent in higher injury severity cases as increases in speed are known to increase the risk of serious and fatal crashes more than for less severe crashes [1]. The findings of this study are therefore as expected in that regard. There were too few fatal cases to consider them separately in the analysis, however, fatal crashes alone would be expected to have even higher levels of speeding than MAIS 3+ crashes. The results therefore suggest that the current estimate of speeding in fatal crashes is a gross underestimate. This is despite having a broader definition that includes inappropriate speed in the estimate in addition to speeding. The current NHTSA estimate may only represent cases of speeding much higher than 10 mph as high levels of speeding may be more easily identified by police.

The vehicles in the sample are biased towards newer vehicles, as this was required for both injury information, and travel speed to be present in the EDR file. It is unknown if the age of the vehicle has an influence on speeding, though it may be thought that older vehicles are more likely to be driven by younger drivers [7] who may be more prone to speeding. Young drivers have been found to be more likely to be "speeders" according to a national survey conducted in the USA [8]. If this is the case the results are an underestimate of speeding in the general population.

The sample does not include heavy vehicles or motorcycles. The NHTSA travel speed survey [3] found that heavy vehicles have higher median speeds but lower 85% percentile speeds than passenger vehicles. Motorcycles are not identified separately in the NHTSA travel speed survey. Speeding, as identified by NHTSA for fatal crashes [4], is more common amongst motorcycles than passenger vehicles, but less common amongst heavy vehicles. While motorcycles represent only a small proportion of the vehicle fleet they are over-represented in serious crashes [9]. The limiting of the dataset to crashes involving only passenger vehicles may have resulted in a slight underestimate in terms of the general population, though it is also quite possible that this made no real difference to the result.

A major limitation of this study is the sample size when breaking down the sample for further analysis. This makes using the NASS-CDS weights to correct for the sampling method difficult, as a small number of crashes can become overly influential on the weighted result. Attempts to correct for this by attenuating the results to the 95th percentile value within the injury severity category still yielded the odd result of MAIS2 crashes having a lower percentage of speeding than MAIS0 and MAIS1, and MAIS3+ crashes, as the 6 crashes with the highest weights were all not speeding in a sample of only 35 crashes. Future work could incorporate more years of the NASS-CDS data to increase the sample size and allow it to be analysed in more detail. The soon to be released Crash Investigation Sampling System (CISS), the successor to NASS-CDS, will provide EDR equipment to all field crash technicians [10] and therefore may provide more EDR data per year of data collection for future studies of this kind.

A further limitation is that the selection criteria were designed for a separate study, and this resulted in the exclusion of some cases that may have been relevant to speeding. One of the selection criteria was that the vehicle had to be a striking vehicle, but the struck vehicle in some crashes may also choose to travel faster than the speed limit (e.g. when it is travelling straight through an intersection). A revised set of selection criteria specific to this type of analysis would increase the number of cases included per year of NASS-CDS data.

Traveling above the speed limit is known to increase both the risk of being involved in a crash and the severity of the crash [1,2]. However, it should not be assumed that the elimination of speeding would result in a reduction in crashes that is equivalent to the percentage of vehicles speeding. Doecke and Ponte [11] conducted a preliminary study that estimated the contribution of speeding to road trauma by using EDR data from NASS-CDS to calculate the new impact speed had the vehicle not been speeding. They applied risk curves to this new impact speed to determine the new injury risk and calculate the overall reductions that could be achieved by eliminating speeding. They found that 22% of crashes could be avoided altogether, MAIS 3+ injuries could be reduced by 62% and MAIS

1 and MAIS 2 crashes could be reduced by 27%. These results were based on only 59 crashes from 2013 therefore their results should be viewed as preliminary. Future work in this area should consider applying the method of Doecke and Ponte (2017) to a large sample of NASS-CDS EDR data in order to robustly estimate the contribution of speeding to road trauma in the USA.

A recent National Transportation Safety Board report [12] highlighted that the key solutions to the problem of speeding in the USA are automated speed enforcement (ASE) and the vehicle technology intelligent speed adaptation (ISA), that are not currently implemented on a wide scale. This study, albeit a pilot study, adds further evidence of the large scale of the problem of speeding in the USA and the road safety benefits that could be gained by wide scale implementation of ASE and ISA.

CONCLUSIONS

EDR data is a useful source of travel speed data that may be used to examine speeding in the USA. It indicates that speeding is a larger problem in fatal crashes than suggested by the current method that uses police reports. Expanding the sample size by using more years of data and calculating the change in impact speed and associated change in injury severity would allow for more robust estimates of the prevalence of speeding and its contribution to road trauma in the USA.

REFERENCES

[1] Elvik R, Christensen P, Amundsen A. Speed and road accidents. An evaluation of the Power Model. Oslo: Institue of Transport Economics; 2004. Available at https://www.toi.no/getfile.php/131013/Publikasjoner/TØI%20rapporter/2004/740-2004/Repsumm.pdf. Accessed October 1, 2018

[2] Kloeden C, McLean A, Moore V, Ponte G. *Travelling speed and the risk of crash involvement. Volumes 1 and 2*. Canberra: Federal Office of Road Safety, Transport and Communications; 1997. Available at http://casr.adelaide.edu.au/publications/subject/?id=317. Accessed October 1, 2018

[3] De Leonardis, D., Huey, R., & Green, J. *National Traffic Speeds Survey III: 2015*. Washington, DC: National Highway Traffic Safety Administration; 2018. Available at https://www.nhtsa.gov/sites/nhtsa.dot.gov/files/documents/812485_national-traffic-speeds-survey-iii-2015.pdf. Accessed October 5, 2018.

[4] National Highway Traffic Safety Administration. *Traffic safety facts, 2016 data: speeding.* Washington, DC: National Highway Traffic Safety Administration; 2018. Available at https://crashstats.nhtsa.dot.gov/Api/Public/ViewPublication/812480. Accessed June 12, 2018.

[5] Niehoff, P, Gabler, H C, Brophy, J, Chidester, C, Hinch, J and Ragland, C. Evaluation of event data recorders in full systems crash tests. Paper presented at: 19th International Technical Conference on the Enhanced Safety of Vehicles (ESV), pp.6–9. Washington, DC.

[6] Samaha, R. R., Prasad, P., & Nix, L. (2013). *Opportunities for injury reduction in US frontal crashes: an overview by structural engagement, vehicle class, and occupant age* (No. 2013-22-0017). SAE Technical Paper.

[7] Anderson, R. W. G., & Doecke, S. D. (2010). The relative age related crashworthiness of the registered South Australian passenger vehicle fleet. *Journal of the Australasian College of Road Safety, 21*(1), 36-46.

[8] Schroeder, P., Kostyniuk, L., & Mack, M. *2011 National survey of speeding attitudes and behaviors.* Washington, DC: National Highway Traffic Safety Administration; 2013. Available at https://www.nhtsa.gov/sites/nhtsa.dot.gov/files/2011_n_survey_of_speeding_attitudes_and_behaviors_811865.pdf. Accessed November 1, 2018.

[9] National Highway Traffic Safety Administration. *Traffic safety facts, 2016 data: motorcycles.* Washington, DC: National Highway Traffic Safety Administration; 2018b. Available at https://crashstats.nhtsa.dot.gov/Api/Public/ViewPublication/812492. Accessed November 1, 2018.

[10] Brophy, B. Upgrades in Technologies for NHTSA's Crash Investigations. 2016. Available at https://www.nhtsa.gov/sites/nhtsa.dot.gov/files/documents/brophy-sae2016-techupgradesforinvestigations.pdf. Accessed 10 October 2018

[11] Doecke, S. D., & Ponte, G. *The safety benefits of limiting ISA: a pilot study using real world crash situations* Adelaide: Centre for Automotive Safety Research; 2017. Available at http://casr.adelaide.edu.au/casrpub/show.php?id=1717. Accessed June 12, 2018.

[12] National Transportation Safety Board. *Safety study: reducing speeding-related crashes involving passenger vehicles.* Washington, DC: National Transportation Safety Board; 2017. Available at https://www.ntsb.gov/safety/safety-studies/Documents/SS1701.pdf. Accessed November 2, 2018.

SIMULATION OF TEST DRIVES BY USING POLICE-RECORDED ACCIDENT DATA AND COMBINING MACROSCOPIC AND MICROSCOPIC ELEMENTS

Pfitzner, Pascal
Erbsmehl, Christian T.
Fraunhofer Institute for Transportation and Infrastructure Systems IVI
Germany

Paper Number 19-0098

ABSTRACT

With the development of autonomous driving functions, the evaluation of their functional safety is becoming increasingly important. Current vehicles are tested with separate simulations or test drives. In order to validate future autonomous vehicles by means of test drives, a substantial number of test kilometers are necessary. In addition, these test drives must be repeated for every new release of the system, which increases the expenses for validation. For this reason, programs that can simulate test drives have a high significance. Previous programs do not include the indispensable combination of routing simulation and accident simulation needed to represent a simulated test drive. Therefore, an approach to combining a macroscopic simulation (routing simulation) with a microscopic simulation (accident simulation) is used in this paper.

When the start location and the destination are given, the macroscopic simulation can compute the test route by means of the OSRM (Open Source Routing Machine) routing application. While driving along the test route, the simulated vehicles pass various locations of real accidents. The relevant data is taken from the accident database compiled by the police of Saxony, Germany.

A selection procedure ensures that only relevant accident situations along the test route are later simulated microscopically. Only if the accident situation is similar to the current situation of the simulated vehicle can the accident situation be simulated microscopically. Therefore, various boundary conditions are used to determine whether there are similarities regarding weather, traffic, light conditions and trajectories of the accident vehicles. To study different variations of the selection procedure, three different concepts are developed and evaluated. The first concept is based on a given test route between start location and destination and a realistic calculation of the travel time. The second concept is also based on a given test route but combines this with a time window for the entire route. The third concept combines an unknown test route, which is calculated between relevant accident locations during the simulation, with a realistic calculation of the travel time. After the evaluation of all three concepts, only the third concept is implemented in the simulation.

Within the microscopic simulation by means of PC-Crash, a relevant accident situation is simulated twice, once without and once with the tested driver assistance system in action. With the help of a collision detection system, a conclusion about the efficiency of the driver assistance system is made. The result is a program that combines completed test kilometers with avoided accident situations to simulate a test drive.

The current program can only be used in Saxony, Germany. For an expansion to all of Europe, comprehensive accident data is necessary. In addition, the selection procedure could be improved by means of georeferenced weather and traffic data. Because of the basic simulation tools, the actual simulation is not designed for quality but rather for quantity. However, high-quality simulation tools can be implemented with little effort. The simulation of test drives is an important challenge, and with the program developed here, an opportunity to solve it is introduced.

OBJECTIVE

In the development process of automated driving functions, the evaluation of their efficiency is unavoidable. Currently, simulations as well as test drives are used for evaluation purposes. With the help of repeated simulations of real accidents, it is possible to estimate whether an accident could have been prevented if the vehicle had been equipped with an Advanced Driver Assistance System (ADAS). Test drives in road traffic or on test tracks, on the other hand, expose the ADAS in question with real or staged situations [1].

In the future, the homologation process for highly automated driving functions and autonomous vehicles will become increasingly important. Currently, the functionality of prototypes is established in long test drives. However, several million test kilometers must be driven in order to obtain proof of safety. This procedure must be repeated after each system modification. This means that the expenses for obtaining proof of safety will increase significantly in the years to come [2].

For this reason, the development of a way to simulate test drives is desirable. In order to state the number of test kilometers driven, it is necessary to specify the route of the simulated vehicle. A suitable simulation solution – from now on called macrosimulation – is used for this purpose. Furthermore, an appropriate selection process for specific accident scenarios is developed within the scope of the macrosimulation. These scenarios are then studied microscopically. This way, it is possible to make a claim about how many of the selected specific accident scenarios could have been prevented by the system under testing. This is achieved with the help of a simulation that maps the interaction of the party who caused the accident and other parties involved in the accident. This simulation will be called microsimulation from now on.

METHODS AND DATA SOURCES

The combination of macroscopic and microscopic simulation elements allows the simulation of a test drive. Using the OSRM navigation application as a macrosimulation tool, the test route can be calculated from given points of origin and destination, and the vehicle's position can be simulated depending on the time. The following elaborations are visualized by the schematic depicted in Figure 1.

During the test drive, the simulated vehicle will be faced with several accident scenarios. The database of police-recorded accident data in Saxony provides the basis for all possible specific scenarios. An integrated, three-level selection process ensures that not only accident scenarios relevant in terms of time and location are considered for microsimulation, but also those that show similarities to the simulated vehicle in terms of traffic situation, weather and lighting conditions, as well as trajectories of the involved parties. The similarities are determined and guaranteed by applying several framework conditions. One example of a framework condition is the limitation of the time of the specific accident scenario to the arrival of the simulated vehicle at the accident location. The smaller the time difference to the specific accident, the greater the similarity of the oscillating traffic volume and the lighting is believed to be.

Three different concepts for the integration of the macrosimulation and the corresponding selection process will be developed and compared.

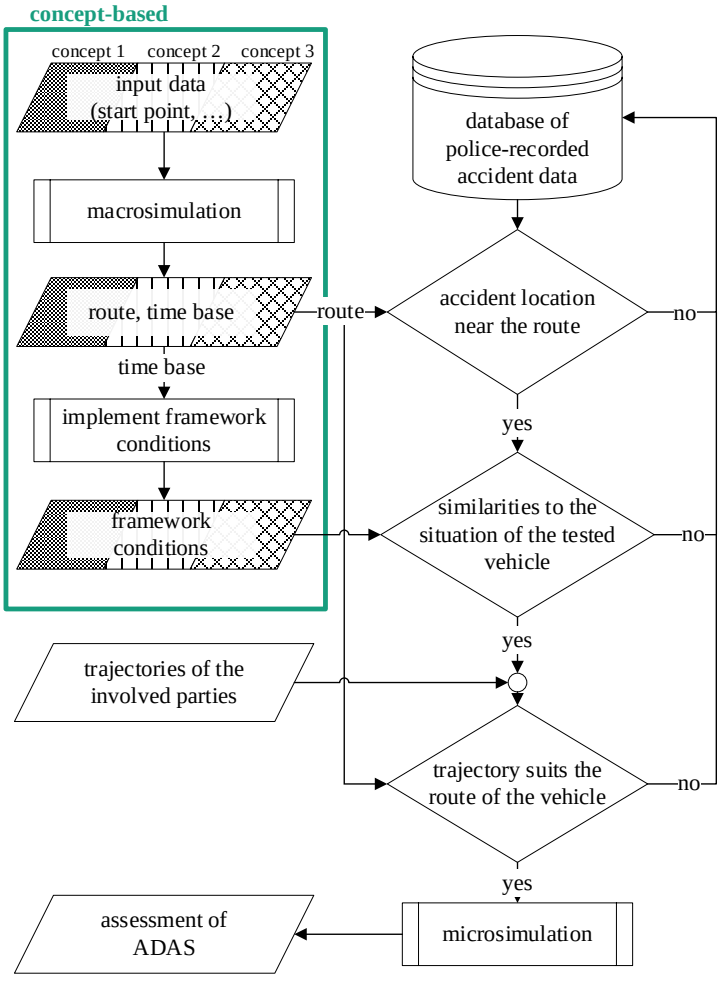

Figure 1: schematic of the selection process

The third and last step of the selection process is based on the intended trajectories of the involved parties. These, as well as the real trajectories, are generated at the Fraunhofer IVI on the basis of the accident data. In order for a certain accident scenario to be selected, one of the intended trajectories needs to correspond with the simulated course of the test vehicle. It is only possible under these circumstances that a vehicle at the same precise location and under similar framework conditions will be involved in an accident similar to the existing concrete accident scenario. If, for example, the simulated vehicle makes a right turn at an intersection where a left-turn accident has occurred, this accident simulation cannot be submitted to the microsimulation.

Within the microsimulation, a statement is made about whether there is a collision between the parties involved. By executing separate simulations with and without a system under testing, it is possible to assess whether the system is able to prevent an accident. In combination with the length of the test route, a claim can be made about test kilometers driven, simulated accidents as well as prevented accidents.

Development of three concepts for the integration of the macrosimulation
Each of the three concepts is based on the macroscopic calculation of a test route between points of origin and destination. The concepts differ in the integration of the macrosimulation and the establishment of framework conditions for the selection process.

Concept 1 adapts a real test drive. The route is known prior to the start of the simulation, meaning that the points of origin and destination are also known. A route is generated between these two points under consideration of any desired number of intermediate points.

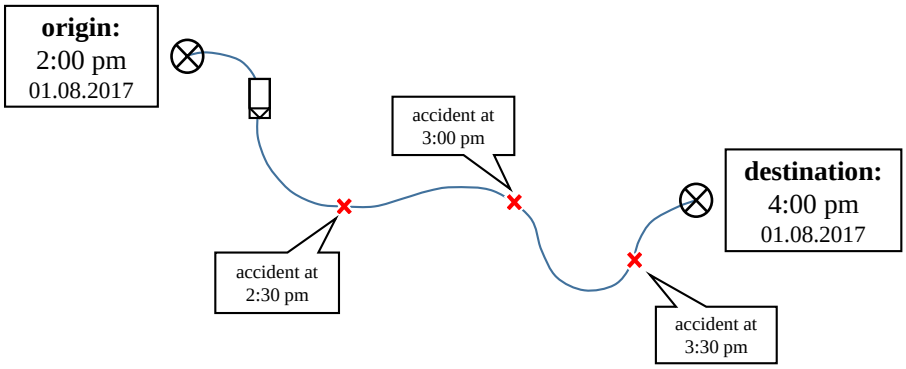

Figure 2: schematic of the first concept

Figure 2 shows the schematic structure of the first concept. The blue line depicts the route from point of origin to point of destination. In concept 1, all accidents along this route with a maximum distance of 15 m to the middle of the road are extracted from the database. The red crosses depict these accident locations along the route. Concept 1 also requires a start date and time, henceforth called the start time stamp. With the help of the start time stamp, it is possible to calculate the position of the test vehicle along the route. The result of this calculation is one arrival time stamp for the point of destination and arrival time stamps for each of the accidents extracted. In addition, each accident also has an accident time stamp describing the date and time at which the accident occurred. The accident time stamp can be extracted from the database of police-recorded accident data. If a simulated vehicle reaches the accident location close to the accident time stamp, the vehicle's situation is similar to the situation. If a simulated vehicle reaches the accident location close to the time of the accident time stamp, its situation is similar to the situation causing the accident. A higher proximity between arrival time stamp and accident time stamp means a higher similarity.

Concept 2 is based on concept 1. Just as in concept 1, a route is generated between the points of origin and destination. This route is shown as blue line in Figure 3.

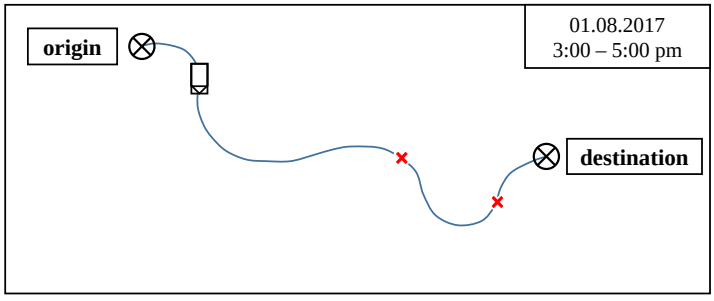

Figure 3: schematic of the second concept

Then, all accidents along the route that are close to the road are looked up. Similar to concept 1, each accident has a time stamp. However, concept 2 does not calculate when a simulated vehicle reaches the accident location. Instead, accidents are selected on the basis of a freely configurable time window. For the example shown in Figure 3, this means that every accident between 3:00 pm and 5:00 pm is selected (red crosses). It is irrelevant in this case whether the simulated vehicle would be able to reach the accident locations in the given time or whether the accidents are depicted in a chronological order. The result of this abstraction is the simulation's loss of direct comparability with real test drives.

Concept 3 is comparable to a real test drive because the calculation of its duration is realistic. However, the drivers do not know their final destination at the start of the test drive. Instead, they receive a new destination after they have reached a given intermediate destination. At the start of the simulation, only the point of origin, the start time stamp and the minimum distance of the test route are known.

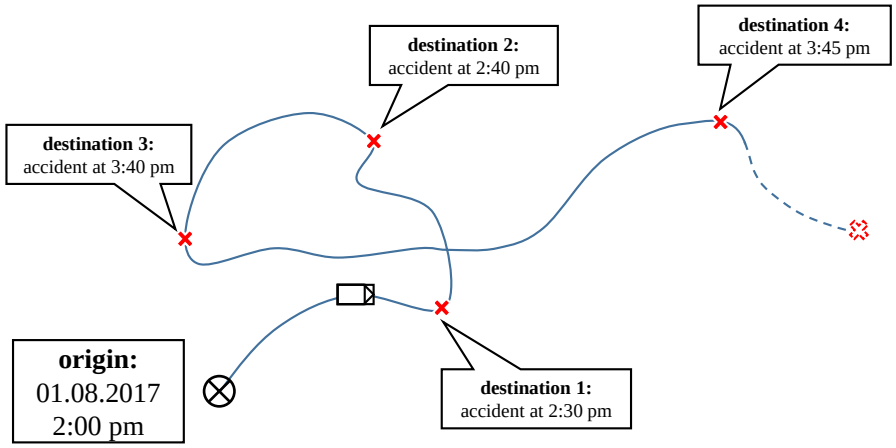

Figure 4: schematic of the third concept

Figure 4 shows the schematic structure of the third concept. The point of origin and the start time stamp are visualized by a black circle with a cross. A pre-defined route, however, needs a destination. To determine a destination, all relevant records are filtered out of the database of police-recorded accidents in Saxony. Then, the distances between the point of origin and all extracted accident location is calculated. The accident location closest to the point of origin becomes the destination of the first route segment (red cross in Figure 4).

An arrival time stamp is calculated for the selected accident location. Based on the arrival time stamp there is an assessment of whether the lighting conditions at the time of arrival are similar and whether the difference between the time of arrival and the time of accident is tolerable. If, considering all framework conditions, the accident scenario is still valid at the simulated vehicle's arrival at the accident location, the scenario can be submitted to the selection process and simulated microscopically.

After this, a destination for the following route segment is determined. The new point of origin is the location of the current accident scenario and the arrival time at the accident location becomes the new start time. As described above, all relevant records are extracted from the database and the distances to potential points of destination is calculated. Again, the closest accident is defined as destination of the current route segment. This loop is continued until the test vehicle has exceeded a predefined number of test kilometers. At this point, the simulation according to the third concept is terminated.

Evaluation of the three concepts

Before the three concepts can be compared to each other, each concept needs to be defined rigidly. For this, each concept is assessed in terms of its possible framework conditions for the selection process so that in the end, each concept is defined by a special combination of rigidly implemented framework conditions. The following three criteria are considered in the specification of the framework conditions.

The first criterion is the number of selected accidents per 1,000 km distance. To determine this figure, the absolute number of selected accidents is divided by the test kilometers driven. According to the statistics on road traffic accidents in the year 2016 compiled by the German Federal Statistical Office (Statistisches Bundesamt, Destatis) [3], about 3,375 accidents per 1 billion kilometers driven occurred in 2016. Or, to put it differently: On average, there was one accident every 296,296 kilometers. This corresponds to 0.003375 accidents per 1,000 km. However, it is not practical to use this figure as an evaluation standard for the first criterion. In order to test a system, a much higher number of accidents per kilometer should be simulated. In order to achieve a compromise between higher accident numbers and the highest possible comparability of vehicle and accident situations, a range of 50 to 100 accidents per 1,000 km is desirable.

The second criterion is the representativeness of the selected accidents within the context of all available police-recorded accident data. The database of accident data recorded by the Saxon police includes, among others, all police-recorded accidents between 2010 and 2016. Each of these accidents is described by characteristic features such as accident category, kind of accident, type of accident and area (urban, rural). This means that the distribution of these features within the Saxon database reflect the general accident situation in Saxony in the past years. It is therefore desirable to achieve an approximation of this distribution within the planned simulated test drive.

The third criterion is the logical comparability of vehicle situation and accident scenario. The repeated simulation of a past accident becomes more comprehensible if the situation of the simulated vehicle and the situation that caused the accident are as similar as possible. Different framework conditions may decrease or increase the similarities between the two situations. Therefore, the framework conditions must be studied in terms of their effects.

After the analysis and subsequent definition of the concepts framework conditions, they can be compared. This process takes into account seven criteria that are weighted differently. After the evaluation of all concepts, it is possible to identify the best one.

Trajectory-based analysis of selected accident scenarios

The selection process for the microsimulation is carried out partly based on concepts (within the concepts) and partly independent from concepts (outside of the concepts). Trajectory-based selection is the part of the selection process that is independent from concepts.

Upon the arrival at a selected accident location, the simulation program examines whether the course of the simulated test vehicle corresponds with the intended course of a party involved in an accident. If the courses correspond, the test vehicle is allowed to simulate the specific accident scenario in the role of this specific party only. Figure 5 shows the schematic of a potential accident scenarios along the test route. The party causing the accident (red) collides with the injured party (blue) while making a left turn. The course of the simulated test vehicle (green), however, does not correspond with either of the two intended courses. In this case, the specific accident scenario was selected within the concept on the basis of framework conditions, but it may not be used within the microsimulation because the course and the trajectories do not correspond. This is the reason why it is important to establish a method for assessing the courses and trajectories of the parties involved in an accident.

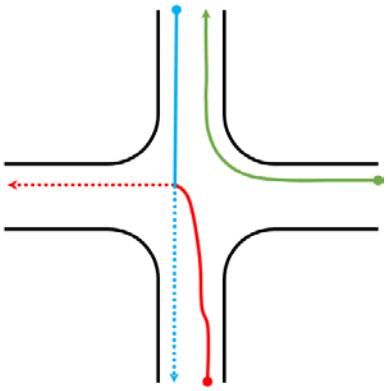

Figure 5: Necessity of the trajectory-based selection

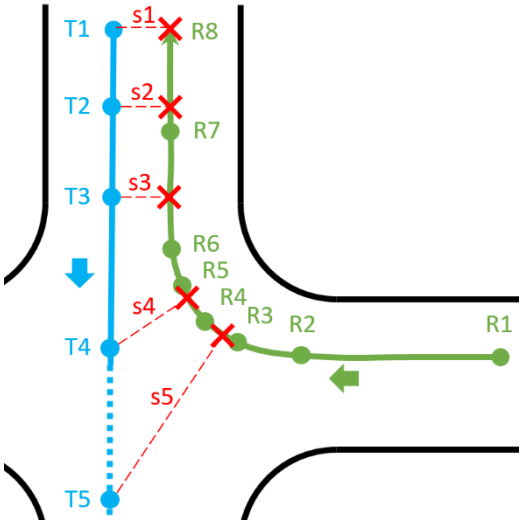

Figure 6: sketch of the solution approach of the trajectory-based selection

The solution of this problem is a method that combines the evaluation of the distance between course and trajectory with the evaluation of the direction of travel. The course and the trajectories are defined by any given number of points represented by geographic coordinates (from now on called supporting points). In Figure 6, these are visualized by the round dots. For each supporting point of the trajectory (blue), the shortest perpendicular distance to the course (green) is calculated (see s_1 to s_5). The resulting vector of shortest distances $\bar{s}$ can be studied in terms of various parameters such as mean value and standard deviation.

In order to compare the directions of travel, it is necessary to analyze the order of the trajectories supporting points (T1 to T5) and their corresponding closest course supporting points (R1 to R8). For this, each trajectory supporting point Tx is matched with the route supporting point Rx that is closest to the point depicted by the red cross in Figure 6. For example, T1 is matched with R8, T2 is matched with R7 and T3 is matched with R6. This way, two vectors are formed that conatin the figures of the matching points (for example: $\bar{T} = [1; 2; 3; 4; 5]$ and $\bar{R} = [8; 7; 6; 5; 3]$).

After that, it is possible to estimate the strength of the linear relation of the two vectors $\bar{T}$ and $\bar{R}$ by using the Pearson correlation ρ according to the Equation 1.

$$\rho = \frac{cov(\bar{T}, \bar{R})}{\sigma_{\bar{T}} * \sigma_{\bar{R}}}, with\ cov(\,) - covariance\ und\ \sigma - standard\ deviation \quad \text{(Equation 1)}$$

In order to test which parameters (mean value, standard deviation, … , ρ) allow the identification of suitable trajectories, a test data set is compiled. The basis of this are 18 different random accidents with known trajectories. For each of the accident locations, all courses in all possible directions are established. Then, a manual assessment is carried out for each of the 256 route-trajectory-pairs of whether they are approximately parallel. If this is the case, a distinction is made between "right direction" and "wrong direction". With the help of several graphic representation methods, it is then possible to determine which parameters allow the identification and selection of suitable trajectories (along the course, right direction).

Microsimulation

The selected accidents are automatically transferred to the microsimulation via an interface and then analyzed. Because the PC-Crash software can easily be integrated by external applications and also supports trajectory-based collision detection, it is used as microsimulation software.

Input data such as the real trajectories of the parties involved in the accident, their speeds and initial locations provide the basis for microsimulation. The maximum allowed speeds of the involved parties can be found in the police-recorded accident data, an uniform movement is assumed. The initial locations of both parties are deduced on the following assumption: the vehicles of both parties collide at the end points of their real trajectories. Based on this assumption, possible initial locations for each party can be established with the help of a reverse simulation along their trajectories that starts at the end points.

The result of the microsimulation consists of two return values. The first return value stores the information whether a collision has occurred without the system under testing, thus error-proofing the process. The second return value gives information about whether the vehicles collide while the system under testing is active. If the first return value is negative (no collision), then no claims can be made about the effect of the system under testing on the basis of this specific accident scenario. If the first return value is positive, a second step describes whether a collision was prevented by the system or not. The system's effects can then be evaluated based on the accidents prevented.

RESULTS

The results of the comparison of the three concepts are depicted in Table 1.

Table 1.
Comparison of the three concepts with the help of a weighted decision matrix

Criterion	Weighting	Concept 1	Concept 2	Concept 3
Comparable with reality	**5**	9	4	9
Accident numbers along the test route	**2**	5	5	9
Options of test route manipulation	**3**	2	2	8
Functionality of long test routes	**5**	3	2	10
Options of influencing the testing environment	**2**	5	9	0
Functionality in case of missing accident data	**4**	10	10	9
Option of expanding the simulation to further regions	**5**	9	9	7
Result [Percentage of maximum points attainable]		**66 %**	**57 %**	**80 %**

Table 1 shows that each of the concepts has its advantages and disadvantages. However, for the simulation of a test drive under the given requirements, the third concept is the most suitable one.

Results of the trajectory-based selection process

The analysis of the parameters for the identification of suitable route-trajectory pairs had the result that no single parameter offers a finite solution. Instead, a combination of the standard deviation and the Pearson correlation coefficient is used. Figure 7 shows which threshold values need to be defined.

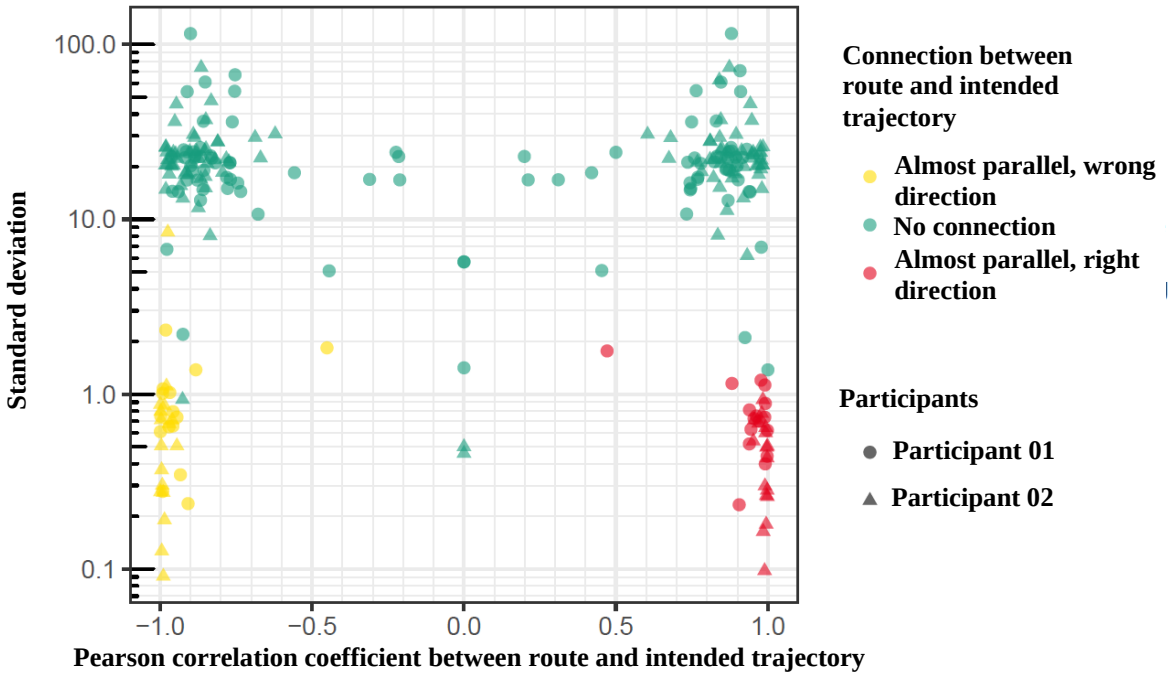

Figure 7: standard deviation and correlation coefficient (256 route-trajectory pairs)

Based on the above image, the trajectory-based scenario selection procedure is implemented as follows: For the examination, the type of road use of the trajectories taken into account is limited to the class of "passenger car". For example, pedestrian trajectories are not allowed. The remaining intended trajectories can be examined with the help of the standard deviation and the correlation coefficient. In 97% of cases, trajectories with a standard deviation $\sigma \leq 3$ and a correlation coefficient $\rho \geq 0{,}8$ are suitable for the current route and go in the right direction.

Example application of the program

The example application demonstrates the entire process of the developed program using a vehicle equipped with an advanced emergency braking system (AEBS). At the beginning of the example application, the input data is defined. The test drive begins on August 1, 2017 at the Fraunhofer IVI in Dresden and covers a distance of 100 km or more. The system under testing is mapped in PC-Crash with the help of a proximity sensor with a range of 80 m, an opening angle of 5 degrees and a cycle time of 100 ms, as well as with an active TTC time to collision monitoring system. If the TTC falls below 1 second, an emergency braking process is initiated.

Within 11 minutes, the program carries out the construction of the route, the selection process and the microsimulation. The resulting test route of 109 km length is visualized in Figure 8 by a transparent green line. It passes through Dresden's urban center as well as through surrounding areas. Along this route, the test vehicle is confronted with 18 selected accident scenarios. 14 of these pass the trajectory-based selection process and are then simulated microscopically. The results are summarized in Figure 9.

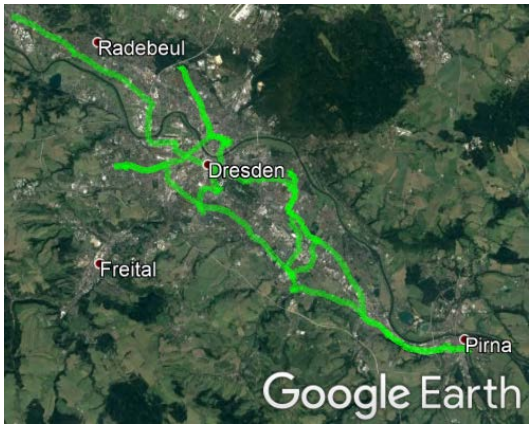

Figure 8: test route of the example application

The 14 simulated accident situations are plotted according to their types of accident and distinguished by color. Only those accident situations that were prevented by the AEBS are marked green. Thus, the efficacy of the AEBS becomes evident with respect to the different types of accident.

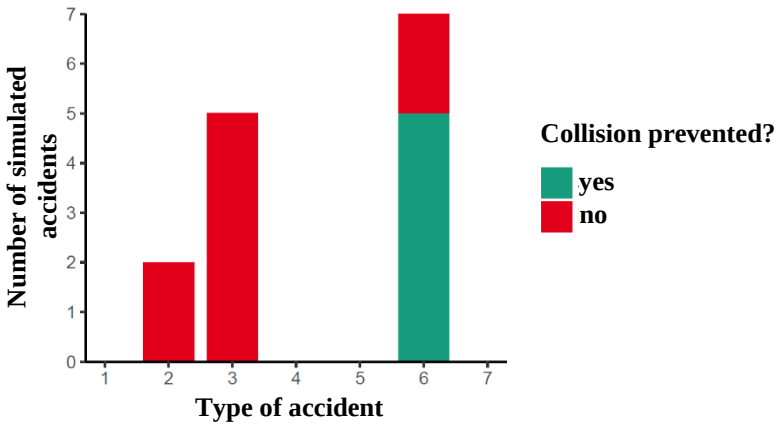

Figure 9: results of the example application, broken down by type of accident

According to Figure 9, the AEBS is able to prevent over 70 % of accidents in parallel traffic (accident type 6) within the simulation. However, no accidents are prevented during turning and during turning/crossing accidents (types of accident 2 and 3). This leads to the conclusion that the AEBS in use is mainly effective in rear-end collisions. Further examination of the simulation files created by the microsimulation confirms this conclusion. Only in the situation of a rear-end collision on a straight road is the injured party detected in time, so that an emergency braking process can prevent the collision. In rear-end collisions in turns and in all other accident situations included in the simulation, the injured party is not detected or not detected early enough.

DISCUSSION

The integration of traffic and weather data would be very beneficial for the area of the macrosimulation. The implementation of other external macrosimulation applications is also conceivable to and the modular design of the program supports this.

The selected variant of microsimulation is able to draw a conclusion about prevented collisions. However, a more detailed realization of sensors and advanced driver assistance system would improve the plausibility of results. Also, no exact input parameter exist for the microsimulation, which is why they need to be deduced with the help of assumptions. Thus, there is a potential for an expansion of the microsimulation. Due to the modular design of the program, the microsimulation could also be realized through the implementation of other simulation programs.

In order to evaluate the simulation of an entire route, the accident selection is studied in terms of representativeness by comparing it to a reference data set. For this, the distribution of the double-digit types of accident of the selected accidents is examined in the context of the distribution of the double-digit accident types of the reference data set. The result of the comparison provides the basis for a two-level score, which is calculated automatically. This score first examines how many of the types of accident are reflected in the accident selection. Subsequently, it evaluates how well the reflected types of accident are represented. The score has values between 0 and 1, where 1 symbolizes a perfect reflection of the overall data set.

The score of the example application was calculated to be 0.38, which means an inadequate representativeness. Although 5 of 14 collisions were prevented, the statement “The AEBS is able to prevent 5 in 14 (35%) accidents” is a misinterpretation. A longer test route with an increased number of simulated accidents would improve chances of a higher score and a more well-founded statement.

CONCLUSION

Due to the necessity mapping test drives in a simulation environment, a method was developed that allows a statement about test kilometers driven and accidents prevented. To achieve this, a simple macroscopic simulation of a test vehicle was combined with a selection process for specific accident scenarios with the objective of transferring selected scenarios from the macroscopic simulation to the microscopic simulation. On the basis of multiple simulation, the latter allows to draw a conclusion about the collision prevention potential of the system tested.

The reduction of effort and expenses for real test drives will be possible with the help of the described method. If comprehensive accident data is available, the expansion of the simulation to additional regions will be possible.

REFERENCES

[1] Kühn, Matthias; Hannawald, Lars:
Verkehrssicherheit und Potenziale von Fahrerassistenzsystemen. in: Winner, Hakuli et. al. - Handbuch Fahrerassistenzsysteme (2015). page 55–70.

[2] Winner, Hermann:
Quo vadis, FAS? in: Winner, Hakuli et al. (Hg.) - Handbuch Fahrerassistenzsysteme, Springer Fachmedien (2015). page 1167–1186.

[3] Statistisches Bundesamt (Destatis):
Fachserie 8 Reihe 7 - Verkehr. Verkehrsunfälle; Wiesbaden. 2016.

FAULT TREE-BASED DERIVATION OF SAFETY REQUIREMENTS FOR AUTOMATED DRIVING ON THE EXAMPLE OF COOPERATIVE VALET PARKING

Valerij Schönemann, Hermann Winner
Institute of Automotive Engineering ,Technische Universität Darmstadt
Darmstadt, Germany

Thomas Glock, Eric Sax
Research and Engineering Center, FZI Research Center for Information Technology
Karlsruhe, Germany

Bert Boeddeker, Sebastian vom Dorff
Research and Engineering Center, DENSO AUTOMOTIVE Deutschland GmbH
Eching, Germany

Geert Verhaeg[1], Fabrizio Tronci[2], Gustavo G. Padilla[3]
TNO[1], Magneti Marelli[2], Hella Aglaia Mobile Vision[3]
Netherlands[1], Italy[2], Germany[3]

Paper Number 19-0099

ABSTRACT

Developing safe vehicle automation systems is crucial for the commercialization of automated driving. One of the major challenges for the release of fully automated driving is functional safety. Automated driving systems explode in complexity due to an infinite number of occurring scenarios. Thereby, the derivation of safety requirements for complex automated driving functions lacks a categorization to tackle the completeness issue. This work presents a structure for a fault tree-based approach to derive safety requirements from safety goals systematically in compliance with the international standard of functional safety for road vehicles known as ISO 26262. The investigation of the state of the art reveals that a functional safety concept for fully automated valet parking (AVP) has not yet been targeted. The methodology is therefore applied on the example of automated valet parking to elaborate a safety concept which was not yet investigated.

Beforehand, the AVP system was split into a manageable amount of relevant functional scenarios to decrease complexity. For each scenario, a Hazard Analysis and Risk Assessment (HARA) was performed. A set of safety goals was elaborated. The approach utilizes a fault tree-based Sense-Plan-Act architecture to achieve a large coverage of possibly derivable safety requirements from safety goals. The sense phase contains the acquisition of sensor data and leads to three uncertainty domains: state, existence, and class uncertainty. The plan segment includes the situation comprehension and action planning. Thereby, the transportation mission can be split into five tasks. The act block represents the execution of the planned trajectory. Longitudinal and lateral vehicle dynamics such as steering, shifting, accelerating, and braking are performed. A violation of a safety goal occurs if at least one of the failure events in the sense-, plan-, and act-phase is present. The methodology is suitable for safety goals which follow the specified Sense-Plan-Act pattern.

INTRODUCTION

The globally leading cause of death among people aged 15-29 in the year 2012 are road traffic accidents [1]. 94 % of crashes can be tied back to human error [2]. In 2015, the United Nations agreed to global goals for sustainable development. The goal “good health and well-being” concerns road safety in which the number of global deaths and injuries from road traffic accidents shall be halved by 2020. Safe automated systems that intervene in case of a proximate accident and release the driver from the responsibility are required. Thereby, functional safety is one of the major challenges for the release of automated driving [3]. An automated driving function shall be harmless in all operating states. The system shall identify hazards and reach a safe location in which the vehicle is no hazard for other participants. The international standard for functional safety ISO 26262 specifies a systematic procedure for designing functionally safe electrical and electronic systems [4]. ISO 26262 and international standards for other domains are derived from the IEC 61508 [5].

Automated systems from different domains have a common denominator: exploding complexity. A nearly infinite number of possible scenarios has to be tested. The European Union (EU) project ENABLE-S3 focuses on the reduction of today’s cost-intensive verification and validation process to establish efficient methods for the commercialization of automated cyber-physical systems. Different approaches have to be targeted in order to cope with the increasing complexity regarding the development of safe automated systems.

A major challenge is to develop a functionally safe distributed system in which independent subsystems share responsibility for the automation task. Such a distributed system is fully Automated Valet Parking (AVP). AVP is realized through cooperation between the automated vehicle and a Parking Area Management system (PAM). The automated vehicle operates driverless and is classified as level 4 of SAE International's taxonomy of driving automation [6]. The use case provides an automated parking procedure. In previous work, a scenario-based methodology for functional safety according to ISO 26262 was presented and applied on the safety analysis of AVP [7]. The following pre-conditions were assumed for AVP:

1. Parking management system and automated vehicle manage the driving task in cooperation.
2. The handing over and requesting back procedure of the automated vehicle to/ from the PAM is instructed via a terminal (human-machine interface, HMI).
3. Manually and automatically operated vehicles are allowed to enter the parking garage.
4. Pedestrians, animals, obstacles, etc. sojourn in the car park.
5. Drivers and passengers have to leave the automated vehicle before AVP is activated.
6. Parking construction prevents dangers caused by running engines.

The described constraints served as an input to break down the system's functional behavior into scenarios. Thereby, the AVP system was split into a manageable amount of relevant functional scenarios to decrease complexity. For each scenario, a Hazard Analysis and Risk Assessment (HARA) is performed. As a result, a more complete set of safety goals was elaborated as indicated in Table 1.

This work is structured as follows: Section 2 contains the related work of functional safety. Section 3 illustrates a structure for a fault-tree-based approach to derive functional safety requirements for automated driving. Thereafter, the presented methodology is applied using the example of fully automated valet parking. Section 4 shows the elaborated safety requirements from safety goals for AVP. Section 5 summarizes the results of the safety requirements and gives a brief outlook for developing a safety concept.

Table 1.
Safety Goals for Automated Valet Parking [7]

ID	Safety Goal	ASIL
SG01	Unintended activation of the valet parking function outside of the PAM-controlled parking area shall be prevented.	D
SG02	The integrity of the communication between the PAM and the vehicle shall be ensured.	D
SG03	The system shall prevent a collision between automated vehicles and persons.	C
SG04	The vehicle shall not start moving during embarkment and disembarkment.	C
SG05	The system shall prevent collisions with other vehicles.	B
SG06	The system shall notify a human supervisor in case of a collision or fire.	B
SG07	The system shall ensure that the vehicle stays within the (statically defined) drivable area during AVP.	B
SG08	The valet parking function shall be disabled if people are inside the vehicle.	A
SG09	The system shall prevent collision of automated vehicles with objects.	A

RELATED WORK

A major challenge for the release of automated driving is the issue of testing. Up to now, only the international standard ISO 26262 illustrates a systematic process for developing functionally safe electrical and electronic systems in the automotive domain. Neither a standard, nor a methodology is specified to elaborate a safety concept specifically for automated driving. However, functional safety as well as a corresponding methodology for developing a safety concept for such complex systems is crucial for the release of automated driving [8].

Alexander et al. [9] combined several existing approaches to develop a methodology for deriving safety requirements for autonomous systems. The authors describe the derivation of safety requirements as a three-stage process. In the first step, harmful events are determined (hazard identification). Causes of the hazards are explored (hazard analysis) and finally safety requirements can be derived from causes. The system is seen as a combination of operators (Combined Autonomous Systems, CAS) in which hazards may occur. High-level capabilities of CAS are determined and hierarchically decomposed in lower level capabilities until these can be analyzed for safety (Hall-May [9]). The authors consider autonomous systems in general. Autonomous systems from other domains will lead to different safety requirements e.g. by comparing automated systems in the health domain with automated driving functions.

The fault tree analysis is a deductive approach starting with a top undesired event and is suggested in the ISO 26262 beside a Failure Modes and Effects Analysis (FMEA) and Hazard and Operability study (HAZOP) for safety analysis. FTA is also used in the nuclear power and aerospace sector. Failure events can be identified by considering Boolean logic. The main advantage of a FTA is that it displays interactions between events in a graphical format [11]. The interaction cannot be seen from a FMEA. A FMEA is more suitable for an inductive failure analysis of components and subsystems. Furthermore, the FTA should contain all failure modes of a FMEA.

Lambert applied a qualitative FTA on a car starting system [12]. Thereby, the applier has to identify the failure modes that cause the top event. Starting from the top undesired event that the car does not start, the author shows a logical progression of undesired events connected via AND and OR logic. However, a vast number of undesired events may occur with increasing system complexity. The elaboration of a FTA for automated driving systems without providing any structure is challenging.

Stolte et al. [13] derived safety goals and functional safety requirements of actuation systems for automated driving by applying a system theory-based methodology. The authors used a System-Theoretic Process Analysis (STPA) to identify unsafe control actions and its causes which serve as an input for a HARA. Furthermore, safety requirements are derived from a control structure and corresponding unsafe control actions. The authors do not determine safety requirements for perception or planning modules of automated vehicles. The trajectory input was assumed to be correct and only actuation systems of automated vehicles were analyzed.

The national project PEGASUS [14] applies a scenario-based approach to reduce driving test distances for a statistical approval of highly automated driving. It is assumed that the majority of the driven mileage is uncritical and only critical scenarios are required to be investigated. Amersbach and Winner [15] proposed a six-layer decomposition of the automated driving function. The six layers are Information Access, Information Reception, Information Processing, Situational Understanding, Behavioral Decision, and Action. A matrix to allocate fail criteria to functional layers and relevant scenarios is built. Fail criteria are identified by using a FTA. Redundant fail criteria that are “subsets or intersecting sets of each other” are combined and thus the testing effort is reduced. Test cases and environments are derived from fail criteria for the use of safety approval. However, the authors propose a different approach and do not relate to the ISO 26262 standard. The interaction of different subsystems is not targeted.

Furthermore, there is still a risk of a violation of a safety goal without any malfunction. It is therefore required to consider the safety of the intended function (SOTIF). A sub-working group was built within ISO 26262 to specify when a target function behaves safely. The results are present in the ISO/WD PAS 21448. This work aims to cover critical scenarios, which are not only a result of malfunction, but also the safety of the intended functionality.

Reschka et al. [16] investigated safety concepts for automated driving without driver monitoring. The analysis leads to high-level safety mechanisms to handle potential hazards for AVP systems. More specific safety requirements are not presented. Bosch and Daimler [17] released the first prototype for infrastructure- based AVP in a mixed traffic parking garage. However, further specification concerning the safety are missing. Chirca et al. [18] and Schwesinger et al. [19] provide mainly a technical description of an AVP service in which safety is not of major focus.

The state of the art reveals that a structure for breaking down highly complex and self-driving automation systems is missing. This work aims to overcome the lack of a recipe for deriving safety requirements from safety goals. This work presents a methodology how such a specification can be achieved by deriving safety requirements for automated driving systematically in compliance with the international standard ISO 26262. The approach utilizes a fault tree-based technique to achieve a large coverage of possibly derivable safety requirements. The issue of completeness is targeted qualitatively by applying a deductive

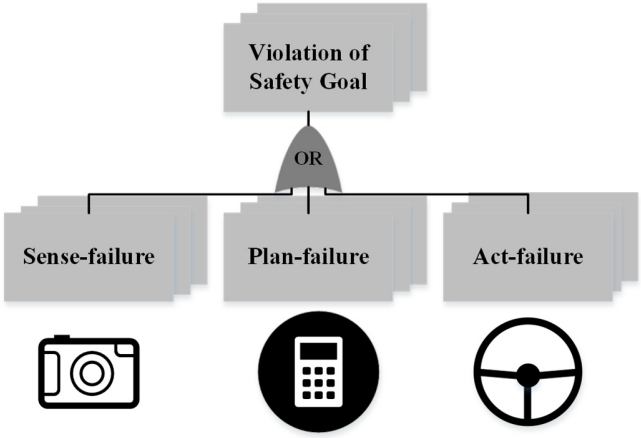

Figure 1. The violation of a safety goal occurs if at least one of the failure events in the sense-, plan-, and act-phase is present.

method. The methodology is applied on cooperative valet parking for which a safety concept is still missing in the state of the art.

METHODOLOGY

The methodology presented in this work provides a path to systematically derive safety requirements from safety goals. A fault tree-based approach is proposed to ensure a more complete set of safety requirements. Sequential robot control architectures are known as Sense-Plan-Act or Sense-Model-Plan-Act architectures. Thereby, the signal processing steps of the sensor data acquisition, the environment modeling, the planning, and finally the actions are executed sequentially. Sequential architecture elements serve for achieving a long-term goal, e.g. the execution of a driving mission [20]. In the following the terms Sense, Plan, Act and the corresponding breakdown into segments are introduced. Figure 1 indicates the safety analysis of a Safety Goal's violation.

Sense: The Sense phase contains the acquisition of sensor data and modelling of the environment. According to Dietmayer et al. [21] detecting static and dynamic objects and physically measuring them as precisely as possible, leads to three uncertainty domains visualized in Figure 2:

- State uncertainty: Represents the measuring errors of physical measured variables, especially the object's dimensions (length, width, height), the object's pose and the object's velocity.
- Existence uncertainty: Outlines the uncertainty whether an object captured by the sensors and mapped into the representation actually exists. This concerns mainly false positives and false negatives. For example, emergency braking should only be executed in case of a high existence probability.
- Class uncertainty: Describes uncertainty of the capability to classify the object's membership in order to predict the object's behavior. Type of object might be for example pedestrians, bicyclists, trucks, or cars. The degree of granularity is dependent on the use case.

Plan: The Plan segment includes the situation comprehension and action planning. The transportation mission can be split into five tasks which are partly computed by today's navigation systems. These five steps are given in Figure 3:

- Mission Planning: In the first step, a mission has to be planned from the current location to the destination.
- Route Planning: A route has to be determined in order to get to the destination.
- Behavior Planning: Selects a sequence of maneuvers by considering other traffic participants, traffic rules and restrictions.
- Maneuver Planning: Maneuvers such as lane changes have to be executed.
- Trajectory Planning: A trajectory has to be calculated to perform necessary maneuvers.

Timing constraints for the start and end of each maneuver and the calculation of the maneuver trajectory have to be specified.

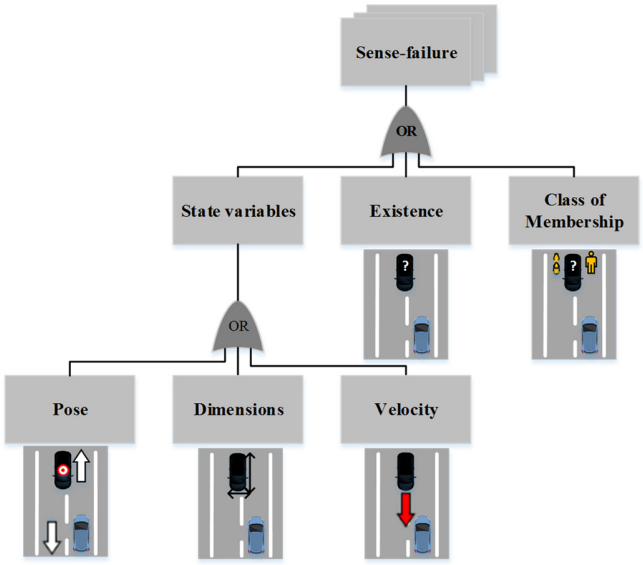

Figure 2. According to Dietmayer [17] an uncertainty in the sense phase occurs if the object's state variables such as the object's pose, the object's dimensions, and the object's velocity are not measured with sufficient precision or if the object's existence or its class of membership are uncertain.

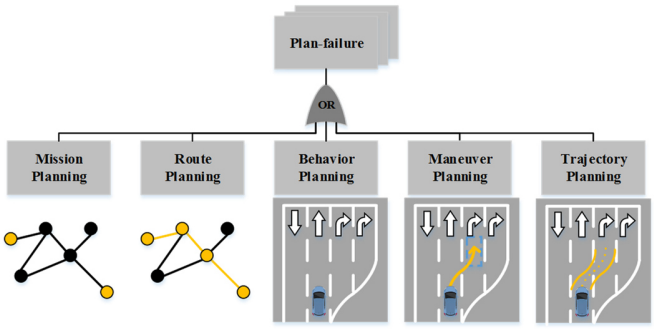

Figure 3. According to Lotz [22] the driving mission can be split into mission planning, route planning, behavior planning, maneuver planning, and trajectory planning. For maneuver and trajectory planning, timing constraints for calculation and execution are crucial.

Act: The Act block represents the execution of the planned trajectory. The following vehicle control inputs are required for performing longitudinal and lateral vehicle dynamics: Steering, shifting, accelerating, and braking. A complete electrification of actuators is mandatory. This is realized by today's X-by-Wire concepts: Throttle-by-Wire, Brake-by-Wire, Shift-by-Wire, and Steer-by-Wire [19]. Thereby, either the targeted steering, shifting, acceleration, and braking parameters are not plausible for the executed maneuver in terms of range and time or corresponding vehicle components are corrupted. The breakdown of possible Act-failures is illustrated in Figure 4.

The presented structure can be further broken down into use case-specific safety requirements. The safety requirements can be derived systematically by covering a more complete set of safety requirements due to the application of a deductive fault tree-based approach. The methodology is not suitable for all derived safety goals since for example C2X-communication does not follow the specified Sense-Plan-Act pattern.

DERIVATION OF SAFETY REQUIREMENTS

In the following, the elaborated methodology is applied to the safety goal "SG03: *The automated driving system shall prevent a collision between automated vehicles and persons*". Furthermore, the derivation is similar for SG05 and SG09 only with a different ASIL inheritance for derived safety requirements and decomposition to architectural elements.

The division in sense, plan, and act leads to the following high-level Functional Safety Requirements (FSR):

- FSR3.1: The system shall detect objects in its required sensor perception area
- FSR3.2: The system shall not plan a harmful trajectory
- FSR3.3: The vehicle shall prevent unintended control actions

Each high-level FSR will be further broken down into low-level FSR.

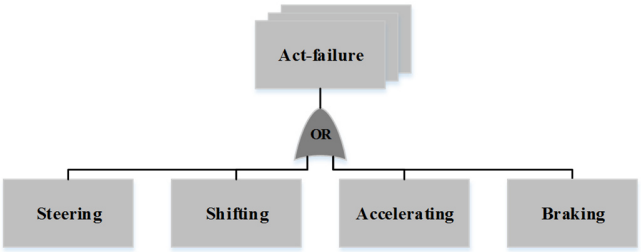

Figure 4. Steering, shifting, accelerating, and braking are primitives that are required for vehicle control mechanisms.

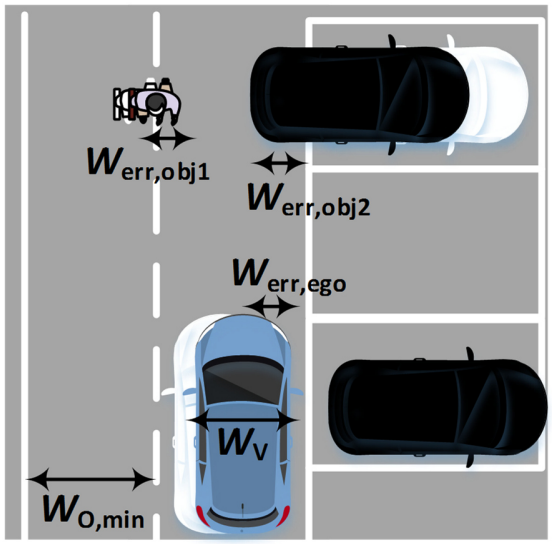

Figure 5. Maximum accepted total error of size determination and object localization is given by the narrowest part in the operational domain and measurement inaccuracies

A. Sense

Since no standard exists specifically for safety requirements of automated driving, other regulations have to be considered as a basis. State uncertainty is represented by the functional safety requirement FSR3.1.1 - FSR3.1.3 of Table 3. and corresponding derived functional safety requirements. The system has to detect the object's position by localizing it. The precision of localization is given by the narrowest part of the operational design domain $W_{\mathrm{O,min}}$, the vehicle width W_{V}, and corresponding measurement inaccuracies W_{err} which may appear on both sides in worst-case. Figure 5 indicates an ego-vehicle driving straight and approaching two objects. Beside the ego-vehicle's localization error $W_{\mathrm{err,ego}}$, the object's localization errors $W_{\mathrm{err,obj}}$ are present. The ego-vehicle assesses a collision-free area due to localization errors, but in reality the ego-vehicle would collide with a traffic participant. The total accepted localization error $W_{\mathrm{err,total}}$ is given by

$$W_{\mathrm{err,total}} \leq W_{\mathrm{err,ego}} + W_{\mathrm{err,obj}} = \frac{W_{\mathrm{O,min}}}{2} - \frac{W_{\mathrm{V}}}{2} \quad \text{(Equation 1)}$$

$$W_{\mathrm{err,obj}} \leq \frac{W_{\mathrm{O,min}} - W_{\mathrm{V}}}{4} \quad \text{for } W_{\mathrm{err,ego}} = W_{\mathrm{err,obj}} \text{ (infrastructure-based)}$$

Considering Germany's road construction regulation and Germany's traffic regulation, a minimum lane width $W_{\mathrm{L,min}} = 2.75$ m [25][26] and a maximum vehicle width of $W_{\mathrm{V,max}} = 2.50$ m [27] can be found. The overall error of size determination and object localization for $W_{\mathrm{err,ego}} = W_{\mathrm{err,obj}}$ shall be less than $W_{\mathrm{err,total}} = (W_{\mathrm{L,min}} - W_{\mathrm{V,max}})/2 = 12.5$ cm and $W_{\mathrm{err,obj}} \leq 6.25$ cm. However, for AVP systems a parking lot width of $W_{\mathrm{P,min}} = 2.75$ m is not profitable for the operator and a minimum parking lot width of Germany's parking garage regulation $W_{\mathrm{P,min}} = 2.30$ m [26] could be considered by not allowing to enter oversized vehicles. In that case, a look on the European's average passenger car size of 2016 could be done [24]. Adding a safety margin of 10 cm for withdrawn car mirrors on each side, we end up with an average vehicle width of around $W_{\mathrm{V,avg}} = 2$ m and therefore an overall error of size determination and object localization of less than $W_{\mathrm{err,total}} \leq (W_{\mathrm{P,min}} - W_{\mathrm{V,avg}})/2 = 15$ cm and $W_{\mathrm{err,obj}} \leq 7.5$ cm.

The object can only be detected if it appears in the system's sensor perception area. Safety-relevant areas of interest for collision avoidance can be specified dependent on the dynamic driving parameters of the engaged traffic participants such as velocities, timing constraints and deceleration capabilities. A definition of an area, in which the perception of objects for collision avoidance is mandatory, has to be given. Furthermore, maneuvers that can occur in the defined operational domain as illustrated in Figure 6 have to be identified. The superposition of the maneuver-based stopping distances shows that the overall safety zone is created by the ego-vehicle's and the object's travelled envelopes given by their widths and stopping distances [28].

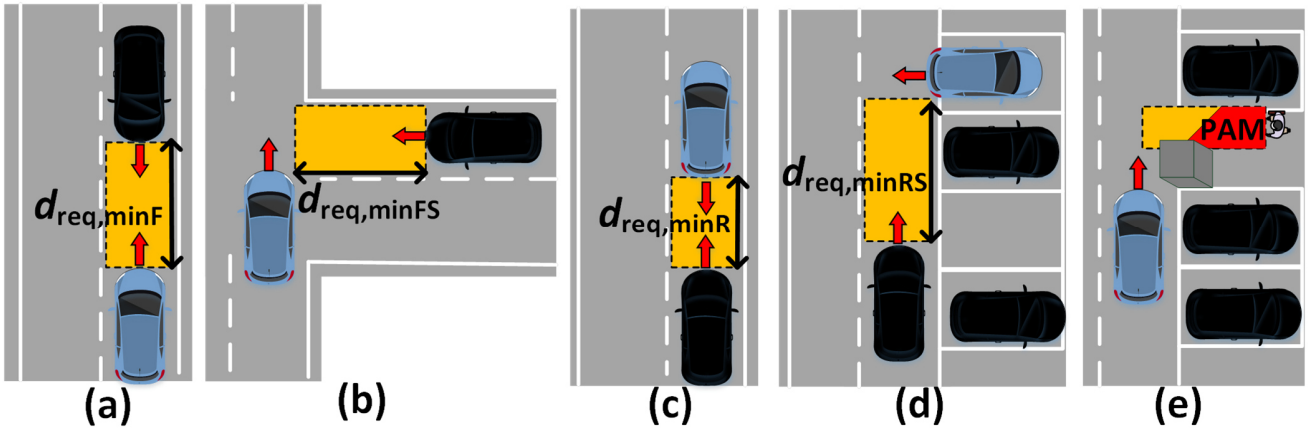

Figure 6. Identified maneuvers that lead to a minimum required sensor perception area: (a) driving straight with potential frontal collision between an automated and manually driven vehicle and both vehicles are braking, (b) intersection crossing and approaching collision partner, (c) driving in reverse with potential rear collision and both vehicles braking, (d) leaving the parking spot in reverse, (e) covered object and required infrastructure support.

The worst-case concerning the stopping distance is defined as a frontal collision of an automated and manually operated vehicle driving with $v_{\max}$ and both vehicles are braking. It is assumed that both vehicles react at the same time. The minimum required sensor range d_{req} is theoretically given by the stopping distance until frontal collision and can be calculated according to

$$d_{\text{req,min}} \geq \left(v_{\text{ego}} + v_{\text{obj}}\right) \cdot \left(\mathrm{t}_{\text{B,lag}} + t_{\text{R,ad}}\right) + v_{\text{obj}} \cdot \left(t_{\text{R,md}} - t_{\text{R,ad}}\right) + \frac{v_{\text{ego}}^2 + v_{\text{obj}}^2}{2 \cdot D_{\min}} + d_{\text{tol}} \qquad \text{(Equation 2)}$$

Thereby, the worst-case constraints are defined as presented in Table 2. Considering rather conservative values of a nearly dry road surface and a resulting minimum deceleration of $D_{\min} = 8\ \mathrm{m/s^2}$, a free running time $\mathrm{t}_{\text{B,lag}} + t_{\text{R,ad}} = 0.5$ s, worst-case driver reaction time $t_{\text{R,md}} = 1.5$ s and $d_{\text{tol}} = 0.5$ m, we get $d_{\text{req,minF}} \geq 27.51$ m. A worst case for a rear collision is a collision at a maximum allowed reverse velocity of the ego-vehicle $v_{\text{ego}} = v_{\text{maxR}}$, an object forward velocity of $v_{\text{obj}} = v_{\text{maxF}}$, and braking of both vehicles. From this, a required sensor range of $d_{\text{req,minR}} \geq 20.88$ m can be calculated. Finally, a worst case for the perception distance to the side is given by crossing an intersection at a maximum allowed intersection crossing velocity of $v_{\text{obj}} = v_{\text{maxI}}$

$$d_{\text{req,minFS}} = d_{\text{req,minRS}} \geq v_{\text{obj}} \cdot \left(t_{\text{B,lag}} + t_{\text{R,obj}}\right) + \frac{v_{\text{obj}}^2}{2 \cdot D_{\min}} + d_{\text{tol}} \qquad \text{(Equation 3)}$$

We end up with a required sensor perception range of $d_{\text{req,minFS}} = d_{\text{req,minRS}} \geq 19$ m. The required sensor perception area to the rear side is actually largest if the vehicle leaves the parking spot backwards. However, since the required sensor perception area to the front is mandatory in many specific situations, the required sensor perception area to the rear side $d_{\text{req,minRS}}$ can be significantly reduced if only reverse parking and forward leaving of the parking bay is allowed. Considering a parking spot length of $L_{\text{P,min}} = 5$ m [26], we can approximate $d_{\text{req,minRS}} \geq L_{\text{P,min}} = 5$ m. Objects that lie within the ego-vehicle's required sensor perception area and are covered, have to be detected by top-mounted sensors of the infrastructure. The elaborated safety zone should adjust its size according to the present velocities in the sensor perception area. The overall required horizontal FoV of 180° in the front and to the rear is required to detect moving objects in the frontal/ rear vehicle area. Elaborated functional safety requirements are shown in Table 3.

Table 2.
Pre-defined Constraints for Automated Valet Parking [28]

ID	Description	Value
C01	Maximum allowed velocities: in forward $v_{\mathrm{max,f}}$, in reverse $v_{\mathrm{max,r}}$, at intersections $v_{\mathrm{max,i}}$	$v_{\mathrm{maxF}} = 30\ \mathrm{km/h}$ $v_{\mathrm{maxR}} = 10\,\mathrm{km/h}$ $v_{\mathrm{maxI}} = 10\,\mathrm{km/h}$
C02	Worst-case expected time delays: system response time from the plausibility check until initiating the brakes $t_{\mathrm{R,ad}}$, driver reaction time $t_{\mathrm{R,md}}$, lag time of the brake $t_{\mathrm{B,lag}}$ given by the response time of the brake $t_{\mathrm{R,b}}$ and the time until buildup of deceleration $t_{\mathrm{B,b}}$	$t_{\mathrm{R,ad}} = 0.3$ s $t_{\mathrm{R,md}} = 1.5$ s $t_{\mathrm{B,lag}} \approx t_{\mathrm{R,b}} + \frac{t_{\mathrm{B,b}}}{2}$ [1]$t_{\mathrm{B,lag}} = 0.2$ s
C03	Minimum expected deceleration $D_{\mathrm{min}} = \mu_{\mathrm{min}} \cdot g$ for object- and ego-vehicle	$D_{\mathrm{min}} = 8\ \frac{\mathrm{m}^2}{\mathrm{s}}$
C04	Safety margin d_{tol}	$d_{\mathrm{tol}} = 0.5$ m

1) Breuer and Bill, 2008

Table 3.
Derivation of FSR3.1: "The system shall detect objects in its sensor perception area."

ID	Functional Safety Requirement
FSR3.1.1	The system shall detect the object's state variables sufficiently accurate.
FSR3.1.1.1	The system shall localize the object's pose $p_{\mathrm{obj.}}$ The error for size determination and object localization shall be less than $W_{\mathrm{err,obj}}$.
FSR3.1.1.1.1	The system shall detect objects in a 180° front and rear horizontal and sufficiently high vertical field of view.
FSR3.1.1.1.2	The system shall detect the object's pose p_{obj} in its minimum required sensor range $d_{\mathrm{req,minF}}$, $d_{\mathrm{req,minFS}}$, $d_{\mathrm{req,minR}}$, and $d_{\mathrm{req,minRS}}$.
FSR3.1.1.2	The system shall determine the object's dimensions length l_{obj}, width w_{obj}, height h_{obj} in its minimum required sensor range. The error for size determination and object localization shall be less than $W_{\mathrm{err,obj}}$.
FSR3.1.1.3	The system shall determine the object's velocity v_{obj} in its minimum required sensor range.
FSR3.1.1.4	The system shall detect objects under all possible environment conditions in the PAM area.
FSR3.1.1.5	The system shall diagnose broken/ covered or misplaced sensors.
FSR3.1.1.6	The system shall detect objects that are covered from the vehicle's view in its minimum required sensor perception area.
FSR3.1.2	The system shall have an ASIL-dependent false positive and false negative rate.
FSR3.1.3	The system's object classification shall not lead to harmful situational interpretation.

B. Plan

The navigation to a specified destination starts with mission planning. The vehicle's position and the destination's position are required for mission planning. Based on the current and the destination's position, todays graph-based search algorithms for road networks determine a route. The computed route shall be composed of up-to-date, accessible, connected road segments that shall be driven in compliance with traffic regulations. The functional safety requirements are equally valid for the lane assignment. Maneuvers such as lane changes are required to reach the destination. The maneuver and the corresponding trajectory shall be feasible, collision-free, and calculated within hard real-time constraints. Thereby, hard real-time is defined as "a missing system response deadline leads to a collision". Start and end of the maneuver have to be defined depending on the maneuver and environmental constraints. Derived functional safety requirements are presented in Table 4.

Table 4.
Derivation of FSR3.2: "The system shall not plan a harmful trajectory."

ID	Functional Safety Requirement
FSR3.2.1	The system shall plan a safe mission.
FSR3.2.1.1	The system shall localize its pose p_{obj}. The error for size determination and localization shall be less than $W_{\mathrm{err,ego}}$.
FSR3.2.1.2	The system shall localize the destination's position. The error for size determination and localization shall be less than $W_{\mathrm{err,obj}}$.
FSR3.2.2	The system shall plan routes on up-to-date, accessible, connected road segments in compliance with traffic regulations.
FSR3.2.3	The system shall assign maneuvers on up-to-date, accessible drivable area in compliance with traffic regulations.
FSR3.2.4	The system shall compute a feasible, collision-free maneuver within hard real-time constraints (= missing deadline leads to a collision).
FSR3.2.5	The system shall plan a collision-free trajectory.

C. Act

Act-failures are not further broken down since an investigation is already done in [13] and state of the art. For the sake of completeness, functional safety requirements are illustrated exemplary in Table 5.

Table 5.
Derivation of FSR3.3: "The vehicle shall prevent unintended control actions."

ID	Functional Safety Requirement
FSR3.3.1	The system shall detect corrupted or uncalibrated actuators and breakdown of necessary vehicle components.
FSR3.3.2	The system shall prevent unintended steering.
FSR3.3.3	The system shall prevent unintended shifting.
FSR3.3.4	The system shall prevent unintended accelerating.
FSR3.3.5	The system shall prevent unintended braking.

Finally, a safety engineer has to control whether a functional safety requirement is not yet covered by another safety goal and should inherit the corresponding safety goal's Automotive Safety Integrity Level (ASIL). The functional safety requirements for the remaining safety goals are shown in Table 6. in the appendix.

CONCLUSION AND OUTLOOK

The state of the art has revealed challenges for automated driving in terms of functional safety. Beside malfunctions, the safety of the intended functionality has to be considered. The derivation of safety requirements for complex automated driving functions leads to the completeness issue. An approach is proposed to derive functional safety requirements in compliance with ISO 26262 according to a deductive fault tree-based methodology for automated driving functions. Functional safety requirements can be derived systematically to target the completeness issue qualitatively. The technique is applied on elaborated safety goals for automated valet parking. Functional safety requirements are derived for all elaborated safety goals. A minimum required sensor perception area could be specified for AVP in which the object's parameters such as pose, dimensions, velocity, existence and class are required to be known. The maximum accepted total error of size determination and object localization could be identified. In future work, functional safety requirements should be assigned to functional blocks of the valet parking system architecture. Thereby, the distribution of functionalities between the automated vehicle and the parking area management system will be targeted and additional test cases will be derived for functional safety requirements to validate the safety concept of automated valet parking.

ACKNOWLEDGEMENT
This project has received funding from the ECSEL Joint Undertaking under grant agreement No 692455. This Joint Undertaking receives support from the European Union's Horizon 2020 research and innovation programme and Austria, Denmark, Germany, Finland, Czech Republic, Italy, Spain, Portugal, Poland, Ireland, Belgium, France, Netherlands, United Kingdom, Slovakia, Norway.

REFERENCES

[1] World Health Organization, "Global status report on road safety 2015," World Health Organization, 2015.

[2] S. Singh, "Critical reasons for crashes investigated in the national motor vehicle crash causation survey," No. DOT HS 812 115, 2015.

[3] W. Wachenfeld and H. Winner, "The Release of Autonomous Vehicles," in Autonomous Driving: Technical, Legal and Social Aspects, M. Maurer, J. C. Gerdes, B. Lenz, and H. Winner, Eds.: Springer, 2016, pp. 425–449.

[4] International Organization for Standardization, "ISO 26262: Road vehicles - Functional Safety," Geneva, Switzerland, 2011.

[5] International Electrotechnical Commission, "Functional safety of electrical/electronic/programmable electronic safety related systems," IEC 61508, 2000.

[6] SAE, "Taxonomy and Definitions for Terms Related to Driving Automation Systems for On-Road Motor Vehicles," Society of Automotive

[7] V. Schönemann and H. Winner et al.," Scenario-based Functional Safety for Automated Driving on the Example of Valet Parking," in IEEE Future Information and Communication Conference, Singapore, 2018.

[8] H. Winner, M. Graupner and W. Wachenfeldt, "How to Address the Approval Trap for Autonomous Vehicles (Keynote)," in IEEE 18th International Conference on Intelligent Transportation Systems (ITSC), Sep. 2015.

[9] R. Alexander, N. Herbert, and T. Kelly, "Deriving safety requirements for autonomous systems," in 4th SEAS DTC Technical Conference, 2009.

[10] M. Hall-May, "Ensuring Safety of Systems of Systems—A Policy-based Approach," PhD Thesis, University of York, 2007.

[11] H. Ross, "Functional Safety for Road Vehicles: New Challenges and Solutions for E-mobility and Automated Driving," Springer Verlag, pp. 115 – 119, 2016.

[12] H. Lambert, "Use of fault tree analysis for automotive reliability and safety analysis," Lawrence Livermore National Lab., CA (US), 2003.

[13] T. Stolte, G. Bagschik and M. Maurer, "Safety goals and functional safety requirements for actuation systems of automated vehicles," 19th IEEE Intelligent Transportation Systems (ITSC), 2016.

[14] German Aerospace Center (DLR), "PEGASUS RESEARCH PROJECT," [Online] Available: http://pegasus-projekt.info/en/home, accessed: March 28th 2018.

[15] C. Amersbach and H. Winner, "Functional Decomposition - An Approach to Reduce the Approval Effort for Highly Automated Driving," in 8. Tagung Fahrerassistenz, 22.-23. November, München, 2017.

[16] A. Reschka, Safety Concept for Autonomous Vehicles, In *Autonomous Driving – Technical, Legal and Social Aspects*, pp. 473–496, Springer Nature, 2016

[17] Automotive World, 2018. Daimler and Bosch jointly premiere automated valet parking in China. From: www.automotiveworld.com/news-releases/daimlerand-bosch-jointly-premiere-automated-valet-parkingin-china/. Accessed: November 2018

[18] M. Chirca, R. Chapuis, and R. Lenain, "Autonomous Valet Parking System Architecture," IEEE International Conference on Intelligent Transportation Systems (ITSC), 2015.

[19] U. Schwesinger, M. Bürki, J. Timpner, S. Rottmann, L. Wolf, ... & L. Heng. Automated valet parking and charging for e-mobility. In Intelligent Vehicles Symposium (IV), pp. 157-164, 2016.

[20] J. Hertzberg, K. Lingemann and A. Nüchter, "Mobile Roboter: Eine Einführung aus Sicht der Informatik," Springer-Verlag, 2012.

[21] K. Dietmayer, "Predicting of machine perception for automated driving," in Autonomous Driving: Technical, Legal and Social Aspects, M. Maurer, J. C. Gerdes, B. Lenz, and H. Winner, Eds.: Springer, 2016, pp. 407-424.

[22] F. Lotz, „Entwicklung einer Referenzarchitektur für die assistierte und automatisierte Fahrzeugführung mit Fahrereinbindung", PhD thesis, Technische Universität Darmstadt, Darmstadt, Germany, 2017, pp. 85-87

[23] A. Cacilo et al. "Hochautomatisiertes Fahren auf Autobahnen–Industriepolitische Schlussfolgerungen" Stuttgart: Fraunhofer-Institut für Arbeitswirtschaft und Organisation IAO , 2015.

[24] International Council on Clean Transportation, "European Vehicle Market Statistics Pocketbook 2017/18." (2017).

[25] Arbeitsgruppe Straßenentwurf, "Richtlinien für die Anlage von Straßen (RAS), Teil Querschnitte (RAS-Q 96)," Forschungsgesellschaft für Straßen und Verkehrswesen, Bonn.(a)(b)(c)(d), 1996.

[26] Bundesministerium der Justiz und für Verbraucherschutz, „Anordnung über den Bau und Betrieb von Garagen (GarBBAnO)," 1990.

[27] Bundesministerium der Justiz und für Verbraucherschutz, "Straßenverkehrs-Zulassungs-Ordnung (StVZO), " 2012.

[28] V. Schönemann, M. Duschek, H. Winner, "Maneuver-based adaptive Safety Zone for infrastructure-supported Automated Valet Parking," 5th International Conference on Vehicle Technology and Intelligent Transport Systems (in publication), 2019.

APPENDIX

Table 6.
Derivation of functional safety requirements for derived safety goals

ID	Safety Goal (SG)/ Functional Safety Requirement (FSR)	SG
SG01	Unintended activation of the valet parking function outside of the PAM-controlled parking area shall be prevented.	
FSR1.1	The system shall detect if the automated vehicle's position is located within the handover zone.	
FSR1.2	The system shall detect if the automated vehicle is in standstill.	SG01
FSR1.3	The system shall have the ability to activate and deactivate the valet parking function.	
FSR1.4	The system shall not activate the valet parking function without user permission.	
SG02	The integrity of the communication between the PAM and the vehicle shall be ensured.	
FSR2.1	The system shall control transmitted safety relevant information for authentication, identification, error correcting, and manipulation. Transmitted data shall be encrypted.	
FSR2.1.1	The system shall add to transmitted safety relevant information a check sum, a signature, a time stamp, and an identifier. Transmitted data shall be encrypted.	SG02
FSR2.1	The system shall receive safety-relevant information in time.	
SG04	The vehicle shall not start moving during embarkment and disembarkment.	
FSR4.1	The system shall detect the embarkment and disembarkment of passengers with its sensors.	
FSR4.1.1	The system shall detect persons in the handover and handback zones.	SG04
FSR4.1.2	The system shall detect if doors are closed.	
SG06	The system shall notify a human supervisor in case of a collision or fire.	
FSR6.1	The system shall detect collisions.	
FSR6.2	The system shall detect fire in the parking garage.	
FSR6.2	The system shall stop the valet parking service by applying an emergency brake of automated vehicles in case of a fire.	SG06
FSR6.3	The system shall notify a human supervisor via a Human Machine Interface.	
SG07	The system shall ensure that the vehicle stays within the (statically defined) drivable area during AVP.	
FSR7.1	The system shall detect if a digital map of the parking garage was transferred.	
FSR7.2	The system shall place the automated vehicle's trajectories within the drivable area.	SG07
FSR7.3	The maximum distance error of the automated vehicle's lateral control with respect to the lane center shall not exceed $W_{\mathrm{err,ego}}$.	
SG08	The valet parking function shall be disabled if people are inside the vehicle.	
FSR8.1	The system shall detect whether people are inside the vehicle.	SG08

DEVELOPMENT OF AN EMERGENCY CONTROL ALGORITHM FOR A FAIL-SAFE SYSTEM IN AUTOMATED DRIVING VEHICLES

Jongmin Lee
Kwangseok Oh
Kyongsu Yi
School of Mechanical and Aerospace Engineering, Seoul National University
Korea

Paper Number 19-0101

ABSTRACT

This paper proposes the concept of automated driving vehicle failsafe system structure. It contains vehicle hardware and software structure design for automated driving vehicle failsafe system. Moreover, it handles the contents fail detection, fault-tolerant control, and emergency braking strategy in case there is no driver intervention in the fail condition of automated driving vehicle. According to the 2017 'AUTOMATED DRIVE SYSTEM 2.0: a vision for safety' report released by the NHTSA, it states that deployment of the crash avoidance system is essential to switch to a minimum hazardous condition in the event of a problem with the self-driving vehicle, or the system cannot operate safely. First, the method used to build the hardware & software of the vehicle was based on the guideline of 'AUTOMATED DRIVE SYSTEM 2.0: Section 1 fallback (Minimal Risk condition)' report released by NHTSA. Second, a method of an algorithm is sliding mode control based fault tolerant control and emergency deceleration control which designed to target SAE International standard J3016 autonomous driving phase 4: automated driving system perform ass aspects of the dynamic driving task, even if a human driver does not respond appropriately to a request to intervene. In this paper, to meet the requirements of autonomous driving phase proposed by SAE International standard J3016 phase 4 and NHTSA safety standard, the hardware configuration was created to ensure that the automated driving vehicle could perform the given task without proper driver intervention. In detection part, hardware (Actuator, Sensor, CAN signal, Upper&Lower controller) and module based failsafe diagnosis method and algorithm were proposed to detect fail condition. In decision and control part, when a failure of an automated driving vehicle is diagnosed, and no driver intervention was detected, the automated driving vehicle failsafe phase is a move to the system error. In the phase of the system error (lower controller), proposed methodologies are utilized. Automated driving vehicle experiments have demonstrated the algorithms as mentioned earlier and failsafe structure. First of all, it is true that not many papers and studies have been done on the failsafe system of an automated driving vehicle. NHTSA's safety report of an autonomous vehicle only contains a "suggestion" that says, "It is a good thing to do this," and has not yet created a rule. However, this paper proposes an automated driving vehicle failsafe system that is not commercialized but has been configured to meet NHTSA's requirements to take into account safety. The proposed failsafe system is applied to the automated driving vehicle, and the vehicle experiment was completed with the proposed algorithm. The proposed system is considered to be very compatible with the subject of the technical session by suggesting the system that meets the NHTSA standards as well as testing control and emergency systems targeted automated driving vehicle phase 4.

INTRODUCTION

Autonomous vehicle research aspect of failsafe and a fallback system is a very necessary and important study. Autonomous vehicles are composed of various sensors, computers, actuators and other types of equipment, and these equipment are configured to communicate together. In terms of fault diagnosis, each of them also needs real-time monitoring and also needs maneuver to be configured in the event of a failure. The algorithm proposed in this paper is an algorithm in the control part that makes an emergency stop when the fault is determined by fault diagnosis system when there is no driver intervention. The control classification was divided into two control categories, longitudinal control, and lateral control. Even if an error occurs that vehicle does not receive normal data from the upper controller that designed to recognition and judgment components of the autonomous driving system, the proposed algorithm only uses the vehicle's chassis information to provide a way for autonomous vehicles to respond safely. The vehicle hardware configuration is divided into upper controllers that responsible for recognition and judgment part and lower controller responsible for control of a vehicle. The lower controller consists of very robust hardware that allows for the safe longitudinal and lateral control in the event of errors in the upper controller.

Therefore, during the autonomous driving phase proposed by SAE International, level 4 suggests: the driving mode-specific performance by an automated driving system complete driving task, even if a human driver does not respond appropriately to a request to intervene.

Figure1. Waymo vehicle redundant Safety-Critical Systems. [1]

The hardware configuration was configured so that the autonomous vehicle could perform the failsafe system task without proper driver intervention. Although there are not many prior studies on the fault diagnosis system of autonomous driving systems was completed, the development of the failure diagnosis system of non-automated vehicles has already been carried out in terms of the failsafe system. YH.J developed the vehicle sensor fault diagnosis and acceptance algorithm and conducted the residual and adaptive threshold fault diagnosis without additional hardware. [3] KS. O conducted a study on the predictive fault diagnosis algorithm using sliding mode observers. [4] Advanced research in failsafe and system construction methods was consulted by overseas automotive OEMs. Google Waymo self-driving vehicles have applied fallback systems. Figure1. is Waymo safety-critical system description. Waymo vehicle's redundant system composed of backup computing, backup braking, backup steering, and a backup power system. [1] Similar to Google Waymo, CRUISE has a backup computer, backup actuator, signal communication redundant and data accumulation system. [2]

HARDWARE-BASED FAIL DETECTION CLASSIFICATION

In this chapter, mainly introduce module based classification of an autonomous vehicle fail detection and maneuver system. Hardware divide into Actuator, Sensor, Upper controller, CAN network and Lower controller. Actuator classifies as steering and throttle/brake. Sensor part composed of Lidar, Radar, and Vision (mono camera). The upper controller contains logic for perception and judgment of entire autonomous driving algorithms and calculates at regular intervals and transmits the calculated values to the lower-controller over real-time communication. CAN communication refers to the overall communication of the vehicle, including many sensors and actuators, vehicle inter communication, and uses a method to conduct real-time monitoring of their values. The Lower Controller consists of algorithms that calculate the relative sub-controller of the overall configuration, the algorithm for path tracking, or the control input that enters longitudinal control in the event of failure.

Sensor fail detection

The hardware fault detection method of the sensor is shown as Figure2. The manufacturer sends a corresponding fault signal from the sensor itself in the event of a fail. Delphi's radar has signals that can find many faults such as sensor communication error, sensor status failed, status blocked, and status over temperature, etc. Communication settings allow users to read the appropriate information. The figure 2. b) is about Ibeo LUX Ridar error and warning messages. Error contents internal error, a motor error, temperature rise, data loss, internal communication error, incorrect scan data, etc. The warning signal that is sent to the user can receive error messages such as internal communication, temperature increase, etc.

4E0	CAN_TX_COMM_ERROR	Indication that the sensor has detected a communication error	False/True	bool	0: False 1: True	False	50ms	MMR
4E1	CAN_TX_XCVR_OPERATIONAL	Sensor Status Radiating 0 = not radiating 1 = radiating	0 to 1	n/a	1	0	50ms	MMR
4E1	CAN_TX_INTERNAL_ERROR	Sensor Status Failed 0 = not failed [] = failed	0 to 1	n/a	1	0	50ms	MMR
4E1	CAN_TX_RANGE_PERF_ERROR	Sensor Status Blocked 0 = not blocked 1 = blocked	0 to 1	n/a	1	0	50ms	MMR

6.1 Error register 1

Bytes	LUX error	Description	Comment
Bit 0	E-SP	internal error	contact support
Bit 1	E-Motor_1	motor fault	contact support
Bit 2	E-Buffer_1	scan buffer transmitted incompletely	decrease scan resolution/frequency/range; contact support
Bit 3	E-Buffer_2	Scan buffer overflow	decrease scan resolution/frequency/range; contact support
Bit 4	E-Meas_1	APD voltage failed	contact support
Bit 5		reserved	
Bit 6		reserved	
Bit 7		reserved	
Bit8…9	E-Temp	Bit 9: APD Over Temperature Bit 8: APD Under Temperature Bit 8 and 9: APD Temperature Sensor defect	provide cooling provide heating contact support
Bit 10	E-Motor_2	motor fault	contact support
Bit 11	E-Motor_3	motor fault	contact support
Bit 12	E-Motor_4	motor fault	contact support
Bit 13	E-Motor_5	motor fault	contact support
Bit14…15		reserved	

6.2 Error register 2

Bytes	LUX error	Description	Comment
Bit 0	E-IF_internal_1	no scan data received.	contact support
Bit 1	E-IF_internal_2	internal communication error	contact support
Bit 2	E-IF_internal_3	incorrect scan data	contact support
Bit 3	E-Configuration_1	FPGA not configurable	contact support
Bit 4	E-Configuartion_2	incorrect configuration data	load correct configuration values
Bit 5	E-Configuration_3	configuration contains incorrect parameters	load correct configuration values
Bit 6	E-Timeout_1	data processing timeout	decrease scan resolution or scan frequency
Bit 7	E-Timeout_2	reset the computation of the environmental model	contact support
Bit8…15	reserved		

6.3 Warning register 1

Bytes	LUX warning	Description	Comment
Bit0	W-CMD	internal communication error	
Bit1	W-Range_1	internal warning	
Bit2	W-Range_2	internal warning	
Bit3	W-low_temperature	temperature too low	warning of insufficient temperature
Bit4	W-high_temperature	temperature too high	warning of exceeding temperature
Bit5	W-Motor_1	internal warning	
Bit6	W-Motor_2	internal warning	
Bit 7	W-Sync	synchronization error	check synchronization- and scan frequency
Bit7…15	RES 7…15	reserved	

6.4 Warning register 2

Bytes	LUX warning	Description	Comment
Bit0	W-IF_CAN	CAN Interface blocked	check CAN bus and CAN connection
Bit1	E-IF_ETH	Ethernet Interface blocked	check Ethernet connection
Bit2	W-CANdata	incorrect CAN message received	check CAN data
Bit3	W-IF_internal_1	incorrect scan data	contact support
Bit4	W-ETHdata	unknown or incomplete data	check Ethernet data
Bit5	W-Command	incorrect or forbidden command received	check command
Bit6	W-Flash	memory access failure	restart ibeo LUX, contact support
Bit7	W-Overflow_1	internal overflow	contact support
Bit8	W-EgoMotion	vehicle data update missing	check CAN vehicle data
Bit9	W-Mounting Position	incorrect mounting parameters	correct mounting position according to OM
Bit10	W-CalcFrequency	no object computation due to scan frequency.	set the scan frequency to 12.5 Hz to receive objects
Bit11…15	reserved		

Figure2. a) Delphi Radar error message b) Lidar IBEO LUX error message[13]

Communication & controller fail detection

Inside the vehicle, communication is via the CAN bus (Controller Area Network) communication protocol is a standard communication specification designed to enable multiple devices to communicate with each other without a host computer. In order to detect errors in CAN signals, it is important to identify characteristics of CAN signals. Using the characteristics that the last value in the event of CAN failure is maintained by the host controller, utilized PC LabVIEW signal processing program, which is a higher control of an autonomous vehicle, can recognize an error about a CAN state that is judged to be a CAN error when the same value is received. The LabVIEW program itself can also detect errors on the CAN signal using a virtual instrument (VI) that detect for CAN errors. VI could find an error where the internal CAN state value is fixed. The upper controller refers to a PC and the lower controller (micro-autobox) that is responsible for control. Fault finding system that recognizes if one system fails while the PC to autobox system sends and receives data over CAN communication in real time.

FAILSAFE CONTROL

In this chapter, mainly address concept of failsafe control and reason of study. The main purpose of this part is to meet the requirements of SAE International level 4 as figure3. the control part that makes an emergency stop when there is no driver intervention after the failure determined by the algorithm.

SAE level	Name	Narrative Definition	Execution of Steering and Acceleration/ Deceleration	*Monitoring* of Driving Environment	Fallback Performance of *Dynamic Driving Task*	System Capability *(Driving Modes)*
***Human driver* monitors the driving environment**						
0	No Automation	the full-time performance by the *human driver* of all aspects of the *dynamic driving task*, even when enhanced by warning or intervention systems	Human driver	Human driver	Human driver	n/a
1	Driver Assistance	the *driving mode*-specific execution by a driver assistance system of either steering or acceleration/deceleration using information about the driving environment and with the expectation that the *human driver* perform all remaining aspects of the *dynamic driving task*	Human driver and system	Human driver	Human driver	Some driving modes
2	Partial Automation	the *driving mode*-specific execution by one or more driver assistance systems of both steering and acceleration/ deceleration using information about the driving environment and with the expectation that the *human driver* perform all remaining aspects of the *dynamic driving task*	**System**	Human driver	Human driver	Some driving modes
***Automated driving system* ("system") monitors the driving environment**						
3	Conditional Automation	the *driving mode*-specific performance by an *automated driving system* of all aspects of the dynamic driving task with the expectation that the *human driver* will respond appropriately to a *request to intervene*	System	**System**	Human driver	Some driving modes
4	High Automation	the *driving mode*-specific performance by an automated driving system of all aspects of the *dynamic driving task*, even if a *human driver* does not respond appropriately to a *request to intervene*	System	System	**System**	Some driving modes
5	Full Automation	the full-time performance by an *automated driving system* of all aspects of the *dynamic driving task* under all roadway and environmental conditions that can be managed by a *human driver*	System	System	System	**All driving modes**

Figure3. SAE International standard J3016, Levels of vehicle automation

Failsafe control description The control part is divided into the longitudinal and the lateral part. Offer a way for autonomous vehicles to respond safely, using the vehicle's chassis information only, even if there is no information on the upper control part, i.e., the recognition and judgment part. The system error situation defined in this paper means network communication is blocked. In this situation, the last value in CAN network is only useful information. A failsafe module proposed in this paper utilized the unique phenomenon of system error and used that useful information to predict and control. System error – supervisor part contains prediction contents. The method used for longitudinal control is to calculate the safe driving distance in real time and transmit to reference deceleration model, and reference model calculates reference distance and reference velocity model for sliding mode control based deceleration and stop the algorithm. It is possible to make a stop within a safe distance through the above method. Lateral control consists of an algorithm that only uses the vehicle chassis information. This algorithm uses last information (desired path) of the upper controller to follow the path using DR to the lateral control algorithm.

The entire module was composed of the failure detection part that finds the failure of the total module, the failure detection part that carries out the classification for the failure, and the control model that is responsible for controlling deceleration with limited information.

Figure4 is hardware concept of the autonomous vehicle including the failsafe module. Considering autonomous vehicle hardware structure, the failsafe module was configured under normal circumstances, the algorithms of the perception, decision, and control algorithm operating in the upper controller. In order to prepare for a fault situation, the algorithms of the prediction in a fail-safe module using information from the upper controller calculate prediction algorithm in real-time. If an error is detected by the error-diagnosis module and no driver intervention is determined, the final information is used to predict and control. The last safety distance (in

normal situation information) received from the upper controller is used in two ways. In the lateral direction, the dead reckoning algorithm will be used to drive the safety path, and in the longitudinal direction, sliding

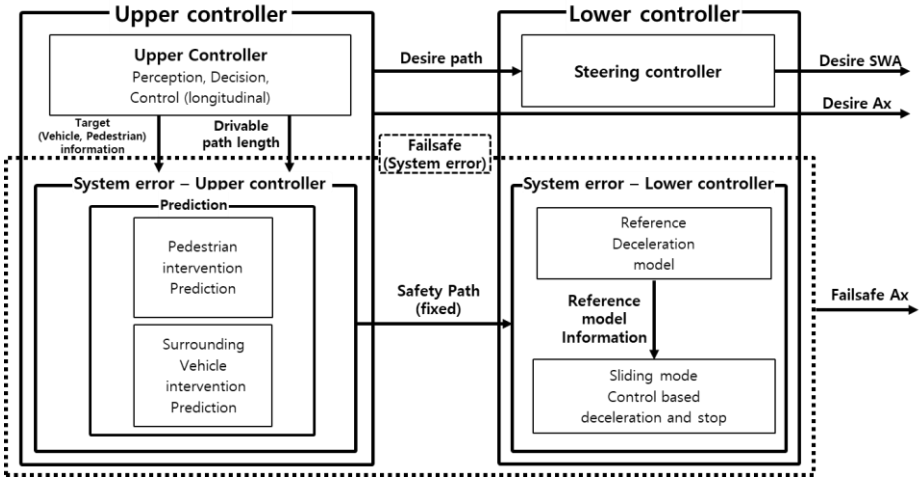

Figure4. Failsafe hardware concept diagram

mode control based deceleration and stop algorithm will be performed.

Methodology in this section, mainly describe System error situation used algorithm. One is defining reference deceleration model another is sliding mode control based deceleration and stop algorithm. The reference deceleration model [1] was determined by the general driver deceleration data which considering driver safety and ride comfort. The first-integrated velocity model and secondary integrated station model were used to construct an algorithm for stopping at safe distances. Pictures and formulas for longitudinal acceleration model, a longitudinal velocity model, and longitudinal distance model. V_x is initial velocity, a_m is maximum used deceleration, $\theta\,(\theta=t/t_d)$ is time ratio, t_d is deceleration time, m is a model variable parameter, r $\left(r=\frac{(1+2m)^{2+\frac{1}{m}}}{4m^2}\right)$ is model parameter. Define a time-varying sliding surface $S(t)$ by the scalar equation $s(x;t)=0$, where $s(\mathbf{x};t)=e\cdot\left(\lambda+\frac{d}{dt}\right)^{n-1}$ and λ is a strictly positive constant. In this controller n =2 and he problem of keeping the scalar $s(t)$ at zero can be achieved by choosing proper control input u, the outside of $S(t)$, $\frac{1}{2}\frac{d}{dt}s(t)^2\le-\eta|s(t)|$ and let equation $s(\mathbf{x};t)=0$.

$$e(t)=S_{ref}(t)-S_{vehicle}(t) \qquad (1)$$

$$s(t)=\dot{e}(t)+\lambda\cdot e(t) \qquad (2)$$

$$V(s(t))=\frac{1}{2}s(t)^2 \qquad (3)$$

In (1) $e(t)$ is an error between the reference station and vehicle station. (3) is Lyapunov function. Differentiating the Lyapunov function

$$\dot{V}(s(t)) = s(t) \cdot \dot{s}(t) \quad (4)$$

For a stable system, the derivative of the Lyapunov function should be negative.

$$\dot{V}(s(t)) = s(t) \cdot \dot{s}(t) = -K \cdot |s(t)| < 0 \quad (5)$$

$$\therefore \ \dot{s}(t) = -K \cdot tan(s(t)) \quad (6)$$

$$\dot{s}(t) = \ddot{e}(t) + \lambda \cdot \dot{e}(t) = -K \cdot atan(s(t)) \quad (7)$$

$$u_{eq} = a_{x,ref} - \lambda \cdot \dot{e}(t) - K \cdot atan(s(t)) \quad (8)$$

design (2) sliding surface. Design sliding surface and calculate control input (8) tracking sliding surface. Control input u_{eq} is a longitudinal acceleration to vehicle SCC module.

<u>Vehicle SCC (Smart Cruise Control) module description</u> SCC (Smart Cruise Control) module is the ADAS system of Hyundai Motor Company. Through the communication operation, longitudinal acceleration, which is the control input put into the SCC module. SCC module is a module that considers safety and ride comfort of drivers. If longitudinal acceleration or deceleration is inserted into the module, the actual input value and vehicle reacts has a time delay. To analyze the characteristics of the delay conducted SCC module delay test. The test method verifies the characteristics of the SCC module by inserting the deceleration value into the module as input during vehicle accelerates and cruising.

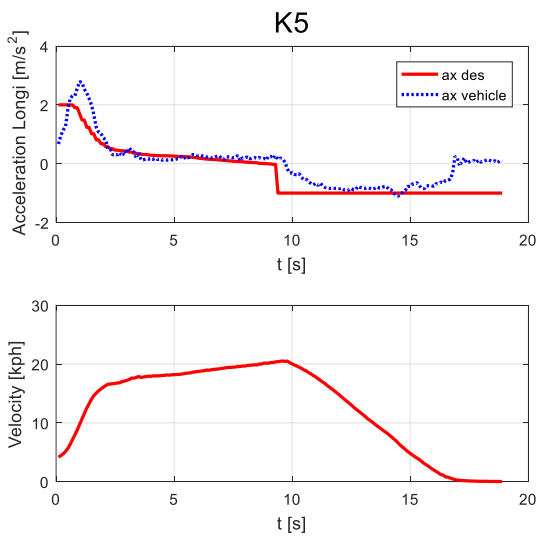

Figure5. K5 deceleration test ($-1m/s^2$, 20kph)

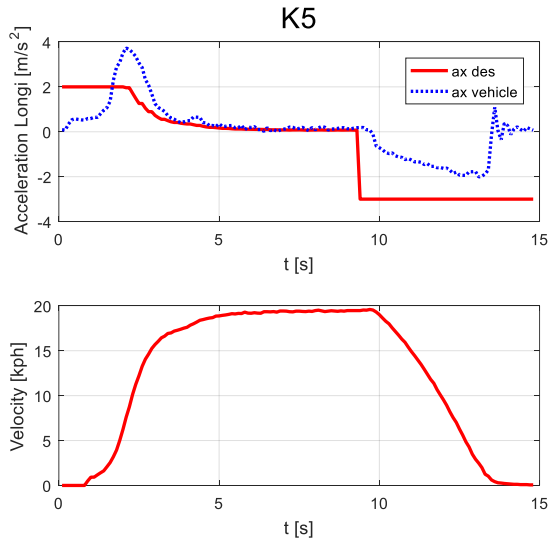

K5 deceleration test ($-3m/s^2$, 20kph)

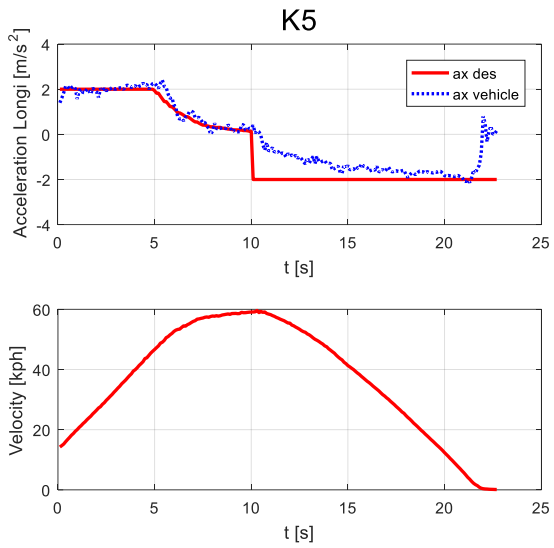

Figure6. K5 deceleration test (-2m/s^2 , 60kph)

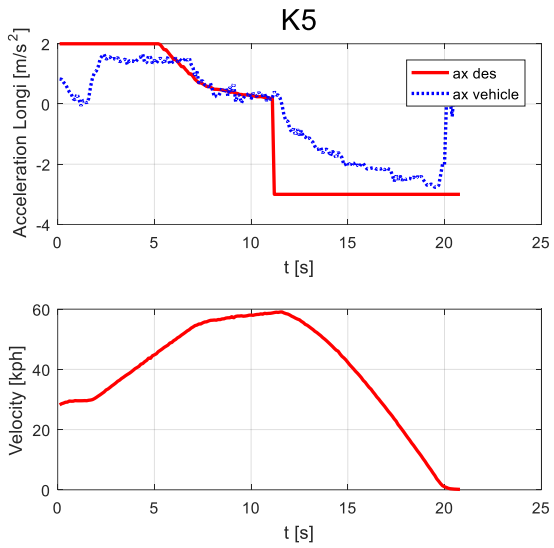

K5 deceleration test ($-3m/s^2$, 60kph)

If the reference model referred to in chapter 'Methodology' is inserted directly into the vehicle SCC module, it can be safely stopped within the specified distance of a simple configuration without the use of other control methods. Therefore, the output of the reference station and reference velocity utilized as control input. As a result, the problem of delay in SCC module extension time resulted in a value different from the value of the reference model to the output of the vehicle. The following chapter is the result of multiple experiments and test data showing that the SCC module has the nonlinear characteristic.

As mentioned above, control inputs were applied in several situations to experiment with nonlinear characteristics of SCC module. The test scenario is set as follow. 1. 20km/h (minus one to minus five) deceleration to stop 2. 40km/h (minus one to minus three) deceleration to stop 3. 60km/h (minus one to minus three) deceleration to stop 4. Acceleration test

K5 vehicle deceleration test for check SCC module delay. Test content contains constant deceleration from $-1m/s^2$ to $-3m/s^2$ when vehicle velocity close to 20 km/h and 60km/h. From test get a conclusion about SCC module delay as follow. First, module exists time delay about 0.1second to 0.5second. Second, module deceleration control input is not severe so couldn't reach command input . In conclusion, the SCC module exists time delay and nonlinear model characteristic.

Sliding Mode Control based deceleration vehicle test For the failsafe control deceleration and stop vehicle test, the following methods were used to conduct the test. The whole vehicle test was conducted in autonomous mode, from beginning to end the experimental scenario was planned and conducted in low-speed area of 20km/h and 30 km/h. Figure7 shows that the vehicle has been tested on autonomous mode from stop → accelerate → stops. The first figure in Figure7 shows the vehicle accelerating to ACC mode up to 30 km/h and the sliding mode control based algorithm operating when failure occurred. The second figure is a comparison of the longitudinal acceleration of the vehicle and the control input (longitudinal acceleration) into the vehicle SCC module.

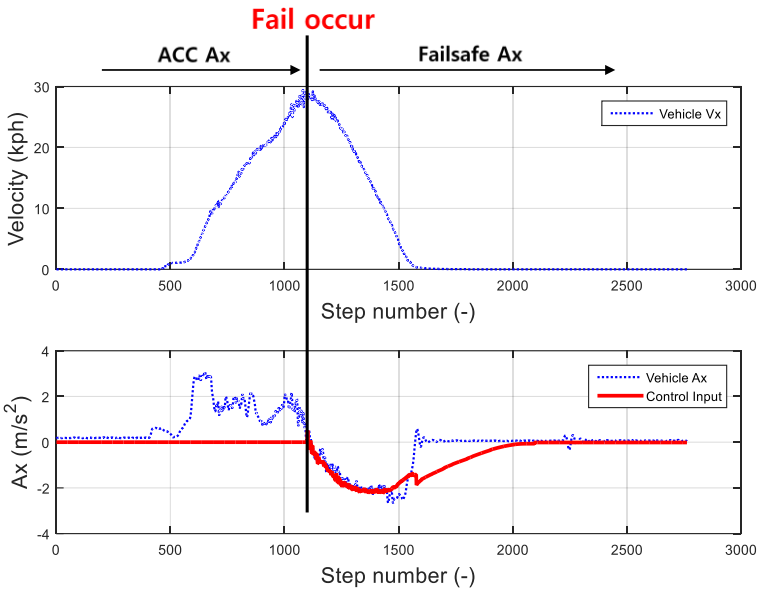

Figure7. Vehicle test scenario – Acceleration to stop

VEHICLE TEST RESULT

The fail-safe module described above chapter is applied to the autonomous vehicle as Figure8. As described in Figure8, a number of algorithm and method have been applied to the actual autonomous vehicle. The alarm system has been constructed to allow the driver to recognize the warning situation in autonomous vehicles. In perception part, 1) Internal CAN communication error in the vehicle, 2) CAN value holding error (for multiple CAN channels), 3) sensor hardware error. These error warning system has been constructed to alert the driver. The proposed automated driving control algorithm is evaluated through computer vehicle tests. In order to evaluate the proposed algorithm on a real test vehicle, Hyundai-Kia Motors K5 is used as a test vehicle platform. Figure 5 shows the test vehicle configuration. The proposed algorithm has been implemented on "dSPACE Autobox", which is used for the real-time application and equipped with a processor board. The hardware components mentioned above communicate through a CAN bus.

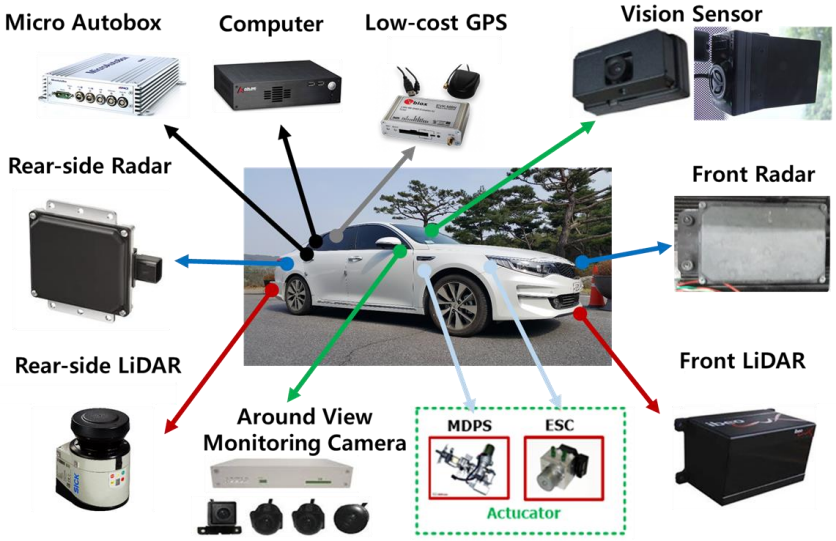

Figure8. Autonomous vehicle hardware configuration

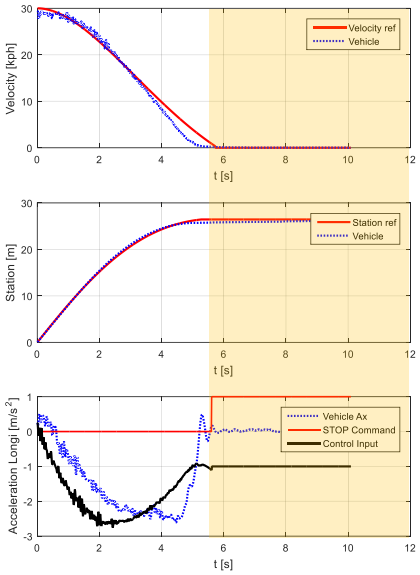

Figure9. Vehicle test result – (a) Velocity (b) Station (c) Vehicle and Control input

Figure9 is vehicle test result near 30km/h. (a), (b) and (c) are respectively the vehicle longitudinal velocity and reference model velocity profile, vehicle station and reference model station, vehicle acceleration and control input, the experiment result shows that the sliding surface follows well through the control input. The yellow section addresses overload problems on SCC modules rather than algorithmic stops and consists of stopping with constant deceleration as the speed decreases for module safety.

CONCLUSIONS

In this paper, in order to meet the requirements of autonomous driving phase proposed by SAE International, the hardware configuration was made to ensure that the driver could perform the autonomous vehicle task without driver proper intervention. In detection part, hardware (Actuator, Sensor, CAN signal, Upper controller, Lower controller) and module (Steering, Throttle/Brake, Lidar, Radar, GPS, CAN signal, CAN status, Chassis CAN) based failsafe diagnosis method and algorithm were proposed to detect fail situation. In decision and control part, when a failure of an autonomous vehicle is diagnosed and no driver intervention was detected, autonomous vehicle failsafe phase is a move to system error in figure4 in the phase of the system error (lower controller), reference station model and reference velocity model was calculated in real-time. Sliding mode controller based deceleration and stop algorithm tracking designed sliding surface. The effectiveness of the proposed automated driving fails situation deceleration algorithm has been evaluated via test-data based simulations and vehicle tests. From the results, it has been shown that the proposed algorithm can provide the robust performance in low speed (20,30kph) condition.

* This work was supported by National Research Foundation of Korea(NRF) grant funded by the Ministry of Science, ICT & Future Planning (NRF-2016R1E1A1A01943543). This work was supported by the Technology Innovation Program (10079730, Development and Evaluation of Automated Driving Systems for Motorway and City Road) and driving environment) funded by the Ministry of Trade, Industry & Energy (MOTIE, Korea). This research was supported by the Korea Ministry of Land, Infrastructure and Transport. It was also

supported by the Korea Agency for Infrastructure Technology Advancement (Project No.: 18TLRP-B117133-03).

REFERENCES

[1] Waymo, Safety Report: ON THE ROAD TO FULLY SELF-DRIVING, 10
[2] GM, SELF-DRIVING SAFETY REPORT, 2018, 11
[3] YH. JEONG and KJ LEE, 2015, “Virtual sensor based vehicle sensor fault tolerant algorithm,” KSME, 1761-1766.
[4] KS. OH, 2017, “Kinematic Model-based Predictive Fault Diagnosis Algorithm of Autonomous Vehicles using Sliding Mode Observer ”, KSME, Vol41 No.10, 931-940.
[5] Kim, B., & Yi, K.: Probabilistic and holistic prediction of vehicle states using sensor fusion for application to integrated vehicle safety systems. IEEE Transactions on Intelligent Transportation Systems, Vol. 15, No. 5, pp. 2178-2190, 2014
[6] Kim, B., Yi, K., Yoo, H. J., Chong, H. J., & Ko, B.: An IMM/EKF approach for enhanced multitarget state estimation for application to integrated risk management system. IEEE Transactions on Vehicular Technology, Vol. 64, No. 3, pp. 876-889, 2015
[7] Kim, B., Son, Y., & Yi, K.: Probabilistic threat assessment with environment description and rule-based multi-traffic prediction for integrated risk management system. In Intelligent Vehicles Symposium (IV), 2015 IEEE. IEEE., pp. 642-647, June 2015
[8] Kim, T., & Jeong, H. Y.: A novel algorithm for crash detection under general road scenes using crash probabilities and an interactive multiple model particle filter. IEEE Transactions on Intelligent Transportation Systems, Vol. 15, No. 6, pp. 2480-2490, 2014
[9] LEE, J., CHOI, J., YI, K., SHIN, M. & KO, B. 2014. Lane-keeping assistance control algorithm using differential braking to prevent unintended lane departures. Control Engineering Practice, 23, 1-13.
[10] Tobias Kessler, Pascal Minnerup, David Lenz, Alois Knoll.: Systematically Comparing Control Approaches in the Presence of Actuator Errors. In Intelligent Vehicles Symposium (IV), IEEE. pp. 11-14, 2017
[11] Jin Li-sheng, Fang Wen-ping, ZHang Ying-nan, Yang Shuang-bin,Hou Hai-jing. : Research on safety lane change model of driver assistant systemon highway. In Intelligent Vehicles Symposium (IV), IEEE, June 2009
[12] Markus Hörwick and Karl-Heinz Siedersberger, Strategy and The architecture of a Safety Concept for Fully Automatic and Autonomous Driving Assistance Systems., In Intelligent Vehicles Symposium (IV), IEEE, June 2010
[13] Ibeo LUX and ibeo LUX systems CAN protocol description,ibeo automotive,2014

HARMONIZED PRE-CRASH SCENARIOS FOR REACHING GLOBAL VISION ZERO

Antonio Lara
Mexico
Jeffrey Skvarce
United States of America
Harald Feifel
Michael Wagner
Germany
Toshihisa Tengeiji
Japan

Continental AG – Division Chassis & Safety

Paper Number 19-0110

ABSTRACT

Crash data are essential for the development and introduction of new of active safety systems. At first, the target population of a new system is evaluated to understand the situations in which the system shall become active. The respective crashes are then analyzed and requirements towards the system development are derived. Finally, an effectiveness evaluation validates the potential benefit of the system in real-world crashes.

Multiple in-depth databases are available for different regions of the world. They are generally based on different crash collection and data coding methods. Thus, comparable data analysis is hard to achieve. This is however necessary for a systematic worldwide approach towards reaching "Vision Zero".

Crash scenarios describe the scene of the crash including the participants and their respective actions and intentions. They are the basis for developing sensor-based active safety systems.

The paper discusses possibilities of analyzing in-depth crash data and deriving harmonized crash scenarios. Different databases and their limitations are considered, and a scenario catalogue is proposed.

This catalogue will enable various stakeholders to compare and analyze crash scenarios of different regions and countries. The catalogue serves as a new and efficient tool to enhance the policy making for vehicles and the development of safety technology to drive "Vision Zero" worldwide.

INTRODUCTION

Crash data are needed to evaluate the benefit of safety systems in real-world crashes. The field-of-action is analyzed in which the system can become active to avoid or mitigate crashes, and essential requirements for the system development are derived. Additionally, the potential effectiveness of the safety system within its defined field-of-action is evaluated. For both development phases, a classification of crashes based on common characteristics, before and during the collision, is needed. Such common characteristics can be the trajectories of crash participants or the actual collision geometrics.

To classify traffic crashes, a set of pre-defined crash scenarios can be used. The commonly used terms scene, situation and scenario differentiate by the added level of detail. A scene describes all players and their local and dynamic properties within the surrounding environment. A situation additionally includes goals and values of the players. Besides the properties of the scene and the situation, a scenario also contains actions of the players and other decisive events [1]. Generally, a crash scenario describes the course-of-events that lead to a traffic crash, based on intentions and movements of the participants and other events and circumstances, at the scene and within the environment of the crash, and including the collision outcome. Thus, crash scenarios are well-suited for the description and definition of a safety system.

Vehicle safety systems are divided into primary, secondary and tertiary systems, with active safety systems (ADAS) addressing the primary safety by performing driver warnings and active interventions in the vehicle dynamics. This is based on a critical assessment due to ego kinematics data and object information provided by

environment sensors. Therefore, a classification of crashes into crash scenarios, that are to be used for ADAS development, should be done using common sensor-relevant properties in the pre-crash phase. These are mainly the positions and movement directions of the crash participants.

Crash types describe the conflicts that lead to traffic crashes. They are generally represented by pictograms which show the first conflict between two traffic participants, regardless whether other participants are involved. Crash types are used to systematically classify and group traffic crashes. Each crash is classified by the respective crash causer and non-causer. The crash types are partly characterized by a very high level of detail [2]. Due to this segmentation they are generally unfavorable to represent the overall crash occurrence in a compact way.

This paper shows a method to cluster crash types into crash scenarios, considering characteristics and limitations of active safety systems. The focus shall be on the usability of the defined crash scenarios during the development of active safety systems. A scenario catalogues is proposed based on the Cyclist-AEB Testing System (CATS) [3]. The method is demonstrated using in-depth databases from four of the biggest markets worldwide (USA, Germany, China, Japan). As an example, traffic crashes between passenger cars and motorcycles are analyzed and visualized.

METHOD

Active safety systems prevent crashes by direct or indirect intervention in the longitudinal or lateral vehicle dynamics based on sensor information in the pre-crash phase. A classification of traffic crashes that is based on the crash type definition is therefore particularly suitable for defining the field-of-action for an ADAS.

For this paper, the authors used data from USA, China and Japan. Depending on the database used, the authors were able to identify variables which classify the crash configuration and are suitable for clustering. Table 1 gives an overview of the databases and the respective variables used for the scenario generation.

Table 1.
Databases used for the analysis and the respective variables for scenario generation

Database	**Country**	**Variables**	**Reference**
GIDAS	Germany	UTYP, UTYPA, UTYPB	[4]
FARS	USA	ACC_TYPE, PEDCTYPE, BIKECTYPE	[6]
ITARDA	Japan	SIP-code	[7]
CIDAS	China	UTYP, UTYPA, UTYPB	[5]

The GIDAS database describes the three-digit crash type UTYP for each recorded crash and classifies the two participants in the causal conflict as UTYPA and UTYPB. In general, the causing crash participant is coded as UTYPA. The exception are crashes with pedestrians, who are always coded as UTYPB regardless of the question of guilt. Based on the parameters UTYP, UTYPA and UTYPB, the crashes are clustered into crash scenarios.

In [8] the methodology to derive a scenario catalogue based on the GIDAS database has been extensively documented. Each step of the methodology is almost exactly applicable to the data found in CIDAS and ITARDA database. The authors propose a scenario mapping for the ITARDA data in Appendix 1. An example for the ITARDA data is given in Figure 1. Note that scenario C1 describes crossing scenarios from nearside, thus left-hand driving in Japan must be considered.

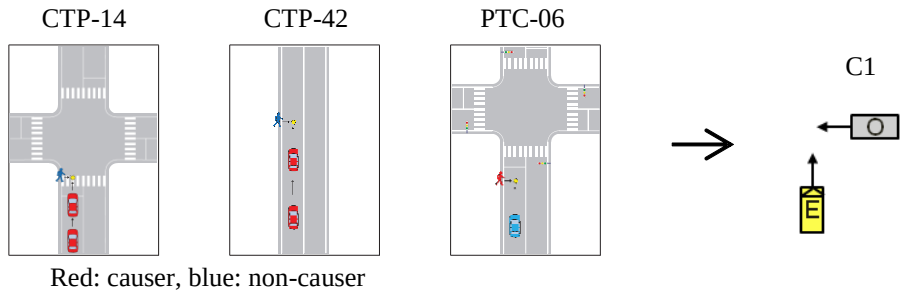

Figure 1. Example of scenario C1 using SIP code an ITARDA data

The FARS database differs in many ways from the previously mentioned databases (GIDAS, ITARADA, CIDAS). Therefore, in this paper the authors propose a methodology to derive a scenario catalogue based on the FARS database. Figure 2 describes the necessary steps of the method when using FARS. In the following text, the authors are using the terminology of FARS variable as described in Appendix 2.

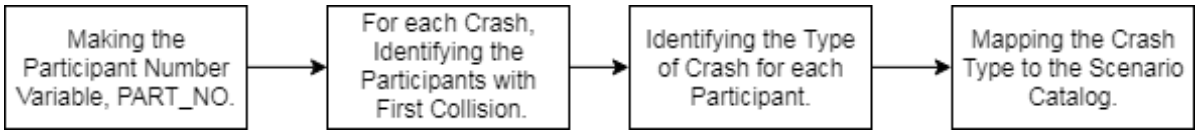

Figure 2. Generation of scenarios based on FARS data

Introduction of a new variable in FARS

The FARS database describes the type of crash at the level of the vehicle for each of the motorized vehicles. It does not contain a causal conflict and it does not contain a participant variable equivalent to the GIDAS data. A comparison of the database hierarchies of both GIDAS and FARS is visualized in Figure 3.

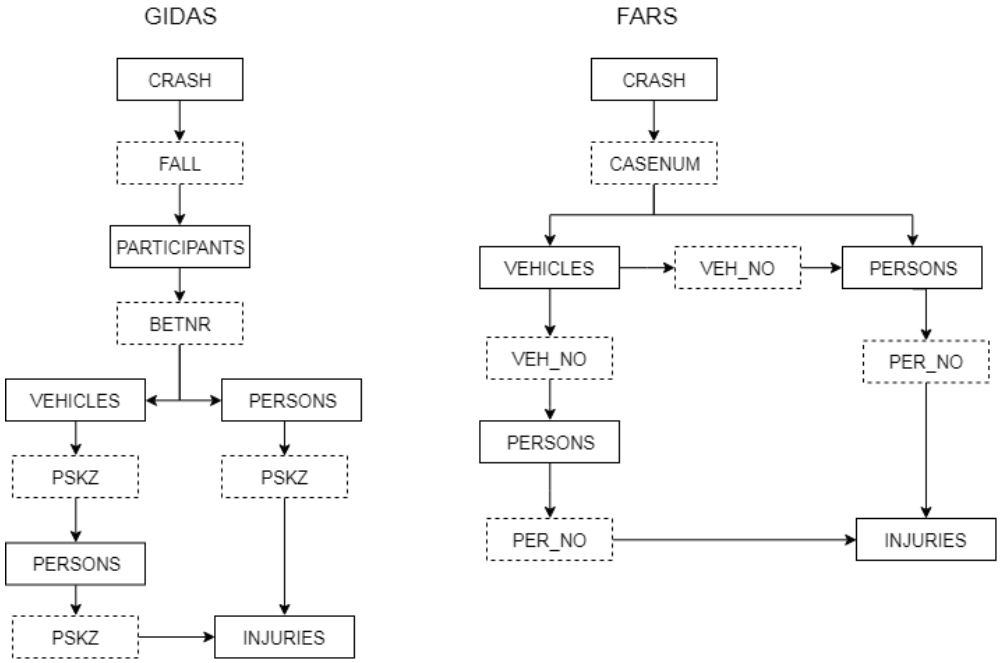

Figure 3. Comparison of GIDAS and FARS database hierarchies

For instances, in GIDAS, a conflict between a vehicle and a pedestrian is classified as a crash between two participants. In contrast, for FARS this would be considered as a single crash given that only one motorized vehicle was involved. To harmonize the data and to be able to apply the proposed scenarios found in [8], one of the primary goals was the introduction of a "participant" layer in the FARS data, which takes the number of the vehicle and the number of the pedestrian/bicyclist in a crash as an input, and then maps them into a participant number.
To this end we merge the person and vehicle data sets. Then for each state cases, the following equation is proposed, and it gives a solution to this problem.

$$Participant\ Number = \begin{cases} \text{VEH_NO (num. of vehicle)}, & If\ \text{VEH_NO} \neq 0 \\ max(\text{VEH_NO}) + PER_NO, & If\ \text{VEH_NO} = 0 \end{cases} \quad \text{(Equation 1)}$$

For the Equation 1, suppose a State Case with n Vehicles, $\{V_1, V_2, \ldots, V_n\}$, and Persons, $\{P_j^k\}$ for k in $\{0,1,..,n\}$, where P_j^k represents the Person j in the Vehicle k; if $k = 0$, the Person is a Pedestrian or Bicyclist.

It follows from the above equation that the participant number is the same for the vehicles. We do not consider the case where $k, j = 0$, since this case reduces to a conflict among motorized vehicles. For $k = 0$, the pedestrians/bicyclist case, that is $\{P_j^0\}_{1 \le j \le m}$, the participant number is $j + n$ for all the j, as n corresponds to the maximum number of vehicles. Hence, the total number of participants is given as follows.

$$\#\{P_j^0\}_{1 \le j \le m} + \#\{V_1, V_2, \ldots, V_n\} = m + n \quad \text{(if } j \neq 0\text{) (Equation 2)}$$

A visualization of the above described process can be found in Figure 4.

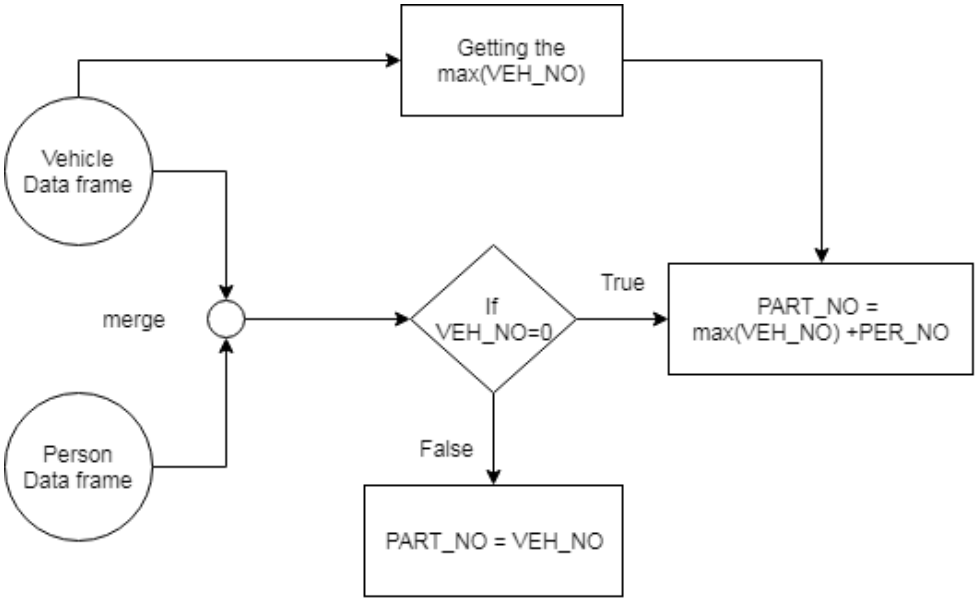

Figure 4. Generation of the participant variable from the number of vehicles and pedestrian.

Table 2 shows the above visualized process for a specific example taken from FARS 2015.

Table 2.
Example for the introduction of a new variable in FARS

ST_CASE	VEH_NO	PER_NO	PART_NO
10712	1	1	1
10712	2	1	2
10712	0	1	3 (*2+1 = max (VEH_NO)+PER_NO)*
10712	0	2	4 (2+2)
10712	0	3	5 (2+3)

Identifying the participants with the first collision

The next step is the identification of the participants with the first collision in a crash to apply the proposed scenarios. Since the authors could not identify a variable indicating the participants directly, this information was obtained using different steps. We select the first two participants in the crash using the lowest possible number in the event variable, EVENTNUM, from the VEVENT data set.

If the first participants are vehicles, we use the VNUMBER1 and VNUMBER2 variables to infer the causal conflict. The limitation with this approach is that this field is only applicable when the event is a collision between two motor vehicles.

If the first participants are a vehicle and pedestrian/bicyclist, we use, depending of the case, PEDCTYPE and BIKECTYPE for the analysis. One of the limitations with this approach is the lack of information to get a complete classification, particularly on the direction of travel of the pedestrian and cyclist. Thus, if there is a doubt about who the causer of the crash could be, the authors assume that the motorized vehicle is the causer of the crash. However, this is regardless of the question of who the (legally) guilty participant of a crash is, like it can be found in GIDAS. The overall process is visualized in Figure 5. To see our assumptions for the cause conflict in the vehicle/pedestrian and vehicle/bicyclist conflict, see Table 2 and Table 3.

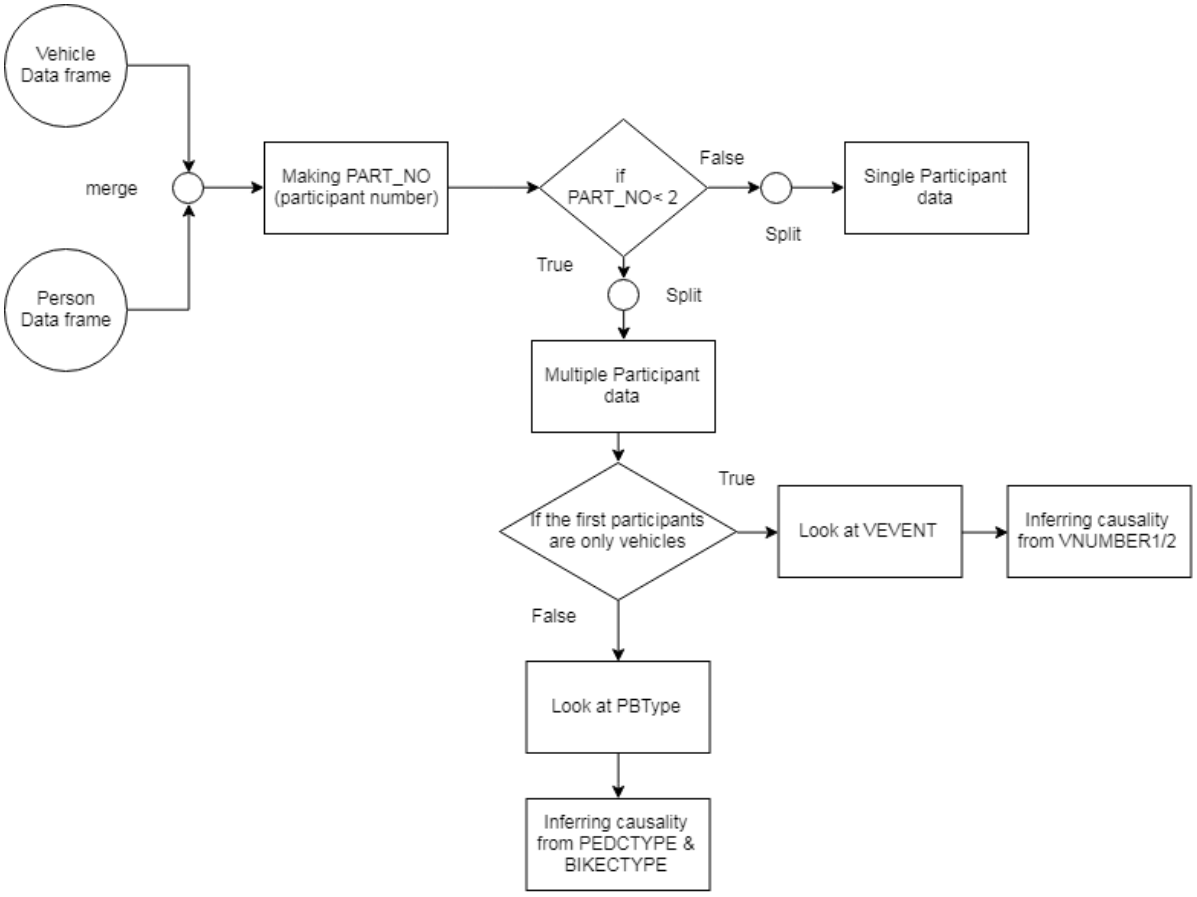

Figure 5. Identifying participants with the first collision in the crash.

Table 3.
PEDCTYPE indicates pedestrian causation in vehicle/pedestrian conflict

PEDCTYPE	Title	Description
160	Pedestrian Loss of Control	is used when the pedestrian stumbled, fell or rolled into path of a vehicle due to surface conditions, medical issue, blackout or unconsciousness, alcohol or drug impairment, falling asleep, or other mishap.
313	Lying in Roadway	is used when the pedestrian is lying in the roadway when involved with a collision with a motor vehicle. This includes someone sitting, getting up, asleep/unconscious, kneeling, etc.
742	Dart-out	is used when the pedestrian walked or ran into the roadway and was involved in a collision with a vehicle where the driver's view of the pedestrian was blocked until an instant before impact. A dart-out can only occur if there is some documented visual obstruction (e.g., parked vehicle, building or vegetation).

Table 4.
BIKECTYPE indicates bicycle causation in vehicle/bicycle conflict

BIKECTYPE	Title	Description
114, 115, 116	Bicyclist Turning Error	is used when the bicyclist made a left turn/right at an intersection or a commercial driveway, cut the corner and entered the opposing traffic lane (travel lane, bike lane, paved shoulder, parking lane) occupied by the motorist.
122, 123, 124	Bicyclist Lost Control	is used when the bicyclist lost control due to mechanical problems, alcohol, drug impairment, surface condition, improper breaking, etc.
142,153, 311, 312, 313, 318, 319	Bicyclist Ride-out	is used when the bicyclist rode from a driveway access into the path of a motor vehicle
155	Bicyclist Ride-Through	is used when the case materials indicate that the motorist had the right-of-way and the bicyclist did not stop at a sign (stop or yield) or flashing light-controlled intersection.
156, 157, 159	Bicyclist Failed to Clear	is used when the bicyclist entered the intersection on green, did not clear the intersection before the signal changed for the cross-street traffic giving those operators the right-of-way, and was involved in a collision with a vehicle whose view was not obstructed by standing or stopped traffic
250	Wrong way/Wrong side	is used when the bicyclist was traveling the wrong way on a one-way roadway or on the wrong side of a two-way roadway and collided with a motor vehicle.

Applying the scenario catalogue to FARS

After these steps, we have a dataset which satisfies all the premises to apply the proposed crash scenarios. An example of the catalogue mapping is shown in Figure 6. For each of the crashes, the solid red point represents the participant to which the scenario "C1" is attributed. Notice that only one of the involved vehicles belongs to the scenario.

Passing the variables in Table 1 of the processed data through the mapping in Appendix 3 results in a list of scenarios for a comparison with other regions.

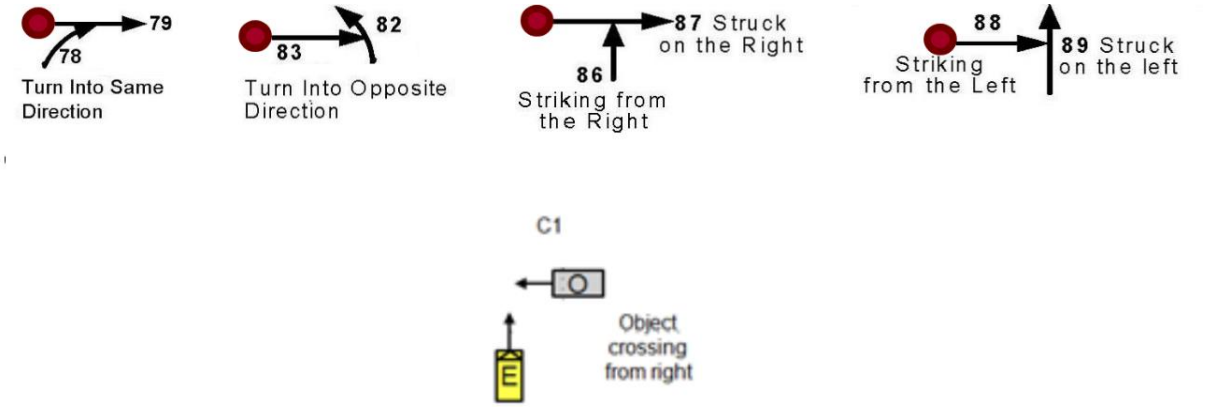

Figure 6. Mapping crash types for scenario "C1" as defined in [8]

RESULTS

FARS describes 92 different crash types for motorized vehicles (ACC_TYPE), 56 for pedestrians (PEDCTYPE) and 78 for bicyclists (BIKECTYPE). This totals more than 220 crash types to describe the overall traffic crashes in the USA. Using a proven methodology [8] this paper shows that with slight modifications for the FARS database a mapping of nearly all FARS crash types to an existing harmonized pre-crash catalogue is possible.

This mapping allows for a reduction of the overall number of crash type categories from over 220 to 22 (-90%). For Japan this reduction is even greater since there are currently 255 SIP-Codes defined in ITARDA (-91%). As for Germany and China there are almost 300 crash types (UTYP) defined in the database, which means a reduction of about 92%. The complete overview of the mapping for the ITARDA variable SIP-Code and the FARS variable ACC_TYPE can be found in Appendix 1 and Appendix 3, respectively. The mapping for GIDAS (UTYP) has already been published in [8].

Besides reducing the number of categories, another benefit of the harmonized pre-crash scenarios can be found in the comparability of traffic crashes between countries, regions, databases, etc. The authors are not aware of any studies that have shown a practical mapping between more than two databases up to this point in time.

To demonstrate the practicability of the harmonized pre-crash scenarios, crashes between passenger cars (including light trucks) and motorcycles were analyzed across four different databases. For this example, the scenarios are clustered further into bundles to simplify the visualization and to allow a better comparability. In Table 5, the scenario bundles are displayed.

Table 5.
Scenario Bundles

Turning farside	Crossing	Runup	Rear	Lane Change	Oncoming same	Oncoming adjacent
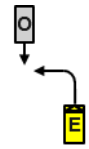	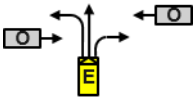	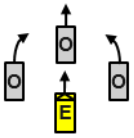		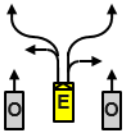		
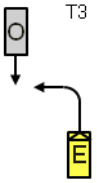	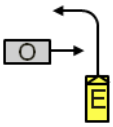			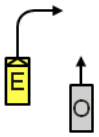		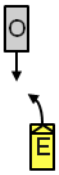
	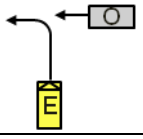	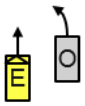		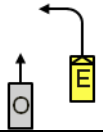		
	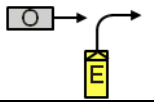	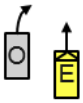		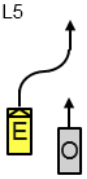		
	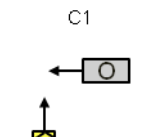					
	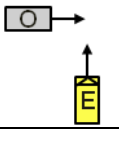					

From the point of view of the cars and the motorcycles, the complete accident occurrence can be presented using the proposed scenario bundles. This shows how the scenario catalogue can be applied to various participants types. In Figures 7 and 8 both, the cars and the motorcycles are depicted in the role of the ego vehicle.

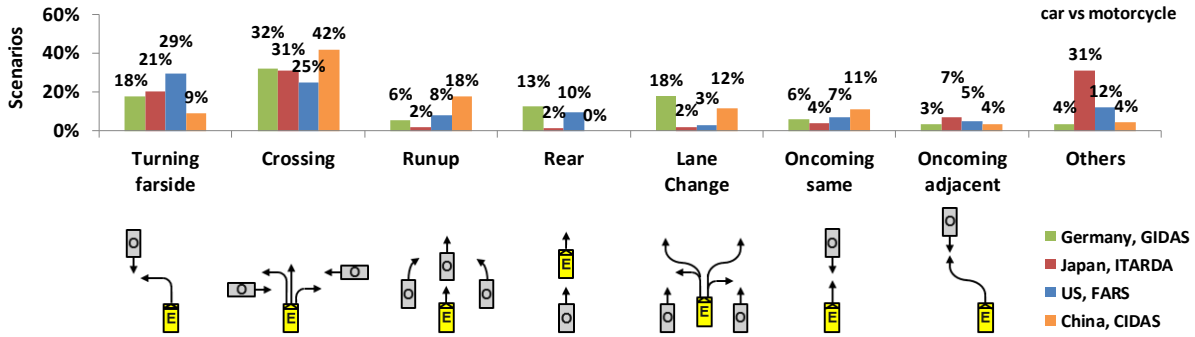

Figure 7. Car perspective: Ego is car, object is motorcycle

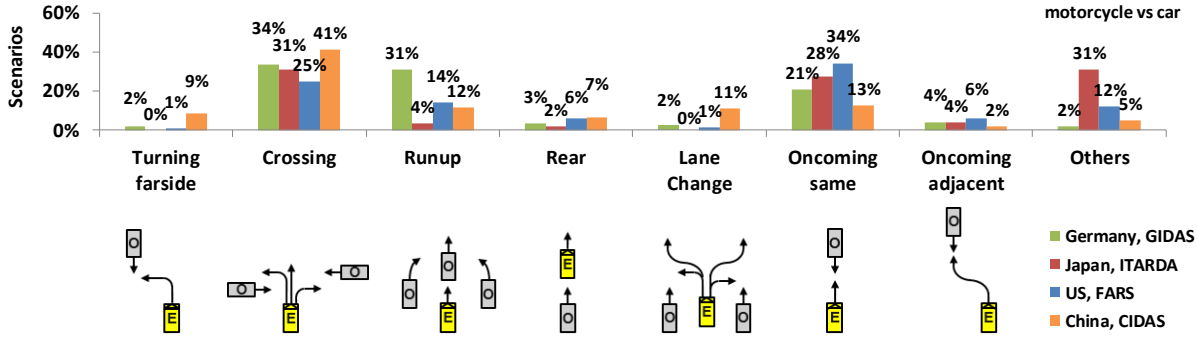

Figure 8. Motorcycle perspective: Ego is motorcycle, object is car

Appendix 4 gives an overview of all scenarios for crashes with car vs. motorcycle participation in four countries (Germany, USA, China, Japan).

At this level of the analysis of traffic scenarios it is already possible to derive the most relevant scenarios for a specific crash constellation. In the example above, "Crossing" scenarios are the most relevant in all four crash databases with "Turning farside" scenarios as second most relevant (Figure 7). Looking from the motorcycle perspective at the same crashes, "Crossing" followed by "Oncoming same" scenarios are the most relevant.

Following this high-level analysis, which can be used for identifying for example consumer test scenarios, data analysts can also take a deeper dive into the existing data to provide input for the requirements of advanced driver assistance systems (ADAS) and of advanced rider assistance systems (ARAS®).

CONCLUSIONS

The crash scenarios are consolidating for regions by combining them into a common form PCAS scenarios. Since the GIDAS and FARS coding hierarchy differs, it requires an extra effort to map the existing data upon the proposed scenarios. The limitations found within the FARS data are as follows:

i) Non-motorized participants (Pedestrian and Bicyclist) do not have a crash type in the ACC_TYPE variable.
ii) Crash type for non-motorized participants needs to be obtained through PEDCTYPE and BIKECTYPE and adjust to each of the cases.
iii) Changes in the data throughout the years (ACC_TYPE is introduced after 2010).

Nevertheless, the methodology presented in this paper shows a systematic way to deal with these limitations.

Since the FARS coding does not explicitly state if the pedestrian or cyclist was at fault (causer), we had to make the choice based on the parameter descriptions (See Table 3 and 4). Mapping results shown in Appendix 3 is

incomplete because we are unable to map directly a FARS value into a PCAS scenario since some values are coded unknown (i.e. specifics unknown, specifics other). However, the authors understand that improvement in the classification as well as the processing of the data still can be made. We may improve the method by using the pre-crash variables to get further details of the critical events which lead to the collision.

Considering the challenge of properly mapping the N/A's presented in Appendix 3, more research is needed to analyze and understand these parameters. We found that our algorithm works for the years 2015 to present; however, the database has significant changes for 2010 and prior which would need further analysis.

The crash scenario catalogue presented in this paper is the result of an analytical approach of available in-depth crash data worldwide. Existing crash classifiers of different databases are used to create a harmonized dynamic scenario description. This enables a comparability of crash research results regardless of regional differences in data collection and coding formats. Therefore, harmonized safety system development and simulation methods and tools can be utilized.

The scenario generation has been demonstrated on four different crash databases. The focus of this paper lays on the US fatality database FARS. The detailed mapping of the German GIDAS crash data is explained in [8], which can also be applied to the Chinese CIDAS data. Due to its simplicity, the Japanese ITARDA SIP crash codes can directly be mapped to the proposed crash scenarios. SIP codes are defined by 255 typical accident types with more than three fatalities; these cover around 80% of fatal accidents in Japan, however, accident types with less than 3 fatalities are not considered.

OUTLOOK

This paper describes a method to cluster crash types to a harmonized set of scenarios, by looking at each crash from the perspectives of the causer and of the non-causer and by considering additional pre-crash information. This inductive approach will naturally leave a quantity of crashes that cannot automatedly be mapped to crash scenarios, since the available classification is not sufficient, see Table 6. To further increase the respective percentages, additional research should be performed to add further available crash parameters. Ultimately, manual re-coding might be needed to reach 100% coverage, which however will be difficult to justify for existing data. It is therefore suggested that the proposed scenario catalogue is introduced as a standard crash parameter to all relevant worldwide databases and is consequently populated for all new cases.

Table 6.
Percentage of crash participants classified by automatic mapping method

Database	**Region**	**Percentage covered**
GIDAS	Germany	75%
FARS	US	70%
ITARDA	Japan	82%
CIDAS	China	75%

The crash scenarios allow for a dynamic crash description from the perspective of the ego vehicle. They include ego movement and object direction, however do not differentiate between possible object intentions. In V2V communication systems, the object intention is communicated over the air, therefore the crash dynamic scenarios should be extended to reflect this extra information. An extension to the scenario definition with additional object intentions is proposed. Table 7 gives an example for scenario C1 "Crossing from right" with added object intentions.

Table 7.
Scenario C1 "Crossing from right" with different object intentions

No object intention	Object going straight	Object turning right	Object turning left
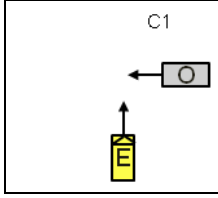	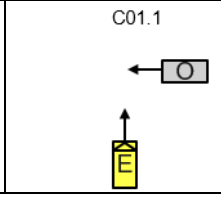	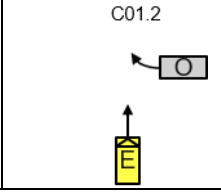	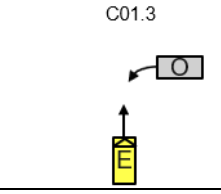

The proposed scenario catalogue has been developed by aggregating crash types from different crash databases. The catalogue does not cover normal driving scenarios that are not crash relevant. To allow the classification of all real-world driving data, such as normal driving, near miss incidents and crashes, the scenarios catalogue is further extended. Therefore, non-crash relevant scenarios are added. Table 8 shows following-scenarios with traffic objects in same or adjacent lanes.

Table 8.
Scenarios L1, L11, L12 "Run-up in same lane", "Following in adjacent lane"

Run-up in same lane	Following in adjacent lane	
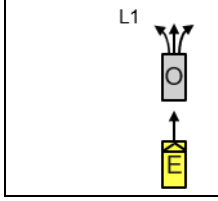	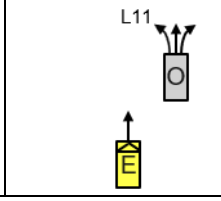	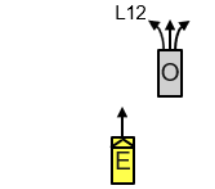

The proposed scenario catalogue should be applied to a maximum number of worldwide crash and naturalistic driving databases (NDD). Table 9 lists several databases that are suggested for further research.

Table 9.
Possible variables for scenario generation in other databases

Database	Region	Variables	Reference
RASSI	India	PRECREV, PRECRA, PRECRB	[9]
iGLAD	Worldwide	ACCTYPE, ACCTYPEA, ACCTYPEB	[10]
SHRP2 NDS	USA	Crash Type	[11]
TUAT NDS	Japan	Incident / Collision Type	[12]

REFERENCES

[1] Ulbrich, S. et.al. 2015. “Defining and Substantiating the Terms Scene, Situation, and Scenario for Automated Driving." In Proceedings of 18th International Conference on Intelligent Transportation Systems (Las Palmas, 2015). IEEE, pp. 982-988.

[2] German Insurance Association (GDV). Accident Types Catalogue 2016. Retrieved from URL: https://udv.de/sites/default/files/tx_udvpublications/unfalltypen-katalog_udv_web_2.pdf

[3] Op den Camp, O., et al. 2017. “Cyclist Target and Test Setup for Evaluation of Cyclist-Autonomous Emergency Braking.” International Journal of Automotive Technology, Vol. 18, No. 6, pp. 1085−1097.

[4] VUFO GmbH. 2017. “Codebook German In-Depth Accident Study.”

[5] CATARC. 2018. “Codebook China In-Depth Accident Study.”

[6] National Highway Traffic Safety Administration. 2017. “Fatality Analysis Reporting Systems (FARS) Analytical User’s Manual 1975 – 2016.” US DOT HS 812 447.

[7] Cabinet Office, Government of Japan. 2018. “Survey on Analysis Method to Estimate Traffic Fatalities Reduction Effect by Automated Driving System.”

[8] Feifel, H. and Wagner, M. 2018. “Harmonized Scenarios for the Evaluation of Active Safety Systems based on In-Depth-Accident Data.” Expert Symposium on Accident Research ESAR 2018.

[9] JP Research India PVT Ltd. 2016. Road Accident Sampling System - India (RASSI) Database Coding Manual.”

[10] IGLAD Technical Working Group. 2018. “Codebook Member Year 2018 Phase III.”

[11] Virginia Tech Transportation Institute. 2015. “SHRP2 Researcher Dictionary for Video Reduction Data.”

[12] Akagi, Y. 2017. "Ontology based collection and analysis of traffic event data for developing intelligent vehicles," IEEE 6th Global Conference on Consumer Electronics, pp.219-223.

APPENDICES

Appendix 1: Scenario mapping Japan for crashes with at least 3 fatalities (SIP code)

Code	Causer	Non-causer	Code	Causer	Non-causer	Code	Causer	Non-causer
CTC-01	C2	C1	CTC-11	On2	N/A	CTC-20	On1	On1
CTC-02	C1	C2	CTC-12	On2	On1	CTC-21	On2	On1
CTC-03	On1	T3	CTC-13	L1	L4	CTC-22	On2	On1
CTC-04	T3	On1	CTC-14	L1	L4	CTC-23	On2	On1
CTC-05	On2	On1	CTC-15	On2	On1	CTC-24	On2	On1
CTC-06	C2	C1	CTC-16	L1	L4	CTC-25	L1	L4
CTC-07	C1	C2	CTC-17	On2	On1	CTC-26	L1	L4
CTC-08	T4	C1	CTC-18	On2	On1	CTC-27	On1	On1
CTC-09	T9	C2	CTC-19	On2	On1	CTC-28	On1	On1
CTC-10	T3	On						

Code	Causer	Non-causer	Code	Causer	Non-causer	Code	Causer	Non-causer
CTM-01	C2	C1	CTM-09	T4	C1	CTM-16	On2	On1
CTM-02	C1	C2	CTM-10	T3	On1	CTM-17	L1	N/A
CTM-03	On1	On2	CTM-11	On2	On1	CTM-18	L1	L4
CTM-04	T5	L2	CTM-12	L5	L3	CTM-19	T4	N/A
CTM-05	T3	On1	CTM-13	T3	On1	CTM-20	L5	L3
CTM-06	C2	C1	CTM-14	On2	On1	CTM-21	T3	On1
CTM-07	C1	C2	CTM-15	L5	L3	CTM-22	L5	L3
CTM-08	T10	C2						

Code	Causer	Non-causer	Code	Causer	Non-causer	Code	Causer	Non-causer
CTB-01	C2	C1	CTB-11	T1	L2	CTB-20	On1	On1
CTB-02	C1	C2	CTB-12	T3	On1	CTB-21	L1	L4
CTB-03	T1	L3	CTB-13	On1	On1	CTB-22	C2	C1
CTB-04	T2	On1	CTB-14	L1	L4	CTB-23	C1	C2
CTB-05	T5	L2	CTB-15	C2	C1	CTB-24	L5	L3
CTB-06	T3	On1	CTB-16	C1	C2	CTB-25	L5	L3
CTB-07	L1	L4	CTB-17	C2	C1	CTB-26	On1	On1
CTB-08	C2	C1	CTB-18	L1	L4	CTB-27	C2	C1
CTB-09	C1	C2	CTB-19	L1	L4	CTB-28	C1	C2
CTB-10	T14	C2						

Code	Causer	Non-causer	Code	Causer	Non-causer	Code	Causer	Non-causer
CTP-01	C2	C1	CTP-18	C1	C2	CTP-35	C1	C2
CTP-02	C1	C2	CTP-19	T1	C2	CTP-36	L1	N/A
CTP-03	T2	C1	CTP-20	T5	C1	CTP-37	L5	L3
CTP-04	T1	C2	CTP-21	T3	C2	CTP-38	L6	L2
CTP-05	T5	C1	CTP-22	L1	N/A	CTP-39	C2	C1
CTP-06	T3	C2	CTP-23	T3	N/A	CTP-40	C1	C2
CTP-07	T3	C2	CTP-24	L5	L3	CTP-41	C2	C1
CTP-08	C2	C1	CTP-25	C1	C2	CTP-42	C1	C2
CTP-09	C1	C2	CTP-26	C2	C1	CTP-43	C1	C2
CTP-10	T3	C2	CTP-27	C1	C2	CTP-44	L1	N/A
CTP-11	L1	N/1	CTP-28	T3	C2	CTP-45	L5	L3
CTP-12	L5	L3	CTP-29	C1	C2	CTP-46	C1	C2
CTP-13	C2	C1	CTP-30	L1	N/A	CTP-47	L1	N/A
CTP-14	C1	C2	CTP-31	T3	N/A	CTP-48	B1	N/A
CTP-15	T5	C1	CTP-32	L1	N/A	CTP-49	B1	N/A
CTP-16	T3	C2	CTP-33	L5	L3	CTP-50	B3	C2
CTP-17	C2	C1	CTP-34	C2	C1			

Code	Causer	Non-causer	Code	Causer	Non-causer	Code	Causer	Non-causer
MTC-01	C2	C1	MTC-06	C1	C2	MTC-10	On2	On1
MTC-02	C1	C2	MTC-07	T4	C1	MTC-11	On2	On1
MTC-03	On1	T3	MTC-08	T3	On1	MTC-12	L1	L4
MTC-04	T3	On1	MTC-09	On2	On1	MTC-13	L5	L3
MTC-05	C2	C1						

Code	Causer	Non-causer	Code	Causer	Non-causer	Code	Causer	Non-causer
BTC-01	C2	C1	BTC-04	C1	C2	BTC-06	L6	L3
BTC-02	C1	C2	BTC-05	C1	C2	BTC-07	L6	L3
BTC-03	C2	C1						

Code	Causer	Non-causer	Code	Causer	Non-causer	Code	Causer	Non-causer
PTC-01	C1	C2	PTC-05	C1	C2	PTC-08	C1	C2
PTC-02	C2	C1	PTC-06	C2	C1	PTC-09	C2	C1
PTC-03	C1	C2	PTC-07	L4	L5	PTC-10	N/A	L1
PTC-04	C2	C1						

Code	Causer	Non-causer	Code	Causer	Non-causer	Code	Causer	Non-causer
HCTC-01	L1	L4	HCTC-04	L1	L4	HCTC-07	L1	L4
HCTC-02	L1	L4	HCTC-05	On2	On1	HCTC-08	On2	On1
HCTC-03	L1	L4	HCTC-06	L1	L4			

Code	Causer	Non-causer	Code	Causer	Non-causer	Code	Causer	Non-causer
HCTM-01	L1	L4						

Code	Causer	Non-causer	Code	Causer	Non-causer	Code	Causer	Non-causer
HCTP-01	C1	C2						

Appendix 2: FARS Terminology

For this paper the following data files and variables are used from FARS, year 2015 (FARS Analytical User's Manual 1975 – 2016).

Accident: This data contains information about crash characteristics and environmental conditions at the time of the crash. There is one record per crash.

> **ST_CASE**: This data element is the unique case number assigned to each crash. It appears on each data file and is used to merge information from the data files together.

Vehicle: This data file contains information describing the in-transport motor vehicles and the drivers of in-transport motor vehicle who are involved in the crash. There is one record per in-transport motor vehicle.

> **VEH_NO**: This data element is the consecutive number assigned to each vehicle in the case. It is used in conjunction with the ST_CASE data element to merge information from vehicle level data files.
>
> **ACC_TYPE**: Identifies the attribute that best describes the type of crash this vehicle was involved in based on the "First Harmful Event" and the pre-crash circumstances.

Person: This data file contains information describing all persons involved in the crash including motorists (i.e., drivers and passengers of in-transport motor vehicles) and non-motorists (e.g., pedestrians and pedal cyclists). There is one record per person.

> **PER_NO**: This data element is the consecutive number assigned to each person in the case (i.e., each occupant, pedestrian, or non-motorists involved in the crash). It is used in conjunction with the ST_CASE data element (and sometimes the VEH_NO data element) to merge information from person level data files.

Vevent: This data file contains the sequence of events for each in-transport motor vehicle involve in the crash.

> **VNUMBER1 & 2**: This data element identifies the "Vehicle Number" (VEH_NO) of this in-transport motor vehicle described in this event. This is the vehicle described in "Sequence of Events" for this event. If Vehicle #1 (V1) impacts Vehicle #2 (V2), then we have at least 2 Vevent records.

VEH_NO	EVENTNUM	VNUMBER1	SOE	VNUMBER2
1	1	1	12	2
2	1	1	12	2

> The explanation of these 2 records is as follows:
> V1 was involved in event 1 where V1 impacts V2
> V2 was involved in event 1 where V1 impacts V2
>
> **EVENTNUM**: This data element is the consecutive number assigned to each harmful and nonharmful event in a crash, in chronological order.

PBType: This data file contains information about crashes between motor vehicles and pedestrians, people on personal conveyances and bicyclists. There is one record for each pedestrian, bicyclist or person on a personal conveyance.

> **PEDCTYPE**: This data element summarizes the circumstances of the crash for this pedestrian.
>
> **BIKECTYPE:** This data element summarizes the circumstances of the crash for this bicyclist.

Using the above variables, the data sets, and the formula 1, we can infer the variable PART_NO (Participant number). Thus, a participant number is a number assigned to each of involved parties in a given crash (pedestrian, bicycle, car type). This shall not be mistaken by the PER_NO or the VEH_NO, however is obtained from these two.

Appendix 3: Scenario mapping proposal for USA (FARS)

Crash Type	Scenario
1	D1
2	D1
3	D1
4	N/A
5	N/A
6	D2
7	D2
8	D2
9	N/A
10	N/A
11	L1
12	O2
13	L1
14	O2*
15	N/A
16	N/A
20	L1
21	L4
22	L4
23	L4
24	L1
25	L4
26	L4
27	L4
28	L1
29	L4
30	L4
31	L4
32	N/A
33	N/A
34	D3*
35	D3*
36	D3*
37	D3*
38	D3*
39	D3*
40	D3*

Crash Type	Scenario
41	D3*
42	N/A
43	N/A
44	L2*
45	L3*
46	L5
47	L6
48	N/A
49	N/A
50	On2
51	On1
52	N/A
53	N/A
54	D3*
55	D3*
56	D3*
57	D3*
58	D3*
59	D3*
60	D3*
61	D3*
62	N/A
63	N/A
64	On2
65	On1
66	N/A
67	N/A
68	T2/T3*
69	On1
70	T1
71	L3
72	T5
73	L2
74	N/A
75	N/A
76	T9
77	C2

Crash Type	Scenario
78	T10
79	C1
80	T14
81	C2
82	T4
83	C1
84	N/A
85	N/A
86	C2
87	C1
88	C1
89	C2
90	N/A
91	N/A
92	B
93	L4*
98	N/A
99	N/A

Note: Scenarios with * indicate that the mapping needs to be optimized.

Appendix 4: Overview of all scenarios for crashes "Car vs. Motorcycle" in four major countries

Car vs. motorcycle crashes from the perspective of the car

Scenario	Share in %			
	Germany (KSI)	**USA (K)**	**China (KSI)**	**Japan (K)**
T1	0.1	0.5	6.0	0.0
T2	0.0	0.0	0.7	0.0
T3	18.1	29.5	9.0	22.8
T4	14.6	9.7	9.0	2.0
T5	9.7	1.8	3.0	0.0
T9	2.2	0.9	0.0	0.0
T10	2.2	0.9	0.7	0.5
T14	0.2	0.2	0.0	0.0
C1	6.4	4.0	13.4	10.8
C2	6.8	9.5	18.7	12.2
L1	3.4	5.8	6.7	2.7
L2	1.5	0.8	9.7	0.0
L3	1.0	1.8	1.5	0.0
L4	12.6	9.6	0.0	1.1
L5	2.6	0.6	2.2	1.6
L6	5.6	0.4	0.7	0.5
On1	5.9	7.2	11.2	9.3
On2	3.4	4.9	3.7	2.5
S1	0.0	0.0	0.0	0.0
S2	0.0	0.0	0.0	0.0
B	1.2	0.2	0.7	0.0
N/A	2.3	11.9	3.0	34.1
Total	**100**	**100**	**100**	**100**

Germany: GIDAS 2005-2018, weighted to national crash statistics

USA: FARS 2015, not weighted to national crash statistics

China: CIDAS 2014 - 2018, not weighted to national crash statistics

Japan: ITARDA 2013, not weighted to national crash statistics

Car vs. motorcycle crashes from the perspective of the motorcycle

Scenario	Share in %			
	Germany (KSI)	**USA (K)**	**China (KSI)**	**Japan (K)**
T1	0.1	0.0	0.7	0.0
T2	0.0	0.0	0.0	0.0
T3	2.3	1.2	8.9	2.3
T4	1.2	0.6	3.0	0.0
T5	0.6	0.1	6.7	0.0
T9	0.0	0.1	3.0	0.0
T10	0.2	0.1	0.0	0.0
T14	0.0	0.2	0.7	0.0
C1	24.8	19.8	25.2	14.0
C2	7.4	4.3	10.4	11.5
L1	12.9	9.6	0.0	0.0
L2	15.4	2.4	4.4	0.0
L3	2.8	2.1	7.4	2.0
L4	3.4	5.9	6.7	2.7
L5	0.9	0.6	0.7	0.0
L6	0.9	0.6	3.0	0.0
On1	20.9	34.4	12.6	31.6
On2	4.0	6.0	2.2	0.7
S1	0.0	0.0	0.0	0.0
S2	0.0	0.0	0.0	0.0
B	0.0	0.0	0.0	0.0
N/A	2.2	11.9	4.4	35.2
Total	**100**	**100**	**100**	**100**

Germany: GIDAS 2005-2018, weighted to national crash statistics

USA: FARS 2015, not weighted to national crash statistics

China: CIDAS 2014 - 2018, not weighted to national crash statistics

Japan: ITARDA 2013, not weighted to national crash statistics

PROSPECTIVE EFFECTIVENESS ASSESSMENT OF ROAD VEHICLE AUTOMATION BASED ON DRIVER PERFORMANCE MODELS

Christian Roesener, Lutz Eckstein
Institute for Automotive Engineering, RWTH Aachen University
Germany

Adrian Zlocki
FKA GmbH
Germany

Paper Number 19-0113

ABSTRACT

One of the major challenges for enabling market introduction of automated driving is to identify risks and benefits of these functions. For this purpose, a new framework for assessing the safety impact of automated driving functions (ADFs) has been investigated. This framework is based on accident- and field operational test- (FOT-) data while using simulations for assessment of ADFs with respect to a certain baseline. According to the German Ethics Commission for Automated and Connected Driving, this baseline has to be human manual driver performance. For modelling of this baseline in simulations, so-called driver performance models are introduced in this publication and incorporated in an overall framework for effectiveness assessment.

The main idea of the developed framework is that the types of driving scenarios, respectively physical accident constellations, do not change with automated driving. However, since ADFs are continuously controlling the behavior of the vehicle, it is possible that ADFs will get involved less frequently in accident scenarios playing a major role at human driving, e.g. rear-end accident scenarios. On the other hand, it is likely that other previously irrelevant accident types will rise. Consequently, the frequency of occurrence and the severity of the addressed driving scenarios may change with automated driving although the types of driving scenarios stay the same. To investigate the change of severity in a driving scenario, accident re-simulations are used. The changes in frequency of occurrence of driving scenarios are analyzed by using traffic simulations. In this work, so-called driver performance models are introduced for modelling human baseline in accident re-simulations. Key findings concerning the structure of these driver performance models are presented.

The developed method and models are applied on two generic ADFs, a generic “Motorway-Chauffeur” (SAE level 3) and a generic “Urban Robot-Taxi” (SAE level 4). The results indicate that, e.g. a Motorway-Chauffeur at a market penetration of 50 % has a potential for reducing about 31 % of all accidents on German motorways resulting in personal injury. This equals 2 % of all accidents on German roads.

INTRODUCTION

In the last decade various automotive functions for supporting the driver have been developed. These so-called advanced driver assistance systems (ADAS) are supporting the driver on different levels of the driving task. Driven by recent developments in algorithms for environment perception and decision making, the ultimate goal of vehicle automation seems to be a solvable task as shown by several demonstrations [1].

However, due to an increasing complexity of decision making algorithms of these complex functions, identifying benefits and drawbacks will be challenging. Hence, new safety effectiveness assessment methods have to be designed which are based on detailed accident-, FOT- and simulation data and that are assessing the ADFs with respect to a certain baseline. Since automated driving will not be able to avoid all accidents on roads, e.g. due to the misbehavior of other traffic participants and physical limits, a baseline for assessment has to be defined. According to the German Ethics Commission for Automated and Connected Driving,

> *"[..] the licensing of automated systems is not justifiable unless it promises to produce at least a diminution in harm compared with human driving, in other words a positive balance of risks [..]"* [2]

Consequently, the reference for safety impact assessment needs to be human driver performance. In order to assess ADFs with respect to human driver performance, this paper introduces a method for safety effectiveness assessment. The basic idea of this framework is that the types of accident constellations and thus driving scenarios do not change with automated driving. However, the severity and frequency of occurrence of these driving scenarios may change with automated driving.

BACKGROUND

For effectiveness assessment of (advanced) driver assistance systems with environment perception, many different methods have been used in the past. All these methods have in common, that they compare driving situations without the system with driving situations, in which the system is activated. One valid approach for determining the effectiveness of ADAS is the accident re-simulation on basis of in-depth accident data, e.g. as applied in [3]. In this case, reconstructed accident scenarios from detailed accident data, such as the German-in-depth accident database (GIDAS) [4], are simulated with and without the considered function. The difference in performance in the situation, e.g. probability of severe injuries, is considered as the benefit of the function. An alternative to re-simulation of single accident situations is provided by stochastic approaches describing the situational variables of a driving scenario by Monte Carlo sampling of synthetic driving situations from probability distributions as presented in [5]. A disadvantage of accident re-simulations is that new induced driving scenarios by automated driving cannot be considered, because these are not represented in the accident data. Another approach for safety impact assessment based on recorded data is the field operational test (FOT) as presented in [5]. Here, huge amounts of driving data without function (control condition) and with activated function (experimental condition) are collected. The effectiveness of the considered function is analyzed by investigating the change in frequency of occurrence of incidents and near-crashes compared to the baseline. For effectiveness assessment of a function in defined situations, driving simulator studies can be used as well. This approach allows a detailed investigation of human driver performance with and without the considered function as demonstrated in [6], but requires a selection of situation parameters to be presented to the drivers. As described previously, ADFs need to be assessed in the whole entity of possible driving situations in their operational design domain. Hence, simulations of these functions in the whole traffic are a promising approach as presented in [7]. However, validation of these simulations remains challenging because of the variety and complexity of models necessary for safety impact assessment.

Based on the available methods presented previously, a suitable method for assessing the effectiveness of road vehicle automation is defined. Although accident re-simulation based on detailed accident data is a valid approach, it will not be suitable for assessing ADFs since this approach is based on previously recorded detailed accident data from human driving. In order to identify new driving situations induced by ADFs, a FOT would be suitable. However, considering the necessary resources difficult to realize. Thus, a holistic approach including accident re-simulations for investigation of changes in severity and traffic simulations for assessing changes in frequency of driving scenarios is developed for effectiveness assessment of ADFs.

FRAMEWORK FOR EFFECTIVENESS ASSESSMENT

Built on previously recorded accident- and FOT-data and extended by simulation data, the effectiveness of a defined ADF is assessed by considering the changes in severity and frequency of addressed driving scenarios, see Figure 1. Based on a definition of the ADF and the addressed driving scenarios the effectiveness fields – all

addressed accidents and relevant driving situations – are identified in the input data. To this end, the absolute number of accidents per driving scenario is extracted form accident statistics for upscaling. By this, the results derived from detailed data can be projected upon the effectiveness on a national level. The parameters spaces (e.g. probability density function of velocity of involved traffic participants) are extracted from in-depth accident- and FOT-data for determination of the changes in severity of driving scenarios due to the function.

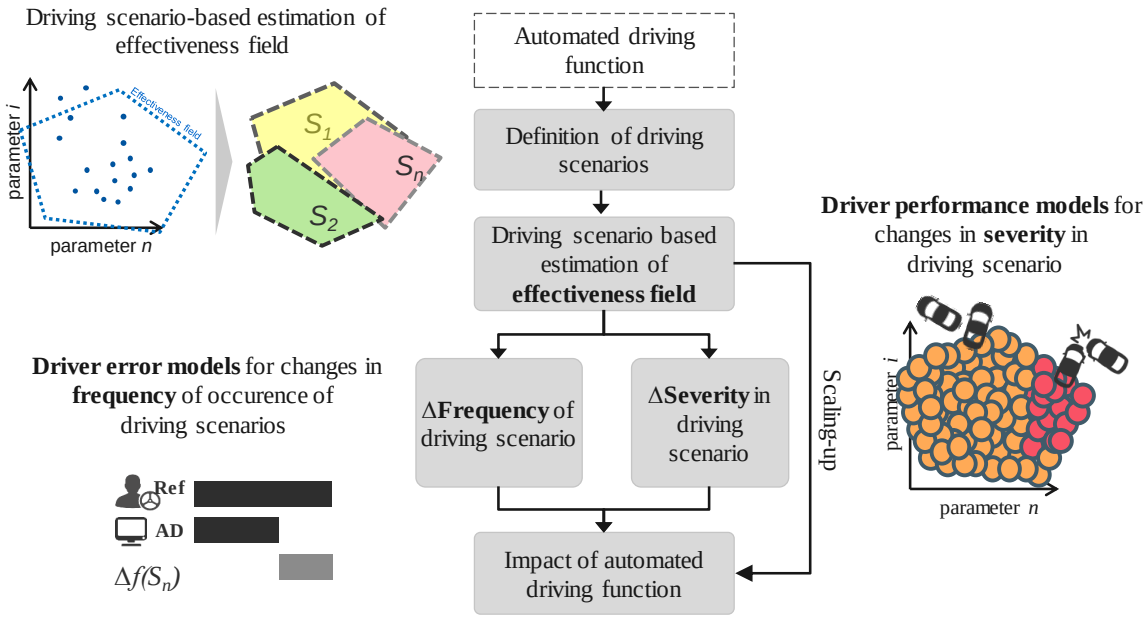

Figure 1. Framework for Effectiveness Assessment of Road Vehicle Automation.

Afterwards, the changes in frequencies of occurrence of the defined driving scenarios are assessed by using traffic simulations. Here, so-called driver error models are used to model critical driving situations in traffic simulations. To identify the changes in severity in the defined driving scenarios, these are simulated with and without ADF while the reference performance is modelled by human driver performance models. The effectiveness E of an ADF in terms of safety can be derived based on a consideration of the accident risk $R_{Scenario}$ by the severity $I_{Scenario}$ and the frequency of occurrence $f_{Scenario}$ for each driving scenario.

$$R_{Scenario} = I_{Scenario} \cdot f_{Scenario}$$

The effectiveness E in a scenario i is defined as the difference of risks ΔR_i.

$$E_i = \Delta R_i = R_{ADF,i} - R_{Human,i}$$

Substituting the risk R_i by severity I_i and frequency f_i results in:

$$E_i = I_{ADF,i} \cdot f_{ADF,i} - I_{Human,i} \cdot f_{Human,i}$$

With the change in severity $\Delta I = I_{ADF}/I_{Human}$ and the change in frequency of occurrence $\Delta f = f_{ADF}/f_{Human}$, the effectiveness E is derived for all scenarios n by:

$$E = \sum_{i=1}^{n} I_{Human,i} \cdot f_{Human,i} \ (\Delta I_i \cdot \Delta f_i - 1)$$

Definition of Driving Scenarios based on Accident Type Catalogue

The developed framework assumes that the defined driving scenarios cover all physical possible accidents constellations. For this purpose, the driving scenarios are derived from the German accident type catalogue [9] that includes a classification scheme for all accidents by a three-digit code built upon decades of experience by the German police. In consequence, almost all accident constellations that are physical possible are included in this catalogue. The considered driving scenarios are derived from this catalogue by assigning each three-digit accident types $UTYP3$ to a driving scenario. This process is illustrated on the example of a "cut-in" driving scenario in Figure 2.

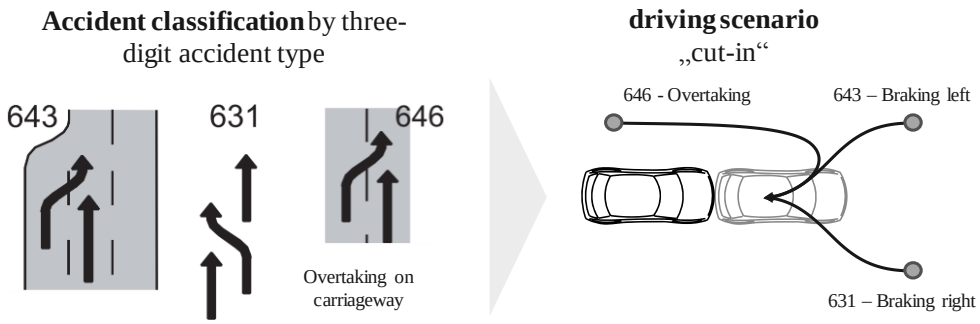

Figure 2. Derivation of driving scenarios based on three-digit accident classification on the example of a "cut-in" driving scenario.

Description of Automated Driving Function

The previously derived driving scenarios are used to describe the functional scope of the assessed ADF. In this sense, to describe an Urban Robot-Taxi, only driving scenarios on urban roads within the operational design domain of the Urban Robot-Taxi will be linked to the function. In addition, functional limitations, e.g. due to environmental conditions (fog, heavy rain, snow) are included in the description of the ADF and can be used to limit the addressed accidents. An exemplary description of an Urban Robot-Taxi is given in Table 1.

Table 1.
Description of automated driving functions and their operational design domain (ODD) on the example of the Urban Robot-Taxi.

Parameter	***Value***
Name	Urban Robot-Taxi
Level of automation according to [SAE16]	4
Sensor view range	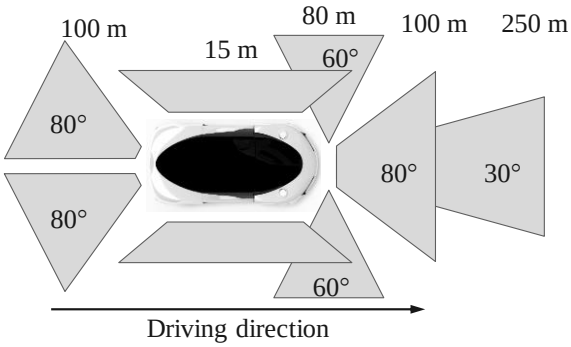
Adressed driving scenarios	• Driving without influence from leading vehicle • Approaching static object • Approaching leading vehicle • Approaching lateral moving object • Approaching traffic jam • Cut-in • Lane change • Turning • Crossing • U-Turn
Road types and speed range	• Inside city-limits: 0 - 50 km/h
Functional limitations	• None

Driving Scenario-based Identification of Effectiveness Fields

After describing the assessed ADFs including their applicable driving scenarios, the effectiveness fields – the accidents and driving situations where the ADFs have a potential impact - are estimated. For in-depth accident data and national accident statistics, the three-digit accident type can be used to select the driving scenarios. FOT-

data is not labelled with a three-digit accident type as it contains time series data. To cluster FOT-data, the driving scenario classification algorithms based on machine learning introduced in [9] can be used. Here, the relative motion included in the three-digit accident type is used to detect the driving scenarios in time series data.

The effectiveness fields can be limited regarding road types and limitations of the ADFs. The classification of driving scenarios results in a number of accidents per driving scenario (see Figure 4) that enables to investigate the change in frequency of the driving scenarios as well as the parameter spaces necessary to determine the change in severity per driving scenario (see Figure 5). Figure 3 illustrates the whole definition process of a driving scenario-based estimation of the effectiveness fields exemplified for a "cut-in" driving scenario.

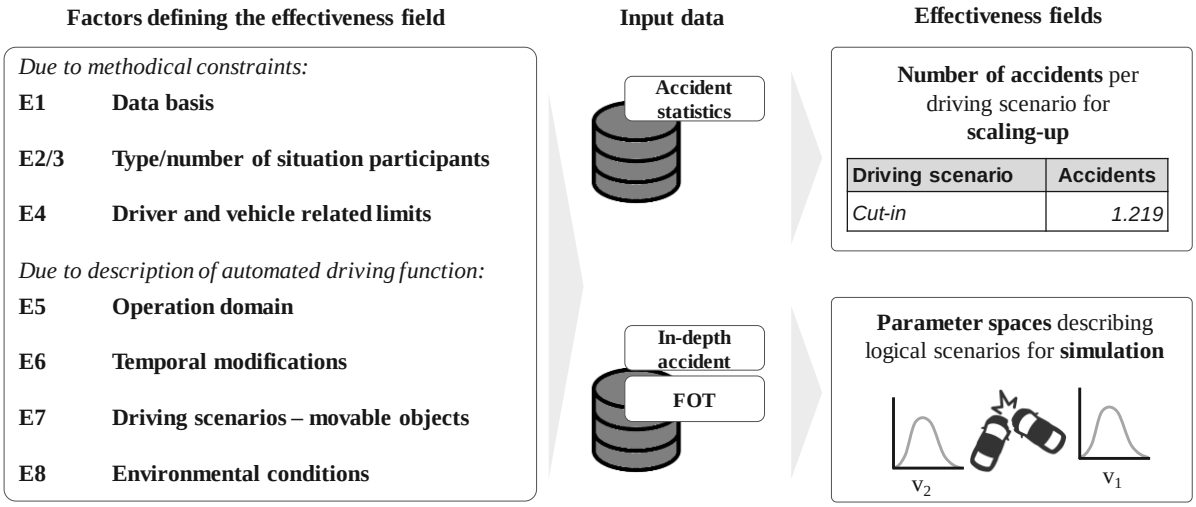

Figure 3. Process for driving scenario-based estimation of effectiveness fields due to methodical constraints and description of the ADF. The effectiveness fields include the number of accidents as well as the parameter spaces per driving scenario.

For example, from all accidents with personal injuries A(P) occurring within city limits in Germany (70 % of all accidents), an Urban Robot-Taxi is addressing 66 %. The other accidents in the domain cannot be addressed due to the reason that driving scenarios are not covered by the functional scope of the automated driving function (14 %), driver and vehicle related limits such as technical failures or alcohol use (3 %) and no car involvement in the accident (17 %), see Figure 4.

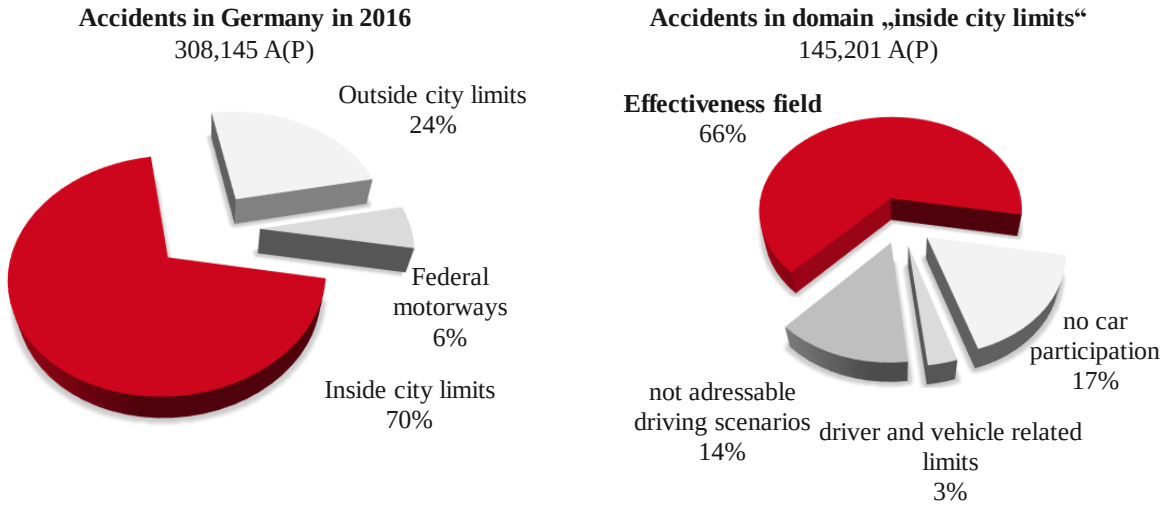

Figure 4. Numbers of addressed accidents resulting from effectiveness field of Urban Robot-Taxi in German national accident statistics DESTATIS.

Next to the number of accidents resulting from the effectiveness fields, the parameter spaces describing the driving scenarios for estimation of the changes in severity are extracted from FOT- and in-depth accident data. The

parameter spaces are represented as Kernel Density Estimation (KDE) obtained from the probability density functions of situational variables of in-depth accident data and FOT-data. Using Monte-Carlo sampling techniques according to [11], concrete scenarios that can be simulated are randomly "drawn" from the logical scenarios. Exemplary parameter spaces of situational variables such as "ego velocity" describing the logical scenario "cut-in" are presented in Figure 5.

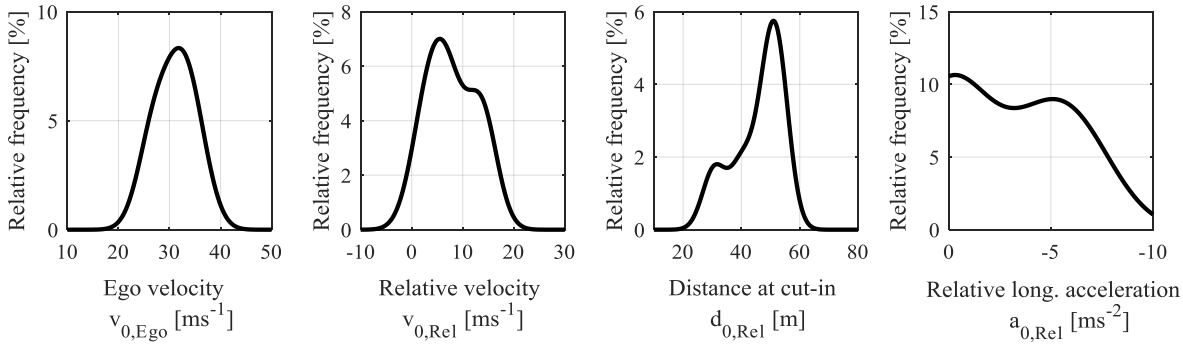

Figure 5. Parameter spaces for describing the logical scenario "cut.in" for estimation of the changes in severity by simulation.

Both number of accidents per driving scenario and the parameter spaces describing the driving scenario for simulation are used in the following to estimate the effectiveness in terms of a change in accidents per driving scenarios.

Driver Error Models in Traffic Simulations for Changes in Frequency of Driving Scenarios

Traffic simulations are used to identify the changes in frequency of occurrence Δf of driving scenarios. For considering the effects within mixed traffic conditions of human driven and automated vehicles, it is distinguished whether a human driven or an automated vehicle has induced or "caused" a certain driving scenario. For example, a human driver cutting-in in front of the automated vehicle can cause a "cut-in" driving situation. In this case, the human driver induced the driving situation while the automated vehicle was involved in it. Based on this principle, a classification scheme for driving situations is introduced, see Table 2.

Table 2.
Types of interactions in driving scenarios in mixed-traffic conditions

Type of interaction	Type of vehicle driving scenario **induced** by	Type of vehicle **involved:**	Illustration
HUM-HUM	Human driver	Human driver	
HUM-ADF	Human driver	Automated driving function	
ADF-HUM	Automated driving function	Human driver	
ADF-ADF	Automated driving function	Automated driving function	

The changes of frequencies for all four defined types of interactions are analyzed by using traffic simulation data of human driven and automated vehicles for several market penetration rates of automated vehicles. For traffic simulation, a 26 km long section of the German motorway A2 around Hanover is used, see Figure 7 (left).

Modelling the behavior of human traffic participants is one of the most crucial parts in traffic simulations. Although a tremendous variety of driver models is available [12], [13], [14] the main purpose of these existing models are traffic flow investigations and not investigations related to traffic safety. The main limitation of the available models is that they do not require to reflect human behavior in critical and uncommon situations but that they have been designed to represent the trained "normal" driving behavior. Special driver models are therefore needed to realistically represent human driving behavior in incident situations.

Consequently, so-called driver error models are developed that are modelling human errors causing incident driving situations in traffic simulations.

To model how humans induce incident situations in traffic simulations, the principles leading to human errors have to be incorporated in the simulation models. The existing driver models, e.g. [14], that assume an ideal recognition and decision of humans, are extended by probabilistic error models that represent uncertainties in recognition and decision. According to the findings of [15], human drivers are able to perceive Time-to-Collision (TTC) and Time Headway (THW) to other objects in their surroundings. For example, the human eye is capable of perceiving the TTC to an object by detecting changes in its retinal projection [15]. A similar principle is assumed for perceiving the THW [15]. For modelling driver errors, it is assumed that the perception of TTC and THW is afflicted with uncertainties. Therefore, the perceived $TTC_{perceived}$ might differ from the real TTC_{real} in a driving situation ending up in a misjudgment of the situation by the driver that can lead to an incident situation, see Figure 6.

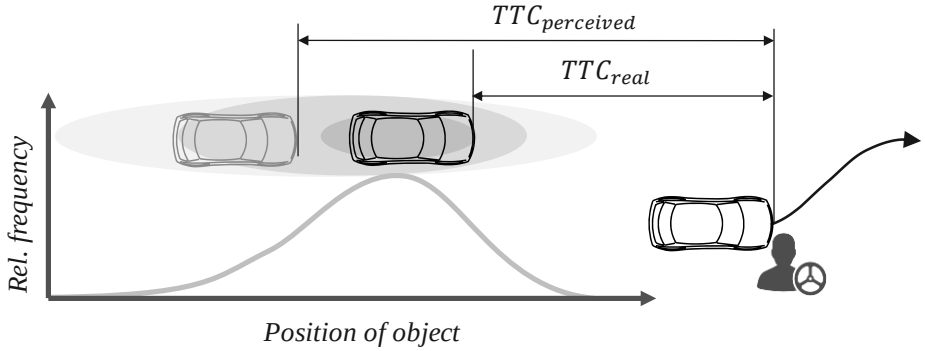

Figure 6. Probabilistic modelling of uncertainties in recognition and decision for the induction of incident driving scenarios.

It is assumed that these uncertainties in recognition of other traffic participants of the driving scenario are gamma distributed. Based on Monte-Carlo sampling [11] of the gamma probability distributions, for each explicit driving situation occurring in simulation uncertainties in THW and TTC can be generated. While most of the sampled uncertainties will be few and not lead to incident situations, potential incident "cut-in" driving situations will occur according to the probability for high uncertainties represented in the gamma probability distributions. The resulting exemplary changes of frequency for an "approaching leading vehicle" driving scenario are shown in Figure 7 (right).

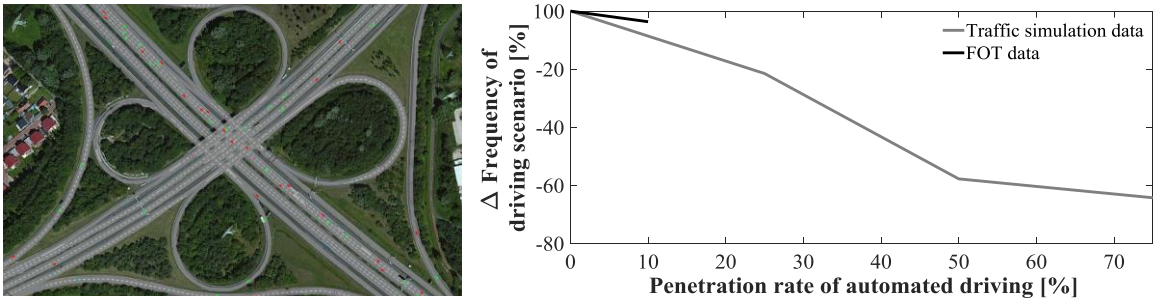

Figure 7. Traffic scenario for estimation of changes in frequencies of driving scenarios (left) and change of frequency of "approaching leading vehicle" driving scenario (right).

Driver Performance Models for Changes in Severity of Driving Scenarios

If an automated vehicle gets involved in an incident driving situation, the changes in severity ΔI induced by the ADF are assessed. For this purpose, driving situations with explicit parameters are simulated with an ADF and with human driver performance models as a reference. The process is illustrated in Figure 8. The difference in performance between human and ADFs is defined as the change in severity. This is measured by the likelihood for severe injuries (MAIS2+) that is derived by injury risk curves based on the relative collision speed. The

parameter spaces resulting from the driving scenario-based estimation of effectiveness fields (see Figure 5) are used to generate concrete scenarios with explicit parameters that can be simulated.

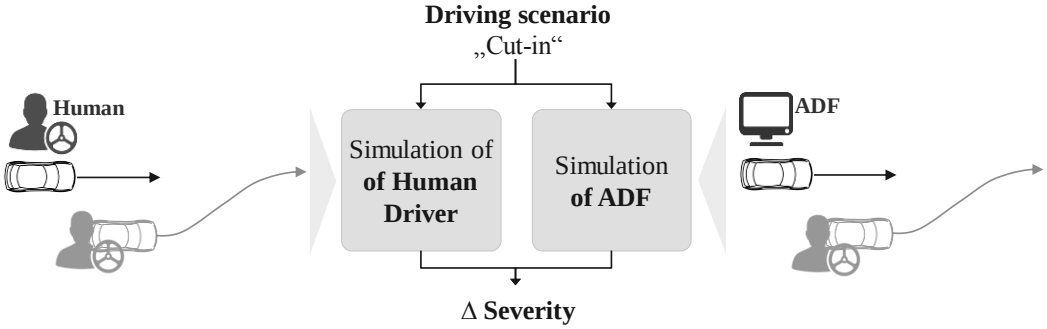

Figure 8. Simulation method for estimating the changes in severity in driving scenarios on the example of a "cut-in" driving scenario.

For human reference performance, quantitative driver models for modelling human driving performance in defined driving scenarios from [16] are used. The structure of the models is split into perception, information processing and action. Human drivers are acting in unexpected driving situations based on their knowledge rather than on the actual situational variables according to [17]. Thus, human action is modelled with an initial feedforward impulse and a feedback control to stabilize the vehicle afterwards. The initial feedforward reaction is described by reaction time and -intensity and is sampled from gamma distributions representing a driver population. The structure of the developed driver performance models is validated based on simulator studies with 35 test subjects [16]. Finally, the developed models are verified based on in-depth accident data for ensuring that they can be applied for the respective driving scenario. The structure of the models is presented in Figure 9.

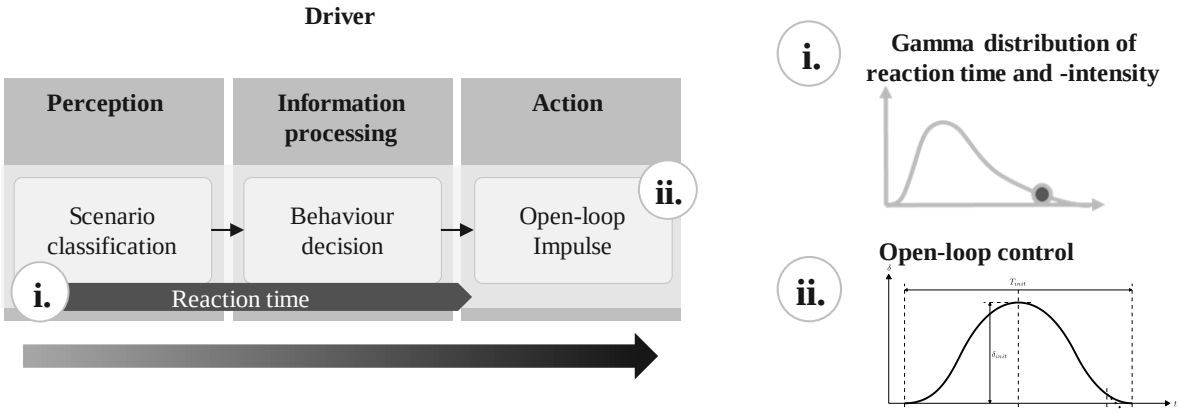

Figure 9. Framework for human driver performance models consisting of perception, information processing and action.

These driver performance models are developed for all covered driving scenarios. For example, in the driving scenario "cut-in" the likelihood for severe injuries (MAIS2+) can be reduced by 42.3 % by the Motorway-Chauffeur.

Effectiveness of Automated Driving Function

Finally, the effectiveness of the automated driving function in the effectiveness field is derived based on the changes in frequencies of all driving scenarios and the changes in severity in all driving scenarios. This process is illustrated on the example of the "cut-in" driving scenario at 50 % market penetration of the Motorway-Chauffeur.

The results of the analysis of changes in frequency of occurrence based on traffic scenario level showed a decrease in accidents by 28.2 %, as presented in Figure 10. According to the traffic simulation (see Section 7.3), human drivers induced all resulting in 71.8 % of accidents on traffic scenario level. From all accidents on traffic scenario level induced by human drivers, 43.5 % are with involvement of a human driver ("HUM-HUM") while the remaining incidents are with involvement of an ADF ("HUM-ADF")

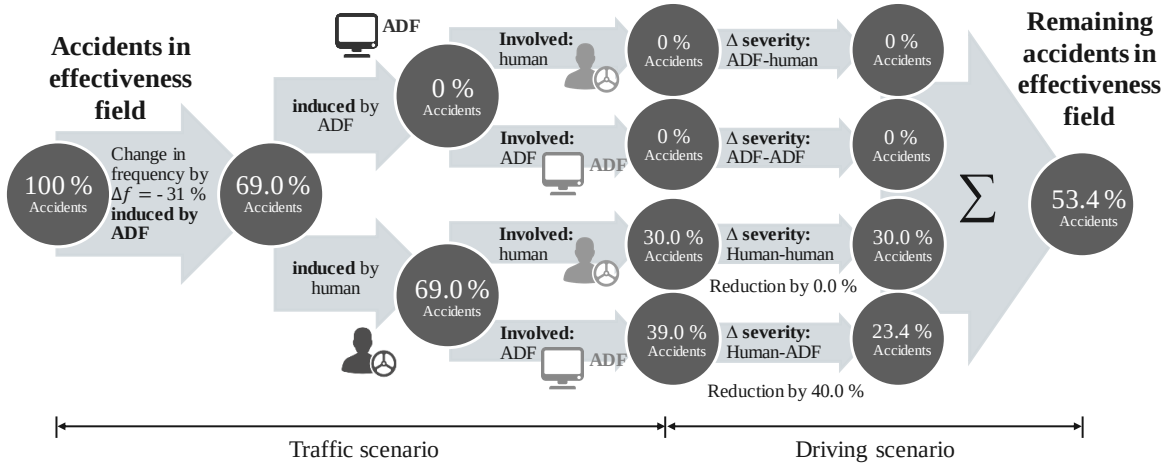

Figure 10. Effectiveness of an ADF on traffic- and driving scenario level on the example of a "cut-in" driving scenario and a market penetration of 50 %.

In the next step, the changes in severity on driving scenario level are analyzed. According to the results of the re-simulation (see Section 7.4), all accidents with involvement of ADF can be reduced by 40 % to 23.4 % of accidents. For the case in which only human drivers were involved, the 31.2 % of accidents do not change with ADF. In total, from the initial 100 % of accidents, the ADFs reduces to 53.4 % of accidents which consequently results in an effectiveness of 46.6 % for the driving scenario "cut-in" at a market penetration rate of 50 %.

RESULTS

The simulation-based estimated effectiveness for the different ADFs is scaled-up on national level for the Federal Republic of Germany. Since the effectiveness of the ADF is determined based on detailed GIDAS accident data that is only available for a limited geographical region in Germany the effects have to be corrected and projected by using the national accident statistics. For this purpose, the correction factors per driving scenario are derived based on the frequency of occurrence of the defined driving scenarios in GIDAS detailed accident and national accident statistics by using the three-digit accident type. On basis of the Urban Robot-Taxi the results presented in Figure 8 will be explained. In the operation domain of the Urban Robot-Taxi 205,321 accidents with personal injuries occurred in 2016. Since only ADFs of passenger cars are considered, just those accidents can be addressed where at least one passenger car is among the first two participants of the accidents. These 36,486 accident cannot be addressed (see light gray area). Furthermore, 47,487 accidents per year are outside the functional limits of the Urban Robot-Taxi (see dark gray area) due to not addressed driving scenarios, alcohol and drug use, technical failures and limitations of the Urban Robot-Taxi (rain, fog, ice, construction sites).

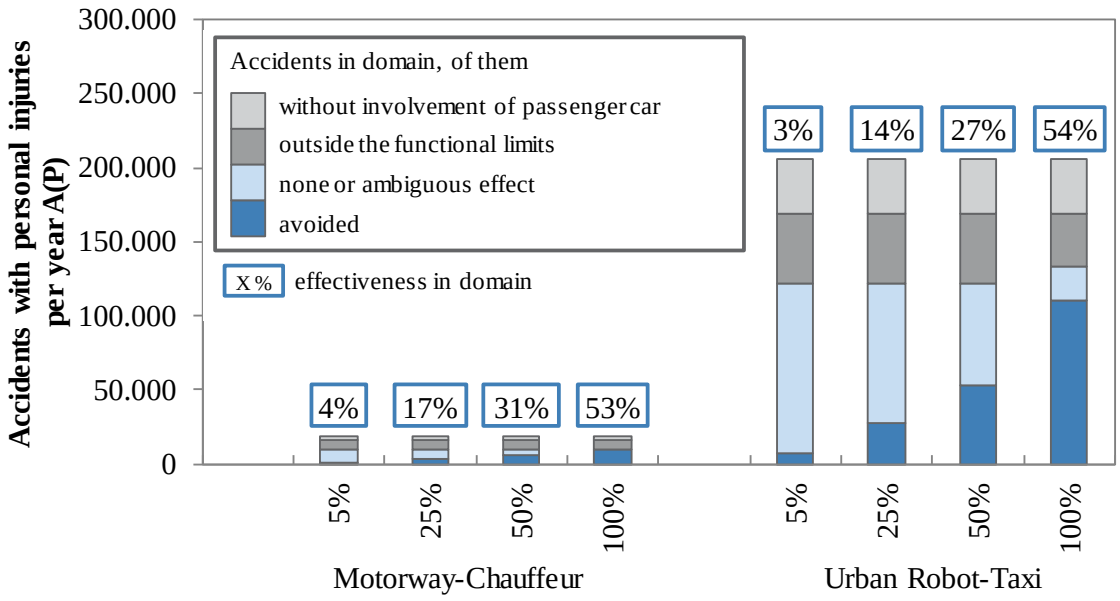

Figure 11. Effectiveness in terms of avoided accidents of Motorway-Chauffeur and Urban Robot-Taxi [18]**.**

The light blue area represents the number of accidents that are potentially addressable, but cannot be avoided according to the simulation results. These are for example accidents that cannot be avoided due to physical constraints. However, the severity of these accidents possibly can be reduced by a reduction of the collision speed. The dark blue area represents the number of avoided accidents. Hence, the Urban Robot-Taxi can avoid 52,517 accidents at a market penetration of 50 %. This equals an effectiveness of 27 % of all accidents in the operation domain.

DISCUSSION

In contrast to existing approaches in literature that define driving scenarios based on ontologies created by expert knowledge, in this work the driving scenarios are derived from the three-digit accident type covering all potential physical accident constellations known to accident research for decades. A set of 13 driving scenarios has been identified from the accident type catalogue. The definition of the driving scenarios by the three-digit accident type reveals tremendous gains. Since both national accident statistics (in five German federal states) and GIDAS in depth accident data feature the three digit-accident type, the driving scenarios can be classified in both types of data. Consequently, both, the number of accidents on national level per driving scenario and the parameter spaces for deriving the change in severity induced by ADFs can be determined with the developed concept. The presented concept in this thesis limited the available number of traffic participants by a number of two that covers 90 % of accidents. A possible enlargement of the presented driving scenarios to cover the remaining 10 % of accidents is to extend the number of traffic participants per driving scenario to more than two. Beyond that, a more detailed clustering into more than 13 driving scenarios can be realized. However, it has to be considered that the efforts for assessment are increasing with the number of driving scenarios.

CONCLUSIONS

According to the statements in [2], automated driving functions need to show a positive risk-balance compared to human driving in terms of traffic safety. Therefore, a framework for effectiveness assessment of road vehicle automation has been introduced in this work. The basic idea of this framework is that the types of accident constellations and thus driving scenarios do not change with automated driving. Though, the severity and frequency of occurrence of these driving scenarios may change with automated driving. Traffic simulations with automated driving functions are investigating the changes in frequency of occurrence. For determination of the change in severity in relevant driving scenarios, accident re-simulations were used. After determining the effectiveness of the automated driving functions, they are projected and depicted over the whole territory of the Federal Republic of Germany. The results indicate that, e.g. a Motorway-Chauffeur at a market penetration of 50 % has a potential for reducing about 31 % of all accidents on German motorways resulting in personal injury. This equals 2 % of all accidents on German roads. The Urban Robot-Taxi can avoid 27 % of all accidents with personal injury within city-limits at a market penetration of 50 %. This equals 17 % of all accidents on German roads.

ACKNOWLEDGEMENT

The research leading to these results has received funding from the German Federal Highway Research Agency (BASt) within the project “Potential Societal Benefits due to increasing Vehicle Automation” FE 82.0626/2015/ERB. Responsibility for the information and views set out in this publication lies entirely with the authors. The authors would like to thank all partners within this project for their cooperation and valuable contribution.

REFERENCES

[1] M. Aeberhard, S. Rauch, M. Bahram, G. Tanzmeister, J. Thomas, Y. Pilat, F. Homm, W. Huber and N. Kaempchen, "Experience, results and lessons learned from automated driving on Germany's highways," *ITS Magazine*, vol. 7, pp. 42-57, 2015.

[2] U. Di Fabio, M. Broy, R. Brüngger and e. al., "Ethics Commission Automated and Connected Driving," *Federal Ministry of Transport and Digital Infrastructure of the Federal Republic of Germany*, 2017.

[3] M. Noort, T. Bakri, F. Fahrenkrog and J. Dobberstein, "SIMPATO - the Safety Impact Assessment Tool of Interactive," in *16th International IEEE Annual Conference on Intelligent Transportation Systems*, The Hague, 2013.

[4] N.N., "GIDAS (German In-Depth Accident Study) Codebook," in *BASt/FAT*, Bergisch-Gladbach, Germany, 2015.

[5] T. Helmer, Development of a Methodology for the Evaluation of Active Safety using the Example of Preventive Pedestrian Protection, Berlin, Germany: Springer, 2014.

[6] M. Benmimoun, A. Puetz, A. Zlocki and L. Eckstein, "euroFOT: Field Operational Test and Impact Assessment of Advanced Driver Assistance Systems: Final Results," in *Proceeding of the FISITA 2012 World Automotive Congress*, 2013, 2013.

[7] H. Schittenhelm, "The influence of situational factors on the reaction time of Motorcar Drivers," in *EVU-Jahrestagung*, Dresden, 2006.

[8] F. Fahrenkrog, "Traffic safety impact assessment for advanced driver assistance systems," in *PhD. Thesis, RWTH Aachen University*, Aachen, 2016.

[9] N.N., "GDV - German Insurance Association," in *Führen und Auswerten von Unfalltypen-Steckkarten*, 2003.

[10] C. Roesener, F. Fahrenkrog, A. Uhlig and e. al., "A Scenario-based Assessment Approach for Automated Driving By using Time-Series Classification of Human Driving Behaviour," in *19th International IEEE Conference on Intelligent Transportation Systems (ITSC)*, Rio de Janeiro, Brasil, 2016.

[11] C. Mooney, "Monte Carlo Simulation," Sage Publications, 1997.

[12] R. Wiedemann, "Simulation des Straßenverkehrsflusses," in *Schriftenreihe des Instituts für Verkehrswesen der Universität Karlsruhe*, Karlsruhe, 1974.

[13] D. Ehmanns, "Modellierung des taktischen Fahrerverhaltens bei Spurwechselvorgängen," in *PhD thesis* , Aachen, RWTH Aachen University, 2003.

[14] U. Sparmann, "Spurwechselvorgänge auf zweispurigen BAB-Richtungsfahrbahnen," in *Forschung Straßenbau und Straßenverkehrstechnik, no 263*, 1978.

[15] D. N. Lee, "A Theory of Visual Control of Braking Based on Information about Time-toCollision," in *Perception (5)*, 1976, pp. 437-459.

[16] C. Roesener, M. Harth, H. Weber, J. Josten and L. Eckstein, "Modelling Human Driver Performance for Safety Assessment of Road Vehicle Automation," in *21st IEEE Intelligent Transportation Systems Conference (ITSC)*, Hawaii, USA, 2018.

[17] J. Rasmussen, "Signals, Signs and Symbols, and other Distinctions in Human Performance Models," in *Pullman: IEEE Transactions on Systems, Man, Cybernetics 13,3*, 1983.

[18] C. Roesener, F. Hennecke, J. Sauerbier, A. Zlocki, D. Kemper, L. Eckstein and M. Oeser, "A Traffic-based Method for Safety Impact Assessment of Road Vehicle Automation," in *12. Uni-DAS Workshop Fahrerassistenzsysteme und automatisiertes Fahren*, Walting, 2018.

[19] N.N., "DESTATIS, Statistisches Bundesamt, Fachserie 8 / Reihe 7 Verkehr," in *Statistisches Bundesamt, Fachserie 8 / Reihe 7 Verkehr, No.: 2080700147004*, Wiesbaden, 2016.

PASSIVE SAFETY IMPROVEMENTS IN CHILD RESTRAINT SYSTEMS PLACED IN REAR SEATS OF VEHICLES BY INTRODUCING A NEW ISOFIX ACCESSORY

Guillermo Ramos
Jose Lagunar
Jesus Casado
Cristina Calvillo
RiveKids Technology SL
Spain

Paper Number 19-0114

ABSTRACT

In a 3-abreast seating configuration whenever there is a child restraint system (CRS) present, and especially if it is an ISOFIX one, occupants of the central position miss the room needed in order to rest their back properly against the backrest making them prone to suffer serious whiplash injuries in frontal or rear crashes or to collide with the adjacent passengers in lateral crashes. This lack of space jeopardizes the safety of all occupants as the restraint systems cannot work properly if the passengers are not correctly seated; more so, it affects further the safety of children making safety belt fastening difficult and uncomfortable and causing their CRS to be removed prematurely from the car to give room for that third occupant.

Most of those problems can be tackled by introducing an accessory to be inserted between the vehicle ISOFIX anchorages and the CRS ISOFIX connectors, which allows to move laterally the CRS, while keeping that ISOFIX connection, from the CRS nominal position to an extreme position where the CRS is shifted aside resting against the door panel, or at least coming quite close to it.

Due to limited resources, full capacity tests have not been possible running 3-abreast configurations. To assess technical feasibility and performance, the device was submitted to the tests specified in the ECE R129 standard, comparing sled tests carried out with the CRS alone (baseline reference case) with those same CRS coupled with the device shifting their nominal position 70 mm towards the door panel to establish potential safety improvements. CRS selection was based on their popularity within the Spanish market, and the tests were performed using both Q6 and Q10 dummies for each combination.

The analysis of the results of the dynamic tests carried out showed improvements in the level of side impact protection. For instance, the average HPC15 (Head Performance Criterion), directly related with the expected level of damage in the event of an impact, measured for the Q6 dummy was 232.76, while the average HPC15 with the same seats moved closer towards the door panel was 225.08, a 3.3% improvement in average with improvements for one of the CRS of up to 22.5%. For the Q10 dummy, the results were similar with an average HPC15 of 103.75 for the stand-alone CRS and an average HPC15 of 99.23 for the CRS coupled with the accessory device, a 4.4% improvement in this case. In every test performed, the resulting values remained below the limits designated in ECE R129 for the injury assessment criteria.

The introduction of this new device could lead to important benefits on the safety of families, and children in particular, by providing an effective use of the central seat by any passenger or additional CRS, while retaining the ISOFIX connection for a CRS placed in a lateral seat. Specifically, side protection could be significantly improved preventing undesired yaw rotations, and the optimized space usage will allow extending the CRS usage period avoiding their premature removal due to the lack of space.

INTRODUCTION

It is estimated by the Spanish Statistics National Institute that, in 2016, there were 180.872 families in Spain with three children between the ages of 0 and 11 and therefore capable of using three CRS or at least two CRS and a third child not requiring one (high occupation scenario). That same year, according to Eurostat figures, an analogous

situation was meet in Germany by 379.000 families, 590.000 families in France and 524.000 in the United Kingdom.

A high occupation in a vehicle rear seat can also occur with 2 children and an adult, usually seated in the central position. In 2016, in Spain there were 1.507.179 households with two children in car-seat age that can be sporadically accompanied by an adult inserted between 2 CRS.

Despite these figures, there are few studies available regarding CRS performance in impact crashes for a 3-abreast configuration in the rear seats. Those studies, based on the analysis of real-world crashes, suggest a reduced risk of injury for children sitting with other occupants compared to children seated alone yielding a kind of protective effect to adjacent occupants for rear seat passengers in side impact crashes (Arbogast et al. [1]; Lund [2]; Maltese et al. [3]).

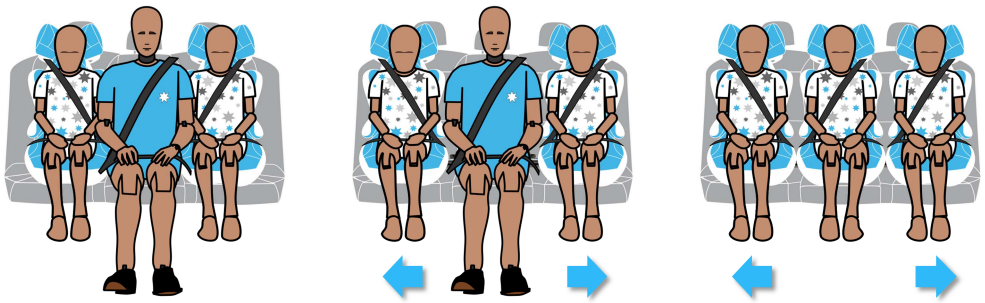

Figure 1. In 3-abreast configurations, ISOFIX CRS take part of the rear central seat invading the space needed to make a safe use of its restraint systems: ISOFIX CRS installed in their nominal position (left), interference with central occupant; CRS shifted aside with ISOFIX accessories giving room to accommodate an adult (middle), or additional CRS (right) in the central place

The limited resources available prevented carrying out confirmatory tests using this type of high occupation environment; instead, as the results presented by Charlton et al. [4], allow us to think that the use of ISOFIX attachments would help reducing the average injury risk level for three passengers in 3-abreast seating position, we focused on analysing the influence of the ISOFIX-attachment coupled with our accessory for the struck side occupant using groups II-III ISOFIX child seats. According to their results, we could anticipate an increase in the risk of injury in side impact crashes for that near-side occupant; an effect we wanted to quantify given that the introduction of an accessory that pushes the CRS towards the door may be deemed as dangerous by the average citizen.

ISOFIX DEVICE

The ISOFIX device developed (Figure 2) is an accessory for CRS that allows them to be displaced laterally, while retaining the ISOFIX connection, in order to maximize the remaining space for other occupants. It is inserted between the vehicle ISOFIX anchorages and the CRS ISOFIX connectors making it possible to position the CRS closer to the vehicle door panel. Thus, it is a device that can have certain regulations between a central position (coincident with the CRS nominal position) and an extreme position (where the CRS is displaced to its maximum, resting against the door panel or at least coming quite close to it) (Figure 3).

Figure 2. RiveMove (RM) device

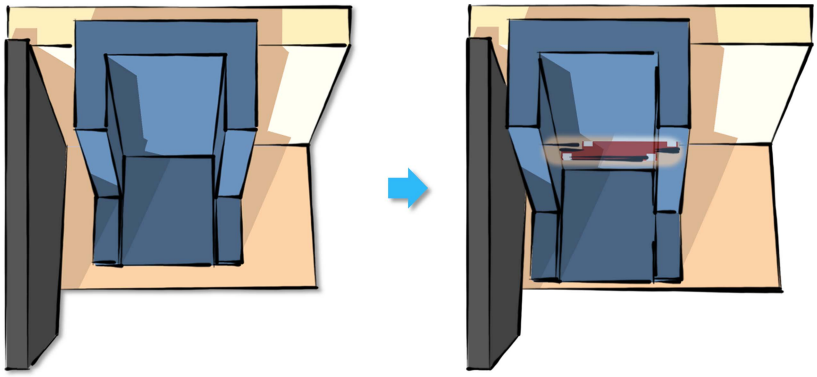

Figure 3. Nominal position (left). Shifted position where the CRS' ISOFIX connectors are attached to the device with a 50mm or 70mm offset towards the door panel (right)

The device designed has been carefully defined to absorb part of the energy put in place in the event of an accident contributing to reduce damage values and increasing the overall safety level for three rear seat occupants. Therefore, the technology is mainly aimed to families that make full use of the rear seat with three occupants and up to 3 CRS.

After installation, the CRS should allow regulating its own ISOFIX connectors' position to avoid undesired forward displacements due to our system's dimensions. Finally, the CRS has to be secured as well using the adult seatbelt available and any anti-rotation device it may have (Figure 4).

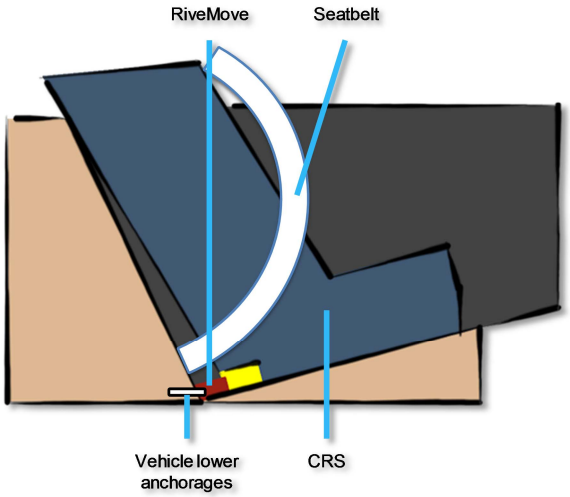

Figure 4. General disposition of the system

METHOD

To assess technical feasibility and performance, the device was submitted to the tests specified in the ECE R129 standard. First, by carrying out a sled test with the CRS alone (right out of the box) to establish the baseline reference case; then, a new seat of the same CRS model coupled with the device shifting their nominal position 70 mm towards the door panel looking for potential safety improvements.

Figure 5. Positioning of the dummy mid-plane at 350mm from the door panel (left), according to ECE R129 specifications for the baseline tests. Displacement aside of the dummy mid-plane closer to the door panel in the CRS+ISOFIX accessory configuration, regulation set at 280mm (right)

The introduction of the device resulted in a displacement forward of the ISOFIX anchorage points that was compensated, depending of the particular CRS, regulating the CRS' ISOFIX connectors to place flush the CRS backrest against the test bench. Something that not always was possible to do as will be mentioned later.

All the dynamic tests were carried out by CSI, S.p.A. with a deceleration sled according to the requirements defined in the ECE R129 standard.

The selection of the groups II-III CRS was based on their popularity within the Spanish market, including the CRS commonly used in the EuroNCAP tests.

RESULTS

The dynamic tests performed included frontal, lateral and rear impacts. For the first two a graphically comparison with the dummy values obtained is shown in the figures below.

Preliminary tests

The first tests conducted where intended to obtain a general knowledge on the modifications introduced by the ISOFIX accessory on the risk of injury for a Q10 dummy submitted to lateral impact. Therefore, a series of tests were defined for two types of CRS in which we could assess the potential differences between the baseline case, the shifted regulation of the device with a 70mm displacement, and an intermediate position with just a 50mm displacement. Their corresponding values are shown in the next figures (from left to right), for the two CRS initially considered.

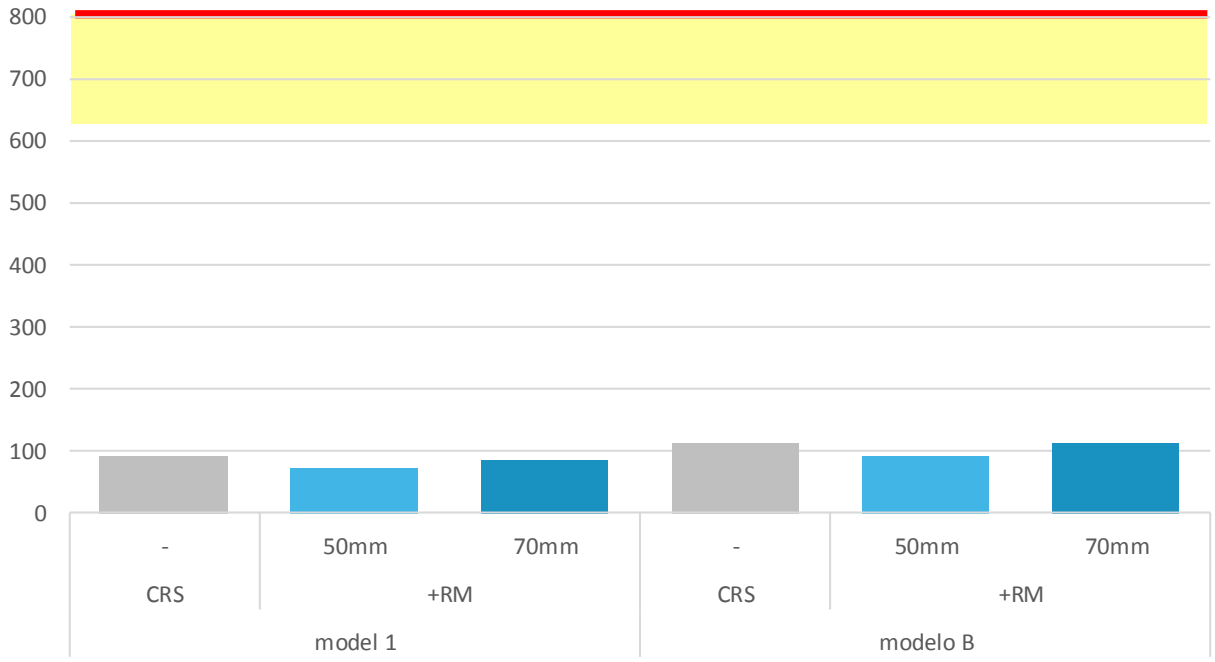

Figure 6. Q10 dummy HPC15 values (lateral impact)

From Figure 6 and Figure 7, it is obvious that the best results are obtained with a lateral displacement of 50mm, whereas a displacement of 70mm still yields better results than the baseline reference but is closer in value. Anyway, we decided to select the 70mm displacement as sort of a worst-case scenario and kept that displacement for the rest of the study as the case against which the baseline reference would be measured.

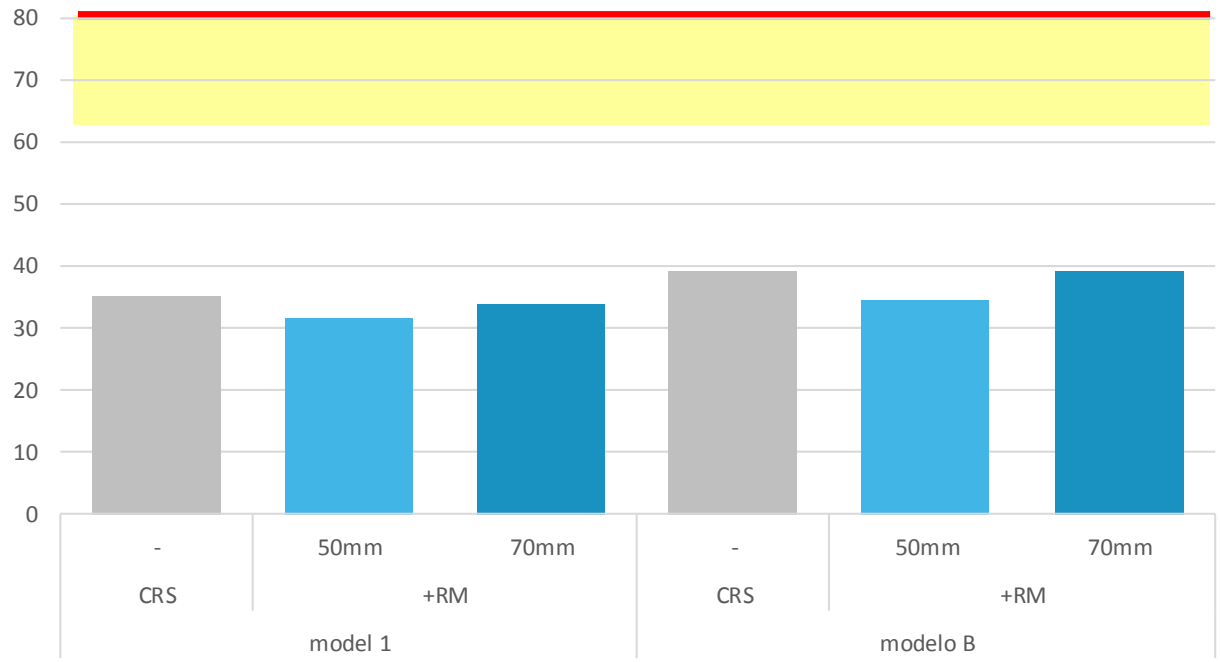

Figure 7. Q10 dummy 3ms head acceleration values (lateral impact)

Q6 dummy

Frontal impacts

For each CRS model tested, the first column presents the CRS-alone dummy readings while the second one gathers the corresponding CRS+ISOFIX accessory value, always with a 70mm displacement towards the door panel.

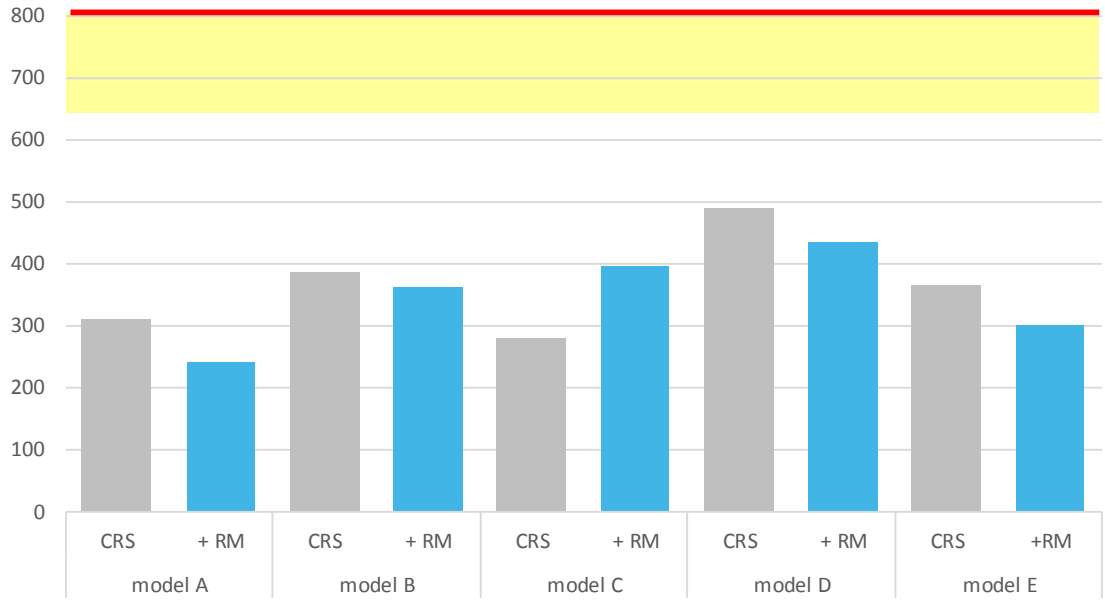

Figure 8. Q6 dummy HPC15 values (frontal impact)

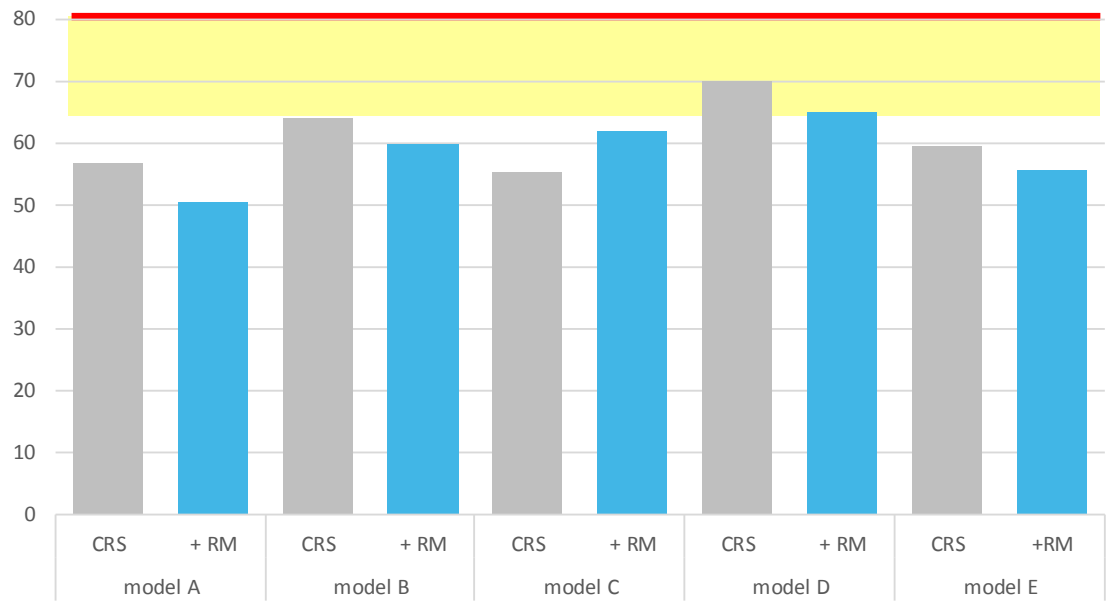

Figure 9. Q6 dummy 3ms head acceleration values (frontal impact)

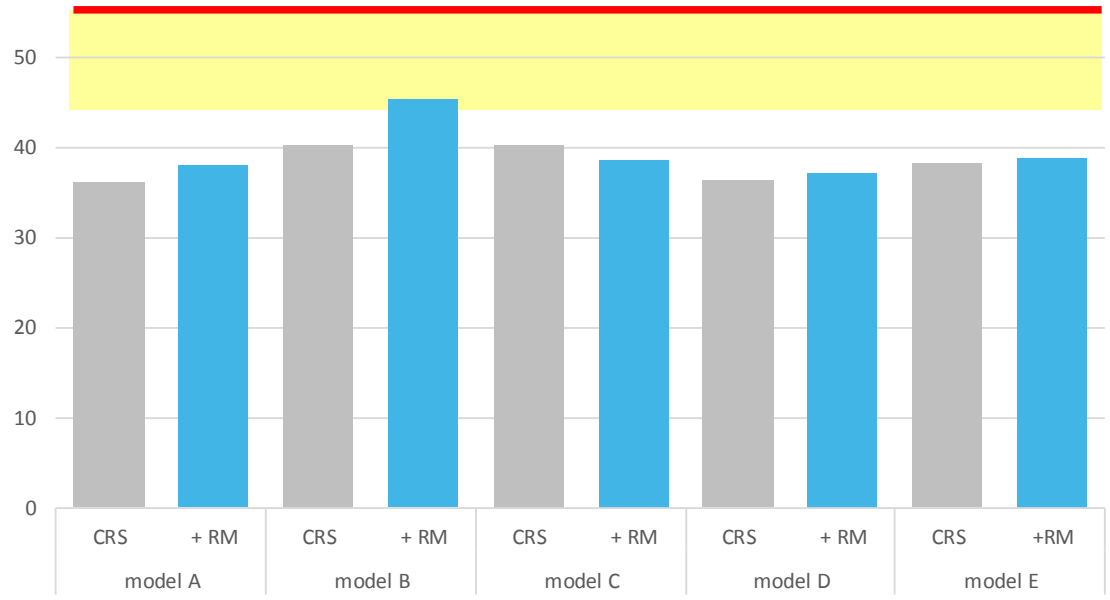

Figure 10. Q6 dummy 3ms chest acceleration values (frontal impact)

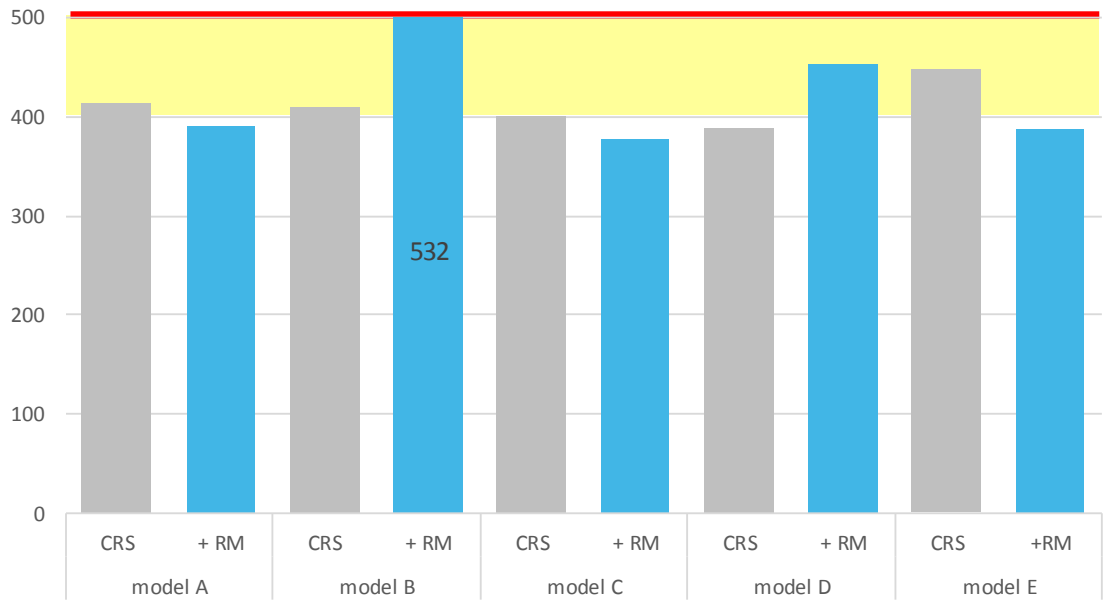

Figure 11. Q6 dummy head excursion X values (frontal impact)

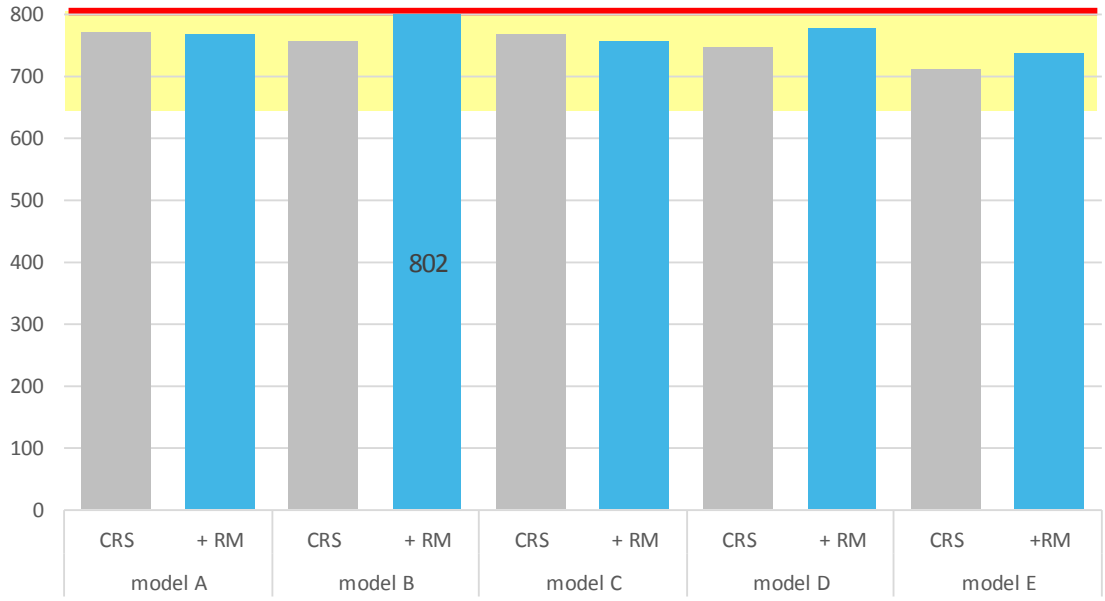

Figure 12. Q6 dummy head excursion Z values (frontal impact)

Generally, the overall performance of the CRS considered is improved by introducing the ISOFIX accessory: PDC15 and 3ms head acceleration values are reduced, with some increase in the 3ms chest acceleration. Regarding head excursion displacements in X and Z axis they're lower for most of the seats.

However, there are two major discrepancies to that statement. First, while the results for the baseline and the displaced configuration were within the average values for the other CRS models, the model C CRS behaved in a totally opposite way to the rest of the seats. Analysing in detail the tests, it was found that its bulky structure combined with the RiveMove device interfered with the anchorage points of the 3-points seatbelt.

The second issue is the excessive values for the head excursion obtained with the model B CRS, surpassing the limits defined in the normative. Model B is a CRS so rigid that prevented reclining the backrest so that it kept a uniform gap, top to bottom with the test bench. The detection of such a problem has led to a new line of work addressing this effect.

Both facts highlight the importance of installing the CRS properly guaranteeing enough space to avoid totally undesired contacts between the child's head and interior elements from the vehicle.

Lateral impacts

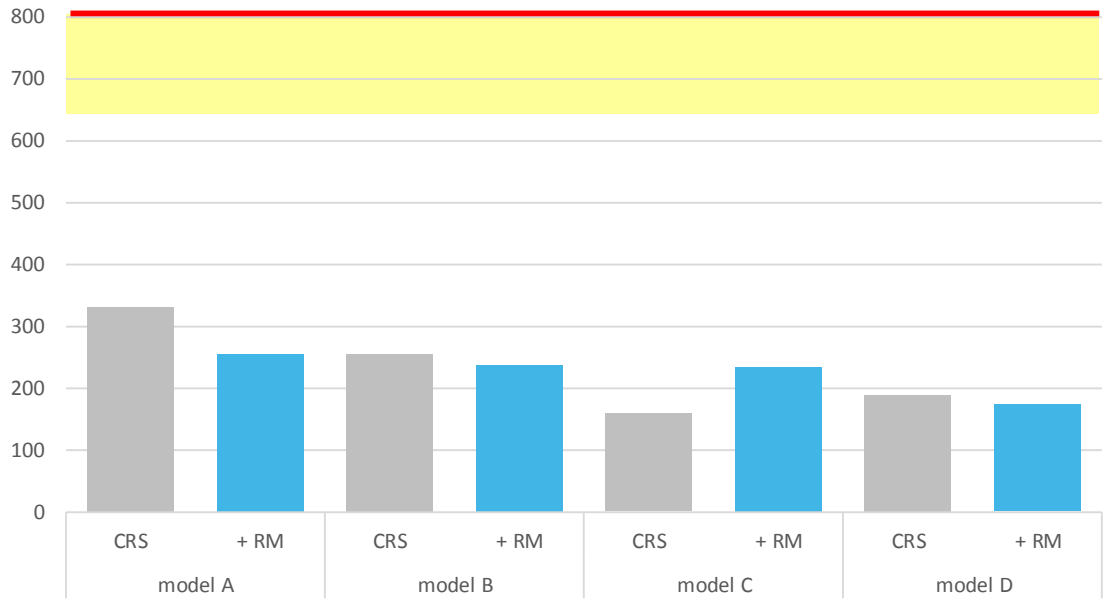

Figure 13. Q6 dummy HPC15 values (lateral impact)

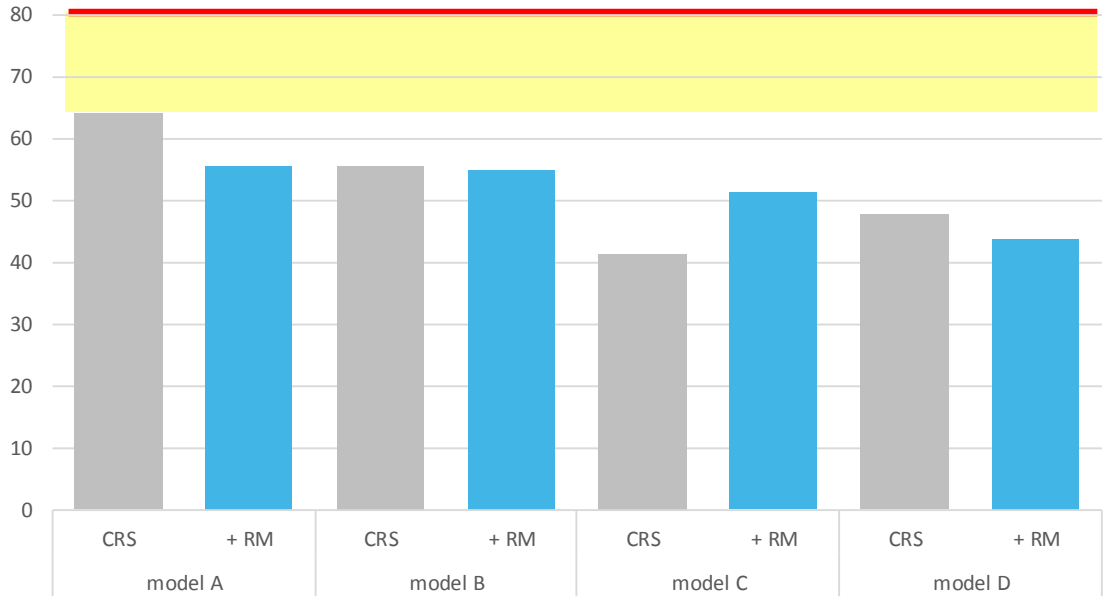

Figure 14. Q6 dummy 3ms head acceleration values (lateral impact)

Again, we face the same opposite behaviour of model C CRS compared to the rest due to the aforementioned interference with the 3-points seatbelt anchorage points. Nevertheless, the resulting values remained closed to the average values obtained with all the other CRS.

Figure 15. Resulting deformation in the RiveMove device (right) after one of the side impact tests

Q10 dummy

Frontal impacts

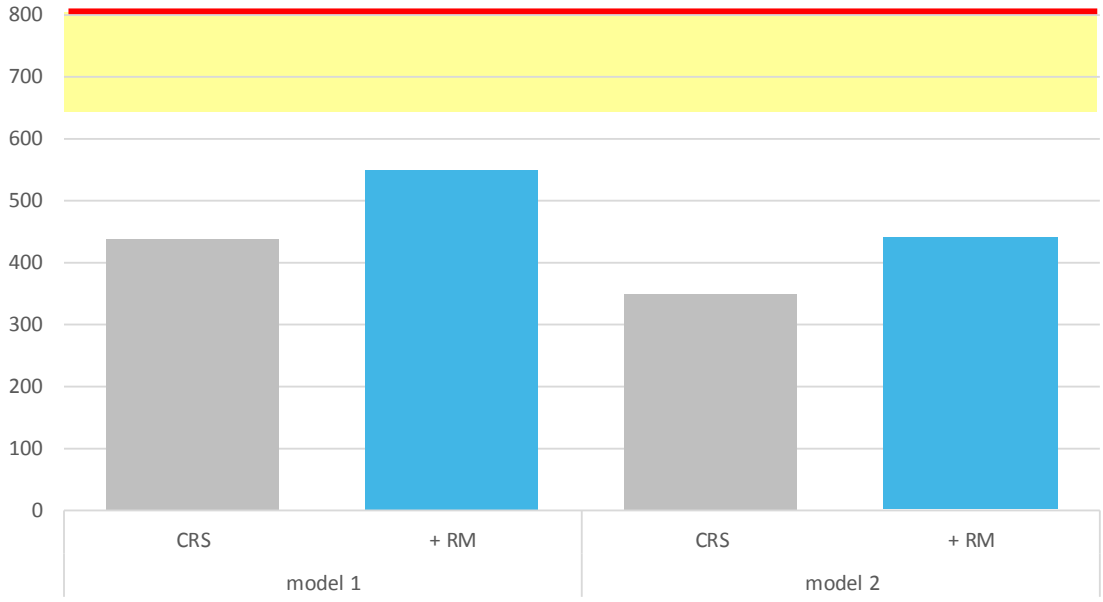

Figure 16. Q10 dummy HPC15 values (frontal impact)

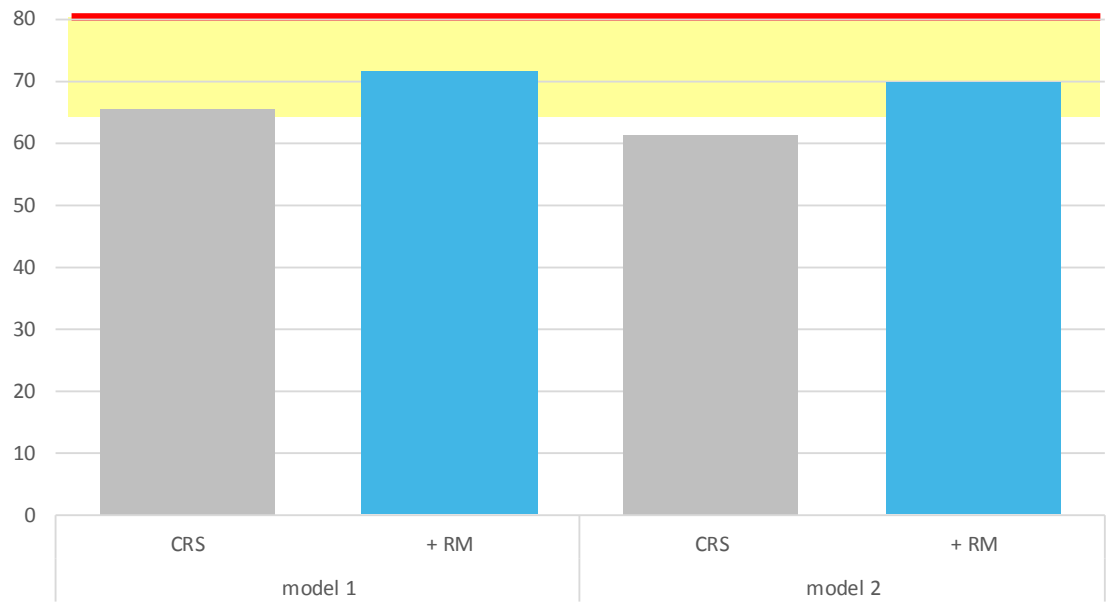

Figure 17. Q10 dummy 3ms head acceleration values (frontal impact)

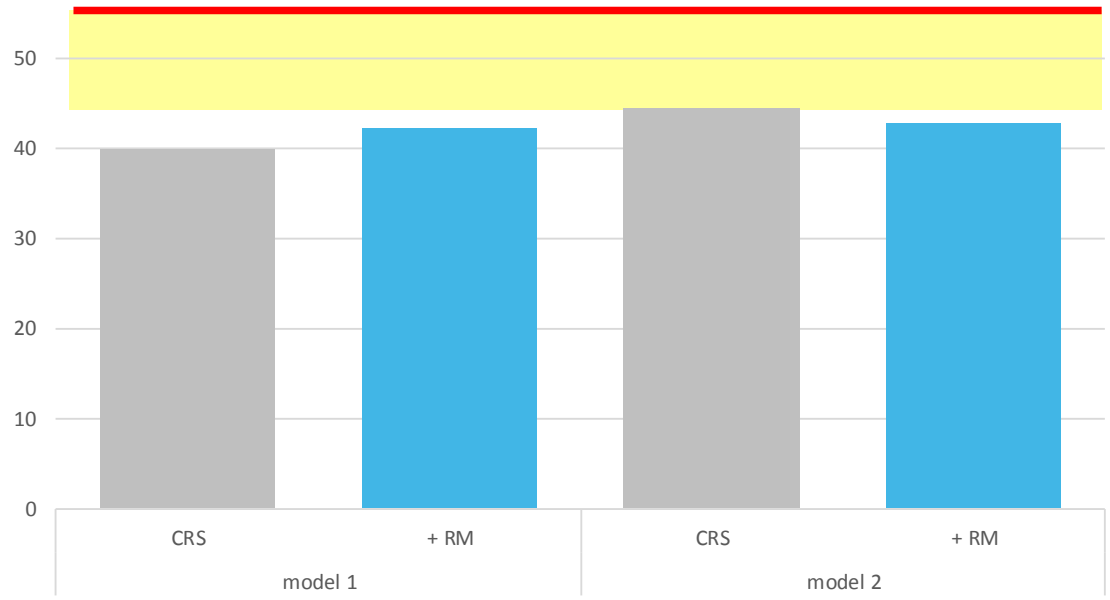

Figure 18. Q10 dummy 3ms chest acceleration values (frontal impact)

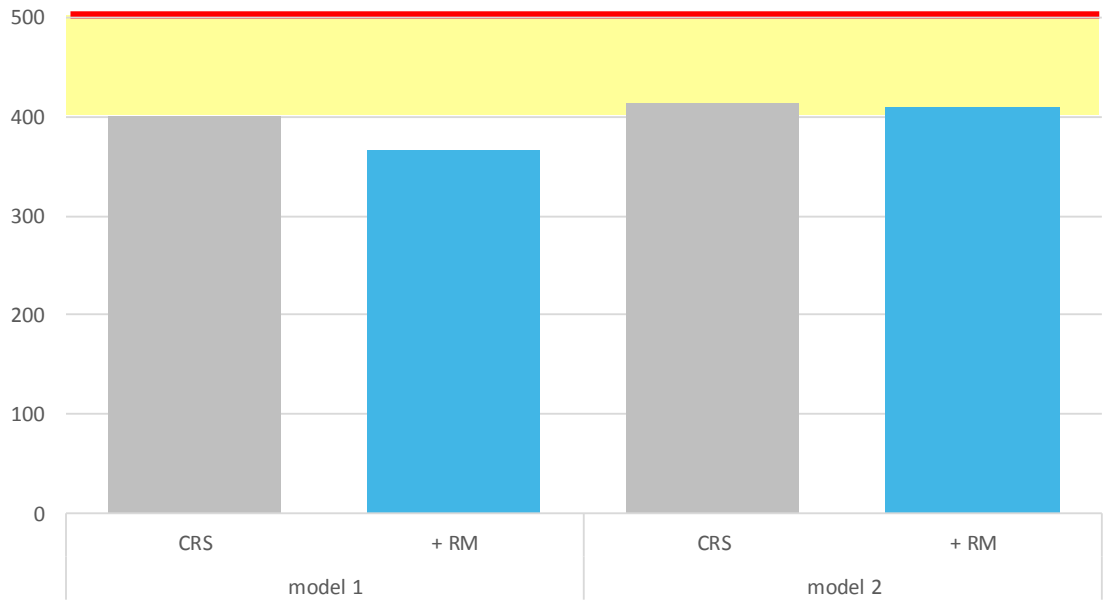

Figure 19. Q10 dummy head excursion X values (frontal impact)

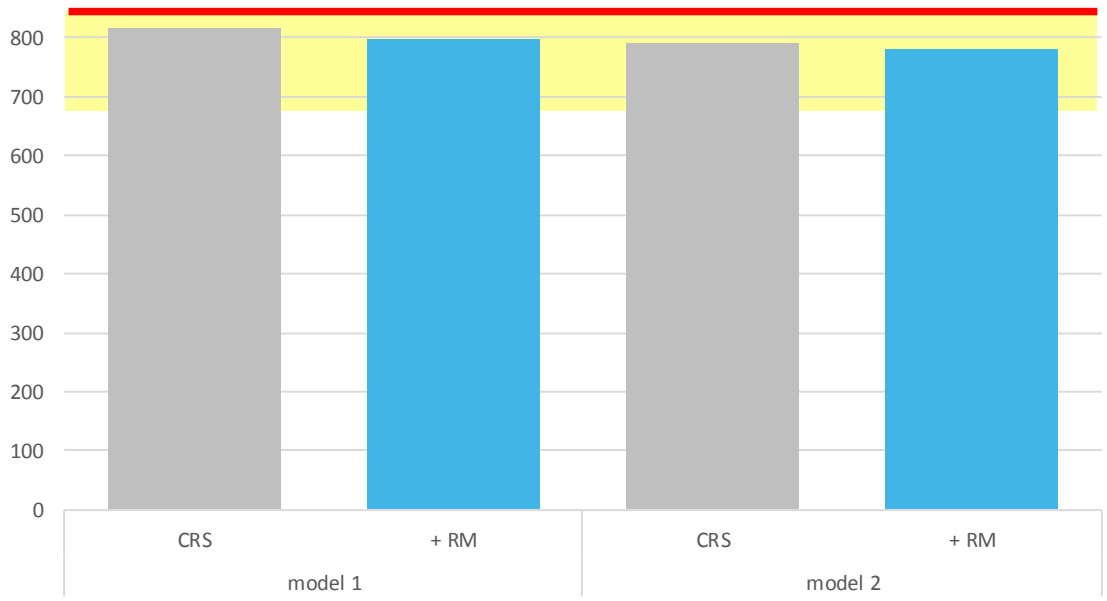

Figure 20. Q10 dummy head excursion Z values (frontal impact)

In this case, the dummy values obtained are worse for the HPC15 and 3ms head acceleration, whereas 3ms chest acceleration results were similar and the head excursion displacements slightly better.

Lateral impacts

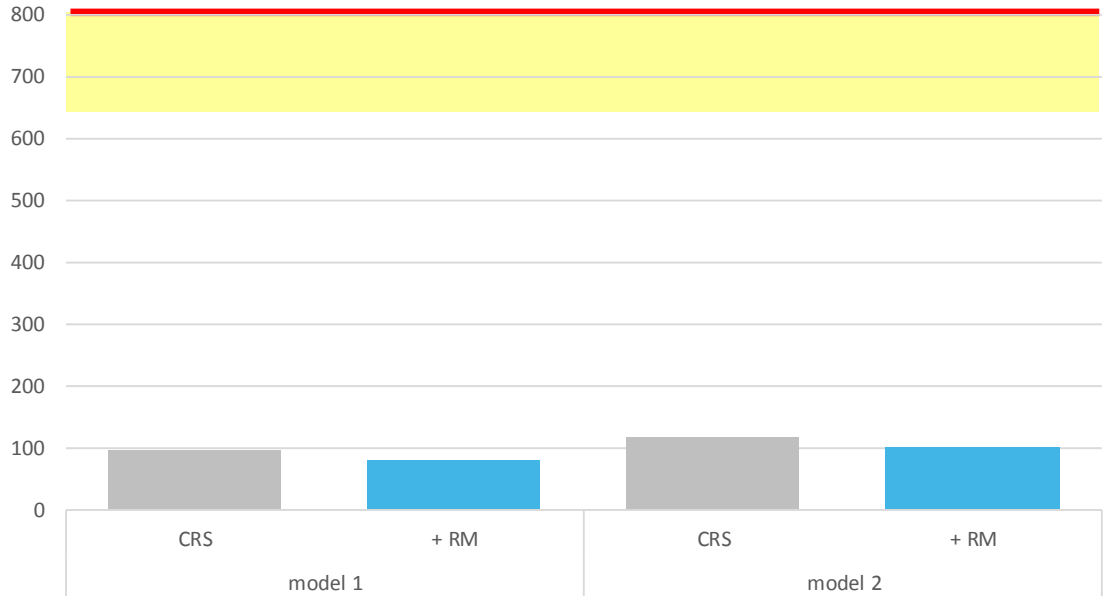

Figure 21. Q10 dummy HPC15 values (lateral impact)

Figure 22. Q10 dummy 3ms head acceleration values (lateral impact)

With the CRS considered, both HPC15 and 3ms head acceleration results were improved compared to the baseline reference in side impacts using the Q10 dummy.

Regardless the size of the dummy and the CRS model used, the injury assessment criteria defined in ECE R129 for frontal and lateral impacts were never surpassed. Obviously not for the baseline references, but also for the CRS coupled with the ISOFIX accessory.

However, once did the head excursion limits were exceeded with a CRS whose backrest couldn't be properly rested against the test bench. It is so important to install properly the CRS and this particular case also proved that not every combination CRS + RiveMove is allowed.

Regarding side impact tests, it also should be mentioned that no head contact with the door panel was registered for any test, nor did the dummy head exceed the vertical plane identified on top of the door panel.

CONCLUSIONS

Unlike what was anticipated from existing bibliography, not only the risk of injury in lateral impact crashes did not increase for the struck-side occupant but the analysis of the results of the dynamic tests carried out showed improvements in the level of side impact protection. Thus, in the considered worst case scenario, with a 70mm displacement towards the door, the average HPC15, directly related with the expected level of damage in the event of an impact, measured for the Q6 dummy was 232.76, while the average HPC15 with the same seats moved closer towards the door panel was 225.08, a 3.3% improvement in average with improvements for one of the CRS of up to 22.5%. For the Q10 dummy the results were similar with an average HPC15 of 103.75 for the stand-alone CRS and an average HPC15 of 99.23 for the CRS coupled with the accessory device, a 4.4% improvement in this case. In every test performed, the resulting values remained below the limits designated in ECE R129 for the injury assessment criteria.

Taking into consideration as well the documented improvement in the general average risk of injury when using ISOFIX attachments for 3-abreast seating configurations, the results obtained show that the introduction of this new device could lead to important benefits on the safety of families, and children in particular, by providing an effective use of the central seat by any passenger (minimizing the possibilities of suffering whiplash injuries) or additional CRS, while retaining the ISOFIX connection for a CRS placed in a lateral seat. Specifically, side protection could be significantly improved preventing undesired yaw rotations, and the optimized space usage will allow extending the CRS usage period avoiding their premature removal due to the lack of space.

REFERENCES

[1] Kristy B. Arbogast; Irene Chen; Dennis R. Durbin et al. 2004. "Injury risk for children in child restraint systems in side impact crashes". IRCOBI Conference – Graz (Austria), 2004

[2] Ulric J. Lund. 2005. "The effect of seating location on the injury of properly restrained children in child safety seats". Accident Analysis & Prevention, volume 37, issue 3, pages 435-439; 2005

[3] Matthew R. Maltese; Irene G. Chen; Kristy B. Arbogast. 2005. "Effect of increased rear row occupancy on injury to seat belt restrained children in side impact crashes". 49th Annual Proceedings, Association for the Advancement of Automotive Medicine; 2005

[4] Judith L. Charlton; Brian Fildes; David Taranto; Ronald Laemmle; Stuart Smith; Anthony Clark. 2007. "Performance of booster seats in side impacts: effect of adjacent passengers and ISOFIX attachment". 51st Annual Proceedings, Association for the Advancement of Automotive Medicine; 2007

DEVELOPMENT OF SAFETY EVALUATION SCENARIOS FOR INFRA-COOPERATED AUTOMATED VALET PARKING SYSTEMS

Seonwook Kim
Heungseok Chae
Yonghwan Jeong
Kyongsu Yi
School of Mechanical and Aerospace Engineering, Seoul National University
Korea

Myungsu Lee
Kyongchan Min
Korea Automobile Testing & Research Institute, Korea Transportation Safety Authority
Korea

Paper Number 19-0123

ABSTRACT

This paper presents an evaluation procedure for an infrastructure based automated valet parking system. Because parking is one of the difficult and complicated tasks for drivers, park assistance system(PAS) has been already developed and commercialized by several auto-manufacturers. As a further step for PAS, researchers are focusing on automated valet parking system which is a fully automated system of PAS and periodically demonstrated their automated parking system. However, from an institutional point of view, evaluation standard and scenarios for automated parking system are progressing slowly compare to the automated driving. Because of specialty that in valet parking system, driver has to get out of the vehicle, most of the developers can not mass produce the system by legal issues. Thus, the necessity of evaluation procedure for parking system rise. Considering many automated valet parking systems are designed with digital map or infrastructure. Thus, in this paper, automated valet parking system cooperating with infrastructure is focused.
To design the evaluation process for automated parking, we divided the parking situation into two sides. 1) Nominal parking process, which is a static obstacle avoiding case related to static factors. 2) Complicated parking process, which is avoiding not only static obstacles but also moving obstacles such as pedestrians. As a valet parking is a very sequential service, to design evaluation items for nominal parking, we considered a procedure of manual parking and divided valet parking process into three different stages. 1) Driving in the parking lot while moving near to the parking space. 2) Parking to the aimed space. 3) Parking out from the space. Finally, the component of nominal parking scenario classified as static factors to test basic parking performance of the target vehicle and addable evaluation scenarios listed up as dynamic factor which can reproduce the complicated and frequent situation that can happen in the parking lot by combining with the nominal scenario. Both the nominal scenario and additional scenarios are organized as an evaluation matrix.

INTRODUCTION

In recent years, research has been carried out vigiriously about advanced driver assistance systems (ADAS) and autonomous vehicle. One of those automated driving technology, automated parking and parking assistant system are one of the close to mass production technology since parking is considered as troublesome and time-consuming task in driving. Thus various of configuration of sensor set for parking assistance[1-5] has been researched, furthermore, some car-makers, such as BMW and Volvo, periodically demonstrated their automated parking system. Now the researchers are aiming the fully automated parking system as a further step of PAS.
At the same time, the regulation and test procedure for active safety also have been researched including well known ADAS systems such as Adaptive Cruise Control (ACC), Traffic Jam Assist (TJA), Lane Keeping Support

(LKS), Lane Change Assist (LCA), Blind Spot Detection (BSD) and Advanced Emergency Braking (AEB)[6,7]. And the target system of the regulations and test protocols has been extended to automated driving and some legal issues hav been eased such as license system that allows automated vehicle driving in some area in normal road. But still, in a sight of automated parking technology, compare to automated driving, some legal issues are left to test and commercialize. Similarly, the research about test procedure for automated parking has plenty of works to do.
In case of Korea, recently standard about the definition of automated valet parking system had been released[8] and some test procedure of KNCAP related to parking situation such as AEB and rear-side access alarming system had been also already released[9]. But still, the detail factors to be consider to test the actual valet parking system has to be defined and have legal issues to evaluate the test procedure. There are some legal amendment for the automated driving on highway and urban road, valet parking has more issues about operating the acceleration/deceleration and steering system of the vehicle without the driver. And the automated valet parking system is still in develop, there are various automated parking related systems from level 2 to 4. Thus, the test scenario would be better if it can manage the automaed parking system widely according to the level or technical coverage of the test target's system. In this paper, the infra-cooperated valet parking system divided into lower level maneuver based on the sequence of valet parking. The typical factors which should be considered in a sight of parking area's enviroment and situation are summarized. Then, we present the actual test case generation by cobiming the factors that can manage based on test site and test target system's needs and coverage. Last of all, the proposed test scenario is verified via computer simulation.

SEQUENCE OF INFRA-COOPERATED VALET PARKING TEST

To evaluate the valet parking test scenario, as a first step, the sequence of the parking should be defined. Excepting the static environment conditions such as shape of target parking lot, the entire valet parking service can be devided into two major items, parking and exit. Parking is a sequence that starts from the predefined zone and ends when the vehicle is parked in empty slot. Compare to parking, exit is a sequence that gets out from the parked slot and comes back to the predefined zone where the vehicle started the parking sequence. In short, exit and parking are the opposite process. More specific items and situation are shown in fig. 1.

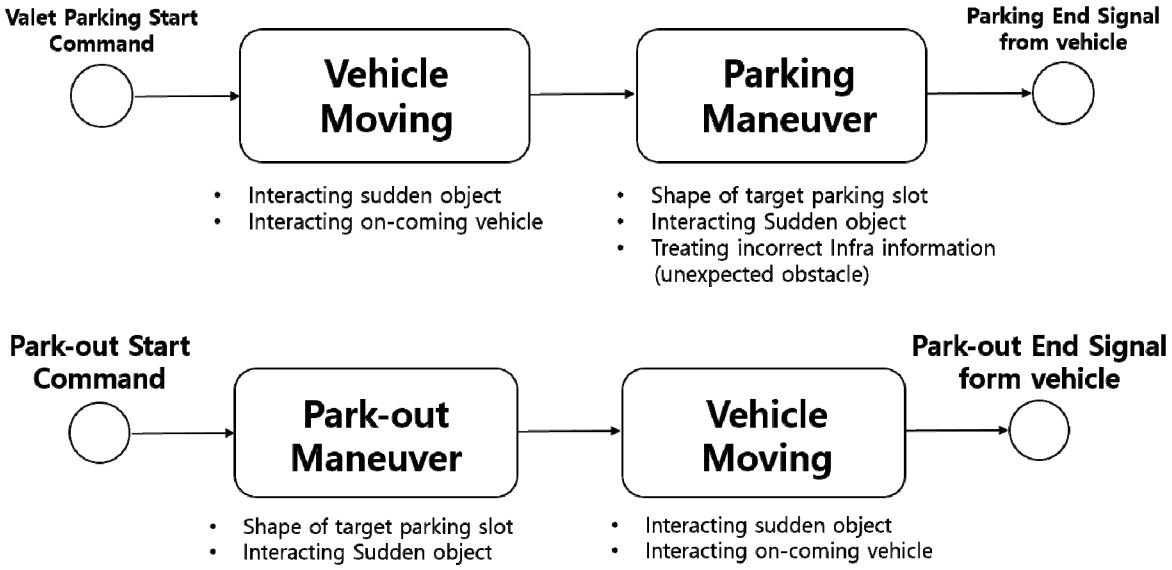

Figure1. Sequence of valet parking service.

Low-level Components for valet parking sequence

The two sequences, parking and exit can be also divided into two phases each. For both sequences, they have same purpose that the vehicle should move from starting point to the end point. The only difference is the fact that parking has to park in, and exit has to get out from the parked slot. Thus they have common phase, the vehicle moving phase. To consider their difference, parking maneuver phase and park-out maneuver phase are divided. In summary, the parking sequence is consisted with vehicle moving phase and parking maneuver phase and the exit sequence is consisted with park-out maneuver phase and vehicle moving phase.

Vehicle moving phase When the vehicle is in vehicle moving phase, it is very similar to the urban road driving cases. The only thing to do is to drive within a designated area, watch out for a collision, and move the vehicle to its destination. To specialize in parking area, vehicle can meet sudden pedestrian or parked out vehicle while driving parking area. Also, unlike to normal driving cases, facing with on-coming vehicle can also occur when two or more vehicles driving in parking area.

Performance evaluation In vehicle moving phase, whether the vehicle is driving within a designated area is the basic object of the phase. The boundary of the designated area is line that divides the parking slot and driving area in this case. It can be easily checked with the trajectory of the vehicle with known vehicle size, or the surround view camera images of the vehicle. Addable scenario item to this phase could be sudden obstacles such as pedestrian or parked out vehicles, which is similar to the urban AEB test scenarios[6]. In parking area, the vehicle should driving their velocity under 10kph, thus the test scenario case only needs for the vehicle speed 10 kph. For the on-coming vehicle interacting case, the subject vehicle has to leave enough space when the on-coming vehicle detected. The width of driving area is at least 6m space in law, thus the half of the space should be opened to on-coming vehicle.

Parking & Park-out maneuver phase Parking maneuver phase is a phase that park the vehicle into the parking slot without collision to the surroundings. Park-out maneuver phase is a phase that get out from the parked slot, which is directly reverse process of the parking. Although these two phases are separated because their region to watch out or consider is different, when we think ideal cases, excepting the moving obstacles, the two sequences have very similar actions, design collision-free path to static surroundings such as wall or other parked vehicles and control the vehicle to track that path. As addable scenarios, pedestrians walking near the selected parking slot, or other moving vehicle in parking area can be considered.

Performance evaluation As the parking and park-out maneuver phase are focusing on the collision and control performance, the major performance to be checked is that the vehicle totally get in to the parking slot or get out from the parking slot without any collision. For parking maneuver, when vehicle ends the parking, the vehicle should be fit in the parking slot well, which means the vehicle should not interfere the parking line. For both parking and park-out phases, the collision should not occur in their progress. For only static obstacle cases, checking the vehicle's trajectory or surround view images of the vehicle would be fine. For the moving obstacle cases, especially for the pedestrians, similar to AEB test, design the expected collision point and check the vehicle actually stops for each cases. For other driving vehicle case in parking area, the test scenarios are representable using reverse case of the rear-side access alarming system test[9].

CONSIDERING FACTORS FOR CO-INFRA VALET PARKING TEST

As shown in the previous chapter, infra cooperated valet parking test, the test condition can divided into static environment condition and dynamic environment condition. Static conditions usually contains weather, road shape, especially for the co-infra parking scenarios, it can be extended to other factors such as surrounding

object placement near the target parking slot, shape of the parking slot. The considered static environment factors are as follows in table 1.

Structural Environment The valet parking test cannot held without the parking lot. Thus the structural factor is one of the considerable element in valet parking. The structural elements starts with whether the parking area is outdoor or indoor. If the parking area is placed outside, than the floor of the area would be automatically 1st floor only case and the global navigating system such as GPS would available. On the other hand, for multi-floor parking area, which is often seen in skyscraper or underground parking lot, the vehicle has to overcome the localization or indoor position problem itself. In short, the structural element is composed with whether the parking area is indoor or not and the parking lot has multi-floor or not.

Shape of target parking slot Shape of the target parking slot is one of the typical condition in parking. Especially for the parking or park-out maneuver, it is directly related to their trajectory generation. And this is the factor that parking has differentiation from driving. There are typically three different types of slots, one is perpendicular parking which is often called as T-parking. Another type is parallel parking, which is often used in road parking. And the last type is diagonal parking, which is usually placed in large parking lot area. The slot's shape condition can be affected from both valet parking system maker and test site. Test sites often have most of them for offer various test cases, but the valet parking technology is still in developing, hence the system or algorithm makers might have limits to their available range in shape type.

Table1.
Static factors of valet parking scenario.

Structural element of parking lot	**Geometric Positional Condition (G)**	**Floor type (F)**	
	• **(G-1) outdoor area (GNSS available)** • (G-2) indoor area (GNSS unavailable)	• **(F-1) Single floor case (floor movement X)** • (F-2) multi floor case (floor movement O)	
Shape of target parking slot (S)	**T parking (S-T)**	**Parallel parking (S-P)**	**Diagonal parking (S-D)**
Object placement near goal (P)	**(P-1) only the target parking slot is empty** (P-2) two slots are empty in a row including target space (P-3) more than three slots are empty in a row including target space		
Correctness of Infra' s information	**Status of infra (I)**	**Unexpected object in target space (O)**	
	(I-1) Normal (target space is empty) (I-2) Error(unexpected obstacle in target space)	• **(O-1) full size vehicle** • (O-2) two wheeled car • (O-3) parking cone *this category only activates in (I-2) case	

Object placement near goal Object placement near goal is the factor that defines the availability of the parking slots near the target slot before the system test starts. The graphical concept of this factor is shown in fig. 2. This category can be very minor change compare to the other categories, because if the valet parking system can solve (P-1) case, which is the only target parking slot is empty, then other cases like (P-2) and (P-3) are automatically available. Although the (P-1) is the most challengeable case among them in vehicle control

side, but as for detecting the actual slot's area, (P-2) and (P-3) become more challengeable case cause the system need to detect the parking lot line and identify the target space among them. Thus, as for the test environments, this factor also has to be considered differently.

Correctness of Infra' s information The testing target system of this paper is infra-cooperating valet parking system. This means that when the total valet parking sequence starts, infra gives the target parking slot to vehicle, and vehicle moves to the point. In a side of testing the vehicle's valet parking system, this factor is considered to check the ability that the vehicle can overcome the wrong information from the infrastructure. When infra gives the information, there would be actually tow cases. First case is the when the information is true, means the slot's actual availability is same with the known information. In this case, there is no extra issues for the scenario and becomes the basic case. On the other hand, if the known information is inconsistent with actual information, that means there is unexpected objects in the target parking slot. The unexpected objects can be other parked full size or two wheeled vehicles, or just banned with parking cone for other issues such as repair work. The situation that the target slot is unavailable seems already enough for vehicle to react, but the vehicle should make a decision that the space is unavailable itself. Thus, similar to the object placement category different types of object represents different condition to detection system of the vehicle.

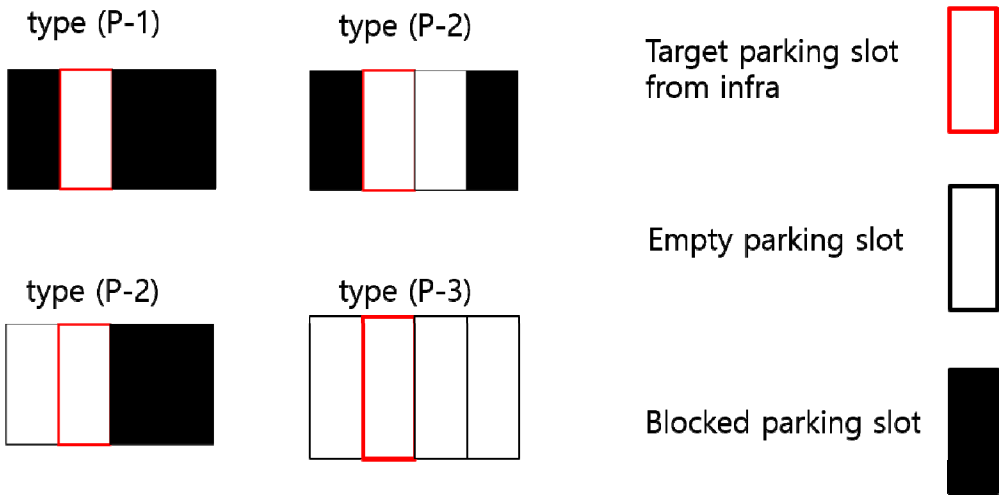

Figure2. Different object placement around target parking slot.

Table2.
Dynamic factors of valet parking scenario.

During vehicle moving phase	**pedestrian (H)**	**Park-out vehicle (J)**	**교행 vehicle (K)**
	(H-1) Adult(8 kph) (H-2) child (5 kph)	**(J-1) 5 kph** (J-2) 10kph	**(K-1) on-coming vehicle(10 kph)**
During vehicle parking& park-out phase	• **(E-1) adult pedestrian crossing the parking slot while in parking maneuver** • (E-2) child pedestrian crossing the parking slot while in parking maneuver • (E-3) other vehicle passing near the parking slot while in park-out maneuver		

Dynamic factors The above components are static factors that are predefined and maintained during for one test case. In contrast, the dynamic factors, in this case the moving objects, also can be represented in each test cases. Most typical moving objects in parking area are pedestrian and other moving vehicles. The dynamic factors can be listed in a similar table form above, which is shown in table 2. Here, we divide up the situations into two low-level component sequences that mentioned in valet parking sequence part. For each moving objects. Thus the factor (H-) and (J-) represents sudden moving objects while the subject vehicle driving the parking area. Factor (K-) shows the on-coming vehicle cases, and the factor (E-) gives the moving object during parking or park-out maneuver.

TEST CASE CONSTRUCTIION

From the previous two sector, we see that the system should be tested with total sequence level, and show the factors that majorly affects to the systems performance in a sight of autonomous valet parking vehicle. Still the valet parking system is in develop, for actual test, some factors can be considered and others are might not. Thus while constructing the actual test scenarios, firstly, define the systems coverage and divide the static and dynamic factors into the test cases. Table 3 and Table 4 shows one example of the test case generation and the following check list of each cases for one floor outdoor condition parking lot with all different type of parking slot shape.

Table3.
Test case/check list generation using static/dynamic factors.

Test case No.	Static Factor Condition	Dynamic Factor Condition
No.1	(S-T)-(G-1)-(F-1)-(P-1)-(I-1)	none
No.2	(S-P)-(G-1)-(F-1)-(P-1)-(I-1)	none
No.3	(S-D)-(G-1)-(F-1)-(P-1)-(I-1)	none
No.4	(S-T)-(G-1)-(F-1)-(P-2)-(I-2)-(O-2)	(H-1)-(J-1)-(E-1)
No.5	(S-P)-(G-1)-(F-1)-(P-2)-(I-2)-(O-2)	(H-2)-(J-2)-(E-3)
No.6	(S-D)-(G-1)-(F-1)-(P-3)-(I-2)-(O-3)	(K-1)-(E-2)

Test case no.	Check list
Common criterion	- Whether the vehicle keep driving in the designated area - Whether the vehicle fit-in the parking slot after parking - Whether the vehicle interfere the parking line in parking/park-out maneuver
No. 1	**- Common criterion only**
No. 2	**- Common criterion only**
No. 3	**- Common criterion only**
No. 4	**- Common criterion** - Whether the vehicle figure out and notive that the target slot is unavailable

	- Whether the vehicle properly stop and avoid collision with moving objects
No. 5	**- Common criterion** - Whether the vehicle figure out and notive that the target slot is unavailable - Whether the vehicle properly stop and avoid collision with moving objects
No. 6	**- Common criterion** - Whether the vehicle figure out and notive that the target slot is unavailable - Whether the vehicle properly stop and avoid collision with moving objects - Whether the vehicle make enough space for on-coming vehicle

In 6 test cases, the first three cases have no any dynamic factors and the other three test cases have dynamic conditions such as sudden pedestrian occurring. Although the test cases are generated based on the test target system's coverage, in order to system successfully perform the valet parking, test cases that only depends on static factors must be satisfied, in this case, test case no. 1-3. Common criterion shows the least conditions for system to be defined as valet parking system. As an extension of these cases, by considering dynamic factors, test case no. 4-6 shows whether the vehicle can react with some sudden objects or frequent situation when other moving objects are in the parking area. Thus the tested system can be differentiated their performance consider to the system that just doing basic operation of valet parking.

SIMULATION TEST RESULT

In this chapter, the simulation of the proposed test scenario is proposed. For this, valet parking algorithm which is presented in previous research is introduced in the first section. Using this valet parking algorithm, computer simulation was conducted using simulation tool MATLAB and Simulink.

Valet Parking Algorithm

In the study of Jeong[10], the reasearch proposed valet parking algorithm focusing on moving obstcle while driving in the parking area. The architercture of the test target algorithm is as follow in fig. 3. Based on the surrounding static/moving obstacle data and digital map, the algorithm infer the intention based on IMM filter and represent the drivable area in parking area by using potential field approach.

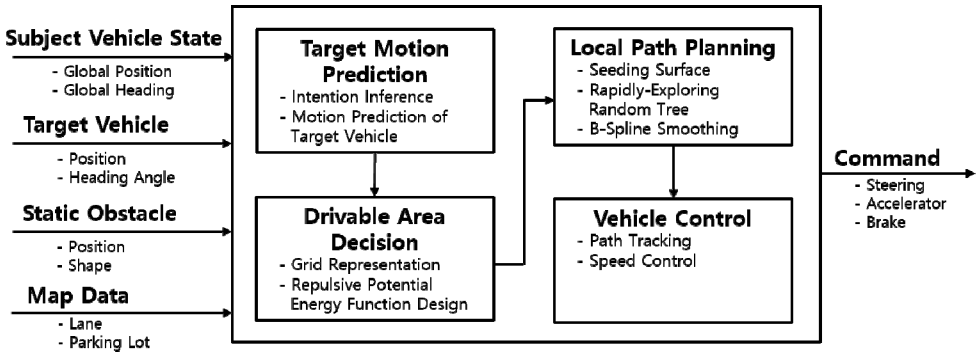

Figure3. Overall architecture of tested Automated Valet Parking

For the detail representation, two different potential energy function is used which is researched by Kim[11]. For the static obstalces or parking line boundary, cleareance based energy function is used which is in equation (1).

$$U_{rep} = \begin{cases} \min\left[U_{rep,\max},\ k \cdot \left(\frac{1}{D} - \frac{1}{Q} \right)^2 \right] & if \quad D < Q \\ U_{rep,\max} & else \end{cases}$$

On the other hand, for the moving object, to imply the velocity information of the object, equation (2) is used.

$$U_{rep} = \begin{cases} k \cdot \exp\left(-\left(\frac{x_{r,p}}{\dot{x}_{r,p}} \right)^2 - \left(\frac{y_{r,p}}{\dot{y}_{r,p}} \right)^2 \right) & if \quad \left\| \rho(x_{r,p}, y_{r,p}) \right\| < \rho_{long} \\ 0 & else \end{cases}$$

While in simulation, the surround representation result of this algorithm can also be used as check the actual collision occur or not for the test case.

Simulation Result

Computer simulation was conducted using simulation tool Carsim and MATLAB/Simulink. In this paper, the simulation result of total progress of Parking into T park slot including on-coming vehicle condition in a snap-shot image form.

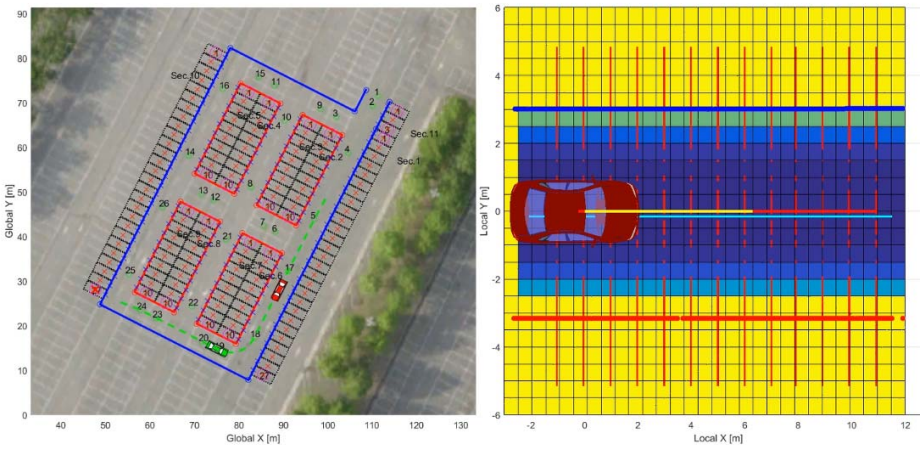

(a) Normal driving before meeting on-coming vehicle

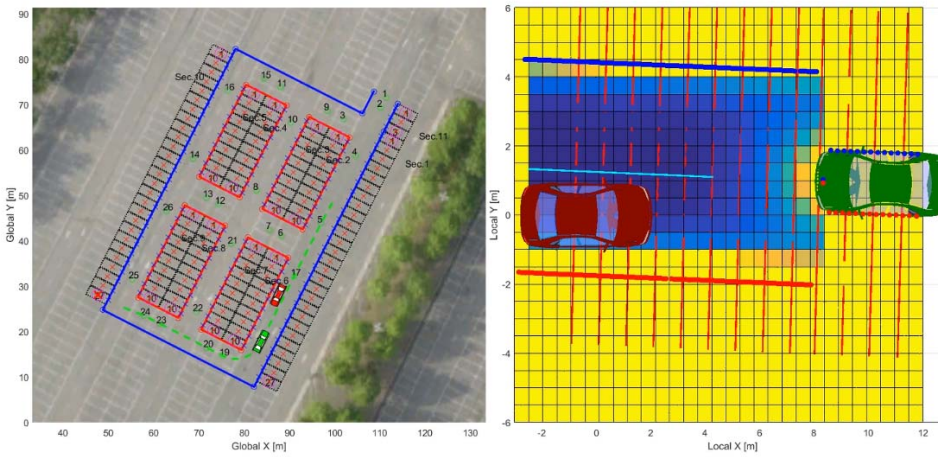

(b) Detect the on-coming vehicle & space generating on-coming vehicle

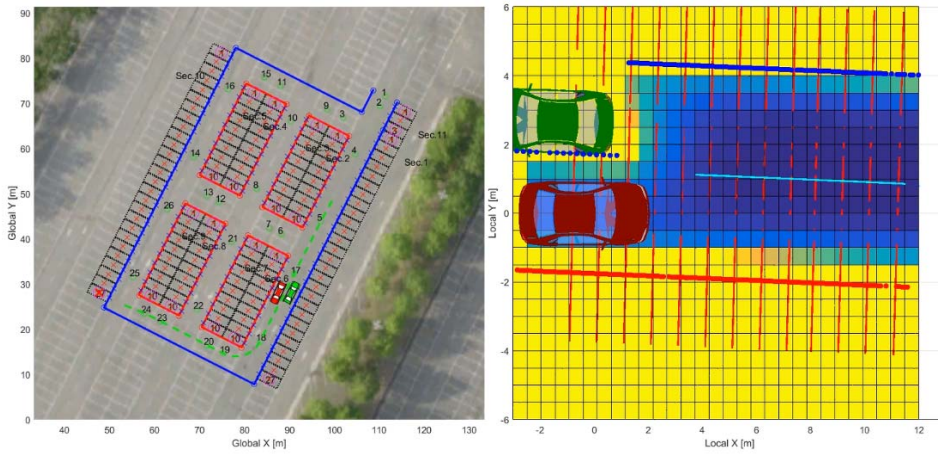

(c) Waiting for on-coming vehicle to pass

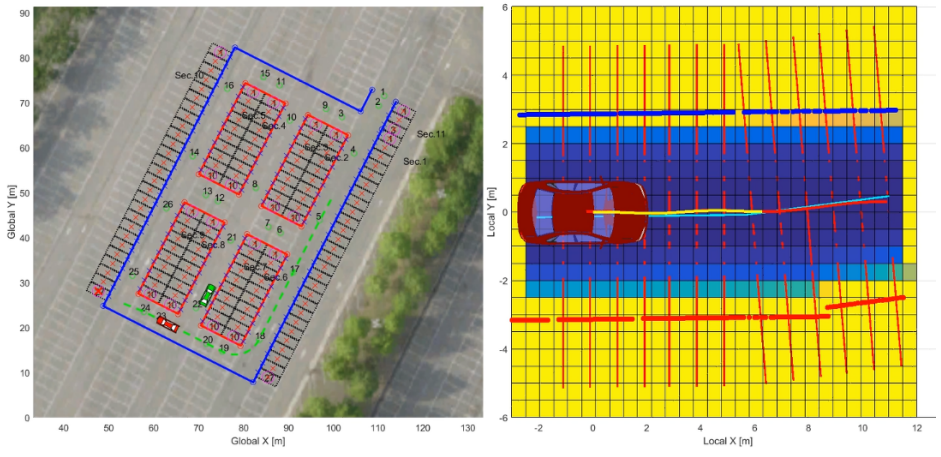

(d) Come back to global trajectory and keep move to goal

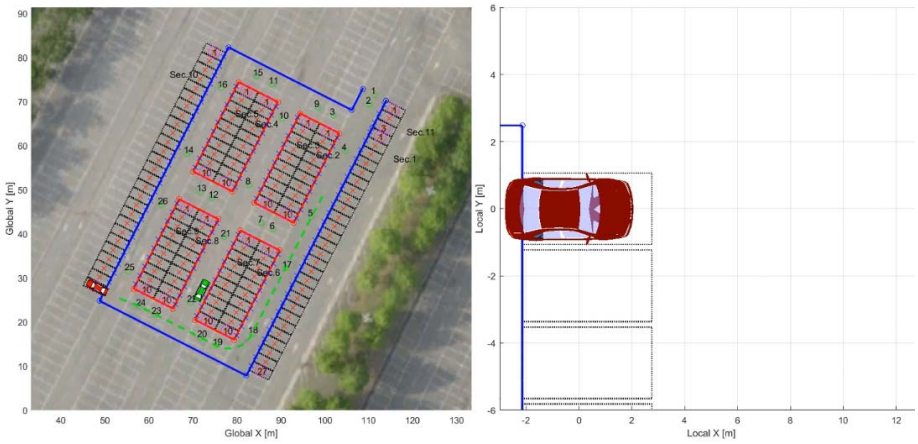

(e) Front side parking with fit-in left/right parking line of the goal

Figure4. Snap shot images of one example of valet parking simulation Testing condition with (S-T)-(G-1)-(F-1)-(P-1)-(I-1), (K-1)

Simulation Case: T- slot parking with on-coming vehicle The simulation result of the parking scenario in fig. 4. As the parking scenarios should check whether collision and interference occur or not, the simulation result proposed with graphical image of global situation to see the progress of total sequence and local coordinate of subject vehicle to check the collision or interference. The static factor condition is (S-T)-(G-1)-(F-1)-(P-1)-(I-1), which means outdoor parking lot with target slot shape T parking, and the information from the infra is correct. For the dynamic factor, (K-1) is applied before the subject vehicle enters the corner point of the global trajectory. The proposed images are mainly focusing on moment when the on-coming vehicle and subject vehicle met. The subject vehicle is shown as red vehicle and the on-coming vehicle is shown as green. Left images show the global position of both vehicle and right side images show the local path and boundary of the environment in local coordinate of the subject vehicle. As the result shows, the subject vehicle avoid the collision with the on-coming vehicle and finally parked into the target slot. Although the used parking algorithm had its coverage parking sequence, the scenario case can be applied as a partial test form.

CONCLUSIONS

In this paper, a procedure for evaluating scenarios for infra-cooperating valet parking system has been developed. The proposed test scenario divide the infra-cooperating valet parking with three sequential phases, vehicle moving, parking, park-out maneuver. To construct the factor matrix of the test condition, several frequent situation that can be face in parking lot area are list up and classified into static condition and dynamic condition. Then as a final step, test cases are generation step is suggested considering the test target system's coverage and the test site's condition, to manage both level 4 parking system and lower level parking assist systems. As an one example, one of the valet parking algorithm is applied with generated test case. The simulation shows that the proposed valet parking test scenario can be applied to one total functional sequence data and check whether the parking system works well including the performance of basic purpose
In order to develop the specific regulation such as rating criteria and detail procedure of each test scenario, additional vehicle experimental test should be conducted with various test cases applied to systems.

* This research was supported by the Korea Ministry of Land, Infrastructure and Transport. It was also supported by the Korea Agency for Infrastructure Technology Advancement (Project No.: 18TLRP-B117133-03); the Technology Innovation Program (10079730, Development and Evaluation of Automated Driving Systems for Motorway and City Road) and driving environment) funded By the Ministry of Trade, Industry & Energy(MOTIE, Korea); National Research Foundation of Korea(NRF) grant funded by the Ministry of Science, ICT & Future Planning (NRF-2016R1E1A1A01943543).

REFERENCES

[1] W. Kim, D. Kim, K. Yi, and H. J. Kim, "Development of a path-tracking control system based on model predictive control using infrastructure sensors," Vehicle System Dynamics, vol. 50, no. 6, pp. 1001-1023 (2012)
[2] C. Wang, H. Zhang, M. Yang, X. Wang, L. Ye, and C. Guo, "Automatic Parking Based on a Bird's Eye View Vision System," Advances in Mechanical Engineering, vol. 6, no. 0, pp. 847406-847406 (2015)
[3] M. Chirca, R. Chapuis, and R. Lenain, "Autonomous Valet Parking System Architecture," pp. 2619-2624 (2015)
[4] M. Kyoung-Wook and C. Jeong-Dan, "Design and implementation of an intelligent vehicle system for autonomous valet parking service," pp. 1-6 (2015)
[5] J. Timpner, S. Friedrichs, J. van Balen, and L. Wolf, "k-Stacks: High-density valet parking for automated vehicles," pp. 895-900 (2015)
[6] Euro NCAP, "Euro_NCAP_2014_AEB_Test_Protocol", 2013
[7] Inseong, Choi, Seongwoo, Cho and Byungdo, Kang, "An Overview on Establishing Safety Assessment Standard of Longitudinal Active Safety System in Korea", ESV 2013-0490
[8] Korean standard association, "Road vehicles — Parking system for autonomous driving vehicles — General requirements and use-cases definition (KS R 1176)", (2017)
[9] Korea Ministry of Government Legislation, "Regulations for Vehicle Safety Evaluation Test" (2016)
[10] Jeong, Yonghwan, et al. "Sampling Based Vehicle Motion Planning for Autonomous Valet Parking with Moving Obstacles." *International Journal of Automotive Engineering* 9.4, pp.215-222. (2018)
[11] K. Kim, B. Kim, K. Lee, H. Chong, B. Ko, and K. Yi, "Vehicle motion control for integrated risk management of automated vehicle," Proceedings of FAST-zero'15: 3rd International Symposium on Future Active Safety Technology Toward zero traffic accidents, pp.229-234 (2015)
[12] J. Seo and K. Yi, "Robust Mode Predictive Control for Lane Change of Automated Driving Vehicles," SAE Technical Paper, No.2015-0148-7191 (2015)
[13] J. Lee, B. Kim, J. Seo, K. Yi, J. Yoon, and B. Ko, "Automated Driving Control in Safe Driving Envelope Based on Probabilistic Prediction of Surrounding Vehicle Behaviors," SAE International Journal of Passenger Cars-Electronic and Electrical Systems, Vol. 8, No. 2015-01-0314, pp. 207-218 (2015)
[14] K. W. Seo, "Smart parking assist system and control method thereof," ed: Google Patents (2013)
[15] Euro NCAP, "Euro_NCAP_2017_Assessment_Protocol-Safety Assist" (2018)

A METHOD FOR SCENARIO RISK QUANTIFICATION FOR AUTOMATED DRIVING SYSTEMS

Erwin de Gelder, Arash Khabbaz Saberi, Hala Elrofai
TNO, Integrated Vehicle Safety Department
5700 AT Helmond The Netherlands

Paper Number 19-0129

ABSTRACT

Recent innovations, such as automated driving and smart mobility, have elevated the safety-criticality of automotive systems due to the impact of these technologies on the traffic behavior and safety. New safety validation and assessment methodologies are required to provide the level of assurance that matches the societal impact of these systems. The objective of this paper is to introduce a novel method for assessment and quantification of the risk of a driving scenario considering the operational design domain. For our proposed method, we assume that a scenario consists of activities (performed by different actors) and environmental conditions that leads to a potentially hazardous consequence. The risk of a driving scenario is the product of the probability of the exposure of a scenario and the severity of the hazardous consequence of that scenario. We introduce a systematic method for calculating the probability of exposure, where we assume a causal relation between the activities that constitute a scenario. By making educated assumptions on the dependencies among the different activities and environmental conditions, we simplify the calculation of the probability of the exposure. For estimating the severity, we employ Monte Carlo simulations. We illustrate the use of our proposed method by applying it to an example of a collision avoidance system in a cut-in scenario. We use naturalistic driving data acquired from field studies on the Dutch highways to determine the risk. The presented example illustrates the potential of our proposed risk estimation method. Using our proposed method, we can compare the safety criticality of various scenarios in a quantitative manner, which can be used as a safety metric for evaluating automated driving systems. This can lead to stronger justification for design decisions and test coverage for developing automated vehicle functionalities.

INTRODUCTION

New developments in the automotive industry towards higher levels of automation are introducing new safety concerns for vehicles. Test procedures and performance measures need to be adapted for evaluation of vehicles with an Automated Driving (AD) system. The safety and reliability of the AD vehicles must be validated in principle for all possible traffic situations that an AD system may encounter on the road, before these systems can be taken into production.

Scenario-based safety validation for automated driving is one of the proposed approaches that is broadly supported by the automotive community. This is reflected in the ISO/PAS 21448:2019 standard on the safety of th intended functionality (SOTIF) [1]. Related projects in Germany (Pegasus [2]), The Netherlands (StreetWise [3]), and Singapore [4] strongly support this approach. Risk assessment is an essential component of the safety validation as it indicates the acceptance criteria of the AD system.

The ISO 26262:2018 [5] captures the state of the art in automotive functional safety. It defines the safety lifecycle and the related safety activities such as Hazard Analysis and Risk Assessment. Other methodologies, such as STPA [6], give guidelines on safety engineering based on systems theory. From the mentioned sources, the only one that offers a framework for measuring risk is ISO 26262. It defines risk as:

Definition 1 (Risk [5]) *The combination of the probability of occurrence of harm and the severity of that harm.*

ISO 26262:2018 gives guidelines to assess risk based on vehicle level hazardous events. A hazardous event is the combination of a vehicle level hazard with operational situation or scenario. It requires analyzing each hazardous event risk individually based on three parameters of Severity, Probability of exposure, and Comparability. The combination of these parameters contributes to constructing the Automotive Safety Integrity Level (ASIL). In this framework, each parameter is quantified in three or four levels that construct the ASIL ranking A, B, C, D, and QM, where ASIL A represents the least critical level and in ascending order, ASIL D the most critical level. Quality Management (QM) means that the identified hazard is not critical enough for the safety processes, and the quality management system of the manufacturer should suffice for reducing the risk. We depict the ASIL ranking graph in Figure 1.

The ASIL methodology for risk assessment relies on the experts' judgments of the three risk parameters. The ISO 26262:2018 provides some general guidelines for assessing these parameters. However, the assessment is for the most part subjective and dependent on the experts who carry it out. Moreover, it is only capable of evaluating the risk of a single (hazardous) event within the context of a generic operational situation.

The alternative methodology proposed in STPA has the means for providing a quantitative risk assessment as it provides the means for connecting the hazard identification to a control system and its characteristics. However, this method skips the risk assessment entirely and does not offer any solutions.

We argue that as the automotive systems move towards higher automation levels, we require more formal methods for risk assessment. By quantifying risk assessment, we reduce the risk of subjective errors in the judgment. Risk quantification is a step towards run-time risk assessment for the autonomous systems.

The objective of this paper is to introduce a method for assessment and quantification of the risk of a driving scenario taking into account the entire operational situations and their relations. This is achieved by calculating the

Controllability C	Probability of Exposure (E)	Severity (S)			
		S0	S1	S2	S3
C1	E1	QM	QM	QM	QM
	E2	QM	QM	QM	QM
	E3	QM	QM	QM	A
	E4	QM	QM	A	B
C2	E1	QM	QM	QM	QM
	E2	QM	QM	QM	A
	E3	QM	QM	A	B
	E4	QM	A	B	C
C3	E1	QM	QM	QM	A
	E2	QM	QM	A	B
	E3	QM	A	B	C
	E4	QM	B	C	D

Figure 1: ASIL risk assessment graph.

Table 1: The terms and definitions.

Term	Definition
Severity	An estimate of the extent of harm to one or more individuals that can occur in a potentially hazardous event [5]
Exposure	The state of being in a driving scenario
Risk	The combination of the probability of occurrence of harm and the severity of that harm [5]
Condition	The constant parameters describing the environmental aspects of the operational design domain[1]
Actor	An element of a scenario acting on its own behalf [8]
Scenario	A quantitative description of the activities of the ego vehicle and other actors and the conditions from the static environment

probability of exposure to a certain scenario through analysis of real-world driving data. Next, we employ simulations to estimate the severity of the potential hazardous consequence of a scenario.

The paper is structured as follows. We first present the proposed method for estimating the risk quantitatively. Next, we perform a case study to illustrate the method using real-world data. We end the paper with a discussion and a conclusion.

PROPOSED RISK ESTIMATION METHOD

In the Hazard Analysis and Risk Assessment (HARA) required by the ISO 26262 standard, the estimation of Automotive Safety Integrity Level (ASIL) is calculated based on a so-called single specific hazardous event [5]. Although the operational situation in which this single event occurs as well as the operating mode are considered in the analysis, still the proceeding and successive events are not taken into account. In this paper, we propose a new method to estimate the risk of a certain scenario considering the whole chain of activities and conditions that constitute the scenario. The estimated risk is based on real-world driving data. To estimate the risk, we quantify the exposure and the severity. In Table 1, we present the definitions of the terms that are used in our proposed methodology.

As explained in Table 1, a scenario consist of a set of conditions and activities, denoted by A and C, respectively. We formulate the exposure as the average number of occurrences of the activities A under the conditions C, denoted by $\lambda_{A,C}$. The severity is the likelihood of the potential hazardous consequence R given the activities A and the conditions C, denoted by the conditional probability $P(R|A,C)$. The risk is computed as the multiplication of the exposure and the severity.

The proposed method is summarized in Figure 2. To compute the exposure, we calculate the likelihood of the conditions, denoted by $P(C)$, and the conditional likelihood of the activities, denoted by $P(A|C)$, based on real-world driving data. This is explained in detail in the next section. For the estimation of the severity, we consider all possible scenarios that are subject to a set of conditions C and consist of the activities A. Therefore, we parametrize the scenarios using the parameter vector θ. Based on the real-world driving data, the probability density function of the parameters, denoted by $P(\theta|A,C)$, is estimated. Next, using simulations, we estimate $P(R|\theta,A,C)$, the likelihood of a potential hazardous consequence R given a parametrized scenario. The details of the estimation of the severity are presented after the details of the estimation of the exposure. Finally, we describe how the risk is estimated based on the estimated exposure and severity.

Calculate exposure

The scenarios are subject to n_C conditions, denoted by $C_1,\ldots,C_{n_C}$. For the sake of brevity, all conditions together are denoted by C, i.e., $P(C_1,\ldots,C_{n_C}) = P(C)$. Many of these conditions might be based on the operational design domain of the AD system and might include conditions with respect to the infrastructure, weather conditions, lighting conditions, and geographical locations.

The first step is to compute the joint probability of the conditions, i.e., $P(C)$. In case these conditions are independent, the probability can be computed by simply multiplying the individual likelihoods for each condition, i.e.,

[1]The operational design domain refers to the "operating conditions under which a given driving automation system or feature thereof is specifically designed to function" [7].

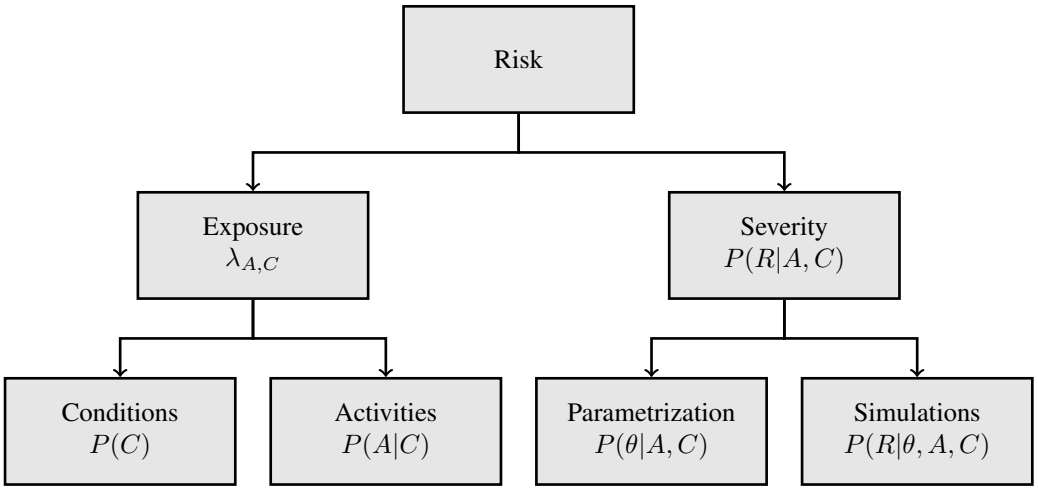

Figure 2: Proposed method for quantifying the risk. The risk is a multiplication of the exposure and the severity.

$P(C) = P(C_1) \cdot \ldots \cdot P(C_{n_C})$. This, however, might not necessarily be the case, which requires either to compute the joint probability or to compute conditional probabilities. In some cases, it might also be reasonable to simply assume that the likelihood of certain conditions are independent.

Note that the the defined conditions might not be the same as the conditions under which the data is collected that is used to compute $P(C)$. This might require additional assumptions, see our case study for examples.

To calculate the exposure, the average number of occurrences of the activities that constitute the scenarios within a certain time interval need to be estimated. Let n_A denote the number of activities, such that $A_1, \ldots, A_{n_A}$ denote the activities. For the sake of brevity, all activities together are denoted by A.

Without loss of generality, we assume that the time interval is an hour. To estimate the number occurrences of the activities, the data for which the conditions C are satisfied are analyzed. The average number of occurrences of the activities A for each hour of driving for which the conditions C are satisfied is denoted by $\lambda_{A|C}$. Next, we can calculate the average number of occurrences of the activities A under the conditions C for each hour of driving:

$$\lambda_{A,C} = \lambda_{A|C} \cdot P(C). \tag{1}$$

Regarding the scenarios consisting of conditions C and activities A, we assume the following:

- The occurrence of one scenario consisting of activities A and conditions C does not affect the probability that a second scenario consisting of activities A and conditions C occurs.
- The rate at which a scenario consisting of activities A and conditions C occurs is constant. I.e., $\lambda_{A,C}$ is constant.
- Two scenarios consisting of activities A and conditions C cannot occur at exactly the same time instant.

Based on these assumptions, the number of occurrences of scenarios consisting of activities A and conditions C is distributed according to the Poisson distribution:

$$P(k \text{ times } A, C \text{ in an hour}) = \exp\left\{-\lambda_{A,C}\right\} \frac{\lambda_{A,C}^k}{k!}. \tag{2}$$

Severity

The first step towards estimating the severity is to parametrize the scenarios with a parameter vector $\theta \in \mathbb{R}^d$. The parametrization enables the generation of infinitely many unique individual test cases that resemble the scenarios found in naturalistic driving [3], [9].

In case the parameters are dependent, which is often the case, it is important that the number of parameters is limited to avoid the curse of dimensionality [10]. This often requires some assumptions. An example is presented in our case study in the next section.

To estimate the probability density function (pdf) of the parameter vector θ, i.e., $P(\theta|A,C)$, either parametric models, non-parametric models, or a combination of the two can be used. In case of parametric models, a certain functional form of the pdf is assumed. For example, it might be assumed that the pdf can be modeled using a Gaussian distribution. In this paper, we present a non-parametric approach using Kernel Density Estimation (KDE) [11], [12]. Using KDE, there is no assumption on the functional form of the pdf because the shape of the pdf is automatically computed. With KDE, the estimated pdf is given by

$$P(\theta|A,C) = \frac{1}{nh^d} \sum_{i=1}^{n} K\left(\frac{\theta - \theta_i}{h}\right). \tag{3}$$

Here, $K(\cdot)$ is an appropriate kernel function and h denotes the bandwidth. From the data, n scenarios are extracted and each scenario is parametrized with θ_i. The choice of the kernel $K(\cdot)$ is not as important as the choice of the bandwidth h [13]. Often, a Gaussian kernel is used, which is given by

$$K(u) = \frac{1}{(2\pi)^{d/2}} \exp\left\{-\frac{1}{2}\|u\|^2\right\}, \tag{4}$$

where $\|u\|^2$ denotes the squared 2-norm of u, i.e., $u^T u$.

The bandwidth h controls the amount of smoothing. For the kernel of Eq. (4), the same amount of smoothing is applied in every direction, although this can easily be extended to a multi-dimensional bandwidth, see, e.g., [14], [15]. There are many different ways of estimating the bandwidth, ranging from simple reference rules like, e.g., Scott's rule of thumb [10] or Silverman's rule of thumb [16] to more elaborate methods; see [13], [17]–[19] for reviews of different bandwidth selection methods.

Let R denote a potential hazardous consequence of a scenario. We define the severity of a scenario with activities A and conditions C as the probability of R, given the activities A and C, i.e., $P(R|A,C)$. We cannot evaluate $P(R|A,C)$ directly, because the outcome of a scenario highly depends on the parametrization θ. Therefore, we estimate $P(R|\theta,A,C)$ through a simulation of the scenario with parameters θ. Using $P(\theta|A,C)$ from Eq. (3), we can compute

$$P(R,\theta|A,C) = P(R|\theta,A,C) \cdot P(\theta|A,C). \tag{5}$$

To obtain $P(R|A,C)$, we need to integrate Eq. (5) over θ, i.e.,

$$P(R|A,C) = \int_{\mathbb{R}^d} P(R|\theta,A,C) \cdot P(\theta|A,C)\,\mathrm{d}\theta. \tag{6}$$

One approach to evaluate the integral of Eq. (6) is to perform Monte Carlo simulations. For sufficiently large N, we have

$$P(R|A,C) \approx \frac{1}{N} \sum_{k=1}^{N} P(R|\theta_k,A,C),\ \theta_k \sim P(\theta|A,C). \tag{7}$$

To improve the accuracy of Eq. (7), importance sampling can be used where the parameters θ are drawn from another distribution with a focus on the critical scenarios, see, e.g., [9].

Calculating the risk

Analogous to the exposure, we define the risk as the number of occurrences of the hazardous consequence R in a scenario consisting of activities A and conditions C in a certain time interval. Let λ denote the average number of these occurrences in an hour of driving. The chain rule of probability tells us that this equals the product of $\lambda_{A,C}$ (i.e., the exposure) and $P(R|A,C)$ (i.e., the severity):

$$\lambda = \lambda_{A,C} \cdot P(R|A,C) \tag{8}$$

Analogous to the number of occurrences of a scenario consisting of activities A and conditions C, we assume that the number of occurrences of a harmful outcome R in a scenario consisting of activities A and conditions C can be modeled using a Poisson distribution:

$$P(k \text{ times } R,A,C \text{ in an hour}) = \exp\{-\lambda\}\,\frac{\lambda^k}{k!}. \tag{9}$$

Using Eq. (9), to calculate the probability of not having the harmful outcome R in a scenario consisting of activities A and conditions C we simply need to use $k = 0$:

$$P(\text{no } R, A, C \text{ in one hour}) = \exp\{-\lambda\}. \tag{10}$$

CASE STUDY

In this section, we present a case study to illustrate the method of quantifying the risk for a cut-in scenario. We will first describe the cut-in scenario and the use case. The actual system for which the risk is computed is presented in next. After these two steps, we will go through the steps of our proposed method.

The cut-in scenario and the use case

We want to quantify the risk for cut-in scenarios that are linguistically described as follows: while the ego vehicle drives at a moderate to high speed while staying in its lane, another vehicle cuts into the lane of the ego vehicle, such that this vehicle becomes the ego vehicle's lead vehicle. Furthermore, the ego vehicle needs to brake to prevent a collision.

For the quantification of the risk, 60 hours of data (see also [9]) are collected by driving a specific route in and between Eindhoven and Helmond, The Netherlands, with twenty different drivers, each driving the route twice. Therefore, it is assumed that the use case of the AD system is driving this route. We will use the data for the estimation of the risk. Hence, we will make use of the following assumption:

Assumption 1 *The recorded naturalistic driving data is representative for what a vehicle with the AD system might encounter along the same route.*

System-under-test

To reduce efforts for the assessment, often simulations are employed. However, even simulations can consume considerable time, as these simulations might run real-time [20] or slower when a higher level of detail is used [21]. For our method, we will simplify the simulations, such that the total required time on a common computer is in the order of minutes. Since we are interested in approximate results, a high level of detail is not required.

To simplify the system-under-test, it is assumed that the system's desired acceleration is similar to the adaptive cruise control defined in [9], i.e.,

$$u(t) = k_{\mathrm{d}}(v(t))(d(t) - \tau_{\mathrm{h}} v(t) - s_0) + k_{\mathrm{v}}\left(\dot{d}(t) - h a(t)\right), \tag{11}$$

with

$$k_{\mathrm{d}}(v(t)) = k_{\mathrm{d1}} + (k_{\mathrm{d2}} - k_{\mathrm{d1}}) \exp\left\{-\frac{v(t)^2}{2\sigma_{\mathrm{d}}}\right\}. \tag{12}$$

Here, v is the speed of the ego vehicle, d denotes the clearance between the ego vehicle and its predecessor, i.e., the vehicle that performs the cut-in. The relative speed is denoted by $\dot{d}$ and a refers to the acceleration of the ego vehicle. The ego vehicle is modeled using a first order model with a time delay, i.e.,

$$\tau \dot{a}(t) + a(t) = u(t - \theta). \tag{13}$$

Furthermore, the deceleration is limited at $-6\,\mathrm{ms}^{-2}$. A description of the constants of Eqs. (11) to (13) are listed in Table 2. The controller runs at 100 Hz.

Note that there is no intervention of a human:

Assumption 2 *The ego vehicle is fully controlled by the automation system as defined by Eqs.* (11) *and* (12)*. Hence, there is no intervention of a human.*

Table 2: The constants used for the simple automation system of Eqs. (11) to (13).

Parameter	Description	Value
τ_h	Desired headway time	2.0 s
s_0	Safety distance	1.5 m
k_d1	Distance gain at high speed	$0.7\,\mathrm{s}^{-2}$
k_d2	Distance gain at low speed	$2.0\,\mathrm{s}^{-2}$
σ_d	Shaping coefficient of distance gain	$5\,\mathrm{ms}^{-1}$
k_v	Speed difference gain	$0.35\,\mathrm{s}^{-1}$
τ	Time constant of the vehicle model	0.1 s
θ	Delay of the vehicle response	0.2 s

Calculate exposure

The cut-in scenarios are subject to the following conditions:

- C_1: The speed of the ego vehicle is within the range of 60 km/h and 130 km/h.
- C_2: There are no restrictions on the weather conditions.
- C_3: There are no restrictions on the lighting conditions.

Obviously, because there are no restrictions to the weather and lighting conditions, we have $P(C_2, C_3) = 1$. For the first condition, we can use the data to estimate the likelihood. The data, however, has been recorded during sunny weather at daylight. Therefore, we need to following assumption.

Assumption 3 *Let C_2' and C_3' denote the conditions of having sunny weather and daylight, respectively. Then we have $P(C_1|C_2, C_3) = P(C_1|C_2', C_3')$.*

From the data, it appeared that $P(C_1|C_2', C_3') = 0.20$. Using Assumption 3, we have

$$P(C) = P(C_1, C_2, C_3) = P(C_1|C_2', C_3') \cdot P(C_2, C_3) = 0.20. \tag{14}$$

The cut-in scenarios consist of the following activities:

- A_1: The ego vehicle is lane following.
- A_2: The target vehicle is driving in an adjacent lane in the same direction as the ego vehicle.
- A_3: After activity A_2, the target vehicle performs a lane change towards the lane of the ego vehicle, such that the ego vehicle needs to brake.
- A_4: The automation system detects the cut-in.
- A_5: After activity A_4, the automation system activates the brakes of the ego vehicle.

The likelihood of the activities A_1, A_2, and A_3 can be estimated using the data. It is assumed that the ego vehicle needs to brake if the target vehicle is driving slower and the headway time is less than three seconds. In case of a slower target vehicle with a larger headway time, the scenario is referred to as a gap closing scenario [22], [23].

For simplicity, we assume the following:

Assumption 4 *The automation system always detects the cut-in and activates the brakes after detecting the cut-in, such that $P(A_4, A_5|A_1, A_2, A_3, C) = 1$.*

Using this assumption, we can compute $\lambda_{A|C}$ by detecting the number of occurrences of the activities A_1, A_2, and A_3 under the conditions C. Based on the dataset, we have $\lambda_{A|C} = 9.9\,\mathrm{h}^{-1}$, i.e., in each hour that the ego vehicle is driving in a speed range of 60 km/h and 130 km/h, there are on average 9.9 cut-ins with the target vehicle driving slower than the ego vehicle, such that the headway time after the cut-in is less than three seconds. From this, it simply follows that

$$\lambda_{A,C} = \lambda_{A|C} \cdot P(C) = 2.0. \tag{15}$$

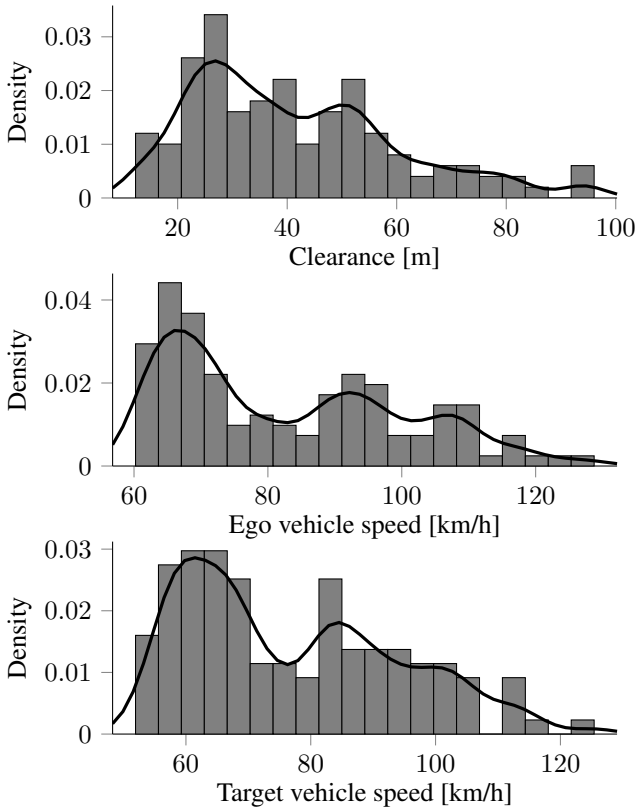

Figure 3: Histogram of the data of the parameters (bars) and their estimated marginal probabilities (lines).

Calculating severity

To limit the number of parameters, we assume the following:

Assumption 5 *The ego vehicle is driving at a constant speed at the moment of the cut-in of the target vehicle, i.e., the moment that the target vehicle enters the lane of the ego vehicle.*

Assumption 6 *The target vehicle is driving at a constant speed.*

Both assumptions can be justified using the data. In case of the ego vehicle, the average acceleration at the moment of the cut-in is $-0.29\,\mathrm{ms}^{-2}$ and the standard deviation equals $0.50\,\mathrm{ms}^{-2}$. In case of the target vehicle, the average deceleration at the moment of the cut-in is $0.05\,\mathrm{ms}^{-2}$ and the standard deviation equals $0.37\,\mathrm{ms}^{-2}$. As a result, the scenario is parametrized using $d = 3$ parameters:

1. The clearance between the target vehicle and the ego vehicle at the moment of the cut-in, i.e., the moment than the target vehicle enters the lane of the ego vehicle.
2. The speed of the ego vehicle at the moment of the cut-in.
3. The speed of the target vehicle throughout the whole scenario.

A histogram of the data of the parameters is shown in Figure 3. The probability density function is estimated using the KDE of Eq. (3) with the Gaussian kernel of Eq. (4). Before applying KDE, the data is scaled, such that the standard deviation equals one for each parameter. We use leave-one-out cross validation to compute the bandwidth h (see also [24]) because this minimizes the Kullback-Leibler divergence between the real underlying pdf and the estimated pdf [13], [25]. The resulting bandwidth equals $h = 0.198$. The marginal probability distributions coming from the resulting joint distribution, i.e. the KDE, are shown in Figure 3 by the black lines.

Let R denote the result of having a collision. Given a certain parameter vector θ, we have $P(R|\theta, A, C) = 1$ if the outcome of the simulation is a collision and $P(R|\theta, A, C) = 0$ otherwise. For the simulation, we used the forward Euler method with a step size of 0.01 s, similar as the sample time of the controller. On a regular computer, approximately 2000 simulations are performed in a second. We performed a million simulations, i.e., $N = 10^6$. In total, 28 simulations ended with a collision, thus, according to Eq. (7), we have:

$$P(R|A, C) = 2.8 \cdot 10^{-5}. \tag{16}$$

Calculating the risk

Let λ denote the average number of collisions with a cut-in scenario as described earlier along the specified route for a vehicle with the automation system as described above. Using Eq. (8), we have:

$$\lambda = \lambda_{A,C} \cdot P(R|A, C) = 5.5 \cdot 10^{-5}\,\mathrm{h}^{-1}. \tag{17}$$

Using Eq. (10), the probability of having no collision in a cut-in scenario as described above during an hour of driving is

$$P(\text{no } R, A, C \text{ during an hour}) = 0.999945. \tag{18}$$

By solving the Poisson distribution of Eq. (9) for λ with $k = 0$, we can also conclude that with 95 % certainty, there will be no collision in a cut-in scenario as described earlier when driving 925 h.

DISCUSSION

We illustrated the applicability of our risk estimation method through an example in the previous section. However, our method has some limitations as well. As an example, many assumptions are made to simplify the calculation of estimated risk or because there are unknowns due to lack of data. These assumptions reduce the accuracy of the estimated risk. Another limitation is that we applied the proposed method for only one type of driving scenario, while the full potential can be better demonstrated by applying the method to a wider range of scenarios.

Despite the mentioned limitations, we believe that our proposed method takes an important step towards objective hazard and risk analysis as we summarize in the following points:

- All the assumptions that were made for estimating the risk are explicit and based on measured data. By making the assumptions explicit, it is much clearer why a certain risk is associated with — in this case — a certain/specific scenario.
- Because our proposed method explicates all the steps and assumptions that lead to a certain estimated risk, it is easily possible to update the risk when more information of the system is known or when more data is available.
- The systematic quantification of the risk provides additional objectified trust in the safety analysis that depends on the availability of data rather than experts judgment.
- The method can be scaled up to be applied to multiple scenarios and operational situations with small modifications.

CONCLUSIONS

As automotive systems move towards higher automation levels, we require formal methods for risk assessment. Currently, however, measuring risk is often based on experts' judgments. Therefore, we propose a method for quantifying the risk assessment as to reduce the risk of subjective errors in the judgment. Our proposed method estimates the risk of a driving scenario while considering the entire operational situations and their relations through analysis of real-world driving data and simulations of the automation system. Our systematic approach for quantifying the risk provides additional trust in the safety analysis, as it depends on the available data rather than experts' judgment.

It remains future work to apply the method for different scenarios to show the full potential of the method. We also aim for extending our method by considering, next to the exposure and the severity, the controllability [26].

REFERENCES

[1] ISO/PAS 21448, "Road vehicles — Safety of the intended functionality," International Organization for Standardization, Tech. Rep., 2019.

[2] A. Pütz, A. Zlocki, J. Bock, and L. Eckstein, "System validation of highly automated vehicles with a database of relevant traffic scenarios," in *12th ITS European Congress*, 2017, pp. 1–8.

[3] H. Elrofai, J.-P. Paardekooper, E. de Gelder, S. Kalisvaart, and O. Op den Camp, "Scenario-based safety validation of connected and automated driving," Netherlands Organization for Applied Scientific Research, TNO, Tech. Rep., 2018.

[4] J. Ploeg, E. de Gelder, M. Slavík, E. Querner, T. Webster, and N. de Boer, "Scenario-based safety assessment framework for automated vehicles," in *Proceedings of the 16th ITS Asia-Pacific Forum*, 2018, pp. 713–726.

[5] ISO 26262-1:2018, "Road vehicles – Functional safety," International Organization for Standardization, Geneva, Switzerland, Tech. Rep., 2018.

[6] N. Leveson, "An STPA primer," MIT, Tech. Rep., 2013.

[7] "Taxonomy and definitions for terms related to driving automation systems for on-road motor vehicles," SAE International, Tech. Rep., 2018.

[8] S. Ulbrich, T. Menzel, A. Reschka, F. Schuldt, and M. Maurer, "Defining and substantiating the terms scene, situation, and scenario for automated driving," in *IEEE 18th International Conference on Intelligent Transportation Systems*, 2015, pp. 982–988.

[9] E. de Gelder and J.-P. Paardekooper, "Assessment of automated driving systems using real-life scenarios," in *IEEE Intelligent Vehicles Symposium (IV)*, IEEE, 2017, pp. 589–594.

[10] D. W. Scott, *Multivariate Density Estimation: Theory, Practice, and Visualization*. John Wiley & Sons, 2015.

[11] M. Rosenblatt, "Remarks on some nonparametric estimates of a density function," *The Annals of Mathematical Statistics*, vol. 27, no. 3, pp. 832–837, 1956.

[12] E. Parzen, "On estimation of a probability density function and mode," *The Annals of Mathematical Statistics*, vol. 33, no. 3, pp. 1065–1076, 1962.

[13] B. A. Turlach, "Bandwidth selection in kernel density estimation: A review," Institut für Statistik und Ökonometrie, Humboldt-Universität zu Berlin, Tech. Rep., 1993.

[14] D. W. Scott and S. R. Sain, "Multi-dimensional density estimation," *Handbook of Statistics*, vol. 24, pp. 229–261, 2005.

[15] Y.-C. Chen, "A tutorial on kernel density estimation and recent advances," *Biostatistics & Epidemiology*, vol. 1, no. 1, pp. 161–187, 2017.

[16] B. W. Silverman, *Density Estimation for Statistics and Data Analysis*. CRC press, 1986.

[17] D. M. Bashtannyk and R. J. Hyndman, "Bandwidth selection for kernel conditional density estimation," *Computational Statistics & Data Analysis*, vol. 36, no. 3, pp. 279–298, 2001.

[18] M. C. Jones, J. S. Marron, and S. J. Sheather, "A brief survey of bandwidth selection for density estimation," *Journal of the American Statistical Association*, vol. 91, no. 433, pp. 401–407, 1996.

[19] S.-T. Chiu, "A comparative review of bandwidth selection for kernel density estimation," *Statistica Sinica*, vol. 6, pp. 129–145, 1996.

[20] S. Shah, D. Dey, C. Lovett, and A. Kapoor, "Airsim: High-fidelity visual and physical simulation for autonomous vehicles," in *Field and Service Robotics*, Springer, 2018, pp. 621–635.

[21] M. R. Zofka, S. Klemm, F. Kuhnt, T. Schamm, and J. M. Zöllner, "Testing and validating high level components for automated driving: Simulation framework for traffic scenarios," in *IEEE Intelligent Vehicles Symposium (IV)*, IEEE, 2016, pp. 144–150.

[22] E. Semsar-Kazerooni, J. Verhaegh, J. Ploeg, and M. Alirezaei, "Cooperative adaptive cruise control: An artificial potential field approach," in *IEEE Intelligent Vehicles Symposium (IV)*, 2016, pp. 361–367.

[23] E. de Gelder, I. Cara, J. Uittenbogaard, L. Kroon, S. van Iersel, and J. Hogema, "Towards personalised automated driving: Prediction of preferred ACC behaviour based on manual driving," in *IEEE Intelligent Vehicles Symposium (IV)*, 2016, pp. 1211–1216.

[24] Duin, "On the choice of smoothing parameters for parzen estimators of probability density functions," *IEEE Transactions on Computers*, vol. C-25, no. 11, pp. 1175–1179, 1976.

[25] A. Z. Zambom and R. Dias, "A review of kernel density estimation with applications to econometrics," *International Econometric Review (IER)*, vol. 5, no. 1, pp. 20–42, 2013.

[26] H. Monkhouse, I. Habli, and J. Mcdermid, "The notion of controllability in an autonmous vehicle context," in *CARS 2015 — Critical Automotive applications: Robustness & Safety*, 2015.

THE EFFECT OF P-AEB SYSTEM PARAMETERS ON THE EFFECTIVENESS FOR REAL WORLD PEDESTRIAN ACCIDENTS

Michael Gruber, Harald Kolk, Ernst Tomasch, Florian Feist, Corina Klug
Graz University of Technology
Austria

Anja Schneider, Franz Roth, Volker Labenski
Audi AG
Germany

Karthikeyan Shanmugam, Magdalena Lindman, Anders Fredriksson
Volvo Car Corporation
Sweden

Paper Number 19-0130

ABSTRACT

The objective of this ACEA funded study was to determine the effect of different pedestrian autonomous emergency braking (P-AEB) systems on the collision speeds of real world pedestrian accidents originating from three different accident databases. The precrash phases of real world passenger car to pedestrian frontal accidents from the in-depth accident databases were investigated using different pre-crash simulation tools. Collision parameters were compared between the original real-world cases and cases with treatment conditions. For treatment simulations, the car was equipped with a virtual generic P-AEB system, triggered at a time to collision (TTC)≤ 1 s. The range of the generic sensor was 80 m and the opening angle was varied between 60°, 90° and 120°. For the braking system, two different brake gradients (24.5 m/s³ and 35 m/s³) were modelled with different decelerations of 0.8 g and 1.1 g. Accidents from the Austrian in-depth accident database CEDATU (n=50), the German GIDAS (n=1084) and Swedish V_PAD (n=68) were used for the baseline. The effect of using different data samples was compared to the effect of assuming different generic AEB system parameters. The best performing P-AEB system (120°, innovative brake system) avoided 42% of the CEDATU cases, while the baseline P-AEB system (60°, standard brake system) avoided 18%. The best performing AEB System was able to avoid 79.4% of the V_PAD sample. The baseline P-AEB avoided in V_PAD at least 66.2% compared to GIDAS with 39.5%. The lower the mean collision speed of the sample, the higher was the benefit of the P-AEB system, as a higher percentage of cases can be avoided. The study shows that system parameters and the selection of accidents can greatly affect the outcome in prospective traffic safety analyses. As a significant reduction of collision speeds was seen in all three data sources, the study highlights the need for a combined vehicle safety assessment instead of a separate evaluation of active and passive pedestrian safety measures.

INTRODUCTION

Pedestrians accounted for 21% of the total road fatalities in the European Union in 2016 [1]. Safety measures addressing pedestrians have not been as effective as those for car occupants. While the total number of road fatalities decreased by 41% in the period from 2007 and 2016, it was only reduced by 36% for pedestrians [1]. It is expected that active safety systems, such as pedestrian autonomous emergency braking (P-AEB) systems will help to avoid or mitigate pedestrian accidents. Studies agree, however, that all accidents cannot be avoided, which is the reason why passive safety systems will be still needed in the future [2–8]. In the Euro NCAP VRU assessment active and passive safety measures are evaluated separately, i.e. in a non-integrative way. However, active safety measures influence the boundary conditions of accidents which were not avoided by the active safety measure. The question is raised of what targets for passive safety measures are relevant for vehicles with P-AEB systems in the future.

The present study was conducted in the framework of the project ProPose, which is funded by ACEA (European Automobile Manufacturers' Association) and addresses the following questions:

1. How many real-world accidents can be avoided with P-AEB systems?
2. Is there a need to consider an update of the speed range addressed by passive safety measures in the future?
3. How does the sensor opening angle and brake characteristic affect the effectiveness of the P-AEB system?

The effect on collision speed for different crash data samples was analyzed in order to suggest input to future pedestrian crash test setups, relevant for the design of passive safety measures. In contrast to other studies, the analyses were examined by comparing results based on three different accident databases.

METHOD

The effectiveness of the conceptual P-AEB systems was determined by means of comparing baseline- (the crash situations without the AEB) with treatment (the same situations but with a concptual P-AEB system) virtual simulations.
Collision parameters of the original real-world cases (w/o P-AEB) were compared to those with a conceptual P-AEB system. The method used in this study is referred to as 'virtual pre-crash simulation'. In the last couple of years this type of investigation gained importance for the evaluation of effectiveness of active safety systems [9–14].
To analyse the effectiveness of P-AEB systems it is crucial that the velocity-time-history is known for the entire duration of the pre-crash phase, where the P-AEB deploys.

Input Data

In this study, the pre-crash phase of real-world passenger car to pedestrian frontal collision accidents from three different in-depth accident databases (Table 1) were investigated using different pre-crash simulation tools. Within the accident databases, the reconstructed accidents including the pre-crash phase are available. In CEDATU (Central Database for In-Depth Accident Study) [15,16] accidents are reconstructed with the software PC Crash on the basis of police-, medical-, witness and court reports, photos and photogrammetric analysis of the accident side. In V_PAD [17] (Volvo Cars Pedestrian Accident Database), the information considered by the crash investigator at Volvo's Traffic Accident Research Team is compiled and the pre-crash phase is digitized in order to provide vehicle paths in relation to vehicle velocities and to the surroundings in a numerical time history data (THd) format. The GIDAS (German In-Depth Accident Study) accidents are recorded on scene and therefore often provide additional information [18]. Apart from regional differences, the three databases are also differing in terms of their case selection criteria: In CEDATU Austrian accidents with at least one injured road user are included, for which access to the court file is given [16]. In GIDAS accidents are selected according to a statistical sampling process [18] from the area around Hannover and Dresden. The V_PAD sample [17] consists of Swedish pedestrian accidents reported to the insurance company Volvia (IF P&C Insurances), where all new Volvo passenger cars in Sweden are insured for at least three years. The different inclusion criteria for the databases are clearly reflected in injury distributions and speed statistics, see Table 1.

Table 1: Comparison of applied data sources, simulation tools and variations

Source	CEDATU	GIDAS	V_PAD
Region	Austria	Hannover, Dresden	Sweden
Number of accidents for simulation	50	1084	68 SCP cases
cases with MAIS 4+ (AIS98)	50 %	7 %	3 %
cases with MAIS 3 (AIS98)	14 %	9 %	10 %
cases with MAIS 2 (AIS98)	24 %	33 %	40 %
cases with MAIS 1 (AIS98)	6 %	45 %	41 %
cases with unspec. MAIS 3+ (AIS98)	6 %	6 %	4 %
Analysed Scenarios	All	All	SCP
Mean initial speed [km/h]	50 (SD=22.9)	35.5 (SD=16.8)	31.5 (SD=17.1)
Mean collision speed [km/h]	47.2 (SD=20.4)	30.7 (SD=14.6)	23.6 (SD=16.3)
Median collision speed [km/h]	45	29.1	20
Simulation tool	X-Rate	rateEFFECT	VCART
Variations	Sensor 1-3; Brake 1-4	Sensor 1, Brake 1	Sensor 1-3; Brake 1-4

Only vehicle-to-pedestrian accidents which comply with the following filter criteria are considered in this study:

- the vehicle is a car or van, mass up to 3.5t,
- the vehicle is moving forward,
- the pedestrian was upright (not laying) prior to the impact,
- the pedestrian was struck by a single vehicle,
- only one pedestrian was involved in the accident,
- the vehicle was not skidding before the crash (but braking vehicles were included),

- Additional filter criterion for CEDATU and GIDAS: the pedestrian was impacted by the front of the vehicle,
- Additional Filter Criteria for V_PAD: the crossing path of the pedestrian was straight (SCP according to Figure 6 in the Appendix were considered).

The conflict situations (according to the classification introduced by Lindman et al. [17], which is explained in detail in Figure 6 in the Appendix) covered in the CEDATU and GIDAS sample, are shown in Figure 1: In the majority (80%) of the CEDATU cases, the pedestrian was crossing the road while the cars were driving straight (SCP). In 60% of the SCP accidents the pedestrian was entering the street straight from the left (far-side) and in 22,5% (9 cases) straight from the right side (near-side). In 20% of the CEDATU cases the pedestrian was either walking in the same direction (SD), oncoming direction (OD) of the, or the car was turning to the left (LT) prior to the impact. In the GIDAS dataset, 84% of the pedestrian were crossing the road while the cars were driving straight (SCP). I the remaining 9% of the GIDAS sample, the pedestrian was walking in the same direction (SD), oncoming direction (OD) of the car or the car was turning left (LT) or to the right (RT) prior impact. For 5%, another conflict situation occurred. In the V_PAD dataset, only conflict situations with a straight crossing pedestrian (SCP) were included. In 68% of the CEDATU and 69% of the GIDAS cases, the accident occurred on dry roads compared to V_PAD, where only 33.8% occurred on dry roads.

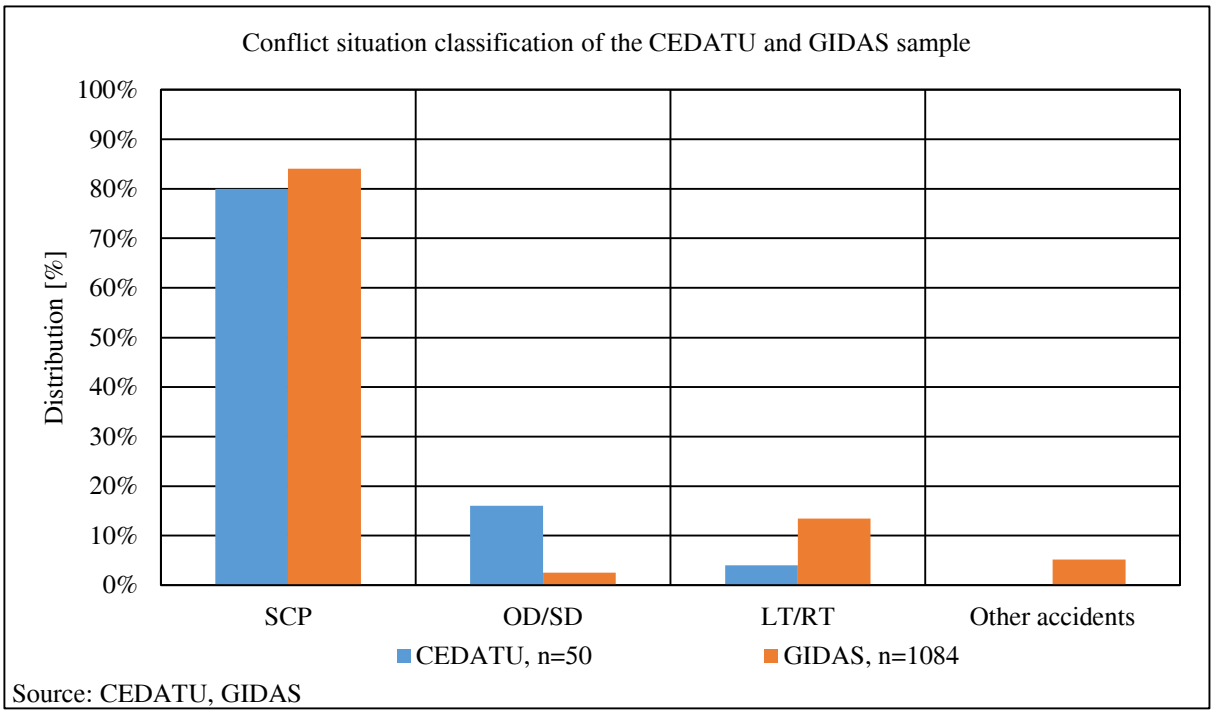

Figure 1. Conflict situations covered in the CEDATU and GIDAS sample. For the V_PAD sample, only SCP crashes were considered.

Virtual pre-crash simulation

The pre-crash phases of reconstructed real-world accidents were rerun within a virtual forward simulation, where the vehicle follows the trajectory and the velocity profile of the reconstructed case until the system reacts. The baseline simulations were compared to treatment simulations, where the vehicles are virtually equipped with an ideal, conceptual P-AEB System having a generic sensor and various braking strategies.

The virtual forward pre-crash simulations in this study were made using three different simulation tools: X-RATE, rateEFFECT and VCaRT: In general, each of them operates on a time-step basis. At each time-step, the tool updates its information (speed, position, rotation, etc.) on dynamic objects by querying the dynamics simulation module. Based on that information, the sensor vision module determines which objects in the environment are visible. The sensor information is then forwarded to the function logic module which represents the P-AEB systems that are simulated by the individual tools. When the function logic module decides to intervene by e.g. braking, appropriate deceleration values are forwarded to the dynamics module for simulation of the next time step. The simulation terminates as soon as the stop criteria are fulfilled (i.e. first collision is detected or maximum simulation time reached).

X-RATE (Extended Effectiveness Rating of Advanced Assistance Systems) is developed by the Vehicle Safety Institute at TU Graz to simulate a variation of different sensor parameters and different active safety systems. It has already been used successfully for several research questions (e.g. pedestrian collision avoidance systems [19], collision mitigation for motorcycles at junctions [20], collision mitigation at intersections [21]) or in combination with traffic flow simulation [22]). X-RATE is developed in MATLAB and operates in conjunction with PC-Crash as driving dynamics simulation core.
rateEFFECT is a tool developed and used by Volkswagen Group to analyse the performance of advanced driver assistance or safety systems in traffic scenarios and to evaluate the effectiveness of active safety systems. The functionality is very similar to X-RATE as the vehicle dynamics and the scenery is based on PC Crash, too. Via a system editor it is possible to define own active systems with predefined or self-developed function blocks. The system configuration generally consists of sensors, algorithms, driver models and actuators. [23,24] The effectiveness assessment is an important procedure during the process of function development and is used for internal and external research questions, latest for the accident analysis done for the effectiveness evaluation of the General Safety Regulation for the European Commission [12–14].
VCaRT (Volvo Cars Research pre-crash simulation Tool) is a MATLAB tool to evaluate the potential of conceptual and ideal crash avoidance/mitigation ADAS. The tool main parts are simulation control, vehicle surrounding, virtual vehicle and collision control. The simulation control synchronizes the execution of the other parts, which can be configured depending on the test to be performed. Elements in the vehicle surrounding are 3-dimensional representations of the objects. The vehicle representation is based on a point-mass-model combined with actuator models that constrains the response on function logic requests. Examples of parameters that can be varied in the sensor model are field of view, sensor position and classification time.

Analysis of results
In order to analyse the potential safety effect of the P-AEB systems, the collision speed was used. It was defined as the speed of the vehicle at the first time step when the pedestrian and the vehicle geometries were intersecting. The mean and median collision velocities as well as the standard deviations (SD) were analysed from the different data sets separately. The mean of the relative reduction ($\overline{\Delta v_{c_rel}}$) of the collision speed was calculated according to Equation (1) as 1 minus the mean value of the case-wise ratio of the collision speed in the treatment simulations ($v_{c-treatment_i}$) and the baseline simulation ($v_{c-baseline_i}$), with n being the number of analysed cases.

$$\overline{v_{c_red_rel}} = 1 - \frac{1}{n}\sum_{i=1}^{n}\frac{v_{c-treatment_i}}{v_{c-baseline_i}} \qquad \text{Equation (1)}$$

Conceptual P-AEB system
The generic sensor of the virtual P-AEB system was positioned 1.8 m behind the vehicle front. The range of the sensor model was set to 80 m. The opening angle of the sensor model was varied between 60° (Sensor 1), 90° (Sensor 2) and 120° (Sensor 3). The sensor vision was implemented by considering vision rays, also described in [25] and checks visibility of objects every 15 ms. The vision rays are emitted horizontally with a resolution of 0.1°, as shown in Figure 2. Intersections of the vision rays and the pedestrian are detected at each time step. If the pedestrian is fully within the sensor area, this is classified and the Time to Collision (TTC) is calculated.
The TTC is calculated by deriving a relative speed vector between the car and the pedestrian at each time step. The algorithm estimates how long it would take until a detected point, moving with the relative speed, contacts the ego-vehicle (car). The minimum time for all detected points is the estimated TTC for this time-step.
The P-AEB is triggered, when the pedestrian is classified (i.e. visible and 100% in the sensor area) for at least 150 ms (acquisition time) and the calculated TTC is ≤ 1 s. The car and pedestrian follow the original trajectory and the acceleration profiles remain unchanged until the AEB takes over.
After getting the AEB trigger signal, a 0.2 s actuator delay is assumed (=reaction time of the brake system).

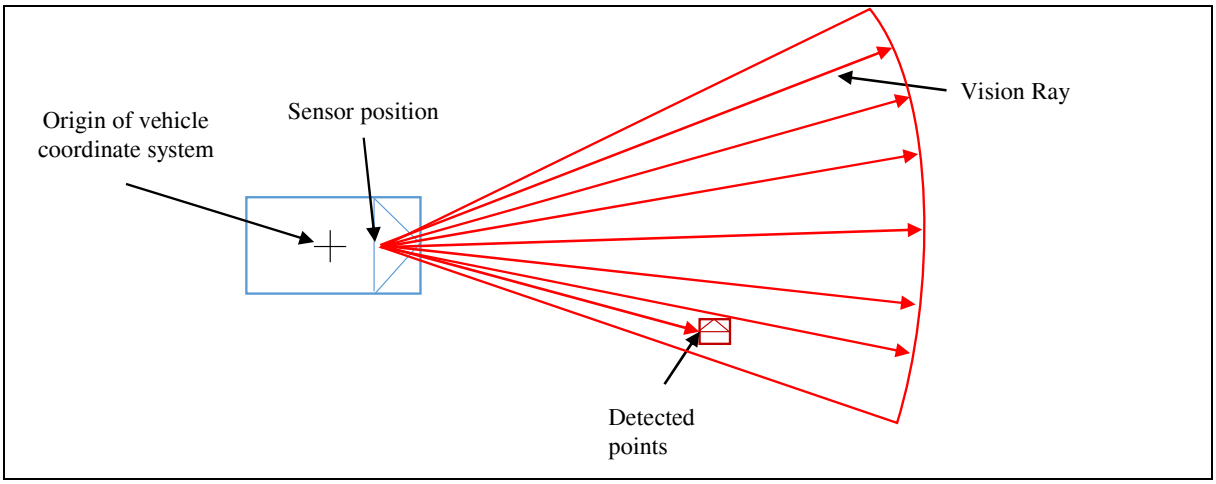

Figure 2. Top view of the sensor vision based on [25]

As brakes are activated, the maximum realisable acceleration is build up. The build-up time depends on the brake gradient of the system (see Equation (2). The results for the build-up times are shown in Table 9 in the appendix.

$$build\text{-}up\ time = \frac{deceleration}{brake\ gradient} \qquad \text{Equation (2)}$$

The maximum deceleration depends on the friction coefficient which in turn depends on the road conditions. Different brake systems were evaluated (Table 2), which differed in terms of braking gradient and maximum realisable deceleration. In total four variations were investigated.

Table 2.
Definition of the braking systems for treatment simulations

	Braking system	Brake gradient	Max. realisable deceleration
Brake 1	Standard	24.5	0.8*g
Brake 2	Standard	24.5	1.1*g
Brake 3	Innovative	35	0.8*g
Brake 4	Innovative	35	1.1*g

The braking profiles of the different braking strategies are shown in Figure 3. After the actuator delay, the deceleration increases with the defined brake gradients to the maximally feasible deceleration.
Brake 1 and Sensor 1 as well as the applied strategy are in accordance with a previous studies [12–14].

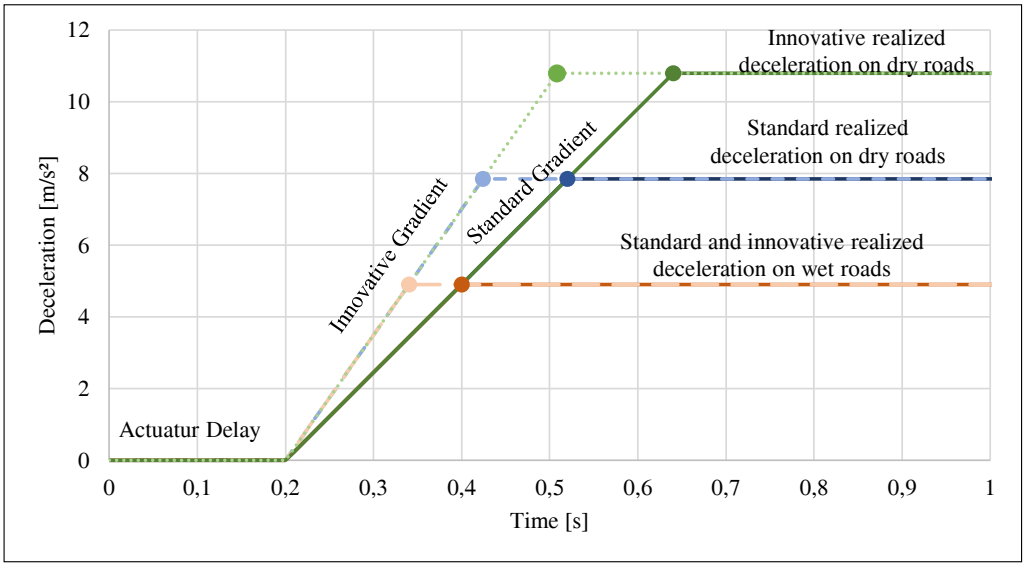

Figure 3. Braking Profile

RESULTS

In total, twelve treatment simulations of every baseline simulation were performed for the CEDATU and V_PAD sample. In GIDAS only one treatment simulation per baseline simulation (with Sensor 1 and Brake 1) was performed.
The results are presented by means of the data sample in this section. Collision speeds and the share of avoided cases of the different treatment simulations are compared to the baseline sample. For avoided accidents the collision speed was set to 0 km/h, resulting in a relative reduction of 100%. Mean and Median values were analysed per braking system for each sensor as well as overall braking systems.

CEDATU Cases

The mean collision speed of the original baseline CEDATU cases was 47.2 km/h (SD=20.4 km/h) and the median 45 km/h. The mean collision speed over all simulated P-AEB strategies was reduced by 55% to 24.9 km/h (SD=22 km/h). The individual results of the treatment simulations are shown in Table 3, depending on the sensor-opening angle and the braking system. The highest reduction of the collision speed $\overline{v_{c_red}}$ (including avoided accidents as accidents with 0 km/h) was observed with Sensor 3 and Brake 4. The baseline collision speed of 47.2 km/h (SD=20.4 km/h) was reduced by 67.1% to 19.2 km/h (SD=22.7 km/h and the median from 45 km/h to 6.7 km/h. Sensor 3 and Brake 4 avoided 21 accidents (42%). The lowest change of the collision speed was observed with Sensor 1 and Brake 1. The reduction was 17.8 km/h (45.5%) and 9 accidents (18%) were avoided. A comparison of Sensor 1 and 2 shows that the difference of the mean collision speed due to the increased sensor angles was 0.1 km/h. A difference of the collision speed of about 0.3 km/h was observed between Sensor 1 and Sensor 3. Sensor 3 avoided one additional accident compared to Sensor 1 or 2. A comparison of Brake 1, 2 and 3 shows that a higher maximum deceleration results in a lower collision speed than a larger brake gradient.
With Brake 1 and Sensor 1 or 2, nine accidents were avoided (18%). When increasing the maximum deceleration to 1.1 g (Brake 2), five additional collisions were avoided (in total 28% avoided accidents). By increasing the brake gradient to 35 m/s³ (Brake 3), two additional accidents were avoided compared to brake 1. Combined with the higher maximum deceleration (Brake 4), a total number of 20 (40%) accidents were avoided.

Table 3.
Results of the CEDATU treatment simulations depending on the sensor opening angle and braking strategy including avoided accidents as accidents with 0 km/h

Sensor strategy	Braking strategy	Median v_c [km/h]	Mean $\overline{v_c}$ [km/h]	Mean reduction $\overline{v_{c_red}}$ [km/h]	Mean rel. reduction $\overline{v_{c_red_rel}}$ [%]	Avoided cases
Baseline		45	47.2 (SD=20.4)	-	-	-
Sensor 1	Brake 1	27.6	29.4 (SD=22.5)	17.8	45.5%	9 (18%)
	Brake 2	19.5	23.8 (SD=22.6)	23.4	56.4%	14 (28%)
	Brake 3	25.1	27.6 (SD=22.5)	19.6	50.0%	11 (22%)
	Brake 4	8.7	19.6 (SD=22.6)	27.6	64.7%	20 (40%)
	Overall	24.2	25.1 (SD=22.9)	22.1	54.1%	
Sensor 2	Brake 1	27.6	29.3 (SD=22.6)	17.9	45.9%	9 (18%)
	Brake 2	19.4	23.7 (SD=22.6)	23.5	56.8%	14 (28%)
	Brake 3	25.0	27.5 (SD=22.6)	19.7	50.2%	11 (22%)
	Brake 4	8.7	19.5 (SD=22.6)	27.7	65.1%	20 (40%)
	Overall	23.0	25.0 (SD=22.9)	22.2	54.5%	
Sensor 3	Brake 1	27.6	29.1 (SD=22.7)	18.1	47.9%	10 (20%)
	Brake 2	19.4	23.5 (SD=22.7)	23.7	58.8%	15 (30%)
	Brake 3	25	27.3 (SD=22.8)	19.9	52.2%	12 (24%)
	Brake 4	6.7	19.2 (SD=22.7)	28.0	67.1%	21 (42%)
	Overall	23.0	24.8 (SD=23.0)	22.4	56.5%	

In Table 4 the results of the CEDATU sample were separated between cases where the pedestrians were coming from the left (far side) or right side (near side).
The mean collision speed of the 24 far side cases was 45.8 km/h (SD=16.9 km/h). The mean collision speed of the treatment simulations of all P-AEB systems was 23.7 km/h (SD=20.5 km/h), with a reduction of 55.7%. Due to the best braking strategy (Brake 4) the collision speed was reduced by 66.8% to 17.5 km/h (SD=19.8 km/h) compared to the least effective braking strategy (Brake 1), for which the mean collision speed was reduced to 28.2 km/h (47.2%). In the simulations with Brake 4, twelve accidents were avoided, while six accidents were avoided with Brake 1. For the far side scenario, no influence of the sensor angle was observed.
The sample comprises nine accidents from the nearside scenario with a baseline mean collision speed of 30 km/h (SD=13.1 km/h). The collision speed was reduced to 11.2 km/h (SD=12.3 km/h) within the simulations with Sensor 1 or Sensor 2, which is a reduction of 61.9%. The simulations with Sensor 3 achieved a collision speed of 10 km/h (SD=12.8 km/), this was a reduction of 73%. With Sensor 1 or 2, at least 3 accidents were avoided (33%). Sensor 3 and braking system 4 was the most effective system as 5 accidents were avoided (55%) and the lowest mean collision speed for treatment simulations (7.2 km/h, SD=11.8 km/h) was observed.

Table 4.
CEDATU treatment simulations for far side and nearside SCP traffic simulation scenarios including avoided accidents as accidents with 0 km/h

		Farside situations (n=24)			Nearside situations (n=9)		
Sensor strategy	Braking strategy	Mean $\overline{v_c}$ [km/h]	$\overline{v_{c_red}}$ [km/h] ($\overline{v_{c_red_rel}}$)	Avoided cases	Mean $\overline{v_c}$ [km/h]	$\overline{v_{c_red}}$ [km/h] ($\overline{v_{c_red_rel}}$)	Avoided cases
Baseline		45.8 (SD=16.9)	-	-	30.0 (SD=13.1)	-	-
Sensor 1	Brake 1	28.2 (SD=20.5)	17.5 (47.3%)	6 (25%)	13.0 (SD=12.7)	16.9 (56.4%)	3 (33%)
	Brake 2	22.4 (SD=20.2)	23.4 (58.6%)	8 (33%)	12.1 (SD=11.9)	17.9 (58.7%)	3 (33%)
	Brake 3	26.8 (SD=20.1)	18.9 (50.1%)	6 (25%)	11.4 (SD=12.4)	18.6 (62.6%)	3 (33%)
	Brake 4	17.5 (SD=19.8)	28.2(66.9%)	12 (50%)	8.4 (SD=11.6)	21.6 (69.9%)	4 (44.4%)
	Overall	23.7 (SD=20.5)	22.0 (55.7%)	-	11.2 (SD=12.3)	18.7 (61.9%)	--
Sensor 2	Brake 1	28.2 (SD=20.5)	17.5 (47.3%)	6 (25%)	13.0 (SD=12.7)	16.9 (56.4%)	3 (33%)
	Brake 2	22.4 (SD=20.2)	23.4 (58.6%)	8 (33%)	12.1 (SD=11.9)	17.9 (58.7%)	3 (33%)
	Brake 3	26.8 (SD=20.1)	18.9 (50.1%)	6 (25%)	11.4 (SD=12.4)	18.6 62.6%)	3 (33%)
	Brake 4	17.5 (SD=19.8)	28.2(66.9%)	12 (50%)	8.4 (SD=11.6)	21.6 (69.9%)	4 (44.4%)
	Overall	23.7 (SD=20.5)	22.0 (55.7%)	-	11.2 (SD=12.3)	18.7 (61.9%)	-
Sensor 3	Brake 1	28.2 (SD=20.5)	17.5 (47.3%)	6 (25%)	11.8 (SD=13.4)	18.1 (67.5%)	4 (44.4%)
	Brake 2	22.4 (SD=20.2)	23.4 (58.6%)	8 (33%)	10.9 (SD=12.5)	19.1 (69.8%)	4 (44.4%)
	Brake 3	26.8 (SD=20.1)	18.9 (50.1%)	6 (25%)	10.2 (SD=12.9)	19.8 (73.7%)	4 (44.4%)
	Brake 4	17.5 (SD=19.8)	28.2(66.9%)	12 (50%)	7.2 (SD=11.8)	22.7 (81.0%)	5 (55.5%)
	Overall	23.7 (SD=20.5)	22.0 (55.7%)	-	10.0 (SD=12.8)	19.9 (73.0%)	-

An influence of the opening angle was observed in two simulated accident cases without sight obstructions at junctions (conflict situation LT/SD and SCP). The relative trajectory of the pedestrian to the vehicle is shown in Figure 4 with black lines. For the first accident (SCP), only the P-AEB with Sensor 3 was able to avoid the accident. In the second case (LT/SD), the AEB was triggered with Sensor 2 and 3 earlier. The System was able to reduce the collision speed by about 23.4% from 25 km/h to 19.4 km/h with the best system (Sensor 3 and Brake 4). In Figure 4, the relative position of the pedestrian to the vehicle is shown for 2 other CEDATU cases as grey line. These two cases with sight obstructions were detected for all sensor angles at the same time.
In another 5 accidents with sight obstructions, the pedestrian was classified at the same time and no influence of the opening angle was observed.

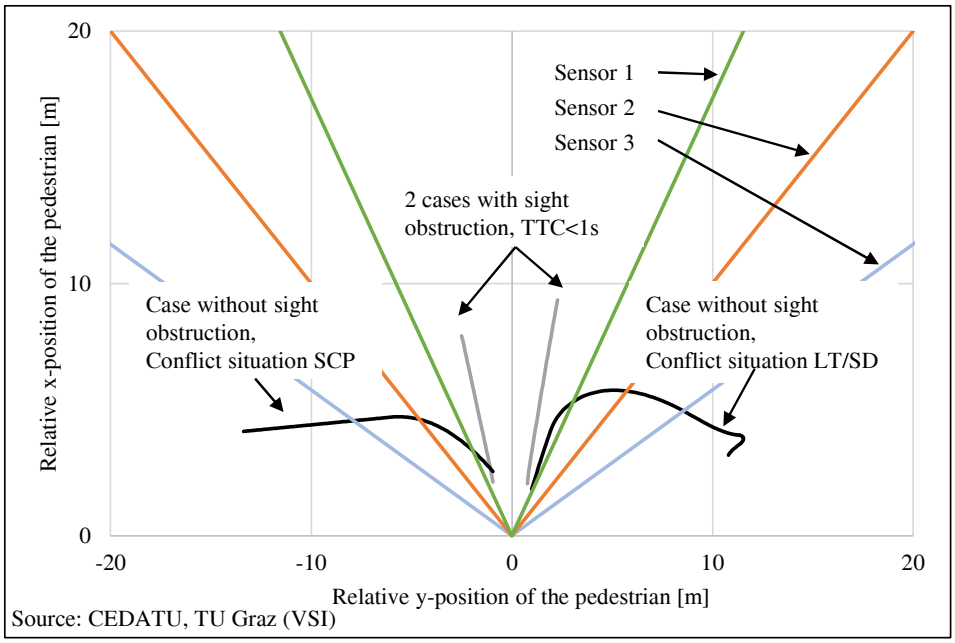

Source: CEDATU, TU Graz (VSI)

Figure 4. Trajectories of the pedestrian relative to the vehicle of CEDATU simulations for four selected cases

GIDAS Cases

The mean collision speed of the original GIDAS cases was 30.7 km/h (SD=14.6). Due to treatment simulations with Sensor 1 and Brake 1 (Table 5), the collision speed was reduced by 17.1 km/h to 13.6 km/h (SD=14.7), which equals a relative reduction ($\overline{v_{c_red_rel}}$) of 57.7%. This system avoided 39.6% of 1078 cases.

Table 5.
Results of the GIDAS treatment simulations depending on the sensor opening angle and braking strategies including avoided accidents as accidents with 0 km/h

Sensor strategy	Braking strategy	Median v_c [km/h]	Mean $\overline{v_c}$ [km/h]	Mean reduction $\overline{v_{c_red}}$ [km/h]	Mean rel. reduction $\overline{v_{c_red_rel}}$ [%]	Avoided cases
Baseline		29.1	30.7 (SD=14.6)	-	-	-
Sensor 1	Brake 1	11.0	13.6 (SD=14.7)	17.1	57.7%	429 (39.6%)

V_PAD Cases

The mean collision speed of the original V_PAD cases was 23.6 km/h (SD=16.3 km/h) and the median 20 km/h. The mean collision speed for all simulated P-AEB strategies was reduced by 70.2% to 7 km/h (SD=22 km/h).
The treatment simulation results are shown in Table 6, depending on the sensor opening angle and the braking system. The highest change of collision speed $\overline{v_{c_red}}$ (including avoided accidents with 0 km/h) was achieved with Sensor 3 and Brake 4. The baseline collision speed of 23.6 km/h (SD=16.3 km/h) was reduced to 5.8 km/h (SD=12.4 km/h). This represents a reduction of 17.8 km/h ($\overline{v_{c_red_rel}}$ =86.6%). The lowest reduction of the collision speed ($\overline{v_{c_red_rel}}$ =79%) was achieved with Sensor 1 and Brake 1. The effect of the different sensors was very small. The mean collision speeds differed by only 0.1-0.2 km/h for all brakes. The results of Sensor 2 and 3 were equal for all brakes. The mean collision speed of Sensor 1 over all braking systems was 7.1 km/h

(SD=13.2 km/h). All braking systems with Sensor 2 and Sensor 3 were able to reduce the collision speed to 7 km/h (SD=13.3 km/h).
A comparison of the braking systems shows that Brake 4 leads to the lowest collision speed for all three simulated sensors. With Brake 2 and 3, differences in standard deviation and number of avoided accidents were observed.
In the simulations with Sensor 1 and Brake 1 at least 45 (66.2%) accidents were avoided, while the number of avoided cases with Sensor 2 and 3 was at least 47 (69.1%). The best system (Sensor 3, Brake 4) avoided 54 accidents (79.4%).

Table 6.
Results of the V_PAD treatment simulations depending on the sensor opening angle and braking strategy including avoided accidents as accidents with 0 km/h

Sensor strategy	Braking strategy	Median v_c [km/h]	Mean $\overline{v_c}$ [km/h]	Mean reduction $\overline{v_{c_red}}$ [km/h]	Mean rel. reduction $\overline{v_{c_red_rel}}$ [%]	Avoided cases
Baseline		20	23.6 (SD=16.3)	-		-
Sensor 1	Brake 1	0	8.2 (SD=13.9)	15.4	79.0%	45 (66.2%)
	Brake 2	0	7.2 (SD=13.3)	16.4	81.1%	48 (70.6%)
	Brake 3	0	7.2 (SD=13.1)	16.4	81.4%	49 (72.1%)
	Brake 4	0	6.0 (SD=12.4)	17.7	83.7%	52 (76.5%)
	Overall	0	7.1 (SD=13.2)	16.5	81.3%	-
Sensor 2	Brake 1	0	8.1 (SD=14.0)	15.6	81.9%	47 (69.1%)
	Brake 2	0	7.0 (SD=13.3)	16.6	84.0%	50 (73.5%)
	Brake 3	0	7.0 (SD=13.2)	16.6	84.3%	51 (75.0%)
	Brake 4	0	5.8 (SD=12.4)	17.8	86.6%	54 (79.4%)
	Overall	0	7.0 (SD=13.3)	16.6	84.2%	-
Sensor 3	Brake 1	0	8.1 (SD=14.0)	15.6	81.9%	47 (69.1%)
	Brake 2	0	7.0 (SD=13.3)	16.6	84.0%	50 (73.5%)
	Brake 3	0	7.0 (SD=13.2)	16.6	84.3%	51 (75.0%)
	Brake 4	0	5.8 (SD=12.4)	17.8	86.6%	54 (79.4%)
	Overall	0	7.0 (SD=13.3)	16.6	84.2%	-

In Table 7 the results of the V_PAD sample were separated in far side and near side scenarios. The mean collision speed of the 32 far side cases was 26.8 km/h (SD=17.8 km/h). The collision speed was reduced to 9.7 km/h (SD=15.3 km/h) with simulations of Sensor 1. The mean relative reduction ($\overline{v_{c_red_rel}}$) was 74%. The simulations with Sensor 2 and 3 achieved a reduction of 80.3 % to a collision speed of 9.4 km/h (SD=15.4 km/h). With Sensor 1, at least 19 accidents (59.4%) were avoided. The most effective System (Sensor 3 and Brake 4) avoided 23 (71.9%) of the 32 far side scenarios and reduced the collision speed about 18.6 km/h (82.6%) to 9.4 km/h (SD=15.4 km/h)
The V_PAD sample comprises 36 nearside scenarios with a baseline collision speed of 20.9 km/h (SD=14 km/h). The collision speed was reduced for all 3 sensors by about 87.7% to 4.8 km/h (SD=10.6 km/h). Brake 1 avoided 26 (72.2%), Brake 2 28 (77.7%) and Brake 3 29 (80.5%) accidents. The best system with Brake 4 avoided 31 of the 36 near side cases (86.1%). No influence of the sensor opening angle for the nearside scenario was observed.

Table 7.
V_PAD treatment simulations for farside and nearside SCP traffic simulation scenarios including avoided accidents as accidents with 0 km/h

		Farside scenario (n=32)			Nearside scenario (n=36)		
Sensor strategy	Braking strategy	Mean $\overline{v_c}$ [km/h]	$\overline{v_{c_red}}$ [km/h] ($\overline{v_{c_red_rel}}$)	Avoided cases	Mean $\overline{v_c}$ [km/h]	$\overline{v_{c_red}}$ [km/h] ($\overline{v_{c_red_rel}}$)	Avoided cases
Baseline		26.8 (SD=17.8)	-	-	20.9 (SD=14.0)	-	-
Sensor 1	Brake 1	10.9 (SD=15.9)	15.8 (71.7%)	19 (59.4%)	5.8 (SD=11.3)	15.1 (85.5%)	26 (72.2%)
	Brake 2	9.9 (SD=15.5)	16.8 (73.4%)	20 (62.5%)	4.8 (SD=10.3)	16.1 (87.9%)	28 (77.7%)
	Brake 3	9.5 (SD=15.0)	17.3 (74.7%)	20 (62.5%)	5.1 (SD=10.8)	15.7 (87.3%)	29 (80.5%)
	Brake 4	8.5 (SD=14.5)	18.3 (76.4%)	21 (65.6%)	3.7 (SD=9.7)	17.1 (90.2%)	31 (86.1%)
	Overall	9.7 (SD=15.3)	17.0 (74.0%)	-	4.8 (SD=10.6)	16.0 (87.7%)	-
Sensor 2	Brake 1	10.6 (SD=16.1	16.1 (77.9%)	21 (65.5%)	5.8 (SD=11.3)	15.1 (85.5%)	26 (72.2%)
	Brake 2	9.6 (SD=15.7)	17.1 (79.7%)	22 (68.8%)	4.8 (SD=10.3)	16.1 (87.9%)	28 (77.7%)
	Brake 3	9.2 (SD=15.1)	17.6 (80.9%)	22 (68.8%)	5.1 (SD=10.8)	15.7 (87.3%)	29 (80.5%)
	Brake 4	8.2 (SD=14.6)	18.6 (82.6%)	23 (71.9%)	3.7 (SD=9.7)	17.1 (90.2%)	31 (86.1%)
	Overall	9.4 (SD=15.4)	17.3 (80.3%)	-	4.8 (SD=10.6)	16.0 (87.7%)	-
Sensor 3	Brake 1	10.6 (SD=16.1	16.1 (77.9%)	21 (65.5%)	5.8 (SD=11.3)	15.1 (85.5%)	26 (72.2%)
	Brake 2	9.6 (SD=15.7)	17.1 (79.7%)	22 (68.8%)	4.8 (SD=10.3)	16.1 (87.9%)	28 (77.7%)
	Brake 3	9.2 (SD=15.1)	17.6 (80.9%)	22 (68.8%)	5.1 (SD=10.8)	15.7 (87.3%)	29 (80.5%)
	Brake 4	8.2 (SD=14.6)	18.6 (82.6%)	23 (71.9%)	3.7 (SD=9.7)	17.1 (90.2%)	31 (86.1%)
	Overall	9.4 (SD=15.4)	17.3 (80.3%)	-	4.8 (SD=10.6)	16.0 (87.7%)	-

Summary of most and the least effective system

In Table 8, the mean reduction of the least effective system (Sensor 1, Brake 1) and the most effective System (Sensor 3, Brake 4) including avoided accidents as accidents with 0 km/h collision speed is shown. The results show a similar reduction of the collision speed for Sensor 1 and Brake 1 for all three databases. In the GIDAS sample, the speed was reduced by 17.1 km/h (57.7%) compared to 17.8 km/h (45.5%) in the CEDATU cases and 15.4 km/h (79%) in the V_PAD cases. With the most effective system (Sensor 3, Brake 4), a higher reduction of the collision speed was observed compared to the least effective System. In CEDATU, a reduction of 28 km/h (67.1%) was observed and in V_PAD, 17.8 km/h (86.6%).

Table 8.
Mean reduction of the collision speed through treatment simulations including avoided accidents as accidents with 0 km/h

	Sensor 1, Brake 1		Sensor 3, Brake 4	
Database	Mean reduction $\overline{v_{c_red}}$ [km/h]	Mean rel. reduction $\overline{v_{c_red_rel}}$ [%]	Mean reduction $\overline{v_{c_red}}$ [km/h]	Mean rel. reduction $\overline{v_{c_red_rel}}$ [%]
CEDATU	17.8	45.5%	28	67.1%
GIDAS	17.1	57.7%	-	-
V_PAD	15.4	79.0%	17.8	86.6%

DISCUSSION

Effect of different data sources

Accident scenarios in different countries can highly differ [26] for various reasons (e.g. different speed limits, country specific regulations, etc.). Thus, it is valuable to include different regions for such kind of investigation. For the present study, three databases were available.

The three different data samples differed in terms of the collision velocities of the accidents. The mean speed in the CEDATU sample was highest with 47.2 km/h, followed by GIDAS with 30.7 km/h and V_PAD with 23.6 km/h. The greater severity of the CEDATU accidents is also obvious from the analysis of the injury severities: In the CEDATU sample, 50% of the pedestrians suffered an injury of severity greater than AIS 4 +. In the GIDAS sample only 7% and the V_PAD sample only 3% of the pedestrians sustained AIS 4+ injuries.

Even if the relative speed reduction is similar in simulations based on the three different data sources, the mean speeds for remaining crashes is lower in V_PAD. The V_PAD sample is based on insurance claim reports, and is thus including a wide range of crash situations. Compared to VRU cases in the police reported sample in STRADA, only 50% of crashes reported to the insurance company were covered by police reports [27]. This is a probable reason why the mean collision speed in this data sample is lower than in the other two data samples. Also, the baseline sample from V_PAD only included SCP crashes that are associated with lower collision speeds than e.g. situations in longitudinal traffic. CEDATU and GIDAS include more severe accident cases and therefore, results based on CEDATU and GIDAS are reflecting higher collision speeds. Differences in initial speed are caused by the original focus of CEDATU on accidents resulting in fatalities (cases before 2008) and different share of conflict situations between the CEDATU and GIDAS datasets.

For all three data sources, information of crashes were collected retrospectively. The collision speeds and trajectories of the baseline simulations are calculated based on accident sketches. However, in GIDAS an accident team is investigating the accident on the spot whereby in CEDATU and V_PAD the data are investigated based on various kinds of reports. In order to compensate for uncertainties in the pre-crash data, robustness analysis of parameters should be performed (e.g. variation of pedestrian- and car speed). This is usually done for baselines from V_PAD, but was not performed in the current study.

Although it was tried to perform analysis as similar as possible, the applied simulation tools were not harmonised. Those differences are discussed within the P.E.A.R.S. initiative [11], which is working on the definition of a harmonised assessment process for effectiveness evaluations.

The results show a similar reduction of the collision speed for all three data sources with the least effective system (Sensor 1 and Brake 1).

Speed range for passive safety measures

To calculate the overall effectiveness, the avoided cases are assigned a collision speed of 0 km/h. Else the effectiveness evaluation would rate systems poorer as they are, because only severe cases remain.

When defining requirements for the passive safety measures, though, it makes no sense to consider avoided cases. Therefore, those were excluded for the definition of requirements to future passive safety measures that is discussed in the following section.

It is remarkable that even for the severe CEDATU sample the least effective P-AEB system (Sensor 1, Brake 1) is able to reduce the mean collision speed to less than 40 km/h, which is the impact speed in current passive safety systems. 63.4% of the unavoided cases would be covered by current pedestrian safety testing. In the V_PAD simulations with the least effective system, 87% of the simulated were below 40 km/h.

The speed distribution (shaded area) and the cumulative speed distribution (lines) of the cases are shown in Figure 5. The baseline speeds include all cases, the treatment simulation only unavoided cases. The analysis show that if it is intended to cover the same ratio of accidents with passive safety measures as today (with vehicles without P-AEB system), the speed considered for the evaluation of passive safety measures can be reduced by at least 34%. With the impact speed at 40 km/h [ref procedure], it would be possible to address a larger proportion of accidents than today. Looking at the results based on the V_PAD sample (although considering only SCP situations) more than 90% of the remaining accidents had speeds below this.

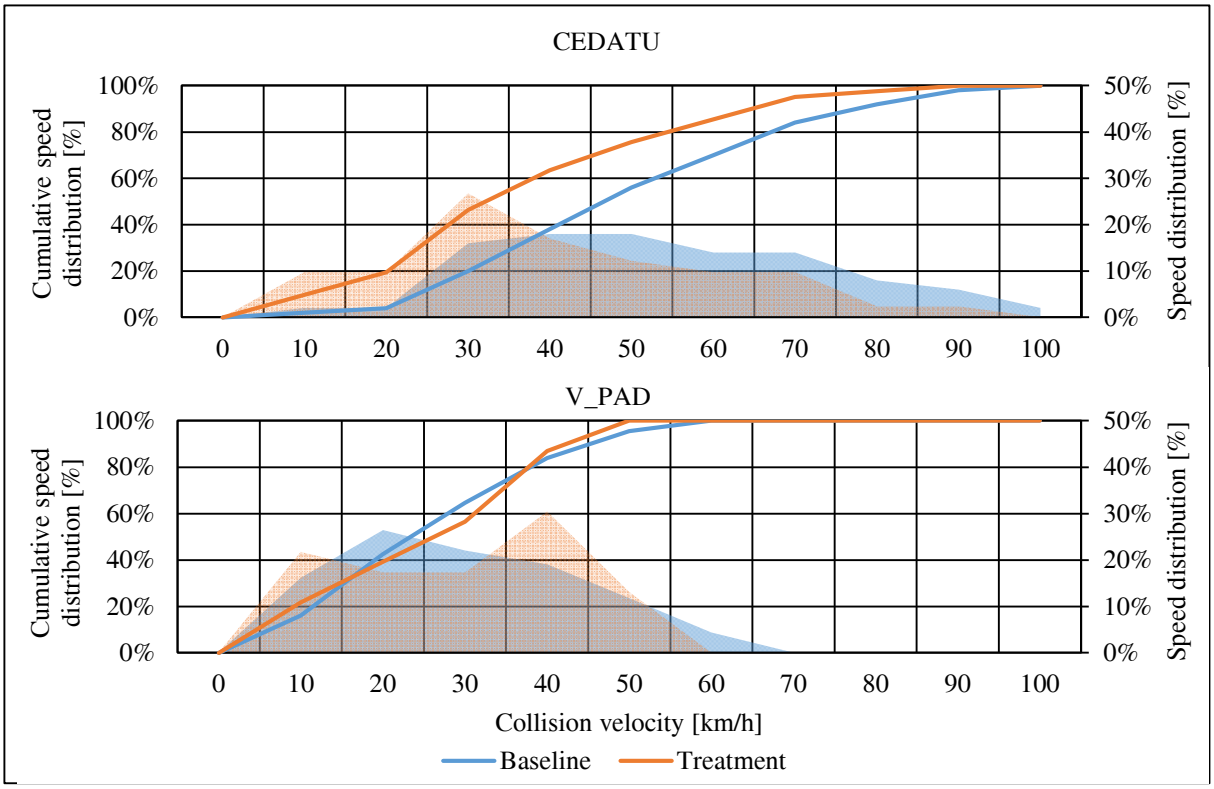

Figure 5. Distribution of the cumulative collision speed for crashes in baseline and unavoided crashes in treatment condition (baseline cases in the treatment not considered)

Effect of opening angle

A similar effect of the sensor opening angle was noticed in treatment simulations of the V_PAD and CEDATU cases. Increasing the sensor angle did affect the results only marginally. Within CEDATU, a sensor opening angle of 120° additionally avoided one accident more (+2%) compared to 60° and 90°. For V_PAD, a sensor opening angle of 90° and 120° avoided 2 additional accidents (+2.9%) compared to 60°.

Effect of braking characteristics

A higher brake gradient (Brake 3 versus Brake 1) leads to two additional (+4%) avoided cases in CEDATU and four additional (+5.8%) in the V_PAD sample. Increasing the maximum realisable deceleration (Brake 1 vs 2 and 3) has a greater effect on the CEDATU cases than on the V_PAD sample.

The effect of the different braking systems depends to a great extent on the sample composition. In the CEDATU sample, 68% of the cases were on dry road, 69% in GIDAS and 33.8% in V_PAD. A comparison of Brake 2 and 3 in V_PAD showed no differences in mean collision speed, while 5.6 km/h in CEDATU.

For real sensors, proper classification and collision detection of moving objects such as pedestrians is a particular challenge. With the ideal generic sensors, in the performed simulations, the pedestrian was classified only when it was 100% in the sensor field of view. Collision detection was based on deriving a relative speed vector between the car and the pedestrian and exact detected positions, while real sensor output is noisy and contains measurement error. The algorithm of the real safety system therefore operates under the assumption that the data is noisy, which leads to different implementations than with an ideal sensor. Furthermore, environmental influences (rain, fog) also negatively affect the visibility of objects, which has not been accounted for in the ideal sensor. Overall, the effects from ideal P-AEB systems that were evaluated in this study can differ from real P-AEB systems.

CONCLUSIONS

Virtual precrash simulations of different ideal and conceptual P-AEB systems using real-world pedestrian cases from three different accident databases as baseline, showed that the lower the mean baseline collision speed in

the data sample, the more accidents were avoided. The maximum deceleration was the most influential P_AEB system parameter on the share of avoided cases and on the collision speed of the remaining cases. With the best system and the least severe data sample, 20% of the accidents/crashes still remained. A drastic reduction of collision speed (min 34%) was observed in all three data samples and this even with the most conservative P-AEB system parameters. This clearly highlights the need for a combined vehicle safety assessment instead of a separate evaluation of active and passive pedestrian safety measures.

ACKNOWLEDGEMENT

The study was funded by the European Automobile Manufacturers' Association (ACEA).

REFERENCES

[1] European Commission, June 2017. Traffic Safety Basic Facts on Pedestrians; Available from: https://ec.europa.eu/transport/road_safety/sites/roadsafety/files/pdf/statistics/dacota/bfs2017_pedestrians.pdf.

[2] Lindman M., Ödblom A., Bergvall E., Eidehall A., Svanberg B., Lukaszewicz T. Benefit Estimation Model for Pedestrian Auto Brake Functionality.

[3] Hummel T., Kühn M., Bende J., Lang A., 2011. Advanced Driver Assistance Systems: An investigation of their potential safety benefits based on an analysis of insurance claims in Germany. Berlin: GDV.

[4] Chen Q., Lin M., Dai B., Chen J., 2015. Typical Pedestrian Accident Scenarios in China and Crash Severity Mitigation by Autonomous Emergency Braking Systems. In: SAE International, editor. SAE 2015 World Congress Proceedings. SAE International.

[5] Strandroth J., Nilsson P., Sternlund S., Rizzi M., Krafft M., 2016. Characteristics of future crashes in Sweden – identifying road safety challenges in 2020 and 2030. In: International Research Council on the Biomechanics of Injury, editor. 2016 IRCOBI Conference Proceedings. IRCOBI, p. 47–60.

[6] Vertal P., Steffan H., 2016. Evaluation of the Effectiveness of Volvo's Pedestrian Detection System Based on Selected Real-Life Fatal Pedestrian Accidents. In: SAE International, editor. SAE 2016 World Congress Proceedings. SAE International.

[7] Luttenberger P., Tomasch E., Willinger R., Mayer C., Bakker J., Bourdet N. et al., 2014. Method for future pedestrian accident scenario prediction. In: Transport Research Arena.

[8] Detwiller M., Gabler H.C., 2017. Potential Reduction in Pedestrian Collisions with an Autonomous Vehicle. In: NHTSA, editor. The 25th ESV Conference Proceedings. NHTSA, p. 1–8.

[9] Jeppsson H., Östling M., Lubbe N., 2018. Real life safety benefits of increasing brake deceleration in car-to-pedestrian accidents: Simulation of Vacuum Emergency Braking. Accid Anal Prev 111:311–20. https://doi.org/10.1016/j.aap.2017.12.001.

[10] Rosén E., Källhammer J.-E., Eriksson D., Nentwich M., Fredriksson R., Smith K., 2010. Pedestrian injury mitigation by autonomous braking. Accid Anal Prev 42(6):1949–57. https://doi.org/10.1016/j.aap.2010.05.018.

[11] Page Y., Fahrenkrog F., Fiorentino A., Gwehenberger J., Helmer T., Lindman M. et al., 2015. A Comprehensive and Harmonized Method for Assessing the Effectiveness of Advanced Driver Assistance Systems by Virtual Simulation: The P.E.A.R.S. Initiative. In: NHTSA, editor. The 24th ESV Conference Proceedings. NHTSA.

[12] Barrow A., Edwards A., Smith L., Khatry R., Kalaiyarasan A., Hynd D., 2018. Effectiveness estimates for proposed amendments to the EU's General and Pedestrian Safety Regulations. 3rd ed. Wokingham, Berkshire, United Kingdom: TRL.

[13] Roth F., Labenski V., Gruber M., Kolk H., 2018. Future Traffic Scenario under Consideration of AEB Systems. In: CARHS, editor. Praxiskonferenz Fußgängerschutz.

[14] TRL, CEESAR, ACEA, September 2018. Accident Analysis.

[15] Tomasch E., Steffan H., 2006. ZEDATU - Zentrale Datenbank tödlicher Unfälle in Österreich - A Central Database of Fatalities in Austria. In: ESAR, editor. 2nd International Conference on ESAR "Expert Symposium on Accident Research". ESAR.

[16] Tomasch E., Steffan H., Darok M. (eds.), 2008. Retrospective accident investigation using information from court.

[17] Lindman M., Jakobsson L., Jonsson S., 2011. Pedestrians interacting with a passenger car; a study of real world accidents. In: International Research Council on the Biomechanics of Injury, editor. 2011 IRCOBI Conference Proceedings. IRCOBI, p. 255–264.

[18] Brunner, Horst, Krettek, Christian, Otte, Dietmar et al., 2003. Scientific Approach and Methodology of a New In-depth Investigation Study in Germany so called GIDAS. In: NHTSA, editor. The 18th ESV Conference Proceedings.

[19] Tomasch E., Sinz W., Hoschopf H., Kolk H., Steffan H., 2015. Bewertungsmethodik von integralen Sicherheitssystemen durch Kombination von Test und Simulation am Beispiel von Fußgängerunfällen. In: 10. VDI-Tagung Fahrzeugsicherheit - Sicherheit 2.0: Berlin, 25. und 26. November 2015. Düsseldorf: VDI-Verlag, p. 157–169.

[20] Michael Gruber, Christian Matt, Ernst Tomasch, Alessio Sevarin, Harald Kolk, Christian Ellersdorfer et al. (eds.), 2018. Effectiveness assessment of a generic collision mitigation system for motorcycles at junctions.

[21] Kolk H., Kirschbichler S.K., Tomasch E., Hoschopf H., Luttenberger P., Sinz W., 2016. Prospective evaluation of the collision severity of L7e vehicles considering a Collision Mitigation System. In: Transportation Research Procedia. Elsevier.

[22] Kolk H., Tomasch E., Haberl M., Fellendorf M., Moser A., Rüther M. et al., 2018. Active safety effectiveness assessment by combination of traffic flow simulation and crash-simulation. In: ESAR, editor. 8th International Conference on ESAR "Expert Symposium on Accident Research".

[23] Hierlinger, Thomas: Dirndorfer, Tobias, Neuhauser T., 2017. A method for the simulation-based parameter optimization of autonomous emergency braking systems. In: NHTSA, editor. The 25th ESV Conference Proceedings. NHTSA, p. 1–9.
[24] Wille J., Zatloukal M., 2012. rateEFFECT - Effectiveness evaluation of active safety systems. In: ESAR, editor. 5th International Conference on ESAR "Expert Symposium on Accident Research", p. 1–41.
[25] Kolk H., Kirschbichler S., Tomasch E., Hoschopf H., Luttenberger P., Sinz W., 2016. Prospective evaluation of the collision severity of L7e vehicles considering a collision mitigation system. In: TRA, editor. 6th Transport Research Arena 2016 (TRA).
[26] Kreiss J., Feng G., Krampe J., Meyer M., Niebuhr T., Pastor C. et al. Extrapolation of GIDAS Accident Data to Europe.
[27] Isaksson-Hellman I., Werneke J., 2017. Detailed description of bicycle and passenger car collisions based on insurance claims. Safety Science 92:330–7. https://doi.org/10.1016/j.ssci.2016.02.008.

APPENDIX

Table 9.
Calculated Build - Up Times

Build-up times	Brake gradient	
Realized Deceleration	24.5 m/s³	35 m/s³
0.5*g = 4.91 m/s²	0.2 s	0.14 s
0.8*g = 7.85 m/s²	0.32 s	0.22 s
1.1*g = 10.79 m/s²	0.44 s	0.31 s

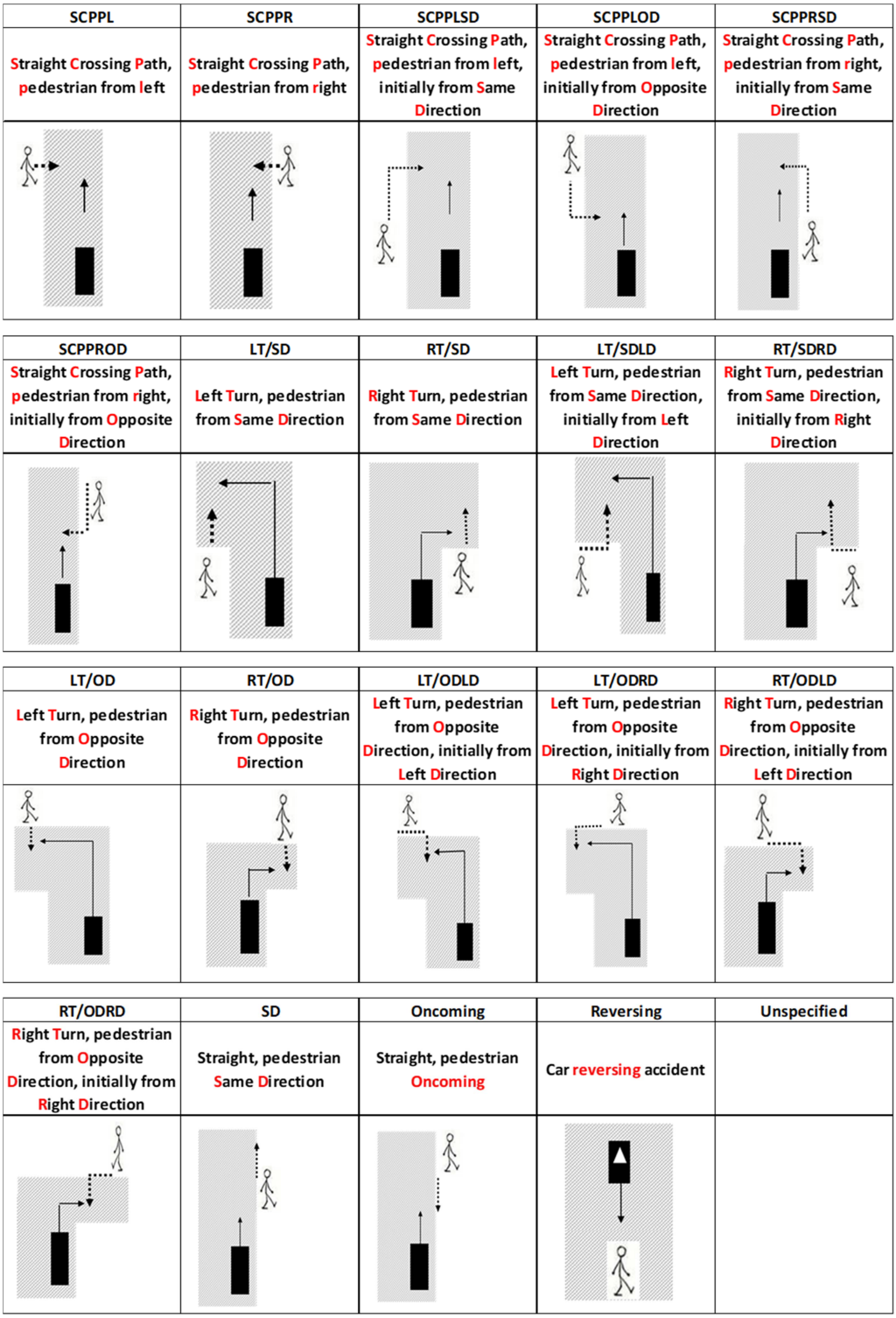

Figure 6: Definition of conflict situations according to Lindman et al. [17]

STRUCTURAL COUNTERMEASURE STUDY ON OBLIQUE OFFSET FRONTAL IMPACT

Mahendran, Paramasuwom
Velayudham, Ganesan
EDAG Inc
United States of America

Harjinder, Singh
United States Steel Corporation
United States of America

Paper Number 19-0131

ABSTRACT

National Highway Traffic Administration (NHTSA) has been investigating an oblique offset frontal impact test. This project evaluates test and simulation results to determine structural changes to reduce occupant compartment intrusion. Review of test results indicated that mid-size Sedans and Pickup trucks showed higher structural intrusions and higher passenger compartment decelerations. Existing Computer Aided Engineering (CAE) models for a mid-size Sedan and Pickup truck were used to evaluate structural changes and the corresponding cost impact to improve performance in the oblique offset test condition. This paper describes the CAE study carried out to study structural reinforcement countermeasures for both the driver and passenger sides of the vehicle in left- and right-side oblique offset frontal impacts. This paper presents the structural mass changes due to reinforcement countermeasures and the cost impact.

INTRODUCTION

The objective of this research was to demonstrate necessary changes to a vehicle's structure and their associated cost in order to reduce the occupant compartment intrusion from NHTSA's oblique offset frontal crash condition. The finite element (FE) models of vehicle to be studied had to meet the structural intrusion requirements for a "Good" or "Acceptable" structural rating in the IIHS small overlap test, "Good" rating in IIHS moderate overlap test rating. The mentioned tests are as shown in Figure1.

The vehicle models chosen for this study were based on the availability of NHTSA oblique test results, and the availability of a good correlated CAE model. The CAE model should be modified with minimum effort to represent the vehicle for the NHTSA oblique test simulation. It also should represent a latest possible production year vehicle meeting NHTSA's 5-star rating as well as "Good" or "Acceptable" rating of IIHS small overlap frontal impact and "Good" rating of IIHS moderate overlap frontal impact.

Therefore, for the passenger car category, the chosen vehicle was the 2014 Honda Accord with "Good" IIHS ratings, 5-star NHTSA rating. The test results of 2014 Honda Accord were obtained from two NHTSA oblique tests.

For the pick-up category, the chosen vehicle was the 2014 Chevrolet Silverado 1500 with 5-star NHTSA ratings. In this case, the IIHS small overlap test results were not available when the model was developed. But IIHS has already conducted two small overlap tests on the 2016 Chevrolet Silverado, so the test results of 2016 Chevrolet Silverado 1500 were used for this study.

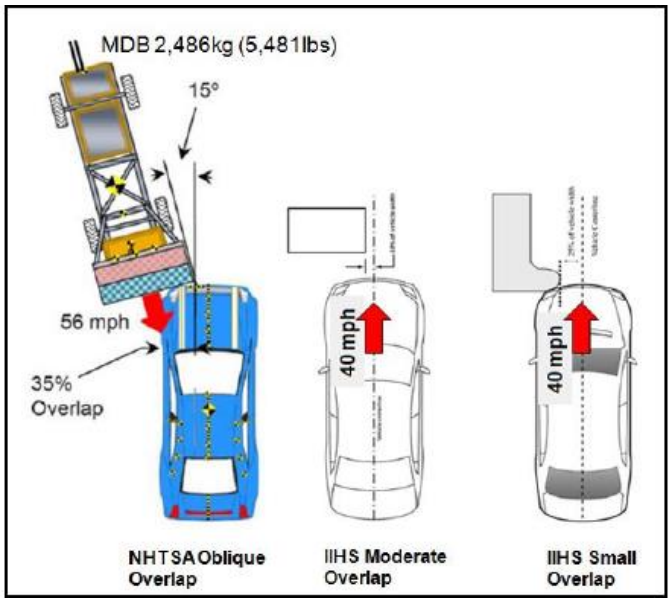

Figure 1. Vehicle Frontal Offset Tests.

During a high-speed crash event, the structural intrusions into the toe pan and dash panel are generally caused by hard contact between the intruding wheel and/or the engine/transmission assembly. In general, there are three methods applied to reduce structural intrusions. First is by absorbing as much energy as possible by the deforming structures. Second is by introducing failure points at key locations to deflect the intruding surfaces away from the critical zones on toe pan and dash panel and finally by reinforcing the passenger compartment by using high strength materials with optimized load paths.

This paper outlines the structural countermeasures undertaken to reduce the instructions by including these three methods. The detailed design of reinforcing components considered manufacturability, joining, and assembly into the vehicle design. Additionally, the cost impact of implementing the countermeasures was also studied.

The technical cost modeling (TCM) approach developed by Massachusetts Institute of Technology's Materials Systems Laboratory research was used in this research to estimate additional cost accrued due to the countermeasures. The TCM application allows consideration of the whole production process from part production, assembly, logistics and overhead cost.

COUNTERMEASURE STUDY

The countermeasure study included two vehicles Honda Accord 2014 and 2014 Chevrolet Silverado 1500. In each vehicle study, the FE model was developed first to obtain a baseline model compared to the corresponding crash tests. Upon validating the baseline model with acceptable correlation in terms of structural intrusions, it was used in the countermeasure development.

Passenger Car – 2014 Honda Accord

The full vehicle FE model of the 2012 Honda Accord which was developed and correlated for NHTSA's study [1] was updated to represent the 2014 MY Honda Accord. A few structural modifications going from 2012 to 2014 vehicle were undertaken by remodeling and updating the 2012 full vehicle model into 2014 full vehicle model. Necessary structural changes were obtained by white light scanning and CAD update of the 2014 vehicle parts accordingly. The details of updating 2012 Honda Accord full vehicle model is out of scope of this paper (it can be found in the NHTSA report [1]).

The updated FE model – 2014 Honda Accord full vehicle model is shown in Figure 2. The 2014 Honda Accord full vehicle model was setup for the following crash load cases.

1. NHTSA Oblique Offset Test (simulating left- and right-side frontal oblique offset)
2. Frontal NCAP Test

3. IIHS Moderate (40%) Frontal Offset Test
4. IIHS Small (25%) Overlap Front Test
5. Lateral NCAP Moving Deformable Barrier Test
6. Lateral NCAP Pole Test
7. IIHS Roof Crush Test
8. IIHS Lateral Moving Deformable Barrier Test

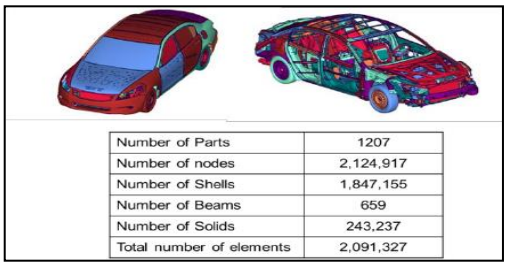

Number of Parts	1207
Number of nodes	2,124,917
Number of Shells	1,847,155
Number of Beams	659
Number of Solids	243,237
Total number of elements	2,091,327

Figure 2. 2014 Honda Accord CAE Model.

LS-DYNA simulations were run for each of the load cases. The simulation results were compared to the available test results. The review of the comparison between the FE results and test results concluded that, the overall correlation was acceptable to use the FE model for the oblique frontal impact requirements:

The details of baseline model development and FE results comparisons with test results can be found in [2]. The correlated FE model was used to identify suitable countermeasures design to reduce the occupant compartment intrusions. The countermeasures were based on observed body structure deformations when subjected to oblique impact on the driver and passenger sides. Higher intrusion values were mainly observed in the mid to lower section of the dash panel impacted by battery and brake booster assemblies on the driver side and by the transmission and engine block on the passenger side of the dash panel. Several CAE iterations were conducted to find the optimal set of structural changes. The recommended changes have to be fine-tuned in such a way that vehicle crash performance is not jeopardized for all other crash requirements, and also to make sure the design-packaging space for other vehicle systems is not violated.

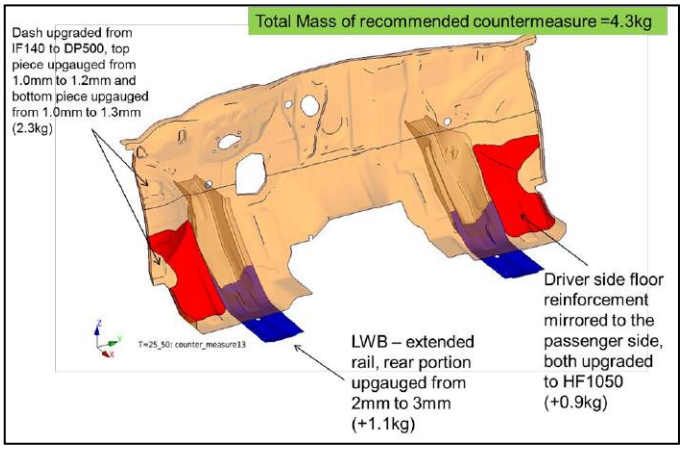

Figure 3. Structural Countermeasures to Reduce Occupant Compartment Intrusions.

The recommended changes are shown in Figure 3. These countermeasures added up to an additional mass increase of 4.3 kg for the entire body structure. These changes are given as follows:

1. The dash panel was changed to a laser-welded blank stamping, with increase in thickness from 1.00 mm to 1.20 mm upper segment and to 1.3 mm lower segment, incurring a mass penalty of 2.3 kg. Its material steel grade was also changed from low-strength steel to higher strength duel phase DP500. The dash panel using the higher grade can be successfully formed. The DP500 grade is a good formable grade with over 20 percent elongation.
2. The front rail extensions (left and right) stamped parts that were positioned under the lower dash panel and front floor panels were converted into laser-welded blank (LWB) stampings with two thicknesses. The

thickness of the rear of this part was increased from 2.00mm to 3.00mm, incurring a mass penalty of 1.1 kg for both parts.

3. The driver side front floor reinforcement panel (shown in red in Figure 3) was duplicated (mirror image) on to the passenger at an additional mass of 0.90 kg. The grade of steel was also changed to advance high-strength steel HF1050/1500 suitable only for hot-stamping.

Figure 4 shows the comparison of the dash panel before countermeasure (Baseline) and after countermeasure (CM). It can be observed that the countermeasure significantly reduced the intrusion levels of the dash below 150mm (>150mm intrusion is shown in red).

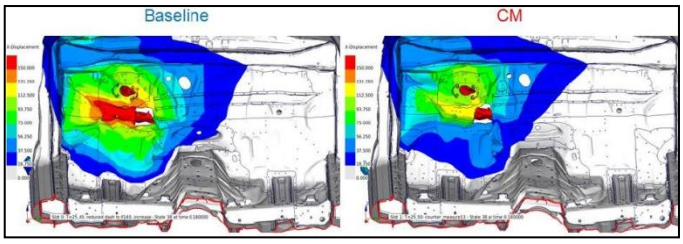

Figure 4. Baseline vs Countermeasure CAE - Dash View.

The countermeasure implementation affected little on the assembly process but significantly on the manufacturing process. Therefore, the manufacturing cost changes were estimated. The manufacturing costs of baseline parts and the corresponding countermeasure parts were calculated using the EDAG's TCM-based cost model mentioned in the introduction section. Incremental manufacturing and assembly costs of the added/subtracted components are summarized in Table 1 and Table 2. The cost of baseline parts weighing 14.73kg was estimated as $35.54 and the cost of countermeasure parts weighing 19.0kg was estimated as $59.91. The total cost increase for the countermeasures is $24.37 ($59.91 - $35.54). Total mass increase for the countermeasures is 4.3 kg (19.0 kg – 14.7 kg).

Table 1. 2014 Honda Accord Baseline Model - Subtracted Parts.

2014 Honda Accord - Baseline Parts						
Item #	Part Name	Qty per Veh	Steel Grade	Mass (kg)	Manufacturing Process	Part Piece Cost
1	Dash Panel	1	Mild 140/270	8.300	Stamping Single Thickness	$14.64
2	Dash Panel Bracket Lh	1	DP 500/800	0.900	Stamping Single Thickness	$3.68
3	Reinforcement Dash Panel Longitudinal Lh	1	Mild 140/270	2.765	Stamping Single Thickness	$8.61
4	Reinforcement Dash Panel Longitudinal Rh	1	Mild 140/270	2.765	Stamping Single Thickness	$8.61
			Total Mass	**14.73**	Total Part Piece Cost	**$35.54**

Table 2. 2014 Honda Accord Countermeasure Model - Added Parts.

2014 Honda Accord - Counter-Measure Parts						
Item #	Part Name	Qty per Veh	Steel Grade	Mass (kg)	Manufacturing Process	Part Piece Cost
1	Dash Panel	1	DP 500/800	10.600	Laser Welded Blank	$26.76
2	Dash Panel Bracket Lh	1	HF 1050/1500	0.900	Hot Stamped Single Thickness	$5.66
3	Dash Panel Bracket Rh	1	HF 1050/1500	0.900	Hot Stamped Single Thickness	$5.66
4	Reinforcement Dash Panel Longitudinal Lh	1	DP 500/800	3.300	Laser Welded Blank	$10.15
5	Reinforcement Dash Panel Longitudinal Rh	1	DP 500/800	3.300	Laser Welded Blank	$10.15
	Additional Assembly Cost					$1.53
			Total Mass	**19.000**	Total Part Piece Cost	**$59.91**

Light-Duty Pickup Truck – 2014 Chevrolet Silverado 1500

A very detailed FE model of the 2014 Chevrolet Silverado 1500 shown in Figure 5 was developed and correlated for NHTSA's lightweighting study [3]

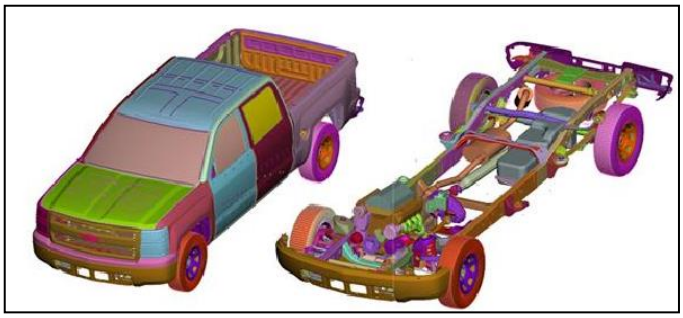

Figure 5. 2014 Chevrolet Silverado 1500 CAE Model.

For this study, the FE model was further modified from four-wheel-drive (4WD) to rear-wheel–drive (RWD) to represent the power train similar to NHTSA oblique-tested vehicles. The front drive differential, front drive shafts and power transfer unit were removed from the FE model as shown in Figure 6.

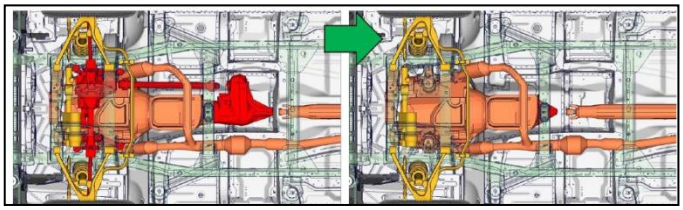

Figure 6. 2014 Chevrolet Silverado 1500 with the Front Wheel Drive Components Shown in Red.

For clarification a comparison of the tested vehicle and the updated FE model is shown Table 3.

Table 3. Oblique Test Vehicle Versus CAE Model.

Description	Tahoe (Test)	Silverado 1500 (Test)	CAE Model Silverado 1500
Model Year	2016	2012	2014
Drive	RWD	RWD	RWD
Engine Size (L)	5.3	4.8	5.3
Tested Weight (kg)	2722	2624	2582
Body Style	SUV	Crew-Cab	Crew-Cab

The FE model was correlated with the following crash load cases prior to using it for countermeasure study for the Oblique Impact:

1. NHTSA Oblique Offset Test (simulating left-side frontal oblique offset)
2. IIHS Small (25%) Overlap Front Test. Similarly, the correlated FE model was used to identify suitable countermeasures design to reduce the occupant compartment intrusions. The countermeasures were based on observed structure deformations when subjected to IIHS small offset and NHTSA oblique impact tests on the driver and passenger sides.

Higher intrusion values were observed mainly in the mid to lower section of the dash panel. The mid dash to lower area was impacted by the left front wheel and transmission on the passenger side. The rearward front wheel base intrusions were reduced by adding additional structure to the frame structure which is shown in red in Figure 7.

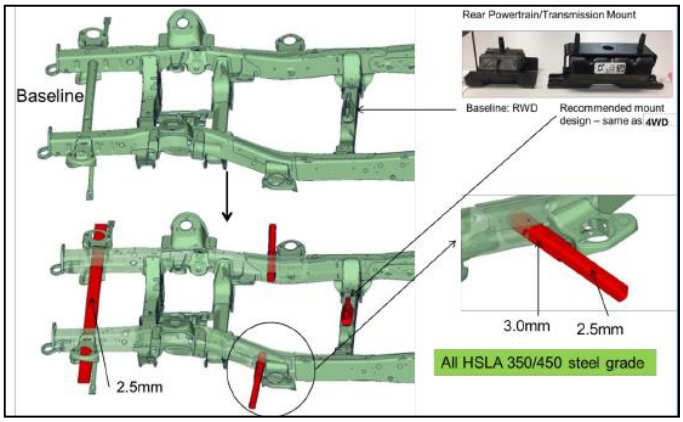

Figure 7. Structural Countermeasures to Reduce Occupant Compartment Intrusions.

Higher deformations were also observed for the IIHS small overlap results as shown in the intrusion chart in Figure 8. The developed countermeasures reduced the intrusion values for both load cases but slightly higher intrusions were found for the IIHS small overlap impact. However, the countermeasures improved the intrusions level within the acceptable range. Therefore, the developed countermeasures were decided still as a successful implementation. The countermeasure changes are shown in Figure 7. It increased the parts weight up to 9.0kg. These changes are symmetrical on the left and right sides of the vehicle. These changes are given as follows:

1. Modified front cross member to extend beyond frame rails, to be positioned in front of the front wheel/tires
2. Front wheel blocker bar positioned in front of the cab front mount
3. Change of the rear powertrain/transmission mount to the more robust design used on the 4WD Chevrolet Silverado 1500. It should be note that the 4WD mount is 1.0 kg heavier than the baseline.

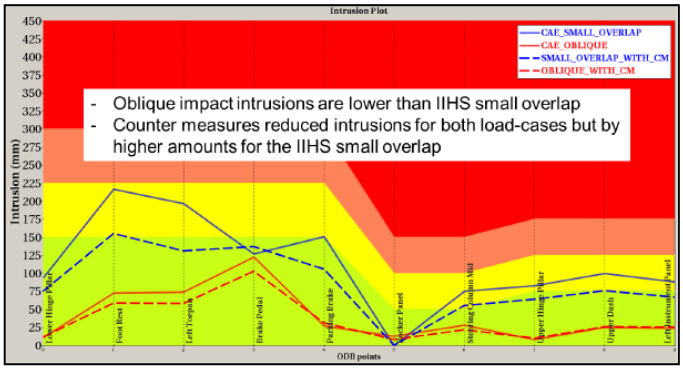

Figure 8. Structural Countermeasures: Reduce Occupant Compartment Intrusions for Oblique and IIHS Small Overlap.

Similar to 2014 Honda Accord, the manufacturing costs were estimated for Chevrolet Silverado 1500. In this case, the countermeasure implementation affected both manufacturing and assembly process. Therefore, both manufacturing and assembly costs of baseline parts and the corresponding countermeasure parts were calculated using EDAG's TCM-based cost model. Incremental manufacturing and assembly costs of the added/subtracted components are summarized in Table 4 to Table 7. From these tables, it can be noted that the total cost increase for the countermeasures is $17.35, total mass increase for the countermeasures is 9.0 kg and the cost impact is $1.93 per kilogram increase of weight.

Table 4. 2014 Chevrolet Silverado Baseline Model - Subtracted Parts.

Silverado Chassis Frame Baseline Manufacturing Costs						
Item #	Part Name	Qty per Veh	Material	Mass (kg)	Manufacturing Process	Part Piece Cost
1	Tube Front Crossmember	1	Mild 140/270	3.29	Hydoform Single Thickness	$5.08
2	Transmission Rear Mount	1	Various	0.65	Various	$2.77
			Total Mass	**3.94**	Total Parts Cost	**$7.85**

Table 5. 2014 Chevrolet Silverado Countermeasure Model - Added Parts.

Silverado Chassis Frame Countermeasures Manufacturing Costs						
Item #	Part Name	Qty per Veh	Material	Mass (kg)	Manufacturing Process	Part Piece Cost
1	Tube Front Crossmember	1	HLSA 350/450	6.50	Roll Form Closed Profile	$7.40
2	Side Frame Tube Inner Upper	2	HLSA 350/450	1.00	Roll Form Open Profile	$1.82
3	Side Frame Tube Inner Lower	2	HLSA 350/450	1.20	Roll Form Open Profile	$2.14
4	Side Frame Tube Outer	2	HLSA 350/450	2.60	Roll Form Closed Profile	$6.08
5	Transmission Rear Mount	1	Various	1.66	Various	$8.12
			Total Mass	**12.96**	Total Part Cost	**$25.56**

Table 6. 2014 Chevrolet Silverado Countermeasure Model - Assembly Cost.

Silverado Chassis Frame Baseline and Countermeasure Assembly Costs				
Item #	Part Name	Number of Fasteners or MIG Weld Length (mm)	Assembly Process	Cost
1	Chassis Frame Baseline	600 mm	MIG Weld	-$0.98
2	Chassis Frame Assembly Counter-Measure	1400 mm (additional assembly steps and fixtures cost)	MIG Weld	$3.78
		4 (washers, step bolts and nuts)	Mechanical Fasteners	$1.86
		Chassis Frame Assembly Cost Increase for the additional Countermeasures		**$4.66**

Table 7. 2014 Chevrolet Silverado Countermeasure Model - Summary Cost and Mass Increase.

Silverado Chassis Frame Baseline Versus. Countermeasure Costs				
Item #	Part Name	Process	Cost	Mass (kg)
1	Chassis Frame (Baseline)	Manufacture	-$7.85	3.94
		Assembly	-$0.98	
		Total	-$8.83	
2	Chassis Frame (Counter-Measure)	Manufacture	$20.54	12.96
		Assembly	$5.64	
		Total	$26.18	
		Δ Cost / Mass	**$17.35**	**9.02**

CONCLUSIONS

The 2014 Honda Accord and 2014 Chevrolet Silverado were chosen to conduct countermeasure implementation for NHTSA's oblique offset frontal impact. Both the vehicle has "good" to "acceptable" rating in IIHS small overlap test and "good" rating in IIHS Moderate overlap test. The FE models for both vehicles were correlated to selected crash load cases. CAE based structural modifications were implemented as countermeasures for oblique offset frontal impact targets. The intrusion levels were achieved within 150 mm target for 2014 Honda Accord and within acceptable range for 2014 Chevrolet Silverado 1500. Also, in case of 2014 Chevrolet Silverado, structural deformation was higher in IIHS small overlap compared to NHTSA's oblique offset frontal impact test. In order to reduce the structural deformation of the 2014 Honda Accord, the structural countermeasures caused 4.3kg of mass increase which in turn increased the cost by $24.37. Whereas, for 2014 Chevrolet Silverado 1500, the countermeasures required 9kg of mass increase and a cost increase of $17.35.

.

REFERENCES

[1] Singh, H., Kabeer, B., Jansohn, W., Davies, J., Kan, C.-D., Kramer, D., et al. (2012). Mass Reduction for Light-Duty Vehicles for Model Years 2017-2025. NHTSA.

[2] Singh, H., Ganesan, V., Davies, J., Paramasuwom, M., Gradischnig, L., Wood, P., et al. (2018). Structural Countermeasure/ Research Program: Mass and Cost Increase Due to Oblique Offset Moving Deformable Barrier Impact Test. NHTSA.

[3] Singh, H., Ganesan, V., Davies, J., Paramasuwom, M., Gradischnig, L., Wood, P., et al. (2016). Mass Reduction for Light-Duty Vehicles for Model Years 2017-2025. NHSTA.

INTERIOR AND RESTRAINT SYSTEMS MODELING FOR OBLIQUE OFFSET FRONTAL IMPACT

Mahendran, Paramasuwom
Velayudham, Ganesan
EDAG Inc
United States of America

Harjinder, Singh
United States Steel Corporation
United States of America

Paper Number 19-0133

ABSTRACT

National Highway Transport Safety Administration (NHTSA) has been investigating oblique offset frontal impact test conditions. This research developed a validated occupant interior and restraint systems that could be used to evaluate the kinematics and injury implications for frontal crash test conditions. The objective was to develop validated oblique offset crash simulations using both Test device for Human Occupant Restraint (THOR) dummy model and human body models. The vehicle selected for this Computer Aided Engineering (CAE) study was a 2014 Honda Accord. The vehicle interior was scanned and modeled and restraint characterization tests were conducted. The occupant interior finite element (FE) model was developed and validated against available test data. FE models for THOR dummies were seated in driver and passenger seats and validated against both left and right oblique offset test results. Subsequently, the 50th percentile FE Human body model from Global Human Body Models Consortium (GHBMC) was seated in the vehicle and the kinematics was compared against the THOR dummy model. The outcome of this study was to develop realistic FE models that could be used to investigate how crash test conditions can affect optimal occupant restraint system design. The results predicted from the CAE simulations of the baseline vehicle model demonstrated similar safety performance to the available vehicle test results in terms of vehicle acceleration and intrusion responses in NCAP frontal, IIHS moderate overlap, IIHS small overlap test procedures, and left and right NHTSA oblique frontal tests. The CAE simulation results compared well with test results for THOR dummy model accelerations and injury criteria. A comparison of occupant kinematics, belt loads and injury criteria against the simulations using the GHBMC model also was done. The CAE simulation results using the GHBMC also compared well with test and CAE results of using THOR dummy model.

INTRODUCTION

The occupant safety performance in some of the newer frontal crash test conditions, particularly oblique frontal crash tests, is dependent on the occupant interaction with the intruding vehicle components and the vehicle restraint system. It is desirable to develop full vehicle finite element models that can be used to study how changes in frontal crash test conditions can affect the occupant interaction with the restraint systems and the occupant injury outcomes. In this research, it was intended to develop a full vehicle finite element model, including the vehicle interior and occupant restraint systems for the driver and front seat passenger simulations using THOR dummy model and human body models.

The selected vehicle for this research was the 2014 Honda Accord as the CAE model was readily available from NHTSA's structural countermeasure program [1]. The chosen vehicle met the structural intrusion requirements of "Good" in both IIHS small and moderate overlap and 5-star in NCAP rating. The test procedure for CAE simulation used involves a high-speed oblique moving deformable barrier (OMDB) hitting a stationary vehicle with a 35-percent overlap at an angle of 15 degree from collinear, in both left and right. This test was conducted to replicate vehicle damage and occupant kinematics based on one of the common configuration crashes with belted occupant fatalities in vehicles with airbags [2].

The oblique frontal crash test currently uses the THOR dummy for evaluating occupant responses in the test vehicles. Currently, there are two finite element models available for THOR dummy. One version is publicly available from the University of Virginia, another is commercially available for lease from Humanetics, Inc. For this study, the University of Virginia THOR dummy model V2.1 of 50th percentile male occupant was used.

Additionally, there is considerable interest in using finite element models of the human body to compare their response and kinematics against the test dummies. Human body models that are commonly used for automotive research include the GHBMC model and the Total Human Model for Safety (THUMS) model from Livermore Software Technology Corporation. For this study the GHBMC 50th percentile male occupant Version 4.5 for LS-DYNA was leased from Elemance, LLC.

This paper describes the stages of CAE modeling and simulations. The initial step in the study was to obtain correlation between the actual oblique offset test performed by NHTSA and the CAE simulation. The parameters observed during the correlation task were THOR dummy model kinematics, airbag deployment and behaviors, seatbelt resistance force and occupant injury measures. When the simulations were correlated, the THOR models were replaced by GHBMC model and comparisons were made between the simulations of using THOR and GHMBC models.

VEHICLE INTERIOR MODEL DEVELOPMENT

The vehicle model was updated with vehicle interior and occupant restraint systems for the driver and front-seat passenger. White light scanned computer aided design (CAD) data for the interior of 2012 MY Honda Accord was used to represent the interior geometry of all relevant parts: instrument/dash panel assembly, center console, driver, and passenger seat. Occupant restraints system included airbags and seatbelts. Airbags and seatbelts were tested by conducting physical tests such as airbag deployment test and seatbelt pull test. They were then validated with the CAE simulations before integrating them in the full vehicle model. The details of FE modeling of interiors and restraint systems testing is out of the scope of this paper.

VEHICLE OBLIQUE OFFSET FRONT TEST SIMULATION – THOR AND HUMAN MODEL (GHBMC)

This test is used to determine the crashworthiness of the vehicle to protect occupants in offset frontal impact crash cases. The test consists of an oblique moving deformable barrier (OMDB) that weighs 2,490.2 kg traveling at a target speed of 90.12 km/h into a stationary vehicle as shown in Figure 1. The struck vehicle is positioned 15 degrees relative to the moving barrier and impacted 35 percent of the left or right side of the vehicle.

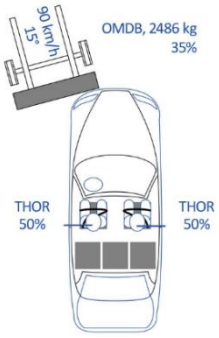

Figure 1. NHTSA Oblique Offset Setup.

THOR dummy model was duplicated into two models to have both driver and passenger. The two THOR dummy models were positioned on the vehicle driver and passenger seat respectively. It should be noted that the seat cushion foams were pre-deformed to accommodate dummies pelvic shape. Two-dimensional (2D) shell element seatbelts were modeled by routing over the shoulder and lap parts of the dummy models. The full vehicle model with the occupant models and restraint systems were checked for standard finite element model quality requirements such as connectivity, time-step and outputs. The model was run in LS-DYNA crash simulation solver for 200 milliseconds.

After the crash simulations with THOR dummy models were performed, using the THOR dummy models, another set of FE model were created by replacing the THOR dummy models by GHBMC models. Likewise, for this purpose, GHBMC model was duplicated into two models, respectively for driver and passenger. Once again, the full vehicle model with GHBMC models were run in LS-DYNA for 200 milliseconds. A comparative simulation results of test, THOR dummy models and GHBMC models are discussed in the following section.

CAE RESULTS DISCUSSION

At first the CAE results of full vehicle model oblique offset frontal impact case using THOR dummy models are compared to the test results. Next, the CAE results of the same using THOR dummy models are compared to CAE results of using GHBMC models.

Figure 2 shows crash simulations using THOR dummy models at 0ms (before crash) and at 120ms (after crash) comparing the test and CAE of THOR dummy models. It can be observed that both driver and passenger airbag deployed at 14ms and curtain airbag deployed in 42ms. Also, at 14ms, the seat belt pre-tensioner fired and tightened any slack defined as length of 25mm. At 120ms the driver dummy's head got sandwiched in between the driver airbag and curtain airbag, meanwhile the passenger dummy's head impacted the dashboard. Overall the kinematics of the CAE simulations and THOR dummy models show good correlation with the test results.

Figure 2. Test vs CAE simulations using THOR dummy models at 0ms (before crash) and 120ms (after crash).

Similarly, Figure 3 shows crash simulations using GHBMC models at 0ms (before crash) and at 120ms (after crash) while comparing THOR dummy models and GHBMC models. It can be observed that the deployment time of airbags and seatbelt pre-tensioner are similar to the simulation using THOR dummy models. In terms of kinematics, the behavior of the GHBMC models was found to be similar to the THOR dummy model except for the seatbelt behavior on the passenger side. Unlike THOR dummy models, in the GHBMC model, the seatbelt did not completely slip off the shoulder, resisting it to impact on the dash.

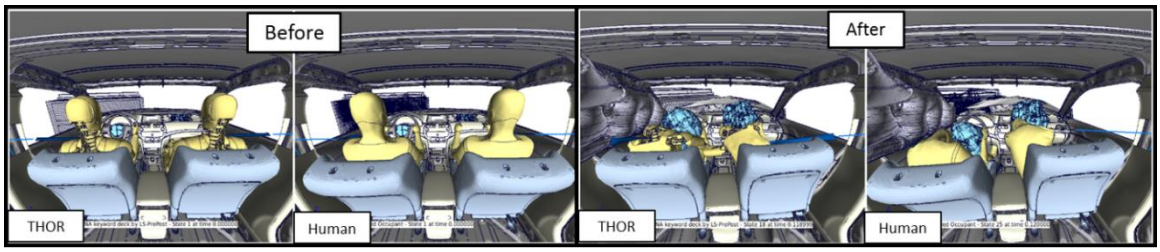

Figure 3. CAE-THOR vs CAE-GHBMC at 0ms (before crash) and 120ms (after crash).

Figure 4 compares the CAE results' head CG acceleration of the driver and passenger with that of test results. For the driver side, the overall trend of the acceleration curves shows a decent correlation among all three events. The passenger side did not correlate well due to the different seat-belt behavior while slipping off the shoulder which was observed in the test. In the THOR dummy model simulation, even though the seatbelt slip-off occurred, the seatbelt still provided some resistance that reduced the head impact to the dash. In the GHBMC model simulation, the seatbelt did not slip-off due to high friction with the skin, hence stopping the GHBMC model from moving forward and contacting the dash.

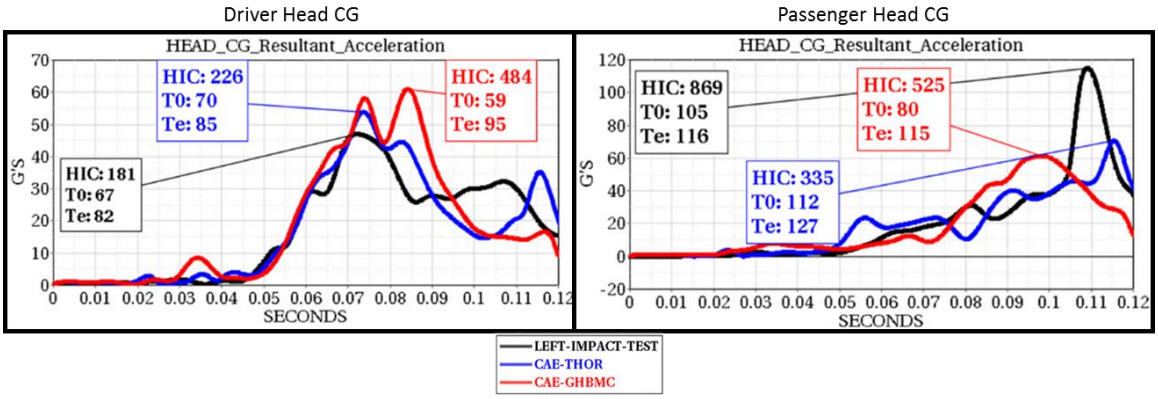

Figure 4. Driver and Passenger Head CG Acceleration.

Figure 5 shows the driver and passenger femur forces. In the THOR dummy model, the force was measured from a beam element that connects two metal sockets moving axially between each other along the femur. In the GHBMC model, the force was taken from a cross-section force of the actual femur bone made of solid elements. The GHBMC model seemed to experience more load through the femur compared to the THOR dummy model.

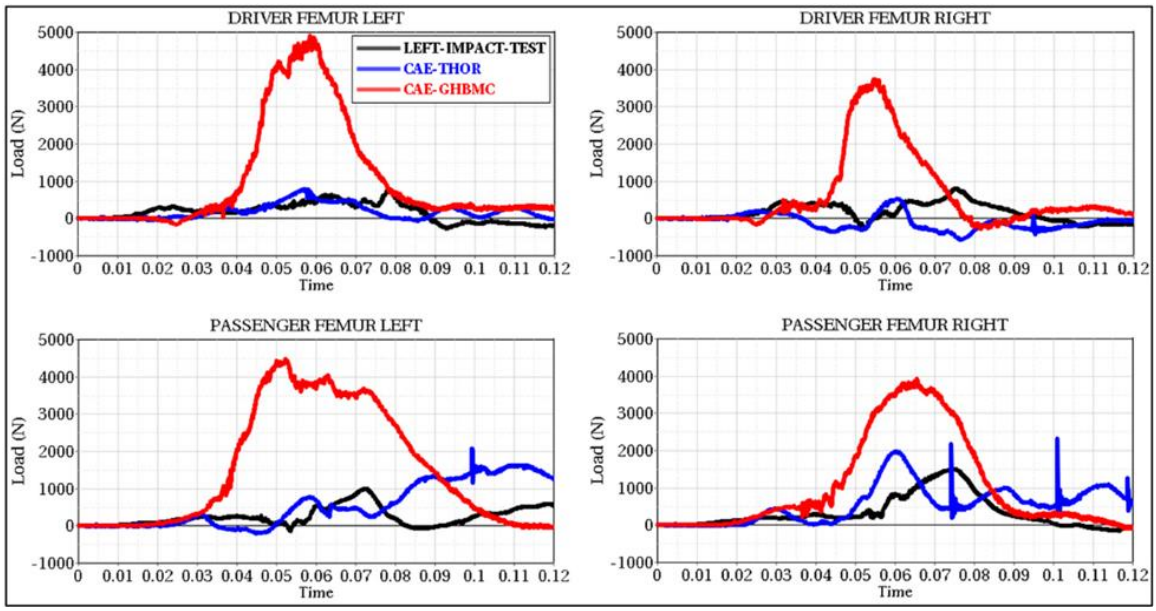

Figure 5. Driver and Passenger Femur Force.

More comparisons such as pelvic accelerations, seatbelt forces, and detailed timeline images of crash and complete right-side impact of oblique offset test can be referred in the full project report [3].

CONCLUSION

Full vehicle finite element models representing 2014 Honda Accord including interior trims and occupant restraints system were developed in this research. The occupant restraint system such as the airbags and seatbelt were tested and validated with the CAE models before they were integrated into the model. The full vehicle used THOR 50th percentile male dummy model to represent both driver and passenger. NHTSA's Oblique Offset front impact test simulations were carried out for both left and right-side impacts. The overall dummy kinematics of THOR dummy model in CAE simulation correlated well with the test. There was a slight difference found in the head to dash interaction due to the difference in seatbelt behavior during the event whether it slipped off the shoulder of the passenger or not. The simulations were repeated by replacing THOR dummy models by GHBMC models. GHBMC models showed similar overall kinematic behavior during the crash event compared to THOR dummy models. Unlike THOR dummy model, in case of passenger side GHBMC model, the seatbelt did not slip off the shoulder due to high friction with the skin, causing it to resist the forward motion. This prevented the GHBMC model head to collide with the dash as seen otherwise in the passenger THOR dummy model. It was also observed that the GHBMC model femur forces were much higher compared to THOR dummy femur forces.

REFERENCES

[1] Singh, H., Ganesan, V., Davies, J., Paramasuwom, M., Gradischnig, L., Wood, P., et al. (2018). Structural Countermeasure/ Research Program: Mass and Cost Increase Due to Oblique Offset Moving Deformable Barrier Impact Test. NHTSA.

[2] Bean, J. D., Kahane, C. J., Mynatt, M., Rudd, R. W., Rush, C. J., & Wiacek, C. (2009, September). Fatalities in frontal crashes despite seat belts and air bags – Review of all CDS cases – Model and calendar years 2000-2007 –122 fatalities (Report No. DOT HS 811 102). Washington, DC: National Highway Traffic Safety Administration.

[3] Singh, H., Ganesan, V., Davies, J., & Paramasuwom, M. G. (2018). Vehicle Interior and Restraints Modeling Development of Full Vehicle Finite Element Model Including Vehicle Interior and Occupant Restraints Systems for Occupant Safety Analysis Using THOR Dummies. NHTSA.

FRONT SEATBACK STRENGTH IMPROVEMENTS STUDY IN REAR CRASH EVENTS

Velayudham, Ganesan
Paraneshkumar, Jayakumar
James, Davies
Wade, Bridges
EDAG Inc.,
USA

Paper Number 19-0134

ABSTRACT

National Highway Safety Administration (NHTSA)'s seat back standard FMVSS No. 207 [1] establishes a minimum strength requirement to reduce occurrence of seat back collapse in rear crash events. NHTSA also has a separate standard for head restraints. FMVSS No. 202a, that is intended to mitigate whiplash injuries in rear end crashes. In general, seat backs in current production vehicles will not significantly deform or collapse when subjected to the FMVSS No. 202a test pulse. Thus, a more severe test impulse would be needed to demonstrate a change in seat back performance in a rear impact. Recently rear crash events had fatal injuries to rear seat occupants that was attributed to the collapse of a front seat back. This study was to study seat back design changes that could reduce seat back motion in high speed rear impact [2]. The Bio-RID II dummy was used for testing and simulation in this study. This paper provides details of seat back strength changes from a baseline 2014 Honda Accord.

INTRODUCTION

In this study, detailed Finite Element (FE) models were developed for manual and power operated seats of 2014 Honda Accord vehicle. The FE models were then validated by comparing them to test results of low speed quasi-static seat back pull test reaffirming similarity between FE seats and test seats. In addition, FMVSS 301 high speed rear impact test [3] and simulations were carried out with rear seat occupant models to investigate front seat back dynamic rotation, post-test deformation and injury measures of rear seat occupant. Structural countermeasures were developed to reduce dynamic seat back rotation beyond 20°. Further countermeasures were verified to ensure no impact on whiplash requirement by comparing results from low speed front seat head restraint test and simulation. The mass and cost changes due to structural updates going from current seat design to improved seat design was also reported. This paper provides brief description of FE seat model developed and countermeasure implementation.

FINITE ELEMENT SEAT MODEL DEVELOPMENT

The vehicle selected for this study was 2014 Honda Accord. Both manual and power seats were considered for investigation. A manual seat with 4-way seat adjustment mechanism and a power seat with 6-way seat adjustment mechanism were used for measurement and testing. In order to develop FE models, the physical seats were scanned and exported to stereolithographic (STL) digital format readable in computer aided design (CAD) tools. The scanned data was processed in CAD tool and meshed in an FE tool accordingly. The thicknesses of the parts were recorded, and the material grades were estimated based on a hardness tests performed on the required seat parts. The scanned CAD data and the FE models of the manual seat and power seat are shown in Figure 1. *Scanned seat and FEA model of Manual and Power seat*. The FE models are also shown in different material grades (provided in the table insert).

Manual Seat | Power Seat

Figure 1. Scanned seat and FEA model of Manual and Power seat

Separate LS-DYNA FE models were developed for manual and power seats by appropriate FE connections and assembling techniques. This included the detailed modeling of kinematic joints of seat mechanism and seat back recliner mechanism; assembling seat cushion foam and recliner mechanism. The seat cushion foam was pre-deformed to accommodate the occupant shape which was used in the later section of FMVSS No. 301 simulations.

SEAT BACK PULL TEST

Seat back strength was chosen as the validation criteria to compare FE seat model with physical test. This test was conducted on the manual seat and power seat without cushions and plastic trim in a quasi-static loading condition. The necessary seat fixtures were fabricated to mount the seat at four seat bolts at the four corners of the seat base. A similar loading method stated in FMVSS No. 207 Rearward Moment (49 CFR 571.207 S4.2d, dated 10/1/2016), was used, but it was applied until the seat collapsed. Load was applied at -9 degree about y axis as shown in Figure *2*.

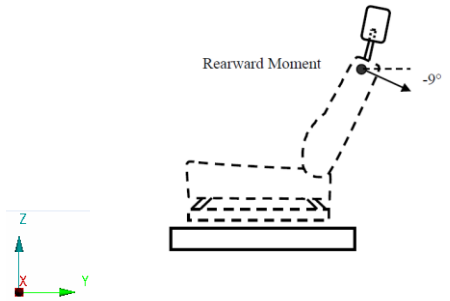

Figure 2. Schematic Diagram of the Seat Back Pull Loading

Load Profile		
Time(second)	Load (N)	Change in Seat back angle(degree)
0	88	0
5	875	1.94
11	875	2.05
51.2	7,151	26.85
132	20,000	40.5

Table 1. Seat Back Pull Load Profile

For understanding purpose, seat back pull test setup of the manual seat is briefly described. Seat back pull test setup is shown in Figure 3. The seat was positioned in full down, full rear track position. Load was applied at mounting plate on top of the seat back frame in rearward direction. The load profile shown in Table 1 was used to pull the seat back. The pull load was applied in the rearward direction from 88 N (at 0 seconds) to 875 N (at 5 seconds), and then the load was maintained for the next 6 seconds (per the FMVSS 207 quasi static seat back strength test).

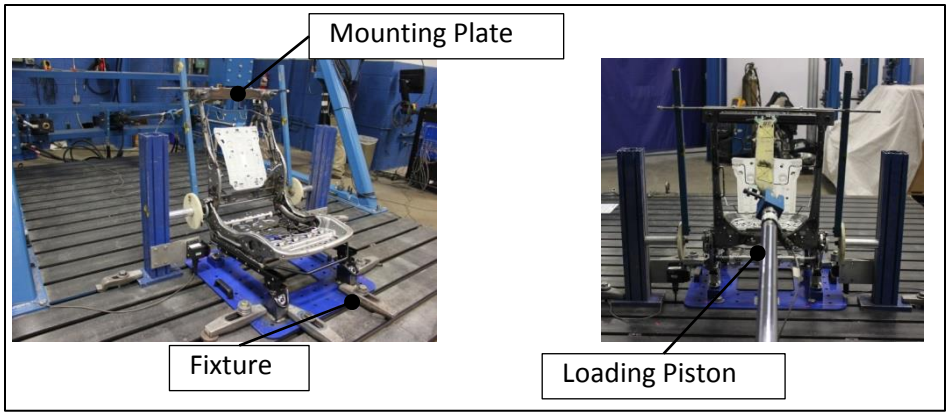

Figure 3. Seat Back Pull Test Seat Setup – Manual Seat

Manual seat post-test and Force-Displacement curve from the test are shown in Figure 4 and Figure 5 respectively.

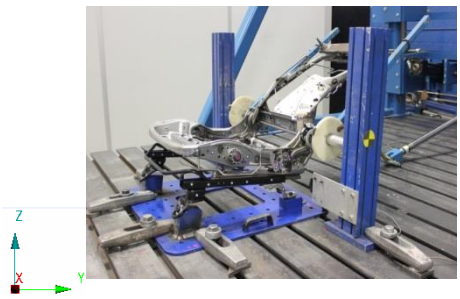

Figure 4. Manual Seat -Post Test

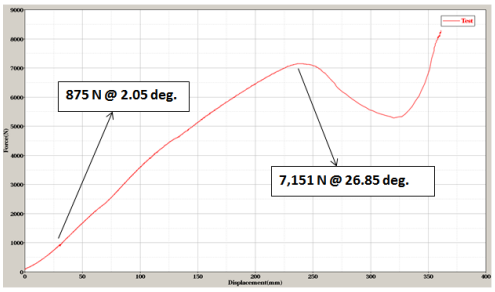

Figure 5. Force vs Displacement curve - Manual Seat

The seat back pull test results of manual seat showed that until 11 seconds there is no deformation or failure. The deformation is observed on the seat bottom frame at the connecting flanges. Significant deformation occurred symmetrically at the seat back frame at the weld joint location. There were no failures or deformation observed on the recliner mechanism. The collapse of the seat started when the seat back angle reached 50.1 degrees from the normal. It was found that the manual seat collapsed at 7,151N.

Similar to the manual seat, the seat back pull test was conducted for power seat in the same full down, full rear track position. Power seat post-test and Force-Displacement curve from the test are shown in Figure 6 and Figure 7 respectively.

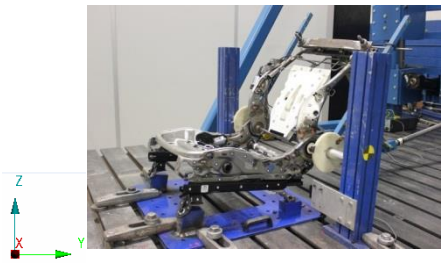

Figure 6. Power Seat -Post Test

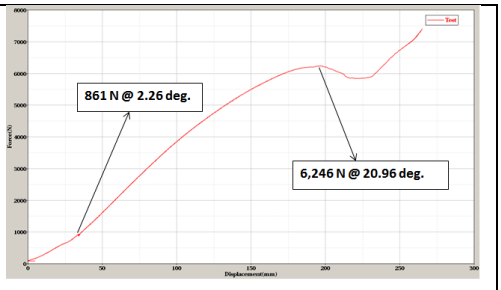

Figure 7. Force vs Displacement curve - Power Seat

The test results showed that there was no deformation or failures observed in the power seat until 11 seconds. Unlike the manual seat, the power seat frame deformed non-symmetrically due to motor and mechanism in the seatback frame. It was found that the power seat collapsed at 6,246N. The left-hand side (LHS) seat frame deformed more than the right-hand side (RHS) seat frame. (LHS) frame collapsed first at 37.1 degrees and (RHS) collapsed later at 20 degrees respectively.

The detailed test reports for both manual seat and power seat has been provided [4].

SEAT BACK PULL TEST SIMULATION

FE simulation of seat back pull test is a quasi-static simulation as per the loading condition. The FE simulation was carried out in quasi-static boundary condition for both manual and power seats. The FE seat models were setup to represent the physical tests accordingly. LS-DYNA simulations were run in implicit mode for 60 seconds. FE simulation results of the manual seat and power seat back were compared with the corresponding physical tests.

Figure 8 shows the global deformation of the collapsed seat frames and the comparison of test and FE simulation at the failed area for manual seat.

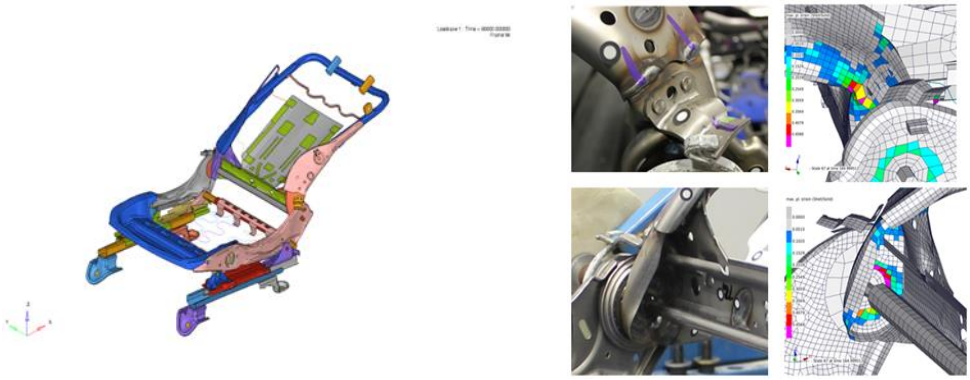

Figure 8. Global deformation of the Seat Frame and Similar Deformation of Test vs FEA – Manual Seat

The gussets folded inward and failed symmetrically in both test and FEA. In addition to the frame deformation, the seat back strength was compared in terms of stiffness or Force-Displacement (FD) plots. The comparison of FD curves of FE simulation and physical test is shown in Figure 9. The FD curve shows a "CORA" [5] correlation rating of about 78%.

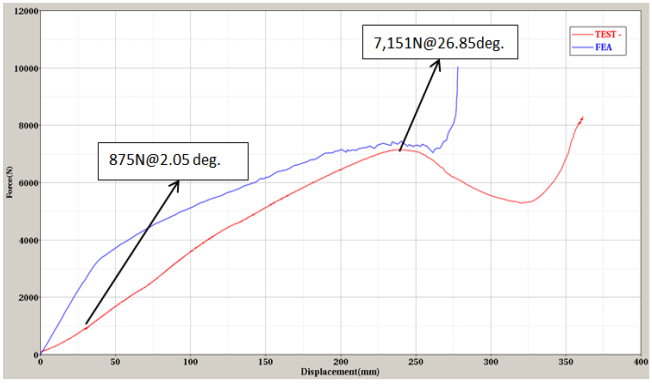

Figure 9. Force vs. Displacement Curves – Manual Seat

Similarly, the power seat FE model was also set up to full down, full rear position by adjusting the seat position mechanism. Same method was followed from the manual seat modeling to set up and run power seat pull test simulation. FE simulation results of the power seat back pull test were compared with the physical test. The gussets folded non-symmetrically due to the motor that is located on the right-side gusset, the (LHS) frame collapsed first at 37.1 degrees and (RHS) collapsed later at 20 degrees respectively. The comparison of FD curves of FE simulation and physical test is shown in Figure 10. The FD curve shows a "CORA" [5] correlation rating of about 78%. Thus, both the manual and power FE seat were modeled with acceptable detail and accuracy.

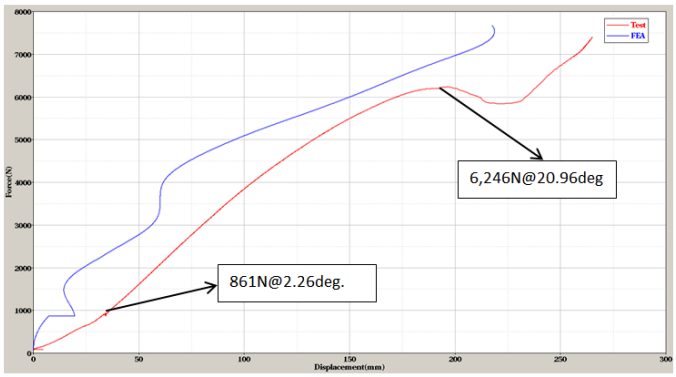

Figure 10: Force vs. Displacement Curves – Power Seat

REAR IMPACT FINITE ELEMENT MODEL DEVELOPMENT

This study was intended to investigate seat design changes to reduce front seat back rotation in rear crash events. It was decided to carry out FE simulations with rear seat passenger using an FMVSS No. 301 crash pulse. Rear impact FE models were developed using a manual seat and a power seat. Each seat model was positioned into an existing 2014 Honda Accord full vehicle model and validated against the sled test results. The rear impact vehicle pulse from 2014 Honda Accord rear impact simulation was used as sled pulse in the test. The sled tests were conducted for both manual and power seats on the physical sleds using this pulse. For example, the rear impact vehicle pulse and the sled test (before and after test) are shown in Figure 11 for manual seat.

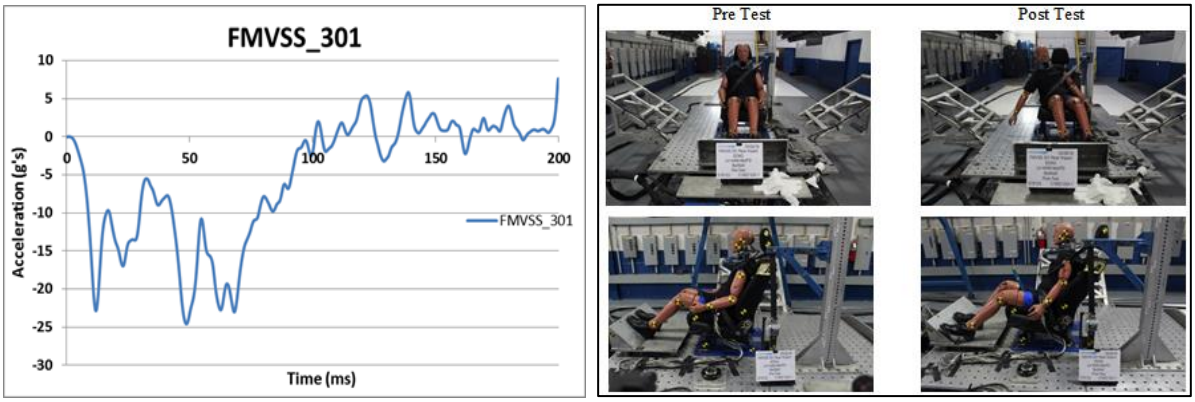

Figure 11.FMVSS No. 301 Rear Impact Vehicle Pulse and Sled Setup

The manual seat was tested in mid track and full down seat position with seat back initial position of 18 degrees. The power seat was tested in full rear track and full down seat position with seat back initial position of 18 degrees. The reason for conducting the sled tests for two different seat positions is to understand the seat back strength requirements for nominal and extreme conditions of occupant seating. Occupant characteristics including head acceleration, neck injury parameters and seat back measurements were recorded appropriately. Measured from the

seat back normal, manual seat recorded a dynamic seat back deflection of 38.4° and post-test static permanent deflection of 9.4°. The test conducted on the power seat recorded a dynamic seat back rotation of 38.5° and post-test static permanent deflection of 9°. The FE animations and physical test video showed similar kinematics. The comparisons of HIC, Nij are listed in Table 2. Similar tests were conducted for the power seat, and the summary of the test and FEA results are also included in the table.

Table 2. FMVSS 301 Sled Test FE Simulations and Test Comparison – Manual Seat and Power Seat

		Manual Seat		Power Seat	
No.	**Injury measures**	**FEA**	**Test**	**FEA**	**Test**
1	HIC 15	80	77	55	76
2	NIJ	0.18	0.28	0.42	0.08

SEATBACK STRENGTH REQUIREMENT

The next step of the research study was to understand the required front seat back strength to avoid interaction with the rear seat occupant and potential injuries in high speed rear crash. For this purpose, first FMVSS No. 301 high speed rear impact simulations were carried out with rear seat occupants using the validated seat models. The Bio-RID II FE dummy model was used as rear seat passenger and positioned on the rear seat behind the driver seat. The necessary rear seat head restraint was modeled and integrated in the full vehicle representation of FE model. Unbelted rear seat occupant condition was chosen to be a worst-case scenario. LS-Dyna simulations were run for both manual and power seat. The front seat back rotation and the interaction of rear seat occupant with the front seat were observed. The FE simulations of both manual and power seat clearly showed that the front seat back impacted on the unbelted rear seat passenger behind the driver seat. The severity of front seat with rear seat occupant interaction is shown in Figure 12. The front seat impact on the rear seat occupant knee showed significant contact and femur force which was above 3.5 kN with the seat back angle of 39 degrees with respect to vertical and knee clearance of only 8.06 mm. Cantor, A. (2000) Seatback Strength and Performance study suggests that safe seat back rotation after crash is 15 degrees from initial position [6]. For this study, 20 degrees of seat back rotation is considered as safe criteria. It can be observed that the seat rotation after impact is greater than 35 degrees which is greater than 20 degrees from initial position. The seat back mechanism will be redesigned to limit front seat rotation.

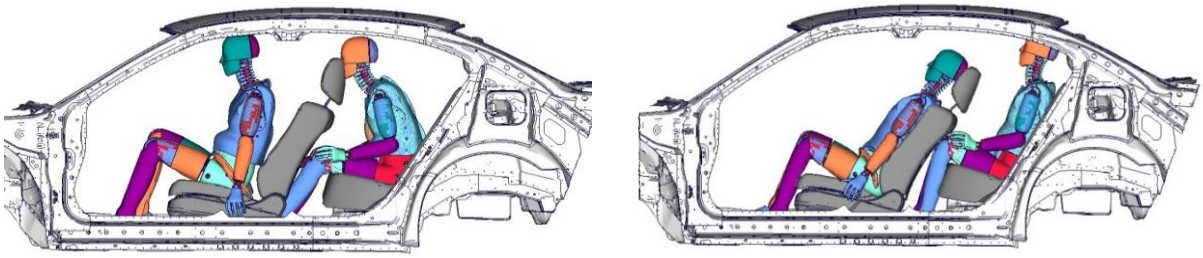

Figure 12. Front Seat Back and Rear Seat Occupant Interaction

SEATBACK STRENGTH IMPROVEMENTS

Having observed that the seat back rotation could contact rear seat passengers in a high speed crash, it was decided to develop necessary structural countermeasures. These countermeasures were implemented on manual and power seat, and FE simulations were run to predict the improvements. Investigation of FE simulation showed that the seat bottom upward movement by the 4-way or 6-way seat mechanism influenced the seat back frame rotation more than the deformation of the seat frame alone. Therefore, Gauge and Grade (2G) optimization was undertaken on the seat bottom frame and bracket members. This approach showed good improvements in reducing the seat back dynamic rotation. The seat bottom frame and mechanism support parts were optimized, and FE simulations were compared with the baseline seats. The gauge and grade changes of the seat bottom frame are shown in Figure 13.

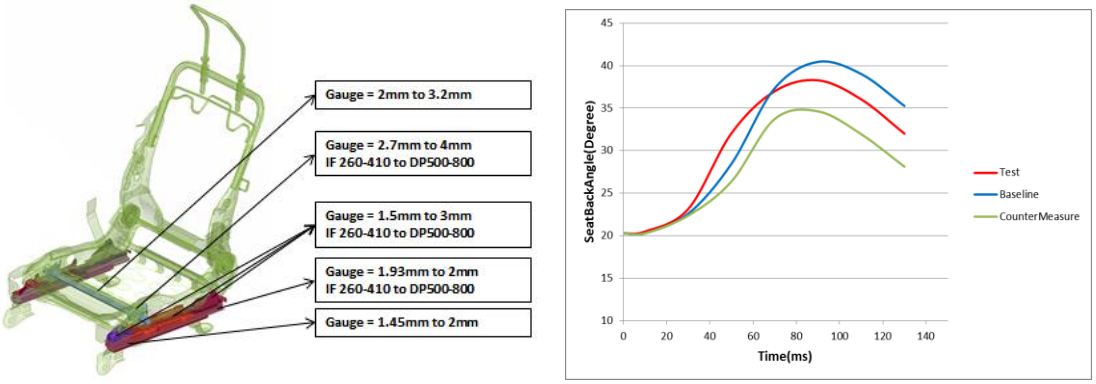

Figure 13. Seat Bottom Countermeasure and Seat Back Angle (Manual Seat)

Finally, the countermeasures were validated by means of FE simulations. The 2G optimized seat models were integrated into the FMVSS No. 301 FE model, and simulations were carried out. The outcome of the FE prediction revealed that the seat back angle, knee clearance and knee impact force of the rear seat occupant were reduced due to the effectiveness of the countermeasure. Table 3 shows a comparative summary of the baseline seats and countermeasure seats. In addition to the seat back rotation angle, seat frame-to-knee clearance and femur forces were also included as target performance criteria. When compared to the respective baseline seats, countermeasure seats showed significant improvements. The manual seat countermeasure showed good knee clearance. The femur force is found to be slightly higher, but 3.1 kN is within acceptable limit as per the knee injury criteria. In case of power seat countermeasure, the improvements are seen in all three criteria.

Table 3. Countermeasure improvements for Manual Seat and Power Seat

			Manual Seat		Power Seat	
No	**Criteria**	**Target**	**Baseline**	**Counter-measure**	**Baseline**	**Counter-measure**
1	Seat back angle	< 35 deg.	39 deg.	35.2 deg.	38 deg.	35 deg.
2	Seat frame to Knee clearance	> 10 mm	8.06 mm	27.68 mm	3.76 mm	17.23 mm
3	Femur force	< 1.5 kN	5 kN	3.1 kN	3.5 kN	1 kN

The countermeasures were similar on the seat bottom frame parts for both manual and power seats. While structural countermeasures were carried out, it was desired to estimate the cost impact of changing the current design. The cost estimation was done for the baseline and countermeasure seats using standard MIT cost model template. The gauge and grade change influenced an increase in the mass of 2.13 kg and corresponding cost increase of $1.94 for the manual seat, and an increase of 1.69 kg and $4.62 for power seat. Cost Impact of the countermeasure seats are shown in Table 4.

Table 4. Cost Impact of Countermeasure Seats

No.	Description	Manual Seat	Power Seat
1	Baseline seat weight (kg)	18.81	23.41
2	Countermeasure seat weight (kg)	20.94	25.10
3	Baseline weight of parts affected (kg)	3.87	4.13
4	Countermeasure weight of parts affected (kg)	6.00	5.82
5	**Δ weight (kg) / seat**	**2.13**	**1.69**
6	Baseline cost of parts affected	$2.24	$ 9.39
7	Countermeasure cost of parts affected	$4.17	$ 14.01
8	**Δ cost / seat**	**$1.94**	**$ 4.62**
9	Cost / kg increase	$0.91	$ 2.73

It is worth mentioning that FMVSS No. 202a low speed requirement was also carried out to confirm that the developed countermeasures do not affect the whiplash requirement without much deviation from baseline or test.

CONCLUSIONS AND RECOMMENDATIONS

The seat back strength improvement study for the driver seat was carried out for manual and power operated seats of 2014 Honda Accord vehicle by utilizing CAE techniques in a systematic approach. The dynamic seat back rotation of the front seat against the rear seat occupant was investigated. It was found from FE simulations that the rear seat occupant exhibited significant injury potentials when the front seat back was rotated more than 20 degrees from initial position. Therefore, the seat back strength was improved by implementing necessary countermeasures on the seat bottom frame parts. Further, these countermeasure changes to manual and power seat show minimal cost impact.

It can be noted that the study was limited to one type of occupant which was 50th percentile male. Front seat strength observation in rear impact scenario and front seat back rotation onto rear seat occupant involved using only Bio-RID II 50th percentile male dummy model. The observation of front seat back dynamic rotation causing potential injuries to rear seat occupant and the countermeasures are based on the occupant injuries of 50th percentile male. However, the severity of the injury can vary depending on different occupant (toddlers, children, adult, etc.) and different riding condition such as belted, unbelted, add-on restraint systems.

REFERENCES

[1] Department of Transportation, National Highway Traffic Safety Administration, “Federal Motor Vehicle Safety Standards; 571.207 Standard No. 207; Seating Systems,” 49 CFR 571.207

[2] Saunders JW, Molino LN, McKoy FL, “Performance of seating systems in a FMVSS No. 301 rear impact crash test.” 18th Enhanced Safety of Vehicles (ESV) Conference; 2003.

[3] Department of Transportation, National Highway Traffic Safety Administration, “Federal Motor Vehicle Safety Standards; 571.301 Standard No. 301; Fuel System Integrity,” 49 CFR 571.301

[4] Ganesan V, J. P. (2018), Front Seat Modeling in Rear Impact Crashes, Troy, EDAG.

[5] Partnership for Dummy Technology and Biomechanics, http://www.pdb-org.com

[6] Cantor, A. (2000), Seatback Strength and Performance, Department of Transportation.

SIMULATION ASSESSMENT OF INJURY TRENDS FOR 50TH PERCENTILE MALES USING POTENTIAL SEATING CONFIGURATIONS OF FUTURE AUTOMATED DRIVING SYSTEM (ADS) EQUIPPED VEHICLES

Vikas Hasija
Rohit Kelkar
Bowhead (Systems & Technology Group)
USA

Erik G. Takhounts
National Highway Traffic Safety Administration
USA

Paper Number 19-000345

ABSTRACT

Occupants in vehicles equipped with automated driving systems (ADS) may sit in various seating positions (e.g. forward facing, rear facing, oblique facing) and at different seatback recline angles. Since forward facing impacts have been studied in detail, the objective of this study was to: A) analyze rear impacts using finite element (FE) human and seat models; B) update the seat model based on lessons learned from part A and then analyze the injury metrics trend for the 50th percentile male occupant: i) at various seatback recline angles, and ii) in different carriage style seating configurations; and C) investigate a potential countermeasure for reducing injury metric values. For analyzing rear impacts, the Total Human Model for Safety (THUMS) FE model along with a FE driver seat model of a Toyota Yaris was used. Simulations were carried out at both low (Delta-V=15 mph) and high (Delta-V=35 mph) speeds to understand the effect of seat hinge stiffness on THUMS kinematics at both speeds. Other design changes such as integrated seat belts and active head restraints were also evaluated. Then injury metrics were analyzed for the 50th percentile male occupant at various seatback recline angles and in different carriage style seating configurations. For this part of the study, Global Human Body Models Consortium (GHBMC) 50th percentile simplified (M50-OS) male FE model was used along with a Honda Accord FE driver seat model. Head Injury Criterion (HIC) and Brain Injury Criterion (BrIC) were used as injury metrics for the head/brain, while max chest deflection was used as the chest injury metric. A potential countermeasure for reducing BrIC was investigated for the seating configuration with the highest BrIC value. From the rear impact study, it was found that having a rigid seat hinge, an integrated seatbelt, and an active head restraint help in reducing the injury metrics. Higher BrIC values were observed at higher seatback recline angles for both frontal and rear impacts. Chest deflection was also higher at higher seatback recline angle for frontal impact but showed an inverse trend for rear impact. For occupants experiencing frontal/oblique-frontal impacts, the BrIC and chest deflection values ranged from 0.75 to 0.81 and from 33 to 45 mm respectively whereas for occupants experiencing rear/oblique-rear impacts, the BrIC and chest deflection values ranged from 0.23 to 0.93 and from 17 to 24 mm respectively. HIC_{15} values were below 300 for the various recline angles and seating configurations investigated except one instance where the head contacted the knee. The potential countermeasure (redesigned head restraint) investigated was effective in reducing BrIC by a third for the case with the highest BrIC value (0.93).

KEYWORDS: Automated driving systems (ADS), human models, head/brain injury, chest injury, carriage style seating configurations

INTRODUCTION

The development of vehicles equipped with automated driving systems (ADS) or self-driving cars is one of the most exciting and important innovations in transportation history. ADS equipped vehicles give occupants the ability to travel from one place to another with minimal or no human intervention depending on the automation level. SAE [1] specifies six automation levels which vary from 0 (no automation) to 5 (full automation). ADS focus on levels 3 through 5, in which human driver can give control to the ADS and is not expected to perform any driving related task for a period of time or it may include no human driver at all [2]. By combining advanced technology with minimal or no human intervention, ADS have the potential to reduce collision incidence. However, there will be

vehicles on the public roadways that will not be equipped with ADS. These vehicles can still crash into ADS equipped vehicles, which makes occupant protection very important.

The occupant compartment of ADS equipped vehicles has been dubbed as the "next living space." These vehicles may have non-traditional seating configurations such as front seats that can rotate to face the rear seat occupants, like a carriage style seating configuration. In addition to having forward-facing and rear-facing occupants, ADS equipped vehicles can have occupants sitting oblique to the length of the vehicle because of the flexibility to orient the front seats by various angles. Also, the occupants in these vehicles do not have to sit up right, they can sit at different recline angles of the seatback. A study [3] was conducted to explore and identify possible seating positions and desired activities in future highly automated cars. They observed that for long drives, with several occupants in the car, there was a desire to rotate the seat to a living room position (like carriage style seating) and for short drives, there was a preference to maintain forward-facing position but with seat reclined to a more relaxed position. The flexibility to rotate and recline the seats to many different positions makes occupant protection for ADS equipped vehicles particularly challenging. Current test procedures and Anthropomorphic Test Devices (ATD) might not be sufficient to evaluate injury risk for all these scenarios. Human FE models are an important tool that can allow assessment of occupant protection for new car interiors with flexible seat arrangements.

In ADS equipped vehicles, occupants may experience different types of impact depending on how they are seated. For example, if occupants are seated in a carriage style seating configuration, an impact to the front of the vehicle will cause occupants in the rear seats to experience frontal impact and occupants in front seats to experience rear impact. Currently, most of the high-speed vehicle impact tests are conducted for frontal impacts (e.g. New Car Assessment Program (NCAP) [4]), where all occupants are seated forward-facing. Low speed rear impact tests are presently conducted, however, for occupant protection in ADS equipped vehicles, high speed rear impact tests need to be conducted as well to evaluate the seats, seatbelt, and to understand the occupant kinematics.

It is the purpose of this paper to use FE human and seat models to:

- evaluate occupant kinematics in both low and high speed rear impacts to identify potential injury modes;
- analyze injury metrics trend at different seatback recline angles;
- analyze occupant kinematics and injury metrics trend in carriage style seating configuration using two occupants in different orientations of the front seat;
- evaluate a possible countermeasure for reducing BrIC.

METHODS

Injury Metrics

The following injury metrics are used in this study:

a) $$\text{BrIC} = \sqrt{\left(\frac{\omega_x}{\omega_{xC}}\right)^2 + \left(\frac{\omega_y}{\omega_{yC}}\right)^2 + \left(\frac{\omega_z}{\omega_{zC}}\right)^2} \qquad (1)$$

where, ω_x, ω_y, and ω_z are the max angular velocities computed at any time about x-, y-, and z-axes respectively. ω_{xC} *(66.25 rad/s),* ω_{yC} *(56.4 rad/s)*, and ω_{zC} *(42.87 rad/s)* are the corresponding critical angular velocities [5]. The time limit for calculation of BrIC was the entire duration of the simulation (150 ms).

b) $$\text{HIC}_{15} = \left\{ \left[\frac{1}{t2-t1} \int_{t1}^{t2} a(t)dt \right]^{2.5} (t2 - t1) \right\}_{max} \qquad (2)$$

where, *t2* and *t1* are any two arbitrary times during the acceleration pulse [6].

c) Chest deflection: It was computed as the absolute maximum of the X displacement of the sternum.

Measurements at the neck have proven to be an issue in both the M50-OS and THUMS model because of the modeling techniques used. Therefore, neck injury criterion (N_{ij}) is not reported in this study.

Crash Pulse

The crash pulse used in this study (Figure 1) was chosen from an oblique test (NHTSA test # 9476), which consists of an Oblique Moving Deformable Barrier (OMDB) traveling at a target speed of 90.1 kph into a stationary mid-size four door sedan (2015 Chevrolet Malibu) positioned at 15 degrees relative to the moving barrier and impacted 35% to the left front of the vehicle. Since the crash pulses for oblique impacts are usually more severe in terms of injury

risk compared to those for frontal impacts at the same Delta-V, the crash pulse was chosen from an oblique test. Figure 1 shows the resultant of the longitudinal and lateral acceleration components only (rotational acceleration components were not considered). This resultant pulse was used for all the simulations.

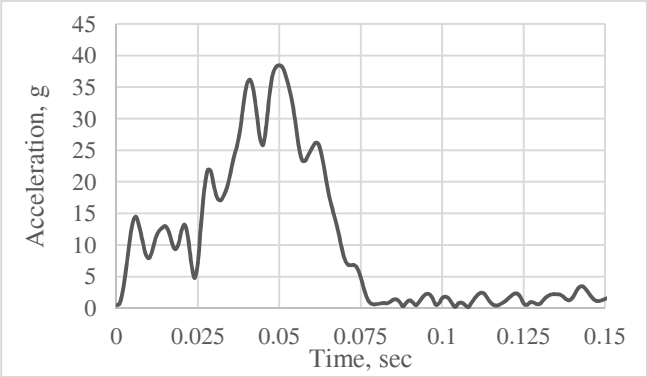

Figure 1. Crash pulse

Model Set-up

All simulations in this study were carried out in a sled type environment. Two different validated 50th percentile FE human models namely THUMS [7] and Simplified GHBMC (M50-OS) [8] along with two different generic FE deformable driver seat models of a 2010 Toyota Yaris [9] and 2014 Honda Accord [10] were used. A validated generic seatbelt system with retractor, pretensioner and load limiter was utilized. The pretensioner and load limiter were set to 1 kN and 3 kN, respectively. The floor was made rigid and no other vehicle structure was used. A sample simulation set-up is shown in Figure 2. All simulations were performed using the general-purpose finite element program, LS-DYNA Version 971 [11].

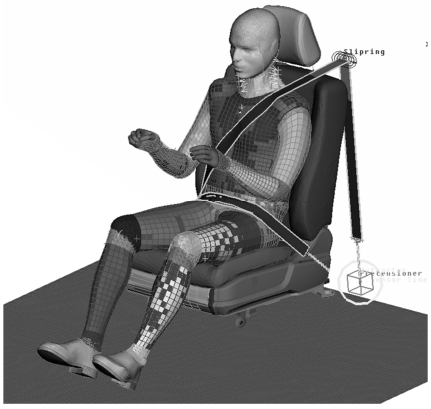

Figure 2. Sample simulation set-up

Analysis

Part 1: Preliminary investigation

This study was carried out to a) evaluate occupant kinematics and injury metrics in both low and high speed rear impacts, and b) explore ways to reduce these injury metrics values. A Toyota Yaris FE driver seat model with THUMS was used for this preliminary analysis. Since no sub system testing or validation was performed on this seat model in rear impacts, a few modifications were made. The bottom seat frame was stiffened and a seat hinge (revolute joint between the seatback and the bottom seat frame, missing in the original model) was created (Figure 3).

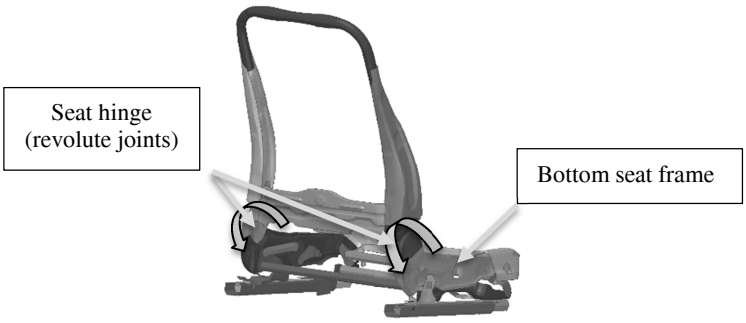

Figure 3. Toyota Yaris FE seat model (seat frame)

A baseline simulation was set up in accordance with a cadaver experiment [12], which consists of a cadaver placed in an experimental seat with non-integrated seatbelt (Figure 4a) and subjected to a rear impact using a 10g acceleration pulse (Delta-V of 15 mph, Figure 4b).

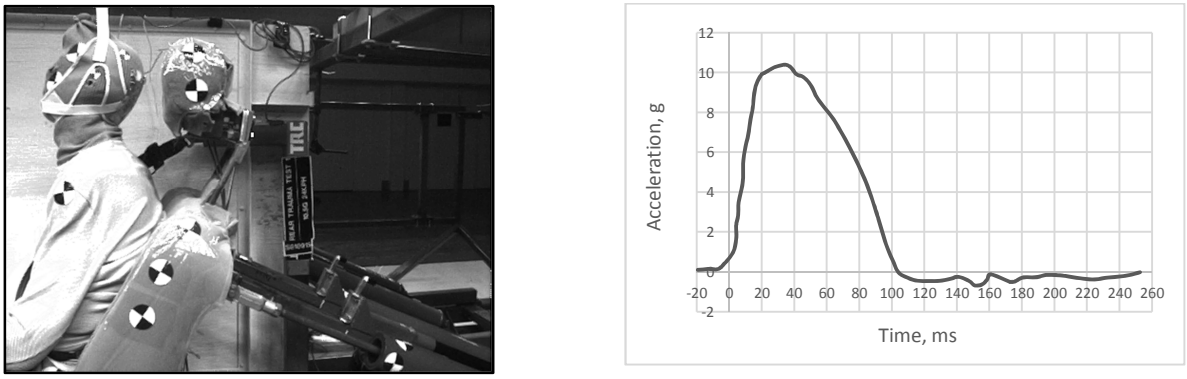

(a) (b)

Figure 4. a) Rear impact cadaver experiment; b) Experimental 10g pulse

THUMS model was positioned in the seat using gravity simulation following which belt creation and fitting was performed in ANSA [13]. Between the experiment and simulation, the seat back recline angle was the same (25^0) but there was slight difference in the seat pan angle (20^0 in experiment compared to 10^0 in simulation). The seat hinge stiffness in the simulations was set close to that of the experimental seat to ensure equivalent seatback rotation during impact. Both the 10g experimental acceleration pulse (Figure 4b, Delta-V=15 mph) and the crash pulse (Figure 1, Delta-V ~35 mph) were applied to the model to study low and high speed rear impacts. Potential injury modes were identified and corresponding values of HIC_{15}, BrIC and chest deflection were recorded. In addition to the simulations performed with a compliant seat hinge (seatback rotates), similar low and high speed rear impact simulations were performed with a rigid seat hinge (no/minimal seatback rotation) to evaluate its effect on the injury metrics (HIC_{15}, BrIC and chest deflection). Also, a head restraint study was conducted wherein the distance between the head and the head restraint was varied (1 mm, 45 mm) to evaluate its effect on the injury metrics. This head restraint study was conducted with a rigid seat hinge and using the crash pulse in Figure 1(Delta-V ~35 mph).

Part 2: Reclined positions and carriage style seating configurations

Compared to the preliminary investigation (Part1) that was performed using a Yaris FE driver seat model and THUMS human model, this part of the study was conducted using a Honda Accord FE driver seat model and simplified GHBMC FE human model (M50-OS). The Honda Accord FE driver seat model was not available to us during the preliminary investigation. Upon availability, the Honda Accord FE driver seat model was compared to the Yaris FE driver seat model. It was observed that the Honda Accord FE seat was modeled in more details especially the seatback compared to the Yaris FE seat, and was thus used for this part of the study. THUMS was replaced with M50-OS because of computational efficiency. M50-OS is computationally more efficient than THUMS (runs in 2.5 hours for a 150 ms event on 40 processors compared to 24 hours for THUMS). As this part of

the study involved time intensive tasks (evaluating multiple human models in the same set up under different impacts, running multiple pre-simulations for adjusting the extremities and positioning the human model in the seat in different recline positions), the switch was made from THUMS to M50-OS.

Based on the lessons learned from the preliminary investigation (Part1), the Honda Accord FE driver seat model was updated i.e. the seat hinge was made rigid, head restraint was moved slightly forward to reduce the distance between the head restraint and the head, and integrated seatbelt was created. This updated seat model along with the M50-OS human model was used to evaluate occupant kinematics and injury metrics in a) different seatback recline positions, and b) two different carriage style seating configurations.

Reclined positions

Two different seatback recline angles, 20° (driving position) and 45° (relaxed position), were evaluated in both frontal and rear impacts. The crash pulse as shown in Figure 1 was used for all the simulations. Gravity simulations were carried out to position the human model in the seat. For seatback recline angle of 20^0, gravity was applied in Z but for seatback recline angle of 45^0, gravity was applied at 45^0 to properly settle the human model in the seat. The final settled positions are shown in Figure 5. The upper extremities of M50-OS were not modified from their default driving position in these simulations. After gravity simulations, belt creation and fitting was performed in ANSA [13].

(a) (b)

Figure 5. Final settled positions for seatback recline angle of a) 20^0, and b) 45^0

A total of four simulations were run (front and rear impact for each recline angle). The injury metrics i.e. HIC_{15}, BrIC and chest deflections were recorded for each simulation to investigate their trend as function of seatback recline angle.

Carriage style seating configurations

For this study, positioning of the human model in the seat was performed in two steps (Figure 6): a) the upper and lower extremities of the human model were adjusted from driving position to relaxed position, and b) this relaxed model was then settled in the seat using gravity simulation. Along with the gravity simulation, the lower extremities were further adjusted to position them as close to the seat as possible to account for the limited legroom in carriage style seating when all seats are occupied.

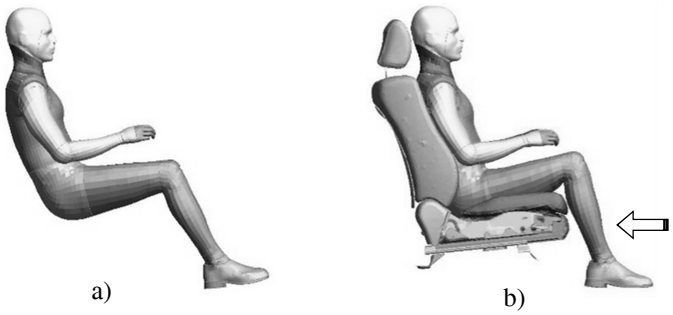

a) b)

Figure 6. a) Relaxed model, and b) Settled model with lower extremities positioned close to the seat

Carriage style seating was evaluated using two M50-OS human models. Two different configurations of the carriage style seating were investigated (Figure 7). In configuration 1, the occupants were positioned at 0° (forward-facing, occupant-1) and 180° (rear-facing, occupant-2) relative to the horizontal axis, whereas in configuration 2, the occupants were positioned at 0° (forward-facing, occupant-1) and 200° (rear-facing-oblique, occupant-2) relative to the horizontal axis. In both configurations, the seatback recline angle was 20°.

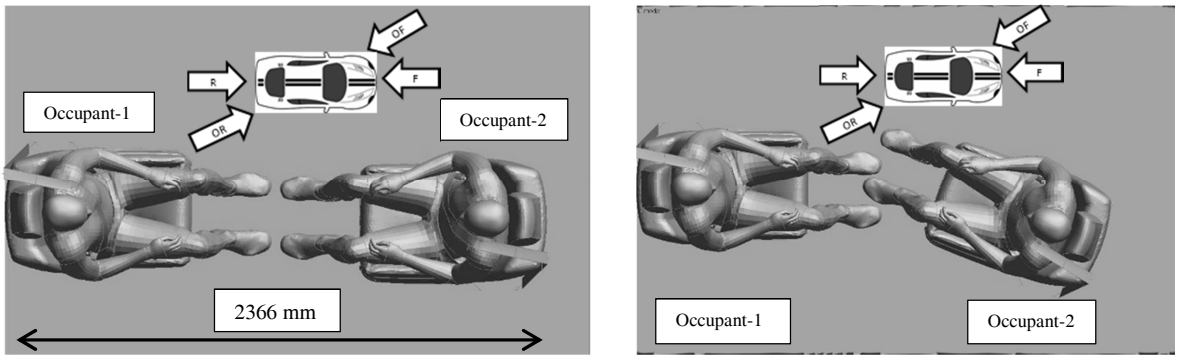

a) b)

Figure 7. Carriage style seating: a) configuration 1, and b) configuration 2

(*Impacts: **F**: Frontal, **OF**: Oblique-frontal, **R**: Rear, **OR**: Oblique-rear)

The two seats were positioned to keep the initial intersection between the feet of the occupants to a minimum. Such seat positioning resulted in the maximum distance of 2366 mm between the seatbacks (Figure 7a). Keeping no/minimal initial feet intersection between the occupants is reasonable since ADS equipped vehicles with carriage style seating are expected to have more legroom compared to the current mid-size sedans and intersection may not be required. For example, the wheelbase (which gives an idea about the size of the occupant compartment) for Mercedes-Benz F015 equipped with ADS [14] with carriage style seating is around 3610 mm compared to 2829 mm for 2018 Honda Accord [15]. This is almost 28% longer. The vehicle structure and its design might pose additional constraints on seating and will be considered in future studies. Four different impacts were simulated for each configuration (Figure 7) for a total of 8 simulations. Impacts simulated were a) frontal; b) oblique-frontal 20°; c) rear, and d) oblique-rear 20°. For all these simulations, the same crash pulse was used (Figure 1).

Part 3: Countermeasure Evaluation

The combination of seating orientation and impact direction that gave the highest BrIC value was identified from Part 2. The cause of high BrIC value was examined and a potential countermeasure was investigated. The high BrIC value was due to a high z-component of angular velocity. To counter this, the head restraint was redesigned. Morphing was performed using ANSA [13] to redesign the head restraint from a nearly flat to a curved shape as shown in Figure 8. This combination of seating orientation and impact direction was simulated again with the countermeasure in place, and the BrIC value was recorded.

Figure 8. Redesigned head restraint

RESULTS

Part 1: Preliminary investigation

The seatback rotation in the rear impact cadaver experiment that was performed using a 10g pulse (Delta-V of 15 mph) was between 30 - 35°. The corresponding simulation showed similar seatback rotation of ~ 30° as well (Figure 9).

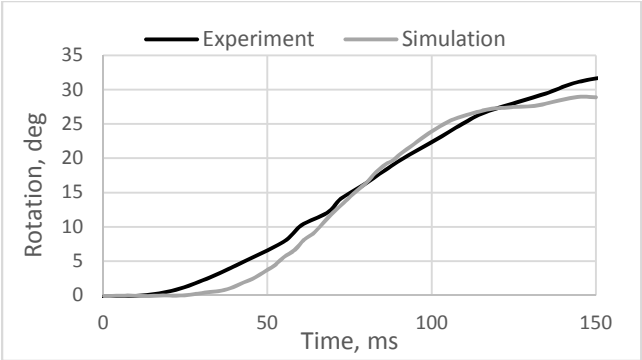

Figure 9. Seatback rotation comparison

The injury metrics observed in the 15 mph and 35 mph Delta-V simulations with a compliant and a rigid seat hinge are shown in Table 1. It can be observed that for both Delta-V's, injury metric values decreased considerably when seat hinge was made rigid. Chest deflection and BrIC were reduced by almost half whereas HIC_{15} was reduced by 15% for lower Delta-V (15 mph). At higher Delta-V (35 mph), the effect of a rigid seat hinge was more pronounced. Each injury metric was reduced at least in half.

Table 1. Injury metrics with compliant and rigid seat hinge

	Delta-V=15 mph			Delta-V=35 mph		
Seat hinge type	BrIC	HIC_{15}	Chest deflection (mm)	BrIC	HIC_{15}	Chest deflection (mm)
Compliant	0.58	92	28	1.85	3466	85
Rigid	0.28	78	15	0.93	490	36

Using a rigid seat hinge, the effect of changing the distance between the head restraint and the head was analyzed. The results are shown in Table 2. BrIC did not change much, however, chest deflection and HIC_{15} decreased by 14% and over 25% respectively.

Table 2. Injury metrics for various distances between head and head restraint

Distance between head-head restraint (mm)	BrIC	HIC_{15}	Chest deflection (mm)
45	0.93	490	36
1	0.90	357	31

Part 2

Reclined positions

The injury metrics for the two seatback recline angles of 20^{0} and 45^{0} in frontal and rear impacts are shown in Table 3. Chest deflection increased with increase in the seatback recline angle for frontal impacts but showed the opposite trend for rear impacts. However, the BrIC value increased with increase in the seatback recline angle for both rear and frontal impacts. HIC_{15} values were below 250 for all the cases except for the frontal impact in driving position (20^{0}), which had a very high HIC_{15} value (1106) due to the head contacting the knee.

Table 3. Injury metrics for various recline angles

	Frontal Impact			Rear Impact		
Recline angle	BrIC	HIC_{15}	Chest deflection (mm)	BrIC	HIC_{15}	Chest deflection (mm)
20^0	0.81	1106	38	0.22	145	21
45^0	0.88	236	44	0.42	166	18

Carriage style seating configurations

The injury metrics for each occupant in the two different seating configurations are presented in Figure 10. The arrows in Figure 10 show the direction of impact with respect to the vehicle (Figure 7). It can be observed that for each impact simulated in this study, the occupants in the carriage style seating experience completely different crash events. For example, an impact to the front of the vehicle causes the rear seat occupants (occupant 1) to experience frontal impact and front seat occupants (occupant 2) to experience rear impact. For clarity, the results are discussed in terms of the type of impact experienced by the occupant. The HIC_{15} value was below 300 for all the cases analyzed. In configuration 1, BrIC and chest deflection were the highest for both the occupants when experiencing oblique-frontal impact. In configuration 2, BrIC was highest for occupant 1 when experiencing frontal impact and for occupant 2 when experiencing oblique-rear impact, whereas chest deflection was highest for occupant 1 when experiencing frontal/oblique-frontal impacts and for occupant 2 when experiencing frontal impact.

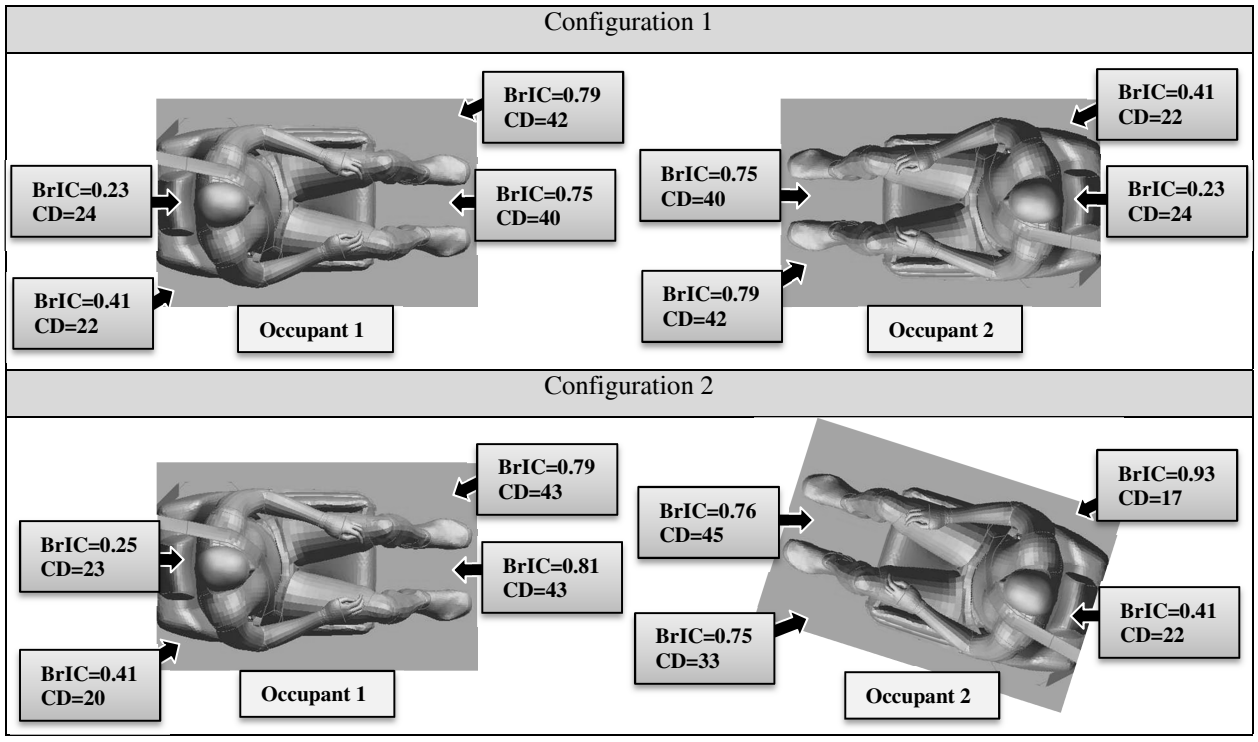

Figure 10. Injury metrics for carriage style seating

(*__CD__=Chest deflection (mm), *__Arrows__ shown indicate the direction of impact w.r.t the vehicle, Figure 7)

Part 3: Countermeasure Evaluation

Of all the seating orientations analyzed in the carriage style seating configurations, occupant 2 positioned at 200° relative to the horizontal in configuration 2 demonstrated the highest BrIC value when experiencing oblique-rear impact (Figure 10). The BrIC values and angular velocities with and without the countermeasure (redesigned head restraint) are shown in Figure 11. It can be observed that the BrIC value reduced by a third with the redesigned head restraint. This reduction was obtained due to a significant decrease in the z-component of angular velocity.

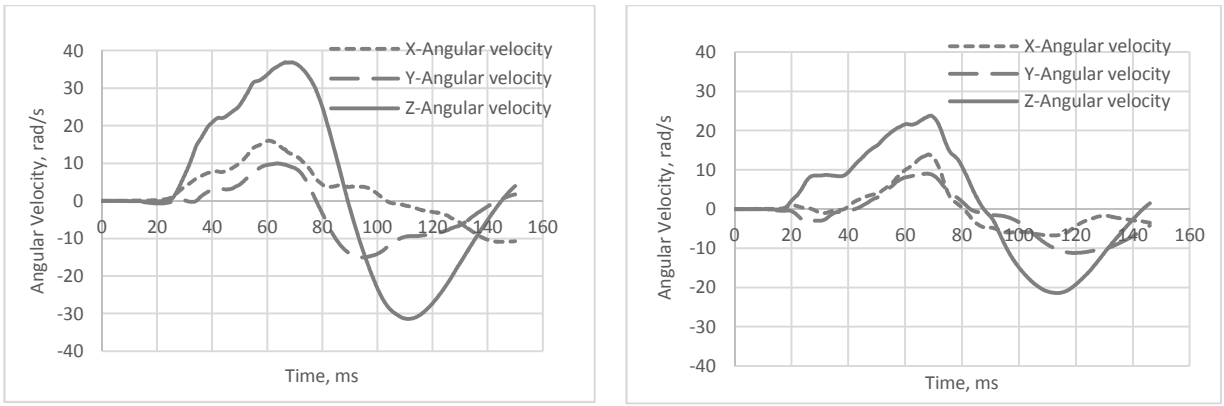

(a) BrIC=0.93 (b) BrIC =0.63

Figure 11. Angular velocities and BrIC with a) standard head restraint and b) redesigned head restraint

DISCUSSION

Rear impacts were evaluated using a Yaris FE driver seat model and the THUMS human model. Initially, only Yaris seat model was available to us and was thus used for this part of the study. Potential injury modes were identified from the low speed (Delta-V =15 mph) and high speed (Delta-V ~35 mph) rear impact simulations. It was observed that when the seat hinge was compliant, the rotation of the seatback allowed occupant ramping along the seatback. This ramping caused the head to whip back and hit/wrap around the head restraint (Figure A1 of Appendix A), which could cause serious head and neck injuries. Similar kinematics were observed in the low speed rear impact cadaver experiment as well where the compliant seat hinge allowed the cadaver to slide up the seatback causing the head to wrap around the head restraint. In this study, the vehicle structure was not considered but excessive ramping may cause the head to contact the car roof, which can also lead to serious head and neck injuries. In addition, the lower legs contacted the seat pan, which may cause tibia and fibula injuries. To mitigate the potential injury modes, the seat hinge was made rigid. It was observed that with a rigid seat hinge, the seat frame and cushion are forced to absorb more energy and as a result the occupant does not accumulate velocity and the ride down begins immediately (Figure A2 of Appendix A). All the injury metrics evaluated in his study were reduced when a rigid seat hinge was used (Table 1). It was also observed that a non-integrated seatbelt (coming from D-ring) does not provide much protection for the occupants in rear impacts. However, a seatbelt integrated with the seat can help mitigate potential injury risk by reducing the occupant ramping along the seatback by restraining the upper body with the shoulder belt. This is beneficial if the seat hinge is compliant. With a rigid seat hinge, the occupant ramping is not as much when the occupant is in the driving position (seatback recline angle of 20^0 to 25^0), however at higher seatback recline angles (45^0, 60^0), there may be significant ramping and integrated seatbelt can help reduce this ramping considerably. It was also observed that having an active head restraint (that can help minimize the distance between the head and the head restraint) in addition to a rigid seat hinge helps in reducing HIC (Table 2).

In this study, lower chest deflection was observed in rear impacts with a rigid seat hinge compared to a complaint seat hinge (Table 1). Yaris seat model was used for this study. Since this seat model was developed for frontal impacts, the seatback was not fully modeled. The seatback consists of just an outer frame on which the cushion is mounted with no supporting structure in the middle of the seatback (Figure 3). During simulations, it was observed that with a complaint seat hinge the upper body loaded the top of the seatback (due to occupant ramping) which is stiff due to the frame underneath whereas with a rigid seat hinge the upper body loaded the upper-middle to middle area of the seatback with no supporting structure behind it causing the seatback cushion to deform more. This may be the reason for lower chest deflections seen in this study with a rigid seat hinge. For rear impacts, stiffness of the seatback supporting structure is an important parameter that was not investigated in this study. This will be done as part of future work with newer FE seat models to better understand the relationship between seat hinge rigidity and chest deflection.

Simulations with higher seatback recline angle showed higher BrIC values for both frontal and rear impacts. It was observed that for frontal impacts, the x- and y-components of angular velocity were higher at higher seatback recline angles leading to higher values of BrIC, whereas for rear impacts, y- and z-components of angular velocity were

higher at higher seatback recline angles. The trend observed is based on limited number of simulations (two for each impact) and needs to be evaluated at more seatback recline angles.

For occupant 1, positioned at 0° relative to the horizontal in both configurations 1 and 2 (Figure 10), there was a difference in the type of impact that had the highest BrIC value. Oblique-frontal impact had the highest BrIC value for occupant 1 in configuration 1 (0.79) compared to frontal impact for the same occupant in configuration 2 (0.81). This difference was due to the feet interaction between the occupants during impact. In configuration 1, since the occupants were positioned face to face with their feet aligned along the horizontal axis, there was feet interaction between them during impact where as in configuration 2 because of different seating orientations of the occupants, there was no feet interaction. The lack of interaction caused the feet of occupant 1 to contact the seat in front of it, thereby changing the kinematics. This change in kinematics caused the head to contact the knee during impact leading to higher BrIC value. The kinematics can be different for different set-ups.

Occupants, when experiencing frontal/oblique-frontal impacts (Figure 10), demonstrated BrIC values in the range from 0.75 to 0.81, and chest deflections in the range from 33 to 45 mm. The lowest chest deflection (33 mm) was for occupant 2 in configuration 2 because of high degree of obliqueness (40° between the seating direction and impact direction). Occupants, when experiencing rear/oblique-rear impacts (Figure 10), demonstrated BrIC values in the range from 0.23 to 0.93 and chest deflections in the range from 17 to 24 mm. Again, occupant 2 in configuration 2 showed the lowest chest deflection (17 mm) because of high degree of obliqueness (40° between the seating direction and impact direction). Chest deflection in frontal/oblique-frontal impacts is due to belt loading whereas in rear/oblique-rear impacts it is due to inertial loading. High degree of obliqueness between the seating direction and impact direction reduces the belt loading on the sternum in frontal impacts and the inertial loading on the seatback in rear impacts leading to lower chest deflection.

The BrIC and chest deflection values for occupants, when experiencing rear/oblique-rear impacts (Figure 10), are quite low. This is due to the rigid seat hinge used in the simulations. A complaint seat hinge would lead to much higher values for rear impacts (Table 1). The actual values here represent those measured by the simplified GHBMC model and are not directly translated to any ATD, i.e. if the chest deflection is about 45 mm, it doesn't mean that if a model of an ATD was used instead of the GHBMC, this value would've been the same.

It can be observed from Figure 10, that there are certain combinations of impact direction and seating orientation which are better than others in terms of BrIC. For occupant positioned at 0^0 or 180^0 relative to the horizontal and experiencing rear/oblique-rear impacts, the BrIC value is very low whereas for occupant positioned at 200^0 relative to the horizontal, the BrIC value is low when experiencing rear impact but very high when experiencing oblique-rear impact. The high degree of obliqueness between seating direction and impact direction causes substantial increase in the z-component of angular velocity, thus increasing the BrIC value. Similar results were observed in Kitagawa study [16], where higher degree of obliqueness gave higher BrIC values in rear impacts. Therefore, while high degree of obliqueness between the seating direction and impact direction reduces chest deflection, it increases BrIC.

Occupants seated in different orientation of the front seat (occupant 2 in configuration 1 and 2, Figure 10), when experiencing frontal/oblique-frontal impacts, did not show any clear trend for the chest deflections nor did they demonstrate any significant changes in the BrIC values. Thus, no seating orientation (180^0, 200^0) stood out as the safest in terms of injury metrics. However, when experiencing rear/oblique-rear impacts (Figure 10), occupant in seating orientation of 180^0 (occupant 2 in configuration 1) demonstrated substantially lower BrIC values compared to occupant in seating orientation of 200^0 (occupant 2 in configuration 2). Although the lowest chest deflection was observed for the occupant in seating orientation of 200^0, the considerable increase in BrIC value outweighs any advantages in terms of chest deflection for this seating orientation. In addition, the chest deflection values are relatively low for rear/oblique-rear impacts (17 to 24 mm) compared to the threshold of 63 mm [6] and may be irrelevant as a selection parameter when choosing safe seating orientation.

The highest value of BrIC obtained in this study was 0.93 for occupant 2 in configuration 2 experiencing oblique-rear impact (Figure 10). The potential countermeasure, modified head restraint, reduced the z- component of angular velocity by more than a third thereby reducing the BrIC value by almost a third as well to 0.63. Although the BrIC value reduced substantially with the countermeasure, occupants in seating orientations of 0^0 and 180^0 demonstrated lower BrIC value (0.41, Figure 10) when experiencing the same impact.

Limitations

- The results presented are limited to the occupant parameters (size, stature, gender) and restraint parameters (seatbelt) used in this study.
- Simulations were run in a sled type environment without any vehicle structure, which may pose additional constraints.
- Only head and chest injury metrics were considered.
- Crash pulse shape was not varied based on PDOF which may affect the results.
- The resultant crash pulse used in this study only considers the longitudinal and lateral components. The results may be different if rotational acceleration components are applied to the model.
- Results presented are based on limited number of simulations and impact types.
- Finally, any outcome from the models is only as good as the models themselves and experimental validation of the results is required, which may be carried out in the future.

Future work may also involve evaluating kinematics and injury metrics for the 50th percentile male by changing the crash pulse, load limiter, occupant location relative to each other (move them closer); simulating carriage style seating configurations for 50th percentile male at different seatback recline angles, and evaluating 5th percentile female in similar scenarios.

CONCLUSIONS

The following observations were made from this study:

- Injury metrics for occupants in rear impacts sitting at various recline angles can be reduced by using:
  - Rigid seat hinge
  - Head restraint positioned close to the head
  - Integrated seatbelts
- Higher seatback recline angles lead to higher BrIC values for both frontal and rear impacts.
- For carriage style seating, occupant interaction during impact can affect the kinematics and hence the injury metrics.
- High degree of obliqueness between the seating direction and impact direction reduces chest deflection but increases BrIC.
- Seating orientations of 0^0 and 180^0 relative to horizontal may be safer for occupants in rear impacts.
- Redesigned head restraint (possible countermeasure) may be useful in reducing BrIC.

REFERENCES

[1] Taxonomy and Definitions for Terms Related to On-Road Motor Vehicle Automated Driving Systems. SAE Information Report (J3016)

[2] https://www.nhtsa.gov/sites/nhtsa.dot.gov/files/documents/13069a-ads2.0_090617_v9a_tag.pdf

[3] Jorlov, S., Bohman, K., Larsson, A. (2017). Seating Positions and Activities in Highly Automated Cars - A Qualitative Study of Future Automated Driving Scenarios. IRCOBI.

[4] The New Car Assessment Program Suggested Approaches for Future Program Enhancements (2007). DOT HS 810 698.

[5] Takhounts, E.G., Craig, M.J., Moorhouse, K., McFadden, J., Hasija, V. (2013) Development of brain injury criteria (BrIC). Stapp Car Crash Journal 57:243-66.

[6] Eppinger, R., Sun, E. et al. (1999) Development of Improved Injury Criteria for the Assessment of Advanced Automotive Restraint Systems – II, NHTSA, USA.

[7] Iwamoto, M., Nakahira, Y., Kimpara, H. (2015). Development and Validation of the Total HUman Model for Safety (THUMS) Toward Further Understanding of Occupant Injury Mechanisms in Precrash and During Crash. Traffic Injury Prevention, Volume16.

[8] Schwartz, D., Guleyupoglu, B., Koya, B., Stitzel, J.D., Gayzik, F.S. (2015) Development of a computationally efficient full human body finite element model. Traffic Injury Prevention.16 Suppl 1: S49-56.

[9] Reichert, R., Park, C-K., & Morgan, R. M. (2014). Development of integrated vehicle-occupant model for crashworthiness safety analysis (Report No. DOT HS 812 087). Washington, DC: National Highway Traffic Safety Administration.

[10] Singh, H., Ganesan, V., Davies, J., Paramasuwom, M., & Gradischnig. (2018). Vehicle interior and restraints modeling development of full vehicle finite element model including vehicle interior and occupant restraints

systems for occupant safety analysis using THOR dummies (Report No. DOT HS 812 545). Washington, DC: National Highway Traffic Safety Administration.
[11] LS-DYNA v.971. Livermore Software Technology Corporation.
[12] Kang, Y.S., Bolte, J.H., Moorhouse, K., Donnelly, B. (2012). Biomechanical Responses of PMHS in Moderate-Speed Rear Impacts and Development of Response Targets for Evaluating the Internal and External Biofidelity of ATDs. Stapp Car Crash Journal.
[13] ANSA, version 17.1.2, BETA CAE Systems.
[14] https://media.daimler.com/marsMediaSite/en/instance/ko/Overview-Mercedes-Benz-F-015-Luxury-in-Motion.xhtml?oid=9904624
[15] http://owners.honda.com/vehicles/information/2018/Accord-Sedan/specs#mid^CV2F5JJNW
[16] Kitagawa, Y., Hayashi, S., Yamada, K., Gotoh, M. (2017). Occupant Kinematics in Simulated Autonomous Driving Vehicle Collisions: Influence of Seating Position, Direction and Angle. Stapp Car Crash Journal.

APPENDIX A: OCCUPANT KINEMATICS

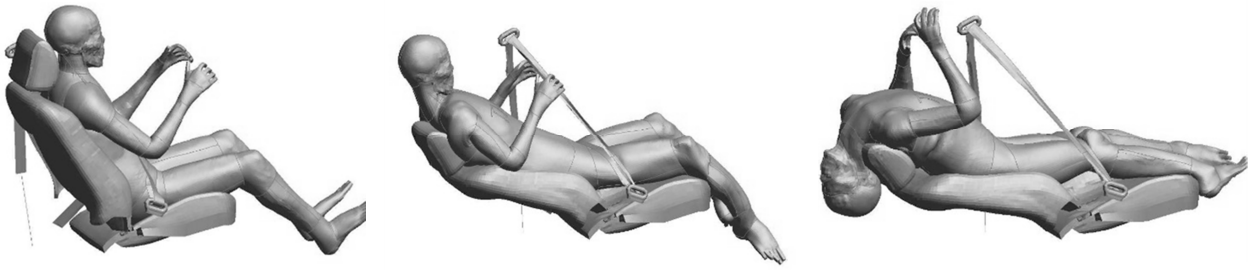

t=0 ms t=78ms t=135ms

Figure A1. Occupant kinematics in rear impact with a compliant seat hinge (Delta-V ~35 mph)

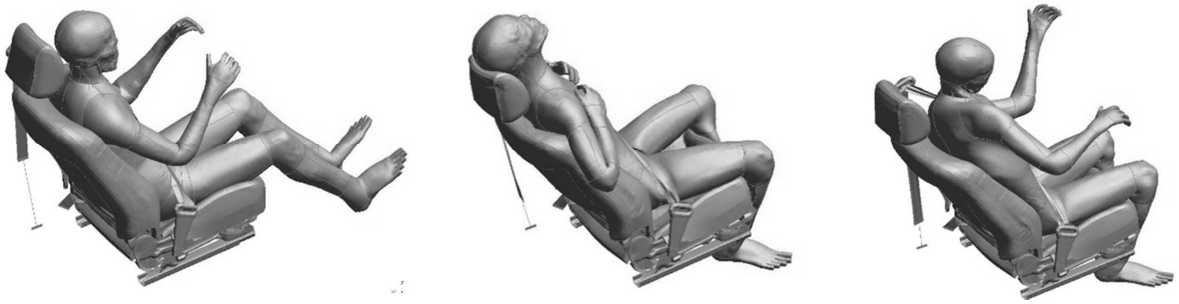

t=0 ms t=78ms t=135ms

Figure A2. Occupant kinematics in rear impact with a rigid seat hinge (Delta-V ~35 mph)

ROLE OF TRAUMATIC SEATBELT FAT STRANDING IN AUTOMOTIVE CRASH INJURY ANALYSIS

Chandrashekhar K. Thorbole
Thorbole Simulation Technologies LLC
United States

Prashant Naik
SKN Medical College, Radiology Department
India

Paper Number 19-0137

ABSTRACT

The seatbelt is a primary and the most important passive safety device protecting occupants in all crash modes. The belt must work in harmony with other passive safety devices such as the frontal airbag, knee bolster and the seat to increase the level of occupant protection in a head-on crash. Failure of any component to restraint the occupant effectively in conjunction with the seatbelt can produce adverse occupant kinematics. Occupant submarining in a frontal crash is an occurrence when the belt moves from the desired stronger skeletal site and loads undesired anatomical location during the forward excursion of the occupant. The focal loading of the abdomen and ribs by the seatbelt produces abdominal and thorax severe injuries.

Subcutaneous fat appears typically darker on the radiographic film with an appropriate window. The focal loading from the seatbelt on the body tends to increase the density of the fat along the course of the seatbelt routing. The increase in the density of fat rises its attenuation and makes the fat appear lighter/whiter on the film. The change in the density, due to traumatic seatbelt loading, can be used in conjunction with other medical and physical evidence to demonstrate the occurrence of submarining. This type of analysis is also useful for the medical provider to take appropriate actions when the trauma patient first appears in the emergency department.

The purpose of this study is twofold: (1) to demonstrate the submarining detection techniques and methodologies using the NHTSA crash-test instrumentation data; and (2) to present real-world crashes as evidence of occupant submarining using fat-stranding analysis in conjunction with other medical and physical evidence.

INTRODUCTION

Automotive passive safety performance in a frontal crash scenario depends on how well the seatbelt and other safety components work together to dissipate occupants kinetic energy while exerting a load on the stronger osseous anatomy[1,2,3,4,5]. However, if the seatbelt transfers load on the body regions such as the abdomen and the ribs, it changes the injury pattern and its severity[6,7]. Occupant submarining in a frontal crash involves slipping of properly placed lap belt from the iliac spine on to the abdomen[8,9]. The traumatic contact between the lap belt and the abdomen as a result of submarining produce direct compressive and shear forces tangential to the abdominal wall exerted by the belt. This force application pattern is evident from the crash testings belt dynamics on the abdomen at the instant of submarining.

The abdominal wall anatomy is composed of skin, superficial subcutaneous fat (Camper fascia), Scarpa fascia and muscle layers separated by their fascia's. The subcutaneous fat, a low dense substance appears darker on the scans due to decreased attenuation. However, with the application of compressive and shear loading on the subcutaneous fat can increase its density in the load application regions. The increase in the density compared to the surrounding local area cause pockets of increased attenuation that appears lighter on the CT scans. Figure 1 shows an example of increased fat density causing increased attenuation making the pockets of fat in the subcutaneous tissue to appear lighter on the CT scan. Figure 2 shows the typical appearance of the subcutaneous fat without any fat stranding.

Figure 1. Subcutaneous fat stranding at the level of seatbelt injury.

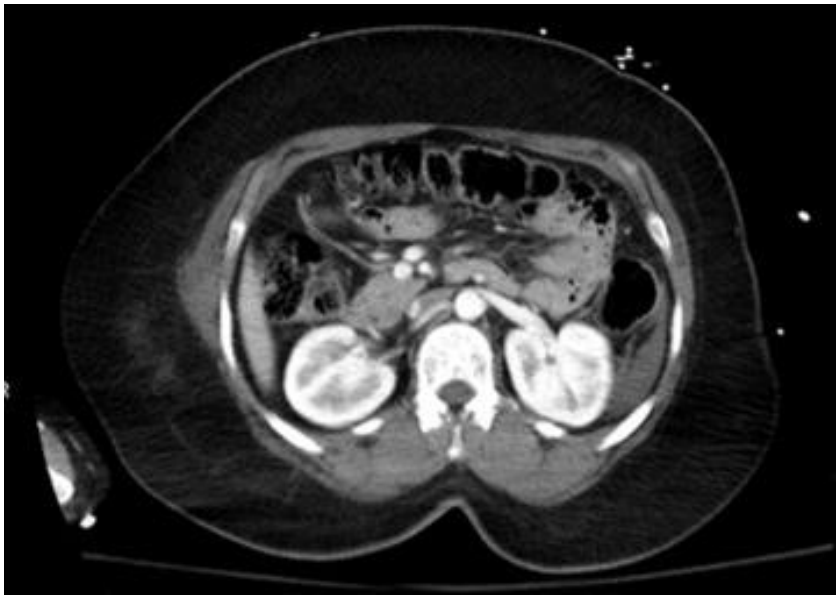

Figure 2. Subcutaneous fat appearance on the CT scan in absence of traumatic fat stranding.

Submarining detection in itself is separate research as submarining prevention. Detection of submarining is mainly challenging due to the use of mechanical crash dummies used for the design and performance evaluation process. The Hybrid III 5th is sensitive to submarining compared to the 50th and the 95th crash dummies[10,11] making it a relative better choice to detect the submarining.

The seatbelt load profile, A.S.I.S load cell output, and the film analysis can be effectively used to detect the occupant submarining or risk of submarining in a frontal crash scenario. The primary objective of this paper is to demonstrate the submarining detection method using standard regulatory test data and to discuss the application of fat-stranding analysis to explain submarining in real-world crashes and factors dictating the outcome.

METHODOLOGY

NHTSA crash-test database [12] is searched for the frontal tests with 5th percentile ATD in the rear seat. Two rigid barrier tests were selected to compare the data and to demonstrate the submarining detection techniques using film and the seatbelt data. Vehicles in both tests belonged to the same class.

Test-1 (NHTSA Test No 9332)

This test involves a 2015 Chevrolet Malibu four-door sedan impacted into a flat rigid barrier at 35 mph (56 kph). Figure 3 shows the film kinematics sequence of the right rear 5th ATD that demonstrates no occurrence of submarining. Figure 4 and 5 show the lap and shoulder belt plots. Figure 6 and 7 shows the right and left ASIS Force plots.

Figure 3. ATD kinematics with no submarining.

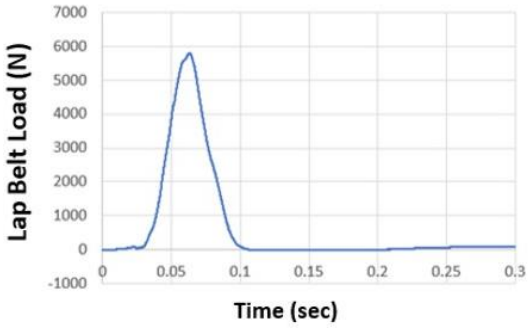

Figure 4. Lap belt load.

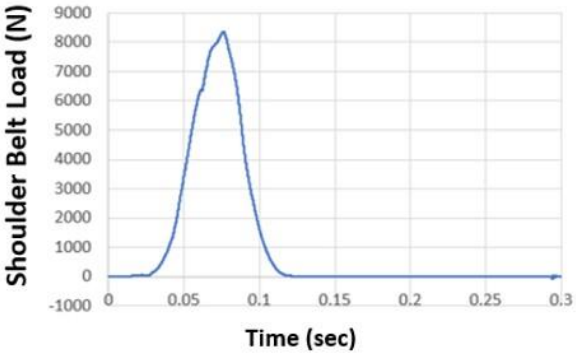

Figure 5. Shoulder belt load.

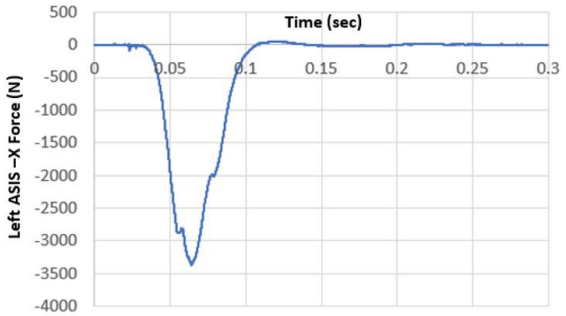

Figure 6. Left ASIS load.

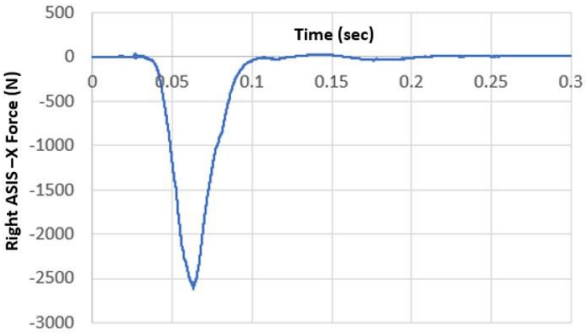

Figure 7. Right ASIS load.

Test-2 (NHTSA Test No 9336)

This test involves a 2015 Mazda 3 four-door hatchback sedan impacted into a flat rigid barrier at 35 mph (56 kph). Figure 8 shows the film kinematics sequence of the right rear 5th ATD that demonstrates no occurrence of submarining. Figure 9 and 10 show the lap and shoulder belt plots. Figure 11 and 12 shows the right and left ASIS Force plots.

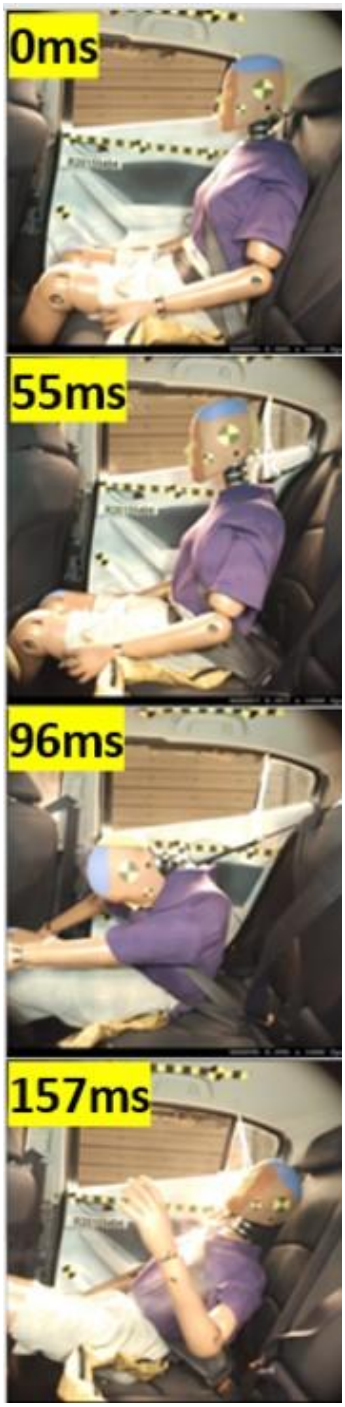

Figure 8. ATD kinematics with submarining.

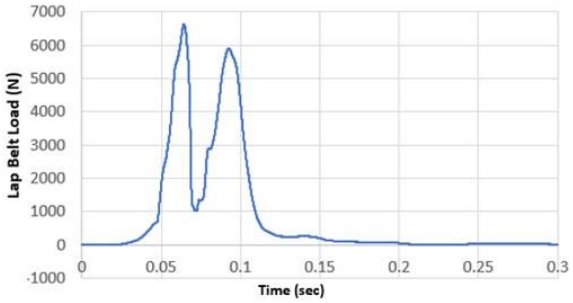

Figure 9. Lap belt load for Mazda 3 test.

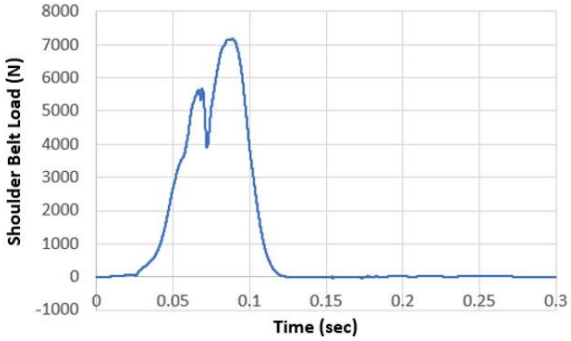

Figure 10. Shoulder belt load for Mazda 3 test.

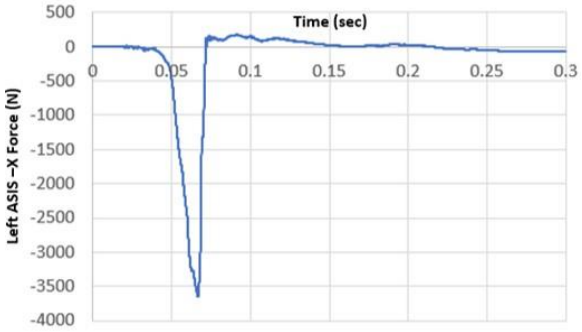

Figure 11. Left ASIS load for Mazda 3 test.

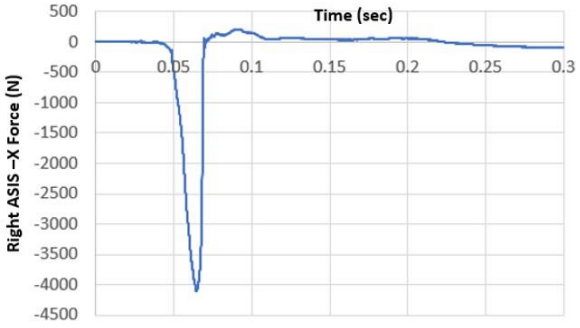

Figure 12. Right ASIS load for Mazda 3 test.

NHTSA TEST COMPARISON

Film Analysis

The film comparison for the ATD kinematics analysis indicates submarining in Test 9336 with 2015 Mazda 3 producing unfavorable ATD kinematics. Test 9332 with 2015 Chevy Malibu shows the favorable occupant kinematics with no submarining of the ATD. The film analysis shows the lap belt kinematics with respect to the ATD pelvis. In the case with submarining, the pelvis rotates backward while moving forward allowing the lap belt to slip from the ASIS zone and migrate upwards and into the abdomen. However, in case of no submarining scenario, the backward pelvis rotation is prevented causing the lap belt to firmly hold on to the ASIS zone during its forward excursion. Figure 13 shows the still image from the film analysis of the Mazda test highlighting the lap belt into the abdominal cavity during the forward excursion of the pelvis. The image also shows the upper torso recline with shoulder point (S-point) lagging behind the H-point. Figure 14 shows the still image from the Chevrolet test highlighting the lap belt on the pelvis during the forward excursion of the pelvis. The image also shows that the shoulder point is not lagging the H-point.

Figure 13. Unfavorable kinematics with submarining.

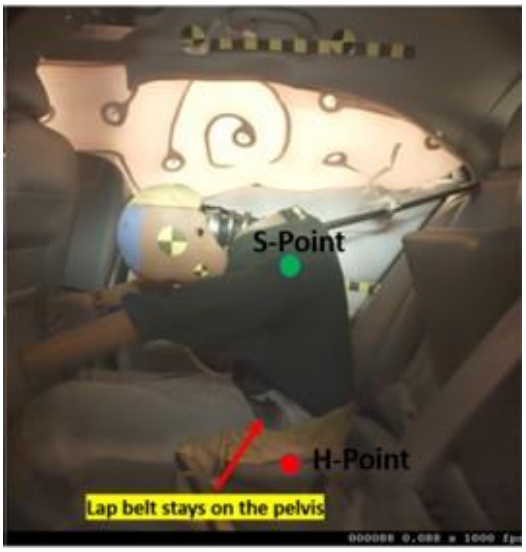

Figure 14. Favorable occupant kinematics without submarining.

Seat Belt Load Analysis
The seat belt load profile, with and without submarining, shows a clear difference. Figure 9 shows the lap belt profile with submarining and Figure 4 without submarining. The belt load profile with submarining always shows a classic hump as visible in Figure 9. This load profile occurs when the pelvis is allowed to rotate backward during its forward excursion on the seat. The backward rotation causes the lap belt to slip from the pelvis causing the drop in the lap belt load. However, the load starts rising once the belt again engages with the abdomen during the ATD's forward excursion. This pelvis rotation kinematics produce the double hump belt load profile. The single loop nature of the belt with the free belt transfer at the latch plate also affects the shoulder belt load profile and demonstrates the hump as shown in Figure 10.

A.S.I.S Load Analysis
The Hybrid III 5th pelvis is equipped with an A.S.I.S load cell capable to measure the belt load and the moment on the pelvis. Figure 15 shows the loaction of the A.S.I.S load cell on the pelvis of the hybrid 5th ATD.

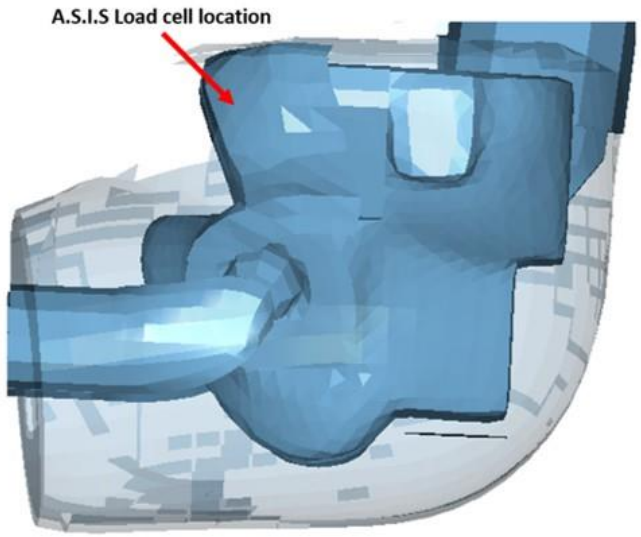

Figure 15. Location of A.S.I.S load cell on the pelvis to measure belt load on the pelvis.

Both tests measured the A.S.I.S loads and moments. In case of submarining, the lap belt slips off from the pelvis producing a sudden drop of the load on the pelvis. Figure 11 and 12 shows the sudden load drop at the right and left A.S.I.S. load cell. With no submarining, the load gradually drops until the ATD starts its rebound as shown in Figure 6 and 7.

REAL WORLD FRONTAL CRASH AND SUBMARINING

In a real-world frontal crash, the occupant's injury pattern in conjunction with a detailed analysis of all other factors provides crucial insight regarding the occupant's motion and injury-producing cause. The subcutaneous fat stranding an increase in its density due to the seatbelt loading can manifest increased attenuation on the CT scan [13,14,15]. The traumatic seatbelt fat stranding observations using CT scan facilitate over-all injury mechanism analysis.

Case Report-1
A 42-year-old female passenger in a right front seat in a mid-size four-door sedan, who was wearing her seatbelt, was involved in a left frontal offset crash. The vehicle EDR data showed 33 mph longitudinal delta V and 11 mph lateral delta-V towards the driver side. She was 5ft 4 inches (164cm) tall and weighed 169 lb (76 kg) at the time of the crash. She sustained head and neck injuries including cervical neck fractures and disruption of posterior ligaments and complex at C1-C2 level with spinal cord injury. Her injury at the C1-2 level is classified as flexion-distraction type injury. She also sustained multiple abdominal injuries including mesenteric defects at mid and distal ileum,1cm

perforation on the lateral border of the cecum and a large right lower abdominal wall traumatic hernia. She also sustained severe bilateral lower lobe atelectasis. Her overall injury pattern and severity was consistent with her submarining on the right front seat. Her CT scan review demonstrated fat-stranding at the hips and the final lap belt position on the abdomen. Figure 16 shows the subcutaneous fat stranding at the A.S.I.S level on the axial CT. Figure 17 shows the corresponding display of fat stranding on the coronal view. Figure 18 shows the fat-stranding at the final displaced position of the lap belt. The lap belt total displacement on the abdomen was 5.2 inches consistent with the marks on the CT scan and her abdominal injuries. Figure 19 shows the schematics of the initial and final belt position with respect to her abdominal injuries. Her submarining produced unfavorable kinematics causing her neck interaction with the shoulder belt producing flexion-distraction injuries at the C1-C2 level.

Figure 16. Axial CT at slightly below A.S.I.S level.

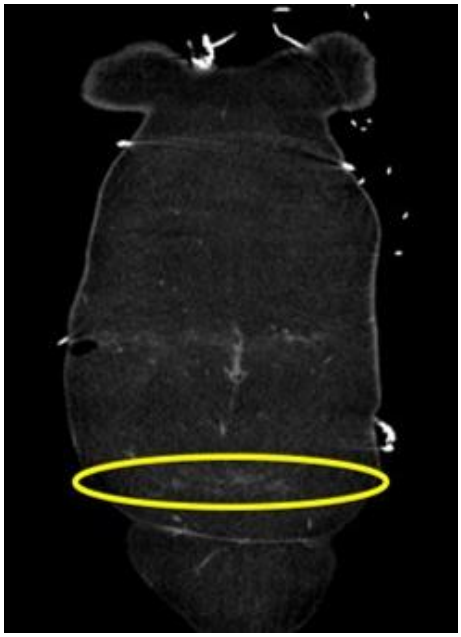

Figure 17. Coronal view of the fat stranding marks at the A.S.I.S level.

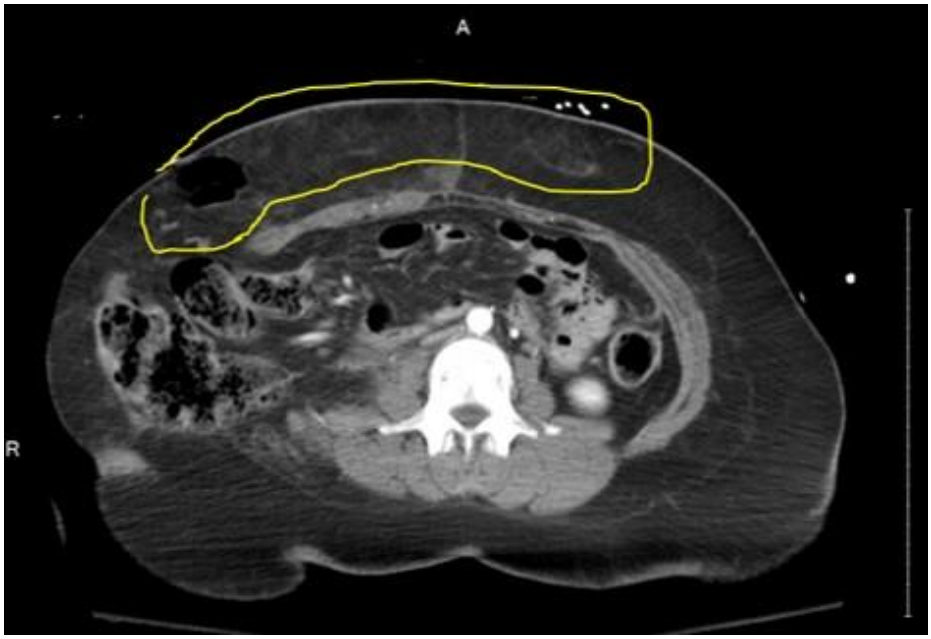

Figure 18. Axial CT at the level of L2-L3 with prominent fat stranding abdominal injuries.

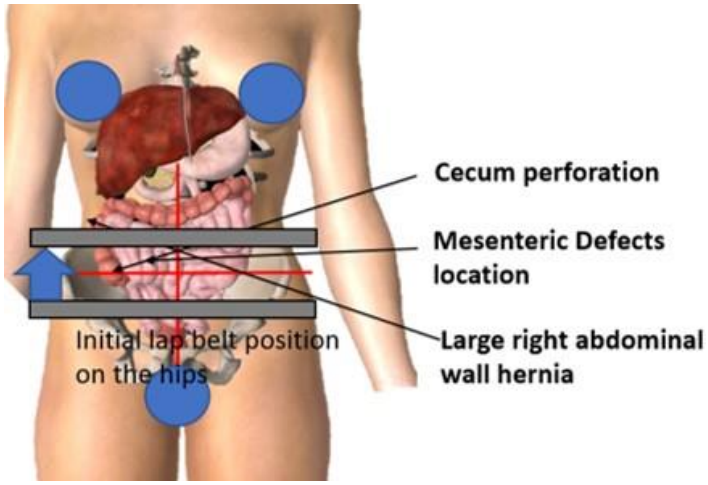

Figure 19. Schematics of the belt movement and abdominal injuries.

Case Report-2

An 11-year-old female passenger in the second row right seat, who had her seatback reclined to approx. 58-60 deg with the vertical, was sleeping with her back on the seatback. She was a properly belted occupant. However, the seatback recline caused her shoulder belt positioned away from her upper torso as the D-ring in this vehicle is mounted on the B-pillar. The frontal crash caused the vehicle to experience a longitudinal change in velocity of 20mph with a minor lateral change in velocity. The seatback recline at the time of crash caused her to submarine under the lap belt. Her acute injury pattern involved clavicle fracture, chance fracture at L2-L3 level in association with several abdominal injuries. She also sustained upper and lower extremity fractures along with facial fractures. Figure 20 shows the axial CT at the level of the chance fracture demonstrating prominent traumatic fat stranding in the anterior abdomen.

Figure 20. Fat stranding at the level of chance fracture.

Figure 21 shows the axial CT at the level of A.S.I.S of the child occupant that shows the fat-stranding. The increase in the fat density at this level confirms the traumatic contact between the belt and the pelvis. However, due to her reclined position, the pelvis failed to hook the A.S.I.S firmly to prevent her slipping under the lap belt. Figure 22 shows the zoomed anterior portion between the left and right A.S.I.S. Figure 23 shows the schematics of lap belt travel on her body.

Figure 21. Fat stranding at the level of A.S.I.S

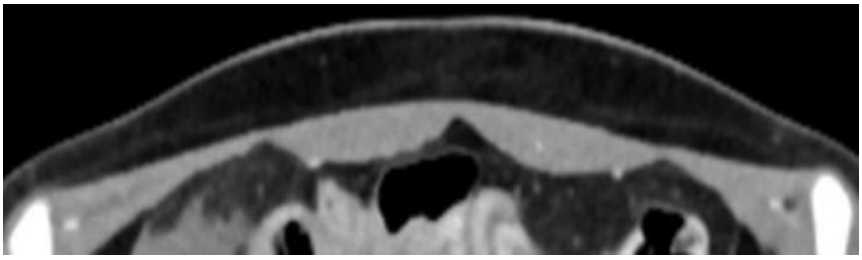

Figure 22. Zoomed image at the level of A.S.I.S demonstrating fat stranding in the subcutaneous fat.

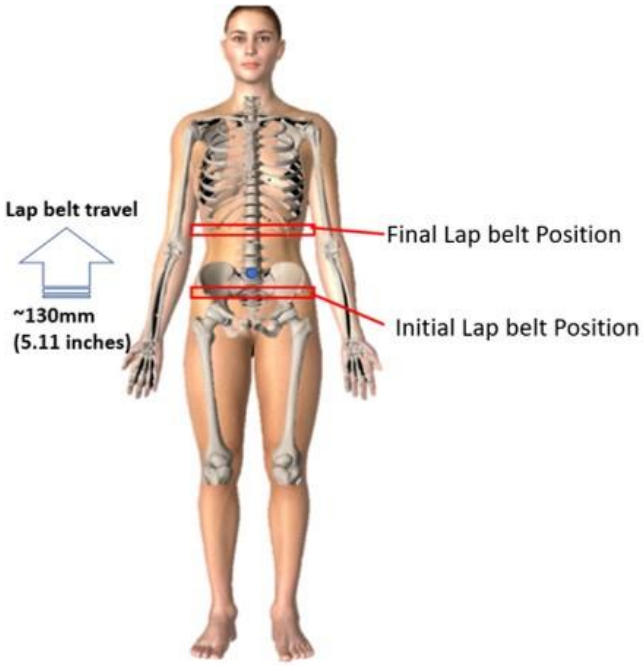

Figure 23. Lap belt displacement from the pelvis to upper abdomen during the crash.

CONCLUSIONS

Occupant submarining in a frontal crash scenario is explained using standard regulatory test data and video. The paper discusses the submarining detection techniques using the film, seatbelt data, and A.S.I.S data. The belt data shows a classic double hump characteristic in the presence of the pelvis backward rotation during its forward excursion on the seat. The film and data analysis show that preventing the backward pelvis rotation during its forward excursion produces overall favorable occupant kinematics by preventing the occupant submarining. This paper shows how the increased attenuation in the subcutaneous fat, below the skin (Camper's fascia) manifest on the CT scan when the belt exerts the compressive and shear loading on the body. Traumatic fat-stranding analysis can be successfully employed in injury causation analysis in conjunction with other available information and data. Seatbelt use, its initial and final position can be determined using the fat stranding analysis.

REFERENCES

[1] Adomeit, Dieter. Evaluation methods for the biomechanical *quality of restraint systems during frontal impact*. No. 770936. SAE Technical Paper, 1977.

[2] Adomeit, D. "SEAT DESIGN-A SIGNIFICANT FACTOR FOR SAFETY BELT EFFECTIVENESS. IN: SEAT BELTS: THE DEVELOPMENT OF AN ESSENTIAL SAFETY FEATURE." In Paper No. 791004, presented at the 23rd Stapp Car Crash Conference, San Diego, CA, October 1979. 2003.

[3] Foret-Bruno, Jean-Yves, et al. "Comparison of Thoracic Injury Risk in Frontal Car Crashes for Occupant Restrained without Belt Load Limiters and Those Restrained with 6 kN and 4 kN Belt Load Limiters." Stapp car crash journal 45 (2001): 205-224.

[4] Adomeit, Dieter, and Alfred Heger. Motion sequence criteria and design proposals for restraint devices in order to avoid unfavorable biomechanic conditions and submarining. No. 751146. SAE Technical Paper, 1975.

[5] Håland, Yngve. "The evolution of the three point seat belt from yesterday to tomorrow." In *IRCOBI Conference, Madrid*. 2006.

[6] Thorbole, Chandrashekhar K. "Seatbelt submarining injury and its prevention countermeasures: How a cantilever seat pan structure exacerbate submarining." Journal of family medicine and primary care 4.4 (2015): 587.

[7] Elhagediab, Ali M., and Stephen W. Rouhana. "Patterns of abdominal injury in frontal automotive crashes." In *16 th International ESV Conference Proceedings*, pp. 327-337. 1998.

[8] Leung, Y. C., C. Tarriere, D. Lestrelin, C. Got, F. Guillon, Manish M. Patel, and Jacques Hureau. "Submarining injuries of 3-point belted occupants in frontal collisions-description, mechanisms and protection." In *Proceedings: Stapp Car Crash Conference*, vol. 26, pp. 173-205. Society of Automotive Engineers SAE, 1982.

[9] Luet, Carole, Xavier Trosseille, Pascal Drazétic, Pascal Potier, and Guy Vallancien. *Kinematics and Dynamics of the Pelvis in the Process of Submarining using PMHS Sled Tests*. No. 2012-22-0011. SAE Technical Paper, 2012.

[10] Couturier, Stéphane, Jacques Faure, Ricardo Satué, Joaquim Huguet, and Julien Hordonneau. "Procedure to assess submarining in frontal impact." In *20th International Technical Conference on the Enhanced Safety of Vehicles (ESV) National Highway Traffic Safety Administration*, no. 07-0481. 2007.

[11] Uriot, Jerome, Pascal Baudrit, Pascal Potier, Xavier Trosseille, Philippe Petit, Hervé Guillemot, Laurent Guérin, and Guy Vallancien. *Investigations on the belt-to-pelvis interaction in case of submarining*. No. 2006-22-0003. SAE Technical Paper, 2006.

[12] https://www-nrd.nhtsa.dot.gov/database/VSR/veh/QueryTest.aspx

[13] Hartka, Thomas, G. Poplin, Kenadeed Hersi, Abigail Booker, and M. Sochor. "Comparison of Visual and CT 3D Reconstructed Abdominal Seatbelt Sign Locations." *TRAFFIC INJURY PREVENTION* 15 (2014): S247-S249.

[14] Hartka,Thomas, 2013 CIREN Presentations " Determination of Seat Belt Use and Positioning with Three-Dimensional CT Fat Volume Rendering in CIREN Frontal Crash Case" https://one.nhtsa.gov/Research/Crash-Injury-Research-(CIREN)/2013-CIREN-Presentations

[15] Thorbole, Chandrashekhar." Traumatic Seat Belt Abdominal Fat Stranding Diagnosis on the CT Scan as a Potential Tool for Injury Causation Analysis" Technical Reference Bulletin 2017, Symposium on International Automotive Technology 2017, Pune, INDIA.

Analysis of the interaction between child occupants and deploying frontal passenger airbag in simulated frontal crashes

Shreyas Sarfare, MS[1], Jalaj Maheshwari, MS[1], and Aditya Belwadi, PhD[1]

[1]Center for Injury Research and Prevention, The Children's Hospital of Philadelphia, Philadelphia, PA

CONTACT: Aditya Belwadi, belwadia@email.chop.edu, 2716 South Street, 13212, Philadelphia, PA 19146

ABSTRACT

Objective: Since the 1990s there has been an emphasis on designing the vehicle airbag system to depower the front passenger airbag to improve the safety of child occupants in the front seat. Recommendations based on first-generation airbag designs varied from switching off PAB to having children less than 13 years of age to be seated in the rear seat. Airbags have evolved over the years and there have been changes to the intensities and deployment characteristics of modern airbags. The aim of the study was to quantify the responses of the 6-year-old ATD installed in child restraint systems seated in the front passenger seating position exposed to a deploying modern front passenger airbag.

Methods: Finite element (FE) models of a 2012 Toyota Camry model (National Crash Analysis Center archives), child seat models (developed internally), a tuned modern front passenger airbag (PAB) (Takata Inc., MI), a Q6 anthropomorphic test device (ATD) model (Humanetics Inc., MI), and a tuned 3-point lap-shoulder belt with pretensioner/retractor (developed internally) were used for the simulations. Seating conditions consisted of a convertible seat in forward-facing harness mode (FFC) with and without a top tether, a highback booster (HBB) and a baseline condition without any child restraint system (No-CRS) in normal seating and a misuse condition with seatbelt behind the back. Models were simulated (N = 12) for NCAP frontal test at 35mph.

Results: Head contact was observed with the instrument panel (IP) in all misuse conditions without PAB (HBB and No-CRS condition with seatbelt behind the back, and FFC without top tether). This contact was eliminated for HBB and FFC seats by the deployment of a PAB. PAB and no-PAB conditions for HBB in normal seating resulted in HIC15 values of 390 and 359 respectively, and resultant head acceleration of 72G and 71G respectively. For FFC with top tether, deployment of PAB resulted in 24.4% reduction in HIC15 (754 to 570) and 12.9% reduction in resultant head acceleration (93G to 81G) as compared to no-PAB condition. For FFC, utilization of top tether resulted in 15.6% reduction in head excursion in the no-PAB condition (471mm to 397mm) and 5.2% reduction (324mm to 307mm) in the case with PAB. In the No-CRS normal usage condition, there was minimal head interaction with the PAB. The PAB and no-PAB conditions showed similar HIC15 (204 and 188 respectively) and resultant head acceleration values (51G for both). In the misuse condition, the Q6 head slid under the deployed PAB and contacted the IP.

Conclusions: In all situations, deployment of PAB provided similar or a relative positive effect as compared to no-PAB condition. There was a clear benefit of using a PAB in all the misuse conditions as it eliminated head contact with the IP. Even in cases where there was no contact with IP (no PAB), usage of PAB resulted in reduced head excursion and comparable or lesser values of HIC. Additional simulation conditions and testing are necessary to explore crash pulses, directions and vehicle/airbag models.

Keywords: Child restraints, Crash dummies, Finite Elements, Front airbags, Front impact, Occupant kinematics

INTRODUCTION

Historically, much attention has been devoted to the interaction between children and frontal passenger airbags. Since the 1990s there has been an emphasis on designing the vehicle airbag system to disable the passenger airbag (PAB) to improve the safety of child occupants. Recommendations vary from switching off passenger airbags to varying airbag deployment intensities based on seating weight. Another initiative in the US was to have all children less than 13 years of age sit in the rear seat. However, these recommendations were based on the designs of first-generation airbags. In the last decade, there have been advancements in airbag inflators and folding techniques with changes in the deployment characteristics of PABs. Additionally, there have been developments in seatbelt restraint systems with the inclusion of pretensioners and load limiters which are designed to work as an integrated system in conjunction with the airbag to further help position the occupant and manage the crash energy. There is a need to explore and quantify the injury potential for children due to a deploying modern front passenger airbag for those in forward-facing child restraints and booster seats in a frontal impact across a range of normal seating and misuse conditions.

These advancements question the validity of the guidelines, based on first-generation airbags, for modern airbag designs. Menon et al. (2003) performed real-world surveillance studies, sled tests, and simulations to explore the interaction of PAB and restrained child occupants in front passenger seat. Their analysis showed that the fatality risk for restrained children was not as high as previously reported for unrestrained children, and that the injuries sustained by restrained children exposed to airbags were mostly not life-threatening. Both sled testing and simulation results suggested a possible benefit of the passenger airbag for restrained children.

Several studies (Winston et al. 2007) have suggested that for certain subgroups of occupants, the front seat is actually safer. These include older adults (Kuppa et al. 2005) and may even extend to young adolescents (Durbin et al. 2015).

Volvo (Heurlin et al. 2016) studied forward-facing pediatric ATDs (Q series dummies - 3YO, 6YO, 10YO) in the front passenger seat exposed to a modern deploying PAB. The hypothesis of the Volvo study was to explore the validity of the front passenger airbag disabling strategy for modern airbag designs and restrained forward-facing children. There was a concern in regard to countries where the airbag deployment was switched off for children, and if forgotten to be turned back on for adults, may compromise the safety of the occupant. The restrained ATDs were

positioned in various seat track positions, booster types and sled tests were conducted for three different crash pulses. Typical misuse conditions such as seatbelt behind the back or under the arm were also considered. The study demonstrated relative positive or comparable effect for activated airbag compared to no airbag. The positive influence of the PAB was relatively more pronounced in the forward seat adjustment positions. In the misuse conditions, the airbag appeared to provide clear benefits to the child. In part based on this work, Volvo changed its recommendation for the use of the airbag cut-off switch (in Europe) for restrained children as front seat passengers in car models with airbag designs as tested in the study. Previously, they recommended switching the airbag off for children less than a height of 140 cm. Now, they recommend the airbag to be switched on (in certain newer model year vehicles with this airbag design) for all forward-facing children.

However, the Volvo study evaluated only children restrained in booster seats. Further exploration across a broader range of child restraints, occupant positioning, and test conditions is required to understand how these findings influence our comprehensive understanding of child occupant protection and the role a frontal airbag can play.

The aim of this study was to quantify the injury potential for restrained children in front of a deploying modern front passenger airbag for frontal impacts. Computational finite element (FE) modeling were used to evaluate the kinetics and kinematics of the pediatric occupant restrained in a forward-facing child restraint and a booster seat (CRSs) installed in the front passenger seating position exposed to a modern passenger airbag.

METHODS

This study utilized a validated Q6 ATD FE model as the occupant. The test environment used was a 2012 Toyota Camry model. The ATD was positioned on booster CRSs and restrained using a 3-point lap-shoulder belt modeled with a retractor and pretensioner in the front passenger seat of the vehicle. Normal seating condition and a misuse condition with the seatbelt behind the back were tested for the study. The models were subjected to a NCAP (New Car Assessment Program) full-frontal barrier impact at 35mph.

The test matrix for this study consisted of a high-back booster CRS (HBB) and a forward-facing convertible seat (FFC). In addition to this, a No-CRS condition was also modeled to simulate a baseline seating condition.

A total of 12 simulations were carried out using an explicit solver in LS-DYNA ver. 971 (LSTC, Livermore, CA) and HyperMesh v17.0 (Altair Inc., MI) as the pre-processor. The simulations were solved on a 16-node computing cluster using a double-precision solver. All post-processing of data was carried out using LS-PrePost v4.5 (LSTC, Livermore, CA).

HIC (Head Injury Criterion), resultant head, chest, and pelvis accelerations, chest displacement, neck forces and moments were extracted and plotted. Head excursion and Nij (Neck Injury) were calculated. All data was filtered as per SAE J211 sign convention and class filter.

Vehicle and Barrier FE Model

The full vehicle FE model chosen for the simulations was the 2012 Toyota Camry obtained from the National Crash Analysis Center (NCAC) archives. The front passenger seat was setup in the foremost possible position to test the extreme condition of the child head impacting the instrument panel (IP). The barrier model used was a rigid wall. This full vehicle model was simulated for a NCAP frontal test at 35mph for a duration of 120ms.

Isolating the front passenger seating compartment

All parts of the vehicle that could potentially come in contact with the occupant seated in the front passenger seating compartment, such as instrument panel (IP), side door trims and window, A-pillar, and the center console, were identified. Interface definitions were used to define surfaces and nodal points of the mentioned components. The displacement and velocity time history data for these components was extracted from the full vehicle crash simulation using Interface cards in LS-DYNA to generate a sub-simulation interface file. The data was saved at a specific frequency (5ms) using the *INTERFACE_COMPONENT option. The subsequent sub-simulations involved only the extracted front passenger seating compartment along with the ATD and CRS. The interface file generated in the main full vehicle crash simulation was then used as a master file to provide the appropriate motion to the extracted components using the *INTERFACE_LINKING option. This technique significantly reduced the computation time as the simulations involving the ATD were carried out using just the extracted front passenger compartment instead of the entire vehicle.

Child Restraint Seats

The CRS models chosen were a high-back booster (HBB) seat and a forward-facing convertible seat (FFC). The CAD data for the CRSs were developed by scanning the seats using an Xbox Kinect Sensor (Belwadi et al. 2015). The FE models for the CRSs were subsequently developed. The HBB was modeled as a rigid material and setup in normal usage conditions as well a misuse condition with the seatbelt behind the ATD's back. The FFC was modeled as a deformable polypropylene plastic material and was used with and without top tether conditions. The child seats were positioned on the front passenger vehicle seat by applying a small force on the CRS and positioning it firmly on the vehicle seat. The FFC was attached to the vehicle seat via a 3-point lap-shoulder belt. Additionally, a No-CRS case was run with normal and misuse conditions. The misuse condition involved the seatbelt behind the ATD's back.

Child Model Positioning

A validated Q6 ATD FE model from (Humanetics Inc., MI) was used for the simulations. The child model was positioned by adjusting the limbs to appropriate positions to get it to fit in the child seat. Further, the ATD was positioned on the CRS by gravity settling. The ATD was installed on the FFC using a 5-point harness, while a 3-point lap-shoulder belt was used for the HBB and No-CRS conditions as per the Federal Motor Vehicle Safety Standard (FMVSS) No. 213 recommendations for ATD positioning.

Seatbelts with Pretensioner and Load-Limiter

After obtaining the most naturalistic ATD placement on the CRS, the lap and shoulder seatbelts were routed over the ATD. A setup of retractor and pretensioner was used along with a load-limiter of 4kN. Sensor models in LS-DYNA were used to trigger the retractor and pretensioner at a specific time to simulate the effect of the vehicle crash.

Front Passenger Airbag (PAB)

Front passenger airbag used for the simulations was provided by Takata Inc. and was modeled as per a 2012 Toyota Camry specifications. All the simulations were carried out with two conditions, with and without PAB.

Final Simulations

After routing the seatbelt, the ATD and the CRS were given an initial velocity of 35mph and the interface file generated from the full vehicle simulation (containing the data for the motion of the components) was assigned to the front passenger seating compartment using interface definitions.

RESULTS

Table 1 lists all injury metrics across all 12 simulations. Head contact was observed with the IP in all misuse seating conditions (seatbelt behind the back for HBB and No-CRS conditions, and convertible seat without top tether). For HBB, this was eliminated when the PAB was deployed. For the convertible seat the head contact was eliminated either by using the CRS with a top tether or deploying the front passenger airbag, or both. However, for the misuse seating condition for No-CRS with PAB, it was observed that the ATD's head slid under the deployed airbag and made contact with the IP. This indicates the potential effectiveness of booster seats.

For the ATD in normal seating condition on a HBB, using a PAB resulted in 13% reduction in HIC36 (from 540 to 471) and 37% reduction in Nij (from 1.2 to 0.75). The upper neck forces and moments saw a reduction of 31% (2790N to 1935N) and 15% (29.2Nm to 24.7Nm) respectively. The values observed for maximum resultant head acceleration and chest displacement were similar in the cases with and without PAB. When seated in misuse condition with the seatbelt behind the back, the PAB provided a clear benefit as it eliminated the head impact with the IP.

For the convertible seat when used with top tether, the deploying PAB resulted in 24% reduction in HIC15 (754 to 570) and 48% reduction in HIC36 (1548 to 805). The resultant head acceleration was reduced by 13% (93G to 81G). The upper neck forces and moments showed reduction of 49% (3347N to 1717N) and 20% (57Nm to 45Nm) respectively. Similarly, the head excursion and IR-TRACC (Infra-Red Telescoping Rod for the Assessment of Chest Compression) chest displacement reduced by 23% (397mm to 307mm) and 40% (17mm to 10mm) respectively when the PAB was deployed. When the convertible seat was used without top tether, there was head impact with the IP in the situation without airbag. This was eliminated when the PAB was deployed.

For normal usage conditions without any CRS, minimal interaction was observed between the ATD and the airbag and thus, the injury metrics were very similar in the cases with and without PAB. However, when the ATD was

seated in the misuse condition with the seatbelt behind the back, there was head impact in both the conditions, i.e., with and without PAB. In the case without PAB, there was direct impact of the ATD's head with the IP, while in the case where the PAB was deployed it was observed that the ATD's head slid under the deployed PAB and made contact with the IP.

In all the conditions, all the injury metrics for the convertible seat were lower for the condition with top tether. For the Q6 seated on a convertible seat without top tether there was contact of the ATD's head with the IP when simulated without PAB. This contact was eliminated when the ATD was restrained on the convertible seat with top tether. When these cases were run with the front passenger airbag, the kinetics and kinematics of the Q6 were very similar (with variation less than 5% for all injury metrics) for the cases of convertible seat with and without top tether.

DISCUSSION

The study is an important step towards understanding kinetics and kinematics of a restrained pediatric occupant in the front passenger seating position across a wide variety of crash, vehicle, and occupant conditions. The conditions simulated in the study were chosen to examine the extreme conditions when a restrained forward-facing pediatric occupant is seated in the front passenger seat. The front passenger seat was modeled in the foremost position to ensure maximum interaction with the deployed PAB, or potential impact with the IP when simulated for conditions without PAB. Additionally, misuse conditions were simulated to examine if the injury risk to the pediatric occupant is increased due to the activation of the front passenger airbag.

In all the misuse cases (the seatbelt behind the back for HBB and No-CRS condition, and FFC without top tether) without airbag where there was head contact with the IP, resulting in extremely high values for HIC and head acceleration (Figure 1). The deployment of PAB eliminated this head contact indicating a clear benefit of airbag where there is contact with the vehicle interiors. In addition to this, the deploying passenger airbag supported in controlling the kinematics of the head and neck as well as the arms of the ATD.

For the scenarios where there was no head contact with IP without the usage of airbag, the kinetics and kinematics of the ATD were comparable to or lesser for the case where the airbag was deployed. The HIC and resultant head acceleration values were similar or lesser for the cases with airbag, while the head excursion was reduced in all the situation when using the PAB.

The airbag also provided support for the head-neck complex of the ATD. In the misuse conditions, the airbag eliminated the head contact with the IP. For the other situations, the deployment of airbag resulted in significant reduction in Nij values (37% reduction for HBB, 7% reduction for convertible seat with top tether, and 17% reduction for the No-CRS condition).

In the No-CRS misuse seating condition with the seatbelt behind the back, head contact was observed with the IP. However, unlike other conditions for HBB and forward-facing CRS, this contact was not eliminated even with the

deployment of the front passenger airbag. The ATD's head was observed to slide under the deployed airbag and make contact with the IP. This suggests the usage of booster seats proves to be significantly more effective than not using a booster seat at all.

LIMITATIONS

There are a few limitations to the study. The study only considers frontal impacts. Further, it is to be noted that only one make/model of highback booster seat and forward-facing CRS was examined in this study. Additional simulation and testing is necessary to explore crash pulses, directions, CRS and vehicle/airbag models.

CONCLUSIONS

The study shows that a deploying modern front passenger airbag provides improved protection to restrained forward-facing pediatric occupants. In all the situations, deployment of PAB provided similar or a relative positive effect as compared to a no-PAB condition. In the cases where there was head contact with the IP without the usage of airbag, the deployment of PAB avoided this head contact. This indicates a clear benefit of using a PAB in situations where there is contact with vehicle interiors. For the cases where there was no head contact with IP even without airbag deployment, the usage of PAB resulted in the reduction of maximum head excursion and comparable or lesser values of HIC. In the misuse condition (shoulder belt behind the back) without any CRS, there was head contact with IP even with airbag deployment. The ATD's head slid under the deployed airbag and impacted the IP. This situation was not observed in any of the studied child restraining seats. This clearly suggest the effectiveness of booster seats as compared to using No-CRS.

ACKNOWLEDGEMENTS

The authors would like to acknowledge the Center for Child Injury Prevention Studies (CChIPS) at The Children's Hospital of Philadelphia (CHOP) and the Ohio State University (OSU) for sponsoring this study and its Industry Advisory Board (IAB) members for their support, valuable input, and advice. The views presented here are solely those of the authors and not necessarily the views of CHOP, CIRP, or the IAB members.

REFERENCES

Belwadi, A., Hanna, R., Eagle, A., Martinez, D., Kleinert, J., & Dahle, E. (2015). Development of a Small Rear Facing Child Restraint System Virtual Surrogate to Evaluate CRS-to-Vehicle Interaction and Fitment (No. 2015-01-1457). SAE Technical Paper.

Durbin DR, Jermakian JS, Kallan MJ, et al. Rear seat safety: variation in protection by occupant, crash and vehicle characteristics. Accid Anal Prev. 2015;80:185-192.

Heurlin, F., Jakobsson, L., & Nilsson, H. (2016). Front Passenger Airbag Benefits for Restrained Forward-Facing Children. In IRCOBI Conference Proceedings.

Kuppa S, Saunders J, Fessahaie O. Rear seat occupant protection in frontal crashes. In: 19th International Conference on the Enhanced Safety of Vehicles. Citeseer; 2005.

Menon R, Arbogast K, Cooper J, et al. Differences in air bag performance with children in various restraint configurations and vehicle types. In: 18th International Technical Conference on the Enhanced Safety of Vehicles, Nagoya, Japan, National Highway Traffic Safety Administration. ; 2003.

Winston FK, Xie D, Durbin DR, Elliott MR. Are child passengers bringing up the rear? Evidence for differential improvements in injury risk between drivers and their child passengers. Annu Proc Assoc Adv Automot Med. 2007;51:113-27.

Table 1: Comparison of injury metrics across simulations

#	CRS	PAB	HIC15	HIC36	NIJ	Max Head Resultant Acc (G)	Max Chest Resultant Acc (G)	Max Upper Neck Forces Fz (N)	Max Head Excursion (mm)	Max Chest Displ (mm)
1	Highback Booster seat	without PAB	359	540	1.20	71.3	76.6	2790.1	303.9	16.8
2		with PAB	390	471	0.75	71.6	95.2	1935.1	243.3	17.0
3	Highback Booster - Misuse condition	without PAB	8508	15035	4.40	1499.5	385.4	8922.8	601.9	5.5
4		with PAB	712	1352	1.53	92.9	80.0	-1208.9	455.0	2.4
5	Convertible seat without top tether	without PAB	3125	3396	1.96	664.3	171.8	2629.7	470.7	11.6
6		with PAB	589	756	1.54	84.2	84.5	1713.4	323.6	11.8
7	Convertible seat with top tether	without PAB	754	1548	1.66	92.7	79.1	3347.0	397.3	16.6
8		with PAB	570	805	1.54	80.5	79.7	1717.3	306.9	10.0
9	No CRS	without PAB	188	323	0.82	51.3	55.6	1983.6	247.8	2.9
10		with PAB	204	314	0.68	50.7	56.2	1722.2	220.3	3.7
11	No CRS - Misuse condition	without PAB	7154	15673	3.78	1553.0	205.9	4095.5	497.9	1.7
12		with PAB	2377	3701	1.98	991.3	101.4	1817.1	496.9	1.8

Note: The simulations with grey markings indicate head contact of the ATD with the instrument panel.

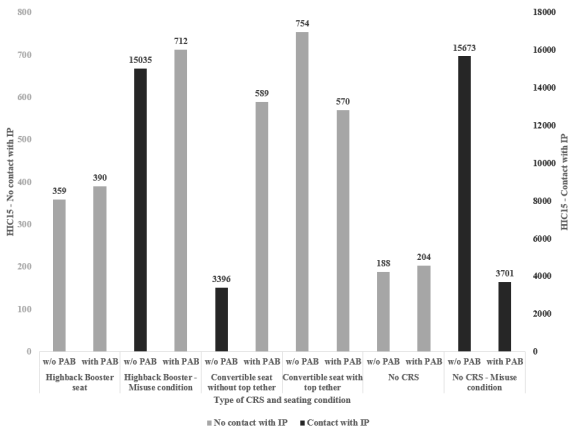
HIC15 - No contact with IP
HIC15 - Contact with IP
359
390
15035
712
3396
589
754
570
188
204
15673
3701
w/o PAB
with PAB
Highback Booster seat
Highback Booster - Misuse condition
Convertible seat without top tether
Convertible seat with top tether
No CRS
No CRS - Misuse condition
Type of CRS and seating condition
No contact with IP
Contact with IP

CALCULATION OF THE POINT OF NO RETURN (PONR) FROM REAL-WORLD ACCIDENTS

Florian, Spitzhüttl
Henrik, Liers
Institute for Traffic Accident Research at Dresden University of Technology (VUFO)
Germany

Paper Number 19-0141

ABSTRACT

Continuing efforts in the field of traffic accident research has led to the development of various active and passive safety systems. They act and influence an incident/accident at different points in time in order to mitigate or avoid a collision. In the event of a collision, the decision to deploy passive safety systems must be made quickly, as the typical activation time is between 10 to 40 ms after the initial contact. However, for future interior/seating concepts and earlier deployment times of restraint systems it is necessary to predict an unavoidable collision much earlier. As the knowledge about this so-called Point Of No Return (PONR) is crucial, this paper introduces an approach to calculate it through using numerical simulation.

This paper uses real world accidents out of the GIDAS (German In-Depth Accident Study) project. The database contains more than 33.000 accidents with personal damage. The reconstruction of the several phases (normal driving, critical situation, pre-crash, in-crash, post-crash) is the basis for the estimation. Therefore, an imminent collision is predicted by simulating the vehicle's possible behavior using a multi body system. If any physically possible vehicle reaction exists that leads to an avoidance of the collision, the PONR has not yet been reached. If all simulation solutions would lead to a collision, the calculations must go one time step backwards. Through an efficient iterative approximation procedure the PONR can be found in a reasonable number of iterations. The approach focuses on the maxima in longitudinal direction (full acceleration or deceleration), in lateral direction (full steering right or left) and in all four combinations of steering and accelerating/decelerating.

The approach can be generally used for all collision types. Here, it is applied to rear-end collisions between two vehicles, highlighting the potential of different avoidance strategies like full deceleration or full steering as a function of time. The distribution of time across all PONRs shows that passive safety measures can be activated prior to the collision in the vast majority of cases. Therefore, occupant protection can be further improved and accidents consequences could be mitigated to a higher degree.

The suggested approach can estimate the PONR for real accidents. An adaption to naturalistic driving data as well as real time estimation is conceivable. This would signify a crucial contribution to the current research on the distinction between accidents and incidents. However, some adaptations would be necessary to enable such calculations. The current simulations are based on idealized acceleration/deceleration and steering behavior, while traffic flow is neglected. Both simplifications lead to an underestimation of the PONR. As the approach is modularized, it can be further developed towards other vehicle behavior maneuvers, specific driver models, or interactions with Advanced Driver Assistance Systems (ADAS).

The PONR is an important value for improved vehicle safety. The developed approach allows to estimate the further potential of passive safety systems with regard to earlier activation times. Furthermore, it can be used to evaluate collision avoidance strategies and to parameterize ADAS.

MOTIVATION AND OBJECTIVE

Traffic accident research and its influence on road safety

Traffic accident research is one of the most important aspects for to reduce road traffic accidents, casualties, fatalities, disabilities, and socio-economic costs. It aims to analyze the causes, sequences, and consequences of accidents; and provides evidence used for future regulations, approaches, technical and infrastructural measures.

Besides national statistics (typically based on sampled police data) in-depth accident investigations are essential to fully understand the accident scenario and to provide appropriate solutions. These initiatives collect as much evidence of accidents as possible to enable analysis of accident causes and to develop approaches for the future mitigation and avoidance of accidents. Collected in-depth accident data is an important source for engineers that aim to develop and improve safety systems. Existing safety measures (e.g. secondary safety measures like belts or airbags) can be further adjusted and optimized on the basis of retrospective data analysis. Additionally, future safety systems or measures and their associated potential benefit can be analyzed by prospective methods, e.g. by virtual simulations. The final goal is the avoidance of accidents. In the transition period, however, one important goal is the mitigation of accidents and the reduction of the consequences to the involved persons by means of integral safety measures. The success of these measures strongly depends on the reliable detection of forthcoming crash events.

Necessity and importance to predict an imminent collision more early

The certainty of an imminent collision as early as possible is very important for effective activation strategies for vehicle safety systems. Passive safety systems usually operate with activation times between 10 to 40 ms after initial contact. Active safety systems activate full when a situation is highly critical or just before a collision. The earlier a system has certainty about an imminent collision the better it can deploy and act without risking a false positive activation. The example of vehicle restraint systems show that an earlier activation can be used to distribute deceleration over a longer distance and to avoid peak loads on the human body. This would significantly contribute to the reduction of thorax and head injuries.

Unfortunately, there is a lack of information for traffic accidents. The need for a model to approximate the point in time, when all available measures must be used to reduce the consequences of a collision is very high. Not only for current vehicles (SAE level 0 to 2 [1]) but even more for vehicles with automated driving functions (SAE level 3 to 5 [1]) and new seat and/or interior concepts more time is crucial to prepare the vehicle and its occupants to an imminent collision.

METHODS AND DATA SOURCES

Point Of No Return (PONR)

The ACEA safety model generally describes a traffic accident in its five phases as seen in Figure 1. Between a critical event at t_{crit} and the collision at t_{coll} exists a theoretical point t_u where the collision is unavoidable. That means, that no reaction can prevent the imminent collision after this point in time (this does not mean that no mitigation is possible). This point represents the Point Of No Return (PONR). It is also known as CU-criterion [3] or time of unavoidability [5].

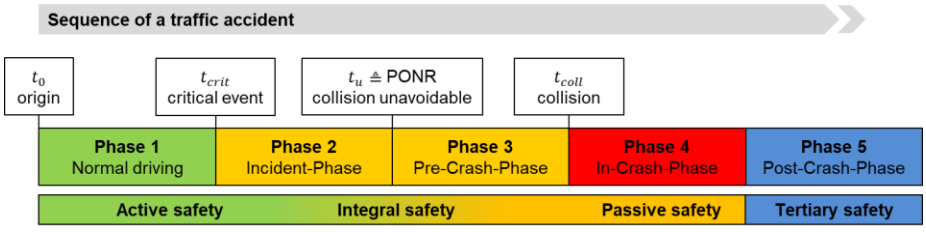

Figure 1. Sequence of a traffic accident based on the ACEA safety model [2]

Limit of vehicle dynamics

Critical events occur very often in road traffic. While most of the incidents return to normal driving states due to proper participant reactions or other influences, the rare case of an accident has led to a collision, as the participant(s) failed to avoid it. At some point earlier, there was the PONR, where the imminent collision is unavoidable through any vehicle behavior.

As the term unavoidable is a final state, the value of the PONR cannot be dependent on the actual or theoretical driver reactions nor on any specific safety system, but rather on physical constraints like the limit of vehicle dynamics. In the case of ground bound vehicles like passenger cars this is mainly the tire-road friction and its transferable force limits as described by the circle of forces (also known as Kamm's Circle) [3], [4]. Figure 2 shows the circle of forces and the vehicle maneuvers model described in the next paragraph. Equation 1 and 2 gives the force and acceleration distribution.

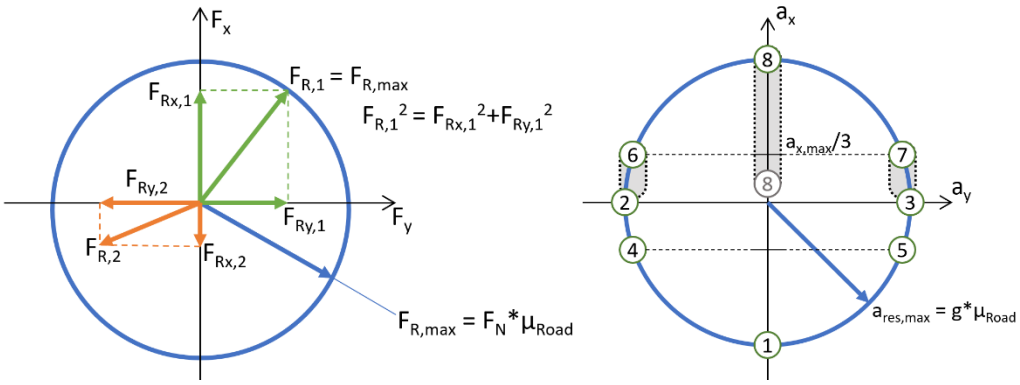

Figure 2. Circle of forces, separation of longitudinal and lateral forces and vehicle maneuvers

$$F_R = \sqrt{{F_{Rx}}^2 + {F_{Ry}}^2} \text{ (Equation 1)}$$

$$a_{xy} = \mu_{road} \cdot g = \sqrt{{a_x}^2 + {a_y}^2} \text{ (Equation 2)}$$

Model for vehicle maneuvers

Unfortunately, the PONR is not measurable and unknown for traffic accidents. There are several model based approaches to approximate vehicle behavior, where especially [6], [7] and [8] must be mentioned. All of these approaches determine the PONR prospectively for idealized situations and cannot be applied directly to real accidents. To determine the PONR for real accidents the development of an advanced model is necessary, taking into consideration the theoretical approaches.

The approach developed for this paper models eight vehicle maneuvers shown in Figure 3, that are able to affect a traffic situation.

In contrast to idealized, generic situations considered in the present approaches (see above), the real situation is a very complex one, including multiple participants, vehicle dynamics, environmental objects and others. Additionally the consideration is a posteriori, as the situation has already taken place. To consider the reactions of the drivers in the actual situation it is necessary to oversteer the reconstructed vehicle behavior with respect to the modeled one at a specific time before the collision. The first point in time when oversteering leads to a collision for all behaviors represents the PONR. This boundary value problem cannot be solved analytically anymore. In contrast, numerical

simulation with a Multi Body System (MBS) is able to solve such a problem, however it is slower and more inaccurate. This paper uses the IPG Carmaker [9]. The variation of the initial vehicle behavior in the accident with the eight modelled ones at specific times is implemented in the simulation environment in Matlab / Simulink [10], [11]

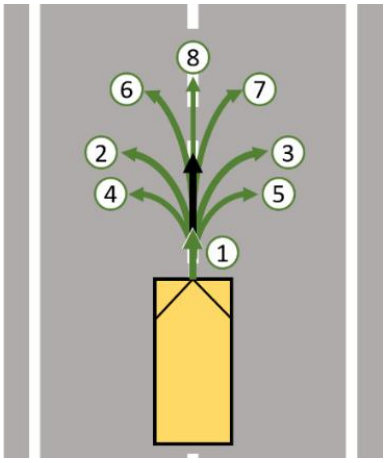

1) longitudinal maximum (full deceleration)
2) lateral maximum (steering left)
3) lateral minimum (steering right)
4) longitudinal min – lateral max combination (deceleration and steering left)
5) longitudinal min – lateral min combination (deceleration and steering right)
6) longitudinal max – lateral max combination (acceleration and steering left)
7) longitudinal max – lateral min combination (acceleration and steering right
8) longitudinal minimum (full acceleration)

Figure 3. Model for vehicle maneuvers to affect a traffic situation or accident

The maneuvers are parametrized with the help of the accident reconstruction. The full acceleration and deceleration use the maximum available grip level on the specific road condition (surface, humidity, pollution etc.) and the extrema of the specific vehicle model (engine characteristics, gearbox and current gear, braking system) which is used in the simulation. The steering behavior is simplified by a clothoid with a constant steering angle velocity of 360°/s, so there is no unit-impulse-sequence but a very severe evasion maneuver. The combination maneuvers split the transferable force into longitudinal and lateral direction in reference to Equation 2 in the proportions given in Equation 3 and 4. Therefore, the maneuver uses a significant steering angle and still has a strong longitudinal deceleration / acceleration.

$$a_x = \frac{1}{3}\mu_{road} \cdot g \text{ (Equation 3)}$$

$$a_y = \sqrt{(\mu_{road} \cdot g)^2 - (a_x)^2} \approx 0.943 \cdot \mu_{road} \cdot g \text{ (Equation 4)}$$

Furthermore, the model contains some uncertainties and a systematic overestimation of vehicle possibilities. This leads to an underestimation of the PONR (meaning it might be closer to t_0) and is addressed in the limitations paragraph.

Approximation method and simulation time efficiency

As already mentioned the PONR is unknown for real-world accidents and there is only the known constraint that it is located before the collision. Considering the criticality of a situation according to [14] as the risk as a function of time, Figure 4 shows that the PONR is the distinction (zero crossing) between a critical situation and an unavoidable collision event. Thereby the exact function is unknown and the approach does not consider the collision severity. To approximate the PONR to a certain precision dt, the model must apply at several time steps backwards from the point of the collision. At every time step there is a dynamics simulation run in forward direction, and the verification of a collision. This would result in a huge number of simulation runs, for what reason time efficient approximation methods are strongly required. Using common values, the simple example in Equation 5 illustrates this requirement, as a four-year calculation time is unacceptable.

$$\Delta t_{sim} = \Delta t_{single-sim} \cdot n_{mnrv} \cdot \frac{\Delta t_{acc}}{dt} \cdot N_{sample} \approx 4.28\, years \text{ (Equation 5)}$$

with

Δt_{sim}	Duration of the entire PONR calculation for the sample
$\Delta t_{single-sim}$	Duration of a single simulation run; assumption: $\Delta t_{single-sim} = 30\ s$
n_{mnrv}	Number of maneuver plus initial simulation; model: $n_{mnrv} = 9$
Δt_{acc}	Duration of the accident simulation; usually: $\Delta t_{acc} \approx 5\ s$
dt	Step size (equivalent to PONR precision); assumption: $dt = 10\ ms$
N_{sample}	Sample size, number of accidents; assumption: $N_{sample} = 1000$

As the requirement for a time efficient simulation is very high, the model uses a combination of several methods. The following sub-paragraphs explain the three major approaches.

Order of avoidance maneuvers: If any maneuver is able to avoid a collision it is not important what the result of the other maneuvers is. As in this case at least one maneuver is able to avoid the collision, the approach obviously did not reach the PONR yet. Thereby the un-simulated maneuvers can be skipped and the simulation moves one time step closer to the collision (in contrast it is not clear if the PONR is already reached unless all maneuvers are not able to avoid a collision). Using this circumstance in combination with the knowledge of maneuver effectiveness from literature and traffic accident research, the model sorts the maneuvers in an efficient way (full braking first, evasion second, acceleration last etc.).

Bisection method: Approximation methods like the Newton's method [15] as well as the Regula-Falsi [15] and others would be promising to determine the described zero crossing. However, they cannot be applied directly as they require an analytical, differentiable function, which is not the case for the function in Figure 4. However, the bisection method [15] is a slower, but appropriate alternative to determine the PONR under these circumstances.

Generally, the bisection method divides the current time interval equally into two parts and verifies the function value. Here, function value means the determination of the collision or the avoidance. The described model uses the bisection method multiple times, so the step size dt_i decreases per iteration i according to Equation 6.

$$dt_i = \frac{\Delta t_{acc}}{2^i} \text{ (Equation 6)}$$

Starting with the duration of the initial accident simulation Δt_{acc} in the interval $[t_0, t_{coll}]$ leads to a necessary number of i iterations to reach a certain precision ε, see Equation 7.

$$i = \log_2\left(\frac{\Delta t_{acc}}{\varepsilon}\right) \text{ (Equation 7)}$$

Using the bisection method solely and assuming typical values of $\Delta t_{acc} \approx 5\ s$ and $\varepsilon = 10\ ms$ leads to $i \approx 8.97$ meaning 9 iterations. The number of necessary iterations is unaffected by the exact position of the PONR within the entire interval $[t_0, t_{coll}]$.

Fixed step size: As accident investigation and especially its reconstruction shows, that the majority of the cases can be avoided by an emergency maneuver within one second before the collision, the model efficiency can be raised by using this knowledge to reduce the number if iterations. A preceding consideration with a fixed step size Δt_{fixed} can roughly determine the PONR position (see Figure 4, orange steps 1. and 2.). Afterwards the described bisection method applies multiple times in the corresponding one-second interval to determine the PONR more accurate (see Figure 4, green step 3.). Thereby the bisection method needs less iterations compared with application on the entire interval $[t_0, t_{coll}]$, see Equation 8.

$$i = i_{fixed} + \log_2\left(\frac{\Delta t_{fixed}}{\varepsilon}\right) \text{ (Equation 8)}$$

Using a fixed step size $\Delta t_{fixed} = 1\ s$ and a precision $\varepsilon = 10\ ms$ is leading to $i = i_{fixed} + 6{,}64$ necessary iterations. Thereby, this combination reduces the number of iterations if the PONR is within the first second prior to the initial collision.

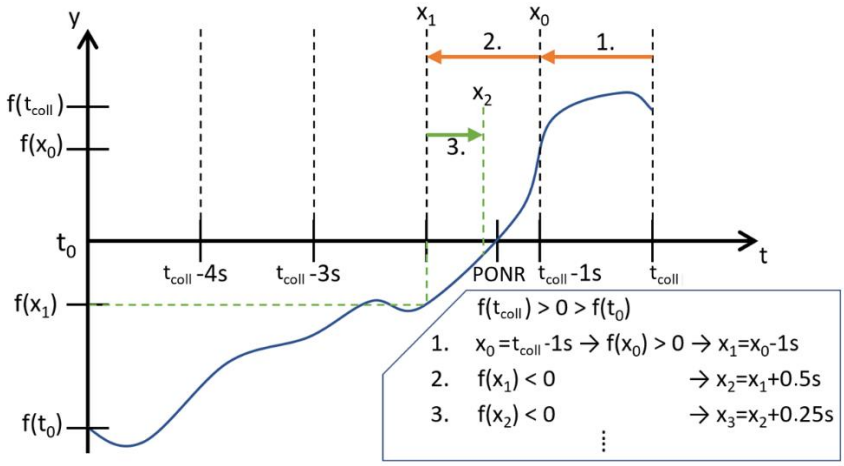

Figure 4. Combined approximation method of fixed step and bisection to determine the PONR

Therefore, a combined approximation method based on a fixed step size (see Figure 4, orange steps 1. and 2.) with a bisection method (see Figure 4, green step 3. multiple times) appears to be the most efficient for the introduced approach. According to reversed Equation 6, this is true for accident simulations with a duration $\Delta t_{acc} > 1.3\ s$.

German In-Depth Accident Study (GIDAS database)

For the analysis accident data from the German In-Depth Accident Study (GIDAS) is used. GIDAS is the largest in-depth accident study in Germany. The data collected in the GIDAS project is very extensive, and serves as a basis of knowledge for different interest groups. Due to a well-defined statistical sampling plan, representative statements for the German accident scenario are possible. Since July 1999, the GIDAS project collects on-scene accident case information in the areas of Hanover and Dresden. GIDAS collects data from all kinds and types of accidents related to personal damage. Approx. 3.500 pieces of information (about vehicles, persons, injuries, infrastructure, environment etc.) are coded in the database per accident on average. Finally, every accident is also reconstructed.

The project is funded by the Federal Highway Research Institute (BASt) and The Research Association of Automotive Technology (FAT), a department of the German Association of the Automotive Industry (VDA). Use of the data is restricted to the participants of the project. However, to allow interested parties the direct use of the GIDAS data, several participation models exist. Further information can be found at www.gidas.org [12].

To ensure representative results, GIDAS data should be weighted towards the German national statistics. This is necessary due to slightly biased data. The investigation teams are not thoroughly informed about all accidents, information about injuries cannot always be obtained immediately and differences in the investigation areas cannot be excluded. The derived conclusions out of a study with weighted GIDAS data can be used for statements that can be considered as representative for the German accident scenario.

The GIDAS dataset is weighted towards the German national traffic accident statistics of the year 2016 on the basis of the parameters accident site (urban, rural), accident severity (accident with slightly, seriously, fatally injured persons) and type of accident (seven different categories).

RESULTS

The presented method of calculating the PONR should be applied to an example accident scenario to provide results out of real accidents. The aim is to use as many comparable accidents as possible to produce significant results. For

this reason, an accident scenario is chosen that frequently occurs in the area of personal injury accidents. The decision is made for rear-end collisions between two cars.

Relevance of rear-end collisions between two cars in German accidents with personal damage
In the first step, the GIDAS dataset (Effective December 31st, 2016) is filtered step by step to check the relevance of this accident scenario. One important filter criteria is the accident year. Here, only accidents of the years between 2005 and 2016 were used as the number and quality of information available in the GIDAS database increased significantly in 2005. Therefore, a total number of 20,148 reconstructed accidents are available as the basis (100 %) for the following analysis (see Figure 5). Next, three further filter steps are applied:

- accident with personal damage, involving at least one passenger car: 16,521 (82.0%)
- thereof: at least one collision between two cars: 6,091 (30.2%)
- thereof: rear-end collision (front of one car strikes preceding car at the back) 2,977 (14.8%)

Although accidents with personal damage are characterized by a tremendous variety in terms of involved road users, vehicle types and collision constellations, the group of "rear-end collisions between two cars" has a quite large relevance. More than every seventh accident with personal damage in Germany (in 2016) belongs to this group (see Figure 5).

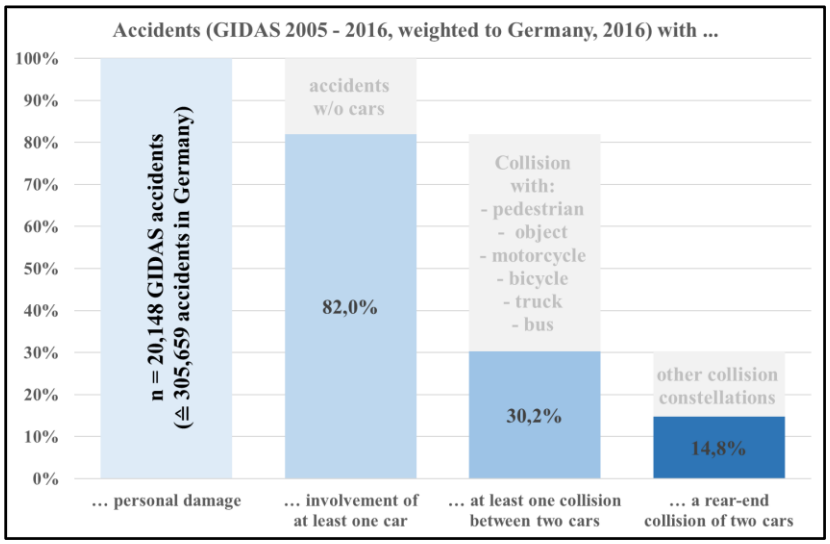

Figure 5. Relevance of rear-end collisions between two cars in German accidents with personal damage

In total, 2,977 GIDAS accidents (representing 45,159 accidents in Germany in 2016) are generally available for further analyses. However, the calculation of the PONR requires some more filtering. On the one hand, some reconstruction parameters are essential for the simulation. On the other hand, the considered accidents should be as similar as possible to the idealized scenario described in Figure 8. Thus, the following filter criteria are additionally used for the creation of the master dataset out of the GIDAS database (used GIDAS variables and codes in brackets):

- collision between participant 1 and 2 in the accident [BETNR < 3]
- first collision for both cars [NRKOLL = 1]
- rear vehicle had a front collision [VDI2 = 1]
- preceding vehicle had a rear end collision [VDI2 = 3]
- collision angle (angle between vehicle's speed vectors) within ± 15° [-15° … KWINK … 15°]
- no skidding or instable vehicle condition prior to the collision [SCHLEU = 2]
- known parameters: initial speed, braking deceleration and distance, collision speed, max. friction value

The filtering process results in 1,878 accidents that meet the above mentioned criteria. Out of these, 1.019 accidents have already been simulated and written into the 2016 Pre-Crash-Matrix (PCM) [13]. So, the basis for the calculation of the PONR are these 1,019 accidents between two cars with a rear-end collision resulting in personal damage

to at least one person. After weighting these accidents to the German national accident scenario of 2016, these accidents represent 1,261 accidents. This means that the considered accident scenario is slightly under-represented in GIDAS.

The following analyses provides a brief characterization of these accidents (using weighted figures).

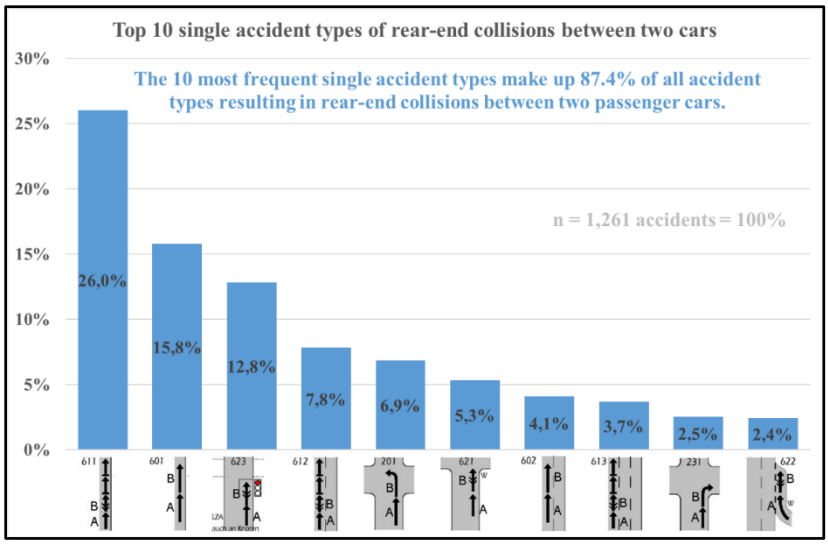

Figure 6. Most frequent single accident types in rear-end collisions between two cars (source: GIDAS)

As expected the most frequent critical situations of the considered accidents are accidents in longitudinal traffic resp. "accidents between vehicles moving along in carriageway" (group 600-699). These represent nearly 84% of all accidents in the master dataset. The remaining accidents are dominated by "Accident caused by turning off the road" which make up another 9.5%.

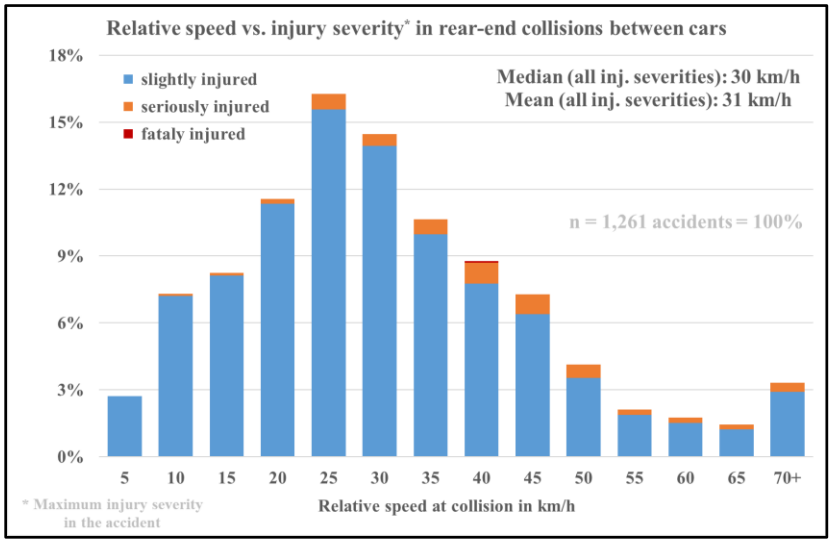

Figure 7. Relative speed vs. injury severity in rear-end collisions between cars (source: GIDAS)

Figure 7 shows the distribution of the relative speed and the documented injury severity of the accident. Here, relative speed is defined as the absolute value of the difference between the velocity vectors of the two cars at the moment of collision. It is not the relative speed at the time of the critical situation. The injury severity is the highest in-

jury severity of the accident. It has to be considered that this injury severity must not necessarily result from the occupants involved in the rear-end collision. It may also come from another collision (in multiple collision accidents) or from another road user that is involved in the accident.

On the one hand, the figures shows the speed differences that occur in rear-end collisions between two cars. However, this diagram tells nothing about the absolute speed level. A relative speed of 30 km/h can occur when a car collides with the back of a standing car or in a highway collision where a car with a speed of 160 km/h collides with a preceding car that is running at 130 km/h. The relative speed is identical but the collision energy may be different.

On the other hand, it can be seen that the vast majority (94.1%) of rear-end collisions leads to slight injuries only. There are only few accidents with serious injuries (5.8%) and only one accident (< 0.1%) at a relative speed of 42 km/h is a fatal one (a highway collision with an old car that resulted in a rollover).

Application on idealized rear-end collisions

To compare the model results with other approaches from literature, that refer to idealized constellations only, the model is applied to the idealized rear-end collision scenario first (see in Figure 8). It is important to point out that "relative speed" in the following chapters as well as in the literature source is the difference between the vehicle's speed vectors prior to the collision (difference between initial speeds) and not (like in the paragraph above) at the moment of the collision.

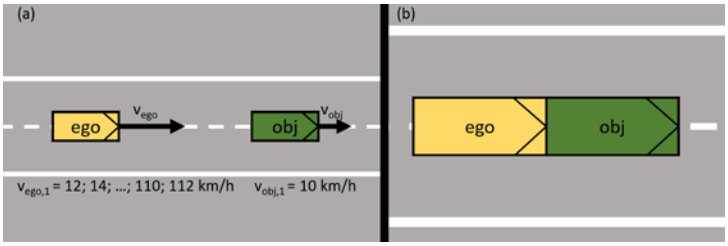

Figure 8. Scheme of the idealized rear-end collision scenario [5]

Figure 9 shows the PONR in seconds (here called t_u) as a function of relative speed between the two vehicles in km/h in the range of 0 to 100 km/h. The results visualize very well the most effective avoidance strategies and the common braking – evading boundary. Considering a decreasing friction value μ_{Road} (left graph), the gradient of the avoidance by braking function is increasing and the bound of the most effective avoidance strategy moves towards lower relative speed. Especially the comparison with Seiniger [8] ($\mu_{Road} = 1.0$) shows very close results and suggests the ability to apply the model for real accidents in a forward simulation. The offset to Reinsch [7] can be explained by differences in the model approach regarding access period of 0.3 s and swell period of 0.7 s.

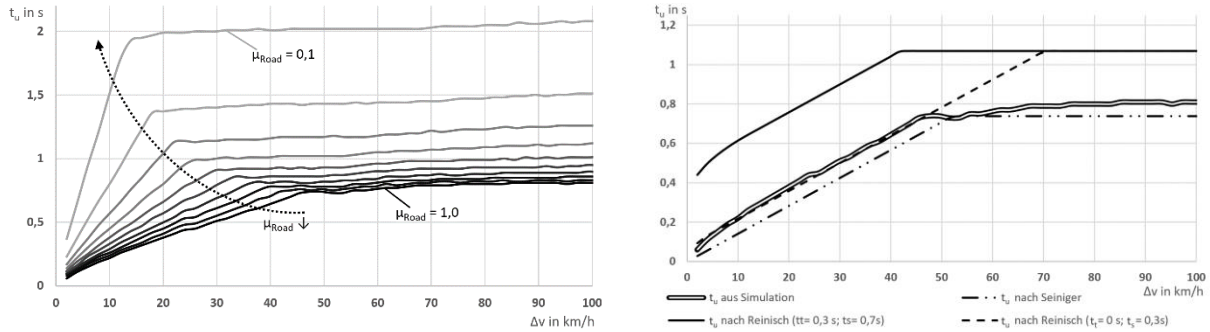

Figure 9. PONR as a function of the relative speed between the two vehicles ([5] in reference to [7] and [8])

Application on real world rear-end collisions

In the second step, the developed model is applied to the 1.019 GIDAS accidents with rear-end collisions of two vehicles as described above. The calculation precision of the PONR is $\varepsilon = 10\ ms$. Even though the described approaches for reducing simulation time are applied, the entire simulation time is around 11.5 days on one CPU and 42.000 iterations are performed (≈ 41 per case). Figure 10 shows the distribution of the calculated PONR rounded to 0.1 s. The large number of PONRs in the area of 0.6 – 0.9 seconds suggests a quite large potential for further safety systems. The low proportions below 0.3 seconds mostly represent low-speed accidents with minor consequences for the occupants. PONR above 1.6 s occur very seldom. These are mainly high speed highway collisions.

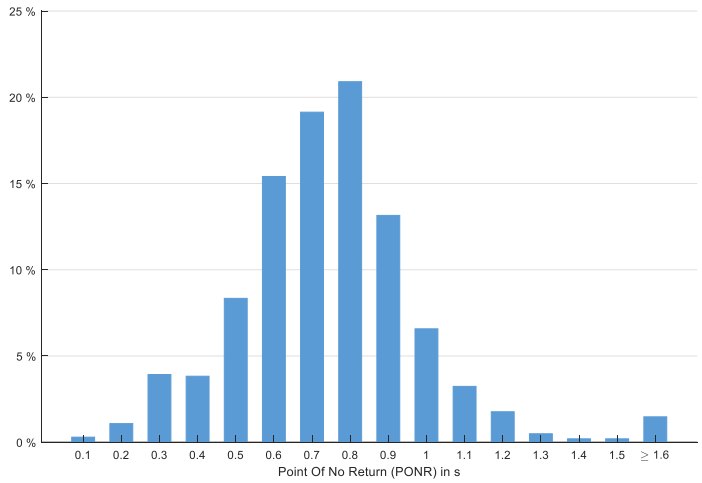

Figure 10. Relative proportions of the calculated PONR for n = 1.019 rear-end collisions from GIDAS

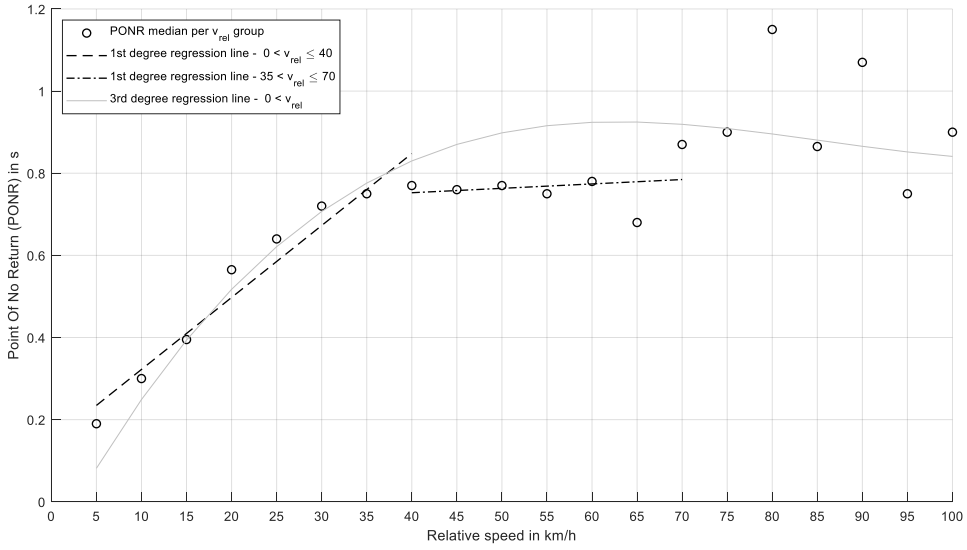

Figure 11. PONR as a function of the relative speed between the two vehicles calculated for n = 1.019 rear-end accidents from GIDAS

Figure 11 shows the calculated PONR as a function of the relative speed between the two vehicles, visualizing the median value per 5 km/h group. The values are unexpectedly close to the idealized scenario in the area of 0 <

$v_{rel} \leq 60$ (compare Figure 9) as the parameter and specific attributes for real accidents spread widely. The sample contains not enough cases above 70 km/h to rely on the calculated values and the PONR is largely spreading.

The most important differences that occur in the real scenario compared to the idealized scenario are:

- Offset of the two vehicles (usually within one lane but not exactly overlapping x-axes)
- Collision angle within ± 15°
- Driving through curves
- Varying μ_{Road} (source reconstruction)
- Approach limit for the steering model at high speed (skidding)

The 1st degree regression lines in the area of $0 < v_{rel} \leq 40$ and $35 < v_{rel} \leq 70$ represent the two avoiding strategies braking and evading respectively, for the majority of the cases. Especially the gradient of the first regression line is in the area of the theoretical approaches even though the μ_{Road} values are highly diverse. The 3rd degree regression line for the entire area must not be over-interpeted and is therefore grayed out. It shows the general behavior only.

LIMITATIONS AND DISCUSSION

The calculated values are based on a theoretical model including limitations as well as neglecting some effects. Even though the model shows significant results, model limits as well as uncertainties must be considered for all interpretations.

Uncertainties of in-depth accident data and reconstruction
In-depth accident investigation and reconstruction as described above is always accompanied by uncertainties [18]. This cannot be avoided, as the event has already been gone when it is considered. The investigation collects as much evidences as available a posteriori and the reconstruction tries to determine the sequence of events leading to the accident and its consequences. Therefore velocities, the coefficient of friction, and other reconstruction parameter must be considered with a certain confidence interval. In addition, the exact driver reactions are estimated based on the drivers statements in combination with the accidents result and all other contributing information. Due to the physical constraints that lead to the limits of vehicle dynamics, the suggested approach is especially sensitive to the coefficient of friction.

Underestimation of the PONR due to model boundaries
The suggested approach describes some model simplifications. Some have been introduced by purpose to avoid an unreasonable extent at this state of the approach, but can be improved in future. It is important to state that probably no regular driver and no real vehicle does reach the model values for acceleration, deceleration, or steering velocities. This is especially true for the reaction period and vehicle access period.

The following model limitations introduce a systematic overestimation of the vehicle's possibilities and therefore an underestimation of the PONR values. This suggests that the actual potential for vehicle safety systems could be even higher than shown in the results.

- Clothoid evasion with constant steering velocity instead of a lane change (e.g. 5th / 7th degree polynom)
- No / low consideration of collisions with the environment or leaving the road
- No consideration of traffic flow

In contrast the assumption that Car2Car or Car2X-communication is completely or partially possible with ideal or noisy signal, leads to the possibility of cooperative avoidance strategies (meaning 8 maneuvers for both vehicles leading to 81 combinations). Under consideration of this subject the current independent approach overestimates the PONR.

Finally, there is the definition on a fixed partition of the maximum transferable force for longitudinal and lateral combined maneuvers (e.g. steering + braking, see Figure 2). Other partitions could lead to a shift of the PONR, but their influence in magnitude as well as direction cannot be predicted at the moment.

Application on other data or other purposes
The suggested approach can estimate the PONR for real accidents. An adaption towards naturalistic driving data as well as real time estimation is conceivable. This would signify a crucial contribution to the current research on the distinction between accidents and incidents. However, some adaptations would be necessary to enable such calculations.

Furthermore, it can be used to evaluate collision avoidance strategies and to parameterize some Advanced Driver Assistance Systems (ADAS). It can also contribute to the estimation of a traffic scenario‘s criticality as a surrogate safety measure. However, friction coefficient values are currently unknown for safety systems and cannot be used for the model parametrization.

CONCLUSIONS

The PONR is an important value to improve vehicle safety as it is the final point where all available safety measures must be activated to avoid personal damage. As this point is not measurable in reality and current analytical approaches are not sufficient to apply on real accidents, this paper introduces an advanced approach using numerical simulation. The developed approach estimates the further potential of passive and integral safety systems regarding earlier activation times. Furthermore, it can be used to evaluate collision avoidance strategies like steering versus braking as well as for parameterization of Advanced Driver Assistance Systems (ADAS).

The calculated PONR as a function of relative speed for a sample of 1.019 rear-end collisions between two cars show significant results compared to the existing analytical approaches in literature. This verifies the applicability of the approach towards traffic accidents at least for the rear-end collision scenario. Further accident scenarios can be treated by the same approach in future. The distribution of all PONR shows that passive safety measures could be possibly activated 0.3 – 1.1 seconds prior to the imminent collision for the majority of the cases. Therefore, occupant protection can be further improved by enabling already existing but unused potentials, and accidents consequences could be mitigated even more.

REFERENCES

[1] SAE International. 2018. SAE J3016: “Taxonomy and Definitions for Terms Related to Driving Automation Systems for On-Road Motor Vehicles”

[2] European Enhanced Vehicle-safety Committee (EEVC). 2006. “Primary secondary safety interaction” EEVC WG 19, p. 12

[3] Winner, H.; et al. 2015. Handbuch Fahrerassistenzsysteme. Wiesbaden: Springer Vieweg

[4] M. Mitschke, H. Wallentowitz. 2014. “Dynamik der Kraftfahrzeuge”. Wiesbaden: Springer Vieweg.

[5] E. Ramin. 2018. “Entwicklung eines Simulationsmodells zur Bestimmung des Zeitpunktes der Unvermeidbarkeit realer Verkehrsunfälle” Diploma Thesis, Institute for Traffic Accident Research at Dresden University of Technology (VUFO) and Chair of Automobile Engineering (LKT) TU Dresden, Supervision: F. Spitzhüttl, M. Köbe, Prof. Dr.-Ing. Günter Prokop

[6] J. Hillenbrand. 2007. “Fahrerassistenz zur Kollisionsvermeidung”. Doctoral Thesis. Karlsruhe Institute of Technology (KIT), Faculty Electrical Engineering and Information Technology.

[7] P. Seiniger; et al. 2012. “Ein validiertes Testverfahren für Notbremssysteme – Ergebnisse des ASSESS-Projekts.” Report.

[8] P. Reinisch. 2012. “Eine risikoadaptive Eingriffstrategie für Gefahrenbremssysteme”. Doctoral Thesis. University of Duisburg-Essen, Faculty of Engineering.

[9] IPG Automotive GmbH, 2016. “CarMaker Reference Manual” www.ipg-automotive.com, Version 5.0.3.

[10] The MathWorks, Inc. 2015. “Matlab, Desktop Tools and Development Environment”, https://www.mathworks.com/help/matlab/

[11] The MathWorks, Inc. 2015. “Simulink User's Guide“, https://www.mathworks.com/help/matlab/

[12] The Research Association of Automotive Technology (FAT), Federal Highway Institute of Germany (BASt). 2019. “German In-Depth Accident Study (GIDAS) “. Retrieved from www.gidas.org

[13] Institute for Traffic Accident Research at Dresden University of Technology (VUFO). 2019. “Pre-Crash-Matrix (PCM) Format Specification v5.0“. Retrieved from https://www.vufo.de/forschung-und-entwicklung/simulationen/

[14] DIN EN ISO 12100. 2011. “Sicherheit von Maschinen - Allgemeine Grundsätze – Risikobeurteilung und Risikominderung”. Beuth.

[15] W. Dahmen und A. Reusken. 2008. “Numerik für Ingenieure und Naturwissenschaftler”, Berlin, Heidelberg: Springer-Verlag.

[16] M. Brännström, E. Coelingh, J. Sjöberg. 2010. “Model-Based Threat Assessment for Avoiding Arbitrary Vehicle Collisions” IEEE Transactions on Intelligent Transportation Systems, S. 658–669.

[17] S. Karrenberg. 2008. “Zur Erkennung unvermeidbarer Kollisionen von Kraftfahrzeugen mit Hilfe von Stellvertretertrajektorien”. Diss. Braunschweig: TU Braunschweig.

[18] H. Burg (pub.). 2017. “Handbuch Verkehrsunfallrekonstrunktion: Unfallaufnahme, Fahrdynamik, Simulation”. Wiesbaden: Springer Vieweg.

RESPONSES OF THE SCALED INFANT HUMAN BODY MODEL IN SIMULATED FRONTAL MOTOR VEHICLE CRASHES

Sophia Tushak
Center for Injury Research and Prevention, The Children's Hospital of Philadelphia
Joint Department of Biomedical Engineering, UNC-Chapel Hill/NC State University
United States

Jalaj Maheshwari
Aditya Belwadi
Center for Injury Research and Prevention, The Children's Hospital of Philadelphia
United States

Paper Number 19-0142

ABSTRACT

Most motor vehicle crash deaths occur among children traveling as passenger vehicle occupants, and proper restraint use and direction of use can reduce these fatalities. There is little to no literature on systematic evaluation on the responses of children under three-years of age in motor vehicle crashes. The study presents the first ever endeavor at developing 18MO, 24MO, 30MO, and 36MO pediatric finite element models from the 6YO PIPER human body model as the baseline and comparing their responses in rear-facing and forward-facing simulations of the same crash pulse conditions in the FMVSS No. 213 test bench and a vehicle seat.

The 6YO PIPER model was scaled down to create anthropometrically accurate models of the 18MO, 24MO, 30MO and 36MO child using the PIPER scaling tool and Snyder anthropometric data. Each model (N=4), along with a convertible car seat and either the 213-test bench or a 2012 Toyota Camry vehicle rear seat was simulated in a full-frontal crash (24G, 120ms pulse). Kinetics and kinematics were extracted and processed as per SAEJ211 metrics.

On the 213-test bench, models in forward-facing configuration showed higher head accelerations, but lower pelvis accelerations for 30MO and 36MO models. Chest displacements were between 84-90% higher in the forward-facing models, with the exception of the 30MO model, which was 35% higher. Neck moments were lower in all rear-facing configurations. Upper neck forces were at least six times higher forward-facing. HIC36 in rear-facing models ranged from 300-344, while HIC36 in forward-facing models ranged from 410-494, showing no linear trend as age increased. Forward-facing head excursions grew over two-fold from their rear-facing counterparts, from an average of 240 to an average of 518. Head trajectories generally followed a longer path in forward-facing models. NIJ for all forward-facing models were five to eight times the values for rear-facing. On the vehicle seat, the forward-facing models showed higher head accelerations for 24MO and 36MO models. Chest displacements were 33-49% higher in forward-facing models, except 36MO, where it was 128% higher. Neck forces and moments were consistently lower for rear-facing models as compared to forward-facing. Upper neck forces were 6.5-9.75 times higher in forward-facing models. HIC36 values were lower in rear-facing, ranging from 335-394, as compared to forward-facing which were 455-624. Head excursions for forward-facing were three times that for rear-facing, except the 36MO model, where it was 1.75 times higher. NIJ for all forward-facing models were six to nine times the values of rear-facing.

Kinetics and kinematics numbers across the board were within IARV limits. Pediatric models in rear-facing configurations generally had lower injury numbers than those in frontal configurations. However, there is no consistent trend seen in injury values as age progresses. This is the first study to conduct a systematic evaluation of the response of children under three years old in frontal motor vehicle crashes.

INTRODUCTION

Motor vehicle crashes (MVCs) are the leading cause of death among children over the age of one [1]. Most knowledge about pediatric injury rates is derived from real-world crash databases, sled testing via anthropometric test devices (ATDs) aged from newborn to 10 years old, and post-mortem human subjects (PMHS), but little has been investigated using computational finite element (FE) analysis and human body models (HBMs) to predict the occurrence of potential injuries in unique crash conditions. Misuse of child restraint systems (CRSs) is a prevalent problem when transporting children. Misuse rates are typically generated from observational studies and vary depending on the sample population included in the analysis. The implications of CRS misuse on injury risk should be assessed using a systematic approach that reduces the number of confounding variables to determine specific injuries associated with misuse.

Current Methods to Assess Injury in Children

Field Databases Despite the gravity of the problem, most of the current knowledge on pediatric injuries from MVCs is obtained from fatal crash reports, and minimal efforts have been made to examine non-fatal crash statistics [2]. Field data can be vague and confusing since the crash reports have many confounding variables, such as the region of the country in which the accident occurred, subject age, car model, impact speed, and crash mode.

Post-Mortem Human Subjects The use of PMHS is common in biomechanical and anatomical assessments of adult populations, but their usage in pediatric populations is far more scarce due to the infrequency of available specimens. The lack of comparable data causes large gaps in knowledge of pediatric injury risk as well as inaccuracies when developing other methods for assessing injury risk, such as ATDs and FE human body models (HBMs).

Anthropometric Test Devices Child ATDs have been used for several decades to study whole-body responses in MVCs. While their biofidelity has improved, they lack the same capacity for anatomical specificity and tissue-level kinematic and kinetic responses as PMHS. Additionally, ATD whole-body responses are only validated for impacts in one direction (frontal, lateral, rear), so their injury outcomes are restrictive to one crash mode.

Finite Element Analysis The newest method of assessing injury in MVCs is FE analysis, which offers a customizable, low-cost, and repeatable computational means to represent the variations due to age and size in different populations [3]. Due to the scarcity of pediatric PMHS and the subjective nature of field data, FE analysis poses an excellent alternative. However, FE responses are based on how the model is defined, so if the model is inaccurate, the responses cannot be trusted. Many existing FE ATD models and HBMs are derived by scaling down adult geometry to child geometry, but this is inappropriate since anthropometric and anatomical differences exist between the two populations [4], namely in the head [5], neck [6], torso [7], and pelvis [8]. The PIPER 6YO Child model is one of the only HBMs developed and validated from child PMHS data. Other similar HBMs, including Wayne State University's CHARM-10 10-year-old model and the Global Human Body Models Consortium's (GHBMC) 6-year-old model, were developed from child PMHS data but are pedestrian models rather than occupant models. Along with the release of the pediatric model, the PIPER project released the PIPER software, a program that continuously scales and quickly positions FE models. This new pediatric HBM and useful program create the potential to accurately predict injuries in children of all ages and sizes in multidirectional impacts.

Misuse of Child Restraint Systems

Previous studies have uncovered a 63-90% CRS misuse rate with at least one installation error [9-14]. Misuse errors vary, and some errors are more detrimental than others. However, the cumulative effect of several small errors can result in the effect of one large error [15-20]. The rear-facing configuration is safest for infants since the CRS protects the anterior loading of the head, neck, torso, and pelvis in the event of a frontal impact car crash by evenly distributing the load across the back face of the CRS and reducing neck flexion, head acceleration, and chest displacement [21]. A convertible CRS allows for effortless transition from rear-facing to forward-facing configurations, but is usually limited to infants under 18 kg. Countries have different recommendations for how long children should remain in rear-facing CRSs. For example, the United States suggests that parents refrain from switching their children to forward-facing until at least the age of 2 years old. Sweden, however, suggests that parents wait until children reach five years old to make the switch. A potentially premature transition may have

severe consequences and could lead to injurious loading or ejection if the belt path is not in the proper orientation for that configuration [21]. A study by Henary et al [22] found a 5.5 times and 1.2 times greater injury risk during side and frontal impacts, respectively, for children under the age of two in forward-facing CRSs. Spinal cord injuries are among the most notable since children's heads are disproportionate in relation to the rest of their body, causing greater head rotation and tensile loads to the cervical spine [21].

Installation angle of rear-facing CRSs is vital. A CRS that is too erect may inhibit breathing if the infant's head is tipped forward. A CRS that is too reclined causes the upward projected force to surpass the reaction force of the back of the CRS, thereby ineffectively restraining the infant. Car seat manufacturers generally suggest a 30 to 45 degree recline angle of the back of the CRS with respect to the vertical axis. For a larger infant, a 30 degree recline may be more appropriate to ensure better crash protection. For a smaller infant, a 45 degree recline is better to allow for ample crash protection, but also discourage the head from leaning too far forward and potentially impairing breathing [21]. Understanding the implications of CRS misuse can provide education for parents as to how severe the consequences of improper installation may be.

Study Goals

Little to no literature on the systematic evaluation of the kinematic and kinetic responses of children under three years of age in MVCs exists. This study presents the first ever endeavor at developing 18MO, 24MO, 30MO, and 36MO pediatric finite element models from the 6YO PIPER HBM and comparing their responses in rear-facing and forward-facing simulations of the same crash pulse conditions in the Federal Motor Vehicle Safety Standards (FMVSS) No. 213 test bench and a 2012 Toyota Camry vehicle seat.

METHODS

The 6YO PIPER Child model was scaled down to create anthropometrically accurate models of the 50th percentile 18MO, 24MO, 30MO and 36MO child using the PIPER scaling tool and Snyder anthropometric data [23]. Each model (N=4), along with a convertible car seat (rear-facing and forward-facing configurations) and either the FMVSS No. 213 test bench or a 2012 Toyota Camry vehicle rear seat was simulated in a full-frontal crash (24G, 120ms pulse) using LS-DYNA (v.971_R8, Livermore Software Technology Company, Livermore, CA) for a total of 16 simulations. Kinetics and kinematics were extracted and processed as per the Society of Automobile Engineers (SAE) J-211 metrics.

Age-Based Scaling

The PIPER 6YO Child model was scaled using the PIPER software (v1.0.1). The 6YO child model was imported into the PIPER program and scaled to 18 month-old (18MO, m=12.6 kg), 24 month-old (24 MO, m=13.7 kg), 30 month-old (30MO, m=14.8 kg), and 36 month-old (36 MO, m=16.0 kg) 50th percentile models. When scaling, one landmark was missing from the thoracic spine, causing a mesh deformity in the upper thoracic spine (Fig.1A). To fix this, the missing landmark was added to the target file in NotePad++ before scaling again in PIPER, without causing a deformity in the mesh (Fig. 1B). The scaled models were exported to be used in finite element (FE) simulations.

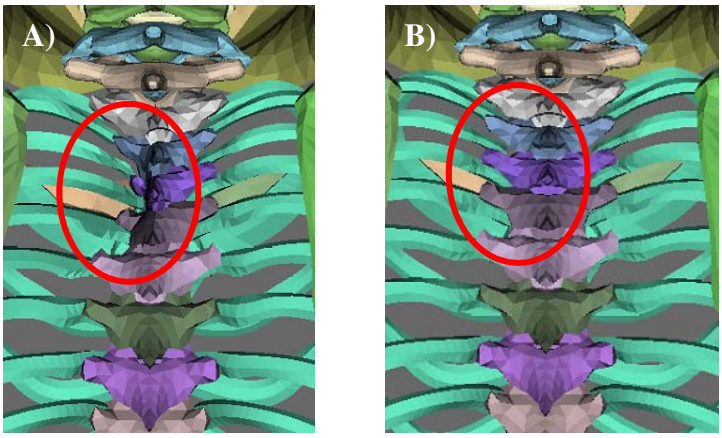

Figure 1. A missing landmark A) causes a deformity in the upper thoracic spine after scaling, B) but was later fixed.

Seat Preparation

A FE model of a convertible car seat (polypropylene plastic: E=10 GPa, $\rho=9e^{-7}$ kg/m^3, $\nu=0.43$, m=8.0 kg) was developed from CAD data in HyperMesh (v.14.0, Altair HyperWorks, Troy, MI). FE models of the convertible car seat and either the FMVSS No. 213 test bench (steel: E=210 GPa, $\rho=6e^{-6}$ kg/m^3, $\nu=0.33$) or a 2012 Toyota Camry rear vehicle seat (plastic: E=1.0 GPa, $\rho=7.11e^{-7}$ kg/m^3, $\nu=0.30$ and foam: E=0.00416 GPa, $\rho=1.01e^{-7}$ kg/m^3, m=6.9 kg) were imported into HyperMesh. The car seat was positioned as close to the bench or seat without contacting it in both forward-facing and rear-facing configurations. The forward-facing car seat was kept at the default position, angled 23.5 degrees with respect to the vertical axis. The rear-facing car seat was rotated to 45 degrees with respect to the vertical axis, as suggested by the car seat manufacturer. The CRS was gravity-settled onto the test bench/Camry seat. All FE simulations were run in LS-Dyna on a 64-node double precision explicit solver. The combined car seat and base model was used in future simulations with the PIPER child models, resulting in models with the car seat and either the FMVSS No. 213 test bench or the Camry seat in forward-facing and rear-facing configurations.

Child Model Preparation

Each scaled PIPER child model (18MO, 24MO, 30MO, and 36MO) was positioned in PIPER. The hips, knees, and ankles were rotated by approximately 15, 20, and 10 degrees, respectively, so that the model could be positioned as close to the car seat as possible to reduce the time required to settle the model. Any mesh deformations accrued during the positioning process were smoothed in PIPER. Following that, the PIPER models were settled into the seat and base using the same method as in the seat preparation.

Simulated Frontal Vehicle Crashes

The settled models underwent seat belt routing. A buckle (steel: E=210 GPa, $\rho=6e^{-6}$ kg/m^3, $\nu=0.33$) was made with 2D elements and placed at the pelvis of the child model in an appropriate location. Using the HyperMesh belt routing tool, a five-point harness consisting of 2D shell elements with a width of 38 mm and 1D connecting elements was generated for each model, with two belts over the shoulders, two belts on the pelvic wings, and one belt between the legs (Fig. 2).

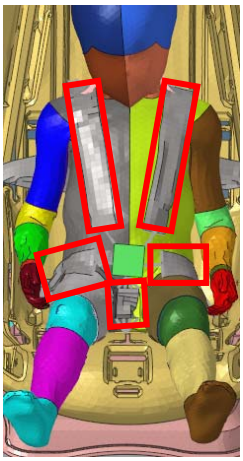

Figure 2. A 2D five-point harness was routed around each model and attached to a 2D buckle via 1D elements.

Once the model was secured in the car seat, the car seat was secured to the base. In the forward-facing configuration, a seat belt with a width of 48 mm was routed from the bottom anchor on the base, through the back of the car seat, and attached to the other bottom anchor on the base. Two additional seat belts were routed from the back anchor on the base, around the top of the base, and attached to the back of the car seat at the top anchor points (Fig. 3A-B). In the rear-facing configuration, a seat belt with a width of 48 mm was routed from the bottom anchor on the base, through the front of the car seat, and attached to the other bottom anchor on the base (Fig. 3C).

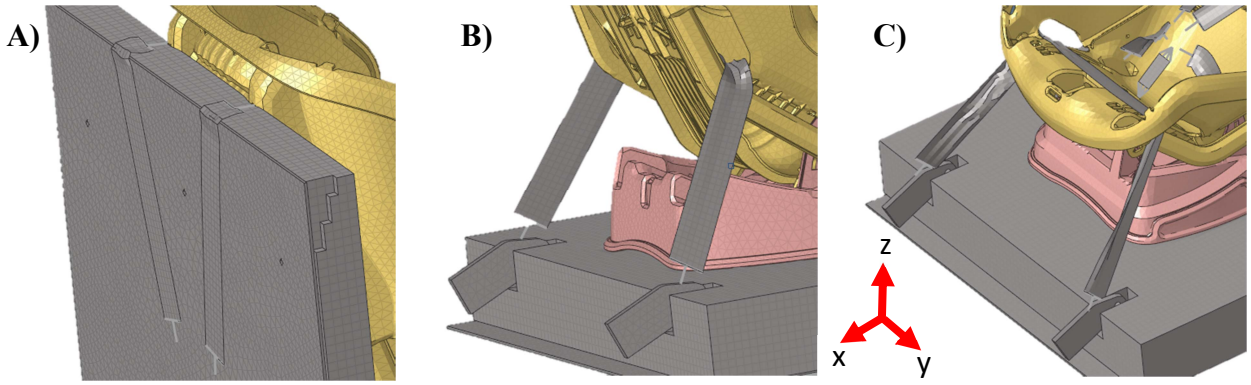

Figure 3. Seat belt routing of the CRS to the FMVSS No. 213 test bench. In the forward-facing configuration, seat belts were secured A) in two locations on the back of the test bench and B) to the two LATCH points on the bottom of the test bench. In the rear-facing configuration, a seat belt was secured C) to the two LATCH points on the bottom of the test bench. Since CRS manufacturers must be able to meet requirements without using a tether under the Federal Motor Vehicle Safety Standard (FMVSS) No. 213 test protocol, a top tether was not used. Similar belt routing was used for the Camry seat.

Model preparation with the Camry seat was set up identical to the 213-test bench, without a pretensioner, retractor, or load limiter. Surface-to-surface contacts were added for the interaction of the seat belt with the child model. Constant gravity was applied in the negative z-direction. The FMVSS No. 213 test pulse (24G) was applied to the base in the x-direction for a duration of 120 ms. Maximum head and pelvis accelerations, chest displacements, lower and upper neck forces and moments as well as head injury criteria (HIC), neck injury criteria (NIJ), and head excursions were extracted and processed as per the SAE J-211 metrics using LS-PrePost (v.4.5, Livermore Software Technology Company, Livermore, CA) and a custom MATLAB code (v.2017, MathWorks, Natick, MA).

RESULTS

Generally, the forward-facing model produced higher injury metrics than the rear-facing models (Table 1). On the FMVSS No. 213 test bench, head accelerations of the 18MO, 24MO, 30MO, and 36MO model in the forward-facing configuration were comparable to the rear-facing configuration, with 1.1-1.2 times (6.6%, 5.6%, 12.3%, and 19.0%, respectively) higher head accelerations. The opposite occurred for pelvis acceleration, where values were 1.1-1.2 times (18.4%, 12.3%, and 16.0%, respectively) higher in the rear-facing 18MO, 24MO, and 30MO models. The 36MO model did not continue this trend, with a pelvis acceleration 1.4 times (73.9%) greater in the forward-facing configuration. Maximum chest displacement ranged from 1.8-1.9 times (84.3-89.7%) higher in the forward-facing 18MO, 24MO, and 36MO models. Maximum chest displacement was substantially lower in the 30MO model, with a value of 1.3 times (34.8%) higher. Lower neck force varied greatly, with the 18MO model showing 0.8 times (17.7%) less force in the forward-facing configuration, the 24MO and 36MO models showing 1.5 and 1.4 times (48.2% and 38.7%) higher forces in the forward-facing configuration, respectively, and the 30MO model showing virtually no difference between the two seating arrangements. Considerably higher differences between forward-facing and rear-facing were seen in upper neck forces: the 18MO, 24MO, 30MO, and 36MO models were almost 15, 12, 7, and 8 times higher, respectively. Lower neck moments were all greater in the forward-facing configuration, with over 11-16 times greater moments. Upper neck moments, while still greater in forward-facing, did not show as great of a difference between seating arrangements (2.8, 3.4, 2.2, and 1.6 times higher for the 18MO, 24MO, 30MO, and 36MO models, respectively). HIC36 for the rear-facing models ranged from 302-344, but were much higher for the forward-facing models, which ranged from 409-494. Generally, the 18MO and 36MO models had higher HIC36 values than the 24MO and 30MO models. Nij ranged from 0.06-0.11 for the rear-facing models, and increased to 0.50-0.63 for the forward-facing models. Both rear-facing and forward-facing Nij were greatest in the 18MO model, lowest in the 24MO model, and similar for the 30MO and 36MO models. Head excursion was 3.4, 2.1, 2.6, and 1.4 times greater in the forward-facing configuration for the 18MO, 24MO, 30MO, and 36MO models, respectively. No correlations could be made between any metric and age of the model.

On the 2012 Toyota Camry seat, the 24MO and 36MO models in the forward-facing configurations showed 1.1-1.5 times (11.4% and 47.3%) higher head accelerations, respectively, while the 18MO and 30MO models showed 1.1 times (9.2% and 7.1%, respectively) higher head accelerations for rear-facing. Pelvis acceleration values were 1.0, 1.2, and 1.7 times (3.0%, 18.3%, and 72.9%) higher in the forward-facing 18MO, 30MO, and 36MO models, respectively. The 24MO model did not continue this trend, with a pelvis acceleration 2.3 times (73.9%) greater in the rear-facing configuration. Maximum chest displacement ranged from 1.3-1.5 times (33.3-48.8%) higher in the forward-facing 18MO, 24MO, and 30MO models. Maximum chest displacement was substantially higher in the 30MO model, with a value of 2.3 times (128.1%) higher. Lower neck force was 1.2-1.3 times (25.1%, 34.8%, and 23.7%, respectively) higher for the 18MO, 30MO, and 36MO models in the forward-facing configuration, and 1.8 times (81.1%) higher for the matched 24MO model. Considerably higher differences between forward-facing and rear-facing were seen in upper neck forces: the 18MO, 24MO, 30MO, and 36MO models were almost 9, 10, 10, and 7 times higher, respectively. Lower neck moments were all greater in the forward-facing configuration, with over 9-20 times greater moments. Upper neck moments, while still greater in forward-facing, did not show as great of a difference between seating arrangements (2.7, 5.0, 5.4, and 2.8 times higher for the 18MO, 24MO, 30MO, and 36MO models, respectively). HIC36 for the rear-facing models ranged from 336-383, but were much higher for the forward-facing models, which ranged from 455-624. HIC36 values varied greatly between models, with no similarities for any two models. Nij ranged from 0.06-0.11 for the rear-facing models, and increased to 0.54-0.64 for the forward-facing models. Both rear-facing and forward-facing Nij were greatest in the 36MO model and similar and lowest for the 24MO and 30MO models. Head excursion was 3.4, 3.3, 3.0, and 1.7 times greater in the forward-facing configuration for the 18MO, 24MO, 30MO, and 36MO models, respectively. No correlations could be made between any metric and age of the model.

Table 1.
Kinematic and kinetic responses of the 18MO (green), 24MO (blue), 30MO (orange), and 36MO (red) models during the simulated frontal crash.

	Max Head Acceleration (G)	Max Pelvis Acceleration (G)	Max Chest Displacement (mm)	Max Lower Neck Fz (N)	Max Lower Neck My (N*m)	Max Upper Neck Fz (N)	Max Upper Neck My (N*m)	HIC 36	Head Excursion	Nij
FF bench	63.2	53.4	30.5	561.0	8.9	1369.1	6.0	494.2	497.8	0.63
RF bench	59.3	65.5	16.5	681.8	0.7	91.6	2.1	306.1	144.6	0.08
FF Camry	58.2	79.4	26.0	828.9	9.0	1350.5	5.0	503.5	543.9	0.60
RF Camry	64.1	77.0	17.5	662.8	0.4	144.7	1.9	382.9	161.7	0.09
FF bench	54.3	53.3	22.9	783.8	10.0	1066.8	5.1	409.9	514.1	0.50
RF bench	51.4	60.8	12.3	528.8	0.9	90.6	1.5	343.1	239.6	0.06
FF Camry	58.7	52.8	18.5	849.4	10.5	1181.2	5.1	468.2	519.4	0.54
RF Camry	52.7	118.9	12.8	469.0	0.3	121.1	1.0	343.5	157.4	0.06
FF bench	64.0	44.0	22.1	746.8	10.2	1119.0	5.1	444.3	520.1	0.52
RF bench	57.0	52.4	16.4	751.7	0.8	165.9	2.3	344.4	200.0	0.11
FF Camry	55.5	62.6	20.6	792.7	9.8	1219.8	4.7	455.3	561.9	0.54
RF Camry	59.8	52.9	15.4	587.9	0.8	126.5	0.9	394.0	186.1	0.06
FF bench	60.9	64.9	27.0	707.1	11.4	1169.2	5.2	471.5	540.3	0.54
RF bench	51.2	45.9	14.3	509.8	0.7	156.9	3.2	302.2	373.6	0.11
FF Camry	71.7	64.1	31.0	844.4	11.4	1420.4	5.8	623.7	556.5	0.64
RF Camry	48.7	37.1	13.6	682.8	1.3	215.7	2.1	335.9	318.8	0.11

Differences between the test bench and Camry seat varied between seating configurations and ages. In the forward-facing configuration, the 18MO model and Camry seat showed an approximate 48% increase in maximum pelvis acceleration and lower neck force and 15% decrease in maximum chest displacement and upper neck moment. In the 24MO model, 10.7% and 14.2% increases in upper neck force and HIC36 values were seen in the Camry seat, while a 19.4% increase in maximum chest displacement was seen in the test bench. A 42.3% increase in maximum pelvis acceleration was seen in the 30MO model with the Camry seat, and a 13.2% increase in maximum head acceleration with the same model and the test bench. The most variation was seen in the 36MO model, with 17.8%, 14.8%, 19.4%, 21.5%, 11.7%, 32.3%, and 19.3% increases in maximum head acceleration, maximum chest displacement, upper neck force, upper neck moment, HIC36, and Nij, respectively. All other metrics showed less than 10% variation between the Camry seat and test bench.

In the rear-facing configuration, the 18MO model and Camry seat showed 17.7%, 58.1%, 25.1%, 11.9%, and 16.5% greater maximum pelvis acceleration, upper neck force, HIC36, head excursion, and Nij, respectively. For the same model, but with the test bench, lower and upper neck moments were 40.0% and 11.4% higher than the model with the Camry seat, respectively. Maximum pelvis acceleration and upper neck moment were 95.6% and 33.6% higher, respectively, in the 24MO model with the Camry seat. Lower neck force and moment, upper neck moment, and head excursion were 11.3%, 61.0%, 32.4%, and 34.3% higher, respectively, in the 24MO model with the test bench. In the 30MO model with the Camry seat, only HIC36 was greater (14.4%), while the lower and upper neck forces, upper neck moment, and Nij were 21.8%, 23.8%, 62.0%, and 44.2% higher, respectively, in the 30MO model with the test bench. Variation was, again, greater in the 36MO model, with lower and upper neck force, lower neck moment, and HIC36 33.9%, 88.2%, 37.5%, and 11.2% larger, respectively, in the model with the Camry seat. Additionally, maximum pelvis acceleration, upper neck moment, and head excursion were 19.3%, 33.3%, and 14.7% greater in the 36MO model with the test bench. All other metrics showed less than 10% variation between the Camry seat and test bench.

Head trajectories varied among seating configurations and ages (Fig. 4). For all four ages, the forward-facing model experienced a longer, wider path. Differences in X position between models in the test bench and Camry seat were relatively small for both seating configurations. The 18MO, 24MO, and 30MO models in the rear-facing configuration, however, experienced differing Z position paths: the models in the Camry seat showed positive Z position throughout the simulations, while the models in the test bench showed negative Z position throughout the simulations (Fig. 4A-C). The Z paths of the 36MO model in the test bench and Camry seat largely differed, with maximum displacements of approximately 220 mm and 40 mm, respectively (Fig. 4D). The largest difference in X displacement between forward-facing and rear-facing was seen in the 18MO model, with maximum displacements of approximately 150 mm and 400 mm, respectively (Fig. 4A).

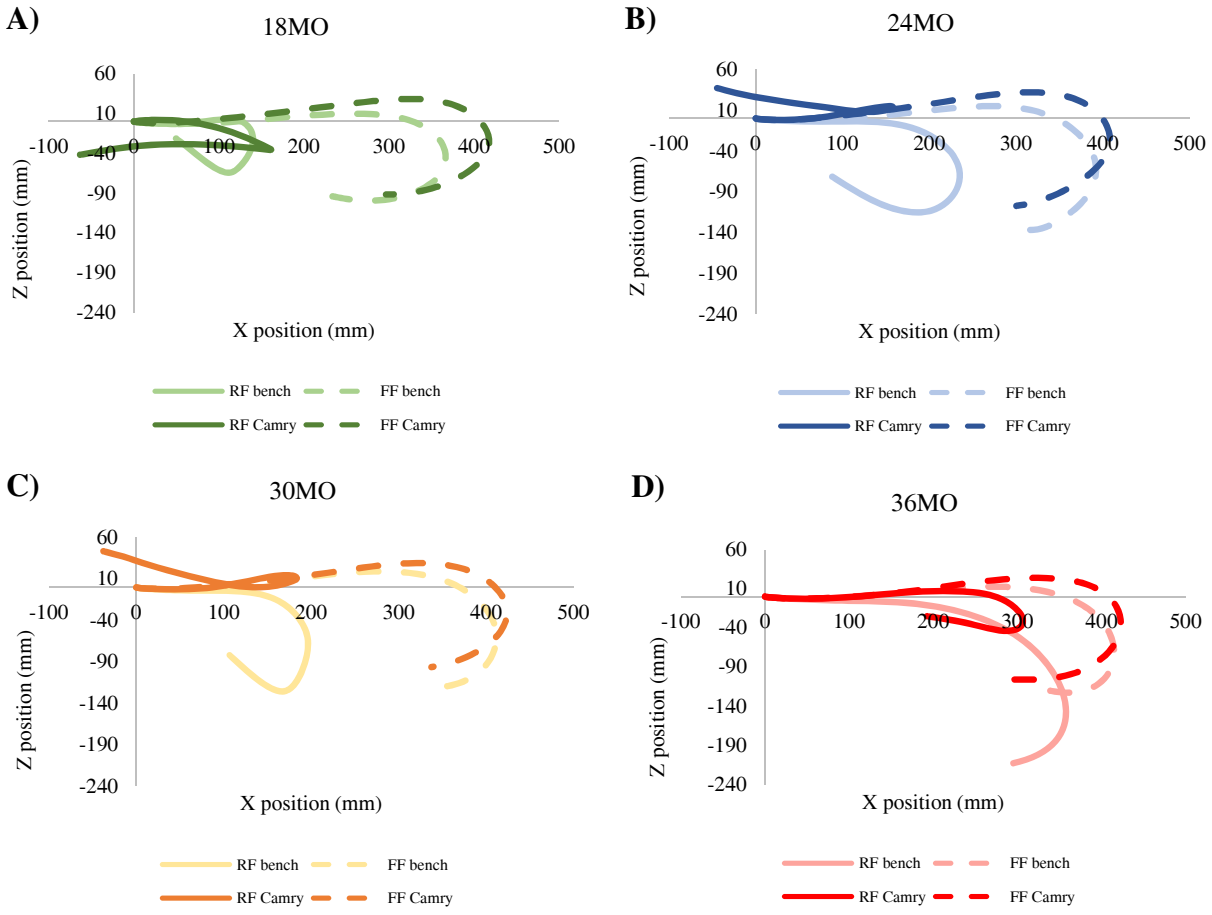

Figure 4. Head trajectories for the A) 18MO (green), B) 24MO (blue), C) 30MO (orange), and D) 36MO (red) during the simulated frontal crash.

DISCUSSION

Head acceleration was relatively similar in forward-facing and rear-facing configurations for all ages, but variation generally increased as age increased. Increased head acceleration was seen in the 36MO model, which may have been due to its higher mass. In the rear-facing configuration, the heavier 36MO model caused increased compression of the CRS into the base, causing the model and CRS to rotate backward at a higher rate with higher head acceleration. Maximum head acceleration occurred at approximately 55 ms for rear-facing, or when the model was restrained against the back of the CRS, and 80 ms for forward-facing, or when the neck reached maximum flexion. Pelvis acceleration did not show a trend with age, as that of the three younger models were higher in rear-facing

compared to the oldest model greatest in forward-facing for those on the test bench, and all but the 24MO had higher pelvis accelerations in forward-facing for those on the Camry seat. This could be due to the model sliding in the CRS after the initiation of the impact. As the load was distributed across the back face of the CRS, some rear-facing models slid back in the CRS and their legs swung back. In forward-facing, the five-point harness restrained the pelvis from any forward motion relative to the rest of the body, but some models slid forward to contact the harness. This space between the CRS and model or buckle and model are not recommended in real life, but was a limitation to the model, as positioning and gravity-settling may have not placed the model in the optimal position for the simulation by creating spaces between the restraints and the models. The maximum pelvis acceleration occurred at around 85-100 ms for the rear-facing configuration, and at around 45-60 ms in the forward-facing configuration, or when the models reached maximum pelvis displacement relative to their starting positions.

Chest displacement were as expected, with forward-facing models having much higher values. In this seating arrangement, the models accelerated forward and compressed against the harness and buckle, causing greater chest deflection than in rear-facing, where the force of the accelerating models was placed on the back of the CRS instead of the harness and buckle.

Lower neck forces were marginally larger in forward-facing models, with the exception of the 18MO model on the test bench. Upper neck forces and both lower and upper neck moments were almost 12, 7, and 2 times greater in forward-facing models, respectively. Forces in the upper neck were far greater than those in the lower neck, but lower neck moments were far greater than those in the upper neck. As the models absorbed energy from the impact, the head and neck whipped forward, causing the lower neck to compress as the upper neck accelerated forward, rotated, compressed, and flexed. As this happened, a large moment was created in the lower neck as the head and upper neck rotated.

HIC36 was greater in all forward-facing models, and corresponds to the increased neck forces and moments of the forward-facing models. Those exhibiting increased head acceleration and extensive neck flexion were more likely to experience a head injury. Similarly, Nij values were at least 5 magnitudes higher in forward-facing models. By the same logic, those with largely greater head accelerations and neck flexion were more likely to receive a neck injury.

Head excursions were approximately doubled or tripled for models in the forward-facing configuration and were generally higher in the younger models. The apparent neck flexion and head rotation in the forward-facing models was likely the reason for largely increased head excursions. Head trajectories followed the same trend, with larger differences in X and Z positions in the younger models (Fig. 4). Along with head acceleration, an increase in model mass likely caused the rear-facing head excursions and trajectories to increase with age. As the mass of the model increased, the compression of the rear-facing CRS into the base increased, causing the model and CRS to increase backwards rotation and head metrics to increase.

In both forward-facing and rear-facing configurations, the 36MO model showed the most variation in injury metrics between simulations with the Camry seat and test bench. Injury metrics were largely inconsistent among seating configurations and ages, with no apparent trends. This could have been due to model and CRS positioning. If the model was not flush against the back of the CRS after gravity settling and the model slid upon impact, then kinematic injury metrics may have been affected. Similarly, if belt routing was not flush against the model or if the pelvis belts slid during the simulation, then results may have been affected for models on either the test bench or Camry seat. Additionally, the test bench is approximately 30 mm shorter in length than the Camry seat, so the CRS partially hung off the test bench, which caused increased compression of the front of the seat in simulations with the forward-facing model and some with the younger rear-facing models. Positioning of the rear-facing models onto the CRS and base was difficult since the legs of the models restricted how close the model and CRS could be to the back of the base. The older models were positioned a relatively far distance from the back of the base and caused the CRS to partially hang off both the test bench and Camry seat. Model positioning was completed in PIPER via lower limb rotation about the hip, knee, or ankle joints. Due to this, the model and CRS were not in the optimal position on the base.

Limitations

Positioning of the rear-facing model was limiting since the joints could only rotate a certain amount before the integrity of the model was compromised. As a result, the CRSs for some models partially hung off the seat so that enough space was available for the legs. For rear-facing models, this created a large gap between the rear-facing CRS seat pan and the back of the base. The elastic modulus of the CRS was increased to 10 MPa to produce simulation stability, so injury metrics are likely not the same as they would be in real life. The simulation setup of the Camry seat lacked a retractor, pretensioner, and load limiter, so the setup may not have been representative of the matched real-world vehicle seat. Additionally, the foam properties of the Camry seat and 213-test bench were not identical and could contribute to differences in responses among the two bases. The objective of this study was to show differences in injury metrics between forward-facing and rear-facing seating arrangements with the same test conditions, so although these limitations created discrepancies between the simulation and real-world conditions, they equally affected results for both seating configurations, and the overall goal was accomplished. The study considered one make and model of CRS and only frontal impacts. Different manufactuers and CRS types (infant, booster) as well as lateral and rear impacts are likely to produce different injury metrics.

CONCLUSIONS

Kinetics and kinematics numbers across the board were within IARV limits. Pediatric models in rear-facing configurations generally had lower injury numbers than those in forward-facing configurations. However, there is no consistent trend seen in injury values as age progresses. This is the first study to conduct a systematic evaluation of the response of children under three years old in forward- and rear-facing seating arrangements in frontal motor vehicle crashes.

REFERENCES

[1] Truong, W. H., Hill, B. W., & Cole, P. A. (2013). "Automobile safety in children: a review of North American evidence and recommendations." *Journal of the American Academy of Orthopaedic Surgeons, 21*(6), 323-331.

[2] Romano, E. & Kelley-Baker, T. (2015). "Child passengers injured in motor vehicle crashes." *Journal of Safety Research, 52*, 1-8.

[3] Rafukka, I. A., Sahari, B. B., Nuraini, A. A., & Manohar, A. (2016). "Child Dummy Finite Element Models Development: A Review." *ARPN Journal of Engineering and Applied Science*, *11*(10), 6649-6656.

[4] Tarrière, C. (1995). "Children are not miniature adults." *International Research Conference on the Biomechanics of Impact (IRCOBI)*. September 13-15, Brunnen, Switzerland.

[5] Roth, S., Raul, J. S., Ruan, J., & Willinger R. (2007). "Limitation of Scaling Methods in Child Head Finite Element Modelling." *International Journal of Vehicle Safety, 2*(4), 404–421.

[6] Ramrattan, N. N., Oner, F. C., Boszczyk, B. M., Castelein, R. M., & Heini, P. F. (2012). "Cervical spine injury in the young child." *European Spine Journal, 21*(11), 2205-2211.

[7] Platzer, P., Jaindl, M., Thalhammer, G., Dittrich, S., Kutscha-Lissberg, F., Vecsei, V., & Gaebler, C. (2007). "Cervical spine injuries in pediatric patients." *Journal of Trauma and Acute Care Surgery, 62*(2), 389-396.

[8] Gray, H., & Clement, C. (1984). *Gray's Anatomy of the Human Body*. New York, NY: Lea and Febinger.

[9] Decina, L. E., & Lococo, K. H. (2005). "Child restraint system use and misuse in six states." *Accident Analysis & Prevention, 37*(3), 583–590.

[10] Decina, L. E., & Lococo, K. H. (2007) "Observed LATCH use and misuse characteristics of child restraint systems in seven states." *Journal of Safety Research, 38*(3), 273–281.

[11] Eby, D. W., & Kostyniuk, L. P. (1999). "A statewide analysis of child safety seat use and misuse in Michigan." *Accident Analysis & Prevention, 31*(5):555–566

[12] Dukehart, J. G., Walker, L., Lococo, K. H., Decina, L. E., & Staplin, L. (2007). "Safe kids checkup events: a national study." *SafeKids Worldwide*, Washington, DC.

[13] O'Neil, J., Daniels, D. M., Talty, J. L., & Bull, M.J. (2009). "Seat belt misuse among children transported in belt-positioning booster seats." *Accident Analysis & Prevention, 41*(3), 425–429.

[14] Ebel, B. E. & Grossman, D. C. (2003). "Crash Proof Kids? An Overview of Current Motor Vehicle Child Occupant Safety Strategies." *Current Problems in Pediatric Adolescent Health Care,* 38-55.

[15] Tai, A., Bilston, L. E., & Brown, J. (2011). "The cumulative effect of multiple forms of minor incorrect use in forward facing child restraints on head injury risk." *International Technical Conference on the Enhanced Safety of Vehicles (ESV).* Paper 11-0118. Washington, DC, June 13-16.

[16] Lesire, P., Cuny, S., Alonzo, F., Tejera, G., & Cataldi, M. (2007). "Misuse of child restraint systems in crash situations – danger and possible consequences." *The Annual Proceedings of the Association for the Advancement of Automotive Medicine, 51*, 207–222.

[17] Weber, K., & Melvin, J. W. (1983). "Injury potential with misused child restraint systems." SAE 831604. Stapp Car Crash Proceedings. Society of Automotive Engineers, Warrendale.

[18] Kapoor, T., Altenhof, W., Snowdon, A., Howard, A., Rasico, J., Zhu, F., & Baggio, D. (2011). "A numerical investigation into the effect of CRS misuse on the injury potential of children in frontal and side impact crashes." *Accident Analysis & Prevention, 43*(4), 1438–1450.

[19] Lalonde, S., Legault, F., & Pedder, J. (2003). "Relative degradation of safety to children when automotive restraint systems are misused." *International Technical Conference on the Enhanced Safety of Vehicles (ESV).* Paper 03-0085. Nagoya, Japan, May 19-22.

[20] Bilston, L. E., Yuen, M., & Brown, J. (2007). "Reconstruction of crashes involving injured child occupants: the risk of serious injuries associated with sub-optimal restraint use may be reduced by better controlling occupant kinematics." *Traffic Injury Prevention, 8*(1), 47–61.

[21] Klinich, K.D., & Manary, M.A. (2015). "Best Practice Recommendations for Protecting Child Occupants." In N. Yoganandan, A. M. Melvin & J. W. Melvin (Eds.), *Accidental Injury: Biomechanics and Prevention* (pp.697-719). New York, NY: Springer.

[22] Henary, B., Sherwood, C. P., Crandall, J. R., Kent, R. W., Vaca, F. E., Arbogast, K. B., & Bull, M. J. (2007). "Car safety seats for children: rear facing for best protection." *Injury Prevention, 13*(6), 398–402.

[23] Snyder, R. G., Schneider, L. W., Owings, C. L., Reynolds, H. M., Golomb, D. H., & Schork, M. A. (1977). "Anthropometry of Infants, Children, and Youths to Age 18 for Product Safety Design." Consumer Product Safety Commission.

TOLERABILITY OF UNEXPECTED AUTONOMOUS EMERGENCY BRAKING MANEUVERS ON MOTORCYCLES - A METHODOLOGY FOR EXPERIMENTAL INVESTIGATION

Nora Leona Merkel
Raphael Pleß
Hermann Winner
Institute of Automotive Engineering, Technische Universität Darmstadt, Otto-Berndt-Str. 2, 64287 Darmstadt Germany

Thomas Hammer
Norbert Schneider
Sebastian Will
Wuerzburger Institut fuer Verkehrswissenschaften (WIVW GmbH), Robert-Bosch-Str. 4, 97209 Veitshoechheim Germany

Paper Number 19-0143

This report is based on parts of the research project carried out at the request of the Federal Ministry of Transport and Digital Infrastructure, represented by the Federal Highway Research Institute, under research project No. 82.0661/2015 [1].
The authors are solely responsible for the content.

Ethical approval for the test track studies was obtained from the Ethics Commission of Technische Universität Darmstadt (reference EK 32/2018).

ABSTRACT

Motorcycle riders are subject to a high risk of suffering severe or fatal injuries. Previous research has identified autonomous emergency braking for motorcycles (MAEB) as one of the most promising technologies to increase safety for riders (e.g., [2]).
Compared to drivers of two-track vehicles, emergency braking maneuvers are much more challenging for motorcyclists. As there is no restraint system such as a safety belt, riders need to support their upper body movement and they need to control and stabilize their vehicle. This requires attention, situation awareness and body tension. Before applying maximum deceleration, the rider has to achieve this 'prepared-for-braking' state.
To generate optimal crash mitigation or even crash avoidance, the velocity should be reduced even before this state is achieved. Therefore, it is necessary to determine applicable preparatory braking profiles. As sudden unexpected braking maneuvers are critical for unprepared riders, there is still a great uncertainty on how high these decelerations can be. The identification of the limits would enable to determine the safety benefit of MAEB, when the full deceleration potential before reaching the 'prepared-for-braking' state is used.
One of the main challenges in MAEB studies is the rider state. On one hand, to evaluate to what extent autonomous interventions can support riders, participants need to be unprepared to receive unbiased results. On the other hand, due to safety and ethical reasons, it is out of question to determine the limits of controllable decelerations with unprepared riders. For this purpose, the experiments within this project are split up:
In a first study with experts, the deceleration limits are identified. The experts are asked to evaluate if different automatically applied braking interventions are controllable for unprepared average riders. By increasing the decelerations until the experts rate them as intolerable for unprepared riders, maximum tolerable decelerations for different braking profiles in real riding scenarios are defined.
In a following participant study, average riders experience a realistic emergency braking scenario (suddenly braking vehicle ahead). The deceleration profiles defined during the expert study are applied. With these experiments, the reaction of the unprepared participants to unexpected autonomous braking maneuvers are analyzed. The result is an evaluation on how partial braking maneuvers can help to reduce the transition time and on the potential decrease of velocity during the transition period.
In a third study, more critical scenarios (different secondary tasks) and the influence of warnings prior to the autonomous braking intervention are investigated on a dynamic motorcycle simulator.
The studies provide empirically obtained data on maximum deceleration values for different automatic braking interventions that are tolerable for average riders in unexpected emergency braking situations. The results also show the maximum amount of velocity – and thus kinetic energy – that can be reduced during the partial automatic braking phase before the maximum deceleration can be applied. The simulator experiments show the influence of different secondary tasks and the effect of visual-auditory warnings. The described method can be used as a reference for future development and configuration of MAEB.

INTRODUCTION

In previous research projects, it has been shown that autonomous emergency braking systems for motorcycles (MAEB) offer a high safety potential to reduce consequences of accidents or even avoid them (e.g., [3]). In these projects, important aspects of MAEB have already been discussed.
Project PISa investigated the influences of braking interventions on the stability of a motorcycle rider on his vehicle [4]. Other studies have shown that low decelerations up to 3 m/s^2 can be applied automatically without making the rider feel like losing control [5]. Within the MOTORIST project the researchers evaluated usual behavior of riders in different braking situations and showed that riders themselves do mostly not use the full deceleration potential [2]. The described projects are examples for a variety of research that has been performed in terms of MAEB. This research is highly important to develop a base line for the design of automatic brake applications.
The contents of the previous work are important aspects for the development and design of autonomous emergency braking systems for motorcycles. In particular, it has been shown that decelerations up to 3 m/s^2 are controllable for motorcycle riders and do not negatively affect the rider‘s postural stability. However, to our knowledge there is no study that determines the maximum autonomous deceleration that is controllable for unprepared riders.

The aim of an AEB is to maximize the reduction of kinetic energy prior to a collision to mitigate the consequences of an accident. In case of an emergency scenario, this requires building up a maximum deceleration as fast as possible. The achievable decelerations are subject to certain limits. Besides the physical limits, these include limits that the rider sets to the applicability. As an integral part of the rider-vehicle system, the rider must be able to control the MAEB intervention. This is essential to avoid destabilizing the vehicle or cause a fall.
The approach of the work described in this paper is based on the assumption that the rider must be in a prepared-for-braking state to be able to control an autonomous maximum deceleration. In order to bring him/her into this state and at the same time being already able to achieve a reduction of speed before reaching the braking readiness, preparatory partial braking maneuvers are used. These partial braking interventions are the main content of the investigations within the project.
The discussed research questions are:

- Can partial braking maneuvers be used to prepare the rider for a maximum deceleration, i.e., to motivate him/her to get to the prepared-for-braking state?
- How fast is the transition to the prepared-for-braking-state completed using different braking profiles?
- What is the potential velocity reduction during the transition phase, i.e. what is the maximum deceleration that is controllable for an unprepared rider?

METHOD

One of the main challenges with investigating MAEB is the fact that on one hand emergency braking situations are always critical scenarios but on the other hand riders need to be unprepared in order to provoke realistic reactions in the studies.
For safety reasons, it is not possible to identify the limits with unprepared participants. Due to this fact, the test track experiments were split up into two studies. First, in an expert study, it was analyzed which decelerations and decelerations profiles would be controllable for average riders. This identification of the deceleration limits was performed with riding instructors and trainers as these people are assumed to be particularly suitable to assessing the skills of unexperienced riders.
However, while the expert study is appropriate for determining the limits of controllable decelerations, it cannot be used to assess the rider reaction because the experts were informed that there will be an automatic deceleration. As mentioned above, riders need to be unprepared to analyze how the partial braking interventions influence the transition to the prepared-for-braking state. Thus, the expert study was followed by a participant study. In this study, average riders were confronted with unexpected emergency braking situations which were followed by autonomous braking interventions according to the deceleration profiles identified in the expert study. The focus was to analyze the riders’ reactions, particularly how different deceleration profiles affect their transition to the prepared-for-braking state. Moreover their subjective evaluation of the interventions was examined.
In the real life experiments, especially those with unprepared motorcycle riders, automatic braking interventions are only applied while going straight (roll angle close to zero) and with the riders’ full attention to the riding situation.
In addition to these two studies, a simulator study was conducted. This simulator study aimed for analyzing the influence of visual-manual distraction on the riders’ ability to control the motorcycle. This offered the opportunity

to analyze potentially critical situations in a controlled environment without exposing the participants to the risk of getting injured.

Figure 1 gives an overview of the performed studies.

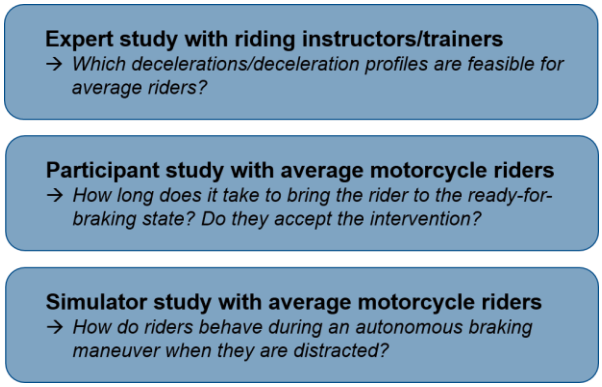

Figure 1. Overview of the performed studies

Test tools

The experiments on the test track were performed with a test motorcycle equipped with a variety of sensors to evaluate the state of the vehicle. These include, e.g., an inertial measurement unit to record translational and rotational accelerations, pressure sensors to monitor the brake pressures and a GPS antenna to track the vehicle.
In order to decelerate the vehicle without an intervention of the rider, the vehicle is equipped with an actuator that operates the foot brake. The test vehicle has a combined brake system. This means that by operating the foot brake, brake pressure is not only built up at the rear wheel, but also at the front. With this setup, automatic decelerations up to 7 m/s^2 can be applied. Figure 2 shows the three implemented braking profiles. The brake actuator is activated via remote control. To ensure that the engine is not stalled and that the rider is not able to accelerate unintendedly during an automatic braking intervention, the clutch is also actuated automatically by an external actuator.

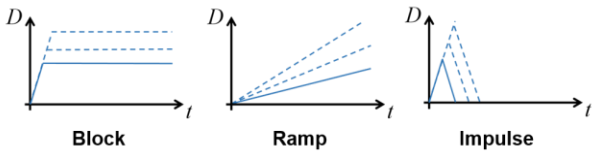

Figure 2. Implemented braking profiles

To evaluate the rider state, additional measurement technology is installed. During the experiment, the rider is equipped with a 3-axis acceleration sensor to analyze the upper body movement. The sensor is mounted on the back at the level of the shoulder blades. To monitor the rider inputs, forces on the handlebar as well as brake actuation, clutch actuation and throttle are also recorded.

Although, the emergency braking shall be unexpected, it should not get the character of a false positive braking intervention. Therefore, it is necessary to create a situation that presents a realistic true positive emergency braking scenario, like a suddenly decelerating target vehicle, to the rider. In order to avoid the risk of collisions between the motorcycle and the target vehicle, the dummy target EVITA (Experimental Vehicle for Unexpected Target Approach) was used. This test tool was developed to allow collision free investigation of anti-collision systems [6]. The dummy target consists of a towing vehicle and a trailer with a vehicle rear. The trailer can be decelerated independently from the front vehicle to simulate a rear-end collision situation. If the time-to-collision (TTC) between the following vehicle and the dummy target gets too short, the trailer is pulled forward to avoid a collision. The system is shown in Figure 3.

Figure 3. Dummy target EVITA

The simulator experiments were carried out at the Würzburg Institute for Traffic Sciences (WIVW). The dynamic motorcycle riding simulator DESMORI is based on a 6-degrees-of-freedom motion base. A real motorcycle body is mounted on the platform so that the rider can operate the virtual motorcycle with authentic control elements (clutch, throttle, brake levers etc.). The simulator allows the rider not only to steer the motorcycle by applying steering torque to the handlebar, but also with shifting his/her body relatively to the motorcycle. The visual representation of the environment is realized by a cylindrical screen (4.5 m diameter, 2.8 m height, 220° horizontal field of view) while sound is displayed via in-helmet speakers. Velocity and acceleration dependent haptic cues are delivered via a G-vest simulating forces to the rider torso [7]. The simulation is implemented in WIVW's simulation software SILAB, the virtual motorcycle is simulated in VI-BikeRealTime (VI-grade).

Figure 4. DESMORI Dynamic Motorcycle Riding Simulator at WIVW

RESULTS

Expert Study

As explained before, the expert study was supposed to identify the limits of deceleration that are controllable for average riders who do not expect an automatic braking intervention. There were three braking profiles (shown in Figure 2) to be investigated:

- block braking (deceleration is built up quickly and then is kept at the required level)
- deceleration ramp (deceleration is built up slowly to a maximum of 7 m/s^2)
- braking impulse (deceleration is only is short to 'wake up' the rider)

For each of the profiles, limits of decelerations or deceleration gradients that can be used in the participant study, needed to be identified. The experts were decelerated by remote control while driving straight ahead and then they were asked to give a rating as to whether the respective braking intervention is reasonable for an average unprepared rider without affecting the controllability of the situation. If the assessment was positive, the deceleration or the deceleration gradient was increased for the next braking maneuver until the braking intervention was classified as no longer acceptable. The varied parameters and the identified limits are summarized in Table 1. A detailed description of the evaluation of the expert study was introduced in [8].

Table 1. Varied parameters

Braking profiles	Varied parameters		Determined maximum
Block braking	Level of deceleration	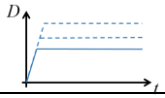	5 m/s²
Deceleration ramp	Gradient	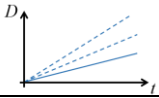	9.1 m/s³
Braking impulse	Level of deceleration	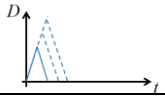	4.7 m/s²

With these results from the expert study, limits for unexpected autonomous decelerations are identified.

Participant Study

With the knowledge of which decelerations are acceptable for average riders, the participant study was carried out. This study examined to what extent the different types of interventions (braking profiles) are suitable to assist the rider in an emergency braking situation and which increase in safety this offers compared to the rider himself/herself carrying out an emergency braking maneuver.

During the experiments, the test persons followed the dummy target EVITA on the test motorcycle at a pre-determined distance (time headway 1.5 s, see Figure 5). The initial velocity for the experiments was 70 km/h. At an appropriate point (correct distance between the vehicles, correct velocity, enough straight track left), the dummy target was decelerated and the remote-controlled braking intervention was triggered synchronously. EVITA served merely to make the automatic braking intervention plausible as true positive for the rider.

The study was carried out with 18 participants. Apart from the braking profiles (block, ramp and impulse), reference experiments without automatic braking interventions were performed in order to create a baseline to evaluate how the autonomous interventions can help to decrease the velocity.

With the aim of receiving unbiased assessments and to avoid habituation effects, only two braking maneuvers are performed per participant. After elimination of the invalid runs, 19 braking maneuvers can be evaluated (5x block, 5x ramp, 5x impulse, 4x reference).

Figure 5. Participant study with EVITA

The following paragraphs summarize the evaluation and the results of the participant study. Figure 6 explains how the measured data is presented for the different braking profiles. The upper diagram always shows the vehicle state. It contains the velocity v and acceleration a_{Vx} as well as the brake pressure at the foot brake $p_{MBC,foot}$ that is automatically built up by the braking actuator. In Figure 6 the vehicle state diagram also shows the target deceleration $a_{Vx,tg}$.

The lower diagram mainly presents the rider state and rider inputs. It shows the acceleration measured at the upper body of the rider a_R, the force on the handlebar F_{hand} and the brake pressure at the front brake $p_{MBC,hand}$ applied by the rider. For comparison purposes for the rider body acceleration, the vehicle acceleration is also shown in this diagram. Diagrams for the impulse profile and for reference scenarios also contain the clutch signal.

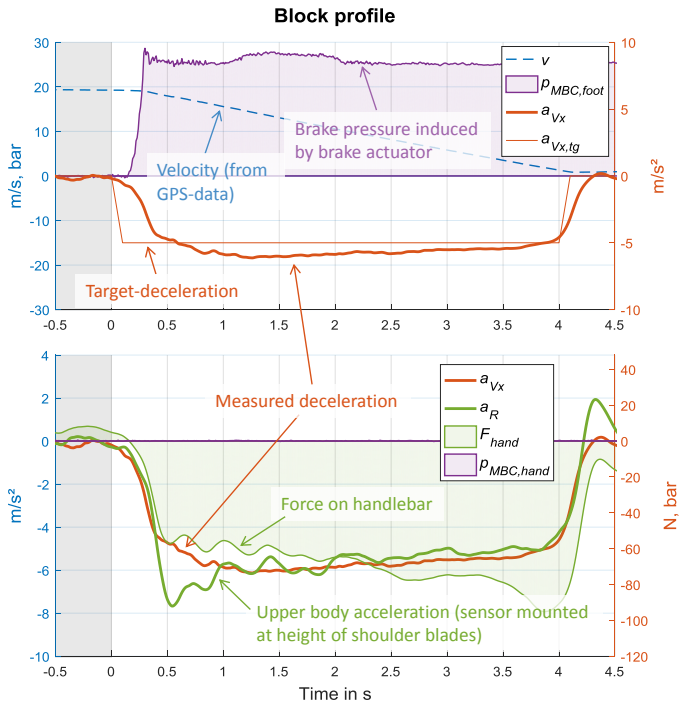

Figure 6. Scheme of measurement data representation

Figure 7 shows the data for a braking maneuver with the block profile. The brake pressure is built up within less than 0.3 s. All block braking maneuvers are analyzed concerning their transition time. The diagram in Figure 7 shows that first, the vehicle deceleration is built up. The deceleration of the rider's upper body then follows with a small time lag. This can be explained by the fact that the upper body is at the first moment moved forward relatively to the vehicle due to the unexpected deceleration. By supporting the resulting force with the arms on the handlebar and straightening the upper body, the upper body deceleration is then adapted to the vehicle deceleration. The transition is considered as completed, as soon as the force on the handlebar or the upper body deceleration does not increase anymore. The earlier of these two points is defined as the end of the transition period.

The mean transition time for the block profile braking maneuvers is at 0.57 s. Within the transition, a mean of 1.48 m/s of velocity reduction can be achieved.

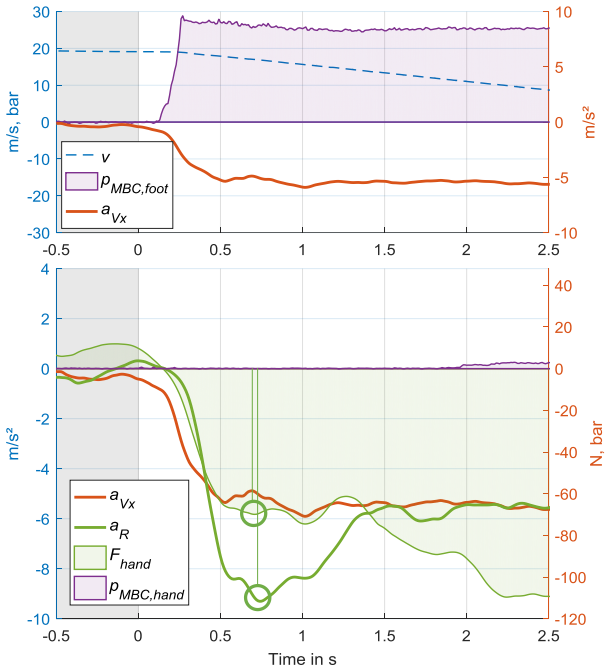

Figure 7. Block profile

Unlike in the block profile, the brake pressure is built up more slowly in the ramp profile braking maneuvers. The built up of the pressure starts at about 0.3 s with a low gradient and then increases progressively, until the target deceleration level of 5 m/s^2 is achieved. The target deceleration gradient (9.1 m/s^3, system-related scattering) starts at about 0.5 s.
The evaluation of the transition period follows the same scheme as for the block profile (see Figure 8). With a mean time of 1.04 s, the transition takes significantly longer than for the block profile. This shows that the block profile appears more effective in terms of motivating the rider to get to the prepared-for-braking state. Due to the slow brake pressure built up, the decrease of velocity is only slightly higher. The mean velocity reduction is 1.69 m/s.

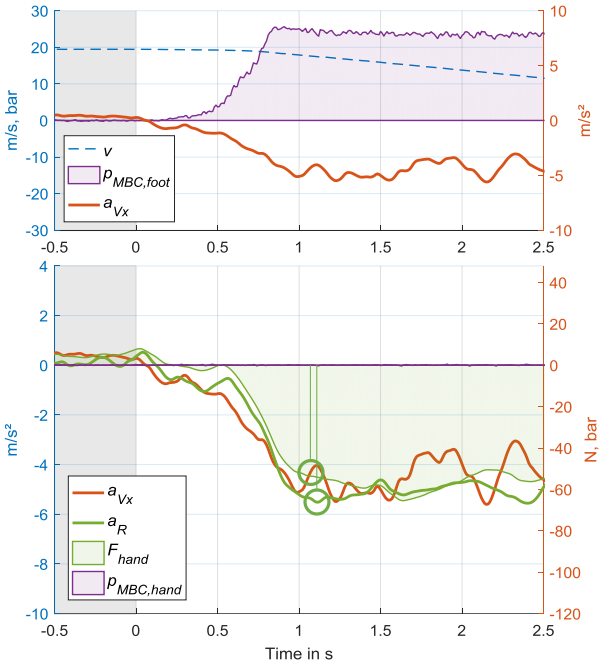

Figure 8. Ramp profile

Unlike the block or ramp profile, the impulse profile only offers a short automatic deceleration without actuating the clutch. Due to the fast increase and decrease of the vehicle deceleration and the resulting pitch movement, the rider is forced to a phase-shifted upper body movement (see Figure 9). Due to the immediate decrease of the deceleration, the upper body swings back. This even results in a pulling force on the handlebar (sign change in the force signal), as the rider needs to retain this movement. Consequently, the force on the handlebar or the no longer increasing upper body deceleration cannot be used as an indicator for the completed transition for the impulse profile.
For the impulse – which is supposed to 'wake up' the rider – the transition is defined as completed, as soon as the rider reacts to the automatic intervention in terms of rider inputs, such as applying the brakes (more than 0.5 bars on the hand- or foot brake) or actuating the clutch (increase of the clutch parameter, see blue marking in Figure 9). The earliest of the inputs represents the end of the transition period for the impulse profile.

The impulse causes a mean transition time of 1.37 s. It is thus longer than the time for the block or ramp profile. Due to the fact that the clutch is not actuated and the deceleration is very short, the velocity is only slightly reduced. The mean velocity reduction is 0.77 m/s.

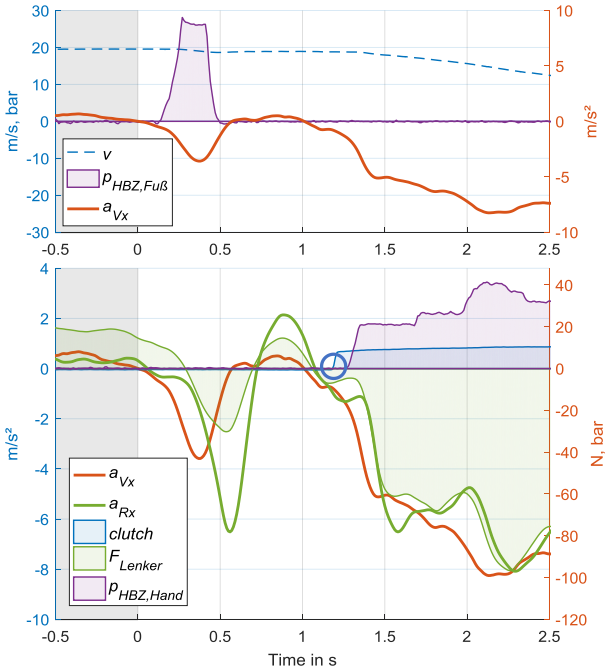

Figure 9. Impulse profile

The reference maneuvers (see Figure 10) were supposed to show how much time the rider needs to initiate a braking maneuver himself/herself after an incident occurs. The incident is represented by the release of EVITA at $t = 0$. The characteristics for the completed transition comply with those for the impulse profile, i.e., the transition is completed as soon as the rider actuates the clutch or the brakes.

In average, it took the participants 1.65 s to react to the deceleration of the dummy target. Within this time, a mean velocity reduction of 0.57 m/s can be observed. This small reduction results from the fact that until the rider reacts, no brake pressure is built up automatically. The deceleration only is only achieved by throttling back.

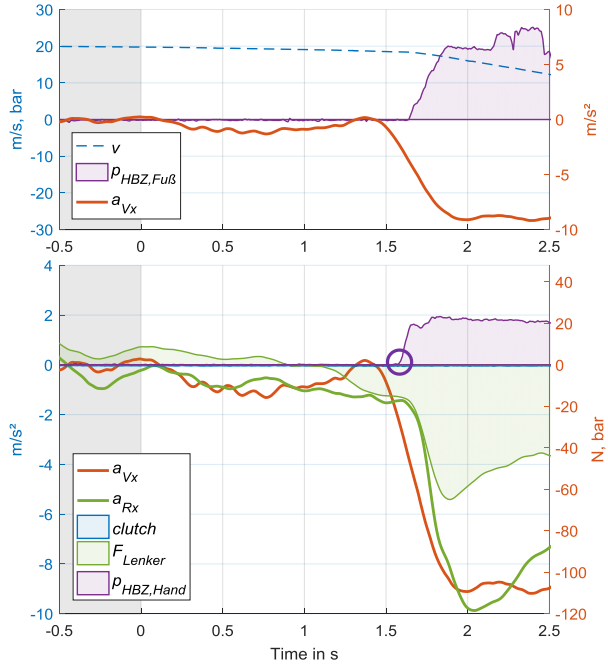

Figure 10. Reference braking maneuver

The test track experiments with participants show that the block profile is the most promising profile in terms of motivating the rider to get ready for full deceleration. The block profile leads to the shortest transition time and at the same time, it leads to the highest velocity reduction within the reference time of 1.65 s. For the ramp and

impulse profile, the transition periods become longer, while the velocity reduction within the reference time decreases.

The velocity reduction within the reference time is calculated based on the assumption that as soon as the transition is completed, the deceleration can be raised to a maximum level. This maximum is not represented by the physical limits of the braking maneuver, but it is set to 7 m/s^2. This deceleration still allows some friction potential in case the rider decides to perform an evading maneuver during the automatic braking.
To determine the potential velocity reduction Δv_{Red} within the reference time T_{Ref} for each braking profile, it is assumed that after the transition period T_{Trans}, the rest of the reference time span is used to decelerate at D_{max} = 7 m/s^2. The calculation is exemplarily shown for the block profile in (Equation 1). Within the transition time of 0.57 s, the velocity is reduced by 1.48 m/s (mean reduction determined during experiments). The rest of 1.08 s within the reference phase are used to decelerate at 7 m/s^2. This results in a total velocity reduction of 9.04 m/s.

$$\begin{aligned}\Delta v_{Red,Block} &= \Delta v_{Trans,Block} + \left(T_{Ref} - T_{Trans,Block}\right) \cdot D_{max} \\ &= 1.48\ \frac{\mathrm{m}}{\mathrm{s}} + (1.65\ \mathrm{s} - 0.57\ \mathrm{s}) \cdot 7 \frac{\mathrm{m}}{\mathrm{s}^2} \\ &= 9.04\ \frac{\mathrm{m}}{\mathrm{s}}\end{aligned} \qquad \text{(Equation 1)}$$

Within the transition time of 0.57 s, the velocity is reduced by 1.48 m/s (mean reduction determined during experiments). The rest of 1.08 s within the reference phase are used to decelerate at 7 m/s^2. This results in a total velocity reduction of 9.04 m/s.
The starting velocity of 70 km/h equals 19.4 m/s. A velocity reduction of 9.04 m/s thus means a decrease of 47 %.

A summary of all test track results including the determined potential velocity reductions is given in Table 2.

Table 2. Summary of test track experiments

Profile	**Mean transition time T_{Trans} in s**	**Mean velocity reduction within transition period Δv_{Trans} in m/s**	**Potential velocity reduction within 1.65 s Δv_{Red} in m/s**
Block	0.57	1.48	9.04
Ramp	1.04	1.69	5.96
Impulse	1.37	0.77	2.73
Reference	1.65	0.57	0.57

Not only the objective assessment of the measured data is important for identifying the potential of MAEB. A safety system can only be successfully engaged, if it is accepted by the users.
For this purpose, the participants were asked to subjectively assess the controllability of the single braking interventions. The rating follows the scale from Neukum et al. [9]. Within this scale, the participant can first classify the intervention on a rough ordinal scale (not noticeable, noticeable, disturbing, dangerous, not controllable) and afterwards refine the assessment within these categories (0 to 10, see Figure 11).
As expected, the participants rated the reference experiments less critical. In these braking maneuvers the brakes were actuated by the riders themselves and thus did not surprise them. The maneuvers were mostly rated at the lower end of the scale within the ‘noticeable’ category. The block profile was also mostly classified in this category. The mean rating for the block (2.8) is only slightly higher than for the reference maneuvers (2.67).
The other two braking profiles (ramp and impulse) were rated more critical. According to the mean rating, the ramp profile still falls into the same category (‘noticeable’) as the block profile and the reference maneuvers. However, there is a greater spread of the ratings and the mean (3.4) is close to the upper border of the category. The ratings for the impulse profile were more critical. The mean rating (4) falls into the ‘disturbing’ category. Although this is the most critical rating, the subjectively experienced criticality is still far away from ‘dangerous’.

The subjective assessment shows that the block profile is not only most promising in terms of transition time and velocity reduction (objective criteria), but also in terms of subjective perception of the criticality of the intervention.

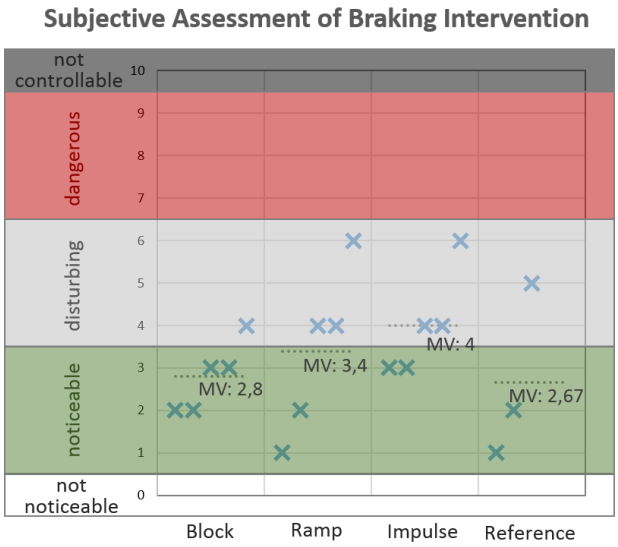

Figure 11. Subjective assessment

Simulator Study

Due to safety reasons, autonomous emergency braking scenarios have usually been tested on the test track while riding straight with full concentration on the riding task. However, MAEB is expected to support the rider especially in situations where the rider is not fully concentrated on the riding task. Thus, the rider might not be in an ideal state (e.g., being visually distracted or not having both hands on the handlebar) to cope with the intervention of an MAEB. Therefore, it is important to investigate the influence of these non-ideal rider states on the controllability of MAEB interventions. For this purpose, a simulator study was conducted. The two main aims of the simulator study were

- to investigate how both-, one- and free-handed riding in combination with visual distraction (eyes not focused on the lead vehicle) affect the riders' behavior and system acceptance in case of an MAEB intervention and
- to assess the potential of a visual-acoustic warning to improve acceptance and controllability of a MAEB intervention.

The test scenario was similar to the test track participant study regarding the primary riding-task. The participants had to follow a lead vehicle in the simulated scenario (with a velocity of 100 km/h) which triggered the autonomous braking maneuver (maximum deceleration of 6 m/s²). To manipulate hand position and visual distraction the riders were instructed to fulfill different secondary tasks which are summarized in the following table:

Table 3. Different secondary tasks used in the simulator study to manipulate hand position and visual attention.

Task	Hand position	Distraction	Implementation
surrogate reference task according to [10]	both handed	visual + manual	controlled via two buttons at the handlebar
operation of a navigation device	one-handed	visual + manual	navigation device mounted at the handlebar
free-handed lateral control	free-handed	manual	simulation of adaptive cruise control for longitudinal guidance

In order to assess the potential of a visual-acoustic warning the riders experienced each condition either with or without a visual-acoustic warning prior to the MAEB intervention in permuted order.

Rider behavior was analyzed by means of brake and clutch operation (i.e., frequency of additional brake reactions and brake reaction time) and steering behavior. Both can be used as indicators for a rider take-over or the rider being back in the control loop. Subjective ratings of controllability based on the scale of [9] were obtained after

each intervention like in the test track studies. In addition, the riders received a questionnaire at the end of the study to assess the acceptance of interventions with/without warnings.

The frequency of additional brake reactions for the front brake lever does not indicate differences between MAEB with or without warnings. In all conditions more than 50% of the riders showed additional brake reactions on the front brake lever (with warning: 57%-61%; without warning: 52%-65%). However, riders in all conditions (both-handed, one-handed and free-handed) respond slightly faster to the autonomous emergency braking of the motorcycle if a warning is presented prior to the onset of the intervention (cf. Figure 12). In addition, the reaction times seem to be more homogenous if a warning has been presented (please note that this interpretation is only based on descriptive data).

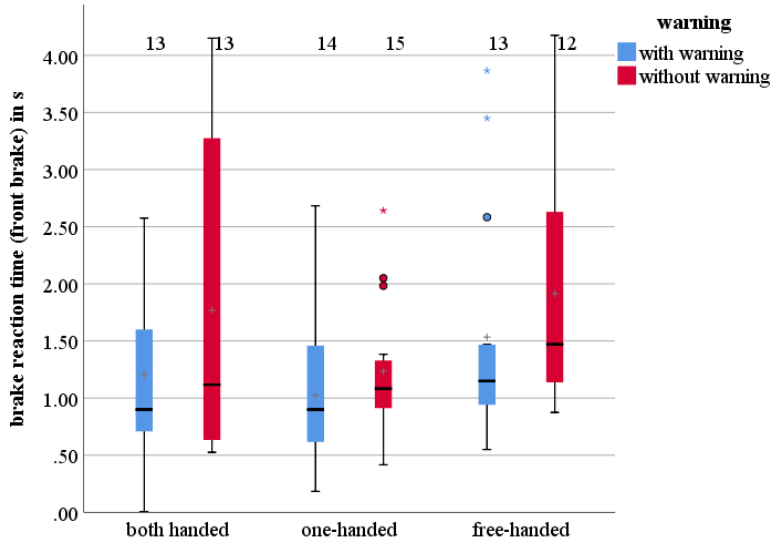

Figure 12. Reaction time depending on warning availability and type of secondary task

The subjective controllability ratings obtained after each intervention show that riders rated autonomous braking interventions with a prior warning as more controllable than interventions without a prior warning ($F(1,120) = 8.99$, $p = .003$)). This is especially reflected in the distribution of the ratings according to the rating categories (cf. Figure 13).

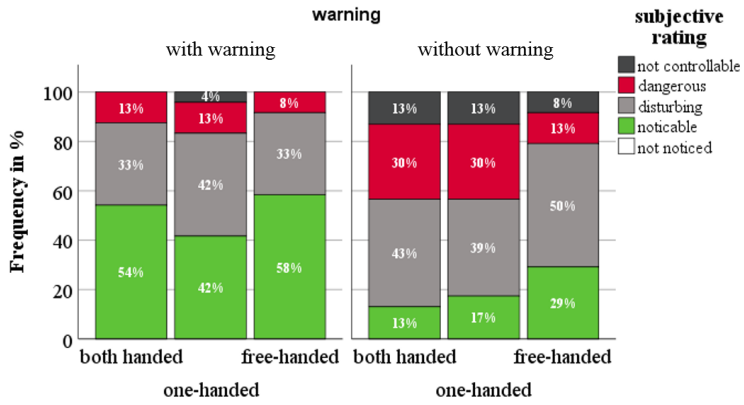

Figure 13. Subjective assessment of intervention controllability depending on warning availability and type of secondary task

The overall rating of acceptance at the end of the study revealed that riders rated autonomous braking interventions with a warning to be *more helpful*, *more relieving* and *safer* compared to interventions with no warning. In addition, the riders showed high consent with the statement that "*the warning made the intervention more controllable*".

Consequently, the results of the simulator study indicate that warnings can not only support the rider in his/her reaction, they also have a positive influence on the acceptance of the interventions. However, it has still to be verified whether the results regarding the effects of warnings can be replicated on a real motorcycle. Furthermore, studies should test how the warning should be designed (visual, auditory, haptic or kinesthetic) to ensure that riders are able to perceive the warning and it's meaning in time to react adequately.

CONCLUSION

With the work described in this paper, a method for the evaluation of controllability and acceptance of autonomous emergency braking for motorcycles has been developed and validated. Furthermore, it has been shown how the prepared-for-braking state of the rider can be detected. The proposed methods prove that automatic braking maneuvers can be applied to and controlled by unprepared riders in participant studies. Thereby, this work provides an important foundation for the future design of MAEB and the assessment and evaluation of its safety potential. The results indicate that the block profile offers the greatest potential to decrease velocity while being well accepted by the riders. This design leads to a high potential of future MAEB solutions. In the tested scenarios with autonomous interventions, the velocity can be reduced by up to 47 % compared to reference scenarios without interventions (due to the delay in the braking response by the rider). In addition, the simulator experiments show that visual-acoustic warnings prior to autonomous braking interventions have the potential to reduce reaction times and further increase the acceptance of the system.

Limitations

So far, the participant study has only been performed at one specific initial velocity (70 km/h) on a specific vehicle. Therefore, it should be considered that the achieved results are only applicable for the setup used in our studies. In addition, we expect that the vehicle geometry has a significant influence on the controllability and acceptance of autonomous braking interventions. Future studies should focus on the influence of the vehicle type, the influence of the initial velocity and the influence of the test scenario (e.g. braking while driving in a straight line vs. braking while cornering).

REFERENCES

[1] Merkel, N. L; Pleß, R; Hammer, T; Schneider, N. and S. Will. “Abschlussbericht zum Projekt BASt FE 82.0661/2015 Automatische Notbremssysteme für Motorräder.”. *Bundesanstalt für Straßenwesen, Project Report, to be published in 2019*

[2] Baldanzini, N; Huertas-Leyva, P; Savino, G. and M. Pierini. 2016. “Rider Behavioral Patterns in Braking Manoeuvres.” Transportation Research Procedia, 14, 4374–4383

[3] Savino, G; Giovannini, F; Baldanzini, N; Pierini, M. and M. Rizzi. 2013. “Assessing the potential benefits of the motorcycle autonomous emergency braking using detailed crash reconstructions.” Traffic injury prevention, 14 Suppl, S40-9

[4] Symeonidis, I; Kavadarli, G; Erich, S; Graw, M. and S. Peldschus. 2012. “Analysis of the stability of PTW riders in autonomous braking scenarios.” Accident Analysis and prevention(49), 212–222

[5] Savino, G; Pierini, M; Grant, R; Frampton, R; Talbot, R; Peldschus, S; Schuller, E; Oudenhuijzen, A; Pauwelussen, J; Scheepers, B; Teerhuis, A; Karanam Venkata, M; Babu, R; Roessler, B; Nanetti, M; Guggia, R; McCarthy, M. and W. Hulshof. 2010. “PISa - Powered two-wheeler Integrated Safety. Development, implementation and testing of PTW integrated safety systems.”. In *ifz Forschungsheft Nr. 14: Tagungsband der 8. Internationalen Motorradkonferenz 2010.* Köln

[6] Fecher, N; Hoffmann, J. and H. Winner. 2015. “EVITA - Das Prüfverfahren zur Beurteilung von Antikollisionssystemen.” In Winner, H., Hakuli, S., Lotz, F. and C. Singer (eds.). *Handbuch Fahrerassistenzsysteme: Grundlagen, Komponenten und Systeme für aktive Sicherheit und Komfort*. Springer Vieweg, Wiesbaden, 197–206

[7] Will S. 2017. “Development of a presence model for driving simulators based on speed perception in a motorcycle riding simulator.” Dissertation, Fakultät für Humanwissenschaften, Julius-Maximilians-Universität Würzburg, Würzburg

[8] Merkel, N. L; Pleß, R; Scheid, K. and H. Winner. 2018. “Einsatzgrenzen automatischer Notbremssysteme für Motorisierte Zweiräder - eine Expertenstudie.”. In *ifz Forschungsheft Nr. 18: Tagungsband der 12. Internationalen Motorradkonferenz 2018.* Köln

[9] Neukum, A; Lübbeke, T; Krüger, H.-P; Mayser, C. and J. Steinle. 2008. “ACC-Stop&Go: Fahrerverhalten an funktionalen Systemgrenzen.”. In *5. Workshop Fahrerassistenzsysteme - FAS2008.* Karlsruhe, 141–150

[10] International Organization for Standardization (ISO). 2012. “14198:2012 Road vehicles - Ergonomic aspects of transport information and control systems - Calibration tasks for methods which assess driver demand due to the use of in-vehicle systems.” ISO/TS 14198

A METHOD TO COMPARE THE SAFETY OF AUTONOMOUS VEHICLES TO HUMAN-DRIVEN NON-EXEMPT MOTOR VEHICLES IN THE UNITED STATES

Lisa Gavin
U.S. Department of Transportation
United States of America

Paper Number 19-0145

ABSTRACT

The objective of this technical paper is to present a method that characterizes autonomous vehicle (AV) safety performance through the application of risk-based validation that leverages existing crash incidence and severity data, physics based model and simulation, and U.S. Federal Motor Vehicle Safety Standard (FMVSS) benchmark metrics. The output of the proposed risk-based methodology is a framework that organizes the number and type of physical tests and model/simulation runs necessary to provide meaningful evidence of AV safety performance statistically equivalent to human-driven non-exempt motor vehicles.

INTRODUCTION

The lure of AVs promises elimination of vehicle crashes, injuries and fatalities. For consumers, passengers, and other road users to embrace AV technology, AVs must perform safely and reliably. A formidable challenge is measuring and quantifying the levels of safety offered by AVs. The debate of how safe is safe enough for AVs has been structured around a mindset of billions of miles traveled.

Common sense dictates the starting benchmark is the current level of safety performance; but how best is this measured? Traditionally, mechanical and physical safety have been measured in terms of compliance with government safety standards. AVs venture beyond this template in that the vehicles are loaded with complex sensor technologies and controlled by software. This paper proposes application of a risk-based methodology that leverages existing knowledge of vehicle performance characteristics and crash problem data with safety metrics to build a framework that compares an overall safety level between nonexempt vehicles and AVs.

Foundational Concepts

Defining AV safety metrics that are recognized and accepted industry wide by all stakeholders is an important first step. Four foundational concepts are in play: AVs must provide an overall safety level at least equal to the overall safety level of nonexempt motor vehicles; the Haddon Matrix, which is the most commonly used paradigm in the injury prevention field; all motor vehicles, including AVs, present as a system of systems; and safety is not reliability.

When determining if a vehicle presents an unreasonable risk to safety, probability of failure, consequence of failure, occurrence and severity of injury are the primary factors to consider. In a probabilistic risk assessment, there is a close relationship between safety and reliability. Yet, safety cannot generally be achieved through component or system reliability alone. The Federal Highway Administration (FHWA) version of the Haddon Matrix [3] illustrates the relationship between four factors of injury (human, vehicle/equipment, physical environment, and socioeconomic) and the phase of injury (pre-crash, crash, and post-crash).

If we consider the vehicle as a system of systems, one system would be the 'driver,' either in human form or in digital technology form. Vehicle systems such as powertrain, steering, braking, suspension, tires, fuel, occupant protection, and exterior lighting exist on all vehicles, whether AV or human driven. The primary differences between AVs and nonexempt vehicles will likely emerge in the driver system, in visibility and glazing systems, and interior human-machine interface (HMI) systems.

A Safety Network can be defined as shown in Equation 1.

$$Safety\ Network = Environment + Vehicle + Driver + Unknowns \quad \text{(Equation 1)}$$

Reliability Concepts

Reliability is considered the absence of failures, and is predicated on how failure is defined. In the context of motor vehicle safety, we can describe a failure rate as both the crash rate and a function of system performance. Adopting the Advanced Product Quality Planning (APQP) and Control Plan manual definitions for reliability and confidence level supports analysis using key risk metrics. Reliability is defined as the probability that an item (i.e., vehicle) will continue to function at customer (i.e., roadway user) expectation levels at a measurement point, under specified environmental and duty cycle conditions. Confidence level refers to the percentage of all possible samples that can be expected to include the true population parameter. Additional reliability concepts include selecting an appropriate reliability distribution, sufficient sample size, and consideration of non-critical failures in the reliability analysis.

Several reliability distributions [7] appear to mirror the crash problem data, such as the binomial distribution, the exponential distribution, the Poisson distribution, and the Pareto distribution. Additionally, the bathtub distribution holds true for AVs in that sensor and camera initialization increases crash risk at the beginning of vehicle deployment. If certain crash avoidance data is collected from AVs, the normal and logistic continuous distributions offer the possibility to include the rate of crash events avoided, plotted as negative severity values. For any reliability distribution, key parameters (e.g., shape, scale, location) need to be confirmed. The distribution most appropriate for AVs may depend on the sample. In this paper, the sample was organized by vehicle classification, and the binomial distribution (with the assumption of replacement) was applied to count the number of successes (i.e., no crash) in a number of independent trials (i.e., VMT); if a crash occurs, then severity outcome is measured as no damage, property damage, injury, or fatality. The number of observations or trials must be sufficiently large.

Crash Problem

Utilizing the U.S. Department of Transportation data collections, databases and published statistical analysis, the crash problem on U.S. roadways in 2016 [4] was reported as 34,439 fatal police-reported crashes, 2,177,000 injury police reported crashes, and 5,065,000 property damage only (PDO) police-reported crashes, 37,461 people killed, 3,144,000 people injured, and 3,174 billion vehicle miles traveled. Additional crashes occurred that were not reported to the police; in 2010, the National Highway Traffic Safety Administration (NHTSA) estimated these unreported crashes as a 59.7% increase in PDO and a 39.7% increase in injury crashes [2]. Figure 1 shows a plot of the 2010 crash incidence versus severity. Ideally, future safety network analyses would be founded on the combined number of police-reported plus unreported crashes.

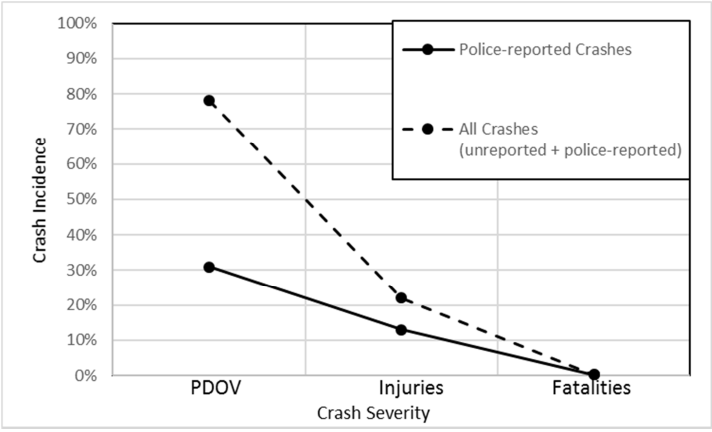

Figure 1. Crash Incidence versus Severity (2010 data; source: DOT HS 812 013)

Table 1 lists the police-reported crash incidence rates using 2016 data. Note that the crash per VMT rate for passenger cars, light trucks and buses are similar in magnitude as the total average. The police-reported crash incidence rate for large trucks is significantly lower, possibly due to these vehicles being operated by trained professional drivers.

Table 1.
Crash Incidence by Vehicle Classification (2016 data; sources: DOT HS 812 580 and [10])

Vehicle Classification	Police-reported Crashes (Fatal + Injury + PDO)	VMT (millions)	1 crash per (VMT)
Passenger Car	7,198,839	1,440,228	200,064
Light Truck	5,010,069	1,409,490	281,331
Large Truck	502,213	287,895	573,253
Motorcycle	129,421	20,445	157,973
Bus	71,227	16,350	229,548
Other/unknown	21,462	Not reported	-
	Total = 12,933,231	Total = 3,174,408	Total = 245,446

In 2015, NHTSA published findings from a statistical analysis of the National Motor Vehicle Crash Causation Survey (NMVCCS) [5], which collected on-scene information about the events and associated factors leading up to crashes involving light vehicles. NMVCCS is a weighted sample of 5,470 crashes, which represents an estimated 2,189,000 crashes nationwide. NHTSA found that the critical reason, which is the last event in the crash causal chain, was assigned to the driver in 94 percent (±2.2%) of the crashes. In about 2 percent (±0.7%) of the crashes, NHTSA found that the critical reason was assigned to a vehicle component's failure or degradation, and in 2 percent (±1.3%) of crashes, it was attributed to the environment (slick roads, weather, etc.). Among an estimated 2,046,000 drivers who were assigned critical reasons, NHTSA found recognition errors accounted for about 41 percent (±2.1%), decision errors 33 percent (±3.7%), and performance errors 11 percent (±2.7%) of the crashes.

METHODOLOGY

A technology-neutral approach to AVs would focus on safety aspects and system safety performance. Shifting the mindset to a system of systems construct with an emphasis on test and evaluation supports quantifying safety in terms of risk and performance. A test and evaluation strategy would include physical testing, modeling, simulation, verification, validation, and accreditation. Stakeholders would use this methodology to generate a sample size of test scenarios to which manufacturers would demonstrate the level of safety. Large statistical sample sizes will only be achieved through physical testing and modeling/simulation. The benchmark would be comprised of a combination of test trials plus simulation runs that vary key performance factors. Reliability theories were developed for aircraft components under a metric of flight time hours and are adapted here to VMT. This method describes how to statistically estimate the level of AV safety without billions of on-road demonstration miles. There exists tremendous opportunity to leverage modeling and simulation along with targeted testing to characterize AV safety performance in terms of a reliability distribution. Modeling and simulation supports enhancing the physical test scenarios through iterations that vary speed ranges, travel direction, traffic density, etc.

Key steps in this analysis are:

- Identify the most relevant set of risk metrics. For example, incidence (number of crashes, severity in terms of fatalities, injuries, and property damage), and vehicle miles traveled (VMT).
- Identify the data needed to support a risk-based analysis. For example, 2,967 billion VMT (2010 data) divided by 6,077,362 police-reported crashes (2010 data) results in 1 crash per 488,205 VMT. The average of 11,866 VMT per registered vehicle (2010 data) multiplied by an estimated average vehicle age of 10.8 years (passenger car vehicles, 2010 data) results in an available test time T_{test} of 128,153.
- Adapt the parametric binomial reliability distribution test by replacing the random variable of Time with vehicle miles traveled (VMT).
- Select the % reliability to be demonstrated. For example, '85% reliable.'
- Select the % confidence level. For example, 'with 90% confidence.'

- Select the number of test failures that can occur in the sample. For example, '1 failure allowed.'
- Calculate the sample size based on VMT and T_{test} to which AV manufactures would demonstrate the AV level of safety.
- Choose trials (e.g., tests and model/simulation runs) that characterize vehicle performance in steering, accelerating, braking, sensor recognition, causes of vehicle control loss, visibility, etc.

In this analysis, the independent test trials correspond to VMT, regardless of vehicle maneuver, speed, etc. An example of the typical resulting output is in the form: a sample size of 11 pedestrian detection system test trials with 0 failures occurring will demonstrate a reliability of 80% at the 90% confidence level. In other words, if the item reliability is < 80%, the chances of passing this test are < 10%.

Test Sample Size

Table 2 is a representative test sample size matrix which was populated by exercising a parametric binomial reliability demonstration test calculator [8] with mission time equal to 1 crash per 488,205 VMT (based on 2010 data) and the available test time equal to 128,153 hours (based on 2010 data). Setting the reliability and confidence levels is a subjective decision. If the current level of safety for nonexempt passenger cars and light trucks is estimated at 85% reliability with 95% confidence, then a test series for equivalent AV safety performance would require a sample size of 425 tests that allows one failure. An alternate approach is to conduct testing until one failure occurs, and then estimate the reliability and confidence level.

Table 2.
Example of a Test Sample Size Calculated using the Parametric Binomial Reliability Distribution

Passenger Cars & Light Trucks	**Confidence with 1 Failure Allowed**					
Reliability	**80%**	**85%**	**90%**	**95%**	**98%**	**99%**
99%	4,325	4,871	5,618	6,851	8,425	9,587
98%	2,152	2,423	2,795	3,409	4,192	4,770
95%	848	955	1,101	1,343	1,652	1,879
90%	413	465	537	654	804	915
85%	268	302	348	425	522	594
80%	196	220	254	309	380	433

Once the test sample size is determined, the test and evaluation strategy can be developed that describes the test scenarios and corresponding specific number of physical tests. Initially, test scenarios can be derived as a mix of existing FMVSS tests and AV sensor suite edge or challenging cases. Examination of sensor algorithms would assist in prioritizing tests and test scenarios that score high in risk assessment parameters probability of failure and consequence of failure. For example, low sun angle is a challenge for camera technologies. Therefore, of the 425 tests, a proportion representative of the risk would be allocated to low sun angle conditions for which the camera technology significantly contributes to vehicle control. Finally, the test and evaluation strategy can be tailored to a specific geographical region, such as state, city, county, geofenced area, or national level.

Building the Safety Framework

Consider building the safety framework by vehicle classification. The U.S. follows a self-certification system of compliance, in which vehicle and equipment manufacturers certify that their products meet applicable standards. Additionally, the manufacturer determines the vehicle classification – e.g., passenger car, large truck, bus, etc. Historically, stakeholders have considered self-certification to be demonstrated through physical test. AVs will likely propel stakeholders toward a new era of targeted physical testing supplemented with extensive modeling and simulation to demonstrate safety.

The values shown in Table 3 represent an example of a safety framework for nonexempt passenger cars and light trucks. The crash risk is derived from reference [9]. The reliability distributions were selected to reflect the network element risk. For example, U.S. DOT data shows high motor vehicle reliability with high confidence as

demonstrated through the low number of crashes caused by vehicle failure, likely buttressed by NHTSA recall authority. The environment – e.g., roadway surface, markings, traffic communications (signage, lighting), etc. - has high reliability with high confidence, however, atmospheric conditions may contribute uncertainty and adversely impact reliability and confidence. Estimating the current level of safety for human drivers of nonexempt vehicles to be 85% reliability with 90% confidence reflects the NVMCCS analysis attributing 94% of passenger car and light truck crashes due to driver error. The unknown/uncertainty element gives stakeholders flexibility to examine competencies and scenarios of interest; for this paper, the reliability distribution of 80% / 85% was assigned as a minimum value.

Table 3.
Example of a Safety Framework for Passenger Cars & Light Trucks

Network Element	Crash Risk [Ref. #]	FMVSS	Reliability Distribution	Number of Tests: Parameter(s)
Environment	2%	301, 302, 303, 304, 305	90% / 95%	109 tests: rain, ice, snow
Vehicle	2%	All Standards	95% / 95%	220 tests: brakes, steering, occupant protection, etc.
Driver	94%	Recognition: 101, 103, 104, 108, 111, 113, 123, 125, 131, 138, 205 Decision: 102, 108, 124, 135, 209, 210, 213, 225, 401 Performance: 105, 106, 109, 110, 116, 117, 118 Non-Performance: 114 Other:	85% / 90%	17 tests: low sun angle 28 tests: speed, curves, intersections 7 tests: lane management, LTAP 3 tests: maneuvers near a “taco truck” with pedestrians 4 tests: see NMVCCS data
Unknown/ Uncertainty	2%	Varies	80% / 85%	37 tests: double parked, orange cone, etc.
				Total = 425 tests

Overall safety by vehicle class allows for differentiation in safety levels. A safety framework for large trucks would vary from Table 3 in the crash risk and reliability distributions, requiring additional data analysis. It is likely that trained professional drivers would be associated with a lower crash risk and a higher reliability distribution for the Driver element, and a safety level higher than passenger cars.

Table 3 shows data parsed into the NMVCCS categories which aligns better with the construct of “level of safety” for AVs because it treats the common vehicle systems (e.g., powertrain, steering, braking, etc.) separate from the Driver, and also allows for refinement of the driver behaviors (e.g., recognition, decision, performance, non-performance, and other). However, the NMVCCS sample is only light vehicles and this distribution cannot be projected directly onto NHTSA GES or CDS estimates for other vehicle classifications. An alternate option could be to parse the test sample by pre-crash scenario (Rear End, Crossing Paths, Road Departure, Pedestrian, Cyclist, etc.) which is a good fit for tracking how crashes occur and factoring system effectiveness.

Successful implementation depends on reaching consensus on the metrics, collecting and sharing relevant AV characterization data, and revisiting at regularly defined intervals.

CONCLUSIONS

All aspects of AV safety and reliability must be demonstrated before candidate AVs are deployed onto public roadways. This proposed methodology establishes a framework to quantify safety performance levels and includes the flexibility to incorporate new data describing driver performance or technological capabilities as AV technology

evolves. To paraphrase Aristotle, the whole framework is greater than the sum of its parts. Blending established engineering concepts from motor vehicle safety, reliability, and systems engineering to form a new approach to specify benchmark test & evaluation scenarios places a reasonable burden on all stakeholders and is achievable well before driving billions of miles.

Table 4 lists one measure of vehicle incidence rates for different types of vehicles. Mindful that VMT and flight hours are not comparable metrics, the promise of AVs may be realized if it follows the trend of automated aviation safety.

Table 4.
Compilation of Vehicle Incidence Data

Vehicle	Incidence Data	
Police-reported Motor Vehicles Crashes	0.0205 crashes/ 10,000 VMT	[Ref. 2]
Estimate for All Motor Vehicles Crashes	0.0457 crashes / 10,000 VMT	[Ref. 2]
CA DMV AV Disengagements	38.6 disengagements / 10,000 AV VMT	[2017 data]
Automated Aviation	0.5 accidents / 1 million take-offs	[Ref. 6]
Commercial Aviation	0.149 accidents / 10,000 flight hours	[Ref. 6]
General Aviation	7.11 accidents / 10,000 flight hours	[Ref. 6]
Customs & Border Patrol Aviation	52.7 accidents / 10,000 flight hours	[Ref. 6]

REFERENCES

[1] Balci, O. and R.G. Sargent. 1981. "A Methodology for Cost-Risk Analysis in the Statistical Validation of Simulation Models." Communications of the ACM 24, No. 4, April 1981: 190-197.

[2] Blincoe, L. J., Miller, T. R., Zaloshnja, E., & Lawrence, B. A. (2015, May). *The economic and societal impact of motor vehicle crashes, 2010. (Revised)* (Report No. DOT HS 812 013). Washington, DC: National Highway Traffic Safety Administration.

[3] Federal Highway Administration (FHWA) website, https://safety.fhwa.dot.gov/hsip/resources/fhwasa09029/app_c.cfm, retrieved March 8, 2019.

[4] National Center for Statistics and Analysis. (2018, September). *Summary of motor vehicle crashes: 2016 data*. (Traffic Safety Facts. Report No. DOT HS 812 580). Washington, DC: National Highway Traffic Safety Administration.

[5] National Highway Traffic Safety Administration. (2008, July). *National Motor Vehicle Crash Causation Survey Report to Congress*. (Report No. DOT HS 811 059). Washington, DC: National Highway Traffic Safety Administration.

[6] Ni, R. and Leung, J. *Safety and Liability of Autonomous Vehicle Technologies*. https://groups.csail.mit.edu/mac/classes/6.805/student-papers/fall14-papers/Autonomous_Vehicle_Technologies.pdf, retrieved March 8, 2019.

[7] O'Connor, A., Modarres, M. and A. Mosleh. (2016). *Probability Distributions Used in Reliability Engineering*. College Park, Maryland: Center for Risk and Reliability.

[8] Reliability Analytics Toolkit website, https://reliabilityanalyticstoolkit.appspot.com/sample_size, retrieved March 8, 2019.

[9] Singh, S. (2015, February). Critical reasons for crashes investigated in the National Motor Vehicle Crash Causation Survey. (Traffic Safety Facts Crash•Stats. Report No. DOT HS 812 115). Washington, DC: National Highway Traffic Safety Administration.

[10] U.S. Department of Transportation, Bureau of Transportation Statistics website, https://www.bts.gov/content/us-vehicle-miles, retrieved March 8, 2019.

[11] Webb, David W. March 2011. "A Comparison of Various Methods Used to Determine the Sample Size Requirements for Meeting a 90/90 Reliability Specification." Army Research Laboratory paper number ARL-TR-5468, https://www.arl.army.mil/arlreports/2011/ARL-TR-5468.pdf, retrieved March 8, 2019.

TITLE: EVALUATION OF AUTOMATIC EMERGENCY BRAKING IN HELPING PREVENT FRONT-TO-REAR CRASHES AMONG TOYOTA MODELS

Rebecca Spicer
Amin Vahabaghaie
George Bahouth
Impact Research, LLC
United States

Paper Number 19-0146

ABSTRACT

This study estimated the effectiveness of Toyota Safety Sense (TSS) in helping prevent front-to-rear collisions among three Toyota models (Avalon, Prius, RAV4). TSS, offered as an option in model year 2016 vehicles, includes a pre-collision warning system with automatic emergency braking (AEB), in addition to lane departure alert and automatic high beam. This study addresses the hypothesis that TSS-equipped vehicles will be less likely to experience a front-to-rear crash (as the striking vehicle) compared to those not equipped with TSS.

Using Toyota-supplied production data linked to police reported crash data from 5 US states (Florida, Louisiana, Michigan, Pennsylvania, Texas) for crash years 2014-2016, the study compared crash rates (crashes per 10,000 vehicle months) of TSS equipped (n= 23,394) versus non-equipped (n= 294,931) vehicles. TSS equipment present per vehicle was identified based on VIN. This study evaluated the impact on front-to-rear crashes where the Toyota was the striking vehicle.

Exposure, using vehicle-months, was computed based on aggregate vehicle sales in the five study states for TSS equipped and non-equipped model year 2014 to 2016 vehicles. The crude rate ratio (CRR) of front-to-rear crash rates where the Toyota was the striking vehicle was calculated as the front-to-rear crash rate for TSS-equipped vehicles divided by the crash rate for non-equipped vehicles.

Given that TSS is optional, it is possible that customers who choose to purchase these safety systems also exhibit different driving and risk-taking behaviors compared to those who do not purchase the safety systems. To address a possible selection bias, sensitivity analysis examined the control outcome of front-end damage in a multi-vehicle crash, excluding the types of crashes targeted by AEB (front-to-rear).

Of the TSS-equipped vehicles, 2.46 per 10,000 vehicle-months (95%CI:1.75-3.17 per 10,000 vehicle-months) experienced a front-to-rear crash as the striking vehicle, compared to 4.55 per 10,000 vehicle-months (95%CI:4.37-4.73 per 10,000 vehicle-months) of the non-equipped vehicles. Therefore, study Toyotas equipped with TSS were 46% less likely to experience a front-to-rear crash as the striking vehicle compared to non-equipped (CRR=0.54; 95%CI:0.40-0.67).

The study found that when the outcome was broadened to include all vehicles with front-end damage in multi-vehicle crashes, TSS-equipped vehicles experienced 17% fewer crashes than non-equipped vehicles (CRR=0.83; 95%CI:0.71-0.94) . However, no significant difference was observed if front-to-rear crashes were excluded (CRR=1.02; 95%CI:0.86-1.16) suggesting that selection bias did not play a significant role in this study.

The TSS option was only available in model year 2016 vehicles, limiting the sample size and follow-up time of TSS-equipped vehicles. Future research that includes additional state data, models and model years, will increase sample sizes and may allow for estimates by model and other crash types.

In conclusion, vehicles equipped with TSS, were nearly half as likely to be the striking vehicle in a front-to-rear crash compared to non-equipped vehicles. This study contributes to the growing evidence of the effectiveness of AEB in helping prevent a significant number of front-to-rear crashes.

INTRODUCTION

The National Motor Vehicle Crash Causation Survey, administered by the National Highway Traffic Safety Administration found that driver error was the critical reason for 94% of crashes [1]. These errors included recognition error (e.g. driver inattention and inadequate surveillance), decision error (e.g. driving too fast for conditions, misjudgment of gap or other's speed), and performance (e.g. overcompensation, poor directional control) and non-performance (e.g. falling asleep) errors.

Advanced Driver Assistance Systems (ADAS) are in-vehicle technologies developed to counteract these driver errors and help prevent crashes or mitigate the severity if a crash occurs. These systems provide drivers timely warnings and some will actively and automatically intervene to help avoid hazardous situations. Examples of ADAS technologies include lane departure warning and active lane keep assistance, blind spot detection, forward collision warning and automatic emergency braking (AEB). In vehicles with pre-collision warning and AEB, the driver is alerted if the speed of the equipped vehicle and the vehicle ahead and the distance from the vehicle or object ahead indicate that a collision is possible. AEB will finally apply the brakes if the system predicts a high probability of a crash to help prevent the collision regardless of driver response.

Many manufacturers offer these technologies as options or standard on some their vehicles. ADAS technologies are the precursor to autonomous vehicles and, depending on the combination of ADAS equipment installed in a vehicle, can allow level 1 through level 3 autonomous driving at the present time [2].

While controlled track and simulated testing of ADAS technologies suggest that they will greatly impact crash involvement rates, real world evidence that characterizes their effectiveness is still limited. Previous evaluations of AEB and other ADAS have found reductions in both injury-involved and, to a lesser extent, all-severity (injury and non-injury) crashes. An evaluation of police-reported crashes in the United States found that vehicles equipped with AEB experienced a 42% reduction in injury front-to-rear crashes and a 39% reduction in all-severity front-to-rear crashes compared to non-equipped vehicles [3]. A meta-analysis of pooled data from multiple countries determined that AEB was associated with a 38% reduction in real-world rear-end crashes [4].

In Toyota vehicles the Toyota Safety Sense (TSS) package includes a pre-collision warning system with AEB, in addition to lane departure alert and automatic high beam. TSS was first offered as an option in some model year 2016 vehicles and standard in most model year 2017 Toyota and Lexus passenger vehicles. Toyota is the frontrunner among manufacturers in the number of model year 2017 vehicles equipped with AEB: 1.4 million vehicles, 56% of its model year 2017 fleet [5].

This study evaluates the effectiveness of TSS among three Toyota models (Avalon, Prius, RAV4) in helping prevent the types of collisions AEB is designed to address: striking another vehicle in a front-to-rear collision. This study hypothesizes that vehicles equipped with AEB will be less likely to be involved in a front-to-rear crash as the striking vehicle compared to non-equipped vehicles.

METHODS

This retrospective cohort study of three Toyota models (Avalon, Prius, RAV4), model years 2014-2016, compares rates in vehicles with TSS versus without TSS in order to estimate the effectiveness of TSS in helping prevent front-to-rear crashes.

Toyota production data was used to compute the aggregate number of vehicles sold in the five study states by model, model year and TSS equipped/non-equipped. Some model year 2014 and 2015 vehicles are equipped with a previous version of the Pre-Collision System. These are not included in the comparison between TSS-equipped vehicles and non-equipped vehicles. Exposure was computed in vehicle-months: the number of vehicles sold multiplied by the estimated number of months on the road. We assumed an average seven months of exposure for the first year of a model year platform; e.g. Model year 2014 vehicles had an average seven months exposure during calendar year 2014.

The study used state police crash reports from five states (Florida, Louisiana, Michigan, Pennsylvania, Texas) for crash years 2014-2016. Vehicles in these five states make up an estimated 23% of U.S. vehicle miles travelled.

The TSS options data were linked at the individual VIN level to the five state police crash report data files, identifying which crashed vehicles were TSS-equipped and which were not. The state police reported crash data included information on the crash type (e.g. front-to-rear, side swipe, angle, etc.) and the location of vehicle damage per vehicle involved.

The outcome evaluated in this study was the subset of crashes targeted by AEB: front-to-rear crashes where the Toyota was the striking vehicle. Using the state police reported crash files, a striking vehicle in a front to rear crash was identified as a vehicle involved in a front-to-rear collision where the Toyota was coded with front-end damage (the striking vehicle) and at least one other vehicle was coded with rear-end damage (the struck vehicle). Figure 1 describes the process. Of all Toyota vehicles involved in a crash ([1] in Figure 1), those involved in multi-vehicle crashes ([2] in Figure 1) were identified. Of the vehicles involved in multi-vehicle crashes, those that experienced front-end damage where identified ([3] in Figure 1). Of these, those involved in a front-to-rear crash ([4] in Figure 1) were defined as the striking vehicle in a front-to-rear crash. Crashes where the Toyota was first involved in a front-to-rear crash as the struck vehicle (rear damage) and subsequently struck a second vehicle from the rear as the striking vehicle were excluded from the evaluation.

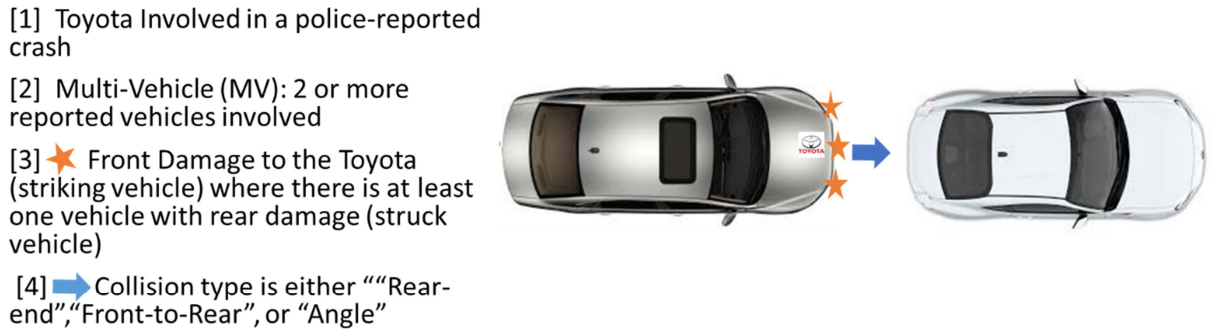

Figure 1. Process for Identifying Crash-Involved Toyotas where Toyota is the Striking Vehicle in a Front-to-Rear Crash

The rate of vehicle involvement in a front-to-rear crash as the striking vehicle was computed as the total number of crashes divided by the total number of vehicle months. Crash rates were computed separately for TSS-equipped and non-equipped vehicles. The state data are a census of police-reported crashes and therefore not subjected to sampling variability. However, to account for random variation, confidence intervals were computed based on the method described by Arias and Smith, 2003 [6].

The crude rate ratio (CRR) for TSS-equipped versus non-equipped vehicles was calculated as the front-to-rear striking vehicle crash rate for TSS-equipped vehicles divided by the crash rate for non-equipped vehicles. Crude rate ratios are interpreted to describe the percent reduction in front-to-rear crashes associated with TSS.

Given that TSS was optional, it is possible that customers who choose to purchase these safety systems also exhibit different driving and risk-taking behaviors compared to those who don't purchase the safety systems. To address a possible selection bias, sensitivity analysis examined two additional outcomes: the broad outcome of front-end damage in a multi-vehicle crash and the subset of these crashes excluding the types of crashes targeted by AEB (front-to-rear where Toyota is the striking vehicle). This control analysis tests the hypothesis that differences in crash rates for TSS (thus, AEB)-equipped vehicles are only observed in front-to-rear crashes.

RESULTS

A combined total 318,325 Toyota Avalon, Prius and RAV4 vehicles, model year 2014-2016, were sold in the five study states. Of these, 23,394 (29%) of the model year 2016 vehicles (the first year TSS was offered as an option) were equipped with TSS (Table 1). Take-rates in model year 2016 vehicles varied; 24% for the Avalon, 28% for the RAV4 and 38% for the Prius.

Table 1
Number of Toyotas Sold in the Study States, by Model Year and TSS Option

Model Year	Without TSS	With TSS	Total
2014	86,401	-	86,401
2015	127,310	-	127,310
2016	81,220	23,394	104,614
Three Model Total	294,931	23,394	318,325

The five state police reported crash files from years 2014-2016 captured 18,454 vehicles involved in crashes among the study cohort of 318,325 vehicles ([1] in Table 2). Of these, 17,402 were vehicles involved in multi-vehicle crashes ([2] in Table 2). Of the vehicles involved in multi-vehicle crashes, 6,076 experienced front-end damage ([3] in Table 2). Of these, 2,749 were involved in a front-to-rear crash ([4] in Table 2), i.e. the striking vehicle in a front-to-rear crash. This outcome was evaluated in this study. Table 2 further presents the number of crashes by state.

Table 2
Number of Crash-Involved Toyotas among the Vehicles Sold in the Study States, by Crash Population and Crash State

Crash Population	Total 5 States	FL	LA	MI	PA	TX
[1] All Crash-Involved Toyotas	18,454	9,534	1,296	1,355	1,116	5,153
[2] Toyotas involved in a Multi-Vehicle (MV) crash	17,402	9,168	1,255	1,130	937	4,912
[3] Toyotas involved in a MV crash with Front-end damage	6,076	3,069	442	472	417	1,676
[4] Outcome Evaluated: Toyota involved in a MV front-to-rear crash with front-end damage (striking vehicle)	**2,749**	**1,282**	**164**	**199**	**155**	**949**

Among the study cohort of 318,325 vehicles, 2,617 (0.82%) were involved in a front-to-rear crash as the striking vehicle. Of the TSS-equipped vehicles, 46 (0.20%) experienced a front-to-rear crash as the striking vehicle, compared to 2,571 (0.87%) of the non-equipped vehicles (Table 3).

To compare crash risk among TSS equipped versus non-equipped, crash rates were computed to account for the overall greater exposure (vehicle-months) of the non-equipped vehicles. Of the TSS-equipped vehicles, 2.46 crashed per 10,000 vehicle-months (95%CI:1.75-3.17), compared to 4.55 crashes per 10,000 vehicle-months (95%CI:4.37-4.73) among the non-equipped vehicles (Table 3).

Therefore, study Toyotas equipped with TSS were 46% less likely to be a striking vehicle in a front-to-rear crash compared to non-equipped (CRR=0.54; 95%CI:0.40-0.67) (Table 3).

Table 3
Number and Rate of Vehicles involved in a Front-to-Rear Crash as the Striking Vehicle, by TSS equipment; Crude Rate Ratio of Vehicles With versus Without TSS

	Number of Striking Vehicle in a Front-to-Rear Crash (A)	Vehicle-Months (B)	Rate Per 10,000 Vehicle-Months C=(A/B)*10,000	Crude Rate-Ratio ($C_{withTSS}$):($C_{withoutTSS}$)
Equipped with TSS	46	187,215	2.46	0.54
Not equipped with TSS	2,571	5,650,834	4.55	

The study found that when the outcome was broadened to include all front-end damaged vehicles in multi-vehicle crashes, TSS-equipped vehicles experienced 17% fewer crashes than non-equipped vehicles (CRR=0.83; 95%CI:0.71-0.94) (Table 4). However, no significant difference was observed for the control crash population where the subset of crashes targeted by AEB (front-to-rear) was excluded (CRR=1.02; 95%CI:0.86-1.16). Table 4 also presents CRR for all crashes and multi-vehicle crashes.

Table 4
Crude Rate Ratio for Crashing Among Vehicles With Versus Without TSS, by Crash Population

Crash Population	Crude Rate Ratio	95% Confidence Interval
[1] All Crash-Involved Toyotas	1.01	(0.94 to 1.08)
[2] Toyotas involved in a Multi-Vehicle (MV) crash	1.00	(0.93 to 1.08)
[3] Toyotas involved in a MV crash with Front-end damage	0.83	(0.71 to 0.94)
[4] Outcome Evaluated: Toyota involved in a MV front-to-rear crash with front-end damage (striking vehicle)	**0.54**	**(0.40 to 0.67)**
Control crash population: MV crash with front-end damage [3] excluding front-to-rear crashes	1.01	(0.86 to 1.16)

CONCLUSIONS

Vehicles equipped with TSS, were 46% less likely to be a striking vehicle in a front-to-rear crash compared to non-equipped vehicles. This study contributes to the growing evidence of the effectiveness of AEB in helping prevent a significant number of crashes.

The control analysis found that differences in crash rates for TSS-equipped vehicles were only observed in front-to-rear crashes. Therefore, selection bias (customers who opt for TSS are safer drivers) did not likely play a significant role in this study. Further research is warranted to explore if the crash reductions in AEB-equipped vehicles found by this and other studies persist once these technologies are offered standard.

This study uses real-world data of a cohort of Toyota vehicles linked to crash events. The strengths of this study include the large sample size of a well-defined vehicle cohort, the ability to identify the individual options for each vehicle, and a well-defined outcome measure.

A limitation of the study is the short (less than one year) follow up of model year 2016 vehicles, limiting the sample size of TSS-equipped vehicles and crashes. In addition, this study uses estimated vehicle-months based on aggregate counts of vehicles by model year.

The current study served as the pilot for a more rigorous Phase 2 study, currently ongoing. Phase 2 uses retail dates of each vehicle to accurately estimate vehicle-months. In addition, Phase 2 expands the field study by incorporating

additional Toyota and Lexus models (Highlander, Corolla, Lexus ES and Lexus RX), more recent model years (model years 2015 to 2017; TSS was standard on model year 2017 vehicles), more recent crash data (years 2015 to 2017) and an additional three states' police reported data. Using the increased sample sizes and accurate computation of exposure at the vehicle level, phase 2 incorporates regression modeling techniques that control for exposure and time and compute adjusted risk ratios to quantify effectiveness. These findings will be reported in the near future.

ACKNOWLEDGEMENT

Toyota Motor Corporation supported this research.

REFERENCES

[1] Singh S. Critical reasons for crashes investigated in the National Motor Vehicle Crash Causation Survey. (Traffic Safety Facts Crash Stats. Report No. DOT HS 812 115). Washington, DC: National Highway Traffic Safety Administration. 2015.

[2] SAE International. Standard J3016 titled Taxonomy and Definitions for Terms Related to On-Road Motor Vehicle Automated Driving Systems. Society of Automotive Engineers. 2014.

[3] Cicchino JB. Effectiveness of forward collision warning and autonomous emergency braking systems in reducing front-to-rear crash rates. Accident Analysis and Prevention. 2017;99(Pt A):14-152.

[4] Fildes B, Keall M, Bos N, Lie A, Page Y, Pastor C, Pennisi L, Rizzi M, Thomas P, Tinvall C. Effectiveness of low speed autonomous emergency braking in real-world rear-end crashes. Accident Analysis and Prevention. 2015;81:24-29.

[5] NHTSA, National Highway Traffic Safety Administration (2017). NHTSA-IIHS Announcement on AEB: Manufacturers make progress on voluntary commitment to include automatic emergency braking on all new vehicles (accesed online, February 1, 2019 at https://www.nhtsa.gov/press-releases/nhtsa-iihs-announcement-aeb)

[6] Arias, E., & Smith, B. L. (2003). Deaths: Preliminary data for 2001. National vital statistics reports (vol. 51, No. 5). Hyattsville, MD: National Center for Health Statistics

AN ANALYSIS OF FACTORS DRIVING THE INCREASES IN TRAFFIC FATALITIES IN THE UNITED STATES

Rebecca Spicer
George Bahouth
Amirfarrokh Iranitalab
Jing Chen
Impact Research, LLC
United States

Kristin Kingsley
Robert Strassburger
Alliance of Automobile Manufacturers
United States

Paper Number 19-0147

ABSTRACT

According to the U.S. Department of Transportation's National Highway Traffic Safety Administration (NHTSA), 37,461 people died in the United States in traffic crashes in 2016, a 5.6% increase in fatalities from 2015. It was the second consecutive year of increasing fatalities following an 8.4% increase from 2014 to 2015. This study applies random-effects generalized linear mixed modeling techniques to examine the association of changes in traffic fatality counts with changes in explanatory factors, by state, between 2005 and 2016. Three regressions modeled different outcomes: 1) passenger vehicle occupant fatalities, 2) pedestrian fatalities, and 3) motorcycle fatalities

Motor vehicle-related traffic fatalities were collected by year and by state using NHTSA's Fatality Analysis Reporting System (FARS). A variety of sources provided measures on explanatory factors. The Fatality counts (outcome) and explanatory factors were then combined as panel data by year (2005-2016) and state (51 states including the District of Columbia). The models tested the association between fatalities and more than seventy explanatory factors including economic, exposure, behavioral and vehicle factors.

The study found that the increases in passenger vehicle fatality counts were associated with increases in vehicle miles traveled (exposure) and an improving economy. In addition, the increase in the population age 65 and older and an increase in the percent of this population in the workforce also was associated with increasing fatality counts. Several behavioral factors were associated with changes in fatality counts, including non-belt use and increased drunk driving. Conversely, improved vehicle safety design was associated with a decline in occupant fatalities. A rise in motorcycle fatalities was associated with increased exposure (motorcycle registrations and overall vehicle miles travelled) and an improving economy. Among pedestrian and motorcycle fatalities, there is some evidence that driver distraction plays a role.

While the quasi-experimental study design does not allow for inferences of causality, the models can be applied to forecast future fatality counts based on expected or observed environmental, behavioral and vehicle factors or to evaluate the potential impact of prospective interventions.

Increased exposure, the improving economy, and behavioral factors drove increases in fatality counts between 2005 and 2016. However, improved vehicle safety design substantially countered these effects, mitigating the increases.

INTRODUCTION

According to the U.S. Department of Transportation's National Highway Traffic Safety Administration (NHTSA), 37,461 people died in the United States in traffic crashes in 2016, a 5.6% increase in fatalities from 2015 the second consecutive year of increasing fatalities following a 8.4% increase from 2014 to 2015 [1]. The data further showed traffic deaths rising across nearly every segment of the population. The last single-year increase of this magnitude was in 1966, when fatalities rose 8.1 percent from the previous year.

These figures come after a decade of progress. Eleven years ago, the number of traffic deaths was nearly 25 percent higher, with 42,708 fatalities reported nationwide in 2005 [2]. In the past two decades, behavioral safety and enforcement programs have helped lower the number of deaths by increasing seat belt use and reducing impaired driving [3][4]. Vehicle improvements, including air bags and electronic stability control, have made substantial contributions to reducing traffic fatalities [5].

Increased exposure in terms of vehicle miles travelled (VMT) does not account for all of the increases. In 2014 there were 1.08 traffic-related deaths per 100 million VMT. This increased to 1.12/ 100 million VMT in 2015 and 1.18/100 million VMT in 2016, a 6.5% and 2.5% change, respectively [1][2]. Changes in fatality counts varied by person type, with non-occupants contributing more to the increases than occupants[2]. The toll was particularly high among and older drivers (age 65+) in 2015 and 2016.

Risk factors for traffic crashes and deaths are fairly well understood. One tool for analyzing an injury event and ways to either prevent the injury or reduce the harm done is the Haddon Matrix. In 1970, William Haddon Jr. proposed a matrix that allows simultaneous consideration of the stages over time of an injury event (pre-, during, and post-event) with all the possible host, agent/carrier, and environment factors involved in the event. Table 1 presents a Haddon Matrix that identifies factors relevant to traffic fatalities. Important person-level factors include restraint use, driver impairment, and driver distraction, age and gender. Important vehicle factors include speed, vehicle size, age and safety design. Environment factors are differentiated as either physical (i.e. road conditions, weather, proximity to emergency medical services) or social (i.e. existing safety laws and economic conditions).

Table 1. Haddon Matrix of factors relevant to traffic deaths

	Person Factors	**Vehicle/Equipment Factors**	**Environment**	
			Physical	**Social/Economic**
Pre-Crash	Driver Experience Impairment Gender Driver condition Risk-taking behavior	Vehicle condition Driving Speed Load characteristics Safety package	Road quality Road characteristics Weather Conditions	Existing laws Enforcement of laws Safety culture Economy Congestion Travel time/Exposure
Crash	Helmet use Restraint use Injury Propensity Health Age	Speed Crashworthiness/safety design of vehicle Vehicle size/Body Type Vehicle condition Type of crash	Road features Type and size of object struck	Laws relevant to human/ vehicle/ physical factors
Post-Crash	Health Age Impairment	Integrity of fuel and battery systems Availability of automated crash notification and GPS locator	EMS response speed and quality Distance to trauma care Availability of rehabilitation programs Accessibility to crash victims	EMS protocols Public support for trauma care and rehab

Changes in these factors will influence the number of crashes or reduce the severity of crashes resulting in fewer fatalities. Depending on the factor or the combination of factors, small changes can have large impacts and vice versa. State or local level policies, laws, enforcement, and education can influence many of these factors.

Engineering approaches (e.g. traffic calming, rumble strips, advanced driving systems in vehicles, vehicle safety design) may also counter some factors.

The growth in the population of motor vehicles and the increase in VMT that accompanies economic growth is associated with an increase in road traffic crashes. According to NHTSA, job growth and low fuel prices were two factors that led to increased driving, including increased leisure driving and driving by young people [2].

Weather and regional demographic distributions are other examples of high-level factors shown to play a role in crash rates. Consistently, studies have shown that increases in temperature are associated with an increase in fatal traffic crashes due to an increase in VMT and exposure for pedestrians, bicyclists, and motorcyclists [6][7].

Nevertheless, even when state characteristics are similar, considerable variability in traffic deaths exists. For example, states with similar populations and seat belt laws have substantially different outcomes with respect to vehicle occupant deaths, seat-belt-use rates, and unbelted vehicle occupant fatalities.

This paper examines the association of these factors with the number of traffic deaths in the United States to identify key factors driving the changes in deaths over the past twelve years. This study quantifies the contribution of high-level factors like the economy and VMT to distinguish the role of key factors relevant to intervention by state and local governments and vehicle manufacturers.

METHODS

This study analyzes changes in traffic death counts in U.S. states from 2005 to 2016 using generalized linear mixed modeling. These regressions model the association of changes in measurable factors (explanatory variables) with changes in traffic death counts by state (outcome variable). Three regressions modeled different outcomes: 1) passenger vehicle occupant fatalities, 2) pedestrian fatalities, and 3) motorcycle fatalities.

Explanatory Variable Selection

The Haddon matrix (Table 1) was used as a guide in selecting explanatory variables to test in the model. To be included in the model, the variable had to be available by state and year. Over seventy variables were tested. These are listed in Appendix A.

Data Sources

Table 2, Table 3, and Table 4 detail the data sources for the outcome, exposure and explanatory variables included in the final models.

Table 2. Data Sources for the Outcome Measure

Measure of Outcome	Data Source and Description
Fatality Counts	Fatal Analysis Reporting System (FARS)

Table 3. Data Sources for Exposure Measures

Measures of Exposure	Data Source and Description
Vehicle Miles Travelled	Highway Statistics, Federal Highway Administration
Population	United States Census Bureau
Number of Vehicles	National Vehicle Population Profile, R.L. Polk
Motorcycle Registrations	Motorcycle Sales Report, 2000-2016, Motorcycle Industry Council

Table 4. Data Sources for Explanatory Measures

Measure of Key Factors	Data Source and Description
U.S. Population Counts, demographic	United States Census Bureau

distributions	
Gross Domestic Product	United States Bureau of Economic Analyses
Employment percentages by age	United States Census Bureau
Average Annual Temperature	National Oceanic and Atmospheric Administration
Motorcycle Registrations	Motorcycle Sales Report, 2000-2016, Motorcycle Industry Council
Alcohol Consumption	National Institute of Alcohol Abuse and Alcoholism
Self-Reported Belt Use	Behavioral Risk Factor Surveillance System, Centers for Disease Control
Self-Reported Drunk Driving	Behavioral Risk Factor Surveillance System, Centers for Disease Control
Observed Driver Handheld Use while Driving	National Occupant Protection Use Survey, National Highway Traffic Safety Administration
Average IIHS crash test rating of vehicle fleet	Insurance Institute for Highway Safety crash test ratings
Average NCAP Score of vehicle fleet	National Highway Traffic Safety Administration, New Car Assessment Program
Percent of vehicle fleet ESC-equipped	Safercar.gov, National Highway Traffic Safety Administration
Average, Median, Vehicle Mass and Mass distribution of state vehicle fleet	National Vehicle Population Profile, R.L. Polk

State motor vehicle traffic deaths counts were tabulated using the NHTSA-administered Fatality Analysis Reporting System (FARS). VMT was tabulated by state using annual data from the Federal Highway Administration. Gross Domestic Product (GDP), based on data from the U.S. Bureau of Economic Analysis, was the primary economic measure included in the final model. United States Census Bureau data provided information on state demographic distributions over time, means of transportation to work, and population employment characteristics.

The Center for Disease Control's Behavioral Risk Factor Surveillance System (BRFSS) provided data on risk behaviors. The BRFSS is a national random digit dial telephone survey. Data are collected at the state level among a representative sample of the population over 18 years of age. Regarding belt use, the survey asks the question: "How often do you use seatbelts in your car?" The possible responses are: always, nearly always, sometimes, seldom, and never. For this study we defined "rarely belted" as those responding "sometimes", "seldom", or "never". Regarding drunk driving, the survey asks the question: "In the past 30 days, have you driven after drinking too much?" with a yes or no response. The BRFSS also includes a question on binge drinking (5 or more drinks for men and 4 or more drinks for women in one drinking session).

Observed belt use data are available by state from the annual National Occupant Protection Use Survey (NOPUS), coordinated by NHTSA. This probability-based survey collects observations on driver and right-front passenger seat belt use. Observations of driver hand held use are also included in the NOPUS and used in this study.

Weather data (precipitation and temperature) were obtained from the National Oceanic and Atmospheric Administration (NOAA). The NOAA maintains and collects data from automated weather stations distributed across all 50 states.

Changes in state laws (in particular alcohol, motorcycle, and graduated drivers licensing) were assessed using information available from the IIHS and the Governors Highway Safety Association.

This study includes a detailed focus on the role of vehicle fleet characteristics (age, safety design, mass disparity). To compute measures of these characteristics, we compiled, by state and year, counts of the vehicle population by vehicle make, model and model year using data published by R.L Polk and Co. Vehicle mass (from NHTSA) and crash testing data (from the Insurance Institute for Highway Safety and from NHTSA's New Car Assessment Program) are available by make, model and model year. IIHS ratings were converted to numeric scores: poor=1, marginal=2, acceptable=3 and good=4. Using these data merged with R.L. Polk vehicle population data (by make, model and model year), the study computed safety-related measures of the vehicle fleet for each state over time. Therefore, changes in these measures represent the improved safety design of new vehicles as they penetrate the fleet. including average IIHS rating, average NCAP rating, average vehicle mass, and fleet age. In addition, we computed several measures of mass disparity to characterize any changing distribution of passenger vehicles by mass.

Other measures tested in the regression models but not included in the final models were obtained from an additional number of data sources: Gasoline prices (from the U.S. Energy Information Administration), driving and walking time per day (from the American Time Use Survey, Bureau of Labor Statistics), drug- and opioid-related fatalities (Multiple Cause of Death File, CDC), number of mobile phone subscribers (Voice Telephone Services Report, Federal Communications Commission).

A full list of measures and data sources is compiled in Appendix A.

Data Preparation

Outcome and explanatory variables were compiled as panel data by year (2005-2016) and state, resulting in 612 observations (12 years x 51 states/DC). Because the scales of the explanatory variables varied dramatically, all variables were standardized and centered. For some data sources the data were missing in one year. In this case, the variable was imputed as the mid-way between the previous year and the following year. No 2016 estimates (last values) were missing in the final analysis.

Statistical Modeling

Generalized linear mixed models (GLMM) were created modeling the relationship between changes in the explanatory variables with fatality counts by year and state. GLMM is an extension of linear mixed models that combines the characteristics of generalized linear models and mixed models. The mixed model includes variables on two levels, time and state. This type of regression is appropriate for panel data with repeated measures over time.

While the outcome variables are count data (count of traffic fatalities), the assumptions for Poisson regression (equality of mean and variance of the outcome variable given the explanatory variables) were not met. Therefore, we used the negative binomial log link function.

Model Specification

GLMMs were fitted at two levels (state and time) using the panel data. The model allows for independent random effects for the intercept and slope for each subject (i.e. state). The model allows for an independent state-level random effect to incorporate the data structure of years nested in a state.

Measures to be included as explanatory variables were collected from multiple sources. Often there was more than one way to measure a key factor; either in different ways by different sources or by defining one source in different ways. For example, we developed three measures of belt use: 1) percent reporting rarely belted, 2) percent reporting always belted in the BRFSS, and 3) the percent observed daytime belted rate reported in the NOPUS. Different measures of the same key factor were tested separately for inclusion in the model. In determining which variable to use in the final model we considered measure's significance in the model and its contribution to model fit (measured by Bayesian Information Criterion, BIC).

Criteria for inclusion in the final model included testing for significance, collinearity, interaction effects, examining the impact on the coefficients of other explanatory variables, and the variable's contribution to model fit. The number of explanatory variables included in the final model was limited to between eight and ten due to the model degrees of freedom. Highly correlated variables (Pearson correlation coefficient>0.8) were not included simultaneously in specifying or in the final model.

This study further estimates the individual contribution of each key factor in the change in fatalities from 2015 to 2016 by applying the model to the known change in that key factor from 2015 to 2016 holding the other variables at 2015 values. For example, the contribution of the change in percent of adults reporting driving drunk is determined by predicting the number of fatalities in 2016 based on the change in this variable where all other explanatory variables remain at 2015 levels. The individual factor contributions by this method are not additive as their effects interact.

RESULTS

Figure 1 presents the counts of traffic-related fatalities over time, by person type. Changes in fatality counts varied by person type, with non-occupants contributing more to the increases than occupants. Fatalities decreased monotonically until 2012. In 2015 and 2016 traffic-related deaths increased again. Increases among non-occupant fatalities were greater than vehicle occupant fatalities. Fatality counts increased by 11.9% and 9.0% among pedestrians in 2015 and 2016, respectively, and 13.7% and 1.3%, respectively, among pedalcyclists. Motorcyclist deaths increased 9.5% and 5.1% in 2015 and 2016, respectively. Passenger vehicle occupant deaths increased 7.5% and 4.7%, respectively.

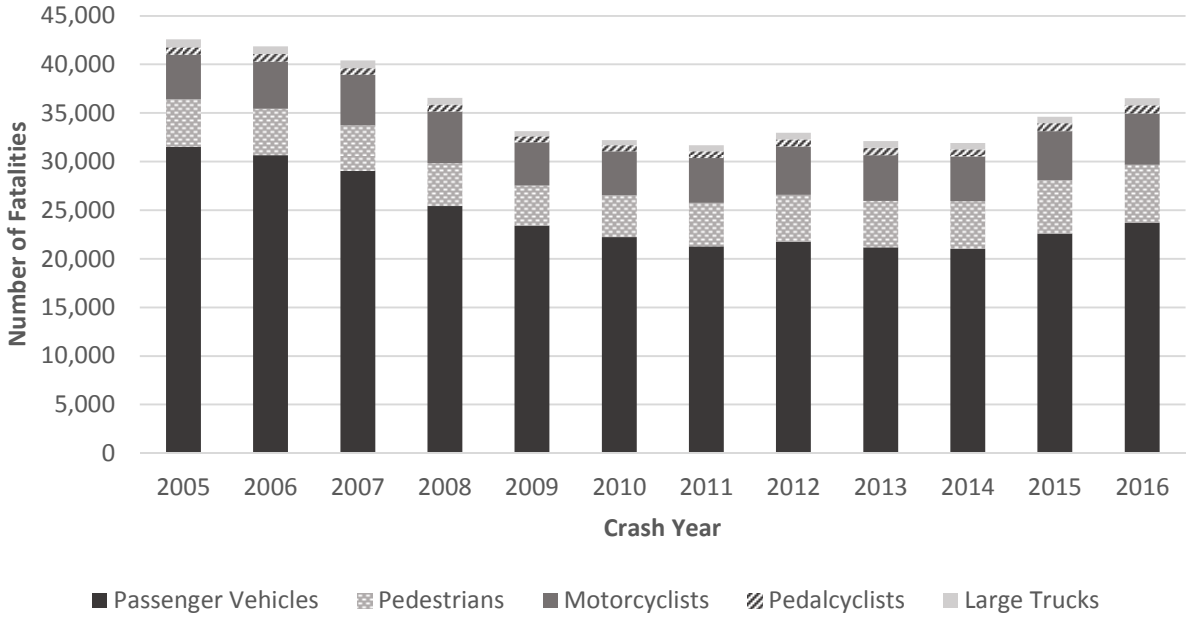

Figure 1. Number of Fatalities by Crash Year and Person Type (Source: Fatality Analysis Reporting System, National Highway Traffic Safety Administration)

Figure 2 plots state VMT versus the count of traffic-related fatalities for the 50 states and Washington D.C. for each of the years between 2005 and 2016. The trendline shows that fatality counts are highly correlated with exposure. However, the points do not cluster tightly around the line indicating that state- and time-related variability in risk exists that is not fully explained by changes in VMT alone.

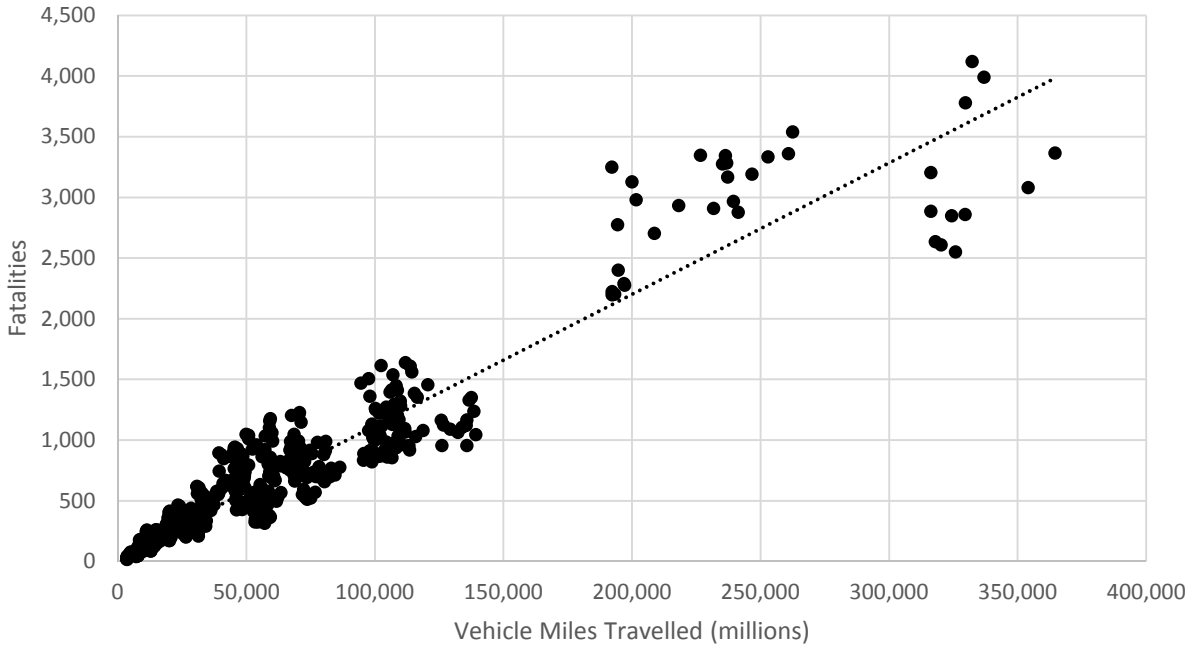

Figure 2. Count of Fatalities Versus Vehicle Miles Travelled, for 50 states and the District of Columbia between 2005 and 2016.

Table 5, Table 6, and Table 7 present the modeled fixed effects parameter estimates of the explanatory variables and the direction of this relationship for passenger vehicle occupant fatalities (Table 5), pedestrian fatalities (Table 6), and motorcycle fatalities (Table 7). "Positive" indicates that as the explanatory variable changes, fatalities change in the same direction; i.e. an increase in the explanatory variable is associated with increasing fatalities, and vice versa. "Negative" indicates that as the explanatory variable changes, fatalities change in the opposite direction; i.e. an increase in the explanatory variable is associated with decreasing fatalities, and vice versa.

Passenger Vehicle Occupant Fatalities

Eight explanatory variables were included in the final model predicting passenger vehicle occupant fatalities (Table 5). The final model controlled for high-level factors related to exposure (VMT per capita), the economy (GDP) and temperature. With the exception of average IIHS rating, all explanatory variables showed a positive association with fatality counts, i.e. an increase in the explanatory variable was associated with an increase in fatality counts. The models found that an increase in the average IIHS rating was associated with a decrease in fatality counts.

Table 5. Fixed Effects Parameter Estimates of Explanatory Variables Included in the Final Model of Passenger Vehicle Occupant Fatalities

Explanatory Variable	Estimate	p-value	Association with Fatalities
Average fleet IIHS Rating	-0.204	< 0.001	Negative
Employment Rate for the Population Age 65+ (%)	0.211	< 0.001	Positive
Population Age 65+ (% of total population)	0.167	< 0.001	Positive
Adults Reporting Rarely Belted (% reporting sometimes, seldom or never wear seatbelt)	0.116	< 0.001	Positive
Adults Reporting Drunk Driving in the past 30 days (%)	0.012	0.016	Positive
Average Temperature (degrees F)	0.137	< 0.001	Positive
VMT per Capita (millions)	0.196	< 0.001	Positive

GDP (Billions)	0.004	0.292	Positive

Pedestrian Fatalities

Nine explanatory variables were included in the final model predicting pedestrian fatalities (Table 6). The final model controlled for high-level factors related to exposure (VMT per capita), the economy (GDP) and temperature. With the exception of percent of workers who walk to work and GDP, all explanatory variables showed a significant positive association with fatality counts. The models found that an increase in the percent of workers who walk to work was associated with a decrease in fatality counts. GDP, however, was included in the model because it significantly modified the effect of VMT in urban areas: increasing urban VMT with a concurrent increase in GDP was associated with a decrease in pedestrian fatalities.

Table 6. Fixed Effects Parameter Estimates of Explanatory Variables Included in the Final Model of Pedestrian Fatalities

Explanatory Variables (Key Factors)	Estimate	p-value	Association with Fatalities
Walk to Work (% of workers)	-0.122	0.012	Negative
% Vehicles with Mass above the U.S. 90th %ile	0.121	0.002	Positive
Observed Using Hand-Held Device (% of drivers)	0.016	0.027	Positive
Population Age 65+ (% of total population)	0.151	< 0.001	Positive
VMT in Urban Areas (% of overall VMT)	0.089	0.140	Positive
Average Temperature (degrees F)	0.175	< 0.001	Positive
VMT per Capita (millions)	0.060	0.060	Positive
GDP (Billions)	0.453	< 0.001	Positive
Police per Million	-0.044	0.005	Negative
Interaction effect: VMT in Urban Areas x GDP	-0.116	0.003	Negative

Motorcycle Fatalities

Eight variables were included in the final model predicting motorcycle fatalities (Table 7). The final model controlled for high-level exposure-related factors (Total VMT and registered motorcycles), economic changes (GDP), motorcycle registrations, and temperature. With the exception of implementing a universal helmet law and population density, all explanatory variables showed a significant positive association with fatality counts. The presence of a universal helmet law was included in the model because it significantly modified the effect of total VMT: the presence of a universal helmet law where there was a concurrent increase in total VMT was associated with decreased fatalities.

Table 7. Fixed Effects Parameter Estimates of Explanatory Variables Included in the Final Model of Motorcycle Fatalities

Variables (Key Factors)	Estimate	p-value	Association with Fatalities
Statewide Universal Helmet Law (1=Yes/0=no)	-0.048	0.513	Negative
Beer Consumption (gallons of ETOH/capita)	0.083	0.002	Positive
Observed Using Hand-Held Device (% of drivers)	0.021	0.008	Positive
Population Density (Population/square mile)	-0.361	< 0.001	Negative
Registered Motorcycles (#)	0.111	0.001	Positive
Average Temperature (degrees F)	0.239	< 0.001	Positive
Total VMT (millions of miles)	0.437	< 0.001	Positive
GDP (Billions)	0.225	0.041	Positive

Interaction effect: Universal Helmet Law x Total VMT	-0.208	0.030	Negative

The models were applied to estimate the contribution of each key factor to changes in fatality counts. Table 8, Table 9, and Table 10 present the estimated change in the number of fatalities between 2015 and 2016 for the observed changed in each individual key factor between 2015 and 2016, holding the other factors constant. (Note: The factor-related contributions by this method are not additive as their effects interact)

In general, high-level factors (i.e. VMT, GDP, Temperature) are related to the highest corresponding changes in fatalities (Table 8, Table 9, Table 10). Increases in non-belt use (reporting rarely belted) and drunk driving (in the past 30 days) were substantial and corresponded to an estimated increase of 220 and 371 occupant fatalities, respectively (Table 8, Table 9). The 2.6% increase in the over-65 population corresponded to an increase in 647 occupant fatalities (Table 8) and 162 pedestrian fatalities (Table 9). The proportion of this population working has increased in the past decade, by 2.3% from 2015 to 2016, and corresponded to an increased 352 occupant fatalities (Table 8). Distracted driving, measured with the NOPUS of observed driver cell phone use, decreased and corresponded with a decline in vulnerable road user fatalities (49 fewer pedestrian fatalities and 60 fewer motorcycle fatalities).

Improved vehicle safety design, as measured by the average IIHS score of the vehicle fleet, was the one factor that corresponded with a substantial decrease in fatalities; 1,325 fewer occupant fatalities. Mass discrepancy, measured by the percent of vehicles in the fleet whose mass is above that of the 90th U.S. percentile declined and corresponded with a decrease of 42 in pedestrian fatalities.

No change, or an insignificant change, in a key factor will not play a role in driving the number of traffic deaths (e.g. no states changed their motorcycle helmet laws between 2015 and 2016).

Table 8. Estimated Individual Contribution of each Key Factor in the Change in Passenger Vehicle Occupant Fatalities from 2015 to 2016

Key Factor	Change 2015 to 2016	Corresponding change in Fatalities
Average IIHS Score	+7.0%	-1,325
Employment Rate for Age 65+ (%)	+2.3%	+352
Population Age 65+ (%)	+2.6%	+647
Adults Reporting Rarely Belted (%)	+6.9%	+220
Adults Reporting Drunk Driving (%)	+14.7%	+371
Average Temperature (degrees F)	+1.5%	+223
Total VMT (millions of miles) per Capita	+1.2%	+293
GDP (Billions)	+1.5%	+417

Table 9. Estimated Individual Contribution of each Key Factor in the Change in Pedestrian Fatalities from 2015 to 2016

Key Factor	Change 2015 to 2016	Corresponding change in Fatalities
Workers who Walk to Work (%)	-1.9%	+18
% Vehicles with Mass above the U.S. 90th %ile	-3.2%	-42
Drivers Observed Using Hand-Held Device (%)	-11.5%	-49
Population Age 65+ (%)	+2.6%	+162
VMT in Urban Areas (%)	+0.9%	+55
Average Temperature (degrees F)	+1.5%	+53

Total VMT (millions of miles) per Capita	+1.2%	+27
GDP	+1.5%	+74

Table 10. Estimated Individual Contribution of each Key Factor in Motorcycle Fatalities from 2015 to 2016

Key Factor	Change 2015 to 2016	Corresponding change in Fatalities
Universal Helmet Law	No change	0
Beer Consumption (gallons/capita)	+0.2%	+9
Drivers Observed Using Hand-Held Device (%)	-11.5%	-60
Population Density (Population/square mile)	+0.8%	-2
Motorcycle Registrations (#)	+2.2%	+2
Average Temperature (degrees F)	+1.5%	+81
Total VMT (millions of miles)	+1.2%	+99
GDP	+1.5%	+45

To gauge the accuracy of the models, we compared the modeled predicted 2016 fatality counts using data from 2005 to 2015 to actual fatality counts (Table 11).

Table 11. Modeled Predicted 2016 Fatality Counts versus Actual 2016 Fatality Counts

Model	Forecasted 2016	Actual 2016	% difference (Forecasted versus Actual)
Passenger Vehicles	23,102 (2.5%)	23,714	-2.5%
Pedestrians	5,671 (5.2%)	5,987	-5.2%
Motorcycles	5,271 (0.2%)	5,286	-0.2%

CONCLUSION

The models presented in this study suggest that observed increases in passenger vehicle fatality counts in 2015 and again in 2016 were driven by measurable changes in vehicle miles of travel (exposure) and an improving economy. Beyond these high-level factors, changes in the elderly population age 65 and older, the percent of this population employed, non-belt use, and drunk driving were associated with increasing fatality counts. However, improved vehicle safety design that accompanied the new vehicles as they entered the fleet substantially countered these effects, thereby tempering fatality increases.

Increases in motorcycle fatalities were associated with increased motorcycle registration, overall VMT (exposure), and an improving economy. Among pedestrian and motorcycle fatalities, there is some evidence that other factors like driver distraction plays a role but could not be easily measured.

DISCUSSION

Newer vehicles, for the most part, receive higher IIHS ratings and NCAP scores. Therefore, IIHS average rating is a surrogate measure of new vehicles penetrating the fleet and the accompanying improving overall safety design. However, it is important to note that the attrition from the fleet of older vehicles without airbags and other safety features is also contributing. The other measure of average safety design, average NCAP score, had the same effect in the models and was collinear with the measure of average IIHS rating. Because both could not be included at the same time, the average IIHS rating was chosen because model fit was slightly better.

The method presented in this paper provides a resource to study the impact of year-to-year changes in factors known to impact fatalities. For vehicle manufacturers the models can be used to examine how vehicle fleet changes are influencing fatality counts in the context of other factors. For example, the models can be applied to estimate fatalities prevented if fleet turnover is accelerated given expected economic changes. This method can be further applied to study how fleet changes influence fatality counts in different crash segments (for example, intersection crashes, rural crashes) to identify opportunities for vehicle safety advancements or detailed follow-up studies.

The models are useful to policy- and decision-makers to identify opportunities for intervention. The resulting models can be applied to forecast future fatality counts, given that a known set of input parameters exists, on at a national level or by state. For example, the model can be applied to predict the number of deaths prevented if seat belt use increased to 95%.

An insignificant change, in a key factor will not contribute to a change in the number of traffic deaths. For example, because there were no changes in universal helmet laws between 2015 and 2016, there was no estimated contribution of this key factor to fatality counts.

Even proven effective countermeasures will not appear to have an impact on fatality counts unless their year to year change is significant. For example, one might expect that the belt use rate should have a large effect on the number of deaths occurring. While safety belts are proven effective in preventing fatalities, no significant change in the belt use rate has been observed in recent years (Enriquez and Pickrell, 2019). However, if safety belt use rates were to increase dramatically to, for example, 95% from their national average of 90%, the impact would be measurable.

The quality of these forecasting models relies on a number of critical factors. First, the data must be available and consistently collected per state for the full study period. A smaller number of training data points would degrade model performance. In many cases data have become available only recently (i.e. self-reported drunk driving), however no historical record exists in earlier years. Next, the homogeneity of each state becomes important for each factor sampled. Since a single value represents each parameter for each state and input year, we assume that this value appropriately represents that condition for the entire state. While this assumption is true in many ways, there are exceptions. For example, average precipitation may provide a useful metric for smaller states while large states may have widely varying conditions depending on the specific region. Depending on the population distribution, these region-specific disparities can be important. A third factor that impacts the quality of models is the representativeness of the data. For example, the model uses observed driver handheld device use as a surrogate for driver distraction. While the use of a handheld device certainly plays a role, it is not the only factor impacting the likelihood of distraction while operating a vehicle.

Finding a suitable measure for some factors was challenging and sometimes not available. In particular, measures of distracted driving, motorcycle helmet use, and speeding were difficult to obtain in a consistent way.

The models generated by this study provide a resource to study the impact of year to year changes in factors known to impact fatalities among passenger vehicle occupants, motorcycle riders and pedestrians.

Limitations

An important limitation of the current study is availability of direct measures to characterize important known risk factors including motorcycle helmet use, distraction, drunk driving and speeding.

In addition, in order to understand any relationship, the measure or a proxy must exist for each state and year. Forecasting the impact of factors that are not yet measurable is also not possible. For example, forecasting the impact of the newest emerging technologies is challenging because limited data exist.

The model examines the relationship of changes in factors with changes in fatality counts. Due to the quasi-experimental design, cause and effect cannot be inferred from the modeled relationships.

ACKNOWLEDGEMENT

This research was supported with funding from the Auto Alliance.

REFERENCES

[1] NHTSA, 2017. Traffic Safety Facts: 2016 Motor Vehicle Crashes: Overview. Washington, D.C.

[2] NHTSA, 2016. Traffic Safety Facts: 2015 Motor Vehicle Crashes: Overview. Washington, D.C.

[3] Kahane CJ (2000). National Highway Traffic Safety Administration. Fatality reduction by safety belts for front-seat occupants of cars and light trucks: updated and expanded estimates based on 1986-99 FARS data. U.S. Department of Transportation; Washington, DC. Publication no. DOT-HS-809-199. Available at http://www-nrd.nhtsa.dot.gov/Pubs/809199.PDF

[4] Fell JC, Beirness DJ, Voas RB, Smith GS, Jonah B, Maxwell JC, Price J, Hedlund J (2016). Can progress in reducing alcohol-impaired driving fatalities be resumed? Traffic Injury Prevention,17(8):771-781.

[5] Farmer CM, Lund AK (2015). The effects of vehicle redesign on the risk of driver death. Traffic Injury Prevention, 16(7):684-690.

[6] Leard B, Roth K (2016). Weather, traffic accidents, and exposure to climate change. Discussion Paper, Transportation Research Board, Washington, DC.

[7] Zlatoper (1991). Determinants of motor vehicle deaths in the United States: a cross-sectional analysis. Accident Analysis and Prevention,23(5):431-436.

[8] Enriquez, J., & Pickrell, T. M. (2019). Seat belt use in 2018 – Overall results. (Traffic Safety Facts Research Note. Report No. DOT HS 812 662). Washington, DC: National Highway Traffic Safety Administration

[9] Fell JC, Jones K, Romano E, Voas R. An evaluation of graduated driver licensing effects on fatal crash involvements of young drivers in the United States. Traffic Injury Prevention,12(5):423-31.

APPENDIX A: MEASURED KEY FACTORS TESTED AS EXPLANATORY VARIABLES IN THE MODELS

CATEGORY	VARIABLE	SOURCE
Weather	Annual Precipitation	National Oceanic and Atmospheric Administration
	Annual Average Temperature	National Oceanic and Atmospheric Administration
Urban/Rural	Urban VMT (million) per Capita	Federal Highway Administration (FHWA)
	VMT in Urban Areas	FHWA
	Urban VMT/Total VMT	FHWA
	VMT in Rural Areas	FHWA
	Rural VMT per Capita	FHWA
Social	Education Level: High School and Higher	United States Census (US Census)
	Police per Capita	US Census
Policies/Laws	Alcohol Policy	Governors Highway Safety Association
	GDL - strength of policy	Insurance Institute for Highway Safety (IIHS); strength based on [9]
	Universal Motorcycle Helmet Law	IIHS
Regulations	FMUSS 214 (side impact protection) implemented	NHTSA
	% of registered vehicles with ESC	R.L. Polk U.S. Vehicle registrations
Economy	Mean Travel Time to Work	US Census
	Gross Domestic Product	Bureau of Economic Analyses

CATEGORY	VARIABLE	SOURCE
	Gas Price per Gallon	Energy Information Administration (EIA)
	Poverty	US Census
	Employment Rate for People 65	US Census
	Population without Health Insurance (%)	US Census
	Average Gas Price per BTU	EIA
	Household Income	US Census
	Employment Rate	US Census
	No Health Insurance	US Census
Exposure	VMT	FHWA (Highway Statistics: 5.4.1. Vehicle-miles of travel, by functional system)
	Total Population	US Census
	Average Driving Minute per Capita per Day	American Time Use Survey
	Number of vehicles	R.L. Polk U.S. Vehicle registrations
	% Who Use Vehicle to Work (Alone)	US Census
	% Who Walk to Work	US Census
	Average Walking Minute per Capita per Day	American Time Use Survey
	Population Density	US Census
	Average Cycling Minute per Capita per Day	American Time Use Survey
	Average Driving Minute per Day for Driver 65	American Time Use Survey
	Total VMT (million) per Capita	FHWA (Highway Statistics: 5.4.1. Vehicle-miles of travel, by functional system)
Demographics	Population age 65 and over	US Census
	Race White%	US Census
	Male Ratio	US Census
	Median age of population	US Census
Car Safety	ESC % of Vehicles on Road	R.L. Polk U.S. Vehicle registrations
	Average IIHS Score	R.L. Polk U.S. Vehicle registrations/IIHS crashworthiness testing
	% of Vehicles with Electronic Stability Control	R.L. Polk U.S. Vehicle registrations
	Vehicle Age 90 Percentile	R.L. Polk U.S. Vehicle registrations
	Average NCAP Score	R.L. Polk U.S. Vehicle registrations/New Car Assessment Program
	Percent of Old Vehicles on Road	R.L. Polk U.S. Vehicle registrations
	Percent of New Vehicles on Road	R.L. Polk U.S. Vehicle registrations
	Average Vehicle Age	R.L. Polk U.S. Vehicle registrations
	Vehicle Age 50 Percentile	R.L. Polk U.S. Vehicle registrations
	Vehicle Age 10 Percentile	R.L. Polk U.S. Vehicle registrations
	Vehicle Age 25 Percentile	R.L. Polk U.S. Vehicle registrations
	Vehicle Age 75 Percentile	R.L. Polk U.S. Vehicle registrations
Vehicle Mass Disparity	Difference of 10th percentile and 90th percentile of Mass	R.L. Polk U.S. Vehicle registrations/NHTSA Safecar.com
	% of Vehicles Below the Bottom 10%	R.L. Polk U.S. Vehicle registrations/NHTSA Safecar.com

CATEGORY	VARIABLE	SOURCE
	National Mass	
	% of Vehicles Above the Top 10% National Mass	R.L. Polk U.S. Vehicle registrations/NHTSA Safecar.com
	Average Mass	R.L. Polk U.S. Vehicle registrations/NHTSA Safecar.com
	Standard Deviation of the Mass of Vehicles on Road	R.L. Polk U.S. Vehicle registrations/NHTSA Safecar.com
	Total % of Vehicles above and below the top 10% and bottom 10% National Mass	R.L. Polk U.S. Vehicle registrations/NHTSA Safecar.com
Belt Use	Self Report Rarely Belted %	Behavioral Risk Factor Surveillance System (BRFSS)
	Self Report NOT Always Belted %	BRFSS
	Self Report Always Belted % for Age 65	BRFSS
	Self Report Always Belted %	BRFSS
	Self Report Rarely Belted % for Age 20-	BRFSS
	Self Report Always Belted % for Age 20-	BRFSS
	Self Report Rarely Belted % for Age 65	BRFSS
	Observed Belted Rate	NOPUS
Alcohol/Drugs	Opioid Related Fatalities	Multiple Cause of Death File, Centers for Disease Control
	Beer Consumption (gallons of ethanol/capita)	National Institute of Alcohol Abuse and Addiction (NIAAA)
	All Beverage Consumption(gallons of ethanol/capita)	NIAAA
	Spirit Consumption(gallons of ethanol/capita)	NIAAA
	Wine Consumption(gallons of ethanol/capita)	NIAAA
	% who Report Binge drinking	BRFSS
	% Self Report Never Drunk Driving	BRFSS
	% Self Report Drunk Driving in Past 30 Days	BRFSS
	Self Report Binge Drinking in Past 30 Days % for Age 65	BRFSS
	Self Report Binge Drinking in Past 30 Days % for Age 20-	BRFSS
Distraction	Phone Subscribers per Capita	FCC (Voice Telephone Services Report) Additional Data
	Phone Subscribers	FCC (Voice Telephone Services Report) Additional Data
	Observed Driver Hand-held Device Use while driving	NOPUS

DISTRACTED DRIVING DETECTION USING ON-BOARD SENSORS

Shigenobu Saigusa
Honda R&D Americas, Inc.
United States of America

Paper Number 19-0148

ABSTRACT

The frequency of distracted driving and its impact on safety is rapidly become a serious social issue. Given that distracted drivers pose an increased crash risk not only to themselves, but also to other road users, it is important to investigate ways to address this growing issue. This research project aims to realize a real-time identification and detection system for distracted driving for use in real-world driving scenarios. Therefore, the main goal of this research is development of a real-time model using on-board sensors, to classify whether the driver of the leading vehicle is distracted or not. This research also investigates the typical types of distracted driving behavior that can be detected by host vehicles (depending on the available sensors) and their key characteristics on driving data pattern.

INTRODUCTION

Safe driving requires drivers' continuous attention on the roadways. Any activities that compete for the driver's attention while driving have the potential to degrade driving performance and can lead to serious consequences for driving safety (Bao et al. 2015; Klauer et al. 2006; Sussman et al. 1985). According to NHTSA data, 3,179 people were killed in crashes that involved distracted driving on the U.S. roadways, which accounts for 10% of all fatalities in 2014 (NHTSA 2015). In addition, 431,000 people were injured in crashes that involved distracted driving, which accounts for 18% of all injuries (NHTSA 2015). The NHTSA report (NHTSA 2015) also indicated that the percentage of fatal and injury crashes due to cell phone use continuously increased over the most recent 5 years, whereas the total number of distraction-affected fatal and injury crashes stayed relatively stable. For example, 2,843 fatal crashes associated with distraction occurred in 2010, among which the percentage of related cell phone use was 12%, whereas in 2013, the total number of distraction-affected fatal crashes was 2,910, and the percentage of related cell phone use in distraction-affected fatal crashes increased to about 14%.

Distracted driving has been an increasing social concern. One of the challenging topics in distracted driving research is to identify and detect distracted driving from surrounding vehicles in a real-world driving setting. With the rapid development of in-vehicle based sensors (e.g., radar and camera), this issue has brought more attention to the transportation safety society including government, OEMs and suppliers. Previous efforts led by Honda have been conducted to develop algorithms to detect and predict lead vehicle's driver states using data from host vehicle sensors (Figure 1). The objective of this study focuses on modifying and prototyping the online detection algorithms to identify distracted driving behaviors on straight road driving. We also developed a prototype system as a pilot test of online detection algorithms.

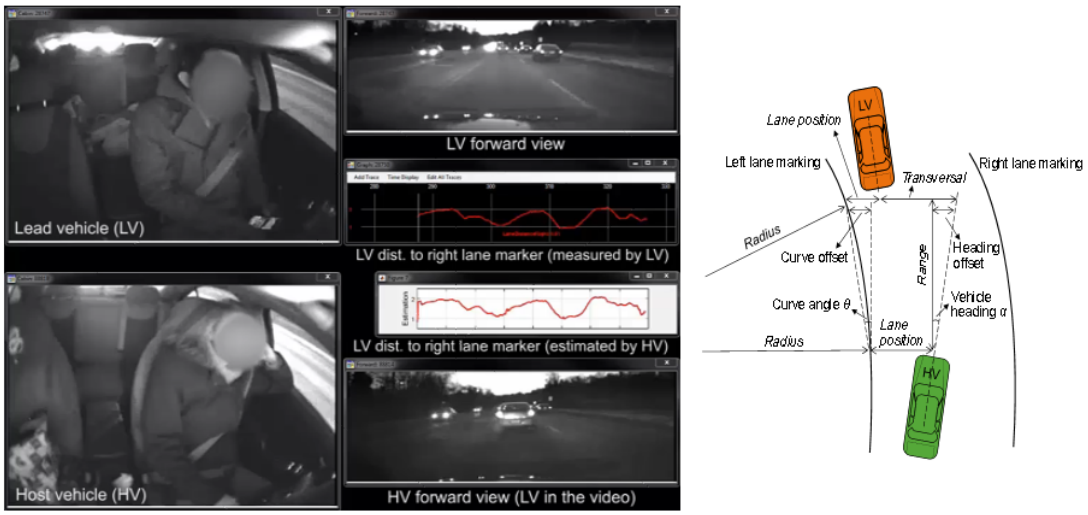

Figure 1. Lead vehicle distraction detection

LITERATURE REVIEW

In this section, a literature search and review was conducted to identify driver behavior models and parameter settings.

- Comparison and evaluation of advanced motion models for vehicle tracking: Schubert, R., Richter, E., & Wanielik, G. (2008, June). Comparison and evaluation of advanced motion models for vehicle tracking. In *Information Fusion, 2008 11th International Conference on* (pp. 1-6). IEEE.
    - The paper introduces 6 tracking models: CV (constant velocity), CA (constant acceleration), CSAV (constant steering angle and velocity). CTRV (constant turn rate and velocity), CTRA (constant turn rate and acceleration), CCA (constant curvature and acceleration) and show their relationship. It discusses 3 model fitting methods: Linear Kalman Filter, Extended Kalman Filter and Unscented Kalman filter. The extended Kalman Filter is the first-order approximation when the transition equation is not linear and the unscented Kalman Filter is the second-order approximation when the transition equation is not linear. In our work, we applied CV, CA and CTRA model. The CV model does not perform well but the CA and CTRA model are useful to detect the distraction driving behaviors. To fit the CA and CTRA model, the Linear Kalman Filter and Extended Kalman Filter are used.
- Two novel metrics for determining the tuning parameters of the Kalman Filter: Saha, M., Goswami, B., & Ghosh, R. (2011). Two novel costs for determining the tuning parameters of the Kalman Filter. *arXiv preprint arXiv:1110.3895*.
    - The paper shows a new approach to determine Q matrix in Linear Kalman Filter and Extended Kalman Filter. It defines J1, J2 as two metrics for determining Q matrix and also defines nq. These parameters are used to tune the Q matrix in Kalman Filters. As nq changes, the values of both J1 and J2 change between these limits of the number of measurements and 0. A large J1 indicates a sensitivity in the RMSE performance but this might also cause the filter to diverge while a large J2 indicates that the filter exhibits robustness for those combinations of the tuning parameters. In our work, we tried the novel metrics but they did not contribute in detecting distraction behaviors. We also tried to minimize RMSE for each of the tracking models but it could not make a fair comparison between these models. As a result, we decided to model the Q matrix based on physical knowledge and then fixed the parameters as the empirical values.

- Unscented Kalman filter design for curvilinear motion models suitable for automotive safety application: Tsogas, M., Polychronopoulos, A., & Amditis, A. (2005, July). Unscented Kalman filter design for curvilinear motion models suitable for automotive safety applications. In *Information Fusion, 2005 8th International Conference on* (Vol. 2, pp. 8-pp). IEEE.
    - The paper derives CTRA model and compares Unscented Kalman Filter with Extended Kalman Filter based on RMSE. In our work, we prefer Extended Kalman Filter rather than Unscented Kalman Filter for simplification.
- A comparative study of multiple model algorithms for maneuvering target tracking: Pitre, R. R., Jilkov, V. P., & Li, X. R. (2005, March). A comparative study of multiple-model algorithms for maneuvering target tracking. In *Proc. SPIE* (Vol. 5809, pp. 549-560).
    - The paper shows 7 multiple model algorithms: AMM (autonomous multiple model), GPB1 (first-order generalized Pseudo-Bayesian), GPB2 (second-order generalized Pseudo-Bayesian), Interacting MM, Reweighted MM, B-Best MM, Viterbi MM. It also compares different algorithms in a target tracking application. In our work, *w*e used AMM model to integrate different tracking models in the Extended Kalman Filter framework.
- An integrated solution for lane level irregular driving detection on highways: Sun, R., Ochieng, W. Y., & Feng, S. (2015). An integrated solution for lane level irregular driving detection on highways. *Transportation Research Part C: Emerging Technologies*, *56*, 61-79.
    - This paper proposes an integrated solution for the lane level irregular driving detection. Access to high accuracy positioning is enabled by GNSS and Inertial Navigation System (INS) integration using filtering with precise vehicle motion models and lane information. The detection of different types of irregular driving behavior is based on the application of a Fuzzy Inference System (FIS). The evaluation of the designed integrated systems in the field test shows that 0.5 m accuracy positioning source is required for lane level irregular driving detection algorithm and the designed system can detect irregular driving styles. In our work, the method is developed for the real road driving data instead of the simulation data. Also, our method does not require strict definitions of distraction behaviors.

METHOD

Our previous works from last years has three parts, one was to identify factors that contribute to distraction detection, the second part was to develop algorithms estimating lead vehicle trajectories by using host vehicle sensors (Feng, Bao, et al., 2017), and the third part was developing the algorithms to detect distracted driving. Table 1 summarizes the detection results from last year.

Table1. Summary of the results from last year work

Dataset	# of Events	Total Mileage	Time threshold	Detection rate	False alarm	False alarm rate
IVBSS (training set)	17	35.26	+-10s	71%	3	1 per 11.75 miles
Safe Pilot (test set)	32	131.85	+-20s	66%	15	1 per 8.79 miles

As the prediction accuracy reached about 66%, there were several limitations from the work last year:

- The previous algorithm (part 3) did not combine with the estimation algorithm (part 2);
- The output of prediction was binary, distracted or not (no probability of distraction);

- The detection rate was not high even in the training dataset;
- Only one test dataset was used for validation.

Based on previous work, the goals of the work of this year are centered on improving detection accuracy (probability based) and combining the lead vehicle trajectory estimation algorithm and distraction detection algorithms. Three models are used in the distraction detection algorithm development, Constant Velocity (CV), Constant Acceleration (CA), and Constant Turn Rate and Acceleration (CTRA) Model. A multiple model algorithm is then developed by integrating the results from the three models to find the best results (Figure 2). The final decision is based on the results from the integrated algorithms.

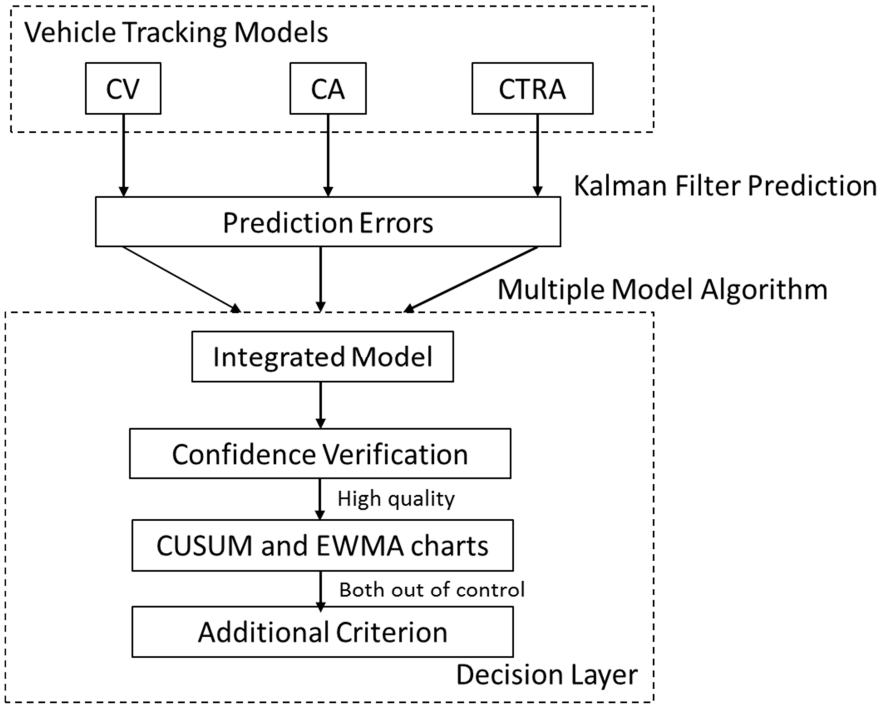

Figure 2. Flow chart of the distraction detection algorithm

KALMAN FILTER MODELING

Kalman Filter method was used to in all three models for the prediction purposes.

Vehicle tracking models

1. Constant Velocity model

We assume the vehicle speed is constant within each sampling interval $\Delta t = 0.1sec$ and use a four-dimensional state vector to formulate the transition equation as:

$$\begin{pmatrix} L_{x,k+1} \\ L_{y,k+1} \\ V_{x,k+1} \\ V_{y,k+1} \end{pmatrix} = \begin{pmatrix} 1 & 0 & \Delta t & 0 \\ 0 & 1 & 0 & \Delta t \\ 0 & 0 & 1 & 0 \\ 0 & 0 & 0 & 1 \end{pmatrix} \begin{pmatrix} L_{x,k} \\ L_{y,k} \\ V_{x,k} \\ V_{y,k} \end{pmatrix} + W = \begin{pmatrix} L_{x,k} + V_{x,k}\Delta t \\ L_{y,k} + V_{y,k}\Delta t \\ V_{x,t} \\ V_{y,t} \end{pmatrix} + W$$

.

where Lx, Ly, Vx and Vy denote longitudinal position, lateral position, longitudinal velocity and lateral velocity, respectively. The W is the process noise following a multivariate normal distribution with mean 0 and covariance matrix Q. The observed signal is denoted by Z, which is related to the state vector via:

$$Z_{k+1} = \begin{pmatrix} 0 & 0 & 1 & 0 \\ 0 & 1 & 0 & 0 \end{pmatrix} \begin{pmatrix} L_{x,k+1} \\ L_{y,k+1} \\ V_{x,k+1} \\ V_{y,k+1} \end{pmatrix} + U = \begin{pmatrix} V_{x,k+1} \\ L_{y,k+1} \end{pmatrix} + U$$

,

where U is the measurement error that follows a normal distribution with mean 0 and covariance matrix R. In other words, only longitudinal velocity and lateral position are observable.

2. Constant Acceleration model

We assume the vehicle acceleration is constant within each sampling interval. Therefore, we introduce 2 more dimensions to describe longitudinal (ax) and lateral accelerations (ay) besides the 4 dimensions in the CV model. The transition equation is written as:

$$\begin{pmatrix} L_{x,k+1} \\ L_{y,k+1} \\ V_{x,k+1} \\ V_{y,k+1} \\ a_{x,k+1} \\ a_{y,k+1} \end{pmatrix} = \begin{pmatrix} 1 & 0 & \Delta t & 0 & \frac{1}{2}\Delta t^2 & 0 \\ 0 & 1 & 0 & \Delta t & 0 & \frac{1}{2}\Delta t^2 \\ 0 & 0 & 1 & 0 & \Delta t & 0 \\ 0 & 0 & 0 & 1 & 0 & \Delta t \\ 0 & 0 & 0 & 0 & 1 & 0 \\ 0 & 0 & 0 & 0 & 0 & 1 \end{pmatrix} \begin{pmatrix} L_{x,k} \\ L_{y,k} \\ V_{x,k} \\ V_{y,k} \\ a_{x,k} \\ a_{y,k} \end{pmatrix} + W = \begin{pmatrix} L_{x,k} + V_{x,k}\Delta t + \frac{1}{2}a_{x,k}\Delta t^2 \\ L_{y,k} + V_{y,k}\Delta t + \frac{1}{2}a_{y,k}\Delta t^2 \\ V_{x,k} + a_{x,k}\Delta t \\ V_{y,k} + a_{y,k}\Delta t \\ a_{x,k} \\ a_{y,k} \end{pmatrix} + W$$

where W is the process noise. Longitudinal velocity and lateral position are the only observable signals, therefore the observation vector Z is written as:

$$Z_{k+1} = \begin{pmatrix} 0 & 0 & 1 & 0 & 0 & 0 \\ 0 & 1 & 0 & 0 & 0 & 0 \end{pmatrix} \begin{pmatrix} L_{x,k+1} \\ L_{y,k+1} \\ V_{x,k+1} \\ V_{y,k+1} \\ a_{x,k+1} \\ a_{y,k+1} \end{pmatrix} + U = \begin{pmatrix} V_{x,k+1} \\ L_{y,k+1} \end{pmatrix} + U$$

,

where U is the measurement error.

3. Constant Turn Rate and Acceleration model

This model can only be used for fitting straight road driving data because the road direction information is not available. The longitudinal acceleration and turn rate are assumed constant. The state vector is $\boldsymbol{x}_{t+1} = [x, y, \theta, v, \omega, a]^T$ representing longitudinal position, lateral position, and vehicle heading angle, longitudinal velocity, yaw rate and longitudinal acceleration, respectively. The transition equation is modelled by a transition function f:

$$\boldsymbol{x}_{t+1} = f(\boldsymbol{x}_t) + u, u \sim N(0, Q);$$

where u is the process noise. The transition function f is calculated according to the physical laws as:

$$
\begin{aligned}
x_{t+\Delta t} &= x_t + \frac{v_t}{\omega_t}(sin(\theta_t + \omega_t \Delta t) - sin(\theta_t)) + \frac{a_t \Delta t}{\omega_t} sin(\theta_t + \omega_t \Delta t) - \frac{a_t}{\omega_t^2} cos(\theta_t) + \frac{a_t}{\omega_t^2} cos(\theta_t + \omega_t \Delta t) \\
y_{t+\Delta t} &= y_t + \frac{v_t}{\omega_t}(cos(\theta_t) - cos(\theta_t + \omega_t \Delta t)) - \frac{a \Delta t}{\omega_t} cos(\theta_t + \omega_t \Delta t) + \frac{a_t}{\omega_t^2} sin(\theta_t + \omega_t \Delta t) - \frac{a_t}{\omega_t^2} sin(\theta_t) \\
\theta_{t+\Delta t} &= \theta_t + \omega_t \Delta t \\
v_{t+\Delta t} &= v_t + a_t \Delta t \\
\omega_{t+\Delta t} &= \omega_t \\
a_{t+\Delta t} &= a_t
\end{aligned}
,
$$

which is a nonlinear function of the state vector. The Extended Kalman Filter approximates the transition function f by using its Jacobian matrix J, where

$$
J = \begin{pmatrix}
1 & 0 & a_1 & a_2 & a_3 & a_4 \\
0 & 1 & a_5 & a_6 & a_7 & a_8 \\
0 & 0 & 1 & 0 & \Delta t & 0 \\
0 & 0 & 0 & 1 & 0 & \Delta t \\
0 & 0 & 0 & 0 & 1 & 0 \\
0 & 0 & 0 & 0 & 0 & 1
\end{pmatrix}
$$

and a's are partial derivative of f with respect to each dimension of the state vector x. This approximation yields $\boldsymbol{x}_{t+1} \approx J\boldsymbol{x}_t + u$. The longitudinal velocity, lateral position and yaw rate are observable on each sampling point. Therefore, we write the observation vector Z as:

$$
\boldsymbol{z}_{t+1} = H\boldsymbol{x}_{t+1} + r = \begin{pmatrix} y_{t+1} \\ v_{t+1} \\ \omega_{t+1} \end{pmatrix} + r, r \sim N(0, R).
$$

Here $H = \begin{pmatrix} 0 & 1 & 0 & 0 & 0 & 0 \\ 0 & 0 & 0 & 1 & 0 & 0 \\ 0 & 0 & 0 & 0 & 1 & 0 \end{pmatrix}$ and r denotes the measurement error.

4. Kalman Filter algorithm

Let X denote the state vector, F denote the transition matrix and Q denote the process noise. The objective of the Kalman Filter is to predict the distribution of X at time k with information from time 1 to k-1 and fit the distribution of X at time k given information from time 1 to k. In the prediction step, we have:

$$
\hat{X}_{k|k-1} = F\hat{X}_{k-1|k-1}
$$

and

$$
P_{k|k-1} = FP_{k-1|k-1}F^T + Q,
$$

Where $\hat{X}_{k|k-1}$ and $P_{k|k-1}$ denote the predicted mean and covariance at time k given information from time 1 to k-1, respectively. We then obtain the pre-fit residuals by comparing the predicted signals with observed signals:

$$
\tilde{Y}_k = Z_k - H\hat{X}_{k|k-1}
.
$$

The corresponding covariance matrix for the pre-fit residuals is calculated as:

$$
S_k = R + HP_{k|k-1}H^T
.
$$

We calculate the optimal Kalman gain and obtain the post-fit distributions by including the information of the observation at time k:

$$K_k = P_{k|k-1} H^T S_k^{-1},$$

$$\hat{X}_{k|k} = \hat{X}_{k|k-1} + K_k \tilde{Y}_k,$$

$$P_{k|k} = (I - K_k H) P_{k|k-1}.$$

The post-fit residual is calculated as $\tilde{y}_{k|k} = Z_k - H\hat{X}_{k|k}$ accordingly.

Kalman Filter parameters

1. R matrix for measurement error

The measurement errors of different signals are assumed independent of each other. The R matrix for different models are hence assumed diagonal matrix with each diagonal element representing the variance of measurement errors of the corresponding signals. In our model, we need to specify the variance of measurement errors of all observable signals, which are longitudinal velocity, lateral position and yaw rate. At the current stage, they take empirical values as 0.01, 0.45 and 0.1.

2. Q matrix for process noise

The process noise is the signal magnitude that is omitted in the transition model. The derivation requires the assumption that the acceleration and yaw rate are random variables within the sampling interval. Specifically, they are assumed to be follow a normal distribution with known mean and variance. In the CV model, we assume the longitudinal and lateral acceleration independently follow normal distribution with mean zero and variance $\sigma_{a,x}^2$ and $\sigma_{a,y}^2$. The Q matrix is derived by comparing CV model with the model with random accelerations, which is:

$$Q_{CV} = \begin{pmatrix} \frac{1}{4}\Delta t^4 \sigma_{a,x}^2 & 0 & \frac{1}{2}\Delta t^3 \sigma_{a,x}^2 & 0 \\ 0 & \frac{1}{4}\Delta t^4 \sigma_{a,y}^2 & 0 & \frac{1}{2}\Delta t^3 \sigma_{a,y}^2 \\ \frac{1}{2}\Delta t^3 \sigma_{a,x}^2 & 0 & \Delta t^2 \sigma_{a,x}^2 & 0 \\ 0 & \frac{1}{2}\Delta t^3 \sigma_{a,y}^2 & 0 & \Delta t^2 \sigma_{a,y}^2 \end{pmatrix}.$$

Similarly, we derive the Q matrix for CA and CTRA model as:

$$Q_{CA} = \begin{pmatrix} \frac{1}{4}\Delta t^4 \sigma_{a,x}^2 & 0 & \frac{1}{2}\Delta t^3 \sigma_{a,x}^2 & 0 & \frac{1}{2}\Delta t \sigma_{a,x}^3 & 0 \\ 0 & \frac{1}{4}\Delta t^4 \sigma_{a,y}^2 & 0 & \frac{1}{2}\Delta t^3 \sigma_{a,y}^2 & 0 & \frac{1}{2}\Delta t \sigma_{a,y}^3 \\ \frac{1}{2}\Delta t^3 \sigma_{a,x}^2 & 0 & \Delta t^2 \sigma_{a,x}^2 & 0 & \Delta t \sigma_{a,x}^2 & 0 \\ 0 & \frac{1}{2}\Delta t^3 \sigma_{a,y}^2 & 0 & \Delta t^2 \sigma_{a,y}^2 & 0 & \Delta t \sigma_{a,y}^2 \\ \frac{1}{2}\Delta t \sigma_{a,x}^3 & 0 & \Delta t \sigma_{a,x}^2 & 0 & \sigma_{a,x}^2 & 0 \\ 0 & \frac{1}{2}\Delta t \sigma_{a,y}^3 & 0 & \Delta t \sigma_{a,y}^2 & 0 & \sigma_{a,y}^2 \end{pmatrix},$$

$$Q_{CTRV} = G \begin{pmatrix} \sigma_a^2 & 0 \\ 0 & \sigma_\omega^2 \end{pmatrix} G^T,$$

$$G = \begin{pmatrix} a_4 & a_3 \\ a_8 & a_7 \\ 0 & \Delta t \\ \Delta t & 0 \\ 0 & 1 \\ 1 & 0 \end{pmatrix}$$

These Q matrices are determined by the standard deviation of longitudinal acceleration, lateral acceleration and yaw rate. Those values are pre-specified based on empirical knowledge, which are 0.3, 0.1 and 0.1, respectively.

Multiple model algorithm

The purpose of using multiple model algorithm is to switch between different tracking models to guarantee the tracking accuracy. The distraction behaviors are detected when none of the models provides an acceptable tracking accuracy. We integrate multiple models based on the residual likelihood. Because the pre-fit residual in a Kalman Filter follow normal distribution with mean 0 and known covariance matrix $S_k^{(i)}$. The likelihood is calculated as the density of the multivariate normal distribution:

$$L_k^{(i)} = f(\tilde{Y}_k^{(i)})$$
$$\tilde{Y}_k^{(i)} = Z_k^{(i)} - H\hat{X}_{k|k-1}^{(i)}$$
$$S_k^{(i)} = HP_k^{(i)}H^T + R \quad ,$$

where i represents the model index (i=1: CV, i=2: CA, i=3: CTRA). Normalizing the likelihood yields weight coefficients for each of the tracking model:

$$w_k^{(i)} = \frac{L_k^{(i)}}{\sum_{j=1}^{3} L_k^{(j)}} \quad .$$

The overall post-fit state vector is then calculated as the weighted average of the post-fit state vector of each of the tracking models as:

$$\hat{X}_{k|k} = \sum_{i=1}^{3} w_k^{(i)} \hat{X}_{k|k}^{(i)} \quad .$$

Control chart methods

1. CUSUM chart for prediction error monitoring

Signal patterns during abnormal driving periods cannot be well explained by the known physical models. We would like to relate the abnormal driving periods with high prediction errors from the fused vehicle tracking models obtained from the multiple model algorithm. Consequently, monitoring the variance of the prediction errors using CUSUM control chart helps detect the distraction behaviors. To calculate the variance, we set the window size as 10, which is to make decision for each consecutive 10-time points. The monitoring statistics are calculated as below:

$$v_i = \frac{\sqrt{|(\tilde{Y}_i - \mu_0)/\sigma|} - 0.822}{0.349} \sim N(0,1)$$
$$\bar{v}_i = \frac{1}{\sqrt{10}} \sum_{t=i+1}^{i+10} v_t \sim N(0,1)$$
$$S_i^+ = \max\{0, \bar{v}_i - k + S_{i-1}^+\}$$
$$S_i^- = \max\{0, -\bar{v}_i - k + S_{i-1}^-\}$$

Here, we set k = 0.5. According to the CUSUM control chart method, a time window is detected whenever the value S_i^+ is greater than the threshold H = 5.

2. EWMA chart for lane offset monitoring

Besides monitoring the error variance, we suggest monitoring the mean shift of lane offset signal at the same time. The lane-offset data is not normally distributed. EWMA control chart is recommended because it is less sensitive to the normality of the data. The monitoring statistic and the control limits are calculated as follows. Similar as CUSUM chart, the decision is made for each 10-time points. A time window is detected whenever the value Z_i is smaller than LCL_i or it is greater than UCL_i.

$$X_i: \text{ lane offset signal}$$

$$Z_0 = \bar{X}_{1:n}, n = 10$$

$$Z_i = \lambda \bar{X}_{(n-1)i+1:ni} + (1-\lambda) Z_{i-1}$$

$$\lambda = 0.2,\ L = 3$$

$$CL_i = 0$$

$$UCL_i = L\sigma\sqrt{\frac{\lambda}{2-\lambda}[1-(1-\lambda)^{2i}]}$$

$$LCL_i = -L\sigma\sqrt{\frac{\lambda}{2-\lambda}[1-(1-\lambda)^{2i}]}$$

Detection decision:

1. Combine CUSUM chart and EWMA chart

CUSUM chart monitors the variance of the prediction errors. It detects the time windows when the driving pattern is not predictable by the fused vehicle-tracking model. False alarms are generated if only CUSUM chart is used and the vehicle is waving around the center lane. EWMA chart monitors the mean shift of the lane-offset signal. It detects the time windows when the vehicle is off the center of the lane. False alarms are triggered if only EWMA chart is used and the driver has a habit of driving close to one of the lane edges. Therefore, we detect a time window if and only if the monitoring statistics are out of the control limits in both the control charts.

2. Evaluate distraction severity

We evaluate the distraction severity using distraction levels defined as below:

- Level = 0.5: EWMA chart generates alarms
- Level = 0.6: CUSUM chart generates alarms
- Level = 0.7: Both the charts generate alarms
- Level = 0.8: Both the charts generate alarms in consecutive two points (2 seconds)
- Level = 0.9: Both the charts generate alarms in consecutive three points (3 seconds)

We generate a distraction alarm for a time window when its distraction severity level is labeled as 0.9. To avoid the circumstances when the algorithm keeps generating alarms, we reset the monitoring statistics to zero in the next time window if a distraction alarm is triggered.

3. Mute the algorithm in special cases

The algorithm is designed for detecting the distraction behaviors during straight road driving only. It is muted in the following cases.

- Lane change: Lane change behaviors give rise to non-continuous lane offset signal patterns, which trigger false alarms. The algorithm is muted whenever a lane change behavior is detected.

- Curve driving: CTRA model cannot track the vehicle when it is in curves unless the vehicle's heading signal is given. When the vehicle's heading signal is not available, we have to assume the vehicle heading is as same as the lane heading, which implies that the algorithm only performs well during straight road driving periods. We mute the algorithm when the lane radius is smaller than 0.00015 meter.
- Low signal quality: the algorithm does not work when the signal measurements or estimation are not reliable. A frequent seen circumstance is that the lane boundary cannot be captured by camera.

RESULTS

When combining the leading vehicle estimation algorithm with the online detection algorithm, we only need to replace the measured signals Z as the estimated signals and change the corresponding observation errors to the estimation errors. The standard deviation of the estimation errors are estimated from the straight road driving segments when the leading vehicle is paired with the host vehicle. It is calculated as the sample variance of the differences between the estimated signals and the measured signals. Table 2. Summaries the detection results from different datasets. A relative high accuracy detection rate was observed.

Table 2. Prediction results summary

#	Dataset	Distracted	Curvature	Lane Change	Paired	Detection	False Alarm	Time between alarm (min)
1	IVBSS	No	Yes	No	No	NA	0/692s	NA
2	IVBSS	Yes	No	Yes	No	6/7	3/470s	2.6
3	IVBSS	No	Yes	Yes	No	NA	47/3880s	1.4
4	Safe Pilot	Yes	Yes	Yes	Yes	4/6	20/2924s	2.4
5	Safe Pilot	No	No	No	No	NA	0/762s	NA

Distracted: whether cell phone uses are observed in the video.

Curvature: whether curvy road segments are included during the trip.

Lane change: whether lane change behaviors are observed during the trip.

Paired: whether a host vehicle and a leading vehicle are paired to test the estimation algorithm.

Detection: detection rate (# of detections / # of total distraction behaviors).

False alarm: false alarm rate (# of false alarms / total driving time in second)

1. IVBSS Training Dataset

Description: This dataset is used to estimate the parameters in the Kalman Filter. No distracted behaviors are included during the trips.

- Parameters: (Trained in IVBSS Training Dataset)
- Standard deviation of observation error of Velocity: 0.45 m/s
- Standard deviation of observation error of Lane Offset: 0.01 m
- Standard deviation of observation error of Yaw Rate: 0.1 degree/s
- Standard deviation of longitudinal acceleration during cruise control: 0.3 m/s2

- Standard deviation of lateral acceleration during cruise control: 0.1 m/s2
- Standard deviation of angle acceleration during straight road driving: 0.1 degree/s2
- Standard deviation of prediction error of Lane Offset from Kalman Filter: 0.0523 m

2. IVBSS Distracted Driving Dataset

Description: Seven events are included in the dataset, each of which has a distraction period. The objective is to detect the distraction behavior during the period.

Parameters: (Trained in IVBSS Training Dataset) Same as 1

3. IVBSS Baseline Driving Dataset for Evaluating the False Alarm Rate (column 8 in the table)

Description: It is used to test the false alarm rate of the purposed algorithm.

Parameters: (Trained in IVBSS Training Dataset) Same as 1

4. Safe Pilot Distracted and Paired Driving Dataset

Description: Both the estimation algorithm and the detection algorithm are tested in the dataset. The estimated signals trigger slightly more false alarms than the directly measured signals. The standard deviations of the estimation errors are estimated based on the driving segments when both the lane quality and estimation confidence are high. In addition, we do not have the estimated yaw rate signal and therefore use the measured signal instead.

Parameters: (Trained in IVBSS Training Dataset and Safe Pilot Paired Driving Dataset)

- Standard deviation of estimation error of Velocity: 0.41 m/s
- Standard deviation of estimation error of Lane Offset: 0.49 m
- Standard deviation of estimation error of Yaw Rate: 0.1 degree/s
- Others: Same as 1

5. Safe Pilot Baseline Driving Dataset for Evaluating the False Alarm Rate (column 8 in the table)

Description: The dataset is used to evaluate the false alarm rate of the detection algorithm. As a result, no false alarm is triggered.

Parameters: (Trained in IVBSS Training Dataset) Same as 1

Table 3. Result comparison between the old and new algorithms

Method	Straight road only?	Length of test events	Paired cases?	Detection Rate	False Alarm Rate
Old	No	Approximately 7032s	No	68%	18/7032s (exclude vehicle passing)
New	Yes	8036s	Yes	77%	70/8036s (include vehicle passing)

CONCLUSIONS

In this work, an integrated multiple models was developed and applied. Control charts were used in the online detection decision. Results showed that a higher prediction accuracy and higher false alarm rate were observed, when compared to the results from previous work (Table 3). Methods and results from this work have provide a promising way and framework to the distracted driving detection. One limitation of this work is that only straight road driving was considered. Future work should be conducted to include curve road driving and how to reduce the false alarm rate.

REFERENCES

[1] Bao S, Guo Z, Flannagan C, Sullivan J, Sayer JR, LeBlanc D. Distracted driving performance measures: spectral power analysis. *Transp Res Rec.* 2015;2518:68–72.

[2] Klauer SG, Dingus TA, Neale VL, Sudweeks JD, Ramsey DJ. The Impact of Driver Inattention on Near-Crash/Crash Risk: An Analysis Using the 100-CarNaturalisticDriving StudyData. Springfield,VA:Virginia Tech Transportation Institute; 2006. DOT HS 810 594.

[3] NHTSA. 2015. Driver Electronic Device Use in 2014. 2015.Washington, DC.DOT HS 812 197.

[4] Sussman ED, BishopH,Madnick B, Walter R. Driver inattention and highway safety. Transp Res Rec. 1985;1047:40–48.

Occupant Injuries Related to Rollover Crashes and Ejections from Recent Crash Data

Jingshu Wu, PhD, Stephen Summers, Stephen Ridella, PhD, Ellen Lee, Thomas Kang, James Myers
National Highway Traffic Safety Administration (NHTSA), Washington, DC
Paper No. 19-0153

ABSTRACT

The goal of this paper is to determine the recent annual occupant populations and trends related to rollover injuries and fatalities, and to assess the risk factors that may have significantly contributed to occupant injuries and fatalities when rollovers and ejections occur. Fatality Analysis Reporting System (FARS) 2004-2017 data were used to obtain the recent occupant fatalities related to rollovers and ejections. National Automotive Sampling System (NASS) – Crashworthiness Data System (CDS) 2013-2015 weighted survey data were used extensively to estimate the occupant injury severities and occupant ejection details associated with rollovers. For rollover cases, the injured body regions (e.g., head, neck, shoulder and back, and chest) and injury contact sources (e.g., vehicle roof, side door, or seat back) were investigated in detail. This study paid close attention to the interaction between the vehicle roof and occupant injuries for the consideration of the requirements from Federal Motor Vehicle Safety Standards (FMVSS) 216a and 226. Finally, occupant injury risk and key risk factors were evaluated using methods of relative risk, including multiple logit model and case-control study. The data analysis using FARS showed a decrease in annual fatalities from approximately 10,500 during 2004-2006 to approximately 7,000 during 2014-2017. Approximately one thirds of all occupant fatalities of light passenger vehicles (Gross Vehicle Weight Rating, GVWR <=10,000 lbs.) are related to rollovers. FARS data also provided the occupant ejection status (complete or partial ejection) and ejection path associated with rollovers. The CDS data indicated that rollovers are strongly associated with the injury sources of vehicle roof, side doors, and seat back/support; rollover crashes also resulted in primarily the injured body regions of head, neck, shoulder/back, and chest. The occupant ejection paths are usually side windows and roof opening. The analytical results also revealed that light trucks /vans, with relatively higher centers of gravity, tend to have relatively higher likelihood of rollover crashes than passenger cars, but passenger cars tend to result in a higher rate of occupant serious injuries (Maximum Abbreviated Injury Scale 3+, or MAIS 3+) than light trucks/vans, if rollovers did occur. Overall this study explored the trends and annual occupant populations related to rollovers and ejections using recent traffic data. Logistic regression model was used, with considerations of multiple risks and confounding factors, to predict the occupant injury relative risks of several key risk factors simultaneously. The analytical results using both FARS and CDS indicated that higher occupant injury risks were especially associated with higher delta-V, unbelted occupant, rollover, ejection, side impact, and older occupant age. This study, utilizing the recent crashes from three main databases of FARS, NASS CDS and NASS General Estimates System (GES), may enrich the understanding of rollover and ejection related occupant injuries.

1. INTRODUCTION AND DATA

National Highway Traffic Safety Administration (NHTSA) has been working constantly to improve vehicle safety and reduce traffic injuries. The total traffic fatalities (including occupants, pedestrians and cyclists) for the past few years are 32,744 in 2014, 35,806 in 2015, and 37,461 in 2016 (approximately 37,133 in 2017 from the recent release). Approximately two-thirds of all traffic fatalities are from the occupants killed of light passenger vehicles (cars and light trucks /vans with GVWR less than 10,000 lbs.), furthermore, approximately one-thirds of those occupant fatalities of light passenger vehicles come from rollover crashes. Vehicle rollover is a very risky crash mode that causes severe injuries to occupants, especially to the head, shoulder & back, face, neck and chest from contacts between occupants and vehicle roofs and side doors, or from ejection out of vehicles.

Rollover crashes have previously been identified by NHTSA as a high safety priority, and work has been done investigating potential countermeasures [1, 2, 3, 4, 5]. Recently enacted FMVSS (and now fully implemented), such as FMVSS 126 (Electronic stability control systems for light vehicles), FMVSS 216a (Roof crush resistance) and FMVSS 226 (Ejection Mitigation), have sought to reduce the incidence of rollovers, improve vehicle crashworthiness during rollovers and reduce the likelihood of ejections during rollovers. Thus, it is of interest to update the previous understanding on rollovers and injury risk, with different vehicles ages and newer data.

Data sources for this study include FARS (which contains a census of all vehicle fatalities), and the two data systems of NASS, e.g., CDS and GES. The general trends of crashes of all vehicle types and injuries of all person types can be obtained from GES, on the other hand, CDS will be most extensively used throughout this study for occupant injury details associated with light passenger vehicles. CDS data have previously been used by many NHTSA researchers to investigate crash injury details and risk factors, such as weighting factor designs of survey data, vehicle damage areas (frontal crash or side impact), occupant seating position and belt use, delta-V, occupant injured body regions, the vehicle components that contacted the occupants within a crashed vehicle, and occupant injuries and time to medical treatments [6, 8, 9, 10, 11, 12, 19]. A similar approach is used for the current research.

CDS contains several independent data files that describe vehicle crashes and occupant injury details. The data file of 'General Vehicle' (GV) provides the crash details related to the towed crashed vehicles (i.e., vehicle type, model year, vehicle weights, delta-V, crash type and rollover status). The data file of 'Occupant Assessment' (OA) provides the occupant information (e.g., occupant age, gender, belt use, drinking status, seating position, ejection and ejection area, injury scales, or MAIS). Similarly, the 'Occupant Injury' (OI) data file provides detailed injured body regions (e.g., head, face, AIS scale, and others) and injury sources of vehicle components (roof, door, B-pillar, seat back, or others). The 'Vehicle External' (VE) file provides the principal crash damage areas (e.g., frontal damage, or side damage, useful for identifying the crash directions and crash modes), and 'Accident' (ACC) data file has information about crash location, road, weather, and case number. Starting in 2009, the CDS system collected crash data only from newer vehicles of age <=10 years old only. Therefore, for this research, the vehicle age was limited to within ten years for most analysis (crash year – model year <= 10). The primary CDS data files related to vehicle crash types and occupant injuries, e.g., 'GV', 'OA', 'VE', 'ACC', or 'OI', can all be sorted and merged together by using 'crash year, PSU, case number, vehicle number, and occupant number'. Statistical Analytical System (SAS) procedures of '*sort*' and '*merge*' are used to sort and link the data files of research interest together for this data flow-chart design. SAS version 9.3 was used for this study. [16, 17]

A detailed flowchart of using CDS data, described in Figure 1, provides the overall approach to examine the research questions. For example, merged "GV+OA" data by using 'crash year, PSU, case number, and vehicle number', with auxiliary information of vehicle external (VE) damages, can answer the questions related to overall occupant fatality and injury, vehicle damage areas, rollover, and occupant seating and maximum occupant injuries (MAIS). In the final step, the correlations, between the occupant injuries and several main independent risk factors, are examined using multiple regression model.

The objectives of this study are to continue the earlier injury research efforts and better understand the injury causes related to rollovers and ejections. Some questions of special interest, step-by-step, are summarized as follows:

- How many occupants (drivers and passengers) of light vehicles died from rollover crashes? FARS data provide complete descriptions of fatalities related to rollovers and ejections.
- How many vehicles (passenger cars and light trucks/vans not more than 10,000 lbs.) are involved in rollover crashes annually? Both GES and CDS data can provide estimates of rollover incidence.
- How many occupants are injured from rollovers annually? CDS data will be used to look at detailed injury severities associated with various vehicle types and crash modes.
- What body regions are commonly injured in rollovers (e.g., an occupant may suffer injuries in several body regions)? What are the most prevalent injury sources (e.g., vehicle roof, side door, B-pillar) that contact occupants in rollovers?
- If rollover and ejection occur, what are the common ejection paths (e.g., roof opening or side windows)?
- If there is an interaction between the vehicle roof and occupant, what are the common injured occupant body regions (e.g., head, neck, spine)?
- More generally, if rollovers, either lateral or longitudinal crashes, and other risk factors are considered simultaneously, what are the relative risks from each factor (e.g., comparing the injury odds of rollover versus non-rollovers, belted vs. not-belted occupants)? This study explores this question using a multiple regression model.
- Finally, FMVSS 216a and 226 have certain impacts on vehicle rollovers /ejections, especially for vehicle models after 2011. This study explores the effect of vehicle age (<=2, <=4, and <=10 years old, respectively), and uses recent CDS data from the past ten years.

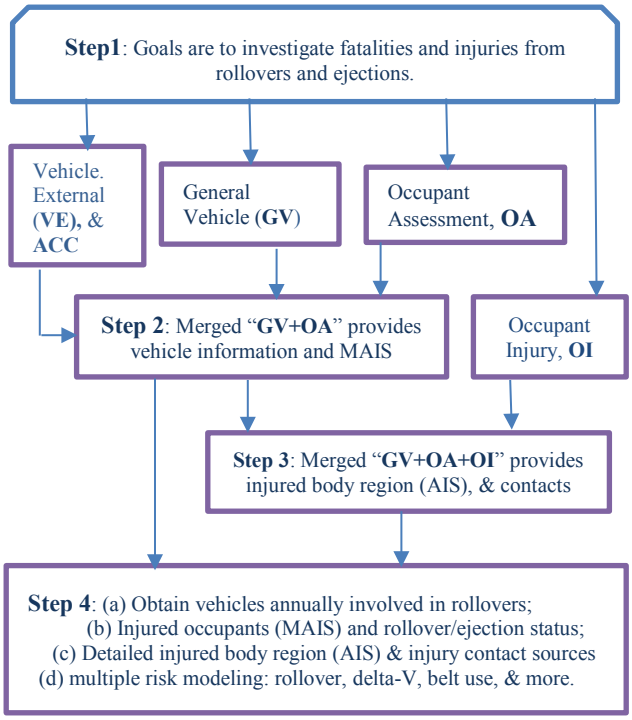

Figure 1: *Data Flow-Chart for obtaining Occupant Injuries related to Rollover and ejection using CDS Data*

A similar but much simpler flow-charts, using FARS or GES data files of 'Accident', 'Vehicle', and 'Person', can be done as Figure 1.

2. OCCUPANT FATALITIES RELATED TO ROLLOVERS AND EJECTIONS

FARS is a census of fatalities resulting from all types of crash modes. Three main data files, 'Accident', 'Vehicle', and 'Person', from the FARS database are used in this analysis. Several variables in FARS are of special interest, such as 'rollover', 'ejection', 'ejection path', and 'injury severity', and these key variables are used to answer various research questions.

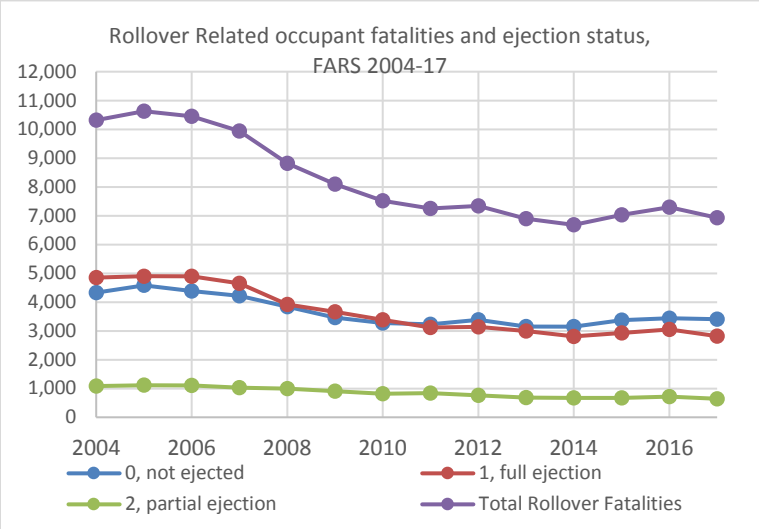

Figure 2: *Rollover-crash related occupant fatalities and ejection status (FARS 2004-2017, car or light truck/van GVWR <=10,000 lbs.)*

Figure 2 provides the rollover-related fatality 14-year trends using FARS 2004-2017 for occupants of light passenger vehicles (cars and light trucks/vans GVWR <= 10,000 lbs.). The total occupant fatalities due to rollover crashes decreased from 10,627 in 2005, to a lower 6,681 in 2014, and then slightly increased to approximately 6,933 in 2017. The annual average of rollover-related occupant fatalities was 8,227 during 2004-2017. Figure 2 shows the ejection status of either 'not ejected', 'partial ejection', or 'full ejection' out of all rollover-related occupant fatalities, and the occupant fatalities include the occupants (driver or passenger) in the motor vehicles-in-transport only (not including the vehicles-not-in-transport).

For passenger cars and light trucks /vans, the percentage (%) of rollover-related occupant fatalities among all occupant fatalities dropped from the high peak of approximately 35% during 2008-09 to the lower values of approximately 31% in 2016 and 30% in 2017, and this percentage decreasing trend was especially obvious during 2011-2017, as shown as Figure 3. The extensive efforts for higher fitment of vehicle stability control and stronger roof designs may have helped to reduce the rollover-related fatality percentage during recent years. [1, 3]

Vehicle rollovers often result in occupant ejections. Figure 4 shows ejection paths of light passenger vehicle occupants during rollovers. The average number of occupant fatalities during ejections out of the roof opening (sunroof, moonroof or others) is 87 during the 14 years of 2004-2017, but this number is higher, 97 and 109, in 2015 and 2016, respectively. Figure 4 also indicates that the 'side windows' are the most frequent ejection path, with an average of 773 fatalities during 14 years. The highest number of fatalities from side window ejection occurred in 2005 (1064), while the lowest occurred in 2016 (593) and in 2017 (576). The occupant fatalities associated with various known ejection paths (e.g., side windows, roof, etc.) are approximately 15% of rollover-related fatalities (unknown ejection paths are commonplace and FARS data contain complete fatalities but only partial injuries).

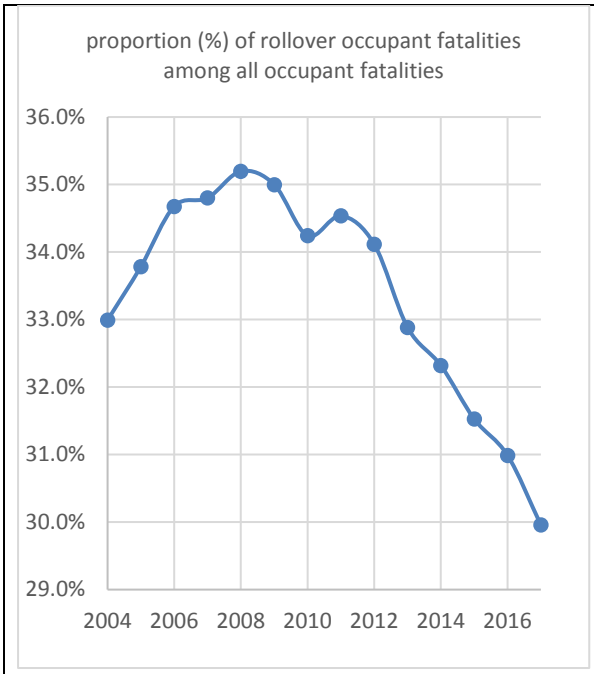

Figure 3: *Proportion (%) of occupant fatalities related to rollover crashes among all occupant fatalities (FARS 2004-17, passenger cars and light trucks/vans GVWR <=10,000 lbs.)*

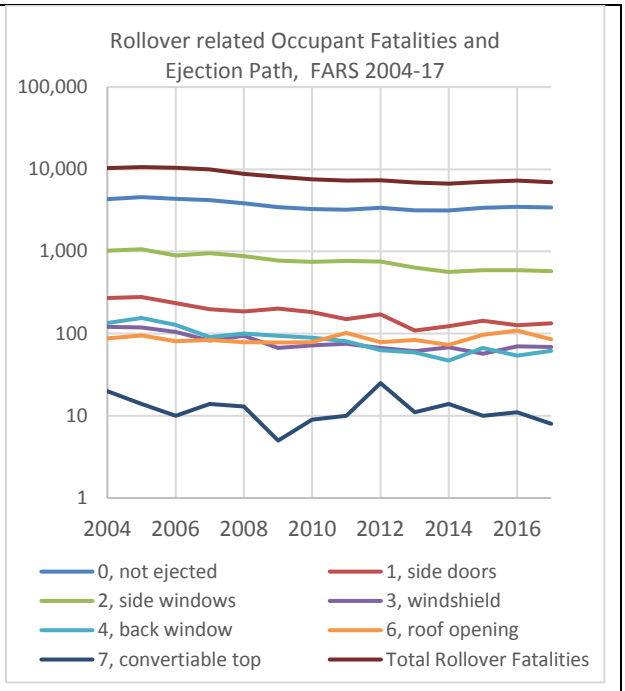

Figure 4: *Ejection paths of occupant rollover fatalities among occupant fatalities (from FARS 2004-2017, for light passenger vehicles <=10,000 lbs.)*

When rollovers occur, belt or restraint use is critically important to occupant safety. Although FARS does not contain details of specific injuries, the data clearly indicate the belt effect by relative comparison of injuries of 'unbelted' occupants versus the 'belted' (Table 1). In Table 1, the unbelted group has a fatal incidence of 70,796/105,521 = 67.1%. However, in the belted group, the fatal incidence is 33,423/84,441 = 39.6%.

Table 1: *Belt use status and occupant fatalities related to rollover crashes (light passenger vehicles GVWR <=10,000 lbs., FARS 2004-2017)*

Belt status	Fatal Injury	Not fatal	Total Occupants
Unbelted	70,796	34,725	105,521
Belted Occupants	33,423	51,018	84,441

Hence, the relative risk (RR) of fatal injury when unbelted versus belted is 0.671/0.396=1.7; and the fatality Odds Ratio (OR) of unbelted versus the belted is 3.1. The interpretation is that an unbelted occupant's odds of fatality are approximately 3 times compared with the belted occupant, if a rollover occurred. In this comparison, only one risk factor (belt use) is considered without considering other risk factors. Similar two-by-two table can be made for heavier vehicles with GVWR over 10,000 lbs. If multiple risk factors of belt use, occupant age, travel speed (crash severity, or delta-V), and rollover are considered simultaneously, a multiple regression approach is discussed in section 5.

3. ROLLOVER TREND FROM GES

To examine how many vehicles are involved in rollovers annually, GES 2006-15 weighted data from 36 Primary Sampling Units (PSU) can provide more general annual trends and populations of crashes of various vehicle types and injuries of all person types. The weighted annual averages of light vehicles and other vehicle types, if involved in rollover crashes during 2006-2015, are listed as Table 2.

Table 2*: Weighted Annual Vehicle Types Involved in Rollover Crashes (GES 2006-15, including all model years)*

Year	combination truck	Single unit truck	bus	car & light truck /van
	GVWR >10,000 lbs.			<=10,000 lbs
2006	9,769	5,645	55	251,543
2007	9,461	5,385	111	263,058
2008	7,303	4,307	67	248,543
2009	6,333	3,117	0	213,675
2010	6,344	2,916	17	189,445
2011	6,343	2,722	233	184,867
2012	8,124	4,442	229	196,236
2013	7,046	3,809	139	184,082
2014	9,047	4,030	20	199,734
2015	6,909	4,698	0	193,349
Total	76,678	41,070	871	2,124,530

The weighted averages of light passenger vehicles (GVWR <=10,000 lbs.) involved in rollovers from GES data may be used as a reference to the similar rollover results from CDS data. [6, 7]

4. ROLLOVER AND INJURED OCCUPANTS FROM CDS

CDS data, that are survey data from 24 PSU and focused on the crashes of light passenger vehicles (GVWR not more than 10,000 lbs.), include details of occupant injuries and vehicle crash conditions. Recent CDS data (from 2013-2015 mainly) are used in this study to explore occupant injuries from rollover crashes. In CDS, occupant injuries are coded using AIS, a numerical scale system by Association for the Advancement of Automotive Medicine (AAAM) to rate

the injury severity (e.g., AIS 0=not injured, 1=minor injury, 2=moderate injury, 3=serious injury, 4=severe injury, 5=critical injury, 6=maximum injury or fatal, 7=injured but severity unknown), although a high percentage of AIS codes are missing or unknown. In CDS data, each occupant injury is assigned an AIS severity level and each injured body region has a maximum severity AIS injury level within that body region. Also, one value of overall Maximum AIS (e.g., MAIS, the maximum AIS severity from all body regions) for each occupant, hence, each occupant has one count of MAIS and may have several regional AIS results. The data flow-chart of Figure 1 is used extensively for CDS data analysis, this flow-chart analyzed the 'top-down' data structure in CDS and searched the vehicle crashes and occupant injury details from 'Accident' to 'Vehicle', then to 'Occupant', and finally 'Injured Body Region' or 'Contact Source' were searched. All listed results are from weighted data calculations (Tables 3-7 and Figures 5-15).

CDS survey data are associated with weighting factor for each crash, the general 'weighted population mean', $\bar{y}$, is defined by following formula: [6, 8, 13]

$$\bar{y} = \frac{\sum_{i=1}^{n} \omega_i y_i}{\sum_{i=1}^{n} \omega_i} \qquad \text{Eq. (1)}$$

where 'y_i' is the value of 'i-th' unit or crash, and 'ω_i' is the weighting factor associated with 'i-th' unit or crash. The weighting factors in CDS came from the three-stage sampling designs, in which the selection of each PSU among 24 PSUs, the probability of crashes selected by police in each PSU, and the selections of various crash severities /types were considered statistically, stage-by-stage. [6, 8]

4.1 Cars and Light Trucks Involved in Rollovers and Occupant Injury Comparison

First, overall numbers of vehicles (passenger cars and light trucks) involved in 'rollover' crashes or 'non-rollover' crashes were obtained. 'Rollovers' were further categorized as "side rollovers 1-3 quarter", "side rollover >=4 quarters" (quarter refers to number of quarter turns during the rollover, each quarter is 90 degrees of revolution), and "end to end rollover /tilt"; non-rollover crashes were categorized as single vehicle plane damaged (front damage, side damage, rear damages or top/under damage), or multiple vehicle planes damaged, as described in Figure 5 and Table 3. Secondly, the number of occupants injured from passenger cars and light trucks was determined, from both rollover and non-rollover crashes (Table 4).

During the years of 2013-2015, approximately 161,000 (annual weighted average including all model years) passenger cars and light trucks were involved in rollover crashes, and rollover crashes comprised approximately 6% of all crashed vehicles of approximately 2.7 million annually, shown in Table 3. Furthermore, Table 3 shows that passenger cars experienced a smaller percentage of rollover crashes (3.7%) among all car crashes than the light trucks (10.3%).

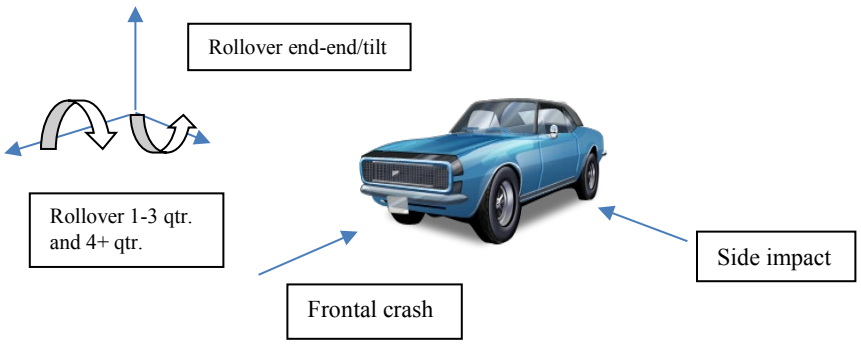

Figure 5: *The rollover types of light passenger vehicles (car or light truck/van in CDS, GVWR <=10,000 lbs.)*

***Table 3**: Annual weighted averages of passenger car and light truck/van crash types ('Rolled' and 'non-Rolled', CDS 2013-2015, GVWR <=10, 000 lbs.*)

Crash Types of Passenger Cars	**Crash Modes of Light Trucks/Vans**
Rollovers 1-3 Quarter: 48,063 Rollovers 4+ Quarter: 19,050 Rollovers end-end: 815 **Total Rolled Cars: 67,928**	Rollovers 1-3 Quarter: 53,225 Rollovers 4+ Quarter: 39,188 Rollovers end-end: 641 **Total Rolled Trucks: 93,054**
single front damage: 229,309 single side damage: 76,927 single rear-damage: 4,796 single top/under damages: 9,904 multiple front damage: 807,459 multiple side damage: 407,182 multiple rear-damage: 194,483 multiple top/under damages: 1,948 **Total non-Rolled Cars: 1,732,008**	single front damage: 103,484 single side damage: 25,215 single rear damage: 529 single top/under damage: 1,636 multiple front damage: 416,958 multiple front damage: 190,947 multiple front damage: 69,461 multiple front damage: 527 **Total non-rolled Trucks: 808,757**

It is known that light trucks or vans, in general, have higher centers of gravity than passenger cars, and Table 3 using CDS 2013-2015 indicated that light trucks or vans tend to rollover more frequently than passenger cars.

The occupant injury rates from passenger cars and light trucks/vans were different, too, which shared the similar trends as vehicle crash data of Table 3. From a perspective of injured occupants within light passenger vehicles, Table 4 indicates that passenger car occupants (injured or not) involved in rollovers count approximately 3.4%, or 83,917 divided by (83,917+2,359,792) of all car crash occupants; while the light truck/van occupants involved in rollover crashes count approximately 10.3%, or 134,146 divided by (134,146+1,170,789). All model years of light vehicles were included in Tables 3, 4.

***Table 4:** Annual weighted Averages of Occupant Injuries (MAIS) of Light Passenger Vehicles (CDS 2013-15, Rollover, 'R', vs. Non-Rollover, 'N')*

Car Occupant Injuries (by MAIS)							
	unknown	MAIS=0	1	2	3 -6	7	Total
R	39,137	16,295	19,557	4,438	2,813	1,676	83,917
N	1,059,612	834,998	347,400	65,381	19,987	32,414	2,359,792
Light Truck/Van Occupant Injuries (by MAIS)							
	unknown	MAIS=0	1	2	3 -6	7	Total
R	90,526	11,923	24,608	3,460	3,037	591	134,146
N	564,165	440,081	128,403	22,698	6,178	9,263	1,170,789

Passenger car occupants are more likely to be seriously injured when in a rollover crash, compared with a non-rollover. Table 4 indicates that approximately 2,813 car occupants are seriously injured (MAIS =3,4,5,6) in rollover crashes annually (weighted data of MAIS 3=1948, MAIS 4=479, MAIS 5=212, MAIS 6=174), which is 4.2% of the total number of injured car occupants in rollovers (MAIS not 0, or 67,622 annually). For non-rollover crashes, approximately 19,987 car occupants are seriously injured (MAIS = 3,4,5,6) (14,532 + 3737 + 1169 + 549), or only 2.7% of all injured car occupants (MAIS not 0, or 730,708 annually) of non-rollover cars. Hence, rollover crashes usually result in more serious injuries than other crash types for car occupants.

For light trucks/vans, seriously injured occupants (MAIS =3,4,5,6) make up of 2.5% of all injured occupants in rollovers (MAIS not 0). For non-rollovers, seriously injured occupants (MAIS = 3,4,5,6) of light trucks/vans are only 0.85% of all injured light truck occupants (MAIS not 0). Thus, in rollover crashes, light truck/van occupants (2.5%) have lower serious injury rate than car occupants (4.2%). This injury severity difference may possibly be due to smaller head room in cars compared with light truck/vans, meaning that the occupant head and /or neck may be more likely injured from contacting the roof in a car. Occupant contacts and injury sources will be examined using CDS

data in a subsequent section of this study. The difference between roof designs and roof strengths associated with car and light truck/van may also contribute to the occupant injury severities, [2, 5] and more future research may shed a light on this challenging topic.

4.2 Rollovers and Ejection Areas of Light Passenger Vehicle Occupants

Since 2009, CDS data collected the crashes from vehicle age<=10 only, hence, the sample sizes could be smaller after 2008. [8] Figure 6 provides yearly trends of occupant injuries (MAIS 2-7) including all vehicle ages and vehicle age <=10 years old, respectively. This study also focuses on the crash data of recent years, 2013-2015.

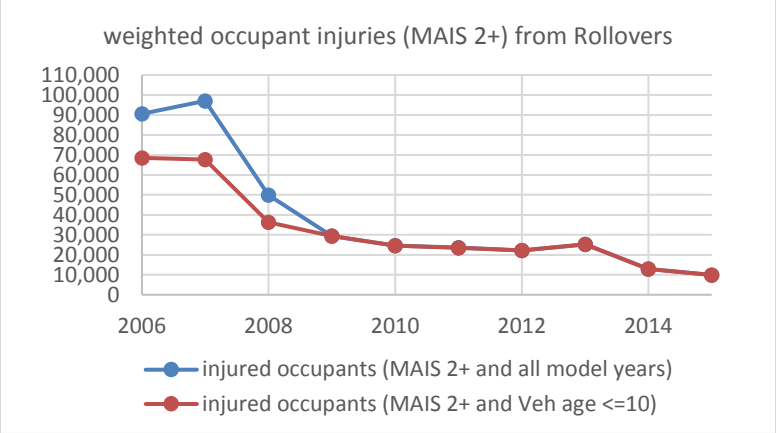

Figure 6: *Weighted occupant injuries (MAIS 2+) related to rollovers (CDS 2006-2015 light passenger vehicles including all model years, and vehicle age <=10, respectively)*

As discussed previously, rollovers are usually associated with occupant ejections. Figure 7 shows annual averages of ejection areas related to rollovers (CDS 2013-2015 including all vehicle model years and occupant injury levels). Occupants were more frequently ejected from the front side windows (left or right) and roof opening. In CDS 'OA' data file, there are four variables that are insightful to rollover and ejection details - 'ejection' (partial or full ejection status), 'ejection area' (windshield, left or right front, or roof, and 'ejection area' in CDS data is similar to the variable of 'ejection path' in FARS data), 'ejection medium' (non-fixed roof, fixed or non-fixed glazing, or integral structure), and 'entrapment' (entrapped or not, jammed door/fire). [20, 21] This paper will not include all related data explorations due to the paper size limit. All CDS data analysis included the occupants who were within the rolled vehicles or ejected, only Table 6 focused on the ejected occupants of rolled vehicles. Also, the CDS analytical results including AIS2+ could have much larger sample sizes than the similar results including AIS 3+ only, and the missing or unknown AIS, ejection status, and several key variables are still commonplace.

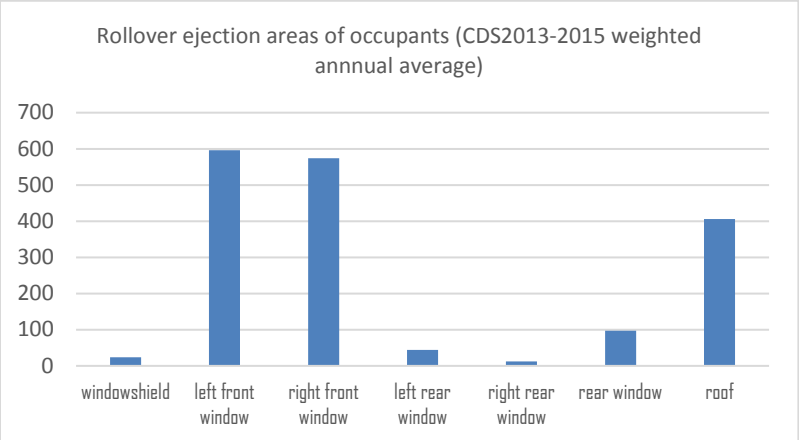

Figure 7: *Annual weighted average of ejection areas related to rollovers (CDS 2013-2015 light passenger vehicles with all model years)*

4.3 Injured Body Regions and Vehicle Contacts Related to Rollovers

When occupants are involved in rollover crashes, they are most frequently injured in the body regions of head, neck, and chest. [2, 3] CDS data of Occupant Injury (OI) contain very detailed descriptions of injured body regions and injury contact sources of vehicle components. Again AIS, a numerical scale system by AAAM to rate the injury severity, is used here to describe the injured body regions. 'OI' data file is merged together with general vehicle (GV) and occupant assessment (OA) data especially during 2013-15 (Figure 1). This study intends to explore several questions about rollover crashes and related injuries: one question may be what are the commonly injured body regions (head, face, chest or others)? What are common injury sources of vehicle components (e.g., roof, door, B-pillar) that contact the occupant in rollovers?

For rollover crashes (including vehicle age <=10 years old), the main injured body regions (AIS 2+) are head, chest, shoulder and back, and neck (Figure 8).

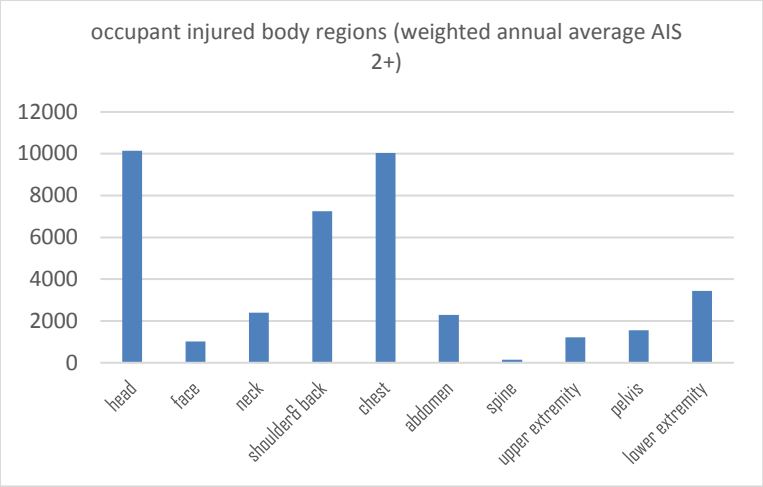

Figure 8: *Annual weighted average of injured body regions (AIS 2+) due to rollovers (vehicle age <=10 years, CDS 2013-2015)*

When a vehicle is involved in a rollover crash, some vehicle components are more likely to contact the occupants (driver and passenger), and these vehicle components become so called 'injury contact sources'. The main injury sources associated with AIS 2+ injuries in rollover crashes are roof, left side door/interior, instrument panel and seat back, as indicated by Figure 9.

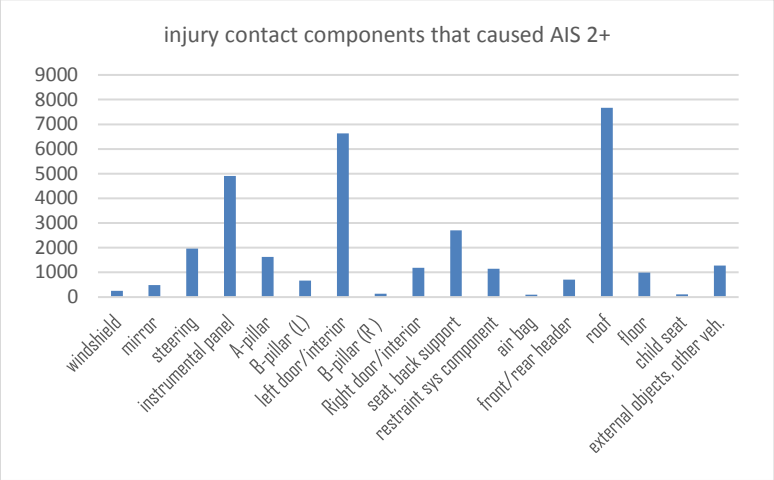

Figure 9: *Annual weighted average of injury vehicle component sources that caused AIS 2+ from rollovers (vehicle age <=10 years), CDS 2013-2015*

4.4 Injured Body Regions by Roof Contact Only Associated with Rollover

Injuries caused by the interaction between occupants and the vehicle roof only, when rollovers occurred, are of special interest in this study. Figure 10 shows the weighted average of injured regions, especially three body regions of head, neck, and shoulder /back, due to contacting the roof during rollovers (vehicle age <=10 years and AIS 2+, CDS 2013-2015). The interaction odds between the roof and head were especially high if a rollover crash did occur.

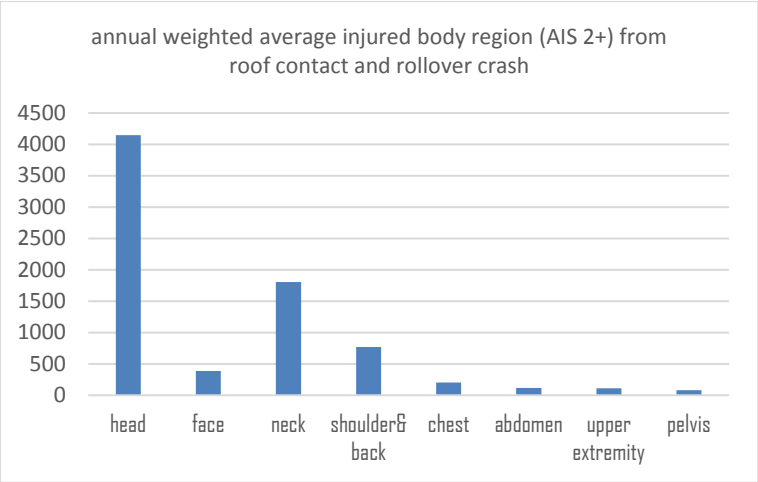

Figure 10: *Annual weighted average of injured regions due to contacting roof only of rolled vehicles (vehicle age <=10 years and AIS 2+, CDS 2013-2015)*

If additional years are included and CDS 2006-2015 data are used, Figure 11 shows that if the roof was the injury source and rollover occurred, the main injured body regions are head, neck, shoulder/back, and face. CDS 2006-2015 data provide a yearly trend of roof caused injured body regions when the vehicles were involved in rollover, where vehicle age, determined by (crash year – model year), is limited not more than ten years old. The weighted annual averages of injured body regions were lower during 2013-2015 than the similar averages of 2006-2009. This study also explored AIS results related to rollovers /ejections with vehicle age under 3-4 years only, but the sample sizes were small especially during 2011-2015 (not listed in this study).

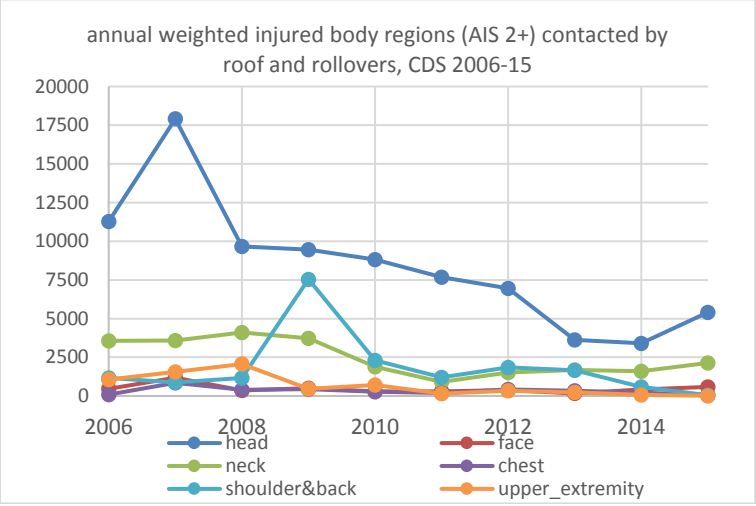

Figure 11: *Annual weighted injured body regions (AIS 2+) related to rollover crashes and roof contact only (vehicle age <=10 years, CDS 2006-15)*

5. ANNUAL TREND OF ROLLOVER INJURIES AND MULTIPLE RISKS

This section explored the yearly trends of rollover-related occupant injuries using CDS 2006-2015. In this trend analysis, MAIS is used to describe the overall maximum severity injury sustained by an occupant during 10-year span. Then a more general correlation investigation of occupant injuries is done by a multiple regression approach, when various risk factors, including rollover, side or longitudinal impact, delta-V, occupant age and belt use, are considered, simultaneously.

5.1 Occupant Injury Yearly Trend from Rollovers

The injured occupants involved in the rollover crashes per year, using MAIS versus calendar year during ten years (CDS 2006-2015), is shown as Table 5 and Figure 12, where only vehicle ages <=10 years old are included. It can be observed that the weighted injured occupants decrease after 2009, the injured occupant number could be even smaller, if only newer vehicles of vehicle ages not older than 4, or 2 years old are included.

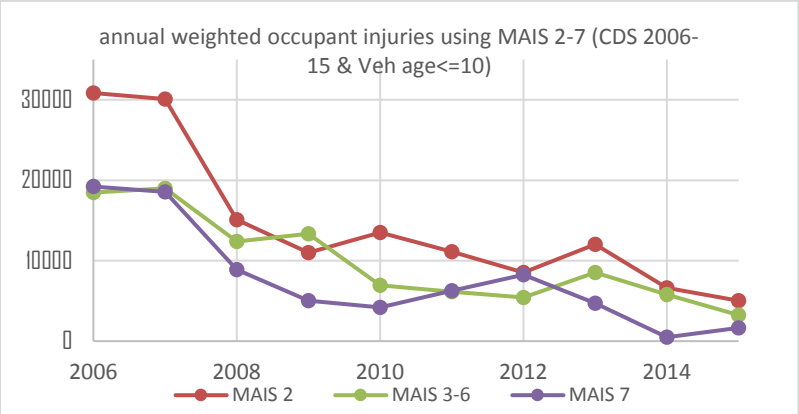

Figure 12: *Annual weighted occupant injuries (MAIS) related to rollovers crashes (CDS 2006-2015 including vehicle age <=10 years only)*

Table 5: *Weighted annual averages of occupant MAIS from rollovers crashes (CDS 2006-15 including vehicle age <=10 years only)*

YEAR	MAIS 1	MAIS 2	MAIS 3-6	MAIS 7
2006	102,036	30,839	18,478	19,210
2007	132,423	30,069	18,984	18,568
2008	125,774	15,106	12,383	8,873
2009	58,890	10,989	13,342	5,043
2010	54,688	13,515	6,916	4,174
2011	38,965	11,128	6,144	6,273
2012	35,849	8,529	5,439	8,235
2013	35,557	12,022	8,529	4,694
2014	71,256	6,622	5,776	483
2015	25,684	5,021	3,237	1,626

Table 6: *annual weighted injuries (MAIS) of both "rolled vehicle and ejected occupant" (CDS 2006-15 and vehicle age <=10 years only)*

YEAR	MAIS 1	MAIS 2	MAIS 3-6	MAIS 7
2006	2022	3325	9159	1996
2007	4751	2930	8412	1835
2008	3416	4409	4868	344
2009	2469	1118	3682	409
2010	2256	1746	2852	300
2011	301	722	2462	169
2012	595	504	1406	118
2013	350	521	1997	252
2014	966	186	331	93
2015	69	678	970	709

Table 5 provides the annual weighted occupant MAIS results including vehicle age <=10 years old. If newer vehicle models are preferred with the consideration of FMVSS 216a and 226, the similar occupant MAIS tables, including vehicle age <=4, and <=2 years old, respectively, are listed in Table 5b and 5c in Appendix.

Occupants involved in a rollover crash, and who were also ejected, are shown in Table 6 (with much fewer occupants than Table 5), and Table 6 provides MAIS for each year (CDS 2006-15, and vehicle ages<=10 years old). The ejection rates of occupants of rolled vehicles were related to their MAIS levels: the MAIS 3-6 group had the highest ejection

rate of 36% approximately, the ejection rate for MAIS 2 was 11% approximately, while MAIS 1 had the lower rate of 2.5% (from Tables 5, 6).

Furthermore, if rollover crashes occurred, following Figures 13-14 show the annual injured occupant body regions (AIS 2+) using weighted CDS data during 2006-2015. It can be observed that head and shoulder /back injuries are most frequent, together with other injured body regions of face, neck, chest, upper and lower extremity areas.

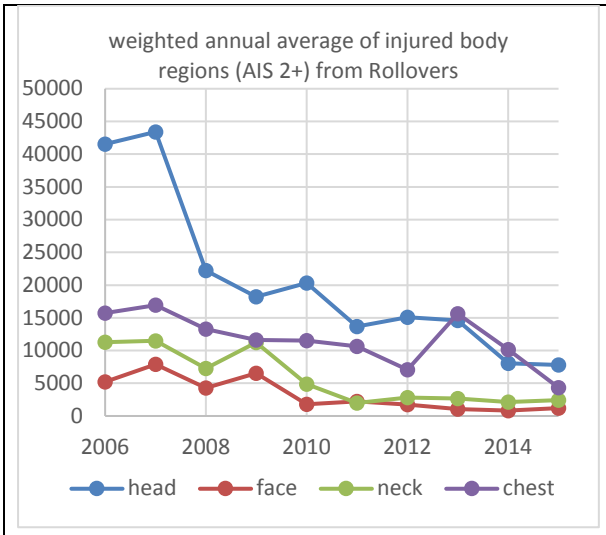

Figure 13: *Annual weighted average of injured body regions (AIS 2+) related to rollover crashes (vehicle age <=10 years, CDS 2006-2015)*

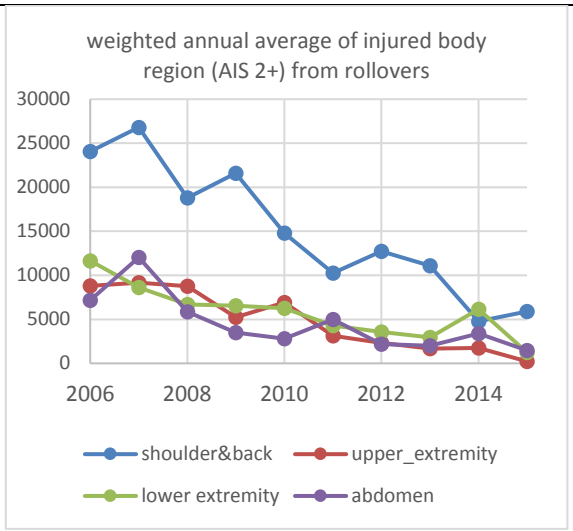

Figure 14: *Annual weighted injured body regions (AIS 2+) related to rollover crashes (vehicle age <=10 years, CDS 2006-2015)*

5.2 Occupant Injury Modeling with Consideration of Multiple Risks Simultaneously

The goal here is to establish a correlation between the occupant injuries (the outcome) and some contributing risk factors (the independent variables). The risk factors may include various crash types (rollover, side or longitudinal impact), delta-V, belt use and others. Many risk factors contribute to occupant injuries simultaneously, and some factors are more significant than others. Most CDS data are categorical data and are convenient to use for logistic regression. The logit model explores the relative risk of two different crash conditions and the impact from each risk factor on occupant injury severities. Some variables in CDS can be treated as binary data, e.g., injured body regions of AIS being '3, 4, 5, 6' were treated as 'serious and fatal injury' case (or '1', dependent variable), while AIS (0, 1, 2, 7) as not-serious case (or '0', dependent variable). Similarly, the common independent factors in the logit model include 'rollovers, or 1' vs. 'not-rollover, or 0', front seating occupant vs. rear-seating, side impact vs. frontal crash. This study also explored the effect of vehicle age on occupant injuries, and vehicle age is determined by (crash year – model year). The regression modeling intended to consider the impacts on occupant injuries from main risk factors, although not all factors can practically be included in this modeling. The modeling data came from CDS 2006-15, including any crash types, all AIS levels, and vehicle age <=10 years.

Several references provide excellent introduction to logistic regression and categorical data analysis.[13 14 17] Statistical correlation between the outcome and the independent variables is described as Eq. (2), from this correlation modeling it is possible to compare the occupant injury severity odds ratios (OR) between two very different crash conditions – for example, these include comparing the effects between rollovers versus not-rollovers; higher Delta-V (>35 MPH) versus lower delta-V; 'not-belted' occupants versus 'belted' occupants; furthermore, to compare side crashed vehicle with frontal crashed one; to compare smaller vehicle size (<3,000 lbs.) with the relatively larger sizes; or to compare older occupant (>65 years old) vs. the younger. This multiple regression model considers the effects of these primary eight risk effects on occupant injuries, simultaneously, as Eq. (2):

$$\ln\left(\frac{p}{1-p}\right) = \beta_0 + \beta_1 VehAge + \beta_2 DeltaV + \beta_3 VehSize + \beta_4 Belt + \beta_5 Rollover + \beta_6 DamageArea + \beta_7 Seating + \beta_8 OccupAge \qquad (2)$$

In Eq. (2), '*ln*' is the natural log sign, 'p' is the probability of 'occupant serious injury (AIS =3,4,5,6)', and '$\frac{p}{1-p}$' is the odds of 'occupant serious injury' versus 'not serious injury'. This statistical modeling, using SAS procedure of '*SurveyLogistic*' [16, 17] that considers the PSU and sampling weights, provides the serious injury odds ratio (OR) results from eight risk factors, as summarized in Figure 15 and Table 7. Missing data are included and SAS procedures usually handle the missing data reasonably well. The large percentage of unknown or missing AIS could make it challenging to build a correlation model. The receiver operating characteristic (ROC) curve is used to give a measure of the predictive accuracy of a logistic regression model, and ROC curve displays the sensitivity and specificity of the model. The area under the ROC curve, measured by 'c statistic', is still relatively low (0.68), and future correlation modeling of using more complete AIS information and with more than eight independent risk factors in Eq. (2) may be desired.

Data Interpretation of Table 7 or Figure 15:
Results indicate that higher occupant serious injury risks are significantly associated with rollover crashes, OR=1.74 (95% confidence interval 1.31 to 2.31, with a significant p-value of 0.0001), e.g., the occupants of rollover vehicles would be 74% more likely seriously injured (AIS 3+) when compared with the occupants of not-rolled vehicles. Similarly, higher injury risk is associated with higher delta-V (>35 MPH, OR=5.59), 'not-belted' (OR=3.26, 95% confidence interval 2.63 to 4.04), side crash (OR=1.54), and older occupant age (OR=2.69). On the other hand, older vehicles (>4 years), seating row, and smaller vehicle size (under 3,000 lbs.) did not have significant impact on occupant injuries (with p-values more than 0.05). Figure 15 clearly indicates that three highest risk factors come from higher Delta-V >35 MPH (driving speed or crash severity), 'not using belt , and old occupants, and rollover crash is also a significant risk factor.

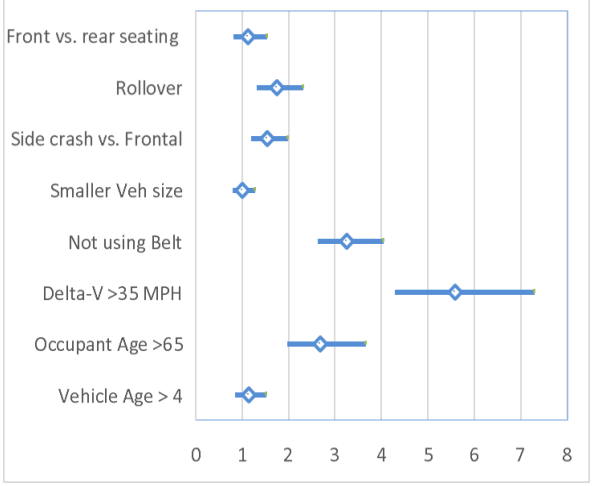

Figure 15: *Odds Ratios (Means and 95% Confidence Intervals) of Occupant Serious Injury (AIS 3+), including several risks simultaneously (CDS 2006-15 vehicle age <=10)*

Table 7*: Odds Ratios (means and 95% Confidence Intervals) of Occupant Serious Injuries (CDS 2006-2015 including vehicle age <=10)*

Effect	Point Estimate	95% Wald Confidence Limits		p-Value
Vehicle Age > 4	1.136	0.849	1.522	0.3910
Occupant Age >65	2.686	1.969	3.664	<.0001
Delta-V >35 MPH	5.591	4.282	7.299	<.0001
Not using Belt	3.257	2.625	4.041	<.0001
Smaller veh size	1.004	0.788	1.279	0.9748
Side impact vs. Frontal crash	1.543	1.197	1.990	0.0008
Rollover	1.740	1.308	2.314	0.0001
Front vs. rear seating	1.123	0.815	1.546	0.4778

6. CONCLUSIONS AND DISCUSSIONS

FARS and CDS data systems were used to explore the occupant injuries related to vehicle rollover crashes and occupant ejections, while GES vehicle data could also be used as a reference to CDS data. This data analysis used a simple approach of 'step-by-step' approach – e.g., from annual occupant fatalities in FARS data to the vehicles involved in rollovers in both GES and CDS data; from the rollover-related occupant injuries with overall MAIS to the detailed injured body regions (AIS) and injury contact sources (roof or side doors). Finally, this study viewed occupant injuries from a bigger picture by considering multiple risk factors simultaneously. Some key findings from this study are –

- The FARS data indicated annual rollover-caused fatalities decreased from around 10,500 in 2004-2006 to approximate 7,000 in 2014-2017, approximately one thirds of all occupant fatalities of light passenger vehicles are from rollover crashes, but the percentage of rollover-related occupant fatalities among all occupant fatalities

dropped sharply during 2011-2017. The number of both rollover and ejection-caused fatalities decreased from approximately 6,000 in 2004-2006 to 3,600 in 2014-2017. The occupant fatalities associated with various known ejection paths (e.g., side windows, roof, etc.) were approximately 15% of rollover-related occupant fatalities.

- CDS 2013-2015 weighted survey data showed approximately 161,000 light vehicles (cars and light trucks/vans, GVWR <=10,000 lbs.) were involved in rollovers (similarly, GES data were also used to estimate the rolled vehicles), and approximately 190,000 occupants of light passenger vehicles were injured (MAIS 1+) annually related to rollovers.
- Rollover crashes tend to be more likely associated with light trucks/vans than passenger cars, and this may be possibly due to higher centers of gravity in light trucks, however, if rollovers did occur, the passenger car occupants were more likely to be seriously injured (MAIS =3,4,5,6) than the light truck/van occupants.
- The CDS data indicated that rollover injuries (especially AIS 2+) were strongly associated with the injury sources of the vehicle roof, side doors, instrumental panes, and seat back/support; and rollover crashes also resulted in primarily the injured body regions of head, shoulder/back, neck, and chest.
- When a rollover crash occurred, contact between occupant and roof primarily caused head injury, as well as neck and shoulder/back injuries.
- The ejection rates of occupants of rolled vehicles were significantly related to their MAIS levels from CDS 2006-15: the MAIS 3-6 group had the highest ejection rate of 36% approximately, the ejection rate for MAIS 2 was 11%, while MAIS 1 group had the lower rate of 2.5%.
- A multiple logit regression was used, with considerations of all crash types and multiple risk factors simultaneously, to predict the occupant injury relative risks of several risk factors, e.g., comparing rollover versus not-rollover, belted occupants versus not-belted, higher delta-V versus lower. It was found that higher occupant injury risks are significantly associated with rollover crash (OR=1.74), delta-V >35 MPH (OR=5.59), not-belted (OR=3.26), side impacts (OR=1.54), and older occupant age >65 (OR=2.69). On the other hand, older vehicles (>4 years), seating position, and relatively smaller vehicle size did not have significant impact on occupant injuries with p-values > 0.05.
- This study paid close attention to data structures and data sorting, data appending vertically and data merging horizontally, logic design of flow-chart, and vehicle crash type identifications using key research variables.
- With consideration of FMVSS 216a and 226 that focused on the newer vehicles after 2011, this study explored the effect of vehicle age and focuses on the recent crash data (CDS 2013-15), the rollover-related occupant injuries, including vehicle age <=2, <=4, and <=10 years old, respectively, are listed, but CDS database is still limited by the sample size, especially if only model years after 2011 are included.
- CDS data analysis is also limited by the high percentages of missing or unknown values of some key variables, such as delta-V, rollover/ejection status, and AIS.
- Overall, this study may enrich the understanding of rollover crashes, ejections and occupant injuries from using recent crash data. Future data analysis, using both NASS Crash Investigation Sampling System (CISS) and Crash Reporting Sampling System (CRSS) data starting since 2016 that are collected from more PSU, may provide more insights of rollover crashes, ejections, and occupant injuries.

7. REFERENCES

1. Summers, S., Willke, D. T., Sullivan, L. K., Duffy, (2007). NHTSA's crashworthiness rollover research program. (Paper No. 05-0279). Proceedings of the 19th International Technical Conference on the Enhanced Safety of Vehicles (ESV), Washington, D.C., June 6-9, 2005.
2. Strashny, A. (2007), "An Analysis of Motor Vehicle Rollover Crashes and Injury Outcomes", DOT HS 810 741, Washington DC.
3. Ridella, S.A. and Eigen, A.M. (2008), "Biomechanical Investigation of Injury Mechanisms in Rollover Crashes from the CIREN Database", *Proceedings of the International IRCOBI Conference on the Biomechanics of Injury*, Bern, Switzerland, pp. 33-47, 2008.
4. Ridella, S.A., Eigen, A.M., Kerrigan, J.R. and Crandall, J. (2009), "An Analysis of Injury Type and Distribution of Belted, Non-Ejected Occupants Involved in Rollover Crashes". *Annals of Advances in Automotive Medicine*, Vol. 53, 2009.
5. Austin, R. (2010), "Roof Strength Testing and real-World roof intrusion in rollovers", DOT HS 811 365.

6. NCSA /NHTSA (1998). *National Automotive Sampling System Crashworthiness Data System Descriptive Summary, 1996-98 Update*, National Highway Traffic Safety Administration, Washington DC.
7. Shelton, T. (1991). "National Accident Sampling System, General Estimates System Technical Note, 1988 to 1990", Report No. DOT HS 807 796. Washington, DC: National Highway Traffic Safety Administration.
8. Zhang, F., & Chen, C-L. (2013). *NASS-CDS: Sample Design and Weights*, (Report No. DOT HS 811 807), Washington, DC.
9. Ridella, S., Kuppa, S., Martin, P., McCullough, C., Rudd, R. W., Scarboro, M. (2007). NHTSA's Vision for Human Injury Research. (Paper Number 07-0043). 20th Enhanced Safety of Vehicles, 2007, Lyon, France.
10. Wu, J., Subramanian, R. & Craig, M. (2013), "The effect of earlier collision notification on Traffic fatality using Survival Analysis", *J. of Traffic Injury Prevention*, 8/2013.
11. Lee, E., Wu, J., Kang, T. and Craig, M. (2017), "Estimate of mortality reduction with implementation of advanced automatic collision notification", *J. of Traffic Injury Prevention*, Vol. 18, 2017.
12. Sharma, D., Stern, S., Brophy, J., & Choi, E-H. (2007), An Overview of NHTSA's Crash Reconstruction Software WinSMASH. (Paper No. 07-0211). 20th Enhanced Safety of Vehicles Conference, France, 2007.
13. Korn, E., & Graubard, B. (1999). *Analysis of Health Surveys*. New York: John Wiley & Sons.
14. Hosmer, D. and Lemeshow (1999), *Applied Logistic Regression*, John & Wiely.
15. Hosmer, D. and Lemeshow (2000), *Applied Survival Analysis*, John & Wiely.
16. SAS Institute (2005), *Categorical Data Analysis using Logistic Regression*, SAS Publishing.
17. SAS Institute (2005), *Design and Analysis of Probability Surveys*, SAS Publishing.
18. Conroy, C., Hoyt, D, Eastman, A.B, etc. (2006), "Rollover crashes: Predicting serious injury based on occupant, vehicle, and crash characteristics", *Accident Analysis and Prevention,* 38 (2006).
19. Kuppa, S., Wang, J. and Haffner, M, "Lower extremity injuries and associated injury criteria", Paper No 457, Proceedings of ESV 2001, NHTSA, US DOT.
20. NHTSA (2018), "Fatality Analysis Reporting System (FARS) Analytical User's Manual", National Center for Statistics and Analysis (NCSA), NHTSA, Washington DC.
21. NHTSA (2014), "National Automotive Sampling System–Crashworthiness Data System (CDS) - Analytical User's Manual, NHTSA, Washington DC.

8. ACKNOWLEDGEMENT

The 1st author appreciates the inspiring inputs from his colleagues, including Dr. Chou-Lin Chen, Dr. Cejun Liu, and Mr. Scott Yon.

9. APPENDIX

Table 5b: *Weighted annual averages of occupant MAIS from rollovers crashes (CDS 2006-15, vehicle age <=4)*

YEAR	MAIS 1	MAIS 2	MAIS 3-6	MAIS 7
2006	35,197	5,180	6,932	6,209
2007	41,239	12,146	6,574	3,043
2008	72,017	7,004	6,217	4,264
2009	18,981	3,102	3,514	591
2010	27,901	3,819	2,349	1,661
2011	16,133	4,064	1,893	546
2012	17,195	3,250	1,998	1,049
2013	9,075	4,287	4,569	2,627
2014	17,540	3,108	1,390	352
2015	15,997	2,998	899	1,007

Table 5c: *Weighted annual averages of occupant MAIS from rollovers crashes (CDS 2006-15, vehicle age <=2)*

YEAR	MAIS 1	MAIS 2	MAIS 3-6	MAIS 7
2006	18,151	2,493	3,245	4,641
2007	23,664	5,894	3,067	955
2008	14,541	2,510	3,642	2,846
2009	7,828	1,611	1,336	314
2010	16,144	2,850	1,409	1,229
2011	8,168	2,148	1,082	395
2012	11,692	1,004	1,132	726
2013	3,319	2,947	1,483	1,423
2014	12,855	1,395	832	352
2015	6,505	1,003	554	666

BRIC AND FIELD BRAIN INJURY RISK

Erik G. Takhounts
National Highway Traffic Safety Administration
USA

Vikas Hasija,
Bowhead (Systems & Technology Group)
USA

Matthew J. Craig
National Highway Traffic Safety Administration
USA

Paper Number 19-0154

ABSTRACT

This study investigates the adequacy of comparing the risk of brain injuries based on the available National Automotive Sampling System/Crashworthiness Data System (NASS/CDS) field data to the risk predicted by Brain Injury Criterion (BrIC) measured from an Anthropomorphic Test Device (ATD) in NHTSA's Research Moving Deformable Barrier (RMDB) oblique tests (fleet). Finite Element (FE) analysis was utilized to simulate crashes with a given range of Principal Direction of Force (PDOF) and change in velocity (Delta-V) to illustrate their effect on the field vs. fleet risk comparison. The simulation based results indicate that BrIC is highly dependent on PDOF and Delta-V. The methods applied for estimating brain injury risk from the simulation results demonstrate the importance of accounting for the distributions of both PDOF and Delta-V when comparing brain injury risk estimates from the field data versus those calculated from fleet testing.

KEYWORDS: BrIC, field data analysis, fleet data analysis, head/brain injury

INTRODUCTION

In this study, we computed the risk of brain injuries based on the available NASS/CDS field data and compared it to the risk predicted by BrIC in FE simulations of various PDOF and Delta-Vs representing a range of frontal crash conditions. Previous analyses of the field data (for example, Laituiri et at., 2016; Prasad et al., 2014) included crashes at PDOFs 11, 12, and 1 o'clock (that is spanning from -40^0 [near side oblique] to $+40^0$ [far side oblique] for the drivers) and the damage extent 3-6 (Delta-V ranging from under 25 mph [approximately 66% of the cases with the 3-6 damage extent] to around 35 mph). The fleet data (NHTSA's RMDB oblique tests) have the PDOF range between $20\text{-}30^0$ for both near and far sides, and the Delta-V span of 31-37 mph.

The purpose of this study is to investigate the adequacy of such comparisons between field and fleet risks when neither PDOF nor Delta-V ranges are comparable between the two datasets. Because of such incompatibility of the Delta-V and PDOF ranges between the two datasets, FE analysis of various frontal crash Delta-V and PDOF was utilized together with PDOF and Delta-V ranges/distributions from fleet and field data to derive adjusted simulation based estimates of brain injury risk.

METHODS

The efforts of this study can be separated into three distinct phases: (1) estimation of brain injury risk from field data; (2) application of a vehicle model and simulation to measure BrIC over a wide range of frontal crash Delta Vs and PDOF values; and (3) application of different filtering/calculation techniques to estimate brain injury risk from simulation data from (2) while considering the range of Delta V observed in fleet testing and the distribution of PDOF in frontal crashes from field data. The third step was done specifically for the purpose of demonstrating limitations that can be present when comparing field and fleet data while not considering the associated ranges and distributions of Delta-V and PDOF in the two data sets.

Field Data Analysis: The inclusion criteria for the ranges of PDOF and Delta-V in the field data analyses in previous studies were rather wide due to a small sample size for the specific PDOF and Delta-V. For the current study, the "field" data is referred to as all NASS/CDS passenger car, light truck and van frontal crash cases with a PDOF of -40^0 to $+40^0$ and Delta-V range between 31 and 37 mph. The brain injury field risk of AIS 2+, 3+, and 4+ (AIS – abbreviated injury scale) was calculated from weighted 2000-2015 NASS/CDS age 15+ belted drivers involved in frontal crashes with a Delta-V range of 31-37 mph and deployed frontal airbags. The case vehicles were restricted to passenger cars, light trucks and vans. Cases with rollovers were excluded. The risk at each AIS level was calculated as the ratio or percent of injury cases to the total weighted case count for the target population described above.

Frontal Crash FE Simulation: An FE model of a mid-size sedan was created and the GHBMC-OS (Global Human Body Modeling Consortium Simplified 50th Percentile Male, v1.8) FE model was utilized to simulate crashes at various PDOFs and Delta-Vs (Figure 1).

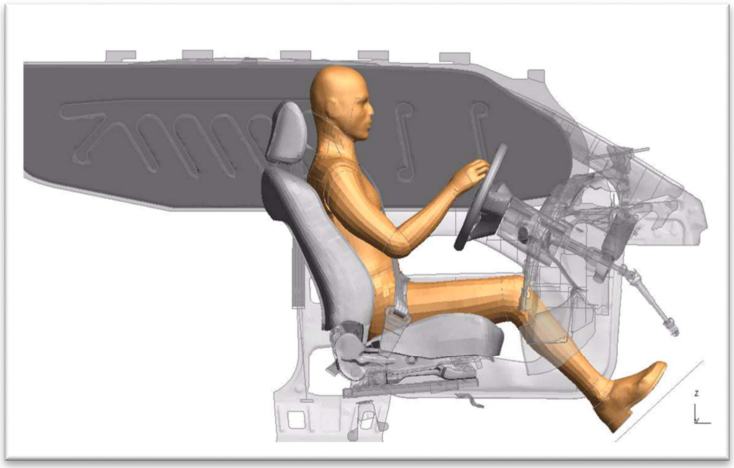

Figure 1: GHBMC-OS 50th % male FE model in a mid-sized sedan.

BrIC values were calculated for each combination of the investigated parameters (Table 1). The simulations were done without any structural deformation of the vehicle model (i.e. were run similar to a model of a sled test). No attempts were made to recreate/reconstruct actual field cases nor replicate the results of a specific crash test. Instead, the model was developed to represent an average passenger car. The range of Delta-V and PDOF values that were simulated overlap what was observed in NHTSA's RMDB oblique fleet testing, where PDOF ranges from 20^0 to 30^0 for both near and far sides, and the Delta-V spans from 31 mph to 37 mph. The simulated PDOF range covers what would normally be defined as a frontal crash in NASS-CDS when considering 11 o'clock to 1 o'clock frontal crashes.

Table 1. Investigated parameters in FE simulation of frontal crashes (MFR is Mass Flow Rate).

Parameters	Baseline value	Range
Delta-V	35 mph	25 mph - 47 mph
PDOF (degrees)	0	-40 (320) to +40
Frontal airbag friction	0.5	N/A
Frontal airbag MFR (scaling factor)	1	N/A
Frontal airbag firing time (ms)	18	N/A
Load limiter (N)	3000	N/A
Side airbag friction	0.5	N/A
Side airbag MFR (scaling factor)	1	N/A
Side airbag firing time (ms)	18	N/A

Estimation of Brain Injury Risk: Using a single set of FE simulation results over a range of applicable frontal crash Delta-V and PDOF (per Table 1), simulation based brain injury risks were calculated while considering the PDOF and Delta-V ranges associated with the respective field and fleet data. Brain injury risk was calculated from the simulated BrIC values using the CSDM based risk functions described in Takhounts et al. (2013).

Three simulation based estimates of brain injury risk were calculated. The first was based on a simple average of BrIC for all simulations from 31 to 37 mph. The second version limited the average risk calculation to the PDOFs observed in NHTSA's RMDB oblique fleet testing (20-30^0). The final method used to estimate risk using the simulated BrIC data considered all simulation data over Delta-Vs of 31-37 mph (same as the first version), but with weighting applied based on the distribution of PDOFs obtained from the NASS/CDS field data for the Delta-V range of 31-37 mph.

RESULTS

Field Data Analysis: The distribution of PDOFs obtained from the NASS/CDS field data was very close to normal with the maximum at 0^0 (full-frontal crashes) representing approximately half of all the crashes (Figure 2). The NASS/CDS filter used to produce Figure 2 was the same as described above for the calculation of brain injury field risk.

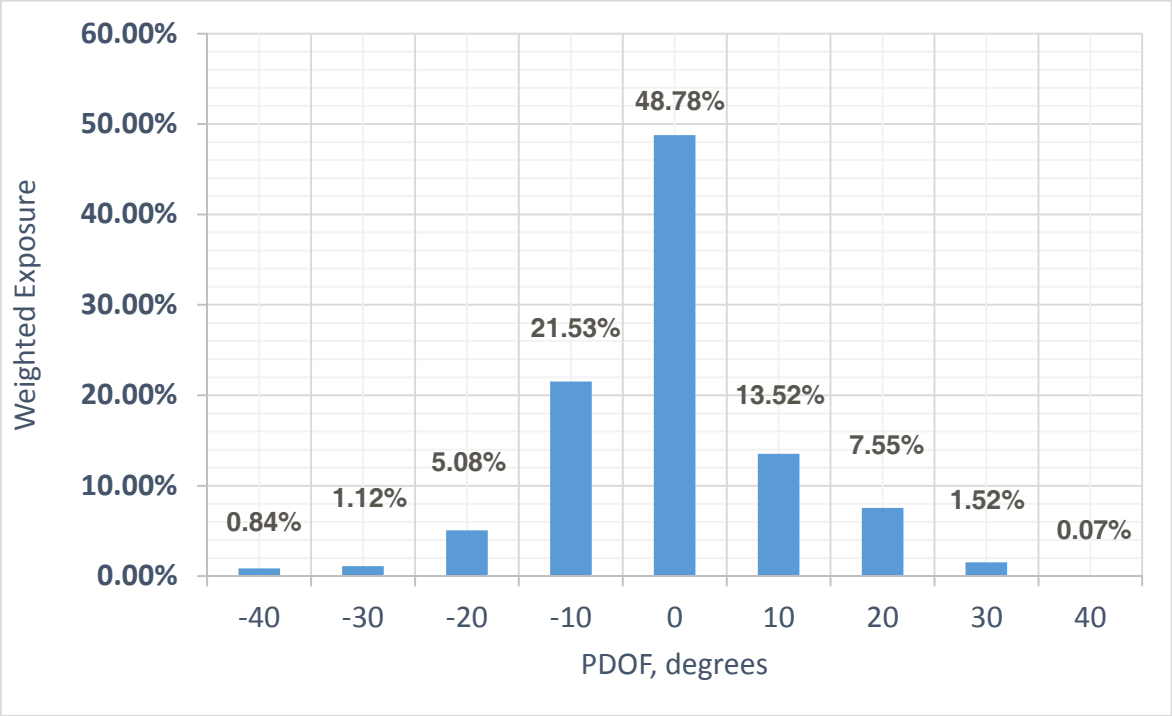

Figure 2: Weighted distribution of PDOF at Delta-V range 31-37 mph from the NASS/CDS field data.

The brain injury field risk from NASS/CDS of AIS2+, 3+, and 4+ for the Delta-V range of 31-37 mph (and PDOF of -40^0 to +40^0) was 7.59%, 3.34%, and 2.40% respectively. All brain injury cases at the three AIS levels were included in the respective risk calculations regardless of whether there was an accompanying skull and/or facial fracture.

Frontal Crash FE Simulation: Table 2 lists the values of BrIC from the simulation results for the parameters and ranges described in Table 1.

Table 2. Values of BrIC computed from the simulations for various Delta-V and PDOF.

DeltaV	PDOF=-40	PDOF=-30	PDOF=-20	PDOF=-10	PDOF=0	PDOF=10	PDOF=20	PDOF=30	PDOF=40
DV 25	0.553	0.688	0.534	0.524	0.462	0.482	0.625	0.699	0.707
DV 27	0.635	0.664	0.506	0.502	0.448	0.485	0.661	0.756	0.747
DV 29	0.713	0.683	0.498	0.481	0.469	0.497	0.661	0.821	0.824
DV 31	0.814	0.784	0.561	0.498	0.505	0.508	0.627	0.896	0.899
DV 33	0.855	0.784	0.619	0.536	0.527	0.519	0.71	1.066	0.9597
DV 35	0.959	0.759	0.593	0.615	0.555	0.548	0.986	1.268	1.008
DV 37	1.07	0.769	0.617	0.796	0.609	0.563	1.29	1.334	1.05
DV 39	1.196	1.05	0.738	0.883	0.62	0.571	1.465	1.3	1.13
DV 41	1.53	1.31	0.872	1.06	0.657	0.609	1.53	1.256	1.3
DV 43	1.693	1.098	0.989	1.23	0.697	0.607	1.61	1.39	1.765
DV 45	1.668	0.948	1.175	1.379	0.698	0.621	1.71	1.768	2.698
DV 47	1.824	1.074	1.31	1.147	0.654	0.651	1.81	2.26	3.95

Estimation of Brain Injury Risk: As previously noted, estimation of brain injury risk given the simulation results presented in Table 1 was done in three different ways.

The first version simply takes the average BrIC from the simulation results (Table 2) across all PDOFs for the Delta-V range of 31-37 mph (as was done by other researchers such as Prasad et al., 2014; Laituiri et at., 2016). The resulting average BrIC of 0.78 corresponds to 48.00%, 24.00%, and 17.00% risk of AIS2+, 3+, and 4+ brain injury (CSDM based injury risk from Takhounts et al. 2013).

The second version considers the same Delta-V range as above but limited to PDOFs of -30 to -20 and 20 to 30 degrees. As previously noted, this represents the range of PDOF observed in NHTSA RMDB oblique crash testing. The resulting average BrIC of 0.854 corresponds to 64.60%, 34.70%, and 25.80% for AIS 2+, 3+ and 4+, respectively, which is approximately an order of magnitude higher than that calculated from the NASS/CDS field data and in the same range obtained directly from the ATDs in NHTSA's RMDB oblique tests. This calculation was made by taking a simple average of BrIC values (from Table 2) for the Delta-V and PDOF ranges noted above (see bold rectangles in Table 2).

The prior two simulation based risk estimates did not consider the frequency or exposure of the respective PDOF/Delta V combinations in the field. Discrepancies in prediction among various studies can occur when the distribution of PDOF in the field is not considered in the calculation of averages. The formula for the average BrIC that includes the distribution of PDOF in the field is:

$$BrIC_{Ave} = \sum_{-\theta}^{+\theta}(\alpha_i BrIC_i), \quad (1)$$

where θ is the PDOF angle ranging from -40 to +40 degrees, α_i is the field exposure for each PDOF given in Figure 2, $BrIC_i$ is the average BrIC for 31-37 mph for each PDOF given in Table 2. For example, for a full-frontal case at 0 degree PDOF, the α_0 = 48.78% = 0.4878, and $BrIC_0$ = (0.505 + 0.527 + 0.555 + 0.609)/4 = 0.549. Average BrIC values for each PDOF at 31-37 mph are given in Table 3.

Table 3. Average values of BrIC (in bold) for the 31-37 mph Delta-V range.

	PDOF (degrees)								
	-40	-30	-20	-10	0	10	20	30	40
Delta-V = 31-37	**0.925**	**0.774**	**0.598**	**0.611**	**0.549**	**0.535**	**0.903**	**1.141**	**0.979**

Taking PDOF exposure from Figure 2 and corresponding values of BrIC from Table 3, the average BrIC calculated from equation 1 is:

$BrIC_{Ave} = \sum_{-\theta}^{+\theta}(\alpha_i BrIC_i)$ = 0.925*0.0084 + 0.774* 0.0112 + 0.598*0.0508 + 0.611*0.2153 + 0.549*0.4878 + 0.535*0.1352 + 0.903*0.0755 + 1.141*0.0152 + 0.979*0.0007 = 0.605.

Note that the sum of α_i in the formula above equals to 1 indicating that all possible PDOF exposures in Figure 2 are accounted for.

The risks of AIS 2+, 3+, and 4+ brain injury for BrIC = 0.605 are 8.08%, 3.40%, and 2.39% respectively. All the presented above values of BrIC (based on CSDM per Takhounts et al. 2013) are tabulated below in Table 4.

Table 4. Risks of AIS2+, 3+, and 4+ brain injury based on the field data and various BrIC values.

	AIS 2+	AIS 3+	AIS 4+
Average Field Weighted Risk for Delta-V 31-37 mph – NASS/CDS	7.59%	3.34%	2.40%
BrIC = 0.78 - simulation based average BrIC for Delta-V 31-37 mph and all PDOF	48.00%	24.00%	17.00%
BrIC = 0.854 - simulation based average BrIC for Delta-V 31-37 mph and PDOFs -30^0 to -20^0 and $+20^0$ to $+30^0$	64.60%	34.70%	25.80%
BrIC = 0.605 - simulation based average BrIC at Delta-V 31-37 mph weighted by the probability of occurrence of crash at each PDOF from -40^0 to $+40^0$	8.08%	3.40%	2.39%

When the average BrIC is calculated per equation 1, i.e., considering the actual PDOF exposure in the field given in Figure 2, as given in the last row in Table 4, the simulation based brain injury risks at various severities are comparable to those taken directly from the field (first row in Table 4).

Other formulas calculate such risks by simply lumping together all the risks at various PDOFs into one simple average without considering the PDOF exposure. Such calculations implicitly assume that the field PDOF exposure is uniform, i.e., a rectangular rather than normal distribution of PDOF given in Figure 2, with equal exposure coefficients in equation 1. However, when PDOF exposure is considered, the risks of brain injury calculated by BrIC are comparable to those obtained directly from the NASS/CDS field data.

Similar considerations are applicable when the range of Delta-V becomes wider (as in Prasad et al., 2014). In this case the Delta-V distribution in the field must be accounted for and equation (1) for calculating average BrIC should be modified (equation 2) to include an additional coefficient representing the Delta-V exposure in the field:

$$BrIC_{Ave} = \sum_{-\theta}^{+\theta}\sum_{dv1}^{dv2}(\alpha_i \beta_j BrIC_{ij}), \quad (2)$$

where βj is the Delta-V exposure at each PDOF, dv_1 and dv_2 are the lowest and highest Delta-Vs under consideration (for example, if all the values of BrIC were used from Table 2, then dv_1 = 25 mph and dv_2 = 47 mph), and $BrIC_{ij}$ is the value of BrIC at a given PDOF and Delta-V. Similarly, for the analysis of the field (and/or fleet) data based brain injury risk, the risks at each PDOF and Delta-V should be weighted according

to equation (2). In the case when such field data resolution is not available (due to small sample size), some averaging may be assumed as was demonstrated above using equation (1). However, when 66% of the cases are under Delta-V of 25 mph (such as the case when considering the damage extent range of 3 to 6 used in Prasad et al., 2014), which corresponds to much lower values of BrIC compared to those at 35 mph (see Table 2), then lumping all the data together and taking a simple average will predictably lead to incorrect assessment of the brain injury risk.

If a brain injury risks comparison between field and fleet data is to be made, then both PDOF and Delta-V ranges in the field and fleet datasets should be the same and the distributions of PDOF and Delta-V that occur in the field must be accounted for in the fleet data.

CONCLUSIONS

Simulation based results indicate:

1. BrIC is highly dependent on Delta-V and PDOF (Table 2).
2. When overall field risk of brain injury is compared to that calculated by BrIC from the fleet data, both Delta-V and PDOF ranges should be comparable between the two datasets and the distributions of PDOF and Delta-V that occur in the field data must be accounted for in the fleet data.
3. When conclusion 2 is satisfied, the brain injury risks for field and fleet are comparable (Table 4).

REFERENCES

[1] Laituri, T.R., Henry, S., Pline, K., Li, G., Frankstein, M., Weerappuli, P (2016) New risk curves for NHTSA's Brain Injury Criterion (BrIC): Derivations and Assessments. Stapp Car Crash Journal, Vol 60; pp 301-362.

[2] Prasad, P., Dalmotas, D., German, A. (2014) The Field relevance of NHTSA's oblique research moving deformable barrier tests. Stapp Car Crash Journal, Vol 58; pp 175-195.

[3] Takhounts, E.G., Craig, M.J., Moorhouse, K., McFadden, J., Hasija, V. (2013) Development of brain injury criteria (BrIC). Stapp Car Crash Journal 57:243-66.

THOR 50M SUITABILITY FOR AUTOMATED VEHICLE CRASHWORTHINESS

Z. Jerry Wang, Jianying Li, Kartik Pallavajhala, Zaifei Zhou
Humanetics Innovative Solutions, Inc.
USA

Jingwen Hu, Kyle Boyle, Mathew Reed
University of Michigan Transportation Research Institute
USA

Paper Number 19-0162

ABSTRACT

The objective of this study is to use finite element (FE) models to understand the differences in response between human body model (HBM) and THOR-50M dummy in reclined seating scenarios that may become more common in automated vehicles. The **T**otal **Hu**man **M**odel for **S**afety (THUMS) v4.01 and Humanetics THOR-50M Anthropomorphic Test Device (ATD) FE model were used in both frontal- and rear-impact scenarios. The seating postures were based on data from a recent volunteer study. Front and rear impacts with seatback angles of 23, 33, and 43 degrees were simulated for a total of six test conditions. A US NCAP midsize sedan pulse was selected for the analysis. A publicly available seat model based on a 2012 Toyota Camry driver seat and a model of a ZF seatbelt system with pre-tensioner and load limiter were used in the study.

Both dynamic and kinematic data were analyzed and compared between the THUMS and THOR models, including motion, load measurements and displacements at numerous anatomical positons and sensor measurement locations. In addition, the seat cushion and seatback contact forces were compared. Due to the anthropometry discrepancies between the two models, the sensor measurement locations in THOR 50M do not necessarily coincide with THUMS anatomical locations. In such case, the anatomical location in THUMS was selected. The responses between the two FE models were similar in some parameters and quite different in others. The study could not determine which FE model has better biofidelity because no biofidelity specifications from Post Mortem Human Subject (PMHS) testing are available for such assessment.

INTRODUCTION

Future Automated Vehicles (AV) may offer new opportunities to restructure vehicle seat configurations to promote riding comfort or interactions among occupants [1]. AV show cars have proposed seat configuration that can be changed to facilitate better interactions between occupants, such as rear-facing in front row, diagonal cross seating, or other orientations. A widely anticipated scenario involves seatback angles that are more reclined for riding comfort or resting. However, these seat configurations pose challenges for the occupant protection. Kitagawa et al [2] studied the influence of seating position, direction and seating orientation on occupant responses with THUMS for autonomous vehicles. The study presented the challenges in various crash scenarios, including the interactions among the occupants in non-traditional seating configurations.

This paper focuses on the existing vehicle fleet with an extended scope, i.e. rearward facing seating. Oblique and side impact scenarios are not covered in this paper. Since there is a lack of PMHS data available for these crash scenarios, finite element model simulations were used to understand the difference between the HBM and the ATD FE models. To the authors' knowledge, none of the FE models have been validated in these seating configurations in crash testing. This analysis focuses on the upper-body kinematics and output from the ATD sensors and the corresponding outputs from THUMS. Lower extremities were not analyzed since there was no vehicle interior representation that would interact with the lower extremities in the study.

METHODS

Analysis Tools

LS-DYNATM Version 971 (Livermore Software Technology Corporation, USA), a general –purposed FE simulation package was used for the analysis. Toyota Camry 2012 driver seat FE model was used for the simulation [3]. ZF seatbelt model with retractor pre-tensioner and load limiter was from a previous project of University of Michigan Transportation Research Institute (UMTRI). THUMS version 4.01 [4] [5] was selected as the HBM and Humanetics THOR-50M FE model v1.6 was used for the comparison analysis.

Occupant Positioning Guidelines

Before the simulation work, a project at UMTRI studied the volunteer seating postures in reclined seatback configurations [6]. The study measured critical landmarks in different seatback angles. A regression model was generated from the human volunteer measurements to represent the occupant seating postures, including head orientation, spine position, pelvic bone orientation and lower leg positions.

THUMS Sensors

Load cell representations were created in THUMS at the corresponding locations in the THOR-50M model. Linear accelerations and angular rate were extracted from THUMS at the corresponding sensor locations in THOR-50M as well. Pre-simulation was used to position the THUMS 4.01 model according to the seating posture defined in [6]. The THUMS head orientation, T1, T4, T8, T12, pelvis orientation, hip joint, knee joints, and ankle joints are prescribed to match the occupant seating postures obtained from UMTRI[6].

ATD Positioning

The ATD was studied in CAD to best match the seating posture defined in [6]. The hip joint was aligned first, then the ATD dummy pelvis was rotated until pelvic bone matched the occupant seating orientation. Next, the lower spine joint was adjusted to match the target spine position, and the upper spine joint was adjusted to match the target head orientation. The thighs were adjusted to match the orientation between the hip and the knee joint center, and finally the lower leg was adjusted accordingly. The ATD thoracic joint setups are summarized in Table 1. The ATD seating postures in various seatback angle are shown in Figure 1. A round bar was placed in the front of the lower leg to prevent the legs from flailing.

Table 1.
THOR-50M thoracic joint pitch positon for each seatback angle

Seatback Angle	Pelvis Angle	Lower Spine Pitch Positon	Upper Spine Pitch Positon
23°	33°	-12° (yellow mark)	0°
33°	36.3°	-3°	0°
43°	39.6°	+6°	-3° (head forward)

a. 23° seatback angle b. 33° seatback angle c. 43° seatback angle

Figure 1. Side views of THOR-50M seating postures at 23°, 33° and 43° seatback angles

For 23° seatback angle positioning, NHTSA NCAP ATD positioning procedure was followed. The pelvis angle was set to 33°, then the lower spine joint was adjusted to best match the occupant spine position, see Figure 1a. It was

observed the head positon is quite off toward the rear direction comparing to Robbins 1983 [7] . This placed the THOR 50M head approximately 39 millimeters behind the UMTRI AMVO 50th male head location.

Crash Pulse

US NCAP mid-size sedan pulse was selected for the simulation, see Figure 2. The delta-V is 56km/hour and the peak acceleration is approximately 43 g. The pulse first returns to zero acceleration after 90 ms.

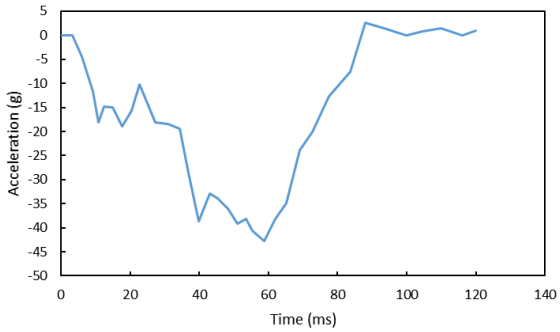

Figure 2. Sled pulse for both forward and rearward facing simulation.

RESULTS AND DISCUSSION

Forward Facing

Kinematics – Trajectory

The kinematics responses of the THUMS and THOR-50M FE models with 23°, 33°, and 43° seatback angles were compared at the head center of gravity location (CG), T1, T4, T12 and pelvis CG locations. The head rotation and the pelvis rotation were calculated from the angular rotational sensors and compared in this study. The THUMS model upper torso bends more than that of the THOR-50M model. The known stiff lumbar of THOR-50M may have contributed significantly to this difference. For the lower torso trajectories, it was noticed the THUMS model's forward motion is much higher than that of THOR-50M at all locations compared.

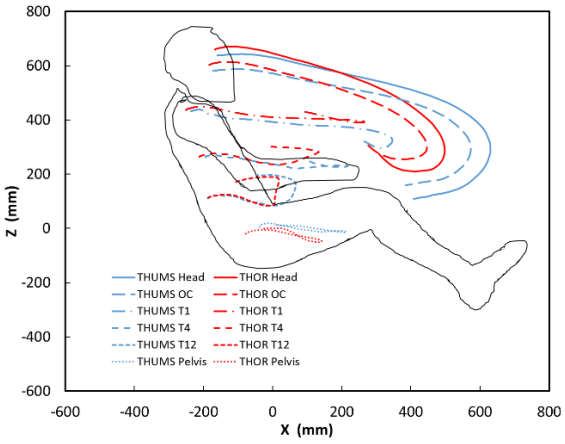

Figure 3. Trajectory comparison between THUMS and THOR-50M for 23° seatback angle, forward facing

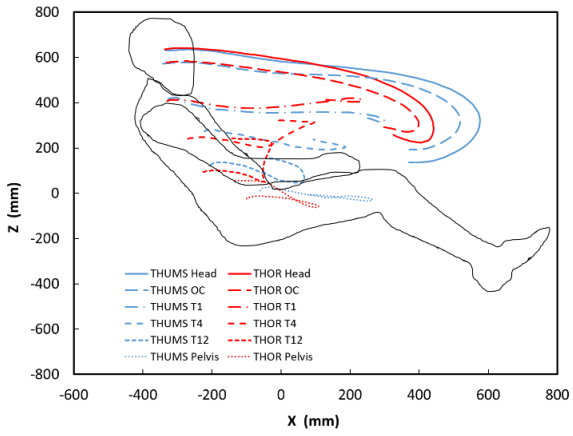

Figure 4. Trajectory comparison between THUMS and THOR-50M for 33° seatback angle, forward facing

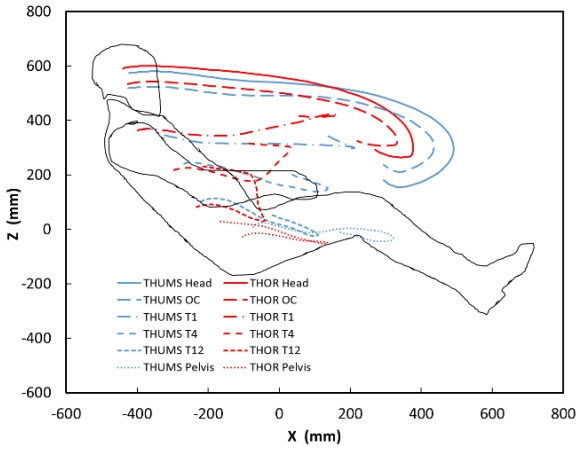

Figure 5 Trajectory comparison between THUMS and THOR-50M for 43° seatback angle, forward facing

Head

The head accelerations and head rotations are shown in Figure 9 through Figure 12 in Appendix I. The head resultant accelerations are very comparable in all three seating postures between THOR-50M and the THUMS models. The spikes near 0.13 second time mark were due to the head-knee contact during the impact, see Figure 9. In x-direction, THOR-50M head rotation started earlier than that of the THUMS model, and its maximum rotation is much lower, see Figure 10. In y-direction, the THOR-50M and THUMS rotations were similar. However, the THOR-50M rotation rose faster later in the event, and the maximum rotations were comparable, see Figure 11. In z-direction, the THUMS head rotation is much faster than THOR-50M, and the maximum rotation is much more than the THOR 50M in 23° and 33° seatback angles. Since THOR-50M dummy neck does not have a human-like low resistance in torsion up to approximately 40 degrees from the neutral forward direction, this could be the reason that the THOR-50M z rotation is less than that of the THUMS.

Thorax Displacement - Upper Left IR-TRACC

The upper left thorax Displacement was caused by the torso interaction with the shoulder belt. In x-direction, the displacement in THOR-50M is higher than THUMS except for the 43° seatback angle configuration, see Figure 13 in Appendix I. In y- direction, the THUMS has much higher displacement, see Figure 14. In z-direction, both THOR-50M and THUMS moved downward, however the displacement magnitude for THUMS is much higher, see Figure 15. The THUMS model results showed more sinusoidal pattern in y and z direction, which also shown in the resultant acceleration. Higher displacement was observed at 43° seatback angle for both THUMS and THOR-50M models, especially in x and y direction, see Figure 13 and Figure 14.

Thorax Displacement - Upper Right IR-TRACC

The upper right thorax displacements were very comparable between THOR and TUMPS in x and z directions during the loading stage, and very different in the unloading stage, shown in Figure 16 and Figure 18 in Appendix I. In y direction, the ribs in both THOR-50M and the THUMS moved toward the right at the beginning, then the THUMS rib moved toward the left while the THOR-50M was still moving toward the right, shown Figure 17.

Thorax Displacement - Lower Left IR-TRACC

The lower left thorax x displacement was significantly lower than THUMS, see Figure 19 in Appendix I. It was noticed that the x-displacement at the corresponding position of the lower left IR-TRACC had positive displacement, which was caused by the internal organ movement when compressed by the seatbelt. It also moved downward by approximate 40 mm (z displacement) for THUMS model, a much higher magnitude than the THOR-50M, shown in Figure 19.

Thorax Displacement - Lower Right IR-TRACC

The lower right thorax x displacement for THUMS was much higher and it moved forward due to the organ movement when compressed by the seatbelt, see Figure 22 in Appendix I. On the contrary, the THOR-50M x displacement was in a much lower magnitude. In y and z directions, the displacement between THUMS and THOR-50M matches closely in the loading stage, see Figure 23 and Figure 24. In the unloading stage, THUMS model has much higher z displacement during the unloading stage, see Figure 24. The THUMS model y displacement was more sensitive to the seatback angle change, especially in the unloading stage, see Figure 23.

Abdomen Displacement

The left abdomen x displacement was similar between THUMS and THOR-50M, see Figure 25 in Appendix I. The x displacements of the THUMS was insensitive to the seatback angle change while the THOR-50M was quite sensitive in contrary. The lateral and vertical displacements were different between the two models, see Figure 26 and Figure 27. However, this is insignificant because of the relatively low magnitude. Similar responses were observed for the right abdomen displacements, see Figure 28 through Figure 30.

Pelvis Rotation and Acceleration

The pelvis y rotation was similar for 23°and 33° seatback angle within the two models. However, the y rotation for 43° seatback angle was in opposite direction for THUMS, see Figure 32 in Appendix I, which was most likely caused by the pelvis bone geometry difference and the lumbar stiffness, which could significantly affect the interaction with seatbelt. The THUMS pelvic bone is narrower than the THOR-50M, the relatively stiff THOR-50M lumbar provided a stronger coupling between the upper torso and pelvis, and therefore influenced the kinematics of the pelvis.

The oscillations of the pelvis acceleration for THUMS was prominent, shown in Figure 34 through Figure 37 in Appendix I. For 23° and 33° seatback angle, the pattern between the two models were comparable when ignoring the oscillations. The pelvis acceleration in x and z directions for 43° seatback angle differed from the other two seatback angles studied. The difference could be caused by the severe submarining behavior in both THOR and THUMS models.

Anterior Superior Iliac Spine (ASIS) Load

It was observed that the THUMS model tends to submarine more than THOR-50M for all three cases, evidenced by the animation and the low ASIS force and moments in both left and right sides, see Figure 38 through Figure 41. THOR-50M model did not submarine in 23° and 33° seatback angles, but submarined in 43° seatback angle.

Belt Force and Seat Pan Force

The belt tractor payout of the THUMS is slightly higher than that of THOR-50M, shown in Figure 42 in Appendix I, implying that the upper torso has more forward motion in THUMS. The shoulder force between the two models were comparable, see Figure 43. The lap belt force and occupant seat pan contact force for THUMPS are slight lower than these of THOR-50M, shown in Figure 44 and Figure 45.

Rearward Facing

In rearward facing cases, the seatback contributed significantly to restraint the occupant. It was found the Toyota Camry 2012 seat yielded during the rearward facing simulation without any reinforcement, which is not of the interest of this study. To address the problem temporarily, the seatback frame was rigidized. The occupant motion was in a much lower scale compared to the frontal impact when the seatback did not yield. The neck motion was largely influenced by the head restraint. There was no effort in this paper to explore the head restraint design options. However, the head restraint was positioned against the back of the head for each analysis.

Trajectories

It was noticed both THUMS and THOR-50M torso moved upward along the seatback, see Figure 6 through Figure 8. The neck ramped up and interacted strongly with the head restraint. The head restraint design is critical for the head and neck protection.

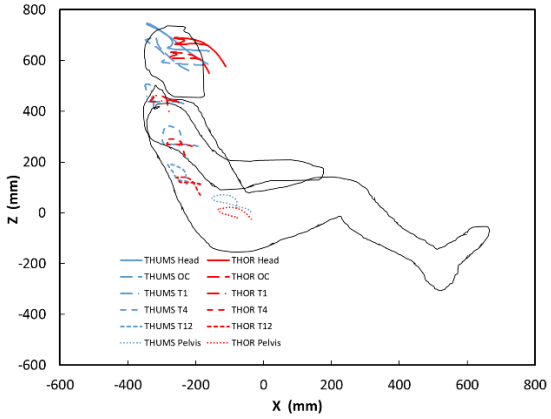

Figure 6. Trajectory comparison of THUMS and THOR-50M in 23° seatback angle, rearward facing

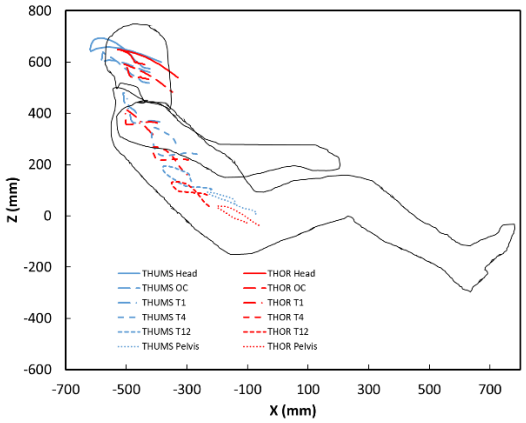

Figure 8. Trajectory comparison of THUMS and THOR-50M in 43° seatback angle, rearward facing

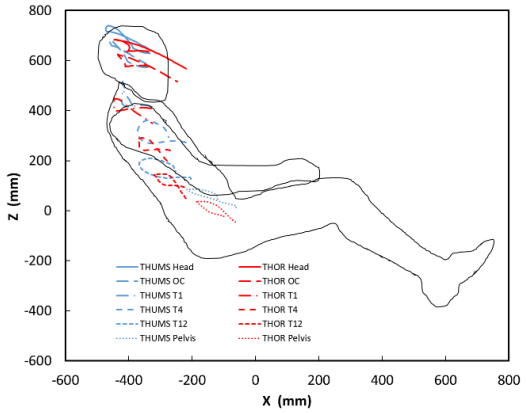

Figure 7. Trajectory comparison of THUMS and THOR-50M in 33° seatback angle, rearward facing

Head

The head acceleration for THUMS at 23° angle is much higher than any other cases in this study, shown in Figure 46 in Appendix II. To the author's knowledge, the biofidelity of both THOR-50M and the THUMS in rear impact was not evaluated in the past, there was not enough information to draw conclusion whether the high resultant head acceleration represents the production seat test data. However, attention should be paid to the head restraint system to address the potential head injury in high-speed rear impact conditions.

The rotations in y direction have similar magnitudes in loading stage and the THUMS rebound in y rotation was much higher, see Figure 48 in Appendix II. For the head rotation in z direction, the THUMS has much higher magnitude than the THOR-50M, see Figure 49. THOR-50M neck torsion response is much more stiffer than a human in the first 45° rotation from neutral forward position, where the human neck experiences a very low resistance in such a range [8][9].

Thoracic Displacement – Upper Left and Upper Right

It was noticed that the thorax displacement in x-direction at the upper left IR-TRACC attachment location is near 40 mm in the rear impact test condition, shown in Figure 50. It reached the peak earlier in THOR-50M than in THUMS, shown in Figure 50. The ribs of THUMS moved upward relative to the spine with a much higher magnitude, while THOR-50M moved downward with a very low magnitude, see Figure 52.

The displacements at upper right IR-TRACC location were similar to these at the upper left IR-TRACC location, see Figure 53 and Figure 55 in Appendix II.

Thorax Displacement – Lower Left and Lower Right

The x displacement at lower left IR-TRACC location was much higher in THOR than in THUMS for 43 degree seatback angle, see Figure 56 in Appendix II, while reversed in z displacement, see Figure 58. The higher the seatback angle is, the higher the thorax displacement. This was most likely due to the interaction with shoulder belt in the upward motion. The occupant torso would be more upright with a higher seatback angle. The displacement in THUMS was very sensitive to the seatback angle change while THOR-50M was much less sensitive.

The displacement at the lower right IR-TRACC was similar to the lower left IR-TRACC except for the y displacement. The y displacement indicated the THOR-50M and THUMS moved opposite directions, see Figure 57 and Figure 60 in Appendix II.

Abdomen Displacement

The abdomen x displacement is comparable between the two models in magnitude, see Figure 62 for the left and Figure 65 for the right side respectively. The THOR-50M stayed plateaued after it reached its maximum while the THUMS recovered back. In y and z directions, the THUMS had much higher displacement magnitudes, moving rightward in y direction and downward in z direction, see Figure 63 and Figure 64 for the left side and Figure 66 and Figure 67 for the right side respectively. It was observed that in the y direction, the displacement moved left (negative), opposite to the THOR-50M motion, see Figure 63 for the left side and Figure 66 for the right side in Appendix II.

Lower Thoracic Spine (Lumbar)

The lower thoracic spine x and z forces were higher, but y force was lower in THOR-50M, shown in Figure 68 through Figure 70 in Appendix II. The lower thoracic spine x force was not very sensitive to the seatback angle change except for THOR-50M with 43° seatback angle, shown in Figure 68. The moment measurement in THUMS were very low, especially in x and y directions, see Figure 71 and Figure 72.

CONCLUSIONS

FE models of the THOR-50M and midsize human male (THUMS) were used to study the occupant impact responses with different seatback angles in both forward and rearward facing configuration. The seating postures were based on a previous volunteer study. A US NCAP pulse with a 56 km/hour delta-V was used for the analysis.

In forward facing condition, the THUMS excursions in head, spine and pelvis were greater than THOR-50M. Head accelerations were comparable between the two models. The head rotation in x and z were higher in THUMS model. For the upper thoracic displacement at IR-TRACC attachment point, the displacements in x direction were similar between the two models. Higher displacements in y and z directions were observed for THUMS model. For the lower thoracic displacement at IR-TRACC locations, THOR-50M measurements were very low and the THUMS had positive x displacement, indicating the expansion instead of compression. This was caused by the organ movement when the chest was compressed. For the abdomen response, the magnitude of the displacement between the two models were comparable. The THOR-50M displacement stayed plateaued after reaching its maximum while THUMS recovered. For the pelvis, the acceleration had similar pattern and the THUMS output showed high oscillation magnitude. THUMS tended to submarine more than THOR-50M. The THOR-50M only submarined in the 43° seatback angle, evidenced by one or a combination of the animation, low ASIS load cell output (lap belt and ASIS engagement), low shoulder belt force and low seat pan force.

In rear facing, torso of the two models were restrained by the seatback and the excursions were relatively low. The head kinematics was strongly influenced by the interaction with the head restraint. The THUMS model had higher head acceleration and rotations. The upper thoracic resultant displacement was approximately 40 mm, which could be indicative of injury risk. THUMS upper thorax had high z displacement with a range 30-48 mm approximately. The lower thoracic displacement for THUMS was sensitive to the seatback angle change, and reached as high as 68 mm with 43° seatback angle. THOR-50M lower thoracic displacement was not sensitive to the seatback angle change. The abdomen displacement was similar in magnitude between the two FE models. The lumbar forces and moments for THOR-50M were much higher than THUMS, especially at 43° seatback angle.

LIMITATIONS

Neither FE model has been validated in reclined seating configurations. Consequently, the results in this study cannot be used to compare the biofidelity of the THUMS and THOR-50M. In addition, the Humanetics THOR-50M model was developed to fully represent the Humanetics THOR-50M ATD responses; no effort was made to improve its biofidelity beyond matching the physical dummy responses.

REFERENCES

[1] Lindman, M., Isaksson-Hellman, I., Strandroth, J., 2017. Basic numbers needed to understand the traffic safety effect of automated cars, IRCOBI Conference 2017, Antwerp, Belgium.

[2] Kitagawa, Y., Hayashi, S., Yamada, K., Gotoh, M., 2017. Occupant kinematics in simulated autonomous driving vehicle collisions: influence of seating positon, direction and angle, Stapp Car Crash Journal, Vol. 61 (November 2017), pp. 101-155.

[3] Reichert, R., Mohan, P., Marzougui, D., Kan, C. et al., "Validation of a Toyota Camry Finite Element Model for Multiple Impact Configurations," SAE Technical Paper 2016-01-1534, 2016, https://doi.org/10.4271/2016-01-1534.

[4] Kitagawa, Y., Yamada, K., Motojima, H., Yasuki, T., 2015. Consideration on Gender Difference of Whiplash Associated Disorder in Low Speed Rear Impact, Proceedings of IRCOBI Conference, pp. 233-245, Lyon, France.

[5] Kitagawa, Y., Yasuki, T., 2013. Correlation among Seatbelt Load, Chest Deflection, Rib Fracture and Internal Organ Strain in Frontal Collisions with Human Body Finite Element Models. Proceedings of IRCOBI Conference, pp. 282-316, Gothenburg, Sweden.

[6] Reed, M.P. and Ebert, S.M. 2018. “Effect of Recline on Passenger Posture and Belt Fit”. University of Michigan Transport Research Institute, Final Report UMTRI-2018-2, September 2018.

[7] Robins, D.H., 1983. Anthropometric specifications for mid-sized male dummy, vol. 2. UMTRI-83-53-2.

[8] Myers B.S., McElhaney J.H., Doherty B.J.m Paver J.G., Nightingale R.W., Ladd T.P. and Gray L., 1989. Responses of the human cervical spine to torsion, Proceedings of the 27th Stapp Car Crash Conference, November 1989.

[9] Kang, Y-S., Stammen, J., Moorhouse, K., Bolte, J., Head and neck responses of post mortem subjects in frontal, oblique, side and twist scenarios. 2018 International Research Council on the Biomechanics of Injury (IRCOBI) Conference Proceedings, 12 – 14 September 2018 – Athens, Greece.

APPENDIX I Forward Facing Data Plots

Head Acceleration and Rotation

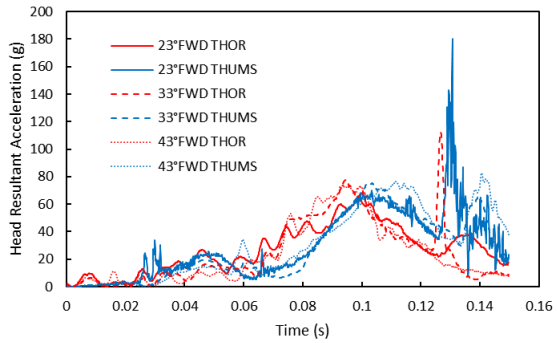

Figure 9. Head resultant accelerations

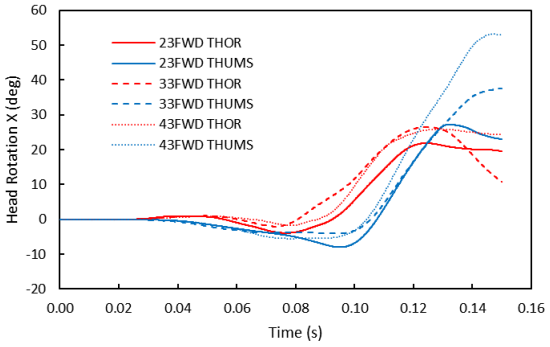

Figure 10. Head rotation x (integrated from angular velocity)

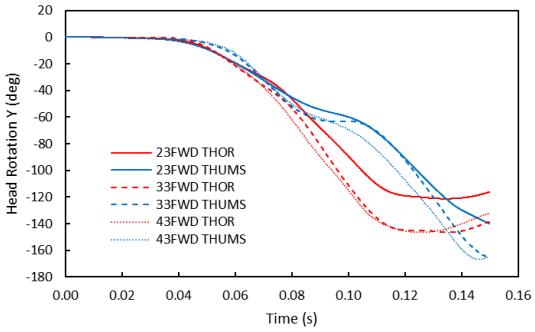

Figure 11. Head rotation y (integrated from angular velocity)

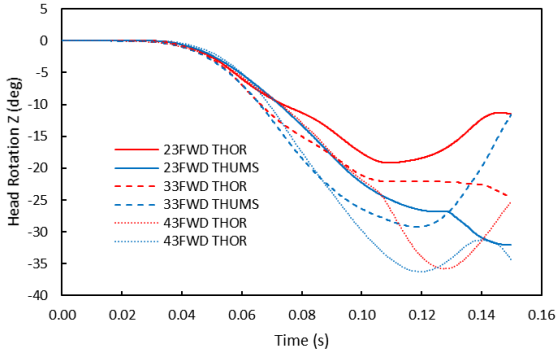

Figure 12. Head rotation z (integrated from angular velocity)

Thorax Displacement – Upper Left and Right

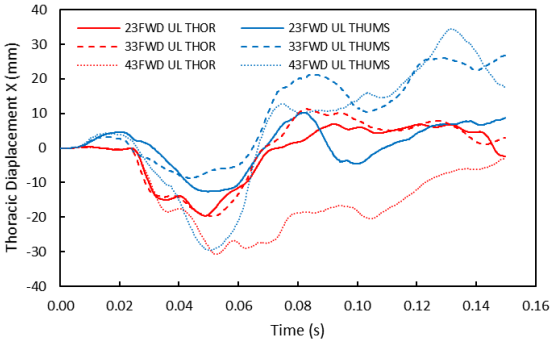

Figure 13. Thorax displacement x at upper left IR-TRACC front attachment point

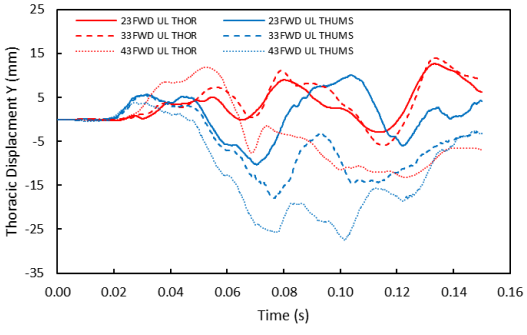

Figure 14. Thorax displacement y at upper left IR-TRACC front attachment point

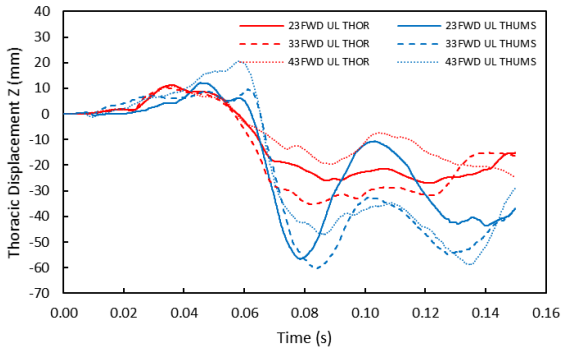

Figure 15 Thorax displacement z at upper left IR-TRACC front attachment point

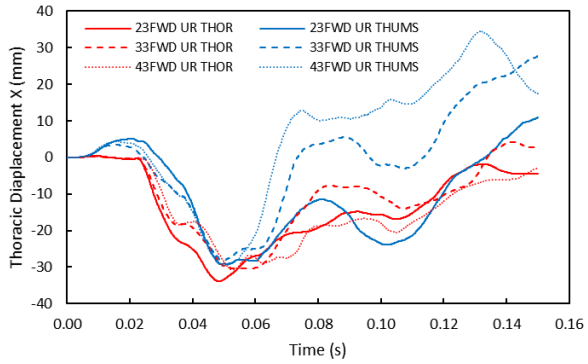

Figure 16. Displacement x at the upper right IR-TRACC front attachment point

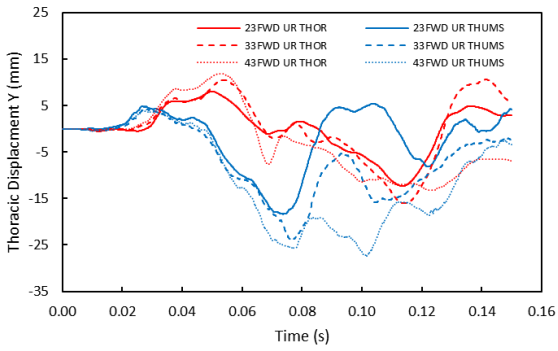

Figure 17. Displacement y at the upper right IR-TRACC front attachment point

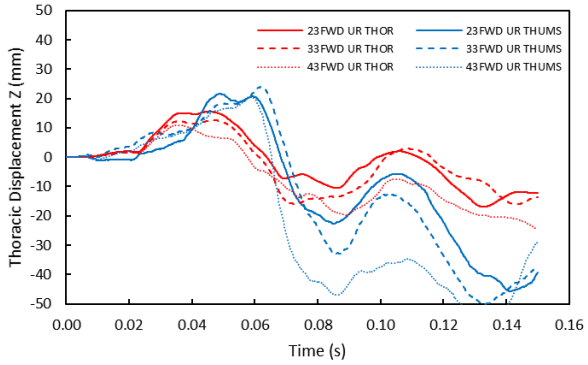

Figure 18. Displacement z at the upper right IR-TRACC front attachment point

Thorax Displacement – Lower Left and Right

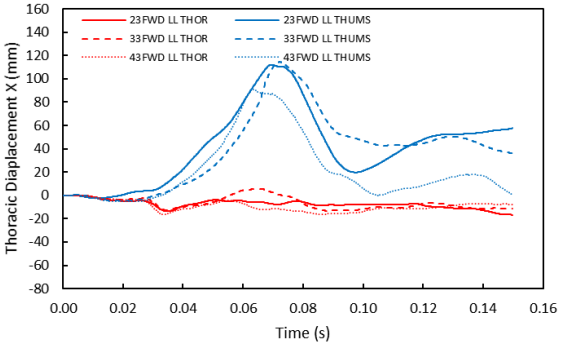

Figure 19. Displacement x at the lower left IR-TRACC front attachment point

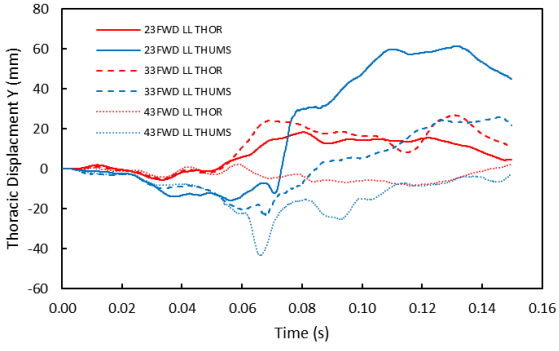

Figure 20. Displacement y at the lower left IR-TRACC front attachment point

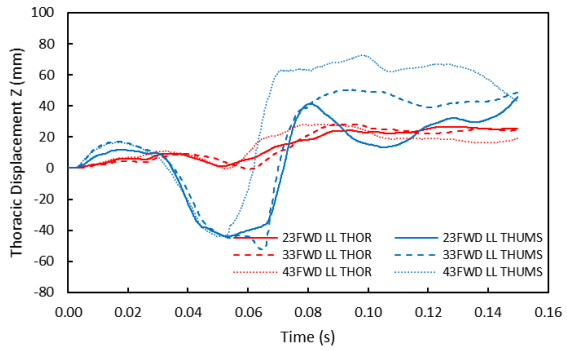

Figure 21. Displacement z at the lower left IR-TRACC front attachment point

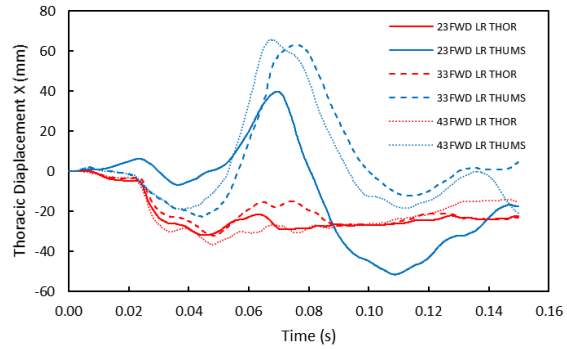

Figure 22. Displacement x at lower right IR-TRACC front attachment point

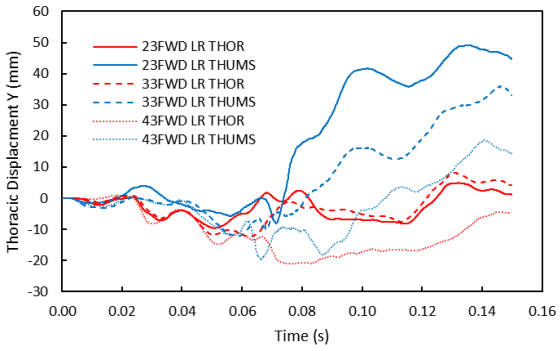

Figure 23. Displacement y at lower right IR-TRACC front attachment point

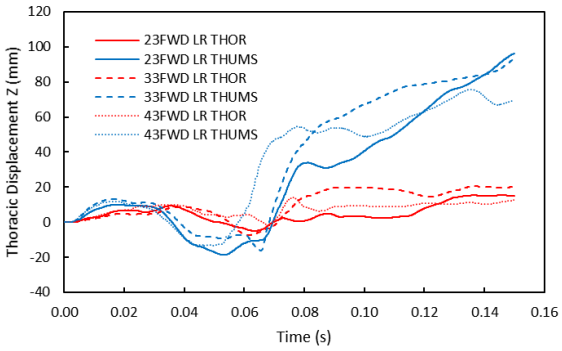

Figure 24. Displacement z at lower right IR-TRACC front attachment point

Abdomen Displacement – Left and Right

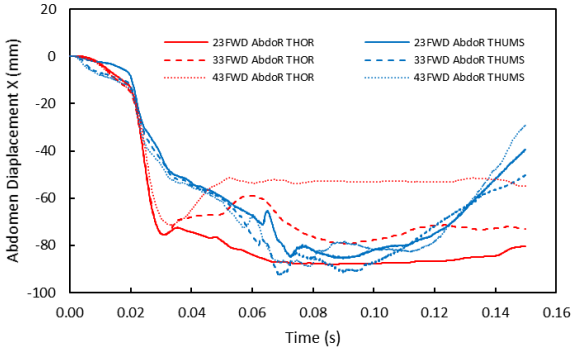

Figure 25. Displacement x at abdomen left IR-TRACC front attachment point

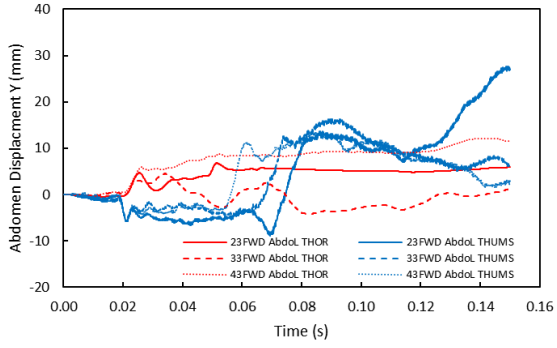

Figure 26. Displacement y at abdomen left IR-TRACC front attachment point

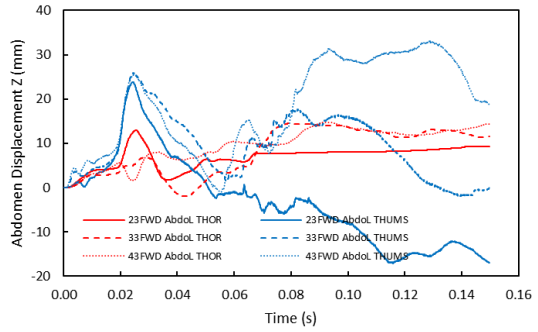

Figure 27 Displacement z at abdomen left IR-TRACC front attachment point

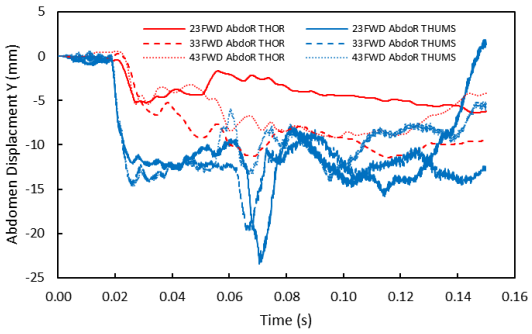

Figure 29 Displacement y at the right abdomen IR-TRACC attachment point

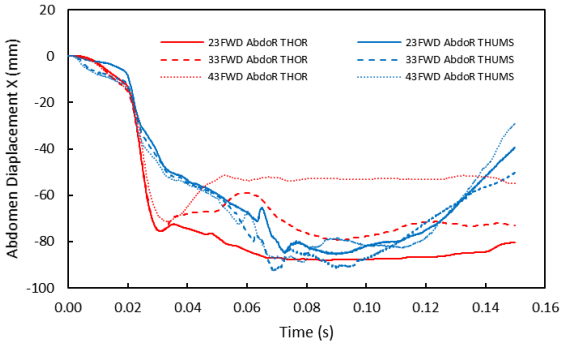

Figure 28. Displacement x at the right abdomen IR-TRACC attachment point

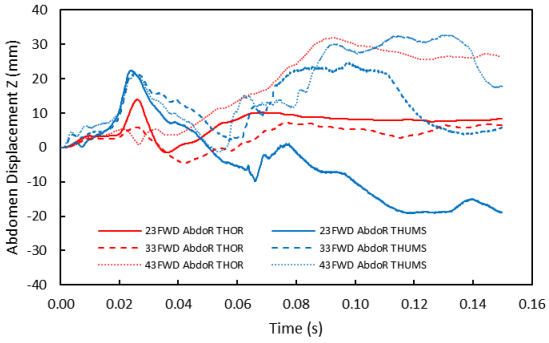

Figure 30. Displacement z at the right abdomen IR-TRACC attachment point

Pelvis

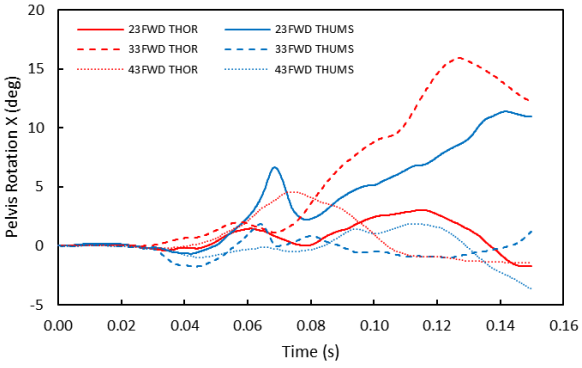

Figure 31. Pelvis bone rotation in x direction (integrated from angular rate)

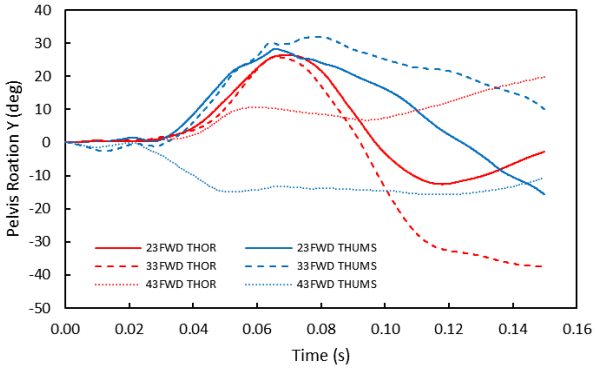

Figure 32. Pelvis rotation in y direction (integrated from angular rate)

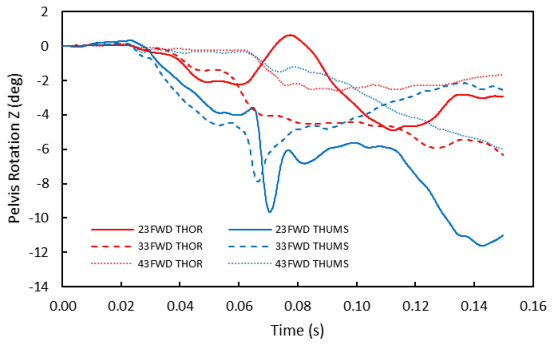

Figure 33. Pelvis rotation in z direction (integrated from angular rate)

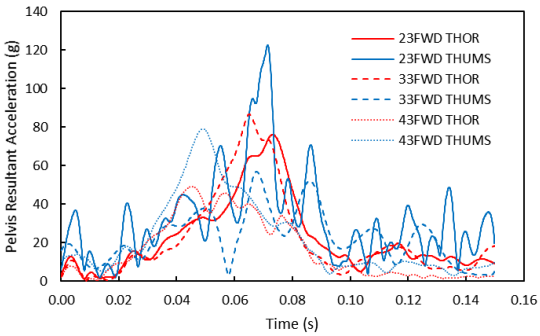

Figure 34. Pelvis resultant acceleration

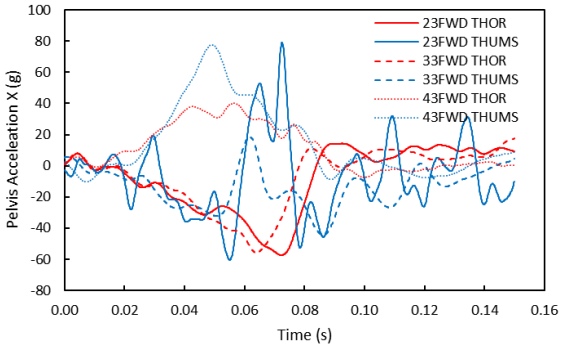

Figure 35. Pelvis acceleration in x direction

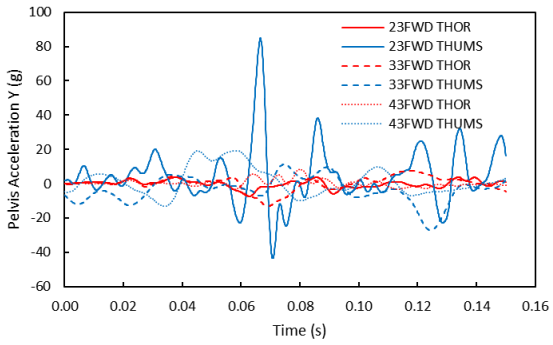

Figure 36. Pelvis acceleration in y direction

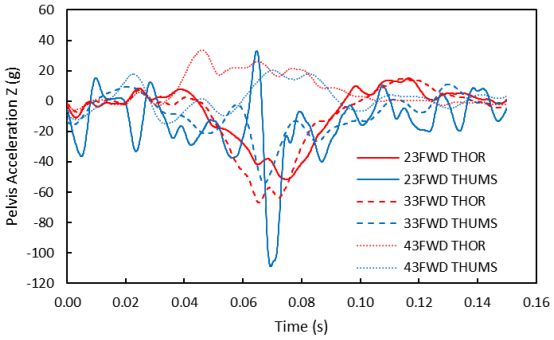

Figure 37. Pelvis acceleration in z direction

ASIS

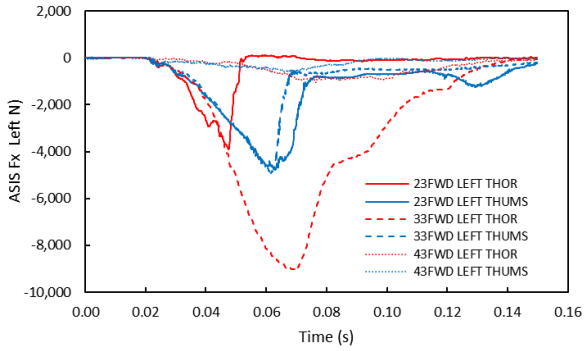

Figure 38. Force in x direction for the left A.S.I.S.

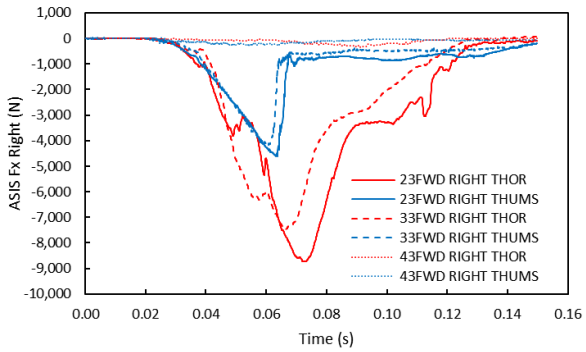

Figure 39. Force in x direction for the right A.S.I.S.

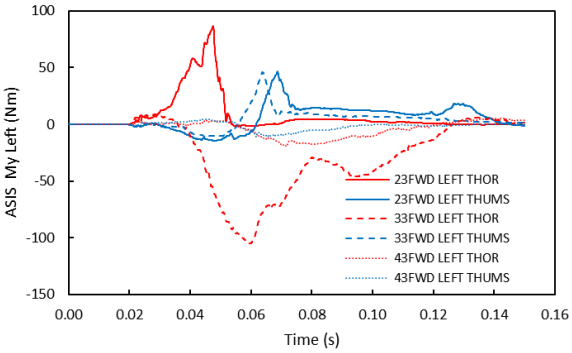

Figure 40. Moment in y direction for the left A.S.I.S

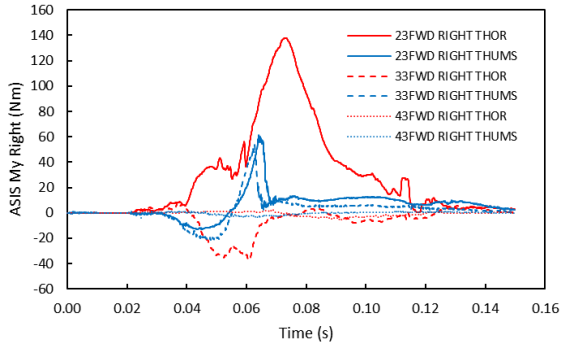

Figure 41. Moment in y direction for the right A.S.I.S.

Seat Belt

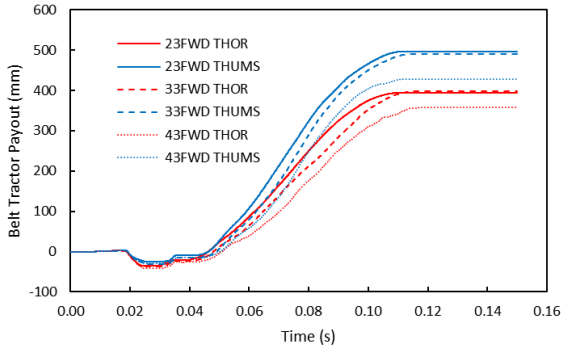

Figure 42. Shoulder belt tractor payout

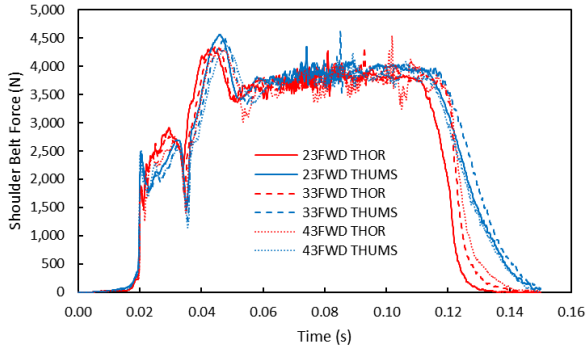

Figure 43. Shoulder belt force

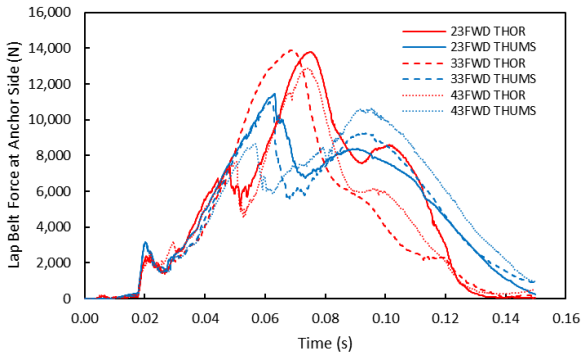

Figure 44. Lap belt force at anchor side

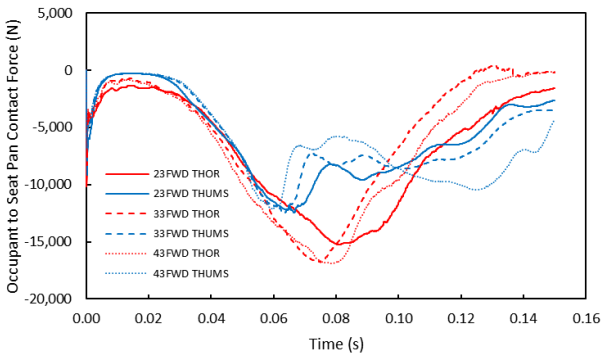

Figure 45. Occupant seat pan contact force

APPENDIX II Rear Facing Additional Plots

Head

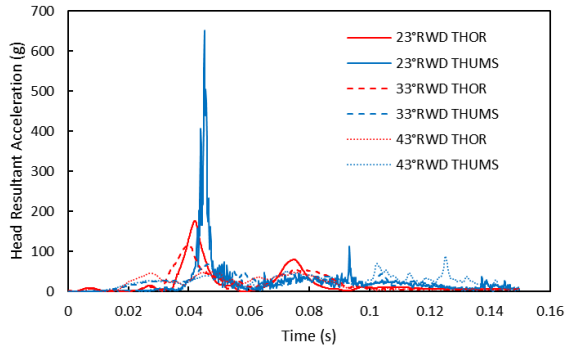

Figure 46. Head resultant acceleration

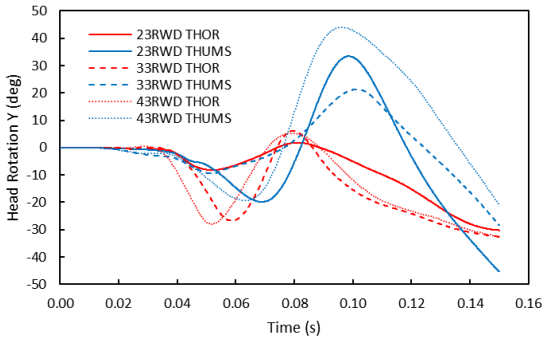

Figure 48. Head rotation y (integrated from angular rate)

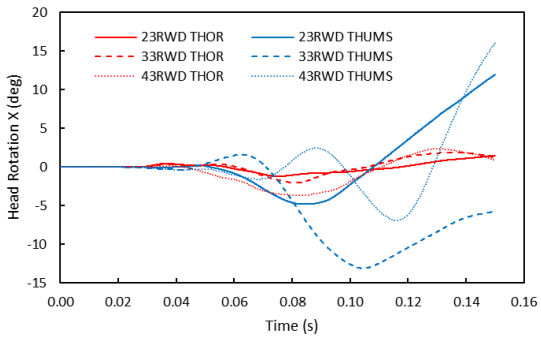

Figure 47. Head rotation x (integrated from angular rate)

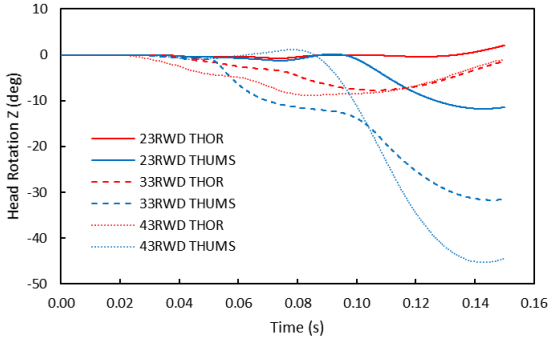

Figure 49. Head rotation z (integrated from angular rate)

Thorax Displacement – Upper Left and Right

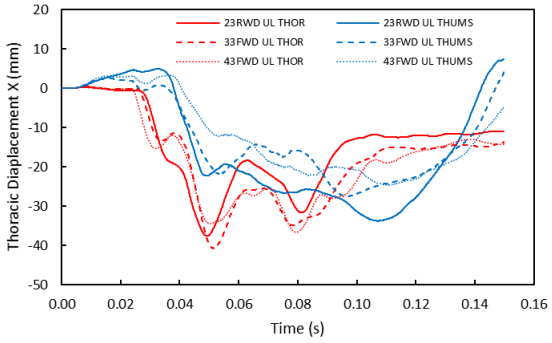

Figure 50. Displacement x at upper left IR-TRACC front attachment location

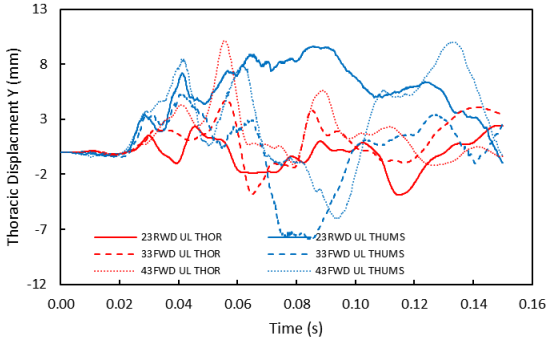

Figure 51. Displacement y at the upper left IR-TRACC front attachment location

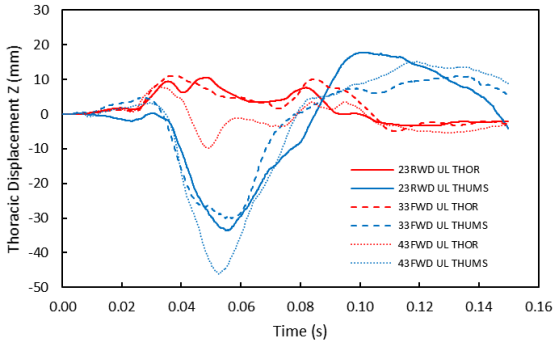

Figure 52. Displacement z at upper left IR-TRACC front attachment location

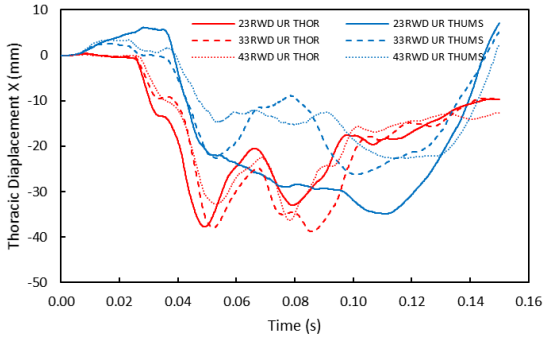

Figure 53. Displacement x at upper right IR-TRACC location

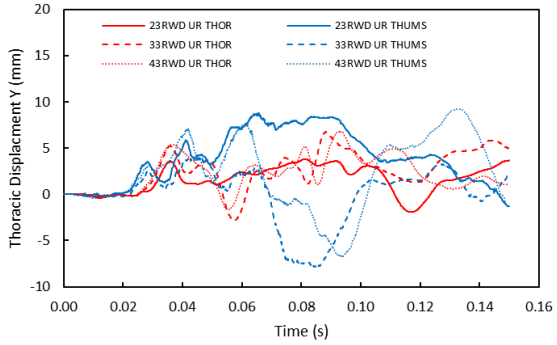

Figure 54. Displacement y at the upper right IR-TRACC location

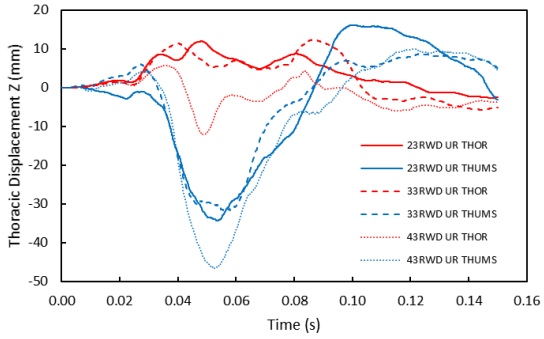

Figure 55. Displacement z at the upper right IR-TRACC location

Thorax Displacement – Lower Left and Right

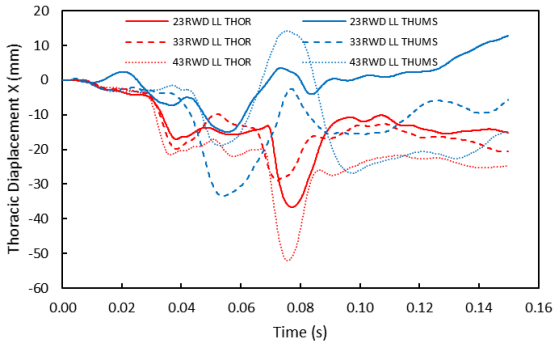

Figure 56. Displacement x at lower left IR-TRACC front attachment location

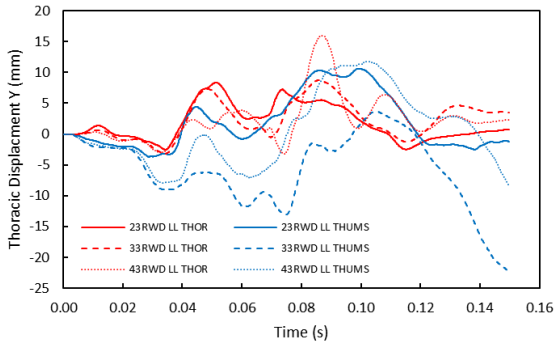

Figure 57. Displacement y at lower left IR-TRACC front attachment location

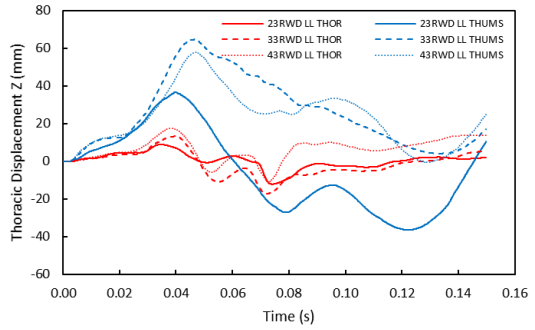

Figure 58. Displacement z at the lower left IR-TRACC attachment location

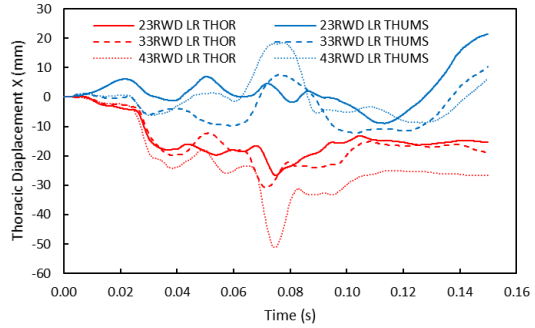

Figure 59. Displacement x at lower right IR-TRACC front attachment location

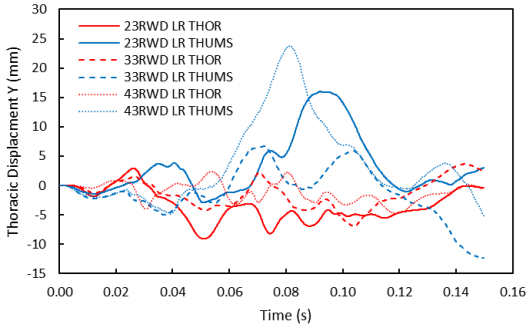

Figure 60. Displacement y at the lower right IR-TRACC front attachment location

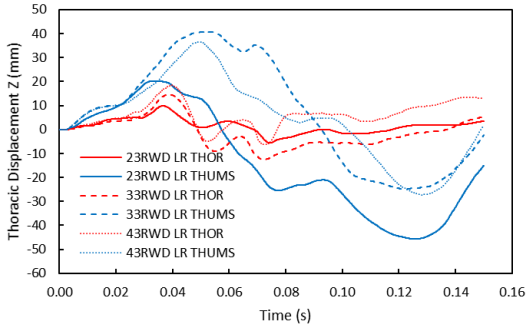

Figure 61. Displacement z at the lower right IR-TRACC front attachment location

Abdomen Displacement – Left and Right

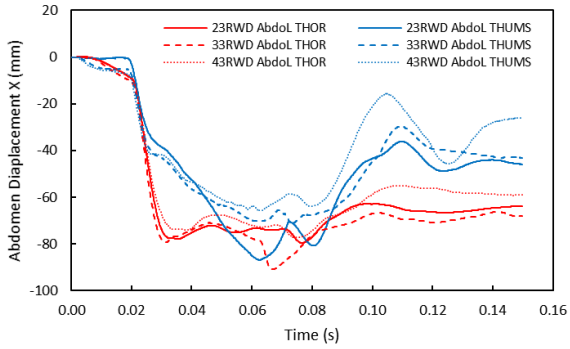

Figure 62. Displacement x at abdomen left IR-TRACC front attachment position

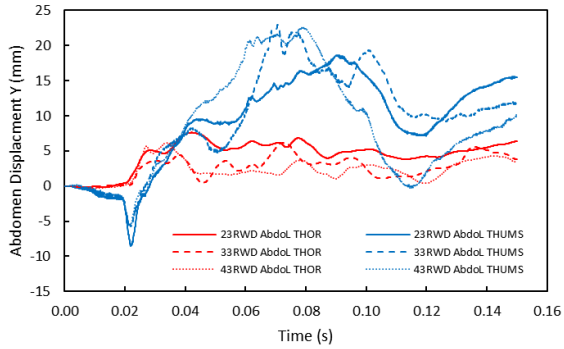

Figure 63. Displacement y at abdomen right IR-TRACC front attachment position

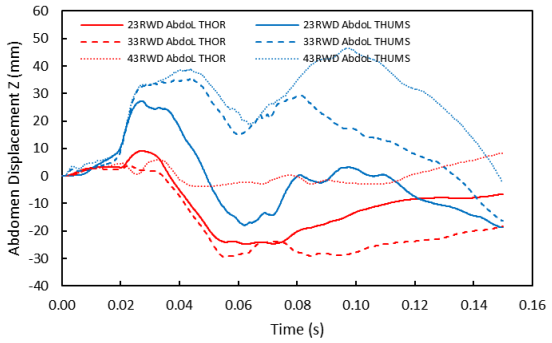

Figure 64. Displacement z at abdomen right IR-TRACC front attachment position

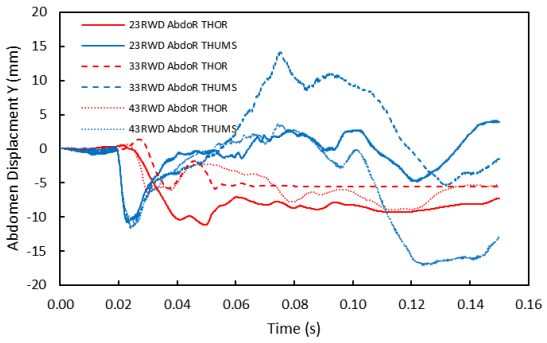

Figure 66. Displacement y at abdomen right IR-TRACC front attachment location

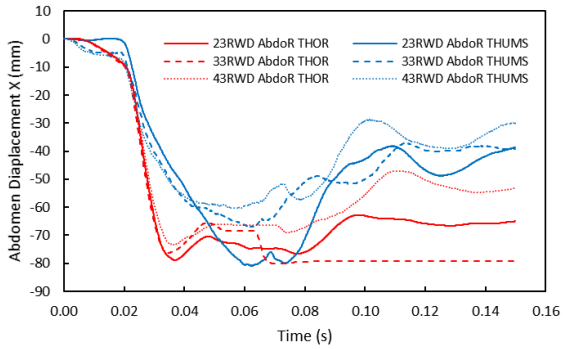

Figure 65. Displacement x at the abdomen right IR-TRACC front attachment location

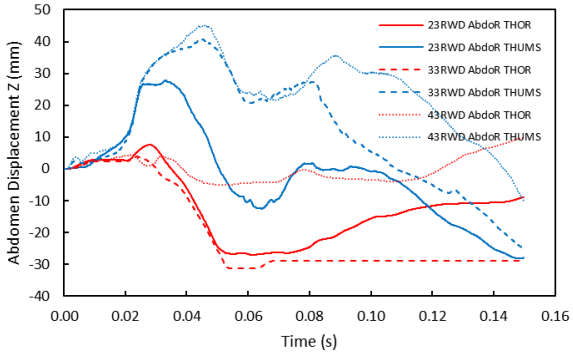

Figure 67. Displacement z at the abdomen right IR-TRACC front attachment location

Lumbar Spine

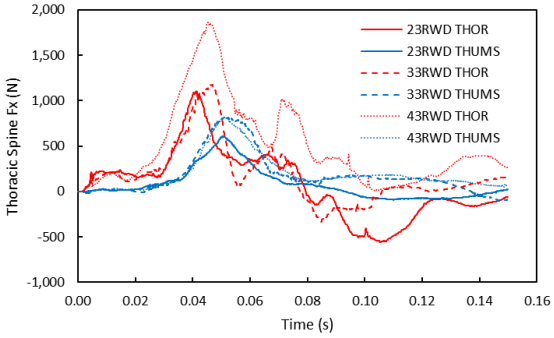

Figure 68. Lower thoracic spine force in x direction

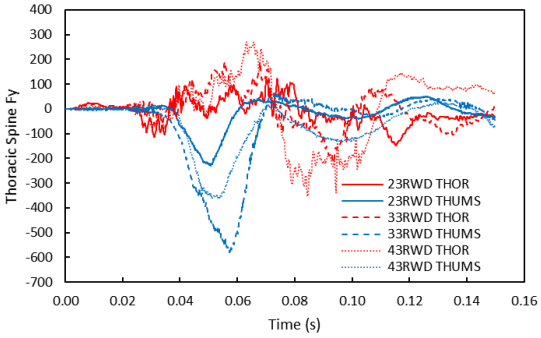

Figure 69. Lower thoracic spine force in y direction

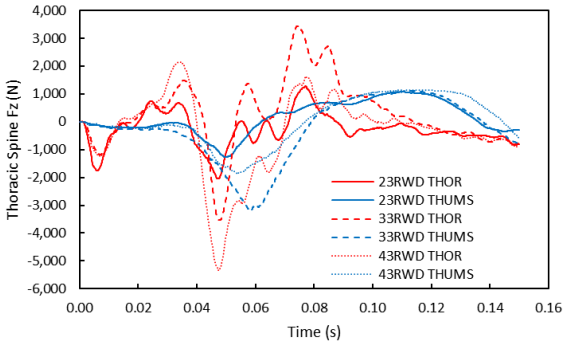

Figure 70. Lower thoracic spine force in z direction

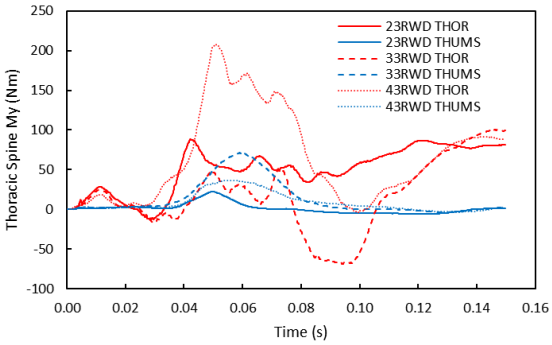

Figure 72. Lower thoracic spine moment in y direction

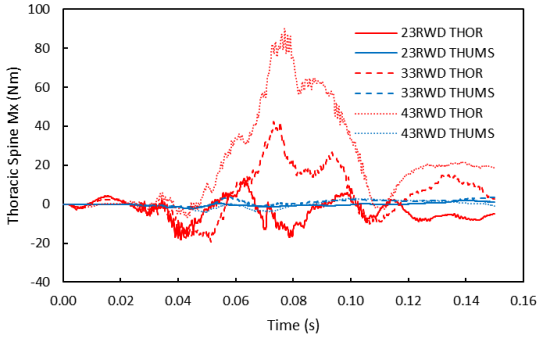

Figure 71. Lower thoracic spine moment in x direction

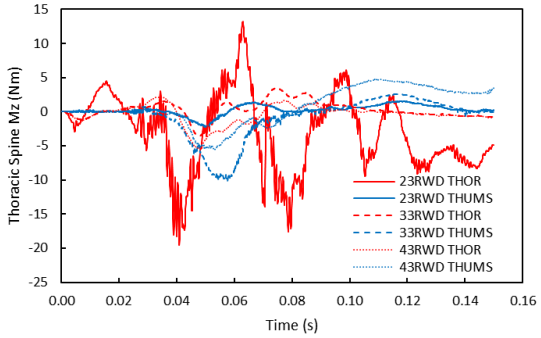

Figure 73. Lower thoracic spine moment in z direction

PROSPECTIVE SAFETY EFFECTIVENESS ASSESSMENT OF AUTOMATED DRIVING FUNCTIONS – FROM THE METHODS TO THE RESULTS

Felix Fahrenkrog
BMW AG
Germany

Lei Wang
BMW AG
Germany

Thomas Platzer
BMW AG
Germany

Alexandra Fries
BMW AG
Germany

Florian Raisch
BMW AG
Germany

Klaus Kompaß
BMW AG
Germany

Paper Number 19-0166

ABSTRACT

The development in the areas of sensors and electronics has been bringing the automotive industry increasingly closer to automated driving in recent years. Automated functions that need to be continuously supervised by the driver are already on the market. Highly automated driving functions (HAD) will enter the market in the near future. The German Ethics Commission for automated and connected driving stated in its report that "the licensing of automated functions is not justifiable unless it promises to produce at least a diminution in harm compared with human driving, in other words a positive balance of risks" [1]. This leads to the question, how the traffic safety effect of automated driving functions can be assessed taking into account possible positive and negative aspects?
This paper introduces comprehensively a method that is used by BMW for the prospective safety assessment of HAD by means of virtual experiments. This method is besides others part of the evaluation and safety assurance activities for HAD. The method is described from the scenario selection via the simulation up to the validation and verification. In contrast to other simulation approaches in this area, which mainly use accident re-simulation, this approach uses Monte-Carlo techniques, in which the initial starting conditions of the simulated driving scenario as well as the parameters of the involved drivers are randomly selected from distributions. These distributions base on accident data as well as on naturalistic driving data. A core aspect of this approach is the stochastic cognitive driver behavior model to describe the behavior of individually different traffic participants in a scenario. In contrast to accident re-simulation based approaches, this approach allows to analyze time-wise larger driving scenarios, which are of importance for HAD, since these functions act throughout the driving within the operational design domain and not only in critical situations.
The method for assessing the safety performance is applied to exemplary HAD. The results cover the positive effects, which are mainly achieved in today known accident scenarios, as well as scenarios, in which potentially new

risks compared to manual traffic can occur. One example for this is the minimum risk maneuver, for which the consequences of different implementation is discussed. Like all other methods (accident analysis, studies in driving simulator or on test track, field operational test) the simulation based approach has advantages and disadvantages. The main criticism is that the assessment is done virtual, which poses the question on the validity of the simulation. In order to tackle this aspect the validation and verification of the method and tool is a key aspect. Therefore, our current conceptual considerations regarding validation and verification are described in this paper.

INTRODUCTION

Since the 1960's different technologies have been introduced in the automobile industry in order to improve the traffic safety, see ***Figure 1***. The first type of technologies were passive safety systems (seat belt, airbag etc.). These technologies mainly aim to reduce the consequences of an accident. The next step were systems that actively try to prevent an accident or at least try to reduce – in case of unavoidable accidents – its consequences prior to the first contact. These systems are known as active safety technologies. Their development started with systems focusing mainly on the vehicle dynamics (e.g. ABS and ESC) in the 80's of the last century. From 2000 onwards further active safety systems entered the market. The systems use the information about environment and surrounding traffic in order to detect an imminent risk and to start countermeasures (e.g. AEB, blind spot detection). The third category of systems in the integrated traffic safety approach are systems that aim to prevent the occurrence of critical driving situations already beforehand. Systems of this category typically take over the control of the vehicle in longitudinal, lateral or both directions. These systems can be categorized by the SAE classification for automated driving [2]. The systems of this category range from advance driver assistance systems (ADAS), like ACC, up to highly automated driving functions (HAD). In particular the latter one is currently a major topic in the development of the automobile industry [3] [4].

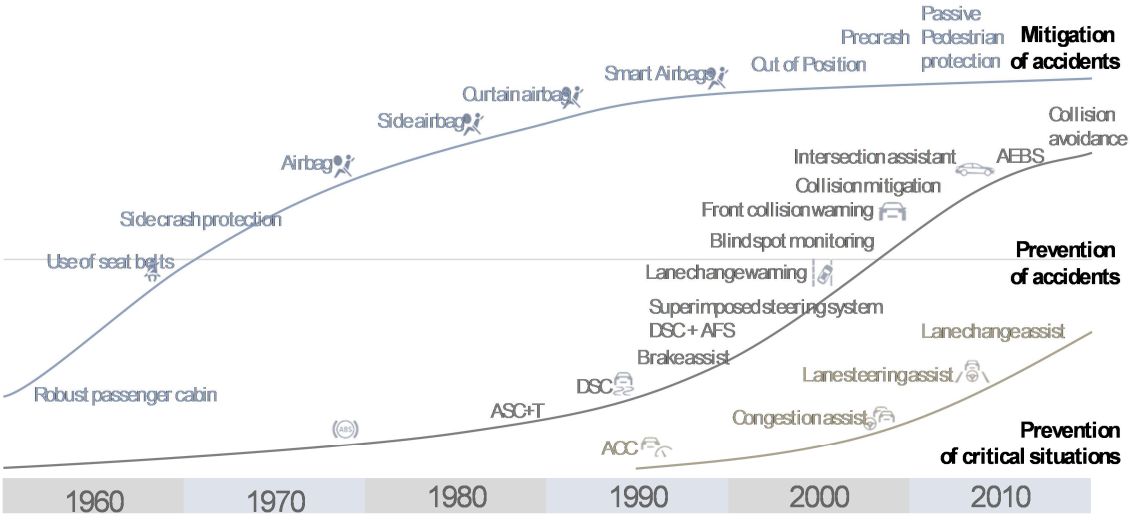

Figure 1. Integrated traffic safety approach [5].

Highly automated driving functions are expected to bring major improvements in terms of traffic safety [6] by avoiding human error related accidents. However, it must be taken into account that accidents are very rare events. Altogether 20.928 accidents occurred on a German motorway in 2017, in which a human was slightly, severely or fatally injured [7]. Considering an annual driving distance of approx. 243 billion kilometers [8] an accident with injured persons occurs statistically on a German motorway only approx. every 11.6 million kilometers. An improvement of traffic safety due to automated driving would become reality once it is proven that accident frequency is less than for human driving. Therefore, the German Ethics Commission on automated and connected driving request in article 3 "…The guiding principle is the avoidance of accidents, although technologically unavoidable residual risks do not militate against the introduction of automated driving if the balance of risks is fundamentally positive" [1]. This poses the question, how a positive balance of risk for automated driving can be

investigated and proven already before real world accident data are available. One method to investigate this balance of risk for automated driving is the prospective safety effectiveness assessment approach.
In the paper different approaches for the prospective safety effectiveness assessment are presented including BMW's simulation based approach for automated driving. This approach is later exemplarily applied for different driving scenarios. Finally, the paper ends with a description of the taken validation and verification approach for this method.

METHODS FOR PROSPECTIVE SAFETY EFFECTIVENESS ASSESSMENT

There are different approaches and tools to determine the effectiveness of a technology on traffic safety. In general the safety effectiveness assessment conducts a comparison of the situation without the technology under assessment (baseline) with the situation with the technology presented in terms of traffic safety.
At this point a distinction between the retrospective and prospective assessment approaches is necessary. The retrospective assessment is conducted after the market introduction of the technology. The assessment is typically done by means of real world accident data [9-11]. The advantage of this method is that it is capable to provide the real world impact of a technology. But there are two challenging aspects for this method. The first one is that confounding factors can hardly be controlled. The second aspect is that it requires a certain penetration rate of the technology, which means, that it cannot be used before a technology is introduced in the market or shortly after its introduction. However, the application of the method in the development is fundamental requirement, if the proof of a positive risk balance is prerequisite for the market introduction of automated driving.
The safety effectiveness assessment of the technology before its market introduction is aimed by the prospective assessment approaches. Basically, four different approaches are known. These are: field operational test (FOT), user studies in a controlled environment (driving simulator or test track), accident analysis and computer simulations. Each of these approaches has its advantages and disadvantages. The FOT approach, which has for instance applied in the euroFOT project [12], analyzes the effects of a technology in real world conditions. However, the approach requires quite high resources and can only be applied once a technology has reached maturity, which allows to test on public roads. Furthermore, due to the low likelihood of accidents, it is rather unlike that a statistical relevant number of accidents is detected in a FOT. For this reason typically surrogate measures (e.g. critical driving situations) are applied in the assessment. Studies with users on test tracks or driving simulators provide detailed information about the interaction of the user with the technology under controlled conditions and without posing the users any risk. This approach has been used in different studies, e.g. by [13]. However, these studies require also a high effort – in particular if the effect of technology should be analyzed in a large number of driving scenarios. In contrast the prospective accident analysis, which for instance has been applied in [14-16], allows to investigate the potential field of application with relative low effort. The drawback is that the approach is limited in the way, how precise the effectiveness of technology can be calculated, since specific effects in driving scenarios cannot be taken in account.
The remaining approach is the computer simulation, which has been used in different studies (e.g. [17-19]). This approach is able to investigate the safety effect of a technology in various driving scenarios at a reasonable effort. The challenging aspect for this approach is that it is done entirely virtually, which poses high requirements for the in the simulation applied models. It is also clear that input data from other tools are required to set up the simulations [20], e.g. accident data, driving simulator data, FOT data or data from naturalistic driving studies (NDS). Within the prospective safety effectiveness assessment by simulation two different approaches are known, see ***Figure 2***.

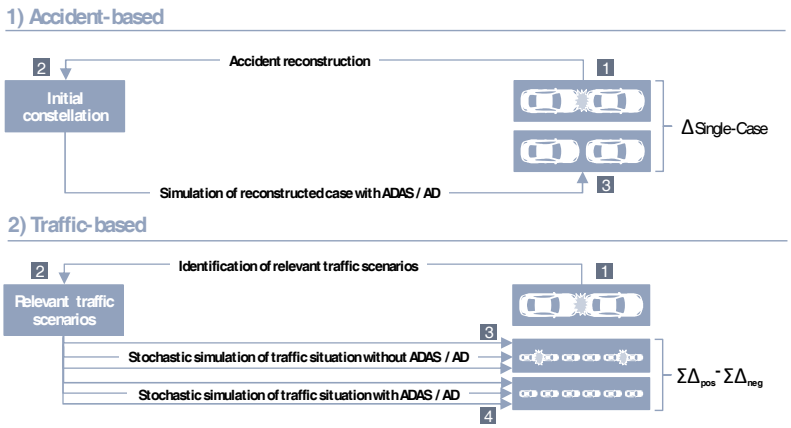

Figure 2. Approaches for the simulation based prospective safety effectiveness assessment.

The first approach is the accident-based approach. For this approach real-world accidents, which have been reconstructed, are simulated considering the technology to be assessed. The trajectory of the simulated traffic agents (combination of driver and vehicle) are derived from the original accident case. A prerequisite of this approach is that detailed reconstructed accidents are available. Examples for the application of this approach are [17] [18] [21-23]. Here, it must be noted that the uncertainty in the reconstruction increases the longer the accident case is reconstructed. Furthermore, this approach allows to investigate only critical situations. A modification of this approach in order to cover a wider range of situations can be accomplished by slightly altering the parameters of the original accident case in order to investigate, how a technology would react under the changed conditions [22] [24] [25].

The second approach is the traffic-based approach, which has been for example applied by [25-27]. Artificial driving scenarios are simulated within this approach. The starting conditions of the driving scenario are stochastically chosen from distributions that are derived from accident data or NDS/FOT data. Thus by means of the distribution the link between the simulated cases and the real world is ensured. In contrast to the accident-based approach no trajectories can be pre-calculated. Therefore, models are required that determine within the simulation the behavior of the traffic participants. For a valid simulation the quality of these models must be ensured. On the one hand there are no limitations in terms of duration and complexity (length of road, involved traffic participants, conducted maneuvers etc.) of the scenarios as for the accident-based approach. And by means of this approach also driving situations can be analyzed that are not critical in the first place, which allows to analyze, whether any false positive reactions of the technology are detected.

Due to the wide range of scenarios that can be analyzed at a reasonable effort BMW has used the traffic-based simulation approach for the prospective safety effectiveness in a wide range of different analyses [28-30] for ADAS. However, HAD poses new challenges for the prospective safety effectiveness assessment. The following sections discuss these challenges as well as the taken measures to solve them.

APPROACH FOR PROSPECTIVE SAFETY EFFECTIVENESS ASSESSMENT OF AUTOMATED DRIVING

The required adaption to apply the method of prospective safety effectiveness assessment by simulation for automated driving functions can be derived from the difference to active safety functions. First, in general each technology can have positive as well as negative effects on traffic safety. The longer the technology is operating the more situations are affected by the technology. Active safety systems, such as AEB, only operate respectively intervene in the driving dynamics once a critical situation is detected. These situations are – of course depending on the individual driving style – rare and short driving situations. In addition, the situations, in which the system is active, are clearly defined. Thus, the situation space can be narrowed down to a few types of situations. Since intervention just starts seconds before the imminent collision, the simulated time frame can rather be short. Also when assessing potential negative consequences it can be focused on situations that are short in time.

For the HAD the nature of the technology leads to different requirement. Here, the function can constantly operate through driving as long as the vehicle is in the operation design domain (ODD). This longer operation time of the HAD means that the simulation needs to cover larger and longer driving scenarios. Since during the drive different

maneuvers occur, it is not enough to focus just on single maneuvers. It is rather required to simulate the entire range from normal driving via critical situations up to the moment of the collision.
Furthermore, challenging driving scenarios for HAD, which might lead to negative impacts on traffic safety, must be paid more attention compared to active safety system for two reasons. First, the longer operation of HAD and by this larger interference with the traffic raise risk of executing not for given situation appropriate actions. The second reason is that HAD leads to new driving scenarios that are not part of the manual driving today. The main example is a driving scenario in which the driver has to take over vehicle control from the function.
A last important aspect for assessment of automated driving is that the function does not only change the severity of a situation as mainly considered for active safety systems, but also can influence the frequency of certain driving scenarios. One example is the passive cut-in maneuver. First experiences on public roads already show an increase of occurrence frequency of this maneuver while driving automated compared to manual driving [30]. Since the safety effect of a technology is described by the change in the severity and the frequency in the relevant driving scenarios, such effects must also be taken into account when assessing automated driving.
These requirements lead to the conclusion for prospective safety effectiveness assessment, which is only one part of the entire test and safety assurances activities of HAD, that an assessment for automated driving is only feasible by means of the traffic-based simulation approach. The accident-based simulation approach is too limited in terms of scenario duration and selection of scenario to ensure a comprehensive assessment. Of course it must be noted that the simulation approach requires different input data. The input data must come from other sources, like accident data, driving simulator data for e.g. describing the overtaking abilities of human drivers as well as FOT and NDS data. In the following relevant aspects of the traffic-based simulation approach as it is applied at BMW are highlighted.

Analyzed scenarios for automated driving

The assessment of automated driving requires consideration of driving situations, which might lead to positive as well as to negative effects in terms of traffic safety. In order to assess these effects the relevant driving scenarios must be identified. However, as stated earlier due the constant operation of HAD driving scenario does not mean that the scenario is limited in time to a few second and to a few involved traffic participants. Driving scenario here means that a larger road section – for instance two kilometers – with depending on the pre-defined traffic flow calculated number of traffic participant is simulated in which the certain driving maneuver or a kind of conflict occurs.
BMW's approach for identifying the scenario to be analyzed bases on three pillars, see **Figure 3**. The first pillar focuses on the driving scenarios for which positive effects of the HAD are expected. These can be derived from the driving scenarios, in which human drivers do not perform well. Typically these are accident situations. The major accident types that occur on German motorways are accidents related to (passive) cut-in, rear-end conflicts at the end of traffic jams, rear-end conflicts in general and single driving accidents, in which one vehicle leave the road not directly involving any other road users.

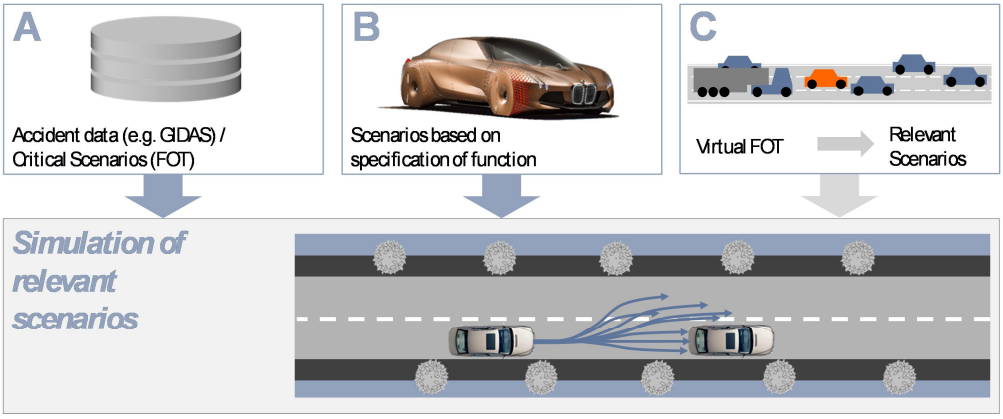

Figure 3. Identification of top scenarios for the assessment of HAD.

The second pillar considers the for the HAD challenging driving scenarios. The scenario can either have positive or negative effects. These driving scenarios are identified by means of analyzing the function itself. With respect to the accident frequency within manual driving, these scenarios are typically less relevant. Due to the uncertainty regarding the HAD behavior, they require more in-depth analysis. Examples are driving scenarios that require an interaction with other road users (e.g. highway entrance, end of driving lane), scenarios in which the HAD needs to take complex decisions (e.g. obstacle in the driving lane) and the already mentioned transition of control scenarios, in which the driver (suddenly) has to take-over the vehicle control from the function.
The last pillar addresses the issue of detecting changes in the frequency of driving scenarios. This is hardly possible by simulating driving scenarios. This requires even larger traffic simulations, in which longer and representative road sections are simulated. Therefore, BMW considers for this purpose a "virtual"-FOT approach, in which traffic scenarios with the HAD are simulated. In a second step relevant driving scenarios are identified in the output data of the simulations. This approach allows to get an understanding how the frequency of certain driving scenarios changes.

Simulation tool openPASS
Naturally, the simulation based approach for the prospective safety assessment requires a simulation tool, in which the simulation are carried out. There are several commercial tools available on the market. However, most of these tools are proprietary software tools that lead to limitations in terms of the required adaptations. Therefore, BMW does use for its approach the open source simulation tool openPASS [31], which is currently jointly developed under the eclipse foundation developed by BMW, Daimler, Volkswagen, Toyota, Bosch, TÜV Süd and ITK-Engineering.
openPASS offers the opportunity to simulate both simulation bases approaches in the prospective safety assessment, namely the accident-based and the traffic-based approaches. The modular framework of openPASS allows to include different models for the different modules, while the open source approach offers a certain transparency. Furthermore, it is possible to use within openPASS the open source interfaces such as openDRIVE, openSCENARIO, OSI and FMI. For the used approach of the HAD assessment the most important aspect of openPASS is that scenario can be simulated with several stochastic variations that could affect the environment, the vehicle, the sensors parameters and the traffic. A last important aspect is the driver behavior model that is addressed in the next section in more detail. Here, the flexibility of openPASS is used by integrating the BMW's driver behavior model in the simulation framework.

Driver Behavior Model
For the traffic-based simulation approach a driver behavior model is an essential building block. A driver behavior for the assessment of HAD is required for two purposes. The first purpose is to simulate the behavior of driver in the automated vehicle in situations, in which the driver must take over the driving task from the function. The second purpose is to describe the behavior of different traffic participants during situations considering the interaction among all relevant traffic participants. In the baseline simulation all traffic participants are controlled by the driver behavior model. In the treatment simulation the model is only relevant for the non-automated agents. Due to the fact that in the assessment a comparison between the baseline and treatment simulation is done, the risks in the baseline simulation should be comparable to the real world. Hence, the driver behavior model should cover the driving ability of a wide range of drivers including accident prevention strategies as well as faulty behavior of human drivers.
The requirement let to the development of Stochastic Cognitive Driver model (SCM) at BMW from 2014 onwards. This driver behavior model is mainly designed for highway traffic. The functional concept of the SCM combines human cognitive processes with stochastic process modeling. The SCM consists of five different sub-modules to represent the behavior of different drivers (information acquisition, mental model, decision making process, action patterns, action implementation). By means of these models it is possible to represent the process from the information acquisition up to steering, braking or acceleration actions by the agent. Due to the stochastic characteristics of the SCM it is guaranteed that agents behave differently in certain driving situations. And it is even possible that the same agent in the same situations reacts differently. By this it is ensured that a wide range of driver behavior is covered by the assessment.
Further developments of the SCM in the recent years covered two aspect. The first aspect is that the model's prediction and anticipated capabilities have been improved in order to ensure a better traffic flow and to reduce the accident rate in passive cut-in maneuvers [32]. The second aspect is the driver characteristics module. This sub-module links driver parameters (age, driven mileage) and states, such as fatigue and stress [33], with the driver parameters of the SCM. It covers individual and inter-individual driver differences and their impact on driver

behavior. In a one-way stochastic process, traffic agents are provided with a set of individual driver characteristics that shift, widen or narrow baseline distributions of stochastic parameters in all sub-modules of the SCM. By this, a broader spectrum of the over-all driver population can be modelled and virtual traffic simulations can be run as realistic as possible. For filling this sub-module with valid data, a driving simulator study has been conducted.
After the general background has been discussed, the next chapter shows exemplarily the application of the method for HAD.

APPLICATION OF METHOD FOR AUTOMATED DRIVING

After presenting the approach this chapter focuses on its exemplary application. For this purpose the effect of an exemplary HAD is analyzed in eight different driving scenarios. The eight different driving scenarios are: 1. Cut-In, 2. Traffic jam, 3. Rear-end accident, 4. Single driving accident, 5. End of Lane, 6. Obstacle in the lane, 7. Highway entrance and 8. Minimum risk maneuver after transition of control. The analysis have been conducted in the context of the European funded research project AdaptIVe [34] and the German funded research project Ko-HAF [35]. The first four scenarios are reported in the section for the accident scenarios, whereas the remaining four are reported in the section for the challenging scenarios.
It must be noted that analyzed HAD is an example function that does not represent BMW's actual implementation.

Analyzed highly automated driving function

The exemplary HAD that is simulated in the following has been implemented according to the **Table 1.** For the minimum risk maneuver that is activated in case the driver does not take over from the function two implementations are analyzed. For the first implementation a moderate deceleration (approx. 2 m/s²) and for the second implementation a strong deceleration (approx. 5 m/s²) is considered.

Table 1.
Specification of analyzed artificial automated driving function.

Category	Operation conditions
Road Type	Motorway
Conditions, when function is deactivated	Invalid environment conditions, end of motorway, defect in vehicle, loss of sensor data, loss of software module(s), construction sites
Covered environmental conditions	Dry condition and light rain in day and night
Speed range	0-130 km/h
Sensor range (front / side left / side right / rear)	200 m / 40 m / 40 m / 200 m
Covered driving maneuvers	Vehicle following in lane, obstacle or VRU on the road, lane change, stop & go driving, speed / time gap adaptation, enter and exit of motorway, minimum risk maneuver
Max. / Min. long. acceleration (normal operations)	4,0 m/s² / -4,0 m/s²
Max. / Min. lateral acceleration (normal operations)	3,0 m/s² / -3,0 m/s²

Safety performance of HAD in accident related traffic scenarios

First the driving scenarios are simulated according to the described method for which a positive effect of the HAD is expected. The change in the accident risk for the automated vehicle compared to the manual driven vehicle are given in **Table 2.** As expected all scenarios show potential to reduce the accident risk.

Table 2.
Results of the simulated accident related traffic scenarios [34].

Driving scenario	Expected mean change of accident rate [Confidence interval]	Accidents within ODD in GIDAS (including accident at speeds outside the operation conditions)
1. Cut-In	-83% [-76%; -90%]	72% (92%)

2. Traffic jam	-40% [-25%; -55%]	80% (89%)
3. Rear-end accident	-73% [-56%; -91%]	69% (96%)
4. Single driving accident	-100%* [-;-]	67% (93%)

The only scenario that has not been covered by the simulation approach is the "single driving accident". In this scenario the vehicle leaves unintendedly the lane or the road. It is expected that as long as a curve is in the ODD and no functional issues occur the function will be able to keep the vehicle in the lane and prevent by this the related accidents.

However, the effect in the driving scenario is only one part of the potential safety effect, since it implies the function can operate under all conditions and is always active. This of course does not meet the truth, since HAD is as described in Table 1 limited in terms of the ODD. In order to consider this limitation the third column in table 3 provides information about the proportion of the GIDAS accident [36] for which the ODD have been fulfilled. Regarding the proportion of the in the ODD included accident there is an uncertainty regarding accident that occur outside the operation speed of the HAD. For these cases either the function is switched on and drivers benefit as calculated or drivers intend to drive faster, which means that he/she switches the function off. This would result in no benefit at all. To a certain extent this is a country specific aspect, which is more relevant in Germany than other countries due to the in terms of speed limit unlimited German motorway. However, the principle question applies to all accidents above the operation speed of the HAD. Regarding the usage of the HAD any statement before market introduction is hardly possible, since the actual usage will depend on the HMI design and user's attitude towards the function.

Safety performance of HAD in challenging traffic scenarios

After the driving scenario with expected positive effect the challenging scenarios are evaluated. Table 3 provides the results of expected mean change of accident rate in the driving scenarios as well as the proportion of accidents in the ODD.

Table 3.
Results of the simulated challenging traffic scenarios [34][35].

Driving scenario	**Expected mean change of accident rate [Confidence interval]**	**Accidents within ODD in GIDAS (including accident at speeds outside the operation conditions)**
5. End of Lane	-14% [-8%; -20%]	67% (83%)
6. Obstacle in the lane	-40% [-34%; -47%]	78% (97%)
7. Highway entrance	-49% [-45%; -53%]	95% (95%)
8. Minimum risk maneuver (moderate deceleration)	+2.6% [+0.2%;+5.0%]	No reference data available
9. Minimum risk maneuver (strong deceleration)	+48.4% [+36.4%;+60.4%]	No reference data available

Simulations show a high variation in the results for the challenging scenarios. For obstacle in lane and highway entrance driving scenario a high potential for the reduction of accident risk is detected compared to the baseline scenario. For the minimum risk maneuver the situation differs. This does not surprise, since compared to normal driving an additional and properly for other traffic participant surprising braking maneuver is induced. For the moderate minimum risk maneuver the accident risk is approximately in the range of manual driving. The minimum risk maneuver with strong deceleration shows a significant increase of the accident risk compared to manual driving. Thus, from traffic safety perspective the deceleration in the minimum risk maneuver should be rather low. However, it is important to note in this context that the technical feasibility of applying a minimum risk maneuver has not been considered in this study. It is obvious that the implementation effort for moderate deceleration is significantly higher than for stronger deceleration, since the time that need to be covered by the maneuver is higher.

VALIDATION AND VERIFICATION PROCESS

Since the present approach for the prospective effectiveness assessment relies on virtual computer simulations, validation and verification is essential to ensure that the simulation provides trustable and reliable results. Within the validation and verification it is checked whether the results of a single model or the entire simulation meet the results of a reference within a pre-defined range. The challenge within the validation and verification for simulation is ensuring correctness of the simulation while keeping the effort for this activity at reasonable level.
Since BMW considers validation and verification as an important aspect for the method of the prospective safety effectiveness assessment, a validation and verification process has been defined for its simulation. The main requirements of BMW's validation and verification process are:

- This process must cover the entire method and all relevant (sub-)modules within the simulation method.
- The process shall be conducted at least once for each model and the entire method.
- It needs to be repeated depending on the changes on the method or on the simulation tool. For this purpose it is distinguished between minor and major changes depending on the impact of a change.
- In case already validated models are used, a further validation or verification of this model is not required.
- The reference shall be selected in accordance with to be validated model and the quality of the reference data.

An overview on models that can be validated and verified by means of different reference is given in the **Table 4.**
Independent of the taken approach, it must be decided in the end whether the output of the validated model is close enough to the reference. For the definition of the criteria the purpose of assessment as well as the quality of the reference data are of relevance. In case explicit criteria (e.g. max. error) are available, it shall be shown that these thresholds are met. This applies also if a certain target range is defined. Here, it can be necessary to break down into permitted inaccuracies per model. In case no explicit criteria is available the quality of a module can be quantified by one of the following approaches:

1) Calculation of a quality indicator (max. error).
2) Quantification of technical deviations between distributions (e.g. effect size).
3) Sensitivity analysis.
4) Explicit declaration of confidence intervals.

Table 4.
Reference data for different models in the validation and verification of simulation models.

Reference	**To be validated simulation model**
Real world effectiveness based on accident data	Entire method, collision model
FOT or NDS	Traffic module, driver behavior module
Test on test tracks	Vehicle module, technology module, driver behavior module
Driving simulator	Driver behavior module
Sensitivity analyses	Vehicle module, technology module
Review against the specification	Technology module
External database / literature	Environment module, driver behavior module, traffic module
Inspection	Collision module
Software tests incl. module, unit, integration and system tests	Simulation control

CONCLUSIONS AND DISCUSSION

This paper presented a comprehensive overview on the prospective safety assessment approach for HAD. The introduction of HAD leads to different challenges for the prospective safety assessment of this technology. In principle, different tools can be applied for the safety assessment. However, considering the advantages and disadvantages the simulation based assessment approach is the most promising approach for this purpose, since it is capable of covering a high variety of driving and traffic scenarios at reasonable effort. Nevertheless, the input of the other tools can and should be used for the correct definition of the in the simulation applied models. In this sense the simulation is a synthesis of knowledge that is gained by the assessment tools.

The key challenges of the simulation approach for the prospective safety assessment approach for HAD are besides the implementation of the function the identification of the relevant driving scenarios, the simulation tool and the driver behavior model. In the paper it has been reported how BMW addresses each of the issues.
Finally, the described method has been applied for an exemplary HAD. The results indicate that HAD can lead to a significant reduction of the accident risk in the specific scenarios within the ODD. For the challenging scenario the situation is not that clear. Here, also new risk in terms of traffic safety can occur. However, the differences in the outcome in terms of accident risk for the two minimum risk maneuvers emphasize the demand for detailed analysis considering the exact technology behavior as well as detailed simulations in this area.
The last challenge in the context is to prove that the derived results are reliable and trustable. Therefore, validation and verification of the method as well as the simulation tool including all models is essential. The paper reported on the taken validation and verification approach for the prospective safety assessment at BMW.

REFERENCES

[1] N.N. 2017. “Ethics commission – automated and connected driving”, Appointed by the Federal Minister of Transport and Digital Infrastructure, Final Report.

[2] N.N. 2018. “Taxonomy and Definitions for Terms Related to Driving Automation Systems for On-Road Motor Vehicles”, SAE International, Document J3016_201806.

[3] Etemad, A., Bartels, A. 2014. “A Stepwise Market Introduction of Automated Driving”, 21st ITS World Congress, Detroit.

[4] M. Aeberhard., S. Rauch, M. Bahram, G. Tanzmeister, J. Thomas, Y. Pilat, F. Homm, W., Huber, W. and N. Kaempchen 2015. „Experience, Results and Lessons Learned from Automated Driving on Germany’s Highways”, Intelligent Transportation Systems Magazine, IEEE, 7(1):42–57.

[5] Martinez von Bülow, R., Raisch, F., 2018. „Driver Assistance System / Highly Automated Driving – Acceptance and Benefit for Customers“, VDA Technical Congress 2018, Berlin.

[6] N.N. 2015. “Automated Driving Roadmap”, ETRAC Task Force “Connectivity and Automated Driving”, Version 5.

[7] N.N. 2018. “Verkehr - Verkehrsunfälle - 2017”, Statistisches Bundesamt (Destatis).

[8] N.N. 2017. „Verkehr in Zahlen 2017/2018”, Bundesministerium für Verkehr und digitale Infrastruktur.

[9] Farmer, C.M. 2004 “Effect of Electronic Stability Control on Automobile Crash Risk”, Traffic Injury Prevention 5, 317–325.

[10] Langwieder, K., Gwehenberger, J., Hummerl, T. 2004. “Sicherheitsgewinn durch ESP Internationale Erfahrung aus Realunfällen“, 1. Tagung Aktive Sicherheit durch Fahrerassistenzsysteme, Munich.

[11] Knoll, P. Langwieder, K. 2006. “Der Sicherheitseffekt von ESP in Realunfällen – Überlegungen zum volks-wirtschaftlichen Nutzen von prädiktiven Fahrerassistenzsystemen”, 2. Tagung Aktive Sicherheut durch Fahrerassistenz, Munich.

[12] Kessler, C., Etemad, A., Alessandretti, G., et al. 2012. “Final Report” euroFOT Deliverable D11.3, Version 1.1.

[13] Breuer, J. 2009. “Bewertungsverfahren von Fahrerassistenzsystemen Handbuch Fahrerassistenzsystem“, Vieweg+Teubner, 1st edition.

[14] Kocherscheidt, H. 2004. “Wege zur Effizienzbetrachtung von Fahrerassistenzsystemen“, 1. Tagung Aktive Sicherheit durch Fahrerassistenz, Munich.

[15] Frost, U. and Keller, H. 1988. “Einschätzung einer Zuordnung von Prometheus-Maßnahmen und Unfalltype“, TU München, Munich.

[16] Dryselius, B. 1990. “Summary Report: Estimation of the Potential Safety Effects of Different Possible PROMETHEUS-Functions” ProGEN Safey Group, Stuttgart.

[17] Van Noort, M., Bakri, T., Fahrenkrog, F., Dobberstein, J. 2015. “SIMPATO - The Sfety Impact Assessment Tool of interactIVe,” IEEE Intell. Transp. Syst. Mag., vol. 20.

[18] Wille, J. M., Zatloukal, M. 2012. “rateEFFECT: Effectiveness Evaluation of Active Safety Systems,” in 5th International Conference on ESAR „Expert Symposium on Accident Research“, pp. 1–41.

[19] Kates, R., Jung, O., Helmer, T., Ebner, A., Gruber, C., Kompass, K. 2010. “Stochastic Simulation of Critical Traffic Situations for the Evaluation of Preventive Pedestrian Protection Systems,” Erprobung und Simulation in der Fahrzeugentwicklung.

[20] Fahrenkrog, F., Zlocki, A., Eckstein, L. 2014. “Bewertung Aktiver Sicherheit: Vom Test zur Wirksamkeitsanalyse“. ATZ, 1(116):34–39.

[21] Lindman, T., Ödblom, M., Bergvall, A. et al. 2010. “Benefit Estimation Model for Pedestrian Auto Brake Functionality”, ESAR - Expert Symposium on Accident Research.
[22] Kolk, H., Tomasch, E., Sinz, W., et al. 2016. “Evaluation of a momentum based impact model and application in an effectivity study considering junction accidents” ESAR - Expert Symposium on Accident Research.
[23] Zauner, C., Tomasch, E., Sinz, W., et al. 2014. “Assessment of the effectiveness of Intersection Assistance Systems at urban and rural accident sites,” ESAR - Expert Symposium on Accident Research.
[24] Kolk, H., Kirschbichler, S., Tomasch, E. 2016. “Prospective evaluation of the collision severity of L7e vehicles considering a Collision Mitigation System”, Transportation Research Procedia, vol. 2016.
[25] Fahrenkrog, F. 2016. “Wirksamkeitsnalanyse von Fahrerassistenzsystemen in Bezug auf die Verkehrssicherheit”, Dissertation RWTH Aachen University, fka mbH Aachen.
[26] Luttenberger P., et al. 2014. “Method for future pedestrian accident scenario prediction”, Transport Research Arena.
[27] Helmer, T., Neubauer, M., Rauscher, S., et al. 2012. “Requirements and methods to ensure a representative analysis of active safety systems”, 11th International Symposium and Exhibition on Sophisticated Car Occupant Safety Systems.
[28] Helmer, T., Scullion, P., Samaha, R., et al. 2011. „Predicting the Injury Severity of Pedestrians in Frontal Vehicle Crashes based on Empirical, In-depth Accident Data”, International Journal of Intelligent Transportation Systems Research, 9(3):139–151.
[29] Helmer, T., Kühbeck, T., Gruber, C., Kates, R. 2012. “Development of an integrated test bed and virtual laboratory for safety performance prediction in active safety systems” FISITA 2012 World Automotive Congress - Proceedings and Abstracts, ISBN 978-7-5640-6987-2.
[30] Rösener, C., 2017, “A Comprehensive Evaluation Methodology for Automated Driving”, AdaptIVe, Final Event 29th June 2017.
[31] N.N., 2019. “openPASS”, https://openpass.eclipse.org/, Eclipse.
[32] Ring, P., Wang, L., Fahrenkrog, F., Jung, O. et al., 2017. „Modelling Cognitive Driver Behavior In The Context Of Prospective Safety Assessment” Aachner Kolloquium, Aachen.
[33] Witt, M., Wang, L., Prokop, G., Kompaß, K. 2017. „Kognitive Fahrerverhaltensmodellierung in der virtuellen Bewertung von Fahrerassistenzsystemen unter Berücksichtigung der Ausprägungen menschlichen Fahrens.“ 8. Tagung Fahrerassistenz, Munich.
[34] Fahrenkrog, F., 2017. “Impact Assessment”, AdaptIVe Final Event, Aachen.
[35] Fahrenkrog, F., 2018. “Prospective Effectiveness Assessment“, Ko-HAF Final Event, Results - Poster, https://www.ko-haf.de, Dudenhofen.
[36] Seek, A.; Gail, J.; Sferco, R.; et al. 2009. ”Development of the accident investigation and data handling methodology in the GIDAS project”, Enhanced Safety of Vehicles Conference, Washington D.C.

SOCIETAL BENEFIT OF AUTOMATIC EMERGENCY BRAKING AND LANE DEPARTURE WARNING SYSTEMS IN LARGE TRUCKS

Jeffrey S. Hickman
Matthew Camden
Alejandra Medina-Flintsch
Richard J. Hanowski
Virginia Tech Transportation Institute
U.S.A.

Brian Tefft, B.[2]
AAA Foundation for Traffic Safety, U.S.A.

Paper Number: #19-0167

ABSTRACT

The objective of this study was to provide scientifically-based estimates of the societal benefits and costs of two large truck advanced driver assistance systems (ADASs): automatic emergency braking (AEB) and lane departure warning (LDW). For each technology, benefit-cost analyses (BCA) were performed for installing the technology on all large trucks (including retrofitting old trucks) and for equipping new large trucks only, and were performed for equipping only single-unit trucks, only combination-unit trucks, and all large trucks. Sensitivity analyses examined three cost estimates, two estimates of system efficacy, and three discount rates. Equipping trucks with LDW systems were found cost-effective under almost all scenarios examined. Results for AEB were mixed. Only the low cost estimate was cost effective for all large trucks regardless of efficacy rate.

BACKGROUND

Recent advances in large truck advanced driver assistance systems (ADASs) have shown promise to mitigate risky driving behaviors or errors, which in turn help prevent large truck crashes. ADASs may use sensors or alerts to warn a driver of a possible collision, actively assume lateral and/or longitudinal control of a vehicle in situations where a driver does not react to the threat of an imminent crash, or improve driver and fleet management. Two of these large truck ADASs include automatic emergency braking (AEB) systems and lane departure warning (LDW) systems,

AEB systems combine a forward-looking sensor, driver alerts, and automatic vehicle braking. These systems are designed to reduce or prevent rear-end collisions in which the large truck strikes another vehicle (and, to a lesser extent, head-on collisions). LDW systems are vision-based, in-vehicle electronic systems that monitor the vehicle's position within the roadway. Based on lane line markings, the LDW system warns a driver if the vehicle deviates or is about to unintentionally deviate outside the lane line. LDW systems are designed to prevent single vehicle roadway departures, sideswipes, opposite sideswipes, and to a lesser extent, head-on crashes.

Although these large truck ADAS may be effective at preventing large truck crashes, there is limited published data on whether they are cost effective. Despite advancements in the effectiveness of these systems, widespread adoption across the transportation industry is slow. Cost effectiveness data is critical for ADAS as this information may increase industry adoption rates and/or government regulators in mandating their use.

Project Objective

The objective of this project was to provide scientifically-based estimates of the societal benefits and costs (i.e., the impacts an ADAS may have across the entire U.S. society if implemented) of two large truck ADASs, including: AEB systems and LDW systems. To accomplish this objective an Expert Advisory Panel informed cost and benefit estimations for these ADASs so a benefit-cost analysis (BCA) could be performed.

METHODS

An Expert Advisory Panel was held on May 17, 2017. This Advisory Panel consisted of six individuals representing various aspects of the trucking industry, including a representative from a commercial motor vehicle carrier, a trucking insurance company, the Federal Motor Carrier Safety Administration (FMCSA), the National Highway Traffic Safety Administration (NHTSA), an ADAS technology vendor, and an industry safety consultant. The purpose of this meeting was to identify the appropriate efficacy rates and costs for each ADAS and the crash types that may be mitigated or prevented by each of the ADASs. When determining the recommended efficacy rates and cost associated with ADAS, the Advisory Panel prioritized recent research, real-world studies, generation of the technology, Federal regulations, efficacy/cost estimates from the U.S. (due to differences in roadway infrastructure, safety culture, and crash rates), and crash reductions for specific crash types (compared to crash reductions to all large truck crashes). Additionally, the Advisory Panel was

conservative in their efficacy estimates. Following this discussion, upper- and lower-bound efficacy rates and low, average, and high costs were selected for each of the two ADAS (Table 1). The efficacy rates selected by the Expert Panel were applied only to the relevant crash types.

Table 1. Advisory Panel Recommended Relevant Crash Types, Efficacy Rates, and Cost

ADAS	Relevant Crash Types	Efficacy Rates	Costs
AEB	Large truck striking rear-end crashes	16% and 28%[1]	$500, $2,500, $3,000[2-4]
LDW.	Single vehicle roadway departures, sideswipes, opposite direction sideswipes, and head-on collisions	30% and 47.8%[3,5]	$500, $1,000, $1,200[3,6-8]

Benefit Cost Analysis Methods

The BCA followed conventional methods used in similar studies to estimate the societal benefits and costs of implementing ADASs in the trucking industry [1-4]. Societal benefits and costs associated with a reduction in crashes with each ADAS were compared to the costs of deploying each ADAS across the entire U.S. fleet of large trucks over an analysis period of 20 years starting in 2018. The benefits included medical-related costs, emergency response service costs, property damage, lost productivity from roadway congestion, and monetized value of quality-adjusted-life-years lost. Costs considered in this study included the purchase and installation costs associated with the ADAS's hardware, maintenance costs of the ADAS, replacement costs of the ADAS, and costs associated with training drivers to use the ADAS, including driver coaching when applicable.

All costs were calculated using information provided by FMCSA (crash costs), the Bureau of Labor Statistics (training costs), costs provided by carriers and technology providers (hardware costs and training requirements), Ricardo's [5] cost and weight analysis, and the Federal Highway Administration, NHTSA, and the Department of Energy (large truck population, large truck population entering the market, vehicle miles traveled, and vehicle age).

To assess the crash reductions (and their associated costs) of each ADAS, national crash databases were used to identify the target population for each ADAS. These crash databases included the Fatality Analysis Reporting System (FARS) and the General Estimates System (GES). The FARS database was used to determine the number of fatal crashes and their associated fatalities and injuries, and the GES database was used as an estimation for injury and property damage only (PDO) crashes. The GES database also was used to estimate the number of injuries as a result of injury crashes. Queries were developed for each ADAS and information was extracted for different vehicle types for a period of 6 years (2010 to 2015).

When filtering the GES and FARS crashes, the research team carefully considered the scenarios where each ADAS could have mitigated or prevented the crash. Specifically, only rear-end crashes where the large truck struck another vehicle were selected for AEB; all large truck road departures, sideswipes, opposite sideswipes, and head-on crashes were selected for LDW. Additionally, the research team used the following GES/FARS variables to further limit crashes that may have been prevented by each ADAS: pre-event movement, critical event, and first harmful event. Finally, all crashes that involved the use of alcohol or drugs by the large truck driver were eliminated.

Two BCAs were performed for each ADAS. The first analyses included retrofitting the entire U.S. fleet of large trucks with the ADAS. This approach assumed all new trucks added to the fleet are equipped with the ADAS and old trucks are retrofitted with the ADAS. These analyses represents the most benefits, but also the largest costs. The second analyses were an annual incremental costs analysis. This approach assumed all new trucks will be equipped with the ADAS (staring in 2018) and no old trucks are retrofitted. Societal benefits were assessed over the life of the truck for both analyses.

Additionally, analyses were performed on different types of large trucks. The first analysis included all class 7 and 8 trucks (gross vehicle weight rating greater than 26,000 pounds). The second was performed only using class 7 and 8 combination unit trucks (CUTs). The third analysis used class 7 and 8 single unit trucks (SUTs). Finally, separate analyses were performed for each ADAS to account for the rate of monetary discount, in the present value, of the cost and benefits in any future year. Following guidance from the Office of Management and Budget [6] analyses were performed using a 0%, 3%, and 7% discount rate.

RESULTS

The BCA results for each of the ADASs are presented below.

Automatic Emergency Braking Systems

AEB systems were evaluated using a low and high efficacy rate (16% and 28%, respectively) and a low, average, and high cost ($500, $2,500, and $3,000, respectively). Table 2 shows the benefit cost ratios (BCRs) for AEB systems when equipping all trucks (new and old). The analyses with a BCR greater than 1.00 indicate the benefits outweigh the costs (highlighted cells in Table 2). For example, the third row in Table 2 shows the results for all large trucks using a high efficacy rate for AEB systems. When the costs of AEB systems are average and the discount rate is 0%, the estimated costs of AEB systems are 9% greater than the estimated benefits. However, when the costs of AEB systems are low and the discount rate is 0%, the estimated benefits of AEB systems are 3.75 times as great as the estimated costs. Overall, only the low cost estimate was found to be cost effective.

Table 2. BCRs for AEB Systems Installed on New and Old Trucks by Vehicle Type, Efficacy Rate, Cost, and Discount Rate

	Low Cost ($500)			Average Cost ($2,500)			High Cost ($3,000)		
	0%	3%	7%	0%	3%	7%	0%	3%	7%
All Large trucks – 28% Efficacy	3.75	3.58	3.37	0.91	0.87	0.82	0.76	0.73	0.69
All Large trucks – 16% Efficacy	2.14	2.05	1.93	0.52	0.50	0.47	0.44	0.42	0.39
Only CUTs – 28% Efficacy	4.11	3.94	3.72	0.99	0.95	0.90	0.83	0.80	0.76
Only CUTs – 16% Efficacy	2.35	2.25	2.13	0.56	0.54	0.52	0.47	0.46	0.43
Only SUTs – 28% Efficacy	3.08	2.92	2.72	0.75	0.72	0.67	0.63	0.60	0.56
Only SUTs – 16% Efficacy	1.76	1.67	1.56	0.43	0.41	0.38	0.36	0.34	0.32

Table 3 shows the BCRs for AEB systems when only equipping new trucks. As shown in Table 3, a low-cost AEB system was cost effective with a 26% efficacy rate. However, the $2,500 and $3,000 AEB system were also cost effective with a 28% efficacy rate.

Table 3. BCRs for AEB Systems Installed on New Trucks Only by Vehicle Type, Efficacy Rate, Cost, and Discount Rate

	Low Cost ($500)			Average Cost ($2,500)			High Cost ($3,000)		
	0%	3%	7%	0%	3%	7%	0%	3%	7%
All Large trucks – 28% Efficacy	6.09	5.67	5.27	1.62	1.49	1.36	1.37	1.26	1.15
All Large trucks – 16% Efficacy	3.48	3.24	3.01	0.92	0.85	0.78	0.78	0.72	0.66
Only CUTs – 28% Efficacy	6.41	5.97	5.54	1.70	1.57	1.43	1.44	1.32	1.21
Only CUTs – 16% Efficacy	3.66	3.41	3.17	0.97	0.89	0.82	0.82	0.76	0.69
Only SUTs – 28% Efficacy	6.09	5.67	5.27	1.62	1.49	1.36	1.21	1.12	1.02
Only SUTs – 16% Efficacy	3.48	3.24	3.01	0.92	0.85	0.78	0.69	0.64	0.58

Lane Departure Warning Systems

LDW systems were evaluated using a low and high efficacy rate (30% and 47.8%, respectively) and a low, average, and high cost ($500, $1,000, and $1,200, respectively). Table 4 shows the BCRs for LDW systems when equipping all trucks (new and old). The results showed that equipping all large trucks or all CUTs with LDW were cost effective regardless of cost, efficacy rate, or discount rate. Additionally, equipping all SUTs with LDW was cost effective with a high efficacy rate regardless of cost or discount rate. However, LDW was only cost effective for SUTs with a low cost.

Table 4. BCRs for LDW Systems Installed on All Trucks by Vehicle Type, Efficacy Rate, Cost, and Discount Rate

	Low Cost ($500)			Average Cost ($1,000)			High Cost ($1,200)		
	0%	3%	7%	0%	3%	7%	0%	3%	7%
All Large trucks – 47.8% Efficacy	4.11	3.92	3.69	2.30	2.20	2.08	1.96	1.88	1.77
All Large trucks – 30% Efficacy	2.62	2.50	2.36	1.47	1.41	1.33	1.25	1.20	1.13
Only CUTs – 47.8% Efficacy	4.83	4.63	4.38	2.70	2.59	2.46	2.29	2.21	2.09
Only CUTs – 30% Efficacy	3.08	2.96	2.79	1.72	1.66	1.57	1.46	1.41	1.33
Only SUTs – 47.8% Efficacy	2.74	2.60	2.43	1.55	1.47	1.37	1.32	1.25	1.17
Only SUTs – 30% Efficacy	1.75	1.66	1.55	0.99	0.94	0.88	0.84	0.80	0.75

Table 5 shows the BCRs for LDW systems when only equipping new trucks. As shown in Table 5, low-, average-, and high-cost LDW systems were cost effective for the lower and upper efficacy rate with all truck types.

Table 5. BCRs for LDW Systems Installed on New Trucks Only by Vehicle Type, Efficacy Rate, Cost, and Discount Rate

	Low Cost ($500)			Average Cost ($1,000)			High Cost ($1,200)		
	0%	3%	7%	0%	3%	7%	0%	3%	7%
All Large trucks – 47.8% Efficacy	6.67	6.21	5.77	3.94	3.65	3.36	3.39	3.13	2.87
All Large trucks – 30% Efficacy	4.26	3.96	3.68	2.52	2.33	2.14	2.16	2.00	1.83

	Low Cost ($500)			Average Cost ($1,000)			High Cost ($1,200)		
	0%	3%	7%	0%	3%	7%	0%	3%	7%
Only CUTs – 47.8% Efficacy	7.53	7.02	6.52	4.45	4.12	3.79	3.83	3.54	3.25
Only CUTs – 30% Efficacy	4.81	4.48	4.16	2.84	2.63	2.42	2.44	2.26	2.07
Only SUTs – 47.8% Efficacy	4.83	4.50	4.18	2.85	2.64	2.43	2.45	2.27	2.08
Only SUTs – 30% Efficacy	3.08	2.87	2.67	1.82	1.69	1.55	1.57	1.45	1.33

DISCUSSION

The current study used efficacy rates from previously published research and identified crashes that may have been prevented through the deployment of an ADAS. Crashes were identified using 2010 to 2015 GES and FARS datasets. BCAs were performed using varying efficacy rates (low and high), vehicle types (all large trucks, only CUTs, and only SUTs), costs (low, average, and high), and discount rates (0%, 3%, and 7%).

Automatic Emergency Braking System Conclusions

The results showed the current pricing/efficacy rate used in this study did not always suggest that AEB systems were cost effective. Only a $500 AEB system was found to consistently be cost effective regardless of which trucks were equipped with the system. Average and high-cost systems were only found to be cost effective occasionally. Additionally, retrofitting old large trucks with AEB systems typically was not cost effective. These results provide insight into the feasibility of government regulation for large truck AEB systems. There was not a strong case for government regulation requiring AEB systems for the entire U.S. fleet of large trucks given the cost/efficacy rates used in this study. However, the analyses showed AEB systems on new CUTs were cost effective with a high efficacy rate regardless of cost. If the cost and efficacy of AEB systems can be maintained (or improved from) at $2,500 and 28%, respectively, regulation may be appropriate.

Lane Departure Warning System Conclusions

The results strongly support the cost effectiveness of LDW systems for all large trucks. Regardless of cost and efficacy rate, LDW systems were shown to be cost effective. These results were likely due to: (1) the relatively low cost of LDW systems compared to other ADASs, and (2) the large number/severity of roadway departures, sideswipes, opposite sideswipes, and head-on crashes that could be prevented with LDW systems. As with the other ADASs, cost effectiveness was higher with regulations only for new large trucks. However, these results would support LDW system regulations for both all trucks (retrofitting and original equipment manufacturer installed) and only new large trucks. Mandating LDW on all large trucks (both new and old) would result in the largest benefits in crashes prevented.

REFERENCES [1] Hickman, J. S., F. Guo, M. C. Camden, A. Medina, R. J. Hanowski, and E. Mabry. *Onboard Safety System Effectiveness Evaluation Final Report.* Report No. FMCSA-RRT-12-012. FMCSA, U.S. Department of Transportation, 2013.

[2] Houser, A., D. Murray, S. Shackelford, R. Kreeb, and T. Dunn. *Analysis of Benefits and Costs of Lane Departure Warning Systems for the Trucking Industry.* Report No. FMCSA-RRT-09-022. FMCSA, U.S. Department of Transportation, 2009.

[3] Murray, D., S. Shackelford, and A. Houser. *Analysis of Benefits and Costs of Forward Collision Warning Systems for the Trucking Industry*. Report No. FMCSA-RRT-09-021. FMCSA, U.S. Department of Transportation, 2009.

[4] Murray, D., S. Shackelford, and A. Houser. *Analysis of Benefits and Costs of Roll Stability Control Systems for the Trucking Industry.* Report No. FMCSA-RRT-090-020. FMCSA, U.S. Department of Transportation, 2009.

[5] Ricardo Inc. *Cost & Weight Analysis for CMB and LDWS for Heavy Trucks*. Report No. NHTSA-2011-0066-0085. NHTSA, U.S. Department of Transportation, 2013.

[6] Office of Management and Budget. *Circular A-4: Regulatory Analysis.* OMB, 2003

Evaluation of the Safety Performance and Weight Reduction Using CFRP Modified Automotive Structures in NHTSA's Frontal Oblique Impact Test

William Hollowell, Ph.D.
WTH Consulting LLC

Rudolf Reichert
Steve Kan, Ph.D.
Chung-Kyu Park, Ph.D.
George Mason University

United States

Paper Number 19-0169

ABSTRACT

In a project conducted for NHTSA during 2016-2017, finite element analysis simulations were conducted representing NHTSA's right and left oblique impact configurations being developed for possible use in the agency's New Car Assessment Program. For the study using this test procedure, simulations were conducted representing an offset moving deformable barrier impacting a stationary 2015 Toyota Camry with a 35 percent overlap and an angle of 15 degrees (from collinear) at a speed of 90 km/h. In the NHTSA project, the model was successfully used to develop structural countermeasures in order to reduce occupant compartment intrusion for the new oblique impact configuration. Higher strength steel materials and modification of component thicknesses allowed the reduction of occupant compartment intrusion by more than 50%. As part of this effort, George Mason University (GMU) calculated mass and relative material expense comparisons to traditional materials. As a result, three optimized models using traditional materials were created. The accomplished reduction of occupant compartment intrusion ranged from 52% to 69% and the associated added mass ranged from 7.3 kg to 17.3 kg. The significant reduction in intrusion was achieved without unintended consequences, i.e., no considerable increases in the vehicle pulse severity for oblique and co-linear crash configurations were observed.

Following these results, the American Chemistry Council (ACC) commissioned this subsequent study to determine if the vehicle could be lightweighted and provide a similar reduction of occupant compartment intrusion for NHTSA's right and left oblique impact configurations using carbon fiber reinforced plastic (CFRP) composite materials. Different thicknesses for relevant components were evaluated and associated reductions in intrusion, associated changes in mass, and associated critical areas with material failure were determined. As a result of using selected components made out of a composite material, a similar reduction in occupant compartment intrusion was achieved in NHTSA's right and left oblique impact configuration as realized for the best high strength steel model. In using the CFRP composite material, the associated change in mass was a reduction of 7 kg of the baseline vehicle as compared to an increase of 17 kg in the baseline vehicle mass when using more traditional countermeasures--higher component thicknesses and use of high strength steel materials.

The developed and incorporated countermeasures using composite materials were also evaluated to determine if they produced unintended consequences in other impact configurations. The developed FE models, which showed reduced occupant compartment intrusion due to components made out of the CFRP composite material in NHTSA's oblique crash configuration, were also evaluated in NHTSA's NCAP full overlap and in the Insurance Institute for Highway Safety (IIHS) partial overlap crash configurations. No unintended consequences were observed when the results were analyzed with respect to vehicle pulse and intrusion when compared to the results using the baseline simulation model.

In addition to the above technical achievements, in partnership with Honda R&D Americas and LSTC; other efforts are underway. These include the development of a material constitutive model of the composite material for use in modeling and subsequent simulation in automotive crash applications. Also, validation efforts using CFRP components will be undertaken.

INTRODUCTION

In fiscal year 2006, Congress directed the National Highway Traffic Safety Administration (NHTSA) of the U.S. Department of Transportation (DOT) to begin the development of a program to examine the possible safety benefits of lightweight Plastics- and Composite-Intensive Vehicles (PCIVs). NHTSA tasked the Volpe National Transportation Systems Center to conduct focused research in cooperation with industry partners from the American Plastics Council (APC), now the American Chemistry Council Plastics Division (ACC-PD).

NHTSA concentrated on the safety-related research issues affecting the deployment of PCIVs in 2020. In 2007, the Volpe Center developed a safety roadmap for future PCIVs and described the approach, activities, and results of an evaluation of potential safety benefits of PCIVs [1,2]. Barnes et al. identified outstanding safety issues and research needs for PCIVs to facilitate their safety deployment by 2020, and recommended three topics pertinent to crashworthiness of PCIVs: (1) material database, (2) crashworthiness test method development, and (3) crash modeling [3].

In 2001, the APC (now the ACC-PD) outlined a Vision and Technology Roadmap for the automotive and plastics industries [4]. In the technology integration workshop in 2005, the ACC-PD provided an expansive safety road mapping effort, examining PCIVs [5]. In 2009, the ACC-PD updated the vision and technology roadmap to outline the industry's action priorities for achieving the technology and manufacturing innovations required to realize PCIVs [6]. In addition, the ACC-PD recommended three research activities: (1) improvement of the understanding of composite component response in vehicle crashes, (2) development of a database of relevant parameters for composite materials, and (3) enhancement of predictive models to avoid costly overdesign [7].

There is an increasing need to investigate opportunities for weight reduction of the vehicle fleet to improve fuel economy and compatibility. However, this should be achieved without sacrificing the current self-protection. Innovative plastics and fiber-reinforced composite materials offer a means to lightweight vehicle structures. The main advantages of composites over the more conventional isotropic materials are the lower density, very high specific strength, and specific stiffness that can be achieved.

In 2014, the ACC-PD updated the Plastics and Polymer Composites Technology Roadmap for Automotive Markets [8] in response to the U.S. Corporate Average Fuel Economy (CAFE) standards in order to develop an effective industry-wide strategy that will extend to 2030 and beyond. The roadmap addresses current barriers and key initiatives to recognize plastics and polymer composites as preferred material solutions that meet automotive performance and sustainability requirements.

As part of implementing the ACC roadmap, the ACC partnered with the George Mason University's Center for Collision and Safety Analysis (GMU/CCSA) to conduct research to evaluate the application of plastics and composites using Computer-Aided Engineering (CAE) simulations. In a previous study, the GMU Team developed a lightweight vehicle by replacing existing steel components with plastics or composite components in a reverse-engineered computer model. To support realistic development, industry partners participated in the project by providing available plastics/composite materials and their application and design. The crashworthiness of the light-weighted components was investigated through impact simulations, both at a component level and at a full vehicle level. The results were documented in Reference [9].

A more specific research task was adopted in this current project. Using computer simulation, an evaluation was conducted to determine if countermeasures using CFRP modified automotive structures in NHTSA's newly developed frontal oblique impact test procedure could achieve a similar reduction in occupant compartment intrusion as countermeasures using high-strength steel materials.

Consumer information crash tests, such as NHTSA's New Car Assessment Program's (NCAP's) full overlap frontal impact and the Insurance Institute for Highway Safety's (IIHS's) small and moderate overlap frontal impacts, have contributed to advance vehicle safety and reduce injury risk in the past. Recent studies have indicated that oblique crashes represent common real-world accident patterns related to belted occupant fatalities [10]. When comparing the number of injuries by body region for oblique and co-linear frontal impacts, it was observed that drivers in left oblique impacts experienced more Maximum Abbreviated Injury Scale (MAIS) 3+ injuries in almost every body region than drivers in co-linear crashes [11].

The Center for Collision Safety and Analysis (CCSA) at George Mason University (GMU) has analyzed sixteen left oblique tests conducted by NHTSA regarding intrusion patterns and related injury risk [12]. Furthermore, 65 oblique and 265 NCAP full overlap tests were analyzed regarding vehicle pulse, intrusion, and injury metrics. While there was no clear trend linking higher intrusion to higher tibia loads, it was found that occupant compartment intrusion, pulse severity, and local effects could contribute to lower extremity injuries. It can be concluded that risk of injury can increase as the maximum intrusion from the occupant compartment increases.

IIHS compared the performance of 25 vehicles in NHTSA's frontal oblique condition and the IIHS small overlap configuration. The selected cars represented a wide range of vehicle sizes. With respect to lower extremity injuries, it was found that 36% (9 cars) of the vehicles exceeded preliminary Injury Assessment Reference Values (IARVs) in the oblique impact, while only 8% (2 cars) exceeded the IARVs for the small overlap configuration [13]. Differences in vehicle pulse and occupant compartment intrusion are considered possible reasons.

The oblique impact test captures the deformations of a significant number of real-world accidents that occur today, and the development of additional countermeasures for restraints and vehicle structure may have the potential to further improve vehicle safety and reduce injury risk in the future. Consequently, NHTSA is considering adopting a frontal oblique impact configuration into its NCAP rating protocol [11].

The developed laboratory test procedure is conducted in combination with a more biofidelic dummy, the Test device for Human Occupant Restraints (THOR) [11]. An Oblique Moving Deformable Barrier (OMDB) was developed to produce target vehicle crush patterns similar to real-world cases [14]. It has a weight of 2,500 kilograms (kg) and impacts a stationary vehicle at a speed of 90 kilometers per hour (km/h). The vehicle is placed at a 15-degree angle and a 35-percent overlap occurs between the OMDB and the front end of the struck vehicle, as shown in Figure 1.

Figure 1 - Frontal Oblique Test Configuration

Crash test results have shown that vehicles may require structural modifications for good performance in NHTSA's frontal oblique test procedure. In a previous project that was funded by NHTSA, the GMU team determined incremental vehicle structural change requirements using steel materials and their associated mass to significantly reduce occupant compartment intrusion.

An available FE model of a 2012 Toyota Camry mid-size sedan was updated and validated using data to represent a 2015 Toyota Camry. The newly generated baseline model correlated well with the New Car Assessment Program (NCAP) full overlap test, NHTSA's left and right oblique impact tests, and with the IIHS small and moderate overlap crash configurations. An iterative process was used to develop countermeasures to significantly reduce occupant compartment intrusion for the left and right oblique impact configuration. No un-intended consequences (i.e., no considerable increase in the vehicle pulses for the oblique and co-linear crash configurations) were observed. The associated added mass was +17 kg using high-strength steel materials [15].

The aforementioned developed FE model and tools were used to determine if similar results (i.e., a similar reduction in occupant compartment intrusion, and no un-intended consequences, such as significantly more severe vehicle crash pulses) could be achieved using composite materials for select components.

OBJECTIVE

The objective of this research was to develop changes using CFRP composite materials to modify a passenger vehicle's structure to provide equivalent performance as the vehicle modified with high strength steel modifications in order to reduce occupant compartment intrusion in NHTSA's oblique frontal crash test condition. Structural countermeasures for both the driver's and passenger's sides of the vehicle for left- and right-side oblique impacts were to be developed.

VEHICLE SELECTION

The vehicle selected for this study was the baseline selected for the NHTSA study using the high strength steels for improving the crash performance in the frontal oblique offset test. Several criteria were used to determine an appropriate vehicle on which to conduct that research. This included evaluation of the number of vehicle sales as a measure of how well it represents mid-size sedans in the United States (US), performance in existing consumer information tests, and availability of an adequate FE simulation baseline model. The vehicle also was required to meet the structural intrusion requirements for a "GOOD" or "ACCEPTABLE" structural rating in the IIHS small overlap crash test, "GOOD" rating in the IIHS moderate overlap crash test, and a 5-Star rating in the NCAP full frontal crash test.

Satisfying the aforementioned criteria, a FE model of a 2012 Toyota Camry, which had been developed by the GMU Team, was used as a starting point. Toyota introduced structural design changes in January 2014. The MY 2012 mid-size sedan FE model was updated accordingly. Figure 2a illustrates the relevant structural differences between MY 2012 and MY 2015. Figure 2b shows (from right to left) a bottom view of the finite element model with an enlarged view of the added bumper reinforcement extension and "spacer" for the simulation model and the physical vehicle.

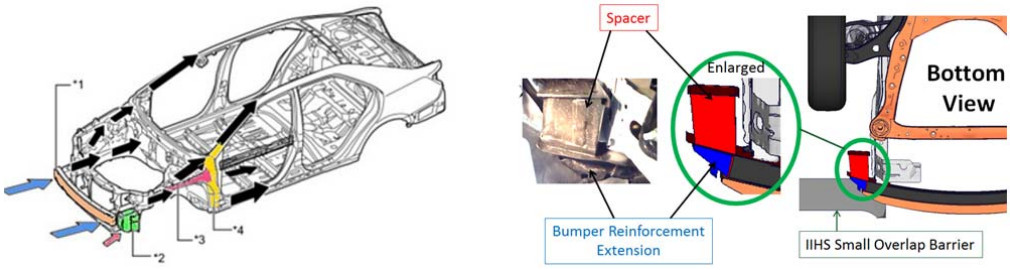

Figure 2 – Design Changes (a) Schematic, (b) "Spacer"

Advanced modeling techniques for the wheel connection were implemented into the FE model to better represent the failure mechanisms and wheel kinematics seen in the IIHS small overlap impact. The added bumper reinforcement extension and spacer interacts with the IIHS small overlap barrier and activates the frontal rail on the driver side. The deformation of the longitudinal rail contributes to the structural crash energy absorption. Full-scale test results showed that the design changes mainly affected performance in the IIHS small overlap impact, while other crash configurations, such as NCAP full overlap and NHTSA left oblique impact, showed similar results for the MY 2012 and MY 2015 vehicles.

All updates were implemented to the driver and passenger side of the FE model. The associated added vehicle mass was equivalent to 9.7 kg and is like the difference in vehicle mass from NHTSA's left oblique test of a MY 2015 vehicle (test #8790, 1450 kg as delivered, 1734 kg as tested) and a MY 2012 vehicle (test #9124, 1443 kg as delivered, 1759 kg as tested).

Test data from the MY 2015 vehicle was used to evaluate the updated FE model. Full-scale crash tests with vehicles that included these changes are called "2015 Toyota Camry" tests in the remainder of this paper. Even though complete information for all the detailed design changes from MY 2012 to MY 2015 was not available, it was determined that the updated FE model does a good job of simulating the performance of the MY 2015 mid-size sedan in the respective crash configurations.

Shown in Figures 3 and 4 are the vehicle's longitudinal (X-axis) acceleration time histories for the left oblique and right oblique simulations versus the test results. Also shown in each figure is the CORA rating value. The CORA values of 0.94 and 0.93 respectively represent a good correlation between the test and simulation results.

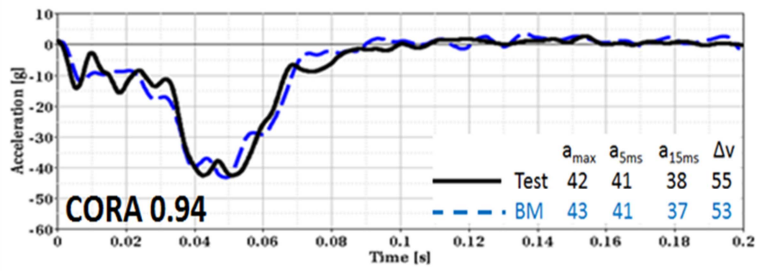

Figure 3 - 2015 Left Oblique Test vs Sim. - Vehicle Pulse

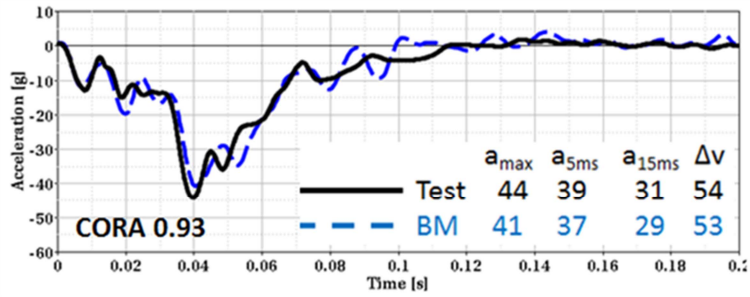

Figure 4 - Right Oblique Test vs Sim. - Vehicle Pulse

All baseline simulations were conducted using this model. It will be called the "2015 Toyota Camry Baseline Model (TCBM)" in the remainder of this paper. For this study looking at CFRP composite structural modifications, the developed structural countermeasures to significantly reduce occupant compartment intrusion were evaluated with respect to the TCBM and to the TCBM with the high strength steel modifications.

CFRP COMPOSITE MATERIAL SELECTED FOR STUDY

In a previous study [16], a braided carbon-fiber thermoset composite material was selected as the steel substitute in the vehicle structures. Many material tests and numerical simulations were conducted to identify its material characteristics for a Carbon Fiber Reinforced Plastic (CFRP). Their results are described in the project report [16]. A brief summary of these is described in this section. The developed and validated material card was used for select components when developing structural countermeasures to reduce occupant compartment intrusion in NHTSA's oblique impact configuration.

Tri-axial braided composites can offer an isotropic design by using axial and angled fiber bundles in a single plan. Braided composites also offer better damage resistance, torsional stability, and bending strength compared to unidirectional or weaved composites. Tri-axial braided composites have been used in the commercial aerospace and automotive industry for over 20 years. They are well suited for components that are of simple geometry and need to provide off-axis as well as unidirectional strength. In addition, various studies using braided composites have been conducted and published.

The selected braided CFRP composite used for the material tests is described as follows. The carbon fiber was Torayca T700S C 12000, manufactured by Toray Carbon Fibers America, Inc. The braid architecture is 0°/±60° 2D triaxial (2D3A), as shown in Figure 5. The axial fiber tows contained 24K fibers. The bias tows contained 12K fibers. The resin was Epon 862 epoxy with an Epikure W curing agent, both manufactured by Momentive.

Figure 5 - 2D3A braided composite: (a) panel, (b) unit cell.

Tension, compression and shear coupon tests were performed in two different directions (axial and transverse) and at four different loading rates. The tension test used two different types of specimens; a standard specimen and a bowtie specimen. A total of 72 coupon tests were conducted. Tube compression tests were performed with three different loading rates. Reference 16 provides a summary of the test data and the material properties used for LSDYNA's MAT58 material cards.

STRUCTURAL COUNTERMEASURES

Three sets of countermeasures using high-strength steel materials were developed to meet the defined design goals in the previous project, funded by NHTSA. The countermeasure model ("CM-Steel") that showed the highest amount of occupant compartment intrusion reduction is discussed in this paper. It serves as reference for the countermeasure model using composite material ("CM-Composite"). Occupant compartment intrusion was reduced by more than 60% compared to the baseline model (BM). Figure 6 presents an overview of the implemented modifications for CM-Steel.

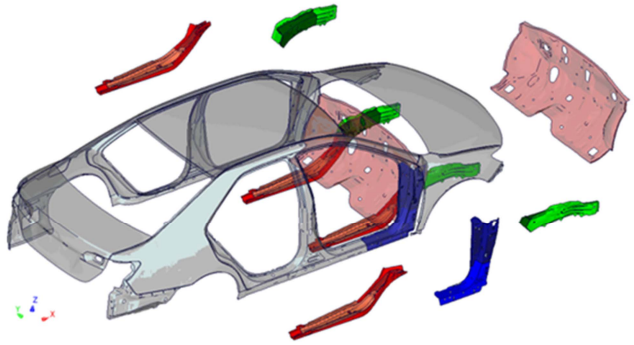

Figure 6 – CM Steel - Structural Countermeasures

The firewall, three components of the right hinge pillar, two parts of the left and right frontal rails, and three parts of the left and right mid-rails were modified.

In order to reduce maximum toe-pan intrusion and local buckling, the material thickness and material strength were increased for the firewall, shown in pink. Material thickness was also increased for three components of the right hinge pillar, shown in blue. For the inner hinge pillar (a) and the middle hinge pillar (b) material strength was also increased. The material strength for the outer hinge pillar (c) was not changed in order to allow the same manufacturing stamping process used for the BM. Changes to the right hinge pillar contributed to reduced intrusion and reduced local buckling, specifically in the right oblique impact. The parking brake on the driver side acts as a reinforcement of the hinge pillar area on the driver side. Therefore, the left hinge pillar components were not changed.

In order to reduce the load induced into the firewall, material thickness for two parts of the left and right frontal rails, shown in green, were marginally reduced. This contributed to reduction in maximum toe-pan intrusion and local buckling.

For this study, the use of CFRP composite material for the development of structural countermeasures to significantly reduce occupant compartment intrusion in NHTSA's oblique impact condition required having a thorough understanding of the crash mechanisms. The baseline vehicle model crash simulations were analyzed with respect to crash mechanisms that specifically contribute to the observed intrusion in left and right oblique impacts.

Local buckling of the firewall was found to be a major factor. Highest intrusion values were observed for toe-pan measurement points in row 1, which represent the most forward and upward locations. It was found that the load transferred through the longitudinal rail contributed to the maximum intrusion values. It can be noted that the load introduced through the frontal rails is being leveraged through the difference in height between the frontal rail and the bottom of the mid-rails. The load introduced through the frontal rail contributes to the maximum intrusion values and local buckling of the toe-pan.

Local buckling of the mid-rails also contributed to the observed occupant compartment intrusion. It was found that there was a significant amount of deformation occurring in the right mid-rail. The parking brake on the driver side is connected to the rocker pillar and the toe-pan area. It acts as a reinforcement of the rocker pillar area on the driver side. Since there is no equivalent component on the passenger side, a significant amount of deformation of the right rocker pillar components was observed in the right oblique impact configuration. Deformation of the rocker pillar components on the passenger side contributed to the maximum occupant compartment intrusion in the right oblique impact.

A firewall support component around the steering column exists on the driver side. The absence of an equivalent firewall support component on the passenger side contributed to the maximum occupant compartment intrusion in the right oblique impact.

As a result of the above analysis, an evaluation was undertaken to determine if a similar reduction of occupant compartment intrusion could be achieved by using the CFRP composite for the firewall component. Three different thicknesses, i.e., 1.2 mm (2 layers), 2.4 mm (4 layers), and 3.6 mm (6 layers) were evaluated. The associated change in vehicle mass for the CM-Composite vehicles compared to the TCBM was -15 kg, -11 kg, and -7 kg, respectively.

RESULTS

Left Oblique Impact

CM-Steel simulation results were compared against the respective BM simulation in NHTSA's left oblique impact configuration. The maximum toe-pan intrusion was reduced by more than 60%. Figure 7 shows a cross-section view of the left passenger compartment. The black line represents the un-deformed "pre-crash" vehicle. The red line represents the deformed shape of the baseline model with high occupant compartment intrusion. The green line shows the deformed shape of the CM-Steel vehicle with a significant reduction of intrusion compared to the BM. The associated change in mass when using countermeasures made out of steel, was +17 kg compared to the BM.

The dark red line represents the CM-Composite 1 vehicle, where a composite material made out of two layers was used for the firewall. Intrusion was as high as for the BM and the associated change in mass was -15 kg. The yellow line shows the CM-Composite 2 vehicle with 4 layers of composite and an associated change in mass of -11 kg. Intrusion was reduced compared to the BM but was still significantly higher than for the CM-Steel vehicle. The blue line represents the CM-Composite 3 vehicle with 6 layers of composite. The respective thickness was 3.6 mm and the associated reduction in mass compared to the BM was -7 kg. Similar reduction of occupant compartment intrusion was achieved with the CM-Composite 3 model compared to the CM-Steel vehicle. However, instead of adding 17 kg to the total vehicle mass when using steel countermeasures, a reduction of 7 kg was achieved when using composite countermeasures. The CM-Composite 3 vehicle will also be called "CM-Composite" in the remainder of this paper.

Figure 7 – Left Oblique Intrusion- Baseline vs. CM-Steel and CM-Composite

Figure 8 shows the vehicle pulse, measured at the rear of the vehicle and processed using a SAE 60 filter. An overall similar vehicle pulse was observed for the CM-Steel vehicle, shown in green, and the CM-Composite vehicle, shown in blue. The maximum peak of both vehicles was only marginally higher than measured for the BM, shown in red. No significant effect with respect to restraint system performance and occupant injury risk due to the introduced structural changes for CM-Steel and CM-Composite was therefore predicted.

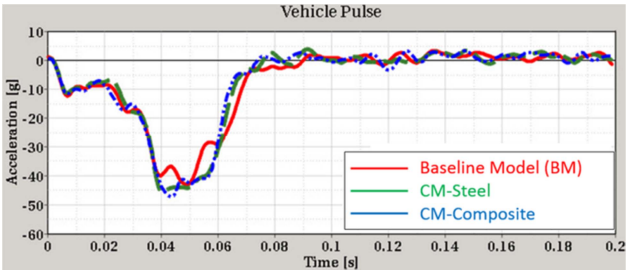

Figure 8 – Left Oblique Vehicle Pulse - BM vs. CM-Steel and CM-Composite

Right Oblique Impact

CM-Steel simulation results were compared against the respective BM simulation in NHTSA's right oblique impact configuration. The maximum toe-pan intrusion was reduced by more than 60%. Figure 9 shows a cross-section view of the left passenger compartment. The black line represents the un-deformed "pre-crash" vehicle. The red line represents the deformed shape of the baseline model with high occupant compartment intrusion. The green line shows the deformed shape of the CM-Steel vehicle with a significant reduction of intrusion compared to the BM. The associated change in mass when using countermeasures made out of steel, was +17 kg compared to the BM. The dark red line represents the CM-Composite 1 vehicle, where 2 layers of composite material were used for the firewall. Intrusion was as high as for the BM and the associated change in mass was -15 kg. The yellow line shows the CM-Composite 2 vehicle with 4 layers of composite and an associated change in mass of -11 kg. Intrusion was reduced compared to the BM but was still significantly higher than for the CM-Steel vehicle. The blue line represents the CM-Composite 3 vehicle with 3 layers of composite. The respective thickness was 3.6 mm and the associated reduction in mass compared to the BM was -7 kg. Similar reduction of occupant compartment intrusion was achieved with the CM-Composite 3 model compared to the CM-Steel vehicle. However, instead of adding 17 kg to the total vehicle mass when using steel countermeasures, a reduction of 7 kg was achieved when using composite countermeasures.

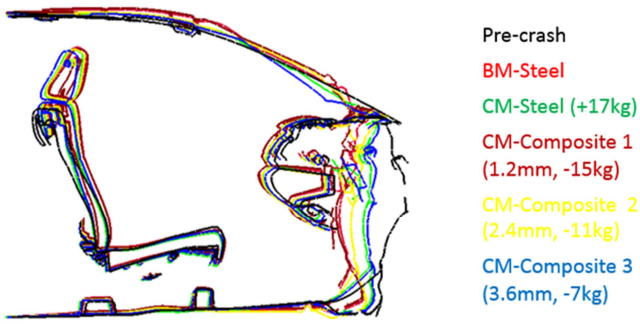

Figure 9 – Right Oblique Intrusion- Baseline vs. CM-Steel and CM-Composite

Figure 10 shows the vehicle pulse, measured at the rear of the vehicle and processed using a SAE 60 filter. An overall similar vehicle pulse was observed for the CM-Steel vehicle, shown in green, and the CM-Composite vehicle, shown in blue. The maximum peak of both vehicles was only marginally higher than measured for the BM, shown in red. No significant effect with respect to restraint system performance and occupant injury risk due to the introduced structural changes for CM-Steel and CM-Composite was therefore predicted.

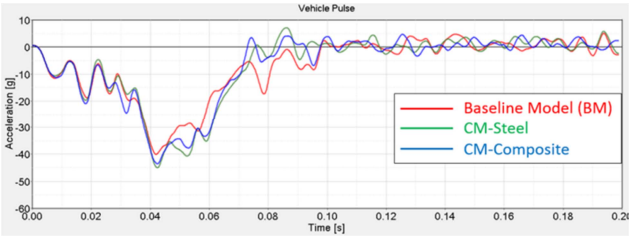

Figure 10 – Right Oblique Vehicle Pulse - BM vs. CM-Steel and CM-Composite

NHTSA NCAP Full Overlap

In the NCAP full frontal configuration, the tested vehicle travels at a speed of 56 km/h with full overlap co-linear into a rigid wall. In the full-scale test, the vehicle is equipped with a 50th percentile male Hybrid III dummy in the driver seat and with a 5th percentile female Hybrid III dummy in the passenger seat. The current NCAP rating is based on injury risk assessment rather than occupant compartment intrusion.

The effect of structural countermeasures developed for NHTSA's oblique impact was evaluated for the NCAP full overlap load case. The CM-Steel vehicle with countermeasures using high-strength steel (+17 kg) and the CM-Composite vehicle with 6 layers (-7 kg) were evaluated with respect to the baseline model.

Figure 11 shows a cross-section view on the driver side. The geometrical shape of the vehicle "pre-crash" is shown in black. The deformed shape of the BM after the vehicle has impacted a rigid wall at 56 km/h is shown in red. The occupant compartment intrusion is smaller than for the oblique impact configurations. The vehicle with countermeasures out of high-strength steel (CM-Steel) is shown in green and the CM-Composite vehicle is depicted in blue. No significant occupant compartment intrusion was observed for either countermeasure models. CM-Steel and CM-Composite resulted in a reduction of occupant compartment intrusion compared to the BM in NHTSA's NCAP full overlap load case.

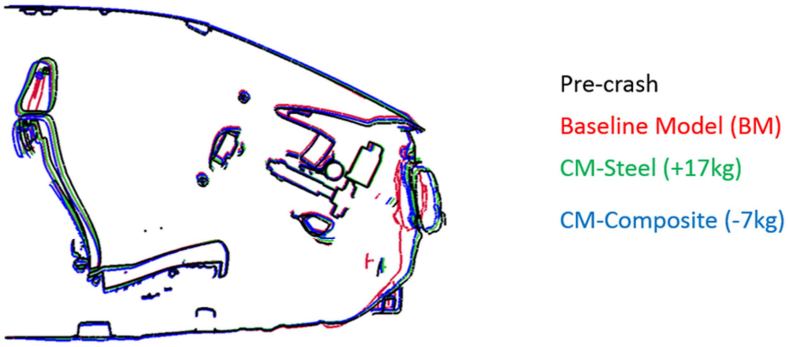

Figure 11 – NCAP Full Overlap – BM vs. CM-Steel and CM-Composite

Figure 12 shows the vehicle pulse, measured at the rear of the vehicle and processed using a SAE 60 filter. An overall similar vehicle pulse was observed for the CM-Steel vehicle, shown in green, and the CM-Composite vehicle, shown in blue. The maximum peak of both vehicles was similar to the BM, shown in red. While the first peak, caused by initial contact of the rigid barrier with the engine, was the same for the BM and CM-Steel, the initial peak was marginally lower for the CM-Composite vehicle. The second peak at about 50ms showed the opposite trend. The CM-Composite vehicle showed a marginally higher peak compared to the BM and CM-Steel. No significant effect with respect to restraint system performance and occupant injury risk due to the introduced structural changes for CM-Steel and CM-Composite was therefore predicted.

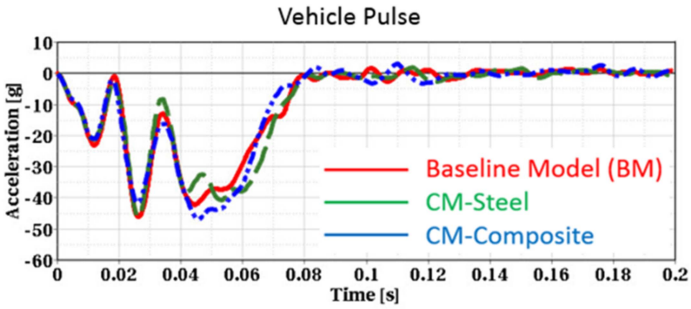

Figure 12 – NCAP Vehicle Pulse – BM vs. CM-Steel and CM-Composite

IIHS Moderate Overlap (40%)

In the IIHS moderate overlap configuration, the tested vehicle travels at a speed of 64 km/h with a 40 percent overlap co-linear into a fixed deformable barrier. In the full-scale test, the vehicle is equipped with a 50th percentile male Hybrid III dummy in the driver seat. The structural rating is based on comparison of intrusion measurements with rating guidelines for the upper and lower occupant compartment.

The effect of structural countermeasures developed for NHTSA's oblique impact was evaluated for the IIHS moderate overlap load case. The CM-Steel vehicle with countermeasures using high-strength steel (+17 kg) and the CM-Composite vehicle with six layers (-7 kg) were evaluated with respect to the baseline model.

Figure 13 shows a cross-section view on the driver side. The geometrical shape of the vehicle "pre-crash" is shown in black. The deformed shape of the BM after the vehicle impact is shown in red. A significant amount of occupant compartment intrusion can be observed for the BM. The vehicle with countermeasures out of high-strength steel (CM-Steel) is shown in green and the CM-Composite vehicle is depicted in blue. No significant occupant compartment intrusion was observed for either countermeasure models. CM-Steel and CM-Composite resulted in a reduction of occupant compartment intrusion compared to the BM in the IIHS moderate overlap load case.

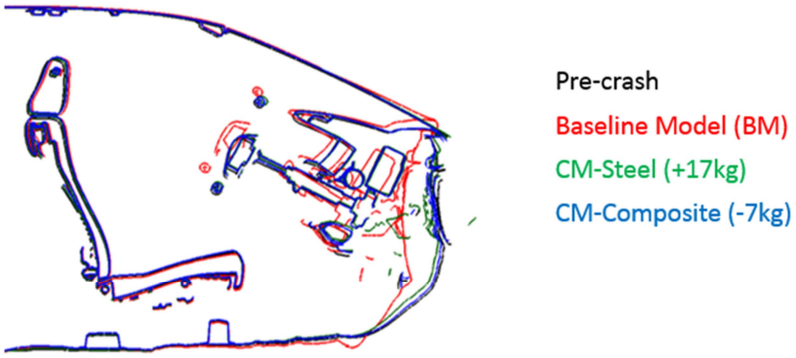

Figure 13 – IIHS Moderate Overlap – BM vs. CM-Steel and CM-Composite

Figure 14 shows the vehicle pulse, measured at the rear of the vehicle. An overall similar vehicle pulse was observed for the CM-Steel vehicle, shown in green, and the CM-Composite vehicle, shown in blue. The maximum peak of both vehicles was similar to the BM, shown in red. The maximum peak of the CM-Steel vehicle was slightly lower than the BM. The peak of the CM-Composite vehicle occurred marginally earlier than the BM. No significant effect with respect to restraint system performance and occupant injury risk due to the introduced structural changes for CM-Steel and CM-Composite was therefore predicted.

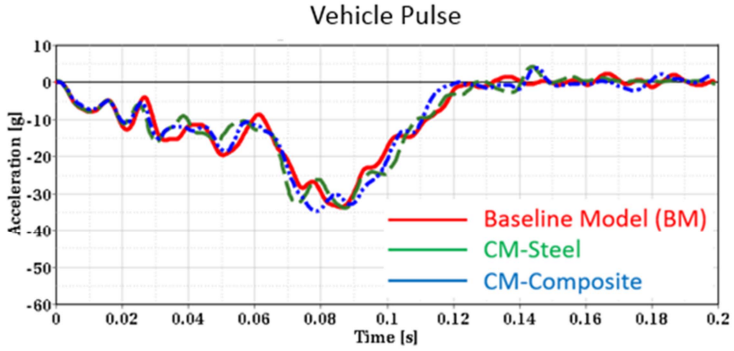

Figure 14 – IIHS MO Vehicle Pulse – BM vs. CM-Steel and CM-Composite

IIHS Small Overlap (25%)

In the IIHS small overlap configuration, the tested vehicle travels at a speed of 64 km/h with a 25 percent overlap co-linear into a fixed rigid barrier. In the full-scale test, the vehicle is equipped with a 50th percentile male Hybrid III dummy in the driver seat.

The effect of structural countermeasures developed for NHTSA's oblique impact was evaluated for the IIHS small overlap load case. The CM-Steel vehicle with countermeasures using high-strength steel (+17 kg) and the CM-Composite vehicle with six layers (-7 kg) were evaluated with respect to the baseline model.

Figure 15 shows a cross-section view on the driver side in the IIHS small (25%) overlap configuration. The geometrical shape of the vehicle "pre-crash" is shown in black. The deformed shape of the BM after the vehicle impact is shown in red. A similar amount of occupant compartment intrusion can be observed for the BM, the vehicle with countermeasures out of high-strength steel (CM-Steel), shown in green, and the CM-Composite vehicle, depicted in blue.

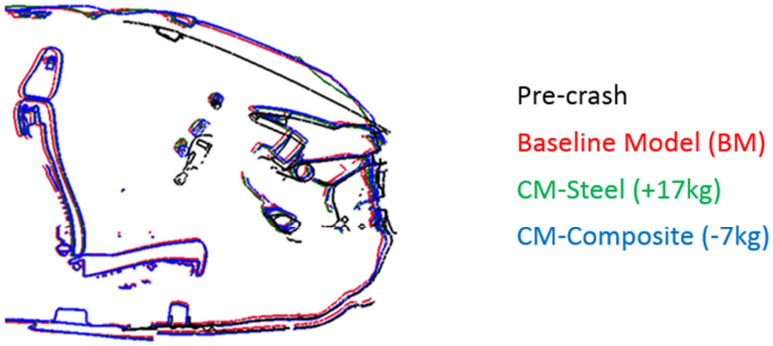

Figure 15 – IIHS Small Overlap – BM vs. CM-Steel and CM-Composite

Figure 16 shows the vehicle pulse, measured at the rear of the vehicle. An overall similar vehicle pulse was observed for the CM-Steel vehicle, shown in green, and the CM-Composite vehicle, shown in blue. The maximum peak of both vehicles was similar to the BM, shown in red. The maximum peak of the BM, CM-Steel vehicle, and CM-Composite vehicle was smaller than for other co-linear impact configurations. No significant effect with respect to restraint system performance and occupant injury risk due to the introduced structural changes for CM-Steel and CM-Composite was therefore predicted.

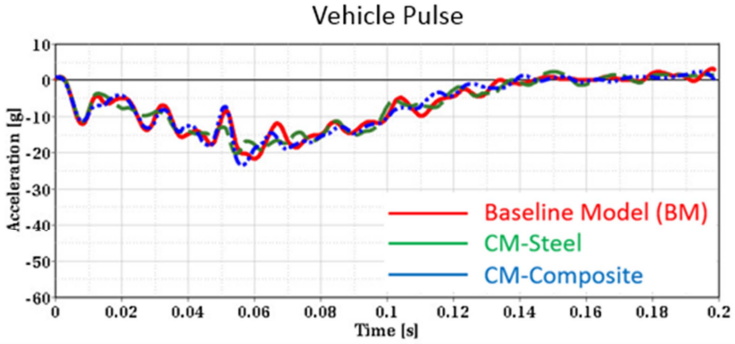

Figure 16 – IIHS SO Vehicle Pulse – BM vs. CM-Steel and CM-Composite

MATERIAL MODEL DEVELOPMENT

In an ongoing effort in cooperation with Honda R&D, a shell element version of Material Model MAT_213 in LS-DYNA for simulation of composites is being developed and validated. Between 2015 and 2018, the National Aeronautics and Space Administration (NASA), the Federal Aviation Administration (FAA), the Arizona State University (ASU), the George Mason University (GMU), and the Ohio State University's (OSU) composite material modeling consortium has sponsored the development of a material law (MAT_213) in the commercial LS-DYNA code for the simulation of composite materials under ballistic loads.

The MAT_213 has some features, such as (1) a deformation model involving elastic and plastic deformations, (2) dependency of strain-rate and temperature, (3) a damage model, (4) a failure model, and (5) a stochastic variation model. The model is driven by tabular data that is generated either using laboratory tests or via virtual testing. However, this material law was implemented for solid elements only.

In cooperation with Honda, GMU is implementing this material law for plane stress conditions so that it can be used by shell elements based on thin shell theory. This will allow for applying the material law to the simulation of thin panels undergoing loads occurring in automotive crash applications.

Current activities includes code development and verification, characterization of a material law for a composite material based on coupon testing, comparison of different discretization techniques when used in conjunction with MAT_213 for solids and/or shells, and validation of the material model based on component testing.

Many coupon tests are required to develop the material parameters of the material model for a particular composite. The developed material model will be validated by component test simulations, such as head form impact test and static/dynamic crush tests.

The material development and validation efforts within the formed consortium is of significant relevance for the research conducted by GMU for ACC. Honda is planning to share this work with plastic and composite material suppliers to allow them to develop material models of their composite products. That way, OEMs can directly use the material models provided from suppliers to be used in crash simulations for component designs and other analyses.

It is anticipated that this new material model will allow for better simulating and predicting the crash performance of components made out of composites in the future. Plastic and composite material suppliers can use methods and tools developed by the GMU Team in previous projects to evaluate their components in relevant crash loading conditions.

CONCLUSIONS

This research project helped to further understand the numerical polymer/composite material models and their CAE applications.

NHTSA found that oblique crashes represent common real-world accident patterns. The risk of injury in oblique impact configurations is often higher than in co-linear crashes. IIHS found that the risk of lower extremity injury was higher in the oblique impact tests compared to small overlap co-linear impact tests. The development of countermeasures for both restraints and vehicle structure for oblique configurations will therefore potentially improve vehicle safety and reduce injury risk in the future. Consequently, NHTSA is considering adopting a frontal oblique impact configuration into its NCAP rating protocol. NHTSA has contracted GMU in a previous project to evaluate structural countermeasures using high-strength steel materials, including associated mass, to reduce occupant compartment intrusion in the oblique impact condition.

A FE model of an appropriate mid-sized passenger vehicle was developed and validated to match the acceleration and intrusion measurements available from full-scale crash tests. Crash mechanisms that specifically contributed to high intrusion in the oblique impact condition were analyzed. Local deformation and buckling of the toe-pan, was found to be mainly responsible for producing high intrusions for both left-side and right-side oblique configurations.

A 60% reduction of the maximum intrusion was defined as the main design goal. Another design goal was to maintain moderate vehicle pulses in all impact configurations as a prerequisite for good restraint system performance and low injury risk in current and future rating tests. A model with a possible set of countermeasures using high-strength steel materials (CM-Steel) was developed. The associated increase in vehicle mass for the CM-Steel vehicle compared to the BM was +17 kg.

In the current project, countermeasures using composite material, i.e., Carbon Fiber Reinforced Plastic (CFRP), were developed to achieve a similar reduction in occupant compartment intrusion (“CM-Composite”). The associated reduction in mass for the CM-Composite was -7 kg compared to the BM and -24kg compared to the CM-Steel vehicle.

The change in vehicle pulse due to the developed countermeasures was not significant for oblique and co-linear impacts. Therefore, no unintended consequences were predicted.

In a parallel effort in cooperation with Honda R&D, a shell element version of Material Model MAT_213 in LS-DYNA for simulation of composites is being developed and validated. This will allow for better simulating and predicting the crash performance of components made out of composites in the future.

REFERENCES

[1] Brecher, A., November 2007, "A Safety Roadmap for Future Plastics and Composites Intensive Vehicles, Report No. DOT HS 810 863, Washington, DC: National Highway Traffic Safety Administration.

[2] Brecher, A., Brewer, J., Summers, S., & Patel S, 2009, "Characterizing and Enhancing the Safety of Future Plastic and Composite Intensive Vehicles," 21st International Conference on the Enhanced Safety of Vehicles, Stuttgart, Germany.

[3] Barnes, G., Coles, I., Roberts, R., Adams, S. O., Garner, D. M., 2010, "Crash Safety Assurance Strategies for Future Plastic and Composite Intensive Vehicles (PCIVs)," Report No. DOT-VNTSC-NHTSA-10-01, Cambridge, MA: Volpe National Transportation Systems Center.

[4] Fisher, M., & Cundiff, B., 2002, "APC Vision and Technology Roadmap for the Automotive Market - Defining Priority Research for Plastics in 21st Century Vehicles," SAE Technical Paper 2002-01-1890, Warrendale, PA: Society of Automotive Engineers.

[5] Fisher, M., Kolb, J., & Cole, S., 2007, "Enhancing Future Automotive Safety with Plastics." Paper No. 07-0451, 20th International Conference on the Enhanced Safety of Vehicles, Lyon, France.

[6] ACC Plastics Division, 2009, Retrieved from "Plastic in Automotive Markets Technology Roadmap – A New Vision for the Road Ahead," Available at www.plasticscar.com/roadmap_fullversion.

[7] ACC Plastics Division. 2009, Plastic and Composite Intensive Vehicles: An Innovation Platform for Achieving National Priorities," Available at www.plastics-car.com/pcivs.

[8] ACC Plastics Division, 2014, "Plastics and Polymer Composites Technology Roadmap for Automotive Markets," Available at http://www.plastics-car.com/Tomorrows-Automobiles/Plastics-and-Polymer-Composites-Technology-Roadmap.

[9] Park, C-K., Achstetter, T., Kan, C-D., Hollowell, W., 2017, "Understanding of Numerical Polymer/Composite Material Models and Their CAE applications," George Mason University Final Report.

[10] Bean, J., Kahane, C., Mynatt, M., Rudd, R., Rush, C., Wiacek, C., 2009, National Highway Traffic Safety Administration, "Fatalities in Frontal Crashes Despite Seat Belts and Air Bags", Report No. DOT HS 811 202.

[11] DOT / NHTSA, December 2015, "New Car Assessment Program (NCAP), Request for Comments," Federal Register Vol. 80 No. 241.

[12] Zhang, R., Reichert, R., Kan, C.-D. and Cao, L., 2015, "Evaluation of driver lower extremity injuries in 16 oblique crashes with THOR", International Journal of Crashworthiness, doi: 10.1080/13588265.2015.1120983.

[13] Mueller, R., 2017, "Comparison of Frontal Crash Modes: IIHS Small Overlap and NHTSA Oblique", Insurance Institute for Highway Safety, SAE Government/Industry Meeting, Washington, DC.

[14] Saunders, J., Craig, M.J., Suway, J., 2011, "NHTSA's Test Procedure Evaluations for Small Overlap/Oblique Crashes," The 22nd International Technical Conference for the Enhanced Safety of Vehicles, Paper No. 11-0343.

[15] Reichert, Rudolf and Kan, Steve, TBD, "Structural Countermeasure Research Program," NHTSA Contract DTNH2215D00005/0001, Final Report to be published.

[16] Park, C-K., Kan, C-D., Hollowell, W., & Hill, S.I. December 2012, Investigation of Opportunities for Lightweight Vehicles Using Advanced Plastics and Composites, Report No. DOT HS 811 692, Washington,

DC: National Highway Traffic Safety Administration. Available at
www.nhtsa.gov/DOT/NHTSA/NVS/Crashworthiness/Plastics/811692.pdf

Comparison of Thorax Responses between the Belted Elderly Occupant Human Body and THOR-50M FE Models under Typical Frontal Crash Test Conditions

Kazuki Hikida, Kazunori Maehara, Hidenori Mikami, Yasuhiro Dokko
Honda R&D Co., Ltd. Automobile R&D Center
Japan

Kazuki Ohhashi
Honda Techno Fort Co., Ltd Affiliation or Company Name
Japan

Paper Number 19-0172

ABSTRACT

In Japan the ratio of traffic accident fatalities of elderly people has been increasing, and the main factor is thorax injury. An elderly human body model (HBM) has been developed to evaluate the vehicle safety systems. At the same time, Test device for Human Occupant Restraint (THOR) ATD that has high bio-fidelity is being used in frontal crash tests including lateral vehicle motion. This paper describes the comparison of the thorax response between an elderly human and THOR 50th percentile male (THOR-50M) under a simulated frontal crash including lateral vehicle motion, and clarifies whether there is the correlation between them, especially, the correlation between the rib fractures of the elderly HBM and the thorax deformation of the THOR-50M.

The elderly HBM and THOR-50M model were compared under the condition of a driver seat position in a left-handed midsized sedan vehicle equipped with a three-point seat belt, a driver airbag, a knee airbag, and a side curtain airbag. The frontal crash motions of Full Width Rigid Barrier (FWRB) at 56 km/h, Offset Deformable Barrier (ODB) at 64 km/h, Small Overlap Test (SOT) at 64 km/h and Oblique Moving Deformable Barrier (OMDB)-to-vehicle crash test at 90 km/h were applied. From the results the thorax responses and deformation were investigated respectively.

The kinematics of each body component was in same trend between the elderly HBM and THOR-50M model in each test condition. For the elderly HBM and THOR-50M model in all the test conditions, the thorax deformation at the upper right was largest among four measurement locations, and that of the elderly HBM and THOR-50M model showed good correlation. In the elderly HBM, the locations of rib fractures were roughly assorted into three regions on the ribcage. The upper left ribs around the belt path in all test conditions, the right ribs around the belt path in FWRB and OMDB, and the lower left ribs in SOT and OMDB were fractured. The R^2 (correlation coefficient) between the number of fractured ribs of the elderly HBM and the overall peak resultant deformation (R_{max}) of THOR-50M was high as 0.83 for total rib fractures over all regions, while that wasn't high as 0.7 or less for those of each region.

The structural differences between the elderly human and THOR-50M such as the ribcage, spine and shoulder were considered to affect the differences of the kinematics and thorax deformation between them under frontal loading with lateral and vertical input.

The comparison results showed a certain correlation between the rib fractures of the elderly HBM and the thorax deformation of THOR-50M, and several differences of the partial thorax responses due to structural differences between humans and THOR-50M. The results of this study suggested that further study for the methods to evaluate detailed thorax injury using THOR-50M should be needed in order to correlate any other indices and possible thorax injuries in the crash conditions with lateral motion.

RESEARCH QUESTION/OBJECTIVE

In recent years, the population ratio of the elderly has been drastically increasing in developed countries such as Japan. Therefore, a lot of the elderly get caught up in traffic accidents. In Japan, the number of traffic accidents has been decreasing. However, the ratio of traffic accident fatalities of elderly people (aged 65 years old and older) has been increasing [1]. The thorax injury due to rib fractures is the main factor of the death of elderly people [2], because the density and strength of bone decrease with age [3]. It is necessary to evaluate the vehicle safety systems for the elderly occupant. Therefore the elderly occupant full body finite element (FE) models were developed to simulate vehicle occupant with restraint systems.

Anthropomorphic Test Device (ATD) has been used for assessing injury values in various countries. The bio-fidelity and measurement capability of ATD has been continuously improved. Test device for Human Occupant Restraint (THOR) ATD is considered to be the next-generation ATD in place of the traditional Hybrid III ATD. In THOR 50th Male (THOR-50M) ATD, the bio-fidelity had been enhanced to simulate human body in response to impact loading by using bio-mechanical data [4] [5]. Especially, the thoracic spine consists of a flexible rubber link and the rib cage has been redesigned to reproduce human rib geometry and structure. In addition, THOR-50M ATD is capable to measure the 3D thorax deformation at four locations with light reflective displacement meter which called the Infra-Red Telescoping Rod for Assessment of Chest Compression (IR-TRACC). Also, THOR-50M FE model has been developed to study the physical mechanical systems.

Some studies were conducted to evaluate the bio-fidelity of THOR-50M ATD in a simulated frontal crash [6] [7]. Recently, Albert et al. [10] showed the improved bio-fidelity of THOR-50M's thorax deformation by comparisons with the Hybrid III ATD and the elderly post-mortem human surrogates (PMHS) in frontal sled tests remarking the overall peak resultant thorax deformation, R_{max}.

For the purpose of reducing traffic fatalities of elderly people, an index to assess the thorax injury of elderly people in detail is necessary. It has not been thoroughly investigated whether the thorax injury of an elderly human under frontal crash including lateral motion can be assessed by THOR-50M ATD yet. This research compared the thorax response between elderly human and THOR-50M ATD under simulated frontal crash including lateral vehicle motion, and clarified whether there is a correlation between them, especially, a correlation between rib fractures of the elderly HBM and the thorax deformation of THOR-50M.

METHODS

Figure 1 (a) shows the elderly occupant full body FE model that is capable of predicting rib fracture, developed by Ito et al.[8] [9] and Dokko et al.[10] [11]. The model was designed to be a representative of elderly humans with an average American male body size (AM50%ile). The age of the elderly occupant FE model was defined as 75 years old. Rib fracture is predicted by 'element elimination' when an element strain reaches the specified fracture strain level. Figure 1 (b) shows the THOR-50th Metric FE model Version 1.4.1 developed by Humanetics Innovative Solution, Inc. [12]. LS-DYNA (Version971 R6.1.2) was adopted as a FEM solver [13].

(a) Elderly occupant full body FE model (b) THOR-50th Metric FE model Version 1.4.1

Figure 1. AM50 occupant FE models

As shown in Fig. 2 (1), in the full vehicle FE model, the elderly HBM and THOR-50M models were seated at the driver seat position of a left-handed midsized sedan vehicle. The simulated vehicle was equipped with a three-point seat belt that had a force limiter, a driver airbag, an outer anchor and a retractor pretensioner, a knee airbag and a side curtain airbag. Figure 2 (2) shows the shoulder belt path on the thorax of the elderly HBM and THOR model. The frontal crash motions of Full Width Rigid Barrier (FWRB) at 56 km/h, Offset Deformable Barrier (ODB) at 64 km/h, Small Overlap Test (SOT) at 64 km/h and Oblique Moving Deformable Barrier (OMDB)-to-vehicle test at 90 km/h were applied. The 6-axis motion of each test condition was made from the data of real collision test results. These models were simulated without the body deformation of a vehicle.

(1-a) Elderly HBM (1-b) THOR-50M model (2-a) Elderly HBM (2-b) THOR-50M model

Figure 2. Occupant and shoulder belt path on the thorax in full vehicle FE models

The elderly HBM and the THOR-50M models were seated at the same position as according to THOR-50M seating procedure [14]. Figure 3 shows the postures of the elderly HBM and THOR-50M model. The measurement locations for each model were set to compare the kinematics of the bodies during collision. The THOR-50M model has measurement locations at the head, the first, fourth and twelfth thoracic vertebrae (T1, T4, T12), and the pelvis. In the elderly HBM model, the head, first and ninth thoracic vertebrae (T1, T9), the second lumbar vertebra (L2) and the pelvis were set so as to be locations close to those of THOR-50M model. The origin of the coordinate system was set at a certain point without deformation in the vehicle body model.

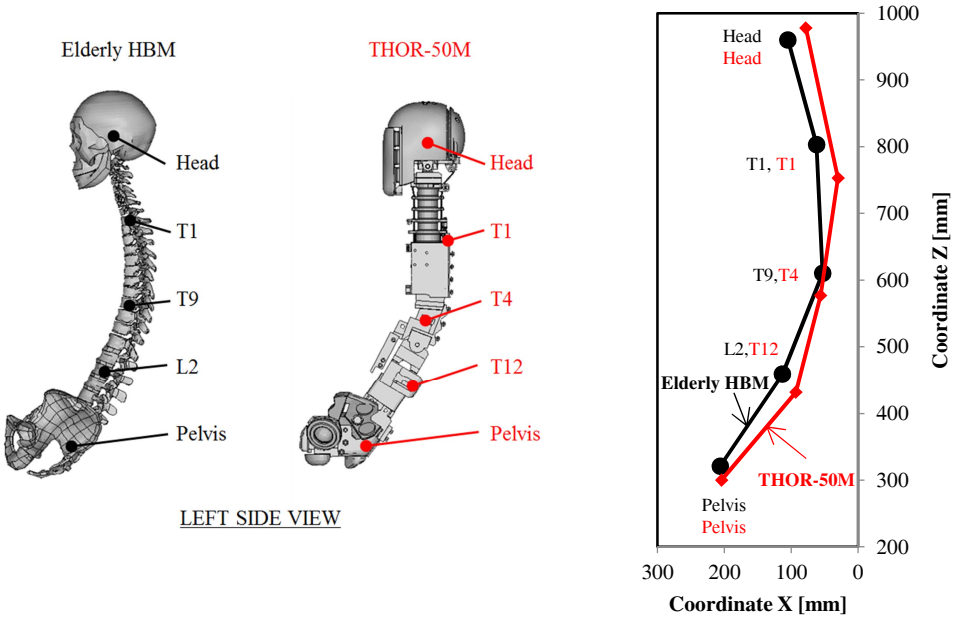

Figure 3. Measurement locations and posture of the elderly HBM and THOR-50M model

Figure 4 shows the measurement locations of thorax deformation of the elderly HBM and THOR-50M model. The 3D thorax deformations of THOR-50M's ribs were measured by the four equipped IR-TRACCs. Aiming at the

places closest to measurement locations of the THOR-50M, the thorax deformations of the elderly HBM were measured at four locations. The upper thorax deformations on both the left and right were measured between the 4th thoracic vertebrae and rib tips, and the lower thorax deformations on both the left and right were measured between the 8th thoracic vertebrae and rib tips.

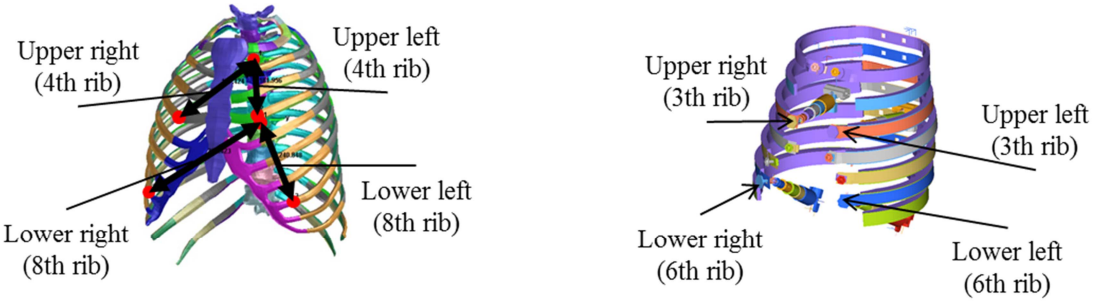

(a) Elderly HBM (b) THOR-50M model

Figure 4. Measurement locations of thorax deformation of the elderly HBM and THOR-50M model

RESULTS

Kinematics of occupant FE model

Figure 5 shows the displacement of the occupant FE models in each test condition. The X, Y, and Z axes were defined as the longitudinal, lateral and vertical directions of the vehicle coordinate system, respectively. For the elderly HBM, the displacement of the head, T1, T9, L2 and pelvis were shown, and for the THOR-50M model, the displacement of the head, T1, T4, T12 and pelvis were shown. The displacements of the occupant FE models until reaching its X-axis maximum at the vehicle coordinate system were shown in each test condition. The kinematics of each body component was in same trend between the elderly HBM and THOR-50M model in each test condition. In FWRB, between the elderly HBM and the THOR-50M model, the X-axis maximum displacement differences of the head and the pelvis were approximately 50mm or less. The X-axis maximum displacement of the thoracic vertebrae (T1, T4, T12) of THOR-50M model was less than those (T1, T9, L2) of the elderly HBM. In such cases with lateral vehicle motion as SOT and OMDB, between the elderly HBM and THOR-50M models, the X-axis maximum displacement difference of the pelvis was approximately 50mm or less. The X and Y-axis maximum displacements of the head and the thoracic vertebrae (T1, T4, T12) of THOR-50M model were less than those (head, T1, T9, L2) of the elderly HBM. Between the elderly HBM and THOR-50M models, the Y-axis maximum displacement differences of the head, thoracic vertebrae and pelvis were approximately 100 mm or less.

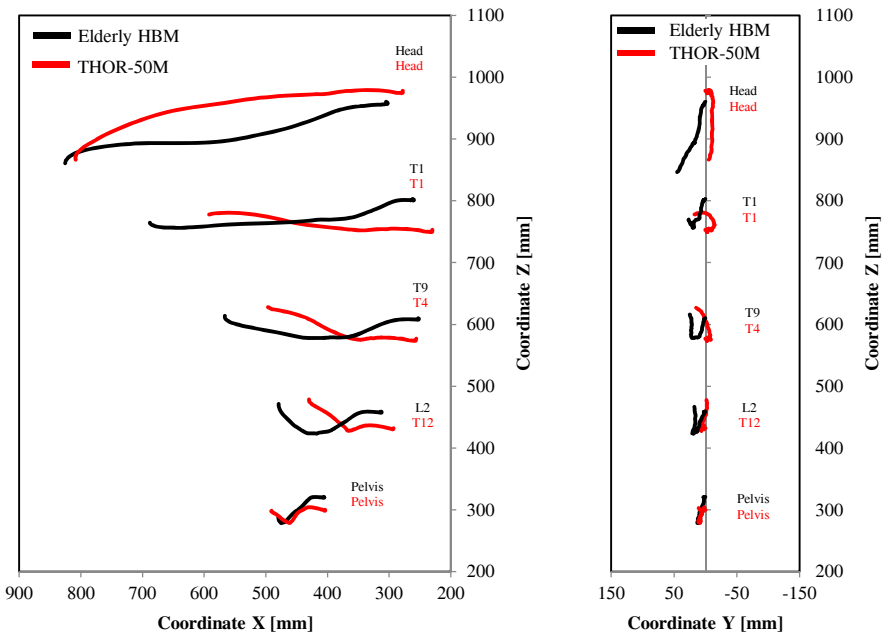
Elderly HBM
THOR-50M
Head
Head
T1
T1
T9
T4
L2
T12
Pelvis
Pelvis
Coordinate X [mm]
Coordinate Z [mm]
Coordinate Y [mm]
LEFT SIDE VIEW
REAR VIEW

(a) FWRB

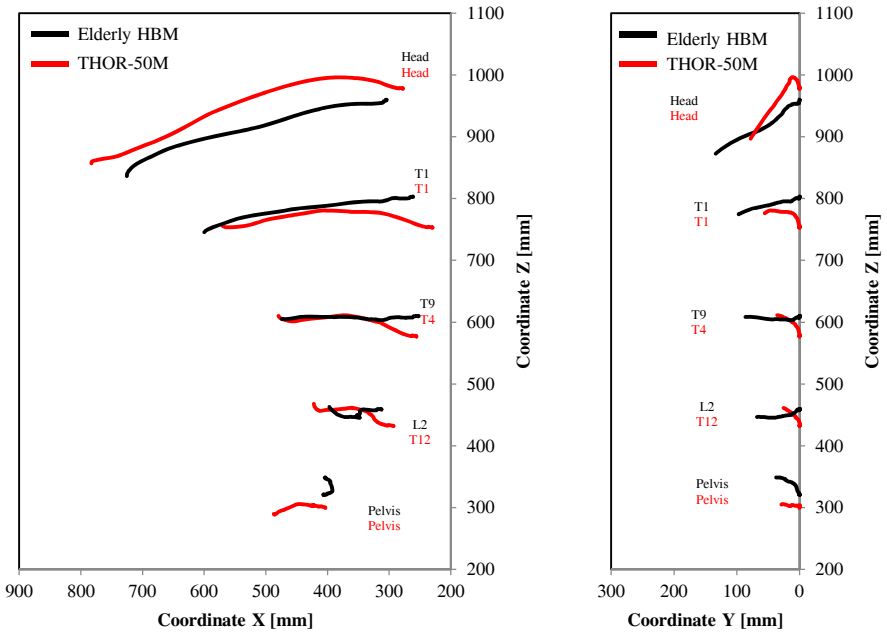
Elderly HBM
THOR-50M
Head
Head
T1
T1
T9
T4
L2
T12
Pelvis
Pelvis
Coordinate X [mm]
Coordinate Z [mm]
Coordinate Y [mm]
LEFT SIDE VIEW
REAR VIEW

(b) ODB

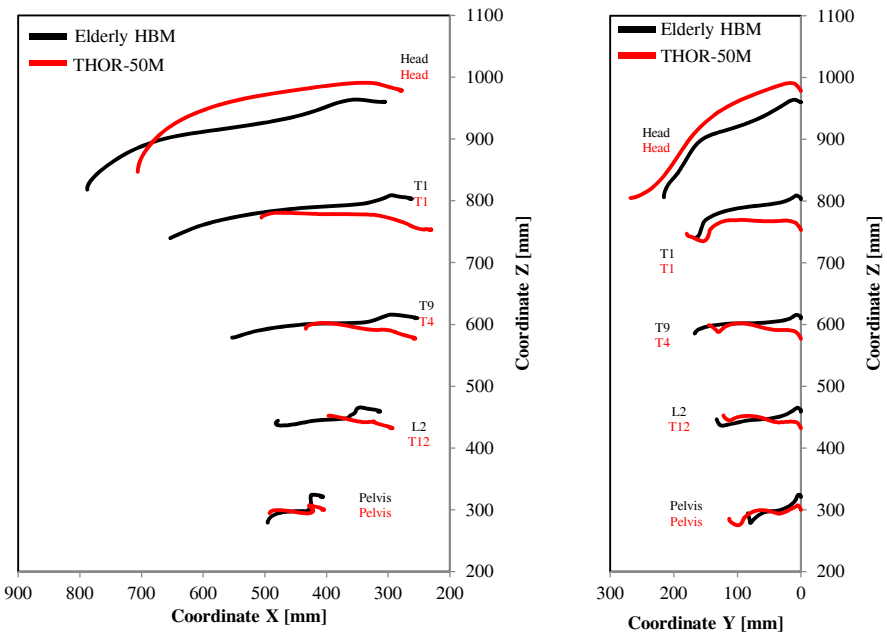

LEFT SIDE VIEW REAR VIEW

(c) SOT

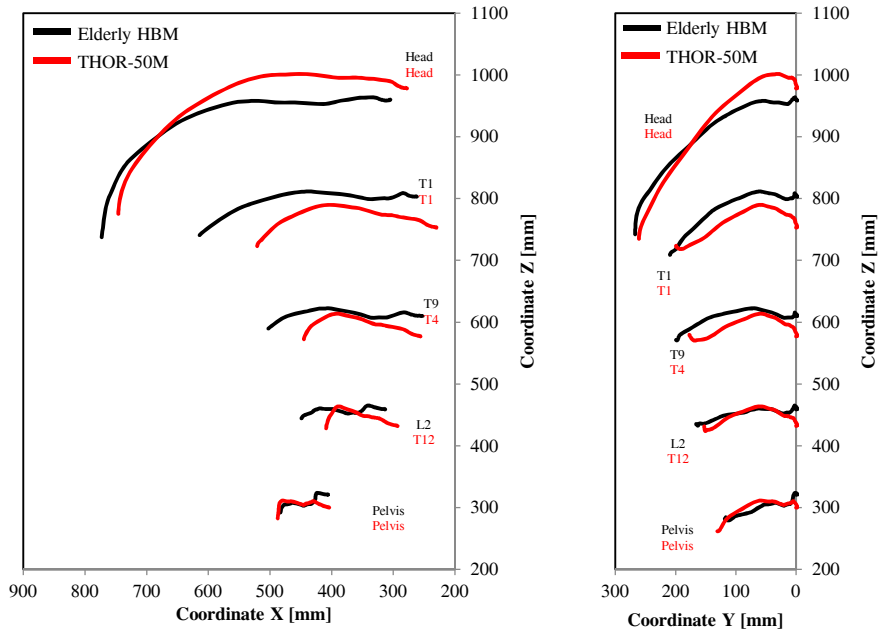

LEFT SIDE VIEW REAR VIEW

(d) OMDB

Figure 5. The displacements of the occupant FE models until reaching its X-axis maximum at the vehicle coordinate system in each test condition

Thorax deformation

Table 1 shows the maximum resultant thorax deformation of the elderly HBM and THOR-50M model in each test condition. Among all test conditions, the thorax deformation of the lower left in OMDB of the elderly HBM showed the maximum value. Figure 6 illustrates the deformed thorax shape and the displacement of the left 8th rib tip of the elderly HBM from the viewpoint fixed at the 8th thoracic vertebra at 0 ms and 105 ms in OMDB. It was observed the expansion of a part of the rib cage appeared that was caused by an inertial force from the abdominal parts moving forward and by an excessive flexion of the trunk during the rebound phase in the crash. Since such a phenomenon of the human model has not been validated and could not be related with thorax deformation, these thorax deformations were omitted from the discussion hereafter in this research and denoted by parentheses in Table 1. For the elderly HBM and THOR-50M model in all test conditions, the thorax deformation at the upper right was largest among the four measurement locations.

Table 1.
Maximum thorax deformation of the elderly HBM and THOR-50M models at four measurement locations in each test condition

	Maximum resultant thorax deformation (mm)							
	Upper right		Upper left		Lower right		Lower left	
Test conditions	Elderly HBM	THOR-50M model	Elderly HBM	THOR-50M model	Elderly HBM	THOR-50M model	Elderly HBM	THOR-50M model
FWRB	55.9	40.4	33.3	17.1	22.9	30.2	43.8	12.7
ODB	53.6	36.5	32.7	17.0	25.4	31.3	46.5	11.5
SOT	56.6	42.0	35.0	17.4	26.6	35.2	49.3	13.9
OMDB	58.0	50.7	52.5	27.5	(50.9)	35.8	(85.4)	25.0

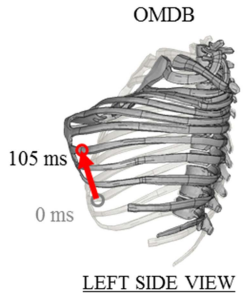

Figure 6. The deformed thorax shape and the displacement of the left 8th rib tip (Arrow) of the elderly HBM from the viewpoint fixed at the 8th thoracic vertebra at 0 ms and 105 ms in OMDB

The thorax deformations were measured at four locations (upper right, upper left, lower right, lower left) for the elderly HBM and THOR-50M model. The correlations of thorax deformation in resultant (Res.), X, Y and Z-axis between the elderly HBM and THOR-50M model at four measurement locations were investigated in all test conditions. As an example, Fig. 7 plots the thorax deformation every 5 ms until either the thorax deformation of the elderly HBM or THOR-50M model have reached its maximum at the upper right thorax in FWRB. The R^2 (correlation coefficient) and the ratio of variability of the approximation straight line that passed the origin were calculated from all results. Figure 8 shows the R^2 of zero or more between the elderly HBM and THOR-50M models, and Fig. 9 shows the ratio of the thorax deformation of the THOR-50M model to that of the elderly HBM, at four locations in each test condition. When focusing on the upper right thorax deformation where there was maximum deformation in all test conditions, the Res., X-axis, and Z-axis thorax deformation had high correlation between the elderly HBM and THOR-50M model. In the upper right thorax deformation, the ratio of variability in X-axis was larger than 1, in Z-axis it was less than 1. In other words, in X-axis the thorax of the THOR-50M model was easier to deform than that of the elderly HBM, in Z-axis it was not. In Y-axis thorax deformation between them didn't show a good correlation. In Y-axis the thorax of THOR-50M model wasn't easier to deform than that of the elderly HBM. In contrast, in the lower left thorax where the belt did not pass directly, there was a low correlation between

them in Res. and all axes. It may be because of too little deformation of both to statistically show a certain correlation.

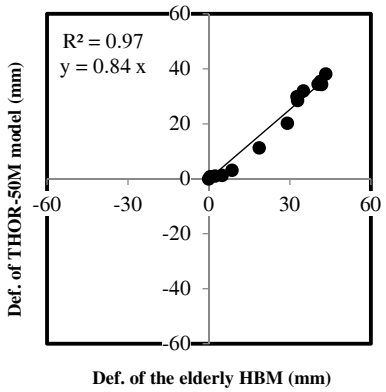

Figure 7. The plots of the thorax deformations every 5 ms until either the thorax deformation of the elderly HBM or THOR-50M model reached the maximum value at the upper right thorax in FWRB

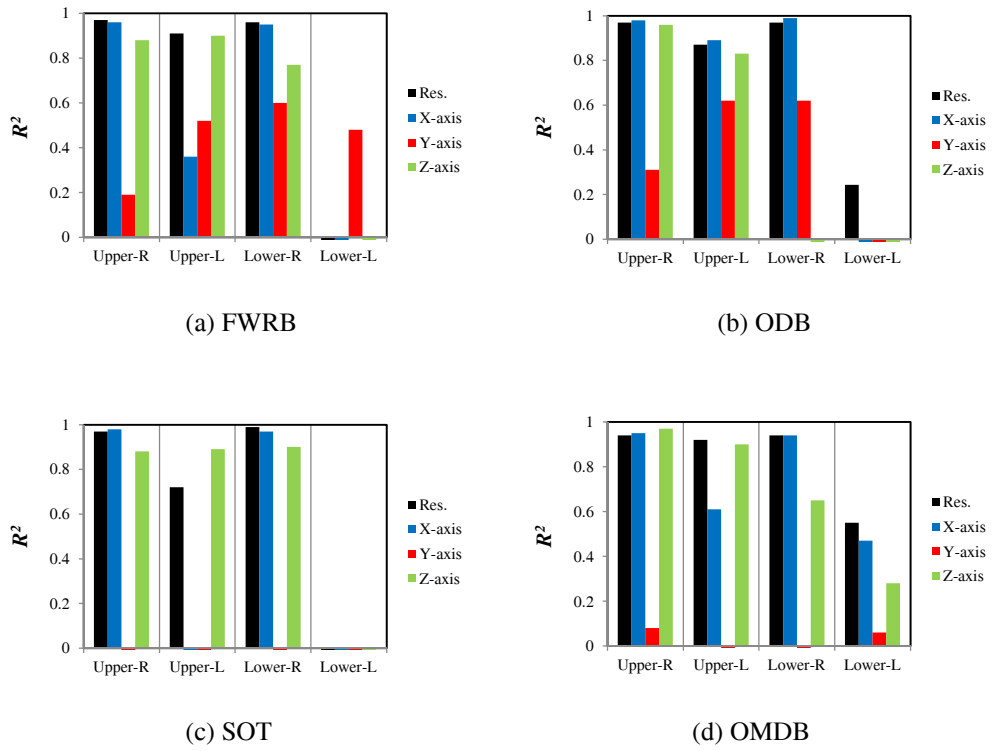

(a) FWRB (b) ODB

(c) SOT (d) OMDB

Figure 8. The R^2 of zero or more between the thorax deformation of the elderly HBM and THOR-50M model in each test condition

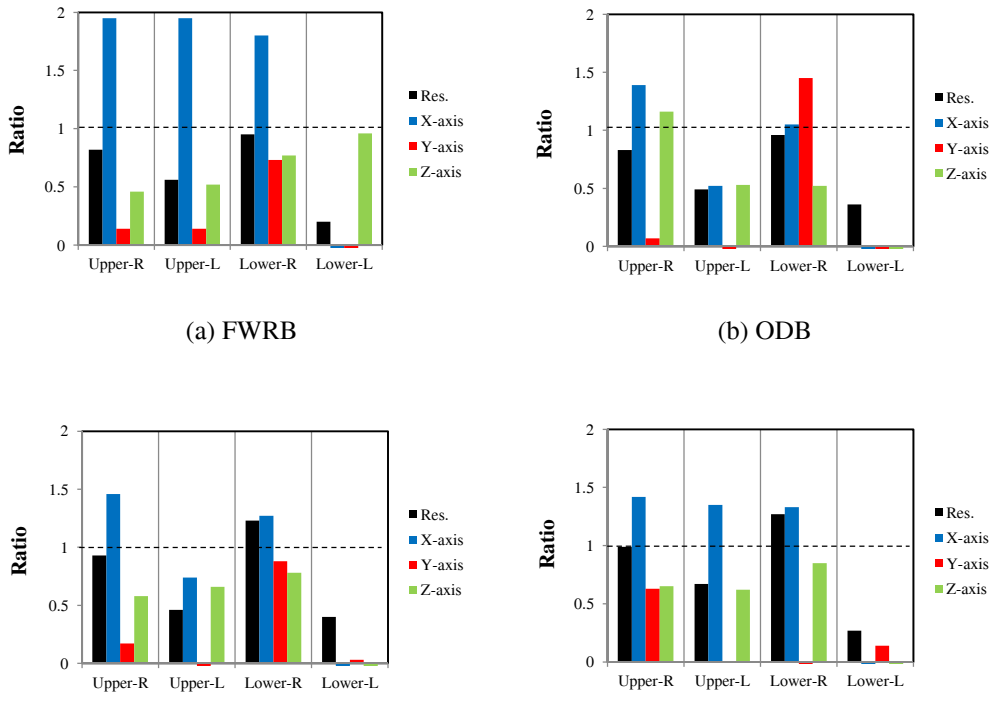

(a) FWRB (b) ODB

(c) SOT (d) OMDB

Figure 9. The ratio of the thorax deformation of the THOR-50M model to that of the elderly HBM in each test condition

Rib fractures of the elderly HBM

Figure 10 illustrates the locations of rib fracture of the elderly HBM in FWRB, ODB, SOT and OMDB. The locations of rib fracture were counted until reaching the maximum thorax deformation of the elderly HBM. In FWRB, the number of fractured ribs was 8 and there were fractured ribs around the right and left shoulder belt path. Both the left and right side ribs were fractured around the lateral. In ODB the number of fractured ribs was 4, the least among the four test conditions, and only left side ribs were fractured. The locations of fractured ribs in SOT were almost same as those in ODB;, in addition, the 9th and 10th ribs of the left side were also fractured. In OMDB the number of fractured ribs was 11 and the largest among the four test conditions. The locations of the fractured ribs were almost same as those of FWRB;, in addition, the 9th and 10th ribs of the left side were also fractured, like SOT. The 1st and 2nd ribs of the right side and the 6th rib of the left side were fractured but happened during the rebound phase after maximum excursion by upward loading from abdominal parts caused by extreme flexion of the body. Since such a phenomenon of the human model has not been validated and could not be related with thorax deformation, these fractures were omitted from the discussion hereafter in this research.

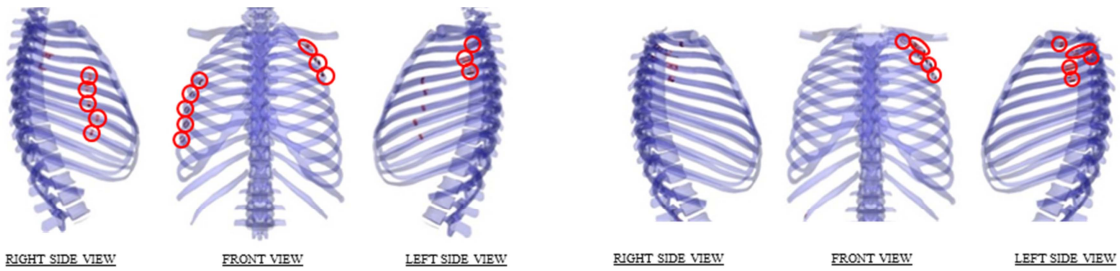

(a) FWRB (b) ODB

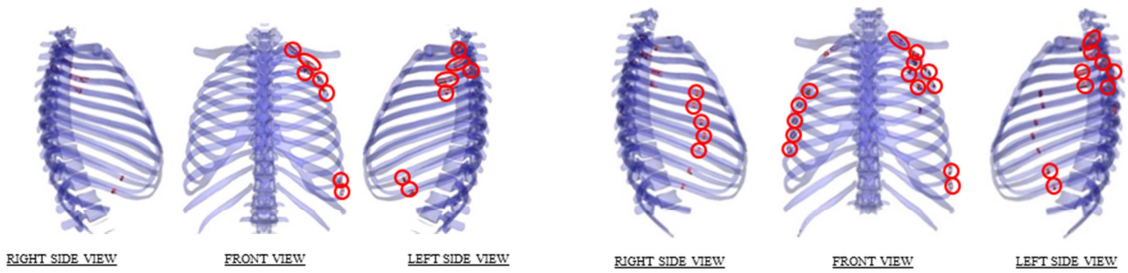

(c) SOT (d) OMDB

Figure 10. The locations of rib fractures of the elderly HBM in each test condition

The correlation between the number of the fractured ribs of the elderly HBM and R_{max} of THOR-50M model

From Fig. 10 the locations of rib fracture were roughly assorted into three regions on ribcage (Region A: the 1st to 8th ribs of left side; Region B: the 1st to 10th ribs of right side; and Region C: the 9th to 10th ribs of left side) as shown in Fig. 11. The correlation between the number of fractured ribs in all regions or each region and R_{max} was investigated.

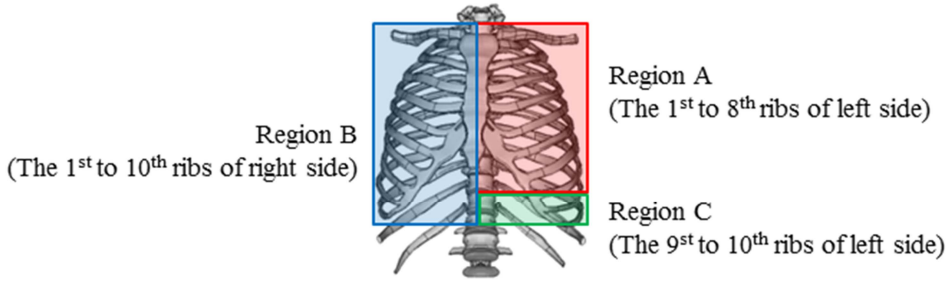

Figure 11. The assorted regions of the ribcage of the elderly HBM to classify the rib fracture locations

Figure 12 plots the number of the fractured ribs of the elderly HBM in all regions or each region and the R_{max} of THOR-50M model. The R^2 between them was calculated from the results of FWRB, ODB, SOT and OMDB. The R^2 in rib fractures of all regions was high as 0.84, while that of each region wasn't high as 0.7 or less.

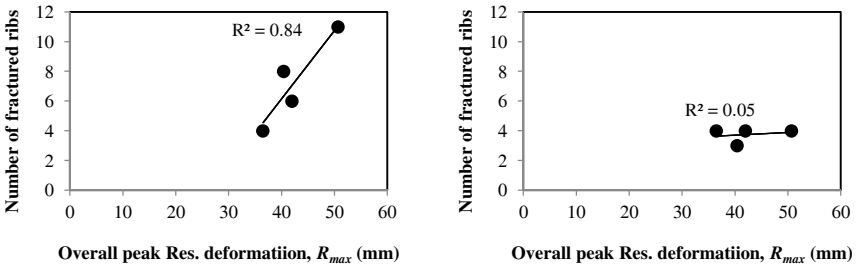

(1) All regions (2) Region A

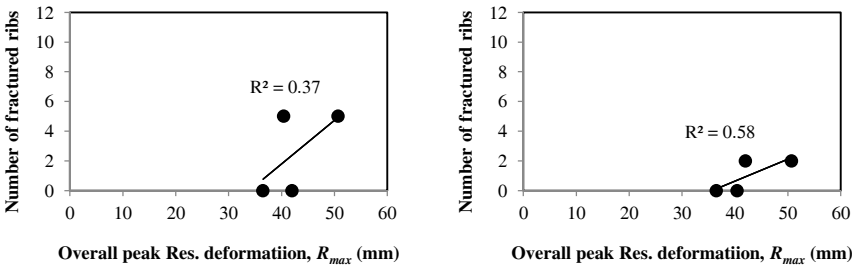

(3) Region B (4) Region C

Figure 12. The correlation between the number of the fractured ribs of the elderly HBM in all regions or each region and the R_{max} of THOR-50M model

DISCUSSION

As the result of Table 1, the measurement location of R_{max} was upper right in all test conditions. In the elderly HBM, the locations of rib fractures were not only around the upper right thorax but also the other thorax areas such as the upper left, lower right and lower left. Therefore, it was analyzed why the rib fractures of the elderly HBM occurred in each region.

Upper left rib fractures (Region A)

As shown in Fig. 10 and Fig. 11, there were the rib fractures of Region A in all test conditions. At the deformation measurement location of the upper left thorax close to the Region A, the ratio of the Res. thorax deformation of THOR-50M model to that of the elderly HBM was low although the correlation of the Res. thorax deformation between them was high, as shown in Fig. 8 and Fig. 9. In order to investigate this reason, these kinematics and thorax responses were compared. Fig. 13 shows the thorax responses of the elderly HBM and THOR-50M model from the viewpoint of the vehicle coordinate system during the SOT collision. It was observed that the clavicle and shoulder of the elderly HBM went down by the shoulder belt loading, while those of the THOR-50M model didn't. The human shoulder is connected to the thorax with the ligaments, muscles and so on. Therefore the shoulder can probably move in a wide range. It was presumed the upper ribs were fractured by the downward and rearward loading by the shoulder belt via the clavicle. Since it hasn't been investigated whether this phenomenon occurs in a real human body, the rib fractures may be peculiar to this elderly HBM. In THOR-50M, structurally the shoulder can move limitedly within a certain range. It was thought that it was hard for the shoulder belt loading to be transmitted from the shoulder to the ribcage because the loading was transmitted from the shoulder to the spine. By these reasons, the upper left deformation of the THOR-50M model might be less than that of the elderly HBM.

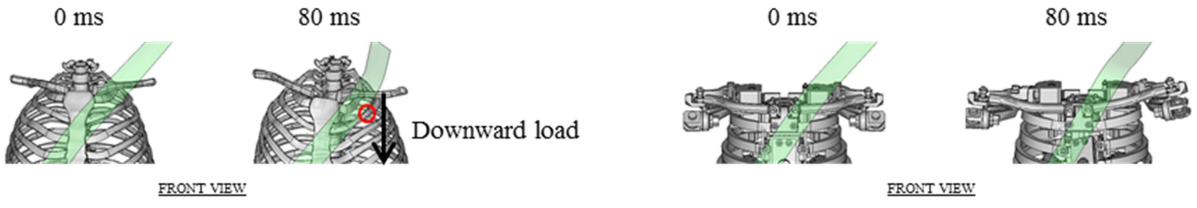

(a) Elderly HBM (b) THOR-50M model

Figure 13. The illustration of the thorax response of the elderly HBM from the viewpoint of the vehicle coordinate system during the SOT collision

Upper and lower right rib fractures (Region B)

As shown in Fig. 10 and Fig. 11, the number of fractured ribs of Region B was much different depending on the test conditions. The rib fractures of Region B occurred in FWRB and OMDB, but none did in ODB and SOT. The correlation between the number of fractured ribs of Region B and the R_{max} of THOR-50M model wasn't high as 0.37, as shown in Fig. 12. In order to investigate this reason, the thoracic kinematics and the deformed thorax of the elderly HBM during collision were observed. Figure 14 shows the trajectories of the 9th thoracic vertebra of the elderly HBM in X-Y plane until reaching the X-axis maximum displacement at the vehicle coordinate system in all test conditions with marking the timing when right side rib fractures have all happened in FWRB and OMDB or the thorax deformation have reached its maximum in ODB and SOT. Among the crash test conditions including lateral vehicle motion such as ODB, SOT and OMDB, the Y-axis displacement of the 9th thoracic vertebra in OMDB was least at each time. Figure 15 illustrates the deformed thorax shape and the shoulder belt path of the elderly HBM from the viewpoint fixed at the 4th thoracic vertebra at the time when right side rib fractures have all happened in FWRB and OMDB or the thorax deformation have reached its maximum in ODB and SOT. The θ represents the angle between the direction of the lower right shoulder belt and the X-axis in X-Y plane of the 4th vertebra. Each time, the θ in FWRB, ODB, SOT and OMDB were respectively defined as θa, θb, θc and θd. The θa and θd (in FWRB and OMDB) were less than θb and θc (in ODB and SOT). Therefore, it was assumed that the forward deceleration of the vehicle in FWRB and OMDB was larger than that in ODB and SOT, and the rearward loading by the shoulder belt to the thorax was applied more due to the occupant moving in the forward direction. When the X component of the shoulder belt load to thorax is large, there may be a possibility that rib fracture tends to occur. It may be necessary to further study the influence that the direction and magnitude of input to the thorax has on the severity of rib fractures.

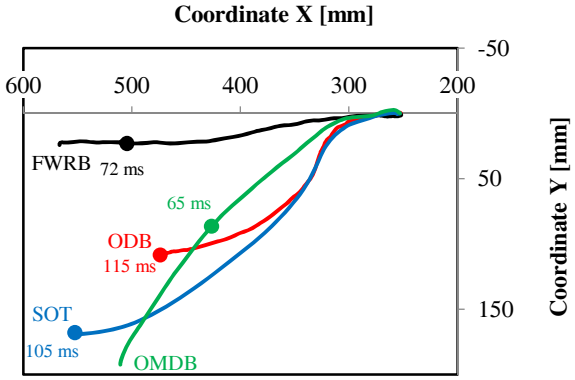

Figure 14. The trajectories of the 9th thoracic vertebra of the elderly HBM in X-Y plane until reaching the X-axis maximum displacement at the vehicle coordinate system in all test conditions with marking the timing when right side rib fractures have all happened in FWRB and OMDB or the thorax deformation have reached its maximum in ODB and SOT

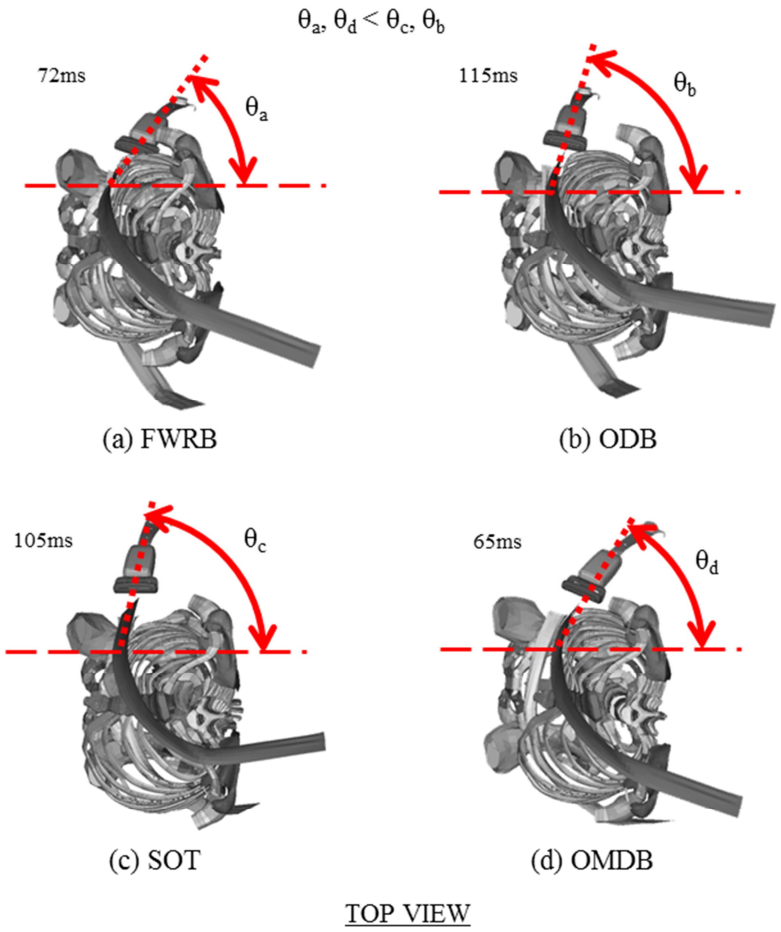

Figure 15. The deformed thorax shape and the shoulder belt path of the elderly HBM from the viewpoint fixed at the 4th thoracic vertebra at the time when right side rib fractures have all happened in FWRB and OMDB or the thorax deformation have reached its maximum in ODB and SOT, with θ representing the angle between the direction of the lower right shoulder belt and the X-axis in the vehicle X-Y coordinate of the 4th thoracic vertebra

Lower left rib fractures (Region C)

As shown in Fig. 10, the ribs around the lower left thorax were fractured in such cases including the lateral vehicle motion as SOT and OMDB. It was observed that the thorax of the elderly HBM contacted the door trim although that of THOR-50M model didn't. The difference of thorax response between the elderly HBM and THOR-50M models is considered to have occurred for following reasons:

Firstly, there was the difference of the thorax maximum displacement in Y-axis between the elderly HBM and THOR-50M models. As shown in Fig. 5, the Y-axis maximum displacements of the thoracic vertebrae (T1, T9, L2) of the elderly HBM were larger than those (T1, T4, T12) of the THOR-50M model in SOT and OMDB. Figure 16 shows the deformed body shapes of the elderly HBM and THOR-50M model and the door trim from the viewpoint of the vehicle coordinate system at 94ms in SOT. The spine of the elderly HBM was curved more outward than that of THOR-50M model. The human spine consists of multiple vertebrae and intervertebral discs. In the elderly HBM, that enables such a flexible motion. In contrast, THOR-50M has only the upper thoracic spine flex joint and lumbar spine flex joint made of rubber as components of the spine. Therefore, it was considered that the spine of the THOR-50M model could bend limitedly.

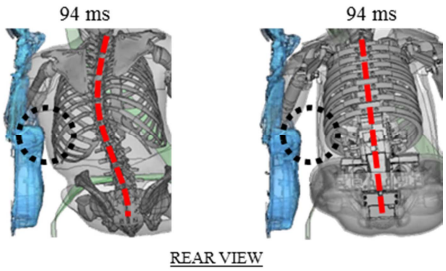

Figure 16. The deformed body shapes and the door trim from the viewpoint of the vehicle coordinate system in SOT

Secondly, there is the difference of the thorax geometry between the elderly HBM and THOR-50M model as shown in Fig. 17. The rib cage of the elderly HBM was created based on the CAD of one elderly individual with the body size close to AM50%ile by Ito et al. [3]. Its geometry showed it had a bit wider around the lower part and a higher bottom than THOR-50M; that made the elderly HBM contact the door trim while THOR-50M didn't reach it.

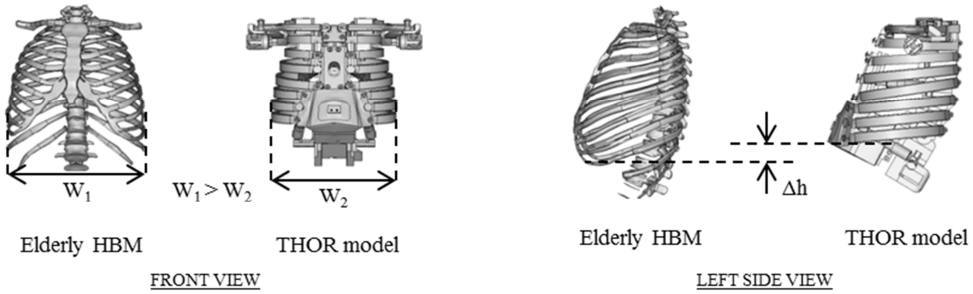

Figure 17. The thorax geometry of the elderly HBM and THOR-50M model

Thirdly, between the elderly HBM and THOR-50M model there was the thorax response difference around the lower left where the shoulder belt didn't pass directly. Figure 18 shows the deformed thorax shapes of the elderly HBM and THOR-50M models from the viewpoint fixed at the 4th thoracic vertebra at 0 ms and 70 ms in SOT. In the elderly HBM, it was observed that the rib cage around the lower left was swollen largely. It is assumed that the forward inertial force of the viscera contributed to this phenomenon. In the THOR-50M model, it is thought that the rib cage hadn't been swollen because THOR-50M has no part simulating human viscera. At the lower left thorax, the correlation of the thorax deformation between the elderly HBM and THOR-50M model might not be high due to the difference of the inertial force by the viscera.

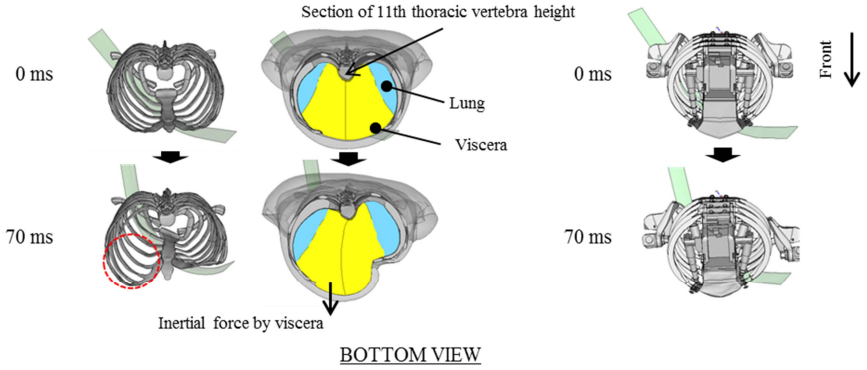

(a) Elderly HBM (b) THOR-50M model

Figure 18. The deformed thorax shapes from the viewpoint fixed at the 4th thoracic vertebra at 0 ms and 70 ms in SOT

Mainly for these three reasons, it was consider that the distance between the thorax of the elderly HBM and the door trim decreased during the collision in SOT and OMDB. The thorax contact to the door trim occurred, and the ribs around the lower left ribs were fractured. The rib fractures and thorax response may be peculiar to this elderly HBM since it hasn't been investigated whether this phenomenon occurs in a real human body.

CONCLUSION

In this research, the comparison of the thorax response between human and THOR-50M under simulated frontal crashes including lateral vehicle motion such as FWRB, ODB, SOT and OMDB was performed, that showed a certain correlation between rib fractures of the elderly HBM and the thorax deformation of THOR-50M. As the results, the following conclusion was obtained.

- For the elderly HBM and THOR-50M model in all the test conditions, the thorax deformation at the upper right was largest among four measurement locations, and that of the elderly HBM and THOR-50M model showed good correlation.
- The number of fractured ribs of the elderly HBM and the overall peak resultant deformation (R_{max}) of THOR-50M model calculated in four crash test conditions showed good correlations. However, the number of the fractured ribs assorted into three regions didn't show a good correlation with R_{max}.
- The upper left ribs of the elderly HBM were fractured by the downward and rearward loading by the shoulder belt via the clavicle. In the THOR-50M model, however, because the shoulder can move within a structurally limited range, such a mechanism of deformation could not be represented.
- A few of right ribs were fractured in FWRB and OMDB, and none was in ODB or SOT. Under the condition of FWRB or OMDB where the occupant moves more forward than ODB or SOT by higher frontal deceleration, there may be a possibility that rib fractures occur due to the higher rearward loading by shoulder belt to the thorax.
- A few of the lower left ribs were fractured in SOT and OMDB because the thorax contacted the door trim in the elderly HBM, while it didn't in the THOR-50M model.

The results of this study suggested that the R_{max} of THOR-50M might be an acceptable index to evaluate an overall severity for the occupant thorax in frontal crash conditions while further study for the methods to evaluate detailed thorax injury using THOR-50M should be needed in order to correlate any other indices and possible thorax injuries in the crash condition with lateral motion. At the current status, when the current THOR-50M measurements are used to evaluate the injury risk, it is important to understand such the characteristics above.

REFERENCES

[1] National Police Agency, 'Traffic Accident Situation', http://www.e-stat.go.jp (2016)

[2] Shimamura M, Ohhashi H, Yamazaki M, 'The Effects of Occupant Age on Patterns of Rib Fractures to Belt-Restrained Drivers and Front Passengers in Frontal Crashes in Japan', Stapp Car Crash Journal, Vol. 47 (October 2003), pp.349-365

[3] Ito, O., Dokko, Y., Ohashi, K., 'Development of Adult and Elderly FE Thorax Skeletal Models', SAE Technical Paper 2009-01-0381, 2009, doi:10.4271/2009-01-0381

[4] Rangarajan, Shams, T.,N.,White, R., Oster, J, Hjerpe, E., Haffner, 'Response of THOR in Frontal Sled Testing in Different Restraint Conditions', IRCOBI Conference Proceedings, (Sept. 1998)

[5] Xu L, Jensen J, Brynes K, Kim A, Agaram V, Davis K, Hultman R, Kostyniuk G, Marshall M, Mertz H, Nusholtz G, Rouhana S, Scherer R., 'Comparative performance evaluation of THOR and Hybrid II', SAE paper no. 2000-01-0161 SAE, Warrendale, PA. (2000)

[6] Richard Kant, Greg Shaw, David Lessley, Jeff Crandall, Dimitris Kallieris, Mats Svensson, 'Comparison of Belted Hybrid III, THOR, and Cadaver Thoracic Responses in Oblique Frontal and Full Frontal Sled Tests', SAE Technical Paper, 2003-01-0160, p. 1-16, (2003)

[7] Greg Shaw, David Lessley, Joe Ash, Jeff Crandall, Dan Parent, 'Response Comparison for the Hybrid III, THOR Mod Kit with SD-3 Shoulder, and PMHS in a Simulated Frontal Crash', Proceeding of the 23rd ESV Conference, Report No.13-0130, (2013)

[8] Devon L Albert, Stephanie M Beeman, and Andrew R Kemper, 'Assessment of Thoracic Response and Injury Risk Using the Hybrid III, THOR-M, and Post-Mortem Human Surrogates under Various Restraint Conditions in Full-Scale Frontal Sled Tests', Stapp Car Crash Journal, Vol. 62 (November 2018), pp. 1-65

[9] Ito, O., Dokko, Y., Ohashi, K., 'Development of the Human Lower Limb FE Models of Adult and Elderly Person Considering Aging Effects', Proceedings, JSAE Annual Congress (Spring), #20085048 (2008)

[10] Dokko, Y., Ito, O., and Ohashi, K., "Development of Human Lower Limb and Pelvis FE Models for Adult and the Elderly," SAE Technical Paper 2009-01-0396 (2009), doi: 10.4271/2009-01-0396.

[11] Dokko, Y., Kanayama, Y., Ito, O., and Ohashi, K., "Development of Human Lumbar Spine FE Models for Adult and the Elderly," SAE Technical Paper 2009-01-0382 (2009), doi:10.4271/2009-01-0382.

[12] Humanetics Innovative Solutions : THOR-50th Metric V1.4.1 LS-DYNA Model Technical Report User's Manual, (2016)

[13] LSTC : LS-DYNA Version 971 R6 User's Manual, (2012)

[14] National Highway traffic Safety Administration, 'Oblique Test Procedure', Docket ID 2015-0119, (2016)

ESTIMATING PRELIMINARY OCCUPANT INJURY RISK DISTRIBUTIONS FOR HIGHLY AUTOMATED VEHICLES WITH RESPECT TO FUTURE SEAT CONFIGURATIONS AND LOAD DIRECTIONS

Felix Ressi
Wolfgang Sinz
Graz University of Technology
Austria

Claus Geisler
Abdulkadir Öztürk
Daimler AG
Germany

Gian Antonio D'Addetta
Heiko Freienstein
Robert Bosch GmbH
Germany

Paper Number 19-0175

ABSTRACT

While highly automated vehicles (HAVs) will be able to reduce the number of accidents significantly by removing human error, some accidents may remain unavoidable – particularly during the transition period. HAVs also promise increased freedom in seat positioning for all passengers, including the driver. A growing amount of literature deals with individual issues of occupant safety in these new positions, but there is currently no comprehensive overview on the effects of combinations of possible future seat positions and vehicle load directions. Addressing this, the aim of this research is to develop a method to quickly highlight key combinations of seat position/inclination and crash load direction with respect to occupant safety for any given interior layout and set of restraint systems. Also, the method should facilitate the evaluation of restraint systems' active principles. Inspired by common safety engineering methods, the proposed approach defines risk as combination of severity, exposure and controllability. To estimate the severity, each restraint system's ability to restrain the occupant – referred to as restraining potential – is defined as mathematical function of relevant parameters, e.g. various seat adjustments and as function of the load direction relative to the occupant. These individual restraining potential functions which can be plotted as 2D-graphs, can then be combined into a total restraining potential for any specific combination of parameters (seat, load direction...). The required interpolation points for these functions are estimated theoretically and checked for plausibility based on finite element (FE) simulations with a human body model (HBM) and compared to literature. Additionally, the space available for occupant displacement (and thus available for dissipation of kinetic energy) is considered and combined with the restraining potential to a measure which is inversely proportional to the severity. The exposure is estimated with a distribution of the main accident types (front/side/rear). While the relevant future distribution is not yet known, estimates from recent literature or current accident data can be used as starting points. With a modular approach, effects of different distributions can easily be analysed by changing this input. Controllability (with respect to the risk definition) is not taken into account in this first implementation, since the approach only considers scenarios where crashes occur and all systems are expected to work faultlessly. Based on the calculated severity and exposure the occupant injury risk is automatically computed for a specific interior and then plotted for all reasonable combinations of seat adjustments. This enables an immediate overview for finding key combinations which should be the focus of in-depth analyses, e.g. detailed FE simulations. The proposed approach should not be seen as a replacement for detailed FEA but as a useful supplement for time and resource efficient preparation of simulation studies concerning the occupant safety of future HAVs. Estimating preliminary occupant injury risks for future HAVs provides an insight to their expected performance which highlights key parameter combinations and can aid the development of relevant regulations and test procedures.

INTRODUCTION

Among other benefits, highly automated vehicles (HAVs) promise a significant reduction of the number of accidents. The important role of human error as accident cause is widely acknowledged but it is hard to determine the actual percentage of accidents which would be prevented if cars drove themselves. A study in 2008 suggested that over 90% of accidents are caused by human error [1], but even removing all human factors does not mean that the number of car crashes is going to be reduced to 10% – particularly not in the short or even mid-term. While the goal has to be to prevent all accidents, at least a significant reduction of accident numbers can be expected with

the introduction of HAVs. Especially accident causes like distraction, driving under the influence of alcohol or drugs, fatigue and cardiac and circulatory troubles – which together accounted for over 40% of all fatal crashes in Austria in 2017[1] [2] – could be removed completely. Still, considering that in 2016 the average vehicle age in the European Union was more than ten years and that as of today fully-automated driving is not available in a series production vehicle, it will take many years until all cars on the roads are HAVs. Particularly during the transition phase, unforeseeable circumstances or the mix of conventional and automated vehicles will produce scenarios in which the accident cannot be avoided by the HAV. In these remaining crashes new challenges for occupant safety emerge due to the increased spatial freedom HAVs can potentially offer to occupants. When the car takes over control and the driver is released from the driving task, he or she essentially becomes a passenger. Passengers in conventional cars are already spending the time during journeys on various other activities. In HAVs, all occupants could read, use their mobile devices, talk to one another, relax or even sleep while being chauffeured by the car. The standard driving position is not ideally suited for most of these activities – especially considering that the "driver" does not need to reach the controls, since the car is driving itself. In a qualitative study by Jorlöv et al. most participants expressed the desire to rotate their seats [3], at least for longer journeys, which suggests that passengers are potentially open to new interior layouts. These new possibilities have motivated many concepts for new seat configurations [4]. Most of these concepts have three ways of adjustments in common. Figure 1 shows a sketch of a seat with a vehicle coordinate system according to ISO 4130:1978 [5] and the three main adjustments: seat rotation β, increased backrest inclination α and longitudinal adjustment ΔX towards the rear of the vehicle.

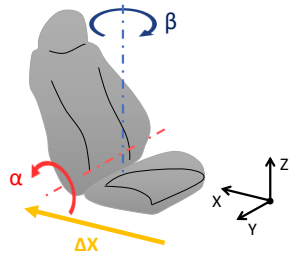

Figure 1. Main seat adjustments for new spatial configurations in HAVs (CS according to ISO 4130:1978).

These new seat configurations motivate a new area of research in the field of occupant safety. While there are many crash test configurations required by laws, regulations or performance assessment programmes for conventional seat configurations around the world, there are currently no mandatory crash tests specifically addressing the possible new seat configurations in HAVs. Instead of establishing mandatory tests, the United States Department of Transportation (US DOT) and the National Highway Traffic Safety Administration (NHTSA) encouraged car manufacturers to demonstrate due care to ensure full protection of all occupants in its Federal Guideline on Automated Driving Systems [6].

In absence of concrete rules or regulations, the key to demonstrate such due care is to determine all relevant load cases for such vehicles and to provide sufficient evidence that all occupants – when exposed to these load cases – experience acceptable injury risks. One way to approach this is to consider two perspectives: external and internal. The external perspective accounts for all external factors affecting the crash-induced loads on the occupants. Equivalently, the internal perspective accounts for all factors inside the vehicle. All of these factors need to be considered since they form the basis of any occupant injury risk assessment – the crucial part of demonstrating due care. Figure 2 illustrates this approach.

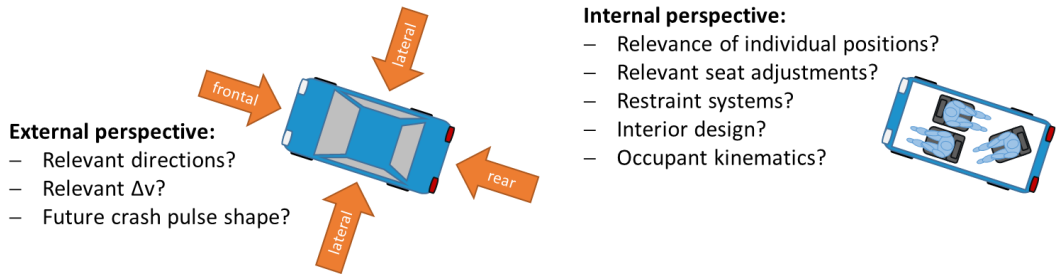

Figure 2. Illustration of the external and internal perspective affecting the loads on an occupant in a HAV.

[1] This number should be seen as an estimation, since it is derived from accident reports forms, compiled by police officers at the accident site. Even if subsequent analyses, e.g. by accident investigators, reveal a different accident cause, the original accident report is often not updated accordingly.

The external perspective encompasses the relevant future impact directions, the kinetic energy of the impact (commonly estimated with the velocity difference pre-/post-collision, Δv) and the shape of the crash pulse, which is the result of the HAV's stiffness and the stiffness of the striking vehicle. All these factors can only be estimated, since highly automated cars are not commercially available yet. Consequently, hardly any field data is available. While data from conventional vehicles can be used, it should be seen as an indication and be updated as soon as new research or data is available. Favarò et al. [7] found that out of 26 crashes involving HAVs in California between September 2014 and March 2017, injuries where only reported in two cases. They also provide a damage distribution for the HAVs, where rear damage accounts for the majority of 62%. Side and front damage only make up 23% and 15% respectively. While the study provides an interesting first glimpse at the issue, the empirical value of the accident distribution must not be overestimated, particularly because it only covers a very limited number of cases. It is only used in the present study exemplarily to provide a starting point.

The internal perspective (see right hand side in Figure 2) depends, to some extent, on the environment. For instance, the importance of a specific restraint system like the curtain airbag for reducing the occupant injury risk is dependent on the load case. In this case, the curtain airbag's importance is much higher in lateral impacts than for example in rear-end crashes. Nevertheless, there are many aspects of the internal perspective which are not reliant on external factors. Examples are the relevance of seat configurations in terms of acceptance by passengers of HAVs or the future interior designs as showcased by many OEMs and suppliers in concept vehicles. This is important since it defines the adjustment ranges of the seat system and the interior layouts which are relevant for further analysis. Since ultimately the focus of the internal perspective is the occupant and specifically it's injury risk for all relevant seat configurations it should be discussed in more detail.

In principle, there are two main approaches to estimate occupant injury risks for a given vehicle concept. One way is physical testing of prototypes e.g. with a sled test setup. Anthropomorphic test devices (ATDs) can be used in these tests to represent and measure the human response to the applied crash loads. While this approach is commonly used in later stages of development, it is often too costly and time-consuming to use it in pre-development, where many configurations need to be evaluated. The alternative, virtual testing, offers many benefits particularly in terms of flexibility and the ease of use for evaluation of large numbers of configurations (once the models are built). Even the Federal Guideline on Automated Driving Systems explicitly states that the demonstration of due care need not be limited to physical testing but may also include virtual vehicle and human body models[2] (HBMs) [6]. Using HBMs in the context of alternative seat configurations is especially interesting for four main reasons, which are discussed in the following paragraphs.

Firstly, commonly used ATDs or crash test dummies were designed to be used in upright seat configurations, as they are for instance defined in current laws and regulations. Many new concepts for future vehicles promote "relax" or "lounge" positions with significantly reclined seatbacks [9–11]. These positions are generally infeasible with state of the art dummies due to the non-adjustable angle between their thighs and their torso. HBMs can theoretically take any position a human can, even if this usually is a time-consuming task.

Secondly, unlike commonly used crash test dummies, most HBMs are validated for multiple loading directions. The dummy used in most frontal crash tests, the Hybrid III 50th percentile male, is only calibrated with frontal crash loading [12]. Likewise, the state-of-the-art side and rear impact ATDs, the WorldSID and the BioRID II, are only validated for lateral (±30°) [13] and rearward impacts respectively [14,15]. The latest frontal ATD, the "Test Device for Human Occupant Restraint", or short THOR, has also not been designed for multi-directional use [16], but could be modified to be comparable to dedicated side impact dummies [17]. While it might currently be the ATD most suited for multi-directional use, it is only validated for frontal impacts [18]. By contrast, state-of-the-art HBMs like the Global Human Body Model Consortium (GHBMC) models or the Total HUman Model for Safety (THUMS) are validated on component and regional level as well as for whole body impacts from various directions [19–22]. This means, they are theoretically able to predict injuries independently of the loading direction [23], which is particularly useful when comparing the effects of seat rotation angles that result in a combination of frontal and lateral loading on the occupant. Their biofidelity depends almost exclusively on the validation quality and is theoretically not limited by design, like in ATDs, where loads can only be measured in sensor positions and often only one loading direction.

Thirdly, human body models offer the possibility to represent human diversity far more accurately than ATDs. Many crash test dummies are only available in one or only a small number of size and weight specifications

[2] Throughout this paper the term 'human body model' refers to models considering the complex human anatomy including a full skeleton, adopting Euro NCAP's definition in their technical bulletin on Pedestrian Human Model Certification [8].

(usually derived from the 50th percentile of a sample population). HBMs can be morphed to represent any individual in terms of anthropometry, body mass index and even age [24].

Fourthly, some HBMs offer the possibility to model muscle activity, also referred to as active human body models (A-HBMs) [25,26]. Muscle activity is most significant during low-g loading conditions like emergency braking or swerving manoeuvres. ATDs passive models and also only validated for high-g loading and therefore not usable under low-g loading conditions. Yet, these scenarios are particularly relevant for HAVs, because if an unavoidable crash is detected by the vehicle, reversible and irreversible safety features could also be deployed before the actual crash itself. This calls for high accuracy occupant models for the pre-crash phase. [27]

While these benefits make HBMs a very interesting option for research in the area of occupant safety for HAVs, there are currently some disadvantages to be considered. The detailed representation of the human body comes at the expense of increased computational resources. State-of-the-art finite element models of HBMs have between 1.9 and 2.5 million elements [25] whereas detailed virtual dummy models have around 0.3 to 0.5 million elements [28,29]. This increases simulation times significantly and automatically raises the computational demands for data storage and post-processing. The other main drawback of HBMs compared to dummies is that results obtained with these simulation models cannot be tested or validated in the physical world directly. Also, while detailed injury analysis is one of their main advantages, more research is needed on strain-based assessment methods. Many body regions are still lacking reliable injury risk functions [30] including the lumbar spine. This body region could become more important for HAVs, since it is going to be subjected to more loading in more reclined seat positions (increased spine compression). Nevertheless, due to the unique insights they can give into kinematics and possible sources of injury, they are an important tool in the current and future occupant safety assessment of HAVs.

Recently, many publications have dealt with various aspects of occupant safety in HAVs and used different models in the process. Table 1 compares these simulation studies with regard to the occupant model and the parameters which were used for variation. In this table, the algebraic signs of all adjustments refer to the sketch in Figure 1, not to the convention used in the individual publications.

Table 1.
Comparison of current literature on occupant safety in HAVs.

Publication	Occupant model	α	β	ΔX	Impact		Interior	Belt routing[3]	Restraints[4]
				[mm]	Dir.[5]	Δv $\left[\frac{m}{s}\right]$			
Kitagawa et al. 2017 [31]	THUMS v4	base	0°, -30°, 180°	-	F	15.56, 11.1, 8.3	yes	D/P	3P-B
		24°, 36°, 48°	0° - 360° (45° steps)				no	D	
Jin et al. 2018 [32]	THUMS v4	base	0°, 90°, 135°, 180°	-	F	15.56	no	D	3P-B
Huf et al. 2018 [33]	THOR	fully reclined	0°	-	F	?	only for β = 180°	D	3P-B, SEMS
	H III 5th	base, fully reclined	0°, 180°						active head & backrest, SEMS
	H III 50th								
	THUMS v3								
	ES2	base	90°						3P-B, CC-B, SIP
Gepner et al. 2018 [34,35]	GHBMC O	25°, 45°, 60°	0°, 30°, 90°, 135°, 180°	-	8[6]	?	yes	P	3P-B, PAB, CAB, SAB
	GHBMC OS								
	THOR	25°, 45°							
Zhao et al. 2018 [36]	GHBMC O	base	0° - 360° (30° steps)	-	F	11.1	no	D	3P-B
Boin 2018 [37]	H III 50th	base	0°, ±30°, ±45°	-	F	16.2	no	D	3P-B, CC-B, Airbelt, improved seat and headrest
	ES2-re		60°, 90°		F	11.1			

[3] P – passenger side (in conventional vehicles), i.e. shoulder belt routed from the right shoulder to the left side of the pelvis; D – driver side, i.e. shoulder belt routed from the left shoulder to the right side of the pelvis.
[4] 3P-B – 3-point-belt; CC-B – criss-cross-belt; PAB – passenger airbag; CAB – curtain airbag; SAB – side airbag; SIP – side impact pad for head, thorax and pelvis; SEMS – seat energy management system.
[5] Impact direction w.r.t. the vehicle (F – front, S – side, R – rear).
[6] Eight impact directions: 0°, ±30°, ±90°, ±150°, 180° with moving deformable barrier, v = 15.56 m/s.

While most of these publications consider the effects of individual seat configurations on occupant kinematics (and sometimes injury risk), there is currently no comprehensive overview on the effects of combinations of future seat configurations under various impact directions. It would be theoretically possible to estimate the effects of changing one parameter based on expertise but changing four parameters at once quickly leads to an unmanageable situation. Therefore, setting up finite element analyses (FEA) is the preferred method. The main issues with this approach are the lack of finite element models which are validated for all the relevant loading conditions and the enormous number of possible combinations. While it is possible to simulate hundreds of combinations individually, finding an efficient approach to prioritise or identify the most relevant ones from an occupant safety perspective could reduce the computational costs and time significantly. Many disciplines are faced with similar tasks of identifying the most significant combination of parameters among a large number of possible combinations. Well known examples for such methods in the area of reliability engineering are the failure mode and effects analysis or the hazard analysis and risk assessment described in ISO 26262 [38]. Theoretically, this could also be an area of application for the growing field of machine learning.

The main objective of the present study was to develop a method to quickly highlight key combinations of seat configurations and crash load directions with respect to occupant safety for any given interior layout and set of restraint systems. Additionally, the method should facilitate the evaluation of restraint systems' active principles. The considered parameters are the seatback inclination (14 discrete angles), the seat rotation (13 discrete angles) and the longitudinal seat adjustment (4 adjustment positions). These are combined with three load cases (front, side and rear crash) to estimate an occupant injury risk for every combination. Multiplying all parameter ranges with one another, this results in 2184 possible combinations. Out of these, all variants with a higher risk value should be prioritised and be the focus of further investigation. Also, some configurations, while being theoretically possible, might not be technically feasible and are actually irrelevant in practise. In this case, the configuration – despite potentially having a high risk value – should be excluded from further analysis and not made available in future vehicles.

METHOD

The general approach to estimate the occupant injury risk distributions is illustrated in Figure 3. First, the seat configuration and vehicle characteristics have to be defined. This information is used to look up the relevant (pre-defined) restraining potentials and compute the available distance to interior surroundings. Similar to the hazard analysis and risk assessment in ISO 26262 [38], the severity can then be estimated and combined with the measures for exposure and controllability to the risk estimate. In this first implementation, controllability is not taken into account, since only scenarios where crashes occur are considered and all systems are expected to work faultlessly.

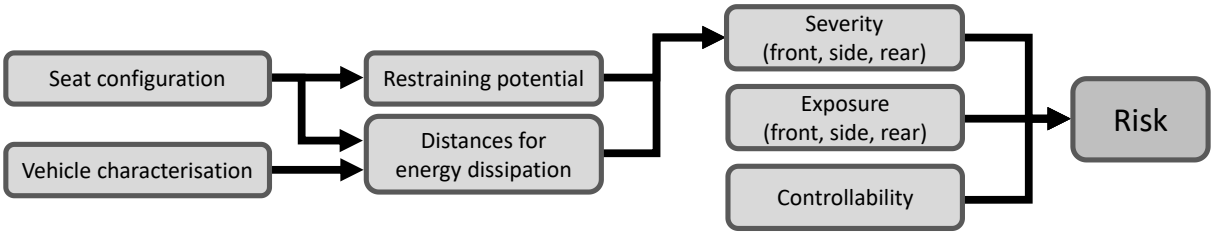

Figure 3. Schematic overview on the general approach to estimate the occupant injury risk distributions.

With respect to the internal/external perspective, this approach focusses mainly on the internal perspective. In this first step, a separate investigation makes sense – in particular to assess the main challenges. Also, at this stage, many factors regarding future accident scenarios are still unknown. The external factors, which are necessary to assess occupant safety within the internal perspective (in particular the accident distributions to estimate the front/side/rear exposure levels), are determined using recent literature. Where this is not possible the factors are estimated with a safety margin following a due care approach. For instance, the future crash severities for HAVs are unknown today, but it could be argued that they will be lower than the severity for conventional vehicles, due to their inherent lack of inattentiveness and lower reaction times. These reduced reaction times would in turn lead to lower collision velocities and hence lower crash severities. Therefore, while the currently mandated crash test severities represent an upper limit which represent a worst case scenario for this study, these are highly relevant for a due care approach.

The following paragraphs explain the individual aspects illustrated in the overview in Figure 3 in more detail.

Seat configuration

The basis of the seat configuration is made of the three adjustments introduced in Figure 1 (seat rotation β, increased backrest inclination α and longitudinal adjustment ΔX). While occupants can theoretically take many

different postures in one seat position, it is assumed, for the purpose of this study, that the occupants H-point matches the equivalent H-point that has been determined for the seat. For reasons of simplicity, this point is also defined as the base point for the seat rotation (angle β) about the Z-axis. Furthermore, the occupant's torso is assumed to be in contact with the backrest and asymmetric postures are not considered. While many activities which are possible in HAVs will involve the occupants holding objects in their hands (mobile devices, books, etc.), a relaxed arm position is assumed (i.e. hands in lap) to reduce the number of variables.

To facilitate future comparisons of configurations with different load cases but similar direction of loading with respect to the occupant the load direction φ is defined. Figure 5 illustrates the relationship between the seat rotation β and the load direction with respect to the occupant φ. For a frontal collision, φ equals β (illustration on left side of Figure 4). For the lateral load case, when the vehicle is struck from the left side (illustration in the middle of Figure 4), φ is defined as $\beta + 90°$. Equivalently, in the rear crash load case, φ is defined as $\beta + 180°$ (illustration on right side of Figure 4).

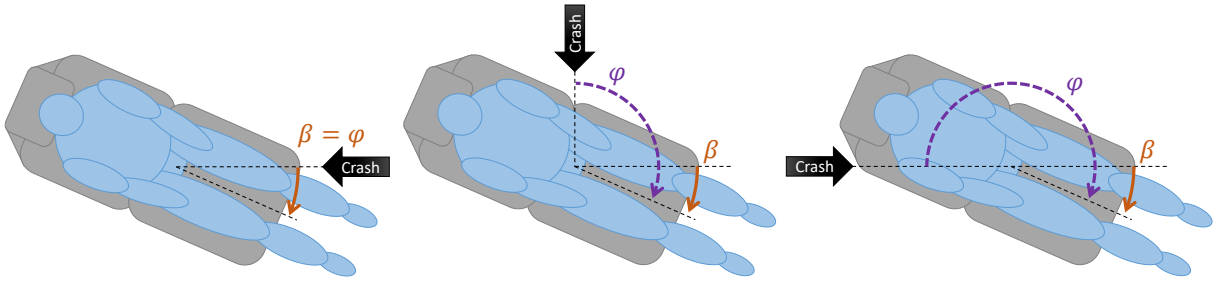

Figure 4. Illustration of the relationship between the seat rotation β and the load direction φ.

To estimate if intersections with the interior occur, parameters describing the seat, its position and its space requirements need to be defined. The most extreme extensions of the seat in X and Y direction, relative to the base point (the H-point), are determined in the following way. The distance between the 50th percentile occupant's pelvis to the head, d_{HP}, is used in combination with the backrest inclination α to calculate the theoretical position of the head-COG (cf. illustration on the left side of Figure 5). From this point, the parameters w_{SB} (width of the seatback at the rear) and d_{HS} (distance between the 50th percentile's head-COG and the back of the seat), shown in the illustration in the centre of Figure 5, are used in combination with the seat rotation β to approximate the two distances s_{S_lat} and s_{S_lon}. These two distances are shown in the illustration on the right of Figure 5.

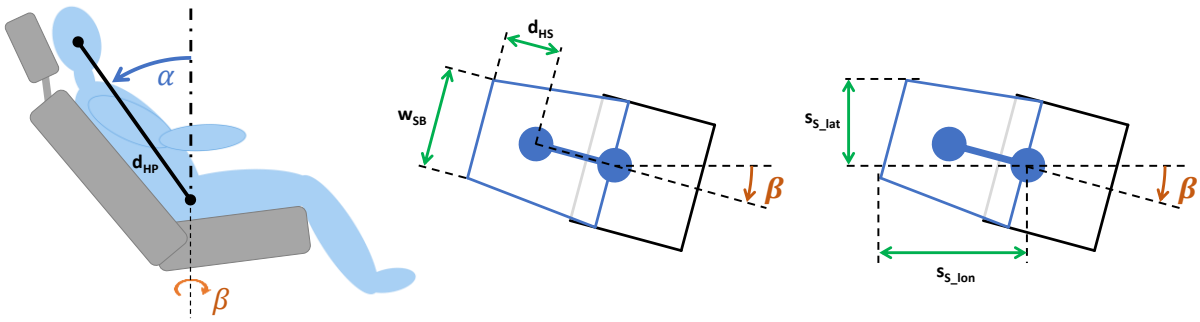

Figure 5. Illustration of the parameters describing the seat configuration and its space requirements.

Vehicle characterisation

To characterise the vehicle, the load cases and the interior dimensions, a number of parameters have to be defined. Also, some general information about the available restraint systems needs to be determined. The restraint systems in the vehicle discussed in the present study are summed up below:

- Standard vehicle seat
- Seat integrated 3-point belt system (with pretensioner and load limiter)
- Frontal airbag (fixed to the vehicle, in other words: independent of seat position)
- Side airbag (seat mounted)
- Curtain airbag (fixed to the vehicle, in other words: independent of seat position)

Figure 6 shows a top view of a vehicle seat, rotated 15° clockwise (angle β) and the distances (green arrows) of the seat H-point to the interior (grey dashed lines). Distance s_{BP_Y} indicates the available space between the seat

H-point and the lateral interior, while s_{BP_X} and s_{BP_-X} indicate the space to the rear and the front of the interior respectively. The longitudinal distances obviously change when the seat is moved to a more rearward position, therefore the distances have to be defined in a base position (which is the standard driving position).

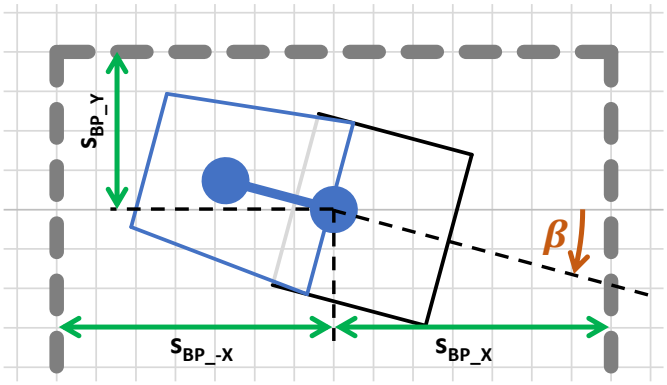

Figure 6. Schematic vehicle seat and interior (top view) with the distances describing the seat position.

These distances, together with the seat rotation, the recline angle and occupant size make it possible to estimate the distances of the occupant's head to the interior – which, in combination with the crash velocity, is later used to determine a theoretical mean deceleration for each load case.

Additionally, these distances are utilized to determine if a certain combination of seat adjustments is feasible in the given interior space around the base position. The example in Figure 7 illustrates that with increased seat rotation, the distance s_{SB_lat} between the seatback and the lateral interior is reduced. Likewise, if the seat is moved towards the rear, distance s_{SB_lon} between the rear of the seat and the interior is reduced. For large enough rotation angles or excessive longitudinal seat adjustments towards the rear the seat would collide with the interior. Configurations which lead to such collisions are not evaluated since they are irrelevant in practise.

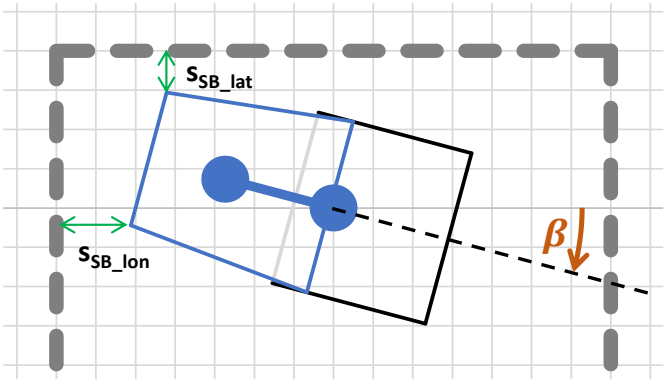

Figure 7. Schematic vehicle seat and interior (top view) with distances between seat and interior.

In addition to these geometric parameters, the load cases have to be defined. The load cases used in the present study consist of a frontal, a lateral and a rear crash, which are characterised by their Δv. The crash severity representing the frontal collision is derived from a full-width crash test with 56 km/h into a rigid wall. Accordingly, the severity for the lateral impact is represented by a crash test with a deformable barrier which is striking the vehicle with a speed of 55 km/h (normal to the vehicle). While a pole crash test is generally the more demanding lateral load case in terms of occupant safety due to its inherently larger intrusions, it is not deemed representative for HAVs. The reason for this is the assumption that the systems in a HAV will be designed in a way that running off accidents (and subsequent lateral collisions with trees or poles) will be avoided. The rear crash is represented by a test mandated for fuel system integrity. In this test a deformable barrier, moving at 80 km/h, strikes the vehicle from the rear. It can be argued that this represents a scenario, where the HAV is struck from behind by an inattentive driver of a conventional vehicle. Since all of these are standard crash tests for conventional vehicles, each represents a kind of upper limit considering the crash severities for HAVs.

Table 2 gives an overview of the defined parameters. The values for the parameters used in the present study can be found in the appendix.

Table 2.
Parameters used to characterise the vehicle interior and load cases.

Parameter	Symbol	Found in	Unit	Comments
occDistHeadPelvis	d_{HP}	Figure 5	m	Distance H-point to COG head[7]
spaceBasePositionX	s_{BP_X}	Figure 6	m	Initially available deceleration space - frontal
spaceBasePositionY	s_{BP_Y}	Figure 6	m	Initially available deceleration space - lateral
spaceBasePositionMinusX	s_{BP_-X}	Figure 6	m	Initially available deceleration space - rear
spaceAvailableY	s_{BP_Y}	Figure 6	m	Available space to the side (for seat rotation)
seatDepthBehindHead	d_{HS}	Figure 5	m	Distance between COG head and rearmost part of the seat
seatBackWidth	w_{SB}	Figure 5	m	Seatback width (at rearmost part)
velocityFront	-	-	m/s	Impact velocity - frontal
velocitySide	-	-	m/s	Impact velocity - side
velocityRear	-	-	m/s	Impact velocity - rear

In short, these parameters are used to estimate if a certain seat configuration is feasible in the proposed interior space and to calculate theoretical mean deceleration levels for the various impact conditions for the risk definition.

Risk definition

The risk definition consists of three elements: severity, exposure and controllability. This concept is loosely based on the risk definition used in ISO 26262 [38]. The most complex aspect is defining the severity in a way which is universal but selective. In other words, it needs to be applicable to all seat configurations while accurately distinguishing differences in potential injury severity between them. In this study, the severity is estimated in the following way. Each restraint system's ability to restrain the occupant – referred to as restraining potential – is defined as mathematical function of relevant parameters. A value of 100% means that the occupant is restrained perfectly just by this single restraint system while 0% means that the occupant is not restrained at all by the considered restraint system. Specifically, this is defined as a function of seat adjustments (recline angle and seat rotation) for every impact direction (front, side, rear). Figure 8 shows the restraining potential (RP) of the seat in a frontal impact as an example. The two plots on the left show the RP as a function of the seat rotation at 25° and 90° recline angle. The two plots on the right show the RP as a function of the recline angle at 0° and 180° seat rotation.

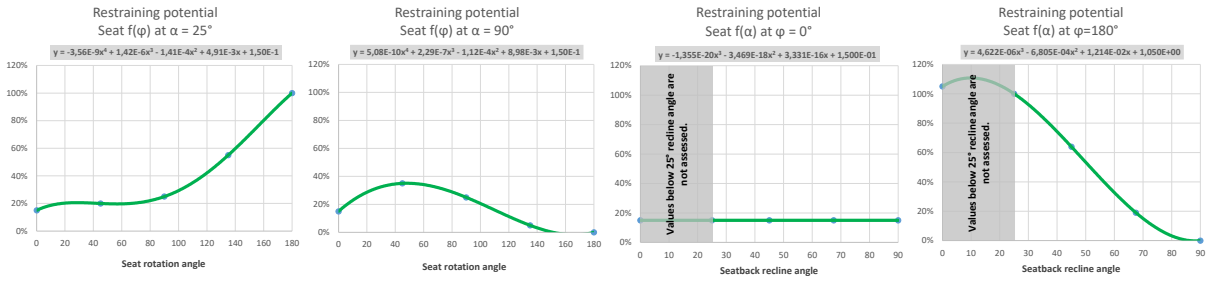

Figure 8. Restraining potential of the seat as a function of recline angle and seat rotation.

The first graph to the left shows that the RP of the seat increases with increasing seat rotation angle. This is based on the fact that with increased area to hold the occupant in position, the seats potential to restrain it is higher. While this is true for a base backrest recline angle of 25°, this is not the case for a fully reclined backrest (second graph from the left in Figure 8). In this configuration, the RP first increases until the seat is rotated 45°, which is the position that is estimated to produce the largest projected contact area between the seat and the occupant. This estimation is based on the assumption that at 45° seat rotation, this contact area comprises of a combination of the seat cushion itself (which is slightly angled backwards) and the side bolsters. For rotation angles above 45°, the RP decreases, because the projected contact area of the seat cushion is reduced, until it is negligible for 180°. It is important to note, that this is only valid for a seat for which the cushion angle is independent of the backrest angle. The second graph from the right shows that the seat's RP is independent of the backrest angle for 0° seat rotation. For 180° of rotation, the RP decreases with increased backrest recline, as the projected contact area is reduced. These curves represent a preliminary implementation which, while checked for plausibility with literature and

[7] This distance is occupant specific. The approximated measures for the Hybrid III dummy family are listed here as an orientation: H305: 590 mm; H350: 670 mm; H395: 704 mm

interim FEA, is subject to be updated in the future. Also, due to the smooth functions, this approach cannot account for phenomena like submarining, which do not occur gradually. Therefore, such effects need to be accounted for separately.

The four curves shown in Figure 8 essentially define the boundaries of a three-dimensional area diagram with the horizontal axes being seat rotation and recline angle, and the vertical axis representing the restraining potential of the seat. Figure 9 shows a plot of this area diagram, where the points between the boundaries are the result of linear interpolation of the four curves. The higher the area in the diagram, the higher the ability of the seat to restrain the occupant. The values, on which this plot is based, form a look-up-table which gives the restraining potential for the seat for any given parameter combination.

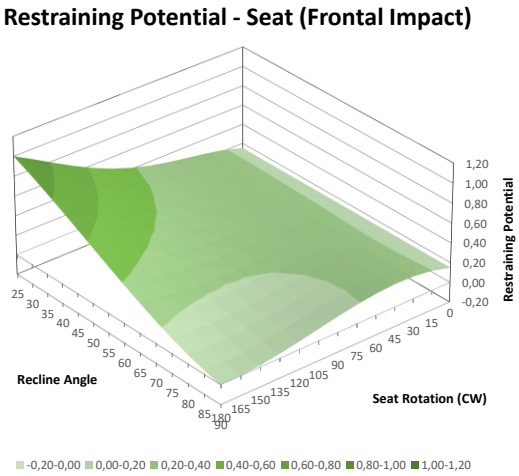

Figure 9. Restraining potential of the seat for frontal impacts as 3D-plot.

The restraint potential is also defined for the lateral and the rear impact condition, resulting in three look-up-tables per restraint system. The whole procedure is applied to the other restraint systems as well – resulting in restraining potentials of the 3-point seatbelt, the frontal airbag, the (seat mounted) thorax airbag and the curtain airbag in all three impact conditions.

The second element of the severity definition considers the estimated distance between the occupant's head and the closest interior parts in the direction of impact. This, together with the assumed impact velocity for each load case, enables the calculation of a mean deceleration. Figure 10 shows a diagram of an occupant in top and side view. The horizontal distance between the head and the pelvis (purple line) only depends on the recline angle α (which is approximated to be identical to the seatback recline angle).

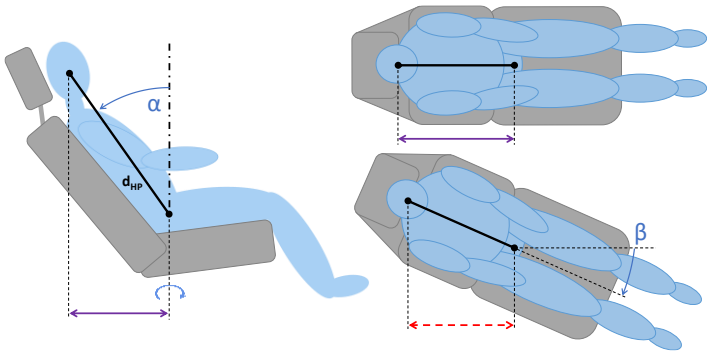

Figure 10. Top and side view of an occupant illustrating the calculation of the longitudinal distance between the head and the seat base point.

Accounting for seat rotation of β degrees about the vertical axis through the hip point, it is possible to calculate the longitudinal distance between the head and the seat base (rotation) point (red dashed line). This enables the estimation of the distance between the occupant's head and the interior for each impact direction. Figure 11 shows this in the form of a simple illustration for a frontal impact, the green distance s representing the total horizontal distance between the head and the interior.

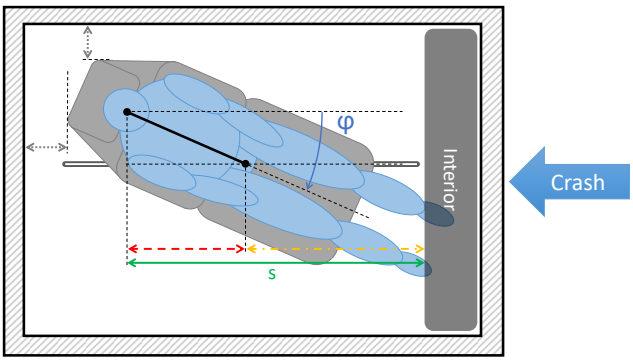

Figure 11. Illustration of the distance s between the occupant's head and the interior for a frontal impact.

This distance s is calculated for each seat configuration. Together with the assumed velocity v for each load case it can be put into Equation 1 to get an estimate of the mean deceleration $\bar{a}$. This is based on the theoretical assumption of uniform linear deceleration for the occupant.

$$\bar{a} = \frac{v^2}{2 \cdot s} \qquad \text{(Equation 1)}$$

Finally, for each individual parameter combination and load case, the quotient of the mean deceleration $\bar{a}$ and the combined restraint potential RP (which is the sum of the individual restraining potentials) equals the severity S (Equation 2).

$$S = \frac{\bar{a}}{RP} \qquad \text{(Equation 2)}$$

More distance in Equation 1 yields a lower mean deceleration and hence a lower severity. Nevertheless, increased distance to those restraint systems which are fixed to the vehicle and therefore do not move with the seat (e.g. the frontal airbag or curtain airbag) is generally not beneficiary. To account for this in the severity value, a modifier is included. If the distance between the head and the restraint which is relevant for the load case exceeds a "maximum range" threshold s_{range}, the modifier is activated. For positions where the distance s is larger than the threshold s_{range}, the adjusted severity S_{adj} is increased linearly, as shown in Equation 3.

$$S_{adj} = \frac{\bar{a}}{RP} + x_{mod} \cdot (s - s_{range}) \qquad \text{(Equation 3)}$$

To make this equation mathematically sound, the modifier has to have the unit s^{-2}, because RP is given in percent and therefore has no units. Since units are not relevant in this context and relative comparisons are more interesting, all the individual severity values are divided by the value obtained for the base seat configuration (cf. Equation 4). This means that in the resulting tables, a severity value of 1 indicates that the severity is equal to that in the base position. Lower and higher values identify reduced and increased severity respectively.

$$S_{norm_R_{\alpha,\beta}} = \frac{S_{adj_R_{\alpha,\beta}}}{S_{adj_R_{0°,25°}}} \qquad \text{(Equation 4)}$$

The normalised severity measure on its own enables the comparison of all relevant seat configurations within one impact direction (examples are shown in Figure 12, Figure 13 and Figure 14). To evaluate the overall risk, exposure and controllability need to be addressed. The exposure is estimated with the distribution of the main accident types (front/side/rear). While the relevant future distribution for HAVs is not yet known, current accident data can be used as a starting point. Effects of different distributions, e.g. for different vehicle types or road types, can easily be analysed by changing this input. Controllability (with respect to the risk definition) is not taken into account in this first implementation, since we only consider scenarios where crashes occur and all systems are expected to work faultlessly (as mentioned in the beginning). Equation 5 shows the formula to calculate the risk which combines the severity of a given seat configuration for each impact direction with its respective exposure E_i.

$$R_i = \sum_{i}^{k} S_{norm_R_i} \cdot E_i = S_{norm_{front}} \cdot E_{front} + S_{norm_{side}} \cdot E_{side} + S_{norm_{rear}} \cdot E_{rear} \qquad \text{(Equation 5)}$$

The formulas above were put into spreadsheets and severity and risk values were calculated for every possible parameter combination.

RESULTS

To get a clearer picture of the underlying effects, the severity charts are discussed individually, before their combination into the overall risk chart which is based on Equation 5.

Figure 12 shows the severity for a frontal impact for two longitudinal seat positions. The chart on the left side shows the severity for the base position; the chart on the right shows the severity for a seat positioned 300 mm towards the rear. The values are relative to the frontal severity in the standard position, which is defined as 0° seat rotation and 25° backrest inclination. Therefore, the frontal severity for this configuration is always 1,0, which stands for the base severity (see top left corner in Figure 12).

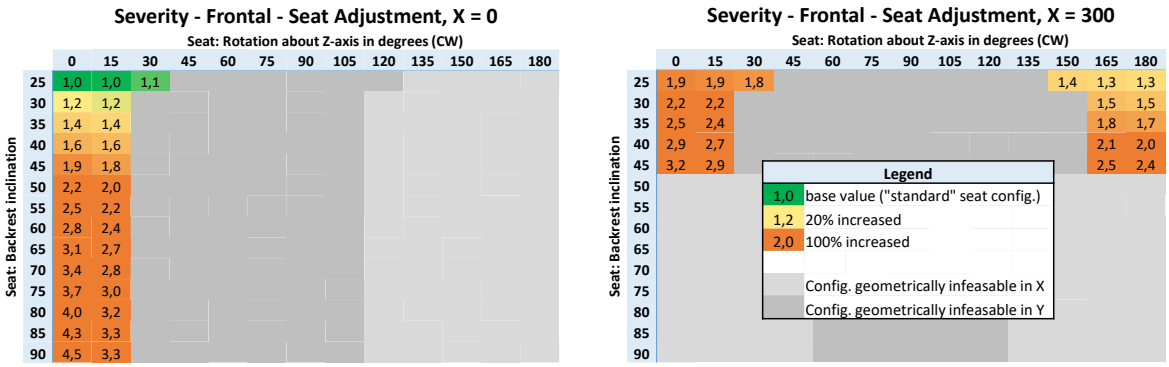

Figure 12. Severity for a frontal impact for two longitudinal seat positions (left: base, right: 300 mm rearward).

The legend on the right side of Figure 12 explains the colour codes. Green values are lower or equal to the base value of 1,0. Yellow values are 20% increased relative to the base position and orange values indicate a risk increase by at least 100%. The light grey areas indicate positions which have not been evaluated because they are not feasible in the given longitudinal vehicle interior space. Areas which are coloured in a darker grey have not been evaluated because there is not enough lateral space in the interior to realise the individual seat adjustment. For instance, in a seat position which is moved 300 mm further rearwards the backrest cannot be reclined as far much as in the base position. On the other hand, for the more rearward adjustment the seat can be positioned in a fully rotated configuration, since – due to the increased distance – the seat back clears the interior in the front of the vehicle.

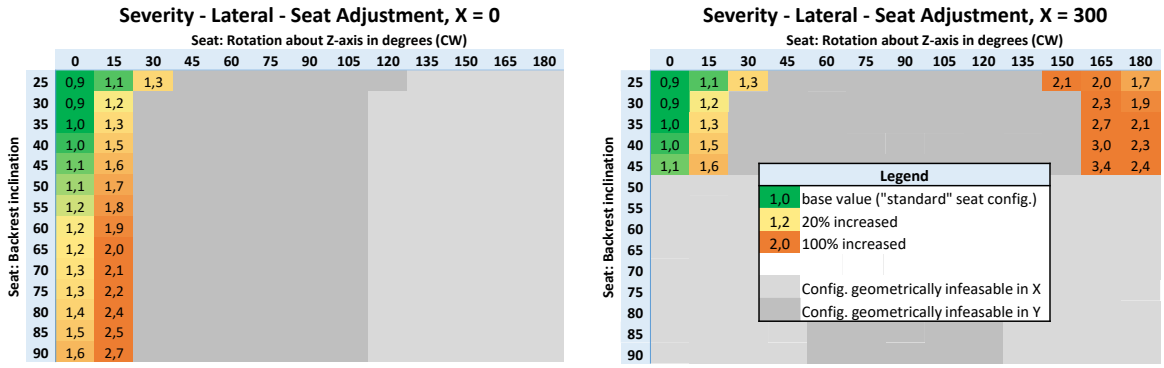

Figure 13. Severity for a lateral impact for two longitudinal seat positions (left: base, right: 300 mm rearward).

Since the interior dimensions do not depend on the load case, the same greyed out areas mark the configurations which are geometrically infeasible.

The equivalent charts for a rear impact load case are shown in Figure 14.

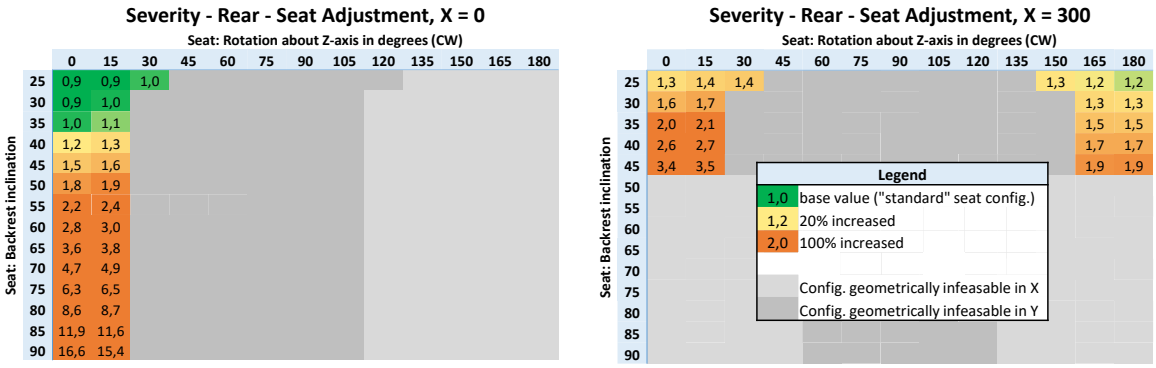

Figure 14. Severity for a rear impact for two longitudinal seat positions (left: base, right: 300 mm rearward).

Utilising Equation 5 and the exposure estimation (62% frontal, 23% lateral and 15% rear crashes) based on the accident data for HAVs by Favarò et al. [7], these severity charts can be combined to the exemplary overall risk charts shown in Figure 15.

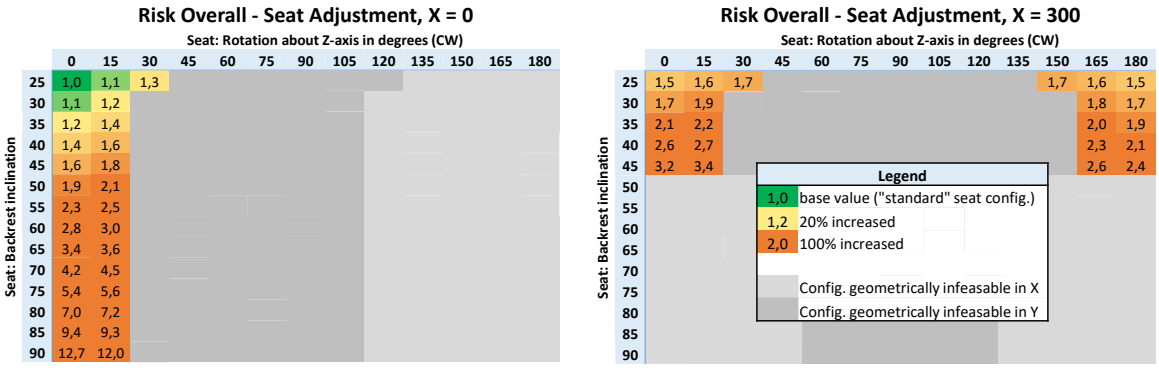

Figure 15. Overall injury risk for two longitudinal seat positions (left: base, right: 300 mm rearward).

The chart shows that the risk increases rapidly for backrest inclination angles above 45°. Also the risk is generally increased by about 50% for a seat position 300 mm further rearward compared to the base position.

Finite element simulations to aid plausibility checks

Individual simulations within a generic vehicle model, based on the detailed finite element model of a mid-size sedan, were set up in order to perform simple plausibility checks for some of the points on the overall risk chart. It was modelled to fit the vehicle characterisation on which the risk distributions shown in above are based. A THUMS v. 4.02 was used to model the occupant. All simulations were performed with LS-DYNA R9.2.0 (Rev. 119543) on a Linux cluster at Graz University of Technology. A view of this model is shown in Figure 16 (only the skeleton with a semi-transparent skin is visualised in this picture to aid belt path analysis).

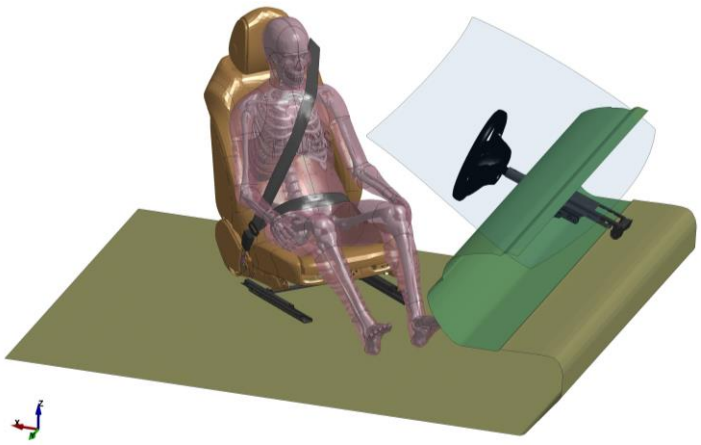

Figure 16. The THUMS v. 4.02 in the generic finite element model with the seat adjusted 300mm towards the rear and rotated by 45°.

In the following discussion, the results of these simulations are compared to the estimation of the preliminary occupant injury risk distributions shown in Figure 15 and the three severity charts (frontal/lateral/rear load case) on which the combined risk chart is based.

DISCUSSION

The comparison of the results obtained with the approach presented in this study and the results from HBM simulations in a generic virtual vehicle model suggest that the estimated preliminary occupant injury risk distributions are plausible.

For the frontal load case, the seatback inclination angles above 40° and increased distances from the frontal airbag system are not ideally covered by current state-of-the-art restraint systems. This seems to be in line with the findings of Kitagawa et al. [31], who presented still images of simulations with recline angles between 24° and 48° without an interior (and therefore without leg support). Submarining occurred in almost all of these cases. The risk charts also suggest that moderate seat rotations (30° or less) seem less problematic, given that there is sufficient leg support. This fits results obtained with the FEA with the HBM which show very similar injury risks for load directions of 0° and 15°. Apart from a 50% increase in BrIC-induced AIS^{3+}-injury risk compared to the 15° position, also the 30° position shows basically the same injury risk values. The simulations also highlighted the importance of the interior dimensions since – similar to Kitagawa et al. [31] – the HBM contacted the windscreen in the frontal load case, when the seat was rotated by 180°.

Since 30° seat rotation is the maximum value which is geometrically possible in the present interior, no significant lateral loading is observed apart from the lateral load case. This load case is currently being re-modelled to incorporate a realistic representation of the intrusions into the cabin. Since there are currently no publications available which present simulation results to compare the risk distribution to, this load case needs to be discussed in more detail once the simulation model is updated. The tendency of increased risk for even slightly increased rotation seems reasonable though, since the occupant's head is significantly closer to the side where the vehicle is struck. Considering intrusions should increase this trend. The increased risk for more or less fully rotated seats (right side in Figure 13) also seems plausible, since the side airbag is only available on the left side of the seat.

For the rear load case, the severity chart in Figure 14 suggests that seatback inclination angles up until 35° are easily feasible – even for seat rotation angles of 15°. Comparing this to the results of Zhao et al. [36] and the FEA conducted for this study, this is not entirely plausible. Zhao et al. found the highest BrIC values for loading angles in the range between 120° and 210° degrees. In the FEA, the BrIC-induced AIS^{3+}-injury risk of the head is increased significantly for 15° seat rotation ($\varphi = 195°$). This needs further investigation, since it is expected, that there is significant influence of the head restraint geometry. Also the trigger times for the seatbelt pretensioners in the FEA seem to be of vital importance – but they cannot be accounted for in the presented approach.

In summary, the approach – in its current implementation – helps to identify key combinations of load cases and interior configurations in which a given set of restraint systems. These can later be the focus of more detailed analyses. The approach can also be used as a preliminary check for feasibility in terms of the basic physical limits. Furthermore, it enables a relative comparison between different concepts (restraint systems, geometric constraints etc.) comparable to a high dimensional occupant load criterion. In this respect it also allows a preliminary estimation of the necessary effort for implementation.

LIMITATIONS

The present study has some limitations. Seat rotation was only considered about a discrete axis, while rotating seats could also swivel and move to the side to allow greater rotation angles in the confined interior space of a vehicle. Also, while different seatback inclination angles were considered the seat cushion angle was not altered. It is likely that seats offering reclining angles above 45° will also alter the seat cushion angle accordingly to provide a comfortable seat position. The occupant posture itself was not considered as a variable. In reality, occupants can take many different postures for any given seat position. A variation of the method could also include the expected distribution or field data of the most relevant seat configurations in order to weight the configurations with higher relevance from an acceptance point of view. The seat could also be moved into a safer position during the pre-crash phase [32], which was not investigated in the present study. To further reduce the loads on the occupants, the seat could be mounted in such a way that energy is dissipated between the seat and the vehicle [33]. This way, less energy is transferred to the occupant. Another area of possible improvement is the representation of intrusions into the cabin. Currently, intrusions are not considered even though they can be significant; particularly in lateral collisions. The approach can also not account for anomalies like submarining. Likewise, configurations which lead to a problematic belt path (e.g. belt slipping off the thorax and up the neck of the occupant) are not detected. While

it is theoretically possible to try to account for these issues via modifiers, it is questionable that all effects can be incorporated. It seems far more reasonable to practise due care when interpreting the resulting charts.

CONCLUSIONS

In this paper a method is presented to quickly highlight key combinations of seat configurations and crash load directions for any given interior layout and set of restraint systems in order to facilitate the evaluation of restraint systems' effectiveness. Estimating preliminary occupant injury risks for future HAVs provides an insight to their expected performance which highlights key parameter combinations and can aid the development of relevant regulations and test procedures. Finally, a first comparison of achieved results with in-depth FE simulations with a HBM showed plausible results and emphasised the validity of this approach in a well-defined range of operation. This method has shown its capability for time and resource efficient preparation of simulation studies concerning the occupant safety of future HAVs.

The presented approach helps to highlight areas in which current restraint systems reach their limits. It is based on a combination of the restraint potential and the mean deceleration for each considered configuration. The overall restraint potential combines the estimates of the individual restraint systems abilities to restrain the occupant while the mean deceleration is estimated based on the impact velocity and the space available for energy dissipation. Both measures are dependent on the seat configuration, interior geometry and load direction and therefore individually evaluated for any combination of the respective parameters. Since more complex effects like submarining can currently not be detected with this approach, they still need to be addressed separately. Nevertheless, the analysis suggests that the current occupant restraint systems need to be adapted or supplemented to ensure ideal occupant safety for increased longitudinal adjustments and more reclined backrest configurations. Moderate seat rotations (less than 30°) on the other hand, seem to be feasible with currently available restraint systems, especially if the headrest design minimises the head rotation in rear-end crashes.

The other aim was to facilitate the evaluation of restraint systems active principles. A visual assessment of the 3D-plots of the individual restraint systems' restraining potential (e.g. Figure 9), clearly shows the restraints system's dependency on the seat configuration. This could help to motivate new active principles by highlighting areas in which current systems lack performance.

Still more work is needed to validate the preliminary occupant injury risk distributions with detailed finite element simulations. This is particularly important with regards to lateral collisions, which are much more complex to model, due to the intrusions into the cabin.

The proposed approach should not be seen as a replacement for detailed finite element analyses but as a useful supplement for time and resource efficient preparation of simulation studies concerning the occupant safety of future HAVs.

ACKNOWLEDGEMENTS

This work was supported by Tech Center i-protect. The authors would also like to acknowledge the use of HPC resources provided by the ZID of Graz University of Technology.

REFERENCES

[1] National Highway Traffic Safety Administration, 2008. National Motor Vehicle Crash Causation Survey: Report to Congress. DOT HS 811 059.

[2] Statistik Austria, 2018. Straßenverkehrsunfälle Jahresergebnisse 2017: Straßenverkehrsunfälle mit Personenschaden. Wien.

[3] Sofia Jorlöv, Katarina Bohman, Annika Larsson, 2017. Seating Positions and Activities in Highly Automated Cars – A Qualitative Study of Future Automated Driving Scenarios. In: International Research Council on the Biomechanics of Injury, editor. 2017 IRCOBI Conference Proceedings. IRCOBI.

[4] Bengtsson O., 2017. Autonomous Vehicle Seats: A User Oriented Concept Design [Bachelor Thesis]. Gothenburg, Sweden: Chalmers University of Technology.

[5] International Organisation for Standardisation, 1978. Road Vehicles - Three-Dimensional Reference System and Fiducial Marks - Definitions. Geneva: International Organization for Standardization.

[6] U.S. Department of Transportation, National Highway Traffic Safety Administration, 2017. Automated Driving Systems 2.0: A Vision for Safety.

[7] Favarò F.M., Nader N., Eurich S.O., Tripp M., Varadaraju N., 2017. Examining Accident Reports Involving Autonomous Vehicles in California. PLoS ONE 12(9). https://doi.org/10.1371/journal.pone.0184952.

[8] Euro NCAP, December 2017. Pedestrian Human Model Certification. 1st ed.(TB 024); Available from: https://cdn.euroncap.com/media/34544/tb-024-pedestrian-human-model-certification-v101.pdf.

[9] C26 | Volvo Cars: Introducing a new symbol of automotive freedom. [January 28, 2019]; Available from: https://www.volvocars.com/intl/cars/concepts/c26.

[10] NIO GmbH. NIO Deutschland - Experience EVE. [January 28, 2019]; Available from: https://www.nio.io/de_DE/visioncar-experience.

[11] Adient plc. Adient unveils new luxury seating concept for level-3 and level-4 automated driving systems. [January 28, 2019]; Available from: https://www.adient.com/media/press-releases/2017/01/09/adient-unveils-new-luxury-seating-concept-for-level-3-and-level-4-automated-driving-systems.

[12] NHTSA, 2008. FMVSS Test Procedure 208-14 - Appendix A: Part 572E (50th Male) Dummy Performance Calibration Test Procedure.

[13] Hynd D., Page M., Bortenschlager K., Been B., van Ratingen M., Pastor C. et al., 2004. Status of side impact dummy developments: WorldSID development. Report number: EEVC WG12 doc 252.

[14] Davidsson J., December 30, 1999. BioRID II Final Report. Gothenburg, Sweden.

[15] Hynd D., Depinet P., Lorenz B., 2013. The repeatability and reproducibility of the BioRID IIg in a repeatable laboratory seat based on a production car seat. Traffic Inj Prev 14 Suppl:95-104. https://doi.org/10.1080/15389588.2013.806987.

[16] Newby N., Somers J.T., Caldwell E.E., Perry C., Littell J., Gernhardt M., 2013. Assessing Biofidelity of the Test Device for Human Occupant Restraint (THOR) Against Historic Human Volunteer Data. In: SAE Technical Paper Series. SAE International, 400 Commonwealth Drive, Warrendale, PA, United States.

[17] Rangarajan N., Shams T., Artis M., Huang T.J., Haffner M., Eppinger R.H. et al., 2000. Oblique and Side Impact Performance of the THOR Dummy. In: International Research Council on the Biomechanics of Injury, editor. 2000 IRCOBI Conference Proceedings. IRCOBI, p. 31–40.

[18] Somers J.T., Newby N., Lawrence C., DeWeese R., Moorcroft D., Phelps S., 2014. Investigation of the THOR Anthropomorphic Test Device for Predicting Occupant Injuries during Spacecraft Launch Aborts and Landing. Front Bioeng Biotechnol 2. https://doi.org/10.3389/fbioe.2014.00004.

[19] Kitagawa Y., Yasuki T., 2014. Development and Application of THUMS Version 4. In: CARHS, editor. 5th International Symposium: Human Modeling and Simulation in Automotive Engineering. carhs.

[20] Schap J.M., Koya B., Gayzik F.S., 2019. Objective Evaluation of Whole Body Kinematics in a Simulated, Restrained Frontal Impact. Ann Biomed Eng 47(2):512–23. https://doi.org/10.1007/s10439-018-02180-2.

[21] Park G., Kim T., Panzer M.B., Crandall J.R., 2016. Validation of Shoulder Response of Human Body Finite-Element Model (GHBMC) Under Whole Body Lateral Impact Condition. Ann Biomed Eng 44(8):2558–76. https://doi.org/10.1007/s10439-015-1546-6.

[22] Katagiri M., Zhao J., Lee S., Kang Y.-S., Nov. 2018. GHBMC M50-O Occupant Response in Moderate-Speed Rear Impacts. 46th International Workshop on Human Subjects for Biomechanical Research.

[23] Fressmann D., June 2016. The THUMS Human Models: Overview. Infotag Human Modeling. Stuttgart.

[24] Hwang E., Hu J., Chen C., Klein K.F., Miller C.S., Reed M.P. et al., 2016. Development, Evaluation, and Sensitivity Analysis of Parametric Finite Element Whole-Body Human Models in Side Impacts. In: The Stapp Association, editor. Stapp Car Crash Journal. Warrendale, PA, United States: SAE International.

[25] Kato D., Nakahira Y., Atsumi N., Iwamoto M., 2018. Development of Human-Body Model THUMS Version 6 containing Muscle Controllers and Application to Injury Analysis in Frontal Collision after Brake Deceleration. In: International Research Council on the Biomechanics of Injury, editor. 2018 IRCOBI Conference Proceedings. IRCOBI.

[26] Kimpara H., Nakahira Y., Iwamoto M., 2016. Development and Validation of THUMS Version 5 with 1D Muscle Models for Active and Passive Automotive Safety Research. Conference Proceedings: Annual International Conference of the IEEE Engineering in Medicine and Biology Society:6022–5. https://doi.org/10.1109/EMBC.2016.7592101.

[27] Iwamoto M., Nakahira Y., Kimpara H., 2015. Development and Validation of the Total HUman Model for Safety (THUMS) Toward Further Understanding of Occupant Injury Mechanisms in Precrash and During Crash. Traffic Inj Prev 16 Suppl 1:48. https://doi.org/10.1080/15389588.2015.1015000.

[28] Panzer M.B., Giudice J.S., Parent D., January 2015. THOR 50th Male Finite Element Model User Manual: Model Version 2.1 for LS-Dyna.

[29] Stahlschmidt S., Huang Y., Usta E., February 9, 2018. Documentation PDB LS-Dyna WorlSID 50th - Version 5: User's Manual Release 0.0 for Model v5.0. Germany.

[30] Klug C., 2018. Assessment of Passive Vulnerable Road User Protection with Human Body Models [Doctoral Thesis]. Graz: Graz University of Technology.

[31] Kitagawa Y., Hayashi S., Yamada K., Gotoh M., 2017. Occupant Kinematics in Simulated Autonomous Driving Vehicle Collisions: Influence of Seating Position, Direction and Angle. In: The Stapp Association, editor. Stapp Car Crash Journal. Warrendale, PA, United States: SAE International, p. 101–155.

[32] Jin X., Hou H., Shen M., Wu H., Yang K.H., 2018. Occupant Kinematics and Biomechanics with Rotatable Seat in Autonomous Vehicle Collision: A Preliminary Concept and Strategy. In: International Research Council on the Biomechanics of Injury, editor. 2018 IRCOBI Conference Proceedings. IRCOBI.

[33] Huf A., Sengottu Velavan S., 26.11 - 28.11.2018. Development of Occupant Restraint Systems for Future Seating Positions in Fully or Semi-Autonomous Vehicles. In: Fraunhofer ICT, editor. Airbag 2018: 14th International Symposium & Accompanying Exhibition on Sophisticated Car Safety Systems.

[34] Lin H., Gepner B., Wu T., Forman J., Panzer M., 2018. Effect of Seatback Recline on Occupant Model Response in Frontal Crashes. Short Communication. In: International Research Council on the Biomechanics of Injury, editor. 2018 IRCOBI Conference Proceedings. IRCOBI.

[35] Gepner B., Lin H., Wu T., Forman J., Panzer M., January 24-26, 2018. The Challenge of Out of Position Occupants for Passive Safety in Automated Vehicles.

[36] Zhao J., Katagiri M., Lee S., Hu J., 2018. GHBMC M50-O Occupant Response in A Frontal Crash of Automated Vehicle. In: CARHS, editor. 7th International Symposium: Human Modeling and Simulation in Automotive Engineering.

[37] Boin M., 2018. Occupant Protection in Alternative Seating Positions. In: DYNAmore, editor. 15th German LS-DYNA Forum.

[38] Hillenbrand M., 2011. Funktionale Sicherheit nach ISO 26262 in der Konzeptphase der Entwicklung von Elektrik/Elektronik Architekturen von Fahrzeugen [Doctoral Thesis]. Hannover, Karlsruhe.

APPENDIX

Table 3.
Values for the parameters used to characterise the vehicle interior and load cases in the present study.

Parameter	Value	Unit	Comments
occDistHeadPelvis	0,67	m	Distance H-point to COG head
spaceBasePositionX	0,40	m	Initially available deceleration space - frontal
spaceBasePositionY	0,50	m	Initially available deceleration space - lateral
spaceBasePositionMinusX	1,00	m	Initially available deceleration space - rear
spaceAvailableY	0,50	m	Available space to the side (for seat rotation)
seatDepthBehindHead	0,20	m	Distance between COG head and rearmost part of the seat
seatBackWidth	0,35	m	Seatback width (at rearmost part)
velocityFront	15,56	m/s	Impact velocity - frontal
velocitySide	8,33	m/s	Impact velocity - side
velocityRear	11,11	m/s	Impact velocity - rear

Car-to-car accidents at intersections in Europe and identification of Use Cases for the test and assessment of respective active vehicle safety systems

Marcus Wisch
Adrian Hellmann
Markus Lerner
Federal Highway Research Institute (BASt), Germany
Thomas Hierlinger
Volker Labenski
Audi AG, Germany
Michael Wagner
Harald Feifel
Continental Teves AG & Co. oHG, Germany
Oana Robescu
Denso, Sweden
Pauline Renoux
Renault, France
Xavier Groult
Valeo, France

Paper Number 19-0176

ABSTRACT

The Intersection 2020 project was initiated to develop a test procedure for Automatic Emergency Braking systems in intersection car-to-car scenarios to be transferred to Euro NCAP. The project aims to address current road traffic accidents on European roads and therefore sets a priority of the identification of the most important car-to-car accidents and Use Cases. Taking into account technological and practical limitations, Test Scenarios are derived from the Use Cases in a later stage of the project.

This paper presents parts of a larger study and provides an overview of common car-to-vehicle(at least four wheels) collision types at junctions in Europe and specifies seven Accident Scenarios from which the three scenarios “Straight Crossing Paths (SCP)”, “Left Turn Across Path – Opposite Direction Conflict (LTAP/OD)” and “Left Turn Across Path – Lateral Direction (LTAP/LD)” are most important due to their high relevance regarding severe car-to-car accidents. Technical details about crash parameters such as collision and initial speeds are delivered. The analysis work performed is input for the definition and selection of the Use Cases as well as for the project’s benefit estimation.

The numbers of accidents and fatalities in accidents at intersections involving a passenger car were shown per intersection type. In both statistics, it was found that accidents at crossroads and T- or staggered junctions are of highest relevance, followed by roundabouts. Focusing on accidents at intersections between one passenger car and another road user shows that around one-third of all accidents and related fatalities could have been assigned to car-to-PTW accidents and one-fifth of all accidents and fatalities to car-to-car accidents.

Regarding car-to-car accidents with at least serious injury outcome 38% out of 34,489 car-to-car accidents happened at intersections. These figures correspond to 18% of the fatalities (4,236 fatalities in total). Considering all intersection types, around half of all related accidents happened in urban environments whereas this number decreased to one-third of all fatalities. Further, the proportion of road fatalities per country occurring at intersections varies widely across the EU. Also, there are proportionately more fatalities in daylight or twilight conditions at junctions.

Use Cases are supposed to be derived from Accident Scenarios and by adding detailed information for example about the road layout, right-of-way and the vehicle trajectories prior to the collision. Instead of applying cluster algorithms to the accident data, a pragmatic approach was finally preferred to create them. Note: Use Cases serve as an intermediate step between the Accident Scenarios and the Test Scenarios which describe the actual testing conditions. Finally, 74 Use Cases were identified. This large number indicates the complexity of intersection crashes due to the combination of several parameters.

INTRODUCTION

General View on Road Traffic Accidents at Intersections

Junctions are intended to operate where vehicles often must share space with other vehicles and pedestrians. Negotiating a junction requires many simultaneous or closely spaced decisions, such as selection of the proper lane; maneuvering to get into the proper position; need to decelerate, stop, or accelerate; and need to select a safe gap [1]. Three- or four-arm non-signalized at grade junctions: These junctions may provide satisfactory road safety level when operating in low traffic volumes and speeds. Traffic islands and pavement marking, delimiting traffic directions and creating special lanes for left turning movements have a positive road safety effect [2]. When traffic volumes increase, it is necessary to establish traffic signals or consider modifications of the junction layout. In urban areas, changing a three- or four-arm level junction into a roundabout may lead to around 30% accidents reduction [3]. Signalized level junctions are the most common junction type in urban areas. Fatal accidents at signalized junctions are predominantly multivehicle [4]. The majority of accidents on signalized junctions concern left-turn vehicle movement or pedestrian's movement. Moreover, a higher accident involvement, in relation to their traffic volumes, may be observed for motorized two-wheelers and bicycles [5].

Roundabouts

Roundabouts have higher capacity than three- or four-arm non-signalized junctions; Roundabouts appear to have considerable safety advantages over other types of at-grade junction and are now being widely used in many countries [6]. However, in some countries they appear to be related to higher accident involvement of motorized two-wheelers and bicycles [5]. Roundabouts reduce the number of injury accidents depending on the number of arms and the previous form of traffic control. There appears to be a larger effect in junctions that used to have yield control than in junctions that used to be traffic controlled. Fatal accidents and serious injury accidents are reduced more than slight injury accidents [7]. Montella et al. reported in [8] that “The use of roundabouts improves intersection safety by eliminating or altering conflict types, reducing crash severity, and causing drivers to reduce speeds. However, roundabout performances can degrade if precautions are not taken during either the design or the operation phase.”

Accident Data

The European project TRACE (funded by the European Commission) also investigated accidents at intersections in the EU-27 [9]. The authors reported that:

- Approx. 43% of all road injuries occur at intersections in EU-27;
- Approx. 70% of intersection accidents occur inside urban area;
- Approx. 80% of intersection accidents occur with at least one passenger car in urban area;
- 45% to 68% of intersection accidents occur at intersections with traffic regulation.

The authors also note issues about the definitions of intersections. For example, “intersections” in the UK include the point where the roads cross plus the 20 m on either side.

The European Commission arranged intersection accident data analyses using the Community Database on Accidents on the Roads in Europe (CARE) and published the results in a special issue of the series “Traffic Safety Basic Facts” [10] in 2015. It was estimated that more than 5,000 people died in road accidents at junctions in the EU in 2013. Note: European figures have to be handled with care as there is no common definition for crashes at junctions in Europe and not all countries provide related figures in the same quality. It was summarised that the proportion of fatalities occurring at junctions is higher on urban roads than on rural roads or motorways and varied widely across the EU. The proportion of fatalities occurring at junctions is highest for pedal cyclists and moped riders, and lowest for HGV, lorry and car occupants. However, proportions change when considering seriously injured casualties. Regarding the light conditions at the point of time of the accidents at intersections, proportionately more fatalities occurred in daylight or twilight compared to dark light conditions. With regard to the weather condition, the proportion of accidents with fatal outcome that occurred at junctions was highest for dry conditions (87%), followed by rainy conditions (7%) and lowest in adverse conditions such as snow.

Accident Clusters and Methods for Identification

Nitsche et al. analysed in [11] accident data from the United Kingdom with the aim to identify critical pre-crash scenarios at T- and four-legged junctions (“crossroads”). The method employed k-medoids to cluster historical junction crash data into distinct partitions and then applies the association rules algorithm to each cluster to specify the driving scenarios in more detail. The study resulted in thirteen crash clusters for T-junctions and six for crossroads. Association rules revealed common crash characteristics, which were the basis for the scenario descriptions. Exemplarily for all clusters, some are detailed:
Cluster T-C1 is the largest cluster with a size of 212 crashes, from which all resulted in slight injury. More than 90 percent of the accidents occurred at T-junctions with a minor road joining from the left. There is no clear indication on the collision type of this cluster. The third largest cluster T-C2 groups collisions while turning,

with a highly significant representativeness of frontal and nearside impacts, all of which occurring at roads terminated by a major road. Powered two-wheelers (PTW) and bicyclists have relatively high frequencies, but the car is still the dominant crash partner. Cluster T-C3 with 62 samples represents car-to-car collisions at roads with minor roads joining from the right, mainly resulting in slight injury. Since there are mainly impacts on the back of the car, this cluster can be seen as rear-end crash group. The second largest cluster Cluster T-C5 indicates rectangular collisions with another car crossing the car's trajectory from the right. Cluster X-C1 is the largest cluster with 142 samples, which mainly includes rear-end collisions. Cluster X-C2 groups situations on crossroads broken by a major road, with high numbers for turning left or right as well as first front impact collisions. Cars and PTWs were mostly involved.

Sander and Lübbe investigated the potential of different clustering methods to define intersection AEB test scenarios [12]. The "study investigates whether clustering methods can be used to identify a small number of test scenarios sufficiently representative of the accident dataset to evaluate Intersection Automated Emergency Braking (AEB). Data from the German In-Depth Accident Study (GIDAS) and the GIDAS-based Pre-Crash Matrix (PCM) from 1999 to 2016, containing 784 SCP and 453 LTAP/OD accidents, were analyzed with principal component methods to identify variables that account for the relevant total variances of the sample.
[…] Test scenarios were defined from optimal cluster medoids weighted by their real-life representation in GIDAS. The set of variables for clustering was further varied to investigate the influence of variable type and character. […] Despite thorough analysis using various cluster methods and variable sets, it was impossible to reduce the diversity of intersection accidents into a set of test scenarios without compromising the ability to predict real-life performance of Intersection AEB. Although this does not imply that other methods cannot succeed, it was observed that small changes in the definition of a scenario resulted in a different avoidance outcome."

Feifel and Wagner described a method to cluster accident types and proposed a catalogue of harmonized pre-crash scenarios [13]. The method uses GDV accident types, that describe the conflict situations which lead to crashes and that classify causer and non-causer participants, respectively [14]. The catalogue describes the dynamic scenarios and allows for all degrees of freedom of the ego and object participants. Looking at each accident from the perspective of the causer and of the non-causer, sensor-equivalent accident types are clustered to pre-crash scenarios. This inductive approach requires in-depth knowledge of the functionality and performance of environment sensors, thus as an advantage the scenarios can be easily mapped to the respective safety systems. It is essential to consider both, the causer and the non-causer perspective, to develop a holistic picture of the traffic accident distribution between two participant types, such as car versus car. Therefore, the number of accident scenarios will be twice the number of accidents. Due to the pre-crash nature of the scenarios, they can ideally be used as a basis for analyzing the target population of an active safety system and for the evaluation of its performance using virtual simulation.

METHODS AND DATA SOURCES

Definitions

Accident Scenarios (AS) describe the basic road layout and basic motions of vehicles (here, at least four wheels each) relative to each other participating in a road traffic accident. Use Cases are derived from accident scenarios by adding detailed information for example about the road layout, right-of-way and the vehicle trajectories prior to the collision. They can be derived using statistical methods such as cluster algorithms applied to the available accident data. Note: Use Cases serve as an intermediate step between the Accident Scenarios and the Test Scenarios which describe the actual testing conditions.

Available datasets for analysis

Various accident datasets have been considered for the data analysis, see Table 1.

Table 1: Accident datasets considered in Intersection 2020

Country / Region	High-level crash data	In-Depth Crash data
Europe	CARE	IGLAD
France	BAAC	-
Germany	DESTATIS	GIDAS
Spain	DGT	-
United Kingdom	STATS19	-

CARE is a Community database on road accidents resulting in death or injury (no statistics on damage-only accidents). The major difference between CARE and most other existing international databases is the level of aggregation, i.e. CARE comprises detailed data on individual accidents as collected by the Member States.
The legal basis for the German Official Road Accident Statistics (DESTATIS) is the law on the statistics on road traffic accidents. Pursuant to this, federal statistics are compiled on accidents due to vehicular traffic on public roads. The national database for injury road traffic accidents in France (BAAC) is initially filled by the police. The data is checked afterwards by local road safety observatories, under the umbrella of the national road safety observatory. The Direción General de Transito or Directorate General of Traffic (DGT) is the official body of traffic in Spain. As part of managing the traffic licenses, traffic safety actions and vehicle registration, it develops different statistics regarding vehicles and traffic issues which are at the disposal of the citizen.
Road accidents on the public highway in Great Britain, reported to the police and which involve human injury or death, are recorded by police officers onto a STATS19 report form. The form collects a wide variety of information about the accident (such as time, date, location, road conditions) together with the vehicles and casualties involved and contributory factors to the accident (as interpreted by the police). The Department for Transport has overall responsibility for the design and collection system of the STATS19 data.
IGLAD was started in 2010 by European car manufacturers and is an initiative for harmonisation of global in-depth traffic accident data to improve road and vehicle safety which has grown greatly during last years. A database was developed containing accident data according to a standardised data scheme that enables comparison between datasets from different countries.
The German In-Depth Accident Study (GIDAS) was founded in 1999 and is a co-operation between the Federal Highway Research Institute (BASt) and the German Research Association for Automotive Technology (FAT). Investigation teams record data of road traffic accidents involving personal injury in two regions of Germany (cities of Hanover and Dresden and their surrounding regions).

Categorization of Intersection types
To assign and categorize road accidents at intersections, their geometries / layouts were required to be grouped. Most countries in Europe distinguish between intersection layouts; however, the comparability among each other is limited. The lowest common denominator was found in the categorization based on an initiative by the EU to create a Community database on road accidents, see Table 2.

Table 2: Categorization of „intersection“ [15]

Categorisation	Description
Crossroad	Road intersection with four arms. Includes arm sections within 20m distance.
Multiple junction	A junction with more than four arms (except roundabouts). Includes arm sections within 20m distance.
Roundabout	Circular road. Includes sections leading to it, within 20m distance.
T or staggered junction	Road intersection with three arms. Includes T, or staggered junction (a junction with an acute angle). Includes arm sections within 20m distance.
Not at grade (interchange)	Not all roads intersect at the same level.
Other	Other junction type not in the list of the previous values. Includes arm sections within 20m distance.
Not a junction	The accident has not occurred at a junction or at a distance greater than 20m from a junction.

Contrarily, in Germany road traffic accidents at intersections are coded by the police using seven pre-defined “characteristics of the accident scene” from which a maximum of three characteristics could be selected per accident. These characteristics are “Intersection”, “T-junction”, “Property entry / exit”, “Steep hill upwards”, “Steep hill downwards”, “Bend” and “Roundabout”. It has to be noted that accidents at roundabouts were coded as accidents at intersections until the year 2015 and only a few federal states provided more details. Since 2016, accidents at roundabouts are coded separately in the national statistics. However, to provide possibilities for direct comparisons with other countries different approaches were considered.

The most promising approach was found in a work by the Fraunhofer Institute IVI which was commissioned by a project partner to conduct a study focusing on accidents at intersections in Germany. Relevant results were kindly provided to the Intersection 2020 project. The analysis referred to 9.7% of accidents classified as intersection accidents by the road accident databases of the police of the four German federal states Saxony, Hesse, Brandenburg and Saxony-Anhalt between years 2010 and 2015. The dataset contained all accidents, hence, including also accidents with material damage only if selected.

CARE analysis

The CARE database has been analysed applying specific filter criteria, see Figure 1. A country selection was required because only 11 countries delivered satisfying data about the abovementioned commonly agreed European definitions of an intersection. For the present analysis accidents with fatalities AND serious injuries were included under the assumption that the structure of type of junction (variable R13) is comparable and even if the total number of serious injuries is not fully comparable between different countries.

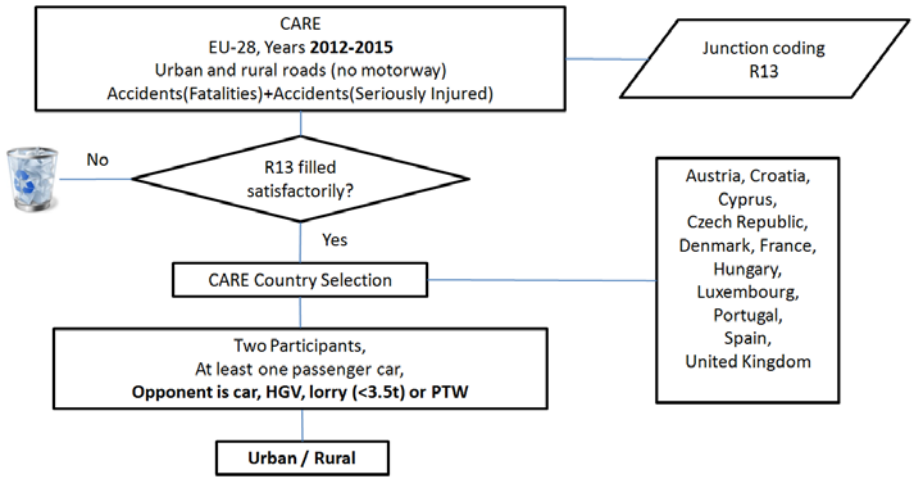

Figure 1: Approach for CARE analysis

Derivation of Accident Scenarios

According to the Federal Statistical Office of Germany "the kind of accident describes of the entire course of events in an accident the direction into which the vehicles involved were heading when they first collided on the carriageway or, if there was no collision, the first mechanical impact on a vehicle" [16]. It can be distinguished between 10 kinds of accidents. To address accidents being of highest relevance for enhanced AEB systems specifically designed for intersection scenarios (and thus considering existing AEB systems, e.g. car-to-rearend systems), it was determined to focus on accidents either assigned to kind of accident 4) Collision with another oncoming vehicle, 5) Collision with another vehicle which turns into or crosses a road or 10) Accident of another kind.

Figure 2 describes the data filter criteria to derive the AS for car-to-car accidents using data from the German national statistics. The focus was on accidents on urban and rural roads (but not on motorways) with at least one killed or seriously injured (KSI) person.

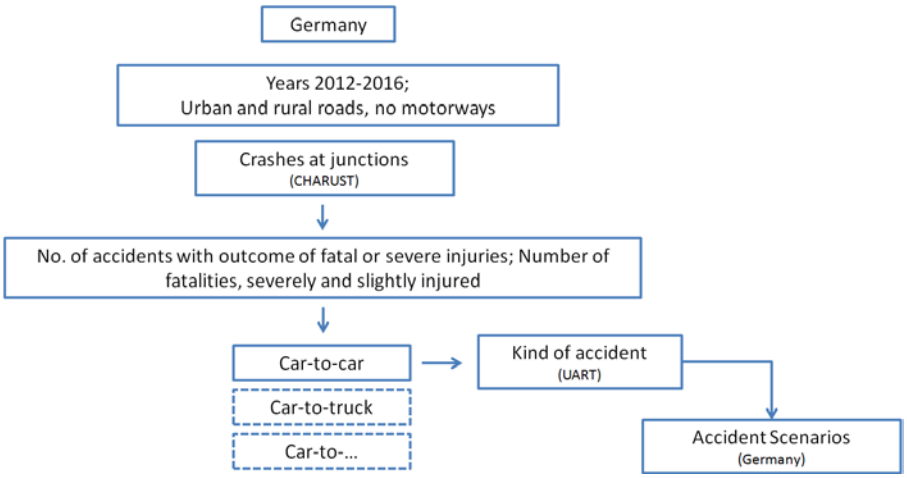

Figure 2: Approach for the derivation of Accident Scenarios from the German national statistics

In the German statistics there are seven types of accidents (coded as type 1 to type 7) describing the conflict situation prior to the accident. Each of these types can be further detailed into sub-types (e.g., accident type

"301"), see also [14]. However, in the German accident statistics this 3-digit accident type information is not available for all federal states of Germany but is provided by 5 (out of 16) federal states (Lower Saxony, North Rhine-Westphalia, Rhineland Palatinate, Saxony-Anhalt and Saarland) which by random, represent the German accident occurrence quite well, as non-published studies have shown. It was concluded that only data from these 5 federal states were used for the subsequent analyses regarding AS.

Various studies have already defined groups of accidents at intersections. Finally, for the purpose of comparisons and for harmonization it was aimed to select the AS of Intersection 2020 considering mainly findings from the US Department of Transport in [17].

Detailed analysis of Accident Scenarios regarding technical parameters
Basic crash parameters have been analysed for the most frequent AS SCP, LTAP/OD and LTAP/LD using GIDAS according to the following filter criteria:

1) Accident years 2005-2016 (GIDAS database version 07/2017)
2) Completed and reconstructed cases
3) Car-to-car (two parties exactly), first major collision
4) Only urban and rural roads, no motorways
5) Two injury severity groups:
    a. Seriously and/or killed car occupants (**KSI**)
    b. Slightly, seriously and/or killed car occupants (**ALL**)

Derivation of Use Cases
Use Cases had to be developed aiming to serve as an intermediate step between the identification of AS and defining the Test Scenarios describing the final testing conditions. A first attempt to generate a proper list of Use Cases based on the available collision data, using clustering algorithms and having the principal goals of the project in mind failed as the application of the statistical models to the data directed quickly into various issues and uncertainties but also similar results as presented in literature, see [12] (note: both datasets were greatly based on the same data source). Further, it became clear that vehicles' trajectories are important but could not be derived from GIDAS and various parameters (e.g., varying lane width, view obstructions), identified as being meaningful, could not be transferred to any Test Scenario for consumer programs in next years for which reasons a pragmatic approach was finally preferred. As a consequence, the GIDAS-based Pre-Crash Matrix (PCM) data was analyzed providing more information for example about the vehicles' trajectories up to five seconds prior to the collision. It was aimed to apply the same filter criteria as used for the GIDAS analysis. Further crucial parameters were identified and investigated. Subsequently, the frequency distributions of these parameters have been evaluated with regard to the pre-crash and the collision phase. Finally, the most relevant ranges of values were considered to be transferred into Use Cases. Use Cases were derived for the most relevant Accident Scenarios.

RESULTS

Accidents on European Roads (CARE analysis)
CARE has been analyzed towards accidents with fatal and/or seriously injured on urban and rural roads per intersection type based on accident years 2013-2015. Various differences were found comparing the information from the 24 countries for which data was available. For example, Ireland and Sweden reported a very high "unknown" rate regarding the crash location whereas countries such as Slovenia reported only a very few severe accidents at intersections and the United Kingdom a comparatively high rate. Germany reported no differentiation in the crash location. However, 11 countries were considered as providing reliable data for the purpose of this study. These 11 countries are: Austria, Croatia, Cyprus, Czech Republic, Denmark, France, Hungary, Luxembourg, Portugal, Spain and the United Kingdom. Figure 3 shows an overview about accidents with exact two collision partners involving at least one passenger car per intersection type. This analysis step revealed a share of accidents at intersections for all countries varying around 40-45%. "Crossroads" were reported most often followed by "T- or staggered junctions" and "roundabouts".

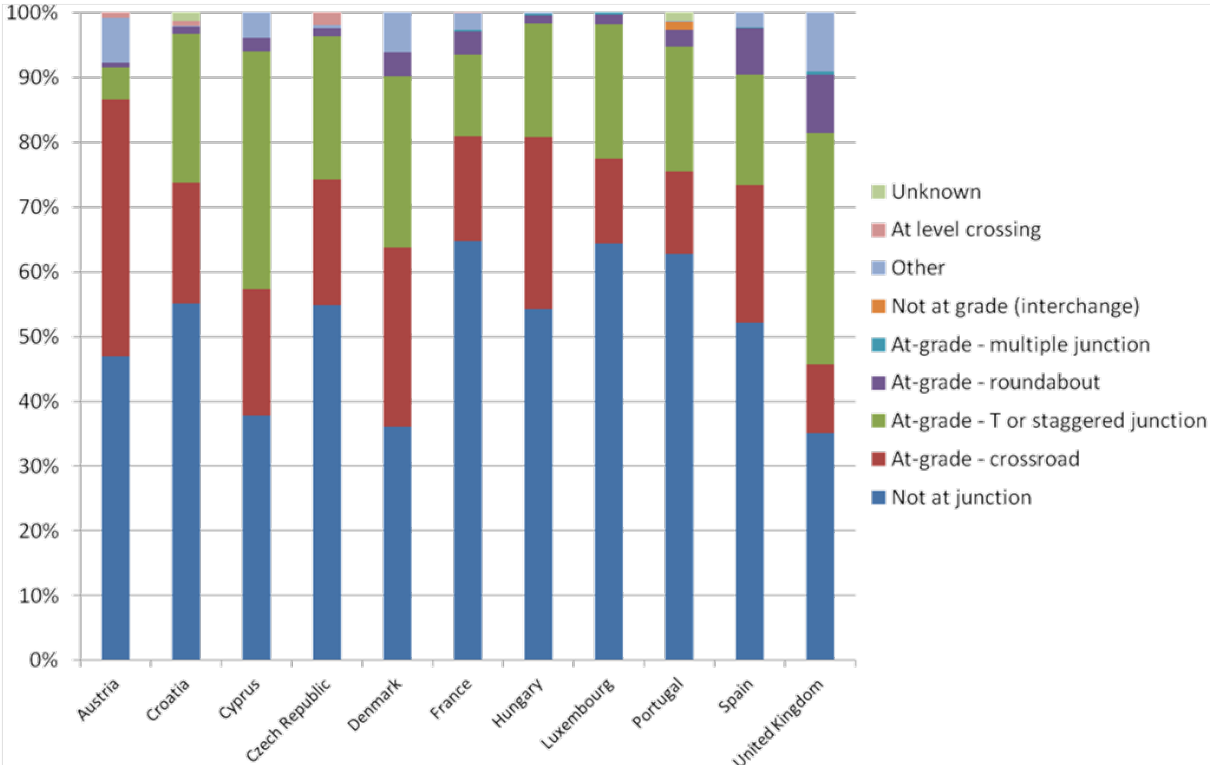

Figure 3: Accidents with fatal and/or seriously injured on urban and rural roads per intersection type, Two crash participants with at least one car, Country selection EU28, 2013-2015

The second analysis step based on CARE data from 2012-2015 and has looked for the number of KSI accidents (N=162,460) and corresponding fatalities (N=15,857) involving one passenger car (incl. taxis) and another road user (differentiating for accidents according to the configurations car-to-car, car-to-lorry, car-to-HeavyGoodsVehicle/Bus, car-to-PoweredTwoWheeler and car-to-RemainingRoadUsers). Omitting the "remaining road users", it was found that car-to-PTW collisions (n=46,195) dominated the number of severe accidents, followed by car-to-car collisions (n=34,489). However, car-to-car collisions dominated the number of fatalities (n=4,236), followed by car-to-PTW collisions (n=2,992).

The numbers of accidents involving at least one passenger car and another road user and the corresponding figures on fatalities are shown per intersection type in Table 3 and Table 4, respectively. In both statistics, it was found that accidents at crossroads and T- or staggered junctions are of highest relevance. Focussing on accidents at intersections between one passenger car and another road user shows that around one-third of all accidents and related fatalities could have been assigned to car-to-PTW accidents and one-fifth of all accidents and fatalities to car-to-car accidents. "Car-to-remain" accidents involve accidents between cars and pedestrians/cyclists.

Table 3: Number of severe intersection accidents with involvement of one passenger car and another road user per intersection type (CARE, EU country selection, 2012-2015)

Number of **KSI accidents** and shares	**Crossroad**	**Multiple junction**	**Roundabout**	**T- or staggered junction**	**Total**
CAR-CAR	**6,354 (9%)**	102 (<1%)	908 (1%)	**5,652 (8%)**	**13,016 (19%)**
CAR-LORRY	934 (1%)	13 (<1%)	116 (<1%)	810 (1%)	1,873 (3%)
CAR-HGV/BUS	868 (1%)	19 (<1%)	174 (<1%)	931 (1%)	1,992 (3%)
CAR-PTW	**8,797 (13%)**	126 (<1%)	2,299 (3%)	**11,209 (17%)**	**22,431 (33%)**
CAR-REMAIN	8,888 (13%)	324 (<1%)	3,624 (5%)	15,013 (22%)	27,849 (41%)
TOTAL					67,161 (100%)

Table 4: Number of fatalities in severe intersection accidents with involvement of one passenger car and another road user per intersection type (CARE, EU country selection, 2012-2015)

Number of **fatalities** and shares	**Crossroad**	**Multiple junction**	**Roundabout**	**T- or staggered junction**	**Total**
CAR-CAR	**396 (10%)**	5 (<1%)	34 (1%)	**321 (9%)**	**756 (20%)**
CAR-LORRY	111 (3%)	0 (<1%)	7 (<1%)	75 (2%)	193 (5%)
CAR-HGV/BUS	156 (4%)	2 (<1%)	19 (1%)	158 (4%)	335 (9%)
CAR-PTW	**464 (12%)**	3 (<1%)	49 (1%)	**605 (16%)**	**1,121 (30%)**
CAR-REMAIN	508 (13%)	12 (<1%)	94 (2%)	758 (20%)	1,372 (36%)
TOTAL					3,777 (100%)

It has to be noted that the aforementioned (and also following) proportions per intersection type may reflect rather the frequency of these intersection types in Europe than certain associated risk factors.

Focusing on car-to-car intersection accidents, Figure 4 shows the distribution of the number of these accidents and fatalities per intersection type for urban and rural roads (without motorways). Considering all intersection types, around half of all related accidents happened in urban environments whereas this number decreases to one-third of all fatalities.

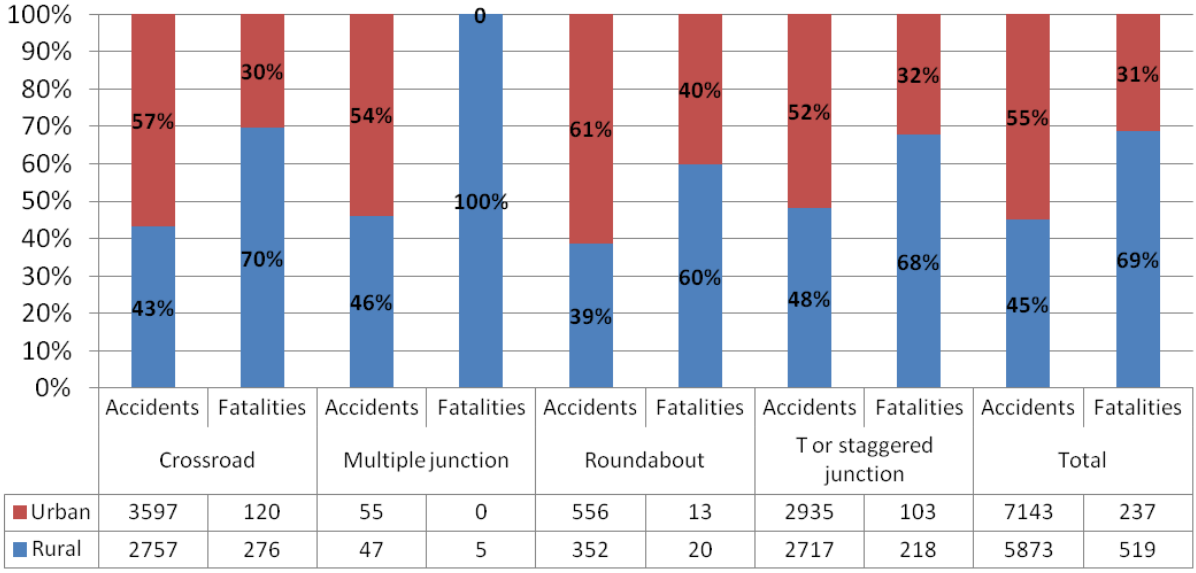

	Crossroad		Multiple junction		Roundabout		T or staggered junction		Total	
	Accidents	Fatalities	Accidents	Fatalities	Accidents	Fatalities	Accidents	Fatalities	Accidents	Fatalities
Urban	3597	120	55	0	556	13	2935	103	7143	237
Rural	2757	276	47	5	352	20	2717	218	5873	519

Figure 4: Shares of accidents and fatalities in car-to-car accidents per intersection type (CARE, EU country selection, 2012-2015), N(accidents)=13,016, N(fatalities)=756

Accidents on European Roads (selected countries)

Since the figures on seriously and slightly injured persons due to road traffic accidents are less reliable on a European level, further analyses of accidents involving exactly two passenger cars (incl. taxis) on urban and rural roads (without motorways) have been conducted accessing national statistics from France, the United Kingdom (UK) and Spain (note: Spain is not distinguishing for “multiple junctions”).

France, UK, Spain

The corresponding analyses concerning France, the UK and Spain are shown in Figure 5 - Figure 7, respectively. Overall, it can be seen that a severe injury outcome is linked with accidents on rural roads which is possibly connected to higher speeds. The proportion of rural environments is considerably higher in France and Spain compared to the UK. Comparing with the CARE analysis, the proportions of the intersection types crossroads and T- or staggered junctions against multiple junctions and roundabouts were confirmed; however, looking in greater depth shows that these proportions are varying a lot between the countries. For example, the shares of severe accidents at crossroads are 63% in France, but 28% in the UK and 50% in Spain and at T- or staggered junctions 30% in France, 66% in the UK and 36% in Spain.

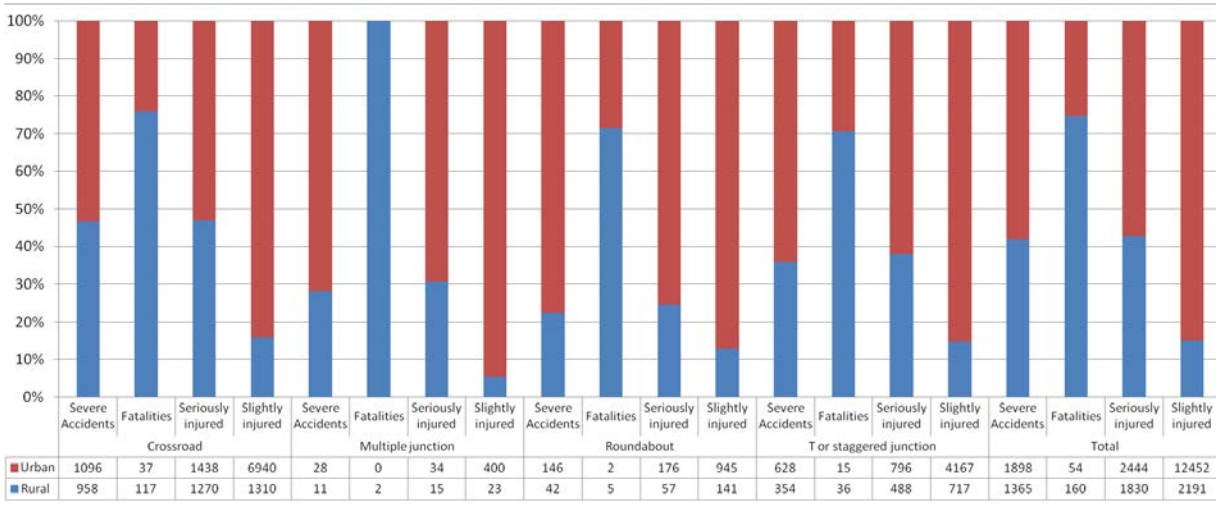

	Crossroad				Multiple junction				Roundabout				T or staggered junction				Total			
	Severe Accidents	Fatalities	Seriously injured	Slightly injured	Severe Accidents	Fatalities	Seriously injured	Slightly injured	Severe Accidents	Fatalities	Seriously injured	Slightly injured	Severe Accidents	Fatalities	Seriously injured	Slightly injured	Severe Accidents	Fatalities	Seriously injured	Slightly injured
Urban	1096	37	1438	6940	28	0	34	400	146	2	176	945	628	15	796	4167	1898	54	2444	12452
Rural	958	117	1270	1310	11	2	15	23	42	5	57	141	354	36	488	717	1365	160	1830	2191

Figure 5: Shares of accidents and fatalities in collisions involving exactly two passenger cars per location and intersection type, excluding the intersection type "other" (BAAC, France, 2012-2015)

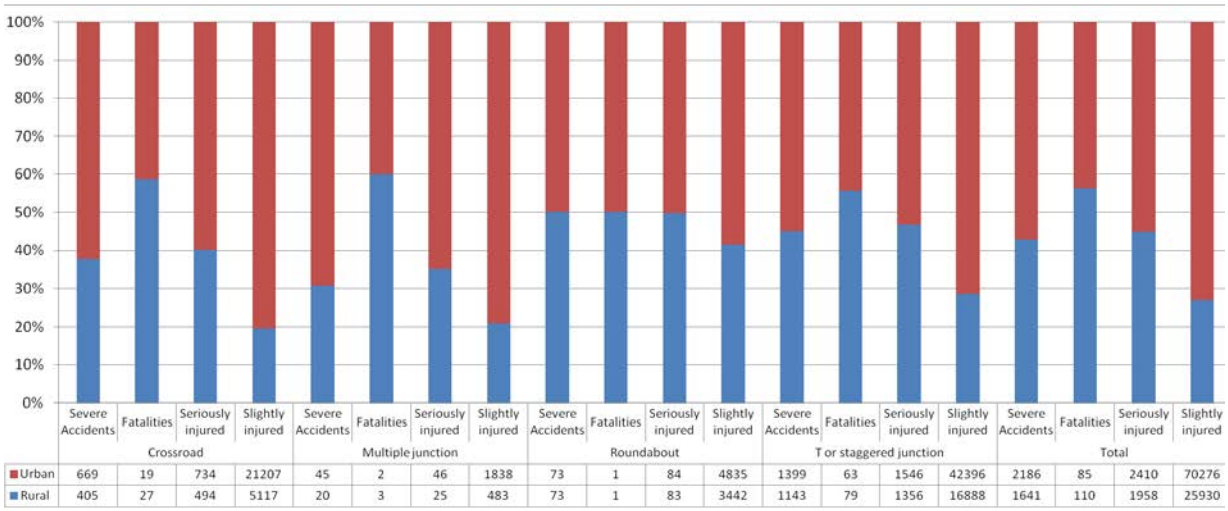

	Crossroad				Multiple junction				Roundabout				T or staggered junction				Total			
	Severe Accidents	Fatalities	Seriously injured	Slightly injured	Severe Accidents	Fatalities	Seriously injured	Slightly injured	Severe Accidents	Fatalities	Seriously injured	Slightly injured	Severe Accidents	Fatalities	Seriously injured	Slightly injured	Severe Accidents	Fatalities	Seriously injured	Slightly injured
Urban	669	19	734	21207	45	2	46	1838	73	1	84	4835	1399	63	1546	42396	2186	85	2410	70276
Rural	405	27	494	5117	20	3	25	483	73	1	83	3442	1143	79	1356	16888	1641	110	1958	25930

Figure 6: Shares of accidents and fatalities in collisions involving exactly two passenger cars per location and intersection type, excluding the intersection type "other" (STATS19, United Kingdom, 2012-2016)

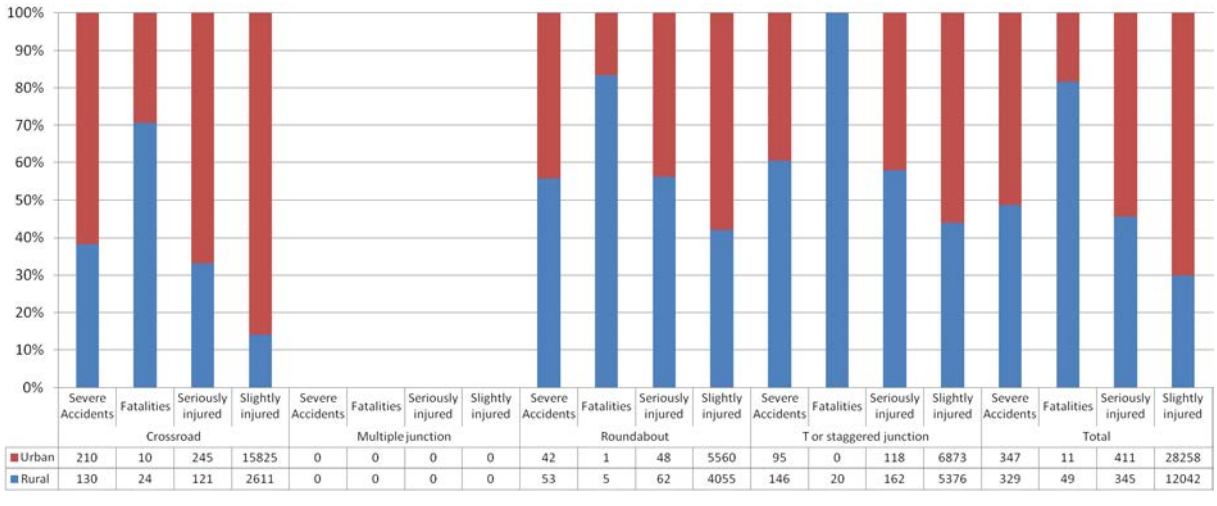

	Crossroad				Multiple junction				Roundabout				T or staggered junction				Total			
	Severe Accidents	Fatalities	Seriously injured	Slightly injured	Severe Accidents	Fatalities	Seriously injured	Slightly injured	Severe Accidents	Fatalities	Seriously injured	Slightly injured	Severe Accidents	Fatalities	Seriously injured	Slightly injured	Severe Accidents	Fatalities	Seriously injured	Slightly injured
Urban	210	10	245	15825	0	0	0	0	42	1	48	5560	95	0	118	6873	347	11	411	28258
Rural	130	24	121	2611	0	0	0	0	53	5	62	4055	146	20	162	5376	329	49	345	12042

Figure 7: Shares of accidents and fatalities in collisions involving exactly two passenger cars per location and intersection type, excluding the intersection type "other" (DGT, Spain, 2013-2015)

Germany

Germany uses a different coding of road traffic accidents at intersections. The study by the Fraunhofer Institute found that more than 50% of all considered accidents have not been assigned any of the introduced seven pre-defined characteristics which means none of these characteristics was found relevant for / influencing remarkably the accidents. However, it was expected that a large amount of these accidents happened at an intersection (even though this was not seen as one of the primary contributing / influencing factors). Hence, the aim of the study was also to analyze as many accident locations as possible and if happened at an intersection, to classify the intersection type by the means of software ("analysis tool") specialized for this purpose.

Concluding, the most common type of intersections is the crossroad with almost 48%, followed by the T-junction with nearly 25%. About 7% are multiple junctions and 6% are double crossroads (at least two lanes per driving direction). For almost 12% of all identified intersection accidents, the respective intersection type remained "unknown". Accidents at roundabouts took place in 2.5% of the accidents. Though, it has to be mentioned that the tool still has limitations in classifying the intersections.

Accident Scenarios

Within Intersection 2020 seven AS were identified and considered for subsequent analyses. The following five AS were considered as being of highest interest, see also Table 5:

- Left Turn Across Path – Opposite Direction Conflict (LTAP/OD)
- Left Turn Across Path – Lateral Direction (LTAP/LD)
- Left Turn Into Path – Merge Conflict (LTIP)
- Right Turn Into Path – Merge Conflict (RTIP)
- Straight Crossing Paths (SCP)

In addition, the AS "Parking / Reversing" (P/R) and the AS "NA" were created. The latter AS comprises situations covered by current AEB systems, situations not addressed by intersection AEB systems or unclear accident courses of events. The assignment of "accident types" to these AS is summarized in the Appendix.

Table 5: Accident Scenarios of highest interest

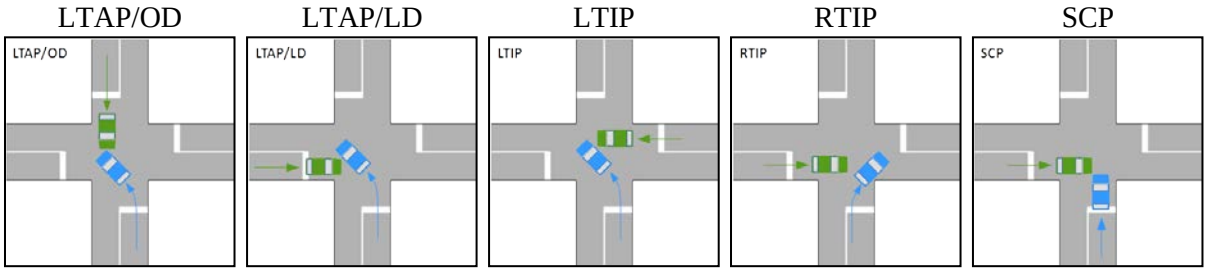

To quantify the relevance of the particular AS considering all injury severity groups (fatally, seriously and slightly injured) an analysis of the subsample of the German national road accident statistics (data from five federal states) was performed and took 8,114 severe car-to-car accidents (at least one seriously injured person) at intersections with 168 fatalities, 10,728 seriously and 7,600 slightly injured casualties into account. To gain a ranking, the numbers of injured casualties were summed up and multiplied with weighting factors established in the European FP7 project ASSESS considering the average casualty injury costs as collected for different European countries [18]. Basically, the approach is based on the Equation 1:

Analytical sum (per scenario) = 1 * number of killed + 0.11 * number of seriously injured + 0.011 * number of slightly injured (Eq. 1)

Accordingly, applying the formula to all available data resulted into the figures and ranking summarized in Table 6. It can be seen that the highest ranked AS is SCP, followed by LTAP/OD and LTAP/LD.

Table 6: Analytical sum of ASSESS approach and ranking of severe car-to-car intersection accidents in Germany (sub-sample) per Accident Scenario

Ranking	AS	Analytical sum of ASSESS approach	Proportion (cumulative)
1	**SCP**	**511.178**	35,7%
2	**LTAP/OD**	**391.423**	27,3%
3	**LTAP/LD**	**286.256**	20,0%
4	NA	161.398	11,3%
5	LTIP	39.770	2,8%
6	RTIP	38.619	2,7%
7	P/R	3.036	0,2%
-	Total	**1,431.680**	100%

In-depth accident data analysis (GIDAS)

Table 7 shows the number of crashes and involved passenger cars per Accident Scenario for both injury severity groups: "slightly, seriously and fatally injured" (ALL) and "seriously and fatally injured" (KSI), for which similar shares were found. Overall, SCP reached highest shares around 40-43%, followed by LTAP/OD (~29-35%) and LTAP/LD (~21-23%). It has to be noted that at this analysis stage, SCP was not split into opposing vehicles approaching from left or right. Comparing the GIDAS figures on severe accidents with those presented in Table 6 by neglecting the additional AS "NA" shows comparable proportions of the AS. It has been concluded that the GIDAS figures represent satisfyingly Germany in this study and thus, no weighting factors are required.

The following results are focusing on the KSI accidents.

Table 7: Number of accidents (involving each two passenger cars) per Accident Scenario for the injury severity groups "slightly, seriously and fatally injured" (ALL) and "seriously and fatally injured" (KSI), highest shares were highlighted in grey, GIDAS 2005-2016, data not weighted

		LTAP/OD	LTAP/LD	LTIP	RTIP	SCP	P/R	∑
KSI	Accidents	76	49	2	2	86	0	215
	%	35.3	22.8	0.9	0.9	40.0	0	100
All	Accidents	464	336	43	44	680	10	1,577
	%	29.4	21.3	2.7	2.8	43.1	0.6	100

LTAP/OD

According to the assignment of accident types to the AS, see Appendix, all LTAP/OD relevant GIDAS cases were grouped leading to 76 KSI and 464 ALL accidents. An overview of the associated accident types showed that for KSI and ALL accidents, accident types 211 and 281 emerged most frequently and covered at least ~95% of all LTAP/OD cases. Accidents assigned to 281 differ to 211 accidents by the existence of a traffic light only.

Hence, all LTAP/OD KSI accidents assigned to accident types 211 or 281 have been analyzed towards the reconstructed driving and collision speeds of both crash participants. The average speeds are shown in Figure 8.

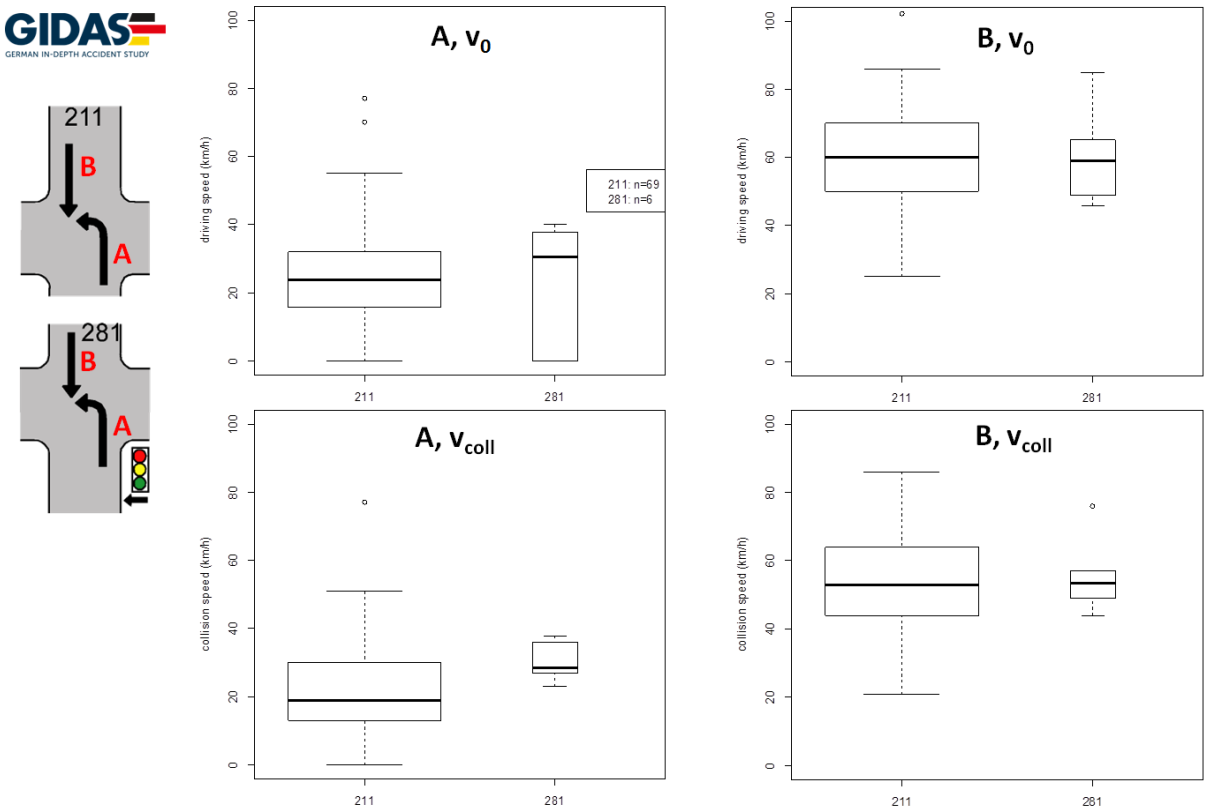

Figure 8: Boxplots of the driving (v_0) and collision (v_{coll}) speeds in LTAP/OD, KSI (N=76)

Table 8 summarizes these speeds approximately regarding their mean 50% (box without whisker), i.e., 50% of the accidents were within the specified speed ranges.

Table 8: Approximated mean 50% driving (v_0) and collision speeds (v_{coll}) of LTAP/OD and LTAP/LD KSI accidents for turning vehicle A and straight going vehicle B as well as of SCP KSI accidents for the entering, not-privileged vehicle A and the crossing privileged vehicle B

	A, v0	B, v0	A, vcoll	B, vcoll
LTAP/OD - KSI	15-35 km/h	50-70 km/h	15-30 km/h	45-65 km/h
LTAP/LD - KSI	05-25 km/h	50-75 km/h	10-20 km/h	40-65 km/h
SCP - KSI	20-50 km/h	30-60 km/h	20-45 km/h	30-60 km/h

However, to specify appropriate test speeds for this AS LTAP/OD a comparison of pairwise speeds was required, i.e., pairs of speeds of vehicles A and B, both involved in the same accident, see Figure 9.

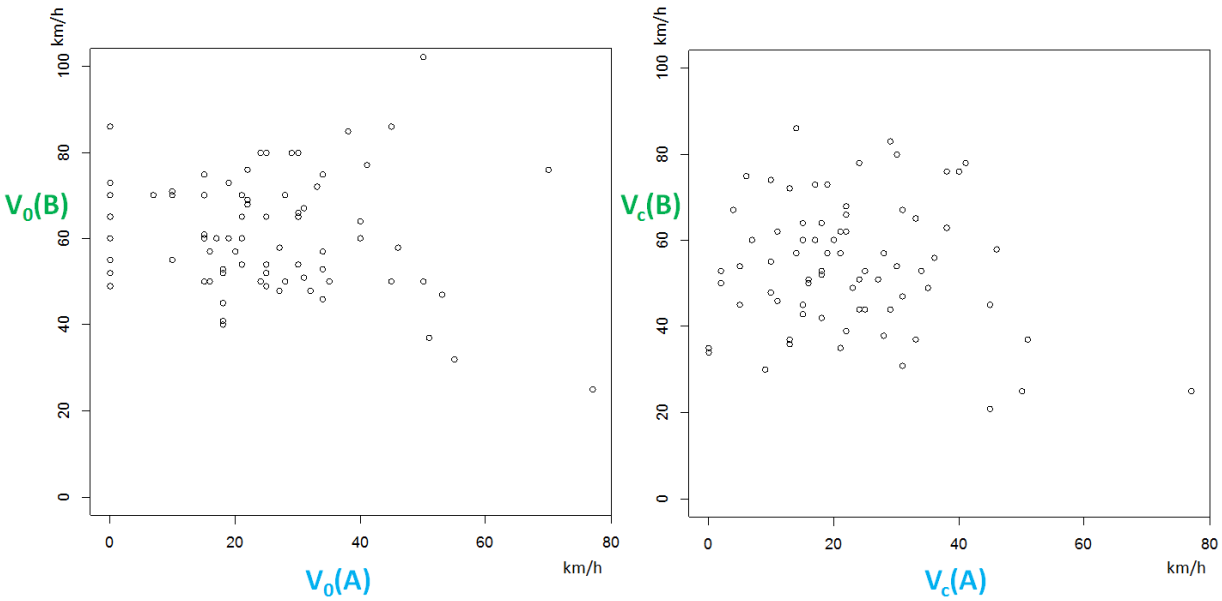

Figure 9: Pairwise driving (v_0) and collision (v_{coll}) speeds in LTAP/OD, KSI (N=76)

In addition, Figure 10 shows the speed change (here difference of a passenger car's driving and collision speed) to identify the basic patterns of accelerations and decelerations in LTAP/OD KSI accidents. Note: visible accelerations and decelerations do not necessarily correlate with initiated accelerating or braking of the driver. Further, the speed changes might have led to smaller or bigger changes in movement as the driving speeds could have been low or high. This is also true for the related figures on the AS LTAP/LD and SCP, see Figure 13 and Figure 16, respectively.

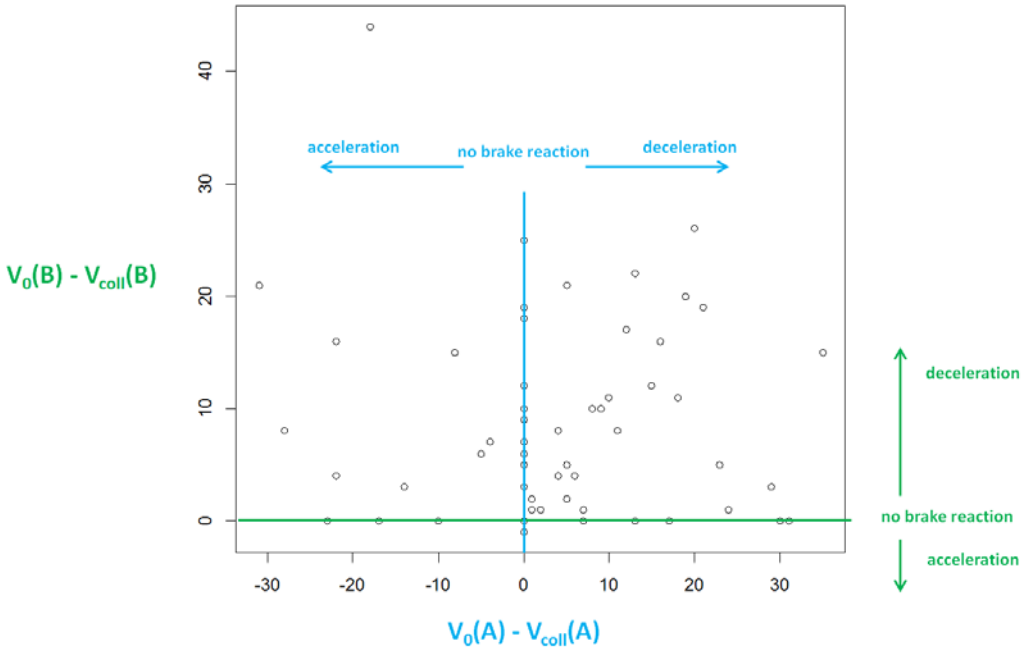

Figure 10: Pairwise speeds - accelerations and decelerations, LTAP/OD, KSI (N=76)

LTAP/LD

According to the assignment of accident types to the AS, see Appendix, all LTAP/LD relevant GIDAS cases were grouped leading to 49 KSI and 336 ALL accidents. An overview of the associated accident types showed that for KSI and ALL accidents, the accident type 302 emerged most frequently and covered at least ~94% of all LTAP/LD cases. Accidents assigned to 312 differ to 302 (accounting for remaining cases) accidents by the driving of another vehicle parallel to the vehicle with right of way.

Hence, all LTAP/LD KSI accidents assigned to accident types 302 or 312 have been analyzed towards the reconstructed driving and collision speeds of both crash participants. The average speeds are shown in Figure 11.

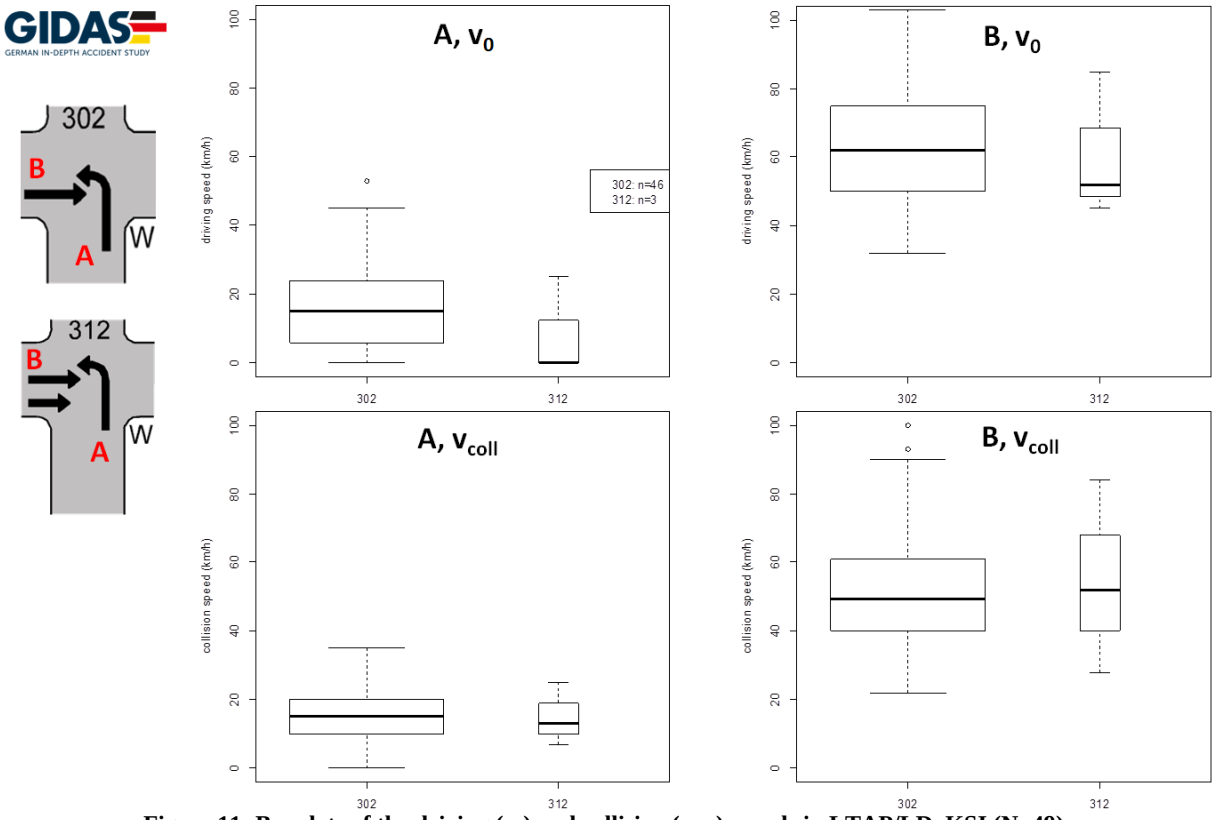

Figure 11: Boxplots of the driving (v_0) and collision (v_{coll}) speeds in LTAP/LD, KSI (N=49)

Table 8 summarizes these speeds approximately regarding their mean 50% (box without whisker), i.e., 50% of the accidents were within the specified speed ranges.

To specify appropriate test speeds for this AS LTAP/LD a comparison of pairwise speeds was required, i.e., pairs of speeds of vehicles A and B, both involved in the same accident, see Figure 12.

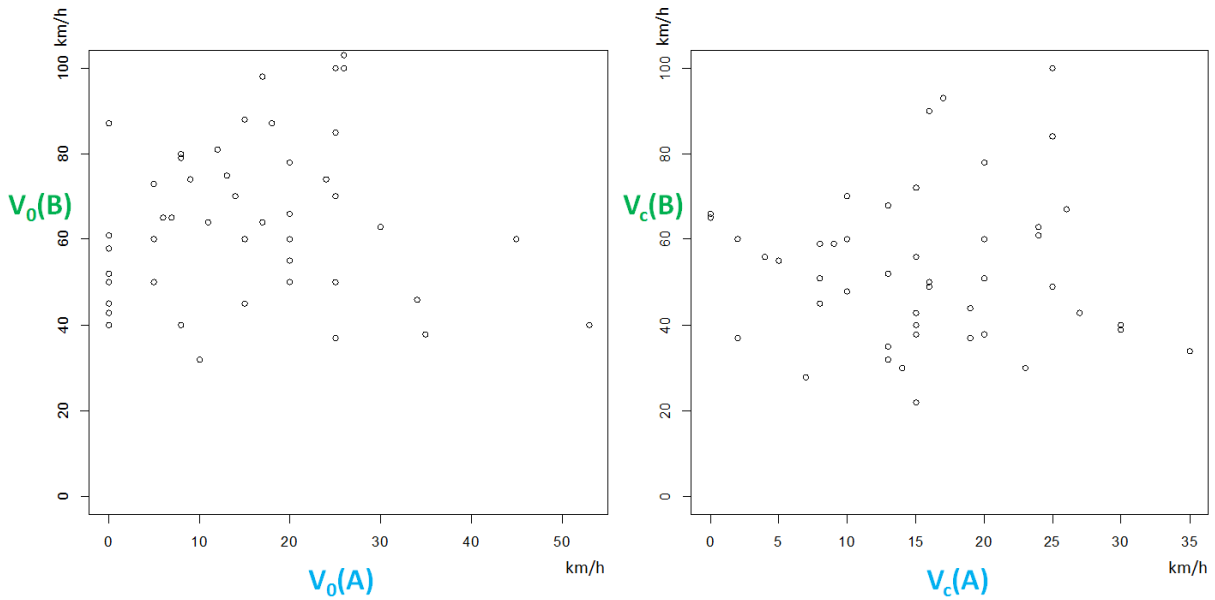

Figure 12: Pairwise driving (v_0) and collision (v_{coll}) speeds in LTAP/LD, KSI (N=49)

Additionally, Figure 13 shows the speed change (here difference of a passenger car's driving and collision speed) to identify the basic patterns of accelerations and decelerations in LTAP/LD KSI accidents.

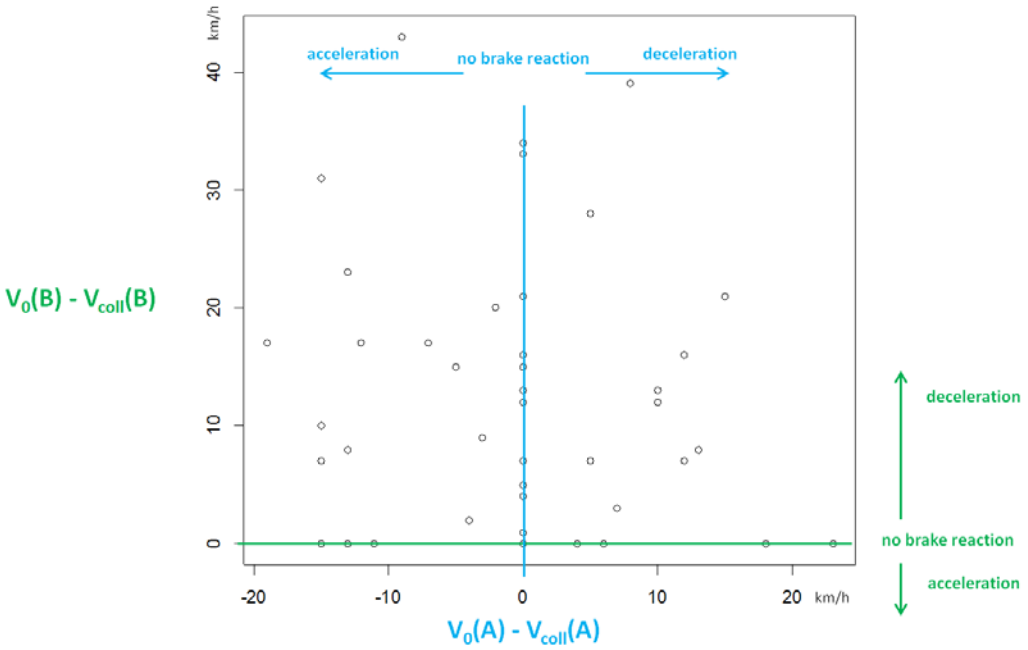

Figure 13: Pairwise speeds - accelerations and decelerations, LTAP/LD, KSI (N=49)

SCP

According to the assignment of accident types to the AS, see Appendix, all SCP relevant GIDAS cases were grouped leading to 86 KSI and 680 ALL accidents. An overview of the associated accident types showed that for KSI and ALL accidents, the accident types 301 and 321 emerged most frequently and covered at least ~92% of all SCP cases. Accidents assigned to 301 differ to 321 accidents by the direction of the privileged vehicle, either approaching from left or right.

Hence, all SCP KSI accidents assigned to accident types 301 or 321 have been analyzed towards the reconstructed driving and collision speeds of both crash participants. The average speeds are shown in Figure 14.

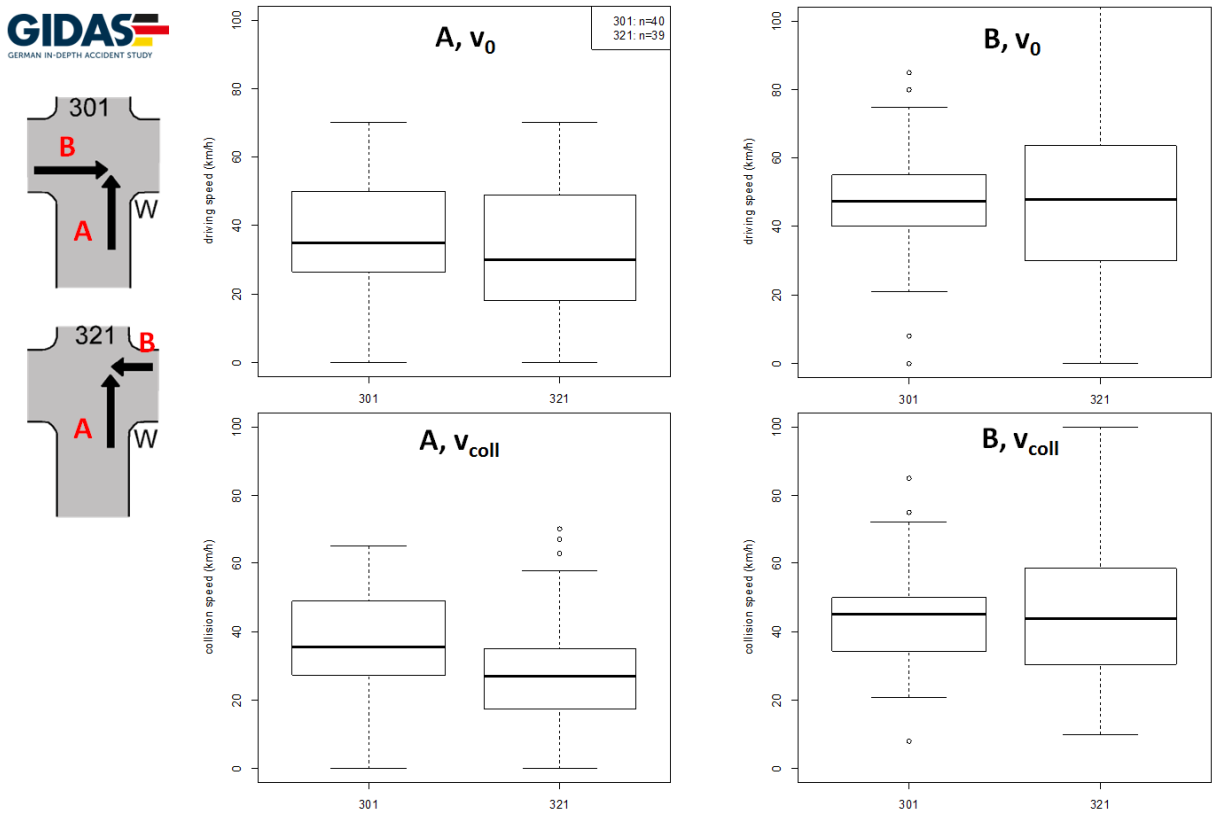

Figure 14: Boxplots of the driving (v_0) and collision (v_{coll}) speeds in SCP, KSI (N=86)

Table 8 summarizes these speeds approximately regarding their mean 50% (box without whisker), i.e., 50% of the accidents were within the specified speed ranges.

To specify appropriate test speeds for this AS SCP a comparison of pairwise speeds was required, i.e., pairs of speeds of vehicles A and B, both involved in the same accident, see Figure 15.

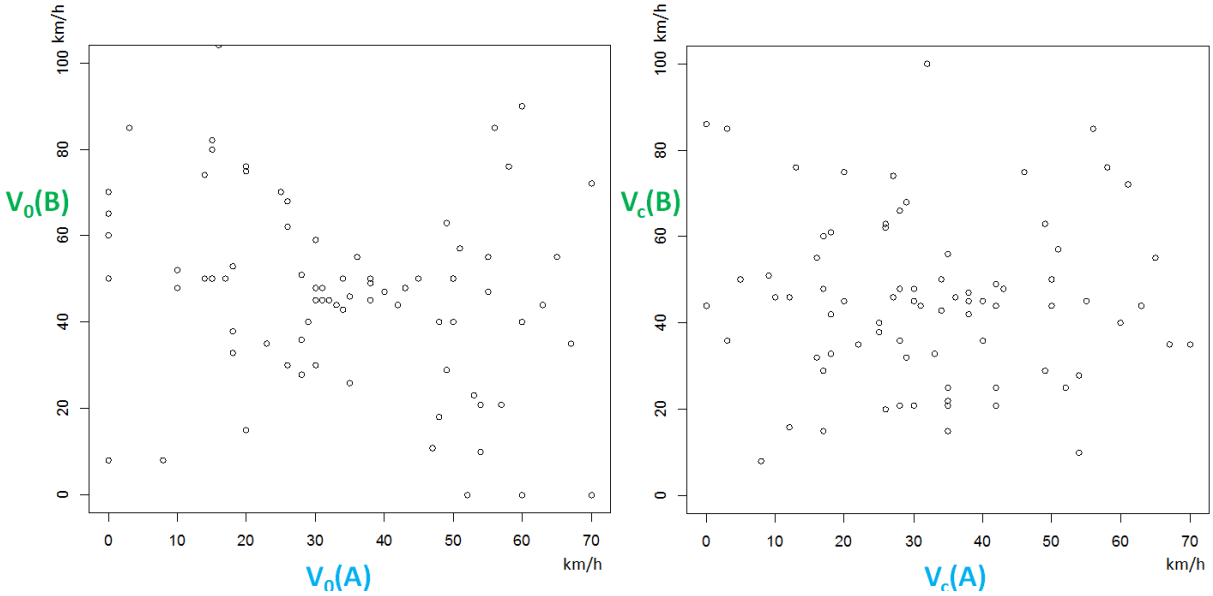

Figure 15: Pairwise driving (v_0) and collision (v_{coll}) speeds in SCP, KSI (N=86)

Additionally, Figure 16 shows the speed change (here difference of a passenger car's driving and collision speed) to identify the basic patterns of accelerations and decelerations in SCP KSI accidents.

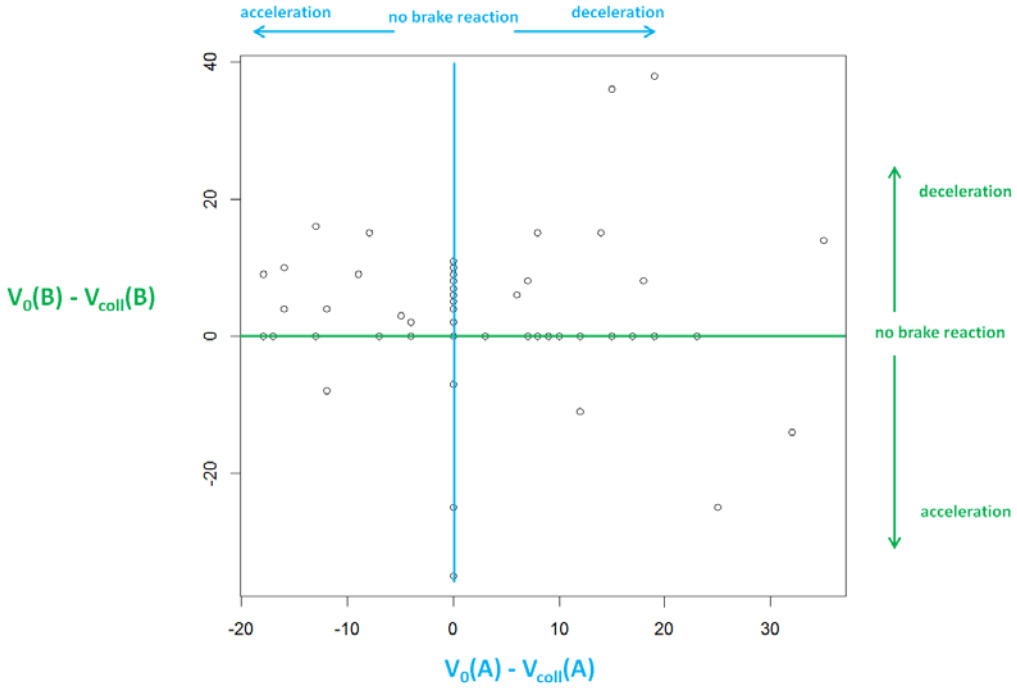

Figure 16: Pairwise speeds - accelerations and decelerations, SCP, KSI (N=86)

Use Cases

Required Parameters

Up to the level of Accident Scenarios, a rather abstract description of the basic movements of the vehicles is given. At the same time, the most important conflict situations at intersections to be addressed by corresponding AEB systems are known. However, when it comes to testing of such systems, scenarios should be representative

with regard to the crucial parameters. The selected parameters for further investigations are listed in Table 9. The principles of the analysis are provided for LTAP/OD in this paper. Analogue gained results for LTAP/LD and SCP were summarized below.

Table 9: Parameters under investigation using the GIDAS-based PCM to derive Use Cases

Parameter	Description / Main reason for consideration
Intersection type	Basic layout of an intersection (crossroad, t-junction etc.)
Right-of-Way	Driving behavior might be affected by the kind of road/traffic regulation
Angles between road arms	To estimate more exactly the relative direction of approach of the collision partners.
Lateral Offset between accident participants	Regarding a turning vehicle, the lateral distance to an oncoming crash opponent before initiating the turn maneuver is of interest. Defining this parameter is required to enable the initial positioning of the two vehicles.
Speed Profiles	To estimate the initial and collision velocities of both collision partners. Initial velocity means the speed at the point in time when the driver recognized the situation to be critical and thus, started a braking or evasive maneuver. In addition, data about the longitudinal acceleration and deceleration is of interest.
Collision Angle	Represents the orientation of two colliding vehicles to each other at the time of the crash. It can be related to the longitudinal axes or to the velocity vectors of the colliding vehicles.
Impact Points/Overlap	To determine the overlap by comparing the impact points for each of the colliding vehicles pair wise.
Turning Radius/Curvature	Relevant for turning vehicles

LTAP/OD - Lateral Offset

The lateral offset of both vehicles in the LTAP/OD could not be extracted automatically from GIDAS. Therefore, the sketches of the corresponding accident sites have been analyzed case-by-case to extract at least the relative positions of the lanes used by the accident participants. In general, the evaluation was performed regarding ALL LTAP/OD accidents; however, if classified as significant during the analysis of certain further parameters, the results for KSI accidents were reported separately. Additionally, the dataset was reduced to those cases that are included in the PCM (version 2016/2), as the associated subset was used in particular to determine the turning radii. Also, only those cases were evaluated where driver of the turning car had to give way to the oncoming traffic, which represented 88 % of all LTAP/OD cases.

Finally, three simplified intersection layouts were identified, see Figure 17. Layout 1 represents a rather clean layout, containing only two lanes in sum (one lane per direction of travel). The lanes are not separated by any other road elements. Layout 2 contains specific lanes (at least for the left turning car). However, as with layout 1, the lanes used by the accident participants are not separated by any other road elements. Layout 3 represents a rather complex geometry, containing a separation between the lanes used by the accident participants due to road elements such as traffic islands or additional lanes, for instance. Compared to layouts 1 and 2, this leads to an additional offset.

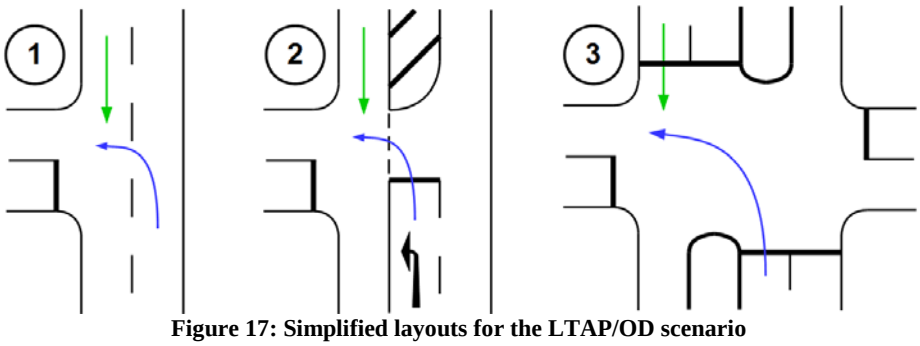

Figure 17: Simplified layouts for the LTAP/OD scenario

The spread of the lane widths and offsets with regard to the layouts 1 and 2 is relatively low. Regarding the offset, the mean 50% is in a range of approximately 3.2 to 3.5 m. It is worth noting that the lane widths also match the most relevant left turn types described in the German recommendations for the construction of rural roads [19].

However, the aforementioned determination of the lateral offset between the vehicles' centers followed the assumption that drivers are using exactly the middle of their lanes. In this context, the actual positions of the

vehicles within the used lanes was checked, finding that drivers tend to use the area facing away from the oncoming traffic. Thus, it was agreed on a lateral offset of 3.7 m for layout 1 and 2.

Looking at layout 3, the lane widths are smaller compared to layouts 1 and 2 which is possibly due to their high relevance in urban areas. On the other hand, the spread of offsets is much higher and also the mean 50 % (approx. 9.5 to 15.5 m). The presence of additional lanes between the accident participants, other road elements like traffic islands as well as tram tracks is a possible reason. Even though the significance is limited considering the small number of 15 cases, the results indicate that the variety of possible road dimensions increases with the complexity of layouts. Thus, the median of the distribution provides at least a minimum of representativeness, which means a lateral offset of around 11.5 m for layout 3, see Figure 18.

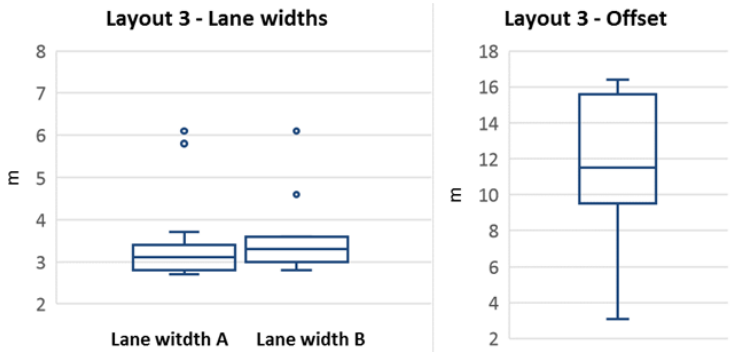

Figure 18: Boxplots of the lane widths of vehicle A (turning vehicle) and B (oncoming vehicle) and the resulting lateral offset for layout 3 (n=15) in LTAP/OD

LTAP/OD - Turning Radius

The dimension of a circle and thus, the radius can be derived by the positions of three points on an associated circular arc. It was considered to cover the arc as completely as possible by choosing the point where the turning maneuver is initiated, the collision point and the point in the middle between the aforementioned points.

Point 1 was identified by evaluating the time to collision (TTC) where the yaw rate ($d\varphi/dt$) of the turning car exceeds a threshold of 5 °/s. Note: 5 °/s is a value that cannot count as disturbance but as a deliberate action from the driver to change his way of travel. The 5 °/s were derived from the 4 °/s found in the literature as a tolerated disturbance from the perspective of a driver, see e.g., [20] and [21].
The TTC of the collision point (point 2) is equal to zero. The TTC related to point 3 is given by the half of the TTC of point 1. Finally, the x and y coordinates for each of the evaluated points in time is given in the PCM, so that the radius (r) can be determined by calculating the center of the circle (O) the three given points have in common. Note: TTC in the context of PCM does not represent the theoretically remaining time before a collision under the assumption of a constant speed, but the actual time lag prior to the crash resulting from the PCM simulation.

Since it was assumed that the radius chosen by turning drivers is also dependent on the presence of certain road elements (especially islands) in the area of the exit roadway, the defined layouts 1-3 were extended. Two additional subcategories (a and b) were defined, distinguishing between such exit road arms with an island in the middle of the roadway and those without, see Figure 19.

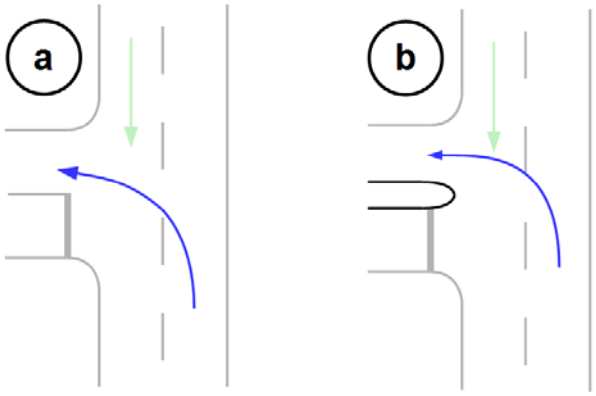

Figure 19: Distinction related to the presence of an island in the middle of the exit roadway

For the evaluation of the turning radii, six clusters (labeled as I-VI) were defined based on the layouts 1-3 and the subgroups a and b. On the one hand, the layouts 1 and 2 were merged, still distinguishing between the location of the accident site (urban/rural) and the presence of islands in the middle of the exit roadway. On the other hand, the distinction in terms of road elements was no longer pursued for layout 3. The resulting clusters and the associated turning radii are given in Table 10.

Table 10: Turning radii for different layout clusters

Cluster	Description	Area	No. of cases	Median radius
I	Layout 1a + 2a	urban	71	20.57
II	Layout 1b + 2b		24	25.41
III	Layout 3		68	19.64
IV	Layout 1a + 2a	rural	7	28.00
V	Layout 1b + 2b		65	21.87
VI	Layout 3		5	21.07

Regarding the urban clusters I and II, it is noticeable that the absence of a traffic island in the exit roadway does not lead to higher turning radii, even though this was expected before (assuming that the curve is cut more often in this case). An explanation might be that within urban areas the roadway width of the exit road arms as such is possibly rather narrow. With regard to the rural clusters IV and V, the results are in line with the expectations, although it has to be mentioned that the number of cases in cluster IV is rather low. Another interesting fact is that the turning radii related to the complex layouts (cluster III and cluster VI) have the lowest values. This leads to the conclusion that separations between the lanes used by the accident participants (like traffic islands for instance) prevent drivers from cutting the curve to a noticeable extent. Overall, it can be stated that across all the clusters there are no particular abnormalities.

LTAP/OD – Speed Profiles

The speed distribution of the turning vehicle for certain points in time prior to/at the collision (TTC=0...5 s) has been analyzed using the GIDAS-based PCM data. Table 11 shows the results for speeds at TTC=5 s and TTC=0 s and the longitudinal accelerations at the time of collision. Due to the small number of cases with regard to cluster IV and cluster VI, only the results of clusters I-III and cluster V are given.

The figures show that there are no particular abnormalities regarding the different clusters/layouts. In nearly all cases the turning vehicle is continuously moving with a speed higher than 5 km/h. Thus, turning vehicles involved in a crash do not seem to stand/wait before initiating the turning manoeuvre. Furthermore, the figures representing the acceleration at the time of collision show that constant speed during the crash is the most relevant situation. The number of cases with a turning vehicle accelerating during the collision is negligible. The remaining share of braking vehicles can have different reasons. Lower absolute values are possibly rather caused by a normal braking behaviour while turning, whereas the higher absolute values might represent emergency braking manoeuvres.

LTAP/OD - Impact Points / Overlap

The location of the main damage on a vehicle can be extracted from GIDAS; however, it does not necessarily describe satisfyingly the collision constellation at the time of collision. Therefore, a pairwise analysis of the impact points of the collision partners was performed enabling an approximation of the vehicles' overlap at the time of collision. In GIDAS the impact point is described by three variables: x_{impact} (distance to the foremost point of the vehicle in the direction of the vehicle's longitudinal axis), y_{impact} (distance to the longitudinal axis of the vehicle in the direction of the vehicle's lateral axis) and z_{impact} (vertical distance to the street surface).

To determine the frequencies of the impact points, a grid with regard to the vehicle contour was defined for the x- and y-directions as shown in Figure 20. The vehicle width was divided into three equal sections, while the vehicle length was divided into parts each of 12.5 % at the front and the rear and three sections each of 25 % for the remaining part. Depending on their location, the sections were labeled with a two digit number (from 11 to 53). In this context, the first digit represents the longitudinal location of the section, while the second digit represents the lateral location. Subsequently, each impact point could be assigned to the respective section.

As a next step, the bivariate frequency distribution with regard to the impact points of the two vehicles involved in the crash can be displayed by drawing a respective table. This makes it possible to identify the most relevant combinations of impact point sections and thus, the approximation of the corresponding overlap between two colliding vehicles.

Table 11: Distributions for speeds and longitudinal accelerations at time of collision for different layout clusters, LTAP/OD

Cluster	Initial velocity (TTC = 5 s)	Velocity at collision (TTC = 0 s)	Longitudinal acceleration at time of collision (in m/s²)
I (n=71)	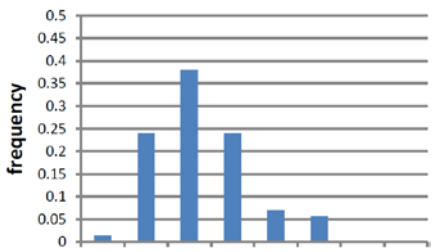	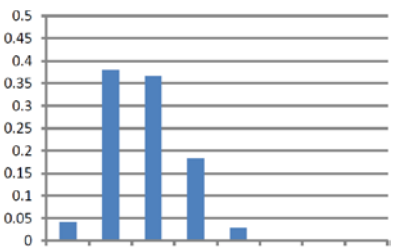	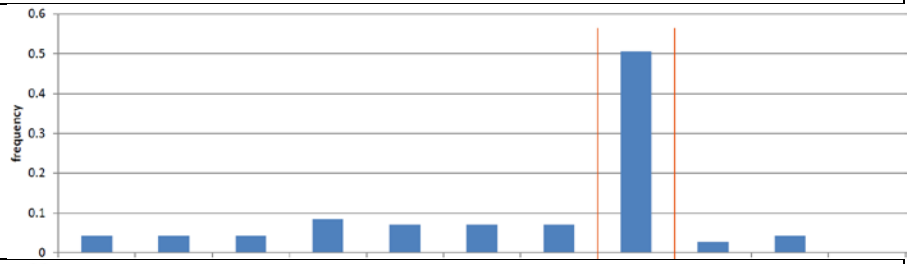
II (n=24)	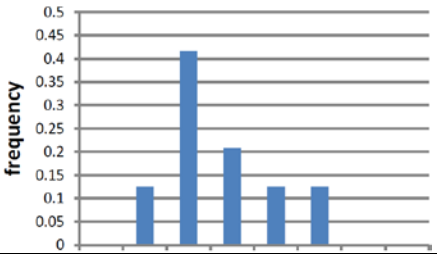	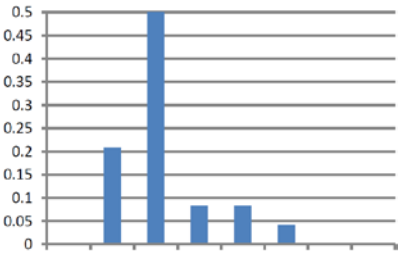	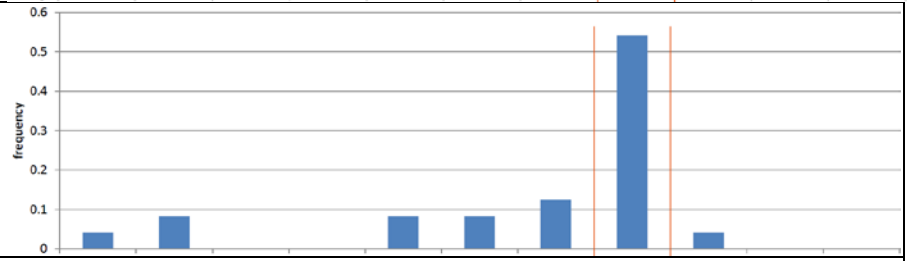
III (n=68)	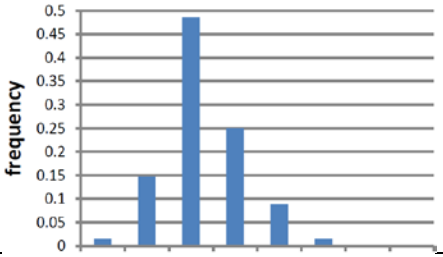	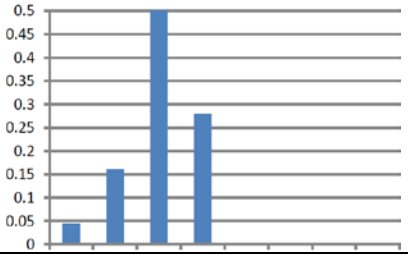	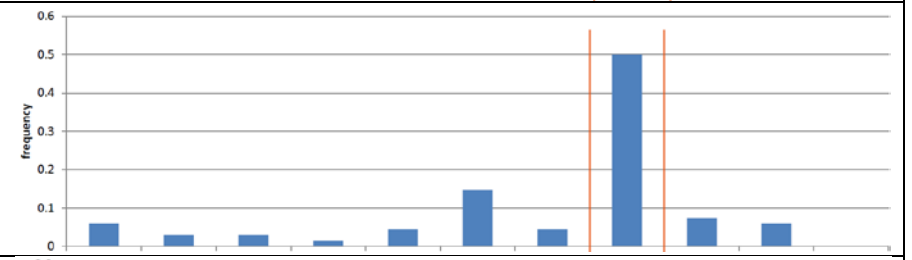
V (n=65)	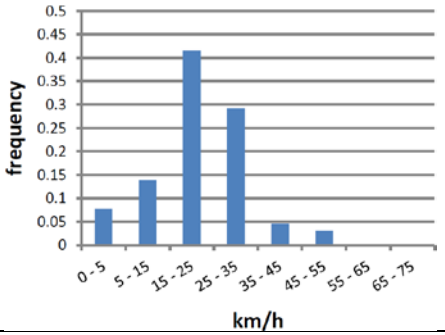	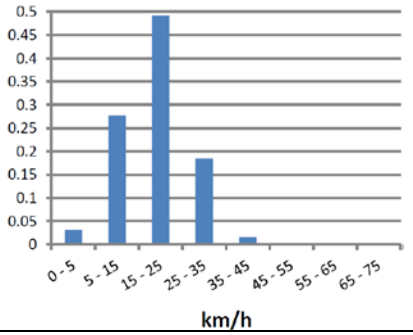	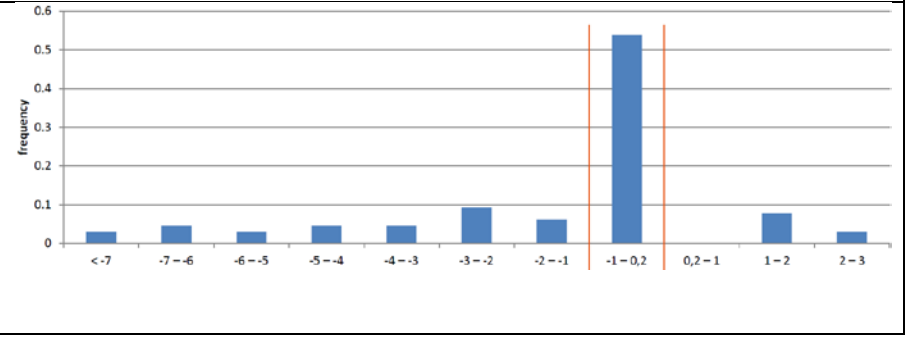

Note: GIDAS also records the point of first contact for each of the colliding vehicles, which could have been a potential variable to be evaluated alternatively. However, small variations of the collision angle might lead to big changes of the contact point. Thus, it was considered that the evaluation of the impact point provides more significant results.

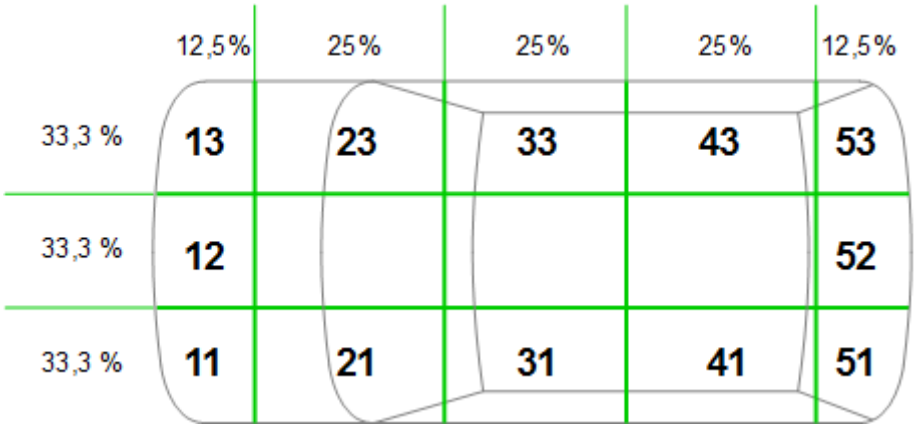

Figure 20: Definition of impact point sections

The notation “section A/section B” is used to address the respective combination of impact sections. For instance, the peak of pairwise impact points can be found at 13/11, representing 32 cases. It should be noted that some of the adjacent entries on the diagonals of the table are related to each other. Figure 21 gives an example: Regarding the initial overlap of both vehicles, combination 11/13 is comparable to combination 12/12, depending on intrusions during the crash phase and varying collision angles.

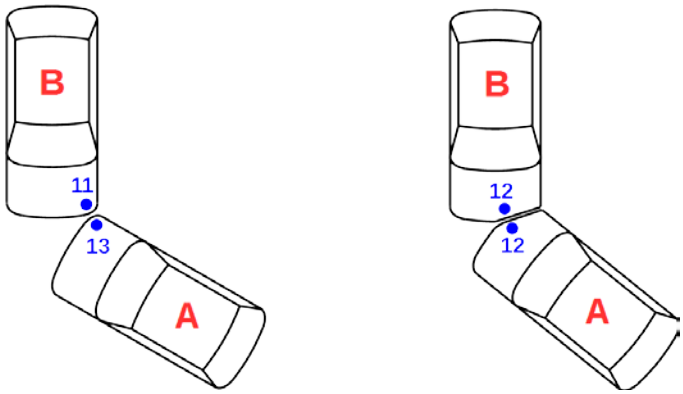

Figure 21: Similar impact point combinations regarding the initial overlap

Evaluations of the frequencies of the impact sections have been performed for “ALL LTAP/OD cases”, “KSI LTAP/OD cases” and “ALL LTAP/OD layout 1+2 cases”. The combinations of impact sections for ALL cases tend to be normally distributed around the above mentioned peak 13/11. Regarding KSI cases, no significant difference to ALL cases could be identified, also due to the small number of cases. Thus, the decision was taken to focus on ALL LTAP/OD cases and on the both most important intersection layouts 1 and 2, see Figure 22 for the respective impact section distribution.

LTAP/OD Layout 1+2 (ALL)			Vehicle B											
			left				front			right				
		Section	51	41	31	21	11	12	13	23	33	43	53	Total
Vehicle A	right	53												0
		43								1				1
		33						1	6					7
		23					1	5	9	2				17
	front	13				1	17	19	7	1				45
		12				5	23	5	2					35
		11		1	1	11	18	1						32
	left	21		1		3	1							5
		31												0
		41												0
		51												0
		Total	0	2	1	20	60	31	24	4	0	0	0	142

Figure 22: Impact points of LTAP/OD for layout 1 and 2, ALL cases

To identify the most relevant combinations of impact sections, a ranking was performed, see Table 12. In this context, the values of the aforementioned similar combinations of impact sections are summed up. All combinations of impact sections which represent at least 50 % of the evaluated cases (indicated by the column "cumulated shares") were considered to be transferred into Use Cases.

Table 12: Ranking of impact point sections for layouts 1 and 2, LTAP/OD

Section combination (veh A/veh B)	Similar section combination (veh A/veh B)	No. of cases	Total	Relative share	Cumulated shares
12/11	11/12, 13/21	23+1+1	25	17.6 %	17.6 %
11/11	12/21	18+5	23	16.2 %	33.8 %
13/11	12/12	17+5	22	15.5 %	49.3 %
13/12	12/13, 23/11	19+2+1	22	15.5 %	64.8 %

Use Cases for LTAP/OD

Branching all LTAP/OD cases as previously described led to the corresponding Use Cases given in Table 13. Note: The mentioned speed ranges represent the middle 50% of the respective distributions, also referred to as interquartile range (IQR). To provide a potential link between the basic shares and the results of high-level accident data, the distributions of intersection types (crossing, t-junction and other types) is given, too. Apart from the possibility of testing several speeds, the combinations of the two layout groups and nine pairwise impact sections already leads to a number of 18 Use Cases.

Table 13: Use Cases for LTAP/OD

	Layout 1+2				Layout 3				
Inters. type	Crossing		T-junction	Other	Crossing		T-junction		Other
Shares (in %)	56.0		40.7	3.3	74.0		24.7		1.3
Lateral offset	≈ 3.7 m				≈ 11.5 m				
Shares (in %)	70 %				30%				
Speed profiles	Vehicle A		Vehicle B		Vehicle A		Vehicle B		
$v_{initial}$ (IQR)	16-30 km/h		47-65 km/h		20-33 km/h		45-53 km/h		
$v_{collision}$ (IQR)	12-25 km/h		38-55 km/h		16-27 km/h		33-50 km/h		
a_x (at collision)	Constant speed		Constant speed		Constant speed		Constant speed		
Impact sections	12/11	13/11	13/11	13/12	13/11	23/13	12/11	11/11	23/12
Shares (in %)	17.6	16.2	15.5	15.5	21.5	12.7	11.4	10.1	10.1

Use Cases for LTAP/LD

Similar to LTAP/OD scenario evaluation, simplified intersection layouts have been defined with regard to the LTAP/LD scenario, resulting in three groups (from a rather clean layout 1 up to a rather complex layout 3). The evaluation of approaching angles as well as turning radii showed that the layouts 1 and 2 are quite similar (median turning radius: ≈ 25 m). In addition, these two layouts represented 89 % of all LTAP/LD cases. Thus, layout 3 was found to be less relevant.

Regarding the speed profiles and accelerations, it was found that vehicle A is driving with low speed (< 5 km/h) in a significant number of cases (about 15 %) compared to the other scenarios. Accordingly, deceleration is not relevant with regard to vehicle A. Looking at vehicle B, constant speed at the time of collision took place in about 34 % of all cases, whereas a braking maneuver was initiated in about 66 % of all cases. The most relevant impact point combinations for the merged layouts 1 and 2 were identified, resulting in four crash constellations.

Branching all LTAP/LD cases finally led to the corresponding Use Cases given in Table 14. The speed ranges represent the middle 50% of the respective distributions (IQR). Apart from the possibility of testing several speeds, the combinations of all identified parameter groups (acceleration and pairwise impact sections) already leads to a number of 24 Use Cases.

Table 14: Use Cases for LTAP/LD

	Layout 1+2 (89 % of all LTAP/LD cases)				
Inters. type	Crossing		T-junction		Other
Shares (in %)	18.5		60.5		21.0
Speed profiles	Vehicle A			Vehicle B	
$v_{initial}$ (IQR)	8-19 km/h			45-61 km/h	
$v_{collision}$ (IQR)	9-16 km/h			37-50 km/h	
a_x (at collision)	Const.	Accel.	Braking	Const.	Braking
Shares (in %)	47.0	32.0	21.0	33.8	66.2
Impact sections	11/13	21/12		11/12	12/23
Shares (in %)	22.4	14.4		11.2	10.4

Use Cases for SCP

First, all SCP cases have been split into two sub-scenarios based on the direction of approach of the prioritized vehicle (from left or right). With regard to the angle of approach, no particular abnormalities were found. Thus, test scenarios with an orthogonal orientation of the vehicles during the entire pre-crash phase can be seen as sufficiently representative for the SCP cases.

Regarding the initial and collision speeds, no significant differences were identified between the sub-scenarios SCP/L and SCP/R. However, looking at the acceleration at the time of collision, specific characteristics have to be taken into account. Significant shares of vehicle A and vehicle B are performing braking manoeuvres in both sub-scenarios. Finally, the most relevant impact point combinations were identified, resulting in four crash constellations for each of the two sub-scenarios.

Branching all SCP cases led to the corresponding Use Cases given in Table 15. The speed ranges represent the middle 50 % of the respective distributions (IQR). Apart from the possibility of testing several speeds, the combinations of the sub-scenarios and the further parameter groups (acceleration and pairwise impact sections) already leads to a number of 32 Use Cases.

Table 15: Use Cases for SCP

	SCP/L				**SCP/R**			
Inters. type	Crossing		T-junction	Other	Crossing		T-junction	Other
Shares (in %)	92.0		6.6	1.4	91.8		7.7	0.4
Speed profiles	Vehicle A		Vehicle B		Vehicle A		Vehicle B	
$v_{initial}$ (IQR)	19-44 km/h		37-52 km/h		25-46 km/h		30-50 km/h	
$v_{collision}$ (IQR)	19-40 km/h		33-48 km/h		21-40 km/h		26-46 km/h	
a_x (at collision)	Const.	Braking	Const.	Braking	Const.	Braking	Const.	Braking
Shares (in %)	75	25	50	50	50	50	50	50
Impact sections	11/13	31/12	21/13	21/12	33/12	23/12	13/11	23/11
Shares (in %)	15.7	15.7	13.6	11.4	14.8	13.9	12.2	11.8

SUMMARY
The Intersection 2020 project was initiated to develop a test procedure for Automatic Emergency Braking systems in intersection car-to-car scenarios to be transferred to Euro NCAP. The project aims to address current road traffic accidents on European roads and therefore sets a priority of the identification of the most important car-to-car accidents and Use Cases. In a later stage taking into account technological and practical limitations, Test Scenarios are derived from the Use Cases.

This report provides an overview of common car-to-vehicle(at least four wheels) collision types at junctions in Europe, specifies seven Accident Scenarios from which the three scenarios "Straight Crossing Paths (SCP)", "Left Turn Across Path – Opposite Direction Conflict (LTAP/OD)" and "Left Turn Across Path – Lateral Direction (LTAP/LD)" are most important due to their high frequencies of severe car-to-car accidents. Technical details about crash parameters such as collision and initial speeds are delivered. The analysis work performed is input for the definition and selection of the Use Cases as well as for the project's benefit estimation.

Various accident datasets from Europe have been analyzed. Two major injury severity groups have been investigated: killed and seriously injured (KSI) and killed, seriously and slightly injured (ALL).

Most countries in Europe distinguish between intersection layouts; however, the comparability among each other is limited. The lowest common denominator was found in the categorization based on an initiative by the EU. However, although these definitions are widely accepted and applied, only a few countries work accordingly.

The numbers of accidents and fatalities in accidents at intersections involving a passenger car were shown per intersection type. In both statistics, it was found that accidents at crossroads and T- or staggered junctions are of highest relevance, followed by roundabouts. Focusing on accidents at intersections between one passenger car and another road user showed that around one-third of all accidents and related fatalities could have been assigned to car-to-PTW accidents and one-fifth of all accidents and fatalities to car-to-car accidents.

Regarding severe car-to-car accidents 38% out of 34,489 car-to-car accidents in Europe happened at intersections. These figures correspond to 18% of the fatalities (4,236 fatalities in total). Considering all intersection types, around half of all related accidents happened in urban environments whereas this number decreased to one-third of all fatalities. It has to be noted that the aforementioned proportions of the number of accidents and fatalities per intersection type may reflect rather the frequency of these intersection types in Europe than certain associated risk factors.

Further results based on the CARE analysis comprised that the proportion of road fatalities per country occurring at intersections varies widely across the EU and that there are proportionately more fatalities in daylight/twilight.

In addition, latest national accident statistics from France, the United Kingdom, Spain and Germany have been analyzed regarding road traffic accidents at intersections. Overall, the results were similar to the ones obtained from the CARE analysis. The shares of accidents in urban areas differed considerably between the countries. Severe car-to-car accidents occurred most often on crossroads and T- or staggered junctions. Contrarily, two-thirds of these accidents were assigned to crossroads in France, but to T- or staggered junctions in the UK and around half of these accidents each to crossroads and T- or staggered junctions in Germany. In Spain, half of the severe accidents occurred on crossroads and one-third on T-or staggered junctions. At roundabouts, severe accidents were similarly proportioned in urban and rural areas. Fatal crashes happened most often in rural areas.

Germany uses a different coding of road traffic accidents at intersections. Also, accidents at roundabouts were coded as accidents at intersections until the year 2015. Since 2016, accidents at roundabouts are coded separately in the national statistics. However, to provide possibilities for direct comparisons with other countries different approaches were considered. The most promising approach was found in a work by the Fraunhofer Institute IVI which developed a tool (commissioned by Toyota Motor Europe) being able to distinguish between different intersection types. Relevant results were kindly provided to the Intersection 2020 project.

Use Cases are supposed to be derived from Accident Scenarios and by adding detailed information for example about the road layout, right-of-way and the vehicle trajectories prior to the collision. A first attempt to generate a proper list of Use Cases based on the available collision data, using clustering algorithms and having the principal goals of the project in mind failed as the application of the statistical models to the data directed quickly into various issues and uncertainties but also similar results as presented in literature. Further, it became clear that vehicles' trajectories are important but could not be derived from GIDAS and various parameters (e.g., varying lane width, view obstructions), identified as being meaningful, could not be transferred to any Test Scenario for consumer programs in next years for which reasons a pragmatic approach was finally preferred. The principles of the Use Case analysis are provided for LTAP/OD in this paper. Analogue gained results for

LTAP/LD and SCP were summarized. Finally, 74 Use Cases were identified. This large number indicates the complexity of intersection crashes due to the combination of several parameters.

Regarding the scenario LTAP/OD two main groups were identified as suitable to assign further characteristics: intersections with adjacent lanes used by the accident participants (layout 1 and 2) as well as intersections with an additional lateral offset between the lanes (layout 3). For the first group, which represents approximately 70 % of all LTAP/OD cases, a lateral offset of 3.7 m was identified. The second group has a larger spread of lateral offsets with a median of around 11.5 m. For both groups the turning radii were analyzed, considering also the location of the accident site and road elements such as islands in the exit roadway. However, no significant differences between the several clusters could be identified. To a certain degree, the same applies to the investigated speed profiles with regard to the turning vehicle. Finally, the most relevant impact point combinations for the case groups could be identified, resulting in four crash constellations for layout 1 and 2 and five crash constellations for layout 3.

Regarding the LTAP/LD scenario, simplified intersection layouts have been defined resulting in three layouts. The evaluation of approaching angles as well as turning radii showed that the layouts 1 and 2 are quite similar (median turning radius around 25 m). In addition, these two layouts represented 89 % of all LTAP/LD cases. Thus, layout 3 was found to be less relevant. Regarding the speed profiles and accelerations, it could be found that vehicle A is driving with low speed (< 5 km/h) in a significant number of cases (about 15 %) compared to the other scenarios. Accordingly, deceleration was not found being relevant with regard to vehicle A. Looking at vehicle B, constant speed at the time of collision took place in about 34 % of all cases, whereas a braking maneuver was initiated in about 66 % of all cases. The most relevant impact point combinations for the merged layouts 1 and 2 were identified, resulting in four crash constellations.

Regarding the SCP scenario, firstly, all SCP cases have been split into two sub-scenarios based on the direction of approach of the prioritized vehicle (from left or right). There were no conspicuous findings with regard to the angle of approach. Thus, test scenarios with an orthogonal orientation of the vehicles during the entire pre-crash phase can be seen as sufficiently representative for the SCP cases. Regarding the initial and collision speeds, no significant differences were identified between the sub-scenarios SCP/L and SCP/R. However, looking at the acceleration at the time of collision, specific characteristics have to be taken into account. Significant shares of vehicles A and B are performing braking manoeuvres in both sub-scenarios. Finally, the most relevant impact point combinations were identified, resulting in four crash constellations for each of the two sub-scenarios.

CONCLUSION

An analysis of car-to-car accidents at intersections in Europe has been conducted based on various datasets. It has to be noted that there is no clear definition of an intersection in Europe. And although definitions for different intersection types were achieved in a European consortium, only a few countries deal with it in the intended manner. Nevertheless, the data quality was sufficient to generate basic results for different European countries. More specific analyses have been performed using data from the German national accident statistics and the German In-Depth Accident Study (GIDAS).

The accident data analysis revealed that three Accident Scenarios are key for further work steps within the Intersection 2020 project (due to their high frequency rates in accidents with severe injury outcome) which are accidents at 1) Straight Crossing Paths (SCP), 2) Left Turn Across Path – Opposite Direction Conflict (LTAP/OD) and 3) Left Turn Across Path – Lateral Direction (LTAP/LD). Most of these accidents occurred under daylight conditions.

For each of these Accident Scenarios, basic crash parameters including the cars' initial and collision speeds were provided supporting the work of selecting appropriate test speeds. The data is also supposed to support the activities around the benefit estimation work in the project.

The presented Use Cases are the basis for the development of Test Scenarios considering their relevance, the transferability to the test track, an economic test environment and the expected performance of the systems to be tested.

To accelerate the market penetration of innovative junction/crossing autonomous emergency functions in state-of-the-art vehicles the consumer protection organisation Euro NCAP will change the assessment for the year 2020 and launch an assessment for technology that addresses the above listed accident scenarios. As an example the announced "car-to-car front turn across path" (CCFtab) test for 2020 will address the LTAP/OD accident scenario and the test is derived from the Use Cases presented in the core of this work. An assessment that addresses the remaining Accident Scenarios is strongly considered or even already announced.

REFERENCES

[1] European Road Safety Observatory, “Roads,” www.erso.eu, 2006.

[2] T. Neuman, R. Pfefer, K. Slack, K. Kennedy, D. Harwood, I. Potts, D. Torbic and E. Kohlman, Guidance for implementation of the AASHTO Strategic Highway Safety Plan - Volume 5: A Guidance for Addressing Unsignalized intersections Collisions, vol. NCHRP Report 500, Transportation Research Board, 2003.

[3] Transport Department, “Design Manual for Roads and Bridges - Geometric Design of Major/Minor Priority Junctions,” London, 1995.

[4] N. Antonucci, K. Kennedy, K. Slack, R. Pfefer and T. Neuman, Guidance for implementation of the AASHTO Strategic Highway Safety Plan - Volume 5: A Guidance for Reducing Collisions at Signalized Intersections, NCHRP Report 500, Transportation Research Board, 2003.

[5] TRL Transport Research Laboratory, “Laboratory Report 1120: Accidents at 4-arm roundabouts,” 1984.

[6] D. O'Cinneide och R. Troutbek, ”At-grade intersections/worldwide review,” i *Transportation Research Circular - International Symposium on Highway Geometric Design Practices*, Boston, 1998.

[7] R. Elvik and T. Vaa, “The Handbook of Road Safety Measures,” Elsevier, 2004.

[8] A. Montella, “Identifying crash contributory factors at urban roundabouts and using association rules to explore their relationships to different crash types,” *Accident Analysis and Prevention 43*, pp. 1451-1463, 2011.

[9] M. Simon, T. Hermitte and Y. Page, “Intersection Road Accident Causation: A European View,” in *Study was part of the European TRACE project*, Enhanced Safety of Vehicles Conference Proceedings, 2009, pp. Paper No. 09-0370.

[10] European Commission, “Traffic Safety Basic Facts on Junctions,” Directorate General for Transport, 2015.

[11] P. Nitsche, P. Thomas, R. Stuetz and R. Welsh, “Pre-crash scenarios at road junctions: A clustering method for car crash data,” *Accident Analysis and Prevention 107*, pp. 137-151, 2017.

[12] U. Sander and N. Lubbe, “The potential of clustering methods to define intersection test scenarios: Assessing real-life performance of AEB,” *Accident Analysis and Prevention 113*, pp. 1-11, 2018.

[13] H. Feifel and M. Wagner, “Harmonized Scenarios for the Evaluation of Active Safety Systems based on In-Depth-Accident Data,” in *Proceedings of the Expert Symposium on Accident Research (ESAR)*, Hanover, 2018.

[14] German Insurance Association (GDV), Accident Types Catalogue 2016, Berlin, 2016.

[15] CARE Database, “CaDaS - Common Accident Data Set,” vol. Version 3.4, 2015.

[16] Statistisches Bundesamt (Destatis), “Verkehrsunfälle 2016,” vol. Fachserie 8 Reihe 7, 2017.

[17] US Department of Transport, “Analysis of Crossing Path Crashes,” DOT HS 809 423 Final Report, DOT-VNTSC-NHTSA-01-03, 2001.

[18] M. McCarthy, H. Fagerlind, I. Heinig, T. Langner, S. Heinrich, L. Sulzberger and S. Schaub, “Deliverable 1.1 - Preliminary Test Scenarios,” European Commission - FP7 project ASSESS, 2011.

[19] Forschungsgesellschaft für Straßen- und Verkehrswesen (FGSV), Arbeitsgruppe Straßenentwurf, “Richtlinien für die Anlage von Landstraßen (RAL) - Ausgabe 2012,” FGSV Verlag, Köln, 2013.

[20] A. Wesp, Analyse fahrerwirksamer Systemauslegungen und -störungen eines Fahrzeugs mit Hinterradlenkung bei gleichzeitiger Fahrerbeanspruchung durch eine Fahraufgabe, TU Darmstadt: Dissertation, 2010.

[21] A. Neukum, E. Ufer, J. Paulig and H. Krüger, “Controllability of Superposition Steering System Failures,” in *Steering.Tech*, Garching (Germany), 2008.

[22] J. E. Bakaba and J. Ortlepp, “Sichere Knotenpunkte für schwächere Verkehrsteilnehmer (“Design of safe intersections for vulnerable road users“),” in *Forschungsbericht Nr. 23*, Berlin, Gesamtverband der Deutschen Versicherungswirtschaft e.V. (GDV) - Unfallforschung der Versicherer, 2014.

[23] C. Flannagan, A. Bálint, K. Klinich, U. Sander, M. Manary, S. Cuny, M. McCarthy, V. Phan, C. Wallbank, P. Green, B. Sui, A. Forsman and H. Fagerlind, “Comparing Motor-vehicle Crash Risk of EU and US Vehicles,” University of Michigan, UMTRI, 2015.

[24] U. Sander, “Opportunities and limitations for intersection collision intervention - A study of real world 'left turn across path' accidents,” *Accident Analysis and Prevention 99*, pp. 342-355, 2017.

[25] J. Sandin, “Analysis of intersection crash statistics to define pre-crash test scenarios for detection sensors,” in *SAFER Report Project Scenariobased testing of pre-crash systems*, Gothenburg, SAFER - Vehicle and Traffic Safety Centre at Chalmers, 2009.

APPENDIX
Assignment of accident types [14] to Accident Scenarios

LTAP/OD

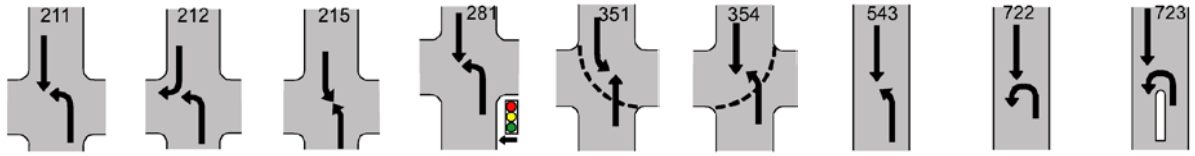

LTAP/LD

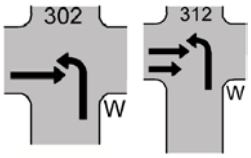

LTIP

RTIP

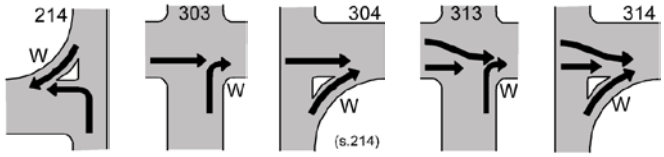

SCP

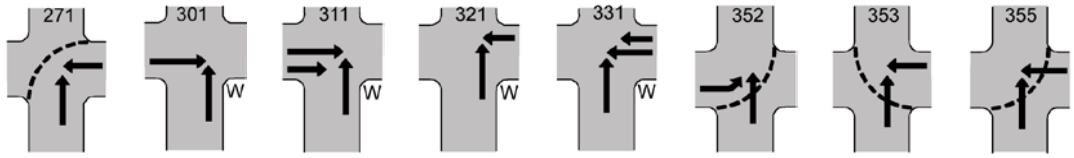

P/R

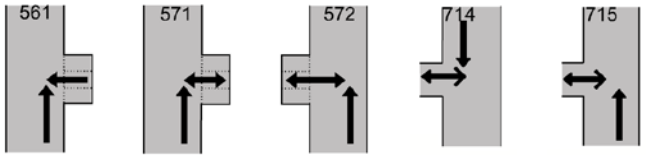

NA (Selection)

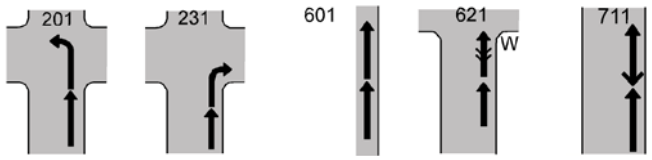

INTEGRATED SAFETY: ESTABLISHING LINKS FOR A COMPREHENSIVE VIRTUAL TOOL CHAIN

Linus Wågström
Alexandros Leledakis
Jonas Östh
Magdalena Lindman
Lotta Jakobsson

Volvo Cars Safety Centre
Sweden

Paper Number 19-0177

ABSTRACT

As technologies for injury prevention and crash avoidance both contribute to injury reduction in car crashes, tools predicting the combined effect of all safety features are needed. This study aims at establishing a computer simulation methodology including two important elements for assessing this combined effect. The first element describes the states of the involved vehicles or objects at crash initiation regarding positions, orientations and velocities as parameters used for crash evaluation. The second element focuses on the car occupant, enabling computationally efficient prediction of occupant position transfer during pre-crash maneuvers. An extended aim is to demonstrate how data flows between these elements in an example case study.

Real-world data from the Volvo Cars traffic accident database (VCTAD) was used as the basis for pre-crash simulations involving two cars, with and without a conceptual autonomous emergency braking (AEB) function. For cases in which the crash was not avoided by the AEB function, the crash configuration was identified. A simplified occupant kinematics model (SOCKIMO) was developed and applied to these remaining crashes, supporting the selection of crash situations to be analyzed in detail. The SAFER human body model (HBM) was used for simulation of the occupant response, providing information on pre-crash kinematics as well as the occupant crash response.

As a result, a novel crash configuration definition for estimating the consequences of car crashes based on preceding events was established. The Volvo parametric crash configuration (VPARCC) definition can be used as a link between pre-crash and crash simulation tools as well as for illustrating sets of real-world accident data and how these change based on maneuvers preceding a crash. SOCKIMO results demonstrated occupant kinematics similar to those of volunteers, and the subsequent simulations using the SAFER HBM showed considerable changes in occupant crash response based on pre-crash vehicle kinematics.

The VPARCC definition can also be applied to collision objects such as trucks or vulnerable road users. The developed SOCKIMO can be used to filter out cases from large crash data sets to be further analyzed with detailed models such as finite element active HBMs. By applying the more detailed HBM, the effects of avoidance maneuvers on occupant kinematics relevant for injury prediction can be evaluated. This approach would not be possible using simplified occupant models only (due to the lack of details) or by using detailed models only (due to the large simulation effort).

The presented methodology for estimating combined safety performance can be used for transferring output from pre-crash simulations to input for crash simulations. The feasibility of combining the individual elements of this methodology was demonstrated in an example case where autonomous emergency braking led to a large change in the crash configuration and was predicted to introduce substantial occupant pre-crash excursion. In this example case, it was shown that the present A-HBM tool is able to cover the complete sequence from pre-crash maneuvers to crash in one single simulation.

INTRODUCTION

Road traffic safety continues to play a major role in the overall health of the world's population. Today, it is the eighth leading cause of death for people of all ages, annually amounting to approximately 1.35 million fatalities worldwide [1]. Continuing to strive for improved safety is therefore in the interest of all stakeholders in road traffic systems. Visions of reducing the number of road fatalities towards zero have been put forward by numerous countries, states and cities [2]. However, recent data suggest that the number of fatalities and injuries on European as well as on U.S. roads has started to level out or even increase [3, 4].

From a vehicle design point of view, a long tradition of improvements has been seen relating to crash safety, i.e. injury prevention in case of a crash occurring. More recently, automated collision avoidance technologies have emerged, raising expectations for a future with autonomous vehicles in which crashes can be avoided. By studying real-world crash data, it can be seen that both systems for injury prevention as well as systems for collision avoidance do have considerable effects on the number of injuries [5]. Developing assessment tools that predictively can quantify how many crashes can be avoided, but also predict the effect on injuries from those remaining, non-avoided, crashes is therefore important for injury prevention in future passenger cars. Today, assessment of the real-world safety performance of a car model is done by analysis of retrospective data, available years after introduction. In addition to this, the effect of safety systems is predicted already before these systems have been put into production. This is done with established methods [6] involving physical crash testing and simulation using computer aided engineering (CAE). For integrated safety, i.e. how safety systems aimed at collision avoidance and injury prevention interact with and complement each other, methods need to be refined in order to make such predictions. The use of virtual tools for integrated safety is therefore a key component in order to predict expected crash outcomes, providing decision-making data for developing the most effective safety systems.

In this process, understanding future crash scenarios and transferring this knowledge into specific crash configurations becomes an important factor. Methods on calculating the effect of collision avoidance systems in terms of injury outcome and accidents avoided or mitigated have been developed. Lindman and Tivesten [7] presented such a method based on available traffic accident data with the aim to support the system development process by offering an opportunity to alternate input parameters, such as, braking (acceleration) level in order to determine the effect of these changes. The method was further refined including the actual system algorithm in a relevant car and sensing model by Lindman et al [5]. These methods include estimations of the consequences of a crash using risk functions based on real-world traffic accident data, by assuming a modified injury risk as a result of reduced crash severity. However, these methods as well as established ways for describing crashes such as using the collision deformation classification (CDC) or principal direction of force (PDOF) [8] were found to lack the level of detail needed to describe subtle relative changes in crash configuration to support CAE studies in the form of structural and occupant finite element (FE) simulations. With a refined description of crash configurations, the effects of collision avoidance interventions can be described and evaluated by simulating a range of traffic situations that are likely to occur. By applying probable distributions of the input parameters, the robustness and sensitivity of the system can be evaluated.

Another context for which the interaction between systems for collision avoidance and injury prevention becomes increasingly important relates to occupant re-positioning due to pre-crash accelerations, regardless from human drivers or autonomous intervention systems. These effects are possible to study in volunteer experiments [9] and it has been found that the muscle activation of car occupants has a considerable influence on the kinematic pre-crash response [10], leading to a need for active human body models (A-HBMs) in order to study these effects using CAE tools. Several approaches to A-HBMs have been made [11, 12] and a potential for use in product development has been demonstrated [13]. The most detailed injury prediction response based on tissue level can be provided by FE HBMs, which however are all computationally intensive. This is even more pronounced when pre-crash maneuvers are considered, these often have a duration of seconds whereas crash simulation typically spans 100-200 milliseconds. It is therefore not seen as feasible to deploy FE A-HBMs directly in larger simulation studies with thousands of cases for estimating the effect of collision avoidance systems. In this context, a computationally efficient model indicating occupant pre-crash motion including effects of muscle tensioning is therefore desired. With such a tool, a number of critical or dimensioning cases could be filtered out from a larger sample set for analysis using FE A-HBMs. From volunteer studies of belted passenger car occupant kinematics during pre-crash maneuvers, it has been observed that the pelvis displacement is small compared to that of the head and torso [14], suggesting a model of only the upper body could be could be useful for studying pre-crash occupant kinematics.

The overall aim of this study is to create a CAE methodology for predicting the combined safety performance from collision avoidance systems (e.g. autonomous emergency braking, AEB) as well as systems for injury prevention (e.g. seatbelts and airbags). Specific aims are to establish two important elements in this simulation methodology. The first element concerns real-world data, and the transfer of real-world pre-crash situations into crash configurations to be used in crash simulations providing insight into occupant protection. The second considers the human occupant, enabling computationally efficient prediction of position transfer between pre-crash situations and crash. An extended aim is to demonstrate how data flows between these elements in an example case study.

THE VOLVO CAE TOTAL SAFETY PERFORMANCE METHODOLOGY

In order to obtain a useful overall methodology based on simulation models, it is of great importance that the individual components can be shown to deliver valid results. The overall validity of this overall methodology will not be possible to prove until validation data is available, i.e. when real-world data can be collected that reflect the actual safety performance. Since this is a process that involves a sufficiently large number of vehicles being put in production and deployed in real-world situations, it could take several years before these effects can be seen. The approach in this study is therefore to assess the validity of each included element in the overall methodology and ensure that each such element delivers realistic results.

A novel methodology is presented for estimating the total safety performance based on CAE tools, i.e. how the effects of countermeasures aimed at injury prevention before and during a crash can be described using computer models in order to summarize these effects for larger sets of traffic scenarios. This is followed by one specific example case which was chosen to demonstrate and further explain the selection process and transfer of data between CAE tools. Focus is placed on the elements that was recently developed in order to bridge gaps and create links in the overall methodology.

Overall description of the methodology

The overall methodology contains seven elements, as displayed in Figure 1. It has its basis in real-world data, and provides output of car occupant response during the complete sequence of events covering both pre-crash and crash phases. When applying the methodology, the process starts with identifying real-world traffic situation datasets relevant for the research question at hand, as illustrated by element 1 and ends with the output that is given from occupant pre-crash and crash simulation in element 7. Each of these and intermediate elements are further described below.

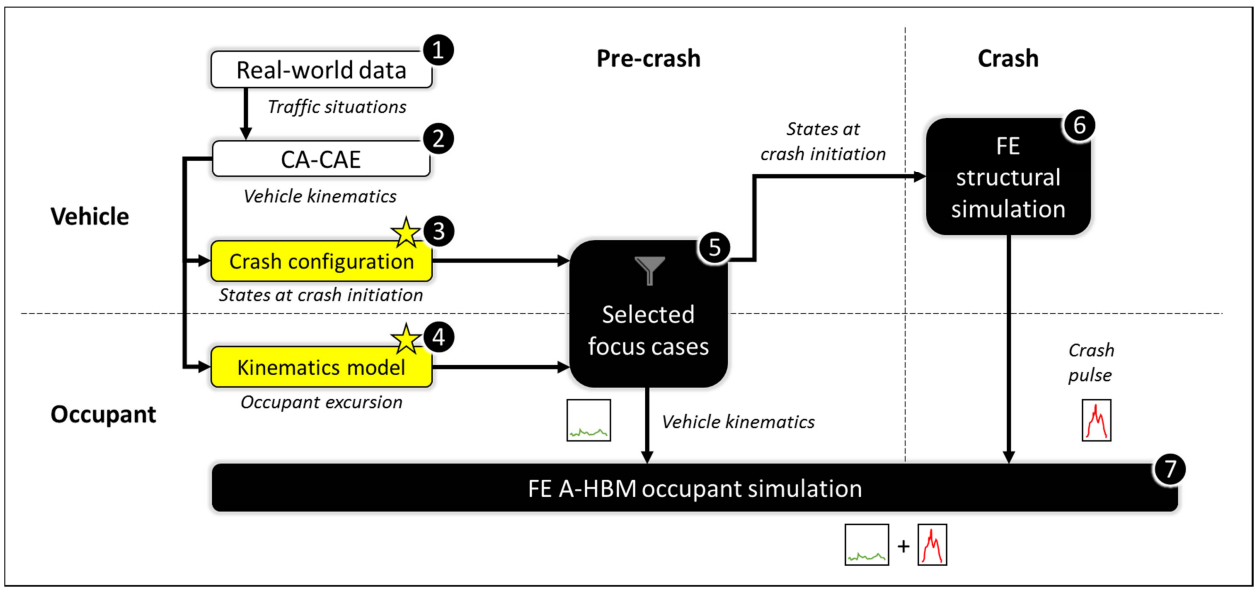

Figure 1. Overview of Volvo CAE total safety performance methodology, with element numbers encircled.

Element 1: Real-world data. Representing a range of real-world traffic situations, a set of data is used as the starting point for this methodology. Each case in this database represents a collision relevant for the research question that will be studied. Information needed for the baseline pre-crash simulation are e.g. vehicle paths in relation to vehicle velocities and to the surroundings in a numerical time history data (THd) format.

Element 2: CA-CAE. In the next step, a "Baseline" pre-crash simulation is performed to reflect the original real-world data. This is then compared to another dataset called "Treatment" which includes the collision avoidance technology to be studied. This tool for collision avoidance CAE (in the following abbreviated to CA-CAE) should include models where sensor and actuator parameters can be adjusted. The CA-CAE tools may also include driver models to simulate how human drivers interact with the vehicle. In its simplest form, the driver model is a path follower that provides driver input in order to make the vehicle follow the time-dependent states given in the real-world data cases. The validity of the CA-CAE tools should be ensured by comparing subsets of pre-crash simulation data to corresponding data collected from physical tests performed on test tracks or public roads.

Elements 3-4: Crash configuration and occupant pre-crash kinematics model. The output from the CA-CAE tools in element 2 are time histories of variables describing the states of all vehicles or objects involved in a crash. If the CA-CAE tools indicate that the collision is avoided, there process will stop after element 2. However in cases where a crash still occurs, the influence of the pre-crash phase needs to described and possibly considered in the crash phase. For this purpose, element 3 in Figure 1 regarding crash configuration and element 4, an occupant pre-crash kinematics model, are defined. These elements describe how the pre-crash phase has influenced the crash configuration as well as how the occupant position may have been affected by the pre-crash phase. They are both marked with a star in Figure 1, and proposals for such elements are presented in separate sections below.

Element 5: Selected focus cases. In the next phase, the methodology allows the user to select certain cases that may be of special interest by filtering out cases where the crash configuration indicates high crash severity, if particular impact locations are identified or if a pre-crash intervention changes the crash configuration to a large extent. Since the number of cases can be extensive, the occupant pre-crash kinematics model is used to further filter out cases where it can be expected that the occupant would experience considerable pre-crash excursion, i.e. displacement due to vehicle accelerations. By selecting this smaller sample of the collision avoidance simulation cases, the simulation effort using the FE A-HBM (element 7) where the pre-crash vehicle kinematics is combined with the crash pulse from the FE structural crash simulation can be substantially reduced.

Element 6: FE structural crash simulation. The purpose of the crash configuration definition is to provide a description of the states of the ego/host vehicle at impact as well as the crash counterpart that can be fed into an FE structural crash simulation of the two objects involved in the collision, or as input to setting up physical crash tests. This simulation could theoretically include also an FE A-HBM, however due to computational efficiency, the structural and occupant crash simulations are normally split into two separate simulations for each case. In this way, output from the FE structural crash simulation can be fed into the complete-sequence (pre-crash and crash) occupant crash simulation using an FE A-HBM, element 7 in Figure 1.

Element 7: FE A-HBM occupant simulation. In this element, the effects of the pre-crash phase and the subsequent crash is studied using an occupant and interior model. For the development of the current methodology, the SAFER HBM occupant model was used. This is a 50th percentile male model based on the THUMS v3 model but substantially updated by the partners of the SAFER Vehicle and Traffic Safety Centre at Chalmers in Gothenburg, Sweden. The head and brain model has been replaced with the KTH head model [15]. The rib cage has been updated with a more detailed model with rib curvature and cortical bone thickness representative of the average 50th male from relatively large sample studies [16, 17]. The cervical and lumbar spine of the model has been updated with non-linear ligament [18] and intervertebral disc models.

The SAFER HBM, Figure 2, has active musculature implemented using Hill-type beam muscle elements controlled by feedback controllers [19]. The most recent update of the active muscle control includes an omnidirectional lumbar and cervical spine controller [20], which enables modelling of both car driver and passenger reflexive and postural responses in pre-crash scenarios.

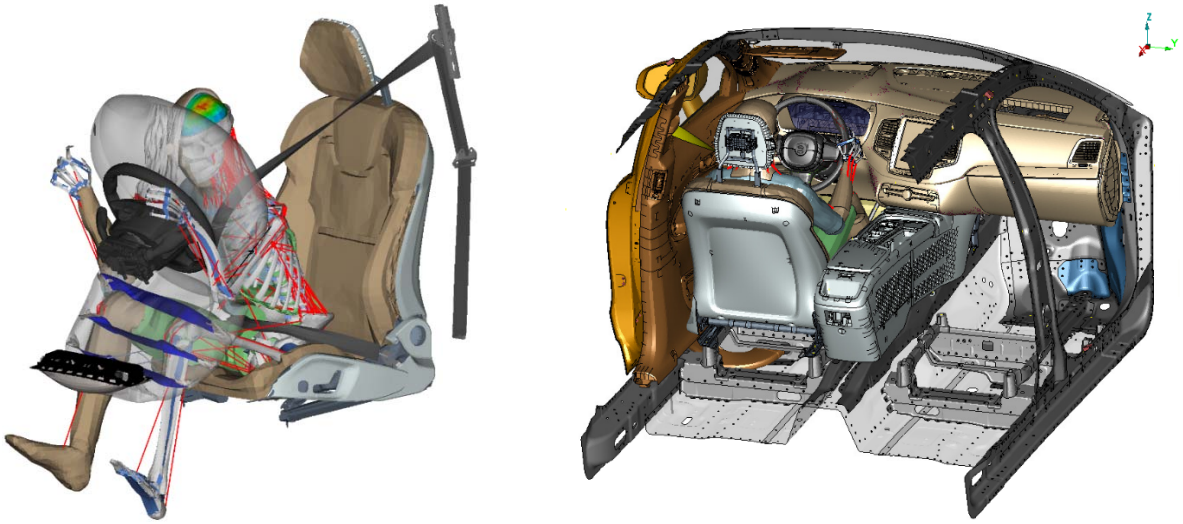

Figure 2: The SAFER HBM in a crash simulation with soft tissues blanked out to show the musculoskeletal structure (left) and overview of the FE vehicle interior model (right).

The vehicle interior used in this study consists of a rigid sled model representing a passenger car body structure where deformable models of the interior components such as seat, steering wheel, instrument panel, airbags and seat belts are included, Figure 2. To simulate the complete sequence of events, three phases are included in the same occupant simulation model as illustrated in Figure 3. The first phase is for HBM stabilization needed for the model to find equilibrium under gravity loading and with active muscles. During this phase which lasts for 300 ms, the rigid sled is stationary. In the following phase of pre-crash vehicle kinematics (PCVK), the maneuver from the CA-CAE pre-crash simulation is given as prescribed motion to the sled. In this study, the PCVK includes three degrees of freedom (DOF): longitudinal and lateral acceleration of the vehicle as well as yaw velocity. The PCVK phase has a duration of 1000 ms when included. In the last phase of the sequence, a crash pulse lasting 200 ms recorded from the FE structural crash simulation, see element 6 in Figure 1, is applied to the rigid sled model using a complete 6 DOF description, i.e. accelerations in all three local directions as well as rotational velocities around the same axes. The SAFER HBM model was used to estimate driver kinematics during the PCVK and the crash.

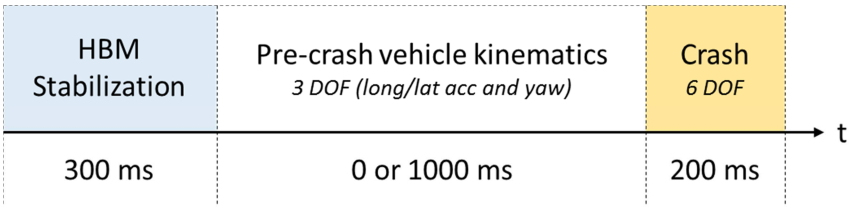

Figure 3. Overview of simulation sequence for pre-crash and crash.

Volvo Parametric Crash Configuration – VPARCC (element 3)

In order to describe and store the states at crash initiation regarding positions, orientations and velocities, the Volvo parametric crash configuration (abbreviated VPARCC) is proposed. In this approach, the first point of contact (FPOC) between two colliding objects is used (for visualization, two identical passenger cars are used here). This part of the crash configuration is to be interpreted as a birds-eye view of the physical appearance of the two objects when first contact occurs. In this definition, the host vehicle serves as the reference system according to SAE [21], where the FPOC is described. Furthermore, the heading direction is defined to coincide with the longitudinal axis of each vehicle, even though in the generalized case the velocity vector at the time of collision may differ from the heading direction in the crash configuration. By utilizing the host center point (HCPO), a counter-clockwise angle around HCPO between the host center plane (HCPL) and the FPOC can be defined as the original host collision point angle (called $HCPA_0$) as illustrated in Figure 4.

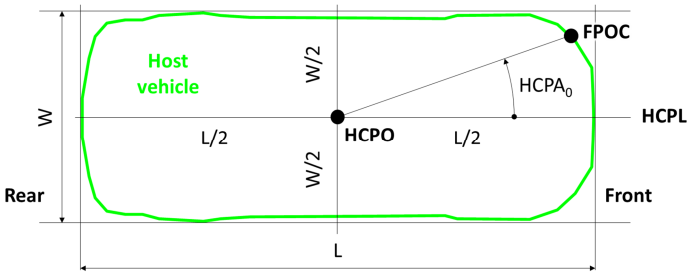

Figure 4. Definition of VPARCC angles in host vehicle

In the same way, the location of the FPOC on the opponent vehicle is defined as the original opponent collision point angle (called $OCPA_0$) using the local reference system of the opponent vehicle. By using a third angle in the horizontal plane, the heading direction of the opponent vehicle is defined relative to the heading direction of the host vehicle. This angle is called the opponent yaw angle (OYA) as indicated in Figure 5.

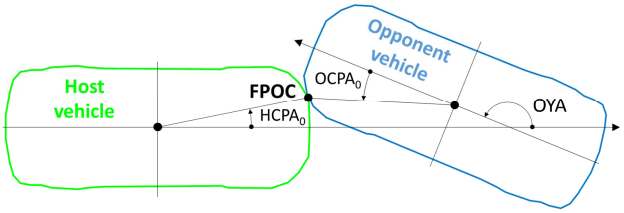

Figure 5. Definition of VPARCC angles in host and opponent vehicle

By using the definitions above, the description of the FPOC in terms of $HCPA_0$ and $OCPA_0$ will be dependent on the vehicle width-to-length ratio. However, a more universal way of describing the angles is sought, therefore the vehicle dimensions including the FPOC are scaled to a square unit car as described in Figure 6. In this way, a transformed host collision point angle (HCPA) is defined for further use. The same procedure is applied to obtain the transformed opponent collision point angle (OCPA).

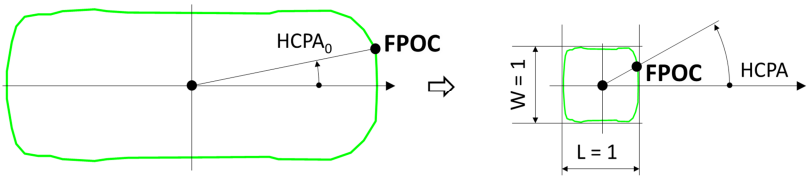

Figure 6. Description of transformation from actual appearance to square unit car system.

The proposed method for describing crash configuration can be used as a tool for visualizing larger sets of crash configuration data to be considered in development of safety systems. In Figure 7, three examples of car-to-car collisions are used to explain how a crash configuration diagram can be created. Figure 7 shows how the transformed host and opponent collision point angles HCPA and OCPA combined with the opponent yaw angle OYA for the impact direction gives a graphic illustration of each crash configuration directly in the diagram. By using a variety of vehicle types, it was seen that their shape generally has a small influence on the crash configuration. However, some crash configurations defined using a rectangular car shape may differ from configurations where a vehicle with rounded corners is used.

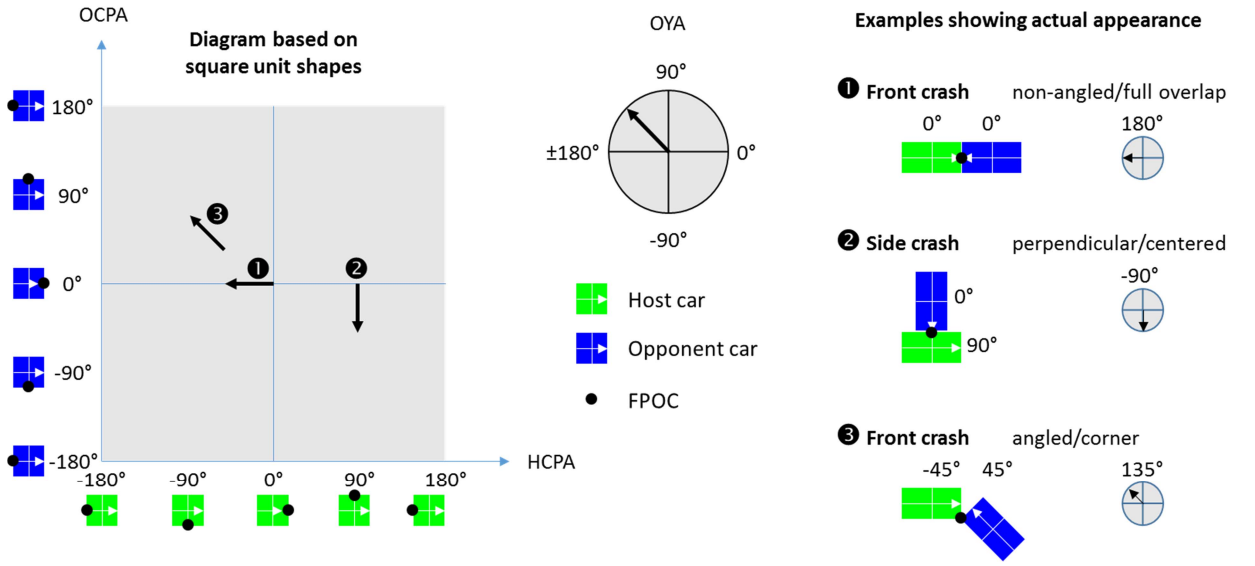

Figure 7. Example of how crash configurations are mapped into a diagram of OCPA vs. HCPA including OYA.

Simplified occupant kinematics model – SOCKIMO (element 4)

As previously stated, pre-crash simulations often consider a large amount of cases, typically more than a thousand for a specific conflict situation. To assess occupant pre-crash kinematics in these large datasets, the need for a computationally efficient model was identified as a tool that at an overall level describes how the pre-crash phase may affect occupant kinematics. In an internal development project it was therefore suggested to describe the upper body of a car occupant as an inverted pendulum constrained in the sagittal plane. This model was used for pure braking scenarios where the effect of AEB interventions could be quantified in terms of occupant pre-crash excursion. In the course of this work, a need for a model useful also in maneuvers including lateral accelerations was identified. This led to the initiation of a master thesis project aiming at describing the occupant as one or more inverted pendula free to move in three dimensions [22]. The studies concluded that a double pendulum model could be employed and using joint stiffness and damping parameters be tuned to fit the response of volunteers.

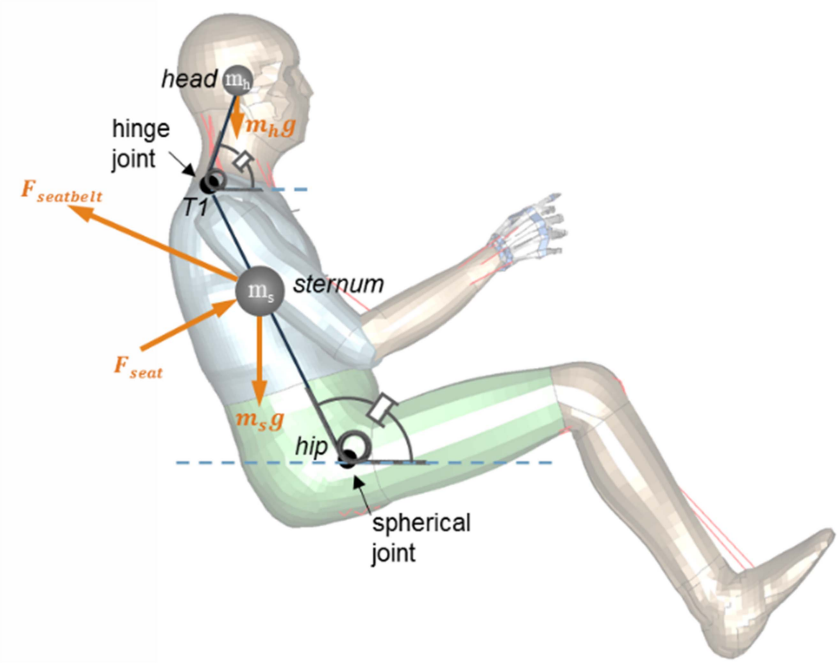

Figure 8. Side view of driver HBM and corresponding simplified mathematical model, from [22].

Figure 8 provides a graphical representation of how the simplified model was implemented. Rigid bodies are assumed between the head center of gravity, first thoracic vertebrae (T1), sternum, and the hip joint. These are positions that were all featured as tracking points in available volunteer data, later used for tuning and validating the model. A lower inverted pendulum was based in the occupant hip joint location and includes a point representing the sternum. At the upper end of the lower pendulum, corresponding to the center of the T1 vertebra, a hinge joint is defined. This hinge joint attaches to the upper pendulum that ends in the head center of gravity. By defining this hinge joint, the upper pendulum is constrained to movement in the plane initially defined by the hip joint, T1 and head center of gravity. Since this plane is updated corresponding to the displacement of the lower pendulum, the head center of gravity is free to move out of the initial sagittal plane.

The seat back was modeled as a contact to prevent the pendula model from tilting rearwards, using contact stiffness based on an FE model representing a typical passenger car seat. Seat belt forces were assumed to be applied in the point representing the sternum on a fixed distance between the hip joint and T1 as illustrated in Figure 8. In both the lower (spherical) joint and the upper (hinge) joint, two parameters were introduced characterizing the stiffness (Nm/rad) and the damping (Nm/rad/s).

In order to find appropriate joint parameters, volunteer tests performed by Chalmers University of Technology [23] were used and the model was tuned accordingly. This process enabled parameter sets representing a range of individual volunteer responses, and the final SOCKIMO included seven different such sets. The tuning process showed that the SOCKIMO can capture not only the magnitude of excursion but also the dynamic response as shown in Figure 9. The combined maneuver for which the model was tuned consisted of steering and braking with maximum accelerations of approximately 0.5 g.

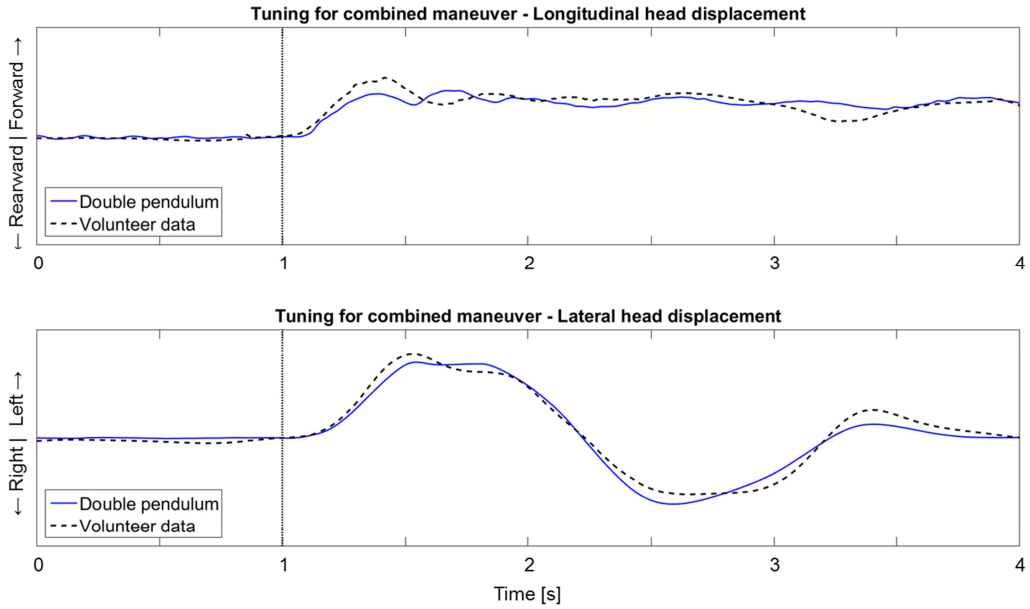

Figure 9. Example of tuned double pendulum model output compared to volunteer data, from [22].

The tuned SOCKIMO was thereafter validated by using a separate data set collected by Graz University data [14] as shown in Figure 10. From these volunteer tests, a corridor representing the and 0.16^{th} and 0.84^{th} quantiles of the response of 25 volunteers was used and compared to the model response.

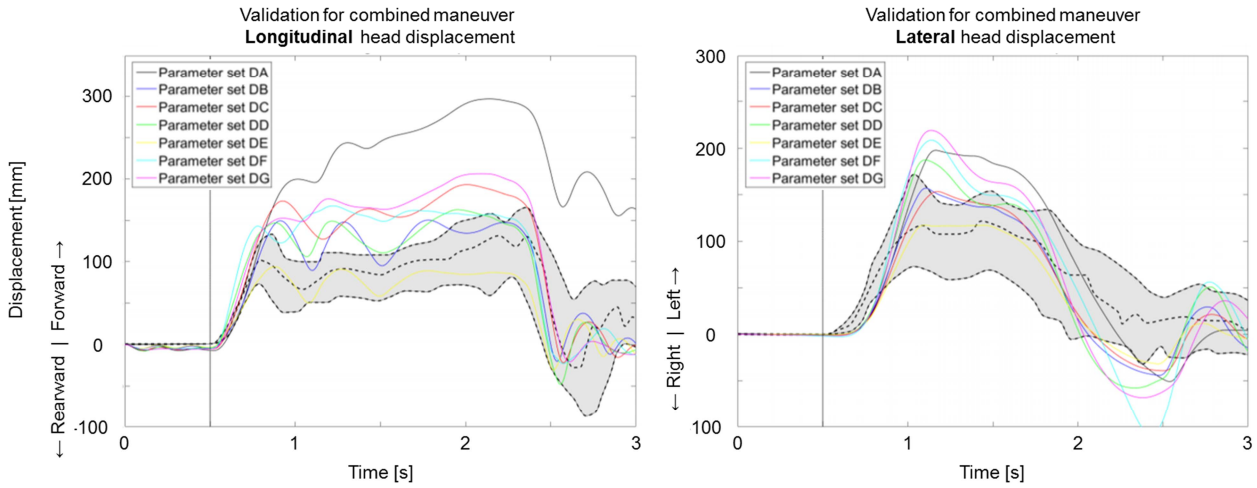

Figure 10. Validation in combined braking and steering maneuver

EXAMPLE CASE

To demonstrate the methodology, an example case was selected from left turn / oncoming direction (LT/OD) conflict situations. These are characterized by the host vehicle turning left in a crossing and is struck by an oncoming vehicle that approaches from the direction opposite to the host vehicle initial direction, i.e. before the turn is initiated.

Case selection (elements 1-6)

In the first stage, the Volvo Cars baseline generation framework was applied. First, crashes in Volvo Cars traffic accident database (VCTAD) were classified and LT/OD crashes were identified. Crash case analysis was performed on the pre-crash phase of each case in detail, and a dataset was generated from all cases. In this dataset, each crash was described numerically in a THd format where each time step, during 15 seconds before the crash or near-crash, depicts the vehicle trajectories, the road environment, the participants and their characteristics. In order to compensate for uncertainties in the data relating to case data quality and contingency of distributions, variations of parameters were implemented as synthetic cases in a THd-batch, comprising in total 940 cases for simulation.

Pre-crash baseline and treatment simulations were performed as a next step. In the baseline setting, all cases resulted in a collision for which the host vehicle impact speed ranged from 4 to 30 km/h, and the opponent vehicle speed ranged from 4 to 131 km/h. By using a conceptual AEB system, a portion of the cases were completely avoided and in another portion there was no effect of the AEB system. In a third portion, mitigation of the crash was achieved by the AEB system. All remaining crashes were analyzed in further detail utilizing the crash configuration depicting method VPARCC and the SOCKIMO, and typical situations were identified for the case study.

The SOCKIMO was used to identify cases with large occupant pre-crash excursions in combination with a substantial crash severity. The SOCKIMO analysis was made with an average of the seven occupant parameter sets, Figure 10. Initially, a maximum SOCKIMO total head excursion above 150 mm during the complete pre-crash maneuver was used as filtering criterion. An additional filtering criterion was used to find one example case for which a substantial crash severity was present. Since the crash severity in the studied cases is highly governed by the impact speed of the opponent vehicle, cases with an opponent speed above 60 km/h were selected, see four encircled candidate cases in Figure 11. A case with a crash configuration notably modified by the AEB intervention was selected, resulting in the example case described in Table 1. Both baseline and treatment cases included a maximum vehicle lateral acceleration of 1.5 m/s² and maximum yaw velocity of 21 deg/s.

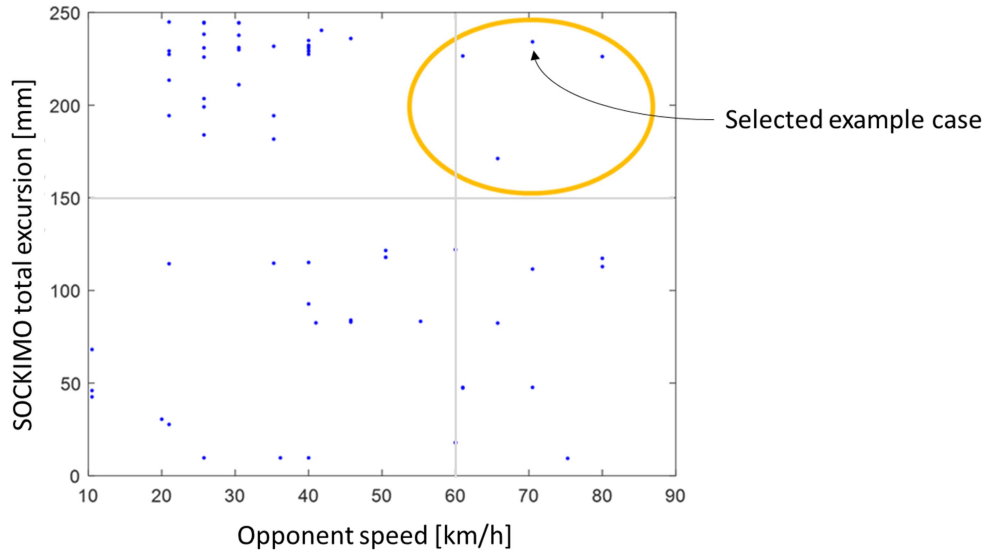

Figure 11. SOCKIMO max head excursion (mean of 7 occupant parameter settings, mm) vs. opponent speed (km/h).

Table 1. Example case crash configurations and AEB description for Baseline and Treatment, respectively.

	Crash configuration						Pre-crash intervention
	Appearance	Host speed (green)	Opponent speed (blue)	OYA	HCPA	OCPA	
Baseline	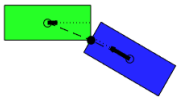	15 km/h	70 km/h	150°	-45°	11°	None
Treatment	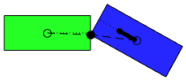	~0 km/h	70 km/h	151°	-6°	45°	AEB: Max longitudinal acceleration 12 m/s²

The selected case was then simulated using the SAFER HBM occupant model positioned in the host vehicle in four different combinations of PCVK and crash pulse as described in Table 2. Simulations BB and TT describe the cases from the CA-CAE tool shown in Table 1, and simulations denoted nB and TB were included in order to study the individual effects of PCVK and crash pulse, respectively. The FE structural crash simulations were performed using two identical mid-size passenger cars to provide the crash pulse needed for the FE A-HBM occupant simulation.

Table 2. Overview of simulations

Simulation code	PCVK	Crash pulse
nB	(none)	Baseline
BB	Baseline	Baseline
TT	Treatment	Treatment
TB	Treatment	Baseline

Output from FE A-HBM occupant simulation – element 7

A clear effect from the pre-crash maneuver as well as crash configuration on driver head trajectory in a vehicle-fixed coordinate system could be seen, Figure 12. The measured effect of the Baseline PCVK is a maximum excursion of 28 mm forward (x) and 44 mm to the right (y). The Treatment PCVK results in a maximum excursion 148 mm forward (x) and 46 mm to the right (y). However, the Treatment PCVK final position is 30 mm rearward (x) and 36 mm to the left (Y) of the origin. A more detailed illustration of the occupant pre-crash kinematic response in the four simulations can be found in Appendix 1.

By further analyzing the head center of gravity trajectories in Figure 12 during the crash phase, it was found that the effect of introducing the Treatment crash had a considerable effect. The Baseline crash pulse introduced a substantial lateral component to the crash pulse, which leads to occupant excursion that has approximately the same magnitude to the right as forward. In the Treatment crash (see Table 1), the opponent vehicle overlaps the host vehicle to a lesser extent, thereby reducing the lateral acceleration component of the host vehicle during the crash phase. The Treatment crash pulse leads to an occupant excursion with low deviation from the vehicle longitudinal direction and increases the lateral excursion only during rebound. Further details on the occupant kinematic response during crash can be found in Appendix 2.

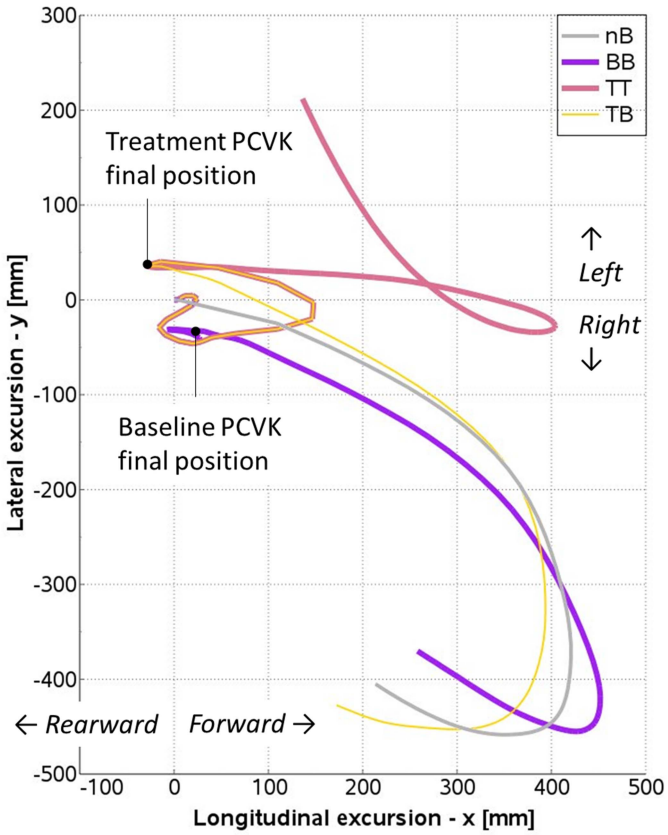

Figure 12. Complete sequence trajectories of SAFER HBM driver head center of gravity, vehicle-fixed coordinate system.

When comparing the three simulations where the Baseline crash pulse was used (nB, BB and TB), it was found that although the initial positions for the crash phase differed, the head trajectory during crash was similar. The maximum lateral head displacement in simulations nB, BB and TB was approximately the same at 450-460 mm. The TB simulation results however suggested that an outboard/rearward initial crash position (i.e. to the left of and behind the origin) led to a longer duration of the interaction with the driver airbag reducing the maximum forward displacement compared to nominal position in the nB simulation. In contrast, the BB simulation results suggested a shorter airbag interaction duration, which was associated with a larger maximum forward displacement.

DISCUSSION

This study aims to describe a CAE methodology that allows for estimation of the combined safety effects from collision avoidance and injury prevention systems. In a demonstration case, combinations of pre-crash maneuver and subsequent crash was presented as an example of the feasibility of the method. The present methodology constitutes a framework for dealing with the large data sets that can be generated through CAE pre-crash simulations of collision avoidance technologies applied to real-world traffic situations. A crash configuration definition for setting up crash simulations or physical crash tests was introduced and a simplified occupant kinematic model for filtering out cases for detailed analysis was presented.

All elements of the methodology are subject to further refinement, for instance the vehicle dynamics model in the pre-crash CAE tool may need further details when studying avoidance maneuvers with significant three-dimensional effects. In this initial study, the SOCKIMO provided an indication of large occupant pre-crash excursion that was also reflected when using the SAFER HBM. For future analyses, the SOCKIMO may need to be further refined along with the interpretation of its output. For some traffic situations, a human body model with more details than the SOCKIMO but not as detailed as an FE HBM may be desirable.

In this study, cases were filtered out when the largest SOCKIMO excursion exceeded 150 mm, regardless when this maximum excursion occurred during the pre-crash maneuver. The excursion at the time of crash initiation may prove to be a better metric for occupant pre-positioning relevant for injury prediction. On the other hand, once a large occupant excursion has occurred, this could be associated with non-linear effects that the SOCKIMO is not able to capture. Such an example could be seat belt interaction where the effect on occupant kinematics could be studied in a more realistic way using the A-HBM, for which also the effect of electrical reversible retractors (ERR) can be studied. There is a risk that the SOCKIMO will point out cases where the occupant excursion is not a problem in terms of predicted injury risk during the crash phase. This depends on the combination of pre-crash maneuver and type of crash. For some crashes, certain pre-crash maneuvers may actually be beneficial for improving the occupant interaction with the restraint system, in some cases unfavorable. Another factor that influences the occupant pre-crash excursion is whether the arms are used for bracing against the steering wheel or other vehicle interior components. In the current implementation, the SOCKIMO is tuned for front seat passengers for which no bracing is present, while the SAFER HBM was run as a driver with hands on the steering wheel and active arm muscles simulating this bracing. This could be one reason why the SOCKIMO head excursion exceeds that of the driver A-HBM. (SOCKIMO ca 230 mm in Figure 11 vs A-HBM approximately 150 mm, Figure 12). An additional reason for this may be found when observing validation data suggesting that several of the seven parameter sets of the SOCKIMO lead to pre-crash motions larger than the volunteer corridors as shown in Figure 10. Occupant excursion as predicted by the SOCKIMO may not be accurate as a prediction of actual occupant excursion but rather as an indicator when comparing sets of pre-crash vehicle kinematic data.

The crash simulation phase in this study was performed using a rigid sled, i.e. assuming no compartment intrusion. Although modern passenger cars often exhibit minimal intrusion, there are and will still be situations where this is not the case. Typically, this assumption could not be made when intrusion occurs in the direct surrounding of the occupant such as in side impacts. In such cases, a deformable sled where intrusions are recorded from full-scale structural FE crash simulations and then applied to the virtual sled with the A-HBM may be useful. Alternatively, the A-HBM can be placed directly in the full-scale model, however this approach is currently judged as unfeasible due to the large simulation effort that would further limit the number of studied cases.

The proposed crash configuration method VPARCC was shown to be sensitive to changes based on pre-crash AEB interventions. Although the provided example case displayed large differences in terms of VPARCC parameters and subsequently significantly different resulting crash pulses, the methodology is detailed enough to describe also subtle geometrical changes in crash configuration not captured in established methods using e.g. CDC [8]. VPARCC was demonstrated in car-to-car crash situations, however it can also be applied to collision objects such as trucks or vulnerable road users. In order for the method to remain generic, the shape of the traffic objects should be defined in such a way that only one point is intersected at a time when a vector is swept the full 360 degrees around the object center as described in the crash configuration section.

The approach in the presented methodology would not be possible using simplified occupant models only since these lack details needed for in-depth analysis of the interaction between the occupant and vehicle interior. In contrast, using only detailed models would lead to a limited ability to cover a wide range of traffic situations due to the great simulation effort associated with FE HBMs. Further methodology validation should be conducted and usage expanded to other combinations of pre-crash maneuvers and crashes.

CONCLUSIONS

A methodology for predicting the performance of safety systems with a combined effect from collision avoidance and injury prevention features was presented. In this process, methods for describing crash configurations was introduced. This method supports detailed descriptions of crashes and is sensitive to changes in configurations based on pre-crash maneuvers. Further, a simplified occupant kinematics model (SOCKIMO) was introduced as a tool for filtering out cases where considerable occupant pre-crash excursion can be suspected to occur. The feasibility of the individual elements of this methodology to function together was demonstrated in an example case where autonomous emergency braking led to a considerable change in the crash configuration and was predicted to introduce substantial occupant pre-crash excursion. In addition, in this example case it was shown that the present A-HBM tool is able to cover the complete sequence of events from pre-crash maneuvers to crash in one single simulation, thereby demonstrating how the tool chain efficiently contributes to evaluating the injury prevention effects from both pre-crash and crash countermeasures in the vehicle.

ACKNOWLEDGEMENTS

This work has been carried out with contributions from FFI-Strategic Vehicle Research and Innovation, by Vinnova, the Swedish Energy Agency, the Swedish Transport Administration and the Swedish vehicle industry.

The authors wish to express their gratitude to Oscar Laudon (formerly Cyrén) and Sofia Johansson for their work on the SOCKIMO in their master thesis project during spring of 2018.

The FE human body model used in this study is a result of collaborative research efforts at SAFER – Vehicle and Traffic Safety Centre at Chalmers, Sweden. The authors would like to acknowledge our research partners, especially Chalmers University of Technology, Autoliv, AB Volvo and KTH (Royal University of Technology).

REFERENCES

[1] World Health Organization, (2018), Global Status Report on Road Safety 2018. ISBN 978-92-4-156568-4.

[2] ITF (2016), Zero Road Deaths and Serious Injuries: Leading a Paradigm Shift to a Safe System, OECD Publishing, Paris.

[3] European Commission, Annual Accident Report, (2018, June). https://ec.europa.eu/transport/road_safety/sites/roadsafety/files/pdf/statistics/dacota/asr2018.pdf.

[4] National Center for Statistics and Analysis. (2018, October), Early estimate of motor vehicle traffic fatalities for the first half (Jan–Jun) of 2018 (Crash Stats Brief Statistical Summary. Report No. DOT HS 812 629). Washington, DC: National Highway Traffic Safety Administration.

[5] Lindman M, et al. (2010), Benefit estimation model for pedestrian auto brake functionality. ESAR conference 2010.

[6] Korner, J. (1989). A method for evaluating occupant protection by correlating accident data with laboratory test data (No. 890747). SAE Technical Paper.

[7] Lindman, M. and Tivesten, E. (2006), A method for estimating the benefit of autonomous braking systems using traffic accident data. SAE 2006-01-0473.

[8] Society of Automotive Engineers (1980), Collision Deformation Classification: Recommended Practice Document SAE J224 MAR80.

[9] Reed, M, et al. (2018), Passenger head kinematics in abrupt braking and lane change events. Traffic injury prevention, 1-8.

[10] Ejima S, et al. (2008), Prediction of the Physical Motion of the Human Body based on Muscle Activity during Pre-Impact Braking. Proceedings of the IRCOBI Conference; Bern, Switzerland.

[11] Matsuda T et al. (2018), Simulation of Occupant Posture Changes due to Evasive Manoeuvres and Injury Predictions in Vehicle Frontal and Side Collisions. IRCOBI 18-81.

[12] Östh J et al. (2015), Muscle activation strategies in human body models for the development of integrated safety, 24th Int. ESV Conf., Paper no. 15-0345, Gothenburg, Sweden.

[13] Östmann, M. and Jakobsson, L. (2016), An Examination of Pre-crash Braking Influence on Occupant Crash Response using an Active Human Body Model. In Proc. IRCOBI.

[14] Huber, P., et al. (2015), Passenger kinematics in braking, lane change and oblique driving maneuvers. In Proceedings of IRCOBI Conference, Sept 9-11 2015, Lyon, France.

[15] Kleiven S (2007), Predictors for traumatic brain injuries evaluated through accident reconstructions. Stapp Car Crash Journal 51.

[16] Choi H-Y, Kwak D-S (2011), Morphologic Characteristics of Korean Elderly Rib. Journal of Automotive Safety Engineering 2.

[17] Shi X, Cao L, Reed MP, Rupp JD, Hoff CN, Hu J (2014), A Statistical Human Rib Cage Geometry Model Accounting for Variations by Age, Sex, Stature and Body Mass Index. Journal of Biomechanics 47(10):227–2285.

[18] Mattucci, SFE and Cronin, DS (2015), "A method to characterize average cervical spine ligament response based on raw data sets for implementation into injury biomechanics models." Journal of the mechanical behavior of biomedical materials 41 (2015): 251-260.

[19] Östh J., et al. (2015), A Human Body Model With Active Muscles for Simulation of Pretensioned Restraints in Autonomous Braking Interventions. Traffic Injury Prevention 16(3): 304–313.

[20] Ólafsdóttir JM (2017), Muscle Responses In Dynamic Events. Volunteer Experiments and Numerical Modelling for the Advancement of Human Body Models for Vehicle Safety Assessment. PhD Thesis, Chalmers University of Technology, Gothenburg, Sweden.

[21] Society of Automotive Engineers (2008), Vehicle Dynamics Terminology, Document SAE J670, JAN2008.

[22] Cyrén, O. and Johansson, S. (2018), Modeling of Occupant Kinematic Response in Pre-crash Maneuvers A simplified human 3D-model for simulation of occupant kinematics in maneuvers - A simplified human 3D-model for simulation of occupant kinematics in maneuvers. Göteborg: Chalmers University of Technology (Master's thesis - Department of Mechanics and Maritime Sciences, no. 2018:57).

[23] Ghaffari, G., et al. (2018), Passenger kinematics in Lane change and Lane change with Braking Manoeuvres using two belt configurations: standard and reversible pre-pretensioner. In Proceedings of the 2018 International IRCOBI Conference on the Biomechanics of Impact, September 12-14, Athens, Greece.

APPENDIX 1

Occupant response in example case during pre-crash maneuver.
Head center of gravity described by red marker and trajectory by thick black line.

From left: Simulations BB / TT / TB (grid size = 100 mm)

APPENDIX 2

Occupant response in example case during oblique crash.
Head center of gravity described by red marker and trajectory by thick black line.

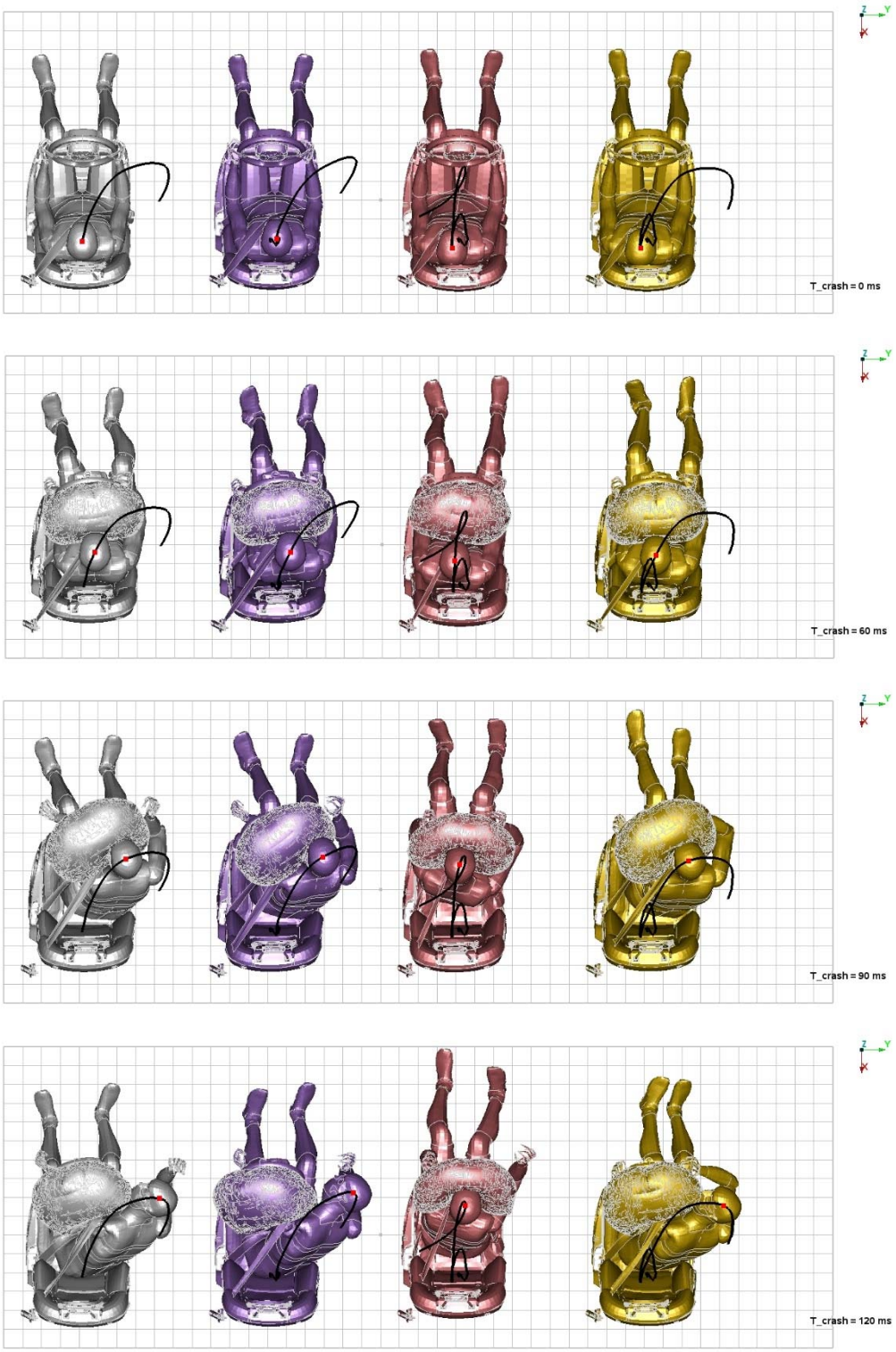

From left: Simulations nB / BB / TT / TB (grid size = 100 mm)

50 years of Mercedes-Benz Accident Research - ready for the next level

Authors: Heiko Buerkle, Jochen Feese
Daimler AG, Sindelfingen, January 2019

Paper ID: 19-0178

Abstract
Mercedes-Benz accident research has been working on product safety for 50 years. The idea to own an accident research investigation center was conceived due to the fact that in 1960s the number of accidents were increasing. The focus was on self-investigated accidents and affiliated data.
In 1969, the Ministry of the Interior provided the mandate for the legitimacy of such accident investigation. Under this mandate, in certain circumstances, the authorized police officials were entitled to report serious accidents involving current Mercedes-Benz vehicles to the accident research center and provide collected data.
One of the first investigated vehicles was a W113, so called Pagode. Required investigation methods were developed immediately. The goal of in-depth investigation was to identify the contributing factors for accidents and injuries and derive possible requirements for research and development. Until 2018, more than 5000 accidents were investigated and reconstructed. Today, some of the major tasks of the accident research are accident-data-analyses and the benefit estimation for future safety systems and innovations.
Accident investigation and reconstruction has changed significantly during the years. Measuring lanes and traces with a tape measure, like it was done in the past, isn't possible anymore due to more traffic on the roads. A modern 3D-laser scanner is being used for this purpose today.
Not only investigating the accident scene has changed, the vehicles themselves have changed significantly. Today, accident research aims at assessing the impact of modern advanced driver assistance systems along with investigating the crash worthiness. Therefore, interpreting all system functions is a new and important task. Modern accident reconstruction software applications can visualize the accident sequence, which can also help to relate the restraint system deployments.
This paper will be discussing the progress of available methods and introduce new approaches for future automated driving applications in road vehicles.
50 years of accident research = 50 years of improvements

Introduction

On a cold, gray winter's day in January 1969, government officials and senior police officers from Baden-Württemberg met up with representatives of the then Daimler-Benz AG for several hours of talks at the state's Interior Ministry. The agenda contained an unusual request added by the automotive company- an appeal for police assistance in reconstructing and analyzing road-traffic accidents involving Mercedes models.
The idea of the development engineers was to use data from real world accidents in order to enhance vehicle-occupant safety. Daimler-Benz had already acquired initial experience in this field during a six-month pilot project held two years previously. During the period January- June 1967, company employees had worked together with police on

the investigation of serious road-traffic accidents that had occurred in the district of Böblingen and on the A8 highway.
The prime aim of the meeting at the Ministry was to place this research project on a broader and most important of all, permanent footing. The reaction was positive, and senior police officers once again signaled a readiness to cooperate. Therefore a communiqué, which was requesting for support, was dispatched to the various departments. The Accident Research Project was officially launched on April 29, 1969, after which the Interior Ministry issued a directive to all the relevant police departments. This directive was telling the police departments to inform Daimler-Benz by telephone of any road-traffic accidents, as well as to allow company representatives to inspect the accident report and question the duty officers on the actual sequence of events. The justification for this measure was as follows: "The Interior Ministry supports the research of Daimler-Benz AG because of its general impact for road safety."
Thanks to successful cooperation with the authorities and the police, the area covered by the Mercedes accident research has been expanded several times over the following years. Today, it stretches from Baden-Baden to Ulm, from Mannheim to Konstanz, and from Tauberbischofsheim to Lindau- almost 200 kilometers across at its widest point.
One of the first investigated vehicles was a W113, so called Pagode.

Mercedes accident researcher in the 1969 till today

Accident researchers on call
50 years of accident research at Mercedes translates into 50 years of meticulous data acquisition and detailed analyses. Today, researchers are called out over 100 times a year to carry out first-hand inspection of serious crashes. Since being set up, Mercedes Accident Research has investigated and reconstructed more than 5,000 traffic accidents.

Examples of investigated Mercedes-Benz models in the 60s/70s

At the accident scene, work generally begins with a set of basic questions: How did the accident happen? What was the position of the vehicles after collision? Are there any traces or skid marks? Today researchers usually use a 3D-laser-scanner to scan the accident scene with all the marks and three-dimensional information of the landscape. During the investigation of the involved Mercedes-Benz vehicle, the researchers ask themselves some questions. How did the crumple zone perform? Is there any deformation of the passenger cell? Were airbags and seatbelt tensioners activated? Is there anything unusual about the interior of the crashed Mercedes model? Were the occupants injured- and if so, what were their injuries? These are some examples of the manifold questions.

The answers to all these questions and additional information is ultimately recorded in a database with more than 1,200 parameters per case. This database also includes dozens of photos, sketches and eye-witness accounts. Once the relevant information has been collected, researchers can systematically reconstruct the actual collision. Assistance is delivered by a computer system that converts the data and 3D-laser-scans gathered at the accident scene for visualization. The researcher is able to reconstruct the actual sequence of events for example by combining the length of traces or skid marks with design data and information on the handling behavior of the damaged Mercedes model. Researchers can then view onscreen how the vehicle moved before, during and after the collision. Furthermore, the computer simulation provides views of the accident scene from different perspectives.
The results are then compared with data from other accidents, thus enabling automotive engineers to gradually compile an exact picture of the typical injuries involved, and acquire the knowledge needed to develop new and even more effective safety systems. Furthermore, the findings of Mercedes Accident Research show the engineers that the brand's longstanding and uncompromising stance on safety is already paying dividends. The analyses of traffic accidents shows, that the risk of being injured when traveling in a Mercedes has been consistently declining for many years now.

Accident researcher when collecting data 1970 and 2018 with the tablet-PC

Technological edge through research

50 years of accident research at Mercedes-Benz have played a major role in preserving the brand's technological edge over rival automakers. That's because engineers are quick to apply this knowledge in a practical manner. Over the years, the findings of such research have repeatedly provided the basis for the development of new and pioneering safety systems:

Interior design

At the end of the 1960s, when Mercedes-Benz first began systematic accident analysis, experts initially focused on improving protection inside the passenger compartment. Although Mercedes models were already then fitted with seatbelts, very few people actually used them. For many front-seat passengers, this carefree attitude led to serious head injuries, resulting from an impact with the steering wheel, instrument panel or windshield. Accident researchers therefore set about identifying dangerous impact points inside the vehicle and suggested improvements to the design of various switches and handles responsible for severe injuries. Likewise, the instrument panel and interior trim materials were also reconsidered with safety in mind. Since then, design engineers have favored energy-absorbing materials.

Some examples of interior improvement in the 90s

Test procedures and body structure

Once the interior had been made safer, the attention of accident researchers and engineers turned toward improving the body structure. Once again, this was the consequence from initial accident analyses.

When reconstructing typical collisions with oncoming traffic, accident researchers quickly realized that vehicles usually hit one another asymmetrically. The result for the front part of the body is that one side is more heavily impacted than the other. Experts describe this type of crash as an offset collision. In around half of all so-called head-on collisions on German roads, the impact actually affects only 30 to 50 percent of the left-hand side of the vehicle front. In a further 25 percent of such collisions, the impact occurs on the passenger side of the vehicle front.

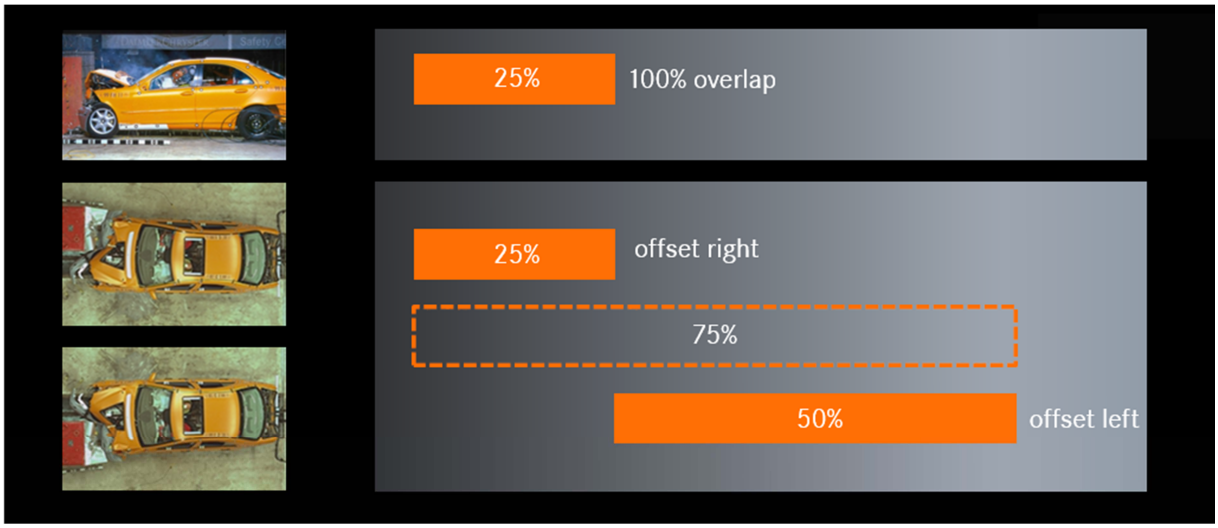

Distribution of frontal collisions (results from the early 90s), 75% of all crashes are offset collisions

This discovery had major consequences for automotive design. Given that a full front-end collision against a flat wall was legally required as a safety test for passenger cars, but only represented a fraction of real world accidents, Mercedes-Benz decided to go further. On the basis of results from the company's own accident research, engineers introduced the first offset crash tests as early as 1974 and went on to develop a design principle that provides high occupant safety even when the vehicle front is subject to extreme partial loads. The solution was realized in form of forked members- rigid longitudinal sections on both sides of the front part of the body structure. Each of these forks in the front of the front wall and toward the side skirts and the drive shaft hump. These cause the force of impact from a collision to spread equally between the hump, floor and side panel, with the result that the passenger compartment remains largely undamaged. The S-class sedans of the W 126 series, as launched in 1979, were the first Mercedes models to feature forked members designed specifically to protect against offset front-end collisions. Today, a new design principle provides an even more effective protection for vehicle occupants- not only in the event of an offset crash.

Mercedes-Benz S-class W 126

Years of continuous accident observation later revealed the need for a further modification of the test procedure, whereupon Mercedes-Benz developed the offset crash test against a deformable barrier. In this test an aluminum structure serves to replicate the crash crumple zone of the opposing vehicle, thereby enabling a more realistic analysis of how the body deforms during impact than is the case with a collision against a rigid concrete or steel barrier. Jointly developed by Mercedes-Benz, the crash test with a deformable barrier is now part of Euro NCAP (New Car Assessment Program) and, as such, compulsory for all new passenger cars in Europe.

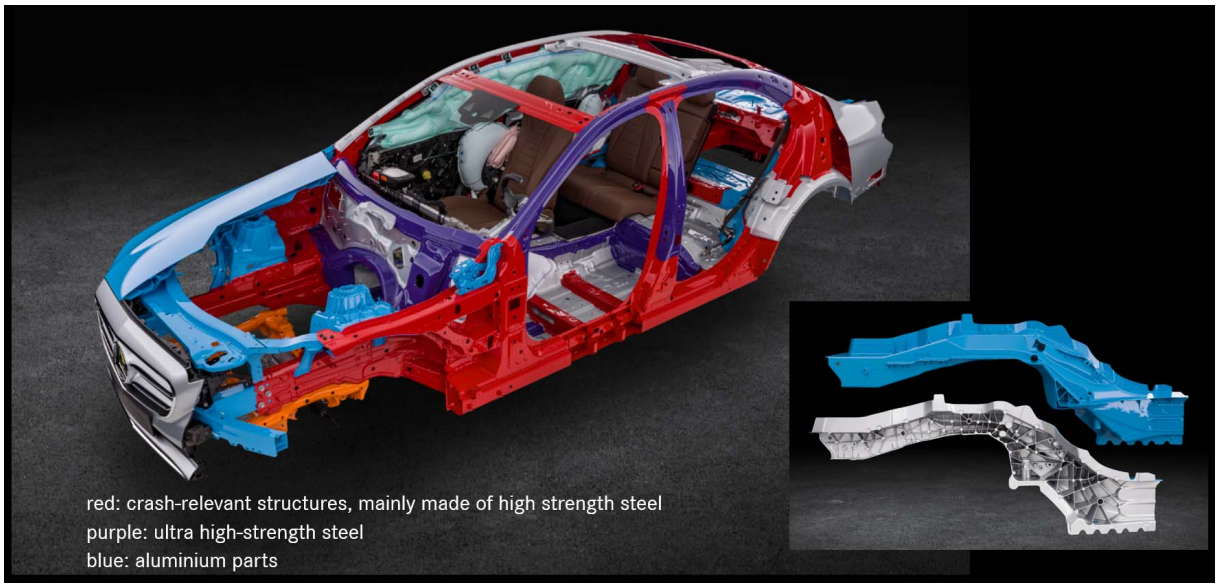

Body in white and restraint systems of a current E-class W213-2018

Seatbelts

Further analysis of real world accidents in the 1970s and '80s led to the development of additional pioneering safety features. The most important of these was the three-point seatbelt, which was first introduced by Mercedes-Benz in 1968 and, along with headrests for the driver and front-seat passenger, became standard equipment in all the brand's models in 1973. The seatbelt remains the most important element of occupant safety and has saved hundreds of thousands of drivers and passengers from death or serious injury over the years.

Once again, however, accident research showed Mercedes engineers that there was still space for improvements. This included enhanced seatbelt geometry as well as fixing the lower mounting point to the frame of the seat. This ensures optimal positioning of the

seatbelt irrespective of the seat's position. In 1971, the Mercedes-Benz 280 SL debuted as the world's first car to feature this important safety feature.

Mercedes-Benz 280 SL, 1971

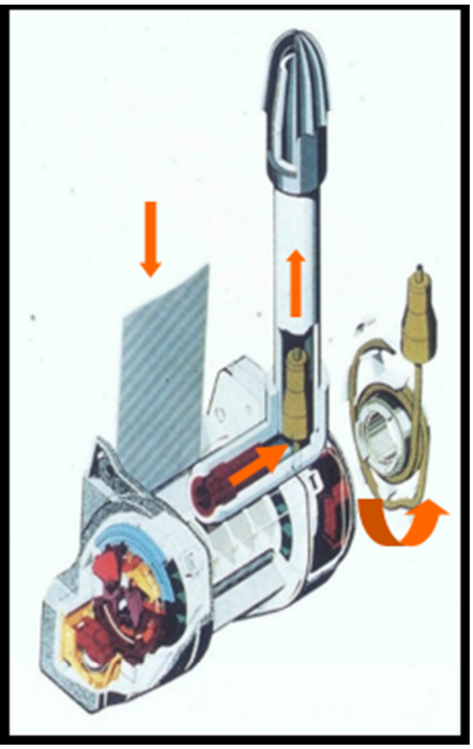

Seatbelt tensioner, 1992

Seatbelt tensioners

It was in the early 1970s that accident researchers first realized that conventional seatbelts were not sufficient to protect vehicle occupants from impact with the steering wheel or instrument panel in the event of a severe front-end collision. The reason for this was the slack in the seatbelt, which results from the design principle of the component, and which Mercedes engineers were able to offset with the invention of the seatbelt tensioner. In the event of a crash, the tensioner tightens the seatbelt in a matter of milliseconds. Development of this practical component began in 1970. After that it was only with subsequent advances in microelectronics, which are required to trigger the mechanism, that the seatbelt tensioner achieved a realistic chance of entering series production. Mercedes-Benz first introduced seatbelt tensioners for the front seats in 1980, and they have been standard equipment in all the brand's passenger car models since 1984.

Today, there is no doubt as to whether this complex development was worthwhile. In the event of a front-end collision, the seatbelt tensioner not only prevents the head and upper body from tilting dangerously forward but also reduces the overall stress load on vehicle occupants.

Front-Airbag

The quality of occupant restraint systems was further enhanced by the development of the airbag- another flash of inspiration on the part of Mercedes engineers and a milestone in safety technology. Development of this pioneering piece of equipment began in 1967. It was patented by Daimler-Benz in October 1971 (DE 2152902 C2) and first introduced into series production at the end of the 1980s, following full 13 years of development and testing. The airbag inflates within milliseconds in the case of a front-end collision to

prevent the driver's head from hitting the steering wheel or instrument panel, thus substantially is reducing the risk of serious injury. Mercedes-Benz has fitted a driver airbag as standard equipment since 1992.
With the launch of the S-class (W220 series) in 1998, Mercedes engineers showed that the airbag can be adapted to deal with different accident situations. The engineers developed an innovative two-phase gas generator that enables the airbag to be inflated in line with the severity of the impact: If the sensor system registers a medium collision, it activates merely the first phase of the gas generator, with the result that the airbag is only partially inflated. If, however, a more severe impact is detected, the first phase is followed by a second phase milliseconds later that further inflates the airbag. This adaptive control system for both the driver and front-seat passenger airbag is today a standard feature of all Mercedes passenger cars.
Mercedes engineers had designed the airbag to supplement the three-point seatbelt. The primary function of which is to provide protection in the event of a front-end collision. Accident research at Mercedes-Benz confirms the wisdom of this approach. Back in the 1970s, around 30 percent of Mercedes car drivers involved in a severe front-end collision suffered life-threatening injuries despite wearing a seatbelt. Today, however, injuries of such a severity are a thing of the past, thanks to the excellent interplay between airbag, seatbelt, seatbelt tensioner and other safety systems.
If these Mercedes accident research results are extrapolated to cover all passenger cars fitted with this technology, it means that the airbag has helped save the lives of more than 2,500 people in Germany alone since 1990. The National Highway Traffic Safety Administration in the United States has ascertained that airbags protect one in three car occupants against serious injury in the event of an accident. Moreover, around one in six drivers and front-seat passengers involved in an accident owe their lives to airbags. Indeed, the airbag has saved the lives of more than 14,200 vehicle occupants in the U.S. since 1987.

Seatbelt force limiters
In the mid-1990s, the analysis of accident reports revealed that standard fitting of airbags and seatbelt tensioners for drivers and front-seat passengers had created scope for further fine-tuning of the restraint system as a whole. In response, Mercedes-Benz developed the seatbelt force limiter, which reduces the restraining force of the seatbelt as soon as vehicle occupants are cushioned by the airbags. This significantly lessens the load on the upper body of front-seat passengers.

Sidebags and windowbags
Mercedes-Benz's longstanding commitment to enhancing occupant safety has had a huge impact: By early 1998, accident researchers were already able to confirm that the risk of suffering life-threatening or fatal injuries in the event of a front-end collision had been substantially reduced over the preceding two decades. Indeed, fatalities among passenger car occupants wearing a seatbelt were almost exclusively limited to extremely severe front-end collisions.
The focus therefore shifted to another type of accident: the side-on collision. The proportion of such collisions among all accidents resulting in serious injury to vehicle occupants had risen continuously since the 1990s. Although only 14 percent in 1985, it had risen to 30 percent by 1995. Similarly, side-on collisions were becoming an increasingly significant cause of fatalities among vehicle occupants: A study by Mercedes Accident Research actually revealed the proportion of all road traffic fatalities involving this type of collision to be 44 percent.

In response to this trend, safety engineers put together a package of measures that included not only stronger door locks and hinges but also special deformable elements and foam padding in the interior trim of vehicle doors. In addition, Mercedes passenger cars were fitted with protective reinforcement in the lower part of the doors. This protection against side impact was further enhanced with the introduction of sidebags in 1995 and windowbags (curtain airbag) in 1998.
The development of the windowbag was based on intensive research at Mercedes-Benz, which had shown that side-on collisions can lead to serious head injuries. Either because occupants are struck by foreign objects entering the vehicle or because the force of the impact causes passenger heads to move outward. A large windowbag, which is inflated along with sidebags and covers the inner surface of the side window, provides effective prevention against this type of injury.

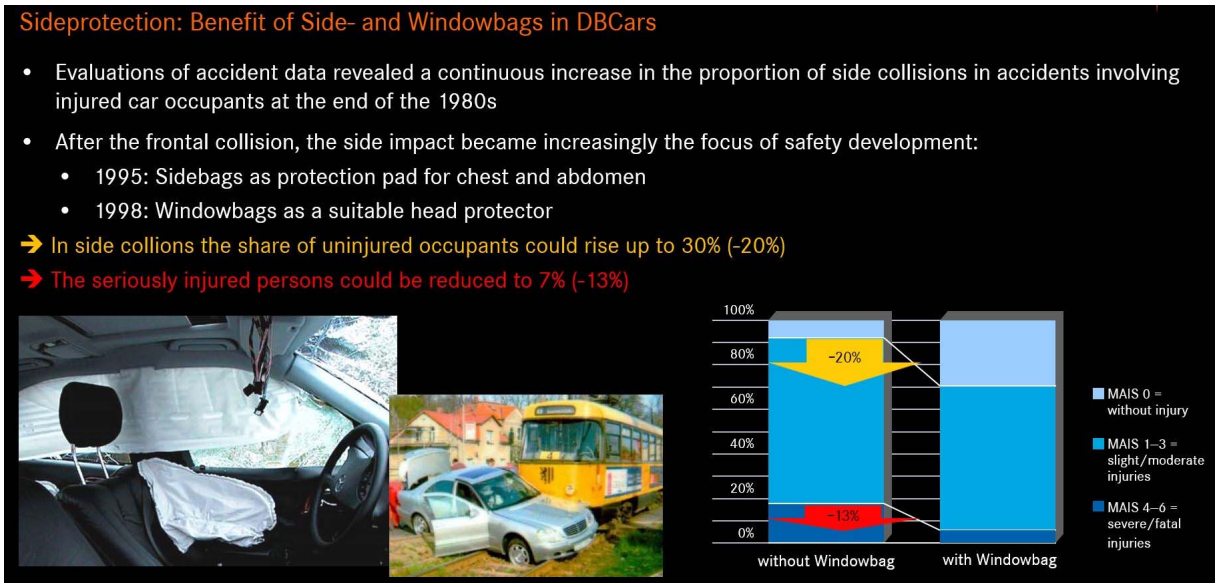

S-class W220 which was hit by a tram (left and middle) and benefit calculation (right)

Mercedes-Benz also developed a similar safety system for its roadsters and convertibles. These models are fitted with special head/thorax sidebags and special headbags to protect the upper body and head of front-seat passengers.

Real world accident, E-class convertible A238 side impact into a tree

Several accidents have shown that there is also a benefit from windowbags in rollovers to protect the occupants. Since 2004, such rollover-sensing sensors are available in many

models. The first model which was standard equipped was the S-Class W221 followed by the E-Class W211.

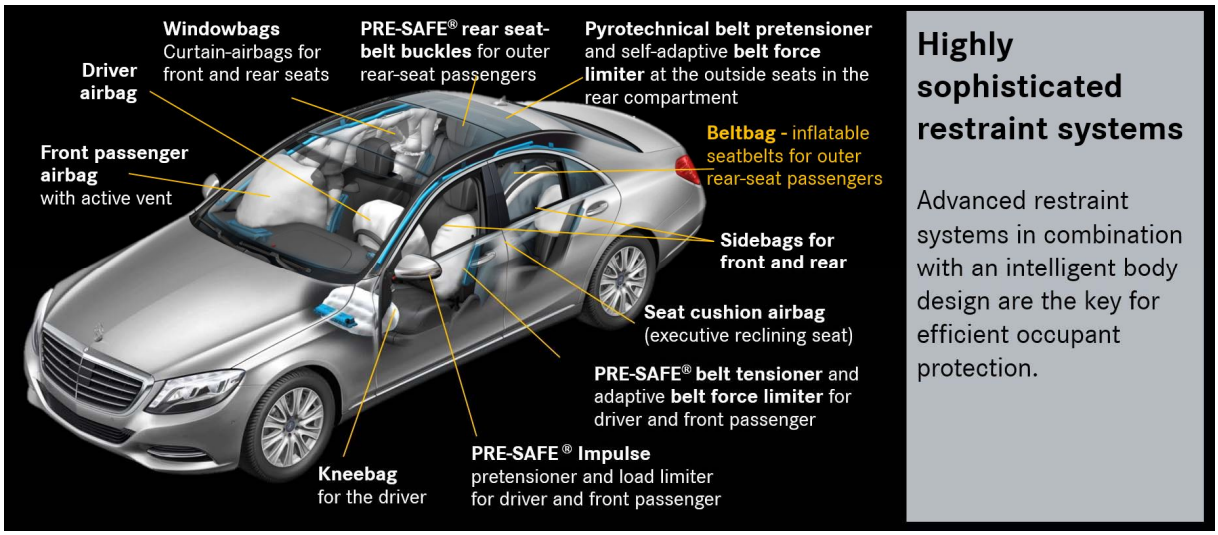

Overview of the current passive safety features in an S-class W222

PRE-SAFE®

Thanks to automatic seatbelts, seatbelt tensioners, airbags and many other innovations, Mercedes models have reached such a high level of safety in recent years that it is hard to find room for significantimprovements using available technology. In other words, new ideas and approaches are required to achieve further advances in occupant safety. Once again, accident research has provided the necessary impetus: Some time ago, experts determined that over two-thirds of all traffic accidents are preceded by a critical driving situation such as skidding, emergency braking, or sudden evasive action- situations that already indicate an imminent collision. In the past, these precious few seconds before the crash could not be utilized for the benefit of passive occupant safety. That's because established protection systems such as seatbelts, airbags and seatbelt tensioners would only engage after impact.

Such insights from accident research led to the development of PRE-SAFE®, an innovative occupant protection system that ushered in a new era in vehicle safety at the end of 2002, and which has since then won a number of awards for Mercedes-Benz. PRE-SAFE® is a preventive system that can anticipate an impending accident and immediately start to prepare the vehicle and its occupants for a possible collision by initiating a precautionary tightening of the seatbelts, for example. It thus makes the best possible use of the brief period before a collision to initiate a variety of preventive safety procedures. A comparison with nature is apt here: PRE-SAFE® gives the car "reflexes." PRE-SAFE® is able to recognize an impending accident because it offers a unique synergy of active and passive safety features. It is connected to the Active Brake Assist and the Electronic Stability Program (ESP®) - standard safety systems which use sensors that can recognize potentially dangerous driving situations and then transmit this information to their control units within milliseconds. Mercedes-Benz also uses this data for the purposes of anticipatory occupant protection, thus creating a new dimension in automotive safety.

PRE-SAFE® has been continuously developed and has now been extended with the functions PRE-SAFE® Sound and PRE-SAFE® Impulse Side, which gives additional safety for the vehicle occupants in real life accidents.

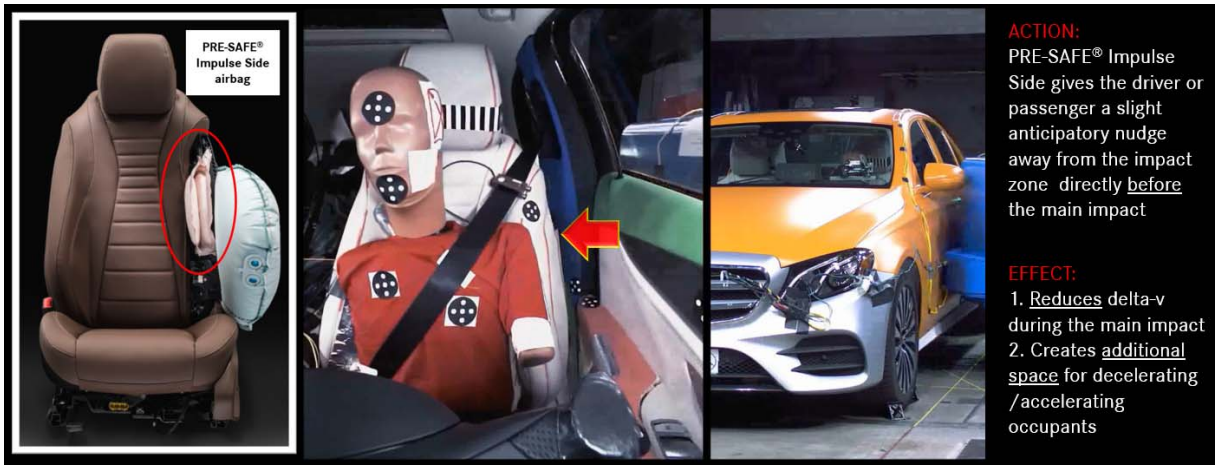

One of the latest PRE-SAFE® functions: PRE-SAFE® Impulse side

Beltbag

The inflatable webbing of the belt, so called beltbag, may reduce the risk of injury to rear passengers in a severe frontal impact by distributing the load on the chest over a larger area. If the crash sensors detect a severe frontal impact, the airbag control unit triggers the deployment of the pyrotechnical seat belt pretensioner along with the beltbag. A gas generator inflates the webbing to almost three times of the width. The larger area of the webbing (contact area) now reduces the pressure on the thorax of the outer rear occupants. This helps to reduce the risk of injury. The system has proved its effectiveness in real world accidents investigated by the Mercedes accident researchers.

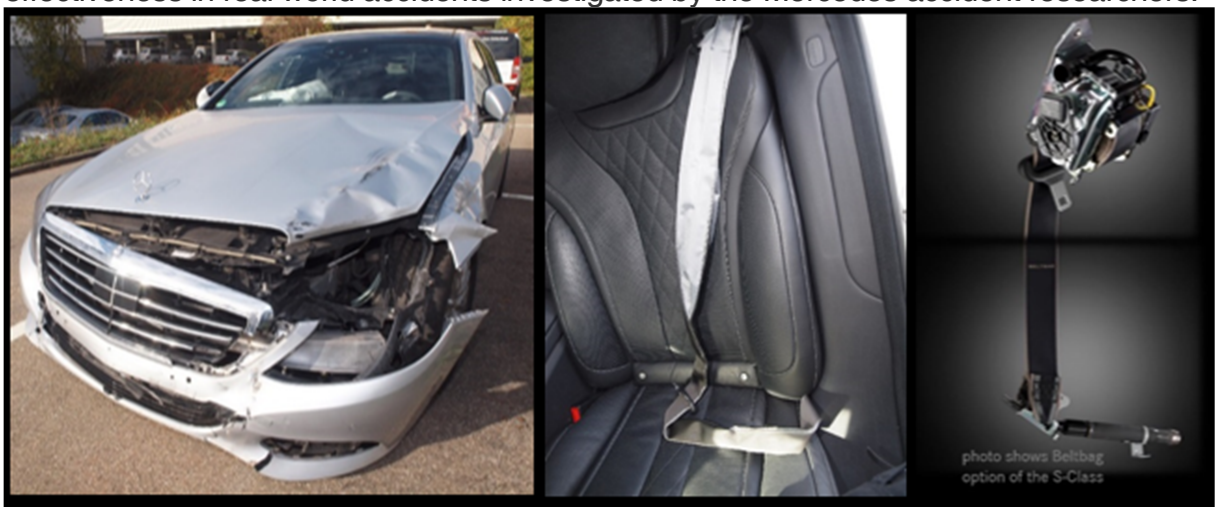

S-class W222 after a frontal collision with beltbag deployment on the left rear seat

Post-Crash functions

Another idea in the 90s was to shut off the motor. No further acceleration due to any issues during and after the crash. After this first Post-Crash function many others were introduced over the years. Only the accident research team is able to validate this functions in the field. An overview of Post-Crash functions in the field is given in the next picture.

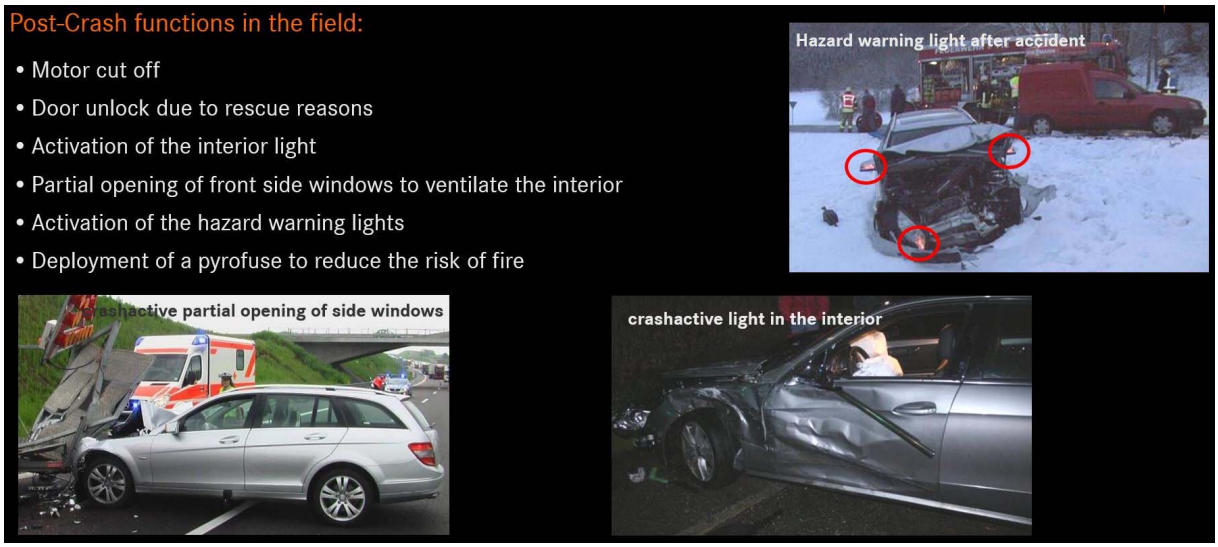

Various functions in different accidents

Investigation Methods

Over the years, the effort of manually creating sketches from the scene was replaced by using a laser scanner and/or satellite-maps with high definition resolution. The more detailed sketches resulting from this method enable more accurate reconstruction and further analyses. This is particularly important for assessing the active safety system functions in the pre-crash phase. Another advantage of the laser scans is the ease of measuring the deformation: the device can overlay the shape of the examined vehicle with the dimensions of a new car and easily determine the deformation.

Using a laser scanner device to investigate the scene requires skilled personnel. Some of the necessary preparation work includes the correct usage of reference points. For that matter, special white and reflecting ball type elements need to be positioned in a way that various scans can be oriented in the post processing phase. At the end, the researcher can decide what type of sketch is most beneficial for his analysis. Either a 3D cloud with all parts of the road and uneven pavement or a simple sketch as a JPG-file for plain sights and easier calculation.

Both methods are used for reconstructions and are more accurate than any handmade sketch.

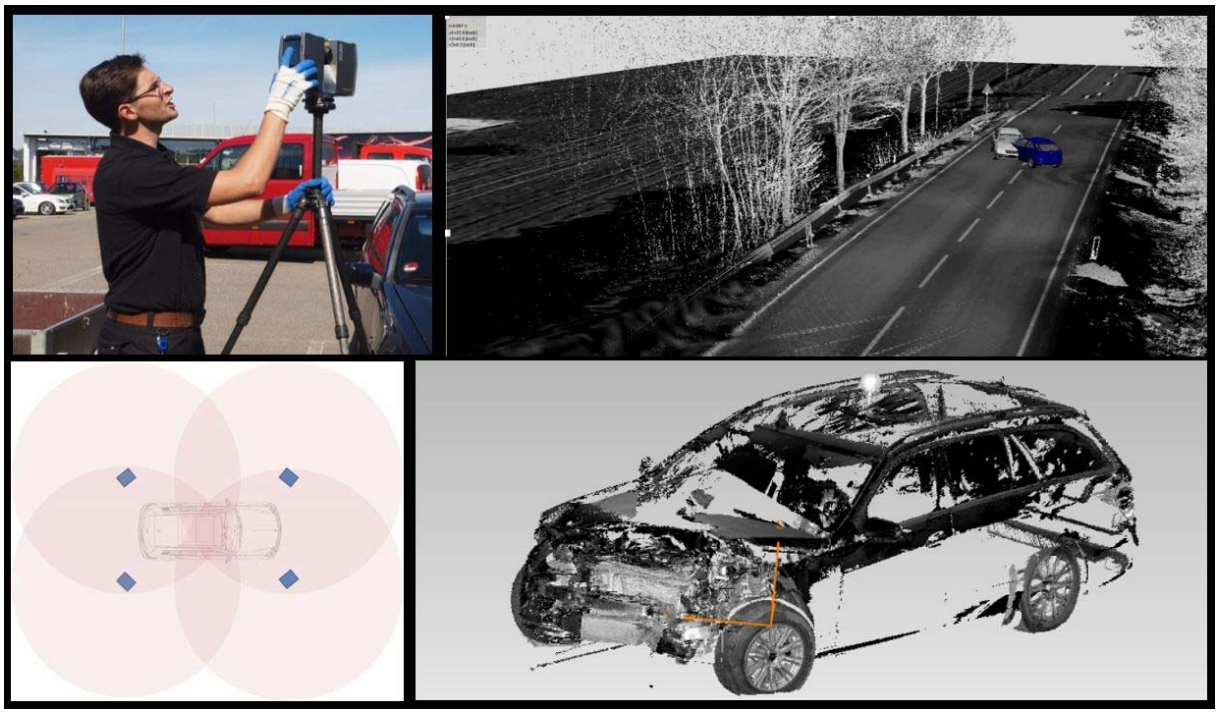

Examples for laser scan usage, vehicle scans and mostly measuring accident scenes

International investigations

Results from different databases around the world show differences in configurations, participants and share of accident data. Due to this issue, a harmonized dataset was created. The project for this standardized data was iGLAD [1]. However, iGLAD currently is not able to fill all the gaps of the worldwide data. The biggest gap is the data from the car itself. To close this gap, it is necessary to also investigate in other markets to identify differences. With this in-depth data from the car, there will be sufficient data for research and development available.

The biggest challenge is the communication and the education in different locations. For that reason, AR technique will be used in the future. With these VUZIX M300 glasses, real-time communication with researchers in different locations can be facilitated. Fast and direct contact with live-video-stream and audio as well as additionally specific data and other important information can be established. Data can quickly be transferred between all participants.

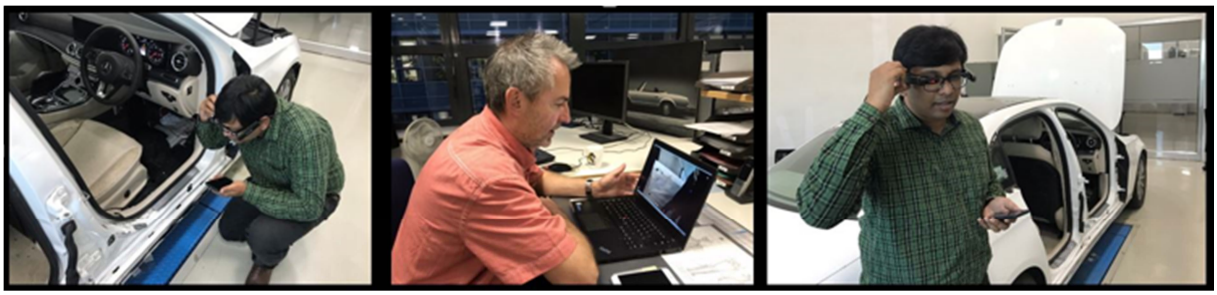

Direct communication between experts around the globe in real time using new AR technology

Conclusion

A wide range of technical innovations contributes to the exemplary safety of Mercedes passenger cars. Many of the patented developments are what set Mercedes models

apart from other cars, thus underlining their role as safety pioneers. And most of them resulted from the findings of 50 years of Mercedes accident research, which helped to safe a significant number of lives.
New technologies like the laser scanner or AR will also change the investigation and reconstruction techniques of real world accidents in the future. This will not only allow to obtain more accident data, even in emerging markets. It will also provide a better chance to find the right solutions to mitigate or even avoid more and more crashes in the future. The need for more safety is documented in the current WHO-status report [2] with 1.35 Mio. of road traffic related fatalities in 2018. The amount of different datasets from several countries brings the opportunity to develop an optimized unique vehicle which can address the most accident-configurations and -severities worldwide.

References:

[1] D. Ockel, J. Bakker, R. Schöneburg, “Internationale Harmonisierung von Unfalldaten; Fortschrittsbericht des FIA /ACEA Projekts iGLAD (Initiative for the Global Harmonization of Accident Data)“, VDI Kongress 2011, Berlin.
[2] WHO, Global status report on road safety 2018

EVALUATION OF THRESHOLD USED BY ADVANCED AUTOMATIC COLLISION NOTIFICATION SYSTEM FOR DISPATCHING DOCTORS TO ACCIDENT SITES

Tomoyuki Miyoshi, Takenori Koase

Toyota Motor Corporation

Japan

Tetsuya Nishimoto

Nihon University

Japan

Hirotoshi Ishikawa

HEM-Net

Japan

Paper Number 19-0179

ABSTRACT

An advanced automatic collision notification system (AACN) called "D-Call Net" started operation in Japan at the end of 2015. D-Call Net reports both the location of the accident and the probability of serious and fatal injuries calculated based on event data recorder (EDR) information such as the collision direction, delta-V, seatbelt usage, and whether multiple impacts occurred. This information is sent simultaneously to fire departments and emergency responders at hospitals operating air ambulances to shorten the duration before a doctor reaches the injured as much as possible. The probability of serious or fatal injury used by D-Call Net was calculated by Toyota Motor Corporation and Nihon University based on 2.8 million items of crash data in Japan. This probability was developed using only driver side data, and is also applied to the passenger side. The recommended threshold for dispatching a doctor to an accident site is currently set to a 5% probability of serious or fatal injury, which means that the under-triage (UT) rate does not exceed 10%. This research investigated 374 accidents notified via D-Call Net to determine whether the current threshold of 5% is appropriate. This investigation found that the UT rate was 0%, the over-triage (OT) rate was 29%, and that the correct judgment was made in 71% of cases. These results satisfy the targets set when operation of the system started (UT: 10%, OT: 61%). This paper also discusses the appropriate threshold for dispatching doctors via D-Call Net to further reduce the rate of unnecessary emergency dispatches.

1. INTRODUCTION

The number of traffic accident fatalities in Japan in 2017 was 3,694 (here, "traffic accident fatality" is defined as a death occurring within 24 hours of an accident). Although this is the lowest number since statistical records began [1], it still represents a significant loss of life. The target set by the Japanese government is lower than

2,500 annual traffic accident fatalities by 2020 [2]. Although the number of fatalities is declining, the rate of decline has fallen off in recent years, and this target will likely be difficult to accomplish (Fig. 1).

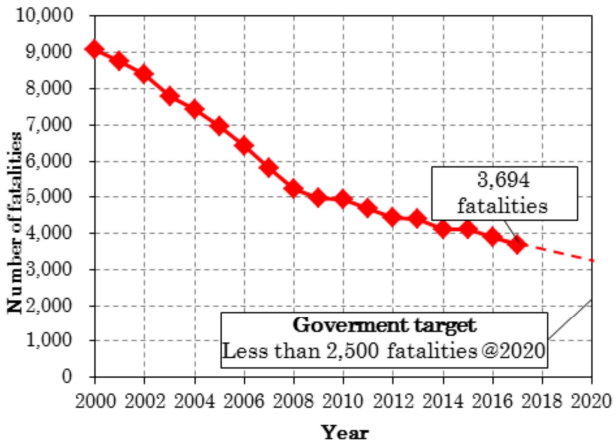

Figure 1. Traffic accident fatality trends in Japan.

Automatic collision notification (ACN) systems and advanced versions of these systems (advanced ACN, or AACN) are being adopted in increasing numbers around the world as telematics technologies become more prevalent. These systems are regarded as an important means of further reducing traffic accident fatalities, and effective application is desirable to promote the effectiveness of post-accident emergency treatment.

In Japan, an AACN system called “D-Call Net” entered full-scale operation in April 2018. This system combines medical and technical information to transmit injury probability information to fire departments and hospitals operating air ambulances, with the aim of reducing the time before medical staff can start emergency treatment (Fig. 2).

The purpose of ACN is to speed up the provision of medical treatment by automatically notifying emergency teams when an accident occurs. These systems facilitate the provision of more appropriate emergency treatment by transmitting data such as the location and the color of the vehicle. However, the effect of these systems in shortening the time before treatment is limited to a 4-minute reduction in accident notification times [3]. The EU mandated the installation of a system called “eCall” in all new vehicles from March 31, 2018. In addition, Russia mandated that new models must be equipped with a system called “ERA-GLONASS” from January 2015. This was extended to all production vehicles from January 2017. Other countries are also studying making ACN systems a legal requirement.

In contrast, D-Call Net automatically transmits information from vehicle event data recorders (EDRs). This system predicts the seriousness of injuries in the accident by applying this data to a mathematical model called an injury prediction algorithm. It then determines whether to dispatch medical staff to the accident site in accordance with the predicted injury severity.

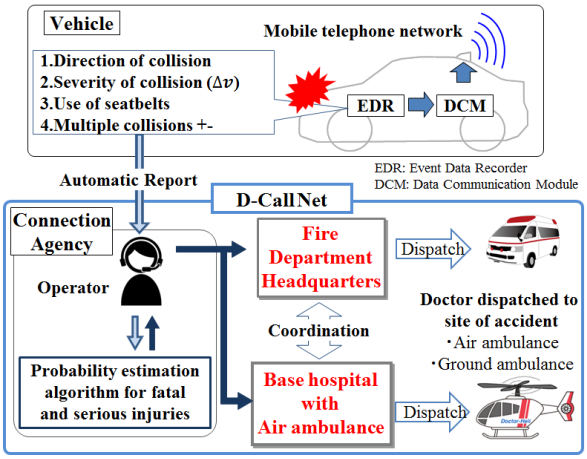

Figure 2. Information transmitted by D-Call Net

If the algorithm predicts that rapid emergency treatment is required, this system automatically transmits the information shown in Fig. 3 directly to base hospitals operating air ambulances through a call center called "HELPNET" (run by an organization called Japan Mayday Service Co., Ltd.). The purpose of dispatching medical staff in air ambulances or medical vehicles to the accident site in this way is to speed up the provision of emergency treatment.

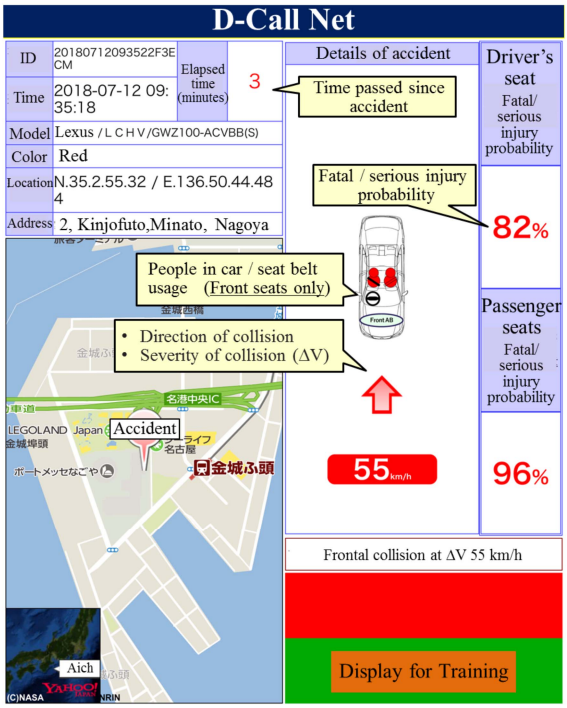

Figure 3. Information transmitted by D-Call Net.

Without this system, the average time required for an air ambulance to reach the accident site and begin treatment is currently 38 minutes. In field tests using vehicles equipped with D-Call Net, treatment was started

in 21 minutes, a saving of some 17 minutes (Fig. 4). It was provisionally calculated that rapid notification of the probability of serious or fatal injury to the occupants of vehicles equipped with the system or other vehicles involved in accidents to fire departments or hospital emergency departments would reduce the number of annual traffic accident fatalities in Japan by 282 people [8]. However, information about the probability of serious or fatal injury is currently limited to front seat occupants of vehicles equipped with the system. It would be beneficial to generate and transmit this information about rear seat occupants, pedestrians, cyclists, and occupants of other vehicles involved in accidents, as well.

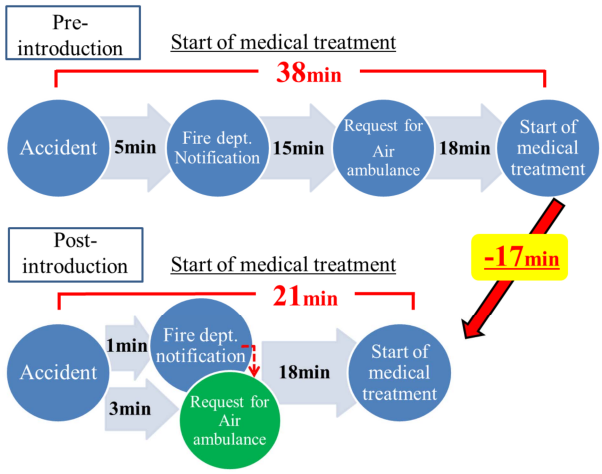

Figure 4. Effect of D-Call Net in reducing treatment start time.

2. OUTLINE OF D-CALL NET SYSTEM

Unlike conventional ACN systems that only transmit vehicle location data to the system operators, D-Call Net calculates the probability of serious or fatal injury to vehicle occupants based on EDR information (such as the collision direction, delta-V (ΔV), seatbelt usage, and whether multiple impacts occurred). This information is sent simultaneously to fire departments and base hospitals operating air ambulances (Fig. 2). The current version of the serious or fatal injury estimation algorithm (Ver. 2015) was created by Toyota Motor Corporation and Nihon University based only on driver seat information from 2.8 million items of accident data in Japan. The same data is also applied to occupants on the passenger side. The recommended threshold for dispatching medical staff to an accident site is set to a 5% probability of serious or fatal injury. After cross-verification with accident conditions in Japan, this threshold was set with the aim of achieving a maximum under-triage (UT) (i.e., when insufficient treatment is provided) rate of 10% and a maximum over-triage (i.e., when more than the minimum necessary care is provided) rate of 61% when the system began operation (Fig. 5) [4].

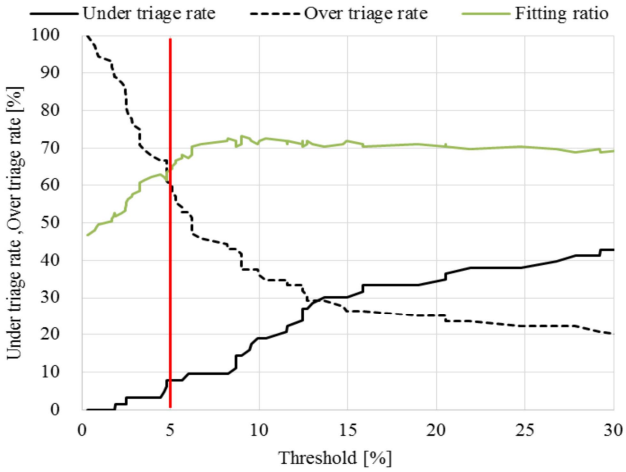

Figure 5. Threshold values of under-triage in Toyota-Nihon University algorithm.

3. APPLICATION TO VEHICLE OCCUPANTS

3.1. Period from Trial to Full-Scale Operation

D-Call Net started trial operations in Japan on November 30, 2015, using vehicles supplied by Honda Motor Co., Ltd. and Toyota Motor Corporation. The system then transitioned to full-scale operation in April 2018. As of the end of January 2019, 374 accidents had been accompanied by notification via D-Call Net (Fig. 6). These real-world accidents were investigated with the cooperation of HELPNET and the Institute for Traffic Accident Research and Data Analysis (ITARDA) to verify the prediction accuracy of D-Call Net.

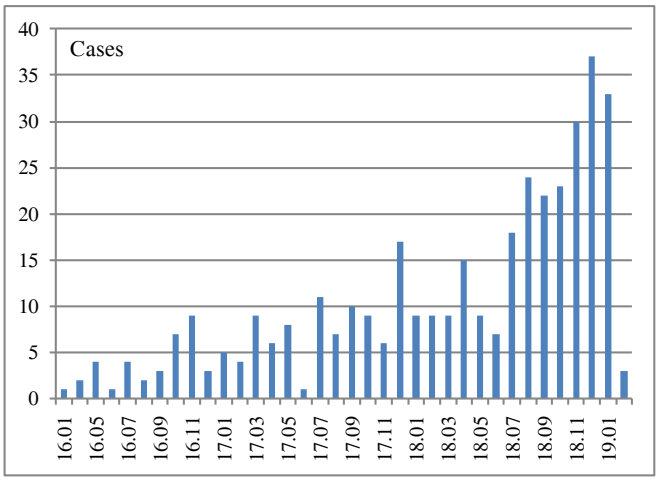

Figure 6. Month-by-month accident occurrence accompanied by D-Call Net notification.

3.2. Evaluation of D-Call Net

The 374 accidents that occurred by the end of January 2019 were analyzed. The results identified an UT rate of 0% and an OT rate of 29%. Furthermore, the correct level of care was predicted in 71% of accidents. These results confirmed that the targets for UT (10% or less) and OT (61% or less) established when the system began operation had been achieved (Figs. 6 and 7).

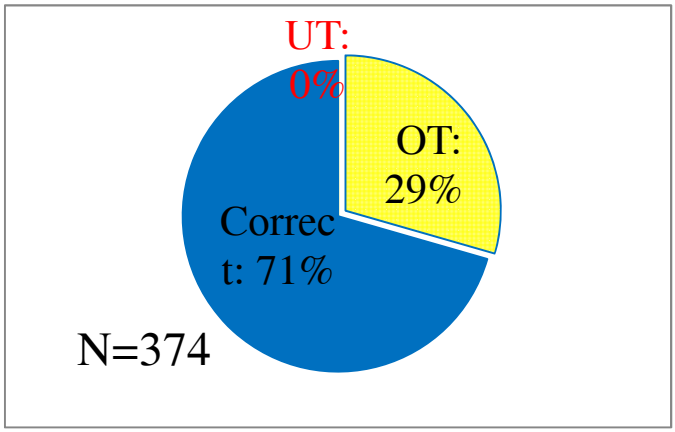

Figure 7. Rate of correct treatment provision by D-Call Net.

A breakdown of the collision types identified 137 frontal collisions, 138 rear-end collisions, and 99 side impact collisions. Over-triage occurred in 54% of the frontal collisions, 13% of the rear-end collisions, and 18% of the side impact collisions, indicating that OT occurs more frequently in frontal collisions (Fig. 8).

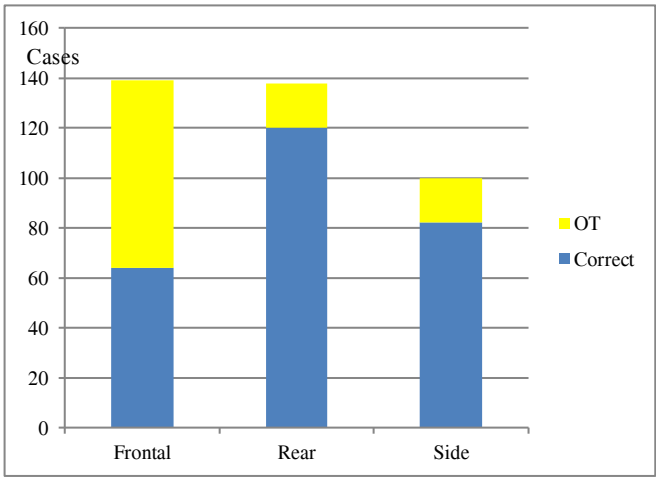

Figure 8. Proportion of OT in each collision type.

Of the 374 accidents, 56 exceeded the threshold for air ambulance dispatch (predicted injury probability of 5%) and required emergency treatment. Of these 56, 17 cases occurred within the time window allowing dispatch of an air ambulance and 39 cases occurred outside this window (Fig. 9). Furthermore, an air ambulance was actually dispatched in only 2 of these 17 cases. The 15 cases in which an air ambulance was not dispatched despite being within the required time window were analyzed. Although hospital transportation was required in these cases, it was determined that dispatch of medical staff to the accident site was not necessary.

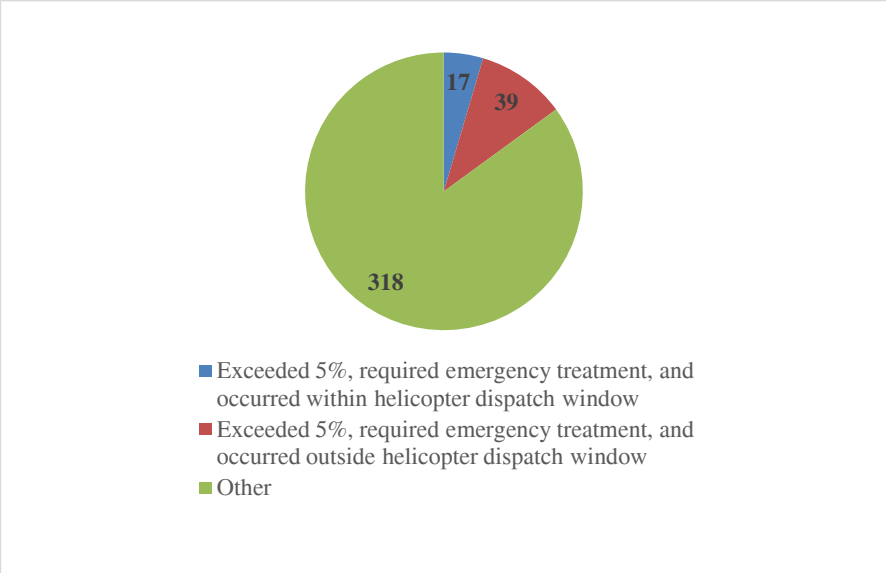

Figure 9. Cases exceeding injury probability of 5% and requiring emergency treatment.

The following section describes the details of these two cases in which an air ambulance was dispatched. Case 1 involved a collision between a mid-sized passenger car (a Toyota Crown) and a mini-vehicle in Chiba prefecture. The driver of the mid-size passenger vehicle suffered whole-body contusions and the driver of the mini-vehicle suffered external injuries (a fractured sternum and fractured right clavicle). Both drivers were taken to a trauma department. This case verified that D-Call Net enables the provision of emergency treatment to occupants of other vehicles in an accident, as well as vehicles actually equipped with the system (Figs. 10 and 11).

Figure 10. Case 1: mid-sized passenger car (Toyota Crown) equipped with D-Call Net.

Figure 11. Case 1: mini-vehicle not equipped with D-Call Net.

The duration before the provision of emergency treatment was as follows. The fire department requested dispatch of an air ambulance 3 minutes after the accident, substantially shortening the time required to reach the accident site. This case highlighted the following issue: Although the helicopter arrived at the accident site as envisioned by the system, it had to wait 17 minutes in the air while the safety of the landing site was secured (Fig. 12).

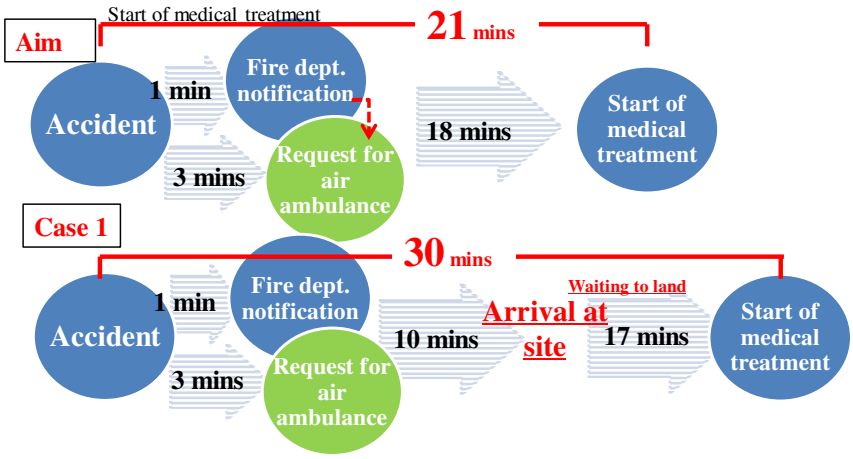

Figure 12. Timetable of case 1.

Case 2 was a collision between a mid-sized SUV (a Lexus RX) and a mini-vehicle pickup truck in Hakodate, Hokkaido (Figs. 13 and 14). Both the driver and passenger seats of the Lexus were occupied. The driver suffered damage to the mesentery tissues and small intestine, and the passenger suffered a burst fracture to the spine. Both were taken to a trauma department. Unfortunately, the occupant of the mini-vehicle pickup truck suffered cardiopulmonary arrest (CPA) before the emergency team arrived and was subsequently confirmed to have passed away. The duration before the provision of emergency treatment was as follows. Dispatch of an air ambulance was requested 11 minutes after the accident, 8 minutes later than the target time of 3 minutes (Fig. 15). This was due to a delay in noticing the D-Call Net information sent to the hospital. This issue must be addressed by, for example, directly sending the information to the mobile telephones of the medical staff.

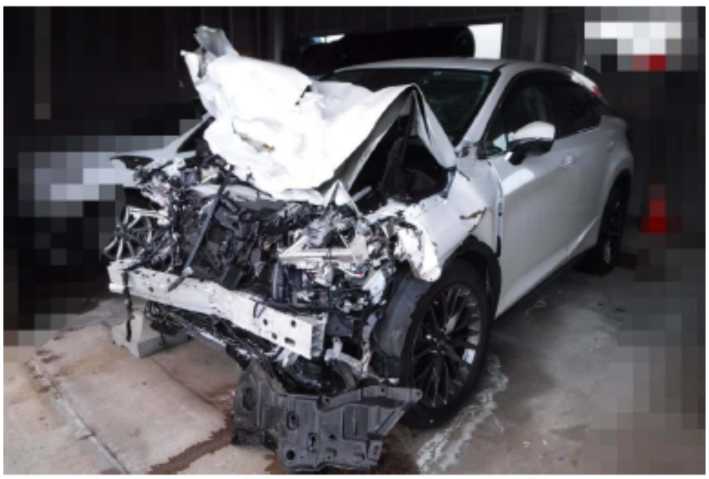

Figure 13. Case 2: mid-sized SUV equipped with D-Call Net.

Figure 14. Case 2: mini-vehicle pickup truck not equipped with D-Call Net.

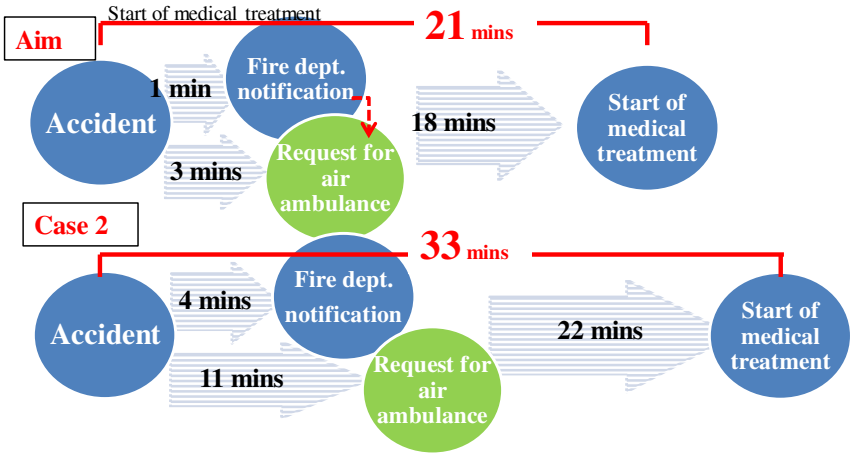

Figure 15. Timetable of case 2.

4. DISCUSSION

The calculated OT rate results for each collision type (Fig. 8) found that OT occurred in frontal collisions more frequently than other collision types. The reasons for this are as follows. The ΔV values of frontal collisions are more widely dispersed at the high end of the ΔV range than side impact and rear-end collisions (Fig. 16). As a result, although the air ambulance dispatch threshold (predicted injury probability of 5%) was exceeded in many frontal collisions, the high OT rate occurred because these accidents actually resulted in less severe injuries.

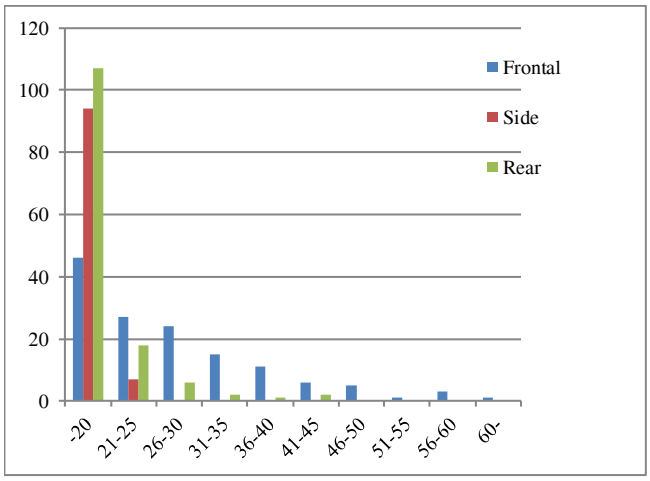

Figure 16. Δ V distribution of each collision type (vertical axis: number of cases, horizontal axis: collision velocity).

Additionally, many of these data cases were acquired from comparatively heavy vehicles (ranging from mid-size passenger cars to large SUVs). However, the current injury prediction algorithm (Ver. 2015) creates a risk curve covering a single category of vehicles ranging from small passenger cars to large SUVs. As a result, it is possible that the severe or fatal injury probability calculated using heavy vehicles may be higher than the real-world injury probability. To verify these suppositions, an algorithm (Ver. 2019) that divides vehicles into more detailed categories was formulated using the most recent year of accident data. Compared to Ver. 2015, which includes two vehicle categories (mini-vehicles and other), Ver. 2019 includes three categories (mini-vehicles, small vehicles, and mid/large vehicles). Figure 17 shows these results. When the OT rate was estimated using the more detailed algorithm (Ver. 2019), the OT rate for frontal collisions fell from 54 to 42%. This shows that the injury prediction accuracy can be improved by adopting more detailed vehicle categories as an algorithm risk factor. In addition to creating more detailed vehicle categories, it is also planned to create risk curves in accordance with the type of collision (frontal, side (near/far), or rear), seating position (driver, front passenger, or rear) to further enhance the accuracy of injury probability prediction.

The results of this verification also identified the following issues.

4.1 Expansion of participating hospitals, including the use of medical vehicles

The results found that 26 of the 108 accidents in which the air ambulance dispatch threshold was exceeded occurred outside the range of participating hospitals with air ambulances, and that 56 cases occurred at nighttime, when air ambulances cannot be dispatched. When D-Call Net started trial operation in November 2015, 9 (out of a total of 53) air ambulances were registered with the system. In the following two-and-a-half years, the number of participating air ambulances has been increased in accordance with HEM-Net (an emergency medical network consisting of helicopters and hospitals). Although the number of participating air ambulances had increased to 45 (approximately 85% of the total) by the end of January 2019, increasing this rate to 100% as quickly as possible is a matter of urgency. Furthermore, since air ambulance operation in Japan is restricted at night, it is extremely important to expand the participation of less-restricted medical road vehicles to help cover accidents that occur after dark.

4.2 Securing of rendezvous points

In case 1, the air ambulance spent 17 minutes above the accident site while the safety of the landing site was secured. To help prevent this situation and bring the medical staff to the patients as quickly as possible, the number of rendezvous points capable of receiving patients quickly and safely must be increased.

Finding ways of addressing these issues will play a major role in further increasing the number of lives saved after traffic accidents. D-Call Net must be used effectively in close cooperation with the relevant government ministries.

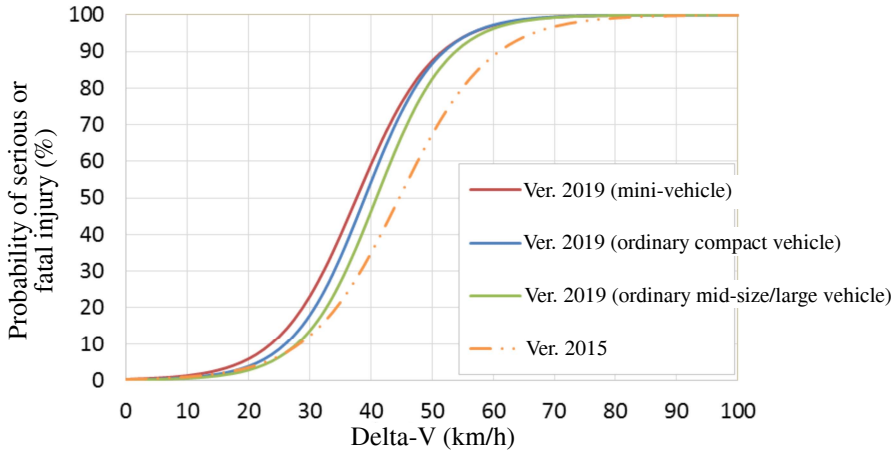

Figure 17. Risk curves for each algorithm version.

6. CONCLUSION

This paper described how the injury prediction accuracy for real-world accidents was verified using vehicles equipped with the D-Call Net system. The results found 374 accidents that used D-Call Net by the end of January 2019. Analysis of these results identified an UT rate of 0% and an OT rate of 29%. The correct level of care was predicted in 71% of these accidents. These results satisfied the targets established when the system

began operation. This paper also described two real-world case studies requiring lifesaving medical treatment, and demonstrated the effectiveness of the D-Call Net system. In the future, it is intended to continue enhancing the serious or fatal injury probability algorithm with the aim of further enhancing the accuracy of injury prediction, and to enlarge the application of D-Call Net in cooperation with the relevant government ministries.

REFERENCES

[1] Japan National Police Agency Report 2017

[2] Cabinet Office, Government of Japan. 2016. “Challenge to New Goals in Road Transport – Preparation of the 10th Traffic Safety Basic Plan (Road Transport).”

[3] Cowley, R.A., Hudson, F., et al. 1973. “An economical and proved helicopter program for transporting the emergency critically ill and injured patient in Maryland.” The Journal of Trauma, 1029-1038

[4] Nishimoto, T. 2017. “Serious injury prediction algorithm based on large-scale data and under-triage control.” Accident Analysis and Prevention, 98, 266-276

[5] Motomura, T. 2017. “The Actual Request from D-Call Net and Activation of Doctor Heli System.” JSAE Journal Vol. 71, 40-44

[6] Toyota Motor Corporation Global Newsroom. 2018. “Advanced Automatic Collision Notification Service, D-Call Net, Expanded Nationwide.” (https://newsroom.toyota.co.jp/en/corporate/22961893.html)

[7] Tominaga, S., Nishimoto, T., et al. 2015. “Injury Prediction Algorithm for AACN Based Japanese Road Accident Data.” JSAE Journal Vol. 46, 925-930

[8] Takayama, S., Ono, K., et al. 2014. “Effect estimation of automatic crash notification system for the reduction of traffic accident fatalities utilizing the Japan trauma data bank.” JSAE Annual Congress, 135, 11-4

[9] Motomura, T. 2018. “Actual doctor-helicopter missions activated by D-Call Net and full scale operation of D-Call Net in Japan.” JSAE Annual Congress (Spring) (Yokohama, Kanagawa Prefecture, May 23-25), 20185252

[10] Kiuchi, T., Ishikawa, H., et al. 2018 “Study on D-Call Net accident cases for the pilot study using in-depth investigation.” JSAE Annual Congress (Spring) (Yokohama, Kanagawa Prefecture, May 23-25), 20185251

DEVELOPMENT OF PORTABLE BREATH-ALCOHOL-DETECTION SYSTEM

Masuyoshi Yamada

Hironori Wakana

Center for Exploratory Research, Research & Development Group, Hitachi, Ltd.
Japan

Paper Number 19-0181

ABSTRACT

A portable alcohol detection system based on exhaled breath analysis has been developed. The system consists of a breath sensor, a smartphone to control the sensor and communicate various data, and a data cloud system. The system can be used to monitor a driver's status from a remote location.
The breath sensor consists of four separate sensors. The first is a water vapor sensor that is used to verify if the applied gas is human breath. The others are semiconductor gas sensors to detect ethanol, acetaldehyde, and hydrogen. The detector is connected to a smartphone, and the driver's alcohol check results are automatically sent to a data cloud system. To prevent abuse of this detector by blowing substitute gas, it can recognize human exhaled breath by detecting small amounts of metabolites as well as saturated water vapor. The ethanol concentration is obtained from the voltages of the three semiconductor gas sensors. Each sensor has a specific sensitivity for ethanol, acetaldehyde, and hydrogen. We apply the differential evolution algorithm to the relationship between each sensor's output voltage and its calibration curve. Then we calculate the ethanol concentration of the human breath. This multi sensor method is more accurate than a single sensor method that only uses one gas sensor to measure ethanol concentration. We also employ an original humidity sensor that was suitably designed to detect highly humid (saturated) water vapor using a comb-shaped electrode pattern.
From our field tests, in which we used more than 30 sets of detectors, we investigated the performance of exhaled breath recognition. When the field test users of our detector did not consume alcohol, their ethanol, acetaldehyde, and hydrogen concentration levels, as a result of natural human metabolism, were 1.8, 1.9, and 0.1 ppm on average, respectively. Based on these data, we set the threshold level on each gas sensor to recognize human breath. As a result, the detector could measure the breath alcohol level within 3 s. It could also successfully distinguish human exhaled breath from ambient air or spray gas.
Since the detector is small (Size: 75 mm(W), 55 mm(D), 20 mm(H), Weight: 20 g, approx.) and connected to a smartphone, it can be used at any time and can contribute to the safety of professional drivers by enabling remote and central management of alcohol test data.
It is possible to connect this detector to a vehicle engine interlock system by wireless communication so that the system can recognize the driver's status, even before they enter a vehicle. This will help prevent drunk driving. We believe that our detector is helpful to decrease alcohol-related accidents and enable remote management of alcohol inspection.

INTRODUCTION

There is a global effort to prevent or stop drunk driving. Therefore, safe driving technology has been extensively researched. In Japan, transportation operators are required to use an alcohol detector to test whether professional drivers are under the influence of alcohol before they begin their shifts [1]. Meanwhile, in the U.S., the National Highway Traffic Safety Administration (NHTSA) has launched and directed the development of ignition interlock technology that connects alcohol detectors to a vehicle's engine [2]. Their systems require drivers to perform the test from the driver's seat once they are already inside the vehicle [3-6]. With our prototype device, drivers can measure their alcohol level from anywhere and, importantly, prior to entering their vehicle. This will reduce the temptation to drive. In addition, our device can confirm if the applied gas is human exhaled breath and simultaneously detect the level of alcohol [7,8]. These advancements will contribute to reducing or eliminating instances of drunk driving.

While our previous prototype allowed the driver to take the test anywhere and prevented tampering by being able to distinguish whether the submitted sample was human breath [7], it had issues such as the possibility of abuse by a substitute taking the test instead of the actual driver, and the need to be able to centrally manage test data from each driver in fleet situations.

To address these issues, we developed a function to prevent the use of substitutes as well as enabling central management of alcohol test data. The developed prototype includes a function to send a facial image to prevent substitution and a data communication system between the smartphone and cloud system.

METHODS

Figure 1 shows an image of the breath-based alcohol detection device and circuit board. The sensor device consists of a water vapor sensor to detect saturated water vapor in human breath and three semiconductor gas sensors to detect ethanol (Nissha FIS, Inc., SB-30), acetaldehyde (SB-33), and hydrogen (SB-19). These sensors are located behind the breath inlet area of a sensor case. The case size is 75 mm (W), 55 mm (D), 20 mm (H), and its weight is approximately 20 g. The device is connected to a smartphone as shown in Fig. 1, and the drivers can measure their alcohol level anywhere including, importantly, prior to entering the vehicle. The alcohol concentration is calculated in the device and then sent to the smartphone. A driver can see his/her alcohol level on the smartphone display, and data is simultaneously sent to a cloud system to be checked by a safety/health officer at a control center. In addition, it is possible to communicate with a vehicle's engine interlock system as developed in a previous prototype [8].

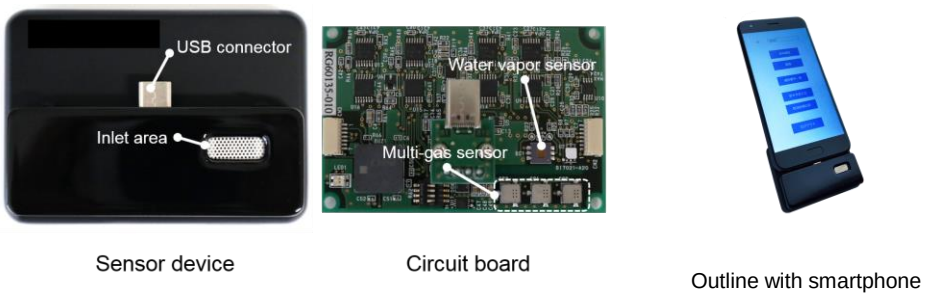

Figure 1. Image of breath alcohol detection device.

Water vapor sensor

Figure 2 shows the schematic of the water vapor sensor, which can detect the saturated water vapor from the exhaled breath with a high degree of sensitivity. When human breath is applied to the sensor, which is an oxide insulator sandwiched between the electrodes, the water vapor from the breath is adsorbed on the insulator, and an electric current flows between the electrodes. When this occurs, the sensor can recognize if the applied gas is human breath. Furthermore, micro comb-shaped electrodes are used to extend the length of the electrodes and decreases the distance between them, thus improving the sensitivity of the sensor. This sensor has a heating layer to prevent condensation before it starts measuring. An AC voltage of ±1.5 V at a frequency of 10 Hz was applied to the voltage electrodes to detect water vapor. This device can detect a small amount of saturated water vapor even though the sensor dimensions are only 1.5 mm × 2.1 mm. As a result, the device is highly portable.

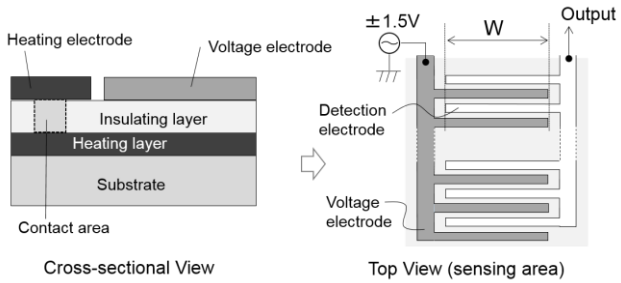

Figure 2. Schematic of water vapor sensor.

Calibration and evaluation

The ethanol concentration in the breath is obtained as follows. After the water vapor sensor acknowledges that a sufficient amount of breath is introduced, maximum voltages of the above-mentioned gas sensors are recorded and sent to a concentration calculation algorithm. This is installed in the circuit board CPU. The algorithm is based on a differential evolutional method [9] and can determine an approximate solution. The relationship between the output sensor voltage and gas concentration are shown as the calibration curve in Fig. 3. The concentrations of ethanol, acetaldehyde, and hydrogen are calculated from the calibration curve and differential evolutional method. The calibration curve was obtained using a thermostatic chamber (100 L) as shown in Fig.4. The temperature and humidity in the chamber were maintained at 34 °C and above 85% for 30 min, respectively.

At each measuring condition, 1 mL of the inside gas was sampled, and each gas concentration was measured by GC-FID.

We also evaluated the effect of the distance of the breath flow path to the gas inlet of the sensor using a breath simulator, as shown in Figure 5. The breath simulator was operated under the following conditions: temperature of 34°C, ethanol concentration of 10 – 150 ppm, breath flow distance of 0 – 40 mm, and gas flow rates of 2.5 – 5.0 L/min. The humidity at the outlet of the simulator was at a saturated water vapor level. We investigated the measurement accuracy of the alcohol concentration, and the dependence of the distance (D) between the outlet pipe and inlet of the sensor.

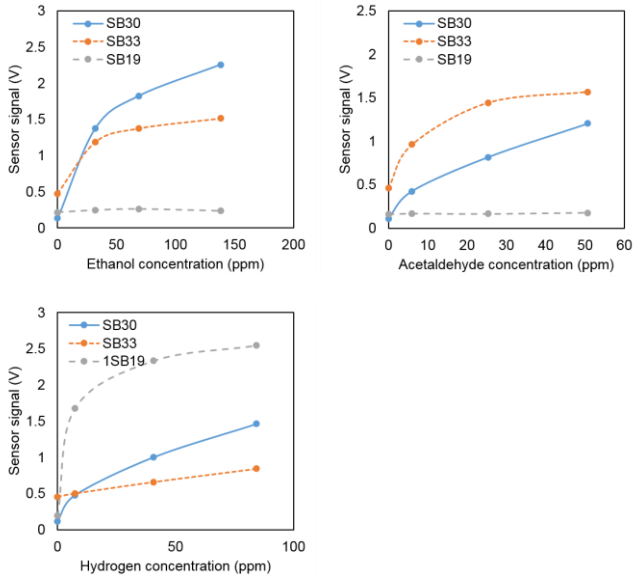

Figure 3. Calibration curves of gas sensors.

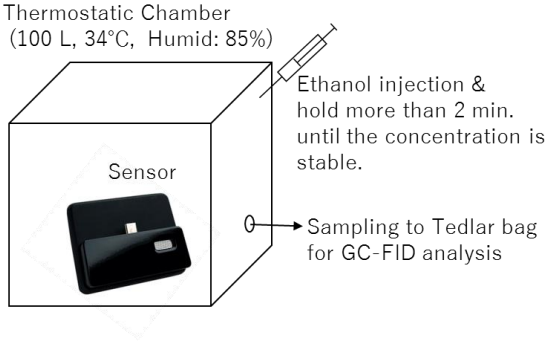

Figure 4. Experimental set up to obtain calibration curve.

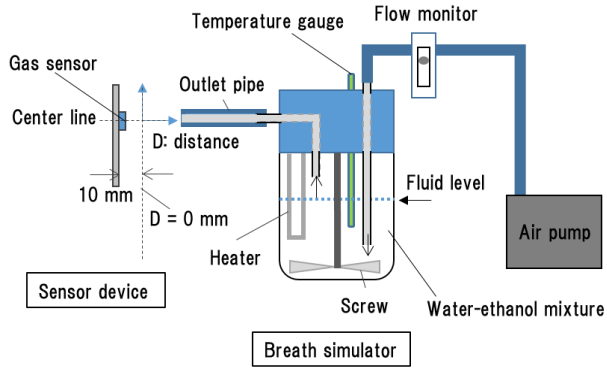

Figure 5. Schematic of a breath simulator system.

RESULTS AND DISCUSSIONS

Breath recognition function

Figure 6 shows an example of the output signal of the water vapor sensor after introducing a human's breath, ambient air, and spray gas. The output signals were obtained at a sampling rate of 1 kHz. The output signal of the water vapor sensor increased with an increase in the amount of exhaled breath and exceeded the level (threshold voltage) for recognizing breath. For ambient air and spray gas, the output signals did not exceed this threshold voltage while introducing gases. The water vapor sensor only reacted to the exhaled breath and not ambient air or spray gas.

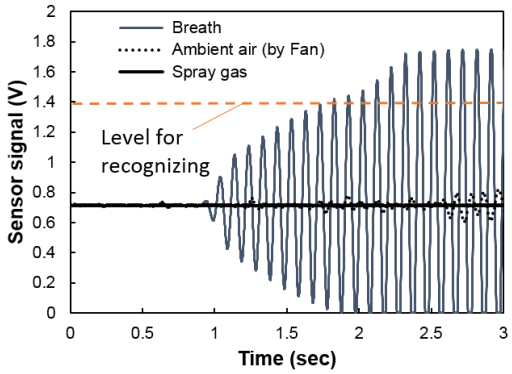

Figure 6. Time dependence of the output signal of water vapor sensor with different sample gases, such as human breath, ambient air, and spray gas.

The gas sensors in our device can also distinguish water vapor from a human breath. Figure 7 shows a comparison of the sensor signals obtained after introducing pure water vapor and human breath. The signals of each gas sensor for the human breath were higher than those obtained for water vapor. This is because the breath includes small amounts of these gases as metabolites. Figure 8 shows the averages and standard variations in ethanol, acetaldehyde and hydrogen concentrations obtained from the breaths of 100 volunteers under non-alcohol conditions. The sensor's threshold levels are determined with these data. Thus, a feature of our sensor device is that it can avoid false detection, which is caused by other gases, such as ambient air and/or water vapor.

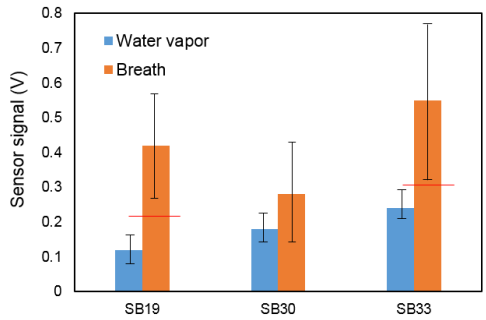

Figure 7. Comparison between water vapor and human breath.

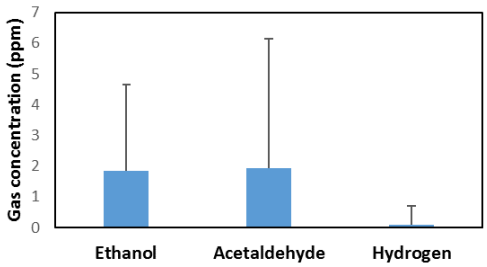

Figure 8. Measured gas concentration in volunteers' breath.

Evaluation of the sensor's applicability

Figure 9 shows the measurement results of an artificial breath, which was introduced using a breath simulator at different distances from 0 to 40 mm. The signal intensity of the ethanol gas sensor (SB30) depends on the distance between the outlet pipe of the breath simulator and the inlet of the sensor device. In the case of distances less than 20 mm, the sensor signals were constant. Therefore, we recommend the sensor to be used at a distance within 20 mm.

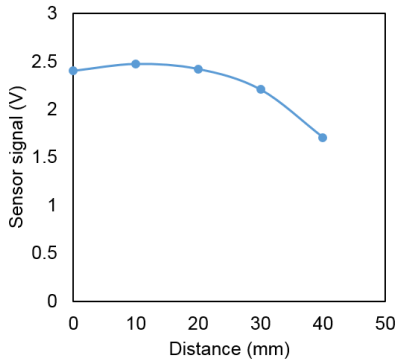

Figure 9. Dependence of ethanol sensor signal on the distance using the breath simulator system.

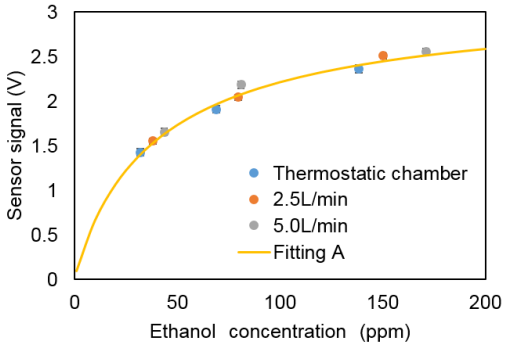

Figure 10. Comparison between the results of the thermostatic chamber and breath simulator.

Figure 10 shows a comparison of the ethanol sensor (SB30) signals measured using a thermostatic chamber and a breath simulator. The distance between the outlet of the breath simulator and the sensor device was 0 mm. "Fitting A" in Figure 10 was obtained using the data from the thermostatic chamber. We investigated the dependence of the sensor signals on the ethanol concentration by applying different gas flow rates at 2.5 L/min and 5.0 L/min using the breath simulator. The experimental results obtained with the breath simulator showed good agreement with the results obtained using the thermostatic chamber (Fitting A). This indicates that the estimated measurement accuracy is less than ±10 ppm.

Breath alcohol detection

Figure 11 shows results of a participant's breath test after they consumed alcohol. The vertical axis represents the output signal of each sensor, while the horizontal axis represents time in seconds. The results were obtained from the participant's exhaled breath after they had consumed 200 mL of wine (alcohol content: 13%). The signal intensity of each gas sensor increased until the end of the exhaled breath and exceeded the legal limit level of 0.15 mg/L (in Japan) immediately. The system exhibited the calculated results of gas concentration within 3 s after the start of breath exhalation.

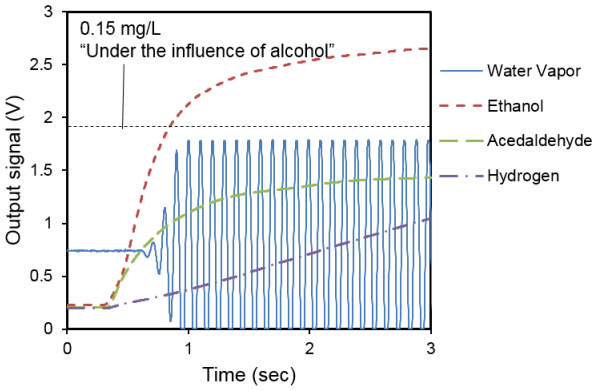

Figure 11. Validation test after consuming alcohol.

CONCLUSION

We have successfully developed a prototype portable alcohol device that is able to distinguish human breath from other gases. This device is capable of distinctively detecting the saturated water vapor and the metabolites from human breath while accurately measuring the alcohol level within 3 s of a driver breathing into the device. We also developed a system that displays the alcohol level measured by the detector on a smartphone and sends the data to a cloud system. A measurement accuracy of ±10 ppm was obtained by introducing an exhaled breath within a distance of 20 mm. We aim to develop our proposed detector to make it more practical for further use.

ACKNOWLEDGEMENT

The authors would like to thank people concerned in Yabu city of Hyogo Pref. for cooperation of our field tests, and Mr. K. Kin of Honda R&D Co., Ltd. for helpful advice.

REFERENCES

[1] http://www.mlit.go.jp/common/000131573.pdf (Japanese edition)

[2] R.P. Compton and J. Hedjund, "Reducing Impaired-driving Recidivism Using Advanced Vehicle-Based Alcohol Detection Systems" in A Report to Congress, National Highway Traffic Safety Administration, Washington, DC, pp. 4-15, 2007.

[3] K. Zaouk, M. Wills, E. Trube and R. Strasssburger, "Driver Alcohol Detection System for Safety (DADSS) – A Status Update," Paper Number 15-0276. Proceedings of the 24nd International Technical Conference on the Enhanced Safety of Vehicles, 2015.

[4] B. Hok, J. Ljungblad, A. K. Andersson, M. Ekstrom and M. Enlund, "Unobtrusive and Highly Accurate Breath Alcohol Analysis Enabled by Improved Mrthodology and Technology," Journal of Forensic Investigation, Vol. 2, Issue 4, 8, 2014.

[5] P. Sanchez, C. R. Zamarreno, M. Hernaez, I. R. Matias and F. J. Arregui, "Exhaled Breath Optical Fiber Sensor based on LMRs for Respiration Monitoring," IEEE SENSORS 2014 Conference, pp. 1142-1145.

[6] L. Cech, M. Nagolu, D. Rumps, B. V. Steeg, D. Treese, B. Laaksonen, S. Tehseldar and T. Ridder, "Introduction of a Solid State, Non-invasive Touch Based Alcohol Sensor," Paper Number 15-0380., Proceedings of the 24tn International Technical Conference on the Enhanced Safety of Vehicles, 2015.

[7] H. Wakana, M. Yamada and M. Sakairi, "Development of Breath-alcohol-detection System," SAE technical paper, 2016-01-1498, 2016.

[8] H. Wakana, M. Yamada and M. Sakairi, "Portable Alcohol Detection System with Breath-Recognition Function," IEEE SENSORS2018 Conference, pp. 939-942.

[9] R. Storn and K. Price, "Minimizing the real functions of the ICEC'96 contest by differential evolution," Proc. Of the International Conference on Evolutionary Computation, pp. 842-844, 1996.

EURO NCAP'S FIRST STEP TOWARDS SCENARIO-BASED ASSESSMENT BY COMBINING AUTONOMOUS EMERGENCY BRAKING AND AUTONOMOUS EMERGENCY STEERING

Richard Schram
European New Car Assessment Programme
Belgium

on behalf of the Euro NCAP Working Group on AEB/AES

Paper Number 19-0128

ABSTRACT

Following the implementation of Autonomous Emergency Braking in the overall safety rating in 2014, Euro NCAP is making its first step towards a scenario-based approach by allowing a driver initiated steering intervention as an alternative to the driver responding to a Forward Collision Warning (FCW) by braking. With this first step, Euro NCAP is acknowledging that there are multiple responses possible to the same threat and that steering, in some cases, may be a better crash avoidance strategy than braking.

Within the Euro NCAP Working Group on AEB/AES, Euro NCAP members, test centers and the automotive industry represented by the ACEA, JAMA, KAMA and CLEPA associations, the first protocols are developed for both AEB Car-to-Car (C2C) and AEB systems, responding to vulnerable road users (VRU). The procedures are an extension to the current AEB C2C and AEB VRU test and assessment protocols, with expected adoption in the rating in 2020. This paper describes both the test and assessment protocols.

BACKGROUND

In 2009, Euro NCAP introduced the overall rating scheme, which allows new technologies to be implemented in the safety assessment of a new vehicle. The new rating scheme consists of four areas of assessment, also called boxes, which together result in a single overall safety rating. The four areas of assessment are Adult Occupant Protection (AOP), Child Occupant Protection (COP), Pedestrian Protection (PP) and Safety Assist (SA).

Over the last few years, the car industry has taken their responsibility and are now fitting active safety systems like AEB as standard on nearly all new models released on the European market.

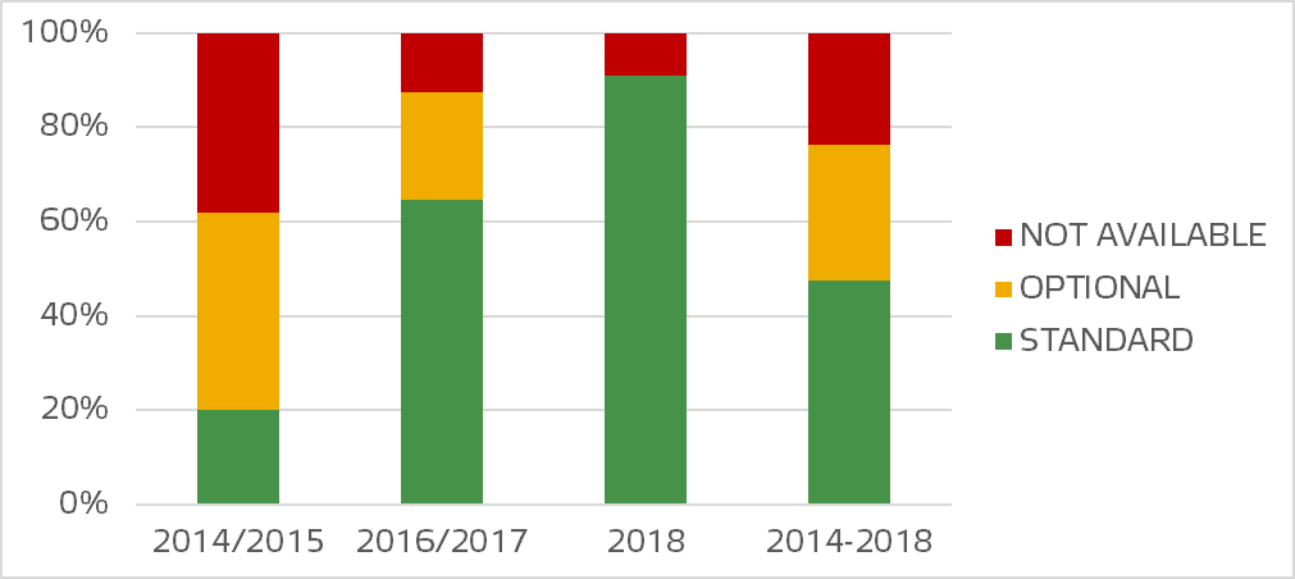

Figure 1. AEB fitment distribution for Euro NCAP tested models

As also the hardware and performance of these safety systems has evolved rapidly, Euro NCAP is now in the position to look for further use cases. With the inclusion of more complex scenarios, a scenario-based assessment instead of a system based assessment seems to be a logical next step in allowing the industry to decide themselves what is the most efficient strategy to avoid or mitigate any critical situation, while at the same time balancing the risk at possible false interventions.

As a first step, Euro NCAP will award so-called Emergency Steering Support (ESS), driver initiated systems that can steer away from a potential impact. The focus is on scenarios where responding to the FCW by steering is seen to be the better solution than hard braking to avoid a possible collision.

As for all Euro NCAP protocols, the development of the test procedure and assessment criteria was done within a collaborative Working Group. The Euro NCAP working Group on AEB/AES involves Euro NCAP members and laboratories, representatives from the car industry and suppliers, and was given the task to deliver extended AEB protocols for both Car-to-Car and Vulnerable Road Users by the end of 2018, for implementation in 2020. The work of the group took advantage of and brought together the results delivered by several research initiatives in Europe that where looking into extending the scope of AEB systems.

EURO NCAP WORKING GROUP

Initiatives

In Europe, several initiatives led by Euro NCAP members and/or laboratories have been running in parallel, all with the same goal of developing test procedures for extended AEB scenarios for both AEB C2C, AEB VRU: INTERSECTION, PROSPECT, MUSE and CATS.

The INTERSECTION project, led by BASt and IDIADA has been specifically set up to develop test procedures for AEB C2C scenarios at intersections, which could be adopted in consumer testing. Accident analysis and driving studies are performed to understand the trajectories and scenario details of accidents between cars occurring on intersections. The group is supported by car manufacturers and suppliers and liaises closely with the PROSPECT project in terms of the intersection layout.

The European Commission sponsored FP8 project PROSPECT (Proactive Safety for Pedestrian and Cyclists) led by IDIADA had the overall objective is to provide a better understanding of VRU-related accidents and to develop, demonstrate and test innovative, (pro) active safety systems for protecting VRUs. The project partners consisted of research institutes, car manufacturers and suppliers, three of which were Euro NCAP laboratories: BASt, IDIADA and TNO. The PROSPECT project ran from 2015 until 2018.[1]

The results of the initiative CATS (Cyclist-AEB Testing System) were already implemented in the 2018 Euro NCAP update when AEB Cyclist scenarios were introduced. Additional scenarios that were judged to be too challenging for 2018 introduction are now added to the list of test scenarios in AEB VRU. The project was supported by another Euro NCAP test laboratory, BASt as well as car manufacturers and suppliers. The additional scenarios will be described in further detail within this paper.

UTAC is leading an initiative looking into specific scenarios for car-to-motorcycle accidents. In addition, the project will develop the necessary test equipment to be able to realistically assess the performance of AEB systems responding to motorcycles. This project is also supported by car manufacturers, suppliers and Euro NCAP laboratories ADAC, BASt, CSI and Thatcham Research. The results of this project will be useful for Euro NCAP planned update in 2022.

The outcome and deliverables of all these initiatives were and will be extensively discussed within the working group and formed the basis for the decision on test scenarios and targets used.

TEST SCENARIOS AND TARGETS

The Euro NCAP 2025 Roadmap indicates several updates in the field of AEB C2C and AEB VRU. With the roadmap as a basis and based on the work done in the different initiatives, some updated and new scenarios are selected for implementation in 2020, and 2022 Euro NCAP rating updates. The sections below will explain the updates in the different areas including a first step into a so-called scenario-based assessment.

AEB Car-to-Car

For Car-to-Car scenarios, the roadmap picks up on the latest technological developments and scheduled for inclusion of a turn across path scenario in 2020 and general crossing scenarios for 2022.

The Car-to-Car Front turn-across-path (CCFtap) scenario represents the case where a driver intends to cross the oncoming lane and either misses or misjudges the speed of an oncoming vehicle. These accidents typically happen in a city environment and at relatively low ego speeds of the vehicle making the turn. In the first step, this scenario is tested at three different test speeds for the VUT (10, 15 and 20km/h) and three speeds for the GVT (30,45 and 55 km/h). Avoidance in these cases can only be reached by a late and harsh intervention of the AEB system as there is not enough time to warn the driver. In 2022, additional crossing scenarios will be added for which the details are being developed in the INTERSECTION project.

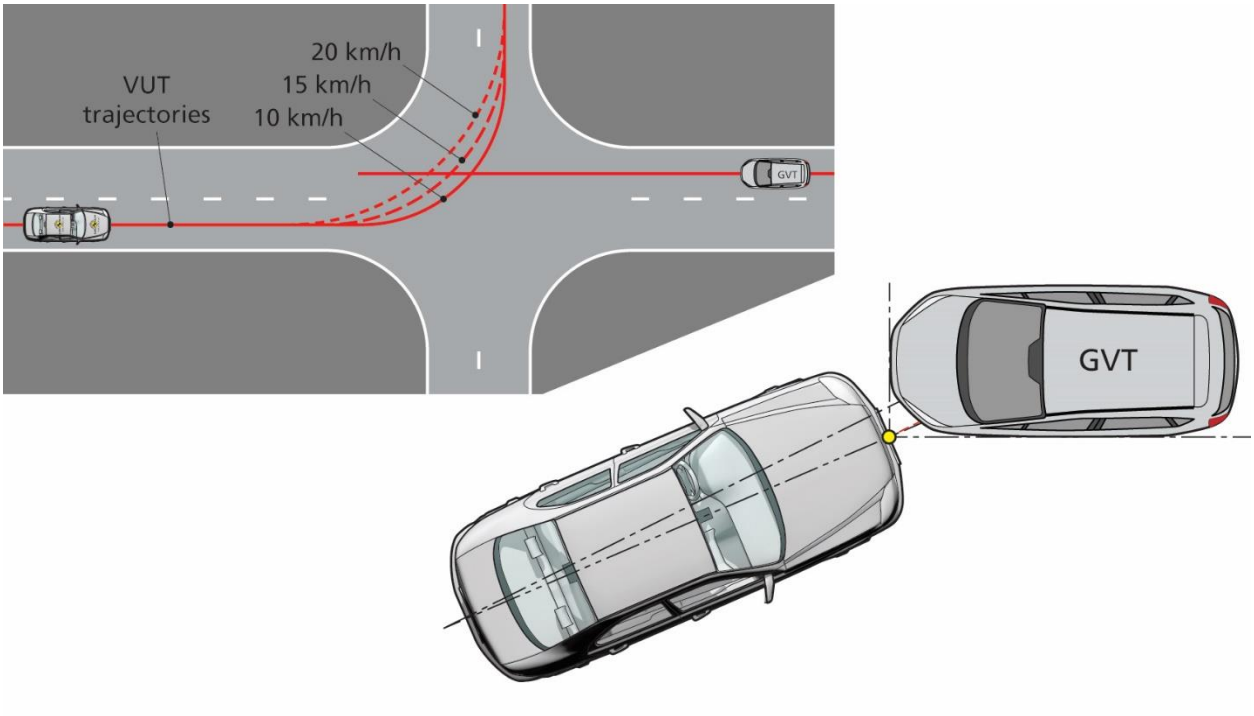

Figure 2. AEB Car-to-Car turn-across-path scenario, CCFtap

AEB Bicyclist

Two additional AEB Bicyclist scenarios are added to the test suite; Car-to-Bicyclist Farside (CBFA) and Car-to-Bicycle Nearside Obstructed (CBNAO). The challenging part of these scenarios, and the reason for implementation in 2020 instead of 2018, is the higher bicycle speed in the CBFA scenario and short detection time for the CBNAO.

In the CBFA scenario, tested at 10-60km/h, the bicycle speed is 20 km/h, which means that the opening angle of the forward-looking sensor(s) has to be increased to be able to detect the bicyclist in due time.

The obstruction in the CBNOA is blocking the sensors to see the cyclist only just before the impact, which means that the AEB system has very little time to respond to the critical situation. As the obstruction, the Euro NCAP WG decided to use two vehicles as a pragmatic method already used in the AEB child scenario.

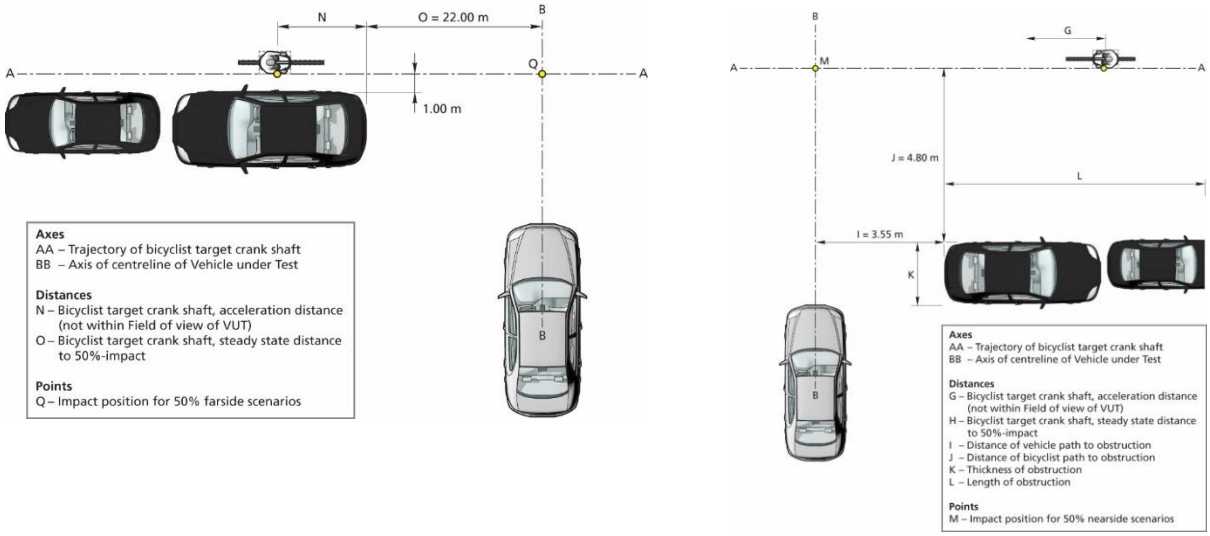

Figure 3. AEB Car-to-Bicycle Farside (CBFA) and Car-to-Bicycle Nearside Obstructed (CBNAO) scenarios

AEB Pedestrian

Rear AEB for cases where a pedestrian is overrun by a vehicle backing up is now also included in the Euro NCAP tests for AEB Pedestrian. Both moving and stationary cases are included where additional rearward sensing hardware is required to be able to detect the pedestrian walking or standing behind the vehicle. The test speeds are very low, 4 and 8 km/h, and the only assessment criteria is full avoidance. To incentivize this technology sufficiently, Euro NCAP awards these tests with two points out of nine points available for AEB Pedestrian.

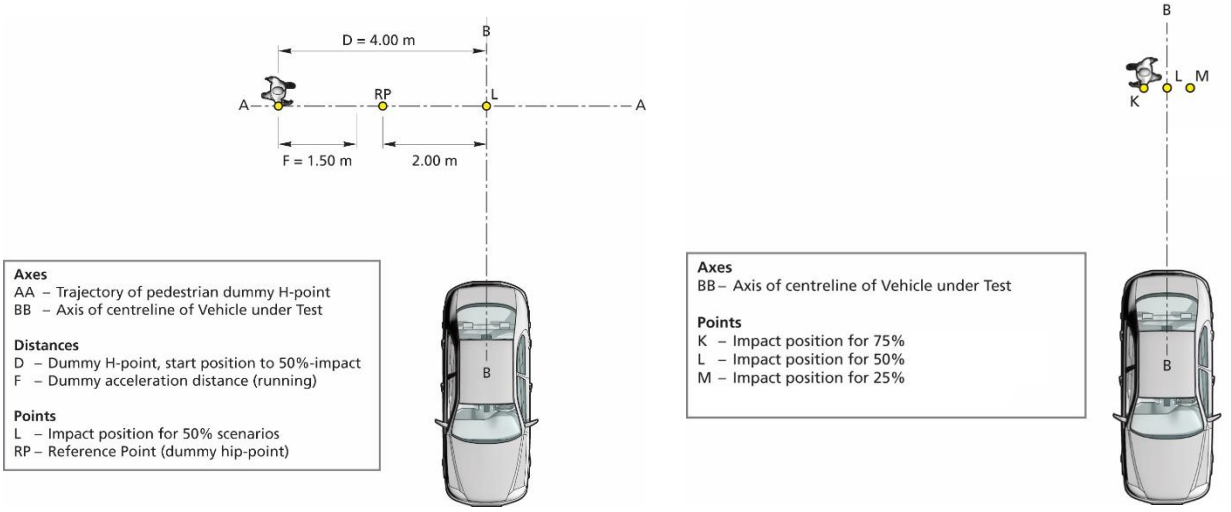

Figure 4. AEB Car-to-Pedestrian Rearside (CPRA) moving and stationary scenarios

Another new scenario in the AEB Pedestrian area is the Car-to-Pedestrian Turning scenarios (CPTA). As mainstream technology expected in 2020 is still limited in its field of view, only cases where the pedestrian walks from the opposite direction are included in the first step. Vehicle turns to both left and right at various speeds are included as shown in Figure 4. The exact specifications of the path relative to lane markings is required to facilitate different lane width's that may be present at the test laboratories.

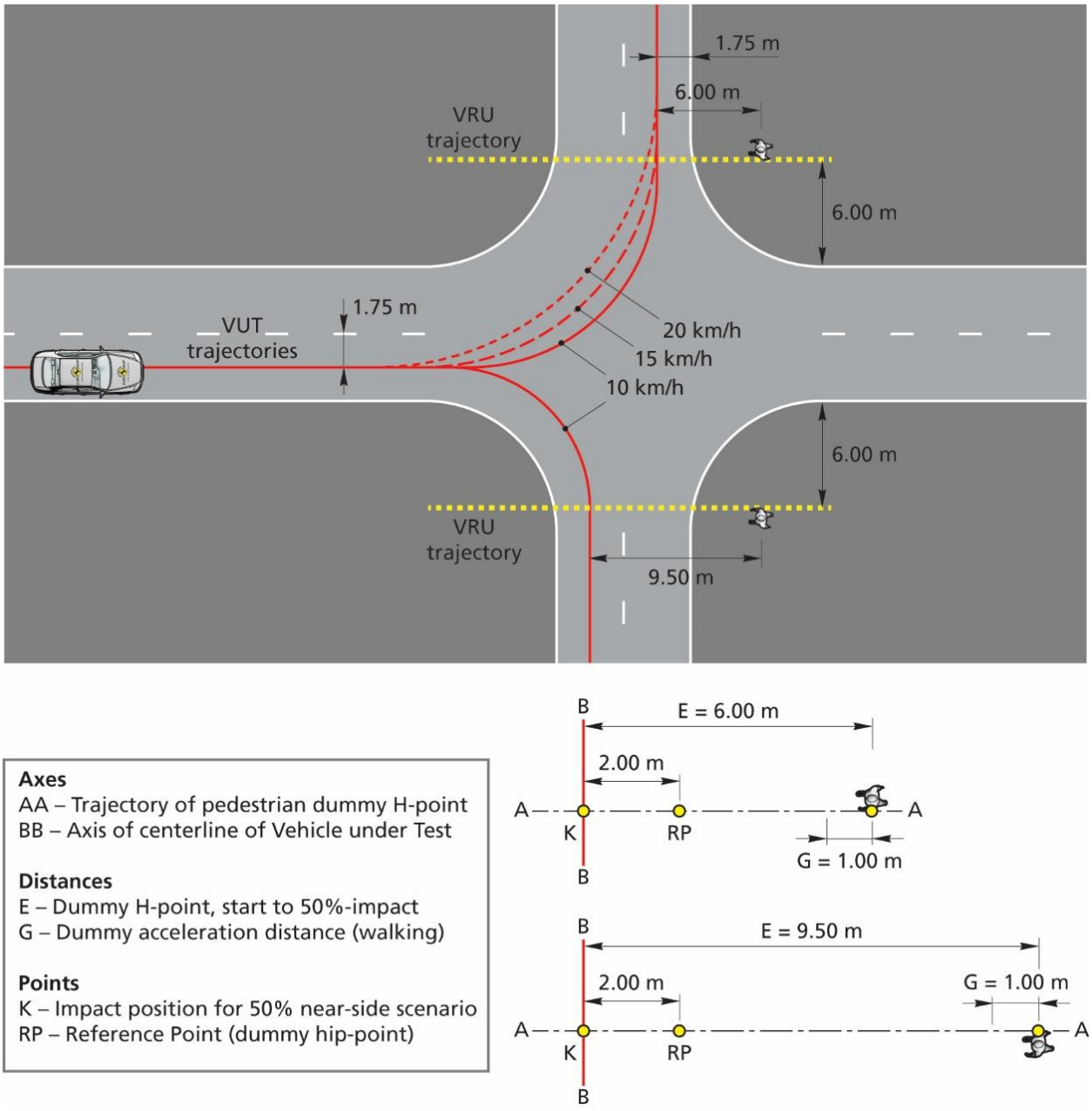

Figure 5. AEB Car-to-Pedestrian Turning (CPTA) scenarios

Emergency Steering Support

The already included Car-to-Car Rear stationary (CCRs) scenario is one of the cases where Emergency Steering Support is recognized as one of systems that help the driver avoiding the crash when responding to the FCW. As steering is most effective in lower overlap cases where minor lateral displacement is enough to avoid the collision, Euro NCAP only allows ESS in the low overlap cases.

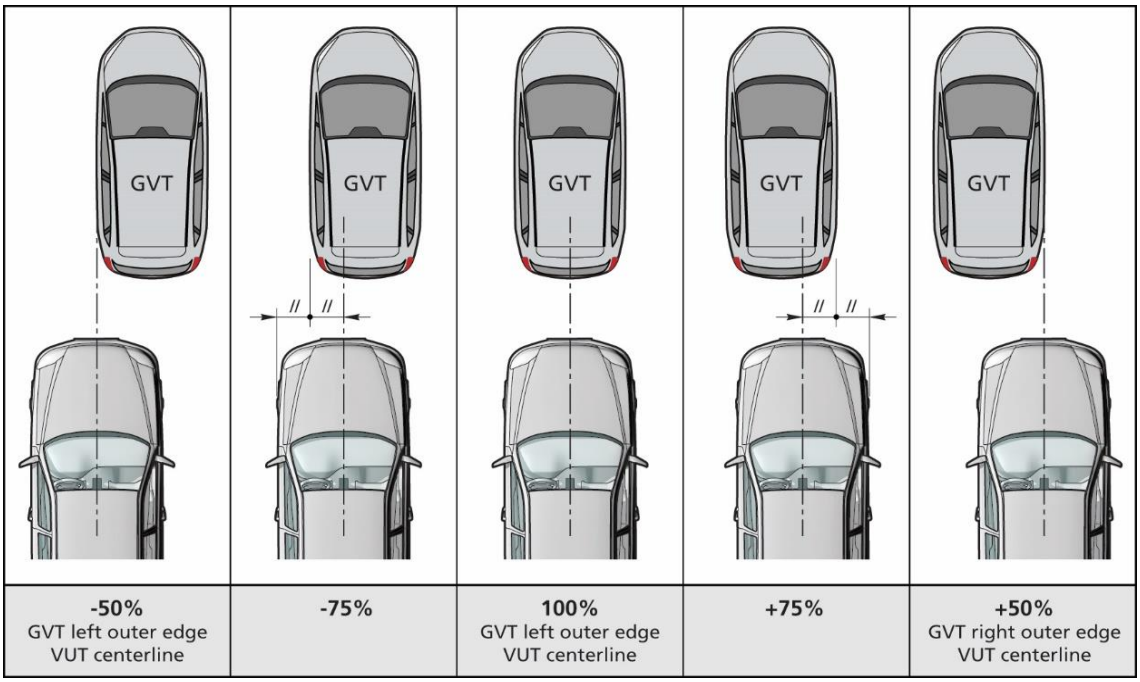

Figure 6. AEB Car-to-Car Rear stationary scenario where ESS is allowed in the -50% overlap case

Emergency Steering Support is allowed in both the longitudinal scenarios of Car-to-Pedestrian and Car-to-Bicyclist at small overlap situations. In these specific scenarios, a small lateral movement is the most adequate intervention to avoid the collision.

A specific test procedure has not been developed yet due to lack of experience with these systems and the large variety in logic within the limited amount of systems currently available on the market. At the moment, Euro NCAP will ask the car manufacturer wishing to have their ESS system performance assessed and included, to show the technical details and provide evidence that in cases of late driver steering intervention, the system will still be able to support the driver by optimizing or guiding the steering maneuver.

DISCUSSION

Test scenarios used for AEB/AES systems are a simplified and standardized representation of accident scenarios to ensure repeatable and reproducible test results. A significant correlation between the test track performance and the performance of the technology in real-life is not guaranteed. Requirements and possible sub optimization need to be constantly reviewed to ensure robust performance that will ensure continuous development of these live saving systems. On the other hand, more complex and more realistic test tools are required to ensure that the test environment are the best possible representation of situations occurring on real roads.

For the longer term, Euro NCAP is working on a more general scenario based approach where as part of the vehicle assessment, the car manufacturer would be asked to provide a performance prediction for all of the (critical) scenarios in a defined database with more complex and more realistic scenarios. To be able to validate the OEM performance, a combination of Vehicle in the Loop tests and simplified tracks would be required.

CONCLUSION

Euro NCAP puts more emphasis on extended capability and robustness of safety assist systems within its 2020 and 2022 rating schemes. Additional scenarios are added to cover a larger portion of accidents happening on the roads.

With the implementation of a combined AEB/AES assessment within the overall safety rating, Euro NCAP takes a first step towards a scenario-based assessment. This will offer the car manufacturer maximum flexibility to develop their active safety systems. With the upcoming General Safety Regulation, Euro NCAP keeps on pushing the performance of these live-saving systems, well beyond regulatory requirements in the years ahead.

REFERENCES

[1] Proactive Safety for Pedestrians and Cyclist, FP8-project PROSPECT, http://www.prospect-project.eu/

3D STROKE CALCULATION AND APPLICATION USING 6-DEGREE-OF-FREEDOM SENSORS

Suk Jae (Steve) Ham, Ben Meyers
Toyota Motor Engineering & Manufacturing North America
United States of America

Paper Number 19-0185

ABSTRACT

Time history of movement (stroke) is crucial information for crash test analysis. The stroke is often calculated from double integration of linear acceleration data when direct measurement by a potentiometer is impossible. But this method may not be accurate for the cases with large rotations. Newer crash tests like IIHS small overlap and NHTSA oblique involve large rotation, creating 3-dimensional (3D) occupant motions compared to front rigid barrier tests which are primarily 2D events. To help overcome some of the challenges posed by newer crash tests, the authors developed a method to calculate accurate 3D motion with 6-DOF (Degree-of-Freedom) instrumentation including angular rate sensors (ARS).

The calculation of accurate 3D position and orientation for a rigid body requires data collection of 6-DOF: linear acceleration (a_x, a_y, a_z) and angular velocity (ω_x, ω_y, ω_z). The mathematical calculation to account for rotation of a rigid body was done by using the screw-axis method. The quaternion was calculated using numerical integration via the 4th-order Runge-Kutta method.

A dynamic component test was designed and conducted with a linear impactor to validate the 3D stroke calculator. The test set up included a 6-DOF sensor pack mounted on a polyethylene stick with an offset. The stick was mounted on a base, which was pushed by a linear impactor with controlled speed. The sensor experienced 3D motion when the stick was decelerated by the base impacting a honeycomb backstop.

This method of 3D rigid body tracking has various crash testing applications. The authors compared occupant head kinematics among three different frontal offset crash modes. A finding of the study was that one test mode resulted in more driver head stroke (relative to vehicle interior) compared to the other two crash test modes. The maximum head stroke, compared to the least, was more by 64% (longitudinal) and 49% (lateral).

BACKGROUND AND PURPOSE

For crashworthiness engineers, time history of ATD (Anthropomorphic Test Devices) movement is necessary information to help analyze the performance of restraint systems. The movement, or stroke, is often calculated from double integration of linear accelerometers when direct measurement by a potentiometer is not available or too difficult. But this double integration method is may not be accurate enough for the ATD motions with large rotations. For example, a 5th%ile Hybrid III ATD in the front passenger seat experiences rotation (pitching) during rebound after loading the front passenger airbag (Figure 1) in NCAP front crash tests. As a simple solution, a 2D rotation matrix can be used for this type of crash test if pitching angular velocity was measured during the test.

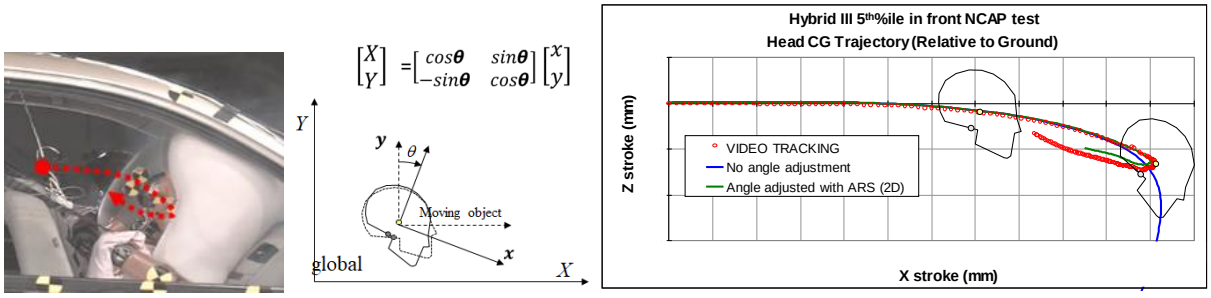

Figure 1. 5th%ile Hybrid III head stroke calculation for front impact crash test.

However, newer frontal crash tests like IIHS small overlap and NHTSA oblique tests, which have less overlap with the impact barriers, involve larger vehicle rotations than full-overlap frontal crash test. These test modes create complex 3D occupant motions compared to front rigid barrier tests. One example is the new NHTSA oblique test shown in Figure 2. In this test, the driver head experiences large rotation and no camera view is good for video tracking. Therefore, getting accurate head movement time history is very challenging. To overcome the challenge to calculate accurate 3D strokes in newer crash tests, the authors developed a calculator to get accurate motion with currently available instrumentation.

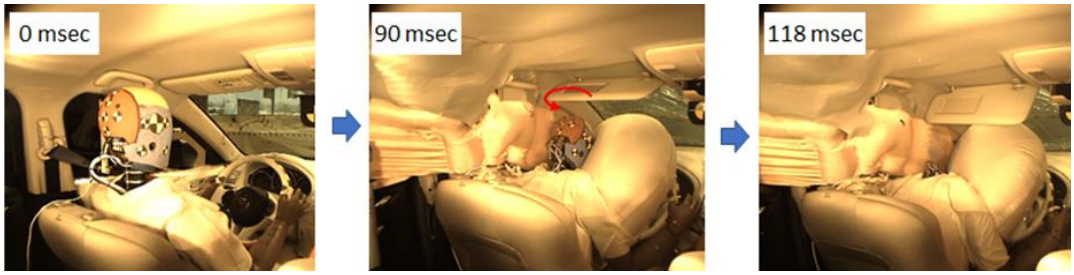

Figure 2. An example of NHTSA Oblique front impact test with large rotation of ATD head [1]

THEORY AND METHOD

To get accurate 3D position of a moving rigid body, like an ATD head in an offset crash test, all three linear accelerations need to be corrected by calculating three Euler angles by using measured angular velocities [2] before time integration or displacement (Figure 3).

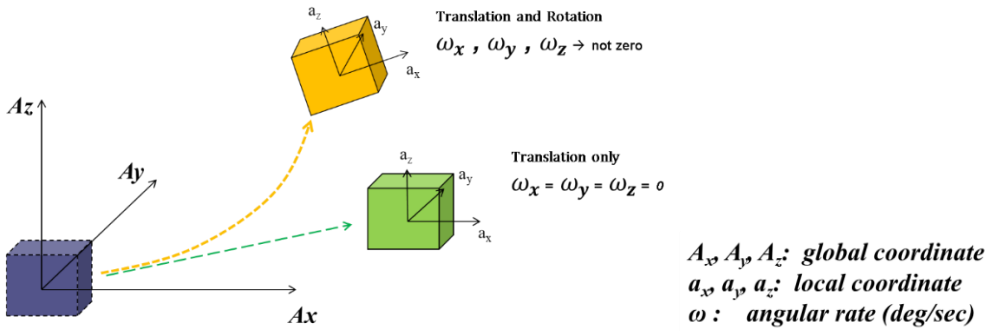

Figure 3. Consideration of angular rates for accurate 3-dimensional motions.

If all three angular velocities (ω_x, ω_y, ω_z, deg/second) are measured, along with linear accelerations, correction of linear acceleration can be done with a 3D rotation matrix **[R]** in figure 4. There are several methods to calculate the rotation matrix, but two methods, successive rotation and screw axis methods [3] were considered in this paper.

$$\begin{bmatrix} X \\ Y \\ Z \end{bmatrix} = [R] \begin{bmatrix} x \\ y \\ z \end{bmatrix}$$

Figure 4. Rotation matrix to adjust linear accelerations (X, Y, Z = corrected with angle and x, y, z = not corrected) [2].

The successive rotation angle method rotates 3 axes continuously to achieve a new position in each time step using angular rate data as shown in Figure 5. It is basically a 3D version of 2D adjustment shown in Figure 1. But this

method has two limitations which are Gimbal lock and complexity of calculation [2]. Gimbal lock is the case when there is more than one solution to the Euler angles calculated from angular velocities. The other challenge point is that this method requires complicated coding which could result in a higher chance of error, leading to a difficult debug process.

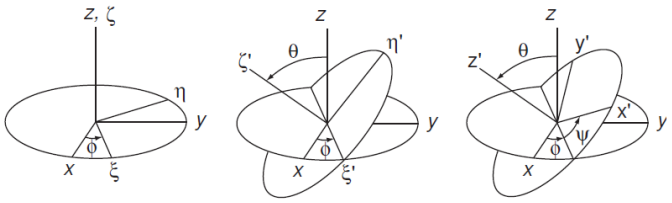

$$[R]= \begin{bmatrix} \cos\theta\cos\phi & \sin\psi\sin\theta\cos\phi-\cos\psi\sin\phi & \cos\psi\sin\theta\cos\phi+\sin\psi\sin\phi \\ \cos\theta\sin\phi & \sin\psi\sin\theta\sin\phi+\cos\psi\cos\phi & \cos\psi\sin\theta\sin\phi-\sin\psi\cos\phi \\ -\sin\theta & \sin\psi\cos\theta & \cos\psi\cos\theta \end{bmatrix}$$

Figure 5. Successive rotation angle method: Euler angles (ϕ, θ, ψ) and associated rotational matrix equation [2], [3].

The problem of Gimbal lock can be resolved by using Euler parameters, which are unit quaternions [2]. The screw axis method uses Euler parameters to calculate the 3D rotation matrix as shown in Figure 6. The unit vector $\vec{u}$ (Figure 6) is the axis for final rotation angle χ resulted from 3 Euler angle rotations. This study used the screw axis method for its simplicity in programming and freedom from Gimbal lock.

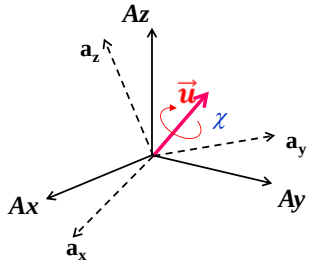

$$q_0=\cos\left(\frac{\chi}{2}\right),\quad \vec{q}=[q_1,q_2,q_3]=\vec{u}\sin\left(\frac{\chi}{2}\right),\quad q_0^2+q_1^2+q_2^2+q_3^2=1$$

$$[R]= \begin{pmatrix} q_0^2+q_1^2-q_2^2-q_3^2 & 2(q_1q_2-q_0q_3) & 2(q_1q_3+q_0q_2) \\ 2(q_2q_1+q_0q_3) & q_0^2-q_1^2+q_2^2-q_3^2 & 2(q_2q_3-q_0q_1) \\ 2(q_3q_1-q_0q_2) & 2(q_3q_2+q_0q_1) & q_0^2-q_1^2-q_2^2+q_3^2 \end{pmatrix}$$

Figure 6. Screw axis method: Euler parameters and rotation matrix equation with quaternions [2], [3]

To get the rotational matrix **[R]**, q_0 and $\vec{q}$ need to be calculated using angular velocities measured in the physical test. Quaternions are a function of angular velocity, and they form a series of ordinary differential equations as shown in Figure 7. Angular velocities ω_x, ω_y and ω_z are measured by ARS on a rigid body.

$$\begin{Bmatrix} \dot{q}_0 \\ \dot{q}_1 \\ \dot{q}_2 \\ \dot{q}_3 \end{Bmatrix} = \frac{1}{2}[Q]\begin{Bmatrix} 0 \\ \omega_b \end{Bmatrix}\quad ,\quad \text{Where, } \omega_b=\begin{Bmatrix} \omega_x \\ \omega_y \\ \omega_z \end{Bmatrix} \text{ and } \quad [Q]=\begin{bmatrix} q_0 & -q_1 & -q_2 & -q_3 \\ q_1 & q_0 & -q_3 & q_2 \\ q_2 & q_3 & q_0 & -q_1 \\ q_3 & -q_2 & q_1 & q_0 \end{bmatrix}$$

Figure 7. Time derivative of quaternions [2]

The authors calculated quaternions using numerical integration via the 4th order Runge-Kutta method [4]. Four unknown variables (quaternions) were expressed as a system of 4 ordinary differential equations, $\boldsymbol{f1}$, $\boldsymbol{f2}$, $\boldsymbol{f3}$ and $\boldsymbol{f4}$ shown below. The authors used MS Excel® to calculate quaternions, the rotational matrix **[R]** and the adjusted position of the rigid body. The inputs were 6-DOF data (3 linear accelerometers and 3 ARS) of two objects (i.e. ATD head and vehicle body) and the outputs are the corrected stroke of both objects.

$$\dot{q}_0 = \frac{-q_1\omega_x - q_2\omega_y - q_3\omega_z}{2} = f1$$

$$\dot{q}_1 = \frac{q_0\omega_x - q_3\omega_y + q_2\omega_z}{2} = f2$$

$$\dot{q}_2 = \frac{q_3\omega_x + q_0\omega_y - q_1\omega_z}{2} = f3$$

$$\dot{q}_3 = \frac{-q_2\omega_x + q_1\omega_y + q_0\omega_z}{2} = f4$$

VALIDATION

To validate the calculation method, a component test was devised to create a complex motion path of a known point. The component test setup allowed for accurate video analysis at multiple angles (top & side) of this point, as seen in Figures 8 and 9. At this known point, a 6-DOF sensor pack was installed. The purpose of the test was to calculate the path of the point using the 3D calculator with the 6-DOF sensor pack, and then compare the calculation result to the known motion of that point based on accurate video tracking.

The component test was comprised of a platform that could slide on tracks toward a rigid wall which would stop the platform's motion. A section of honeycomb was fixed to the wall to reduce the peak g experienced by the platform. A 5/8" diameter flexible plastic (polyethylene terephthalate) shaft approximately 2 feet in length, extending vertically, was attached to the platform. At the top of the shaft was a plate where the 6-DOF pack was mounted. The sensor pack was aligned to the platform so that the platform's sliding motion would be the X-axis, vertical from gravity would be the Z-axis, and the remaining orthogonal axis would be the Y-axis. A cantilever mass was attached to the shaft, offset in the Y-axis at a height of 18" from the base. The purpose of the mass was to introduce a twisting motion of the shaft when the platform was stopped by the rigid wall.

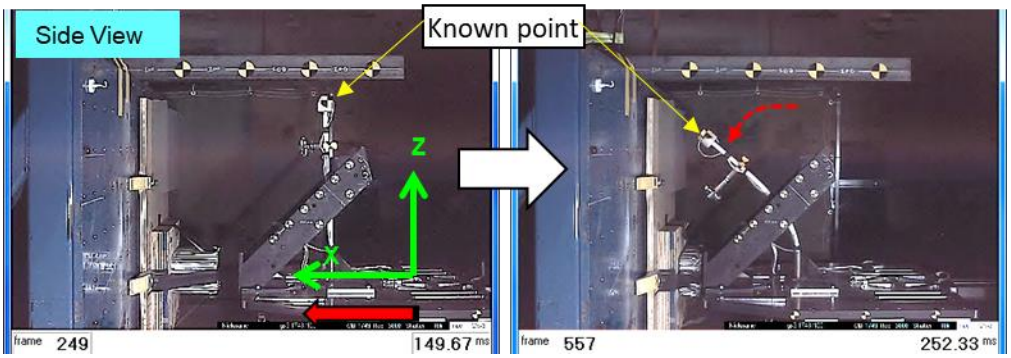

Figure 8. Side view of component test before impact with the rigid wall (left) and when the shaft is at peak forward rotation (right).

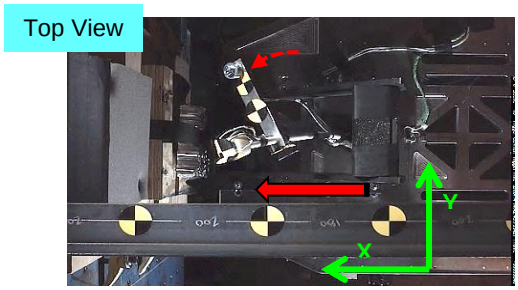

Figure 9. Top view of component test showing axial rotation of the shaft.

The result of the component test matched the calculation result explained in this paper as shown in Figure 10. Red color is the calculated stroke and blue is by video analysis. The calculated stroke data showed close correlation to video analysis. For comparison, the calculation result without 3D angular correction is also shown (green).

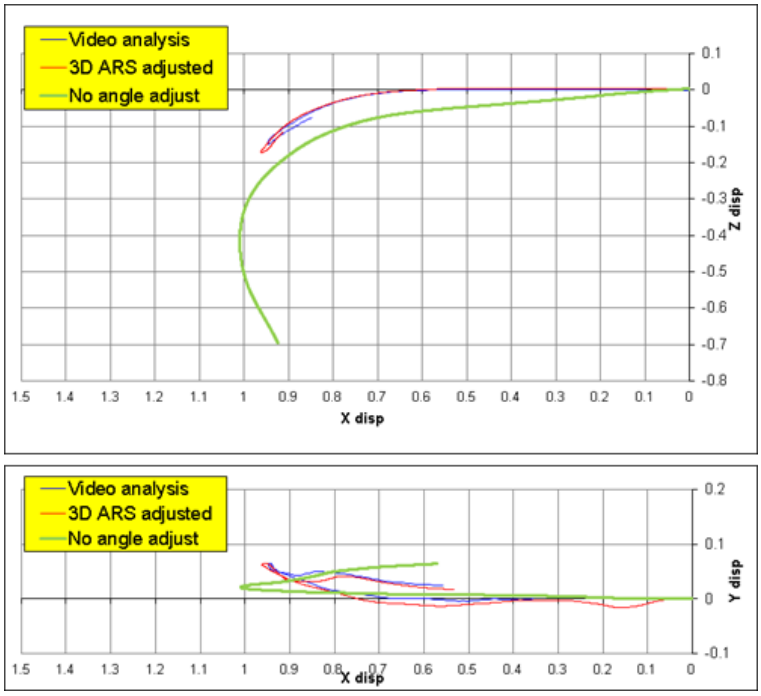

Figure 10. Comparison of results observed by video analysis vs 3D angular rate (ARS) correction calculation method vs original calculation method without angle adjust.

APPLICATION EXAMPLES AND DISCUSSIONS

The authors applied the 3D calculation method to two crash tests. The first application was a comparison of the front passenger head trajectory in an NCAP frontal impact sled test. In most cases, off-board video tracking can provide accurate head stroke information but, in some cases, the video target on the head C.G. becomes invisible due to the passenger airbag or the side curtain airbag blocking the camera view. In either case, 3D stroke calculation can be an alternative to video tracking. Figure 11 shows an example of this application to a front NCAP case study. As shown in Figure 11, maximum head stroke in the longitudinal and vertical axis are distinguishable from test to test, even though the head target was not visible.

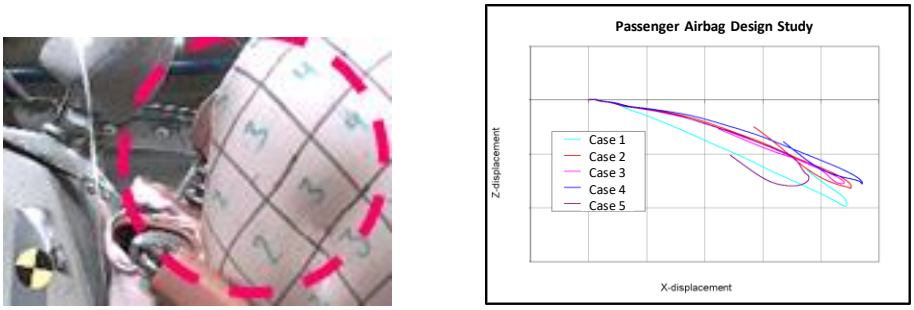

Figure 11. Example of head stroke analysis (Hybrid III 5th%ile head stroke in front NCAP sled test).

Another example was to compare a driver ATD head motion in three different frontal offset crash modes (TESTS A, B and C). The goal was to compare the maximum head stroke (relative to vehicle) in three (x, y and z) directions. The three test modes had different impact speeds, barrier types and amounts of overlap. Two of the tests used Hybrid III 50th%ile and the other used a THOR 50th%ile. All three tests were done with the same vehicle model for direct comparison. Data from 6-DOF sensors were measured for both the ATD head and the vehicle floor to calculate relative stroke. Head stroke results in side and top views are shown in Figure 12. In the case of TEST A, it had the largest stroke observed in all three directions. Compared to test B, maximum stroke was greater by 64% in the longitudinal direction and 49% in the lateral direction. Also, the head moved up (relative to vehicle interior) in early timing due to vehicle pitching.

The application is not limited to the examples shown in this paper. Crash tests with large vehicle rotation can get benefit from this 3D calculator as long as 6-DOF data were measured properly.

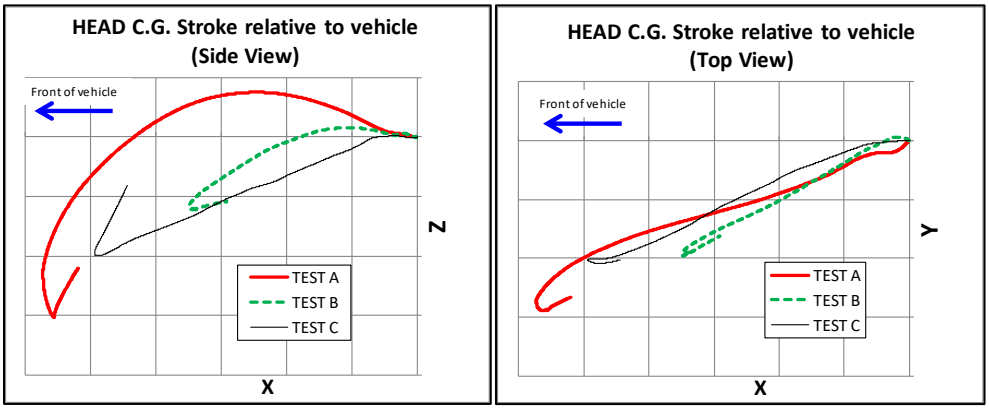

Figure 12. Example of head stroke calculation method – Comparison ATD head CG stroke relative to vehicle for three different frontal offset crash modes.

CONCLUSION

The 3D stroke calculator was developed using the screw-axis method and 4th-order Runge Kutta integration in this study. The calculator was validated by component testing, which demonstrated more accuracy than double-integration methods without angular correction. Example studies using the 3D calculator provided accurate stroke of an ATD head relative to the vehicle which could be valuable data for occupant restraint strategy and performance analysis. Furthermore, this 3D calculator could be used on any two rigid-body system with 3D rotational kinematics as long as 6-DOF sensor data and initial condition are measured.

LIMITATIONS

Theoretically, the method looks promising but there are limitations in actual application. The first limitation is that accurate initial conditions (position and angle relative to the ground) are necessary because this method is a typical initial value problem with explicit time integration. Also, the authors observed that the ARS could give invalid data if the ARS did not include shock-resistance feature or if the sensor mount location on the vehicle was involved in local deformation. The authors recommend the use of shock-resistant ARS mounted in an area with no deformation on the vehicle.

REFERENCES

[1] National Highway Traffic Safety Administration, "Vehicle Crash Test Database" (https://www-nrd.nhtsa.dot.gov/database/VSR/veh/QueryTest.aspx). Accessed on FEB 13, 2019.

[2] A. L. Schwab, "How to draw Euler Angles and Utilize Euler Parameters". ASME 2006 IDETC/CIE, 2006.

[3] TNO, MADYMO version 5 theory manual, 1999.

[4] Chapra, S. C., Canale,R.P, Numerical Methods for Engineers, 6th ed., page 707~737, McGraw-Hill, New York, N.Y., 2010.

[5] Jianping Wu et al, "Using Triaxial Angular Rate Sensor and Accelerometer to Determine Spatial Orientation and Position in Impact Tests", SAE 2009-01-0055.

OPTIMIZATION OF FRONT END STRUCTURES FOR IIHS SMALL OVERLAP FRONTAL CRASH TEST

Guofei Chen and Ming F. Shi
United States Steel Corporation
USA

Tau Tyan
Ford Motor Company
USA

Paper Number 19-0188

ABSTRACT

The Insurance Institute for Highway Safety (IIHS) introduced a small overlap rigid barrier (SORB) crash test in 2012. In the IIHS SORB tests, the rigid barrier primarily impacts a vehicle's outer edges instead of the main longitudinal structures traditionally designed to absorb frontal impact energy. Due to the test condition, the front wheels are often forced to move rearward and into the footwell, contributing to significant and localized intrusion in the occupant compartment. To investigate the design countermeasures for such a severe test mode, the full vehicle model developed in the final phase of the Future Steel Vehicle (FSV) program by WorldAutoSteel was adopted as a baseline. In this study, innovative countermeasure design concepts for the front end structures, especially bumper beam, shotgun, front rail, A-pillar, hinge pillar, and rocker, were proposed and optimized with the FSV full vehicle model. The optimized designs helped the vehicle slide away from the small overlap rigid barrier and converted more impact energy to vehicle kinetic energy. When used together with ultra high strength steel (UHSS), the intrusion into the occupant compartment was reduced and the overall structural rating was improved from “Marginal” to “Good” in the SORB test. In the meantime, the design concepts reduced intrusion in the IIHS 40% overlap deformable barrier (ODB) test and maintained a similar crash pulse in the US-NCAP full frontal crash test. The potential mass reduction opportunity with the design concepts and UHSS was also evaluated.

INTRODUCTION

Over the last several decades, tremendous progress in vehicle frontal crash performance has been achieved. The automotive community has made considerable efforts in developing optimized crumple zone structures with higher strength materials such as advanced high strength steels (AHSS) to absorb the crash energy.

In 2012, the IIHS released the more demanding frontal offset test named the small overlap rigid barrier (SORB) crash test [1, 2]. The new test, which is used in addition to the 40% overlap deformable barrier (ODB) test introduced in 1995, subjects only 25% of the front end of the vehicle to a 64.4 km/hr (40 mph) impact into a 1524-mm-tall (5 feet) rigid barrier. The new test is far more demanding on the vehicle structures than the 40% ODB test. What makes the small overlap crash test so challenging is that the outer front wheel receives the impact forces first rather than the more central crash absorbing structures such as the longitudinal structural members. The crash forces are concentrated on the front suspension, the firewall, the hinge pillar and the base of the A-pillar, which are not traditionally designed to absorb and dissipate crash forces in a front impact.

The vehicle performance in the IIHS small overlap frontal crash test is rated based on three categories: restraints and dummy kinematics, dummy injury measures, and vehicle structural performance [3]. Since the release of the IIHS SORB crash test protocol, the IIHS has evaluated numerous midsized and small cars, with few vehicles earning the top rating of good, particularly due to the structural performance rating. Most of the vehicles on the road in 2012 could not meet the targets for a ‘good’ rating in this test and all vehicle manufacturers started incorporating counter measures to improve SORB performance [4].

The advancement in computer optimization technologies and the availability in higher strength of AHSS in GigaPascal-strength levels provide opportunities to develop countermeasure designs to improve the overall

structural rating in the SORB crash test. In this study, a full vehicle finite element model was utilized in the SORB crash test simulation to identify the critical components contributing to the performance in the SORB crash event. Innovative countermeasure design concepts with ultra high strength steels (UHSS) were developed and optimized for the front end structures, especially bumper beam, shotgun, front rail, A-pillar, hinge pillar, and rocker. The potential vehicle weight reduction opportunity with the optimized design concepts and UHSS was also evaluated.

SORB CRASH SIMULATION MODEL

The full vehicle finite element model developed in the final phase of the Future Steel Vehicle (FSV) program [4] by WorldAutoSteel in 2011 was adopted as the baseline in this study, as shown in Figure 1. The FSV features optimized AHSS body structure designs that reduce mass by more than 35 percent over a baseline ICE body structure adjusted for a battery electric powertrain. More than 20 new AHSS grades, representing materials expected to be commercially available in the 2015 – 2020 technology horizon, are applied in the FSV final concept designs. The material portfolio includes dual phase (DP), transformation-induced plasticity (TRIP), twinning-induced plasticity (TWIP), complex phase (CP) and hot formed (HF) steels, which are the newest in steel technology offered by the global industry. The FSV uses 97 percent HSS and AHSS with nearly 50 percent of the steels at GigaPascal-strength levels.

The FSV front end structures feature:

- A front rail sub-system with the optimized section shape of the rails that improved crash energy management while reducing mass. It was manufactured using a laser welded blank with varying gauges of TRIP material.
- A shotgun sub-system resembling a shotgun-type rifle that provided enhanced performance in both full frontal and offset crash simulations. The shot gun was designed with a three-piece hot formed steel tailor welded blank of varying thicknesses.

The FSV final concept designs met a broad list of global crash and durability requirements, including the US-NCAP and the IIHS 40% ODB frontal crash criteria. Since FSV was developed before the SORB crash test was introduced in 2012, the SORB crash test was not considered in the FSV program.

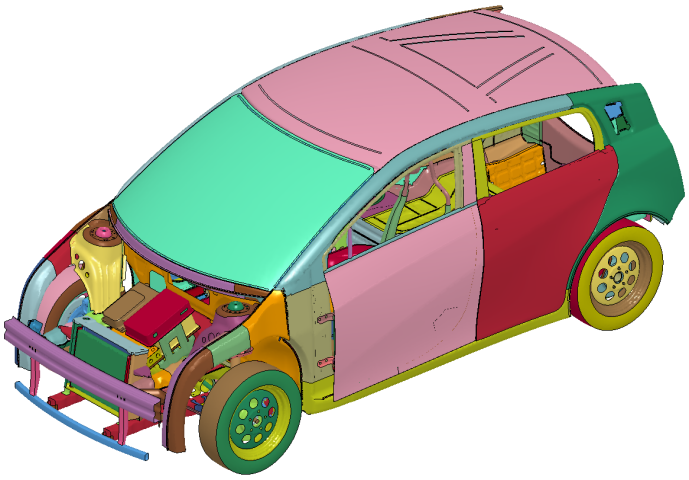

Figure 1. FSV full vehicle finite element model

In this study, the crash simulation model for the SORB test was developed using the FSV final concept design as the baseline, as shown in Figure 2. The vehicle was aligned with a rigid barrier such that the right edge of the barrier face is offset to the left of the vehicle centerline by 25 percent of the vehicle's width [2]. The vehicle crashed into the 1524-mm-tall (5 feet) rigid barrier at 64.4 km/hr (40 mph) speed.

The structural rating is based on intrusion measurements on selected points at the lower occupant compartment and the upper occupant compartment [2, 3]. The lower occupant compartment points include the lower hinge pillar, footrest, left toepan, brake pedal, parking brake pedal, and rocker panel measurements. The upper occupant compartment points include the steering column, upper hinge pillar, upper dash, and left instrument panel. The intrusion measurements for the FSV in the SORB crash simulation are shown in Figure 3. The subrating for the lower occupant compartment is "Good" and the subrating for the upper occupant compartment is "Marginal", therefore the overall structural rating for the FSV is "Marginal" in the SORB crash test.

Table 1 lists the top seven components in crash energy absorption in the SORB crash test along with the steel grades and gauges used in the FSV baseline design. As the front rail crash tip is located outside of the rigid barrier, the shotgun becomes the most important component to engage with the barrier and absorb the crash energy. Other critical components include the front rail rear, rocker, wheel rim, hinge pillar and A-pillar when the front wheel is forced to move rearward and crash into the footwell of the occupant compartment. The bumper beam absorbed less crash energy than those of other components because the bumper beam in the FSV design is short and located at the arc portion of the rigid barrier. The bumper beam immediately slid away from the barrier in the SORB crash test, resulting in reduced crash energy absorption. However, as the first structural member to engage with the crash barrier, the importance of the bumper beam should not be underestimated. A sensitivity study was conducted on the bumper beam length effect. Figure 3 shows that the intrusion into the occupant compartment decreased when the bumper beam was extended outward to align with the body width. The extended bumper beam enlarged the impact zone to help absorb more impact energy and increase vehicle lateral movement.

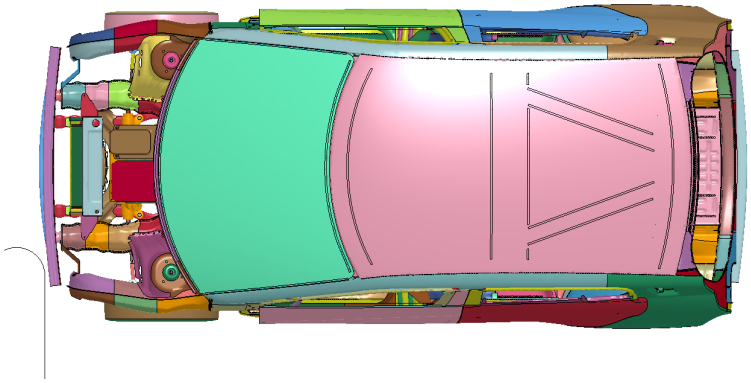

Figure 2. FSV crash simulation model for the SORB test – top view

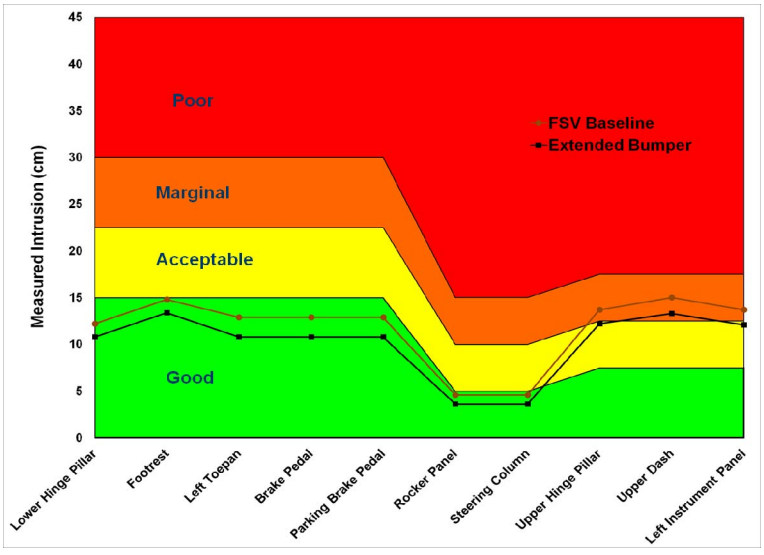

Figure 3. The effect of bumper beam extension in the SORB crash test

Table 1.
Top components in SORB crash energy absorption

Part Name	Material	Gauge (mm)	Energy Absorbed (kJ)	Percentage (%)
Shotgun	HF1550	1.0/1.2/1.5	17.80	11.41
Front Rail	TRIP980	1.8/2.0/1.9/1.8	9.00	5.77
Rocker	CP1470	1.0	8.85	5.67
Wheel Rim	HSLA350	2.0	7.56	4.85
Hinge Pillar	DP780	1.2	6.55	4.20
A-Pillar	HF1550	0.7	5.64	3.62
Bumper Beam	DP780	1.0	3.46	2.22

DESIGN OPTIMIZATION FOR THE SORB

In this study, the bumper beam, shotgun, front rail, A-pillar, hinge pillar, and rocker were selected in the design optimization, including geometry, gauge and steel grade optimization. Before the geometry optimization, the FSV front end structures were modified. The bumper beam was extended outward and the shotgun was extended forward into the extended bumper beam. Then, the shot gun was connected with the front face of the extended bumper beam by bolt joints or spot welds to strengthen the front end side structures so that both the shot gun and the bumper beam can engage with the barrier earlier during the initial impact. As a result, the impact loads could be distributed to the upper and lower body structures. In addition, more impact loads could be transferred to the non-impact side than a traditional design with only the front rails connected to the bumper beam.

The shape variables in the geometry optimization include the extension length of the bumper beam and the transition shape of the shotgun from the body side to the bumper beam. The objective of the optimization is to improve the overall SORB structural rating to “Good” from “Marginal” in the FSV baseline design without mass penalty. In the meantime, the baseline design is optimized to maintain or enhance crash performance in the IIHS 40% ODB and US-NCAP full frontal crash tests. HyperStudy® optimization software and LS-DYNA® nonlinear finite element software were utilized together for the geometry, gauge and steel grade optimization [5, 6].

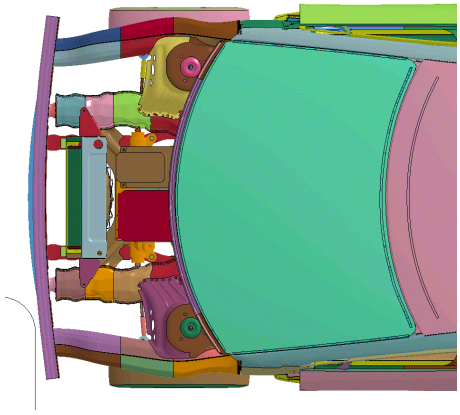

Figure 4. Connection between the shot gun and the extended bumper beam

OPTIMIZED DESIGN CONCEPTS

An optimized design concept for the SORB crash test is shown in Figure 5. It features:

- An extended bumper beam at both ends. The bumper beam was extended as far as possible to align with the body width. The extended bumper beam would enlarge the impact zone to help absorb more crash energy and increase vehicle lateral movement.
- A new connection between the shotgun and the front face of the extended bumper beam. The system with the bumper beam integrated both the shotgun and front rail would strengthen the front end side structures,

engage the shotgun with barriers earlier, distribute impact load to upper and lower body structures, and transfer more impact load to the non-impact side than traditional design with only front rails connected to the bumper beam.

- A shape optimized shotgun with a "snake-shaped" transition from the body side to the corner of the rigid barrier. The optimized shape of the shotgun would increase the vehicle lateral movement by helping the vehicle slide away from the barrier and converting the impact energy to the vehicle kinetic energy. Figure 6 shows the comparison of vehicle lateral movement of the optimized new design with the FSV baseline in the SORB crash test.

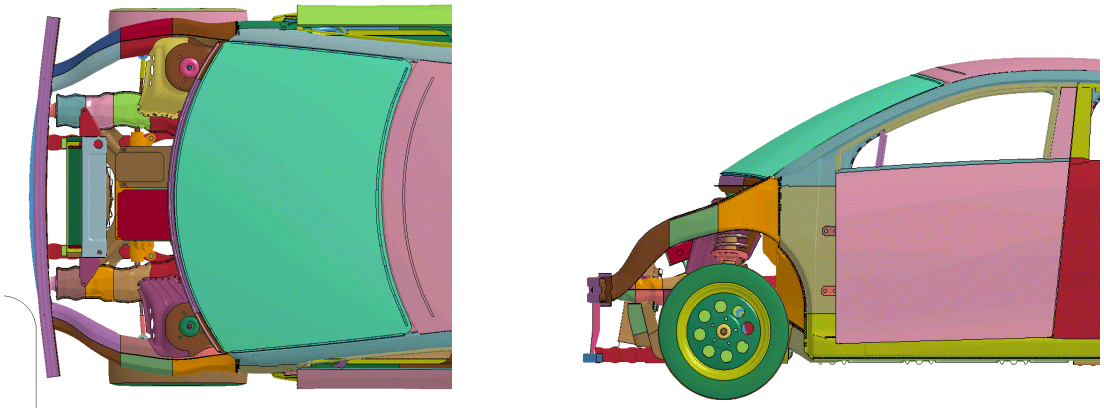

(a) Top view *(b) Side view*

Figure 5. An optimized design concept for the SORB crash test

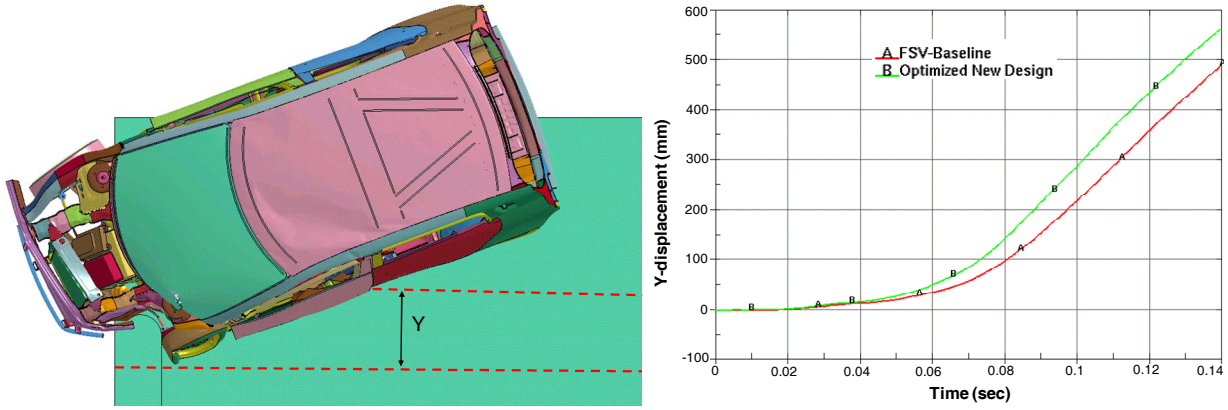

(a) Vehicle lateral movement *(b) Comparison*

Figure 6. Comparison of vehicle lateral movement in the SORB test

Figures 7 and 8 show the comparison in the vehicle deformation and intrusion into the occupant compartment from the SORB test, respectively. Since the optimized new design helped the vehicle slide away from the SORB, less deformation was observed at the shotgun, hinge-pillar, rocker, roof rail and tire in the optimized new design. As a result, the intrusion into the occupant compartment was reduced, and the overall SORB structural rating was improved to "Good" from "Marginal" in the FSV baseline design.

The optimized shotgun and bumper beam also helped transfer the impact force to the non-impact side and reduced deformation/intrusion on the impact side in the IIHS 40% ODB frontal crash test, as shown in Figure 9(a). The intrusion was improved further to a "Good" structural rating with a higher probability and confidence level.

As both the front rails and the shotgun are connected to the bumper beam, one concern is that the front-end structures may be too stiff and can deteriorate the vehicle crash performance such as the deceleration pulse in the US-NCAP frontal crash test. Figure 9(b) shows the optimized new design had similar pulse responses in the NCAP full frontal test to that of the FSV baseline design, allowing similar occupant responses. This was achieved by slightly reducing the gauges of the front rails, as shown in Table 2, to balance the stiffness of the front rails and the shotgun as both of them were connected to the bumper beam.

Table 2 compares the materials, gauges and mass between the optimized new design and the FSV baseline design for some key components. More ultra high strength steels (UHSS) such as TRIP980 and HF1550 were used in the optimized new design. The total mass of the optimized new design remains similar to that of the FSV baseline with the intrusion reductions in both the IIHS SORB and the 40% ODB crash tests.

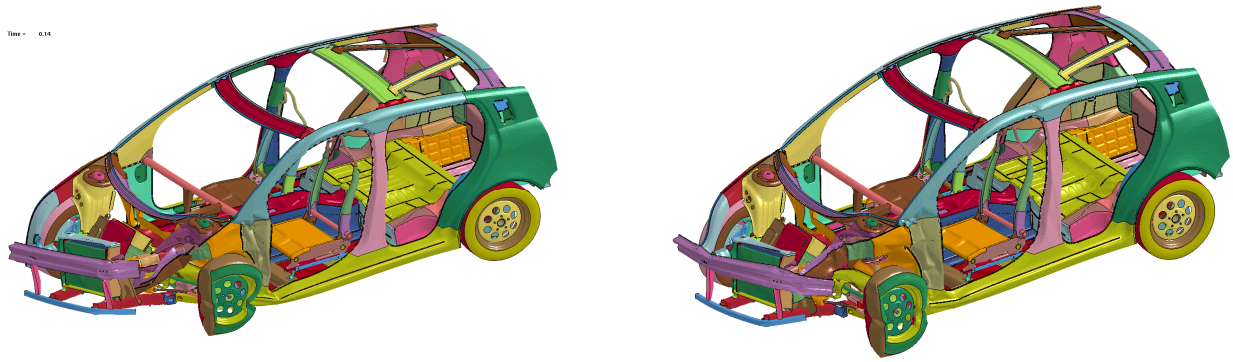

(a) FSV baseline *(b) Optimized design for SORB*

Figure 7. Comparison of vehicle deformation in the SORB test

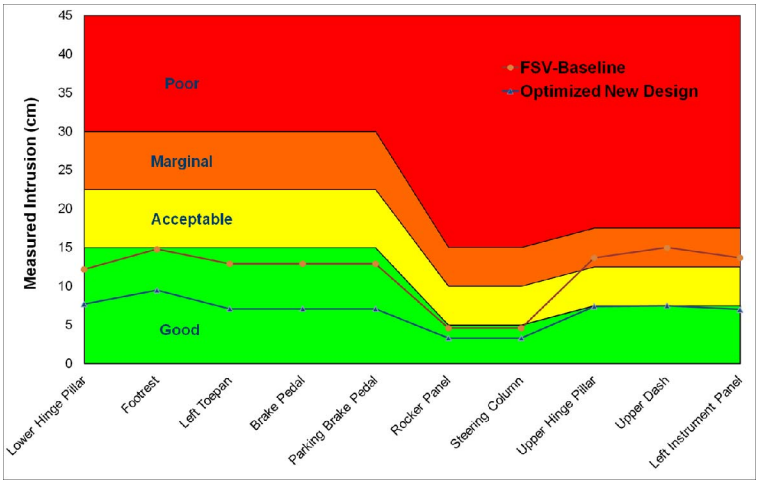

Figure 8. Comparison of intrusion in the SORB test

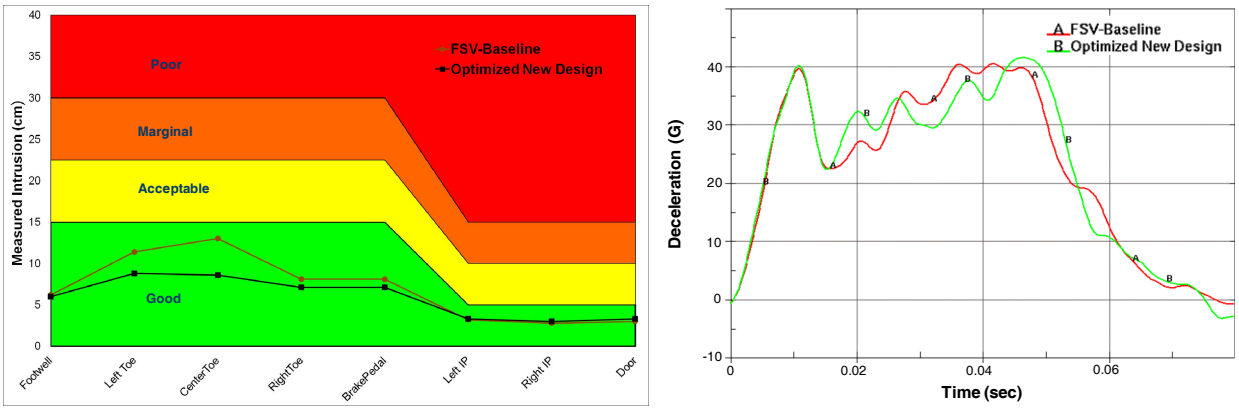

(a) IIHS 40% ODB *(b) US-NCAP*

Figure 9. Comparison of crash performance in the IIHS 40% ODB and the US-NCAP tests

Table 2.
Optimized materials and gauges for key components

	FSV-Baseline			Optimized New Design		
Part Name	**Material**	**Gauge (mm)**	**Mass (kg)**	**Material**	**Gauge (mm)**	**Mass (kg)**
Shotgun	HF1550	1.0/1.2/1.5	8.9	HF1550	1.2/1.2/1.3	8.5
Bumper Beam	DP780	1.0	3.7	HF1550	0.8	3.5
Rocker Reinf	CP1470	1.0	11.9	CP1470	1.2/1.0	12.7
Rocker Outer	DP590	0.8	6.2	TRIP980	0.8	6.2
Hinge Pillar Inner	DP780	1.2	3.3	HF1550	1.2	3.3
Hinge Pillar Outer	DP590	0.8	2.5	TRIP980	0.8	2.5
A-Pillar Inner	HF1550	0.7	1.7	HF1550	0.7	1.7
A-Pillar Outer	DP590	0.8	5.3	TRIP980	0.8	5.3
Roof Rail Inner	HF1550	0.95/0.8	2.1	HF1550	0.95/0.8	2.1
Roof Rail Reinf	HF1550	0.7	4.1	HF1550	0.7	4.1
Front Rail	TRIP980	1.8/2.0/1.9/1.8	18.7	TRIP980	1.8/1.9/1.8/1.8	18.5
		Total Mass (kg)	**68.4**			**68.4**

It is noticed from Figure 7(b) that the front wheel was still forced rearward into the footwell, causing the deformation of the rocker and hinge pillar. To alleviate the impact from the front wheel, a second design concept was proposed based on the previous design concept by optimizing the directions the bumper beam to be extended. As shown in Figure 10 for optimized design concept #2, the straight outward extension in the previous design concept was modified by extending the bumper beam:

- Rearward to be as close as possible to the front edges of the front wheel;
- Downward to be as close as possible to the centerline of the front wheel.

During the impact in the SORB test, the extended bumper beam is intended to move rearward to contact with the outer edges of the front wheel and subsequently to turn the front wheel outward. To turn the front wheel more effectively, the bumper beam was designed with a tailor-welded-blank (TWB) or two parts joined together with a relatively stiffer outside portion.

Figure 11(a) shows the deformation of optimized design concept #2 in the SORB test. As the intended design, the front wheel was turned outward by the bumper beam to reduce the direct impact force from the front wheel to the rocker and hinge pillar. When compared to the deformation of optimized design concept #1 shown in Figure 7(b), optimized design concept #2 had less deformation in the rocker, hinge pillar and the roof rail. Consequently, the intrusion into the occupant compartment was reduced by 2 cm, as shown in Figure 11(b). Optimized design concept #2 further improved the structural rating to "Good" for the upper occupant compartment with higher probability and confidence level, enabling mass reduction while maintaining the "Good" overall structural rating.

Materials and gauges for the two optimized design concepts are compared in Table 3. In optimized design concept #2, the gauges of the bumper beam were increased to 1.2 mm for its outside portions, while the front and middle portions of the TWB shotgun were downgauged to 0.6 and 0.8 mm, respectively. Because concept #2 changed the front wheel kinematics, the front portion of the TWB rocker reinforcement and the rocker outer could be downgauged by 0.1 mm. Total mass reduction of 1.3 kg was achieved with optimized design concept #2, while maintaining the "Good" overall structural rating.

THE NEXT GENERATION AHSS

The current study focused on the countermeasure design optimizations using the available steels grades used in the FSV vehicle model. Since then, the next generation AHSS with an excellent combination of strength and ductility have become available and been commercialized. For example, U. S. Steel's third generation steel with 980 MPa minimum tensile strength (980 XG3^{TM} steel) has comparable crash performance to HF1550 with minimum weight penalty [8, 9]. It was demonstrated that same gauged 980 XG3^{TM} steel could replace hot formed HF1550 steel for hinge pillars for a sedan with complex geometry, and achieved a "Good" rating in IIHS SORB crash test [9]. The benefits of cold-stamping versus hot-stamping include cost reduction and improved corrosion protection.

Other currently available next generation AHSS are:

1. Super high formable steel with 1180 MPa minimum tensile strength (1180SHF);
2. Martensitic steel with 1500 MPa minimum tensile strength (MS1500);
3. Martensitic steel with 1700 MPa minimum tensile strength (MS1700);
4. Dual phase steel with 1470 MPa minimum tensile strength (DP1470).

Table 4 shows the potential material recommendation with the next generation AHSS, which have equivalent strength and improved ductility compared to the steel grades used in the FSV model. 980 XG3^{TM} steel can be used to replace HF1550 and TRIP980 for the shotgun, hinge pillars, A-pillar outer, front rail and rocker outer. The HF1550 bumper beam, rocker reinforcement and roof rail can be replaced with MS1500/MS1700, DP1470 and 1180SHF, respectively. The flow stresses of the cold-stamped 980 XG3^{TM} and 1180SHF parts can match that of the hot-stamped HF1550 parts when the work and bake hardening effects are considered. The 980 XG3^{TM} and 1180SHF steels also demonstrate greatly improved fracture resistance performance during crash events because their fracture limit strains are significantly higher than that of HF1550 [10, 11]. It is expected to achieve similar crash performance with the next generation AHSS for the two optimized designs shown in Table 3 at similar mass savings, but reduced costs.

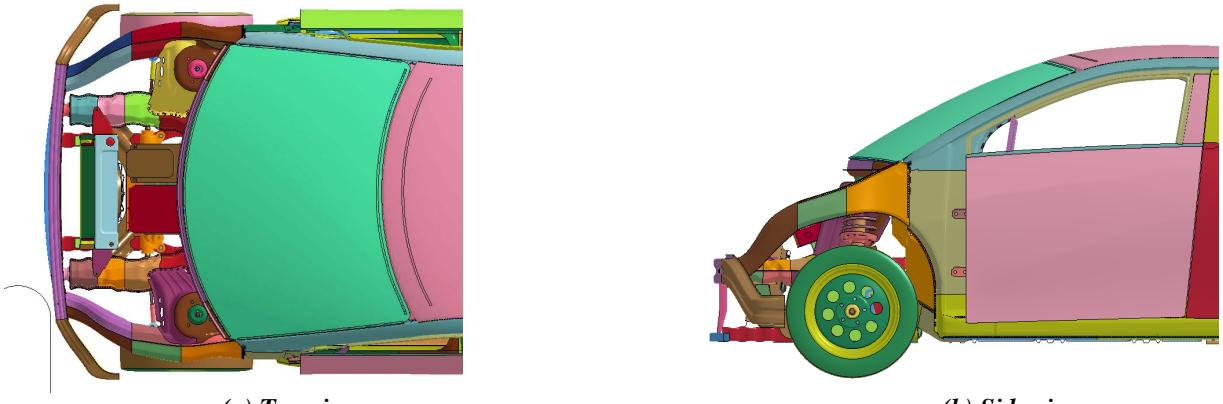

(a) Top view ***(b) Side view***

Figure 10. Optimized design concept #2 for SORB

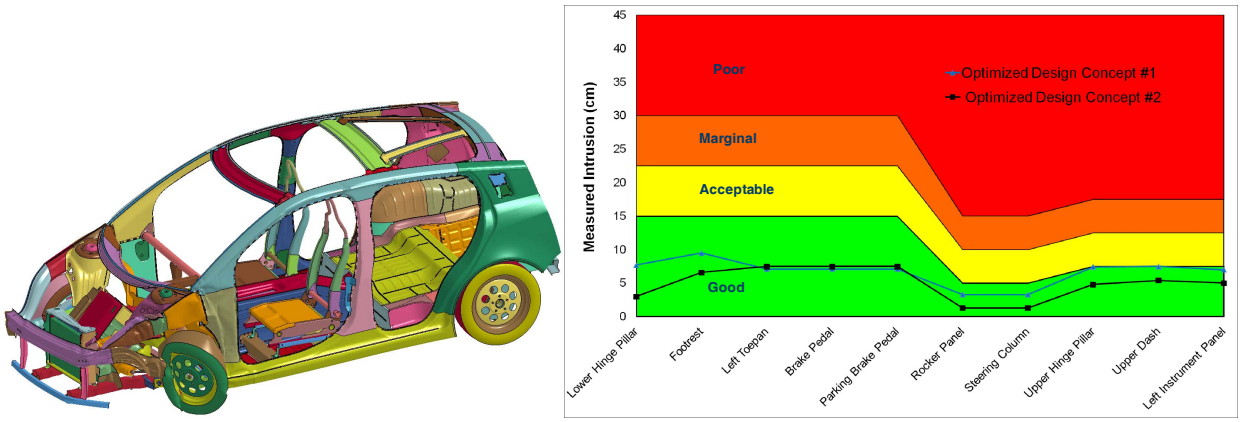

(a) Deformation *(b) Intrusion*

Figure 11. The optimized design concept #2 in the SORB test

Table 3.
Materials and gauges for the two optimized design concepts

	Optimized Design Concept #1			Optimized Design Concept #2		
Part Name	**Material**	**Gauge (mm)**	**Mass (kg)**	**Material**	**Gauge (mm)**	**Mass (kg)**
Shotgun	HF1550	1.2/1.2/1.3	8.5	HF1550	0.6/0.8/1.3	6.2
Bumper Beam	HF1550	0.8	3.5	HF1550	0.8/1.2	5.6
Rocker Reinf	CP1470	1.2/1.0	12.7	CP1470	1.1/1.0	12.4
Rocker Outer	TRIP980	0.8	6.2	TRIP980	0.7	5.4
Hinge Pillar Inner	HF1550	1.2	3.3	HF1550	1.2	3.3
Hinge Pillar Outer	TRIP980	0.8	2.5	TRIP980	0.8	2.5
A-Pillar Inner	HF1550	0.7	1.7	HF1550	0.7	1.7
A-Pillar Outer	TRIP980	0.8	5.3	TRIP980	0.8	5.3
Roof Rail Inner	HF1550	0.95/0.8	2.1	HF1550	0.95/0.8	2.1
Roof Rail Reinf	HF1550	0.7	4.1	HF1550	0.7	4.1
Front Rail	TRIP980	1.8/1.9/1.8/1.8	18.5	TRIP980	1.8/1.9/1.8/1.8	18.5
		Total Mass (kg)	**68.4**			**67.1**

Table 4.
Material recommendations with the next generation AHSS

Part Name	FSV Material	Next Gen AHSS
Shotgun	HF1550	980 XG3™
Bumper Beam	HF1550	MS1500/MS1700
Rocker Reinf	CP1470	DP1470
Rocker Outer	TRIP980	980 XG3™
Hinge Pillar Inner	HF1550	980 XG3™
Hinge Pillar Outer	TRIP980	980 XG3™
A-Pillar Inner	HF1550	1180SHF
A-Pillar Outer	TRIP980	980 XG3™
Roof Rail Inner	HF1550	DP1470
Roof Rail Reinf	HF1550	1180SHF
Front Rail	TRIP980	980 XG3™

CONCLUSIONS

In this study, two optimized countermeasure design concepts for the front end structures were developed for the IIHS SORB crash test. The optimized designs helped the vehicle slide away from the SORB, turned the front wheel outside and converted more impact energy to vehicle kinetic energy. The intrusion into the occupant compartment was reduced and a "Good" overall structural rating was achieved in the SORB test with the optimized design concepts. The optimized design concepts also reduced the intrusion in the IIHS 40% ODB frontal crash test and maintained a similar crash pulse in the NCAP full frontal crash test. The improved crash performance in the IIHS SORB and the 40% ODB frontal crash tests were achieved without mass increase. When used together with UHSS, a potential mass reduction of 1.3 kg could be realized with the optimized design concepts. The potential material replacement with the next generation AHSS is recommended at reduced costs.

REFERENCES

[1] C. Sherwood, J. Nolan and D. Zuby. 2009. "Characteristics of Small Overlap Crashes," 21st Enhanced Safety of Vehicles (ESV) Conference, paper no. 09-0423.

[2] Insurance Institute for Highway Safety. 2014. Small Overlap Frontal Crashworthiness Evaluation, Crash Test Protocol (Version III), May 2014, Arlington, VA.

[3] Insurance Institute for Highway Safety. 2012. Small Overlap Frontal Crashworthiness Rating Protocol (Version II), Rating Guidelines for Restraints and Dummy Kinematics, Injury Measures, and Vehicle Structural Performance, Weighting Principles for Overall Rating, December 2012, Arlington, VA.

[4] E. Elliott, C. Roche and J. Reddy, "Small Overlap Impact Countermeasure-Front Door Hinge Pillar Dual Box," SAE Technical Paper 2016-01-0142, 2016, doi:10.4271/2016-01-0142.

[5] J. Shaw, Y. Kuriyama and M. Lambriks. 2011. "Achieving a Lightweight and Steel-Intensive Body Structure for Alternative Powertrains," SAE Technical Paper 2011-01-0425, 2011, doi:10.4271/2011-01-0425.

[6] G. Chen, M. Shi, and T. Tyan. 2009. "Cross-Section Optimization for Axial and Bending Crushes Using Dual Phase Steels," SAE Int. J. Mater. Manuf. 1(1):537-547, 2009, doi:10.4271/2008-01-1125.

[7] G. Chen, M. Shi, and T. Tyan. 2012. "Optimized AHSS Structures for Vehicle Side Impact," SAE Int. J. Mater. Manf. 5(2):304-313, 2012, doi:10.4271/2012-01-0044.

[8] T.M. Link, and B.M. Hance, "Axial and Bending Crash Performance of Advanced High-Strength Steels," Intl. Symp. On New Developments in Advanced High-Strength Steels, 19-30, AIST 2017, Keystone, CO.

[9] P. McKune, A. Khutorsky and K. Butala, "Replacing Press Hardenable Steel with 980 MPa Generation 3 Steel for Automotive Pillars," SAE Technical Paper 2018-01-0117, 2018, doi:10.4271/2018-01-0117.

[10] X. Chen, G. Chen and L. Huang, "Validation of GISSMO Model for Fracture Prediction of a Third Generation Advanced High Strength Steel," SAE Technical Paper 2018-01-0107, 2018, doi:10.4271/2018-01-0107.

[11] X. Chen, G. Chen, L. Huang and M.F. Shi, "Calibration of GISSMO Model for Fracture Prediction of A Super High Formable Advanced High Strength Steel," 15th International LS-DYNA User Conference, June 2018, Dearborn, MI.

ACKNOWLEDGEMENT

The authors would like to thank United States Steel Corporation and Ford Motor Company for permission to publish this manuscript.

DISCLAIMER

The material in this paper is intended for general information only. Any use of this material in relation to any specific application should be based on independent examination and verification of its unrestricted availability for such use and a determination of suitability for the application by professionally qualified personnel. No license under any patents or other proprietary interests is implied by the publication of this paper. Those making use of or relying upon the material assume all risks and liability arising from such use or reliance.

DIFFERENT APPROACHES TO THE NEW REGULATORY CHALLENGES FOR CONNECTED AND AUTOMATED VEHICLES (CAV)

Lafuente, Ignacio; Tobar, Marta; Luján, Carlos; Martínez, Estrella
IDIADA Automotive Technology S.A
Spain

Paper Number 19-0192

ABSTRACT

Automated Driving (AD) is foreseen to be one of the major social and technological challenges in the coming years. Many manufacturers are developing new models with cutting-edge functionalities, which are not included in the scope of the current regulatory framework. Apart from demonstrating their know-how and expertise on AD, their willingness to sell their AD models in the European market is accelerating the rule-making system. However, what is the roadmap for the European regulatory framework? Policy makers and regulatory bodies are pushing their boundaries at all levels (national and international) in order to introduce modifications in existing regulations. These regulations will enable the introduction of these new functionalities into the market. Without decreasing the standards of safety and security, the implementation of a clear and harmonized regulatory framework and approval process is extremely necessary.

The last amendments of the UN Regulation nº79 related to steering equipment or the creation of new standards such as the ISO 21448 regarding Safety and Intended Functionality (SOTIF) are examples of recent efforts from the regulatory bodies to achieve this goal. The aim of this paper is to show the state of the art of the regulatory framework regarding automated driving. In order to provide a thorough understanding of the forthcoming amendments and new standards, the different challenges that the European Commission (EC) / United Nations Economic Commission for Europe (UNECE) are facing will be analysed, as well as the different approaches to be considered by the international regulatory bodies.

Finally, as a result of this research, the conclusions will be presented as considerations and proposals for all players involved in this change of paradigm: users, manufacturers, approval authorities and technical services.

INTRODUCTION

The deployment of new advanced technologies and new needs in our society is resulting in a change of paradigm when talking about transport modes. This change of paradigm is resulting in new vehicle concepts, new business cases and new propulsion technologies. Nowadays, all manufacturers are developing models with more advanced functionalities, moving forward to more highly automated vehicles. New actors are also involved in these new vehicle concepts in order to provide highly automated or even autonomous vehicle prototypes.

However, the current European Regulatory Framework does not permit the deployment of highly automated and autonomous cars because its regulations are not totally adapted to the new technologies and functionalities that are being introduced in their new prototypes. Differently from other regions in the world, in Europe vehicles must fulfill a list of particular regulations depending on their category before being commercialized. Through type-approving a particular vehicle, its safety and reliability are ensured.

In particular, regulations are being created and modified following a specific procedure in the discussion groups of the United Nations European Commission for Europe (UNECE), in Geneva, and the European Commission (EC), in Brussels.

Discussion groups
Discussion groups are groups of representatives from the Member States and experts from organizations and stakeholders. They meet periodically and when a specific subject needs more focus, smaller or specific groups are created in order to deal with it during a specific period of time. Several groups have been discussing autonomous driving, agreements on vehicle characteristics and rules for road traffic. Some are regulatory groups which are

continuously improving their agreements, while others are discussion groups looking for the implementation of new technologies in the official rules.

Although both organizations, UNECE and EC, have a similar procedure of regulatory making, their structure and methodology strategies differ.

UNECE - Geneva: At the UNECE, the Transport Division holds the Inland Transport Committee which is in charge of road, rail and river transport. The Inland Transport Committee is organized in subsidiary bodies known as Working Parties (WP). Each WP deals with a specific subject; e.g. WP.1 is the Global Forum for Road Traffic and WP.29 is the World Forum for Harmonization of Vehicle Regulations. This last one is working on the adaptation and/or creation of regulations in order to enable the introduction of innovative technologies in the vehicle. The main goal is to make vehicles safer and more environmentally sound. Figure 1 below shows the structure of the UNECE.

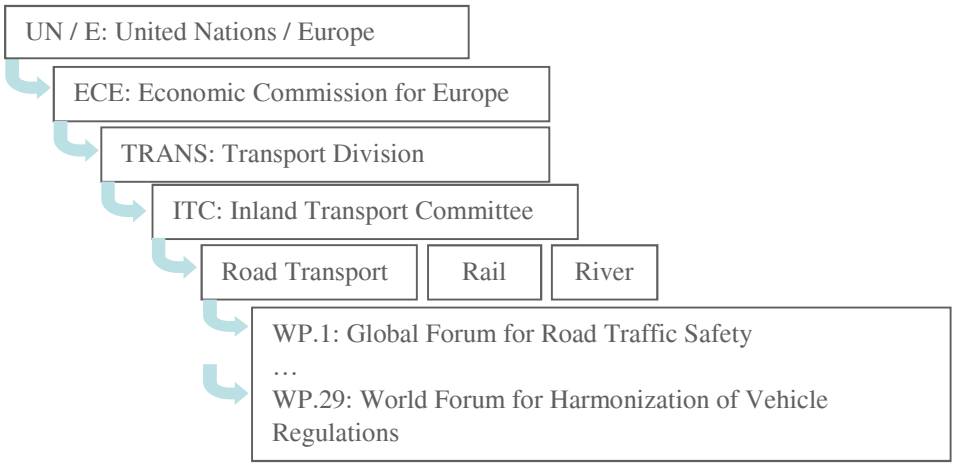

Figure 1. UNECE structure

European Commission – Brussels: In April 2016, 28 EU transport ministers signed the Declaration of Amsterdam, where all parties agreed the next necessary steps for the development of self-driving technologies. In the Amsterdam Declaration it is acknowledged that connected and automated vehicle technologies offer great potential to improve road safety, traffic flows and the overall efficiency and environmental performance of the transport system [1].

In this Declaration, actions needed to be done by the EU are outlined and described. These actions are grouped into four main pillars and are identified as follows:

- Development of a shared European strategy on connected and automated driving while strengthening the links between existing platforms such as the Cooperative Intelligent Transport Systems Platform (C-ITS), Gear 2030 and the Round Table on Connected and Automated Driving
- Continuation of the C-ITS platform for the deployment of interoperable C-ITS in the EU
- Review of the EU regulatory framework to support the development and use of automated and connected driving
- Development of a coordinated approach towards research and innovation activities in the field of connected and automated driving. As an example, at the Digital Day in Rome on March 2017, European countries signed a Letter of Intent to further intensify their cooperation on cross-border testing of automated road transport. Such cross-border tests will notably build on pilot projects funded under Horizon 2020

Cooperative Intelligent Transport Systems (C-ITS) Platform, created in early 2014, is a group that involves national authorities, C-ITS stakeholders and the Commission. Its objective was to develop a shared vision on the interoperable deployment of cooperative ITS in the EU. C-ITS allows road users and traffic managers to share information, "communicating" between them, and use it to coordinate their actions. In addition to what drivers can immediately see around them, and what vehicle sensors can detect, all parts of the transport system are thus able to share information.

The outcome of the C-ITS feeds the discussions held in the GEAR 2030 High level group on highly-automated vehicles. This high-level group was launched on January 2016 by the European Commission to ensure a coordinated approach and to address the challenges faced by the European automotive industry.

Its purpose is to build political support in order to help the automotive industry to quickly adapt to challenges from globalization, changing mobility patterns, digitalization, and environmental expectations, gathering industry and NGOs (CEOs level) and policy makers (Ministers and relevant Commissioners). Their work focuses on the adaptation of the value chain to new global challenges, automated and connected vehicles, and international harmonization and global competitiveness.

One of the most important actions taken by the GEAR 2030 group is the revision of the current legislation to enable autonomous driving. One of the conclusions of its final report submitted at the end of 2017 [2] was the revision by the Member States of their national traffic rules systems and the reporting in order to support converging approaches across the EU. Also, in this report, it was concluded that all Member States should confirm in the UNECE that the 1949 Geneva Convention and the 1968 Vienna Convention on Road Traffic were compatible with the safe use of automated vehicles with a driver expected by 2020 (level 3 and 4).

More recently, at the end of 2018, the Commission (in particular DG JRC and DG GROW) held the 1st Technical Workshop on new approaches for AD vehicle certification. The objective was to join Industry, Technical Services and Approval Authorities, so as to define a common strategy for the Safety Assessment of Automated Vehicles. The definition of this strategy will be continued in its 2nd workshop on March 2019.

UPCOMING CHALLENGES FOR REGULATORY BODIES

Historically, the UNECE Agreement on 1958, concerning the Adoption of Harmonized Technical United Nations Regulations for Wheeled Vehicles, and the EU Directive 70/156/EEC on the approximation of the laws of the Member States relating to the type-approval of motor vehicles and their trailers (later derogated by the Directive 2007/46 first and Regulation (EU) 2018/858 later), set the regulatory framework and the basis for the type-approval process as it is known nowadays.

For a Technical Service, and for a homologation engineer in particular, the task of type-approving a vehicle or component has always been a clear and unambiguous activity. Nevertheless, manufacturers are including more and more advanced systems in their vehicles, sometimes out of the scope of the regulations. This leads to an increasing responsibility for the person signing a homologation because the decision to sign or not sign is not as evident as always.

From a Technical Service's point of view, a group of "Main Challenges" have been identified. These challenges are being faced by policy makers and regulatory bodies, and current discussions held in WP.29 turn around the topics presented in the sections described below.

Challenge 1 – The time scale of legislation procedure and restructuring
The groups of experts such as the GRRF have been actively working on the creation of new proposals for regulations according to the recommendations received from the ITS/AD informal group of the WP.29.

These two groups have always been working in coordination, but the introduction of new players with disruptive technologies has increased the gap between their evolutions in time. While regulatory bodies have always evolved at a constant pace, traditional manufacturers and new player technologies are increasing their complexity exponentially.

This acceleration has led to the creation of dedicated task forces and specific working groups in the UNECE WP29 structure (see Figure 2). The GRVA "Groupe Rapporteur pour Véhicules Autonomes" (*Groups of Experts on Automated Driving*) was created in June 2018, mainly focused on encompassing activities for automated, autonomous and connected vehicles. Even though there was an Informal Working Group on Intelligent Transport Systems-Automated Driving (IWG ITS/AD), the resources were not enough to respond to the current market needs. For this reason, the organization took this decision and convened its 1st meeting on September 2018. These changes, promoted by the international regulatory bodies, were clear evidence of the willingness to adapt their structure to a more appropriate one according to the current automotive sector.

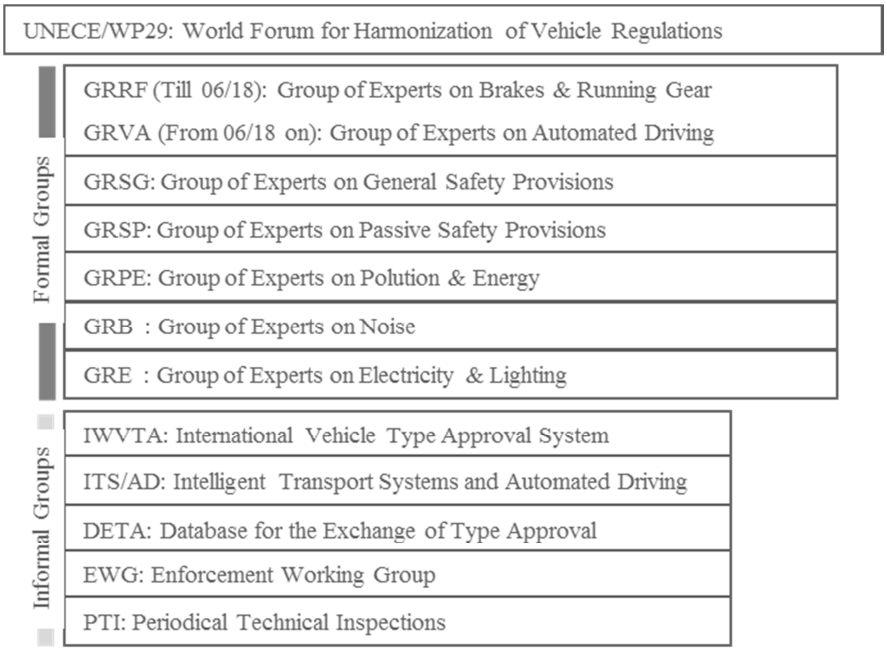

Figure 2 WP.29 Structure

For example, in order to deal with the new functionalities of the steering equipment, an informal group belonging to the GRRF was created in 2015. This informal working group was named the Automatically Commanded Steering Function (ACSF) working group.

Since its creation, the UN Regulation No. 79, dedicated to steering equipment, has been amended several times. In October 2017, the 2nd series of amendments came into force. This series brought new regulation concepts such as the division of automatically commanded steering functions into categories (A, B1, B2, C, D and E), depending on their level automatization and/or the introduction of the Corrective Steering Function (CSF). As the 2nd series only regulated the functions of category A and B1, the policy makers started working on new amendments. For this reason, a new series of amendments came out in 2018. The 3rd series of amendments will entry into force in new type approvals on 1st September 2019, bringing into place legislation functions of category C, a specific CEL in Annex 6 and the introduction of the Emergency Steering Function (ESF). Figure 3 below shows the main introductions of each series of amendments.

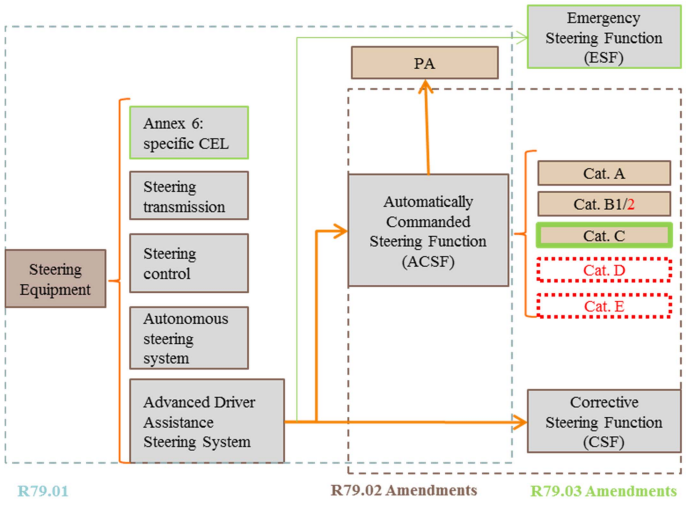

Figure 3 Series of amendments of UN Regulation 79

In last ACSF meeting, held in January 2019 in Hanghzhou [3], a proposal for Technical Requirements for an Automated Lane Keeping System was submitted. This new regulation should address the technical requirements for SAE Level 3 vehicles. According to the National Highway Traffic Safety Administration (NHTSA), SAE level 3 represents Conditional Automation, which means that the driver is a necessity, but is not required to monitor the environment. The driver must always be ready to take control of the vehicle with notice [4].

Challenge 2 – Time scale of the type-approval process

The current type-approval process consists of several predefined and standardized steps where the length of these steps is well known. Depending on the manufacturer and the workload of the technical services, this duration might change but, in the long term, it can be considered a steady process. This means that if the manufacturer is planning a new model release, the homologation process is a phase of about 6 months and they can schedule it in their plan.

This traditional process is divided into five primary phases or steps: technical documentation receipt, definition of the worst case to be tested, prototype receipt, tests performance and report drafting to get the certificate from the ministry.

However, with the upcoming change of paradigm, more stages will be incorporated to the type-approval process including new phases and aspects such as ISO 26262 for functional safety of electrical or electronic systems, Cyber-Security and Over the Air updates monitoring, simulations, among others. The introduction of more phases will increase the whole duration of the process.

This process will be reduced once the process is optimized (ISO 26262 for instance, could be shared between models) so some stages could be shared for the same manufacturer.

Determining how long the whole process is going to take is still unknown. That is why, it is important for manufacturers to consider this time factor when planning to launch their product on the market.

Challenge 3 – The role of the driver

The role of the "driver" as known nowadays is under discussion. According to the Convention on Road Traffic of Vienna of 1968 [5], the concept "driver" is defined as *any person who drives a motor vehicle or other vehicle (including a cycle), or who guides cattle, singly or in herds, or flocks, or draught, pack or saddle animals on a road.*

Nowadays, it is compulsory to get a driving license to drive a motor vehicle, which is granted by the traffic authority of each country. In the case of Europe, the driving license enables you to drive through any Member State of the European Union.

However, the upcoming change in AD vehicles is the new role of the "driver" or, preferably, the lack of it. Instead of drivers, experts are using other expressions like users or operators. So, one could think that if no one is in control of the vehicle, there is no need to own a driving license to use it. But, somehow, it must be ensured that the vehicle fulfils the road traffic rules and understands the signals or daily life events on the road such as road works, heavy rain, the approach to a flock of sheep, etc.

Experts are considering new ways to ensure that the vehicle fulfils and understands the general traffic laws. This consideration or proposals are further detailed in the chapter *Considerations and proposals to certificate the vehicles of the future* (page 8).

Challenge 4 – The gap between technology and legislation
The current applicable Directive 2007/46/EC [6] includes an article that specifies the requirements for type-approval exemptions; *Article nº 20 Exemptions for new technologies or new concept,* where Member States may, on application by the manufacturer, grant an EC type-approval in respect of a type of system, component or separate technical unit that incorporates technologies or concepts which are incompatible with one or more regulatory acts listed in Part I of Annex IV of the mentioned Directive.

This means that if a manufacturer has a model which does not fulfil one of the regulations necessary to grant a type approval, they can use this Article 20 as an alternative.

Member States may issue a temporary approval valid only in its territory, providing the following information to the Commission and other states:

- The reasons why the technologies or concepts in question make the system incompatible with the requirements
- A description of the safety and environmental considerations concerned, and the measures taken
- A description of the tests, including their results, demonstrating that, by comparison with the requirements from which exemption is sought, at least an equivalent level of safety and environmental protection is ensured

Published on May 2018, the new Regulation (EU) 2018/858 [7], has adopted this article in Article 39 and it will enter into force on 2021.

However, the forthcoming vehicle technologies cannot be considered as exemptions themselves, regulations will have to evolve in order to overcome their actual limitations.

Challenge 5 – Societal acceptance of the "unknown" level of risk
The number of accidents in developed countries has been decreasing in recent years. According to the Eurostat, there were 50 road traffic victims in total per million inhabitants in the EU Members [8].

The defenders of AD vehicle deployment argue that the introduction of AD vehicles in the vehicle park will lead to a reduction of traffic fatalities. The even more optimistic claim is that it is the only plausible strategy to get to zero traffic fatalities.

Although the long-term benefits of AD are unquestionable and probably true, experience has shown that it is not plausible to prevent accidents during the implementation process. For this reason, even if the final objective is to get zero fatalities, the way to achieve this goal is not clear. It depends on the society and institutions to declare the number of fatalities that can be accepted and in which period. The level of exigency of society will impose the complexity or number of regulations regarding AD legislation.

If the authorities decide to accept a temporary increase in road fatalities before achieving the turning point; they will also have to establish a limit in terms of time and number of accidents/fatalities.

Challenge 6 – Change of paradigm in passive safety
One of the remarkable changes that will be introduced is the concept of "living mode". This new method of transport will replace the existing "transport mode" by creating new experiences while being in a vehicle.

Using the phone, sleeping or even writing emails while going to work or on holiday will be a reality in the near future. But, even if road fatalities are supposed to tend to zero, the safety of vehicle users cannot be decreased. This means that manufacturers will have to include new passive safety systems. Airbags, seat belts, head supports, etc. will have to be redesigned and redefined.

In addition, it will be necessary to do new research into human injuries in case of accident. The main reason is that passengers will be able to "sit" in new positions adopting postures that could lead to more harmful injuries if an accident occurs.

In parallel, other systems such as lighting and signalling will need to be adapted. The International Automotive Lighting and Light Signalling Expert Group, named GTB, presented in the las GRE meeting the signalling requirements for automated and autonomous. Their objective is to take this opportunity to consider a global solution, instead of letting national authorities reach their own conclusions. For this reason, in last GRE they proposed to create a Special Interest Group to deal with this in conjunction with other stakeholders.

Challenge 7 – Dealing with disruptive transitions
A key factor to guarantee the success of the deployment of AD vehicles in the current traffic network is the management of the transition period. AD vehicles, standard cars, buses, trucks, pedestrians and other multiple vehicles and modes of transport will cohabit on the roads.

Although this transition will wake up public opinion and generate controversy, this is not the first transition seen in the cities. Not so many years ago, people experienced the transition from horses to cars. The late 19th and early 20th centuries were actually the age of streetcars. In the US, for example, the first cars appeared between 1920 and 1939 and their presence increased very fast leading to changes in the transport infrastructure and network.

However, is it possible to predict how many years take to replace the worldwide car fleet? In 2016, there were around 88 million passenger cars and light commercial vehicles sold worldwide, according to the study "National car data" presented by Macquarie Research in January 2017 [9]. According to the automotive trade journal Ward's Auto, it is estimated that by 2035 a record of 2 billion cars will be beaten. Considering these two factors, it can be easily estimated that it would take, at least, 23 years to fully replace the car fleet, considering only passenger car and light commercial vehicles.

This means that, even if the trends are met and there is not any unexpected event, AD vehicles will have to live together with all other transport modes without causing a catastrophe.

Challenge 8 – User awareness of new technologies
Linked to the societal acceptance of AD vehicles, another challenge for AD manufacturers are societal awareness of the technology.

Even if new generations (known as Gen Z, iGen or Centennials) are very used to disruptive technologies, AD vehicles are supposed to be available to everyone. This means that it is necessary to make sure that all drivers, the new ones and the existing ones, understand well all functionalities.

In addition, it is not enough to ensure that the user knows what a particular functionality does. It is important to make sure that this person clearly knows the limits of the system and he/she is aware of his/her responsibilities. For instance, if someone is using a functionality of SAE 3, that can be activated or deactivated, it must be clear when the vehicle must be under the control of the driver and who is the ultimately responsible in each mode of use.

A misuse caused by misunderstandings or unawareness of the technologies used in the roads can easily lead to accidents and fatalities that must be avoided.

Challenge 9 – Cyber-security and planned obsolescence
It is widely held that certain gadgets, cars and other devices have deliberately short lifespans. This is known as planned obsolescence. In smartphones, for example, the software updates are usually only available for the latest versions, which force the user to buy a new model of smartphone. As a result, manufacturers can sell more units and increase their sales. This situation could be transposed to vehicles. Instead of having a car that can run for more than 30 years, new vehicles could include systems that become obsolete after a limited period or use.

On the other hand, cyber-security is an issue that highly concerns the international regulatory bodies. Today, cybersecurity is present in everyone's life. In the automotive sector, as ADAS depends on an array of electronics, sensors, etc., these systems could lead to safety risks to passengers and other pedestrians if a minimum high standard of security and safety is not guaranteed.

Since December 2016, a new Task Force on Cyber Security and Over The Air issues was created. At the end of 2018, the Test Phase for draft UN Regulation on Cyber Security and Software Updates was presented. The aim of this "test phase" is to provide some guidelines on how to assess the regulatory requirements and verify the effectiveness of the regulation while verifying at the same time that Approval Authorities and Technical Service are able to reach the same conclusions based on identical OEM documentation [10].

Challenge 10 – Adaptation of the vehicle life cycle
Considering the standard cycle of a vehicle in Europe, this is basically divided into the following phases: initial assessment, homologation and authorization, Conformity of Production (COP), in-use compliance and Product Technical Inspection (PTI). With the new Regulation (EU) 2018/858 [7] new priority focus has been pointed out: Market Surveillance (MS) and Continuous Technical Inspection (CTI).

Since September 2015, when the Diesel gate scandal came out, market surveillance has become essential to avoid more cases like this one.

Furthermore, the fact that software updates and communications between the vehicle and other agents (V2X, V2V, V2I) will probably be over the air, approval authorities and policy experts consider it is important to have a CTI to authorize manufacturers to modify the vehicle software after approval.

CONSIDERATIONS AND PROPOSALS TO APPROVE THE VEHICLES OF THE FUTURE

Nowadays, five approaches are being considered to face the future of the homologation process. These five proposals are:

1. Classic homologation: Where a limited number of relevant test cases are selected, respecting the criteria of representativeness, repeatability and statistical relevance. These tests are supposed to be performed in proving grounds at the Technical Services, and according to all the vehicle regulations.

2. Real-world test drive: In this case, two different approaches can be chosen; through mileage validation or through the "digital driving license" concept. On the one hand, the mileage validation process is based on the idea that the vehicle is considered approved if it drives "X" kilometres without accidents. On the other hand, the digital driving license is based on the concept that the vehicle should be approved if it is able to pass a certain circuit that is representative of the real world. While the first process' limitation is clearly its expensiveness in terms of time and costs, the drawback of the second option is the difficulty of choosing a relevant representative circuit for the vehicle.

3. Simulation: This method enables to virtually test a very extensive list of test cases in a short period of time. Although programming the scenarios can be very expensive in terms of time and costs, once they are created the exploitation of the scenarios will help reduce time and cost validation.

4. Audit – Process oriented: The audit can be at three different levels: organizational, quality and assessment. The first one, the organizational audit, ensures that the vehicle manufacturer developing team is organized according to functional safety standards. The second one, the quality audit, guarantees that the AD function that is being validated has been developed according to ISO 26262, which sets the functional safety standards minimizing the safety risks due to malfunction of the vehicle hardware/software functions. The third one, the assessment, guarantees that the functional safety has been correctly considered in the function development.

5. Manufacturer declaration: Last but not least is to trust the vehicle manufacturer by means of a "manufacturer declaration" or "self-certification". This way to proceed is the one used in some countries such as the US to certify the vehicles sold in their country.

According to the International Organization of Motor Vehicle Manufacturer (OICA) [11] , automated and autonomous vehicles will need to follow a "Multi-Pillar" certification approach. Due to the difference in the scenario probability of occurrence in real-world traffic, an assessment considering only one approach (for instance Real World Test Drive) would imply to test the "typical" traffic scenarios. Thus, more critical scenarios would not be tested. Each approach has pros and cons and, probably, there is not a correct unique solution, but a combination of all the previous.

CONCLUSIONS

Until 2018, the homologation process has been clear and unambiguous. Signature decision was a consequence of an objective procedure. But, from now on, with the deployment of AD vehicles, their technologies and the huge number of functionalities and scenarios to be tested make the traditional validation process unaffordable in cost and time.

For this reason, five approaches will have to be considered all together: classic homologation, real-world test drive, simulation, manufacturer declaration and audit. In combination or not, the decision of how AD vehicles will be approved will be crucial for the proper deployment of these vehicles.

In overall terms, AD vehicles will bring a change of paradigm with lots of new challenges that all players (rule-makers, approval authorities, Technical Services, manufacturers and users) will have to solve in cooperation. Rule-makers will have to establish clear and objective procedures and prescription to avoid grounds of flexible interpretation. Approval authorities will have to define clear and harmonized designation rules and homologation processes, including COP and audit requirements. Technical Services must be technically competent and strictly follow rules and procedures. Manufacturers will have to present their prototypes, solutions and information in a way compatible with homologation. And users, even if for the moment they are not playing an active role, will have to cooperate to guarantee that the technology is not misused.

It seems that first steps have already been done to coordinate all players and come out with results in the near future. The reorganization of the WP.29 creating the GRVA working group on AD and the release of the new Regulation (EU) 2018/858 on Type Approval are clear examples of the efforts that international bodies are making to promote the proper deployment of automated driving vehicles on the roads worldwide.

REFERENCES

[1] Declaration of Amsterdam on "Cooperation in the field of connected and automated driving", 14 April 2016. Available on: https://www.regjeringen.no/contentassets/ba7ab6e2a0e14e39baa77f5b76f59d14/2016-04-08-declaration-of-amsterdam---final1400661.pdf

[2] GEAR 2030 High Level Group on the Competitiveness and Sustainable Growth of the Automotive Industry in the European Union, Final Report - 2017. Available on: http://www.europarl.europa.eu/cmsdata/141562/GEAR%202030%20Final%20Report.pdf

[3] Consolidated version after 20th meeting of IWG on ACSF. Informal Group on ACSF-21-03. Available on: https://wiki.unece.org/display/trans/ACSF+21st+session

[4] The Road to Full Automation, NHTSA. Available on: https://www.nhtsa.gov/technology-innovation/automated-vehicles-safety

[5] Convention on Road Traffic, Vienna 8 November 1968. Available on: https://www.unece.org/fileadmin/DAM/trans/conventn/crt1968e.pdf

[6] Directive 2007/46/EC, 5 September 2007 (page 12). Available on: https://eur-lex.europa.eu/legal-content/EN/TXT/PDF/?uri=CELEX:32007L0046&from=ES

[7] Regulation (EU) 2018/858, page 38, 30 May 2018 (page 38). Available on : https://eur-lex.europa.eu/legal-content/EN/TXT/PDF/?uri=CELEX:32018R0858&from=EN

[8] European Commission, "Over 25000 victims of road accidents in the EU in 2016". Available on: http://ec.europa.eu/eurostat/web/products-eurostat-news/-/EDN-20171119-1?inheritRedirect=true

[9] National Car Data, Macquarie Research January 2017. Available on: http://static.macquarie.com/dafiles/Internet/mgl/global/shared/about/investors/reports/2017/interactive/assets/pdfs/Macquarie-Group-AR2017-report.pdf

[10] Test Phase for draft UN Regulations on Cyber Security and Software Updates. Informal Document TFCS14-11, OICA. Available on: https://wiki.unece.org/pages/viewpage.action?pageId=73924689

[11] Future Certification of Automated Driving Systems, OICA. Informal Document GRVA-02-27. Available on: https://www.unece.org/fileadmin/DAM/trans/doc/2019/wp29grva/GRVA-02-27e.pdf

COMPARISON OF HIGHER SEVERITY SIDE IMPACT TESTS OF IIHS-GOOD-RATED VEHICLES STRUCK BY LTVS AND A MODIFIED IIHS BARRIER WITH THE CURRENT IIHS SIDE TEST AND REAL-WORLD CRASHES

Becky C. Mueller
Raul A. Arbelaez
Matthew L. Brumbelow
Joseph M. Nolan
Insurance Institute for Highway Safety (IIHS)
United States of America

Paper Number 19-0193

ABSTRACT

Since 2003, the Insurance Institute for Highway Safety (IIHS) has rated side impact crashworthiness based on tests involving a 1,500 kg moving deformable barrier (MDB) with the geometry of pickups and SUVs (LTVs) striking the side occupant compartment of a stationary vehicle with driver and rear passenger SID-IIs dummies. Previous examinations of real-world side crashes revealed that one quarter of 2016 side crash fatalities were in good-rated vehicles, suggesting that more improvements in side crashworthiness may be necessary. Research focused on injured occupants suggests that a higher severity test in a similar configuration may be the most effective at driving continued crashworthiness improvements relevant in real-world crashes. This study investigates how well the IIHS MDB impact and injury patterns replicate those observed in modern striking LTVs in a higher severity laboratory test.

Four recently designed good-rated vehicles were impacted by an MDB, a pickup, and an SUV at 50 km/h and 60 km/h. Two vehicles, the Toyota Camry and Volkswagen Atlas, were chosen because they had very low structural intrusion measures at the B-pillar in the current (or established) IIHS test, with 22 and 32 cm of survival space for the driver, respectively. Two vehicles, the Honda Accord and Infiniti QX50, were chosen because their survival space measures were on the borderline of a good/acceptable rating, with 14 cm and 15 cm of survival space, respectively.

Data collection included external and internal measurements along the side structures of the vehicles. All other measures and test setup were conducted according to the current IIHS side test protocol. Observations from the crash tests were compared with real-world higher severity crashes involving good-rated vehicles with configurations like the IIHS test to understand the potential real-world benefit of a new crash test configuration.

The MDB produced vehicle kinematics, deformation, and injury patterns that were not representative of striking LTVs. LTVs loaded the struck vehicles with force concentrations at the striking vehicle's front longitudinal structures while MDBs loaded vehicles more uniformly, both vertically and laterally. Dummy injury patterns were consistent with the deformation patterns; elevated pelvis/femur injury risk was present when struck by the LTVs and elevated head and chest injury risk was present when struck by the MDB.

The four good-rated vehicles exhibited a range of performance when struck by the LTVs, suggesting that a different test configuration, speed, or crash partner may highlight those differences in performance among the current good-rated vehicles. Additionally, MDB tests at 60 km/h revealed dimensional limitations of the barrier that must be addressed prior to further higher speed barrier research.

The current research suggests that increases in severity – mass or speed – of the current MDB would not necessarily encourage vehicle countermeasures that would confer benefit to occupants in real-world side impacts. To encourage relevant real-world design changes, the MDB must be redesigned to replicate the damage and injury patterns of current LTVs in a field-representative impact condition. This test configuration could potentially address an additional 10% of real-world, injury-causing side crashes.

BACKGROUND

The Insurance Institute for Highway Safety (IIHS) began its side crashworthiness evaluation program in June 2003 [1]. SID-IIs dummies are placed in the driver and left rear seating positions of the subject vehicle, and a perpendicular moving deformable barrier (MDB) strikes the left side of the vehicle at 50 km/h [2].

The IIHS MDB was designed to represent the front end of a midsize SUV or large pickup truck, but with a mass (1,500 kg) closer to a small SUV or midsize car. The test evaluation criteria include assessments of dummy injury measures, head protection (which was especially important when few vehicles had standard head-protecting side airbags), and structural intrusion of the occupant compartment as assessed by driver survival space. Vehicles are assigned an overall rating based on a combination of assessment criteria in one of four categories ranging from best to worst protection: good, acceptable, marginal, or poor.

The IIHS side crash test was more challenging to vehicle structures than other regulatory and consumer information tests that were being conducted in 2003. The MDB was heavier, had a higher ride height (compared with the NHTSA and Euro NCAP MDBs), and had a chamfered front end. The combination resulted in B-pillar loading and intrusion that was more severe and matched real vehicle-to-vehicle crash deformation better than other MDBs in use at the time [3]. Although the IIHS test was considered very severe for its time, an early comparison of the IIHS side test with real-world vehicle-to-vehicle side crashes indicated that 70% of serious injury (MAIS 3+) crashes and 90% of fatal side crashes exhibited more intrusion than the average IIHS crash test configuration [4] (Figure 1).

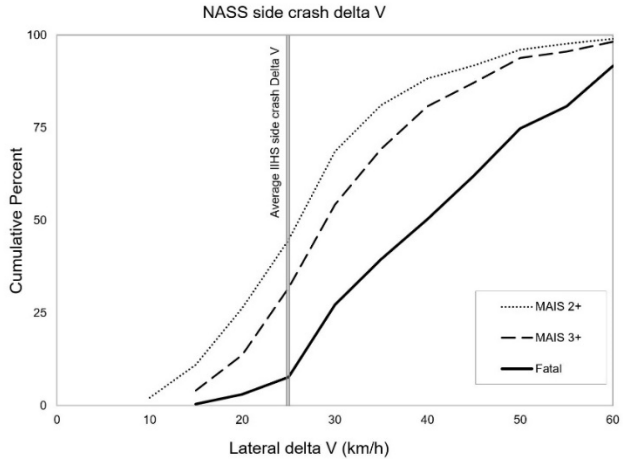

Figure 1. Delta V of side crashes causing injury and fatalities (from "Delta Vs for IIHS side impact crash tests and their relationship to real-world crash severity" by R.A. Arbelaez, B.C. Baker, and J.M. Nolan [2005])

The IIHS side crash test configuration also encouraged the installation of head-protecting side airbags, shown to reduce death risk in near-side crashes [5], which prior to 2003, were not available on most vehicle models or only available as an optional safety feature. The IIHS test encouraged fitment of these airbags because in vehicles without head-protecting side airbags, the front of the MDB often struck the dummy's head, a result of the smaller statured SID-IIs dummy combined with the higher front end of the MDB. To improve ratings, vehicle manufacturers strengthened vehicle side structures and fit head-protecting side airbags, initially as optional equipment and eventually as a standard safety feature by 2009. Since 2014, over 95% of new vehicles rated by IIHS earned a good side crash rating. In 2016, 40% of registered vehicles had a good rating, and this proportion of good-rated vehicles will continue to increase as older vehicles are retired from the fleet. Driver fatality rates in 1–3 year old vehicles have dropped from 22 per million registered vehicles in 2005 to 7 per million in 2017 [6] and declines may be largely attributable to improvements in vehicle crashworthiness [7, 8] (Figure 2). Despite the improvements made in side crash protection and the continued increase of good-rated vehicles in the fleet, side crash fatalities have increased slightly in recent years, leaving open the possibility that modifications to the existing side impact test could further real-world crashworthiness improvements.

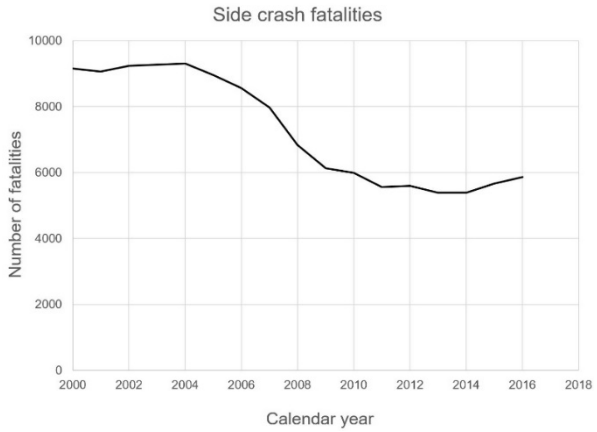

Figure 2. Trends in side crash fatalities in the United States from 2000–2016 (data retrieved from NHTSA's Fatality Analysis Reporting System [FARS])

Using methods analogous to the Teoh and Lund study [9], a 2019 analysis by Teoh and Arbelaez was conducted with the latest years of available crash data (2000–2016) but focused on the effects of crash test measures rather than component ratings [10]. Table 1 shows that reductions in crash measures are strongly associated with reductions in real-world death risk, indicating that the level of each measure matters, not just achieving a certain ratings threshold. B-pillar intrusion (survival space) showed the most promise in terms of both risk reduction and room for improvement among rated vehicles on the road. Results demonstrate that one way to improve vehicle performance in side crashes is to change the minimum criteria for good component ratings, even without changing the fundamentals of the crash test.

Table 1.
Percent changes in real-world left-side impact death risk associated with the IIHS side crash test

Test measure	Reduction in measure	Reduction in death risk
B-pillar intrusion	10 cm	25%
HIC-15	100	8%
Maximum shoulder deflection	10 mm	10%
Average rib deflection	10 mm	12%
Maximum rib deflection	10 mm	12%
Maximum rib deflection rate	1 m/s	9%
Maximum rib V*C	0.5 m/s	14%
Acetabulum force	1 kN	7%
Iliac force	1 kN	9%
Combined pelvic force	1 kN	8%

Note. All values are statistically significant at the 0.01 level.

Evaluation crash tests should be based on real-world crash conditions to best develop effective countermeasures against real-world injuries. A 2015 IIHS study focused on crashes that produced serious or fatal injuries to occupants in vehicles with good ratings [11]. Queries of the National Automotive Sampling System Crashworthiness Data System (NASS-CDS) and Crash Injury Research and Engineering Network (CIREN) identified 109 occupants in crashes from 2005–2012. Differences between the real-world crashes and the IIHS test were categorized through in-depth analysis of each case. Table 2 shows the potential for various changes to the IIHS test configuration to affect the injury outcome for the study population. No single change to the current test configuration would have been relevant to more than approximately 25% of the occupants. When considering combinations of two changes, a more severe test combined with a forward-shifted impact point (relative to the existing IIHS configuration), assessment of far-side occupant injuries, or modified injury criteria had the greatest potential relevance. Upon further examination of the far-side occupant cases, configurations included a large number of unbelted and out-of-

position occupants and a variety of alignments and crash severities, which would be difficult to capture in a single test configuration.

Another IIHS study [12] explored whether the occurrence of real-world injury in a crash with an impact location forward of the current IIHS test can be identified in the laboratory, how injury risk in such a configuration compares with the current IIHS test, and whether current vehicle designs already offer improvements over the vehicles in the real-world cases (median model year was 2007). The laboratory tests were successful in replicating the damage and injury patterns seen in the real-world case. It also determined that the risk factors observed in this configuration were mitigated in the newer generation of the vehicle with more recent crashworthiness improvements. This test series further concluded that a higher severity crashworthiness evaluation would be more likely to encourage improvements in the current fleet than one with a forward-shifted impact point.

Table 2.
Potential relevance of test changes to real-world cases

Change or combination of changes	Case occupants affect (%)
Adjust injury criteria	9
Include a far-side occupant	9
Increase severity	17
Shift the impact location forward	28
Increase severity and adjust injury criteria	26
Increase severity and include a far-side occupant	37
Increase severity and forward impact location	62

OBJECTIVE

Currently, IIHS is exploring potential modifications to the side impact crash test to address real-world injuries occurring in vehicles with good performance in the existing test. Previous examinations of real-world side crashes with injured occupants suggest that a higher severity test in a similar configuration may be the most effective at achieving this aim. This study investigates how well the IIHS MDB impact and injury patterns represent those observed in modern pickup and SUV striking vehicles in a laboratory test.

METHODS

Laboratory crash tests

Four recently designed IIHS-good-rated vehicles were impacted by various crash partners at 50 km/h and 60 km/h (Table 3). Two vehicles, the Toyota Camry and Volkswagen Atlas, were chosen because they had very low structural intrusion (greater survival space) measures at the B-pillar in the ratings test, 22 and 32 cm respectively. Two vehicles, the Honda Accord and Infiniti QX50, were chosen because their structural intrusion measures were on the borderline of a good/acceptable rating, 14 cm and 15 cm, respectively.

Striking vehicles were chosen from popular modern vehicles with a focus on pickups and SUVs (LTVs), which the MDB was originally designed to best represent. In addition, one midsize car partner was chosen to understand how cars compare with the MDB. The MDB mass was increased to 1,900 kg, the registration-weighted mass of midsize SUVs in the U.S. market (Figure 3). Registration-weighted mass was calculated based on curb mass from the vehicle information databases maintained by the Highway Data Loss Institute [13] and vehicle registration data from IHS Automotive. The test speed for the striking vehicles was either 50 km/h or 60 km/h. All data were compared with results from the baseline IIHS side test in the 50 km/h, 1,500 kg MDB configuration. Data for comparison included high speed video analysis, dummy sensor measures, and pre- and postcrash static measurements on the vehicle.

Table 3. Test Matrix

	Striking Vehicle					
	60 km/h				50 km/h	
	F-150	Pilot	Camry	MDB	MDB	F-150
	2,200 kg	1,900 kg	1,500 kg	1,900 kg	1,500 kg	2,200 kg
Camry	X	X	X	X	X	X
Accord				X	X	X
Atlas	X	X		X	X	
QX50				X	X	

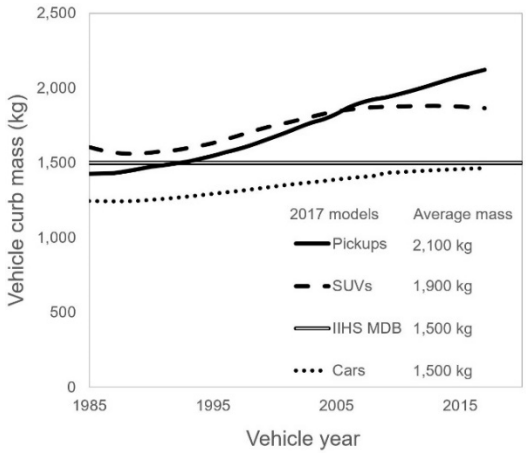

Figure 3. Vehicle curb mass over time based on weighted vehicle registrations (data provided by the Highway Loss Data Institute)

Vehicle tests were setup following the IIHS side impact crash test protocol [2] with the following modifications:

- For striking vehicle partners, a Hybrid III midsize male dummy was installed in the driver and pre- and postcrash measurements of the bumper bar were taken.
- For tests with the MDB, pre- and postcrash measurements of the honeycomb profile were taken at the bumper, mid-barrier height, and top of the barrier.

Adding the extra 400 kg on the MDB resulted in a new center of gravity location and moments of inertia, as shown in Table 4. Striking vehicles were positioned so that the vehicle's centerline aligned with the calculated impact reference distance (IRD) from the front axle to MDB centerline in the test protocol (Table 5).

Table 4. MDB Characteristics

Characteristics	1,500 kg MDB	1,900 kg MDB
CGx rearward of front axle (mm)	990	1,056
CGy from vehicle centerline (mm)	0	0
CGz (mm)	566	530
Ix (kg-m^2)	542	572
Iy (kg-m^2)	2,471	2,560
Iz (kg-m^2)	2,757	2,870

Table 5. Impact reference distance (IRD) from front axle to striking vehicle centerline

Vehicle	IRD (mm)
Camry	1610
Accord	1614
Atlas	1648
QX50	1597

For the struck vehicle, setup followed the IIHS side impact test protocol and UMTRI ATD Positioning Procedure [14] with the addition of pre- and postcrash measurements taken along the side of the vehicle to compare deformation patterns (Figure 4).

Figure 4. Measurement locations for external crush

In addition, pre-and postcrash measurements were taken vertically along the driver-door trim at locations matching the UMTRI ATD Positioning Procedure H-point positions of the Hybrid III 5th female and Hybrid III 50th male dummies [14] to compare localized loading for different-sized occupants (Figure 5).

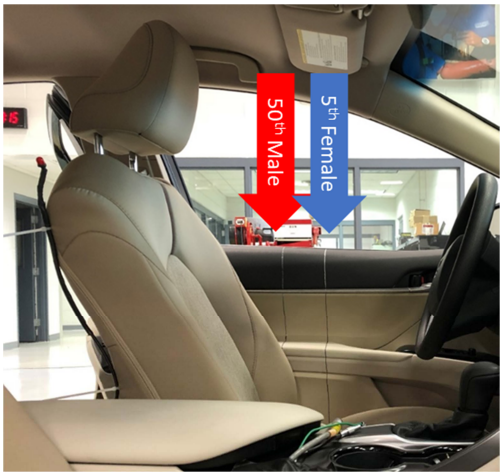

Figure 5. Door trim vertical measurements of crush at the location of dummy H-points

Real-world higher severity crashes
NASS and CIREN cases from Brumbelow et al. [11] categorized as higher severity crashes with similar impact locations as the IIHS side impact test were further examined to relate real-world crash observations to this study's laboratory tests. A list of cases is shown in Appendix C.

RESULTS

Laboratory crash tests
High-speed video footage indicated different vehicle dynamics between vehicle partners and the MDB. The struck vehicles rolled away from the MDB (positive roll, as defined by SAE [15]), while struck vehicles rolled toward (negative roll) all three of the striking vehicle partners. This pattern was observed in all four struck-vehicle models in this study. An example of these kinematic differences is shown in Figure 6 with the Toyota Camry.

Figure 6. Vehicle dynamics comparison between Toyota Camry struck by the MDB (left) and Ford F-150 (right) at 60 km/h during maximum roll

Vehicle deformation patterns were compared using measurements along the outside and inside door and B-pillar structures of struck vehicles. Appendix A has a summary of structural measurements for the striking and struck vehicles. Striking LTVs created a distinct "M" shape in the sides of struck vehicles when compared in a plan view (Figure 7). Whether the striking vehicle was a pickup, an SUV, or a car, they all produced the characteristic 'M' shape deformation pattern to varying degrees. The test configuration aligns the stiffer frame rails with the middle of the struck vehicle doors and the comparatively less stiff bumper center with the B-pillar.

In contrast, the uniform shape and stiffness of the MDB center section created relatively evenly shaped loading into the sides of the struck vehicles (Figure 7). For the MDB impacts, the maximum crush measured at the mid-door height varied by only 6 cm from the crush measured at the B-pillar, compared with a 12- to 19-cm differential in the LTV impacts. Vertically, the MDB resulted in only 2 to 5 cm less crush at the beltline than mid-door, while the LTV and car partners produced 9 to 17 cm less crush. The greater crush at mid-door height aligns with the striking vehicle's frame rails. These trends in vertical deformation patterns are shown in Figure 8.

Survival space measured relative to the driver seat centerline, near the theoretical H-point positions of a 50th male and 5th female dummy was less than at the B-pillar in all tests, with the lowest survival space measures recorded at the 5th female location, the furthest from the B-pillar (Figure 9). The largest differences were seen with LTV partner vehicles, with 7 to 19 cm more intrusion at the 5th female location than measured at the B-pillar. For the four vehicles in this study, the B-pillar is located, on average, 41 cm rearward of the 5th female driver dummy's H-point line. The difference between the measurement and occupant location becomes even more pronounced in two-door vehicles, where the B-pillar was an average of 57 cm rearward of the vehicle occupant being evaluated in a sample of two-door vehicles tested at IIHS. While repeatability of measuring door-trim deformation is suspect, consideration should be made for new test rating criteria to capture the magnitude of intrusion directly at the occupant location to better relate to real-world injuries.

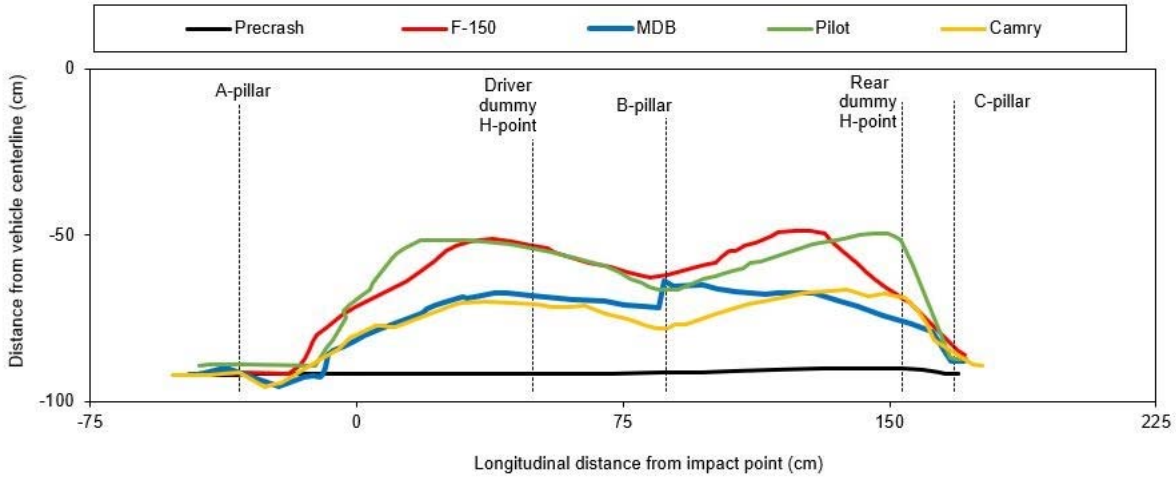

Figure 7. Comparison of external crush along the struck vehicle doors for the Toyota Camry struck by different vehicle partners at 60 km/h

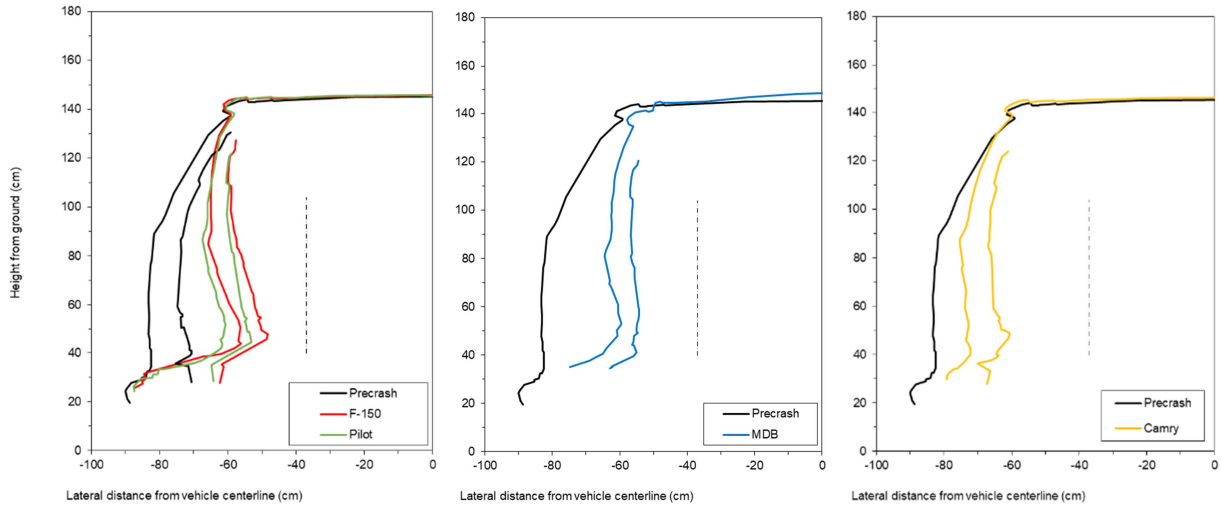

Figure 8. Comparison of B-pillar vertical deformation in Toyota Camry tests

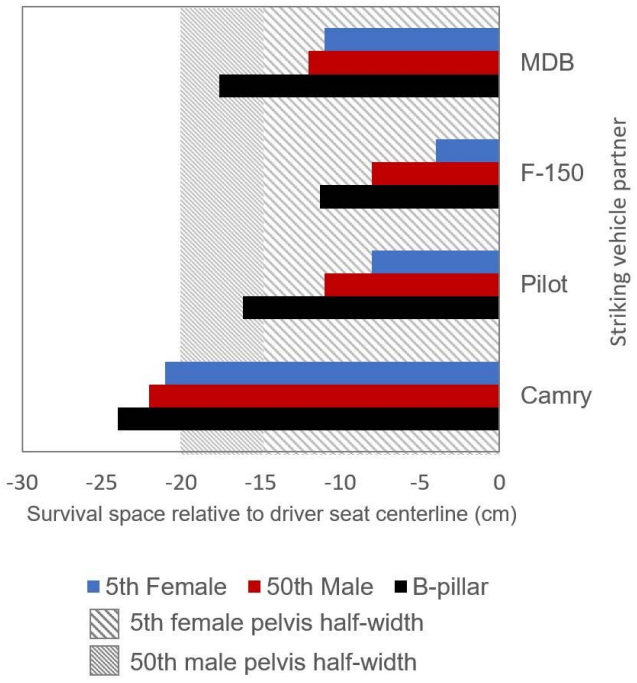

Figure 9. Comparison of occupant survival space measurements for 60 km/h striking vehicles against the Toyota Camry

The effects of crash energy on performance for the Toyota Camry when struck by the F-150 and MDB are shown in Figure 10. The 10 km/h increase in speed for the F-150 test pair represents a 44% increase in energy and resulted in a 50% increase in intrusion on the Camry. In comparison, increasing the MDB mass and speed represented an 82% increase in energy yet resulted in only a 20% increase in intrusion. These specific comparisons highlight the observations that the MDB distributes loading over a broader area of the side structure than the striking LTV.

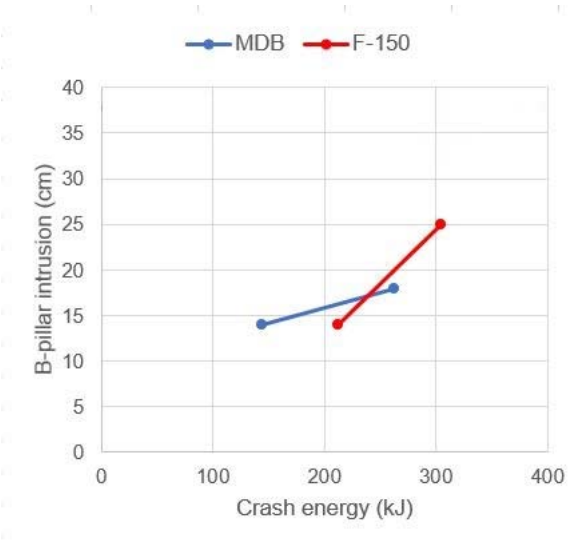

Figure 10. Crash energy and vehicle structural performance for Toyota Camrys struck at 50 km/h and 60 km/h

Peak injury measures from the driver and rear passenger SID-IIs dummies are summarized in Appendix B. General injury patterns in the Toyota Camry tests are illustrated in Figure 11. Striking vehicle partners caused vertically lower structural intrusions and dummies recorded elevated pelvic and femur injury measures, while dummies in the MDB partner tests had elevated head and chest measures.

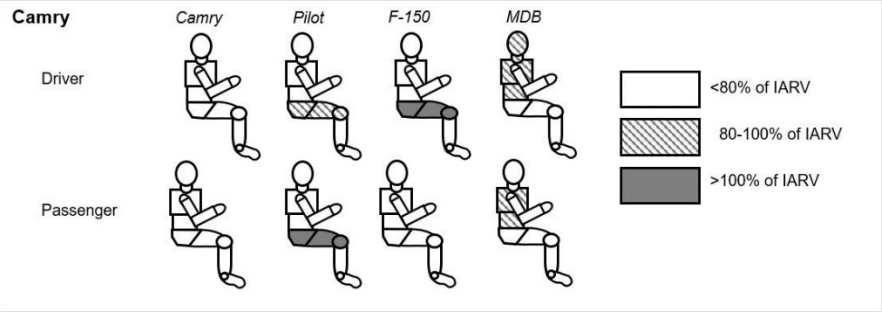

Figure 11. Injury patterns in Toyota Camry tests conducted at 60 km/h

Real-world higher severity crashes

Laboratory test results of impact and injury patterns were compared with observations from field data. NASS and CIREN cases from Brumbelow's 2015 study (Appendix C) that may benefit from vehicle countermeasures designed for a 60 km/h test were identified. Pockets of localized deformation observed in the laboratory tests with striking LTVs were also observed to varying degrees in more than half of the field cases. Maximum crush in real-world crashes was typically higher than measured in this series of laboratory tests (Figure 12). This suggests either that the real-world crashes involve speeds higher than 60 km/h or that the vehicles in this sample, which were older than those in the test series, had weaker side structures. The latter possibility is suggested by the field-study vehicles having lower structural ratings in the standard IIHS evaluations than vehicles chosen for laboratory tests. Dummies in the laboratory LTV-striking vehicle tests had pelvic injury measures suggesting a high risk of injury, consistent with the occurrence of pelvic injury seen in the majority of the field cases. However, the laboratory LTV tests did not reveal high chest injury risk, which was sustained in more than half of the field cases. Laboratory LTV tests did not predict high risks of head injury, consistent with the low frequency of head injuries observed in the field. For the two field occupants with head injuries, it is suspected that curtain airbags were not fully effective in preventing head contact with the striking pickups, resulting in contact through the airbag.

Laboratory MDB-striking-vehicle tests showed mixed trends when compared with field data. Relatively uniform loading across the struck vehicle's side was seen in about half of the field cases, but vertically, intrusion patterns were more consistent with LTV laboratory tests, with maximum crush concentrated at mid-door height and significantly less at higher locations. Dummies in the MDB tests did not reveal high pelvic injury risk, despite the large frequency seen in field cases. Conversely, the MDB tests typically predicted high risks of head injury, but the field cases typically did not. Dummies in the MDB tests were consistent with field observations for chest injury risks.

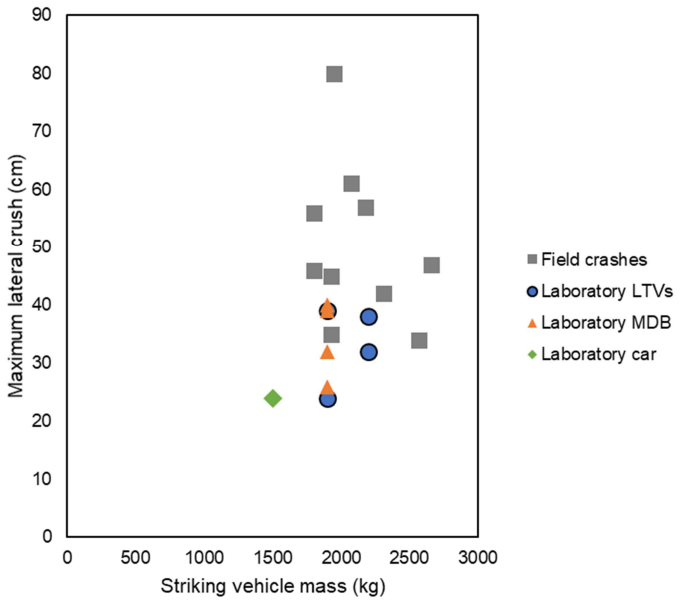

Figure 12. Vehicle maximum crush for seriously injured real-world occupants in side crashes with a striking LTV that may benefit from a higher severity ratings test compared with laboratory tests conducted at 60 km/h

DISCUSSION

In the 1990s, field evidence was clear that occupant injury risk in side-struck vehicles was significantly higher when the striking vehicle was a pickup or an SUV. IIHS developed its side barrier to mimic this elevated risk and encourage automakers to improve occupant protection. The structural changes, plus the fitment of side head-protecting airbags that resulted, have been very effective at reducing side impact fatalities.

The efforts in the current study suggest that the simplistic barrier design conceived in the late 1990s is no longer replicating the deformation and injury patterns of current striking LTVs. Design requirements in regulatory and consumer information tests in the 1990s did not necessitate structural improvements of vehicle sides to perform well, but current testing requirements require consideration for stronger vehicle structures. Consequently, the lack of fidelity of the IIHS MDB to real LTV front structures was not as apparent as the present tests show. Current side designs now tend to fend off the MDB by carrying large loads through the B-pillar, door sill, and roof rail. However, the fronts of modern vehicles are stiffer at the frame rail locations while sections outside and in the middle are softer, contrasting with the MDB's uniform stiffness. Thus, the strongest parts of vehicles' sides do not align with the stiffer portions of the striking vehicles' fronts, so less load can be carried by the B-pillar, door sill, and roof rail than is apparently the case when struck by the IIHS MDB. Additionally, the MDB is loading A-pillars and lower rear door frames of the struck vehicles, which is not seen with LTV striking vehicle comparisons (Figure 13).

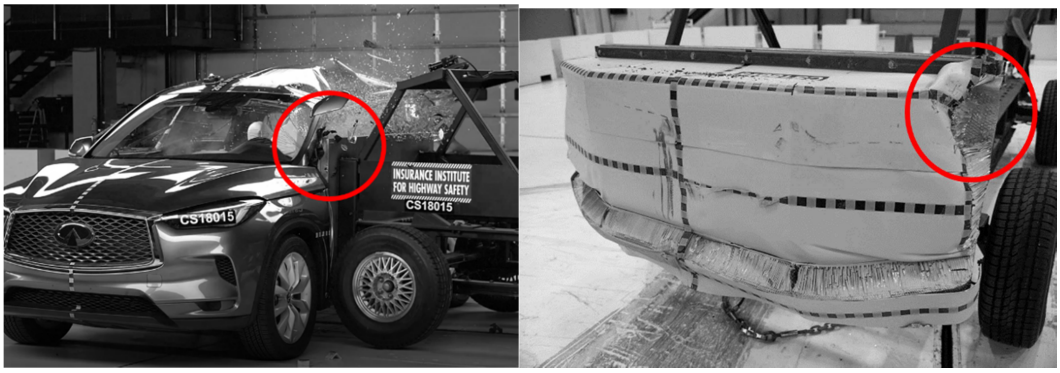

Figure 13. Barrier crush in the 60 km/h Infinity QX50 test highlights significant loading at the barrier's edges that do not occur in laboratory LTV tests

Vehicles in this study had a range of performance in higher severity tests. The two vehicles with the strongest B-pillar structures (Camry and Atlas) performed appreciably better than their borderline good B-pillar structure comparison vehicles (Accord and QX50) in comparative tests with real striking vehicles. Differences were more dramatic in the 60 km/h MDB configuration, where the Camry had an additional 9 cm of survival space compared with the Accord and also, the Atlas had 17 cm more survival space compared with the QX50. The higher levels of intrusion in the Accord and QX50 tests corresponded to much higher risks calculated for head and chest injuries compared with the Camry and Atlas. The 50 km/h F-150 tests, with a crash severity closer to the IIHS ratings test, did not differentiate vehicle structural performance between the Camry and the Accord, but indicated that these vehicles provide different levels of pelvic protection for occupants, with pelvic injury risks up to 115% of the good-acceptable boundary for the Camry and 165% for the Accord. In comparison, for the IIHS ratings tests, neither vehicle indicated deficiencies for pelvic protection, where dummies in both vehicles measured pelvic injury below 70% of the good-acceptable boundary. A different test configuration, speed, or crash partner may capture that modern vehicles with good IIHS side impact ratings have a range of occupant protection in higher severity side crashes.

A future IIHS side crash test must be able to replicate real-world damage and injuries to encourage effective crashworthiness improvements beyond those developed for the current evaluation. IIHS is investigating barrier modifications that will better replicate common LTV crash partners in terms of mass and front-end structure. Damage patterns and injuries from real-world crashes correspond to results from 60 km/h tests with LTV partners better than tests with the current MDB. The localized pockets of door deformation observed in all LTV partner tests were seen to varying extents in about half of the real-world cases with LTV partners. Cases with more uniform loading typically had torn B-pillars, suggesting weaker B-pillar structure (many of the real-world vehicles had acceptable-rated B-pillar structure) or that these crashes had significantly more energy than the laboratory tests. Serious pelvic injuries occurred in 70% of the real-world cases (Figure 14), and LTV laboratory tests indicated risks to this body region while MDB tests did not. In contrast, the incidence of real-world chest injuries was better reflected by MDB test results. However, this may indicate that the current injury criteria can be further improved, as Teoh and Arbelaez [10] showed a 10-mm reduction in peak deflection related to a 12% increase in survivability. Additionally, rating criteria should include considerations for an elderly risk curve to provide benefit for chest-injured occupants over 60 years old. Low head injury risks from the LTV tests better agreed with the low number of real-world observations of head injury than the higher head injury risks observed in the MDB tests. A higher speed test with the current MDB could encourage countermeasures targeting body regions where the fewest amount of injuries are occurring while potentially ignoring areas of greater concern. An MDB that better replicates modern LTVs is needed to appropriately address real-world injuries. A higher speed test with a redesigned MDB could potentially address an additional 10% of real-world injury-causing side crashes. Vehicle design changes made in response to such a test would need to be evaluated for their potential to reduce protection in the more common lower severity crashes where much improvement already has been achieved.

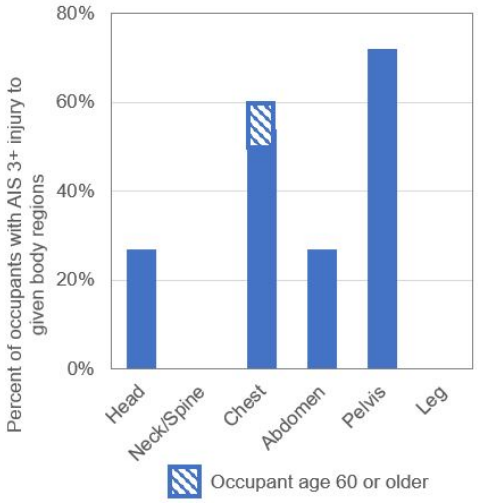

Figure 14. Injured body regions for seriously injured real-world occupants in side crashes with striking LTV partners that may benefit from a higher severity ratings test

CONCLUSIONS

The current IIHS side impact test, developed in 1999–2002, has encouraged side crashworthiness improvements that have significantly reduced driver fatality rates in side impact crashes. Findings from this research suggest that further improvements could be encouraged. Options such as a higher severity crash test show promise. To achieve this, the IIHS MDB needs modifications to better replicate the deformation and injury patterns caused by LTVs.

REFERENCES

[1] Insurance Institute for Highway Safety. (2003, June 28) First side impact tests: How 12 small SUVs fared. Status Report, 38(7). Retrieved from https://www.iihs.org/iihs/sr/statusreport/article/38/7/1

[2] Institute for Highway Safety. (2017) *Side impact crashworthiness evaluation: Crash Test Protocol (Version X)*, Arlington, VA

[3] Arbelaez, R.A., Dakin, G.J., Nolan, J.M., Dalmotas, D.J., and Tylko, S. (2002) IIHS side impact barrier: Development and crash test experience. *Proceedings of the 2002 Vehicle Safety Conference* (May 2002). Institution of Mechanical Engineers, London, England.

[4] Arbelaez, R.A., Baker, B.C., & Nolan, J.M. (2005) Delta Vs for IIHS side impact crash tests and their relationship to real-world crash severity. *Proceedings of the 19th International Technical Conference on the Enhanced Safety of Vehicles (ESV)*, Paper Number 05-0049. National Highway Traffic Safety Administration, Washington DC.

[5] McCartt, A.T., & Kyrychenko, S.Y. (2007). Efficacy of side airbags in reducing driver deaths in driver-side car and SUV collisions. *Traffic Injury Prevention, 8*(2), 162–170.

[6] Insurance Institute for Highway Safety. (2018). Fatality Facts: Passenger Vehicle Occupants [Web page]. Arlington, VA. Retrieved from https://www.iihs.org/iihs/topics/t/general-statistics/fatalityfacts/passenger-vehicles

[7] Farmer C.M., & Lund, A.K. (2006). Trends over time in the risk of driver death: what if vehicle designs had not improved? *Traffic Injury Prevention, 7*(4), 335–342.

[8] Farmer, C.M., & Lund, A.K. (2015). The effects of vehicle redesign on the risk of driver death. *Traffic Injury Prevention, 16*(7), 684–690.

[9] Teoh, E.R., & Lund, A.K. (2011). IIHS side crash test ratings and occupant death risk in real-world crashes. *Traffic Injury Prevention, 12*(5), 500–507.

[10] Teoh, E.R., & Arbelaez, R.A. (2019). *Association between data collected in IIHS side crash tests and real-world driver death risk, and opportunities to improve the current test*. Arlington, VA: Insurance Institute for Highway Safety.

[11] Brumbelow, M.L, Mueller, B.C., & Arbelaez, R.A. (2015) Occurrence of serious injury in real-world side impacts of vehicles with good side-impact protection ratings. *Traffic Injury Prevention, 16*, S125–S132.

[12] Brumbelow, M.L, Mueller, B., Arbelaez, R.A., and Kuehn, M. (2017) Investigating potential changes to the IIHS side impact crashworthiness evaluation program. *Proceedings of the 25th International Technical Conference on the Enhanced Safety of Vehicles (ESV)*, Paper Number 17-0083. National Highway Traffic Safety Administration, Washington DC.

[13] Highway Loss Data Institute. (2018) Vehicle information database. Arlington, VA.

[14] Insurance Institute for Highway Safety. (2004). *Guidelines for using the UMTRI ATD positioning procedure for ATD and seat positioning (Version V).* Arlington, VA.

[15] Society of Automotive Engineers. (1994, December). *Surface vehicle information report: Sign convention for vehicle crash testing* (SAE Standard J1733). Warrendale, PA. Retrieved from https://law.resource.org/pub/us/cfr/ibr/005/sae.j1733.1994.html

APPENDIX A: VEHICLE DEFORMATION

Table A1. Measurements of external crush along the struck vehicle side profile (cm)

	Lower door			Mid-door				Upper door			
	Driver H-point	B-pillar	Passenger H-point	Driver H-point	B-pillar	Passenger H-point	Max	Driver H-point	B-pillar	Passenger H-point	Max
F150	23	21	15	31	16	20	34	14	20	13	20
Pilot	13	12	16	23	12	20	31	7	6	16	14
MDB	12	16	17	33	28	17	33	27	25	15	30
F150	2	2	1	39	30	20	43	17	15	18	27
Pilot	2	2	1	37	25	38	42	25	13	27	33
MDB	0	2	4	24	28	14	28	21	17	15	23
Camry	9	9	4	22	14	21	25	3	7	9	13
50km/h F150	18	7	12	31	20	20	38	11	10	16	25
MDB	5	9	9	39	36	31	39	37	29	23	37
50 km/h F150	18	6	28	35	19	24	37	20	8	20	27
MDB	14	12	9	39	35	31	41	38	38	28	38

Table A2. Struck vehicle survival space comparison at interior locations relative to the driver seat centerline aligned longitudinally with the theoretical 5th female H-point, 50th male H-point, and centerline of the B-pillar structure as used for rating vehicles (cm)

		5th Female	50th Male	B-pillar
Camry	50 km/h MDB			-22
	F-150	-4	-8	-11
	Pilot	-8	-11	-16
	MDB	-11	-12	-18
	Camry	-21	-22	-24
	50 km/h F150	-13	-23	-22
Atlas	50 km/h MDB			-32
	F-150	-7	-11	-26
	Pilot	-22	-23	-32
	MDB	-6	-9	-21
Accord	50 km/h MDB			-15
	50 km/h F150	-16	-17	-21
	MDB	-5	-7	-9
QX50	50 km/h MDB			-14
	MDB	-4	-5	-4

APPENDIX B: DUMMY INJURY MEASURES

Table B1. Peak driver dummy injury measures

		Camry						Atlas					Accord			QX50	
		60 km/h				50 km/h		60 km/h			50 km/h	60 km/h	50 km/h			60 km/h	50 km/h
	Reference	F150	Pilot	MDB	Camry	MDB	F150	F150	Pilot	MDB	MDB	MDB	50 F150	MDB		MDB	MDB
Resultant acceleration (g)		70	69	82	36		56	32	21	109		110	42			88	
Resultant acceleration (3ms clip, g)		66	66	80	36		54	29	20	92		106	38			84	
HIC15	779	412	434	723	107	334	276	65	26	696	63	1291	116	316		791	159
X shear force (kN)		-0.4	-0.4	-0.6	-0.3		-0.3	-0.4	-0.2	-0.5		-0.8	-0.4			-0.4	
Y shear force (kN)		0.5	0.4	-0.4	0.3		0.3	0.5	0.3	0.6		-0.4	-0.3			0.4	
Tension (kN)	2.1	1.4	1.4	1.5	0.8	0.9	0.8	1	0.6	1.6	0.7	1.4	1	0.9		2	1.4
Compression (kN)	2.5	0.5	0.9	0.1	0.2	0.2	0.3	0.2	0.1	0.6	0.4	0.1	0.2	0.1		0.4	0.3
X moment (Nm)	±67	-58	-45	-35	-18		-38	34	-10	29		-39	-46			-27	
Z moment (Nm)	±39	-22	-25	-18	16		-21	24	15	-17		-32	-11			-23	
Lateral deflection (mm)	60	30	39	53	15	29	19	24	24	49	23	61	13	53		61	42
Lateral force (kN)		1.6	1.6	2.1	1	1.2	1.3	1.4	1.4	2	1.1	4.8	0.8	1.5		5.2	1.7
Rib 1 deflection (mm)	34	25	29	46	9	27	15	12	11	32	21	58	17	42		58	33
Rib 2 deflection (mm)	34	23	30	40	12	28	14	17	14	31	19	54	18	37		57	36
Rib 3 deflection (mm)	34	29	35	42	16	30	20	22	18	36	17	52	20	34		56	37
Rib 4 deflection (mm)	32	33	37	36	21	28	25	23	21	46	17	43	17	29		45	32
Rib 5 deflection (mm)	32	38	40	34	25	29	33	23	22	40	16	37	21	28		35	27
Maximum Rib Deflection		38	40	46	25	30	21	23	22	46	21	58	19	42		58	37
Average rib deflection (mm)		29	34	41	16	28	21	19	17	37	18	49	21	34		50	33
Rib 1 deflection rate (m/s)	8.2	1.97	1.55		0.74	2.8	1	1.48	1.18	1.85	1.82	6.27	1.28	4.12		5.98	4.86
Rib 2 deflection rate (m/s)	8.2	2.22	1.36	3.94	0.76	2.4	1.14	1.82	1.52	2.04	1.75	6.23	1.12	3.63		6.58	4.21
Rib 3 deflection rate (m/s)	8.2	2.42	1.91	3.82	1.5	2.4	1.34	2.4	2.15	2.68	1.84	5.32	1.4	3.18		6.14	3.89
Rib 4 deflection rate (m/s)	8.2	3.11	2.12	3.1	1.63	2.1	2.13	2.25	2.37	2.98	2.14	3.32	1.98	3.08		3.56	3.75
Rib 5 deflection rate (m/s)	8.2	2.82	2.42	2.93	1.66	3.6	2.47	2.25	2.52	2.39	1.89	4.33	3.63	5.03		3.2	3.65
Rib 1 VC (m/s)	1	0.27	0.28	0.85	0.02	0.33	0.08	0.08	0.07	0.33	0.17	1.6	0.12	0.59		1.16	0.61
Rib 2 VC (m/s)	1	0.22	0.27	0.78	0.04	0.33	0.07	0.17	0.11	0.31	0.17	1.68	0.1	0.56		1.35	0.6
Rib 3 VC (m/s)	1	0.37	0.33	0.82	0.09	0.34	0.12	0.3	0.18	0.48	0.16	1.51	0.17	0.54		1.41	0.54
Rib 4 VC (m/s)	1	0.55	0.41	0.61	0.16	0.28	0.28	0.27	0.27	0.72	0.11	0.67	0.11	0.32		0.69	0.28
Rib 5 VC (m/s)	1	0.58	0.44	0.58	0.19	0.31	0.42	0.22	0.29	0.48	0.1	0.46	0.13	0.31		0.42	0.25
Lateral acceleration (g)		152	52	54	66		96	29	9	74		33	148			79	
Iliac force (kN)	4	0.5	3	0.3	2	1.3	1.9	2.9	1.6	0.4	1.2	1.7	1.7	1.1		2.4	1.2
Acetabulum force (kN)	4	3.2	2.6	1.6	1.8	1.4	2.7	3	3.1	2.4	2.3	1.5	4.5	0.9		1.4	1.2
Combined Acetabulum and Ilium force (kN)	5.1	3.7	5.2	1.9	3.7	2.6	4.6	5.6	4.6	2.8	3.5	2.7	5.3	1.3		3.7	2.3
Distal femur Y force (3ms clip, kN)	±3.9	-3.6	-1.1	-0.7	-0.5	-0.4	-0.4	-1.2	-0.5	-1.1	0.5	-0.9	-0.6	0.8		-1.3	-0.6
Distal femur X moment (3ms clip, Nm)	±356	563.7	199.1	103.6	147.9	50	247.8	138.1	52.7	120.1	40	130.9	386.7	53		186.2	94
Distal femur Y moment (3ms clip, Nm)	±356	-74.4	85.5	62.3	34.9	122	52.9	-28.1	-13.4	38.8	16	71.1	53	137		51.9	32

Table B2. Peak passenger dummy injury measures

		Camry						Atlas				Accord			QX50	
		60 km/h				50 km/h		60 km/h			50 km/h	60 km/h	50 km/h		60 km/h	50 km/h
	Reference	F150	Pilot	MDB	Camry	MDB	F150	F150	Pilot	MDB	MDB	MDB	50 F150	MDB	MDB	MDB
Resultant acceleration (g)		46	49	66	45		47	53	49	51		66	51		72	
Resultant acceleration (3ms clip, g)		43	48	65	44		46	53	48	48		63	51		70	
HIC15	779	171	226	425	176	151	176	258	206	199	57	379	233	111	463	90
X shear force (kN)		-0.1	0.1	0.3	0.1		-0.1	-0.3	-0.3	-0.2		0.3	0.3		-0.2	
Y shear force (kN)		-0.5	-0.4	-0.2	-0.2		-0.3	-0.2	0.3	0.3		0.4	-0.3		-0.4	
Tension (kN)	2.1	0.4	0.6	0.2	0.2	0.1	0.2	0.7	0.8	0.3	0.1	0.9	0.4	0.3	0.6	0.4
Compression (kN)	2.5	0.5	0.3	0.5	0.5	0.5	0.5	0.3	0.4	0.5	0.5	0.2	0.6	0.5	0.9	0.6
X moment (Nm)	±67	-23	-31	-28	-17		-14	-42	-48	-50		-48	-30		-37	
Z moment (Nm)	±39	-21	-25	-23	-17		-18	-13	16	-19		-20	-24		-20	
Lateral deflection (mm)	60	22	23	38	25	22	22	31	21	25	17	52	43	36	38	25
Lateral force (kN)		1	0.7	1.7	1.2	0.9	0.9	1.4	1	1.5	1	1.7	0.9	0.9	2.4	1.5
Rib 1 deflection (mm)	34	24	27	34	31	24	25	23	19	21	15	57	45	41	31	17
Rib 2 deflection (mm)	34	23	27	38	31	26	21	20	17	18	11	49	33	30	22	14
Rib 3 deflection (mm)	34	24	29	39	33	24	23	32	21	15		38	16	15	13	14
Rib 4 deflection (mm)	32	22	24	38	29	20	21	48	48	42	23	25	5	17	32	33
Rib 5 deflection (mm)	32	24	27	28	30	21	25	54	57	52	34	26	7	15	56	46
Maximum Rib Deflection		24	29	39	33	26	23	54	57	52	34	57	45	**41**	56	**46**
Average rib deflection (mm)		24	27	35	31	23		35	32	29	21	39	21	**24**	31	**25**
Rib 1 deflection rate (m/s)	8.2	1.4	1.62	2.12	1.4	1.4	0.93	2.62	3.54	2.43	2.04	6.36	3.49	2.95	2.92	1.73
Rib 2 deflection rate (m/s)	8.2	1.45	1.6	2.2	1.76	1.6	0.97	2.56	3.38	2.42	1.98	5.56	2.37	2.44	2.64	1.64
Rib 3 deflection rate (m/s)	8.2	1.61	1.84	2.15	2.27	1.3	1.27	2.49	2.69	1.68		4.35	1.95	1.56	1.85	1.52
Rib 4 deflection rate (m/s)	8.2	1.69	1.92	2.19	2.03	1.1	1.45	4.09	3.34	3.5	2.05	3.48	1.15	3.48	2.63	2.39
Rib 5 deflection rate (m/s)	8.2	1.69	1.93	1.84	2.1	3.9	1.52	5.5	4.91	4.23	2.73	4.97	0.93	2.22	3.7	3.19
Rib 1 VC (m/s)	1	0.19	0.22	0.38	0.26	0.19	0.14	0.23	0.3	0.21	0.16	2.06	0.76	0.51	0.35	0.12
Rib 2 VC (m/s)	1	0.2	0.23	0.49	0.24	0.22	0.1	0.21	0.26	0.17	0.09	1.39	0.3	0.32	0.18	0.1
Rib 3 VC (m/s)	1	0.22	0.29	0.45	0.3	0.18	0.14	0.35	0.32	0.08		0.78	0.14	0.12	0.06	0.1
Rib 4 VC (m/s)	1	0.19	0.27	0.49	0.23	0.12	0.14	0.82	0.92	0.73	0.22	0.45	0.02	0.2	0.38	0.42
Rib 5 VC (m/s)	1	0.21	0.28	0.29	0.23	0.14	0.18	1.01	0.97	0.96	0.49	0.38	0.04	0.13	0.8	0.59
Lateral acceleration (g)		137	165	76	83		105	95	88	73		110	77		74	
Iliac force (kN)	4	1.2	1.7	0.9	1.1	0.9	0.6	0.5	0.4	1.6	0.3	0.7	0.1	0.1	0.5	0.7
Acetabulum force (kN)	4	2.3	6.1	1.6	2.4	1	4.6	5.8	5.3	1.8	1.8	0.7	2.9	0.5	1.7	0.5
Combined Acetabulum and Ilium force (kN)	5.1	3.4	7.8	2.4	3.5	1.7	5.1	6.1	5.6	2.9	1.9	1.3	2.9	0.6	2.1	1
Distal femur Y force (3ms clip, kN)	±3.9	1.2	-0.5	0.4	0.8	0.2	-0.7	-0.5	-0.9	-0.4	0.6	-2.3	1.1	0.7	-1.8	-1.3
Distal femur X moment (3ms clip, Nm)	±356	232.4	143.3	106.9	111.8	-31	168.6	187.9	85.9	105.6	29	636.5	420	28	205.9	140
Distal femur Y moment (3ms clip, Nm)	±356	-160.3	52.8	25.8	30.9	89	-85	-39.8	43.9	-21	16	-269.5	-193.7	206	19.2	32

APPENDIX C: NASS AND CIREN CASE LIST

Table C1.
Crashes that may benefit from a higher speed crash test

Case ID	Crash partner	AIS 3+ injured body regions
781136585	LTV	Abdomen, pelvis
2011-73-024	Heavy vehicle	Chest (elderly)
2007-81-048	Fixed object	Leg
133129	LTV	Abdomen, pelvis
352203868	Car	Chest, pelvis
338071752	LTV	Chest, pelvis
2007-48-216	LTV	Pelvis
2010-75-043	LTV	Chest, pelvis
2009-12-289	Car	Chest (elderly)
842005511	LTV	Head, chest, abdomen, pelvis
2012-73-118	LTV	Chest
2012-78-139	LTV	Chest, pelvis
852153529	LTV	Chest (elderly)
2011-09-091	LTV	Head
554160123	LTV	Head, pelvis

Table C2.
Crashes too severe to benefit from a higher speed crash test

Case ID	Crash partner	AIS 3+ injured body regions
160151944	LTV	Pelvis
2009-79-003	Fixed object	Head, spine, chest
2009-11-180	Fixed object	Head, spine chest, abdomen
2007-09-135	Fixed object	Head
2009-09-185	Fixed object	Chest, abdomen, pelvis
2011-81-080	Fixed object	Head, chest
2009-79-180	Car	Chest
2006-09-173	Car	Head, neck, chest
2009-43-041	Fixed object	Chest
2007-74-123	Fixed object	Chest
2007-11-067	Heavy vehicle	Head, chest, abdomen
2007-45-174	Fixed object	Head
2011-11-187	Heavy vehicle	Chest
2012-48-109	Heavy vehicle	Head, chest, abdomen
2012-49-052	Fixed object	Head

DEVELOPMENT OF A MODULAR TOOL FOR SAFETY ASSESSMENTS OF HUMAN-MACHINE-INTERACTION FOR ASSISTED DRIVING FUNCTIONS (SAE LEVEL 2)

André Wiggerich
Federal Highway Research Institute (BASt),
Germany

Paper Number 19-0195

ABSTRACT

Per definition, SAE Level 2 (L2) Systems perform both the lateral and longitudinal vehicle motion control with the expectation that the driver completes the Object and Event Detection and Response (OEDR). Since every system performs also parts of the OEDR itself and this amount of OEDR also varies between different L2 systems depending on the intended system design, it cannot be taken for granted that drivers automatically understand their roles and responsibilities in interaction with the system. Especially highly reliable L2 systems performing a greater amount of OEDR while at the same time requiring only little driver input over time can make it difficult for drivers to correctly identify their role and responsibility.

Until now, neither application-oriented assessment methods nor design guidelines for OEDR related system design features taking safety of human-machine-interaction into account are available. The objective is therefore to deliver a standardized tool for the assessment of human-machine-interaction-related safety of vehicles with L2 systems currently available on the market. To evaluate the impact of different system design aspects on safety of human-machine-interaction and also to be able to differentiate between system designs, a holistic, standardized and application-oriented assessment procedure is proposed. The novel tablet-based assessment tool focuses not only on available standards and guidelines but measures also concrete user behaviour and user understanding in interaction with the L2 systems. The aim is to gain further insights which cannot be measured directly by simple checklist instruments.

For preparation, based on international standards, literature reviews and expert consultations, a first checklist-based expert-evaluation for currently available vehicles with L2 systems was developed. These assessments are focusing on different sources of user information (e.g. user manual), human-machine-interface design as well as the prevention of unintended use by different driver monitoring techniques. The checklist-tool was developed in cooperation with experts of different EuroNCAP test laboratories and validated in a common expert workshop to gain high level of standardization and agreement. However, to assess safety of human-machine-interaction holistically beyond these rather explicit forms of information design criteria, also implicit forms of driver-vehicle-communication via vehicle dynamics, functional behavior or reliability play an important role and should be taken into account. Therefore, the main and novel methodological aim is to consider also interaction related processes regarding user´s understanding of roles and responsibilities when applying automated driving functions as well as user´s awareness of automation modes or traffic situations in the modular tablet-based assessment tool.

INTRODUCTION

Safety of continuously automating functions strongly depends on and results from successful driver-vehicle-interaction. This effect is particularly strong in case of parallel automation as provided by SAE Level 2 (L2) systems. The human driver and the respective functions can be considered as socio-technical systems requiring prolonged collaboration to ensure safety and enhanced comfort. Vehicle automation in this case is not simply relieving drivers of routine tasks by replacing him or her with continuously automating functions but introducing also new tasks and responsibilities [1]. According to SAE J3016 Assisted Systems (SAE L2) can be defined as "the sustained and ODD [Operational Design Domain]-specific execution by a driving automation system of both the lateral and longitudinal vehicle motion control subtasks of the DDT [Dynamic Driving Task] with the expectation that the driver completes the OEDR [Object and Event Detection and Response] and supervises the driving automation system" [2, p.17]. This means that the system continuously assists the driver in performing the lateral and longitudinal vehicle motion control, for example by combining adaptive cruise control (ACC) and lane centering functions. The driver performs the part of the DDT not performed by the system (mainly the OEDR), supervises the system and intervenes as necessary to maintain safe operation of the vehicle. Nevertheless, every system performs also parts of the OEDR itself, for example reducing speed if a vehicle in front slows down or providing steering torque if lane markings indicate a curve. This amount of OEDR performed by the system and the expectation that the driver completes the remainder of OEDR varies between

different systems and depends largely on the intended system design [3]. In order to create recommendations and assessment criteria for human-machine-interaction in line with this variation, the first objective is to determine different L2 assessment categories with different interaction related requirements.

HOW USERS UNDERSTAND DRIVING AUTOMATION

The driver´s understanding of his/her role and tasks within the interaction with the L2 system can be described by the term mental model, a "rich and elaborate structure, reflecting the user´s understanding of what the system contains, how it works, and why it works that way" [4, p. 12]. The concept of mental models is strongly related to various psychological constructs and cognitive processes, for example attention and perception, situational awareness, learning and experience, problem solving or trust, reliance and acceptance [5, 6]. The development of a correct mental model concerning the driver´s role in interaction with and concerning the functionality of a continuously automating function is one of the most important requirements for safe and adequate use, trust and acceptance [7]. Inaccurate mental models on the other hand are linked to inadequate monitoring behavior [8]. A key human factors issue for L2 systems in terms of mental models is therefore to support drivers develop appropriate reliance on the system, make drivers understand that in terms of secondary task involvement it is not different to manual driving and that the system is not capable of performing all driving situations safely and therefore can fail immediately [1].

Humans and Automation

Meta-analyses show that the effect of automation on human performance in general depends largely on the degree of automation [9]. Although higher levels of automation have been found to improve routine task performance and workload, it negatively affected performance in case of system failures or unexpected events as well as situational awareness in this case. The authors therefore conclude that if manual performance by the human operator is required at some time, as it is by definition for L2 systems, the automation should be designed to keep the operator involved in the decision and action selection as well as the action implementation tasks [9]. Active task involvement, for example by a functional design requiring prolonged hands-on collaboration, seems to be more effective than only passive task involvement, for example by only visual monitoring of displays and traffic situations, and may help the driver understand his/her role in interaction with the system correctly [1]. This involvement seems to be of particular importance, since the performance reduction is often reported to be related to reduced monitoring behavior of the human operator. In this case, it is difficult for humans to monitor a reliable system permanently or to be out of the loop for some short time and then intervene immediately to perform difficult and critical tasks. Therefore, especially for L2 systems, as Seppelt and Victor [1, p. 140] conclude, it is important to consider that "the better the automation, the less attention drivers will pay to traffic and the system, and the less capable they will be to resume control".

Based on the definition of Merat and colleagues [10] the driver using any L2 function should be at least *On the Loop*, which means that he/she is not physically in control of the vehicle but continuously monitoring the driving situation. This driving situation does not only comprise the surrounding environment and traffic but also the performance of the automated driving function. The authors describe the concept of being *In, On* or *Out of the Loop* as a continuum rather than a distinct state which requires a lot of experience and knowledge for a driver to handle all situations safely and at the same time gain a maximum of comfort. Since the intensity of cognitive control may be different in different driving situations, the driver needs experience on a meta-level when to invest how much cognitive effort. In manual driving this is a well trained routine task. Drivers normally know when extensive monitoring is required and automatically decide from a moment to moment basis. When using automated or assisted driving functions this automatic decision may be interrupted. Since the driver is not physically in the control loop this makes it somehow more difficult to assess all driving related information immediately and correctly. Human-machine-interaction in this case is not limited to visual or auditory information communicated via displays and speakers only but in broader sense also includes every kind of information processing between the human being and the vehicle [11]. Besides rather explicit forms of information design in display and control elements, also implicit forms of communication, for example vehicle dynamics or system behavior and reliability within different situations and contexts as well as any haptical communication (e.g. how strong is the steering wheel resisting input of human driver when the system is active) play an important role.

Roles and Responsibilities in redundant parallel automation

It cannot be taken for granted that drivers automatically understand their roles and responsibilities when using continuously automating functions. Knowledge concerning system limitations as well as reacting correctly towards potential hazardous situations is the result of an extended learning process [12]. Especially the

redundant parallel automation of L2 functions can be ambiguous, since the proportion of OEDR performed by the system depends largely on the system design and its limitations. Even when driving the same route every day, the same system can behave completely different depending on different situational factors, for example weather, lighting, surrounding traffic or speed conditions. Furthermore, the relationship between the designer and the user of the function is of specific relevance. Designers of automation expect users to behave in a certain way to interact appropriately with the function to ensure safe and comfortable use. However, these assumptions or expectations can diverge from the way users actually behave and interact with the automation [13]. Therefore, trust and reliance need to be carefully taken into account when designers define the ideal or intended use or try to anticipate the actual use of automation. A safe human-machine-interaction strategy should make sure that designers and drivers have one common understanding about how to make use of the respective function.

MISCONCEPTIONS AND HUMAN FACTORS PROBLEMS RELATED TO ASSISTED DRIVING

Misconceptions regarding these basic functionalities can lead to dangerous situations and accidents as for example the fatal crash of a Tesla Model S operated in Autopilot mode in May 2016 in Florida (investigated by the US National Transportation Safety Board (NTSB)) has demonstrated [14]. The Tesla driver was travelling with active Autopilot on a US highway when an oncoming semitrailer truck crossing his travel lanes to make a left turn into a local road. The Tesla crashed into the right side of the semitrailer and went underneath it. The roof of the car was torn off. The driver died in the accident. The agency concludes that the Autopilot system did not brake for the crossing truck because it was not designed to do so, but that the driver´s pattern of use of the Autopilot system suggests a misunderstanding of his role in interaction with the system as well as over-reliance on the system´s capabilities [14]. As a result, the driver did not pay as much attention as required in the respective situation and did not react to the crossing truck. The Autopilot system on the other hand was not able to monitor the driver´s inattention and intervene effectively.

Besides these tragic misconceptions, at the same time more and also more different kinds of continuously automating functions requiring collaboration between the human operator and the vehicle appear and will come to the market in the foreseeable future [11]. Here, a common trend is observable that small and simple tasks formerly performed manually by the driver are now automated and performed by a continuously automating function. The BMW Driving Assistant Plus in the BMW 5 Series 2016 Version for example was able to adapt speed to traffic sign recognition if the driver confirmed via control input and was not able to adapt speed (based on GPS information or camera detection) prior to entering a curve or in front of a roundabout. The 2019 Version of the System, now called Driving Assistant Professional, for example in the X5 (2018) or 3 Series (2019) is able to adapt speed to traffic sign recognition without any driver input (if this option is chosen by the driver) and is also able to adapt speed prior to entering a curve or in front of a roundabout. The Tesla Autopilot Software Update 9.0 in the US is introducing a function called “Navigate on Autopilot” [15]. The function “guides a car from a highway’s on-ramp to off-ramp, including suggesting and making lane changes, navigating highway interchanges, and taking exits” [15]. Although Tesla strongly claims that the driver is always responsible and should pay attention while using this function, it is obvious that the driver is taken even further out of the DDT (because more OEDR is performed by the function) and pushed into a passive monitoring task with less frequent interactions.

Altogether, these are only small and very simple changes but represent a common trend: Tasks formerly performed by a human driver are now automated, which at first sight seems to be an enhancement in system performance, but as was already mentioned: “the better the automation, the less attention drivers will pay to traffic and the system, and the less capable they will be to resume control” [1]. Therefore, just because it is technically possible to automate an even small and very simple task, from a human factors perspective it is not always beneficial to do so.

Automation related task changes

The example of the system automatically reducing speed prior to entering a roundabout demonstrates different human-machine-interaction related problems or concerns: First, the feedback a driver gets in this situation is reduced and/or qualitatively different compared to approaching a roundabout driving manually. Besides purely visual information of the road scene or vehicle displays, the manual driver perceives also proprioceptive feedback, for example the feelings of reduced speed because of his/her actions in pressing the brake pedal. When the system is reducing speed (“feet-off”), only visual information is left, which can make it more difficult to assess the situation and decide whether to brake or speed up in case another car is already driving in the roundabout [16]. The automation in this case distances the driver from the process of approaching a roundabout,

a very ordinary task in daily driving can be more challenging just because a source of informal or implicit feedback is taken away.

Second, to monitor an automated system approaching a roundabout is basically a passive observation task where at the end the driver has to decide whether to do something, for example to brake or speed up, or to let the automation control the speed through the roundabout. This task is qualitatively very different compared to monitoring the situation actively when controlling the vehicle manually [17, 18]. In the manual control condition, perception actively supports control actions, and control actions guide the way of perception [19]. However, this process is disrupted by only monitoring automation guiding the vehicle.

Third, the driver´s mental model may be inadequate to guide expectations and control inputs. For example, the automation control algorithm in the described situation approaching a roundabout could be designed to decrease speed early and continue with a constant low speed into the entrance of the roundabout without further deceleration or acceleration. However, a driver´s manual control strategy as well as his/her mental model of the function and situation might be very different. Anticipating vehicle actions as well as system limits may therefore be complicated or even fail in this case [20]. Previous experiences and well developed mental models simplify the interaction but it needs some time and learning until they are developed holistically [7].

Last, by developing functions which automate very easy and ordinary tasks of a human driver, as slowing down when approaching a roundabout, designers are running the risk of creating clumsy automation. The term refers to a concept where automation makes easy task easier, but harder task harder [21]. As Bainbridge [22] reports, users are often left with the most difficult tasks of a certain operation because designers are not able to automate them. However, because easy tasks are automated, the user is disrupted from the process and the context of performing the operation as a whole, which makes it difficult to respond correctly to the left over difficult tasks only. Reducing speed when approaching a roundabout is a simple task and the decision to brake or speed up depending on the traffic inside the roundabout often is done in one go with it. However, performing the decision task only without feet on brake or accelerator pedal before is a change in the structure of the task, which can make this isolated task more complicated compared to performing the whole task at once.

The mentioned problems or concerns do not necessarily mean that a function reducing speed prior to entering a roundabout is something bad or dangerous per se. It is intended to demonstrate that vehicle automation, even when focusing only at L2 functions, is a continuum of automating different tasks of driving. Since the driver is always responsible for safe driving when using these functions, he/she is supposed to perform all tasks the function is not designed for and also to intervene if the function makes a mistake. These two tasks are structurally different to driving manually, which can make it harder for drivers to behave correctly, especially in difficult or accident-prone driving situations, which in general occur very rarely.

Automation mode related problems and driver behavior

Besides these problems related to the concrete task execution of driving, also errors concerning the perception and understanding of the automation mode or status can occur. The aspects of mode confusion and mode related errors basically result from two factors: poor monitoring behavior combined with poor feedback. Research concerning automation in aviation shows that unexpected mode changes of autopilot systems often surprise pilots and sometimes even remain unnoticed [23]. In automated driving similar problems could arise. Therefore, feedback as well as an intuitive monitoring strategy should support the driver in understanding the current system mode or state and help him/her to be able to react immediately to system initiated mode changes.

Negative effects of automation can also result on a behavioral level. Behavioral adaptation is a phenomenon well known by social-psychologists. Diffusion of responsibility, also called the bystander effect or pluralistic ignorance, describes an instance of behavioral adaptation where a person is less likely to act and take responsibility in a certain situation (e.g. an emergency) if other persons are present or available which could probably also take responsibility [24]. The effect is linked to lower performance of individuals working in groups and can also be transferred to human-machine-interaction related tasks where the human operator and the machine are working together. Hence, with respect to driving automation, subjective responsibility diffusion can lead to drivers spending less effort in controlling and monitoring the driving situation while the automation is active, since these tasks are also at least partially performed by the machine. Clear communication of roles and responsibilities can only support drivers in monitoring and interacting with the system whilst holistic L2-design designated to sustained driver involvement is the most promising approach.

DEVELOPMENT OF A MODULAR ASSESSMENT TOOL FOR ASSISTED DRIVING FUNCTIONS

Taking the afore-mentioned human factors related problems and concerns as well as the available guidelines, standards and assessment criteria into account, it becomes clear that assessment of safety of human-machine-interaction for the large bandwidth of L2 systems currently available on the market is not as easy as it might seem at first sight. Therefore, the first aim of this research is to develop and validate standardized assessment instruments which focus on two aspects: 1. design of the human-machine-interface (HMI) as well as 2. design of the functional behavior per se (e.g. functional reliability, steering quality, automated tasks, etc.) from a human factors perspective. The second aim is to deliver guidelines and requirements for the functional design of automated driving functions taking not only HMI design principles into account but also the influence of implicit information on the development of mental models and driver behavior. To do so, measures and instruments focusing on these aspects have to be developed first.

A first collection of standards, guidelines and best practices regarding the design of rather explicit forms of communication via classical visual-auditory or visual-vibrotactile HMIs for automated driving functions can be found in the recent paper of Naujoks and colleagues [25]. However, taking also implicit forms of communication via functional behavior into account two problems arise: First, no guidelines or standards concerning this form of driver-vehicle-interaction are available in the field of automated driving so far. Second, also methods measuring the influence of system settings or behavior on the driver´s mental model and behavior are not available so far.

Due to its various facets especially the measurement of a driver being *On the loop* is difficult [10]. Since the driver is not physically in control of the vehicle a detection of drivers' physical activity based on in-vehicle sensors seems insufficient. Many studies on automated driving therefore focus on measuring drivers' visual behavior and try to assess quality and quantity of monitoring behavior by analyzing gaze or fixation patterns with eye-tracking camera systems. Nevertheless, since monitoring traffic situations and system performance and reacting to an upcoming system limit are very complex cognitive tasks, relying only on eye-tracking measurements doesn´t reflect this process adequately [8]. Observing driver behavior as well as interviewing drivers about their understanding may support the assessment of the quality of monitoring behavior. However, without further standardization or routine this methodology can be very time and resource consuming in preparation, execution and analysis of required driving trials with subjects. Such tools are therefore mainly used in research projects but seem to be inappropriate for applied contexts, for example in NCAPs or type approval, at first sight. Therefore the development of a standardized modular assessment tool including observations and interviews of drivers and focusing on the special needs of applied contexts is proposed. The aim is to bundle advantages of different methods without unnecessarily inflating the effort but at the same time reaching a reliable and valid assessment result.

Checklist-based expert evaluation

Based on international standards, literature reviews and expert consultations, a first checklist-based expert-evaluation for currently available vehicles with L2 systems was developed. These assessments are focusing on different sources of user information (e.g. Is the correct use of the function described precisely and in plain language in the user manual and is it in general easy to read?), human-machine-interface design (e.g. Is the activation straightforward?, Does the driver get appropriate feedback about current status?) as well as the prevention of unintended use by different driver monitoring techniques (e.g. Does the system effectively promote proper use by means of driver monitoring?). The checklist-tool was developed in cooperation with experts of different Euro NCAP test laboratories and validated in a common expert workshop to gain high level of standardization and agreement.

Results indicate that at least two different kinds of L2 systems can presently be identified: One category of systems (category A), which only support drivers to some extent by providing limited steering torque, as well as another category of systems (category B), which enhance assistance and actively reduce frequency of driver response execution by precise adaptation of speed and/or steering torque required at specific road sections (e.g. by means of GPS-based digital maps or vehicle fleet based learning algorithms). The co-operative systems of category A involve drivers in the driving task by design. The systems allow and require driver input, for example steering in curves. Driver out of the loop phenomena are less likely to occur because of the need for the driver to permanently interact with the system. Experience of system limitations is clear and frequent. Driver disengagement from the driving task is prevented by prolonged hands-on cooperation with the system. Driver activity (e.g. steering) in this case is seen as an indicator of driver attentiveness. Since a greater amount of OEDR is performed by the driver, requirements regarding human-machine-interaction are lower compared to systems which relieve the driver more frequently from performing OEDR. A basic status indication as well as simple hands-on detection in this case may be sufficient to keep the driver focused on performing the DDT.

Systems of the other category B offer drivers a broader use and comfort, but at the same time from a safety perspective require additional measures to actively keep the driver in the loop. Driver engagement and activity have to be ensured since often no permanent interaction with controls (e.g. steering wheel) is required. Since a larger amount of OEDR is performed by the system (compared to systems of the other category), the driver may experience greater difficulties in understanding the permanent role of parallel OEDR execution. Driver out of the loop phenomena are likelier if no additional instruments are implemented to keep the driver interacting with the vehicle or responding to objects and events in the driving environment. A goal-oriented and effective status feedback and warning strategy has to be defined to make sure that drivers are able to react immediately and appropriately even in rare events. However, especially for these systems it is difficult to assess the safety of human-machine-interaction by means of a checklist based method only, because there is a fine line between driver In, On or Out of the Loop if no permanent interaction and hands-on collaboration is required. Assessments of a driver´s correct understanding of his/her role and responsibility cannot be carried out by HMI design checklists only.

Development of a tablet based observation and interview tool

Since the described checklist based procedure is focusing on design criteria only, further assessments should also include observational and interview measures of user studies taking into account interactional processes regarding users' understanding of roles and responsibilities when applying automated driving functions as well as users' awareness of automation modes or traffic situations. A first standardized observational tool for assessing safety of human-machine-interaction for automated driving is currently being validated in a simulator study. The semi-automated, tablet based application allows human factors experts to directly observe and assess the interaction of naïve users with any automated driving function. This scenario based procedure allows the observation of interactional behavior in average traffic situations. For example the matter of assessment might be whether a driver distracts him/herself or is unsure about how to put his/her hands on the steering wheel while the system is active. Based on these observations conclusions concerning reactions in difficult situations can be drawn and also observed. Three observation categories (system control related problems, general vehicle guidance related problems, system monitoring behavior and misuse) with different observable behavior patterns are proposed. A general rating of driver-vehicle-interaction performance based on the rating scale of Neukum and Krüger [26] can be used to assess the accomplishment of interaction related critical and non-critical situations, for example activation or deactivation of system, monitoring behavior while system is active or reaction in case of system limits. Besides observation, the tool also supports the assessor's decision by delivering standardized questionnaire items. These items focus on the role and understanding of the driver in certain situations as well as on trust, comfort and usability. Results of the validation of the whole tool will be published in the near future.

CONCLUSION

L2 systems require the driver to perform the part of the DDT not performed by the system (mainly the OEDR), supervise the system and intervene as necessary to maintain safe operation. Since every system performs also parts of the OEDR itself and this amount of OEDR varies between different systems and depends largely on the intended system design, it cannot be taken for granted that drivers automatically understand their roles and responsibilities. Misconceptions on the other hand can lead to dangerous situations and accidents and should therefore be avoided by safe human-machine-interaction design. However, a common trend is observable that small and simple tasks formerly performed manually by the driver are now automated and performed by a continuously automating function. This kind of automation changes the structure of the whole task of safe interaction and can make it difficult for drivers to react if something unexpected happens. Therefore, to assess safety of human-machine-interaction holistically, different assessment methods should be taken into account. This includes besides rather explicit forms of information design criteria in display and control elements also implicit forms of communication via functional behavior and task reliability. The aim of this research is to develop on the one hand standardized methods for measuring and assessing the influence of these implicit forms of information on human-machine-interaction as well as on the other hand guidelines and requirements for the functional design of automated driving functions taking not only HMI design principles into account but also the influence of implicit information on the development of mental models and driver behavior.

REFERENCES

[1] Seppelt, B. D., and Victor, T. W. (2016). “Potential solutions to human factors challenges in road vehicle automation” In G. Meyer and S. Beiker (Eds.): Road Vehicle Automation 3 (pp. 131-148). Springer, Cham.
[2] SAE International Standard J3016. (2016). “Taxonomy and Definitions for Terms Related to On-Road-Motor Vehicle Automated Driving Systems”
[3] Seppelt, B., Reimer, B., Angell, L., and Seaman, S. (2017). “Considering the Human across Levels of Automation: Implications for Reliance” Proceedings of the Ninth International Driving Symposium on Human Factors in Driver Assessment, Training and Vehicle Design, June 26-29, 2017, Manchester Village, Vermont. Iowa City, IA: Public Policy Center, University of Iowa, 2017:228-234.
[4] Carroll, J. M., and Olson, J. R. (1987). “Mental models in human-computer interaction. Research Issues About What the User of Software Knows” Washington, D.C.: National Academy Press.
[5] Beggiato, M., Pereira, M., Petzoldt, T., and Krems, J. (2015). “Learning and development of trust, acceptance and the mental model of ACC. A longitudinal on-road study.” Transportation research part F: Traffic psychology and behaviour, 35, 75-84.
[6] Kazi, T., Stanton, N. A., Walker, G. H., and Young, M. S. (2007). “Designer driving: drivers’ conceptual models and level of trust in adaptive cruise control.” International Journal of Vehicle Design, 45(3), 339-360.
[7] Beggiato, M., and Krems, J. F. (2013). “The evolution of mental model, trust and acceptance of adaptive cruise control in relation to initial information.” Transportation research part F: Traffic psychology and behaviour, 18, 47-57.
[8] Victor, T. W., Tivesten, E., Gustavsson, P., Johansson, J., Sangberg, F., and Ljung Aust, M. (2018). “Automation expectation mismatch: incorrect prediction despite eyes on threat and hands on wheel.” Human factors, 60(8), 1095-1116.
[9] Onnasch, L., Wickens, C. D., Li, H., and Manzey, D. (2014). „Human performance consequences of stages and levels of automation: An integrated meta-analysis.” Human factors, 56(3), 476-488.
[10] Merat, N., Seppelt, B., Louw, T., Engström, J., Lee, J. D., Johansson, E., ... and Keinath, A. (2018). “The “out-of-the-loop” concept in automated driving: Proposed definition, measures and implications.” Cognition, Technology & Work, https://doi.org/10.1007/s10111-018-0525-8
[11] Carsten, O., and Martens, M. H. (2018). „How can humans understand their automated cars? HMI principles, problems and solutions.” Cognition, Technology & Work, https://doi.org/10.1007/s10111-018-0484-0
[12] Larsson, A. F., Kircher, K., and Hultgren, J. A. (2014). “Learning from experience: Familiarity with ACC and responding to a cut-in situation in automated driving.” Transportation research part F: Traffic psychology and behaviour, 27, 229-237.
[13] Lee, J.D. and Seppelt, B.D. (2012). „Human Factors and Ergonomics in Automation Design” In G. Salvendi (Ed.): Handbook of Human Factors and Ergonomics, 4. Edition (pp. 1615-1642). John Wiley & Sons.
[14] National Transportation Safety Board (NTSB) (2017). “Collision Between a Car Operating With Automated Vehicle Control Systems and a Tractor-Semitrailer Truck Near Williston, Florida May 7, 2016.” Accident Report NTSB/HAR-17/02 PB2017-102600 Notation 56955, Adopted September 12, 2017.
[15] Tesla Motors Inc. (2018). “Introducing Navigate on Autopilot”. https://www.tesla.com/de_DE/blog/introducing-navigate-autopilot
[16] Wickens, C. D., and Kessel, C. (1981). „Failure detection in dynamic systems.” In J. Rasmussen and W.B. Rouse (Eds.): Human detection and diagnosis of system failures (pp. 155-169). Springer, Boston, MA.
[17] Gibson, J. J. (1962). “Observations on Active Touch.” Psychological Review, 69, 477–491.
[18] Eprath, A. R., and Young, L. R. (1981). “Monitoring vs. Man-in- the-Loop Detection of Aircraft Control Failures.” In J. Rasmussen and W.B. Rouse (Eds.): Human detection and diagnosis of system failures (pp. 143-154). Springer, Boston, MA.
[19] Flach, J. M., and Jagacinski, R. J. (2002). “Control Theory for Humans”, Lawrence Erlbaum Associates, Mahwah, NJ.
[20] Goodrich, M. A., and Boer, E. R. (2003). “Model-Based Human-Centered Task Automation: A Case Study in ACC System Design.” IEEE Transactions on Systems, Man and Cybernetics, Part A, Systems and Humans, Vol. 33, No. 3, pp. 325–336.
[21] Wiener, E. L. (1989). “Human Factors of Advanced Technology (“Glass Cockpit”) Transport Aircraft,” NASA Contractor Report 177528, NASA Ames Research Center, Wilde, Moffett Field, CA.
[22] Bainbridge, L. (1983). “Ironies of Automation.” Automatica, Vol. 19, No. 6, pp. 775–779.
[23] Sarter, N. B., and Woods, D. D. (1995). “How in the World Did We Ever Get in That Mode? Mode Error and Awareness in Supervisory Control.” Human Factors, Vol. 37, 1, 5–19.
[24] Darley, J. M., and Latané, B. (1968). “Bystander intervention in emergencies: diffusion of responsibility.” Journal of personality and social psychology, 8(4), 377-383.

[25] Naujoks, F., Wiedemann, K., Schömig, N., Hergeth, S., and Keinath, A. (2019). „Towards guidelines and verification methods for automated vehicle HMIs." Transportation research part F: Traffic psychology and behaviour, 60, 121-136.
[26] Neukum, A., and Krüger, H. P. (2003). Fahrerreaktionen bei Lenksystemstörungen–Untersuchungsmethodik und Bewertungskriterien. VDI-Berichte, 1791, 297-318.

Euro NCAP - New Frontal Impact Test with Mobile Progressive Deformable Barrier (MPDB)

Volker Sandner
ADAC e.V.
Germany

Michiel van Ratingen, James Ellway
Euro NCAP
Belgium

On behalf of the Euro NCAP Frontal Impact Working Group

Paper Number 19-0196

ABSTRACT

In 2015 Euro NCAP announced that the current offset deformable barrier frontal impact test procedure would be revised and a frontal impact working group was set-up to develop the new procedure. The aim was to bring together individual research efforts by FIMCAR [1], ADAC and other organisations [2,3] on the development of a 'moving barrier to vehicle' frontal impact test and derive common specifications for the new Euro NCAP test and assessment procedure from this. In partnership with the European Enhanced Vehicle safety Committee (EEVC), Euro NCAP examined the extent to which the advanced frontal THOR-M ATD is ready and suitable for use in this new test procedure. The overall results of the accident analyses, the specification of the test setup and the definition of the barrier were reported at the ESV 2017 in Detroit [4]. In the subsequent stage, the group focussed on the assessment criteria for the THOR dummy, the compatibility assessment and the full-scale evaluation of the procedure. Several round robin tests were organised to check the feasibility and repeatability of the method, in particular with regards to the THOR dummy and the barrier scanning. The group has released the final test and assessment protocols in 2018 for adoption in 2020, but will continue to monitor relevant developments, in particular related to dummy hardware and certification updates.

BACKGROUND

In the first phase of work of the group, the basic foundations for the definition of the new frontal mobile barrier test were laid, especially test parameters like impact speed overlap, mass of the barrier, the definition of the mobile barrier face and the dummy positioning in the test vehicle. The new test is aiming at improving the biomechanical assessment of critical body region risk at injury and at assessing, for the first time, vehicle compatibility. As NHTSA has postponed the introduction of the new US NCAP that was announced in 2016, Euro NCAP will most likely be among the first world-wide to use the advanced THOR-M dummy as part of their assessment of vehicle's crashworthiness. Several relevant documents pertaining the specification and certification of the latest dummy hardware remain unreleased by NHTSA until this date, which meant that the working group had to verify the latest built-level dummy's repeatability and reproducibility and make some practical decisions regarding certification. Beside the dummy specification, injury criteria and the upper and lower reference values (limits) for the rating needed to be set. The biggest challenge, however, was to agree on the method by which vehicle compatibility could be assessed and included in the safety rating. Finally, the complete test procedure by R&R testing needed to be validated, so several test series were carried out in the Euro NCAP accredited laboratories to verify the test setup and assessment and to proof the test's reproducibility in different labs with the same result.

TEST SPECIFICATION

The actual car-to-barrier test specification was agreed in 2016 with both the vehicle and the barrier approaching at 50kph (MPDB). The test vehicle is equipped with a THOR 50th percentile male dummy (THOR 50M) on the driver seat and a Hybrid III 50th percentile male dummy (H-III 50M) on the front passenger seat. In the second row, a Q10 dummy is placed on the struck side while the Q6 dummy is seated on the non-struck side, the results of which are used for the Child Occupant Protection assessment in Euro NCAP. The overlap is moderate at 50 percent of the total vehicle width. The moving trolley carries a progressive deformable barrier [5,6] on the front outboard side and has a mass of 1400kg (Figure 1).

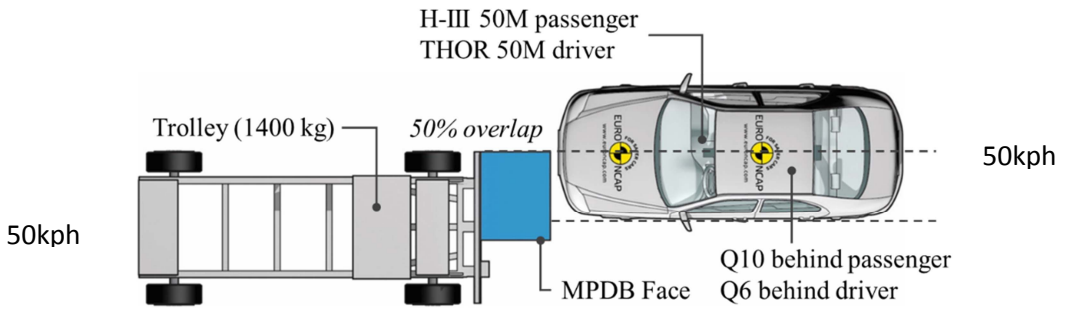

igure 1: Impact condition of the MPDB test

ASSESSMENT CRITERIA

Euro NCAP has carried out the frontal offset deformable barrier (ODB) testing for more than 20 years. During this time, there have only been minor changes to the assessment of the vehicle performance. From the beginning, the test score was based on actual dummy scores (based on injury limits) and so-called modifiers, which can reduce the number of scored points from the dummy values, due to observations made in the high-speed films, dummy traces or based on structural problems in the vehicle such as deformation or potential risks for the passengers. This kind of assessment, which is also used in other full-scale tests, was also followed for the new MPDB test. With the assessment of the barrier/trolley performance for compatibility, a new modifier was introduced for the overall frontal performance of the tested vehicle.

Approach

Euro NCAP's assessment of driver and passenger occupant protection will be based on dummy values, derived from lower and higher performance limits against a set of dummy criteria, and restraint and structural modifiers, such as airbag failure, pedal intrusion etc. Contrary to Hybrid-III, there are few industry accepted injury limits for THOR available and there is still a lack of information of injury risk curves or dummy limits published in the scientific community. The group analysed data from the round robin tests, ongoing research, publications and studied comparable tests between the Hybrid-III 50M and the THOR 50M to find correlations and set the first criteria and limits for the THOR 50M dummy.

THOR Assessment Criteria

The initial list of criteria included more or less all parameters which have been considered by NHTSA, with the exception of those related to the THOR-LX as Euro NCAP has decided to use the Hybrid III 50% lower legs in the first step. These criteria are:

- HIC15
- BrIC/SUFHEM (monitoring)
- Neck forces and torque
- Chest displacement / Rmax
- Abd compression
- Left acetabulum load
- Right acetabulum load
- Left femur force
- Right femur force
- Left knee shear displacement
- Right knee shear displacement
- Left tibia index
- Right tibia index
- Left tibia compression
- Right tibia compression
- Pedal rearwards displacement

Lower Leg, Knee and Femur At the time that the group defined the THOR 50M specification in 2016, the decision was taken not to adopt the LX-legs, due to the status of the development of the legs, the high costs of obtaining and certification of the legs, and the relative low priority of lower leg injuries in the field. So, the Hybrid-III 50M lower legs were applied to the THOR femurs, including the knee slider of the Hybrid dummy. With the use of the Hybrid III parts, also the current Hybrid III 50M dummy criteria and upper and lower performance limits could be used for assessment. This includes the Tibia Index, the Tibia Force F_z and the knee slider performance. Euro NCAP also continues to monitor pedal rearward displacement and foot well

behaviour as part of the modifier assessment, a practical measure that has been an effective way to minimise the risk at foot and lower leg injuries in practice.

The other parts of the THOR assessment in the lower extremity area are the femur and the acetabulum. The Femur load is also based also on the Hybrid III 50M value and is evaluated in used in the compression phase. A preliminary NHTSA publication showed comparable values for H-III and THOR so the higher performance limit was set to 3,8kN and the lower performance limit to 9,07kN. The acetabulum calculation takes the resultant force of F_x, F_y and F_z into account. Often the tension force F_x produces higher values than the compression force, but tests have shown that the compression force is the driving factor of injuries in the acetabulum region. Due to this fact, high resultant values of the acetabulum might not be problematic for the passenger as this will be result of the tension force primarily. To solve this issue, the Euro NCAP acetabulum calculation foresees that the resultant force is only calculated in the phase when F_x shows compression. The proposed limits were set to 3.28 as lower performance and 4.1 as higher performance limit.

Chest and Abdomen Actual crashes analysed by the group showed that chest and abdominal injuries are still the most common injuries in frontal impacts on European roads. This was the main motive to introduce THOR in the new frontal test. This dummy was designed to be more biofidelic in the chest and abdomen area than the Hybrid III dummy. The interaction with the restraint systems is expected to be more humanlike, due to its higher spine flexibility and improved anthropometry. Despite these advantages, however, the idea of using an advanced chest injury risk criterion of based on a combination of chest compression and geometric deformation, such as the PCA-score, turned out to be premature, as there is still work ongoing and only limited data are available to support biomechanical limits. In the introduction phase, the maximum deflection R_{max} will be the assessed criterion in the chest region. All ribs will be evaluated, while the rib with the highest compression is driving the assessment. The results of the SENIORS project [7] and the internal test runs of MPDB test from Euro NCAP were used to set acceptable upper and lower performance limits. It was also understood that the current vehicles tested were not optimized for the new dummy and future performance in cars will likely show better results. Based on these studies, the lower performance limit was set to 35mm, while the higher performance limit of 60mm is used.

Unfortunately, even less information is currently available regarding abdominal injury risk. Due to this fact, and primarily based on the experience in the full-size crashes, only the upper performance limit was defined, which will allow to Euro NCAP to identify vehicles showing elevated submarining risk. In addition, ASIS load cells will help to detect issues in performance of the lap belt section.

Head and Neck The current Euro NCAP assessment of the head includes the HIC_{15} and the 3ms resultant acceleration, taken from the dummy measurement. Both criteria will be also used with the THOR dummy as there is no influence of the dummy construction which might influence these criteria. These criteria however are not adequate to accurately assess brain injury risk and therefore additional criteria are under discussion for AIS 2+ injuries in front impact crashes. As further research is needed on this topic, Euro NCAP delayed the introduction of a brain injury risk criterion to 2022. In the meanwhile, it will monitor several possible criteria such as BrIC, UBrIC and criteria which include simulation models i.e. SUFHEM. HIC_{15} lower (500) and upper (700) values will be applied as well as the resultant acceleration 3ms limits of 72g for the lower performance limit and 80g for the upper performance limit.

For the neck, Nij was not adopted. Instead, neck forces and bending moments are used for assessment, as is the case for the Hybrid HIII 5F and 50M. Comparing MPDB tests with the THOR and Hybrid III dummies, it was found that the neck tension force F_z correlates well between these two dummies and could be transferred to the THOR assessment, with a lower performance limit of 2.7kN and an upper performance limit of 3.3kN. This correlation could also be seen in certification tests, while shear force F_x and extension moment M_y did not show such correlation whether in certification or in vehicle crash tests. Euro NCAP continues to study the neck injury criteria and currently proposed limits remain to be confirmed at time of submitting this paper.

The situation with neck injury assessment is exacerbated by continuing neck certification issues as several production level THOR necks have not been passing the certification corridor that was previously agreed with the dummy manufacturer. This issue needs to be solved first, before final values for upper and lower performance of neck criteria can be defined.

In Table 1 all relevant criterion, with upper and lower limits are shown, as well as the point's calculation. The assessment is based on the worse scoring parameter of each individual body region and the overall score on the

worst scoring body region of the driver and the passenger. The passenger scoring remains unchanged from the ODB assessment in 2019.

Table 1

Injury criteria for THOR 50M ATD

Body Region	Criterion	Unit	Upper	Lower	Scoring*
Head	HIC15		700	500	4 points
	SUFEHM				
	BrIC				
	A Resultant 3ms	g	80	72	
Neck	Fx	kN	3.1	1.9	
	Fz	kN	3.3	2.7	
	My	Nm	57	42	
Chest & Abdomen	Chest compression / Rmax	mm	60	35	4 points
	Abdominal Compression	mm	88		
Knee, femur, pelvis	L/R Acetabulum	kN	4.1	3.28	4 points
	L/R Femur compression	kN	9.07	3.8	
	L/R Knee shear displacement	mm	15	6	
Lower leg	L/R Tibia index		1.4	0.4	4 points
	L/R Tibia Compression	kN	8	2	

**Based on worst-case parameter*

Dummy Certification

With the introduction of the Service Built Level (SBL) B of the THOR 50M, also a certification procedure needed to be established. The lower leg and knee certification is based on the Hybrid III certification but from the femur to the head, a new set of certification procedures and limits were proposed, based on the THOR 50M, Qualification Procedure Manual 2016. This procedure is defined in the TB26 [8] of Euro NCAP.

COMPATIBILITY ASSESSMENT

Rationale

Former research on compatibility has identified mass differential, stiffness of front structures and geometric alignment as the parameters most influencing vehicle incompatibility. The impact scenario of the proposed MPDB with 180° impact angle, will lead to a nearly vertical loading of the barrier, which enables a good calculation of the energy transfer into the barrier and measurement of the footprint in the barrier. ADAC previously used this scan in their assessment to rate the geometry and the stiffness of the tested vehicle [9], see Figure 2. The idea behind this assessment is to rate the homogeneity of the front structure. The flatter the surface, the better the load spread.

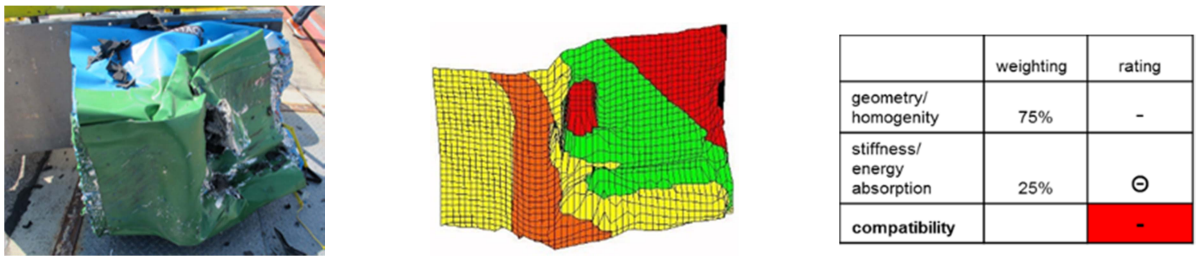

Figure 2. PDB barrier scan and compatibility assessment by ADAC

To investigate both the longitudinal and the area outside of the longitudinal, an assessment area is defined on the barrier front which depends on the vehicle width. The standard deviation of the intrusion in this assessment area is calculated, see Figure 3. The intrusion measurement is done by scanning the barrier footprint after the test. This is the first part of the assessment, reflecting geometry/ homogeneity.

The second part of the assessment is the deceleration of the mobile barrier and the energy absorption of the deformable element in the assessment area. The idea behind is to decelerate the trolley as slowly as possible, to avoid unnecessary loading of the partner car. Also, the less energy the test vehicle puts in the barrier the less energy the partner car needs to absorb. If stiff front-end vehicle parts bottom out the barrier, there will be an additional downgrading modification of the assessment. For this, a maximum intrusion of 633mm is proposed. The penetration of 633mm results in the maximum deformation of the first and the second honeycomb element and the block length of the honeycomb material and no deformation of the last element.

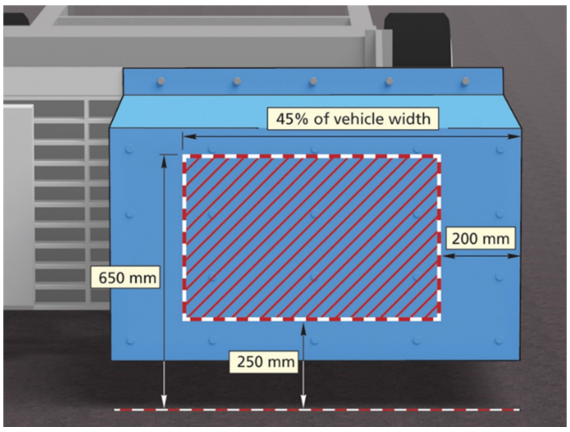

Figure 3. Compatibility assessment zone

The points distribution and the potential impact of the compatibility modifier on the rating was chosen to maximise the incentive for vehicle manufacturers to improve their structures, given what is feasible in a relatively short period. A good interaction between the different front structures is essential to activate the crash zones and to reduce the impact energy. Examples of a good geometric design, which helps to distribute the loads in several levels and also outside the longitudinal, are already available on the market and are easier to adopt than totally new crash energy management systems, which will take longer to implement and must be designed early in the construction process. Hence a weighting of the various rating elements was chosen that would incentive compatibility improvements in the fleet in a faster way.

The main elements used in the assessment were barrier scanning and calculation of the footprint and standard deviation, and the energy management of the barrier and trolley deceleration. As there was no clear proof from the accident data which of these two criteria should be prioritised, both are rated equally. Some of the vehicles tested, however, had very stiff longitudinal frames, which was seen to be critical in car to car impacts. Their localised “punch” effect could be reproduced in the MPDB test, however as this results in a relatively small area of penetration, this issue is not necessarily adequately reflected by the standard deviation. Therefore, it was decided to have this separately assessed and penalised in the score. Finally, the Occupant Load Criterion [10] was considered as the best way to evaluate energy management by assessing the vehicle stiffness indirectly with the barrier deceleration pulse.

In summary, the three agreed parameters for assessing the compatibility were:

- Standard deviation (SD) of the post-test barrier measurement,
- Occupant load criterion (OLC), according the deceleration pulse of the barrier,
- Bottoming out, measured by intrusion depth of the honeycomb.

Standard Deviation (SD)

The homogeneity measurement is based on standard deviation (SD) of the measurement of the intrusion depth in the assessment zone (Figure 4). The assessment zone was taken over from the original ADAC rating as there was a lot of experience of testing vehicles against progressive deformable barriers faces. Due to the movement of the vehicle after the impact, the outboard side of the barrier will be loaded sideways, and the honeycomb faces are bent instead of compressed. This will result in a different deformation, so a distance of 200mm is excluded from the outboard side to the assessment zone. Due to issues in the upper and lower area,

resulting from behaviour of the cladding sheet, the lower rating area was set to 250mm from ground, while the upper area was set to 650mm from the ground. The width is based on 45% of the vehicle width.

The standard deviation is defined as the spread around the mean intrusion that covers 68.2% of all measured intrusion points. The bigger the standard deviation the bigger the spread of the intrusion points and the less the homogeneity of the structure. Steps in the deformation zone, such as single cross members, no structure in front of the road wheel etc. could be detected. The assessment of the SD is based on a linear scale from 50mm, higher performance limit, to 150mm, which is the lower performance limit.

Reproducibility of the scanning method to ensure that the scanning process and the used tools produced repeatable and reproducible SD results, the labs were trained how to deal with different deformed elements, ruptured barrier etc. Solutions were worked out to treat problems during scanning such as reflexions, open hexagons, etc. After that, one barrier was sent out to 5 different Euro NCAP accredited laboratories to perform a scan round-robin test. The barrier of the round robin was scanned in the individual labs, with different equipment and test crew. The results are shown in Table 2 as well as the different scans in Figure 4.

Table 2

SD of barrier scans measured at different labs

Laboratory	Standard Deviation Measured (mm)
Lab1	42
Lab 2	42
Lab 3	41
Lab 4	42
Lab 5	41

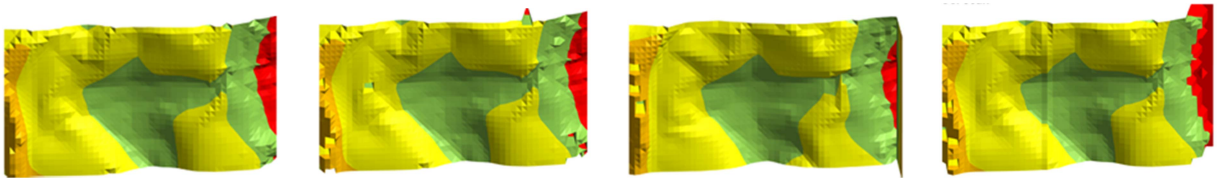

Figure 4: Barrier scans round robin results for 4 out of 5 laboratories

Occupant Load Criterion (OLC)

The occupant load criterium is based on the measured deceleration in the CoG of the trolley during the impact. After filtering the deceleration signal with CFC 180, the pulse should be integrated with the following equation to derive the velocity course of the barrier.

$$V_t = \int A_X(t)\, dt + V_0$$

Where V_0 is the initial velocity of the barrier at t = 0s. $OLC_{SI\text{-}unit}$, t_1 and t_2 can by calculated by the following equation system:

$$\begin{cases} \int_{t=0}^{t=t_1} V_0\, dt - \int_{t=0}^{t=t_1} V(t)\, dt = 0.065 \\ \int_{t=t_1}^{t=t_2} \left(V_0 - OLC_{SI-unit} \times (t - t_1)\right) dt - \int_{t=t_1}^{t=t_2} V(t)\, dt = 0.235 \\ V_0 - OLC_{SI-unit} \times (t_2 - t_1) = V(t_2) \end{cases}$$

Where t_1 is the end of the free flight phase of a virtual dummy on the trolley along a displacement of 0.065m and t_2 is the end of the restraining phase of a "virtual occupant" on the trolley along a displacement of 0.235m after the free flight phase, resulting in a total displacement of 0.300m for the virtual occupant (Figure 5). For the compatibility assessment the OLC is converted into SI units (1g= 9,81m/s2). The OLC is evaluated using a sliding scale from 25g higher performance limit to 40g lower performance limit.

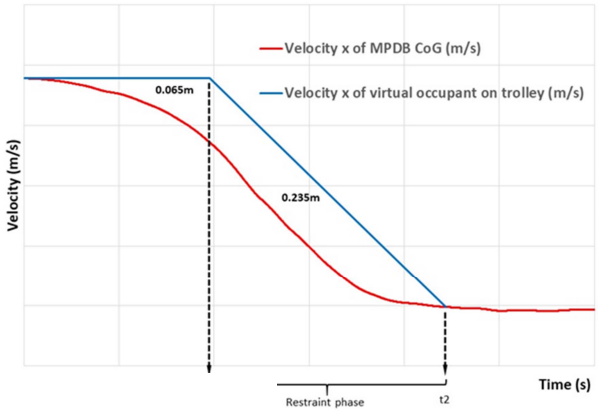

Figure 5. OLC and trolley velocity

Bottoming Out

Bottoming out defines an area where a structure of the vehicle penetrated the barrier more than 630mm in depth and a width of more than 40mmx40mm.

Compatibility Modifier

In the Euro NCAP rating scheme, maximum 16 points can be gained in the MPDB test, if all dummy criteria stay below the higher performance limits and no modifiers are applied. The contribution to the Adult Occupant Protection is half of that score, so a maximum 8 points, similar to the 8 points contribution of the Full-width frontal test.

The result of the compatibility assessment will be applied as a modifier to the total score of the MPDB test. The maximum modifier will be 8 points and will reduce the number of scored points of the occupant rating. In the first phase from 2020 to 2022, the result of the modifier will be limited to maximum of 4 points however to allow industry to adjust their vehicles step-wise. Both, the standard deviation (SD) and the OLC are assessed with a sliding scale with the upper and lower limits mentioned above. The bottoming out modifier is then added to the result. The general scoring rational is shown in Figure 6.

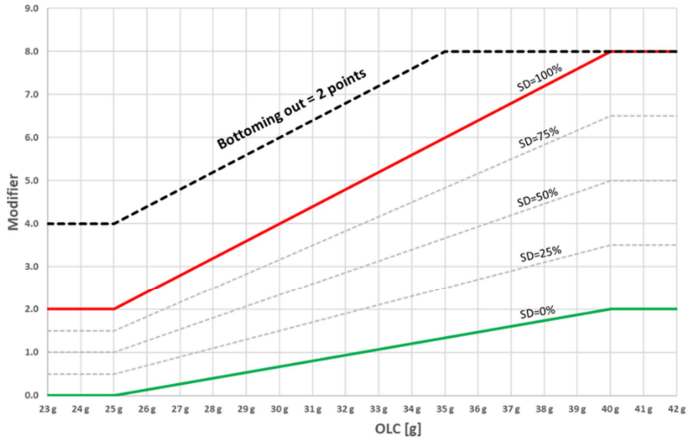

Figure 6. General scoring rational [8]

VERIFICATION TESTS

A final check of the assessment procedure was carried during a final round robin full-scale test series. As part of this series, two pairs of vehicles were tested in different labs to check the test variation in setup, dummy results and compatibility assessment. The vehicles tested twice were the 2017 5-stars rated Honda Civic and the 2017 5-stars rated Ford Fiesta. Other vehicles were chosen to represent, different types of vehicles. Large SUV, smaller SUV, Supermini´s as compact class cars were included. All cars were tested to assess the dummy values and the compatibility modifier. The following table is showing all tested vehicles during the 2nd round robin tests carried out in 2018.

Table 3

Full-scale validation MPDB test series: cars models, labs and barrier suppliers

Model	Description	Lab	Barrier face
Honda Civic	5-star compact class (expected to show good compatibility assessment)	ADAC	Cellbond
		IDIADA	Cellbond
Ford Fiesta	5-star car used for validation tests (expected to show moderate compatibility)	BASt	AFL
		TASS	AFL
Jeep Renegade	Compact 5-star SUV	CSI	Cellbond
Jag E-Pace	Compact 5-star SUV vehicle (expected moderate compatible structure)	TASS (Thatcham)	AFL
Renault Clio	Supermini 5-star (expected to show good compatibility)	UTAC	AFL
Audi Q5	Large 5-star off-road vehicle, representing SUVs (expected not to have a compatible structure)	ACTS/CLEPA	Cellbond

Dummy Results

In the initial phase of the working group's research, several R&R tests were carried out including sled tests, vehicle tests and certification tests to verify the reproducibility and durability of the latest THOR 50M and to identify what updates to the dummy would still be needed. Since then, several improvements were adopted, related to the dummy hardware, handling and certification. The largest step forward was the definition of a Service Built Level of the dummy, because up until that time many of the THOR dummies in the field were of a different built status, causing much confusion and frustration amongst the user community. During the round robin validation tests, all THOR 50M dummies were brought up to SBL-A (later followed by B) to avoid unnecessary discussions and wasting valuable resources.

In the first set of cars, two 2017 Honda Civic were used, a five-star Euro NCAP car with an ODB assessment score of 7.1 pts. This car was tested in 2 different labs, with 2 different THOR dummies on the driver seat. The overall results showed that there was no significant change in performance in the head/neck and knee/femur/pelvis area between the two lab results. The lower legs, which showed in the ODB test good results scored 0, respectively 0,09 points, in the MPDB tests, due to the values of the lower Tibia Index, which was unexpected. On the other hand, the chest deflection, Rmax showed a chest injury risk that was significantly higher than in the original ODB with the Hybrid III, as anticipated. The deflection values between the two MPDB tests were significant different owing to different belt behaviour as could be observed in high speed video. All other values showed equivalent results, as shown in Table 4.

Table 4

Full-scale validation MPDB test results: Paired comparisons

	Honda Civic (2017)		Ford Fiesta (2017)	
	IDIADA	ADAC	BAST	TASS
Head & Neck	4.00	4.00	4.00	4.00
Chest & Abdomen	0.80	2.02	0.26	0.11
Knee, femur, pelvis	4.00	4.00	4.00	4.00
Lower Leg	0.00	0.09	2.67	2.15
Total	8.80	10.11	10.93	10.27

The second set of cars that were tested under the same condition but in different labs, was the 2017 Ford Fiesta.
In the 64kph ODB test with the Hybrid III dummy on the driver seat, the overall performance was excellent, scoring 7.7 points out of 8 points. In the MPDB test, the Ford Fiesta scored less points in the chest and the lower leg area. The results of both test labs matched quite well.

A similar conclusion could be drawn from the remaining vehicles tested in this series. As expected from the THOR 50M the chest area is the predominant cause for points reduction, followed by the lower leg area. Even the larger cars such as the Jaguar E-pace and the Audi Q5 demonstrated weaker performance in the chest area, sometimes exceeding the lower performance limit significantly. Higher Tibia Index values were the main cause for lower scores in the lower legs. All results of the round robin 2 could be seen in Table 5.

Table 5

Full-scale validation MPDB test results: All cars

	Honda Civic	**Honda Civic**	**Ford Fiesta**	**Ford Fiesta**	**Jeep Renegade**	**Renault Clio**	**Jaguar E-Pace**	**Audi Q5**
	IDIADA	ADAC	BASt	TASS	CSI	UTAC	TASS	ACTS
Head & Neck	4.00	4.00	4.00	4.00	4.00	4.00	4.00	4.00
Chest & Abdomen	0.80	2.02	0.26	0.11	2.58	0.00	2.71	0.00
Knee, femur, pelvis	4.00	4.00	4.00	4.00	4.00	2.01	4.00	4.00
Lower Leg	0.00	0.09	2.67	2.15	3.64	0.93	3.49	2.67
Total	8.80	10.11	10.93	10.27	14.23	6.94	14.20	10.67

Compatibility Assessment

All vehicles in the previous and final validation test series were rated according the agreed version of the compatibility assessment. Figure 7 shows the modifier on the LHS according the OLC on the x-axis. The red line shows the SD of 100% and the green line at 0%. The overall results show a wide spread of results, but also the differences between vehicle classes.

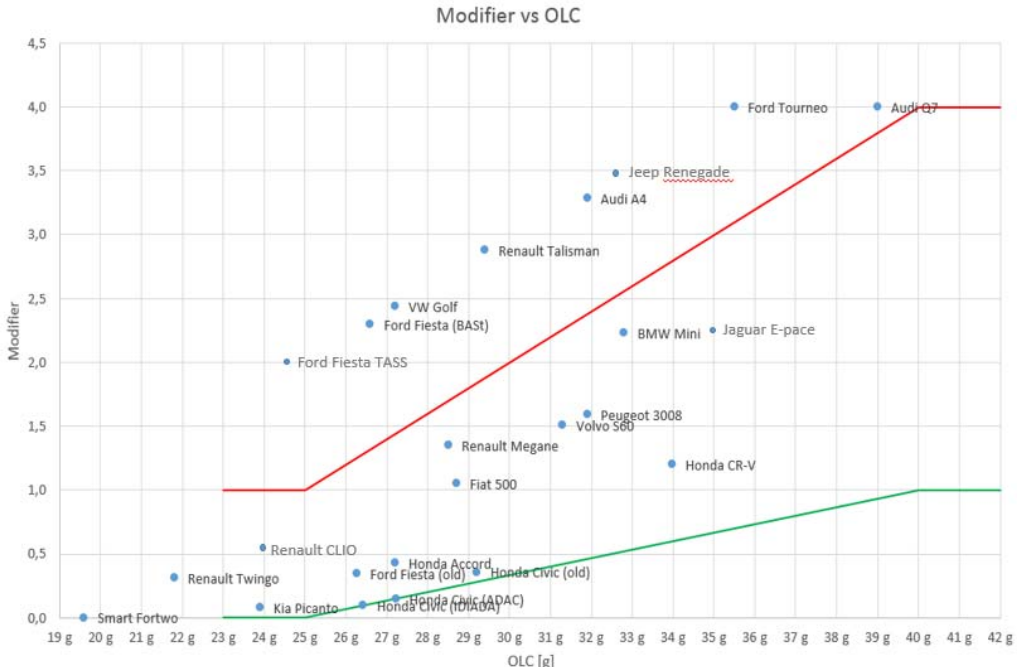

Figure 7. Compatibility Rating for cars tested in first and second validation test series

Small SUV`s such as the Jeep Renegade, the Jaguar I-Pace and the Honda CR-V, show a significantly drop in modifier scoring, even their OLC is more or less the same. On the other hand, vehicles of the same mass show a reduction in OLC, which means with a different front structure the accident partner could be loaded less. Examples are the Audi A4, the Renault Megane and the Honda Accord, while the Audi showed the highest OLC.

Both test pairs of Fiesta and Civic show a good reproducibility of the compatibility assessment. In different test labs, and with cars not being designed for this load case, the overall compatibility result shows only minor differences. In the case of the Fiesta it is 0.1 points difference, while in the Civic test it is only 0.05 points difference. Even as the footprints in the Ford Fiesta test were not exactly identical, due to a slightly different behaviour of the front cross member, the overall compatibility assessment itself is not really affected, which demonstrates that the method of the assessment itself is robust. In case of the Honda Civic, both footprints also showed nearly identical measures (Figure 8). Bearing in mind the small variations that can occur in the scanning process, the overall compatibility assessment shows to be repeatable and robust.

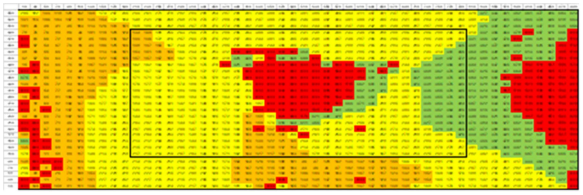		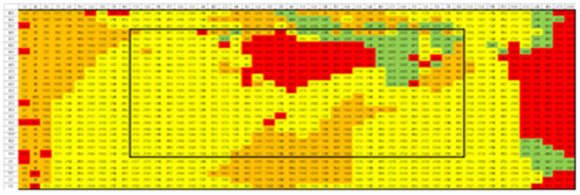	
2017 Ford Fiesta (BASt)	SD: 148 OLC: 26.6 Bottoming out: -2 Overall: -2.1	2017 Ford Fiesta (TASS)	SD: 158 OLC: 24.5 Bottoming out: -2 Overall: -2.0
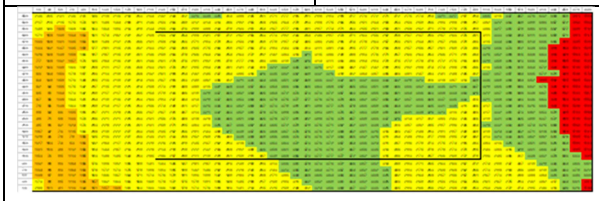		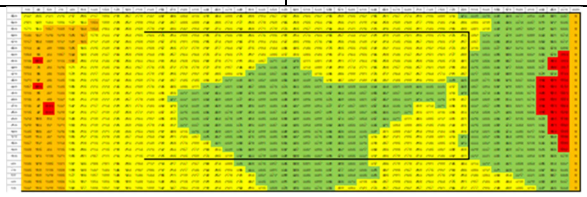	
2017 Honda Civic Fiesta (IDIADA)	SD: 42 OLC: 27.2 Bottoming out: 0 Overall: -0.15	2017 Honda Civic Fiesta (ADAC)	SD: 45 OLC: 26.4 Bottoming out: 0 Overall: -0.1

Figure 8. Comparison of barrier scans from full-scale tests

CONCLUSIONS

In the second and final phase of the development of a new frontal impact test with a mobile barrier, the work has focussed on dummy criteria, dummy certification and the new compatibility assessment. As there was only limited information available on the THOR-dummy injury risk curves, sled and full-scale crashes were carried out to find appropriate upper and lower limits of the different body regions that could be applied from 2020 onwards. Some practical considerations were used to decide on the limits. The repeatability and reproducibility of the dummy in certification tests was also studied and certification corridors for THOR 50M use for Euro NCAP testing were agreed.

The definition of a built level allowed the group to carry out round robin tests to validate the procedure, criteria and also to confirm the reproducibility of the test. The results showed that under the new configuration of this frontal test, the THOR was usable and durable. The chest and lower leg will be the more demanding body regions for the future assessment, as nearly all the cars showed lesser performance in this area compared to the ODB results. It appears that the chest result was influenced by the THOR chest behaviour, the restraint

systems not being developed to accommodate for the more flexible rib cage. The lower leg result seems to be caused by the new test condition, as there was no change in the legs themselves (i.e. Hybrid III legs).

After decades of discussions on compatibility and possible ways to assessment it, a way was agreed in the Euro NCAP frontal impact group to rate the compatibility of test vehicles. Internal test series have shown that the barrier and deceleration assessments correlate with car to car crashes. R&R work in the group, carried out together with suppliers and vehicle manufactures, show a stable test procedure with repeatable and reproducible results. Even the assessment criteria may need further consideration in future, the first step was undertaken to use this test device in a consumer test program.

More work will be undertaken by Euro NCAP in the way to assess brain injuries and improve chest assessment taking the whole chest loading into account. Even without these advanced criteria, however, it is expected that the introduction of the new test will still promote the development of better restraint systems.

ACNOWLEDGEMENTS

Members of the FIWG are:

Sandner Volker, ADAC (WG Chairman)
Ellway James, Euro NCAP (Secretary)
Michiel van Ratingen, Euro NCAP
Tobias Langner, BASt,
Ammerlaan Hans, NL-MOT-RDW
Baroncelli Luca, CSI
Broscheidt Michael, Audi
Herpich Thomas, TRW
Langner Tobias, BASt
Lázaro Ignacio, IDIADA
Lepretre Jean-Philippe, UTAC CERAM
Thorsten Kerz, Opel
Ratzek Andreas, ADAC
Thompson Alex, Thatcham
van Montfort Sjef, TNO
van Slagmaat Marc, Autoliv
Jeremy Magniez , UTAC CERAM
Weimer Christoph, Hyundai

The working group would also like to that the support of David Hynd, Chairman of the TEFIRE group, the barrier manufacturers who have contributed to the development of the MPDB specification: Cellbond, AFL and Plascore, and the dummy manufacturers Humanetics Innovative Solutions and Cellbond ATD.

REFERENCES

[1] Johanssen H et al. 2012 “Documentation for a frontal impact and compatibility assessment approach: Part II”.

[2] VC Compat report, 2006. “Improvement of Vehicle Crash Compatibility through the development of Crash Test Procedures”.

[3] Saunders et al, 2012. “Moving Deformable Barrier Test Procedure for Evaluating Small Overlap/Oblique Crashes.” SAE paper number 2012-01-0577.

[4] Sandner V. 2017. “Euro NCAP Frontal Impact Working Group Report.” In Proceedings of the 25th ESV Conference, paper number 17-0206.

[5] Sandner et al, 2015. “MPDB-Mobile offset progressive deformable barrier.” In Proceedings of the 24th ESV Conference, paper number 15-0389.

[6] Euro NCAP. 2016. “Mobile Progressive Deformable Barrier Face Specification” Technical Bulletin TB022.

[7] European Commission 2018. “SENIORS project report” www.seniors-project.eu/

[8] Euro NCAP. 2018. *“THOR Specification and Certification”* Technical Bulletin TB026, v1.0.

[9] ADAC 2016 Compatibilty Crash, Test report, Andreas Ratzek 2016

[10] J. Metzger, L. Kübler, S. Gargallo. 2010. “Characterization and Evaluation of Frontal Crash Pulses for USNCAP” In Proceedings of the 10th International Symposium and Exhibition on Sophisticated Car Occupant Safety Systems”, Airbag 2010 Conference.

BIOMECHANICAL VALIDATION OF A NEW BIOFIDELIC DUMMY

Schäuble, Andreas
DEKRA Automobil GmbH
Germany

Weyde, Michael
Büro für Unfallrekonstruktion Berlin
Germany

Paper Number 19-0197

ABSTRACT

In order to improve the preciseness in pedestrian-vehicle accident reconstructions, a new biofidelic dummy had been developed. The objective of this work was to biomechanically validate the biofidelity of this new kind of anthropomorphic testing device. Therefore, nine crash tests have been conducted with the biofidelic dummy and the results were compared with four crash tests earlier performed with the Žilina dummy, an anthropomorphic testing device widely used in accident research due to its low cost and robustness, cadaver tests obtained from published research papers and 21 real-world pedestrian accidents.

The trajectories of both anthropomorphic testing devices were computed and compared with those of cadaver tests, highlighting that the biofidelic dummy performs much more human-like than the Žilina dummy.

Damages to the vehicle's front caused by both anthropomorphic testing devices and real pedestrians were compared with each other, as realistic damages are very important for reconstruction purposes. It can be shown that the biofidelic dummy causes damages similar to those a pedestrian would cause in an accident of similar severity, whereas the Žilina dummy causes damages which are far too severe, which may mislead the expert witness to assume an impact velocity which is too slow.

The C-ratio, defined as closing speed over collision speed, was computed for both anthropomorphic testing devices, showing that the two deliver similar results. Computing the dynamic, time-dependent C-ratio, however, highlights differences in the kinematics and dynamics of the two anthropomorphic testing devices.

The throw distances of both anthropomorphic testing devices were compared with throw distance charts developed in-house by DEKRA based on experiments with the Žilina dummy and well-documented real-world accidents. The results show that the biofidelic dummy's behaviour is good.

Finally, the damages to the biofidelic dummy were analysed and transcribed to injuries of a human being. These "biofidelic dummy injuries" were compared with injuries of real pedestrians, focusing on five injuries, which can be used for reconstruction purposes. In general, the "injuries" of the biofdelic dummy correspond well with those of the pedestrian.

NOMENCLATURE

Acronyms

ADR	-	accident data recorder
ATD	-	anthropomorphic testing device
PMHS	-	post-mortem human subject

Symbols

C	-	ratio between closing speed and collision speed
$C(t)$	-	dynamic, time-dependent C-ratio
$C(t)_P$	-	dynamic, time-dependent C-ratio of the pelvis
$C(t; P)$	-	dynamic, time-dependent C-ratio relative to the pelvis
$C(t; P)_F$	-	dynamic, time-dependent C-ratio of the foot relative to the pelvis
$C(t; P)_H$	-	dynamic, time-dependent C-ratio of the head relative to the pelvis
CoM	-	centre of mass
e	-	coefficient of restitution

INTRODUCTION

While severe vehicle-vehicle accidents usually not only cause distinctive damages as well as scratch marks on the road surface, even lethal pedestrian-vehicle accidents often lead neither to significant traces on the road surface nor to a damage pattern which allows precise reconstruction of the vehicle's collision speed. This lack of evidence often complicates the work of experts reconstructing such kinds of accidents. Therefore, a need existed to improve the preciseness of accident reconstruction when pedestrians had been involved.

In order to achieve an improvement in accident reconstruction in this field, there seemed to be a need for a surrogate of an ATD, which was able to deliver realistic vehicle damages as well as damages on itself, which allow finding a correspondence between dummy damages and injury probability. As such, a team of students under the guidance of one of the others had developed a biofidelic dummy. This dummy was designed to cause realistic vehicle damages and furthermore to cause damages to itself comparable to typical injuries, which pedestrians sustain in a similar impact with a vehicle, in order to use the data gathered by conducting crash tests to reconstruct real pedestrian-vehicle accidents.

The objective of this research was to analyse and verify the biofidelity of this human surrogate in pedestrian-vehicle crash tests.

METHODS AND USED EQUIPMENT

DEKRA has conducted nine crash tests with the biofidelic dummy in conjunction with AXA Insurance in Wildhaus, Switzerland in the summer of 2018. The results have been compared with crash tests using the Žilina dummy, a dummy widely used in accident reconstruction due to its robustness and low price, and results of cadaver tests obtained from published research papers as well as 21 well-documented real-world pedestrian accidents. See table 1 for an overview of the crash tests.

The crash test videos have been analysed by the programme "Falcon" to obtain the dummy trajectories and the C-ratio. The frame rate of the videos is 500 pictures/s. Time is set to zero at the point of first contact between the dummy and vehicle, which is visualised by means of a light signal mounted on top of the vehicle. The coordinate system, which is required for the programme to make its calculations, has its origin at the first target on the vehicle. The *x*-direction faces in the direction of travel, while the *y*-direction faces upwards. The dummy targets, used by the programme to track the dummy movements, had to be applied manually to the dummy within the programme. Targets were applied to the head, hip and foot. Each body region was analysed three-times and the average value was calculated, in order to reduce any errors stemming from manually placing the targets on the dummy. Every 10th picture has been analysed, i.e. the time interval between the different measurements is 0.02 s. "Falcon" provides "txt"-files as data output, which have been uploaded into "Excel", with which the lines have been drawn. The final trajectory graphs have been created with "CorelDraw".

"Autopsies" have also been performed on the biofidelic dummy, in order to obtain the damages the dummy sustained during the crash tests and to translate those damages to comparable injuries of a human being.

Table 1.
Overview of the crash tests

crash test	vehicle	collision speed	braking	dummy
wh18.22	BMW 1 Series 2004	75 km/h	pre-crash	biofidelic
wh18.23	BMW 1 Series 2004	99 km/h	in-crash	biofidelic
wh18.24	VW Touareg 2003	75 km/h	pre-crash	biofidelic
wh18.25	VW Touareg 2003	99 km/h	in-crash	biofidelic
wh18.26	VW Passat Variant 2006	75 km/h	pre-crash	biofidelic
wh18.27	VW Passat Variant 2006	99 km/h	in-crash	biofidelic
wh18.28	Mercedes A-Class 2005	72 km/h	pre-crash	biofidelic
wh18.29	Mercedes A-Class 2005	96 km/h	in-crash	biofidelic
wh18.34	VW Touareg 2003	27 km/h	in-crash	biofidelic
wh08.27	Ford Galaxy 1998	40 km/h	pre-crash	Žilina
wh08.28	BMW 523i 1998	40 km/h	pre-crash	Žilina
wh08.29	Toyota Avensis 1998	40 km/h	pre-crash	Žilina
wh10.12	Fiat Punto 1996	55 km/h	late or unbraked	Žilina

CRASH TEST DUMMIES USED IN ACCIDENT RECONSTRCUTION

Žilina dummy

The Žilina dummy was developed at the University of Žilina in the Slovak Republic, and represents a 50th percentile male.

In contrast to the more sophisticated ATDs used by the automotive industry, instrumentation is limited to the chest [1]. This ATD is based on a metal skeleton covered by hard plastic, and the joints can be fastened to enable an upright posture.

Biofidelic dummy

The first prototype had a wooden skeleton, which was held together by stapled straps, covered by a tissue surrogate made of a mixture of silicone and acrylic. The special feature of this ATD tissue are the pseudoelastic properties similar to human tissue. Under the application of an external force, the tissue behaves plastically, while its properties are elastic as soon as the force is removed. The skin was represented by a 3 mm thick wet suit, which is covered by latex to increase the elasticity and tensile strength. Moreover, the wet suit is not only used as a skin surrogate, but also as a means of additional fixation of the tissue parts.

In order to further improve the anthropometry and biofidelity of this 50th percentile male ATD, the current version has no longer wooden bones, but a mixture of epoxy resin and aluminium powder is used. This mixture allows for the fabrication of ATD bones, which better resemble human bones in their shape and mechanical properties. The tissue parts are now made of a two-component silicone instead of a mixture of silicone and acrylic. A wet suit, covered with latex, is still used as the skin surrogate.

RESULTS AND DISCUSSIONS

Dummy trajectories

The dummy trajectories were obtained for each crash test. However, the main characteristics are only explained based on one vehicle for each the biofidelic and Žilina dummy, as the differences between different vehicles are not that stark.

Biofidelic dummy Figure 1 displays the dummy trajectories of the crash tests wh18.22 and wh18.23. The "suck-below" effect, where the pedestrian's foot is sucked below the vehicle's front-end spoiler due to friction and inertia forces, becomes more accentuated with an increase in collision speed. This effect can induce large bending and shear forces close to the talocalcanean joint. The magnitude of this "suck-below" effect further influences the kinematics of the lower extremities. While the legs are catapulted higher into the air at the lower

collision speed, the lower extremities remain rather stuck to the vehicle's front due to the larger "suck-below" effect at the higher collision speed.

In the meantime, however, the ATD's torso is accelerated and moves along the vehicle's contour, leading to extensive stretching. Without the wet suit, the biofidelic dummy would most likely have been torn apart. The probability of dismemberment was analysed by [2]. They report a probability of dismemberment at a collision speed of 100 km/h of 0.281947 as mean, 0.157408 as lower and 0.514652 as upper value. The extensive stretching behaviour of the biofidelic dummy therefore does not seem to be unrealistic, but due to a lack of cadaveric tests at such high collision speeds it is difficult to assess the exact biofidelity of that behaviour.

In crash test wh18.22, the ATD's thigh is pushing backwards the left headlight assembly. This creates a sharp edge at the front part of the left fender. As the biofidelic dummy continues to slide onto the bonnet, this sharp edge pierces the ATD's leg. Such injuries are known from real-world accidents.

The head ultimately still impacts the windscreen at 70 km/h, while the head impacts the roof leading edge at 100 km/h. Hence, the head moves further along the vehicle's contour with an increase in collision speed.

The hip is also further elevated at the higher collision speed, partially due to the extensive stretching behaviour of the biofidelic dummy.

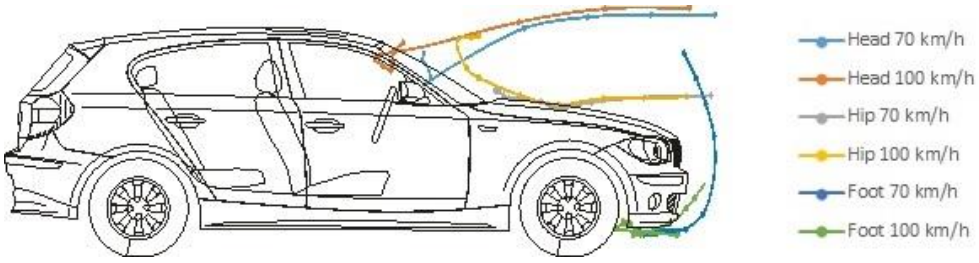

Figure 1. Dummy trajectories of crash tests wh18.22 and wh18.23.

Žilina dummy Figure 2 displays the dummy trajectories of crash test wh08.27.
Here, the "suck-below" effect is much less pronounced. This has two reasons. Firstly, the collision speed of 40 km/h is much lower than the collision speeds of 70 km/h and 100 km/h used with the biofidelic dummy, meaning that the effect is automatically less accentuated. Secondly, the Žilina dummy is made of steel. Thus, the ATD's bones bend less than those of the biofidelic dummy and can further not huddle against the vehicle's contour in the same way as the latter's one. The lower extremities are immediately catapulted away from the vehicle and the ATD rotates onto the bonnet around its *CoM*.

The legs' collision with the bumper is elastic. A speed for the measured leg of 44.87 km/h was recorded 0.02 s after impact. Considering that the collision speed was 40 km/h, this leads to a coefficient of restitution of e=1.12. Normally, however, $e \leq 1$, but the determination of the ATD's velocity by means of the programme "Falcon" is afflicted with minor errors. Thus, it can be concluded that the collision is perfectly elastic. Human tissue, however, is pseudoelastic. The tissue surrogate of the biofidelic dummy therefore exhibits pseudoelastic properties. In crash test wh18.22, the determined coefficient of restitution is e=0.63. This explains why the legs of the biofidelic dummy huddle against the vehicle's contour. The impact force causes the dummy tissue to deform and the impact energy is absorbed due to this plastic behaviour, which means that less energy is available for the legs to be catapulted away.

As the torso of the Žilina dummy rolls onto the bonnet, the ATD props itself on its arm, before the head subsequently impacts the windscreen. The rotation around the *CoM* continues.

In general, the ATD remains stiff throughout the whole impact and there is no stretching behaviour as compared with the biofidelic dummy.

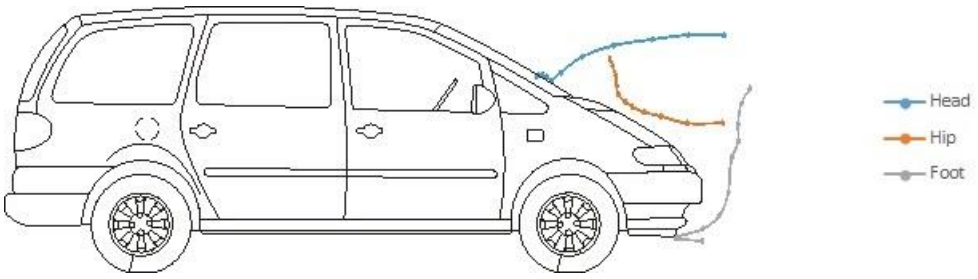

Figure 2. Dummy trajectories of crash test wh08.27.

Comparison with PMHS-tests In order to validate the biofidelity of the trajectories of both the biofidelic and Žilina dummy, the findings were compared with PMHS-tests published in research papers.

[3] conducted four PMHS-tests. They used a mid-sized sedan and a small city car, and the collision speed was 40 km/h. The four cadavers were male and exhibited no pre-existing fractures, lesions or other bone pathology, though three of the subjects had poor bone mineral density.

Figure 3 displays the trajectories of the PMHS-tests using the mid-sized sedan, the biofidelic dummy tests with the VW Passat, and the Žilina dummy test with the Toyota Avensis. The VW Passat and the Toyota Avensis were chosen for comparison as they should equal the mid-sized sedan in weight the most and should also have a similar front-end geometry. However, the different collision speeds must be taken into account, making a direct comparison somewhat complicated.

The PMHSs exhibit the "suck-below" effect similar to the ATDs, before the lower extremities rebound and swing upwards. The trajectories of the PMHSs' lower extremities resemble a circle, while the Žilina dummy's foot swings upwards much steeper. The trajectory of the biofidelic dummy's foot resembles rather the PMHSs, though the lower extremities slide off the front-end in course of the impact, which makes a direct comparison somewhat difficult. Considering the head and hip, no stark contrasts can be determined between the PMHSs and ATDs. The only major difference is that the Žilina dummy's head did not impact the bonnet/windscreen, as the dummy propped itself on its arm.

[3] further computed the body part trajectories relative to the pelvis as shown in figure 4. Figure 5 depicts the dummy trajectories relative to the pelvis of the biofidelic and Žilina dummy. The trajectories of the heads of both ATDs form a cloud and there are no major differences between the individual trajectories, even though the collision speeds are quite different between the biofidelic and Žilina dummy. Considering the feet of the two ATDs, however, two different clusters are formed. The feet of the Žilina dummies swing upwards much faster, also inducing a faster hip rotation, while the feet of the biofidelic dummies swing upwards much slower. At the beginning, these trajectories are also pretty vertical, which is explained first by the "suck-below" effect, second by the huddling of the lower extremities against the front-end structure and third by the stretching of the lower extremities.

Thus, there are hardly any differences in the head trajectories relative to the pelvis between the biofidelic and Žilina dummy. However, the upper body kinematics are still different. Regarding the lower extremities, though, there are stark differences. These are primarily explained by the fact that the biofidelic dummy is a pseudoelastic body, while the Žilina dummy is an elastic body.

Comparing the trajectories of the ATDs with the PMHSs, bearing in mind that the collision speeds differ, the trajectories of the biofidelic dummy match those of the PMHSs more than the Žilina dummy does. The lower extremities of the PMHSs swing upwards in a slower fashion just as the biofidelic dummy does, being explained by a prolonged contact phase between the PMHS's lower extremities and the vehicle's front-end compared to the Žilina dummy, as the human body is a pseudoelastic body as well.

[4] conducted three PMHS-tests at 40 km/h with a small sedan. Figure 6 shows the crash sequence of one of these tests compared with one biofidelic dummy test and Žilina dummy test. These two ATD tests have been chosen for comparison purposes due to the same reasons as above. While the Toyota Avensis has the same collision speed of 40 km/h as the PMHS-test, it is stressed again that the collision speed of the VW Passat is much higher at 75 km/h. The different kinematics of the Žilina dummy can be easily noted, especially the fact that the chest props

itself on the arm and thereby lifts the waist off the bonnet. The biofidelic dummy, on the other hand, huddles against the vehicle's contour.

Thus, it can be concluded that the trajectories of the biofidelic dummy are much more human-like than those of the Žilina dummy. In particular, the "propping" effect of the latter is unnatural. These findings come, however, with the caveat that the collision speeds are quite different. Nonetheless, the tendency that the biofidelic dummy behaves more humanoid cannot be dismissed.

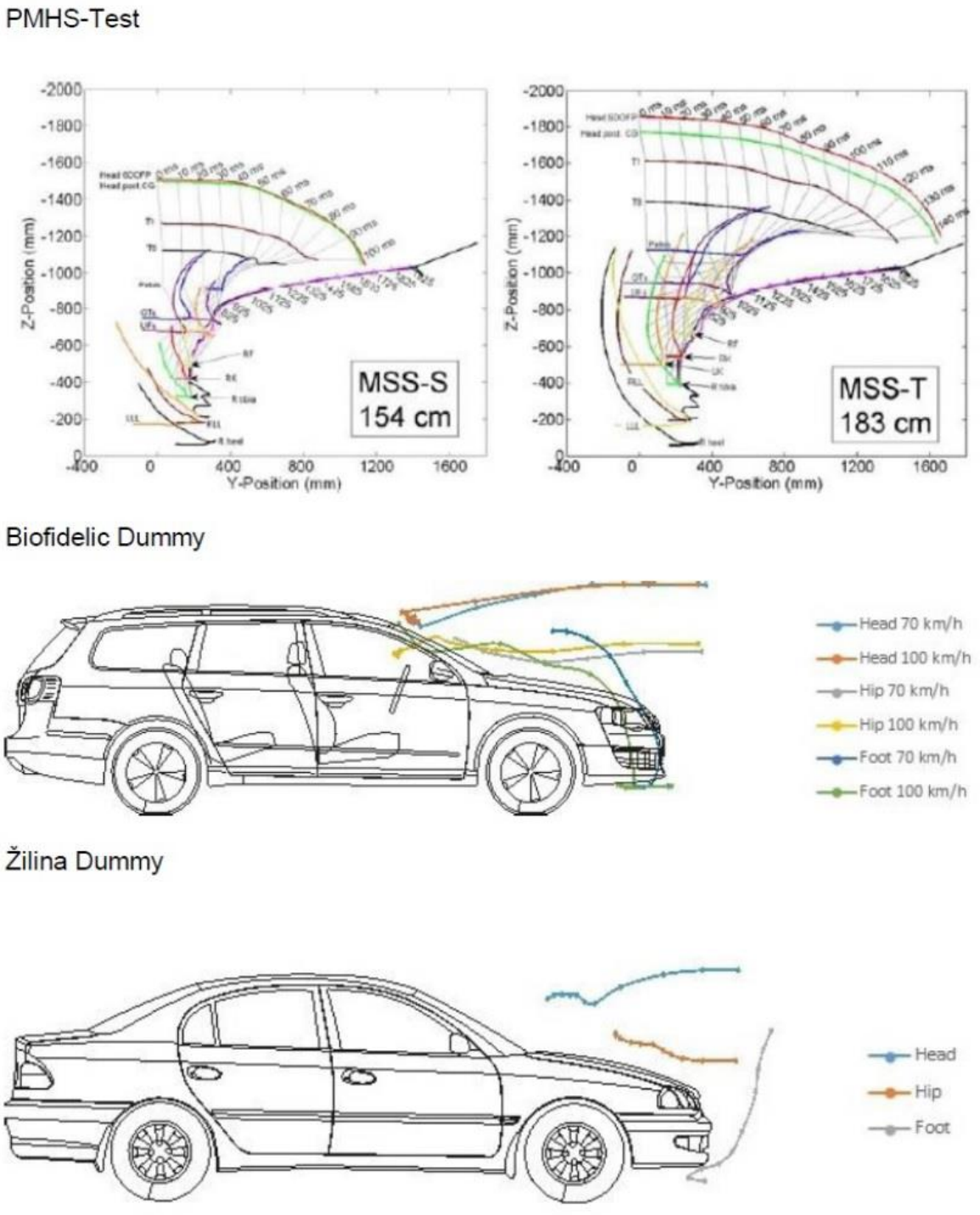

Figure 3. Comparison between trajectories of PMHS, biofidelic dummy and Žilina dummy. Top: MSS-S: mid-sized sedan small subject (body height); MSS-T: mid-sized sedan tall subject (body height) [3]. Middle: crash tests wh18.26 and wh18.27. Bottom: crash test wh08.29.

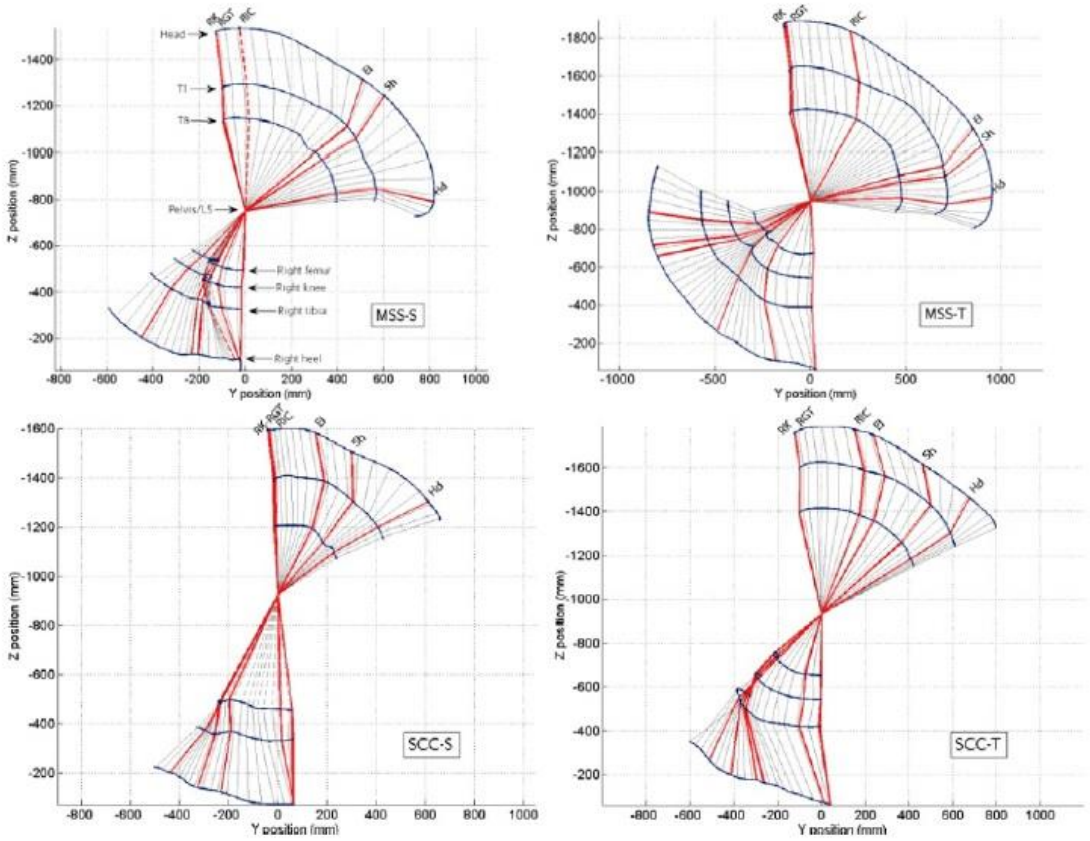

Figure 4. PMHS trajectories relative to the pelvis. MSS-S: mid-sized sedan small subject; MSS-T: mid-sized sedan tall subject; SCC-S: small city car small subject; SCC-T: small city car tall subject [3].

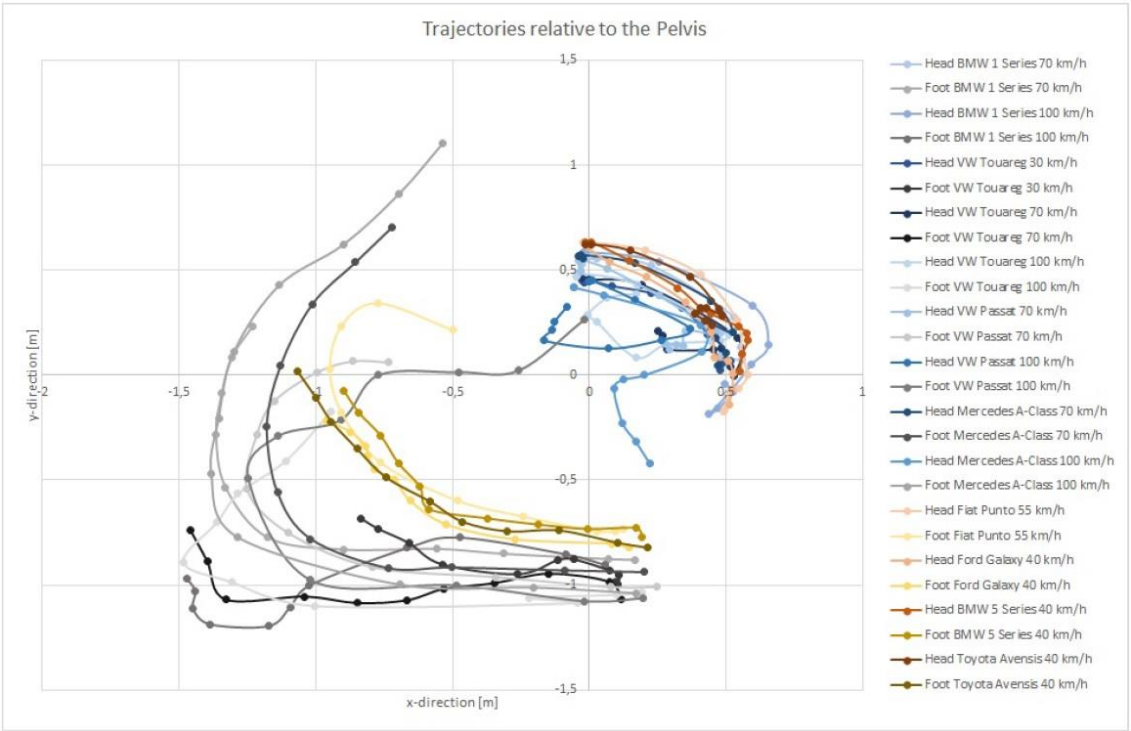

Figure 5. ATD trajectories relative to the pelvis. Blue: biofidelic dummy's head; Grey: biofidelic dummy's foot; Orange: Žilina dummy's head; Gold: Žilina dummy's foot.

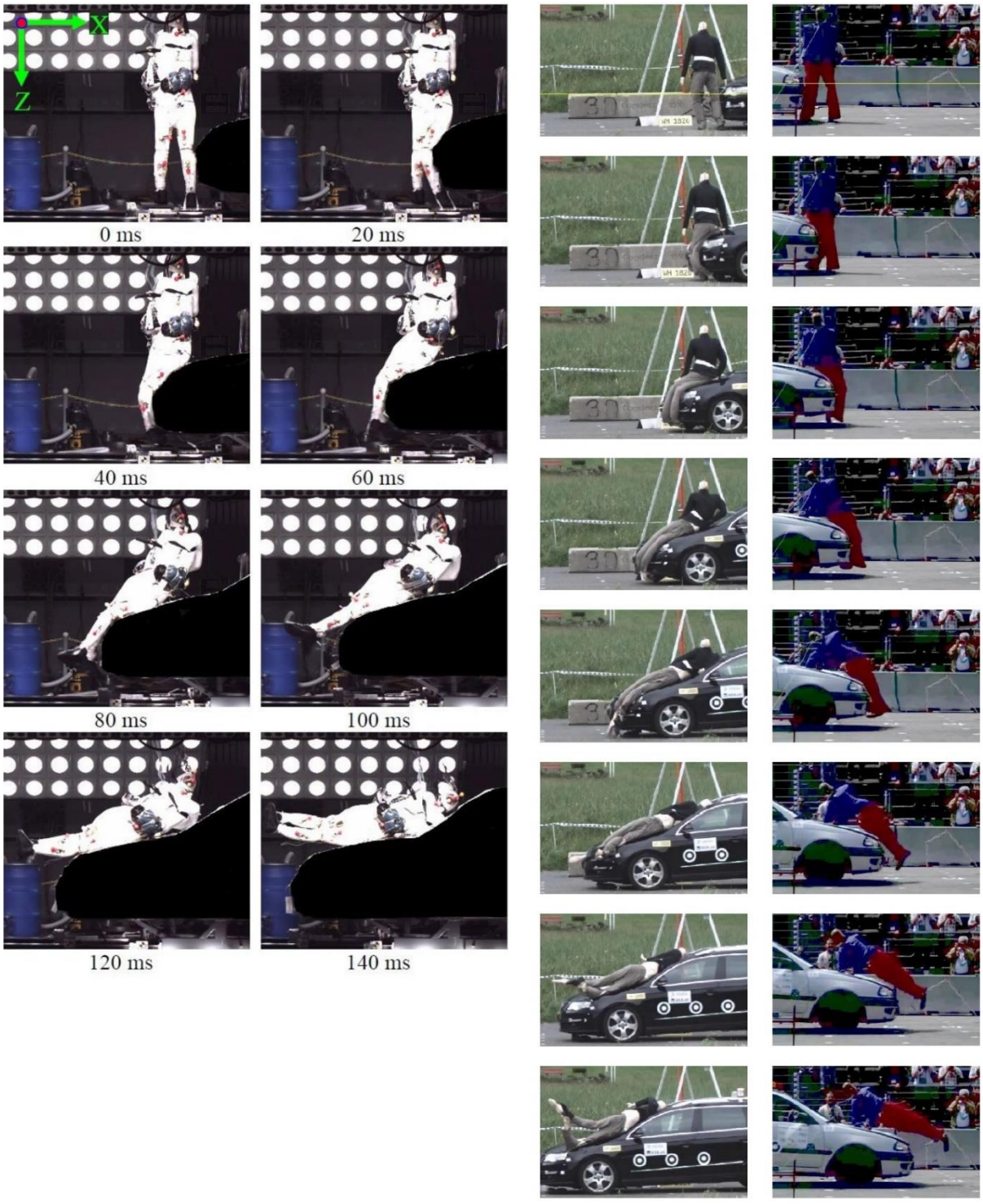

Figure 6. Crash sequences of a PMHS (left) [4], biofidelic dummy (middle) and Žilina dummy test (right) at 20 ms intervals.

Vehicle Damages
For reconstruction purposes, it is very important that the vehicle damages caused by the ATD are comparable to those caused by the pedestrian. Of the nine crash tests with the biofidelic dummy, only crash tests wh18.22 and wh18.26 are comparable to two of the analysed real-world accidents. The collision speed, dummy/pedestrian height and weight are still within an acceptable deviation.

Considering the Žilina dummy, all four crash tests are considered, even though the collision speed is much lower.

Next to the different collisions speeds and differences in dummy and pedestrian anthropometry, differences in front-end geometry and local vehicle stiffness should also be born in mind.

Biofidelic dummy vs. pedestrian The damages to the bonnet leading edge caused by both the biofidelic dummy and the two pedestrians are shown in figure 7.

Figure 7. Vehicle damages biofidelic dummy vs. pedestrian. Top Left: wh18.22; Bottom left: wh18.26; Top right: accident 1: Bottom right: accident 2.

In both accidents, the thigh and hip rolled over the bonnet leading edge and onto the bonnet causing the damages as seen in figure 7. The bonnets are slightly indented and the headlight assembly of the BMW is pushed backwards.

Considering the two crash tests, the damages were also caused by the thigh and hip. As in the real-world accidents, the bonnets are slightly indented and the headlight assembly of the BMW is pushed backwards too with the glass being fractured.

The damages produced by the biofidelic dummy match those caused by the two pedestrians pretty well.

Žilina dummy vs. pedestrian The damages to the bonnet leading edge caused by both the Žilina dummy and the two pedestrians are shown in figure 8.

Even though the collision speed is much lower in the crash tests, the damages are much more intense. The thigh and hip of the Žilina dummy indented the bonnet leading edge much further than the two pedestrians did. Moreover, the bonnet is bulged by this impact, before the chest of the ATD indents it much deeper than the pedestrians did. The pattern of the damages is completely different and cannot be compared with the two real-world accidents.

As the Žilina dummy is a rigid body, it can also cause scratch marks on the bonnet or even lacerate metal parts of the vehicle. A human being cannot cause such damages.

The Žilina dummy causes damages that are much more intense even at a lower collision speed. Hence, it can be concluded that the Žilina dummy does not produce realistic damages and would suggest a lower collision speed when compared with a similar real-world accident.

Figure 8. Vehicle damages Žilina dummy vs. pedestrian. Top left: wh08.27; Upper left: wh08.28; Lower left: wh08.29; Bottom left: wh10.12; Top right: accident 1; Bottom right: accident 2.

C-ratio

The C-ratio is defined as the closing speed over collision speed, and is an important parameter in accident reconstruction.

In practice, the C-ratio is determined using the pedestrian's anthropometric data and the vehicle's geometry. This geometrical C-ratio is determined using an internal DEKRA programme.

Here, it shall be analysed in how far the ATD's C-ratio determined using the geometrical approach matches the one determined by using crash test video analysis. The C-ratio is determined by evaluating the *CoM*'s speed at just that moment when the whole ATD detaches from the vehicle. Table 2 lists the determined C-ratios.

Table2.
C-ratios (the smallest deviation is marked in red)

crashtest	C	geometrical C	geometrical C 5%	geometrical C 10%	geometrical C 15%	ΔC	ΔC 5%	ΔC 10%	ΔC 15%	ΔC%	ΔC% 5%	ΔC% 10%	ΔC% 15%
wh18.22	90	74	78	82	86	-16	-12	-8	-4	-17,78	-13,33	-8,89	-4,44
wh18.23	100	72	76	80	84	-28	-24	-20	-16	-28,00	-24,00	-20,00	-16,00
wh18.24	95	87	91	95	99	-8	-4	0	4	-8,42	-4,21	0,00	4,21
wh18.25	80	86	90	94	98	6	10	14	18	7,50	12,50	17,50	22,50
wh18.26	97	73	77	81	85	-24	-20	-16	-12	-24,74	-20,62	-16,49	-12,37
wh18.27	100	73	77	81	85	-27	-23	-19	-15	-27,00	-23,00	-19,00	-15,00
wh18.28	77	72	76	80	84	-5	-1	3	7	-6,49	-1,30	3,90	9,09
wh18.29	93	71	75	79	83	-22	-18	-14	-10	-23,65	-19,35	-15,05	-10,75
wh18.34	87	87	91	95	99	0	4	8	12	0,00	4,60	9,19	13,79
sum										**15,95**	**13,66**	**12,22**	**12,02**
wh10.12	90	72	76	80	84	-18	-14	-10	-6	-20,00	-15,56	-11,11	-6,67
wh08.27	102	79	83	87	91	-23	-19	-15	-11	-22,55	-18,63	-14,71	-10,78
wh08.28	70	68	72	76	80	-2	2	6	10	-2,86	2,86	8,57	14,29
wh08.29	66	72	76	80	84	6	10	14	18	9,09	15,15	21,21	27,27
sum										**13,63**	**13,05**	**13,90**	**14,75**

C is the C-ratio determined by means of video analysis and is the reference value. Depending on the impact characteristics, a correction factor of between 5% and 15% is applied to the geometrical C-ratio. This is marked as "geometrical *C* 5%", for example. The difference between the two C-ratio values is marked with Δ*C*, while the percentage-wise difference with Δ*C*%. A "minus" indicates that the value is less than the reference value.

While the deviation in sum decreases with an increase of the correction factor for the biofidelic dummy, the deviations are more or less the same for the Žilina dummy, though the correction factor of 5% exhibits the smallest deviation. The respective deviation is sum with no correction factor and a 5% correction factor for the biofidelic dummy is higher compared to the Žilina dummy, while the deviation in sum is lower for the biofidelic dummy compared to the Žilina dummy with a correction factor of 10% and 15%, respectively.

Regarding the biofidelic dummy, positive deviations only occur in crash tests conducted with the VW Touareg and Mercedes A-Class. Looking at the Žilina dummy, positive deviations occur in the crash tests with the BMW 5 Series and the Toyota Avensis.

Considering the biofidelic dummy, Δ*C*% ~25 for all the cases where the ATD hit the roof leading edge and remained attached to it for at least a short time. In crash test wh18.28, the ATD impacted the roof leading edge, but detached immediately. As the different correction factors are applied, the values for Δ*C*% all decrease in a similar pattern.

How different front-end geometries and the fact that the roof leading edge has been impacted affect this behaviour merits further investigation.

Dynamic, time-dependent C-ratio While the C-ratio is a single value determined at the point of ATD detachment, the dynamic, time-dependent C-ratio, *C(t)*, is the fraction between closing speed and collision speed at any point of time. It visualises how the ATD/pedestrian gains energy, and hence speed, during the primary impact, and how the impact energy is then slowly absorbed during the secondary and tertiary impacts. Figures 9, 10 and 11 show the dynamic, time-dependent C-ratio for the head, hip and foot, respectively.

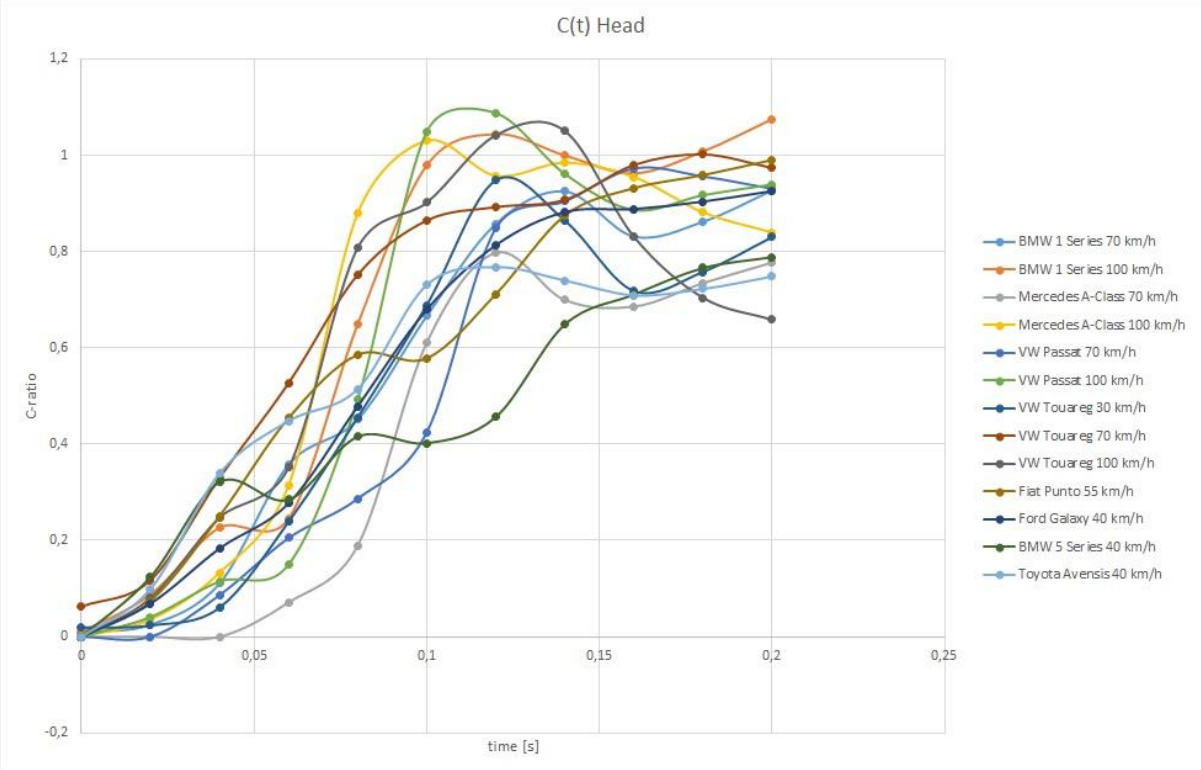

Figure 9. C(t) of the head.

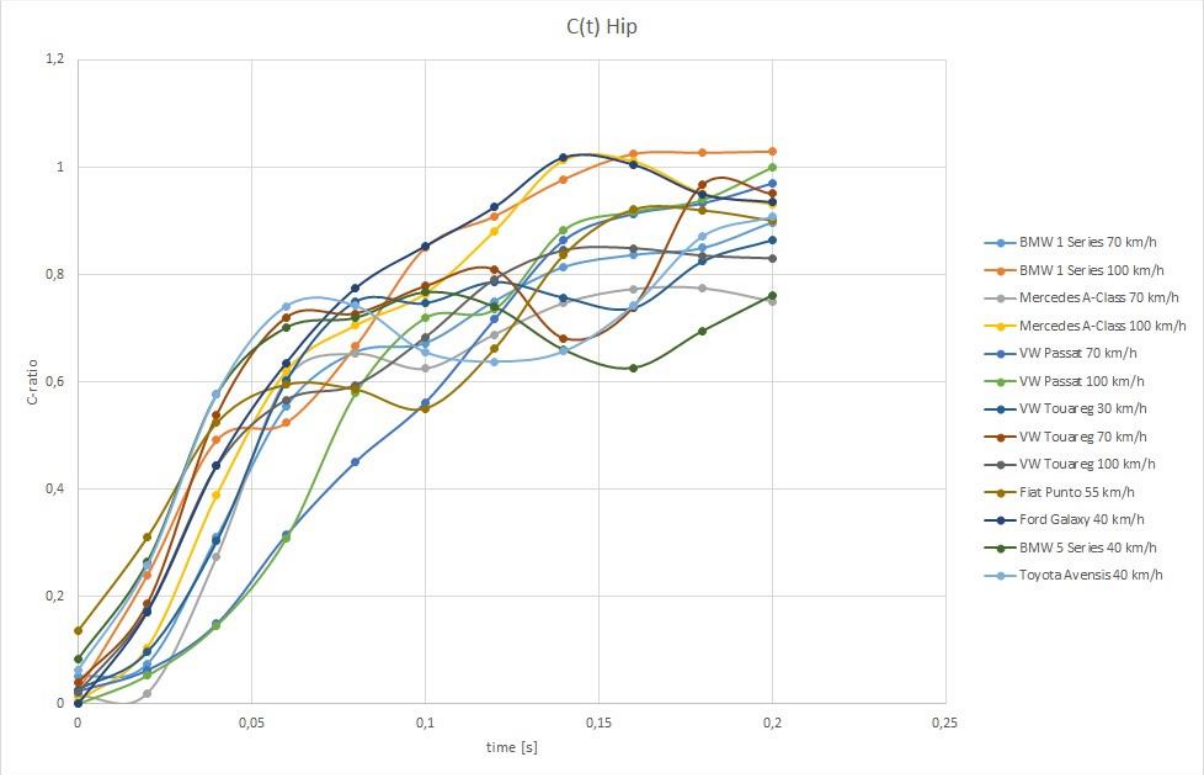

Figure 10. C(t) of the hip.

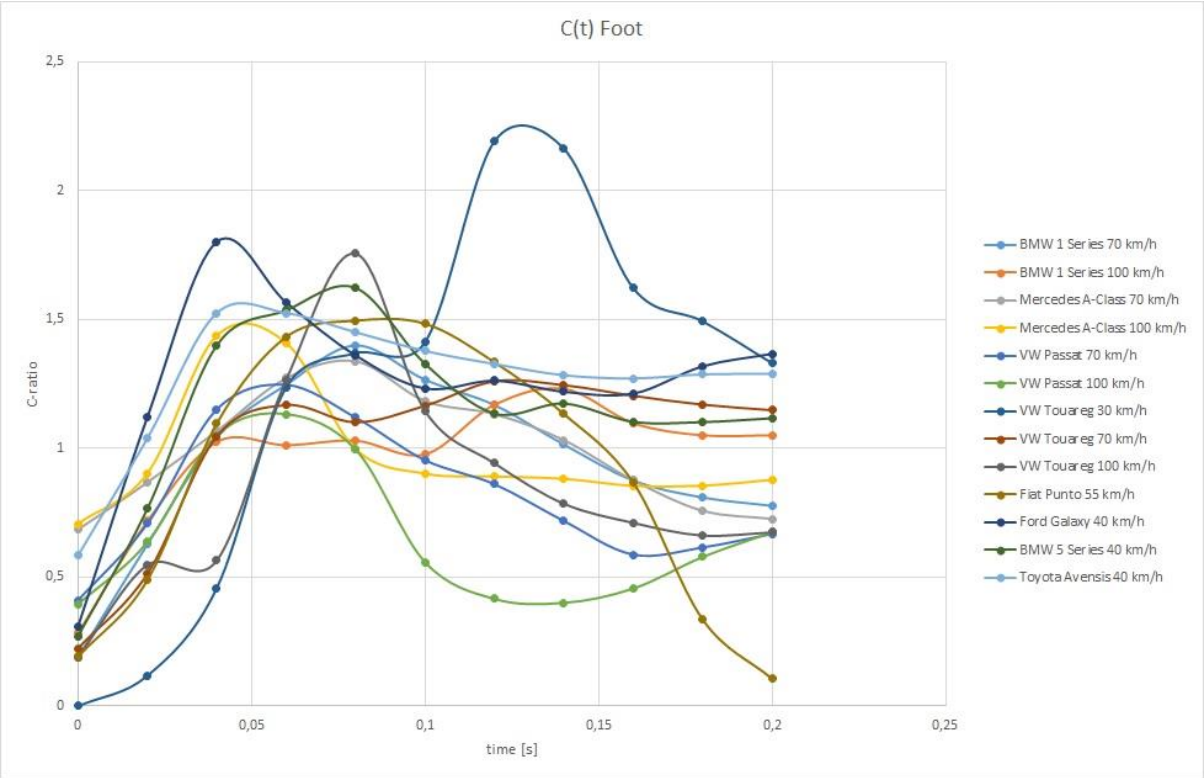

Figure 11. C(t) of the foot.

Considering the head and hip of the biofidelic dummy, certain patterns can be spotted, while the response of the foot seems to strongly depend on the specific front-end geometry and the subsequent dynamics and kinematics of the ATD. Especially the magnitude of the "suck-below" effect seems to influence the behaviour, as well as whether the leg is pierced by any sharp edges such as in crash tests wh18.22 and wh18.26. The shapes of the "head-curves" and "hip-curves" are oftentimes relatively similar for the different collision speeds when impacted by the same vehicle. With an increase in collision speed, they only shift more towards the left and upwards as shown in figure 12.

Figure 12. C(t) of the head when hit by the BMW 1 Series (biofidelic dummy).

Considering the same body part, e.g. the head, at the same collision speed, the shapes of the curves are relatively similar, though the different front-end geometries do have an influence on *C(t)* as shown in figure 13.

In comparison to the biofidelic dummy, the different curves have unsurprisingly a much steeper slope for the Žilina dummy. As the Žilina dummy is an elastic body, less energy is absorbed by the impact itself, and hence the ATD gains more energy compared to the biofidelic dummy, resulting in a steeper increase in speed, especially regarding the lower extremities. However, similar to the biofidelic dummy, there seems to be no recognisable pattern for the lower extremities. For the head and hip, the shape of the curves is relatively similar to each other at the same impact speed with some influence of the front-end geometry as shown in figure 14. Note, however, that the Fiat Punto has a slightly higher collision speed.

Dynamic, time-dependent C-ratio relative to the pelvis As with the dummy trajectories relative to the pelvis, the dynamic, time-dependent C-ratio, *C(t)*, of the head and foot can also be analysed relative to the pelvis.

Plotting *C(t; P)* over time, it can be seen that the heads of both the biofidelic and Žilina dummy behave in similar ways, while there is hardly any pattern discernable considering the feet (see figure 15). The shape of the head's *C(t; P)*-graph resembles more or less a sine curve with decreasing amplitude. The only exception constitutes crash test wh18.34, i.e. a biofidelic dummy being hit by a VW Touareg at 30 km/h.

Figure 16 depicts *C(t; P)* plotted over distance. Here, a much more distinct pattern can be discerned considering the heads and feet measured relative to the pelvis.

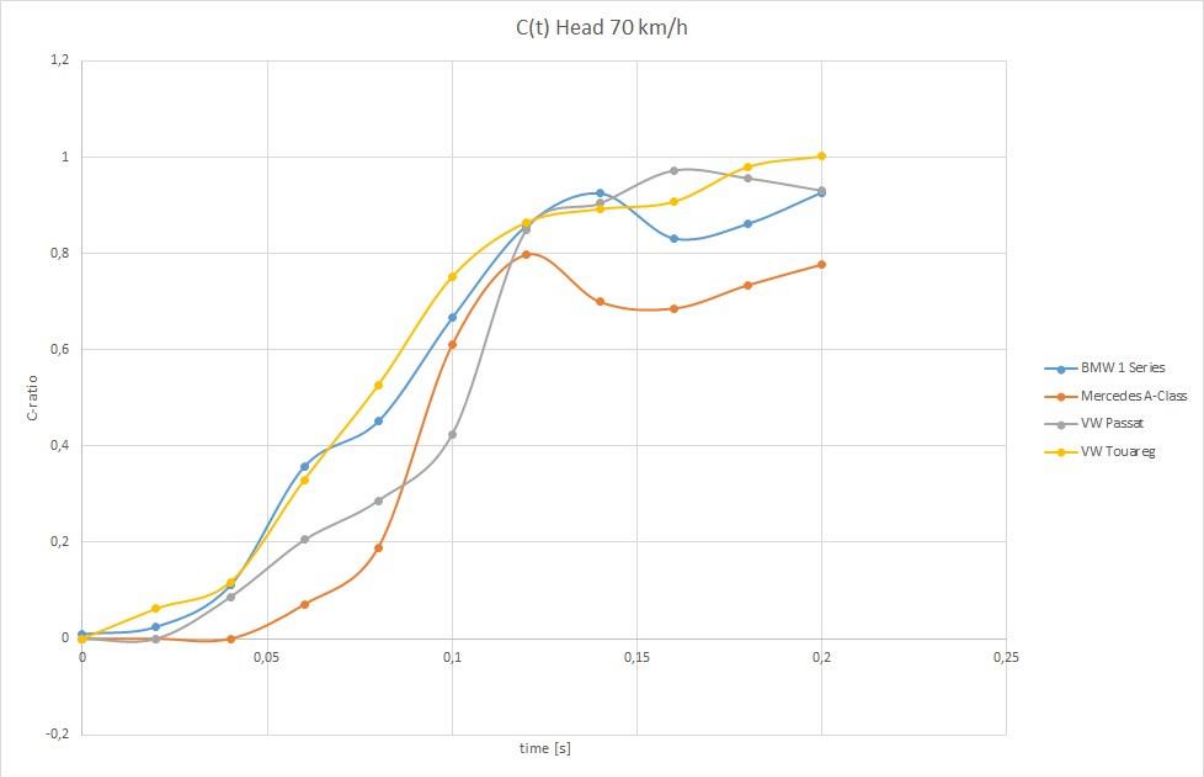

Figure 13. C(t) of the head at 70 km/h (biofidelic dummy).

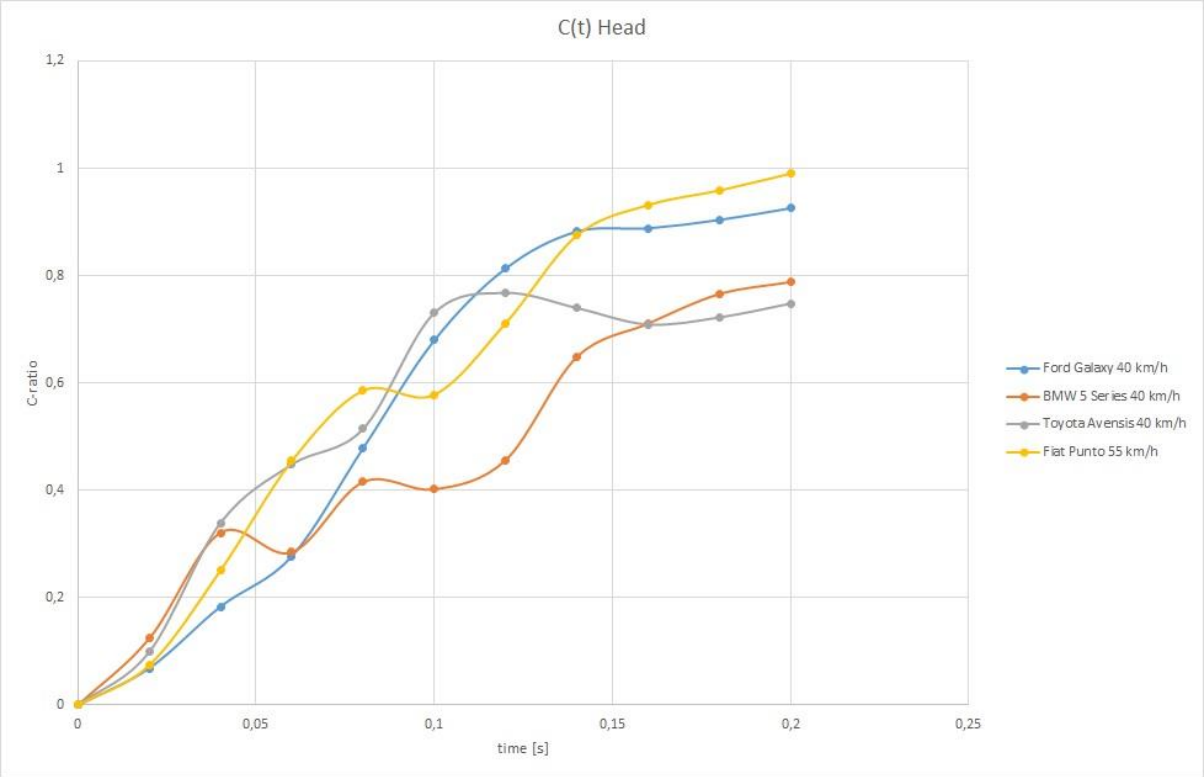

Figure 14. C(t) of the head (Žilina dummy).

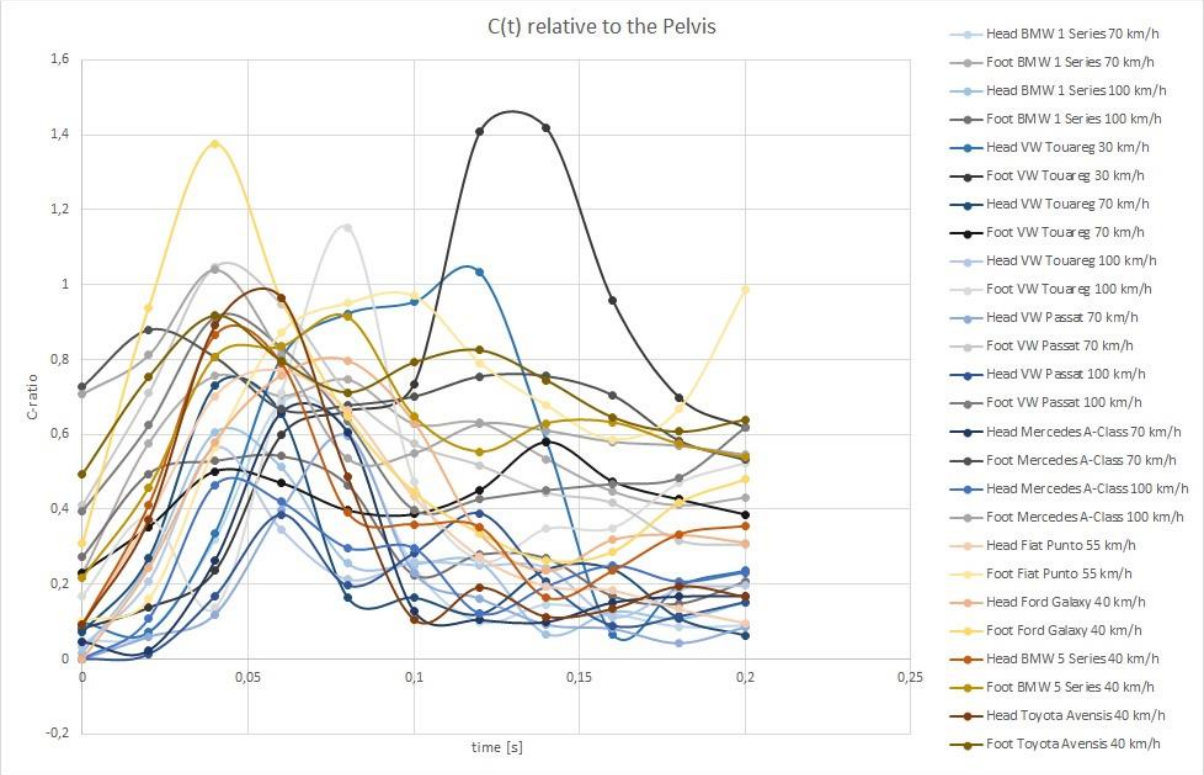

Figure 15. C(t) relative to the pelvis plotted over time. Blue: biofidelic dummy's head; Grey: biofidelic dummy's foot; Orange: Žilina dummy's head; Gold: Žilina dummy's foot.

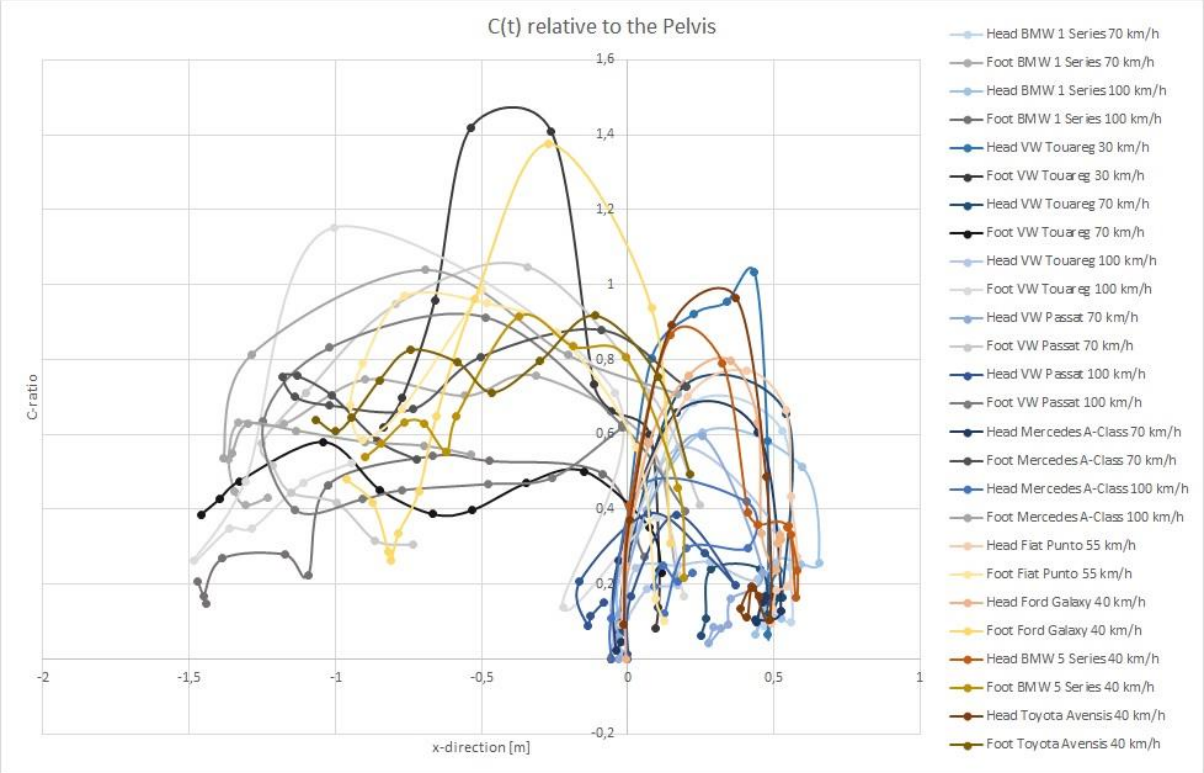

Figure 16. C(t) relative to the pelvis plotted over distance. Blue: biofidelic dummy's head; Grey: biofidelic dummy's foot; Orange: Žilina dummy's head; Gold: Žilina dummy's foot.

First, this graph visualises the kinematics and dynamics of the ATDs, which the first one does not. It is shown that, relative to the pelvis, the head is accelerated towards the striking vehicle, while the lower extremities are accelerated away from the vehicle. However, the behaviour of the different heads is very similar. The graphs resemble a negative square parabola, i.e. the head first experiences a positive acceleration relative to the pelvis and then a negative one. As *C(t; P)* is a ratio, one can argue that the heads experience a similar relative acceleration irrespective of collision speed and front-end geometry. On the other hand, the behaviour of the feet does not allow for any discernable patterns. Neither the biofidelic nor the Žilina dummy exhibit a distinct pattern, nor are there any particular characteristics concerning the collision speed or front-end geometry. The dynamic, time-dependent C-ratio of the foot relative to the pelvis seems to exhibit a completely random behaviour.

From this analysis, it can be concluded that the first collision between the striking vehicle and the pelvis is the primary determining factor considering the dynamics and kinematics of the ATD, and hence most possibly the pedestrian. As the heads exhibited more or less the same relative accelerations, the impact of the pelvis may thus have a direct influence on the injury mechanism and severity of the injuries to the head/neck complex. As the graphs resemble a negative square parabola and thus first exhibit a positive slope followed by a negative slope, the head first experiences an acceleration relative to the pelvis which is followed by a deceleration. As $C(t; P)_H$ is dependent on the pelvis, one can deduce that if $C(t)_P$ increases, $C(t; P)_H$ will increase too, i.e. the head will impact at a higher speed. Consequently, by reducing $C(t)_P$, the severity of head injuries may be reduced. As the head and pelvis are "connected" by the chest, the severity of chest injuries may possibly be lowered, too. $C(t)_P$, and thus $C(t; P)_H$, may be lowered by increasing the detaching time, i.e. allowing for greater deformation at the site of pelvis impact. Therefore, the local vehicle stiffness around the bonnet leading edge may be a decisive factor influencing both the kinematics and dynamics, as well as the injury mechanisms and injury likelihood of the upper body.

The influence of the pelvis on the head is much greater than on the lower extremities. Considering the latter, the magnitude of the "suck-below" effect and the height of the bonnet leading edge may have a decisive influence. While the front-end geometry seems to have a minor effect on the behaviour of the head relative to the pelvis, the influence on the lower extremities relative to the pelvis is much greater. The variability of $C(t; P)_F$ may also be explained by the anatomy of human beings. While the head and pelvis are "connected" to each other via the rather rigid spinal column, the feet and pelvis are "connected" to each other via the legs, which allow for greater relative movements.

[3] already concluded by means of PMHS-tests that the motion of the pelvis has an effect on the kinematics of both the upper body and lower extremities. These findings warrant further investigation.

Throw distance

Given that both the final position of the pedestrian as well as the point of collision are known, the throw distance can be used to determine the collision speed.

Throw distance charts have been developed by DEKRA based on crash tests with the Žilina dummy and results from well-documented real-world pedestrian accidents. Different throw charts have been developed for complete, partial and streaking hits. Considering complete hits, one has to further distinguish between pre-crash and in-crash braking.

Regarding the four pre-crash braking crash tests with the biofidelic dummy, two of the throw distances lie within the boundaries, while one lies just above the upper boundary and the fourth throw distance lies outside of the empirically developed corridor. However, DEKRA accident analysts deemed the deviation still being within an acceptable range. The three pre-crash braking crash tests with the Žilina dummy are also marked in the chart. Two of the three distances lie just below the lower boundary, while one lies outside the corridor. As the deviation is unacceptably high, data from the ADR have been analysed. The data highlight the fact that the brakes were not applied with full force, and hence the ATD was not catapulted away from the vehicle, but "travelled" with the vehicle for a prolonged time. This falsified the throw distance, which is why the Ford Galaxy must be excluded. Figure 17 shows the throw distance chart for complete hits and pre-crash braking.

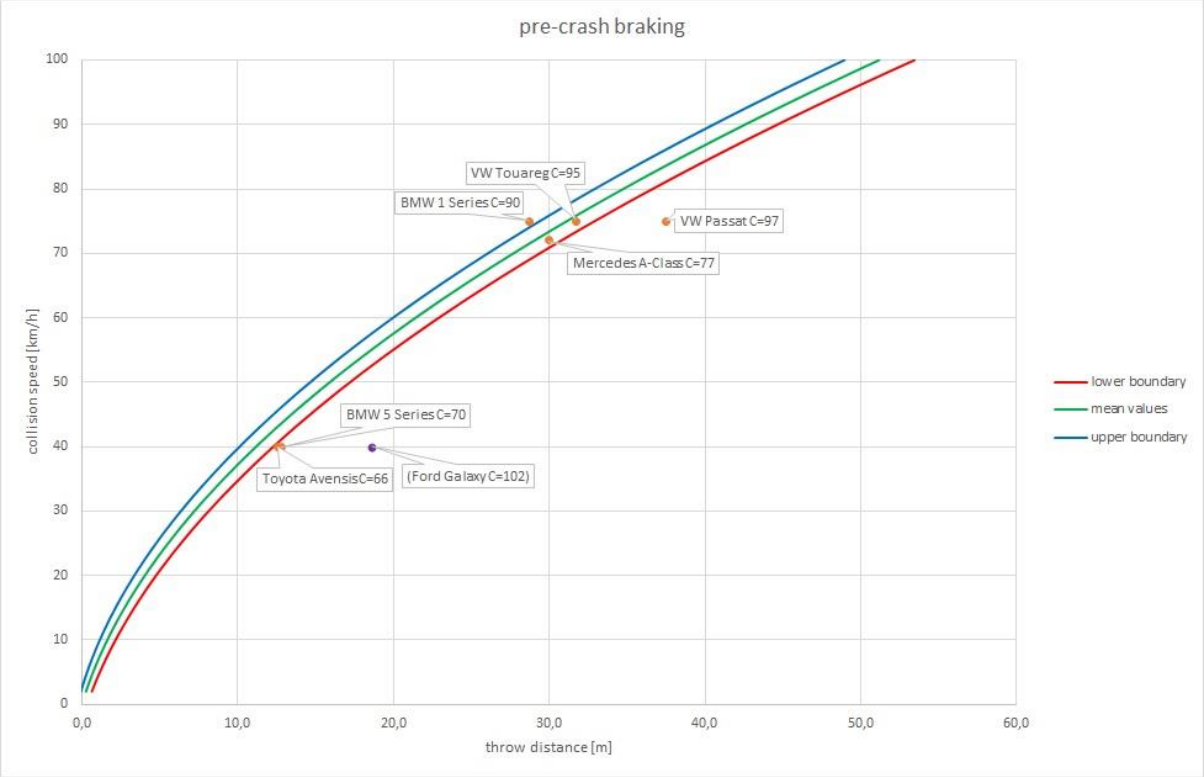

Figure 17. Throw distance chart for complete hits and pre-crash braking.

Considering in-crash braking, only three of the four crash tests conducted with the biofidelic dummy can be analysed. In crash test wh18.27, the ATD penetrated the windscreen and got stuck. While the throw distance for the Mercedes A-Class lies within the boundaries, the throw distance for the BMW 1 Series lies outside the boundaries, but still within an acceptable range according to DEKRA accident analysts. Regarding the VW Touareg, however, the deviation is by far too big. But, by further analysing the dynamics and kinematics of the ATD in this crash test, one realises that the ATD begins to slide off the fender quite immediately after impact and the complete hit hence becomes a partial hit. The throw distance lies well within the boundaries for partial hits. Thus, crash test wh18.25 is a special case, as the impact constellation equals to a complete hit, but turns into a partial hit due to the ATD kinematics and dynamics. This is explained by the flexibility of the biofidelic dummy. Like a human, the biofidelic dummy allows for torsional movement of the upper body relative to the pelvis. Thanks to this torsional movement of the upper body, the pelvis was turned sideways and thus slid off the fender. On the other hand, the Žilina dummy does not allow for such movements as a rigid body. Figure 18 displays the throw distance chart for complete hits and in-crash braking, and figure 19 depicts the throw distance chart for partial hits.

It can be concluded that both the biofidelic and Žilina dummy "produce" expected throw distances. However, as the throw distance charts have been developed partially based on crash tests with the Žilina dummy, the charts are slightly biased towards the Žilina dummy. Nonetheless, the results from the biofidelic dummy are very pleasing and further corroborate the validity of the throw distance charts.

"Dummy injuries"

"Autopsies" of the eight biofidelic dummies have been conducted at the "Bureau for Accident Reconstruction Berlin".

The damages of the biofidelic dummies have been determined by dismembering the ATDs and these damages have then been translated into respective injuries of a human being. It must be noted, however, that only bone fractures have been analysed, as the biofidelic dummy cannot mimic injuries to tissues and organs.

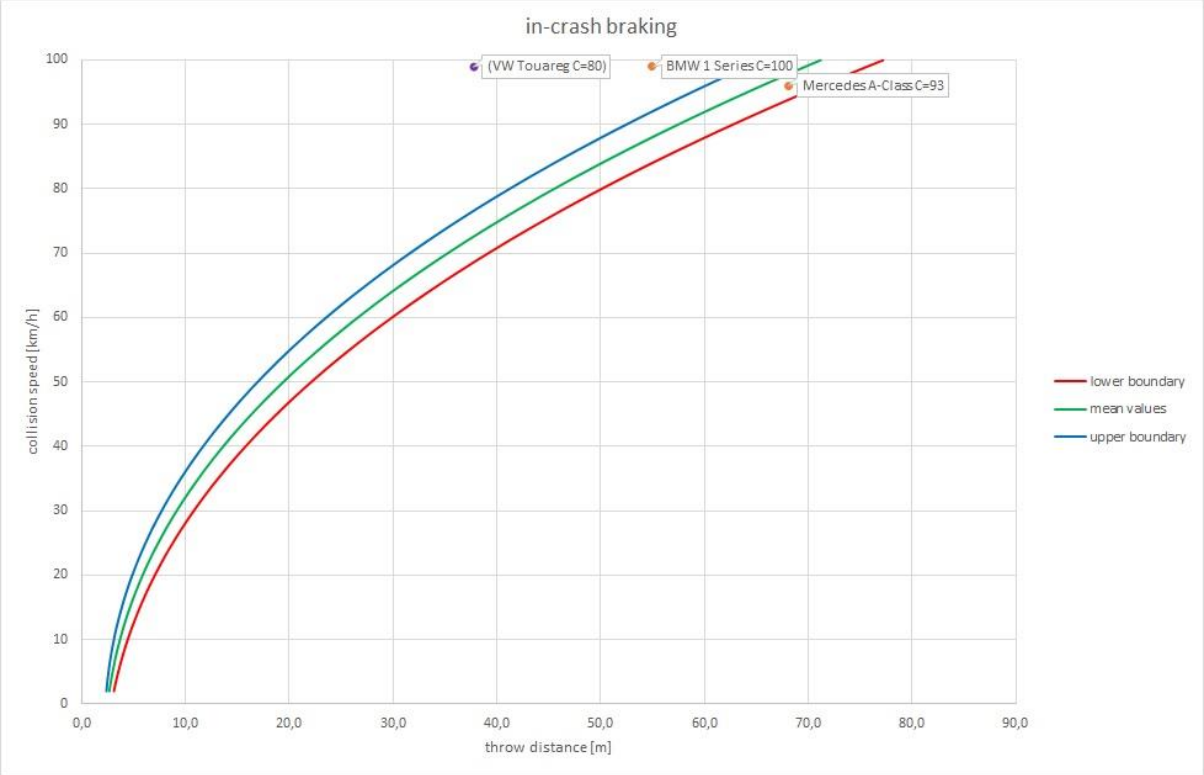

Figure 18. Throw distance chart for complete hits and in-crash braking.

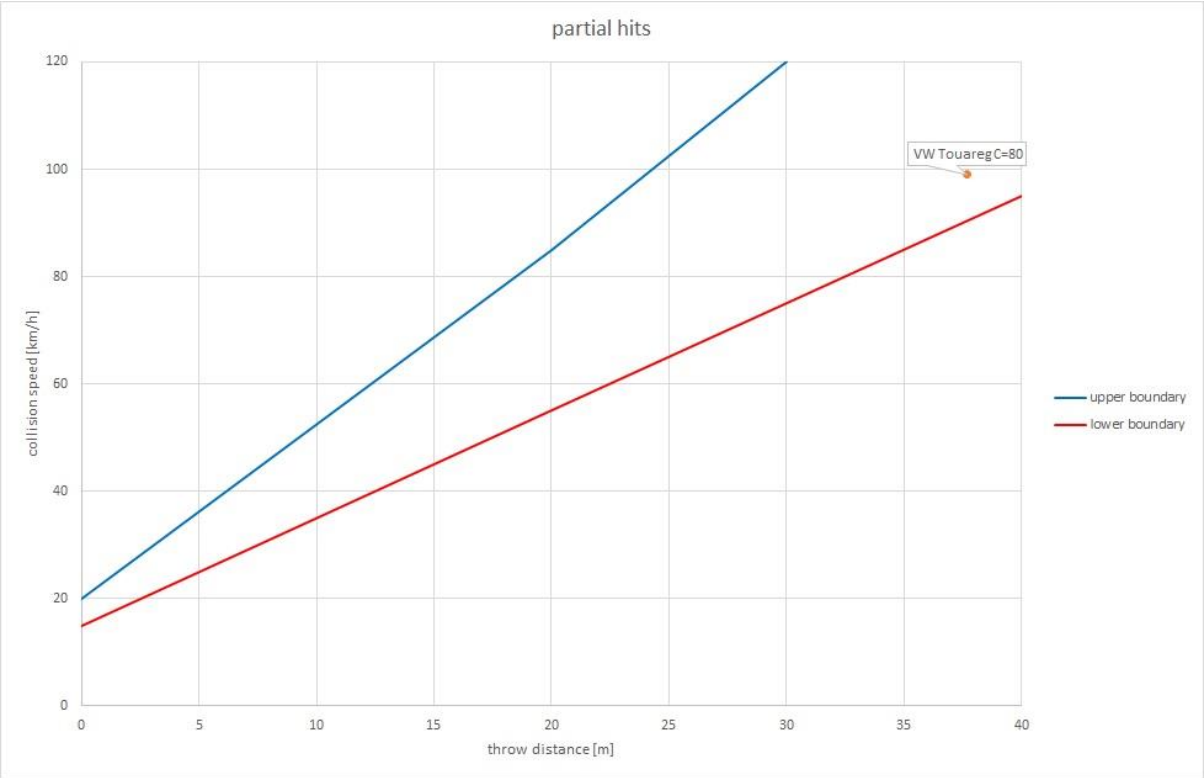

Figure 19. Throw distance chart for partial hits.

In [5], one of the authors analysed the correlations between collision parameters, vehicle damages and pedestrian injuries and concluded that the fracture patterns of long bone fractures in the lower limbs, knee joint injuries, injuries to the ankle, pelvic injuries and head injuries can be used for reconstruction purposes. The following analysis of the biofidelic dummy's "injuries" therefore focuses on these injuries, because the main area of use of this ATD will be in accident reconstruction. Figure 20 shows an overview of the "autopsy" of the biofidelic dummy used in crash test wh18.25.

Figure 20. Overview of the "autopsy" of the biofidelic dummy used in crash test wh18.25.

Fracture patterns of the lower leg's long bones The characteristic wedge-shaped fracture pattern, known as the Messerer's wedge fracture, can be often found in pedestrians hit by a vehicle [6]. The apex points in the direction of the vehicle's velocity vector and is thus indicative of the direction of impact.

While the fracture of the biofidelic dummy's lower leg does not exhibit the characteristic two faces of the Messerer's wedge fracture with the apex showing in the impact direction, a unique fracture pattern can be still observed. Initially, the fracture surface is flat and then ends with a protrusion on one of the two fracture surfaces. As with the apex of the Messerer's wedge fracture, this protrusion always indicates the impact direction.

Bone is a heterogeneous material, whereas the ATD's bones are made of a homogeneous material with similar strength. This difference explains the different fracture patterns observed in human beings and the biofidelic dummy. Notwithstanding, the biofidelic dummy exhibits a fracture pattern comparable to the Messerer's wedge fracture which can be used as a supporting factor in determining the impact direction. Figure 21 shows the fracture pattern observed in the biofidelic dummy used in crash test wh18.23.

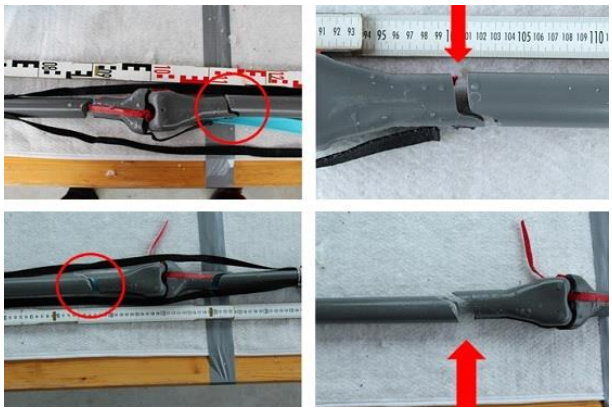

Figure 21. Messerer's wedge fracture in the biofidelic dummy used for crash test wh18.23 (Top: Left side; Bottom: Right side; Red circle: Location of wedge-shaped fracture; Red arrow: Impact direction).

Knee joint injuries The knee injuries sustained by the pedestrian can be classified according to their mechanism, namely avulsive or compressive. The resulting injuries to the condyles, the collateral ligaments and the cruciate ligaments are indicative of the impact direction. While valgus flexion was primarily found in lateral hits, varus flexion was found in medial ones.

The biofidelic dummy's knees have a very humanoid anatomy. The biofidelity of the dummy's knee joint injuries is analysed by means of the left knee joints of the ATDs used in crash tests wh18.23 and wh18.25, which are shown in figures 22 and 23. The underlying injury mechanism is varus flexion.

Figure 22. Knee injury of the biofidelic dummy used in crash test wh18.23 (Left: Front view; Right: Rear view; Red arrow: Impact direction).

Considering crash test wh18.23 and figure 22, the black tape, representing the lateral collateral ligament, has been torn off the femur. The tapes are glued to the bones. Here, the attachment site was weaker than the tape itself, which is why the tape was torn off and did not rupture. In reality, however, the ligament would rupture. Nonetheless, this damage to the biofidelic dummy's knee can be interpreted as a ruptured lateral collateral ligament. Moreover, both the anterior and the posterior cruciate ligaments are frayed. These "injuries" coincide with those found by [7] in human beings.

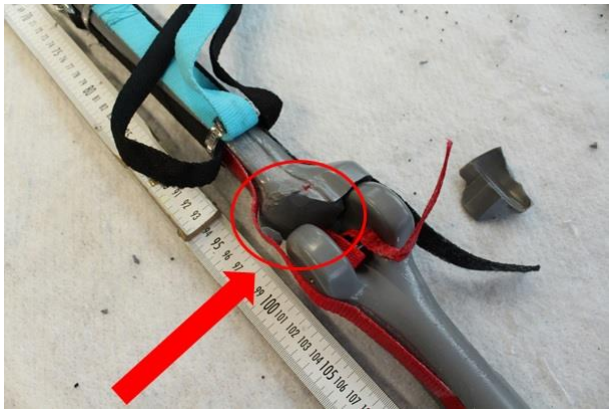

Figure 23. Rear view of the knee injury of the biofidelic dummy used in crash test wh18.25 (Red circle: Location of medial tibial condyle fracture; Red arrow: Impact direction).

Considering crash test wh18.25 and figure 23, the induced bending was even stronger, resulting in the fracture of the medial tibial condyle. In addition, the lateral collateral ligament as well as both the anterior and posterior cruciate ligaments were ruptured. The medial collateral ligament was also frayed by the impact.

Injuries to the ankle The "injuries" to the biofidelic dummy's ankle cannot be analysed as of yet, as the ankle's anatomy is not humanoid at all. The foot, made of rubber, is simply screwed into the lower leg.

Pelvic injuries Pelvis injuries seem to be more common in pedestrians, who have been run over, than in those hit close to an upright posture.

[8] determined that injuries to the sacroiliac joint were the best parameter to determine the side of impact in case of lateral hits, and were found to occur, with very few exceptions, on the side of direct impact.

Of the eight biofidelic dummies tested, only those used in crash tests wh18.24 and wh18.26 exhibited fractures of the right sacroiliac joint, while those used in crash tests wh18.28 and wh18.29 exhibited fractures of the left sacroiliac joint. Figure 24 displays the fractures of the right sacroiliac joint, whereas figure 25 displays the fractures of the left sacroiliac joint.

Figure 24. Fracture of the right sacroiliac joint of the biofidelic dummy (Left: Crash test wh18.24; Right: Crash test wh18.26; Red circle: Location of fracture; Red arrow: Impact direction).

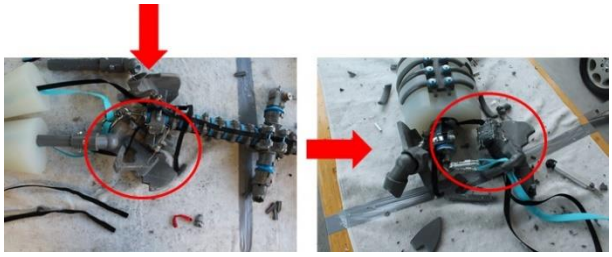

Figure 25. Fracture of the left sacroiliac joint of the biofidelic dummy (Left: Crash test wh18.28; Right: Crash test wh18.29; Red circle: Location of fracture; Red arrow: Impact direction).

The "injuries" to the sacroiliac joint found are in concordance with those reported by [8]. However, only two "injuries" occurred at the direct side of impact, while the other two occurred at the opposite side of impact.

The biofidelic dummies used in crash tests wh18.25 and wh18.27 sustained "injuries" to the ilium very close to the sacroiliac joint. Both biofidelic dummies sustained a fracture to the right ilium. As these "injuries" are so close to the sacroiliac joint, they could be considered as sacroiliac injuries for reconstruction purposes. The fractures of the left and right ilium of the biofidelic dummy used in crash test wh18.23 are further away from the respective sacroiliac joints and can hence hardly be considered as "injuries" to the sacroiliac joint region. This classification, of course, is somewhat subjective. Obviously, the design of the biofidelic dummy and the way it is constructed influence the "injury" patterns. Figure 26 shows the fracture to the ilium within the sacroiliac joint region, while figure 27 shows the fracture to the ilium outside the sacroiliac joint region.

Figure 26. Fracture of the ilium next to the sacroiliac joint of the biofidelic dummy (Left: Crash test wh18.25; Right: Crash test wh18.27; Red circle: Location of fracture; Red arrow: Impact direction).

Thus, of the six "injuries" to the sacroiliac joint region, four occurred at the direct side of impact and two at the opposite side of impact. Though the sample size is too small to make a valid statement, these findings suggest that injuries to the pelvic region are less reliable for reconstruction purposes than those to the knee joint for example.

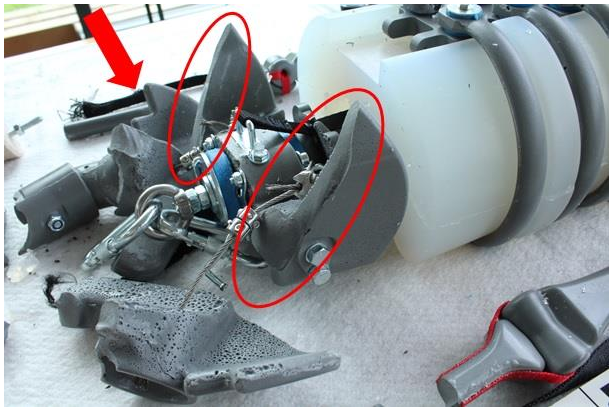

Figure 27. Fracture of the left and right ilium of the biofidelic dummy used in crash test wh18.23 (Red circle: Location of fracture; Red arrow: Impact direction).

"Injuries" to the biofidelic dummy's acetabulum were also frequently noted. According to [8], these injuries, however, are less useful for reconstruction purposes. Nonetheless, the damages of the biofidelic dummies' acetabulums are largely in concordance with the injury mechanism as described by [8]. However, bony split-offs have also been noted at the left acetabulum, i.e. the opposite side of impact.

All in all, the "injuries" to the pelvic region seem to be pretty realistic and are largely in concordance with those reported in literature. Still, many "injuries" were found on the left side of the biofidelic dummy. According to [8], though, pelvic injuries rather occur on the direct side of impact, i.e. the right side of the biofidelic dummy. In how far the design and the construction of the biofidelic dummy's pelvis influence the injury patterns requires further investigation. While many tendons and ligaments support the human pelvic region, the ATD's pelvic region is not supported.

Head injuries As with injuries to the ankle, head injuries cannot be analysed as of yet. This is due to the rigid design of the head. The latest design consists of one cast component with a cavity at the base of the skull. Inside of this rectangular cavity sits the mount of the spinal column. As this mount is more or less a rigid rectangular block, it props up the skull. Thus, the overall design of the cranium is so rigid that it does not break.

One example is the biofidelic dummy used in crash test wh18.25. Here, the ATD was hit at 99 km/h and the head impacted the A-pillar. The only "injuries" the ATD sustained to the head can be described as a laceration of the latex/wet suit with abrasions on the os parietale beneath. In reality, the skull would have fractured, resulting in severe injuries to the brain which would not have been survivable with an extreme likelihood.

Comparison with real-world pedestrian accidents As with the vehicle damages, crash tests wh18.22 and wh18.26 are compared with two real-world pedestrian accidents. The considered accidents are the same.

Without comparing every single injury, it can be noted that overall the injuries of the biofidelic dummy match those of the pedestrians pretty well. Both the pedestrians as well as the biofidelic dummies suffered injuries to the thorax, shoulder region, pelvic region, and the lower extremities.

Obviously, one must consider that the pedestrians and ATDs each collided with different vehicles. Furthermore, the individual fitness of a human being also affects their biomechanical response, explaining variations in the injury patterns. The exact kinematics and dynamics throughout the collision further influence the biomechanics and a crash test will never be able to exactly imitate those.

Nonetheless, it can be concluded that the biofidelic dummy exhibits very similar injuries to pedestrians when considering fractures. As of yet, the biofidelic dummy cannot mimic tissue and organ injuries. Figure 28 displays the different injury diagrams.

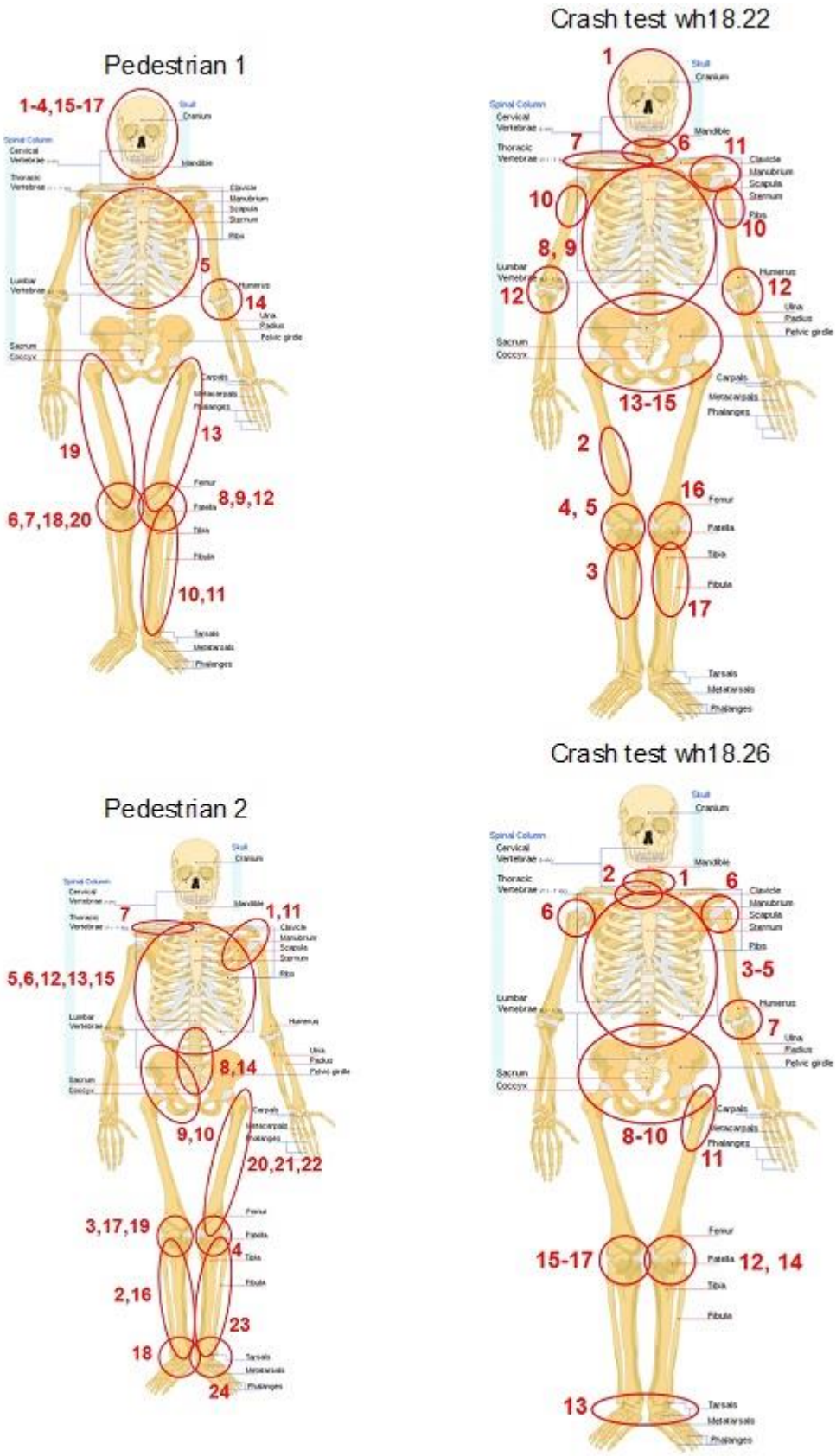

Figure 28. Comparison of injuries between pedestrian and biofidelic dummy.

LIMITATIONS

While the representational crash tests conducted by DEKRA and AXA Insurance with the biofidelic dummy were performed at roughly 70 km/h and 100 km/h, the Žilina dummy and cadaver tests had been conducted at roughly 40 km/h. This makes a direct comparison somewhat complicated due to different impact energies. But former crash tests had been conducted successfully with the Žilina dummy as well as the biofidelic dummy at impact speeds between roughly 40 km/h and 75 km/h. Nonetheless, different vehicles were used, which also has an impact on dummy/cadaver dynamics and kinematics.

As the dummy targets were placed manually on the ATDs in the video analysis programme "Falcon", the determination of the trajectories and C-ratios is further afflicted with minor inaccuracies. However, each value was computed three times and the average has been taken, in order to minimize the inaccuracies as much as possible.

The biofidelic dummy can further only mimic fractures and not injuries to tissues and organs.

CONCLUSIONS

The biofidelic dummy already exhibits a high degree of biofidelity. Its trajectories are comparable with those of PMHSs and this ATD also creates realistic vehicle damages. This allows to more correctly determine the collision speed. The obtained C-ratios are also good and the deviations to those obtained by the Žilina dummy are minimal. It can be concluded that the current procedure of determining the geometrical C-ratio based on the Žilina dummy is still valid and can be further used. The method should only be revised, in order to further refine the correctness of the results. This, however, merits further investigations. The throw distances obtained with the biofidelic dummy are good. The unique feature of the biofidelic dummy is its ability to mimic injuries a pedestrian would suffer in a pedestrian-vehicle accident of similar severity. The "injuries" of the ATD resemble those of a pedestrian pretty well, especially those of the knee joint. Thus, the biofidelic dummy enables expert witnesses to reconstruct a pedestrian-vehicle accident and to obtain realistic vehicle damages, throw distances and injuries. This opens up new possibilities in the field of accident reconstruction.

As long as the mechanical loading parameters need to be determined in a certified way, however, there is no way around the sophisticated ATDs of the like of Hybrid-III dummy, THOR dummy and POLAR dummy.

REFERENCES

[1] Knape, M. 2016. "Weiterentwicklung eines biofidelen Fußgänger-Dummys zur realistischen Schadenerzeugung an Fahrzeugen bei experimentellen Simulationen von PKW/Fußgängerkollisionen". Technische Universität Berlin. (Master's thesis)

[2] Kolla, E., Korbel, T., Imrich, L., Kubjatko, T., & Mackovicová, L. 2017. "Correlation "impact velocity-specific pedestrian injuries" for reconstruction of pedestrian accidents". Proceedings of the 26th Annual Congress of the European Association for Accident Research and Analysis, 213-224.

[3] Subit, D., Kerrigan, J., Crandall, J., Fukuyama, K., Yamazaki, K., Kamiji, K., & Yasuki, T. 2008. "Pedestrian-Vehicle Interaction: Kinematics and Injury Analysis of four full-scale Tests". Proceedings of the 2008 IRCOBI Conference – Bern (Switzerland), 275-294.

[4] Kerrigan, J. R., Murphy, D. B., Drinkwater, D. C., Kam, C. Y., Bose, D. & Crandall, J. 2005. "Kinematic Corridors for PMHS tested in full-scale Pedestrian Impact Tests". University of Virginia Center for Applied Biomechanics.

[5] Schäuble, A. 2018. "Analysis of Pedestrian Accidents - Correlations between Collision Parameters, Vehicle Damages and Pedestrian Injuries". Vienna University of Technology & DEKRA. (Project report)

[6] Hartwig, S. 2016. "Personenschäden im Straßenverkehr: Unfallanalyse, Medizin und Recht. (W. H. M. Castro, M. Becke & M. Nugel, Eds.). C. H. Beck.

[7] Teresinski, G., Madro, R. 2001. "Knee joint injuries as a reconstructive factors in car-to-pedestrian accidents". Forensic Science International, 124, 74-82.

[8] Teresinski, G., Madro, R. 2001. "Pelvis and hip joint injuries as a reconstructive factors in car-to-pedestrian accidents. Forensic Science International, 124, 68-73.

ASSESSING INJURY RISK OF CAR OCCUPANTS ON REARWARD FACING SEATS IN A FULL FRONTAL IMPACT – SLED TESTS IN A GENERIC TEST ENVIRONMENT

Harald Zellmer
Felix Manneck
Autoliv B.V. & Co. KG
Germany

Paper Number 19-0201

ABSTRACT

With the introduction of fully-automated vehicles, new seating configurations of the passenger compartment has been proposed. Rearward facing front seats are considered to provide so-called living room seating. At least as long as conventional and fully-automated vehicles share the same roads in mixed traffic, crashes may occur. Occupant protection on a rearward facing seat must therefore be on the same level as on a forward facing seat to comply with legal requirements. In order to assess dummy response on a rearward facing seat in a 56 km/h full frontal impact, sled tests were performed, analysed, and discussed.

A total of 23 sled tests in three series with a Hybrid III 50th percentile adult male dummy were performed to simulate a vehicle frontal impact against a rigid barrier at impact speeds up to 56 km/h. In the first test series, a serial vehicle seat was used, but it showed already considerable deformation at an impact speed of 40 km/h. Therefore, a generic concept seat was developed. In the second test series, the concept seat was tested and tuned to enable it to perform tests at the target impact speed of 56 km/h. In the third series, tests to investigate repeatability were performed. Dummy loadings at 56 km/h were compared with reference values from legislation and literature. Focus was set on thorax and lumbar spine loadings.

For a qualified interpretation of dummy loadings and the performance of the restraint system, the crash was divided into three phases: (1) impact phase until the maximum dummy rearward displacement, (2) dummy rebound before interaction with the seat belt, and (3) dummy in rebound and interaction with the seat belt. The impact phase (1) is characterized by the highest 3 ms chest acceleration, close to 60 g in 56 km/h tests. Notably, this was the loading closest to the injury assessment reference value (IARV). The lumbar spine was mainly loaded in compression with forces rising up to 5.8 kN. Chest deflection of about 8 mm was caused by inertia of the dummy rib cage. The rebound phase before interaction (2) did not show any substantial dummy loading. The rebound interaction phase (3) was influenced by the seat belt system, chest deflection ranged from 5 mm in the test with lap belts to 19 mm in the test with two crossed shoulder belts (crisscross belt). The viscous criterion was below 0.1 m/s in all tests. Overall, the tests showed good repeatability and the ability of the generic concept seat to control dummy kinematics.

A limitation of our study is, that only full frontal loading directions were studied, dummy kinematics of oblique impact direction, simulating e.g. $\pm$30° impacts to the barrier, were not included. The head rest was not in focus of our investigation and the head was fixed to the head rest without any gap in between.

INTRODUCTION

The development of automated driving systems of SAE levels 4 and 5 [1] allows for new seating options in automobiles. Swivel front seats are desirable to provide so-called living room seating [2]. With this, the front row passengers would sit on a rearward facing seat. At least as long as conventional and fully-automated vehicles share the same roads, crashes may occur. Occupant protection on a rearward facing seat must therefore be at least on the same level as on a forward facing seat.

Although few car models are equipped with rearward facing seats, e.g. Volkswagen Caravelle, Mercedes Viano, or several models of ambulance cars and motorhomes, almost no accident analysis focusing on adult car occupants on rearward facing seats is published. An analysis of the German In-Depth Accident Study (GIDAS) identified only five cases with rearward facing adult occupants in ECE M1 vehicles. Only one occupant on a

rearward facing seat was injured (MAIS 2), but in all collisions the speed change Δv of the impacted vehicle was below 25 km/h [3].

Sled testing in this occupant loading direction is mainly to determine neck injury risk in low speed rear impacts. Further, some studies were performed to determine injury risk in so-called high speed rear impacts with a Δv of up to 40 km/h [4, 5]. Pulses for these studies are to represent loadings in a car to car rear impact and are much softer than pulses in a frontal car to car or car to barrier collision at the same Δv.

Recently simulations with the human FE model THUMS on rearward facing seats in full frontal impact conditions were performed. Kitagawa et al. [6] described occupant kinematics on rearward facing and conventional seats, Xin Jin at al. [7] compared injury risk in different loading directions and concluded that the rearward facing seating position has the lowest injury risk.

The scope of our work was to study occupant loading on rearward facing seats in sled tests. For this, we established a generic test environment. The initial requirements were as follows:

1. The test setup should be sufficiently stable to withstand a stiff crash pulse taken from a small vehicle in a full frontal crash according to FMVSS 208 [8] at 56 km/h.
2. The rearward displacement of the back rest during crash should be adjustable and limited to about 200 mm rearward displacement in order to avoid possible occupant head contact to the windscreen.
3. The environment should be simple in order to build up and validate a finite element model for further investigations.

The dummy used for the investigation was a Hybrid III 50th percentile adult male. For the rearward loading direction of this dummy, injury reference assessment values (IARV) only exist for low speed rear impact. These are however to protect from AIS 1 injuries and are thus not applicable for high speed impacts we are looking at. In a first assumption, we applied IARV for the frontal impact of this dummy. It must be pointed out, that this can only be a first approach as the dummy was not validated for this loading direction. In the first step, we were concentrating on injury assessment of chest and lumbar spine as loading to these body parts mainly dependent on the back rest performance. Head and neck loadings are mainly dependent on the head rest and should be investigated in a next step. As a guideline, IARV given in European or US legislation were taken into account first, the respective lower value was taken as our reference for this paper. For the chest the 3 ms chest acceleration clip of 60 g was taken from FMVSS 208 [8], for chest deflection and the viscous criterion the values were taken from ECE-R 137 (42 mm and 1 m/s) [9]. No reference values in automotive regulations exist for the lumbar spine forces. For helicopter emergency landing the European Aviation Safety Agency (EASA) specifies a limit in compression of 6674 N [10]. An internal specification of General Motors (GM) [11] specifies 12.2 kN in tension and 6.4 kN in compression. The compression value is well comparable to the EASA requirement and was used together with the value for tension as reference in this paper.

To have control of all loadings to the dummy we also used IARV for other body parts. A list of all used IARV and its source can be found in the Appendix.

METHOD

All the tests were performed on a deceleration sled using either a hydraulic brake or a bending bar brake to generate the crash pulse. The seat was mounted to the sled and a Hybrid III 50th percentile male dummy placed on it.

In the first tests series, a serial production seat was used. The dummy was seated according to the definition in [12]. The speed was increased until a Δv of 40 km/h was reached. Already at Δv of 40 km/h a considerable deformation of the seat back occurred and it was decided to design and build a generic seat which could withstand a Δv of at least 60 km/h which compares to a barrier impact speed of 56 km/h.

Figure 1 shows the generic concept seat that was designed and built. It consists of a stiff seat pan which has a steel frame with a surface of acrylic glass and a back rest which has a frame of standard aluminium profiles. This was chosen in order to easily replace in case of damage in crash. The seat back frame has a polycarbonate shell surface to support the back of the dummy. All the surfaces which are in contact with the dummy have a padding of at least one layer of comfort foam. In the second test series, which was the first one with the generic seat, a standard head rest supported by an aluminium frame at its back was used. This design showed not to be

very reliable and in the third test series a stiff steel frame head rest was implemented. It has a wooden plate towards the dummy's head and three layers of comfort foam. The dummy head is taped to the head rest to avoid a gap between both. The back rest is fixed to the sled ground plate by ball bearings at both sides. The torso angle of the dummy is set to 25°. A controlled rearward displacement of the back rest during crash is provided by each two layers of seat belt webbing of 12% elongation at 10 kN and of a length of 1200 mm on both sides of the back rest. The other side of the webbing is fixed to a steel frame mounted to the sled. At the upper cross member of the back rest, seat belt systems can be mounted at each side.

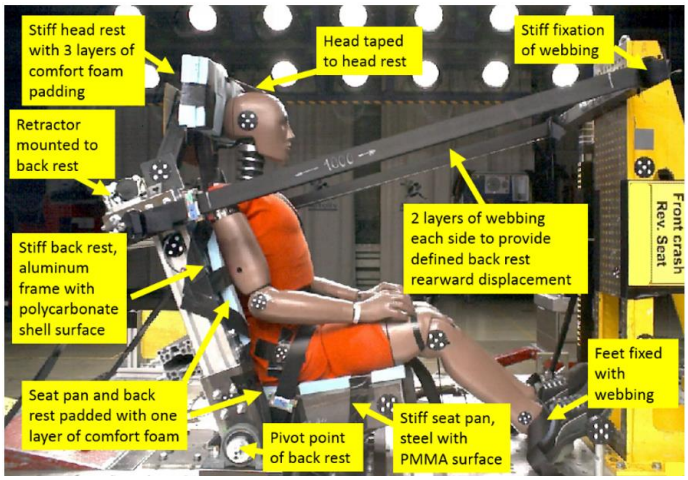

Figure 1. Generic seat in its final version

TEST SETUP

In test series 1, the standard production seat was used. In the first four tests, Δv was increased from 17 km/h as given in FMVSS 202a [12] to 40 km/h. A standard three point belt system was used with the upper shoulder belt fixed to a stiff B-pillar mounted on the sled and the lower anchorages fixed to the seat. At a Δv of 40 km/h, the deformation of the seat back was so large that no further increase in speed was done. The dynamic rear displacement at the upper end of the back rest was with 250 mm above our target of 200 mm. In order to study influencing parameters, three more tests at Δv of 40 km/h were performed, this included the variation of the back rest angle and of seat belt parameters. To investigate the influence of the back rest angle, the back rest was set to its most upright position with otherwise identical parameters to the previous test. The influence of the belt restraint system was investigated in two further tests: One test was done with a lap belt only, the other with two crossed shoulder belts (crisscross belt without lap belt portion) attached directly to the top of the seat and to the anchor plate on the seat frame.

The second tests series was performed with the generic seat. In the first six tests, the speed was increased from a Δv of 40 km/h in 5 km/h increments to about 60 km/h and an occupant load criterion (OLC) [13] of about 36 g. A seat-integrated three-point belt system was used in the tests, mounted to the upper cross member of the back rest. The tests allowed further improvements to be made. There were among others the stiffening of the production head rest and the optimisation of the webbing parameters for the controlled back rest rearward displacement. After six tests, the target Δv of 60 km/h and OLC of 36 g was attained and two additional tests to study the influence of the restraint system were performed, cf. Table 2. The additional belt systems tested were a lap belt only system and a standard 3-point belt with additional shoulder belt at the other shoulder (crisscross belt).

The focus of test series 3 was to determine repeatability and to provide reliable data for the validation of a finite element model. In contrast to the first two series, in which the crash pulses were generated by a hydraulic brake system, the tests in series 3 were performed with a bending bar brake system. This provided a better repeatability of the crash pulses. The pulse chosen had an OLC of 31.5 g and thus was softer than the pulse used in series 3. The first two tests in this series were performed with a seat belt retractor pretensioner. The second two tests were without belt system and performed mainly for the FE model set-up. A pairwise comparison of the tests data already showed a good repeatability. Therefore, a series of four identical tests were performed with a standard three point belt system to better quantify repeatability.

TEST RESULTS

The results of test series 1 are shown in Table 1. Tests 1.1 to 1.4 were performed to access the limit of the seat. It was decided not to exceed Δv of 40 km/h and a small parameter study was done at this speed. All injury assessment values (IAV) were well below its reference values. As can be seen in test 1.5, a more upright seating position slightly reduced chest acceleration. The lumbar spine was mainly loaded in tension, in test 1.6 the dummy was belted only with a lap belt which increased lumbar spine tension, in test 1.7 the dummy was mainly restrained with a shoulder belt at each side. This decreased tension in the lumbar spine. However, the effect was not as big as expected, the main restraint of the dummy was provided by the seat itself. It is interesting to mention, that we measured not only chest deflection but also chest extension. This was possibly due to the back rest frame which pushed the dummy ribs forward. At higher Δv a part of the effect is compensated by the inertia of the ribs being pushed backwards in the crash.

Table 1.
Test series 1, test setups and injury assessment values

Test	ΔV	Backrest Angle (Torso Angle)	Belt System	Chest 3 ms / g	Chest defl. / mm	Chest ext. / mm	Lumbar spine tension / kN	Lumbar spine comp. / kN
1.1	17.3 km/h	22.1° (25°)	Normal Seat Belt	18	3	12	1.1	0.3
1.2	24 km/h	22.1° (25°)	Normal Seat Belt	27	4	14	1.4	0.8
1.3	33 km/h	22.1° (25°)	Normal Seat Belt	30	6	3	1.2	0.7
1.4	40 km/h	22.1° (25°)	Normal Seat Belt	31	0	4	1.9	0.2
1.5	40 km/h	15.6° (N/A)	Normal Seat Belt	27	1	3	1.9	0.3
1.6	40 km/h	22.1° (25°)	Lap Belt only	31	0	8	2.3	0
1.7	40 km/h	22.1° (25°)	CrissCross w/o Lap Belt	29	1	5	1.3	0.3

The test parameters of test series 2 are shown in Table 2. Injury assessment values are not given in the table, as several parameters of the seat were changed in the first six tests. In tests 6 to 8 the same belt parameters as in test series 1 were investigated.

Table 2.
Test series 2, test setups

Test	ΔV	OLC	Belt System
2.1	40 km/h	20.0 g	Seat integrated 3-point belt
2.2	45 km/h	24.7 g	Seat integrated 3-point belt
2.3	50 km/h	29.9 g	Seat integrated 3-point belt
2.4	55 km/h	28.0 g	Seat integrated 3-point belt
2.5	~ 60 km/h	33.5 g	Seat integrated 3-point belt
2.6	60 km/h	36.1 g	Lap Belt only
2.7	60 km/h	36.6 g	Seat integrated CrissCross Belt
2.8	60 km/h	35.2 g	Seat integrated 3-point belt

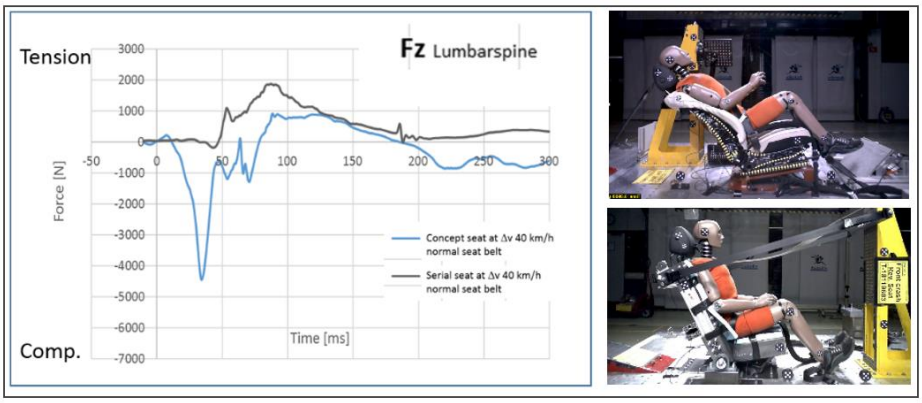

Figure 2. Comparison of lumbar spine forces of tests at Δv 40 km/h with the serial and the generic seat. The upper right picture shows the serial seat at its maximum spine tension (90 ms), the lower right picture the concept seat at its maximum compression at 34 ms

First it has to be mentioned that the dummy kinematic in the generic seat differed from that in the serial seat (Figure 2). In the serial seat the spine was mainly loaded in tension, the dummy pelvis was restrained by the seat back and the upper part of the torso could move up. The generic seat back has a plain surface and the whole body could freely move up. The pelvis pushed the torso and caused compression in the spine.

In contrast to the serial seat, the concept seat showed a considerable rebound of the back rest which is due to elasticity in the webbing and the dummy fell in to the restraint system in rebound. Therefore, it is useful to divide the crash into three phases, similar as earlier done for the low speed rear impact [14]:

Phase 1: From the beginning (t = 0 ms) to the time when the maximum shoulder/arm-joint rearward displacement occurs, this is at about 60 ms in series 2 & 3 with Δv 60 km/h.

Phase 2: From the end of Phase 1 until the shoulder/arm-joint passes its initial x-plane position (relative to the sled) or the dummy starts to be restraint by the seat belt (whatever occurs first), in series 2 & 3 the first happend at about 100 ms.

Phase 3: From end of Phase 2 until the end of the dummy loading at about 300 ms.

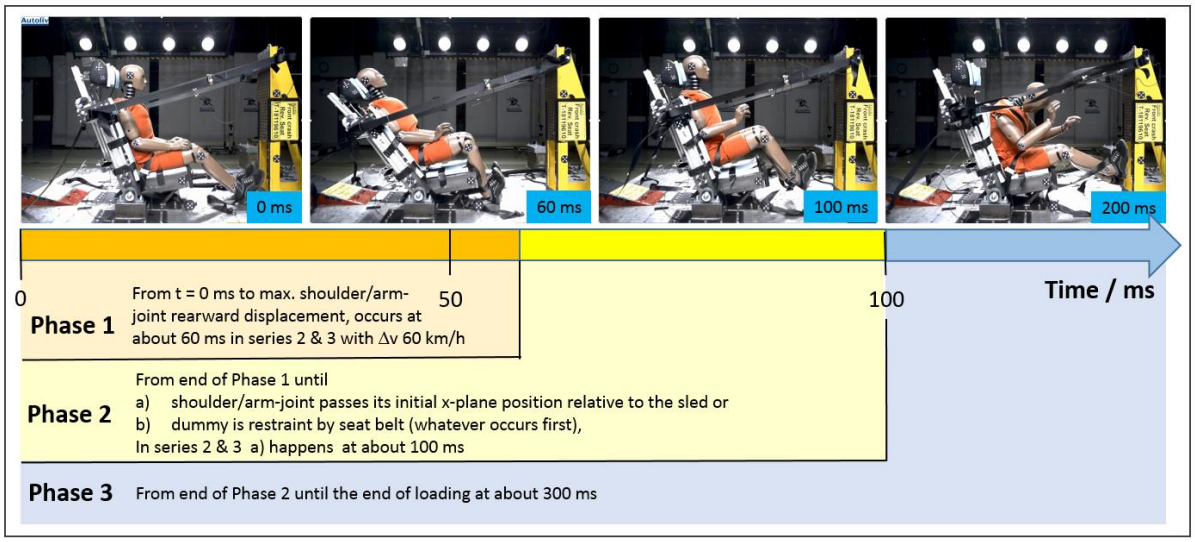

Figure 3. The three phases of the crash

In the further discussion we will focus on injury values for Phases 1 & 2 and will mention values of Phase 3 only when appropriate. Table 3 lists the tests with Δv 60 km/h of test series 2. It is seen that chest acceleration was close to its legal limit in all three tests, lumbar spine compression came up to of 80% of its IARV of 6.4 kN. All other values were uncritical. The influence of the belt system to the injury assessment values was small. The maximum of chest deflection was reached in Phase 3. It was dependent on the seat belt and ranged from 5 mm for the lap belt and 19 mm for the crisscross belt.

Table 3.
Test series 2, injury assessment values

0 < t ≤ 100 ms				Test-No.								
				Test 2.6 Lap Belt only			Seat integrated CrissCross Belt			Test 2.8 Seat integrated 3-point belt		
Region	Criterion		IARV	Value	% IARV	time /ms	Value	% IARV	time / ms	Value	% IARV	time / ms
Chest	3 ms clip	[g]	60	62	103	42 - 45	58	97	43 - 46	60	100	42 - 45
	Deflection	[mm]	42	6	15	37	12	28	64	7	16	39
	V*C	[m/s]	1	0,06	6	37	0,08	8	61	0,07	7	41
Lumbar spine	Tension $F_{L,ZT}$	[kN]	12,2	2,6	21	82	1,1	9	95	1,7	14	83
	Compression $\lvert F_{L,ZC} \rvert$	[kN]	6,4	4,8	76	26	5,1	79	26	5,3	83	27

The main focus of test series 3 was to investigate repeatability and to provide realiable data for the validation of a FE model. The setups of series 3 are listed in Table 4. A total of eight tests were performed with three different belt systems. As in test series 2, the differences between the belt systems in crash Phases 1 & 2 were not very pronounced and should not be discussed here further.

Table 4.
Test series 3, test setups

Test	ΔV	OLC	Belt System
3.1	60 km/h	32.0 g	Seat integrated 3-point belt with pretensioner fired at 0 ms
3.2	60 km/h	31.5 g	Seat integrated 3-point belt with pretensioner fired at 0 ms
3.3	60 km/h	31.4 g	no belt system
3.4	60 km/h	31.8 g	no belt system
3.5	60 km/h	31.6 g	Seat integrated 3-point belt
3.6	60 km/h	32.2 g	Seat integrated 3-point belt
3.7	60 km/h	31.6 g	Seat integrated 3-point belt
3.8	60 km/h	31.2 g	Seat integrated 3-point belt

The tests with the seat integrated 3 point belt were performed four times under the same condition. The time histories of chest acceleration and lumbar spine forces showed a good repeatability, cf. Figure 4. Deviations in lumbar spine forces were slightly bigger (especially close to the peaks at about 30 ms and 60 ms) and indicated a slight "complex" behavior, which is probably due to the friction between dummy and seat back. To further illustrate repeatability, in Figure 5 all IAV are listed. As along as the IAV were above 40% of its respective IARV, the relative standard deviations were below 5% except for the lumbar spine compression.

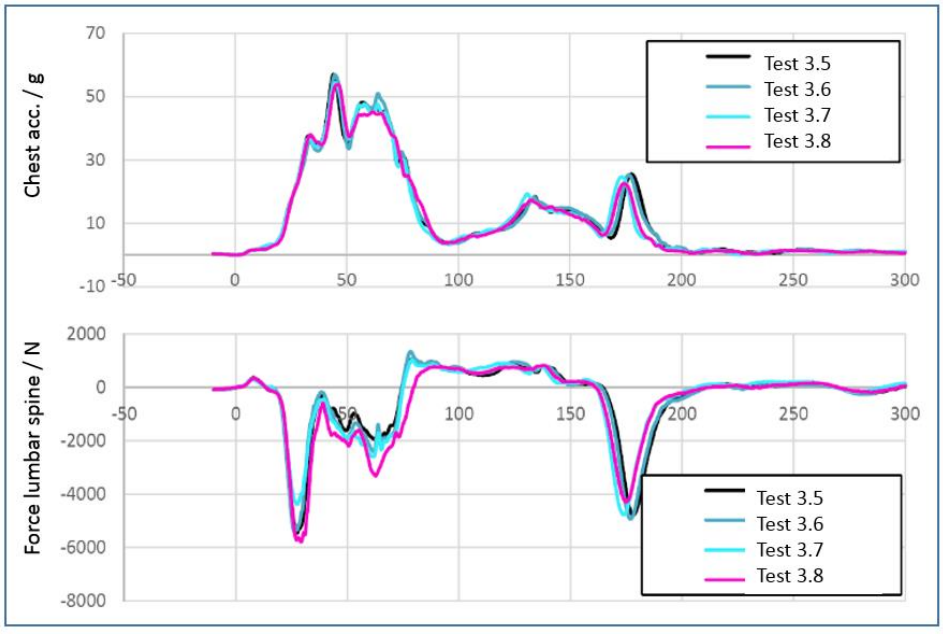

Figure 4. Time histories of chest acceleration and lumbar spine forces, 4 repeatability tests from series 3

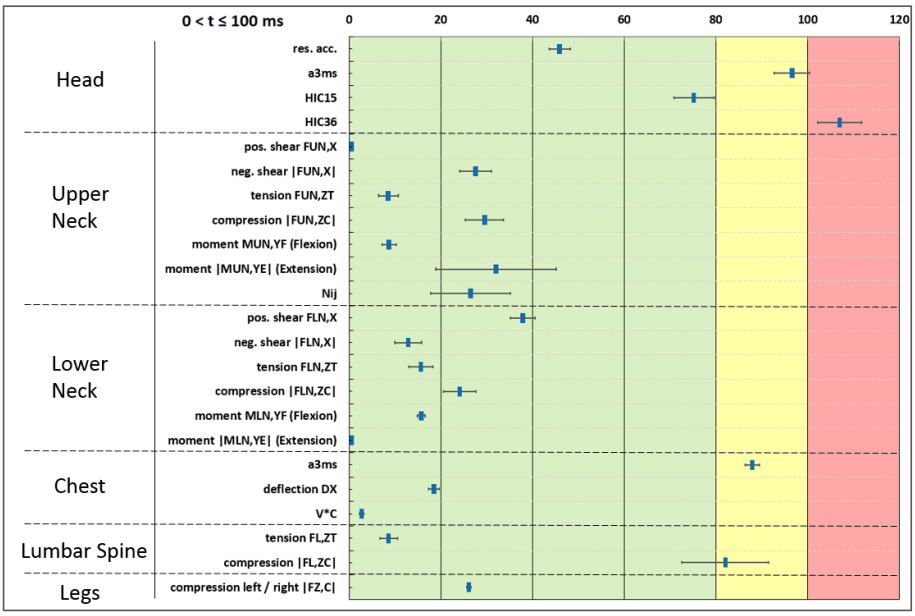

Figure 5. Test series 3, IAV in Phases 1 & 2, mean ± one standard deviation in % of IARV, four repeatability tests, the respective reference values are listed in the Appendix

DISCUSSION

One of our initial requirements to the generic test setup was, that the rearward displacement of the back rest was limited to avoid possible head contact of the occupant to the windscreen. This resulted in a relatively upright torso angle of the dummy during impact, even more upright than in the serial seat at Δv of 40 km/h, cf. Figure 6. Loading the occupant in this upright posture with such a stiff crash pulse requires further research and the dummy values can only be a rough indicator for possible injuries.

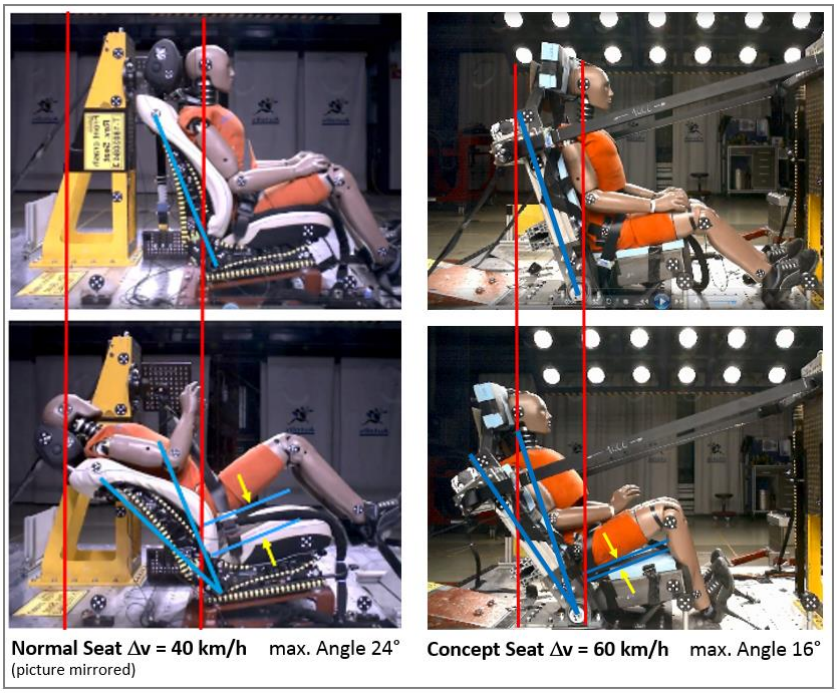

Figure 6. Comparison of the serial seat (left) and the generic (right) seat at maximum dummy rearward displacement

With the slightly stiffer crash pulse of test series 2, injury assessment values for chest acceleration and lumbar spine compression were close to its limits. With the slightly softer pulse of series 3, they reached about 80% to 90% of the limits, cf. Figure 5. It is also shown that injury values for the head were close to its respective reference values, but it again has to be mentioned that the dummy head is not validated for this impact direction. As we used an idealistic head rest without any initial gap between head and head rest, optimising the head rest for the rearward facing occupant may become a challenge. As shown in Figure 5, IAV for all other body regions were well below 40% of its limits. This is a good indicator that the generic test environment is suitable for testing, as test values are not masked by hard impacts of dummy parts to the seat. Chest deflection reached its maximum in Phase 3 and was dependent on the belt system. Values went up to 19 mm and were in good distance to its IARV. It is interesting to mention, that chest deflection in Phase 1 and 2 (0 ms to 100 ms) was mainly due to the inertia of the dummy ribcage, cf. Figure 6. The deflection went up to 7 mm and is the same for the tests with or without seat belt. A simple spring damper simulation with parameters for the thorax and ribcage from literature [15] yielded similar results.

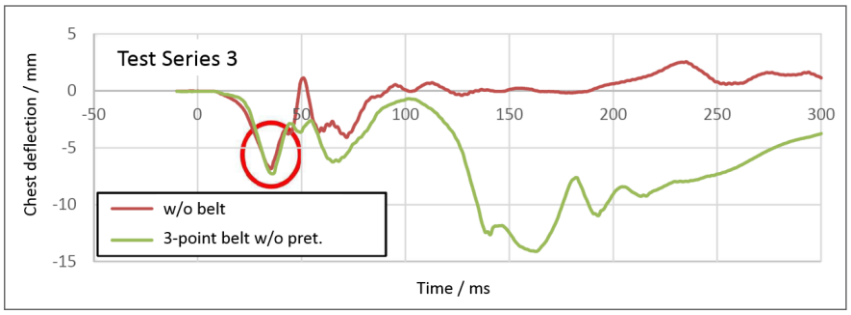

Figure 6. Test series 3, chest deflection with and without seat belt

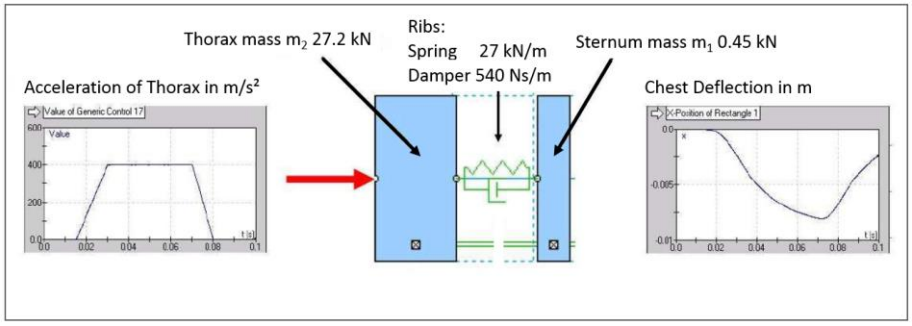

Figure 7. Spring damper model of dummy chest, parameters taken from [15]

As a next step in our investigation it is planned to build up and validate a finite element model of the generic test environment. In addition to the Hybrid III, response of a THOR 50th percentile male dummy and the THUMS human model should be investigated. Following steps using the FE models would include the study of the influence of back rest force to deflection characteristics both in impact as well in rebound. This should be optimised for dummy kinematics and loading. As described before, the influence of the seat belt system in Phases 1 & 2 is small. This is mainly due to a considerable amount of belt slack which is generated in the lap belt portion by initial dummy movement towards the seat back. A seat belt pretensioner at the anchor plate and buckle could eliminate this slack and the lap belt could properly restrain the dummy pelvis and prevent the whole dummy torso to move upwards during impact. This may also help to reduce lumbar spine compression. In the following step, the seat belt system restraint performance in Phase 3 may be optimised.

It has to be pointed out here that there is a need of reliable IARV for this loading direction and a common agreement on which dummy or human model to be used to evaluate the occupant protection.

As limitation of our study it should be mentioned that only full frontal loading directions were studied, dummy kinematics of oblique impact direction, simulating e.g. ±30° angled impacts to the barrier, were not included. As the head rest was not in focus of our investigation, the head was fixed with tape to the head rest without any gap in between.

CONCLUSION

A generic sled test and simulation environment for vehicle frontal impacts at a Δv of up to 60 km/h with occupants on rearward facing seats was developed and evaluated. The repeatability was investigated in four repeated tests, the relative standard deviations showed to be mostly below 5% of the repective injury assessment value and can be considered as good. The injury assessment value closest to its reference value showed to be chest acceleration, second was lumbar spine compression with about 80% of its limit. Peak chest deflection occurred in rebound and was below 20 mm.

REFERENCES

[1] SAE Standard J3016. 2016. "Taxonomy and Definitions for Terms Related to On-Road Motor Vehicle Automated Driving Systems;" SAE, 30.09.2016

[2] Sofia Jorlöv, Katarina Bohman, Annika Larsson. 2017. "Seating Positions and Activities in Highly Automated Cars – A Qualitative Study of Future Automated Driving Scenarios;" Proceedings IRCOBI Conference, Antwerp, Belgium

[3] Harald Zellmer, Nils Lubbe, Ulrich Sander. 2018. "Assessing the Injury Risk of Car Occupants on Rearward Facing Seats – An Analysis of GIDAS Cases;" 8th ESAR Conf. Hannover, Germany

[4] James W. Saunders III, Louis N. Molino, Shashi Kuppa, Felicia L. McKoy. 2003. "Performance of Seating Systems in a FMVSS No. 301 Rear Impact Crash Test"; Proceedings 18th ESV-Conference, Nagoya, Japan

[5] David C. Viano, Chantal S. Parenteau, Roger Burnett, Priya Prasad. 2017. "Occupant Responses in Conventional and ABTS Seats in High-Speed Rear Sled Tests;" Traffic Injury Prevention.

[6] Yuichi Kitagawa, Shigeki Hayashi, Katsunori Yamada, Mitsuaki Gotoh. 2017. "Occupant Kinematics in Simulated Autonomous Driving Vehicle Collisions: Influence of Seating Position, Direction and Angle;" Stapp Car Crash Journal, Vol. 61

[7] Xin Jin, Haibin Hou, Ming Shen, Hequan Wu, King H. Yang. 2018. "Occupant Kinematics and Biomechanics with Rotatable Seat in Autonomous Vehicle Collision: A Preliminary Concept and Strategy"; Proceedings IRCOBI Conference, Athens, Greece

[8] National Highway Traffic Safety Administration. Federal Motor Vehicle Safety Standard No. 208. "Occupant Crash Protection"; 49 CFR 571.208, 2013

[9] ECE-Regulation No. 137-01: "Uniform Provisions Concerning the Approval of Passenger Cars in the Event of a Frontal Collision with Focus on the Restraint System;" Amendment Level 01 Supplement 1, Feb. 2017

[10] European Aviation Safety Agency (EASA): "Certification Specification and Acceptable Means of Compliance for Large Rotorcraft"; Certification Specification 29, Amendment 4, 2016

[11] General Motors (GM): "Occupant Performance Evaluation Consideration Book (Blue book);" Document #SRC-1000G, USA. Version 3, Revision 0, May 1998

[12] National Highway Traffic Safety Administration, Federal Motor Vehicle Safety Standard No. 202a: "Head Restraints"; 49 CFR 571.202a, 2009

[13] L. Kübler, S. Gargallo, K. Elsäßer. 2009. "Frontal crash pulse assessment with application to occupant safety;" ATZ worldwide Volume 111, Issue 6

[14] Markus H. Muser, Felix H. Walz, Harald Zellmer. 2000 "Biomechanical Significance of the Rebound Phase in Low Speed Rear End Impacts;" Proc. IRCOBI Conf., Montpellier, France

[15] Jeff Crandall, Zhiquing Cheng, W. D. Pilkey. 2000. "Limiting performance of seat belt systems for the prevention of thoracic injuries;" Proceedings of the Institution of Mechanical Engineers Part D, Journal of Automobile Engineering 214(2):127-139

[16] Harold J. Mertz, Annette L. Irwin, Priya Prasad. 2016. "Biomechanical and scaling basis for frontal and side impact injury assessment reference values;" Stapp Car Crash Journal, Vol. 60

APPENDIX

Injury assessment reference values (IARV) used for the rating of repeatability

	Injury Criterion	IARV	Source	
Head	res. acc.	180 g	Mertz 2016	[16]
	a3ms	80 g	ECE-R 137	[9]
	HIC15	700	FMVSS 208	[8]
	HIC36	1000	ECE-R 137	[9]
Upper Neck	pos. shear FUN,X	3.1 kN	ECE-R 137	[9]
	neg. shear |FUN,X|	3.1 kN	ECE-R 137	[9]
	tension FUN,ZT	4.17 kN	ECE-R 137	[9]
	compression |FUN,ZC|	4.0 kN	FMVSS 208	[8]
	moment MUN,YF (Flexion)	190 Nm	Mertz 2016	[16]
	moment |MUN,YE| (Extension)	57 Nm	ECE-R 137	[9]
	Nij	1	FMVSS 208	[8]
Lower Neck	pos. shear FLN,X	3.1 kN	Mertz 2016	[16]
	neg. shear |FLN,X|	3.1 kN	Mertz 2016	[16]
	tension FLN,ZT	4.17 kN	Mertz 2016	[16]
	compression |FLN,ZC|	4.0 kN	Mertz 2016	[16]
	moment MLN,YF (Flexion)	380 Nm	Mertz 2016	[16]
	moment |MLN,YE| (Extension)	194 Nm	Mertz 2016	[16]
Chest	a3ms	60 g	FMVSS 208	[8]
	deflection DX	42 mm	ECE-R 137	[9]
	V*C	1 m/s	ECE-R 137	[9]
Lumbar Spine	tension FL,ZT	12.2 kN	GM Blue Book 1998	[11]
	compression |FL,ZC|	6.4 kN	GM Blue Book 1998	[11]
Legs	compression left / right |FZ,C|	9.07 kN	ECE-R 137	[9]

INJURY RISK-BASED CRITERIA FOR THE APPLICATION OF ADAPTIVE LOGIC TO ADAS SYSTEMS

Dario Vangi
Antonio Virga
Michelangelo-Santo Gulino
Università degli Studi di Firenze, Department of Industrial Engineering, Via di Santa Marta 3, Florence, 50139 Italy

Paper Number 19-0204

ABSTRACT

Performance improvement of advanced driver assistance systems (ADAS) yields two major benefits: an increasingly fast progress towards autonomous driving and a simultaneous advance in vehicle safety. The high safety level provided by ADAS result primarily from the possibility to avoid possible impacts in correspondence of critical road scenarios. Nevertheless, specific obstacles (e.g., stationary vehicles, buildings) can interpose between the opponent vehicles and the working field of the sensors, weakening their functions: in these particular conditions, the impact can be inevitable (inevitable collision state – ICS). The systems currently available on the market are not capable to properly handle an ICS, because its occurrence is not conceived.

In the present work intervention criteria for ADAS are introduced which are based on the vehicle occupants' injury risk (IR), particularly useful in case of ICS. In a critical road scenario, the ADAS must first avoid the impact with maximum margin (maximum clearance between vehicles) and, in case of ICS, minimize impact severity and IR. Referring to a system capable of intervening on braking and steering, the ADAS must monitor the surrounding and act on the degrees of freedom adapting to the possible evolution of the scenario, following an adaptive logic. The sequence of optimal interventions based on such adaptive logic tends toward the best possible outcome.

The context (model-in-the-loop) of the adaptive intervention employing the proposed criteria is first introduced, proposing a solution for testing its actual functioning (software-in-the-loop) with a view to its physical implementation (hardware-in-the-loop). The major criticality of the approach consists in the impact phase reconstruction, because IR is also a function of post-impact parameters (e.g., the velocity change ΔV experienced by the vehicle in the crash).

To highlight the potential benefits offered by an adaptive ADAS and to monitor its behavior, a software has been developed based on the software-in-the-loop solution introduced. The best intervention selection is based on a database filled with results of simulations: the outcomes associated to each braking and steering intervention are summarized in the database, for many critical scenarios; the ADAS retrieves information from the database and, through IR-based criteria, selects the most favorable action. Testing the logic functioning in correspondence of three critical road scenarios in which two vehicles are involved, at each instant it is observed that the developed intervention logic aims at creating eccentrical impact configurations, associated to low ΔV; the low values of resulting impact severity demonstrate how the intervention criteria based on IR represent an important tool for the development of increasingly performing ADAS devices.

INTRODUCTION

The Vision Zero program of the European Community [1] actually represents an important reference for the advance of the automotive industry: the objective is the development of vehicles capable of assuring an increasing level of safety, allowing to reduce road fatalities to zero within 2050. Current design is based on the increase of vehicle's passive safety (e.g., its crashworthiness [2]) and, to a greater extent, in the performance of its active safety equipment. In fact, advanced driver assistance systems (ADAS) allow to primarily reduce the probability for an impact between vehicles to occur [3], by functions as the autonomous emergency braking (AEB [4]). In recent vehicles the integration between many ADAS functions is frequently observed, aimed at providing a higher safety level as a consequence of the higher degree of automation achieved: in the case autonomous vehicles are referred to, this complex ensemble of functions is identified as automated driving system (ADS [5]).

SAE standard [6] expresses the automation level of a vehicle, based on the tasks performed by ADAS functions it is constituted of. While SAE 4-5 prototypes exist, the vehicles used on the road with highest level of automation belong to SAE 3: in case of danger, the driver must be ready to take over control in place of the ADS, which however can manage the entire driving process (handover) [7]. The ADS can intervene primarily on two degrees of freedom of the vehicle:

- longitudinal acceleration – the intervention results in the change of the vehicle running speed; the most typical example of intervention on the vehicle longitudinal acceleration consists in the AEB activation, by which the vehicle decelerates employing the maximum available adherence (100%);
- transversal acceleration – the system action aims at modifying the vehicle degree of steering: systems as the lane keeping assist (LKA [8]) or the more recent autonomous emergency steering system (AESS [9]) allow to respectively correct the vehicle trajectory in case of deviation from the lane center and to avoid impacts with obstacles on the carriageway.

The simultaneous action on the two accelerations are mainly limited by the Kamm circle [10], or analogously by the vehicle limits of longitudinal and transversal adherence (friction ellipse [11]). Due to issues linked to their ethical acceptability [12], the interventions aimed at increasing the speed of the vehicle are usually excluded.

Currently, ADAS devices contribute to fatality reduction insisting on three main factors: a) the number of collisions between vehicles, b) the impact severity and c) the injury entity [13]. First, the number of collisions is reduced by the intervention on steering and braking to avoid the collision, by ADAS devices which are momentarily developed to intervene on a straight road; nevertheless, collisions in correspondence of intersections often occur, are much more complex and result in more critical scenarios in respect to straight roads. In these circumstances, the ADAS cannot prevent many accidents from occurring, but it can intervene to minimize the impact severity. An ADAS intervention aimed at reducing the closing velocity at collision V_r is intuitively the best option to minimize the impact severity; however, V_r only partially affects the severity and injury associated to the collision, which mainly depend on the acceleration experienced by the occupants [14]. An alternative parameter to the occupants' acceleration is the velocity change ΔV sustained by the vehicle in the impact: ΔV associated to real accidents can be more easily retrieved from in-depth accident databases, and is strongly correlated to injury risk (IR) [15].

The ADAS devices currently available on the market perform no evaluation on severity of an impending impact; therefore, they do not allow for road safety optimization acting on all the three factors cited above. Inevitable collision states (ICS [16]) correspond to conditions in which any action by the ADAS or the driver does not allow to avoid the impact, as a consequence of low time to collision (TTC). Different reasons contribute in making ICS a reality in the current road environment. First, a circulating fleet with average age of 11 years is observed on European roads [17], with co-existence of vehicles with different SAE levels of automation: in such context, communication between vehicles (V2V [18]) will be limited also in the near future, and recognition of the opponents will totally depend on the sensors efficiency. In contrast, obstacles such as stationary vehicles or buildings concur in limiting the effectiveness of ADAS sensors, in terms of depth of field [19]: this can result in a retarded identification of approaching vehicles, with consequent TTC not compatible with collision evitability.

The present work discusses an ADAS activation logic based on intervention criteria which minimize IR for the occupants. Specifically, a system constituted by autonomous steering and braking functions is referred to, which are capable of jointly intervening to avoid the impact as a priority and, in case of ICS, to minimize IR. The choice of optimal maneuvers is adaptively carried out, i.e., the choice is evaluated at each time step monitoring the environment by sensors. The choice of optimal maneuvers varies with the external scenario, considering for instance the possible maneuvers of the opponent vehicle or additional changes in the road environment (e.g., due to vulnerable road users). In the manuscript the main technical solutions for the application of IR-based criteria to ADAS are highlighted, showing the main implications from the software and hardware point of view resulting from such integration. Through a

simulation program specifically developed, the behavior of an ADAS implementing these criteria is exemplified in some cases of ICS between vehicles.

MATERIALS AND METHODS

Referring to well-established practices in the design of ADAS devices [20], in the present Section the elements necessary for the implementation of IR-based criteria are evidenced: first, the context of ADAS intervention is defined (model-in-the-loop); then a technical solution for the simulation of such intervention is proposed (software-in-the-loop), with a view to its eventual physical implementation (hardware-in-the-loop). For convenience, in the following the term "adaptive ADAS" is employed to indicate a device capable of adapting in real time to changes in the external conditions, employing IR-based criteria to intervene by braking and steering.

Model-in-the-loop definition

Model-in-the-loop (MiL) is a representation of the context in which the ADAS operates, fundamental to efficiently establish the ADAS functional requirements in software and hardware terms. ADAS interfaces with the external environment by sensors, scanning the key elements by different technologies (typically LIDAR and RADAR [21]); the most recent vehicles are equipped with scanning systems with an aperture angle higher than 300°, with more than 170° in the sole portion in front of the vehicle [19]. If combined with an appropriate depth of field (field of view), an angle of 170° allows to identify all road criticalities.

Detection of a critical scenario mainly depends on the algorithm employed by the ADAS manufacturer. Generally the TTC, which tends to non-linearly shorten while the vehicle approaches [22], is an efficient danger indicator of the specific road situation: for instance, the decision logic for the intervention by forward collision warning (FCW) and AEB is generally based on TTC evaluation. The ADAS activates its functions only at specific values of TTC, and in particular when the reaction time of the driver is no more compatible with the impact avoidance [10]. The key elements for the correct functioning of an adaptive ADAS (functional requirements) can be summarized by the scheme in Fig. 1.

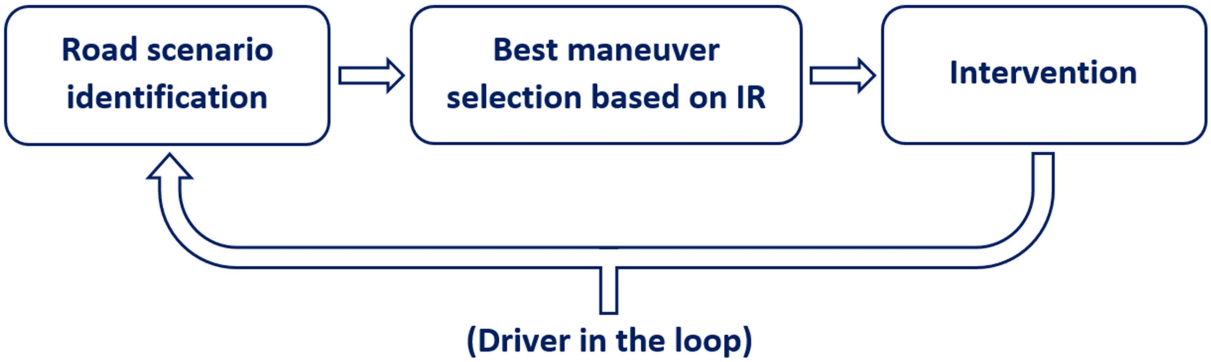

Fig. 1. MiL functioning scheme of an adaptive ADAS.

The system, through sensors, must define the road environment identifying the boundary conditions. Let us consider a planar visualization of the road environment as the one in Fig. 2, in which y corresponds to the longitudinal direction of motion for vehicle A (on which the ADAS is implemented) and x its perpendicular. At a specific TTC, the main parameters of the surrounding environment which can be extracted by sensors attain coordinates x,y and the heading h of an opponent vehicle B, as well as the components of B velocity along the axis (V_x e V_y); these velocities are to be intended in relative terms: since vehicle A velocity is known for the ADAS system, the absolute velocity of vehicle B can be directly obtained. Information regarding the dimensions can be employed to establish the type of vehicle, its class and eventually to derive a plausible mass [23].

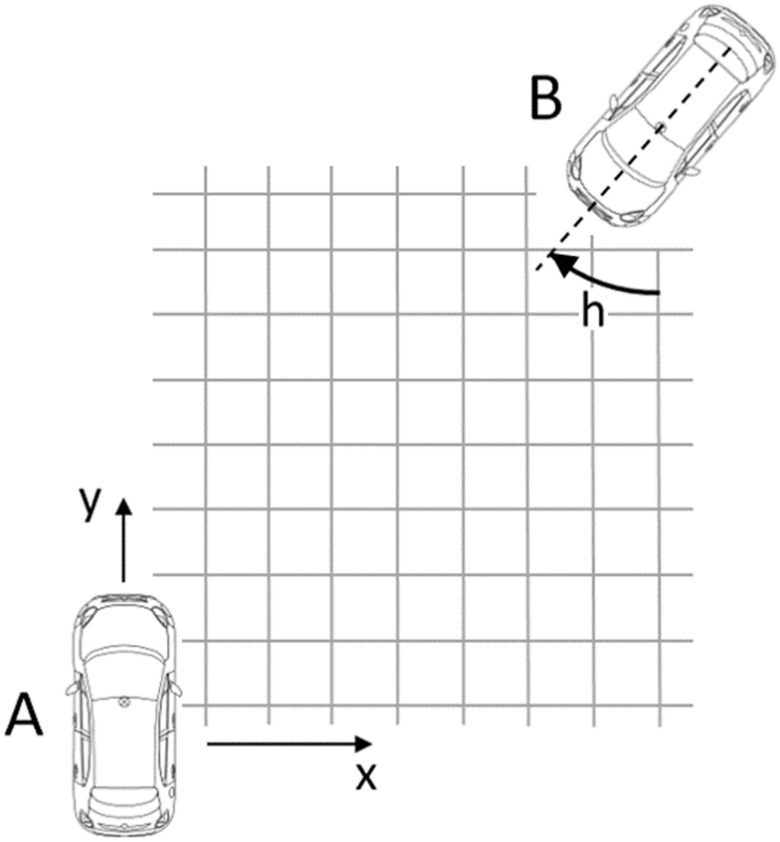

Fig. 2. Planar scheme of the road environment: the ADAS sensors of vehicle A allow to determine *x,y* coordinates, heading *h* and velocity components of the generical opponent vehicle B.

The maneuver to undertake must be selected as a function of predefined criteria: in such context, activation must primarily avoid the collision, with a value of clearance (minimum distance reached between the vehicles during their free motion) as high as possible; in case this is not possible (ICS), the system must minimize IR for the occupants. The autonomous application of the maneuver chosen in terms of braking and steering is carried out by the electro-mechanical components of the vehicle, by systems as brake-by-wire or steer-by-wire [24]. Once these phases have been accomplished, the ADAS scans once more the surrounding to monitor its evolution and adapt consequently, considering also the eventual actions undertaken by the drivers of both vehicles (driver-in-the-loop [25]). If the time step between two scans is sufficiently low (e.g., 0.1 s) changes to the surrounding are already comprehensive of drivers' intervention: in this case, it is not necessary to foresee the scenario evolution making use of complex driver models [26].

Software-in-the-loop solution

Once defined the functional requirements of the adaptive ADAS by MiL, a software-in-the-loop (SiL) is necessary to transpose them in a virtual environment and test the ADAS functioning. The SiL must allow to simulate the ADAS functioning according to the concepts reported in the V-model [27] of Fig. 3. First, the ADAS derives information regarding the environment by sensors, thus defining the scenario by position, velocity and dimensions of the vehicles. Then, for the specific scenario the ADAS must be capable of simulating each possible intervention, deriving the related outcome and identifying the best maneuver (maximum clearance or minimum IR). The best maneuver is subsequently undertaken and the vehicles are subject to a motion which is dependent on the time step selected for the analysis, as well as the degree of braking and steering for each vehicle; the response of braking and steering system is not instantaneous, and a setting time to the desired value should be accounted for: for instance, for tyre steering actuators, typical values are 45°/s [28]. The iterative cycle starts once more, with the identification by sensors of new position and velocity of the opponent.

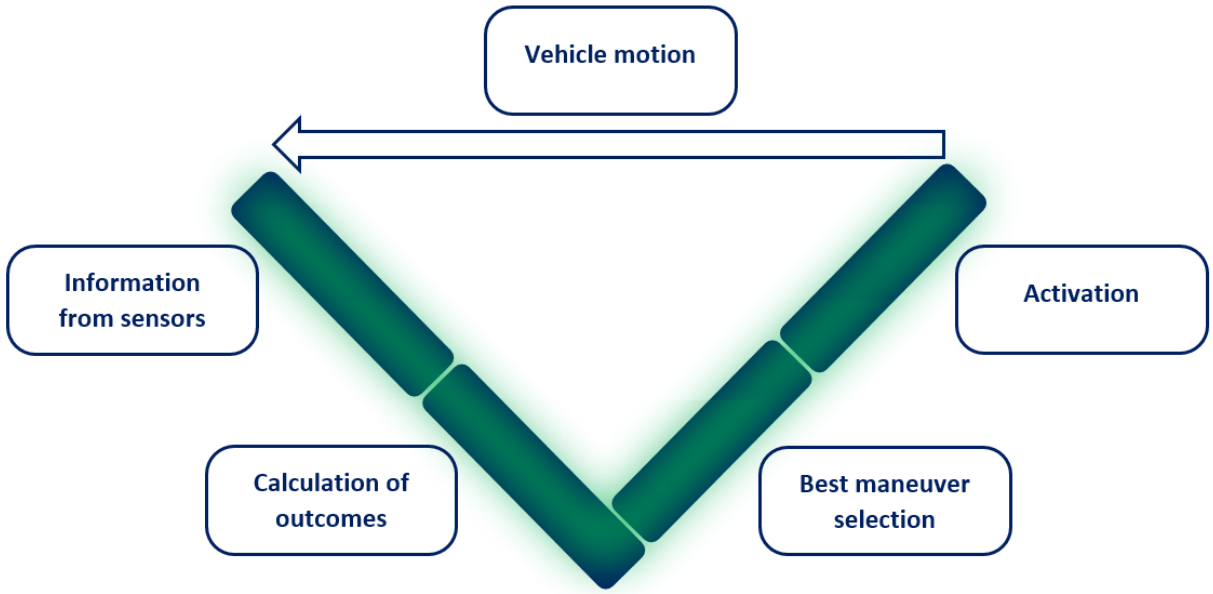

Fig. 3. SiL functioning scheme of an adaptive ADAS.

For calculation of outcomes associated to each maneuver, starting from a specific scenario, it is necessary to simulate each possible braking and steering intervention. The simulation of kinematics (free motion of vehicles) is primarily significant: if no impact between vehicles occurs, the system must identify the resulting clearance. If the maneuver results in an impact, IR derivation is obtained simulating also the impact phase: as visible in Fig. 4, IR depends in fact on the impact type, on occupant's position and on ΔV [29], which is a typical post-impact parameter; the logistic regression curves are referred to a values of Maximum Abbreviated Injury Scale equal to or higher than 3 (MAIS 3+). Even if approximated methods [30] exist for the calculation of impact severity starting from sole pre-impact parameters (as V_r in rear-end collisions [31]), simulation of the impact phase remains the most accurate solution for a correct estimate of ΔV.

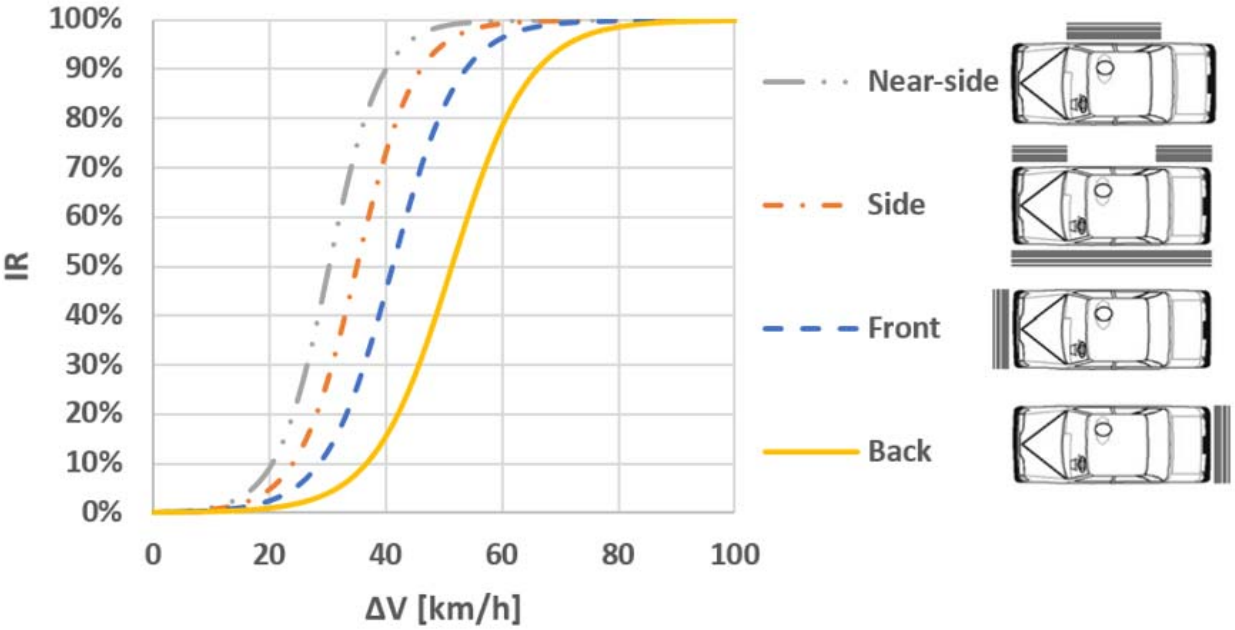

Fig. 4. IR curves as a function of ΔV, impact area and position of the occupant (modified from [29]).

The impact phase between vehicles can be simulated through different calculation methodologies, i.e., through analytical models, finite element method (FEM), multi-body systems (MBS) and reduced order dynamic models. Analytical methods are typically based on impulse-momentum models and allow to solve the problem analytically at the cost of strong approximations, mainly deriving from the choice of a plane and a center of impact [32]. FEM and

MBS are employed in the accurate reconstruction of impacts, for instance in vehicle crashworthiness analysis [33]: calculation time for the single impact configuration between vehicles is in this case high, typically variable between an hour and a day with modern calculators. In such a context, the use of special-purpose RODM is justified, featuring intermediate characteristics of calculation time and accuracy in respect to analytical methods and FEM/MBS [34]. For the simulation of the event, vehicles of equal mass can be considered; through appropriate corrective coefficients, it is possible to calculate the outcomes of impacts between vehicles of different categories (e.g., sport-utility vehicles, vans, etc.).

Once the results of simulations for the possible maneuvers are available for the specific critical scenario, the activation logic is capable of associating a specific value of clearance (collision avoided) or IR (collision not avoided) to each braking and steering intervention. Such capability is summarized in an intelligible way by the map of outcomes reported in Fig. 5, whose analysis allow the ADAS to select the best intervention in the specific critical scenario. In case the the clearance is defined by negative values of IR, the problem of finding the best intervention simplifies to the identification of minimum IR. At a graphical level, if in the map of Fig. 5 green colored areas are present (impact evitability), the system will activate preferring interventions corresponding to dark green; in case only red colored areas are present (ICS), the system will intervene selecting light red areas (low IR).

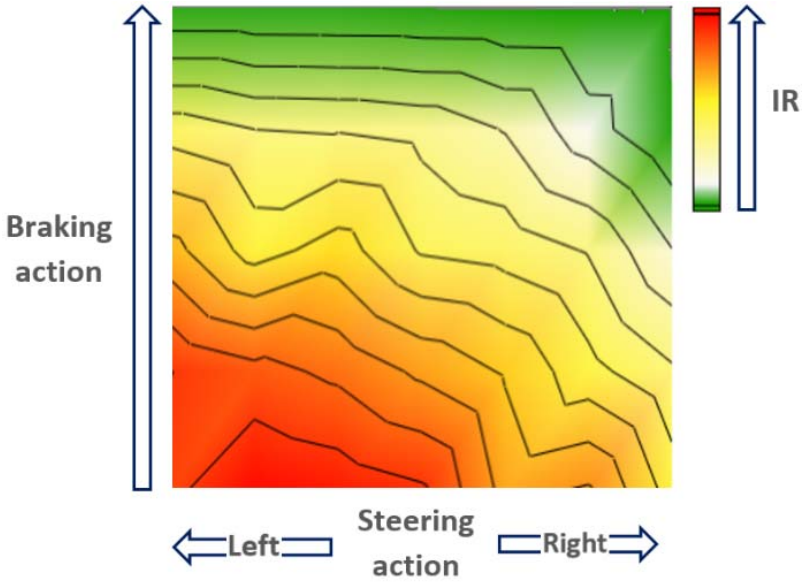

Fig. 5. Map of outcomes for a generic critical scenario, which summarizes the values of IR associated to each braking and steering intervention by an adaptive ADAS.

Hardware-in-the-loop proposals

SiL functions can be converted in two different forms of hardware-in-the-loop (HiL), as a function of the final use: an instrument to evaluate different ADAS logics (e.g., AEB, AESS or their combination) or an actual ADAS to be implemented on-board the vehicle. In the first case, in which the objective is to compare the performances of different ADAS functions by simulation, calculation time has low relevance; on the other hand, in the second case the adaptive ADAS must determine the outcomes associated to all possible interventions in a time which is compatible with the scanning time ofthe scenario. This requirement cannot currently be satisfied even employing RODM: the impact phase reconstruction process is highly time consuming, while the scanning of the scenario occurs in a time close to 0.1 s. The time for scanning mainly depends from the type of sensors and how they are mutually integrated (sensor fusion [35]). For such reason, in the view of an on-board implementation, it can be convenient to refer to a database filled with the results of simulations, from which the adaptive ADAS can easily extract the best maneuver associated to a critical scenario. In this case, the time required to identify the best maneuver corresponds to the sole time of access to the database (some milliseconds).

The functioning of the hardware system which includes the IR-based criteria can be outlined as in Fig. 6. In a specific instant, the ADAS determines by sensors the position and heading of the opponent vehicle, its velocity and its dimensions. The ADAS identifies the outcomes corresponding to different possible maneuvers, calculating IR for the occupants (or retrieving it from the database) and identifying the best intervention. By electronic systems, the information is converted in a steering angle and a braking level to be applied. Then, the system reiterates the process:

the position of the opponent and its velocity identified by sensors differ from the ones at the previous time step, defining thus a new critical scenario that the system should optimally handle.

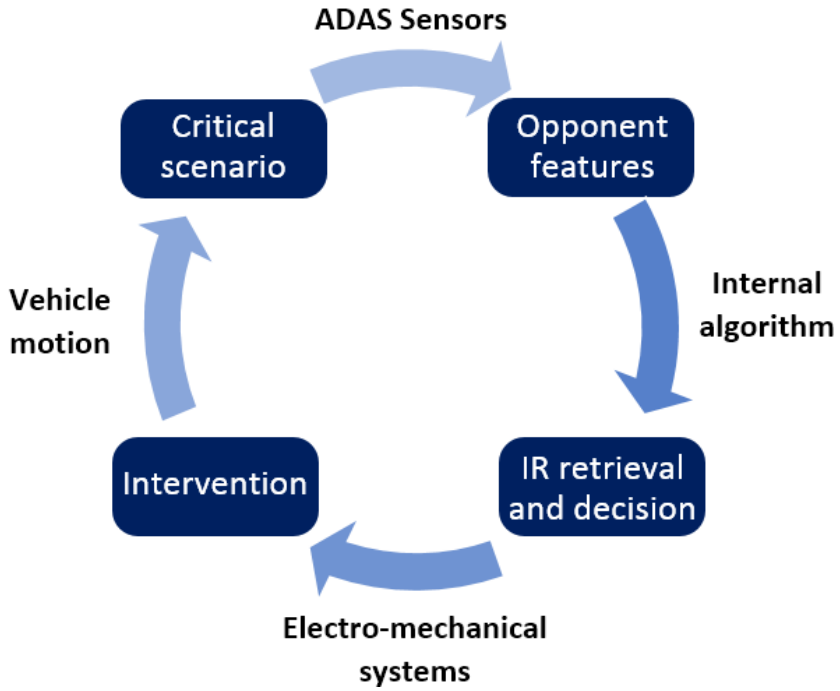

Fig. 6. HiL functioning scheme of an adaptive ADAS.

RESULTS

To highlight the potential of an adaptive logic of intervention in terms of road safety enhancement, the development of an appropriate virtual environment for the SiL implementation is required, allowing to simulate the process in Fig. 3. As reported in the previous Section, the fundamental part of such cycle is the outcome retrieval associated to the single activation: with a view to an HiL implementation on-board the vehicle, by a RODM software [36] a database including the outcomes associated to each braking and steering maneuver has been compiled, for many critical scenarios. The RODM simulation software, implemented in a LabVIEW™ environment, is based on the discretization of the sole vehicle perimeter through 2D beam elements, with constitutive equations similar to the ones employed in FEM models. For an in-depth description about the functioning of the RODM, refer to a previous work [37].

To comprehend which scenarios are included the database, let us refer to Fig. 2: hypothesizing the position of vehicle A always coincident with the origin of the axes, in Tab. 1 is reported the discretization of velocity for A and B, position and heading of B, intervention on steering and braking of A. The maximum distance between the vehicles is considered equal to 14 m: considering vehicles moving at 50 km/h, a maximum TTC equal to 1.0 s can be deduced for the scenarios making up the database; the number of simulated scenarios totals more than 50,000. The model for vehicle A and B is the same: the vehicle belongs to the C segment, with a length equal to 4.2 m, width 1.8 m, wheelbase 3.5 m and mass 1300 kg. The road-tire coefficient of friction is assumed equal to 0.8, and a complete braking corresponds thus to a deceleration of 8 m/s^2. Calculation time for the single simulation with the RODM software is about 1.5 s. For the single simulation, the velocity and the heading of the opponent vehicle are considered constant.

Tab. 1. Parameters which define the space of critical scenarios and interventions, making up the database.

Parameter	Vehicle	Minimum Value	Maximum Value	Step
X coordinate (m)	B	0	14	2
Y coordinate (m)	B	0	14	2
Longitudinal velocity (km/h)	A	10	70	5
Longitudinal velocity (km/h)	B	10	70	5
Heading (°)	B	70	110	10
Steering angle (°)	A	-9 (left)	+9 (right)	3
Braking level (%)	A	0	100	25

To monitor the behavior of the adaptive ADAS and the actual employment of the criteria, three case studies regarding critical scenarios in correspondence of intersections are referred to: for each case study, the parameters related to the velocity of the two vehicles and to the position and heading of the opponent are summarized in Tab. 2; from accident database analysis, it is estimated that those case study represent approximately 30% of the real accident scenarios. In the three case studies, the scenario evolves due to the intervention of the driver in vehicle B. Vehicle B initially moves perpendicularly to A in all three cases; vehicle A heading is null by definition. It is assumed that the input provided by the ADAS reaches instantaneously the electro-mechanical component. The time elapsed between two successive scans of the scenario by sensors is assumed equal to 0.1 s.

Tab. 2. Parameters which define the analyzed case studies.

Parameter	Case study 1		Case study 2		Case study 3	
	Vehicle A	Vehicle B	Vehicle A	Vehicle B	Vehicle A	Vehicle B
X coordinate (m)	0	13	0	10	0	12
Y coordinate (m)	0	11	0	8	0	9
Longitudinal velocity (km/h)	50	50	50	50	50	50
Heading (°)	0	90	0	90	0	90

Case study 1

It is considered that vehicle B driver does not notice the presence of A while performing a left steering maneuver. In 0.2 s, the steering action on vehicle B tires changes from 0° to -9° (adherence limit). The history of steering and braking actions for A according to IR-based criteria is reported in Fig. 7. Between 0.1 s and 0.3 s the outcome map indicates that there is the possibility to avoid the impact by left steering, and the system acts accordingly. Because of the motion of B towards A, between 0.3 s and 0.4 s the ADAS detects that the scenario corresponds to an ICS: the system adapts with a 100% braking, to reduce the collision velocity. In the subsequent instants, the system determines that a 100% braking action would imply an impact at lower velocity, but with low eccentricity: in this case high ΔV would result, because most of the energy would be converted in translation rather than rotation. The brake is thus released to create an eccentrical impact configuration, moving the impact point towards the rear extremity of vehicle A.

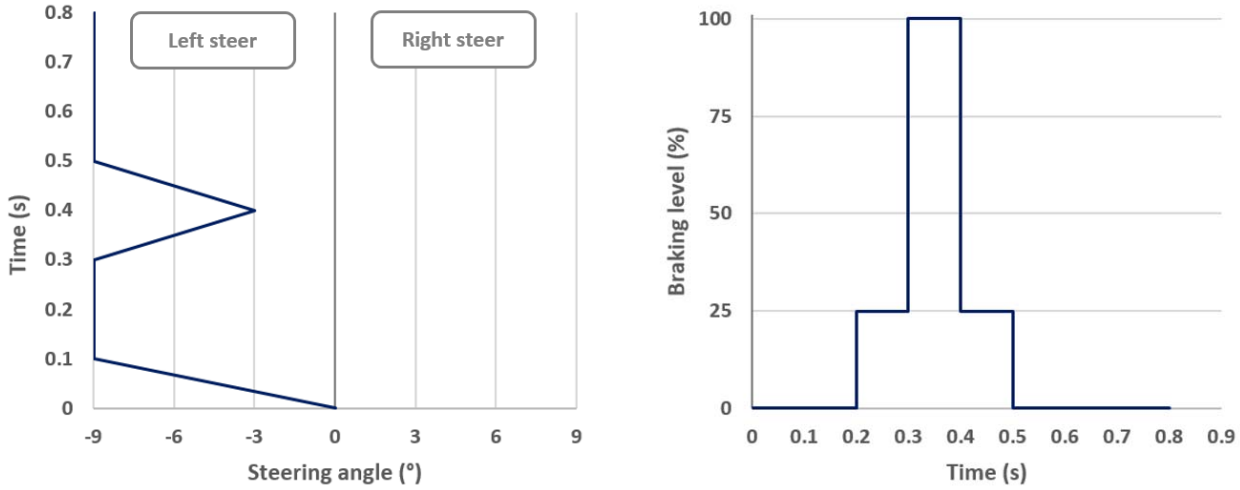

Fig. 7. Case study 1: history of the adaptive ADAS actions on braking and steering.

Case study 2

It is assumed that vehicle B applies a right steering evasive maneuver, according to the typical behavior of a driver [38]; in a time interval of 0.2 s, the steering action on vehicle B tires changes from 0° to +9° (adherence limit). The impact is inevitable from the beginning and the system, as a priority, tries to increase the impact eccentricity by steering and braking. Then (from 0.2 s to 0.4 s), the ADAS detects that vehicle B tries to avoid the collision, and that the release of brake creates an eccentrical impact configuration. Lastly (from 0.4 s to 0.6 s), the system acts with 100% brake to reduce V_r.

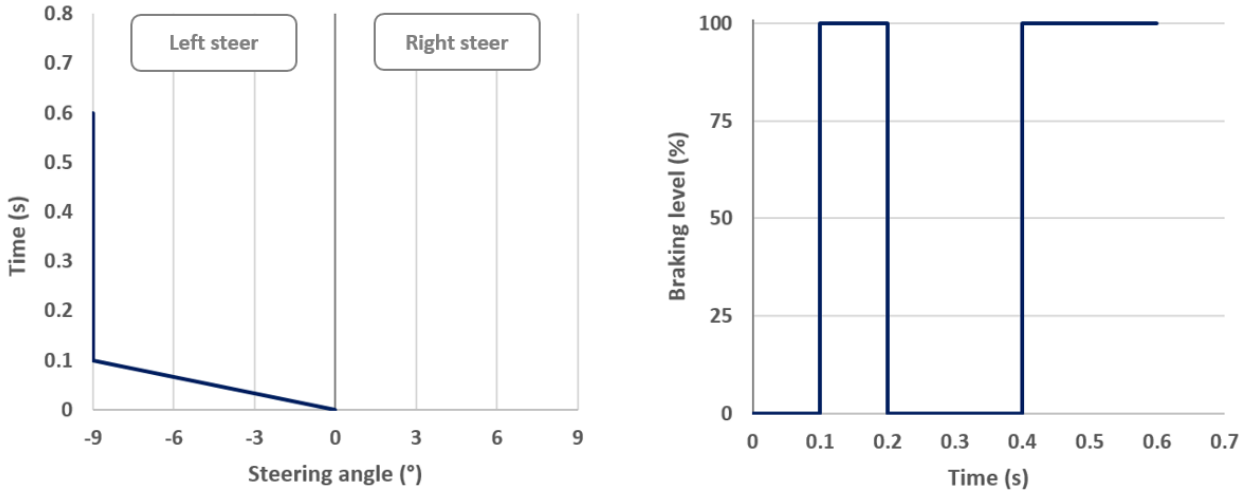

Fig. 8. Case study 2: history of the adaptive ADAS actions on braking and steering.

Case study 3

It is assumed that vehicle B brakes as soon as vehicle A has been identified: in 0.2 s, the braking action of vehicle B changes from 0% to 75% (typical braking action of a driver, with deceleration equal to 6 m/s^2 [38]). The scenario corresponds from the beginning to an ICS, and the system, as a priority, tries to get around vehicle B by left steering (from 0.1 s to 0-4 s in Fig. 9); the system reduces V_r by a 100% braking action only when vehicle A position is compatible with an eccentrical impact (from 0.4s to 0.7 s).

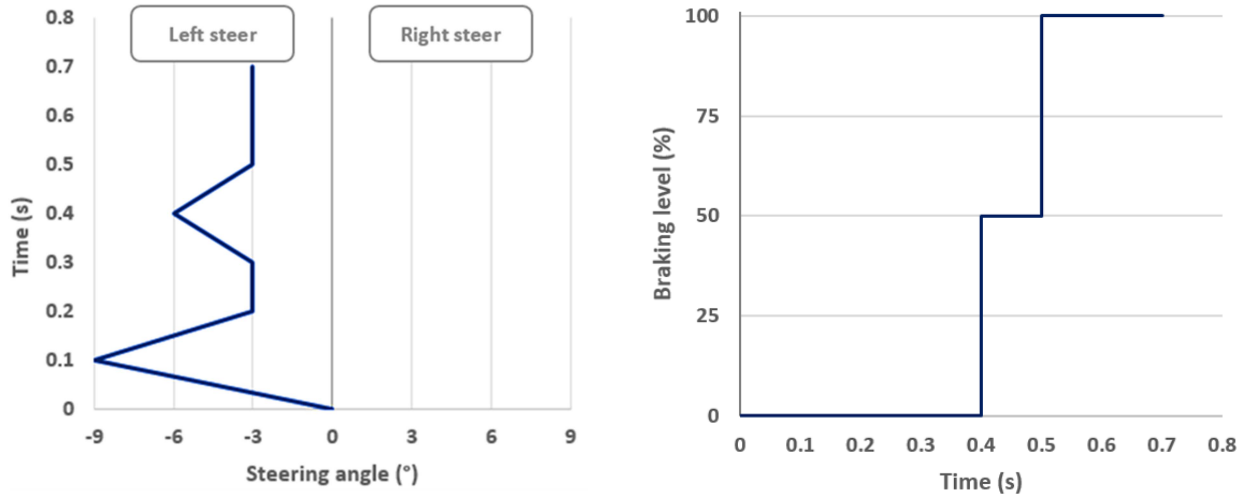

Fig. 9. Case study 3: history of the adaptive ADAS actions on braking and steering.

DISCUSSION

In Fig. 10 the impact configurations for the three case studies are reported, in case the system does not intervene (a), intervenes by 100% braking (b), intervenes by adaptive logic (c). In case study 1-2 the adaptive logic leads to impact configurations similar to the ones associated to the lack of intervention. The use of the adaptive logic implies the involvement of the compartment in the impact: employing the convention in Fig. 4, assuming occupants' presence on the right side of the vehicle, the impact belongs to the "near-side" type with highest potential severity. In reality,

activation of the system converges toward impact configuration with higher eccentricity (lower ΔV) in respect to a 100% braking action. In case study 3, besides a higher ΔV, a different type of impact will result, passing from "side" in case of adaptive logic to "near-side" in case of 100% braking action. Overall, the combined intervention on braking and steering according to IR-based criteria efficiently contributes to the impact severity decrease.

	(a) No intervention	**(b) 100% braking**	**(c) Adaptive logic**
Case study 1	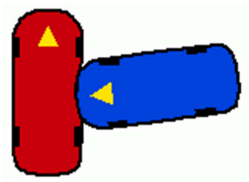	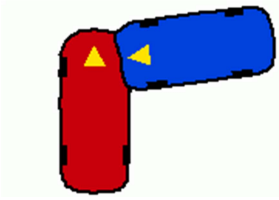	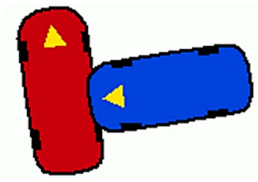
Case study 2	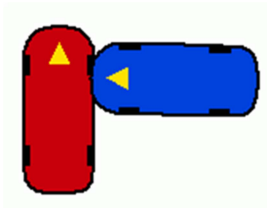	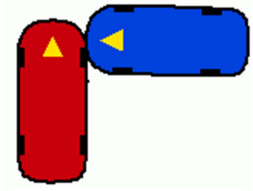	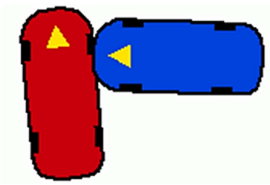
Case study 3	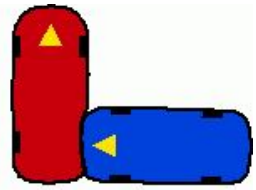	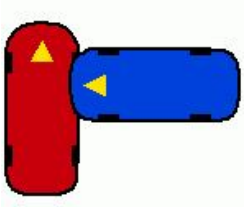	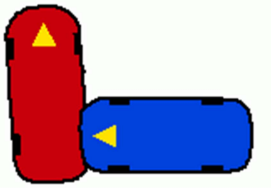

Fig. 10. Impact configurations for case study 1-3, as a function of the intervention logic employed.

Information related to impact configuration can be analogously expressed by means of the crash-momentum index (CMI) [39]. CMI represents the impact eccentricity: the lower the CMI, the more eccentrical the impact. Based on post-impact parameters [40], it can be expressed as $CMI=\Delta V/V_{r_PDOF}$, where V_{r_PDOF} represents the V_r component along the principal direction of force (PDOF) at the collision instant: ΔV is thus the combination of impact eccentricity and closing velocity. From the definition of CMI derives that a decrease in V_r (e.g., by AEB) can result in no substantial benefit in terms of impact severity: if V_r decreases but its component along the PDOF does not (or CMI increases), a 100% braking action can be not effective in lowering ΔV. It is possible to represent the impacts of Fig. 10 in the CMI-V_{r_PDOF} plane [40], resulting in the situation shown in Fig. 11. Distinguishing between the possible ADAS interventions following Fig. 10 convention, it is evidenced that the adaptive logic (c) involves ΔV always lower in respect to the 100% braking condition (b), because of the lower CMI; in such cases, the "No intervention" logic (a) is preferable to a 100% braking action.

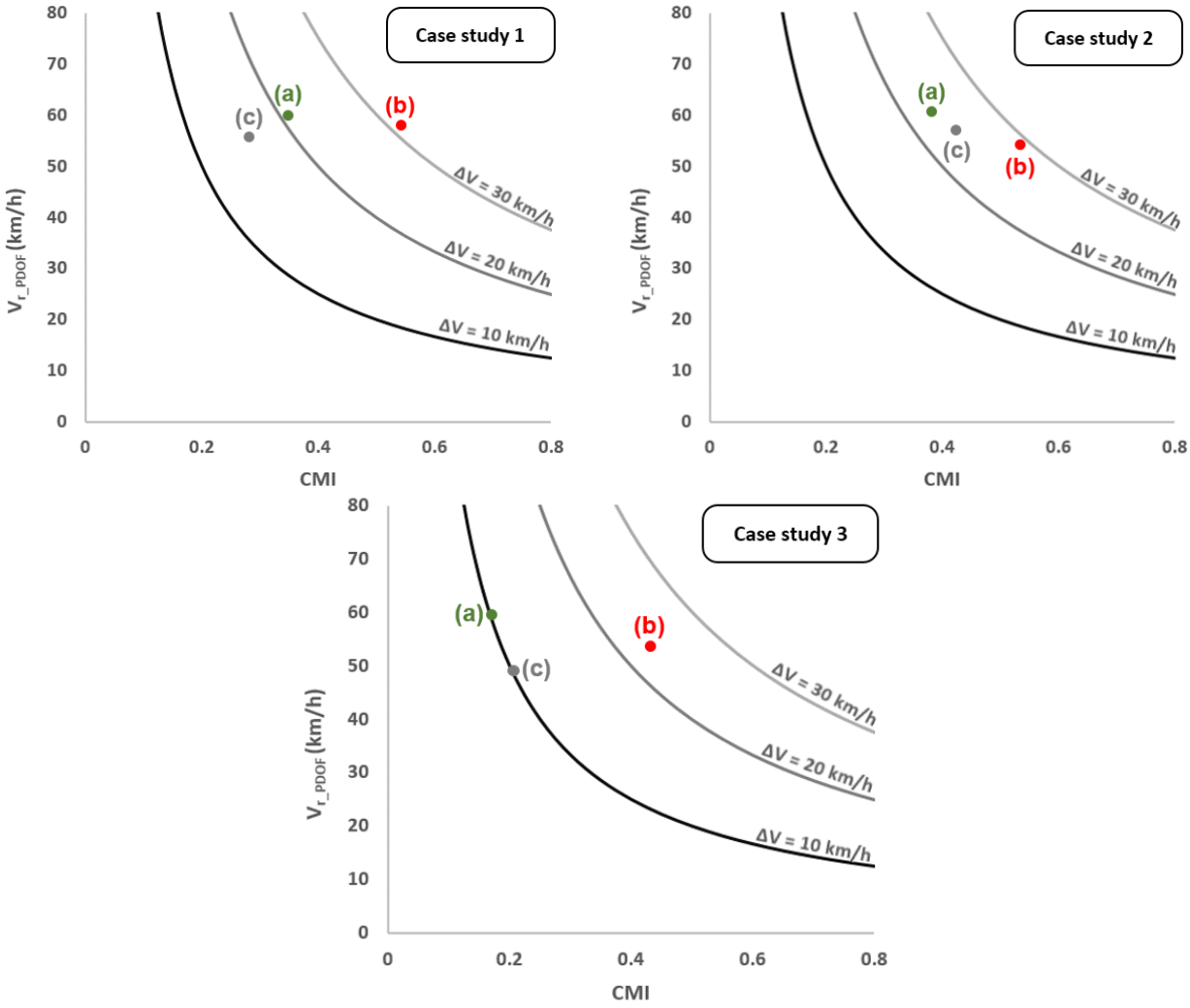

Fig. 11. Representation of the impacts on the CMI-V_{r_PDOF} plane for case study 1-3, in case of no intervention (a), 100% braking action (b) and adaptive logic (c).

In Tab. 3 the outcomes in terms of IR for each case study are reported, based on the logic selected for activation. Coherently with the above expressed concepts, the adaptive logic implies a lower IR value in comparison to the other intervention logics. The maximum benefit deriving from the use of the criteria is evidenced in case study 1: IR deriving from the use of the adaptive logic is equal to 4% (ΔV=16 km/h), instead of 34% obtained by the 100% braking action intervention (ΔV=32 km/h).

Tab. 3. Outcomes in terms of IR associated to each case study, based on the ADAS logic selected for activation.

Case study	Intervention	IR
1	No intervention	9%
	100% braking	34%
	Adaptive logic	4%
2	No intervention	20%
	100% braking	41%
	Adaptive logic	19%
3	No intervention	1%
	100% braking	16%
	Adaptive logic	1%

CONCLUSIONS

The present work analyses solutions for ADAS activation based on criteria for the minimization of injury risk (IR) and clearance. In this work are shown the characteristics and tools required for the application of such criteria to adaptive logics, allowing the ADAS to adapt to the scenario evolution. Three case studies are examined to demonstrate the criteria effectiveness, comparing the solutions with current ADAS activation logics.

A special developed software is firstly introduced, set up to analyze the behavior of an ADAS device implementing the IR-based criteria: the software is based on a database filled with outcomes associated to combined interventions on braking and steering, in many critical scenarios; since the injury outcome (i.e., IR) depends on the velocity change ΔV experienced by the vehicle in the eventual impact, the database has been compiled using a reduced order dynamic model to simulate the impact phase between the vehicles. The use of a database allows to identify the best intervention in a short time, i.e., the time necessary to access to the database (some milliseconds): this solution is to be preferred with a view of an on-board vehicle implementation of the criteria. Referring to some case studies, it has been proven that the IR-based criteria for ADAS activation allow the vehicle to optimally handle highly critical road scenarios, and in particular ICS: adapting to the scenario evolution resulting from the opponent vehicle's driver actions, the system leads to eccentrical impact configurations; this is compatible with low values of ΔV, and IR as a consequence.

Even though explorative, the present work evidences the advantages deriving from the use of the proposed criteria and how the ADAS implementing such criteria can be further optimized. Currently, as a priority, the simulated intervention minimizes IR for the vehicle on which the ADAS is implemented: minimization of IR for the opponent vehicle is also possible, as well as the average IR between the two vehicles. Including IR for the opponent among the intervention criteria, their application field could be further expanded, considering that IR curves for different types of vehicles (e.g., motorcycles) or vulnerable road users can be found in literature. Furtherly, the discussion can also be expanded to IR curves associated to MAIS lower than 3 (e.g., MAIS 2+), thus including lower degrees of injury: this would allow to limit the number of serious injuries and also moderate injuries, allowing to amplify the overall effects on road safety.

REFERENCES

[1] European Commision, "Roadmap to a Single European Transport Area – Towards a competitive and resource efficient transport system", Brussels, 2011.

[2] K. T. Gursel and N. Nane, "Non-linear finite element analyses of automobiles and their elements in crashes", *Int J Crashworth,* vol. 15, n. 6, pp. 667-692, 2010.

[3] R. Spicer, A. Vahabaghaie, G. Bahouth, et al., "Field effectiveness evaluation of advanced driver assistance systems", *Traffic Inj Prev,* vol. 19, n.S2, pp. 91-95, 2018.

[4] J. B. Cicchino, "Effectiveness of forward collision warning and autonomous emergency braking systems in reducing front-to-rear crash rates", *Accid Anal Prev,* vol. 99 (2017), pp. 142-152, 2017.

[5] O. S. M. Gani, Y. P. Fallah, G. Bansal et al., "A study of the effectiveness of message content, length, and rate control for improving map accuracy in Automated Driving Systems", *IEEE Trans Intell Transp Syst,* vol. 20, n. 2, 2019.

[6] J3016_201401:2014, "Taxonomy and definitions for terms related to driving automation systems for on-road motor vehicles", SAE, Warrendale, PA, 2018.

[7] P. L. Morgan, C. Alford, C. Williams, et al., "Manual takeover and handover of a simulated fully autonomous vehicle within urban and extra-urban settings", *Advances in Intelligent Systems and Computing,* vol. 597, pp. 760-771, 2018.

[8] B. Zhong, H. Chen, J. Chen, et al., "Study on important indices related to driver feelings for LKA intervention process", *SAE Technical Paper,* n. 2018-01-1586, 2018.

[9] N. M. Corporation, "Autonomous Emergency Steering System", [Online]. Available: https://www.nissan-global.com/en/technology/overview/autonomous_emergency_steering_system.html. [Accessed 6 March 2019].

[10] N. Kaempchen, B. Schiele and K. Dietmayer, “Situation Assessment of an Autonomous Emergency Brake for Arbitrary Vehicle-to-Vehicle Collision Scenarios”, *IEEE Trans Intell Transp Syst,* vol. 10, n. 4, pp. 678-687, 2009.

[11] R. M. Brach and M. R. Brach, “The Tire-Force Ellipse (Friction Ellipse) and Tire Characteristics”, *SAE Technical Papers,* vol. 01, n. 0094, pp. 1-10, 2011.

[12] S. Nyholm and J. Smids, “The ethics of accident-algorithms for self-driving cars: an applied trolley problem?”, *Ethic Theory Moral Prac,* vol. 19, pp. 1275–1289, 2016.

[13] A. Kullgren, “Dose-response models and EDR data for assessment of injury risk and effectiveness of safety systems”, in *Proceedings of the IRCOBI Conference*, Bern, Switzerland, 2008.

[14] D. J. Gabauer and C. H. Gabler, “Comparison of roadside crash injury metrics using event data recorders”, *Accid Anal Prev,* vol. 40, n. 2008, pp. 548-558, 2008.

[15] D. Vangi, M. S. Gulino and C. Cialdai, “Coherence assessment of accident database kinematic data”, *Accid Anal Prev,* vol. 123, pp. 356-364, 2019.

[16] T. Fraichard and H. Asama, “Inevitable Collision States - A Step Towards Safer Robots?”, in *IEEE/RSJ Int Conf on Intelligent Robots and Systems*, Las Vegas, NV, US, 2003.

[17] E. A. M. Association, “Average Vehicle Age”, [Online]. Available: https://www.acea.be/statistics/tag/category/average-vehicle-age. [Consultato il giorno 6 March 2019].

[18] T. Hirose, Y. Ohtsuka and M. Gokan, “Activation timing of a collision avoidance system with V2V Communication”, *SAE Technical Paper ,* n. 2017-01-0039, 2017.

[19] J. Gunnarsson, L. Svensson, L. Danielsson and F. Bengtsson, “Tracking vehicles using radar detections”, in *Proceedings of the 2007 IEEE Intelligent Vehicles Symposium*, Istanbul, Turchia, 2007.

[20] S. H. a. M. Krug, “Virtual Integration in the Development Process of ADAS”, in *Handbook of Driver Asssitance Systems*, CH, Springer International Publishing, 2016, pp. 160-175.

[21] M. Taraba, J. Adamec, M. Danko, et al. , “Utilization of modern sensors in autonomous vehicles”, in *ELEKTRO*, Mikulov, CZ, 2018.

[22] M. Saffarzadeh, N. Nadimi, S. Naseralav, et al., “A general formulation for time-to-collision safety indicator”, *Proceedings of the Institution of Civil Engineers,* vol. 166, n. 5, pp. 294-304, 2013.

[23] S. Liu, Y. Huang and R. Zhang, “Obstacle recognition for ADAS using stereovision and snake models”, in *IEEE 17th International Conference on Intelligent Transportation Systems (ITSC)*, Qingdao, CN, 2014.

[24] A. Balachandran and J. C. Gerdes, “Artificial steering fell design for steer-by-wire vehicles”, in *7th IFAC Symposium on Advances in Automotive Control*, Tokyo, J, 2013.

[25] V. Banks, E. Shaw and D. R. Large, “Keeping the Driver in the Loop: The ‘Other’ Ethics of Automation”, in *Proceedings of the 20th Congress of the International Ergonomics Association (IEA 2018)*, Florence, IT, 2018.

[26] Y. V. Tan, M. R. Elliott and C. A. C. Flannagan, “Development of a real-time prediction model of driver behavior at intersections using kinematic time series data”, *Accid Anal Prev,* vol. 106, pp. 428-436, 2017.

[27] BMI, “V-Modell XT”, 2013. [Online]. Available: https://www.cio.bund.de/Web/DE/Architekturen-und-Standards/V-Modell-XT/vmodell_xt_node.html. [Accessed 6 March 2019].

[28] Y. Yao, “Vehicle steer-by-wire system control”, *SAE Technical Paper,* n. 2006-01-1175, 2006.

[29] C. Jurewicz, A. Sobhani, J. Woolley, et al., “Exploration of vehicle impact speed – injury severity relationships for application in safer road design”, in *6th Transport Research Arena*, Warsaw, PL, 2016.

[30] I. Han, “Analysis of vehicle collision accidents based on qualitative mechanics”, *Forensic Sci Int,* vol. 291 (2018), pp. 53–61, 2018.

[31] B. Dávid, G. Láncz and G. Hunyady, “Real-time behaviour planning and highway situation analysis concept with scenario classification and risk estimation for autonomous vehicles”, *Designs,* vol. 3(1), 2019.

[32] H. Kolk, E. Tomasch, W. Sinz, J. Bakker and J. Dobberstein, “Evaluation of a momentum based impact model and application in an effectivity study considering junction accidents”, in *7th International Conference on ESAR "Expert Symposium on Accident Research"*, Hannover, DE, 2016.

[33] L. Sousa, P. Veríssimo and J. Ambrósio, “Development of generic multibody road vehicle models for crashworthiness”, *Multibody Syst Dyn,* vol. 19, n. 1-2, pp. 133-158, 2008.

[34] Y. Le Guennec, J. P. Brunet, F. Daim, et al., “A parametric and non-intrusive reduced order model of car crash simulation”, *Comput Methods Appl Mech Engrg,* vol. 338, pp. 186-207, 2018.

[35] M. Darms, “Data fusion of environment-perception sensors for ADAS”, in *Handbook of driver assistance systems*, CH, Springer, 2016, pp. 549-566.

[36] D. Vangi, F. Begani, M. S. Gulino et al., “A vehicle model for crash stage simulation”, in *IFAC PapersOnLine*, Vienna, AT, 2018.

[37] D. Vangi, F. Begani, F. Spitzhüttl et al., “Vehicle accident reconstruction by a reduced order impact model”, *Forensic Sci Int,* 2019 (in press).

[38] J. M. Scanlon, K. D. Kusano and H. C. Gabler, “Analysis of Driver Evasive Maneuvering Prior to Intersection Crashes Using Event Data Recorders”, *Traffic Inj Prev,* vol. 16, n. 2, pp. 182-189, 2015.

[39] M. Huang, Vehicle Crash Mechanics, I ed., Boca Raton, FL: CRC Press, 2002.

[40] D. Vangi, M. S. Gulino, A. Fiorentino, et al., “Crash momentum index and closing velocity as crash severity index”, *Proc IMechE Part D: J Automobile Engineering,* pp. 1-9, 2019.

NEW SAFETY STANDARDS FOR MOTORISED MOBILTY DEVICES IN AUSTRALIA

Michael Paine

David Paine

Vehicle Design and Research Pty Limited, Australia

Paper Number 19-0205

ABSTRACT

A motorised mobility device (MMD) is primarily intended as assistive technology for people with limited mobility. MMDs include powered wheelchairs and mobility scooters. In recent years concerns have been raised about the number of fatal and serious incidents with these devices in Australia. These incidents are not reliably recorded in crash reporting systems but special studies indicated that several hundred Australians are hospitalised each year due to incidents involving MMDs. A review using the safe-systems approach resulted in recommended minimum safety requirements for the design of MMDs intended to be used on footpaths/sidewalks and other public infrastructure. In 2018 Standards Australia published a new Technical Specification settings out these requirements. This paper provides background on the development of these requirements.

INTRODUCTION

In 2012 Austroads, the peak organisation of Australian and New Zealand road transport and traffic agencies, began a review of the safety of MMDs. This followed on from a review by Vicroads in 2009 and a project initiated by the Australian Competition and Consumer Commission (ACCC), as well as concerns expressed by road transport agencies about the safety of MMDs.

RESEARCH FINDINGS

A study commissioned by the ACCC estimated that between 2006 and 2008 the average number of hospitalisations involving MMD users was at least 350 per year. It was found that injury-causing incidents with MMDs were poorly reported by road crash data systems (i.e. police-reported data) and hospital recording systems. Recording of fatalities was more reliable due to the coronial process and between 2000 and 2010 there were 62 fatalities recorded in Australia (Gibson 2011, VISU 2006), although some were medically-related.

In 2008 it was estimated that about 80,000 MMDs were in use across Australia (Griffiths 2010). There is considerable uncertainty about current numbers but it is thought to exceed 200,000 because the number in use appears to be doubling every five years, based on trends with registration of MMDs in Queensland - the only State that requires MMDs to be registered for footpath use.

It was found that the serious crash risk was much higher than conventional vehicles in terms of kilometres travelled. There are numerous reasons for this relatively high rate, including frailty of some users and low annual kilometres travelled but the findings support the need to minimise the consequences of human error or misjudgement through the clever design of MMDs.

In accordance with the safe-systems principles it was concluded that MMD construction requirements were appropriate and that these should be based closely on an existing Australian Standard AS/NZS 3695.2:2013 "Requirements and test methods for electrically powered wheelchairs (including mobility scooters): 2013". However it was recognised that some aspects of that standard were too onerous for the intended application (leading to unnecessary compliance costs) and that some extra requirements were needed to address safety and access issues not adequately covered by the standard.

Overseas standards were also found to be incomplete for the purpose of safe use of MMDs on footpaths but they contained some useful and innovative ideas that were incorporated into the proposed technical requirements.

DEVELOPMENT OF A TECHNICAL SPECIFICATION

After consultation with Standards Australia and stakeholders it was decided that a Standards Australia Technical Specification (SATS) was an appropriate method for publishing the desired technical requirements.

A key reason for this decision was that demonstrating compliance with a Technical Specification is much less onerous than having a product certified to an Australian Standard. During the Austroads review it was recognised that a simple labelling system, where the manufacturer claimed conformity with published technical requirements, would be enforceable under Australian Consumer Law. Therefore there could be reasonable assurance that a product met safety requirements without the resources needed for third-party certification.

An existing Standards Australia committee, highly experienced in assistive technology requirements, took on the task of drafting the SATS.

The result was SATS 3695.3:2018 "Wheelchairs: Requirements for designation of powered wheelchairs and mobility scooters for public transport and/or road-related area use". Standards Australia published the SATS in mid-2018.

CONTENTS OF THE TECHNICAL SPECIFICATION

The SATS refers to many of the requirements set out in AS/NZS 3695.2:2013. In brief, the TS requires MMDs to demonstrate dynamic and static stability on slopes, limits the dimensions and mass of devices, introduces a slow speed switch for devices that can exceed 6km/h, and requires that devices can negotiate uneven surfaces and obstacles.

Stability on slopes

AS/NZS 3695.2:2013 recognises three classes of MMD (paraphrased):

- Class A are primarily intended for indoor use and are not necessarily capable of negotiating outdoor obstacles
- Class B are relatively compact and are intended for indoor and outdoor use
- Class C are large and are primarily intended for outdoor use

Class B requirements were found to be the most appropriate to safety requirements for MMDs used on footpaths. This required the device to be tested on a 6 degree slope as a minimum for dynamic stability (e.g. turning on a slope) and 9 degrees for static stability (e.g. remaining stationary on a slope and for parking brake performance).

For devices intended for use on public transport a 7.1 degree slope was found to be appropriate for dynamic stability tests, based on Australian Disability Standards For Accessible Public Transport (DSAPT) (e.g. boarding ramps).

Speed

Each Australian state and territory sets its own road rules. These are based on the ARR, which are intended as a template for those road rules. For road rule purposes MMDs and their users are treated as pedestrians, provided that the maximum speed on level ground does not exceed 10km/h. This requirement has applied for more than 20 years.

A review of the speed issue included an analysis of sight distances needed to avoid a collision. This was based on established road design practices that took into account reaction times and braking distances. In the case of low speed situations it was also necessary to account for forward projection - the distance from the person's eyes to the front of the device (Figure 1). Because MMDs are often used amongst frail pedestrians the calculations were based on total collision avoidance.

Based on this analysis it was found that the speed of

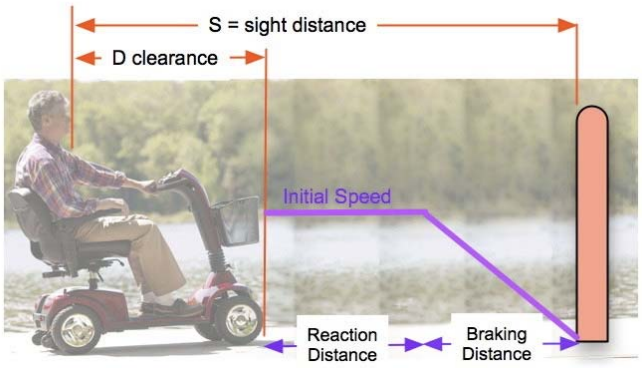

Figure 1. Stopping scenario

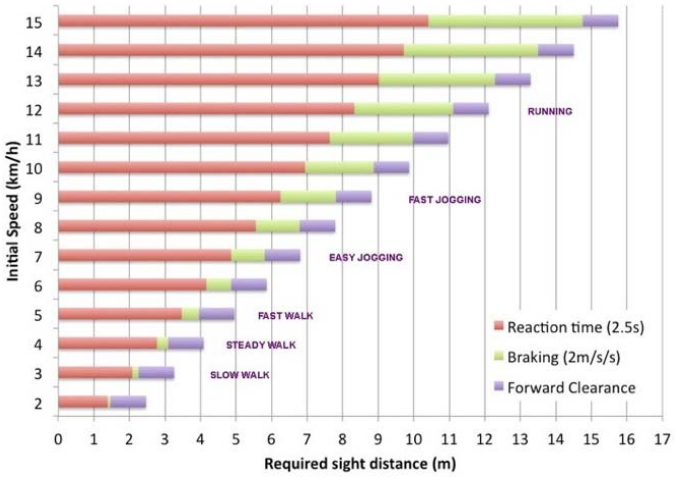

Figure 2. Relationship between speed and sight distance

travel in km/h should not exceed the available sight distance in metres (Figure 2). For example, a sight distance of 5m, typical of uncrowded footpaths, requires a travel speed of no more than 5km/h. It was found that 10km/h (i.e. 10m sight distance) was an appropriate maximum speed for MMDs using footpaths and other public infrastructure but they should travel at much slower speeds in crowded areas.

It was also recognised that, at these relatively low speeds, any motorised wheeled device gives a poor

perception of speed compared with ambulation, where gait is a reliable indicator of speed (labels on Figure 2). This has been addressed by requiring a low speed switch that limits the MMD to 5km/h. The switch is not required if the MMD has a maximum speed not more than 6km/h. Most MMDs in the United Kingdom that are capable of exceeding 4mph (~6kmh) are required to have a low speed switch (Figure 3).

Figure3. Low speed switch

Unladen mass and dimensions

The ARR require MMDs to have an unladen mass no more than 110kg. It is apparent that many MMDs in use in Australia exceed this limit and several Australian states have increased this to 150kg in their regulations. The review looked at this issue.

It is desirable that the laden mass (MMD, user and luggage) does not exceed 300kg based on infrastructure and equipment capacities (e.g. ramps and lifts). Based on anthropometric data and a survey of devices in use an unladen mass limit of 170kg was considered to be appropriate for mobility scooters in the SATS. In recognition of the issues associated with medical needs, powered wheelchairs have no limit on unladen mass but are recommended to not exceed 300kg laden mass.

Maximum width and length were based mainly on the design parameters of infrastructure and public passenger vehicles (Standards Australia 2010, Austroads 2009). For general infrastructure MMDs must not exceed 850mm in width and 1500mm in length.

For MMDs intended to be conveyed by public transport the maximum width is 740mm and length depends on swept path and manoeuvrability tests specified in the SATS. There are several other requirements that apply to these "blue label" MMDs (Figure 5) to ensure improved compatibility with mass-transit vehicles. These requirements took into account the accessibility and allocated space requirements of the DSAPT that apply to public passenger vehicles in Australia.

Obstacles and hazards

AS/NZS 3695.2:2013 includes tests for safely negotiating obstacles and others hazards. Class B MMDs are tested with 50mm high obstacles and 30mm ground unevenness.

In addition the SATS has a test for traversing a pavement gap 75mm wide, such as those found at railway level crossings. There is also a test for lateral stability if one wheel of the MMD drops down a step transition 50mm high that is parallel to the pathway (some incidents involve an MMD suddenly swinging into an adjacent traffic lane when this occurs).

Labelling conforming MMDs

The SATS describes the content of user information to be provided with new MMDs and the specifications of a label to be affixed to the device. The label includes the words "This product conforms with SA TS 3695.3" (Figures 4 & 5). This wording is associated with Australian Consumer Law that, in effect, requires products sold in Australia to be fit-for-purpose.

Figure 4. White Label for footpath use
(© Standards Australia)

Figure 5. Blue Label for compatibility with suitable public passenger vehicles (© Standards Australia)

Now that the SATS is published MMD manufacturers are able to test their products and claim that they conform with the requirements of the SATS. In this way they can ensure the product is suitable for use on footpaths and other public infrastructure and so is fit-for-purpose.

Similarly, purchasers of MMDs can choose a product that meets their needs by checking for the presence of and the colour of the label.

CONCLUSIONS

Incidents involving MMDs are not reliably reported in Australia and this seems to also be the case elsewhere. Specially-commissioned injury research in Australia found a high serious injury rate (e.g. per kilometre travelled) compared with other motorised transport. While there are several reasons for this there is a strong case for a safe-systems approach where the MMD design and construction minimise the consequences of human error or misjudgement.

The number of MMDs in use in Australia is likely to be doubling very five years as the population ages and people seek to retain their mobility.

Until recently very little attention has been paid to the safe design of MMDs and the market is effectively unregulated. While clearly the assistive technology industry is experienced and provides suitable products (ATSA 2011) there is, in effect, nothing to prevent inexperienced, unqualified people from selling inferior products in Australia.

The development and publication of SATS 3695.3 is a major step in efforts to address this safety issue.

User behaviour is another matter...

Figure 6. Only in Australia!

REFERENCES

ATSA (2011) Code of Practice for the Australian Healthcare and Assistive Technology Products and Services Industry, Assistive Technology Suppliers Association Inc, June 2011 version 1.02

Austroads (2009), Guide to Road Design – Part 6A: Pedestrian and Cyclist Paths, ISBN 978-1-921551-81-9

Bradley C and Pointer S (2009). Identifying injuries in Australia due to mobility scooters: Incidence, severity and common characteristics (presentation to ACCC)

DSAPT (2002) Disability Standards for Accessible Public Transport 2002, Attorney- General's Department, Canberra (revision pending).

Gibson K, Ozanne-Smith J, Clapperton A, Kitching F & Cassell E (2011). Targeted study of injury data involving motorised mobility scooters. A report commissioned by the Australian Competition and Consumer Commission by Monash University

Griffiths M, Bailey W and Paine M (2010), Review of Motorised Mobility Devices, report prepared for Vicroads.

Standards Australia (2010) AS/NZS 1428.1:2009 Design for access and mobility - General requirements for access - New building work and Disability (Access to Premises - Buildings) Standards 2010

Standards Australia (2013) AS/NZS 3695.2:2013 "Wheelchairs. Part 2: Requirements and test methods for electrically powered wheelchairs (including mobility scooters)"

UK Dept for Transport, (2010), Consultation on proposed changes to the laws governing powered mobility scooters & powered wheelchairs

VISU (2006) Consumer product-related injury (2): Injury related to the use of motorised mobility scooters, Hazard (Edition No. 62), Summer - Autumn 2006, Victorian Injury Surveillance Unit , Monash University Accident Research Centre

ACKNOWLEDGEMENTS

This work was undertaken by Austroads to support the preparation of appropriate safety requirements for MMDs in the form of the SATS. Standards Australia Committee ME067 drafted the SATS. The authors participated in that task.

DISCLAIMER

This paper represents the authors' views and does not represent the views or policy of any organisation.

Research on skillful drivers' merging behaviors and statistical analysis of traffic lane flow for an investigation of automatic merging assessment method

Eiji, Nunobiki
Kota, Harada
Yoichi, Kondo
Koei, Minami
Toyota Motor Corporation
Japan

Paper Number 19-0207

ABSTRACT

AM (Automatic Merging) is a driving support system which helps drivers to merge into a traffic lane. It is required to set its performance assessment method to see whether it meets people's driving style of each country or region. In this paper, we propose methodologies to set suitable assessment method of AM (target performances and test conditions) which can be applied in each country or region. As for target performances, suitable ones are set by studying Japanese skillful drivers' merging behaviors on highway and on test track. As for test conditions, a new method is proposed to calculate the possibility that a merging vehicle encounters a difficult situation by analyzing traffic camera and cloud data, which allows us to set reasonable test conditions as "X%ile difficulty" of real environment. These methodologies can be applied not only in Japan but also in other countries or regions.

INTRODUCTION

Demand for AD (automated driving) is increasing rapidly. AM (Automatic Merging) is one of the most complex functions of AD. It helps drivers to merge into a traffic lane, and it is the essential function to achieve automated driving from entrance to exit of highway. Various kinds of researches on function of AM have been reported [1] [2] [3]. Then performance of AM should also be considered in order to provide reliable and comfortable AM. However, its performance assessment method hasn't been generalized yet. Additionally, it should be applied to each country or region because traffic conditions varies among them and AM interacts with other vehicles more than the other ADAS functions do. In this paper, we propose methodologies to provide an assessment method (target performances and test conditions) of AM which can be applied in each country or region. In chapter 1, AM target performances are set as "equal to skillful drivers" by modeling their merging behaviors. In chapter 2, reasonable AM test conditions are set by analyzing the traffic flow of 1st lane (the lane being merged) of real environment.

Definitions

Figure 1 shows the definitions of terms and variables. Explanations of each term/variable are listed in Table 1.

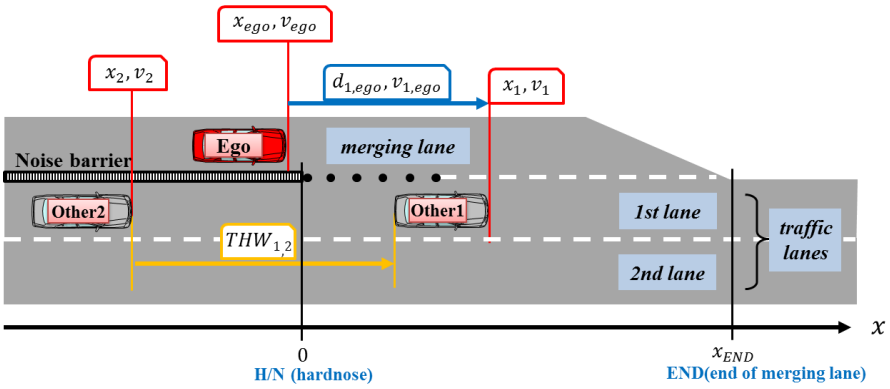

Figure 1. Definitions of terms and variables

Table 1. Definitions of terms and variables

Term/ Variable	Definition
1st lane	The nearest traffic lane to the merging lane.
END	End of merging lane.
H/N	Hardnose. In this paper, it is assumed that the ego-vehicle driver cannot see other vehicles on traffic lanes until he/she passes this point.
x_{ego}, x_1, x_2, x_{END}	Position on x-axis of each vehicle or point.
v_{ego}, v_1, v_2, v_{END}	Velocity of each vehicle or point.
$d_{A,B}$	Relative distance between each vehicle or point. *e.g.* $d_{END,ego} = x_{END} - x_{ego}$
$THW_{A,B}$	Time headway between each vehicle. *e.g.* $THW_{ego,2} = (x_{ego} - x_2)/ v_2$

1. Target performance setting by studying skillful drivers' merging behaviors

Our basic idea of target performance (T/P) is "equal to skillful drivers." Table 2 shows the list of the target performances of AM. The classification is composed of "reliability" and "comfort." "Reliability" means whether the driver can trust AM without feeling uneasy. "Comfort" means whether the driver can feel comfortable. The viewpoints are listed by discussing with skillful drivers based on each classification. Then KPIs (Key Performance Indicators) corresponding to each viewpoint were proposed. Based on these KPIs, all of the target performances were set by analyzing skillful drivers' behaviors on highway or highway-modeled test track. In this paper, "margin to other vehicles on 1st lane (static)" and "which space to merge" are explained as examples.

Table 2 List of target performance for AM

Classification	Viewpoint		KPI	Study method
Reliability	***Margin to other vehicles on 1st lane***	***(Static)***	Restricted area for other vehicles [m] (& THW[s])	Study of skillful drivers' behaviors on highway
		(Dynamic)	Minimum TTC to the other vehicles [s]	
	Margin to the lane end edge	(Static)	Restricted area for end edge[m]	
		(Dynamic)	Minimum TTC to the lane end edge[s]	
	Which space to merge (in front of / behind other vehicle)		Judgment formula composed of $d_{1,ego}$, $v_{1,ego}$, v_{ego}, x_{END}	Study of skillful drivers' behaviors on highway-modeled test track
Comfort	Longitudinal motion		Long. acceleration [m/s^2]	Study of skillful drivers' behaviors on highway
			Long. jerk [m/s^3]	
	Lateral motion		Lat. acceleration [m/s^2]	
			Lat. jerk [m/s^3]	

1-1. T/P example 1: Margin to other vehicles on 1st lane (static)

Concept & Data collection

This target performance provides "how close the ego-vehicle can be to other vehicles on traffic lanes." Our aim is to make the target performance as "equal to skillful drivers." Then a public road test was carried out to acquire the data of skillful drivers' behaviors. The test vehicle was equipped with external sensors such as lidar for all directions. The test was carried out mainly on Shutoko (urban highway in Tokyo) which is one of the busiest highways in Japan. Three skillful drivers who have Toyota's advanced licenses drove the vehicle. They drove not trying to make passengers feel uneasy or uncomfortable. It is because skillful drivers can drive either aggressively or smoothly, and obviously AM should follow the latter way. Additionally, we tried to record if the driver or the passengers (who are also skillful drivers) judged the merging behavior was not ideal, but eventually it never occurred. The test was carried out for three days, and 102 merging cases were collected. In this paper, 22 cases of stop & go traffic jam situation are excluded because the driver's strategy would be different from that of non-traffic jam situation.

Analysis & Result

We set the target performance as the "minimum margin area" of the skillful drivers' merging behaviors. As a first step, we analyzed the skillful drivers' each merging case. Each case was extracted from when the ego-

vehicle passed a hardnose to when it passed end of merging lane. See Figure 2 as an example. In this case, ego-vehicle merged from right to left while 4 other vehicles were driving on the traffic lanes (Figure 2a). Red points in Figure 2b shows the trajectory of the lidar points. Then these points were extended to longitudinal and lateral direction to obtain the edge of the other vehicles (Figure 2c). The obtained white area is the area where the ego-vehicle's driver didn't allow the other vehicles to enter in this case. As a second step, a heatmap of other vehicles' existence possibility was obtained by superimposing each case and dividing it by the number of merging cases (Figure 3). Note that each case is flipped horizontally because there was no significant difference between cases of merging to left and to right. Figure 3a shows the result with lateral position and longitudinal position axis, and Figure 3b shows the result with lateral position and THW axis. Note that negative THW means that to the following vehicle, and there is no THW in the side area of ego-vehicle. The area surrounded by red line is the area where the other vehicles never entered. This is the target performance of AM as "restricted area for other vehicles to enter." In addition, we also conducted a study with the same method in Michigan. The result is also shown in Figure 3 as the areas surrounded by white dotted lines. Here we can see the difference between two regions. This shows that suitable target performances would be different among regions or countries.

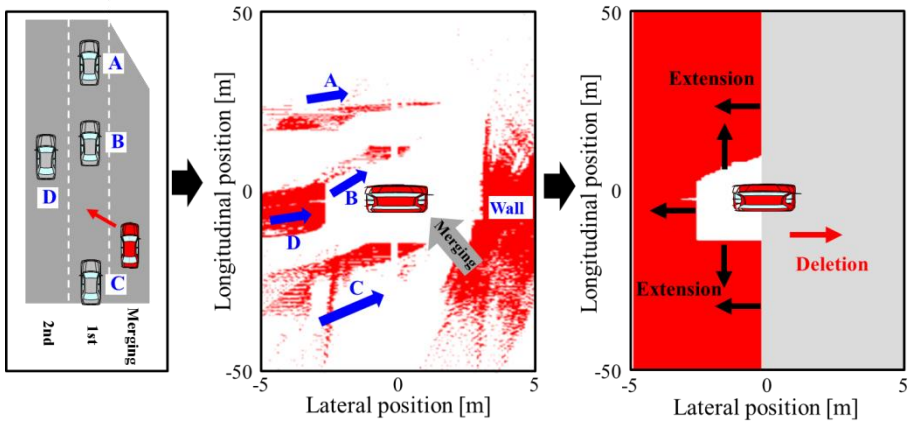

[a] Overview *[b] Trajectory* *[c]Edge extraction*

Figure 2. Analysis method of restricted area (1 case example)

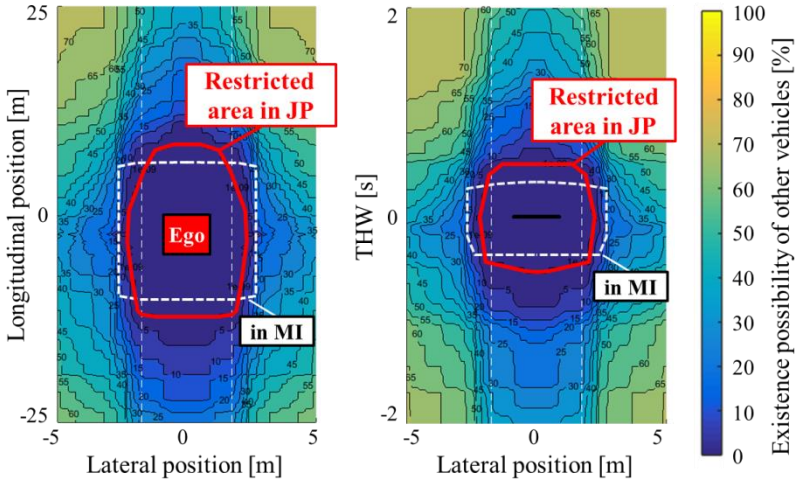

[a] Distance-based *[b] THW-based*

Figure 3. Restricted area for other vehicles

1-2. T/P example 2: "Which space to merge"

Concept & Data collection

This target performance provides "which space should the ego-vehicle merge, in front or behind of a vehicle on 1st lane" when driver recognizes the vehicle on 1st lane at H/N position. The purpose is to avoid uneasy or strange feeling caused by AM's judgment different from drivers' own. Then skillful drivers' behaviors were

studied with controlled conditions of one other vehicle. The test was conducted on a test track for test efficiently. Tests were conducted with varied conditions as shown in Table 3. The test track was modeled as a typical merging lane of interurban highway in Japan. Initial v_{ego}, v_1 and $d_{1,ego}$ means those of when the ego-vehicle passes H/N. As for velocity, in this paper, we focused on the condition that the ego-vehicle's velocity is lower than or equal to the other vehicle's because it is the most common situation in Japan. Then the drivers scored from 1 to 5 in each test case to describe their judgment as defined in Table 4. For example, the driver scored "1" when he/she judged that ego-vehicle must merge in front of the other vehicle. All of the drivers' scoring are shown in Figure 4.

Table 3. Test conditions for the study

Length of merging lane (x_{END})[m]	Speed limit assumption of 1st lane [kph]	Initial v_{ego} [kph]	Initial v_1 [kph]	Initial $d_{1,ego}$ [m]	Total number of test cases
220	100	40 to 60	60 to 120	-180 to 10	92

Table 4. Definition of scoring

Evaluation score	Definition
1	Must merge in front
2	Better to merge in front
3	Cannot decide whether
4	Better to merge behind
5	Must merge behind

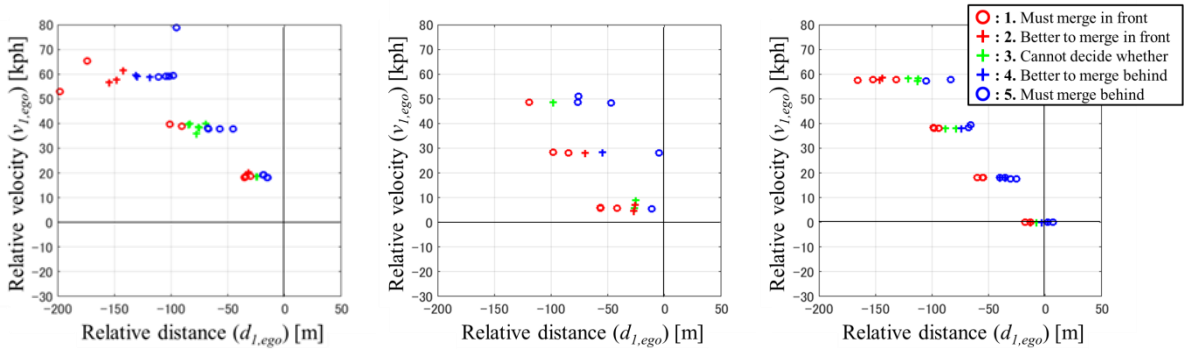

[a] v_{ego} = 40kph ***[b] v_{ego} = 50kph*** ***[c] v_{ego} = 60kph***

Figure 4. Judgment of skillful drivers

Analysis & Result

We set the target performance as "ego-vehicle must merge in front/behind if the skillful drivers judge it as must." Here, the target performance based on driver's judgment models is proposed as below.

(i) Must merge behind if Equation 1 is satisfied. (*Merge behind model*)

$$F_b = w_{b1}d_{1,ego} + w_{b2}v_{1,ego} + w_{b3}v_{ego} + w_{b4}x_{END}\frac{v_{1,ego}}{v_{ego}} + C_b > 0 \quad \text{[Equation 1]}$$

(ii) Must merge in front if Equation 2 is satisfied. (*Merge in front model*)

$$F_f = w_{f1}d_{1,ego} + w_{f2}v_{1,ego} + w_{f3}v_{ego} + w_{f4}x_{END}\frac{v_{1,ego}}{v_{ego}} + C_f < 0 \quad \text{[Equation 2]}$$

(iii) No requirement if neither of them is satisfied.

Here, $d_{1,ego}$, $v_{1,ego}$, v_{ego}, x_{END} are the variables defined in Table 1, and w_* is the weight of each variables. To identify the parameters of each model, Support Vector Machine (SVM) [4] is adopted. Parameters of *Merge in front model* are identified by dividing the score "1" from "2, 3, 4, 5" and those of *Merge behind model* are identified by dividing the score "5" from "1, 2, 3, 4" respectively. Then the suitable parameters for each model were obtained. Figure 5 shows the fitting result of the each model. The blue-colored area means "must merge behind", the red-colored area means "must merge in front", and the non-colored area means "no requirement."

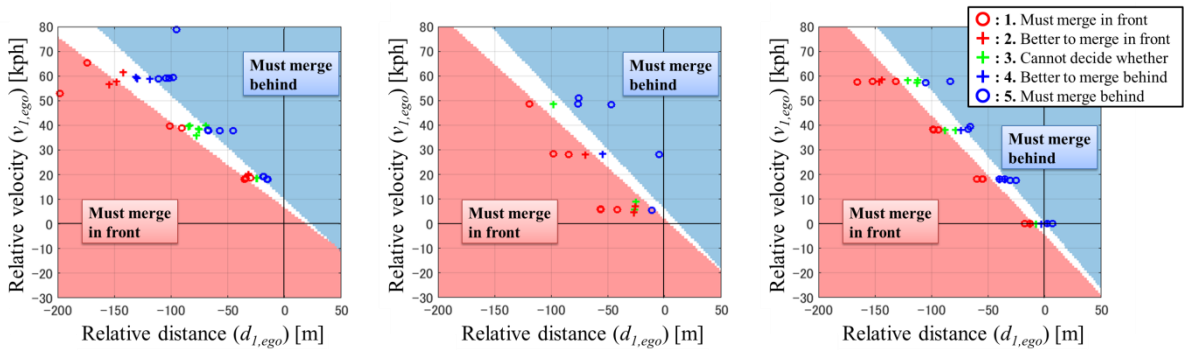

[a] v_{ego} = 40kph *[b] v_{ego} = 50kph* *[c] v_{ego} = 60kph*

Figure 5. Fitting result of each model

To evaluate the accuracy of the obtained model, three accuracy indexes: precision, recall, and F-measure are calculated. These values of *Merge in front model* and *Merge behind model* are shown in Figure 6a. The model accuracy is high considering that human judgment is sometimes inconsistent even under the same condition. Additionally, these values of *Merge in front model* are lower than those of *Merge behind model*. It implies that it is more difficult for human to judge consistently as "merge in front" than as "merge behind" because the 1st lane vehicle is further away.
The same methodology was also applied to urban-highway-modeled merging test which has a shorter length of merging lane (140m). Then the similar fitting result was obtained, and the fitting accuracy was as high as that of interurban-highway-modeled merging test (Figure 6b).

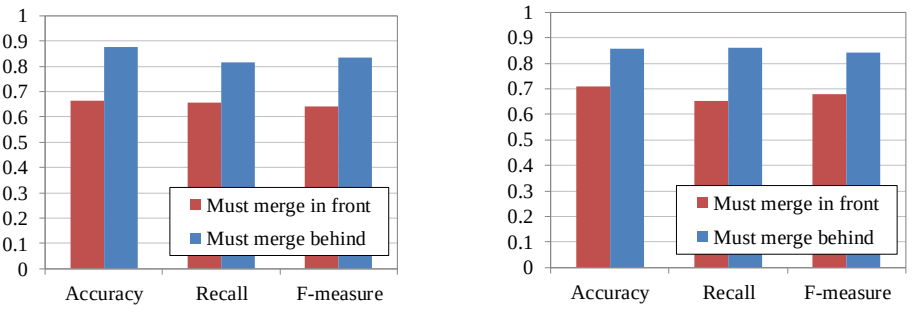

[a] Interurban model *[b] Urban model*

Figure 6. Fitting accuracy of each model

2. Test condition setting by studying 1st lane traffic flow

The conditions of 1st lane vehicles play a key role in AM evaluation. For example, it is obviously more difficult to merge when there are the other vehicles on 1st lane with close distance than when there is no other vehicle. Then reasonable and rather difficult test conditions should be set for effective evaluation of AM. In this chapter, we aim to set suitable ones by studying 1st lane traffic flow of real environment.
First of all, we have to consider what difficult conditions are. There would be two types of traffic situation: traffic jam and non-traffic jam. In this paper, we focus on the difficulty of non-traffic jam situation. Then, we assume that it would be difficult for drivers to merge in the conditions below:

- *(C1)* There is a 1st lane vehicle in a position where the ego-vehicle driver cannot judge which space to merge immediately. (Then the driver would have to drive long distance to merge.)
- *(C2)* There is another vehicle near the vehicle described in *C1*.

Figure 7 shows an image of these conditions.

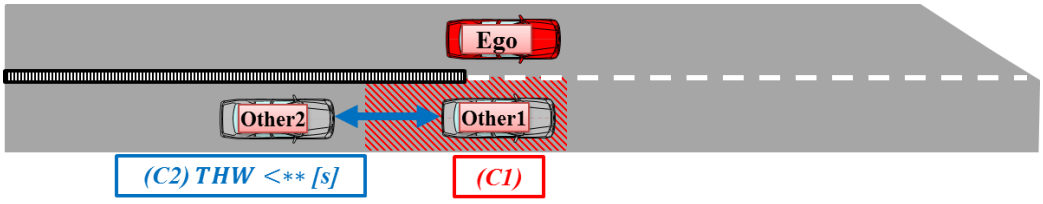

Figure 7. Difficult conditions for merging

With this assumption, a possibility to encounter such a difficult situation can be calculated. We call it "difficult possibility (P_{dif})." It is calculated by following equation.

$$P_{dif} = P(C1 \cap C2) \qquad \text{[Equation 3]}$$

As for the condition *C1*, it can be modeled as no requirement area of "which space to merge" (described as white areas in Figure 5) because drivers within this area have to drive further. Furthermore, it would be also difficult for AM because it should switch its judgment within this area. Then, it is important to clarify how often these conditions (*C1* and *C2*) appear in the real highway. Then traffic camera data was analyzed for this purpose because it allows us to obtain the traffic flow on 1st lane quite directly without losing statistical information. Two interchanges (Higashi-Ikebukuro and Kasugai) are chosen to study the traffic flow of urban and interurban highway (Figure 8). Table 5 and Figure 9 show the overview of traffic camera data. Note that the traffic jam situation (1st lane velocity < 30kph) was excluded in this paper.

[a] Higashi-Ikebukuro (urban) ***[b] Kasugai (interurban)***

Figure 8. Traffic camera image

Table 5. Traffic camera data overview

No.	Interchange	Highway	Speed limit on 1st lane [kph]	Shooting time [hour]	Number of vehicles on 1st lane	Average number of vehicles [Num. / hour]
1	Higashi-Ikebukuro	Shutoko (urban)	60	10.4	7758	746.0
2	Kasugai	Tomei (interurban)	100	11.1	5375	484.2

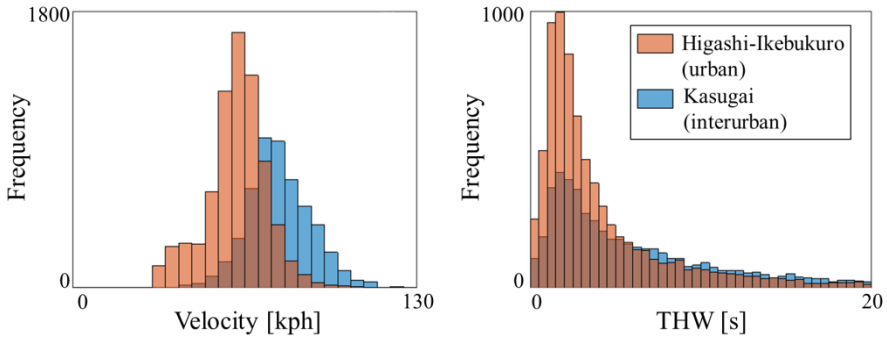

Figure 9. Traffic camera data overview

With these data, P_{dif} can be calculated by following equation with the assumption that the data distribution of sampled period is equal to that of the population.

$$P_{dif} = \frac{t(C1 \cap C2)}{t_{total_cam}} \qquad \text{[Equation 4]}$$

Here, *t(C*)* is the accumulated time when the condition *C** is satisfied, and t_{total_cam} is the total time of traffic camera data. To calculate *t(C1 ∩C2)* with Equation 1 and 2, it is assumed that ego-vehicles appear at every moment at the hardnose with initial velocity. The initial velocity should be set as AM's setting considering that the purpose is to set reasonable test conditions. Here, it is supposed that AM's initial velocity is 50kph at Higashi-Ikebukuro and 60kph at Kasugai, for example. Figure 10 shows the result of P_{dif} calculation. The horizontal red line shows *P(C1)*. The blue line shows the cumulative distribution *of* P_{dif} as a function of $THW_{2,1}$ (as *C2*). With this result, reasonable AM test conditions can be set by setting reasonable value of P_{dif}. For

example, if we assume that AM test condition should be set as difficult as "P_{dif} =1%" of real environment, corresponding $THW_{2,1}$ is 1.07[s] for Higashi-Ikebukuro (urban highway), and 1.54[s] for Kasugai (interurban highway). The set $THW_{2,1}$ is shorter at Higashi-Ikebukuro than at Kasugai even with the same P_{dif} because the 1st lane traffic is heavier in Higashi-Ikebukuro than in Kasugai. (In other words, it is more frequent to encounter a difficult situation in Higashi-Ikebukuro than in Kasugai.)

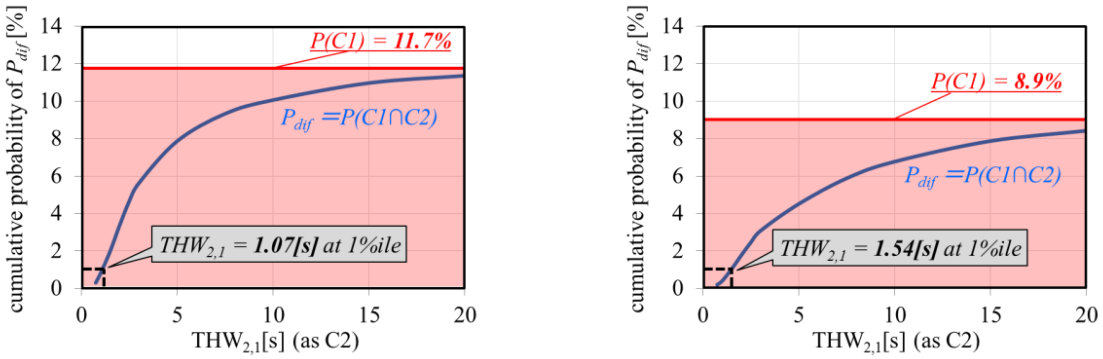

[a] Higashi-Ikebukuro (urban) *[b] Kasugai (interurban)*

Figure 10. Result of difficult possibility calculation

With this method, it would be possible to make reasonable test conditions corresponding to every merging lane of real environment. However, it is unfeasible to collect traffic data of every merging lane by methods such as traffic camera. Then we kept studying to seek an alternative method as following.

$\hat{P}_{dif}$ is defined by the following equation.

$$\hat{P}_{dif} = P(C1) * P(C2) \qquad \text{[Equation 5]}$$

Figure 11 shows the comparison between P_{dif} and $\hat{P}_{dif}$ of each interchange. Their values match well, which means it is possible to suppose that conditions *C1* and *C2* are almost independent of each other when velocity is higher than 30kph.

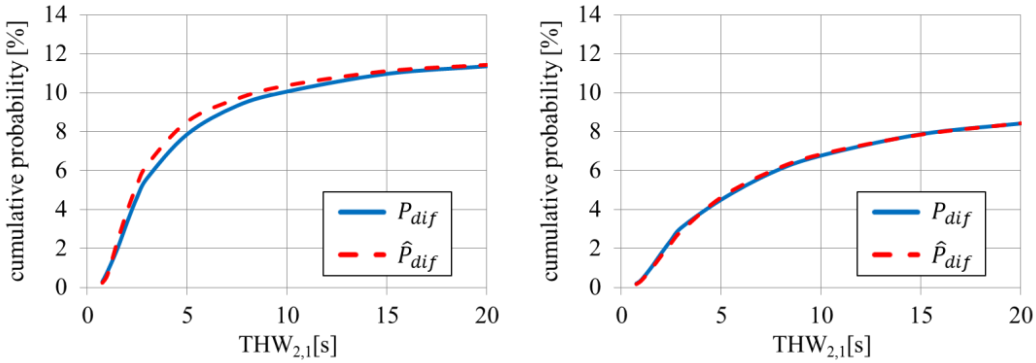

[a] Higashi-Ikebukuro (urban) *[b] Kasugai (interurban)*

Figure 11. Comparison of P_{dif} and $\hat{P}_{dif}$

The following equation is obtained from this result.

$$P_{dif} \cong \hat{P}_{dif} \qquad \text{[Equation 6]}$$

Then, we assume a data sampling method that some of vehicles can send v_{ego} and *THW* to data cloud (Figure 12). Note that, unlike traffic camera data analysis, it is impossible to obtain the data of all vehicles on 1st lane through the sampled period.

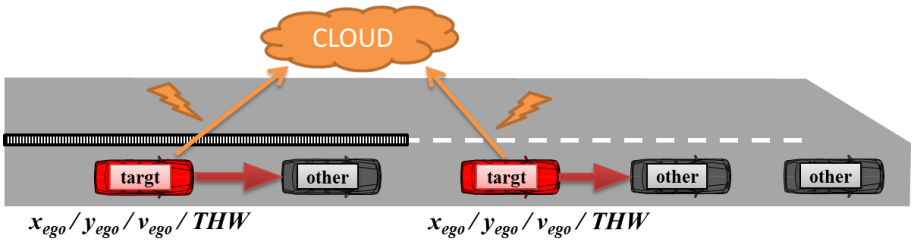

Figure 12. Data collection by cloud

With this kind of method, *P(C1)* and *P(C2)* can be also calculated as following equations with assumption that v_{ego} and *THW* distributions of sampled vehicles are equal to those of the population.

$$P(C1) = \frac{t_{sample}(C1)}{t_{total_sample}} * \frac{N_{AVE_population}}{N_{AVE_sample}} \qquad \text{[Equation 7]}$$

$$P(C2) = \frac{t_{sample}(C2)}{t_{total_sample}} \qquad \text{[Equation 8]}$$

Here, $t_{sample}(C^*)$ is accumulated time when the condition C^* is satisfied by sampled vehicles, t_{total_sample} is total time of data-sampled period, $N_{AVE_population}$ is number per unit time of vehicles of the population, and N_{AVE_sample} is that of sampled vehicles. Note that $N_{AVE_population}$ can be obtained from public database of each region or country. For example, those data of major road junctions in Japan are open to public by MLIT of Japan [5]. Finally, it is possible to calculate P_{dif} of each merging lane of real environment by Equations 5-8 with this kind of data collection method.

CONCLUSION

New methodologies are proposed to determine "target performances" and "test conditions" for Automatic Merging (AM). As for target performances, skillful drivers' merging behaviors were studied and modeled as what AM should follow. It was found that one of the target performances is different between in Japan and in Michigan. As for test conditions, a new method is proposed to calculate the possibility that a merging vehicle encounters a difficult situation by analyzing traffic camera and cloud data, which allows us to set reasonable test conditions as "X%ile difficulty" of real environment. In addition, another analysis method using cloud data is also proposed as a substitute for traffic camera analysis. These methodologies proposed in this paper would help us to set suitable target performances and test conditions for each country or region.

REFERENCES

[1] P. Kachroo and Zhijun Li. "Vehicle merging control design for an automated highway system." *Proceedings of Conference on Intelligent Transportation Systems* (1997): 224- 229.

[2] Xiao-Yun Lu and K.J. Hedrick . " Longitudinal control algorithm for automated vehicle merging." *Proceedings of the 39th IEEE Conference on Decision and Control* (2000). 450- 455 vol.1.

[3] H. Liu, W. Zhuang, G. Yin, Z. Tang and L. Xu. "Strategy for heterogeneous vehicular platoons merging in automated highway system." *Chinese Control And Decision Conference* (2018): 2736- 2740.

[4] U. Fayyad. "A tutorial on support vector machines for pattern recognition." *Data Mining and knowledge diccovery*, (1998): 2, 121- 167.

[5] Ministry of Land, Infrastructure, Transport and Tourism, "Road Traffic Census 2015", http://www.mlit.go.jp/road/census/h27/

APPLYING LANE KEEPING SUPPORT TEST TRACK PERFORMANCE TO REAL-WORD CRASH DATA

Christopher Wiacek
Garrick Forkenbrock
Mark Mynatt
National Highway Traffic Safety Administration
USA

Kellen Shain
Alpha Technology Associate, Inc.
USA

Paper Number 19-0208

ABSTRACT

Lane Keeping Support (LKS) is an advanced driver assistance system (ADAS) technology intended to prevent a vehicle from drifting out of its travel lane. To assess the potential for LKS to reduce real-world crashes where the driver drifts out of their travel lane, test track performance was compared with the real-world crash data.

Five light vehicles equipped with LKS were evaluated on the test track using Lane Keeping Assist (LKA) test methods contained within the Euro NCAP Test Protocol - Lane Support Systems. Specifically, the procedures to evaluate a vehicle's response to an imminent departure over a solid white line were used; tests to evaluate LKS system response to an unmarked road edge were not performed. These tests identified performance differences between the vehicles, and were somewhat dependent on the lateral velocity used during test conduct.

Results from these tests were compared to relevant fatal crashes in the National Motor Vehicle Crash Causation Survey (NMVCCS) survey conducted by the National Highway Traffic Safety Administration from 2005-2007, and the agency's new Crash Investigation Sampling System (CISS). A review of the fatal 2005 – 2007 NMVCCS and 2017 CISS lane/roadway departure cases was performed to classify the shoulder type present on the side of the roadway from which the subject vehicle first departed from, and to estimate the shoulder width just after the departure, where applicable. The objective of this effort was to estimate whether LKS interventions could have potentially amended the real-world pre-crash path of the subject vehicle in the vicinity of the lane departure, given the system performance observed on the test track.

When the test track performance of the vehicles was considered in the context of the road shoulder widths and road/lane/shoulder characteristics present in the 43 fatal NMVCCS and 50 CISS crashes analyzed for this paper, estimating whether LKS could have affected the crash outcome was found to depend on a number of factors. From an input perspective, the lateral velocity of the vehicle as it is directed toward the boundary of the lane, and whether that boundary is comprised of a clearly defined painted line or simply a pavement edge, has the potential to affect whether an LKS intervention can even be expected.

Even if the input conditions are such that a vehicle's LKS activation criteria are satisfied, then the ability of the system to effectively address the pre-crash scenario is relevant, yet can depend on a number of factors. The amount of lateral deviation before or beyond the lane line and/or road edge, and the implications of it being too large, are important considerations. In the case of a right-side departure away from the travel lane, excessive lateral deviation may result in at least part of the vehicle leaving the paved roadway. Similarly, left-side departures with excessive lateral deviation have the potential to increase the risk of a head-on crash.

INTRODUCTION

Lane Departure Warning (LDW), Lane Keeping Support (LKS), and Lane Centering Control (LCC) are three advanced driver assistance system (ADAS) technologies intended to prevent vehicles from drifting out of their travel lane. All three systems utilize a camera-based vision system to monitor the vehicle's lateral position with respect to the roadway. Depending on the system design and system's level of intervention authority, the technology is intended to warn the driver that they are leaving the travel lane, redirect the lateral path of the vehicle to stay in the lane, or continuously maintain the lateral position of the vehicle within the lane of travel.

The run-out-of-lane pre-crash scenarios identified by Swanson, et al were used to estimate the target crash population of the ADAS systems discussed in this paper [Swanson, 2018]. In this work, a combination of the National Automotive Sampling System (NASS) General Estimates System (GES) and Fatality Analysis Reporting System (FARS) 2011-2015 crash databases were used to examine all police-reported crashes involving a light vehicle in the critical event of the crash or in the event that occurred which made the crash imminent. Light vehicles include all passenger cars, vans, minivans, sport utility vehicles, or light pickup trucks with gross vehicle weight ratings less than or equal to 10,000 pounds. Common crash types were analyzed to produce a list of representative pre-crash scenarios based upon NHTSA pre-crash variables (i.e., the pre-crash movement or the vehicle's action prior to an impending critical event or prior to impact if the driver did not make any action). From the pre-crash scenarios identified in the report, Table 1 lists those relevant to the inadvertent run-out-of-lane crash problem. This approach identified, on average, over 760,000 run-out-of-lane crashes annually; over 9,600 of which were fatal.

Table 1.
2011 – 2015 FARS and GES run-out-of-lane light vehicle target population

Scenario	Avg FARS	Avg GES
Road edge departure/No Maneuver	6,284	472,182
Opposite Direction/No Maneuver	2,983	96,095
Drifting/Same Direction	196	120,223
Object/No Maneuver	151	80,088
Total	9,615	768,588

To assess the potential effectiveness of countermeasures intended to prevent run-out-of-lane crashes, Wiacek, et al performed a study to better understand why drivers depart the roadway and under what conditions and circumstances the crashes occur [Wiacek, 2017]. Using fatal crashes from the National Motor Vehicle Crash Causation Survey (NMVCCS), this study identified 72 cases where the result of a subject vehicle departing the travel lane resulted in a crash where an occupant in an involved vehicle sustained fatal injuries. Of these, 43 cases where the subject vehicle drifted out of the lane and crashed were used to assess the real-world applicability of LDW/LKS/LCC crash avoidance technologies.

The study concluded that a robust LKS/LCC system with sufficiently high lateral control authority could have effectively prevented many of the 43 cases reviewed. In other words, unless there were other factors present which prevented the driver from reengaging in the driving task, a robust LKS/LCC system would likely have prevented the driver from running out of the lane, which started the chain of events that led to the fatal crashes. The study suggested that LKS/LCC systems appear to have more potential in crash reduction than LDW since the systems do not rely on alert modality effectiveness or driver responsiveness. Additionally, the mentioned the environmental and roadway conditions at the time of the crash would likely not have compromised the performance of the vision system to detect the roadway boundary at the moment the vehicle left the lane.

This paper builds upon the earlier work by comparing measured test track performance of vehicles equipped with LKS systems with the real-world crash data. The purpose was to measure the performance of the LKS systems under controlled conditions and estimate how the systems may have addressed the driving conditions preceding known crashes. The goal in doing this is to assess the efficacy.

Five light vehicles from different manufacturers were tested using Lane Keep Assist (LKA) test methods contained within the European New Car Assessment Programmed (Euro NCAP) Test Protocol - Lane Support Systems [Euro NCAP, 2015] to assess technology implementation differences. Euro NCAP uses LKA to describe systems NHTSA would describe as having LKS. For the sake of this paper, the terms can be used interchangeably. The following vehicles were tested:

- 2017 Cadillac CTS
- 2017 Ford Fusion
- 2017 Mercedes Benz C300
- 2017 Toyota Prius Prime
- 2017 Volvo XC90

For each vehicle, the test track performance was used to assess if the vehicles' LKS systems intervened, whether the interventions corrected the vehicle's heading back to the travel lane, and the maximum lateral deviation from the test lane line marking.

In addition to the vehicle tests, the crash data were also surveyed to assess how the technology would apply to the real-world. First, the 43 fatal NMVCCS cases from the previous study were reanalyzed. For each crash, on the side of the lane or roadway departure, the shoulder width of the road was estimated. To be consistent with the Euro NCAP LKA test procedure, the shoulder width measurement was estimated from the inside edge of the lane marking to the edge of the road surface. In those crashes where the shoulder width was not relevant because of the crash type or roadway surface, the side of the roadway or lane of travel was characterized.

Lastly, using the same methodology, a review of the run out of the lane fatal data was also analyzed using the 2017 NHTSA Crash Investigation Sampling System (CISS). CISS, which began pilot data collection is 2016, replaced the retired National Automotive Sampling System Crashworthiness Data System (NASS-CDS) as NHTSA's nationally-representative investigation-based data collection program. For these 50 cases, the shoulder width was measured or the side of the lane/roadway departure or was characterized. The results of this analysis will be presented and discussed in the context of the five vehicles tested.

VEHICLE TESTING

Test Procedure

The Euro NCAP LKA test procedure uses a series of trials performed with iteratively increasing lateral velocities towards the desired lane line. For all tests, a robotic steering controller was utilized to increase the repeatability of the procedure and reduce variability associated with manual steering inputs. Although the Euro NCAP LKA test protocol does not specify use of robotic steering controller, it does require tight path tolerances be satisfied by the vehicle as it approaches the desired lane marking during testing.

Pretest conditions

For each subject vehicle (SV), prior to testing, the vehicle manufacturers were asked to complete pre-test forms that included information to determine if any system initiation testing must take place prior to conducting the performance testing. If system initialization testing was needed, the vehicle manufacturer provided the recommended instruction to initialize the system.

Once the system was initialized, the SV's tires and brakes were pre-conditioned using a series of start and stops at predefined speeds and brake decelerations.

Test Maneuver

Each LKS trial began with the SV being driven at 72 km/h down a straight lane delineated by solid white and dashed white lines. The SV path was initially parallel to the lane lines, with an offset from the solid white line that depended on what lateral velocity would be used later in the maneuver (Figure 1).

After a short period of steady state driving, the steering machine was used to adjust the heading of the SV towards the solid white lane line using a path defined by a 1200 m radius curve. The amount of time the SV path remained on this curve depended on the lateral velocity desired for the test trial, and the heading angle

associated with it. Once these parameters had been achieved, the steering machine returned the handwheel angle to zero, and was decoupled from the SV so as to allow the SV handwheel to move freely and independently.

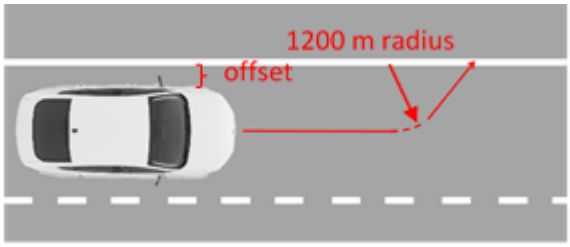

Figure 1. Left lane departure for LKS test

The lateral velocity of the SV approach towards the solid lane line (from both the left and right directions) was iteratively increased from 0.1 m/s. If acceptable LKS performance was realized, the lateral velocity used for the next trial was increased by 0.1 m/s. This continued until the SV was no longer able to satisfy the LKS performance criteria or until a maximum lateral velocity of 1.0 m/s was reached. The tests performed with lateral velocities from 0.1 - 0.5 m/s were used for the Euro NCAP performance assessment protocol, whereas those >0.5 m/s were used for research purposes. [Euro NCAP, 2015]

LKS Validity Criteria
The following validity criteria were applied to each test trial to insure the tests were properly performed:

- SV Speed: 72 km/h ± 1.0 km/h
- Lateral deviation from test path: ± 0.05 m
- Lane departure lateral velocity: ± 0.05 m/s from target lateral velocity
- Steering wheel velocity: ±15 deg/sec

LKS Performance Criteria
Acceptable LKS performance occurred when SV did not cross the inboard leading edge of the solid lane line by more than 0.4 m.

Results
The results from the five vehicles tested under the conditions described above will be presented. A summary of the data by vehicle and test condition is presented in Table 2. Per the test condition, the maximum lateral deviation is noted. Positive values indicate the maximum lateral deviation occurred prior to the vehicle crossing the inboard edge of the lane line. A negative value indicates the maximum lateral deviation occurred after the vehicle crossed the inboard line edge. No LKS intervention (No LKS) is noted on the summary table, as well as if a vehicle was not tested under a given condition (NDT).

Tests Performed with Lateral Velocities from 0.1 – 0.5 m/s
Of the five vehicles tested, only the Cadillac CTS and the Volvo XC90 satisfied the performance criteria for the first five lateral velocity iterations during both the left- and right-side lane line approaches. In the case of the Volvo XC90, the maximum lateral deviation occurred prior to the vehicle crossing the lane line, as indicated by the positive values in Table 2.

The Mercedes C300 satisfied the performance criteria during tests conducted with lateral velocities up to 0.3 m/s during left- and right-side approaches.

The Ford Fusion and Toyota Prius had asymmetrical performance where, under certain test conditions, the vehicles satisfied the performance criteria on one side but not the other for the same lateral velocity.

The Ford Fusion did not satisfy the performance criteria on the left-side approaches when lateral velocities of 0.1 and 0.4 m/s were used, but did for each right-side approach. For this vehicle, LKS did not activate during

trials performed with a lateral velocity of 0.1 m/s (three repeated trials were performed, each with the same outcome) and while LKS did activate during the test performed with a 0.4 m/s lateral velocity, maximum lateral displacement exceeded 0.4 m.

The Toyota Prius satisfied the performance criteria at 0.2 m/s and 0.3 m/s on the right side, but exceeded the maximum lane deviation limit of 0.4 m on the left side.

Tests Performed with Lateral Velocities from ≥0.6 m/s

LKS interventions were observed during tests performed with lateral velocities of 0.6 to 0.9 m/s for three of the five vehicles tested in this paper. The Volvo XC90 satisfied the LKS performance criteria during left- and right-side approaches for lateral velocities up to 0.7 m/s, and only on the left side at 0.8 m/s. No further testing was conducted with the Volvo XC90.

The Cadillac CTS satisfied the LKS performance criteria during left- and right-side approaches performed with a lateral velocity of 0.6 m/s. Although LKS interventions were observed during left- and right-side approaches using lateral velocities up to 0.9 m/s, the vehicle exceeded the maximum lateral deviation threshold.

The LKS system on the Ford Fusion intervened when tested at the lateral velocity of 0.5 m/s, but the vehicle exceeded the maximum lateral deviation threshold on both the left- and right-side approaches. No further testing was conducted at higher lateral velocities.

For the Toyota Prius, testing at higher lateral velocities was only conducted on the right side because the performance criteria was not satisfied at lower lateral velocities during left-side approaches. The vehicle satisfied the maximum lateral deviation at 0.6 m/s, exceeded the criteria at higher lateral velocities on the left-side approach tests.

The Mercedes C300 was only tested on the right side at the lateral velocity of 0.5 m/s. The LKS did not engage during this trial, and no further testing was conducted. No vehicles were tested with lateral velocities at or above 1.0 m/s.

Figures 2 and 3 illustrate the performance differences among the five test vehicles during tests performed with the various lateral velocities. Lateral deviations greater than those specified by the LKS performance criteria are shaded in blue.

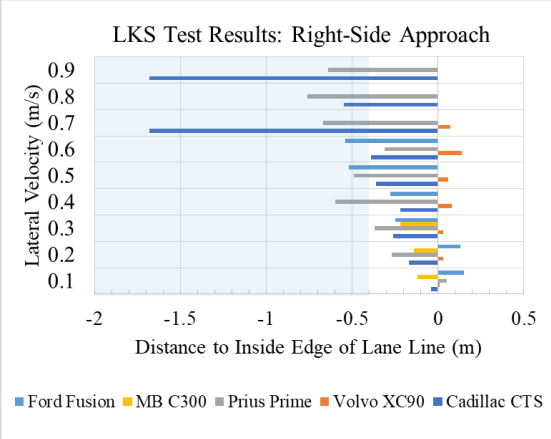

Figure 2. LKS test results – right side departure

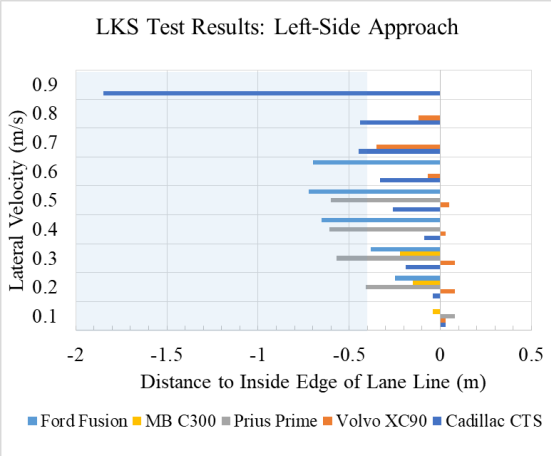

Figure 3. LKS test results – left side departure

Table 2.
Summary of test results by vehicle and test conditions

Maximum Lateral Deviation (m)	Lateral Velocity (m/s)	0.1		0.2		0.3		0.4		0.5	
		L	R	L	R	L	R	L	R	L	R
	Cadillac CTS	0.03	-0.04	-0.04	-0.17	-0.19	-0.26	-0.09	-0.22	-0.26	-0.36
	Ford Fusion	No LKS	0.15	-0.25	0.13	-0.38	-0.25	-0.65	-0.28	-0.72	-0.52
	Mercedes Benz C300	-0.04	-0.12	-0.15	-0.14	-0.22	-0.22	No LKS	No LKS	No LKS	No LKS
	Toyota Prius Prime	0.08	0.05	-0.41	-0.27	-0.57	-0.37	-0.61	-0.6	-0.6	-0.49
	Volvo XC90	0.03	0.01	0.08	0.03	0.08	0.03	0.03	0.08	0.05	0.06
		0.6		0.7		0.8		0.9		1.0	
		L	R	L	R	L	R	L	R	L	R
	Cadillac CTS	-0.33	-0.39	-0.45	-1.68	-0.44	-0.55	-1.85	-1.68	DNT	DNT
	Ford Fusion	-0.7	-0.54	DNT	DNT	DNT	DNT	DNT	DNT	DNT	DNT
	Mercedes Benz C300	DNT	No LKS	DNT	DNT	DNT	DNT	DNT	DNT	DNT	DNT
	Toyota Prius Prime	DNT	-0.31	DNT	-0.67	DNT	-0.76	DNT	-0.64	DNT	DNT
	Volvo XC90	-0.07	0.14	-0.35	0.07	-0.12	DNT	DNT	DNT	DNT	DNT

Figures 4 and 5 are screen shots from test video recorded during right-side approaches performed with a lateral velocity of 0.7 m/s, for the Volvo XC90 and the Cadillac CTS, respectively. LKS intervened during both trials. The maximum lateral deviation recorded for the Volvo XC90 was 0.07 m from the inboard edge of the lane marking (able to satisfy the LKS performance criteria), whereas it was 1.68 m for the Cadillac CTS (unable to able to satisfy the LKS performance criteria). The white arrows shown in Figures 4 and 5 indicate the reference lane marking.

Figure 4. Point of maximum lateral deviation observed during a right-side approach test performed with the Volvo XC90 and a 0.7 m/s lateral velocity

Figure 5. Point of maximum lateral deviation observed during a right-side approach test performed with the Cadillac CTS LKS and a 0.7 m/s lateral velocity

REAL-WORLD SHOULDER WIDTH ANALYSIS

A review of the fatal 2005 – 2007 NMVCCS and 2017 CISS lane/roadway departure cases was performed to classify the shoulder type present on the side of the roadway the subject vehicle first departed its travel lane, and to estimate the shoulder width just after the departure, where applicable. The objective of this effort was to estimate whether LKS interventions could have potentially amended the real-world pre-crash path of the subject vehicle near the lane departure, given the system performance observed on the test track.

NMVCCS Lane Width Analysis

Method To establish a baseline, the 43 previously analyzed fatal NMVCCS cases were reassessed. For these cases, it was previously established that the subject vehicle drifted out of the lane, resulted in a fatal crash, and was relevant to assessing the real-world applicability of LDW/LKS/LCC crash avoidance technologies. All the cases were reviewed and the side of the initial lane or roadway departure was identified. Once identified, the shoulder width distance was estimated for the side of the roadway departure. Examples will be discussed below followed by the results of the analysis.

To be consistent with the measurement convention used in the Euro NCAP LKA test procedure, and with the data reported in Table 2, the shoulder width estimates extracted from the NMVCCS and CISS cases were referenced from the inside edge of the lane marker to the end of the road surface at the location of the lane departure.

The side of the roadway was also characterized in those cases where a lane marking or shoulder was not present, such as when the vehicle traveled into an adjacent lane, rural or local roads where there were no markings and only a road edge and, intersections or when a curb was present that define the edge of the useable road surface.

Examples In NMVCCS Case Nos. 2006-045-063 and 2007-78-071 the drivers drifted out of the lane on the left side. For these types of cases the road shoulder width measurement was estimated from the inside edge of the lane marker to the end of the road surface. This was conducted by examining the scene diagram and the scene photos, using the lane line width as the reference for the measurement. (Figures 6 and 7)

Figure 6. NMVCCS Case No. 2006-045-063 shoulder width

Figure 7. NMVCCS Case No. 2007-078-071 shoulder width

NMVCCS Case No. 2005-76-035 is an example where the subject vehicle departed the lane of travel into the "adjacent lane." In this case the driver drifted over the center line and departed the road on the left resulting in a rollover (Figure 8).

Figure 8. NMVCCS Case No. 2005-76-035 adjacent lane on the left

NMVCCS Case No. 2005-11-61 is an example of crash where the vehicle was traveling a straight, level, two-way, rural gravel roadway with no painted lines (Figure 9). The subject vehicle drifted and exited the roadway to the right. This type of roadway was characterized by its "road edge."

Figure 9. NMVCCS Case No. 2005-11-61 road edge example

NMVCCS Case No. 2007-49-043 is an example of a roadway where there was no lane marking and just a curb at the end of the road surface on the side the vehicle departed the travel lane. In this case the subject vehicle was traveling east in left lane. After traveling through an intersection, the subject vehicle drove off the road to the left onto the curbed median striking a light pole (Figure 10). This crash also has some characteristics similar to the intersection crashes that were identified in the CISS data, and will be discussed later in this paper.

Figure 10. NMVCCS Case No. 2007-49-043 curb example

Results Using the method described above, the results of the analysis of the 43 NMVCCS cases are provided in Figure 11. For this analysis, the shoulder width measurement data was grouped by 0.1 m increments up to 0.4 m.

The data show that in 16 of the 25 crashes where a shoulder was present on the side of the road, and the vehicle departed the lane, the shoulder was greater than 0.4 m. In nine of the crashes, the shoulder width was equally distributed between the "greater than 0.1 m" and "equal to 0.4 m or less" groupings. There were no crashes where the shoulder was 0.1 m or less.

In this data set, there were three crashes where the subject vehicles left the road with no lane markings on the side of the roadway departure. It should be noted that in these cases, there was a clearly-defined road edge. Lastly, in 14 cases the vehicle drifted into the adjacent lane. These crashes resulted in the vehicle leaving the roadway after crossing into the oncoming lane or drifting into oncoming traffic

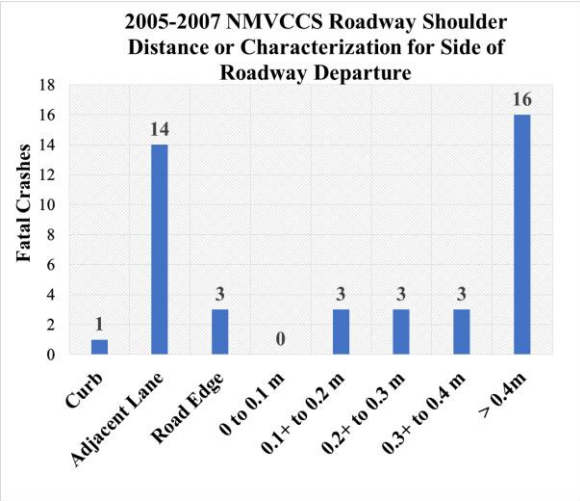

Figure 11. 2005 – 2007 NMVCCS roadway shoulder distance or characterization

CISS Lane Width Analysis

Method A second analysis of the real-world crash data was conducted using NHTSA's CISS. In response to a congressional directive to modernize its nationally representative crash databases, NHTSA concluded that the NASS-Crashworthiness Data System (NASS-CDS) program would be retired and replaced with the CISS. The new CISS program was designed to provide many improvements from its predecessor including, obtaining more accurate scene and vehicle measurements. [Mynatt, 2017] In addition to the improved measurement, the 2017 CISS dataset was the first year collected for the program. Given the NMVCCS data was older, the newer data could provide insight into changes to the roadways with respect to the efficacy of LKS.

As with the NMVCC study, all fatal cases from the 2017 CISS dataset that met the following Crash Type Code were selected: 01, 02, 04, 05, 06, 07, 09, 10, 44, 45, 46, 47, 48, 49, 50, 51, 52, 53, 64, 65, 66, and 67 (a chart explaining the crash types is provided in the Appendix of this paper). As with the NMVCCS case selection, the intent was to capture fatal crashes resulting from the vehicle leaving the original travel lane. The CISS cases are also provided in the Appendix.

Fifty-seven cases met the criteria, however, upon review of the data, seven cases were excluded from the final analysis because the subject vehicles were traveling the wrong way on a one-way street or the vehicle lost control prior to departing the roadway. There were 50 cases in the final data set.

In CISS, all the crash scene measurements are now collected in three-dimensions using a Nikon Total Station electronic measuring devices, coupled with FARO® Blitz software. [Mynatt, 2017] As discussed in the NMVCC section, the cases were reviewed, and the side of the initial lane or roadway departure was identified. The NMVCCS shoulder width measurements were estimated using the scene diagrams and photos. In CISS, the shoulder widths were measured in the Blitz diagramming software near the roadway departure location. It should be noted that beginning in 2018, shoulder width measurements in CISS are coded in the data file. As with the NMVCCS cases, the side of the roadway departure was also characterized when applicable. Examples of the roadways will be provided below followed by a summary of the results.

Examples CISS Case No. 1-13-2017-127-01, the subject vehicle initially departed its lane of travel on the right side prior to returning and departing the lane on the left side, resulting in a crash with a vehicle traveling in the adjacent lane. (Figure 12). In this case, the lane departure occurred on a highway whose shoulder width was measured from the inboard edge of lane line to the end of the road surface on the far right.

Figure 12. CISS Case No. 1-13-2017-127-01 shoulder width example

CISS Case No. 1-19-2017-113-01 is an example of a vehicle leaving the lane of travel into the adjacent lane. In this case the subject vehicle was traveling east on the highway, departing the lane on the left. The vehicle departed the roadway on the left where it struck a concrete driveway, and rolled over before coming to rest on its side (Figure 13).

Figure 13. CISS Case No. 1-19-2017-113-01 adjacent lane

CISS Case No. 1-32-2017-013-01 was categorized as a vehicle parked on shoulder. In this case the subject vehicle was traveling on a major highway. The vehicle departed the roadway to the right, entering the road shoulder. The front of subject vehicle impacted the rear of a parked vehicle on the shoulder (Figure 14).

Figure 14. CISS Case No. 1-32-2017-013-01 parked vehicle

CISS Case No. 1-33-2017-025-01 is an example of a crash that occurred at an intersection. In this case, the subject vehicle drifted out of the travel lane into the adjacent lane. This occurred at an intersection where there were no lane markings. The vehicle proceeded to travel until it impacted a vehicle traveling in the opposite direction. Figure 15 shows the approach for the subject vehicle and the lack of lane markings at the intersection on the left side.

Figure 15. CISS Case No. 1-33-2017-025-01 intersection example

CISS Case No. 1-28-2017-046-01 is an example where there were no lane markings on a gravel road but a discernable road edge. In this case, the subject vehicle was negotiating a right curve. The vehicle departed the roadway to the left side and impacted a tree on the left side of the vehicle (Figure 16).

Figure 16. CISS Case No. 1-28-2017-046-01 road edge example

Results The results of the shoulder width measurements and roadway departure characterization for the 50 CISS cases are presented in Figure 17. As with the NMVCCS analysis, the shoulder width measurement data were grouped by 0.1 m increments up to 0.4 m.

The data show that in 16 of the 19 crashes where a shoulder was present on the side of the road, and the vehicle departed the lane, the shoulder width was greater than 0.4 m. In three of the crashes, the shoulder was greater than 0.1 m wide but equal to 0.3 m or less. There were no crashes where the shoulder was 0.1 m or less.

In this data set, there were seven crashes where the subject vehicle left the road with no lane markings on the side of the roadway departure. It should be noted that in these cases, there was a clearly defined road edge. There were four cases where the vehicle drifted out of the lane at an intersection where the lane markings were not present. In 18 cases, the vehicle drifted into the adjacent lane. As with the NMVCCS cases, generally these crashes resulted in the vehicle leaving the roadway after crossing into the oncoming lane or drifting into oncoming traffic. Lastly, there were two cases (CISS Case Nos. 1-32-2017-013-01 and 1-28-2017-039-01) where the subject vehicles impacted a vehicle parked on the shoulder.

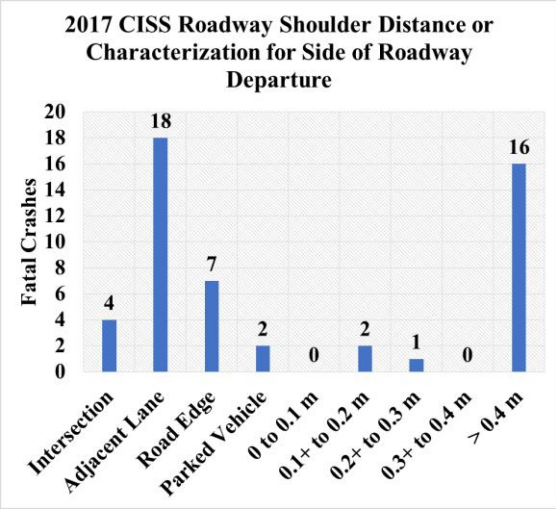

Figure 17. 2017 CISS roadway shoulder distance or characterization

DISCUSSION

This section will discuss the results of five vehicles tested with the Euro NCAP LKA procedure (i.e., those described earlier in this paper) in the context of the analysis of the real-world fatal crashes. Specifically, given the performance of the vehicles under the test conditions, discussion will be focused on whether the fatal crashes could have been potentially prevented for those cases where there was a shoulder, road edge, and adjacent lane.

With respect to the roadway shoulder width, NMVCCS and CISS results (which encompassed 93 fatal crashes that were collected approximately 10 years a part) were consistent and showed similar distributions. For that reason, the combined results are presented in Figure 18.

These real-world data were not assessed for the dynamic state of the vehicle and the lateral velocity of vehicle prior to the roadway departure. Any attempt to correlate that lateral velocity was beyond the scope of the study. It is also assumed that the travel speed of the subject vehicles met or exceeded the minimum activation speed for the LKS. The cases were identified by the vehicle appearing to drift out of the lane, and quantifying the shoulder width when applicable or characterization of the side of the roadway departure.

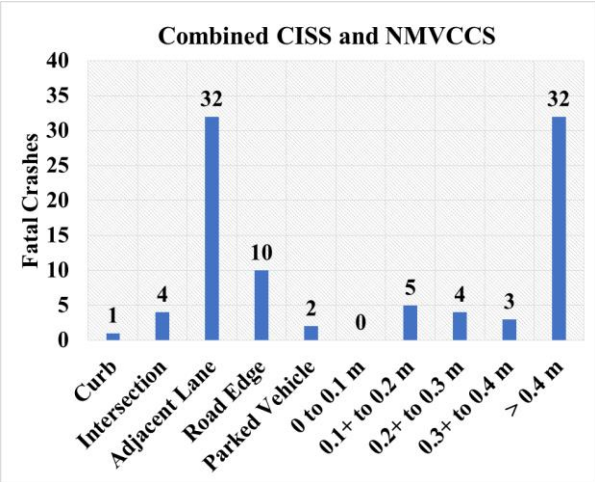

Figure 18. Combined CISS and NMVCCS roadway shoulder distance or characterization.

Lane Departure with Shoulder
CISS Case No. 1-19-2017-041-01, is an example of a roadway with a narrow shoulder that only an LKS that allows very limited lateral deviation from the travel lane would be expected to prevent at least part of the subject vehicle from departing the roadway. The subject vehicle in this example was traveling west and departed the roadway to the right. The vehicle, traveled down an embankment, across an adjacent roadway prior to impacting a tree.

From Figure 19, the shoulder width was measured in CISS to be approximately 0.15 m. The test track data previously presented in Table 2 indicated that only the Volvo XC90 LKS interventions consistently (i.e., over a wide range of lateral velocities) prevented right-side lateral deviations below that distance. Except for the lower lateral velocity conditions, the other test vehicles generally exceeded a lateral deviation of 0.15 m.

Figure 19. CISS Case No. 1-19-2017-041-01 vehicle approach

Lane Departure without Lane Markings
There were 10 crashes identified where there were no lane markings on the road or on the side of the road departure.

It is unknown whether any of the five vehicles tested were equipped with LKS systems capable of intervening in response to a circumstance where a lane departure is imminent, but only a road edge is present (i.e., no lane marker), as such conditions were not evaluated on the test track in this study. Euro NCAP has adopted a test procedure that includes a limit of 0.1 over a road edge, as shown in Figure 20 using a test procedure similar to the LKS test described earlier but without the lane line. [Euro NCAP, 2017]

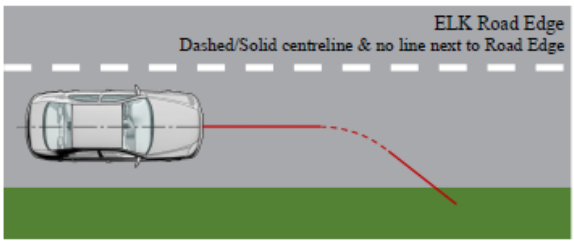

Figure 20. Euro NCAP road edge test condition

CISS Case No. 1-19-2017-097-01 is an example of a road edge case. In this fatal crash, the subject vehicle departed the roadway to the right where there was a disparate lane line and a discernable road edge (Figure 21). After departing the roadway, the vehicle traveled down a steep embankment, striking one or multiple trees and rolling over before coming to final rest. To prevent this type of crash, it is expected the most effective LKS intervention would occur prior to the vehicle leaving the road since pavement provides greater lateral force (turning) capacity than an unpaved deformable surface. With regards to intervention proximity to a lane line, the Volvo XC90 test track performance was indicative of this kind of operation; preventing the

vehicle from traveling past the line in each of the right-side approaches. However, and as previously stated, it is unknown whether the Volvo XC90 LKS system has been configured to respond to an imminent road edge departure which, in this case, is essentially a lane departure without a clear marking delineating the right side of the lane. This case provides evidence of why it may be important for an LKS system to address lane and road departures, to maximize the overall potential safety benefits provided by these systems during real-world driving where clear markings are not always present.

Figure 21. CISS Case No. 1-19-2017-097-01 vehicle approach

Lane Departure into Adjacent Lane

Thirty-two of the ninety-three crashes shown in Figure 18 involved the subject vehicle drifting out of the initial travel lane into an adjacent lane. Crashes that involve the subject vehicle drifting out of its lane result in head-on crashes with an oncoming vehicle or a road departure from the adjacent lane.

With respect to LKS and the vehicles tested, it was determined that the roadway width in the adjacent lane was not a limiting factor as it exceeded the 0.4 m performance criteria. Specifically, for the single vehicle crashes where the vehicle departed the road on the right side, many of the same observations that were discussed in the shoulder width section remain true with respect to the performance of the LKS. If the LKS engaged in the test condition, depending on the lateral velocity, the LKS may have been effective in preventing many of these adjacent lane crashes that did not involve another vehicle traveling in the opposite direction.

Of the 32 adjacent lane cases, over half were head-on crashes. Ten were identified in NMVCCS and eight in CISS. The analysis performed for this paper did not explore the location of the vehicles involved in head-on crashes relative to the lane marking at impact. However, assuming the opposing vehicle does not travel into the subject vehicle's lane, and if it can be assumed that if the subject vehicle's LKS does not allow the subject vehicle to cross into the adjacent lane, the head-on crash would likely not occur.

CISS Case No. 1-28-2017-032-01 is example where the subject vehicle encroaches into the adjacent lane and is involved in a fatal head-on collision. The subject vehicle was traveling west on a two lane non-divided roadway. A large truck was traveling east on the same roadway. The subject vehicle entered the truck's lane, and a head-on impact resulted (Figures 22 and 23).

Figure 22. CISS Case No. 1-28-2017-032-01 vehicle approach

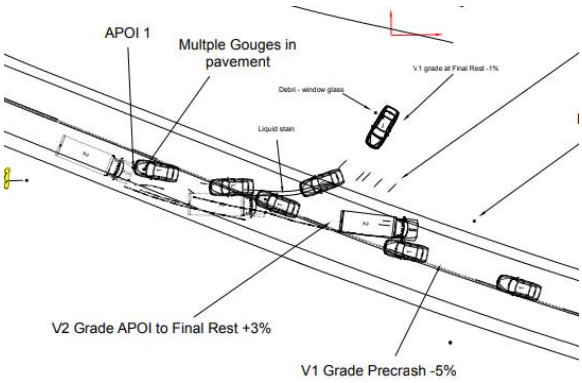

Figure 23. CISS Case No. 1-28-2017-032-01 scene diagram

Figure 24 presents the damage incurred by the subject vehicle. Based upon the crush pattern and interaction with the truck, the subject vehicle likely crossed over the centerline and into the adjacent lane by well over the 0.4 m allowance specified in the Euro NCAP LKA performance criteria.

Figure 24. CISS Case No. 1-28-2017-032-01 front end crush of subject vehicle

Other Lane Departure Cases

There were four crashes that occurred at intersections where there were no lane markings leading up to the location of the lane departure. It was apparent for each case, the subject vehicle was not turning and proceeding through the intersection. Otherwise, lane markings were present leading up to the intersection.

As discussed earlier (NMVCCS Case No. 2007-49-043) there was one crash where there were no lane markings on the side of the roadway departure and the road edge was delineated by a curb, over which the subject vehicle travelled. It is unknown how LKS may have affected the outcome of these crashes where the lane markings are not present.

Lastly, there were two cases (CISS Case Nos. 1-32-2017-013-01 and 1-28-2017-039-01), involving a vehicle parked on the shoulder. The assessment of the LKS performance was similar to the adjacent lane, head-on

crashes discussed earlier. The effectiveness of the LKS is dependent on how far the vehicle deviates into the shoulder and the location of the parked vehicle. The only way to assure the crash is avoided during an imminent lane departure is to prevent or minimize how far the vehicle encroaches into the roadway's shoulder.

CONCLUSION

Five light vehicles equipped with LKS were evaluated on the test track using methods from the Euro NCAP LKA test procedure. Specifically, the procedures evaluated a vehicle's response to an imminent departure over a solid white line; tests to evaluate LKS system response to an unmarked road edge were not performed. These tests identified performance differences between the vehicles, and were somewhat dependent on the lateral velocity used during test conduct.

When the test track performance of the vehicles was considered in the context of the road shoulder widths and road/lane/shoulder characteristics present in the 43 fatal NMVCCS and 50 CISS crashes analyzed for this paper, estimating whether LKS could have affected the crash outcome was found to depend on a number of factors.

From an input perspective, the lateral velocity of the vehicle as it is directed toward the boundary of the lane, and whether that boundary is comprised of a clearly defined painted line or simply a pavement edge has the potential to affect whether an LKS intervention can even be expected.

Even if the input conditions are such that a vehicle's LKS activation criteria are satisfied, the ability of the system to effectively address the pre-crash scenario depends on a number of factors. The amount of lateral deviation before or beyond the lane line and/or road edge, and the implications of it being too large, are important considerations. In the case of a right-side departure away from the travel lane, excessive lateral deviation may result in at least part of the vehicle leaving the paved roadway. Similarly, left-side departures with excessive lateral deviation have the potential to increase the risk of a head-on crash.

REFERENCES

[1] Swanson, E., Foderaro, F., Yanagisawa, M., Najm, W. & Azeredo, P., Statistics of Light-Vehicle Pre-crash Scenarios Based on 2011-2015 National Crash Data, Report No. DOT HS (In Press), National Highway Traffic Safety Administration, Washington, DC, 2018.

[2] Wiacek, C., Fikenscher, J., Forkenbrock, G., Mynatt, M. and Smith, P., Real-World Analysis of Fatal Run-Out-Of-Lane Crashes Using the National Motor Vehicle Crash Causation Survey to Assess Lane Keeping Technologies, 25th Enhanced Safety of Vehicles Conference 17-220, 2017.

[3] European New Car Assessment Programme (Euro NCAP) Test Protocol – Lane Support Systems, Version 1.0, November 2015.

[4] European New Car Assessment Programme (Euro NCAP) Assessment Protocol – Safety Assist, Version 7.0, November 2015.

[5] Mynatt, M., and Brophy, J., Improved Field Measurements in NHTSA's CISS Program, Proceedings of the 25th International Technical Conference on the Enhanced Safety of Vehicles, Paper Number 17-0174, 2017.

[6] European New Car Assessment Programme (Euro NCAP) Test Protocol – Lane Support Systems, Version 2.0, June 2017.

[7] European New Car Assessment Programme (Euro NCAP) Assessment Protocol – Safety Assist, Version 8.0.2, November 2017.

Appendix

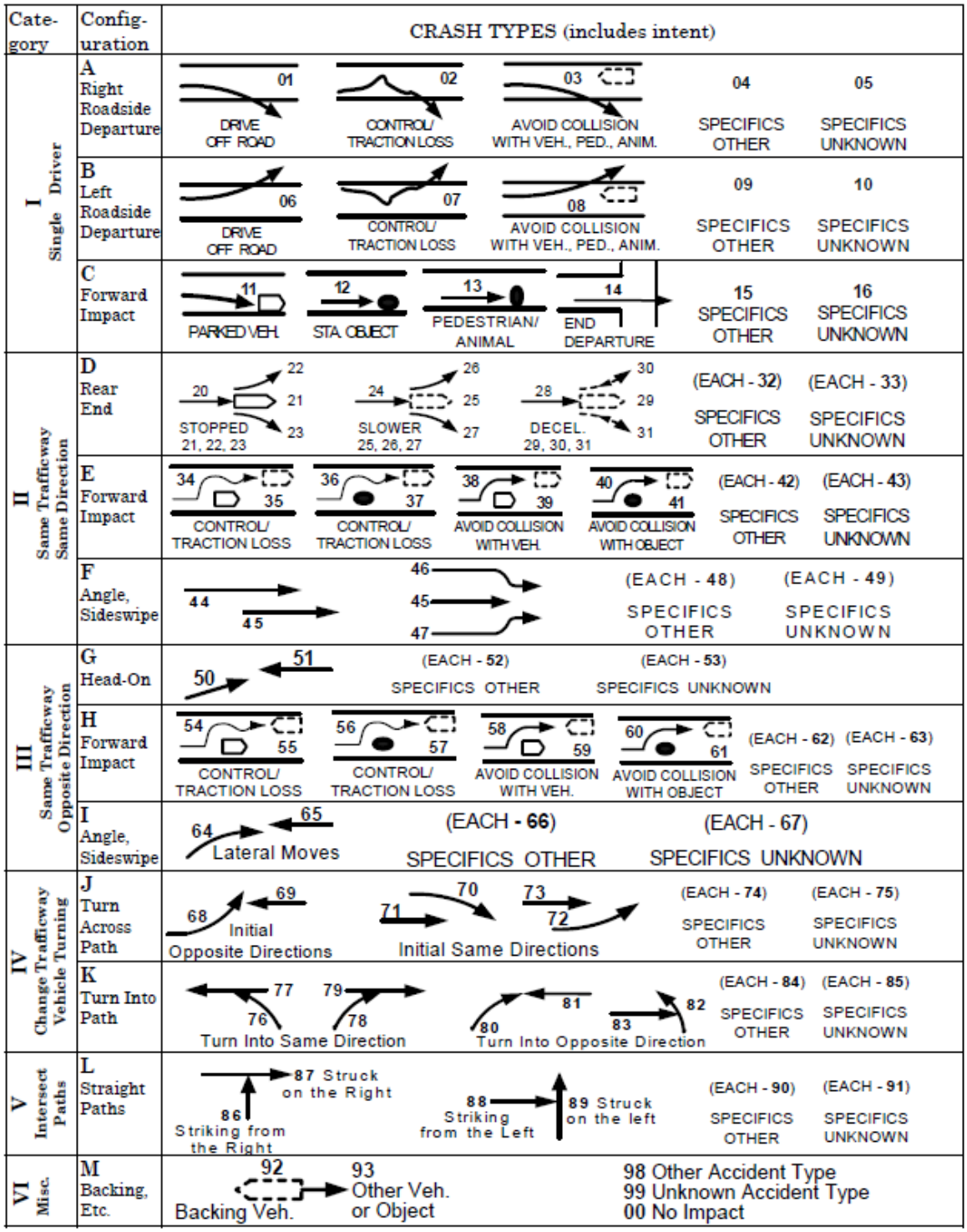

Figure A1. Crash type descriptions.

Table A1. CISS Cases

Case Number	Charcterization	Case Number	Charcterization
1-19-2017-041-01	0.15 m	1-22-2017-036-01	Adjacent lane
1-11-2017-020-01	0.18 m	1-19-2017-048-01	Adjacent lane
1-22-2017-050-01	0.3 m	1-13-2017-008-01	Adjacent lane
1-23-2017-064-01	0.48 m	1-24-2017-014-01	Adjacent lane
1-32-2017-152-01	0.6 m	1-22-2017-046-01	Adjacent lane
1-22-2017-083-01	0.82 m	1-16-2017-048-01	Adjacent lane
1-20-2017-006-01	0.85 m	1-28-2017-032-01	Adjacent lane
1-22-2017-119-01	0.87 m	1-11-2017-033-01	Adjacent lane
1-20-2017-042-01	0.92 m	1-20-2017-084-01	Adjacent lane
1-18-2017-054-01	0.96 m	1-25-2017-024-01	Adjacent lane
1-19-2017-029-01	1.03 m	1-20-2017-103-01	Adjacent lane
1-22-2017-062-01	1.27 m	1-33-2017-090-01	Adjacent lane
1-17-2017-086-01	1.3 m	1-23-2017-102-01	Adjacent lane
1-22-2017-052-01	1.32 m	1-19-2017-113-01	Adjacent lane
1-28-2017-008-01	1.33 m	1-21-2017-074-01	Adjacent lane
1-30-2017-094-01	1.69 m	1-18-2017-073-01	Adjacent lane
1-20-2017-013-01	1.95 m	1-23-2017-130-05	Adjacent lane
1-20-2017-024-01	2.0 m	1-17-2017-095-01	Adjacent lane
1-13-2017-127-01	3.0 m	1-28-2017-046-01	road edge
1-32-2017-013-01	Parked Vehicle	1-28-2017-047-01	road edge
1-28-2017-039-01	Parked Vehicle	1-28-2017-048-01	road edge
1-33-2017-025-01	Intersection	1-19-2017-097-01	road edge
1-24-2017-029-01	Intersection	1-22-2017-104-01	road edge
1-11-2017-017-01	Intersection	1-12-2017-070-01	road edge
1-22-2017-059-01	Intersection	1-19-2017-140-01	road edge

NEW DRIVER SAFETY CONCEPT FOR AUTOMATED AND MANUAL DRIVING MODE

Claus Geisler
Prof. Dr.-Ing. Rodolfo Schöneburg
Jochen Feese
Eric Gärtner
Abdulkadir Öztürk
Dr. Julien Richert
Jürgen Warwel
Mercedes-Benz Cars, Daimler AG
Germany

Paper Number 19-0210

ABSTRACT

After ten years Mercedes-Benz is presenting once again an ESF (**E**xperimentales **S**icherheits**f**ahrzeug / Experimental Safety Vehicle) – the ESF 2019. This research vehicle, based on a series production vehicle, represents a platform of safety innovations

In highly automated vehicles, the driver seat occupant is no longer required to maintain a standard driving posture while the vehicle is operating in automated driving mode. This enables new interior concepts with more flexibility and seating comfort, depending on the specific driving situation and responsibility. During automated driving mode, the driver has the option to choose more flexible seating positions to relax, work or enjoy the entertainment system. The visitors of the ESV exhibition will get a chance to experience this safety concept.

The option to choose a more relaxed seating position compels further consideration of occupant safety. The new flexible seating positions are expected to provide the same level of crash worthiness that is known from current standard seating positions for manual driving. For future car concepts, the safety systems need added flexibility to enable new situations beyond the standard driving position.

AUTOMATED DRIVING OFFERS CHANCES FOR NEW SAFETY CONCEPTS

Automated Driving is the current megatrend for future automobiles throughout the automotive industry. Automated Driving will create opportunity for new use-cases which will lead to new vehicle and interior concepts. While these new concepts will provide comfort and convenience benefits to the occupants, it is also necessary to develop a safety concept that provides the user with robust protection from injury in a crash, regardless of whether the vehicle is being operated manually by a human driver, or is being operated automatically by an ADS. It can be expected that the design process for automated vehicles incorporates a safety-oriented, defensive driving style, developed to avoid at-fault crashes with other road users, while avoiding or mitigating crashes caused by others. But due to various factors such as physical limits of vehicle response or the behavior of other road users, it is vital to understand that ADS-operated vehicles might still be involved in vehicle crashes. Thus crash worthiness will still have to be considered, even for vehicles capable of driverless operation.

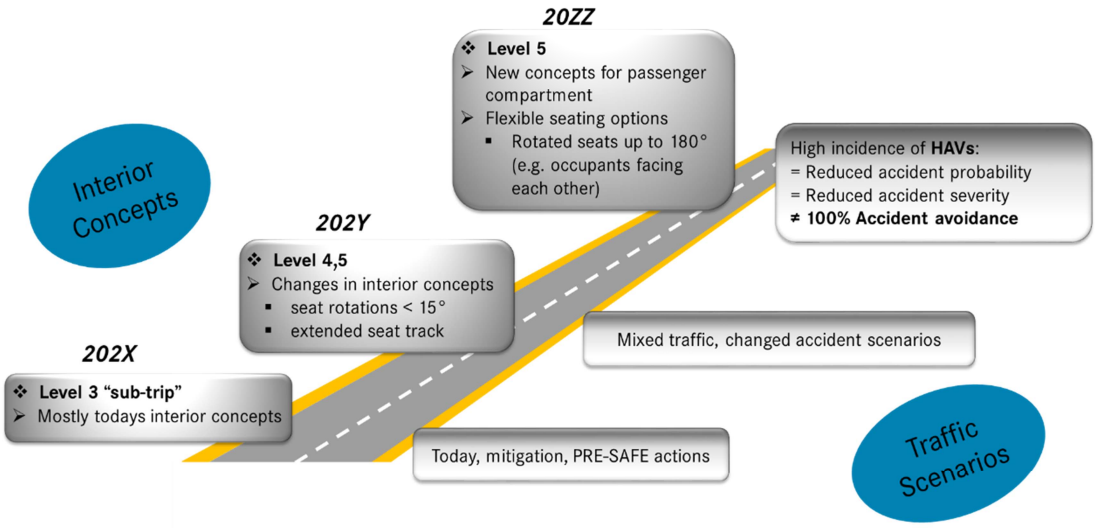

Figure 1. Automated driving from today's perspective

Impact of automated driving levels for safety concepts

Today's driving and safety concepts are based on a manually controlled vehicle, where the driver might also be assisted by advanced driver assistance systems that can enhance comfort and safety. An example is the radar-based collision avoidance system with functions such as distance warning, forward collision warning, dynamic brake support and even automated emergency braking. Although these systems are able to mitigate or avoid certain types of crashes, the driver always has the full responsibility for safe operation of the vehicle while driving in manual mode. Similarly, in future Level 3 conditionally automated driving modes where a driver must operate the vehicle for at least part of every trip, the driver is expected to remain able, alert, and responsive to requests to resume driving, issued by the vehicle. In both cases, the driver needs to maintain a seating position which enables manual or assisted driving.

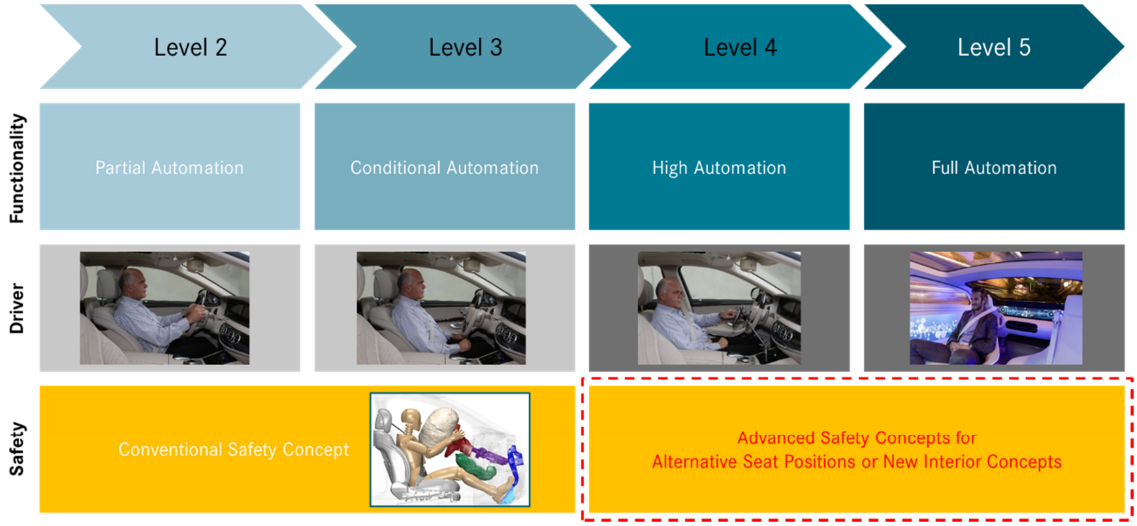

Figure 2. Driver safety concepts are depending on automated driving level

Safety during automated driving:

At Mercedes-Benz we develop highly and fully automated driving (SAE level 4/5) in urban environments at the one hand and on the other we develop the next generation of technologies for driver assistance systems and highly automated driving on highways (SAE Level 3 and Level 4).

This progress has an impact on seating configurations in future vehicles. For one thing occupants are expected to be seated as they would in a conventional taxi cab. Thus the safety systems would be comparable to those in current vehicles. Then in the continuing evolution of automated driving, ADS-operated vehicles will feature new interior concepts including seats that can be rotated 180° from conventional positions and thus allow living room-style seating, as demonstrated by Mercedes-Benz within the research car F015 [1], depicted below. These interior concepts are creating new options for interior stylists, but are also creating new challenges for safety engineers as they develop safety concepts for the future.

Figure 3. Mercedes-Benz F015 - New interior concepts for automated driving [2]

New interior concept for automated driving level 4: The 2019 Mercedes-Benz Experimental Safety Car presents innovative safety concepts for level 4 ADS-equipped dual-mode vehicles that enable either manual driving, or automated driving within specific operational domains. With this type of vehicle, the driver can decide whether to operate it in a traditional, manual mode using steering wheel and control pedals, or take advantage of available automated driving modes. To achieve the full benefit of a highly automated driving mode, Mercedes-Benz seeks to provide more space and comfort for the customer by offering more flexible seating positions to relax, work or further enjoy the entertainment system with improved visibility of the available displays.

CONCLUSIONS

Highly automated driving will offer more options and flexibility for a driver, who can become a passenger when the vehicle is operated in automated driving modes. Not being required to remain in a driving-ready seating position enables more comfortable and relaxing seating and interior options. The new 2019 Mercedes-Benz Experimental Safety Vehicle, displayed at the ESV Safety Conference 2019 in Eindhoven, NL will show new solutions with regard to occupant safety.

REFERENCES

[1] Mercedes-Benz F 015 Concept Car, CES Las Vegas 2015.

[2] Mercedes-Benz ESF 2009 @ ESV Conference 2009 Stuttgart, Prof. Dr.-Ing. Schöneburg, Baumann, Fehring

EVALUATION OF AEB EFFECTIVENESS USING COUNTERFACTUAL SIMULATIONS OF SHRP2 NATURALISTIC CRASHES

Thomas Seacrist, Ethan C Douglas, Valentina Graci, Helen S Loeb
The Children's Hospital of Philadelphia
USA

Ridhi Sahani
Bucknell University
USA

Gregory Chingas
Duquesne University
USA

Paper Number 19-0213

ABSTRACT

Motor vehicle crashes remain a significant problem in the US and worldwide. Automatic emergency braking (AEB) is designed to mitigate the most common crash mode: rear-end striking crashes. However, assessing the efficacy of AEB in real-world crash scenarios is challenging given that avoided crashes are rarely documented except during naturalistic driving studies. Unfortunately, a large-scale naturalistic driving study involving AEB-equipped vehicles has yet to be conducted. In the absence of such data, AEB can be evaluated in real-world crash scenarios by retrospectively adding AEB to naturalistic crash data using counterfactual simulations. Previous counterfactual simulations have purported the potential benefit of AEB; however these studies often make simplified assumptions about vehicle dynamics. To this end, the current study aimed to conduct the most realistic AEB counterfactual simulations to date by using measured host and lead vehicle dynamics data and vehicle-specific AEB deceleration profiles as well as accounting for driver reaction and environmental conditions. The SHRP2 Naturalistic Driving Study was reviewed to identify rear-end striking crashes among teen (16-19 yrs), young adult (20-24 yrs), adult (35-54 yrs), and older (70+ yrs) drivers. Forty rear-end striking crashes that had reliable radar data were identified to serve as a basis for counterfactual simulations. Real-world AEB deceleration profiles were taken from IIHS AEB test data. IIHS AEB tests were matched to SHRP2 vehicles by selecting the most recent IIHS AEB test of the same make and vehicle class. AEB onset for SHRP2 crashes was based on a brake threat number (BTN) algorithm. The BTN was adjusted to match IIHS measured AEB onsets using minimum RMSE. AEB curves were then adjusted to match the speed of the subject vehicle at AEB onset. AEB deceleration curves were also scaled based on road surface conditions. Driver reaction was accounted for by beginning the deceleration curve at the current driver-initiated braking level. Counterfactual simulations were conducted using MATLAB to determine if AEB would have prevented the rear-end striking crash. AEB was found to be very effective, preventing 80% of rear-end striking crashes; greater than previously reported. Half of all crashes that were not prevented by AEB occurred during poor weather conditions. This study provides the most realistic counterfactual evaluation of AEB to date, utilizing real-world crash dynamics, driver reaction, road surface conditions, and measured AEB deceleration pulses. These data suggest that AEB is very effective at preventing rear-end striking crashes.

INTRODUCTION

Motor vehicle crashes continue to be a significant problem in the United States and worldwide. While the National Center for Statistics and Analysis found a decrease in the number and rate of fatal crashes in 2017 [1] as well as for the first half of 2018 [2] – bringing the US out of a multi-year increase in fatal crashes – motor vehicle crashes remain a leading cause of death for those 65 years and younger as well as the second leading cause of unintentional injury-related deaths [3]. Globally, road traffic fatalities remain a leading cause of death, particularly among low to middle-income countries [4].

Advanced driver assistance systems (ADAS), such as forward collision waring and lane keeping assist, have the potential to mitigate these crashes, reducing overall crash severity, injuries, and deaths. Previous injury reduction models have suggested that ADAS can prevent up to 57% of crashes and resulting injuries [6-12]. Automatic emergency braking (AEB) is designed to mitigate the most common crash mode: rear-end striking crashes. However, assessing the efficacy of AEB in real-world crash scenarios is challenging given that avoided crashes are rarely documented except during naturalistic driving studies. Several studies have attempted to illustrate the effectiveness of AEB using statistical models or counterfactual simulations. However, these studies have several limitations including (1) being based on archival data such as police reports and insurance claims which lack real-world vehicle dynamics data, (2) have used idealized AEB deceleration profiles including step or ramp pulses and have assumed constant jerk, (3) have assumed a static lead vehicle, and (4) have *not* accounted for road conditions or driver reaction. Naturalistic driving studies offer a unique opportunity to provide real-world data on these variables, which can serve as inputs for more realistic counterfactual simulations.

The Strategic Highway Research Program 2 (SHRP2) Naturalistic Driving Study (NDS) offers a unique opportunity to evaluate the potential efficacy of AEB on real-world crash scenarios. SHRP2 crashes include vehicle dynamic data such as radar data, vehicle velocity, and vehicle acceleration [13], which can be used to provide more realistic inputs to counterfactual simulations. Additionally, the Insurance Institute for Highway Safety conducts test-track-based AEB evaluations of currently available vehicles and provides year/make/model specific information on deceleration profiles and activation times through IIHS TechData [14]. Therefore, the current study aims to evaluate to efficacy of AEB by recreating SHRP2 rear-end striking crashes with the presence of AEB using measured deceleration profiles to determine if the application of AEB would have effectively prevented rear-end crashes.

METHODS

This study protocol was approved by the Institutional Review Board at the Children's Hospital of Philadelphia.

SHRP2 Dataset

A subset of the SHRP2 NDS data set was obtained via a data use license with the Virginia Tech Transportation Institute (VTTI). Scene videos, incident type, and times series data pre- and post-event including vehicle velocity, acceleration, and radar data were obtained for all crashes (n=1317) previously identified by VTTI for four age groups: teens (16-19 yrs), young adults (20-24 yrs), adults (35-54 yrs), and older adults (70+ yrs). Time series data ranged from 20 s prior to 10 s post event and were collected at 10 Hz.

Data Reduction

Rear-end striking crashes were defined as events where the subject vehicle contacted a lead vehicle. Rear-end striking crashes were identified using scene videos and event narratives by two independent video coders. Any discrepancies were reconciled by the study team. Rear-end striking crashes were then reviewed for reliable radar data. Events with missing or unreliable radar data were excluded from the analysis. Event data including vehicle velocity and acceleration, relative distance to the lead vehicle, and road surface conditions were used to conduct counterfactual simulations.

AEB Counterfactual Simulations

The SHRP2 database includes the year, make, and classification (*car, SUV/crossover, pickup, truck, van*) for each vehicle involved in the NDS. To generate realistic AEB deceleration profiles, measured deceleration curves for 20 kph and 40 kph AEB tests conducted by the Insurance Institute for Highway Safety (IIHS) [14] were downloaded

from IIHS TechData (https://techdata.iihs.org) and used as inputs for the counterfactual simulations. IIHS AEB tests were matched to each SHRP2 rear-end striking events by selecting the most recent IIHS AEB test with the same vehicle make and classification. If a particular make or classification was not tested by IIHS or the SHRP2 subject vehicle was no longer in production, a classification-matched vehicle from the parent OEM was selected.

A brake threat number (BTN) algorithm [15] was used to determine the onset of AEB for each rear-end striking event. To increase the accuracy of the BTN algorithm, the BTN activation curve was scaled to match the AEB onset times measured during the IIHS AEB tests. Goodness of fit of the BTN activation curve was assessed using a minimum root mean square error (RMSE) criteria.

If the vehicle velocity at the time of AEB onset was ≤ 20 kph, the 20 kph IIHS AEB tests were used for the counterfactual simulation. Contrarily if the vehicle velocity at AEB onset was >20 kph, the 40 kph IIHS AEB tests were used. Counterfactual simulations were conducted in MATLAB 2015a. To account for changes in the AEB deceleration profile due to road surface conditions, the deceleration profile was scaled by a road surface friction factor [16]: dry=1.0, wet=0.7, snowy=0.3, icy=0.1. To account for the driver's braking reaction prior to AEB onset, the AEB deceleration curve was initiated at the vehicle's current braking level. To ensure that AEB deceleration profile was proportional to the subject vehicle's velocity at the time of AEB onset, the deceleration curves were either (1) truncated by proportionally scaling down the AEB curve in both magnitude and duration or (2) extrapolated by extending the steady-state portion of the AEB deceleration using a spline fit.

To simulate changes in vehicle dynamics due to AEB activation, the following equations were used:

$$V_{aeb}(t) = \int_{t_{aeb}}^{t_{crash}} A_{aeb}(t) + V_{SV}(t_{AEB}) \qquad \text{(Equation 1)}$$

$$X_{aeb}(t) = \int_{t_{aeb}}^{t_{crash}} \left(V_{SV}(t) - V_{aeb}(t)\right) + X_{LV}(t) \qquad \text{(Equation 2)}$$

$t_{aeb} \le t \le t_{crash}$

t_{aeb} = time of AEB activation
t_{crash} = time of original SHRP2 crash
A_{aeb} = subject vehicle acceleration with AEB
V_{SV} = velocity of subject vehicle
V_{aeb} = velocity with AEB activation
X_{LV} = relative distance to lead vehicle
X_{aeb} = relative distance to lead vehicle with AEB activation

If V_{aeb} reached zero prior to the time of the original SHRP2 crash, it was concluded that AEB prevented the crash. If the addition of the AEB deceleration caused the simulation to extend beyond the time of the original SHRP2 crash, the lead vehicle velocity was assumed to be constant and the equations below were used:

$$V_{aeb}(t) = \int_{t_{crash}}^{t} A_{aeb}(t) + V_{SV}(t_{AEB}) \qquad \text{(Equation 3)}$$

$$X_{aeb}(t) = \int_{t_{crash}}^{t} \left(V_{LV}(t_{crash}) - V_{aeb}(t)\right) + X_{AEB}(t_{crash}) \qquad \text{(Equation 4)}$$

If V_{aeb} reached zero and $X_{aeb} > 0$, it was concluded that AEB prevented the crash.

RESULTS

A total of 99 rear-end striking crashes among 95 drivers were identified from the four age groups. Among these rear-end striking crashes, 30 events had no radar data. An additional 29 events were removed due to unreliable radar data. The final dataset for counterfactual simulations consisted of 40 rear-end striking crashes.

Exemplar counterfactual simulations for a prevented and non-prevented rear-end striking crash are shown in Figure 1. AEB was found to be very effective, preventing 80% (n=32) of simulated SHRP2 rear-end striking crashes with reliable radar data. Half (4 of 8) crashes that were *not* prevented occurred during poor weather conditions.

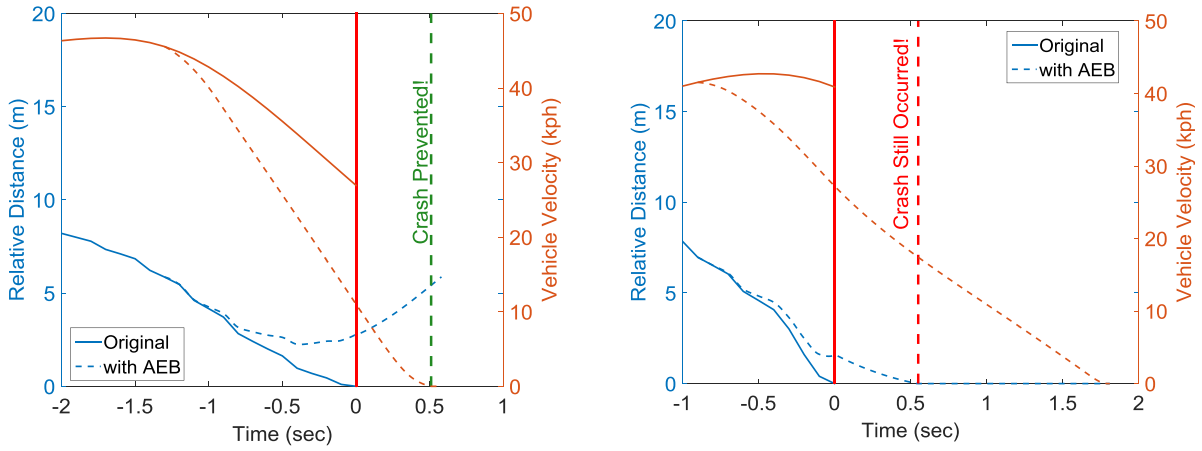

Figure 1. Exemplar prevented crash (left) and non-prevented crash (right).

LIMITATIONS

Several limitations warrant discussion. First, AEB is typically coupled with forward collision warning (FCW). The current study assumed the FCW did not alter the driver's reaction to the crash. Consequently, these counterfactual simulations represent the "worst-case" scenario for AEB. Of note, drivers executed an evasive braking maneuver in 33 (82%) of the simulated rear-end striking crashes. Furthermore, among the seven events where the driver had no evasive maneuver, AEB was capable of preventing all seven crashes. Consequently, the influence of FCW on these results is likely limited. The current study also assumed AEB activated at all speeds. However, this is not the case with all manufacturers. While some OEMs are releasing high-speed FCW and AEB systems, most low to moderate speed systems have a peak AEB activation speed of 36 mph. Consequently, the current study represents the potential of high-speed AEB to prevent rear-end striking crashes. Finally, radar data were only available for a subset (40%) of rear-end striking crashes. This possibly introduced selection bias because this subset may not be representative of all rear-end striking crashes in SHRP2.

CONCLUSIONS

To our knowledge, this study represents the most realistic counterfactual simulations of AEB effectiveness to date – utilizing measured vehicle dynamics, driver reaction, and road conditions from naturalistic data as well as measured AEB deceleration pulses. Our findings suggest that AEB is very effective at preventing rear-end striking crashes. However, AEB was less effective for crashes that occurred in poor weather conditions.

ACKNOWELDEMENTS

The authors would like to acknowledge the National Science Foundation (NSF) Center for Child Injury Prevention Studies IU/CRC at the Children's Hospital of Philadelphia (CHOP) and The Ohio State University (OSU) for sponsoring this study and its Industry Advisory Board (IAB) members for their support, valuable input, and advice. This material is also based upon work supported by the National Science Foundation under Grant Number EEC-1460927. The views presented here are solely those of the authors and not necessarily the views of CHOP, CIRP, OSU, the NSF, or the IAB members.

REFERENCES

[1] National Center for Statistics and Analysis. (2018a, October). 2017 fatal motor vehicle crashes: Overview. (Traffic Safety Facts Research Note. Report No. DOT HS 812 603). Washington, DC: National Highway Traffic Safety Administration.

[2] National Center for Statistics and Analysis. (2018b, October). Early estimate of motor vehicle traffic fatalities for the first half (Jan–Jun) of 2018 (Crash•Stats Brief Statistical Summary. Report No. DOT HS 812 629). Washington, DC: National Highway Traffic Safety Administration.

[3] Webb, C. N. (2018, February). Motor vehicle traffic crashes as a leading cause of death in the United States, 2015 (Traffic Safety Facts Crash•Stats. Report No. DOT HS 812 499). Washington, DC: National Highway Traffic Safety Administration.

[4] World Health Organization. Global Status Report on Road Safety. Geneva, Switzerland: WHO Press; 2015.

[5] Kusano KD, Gabler HC. Potential occupant injury reduction in precrash system equipped vehicles in the striking vehicle of rear-end crashes. Ann Adv Auto Med. 2010;54:203–214.

[6] Rosen E, Kallhammer J, Eriksson D, Nentwich M, Fedriksson R, Smith K. Pedestrian injury mitigation by autonomous braking. Accid Anal Prev. 2010;42:1949–1957.

[7] Edwards M, Nathanson A, Carroll J, Wisch M, Zander O, Lubbe N. Assessment of integrated pedestrian protection systems with autonomous emergency braking (AEB) and passive safety components. Traffic Inj Prev. 2015;16(Suppl1):S2–S11.

[8] Edwards M, Nathanson A, Wisch M. Estimate of potential benefit for Europe of fitting autonomous emergency braking (AEB) systems for pedestrian protection to passenger cars. Traffic Inj Prev. 2014;15:S173–S182.

[9] Kusano K, Gorman TI, Sherony R, Gabler HC. Potential occupant injury reduction in the U.S. vehicle fleet for lane departure warning–equipped vehicles in single-vehicle crashes. Traffic Inj Prev. 2014;15 (Suppl):S157–164.

[10] Searson DJ, Anderson RWG, Hutchinson TP. Integrated assessment of pedestrian head impact protection in testing secondary safety and autonomous emergency braking. Accid Anal Prev. 2014;63:1–8.

[11] Fildes B, Keall M, Bos N, Lie A, Page Y, Pastor C, Pennisi L, Rizzi M, Thomas P, Tingvall C. Effectiveness of low speed autonomous emergency braking in real-world rear-end crashes. Accid Anal Prev. 2015;81:24-29.

[12] Cicchino JB. Effectiveness of forward collision warning and autonomous emergency braking systems in reducing front-to-rear crash rates. Accid Anal Prev. 2017;99A:142-152.

[13] Hankey JM, Perez MA, McClafferty JA. Description of the SHRP2 Naturalistic Database and the Crash, Near-Crash, and Baseline Data Sets. Task Report. Blacksburg, VA: Virginia Tech Transportation Institute; 2016.

[14] Insurance Institute for Highway Safety (IIHS). Autonomous Emergency Braking Test Protocol (Version I). October 2013. https://www.iihs.org/iihs/ratings/technical-information/technical-protocols.

[15] Brännström M, Sjöberg J, Coelingh E, 2008. A situation and threat assessment algorithm for a rear-end collision avoidance system. In: Proceedings of the Intelligent Vehicles Symposium, 2008 IEEE, Eindhoven, Netherlands, 102–107.

[16] Gustafsson F. Slip-Based Tire-Road Friction Estimation. Automatica, 1997; 33(6): 1087-1099.

HANDLING OF CHILD RESTRAINT SYSTEMS (CRS) WITH SPECIAL FOCUS ON MISUSE

Matthias Kühn
Thomas Hummel
German Insurers Accident Research
Germany

Gerd Müller
Technical University Berlin
Germany

Wolfgang Fastenmeier
Institute for applied Psychology Munich
Germany

Paper Number 19-0214

ABSTRACT

The purpose of the presented study was to analyse the actual situation of children safety in cars with special focus on the misuse topic. In order to completely cover all relevant aspects of misuse both data on the frequency, severity and types of misuse and the underlying knowledge, attitudes and skills of the users were recorded. Thus, a threefold concept of observation and inquiry was constructed. First of all misuse of CRS was observed in public areas such as shopping centres, schools, road side restaurants etc.. The form which was used to classify the misuse configurations was based on the approved form already used in previous studies, but was enhanced further on. Subsequently (by telephone interview) a questionnaire was used to get more information about the misuse-relevant situational context, motives and knowledge of the users.
The field observations were conducted in Greater Berlin and Greater Munich and comprised n=1,076 cases which makes this study the largest sample ever. All relevant driving purposes (shopping, leisure activities, kindergarten, school) and all relevant weather conditions from July 2016 to September 2017 were included in the observations.
In 1,046 cases the children had been secured in CRS, about 30 % thereof in ISOFIX-systems. The misuse rate was 47 %, i.e. the first time ever below 50 %. Misuse rates depend significantly on the type of CRS: Higher misuse rates for group 0/0+ and group 1 CRS, typically where installing and securing are two separate actions, and lower misuse rates for group 2/3 CRS. This indicates that especially younger children are in danger not to be secured properly. ISOFIX-systems are significantly better than all other types of CRS. One negative effect compared to the previous studies is that misuse severity is increased. Misuse with heavy or severe impact on the protective capability was most likely to occur to Rearward Facing Systems like car beds and least probably/likely to booster seats and booster cushions, respectively. As far as misuse influencing factors are concerned the results are in analogy to the previous studies: Bad weather conditions, change of clothes, short trips < 10 minutes and related driving purposes such as driving to kindergarten and school, short transactions and going home lead to significantly higher misuse rates.
It can be stated that both the majority of the users are convinced of the protective effects of CRS and the sensibility for safety issues is enhanced. Not only parents are target groups, but also the children themselves have their own subjective needs and attitudes towards being secured in CRS, as they are an active part in CRS-use.
Finally recommendations for the improvement of child safety in cars are developed. They are addressed to car and CRS-manufacturers, authorities, traffic safety councils and Research. It is essential to continually learn about frequent misuse of CRS in order to improve the ease-of-use of CRS and communicate it to the relevant target groups.

INTRODUCTION

Many people these days are highly dependent on cars to get them where they want to be when they want to be there, and it goes without saying that they also want to take their children with them. The safety features of vehicles are designed for adult occupants. Consequently, special safety equipment has to be used for children (child restraint systems – CRSs).
The protection offered by child seats has improved constantly since they became mandatory in 1993. Although a wide range of different models are available, it can reasonably be said that even the simplest and cheapest seats offer adequate protection in theory. The main problem in connection with child seats is misuse. Studies have repeatedly shown that around two-thirds of all child seats are used incorrectly [1–5], which can considerably reduce or even nullify the protection they provide.
The misuse of child seats and the associated problems should therefore be continually examined. Since the last major field study conducted in Germany and elsewhere in Europe [5], circumstances have fundamentally changed. The ISOFIX system is now a statutory requirement for affixing the child seat to the vehicle, and new legislation on the approval of child seats (ECE-R 129) has come into force.
Consequently, the purpose and goal of this study of misuse is both to give a current picture of the use of child seats and to ascertain whether the action taken in the past to improve child safety in cars has been effective. In terms of its scope, this study sets a new benchmark. With over 1,000 cases examined, it is significantly more comprehensive than all previous field studies on this issue in Germany.

DESCRIPTION OF THE FIELD RESEARCH ON MISUSE

This research project examined the frequency and seriousness of misuse in reality. In addition, brief interviews were conducted with the drivers of the cars. Depending on the willingness of the person interviewed, an in-depth telephone interview was conducted as well.

Research tools

In order to learn as much as possible about all the interesting aspects of misuse, data was collected on the frequency, seriousness, etc. of misuse as well as on the underlying knowledge, attitudes and capabilities of the users. Two research tools were developed to record forms of misuse, the motives underlying them and relevant contextual conditions in the field. Both of these tools – an observation sheet and a questionnaire for the subsequent survey – are based on the hypotheses developed in the course of systematizing the causes of misuse in previous studies.

Observation sheet The observations, which were recorded at various locations (e.g. supermarket, leisure facilities, kindergarten, school), focused on misuse. The observation sheet documented the weather conditions and location and had a total of four sections: information on the vehicle and occupants, information on the person interviewed, information on the child, child restraint system (CRS) and misuse and, lastly, questions about the misuse identified.

Forms of misuse Any deviation from the intended way of using a child restraint system that could reduce the level of protection offered is interpreted here as misuse or incorrect use. The check list (further) developed in the previous projects was used to record the misuse observed. The seriousness of the misuse (minor, moderate, serious) was rated a priori only for selected forms of misuse; all others were rated subsequently.
The code book has three sections. The possible types of error for Group 0/0+ seats are listed in the first section, the error types for Group 1 seats in the second section and the error types for Group 2/3 seats in the third section. This also applies to the seat models approved after ECE-R 129.

Questionnaire The subsequent survey once misuse had been identified for all the children in the vehicle was designed to record contextual conditions, the reasons why people did what they did and action-related elements of knowledge. The questionnaire for the subsequent survey included questions about the purchase and fitting of the child seat and about securing the child in the child seat.

The observation and survey tools were subjected to preliminary tests in advance of the field research in order to check them against the criteria of consistency, comprehensibility and acceptance. Based on experience in previous studies, the observation and survey components were separated. As a result of the time it took the subjects to complete the survey (approx. 30 minutes) in previous studies, there were considerable problems getting them to accept it, and this cast doubt on whether the research could be completed. Consequently, a subsequent telephone survey very soon afterwards (i.e. two to three days later) was suggested to the subjects as an alternative to an on-the-spot survey.

Conducting the field research

The field study was started following the successful conclusion of the preliminary tests at the end of June 2016 and completed in June 2017. The data collected was evenly distributed throughout this period (figure 1).

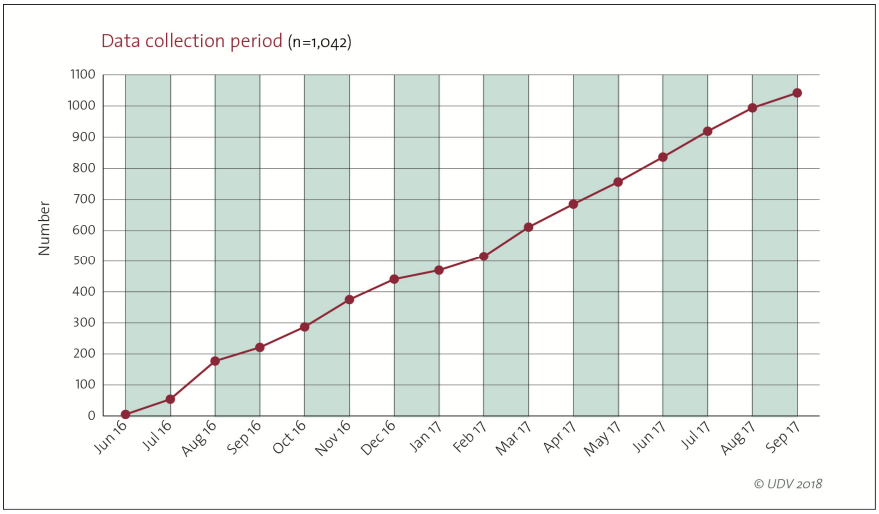

Figure 1: Research period

The securing or otherwise of a total of 1,076 children in cars was recorded. 1,042 of them were secured in a child seat, while 34 were not secured. The children were most often in Group 2/3 seats (n=472), followed by Group 1 seats (n=372) and Group 0/0+ seats (n=198). The study was conducted at selected locations in the greater Berlin and Munich areas. Figure 2 shows an overview of the survey locations. These included both urban areas and locations in the commuter belt as well as cities some distance away (e.g. Leipzig, Potsdam, Augsburg and Rosenheim). The selection of different locations ensured that different journey purposes were taken into account in the study (shopping, kindergarten and school runs, leisure).

The initial criterion for selecting the subjects was that people stopped at these locations at a given time and were driving with children aged up to 12 years old. The aim was to take a random sample and include all child restraint system types in the study. The drivers were generally approached by the observers, who then explained to them what the study was about. When the drivers declared that they were willing to take part, one of the observers collected the general information required by the observation sheet. At the same time, the second observer checked how well the children were secured in the child restraint system and how well the seat was secured to the vehicle. They then either conducted the survey on the spot for all the children in the vehicle or arranged a telephone appointment for the survey in the next few days. An average of 15 to 20 minutes per vehicle was required when the survey was conducted on the spot. This varied depending on the number of children secured in the vehicle.

Compared to previous studies, there were a significantly larger number of cases in the field research (figure 3). The large data set of 1,042 cases also permits a detailed analysis for specific lines of questioning, allowing reliable results to be obtained.

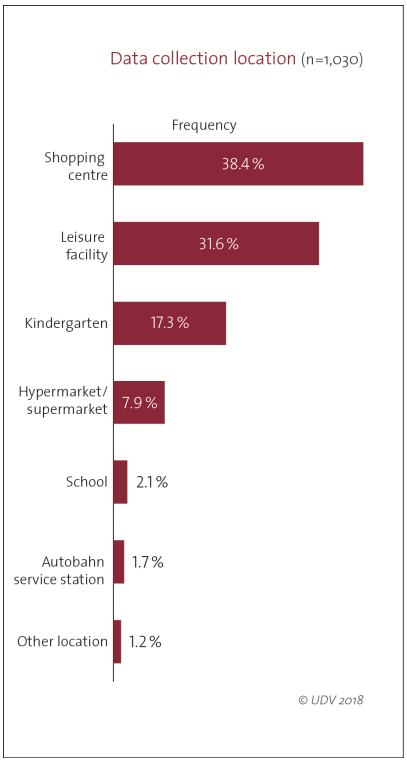

Figure 2: Location in the study

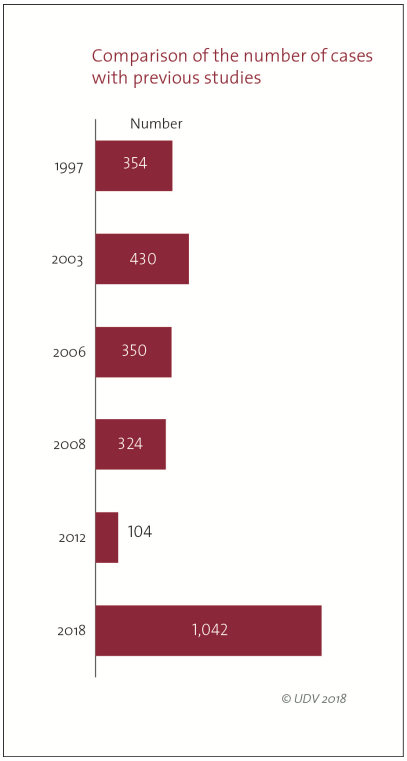

Figure 3: Comparison of the number of cases with previous studies [1–5]

RESULTS OF THE FIELD RESEARCH

Description of the sample

The sample is described in terms of the children studied, the vehicles involved, the vehicle occupants and the child seats used. There were two to six people in each vehicle. In almost two-thirds of the vehicles in the study, there were two or three people. There were one to four children under 12 years of age (i.e. children who are supposed to be secured in a child seat) in the vehicles studied. In over 80 percent of the vehicles, however, there were no more than two children. 47.3 percent of the 1,042 children were female and 52.7 male. The children ranged in age from one month to 12 years old. Figure 4 shows the age distribution of the children.

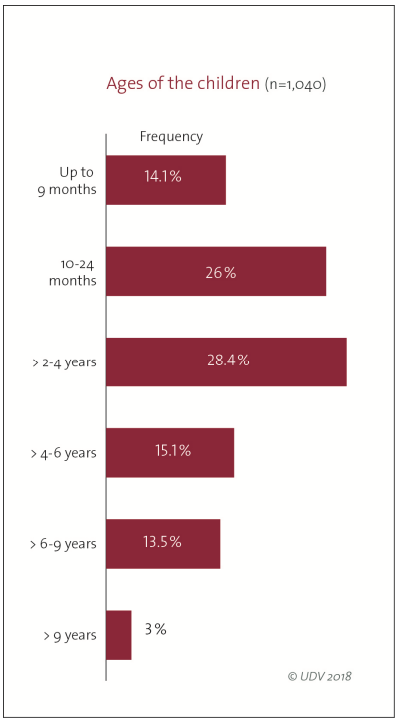

Figure 4: Age distribution of the children under 12 years of age

As mentioned above, an approach was generally made to the drivers of the vehicles. 58 percent of the interview partners were the mother of the child/children, 33.7 percent were the father, 5.4 percent were a grandparent, and 2.9 percent were another relation or friend (see figure 5).

Child restraint system Groups 2/3 and 1 were most common with 45.3 percent and 35.7 percent, respectively; Group 0/0+ accounted for 19 percent. 90.4 percent of the child restraint systems used were compliant with the ECE 44.04 standard, and 7.9 percent with the ECE 44.03 standard. Only 0.3 percent were compliant with the outdated ECE 44.02 standard, and 1.4 percent with the new ECE-R 129 standard. Most of the child restraint systems (80 percent) were fastened with a three-point automatic seat belt. An ISOFIX system was used in 20 percent of the cases. In only four cases was an integrated child restraint system used.

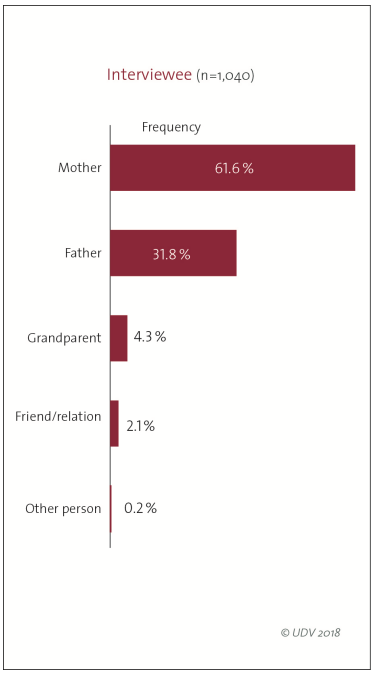

Figure 5: Interviewees

Results of the misuse observations

General investigation of misuse 52.4 percent of the total of 1,042 children were correctly secured, and 47.6 percent were incorrectly secured. The misuse rate is thus under 50 percent for the first time in this kind of study (figure 6). The misuse rate for child seats has dropped significantly.

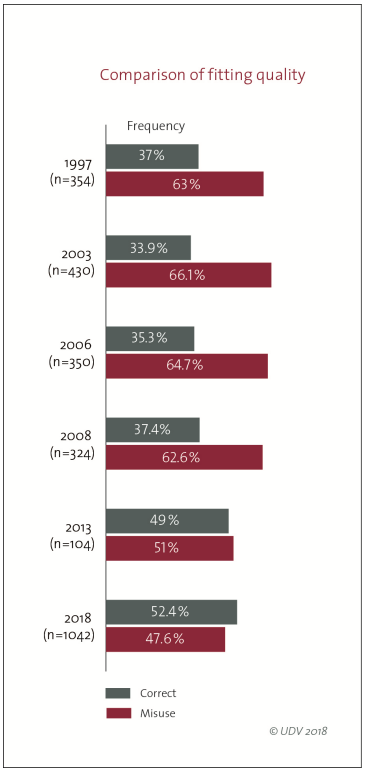

Figure 6: Comparison of the misuse rate with that of previous studies [1–5]

Half of all the observed misuse was rated serious, 35 percent moderate and 15 percent minor. Compared to previous studies, the frequency of misuse is significantly lower overall, but the seriousness of the misuse identified is higher (figure 7). Progressive developments in modern child restraint systems are ensuring that some widespread, long-standing forms of misuse can be avoided really quite easily. When misuse does occur, however, it is comparatively serious.

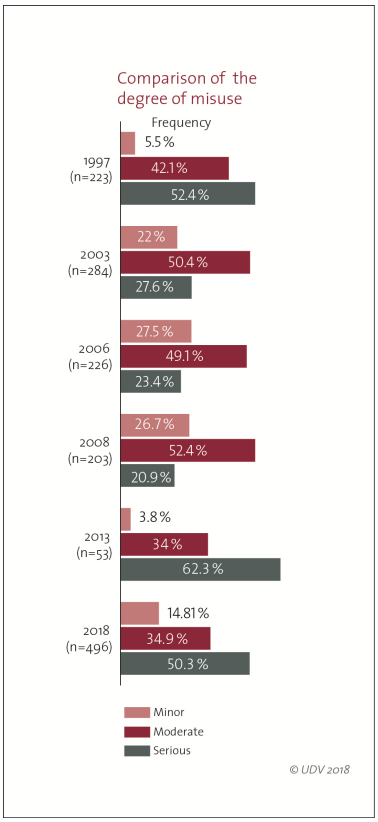

Figure 7: Comparison of the degree of misuse with that of previous studies [1–5]

When the misuse rate is broken down across the different groups of child restraint systems, it varies greatly. Misuse occurs in Groups 0/0+ and 1 significantly more frequently than in Group 2/3 (figure 8) ($p=0.004$). The main reason for this is that it is significantly easier to secure a child in a Group 2/3 seat, since in this case the child and child seat are secured together by means of the seat belt. In the other two child restraint system groups, the child seat generally has its own belt system for securing the child in the seat, and the seat is fitted in the vehicle separately.

Various factors are examined below that may contribute to misuse. For example, bad weather with rain significantly increases the misuse rate (figure 9) ($p<0.001$). It seems likely that, when it is raining, people secure their children very quickly and imprecisely. Consequently, they are not secured as well.

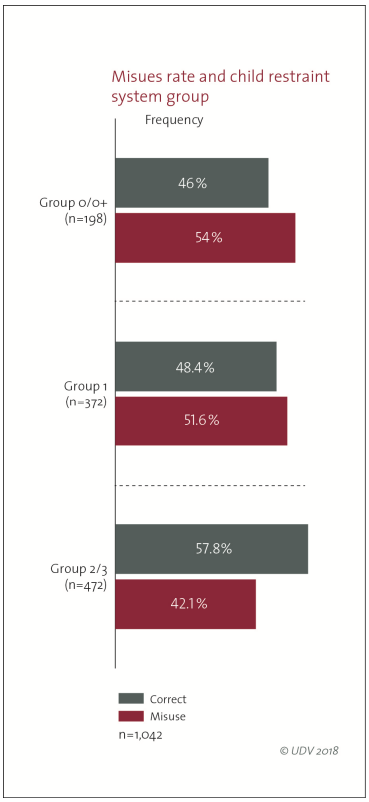

Figure 8: Misuse rate depending on child restraint system group

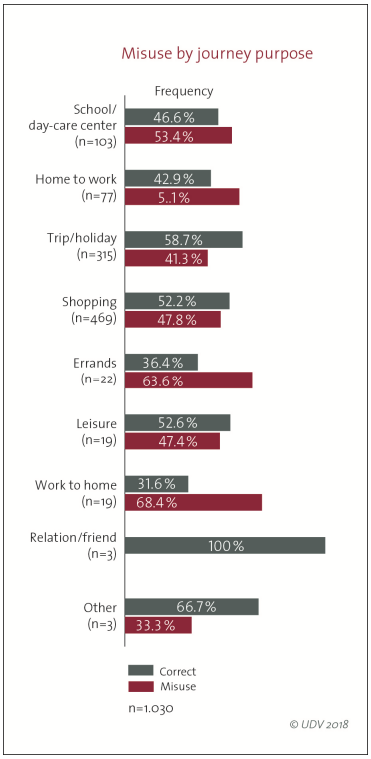

Figure 9: Misuse depending on weather

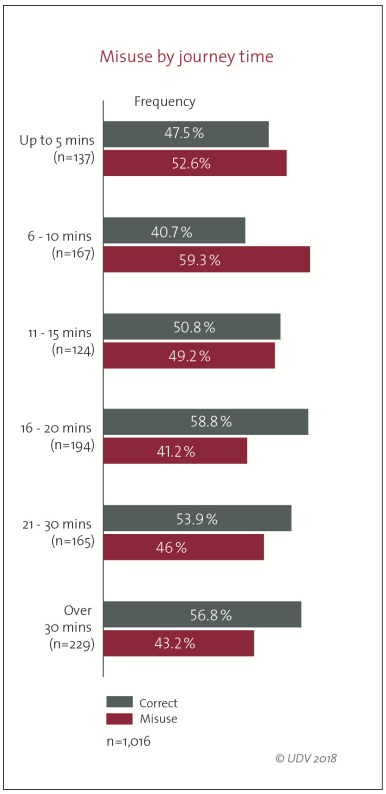

Figure 10: Misuse depending on journey duration

The journey duration also significantly affected the misuse rate. As found in previous studies, significantly more errors were made for short journeys of up to 10 minutes than for longer journeys (figure 10) (p=0.013). There is evidently still a widely held assumption that securing a child properly is less important for short journeys.

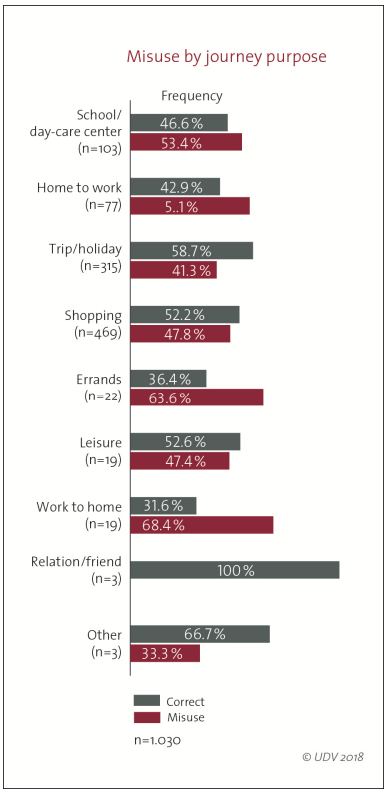

Figure 11: Misuse depending on the purpose of the journey

A significant relationship was also found between the purpose of the journey and the frequency of misuse. Journeys that tend to involve a lot of rushing about and in which time appears to be short are also associated with a higher rate of misuse (figure 11) (p=0.016). This is particularly clear for journeys to and from school or kindergarten and for errand-related journeys.

There are significantly more child restraint systems affixed to the vehicle by means of ISOFIX in this study than previous studies. This trend has a very direct impact on the frequency of misuse. As can be seen in figure 12, there is very significantly less misuse in connection with ISOFIX seats than with child seats secured by means of a three-point seat belt (p=0.000). This illustrates the positive impact of a technical standard with which vehicles and child restraint systems have increasingly complied in recent years.

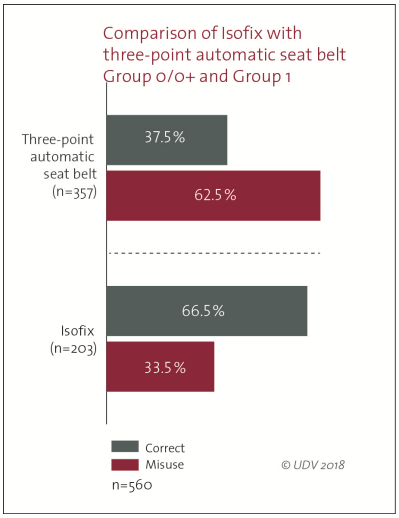

Figure 12: Comparison of ISOFIX and three-point automatic seat belt in Groups 0/0+ and 1

A highly significant relationship was also found between the misuse rate and citizenship of the interviewee (generally the person securing the child) (figure 13). The misuse rate was significantly higher among those who were not German citizens (p=0.000). People from south-eastern Europe, Turkey and Arab countries featured particularly strongly in this group. The interviews conducted repeatedly showed that the effect described has particularly cultural causes. It is thus all the more necessary to continue to develop and implement ways of addressing people of these other nationalities and convincing them of the importance of securing children in vehicles properly.

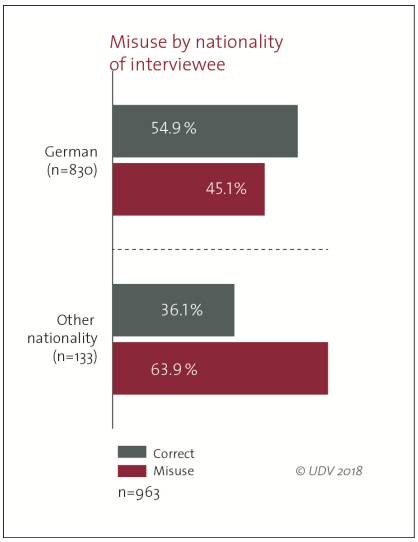

Figure 13: Misuse rate by nationality of the interviewee

Errors fitting the child restraint system Fitting errors are examined in some depth below. Fitting errors are errors that occur when fitting the child seat in the vehicle. These errors are completely different from securing the child in the seat.

Fitting errors with Group 0/0+ seats are dominated by errors in connection with the car's seat belt. These are, in particular, a slack seat belt, failure to use the guides for the seat belt and mixing up the lap and shoulder belts (table 1). Depending on their extent, all three of these errors are classed as serious misuse. Mixing up the shoulder and lap belts essentially means that the child and child seat are not secured in the car. The three types of misuse mentioned have two important factors in common. There pose a considerable risk of injury to the children, and they can be effectively avoided if ISOFIX is used.

Table 1.
Top five fitting errors in Group 0/0+ (n=145)

Top five fitting errors in Group 0/0+ (n=145)

Fitting errors in Group 0/0+	Frequency (%)
Seat belt slack	24.8
Belt guide not used	19.3
Lap and shoulder belts mixed up	16.6
Carrying handle incorrectly positioned	9.7
Seat belt twisted	7.6
Other errors	22.1

Failure to disable the passenger airbag when a baby car seat is fitted in the front passenger seat counts as a particularly serious error with Group 0/0+ seats. Although there are numerous warnings about this in the vehicle's interior, and this point is a separate offense in the German catalog of fines (Bkat), the airbag was not disabled in almost 15 percent of the cases in which an infant car seat was fitted in the front passenger seat. This is all the more remarkable due to the fact that disabling an airbag is generally very easy in modern vehicles. Accidents in which the infant car seat is hit by a triggered airbag can cause considerable injuries to the child.
Mixing up the shoulder and lap belts also occurs very frequently, accounting for 16.6 percent of the cases. This happens when the lap belt is fed behind the infant car seat, and the shoulder belt goes over the child at the front. If this error is made and there is a frontal collision, the infant car seat with the child in it is thrown forward unimpeded and – depending on where it is fitted – crashes against the dashboard or the backrest of the front seat. The associated deceleration force is correspondingly high and subjects the child to heavy loads.
There is a very similar picture for fitting errors with Group 1 seats. In this group, too, problems occur, above all, when people use the seat belt incorrectly (table 2). The most common problem is slackness in the seat belt, which was found in almost half of all Group 1 seats examined. Slackness in the seat belt is rated with different degrees of severity depending on its extent. In the great majority of these cases, the slackness in the seat belt was serious (63 percent, compared to 26 percent for moderate slackness and 11 percent for minor slackness). This considerably reduces the protection offered by a child restraint system and can result in serious injuries to the child.

Table 2.
Top five fitting errors in Group 1 (n=225)

Top five fitting errors in Group 1 (n=225)

Fitting errors in Group 1+	Frequency (%)
Slackness in the seat belt	49.3
Seat belt twisted	12.9
Belt guide not used	10.2
Seat belt buckle not or incorrectly used	4.4
Isofix without anti-rotation feature	4.0
Other errors	19.1

This error and the other three errors listed in table 2 are also reliably prevented by ISOFIX. It is noteworthy that the fifth most common error is directly connected to the fitting of Group 1 ISOFIX seats. In 4 percent of all Group 1 seats, the anti-rotation feature (i.e. the top tether) was not used. This error is rated serious in the code book. This illustrates once more that, in spite of how simple it is to use ISOFIX overall, the use of anti-rotation features presents people with problems. It seems there is further room for improvement here.
The picture is not quite as clear for fitting errors with Group 2/3 seats (table 3). Many different errors were observed, each of which occurred only infrequently. Generally speaking, however, there is less to bear in mind when fitting these seats, since the seat is secured in the vehicle together with the child.

Table 3.
Top six fitting errors in Group 2/3 (n=35)

Top six fitting errors in Group 2/3 (n=35)

Fitting errors in Group 2/3+	Frequency (%)
Blanket (or similar) under child restraint system	11.4
User's own solution	11.4
Interaction problem with headrest (of vehicle)	11.4
Impermissible fitting position	5.7
Child restraint system damaged	5.7
Isofix not engaged on the belt buckle side	5.7
Other errors	48.6

Errors securing the child The child is secured in the child seat either by means of the child restraint system's own belt system, an impact shield that belongs to the child restraint system or the vehicle's seat belt, which secures both the child restraint system and the child. Errors observed in connection with this are described in this section.
In the case of Group 0/0+ child restraint systems, slackness in the seat's integrated belt system is by far the most common problem. This error accounted for over 90 percent of all errors when securing babies in Group 0/0+ seats. Depending on the extent of this error, the effects in the event of an accident vary. If the belt is so slack that the shoulder belt can slip over the shoulders and the baby can slip under the belt, in the worst-case scenario the baby is essentially not secured and can be ejected from the child restraint system unimpeded. Other kinds of error were only very infrequent.
Slackness in the seat belt was also the most common problem with Group 1 seats, accounting for 90 percent of all errors made securing the child. Here, too, this error is particularly serious when the shoulder belt runs the wrong side of the child's shoulders and thus doesn't restrain the upper body. The upper body folds forward, and the child is only held back by the lower section of the child restraint system belt. The forces to which the abdominal area is subjected are then all the greater, which can lead to very serious injuries.
Slackness in the lap belt was also the most common error made when securing children in Group 2/3 seats (table 4). In addition, a large number of errors were made with the belt path of the vehicle's seat belt. Some are characterized as minor errors in the code book, such as the headrest of the child restraint system being set too high. Other forms of misuse, however, can have severe consequences and are therefore categorized as serious. These include running the shoulder belt under the child's shoulder, for example, so that it can no longer hold back the child's upper body. As described for Group 1 seats, this can also lead to serious abdominal injuries.

Table 4.
Errors securing children in Group 2/3 seats by frequency

Errors securing children in Group 2/3 seats by frequency

Securing errors in Group 2/3+	Frequency (%)
Lap belt slack	44.8
Seat belt twisted	11.5
Shoulder belt slack	9.4
Lap belt not inserted in the guide on the buckle side	9.4
Shoulder belt not inserted in the guide on the anchorage side	8.6
Lap belt not inserted in the guide on the anchorage side	4.7
Shoulder belt clamped under arm	2.9
Belt in contact with neck	2.1
Child seat headrest too high	1.8
Shoulder belt inserted in the guide on the buckle side	1.6

ASSESSMENT OF THOSE SECURING THE CHILDREN

After the on-the-spot checks, the people securing the children were interviewed. Over 80 percent of them responded in the affirmative to the question, “Do you believe that everything was properly secured?” It is striking, however, that over 70 percent of those who were found to have made errors were also convinced that they had done everything correctly (figure 14).

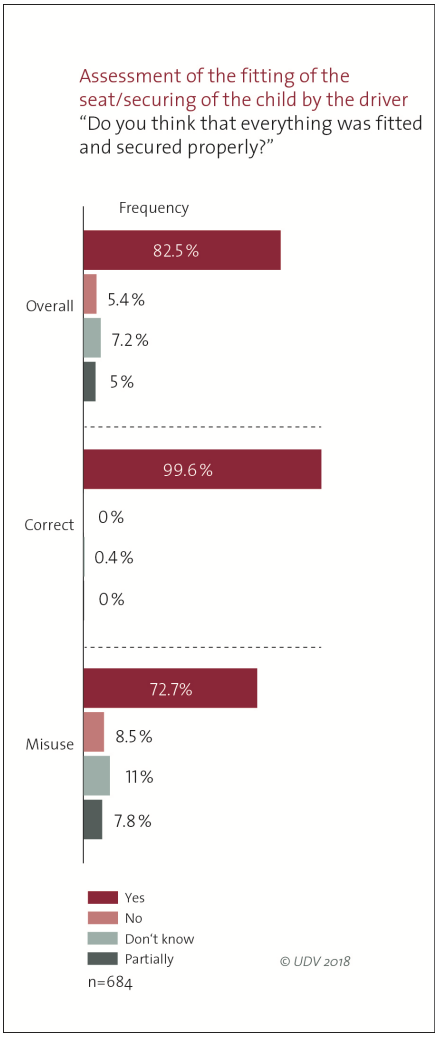

Figure 14: Assessment of how well the child is secured by the driver

When the observers identified misuse, the subjects were asked to assess the extent to which this had compromised safety: 26 percent believed there was no reduction in safety, 13 believed there was a slight reduction, while 9 percent and 14 percent believed there was a substantial or severe reduction, respectively. 37 percent could not come up with an assessment and stated that they didn't know. If you examine the assessments given for each of the child restraint system groups, the answers given are largely congruent. As shown in figure 15, a considerable portion of the interviewees were of the opinion that misuse of the child seats would have no consequences of any kind in terms of their protective effect: This sub-group accounted for almost 20 percent of interviewees in cases of serious misuse, over 30 percent in cases of moderate misuse and 40 percent in cases of minor misuse. Only a small number of them gave a realistic assessment of the associated risks.

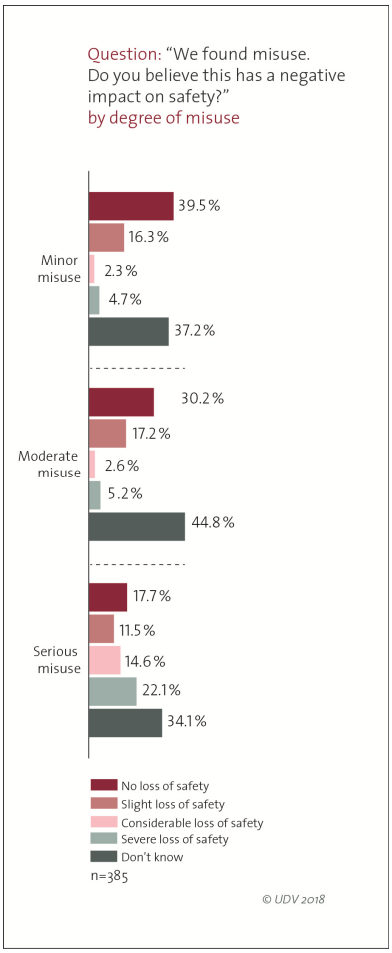

Figure 15: Answer to the question as to the effect of the identified misuse on safety

In reply to the question as to the causes of the misuse identified, the interviewees most often answered that it was due to unconscious negligence (table 5). Further quantitatively significant causes were gaps in knowledge about the correct use of the child restraint systems, insufficient or false information about the correct use of the systems, the shortness of the journey, the desire to improve the comfort of the child, clothing-related misuse, the child being allowed to secure itself and conscious negligence. Points such as technical problems, laborious fitting, etc. played a comparatively minor role.

Table 5.
Causes of misuse by frequency (multiple responses possible) n=321

Causes of misuse by frequency (multiple responses possible) n=321

Causes of misuse	Frequency (%)
Unconscious negligence	32.9
Lack of knowledge	10.1
Short journey	9.1
Insufficient/false information	6.2
Improvement of the child's comfort	5.9
Short journey	5.5
Time pressure	5.3
Conscious negligence	4.3
Technical	3.5
Clothing related (thick/thin)	3.2
Resistance from the child	3.2
Laborious to fit the seat/secure the child	2.7
Second/other car, switch of vehicle	2.2
Multiple children	1.4
Change of seats	0.3
Other reasons	4.3

POSSIBLE MEASURES/SUGGESTED IMPROVEMENTS AND RECOMMENDATIONS

Based on the empirical results of the previous studies referred to above, systematic recommendations and demands have been made to those with key responsibility for the safety of children in cars. A number of these recommendations have been implemented over the years, and they have undoubtedly contributed to the reduction in the misuse rate found in this study. Nevertheless, some recommendations for dealing with the problem of misuse have not, or not yet, been implemented.

Recommendations to manufacturers of child restraint systems and vehicles

As the current study shows, ISOFIX anchorages dramatically reduce the potential for misuse when fitting child restraint systems. The use of ISOFIX must therefore continue to be encouraged.

Although instruction manuals and pictograms are rated positively by a large majority of child restraint system users in terms of their clarity and information content, at the same time many users are still not able to recognize misuse as such. This indicates shortcomings of these instructions in terms of practical relevance, which must therefore be improved. To optimize comprehensibility and clarity, instruction manuals and pictograms must be conceived and designed in such a way as to allow any user to use the child seat correctly.

As of a certain age, children actively engage with their child seat, want to make it (more) comfortable or just work out how it all works. Interference by children is thus a significant source of misuse. To prevent children from interfering with the belt buckle, it should be fitted with a mechanism that functions as a child lock. It would be conceivable to fit a sensor that would identify such interference and notify the driver.

Problems with belts – particularly slackness – are the most frequent sources of misuse. Systems for preventing slackness in the seat belt and child restraint system harness should therefore be improved and distributed.

The next two recommendations are based not on the empirically obtained data of this field study; they come from systematic observations and experiences of the interviewers on the spot. They therefore shouldn't go unmentioned here.
Interviewees quite frequently reported that they had seen instruction videos on fitting their child restraint system and securing their child to the seat and had found these very helpful. Other people expressed the wish for videos like this for their child seat model. It is therefore recommended that there should be comprehensible and easily accessible instruction videos that explain how to use the child restraint system for all child seat models.

Recommendations to the legislative and executive branches of government
As mentioned above, pictograms on child restraint systems are important sources of information for users. It is up to legislators to make pictograms mandatory on child restraint systems.
The media undoubtedly have an important role to play in providing information to child restraint system users. However, the information provided is often relatively one-sided, because it tends to focus on subjects such as crash tests. Approval tests should address more than just this aspect; further requirements should also be defined, such as: a list of criteria for suitable child restraint systems, a list of key forms of misuse and criteria for the suitability of child restraint systems. In addition, an attempt should be made to break up this one-sided reporting in the media through suitable measures (e.g. regular newsletters to journalists specializing in this area and workshops for them).

Recommendations for research and consumer protection
Specialist shops and advisers play an important role in providing information both in advance of a purchase and when a child seat is purchased. At the same time, the results of this and previous studies indicate that the advice given on child seats is very uneven, and frequently not all the relevant aspects are addressed.
Together with the chambers of industry and commerce, binding standards should be developed for the provision of specialist advice in advance of the purchase of child seats that, in addition to providing general information on securing children in child seats, must also provide information on system-specific peculiarities. Particular importance should be attached, and particular emphasis given, to the problems of misuse. General information is not enough; instead, the specific possibilities of misuse with the child seats a customer is interested in and how to avoid this misuse should be demonstrated. As part of such a procedure, a test fitting would of course be included whenever specialist advice was offered.
Foreign citizens living in Germany were not the focus of this study, but systematic observations in the course of the field research demonstrated that foreign parents (in particular those of south-eastern and southern European origin) must continue to be regarded as a particularly problematic group when it comes to securing children in child seats. This is true not just in terms of misuse but also in terms of non-compliance with the mandatory requirement to secure children under 12 years of age in child seats. Particular aspects have to be taken into account with foreign users: their sociocultural heterogeneity and language barriers, for example. In addition, the recognized authorities in these communities (e.g. cultural centers, religious communities, foreign-language media) must be included in order to legitimize any campaigns, and at the same time their help must be enlisted to identify suitable people who can help spread the message. It should be noted in this connection that friends and family have an important role to play.
It is essential that information and awareness-raising campaigns provide both general and system-specific information on the correct way to secure children in vehicles. Information on the danger of different forms of misuse and their portrayal in detail should receive the same priority.

REFERENCES

[1] Langwieder, K.; Stadler, P.; Hummel, Th.; Fastenmeier, W.; Finkbeiner, F.: "Verbesserung des Schutzes von Kindern in Pkw" (Improving the safety of children in cars), BASt report, issue M37, Bergisch Gladbach, 1997

[2] Hummel, Th.; Finkbeiner, F.; Roselt, Th.: "Kinder im Auto. Studie zur Verwendung von Kinderschutzsystemen und Verbesserungspotentiale durch ISOFIX" (Children in cars. Study of the use of child restraint systems and the potential for improvement using ISOFIX), Berlin: Verkehrstechnisches Institut der Deutschen Versicherer, 2003

[3] Fastenmeier, W.; Lehnig, U.: “Fehlerhafte Nutzung von Kinderschutzsystemen in Pkw” (Misuse of child restraint systems in cars), BASt report, issue M178, Bergisch Gladbach, 2006

[4] Hummel, Th.; Finkbeiner F.; Kühn, M.: “Misuse of Child Restraint Systems – A 2008 Observation Study in Germany”, 6th International Conference Protection of Children in Cars, 4-5 December 2008, Munich, Germany

[5] CASPER project: Child Advanced Safety Project for European Roads, D3.1.2: Report on effect of misuse and related items, 2012

DEVELOPMENT OF A HYBRID MUSCLE CONTROLLER FOR AN ACTIVE FINITE ELEMENT HUMAN BODY MODEL IN LS-DYNA CAPABLE OF OCCUPANT KINEMATICS PREDICTION IN FRONTAL AND LATERAL MANEUVERS

Oleksandr V. Martynenko
Fabian T. Neininger
Syn Schmitt
Institute for Modelling and Simulation of Biomechanical Systems,
Stuttgart Research Center for Simulation Sciences, University of Stuttgart
Germany

Paper Number 19-000215

ABSTRACT

Automotive safety has made a definite shift towards the continually increasing use of active safety systems in standard and highly automated vehicles (HAV) with a crucial need for the development of tools to supplement the assessment of such systems. Finite Element Human Body Models (FE HBMs) emerge as an innovative pre-requisite for this process in a virtual toolchain. Traditional passive HBMs were developed for in-crash simulations and are not suitable for straightforward use in the pre-crash phase because of inappropriate soft tissues response in low gravity scenarios and the absence of active muscle elements with a proper controller.

The current contribution covers some transformation issues from passive to active behavior for HBM and focuses on the development of a physiologically motivated controller for the whole HBM utilizing standard LS-DYNA keywords. The controller operates with the contraction dynamics of *MAT_MUSCLE material (also referenced as *MAT_156) through Hatze's activation dynamics and is capable of resembling a valid occupant response during maneuvers.

The proposed neural control model is a form of intermittent control and based on the assumption that the central nervous system governs the controlled motion through shifting between particular states of the musculoskeletal system – so-called "equilibrium points", where equilibrium of all acting external and internal forces is presumed for a resulting desired position. A hybrid formulation of the controller allows for taking closed-loop muscle stimulation (target muscle lengths "λ") as well as open-loop stimulation ("α") into account.

Previous to the whole body application, the equilibrium point hybrid controller (EPHC) approach was validated separately for some parts of the body only. Posture control capability was investigated by tracking motion speed, maximum muscles activation level and the effect of co-contraction. Subsequently, the full HBM simulations were carried out for lane change and 1g braking scenarios retrieved from the experimental database of the Occupant Model for Integrated Safety Project (OM4IS). A modified Total HUman Model for Safety (THUMS) model was correlated to a matched size volunteer with the comparison of head and torso excursions to appropriate experimental corridors.

Each single body region model was validated with in vivo kinematics and dynamics enabling an integration of the single body parts into the entire HBM. Measured maximal deviations for the whole HBM reside within the experimental corridors and correlate well with the volunteer.

The proposed approach permits modeling of active and reactive human responses with the help of an existing passive FE HBM after adequate adaptation of the model, muscle elements insertion and controller parameters tuning. Such model paves the way for the evaluation of new HAV interior concepts and the development of advanced vehicle safety systems.

INTRODUCTION

Crash tests with anthropometric test devices were historically inevitable for the design and test of automotive safety systems. However, stunningly fast development in simulation technologies not only increased computational power and simulation speed but also led to better, more valid digital models for studying the crash scenarios. The idea of using virtual human body models (HBM) emerged as a consequence of such advances realizing the benefits of virtual tests with higher biofidelity, compared to the commonly used virtual dummy models. Today, HBMs provide a vast application field in automotive safety system development, more and more penetrating from the in-crash phase studies into the pre-crash considering active human behavior, e.g., reflexes and simple movements.

As the primary simulation method nowadays in the automotive industry is the finite element (FE) analysis, regularly used state-of-the-art HBMs were implemented applying FE tools and validated for in-crash scenarios, basing mostly on the cadaver studies implying high loads during impact. Accordingly, such models are passive by their nature and are not suitable for straightforward application in the pre-crash phase for two main reasons: inadequate soft tissue response in low g scenarios and absence of active muscle elements with appropriate biological muscle controller. We hypothesize that it is possible to simulate active and realistic human motion with the currently available human body models after accurately solving these issues.

It is proven that muscle activity has a significant impact on the occupant kinematics during typical pre-crash events including braking or evasive maneuvers [1-3]. In recent years, there has been an increasing amount of literature on the aHBM development using different types of models and implementing different muscle activation strategies [4]. However, the number of the existing whole body FE aHBMs is still limited. THUMS v.5 model with a proportional-integral-derivative (PID) muscle controller including two controls for 16 three-dimensional joint angles and two reaction forces from a steering wheel and pedals was introduced in [5]. SAFER A-HBM model [6], which is based on the earlier THUMS v.3 [7], uses similar PID feedback controllers, but limited to seven relative angles between body parts. In contrast to mentioned models, λ-controller was adopted in reactive THUMS-VW model [8] to control around 600 muscles governed by 66 separate controllers. Despite the long development process and validation with many test cases these models still have some drawbacks in simulations of the whole crash sequence, with the main reason being lack of the omni-directionality. Consequently, there is a clear need for further developments of whole body aHBM with omni-directional controllers capable of combined maneuvers simulations.

The purpose of this study is the application of the macroscopic Hill-type [9] muscle modeling approach to activate a modified FE HBM also based on the THUMS v.3 [7]. Currently, such models reveal high joint and tissue stiffnesses which first have to be reduced. Henceforth this model was used with the aim to perform a simulation predicting occupant kinematics behavior according to the experimental data from the Occupant Model for Integrated Safety (OM4IS) project [1]. The hybrid equilibrium point controller (hybrid controller) proposed in [10] was adopted as a muscle control strategy including physiological Hatze's activation dynamics [11] interacting with contraction dynamics from the *MAT_MUSCLE in LS-DYNA R7.1.3 software [12]. All functions serving the controller needs were implemented inside LS-DYNA utilizing standard keywords to increase industrialization possibilities.

METHODS

Adaptation of the soft tissue response

One of the main prerequisites for active human body models (aHBM) is an adequate soft tissue response in low g load scenarios which are predominant in the pre-crash phase. As mentioned above, passive HBMs are found to be excessively stiff. Thus, 50th percentile average occupant THUMS v.3 model was modified according to the procedure described in details in [13] to reproduce passive "relaxed" human occupant behavior with not active muscle elements included to fit experimental corridors given in [1]. According to the given study, "relaxed" state means fitting the corridor defined by displacement of the head center of gravity (CG) from volunteers with minimal muscle activity during 1 g braking loading pulse. The model adaptation includes mesh refinement in several body regions, a modification of connections between skin and some other parts, and the revision of the elastic modulus for specific soft tissues within physiological limits given in the literature.

Implementation of the biological muscle controller

Hybrid Equilibrium Point Controller: The neural control model used in this contribution is a form of intermittent control [14]. It is based on the assumption, that the controlled motion is governed by the central nervous system (CNS) through shifting between individual states of the musculoskeletal system (so-called "equilibrium points", EPs). In such an EP the equilibrium of external and internal forces acting on the body is reached resulting in the desired body posture. For the hybrid EP control approach [10,15], the motor command consists of two terms:

λ part – closed-loop feedback controller signal: Is based on the control of each of the body muscles target lengths. It could be known to the CNS by mapping of joint angles to associated muscles and could be stored in the memory as the magnitude of a respective signal from muscle spindles and Golgi tendon organs and obtained through learning process during an ontogenesis [16,17].

α part – open-loop feedforward controller signal: Could be generated directly by the CNS to compensate existing external loads, to hold the desired body posture or to reach a certain position in a specific manner, e.g. very fast, and could be governed via visual feedback or other internal sensors not directly associated with the muscle itself [18].

Herewith, the total neuronal stimulation signal from the CNS could be defined mathematically as a combination of the closed-loop signal and open-loop signal (Equation 1). Signal values are varying inside the interval [0...1], where "0" is no muscle stimulation at all and "1" is a fully stimulated muscle. It should be noted here, that full stimulation is a theoretical upper limit, and maximum voluntary stimulation is below "1".

$$u_{hybrid}^{total}\Big|_0^1 = u_{\lambda}^{closed} + u_{\alpha}^{open} \qquad \text{(Equation 1)}$$

To simplify the use of this method in industrial applications and to allow for intuitive and easy handling, the controller code was implemented within LS-DYNA software using standard keywords *DEFINE _FUNCTION, *DEFINE_CURVE and *DEFINE_CURVE_FUNCTION in combination with C programming language for missing functionality. Since LS-DYNA provides no capabilities presently to solve user specified differential equations directly inside the program code, a prescribed velocity of the specially created nodes (*BOUNDARY_PRESCRIBED_MOTION keyword) was used for retaining old variable values from the previous load step, which are needed for numerical integration over time and muscle neural delay implementation. A flowchart of the controller logic and its incorporation in combination with the LS-DYNA muscle material model *MAT_MUSCLE is presented in Figure 1, where α represents the open-loop part of the controller signal, and not the α motor neuron signals. Other corresponding symbols could be found in Table 1.

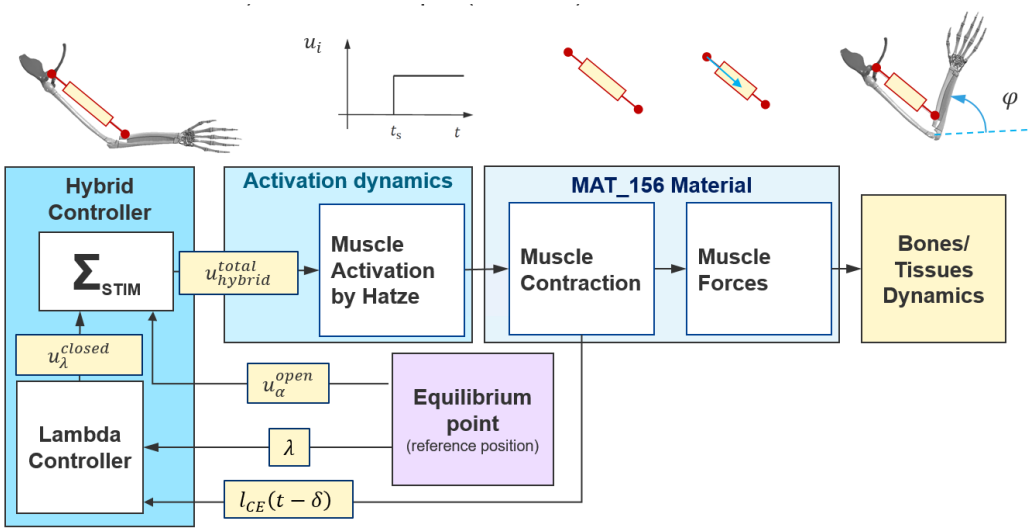

Figure 1. Flowchart of the muscle controller code shown for the single muscle element only.

As seen from the given chart, the implemented controller uses delayed actual muscle length value $l_{CE}(t-\delta)$ as a feedback signal compared to the target length of the muscle λ and a predefined stimulation u_{α}^{open} as a feedforward signal. Both inputted values of λ and u_{α}^{open} are defined by the equilibrium point (reference position) given in the simulation time and were retrieved from existing experimental data [1] a priori to simulation runtime.

Muscle length signal has a delay due to the time of sensory impulse traveling from muscle spindle through the nerve to the control center and back. The muscle spindle belongs to the group of proprioceptors and corresponds to the organ of perception inside the muscle belly. This organ has the functionality similar to a closed-loop PD-controller because muscle tissue itself shows visco-elastic behavior [10]. Thus, the equation of the λ-controller part could be written in the following form (Equation 2) with the corresponding symbols shown in Table 1.

$$u_{\lambda}^{closed}\Big|_0^1 = \frac{k_p}{l_{CEopt}} \cdot [l_{CE}(t-\delta) - \lambda] + \frac{k_d}{l_{CEopt}} \cdot v_{CE}(t-\delta) \qquad \text{(Equation 2)}$$

From the given relation it is evident that deviations in targeted and actual muscle lengths in connection with the contraction speed result in increased muscle stimulation. The main advantage of λ-control is that the forces needed to reach a target position are calculated during the motion, and no inverse problem has to be solved. Thus, switching between different intermediate postures during simulation time is done by changing the muscle's target lengths without any modifications in the controller code. This allows intuitive and easy handling in industrial applications.

Table 1.
List of the Parameters and Corresponding Symbols Used Within the Controller Code

Symbol	Parameter Definition	Value
t	Current simulation time	Calculated in runtime
δ	Neural delay of the muscle signal	Preset value
v_{CE}	Contraction velocity of the contractile element (muscle fiber)	Calculated in runtime
l_{CE}	Actual length of the contractile element (muscle fiber)	Calculated in runtime
l_{CEopt}	Optimal length of the contractile element (muscle fiber)	Preset value
λ	Target length of the muscle	Preset value
k_p	Proportional controller gain	Preset value
k_d	Differential controller gain	Preset value
γ	Free calcium ion concentration in the muscle	Calculated in runtime
$\dot{\gamma}$	Time derivative of free calcium ion concentration	Calculated in runtime
γ_{min}	Initial calcium ion concentration	Preset value
u_{hybrid}^{total}	Total muscle stimulation level from the controller	Calculated in runtime
u_{λ}^{closed}	Stimulation signal from closed-loop feedback controller part	Preset value
u_{α}^{open}	Stimulation signal from open-loop feedforward controller part	Preset value
a	Muscle activation level or activity	Calculated in runtime
a_{min}	Minimal muscle activation level	Preset value

Activation Dynamics: Physiological muscle activation dynamics introduced in [11] is used for a transfer of the total stimulation signal u_{hybrid}^{total} from the Hybrid controller into muscle activation level a, which could be directly inputted as a constant value or a continuous function (load curve) to LS-DYNA material *MAT_MUSCLE. The activation signal is calculated in the controller code in two steps: 1) the free calcium ion concentration is calculated by an integration of a first-order differential Equation 3 with an explicit Euler scheme (Equation 4); 2) this result is fed afterwards in an Equation 5 to calculate the resulting muscle activation with relation to renormalized factor for length dependency.

$$\dot{\gamma} = m \cdot (u - \gamma) \qquad \text{(Equation 3)}$$

where $m = 0.01\ (1/ms)$ – Hatze's activation frequency constant.

$$\gamma_{n+1} = \gamma_n + \dot{\gamma}_n \cdot dt \quad \text{(Equation 4)}$$

taking into account $\gamma(0) = \gamma_{min}$.

$$a(t) = \frac{a_{min} + [\rho(l_{CErel}) \cdot \gamma(t)]^{\nu}}{1 + [\rho(l_{CErel}) \cdot \gamma(t)]^{\nu}} \quad \text{(Equation 5)}$$

where $\rho(l_{CErel}) = \rho_c \cdot \frac{l_\rho - 1}{l_\rho / l_{CErel} - 1}$ is Hatze's length dependency function with respective constants $\rho_c = 9.10$, $l_\rho = 2.9$ and $\nu = 2.0$ taken from [19].

Contraction Dynamics: The muscle's contraction dynamics is incorporated into LS-DYNA material *MAT_MUSCLE [12] and generates active force from contractile element according to the law shown in the Equation 6.

$$F_{CE} = \sigma_{max} \cdot a(t) \cdot f_l(l) \cdot f_v(v) \quad \text{(Equation 6)}$$

where σ_{max} – is a generated peak stress for the muscle, $a(t)$ – is a muscle activation level calculated in the Equation 5, $f_l(l)$ – is a force-length relation in the exponential form taken from [15] and $f_v(v)$ – is a force-velocity relation in a hyperbolic form also from [15] (Figure 2). Additionally, the force generated by the muscle finite element is influenced by passive and damping components. The values of generic parameters used in *MAT_MUSCLE for all muscles along with appropriate references are reported in Table 2 below.

Table 2.
Generic Muscle Parameters for LS-DYNA Material *MAT_MUSCLE

Parameter	Description	Value (units)	Source
PIS	Peak Isometric Stress	0.001 (GPa)	[20]
SRM	Maximum Strain Rate	0.005 (ms-1)For Hand muscles	[21]
		0.0022 (ms-1) For Torso and Neck muscles	[21]
SVS	Force-Length Relation	Load curve Input	[15]
SVR	Force-Velocity Relation	Load Curve Input	[15]
SSP	Stress vs. the Stretch Ratio	Load Curve Input	[15]

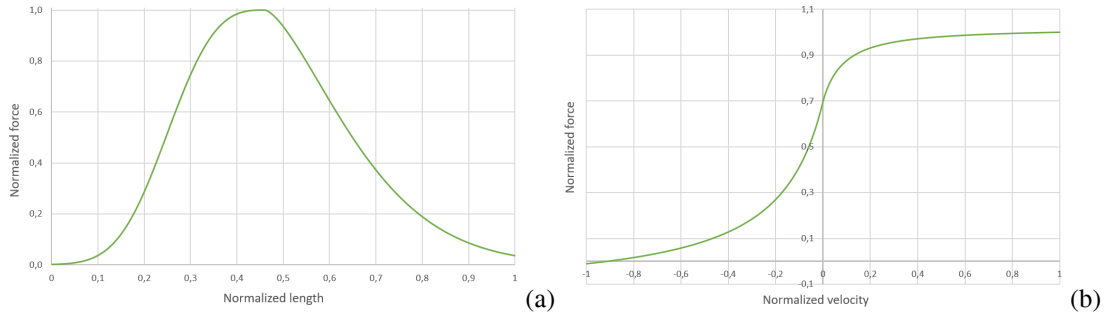

(a) (b)

Figure 2. Force-length (a) and force-velocity (b) relations used for all muscles according to [15].

Insertion of the muscle elements into the HBM

About 370 muscles from the human body were added subsequently into aHBM for the current study. Among them: 180 muscles were added to the neck, 150 – to the thoracic region and 40 – to upper extremities. All these muscles are represented by one-dimensional truss elements (*ELEMENT_BEAM, formulation ELFORM=3) with assigned material *MAT_MUSCLE. In order to give them the necessary anatomical and physiological properties such as origin and insertion nodes, optimal muscle length and physiological cross-sectional area (PCSA), these values were obtained from complementary literature sources [22-25].

Occupant Model for Integrated Safety Project Experimental Data

OM4IS project major objective was to gather a comprehensive collection of vehicle and occupant kinematic data based on results from human volunteers seated in the passenger position undergoing different driving maneuvers. Among them were emergency braking from two different speeds, lane change maneuvers to both sides and combined ones. This data was published in several sources prior to our study and represents an excellent base for the aHBM validation. Load□case results for emergency braking from 50 km/h and lane change, where a combination of lateral and frontal accelerations occurred, given in [1] are used in this contribution to validate the whole body model.

RESULTS

Validation at the body region level

To validate the proposed hybrid controller a simple multibody musculoskeletal model similar to the one proposed in [10] was built. This model consists of three rigid bodies including bones and eight truss elements representing muscles (4 flexors and 3 extensors) which actuate the elbow joint. The elbow flexion movement from 45deg to 145deg was simulated according to the given test set-up. This experimental source was taken because it offers a clear test setup, which is easy to reproduce in a simulation environment. Additionally, only one joint is actuated which allows a fine-tuning of the controller parameters. The resultant model was retrieved from THUMS model [7] by separating the bone parts and adding a revolute joint for the elbow with the stiffness of 0.6 kN·mm/rad specified according to [21] (Figure 3). A physiological muscle routing was not implemented, hence a supplementary rigid beam with the total length of 20mm was connected to the ulna bone to enable the triceps muscle elements connection.

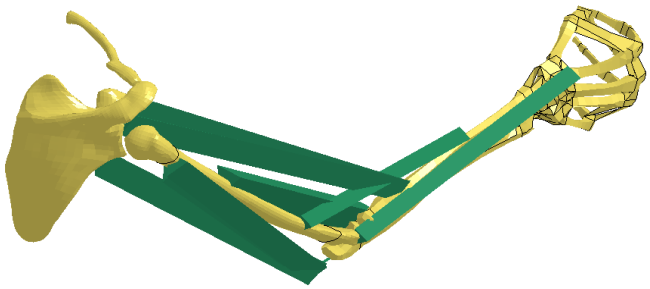

Figure 3. Multibody arm model with inserted muscles.

The structure of the hybrid controller includes feedforward and feedback components. Therefore, input signals for both have to be set.

Deriving control signals for the feedforward α part: Open-loop stimulation signal is governed directly by the CNS to switch between EPs and in current study intended mainly to hold the position or to compensate existing external loads by the muscle co-contraction. By definition, the static equilibrium is considered in any of the EPs resulting in constancy of the angular velocity and acceleration which should be equal to zero [15] (Equation 7).

$$\dot{\varphi}_i = 0 \text{ and } \ddot{\varphi}_i = 0 \quad \text{(Equation 7)}$$

These equalities could be rewritten in a form of moment equilibrium over the joint

$$\sum_{i=1}^{n} M_i = 0 \quad \text{(Equation 8)}$$

For the case when external loading is absent, taking into account definitions of the muscle moment $M_i = \vec{r}_i \cdot \vec{F}_i$, moment arm $r_i(\varphi) = \frac{\partial l_{Mus,i}}{\partial \varphi}$ and linear force from the element with *MAT_MUSCLE material $F_i = a_{i,\alpha} \cdot PCSA_i \cdot \sigma_{max} \cdot (\sigma_{SVS} + \sigma_{SSP})$ the equation for finding muscle activation levels $a_{i,\alpha}$ for α part of the hybrid controller could be derived:

$$\sum_{i=1}^{n} \left(\frac{\partial l_{Mus,i}}{\partial \varphi} \cdot a_{i,\alpha} \cdot PCSA_i \cdot \sigma_{max} \cdot (\sigma_{SVS} + \sigma_{SSP})\right) = 0 \text{ (Equation 9)}$$

This system of linear equation of n variables for muscle activation levels $a_{i,\alpha}$ could be solved for stimulation levels $u_{i,\alpha}^{open}$, which would be used as an input signal for the controller, by coupling it with the Equations 3 and 5. It results in a manifold of solutions, that could be constrained by applying additional conditions governed by the desired co-contraction in the muscles defining the respective joint stiffness. Higher co-contraction (muscle activation levels) leads to higher apparent joint stiffness slowing the movement velocities and vice versa. A list of all symbols with definitions used in the calculations is given in Table 3.

Table 3.
List of Symbols Used in Calculations

Symbol	Definition	Value
M_i	Moment generated by the muscle	Calculated in runtime
r_i	Instantaneous moment arm of the muscle	Calculated in runtime
F_i	Force generated by the muscle	Calculated in runtime
$l_{Mus,i}$	Length of the muscle	Derived in range of motion
φ_i	Joint angle	Preset value
$\dot{\varphi}_i$	Angular velocity of the joint	Calculated in runtime
$\ddot{\varphi}_i$	Angular acceleration of the joint	Calculated in runtime
$u_{i,\alpha}^{open}$	Muscle stimulation level from the feedforward α controller	Calculated in runtime
$a_{i,\alpha}$	Activation corresponding to the $u_{i,\alpha}^{open}$	Calculated in runtime
$PCSA_i$	Physiological cross sectional area of muscle	Calculated in runtime
σ_{max}	Peak isometric stress	Calculated in runtime
σ_{SVS}	Normalized stress generated by contractile element	Read from SVS curve
σ_{SSP}	Normalized stress generated by parallel elastic element	Read from SSP curve

Deriving control signals for the feedback λ part: The closed-loop stimulation signal in real muscle builds on the interaction of muscle spindles and Golgi tendon organs from the sensory side and α- and γ- motoneurons from the actuator side. From the technical perspective, such a system is based on the PD feedback control with the target to maintain the desired muscle length (Equation 2). Thus, before any analysis, it is crucial to preset the target muscle length as a variable for the controller to function. The straight forward way to find these values is to run the pre-simulation that brings the model into the desired state and measure the obtained muscle elements length knowing the attachment nodes. Such procedure was done for the arm model built and elbow flexion from 45deg to 145deg. Target length obtained and applied in the simulation for different muscles over time are shown in Figure 4.

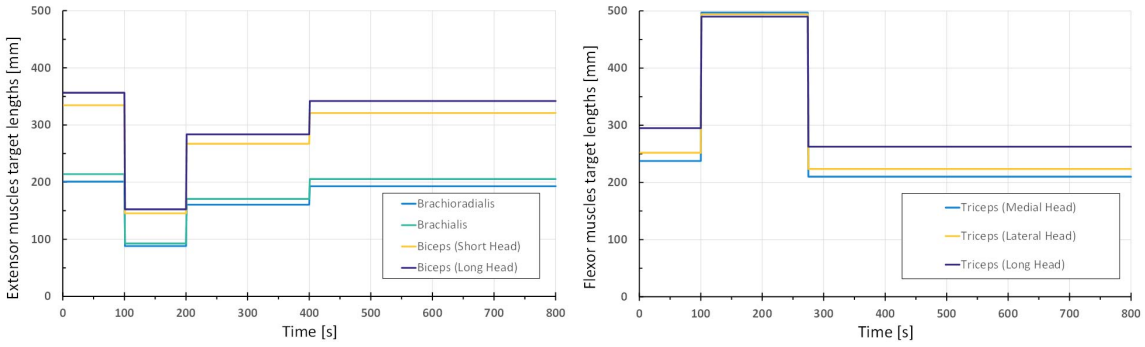

Figure 4. Muscle target lengths (feedback controller input signals λ) used for flexor and extensor muscles.

Simulation results for the arm model: FE arm model simulation results show a good correlation with the volunteer kinematics (Figure 5). A mismatch in a joint stiffness of the multi-body model compared to the human arm could explain small difference in a curve slope, thus higher speed of the simulated movement. Likewise, the lower joint stiffness in the model can also be a reason for a broader range of joint angles achieved.

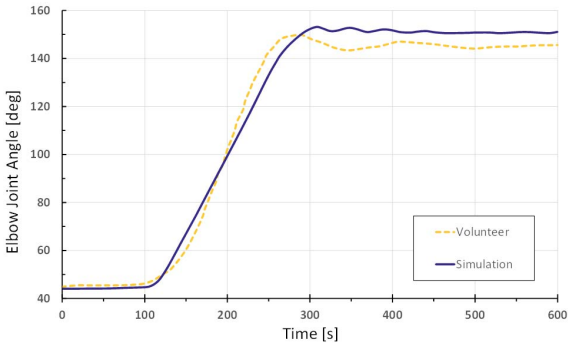

Figure 5. Comparison of elbow joint kinematics for the hybrid controller and volunteer response from [10].

Validation at the HBM level

After successful validation at the body region, the level of the study was extended to the whole HBM level. As a validation basis volunteer tests conducted in the OM4IS project [1] described shortly above was used. Braking and lane change scenarios were chosen for the current study. Data available for the comparison includes vehicle acceleration, head (at ear level) and torso (at T5 level) excursions. A model setup that is similar to the real world test was represented in the simulation environment. AHBM with seatbelt applied is seating in the reference seat in front passenger occupant position with the corresponding maneuver motion pulse applied (Figure 6).

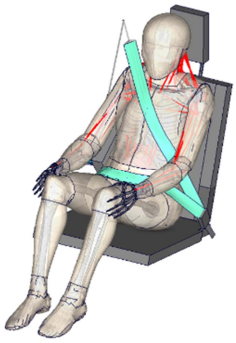

Figure 6. Simulation setup for the sled tests.

Open-loop stimulations $u_{i,\alpha}^{open}$ capable of maintaining the sitting posture with muscle co-contraction were determined and input, following by automatic calculation of closed-loop stimulation $u_{i,\lambda}^{closed}$ according to the procedure described above depending on the validation case.

Emergency braking: Following the experiment, a deceleration pulse to zero of the vehicle with the initial velocity of 50 km/h was applied to the sled. Feedback λ-controller was activated starting from the 10% of the peak pulse value and attaining 80-90% of the initial muscle length set as targets in the most distant body deflections. Choice of the muscle target lengths λ was performed according to suggestions given in [16].

Simulation results carried out for whole HBM with the functioning controller (referenced as active HBM) and without it (referenced as passive HBM) are shown in Figure 7. Head and torso centers of gravity (CG) excursions in the sagittal plane of the body were measured and compared to the experimental corridors. As seen from the results, almost for the whole observed maneuver time the aHBM excursions are lying inside the corridor measured for volunteers, being outside after HBM's contact with the seat on the ending phase. It could be explained by the influence of the contact parameters between the model's back and seat surface, which need to be tuned more precisely. Passive HBM is outside of the corridor for the initial phase and close to the margin later, having the same problem with a contact in the end.

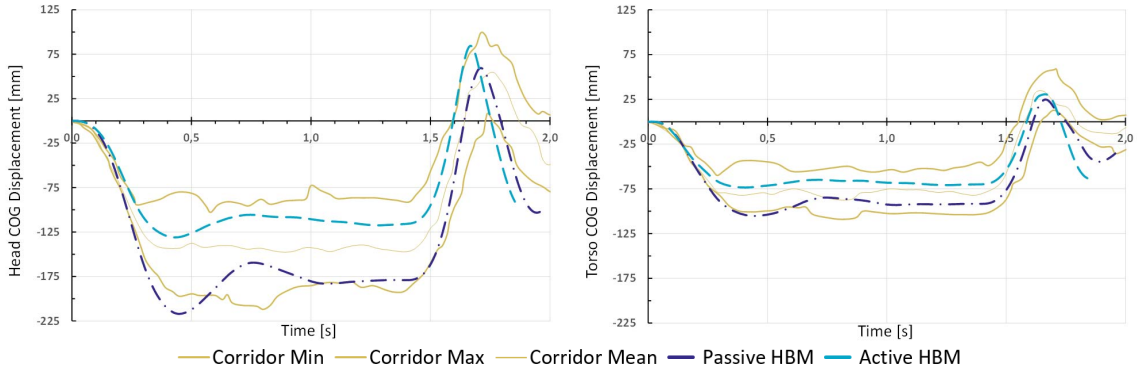

Figure 7. Comparisons of head and torso CG excursions during emergency braking maneuver and volunteer response corridor from [1].

Lane change: Lateral acceleration pulse of the vehicle with the longitudinal velocity 50km/h was applied to the sled. Feedback controller was active from the start and muscle target lengths λ were reversed at the point where the acceleration changes its direction with the pulse slope 0.

Simulation results are available in Figure 8, where head and torso CG excursions in the coronal plane of the body compared to the experimental corridors are given. In the same way, as observed for previous validation case, aHBM has less excursions with respect to the measurement corridor compared to a passive one. Due to the λ controller advantage to control each muscle length individually, additional volunteer muscle activity in order to avoid contact with the B-pillar was mimicked correctly. Head excursion being severely out of the corridor could be explained by the absence of physiological muscle routing in the neck, which is addressed in the DISCUSSION. Besides, more accurate assignment of target lengths to muscle groups responsible for neck flexion and lateral flexion of the lumbar spine could improve the aHBM kinematics. Further studies are needed in this direction.

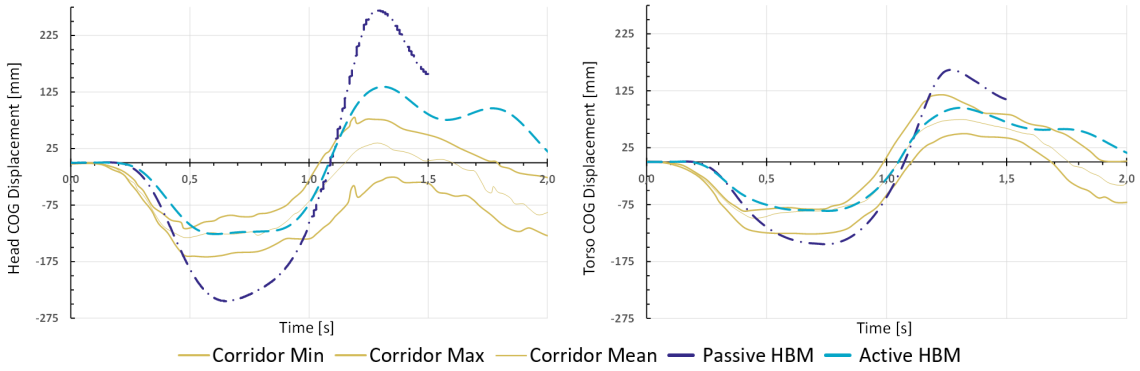

Figure 8. Comparisons of head and torso CG excursions during lane change maneuver and volunteer response corridor from [1].

DISCUSSION

The hybrid controller coupled with Hatze's activation dynamics represents physiological control of the muscle elements, which have been validated initially with an arm model. Obtained knowledge and original findings were extended to other body parts first and finally to the whole HBM. The suggested controller shows the capability to generate motion with appropriate muscle activation signals both in 1g braking and lane change scenarios, although the last one is considered to be a demanding task because of a switch in a muscle activity into opposite directions during the same event. This issue was successfully addressed with the proper combination of target lengths set to the muscles and governed by the hybrid controller, producing movements fast enough and similar to the volunteers.

As an additional outcome of the study, the importance of correct environment modeling according to the test protocol should be mentioned. The interior of the test vehicle should be replicated with all possible details since the seat and the seatbelt interact with the aHBM and produce additional contact forces and reactions, which affect the controller functioning.

Despite the good correlation with the experiments obtained, certain improvements need to be implemented in the aHBM and the hybrid controller. First of all, LS-DYNA material *MAT_MUSCLE that is currently used in a truss muscle elements lacks the serial elastic element representing elasticity of tendons, which was proven to have an important role for muscle modeling in some works [26,27]. Secondly, one of the current model limitations is the absence of muscle routing in some regions representing physiological muscle path including wrapping around joints. Such a modeling approach allows fulfilling of the correct line of action for the muscle, thus producing correct moment arms around the joints as shown in [28]. Thirdly, the current study does not include full activation calculation from the hybrid controller for the leg muscles, because the experimental data lacks the contribution of leg muscles in the motion studied in the study used [1]. Fourthly, the last conditionality applied in the current simulations is the absence of the gravity loading due to limitations of underlying passive HBM. Normally, due to the hybrid controller formulation, it would not affect the functioning itself, rather it will change the muscle activation levels produced and their correspondence for different muscle groups. These limitations designate trends for future work.

CONCLUSIONS

A further step towards an omnidirectional aHBM was made in this study. Such a model could be widely used for integrated safety systems development and accident whole sequence studies. Proposed physiological muscle activation hybrid controller is capable of resembling occupant kinematics in low-speed events, which was validated against experimental tests for 1g braking and lane change maneuvers from the OM4IS project. Besides, suggested control strategy allows to perform modeling of active and reactive human responses for other maneuvers by tweaking the controller parameters in conformity with the desired movement to be simulated. As a next ambitious goal one can set is a simulation of combined maneuvers where acceleration in two directions simultaneously is employed.

ACKNOWLEDGEMENTS

This work was supported by the German Research Foundation (DFG) within the Cluster of Excellence "Data-Integrated Simulation Science" (EXC 2075) at the University of Stuttgart and Tech Center i-protect.

The authors want to thank Atul Mishra, Pronoy Ghosh and Shubham Kulkarni for helpful discussions, useful advice, broad knowledge and valuable assistance with LS-DYNA simulations; Christian Mayer and Ravi Kiran Chitteti for comprehensive support and constructive collaboration.

REFERENCES

[1] Huber, P., Kirschbichler, S., Prüggler, A. and Steidl, T., 2015. “Passenger kinematics in braking, lane change and oblique driving maneuvers.” In Proceedings of the IRCOBI Conference (Lyon, France, September 9-11), 783-802.

[2] Muggenthaler, H., Adamec, J., Praxl, N. and Schönpflug, M., 2005. “The influence of muscle activity on occupant kinematics.” In Proceedings of the IRCOBI Conference, (Prague, Czech Republic, September 21-23), 313-323.

[3] Olafsdottir, J.M., Östh, J., Davidsson, J. and Brolin, K., 2013. “Passenger kinematics and muscle responses in autonomous braking events with standard and reversible pre□tensioned restraints.” In Proceedings of the IRCOBI Conference, (Gothenburg, Sweden, September 11-13), 602-617.

[4] Östh, J, Brolin, K, Ólafsdóttir, JM, Davidsson, J, Pipkorn, B, Jakobsson, L, Törnvall, F and Lindkvist, M., 2015. “Muscle activation strategies in human body models for the development of integrated safety.” In

Proceedings of the 24th International technical conference on the enhanced safety of vehicles (ESV), Gothenburg, Sweden.

[5] Kato, D., Nakahira, Y. and Iwamoto, M., 2017. "A study of muscle control with two feedback controls for posture and reaction force for more accurate prediction of occupant kinematics in low-speed frontal impacts." In Proceedings of the 25th International technical conference on the enhanced safety of vehicles (ESV), Detroit, USA.

[6] Östh, J., Brolin, K. and Bråse, D., 2014. "A Human Body Model with Active Muscles for Simulation of Pretensioned Restraints in Autonomous Braking Interventions." Traffic Injury Prevention, 16(3), 304–313.

[7] Iwamoto, M., Nakahira, Y., Tamura, A., Kimpara, H., Watanabe, I. and Miki, K., 2007. "Development of advanced human models in THUMS." In Proceedings of the 6th European LS-DYNA Users' Conference, Gothenburg, 47-56.

[8] Sugiyama, T., Weber, J., Sandoz, B. and Bensler, H.-P., 2018. "Validation of a Reactive Finite Element Human Body Model under Moderate Lateral Loading", In Proceedings of the 7th International Symposium on "Human Modeling and Simulation in Automotive Engineering," October 18-19, Berlin, Germany.

[9] Hill, A.V. "The heat of shortening and the dynamic constants of muscle" 1938. Proceedings of the Royal Society of London. Series B - Biological Sciences. The Royal Society, 126(843), pp. 136–195.

[10] Kistemaker, D. A., Van Soest, A. (Knoek) J. and Bobbert, M. F. 2006 ."Is Equilibrium Point Control Feasible for Fast Goal-Directed Single-Joint Movements?", Journal of Neurophysiology. American Physiological Society, 95(5), pp. 2898–2912.

[11] Hatze, H. 1977. "A myocybernetic control model of skeletal muscle." Biological Cybernetics. Springer Nature America, Inc, 25(2), pp. 103–119.

[12] LS-DYNA Keyword User's Manual Volume I, LS-DYNA R7.1 (r:5471). Livermore: Livermore Software Technology Corporation; May 26, 2014.

[13] Shelat, C., Ghosh, P., Chitteti, R. and Mayer, C., 2016. ""Relaxed" HBM–an Enabler to Pre-Crash Safety System Evaluation." In Proceedings of the IRCOBI Conference (Malaga, Spain, September 14-16), 239-247.

[14] Gawthrop, P., Loram, I., Lakie, M. and Gollee H., 2011. "Intermittent control: a computational theory of human control." Biological Cybernetics. Springer Nature, 104(1–2), pp. 31–51.

[15] Bayer, A., Schmitt, S., Günther, M. and Haeufle, D.F.B., 2017. "The influence of biophysical muscle properties on simulating fast human arm movements." Computer Methods in Biomechanics and Biomedical Engineering. Informa UK Limited, 20(8), pp. 803–821.

[16] Feldman, A. G. and Levin, M. F. 2009. "The Equilibrium-Point Hypothesis – Past, Present and Future." in Advances in Experimental Medicine and Biology. Springer US, pp. 699–726.

[17] Martynenko, O., Schmitt, S., Bayer, A., Blaschke, J. and Mayer, C., 2017. "A movement generation algorithm for FE Human Body Models." PAMM. Wiley, 17(1), pp. 201–202.

[18] Bizzi, E., Hogan, N., Mussa-Ivaldi, F.A. and Giszter, S., 1992. "Does the nervous system use equilibrium-point control to guide single and multiple joint movements?" Behavioral and Brain Sciences. Cambridge University Press (CUP), 15(4), pp. 603–613.

[19] Rockenfeller, R., Günther, M., Schmitt, S. and Götz, T., 2015. "Comparative Sensitivity Analysis of Muscle Activation Dynamics." Computational and Mathematical Methods in Medicine. Hindawi Limited, 2015, pp. 1–16.

[20] van der Horst, M.J., Thunnissen, J.G.M., Happee, R., van Haaster, R.M.H.P. and Wismans, J.S.H.M., 1997. "The Influence of Muscle Activity on Head-Neck Response During Impact." In: SAE Technical Paper Series, 12 November 1997. SAE International.

[21] Östh, J., Brolin, K. and Happee, R., 2012. "Active muscle response using feedback control of a finite element human arm model." Computer Methods in Biomechanics and Biomedical Engineering. Informa UK Limited, 15(4), pp. 347–361.

[22] Borst, J., Forbes, P. A., Happee, R. and Veeger, D., 2011. "Muscle parameters for musculoskeletal modeling of the human neck." Clinical Biomechanics. Elsevier BV, 26(4), pp. 343–351.

[23] Christophy, M., Faruk Senan, N.A., Lotz, J.C. and O'Reilly, O.M., 2011. "A Musculoskeletal model for the lumbar spine." Biomechanics and Modeling in Mechanobiology. Springer Nature, 11(1–2), pp. 19–34.

[24] Standring, S. Gray's anatomy: the anatomical basis of clinical practice. Philadelphia: Elsevier Limited, 2016.

[25] Östh, J., Brolin, K., Carlsson, S., Wismans, J. and Davidsson, J., 2012. "The Occupant Response to Autonomous Braking: A Modeling Approach That Accounts for Active Musculature." Traffic Injury Prevention. Informa UK Limited, 13(3), pp. 265–277.

[26] Kleinbach, C., Martynenko, O., Promies, J., Haeufle, D.F.B., Fehr, J. and Schmitt, S., 2017. "Implementation and validation of the extended Hill-type muscle model with robust routing capabilities in LS-DYNA for active human body models." BioMedical Engineering OnLine. Springer Nature America, Inc, 16(1).

[27] Günther, M., Schmitt, S. and Wank, V., 2007. "High-frequency oscillations as a consequence of neglected serial damping in Hill-type muscle models." Biological Cybernetics. Springer Nature, 97(1), pp. 63–79.

[28] Hammer, M., Günther, M., Haeufle, D.F.B. and Schmitt, S., 2019. "Tailoring anatomical muscle paths: a sheath-like solution for muscle routing in musculo-skeletal computer models." Mathematical Biosciences.

ADVANCED REAR SEAT SENSING – FURTHER IMPROVING OCCUPANT SAFETY, USING RF TECHNOLOGY

Peter Larsen
Thierry Mousel
IEE S.A.
Luxembourg

Paper Number 19-0217

ABSTRACT

Building on previously developed VitaSense technology, IEE has developed a single sensor, which is integrated behind the headliner of the vehicle, and can serve multiple detection purposes. The new low-power 79 GHz RF sensing unit is used as Occupant Detection Sensor (ODS) while driving, and makes this information available to the vehicle, as input for advanced seat belt reminder (SBR) systems. After the drive, the sensor keeps operating, and can thus detect left-behind occupants, including sleeping new-born children. The standalone sensor is hence capable to address two different functionalities playing a role in the Euro NCAP star rating. Advanced rear seat SBR is incentivised since 2018, and "Child Presence Detection" will become part of the rating scheme in 2022. As "VitaSense+ODS", the sensor addresses two rear seat safety issues: a) seat belt usage in the rear seats tends to be at least 10-15% lower than in the front seats, in some regions of the world even significantly worse; b) in-vehicle heatstroke of unattended infants and children in cars, which in 2018 reached a new record in the US with 51 resulting fatalities. Based on the driving tests performed, and static child detection tests, the 79 GHz RF sensing method has been found to be robust. It is important to note that the system presented serves as a reminder, which does not ensure the prevention of rear occupant injury or heatstroke fatalities per se.

INTRODUCTION

The protection of occupants in the front seats of light vehicles has reached a remarkable level. In the rear seat, however, there is still a significant potential for improvements. More and more vehicles are nowadays equipped with seat belt tensioners and load limiters on the rear seats too, but may occupants do not benefit from those modern restraint systems when they are unbelted. Seat belt usage in the rear seats tends to be at least 10-15% lower than in the front seats, in some regions of the world even significantly worse [1]. Advanced rear seat SBR systems with occupant presence detection have started to enter the market. Capable of triggering an audio-visual alert at the start of the journey, they can be expected to positively influence the seat belt wearing rates on the rear seats.

Another issue, that is predominantly of concern for children in the rear seats, is in-vehicle heatstroke, resulting in 51 child deaths in 2018 in the U.S. alone [2]. At the ESV conference 2017, IEE published a paper on VitaSense [3], capable of detecting even sleeping infants and thus support the vehicle in triggering alerts or initiating countermeasures. Based on radiofrequency signals in the 24 GHz ISM band, the first-generation VitaSense could, however, not be used to support an SBR function.

The novel sensing solution, presented in this paper, is a vehicle-integrated standalone sensor covering both functionalities described above: seat belt reminder and child presence detection. A low-power 79 GHz RF sensor is capable of detecting the seating position of adult rear seat occupants during a journey, and after the vehicle has been parked, it checks whether an occupant may have been left unattended.

REAR SEAT SAFETY ISSUES

Unbelted Occupants

Unbelted rear seat occupants remain a safety issue, as belt wearing rates continue to be lower than those on the front seats. The 2016 National Occupant Protection Use Survey (NOPUS) [4] states that seat belt use in the rear seat was only 80.6%, while on the front seats it reached 90.1%. A study published in 2014 by IIHS and The Children's Hospital of Philadelphia [5], found that unrestrained rear-seat occupants are nearly eight times as likely to sustain a serious injury in a crash as restrained rear-seat occupants. 2017 data from the Fatality Analysis Reporting System (FARS) shows 1341 fatally injured rear seat occupants aged 12 years and older. More than half of them, 801 (59,7%) did not wear their seat belts. Unbelted rear seat passengers can also be a threat for front seat passengers, slamming into them or pushing against the front seat backrest. Driver fatality risk doubles in such scenarios, according to a study of the University of Virginia [6].

Classification: General

Seat belt reminders on rear seats
Simple seat belt reminder (SBR) systems monitoring the belt status on the rear seats and providing a visual information to the driver at the start of the journey are already widespread in Europe due to Euro NCAP incentives. Starting September 2019, such systems will become a type-approval requirement for passenger cars in the European Union. In the US, however, such systems are much less available. In 2015 only 3 percent of new passenger cars had them fitted. More advanced SBR systems, including rear seat occupant detection allowing to trigger audio-visual warnings, have recently started to enter the markets in Japan (2014) and Europe (2017). Hence, rear seat occupant sensing is gaining relevance, and new non-seat-based sensing technologies may be a useful sensing alternative.

In-Vehicle Heatstroke
2018 marked a sad record with 51 in-vehicle heatstroke fatalities in the US. On average there were 38 fatalities per year in the timeframe 1998 – 2018. The victims were either forgotten (54%) or knowingly left (18%) in the car, and some gained access (26%) to unlocked vehicles. A large majority of the heatstroke victims are aged 2 years or younger (74%), and they are mostly "forgotten" or "knowingly left". The "gained access" type of incidents typically occurs for children aged 3 and older. They manage to access the vehicle but do not get out anymore e.g. due to child safety door locks. Infants easily fall asleep in a car, and so they can easily be out of the mind of the driver. In addition, it is known that changes in the daily routine, stress, distractions or misunderstandings play a key role in the situations when children are forgotten in a car. When children are knowingly left in a car, the caretaker either underestimates the risks or falsely assumes to be back soon enough. In-vehicle heatstroke fatalities occur anywhere in the world; however, they are not systematically documented outside of the US.

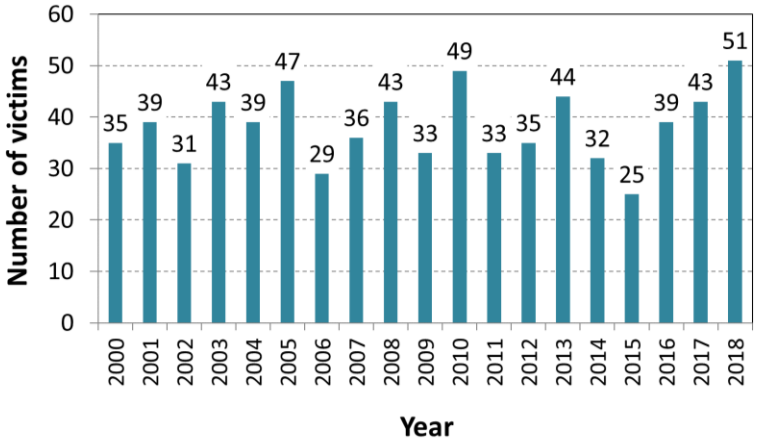

Figure 1. Overview on yearly in-vehicle heatstroke fatalities in the US

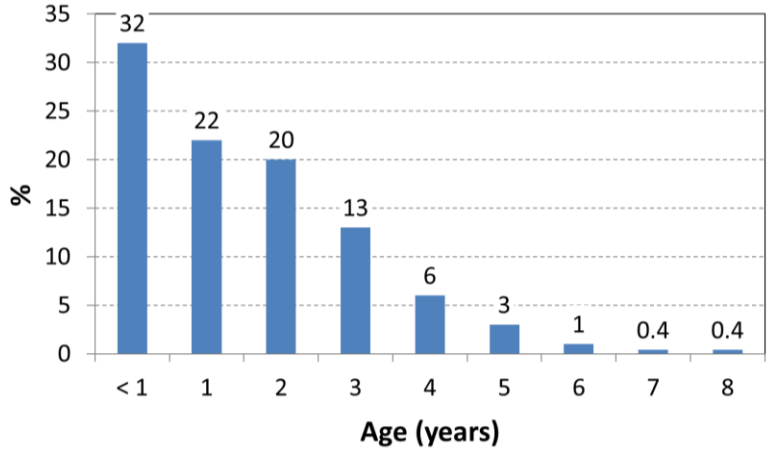

Figure 2. Share of heatstroke victims by age group

Classification: General

NCAP INCENTIVES

NCAP's are frequently having a lead role in promoting novel vehicle safety solutions. Usually being announced in roadmap documents, these new functions then make it into the rating scheme, where they help to improve the vehicle's safety ratings if the functionality complies with the NCAP protocol.

Advanced Rear Seat SBR

In 2011, Japan NCAP took a leading role in defining incentives for rear seat SBR systems capable to trigger an audio-visual warning at the start of the journey. Such a function, known since more than 20 years for the front passenger seat, requires occupant detection technology. In 2014, a first vehicle scored points for such an advanced rear seat SBR system.

Euro NCAP offers incentives for advanced rear seat SBR systems since 2018. Vehicles can score 0.5 point in the "safety assist" category for the advanced rear seat SBR, while a simpler belt status information function scores 1.5 points. In the first assessment year, a remarkable share of 38% of the tested vehicles already offered an advanced rear seat SBR function. In 2020, Euro NCAP will increase the relevance of the advanced function, by allocating 1 point (while the belt status SBR score will decrease to 1 point). The incentives will also be applicable for Australasia NCAP, having aligned their rating with Euro NCAP in 2018.

ASEAN NCAP is the latest NCAP having announced incentives for advanced rear seat SBR in 2021, as part of their Roadmap 2021-2025.

Child Presence Detection

In its Roadmap 2025, Euro NCAP has announced the introduction of incentives for Child Presence Detection in 2022. As for SBR, this will also be applicable to Australia NCAP. Four points will be available in the "vehicle-based assessment" part of the child safety protocol [7]. Some of the elements allowing to score today up to four points in the vehicle-based assessment will be removed or downgraded in order to allow for the integration of the four Child Presence Detection points.

Functional requirements and scoring details are currently under discussion in a dedicated Euro NCAP working group. The assessment protocol will consider how the assumed or actual presence of a child is evaluated (indirect vs. direct systems), what warnings or countermeasures the vehicle can initiate, and whether an escalation of warnings is possible. One general principle has been agreed on: the better the Child Presence Detection system and the more effective the vehicle's countermeasure warnings and interventions, the higher the score. Target is to have a finalised protocol by the end of 2020.

Another NCAP having decided to address in-vehicle heatstroke fatalities is ASEAN NCAP, having announced incentives for 2021 in their Roadmap 2021-2025 document.

THE RF SENSING SYSTEM

Building on previously developed VitaSense technology, IEE has developed a single sensor, which is integrated behind the headliner of the vehicle, and can serve multiple detection purposes. The new low-power 79 GHz RF sensing unit is used as Occupant Detection Sensor (ODS) and makes this information available to the vehicle, as input for advanced seat belt reminder (SBR) systems. After the drive, the sensor keeps operating, and can thus detect left-behind occupants, including sleeping new-born children – a function called UCD (Unattended Child Detector) by IEE.

Developing an occupancy detection function is not as evident as it may sound: It is important to understand the functional requirements in a vehicle, which is at standstill, going slowly on a smooth road or driven off-road. Setting up use cases for simple static occupancy presence sensing or using test procedures that were developed for another technology may not be appropriate.

Test procedures have thus been developed, which take vehicle use cases into consideration. These test procedures contain an element of static and dynamic vehicle situations. The static tests involve measurement of occupants in nominal and due-care positions, as well as specific objects, which the end customer would place in the rear seat under normal circumstances. The objects include back-packs, laptop bags, amongst others.

Classification: General

Based on the driving tests performed, and static detection tests, the module's sensing method has been found to be robust.

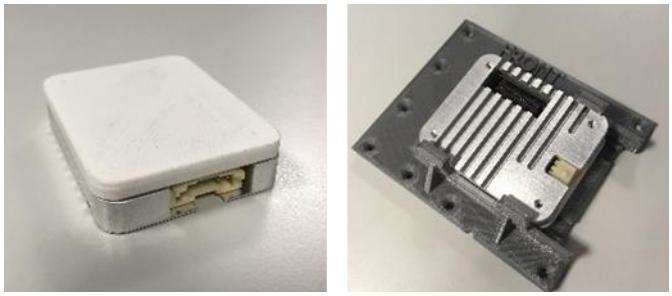

Figure 3. VitaSense+ODS RF sensing unit (40 x 48 12 mm)

To ensure a satisfactory user experience, it was found that a system should be allowed to react to state changes only after a certain qualification period, to allow for people and objects moving around, but not actually changing seating position. Likewise, the occupancy status change while driving will have to be slightly delayed, because occupants must be allowed to move around, reach out for something, without potentially getting an unnecessary seat belt reminder warning.

The Unattended Child Detection function is implemented in a similar manner to our previous generation sensor, which means that it properly detects a range of occupants, including sleeping new-born children. This sensor function is only activated after the vehicle has reached a condition where there is risk of entrapment, e.g. when the driver locks the car after leaving. Typically, presence is detected within a few seconds. To cover specific circumstances, like children holding their breath for a period, the sensor typically operates for 60 seconds.

CONCLUSIONS

The standalone 79 GHz RF sensor can address two different functionalities that will help to improve rear seat occupant safety and thus save lives. In addition, both functionalities will play an important role in improving the Euro NCAP star rating. Advanced rear seat SBR is incentivised since 2018, and "Child Presence Detection" will become part of the rating scheme in 2022.
Based on the driving tests performed, and static child detection tests, the 79 GHz RF sensing method has been found to be robust. The 79 GHz RF sensor successfully detects rear seat occupants while driving and meets requirements for non-detection of objects on the seat, meaning that the sensor can be used as an occupancy detection sensor for an advanced rear seat belt reminder, capable of initiating an audio-visual warning at the start of the journey. When the vehicle is parked, the sensor can even detect the small breathing movements of a sleeping baby and can detect the child under difficult circumstances, such as through the sunshade of a rearward-facing child seat. As the sensor is vehicle-based, the child is detected independent of the specific child seat used, and the vehicle's infrastructure can be used to ensure appropriate countermeasures.
It is important to note that the system presented serves as a reminder, which does not ensure the prevention of rear occupant injury or heatstroke fatalities per se.

REFERENCES

[1] T. Mousel, K. Ueda and M. Takahashi, "Advanced seat belt reminder system for rear seat passengers," *ESV 2015,* paper 15-0018.

[2] «Heatstroke Deaths of Children in Vehicles,» [Online]. Available: http://noheatstroke.org/.

[3] T. Mousel, P. Larsen and H. Lorenz, "Unattended children in cars - Radiofrequency-based detection to reduce heat stroke fatalities," *ESV 2017,* paper 17-0039.

[4] NHTSA, "DOT HS 812 463 Occupant Restraint Use In 2016: Results from the NOPUS controlled intersection study," May 2018.

[5] Insurance Institute for Highway Safety, "Laying the groundwork for safety improvements for back-seat occupants," *Status Report,* December 2014.

[6] Insurance Institute for Highway Safety, "Unbelted," *Status Report,* August 2017.

[7] Euro NCAP, "Euro NCAP Rating Review 2018 - Report from the Ratings Group," November 2018.

Classification: General

A USABILITY STUDY OF SEATBELT BUCKLE ACCESSIBILITY FOR ELDERLY OCCUPANTS

Niharika Bandaru
Christopher Sarros
Aaron Latour
TRQSS, Inc.
Canada

Paper Number 19-0218

ABSTRACT

Elderly occupants form a sub-group in the population spectrum that is often categorized as "vulnerable" in the automotive industry. By 2050, the segment of the population aged 60+ is expected to approximate 26%, which reinforces the importance of developing more adaptable safety technologies that provide optimal and accessible restraint. Following previous research where we analyzed the performance of motorized adjustable buckles in increasing the ease of access to recessed belt buckles for children in booster seats, we extended the examination to study their applicability to elderly occupant comfort and safety.
Thereby, the objectives were:

1. Perform a series of usability studies to prove that the current industry trend of recessed buckles is causing accessibility issues.
2. Attempt to confirm if motorized adjustable buckles improve latching performance while maintaining the intended geometry, given the previous objective was proven true.

A series of studies were conducted with a fixture that simulated the rear right side seat of a mid-sized sedan. The fixture was equipped with a motorized adjustable buckle which replicated two buckle modes – recessed and elevated. Occupants were asked to latch themselves with the buckle in both positions. Observations were made of the number of latch attempts, latching times, occupant preferences, and difficulty levels. The data shows a statistically significant difference for the mean latching attempts and durations between the two buckle modes (recessed and elevated). Objective feedback collected from the occupants shows that a majority of the sample population preferred the elevated mode. However, a strong explanation by the predictor variables (age, sex, weight, standing height, sitting height, arm length, arm to buckle length, and location) of response variables (latch attempts and durations, and buckle preferences) could not be established, unlike our previous study where strong correlations were found. This study's results indicate that elderly occupants are influenced by categorically different factors than children, as variables like age, weight, height, and sex had a limited influence on the outcome of the study. Observations and analyses conducted during the trials point towards more subjective factors that may have had a greater impact on the outcomes; predominantly general health, which can be arbitrary and indifferent to the predictors that were considered in this study. Furthermore, a singular seating configuration was used in this study. More permutations of seat sizes and buckle mounting types will aid in confirming this study's hypotheses.

INTRODUCTION

Elderly occupants are a sizeable and growing segment of the world population. The populations of U.S., Japan, and many other countries are "aging" at historically rapid rates, in the sense that the percentage of the population exceeding 60, 70, and 80 years is larger than at any previous time, and projected to continue to increase for the next few decades[1]. Elderly occupants often face challenges in daily activities due to a myriad of possible physical challenges, and seatbelt latching falls in that umbrella.

In view of this, it becomes pertinent that the automotive safety industry prioritizes elderly occupant restraint. Geometrical configurations of seatbelts are important in providing optimal seatbelt accessibility and comfort, along with restraint performance. Therefore, following previous research where the performance of motorized adjustable buckles in increasing the ease of access to recessed belt buckles for children in booster seats was studied, the analysis was extended to study their applicability to elderly occupant comfort and safety.

Buckle configuration is one issue, where certain car manufacturers have chosen to recede buckles of rear seats further into the seat, possibly to maintain a low Lap-Shoulder point and improve lap belt restraint. This was studied with respect to children in booster seats previously, where it was found that lower buckle heights were indeed causing challenges for buckle accessibility [2]. Following that, the first objective of this paper was to conduct a series of usability studies to examine if a recessed or a relatively more elevated belt buckle configuration was favourable to elderly occupants in terms of accessibility when latching a seatbelt. The second, based on the outcome of the first objective, was to study the effectiveness of a motorized adjustable buckle as a possible solution to increasing accessibility and providing a more comfortable seatbelt configuration to a vulnerable and increasing elderly occupant demographic while simultaneously maintaining the manufacturer's intended buckle position.

METHOD

The method for this study can be divided into three segments: buckle surveying, wherein outboard rear seat buckles of various makes and models were surveyed; usability studies, wherein elderly volunteers meeting pre-determined constraints participated in a series of buckle use trials; and data analysis, where data collected from the usability studies was examined to determine if the posited hypotheses were true.

Buckle Survey

A buckle survey was conducted in the previous study establishing a database of buckle positions and geometries from various vehicles [2]. The data from the surveys was used to help determine the need for a motorized adjustable buckle as postulated in the hypotheses, and to establish buckle configuration for the fixture used in the study. The chosen buckle was to be of a sturdy, inflexible mounting structure that was consistent with the sturdiness of the motorized adjustable buckle (see Figure A1 in Appendix for different buckle mounting types) [2]. Metal anchor strap type buckles and buckles with stiff boots of various vehicle makes and models were measured (refer to Table A1 in Appendix), and a buckle configuration from MY2016 was chosen for the fixture, which was maintained for this study. The previous buckle survey database was expanded to include vehicles of MY 2017-2019 to study further receding trends in buckle configurations.

The chosen seat position was the outboard 1st rear row passenger seat. The chosen seat position was based on buckle survey results where recessed belt buckles were more frequently found in the rear seats than in the front seats, as well as to maintain testing continuity consistent with the previous study where the outboard rear seat was the position of choice for the study. The following buckle configuration data of outboard 1st rear row buckles in vehicles was collected (Figures 1a, 1b):

1. Exposed buckle height (H)
2. Distance from seat back to face 1 of buckle (L')
3. Distance from seat back to face 2 of buckle (L)
4. Maximum seat base width (B)
5. Center of seat to buckle (C)[2]

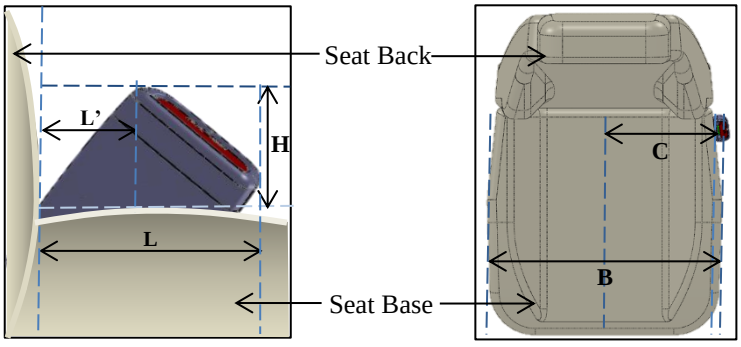

Figure 1a *Figure 1b, Top View of Seat*

Figure 1: Buckle Measurements (Figure 1a), Seat Measurements (Figure 1b).

Usability Study:

The intentions of this activity were to address the following questions:

(a) Do recessed buckles pose accessibility issues for elderly occupants in rear seats?

(b) How do they fare in comparison to elevated buckles?
(c) How does the data vary between occupants of various age groups, heights, weights, genders etc.?
(d) Are motorized adjustable buckles a viable solution?

Following the buckle surveys, volunteers were invited to participate in usability studies conducted across Windsor-Essex County, Canada, at retirement residences and seniors clubs. The details of the studies are as enumerated below:

Mounting Fixture A mounting fixture emulating the outboard rear row seating position of an average mid-sized sedan (Toyota Camry), which was used in previous research that sets precedent to this study [2], was used as shown in Figure 2. An informal survey of popular online automotive websites [3, 4] helped inform the choice of vehicle that the fixture was modelled after. The chosen seat was determined by a seat survey conducted among various vehicles in MYs 2010-2016 (refer to Table A1 in Appendix). A shelf-mount seatbelt retractor assembly was placed over the right shoulder of the car seat. The WSIR (Webbing Sensitive Inertial Response), VSIR (Vehicle Sensitive Inertial Response), and Automatic Locking Retractor (ALR) features were disabled to avoid interference due to locking during the study [2].
An electronically driven motorized belt buckle that replicated two buckle modes – recessed and elevated – was positioned to the left of the vehicle seat (Figures 3a, 3b). In the recessed mode (Figure 3a), the buckle was positioned at L' = 1cm, L = 5cm, H = 1 cm, and C = 22.5cm, which was based on the motorized adjustable buckle geometry, vehicle seat geometry, and buckle survey results for MY 2016. In its elevated mode (Figure 3b) the buckle extends outwards and diagonally upwards by 50mm and 13 degrees. The buckle was connected to a power supply and a switch that allowed the researcher to switch the buckle positions between trials [2].
The right side of the fixture was required to be completely adjacent to a wall (or any planar surface). This was to simulate the vehicle door, so as to recreate the vehicular environment for the test subjects and ensure test fidelity [2].

Figure 2: Mounting fixture used for the usability study.

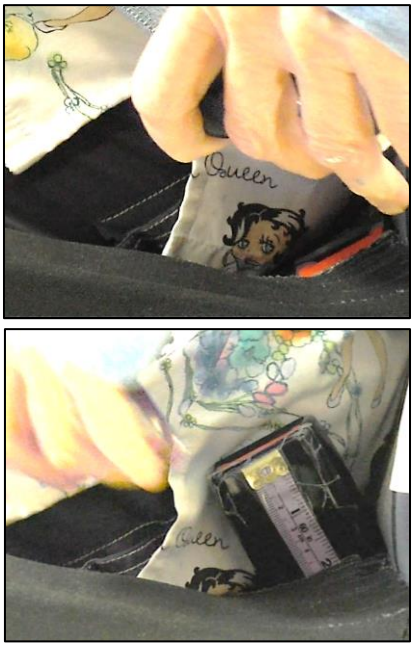

Figure 3: Buckle in recessed mode (3a), and buckle in elevated mode (3b).

Study Constraints The selection process involved picking consenting participants from local retirement residences and seniors clubs. All research ethics guidelines as defined in the Tri-Council Policy Statement by the Panel on Research Ethics [5] were adhered to in this process. Qualifications for candidates participating in the usability study were deemed as follows:

- Age: The occupant was to be 65 years old or above (residents and members at the surveyed locations were 65 or older)

- Height, weight: No restrictions on height or weight were enforced.

It was also required that the participant was able to independently latch themselves with a seatbelt, without the need for assistance.

Study Apparatus The following tools were employed:

- Two video recording devices, one with slow motion and frame by frame recording capabilities (60 fps), were used for this study. The slow motion device was placed directly in line with the buckle, on the left side of the fixture. The slow motion video recordings were used to analyze latch attempts, latch duration, and hand movements. The second recording device was placed diagonally opposite and across from the fixture. These recordings were used to study the overall behaviour of the participants during the trials as well as any other observational data.

- An electronic weighing scale

- Two 60-in soft tape measures; one was taped to a wall for height measurements and the second was used for arm length measurements.

- Two 3ft retractable metal tape measures; these tape measures were inserted into slots created in the roof of the mounting fixture and used to take "Sitting Height" and "Shoulder to Buckle" measurements [2].

Study Procedure The study procedure was replicated from previous research on seatbelt compatibility for occupants in booster seats, and was largely unchanged [2]. The participant was first asked to state their name, age, gender and whether they were currently using a belt extender.

Next, they were weighed and their arm length (straight line distance from the edge of their shoulder to the tip of their longest finger, (A)) and standing height (h) measurement/s were recorded (Figure 4).

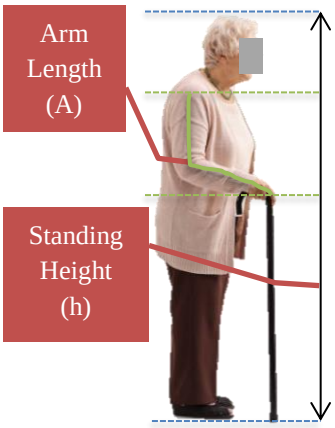

Figure 4: Standing Height and Arm Length Measurements.

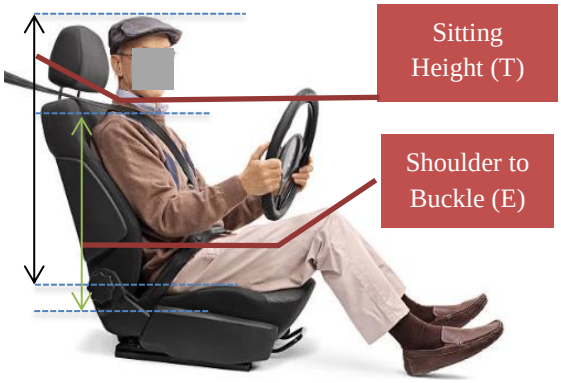

Figure 5: Sitting Height and Shoulder to Buckle Measurements.

The participant was then asked to seat themselves in the fixture while "Sitting Height" (distance from the top of the head to the center of the seat base, (T)) and "Shoulder to Buckle" (straight line distance from the edge of their shoulder to the top surface of the buckle, (E)) measurements were taken (Figure 5). Two slots were cut out in the roof of the fixture to incorporate one tape measure each. One would be used to measure "Roof to Head length" (R) and the other to measure "Roof to Shoulder" (S). These measurements were subtracted from the "Roof to Seat Base" (93cm) and "Roof to Buckle" (92cm) measurements, which were measured beforehand, to obtain T and E measurements. Next, inquiries pertaining to the participant's seatbelt wearing habits were made – if they could use the seatbelt themselves, or if assistance was needed owing to physical or medical restrictions. This was done to obtain an informal awareness of the participant's latching routine and to determine whether they were qualified to participate in the study. Data pertaining to the use of belt extenders was also collected, to establish if buckle accessibility was a common problem which would in turn help determine the need for a more effective solution. In

the cases where the participant independently latched themselves occasionally, they would be encouraged to repeat that for the study, but if the participant always requires assistance and repeatedly struggled with extracting the webbing, maintaining their grip on the slip tongue and/or with the general logistics of using a seatbelt during the trials, they were ultimately disqualified [2].
The protocol for the trials was as follows:

1. Each participant was asked to familiarize themselves with the setup and practice extracting the webbing before the commencement of the trials.
2. There were two trials for each participant – Trial A and Trial B, one for each buckle mode (recessed and elevated).
3. The participants were asked to latch the seatbelt, first for Trial A. After Trial A, the researcher would switch the position of the buckle unbeknownst to the occupant, and ask them to repeat Step 3 for Trial B. They were not informed of the changing buckle modes between the trials (the change point of the study) so as to prevent any presumptive biases.
4. Trials A & B were recorded separately on both recording devices for each participant.
5. Any unique behaviour was observed and recorded [2].

It is important to note that the order of the buckle modes was alternated between participants, as shown in the following example trial matrix:

Table 1.
Usability Study Trial Matrix

Participant #	Trial A	Trial B
1	1	2
2	2	1
3	1	2
4	2	1
5	1	2

1	Recessed
2	Elevated

This was done in order to eliminate any influence a consistent order may have had over the latch attempts and latch durations.
The data collected from the study can be found in the Appendix in Table A2. Figure A3 in the Appendix shows images taken during the course of the study.

Analysis
Data assessment was performed in three phases:

Paired t Tests The buckle video recordings from the usability study were evaluated to obtain the number of latch attempts, total latch duration, and a third parameter of buckle find time, for Trial A & Trial B of each individual participant. The statistical software Minitab [6] was used for the purpose of conducting Paired t Tests for the following groups:

- Latch Attempts (Recessed) vs Latch Attempts (Elevated)
- Latch Duration (Recessed) vs Latch Duration (Elevated)
- Buckle Find Time (Recessed) vs Buckle Find Time (Elevated)

The definition of Latch Attempts is consistent with previous research [2]. Latch Attempts were defined as follows:
One Latch Attempt:

- A single, deliberate, and continuous downward movement of the slip tongue resulting in a singular interaction with ANY buckle surface (buckle top, PRESS button, buckle sides, buckle slot etc.). This downward movement would be followed by a distinctive upward/retracting movement in the case of an unsuccessful latch attempt.

- A single, deliberate, and continuous movement in the buckle region outside of the buckle, below reference line 1 for the recessed mode and reference line 2 for the elevated mode (Figure 6a, 6b). The slip tongue would interact with a single non-buckle surface (seat base, seat back).
- A single, deliberate, and continuous movement in the buckle region outside of the buckle, below reference line 1 for the recessed mode and reference line 2 for the elevated mode, with zero interactions with any surfaces [2].

For the purpose of distinguishing between a continuous and an irregular latch attempt, it was decided that certain motions would be counted as "Half latch attempts".
Half Latch Attempt:

- A deliberate and continuous downward movement of the slip tongue resulting in insertion into the buckle slot after a brief, unintended interaction with the PRESS button or the buckle cover. The insertion would be 1 latch attempt and the brief interaction with the PRESS button or the buckle cover, a half attempt.
- A deliberate but interrupted downward movement of the slip tongue into the buckle slot where the movement of the slip tongue involves brief hesitation but no visible retraction [2].

In exceptional cases, latch attempt analysis was subjective where an attempt stretched outside the definition of a full or half latch attempt.

Latch Duration was defined as the difference between the start time and end time during the course of attempting to latch into the buckle. Latch start and end times for each mode were defined as follows:
Recessed mode: The start time of the event was defined as the instance when any surface of the slip tongue would coincide with the top edge of reference line 1 (Figure 6a) and the end time of the event was defined as the moment when the PRESS button on the buckle reemerged after a successful latch (±1 frame).
Elevated mode: The start time of the event was defined as the moment when any surface of the slip tongue would coincide with the top edge of reference line 2 (Figure 6b) and the end time of the event was defined as the moment when the PRESS button on the buckle re-emerged after a successful latch (±1 frame). There were cases wherein the participant retracted the seatbelt or removed the slip tongue from the video recording frame to adjust their grip on the slip tongue. In these cases the time during which the slip tongue was out of the frame was subtracted from the overall duration. Cases where the tongue or buckle views were obstructed by the participant's hand were disqualified [2].

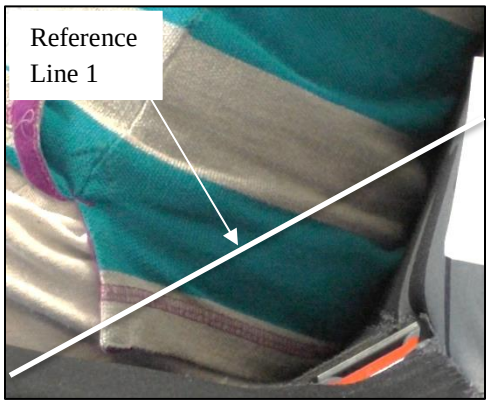

Figure 6a: Buckle in recessed mode and Reference Line 1.

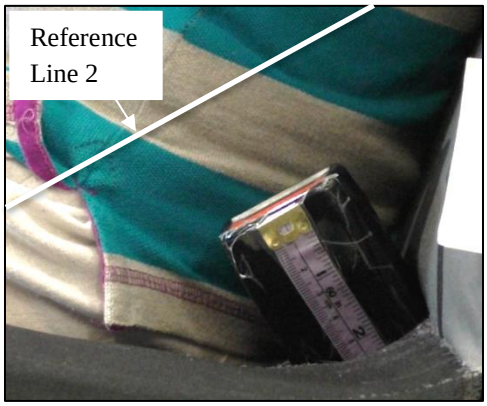

Figure 6b: Buckle in elevated mode and Reference Line 2.

Buckle Find Time: An additional third component was added to the analysis which was not a significant factor in the previous research with child occupants – buckle find time. It was observed that some elderly occupants tended to actively locate the buckle, with the slip tongue outside the buckle area and/or use their hands without a slip tongue. This tendency manifested at the start of the trials and/or during the course of latch attempts, and could not be counted into the latch duration factor owing to the fact that the occupants were trying to locate the buckle and not attempting to latch (Figure 7).

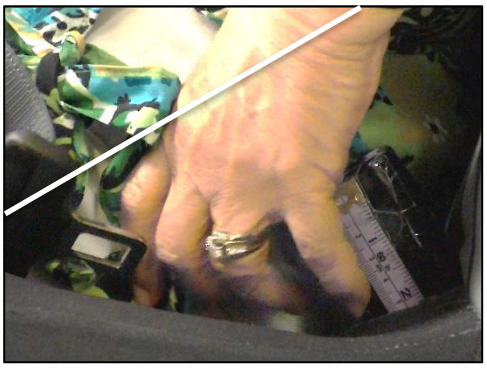

Figure 7: Occupant trying to locate buckle (Buckle Find Time).

Buckle Find Time was the difference between the start and end times of attempting to locate the buckle.

Recessed mode: The start time was the moment when the occupant introduced their hand or the slip tongue below reference line 1 and used either to visibly "find" the buckle without attempting to latch and the end time of the event was defined as the moment when the hand was raised above said reference line or when the slip tongue was used for latching attempts.
Elevated mode: The start time was the moment when the occupant introduced their hand or the slip tongue below reference line 2 and used either to visibly "find" the buckle without attempting to latch and the end time of the event was defined as the moment when the hand was raised above said reference line or when the slip tongue was used for latching attempts.

Reference lines: Reference line 1 was placed 50mm above the top edge of the buckle in recessed mode. Reference line 2 was placed 50mm above the top edge of the buckle in elevated mode. 50mm is the length by which the buckle extends from the recessed mode.

Regression Latch Attempts, latch durations, buckle find times, and individual preferences (recorded retrospectively for each participant) for each buckle mode were regressed against various predictor variables to understand which of these had the strongest influence on the outcomes, and how.
The predictor variables, along with the nature of each predictor that were considered for the regressions were:

- Age (years) - Continuous
- Weight (kg) - Continuous
- Sex (M/F) - Categorical
- Standing Height (cm) - Continuous
- Sitting Height (cm) - Continuous
- Arm Length (cm) - Continuous
- Shoulder to Buckle (cm) - Continuous
- Location - Categorical

Participant buckle preferences were noted after the trials. Responses were categorized into four groups:

- No preference
- Recessed mode
- Elevated mode

- Either

Factors like Standing Height and Sitting Height, that are expected to show a fair degree of correlation between one another, showed only a 50.1% regression value, which meant only about half of the variation in Standing Height was explained by Sitting Height in a linear model. The factor of regression showed that Sitting Height did not pose a strong enough threat as a repeating or confounding factor to Standing Height, and was therefore retained as an explanatory variable (refer to Figure A7a in Appendix). A similar explanation can be attributed to when comparing Arm Length and Shoulder to Buckle measurements. While a small positive correlation was achieved, very little of the variation in Arm Length was explained by Shoulder to Buckle length, and both factors had to be retained as possible explanatory factors (refer to Figure A7b in Appendix).
Weight is an independent variable, which unlike in preceding research with children in booster seats, proved to be a stronger explanatory factor, and was therefore also retained as a predictor variable for regression assessments.

Observational Analysis Video recordings of the test subjects during the trials were studied to identify any behavioral differences between the trials for each subject. Specifics are:
1. The test subject being Out of Position while attempting to latch
2. The extent to which test subjects may have to rotate their bodies to visually access the buckle
3. Any other idiosyncrasies or struggles associated with performing a latch

These observations would further assist in gauging the relative ease or difficulty for the test subjects in latching themselves in the different modes.

RESULTS

Total count of participants from all of the locations was 123. The total sample size for overall analysis was 112, after removing participants that did not meet the study requirements (as enumerated in Table A2 of Appendix) and occupants who failed to independently perform a latch during the trials. Latch Attempts, Latch Duration, and Buckle Find Time were evaluated separately due to different sample sizes, attributed to the following reasons:

1. At the time of latching, the re-emergence of the PRESS button on the buckle was blocked by a participant's hand/s, making it difficult to determine the Start and End times for Latch Duration assessment. However, distinct visible hand movements made it viable to count latch attempts, which were not affected when the buckle view was blocked.
2. Conversely, instances where hand movements for latch attempts were too incoherent, but Latch Duration Start and End times were still decipherable were disqualified for Latch Attempt analysis only.
3. The total sample population that met the study requirements qualified for Buckle Find Time analysis, unless the occupant failed to perform a latch independently and external support was required to do so.

Therefore, participants not meeting the individual requirements of a certain dependent variable were excluded from that dataset only, and considered in the other datasets given that they satisfied their respective conditions. Table A3 in the Appendix shows the final results for Latch Attempt, Latch Duration, and Buckle Find Time datasets. Figures A8-A24 in the Appendix show charted results. Paired t Test evaluations were performed on these data groups using the statistical software Minitab [6].

Paired t Tests:

Outlier fences for Latch Attempt and Latch Duration datasets were calculated using the 1.5*IQR rule, as follows:

Table 2.
Outlier Fences for Latch Attempts in Various Categories.

Group	Sub-group	Latch Attempt Difference	
		LL	UL
Overall	-	-11.3	17.2
Age	65-69	-13.6	21.9
	70-79	-10.6	15.4
	80-89	-9.4	13.6
	90-98	-14	22
Sex	Male	-10	17
	Female	-11.2	16.3
Trials	Rec. first	-10.1	15.4
	Elv. first	-12.8	19.3
Location	Study Site 1	-1	3
	Study Site 2	-11.9	28.6
	Study Site 3	-27.4	22.1
	Study Site 4	-8.8	14.3
	Study Site 5	-11	17

Note: LL – Lower Limit, UL – Upper Limit

Table 3.
Outlier Fences for Latch Duration in Various Categories.

Group	Sub-group	Latch Duration Difference	
		LL	UL
Overall	-	-12.6	17.5
Age	65-69	-14.1	41.9
	70-79	-8.6	24.8
	80-89	-1.5	10.3
	90-98	-3.7	13.3
Sex	Male	-3.9	15.4
	Female	-4.4	14.4
Trials	Rec. first	-5.3	16.7
	Elv. first	-1.8	12.3
Location	Study Site 1	-3.2	7.7
	Study Site 2	-32.2	51.2
	Study Site 3	-90.3	62.2
	Study Site 4	-7.7	13.9
	Study Site 5	-14.9	21.6

Note: LL – Lower Limit, UL – Upper Limit

All negative lower fences are a result of the outlier calculation process. The Latch Attempts and Latch Duration variables are positive counts that start at zero. Therefore all negative lower outlier fences can effectively be rounded up to a "0". All outliers from this evaluation were excluded and Paired t Test analyses were performed using the resulting data. It is vital to note that only the initial outliers were removed and any subsequent outliers calculated by Minitab were not excluded.

The 1.5*IQR rule based outlier fences were not applied to the Buckle Find Time dataset, as the number of cases where the Buckle Find Time was zero superseded the number of cases with recorded times > 0s. This resulted in the latter set of cases resulting as outliers, which is misleading. Excluding all of the 0s Buckle Find Time cases, resulted in the remainder 26 cases with recorded times >0s showing no outliers. This scenario was ideal, but not truly representative of the population. Therefore, a decision was made to analyze the combined results of both scenarios, but without the application of outlier fences.

Table 4.
Paired t Test Results for Mean Latch Attempts in Various Categories.

Latch Attempts					
Group	Sub-group	Sample Size	Paired Diff μ	% Diff	P-value
Overall	-	100	2.9	29.2	<0.001
Age	65-69	12	4.25	49.3	0.008
	70-79	37	2.3	29	0.002
	80-89	29	2.14	20.7	0.005
	90-98	23	4.9	34.5	0.001
Gender	M	27	2.8	26.1	0.005
	F	73	2.9	30.5	<0.001
Trials	Rec. first	54	2.5	27.6	<0.001
	Elv. first	47	3.7	32.9	<0.001
Location	Study Site 1	5	1.4	14	0.404
	Study Site 2	13	6.3	45.9	0.005
	Study Site 3	15	-3.3	-27.2	0.815
	Study Site 4	46	2.7	34.6	0.001
	Study Site 5	27	2.8	23.6	0.005

Note: Alpha risk level for P-values: 0.05

Table 5.
Paired t Test Results for Mean Latch Duration in Various Categories.

Latch Duration (s)					
Group	Sub-group	Sample Size	Paired Diff μ	% Diff	P-value
Overall	-	97	2.5	21.9	<0.001
Age	65-69	12	4.4	46.2	0.013
	70-79	37	1.6	19.3	0.067
	80-89	29	2.3	17.6	0.030
	90-98	22	4.7	25.9	0.013
Gender	M	27	4.3	31.8	0.002
	F	70	1.9	17.5	0.003
Trials	Rec. first	53	3	26.9	<0.001
	Elv. first	45	1.5	13.3	0.033
Location	Study Site 1	5	11.1	57.5	0.2
	Study Site 2	15	11.2	43.2	0.021
	Study Site 3	16	-16.5	-117	0.970
	Study Site 4	44	2.6	33	<0.001
	Study Site 5	26	2.3	15.6	0.060

Note: Alpha risk level for P-values: 0.05

All P-values > 0.05 were determined insignificant for the analysis of study trial results. Result examples for the aforementioned categories can be found in the Appendix on Pages xii-xxi. Sample sizes were large enough for most categories, and normality was not an issue; however for categories where the sample size < 20 (highlighted in red under Sample Size column in Tables 4, 5), normality could not be established, and more data would provide greater significance to the results.
Paired Difference μ for Latch Attempts is the difference between Mean of Latch Attempts (Recessed) and Mean of Latch Attempts (Elevated). Paired Difference μ for Latch Duration is the difference between Mean of Latch Duration (Recessed) and Mean of Latch Duration (Elevated). P-values remain largely under the alpha risk level of 0.05, other than a few exceptions (as highlighted in red under P-value column in Tables 4, 5).

The following outcomes were obtained from data analysis:

Latch Attempts

- The mean latch attempts for the recessed mode would be greater than mean latch attempts for the elevated mode in a population with a 99.99% significance.
- For the study sample size, there was a 29.2% decrease in mean latch attempts in the elevated mode in comparison to the recessed mode.
- The data shows a 95% confidence in the mean latch attempts in the recessed mode being greater than 2.09 attempts in comparison to the mean latch attempts in the elevated mode.
- Percentage differences between recessed and elevated mode latch attempts for the age sub-group ranged from 20.7-49.3%. However, the increase in percentage difference was not proportional to rise in age, and normality could not be established in the case of 65-69YO occupants, with a sample size of only 12 participants.
- A small percentage difference in latch attempts was observed in the female occupant sub-group (30.5%) in comparison to their male counterparts (26.1%). However, the sample size for females was over twice that

of males. This large difference in participation accounts for a more representative average value in the case of the females, and more comparative variance in the case of the males.

- A small percentage difference in latch attempts was observed between "Recessed Mode first" versus "Elevated Mode first" categories, with the latter showing a slightly higher percentage difference. This means that on average, participants that had the order "2, 1" (refer to Table 1) showed a slightly greater improvement between latch attempts in comparison to those who performed according to the order "1, 2".
- Location based results varied from -27.2 – 45.9%, which is a fairly large range. However, sample sizes from trials at *Study Site 1, 2, and 3* were too small to establish normality, which means the P-values are less accurate than required to determine significance in a population.
  However, trials from *Study Site 4*, and *5* showed a percentage difference of 34.6% and 23.6% respectively, with significant P-values.

Latch Duration

- The mean latch duration for the recessed mode would be greater than mean latch duration for the elevated mode in a population with a 99.99% significance.
- For the study sample size, there was a 21.9% decrease in mean latch duration in the elevated mode in comparison to the recessed mode.
- The data shows a 95% confidence in the mean latch duration in the recessed mode being greater than 1.51s in comparison to the mean latch duration in the elevated mode.
- Percentage differences between recessed and elevated mode latch durations for the age sub-groups ranged from 17.6-46.2%. However, the increase in percentage difference was not proportional to rise in age, and normality could not be established in the case of 65-69YO occupants, with a sample size of only 12 participants. The P-value was slightly outside of the established alpha risk level of 0.05 in the case of the 70-79YO category, owing to a single unusual outlier (refer to Page xviii in Appendix) which was a subsequent outlier after the first round of outlier eliminations. Owing to this explanation, the Paired μ result for this category was still considered as significant.
- A large percentage difference in mean latch duration was observed between the female occupant category (17.5%) and the male occupant category (31.8%). However, the sample size for females was over twice that of males, and such a large difference needs to be accounted for. The female category result is a more representative average owing to the large sample size, and the male result is less normalized than its female counterpart.
- A difference of 6% was observed between the "Recessed Mode first" and "Elevated Mode first" categories, with the former showing a higher percentage difference (53%). Both categories had comparable sample sizes. This means that on average, participants that had the order "1, 2" (refer to Table 1) showed a slightly greater improvement in latch duration in comparison to those who performed according to the order "2, 1".
- Location based results varied from -117 – 57.5%. This unusual range can be attributed to the small sample sizes at *Study Site 1, 2, and 3*, which resulted in extreme and insignificant data.
  However, trials from *Study Site 4*, and *5* showed a percentage difference of 33% and 15.6% respectively. The P-value for *Study Site 5* is slightly greater than the established alpha risk level of 0.05, owing to a single unusual outlier (refer to Page xx in Appendix) which resulted after the first round of outlier eliminations. Owing to this, the Paired μ result for this category was still deemed significant.

Buckle Find Time Only two Paired t Tests were performed for Buckle Find Time (BFT) calculations: 1) Entire sample size, and 2) Sample size where either buckle mode trial had a result >0s. The results for these calculations are as shown below:

1. Entire sample size

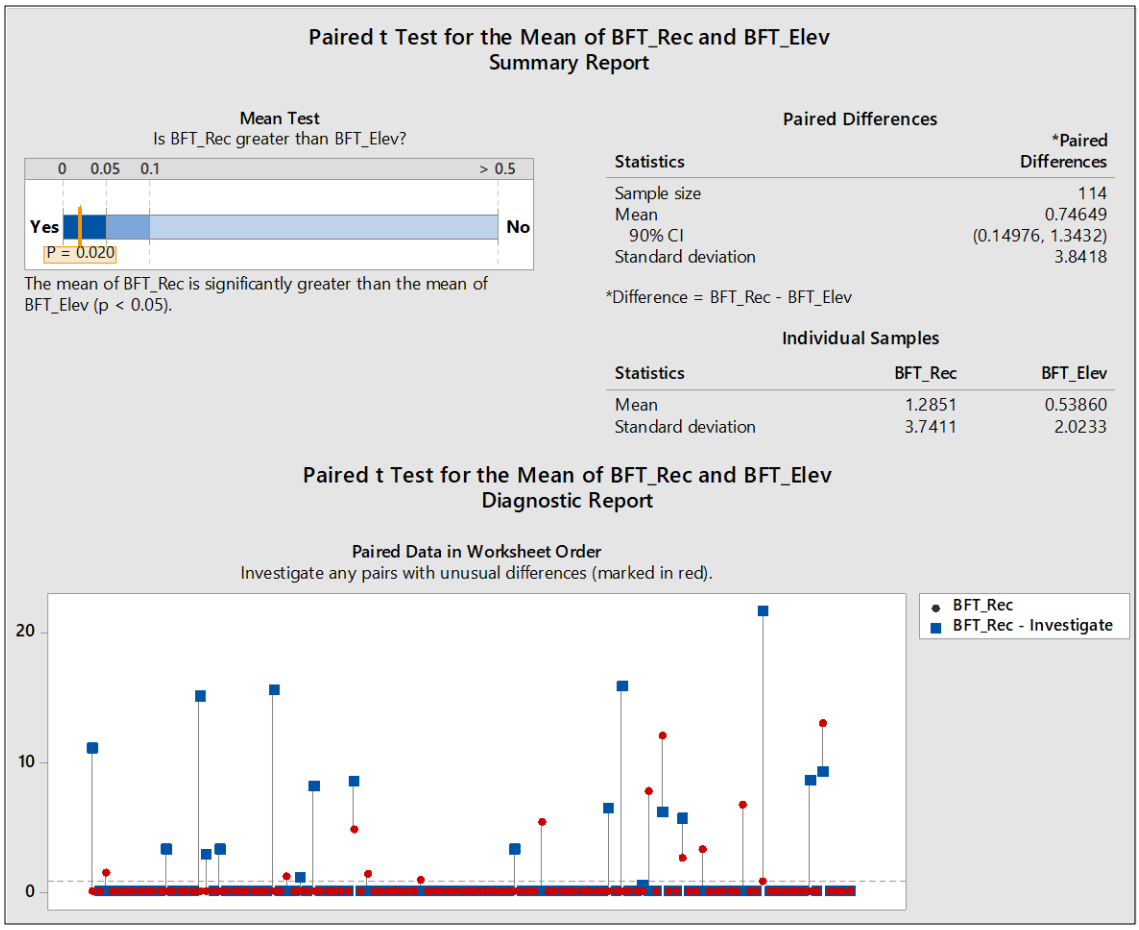

Figure 8: Paired t Test results of Buckle Find Time (Recessed) vs Buckle Find Time (Elevated) for the entire sample size.

As seen above, almost all of the pairs where BFT = 0s for both recessed and elevated mode (here forth referred to as "No Result Data") trials have been determined as outliers, with the addition of some pairs where either trial (recessed or elevated) with measurements >0s. The Paired μ difference is marginal at 0.75s. This data is significantly representative of a population as the P-value is <0.05, but the result is insignificant in terms of representing a study sample that did spend time locating the buckle.

2. Sample size = 26 (Pairs where either trial (recessed or elevated) > 0s)

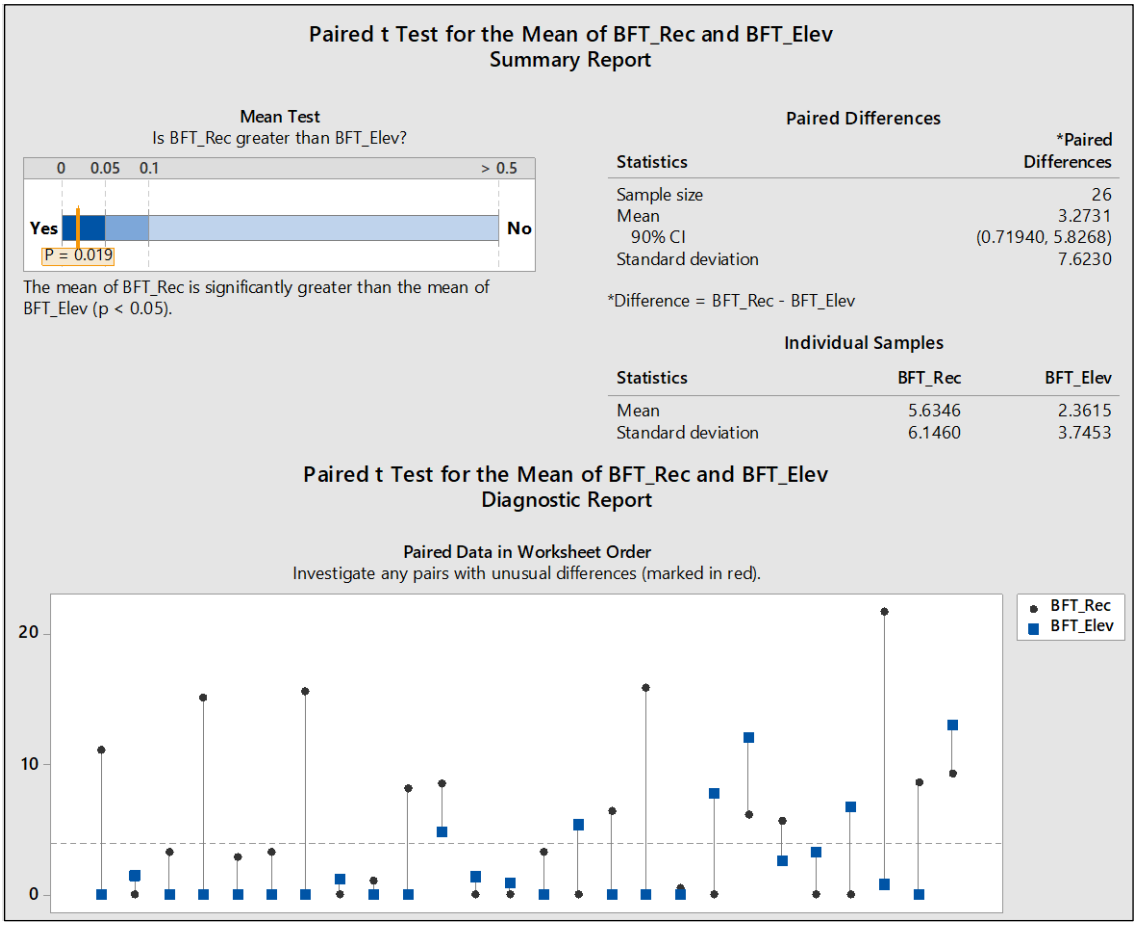

Figure 9: Paired t Test results for Buckle Find Time (Recessed) vs Buckle Find Time (Elevated) for sample size = 26.

Upon the removal of No Result Data, the sample size is reduced to 26 and the Paired μ difference between recessed mode and elevated mode BFTs = 3.27s, where the mean BFT for the recessed mode was higher. A P-value of 0.019 establishes this result as significant in a population. With the removal of No Result Data, the outlier fences readjust themselves, and no outliers are found. The percentage difference of 58.1% between recessed and elevated mode BFTs is significant for the sub-group in a population that spends time finding the buckle prior to attempting to latch. Further evaluations based on age, gender, buckle mode order, and location were not performed for BFT owing to the small, insignificant sample size that would be generated for each category.

Regression

Multiple variable regressions, were performed between the various predictor and dependent variables to determine which factors explained the variance in the data. Only the initial set of residuals calculated by Minitab was removed and any subsequent residuals were not excluded. Examples of individual response variable regressions can be found on Pages xxii-xxviii of the Appendix.

The dependent variables were Latch Attempts, Latch Duration, Buckle Find Time, and Preference.

The following were the results of the regression analysis:

Table 6.
Results of Regression Analysis.

Response Var.	Predictor Var. in Model	r^2 (%)	P-value
LA Rec.	Age, Weight, Shoulder to Buckle, Location	27.44	0.002
LA Elv.	Age, Weight, Sitting Height	16.89	<0.001
LD Rec.	Age, Weight, Sitting Height, Location	33.87	<0.001
LD Elv.	Age, Weight, Sitting Height, Location	44.58	<0.001
BFT Rec	Arm Length, Location	21.65	0.002
BFT Elv	Standing Height, Location	67.73	0.011
Preference	Location	29.19	<0.001

Note: LA - Latch Attempts, LD – Latch Durations, BFT – Buckle Find Times

The predictor variables in the model for each multiple regression of each individual response variable vary. In each case, the regression model included the predictor variables that explained the variance in the output values the most, without overfitting. P-values in each case are < 0.05, which means all of the models are significant in a population. The following were the results of the regressions:

- Age, Weight, and Location are the predominant predictor variables. Location is the most consistent among all the predictor variables, contributing the most new information to explain the models (refer to Figures A18-A24 in Appendix).
- The predictors are able to explain variance to only a certain extent, reaching a peak r^2 of 67.73% in the case of BFT Elevated. Latch Attempt Elevated is the least explained model for the given predictors with an r^2 of 16.89%.
- Gender does not explain or contribute to the results of the study discussed within the scope of this research paper.
- Location supersedes the other predictors in explaining almost all the models (refer to Figures A18-A24 in Appendix).
- This data will help analyze what factors play the most influence in determining whether an elderly occupant benefits from a motorized adjustable buckle or not.
- Parameters outside of the scope of this study were responsible for the unexplained variance in the models.
- This data will help examine other factors not included in the regression models that may have been responsible for the recorded outcomes. It will also help analyze if adjusting these factors would increase or decrease Latch Attempts, Latch Durations, Buckle Find Times and change Buckle Preferences in future studies.

Buckle Preferences:

Buckle preference data that was collected from each participating individual revealed information that supports the results of the Paired t Tests.

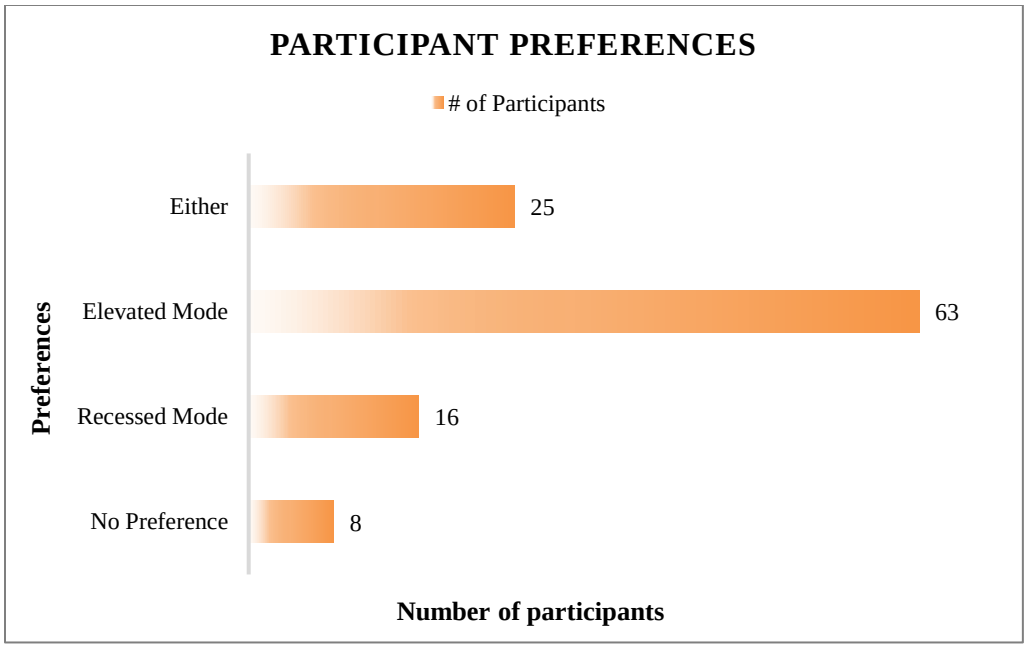

Figure 10: Participant buckle preference results, sorted by preference type.

Occupants were not informed of the changing buckle mode nor the trial order, which removes a considerable amount of bias from the preference results. Some occupants preferred neither buckle mode ("No Preference"), which means that both buckle modes were disliked, and others preferred either buckle mode ("Either"), which means that both buckle modes were equally liked. Of note is that the number of participants whose preference was either buckle mode was greater in number than those who exclusively preferred the recessed buckle mode. Participants overwhelmingly preferred the elevated mode over the recessed mode.

Other Observations:

Supplementary observations recorded during the study trials provide some insight into participant idiosyncrasies and latching patterns, those which have not or cannot be accounted for in statistical analyses.

- It was observed that overweight or obese occupants (BMI >25, Table A2 in Appendix) tended to prefer the elevated buckle mode, owing to a wider spanning lap.
- Most participants did not use a belt extender in their daily lives (refer to Table A2 in Appendix).
- There was a much higher participation from females than males.

DISCUSSION

A notable observation from the trials and analyses is the comparative performance of the elderly population versus the children in booster seats. While the overall latch attempt performance was relatively similar (as seen in Table 7 below), there was a noticeable increase in latch duration percentage difference in the case of the elderly sample population. Paired Difference µs were also relatively higher for multiple sub-categories in the case of the elderly cohort, as seen in the table below, where Paired Difference µ results of the two studies have been conditionally formatted separately for Latch Attempts and Latch Duration (separation of variables indicated by black boxes in table below), with a green to red gradient (green being the lowest and red being the highest value). Graphs comparing the results of both studies can be found in the Appendix.

Table 7.
Comparative analysis of children (in booster seats) versus elderly cohort performances (Latch Attempts and Latch Duration).

		Latch Attempts (Children)		Latch Attempts (Elderly)		Latch Duration (Children)		Latch Duration (Elderly)	
Group	**Sub-group**	**Sample Size**	**Paired Diff μ**	**Sample Size**	**Paired Diff μ**	**Sample Size**	**Paired Diff μ**	**Sample Size**	**Paired Diff μ**
Overall	-	112	1.83	100	2.9	96	1.21	97	2.5
Gender	M	67	1.3	27	2.8	57	0.67	27	4.3
	F	45	2.42	73	2.9	38	1.77	70	1.9
Trials	Rec. First	57	1.97	54	2.5	46	1.54	53	3
	Elv.First	55	1.69	47	3.7	50	0.91	45	1.5
		Latch Attempts				**Latch Duration**			
		Sample Size		**Paired Diff μ**		**Sample Size**		**Paired Diff μ**	
	Children								
Age	4	23		2.97		22		3.55	
	5	23		2.78		18		4.43	
	6	24		1.38		22		0.63	
	7	25		0.8		22		0.62	
	8	19		1.18		17		0.64	
	Elderly								
	(65-69)	12		4.25		12		4.4	
	(70-79)	37		2.3		37		1.6	
	(80-89)	29		2.14		29		2.3	
	(90-98)	23		4.9		22		4.7	

Location played an important role in explaining the variance in various regression models. This can be explained by different underlying factors that govern the participants at each location, like:

1. Whether the location was a retirement residence (which was 4 out of the 5 locations surveyed) or seniors' activity club.
2. The level of fitness or daily physical activity that participants from each location were accustomed to.
3. Average health of participants at any given location.

It was noticed that the seniors' activity club (Study Site 4) generated the most participants out of all the surveyed locations (Tables 4, 5). Participants at this location seemed more agile and active, in comparison to the long term residents of the retirement residences whose mobility and cognition seemed to be more compromised due to various health reasons (possibly Parkinson's disease, Alzheimer's disease, early stages of cataract, etc.). As location dominated age as a stronger predictor variable in most of the regression results, it draws into attention the fact that the overall health for elderly participants is a possibly stronger factor in latching performance than how old they may be. There is no singular, straightforward measure for "Health", as participants could suffer from a variety of medical afflictions of various degrees, with multiple issues affecting the same individual sometimes, compounding the degree of their inflexibility and immobility. Therefore, direct correlations could not be established between "Health" and Latch Attempts, Latch Duration, or Buckle Find Time.

Another observation that needs to be addressed is the ratio of female to male participants in the study. A total of 90 females participated as opposed to 33 males, a very high and disproportionate ratio. This can be appropriated to the established fact that females enjoy a lower mortality rate than men [7-9], which increases in significance with increase in age. Females are also more robust than their male counterparts at all ages [7], which justifies a relatively higher level of enthusiasm in partaking in activities. However, in order to obtain a more balanced comparison of results with respect to the study conducted, a bigger sample size of male participants would have been favourable.

It was also observed that the 65-69YO age category had the lowest number of participants among all the age groups. This can be attributed to a lower number of residents and members pertaining to that age group at the locations that were surveyed.

Similar to the previous study, the input variables (Latch Attempts, Latch Duration, and Buckle Find Time) had to be individually examined, as they had a low P-value, little co-relation, or insufficiently explained for variance when regressed against one another (Figures A25-A29 in the Appendix). The plausible reasons for this could be:

- Multiple latch attempts can be performed in a short span of time, as demonstrated by some older occupants.
- A single latch attempt can be performed over a relatively long time span, as demonstrated by some younger occupants.
- Not all the participants spent time finding the buckle prior to attempting to latch, which meant Buckle Find Time is a separate measurement from Latch Duration.

As discussed via regression analysis, other variables outside the scope of this study need to be examined to justify the unexplained variance in the data. Other potential predictors could be:

1. Vehicle make
2. Buckle anchor type
3. Seat back angle
4. Seating position (FR RH, RR CTR etc.)
5. Latch force
6. Medical conditions

LIMITATIONS

Certain aspects of data collection used in this analysis may have introduced unintended variability to the estimates. Due to a need for further assessments using more configurations, the results cannot be considered universally representative of the randomly sampled test subjects.
The limitations associated with this study are as follows:

- Only one buckle configuration in the recessed mode was studied. Further studies using the best and worst case buckle benchmarking data would provide insight into latching tendencies.
- Only one buckle configuration in the elevated mode was studied (50mm height increase). Further studies into higher buckle lengths would help analyze the optimum buckle height for latching.
- One seating configuration was used - midsize right hand rear row sedan seat. Varying combinations of seat sizes and buckle types would have to be studied.
- Only eight predictor variables were taken into account. Changing the seating configuration, seat position, and other factors outside the scope of this study may influence the results of future evaluations.
- In the cases of some occupants, assistance was provided with the webbing feed, as they visibly struggled to completely extract the webbing themselves. The amount of webbing provided was not measured in each case, and this randomness could have introduced some variability.
- Some occupants' communicated preference for buckle mode was in direct contradiction to their performance during the trials. This bias was typically because of the type of buckle the occupant was accustomed to in their daily lives.
- Any medical issues limiting the performance of participants was a significant factor in this study, as discussed in the Discussions segment of this paper.

CONCLUSION

The analysis in this paper justifies the first hypothesis posed in this paper: the recessed buckle position is more difficult to use than the elevated buckle position for elderly occupants in a population, as demonstrated by the differences in Latch Attempt, Latch Duration, and Buckle Find Time results, under similar circumstances as adopted by this study.
It was also observed that an increase or decrease in percentage differences in performances were not directly proportionate to an increase in age. Females showed a greater percentage difference in latch duration than males, but similar performances in the latch attempt category; however, a larger male participant sample size is imperative to establish comparative and significant results. Trial mode order saw that participants that had the order "2, 1" in the Latch Attempt category showed little difference in performance than the ones that had the order "1, 2". This was the opposite case with respect to the Latch Duration category, where percentage difference in performance spikes, with participants that had the order "1, 2" showing more improvement than the ones who had the order "2, 1".
Occupants that spent time finding the buckle prior to latching, showed an improvement when switched over from the recessed mode to the elevated mode. However, only a small percentage of individuals in the population displayed the tendency to visibly locate the buckle prior to attempting to latch.
Elderly occupants showed a greater improvement when switched from recessed to elevated mode than children in booster seats in the Latch Attempt and Latch Duration categories, for comparable sample sizes.

However, elderly occupants were governed by different predictors than their younger counterparts. Age played a prominent role in dictating the latching patterns of children in booster seats, whereas it played a meandering role in case of the elderly, who were influenced more by the location of the study, which was an indirect measure of their fitness levels.
The chosen predictors played a comparatively smaller role overall in influencing the latching performances and preferences of the participants, relative to the results of the previous study. Factors outside of the scope of this study need to be examined to elucidate the unexplained variance in the regression models.

The data from this analysis shows that the usage of a motorized adjustable buckle demonstrations a clear benefit to improving accessibility for the elderly while maintaining the manufacturer's intended buckle position. These findings confirm the second hypothesis proposed in this study for the conditions that participants were examined under. A further examination including different configurations and variable factors is required to advance a universal confirmation of the hypotheses.

REFERENCES

[1] Reed, M., Ebert, S., & Hallman, J. (2013). Effects of driver characteristics on seat belt fit. *Stapp Car Crash Journal*, *57*, 43-57. Retrieved from https://www.ncbi.nlm.nih.gov/pubmed/24435726#

[2] Bandaru, N., Sarros, C., & Latour, A. (2017). A Usability Study of Seatbelts in Conjunction with Booster Seats. In *25th International Technical Conference on the Enhanced Safety of Vehicles (ESV)*. Detroit, Michigan: National Highway Traffic Safety Administration. Retrieved from http://indexsmart.mirasmart.com/mwg-internal/de5fs23hu73ds/progress?id=AgUPWLUY_VMgJgHbofBd-AkjTPJwEGIMv0enwL5uZ2g,

[3] J.D. Power. (2019). Retrieved from https://canada.jdpower.com/

[4] Product Reviews and Ratings - Consumer Reports. (2019). Retrieved from https://www.consumerreports.org/cro/index.htm

[5] TCPS 2 :: The Interagency Advisory Panel on Research Ethics (PRE). (2019). Retrieved from http://www.pre.ethics.gc.ca/eng/policy-politique/initiatives/tcps2-eptc2/Default/Austad, S. (2006). Why women live longer than men: Sex differences in longevity. *Gender Medicine*, *3*(2), 79-92. doi: 10.1016/s1550-8579(06)80198-1

[6] Minitab Inc. (2010). Minitab Statistical Software (Version 17) [Windows]. State College, Pennsylvania.

[7] Austad, S. (2006). Why women live longer than men: Sex differences in longevity. *Gender Medicine*, *3*(2), 79-92. doi: 10.1016/s1550-8579(06)80198-1

[8] Glei, D., & Horiuchi, S. (2007). The narrowing sex differential in life expectancy in high-income populations: Effects of differences in the age pattern of mortality. *Population Studies*, *61*(2), 141-159. doi: 10.1080/00324720701331433

[9] Zarulli, V., Barthold Jones, J., Oksuzyan, A., Lindahl-Jacobsen, R., Christensen, K., & Vaupel, J. (2018). Women live longer than men even during severe famines and epidemics. *Proceedings Of The National Academy Of Sciences*, *115*(4), E832-E840. doi: 10.1073/pnas.1701535115

[10] Brown, J., Coxon, K., Fong, C., Clarke, E., & Keay, L. (2013). Seat belt wearing characteristics of drivers aged 75 years and older. *23rd International Technical Conference On The Enhanced Safety Of Vehicles (ESV)*. Retrieved from https://www-esv.nhtsa.dot.gov/Proceedings/23/files/23ESV-000389.PDF

[11] Zhang, J., Lindsay, J., Clarke, K., Robbins, G., & Mao, Y. (2000). Factors affecting the severity of motor vehicle traffic crashes involving elderly drivers in Ontario. *Accident Analysis & Prevention*, *32*(1), 117-125. doi: 10.1016/s0001-4575(99)00039-1

[12] OEM Seatbelts, (2017). 3 Point Retractable Seat Belt With 8.5" End Release Cable Buckle. Retrieved from https://oemseatbelts.com/products/3-point-retractable-seat-belt-with-end-release-cable-buckle?variant=28008482179

[13] Mewes, C. (2013, March 25). Car Seat. Retrieved March 01, 2019, from https://grabcad.com/library/car-seat--8

[14] Ljupco. (2017, June 6). Full length profile shot of a mature woman with a cane waiting in... Retrieved from https://www.istockphoto.com/ca/photo/mature-woman-with-a-cane-waiting-in-line-gm693321828-128018929

[15] Ljupco. (2016, March 29). Senior holding a steering wheel seated on a car seat fastened with... Retrieved from https://www.istockphoto.com/ca/photo/senior-driving-seated-on-a-car-seat-gm515803642-88669887

APPENDIX

Table A1.
Buckle and Seat Width Measurements

				Seat		Buckle		
#	**Year**	**Make**	**Model**	**B (cm)**	**C (cm)**	**H (cm)**	**L (cm)**	**L' (cm)**
1	2019	Toyota	C-HR	51	18	3	4.5	1
2	2019	Nissan	Kicks	46	15.5	0	9	4.5
3	2019	Mazda	CX-5	53	20.5	1.25	7	3
4	2019	Mazda	CX-3	40.5	17	2	7.5	4
5	2019	Mazda	CX-9	55	19	2.5	5.5	1
6	2019	Mazda	6	55	21	3	6.5	2.5
7	2018	Chevrolet	Silverado	51	21	3	11	6.5
8	2018	Chevrolet	Silverado LT	51	23	4	6	1
9	2018	Ford	F150-Ext. Cab	49	19.5	7	7	2.3
10	2018	Mazda	3	54	18.7	1.2	6.5	2
11	2018	Mazda	CX-5	46	19	2	7	3
12	2017	Chevrolet	Silverado	51	21	3	11	6.5
13	2017	Nissan	Maxima	52	17	6	7.5	3
14	2017	Nissan	Pathfinder	51	22.5	1.75	14.5	10
15	2017	Hyundai	Elantra	56	21	2	5	1
16	2017	Buick	Encore	48.5	17	6	13	9
17	2017	Chrysler	Pacifica	46.5	23.25	2.6	6	2.6
18	2017	Ford	Fusion	50	22.5	6	4.5	0
19	2017	Toyota	Sienna	59	24	4.5	7.5	3.5
20	2017	Honda	Accord	51	18	8	11	7
21	2017	Honda	CR-V	51	19	2	6.5	1.5
22	2017	Ford	Escape	46	16.5	4	8	3.5
23	2016	Dodge	Caravan	52	21	5	9.5	5.5
24	2016	Dodge	Dart	54	22.5	0.5	8	4
25	2016	Ford	Escape	46	16	5	8.5	4.5
26	2016	Ford	Focus	50	22	4.5	6	2
27	2016	Ford	Fusion	55	23	6.5	5	1.5
28	2016	Hyundai	Sonata	49	20	4.5	7	3
29	2016	Jeep	Cherokee	52	20	3	8	4
30	2016	Jeep	Grand Cherokee	50.5	20	1	8.5	4.7
31	2016	Mazda	3	49.5	24.25	3.5	7	2
32	2016	Mazda	CX-5	53	22.5	4	6	1.5
33	2016	Nissan	Rogue	52.5	22.25	3.8	12.5	8.5
34	2016	Chrysler	200	48	20	6	6	2.5
35	2016	Nissan	Maxima	38.5	19.25	6.5	5.2	1.8
36	2016	Chrysler	Town & Country	50	20	4.5	6	3
37	2016	Kia	Optima	39.5	N/A	7.8	7	3
38	2016	Mazda	CX-3	48	18	2	11.5	7
39	2016	Volvo	XC90	51.8	N/A	10	7	3
40	2016	Honda	HR-V	51.8	15.54	10	7	3
41	2016	Mercedes	GLC	46.5	19.5	4.5	9	5
42	2016	Toyota	RAV4	52.5	19	6	10.5	4.5

43	2015	Dodge	Caravan	47.0	21.5	5.0	5.0	0.0
44	2015	Ford	Escape	46.0	16.2	3.0	8.0	3.0
45	2015	Mazda	3	51.0	18.5	1.5	6.5	2.0
46	2015	Jeep	Cherokee	52.0	20.0	4.0	8.0	5.0
47	2015	Fiat	500L	41.0	15.0	5.0	18.0	13.0
48	2015	Ford	Fusion	48.5	18.0	5.5	5.5	1.0
49	2015	Toyota	Sienna	58.5	24	7.5	11	4
50	2015	Ford	Focus	50.0	22.3	4.5	5.3	1.5
51	2015	Chrysler	200	51.2	22.8	2.0	7.0	2.5
52	2015	Toyota	RAV4	52.0	19.5	4.4	10.8	5.8
53	2015	Chrysler	Town & Country	52.4	21.0	5.0	8.0	4.0
54	2015	Ford	Edge	50.0	20.0	-3.0	2.1	-2.7
55	2014	Chevrolet	Cruz	50.0	17.0	3.5	12.0	6.0
56	2014	Jeep	Cherokee	54.0	21.0	3.4	10.0	6.0
57	2014	Jeep	Grand Cherokee	50.5	19.0	0.0	11.0	7.5
58	2014	Ford	Fusion	47.0	18.0	5.0	5.0	0.0
59	2014	Dodge	Caravan	51.0	23.2	5.0	8.5	4.5
60	2014	Ford	Focus	51.0	23.5	5.3	5.1	1.5
61	2014	Ford	Escape	47.0	19.0	3.8	7.4	3.0
62	2014	Mazda	3	55.0	20.5	0.0	6.5	2.0
63	2013	Ford	Escape	46.0	17.0	3.0	7.5	3.0
64	2013	Ford	Focus	50.0	16.0	4.0	6.0	1.0
65	2013	Chevrolet	Cruz	49.0	17.5	4.0	12.0	6.0
66	2013	Chrysler	Town & Country	52.4	21.0	5.0	8.0	4.0
67	2013	Hyundai	Elantra	50.0	25.0	4.0	5.0	1.0
68	2013	Dodge	Dart	51.5	19.0	2.3	6.0	2.0
69	2013	Chevrolet	Malibu	51.5	23.0	4.0	12.2	7.7
70	2013	Ford	Fusion	50.0	22.0	5.5	4.3	0.7
71	2012	Dodge	Caravan	51.0	22.8	5.0	7.5	3.5
72	2012	Dodge	Dart	51.0	20.0	1.5	7.0	3.0
73	2012	Chrysler	300	50.0	17.0	5.5	5.0	0.0
74	2012	Jeep	Cherokee	49.0	17.0	0.0	9.0	4.5
75	2012	Ford	Focus	50.0	18.0	3.5	5.7	1.0
76	2012	Chevrolet	Cruz	49.5	17.0	5.0	12.0	8.5
77	2012	Dodge	Caravan	51.0	22.8	5.0	7.5	3.5
78	2011	Jeep	Cherokee	49.0	18.0	0.0	9.0	5.0
79	2011	Dodge	Caravan	52.0	21.0	4.0	7.6	4.0
80	2010	Dodge	Caravan	51.5	21.5	4.1	8.5	4.5

Note: All measurements based on in house benchmarking and are not reflective of vehicle design conditions.

Figure A1a

Figure A1b

Figure A1c

Figure A1: Metal anchor strap type buckle mount (Figure A1a), Cable type buckle mount [12]; Figure A1b), Webbing type mount (Figure A1c).

Figure A2a

Figure A2b

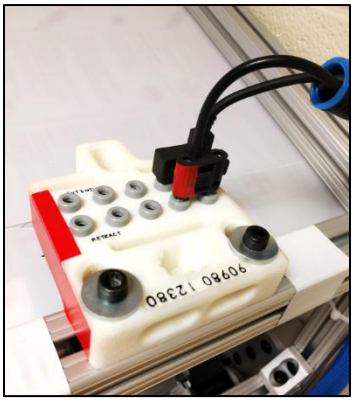

Figure A2c

Figure A2: Mounting fixture and study setup (Figure A2a), Rear view of mounting fixture (Figure A2b), Buckle switch (Figure A2c).

Figure A3: Participants of the usability study.

Table A2.
Data Collected from Usability Study

#	Age	Sex	Belt Extender	Weight (kg)	h (cm)	BMI	A (cm)	R (cm)	T (cm)	E (cm)
1	77	F	N/A	55.84	155	23.24	74.93	17.5	75.5	49.5
2	65	F	N/A	76.18	173	25.45	76.2	5	88	63
3	85	F	N/A	65.83	113	51.55	68.58	18	75	49.5
4	72.9	M	N/A	105.78	186	30.58	81.28	4.5	88.5	62.5
5	72	F	N/A	76.73	118	55.10	62.23	14	79	53
6	77	F	N/A	69.46	163	26.14	71.12	12	81	52.5
7	71	M	N/A	59.02	178	18.63	74.93	9.5	83.5	55.5
8	77	F	N/A	60.38	172	20.41	71.12	10	83	55
9	87	M	N/A	77.18	178	24.36	66.04	7	86	56.5
10	70	F	N/A	69.46	164	25.83	71.12	7.5	85.5	57
11	72	M	N/A	84.90	188	24.02	69.85	3.5	89.5	61
12	72	F	N/A	80.36	155	33.45	66.04	13	80	57.5
13	84	M	N/A	65.38	165	24.01	71	12.5	80.5	52.5
14	74	F	N/A	74.00	165	27.18	71.12	10.5	82.5	58.3
15	80	F	N/A	54.48	154	22.97	66.04	13.5	79.5	53
16	82	F	N/A	52.66	169	18.44	72.39	13.5	79.5	50.5
17	75	F	N/A	66.74	163	25.12	71.12	11.5	81.5	56
18	76	F	N/A	68.55	163	25.80	66.04	12	81	56
19	75	F	N/A	95.34	176	30.78	74.93	12.5	80.5	54
20	70	F	N/A	78.09	164	29.03	69.85	6	87	60.5
21	69	F	N/A	73.55	160	28.73	64.77	13.5	79.5	56
22	77	F	N/A	68.55	152	29.67	62.23	14	79	53
23	66	F	N/A	80.81	177	25.79	71.12	6.2	86.8	59
24	83	F	N/A	89.44	147	41.39	63.5	19.6	73.4	49.5
25	79	F	N/A	75.36	165	27.68	59.69	8	85	58
26	71	F	N/A	80.36	165	29.52	69.85	12	81	55
27	68	M	N/A	85.81	193	23.04	76.2	0	93	62.5
28	70	M	N/A	81.27	175	26.54	68.58	6	87	59
29	72	F	N/A	65.38	153	27.93	66.04	17	76	49.7
30	76	F	N/A	67.19	152	29.08	64.77	18	75	48
31	69	M	N/A	65.83	166	23.89	67.31	9	84	58.5
32	68	F	N	57.84	158	23.17	63	15	78	53.6
33	75	F	N	49.21	154	20.75	60	16	77	50
34	75	F	N	61.93	163	23.31	65	14.5	78.5	49
35	68	F	N	67.92	168	24.06	67	11	82	54.5
36	86	F	N	62.74	165	23.05	73	15	78	51.8
37	80	F	N	65.47	155	27.25	66	17	76	51.6
38	82	F	N	69.92	169	24.48	72	10	83	58
39	82	F	N	97.97	169	34.30	77	14.2	78.8	51

40	71	F	N	81.08	167	29.07	68	9.5	83.5	57
41	68	F	Y	74.82	163	28.16	71	22	71	47
42	90	F	N	60.84	164	22.62	67	15.6	77.4	51.8
43	77	F	N	62.83	160	24.54	65	13	80	54.5
44	78	F	N	76.91	167	27.58	64	9.5	83.5	54.5
45	74	M	N	75.18	174	24.83	74	8.2	84.8	57
46	72	F	N	65.56	175	21.41	76	6.5	86.5	57.5
47	73	F	N	74.91	159	29.63	64	11.5	81.5	56
48	75	F	N	74.55	172	25.20	67	6.5	86.5	60
49	73	F	N	72.82	159	28.80	65.5	12	81	53
50	71	F	N	86.44	152	37.41	69	16	77	50.7
51	72	M	N	75.45	171	25.80	71	10.5	82.5	52
52	88	F	N	66.28	175.5	21.52	77.5	10.4	82.6	54.8
53	92	F	N	50.39	158	20.19	74	18.5	74.5	50
54	96	F	Y	48.94	150	21.75	70	21	72	46.5
55	69	F	N	94.52	164	35.14	74	7	86	59
56	81	M	N	67.01	170	23.19	75	9	84	58
57	70	F	N	59.93	159	23.70	71.5	14.2	78.8	51.5
58	66	F	N	74.55	167	26.73	74	13	80	54
59	81	F	N	69.01	157	28.00	67	17.5	75.5	51.9
60	75	F	N	82.81	164	30.79	71	10	83	54.5
61	88	F	N	82.36	173	27.52	77	13	80	54
62	84	M	N	82.17	170	28.43	78	10.5	82.5	55
63	90	M	N	84.17	180	25.98	78	7.5	85.5	62
64	96	F	N	60.11	150	26.72	68	18.5	74.5	48.5
65	83	F	N	66.47	148	30.34	62	19.4	73.6	50
66	65	F	N	65.83	157.5	26.54	74	13.5	79.5	51
67	94	M	N	70.64	169	24.73	77	7	86	55
68	65	F	N	66.10	168	23.42	68	11	82	50
69	85	F	N	59.20	156	24.33	75	20.5	72.5	44.8
70	84	M	N	66.37	182	20.04	75	6.5	86.5	59
71	83	M	N	102.33	178	32.30	77	7.5	85.5	59.5
72	93	F	N	54.84	152	23.74	70	21	72	47.5
73	91	M	N	76.18	176	24.59	75	8.5	84.5	57.5
74	89	M	N	72.64	166	26.36	69	8.5	84.5	56
75	92	F	N	49.58	152	21.46	69	18.5	74.5	49.5
76	87	F	N	62.02	156	25.48	67	18	75	48
77	90	M	N	70.10	170	24.26	76	10	83	55.5
78	93	F	N	78.27	157	31.75	65	18.5	74.5	48
79	88	F	N	63.74	164	23.70	70	14	79	52
80	88	F	N	70.55	164	26.23	75	15.5	77.5	50.5
81	80	F	N	45.58	155	18.97	64	16	77	50
82	71	F	N	51.21	150	22.76	58	21	72	46

83	90	F	N	62.92	151	27.60	68	21	72	49.5
84	98	M	N	84.72	163	31.89	74.5	20	73	52
85	77	F	N	64.65	156	26.57	72	19.5	73.5	47.5
86	73	M	N/A	88.17	164	32.78	70	15.5	77.5	50
87	84	M	N	66.74	247	10.94	76	0	93	63
88	83	M	N	74.37	175.5	24.14	75	10	83	53
89	79	F	N	51.30	167	18.40	71.5	15	78	50.5
90	91	F	N	67.92	164	25.25	63	10	83	52
91	80	F	N	46.76	152	20.24	61	20	73	48
92	83	F	N	55.48	163	20.88	68	14	79	53
93	85	F	N	91.53	158	36.66	65	12	81	52
94	90	F	N	42.68	161	16.46	68.5	13.2	79.8	52
95	90	M	N	61.29	169	21.46	73.5	15	78	48
96	94	F	N	47.13	156	19.36	63	16	77	50
97	92	M	N	85.90	172	29.03	70.5	9.5	83.5	55
98	84	M	N	94.25	168	33.39	66.5	10	83	56
99	95	M	N	60.11	168	21.30	71	15	78	54
100	91	F	N	98.06	165	36.02	65.5	13	80	56
101	92	F	N	44.58	161	17.20	65	12	81	54
102	90	F	N	43.40	162.5	16.44	64.5	19	74	48.5
103	96	F	N	63.20	159	25.00	67.5	20	73	47.5
104	90	F	N	63.02	165	23.15	74	13.5	79.5	53
105	72	F	N	69.46	167.5	24.76	70.5	12.5	80.5	54
106	82	M	N	71.10	175	23.22	73	11	82	53
107	82	M	N	128.03	175	41.81	71	10	83	58
108	97	F	N	72.55	159	28.70	67	18.5	74.5	51
109	88	F	N	78.36	157	31.79	61	18.5	74.5	48
110	85	M	N	81.90	168	29.02	66	16	77	57
111	76	F	N	57.48	158	23.02	63.5	18.5	74.5	48.5
112	87	F	N	62.20	161	24.00	64	15	78	51

Table A3.
Trial Latch Attempts and Latch Duration Results

#	Trial A	Trial B	Preference	# of LA(Rec.)	# of LA(LUB)	LA Diff	LD (Rec)	LD (LUB)	LD Diff	BFT (Rec.)	BFT (LUB)	BFT Diff
1	2	1	1	8.5	3	5.5	00:07.5	00:03.5	00:04.0	00:00.0	00:00.0	00:00.0
2	1	2	2	3	4	-1	00:04.6	00:05.8	-00:01.2	00:11.1	00:00.0	00:11.1
3	1	2	2	6	6.5	-0.5	00:06.1	00:04.7	00:01.4	00:00.0	00:00.0	00:00.0
4	2	1	1	4	12	-8	00:04.0	00:12.7	-00:08.7	00:00.0	00:01.2	-00:01.2
5	1	2	2	9	5	4	00:08.0	00:02.6	00:05.5	00:00.0	00:00.0	00:00.0
6	2	1	1	3	3	0	00:03.1	00:02.7	00:00.4	00:00.0	00:00.0	00:00.0
7	2	1	2	10	5.5	4.5	00:11.6	00:05.1	00:06.4	00:02.9	00:00.0	00:02.9

8	1	2	2	7.5	1.5	6	00:04.2	00:01.9	00:02.3	00:00.0	00:00.0	00:00.0
9	1	2	2	13	10.5	2.5	00:12.5	00:08.1	00:04.4	00:00.0	00:00.0	00:00.0
10	2	1	2	6	3	3	00:02.7	00:04.2	-00:01.5	00:00.0	00:00.0	00:00.0
11	2	1	1	3.5	5.5	-2	00:08.8	00:03.0	00:05.9	00:00.0	00:00.0	00:00.0
12	1	2	2	11	4	7	00:10.6	00:04.5	00:06.1	00:00.0	00:00.0	00:00.0
13	2	1	2	19	12.5	6.5	00:21.1	00:12.7	00:08.3	00:00.0	00:05.4	-00:05.4
14	1	2	2	12	6	6	00:09.7	00:03.9	00:05.8	00:00.0	00:00.0	00:00.0
15	1	2	1	2.5	3	-0.5	00:02.4	00:02.3	00:00.1	00:00.0	00:00.0	00:00.0
16	2	1	3	2.5	3.5	-1	00:03.7	00:03.1	00:00.6	00:00.0	00:00.0	00:00.0
17	2	1	1	4.5	21	-16.5	00:05.3	00:32.1	-00:26.8	00:00.0	00:00.0	00:00.0
18	2	1	2	8	1.5	6.5	00:06.8	00:02.5	00:04.3	00:00.0	00:00.0	00:00.0
19	1	2	2	9	5.5	3.5	00:06.8	00:03.9	00:02.9	00:00.0	00:00.0	00:00.0
20	1	2	2	6.5	3.5	3	00:09.2	00:03.2	00:06.0	00:00.0	00:00.0	00:00.0
21	1	2	1	4	2.5	1.5	00:06.3	00:03.0	00:03.3	00:00.0	00:00.0	00:00.0
22	2	1	2	6.5	3	3.5	00:07.8	00:03.4	00:04.3	00:00.0	00:00.0	00:00.0
23	1	2	2	2.5	4	-1.5	00:03.9	00:03.3	00:00.7	00:00.0	00:00.0	00:00.0
24	2	1	3	4	4	0	00:03.3	00:04.9	-00:01.6	00:00.0	00:00.0	00:00.0
25	1	2	2	3.5	4	-0.5	00:05.8	00:04.0	00:01.8	00:00.0	00:00.0	00:00.0
26	1	2	2	25	5.5	19.5	00:38.7	00:06.7	00:32.0	00:00.0	00:00.0	00:00.0
27	2	1	2	8	3	5	00:05.8	00:04.4	00:01.4	00:00.0	00:00.0	00:00.0
28	1	2	2	6	4	2	00:04.3	00:03.6	00:00.7	00:00.0	00:00.0	00:00.0
29	2	1	2	13.5	10	3.5	00:13.3	00:07.5	00:05.8	00:00.0	00:00.0	00:00.0
30	1	2	1	15	9	6	00:10.7	00:13.8	-00:03.0	00:00.0	00:01.4	-00:01.4
31	2	1	2	4	4	0	00:05.8	00:04.5	00:01.3	00:03.3	00:00.0	00:03.3
32	1	2	2	12	3.5	8.5	00:12.9	00:03.1	00:09.8	00:00.0	00:00.0	00:00.0
33	2	1	3	16	5.5	10.5	00:10.8	00:05.8	00:05.0	00:00.0	00:00.0	00:00.0
34	1	2	2	4	9	-5	00:05.4	00:10.7	-00:05.3	00:00.0	00:00.0	00:00.0
35	2	1	2	12	3	9	00:15.3	00:05.7	00:09.5	00:00.0	00:00.0	00:00.0
36	1	2	2	6	3.5	2.5	00:07.6	00:04.1	00:03.5	00:00.0	00:00.0	00:00.0
37	2	1	2	2.5	2	0.5	00:02.7	00:02.3	00:00.4	00:00.0	00:00.0	00:00.0
38	1	2	2	14	2.5	11.5	00:10.8	00:03.7	00:07.1	00:00.0	00:00.0	00:00.0
39	2	1	3	11.5	10	1.5	00:10.3	00:10.3	00:00.0	00:00.0	00:00.0	00:00.0
40	1	2	1	7	9	-2	00:06.2	00:12.9	-00:06.6	00:03.3	00:00.0	00:03.3
41	1	2	3	6.5	8.5	-2	00:05.0	00:06.3	-00:01.3	00:00.0	00:00.0	00:00.0
42	2	1	3	5	5	0	00:03.5	00:06.2	-00:02.7	00:00.0	00:00.0	00:00.0
43	1	2	2	7	6	1	00:14.1	00:08.1	00:06.0	00:00.0	00:00.0	00:00.0
44	2	1	2	7	3	4	00:06.8	00:04.4	00:02.4	00:00.0	00:00.9	-00:00.9
45	1	2	3	15	6.5	8.5	00:20.8	00:05.1	00:15.7	00:08.1	00:00.0	00:08.1
46	1	2	2	4	2	2	00:04.0	00:01.5	00:02.5	00:00.0	00:00.0	00:00.0
47	2	1	3	9	6	3	00:19.1	00:12.9	00:06.2	00:02.9	N/A	N/A
48	2	1	2	6	1	5	00:03.2	00:02.6	00:00.7	00:00.0	00:00.0	00:00.0
49	1	2	2	11	8.5	2.5	00:15.1	00:22.7	-00:07.6	00:00.0	00:00.0	00:00.0
50	2	1	3	4	6	-2	00:03.0	00:06.1	-00:03.1	00:00.0	00:00.0	00:00.0

51	1	2	2	7	9	-2	00:07.7	00:11.0	-00:03.3	00:15.6	00:00.0	00:15.6
52	1	2	2	4	5	-1	00:08.1	00:03.5	00:04.6	00:00.5	00:00.0	00:00.5
53	2	1	2	5.5	11.5	-6	00:06.3	00:12.4	-00:06.1	N/A	00:00.0	N/A
54	2	1	3	2	23	-21	00:02.9	01:13.0	-01:10.1	00:09.3	00:13.0	-00:03.8
55	1	2	2	24	11.5	12.5	00:30.2	00:13.2	00:17.1	00:00.0	00:00.0	00:00.0
56	2	1	2	12.5	52	-39.5	00:18.7	01:20.3	-01:01.6	00:00.0	00:00.0	00:00.0
57	1	2	2	4.5	4	0.5	00:03.0	00:02.4	00:00.6	00:15.1	00:00.0	00:15.1
58	2	1	3	17.5	5.5	12	00:16.8	00:06.5	00:10.3	00:00.0	00:00.0	00:00.0
59	1	2	2	40	46.5	-6.5	N/A	N/A	N/A	N/A	00:00.0	N/A
60	1	2	1	12.5	58.5	-46	00:25.9	01:27.0	-01:01.2	00:08.5	00:04.8	00:03.7
61	2	1	3	13.5	29.5	-16	00:23.9	00:47.7	-00:23.7	00:07.8	N/A	N/A
62	2	1	3	9.5	7	2.5	00:08.4	00:06.8	00:01.5	00:00.0	00:00.0	00:00.0
63	1	2	2	13.5	5	8.5	00:13.8	00:07.4	00:06.4	00:00.0	00:00.0	00:00.0
64	1	2	3	11.5	5	6.5	00:15.6	00:03.8	00:11.8	00:00.0	00:00.0	00:00.0
65	2	1	2	47	7.5	39.5	01:00.8	00:06.0	00:54.8	00:03.3	00:00.0	00:03.3
66	1	2	2	6	2	4	00:03.0	00:01.9	00:01.2	00:00.0	00:00.0	00:00.0
67	2	1	2	21	6.5	14.5	00:28.1	00:05.9	00:22.2	00:00.0	00:00.0	00:00.0
68	1	2	2	4	1	3	00:03.4	00:03.1	00:00.3	00:00.0	00:01.5	-00:01.5
69	1	2	2	14	5.5	8.5	00:21.1	00:03.4	00:17.6	00:00.0	00:00.0	00:00.0
70	2	1	1	15	5	10	00:16.3	00:07.7	00:08.6	00:00.0	00:00.0	00:00.0
71	1	2	3	10.5	6	4.5	00:10.8	00:09.8	00:01.0	00:00.0	00:00.0	00:00.0
72	1	2	2	8.5	4.5	4	00:14.6	00:03.0	00:11.7	00:00.0	00:00.0	00:00.0
73	2	1	3	11.5	18.5	-7	00:08.9	00:16.7	-00:07.8	00:00.0	00:06.7	-00:06.7
74	1	2	3	5.5	4.5	1	00:02.9	00:05.0	-00:02.2	00:00.0	00:00.0	00:00.0
75	2	1	2	21.5	14	7.5	00:46.6	00:17.6	00:29.0	00:21.7	00:00.8	00:20.9
76	2	1	1	5	7.5	-2.5	00:06.1	00:10.2	-00:04.1	00:00.0	00:00.0	00:00.0
77	1	2	2	27	7	20	00:54.1	00:10.2	00:43.9	00:00.0	00:00.0	00:00.0
78	2	1	1	29	14.5	14.5	00:22.1	00:20.6	00:01.5	00:00.0	00:00.0	00:00.0
79	1	2	0	7.5	7	0.5	00:10.0	00:06.5	00:03.6	00:00.0	00:00.0	00:00.0
80	2	1	0	25.0	6	19	01:06.4	00:09.0	00:57.4	00:06.1	00:12.0	-00:05.9
81	1	2	0	5.5	4	1.5	00:04.7	00:03.1	00:01.7	00:00.0	00:00.0	00:00.0
82	1	2	0	6	5	1	00:06.0	00:05.0	00:00.9	00:00.0	00:00.0	00:00.0
83	2	1	0	6	21	-15	00:09.3	00:17.4	-00:08.1	00:00.0	00:03.3	-00:03.3
84	2	1	0	27.5	17.5	10	00:57.2	00:45.6	00:11.6	00:00.0	00:00.0	00:00.0
85	2	1	1	3	6	-3	00:02.0	00:17.3	-00:15.3	00:00.0	00:00.0	00:00.0
86	1	2	2	12	5	7	00:16.3	00:03.8	00:12.5	00:01.1	00:00.0	00:01.1
87	2	1	2	12.5	12	0.5	00:13.9	00:11.4	00:02.5	00:00.0	00:00.0	00:00.0
88	1	2	2	7	5	2	00:13.8	00:05.3	00:08.4	00:00.0	00:00.0	00:00.0
89	2	1	3	3	2	1	00:02.9	00:01.9	00:01.0	00:00.0	00:00.0	00:00.0
90	1	2	2	10	4.5	5.5	00:12.3	00:03.6	00:08.7	00:00.0	00:00.0	00:00.0
91	2	1	2	9	7	2	00:05.7	00:03.3	00:02.4	00:00.0	00:00.0	00:00.0
92	1	2	3	9	14	-5	00:08.4	00:20.6	-00:12.2	00:00.0	00:00.0	00:00.0

93	2	1	2	15	10	5	00:15.4	00:12.9	00:02.5	00:00.0	00:00.0	00:00.0
94	1	2	3	2	3	-1	00:03.3	00:04.8	-00:01.5	00:00.0	00:00.0	00:00.0
95	2	1	0	6	10	-4	00:08.6	00:09.8	-00:01.2	00:00.0	00:00.0	00:00.0
96	1	2	2	18	4.5	13.5	00:46.0	00:04.5	00:41.5	00:00.0	00:00.0	00:00.0
97	2	1	2	8	5.5	2.5	00:07.7	00:06.9	00:00.8	00:00.0	00:00.0	00:00.0
98	1	2	2	12.5	7.5	5	00:21.4	00:05.7	00:15.7	00:00.0	00:00.0	00:00.0
99	2	1	3	8	7.5	0.5	00:15.0	00:10.0	00:04.9	00:00.0	00:00.0	00:00.0
100	1	2	2	10	5.5	4.5	00:08.0	00:04.9	00:03.1	00:00.0	00:00.0	00:00.0
101	2	1	0	11	4.5	6.5	00:12.9	00:05.1	00:07.9	00:00.0	00:00.0	00:00.0
102	1	2	2	5.5	4.5	1	00:08.1	00:03.5	00:04.6	00:00.0	00:00.0	00:00.0
103	1	2	1	9	9.5	-0.5	00:21.7	00:16.6	00:05.2	00:00.0	00:00.0	00:00.0
104	1	2	2	11.5	8	3.5	00:10.7	00:04.4	00:06.2	00:00.0	00:00.0	00:00.0
105	2	1	2	13	5	8	00:11.4	00:04.7	00:06.7	00:00.0	00:00.0	00:00.0
106	2	1	2	32	8.5	23.5	00:34.4	00:08.1	00:26.3	00:00.0	00:00.0	00:00.0
107	1	2	1	10.5	11.5	-1	00:09.6	00:13.8	-00:04.2	00:00.0	00:00.0	00:00.0
108	2	1	3	48.5	39.5	9	01:04.6	01:09.4	-00:04.8	00:00.0	00:00.0	00:00.0
109	1	2	3	12	42	-30	00:30.3	01:30.6	-01:00.3	N/A	N/A	N/A
110	2	1	2	9	7	2	00:11.9	00:08.4	00:03.5	00:00.0	00:00.0	00:00.0
111	1	2	3	7	17	-10	00:06.0	00:16.3	-00:10.3	00:00.0	00:00.0	00:00.0
112	2	1	3	18	8	10	00:16.8	00:15.5	00:01.3	00:00.0	00:00.0	00:00.0

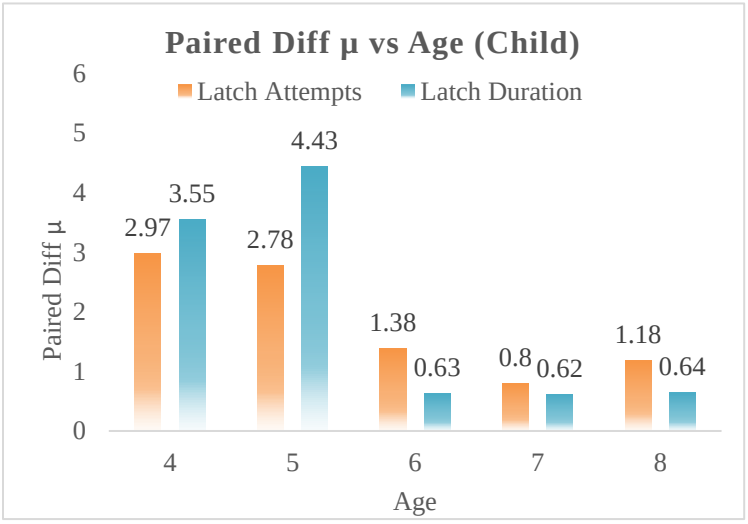

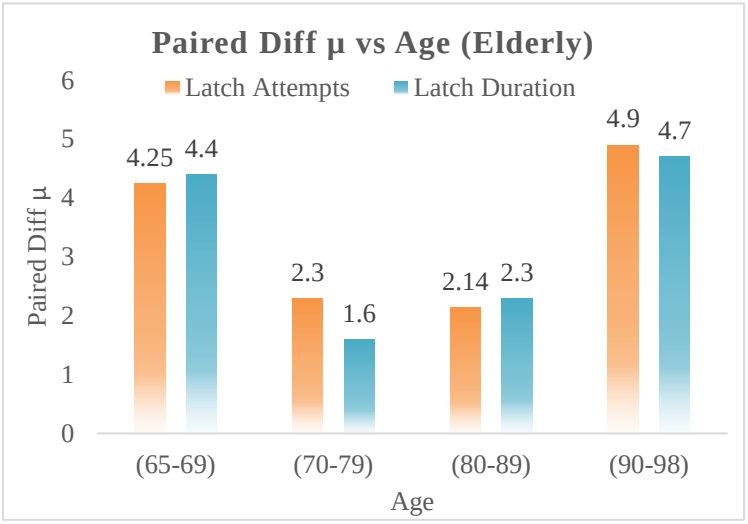

Figure A4: Graphs comparing Paired Diff μ vs Age for Latch Attempts and Latch Duration for Children and Elderly Cohorts.

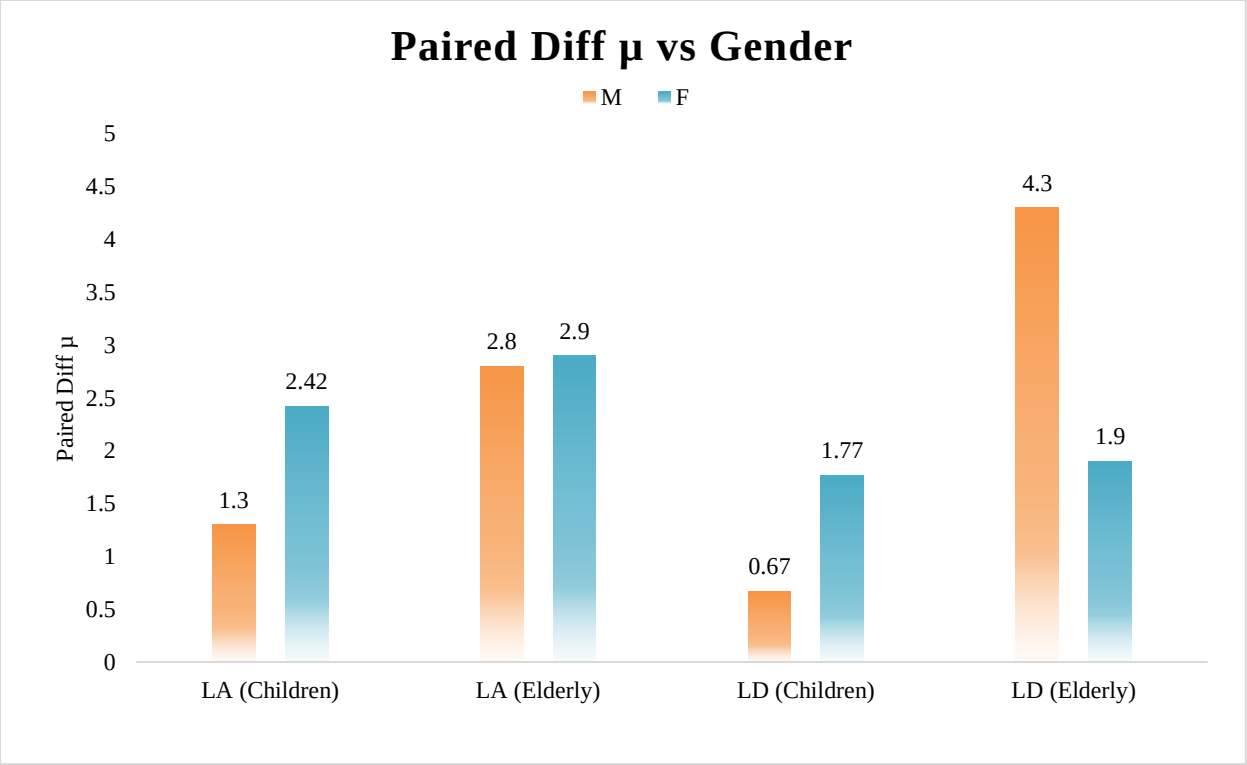

Figure A5: Graph showing Paired Diff μ vs Gender for Latch Attempts and Latch Duration for Child and Elderly Cohorts.

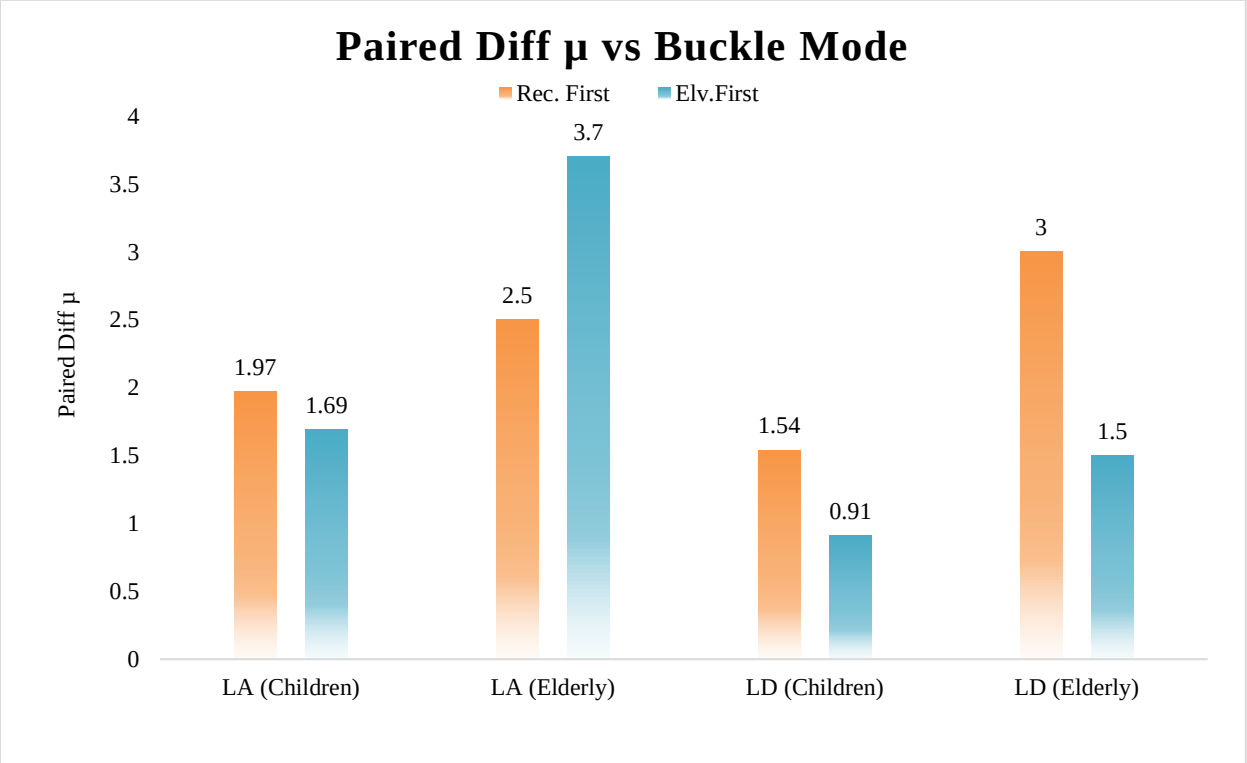

Figure A6: Graph showing Paired Diff μ vs Buckle Mode for Latch Attempts and Latch Duration for Child and Elderly Cohorts.

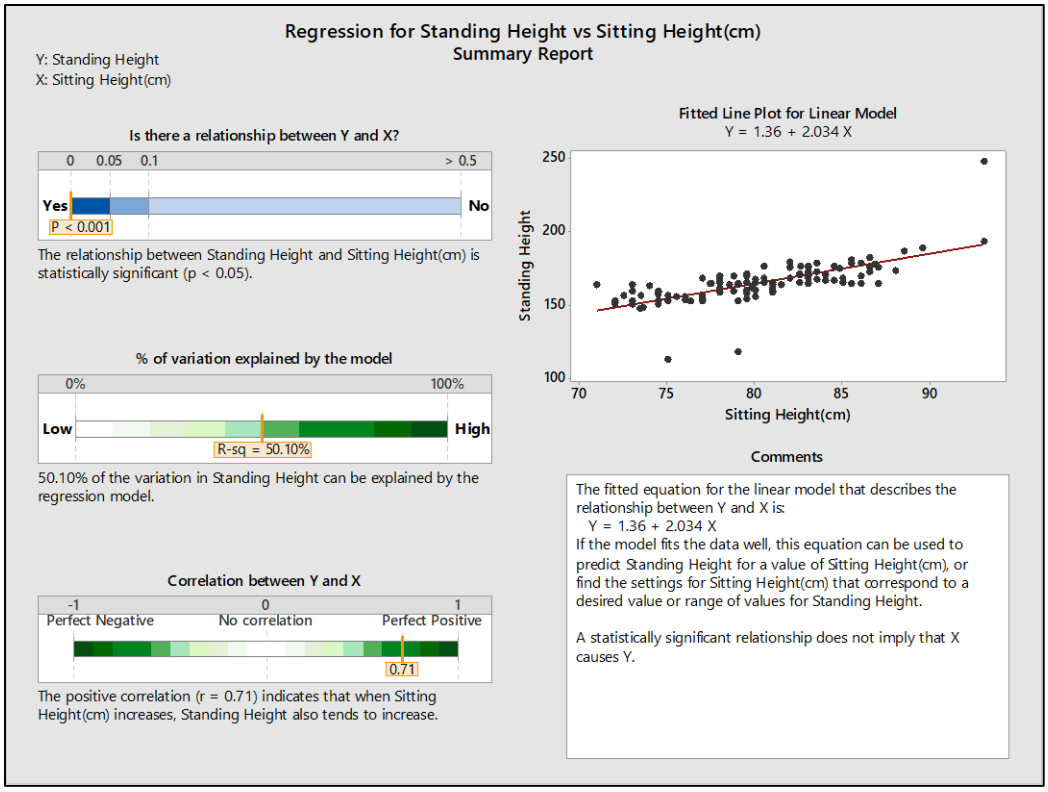

Figure A7a

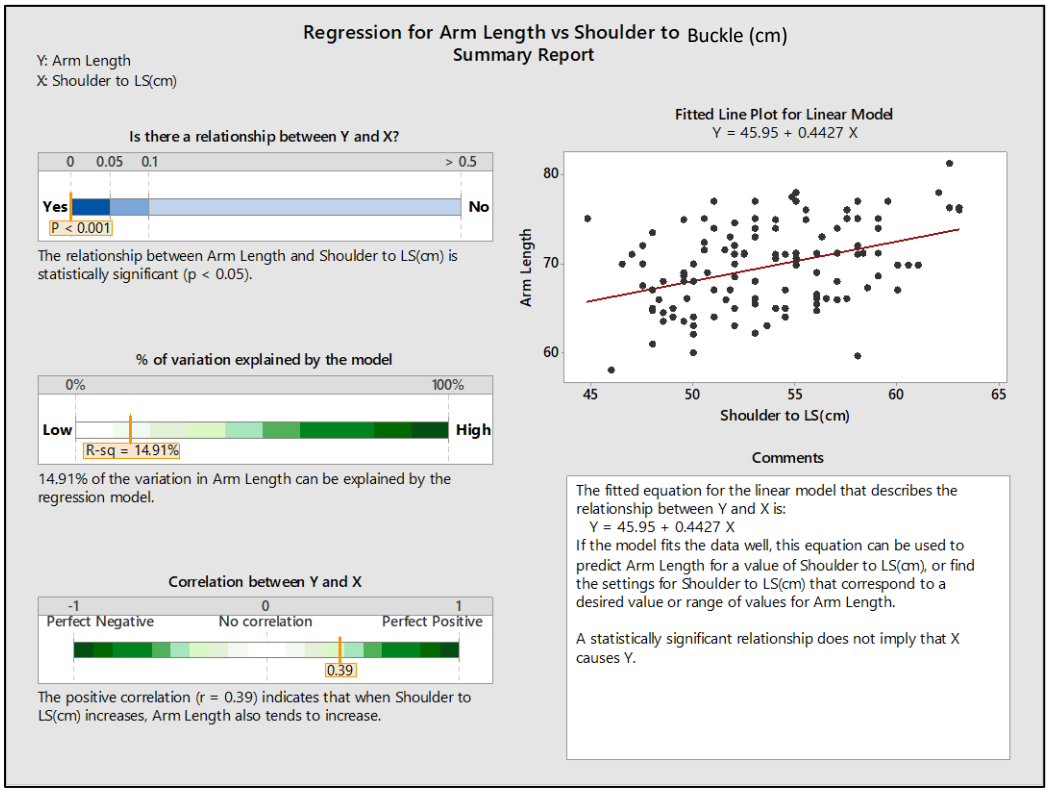

Figure A7b

Figure A7: Simple Regressions; Standing Height vs Sitting Height (Figure A7a), Arm Length vs Shoulder to Buckle (Figure A7b).

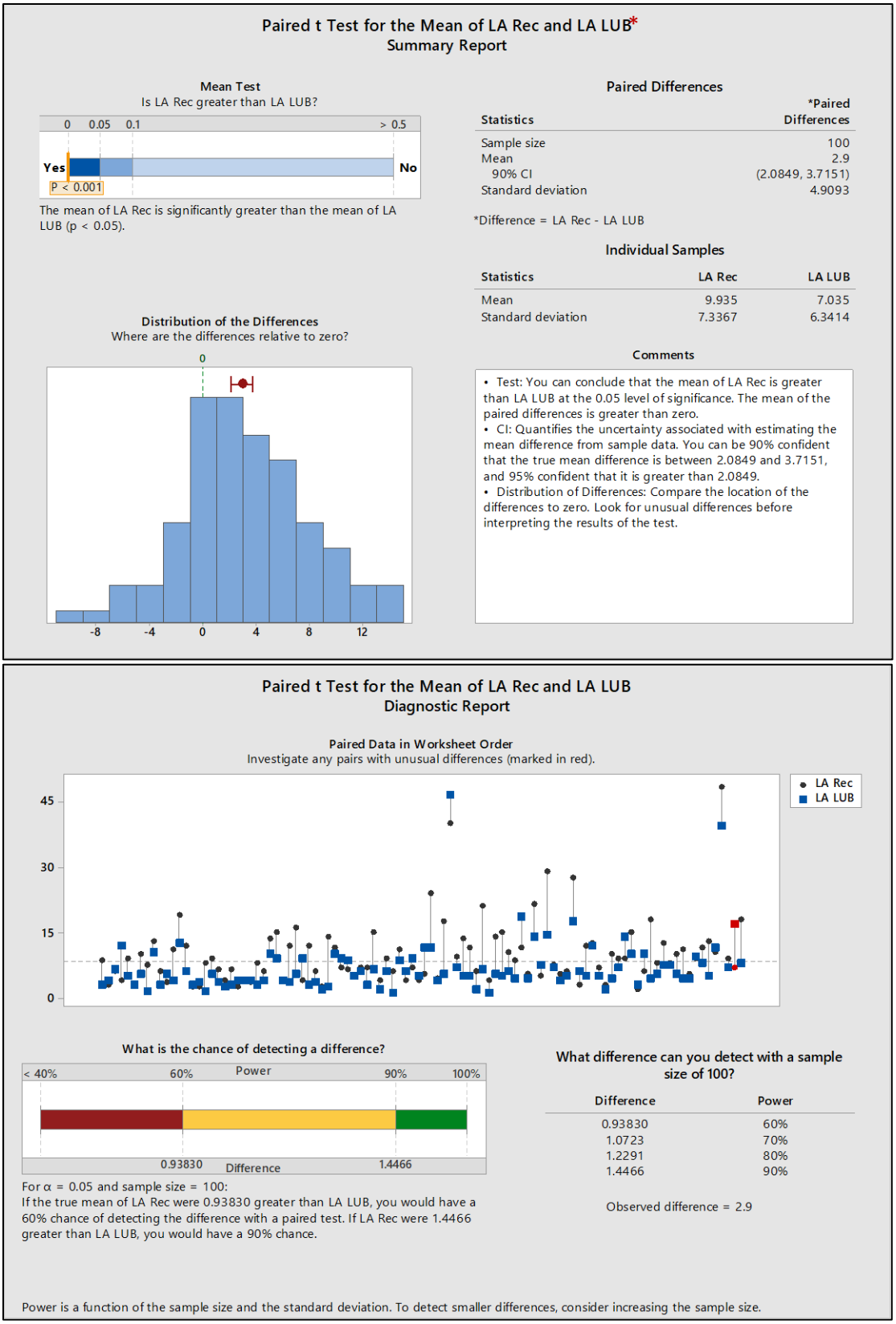

Figure A8: Paired t Test for OVERALL Sample - Latch Attempts.

**Note: For all intents and purposes, "LUB" is the same as "Elevated".*

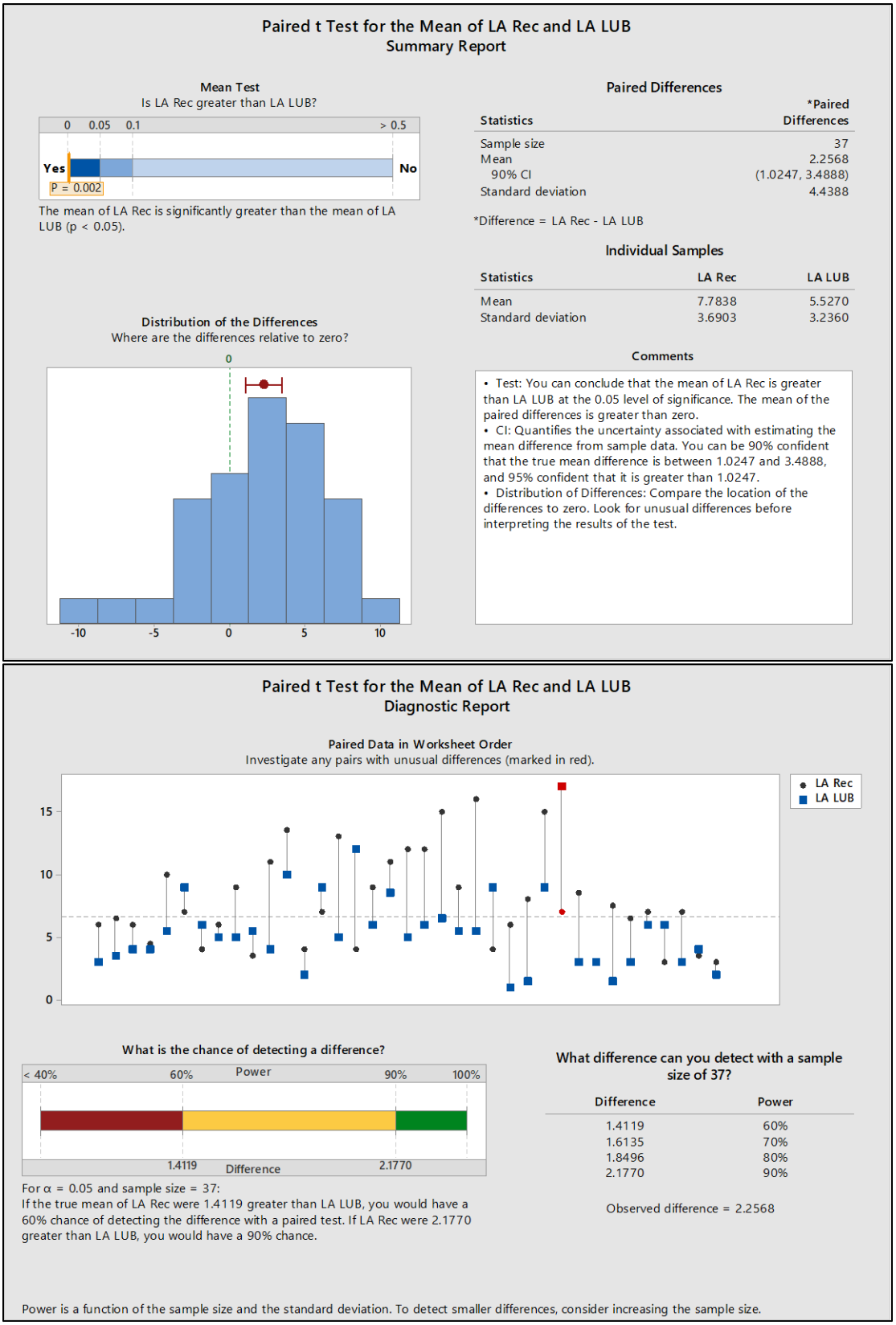

Figure A9: Paired t Test for Age 70-73 Sample – Latch Attempts.

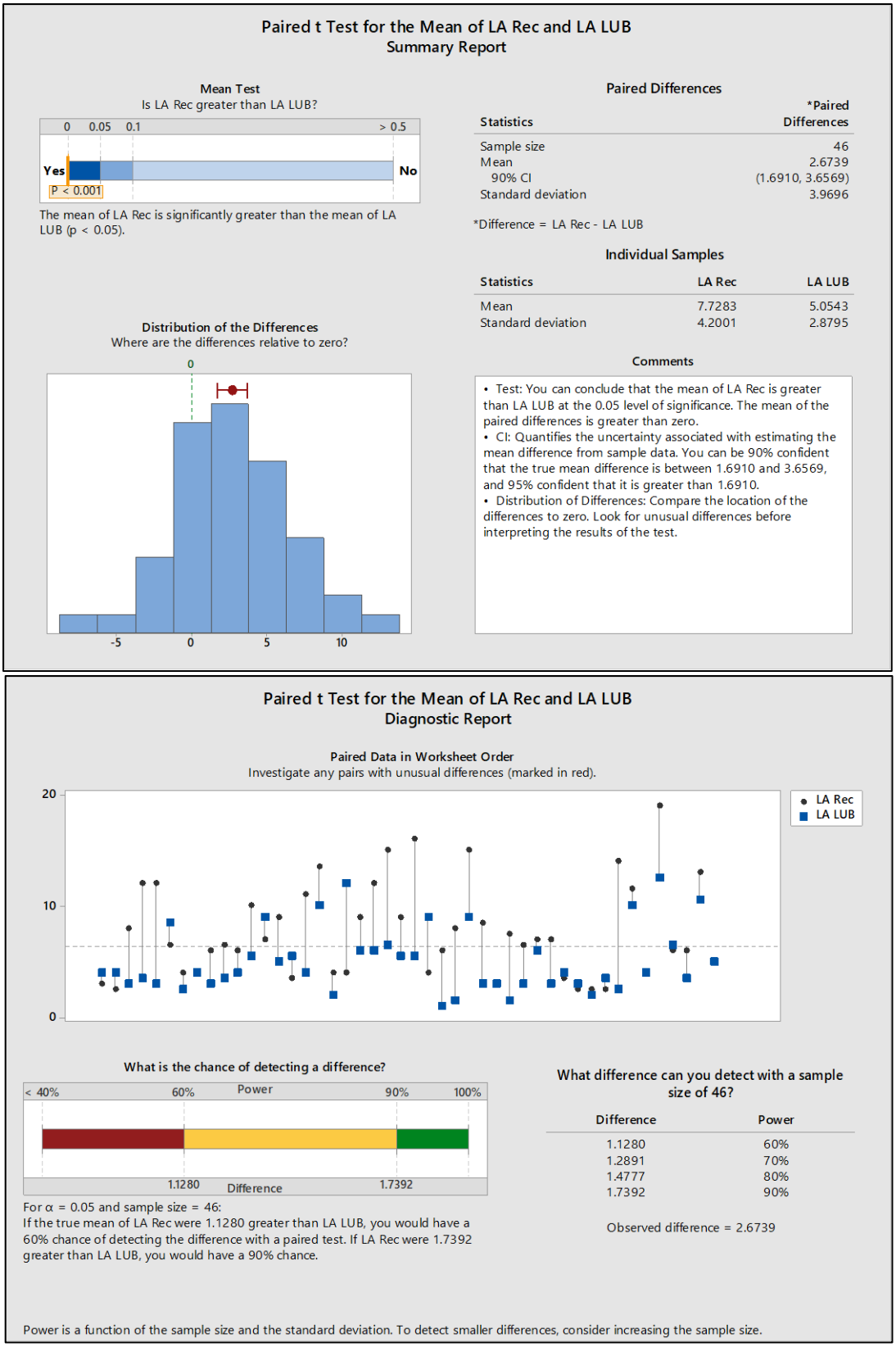

Figure A10: Paired t Test for Study Site 4 Sample - Latch Attempts.

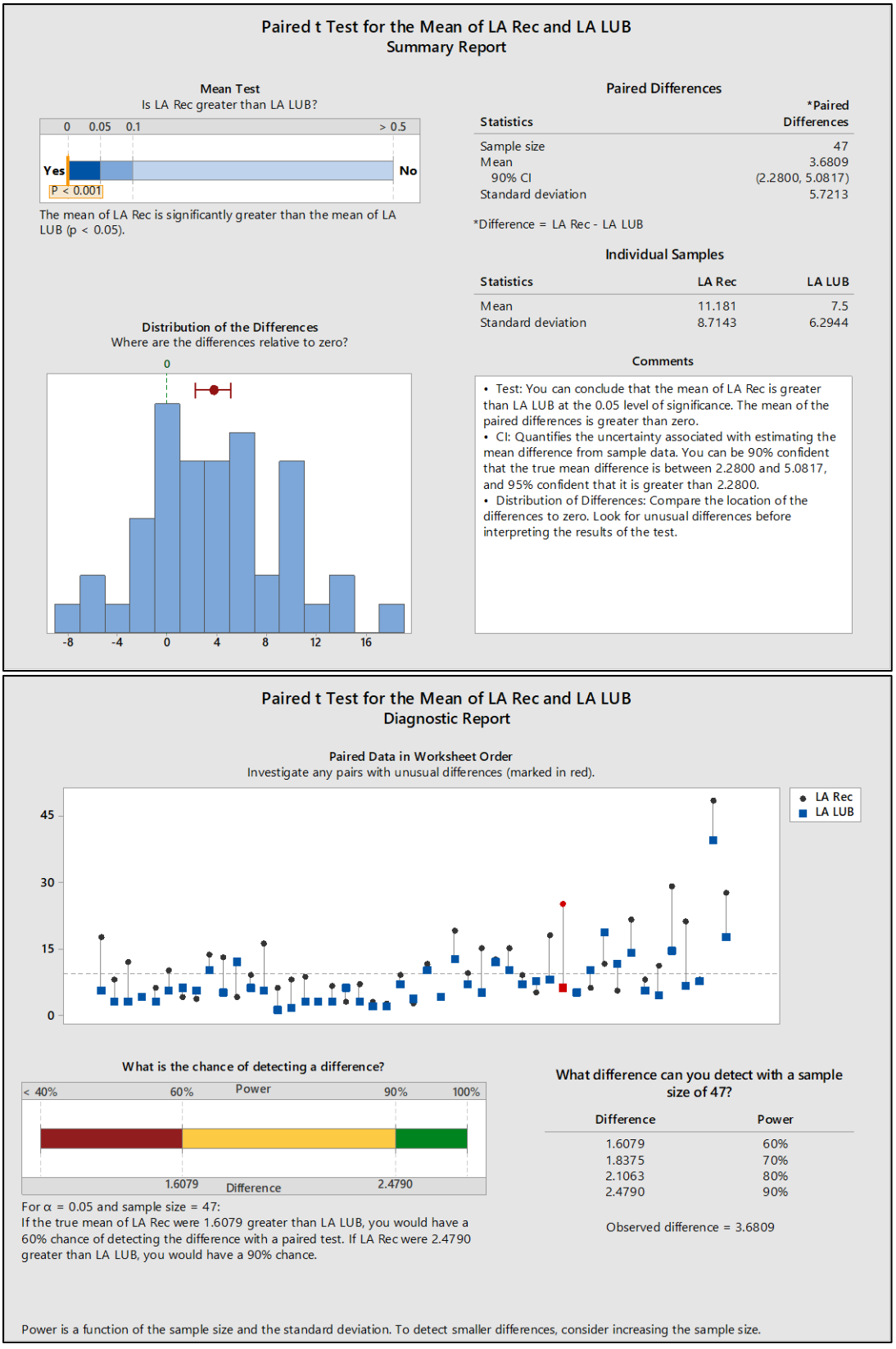

Figure A11: Paired t Test for Elevated Mode First – Latch Attempts.

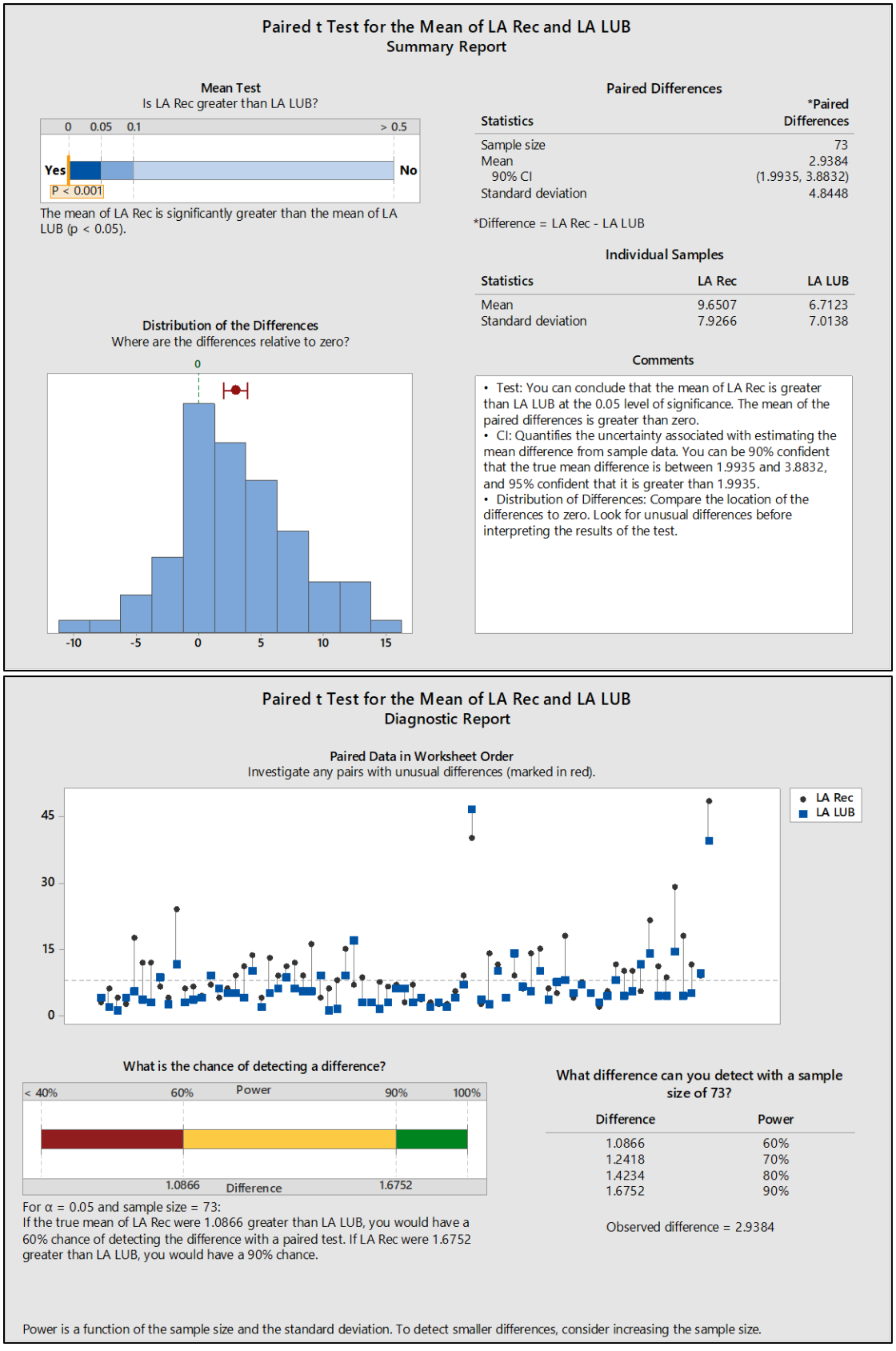

Figure A12: Paired t Test for Females – Latch Attempts.

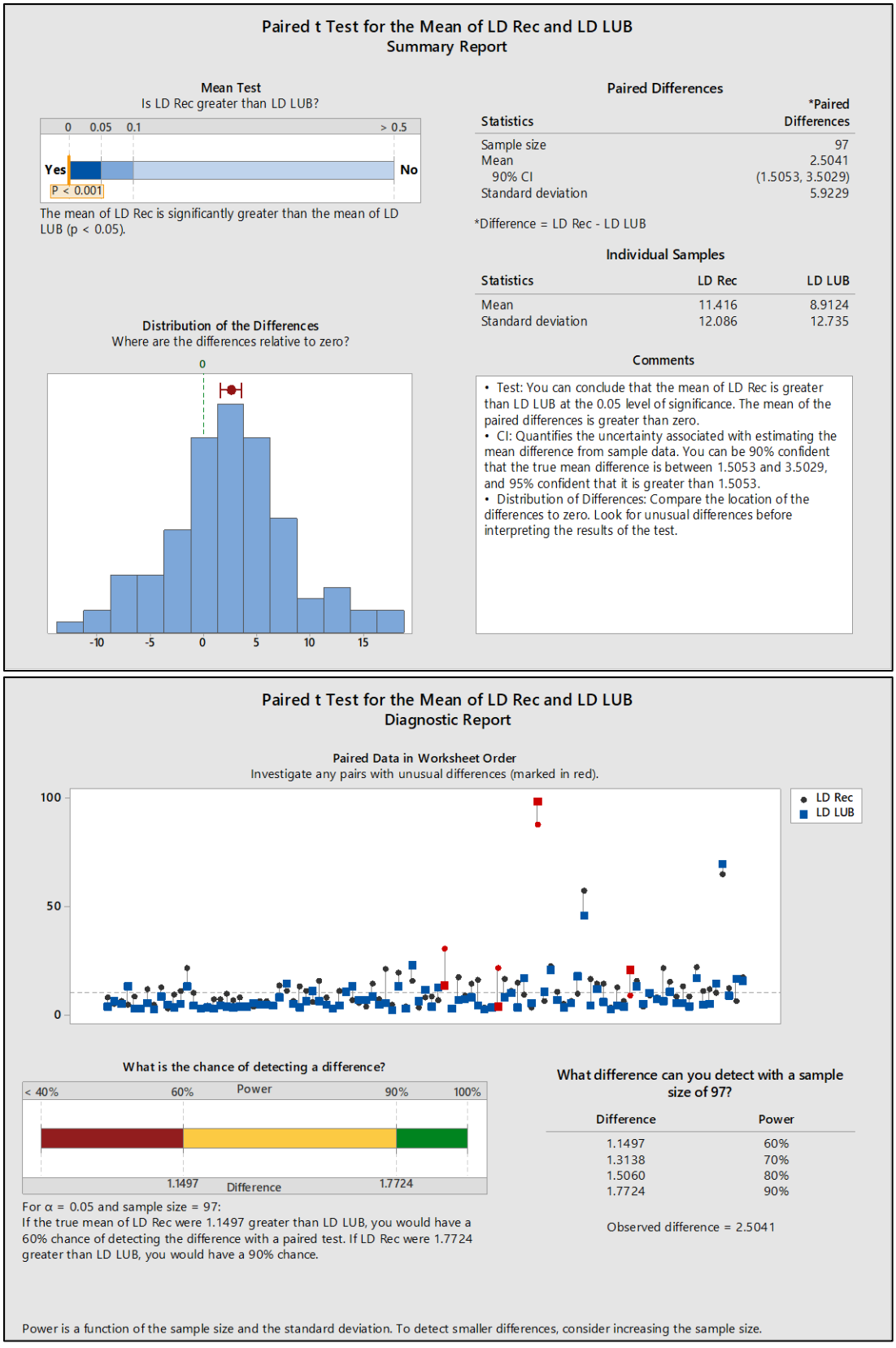

Figure A13: Paired t Test for OVERALL Sample – Latch Duration.

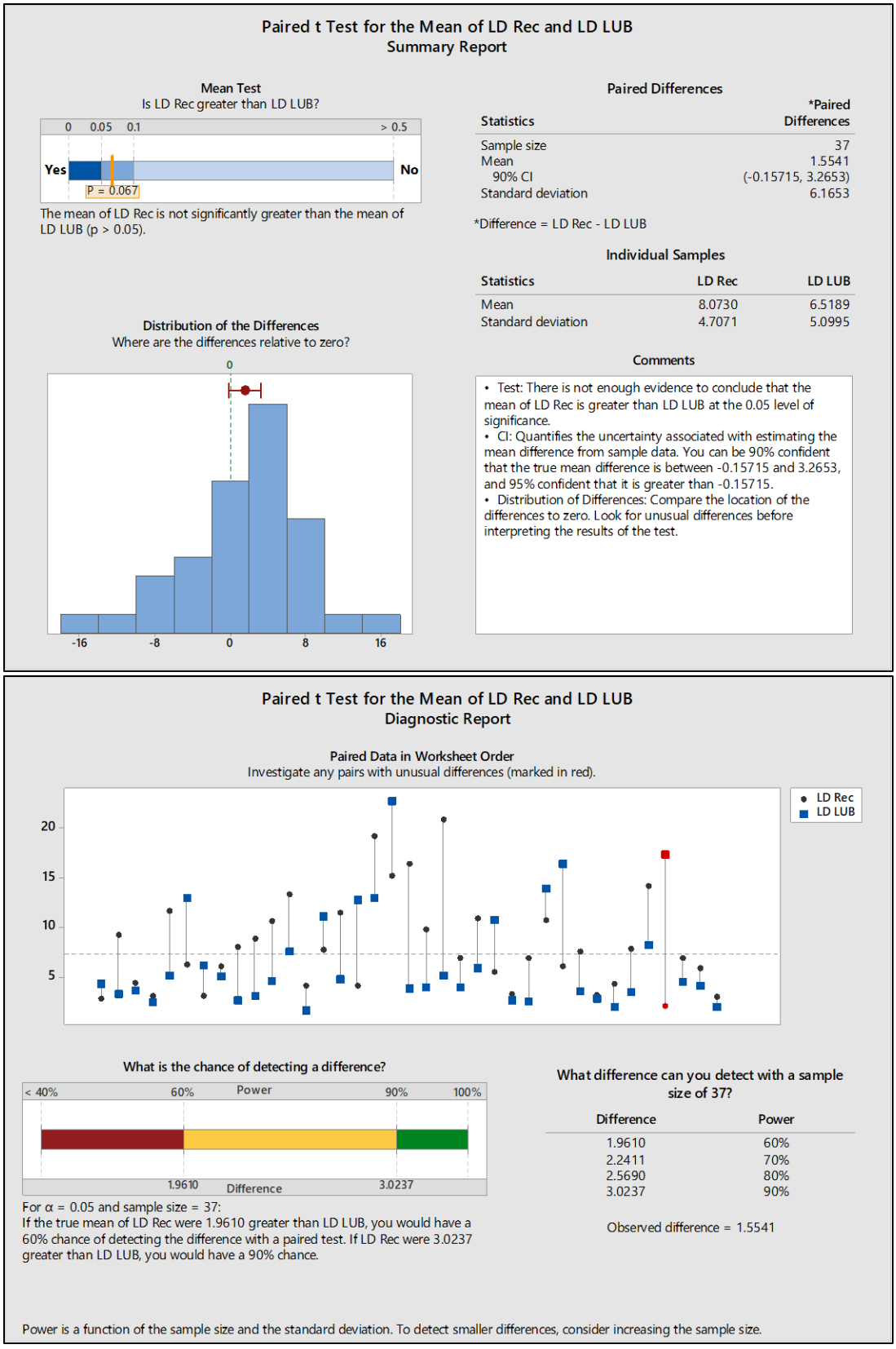

Figure A14: Paired t Test for Age 70-79 Sample – Latch Duration.

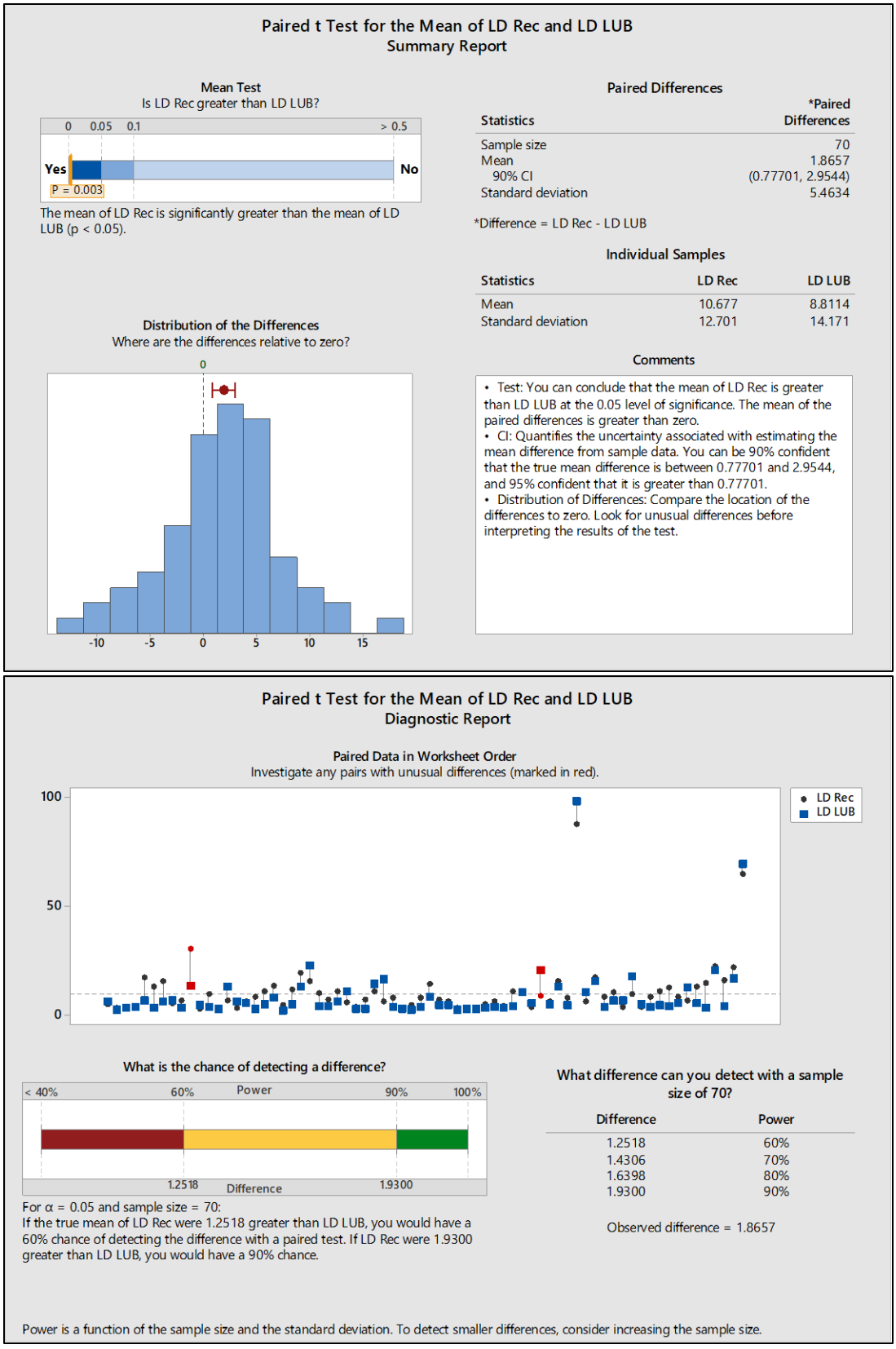

Figure A15: Paired t Test for Female Sample – Latch Duration.

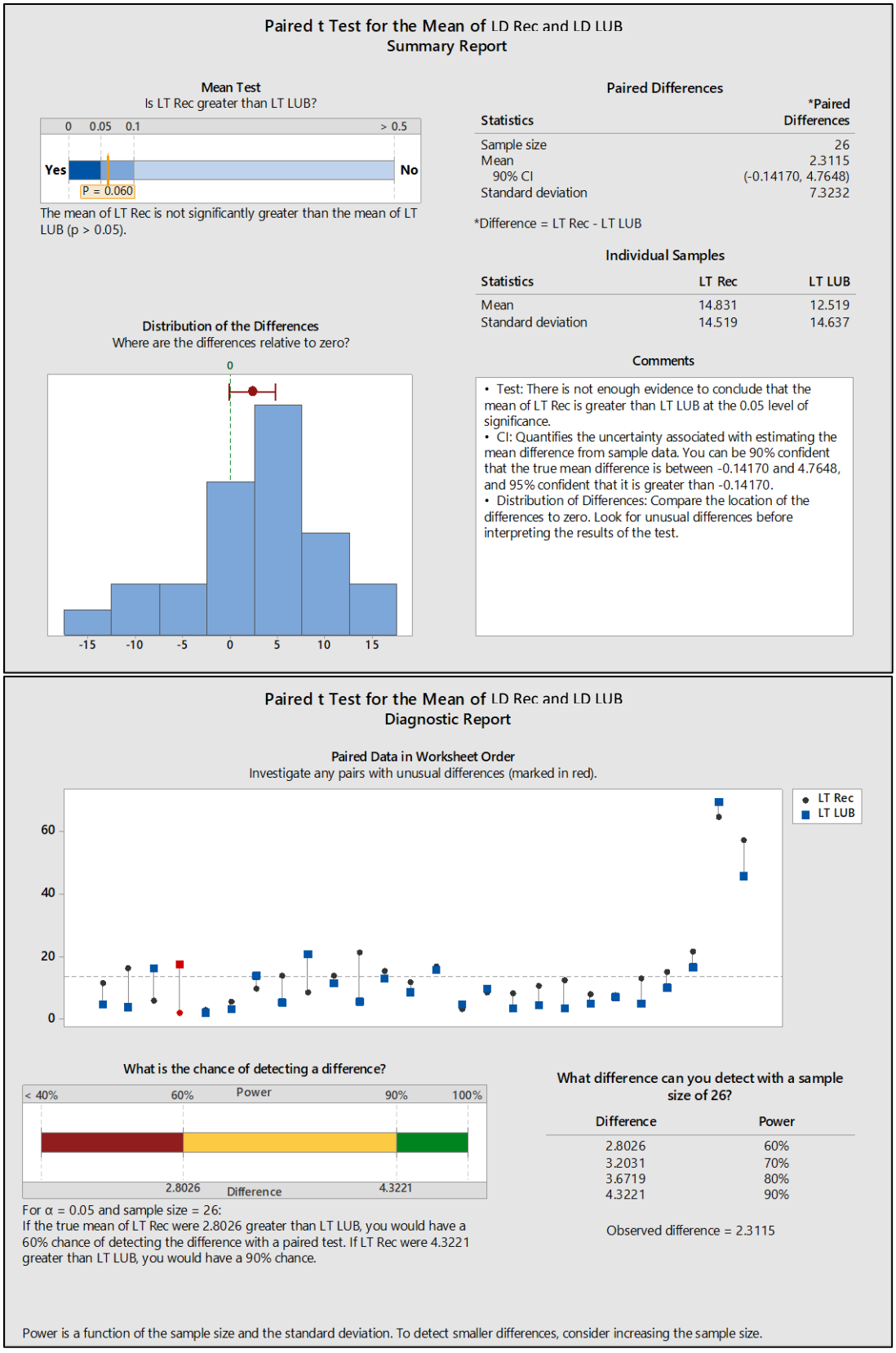

Figure A16: Paired t Test for Study Site 5 – Latch Duration.

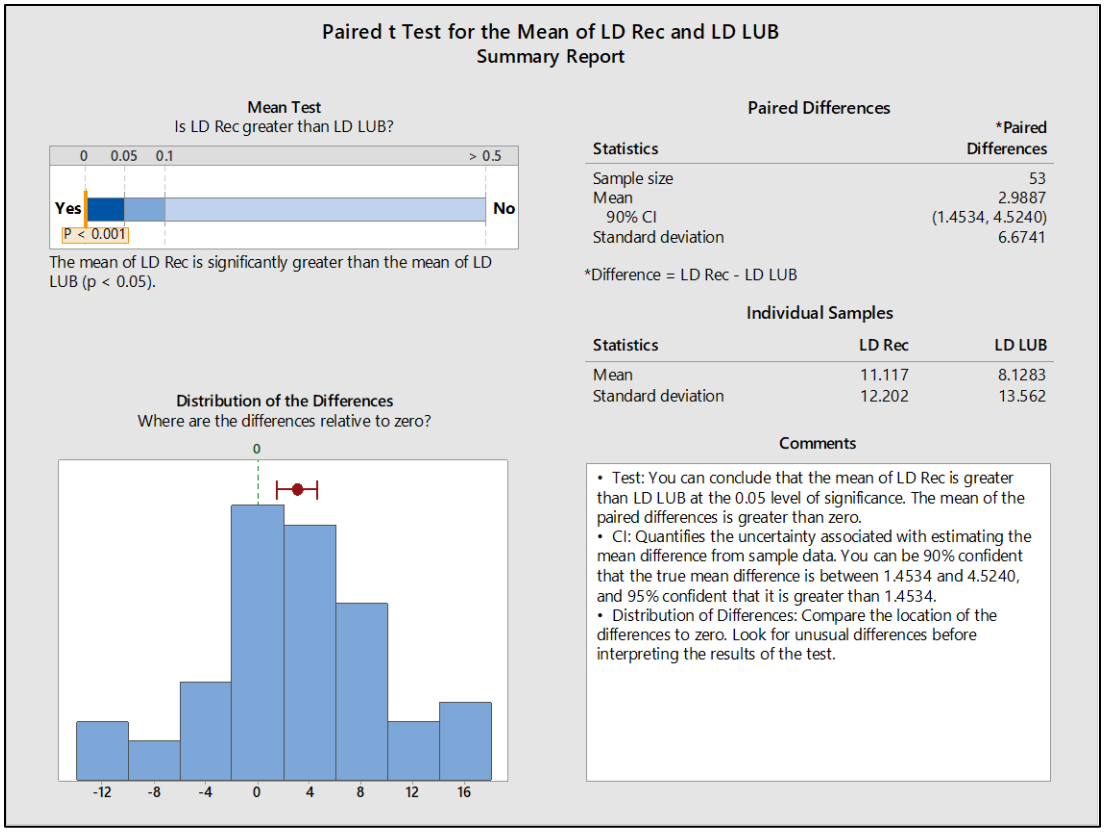

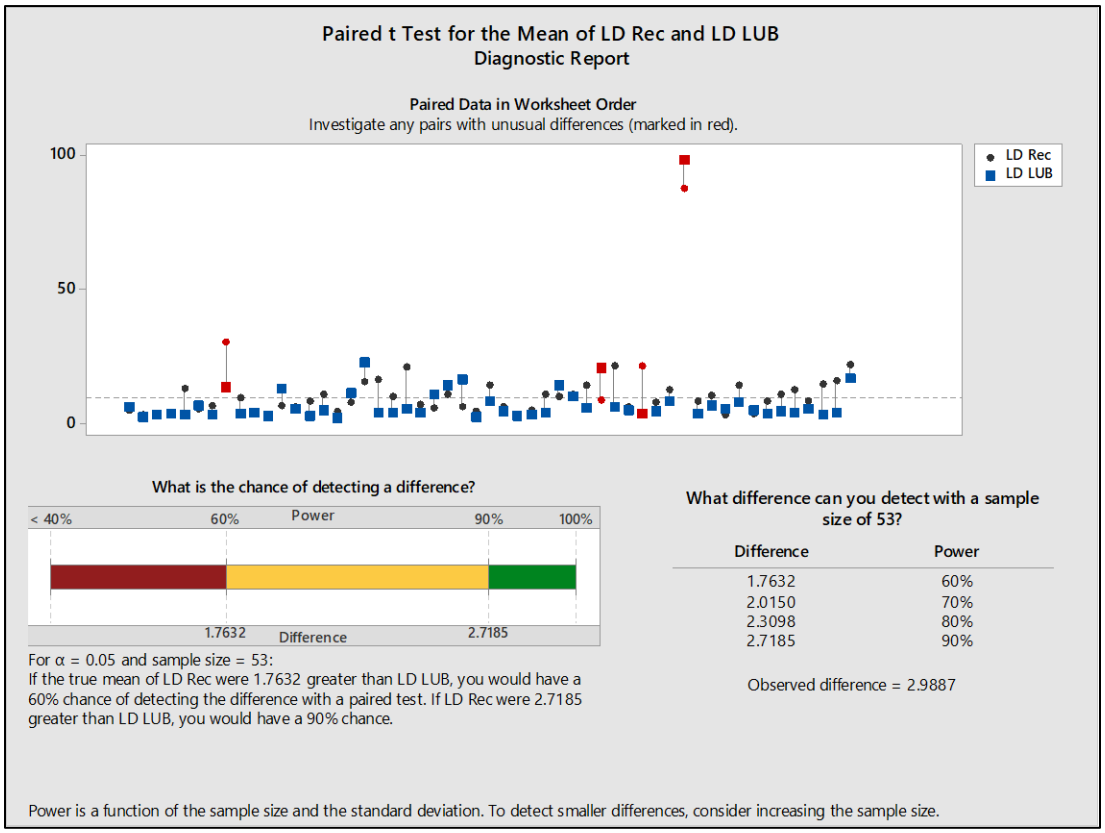

Figure A17: Paired t Test for Recessed Mode First – Latch Duration.

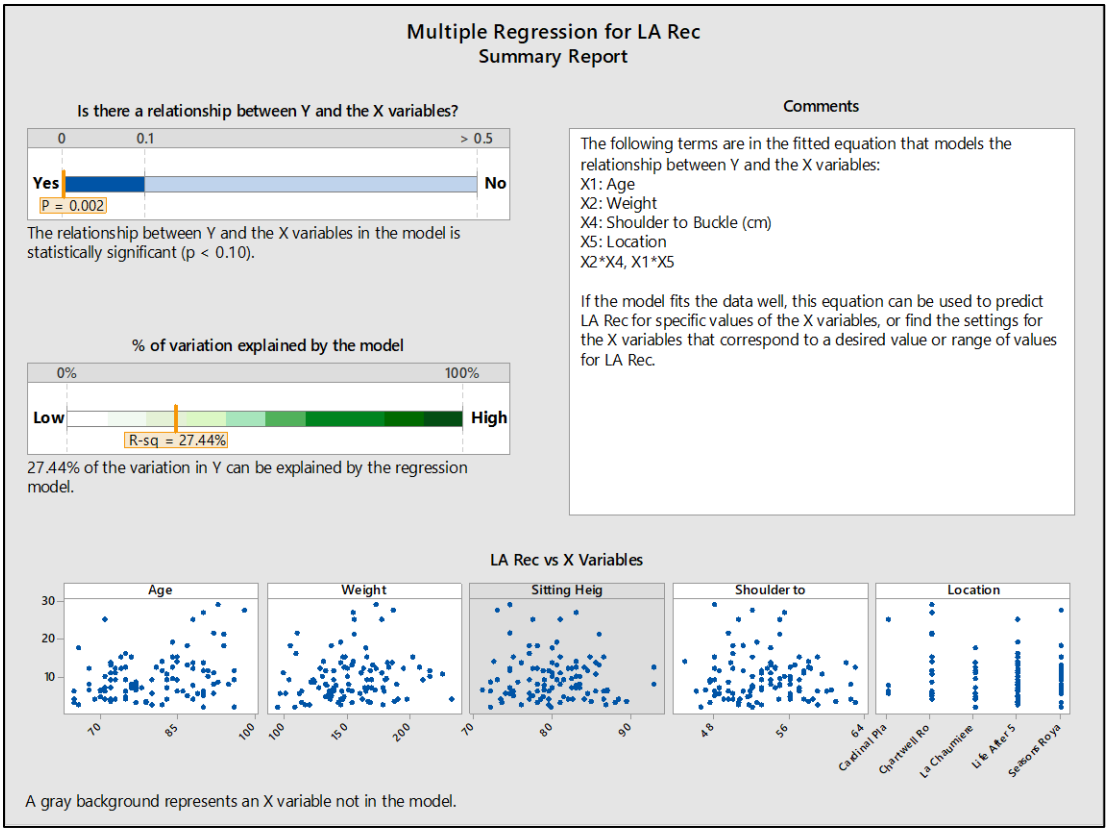

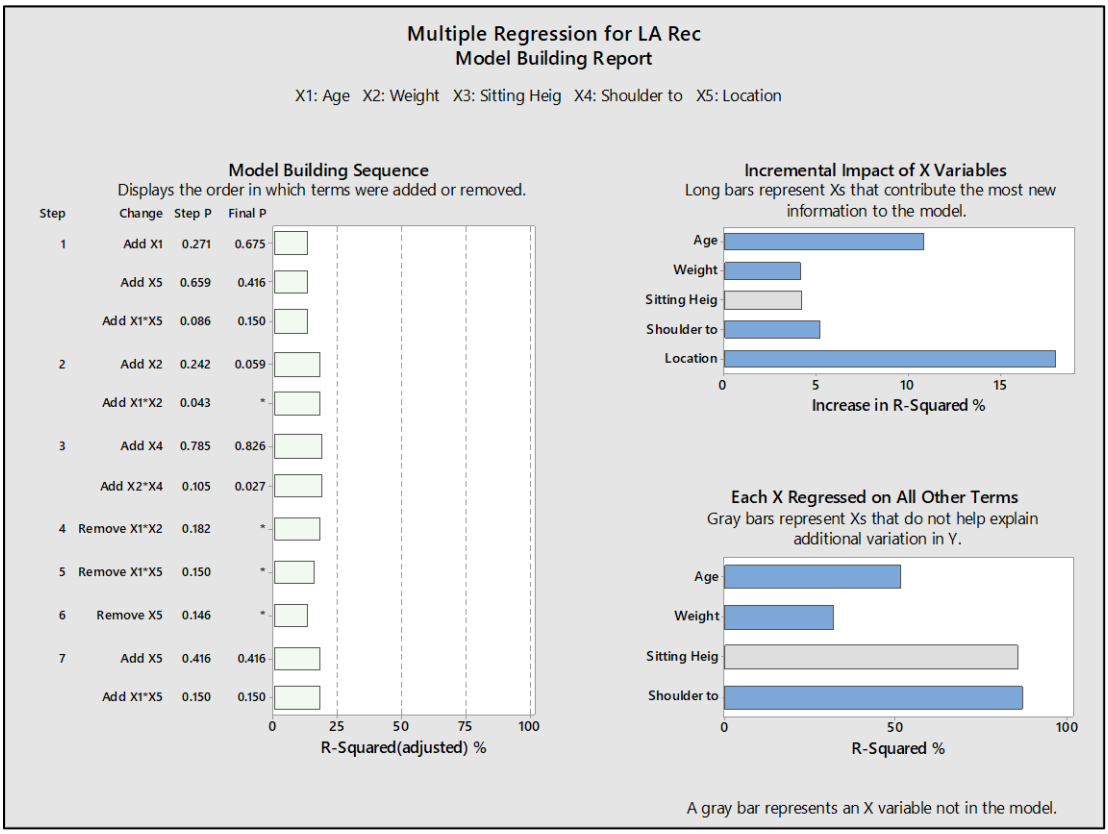

Figure A18: Regression Analysis for Latch Attempts – Recessed.

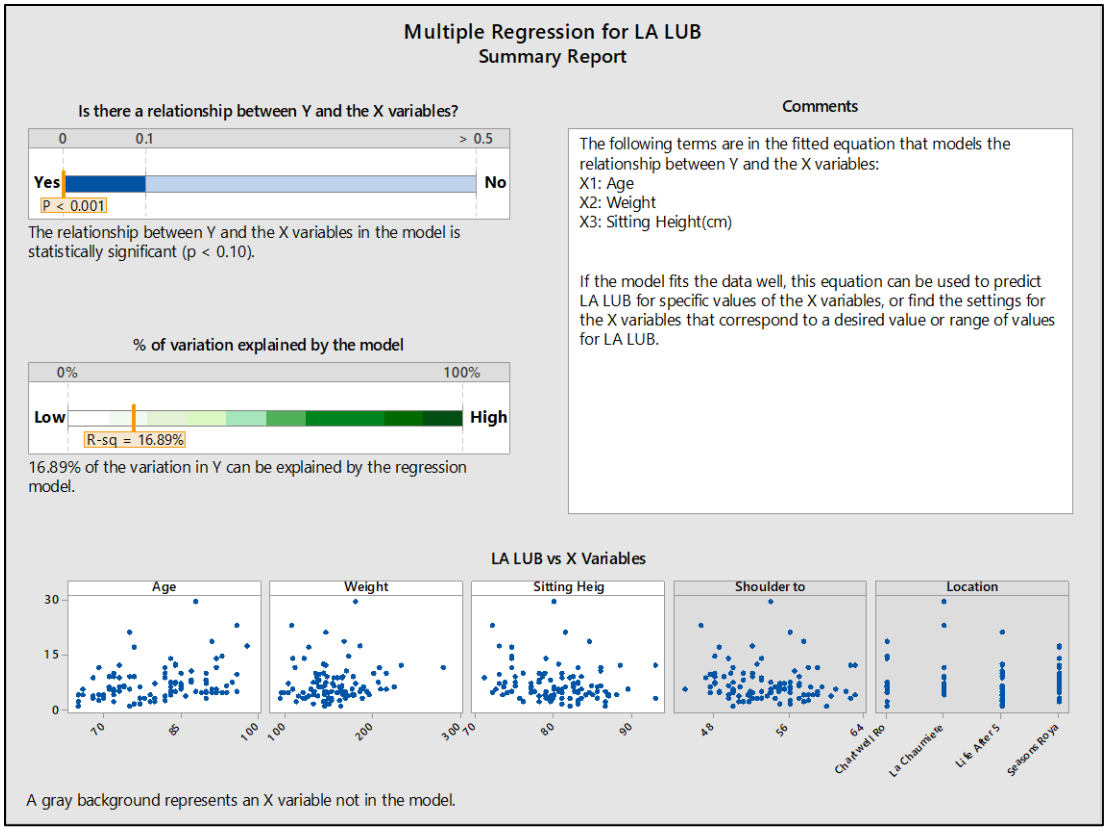

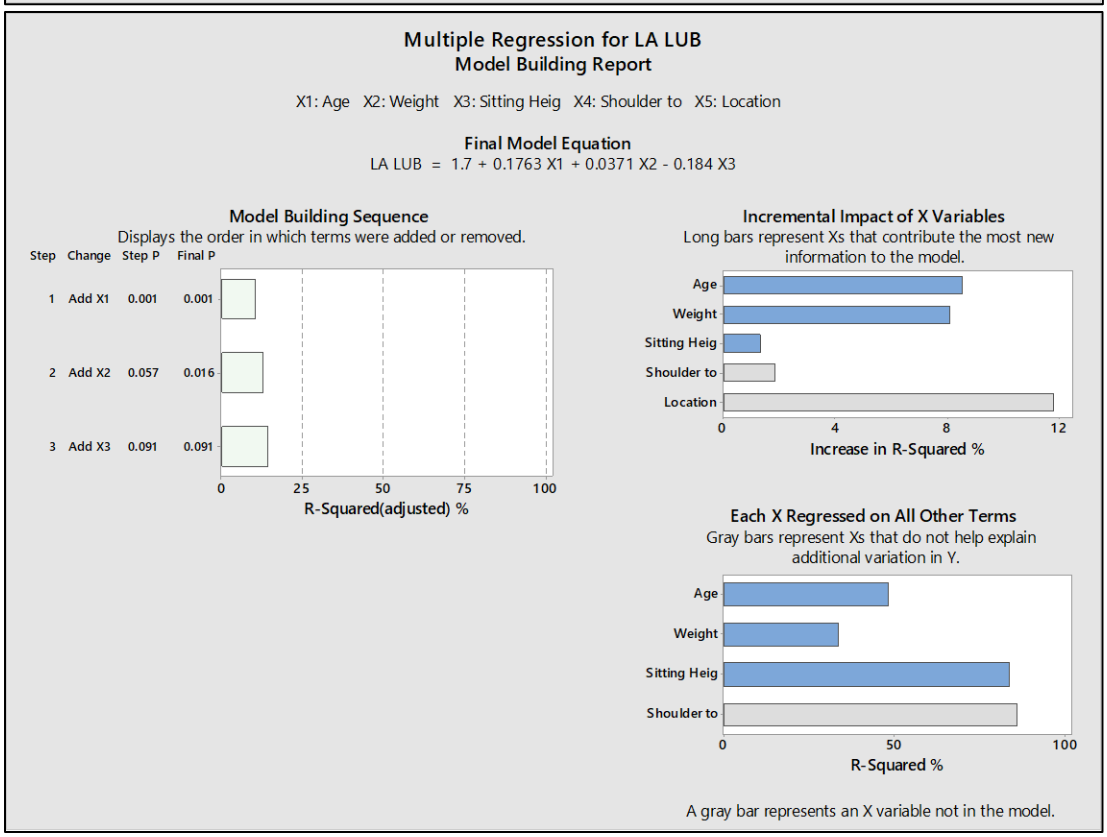

Figure A19: Regression Analysis for Latch Attempts – Elevated (LUB).

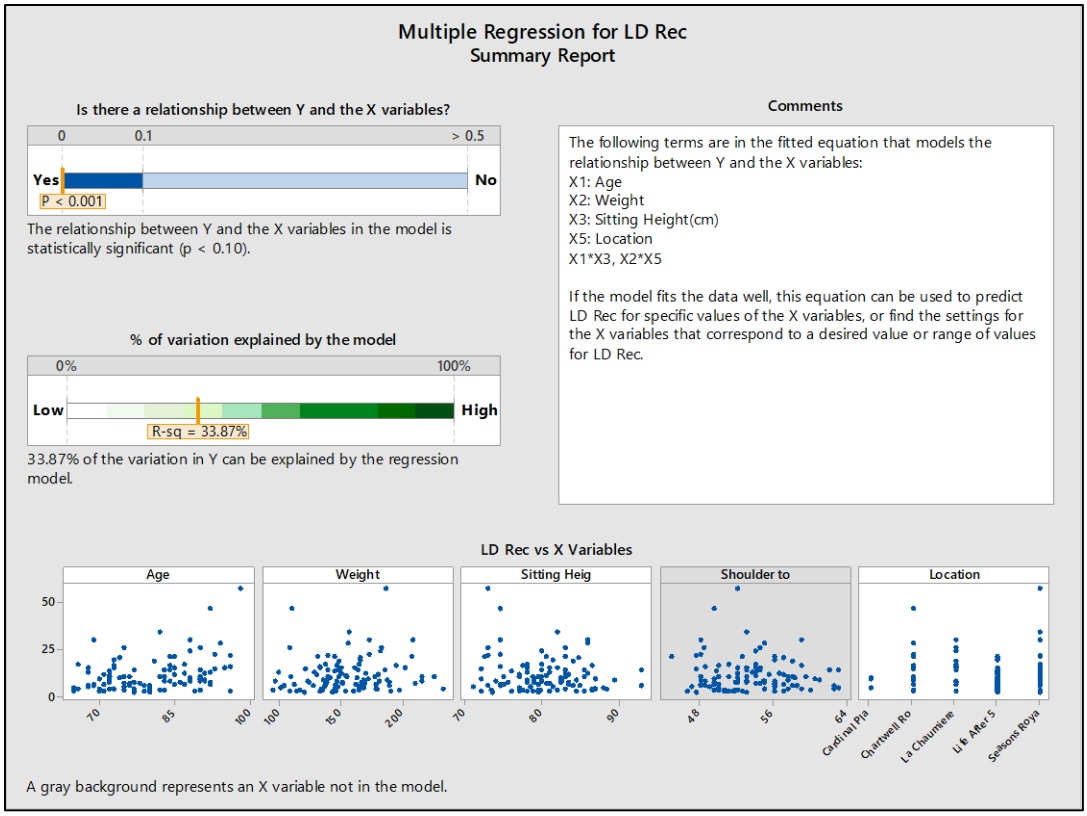

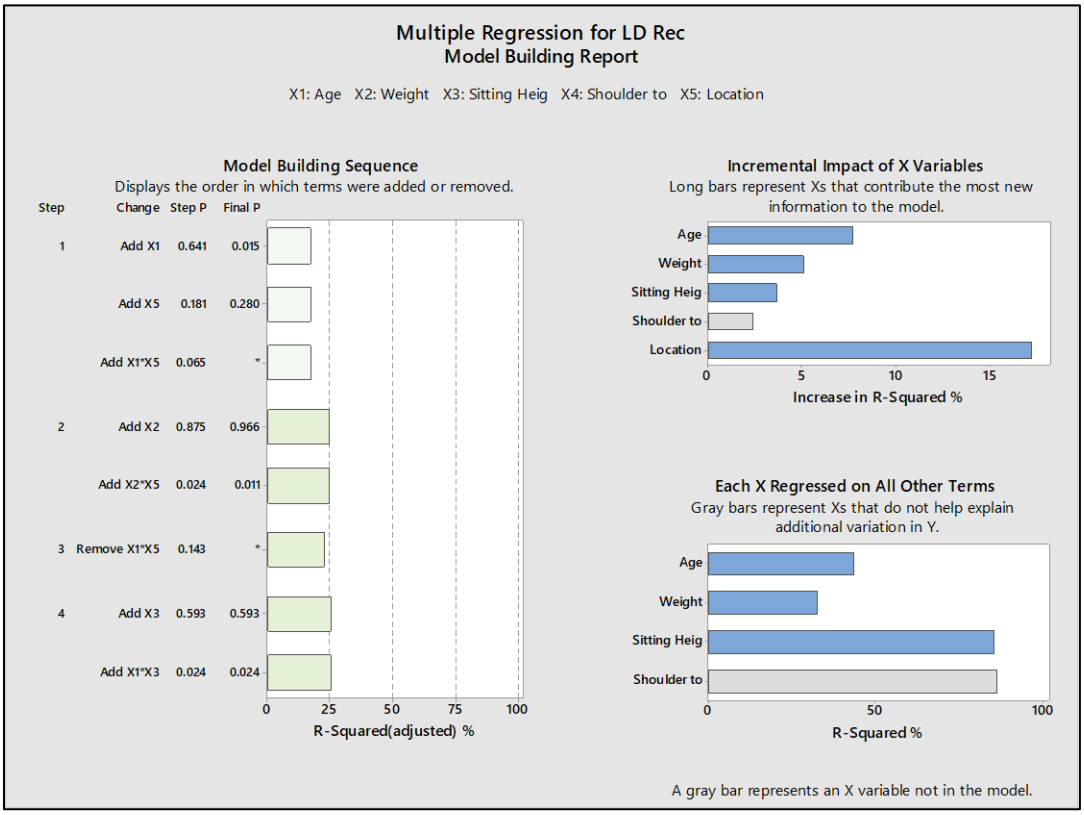

Figure A20: Regression Analysis for Latch Duration – Recessed.

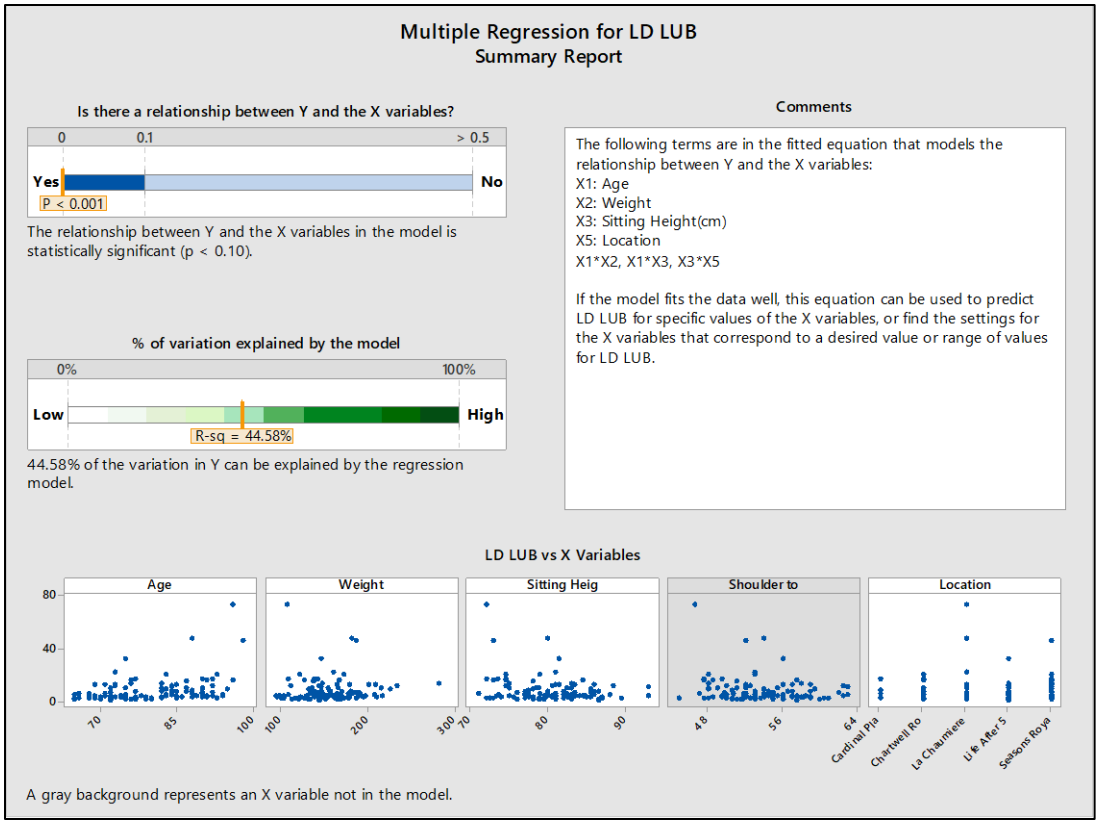

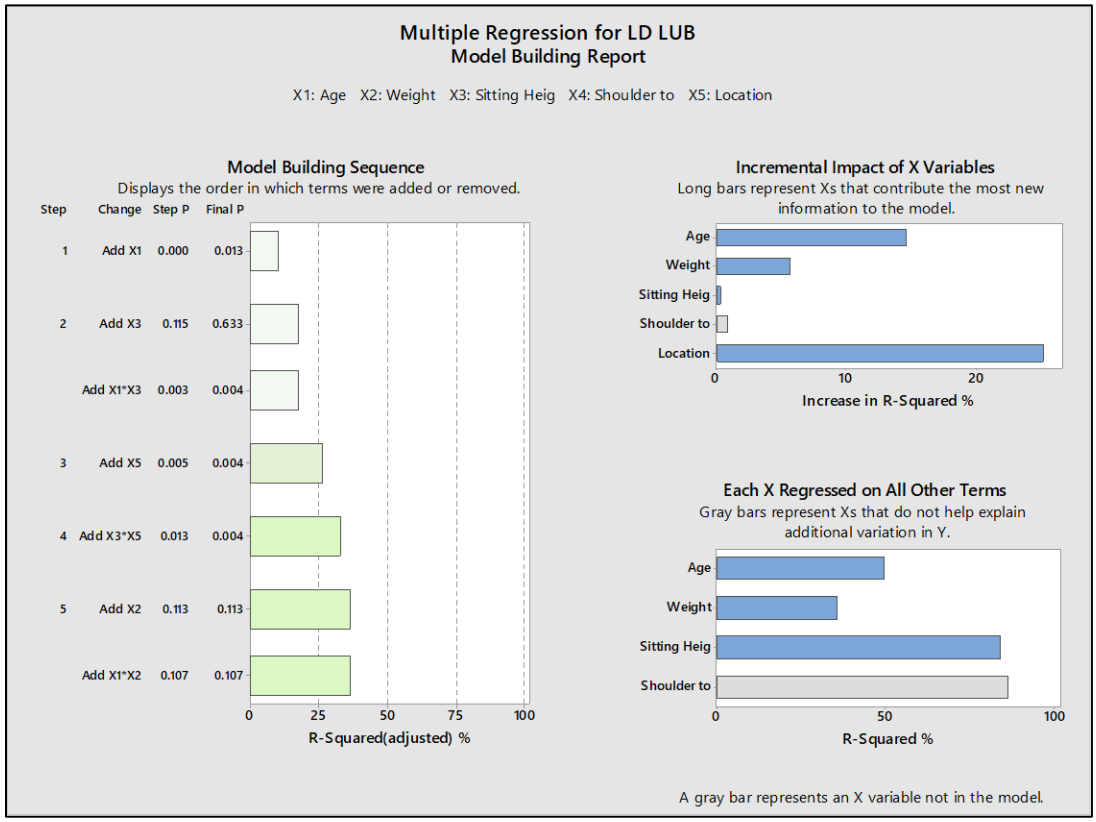

Figure A21: Regression Analysis for Latch Duration – Elevated (LUB).

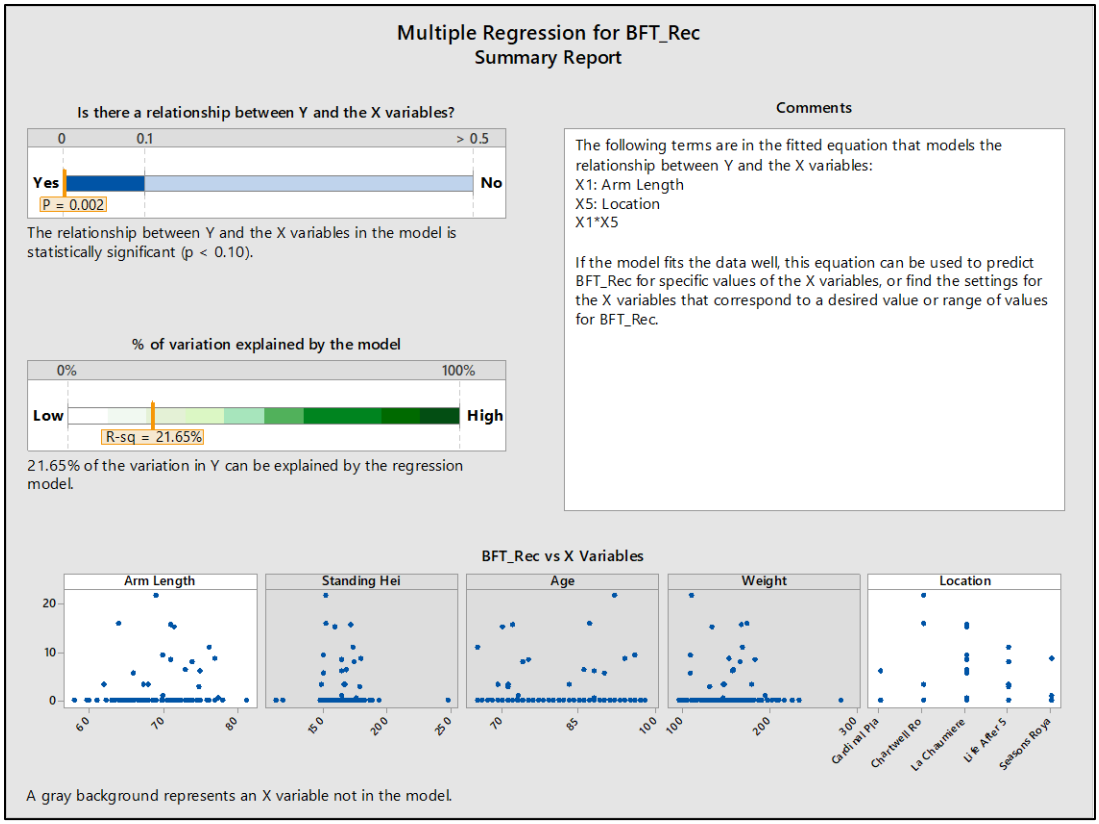

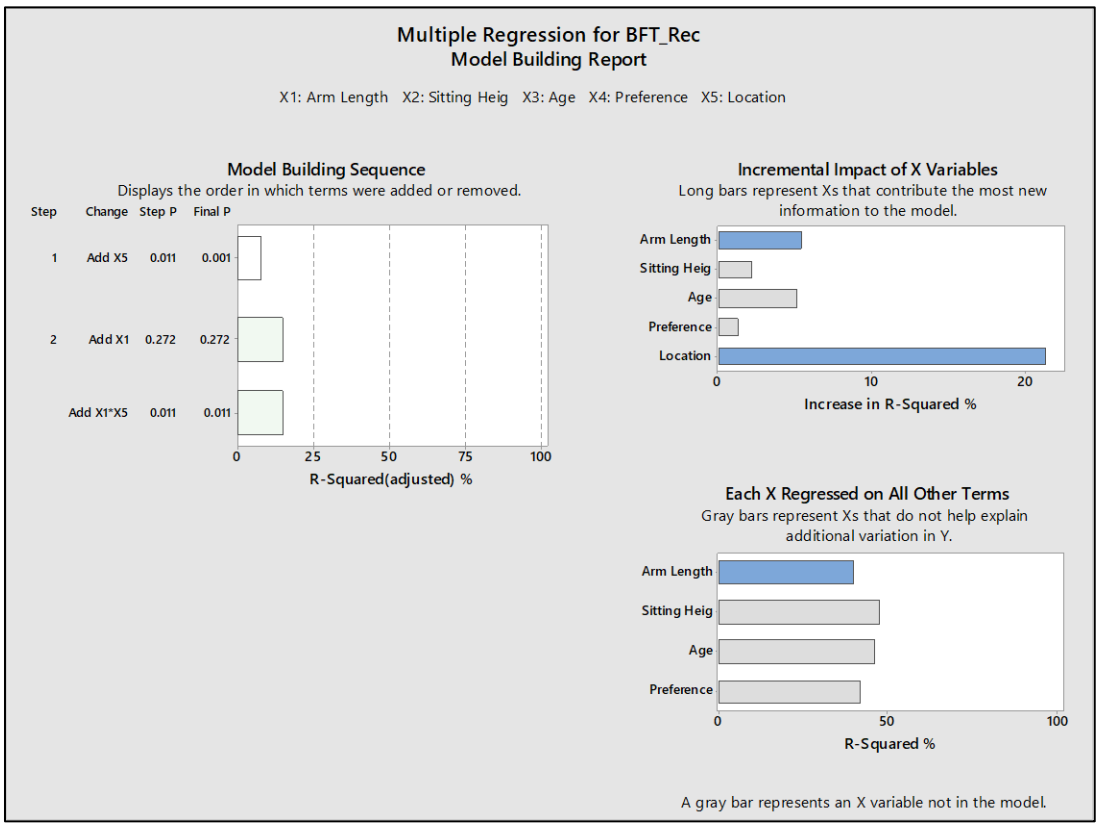

Figure A22: Regression Analysis for Buckle Find Time – Recessed.

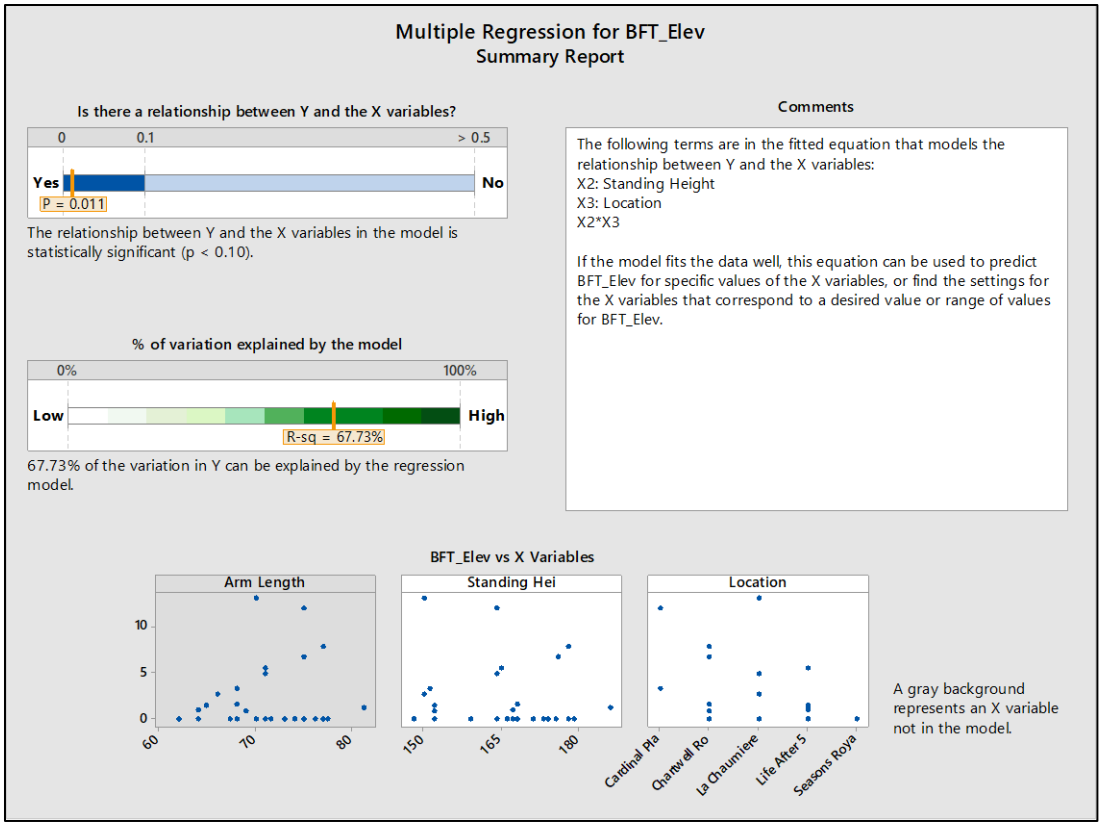

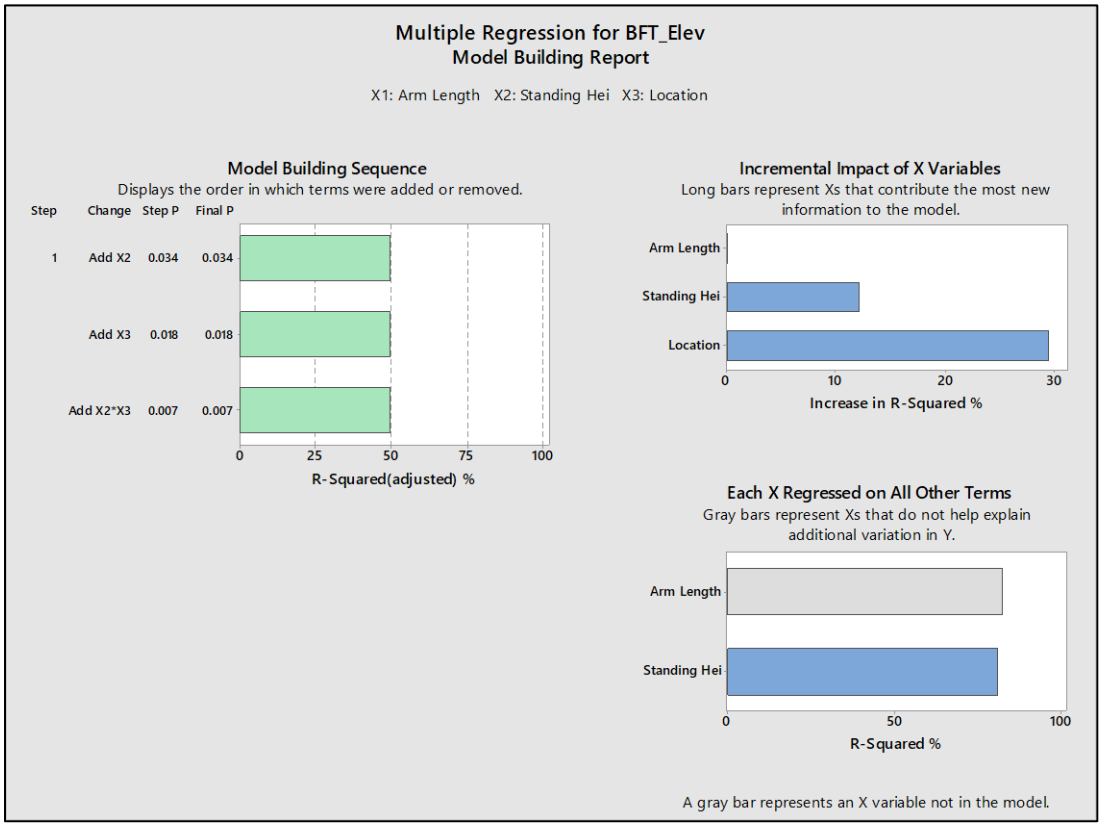

Figure A23: Regression Analysis for Buckle Find Time – Elevated.

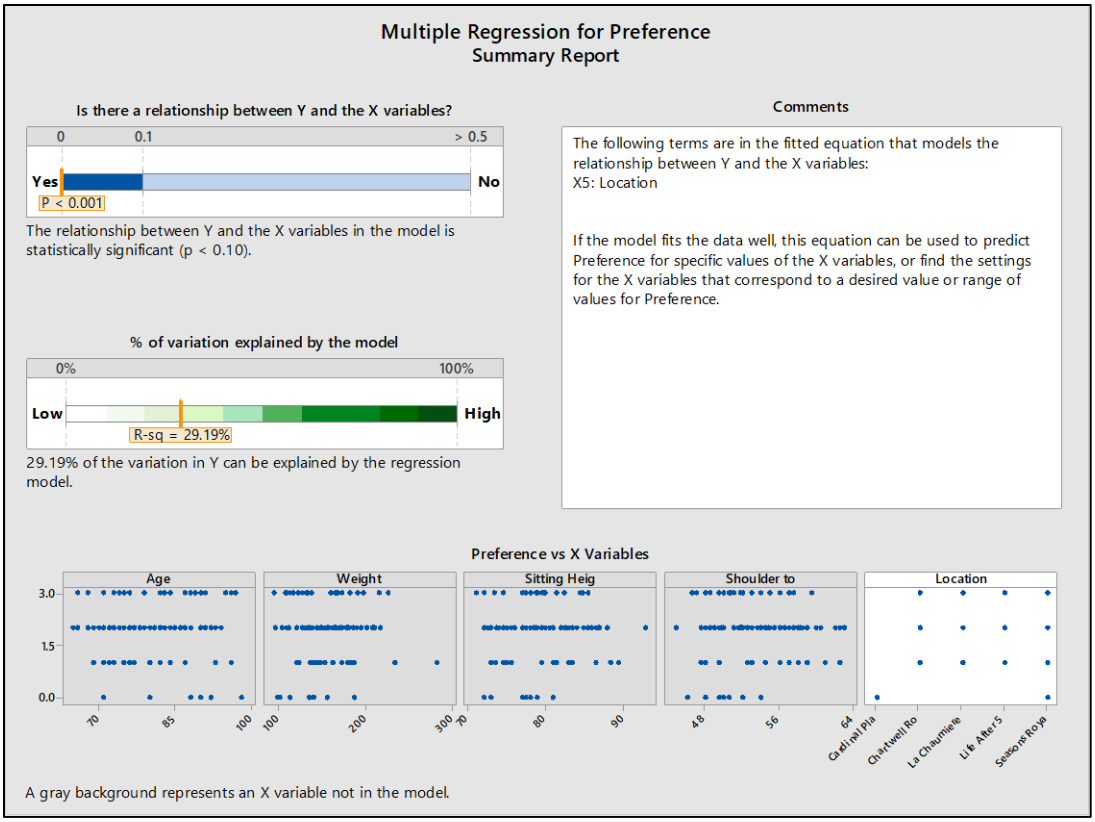

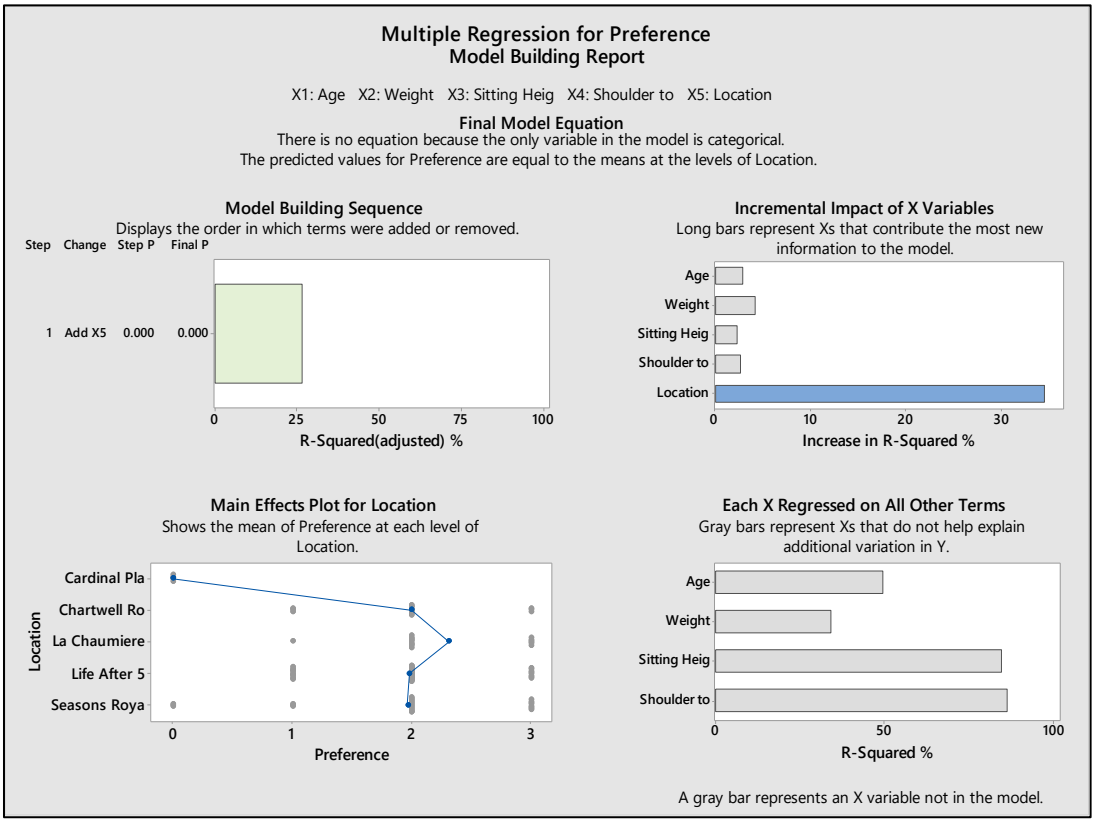

Figure A24: Regression Analysis for Buckle Preference.

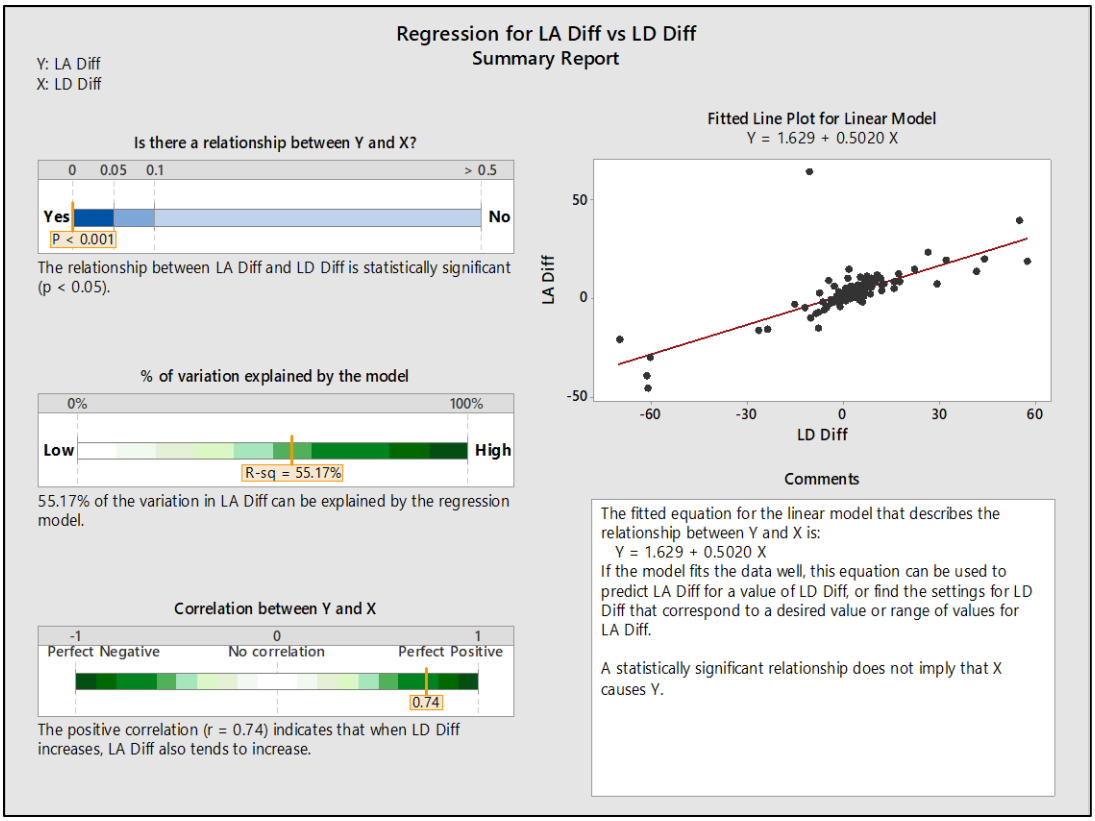

Figure A25: Regression Analysis for Overall Latch Attempts vs Latch Duration Results

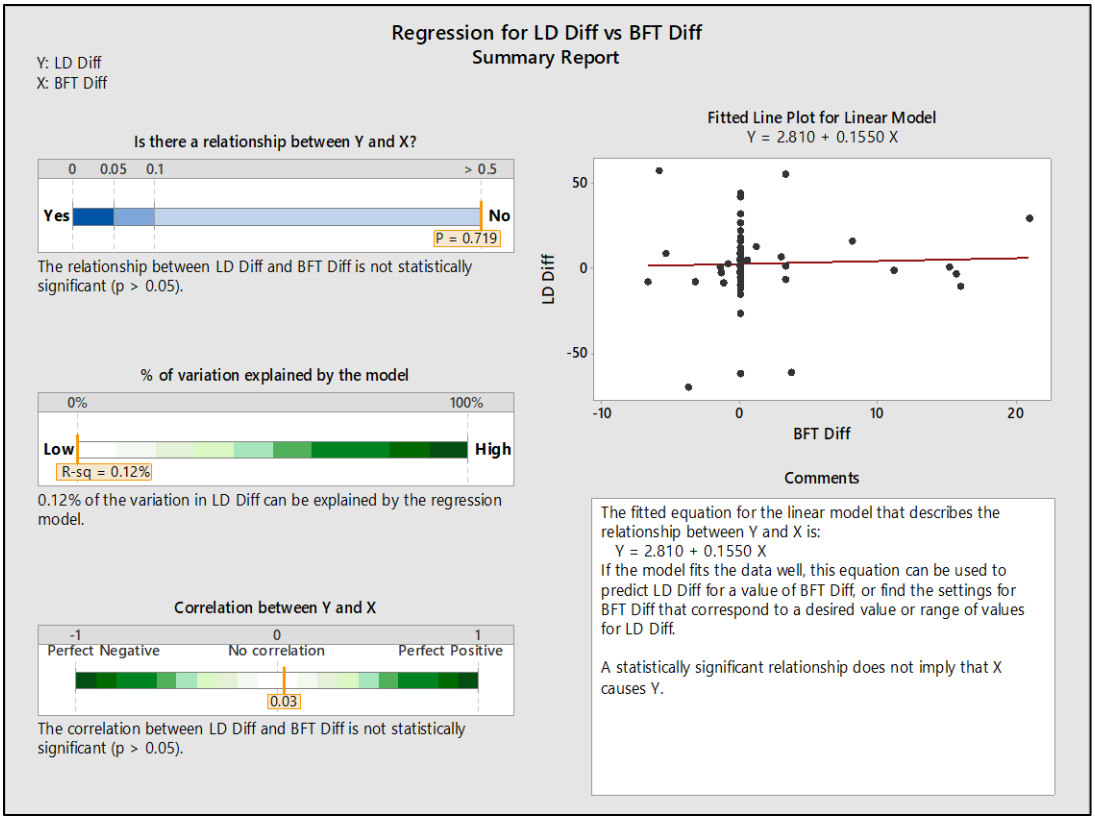

Figure A26: Regression Analysis for Overall Latch Duration vs Buckle Find Time Results

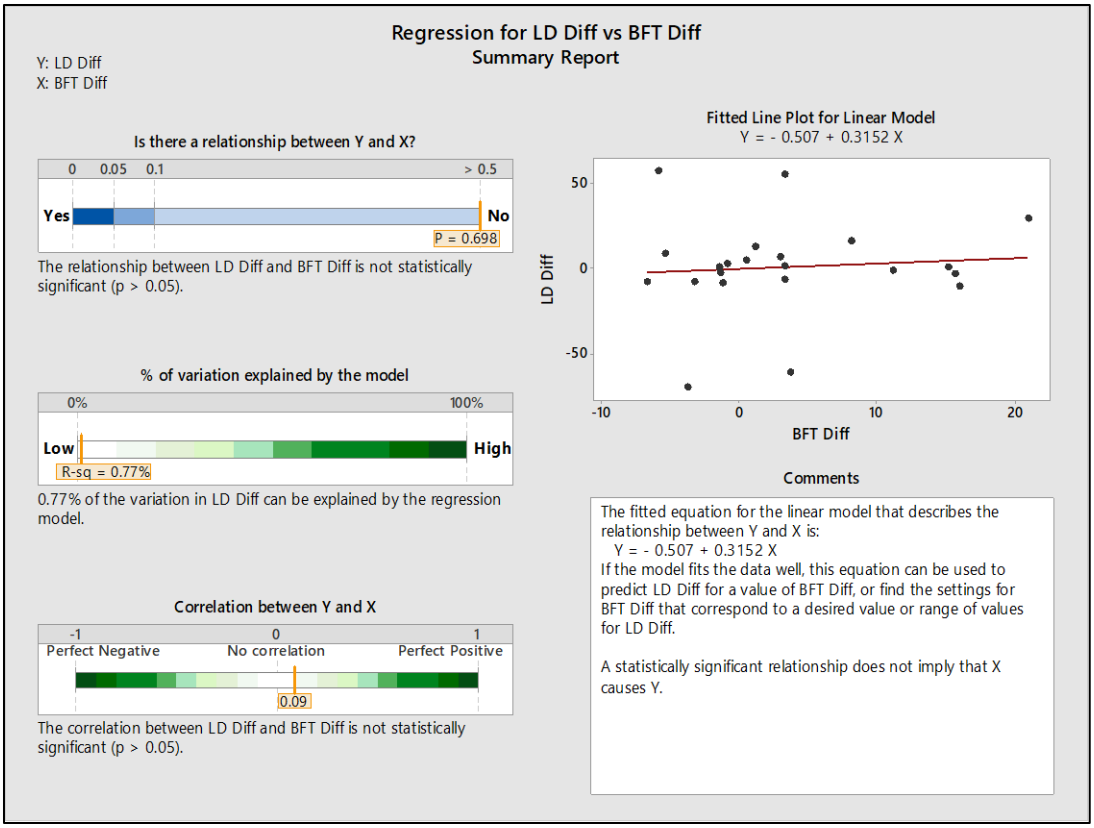

Figure A27: Regression Analysis for Latch Duration vs Buckle Find Time Results (for BFT Sample Size =26)

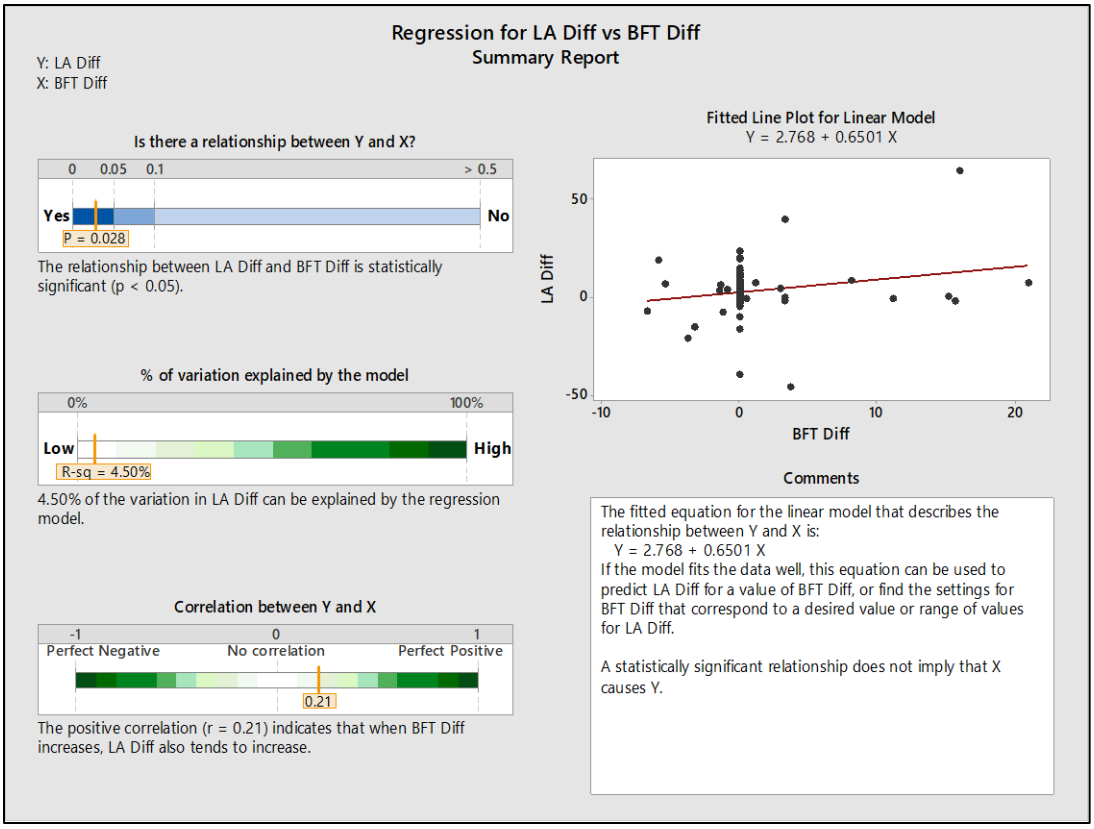

Figure A28: Regression Analysis for Overall Latch Attempts vs Buckle Find Time

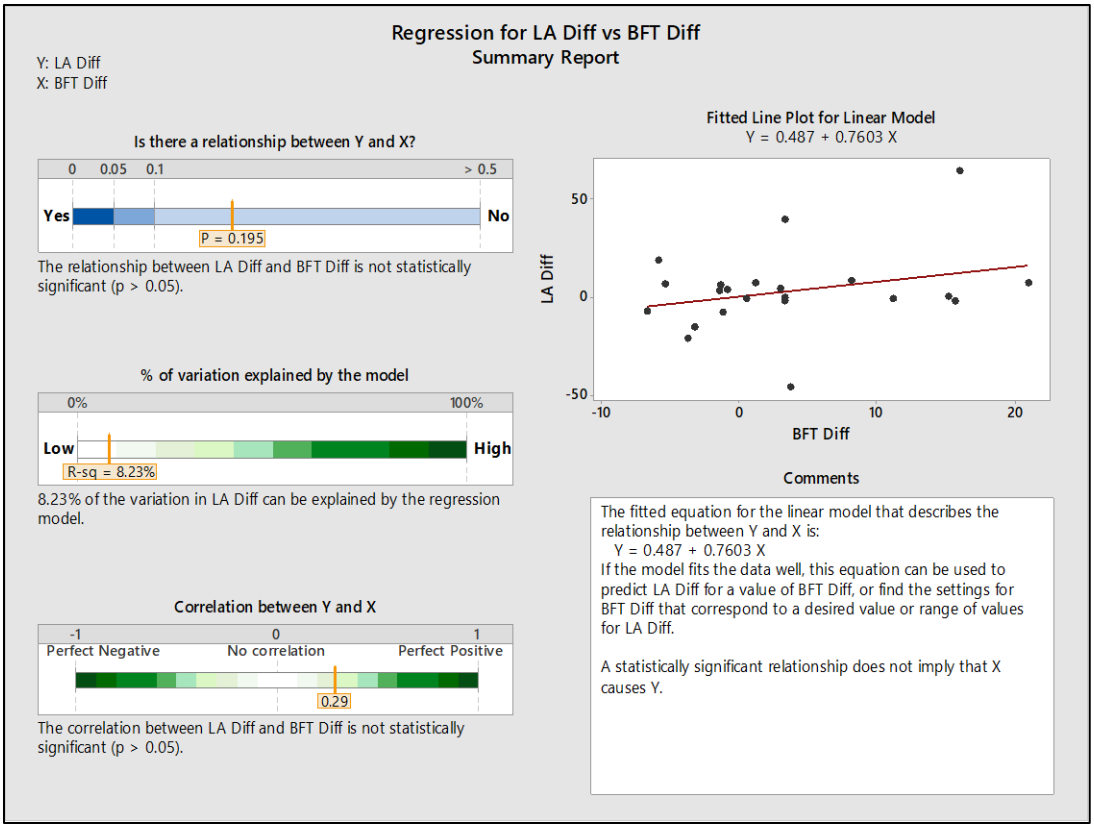

Figure A29: Regression Analysis for Latch Attempts vs Buckle Find Time (for BFT Sample Size =26)

DEVELOPMENT OF TRAILER IDENTIFICATION SYSTEM FOR IMPLEMENTATION OF VEHICLE SAFETY COMMUNICATIONS IN ARTICULATED TRACTOR-TRAILERS

Alrik L. Svenson
National Highway Traffic Safety Administration
United States

Loren Stowe
Virginia Tech Transportation Institute
United States

Paper Number 19-0221

ABSTRACT

Develop and demonstrate methods by which a vehicle safety communications system on a heavy vehicle tractor can automatically determine the geometric parameters of the trailer being towed. This information is required to assemble a Basic Safety Message (BSM) that conveys the dynamically changing position of an articulated tractor-trailer combination vehicle to surrounding vehicles. A review of existing object-detection technologies and the means to extract the trailer parameters from these technologies was conducted. The classes of trailers with highest market penetration were identified and used in the development process of the trailer detection system so as to maximize the applicability to a majority of trailers on the road today. Using the required trailer descriptive parameters defined in the previous study, accuracy requirements were developed. These were derived based on the light vehicle requirements for Vehicle-to-Vehicle (V2V) communication specified in SAE J2945/1. Trailer-identification related data were collected using LiDAR (2D and 3D), radar, camera (monocular, stereo and thermal), and ultrasonic sensors. Subsequent evaluation of the data resulted in the selection of a subset of these technologies for development into a prototype system. The final system technologies included: camera (stereo and monocular), LiDAR (2D and 3D), and ultrasonic. The 3D LiDAR based measurement system developed was able to accurately detect and measure the trailer parameters for box and tanker style trailers which accounts for nearly 90 percent of the trailers in use on roadways in the United States. Also demonstrated were trailer identification solutions based on other technologies. The camera-based solution provided a less robust means than the 3D LiDAR while the ultrasonic and 2D LiDAR was found to be applicable for fixed axle trailers only. The system designs did not require any special trailer markings or input from the driver. In addition, a simpler alternative solution for some fleet applications was developed that utilized markings (AprilTags) placed on the trailer for identification. This research demonstrated that there were methods to determine trailer parameters automatically for use in vehicle safety communications systems on articulated heavy vehicles. The system developed in this study allowed for a sufficiently accurate representation of the position of tractor-trailers during turning maneuvers in the BSM. This is important for effective implementation of safety applications based on vehicle safety communications.

RESEARCH QUESTION / OBJECTIVES

Figure 1 shows a typical turning scenario. The solid purple represents the actual path of the truck and trailer and the grey shadowed area shows the position for the trailer in the light vehicle BSM. For the car in the left lane with no traffic ahead, this representation would communicate a vehicle ahead, resulting in a possible warning (false positive). The car in the right lane would be told there was greater distance between them and the trailer than actually exists and therefore may not receive a warning that should have been issued (false negative).

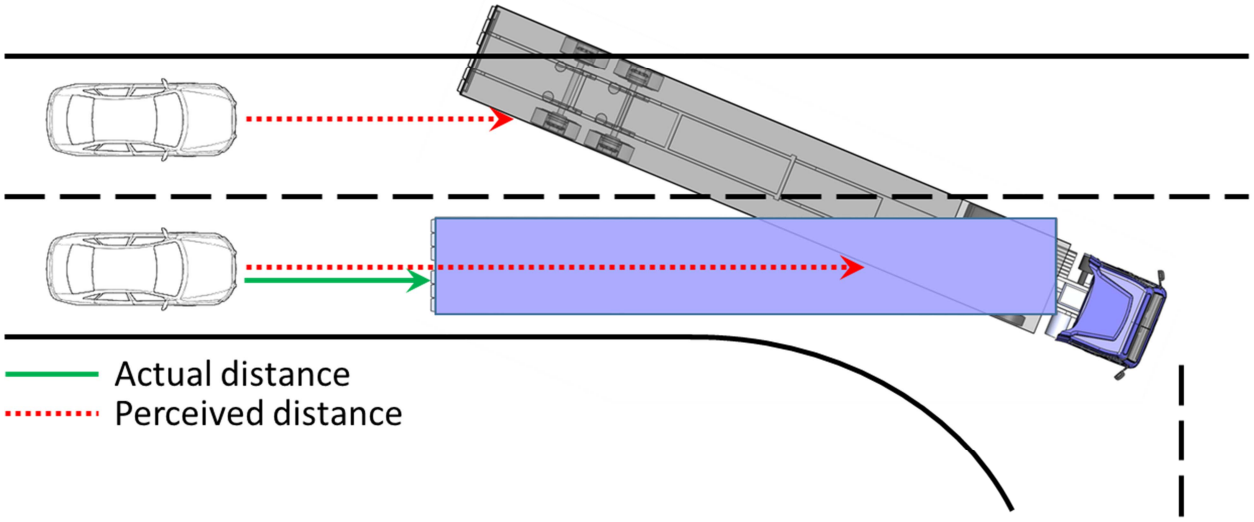

Figure 1. Single-body BSM Challenge for Articulated Vehicles During Low-Speed, Cornering

Previous research [1] showed that representing the trailer as a second vehicle was the most effective means of accurately representing the trailer to surrounding vehicles. Position and heading of the trailer was calculated based on the trailer geometry (length and pivot locations) and the kinematics of the tractor. A new data frame was proposed to transmit the information associated with the trailer.

The objective of this research was to develop and demonstrate methods by which a vehicle safety communications system on a heavy vehicle could automatically determine the trailer parameters needed to populate the content of the proposed Basic Safety Message (BSM).

METHOD

This project built on prior research which resulted in a proposed two-part BSM for heavy vehicle tractor-trailers [1]. The BSM developed in that study treats the trailer as a unique vehicle on the road during low-speed turning maneuvers. During these conditions, the system uses the trailer length and the two pivot locations (fifth-wheel and axle positions) along with the kinematics of the tractor to solve for the position and orientation of the trailer.

In order to develop a system to identify these three parameters, this research defined the scope of the project including the vehicle configurations and the target performance parameters the system needed to obtain. Then a technology survey was performed to identify applicable technologies for the system. These technologies were tested to determine which ones were most likely to meet the system requirements and then integrated into a test bed for evaluation. Based on this initial evaluation, the best performing sensors were selected for integration, testing, and demonstration.

CONSTRAINTS

Scope

One of the guiding principles of this research was that the final system was practicable for the trucking industry. Consequently, the scope of the project focused on the market segment that would impact the largest number of the tractor-trailers on the road. This kept the primary investigation to single trailer trucks, though the potential efficacy of the methods developed to work with multi-trailer heavy vehicles was included in the evaluation. Similarly, rather than trying to develop a solution that would work for all single-trailer truck configurations, including all the variations of load and trailer types, this research surveyed focused on the truck tractor market segment in the U.S. to ensure the development effort was applied toward the largest number of trailers currently on the road.

To accomplish this, annual trailer sales [2] were reviewed to provide an estimate of the trailers on the road. Functional categories were defined consistent with extracting the parameters pertinent to the project from sensor data. For example, box van presents a rectangular feature with straight lines that fall in a common plane. Similarly, container chassis and dump trailers present similar features. Consequently, these trailer types were grouped into the same class. The following list presents the categories shown in Table 1, which group types of trailers based on similarities in how the trailer parameters would be extracted from sensor data.

- Box = dry van + reefer + container chassis + dump
- Flatbed = flatbed + platform + low bed
- Tanker = tanks + dry bulk
- Other = those not included above

Table 1.
Distribution of Trailers Based on Annual Sales

Class	Box	Flatbed	Tanker (round)	Other
Number	285952	36787	15062	2147
Percent	84%	11%	4.5%	0.5%

Performance requirements
To set the performance requirements for the system, the operational conditions were considered along with the performance requirements of the V2V system as a whole. In particular, accuracy targets for length, axle position and 5th wheel or hitch position as they relate to the BSM elements of vehicles size, position and heading were determined.

SAE J2945/1 [3] provides system requirements for light vehicle, on-board V2V systems. This is currently the only published standard that provides function and performance requirements. It was therefore used as a starting place to identify minimum performance criteria for the trailer measurement system. Table 2 provides the requirements from SAE J2945/1 that were relevant to the trailer parameters.

Table 2.
Relevant SAE J2945/1 Requirements for Light Vehicles

Parameter	Value	Description	Primary Mapping to Heavy Vehicle
vPosAccuracy	1.5 m	2D position accuracy* of vehicle reference point	Axle location
vHeadAccuracyB	3 deg.	Heading accuracy* when speed is less than vHeadingSpeedThresh	Heading used to calculate other parameters
vHeadingSpeedThresh	45 km/h	Speed threshold for heading accuracy requirement	Relevant speed
vSizeAccuracy	0.2 m	Length and width accuracy requirements	Length

* Must be accurate to within the value of the vehicle's actual position or heading (respectively) for over 68 percent of the test measurements in open sky conditions.

However, as these specifications are for light vehicles, they had to be translated into values that were pertinent for a heavy vehicle and specifically to the trailer parameters necessary for populating the values for the two-part BSM. For example, vPosAccuracy is the accuracy requirement for the positioning subsystem, which includes at a minimum a GNSS (Global Navigation Satellite System). The average light vehicle width is around 1.8 m (6 ft.) which, for a standard 3.7 m (12 ft.) lane width, provides lane level accuracy. To get lane level accuracy for a 2.6 m (8.5 ft.) wide tractor-trailer (TT) would require a positional accuracy closer to 1.1 m (3.6 ft.). Note that this is trying to meet the intent of the current standard for lane level accuracy and is not under the constraints of the GNSS

performance. The 1.1 m value was then used as one of the parameters in the simulation model to determine the required accuracy for the pivot location. Table 3 provides a summary of the accuracy requirements for the measurement system.

Table 3.
Summary of Measurement Requirements

Parameter	Value	Comments
Length	≤ 0.5 m (20 in.)	Most common trailer lengths are > 2 ft. (0.61 m) different so the practical requirement is 1–2 ft. (0.3 - 0.61 m).
Axle position/ trailer wheelbase	1.3 m (52 in.)	Primarily effects lateral position of trailer during turning maneuvers.
5th wheel/hitch location	< 1.1 m (43 in.)	Primarily effects longitude position but since this moves the pivot point on the tractor, it also changes the directional input for the trailer.
Angle	< 3 deg.	Used to derive pivot locations rather than provide heading.

SYSTEM DESIGN

Figure 2 shows a block diagram of the entire measurement system, including the components independent of the measurement subsystem being developed. On the left of the figure, different trailer types are listed. Those not greyed out were evaluated during the course of the study. The information path between the trailer and sensors is filtered through the environmental conditions that occur during normal operation of heavy vehicles. These include lighting conditions, weather (e.g., rain, snow, fog), road grime, site impurities (e.g., oil, grain dust), and anything else that could influence the quality of the data.

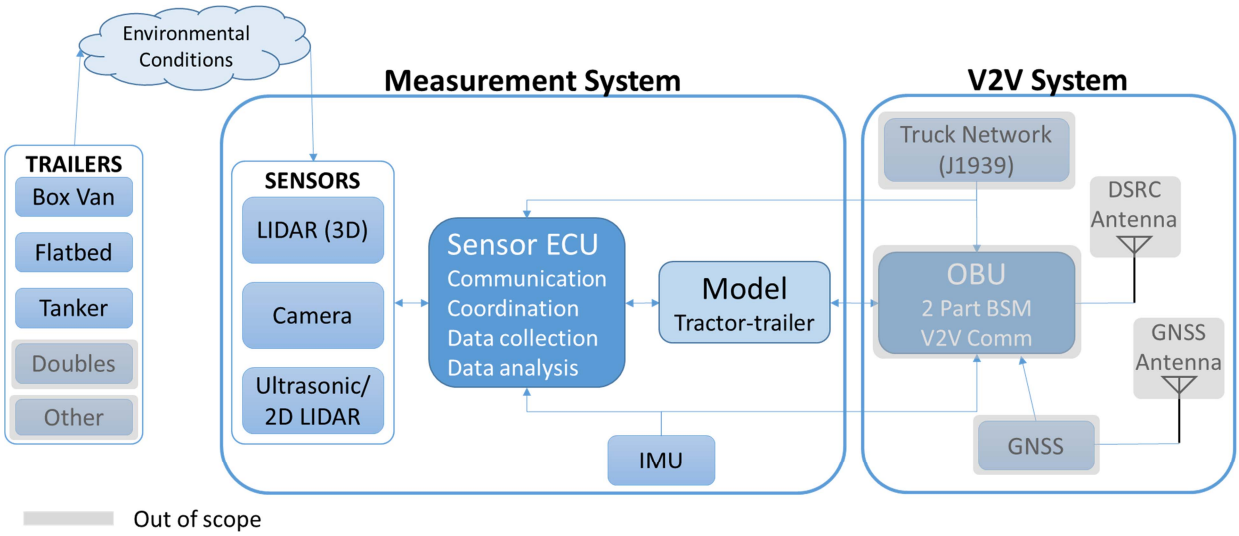

Figure 2. System Block Diagram

The effort for the system design focused on three primary components: the system software, sensors, and data processing. The system software resides on the sensor ECU and is responsible for the communication and coordination with the different system components, data collection from the different sensors, data storage, analysis of the data to extract the trailer parameters, and display of the information. System software and analysis methods will be discussed later in separate sections.

The sensors used in the study were evaluated on their ability to successfully address the different trailers and environmental conditions. For the initial evaluation, a wide array of sensors beyond what is shown in Figure 2 were examined. In addition to those that could measure the three trailer parameters, sensors that provided two or more distance measurements to the front of the trailer were evaluated. While this does not provide a measure of trailer length, for trailers with fixed axles at the rear of the trailer (e.g., tankers, bulk, dump), distance measurements along with tractor data required for the BSM allows calculation of the pivot locations (5th wheel and axle location). Trailer length could then be estimated by adding additional length to the effective axle location determined from trailer angle. This type of system could provide an alternative for trucking fleets that only haul fixed axle trailers and may be more appropriate for some environments. It may also require an additional step to tune the length factor based on the typical trailer within a fleet (e.g., fuel tankers). In addition to the trailer sensors, an IMU was included to provide truck data, in particular yaw.

Sensor Evaluation

In addition to collecting data with a heavy truck tractor and trailer, data were collected with a sensor suite at the Troutville weigh station on U.S. Interstate Route 88 (I-88) just east of Roanoke, VA. Data collection at different times of day starting at dawn and going to dusk was conducted to ensure a broad selection of lighting conditions. In addition to a stereo camera and LiDAR, two high-resolution digital SLR cameras were used to capture images at an angle and perpendicular to the trucks. Images from the latter provided a means to measure trailer length. A light gate was used to trigger the sensors as a truck entered the weigh station. This resulted in the collection of approximately 6,000 images on 2,000 different trucks. Of these, 5,000 were used in developing machine learning algorithms.

These data, along with the data collected on the tractor and trailer, were used in the sensor selection prior to the implementation. The following summarizes the results from the data collection performed during the system design effort. After that follows a description of the criteria used in creating the evaluation matrix that was assembled to help determine which sensor(s) would be used during implementation of the system concept.

Cameras The camera configurations tested during the system design performed as expected in most instances. Cameras are inherently sensitive to low light and low contrast conditions and this bore itself out in running classical machine vision techniques on the data. The trailer used in testing was white except at the rear where there was a collage of different images. This varied background often blended in with the surroundings. To address this fundamental challenge, optical flow was used to isolate pixels based on the motion of the trailer. Optical flow works by looking at consecutive frames and calculating the movement of pixels from one frame to the next. This provides an indication of the rear of the trailer as well as a means to identify pixels in the image associated with the trailer. These pixels can then be segmented into a single entity.

Figure 3 provides an example where the dark section of the end of the trailer looks like the yard and the building on the other side of the street and the street looks similar to the light portion of the trailer (first frame). Consequently, when a simple clustering is performed, the algorithm gets confused and lumps the street and the landscape in with the trailer (second frame). However, when the results from optical flow are used in conjunction with the clustering, the trailer is easily segmented out from the rest of the image (third frame).

Figure 3. Example of Trailer Blending in with Background

While this does not solve the problem of determining the trailer parameters, it does provide a means to extract the parameters.

In addition to having a relative motion that is different from the background, the trailer also has a predictable procession in the image through the turn. Figure 4 shows a sample of images taken during a turn. During the first half of the turn, the trailer moves from right to left in the image. Once it reaches the apex of the corner (lower left), the trailer starts to move left to right.

Figure 4. Procession of Trailer in Image during a Turn

By looking at the pixel velocities throughout the turn, the rear of the trailer can be identified. Figure 5 shows an example of this. In this analysis, the horizontal components of the pixel velocities were used. Red indicates pixels moving to the right and blue indicates pixels moving to the left in the image. The truck is past the apex of the corner so the trailer is moving back in line with the tractor, and thus is moving to the left. The black area above the trailer shows the boundaries of areas with different pixel velocities. The top of the trailer and the back of the trailer both appear as boundaries; however, the correct boundary is easy to identify given the relative strength of the lines and the fact there is only one vertical line.

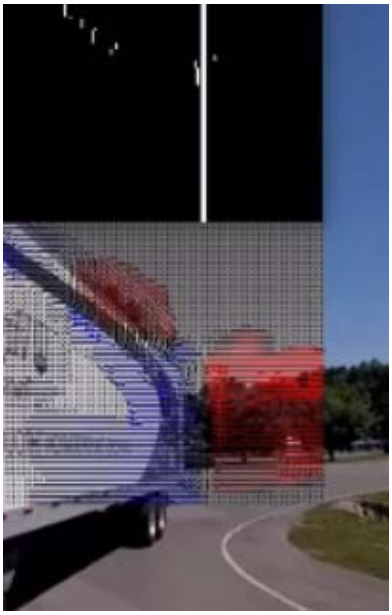

Figure 5. Identification of the End of the Trailer Using Optical Flow

As discussed previously, knowing the lateral position of the end of the trailer does not provide sufficient information to determine the length. However, with additional kinematic data from the truck or a sensor to measure angle, the length can be determined.

LiDAR The 3D LiDAR provided the most consistent results during the evaluation stage. The primary weakness was the cost. However, due to the push from automated vehicle development, the development of new, low cost units helped neutralize some of the cost considerations. 2D LiDAR provides a low cost alternative but does not provide sufficient data density to accurately determine length. The application of 2D LiDAR is therefore limited to trailer heading measurements.

Radar Two radar systems were evaluated. The first system was evaluated by the manufacturer of a light vehicle trailer length detection system. This system was designed to extend the functionality of a blind spot warning system when pulling a trailer, and automatically determines the length of the trailer rather than requiring the user to input the length. The system worked by picking up the motion of features of the trailer during a "significant/dynamic turning maneuver." This information was then used to calculate the hitch to axle length of the trailer. The manufacturer performed additional testing to evaluate the effectiveness for heavy vehicles which revealed potential challenges to extending the technology to heavy vehicles. First, the motion of the trailer was slower with small trailers, making it more difficult to see the relative motion in the radar signature. Second, a large, flat, rectangular box van provided a poor reflective target for the radar. The expected outcome for the axle length measurement was < 1m standard deviation or 68 percent of the measurements would be within $\pm$1 m ($\pm$3.3 ft.). Unfortunately, this was outside the acceptable accuracy for the BSM.

The second radar evaluation was set up to determine if a radar could identify the tires on the trailer. The hypothesis was that since the top and bottom of the tires are moving at equal but opposite directions, the relative velocity may be sufficient to be seen apart from the trailer. The first test performed was with the radar stationary as the truck drove past. With this configuration, the radar was able to pick up the tires on the trailer. However, when the radar was mounted to the tractor, the tires were no longer distinguishable.

While it may be possible to tune the signal processing of the radar data to extract trailer parameters, the amount of development that would be required was outside of the scope of the project.

IMPLEMENTATION

The primary sensors selected were 3D LiDAR, with the goal to improve the point cloud analysis and the single camera solution. For the latter, the stereo camera was used to collect the data so that both image sources were available for future development. Secondary sensors were the 2D sensor options of single plane LiDAR and ultrasonic sensors. Figure 6 shows the placement of the sensors on the tractor. The graphic is a simplified representation of the truck that was created to aid in the visualization of the real time data display. The sensor locations were based on the physical measurements of the actual tractor. The LiDAR was mounted at the top of the doorframe, the camera on the bottom of the passenger mirror, and the ultrasonic sensors and 2D LiDAR on the back of the cab.

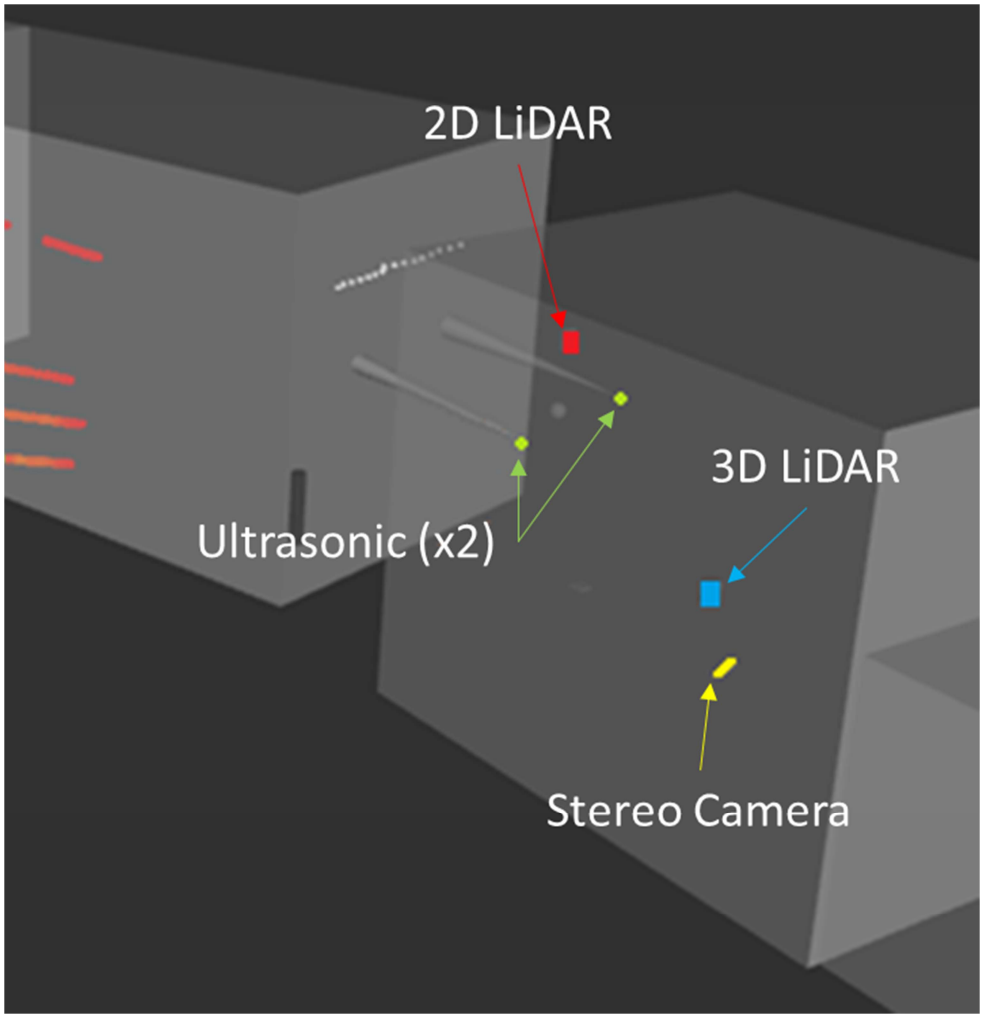

Figure 6. Sensor Placements on Tractor

All sensor data were displayed in real time. The 2D LiDAR output appeared as white dots on the front of the trailer, with each dot representing the output of one of the beams. Similarly, for the ultrasonic sensors, the output appeared as cones, which changed in length based on their returned values. For the stereo camera, both channels were recorded but only one of the video channels was displayed.

To demonstrate the functionality of the system as well as provide context to discuss specific development efforts, the flow diagram in Figure 7 shows the operation of the system and describes the solutions that were implemented. It should be noted that the system was designed as a proof of concept rather than a prototype of a commercial product. Consequently, some of the details were intentionally left out of the development. For instance, the first decision block evaluates whether the trailer is new or not. The most simplistic solution to this step is to assume a new trailer on start up. However, a more robust method might be to monitor the acceleration of the cab to identify the signature impulse that occurs when a tractor connects to a trailer. However, as this step does not preclude the demonstration of the measurement of the trailer parameters, the system was set to default to a new trailer on startup.

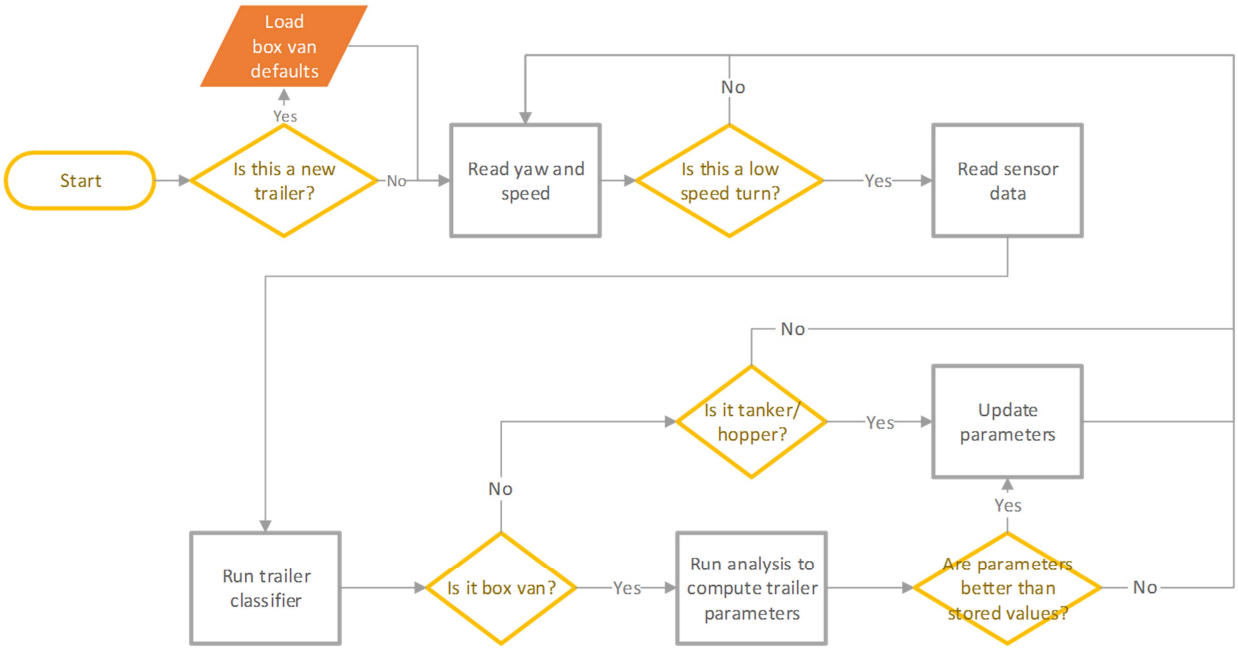

Figure 7. System Flow Diagram

Initialization

The first step in the algorithm is to initialize the system. As stated before, the default condition for this step is that the trailer is new. Therefore, the system initializes the trailer parameters with the following default values (Table 4) for a box van, as this is the most common type of trailer on the road.

Table 4.
Default Trailer Parameters

Trailer Parameter	Default Value	Comment
Length	53 ft.	The most common length of box van used is 53 ft., which is also the longest standard size. If this value is wrong, false rather than missed warnings will occur.
Axle position	0 ft. forward	This gives the trailer the longest wheel base possible, resulting in greater off-tracking.
5th wheel position	0 ft. (middle)	The midpoint minimizes the likelihood of exceeding the 1.1 m position error.

The system then monitors the yaw and speed of the tractor to determine if it is performing a low speed maneuver. Since the ECU was not tied into a V2V system nor the vehicle network, yaw was used. If yaw exceeds a threshold (0.2 rad), the next step was to read the data from the sensor suite.

The data from a single camera were used to run a trailer classifier to classify the trailer into one of four types: box van, tanker/hopper, double, or flat/other. The classifier was based on a convolutional neural network developed using the images from the data collection.

The output from the classifier directs the sensor data to the associated analysis module to extract the trailer parameters. The analysis for the other two trailer classes were not developed in this study, but the structure is in place to accommodate additional classes and associated analysis techniques.

Figure 8 provides a snapshot of the real time display collected during testing with different length trailers. The trailer in this example is a 45 ft. box van. The length displayed, which was extracted from the LiDAR data, is 44.81 ft. (13.66 m)

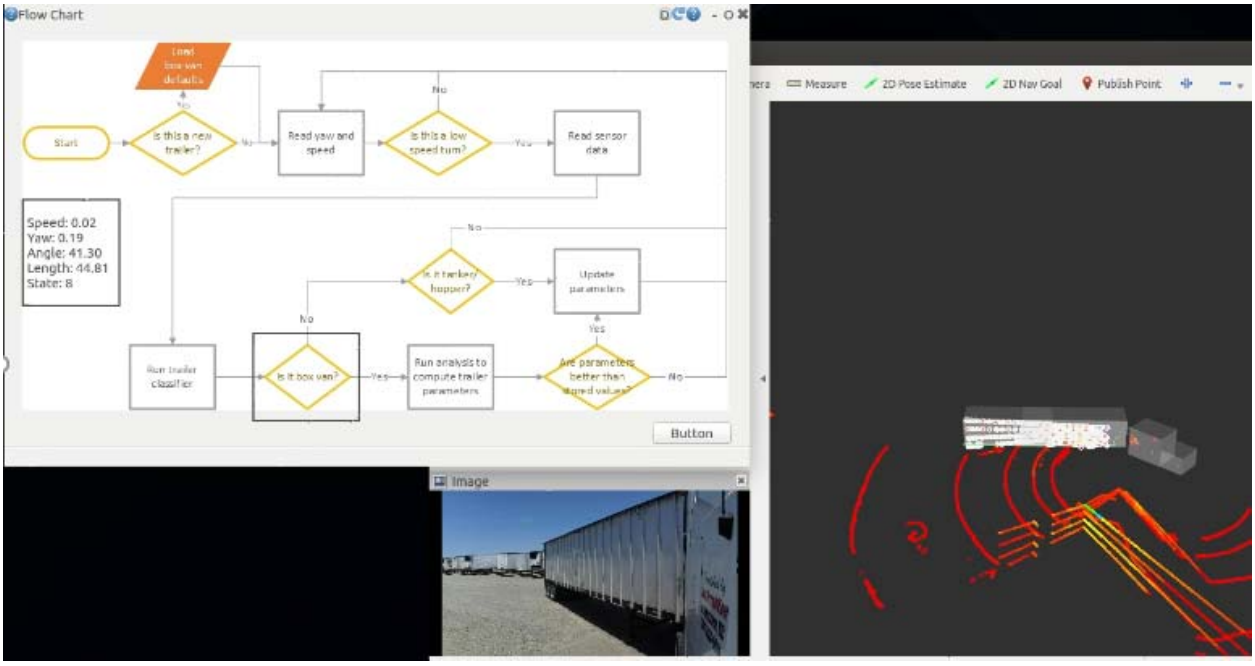

Figure 8. Example Output for 45 ft. Box Van

While the system collected the five sensor channels, the trailer parameter estimation for real time display was based on the point cloud data from the LiDAR. While the stereo vision camera can also produce point cloud data, the LiDAR provided cleaner data that yields better results. The single camera data were processed offline. While identification of the trailer is robust, determination of the trailer length consistently, turn after turn at the accuracy requirements identified, was a challenge. However, each turn provided an opportunity to collect more data and refine the trailer parameters if deemed appropriate.

Marked trailer Implementation

In order to demonstrate more than one solution, an alternative was developed that used special markings on the trailer. This option was included to determine the cost and benefit of this type of system over the type of non-contact system described previously.

One direct method evaluated for detecting the angle of the trailer used unique visual fiducial called AprilTags. Commonly used in augmented reality and robotics, these two-dimensional bar codes were easily detected by a camera system and directly provided pose. The pose information collected by the AprilTags included the X, Y, Z position and roll, pitch, yaw orientation parameters for each tag. Multiple AprilTags could be detected by a single camera because they each contained a unique pattern that corresponded to an identification number.

To track the pose of the trailer, a camera system was mounted on the rear of a heavy truck to observe the front of the attached trailer. An AprilTag fiducial was placed on the front of the trailer so that it could be continuously observed by the camera system during straight and turning maneuvers. A coordinate frame was established to correlate the camera's position to the detected fiducial at every timestamp. As the truck traversed straight paths and turns, the detected fiducial provided the pose information as an output. The most important pose parameter is the yaw angle, which directly correlates to the angle of the trailer relative to the camera. A more accurate measure of the trailer's angle from this extracted yaw angle required further transformations to the truck's axle or other defined coordinate frame. The tracked fiducial output was demonstrated on a closed test loop showing constant updates of the trailer's angle. The AprilTags were used due to their simplicity and existing software tools, but any picture or pattern can be

converted and calibrated into a fiducial for tracking by a camera system. Figure 9 provides an example of the application of the AprilTag, including the position of the tag and the results of the tag tracking.

Figure 9. Example of Output from AprilTags

The camera requirements were relatively low, so an inexpensive camera solution could be used. In addition, the method was robust in terms of placement of both the camera and the tags. One embodiment of this solution could be for a fleet to place these markers on their trailers. The code itself could be associated with a given length so that in addition to measuring the angle of the trailer, which provided heading as well as a means to determine pivot locations, the system would also know the length of the trailer from the marker. Another embodiment would provide drivers with a selection of tags that they would then place on the front of a trailer during hook up. They would be responsible for selecting the tag with the correct associated length.

While still being subject to the same weaknesses of other camera systems, this system provided a lower cost alternative to the fully automated system. The tradeoff is that it required more operator interaction to ensure the proper tag was on the trailer and that the tag was clean of debris. However, for small fleets or owner-operators, this tradeoff may allow these fleets to implement a more economical V2V solution.

RESULTS

Figure 10 shows a single frame of the output for 33 ft., 45 ft., and 53 ft. trailers. The return from the LiDAR data turned white when it identified the side of the trailer. The length of the trailer was then updated to reflect the length calculated from the data. The system was able to identify the trailer and extract its length and angle.

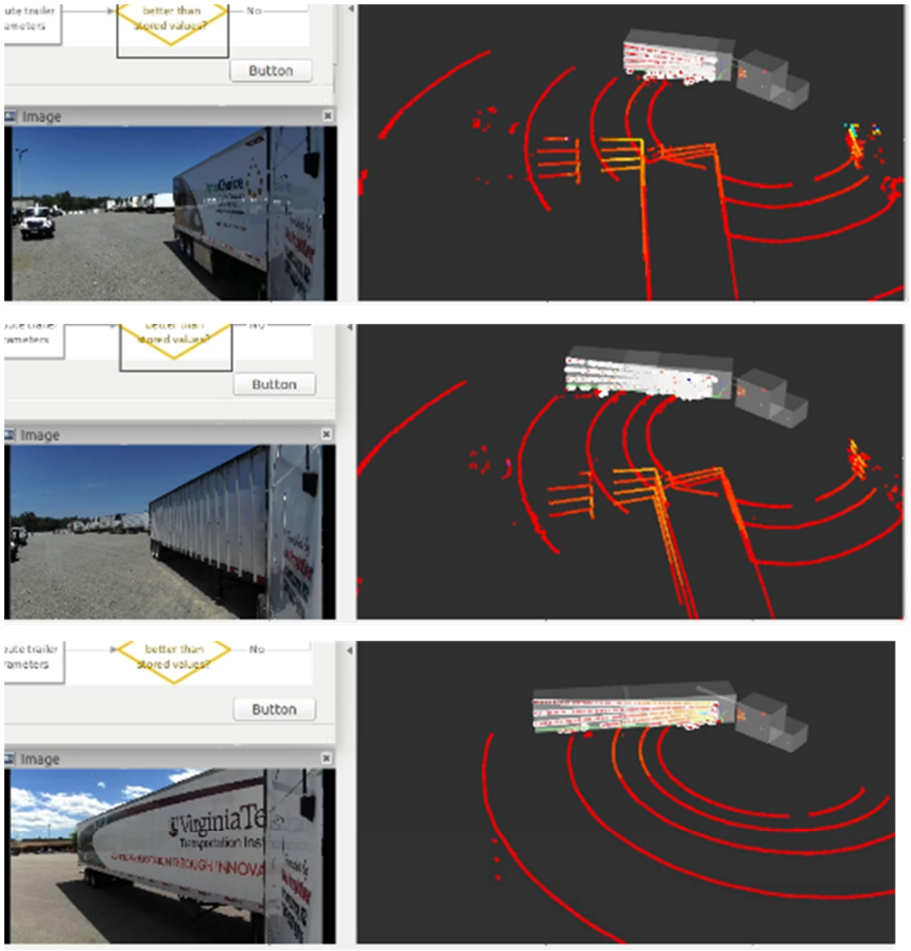

Figure 10. Display of Single Frame from System Output for 33 ft., 45 ft., and 53 ft. Trailers

The plots in Figure 11 show the results for a simple turn with a 53 ft. trailer. The lower value on the left plot, approximately 10 degrees, indicates the minimum angle that the system was able to extract from the trailer measurement data. The right plot shows the time for the measurement to settle in to its final value.

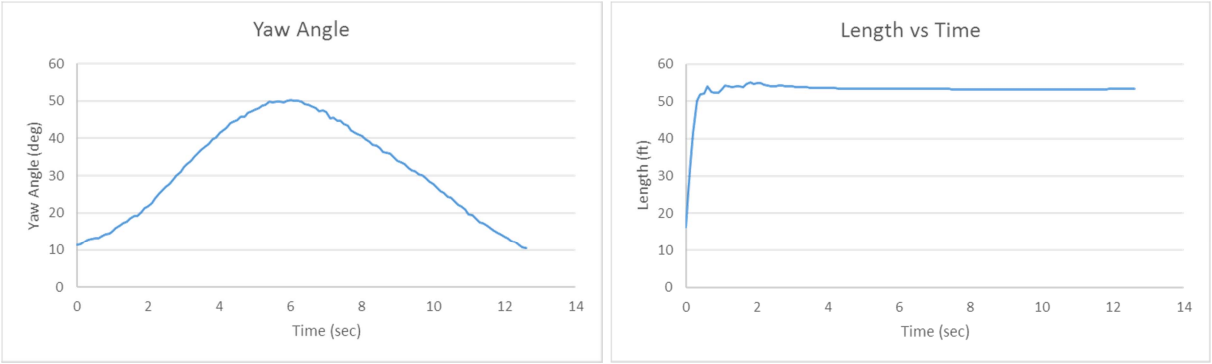

Figure 11. Length as a Function of Yaw Angle

Within a few seconds of a turn with a high enough trailer angle, the trailer length settles into the final value within a few seconds.

Figure 12 shows the results from the tanker trailer. In addition to the angle and length, the system state is shown below as an indication of when the system is and is not reading data from the sensor suite. The red lines indicate the length requirement from Table 3 as applied to this trailer.

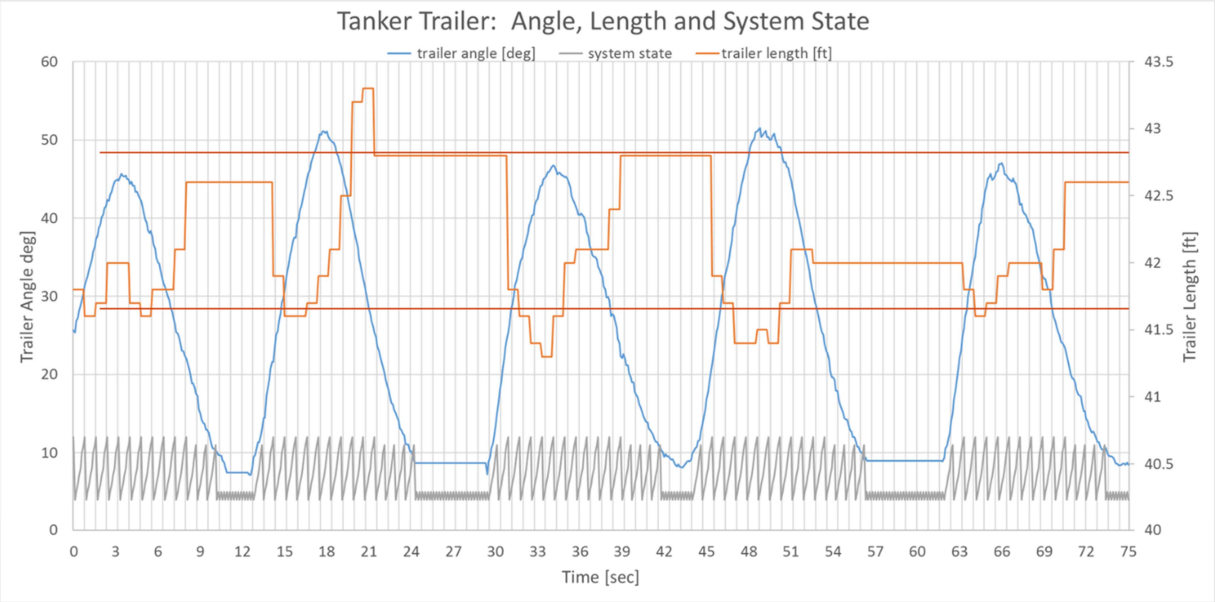

Figure 12. Trailer Length and Yaw Angle for Tanker Trailer

As expected, the tanker trailer results are noisier than for the box van. However, the system still provides adequate results for the BSM.

Results from the camera proved more challenging. The primary factors affecting the results were identification of the edges of the trailer, which were affected by lighting (e.g., shadows, low contrast, occlusions).

Based on a single frame from 45 turning events, with three different trailer lengths, approximately 50 percent of edge detections were within 2 ft. (0.61 m), 30 percent of edges were incorrectly identified, and 20 percent of detections were outside of the acceptable range. Applying the analysis to the entire video sequence during the turn and applying statistical analysis to reject outliers and provide an indication of the quality of the measurements would improve the performance of the method. In addition, given the method's sensitivity to changing light, it would provide a sample across a wider variety of lighting and backgrounds and therefore not be dependent on a single sample.

The ultrasonic, 2D LiDAR and the marked trailer solution (AprilTags) demonstrate solutions that can provide trailer heading information. However, trailer length would have to be obtained through a secondary method. For AprilTags or similar defined tag, trailer length can be associated with a given tag design. For flat trailer surfaces, the ultrasonic and 2D LiDAR perform similarly. While 2D LiDAR is more expensive than ultrasonic, the additional measurement points give additional data from which to calculate the heading. This allows for application with a variety of trailer types and over a large heading range. AprilTags require a human to mark the trailer prior to operation but does provide lower cost solution compared to 2D LiDAR that could be applied to many trailer categories.

DISCUSSION AND LIMITATIONS

While the 3D LiDAR sensors provided the best performing solution tested, they are currently comparatively high in cost. However, with the focus on future automated driving systems, the rapid development of new lower cost sensor solutions is occurring. Consequently, it is expected that cost effective LiDAR sensors could soon be available for use in heavy vehicle V2X applications.

The 2D sensors (ultrasonic and 2D LiDAR) and the marked trailer method provide three different potential solutions to provide trailer heading information. If trailer length is known through some other means, these lower cost alternatives demonstrated provided the opportunity to broaden the adoption of vehicle safety communications by trucking fleets that may otherwise choose not to integrate the technology. However, the lower cost AprilTags have the limitation that they require a human to mark the trailer prior to operation.

CONCLUSIONS

The study described in this paper developed a system that detected and measured the trailer parameters required for populating the elements of the 2-body BSM for box type trailers (dry vans, refrigerated, intermodal trailers, and other enclosed trailers) which account for over 80 percent of the trailers on U.S. roads. Table 5 provides a brief summary of the primary concepts developed and demonstrated.

Table 5.
Overview of Results for Primary System Concepts

Concept	Strengths	Weaknesses
3D LiDAR	• Provides all three trailer parameters • Robust measurements • Works in low/no-light conditions • Provides for other safety functionality (e.g. blind-spot warning)	• Requires significant turning maneuver (>10 degrees) • Cost currently higher than other sensors
Camera (no trailer modification)	• Provides all three trailer parameters • Low cost • Provides for other safety functionality (e.g. blind-spot warning)	• Requires significant turning maneuver (>10 degrees) • Increased processing requirements • Accuracy sensitive to lighting
Camera (with trailer modification)	• Provides all three trailer parameters • Low cost • Results for low turning angles • Robust measurements	• Requires modification of trailer • Sensitive to lighting • No additional safety functionality

REFERENCES

[1] Svenson, A. L., Peredo, G., & Delgrossi, L. (2015). Development of a Basic Safety Message for Tractor-Trailers for Vehicle-to-Vehicle Communications. In 24th International Technical Conference on the Enhanced Safety of Vehicles (ESV) (No. 15-0379).

[2] Schenck, P. (2016, March 4). *2015 Trailer Production Figures Table*. Retrieved from Trailer Body Builders: http://trailer-bodybuilders.com/trailer-output/2015-trailer-production-figures-table.

[3] Surface Vehicle Standard – On-Board System Requirements for V2V Safety Communications, SAE J2945/1, Warrendale, PA: Society of Automotive Engineers, March 2016.

HOW CLOSE TO ZERO CAN VOLVO CARS GET BY 2020? AN ANALYSIS OF FATAL CRASHES WITH MODERN VOLVO PASSENGER CARS IN SWEDEN

Matteo Rizzi
Per Hurtig
Swedish Transport Administration
Sweden

Simon Sternlund
Anders Lie
Swedish Transport Administration and Chalmers University of Technology
Sweden

Claes Tingvall
ÅF Sweden and Chalmers University of Technology
Sweden

Paper number 19-0223

ABSTRACT

In 2008 Volvo Cars set out its vision - by 2020 no one should be killed or seriously injured in or by a new Volvo car. Today, 2020 is very close and it is possible to assume most of the safety technologies that will likely be fitted in Volvo cars by then. The objective of the present study was to estimate how close to zero fatalities Volvo Cars can get in Sweden by 2020.

The Swedish Transport Administration (STA) carries out in-depth studies of all road fatalities in Sweden. Cases involving at least one modern Volvo car were extracted for the period 2010-2017 (MY 2010 and onwards, excluding the C30, S40 and V50 models) and analyzed retrospectively (n=62). The yearly average number of fatalities in Sweden during 2010-2017 was 2.8 for occupants in Volvo cars and 5.0 for either occupants in other vehicles or VRUs impacted by Volvo cars, respectively.

The actual fitment of safety technologies was investigated among the Volvo cars involved in these crashes. The basic assumption was that by 2020 the boundary conditions in each crash would be unchanged, but the Volvo car would be a MY 2020 and therefore would be fitted with the same safety technologies as the V60 MY 2019. An assessment was then made of whether a certain technology could have prevented the crash or substantially reduced the crash severity in 2020. Cases involving extreme violations such as excessive speeding, were included in the analysis but presented separately. It was also assumed that no major improvements in crashworthiness would be introduced between the analyzed Volvo models and Volvo cars MY 2020.

The analysis showed that almost half of the fatalities in and by Volvo cars could have been prevented with the safety technologies fitted on the V60 MY 2019. It was also found that most of the fatalities that could not be prevented with a V60 MY 2019, occurred in crash scenarios where at least one safety technology was relevant, although the current performance was estimated not to be sufficient to prevent the fatality. Only three cases occurred in crash scenarios without any relevant existing safety technology.

It should be kept in mind that that these results were based on retrospectively upgrading already relatively safe cars to the following generation. This suggests that reducing fatalities by almost 50% through the introduction of only one new car generation would be a very impressive achievement. It is also important to note that these results were based on the assumption that the road infrastructure, speed limit and crash opponents would be unchanged. Clearly, taking safety improvements in the road infrastructure and other vehicles into account would result in an even higher reduction of fatalities in and by Volvo cars by 2020.

In conclusion, regardless of whether Volvo's vision will be achieved by 2020 or not, it is very important to set road safety targets, develop new solutions and follow up the results, also for a car manufacturer.

INTRODUCTION

Setting targets for the number of fatalities and serious injuries in road traffic crashes has been a tradition for jurisdictions, regions and even globally. Since some years, starting in Sweden in 1997, long-term targets have been set based on Vision Zero. In this vision, the ultimate objective is to develop the entire road transport system to be forgiving, by adopting the principle of the failing and fragile human. The design philosophy is to reduce human mistakes, but if they still occur, the system is forgiving. Several layers of technology must be in place to bring driving back to normal, or prepare for a crash that is survivable and not causing long-term injury. To develop a safe road transport system is a matter of merging a number of factors and components of the system together to act in a way that protects the road users. In particular the amount of kinetic energy, i.e. speed, must be limited to the inherent safety of the protective systems.

Vision Zero, sometimes called Safe System, has been adopted by many stakeholders across the world. Individual countries, the EU, the UN, the US, and many cities nowadays develop their transport systems according to the policy, and for example the EU has even set a year for reaching ”close to zero deaths” (2050; EC, 2011). Already in 2008, Volvo Cars set a Vision Zero target, and also set a date for when it should be reached (model year 2020; Volvo Cars, 2009). In doing so, Volvo was the first car manufacturer to set a target of this kind, and still seems to be alone in having a target year for its completion. Therefore, it is of great interest to estimate how close to zero Volvo Cars will be in 2020. From the issue of automated cars it is also of great interest to study the latest safety systems, although a manually driven car is far from automated driving when it comes to the ”freedom” of the driver to drive the car outside its design envelope including basic traffic rules.

The target by Volvo Cars does not seem to be set with any restrictions concerning risk factors, when and where it applies. In some of the communication it has even been expressed in a way that it also includes road users outside the Volvo car, i.e. “seriously injured or killed in or by a new Volvo” (Volvo Cars, 2009). In a broader context, the value of the vehicle to solve almost the entire road safety problem is at stake, and therefore needs to be studied carefully as it would have a massive impact on the choice, investments and management of safety countermeasures.

OBJECTIVE

The objective of the present study was to estimate how close to zero fatalities Volvo Cars can get in Sweden by 2020.

DATA SOURCE

The Swedish Transport Administration (STA) has been carrying out in-depth studies of all road fatalities since 1997. Crash investigators at the STA systematically inspect the vehicles involved and record direction of impact, vehicular intrusion, seat belt and helmet use, airbag deployment, tyre properties, etc. The crash site is also inspected to investigate road characteristics, collision objects, etc. Further information is provided by forensic examinations, witness statements from the police and reports from the emergency services (STA 2005). Collision speeds are generally derived by vehicular deformation, and the initial driving speed is mostly based on eye-witness accounts, brake skids, etc. Pre-crash braking is also coded based on eye-witness accounts, brake and skid marks. The final results of each investigation are normally presented in a report. Because all fatal crashes are included in the sampling criterion, the material can be considered fully representative for Swedish road fatalities and possibly even for Northern Europe at large.

MATERIAL AND METHODS

Fatal crashes involving at least one Volvo car of model year (MY) 2010 and onwards were extracted for the period 2010-2017. The C30, S40 and V50 models were excluded as they were based on older platforms with limited safety technologies. This selection process resulted in a total of 57 cases: 18 fatal crashes with 22 fatally injured occupants in modern Volvo cars were found. Further 39 fatal crashes with 40 fatally injured occupants in other motor vehicles or vulnerable road users (VRU) were identified (see Table 1). The yearly average number of fatalities in Sweden during 2010-2017 was 2.8 for occupants in Volvo cars and 5.0 for either occupants in other vehicles or VRUs impacted by Volvo cars, respectively.

Table 1.
Number of fatalities <u>in and by</u> Volvo cars MY ≥ 2010 in Sweden during 2010-2017. C30, S40/ V50 models excluded

road user type	**fatalities *<u>in</u>* Volvo cars**	**fatalities *<u>by</u>* Volvo cars**
car drivers	16	17
car passengers	6	1
pedestrians		12
PTW riders		6
cyclists		2
electric wheelchairs		1
HGV occupants		1
Total	22	40
average per year (2010-2017)	**2.8**	**5.0**

The actual fitment of safety technologies (for instance rear-end Autonomous Emergency Braking, Lane Departure Warning etc.) for each of the Volvo cars involved in these 57 crashes was investigated and retrospectively upgraded to the equipment of the V60 MY 2019. In other words, the analysis was based on the assumption that by 2020 the boundary conditions in each crash would be unchanged (i.e. the road infrastructure, speed limit and crash opponents would be the same). However, the Volvo car would be a MY 2020 and therefore would be fitted with the same safety technologies as the V60 MY 2019. These are as follows (Volvo Cars 2019a):

- Active Bending Lights
- Adaptive Cruise Control (ACC)
- Autonomous Emergency Braking (AEB)
    - Low-speed rear-end
    - Left-turn crossing with oncoming traffic
    - Head-on
    - Large animal detection
    - Pedestrian and cyclist detection
    - Post-crash
- Blind Spot Detection
- Cross Traffic Alert with AEB
- Driver Alert Control
- E-call
- Electronic Stability Control (ESC)
- Emergency Steering Support (individually brakes one or two wheels to reinforce the steering wheel input in an evasive maneuver)
- Forward Collision Warning (FCW)
- Lane Support (Oncoming Lane Mitigation and Lane Keeping Aid)
- Rear Collision Warning
- Run-Off road Mitigation
- Seat Belt Reminder (SBR)
- Tire Pressure Monitoring System

An assessment was then made of whether at least one of the above technologies could have prevented the crash or substantially reduced the crash severity. To handle the issue of subjectivity in such assessments, each case was discussed in a group of at least three road safety analysts until consensus was reached. Cases involving extreme violations were included in the analysis but analyzed separately. In the present study, extreme violations were defined as clear and intentional violations of basic traffic rules, for instance extreme speeding or unbelted occupants despite SBRs. It was also assumed that no major improvements in crashworthiness would be introduced between the analyzed Volvo models and Volvo cars MY 2020.

RESULTS

The majority of the fatal crashes involved the S80/V70/XC70 models (60%, see Table 2). All of the analyzed cars were fitted with ESC and SBR in the front seats. While 65% were fitted with low-speed AEB for rear-end

collisions (City Safety), only 13% had the optional Driver Support safety package including a number of technologies such as ACC, Lane Departure Warning (LDW) and/or Lane Keeping Assist (LKA), Driver Alert Control, Pedestrian Detection and Blind Spot Detection (see Table 3). The V40s were fitted with pedestrian airbag.

Table 2.
Number of Volvo car models MY ≥ 2010 included in the analysis

Volvo model	fatalities *in* Volvo cars	fatalities *by* Volvo cars
S60/V60	7	5
S80/V70/XC70	14	23
V40	1	5
XC60		6
XC90 MY 2016		1
Total	**22**	**40**

Table 3.
Fitment of safety technologies among the Volvo cars included in the analysis

Safety technology	fatalities *in* Volvo cars	fatalities *by* Volvo cars	% fitment
ESC	22	40	100%
SBR front seats	22	40	100%
City Safety (AEB low-speed rear-end)	13	27	65%
Driver Support Package	1	7	13%

It was also found that 37% of the Volvo cars were privately owned. Further 57% were either company cars, leased cars or rental cars. Information on ownership was missing in 6% of cases.

The analysis showed that 16 of the 22 fatalities in Volvo cars occurred under normal driving conditions (73%), see Figure 1. The remaining six cases involved clear violations, mostly excessive speeding. It was assessed that a total of ten fatalities (45%) could have been prevented with a Volvo V60 MY 2019 safety equipped vehicle (9 of these occurred under normal driving conditions). In one case, this assessment was not possible due to partly missing information.

With regard to the fatalities by Volvo cars, similar results were found: 34 fatalities occurred under normal driving conditions (85%, see Figure 2). A total of 17 fatalities (42%) were assessed to be potentially prevented by a Volvo V60 MY 2019 (16 of these occurred under normal driving conditions). In two cases, the available information was not sufficient to make such an assessment.

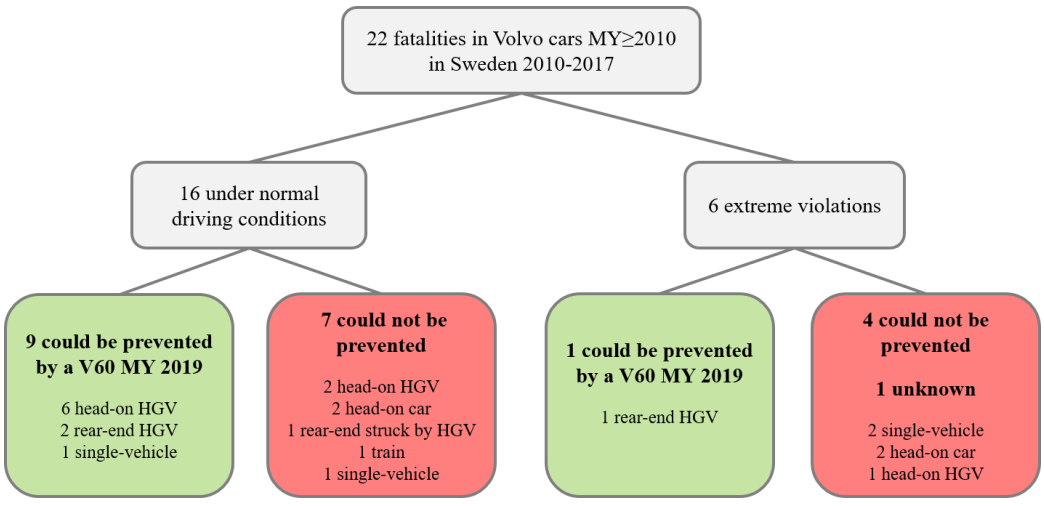

Figure 1. Number of fatalities in Volvo cars MY ≥ 2010 in Sweden during 2010-2017 that could have been prevented in a V60 MY 2019.

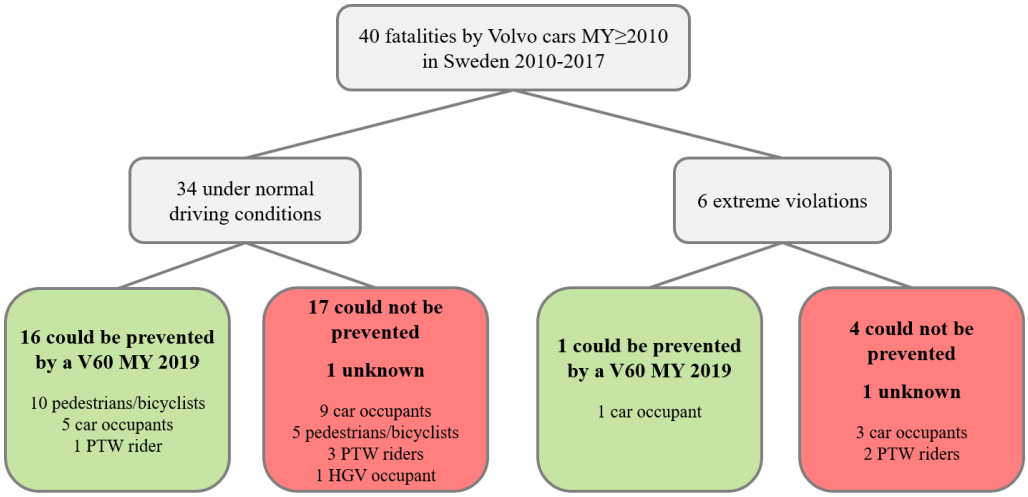

Figure 2. Number of fatalities <u>by</u> Volvo cars MY ≥ 2010 in Sweden during 2010-2017 that could have been prevented by a V60 MY 2019.

The reductions shown in Figure 1 and 2 would correspond to approximately 1.4 fatalities in Volvo cars and 2.6 by Volvo cars per year in Sweden. The technologies that could have prevented the fatalities in and by Volvo cars are listed in Table 4. Among fatalities in Volvo cars, the most effective technology was Lane Support (n=7), followed by ACC and Driver Alert Control (n=3, respectively). However, it is important to note that several crashes could have been prevented by more than one technology, which explains why the sum of the individually prevented fatalities shown in Table 3 is higher than 10.
Among fatalities by Volvo cars, the most effective technology was estimated to be AEB with pedestrian and cyclist detection (n=10), followed by AEB head-on (n=5). In two cases, it was estimated that the combination of AEB with pedestrian detection and improved crashworthiness could have prevented the fatality, at least theoretically. However, such assessment was considered too uncertain to be included among the prevented fatalities.

Table 4.
Number of fatalities that could have been prevented by different technologies

	fatalities *<u>in</u>* Volvo cars	**fatalities *<u>by</u>* Volvo cars**
ACC	3	
AEB head-on	2	5
AEB post-crash		1
AEB with large animal detection		1
AEB with pedestrian and cyclist detection		10
Driver Alert Control	3	
Emergency Steering Support	2	1
Lane Support	7	
Not prevented	*11*	*21*
Unknown	*1*	*2*
Total without double counting	**22**	**40**

As shown in Figures 1 and 2, it was assessed that a total of 32 fatalities in and by Volvo cars could not be prevented with a V60 MY 2019. Among these 32 fatalities, it was found that 20 (16 under normal driving conditions) occurred in crash scenarios where at least one safety technology was relevant, although the current performance was estimated not to be sufficient to prevent the fatality. The most common ones were AEB head-on (n=10) and AEB with pedestrian and bicyclist detection (n=3), in cases where detection was highly likely but impact speeds were too high to be reduced to survivable levels with the current levels of autonomous emergency braking. In further six cases (five under normal driving conditions) the Volvo driver did brake and/or swerve to such an extent that the potential of AEB or Emergency Steering Support was considered to be minimal. In further three cases no technologies were estimated to be effective to any great extent due to extreme violations. Finally, the remaining three cases occurred in crash scenarios without any relevant safety technology. These

were a rear-end collision where a Volvo car was struck from behind by a PTW, a collision with a train at a railway crossing and a single-vehicle crash involving understeering in very slippery road surface conditions.

As shown in Table 3, eight fatalities (six under normal driving conditions) involved a Volvo car fitted with the optional Driver Support safety package. It was found that seven crashes occurred in crash scenarios where no relevant safety technologies were included in such safety package. These were:

- three unintentional lane drifting by an oncoming car, resulting in head-on collisions
- one intentional overtaking by the Volvo car, resulting in a head-on collision
- one reversing collision with a pedestrian
- one collision with a moose, resulting in the moose being ejected into an oncoming vehicle
- one single-vehicle crash involving understeering in very slippery road surface conditions

In one case, a pedestrian was killed by a Volvo car fitted with AEB with pedestrian detection. However, loss-of-control due to very slippery conditions had occurred prior to the collision with the pedestrian, which made the AEB detection and activation impossible.

Finally, it was also found that if the passenger car opponent had been fitted with ESC and Lane Support, further three fatalities in Volvo and six fatalities by Volvo cars could have been prevented, respectively. This would correspond to approximately 58-59% reduction of fatalities in and by Volvo cars. It should be also noted that most HGV in this study lacked all sorts of relevant safety technologies, and that ESC and ACC on HGV could potentially prevent further two fatalities in Volvo cars (for a grand total of 68% reduction, if combined with ESC and Lane Support on the passenger car opponents).

DISCUSSION

The present paper analyzed Swedish in-depth data from fatal crashes involving modern Volvo cars (MY $\geq$ 2010) to understand how close to zero fatalities Volvo cars can get in Sweden by 2020. It was estimated that almost half of the current fatalities in and by Volvo cars could be prevented with a V60 MY 2019 safety equipped vehicle, which suggests that Volvo's vision will not be achieved in Sweden by 2020. However, it should be kept in mind that these results were based on retrospectively upgrading already relatively safe cars to the following generation. When this aspect is taken into account, it could be argued that reducing fatalities in and by a car by almost 50% through the introduction of only one new generation would be a very impressive achievement.

The present study has a number of limitations that need to be discussed. First of all, it should be clear that the results were based on two main assumptions. Firstly, Volvo cars MY 2020 would be fitted with the same safety technologies as the V60 MY 2019, and secondly, no major improvements in crashworthiness would be introduced between the analyzed Volvo models and Volvo cars MY 2020. While these assumptions do not seem unreasonable, it is evident that they directly affect the results.

STA in-depth studies are fully representative for Sweden, and possibly for Northern Europe at large. However, it is important to note that Swedish conditions may differ from other regions of the world. The Swedish market accounts for approximately 10% of Volvo's global market (Volvo Cars 2019b; Bil Sweden 2019). Therefore, caution should be used before generalizing the present results to a global level. Another limitation is that in this kind of retrospective analyses it is difficult to take into account any behavioral effects that may possibly follow from some technologies. On the other hand, analysis of the eight fatalities involving the Driver Support Package did not suggest any clear behavioral adaptation due to the presence of optional safety technologies. Clearly, it will be essential to follow up the real-life safety performance of the V60 model to understand how accurate the present results are.

Another important point to discuss is that the present paper exclusively analyzed the potential benefits of safety improvement in Volvo cars. In other words, no improvements among other vehicles, mostly passenger cars, but also in the road infrastructure were taken into account. This aspect can be seen as both a strength and a limitation at the same time. It is well-understood that the general car development is towards safer and safer cars, and that new cars from other manufacturers than Volvo are also fitted with several safety technologies, as shown in the latest Euro NCAP test results (Euro NCAP 2018). Some of these technologies could contribute to avoid fatalities in and by Volvo cars as well. For instance, unintentional lane drifting by oncoming vehicles could be prevented with Lane Support, thus preventing head-on collisions where the crash severity is too high for the current AEB head-on. At the same time, it could also be argued that the safety standards of Swedish roads are being constantly revised and that a portion of such head-on collisions with high crash severity will be progressively addressed by safer road infrastructure. All of these aspects suggest that the present results may be an

underestimation, at least in the long-term Swedish prospective. On the other hand, from a more global prospective it could be more difficult to achieve Volvo's vision by relying on a high market penetration of new safety technologies in other vehicles, and/or on a significant safety improvement of the road infrastructure. Therefore, it may be also a strength to focus on the potential benefits in Volvo cars to provide better guidance for future safety development.

It is also important to briefly discuss the relevance of different types and degrees of violations for the future development of vehicles. In the present study, 20% of the fatalities involved extreme violations, which is in line with previous findings on the frequency of extreme violations in all fatal crashes in Sweden (Lie et al 2001). In the present material, the majority of such extreme violations were excessive speeding. It seems reasonable to argue that in the future extreme violations will account for an increasingly proportion of all car fatalities, since crashes under normal driving conditions can be expected to be reduced to a larger degree by vehicle and infrastructural safety improvements. Therefore, it will probably become even more important in the future to detect and properly address reckless driving. Also, the potential of addressing milder (or even tolerated) violations such as driving at 90 km/h in an 80 km/h speed area should not be underestimated.

The present results are also relevant for the issue of automated driving. While such a vehicle implicitly does not drive recklessly, drivers of other vehicles might do, thus creating a problem for the automated car. It is also obvious that the automated car, if driven as the cars involved in the current study, would not be able to eliminate all fatalities with vulnerable road users. Obstructed pedestrians are a challenge also for automated cars. This could potentially partly be solved by cautious driving by the automated cars. The way the automated car is driven is therefore crucial for the performance of the safety technology.

Concerning the issue of safety management, it seems like a very good idea to set targets, develop technologies and follow up the results also for a car manufacturer. This gives opportunities for the outside community to monitor the progress and to understand what is needed from the rest of the community to act. This is well in line with both the road safety management system ISO 39001 (STA, 2015) as well as the Sustainable Development Goals (SDG) in the 2030 Agenda (UN, 2015). Communicating targets and outcome is a fundamental piece in both these instruments.

Conclusions

In summary, by analyzing Swedish in-depth data from fatal crashes involving modern Volvo cars (MY $\geq$ 2010), it was found that:

- The yearly average number of fatalities in Sweden during 2010-2017 was 2.8 for occupants in Volvo cars and 5.0 for either occupants in other vehicles or VRUs impacted by Volvo cars, respectively.
- It was estimated that these fatalities could be almost halved with the safety technologies fitted on the following car generation, the V60 MY 2019. This would correspond to approximately 1.4 fatalities in Volvo cars and 2.6 by Volvo cars per year in Sweden.
- It was also found that most of the fatalities that could not be prevented with a V60 MY 2019, occurred in crash scenarios where at least one safety technology was relevant, although the current performance was estimated not to be sufficient to prevent the fatality.
- Only three cases occurred in crash scenarios without any relevant existing safety technology.
- These results are based on the assumption that the road infrastructure, speed limit and crash opponents would be unchanged. Clearly, taking safety improvements in the road infrastructure and other vehicles into account would result in an even higher reduction of fatalities in and by Volvo cars by 2020.
- In conclusion, regardless of whether Volvo's vision will be achieved by 2020 or not, it is very important to set road safety targets, develop new solutions and follow up the results, also for a car manufacturer.

REFERENCES

Bil Sweden (2019). *Definitiva nyregistreringar under 2018* (in Swedish; definitive new registration in 2018). Available at: www.bilsweden.se/statistik/nyregistreringar_per_manad_1/nyregistreringar-2018/definitiva-nyregistreringar-under-2018 Accessed February 1st, 2019.

EC, European Commission (2011). Roadmap to a single European transport area – towards a competitive and resource efficient transport system. SEC (2011) 391 final, Brussels, Belgium.

Euro NCAP (2018). Press release. Available at: www.euroncap.com/sv/press-media/pressmeddelanden/the-best-in-class-of-2018/ Accessed February 1st, 2019.

Lie A, Tingvall C (2001). Governmental status report, Sweden. 17th ESV Conference, Amsterdam, the Netherlands, June 4th-7th, 2001.

STA, Swedish Transport Administration (2005). In-depth studies of fatal accidents save lives. Borlänge, Sweden. Available at: publikationswebbutik.vv.se/upload/1483/88654_in_depth_studies_of_fatal_accidents_save_lives.pdf Accessed November 4th, 2014.

STA, Swedish Transport Administration (2015). ISO 39001 - Management system for traffic safety. Available at: https://www.trafikverket.se/en/startpage/operations/Operations-road/vision-zero-academy/Vision-Zero-and-ways-to-work/iso-39001/ Accessed February 1st, 2019.

Volvo Cars (2009). 2008/09 Corporate report with sustainability. Available at: group.volvocars.com/sustainability/publication-list Accessed February 1st, 2019.

Volvo Cars (2019a). *Utrustning och funktioner för Volvo V60* (in Swedish; equipment and functions for Volvo V60). Available at: www.volvocars.com/se/bilar/modeller/v60/specifikationer/utrustning# Accessed February 1st, 2019.

Volvo Cars (2019b). Retail sales by car model. Available at: www.media.volvocars.com/global/en-gb/corporate/sales-volumes Accessed February 1st, 2019.

UN, United Nations (2015). Transforming our world: the 2030 Agenda for sustainable development. Available at: https://sustainabledevelopment.un.org/content/documents/21252030%20Agenda%20for%20Sustainable%20Development%20web.pdf Accessed February 1st, 2019.

ACCIDENTS INVOLVING CARS IN AUTOMATED MODE – WHICH ACCIDENT SCENARIOS WILL (NOT) BE AVOIDED BY LEVEL 3 SYSTEMS?

Matthias Kuehn
Jenö Bende
German Insurers Accident Research
Germany

Paper Number 19-0224

ABSTRACT

In the coming years systems will become available that will be able to drive in automated mode for certain periods of time but will only be able to handle selected situations. This is referred to as conditional automation (level 3), whereby the driver no longer has to monitor the vehicle continuously but does have to take control on request when the limits of the automation driving system are reached. What we can say today is that vehicles with different levels of automation will be sharing the roads with manually driven vehicles in the foreseeable future. It is still unclear whether automated vehicles sharing the road with manually driven vehicles will lead to additional road safety risks (mixed traffic). With the presumption that vehicles will still be involved in accidents while they are driving in automated mode, following question arises: how will these accidents look like in the future? The German Insurers Accident Research therefore analyzed the impact of automated driving on motorway accidents. For this study, the UDV used its own accident database (referred to as the UDB) which contains a representative cross-section of all third-party vehicle claim files of the insurers involving personal injury and at least € 15,000 total claim value. The analyzed pool consists of accidents which occurred between 2007 and 2013. In a first step, relevant accident scenarios were determined based on all motorway accidents involving cars in the data pool. In a second step, generic automated driving functions and their characteristics were defined. Thereby, starting with driver assistance and comfort systems (DACS), automation Level 3 and 4 were defined and analyzed. By means of a case-by-case analysis the theoretical benefit potential of these systems was evaluated. Results of the analyses are: It can be expected for the future that cars driving in automated mode will still be involved in accidents. An active Level 3 function as described above could prevent up to 6% more motorway accidents than modern cars equipped with DACS. But negative effects that haven't been quantified up to know may decrease this potential significantly. With these systems it can anticipated that the frequency of rear-end accidents will decrease. But accidents caused by lane change will remain a big challenge for the automated driving systems. With a Level 4 system which drives in automated mode a total of 21% of all motorway accidents were considered as avoidable. The approach used in the study is based on limited knowledge on automated driving available today. It can be stated that the driver is the most critical part up to Level 4 automated driving. Starting with Level 4 this uncertainty will be nearly eliminated. A significant change in the accident situation can be expected only from systems with a very high level of automation (Level 4+) which exclude the driver from the driving task completely. But even with a Level 4 system, accidents will still happen in the future, e.g. due to mixed traffic.

INTRODUCTION

Automated driving is regarded as the future of mobility. It is expected to make traffic flow more efficiently and reduce the number of road accident victims as well as emissions and traffic jams. This will be more of a multi-dimensional, gradual transition than a rapid change. The new technology will be available in both cars and commercial vehicles. Currently, these vehicles offer either Level 2 (partial) or, in the near future, Level 3 (conditional) driving automation, which is typically active only on motorways [1]. As the development of the technology continues, vehicles with higher levels of automation that are also suitable for use in other situations, not just on motorways, will gradually become available. The situation is somewhat different with parking functions. Here, development may proceed more quickly toward highly automated functions. What we can say today is that vehicles with different levels of automation will be sharing the roads with manually driven vehicles in the foreseeable future. This development will affect both cars and commercial vehicles.

GERMAN INSURERS ACCIDENT DATABASE

The accident database of the German Insurers Accident Research (referred to as the UDB) is a database that was set up for accident research purposes. The data collected is conditioned for interdisciplinary purposes for the fields of vehicle safety, transport infrastructure and traffic behavior. The contents of the claim files from the insurers form the basis of the UDB. Only third-party vehicle claims involving personal injury and at least € 15,000 damage costs have been taken into account for the GDV accident database. Cases involving only damage to property and less serious accidents involving personal injury (damage costs < € 15,000) are not included in the UDB

The data sample used in this analysis consists of a total of 3,029 accidents that occurred between the years 2007 and 2013 and involved at least one passenger car. A total of 4,845 cars excluding vans were involved in these accidents. Motorway accidents make up 11% (n=346 relevant cases with n=709 involved cars) of these accidents. All types of traffic involvement were taken into account as the collision parties for the car (cars, trucks, buses, motorcycles, bicycles and pedestrians) as well as single car accidents. Single car accidents are, however, underrepresented, as cases in which there is no injury or damage to a third party are not brought to the attention of GDV.

MOTORWAY ACCIDENTS INVOLVING CARS IN THE UDB

The n=346 motorway accidents in the UDB were broken down in:

- accidents where a car was responsible for the crash (which make up 25% of all involved cars)
- accidents where at least one car was involved but not responsible for the crash (which make up 75% of all involved cars).

Out of these 346 accidents, a total of 146 cases where the car was responsible for the crash and 244 cases where the car was not responsible for the crash have been analyzed. The fact that more than one car may be involved in an accident led to multiple counting, i.e. the same case can be counted more than once.

Motorway accidents where the car was the main responsible

Motorway accidents can be described in different ways. The most common method is by using the parameters “Type of accident” [2] and “Kind of accident” [3]. In this study, a combination of both parameters was used first for a rough classification of the UDB accidents in scenarios and, in addition, a case-by-case analysis was performed in order to break them down in sub-scenarios. The type of first conflict between the case-car and another vehicle was the decisive factor in this matter.

Two major scenarios were found to be predominating and these acount for a total of 88% of all n=164 motorway accidents caused by a car. These are:

- “rear-end accidents” (51%) and
- “lane change accidents” (37%).

There is also a small group of “other” accidents (13%) which can not be put in patterns. These are conflicts with crossing animals, for instance, or rear-end collisions where the case-car was hit from behind after a lane change. Since the vehicle coming from behind was very fast and/or far away at time of lane change, these accidents were not assorted to the group of lane change accidents.

Rear-end accidents are characterized by the fact that the case-car is involved in one or multiple collisions after a conflict with a moving or stationary vehicle in front of it in the same lane. In most of the cases the driver of the case-car oversaw the vehicle ahead or failed reacting properly when approaching it.

Lane change accidents are characterized by the fact that the case-car is involved in one or multiple collisions after having left either intentionally (lane change in order to avoid a rear-end collision with the vehicle ahead) or unintentionally (e.g. due to driver distraction, fatique) its own driving lane.

A closer look at the sub-scenarios shows that:

- Unintentional lane changes of the case-car represent the most frequent sub-scenario and account for one third of all all motorway accidents caused by a car.
- Rear-end conflicts with a stationary vehicle, as typical for congestion related situations, are the second most frequent sub-scenario and make up 31% of all mtorway accidents caused by a car.

Motorway accidents that were caused by a car (n=164)			
Accident scenarios from the view of the case-car that caused the accident (x)		n	%
Total accidents		164	100
Rear-end		83	51
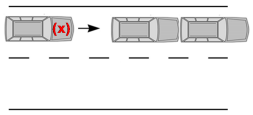	Conflict between the case-car and a stationary vehicle in front in the same lane	51	31
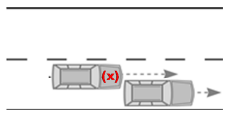	Conflict between the case-car and a vehicle moving ahead in the same lane	32	20
Lane change		60	37
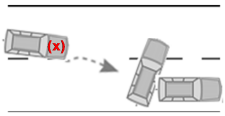	Conflict between case-car and another vehicle in the same or another lane caused by an unintentional lane change of the case-car	54	33
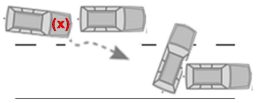	Conflict between case-car and another vehicle caused by an intentional lane change of the case-car due to a vehicle on the same lane	6	4
Others		21	13
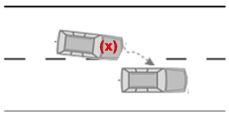	Other conflicts (e.g. lane change of the case-car due to another lane changing vehicle or case-car being hit by a vehicle from the adjacent lane)	21	13

Figure 1. Motorways accidents caused by a car and their classification in scenarios and sub-scenarios

Motorway accidents where the car was involved but not responsible

The groupf of accidents where the car was involved but not responsible for the crash build the second pool. It contains 244 accidents and makes up a larger proportion within all motorway accidents invoving a car in the UDB (n=346).

A short overview of the main and sub-scenarios (Figure 2) reveals a picture which is similar to that observed for accidents with the car being responsible. Rear-end-collisions have the highest share, accounting for 51% of the cases being followed by the group of lane change accidents with a share of 41%.

Motorway accidents that were not caused by a car (n=244)			
Accident scenarios from the view of the case-cars that were invovled but not responsible for the accident (x)		n	%
Total accidents		164	100
Rear-end			
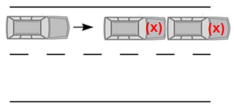	Another vehicle collides with the case-car which is standing in the traffic in the same lane	79	32
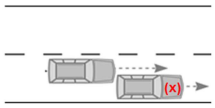	Another vehicle collides with the case-car which is moving ahead in the same lane	46	19
Lane change			
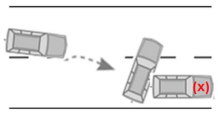	Another vehicle collides with the case-car after a lane-change (different collision constellations possible)	99	41
Others			
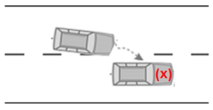	Other conflicts (e.g. case-car is hit by a vehicle that is moving on the adjacent lane)	20	8

Figure 2. Motorways accidents caused by a car and their classification in scenarios and sub-scenarios

CATEGORIZING AND DISTINGUISHING BETWEEN MODERN ASSISTANCE AND AUTOMATED FUNCTIONS

The discussion around automated driving requires a clear understanding of the attributes and capabilities of the functions involved. Driving can be subdivided into navigation, vehicle control and stabilization tasks [4]. According to this model, the navigation level is about route planning, the vehicle control level involves the driver comparing the goal with the current situation (i.e. dynamic driving), and the stabilization level is about controlling deviations in a closed loop system.

Assistance and automation functions operate on the vehicle control level. There are three different modes of action here [5]: informative and warning functions, continuously automating functions and temporarily intervening systems (see table 1). This approach has the advantage that a distinction can be drawn between advanced driver assistance systems and automated driving functions. Even among advanced driver assistance systems, there are differences that are clearly based on their mode of action. Mode of action B describes the levels of automation under discussion (see table 2). Level 1 covers only advanced driver assistance systems that handle longitudinal and lateral control. These

are the proximity control system and the lane-keeping assist system. The lane-departure warning system, on the other hand, comes under mode of action A/2.

Mode of action A Informative and warning functions	Mode of action B Functions offering continuous automation	Mode of action C Systems that intervene temporarily in accident-prone situations
Take effect exclusively and "indirectly" through the driver: 1. Status information, e.g. traffic-sign recognition 2. Abstract warning, e.g. lane-departure warning system 3. Concrete warning, e.g. • Blind-spot detection system or • Collision warning system	Have a direct effect on vehicle control, can always be overriden. Definition according to SAE J3016 [1] or VDA/BASt [4]	Preventive machine intervention with a negative situation forecast, e.g. • Emergency brake assist system • Emergency steering assist system

Table 1. Assistance and automation functions on the vehicle control level [4]

Nomenclature	Driving tasks of the driver by level of automation
Full automation **Level 5**	The system takes full control of driving on all road types and in all speed ranges and environmental conditions
High automation **Level 4**	The system takes over full lateral and longitudinal control in a defined application
Conditional automation **Level 3**	The system takes over lateral and longitudinal control for a certain period in specific situations
Partial automation **Level 2**	The system takes over lateral and longitudinal control (for a certain period and/or in specific situations)
Driver assistance **Level 1**	The driver has constant lateral or longitudinal control. The other driving task is handled by the system within certain limits (e.g. adaptive cruise control (ACC) system, lane-keeping assist system).
No automation **Level 0**	The driver drives constantly (for the whole journey) with both longitudinal control (acceleration and breaking) and lateral control (steering).

Table 2. Levels of automation in accordance with SAE J3016 and VDA/BASt [1,6]

METHOD DESCRIPTION

An overview of the analysis method and some specifications related to the automated driving systems will be given in the following.

For each motorway accident in the UDB, the car that caused the accident was defined as the case-car. In a case-by-case analysis, the safety potential was estimated for driver assistance and comfort systems (DACS) and two levels of automated driving. The cases were analyzed using the "What would happen if..." method. The prerequisite for this is the assumption that none of the analyzed case-cars involved was using an automated function or any DACS at that time. This approach considers the course of the accident as it happened in reality and contrasts it with the course of the accident as it would have been with the case-car driving in automated mode or with DACS. This makes it possible to determine the influence an automated ride would have had on the course of the accident. The original driver behaviour was taken into consideration, as far as it was possible. For each case it was assumed that during the automated ride the driver of the case-car would have behaved in the same way as he did before the original accident.

The challenging part was to define the automated driving functions and implement them in the analyses. An attempt was made to use the knowledge on the system definitions gained from the previous chapter. However, this could not be done in that detail as described in Table 1 and Table 2. When speaking of retrospective accident analysis, a clear distinction between DACS and automation systems is almost impossible. It could not always be determined which system would have intervended first in case of an accident: DACS or the automated system. The "What would happen if..." method uses the assumption that the case-car was driving in automated mode right before the accident, but does not consider earlier traffic events that could have been influenced by the automated ride.

With this limitations and being aware of the fact that we were not exactly in line with the definitions in Table 2, three degrees of systems were defined and their boundary conditions were set. It was assumed that every case-car (and no other vehicle involved) was equipped with following driver assistance and comfort systems (DACS):

- Adaptive cruise control (ACC),
- Emergency braking assist,
- Lane keeping assist and
- Blind spot detection system.

In simply terms spoken, these four DACS are pieces of a Level 1 and in combination a Level 2 automated driving mode. Additonal two more levels were then defined by succesively adding more attributes and capabilities. These levels were Level 3 and Level 4. Table 3 gives a short description of the systems with their boundary conditions.

It has to be underlined that with this method no differentiation could be made between DACS, Level 1 and Level 2. These differences lie mostly in the Human-Machine-Interface – with the full responsibility of the driver - and not in technical details of the systems. These human based differences can also not be adressed with the tool of a retrospective accident analysis. In the following parts of this paper, the term DACS will therefore be used for this group of systems.

It was possible to distinguish between these DACS, Level 3 and Level 4. The differences in the functionalities can be basically described by the situations that can be handled by the systems. But the most crucial difference between DACS and Level 3 was that, for DACS, the driver behaviour”overwrote” the system functionality in certain situations. This was not done for a Level 3 system because, according to the definitions, the driver was not monitoring during the automated ride. Following aspects were essential when declaring no safety potential to the systems:

- System reaches its technical boundaries (see Table 3)
- System is not activated or manually switched off by the driver
- Unforseen environmental or car related events (aquaplaning, tire blow, technical failure of the car).

The analyses did also not consider following aspects that could lead to negative effects for road safety but which are not quantified yet:

- Take-over request to the driver [7]
- Negative effects initiated by the automated ride that could lead to other accidents (e.g. fatique) [8]
- Different driver behaviour due to mixed traffic.

<table>
<tr>
<td>Assumptions for DACS:

o System maintains longitudinal and lateral drive, but no lane change
o Driver can override or switch off the system
o Driver acts / monitors the system continuously (hands on the steering wheel)
o System performs braking manoeuvers but no evasive steering manouvers (only warning)
o System has no safety potential in following cases:
▪ Construction sites
▪ Joining or leaving the motorway
▪ Steering mistake by the driver
▪ Alcohol, fatigue and physical issues of the driver
▪ Technical failure of the car
▪ Extreme weather conditions (strong rain, aquaplaning).</td>
<td>Assumptions for a Level 3 automated driving function:

o System operates up to 130 kph (not considered in this analysis)
o System maintains longitudinal and lateral drive (except: entering and leaving the motorway)
o Driver can override or switch off the system
o System performs braking, lane change (evasive) and overtaking manouvers
o Driver is not required to monitor the system
o Driver receives a take-over-request in critical situations
o System has no safety potential in following cases:
▪ Construction sites
▪ Joining or leaving the motorway
▪ Alcohol and severe physical issues of the driver
▪ Technical failure of the car
▪ Extreme weather conditions (strong rain, aquaplaning).</td>
</tr>
<tr>
<td colspan="2">Assumptions for a Level 4 automated driving function:

o System operates up to 130 kph (not considered in this analysis)
o System maintains longitudinal and lateral drive (incl. entering or leaving the motorway)
o Driver can override or switch off the system
o System performs braking, lane change and overtaking manouvers
o Driver is not required to monitor the system
o System performs braking and evasive manouvers
o In critical situations, the system initiates a minimal risk manouver
o Systems has no safety potential in following cases:
▪ Technical failure of the car
▪ Extreme weather conditions (strong rain, aquaplaning).
▪ Collisions with other vehicles that approach from the site or from behind</td>
</tr>
</table>

Table 3. Boundary conditions for the three defined levels of automation in the UDB analysis

SAFETY POTENTIAL FOR SELECTED LEVELS OF AUTOMATION

The safety benefits were calculated for each of the systems separately and were then put in relation to the different accident pools (see Table 4).

A modern car equipped with DACS could achieve a safety potential of 21% on motorways. This underlines the important part of driver assistance systems for road safety. As already mentioned before, with this method, this equals the safety benefit of a Level 1 and Level 2 system. That means that no additional safety benefits can be expected for Level 1 and Level 2 but negative effects might lead to less benefit at this point (see Figure 3).

Related to all motorway accidents involving a car, an additional safety potential of +6% could be achieved by a Level 3 system. This "ad on" is small and can be explained by the fact that a Level 3 system still has to rely on the driver as a back-up when the technical boundaries of the system are reached (see also Table 3). And it has to be put in contrast to possible negative effcts caused by a Level 3 system.

A nearly maximum safety potential of additional +21% can be achieved by a high automation level (Level 4), which requires no driver monitoring or driver intervention at all during the autonomous ride. Even here, possible negative effects (mixed traffic) must be considered. According to the analyses, with a Level 4 system, more than half of all motorway accidents caused by a car would still remain unavoidable, for instance.

If these benefits are put in relation to the larger accident pools, their amount will decrease. Related to all accidents involving a car in the UDB, for instance, the achievable safety potential for a Level 3 system system is 0.7% and even with a Level 4 maximum 2.4% more car accidents could be avoided.

Systems		**Safety benefit [%] in terms of avoidable accidents as an "ad-on" to the achievable benefits by ADAS**			
		Motorway accidents involving a car (n=346)	Motorway accidents caused by a car (n=164)	All accidents involving a car (n=3,029)	All accidents caused by a car (1,834)
DACS		**21%**	**45%**	**2.5%**	**4.0%**
Level 3	additional	**6%**	**12%**	**0.7%**	**1.1%**
Level 4		**21%**	**45%**	**2.4%**	**4%**

Table 4. Achievable safety benefits for analyzed levels of automated driving functions in relation to the different accident pools – the numbers for Level 3 and 4 represent the additional benefits in comparison with DACS

For those accidents that were caused by a car on motorways, Table 5 gives a differentiated view of the achievable safety benefits for the two main accident scenarios. DACS could avoid 80% of all rear-end accidents in the case material but only 10% of the lane change accidents. This is not surprizing because it reflects what DACS in modern cars can already achieve. Todays DACS already overcome most rear-end conflict situations. But most lane change situations are still critical for them [9].

In comparison to DACS, the additional benefit of a Level 3 system can be derived from better skills in the form of dealing with lane change situations. In the analyzed case material, a Level 3 system could avoid only few more rear-end accidents (factor 1.1) but nearly three times more lane change accidents than DACS (see Table 4). For a Level 4 system there is almost no difference between the share of the two scenarios. Due to the exclusion of the driver from monitoring/intervening during the automated ride, a Level 4 system will be able to overcome all types of conflicts in longitudinal traffic properly, i.e. a lane change will be also no problem anymore for self-caused accidents.

Motorway accidents that were caused by a car (n=164)					
Accident scenarios	n	%	avoidable accidents [%]		
			DACS	**Level 3**	**Level 4**
	164	100	**35**	**49**	**91**
Rear-end	83	51	**80**	**87**	**98**
Lane change	60	37	**10**	**27**	**97**

Table 5. Achievable safety benefits for selected automation levels in the UDB

DISCUSSION - ACCIDENTS AND AUTOMATED DRIVING?

One major outcome of the analyses is that there still will be accidents caused by the car during a Level 3 automated ride in the future, regardless the achievable safety benefits of the system. The main reason is that an automated ride with a Level 3 system will still need the driver in terms of intervening in the event of critical situations.

The fundamental problem in connection with constant monitoring coupled with intervention in the event of critical situations is based on a human characteristic investigated by psychologists over 100 years ago [10]. The resulting Yerkes-Dodson law describes the general relationship between a person's ability to perform well and their state of physiological and mental arousal. When a person has a low level of arousal, their performance remains at a minimum level. As the person becomes more aroused, their performance increases up to a maximum level. If arousal increases beyond that, performance starts to drop again until it reaches a similar minimum level to the level at low arousal (Figure 3). Put simply, this means that people perform demanding tasks best with a moderate level of arousal. Driving a car is such a task. Monotonous tasks, like driving down a perfectly straight road with no traffic, can result in a low level of performance or failure. Monitoring a Level 2 system is one such task. Equally, if a driver is overtaxed, the result will be poor performance and even failure. Suddenly being requested to take over control from a Level 3 system would be an example of this.

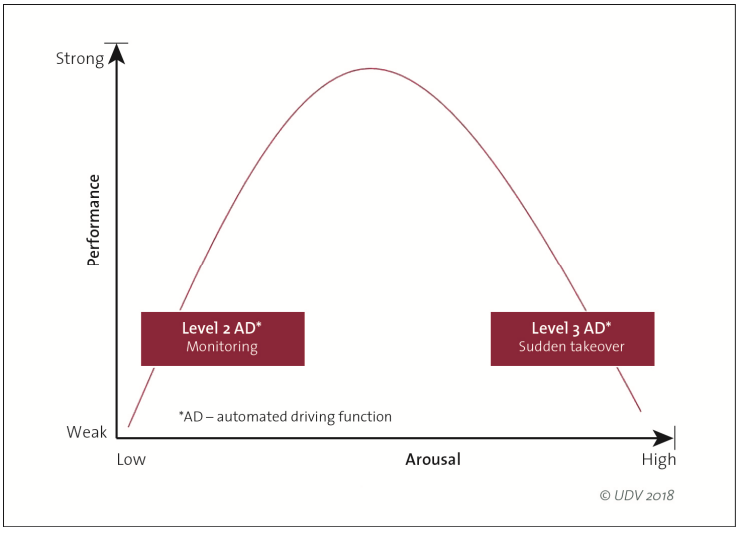

Figure 3. Simplified representation of the Yerkes-Dodson law in connection with automated driving [10]

CONCLUSIONS

The analyses revealed that 11% of all accidents involving a car occur on motorways. For accidents that were caused by a car, safety benefits were determined based on two levels of automated driving. The most substantial benefit in terms of 21% avoidable acidents can be expected from modern assistance and comfort systems (DACS) if these consist of an emergency breaking assist, a lane change assist, a blind spot detection system and an adaptive cruise control.

In comparison to modern cars equipped with DACS, an additional benefit of +6% could be expected for a Level 3 system in terms of avoidable accidents on motorways. Compared to the benefits of DACS, this level of automation might have a higher benefit because it will be able to avoid more lane change accidents. Nevertheless it has to be considered that there could be negative effects on road safety caused by a Level 3 system. Up to know, these effects have not been quantified yet. But studies indicate that they should not be underestimated and that these negative effects might reduce the additional positive benefits. In total, Level 3 systems might have no additional positive effects at all.

It can be predicted that cars driving in a Level 3 automated mode will still cause accidents on motorways in the near future. And they will also be even more often involved in accidents without their own fault. The most critical part for a Level 3 in the future will still be the driver. The majority of those accidents that can not be avoided by a Level 3 system will be lane change accidents.

Only a Level 4 system will provide a high benefit in terms of additional 21% avoidable accidents compared to a Level 3 system. This is because a Level 4 system will be able to handle almost all traffic situations properly but most importantly, the critical part “driver” will be nearly eliminated during the automated ride. Nonetheless, even with a Level 4 system, a large proportion motorway accidents involvoing a car will still remain unavoidable. In this context, possible negative effects of mixed traffic are not considered here.

From the view of the German Insurers, highly automated vehicles (Level 4) could bring great benefits in terms of road safety if they functioned flawlessly under all conditions within their intended scope. Until such time as these systems come onto the market, drivers of manually controlled vehicles should benefit in terms of road safety from continual improvements in driver assistance systems.

REFERENCES

[1] SAE International: Taxonomy and Definitions for Terms Related to Driving Automation Systems for On-Road Motor Vehicles. SAE Standard J 3016, revised version of September 2016.

[2] Federal Statistical Office (2018): Road traffic accident statistics. Wiesbaden

[3] GDV: Accident type catalogue - A guide to determine the accident type. Köln, 1998

[4] Donges, E.: “Driver Behavior Models” in the Handbook of Driver Assistance Systems. Published by: Winner, Hakuli, Lotz, Singer, 3rd Edition. Springer Fachmedien, Wiesbaden 2015. D., Bohle, W., Maier, R., Enke, M., Pohle, M., Zimmermann, F., Ortlepp, J. and M. Schreiber. 2015.

[5] Gasser, T.M., Frey, A. Th., Seeck, A., Auerswald, R.: “Comprehensive Definitions for Automated Driving and DACS”. 25th ESV Conference, Detroit, June 5 to 9, 2017.

[6] Verband der Deutschen Automobilindustrie: Automatisierung – Von Fahrerassistenzsystemen zum automatisierten Fahren (Automation – from advanced driver assistance systems to automated driving). VDA Magazin, Berlin 2015.

[7] UDV: Takeover times in highly automated driving. Compact accident research No. 57, Berlin 2017.

[8] UDV: Tiredness and level 3 - automated driving. Compact accident research No. 70, Berlin 2017.

[9] EuroNCAP, test results for automated functions, October 25th, 2018. http://www.safetywissen.com/#/object/A11/A11.9gq7369919x53lipnvi54019y6ltul63675990019/safetywissen?prev=%2Fnews%2FSAFETYNEWS%2F

[10] Yerkes, R.M. & Dodson, J.D. (1908). The relation of strength of stimulus to rapidity of habit-formation. Journal of Comparative Neurology and Psychology, 18, 459– 482.

BMW'S SAFETY GUIDELINES FOR THE TESTING AND DEPLOYMENT OF AUTOMATED VEHICLES

Paul Daman
BMW AG
Germany

Dr. Martin Götze
BMW AG
Germany

Dr. Christian Gold
BMW AG
Germany

Prof. Klaus Kompass
BMW AG
Germany

Paper Number 19-0226

ABSTRACT

As automobile manufacturers take the leap from Advanced Driving Assistance Systems and implement Automated Driving Systems into their vehicles, certain aspects of vehicle safety become increasingly important. Whereas in today's level 2 automation, the human driver is involved in the dynamic driving task, in level 3 and above, more technological measures are necessary to ensure safety, therefore requiring a newly designed electronic architecture. Nonetheless, analysis of human factors remain a key element to ensure the safe operation of the vehicle. Though conventional techniques may be employed to solve some of these challenges, others require new tools to be developed. In the absence of an international standard, the foundation for discussions of completeness is missing. With an expert analysis of topics and tools a focus can be brought into discussions and serve as a basis for further development. This analysis may also lead to uncover areas where final answers and methods are missing, but serves also to identify areas where effort must be concentrated. When members of the industry apply these principles to the development of automated driving systems, the number of accidents will be minimized following the testing and deployment of this new technology, therefore maximizing safety and customer acceptance.

This submission represents the culmination of multiple sessions within industry, but also with contracting parties and government agencies with the goal of the creation of a comprehensive list of guidelines for the safe development of automated driving systems.

BMW has defined 12 different areas that have been focused into guidelines for the development of a vehicle with a safe automated driving system. These areas include topics from functional safety through the human factors aspects of system handovers to the consideration of passive safety.

While the 12 guidelines are selected to be a comprehensive list of safety topics, they are general in form and do not contain the details necessary to apply it as a blue print for the development. As these automated driving systems are not on the roads in appreciable numbers, the data from real world events are missing. Also the projects to develop the methods to generate and analyze data are still underway, which also forces some guidelines to remain broadly formulated.

The proposed guidelines concentrate the capabilities and limitations of today's safety evaluation for vehicles when applied to automation. By following the guidelines, the industry can ensure that this technology meets an acceptable level of safety when it comes to market.

INTRODUCTION

Automation has defined many areas of development for the past decades and will continue for many to come. From the automation of our digital daily planner to the robots used in manufacturing, our lives have been enabled to move more comfortably, faster and in many ways safer. This trend also continues in the cars we drive. Many areas secondary to the driving task such as automatic climate control and lighting simply make it easier for the driver to drive. Other areas of assistance have a more direct influence on safety as they take action to apply corrective measures to the brakes or steering to avoid an accident at the last moment. Still other features also actuate the brakes, accelerator and steering, but to increase comfort through constant input. Not surprising, these features are all examples of what are called Advanced Driver Assistance Systems, as they assist the driver, who remains in control and responsible at all times.

Based on German accident statistics [1], the errors that these human drivers make cause over 98% of recorded accidents. For that reason, further automation sounds like it would be a simple answer to have a major effect on the worldwide number of accidents. Many have claimed that removing the human from the equation would quickly result in safer streets. After further analysis of the statistics, it is apparent just how challenging this task would be. Overall, accidents are actually quite rare occurrences. Again according to German statistics, once the total life time mileage of 700,000km is taken into account, there is an average distance of approximately 300,000 km between two accidents with any severity. This number raises to 228 million km if fatal accidents are considered, and the distance increases to even 661 million km if we solely look at highways.

These statistics show that the human drivers are actually quite adept at handling the complexities of on-road traffic, and the endeavor of creating technology to accomplish this much is quite daunting. Just reaching this level could be considered difficult enough, but in June 2017, the German Ethical Commission [2] recommended that manufacturers show that the technology used to automate the vehicles perform better than the statistics indicate humans do today. Whereas humans have an amazing capacity to use intuition and anticipation for complex situations, technology has the advantage of offering a 360° view of surroundings, simultaneously processing the information and does not fatigue. When it comes to a safe development of automated vehicles, we need to understand and learn from both the capabilities and limitations of the human driver, while simultaneously taking the risks into account that may emerge from their interaction with an automated vehicle. That could be the handover between a driver and the automated vehicle, or the interaction of road users in a mixed traffic scenario. Therefore, even with higher levels of automation, taking the human factors into account is key to generate a safe system.

To better understand where automation technology in automobiles currently stands, as well as the areas that development is currently engaged in, a brief review of the accepted definitions is necessary. Presently in its 3rd iteration, SAE J3016 [3] is the internationally agreed upon standard to define different levels of automation. While a detailed discussion on the wide range of topics described in the standard is beyond the scope of this paper, several terms shall be described here and referred to in the guidelines. Divided into 6 discrete levels of automation and based upon the separation of tasks required to drive a vehicle, one of the key areas is the operative control of longitudinal and lateral systems (accelerator, brake, steering) which is referred to as the Dynamic Driving Task (DDT). Independent of whether the system or the human is performing this control, the decisions necessary are based on the recognition of objects and events that occur surrounding the vehicle (Object and Event Detection and Recognition- OEDR). In order to group the conditions such as environmental, geographic or similar which are necessary for the system to operate, the term Operational Design Domain (ODD) has been generated.

Level	Name	Narrative definition	DDT		DDT fallback	ODD
			Sustained lateral and longitudinal vehicle motion control	OEDR		
Driver performs part or all of the *DDT*						
0	No Driving Automation	The performance by the *driver* of the entire *DDT*, even when enhanced by *active safety systems*.	*Driver*	*Driver*	*Driver*	n/a
1	Driver Assistance	The *sustained* and *ODD*-specific execution by a *driving automation system* of either the *lateral* or the *longitudinal vehicle motion control* subtask of the DDT (but not both simultaneously) with the expectation that the *driver* performs the remainder of the *DDT*.	*Driver* and *System*	*Driver*	*Driver*	Limited
2	Partial Driving Automation	The *sustained* and *ODD*-specific execution by a *driving automation system* of both the *lateral* and *longitudinal vehicle motion control* subtasks of the *DDT* with the expectation that the *driver* completes the *OEDR* subtask and *supervises* the *driving automation system*.	**System**	*Driver*	*Driver*	Limited
ADS ("*System*") performs the entire *DDT* (while engaged)			*System*	**System**	*Fallback-ready user (becomes the driver during fallback)*	Limited
3	Conditional Driving Automation	The *sustained* and *ODD*-specific performance by an *ADS* of the entire DDT with the expectation that the *DDT fallback-ready user* is *receptive* to *ADS*-issued *requests to intervene*, as well as to *DDT performance-relevant system failures* in other *vehicle* systems, and will respond appropriately.				
4	High Driving Automation	The *sustained* and *ODD*-specific performance by an *ADS* of the entire *DDT* and *DDT fallback* without any expectation that a *user* will respond to a *request to intervene*.	*System*	*System*	**System**	Limited
5	Full Driving Automation	The *sustained* and unconditional (i.e., not *ODD*-specific) performance by an *ADS* of the entire *DDT* and *DDT fallback* without any expectation that a *user* will respond to a *request to intervene*.	*System*	*System*	*System*	**Unlimited**

Figure 1, table of SAE Automation levels [3]

Today, the technology available on large scale production vehicles allows a maximum of level 2 partial driving automation. As the driver is still responsible for the object and event detection the system can actually only assist them in driving the vehicle. The fact that this responsibility is transferred to the system in level 3 and beyond leads to a paradigm shift and a technological quantum leap is necessary to attain it. For simplification, systems capable of level 3 functionality and beyond can be referred to as Automated Driving Systems (ADS)[3]. As discussed in WP29 of UNECE [4] one of the major changes that an ADS brings is that at these levels of automation, activities secondary to the driving task would be explicitly allowed to be undertaken by the driver. Since the system performs the DDT, the driver no longer has this responsibility and is free for other activities such as watching a film on the vehicle displays. The driving task is no longer considered the primary task of the driver in these scenarios, therefore, secondary tasks are also referred to as Non-Driving-Related-Tasks, or NDRTs [5].
It is widely acknowledged that transition between level 2 and level 3 is not trivial [6], and for that reason a common language is necessary to discuss the challenges both inside and outside of the automotive industry. Expert groups within BMW gathered topics and clustered them to generate a comprehensive list of 12 guidelines for the development of automated driving systems. Through review of other recommendations and publications from government bodies or consumer associations such as NHTSA [7], Thatcham Research [8], NTSB [9], GDV [10], the German StVG [11] and the German Ethical Commission [2], it was found that there was much communality between the collections. Nonetheless, additional aspects as well as new viewpoints are introduced here.
To organize BMWs 12 guidelines, an arrangement in three overall groups with common areas of influence were found. The first four guidelines represent technological areas necessary for the system. As in all three groups, though initially simple in form, the details to develop the answer are currently engaging the entire automotive industry. Next is the area of human factors which are also extremely important even for higher levels of automation. While the last four guidelines do not directly create requirements for the automation system, they are areas necessary to be addressed during development of vehicles.

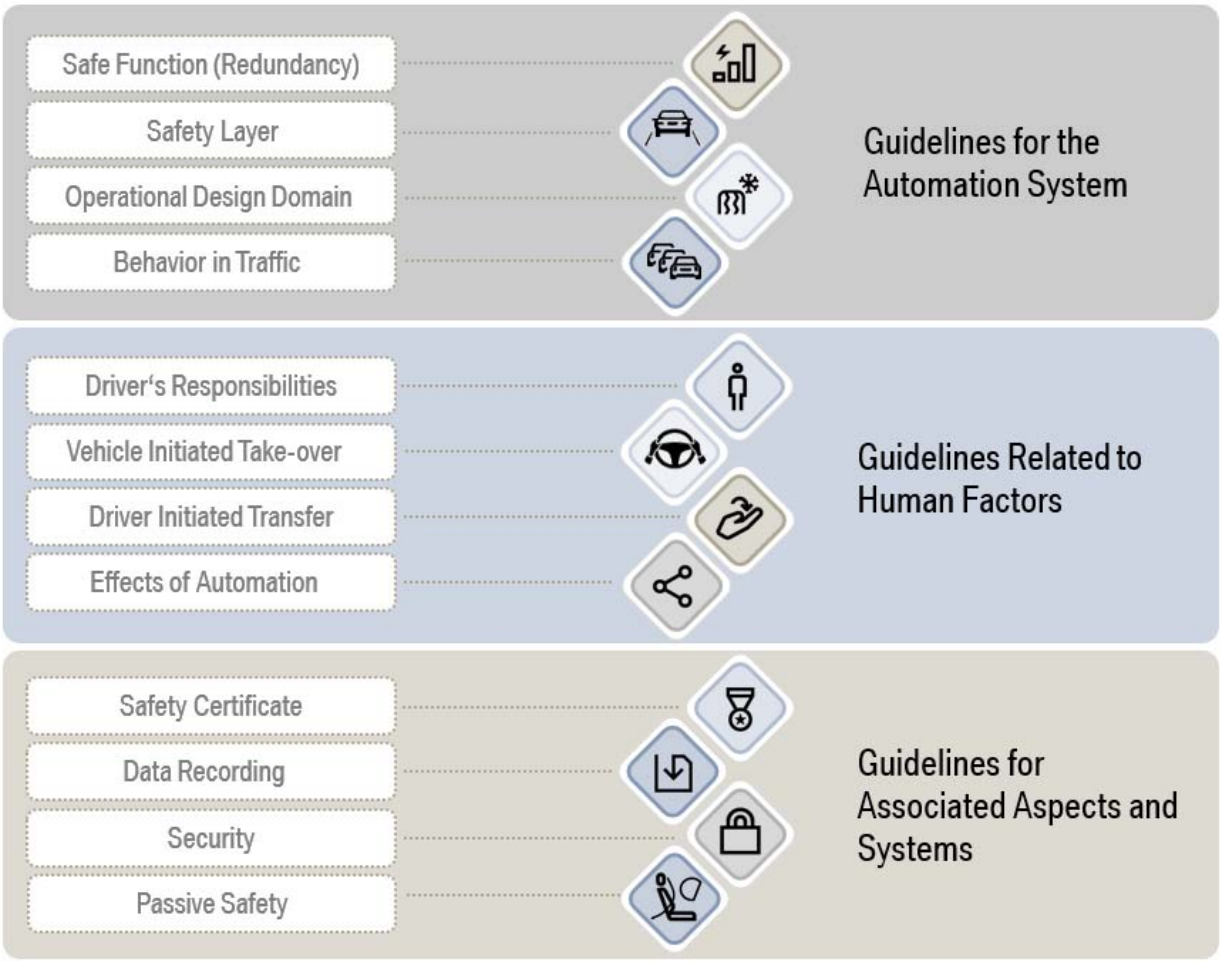

Figure 2 – BMW's 12 Guidelines for Safe Automated Driving Systems

GUIDELINES FOR AUTOMATED SYSTEMS

1. Safe Function (Redundancy)

With automotive systems becoming ever more complicated, the concepts gathered under the term functional safety have become ubiquitous in all areas of automotive development. Either bundled under automotive best practices as ISO 26262-Road Vehicles Functional Safety [12] or other standards from other industries and the military, the processes as well as the measures which result from them have an even higher relevance for automated driving systems. In this list of guidelines, the following aspects gather two of the key elements.

Dealing with Degradation

If system components relevant to the function or individual functions become non-available, the automation system must be capable of compensating or ensuring a sufficient time budget for safe transfer of control to the driver.

This aspect embodies one of the major differences between how a level 2 and level 3 or higher automated driving system must be capable of reacting. As mentioned above, level 2 systems merely assist the human driver and therefore the driver must react if the system does not respond to a relevant object or event. For this reason they can never completely relinquish control and if an aspect of the assistance is no longer available, the driver continues to drive. Once the driver is involved in NDRTs at Level 3+, additional time is necessary before they can resume the responsibility of the DDT from the ADS.

While some have called for redundancy to be the only option to deal with the risk emerging from a degradation, there are also other strategies which can be followed to ensure a safe system behavior. As such, simply the reduction of speed, or avoiding a lane change are two examples of strategies to safely increase the time and reduce risks when aspects of the automated driving function are no longer available. The key is that some form of compensation is necessary.

Fail Operational

The loss of sub functions or system components shall not lead to a safety critical situation.

Continuing along the same idea is that if any component or portion of the system fails, the result shall not be safety critical. This applies to both hardware malfunction which could come from mechanical damage or software/electronic errors.
Due to the new vehicle architecture necessary to fulfill this higher requirement, a level 3+ system is intrinsically different to a level 2 system, independent of the increased competence of the object detection and reaction. For that reason, a system designed as level 2 cannot become a level 3 system simply due to improvements in software. It is the way the system is networked and the measures in the actuators that make it inherently different.

2. Safety Layer

To reduce the frequency of critical situations, automated driving systems of every level are generally designed to drive defensively. Unfortunately even at a reduced frequency, these events will occur and the system must react.

Safety Layer

The automation system must recognize system limits, especially those that do not allow a safe driver take-over, and react to minimize the risk.

There has been a misunderstanding of level 3 automated driving systems in exactly this area. As stated in SAE J3016, it is expected that the fallback ready user regains control in short notice when the system requests it. Of course they are likely performing a task unrelated to driving, so the reaction by the human to an emergency situation may not be possible or inadequate [13]. Further has to be considered that the driver may need additional time for executing the required maneuver to react to the event. For this reason, even in a level 3 system, the system must react to minimize the risk of situations where a transition to the driver is not possible or reasonable, in order to reach an acceptable safety level.
This safety layer must be present below the system carrying out the long term control. Using humans as an analogy, we all have a cognitive layer that allows us to perform complicated activities. As critical situations are rare, a majority of the time is processed in this area. In emergency situations, a faster reaction is necessary to reduce following risk. This is akin to the nervous system, which must quickly react.
Just as human senses provide the information for these quick reactions, the sensors in automated driving systems provide the information for this layer. Therefore, these active safety systems can be found in all levels of automation, though their importance increases in level 3 and above.
Though discussed in further detail in the following section, other system limits may be observed and recognized by the system which are not immediately time critical, as illustrated in Figure 3. For this reason, the fallback ready user of a level 3 system must be able to intervene in these situations with a time allowance on the order of seconds.

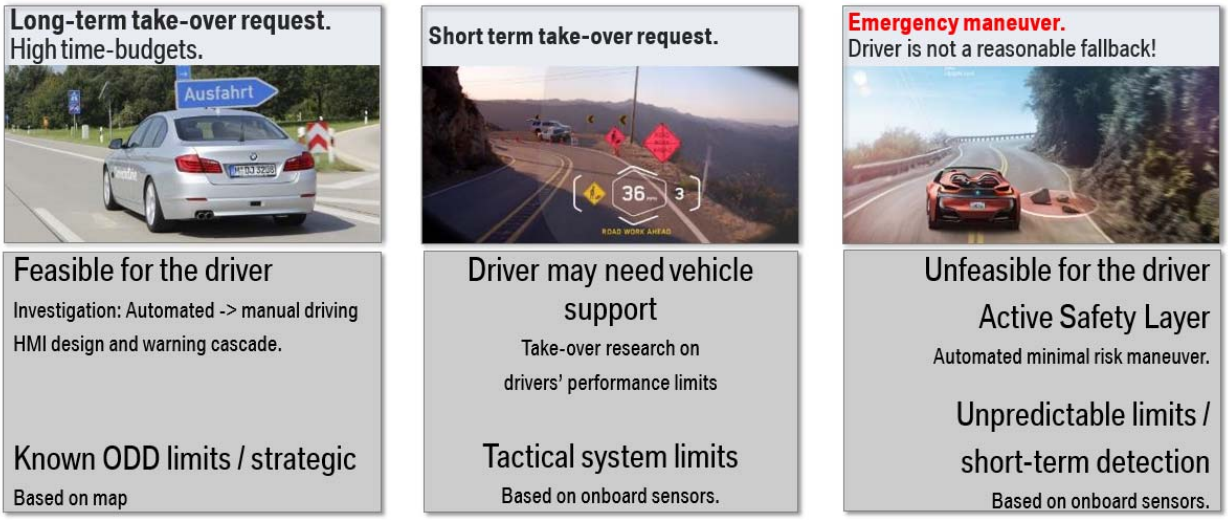

Figure 3 – Comparison of emergency maneuver with other situations

3. Operational Design Domain

Another driving force behind the requirements on the system for higher levels of automation originate in the definition of the operational design domain (ODD). As previously mentioned, the ODD as defined by SAE J3016 is the collection of conditions where the system is designed to operate. Examples can be geographic as in the country or state, environmental as from sunshine to snow, or a collection of roadway characteristics such as a divided highway. As the function is designed to operate safely in this domain, sensors shall confirm at all times that the vehicle is still in that domain.

ODD recognition

As soon as system limits, which restrict the safe functionality of the automation system, are recognized, the system must react to compensate, or request a take-over from the driver with adequate time reserve.

Since the automated driving system is limited to an ODD and while activated in this domain, it is responsible for vehicle control until it requests the fallback ready user to intervene. While this may sound trivial, in lower levels of automation, it is ultimately the driver's responsibility to recognize when the limits are reached. The system may provide assistance to that effect, but only higher levels of automation need to definitively register the limits as a reaction is necessary.

Manage typical situations

The automated driving system must take situations into account, which can typically be expected to be encountered in the ODD and address the risks that may result.

The sensor arrays of vehicles equipped with automated driving systems need to register and classify much more than only the most common objects and the situations they are associated with. Even when they only make up a small percentage of the time spent on the road, there are a multitude of events such as an unexpected lane change, which happen often enough that they cannot be considered unusual. The system shall therefore be able to deal with all situations that are foreseeable to occur within the ODD which have an inherent risk of relevant magnitude.

4. Behavior in Traffic

In the near future, production vehicles capable of conditional automated driving will be on the road. Nonetheless that will only be the beginning of the phase of mixed driving with some conventional vehicles and some automated vehicles sharing the road. Even in today's traffic with solely conventional vehicles, one contributing factor to safe driving is the relatively similar behaviors of most drivers.

Manners on the road

The behavior of the automated function needs to not only be comprehendible to the surrounding road users, but also predictable and manageable.

As mentioned in the introduction, human drivers are often able to apply their intuition and anticipate the actions of other road users based on their experiences. This predictability allows for traffic flow and cooperation between drivers with remarkably limited possibilities for communication. For instance, on the highway using only turn indicators and brake lights, a somewhat complicated coordination of maneuvers can be accomplished to allow a lane change in traffic. Additional lines of communication may even create confusion as human drivers learn how to interpret new signals. Furthermore, an unobtrusive behavior of the automated system reduces the implications emerging from new interaction patterns of a mixed traffic environment.

Conforming to Rules

The applicable traffic rules are to be taken into account.

One method to ensure that driving behavior is similar among drivers is to establish rules. These traffic rules have developed over the last century of human driven vehicles and are often based on human traits such as average reaction time and visibility. Even with these rules there is room for interpretation of the applicable law and in certain situations, drivers are allowed to deviate to a certain extent in some aspects. This poses the question as to whether these rules apply to vehicles with automated driving systems with faster reaction times, a 360 degree field of view, and sensors such as radar, and how the applicable law is interpreted for ADS. As our society develops, the rules and interpretations may change, but the algorithms behind the automated driving systems need to bear them in mind.

GUIDELINES RELATED TO HUMAN FACTORS

5. Driver's Responsibility

Depending on the level of automation being offered by a vehicle, the driver's responsibilities may change. At lower levels, the driver is responsible for all actions of the vehicle except those attributed to a defect. At the highest level, the driver can be relegated to an operator. For the portions of the trip where it is active, an ADS is responsible for all parts of the DDT, but at a minimum the driver needs to ensure that vehicle maintenance has been taken care of. Other responsibilities of the driver may include a reaction after the failure of a suspension component, the correct loading of cargo and maintaining an appropriate seating position if a takeover may be necessary. Complicating matters further, a single vehicle can offer multiple levels of automation depending on the situation. For instance in one operational design domain limited to the highway, there may be a level 3 function available, but once the vehicle is in an urban environment only level 2 or 1 functions may be available.

Responsibilities

The portions of the driving task which remain under the driver's responsibility must be clearly communicated to him/her.

From passages in the owner's manual to the way information is displayed in the vehicle, the manufacturer shall take care to take advantage of the various lines of communication so that the driver understands their responsibilities and act accordingly.

Driver's State

To promote safety, systems need to be integrated that support the driver to recognize driver conditions that are not acceptable.

Though it does not obviate the driver's awareness of their responsibilities, technology can assist the driver if they are presenting characteristics, which conflict with system requirements on the driver. For instance, by using information provided by simple seatbelt contacts, the system can provide a reminder to the driver that they may not leave their seat. Nevertheless, as it is not possible to reliably detect all forms of misuse, no technology can replace the driver's conscious heeding of their responsibilities.

Mode Awareness

The automated function must ensure that the currently active driving mode can be recognized explicitly and unmistakably at any time. If the driver must react, this must be clearly communicated.

As the single vehicle can offer multiple modes of operation, the driver must be aware of which level of automation is currently operational in the vehicle, in order to enable a correct use of the respective assistance or automation system. Through countless hours of simulator studies [14], measures are being defined and implemented in the human machine interface to give this awareness to the driver. While a level 2 system could expect the driver to recognize the necessity to take action, higher levels of automation must communicate whether there is a need for it.

6. Vehicle initiated handover

Even for higher levels of automation, the vehicle may request that a driver take over control of the vehicle. One example is when a portion of the trip is no longer within the system's ODD, and the driver simply would need to once again takeover with the vehicle controls. Other extenuating circumstances may require a takeover in vehicle concepts without conventional controls in level 4. Here the human requested to drive the vehicle may do so remotely, continuing to use the vehicle's sensors and actuators.

Minimal Risk Condition

If the driver does not comply with a take-over request, the ADS must perform a maneuver to minimize risk. The correct maneuver depends on the situation.

Though the reasons for initiating a handover may vary, automated driving systems need to follow a strategy between the time that the request is given and when the driver takes control. Depending on the technology available on the vehicle as well as the situation, the reaction can be as simple as reducing speed to reduce the risks, or as complicated as changing lanes and pulling over to a safe harbor parking space. It is important to note that this minimal risk condition may have a different character depending on whether it is an emergency maneuver, triggered by a loss of sub functions or system components, or a long term take-over request (Figure 3).

Take-Over requests

Handovers must be manageable for the driver.

Hand in hand with the safety layer, time critical emergency situations would not be manageable if the driver is requested to take over in those situations. As with other guidelines associated with human factors, studies taking place in simulators [13] and other controlled environments indicate what time budget and take-over scenario is manageable for the average driver [15] and how an adequate take-over request should be designed [16], and how control elements and human machine interfaces [17] can be adopted to support the driver in taking over control.

7. Driver initiated transitions

Often neglected when considering automated driving systems, there are situations when a driver would want to regain control of the vehicle. A simple example would be to have the full driving experience along an engaging stretch of road. However, there are situations where the driver may touch the controls without actually desiring to regain control.

Take-Over (driver)

Activating and deactivating the automated driving system requires explicit driver‘s intent.

Differentiating the intent can mean the difference between accidentally contacting one of the driver controls (i.e. steering wheel) while reaching for an object, and explicitly taking the wheel to negotiate a curve. Relinquishing control in the former could result in a critical situation. While the driver should be able to take-over control if he intends to do so, an unintended take-over could result in a handover to a driver who is not ready or able to take on the driving task. For that reason concepts must be developed to differentiate between the two situations. Furthermore, there is a wide range of vehicle functions relevant or connected to the functioning of the ADS. Driver interaction with those functions should neither lead to an inexplicable hand-over, nor to a safety relevant change of the ADS state.

8. Effects of Automation

Made evident from other industries with high levels of automation, such as the commercial aviation industry, humans adapt to the automation they experience.

Effects of Automation

> In the overall evaluation of system safety, effects on the driver due to automation need to be taken into account, even when they occur after the automated portion of the drive has ended, when a direct link to the drive while automated can be drawn.

Studies continue to be performed to analyze these effects in the automotive context [18]. Acknowledging that these occur is the first step to implementing measures to counteract them. These measures may include optimizations to the human machine interface [19], which further support mode awareness.

GUIDELINES FOR ASSOCIATED ASPECTS AND SYSTEMS

9. Safety Assessment

In addition to BMW's long history of striving to improve road safety, the German Ethics Commission [2] has also tasked the automotive industry to ensure that the automated driving system, which in some ways replaces the driver in performing the DDT, is safer than the average driver.

Safety Assessment

> Verification and validation shall be used to ensure that the safety goals are met, in order to reach a consistent improvement of the overall safety balance, while minimizing new risks induced by the automation system.

In order to compare the performance of the system to that of human drivers, methods are being developed to quantify and assess how they perform. Simulation and prospective safety analysis [20] is playing a key role in generating the data. As this task effects a multitude of companies and institutions developing this technology, several cooperation projects have been initiated. One showing promise to deliver some of the answers is the PEGASUS project [21] supported by the German state. Summarized in Figure 4, a process of scenario collection, abstraction, database generation and validation is described. An international project titled L3 Pilot [22] is also poised to deliver pieces to the puzzle in quantifying safety and performance.

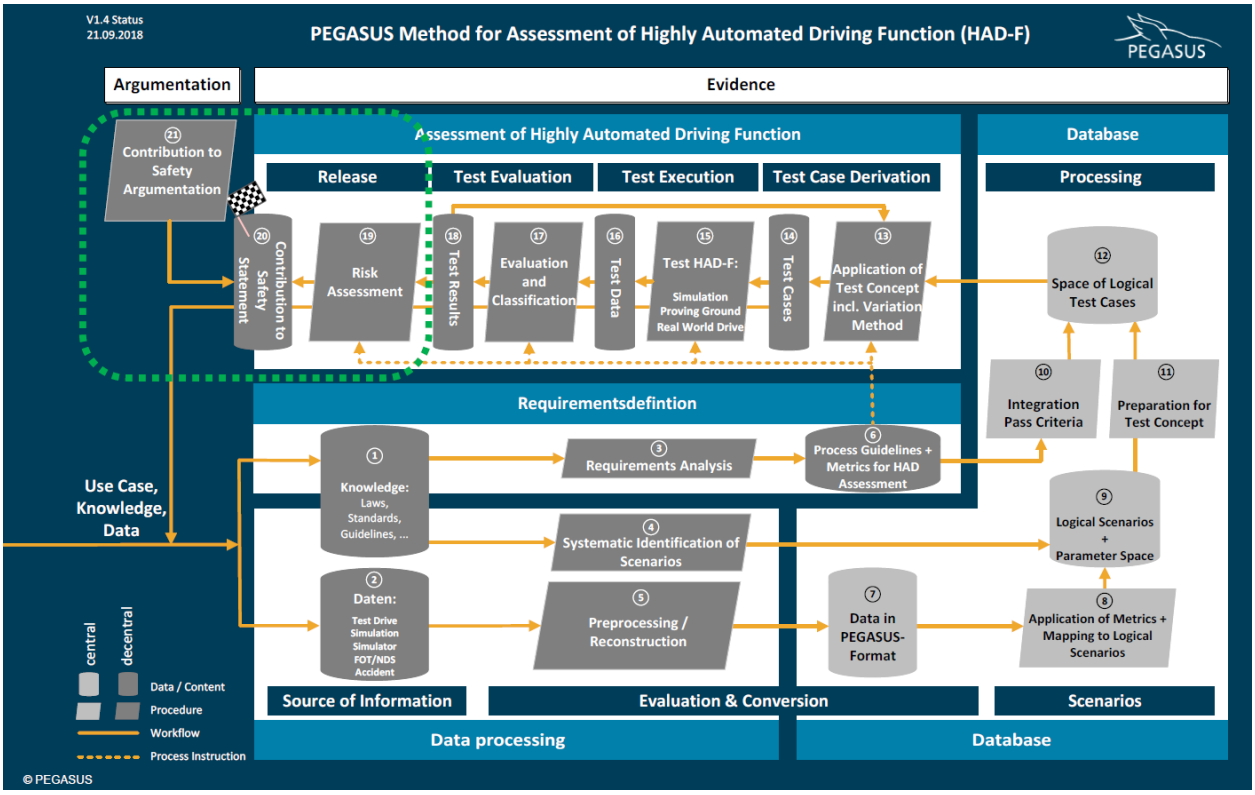

Figure 4 Summary of the Pegasus method [13]

10. Data Recording

Even with today's conventional vehicles, some markets have required that data is recorded in the event of an accident or similar situation. Information about the scenario leading up to the accident can be provided by the driver. Once the driver is no longer performing the DDT, this information will have to be recorded by the system.

Data Recording

While conforming to the applicable data privacy laws, automated vehicles shall record the relevant data pertaining to the status of the functions when an unusual event is recognized.

Just as the today's driver is responsible for driving, their memory serves to aid in reconstructing what happened during a critical or emergency situation. Once this responsibility is transferred to the technology, it must also have the equivalent of a memory to provide information in those situations. As this data contains details, in accordance to privacy laws, access to the data will be limited.

11. Security

In a world of ever increasing connectivity, security is tantamount for information to only flow between appropriate places. In the financial industry or even online trade, the penalty for inadequate security is financial difficulties. In the automotive world, the consequences can be much more drastic.

(Cyber-) Security

When offering an automated driving function, steps shall be taken to protect the function from threats.

With a history of connectivity, BMW has been addressing cyber security for decades. As control systems for the steering and brakes for even level 0 and 1 systems depend on the flow of information from sensor to actuator for a safe operation, even hardware access points are taken into account. Automated driving systems pose additional challenges as the actuators have even higher capabilities and the driver is further removed from the driving task. Just as the attacks evolve from year to year, so must the defense as security directly effects safety.

12. Passive Safety

A motivation for the development of automated driving systems is the overall reduction of accidents which take place on public roads. Nonetheless due to unforeseen circumstances, unfortunately accidents will still occur and the passive safety necessary to protect the occupants will be necessary.

Crash Scenarios

The vehicle layout shall accommodate modifications to crash scenarios brought about by vehicle automation.

The accident statistics stored in all of the databases around the world are generated by vehicles driven by human drivers. The accidents involving automated vehicles will be fewer in number, but it is likely that there will be a shift in the distribution. For that reason, a re-evaluation of relevant scenarios for the development of passive safety systems will be necessary.

Alternative Seating Position

Occupant protection shall be ensured even when new uses for the interior are made possible by automation.

When the driver no longer needs to be involved in the dynamic driving task, new interior possibilities arise for the driver to fully take advantage of the situation. These new interior configurations will also need to be taken into account during the development and verification of passive safety systems.

CONCLUSION

Though there is still much work to be done in the development of large scale automated driving systems, BMW's 12 guidelines for automated driving systems establish a framework and a baseline. Building upon them, a collective discussion can occur both within the industry as well as with important stakeholders outside. This discussion is necessary as questions still remain, and in order to answer them, research continues to take place. Together this common understanding will help bring us forward to a safer future.

REFERENCES

[1] N.N. 2018. “Verkehr - Verkehrsunfälle - 2017”, Statistisches Bundesamt (Destatis).

[2] N.N. 2017. “Ethics commission – automated and connected driving”, Appointed by the Federal Minister of Transport and Digital Infrastructure, Final Report.

[3] N.N. 2018. “Taxonomy and Definitions for Terms Related to Driving Automation Systems for On-Road Motor Vehicles”, SAE International, Document J3016_201806.

[4] N.N. 2017. „Proposal for the Definitions of Automated Driving under WP.29 and the General Principles for developing a UN Regulation on automated vehicles”, Informal Working Group (IWG) on Intelligent Transport Systems / Automated Driving (ITS/AD), UNECE.

[5] Zeeb, K., Buchner, A., & Schrauf, M. 2016. „Is take-over time all that matters? The impact of visual-cognitive load on driver take-over quality after conditionally automated driving.” Accident analysis & prevention, 92, 230-239.

[6] Petermann, I., & Schlag, B. 2010. „Auswirkungen der Synthese von Assistenz und Automation auf das Fahrer-Fahrzeug System“, Proceedings of the AAET, 257-266.

[7] N.N. October 2018. “Preparing for the future of Transportation; Automated Vehicles 3.0”, U.S. Department of Transportation.

[8] N.N. July 2017. “Regulating Automated Driving the UK Insurer View”, ABI and Thatcham Research.

[9] N.N. 2017. “Collision Between a Car Operating With Automated Vehicle Control Systems and a Tractor-Semitrailer Truck Near Williston, Florida, May 7, 2016”, NTSB/HAR-17/02.

[10] N.N. 2018. “Technische Aspekte des automatisierten Fahrens und Verkehrssicherheit“, Gesamtverband der Deutschen Versicherungswirtschaft e. V.

[11] N.N. 2018. „Strassenverkehrsgesetz (StVG) §1a Kraftfahrzeuge mit hoch- oder vollautomatisierter Fahrfunktion“, Bundesgesetzblatt.

[12] N.N. 2018. “ISO 26262 Road vehicles – Functional safety”, International Organization for Standardization.

[13] Gold, C., Damböck, D., Lorenz, L., & Bengler, K. (2013). “Take over!” How long does it take to get the driver back into the loop? Proceedings of the Human Factors and Ergonomics Society Annual Meeting, 57(1), 1938–1942. https://doi.org/10.1177/1541931213571433

[14] Feldhütter, A., Segler, C., & Bengler, K. 2018. „Does Shifting Between Conditionally and Partially Automated Driving Lead to a Loss of Mode Awareness?”, In N. A. Stanton (Ed.): SpringerLink : Bücher, Advances in Human Aspects of Transportation: Proceedings of the AHFE 2017 International Conference on Human Factors in Transportation, July 17-21, 2017, The Westin Bonaventure Hotel, Los Angeles, California, USA (pp. 730–741). Cham: Springer.

[15] Gold, C. G. 2016. “Modeling of take-over performance in highly automated vehicle guidance”, (Doctoral dissertation, Technische Universität München).

[16] Kerschbaum, P., Lorenz, L., & Bengler, K. 2014. „Highly automated driving with a decoupled steering wheel”, In Proceedings of the human factors and ergonomics society annual meeting (Vol. 58, No. 1, pp. 1686-1690). Sage CA: Los Angeles, CA: Sage Publications.

[17] Lorenz, L., Kerschbaum, P., & Schumann, J. 2014. „Designing take over scenarios for automated driving: How does augmented reality support the driver to get back into the loop?” In Proceedings of the Human Factors and Ergonomics Society Annual Meeting (Vol. 58, No. 1, pp. 1681-1685). Sage CA: Los Angeles, CA: SAGE Publications.

[18] Bainbridge, L. 1983. “Ironies of automation. In Analysis, Design and Evaluation of Man–Machine Systems” (pp. 129-135). Pergamon.

[19] Van den Beukel, A. P., van der Voort, M. C., & Eger, A. O. 2016. „Supporting the changing driver’s task: Exploration of interface designs for supervision and intervention in automated driving”, Transportation research part F: traffic psychology and behaviour, 43, 279-301.

[20] Fahrenkrog, F. 2016. „Wirksamkeitsnalanyse von Fahrerassistenzsystemen in Bezug auf die Verkehrssicherheit”, Dissertation RWTH Aachen University, fka mbH Aachen.

[21] Form, T. 2018. “PEGASUS Method for Assessment of Highly Automated Driving Function”, SIP-adus Workshop 2018, 13-15 November 2018, Tokyo International Exchange Center, Tokyo, Japan.

[22] N.N. 2018. “L3Pilot Driving Automation, Piloting Automation on European Roads”, Self-driving vehicles: European automotive R&D leading the global race, Brussels, Belgium.

ESTIMATION OF POTENTIAL SAFETY BENEFITS FOR PEDESTRIAN CRASH AVOIDANCE/MITIGATION SYSTEMS IN LIGHT VEHICLES

Mikio Yanagisawa
Philip Azeredo
Wassim Najm
Volpe National Transportation Systems Center
USA

Stephen Stasko
National Highway Traffic Safety Administration
USA

Paper Number 19-0227

ABSTRACT

This report presents and exercises a methodology to estimate the effectiveness and potential safety benefits of production pedestrian crash avoidance/mitigation systems. The analysis focuses on light vehicles moving forward and striking a pedestrian with the front of the vehicle in the first event of a crash without attempting any avoidance maneuver in two priority scenarios: 1) vehicle going straight and pedestrian crossing the roadway and 2) vehicle going straight and pedestrian in or adjacent to the roadway, stationary or moving with or against traffic. System effectiveness is estimated for crash avoidance and crash severity mitigation. Safety benefits are projected in terms of annual reductions in the number of police-reported vehicle-pedestrian crashes, fatal vehicle-pedestrian crashes, and injured pedestrians at Maximum Abbreviated Injury Scale 2-6 and 3-6 levels. The methodology relies on target baseline crashes obtained from the 2011 and 2012 General Estimates System and Fatality Analysis Reporting System crash databases, system performance data from characterization track tests, and basic kinematic computer simulation of vehicle-pedestrian conflicts.

INTRODUCTION

From 2007 to 2016, there have been 350,408 fatalities on public roadways according to the National Highway Traffic Safety Administration (NHTSA) Traffic Safety Facts [1]. Over the last few years, the increase in population, licensed drivers, registered vehicles, and vehicle miles travelled has led to a rising trend in police-reported (PR) crashes and fatal crashes [2]. Figure 1 shows the number of pedestrian fatalities during this timeframe, as well as an upward trend in pedestrian fatalities as a percentage of total roadway fatalities. This trend may be caused by a variety of factors. This paper investigates the use of pedestrian crash avoidance/mitigation (PCAM) systems and their potential to ameliorate this trend.

PCAM systems are vehicle-based, forward-looking pedestrian detection systems that alert drivers of potential vehicle-pedestrian crashes and/or apply automatic emergency braking (AEB) to prevent potential vehicle-pedestrian crashes. This paper focuses on crashes that involve light-vehicles (i.e., passenger cars, vans and minivans, sport utility vehicles, and light pickup trucks with gross vehicle weight rating under 10,000 pounds) moving forward, striking a pedestrian in the first event of the crash, and not attempting any avoidance action.

This paper describes and exercises a methodology to estimate potential safety benefits associated with PCAM systems in terms of crash avoidance and crash mitigation measures.

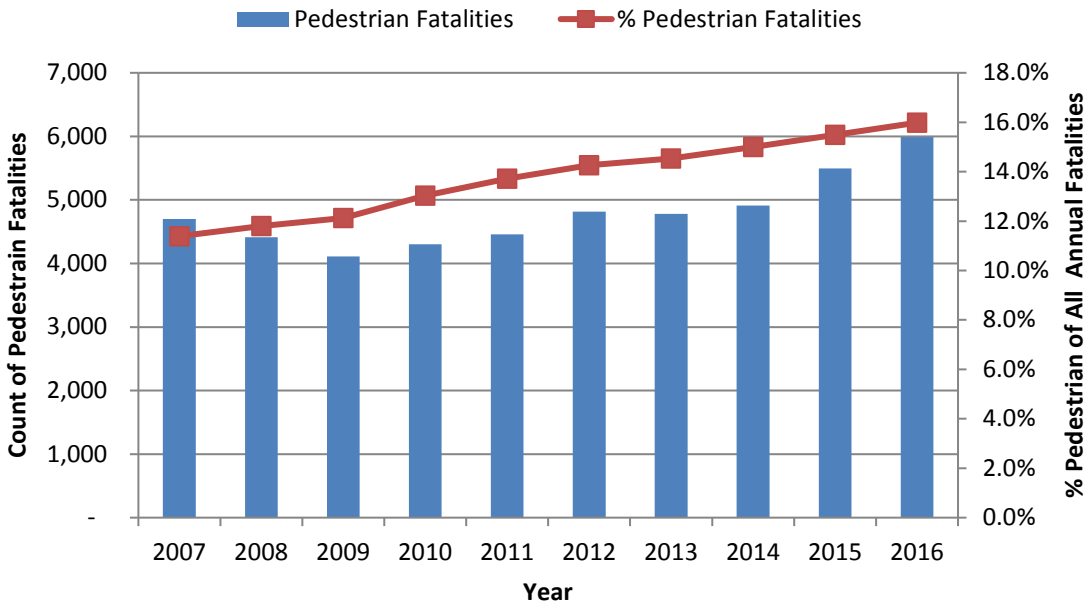

Figure 1. Annual Traffic-Way Pedestrian Fatalities in the United States.

Pedestrian Pre-Crash Scenarios

Historical research identified and prioritized vehicle-pedestrian pre-crash scenarios that PCAM systems could potentially address, and facilitated the development of test scenarios [3]. Four vehicle-pedestrian pre-crash scenarios were recommended as target scenarios based on the analysis of NHTSA's National Automotive Sampling System (NASS) General Estimates System (GES) and Fatality Analysis Reporting System (FARS) crash databases from 2005 through 2009 [4][5]. These four priority pre-crash scenarios are depicted and described in Figure 2. An updated analysis using 2011 and 2012 GES and FARS data provided similar results, giving evidence that the top priority vehicle-pedestrian pre-crash scenarios remained prominent from 2005 to 2012 [6].

From 2011 to 2012, there was an annual average of 62,917 vehicle-pedestrian PR crashes in the GES data that involved a light-vehicle striking a pedestrian in the first event. Based on similar criteria, FARS data provided an annual average of 3,337 fatal vehicle-pedestrian crashes. However, PCAM systems may only target a subset of these crashes. PCAM-addressable crashes involve the light vehicle moving forward and striking a pedestrian with the front of the vehicle and the driver attempting no avoidance maneuver. These criteria are selected because PCAM systems are considered forward facing vehicle-based sensing systems and driver action may significantly alter vehicle dynamics and system performance after the critical event (e.g., loss of control, unintended secondary events, and system suppression). As a result, the average annual number of all PR PCAM-addressable crashes amounts to about 21,000 crashes based on GES statistics, and about 2,200 annual fatal PCAM-addressable crashes from FARS data. The four priority pre-crash scenarios represent the most common vehicle-pedestrian crashes from 2011 to 2012, in terms of PR and fatal crash frequency as shown in Table 1. These four scenarios account for 90 percent of all GES and 97 percent of all FARS PCAM-addressable vehicle-pedestrian crashes. Thus, this paper focuses on the top four pre-crash scenarios as described by the previously published PCAM research (i.e., S1, S2, S3, and S4 in Figure 2).

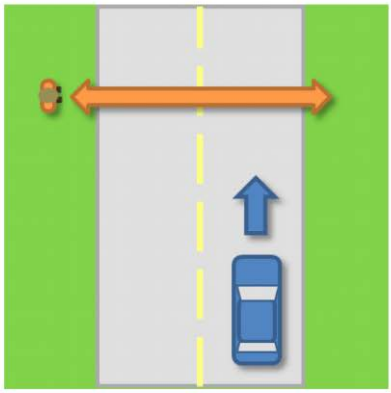

Scenario 1 (S1)
S1 - Vehicle going straight and pedestrian crossing the road

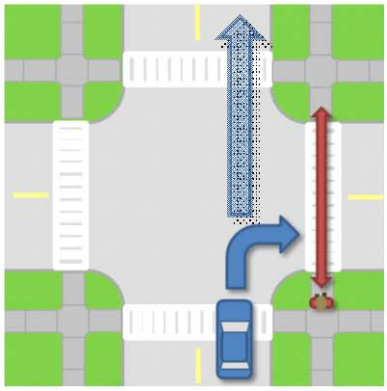

Scenario 2 (S2)
S2 - Vehicle turning right and pedestrian crossing the road

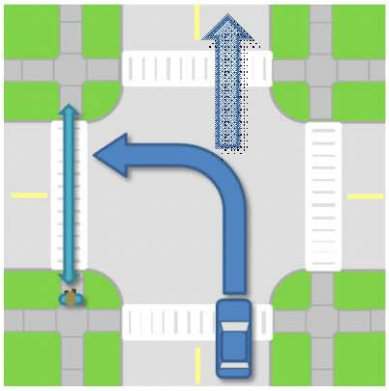

Scenario 3 (S3)
S3 - Vehicle turning left and pedestrian crossing the road

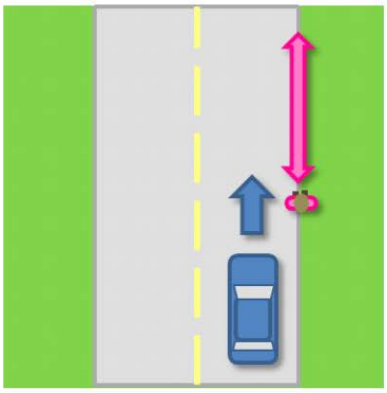

Scenario 4 (S4)
S4 - Vehicle going straight and pedestrian walking alongside the road with/or against traffic

Figure 2. Four Priority PCAM Pre-Crash Scenarios Defined from NHTSA Crash Databases.

Table 1.
Breakdown of PCAM-Addressable Crashes into Priority Pre-Crash Scenarios from 2011-2012.

Scenario	Vehicle Maneuver	Pedestrian Maneuver	GES Frequency		FARS Frequency	
S1	Going Straight	Crossing Roadway	7,481	35.5%	1,396	64%
S2	Turning Right	Crossing Roadway	2,264	10.7%	24	1%
S3	Turning Left	Crossing Roadway	6,200	29.4%	87	4%
S4	Going Straight	Walking along Roadway, with/against Traffic	2,950	14.0%	620	28%
Other Scenarios (~60 Additional)			2,195	10.4%	66	3%
Annual Average Total PCAM-Addressable			**21,090**		**2,193**	

*PCAM-addressable crashes are crashes involve a light-vehicle striking a pedestrian with the front of the vehicle in the 1st event of a crash, with no avoidance maneuver

Previous Research

Previous research studies have employed various methods on available data sources to estimate the efficacy of various advanced pedestrian safety systems, both active and passive. Two studies used the German In-Depth-Accident-Study (GIDAS) to estimate passive, active, and combination safety systems. The first study used GIDAS data to estimate the effectiveness of a 40-degree field of view (FOV) pedestrian AEB system [7]. A total of 243 pedestrian cases within a good FOV and no obstruction from the 1999-2003 GIDAS were identified. This study estimated new impact speeds based on variations in specific parameters to estimate the reduction in fatal and severely injured pedestrians. The duration of the braking event was a critical parameter variation. The average braking duration for drivers was 0.67 second, whereas the AEB system (≤ 0.6 g) had an average braking duration of 1.4 seconds. The results showed that the effectiveness at reducing fatally injured pedestrians in frontal collisions reached 40 percent, with a marginal increase in effectiveness with increased FOV. Nearly 80 percent of the fatality reduction came from cases where the driver had not braked. The second study estimated benefits of using passive (deployable airbag) and active (AEB) countermeasures to mitigate head injuries in pedestrian impacts [8]. This research used 68 GIDAS cases filtered for frontal impacts with pedestrians with severely injured heads. A series of equations and simulations estimated an average impact speed of 48.7 km/h (30.3 mph) in these target cases. Effectiveness estimates were presented for the active, passive, and integrated (active and passive) countermeasure systems. Results showed that the integrated system had an increased potential to reduce pedestrian head injuries as compared to either the active or passive system used alone. Effectiveness values ranged from 11 percent to 64 percent depending on the countermeasure parameters or the type of system modeled: active, passive, or integrated.

A major supplier for video sensing hardware and software used crash data from the Institute for Traffic Accident Research and Data Analysis (Japan) (ITARDA) to estimate the effectiveness of their product in vehicle-pedestrian crashes by identifying specific vehicles and their respective installation rate (none, version 1, or version 2) [9]. This empirical method did not provide explicit results, although basic calculations can provide crash avoidance effectiveness estimates derived from this work ranging from 75 to 88 percent. Furthermore, this study identified common reasons for deactivation based on US survey results, including: low sun angle (80%), followed by heavy precipitation (44%) and fog (17%).

A major car manufacturer used naturalistic driving data to describe pedestrian behavior, conduct track tests, and estimate crash avoidance rates [10]. The naturalistic driving data encompassed 110 vehicles that traveled 1.44 million miles in Indianapolis for one year. There were a total of 1,762 videos of potential conflicts with pedestrians. A distribution of time-to-collision (TTC) versus the number of cases was calculated and cumulative results showed a mean value of 4.43 seconds TTC when a vehicle-pedestrian conflict began. The lateral distances from the left and right side of the vehicle to the pedestrian (at the appearance point) were also calculated, showing means of 6.55 and 5.21 meters, respectively. Track tests of a vehicle equipped with a stereo camera and millimeter-wave radar showed variations in avoidance rate, based on scenario (e.g., pedestrian direction, vehicle motion, light condition, pedestrian size, and pedestrian motion). Preliminary results provided a wide range of effectiveness, including an avoidance rate of 84 percent when the vehicle was turning and an avoidance rate of 35 percent when the mannequin was darting (running).

The review of methods and results proved that a variety of potential data sources and methods may be used to estimate the effectiveness of PCAM systems. Further, as no two analyses are identical (e.g., variations in data sources, modeling, simulation, system algorithms), common elements were identified, including:

- *Crash data*: Understanding of the crash data provides valuable information, including pre-crash scenarios, initial conditions, and baseline measures.
- *Harm curves*: Derived from historical crash data to correlate impact speed to pedestrian injury. These curves help quantify benefits (e.g., crashes, fatalities, and injuries).
- *Operational capabilities*: Understanding the capability of the PCAM system can account for issues that arise when attempting to estimate system effectiveness, such as obstructions, bad weather, speed thresholds, and overall technological capability.
- *Driver and system performance data*: Incorporate driver performance (e.g., reaction time and braking level) and system performance (e.g., activation times, braking levels, driver-system interaction). Warnings systems have different driver-system interactions compared to AEB, thus varying input data and modelling.

- *Simulation or modelling (crash reconstruction or conflicts)*: A method to compare baseline results to treatment results, such as superimposing a PCAM system over historical crashes (reconstructed, probability of baseline crash = 1) or similar crashes in a simulation (probability of a baseline crash ≠ 1). These can use hypothetical systems and conflicts when real-world crash data comparisons are not available.
- *Crash avoidance and/or speed reduction*: Results from baseline to treatment comparison to quantify system effectiveness and safety benefits for crash avoidance and pedestrian injury mitigation.

These elements are identified as core elements for the methodology, each requiring specific data sources and analysis.

APPROACH

The general methodology for estimating PCAM safety benefits is derived from a method previously used for vehicle-to-vehicle (V2V) based crash warning systems in support of NHTSA research efforts assessing the safety impact of V2V technology [11].

Basic Equations

A series of basic equations define the methodology, dictating a minimum set of data parameters. These data parameters determine what data sources can be incorporated into the methodology and further identify the need for basic assumptions.

Crash Avoidance The general equation of safety benefits and system effectiveness for crash avoidance is presented in Equation **(1)** [12].

$$B_A = N_C \times E_A \quad (1)$$

The equation provides a potential safety benefit for PCAM systems, in terms of the annual reduction of vehicle-pedestrian crashes avoided, $\mathbf{B_A}$, based on the crash avoidance effectiveness, $\mathbf{E_A}$, and annual number of target crashes addressed by a PCAM system, $\mathbf{N_C}$. The crash avoidance effectiveness is broken down further, into two distinct ratios, as seen in Equation **(**2**)**.

$$E_A = 1 - \frac{EM_{PCAM}}{EM_{Base}} \times \frac{CP_{PCAM}}{CP_{Base}} \quad (2)$$

The exposure measure, **EM**, refers to the probability that a vehicle enters into a vehicle-pedestrian conflict. The ratio, comparing with and without ($\mathbf{EM_{PCAM}}$ and $\mathbf{EM_{Base}}$, respectively) will provide a positive safety benefit if vehicles are less likely to enter a vehicle-pedestrian conflict with a PCAM system compared to without any assistance. This measures the ability of a system to reduce the occurrence of conflicts in normal driving, typically derived from long-term naturalistic driving [13]. The crash probability, **CP**, refers to the probability that a collision occurs given that a vehicle-pedestrian conflict has been encountered. The ratio, comparing with and without ($\mathbf{CP_{PCAM}}$ and $\mathbf{CP_{Base}}$, respectively) will provide a positive safety benefit if vehicles are less likely to strike a pedestrian with a PCAM system compared to without. This measures the ability of a PCAM system to reduce the likelihood of a crash, given that the vehicle has entered into a conflict [13]. Given the current state of data, minimal naturalistic driving and vehicle-pedestrian conflict (e.g., non-crash) data is available, making **EM** difficult to quantify. For this reason, it is assumed that vehicles would have the same exposure to vehicle-pedestrian conflicts whether or not a PCAM system is installed, neutralizing the **EM** ratio to 1. Furthermore, based on the state of the crash data, it is appropriate to use a crash reconstruction method, superimposing PCAM system performance on historical crashes. Using this method, the historical baseline crash rate is 1, as all conflicts resulted in a crash ($\mathbf{CP_{Base}}$ = 1). These assumptions simplify Equation **(**2**)** to Equation **(**3**)**.

$$E_A = 1 - CP_{PCAM} \quad (3)$$

Based on the core elements defined earlier and the parameters identified within the equations, data needs have been relegated to crash data to determine target crash populations, $\mathbf{N_C}$, and a baseline set of crashes to reconstruct, along

with human behavior and system performance data to determine the likelihood of a crash given system intervention, $\mathbf{CP_{PCAM}}$.

Crash Mitigation In addition to crash avoidance, a PCAM system may potentially reduce any resulting harm to the pedestrian by reducing the vehicle's travel speed prior to impact through improved driver response or automatic vehicle control. Similar to Equation **(**1**)**, the equation to estimate the reduction in pedestrian injury is provided in Equation **(**4**)**.

$$\boldsymbol{B_M = N_I \times E_M = N_I \times \{E_A + E_W \times (1 - E_A)\}} \quad \textbf{(4)}$$

The equation provides a potential safety benefit for PCAM systems in terms of the annual pedestrian injuries mitigated, $\mathbf{B_M}$, based on the crash mitigation effectiveness, $\mathbf{E_M}$, and annual number of pedestrians injured, $\mathbf{N_I}$. Since any crash avoided would inherently avoid all subsequent pedestrian injuries, crash mitigation effectiveness, $\mathbf{E_M}$, has to account for crash avoidance effectiveness, $\mathbf{E_A}$, and assess the effectiveness of injury reduction, $\mathbf{E_W}$, based on the resulting crash's impact speed. The method to estimate injury reduction effectiveness is shown in Equation **(**5**)**.

$$\boldsymbol{E_W = 1 - \frac{H(PCAM)}{H(Base)}} \quad \textbf{(5)}$$

The equation uses crash data to correlate impact speed and resulting pedestrian injury in a ratio comparing the pedestrian harm induced given a crash, with and without a PCAM system (**H(PCAM)** and **H(Base)**, respectively). Given the above set of equations, crash data can be used to obtain additional information on the annual number of pedestrians injured, $\mathbf{N_I}$, and to correlate impact speeds to pedestrian injury. Results from the crash reconstruction simulation can be used to determine impact speed with PCAM intervention.

Based on the above data parameters needed within the basic equations and the above core elements, the developed method is broken down into four key steps:

1. Identify and describe PCAM systems. This step identifies current and near-term production PCAM systems and describes their operational boundaries and capabilities. This includes operational design domain, countermeasure profiles, and driver-system interaction algorithms.
2. Identify data needs and data sources. This step uses the core elements to identify the priority data parameters and respective data sources, then performs a query and analyzes the data. This step assesses baseline conditions and treatment data (i.e., driver behavior with warning, system performance). Further, this step is setup to propose and execute a method to collect supplemental data, if feasible and necessary.
3. Run simulation and estimate effectiveness. Based on a preliminary assessment of the available data, it is appropriate that a crash reconstruction simulation, superimposing PCAM systems on historical crash cases, be used to estimate the effectiveness of PCAM systems.

PCAM SYSTEMS

A technology scan of public literature (e.g., media publications, owner's manuals, publicized testing) was used to understand the functionality and operational conditions of current and near-term production PCAM systems. The dynamics of a vehicle-pedestrian crash offer several intervention or countermeasure opportunities for PCAM systems. Table 2 shows the results of the technology scan of active PCAM systems. Since public literature was used, specific details on system capabilities and limitations were not available (e.g., warning suppression techniques, minimum and maximum thresholds for activation). The PCAM systems identified utilize various forms of technology. However the analysis conducted within this paper is independent of technological implementation.

Table 2.
Number of Active PCAM Systems (Current and Near-Term) Identified and Reviewed from Technology Scan.

PCAM System Type (Countermeasure Profile)	Warning Issued To		
	Driver	Pedestrian	No Warning
Warn Only	4	1	
Warn and Brake Assist	2		
Warn and Automatic Brake	3		
Brake Assist Only			1
Warn, Automatic Brake and/or Steer	2		

As noted earlier, the variations in countermeasures may require different data sets. For example, a warning to the driver would require system performance and driver response data, whereas an AEB-only system requires only system performance data. After assessing the various PCAM systems and associated driver-vehicle interactions, this analysis considers the potential safety benefits for the following three[1] PCAM systems:

- AEB only systems,
- Warning + first braking response between AEB or driver, and
- Warning + best braking response between AEB and driver.

Incremental benefits are determined by adding driver response to a warning issued prior to AEB activation. For example, a system would alert the driver, via warning, that a vehicle-pedestrian crash is imminent. This warning would elicit a driver response, but if a driver does not respond appropriately, AEB may initiate. This driver-vehicle interaction requires specific input data for the multiple components of the system. To encompass potential driver-vehicle interaction and system suppression methods, two logic systems are implemented when both driver and AEB are simultaneously activate:

- *First Braking*: Assumes that once braking has been initiated (by driver or AEB), it remains constant for the remainder of the event, regardless of magnitude. This assumes that any initial response suppresses secondary responses (i.e., driver is in control means no AEB is necessary, or AEB activation assumes the driver will never respond).
- *Best Braking*: Assumes that if both braking inputs are active (driver and AEB), the system uses the higher input to maximize braking effectiveness. If only one braking input is active (AEB or driver), then the system uses the active input. This system attempts to maximize effectiveness with the earliest and then the best braking response.

The driver-system interaction variations will provide a system effectiveness range, with the '*AEB Only*' system providing a lower-limit range, while the addition of a warning to the driver may provide incremental benefits (as a driver may react earlier and/or brake harder than AEB).

DATA SOURCES

The next step of the methodology is to identify potential data sources for the necessary data parameters, then query and analyze these data sources. Within this step, if a data parameter could not be quantified from available data sources, additional data collection methods can be proposed and executed.

[1] Minimal information and data was found on the pedestrian warning and automatic steering countermeasure, therefore these countermeasures were excluded from this analysis.

National Crash Data

Historical crash data at the national level are available from NHTSA's GES and FARS crash databases. The GES provides a national representation of police-reported crashes in public traffic-ways, accumulating a sample of police-reports and incorporating associated variables into the data. The FARS provides a complete census of crashes on public roadways that resulted in a fatality within 30 days. These crash databases contain variables, codes, and relevant statistics that help to quantify and characterize the baseline pedestrian crash problem addressed by PCAM safety systems. The crash databases also contain details to specifically characterize each crash, including pre-crash scenario, travel speeds, environmental conditions, driver factors, and attempted avoidance maneuvers. Details surrounding the crash allow for an accurate depiction of the driving conflict, supporting a crash reconstruction simulation. PCAM-addressable crashes only include crashes where a forward moving light-vehicle struck a pedestrian with the front of the vehicle in the first event of the crash and the driver attempted no avoidance maneuver.

The PCAM-addressable criteria aim to encompass the operational capabilities of PCAM systems and their aimed effectiveness. Due to limited information on system performance with driver input (e.g., driver pressing the brake pedal may suppress AEB activation), attempted avoidance maneuvers were not considered. Impaired drivers may not react to a warning but an AEB component (if applicable) may be designed to still activate; therefore, impaired drivers were considered for this analysis. The following definitions were used to obtain the target baseline crashes:

- Light-Vehicle: The use of the vehicle body type variable in the crash databases identifies passenger cars, vans and minivans, sport utility vehicles, and light pickup trucks with gross vehicle weight rating less than 10,000 pounds.
- Pedestrian: Any person on foot, walking, running, jogging, hiking, standing still, sitting, or lying down, excluding any person on a personal conveyance such as personal mobility device or rideable toy.
- First Event: Crash data provide a series of critical events for the crash, regardless of injury or damage sustained (or lack thereof). The first listed critical event of the crash is considered.
- Vehicle Moving Forward: Crash data provide pre-event movement of the vehicle, prior to the driver's realization of an impending critical event. Movements listed as no driver, stopped, backing, parking related, or unknown are excluded.
- Area of Impact: Crash data provide the area of impact of the vehicle. Only crashes that identified the front of the vehicle to be struck (i.e.., 11, 12, and 1 o'clock values) are considered.
- Avoidance Maneuver: Crash data provide the attempted avoidance maneuver of the vehicle in recognition of the critical pre-crash event. Only crashes with 'no avoidance maneuver' attempted by the vehicle are incorporated.

In addition to the statistics provided earlier in Table 1, these PCAM-addressable crashes resulted in approximately 13,000 injured persons at the Maximum Abbreviated Injury Scale (MAIS) 2^+ levels and 7,000 injured pedestrians at MAIS 3^+ levels. A conversion matrix was used to convert injury scales, from the GES KABCO injury into a MAIS injury [14]. Further, FARS is used to get the actual count of persons killed in target crashes and included in the KABCO-MAIS conversion. Table 3 shows the breakdown of these injuries into the priority pre-crash scenarios.

Table 3.
Breakdown of PCAM-Addressable Pedestrian Injuries into Priority Pre-Crash Scenarios from 2011-2012.

Scenario	Vehicle Maneuver	Pedestrian Maneuver	MAIS 2+	% of MAIS 2+	MAIS 3+	% of MAIS 3+
S1	Going Straight	Crossing Roadway	2,682	49.9%	1,879	56.9%
S2	Turning Right	Crossing Roadway	274	5.1%	92	2.8%
S3	Turning Left	Crossing Roadway	883	16.4%	333	10.1%
S4	Going Straight	Walking Along/Against Traffic	1,207	22.4%	860	26.0%
Other Scenarios (~60 Additional)			330	6.1%	141	4.3%
Total Injuries from PCAM-Addressable Crashes			**5,376**		**3,305**	

Injury Curves Injury probability curves aim to predict the probability of a pedestrian injury occurring given an impact speed. These curves are used to measure crash severity by correlating injury levels to impact speeds from historical crashes. Injury probability curves are derived from 2011 and 2012 GES and FARS data. Similar criteria as the above crash data are used, and the vehicle travel speed and resulting pedestrian injury are obtained to determine the injury probability for five-mph incremental speed bins. [2] It is important to note that travel speed information is mostly unavailable in the GES and FARS data where approximately 80 percent of crashes had unknown travel speed information. Results from this query are fed into a regression model to determine functions for the various harm curves. These smoothed curves from developed functions help mitigate anomalies found with smaller data sets and aid in eliminating unusual spikes in data. Figure 3 illustrates the results from the regression model.

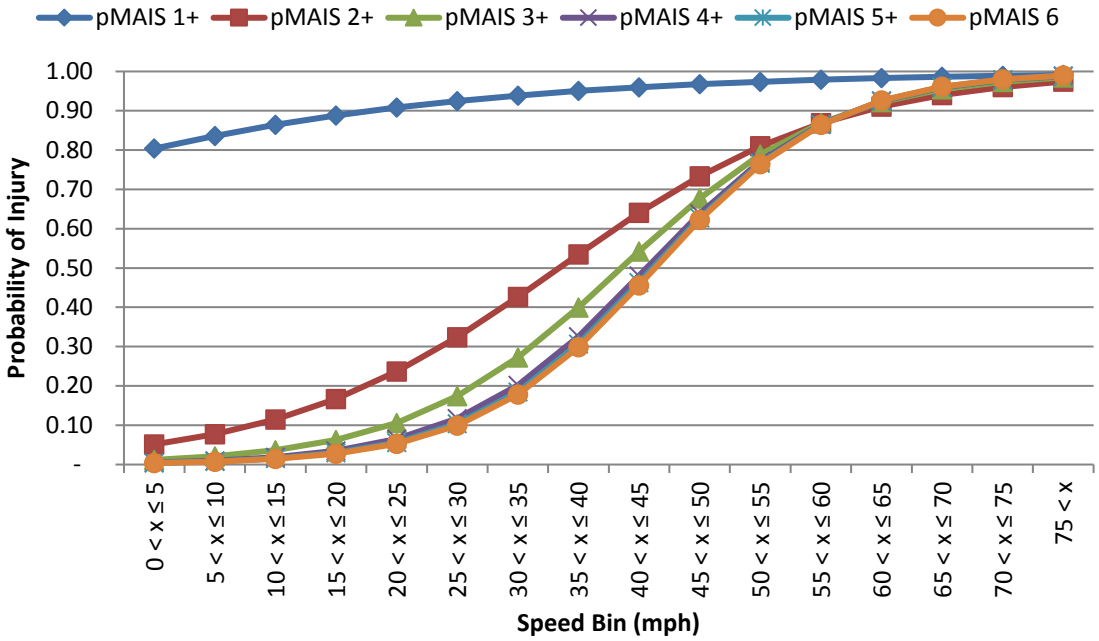

Figure 3. Plots of Pedestrian Injury Cumulative Probability Functions from Regression Model.

The probability for a certain injury level is simply the difference of two MAIS+ probabilities. For example, $p_{MAIS1} = p_{MAIS1+} - p_{MAIS2+}$ and $p_{MAIS2} = p_{MAIS2+} - p_{MAIS3+}$. The injury mitigation analysis in this report focuses on the MAIS 2+ and MAIS 3+ injury levels.

Special Crash Investigation

National crash databases contain an abundance of cases but lack detailed information on the dynamics of the crash. These databases rely on available police reports and witness statements to detail the pre-crash information (e.g., motions, speed, and critical events). Approximately three quarters of GES cases that could be addressed by PCAM systems do not have travel speed information (coded as 'unknown'). Further, detailed information on the pedestrian motion is not readily available (e.g., left-to-right or right-to-left of the vehicle, when crossing the road). From the available information, accurate depictions of the crash become difficult, relying on multiple assumptions. A crucial missing element is the amount of time the pedestrian spent in view of the driver/vehicle, within the roadway, and in the vehicle's intended path. One might assume, for maximum effectiveness, PCAM systems may attempt to maximize accuracy and responsiveness, while minimizing the number of nuisance and false activations. As part of

[2] Travel speed may not be equivalent to impact speed; and crash databases do not contain impact speed and have limited availability of travel speed. Travel speed is the vehicle's speed prior to conflict and could be used if no attempt to avoid a crash was made.

the data identification task, a special crash investigation (SCI) team at NHTSA was tasked to investigate the detailed dynamics of an S1 scenario.[3]

The resulting database contains over 50 recorded variables for 43 relevant vehicle-pedestrian crashes where investigators were able to examine the crash in detail and estimate a comprehensive list of details that depict the exact kinematics of the crash. A list of variables obtained can be found in the Appendix. It is important to note that these 43 cases could not be incorporated into this methodology for numerous reasons (e.g., small sample size with wide range of results, bias towards severe injuries, not nationally representative). However, the data obtained provided detailed cases where PCAM systems could provide a benefit. The focus of the investigation was to determine TTC for the vehicle when the pedestrian was revealed to the driver (or would be PCAM system). Figure 4 details the TTC measure in a vehicle-pedestrian conflict.

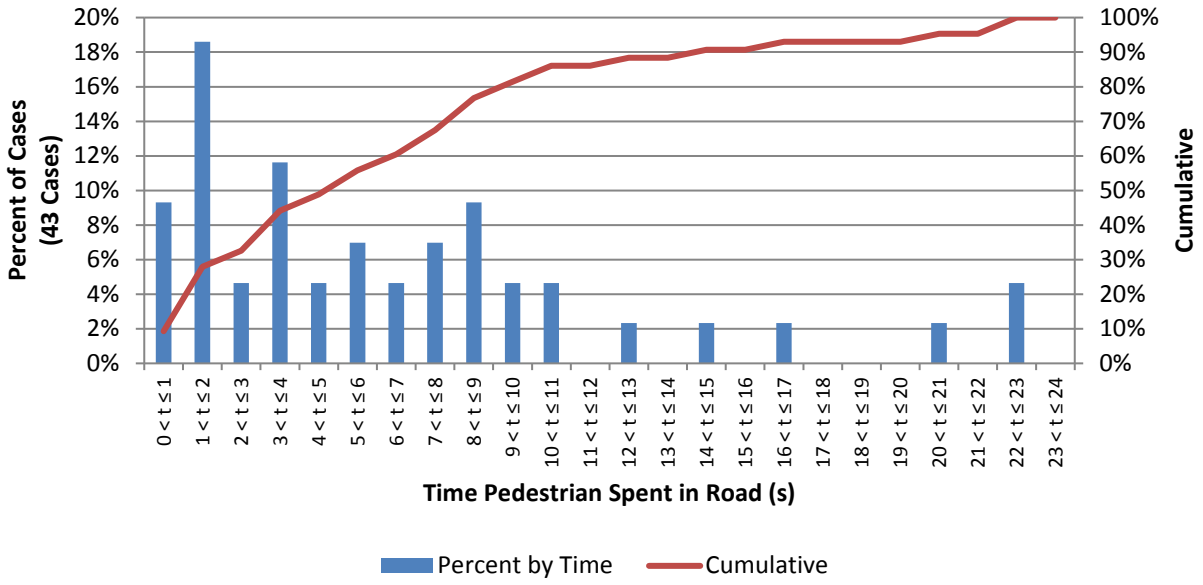

Figure 4. Distribution of Pedestrian Reveal TTC in S1 from SCI Database.

The information provides a wide TTC range, estimating a pedestrian being visible from under 1 second to as much as over 20 seconds. The majority of crashes had TTC values under 6 seconds, accounting for 55.8 percent of the crashes. Although the cases could not be used directly in the benefits model, the wide range signifies a potential for PCAM benefit. In cases with low TTC (less than 1 second), PCAM systems may have a difficult time detecting and identifying pedestrians, warning the driver, and/or applying AEB; this accounts for less than 10 percent of the cases. On the other end, in cases with a high TTC (greater than 6 seconds), PCAM systems may have ample time to detect, identify, and/or apply AEB, as this may be well beyond the longitudinal range of the technology used in PCAM systems. Furthermore, these cases identified drivers that were unable to detect, identify, and/or react to the conflict appropriately (e.g., distracted drivers, impaired drivers/pedestrians, or poor lighting conditions, dark pedestrian clothing). These drivers may potentially benefit from a warning, drawing attention to the pedestrian and aiding the driver in reacting appropriately.

Test Data

A crucial data source for estimating system effectiveness is system performance data. System performance data were obtained from characterization test runs conducted at the Transportation Research Center Inc. (TRC) in East Liberty, Ohio by NHTSA's Vehicle Research and Test Center (VRTC) [15]. Three production vehicles equipped

[3] S1 was selected due to its potential variations on circumstances, high frequency, and injury rates. It is assumed in S4 that the pedestrian is already walking or standing in the vehicle's path, and therefore is limited by technological capabilities (e.g., a driver or PCAM system would be able to monitor an S4 situation as long as the pedestrian is within range).

with PCAM systems were tested in S1 and S4 priority pre-crash scenarios, varying multiple parameters (e.g., pedestrian size, pedestrian speed, pedestrian direction/orientation, lighting, obstructions, vehicle speed, and overlap).[4] Vehicle speeds ranged from 15 to 45 mph. Detailed time-history data were collected for each test run and analyzed for 20 variables, including speeds, distances, warning activation time, AEB activation time, and resulting impact. After assessing the testing conditions and correlating respective testing conditions to crash data, the six distinct test scenarios shown in Table 4 were used for the benefits method. For other scenarios, since empirical test data could not be applied to crash data, system effectiveness was conservatively set to 0. This implies that PCAM systems would not have an immediate benefit. Further research, testing, and analysis would be required to revise this assumption.

Table 4.
Priority PCAM Testing Setups that Correlate to Crash Data and Associated Number of Test Runs and No Impact Results (All Vehicle Speeds* and Vehicles).

Name	Scenario	Pedestrian Size	Pedestrian Speed	Pedestrian Direction	Lighting	Obstruction	Number of Tests	'No Impact' Results
S1-A	S1	Adult	3.1 mph	Right-Left	Day	No	497	397
S1-B	S1	Adult	4.9 mph	Right-Left	Day	No	265	90
S1-C	S1	Child	3.1 mph	Right-Left	Day	No	194	167
S1-D	S1	Child	3.1 mph	Right-Left	Day	Yes	108	42
S4-A	S4	Adult	Stationary	Stationary	Day	No	403	325
S4-B	S4	Adult	3.1 mph	Away	Day	No	202	183

*Speeds ranged from 15 to 45 mph

Analysis of the resulting data provides characteristics of the various PCAM systems. Various parameters were analyzed, including correlating AEB activation time to vehicle speed and average AEB level to vehicle speed, as seen in Figure 5 and Figure 6, respectively. Each production vehicle was analyzed anonymously, labeled as original equipment manufacturer (OEM) 1 to 3. Additional parameters were analyzed for each of the six test scenarios and production vehicles to help in characterizing the system.

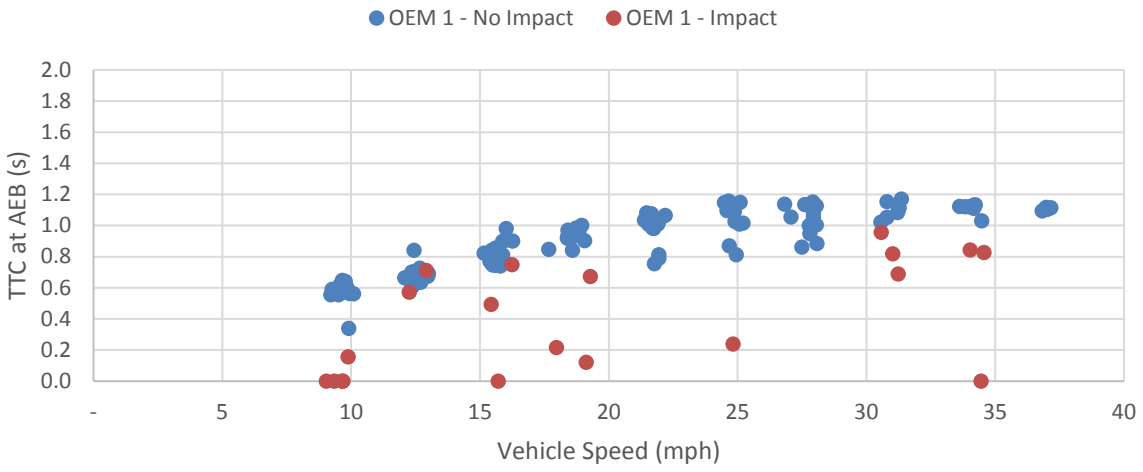

Figure 5. Test Run Results for Production Vehicle 1, Comparing AEB Activation Time to Vehicle Speed in S1-A.

[4] Overlap refers to point on the front bumper where the pedestrian is projected to impact, given no PCAM intervention.

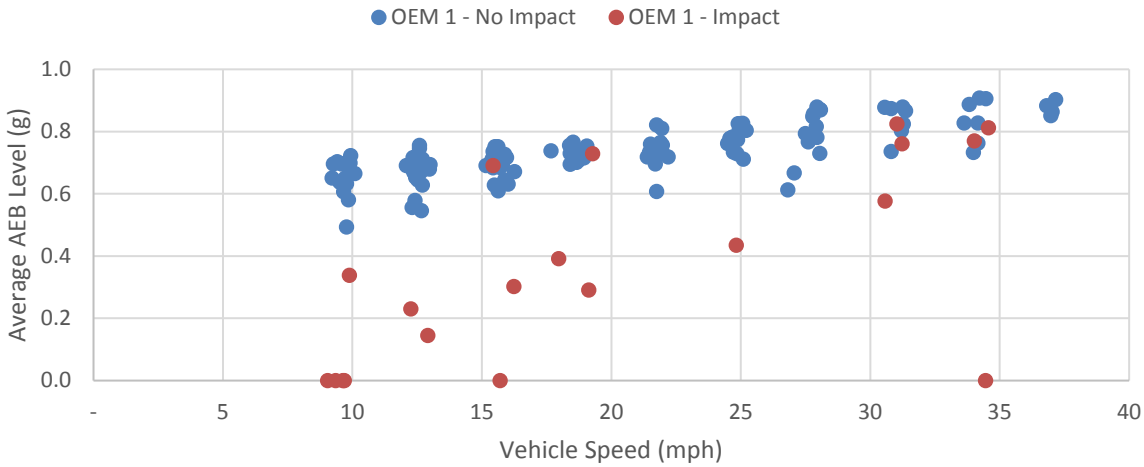

Figure 6. Test Run Results for Production Vehicle 1, Comparing Average AEB Level to Vehicle Speed in S1-A.

Test results show that there is a relationship between AEB activation time and level to vehicle travel speed. This intuitively makes sense, as more time and braking power are needed for the vehicle to come to a complete stop within the finite detection range of the system. Further, it can be seen that although AEB timing and braking varied, there is an overlap in AEB performance and vehicle travel speed and the end result (impact or no impact). In the S1 test setup, the various combinations of conditions allow for the vehicle to stop after the pedestrian's travel path and still avoid the impact (i.e., vehicle slowed enough to allow pedestrian to finish crossing). Even if an impact occurred (potentially due to insufficient AEB) vehicle speed reductions were observed, resulting in lower impact speeds with the pedestrian. Finally, as shown in the figures, in some instances the PCAM system did fail to activate, resulting in an impact at full speed. The test data provided empirical data that were used to estimate system effectiveness.

Human Behavior

Information on driver behavior was obtained from previous research studies, determining driver responses in conflicts with the presence of a warning. Driver performance is incorporated into the treatment data to determine incremental benefits when a warning is issued, along with AEB. As seen in Table 5, based on earlier studies, driver reaction time was estimated as a lognormal distribution with a mean of 1.1 seconds and standard deviation of 0.3 [16]. Also in Table 5, driver braking level was estimated as a normal distribution curve with a mean of 0.5 g and a standard deviation of 0.1 [17]. Only treatment data are necessary, as the benefits method uses a crash reconstruction method. This assumes that all baseline conflicts resulted in a crash regardless of driver response. These parameters are incorporated into the Monte Carlo simulation independently.

Table 5.
Driver Performance Measures in Response to a Warning

Inputs:	Min	Max	Mean*	Std. Dev.*	Distribution Type
Host Driver Reaction Time In Control (s)	0	5	1.1	0.3	Log Normal
Host Driver Deceleration In Control (g)	0.25	0.75	0.5	0.1	Normal

*Mean and standard deviation are based on sample data not population

RESULTS

Results from the benefits model provided information on a PCAM's potential ability to avoid pedestrian crashes and mitigate pedestrian injury through impact speed reduction in unavoidable crashes. The results were derived from crash probability in Equation **(**3**)** and the resulting impact speed to determine pedestrian injury in Equation **(**5**)**. The parameters in these equations were obtained from a crash reconstruction simulation, superimposing empirical PCAM system performance data onto historical vehicle-pedestrian crash cases.

Simulation
A Monte Carlo simulation model exercises general kinematic equations in conjunction with driver and system performance data to determine the probability of a crash and the resulting impact speeds given a crash. Kinematic equations were derived from previous research for the four priority pre-crash scenarios [6]. This simulation reconstructed historical 2011 and 2012 PCAM-addressable GES and FARS crashes and superimposed PCAM system test data and driver performance distribution data to determine the outcome with PCAM intervention.

Initial conditions for the simulation are described by vehicle location, size and speed, pedestrian location, size, and speed, and environmental conditions (e.g., lighting and obstructions). Driver and system performance data are described by driver reaction time, driver braking level, system activation time, and system braking level. The simulation was run for 100,000 iterations.[5] Each iteration cycles through historical crashes and superimposes PCAM system performance data directly from the test data. PCAM system performance data were tied to historical crashes by correlating the initial conditions (e.g., vehicle speed, pedestrian speed). For example, a crash reporting vehicle travel speeds of 25 mph with a pedestrian walking across the road in the daylight with no obstruction was superimposed with S1-A test data (vehicle speeds of 25 mph), as this scenario is representative of this crash case.

System Effectiveness
System effectiveness is estimated as a range of values, in terms of crash avoidance and injury mitigation, for the three systems types defined earlier, three production vehicles, and six testing scenarios. A refined target crash population is presented in Table 6 representing the historical crashes that may be addressed by PCAM systems in the six distinct testing scenarios, as effectiveness cannot be accurately assessed for other conditions. Costs are calculated from NHTSA economic analyses and are based on 2010 economic costs [14].

Table 6.
Annual Average Number (2011 to 2012) of Target Crashes, Injuries, and Costs (2010$).

Scenario Name	GES Crashes	FARS Crashes	Costs (2010 $M)	MAIS 2+		MAIS 3+	
				Pedestrians Injured	Costs (2010 $M)	Pedestrians Injured	Costs (2010 $M)
S1-A	4,582	838	$ 8,393	1,576	$ 8,269	1,111	$ 8,083
S1-B	-	1	$ 5	1	$ 5	1	$ 5
S1-C	796	35	$ 433	150	$ 408	72	$ 377
S1-D	279	9	$ 124	52	$ 115	24	$ 104
% PCAM-Addressable S1	**76%**	**63%**	**64%**	**66%**	**63%**	**64%**	**63%**
S4-A	300	100	$ 967	160	$ 959	125	$ 945
S4-B	471	72	$ 763	187	$ 750	120	$ 723
% PCAM-Addressable S4	**26%**	**28%**	**28%**	**29%**	**28%**	**28%**	**28%**

From these target crashes, a subset of crashes are identified with enough data to allow for a suitable crash reconstruction. The main factors in eliminating crashes included missing information about vehicle travel speed and pedestrian motion and speed. These specific crashes were then used to determine a baseline harm curve, as described earlier (National Crash Data), for use in Equation **(5)**.

Crash Avoidance The results for crash avoidance system effectiveness are presented in Table 7, based on 100,000 iterations within the Monte Carlo simulation. Results are presented for the various production vehicles using the AEB system logic (i.e., only AEB activates without any driver warning). It is important to note that this system logic is presented because it was determined from the test data that the difference between driver warning and AEB activation was minimal (average less than 1 second) and a driver would not be able to react to the warning prior to the AEB activation. Simulation results confirmed this, as there was minimal crash avoidance effectiveness differences between the three system logic variations.

[5] A sensitivity analysis was performed to determine the number of iterations for the simulation to enter a stable state. After 2,500 iterations, this analysis entered a steady state within a ± 0.2 percent range.

Table 7.
Crash Avoidance Effectiveness of PCAM Systems for Three Production Vehicles (AEB Only) and Two Crash Databases.

Scenario Name	GES			FARS		
	OEM 1	OEM 2	OEM 3	OEM 1	OEM 2	OEM 3
S1-A	76%	75%	40%	52%	49%	7%
S1-B	N/A*	N/A*	N/A*	10%	68%	0%
S1-C	90%	70%	64%	37%	36%	12%
S1-D	20%	22%	39%	0%	0%	9%
S4-A	49%	64%	53%	39%	51%	34%
S4-B	70%	100%	95%	22%	59%	46%

*No GES crashes met conditions to be reconstructed

Based on the initial conditions and system performance data, the various production vehicles were successful in avoiding many crashes, although they demonstrate lower performance with faster pedestrian speeds and obstructions. Further, results prove that not all crashes are avoidable but a reduction in impact speeds may provide an additional safety benefit.

Crash Mitigation An output of the Monte Carlo simulation is to report the impact speed of the resulting vehicle-pedestrian crash. A distribution of these impact speeds is compared to the baseline impact speeds to determine the potential for reduced pedestrian harm. Figure 7 illustrates an output of the simulation, showing the various distributions of impact speeds for a production vehicle in the S1-A testing scenario within the GES crash reconstructions. Distributions of impact speeds were smoothed using regression modelling to account for data anomalies.

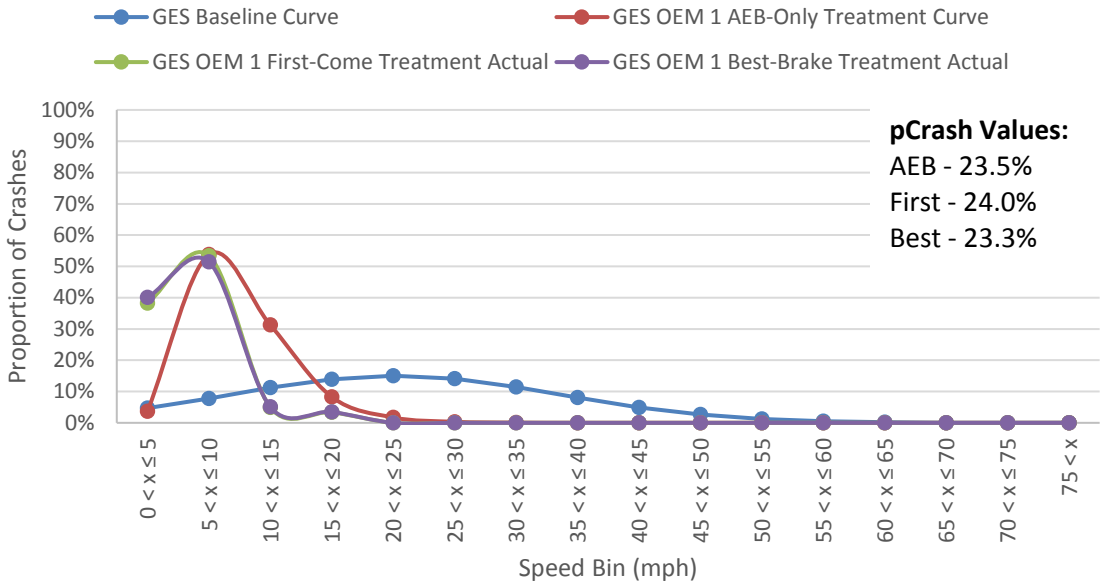

Figure 7. Plots of Functions Comparing Baseline and Treatment Impact Speeds for Production Vehicle 1 in a S1-A Test with GES Crashes.

Results show a distinct shift in the average impact speed, reducing speed from 20-25 mph to 5-10 mph. An impact speed reduction of 15 mph can have a profound effect on mitigating injuries, dropping potential pedestrian injuries from severe to minor. Further, as shown in Figure 7, crash mitigation effectiveness accounts for the crashes avoided, including the 24 percent of crashes avoided, effectively eliminating all subsequent pedestrian injuries (Equation **(4)**).

Crash mitigation effectiveness for the three production vehicles using the AEB system logic (i.e., only AEB activates without any driver warning) is shown in Table 8. Similar to crash avoidance, the minimal difference in AEB activation and driver warning provided small variations in effectiveness.

Table 8.
Crash Mitigation Effectiveness of PCAM Systems for Three Production Vehicles (AEB Only) and Two Crash Databases.

PCAM Scenario	Harm Measure	GES			FARS		
		OEM 1	OEM 2	OEM 3	OEM 1	OEM 2	OEM 3
S1-A	MAIS 2+	92%	91%	72%	91%	88%	67%
	MAIS 3+	96%	96%	83%	96%	94%	79%
S1-B	MAIS 2+	N/A*	N/A*	N/A*	65%	88%	46%
	MAIS 3+	N/A*	N/A*	N/A*	77%	92%	54%
S1-C	MAIS 2+	89%	79%	46%	83%	79%	64%
	MAIS 3+	90%	83%	38%	91%	87%	76%
S1-D	MAIS 2+	54%	65%	73%	41%	68%	73%
	MAIS 3+	65%	77%	82%	52%	84%	87%
S4-A	MAIS 2+	84%	88%	87%	83%	86%	80%
	MAIS 3+	89%	92%	93%	89%	91%	87%
S4-B	MAIS 2+	92%	100%	98%	78%	89%	85%
	MAIS 3+	96%	100%	99%	86%	93%	91%

* No GES crashes met conditions to be reconstructed

Safety Benefits

PCAM systems can potentially provide a wide range of safety benefits, depending on the initial conditions and the system algorithms. Table 9 presents the crash avoidance effectiveness for the six scenarios tested. The range is defined by the three production vehicles and the two sets of crash reconstruction databases; however as noted earlier, only AEB is used for this effectiveness (i.e., no driver warning). The resulting benefits are determined from Equation **(**1**)** using the values from Table 6 and Table 7. These crashes translate to savings in billions of dollars and hundreds of equivalent lives saved (i.e., a metric that translates comprehensive costs into a reduction in pedestrian fatalities).

Table 9.
Annual PCAM-Addressable Crash Mitigation Safety Benefits (AEB Only).

PCAM Scenario	Crash Avoidance Effectiveness	GES Crashes Reduced	FARS Crashes Reduced	Costs Reduced (2010 $M)	Equivalent Lives Saved
S1-A	7% - 76%	318 - 3,503	58 - 641	$ 582 - 6,417	64 - 702
S1-B	0% - 68%	N/A*	N/A*	$ 3*	N/A*
S1-C	12% - 90%	93 - 713	4 - 31	$ 51 - 388	6 - 42
S1-D	0% - 39%	0 - 108	0 - 3	$ 48	5
Total Effectiveness of PCAM Addressable S1	**7% - 77%**	**411 - 4,324**	**62 - 675**	**$ 633 - 6,856**	**69 - 750**
S4-A	34% - 64%	103 - 192	34 - 64	$ 332 - 618	36 - 68
S4-B	22% - 100%	105 - 471	16 - 72	$ 170 – 763	19 - 83
Total Effectiveness of PCAM Addressable S4	**27% - 86%**	**208 - 663**	**50 - 135**	**$ 501 - 1,380**	**55 - 151**

*Only 1 FARS case was identified over two years, this benefit is simply the effectiveness multiplied by the average annual comprehensive cost (one half comprehensive cost of one fatality).

Table 10 presents the injury mitigation effectiveness for the six scenarios tested. Similar to crash avoidance effectiveness estimates, the wide range of crash mitigation effectiveness is obtained from the three production vehicles and two crash reconstruction databases. Further, crash mitigation effectiveness estimates incorporate the crash mitigation effectiveness. Again, results are only provided for AEB only. Metrics used to estimate injury mitigation benefit are annual reduction of pedestrians injured at MAIS 2^+, MAIS 3^+, comprehensive costs, and the number of equivalent lives saved.

Table 10.
Annual PCAM-Addressable Crash Mitigation Safety Benefits (AEB Only).

PCAM Scenario	Harm Measure	Crash Mitigation Effectiveness	Injuries Reduced	Costs Reduced (2010 $M)	Equivalent Lives Saved
S1-A	MAIS 2+	67% - 92%	1,051 - 1,448	$ 5,514 - 7,594	603 - 830
	MAIS 3+	79% - 96%	873 - 1,068	$ 6,347 - 7,767	694 - 849
S1-B	MAIS 2+	46% - 88%	N/A*	$ 2 – 4*	N/A*
	MAIS 3+	54% - 92%	N/A*	$ 2 – 4*	N/A*
S1-C	MAIS 2+	46% - 89%	69 - 133	$ 188 - 364	21 - 40
	MAIS 3+	38% - 91%	27 - 65	$ 143 - 344	16 - 38
S1-D	MAIS 2+	41% - 73%	21 - 38	$ 47 - 84	5 - 9
	MAIS 3+	52% - 87%	12 - 21	$ 54 - 91	6 - 10
Total Effectiveness of PCAM Addressable Total S1	**MAIS 2+**	**64% - 91%**	**1,142 - 1,620**	**$ 5,751 - 8,046**	**629 - 880**
	MAIS 3+	**76% - 96%**	**912 - 1,154**	**$ 6,547 - 8,206**	**716 - 897**
S4-A	MAIS 2+	80% - 88%	128 - 141	$ 764 - 844	84 - 92
	MAIS 3+	87% - 93%	109 - 116	$ 822 - 881	90 - 96
S4-B	MAIS 2+	78% - 100%	145 - 187	$ 581 - 750	64 - 82
	MAIS 3+	86% - 100%	103 - 120	$ 621 - 723	68 - 79
Total Effectiveness of PCAM Addressable Total S4	**MAIS 2+**	**79% - 94%**	**273 - 329**	**$ 1,346 - 1,594**	**147 - 174**
	MAIS 3+	**86% - 97%**	**212 - 236**	**$ 1,443 - 1,604**	**158 - 175**

*Only 1 FARS case was identified over two years, this is benefit is simply the effectiveness multiplied by the average annual comprehensive cost (one half comprehensive cost of one fatality).

Overall PCAM systems could provide a crash avoidance effectiveness of 78 percent, as shown in Table 11. Further, the table shows if a crash occurs, PCAM systems may provide injury mitigation effectiveness of 92 and 96 percent for pedestrians injured at MAIS 2^+ and MAIS 3^+, respectively. The table only shows the highest crash avoidance and crash mitigation effectiveness observed from the simulation and the correlating benefit.

Table 11.
Best Observed Effectiveness and Safety Benefits for PCAM-Addressable Crashes.

Scenario	Crash Avoidance Effectiveness	GES Crashes Reduced	FARS Crashes Reduced	Costs Reduced (2010 $M)	Equivalent Lives Saved
S1	76.4%	4,324	675	$ 6,857	750
S4	85.9%	663	135	$ 1,380	151
Total System	**77.6%**	**4,987**	**810**	**$ 8,237**	**901**

Scenario	Harm Measure	Crash Mitigation Effectiveness	Pedestrian Injuries Reduced	Costs Reduced (2010 $M)	Equivalent Lives Saved
S1	MAIS 2+	91.0%	1,620	$ 8,046	880
	MAIS 3+	95.6%	1,154	$ 8,206	897
S4	MAIS 2+	94.5%	329	$ 1,594	174
	MAIS 3+	96.5%	236	$ 1,604	175
Total System	**MAIS 2+**	**91.6%**	**1,948**	**$ 9,640**	**1,054**
	MAIS 3+	**95.8%**	**1,391**	**$ 9,810**	**1,073**

CONCLUSION

This paper developed and applied a methodology to estimate potential safety benefits for existing and near-term production PCAM systems. These systems are vehicle-based pedestrian detection systems that can warn drivers and/or automatically apply the vehicle brakes to avoid a collision or reduce the impact speed. This paper addressed current and near-term production PCAM systems with driver warning and AEB. Safety benefits were estimated in terms of reductions in the number of all annual vehicle-pedestrian crashes, annual vehicle-pedestrian fatal crashes, and annual injured pedestrians at MAIS 2^+ and MAIS 3^+ levels, annual comprehensive costs, and annual equivalent lives.

Data sources available at the time of this analysis included national crash databases, test track data, and human behavior information. Additional data were collected using a NHTSA SCI team to detail the dynamics of historical pedestrian crashes, specifically the amount of time the pedestrian was visible to the driver. A crash reconstruction simulation superimposed with empirical PCAM system data was conducted to determine crash avoidance effectiveness and any reduction in impact speed if a crash occurred.

Overall, the methodology presented in this paper relied on the availability and accuracy of real-world data. Ideally, safety benefits would be estimated from empirical crash data over the course of multiple years, comparing crash statistics of vehicle-pedestrian crashes without a PCAM system to crashes with a PCAM system. However, with the current state of crash data and collection methods, information is unavailable to estimate PCAM safety benefits in this method. Future considerations may be made to amend the data collection method to address any deficiencies in the crash data. Therefore, this methodology supplemented historical crash data with objective testing of production vehicle systems and previous literature/research. This information was input into a Monte Carlo simulation to compare historical vehicle-pedestrian crashes with synthetic crashes, superimposing PCAM system performance on these historical crashes. Using this method and the limited data available, safety benefits estimates are presented at a high level.

For this study, objective testing was limited to only three production vehicle systems under six specific conditions. The performance of these three systems was not indicative of system performance for other vehicle systems using other technology. Furthermore, as the technology within PCAM systems continues to improve over time, these three systems may not be representative of all current or future technology. Moreover, the limited objective testing conditions may not take advantage of the full operational capabilities of these PCAM systems. Due to the unknown performance of PCAM systems in other scenarios (i.e., S2 and S3) and other conditions (e.g., adverse weather or minimal lighting conditions), it could not be assumed that PCAM systems will have a positive (or negative) safety

benefit. Not being able to correlate testing conditions to historical crashes required this analysis to take a conservative approach and assume that a significant amount of crashes may not be addressed by a PCAM system (e.g., no safety benefit for crashes in the dark). Additionally, limited information on driver-vehicle interaction of these PCAM systems required this analysis to generalize the interaction with three simplified system logic approaches.

This paper summarizes a multi-year effort of data collection and analysis, as such this paper only describes the methodology and presents a portion of the entire data analysis [18]. The full report with data and analysis can be found at: https://www.nhtsa.gov/document/estimation-potential-safety-benefits-pedestrian-crash-avoidance-mitigation-systems

REFERENCES

[1] National Center for Statistics and Analysis. (2018, March). Traffic Safety Facts: Pedestrians (Report No. DOT HS 812 493).Washington, DC: National Highway Traffic Safety Administration.

[2] National Center for Statistics and Analysis. (2018, September). Traffic Safety Facts: Summary of Motor Vehicle Crashes (Report No. DOT HS 812 580).Washington, DC: National Highway Traffic Safety Administration.

[3] Yanagisawa, M., Swanson, E., & Najm, W. G. (2014, April). Target Crashes and Safety Benefits Estimation Methodology for Pedestrian Crash Avoidance/Mitigation Systems (Report No. DOT HS 811 998). Washington, DC: National Highway Traffic Safety Administration.

[4] National Center for Statistics and Analysis. (2014, December). National Automotive Sampling System (NASS) General Estimates System (GES) Analytical User's Manual 1988-2013 (Report No. DOT HS 812 091). Washington, DC: National Highway Traffic Safety Administration.

[5] National Center for Statistics and Analysis. (2015, April). Fatality Analysis Reporting System (FARS) Analytical User's Manual 1975-2013 (Report No. DOT HS 812 092). Washington, DC: National Highway Traffic Safety Administration.

[6] Swanson, E., Yanagisawa, M., Najm, W. G., Foderaro, F. & Azeredo, P. (2016, August). Crash Avoidance Needs and Countermeasure Profiles for Safety Applications Based on Light Vehicle-to Pedestrian Communications (Report No. DOT HS 812 312). Washington, DC: National Highway Traffic Safety Administration.

[7] Rosén, E., Källhammer, J.-E., Eriksson, D., Nentwich, M., Fredriksson, R., & Smith, K. (2010). Pedestrian Injury Mitigation by Autonomous Braking. Accident Analysis and Prevention, 42, 1949–1957.

[8] Fredriksson, R. (2015, January). Potential Head Injury Reducing Benefit of Combining Passive and Active Pedestrian Protection Systems [presentation]. 2015 SAE Government-Industry Meeting. Washington, DC.

[9] Shibata, E. (2015, January). Next Generation EyeSight® and Future Strategy [presentation]. Subaru. 2015 SAE Government-Industry Meeting. Washington, DC.

[10] Sherony, R. (2015, January). Pedestrian Pre-Collision System (PCS) Test Mannequin and Test Method Development [presentation]. Toyota. 2015 SAE Government-Industry Meeting. Washington, DC.

[11] Harding, J., Powell, G., Yoon, R., Fikentscher, J., Doyle, C., Sade, D., Lukuc, M., Simons, J., & Wang, J. (2014, August). Vehicle-to-Vehicle (V2V) Communications: Readiness of V2V Technology for Application (DOT HS 812 014). Washington, DC: U.S. Department of Transportation, National Highway Traffic Safety Administration.

[12] Najm, W.G., and daSilva, M.P. (2000, May). Benefits Estimation Methodology for Intelligent Vehicle Safety Systems Based on Encounters with Critical Driving Conflicts. ITS America 10th Annual Meeting and Exposition. Boston, MA.

[13] McMillan, N.J., Christiaen, A.-C., & Stark, G.V. (2001, November). Estimating Safety Benefits for the IVI Generation 0 Field Operational Tests. Paper No. 01TB-59. 2001 SAE International Truck & Bus Meeting & Exposition. Chicago, IL.

[14] Blincoe, L., Miller, T.R., Zaloshnja, E., & Lawrence, B.A. (2015, May). The Economic and Societal Impact of Motor Vehicle Crashes, 2010 (Revised) (DOT HS 812 013). Washington, DC: U.S. Department of Transportation, National Highway Traffic Safety Administration.

[15] Albrecht, H. (2017, January). Objective Test Procedures for Pedestrian Automatic Emergency Braking Systems [presentation]. 2017 SAE Government-Industry Meeting. Washington, DC.

[16] Olson, P.L., Cleveland, D.E., Fancher, P.S., Kostyniuk, L.P., & Schneider, L.W. (1984, June). Parameters Affecting Stopping Sight Distance. NCHRP Report No. 270. Washington, DC: Transportation Research Board (TRB).
[17] Kiefer, R.J., Cassar, M.T., Flannagan, C.A., Jerome, C.J., & Palmer, M.D. (2005, August). Surprise Braking Trials, Time-to-Collision Judgments, and "First Look" Maneuvers Under Realistic Rear-End Crash Scenarios (DOT HS 809 902). Washington, DC: U.S. Department of Transportation, National Highway Traffic Safety Administration.
[18] Yanagisawa, M., Swanson, E., Azeredo, P., and Najm, W.G. (2017, April). Estimation of Potential Safety Benefits for Pedestrian Crash Avoidance/Mitigation System (Report No. DOT HS 812 400). Washington, DC: National Highway Traffic Safety Administration

ACRONYMS

AEB	automatic emergency braking
CP	crash probability
EM	exposure measure
FARS	Fatality Analysis Reporting System
FOV	field of view
GES	General Estimates System
GIDAS	German In-Depth-Accident-Study
ITARDA	Institute for Traffic Accident Research and Data Analysis
MAIS	maximum abbreviated injury scale
NASS	National Automotive Sampling System
NHTSA	National Highway Traffic Safety Administration
OEM	original equipment manufacturer
PCAM	pedestrian crash avoidance/mitigation
PR	police-reported
SCI	Special Crash Investigation
TRC	Transportation Research Center
TTC	time-to-collision
V2V	vehicle-to-vehicle
VRTC	Vehicle Research and Test Center

APPENDIX

Figure 8. Detailed List of Variables Obtained from NHTSA'S SCI Team for 43 Vehicle-Pedestrian Crashes

Variable	Description
Year	Year of the crash
State	U.S. state of the crash
# Ped. Involved	Number of pedestrians hit by the vehicle
Ped. Age Group(s)	Age of the first pedestrian hit (years) – if multiple pedestrians, another field
Ped. Injuries	Pedestrian injury level on KABCO scale
Weather	Current weather at the time of the crash
Lighting	Lighting at time of crash (e.g., daylight, dark, dark w/ lighting)
Road Surface Condition	Coefficient of friction on road at the time of crash
Speed Limit	Posted speed limit on the road of the crash (km/h)
Intersection?	Did the crash occur at an intersection? (Y/N)
Roadway Alignment	Road alignment (e.g., straight, curve)
Roadway Grade	Roadway grade
Traffic Control	Traffic control at the crash location (e.g., lights, stop sign, none)
Veh. Pre-Crash Man.	Vehicle maneuver in the pre-crash scenario
Veh. Avoidance Man.	Vehicle attempted avoidance maneuver (e.g., brake, steer, brake and steer)
Travel Lane #	The vehicle travel lane (numbered left to right of driver)
Veh. Speed	Vehicle pre-crash speed (km/h)
Veh. Speed Range	Potential error range on the pre-crash vehicle speed (km/h)
Distance from Ped.	Vehicle distance from pedestrian when the pedestrian entered the road (m)
Veh. Dist. Range	Potential error range on vehicle distance from pedestrian (m)
Driver Vision Obstructed?	Was the driver's vision obstructed?
Vision Obstruction	What obstructed the driver's vision?
Driver Eyes Off Road?	Were the driver's eyes off the road?
What Driver Looked At	What was the driver looking at if the eyes were off the road?
Ped. Man. Pre-Crash	Pedestrian's pre-crash maneuver (e.g., crossing road, walking, jogging, standing)
Ped. Avoidance Man.	Pedestrian avoidance maneuver (e.g., walk, run, yell, none)
Ped. Location Pre-Crash	Pedestrian's pre-crash location
Ped. Speed	Pedestrian's movement speed (km/h)
Ped. Direction	Direction of pedestrian movement (left-right or right-left of vehicle)
Ped. Vision Obscured?	Was the pedestrian's vision obscured?
Ped. Vision Obscured by?	What obscured the pedestrian's vision?
Ped. Impaired?	Was the pedestrian impaired? (include description of impairment)
Ped. Inattention?	Was the pedestrian inattentive?
Ped. Inattentive Because?	Why was the pedestrian inattentive?
Distance Away from Roadway OR **Line of Sight of Car**	Vehicle distance from pedestrian when the pedestrian entered the road or was first visible (m)
Location of impact	Where the impact happened (e.g., roadway, crosswalk)
Travel Lane Location of Impact	The lane of impact (numbered from left to right of vehicle)
Distance From Curb	How far from the curb the impact happened (m)
Before, Middle, After Int.?	Did the impact occur before, inside of, or after the intersection?
Area of Impact on Veh	Part of the vehicle that made contact with pedestrian
Distance Traveled by Veh.	Vehicle distance from pedestrian when the pedestrian entered the road (m)
Time Ped. Spends in Roadway	Time the pedestrian spent in the roadway visible and in path of vehicle (s)
Related Factors/Causal Factors	Any related factors that may have contributed to the crash?
PCAM Warning Helpful?	Would a PCAM warning have been helpful for this crash?
PCAM Automatic Braking Helpful?	Would AEB have been helpful for this crash?
PCAM Automatic Steer Helpful?	Would automatic steering have been helpful for this crash?
Summary	Written description of the entire crash scenario
Scene Diagram and photos	Diagram of crash scene and picture of vehicle (contact area, damage) and scene (location)
GPS Coord.	GPS coordinates of the scene of the crash
Impact Speed	Vehicle impact speed (km/h)
Final Rest v1 and p1	How far the vehicle and pedestrian moved after impact until it came to a stop (m)

DEVELOPMENT OF AN FE MODEL FOR FLEXPLI WITH UPPER BODY MASS FOR ENHANCED PEDESTRIAN SAFETY ASSESSMENT

Chirag, Shah
Humanetics Innovative Solutions, Inc.
USA

George, Hu
Humanetics China
China

Mark, Burleigh
Humanetics Innovative Solutions, Inc.
USA

Paper Number 19-0228

ABSTRACT

The FlexPLI GTR tool has been implemented with an Upper Body Mass (UBM) representing portion of the torso mass, hip joint rotation and the response time lag between leg and the upper body during pedestrian to vehicle accidents.

The new FlexPLI GTR UBM tool improves the test method at the end of the bumper test area of vehicle by eliminating unrealistic rotation of the FlexPLI GTR without UBM, bringing it closer to human lower extremity kinematics and loading. The tool is an enhancement to the current dummy technology by improving the pedestrian safety. The key benefit is that the UBM can be added to the existing standard FlexPLI GTR hardware being used in the current test procedures.

The FlexPLI GTR UBM finite element (FE) model is developed and validated against a selected test condition. The geometry and connectivity for the FlexPLI GTR UBM FE model are obtained from the hardware design. Material testing was carried out to obtain the material properties and implementation to the FE model for the rubber element representing the hip joint stiffness during rotation of upper body mass.

The initial findings of the FlexPLI GTR UBM FE model reveal that the model showed promising predictability for the simulated load-case.

INTRODUCTION

In US, on an average a pedestrian was killed nearly every 1.5 hours in traffic crashes and accounted for 16% of all traffic fatalities in 2016 [1]. In the same year, 5320 pedestrian died in road accidents in the EU which is 21% of all road fatalities [2]. The lower limb was found to be the most frequently injured body region with AIS 2 to 6 level injuries in 32.6% of pedestrian accidents worldwide.

In 1998, the European Enhanced Vehicle-Safety Committee proposed a test procedure to assess protection to the lower extremity of a pedestrian during a collision [3]. A legform Impactor composed of rigid long bones was utilized in this procedure. As opposed to a legform impactor with rigid bone parts, the Flexible Pedestrian Legform Impactor (FlexPLI) is more biofidelic especially for its long bone parts, which have human-like bending characteristics [4]. The FlexPLI also provides extended injury assessment capabilities, including long bone bending moment at multiple locations and knee ligament elongations in comparison to other pedestrian legforms [4].

In 2005, the FlexPLI Technical Evaluation Group (Flex-TEG) was settled under the ECE/WP29/GRSP/Informal Group on Pedestrian Safety in order to evaluate FlexPLI hardware performance. Another objective of the FLEX-TEG was to assess the impactor as a regulatory purpose test tool for a Global Technical Regulation on Pedestrian Safety (PS-GTR). The Japan Automobile Manufacturer Association, Inc. (JAMA) and Japan Automobile Research

Institute (JARI) continued to improve and upgrade FlexPLI, and in 2007 the 5th version, called Type GT (FlexPLI-GT) was produced. After the settlement of the Flex-TEG, the FlexPLI GT was evaluated and improved its performance, and the final 6th version, type GTR (FlexPLI GTR), was agreed by the FLEX-TEG members in April 2008 representing leg of the 50th percentile male right leg [5].

The FlexPLI GTR used in the current pedestrian regulatory and consumer programs is focused on assessing injuries to tibia bone and knee ligaments during a pedestrian car collision. The tool has been revised under the European Union (EU) project SENIORS (Safety-ENhancing Innovations for Older Road userS) to implement an Upper Body Mass (UBM) to the standard FlexPLI GTR hardware.

The current efforts describe the development of the FlexPLI GTR UBM finite element (FE) model and validation of the model against a selected test condition.

METHODS

The fully validated FE model for the regulated FlexPLI GTR impactor model as depicted in Figure 1 was available [6]. The FlexPLI GTR regulated model comprises of three regions: Femur, Knee Blocks and Tibia. These three regions are wrapped with neoprene and rubber covers representing the flesh of the legform. Fundamental structures for the femur and tibia regions are constructed segmental with bone cores at the center to achieve bending flexibility representing human like responses during pedestrian crashes. The knee region is comprised of two knee blocks representing condyles like a human knee. Springs and cables are used to replicate the ligaments of the knee.

The geometry and connectivity for the UBM model were obtained from the hardware design (Figure 2(a)) and modeled in detail. Material testing was carried out to obtain the material properties, and implementation to the FE model, for the rubber element (Figure 2(a)) that represents the hip joint stiffness during rotation of the UBM.

The combined model is referred to hereafter as the FlexPLI GTR UBM model and is shown in Figure 2(b). The FlexPLI GTR UBM model (Figure 2(b)) comprises a total of 233K nodes and 340K elements. The total model mass is 19.6 kg within the hardware tolerance limits. The initial time-step size for the model is 0.78 micro-second, which is in line with the common industry practices.

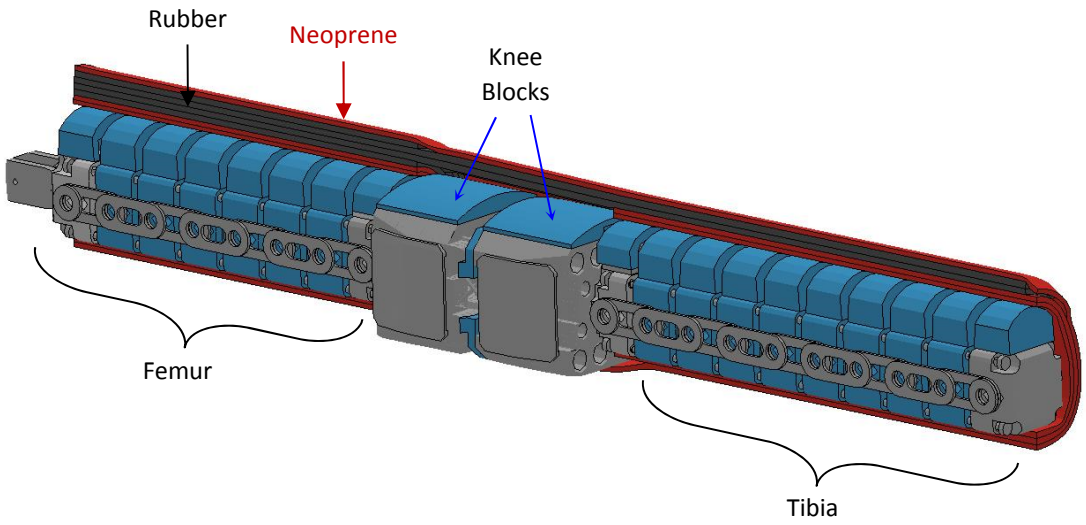

Figure 1. FlexPLI GTR Model.

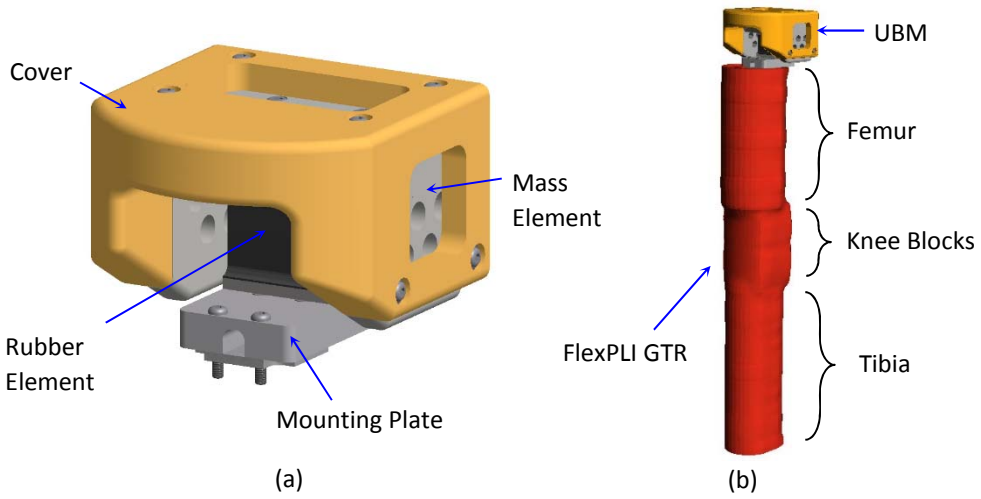

Figure 2. UBM Design (a), and the FlexPLI GTR UBM FE model (b)

INSTRUMENTATION

The FlexPLI GTR UBM model has all the instrumentations for femur, tibia and knee regions, including all available optional channels based on the FlexPLI GTR tool in the current test procedures.

The femur and tibia bone cores have strain gauges used at top and bottom surface of the bone core to measure bending moments in the bones at several locations (Figure 3).

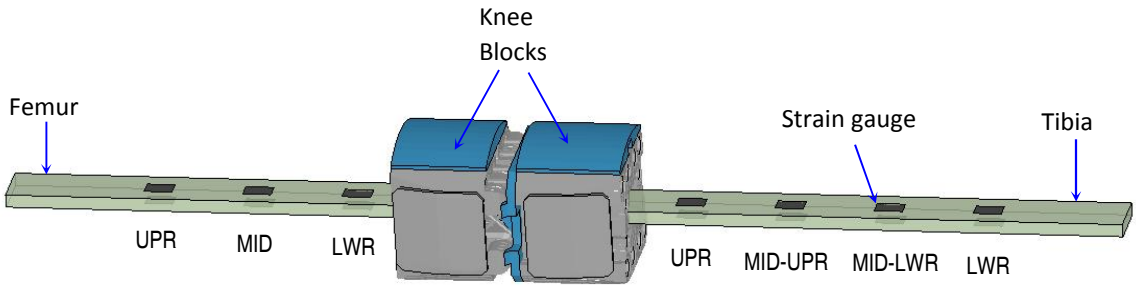

Figure 3: FlexPLI GTR UBM model bone cores with bending moment measurement capabilities

The FlexPLI GTR UBM knee model is shown in Figure 4. The knee has two blocks or condyles, one attaching to femur and the other attaching to the tibia. The condyle surface on the tibia block has nylon material to reduce friction and to avoid metal to metal contact. Four kinds of ligament cables, ACL (Anterior Cruciate Ligament), MCL (Medial Collateral Ligament), PCL (Posterior Cruciate Ligament) and LCL (Lateral Collateral Ligament) are modeled to measure knee ligament elongations at ACL, MCL, LCL and PCL locations as depicted in Figure 4.

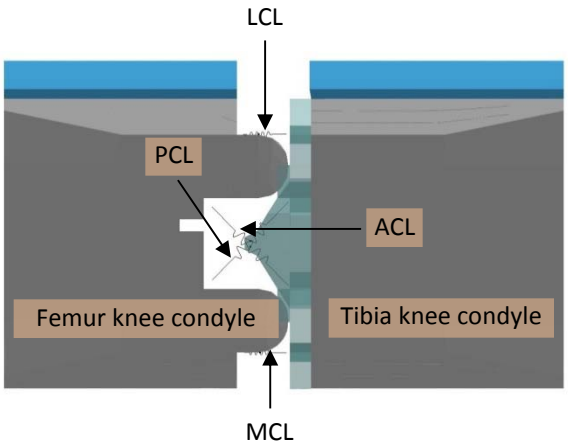

Figure 4: FlexPLI GTR UBM knee model with knee elongation measurement capabilities

VALIDATION

The FlexPLI GTR UBM model was validated against a test condition for a sedan-like vehicle front profile, referred to as SAE buck [7], using the FlexPLI GTR UBM hardware at 0-degree orientation with perpendicular line to the bumper of the SAE buck (Figure 5(a)). The FlexPLI GTR UBM hardware impacted the stationary SAE buck at the impact velocity of 11.1 m/s. All the standard moment output within tibia and femur, knee elongations were recorded during the test and used for validation of the FE model. The model was set up to exactly mimic the test condition as depicted in Figure 5 (b).

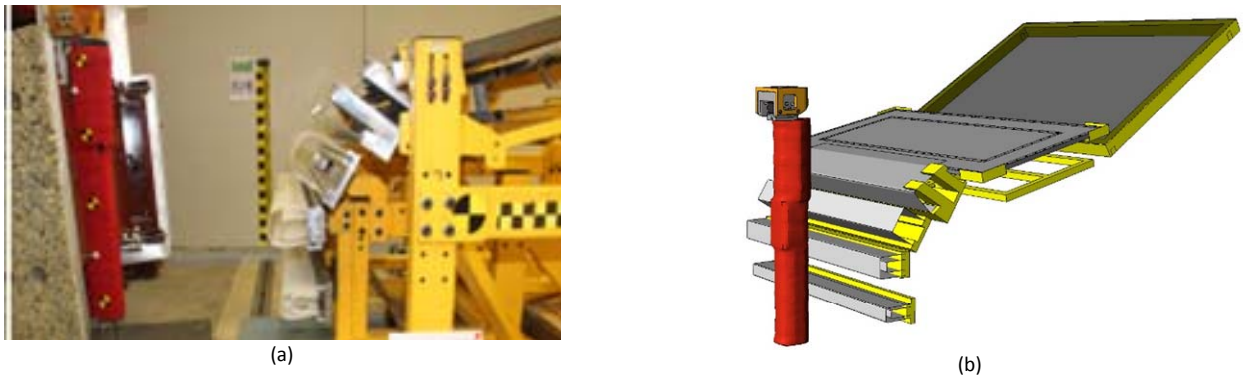

Figure 5. SAE buck test condition for the (a) FlexPLI GTR UBM and (b) FE model setup.

The model response was compared against the hardware output for the femur moments (Figure 6), tibia moments (Figure 7), and knee ligament elongations (Figure 8) injury output measurements. The initial findings of the FlexPLI GTR UBM FE model reveal that the model showed promising correlation for the simulated load case.

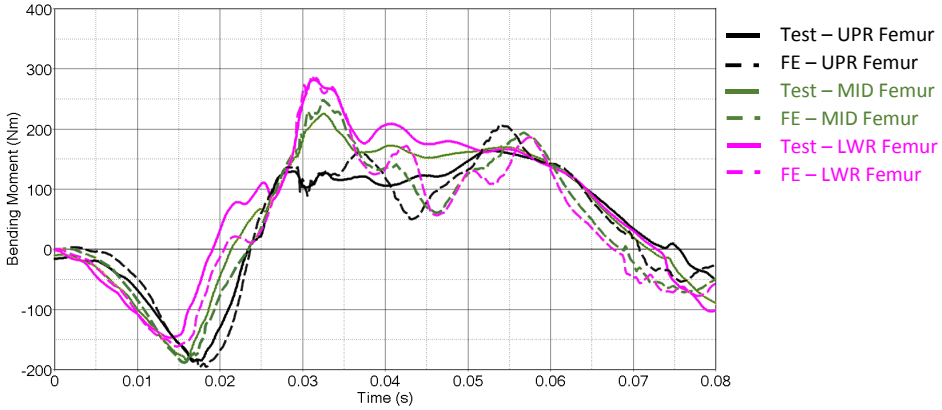

Figure 6: Femur moment for SAE buck test versus FlexPLI GTR UBM FE model predictions

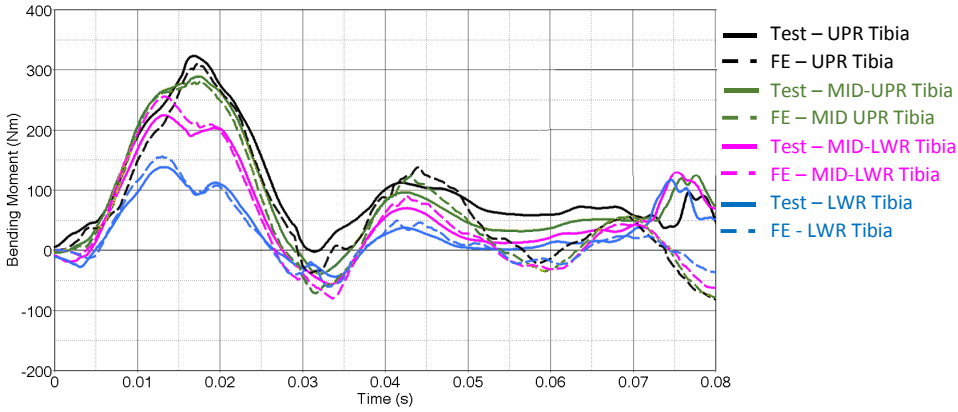

Figure 7: Tibia moment for SAE buck test versus FlexPLI GTR UBM FE model predictions

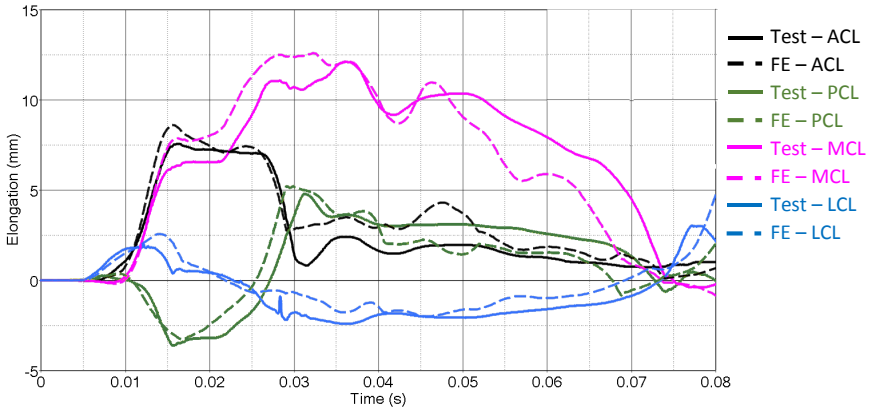

Figure 8: Knee Ligament Elongation for SAE buck test versus FlexPLI GTR UBM FE model predictions

CONCLUSIONS

The FlexPLI GTR UBM tool enables the assessment of the injury risk for the femur, closer to human-like lower extremity injury, and also the assessment of vehicles with a higher front profile. The FlexPLI GTR UBM FE model is currently being validated against a selected load case and will be further validated against additional load cases as they become available.

REFERENCES

[1] NHTSA 2016. “Traffic Safety Facts”, DOT HS 812 493.

[2] European Commission 2018. “Traffic Safety Basic Facts on Pedestrians”, European Commission, Directorate General for Transport, June 2018.

[3] European Enhanced Vehicle-safety Committee 1998. “Improved test methods to evaluate pedestrian protection afforded by passenger cars”, EEVC Working Group 17.

[4] Konosu A. and Tanahashi M. 2005. “Development of a biofidelic Flexible Pedestrian Leg-form Impactor (FLEX-PLI 2004) and Evaluation of its biofidelity at the Component and at the Assembly Level”, SAE paper No. 2005-01-1879.

[5] UN/ECE/WP29/GRSP/INF-GR-PS/Flex-TEG 2008. “First Technology Safety Systems Design Freeze Status FLEX-PLI GTR Development Mechanical Design”, TEG-054-Rev. 1, http://www.unece.org/trans/main/wp29/wp29wgs/wp29grps/pedestrian_FlexPLI.html

[6] Technical Document 2016. “FlexPLI GTR Regulated V1.0.2 Model Technical Report”, Humanetics Innovative Solutions, Inc.

[7] Pipkorn B., Forsberg C., Takahashi Y., Ikeda M., Fredriksson R., Svensson C., and Thesleff A. 2014. “Development and Component Validation of a Generic Vehicle Front Buck for Pedestrian Impact Evluation”, IRCOBI.

DEVELOPMENT OF A SIDE IMPACT CRASH USING INTEGRATED SYSTEM

Raeick Jang, Seokmin Lee, Baeyoung Kim, Yoohoon Choi, Doowon Yang
Hyundai Mobis
KOREA

Paper Number. 19-0229

ABSTRACT

It was judged that it was difficult to prevent passenger injuries caused by vehicle intrusion into a side impact only with conventional airbags. So we considered ways to avoid intrusion. Existing restraint systems are not sufficient to prevent injury caused by vehicle intrusion during side impact. In this thesis, we considered ways to improve passenger injuries by applying new lateral air bag technology using the active system to improve injury caused by vehicle intrusion into existing and new collisions.

INTRODUTION

The system using the active system is as follows.

Stage 1 uses sensors in the vehicle to predict the collision velocity and time of the MDB. It uses a frontal sensor or a lateral sensor to recognize the MDB and signal the ACU.

Step 2 serves to signal the active airbag (different from the existing airbag) in the ACU.

Step 3 operates the active air bag or other system to create a change in passenger movement. There can be many ways.

There are airbags located in the seatback side bolsters, airbags located in the lower section of the seat cushion, two simultaneously operated airbags and a structure that pushes the seat sideways.

Step 4 were tested to verify that actual passenger injuries had an improvement.

It is fully possible to recognize a car that will collide with the sidewall. Unlike the various crash conditions that could occur in a real accident, the prescribed car crash conditions were not difficult to recognize. Based on the sensing results, it was also possible to even implement the signals from the ACU and the airbags. Signaling the air bag from the ACU has varied passenger movement.

First, passenger movement was different depending on the kinds of the inflator deploying the airbags, and the required amount of movements was obtained through CAE. Static testing was conducted in a variety of ways to change actual dummy movement based on the results obtained from the CAE. It was implemented mainly under the design conditions of seats and airbags, and the required passenger movements were calculated and the airbags were developed. The purpose of this paper is to reduce injuries caused by vehicle intrusion by recognizing the difference in passenger movement before side impact. Implementing this required the use of various systems.

Seat bolsters and seat cushions have a form which is in contact with passengers and require a structure to maintain the restraint's resistance. There were also various structures in the seat cushion, which caused difficulties in designing mass-production that avoided them.

Nevertheless, tests were conducted using various structures to improve side impact by utilizing various products. In this paper, airbag-based testing was conducted.

Side Impact Crash

Generally, the side impact mode increases the injury by intrusion of the body. Vehicle intrusion changes depending on collision modes, collision speed, and the like. The modified North American side impact mode and IIHS crash mode change dummies and impact speeds and can be sensitive to body infiltration as well as chest injuries as well as pelvic injuries. First, NCAP in North America is scheduled to change its dummy, which is expected to increase pelvic injuries. The IIHS test requires changes in impact velocity and dummy to improve chest and pelvic injury

US Side Impact Crash Test Result

As a result of the actual vehicle test with the MID size vehicle, the chest and sacroiliac load was high in the new world SID Dummy

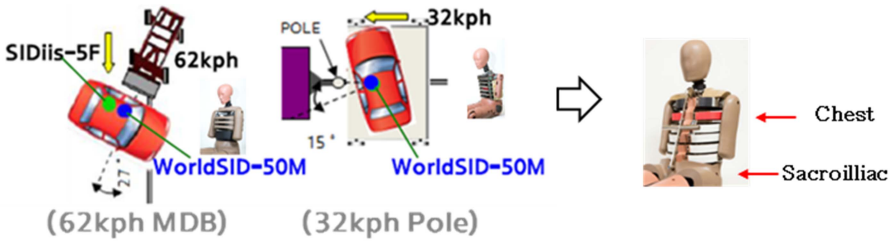

Figure 1. US NCAP crash test.

Table 1.
US NCAP crash test result.

	Rib Deflection	Sacroiliac Force
MDB	19mm (1.0)	2534N (0.78)
POLE	39mm (0.47)	3183N (0.35)

IIHS Side Impact Crash Test Result

IIHS new crashes also resulted in higher chest and pelvic injuries, depending on the velocity of increase and the changed MDB. As the velocity increases, the collision energy increases and the penetration rate increases, leading to an increase in passenger injury

Figure 2. IIHS crash test.

Table2.
IIHS crash test result.

Speed	Dummy	Overall Rating	Injury(Front)	
			Chest	PELVIS
50 km/h	SIDⅡ	G	A	G
50 km/h	W-SID	G	G	G
60 km/h	W-SID	M	P	M

Major Impact of Collision Score

As the MDB velocity increases, the slope and maximum value of the passenger injury increase. The head, chest and pelvis and vehicle showed the same tendency. In conclusion, it was judged that passenger space was enough to avoid vehicle intrusion. The graph below shows the tendency of bust injury according to increase of collision speed and crash severity, and it can be considered to represent not only chest injury but also all injuries

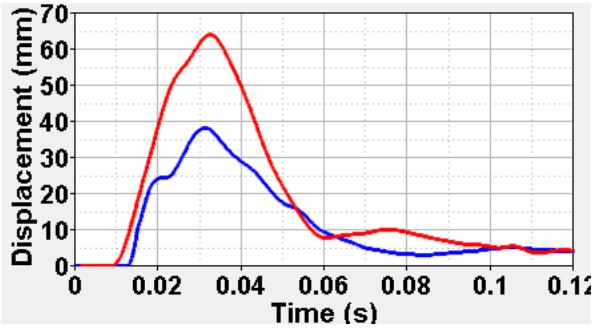

Figure 3. Increased severity

Integrated System Airbag (Reusable)

The purpose of this paper is to develop an air bag system in conjunction with active systems. In this paper, airbag-focused research activities will be recorded. In the conventional side collision mode, the airbag is activated after collision with the MBD. It is not possible to use seat as well as airbag after vehicle breakage and airbag deployment. However, the use of active systems requires the reuse of airbags and seats because airbags can operate even when no collisions occur. The products for the test that have been made this time are as follows. Inflators used compact hybrid type and cold gas. Airbag cushion products are rib bolster product, seat cushion product, seat back product, and combined product. The hybrid small-size Product and cold gas inflator were judged to be reusable cushions and were used in actual tests. Such an inflator would be very advantageous not only in terms of price but also in terms of reliability

Other company applications (References)

Before starting this study, I have investigated existing developed or already mass-produced Products. mercedes-benz developed and produced an active passive integrated airbag called Pre Safe Impulse, and Audi developed a side active passive integration system through vehicle control. Both products are in conjunction with active safety to protect passengers after impact. In this paper, we have conducted additional tests based on existing developments and have conducted better performance or more various tests. We also used HIP SAFE airbags for elderly care made by HELITE. It is a product designed to protect the elderly, etc. It is a concept to protect passengers by sensing the pedestrians that fall when the pedestrians fall and activating the airbag.

The existing articles were used to identify active side systems as beneficial to passenger injuries. (Refer to the articles or products on the market for reference.)

This project is similar to the above products because it is an air bag system for passenger protection of side collision using active system.

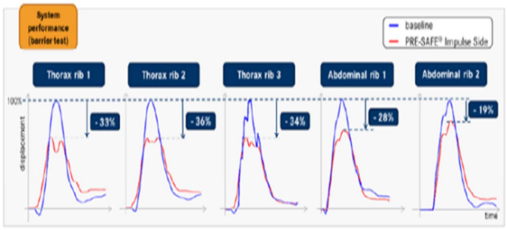

Figure 5: Benefit of PRE-SAFE® Impulse Side in barrier test configuration

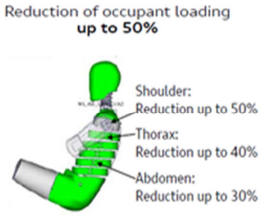

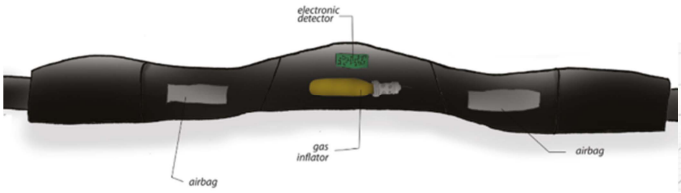

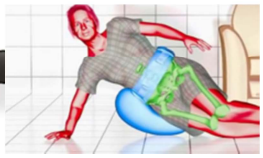

Figure 4. References

MAIN SUBJECT

The main purpose of the study is to improve passenger injuries in side crash tests and side crash room accidents. As mentioned above, major injuries were caused by vehicle intrusion, and it was also found that passenger injuries could be improved if the vehicle intrusion could be avoided. The main goal is to develop products that work in conjunction with the active system to operate the airbag, minimize the impact on the seat, and secure passenger and vehicle infiltration spaces to prevent injury from vehicle intrusion

Method

The main purpose of the study is to improve passenger injuries in side crash tests and side crash room accidents. As mentioned above, major injuries were caused by vehicle intrusion, and it was also found that passenger injuries could be improved if the vehicle intrusion could be avoided. The main goal is to develop products that work in conjunction with the active system to operate the airbag, minimize the impact on the seat, and secure passenger and vehicle infiltration spaces to prevent injury from vehicle intrusion. Side and diagonal sensors are used to sense the collision of the opponent vehicle and receive a signal from the ACU. The ACU signals the ACU before the collision to move passengers to reduce passenger injuries by avoiding vehicle intrusion after the collision. The approximate active system is shown below, and in this paper we refer to the airbag as the center..

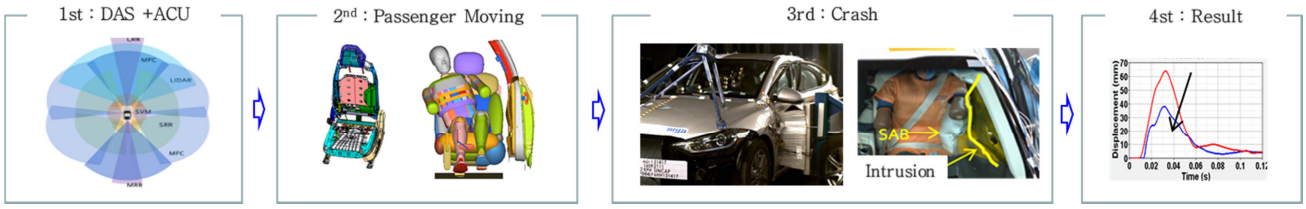

Figure 5. Operating system

CAE Test Result

We conducted analytical tests to find a better concept. The # 1 (RIB) product is mounted on the side bolster on the seat and pushes the dummy shoulder, while the # 2 (RIB & BACK) pushes the shoulder and back. The # 3(HIP) product raised the hips on one side and the # 4(SEAT MOVE) slid the seat sideways to try to figure out the passenger injury trend. It is medium-sized vehicle standard and MDB 62kph speed. The passengers were moved on a static basis without moving them by time zone. Tests were conducted on the four Products, and the tendency that chest injuries were improved with more dummy movements was identified. All four Products were similar, so the actual single item test and the sled test proceeded. It was also confirmed whether the injured Sacroiliac (Pelvis) injuries.

All analytical tests were performed on the basic posture, the 30mm movement, and the 100mm movement. As the distance from the door (or car body) increases, the injury tends to improve. Based on the results, all the products were manufactured, and single item tests and crash tests were conducted. Especially, it was confirmed that not only the improvement of the chest but also the improvement of the pelvic side load, which is a future issue.

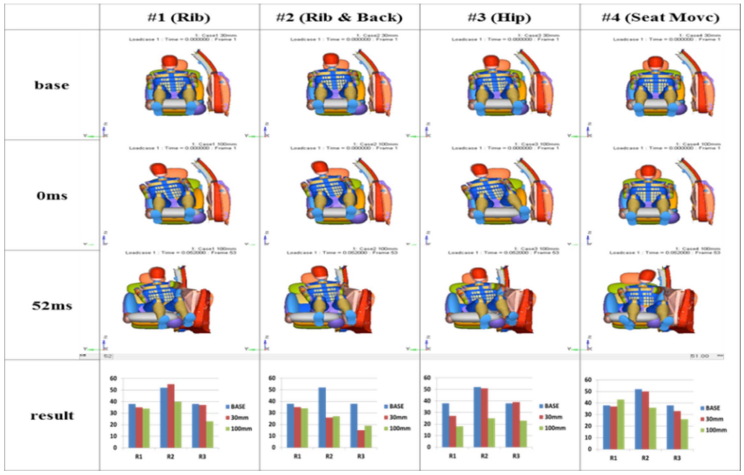

Figure 6. Passenger CAE / Rib injuries results and video

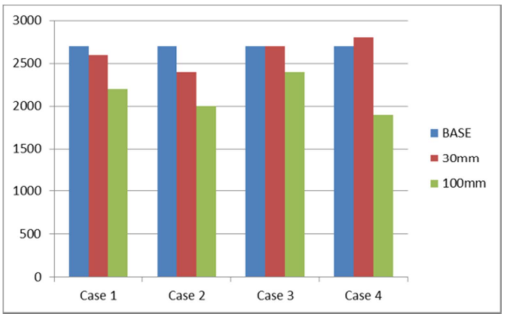

Figure 7. Passenger CAE / Sacroiliac injuries results

Airbag and Inflator (Reusable) and Seat

The actual products of the airbag are as follows. The seat uses the standard Product of the mass production model, the passenger hips and the back side have a hot wire, and the side bolster side has a guider. Airbags were installed on the side bolsters to minimize heat distortion, and it was not difficult to install the airbags on the side bolsters. Based on the CAE results, the actual product was manufactured as follows. The rubber hose connected to the inflator outlet is used as needed, and it can be used when the inflator temperature.

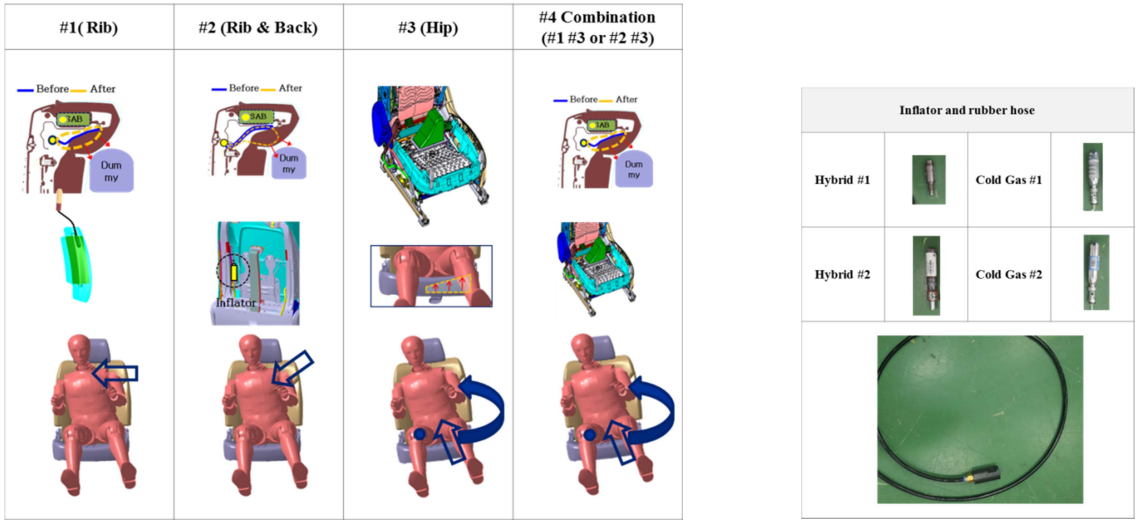

Figure 8. Actual product shape and dummy movement

Static Deployment Test with World SID Dummy

Static tests were conducted based on the above Products. It is to judge the moving distance of the actual world SID dummy and to check the effect and then to perform the collision test. The most effective Products are the combination of COLD GAS inflator and rib cushion, and the cold gas and combination product. The greatest amount of movement was in the dummy. Especially, the combination of RIB cushion and COLD GAS showed 30mm of pelvis .

	Rib (#1)		Rib & Back (#2)		Seat Cushion (#3)		Combination	
							#1 #3	#2 #3
	Hybrid Small	Cold Gas #1	Hybrid Mid	Cold Gas #2	Cold Gas	Hybrid Mid	Cold Gas #1	Cold Gas #1
0ms	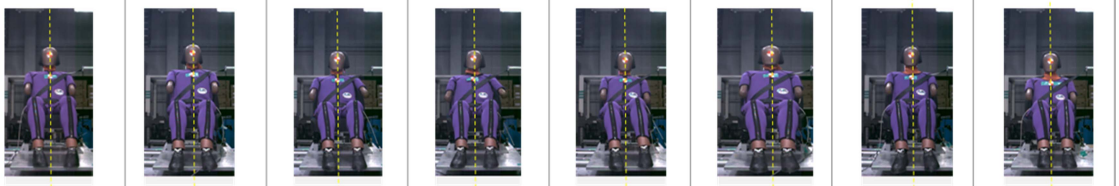							
100ms								
Chest Move	30mm	100mm	20mm	30m	60mm	30mm	100mm	100mm
Pelvis Move	15mm	30mm	0mm	15mm	20mm	30mm	30mm	30mm

Figure 9. Dummy Movement

During the static test, the dummy injuries were found to be 2.5 mm in the chest displacement and the Sacroiliac was also in the level of 260, confirming that the injuries were not affected. Also, there was no difference in dummy movement when wearing the belt and when not wearing it..

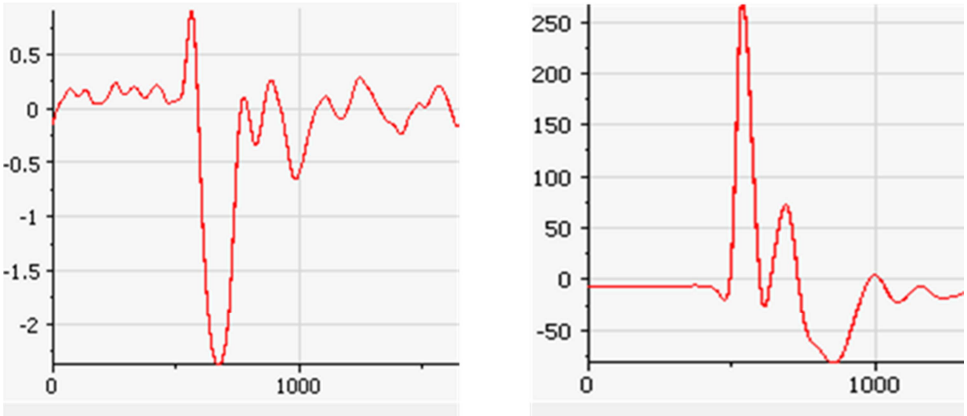

Figure 10. Static test dummy injury

Sled Test Condition

The sled test and the actual vehicle test may have different conditions. Vehicle intrusion and collision waveforms of the actual vehicle do not coincide with the sled test. However, we prepared the base test by using the sled technique

to match the actual vehicle and waveforms as closely as possible. Seats, trimmings, and dummy seating are identical to the drawing conditions. It is equipped with belt and SAB, both of which are in production Products. One side of the seat did not tighten the bolt, and the jumping of the vehicle was reproduced. The interior space of the door trim was filled with rigid blocks to reproduce the collision energy increase due to possible vehicle intrusion. The time for the Pre Safe SAB to operate is 80ms before impact. This is considered to be a sufficient time when the connection well.

Sled Test Result

As shown in the bar graph, the RIB # 1 product and COMBINATION (# 1, # 3) injuries are better than the base test. This shows that the more the dummy movement amount, the less the injury. Especially for RIB # 1, PRE SAFE SAB shows the best performance with just one. For the RIB # 1 Product and COMBINATION (# 1 # 3), the SACROILIAC score is also improved. In the RIB # 1 Product and COMBINATION (# 1 # 3), SACROILIAC injury is expected to be improved by the effect of moving the dummy pelvis. However, it is expected that further improvement will be achieved if the structure avoids interference with the armrest portion of the door trim.

Especially, in case of # 1 (RIB) Product, the maintenance effect of cold gas inflator was excellent in pushing dummy chest from the beginning with good pressure.

PRE SAFE	BASE	#1 Rib	#2 Rib & Back	#3 Hip	#4 Combi. (#1 #3)	#5 Combi. (#2 #3)	#6 Seat Moved 100mm
	N/A	Cold Gas #1	Hybrid Mid	Hybrid Mid	Cold Gas #1	Cold Gas #1	N/A
0ms							
80ms							
RIB1(mm)	30	5	12	14	9	10	14
RIB2(mm)	44	20	34	20	10	32	32
RIB3(mm)	17	5	8	14	12	8	16
SACROILIAC (N)	4193	2996	3949	4598	2989	3606	4097

Figure 11. Dynamic Sled test dummy injury

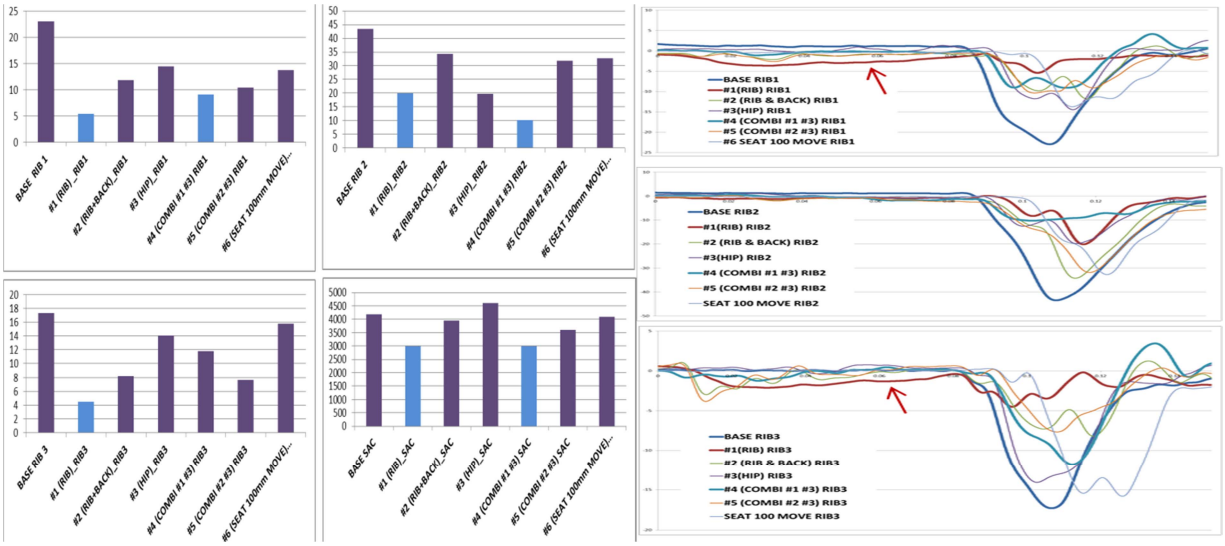

Figure 12. Dynamic Sled test dummy injury graph

It was confirmed that sacroiliac was improved by about 30% in # 1 and # 4 compared with base test. Both specs were a product with a large underbody movement. The # 1 Product shows that the lower body's Moment Z is higher and the pelvis is twisted relative to the Z axis. In the # 4 Product, Moment Y and Moment Z were changed at the same time, lifting their buttocks and making contact with the armrest part of the door trim, so that the improvement was less than expected, but the improvement may be different depending on the shape and position of the armrest.

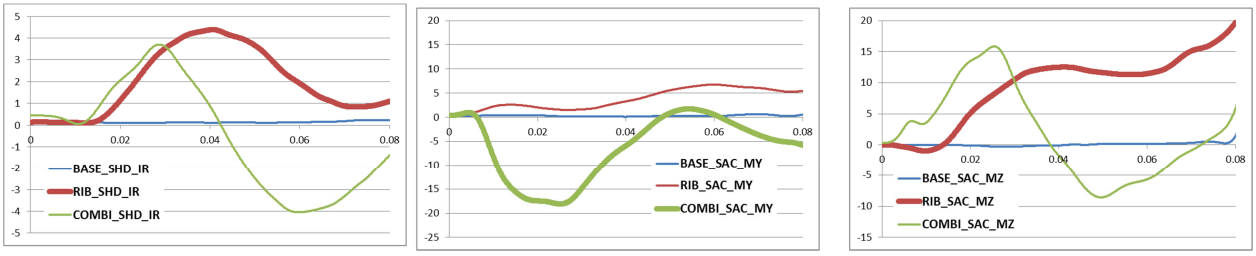

Figure 13. Sensor values for prediction of chest and pelvic movement

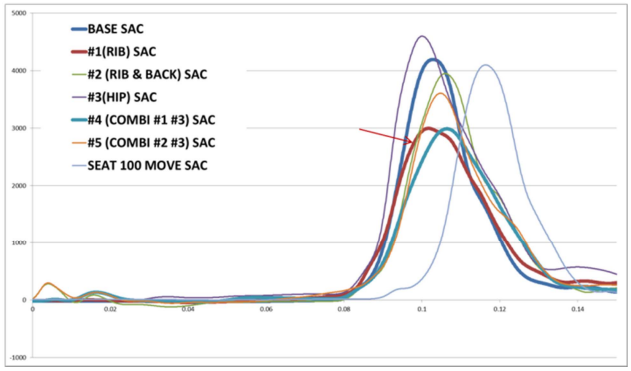

Figure 14. Sacroiliac Injury Graph

Compared to the base test, the injured products have a dummy motion changed (80 ms) before collision with the vehicle. In the case of the RIB Product, the angle of the shoulder was changed and the rotation of the pelvis in the Z axis was largely affected. In the case of the combination Product, the direction of the Y axis was largely affected. Although we could not quantitatively understand the amount of movement and injury of the dummy, it was confirmed that the dummy movement amount was large

CONCLUSIONS.

In this paper, we applied the concepts of existing products and conducted new tests. It was confirmed through CAE and test that major injuries of the chest and sacroiliac injury were improved by the movement of the dummy before the collision at the side collision. Especially, PRE SAFE SAB attached to the chest seat bolster showed that not only chest injuries but also pelvis movements improved pelvic side injuries.

We did not carry out the actual vehicle test linked to the active system, but we will improve the completeness of the product through the actual vehicle test connected with the active system.

We examined ways to improve side impact considering future integration systems. There are already a number of studies being conducted that incorporate active and passive activities, and further progress is expected. We hope that products will be developed that can not only assess conflicts but also respond to accidents by integrating active activities and hands.

REFERENCES

Make sure “references” style is selected. It will automatically number

[1] Michael Fehring. 2017. “Effectiveness Potential of PRE-SAFE® Impulse Using the Scenario of a Major Accident at an Intersection as an Example.” ESV 2017

[2] Christian Weiss,. 2018. “Pre sense side : Innovation for advanced occupant protection in side collisions” Airbag 2018

[3] B.C. Mueller 2018. “ Development of an updated IIHS side impact crash test program” Airbag 2018

THE GEOMETRICAL RELATIONSHIP BETWEEN THE LAP BELT AND OCCUPANTS' ANTERIOR SUPERIOR ILIAC SPINE

Koji Mizuno
Wataru Hatano
Ryoichi Yoshida
Nagoya University
Japan

Yutaka Nakajima
Yoshihiko Tanaka
Takanari Muroya
Ryota Ishigaki
Autoliv Japan
Japan

Paper Number 19-0230

ABSTRACT

The restraint of the pelvis by the lap belt is a prerequisite for occupant protection in a 3-point seatbelt system. If the lap belt slips over the anterior superior iliac spine (ASIS), the lap belt can penetrate the abdominal area during impact, leading to abdominal injuries. Many studies of this phenomenon (known as submarining) have focused on cases in which the lap belt is initially positioned correctly, but slips off due to the dynamics of impact. However, lap belt riding over the iliac bone can also occur when the lap belt is placed on the abdomen from the beginning, without overlapping the iliac crest. In this research, the relationship of the lap belt to the ASIS of seated occupants was investigated, first by statically measuring the initial lap belt-ASIS overlap in a group of volunteers and then by using FE analysis to assess the dynamic interaction of the lap belt with ASIS during test-sled crash simulations.

The lap belt-ASIS overlap of ten volunteers was measured as they sat in a small car's rear seat (where the lap belt anchor is further back). The lap belt did not overlap with the ASIS for four volunteers: of these, three had a body mass index (BMI) of less than average (that is, <24.1 kg/m^2). Further measurements of 20 male volunteers sitting in a rigid seat were conducted to examine the factors which affect the lap belt-ASIS overlap. When volunteers sat in an upright posture, the overlap increased as the height of the ASIS relative to the thigh increased. When they sat in a slouching posture, for low-BMI volunteers the lap belt was located higher on the (flat) abdomen and the overlap of the lap belt with the ASIS tended to decrease.

FE analysis was carried out for rear seat occupants whose ASIS was located at the torso-thigh junction. For the occupant with a protruding abdomen, even though the lap belt did not initially overlap the ASIS, during impact the lap belt was pulled rearward and down; there was sufficient time for the lap belt to interact with the ASIS. However, for the occupant with a flat abdomen, since the abdomen fore-aft diameter and the flesh thickness on the ASIS was small, there was not enough time for the lap belt to interact with the ASIS even though the lap belt was pulled downward, and the lap belt penetrated into the abdomen. Thus, for low-BMI occupants in the rear seat both the initial lap belt-ASIS overlap and the dynamic interaction of the lap belt with the ASIS during vehicle deceleration tend to be insufficient for effective restraint of the pelvis.

INTRODUCTION

The lap belt's ability to restrain the pelvis is a key factor in protecting car occupants during a head-on impact. The lap belt should remain on the forward edge of the iliac wing, and the anterior superior iliac spine (ASIS) works as a hook. When the lap belt slips off the ASIS, the lap belt can translate to the abdomen (a phenomenon known as

submarining) and cause serious injuries. Many studies have investigated the mechanics and parameters which cause submarining [1-5]. During impact, the pelvis rotates rearward because of the inertial force of the lower extremities; if the tangential force of the lap belt along the forward edge of the iliac wing is larger than the maximum friction force, the lap belt slips off the ASIS [1,2]. Thus the angle of the lap belt relative to the pelvis is a criterion for predicting submarining [2]. The submarining occurrence factors and countermeasures for preventing submarining are listed by Östling et al. [5] as: 1. the initial position of the occupant (e.g., slouched or reclined); 2. the relative position of the lap belt and the occupant (e.g., fore/aft position of the lap belt anchorages); 3. restraint system conditions (levels of initial slack in belt and pre-tensioning); 4. seat pan design, geometry and stiffness; and 5. leg/knee support.

Many studies focused on the submarining that occurs when the lap belt initially interacts with the iliac bone, but slips off the ASIS and rides over the iliac crest during impact. However, the lap belt riding over the iliac crest can also occur if the lap belt is poorly positioned initially. The placing of the lap belt on the pelvis depends on lap belt geometry, occupant posture and seatbelt slack [3]. In addition, it has been pointed out that occupants should be careful to wear the lap belt correctly on the pelvis [3].

It is believed that, in general, the lap belt overlaps with the ASIS of occupants when they fasten their seatbelt carefully and correctly. In crash tests with the commonly used Hybrid III dummy, the ASIS is higher than the torso-thigh junction in the initial sitting posture, and the lap belt usually overlaps the ASIS [7]. With the standard restraint systems, the lap belt usually interacts with the Hybrid III's ASIS during impact and submarining does not occur. In offset frontal impact tests conducted by JNCAP (Japan New Car Assessment Program), the scores of the Hybrid III AF05th in the rear seat are reduced if submarining occurs, which is decided based on the drop of the ASIS load cell force. In JNCAP tests from 2010 to 2016, submarining occurred on both sides of the ASIS in one car, and on the inboard side of the ASIS in three of 99 cars.

Some studies investigated the lap belt path with respect to the human ASIS. Wells et al. [8] surveyed volunteers, reporting that lap belt-ASIS overlap was frequently insufficient. 42% of the lap belt centerline was above the ASIS, and 89% partly overlap the ASIS. Reed et al. [9] measured the lap belt position with respect to the ASIS of volunteers. In obese occupants, the lap belt was further away (in the anterosuperior directions) from the ASIS. Another study reported that the lap belt was positioned lower relative to the ASIS in the Hybrid III AM50th and AF05th dummies than in volunteers [10]. Hence, crash tests using the Hybrid III dummies are likely to overestimate the effectiveness of the lap belt at preventing submarining in humans; the lap belt layout may not be adequately assessed in these tests.

The lap belt's interaction with the ASIS has been investigated for obese occupants. In accident analysis, no clear tendency was observed for the frequency of abdominal injuries caused by the lap belt to increase with BMI [11]. Using cadavers to test for comparisons between obese and non-obese occupants, Kent et al. [12] showed that the forward displacement of the pelvis of the obese occupant was greater before the lap belt interacted with the ASIS. Using accident data, Hartka et al. [13] surveyed the location of subcutaneous injuries caused by the lap belt to front-seat occupants in vehicle frontal collisions. They examined computed tomography scans of the abdomen for evidence of the radiographic seatbelt sign. As BMI increased, the anterior displacement of the radiographic seatbelt sign relative to the ASIS increased, whereas the superior displacement decreased. They postulated that the lap belt applied rearward and downward force to the obese occupant (toward the anchor), and that the lap belt interacted with the ASIS during impact, even though the lap belt did not initially overlap the ASIS. Although many research studies focused on occupants of standard-size and obese, there is a little research which examined the pelvis restraint by a lap belt for thin occupants. Izumiya et al. [6] investigated pelvis locations using X-ray image for 85 volunteers in standing and seated postures, and found that low-BMI occupants tend to have kyphosis of the lumbar spine along with the rear-inclined pelvis. They also conducted an FE analysis of a low-BMI occupant model with the pelvis in an initially reclined posture in a rear seat. The pelvis rotated rearward during impact and the lap belt slipped off the ASIS, although they initially interacted.

In this research, the interaction between the lap belt and the ASIS was investigated based on volunteers' measurements (statically) and finite element (FE) simulations (dynamically). We focused on rear seat occupants for two reasons. One is that once the lap belt has slipped off the ASIS, severe submarining can occur because the knees

are not stopped by the instrument panel, as they would be in the front seat. The second reason is that the lap belt-ASIS overlap may be inadequate since the lap belt anchors in the rear seat tend to be very far back, creating a shallow lap belt angle. In this research, the actual situation was first investigated by measuring the lap belt-ASIS overlap of ten male volunteers seated in the rear seat of a small car. Next, to understand the factors which affect the overlap, 20 volunteers sat in a simple rigid seat, and the relationship between anthropometry and lap belt-ASIS overlap was examined. Finally, a human FE model was used to examine the dynamic interaction of the lap belt with the ASIS. The research and the procedure for obtaining the anthropometric measurements of volunteers were both approved by the ethics committee of the School of Engineering, Nagoya University (Document Number 18-1).

THE LAP BELT-ASIS OVERLAP FOR OCCUPANTS OF A SMALL CAR

The geometrical relationships between the lap belt and the ASIS were measured for ten volunteers (Table 1) and two human surrogates, Hybrid III and THOR. The volunteers wore a thin, full bodysuit and sat on the rear seat of a small car. They were directed to sit and place the shoulder belt and lap belt by themselves as usual. The volunteers' ASIS coordinates were measured with a FaroArm coordinate measuring machine. The lap belt's upper and lower edges were also measured along its path. The ASIS location was identified by a medical doctor. The ASIS position was expressed by its projection onto the lap belt: the ASIS point was extended in the vehicle-forward direction until it intersected with the lap belt.

Figure 1 shows the sitting posture of Volunteers 1, 4, and 10, THOR, and Hybrid III. Note that the volunteers were arranged in ascending order of body mass index (BMI). The bottom edge of the lap belt is fitted around the torso-thigh junction at the ASIS for Volunteers 1 and 4 (Figure 1(a) & (b)). The ASIS is above the top edge of the lap belt for Volunteer 1 and Hybrid III. However, for Volunteer 10, who has a high BMI (30.6 kg/m^2), the top edge of the lap belt is fitted around the torso-thigh junction at the ASIS, and the lap belt was fitted in front of the ASIS, as shown in Figure 1(c). This lap belt path is similar to THOR's (Figure 1(d)).

Figure 2 shows the distance of the right and the left ASIS from the bottom edge of the lap belt of inboard (buckle) and outboard side in the rear seat. The ASISs of four volunteers (Nos. 3, 4, 5, and 8) were below the lap belt's bottom edge (poor lap belt fit, which would lead to submarining in the event of a crash); three of them, Volunteers 3–5, had BMIs of less than 23.6 kg/m^2. In the sitting posture in the rear seat, the ASISs of Volunteers No. 3, 4, 5, 8, and 9 and the dummy THOR were positioned on the torso-thigh junction. However, for THOR half of the lap belt overlapped with the ASIS because the lap belt was placed forward, due to the protruding abdomen. In contrast, the pelvic height was high enough that the ASIS was above the torso-thigh junction for the other volunteers (Nos. 1, 6, and 7) and Hybrid III; as a result, more than two-thirds of the lap belt overlapped with the ASIS. The height of the ASIS relative to the torso-thigh junction is probably an important parameter to determine the lap belt-ASIS overlap.

Table 1. Volunteer height and weight sat in the rear seat of small car

No.	Height (cm)	Weight (kg)	BMI (kg/m^2)	Age
1	172	60	20.3	23
2	174	64	21.1	28
3	176	72	23.2	25
4	171	68	23.3	24
5	177	74	23.6	65
6	163	63	23.7	35
7	174	73	24.1	27
8	177	79	25.2	33
9	173	80	26.7	36
10	179	98	30.6	42
Ave.	173.6	73.1	24.1	33.8

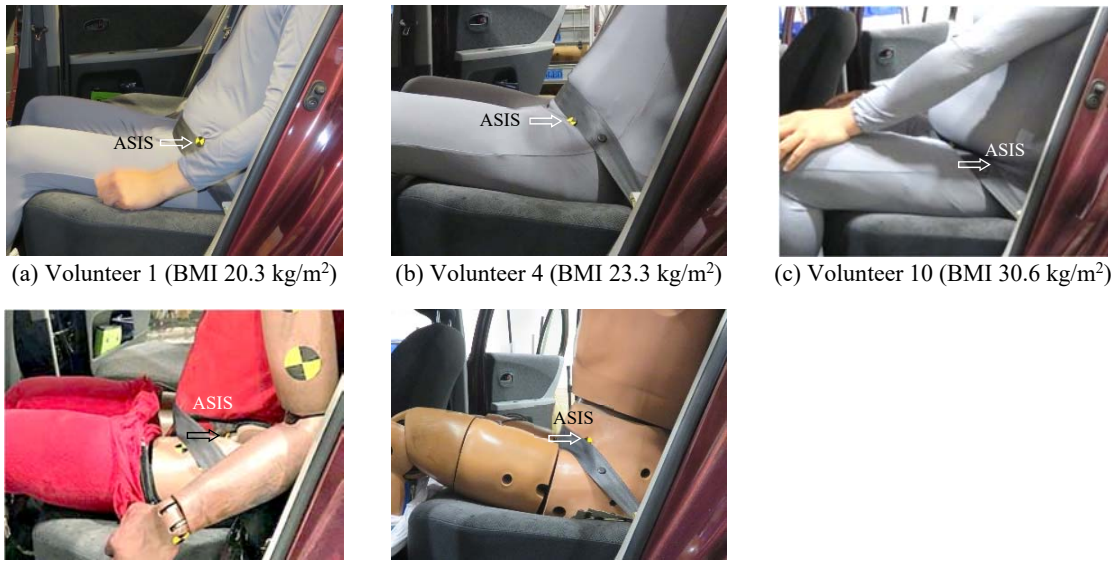

(a) Volunteer 1 (BMI 20.3 kg/m^2) (b) Volunteer 4 (BMI 23.3 kg/m^2) (c) Volunteer 10 (BMI 30.6 kg/m^2)

(d) THOR (e) Hybrid III

Figure 1. The lap belt and ASIS locations in volunteers, THOR and Hybrid III in the rear seat of a small car.

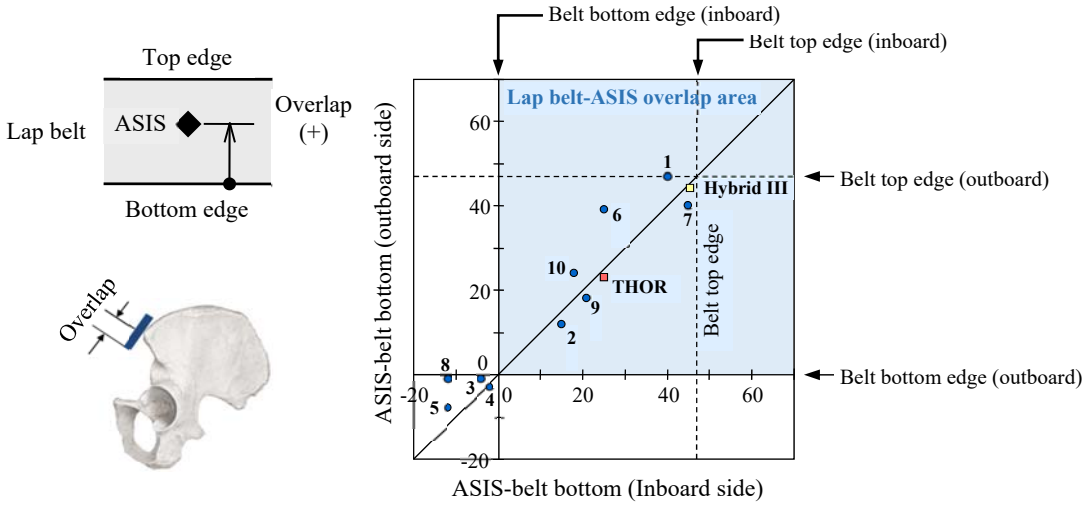

Figure 2. The distance of the ASIS from the bottom edge of the lap belt of inboard (buckle) and outboard side in the rear seat. The blue circles represent the volunteers (numbered w.r.t. BMI) and the squares the test dummies.

FACTORS AFFECTING LAP BELT-ASIS OVERLAP OF OCCUPANTS

A simple rigid seat was used to examine basic factors which affect the lap belt-ASIS overlap. The seat's width, depth, and height was 400 mm, 500 mm, and 550 mm, respectively. Twenty male volunteers sat in an upright posture placing a 3-point seatbelt by themselves (Figure 3). In addition, they also sat in slouching posture so that the pelvis was moved forward by 100 mm. Their BMIs ranged from 17.6 to 32.1 kg/m^2 (average 24.2). The relative positions of thigh, ASIS, and lap belt were measured by a FaroArm coordinate measuring machine. For three of the volunteers (Volunteer 2, 13 & 20), additional measurements were conducted: body outer shape was measured by a 3D LED scanner (Artec Eva), and all measurements were repeated after both lap belt anchors were moved forward by 100 mm from the standard anchor positions.

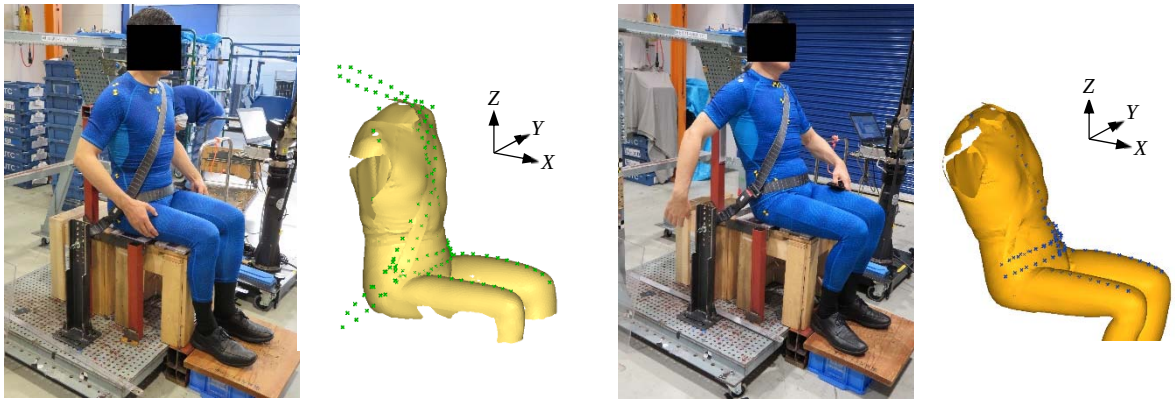

(a) Pelvis position 0 mm (b) Pelvis position 100 mm

Figure 3. Measurements of volunteer in a rigid seat. From the origin of the seat (center of cross line of seat and seat back), the coordinates of the outer and inner belt anchors were x=21 mm, y=284 mm, and z=-50 mm and x=-46 mm, y=-274 mm, and z=-23 mm, respectively. 3-dimensional shape was made by 3D scanner, and points were measured by coordinate measuring machine.

Anthropometry

The lap belt path depends on the anthropometry of the occupant. The anthropometric parameters abdomen fore-aft diameter, ASIS position, and thigh height were examined based on BMI (see Figure 4). Thigh height was measured at the torso-thigh junction in the sagittal plane of the ASIS. Accordingly, the ASIS height relative to the thigh indicates the protrusion of the ASIS from the torso-thigh junction.

Figure 5 graphs the abdomen fore-aft diameter against the BMI for all volunteers. Each circle in the figure corresponds to a volunteer (as before, numbered in order of ascending BMI). The fore-aft diameter of the abdomen increases as BMI increases. The heights of the left and right thighs also increase with BMI for both pelvis positions (Figure 6). However, the correlation of thigh height with BMI is lower for the 100-mm forward pelvis position than for the original position. Figure 7 shows the ASIS height plotted against the BMI. The ASIS heights do not depend significantly on the BMI. Comparing Figure 7(a) to (c) and Figure 7(b) to (d) makes it clear that the ASIS heights do not change significantly, even though the pelvis posture angle changes when the pelvis moves forward 100 mm. As shown in Figure 8, the ASIS height relative to the thigh decreases with an increase in BMI, because thigh height increases with BMI whereas the ASIS height has little relation to BMI. This correlation exists for both pelvis positions (0 mm and 100 mm).

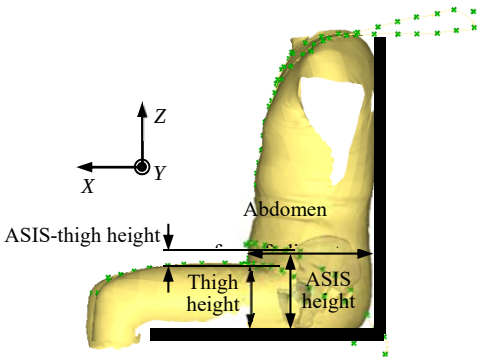

Figure 4. Anthropometric measurements

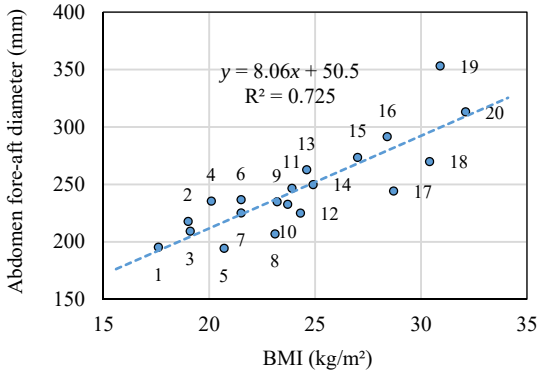

Figure 5. Abdomen fore-aft diameter vs. BMI. The blue circles are volunteers, numbered by increasing BMI.

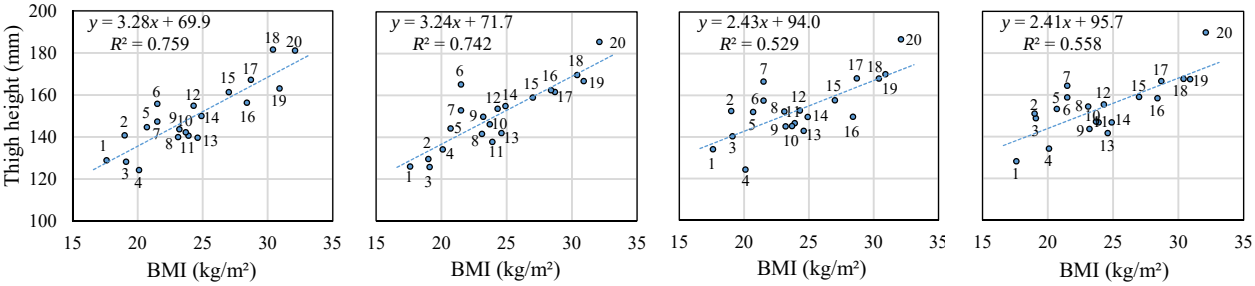

(a) Pelvis position 0 mm (left thigh) (b) Pelvis position 0 mm (right thigh) (c) Pelvis position 100 mm (left thigh) (d) Pelvis position 100 mm (right thigh)

Figure 6. Left and right thigh height vs. BMI

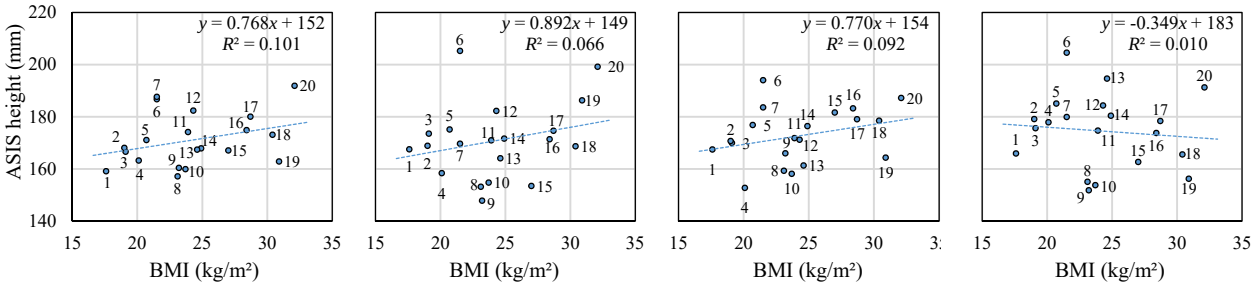

(a) Pelvis position 0 mm (left ASIS) (b) Pelvis position 0 mm (right ASIS) (c) Pelvis position 100 mm (left ASIS) (d) Pelvis position 100 mm (right ASIS)

Figure 7. Left and right ASIS height vs. BMI

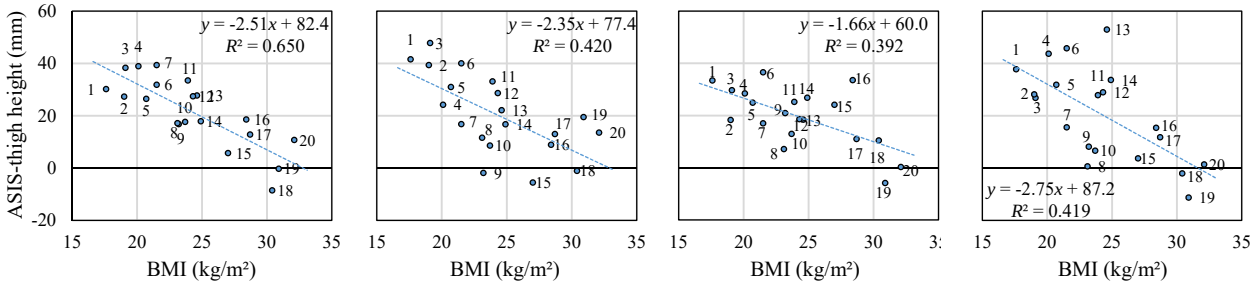

(a) Pelvis position 0 mm (left ASIS) (b) Pelvis position 0 mm (right ASIS) (c) Pelvis position 100 mm (left ASIS) (d) Pelvis position 100 mm (right ASIS)

Figure 8. Left and right ASIS height relative to thigh vs. BMI

Lap Belt Path

The surface shape of the 3D body image was developed and modified using Artec Studio 10 Professional and Geo Magic Design X software from a scan of Volunteer 2, 9 and 19. Shell elements were generated on the surface of the body surface in automatic meshing by Altair Hyper Mesh. The shell elements and seat belt elements of the lap belt were made to fit on the shell elements of body surface using a seatbelt fitting interface in LS-PrePost. The shell elements were used in the area where the lap belt fitted the body in curved surface. Five lap belt paths (P1–5) were made with different belt path heights while inboard and outboard anchor points were fixed. Each path was raised by 20 mm in the midsagittal plane: P3 is made to follow the actual lap belt path. P1 and P2 are below—and P4 and P5 are above—the actual path (Figure 9). The distance (error) between the centerlines of the lap belt elements and of the actual lap belt in the same sagittal plane (*xz*-plane) was calculated. Lap belt length was compared for all five paths in the standard upright position, the slouched position, and the slouched position with both belt anchors moved forward.

Figure 10 shows the average distance between the lap belt fitted on the body surface and the actual lap belt path of Volunteer 2. For the pelvis position 0 mm and the anchor position 0 mm (Figure 10(a)), the farther each path is from the actual, the longer it becomes. That is, P3 is the shortest and the others are all longer. Wearing the lap belt in the shortest path was also true for Volunteer 9 and 19, therefore, many occupants probably fit their lap belt with the shortest total lap belt length, since the actual path was taken from volunteers' freely chosen belt path. However, when the pelvis is positioned 100 mm forward (Figure 10(b)), the total belt lengths for P2, P3, and P4 are comparable, and the lap belt paths are probably unstable. The belts in P3 could slide up to the P4 path on the abdomen. In the forward anchor position with pelvis forward, P2 is shorter than P4, so in the former the lap belt will not be able to slide up to the abdomen, but will remain on the thigh (Figure 10(c)).

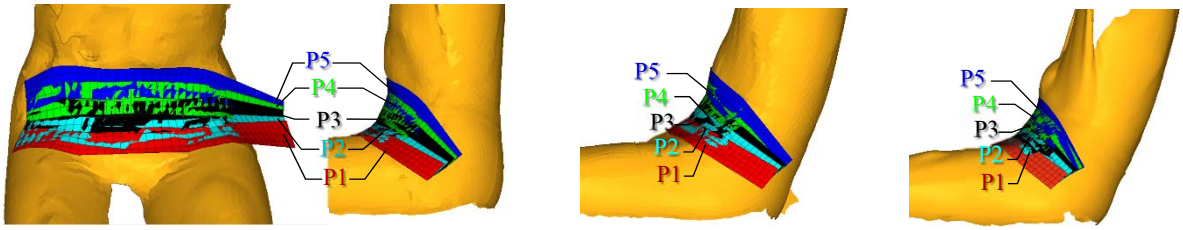

(a) Pelvis position 0 mm
Anchor position 0 mm

(b) Pelvis position 100 mm
Anchor position 0 mm

(c) Pelvis position 100 mm
Anchor position 100 mm

Figure 9. Lap belt fitting on the body surface of Volunteer 2 with a low BMI (19.0 m/kg^2)

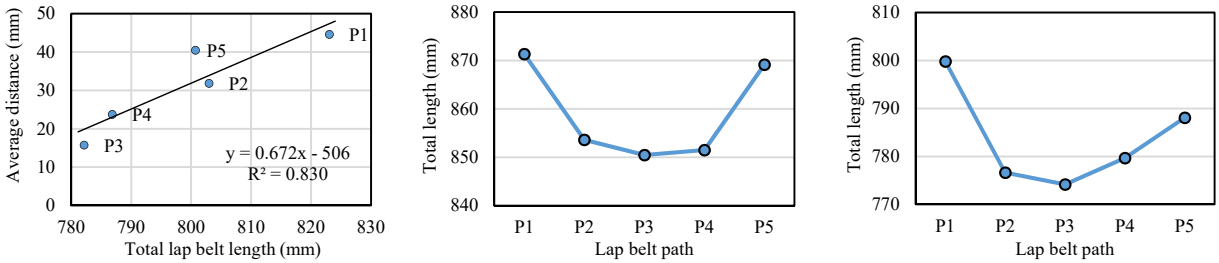

(a) Pelvis position 0 mm
Anchor position 0 mm

(b) Pelvis position 100 mm
Anchor position 0 mm

(c) Pelvis position 100 mm
Anchor position 100 mm

Figure 10.(a) The average distance of the five lap belt paths from the actual lap belt path (pelvis position 0 mm, anchor position 0 mm) for Volunteer 2; (b) & (c) total lap belt lengths for the five belt paths (pelvis position 100 mm and anchor position 0 mm and pelvis position 100 mm and anchor position 100 mm, respectively.

Lap Belt-ASIS Overlap

The height of the lap belt-ASIS overlap (z axis) for each of the 20 volunteers is plotted against BMI in Figure 11, and against ASIS height relative to the thigh in Figure 12. Left and right ASISs are considered separately. Figure 11(a) and (b) show that the lap belt-ASIS overlap decreases as BMI increases for the upright position (pelvis at 0 mm), although the correlation coefficient is small. (Recall that as seen in Figure 8, the ASIS height relative to the thigh decreases with BMI, which indirectly influences the overlap.) However, when the overlaps for the slouching posture are compared (Figure 11(c) & (d)), it is clear that the lap belt-ASIS overlap increases as BMI increases. As shown in Figure 11, the slope of the approximation line of lap belt-ASIS overlap vs. BMI changes from negative to positive when the pelvis is 100 mm more forward, although the correlation coefficient is small. Figure 12(a) and (b) show that, in the upright posture (pelvis position 0 mm), the lap belt-ASIS overlap is proportional to the ASIS height

relative to the thigh. This relation is probably due to the fact that the lower edge of the lap belt is located at the torso-thigh junction. However, for the slouched posture (Figures 12(c) & (d)), there does not appear to be a correlation between the two variables. These results suggest that there is a tendency for the lap belt-ASIS overlap to be sufficient in the upright posture for low-BMI occupants and decrease in the slouching posture. Whereas for high-BMI occupants, the overlap is stable, irrespective of torso angle.

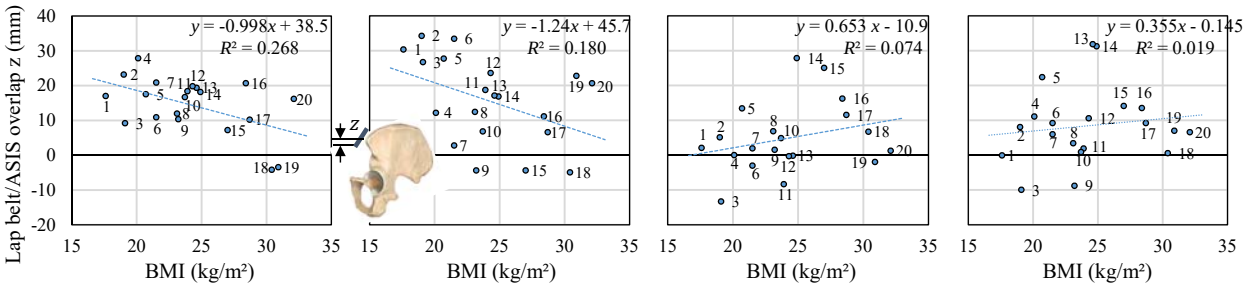

(a) Pelvis position 0 mm (left ASIS) (b) Pelvis position 0 mm (right ASIS) (c) Pelvis position 100 mm (left ASIS) (d) Pelvis position 100 mm (right ASIS)

Figure 11. Lap belt-ASIS overlap height (z) vs. BMI

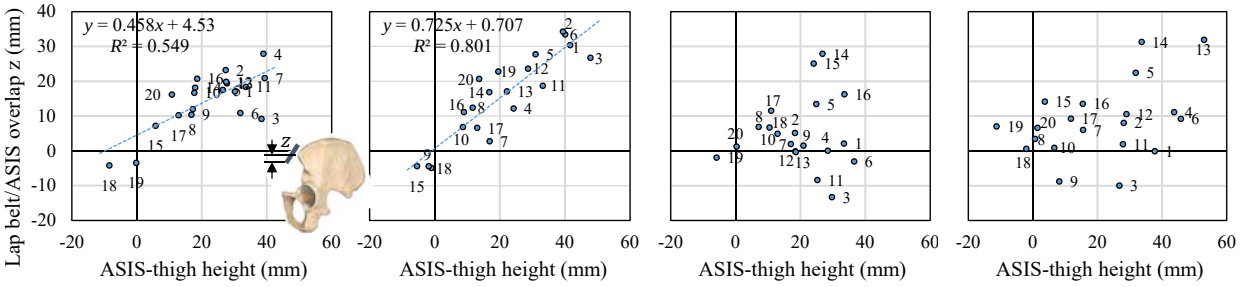

(a) Pelvis position 0 mm (left ASIS) (b) Pelvis position 0 mm (right ASIS) (c) Pelvis position 100 mm (left ASIS) (d) Pelvis position 100 mm (right ASIS)

Figure 12. Lap belt-ASIS overlap height (z) vs. ASIS-thigh height

The photographs in Figure 13 show the lap belt paths of Volunteer 1 (low BMI, 17.6 kg/m^2) and Volunteer 19 (high BMI, 30.6 kg/m^2) for both pelvis positions. In the slouching position, Volunteer 1's lap belt shifted upward onto the flat abdomen, but Volunteer 19's lap belt remained in position under the abdomen. Figure 14 shows the height differences in the lap belt bottom edge for all volunteers in both pelvis positions: the difference is larger for lower-BMI volunteers. All volunteers placed the lap belt around their lower abdomen in the upright posture. However, the low-BMI occupants' belts shifted upward when they slouched. This upward shift probably explains why the lap belt-ASIS overlaps decreased (Figure 11(c) & (d)).

(a) Volunteer 1 Pelvis position 0 mm (b) Volunteer 1 Pelvis position 100 mm (c) Volunteer 19 Pelvis position 0 mm (d) Volunteer 19 Pelvis position 100 mm

Figure 13. Lap belt path in pelvis position of 0 and 100 mm for thin volunteer and obese volunteer

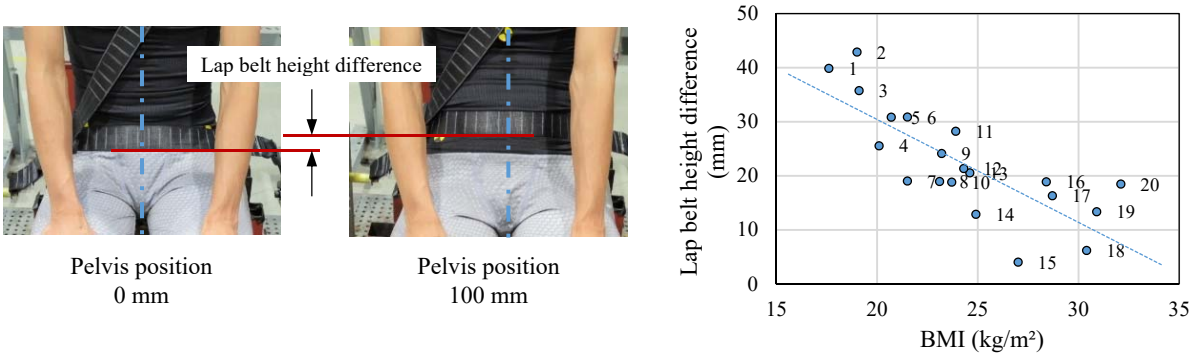

Figure 14. Height differences in lap belt bottom edge from pelvis position of 0 to 100 mm (Volunteer 1)

FE ANALYSIS

The lap belt-ASIS interaction during impact, for occupants with the ASIS locating above and at the torso-thigh junction, was investigated by FE analysis. The model, representing an occupant in the rear seat, consists of a seat, 3-point seatbelt and occupant (Figure 15). THUMS (Total Human Model for Safety) version 3 was used for the human FE model. The friction coefficient between the lap belt and the occupant affects the slip of lap belt on the occupant, and it was 0.3 in this simulation. The crash pulse in the sled was selected to mimic the acceleration of a small car in a full-frontal impact test at a velocity of 50 km/h. Table 2 presents the simulation matrix.

To examine the influence of body habitus on the lap belt's interaction with the ASIS, three different habitus were prepared; for simplicity, only thigh diameter and abdominal shape were modified. Five models were created: Models 1–3 differed in habitus, and Models 4 and 5 used the third habitus and made changes to the lap belt. The ASIS of Model 1 (the original THUMS) when seated was higher by 3 mm (measured vertically, along the z axis) than the torso-thigh junction. Model 2 was the habitus with the ASIS at the torso-thigh junction. To achieve the correct dimensions, the upper thigh diameter was made 20 mm larger than that of Model 1. The ASIS was lower than the bottom edge of the lap belt by 9 mm in the vertical direction (z). In Model 3, which represents an occupant with a flat abdomen, the fore-aft diameter of the torso was reduced to 232 mm from Models 1 and 2 (256 mm). Because it is known that the forward location of the lap belt anchor is effective for improving the lap belt's interaction with the ASIS— preventing submarining [1,2,5]—the seatbelt system was changed in Models 4 and 5. In Model 4, the two anchors were moved forward by 100 mm. In Model 5, a pretensioner model was also attached at each anchor, and the lap belt was pulled toward the lap belt direction by 25 mm at 12 ms in Model 5.

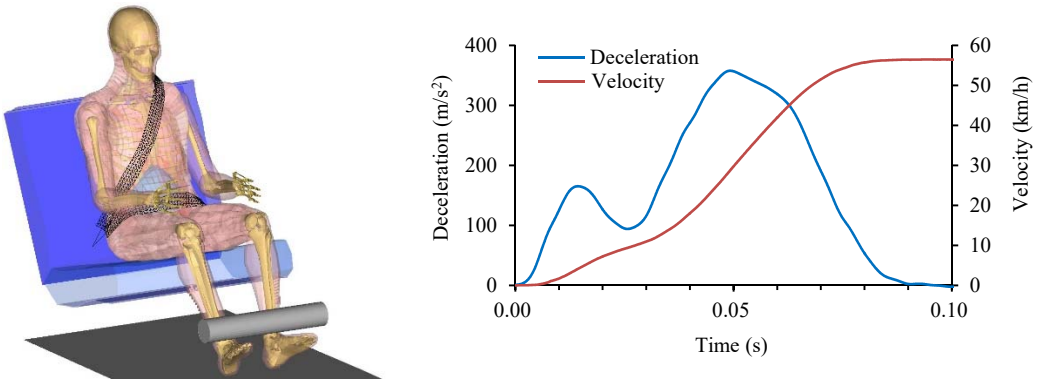

Figure 15. Rear seat occupant model (left), and acceleration pulse and velocity change simulating impact velocity of 50 km/h (right)

Table 2. FE occupant model

Model	Human model	Lap belt anchor	ASIS height w.r.t. lap belt bottom (Δz)
Model 1	Original THUMS (protruding abdomen)	Original	3 mm
Model 2	Large diameter thigh, Protruding abdomen	Original	-9 mm
Model 3	Large diameter thigh, Flat abdomen	Original	-12 mm
Model 4	Large diameter thigh, Flat abdomen	Lap belt anchor 100 mm forward	-14 mm
Model 5	Large diameter thigh, Flat abdomen	Lap belt anchor 100 mm forward Buckle and lap belt pretensioners	-14 mm

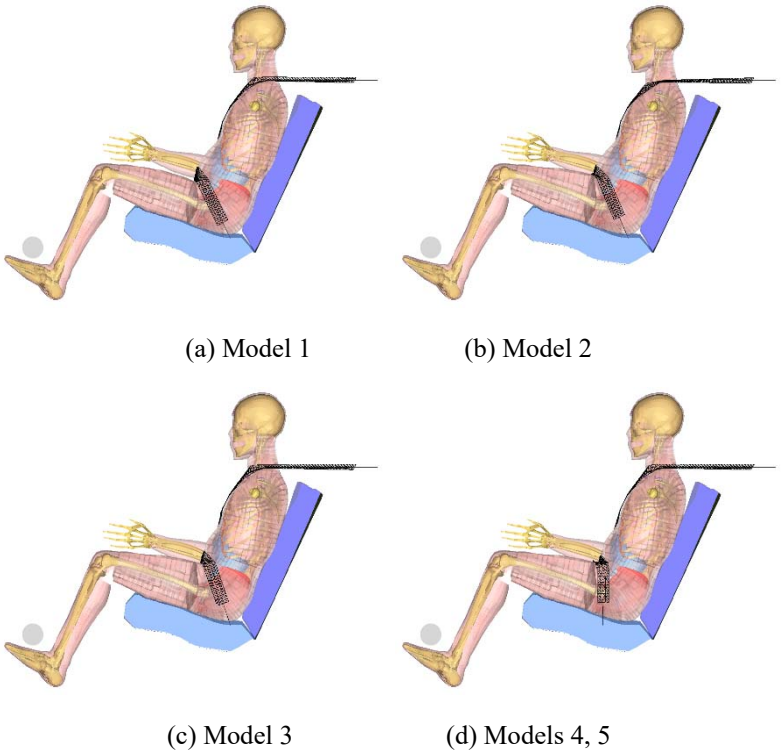

(a) Model 1 (b) Model 2

(c) Model 3 (d) Models 4, 5

Figure 16. Occupant models

The lap belt-ASIS interaction for the five FE models at 75 ms after impact is shown in Figure 17. The lap belt interacted with the ASIS in the original THUMS (Model 1). Even in Model 2, whose ASIS is located at the torso-thigh junction, the middle of the lap belt in the webbing width direction interacted with the ASIS (Figure 17(b)). Although the overlap was less than in Model 1 (in fact, the lap belt did not overlap with the Model 2's ASIS in the initial condition), during the impact the lap belt interacted with the ASIS. The lap belt, pulled down and rearward, stayed on the lower abdomen while the pelvis moved downward in the seat cushion. On the other hand, in Model 3, with a flatter abdomen (the lap belt was closer to the ASIS), even though the lap belt pulled downward during impact, the lap belt rode over the iliac crest because the thickness of flesh tissue on the ASIS was small: the lap belt was positioned above the ASIS initially and there was not enough time for the lap belt to interact with the ASIS during impact. Notably, the lap belt applied force to the abdomen and the lumbar spine flexed due to the concentrated force of the lap belt.

In Model 4, the lap belt anchors were positioned 100 mm forward compared to previous models. The lap belt applied force to the pelvis in a steep downward angle, interacting with the ASIS. In Model 5, the pretensioned lap belt interacted with the pelvis earlier (in the initial phase of deceleration) and reduced the pelvis' forward displacement, compared to Model 4. The pelvis' rearward posture angle was smaller and the lap belt angle steeper for Models 4 and 5 compared to Models 1 and 2, which indicates that the lap belt with anchor in the forward position is stable to interact with the ASIS compared to the standard anchor position [2].

The forward displacement of pelvis (sacrum) for the five models is shown in Figure 18. That of Model 1 is the smallest (199 mm). The pelvis forward displacement is large for Model 3 (260 mm) since the lap belt did not interact with the pelvis at all. In Model 4, the pelvis forward displacement is also large (263 mm) because the lap belt and buckle anchors were positioned more forward. The lap belt angle is steeper and the force component of the lap belt in the rearward direction is too small to decelerate the pelvis effectively. The forward displacement of the pelvis was reduced to 237 mm by the pretensioners in Model 5.

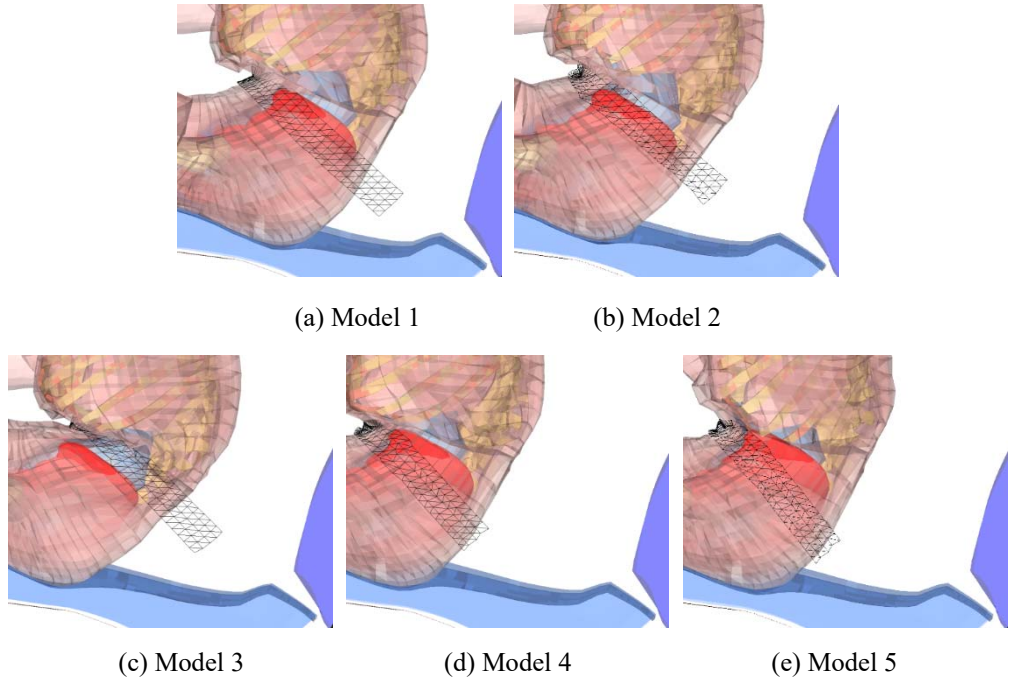

(a) Model 1 (b) Model 2

(c) Model 3 (d) Model 4 (e) Model 5

Figure 17. Lap belt interaction with the ASIS (75 ms)

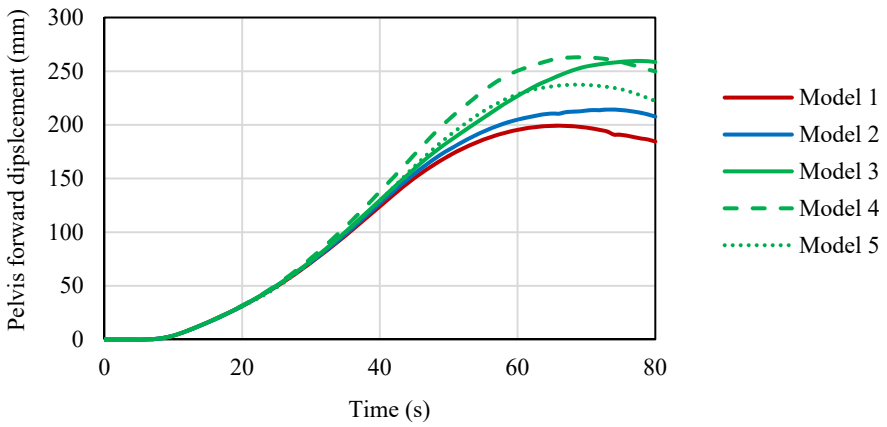

Figure 18. Pelvis forward displacement of FE models

DISCUSSION

In this study, the lap belt-ASIS overlap was examined for ten volunteers sitting in the rear seat of a small car and on a rigid seat. The overlap was relatively small for four out of ten occupants. The overlap tended to be large for low-BMI volunteers in the upright posture, while it decreased in the slouching posture (forward pelvis position). Several volunteers participated in both the rear-seat and the rigid-seat measurements. Figure 19 compares a volunteer (BMI 23.2 kg/m^2) seated in the rear seat of a small car and in the rigid seat. In the 100-mm pelvis forward position in the rigid seat, the pelvis inclines rearward under the lap belt because of the slouched torso. The lap belt path when the volunteer is in the rear car seat is similar to that of the rigid seat with the pelvis forward position. This is probably why low-BMI volunteers tended to have poor lap belt-ASIS overlap both in the rear seat of a small car and in the rigid seat in the pelvis forward position. Some low-BMI occupants sit on the seat with kyphosis of the lumbar spine and the rear-inclined pelvis (Figure 19 (a) & (c)). This posture was pointed out for thin occupants by Izumiya et al. [6]. Thus it is likely that low-BMI occupants rotate their pelvis rearward under the lap belt in the rear seat, and the lap belt-ASIS overlap decreases, as was observed in this study.

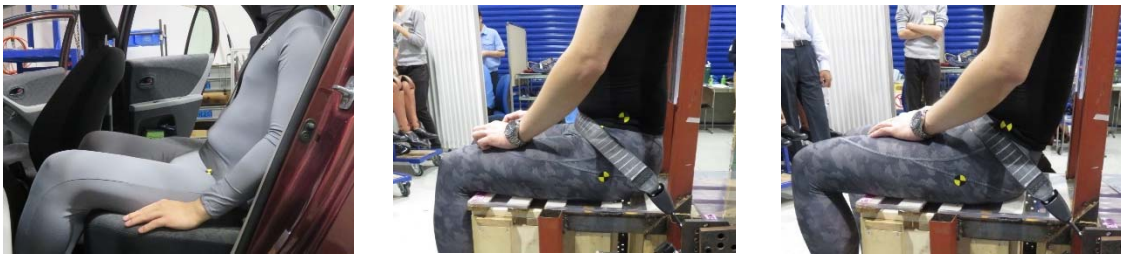

(a) Small car

(b) Rigid seat
(forward position 0 mm)

(c) Rigid seat
(forward position 100 mm)

Figure 19. Volunteer 9 (BMI 23.2 kg/m^2) seated in the rear seat of a small car and in the rigid seat

Based on accident analysis by Hartka et al. [13], the lap belt caught the ASIS for obese occupants in collisions, even though the lap belt overlap with the ASIS of obese occupants are poor in Reed's study [9]. Their results might be consistent with the interaction behavior of the lap belt and ASIS for the original THUMS with protruding abdomen during impact in this study: the protruding abdomen meant the lap belt was further from the ASIS, and thus took more time to move downward as the pelvis rotated, so the lap belt could interact with the ASIS. As shown in Figure 1(c), the lap belt of the THOR dummy is in front of the ASIS because of the protruding abdomen. The lap belt can interact with the ASIS during impact even though the ASIS is located at the torso-thigh junction [7]. In contrast, for the flat abdomen occupant (Model 3), since the abdomen fore-aft diameter is small and the thickness of flesh tissue on the ASIS is small, there was not enough time for the lap belt to catch the ASIS. Model 3 has a thick thigh like a sport man with strong muscle of thigh such as Volunteer 4 sitting in the rear seat (Figure 1(b)). The geometrical relation between the lap belt and the ASIS for Model 3 can be applied for low-BMI occupants with flat abdomen and the bottom of the lap belt placed above the ASIS.

The static measurement in the rigid seat showed that the lap belt can shift up to the abdomen (above the ASIS) in low-BMI occupants in the pelvis forward position, with the standard belt-anchor location (Figure 10(a) & (b)). However, the lap belt will not shift to the abdomen of low-BMI occupants if the lap belt anchor is positioned forward (see Figure 10(c)). On impact, the forward anchor position could cause the lap belt to catch the ASIS, because the lap belt pulled steeply downward during impact. Thus, the anchor-forward position provides a benefit for the lap belt-ASIS interaction. On the other hand, the pelvis displacement is large. Insufficient pelvis restraint can also increase the deflection of the lower chest on the buckle side, since the large lap belt force in the final stage of a crash is transmitted to the shoulder belt through the slit of the tongue plate [7]. In the FE analysis, the lap belt and buckle pretensioners effectively reduced the pelvis forward displacement. However, it should be noted that the forward lap belt anchor locations can worsen the accessibility of rear car seats.

In this study, low-BMI occupants tended to have small lap belt-ASIS overlap in the initial posture; further, FE analysis indicated that the lap belt did not catch the ASIS for these occupants during impact. According to Izumiya's study [6], even though the lap belt interacted the ASIS, submarining inclined to occur for low-BMI occupants because of their initial reclined posture of pelvis. Consequently, the initial overlap—and, more critically, the lap belt-ASIS interaction during impact—can be insufficient for the pelvis restraint of low-BMI occupants.

LIMITATION

The ASIS locations were identified by medical doctors. However, it is difficult to determine the correct position of ASIS because the ASIS has a rounded shape and the high BMI occupants have thick soft tissue on the ASIS. Thus, the ASIS positions can include errors in measurements. The geometry and material properties of the soft tissue of THUMS and its modified FE model were not validated to investigate the movement of the lap belt over the ASIS.

CONCLUSIONS

In this research, the bottom edge of the lap belt relative to ASIS (anterior superior iliac spine) point overlap for volunteers seated in the rear seat of a small car and in the a simple rigid seat was measured. FE analysis was also conducted for the rear seat occupant whose ASIS was located at the torso-thigh junction.

- The bottom edge of the lap belt did not overlap with the ASIS for four of ten volunteers seated in the rear seat of a small car. Three of them had BMIs lower than the volunteer average.
- When volunteers sat in an upright posture in a simple rigid seat, the overlap of the lap belt increased with the vertical height of the ASIS relative to the thigh height. For low-BMI volunteers in the slouched 100 mm forward pelvis posture, the lap belt moved up to the flat abdomen and the lap belt-ASIS overlap tended to decrease.
- FE simulations, using morphed THUMS model, of the occupant with the morphed flat abdomen and ASIS locating at the torso-thigh junction by morphed thighs showed that the lap belt did not interact with the ASIS at all during impact. For the occupant with the protruding abdomen, although the lap belt did not initially overlap with the ASIS, it did during impact since the lap belt was pulled downward and the extra distance provided by compression of the thigh tissue meant there was time for the lap belt to interact with the ASIS.

REFERENCES

[1] Leung, Y.C., Tarrière, C., Fayon A., Mairesse P., Banzet P. 1981. "An Anti-Submarining Scale Determined from Theoretical and Experimental Studies Using Three-Dimensional Geometrical Definition of the Lap-Belt." Proc. 25th Stapp Car Crash Conference, 685-729

[2] Horsch, J.D., Hering, W.E. 1989. "A Kinematic Analysis of Lap-Belt Submarining for Test Dummies." Proc. 33rd Stapp Car Crash Conference, 281-288

[3] Leung, Y.C., Tarrière, C., Lestrelin, D., Hureau, J., Got, C., Guillon, F., Patel, A. 1982. "Submarining Injuries of 3 Pt. Belted Occupants in Frontal Collisions – Description, Mechanisms and Protection." SAE paper 821158, 26th Stapp Car Crash Conference

[4] Rouhana, S.W., Horsch, J.D., Kroell, C. 1989. "Assessment of Lap-Shoulder Belt Restraint Performance in Laboratory Testing." SAE paper 892439, 33rd Stapp Car Crash Conference

[5] Östling M., Sunnevång C, Svensson C., Kock H.O. 2017. "Potential Future Seating Positions and the Impact on Injury Risks in a Learning Intelligent Vehicle (LIV)." VDI-Tagung Fahrzeugsicherheit, Berlin, Germany

[6] Izumiyama, T., Nishida, N., Iwanaga H. et al. 2018. "The Analysis of an Individual Difference in Human Skeletal Alignment in Seated Posture and Occupant Behavior Using HBMs." IRCOBI Conference

[7] Mizuno K., Yoshida R., Nakajima Y. et al. 2018. "The Effects of Inboard Shoulder Belt and Lap Belt Loadings on Chest Deflection." Stapp Car Crash Journal, 62, 67-91

[8] Wells, R.P., Norman, R.W., Bishop, P., Ranney, D.A. 1986. “Assessment of the Static Fit of Automobile Lap-Belt Systems on Front-Seat Passengers.” Ergonomics 29(8), 955-976
[9] Reed, M.P., Ebert-Hamilton, S.M., Rupp, J.D. 2012. “Effects of Obesity on Seat Belt Fit.” Traffic Injury Prevention, 13(4), 364-372
[10] Park, J., Ebert, S.M., Reed, M.P., Hallman, J.J. 2018. “Comparison of Three-Point Belt Fit between Humans and ATDs in Rear Seats.” Traffic Injury Prevention, 19(sup1), S65-S69
[11] Desapriya, E., Giulia S., Subzwari S. 2014. “Does Obesity Increase the Risk of Injury or Mortality in Motor Vehicle Crashes? A systematic Review and Meta-Analysis”, Asia-Pacific Journal of Public Health, 26(5), 447-460
[12] Kent R.W., Forman J.L., Bostrom O. 2010. “Is There Really a “Cushion Effect”?: A Biomechanical Investigation of Crash Injury Mechanisms in the Obese,” Obesity, 18, 749-753
[13] Hartka, T.R., Carr H.M., Smith B.R., Melmer M., Sochor M.R. 2018. “Does Obesity Affect the Position of Seat Belt Loading in Occupants Involved in Real-World Motor Vehicle Collisions?” Traffic Injury Prevention, 19(sup1), S70-S75

INJURY MECHANISM AND EVALUATING METHODS FOR SMALL OVERLAP AND OBLIQUE FRONTAL CRASHES

Akihiro Ishida, Satoshi, Takizawa
Honda R&D Co.,Ltd. Automobile R&D Center
Japan

Paper Number 19-0232

ABSTRACT

According to a National Highway Traffic Safety Administration (NHTSA) study, small overlap and oblique frontal crashes account for 25% of fatal accidents in the United States. This is a large proportion, and comprises the accident mode with the highest fatality rate. The fact that occupants collide with the cabin is a factor in this. The purpose of the present research is to recreate the injuries that occur to occupants in actual accidents involving small overlap and oblique frontal crashes, and to formulate a method for evaluating them. By enhancing vehicle body performance and occupant restraint performance, the goal is to reduce fatalities and injuries. In order to verify the circumstances of injury during small overlap and oblique frontal crashes, crash simulations were performed by numerical computation. A human body model was also placed in the driver's seat to verify the occupant movement and extent of injury. The oblique mode that the NHTSA is slated to adopt was first verified using numerical simulation, but collision on the occupant's chest could not be confirmed. For the present research, therefore, verification of the angle and speed parameters was carried out so that occupant movement could be recreated in a way that conformed to actual accident circumstances. The result of simulation was that occupant movement with respect to the vehicle together with vehicle body deformation showed the occurrence of collision with the occupant's chest when the evaluation vehicle (a passenger car) was impacted by an OMDB with an overlap (LAP) of 25%, at an angle of 30°, and at a speed of 110 km/h. The collision occurred in the same place, with injury to the same areas, and with the same degree of injury as shown under actual accident circumstances in a small overlap and oblique frontal crash. In light of these results, it was confirmed that injuries would be reduced by increasing the body strength of the evaluation vehicle to reduce deformation and by installing air bags on doors where oblique loading affected occupant movement. Numerical simulation of the above modes was performed using a passenger car that received the highest evaluation from the Insurance Institute for Highway Safety (IIHS). While vehicle body deformation was evaluated at the GOOD level even in oblique mode (in-house data), vehicle body deformation increased and occupant chest collision occurred that resulted in AIS4+ level injuries. This method of evaluation was confirmed to offer possibilities for evaluation of small overlap and oblique frontal crashes that conforms to actual accidents, and for evaluation that may further reduce fatalities and injuries. The effectiveness with respect to these injuries of measures taken through restraint devices and the vehicle body by means of numerical simulation using a human body model was verified. The results confirmed that combining vehicle body and restraint device measures had the effect of reducing injuries.

INTRODUCTION

Attention in the United States is being focused on small overlap and oblique frontal crashes because these types of crashes often result in fatal accidents even though the vehicle has the most up-to-date body technology and safety equipment. According to an NHTSA study, small overlap and oblique frontal crashes account for 25% of fatal accidents in the United States, which is a large proportion, making this the accident mode with the highest fatality rate [1]. According to Rudd et al. [2] it has been reported that in small overlap and oblique frontal crashes, 45% of AIS3+ injuries to occupants in the driver's seat are to the chest and 38% to the head. It is clear that causal factors in those injuries to the head are collision with the A-pillar, and to the chest, collision with the door, resulting in the large proportions of these injuries. One distinctive feature in the case of the chest, in particular, is that the ribs on the non-belted side collide with the door, causing fracture injuries. It is reported more chest injuries with the door as a factor in small overlap crashes than in co-linear crashes, and they consider these to be the result of the occupant's lateral motion and deformation of the vehicle body. Iraeus et al. [3] defined the crash mode accompanied with lateral movement as an oblique mode. They studied the mechanism of chest injury during oblique crashes using a human body model, and indicated that fractures occured when the load input from the seatbelt caused the body to bend in a longitudinal direction so that the rib cage bulgeds outward on the side, and the lateral motion of the body caused that side to crash into the door trim, resulting in fracture. There are also the findings in Lindquist et al. [4] and Brumbelow et al. [5] that the sites of fractures that occur in small overlap crashes in real-world accidents extend throughout the entire left side (ribs 1 to 12), with a particularly large number in ribs 1 to 10, which attach to the sternum.

In order to achieve further advances in vehicle body safety performance with regard to small overlap and oblique frontal crash accident patterns, and to reduce the distinctive injuries in such types of accidents, the Insurance Institute for Highway safety (IIHS) initiated a new evaluation in 2012 for the purpose of reducing injuries from small overlap and oblique frontal crashes. The SOT (Small Overlap Test) evaluation tests of the IIHS involve crashing a vehicle into a rigid barrier with 150-mm curvature on the corners at a speed of 64 km/h and the front end offset 25%. The NHTSA is considering revision of the New Car Assessment Program (NCAP) with a test method(Oblique test) using an Oblique Moving Deformable Barrier (OMDB) with attached aluminum honeycomb that collides with the test vehicle at a speed of 90 km/h and at an angle of 15° with a 35% offset in a small overlap crash for evaluation.

The present research sought a reduction in fatalities and injuries by focusing attention on the chest, in particular, as the location of injuries in small overlap and oblique frontal crashes, and devised an evaluation method that could enable reduction of those injuries. A numerical simulation was first implemented using a passenger car in the oblique test that is currently scheduled to be adopted for the NCAP. This approach used an adult male human body finite element (FE) model to verify the occurrence of the occupant’s chest collision with interior car body, and it sought test configurations that would recreate the injuries sustained in actual small overlap and oblique frontal crash accidents. It also used an OMDB FE model to verify configurations that make it possible to evaluate the vehicle. Directions to be taken in measures addressing this issue of injuries to the chest were examined in terms of both vehicle body and restraint device measures necessary for reducing future fatalities and injuries.

METHODS AND RESULTS

Reproducibility of chest injury by Oblique test

Crash simulations were conducted by numerical simulation using an explicit FE code. LS-DYNA(v971 6.1.2) to verify the actual injuries sustaied in small overlap and oblique frontal crashes. A human body model was setted on the driver's seat (DR) to verify the occupant movement and extent of injury. The human body model used for this was an adult male model developed by Ito et al.[6]. Current human body models only allow for whole body movement and fracture prediction, and cannot be used for direct evaluation of more serious (life-threatening) injuries to internal organs. Evaluation was therefore performed according to the number of fractured ribs predicted by the numerical simulation from the relationship between the rib fractures throughout the chest of the L side which is characteristic of the chest injury indicated by the abobe-mentioned past study. The simulation was first conducted through a configuration of the oblique test protocol scheduled to be adopted by the NHTSA[7]. The vehicle used for verification was a 2011 model year small passenger car. The vehicle model had a driver air bag and a 3-point seat belt as a restraint device. Figure1 shows the configuration

.

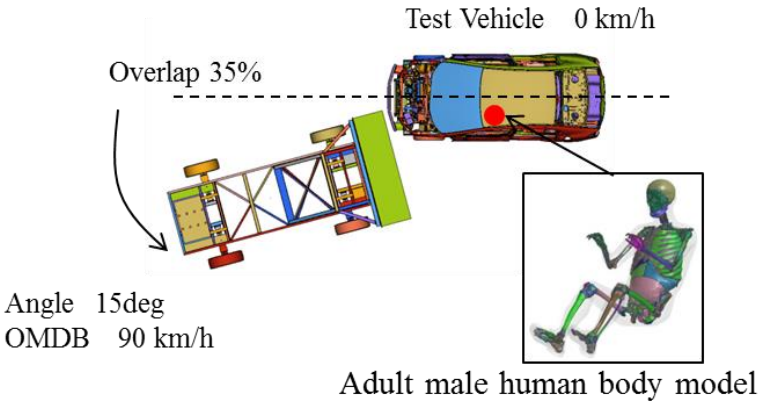

Figure1. Test configuration of Oblique

Figure 2 shows the results from confirmation of the vehicle body deformation, the movement of the human body model, and the number of bones fractured. A distinctive feature of chest injuries in actual small overlap and oblique frontal crash accidents was fractures on the non-belted side (left side) caused by collision with the door trim. However, collision with the door trim did not occur in the vehicle used for verification. The result showed three fractures concentrated in the lower part of the ribcage at #10, #11, and #12 ribs on theleft side. The injuries sustained here differed from the chest injuries that occurred in actual small overlap and oblique frontal crash accidents, where fractures occurred a particularly large number in ribs 1 to 10.

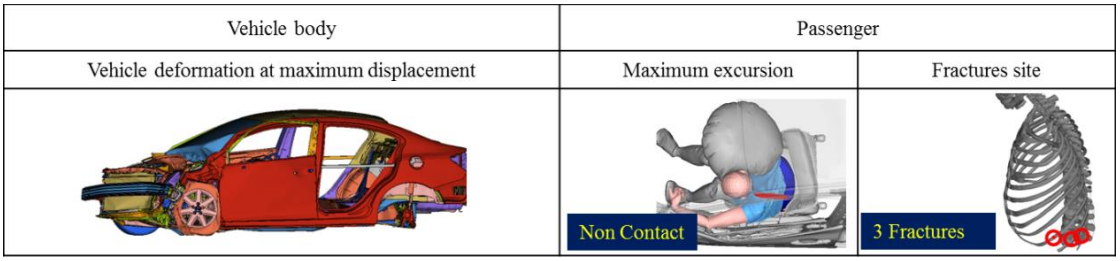

Figure2. CAE Result of vehicle deformation and passenger injury

In the results obtained by Saunders et al.[8] confirming the reproducibility of Vehicle to Vehicle(VtV) and OMDBtV, configurations that provide high reproducibility of the toepan were selected for the configuration of the oblique mode that is currently scheduled to be adopted. These are configurations that place an emphasis on evaluation of tibia injuries, which are numerous in small overlap and oblique frontal crashes. According to Saunders et al. [8], the interaction of longitudinal members of own vehicle and opponent vehicle also influences the A-pillar displacement and accompanying chest injuries. In the case of modes in which there is no engagement of longitudinal members with the opponent vehicle, they indicate a high degree of reproducibility in the A-pillar. In order to reproduce actual accidents resulting in chest injury, deformation of the vehicle body (particularly the A-pillar) needs to be made to more closely resemble what happens in actual accidents. With a view to reproduction of chest injury, therefore, which is the purpose of this verification, the overlap was changed from 35% to 25% so that this would not be a mode that is no engagement between longitudinal members. Other elements of the configuration are the same as shown above. Figure 3 shows the appearance of the vehicle body during the crash.

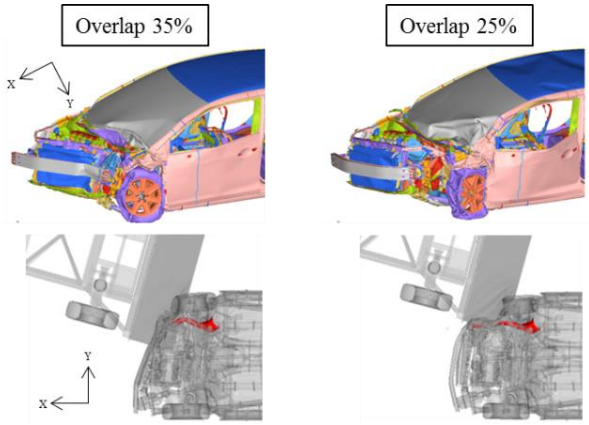

Figure3.Comparison of vehicle body deformation betweem overlap 35% and 25%

The result of numerical simulation with the overlap changed to 25% resuled in a mode in which engagement with the outer side of the longitudinal members did not occur, and there was increased deformation of the upper portion of the A-pillar. Although the increased deformation of the A-pillar also tended to increase the deformation of the door, this did not occur to the extent that the occupant would collide with the door trim. Occupant collision with the door trim did not occur, and no change was seen in the number of fractures or fracture sites. Figure 4 shows the occupant movement and fracture sites.

Passenger movement		Fractures site	
Overlap 35%	Overlap 25%	Overlap 35%	Overlap25%
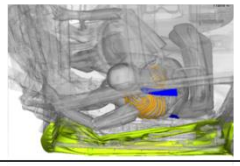	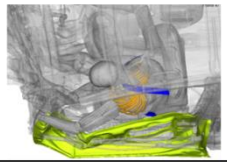	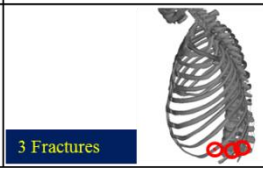 3 Fractures	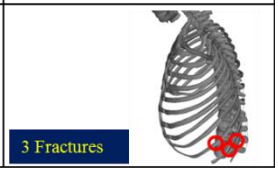 3 Fractures

Figure 4. Comparison of passenger movement and fracture sites betweem overlap 35% and 25%

Reproduction of accident situation

Among the causal factors in the collision of occupant and door trim are the amount of intrusion by the vehicle body and the occupant movement that accompanies vehicle body movement (lateral slide). These are considered to be important parameters. The capability of this mode to reproduce actual accidents was verified by taking three points as tuning parameters. These three points were that overlap was such that it would not depend on longitudinal members, that the angle was such that occupant movement that becomes an impact with the door trim was reproduced, and that the level of kinetic energy (speed) was such as to result in a collision. In order to calculate the configuration for an OMDB, VtV computer simulation was first used to verify that this mode would reproduce the injuries sustained in actual accidents. A 2 ton class SUV was used as a vehicle with a weight ratio to the passenger car of 1:1.6. Figure 5 shows a graph of the estimated number of accidents according to the own vehicle/opponent vehicle weight ratio, as obtained from NASS-CDS accident data (1320 cases from 2000 to 2013). Based on this graph, the ratio of 1:1.6 is positioned to include more or less the entire range of accidents that occur(99%). Next, for the purpose of configuring the speed, Fig. 6 shows the barrier equivalent velocity (BEV) on the horizontal axis and the estimated number of actual accidents on the vertical axis on the left. The average AIS value in the speed range of those accidents is shown on the vertical axis on the right. It is apparent from Fig. 6 that the average extent of injury increases abruptly in the 60-70 km/h speed range, rising to around 4 or less on the Maximum Abbreviated Injury Scale (MAIS). Since an injury rated as AIS4+ is severe, efforts were directed to this region in order to reduce fatalities and injuries. When a BEV of 60-70 km/h is expressed as ΔV, it is the equivalent of approximately 80 km/h.

According to the NHTSA accident study results, this covers 80% of the range of speeds that involve fatal accidents.[1].

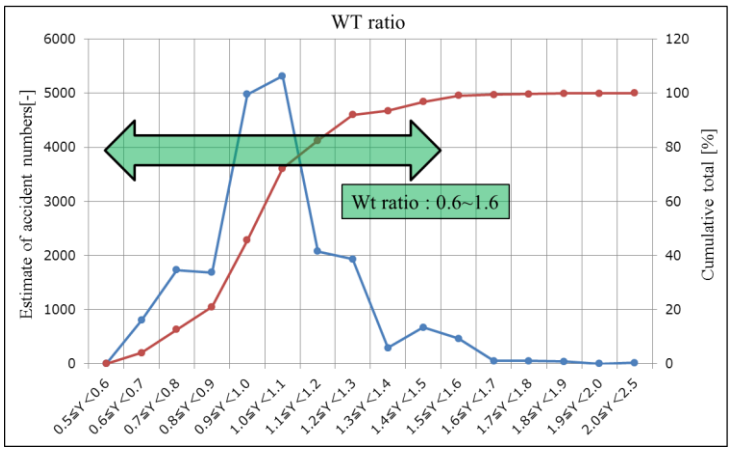

Figure5.The number of accidents by Wt ratio(Opponent vehicle/Own vehicle) in US

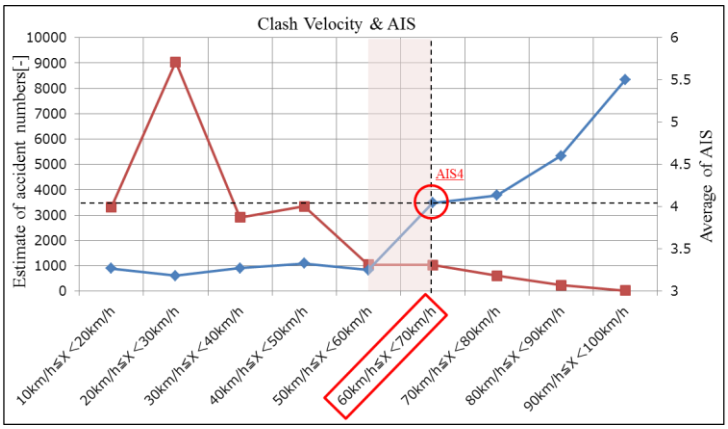

Figure6.The number of accidents and AIS average by BEV

Since the angle results in occupant movement in the direction of the door, the angle was changed from the 15° chosen for the oblique test to 30° with the aim of having the occupant move into a region where the occupant cannot be protected by the driver (DR) air bag that is intended for a conventional frontal crash. The overlap was set to 25% so as to avoid interference by longitudinal members. Figure 7 shows the configuration.

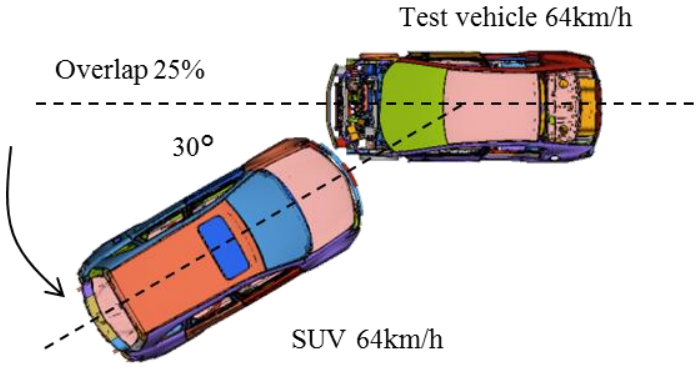

Figure7. Test configuration of VtV

Figure 8 shows the appearance of vehicle body deformation obtained through computer simulation. No engagement between longitudinal members occurred, and the bumper beam of the large vehicle (SUV) therefore collided directly with the A-pillar portion of the test vehicle. Increasing deformation of the A-pillar was accompanied with increasing deformation of the door, so that the door intruded into the occupant compartment space. Figure 9 shows the similar category of vehicle body deformation obtained from NASS-CDS as an example of a small overlap and oblique frontal crash compared with CAE result. Energy could not be absorbed by longitudinal members, and the progressive interference of the opponent vehicle with the A-pillar portion increased the load on the occupant compartment so that the upper portion of the A-pillar became deformed. It is apparent that the deformation mode obtained by computer simulation closely resembles the mode of deformation that occurs in actual accidents.

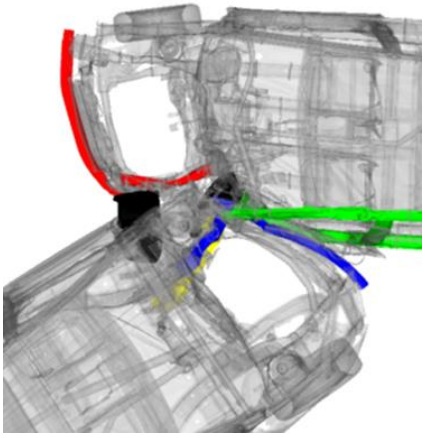

Figre 8. No engagement of the longitudinal structure

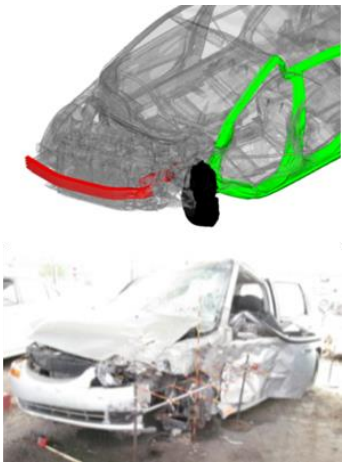

Figure9.Comparison of CAE result and example of small overlap actual accident

Next, in the interest of evaluating chest injury in small overlap and oblique frontal crashes, the deformation shown in VtV was reproduced using OMDB and the capability of reproducing the injury sustained by the occupant's chest in actual accidents was confirmed. In order to have the same vehicle body deformation mode, the overlap and angle were fixed and the speed parameter was tuned to conduct verification. Displacement equal to VtV was defined as the target, and X-Y deformation was confirmed using "toepan_center," " toepan_L," and "A-pillar" as judgment criteria. In order to confirm whether the injuries sustained in small overlap and oblique frontal crashes were successfully reproduced, the occupant contact location and number of fractures were confirmed. The speed of the vehicle crashed into was fixed at 0 km/h and confirmation was conducted in three levels with the OMDB crashed into the vehicle at 10-km/h increments from 90 km/h to 110 km/h. The point at which the computer simulation results were equal to or better than VtV for the OMDBtV at every deformation measurement point was when the OMDB was crashed at a speed of 110 km/h. Figure 10 shows the deformation and occupant movement that the OMDB was crashed at a speed of 110 km/h. Unlike VtV, the mode of large vehicle bumper beam directly impacting the A-pillar could not be reproduced with the OMDB. In the course of proceeding until A-pillar deformation was equal, therefore, the displacement in other regions tended to be greater than in VtV. Occupant movement was the aim of the 30° angle, and the direction was into an area not protected by the front air bag and in the direction of the door, where it coincided with the direction of intrusion by the door so that the chest came in contact with the door trim. This collision resulted in fractures of the ribs, and the result was that the contact sites and number of fractures were the same as the results given for actual accidents. This successfully indicated the possibility that evaluation of chest injury in small overlap and oblique frontal crashes using OMDB could yield the same phenomena as injuries sustained in actual accidents when the OMDB was crashed into the test vehicle at a speed of 110 km/h, an overlap of 25%, and an angle of 30° in the Small Overlap & Oblique (SOO) configuration.

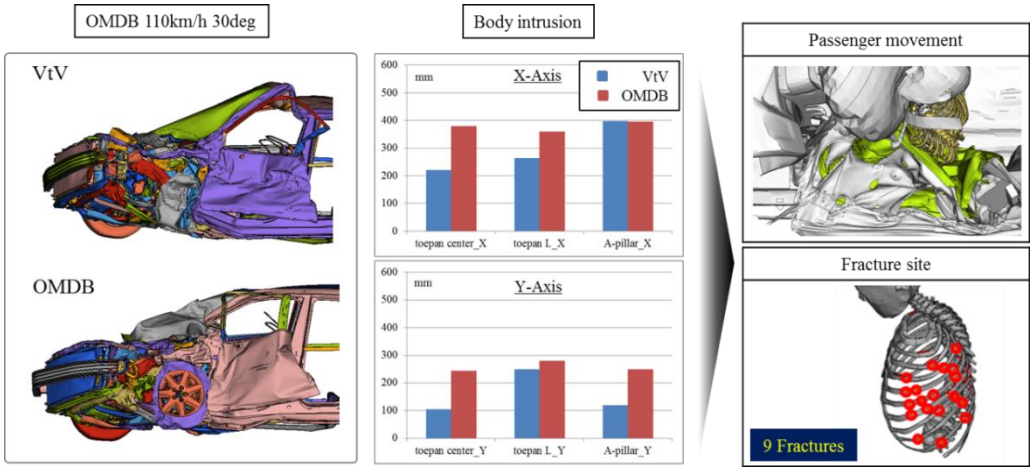

Figure10. VtV and OMDBtV Comparison

Comparison of Oblique test and SOO mode

A comparison of SOO mode and oblique mode was made using the vehicle that was tested for the present research. Figure 11 shows the various mode configurations.

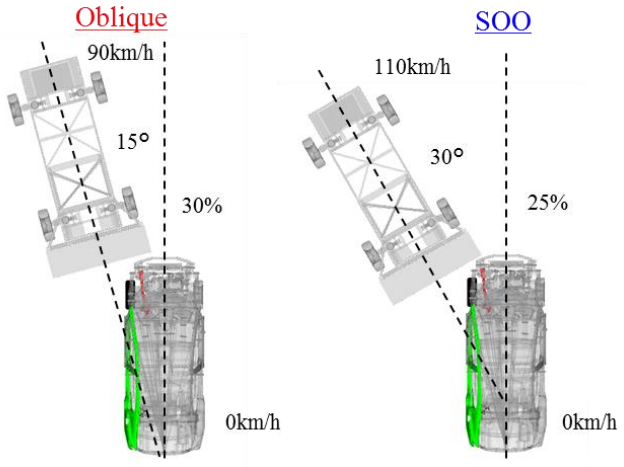

Figure11. Test configurations of Oblique test and NEW vehicle test

The comparison was made in terms of the evaluation vehicle ΔV, which indicates the severity to the occupant. Figure 12 shows ΔV of SOO mode and oblique mode. In oblique mode, the evaluation vehicle ΔV was 64 km/h, while in the SOO mode indicated in the present research, the ΔV was 78 km/h, which places the occupant in a severe situation. However, it was confirmed that ΔV corresponding to 80 km/h was achieved, which was the target, given that the purpose of the present research was to reduce fatalities and injuries. Comparison was then made of deformation in each area of the vehicle body. The comparison was made using the STRUCTURE index defined by IIHS as a reference index for the purpose of the comparison. Figure 13 shows the results of deformation at the measurement points where IIHS evaluation is performed[9].

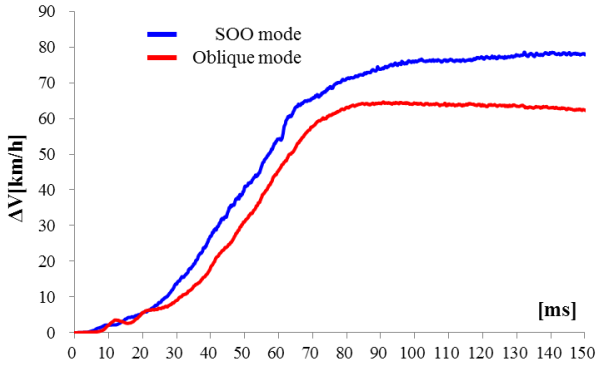

Figure12. ΔV of SOO mode and oblique mode

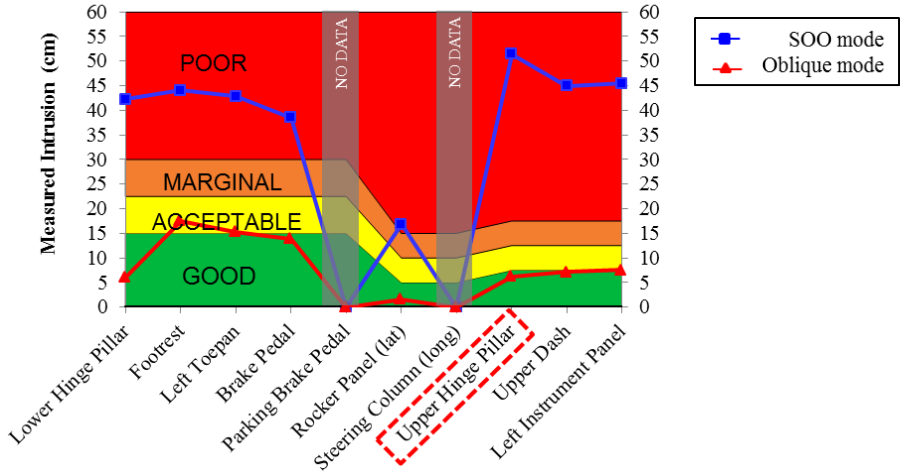

Figure13.Occupant compartment intrusion (IIHS evaluation)

Deformation tended to increase significantly in SOO mode in all regions. Deformation of the A-pillar was particularly conspicuous, and there was an increase of 45 cm in the upper portion of the A-pillar relative to the oblique mode. The contribution of the angle, speed, and overlap parameters was confirmed assuming that the deformation of 45cm was 100%. It was found that changing the angle from 15° to 30° produced 24% of the total increase, changing the speed from 90 km/h to 110 km/h produced 57% of it, and changing the overlap from 35% to 25% produced 19% of the increase in deformation. The increase in deformation due to speed was the result of the increase in input energy. In the case of overlap, energy absorption by longitudinal members did not take place, and the resulting increase in load on the occupant compartment caused the increase in deformation. The causal factors in the increased deformation due to the angle were examined in terms of the appearance of intrusion shown in Fig. 14.

Figure14. Comparison of Oblique test(left) and SOO test(right)

In oblique mode, the angle is shallower than in SOO mode so that the load is distributed through the tire to the side sill. It is apparent that in the NEW mode, however, the tire is turned over on its side so that the load is not transmitted to the side sill, and instead the honeycomb portion of the OMDB impacts directly against an A-pillar portion. When the angle is deeper, the distribution of load toward the rear of the vehicle body is reduced, and the extent to which a load path is not formed is the extent of increase in deformation. Figure 15 shows vehicle body acceleration in the Y direction when numerical simulation of the oblique mode is performed with the speed fixed at 110 km/h and the angle set variously to 7°, 15°, and 30°. In light of the timing of the OMDB honeycomb contact with the A-pillar portion, there is an increase of acceleration in the Y-axis direction and the vehicle body movement shifts in the Y direction. This increase in acceleration is accompanied by occupant movement in the direction of the door, which is a movement counter to the vehicle. These results show that setting the angle at 30° causes acceleration in the Y direction to increase suddenly. This is further indication of the need for a crash angle that can cause the tire to turn over on its side and induce direct impact against the A-pillar. Since collision by the occupant with the door trim occurs at this angle, 30° appears to be appropriate.

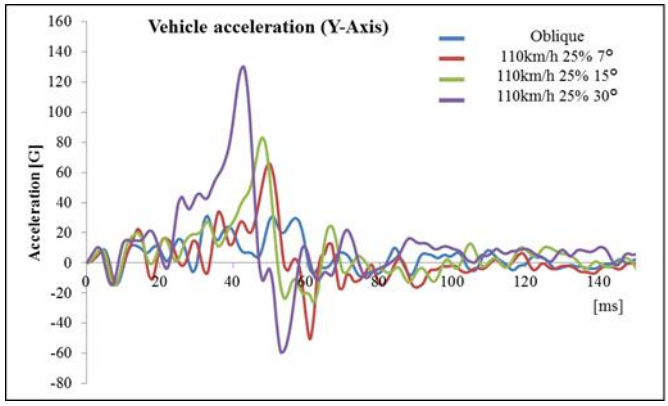

Figure15.Comparison of vehicle acceleration(Y) according to crash angle

Evaluation of SOO mode for SOT GOOD model

Up to this point, verification has been conducted using an 11M small passenger car. Research was continued using a midsize passenger car, which received a GOOD evaluation in the SOT implemented by IIHS in 2018, to confirm how the small overlap and oblique frontal crash is positioned with regard to chest injury. Although it is according to in-house data, the vehicle body in this model yielded vehicle body deformation at a level that was GOOD in terms of the SOT index even in oblique mode.Computer simulation was carried out with the configuration of 25% overlap, 30° angle, and 110 km/h speed that has been verified up to this point. Figures 16 and 17 show comparisons of the deformation and the appearance of the deformation produced with that configuration. By comparison with the SOT and oblique test configurations, the SOO configuration showed an overall tendency toward increased deformation. This was especially conspicuous in the A-pillar portion where there was a tendency to increase to the level rated POOR in the IIHS index. The reason for this was the same as in the verification performed using the 11M small passenger car, which is that the tire was turned over on its side and the OMDB honeycomb impacted directly against the A-pillar. It was found from these results that in the SOT that is presently adopted as well as in the oblique mode that is scheduled to be adopted, there is a possibility that vehicle body performance is inadequate with respect to chest injury even in a vehicle body that has the highest ranking of self-protection performance. In other words, the possibility that chest injury caused by contact of the chest with the door trim may not be comprehensively avoidable became clear. In order to pursue reduction of chest injuries and reduction of fatalities and injuries, it would be necessary to implement evaluation in SOO mode that reproduces actual accident circumstances and proceed to devise countermeasures.

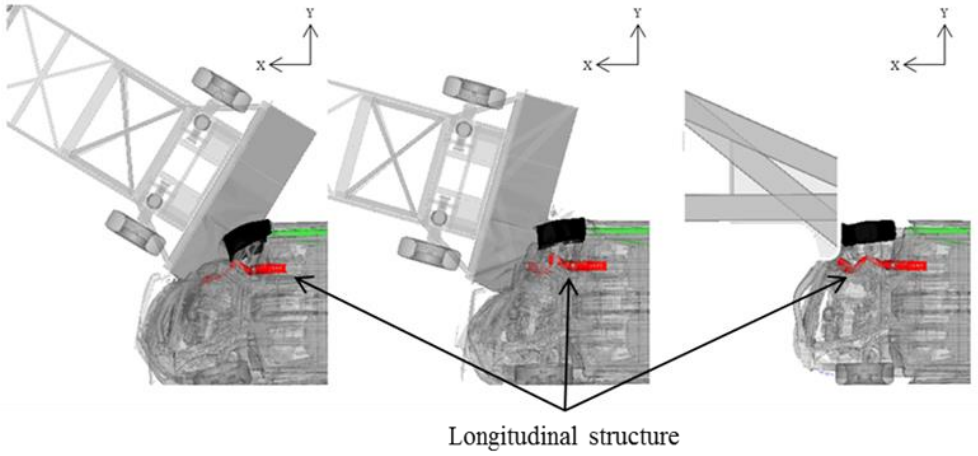

Figure16.Deformation of longitudinal structure (left:SOO,Center:Oblique,Right:SOT)

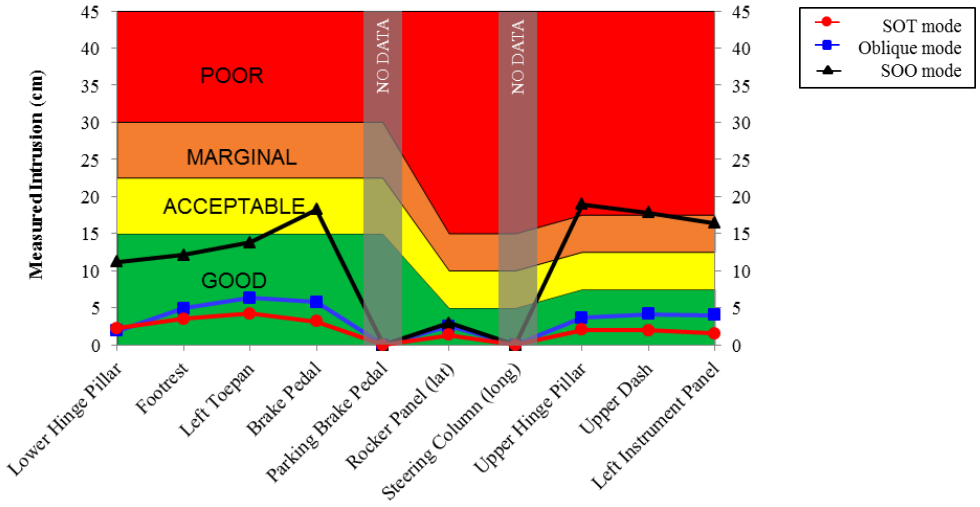

Figure17.Comparison of occupant compartment intrusion

Reduction of chest injury in small overlap and oblique frontal crashes

Body strengthening In investigating approaches to countermeasures, verification was first implemented for countermeasures on the vehicle body side intended to reduce vehicle body deformation. Taking the 11M small passenger car as a baseline, the thickness was changed at five places on members that contribute significantly to vehicle body deformation. For all five parts, the thickness was increased in increments of one rank (RNK) of 0.2 mm each. The OMDB was then crashed into the 11M small passenger car in SOO configuration and computer simulation was performed. Figure 18 shows the vehicle body strengthening areas and a plot of the maximum displacement of the A-pillar portion. As noted above, the 18 M midsize passenger car has the newest vehicle body performance and is positioned at the IIHS GOOD level. The deformation to this 18M midsize passenger car is plotted on the right of the figure. The deformation that occurred at strengthening to the fourth rank (4RANK) showed the same extent of intrusion into the vehicle body as in the 18M midsize passenger car. When further strengthening was applied to raise this to the seventh rank (7RANK) above the BASE, confirmation of occupant movement and occurrence or otherwise of fractures showed that contact with the door was still occurring and fracture injuries were found. Figure 19 shows the fracture status of the respective occupants. The movement of the

respective occupants in the Y direction counter to the vehicle movement is shown in Fig. 18. Although doing such strengthening is not a realistic possibility in terms of the marketability of the vehicle body, even if the rigidity of the vehicle body were to be increased to the point of making it so rigid that the vehicle framework did not undergo any deformation at all, then the vehicle body would rotate by an amount that is in inverse proportion to the decrease in intrusion. It was confirmed that the movement of the occupant in the Y direction would therefore increase, and contact with the door could not be avoided. Although the number of fractures decreased, this resulted in a total of six fractures in ribs 5 to 11, with the lateral load input causing the fractures being concentrated in the ribs on the left side and to the rear from the very left. These fractures are reason for concern about injury to internal organs. It was confirmed, therefore, that there is a limit to countermeasures consisting of increased strengthening of the vehicle body against small overlap and oblique frontal crashes.

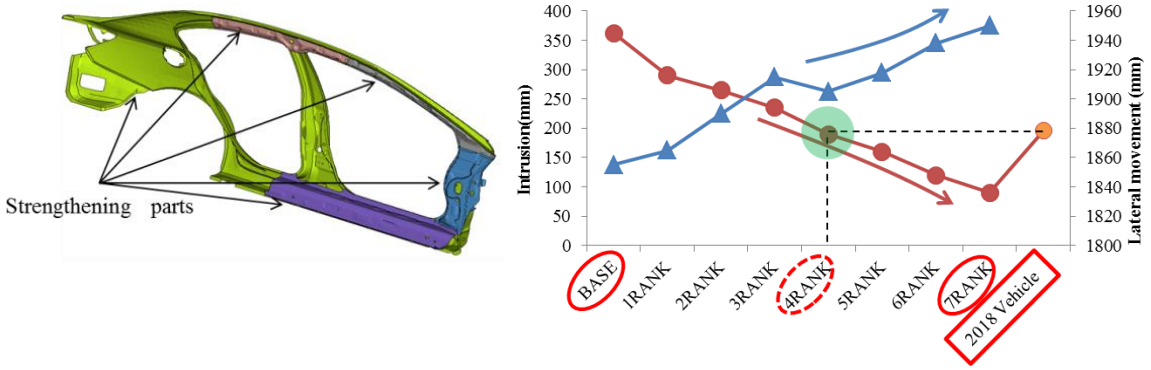

Figure18. Occupant compartment intrusion and occupant movement to lateral direction by body strengthening(left:strengthened parts)

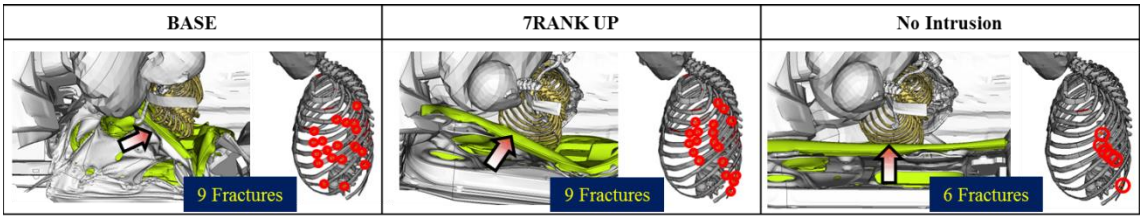

Figure19.Effect of body strengthening on occupant

Restraint device Verification of the possibility of countermeasures using restraint devices was carried out next. The area that the chest comes in contact with in small overlap and oblique frontal crashes is a blind spot in the area protected by conventional driver (DR) air bag and side air bag. Conceivable methods for addressing this are enlarging the side air bag and enlarging the curtain air bag. The purpose here, however, was to confirm effectiveness against fractures of the ribs. For the present research, therefore, a simple check was made to confirm the magnitude of the effect from installing a side air bag in the door front (FR) portion. Figure 20 shows a conceptual image of the installation and air bag deployment. Figure 21 shows the chest fractures of the computer simulation results. Where nine fractures occurred when there were no air bag in place, adding the air bag resulted in eight fractures, not significantly reducing the number of fractures. However, a check of the way the chest deflection when the fractures occurred showed that in the BASE configuration, the chest crashing against the hard structure of the door caused a load to be applied from the outside toward the internal organs locally so that the ribs were bent in toward the inside of the body. Adding the air bag changed the direction in which the ribs were bent to the opposite direction, away from the internal organs. In the former, there is a high possibility that the fracture end damages the internal organs.

This showed the possibility that the use of the air bag may mitigate the load input locally as well as the extent of injury. The effect of not taking countermeasures on the vehicle body side was confirmed as part of the present research, but for the future, it will be necessary to reduce the number of fractures by adding restraint devices that have been optimized for the characteristics of the air bag, thereby securing a survivable space by combining this approach with vehicle body countermeasures.

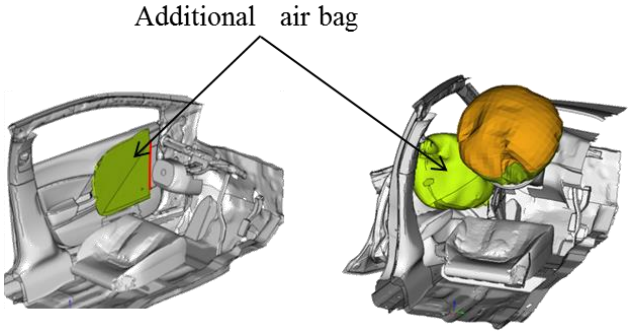

Figure20. Energy absorbing parts for oblique

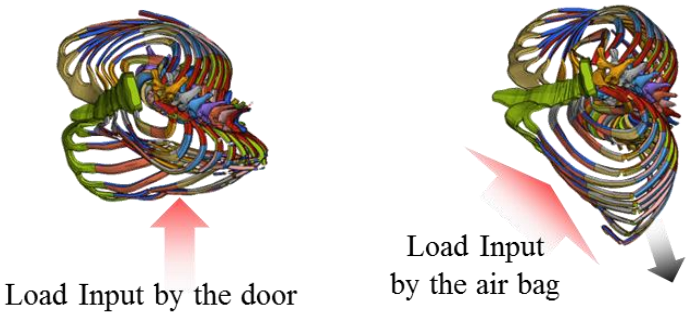

Figure21. Effect of restraint device on occupant(Left:BASE,Right:With air bag)

DISCCUSSION

Taking the view that, for the purpose of reducing fatalities and injuries, it would be necessary to establish evaluation methods that conform to actual accident circumstances, the present research focused on chest injuries during small overlap and oblique frontal crashes and sought modes that would recreate those injuries. With a view to achieving evaluation, configurations using the OMDB were calculated. The modes described above are quite severe when viewed from the perspective of ΔV in existing evaluation test configurations. However, the reason for this is that the present research has the purpose of concentrating attention on chest injuries in order to reduce further fatalities and injuries. According to the computer simulation, performing verification with severe configurations (weight, speed, angle) that systematically include actual accidents has made it possible to identify mechanisms of chest injury in actual small overlap and oblique frontal crash accidents.

The examination of countermeasures against chest injuries in small overlap and oblique frontal crashes has clarified directions for future countermeasures. There are limits to the reduction in injuries that can be achieved by strengthening the vehicle body, and it will be necessary for countermeasures that go beyond the conventional front and side restraint devices to include combinations with airbags for use in oblique crashes. This indicated the possibility that measures against chest injury may be inadequate even if vehicle body performance supports SOT, including the oblique mode that is currently scheduled to be adopted. Further advances are called for in vehicle body and restraint devices. For that purpose, however, achieving widespread adoption of restraint devices in the necessary areas will be a challenge as long as there is no evaluation of modes involving collision with the chest. The present

research has not gone beyond verification using two passenger cars, which are small and midsize vehicles, and this does not suffice for proposing a complete evaluation method. For the future, it will be necessary to establish an evaluation method with the chest injury perspective. The research that will be needed for that purpose extends beyond the verification of test modes in the present research that conform to actual accident circumstances by the use of a human body model. It will be necessary to conduct future examination of the possibility of using the THOR anthropomorphic test devices (ATD) for appropriate measurement and evaluation of the characteristic displacement in the Y direction that is found in small overlap and oblique frontal crashes.

CONCLUSION

The present research used computer simulation to identify configurations that reproduce chest injuries from actual small overlap and oblique frontal crash accident circumstances.

・Overlap (LAP) 25%: This mode does not depend on energy absorption by longitudinal members.

・Angle 30°: This angle enables reproduction of occupant movement.

・Speed 110 km/h: The crash energy at this speed results in collision between the occupant and the cabin.

It was confirmed that by tuning the above three points, it was possible to reproduce the collision between chest and door trim that is a distinctive characteristic of chest injury under actual accident circumstances. These injuries were also subjected to numerical simulation using a human body model, and by this means the effectiveness of countermeasures utilizing the vehicle body and restraint devices was confirmed. This indicated that countermeasures that only strengthen the vehicle body have their limits, so that a combination with countermeasures utilizing restraint devices is needed.

REFERENCES

[1] NHTSA,” Fatalities in Frontal Crashes Despite Seat Belts and Air Bags”,2009

[2] Rodney W. Rudd, Mark Scarboro, James Saunders,” INJURY ANALYSIS OF REAL-WORLD SMALL OVERLAP AND OBLIQUE FRONTAL CRASHES”,2011 ESV, Paper Number 11-0384

[3] Johan Iraeus, Sofie Wistrand, Bengt Pipkorn,” Evaluation of Chest Injury Mechanisms in Nearside Oblique Frontal Impacts”,2013

[4] Mats O. Lindquist, MSc, Andrew R. Hall, BEng, and Ulf L. Björnstig, MD,phD,”Kinematics of belted fatalities in Frontal Collisions:A New Approach in Deep Studies of Injury Mechanisms”,2006 J Trauma,61:1506-1516

[5] Matthew L. Brumbelow, Charles M. Farmer,”Real-World Injury Patterns Associated With HybridⅢ Sternal Deflections in Frintal Crash Tests”,Traffic Injury Prevention,2013,14:807-815

[6] Osamu Ito, Yasuhiro Dokko, Kazuki Ohashi, “Development of Adult and Elderly FE Thorax Skeletal Models”, 2009 SAE, No2009-01-0381

[7] NHTSA,” LABORATORY TEST PROCEDURE FOR OBLIQUE OFFSET MOVING DEFORMABLE BARRIER IMPACT TEST”,2015,Docket NTHSA-2015-0119

[8] James Saunders, Matthew J. Craig, Jeffrey Suway” NHTSA’S TEST PROCEDURE EVALUATIONS FOR SMALL OVERLAP/OBLIQUE CRASHES”,2011 ESV, Paper Number: 11-0343

[9] IIHS,”Small Overlap Frontal Crashworthiness Evaluation Crash Test Protocol(Version VI)”,2017,

PHOTOGRAMMETRY AND MOTION ANALYSIS METHODOLOGIES FOR DUMMY HEAD BEHAVIOUR OBSERVATION

David, Company Molina
Applus IDIADA Group
Spain

Paper Number 19-0233

ABSTRACT

While the airbag is essential for occupant protection, is it also an obstacle to visualizing the distance between the dummy head and rigid objects on the car or other occupants. During the restraint system development process, it is important to understand where the dummy head is in order to modify the restraint systems and avoid bottoming out.

Photogrammetry and motion analysis combined with 3D software enables the minimum distance between the 3D scanned dummy head and any other 3D surface to be calculated. Using the videos from the high-speed cameras the 3D position of any visible point can be obtained. As the head is a rigid object, it is possible to determine where the entire head is relative to the steering wheel with just the position of any point on the back.

With the arrival of 3D high-resolution scanners, HD high-speed cameras and new tracking algorithms, the results obtained from this methodology have increased in precision up to the millimetre scale. This methodology shows the behaviour of a rigid object during a crash or sled test in a 3D environment and can be used as a strong tool in passive safety laboratories. In this particular case, displacement and rotations of the head dummy relative to the car coordinate system determine if the head is too close to the dashboard, "B" pillar, steering wheel, etc.

This methodology requires two high-speed cameras. During a passive safety development process, it is essential to have all high-speed cameras available to monitor critical parts of the car. To reduce the number of cameras required to calculate the behaviour of the head relative to the car, the 6DoF tracking method can be used. This method uses the static position of a group of points in a rigid object to calculate the 3D rotation and displacement of the centre coordinate system. There are some difficulties that limit this process, which will be dealt with here.

This methodology is not commonly applied in every test, usually because the two cameras and the digital process required increase the cost of the crash or sled test. Reducing the number of cameras needed to only one can reduce the cost of this methodology and its implementation for all related tests. Also, there is the possibility of calculating this methodology by using on-board cameras, which is very helpful when the car deploys the curtain airbag.

With the coming of the autonomous car, the Passive Safety Department must have all measurement tools available to understand how dummies behave inside new car morphologies. This tracking methodology could us help to understand how dummies interact with rigid parts of the car in order to modify the restraint systems so as to be adapted to new technologies.

INTRODUCTION

Currently, due to the introduction of new regulations such as Euro NCAP Far Side or the development of future occupant protection systems regarding autonomous driving such as the OSCCAR project or NHTSA protocol modifications, experimental restraint systems to prevent occupant injuries are appearing, and the airbag has become one of the most important passive safety protections inside the car.

The development process of the airbag morphology, time of deployment, vent-hole strategies, etc. are some of the most important parts during occupant protection development. If the airbag has not been tested correctly, bottoming out of the airbag will cause serious injuries to the occupant's head. To avoid bottoming out it is necessary to know the position of the head with respect to any rigid part behind the airbag during the crash test.

It is impossible to understand the distance between the head and the rigid parts by looking at the movies because the airbag is always in the way. Although it is known when the head has hit a rigid part by looking at the accelerometers and neck load-cell results, this information only tells us if it has hit or not. It is difficult to understand the behaviour of the head or the minimum distance between the head and any rigid part of the car. The following study on photogrammetry resolves these difficulties and helps the development of efficient restraint systems by exploring the behaviour of the head during crash and sled tests.

EVALUATIONS FOR DUMMY HEAD POSITION ANALYSIS

There have been different ways of comparison and measurements to try to understand how the airbag was working related to bottoming out, but none have enough accuracy or repeatability to truly inform about the behaviour of the head or its minimum distance between the rigid parts of the car.

Acceleration to Displacement

As this paper is based on film positional calculation, this section will not enter into too much detail. It will just mention the common problems regarding obtaining a dummy head position using acceleration data and clarify that this particular method is discarded for this case.

The use of accelerometer data is a common procedure for calculating the displacement of an object. But that does not mean it is a perfect, accurate solution. A position cannot be calculated directly from an accelerometer. It is necessary to calculate a displacement regarding the first position offset of the head. This is the first problem regarding accelerometer to displacement calculation.

Double integral from acceleration samples will provide a displacement difference from one state to the next relative to the frequency data acquisition. This means that one displacement calculation needs four data acceleration samples. As with all calculations, acceleration has an uncertainty that will be accumulated on every displacement result.

When this calculation is made from the centre of gravity (COG) of the dummy head, we can say that this calculation is relative to the entire head as a solid object. To determine the direction of the tri-axial accelerometer it is necessary to mount a gyroscope on the COG dummy head.

As the accelerometer inside the head can rotate in very different ways, the gyroscope calculation must notify the direction of the head. As with the acceleration, the angular velocity of the gyroscope also has an uncertainty that will be added to the previous. Vibrations and small errors will add more uncertainty to the displacement calculation.

Other related problems are the position of the accelerometers and gyroscope between each other and the COG. The calculations to fix these offsets will increase the uncertainties.

Because the final objective is to compare the head against any rigid part of the car, the displacement calculated must be relative to the coordinate system of the car. That will add another problem, as the car moves in a different direction to the head and should also be calculated by the sensors on the car.

FILM BASE DUMMY HEAD POSITION ANALYSIS

The analysis of the head bottoming out or rollerblading the airbag during a crash test is an important matter for occupant protection. The airbags are changing their morphology functionalities because of newly arriving protocols. The complexities of the new crash tests and new dummies, such as the Small Overlap and the THOR dummy, are demanding more precise and fast tools to analyse the behaviour of the dummy.

The Minimum Distance of the Head (MDH) is the calculation performed by the combination of photogrammetry and 3D software to find the minimum distance between the dummy head and a rigid object. This calculation provides the information needed to understand how the head is performing against the rest of the car.

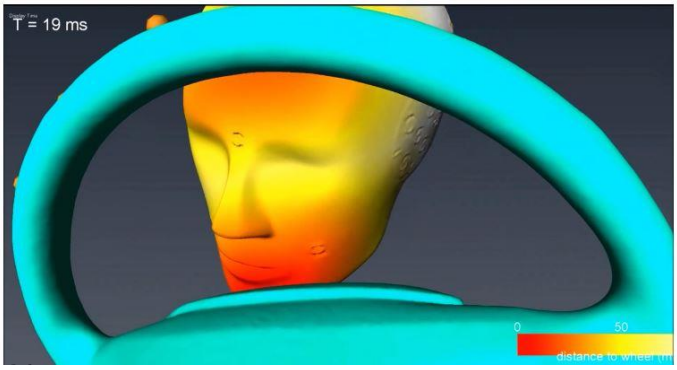

Figure 1. Calculation of the minimum distance between a scanned dummy head and steering wheel.

The dummy head position calculation is based on the 3D position of three points on the head. The position is relative to the car's coordinate system. For a better understanding of the dummy head behaviour, the application exports an animation of the head and the solid object to be compared with. This animation is the real movement of the head relative to the car in a 3D software environment.

A 3D scanner is used to provide the 3D mesh of the dummy head and the parts of the car that will be compared to the head. It is very important that the head is scanned, because the 3D points position are relative to the surface of the real object. When the animation is completed, the complete mesh vertices of the head mesh are measured the distance against any other mesh on the test, such as the steering wheel or the pole barrier.

3D Tracking

To deal with the demand for more accurate tools to understand the behaviour of a dummy head during crash and sled tests, a film analysis using photogrammetry and centre point detection on the movies recorded during the test was developed. This tool has the requirement of placing two cameras with different angle relative to the point that will be measured.

The combination of photogrammetry and centre point detection on two synchronized cameras provides three coordinates of the same exact point. The calculated point must be viewed by the two cameras. And at least four reference points in a cube form must be viewed by the two cameras. This calculation is commonly named as 3D Tracking.

There are different types of algorithms to detect the centre of a real point represented as white and black pixels on the movie. But the most important matter is that the algorithm provides a subpixel position. The algorithm gathers information of contrast pixels and calculates where the centre of the target inside the pixel is. The uncertainty of this measurement will be represented as a percentage gap of the pixel. Further on, the paper will mention the uncertainties of the most common algorithms.

Reference to a Coordinate System A high-precision machine is used to calculate positions of targets with respect to the coordinate system of the car. The centre of the target is represented by a point or intersection, depending on the type of target. The 3D position of the target centre will be used as a reference to calculate the camera orientation with respect to the coordinate system of the car.

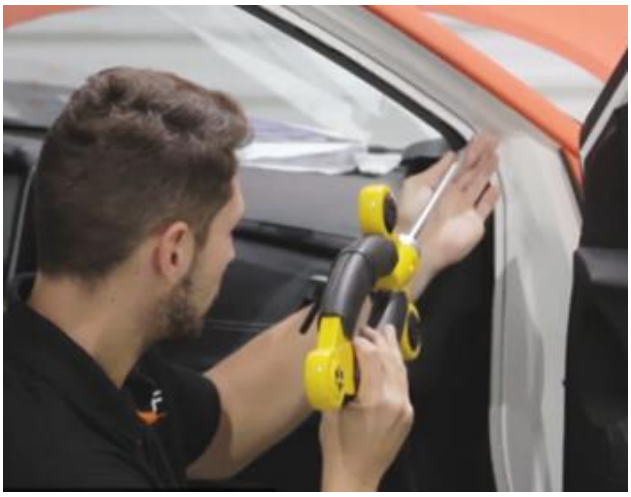

Figure 2. Measurement of 3D points on the car by a CMM operator.

The camera orientation is used to calculate the 3D position of any point on the image. Two cameras between 20–45º of difference are needed to calculate the position of any 3D point on the picture. The point position on the picture compared to the reference points determines the camera orientation that will enable the calculation of the 3D position of any visible point by the two cameras.

Camera orientation can be static or dynamic. The static camera orientation fixes an orientation to one frame of the video. These make it possible to calculate how a point moves with respect to a fixed coordinate system. A dynamic camera orientation has the same calculation, but with respect to a moving coordinate system. Tracking of the reference points must be done to perform a dynamic camera orientation. The dynamic coordinate system also helps to counteract the camera vibration.

On the minimum distance to head calculation, a dynamic camera orientation is required to represent the movement of the head with respect to the car's coordinate system. The final real animation head will be represented as if the head was moving towards the car and the car was static. This procedure reduces time consumption and the number of cameras.

Photographic Quality Strategic position of the cameras and targets is essential to ensure that the tracking quality of the points is the best possible. As well as the camera position, the filming configuration will also increase the accuracy. It is required to reduce the ghosting effect of the picture to a minimum to avoid having pixels represented as something that they are not in reality.

Regarding the pixel information, depending on the video format, the pixels could have false information generated by the compression of the file format. Software must read RAW formats of the movie to avoid this kind of problem. Cameras must not interpret the reality; they must show exactly the light information that is arriving to the camera frame.

Post-processing the video files must be done carefully, as any deformation will change the pixel information and the calibration coordinates of the camera, affecting the photogrammetry calculations. Cutting or extending the number of pixels will also affect the camera calibration. Further on, the paper will mention how camera calibration is performed.

The lens quality provides better light information arriving to the camera frame. Best quality glass on the lens will enable more realistic information and less aberration light caused by the lenses. The aberration caused by the lens can provide different pixel information more common in the perimeter of a bad quality lens mount.

The contrast between pixel information determines a figure of a target. That difference is used by the algorithms to provide centre target detection. A high dynamic range camera provides more information that the user will use to

obtain a better contrast. The target quality printing is also important to have true black printing for a better contrast light.

Distance between the object and the image and lens distance is important to have a smaller pixel representation of the reality. The precision of the point detection is calculated by a percentage of the pixel size, so the smaller the representation of the reality as a pixel, the smaller the error.

Camera-Lens Calibration A calibration panel is normally used to calibrate a lens and camera group. This panel is prepared with measured targets. Different angle captures are taken to provide the maximum information to the calibration software. The differences between the real position of the targets and the positional targets on the picture are the information needed to provide a calibration file. Those files are unique for each camera and lens group.

Figure 3. Calibration panel and high-speed camera with exchangeable lenses.

The Wand calibration method is an alternative calibration process that provides 100 times more points than the calibration panel. To perform this methodology, it is required to use a "Wand Calibration" that has a measured and calibrated distance between two lighting balls that will be filmed by two cameras.

The camera lens calibration is important to provide the same uncertainty result in any part of the image. All lenses modify the light coming into the camera and deform the image. They must be calibrated to inform about this deformation on the photogrammetry algorithms. The calibration is very important to have the best accuracy possible.

3D Scanner Surface New technologies and lower cost of high-resolution cameras have provided the possibility of 3D hand scanner to be available for everyone. The scanner consists of the representation of every impurity of a real object as a point. A consecutive high quantity of points will generate a consistent 3D mesh.

The 3D mesh provides the information of any point of the real surface. Comparing any point of the 3D digital surface of the head against the car surface can provide the calculation of the minimum distance. Because we are calculating the position of the head on every frame of the crash test movies, the behaviour and minimum distance will be calculated at every state during the crash test.

Figure 4. Head dummy to 3D mesh performed with a scanner.

3D Point Displacement Calculation The 3D position of at least three targets on the dummy head is used to calculate the exact position of the full head with respect to a coordinate system. To achieve the real animation of the head, high-speed videos of the test are used. Normally a 1000 frames per second movie is used, having a sample position of the head at each millisecond.

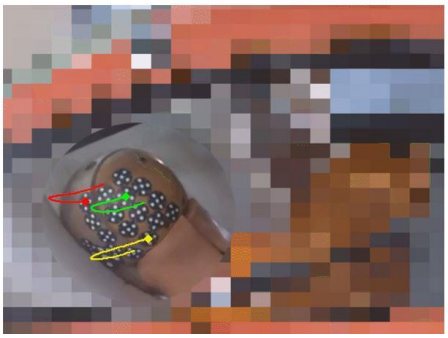

Figure 5. Trajectory of three points. Consecutive point position represented as a curve.

Tracking a point on the movie requires an algorithm that follows the same pattern for every sample. A revolutionary new algorithm has the possibility to follow the same pattern with 1% uncertainty of the pixel. That means that if the pixel represents 1 mm of the reality, the uncertainty will be 0,01 mm.

6DoF Point Displacement Calculation The 3D position of the head can also be calculated by only one camera. This methodology requires non-deformable objects and known position of the points to be measured. The Six Degree of Freedom (6DoF) algorithm uses at least four points of a rigid object to calculate its position. The methodology that the 6DoF uses to calculate the 3D position of the points is able to measure points not visible in the movie.

The 6DoF methodology requires the static measurement of all the points on the rigid object. These measurements must be referred to the same coordinate system. At least four of these points must be seen on movie to be tracked. If the points disappear but other points are visible instead, those can be used as new ones to continue the calculations. All the points measured on the rigid body will have 3D position during the time that at least four points were tracked.

The difficulties of the 6DoF methodology are mostly referred to the coordinate system. The final objective is to compare the car against the head dummy, therefore both of them must be on the same coordinate system. Until now the 6DoF algorithms worked on one coordinate system. A recent improvement allows two different coordinate systems to be compared. The update has an important impact on the camera preparation of a crash test: the number of cameras can be reduced to half and it facilitates the camera framing. Also, it opens the possibility to use on-board cameras.

Tracking point algorithms The tracked points on the head dummy must be exactly the same point on both camera views. The tracking algorithms calculate the centre point of the target with high precision. Then the followed points must be perfectly fixed to the same point in reality, then tracking algorithms work to ensure that these followed points have the best accuracy possible.

This algorithm calculates the position of the target by every frame so there are not cumulative errors on the calculated position of the point. That is essential to avoid problems of wrong displacements of the points. At every frame the position of the point is referred to the coordinate system of the car.

Table 1.
This table represents the uncertainty of the most used tracking algorithms

Point Detection Algorithm	Uncertainty (% of the pixel)
Correlation	50%

Centre of Gravity	20%
MXT	20%
Quadrant symmetry	10%
Correlation advanced	1%

Computation Minimum Distance Every three point's position on the head is represented as a virtual state of the head. The representation has the orientation of the virtual 3D head mesh with respect to the vehicle. The head will have the rotation and position as in the real crash test but in the virtual environment. From the calculation of three points of the head at every frame of the picture and then represented as a step of displacement on a virtual software program, it will have the exact animation head as in reality.
The point's position head are calculated relative to the vehicle at every movie frame using the dynamic coordinate system. On the animation "GIF", the vehicle will be represented as if it were not moving and the head will be moving along with respect to the car.

The minimum distance is the resultant of the 3D distances to the objects around the head dummy. This calculation is represented as a graphic of minimum distance by time.

Because the orientation of the camera to the vehicle is previously calculated, it is possible to represent the 3D head animation overlap with the video file. This file provides the visualization of the full head coordinated with the rest of the video and provides the opportunity to observe and understand the behaviour of the head and the airbag.

As long as this methodology is performed in every development test, it is possible to compare the behaviour of the head dummies for different types of restraint systems. The evolution of minimum distance graphs is also a tool to be determined when and how the head is acting towards the object it is compared to. This kind of analysis provides the information needed to provide the changes to the restraint systems on a development process of the car.

VALIDATION PROCESS

Validation of the full process determines the precision of this analysis, depending on every aspect that was analysed in this paper. The uncertainty is less than ~1.5mm in perfect conditions. This precision is achieved by carefully preparing all influence parameters of the measurement.

A full process validation test with different conditions is performed to determine if the final result, minimum distance comparison, has the best result possible. As well as providing a perfect condition environment and non-destructive test that allows repetitive tests.

The validation will prove if the resultant of minimum distance is the correct one. Two scanned parts, head and a plane surface, are filmed with a known distance object in between. The minimum distance result should be the same as that object, 14.9mm in this case. The best result achieved in these tests is 13.51mm, a 9.3% uncertainty.

Improvements for Better Accuracy

To provide the perfect accuracy in the calculations many tests were performed and three variables were tested: 3D mesh model, the angle between cameras and the tracking algorithms.

Angle Between Cameras On a 3D methodology, the angle between the two cameras will provide the best results in a 90º difference. But at that differential degree, the flat sticker target will not be seen by the two cameras. So the best degree condition will offer a good visibility of the target and enough angle to calculate the 3D position. It is proven that a 20º differential is ideal for providing perfect tracking and 3D position of the point. Less than 20º will produce high errors on the perpendicular to the camera axis.

The 6DoF methodology does not have this angle problem, but can be compared to the triangulation of the points measured. The four points tracked on the head must be as separated as possible between them. That will provide the triangulation needed to calculate the position of the coordinate system with more efficiency. If the points tracked are too close to each other, the small errors of the tracking algorithm will affect the 6DoF calculation more.

The tests performed regarding the 6DoF accuracy in the same conditions as the 3D methodology has proven that the last one is the most accurate. The 6DoF has a 13% increase uncertainty respect to the 3D methodology.

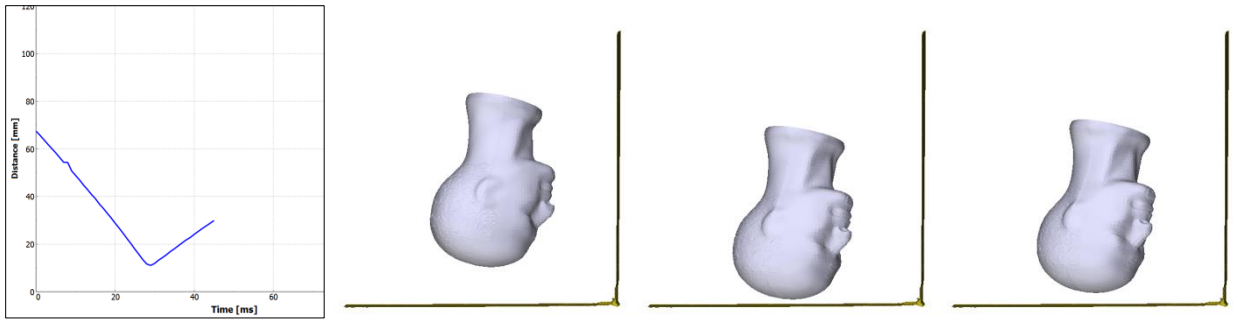

Figure 6. Minimum distance head graph representation. 6DoF tracking methodology. Followed by three states of the animation. The centre state is the minimum distance.

Tracking Algorithms The best tracking algorithm must be defined by the user taking into consideration the conditions of the movie. It is essential, as shown in the next graphs, that some tracking algorithms provide noise to the result.

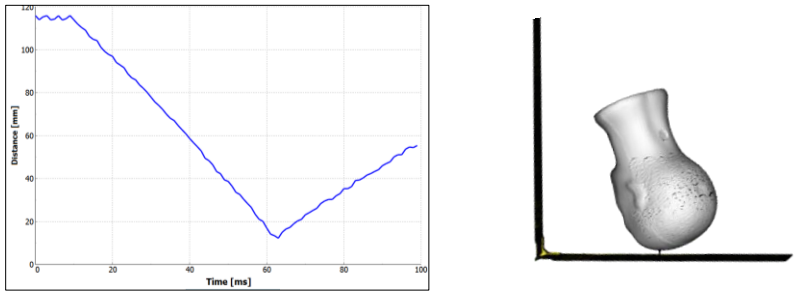

Figure 7. Minimum distance head graph representation. This tracking was performed by an MXT algorithm (20% uncertainty). The animation has noise and can be noticed on the graph.

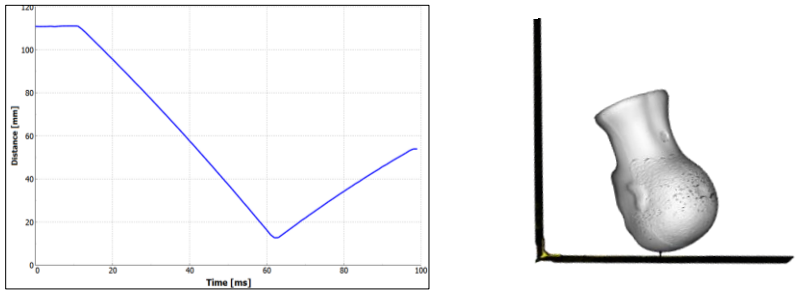

Figure 8. Minimum distance head graph representation. This tracking was performed by a correlation advanced algorithm (1% uncertainty). The noise was reduced dramatically and represents a faithful animation.

Choosing the right algorithm will increase accuracy, a 3.4% incremental accuracy in this test. The benefit may not be much, but the animation of the head is represented with higher precision. The comparison between different animation, movie or even simulation occupant behaviour will be more efficient.

3D Mesh Model The 3D mesh model is related to the 3D scanned surface of the head. The comparison to calculate minimum distance is related to the nodes of the mesh. Part of the uncertainty of the minimum distance is related to the separation of the nodes. The 3D mesh should have the most compacted node mesh possible to reduce the uncertainties. It is important to notice how the mesh is calculated. Increasing the mesh density by software calculations instead of the point cloud from the scanner, could generate more uncertainties.

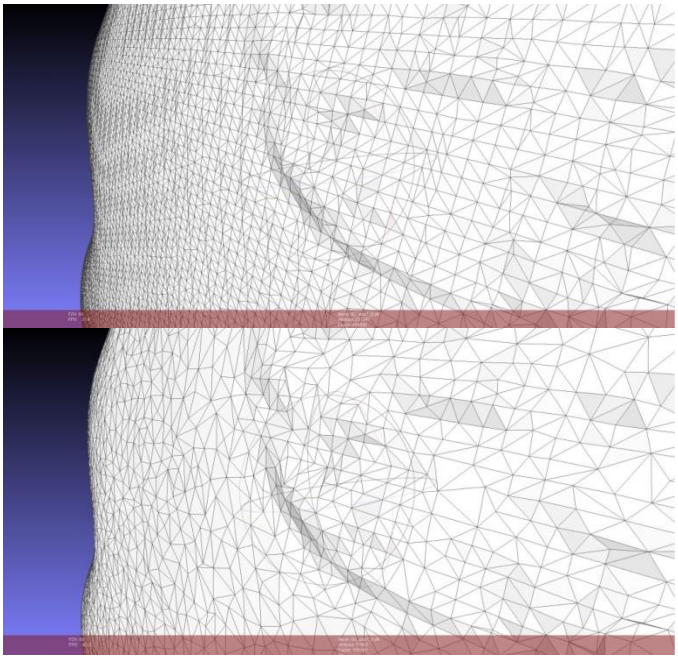

Figure 9. Mesh density comparison. Above picture represents a directly exported mesh from the scanner, above a reduced mesh density. The first has more precision result and the second will process faster.

The validation process notices that these changes provide a 4.8% incremental accuracy. This was the best result yet, with a total of 9.3% uncertainty, in this particular case it is around 1.5mm uncertainty.

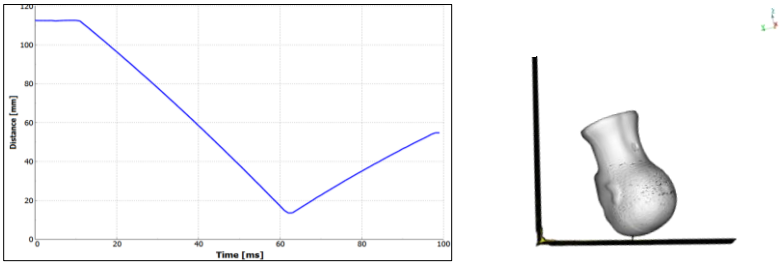

Figure 10. Minimum distance head graph representation. This graph should be compared with figure 8. The mesh used here is the original taken directly from the scanner.

CONCLUSIONS

Photogrammetry and motion analysis is becoming an important tool to analyse crash and sled tests for occupants and the vehicle itself. The minimum distance to the head tracking methodology is becoming an important assessment to provide the right information and allow comparison of different configuration tests and restraint systems.

Improvements in this methodology are continually being made and more improvements will be made in the future. On-board tracking is a big step forward as many different tests will be introduced with autonomous driving as the complexity of new car models with new occupant positions will need a fast and accurate way to analyse restraint systems. This tool could help many development procedures.

ESTIMATION OF EFFECT OF CROSSING SCENARIO AEB SYSTEM TO HELP REDUCE TRAFFIC ACCIDENTS

Akitoshi Minemura, Takashi Hasegawa

Toyota Motor Corporation

Japan

Paper Number 19-0234

ABSTRACT

Advanced safety technologies such as automated emergency braking (AEB) systems are key technologies for helping to reduce traffic accidents. This study quantifies crossing scenario accident types by analyzing traffic accident databases from various countries. It then calculates the delta-V reduction collision velocity obtained by a proposed crossing scenario AEB system, and estimates the benefit of the proposed crossing scenario AEB system.

INTRODUCTION

To help reduce traffic accident fatalities and casualties, national governments, industries, and manufacturers are working with the guidance of regulations and assessments to enhance vehicle safety and to popularize devices and systems that help to ensure an even safer traffic environment [1]. In recent years, several advanced safety technologies have begun to enter wider use, including automatic emergency braking (AEB) systems that detect vehicles or pedestrians in front of the driver's vehicle, as well as lane departure warning (LDW) and lane keeping support (LKS) systems that help the driver to keep the vehicle inside the driving lane. Some vehicle models are also installed with AEB systems that provide support when driving through intersections (in this paper, these systems are referred to as "crossing scenario AEB systems").

This paper focuses on crossing scenarios and discusses the effects of crossing scenario AEB systems in helping to further reduce accidents, fatalities, and casualties. First, this paper analyzes accident data from various countries, and quantifies the types of crossing scenario accidents and the speed distributions of vehicles involved in frontal and side impact collisions. It then uses the National Automotive Sampling System Crashworthiness Data Set (NASS CDS) from the U.S. to identify the relationship between collision velocity and the rate of severe injuries in vehicles damaged at the side. Finally, this paper proposes specifications for an AEB system and calculates the changes in collision velocity with and without system activation in a crossing scenario. These results can be combined to estimate the reduction in severe injuries due to system activation, providing greater impetus to the development of future AEB systems capable of further mitigating damage in crossing collision scenarios.

RESEARCH INTO CROSSING ACCIDENTS

This section analyzes accident data from various countries and discusses the characteristics of crossing scenario accidents.

Country-by Country Breakdown of Fatalities and Casualties

Accident fatality and casualty data of people involved in accidents in three different countries (Japan, the U.S., and Germany) is analyzed below. First, Figs. 1 and 2 compare the proportions of accidents resulting in a fatality or casualty in each country.

It is evident that accident proportions are different even in developed countries. Since vehicle safety performance and education levels in these countries are similar, differences in the road environment may be assumed as a possible cause. For example, in the case of fatal accidents, Japan has a high proportion of pedestrian fatalities (37%), whereas car occupants account for a high proportion of fatalities in the U.S. (66%). The results for Germany are between Japan and the U.S. Accordingly, accident investigations were conducted in each country to help enhance vehicle safety from a global standpoint.

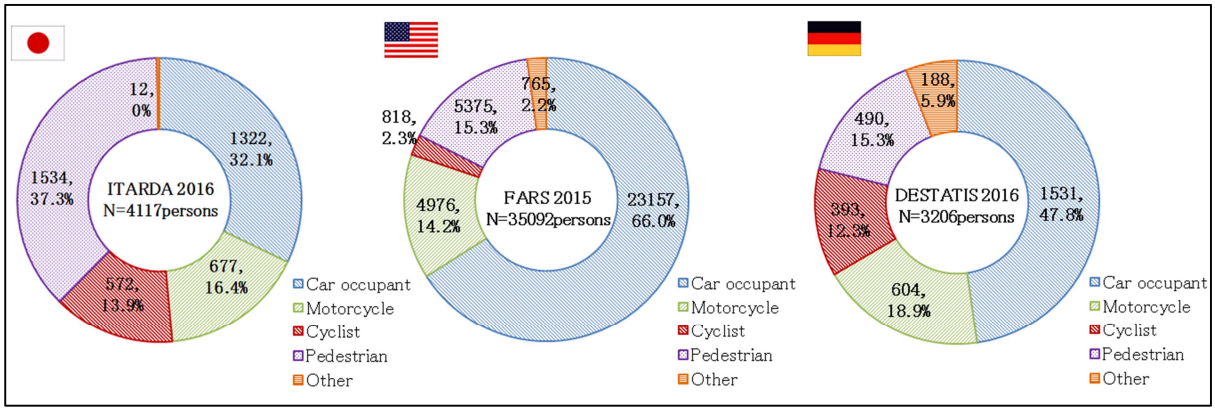

Figure 1. Comparison of proportion of fatalities in Japan, the U.S., and Germany.

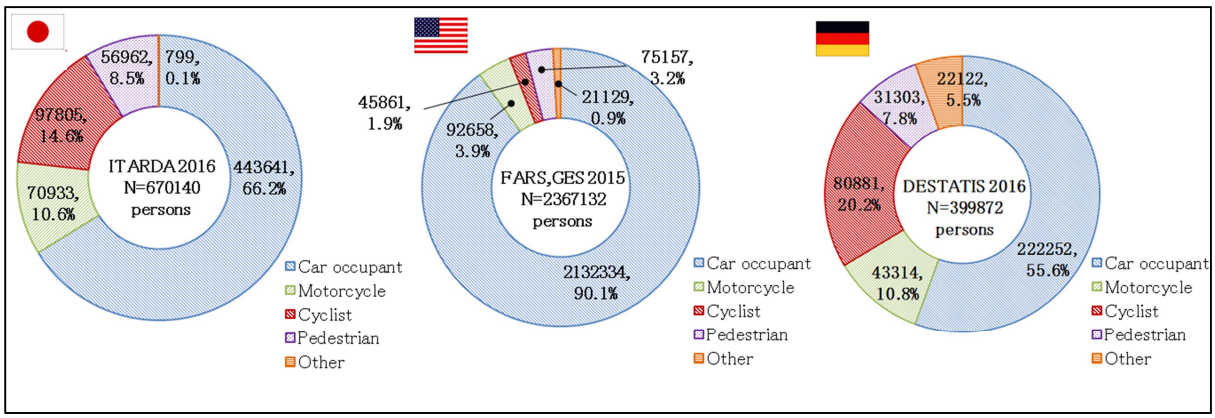

Figure 2. Comparison of proportion of casualties in Japan, the U.S., and Germany.

Proportions of Accidents Leading to Fatalities and Casualties in each Country

Figures 3 and 4 show the proportions of accident types leading to fatalities and casualties. These graphs break down the accident proportions shown in Figs. 1 and 2 into more detailed accident type information. The proportions of crossing scenario accidents involving cars are highlighted in red.

Figure 3 shows the proportions of accident types resulting in a fatality, with the most prevalent type on the left. In the U.S., the proportion of fatal crossing scenario accidents involving cars is approximately 8%, higher than in Japan and Germany, in which the proportion is approximately 4%. Figure 4 shows the proportions of accident types resulting in a casualty, with the most prevalent type on the left. In Japan, the proportion of crossing scenario accidents involving cars and resulting in a casualty is 12%. This is the second most common accident type, after rear-end collisions. In the U.S., the figure is 19%, which is also second only to rear-end collisions. In Germany, the proportion of this accident type is 10%, the third most common accident type after rear-end collisions and loss of control. These figures indicate that crossing scenario accidents result in a comparatively high number of accidents in all countries.

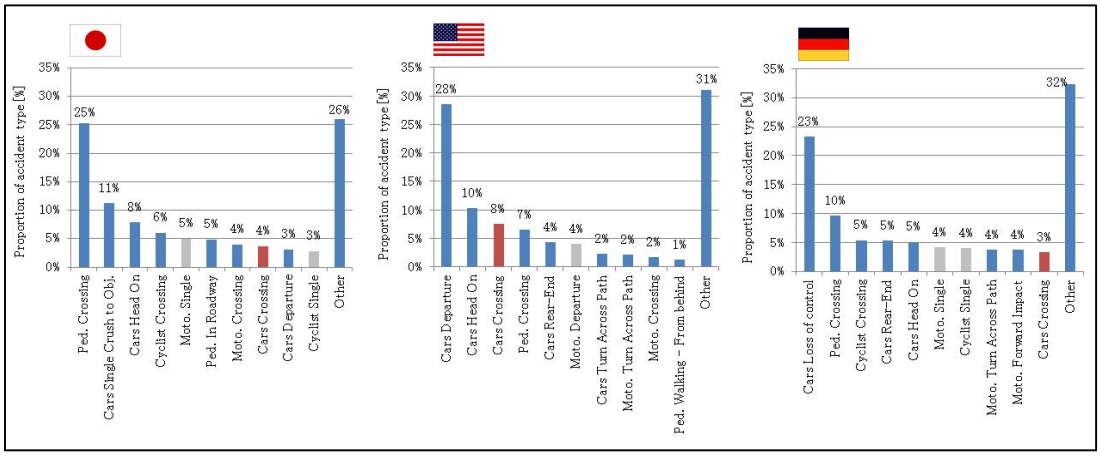

Figure 3. Fatalities: proportion of accident types.

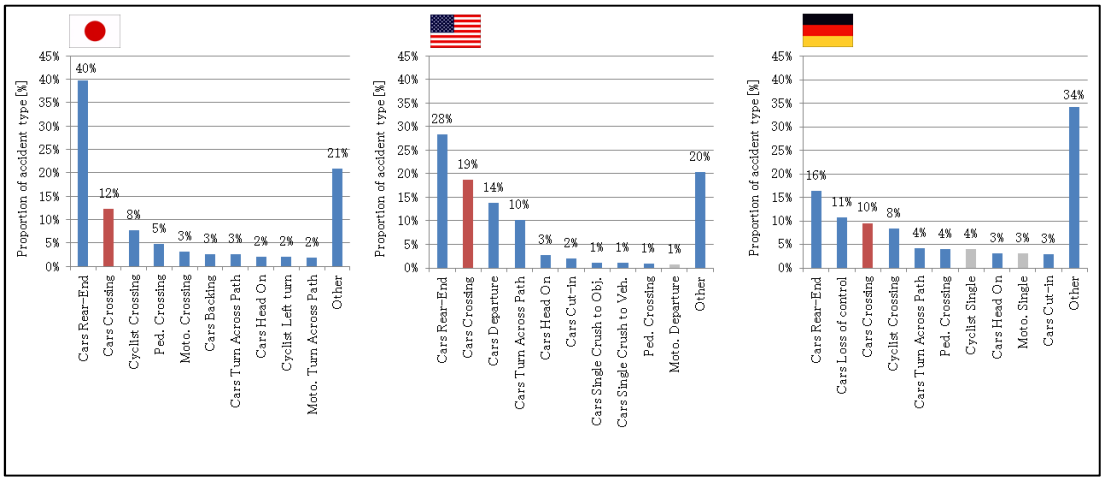

Figure 4. Casualties: proportion of accident types.

Locations of Crossing Scenario Accidents

To identify the circumstances of crossing scenario accidents in more detail, Fig. 5 shows the locations of such accidents that result in a casualty. In all three countries, a high proportion of these accidents occurs at intersections, with only a limited proportion occurring elsewhere. This result highlights the importance of prioritizing accidents at intersections in efforts to mitigate crossing scenario accidents.

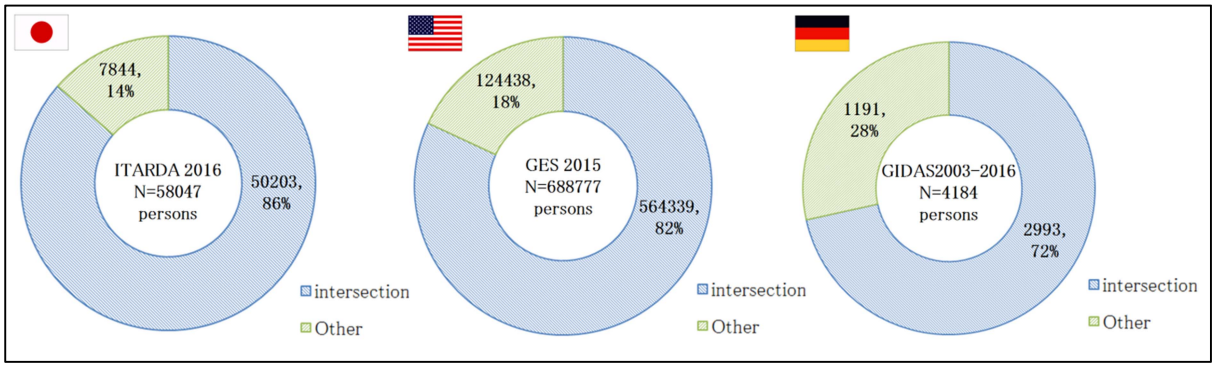

Figure 5. Comparison of proportion of crossing scenario accident locations.

Vehicle Speeds in Crossing Scenario Accidents

Finally, the distribution of vehicle speeds in crossing scenario accidents was analyzed. The results described above found that crossing scenario accidents accounted for a high proportion of casualties in all three countries, as well as a relatively high proportion of fatalities in the U.S. Subsequently, to supplement the fatality data and obtain a sufficiently large data set, this research analyzed accident data from the U.S. with a maximum abbreviated injury scale score of 3 or higher (MAIS3+) and accident data from Germany of people killed or seriously injured (KSI).

Figure 6 shows the distribution of vehicle speeds in crossing scenario accidents resulting in KSI. The X axis shows the speed of the vehicle damaged at the side and the Y axis shows the speed of the vehicle damaged at the front. The data for Germany covered fourteen years of accidents and was converted to show the number of casualties on an annual basis. In many cases in both the U.S. and Germany, the speed of the vehicle damaged at the front exceeded the speed of the vehicle damaged at the side.

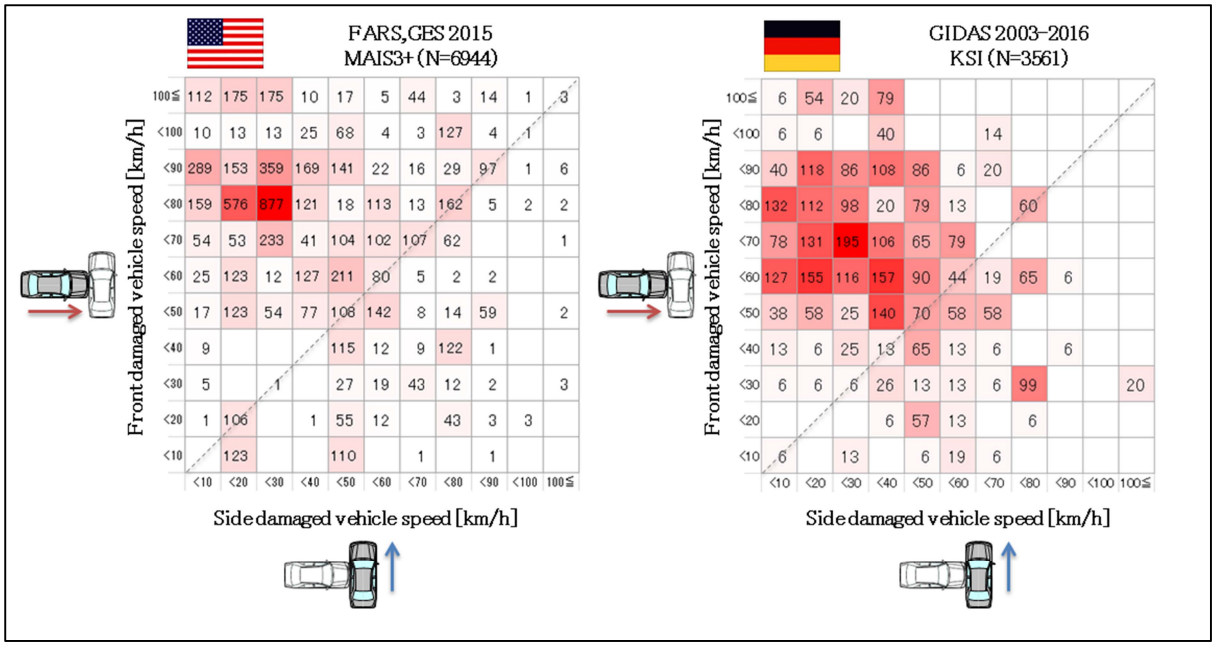

Figure 6. Speed distribution of crossing vehicles in the U.S. and Germany.

ESTIMATION OF EFFECT OF CROSSING AEB SYSTEM

This section calculates the potential effect of a crossing scenario AEB system based on the relationship between changes in collision velocity and the risk of severe injury. Using the results described above, an AEB system capable of mitigating crossing scenario accidents would require additional forward monitoring sensors for vehicles traveling at high speed that can detect potential collision objects in front of the vehicle at longer distances, and wider angle forward or side sensors for vehicles traveling at a lower speed that may be struck in the side. As of 2018, forward sensors have achieved wider commercialization than side sensors. Furthermore, if a vehicle brakes before a potential side impact collision but cannot avoid the collision, then the collision point will change. This will affect the damage caused by the collision in accordance with the positional relationship with the occupant compartment. This means that braking by a vehicle before a potential side impact collision requires more accurate collision point prediction technology. Therefore, this section focuses on AEB activation by vehicles traveling at high speed before a potential frontal collision. In addition, the angle of view of most current forward sensors is between ±20 and ±30 degrees, and it is feasible that this may expand to ±45 degrees in the near future. Assuming the widespread adoption of such advanced sensors, an AEB system was proposed that activates in scenarios in which the other vehicle is driving toward the same location as the driver's vehicle at the same relative speed or lower. The potential effect of such a crossing scenario AEB system is calculated below.

Relationship between TTC Judgment of Crossing Scenario AEB System and Deceleration

This section calculates the relationship between the TTC judgment of the proposed crossing scenario AEB system and the amount of deceleration.

This study assumed the following braking characteristics. Figure 7 shows the time sequence characteristics.

Time from judgment to brake activation: 0.2 sec

Jerk to maximum deceleration: 18.0 m/s^3

Maximum deceleration: 9.0 m/s^2

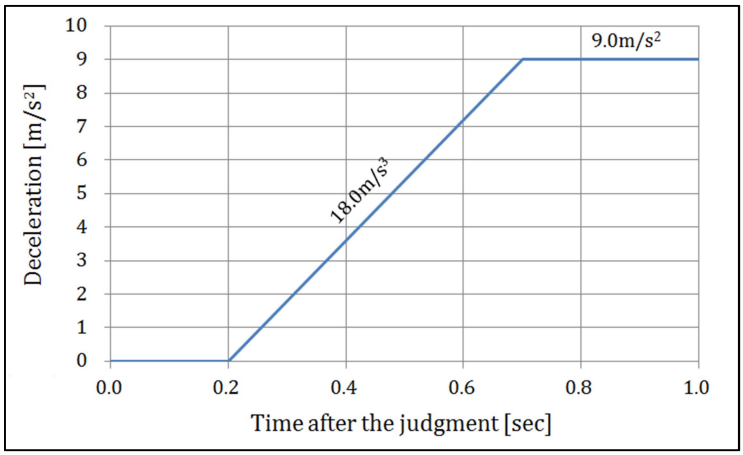

Figure 7. Assumed braking characteristics.

The activation timing of the crossing scenario AEB system was determined as follows. In the case of a crossing scenario, the other vehicle might stop before the potential path of the driver's vehicle. The judgment timing for this eventuality depends on the speed of the other vehicle and the relative vehicle position. Assuming that a collision can be avoided by the other vehicle reducing speed, the time to collision (TTC) with the driver's vehicle was estimated regardless of the behavior of the other vehicle. The estimation was carried out using the conditions shown in Fig. 8. Figure 9 shows the results. When the speed of the other vehicle and the overlap rate are low, it is necessary to delay the AEB activation judgment until a relatively shorter TTC. Assuming brake activation occurs at an overlap rate of 20% or higher, the TTC was estimated as 0.9 sec under the most severe conditions (speed of other vehicle: 10 km/h, overlap rate: 20%). Consequently, the AEB activation timing was set to TTC = 0.9 sec.

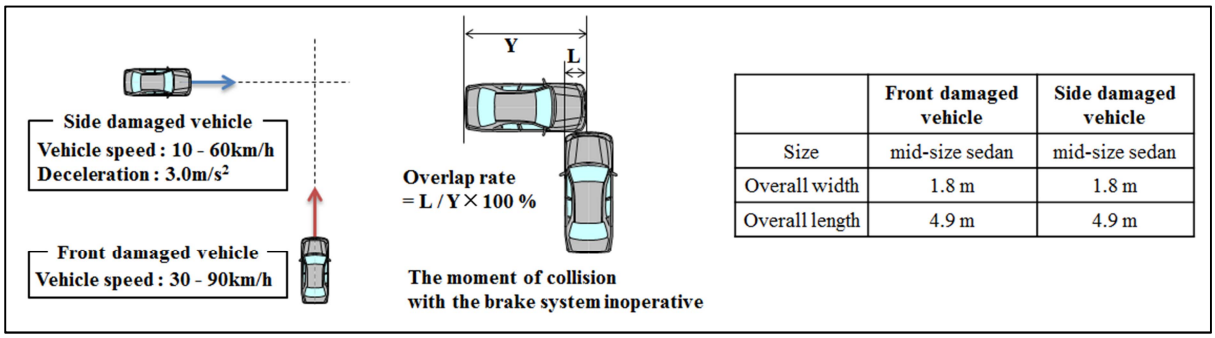

	Front damaged vehicle	Side damaged vehicle
Size	mid-size sedan	mid-size sedan
Overall width	1.8 m	1.8 m
Overall length	4.9 m	4.9 m

Figure 8. Defined overlap rate.

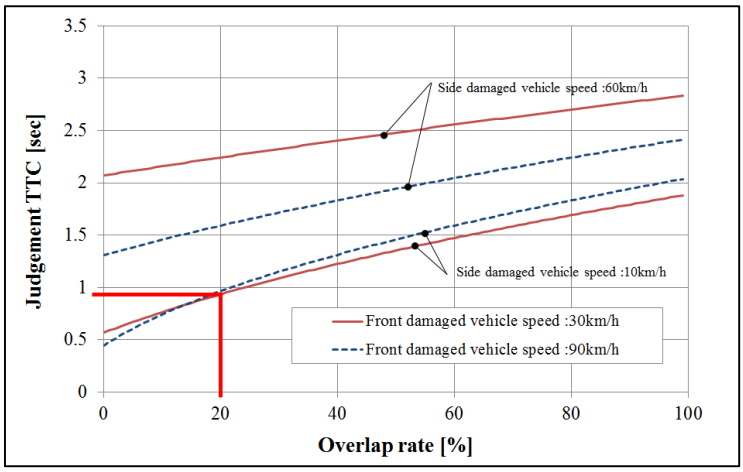

Figure 9. Relationship between overlap rate and TTC judgment.

Next, the relationship between the initial speed and amount of deceleration was estimated. This estimation assumed the braking characteristics shown in Fig. 7 and an activation timing of TTC = 0.9 sec. Under these conditions, a collision can potentially be avoided when the driver's vehicle is traveling up to a speed of 30 km/h. At higher speeds, the proposed system can potentially reduce the collision velocity.

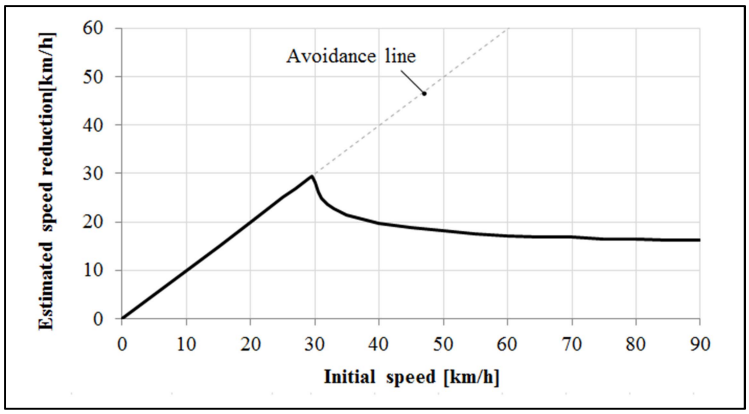

Figure 10. Defined deceleration characteristics.

Change in Collision Velocity and Calculation of Approximate Severe Injury Risk Reduction Effect

This section assumes a case in which the crossing scenario AEB system reduced the collision velocity but could not completely avoid a collision. To estimate the potential damage mitigation effect, the relationship between the collision delta-V (ΔV) and severe injury risk was analyzed. Although similar research has been carried out in the past [2][3], this paper uses NASS CDS data from 2009 to 2013. Reflecting the recent spread of side airbags, this relationship was analyzed based on MAIS3+ accidents in which the side airbags deployed.

First, the data was filtered under the conditions listed in Table 1. These conditions narrow down the analyzed accidents to near side collisions with occupants present in the front seats. The analysis was also limited to models from the 2007 model year or newer, which are expected to have a relatively high side collision

performance, and included only accidents in which the side airbags deployed. After filtering, data from 108 injured people was analyzed in accordance with the change in collision velocity.

The thin line in Fig. 11 shows the results of severe injury rate analysis using this methodology. In addition, the severe injury risk P (ΔV) was approximated using the method of maximum likelihood from the logistic regression line calculated by Equation 1. This approach uses the analytical methodology described in a previous report [4]. This result is shown by the thick line in Fig. 11.

$$P(\Delta V) = \frac{1}{1+e^{-b(\Delta V - c)}} \qquad \text{(Equation 1) [4]}$$

The severe injury rate increases from ΔV = 25 km/h, and the reduction effect eases once the ΔV value exceeds 50 km/h.

Table 1.

Filtering Code of Near Side VTV Collisions with Occupants in Front Seats

TOWPAR	1		Towed	
VEHFORMS	2		2 vehicle forms	
EVENTS	1		1 event	
ROLLOVER	0		No rollover	
DOF1	8,9,10,49,50,68,69,70,88,89,90	2,3,4,62,63,64,82,83,84	Struck Leftside	Struck Rightside
GAD1	L	R		
MODELYR	2007-2014		Later than '07MY	
SEATPOS	11	13	Driver's seat	Front Passenger seat
BAGDEPOT	1		Air bag deployed,other than first seat frontal	

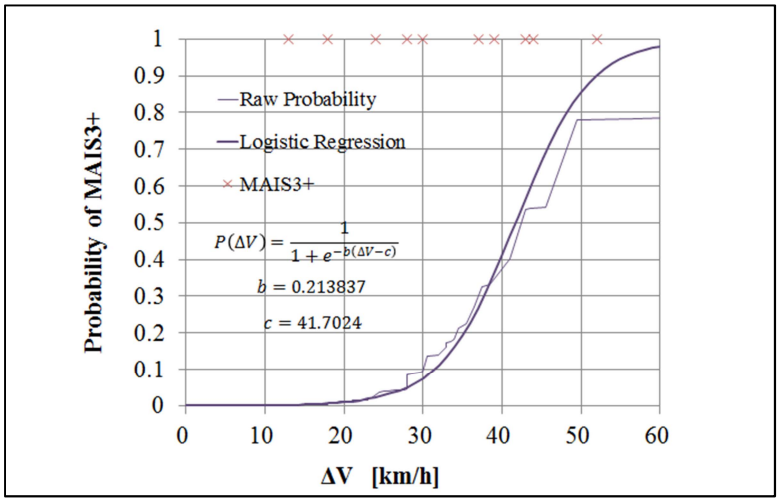

Figure 11. Relationship between normalized collision ΔV and probability of MAIS3+.

Calculation of Approximate Severe Injury Reduction Effect of Crossing Scenario AEB System

This section estimates the potential effect of the crossing scenario AEB system in reducing the number of severe injuries in vehicle-to-vehicle (VTV) side impact collisions by lowering the collision velocity.

The calculation assumptions were as follows. The crossing scenario AEB system was activated in only the driver's vehicle (i.e., the vehicle damaged at the front), the activation object was defined as other vehicles approaching at the same relative speed as the driver's vehicle or lower, the activation timing was set to TTC =

0.9 sec, the deceleration was set based on Fig. 10 to avoid a collision at a maximum speed of 30 km/h, and the amount of deceleration was set to 16 km/h or more from a maximum speed of 90 km/h.

Since the severe injury probability described in the previous section was analyzed based on ΔV, estimation of the reduction in severe injuries must be converted from collision velocity to ΔV. This conversion was carried out based on the assumptions shown in Fig. 12.

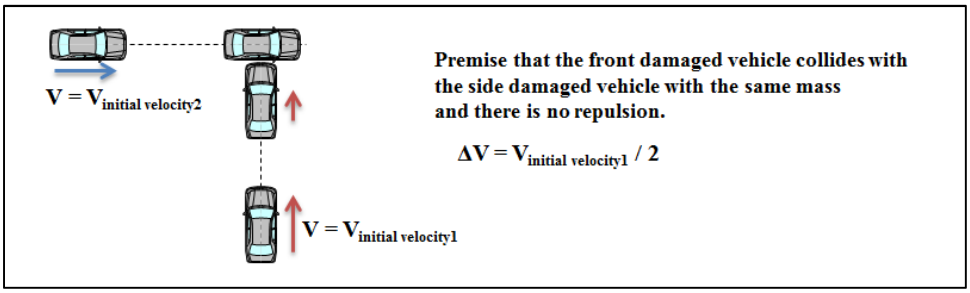

Figure 12. Defined collision ΔV.

Next, the circumstances immediately before the collision were investigated to examine the proportion of conditions in which the AEB system might have a potential effect. First, 2015 data from the Fatality Analysis Reporting System (FARS) run by the National Highway Traffic Safety Administration (NHTSA) in the U.S. was filtered as shown in Table 2. This procedure obtained data pertaining to 830 people. Additionally, as shown in Table 3, the data was categorized in accordance with the presence of avoidance maneuvers by the driver and vehicle stability immediately before the collision. Figure 13 shows these results. This figure indicates that the driver performed no avoidance maneuvers and that the vehicle was stable in 64.1% of accidents. Factoring in this figure, the AEB system activation rate in the U.S. was set to 64%.

Table 2.

Filtering Code of Near Side VTV Collisions (FARS 2015)

INJ_SEV	3,4	Suspected Serious Injury,Fatal Injury
BODY_TYP	1,2,3,4,5,6,7,8,9,10,11,14,15,16,17,19,20,21,22,28,29, 30,31,32,33,39,40,41,45,48,49,50,51,52,55,58,59, 60,61,62,63,64,66,67,68,71,72,78,79,	Passenger Cars,Light Trucks&Vans, Large Trucks,Buses
Ego's IMPACT1	1,11,12	Front
Opposite's IMPACT1	8,9,10,2,3,4	Left or Right
VE_FORMS	2+	VTV
P_CRASH3	1,2,3,4,5,6,7,8,9,10,11,12,98	No Avoidance Maneuver, Braking,Steering,Accelerating,Other Actions

Table 3.

Classification Code for Pre-Event Driver Maneuvers and Vehicle Stability (FARS 2015)

P_CRASH3	P_CRASH4	
1	1	No avoidance maneuver and no skidding
1	2,3,4,5	No avoidance maneuver and skidding
2,3,4,5,6,7,8,9,10,11,12,98	1	avoidance maneuver and no skidding
2,3,4,5,6,7,8,9,10,11,12,98	2,3,4,5	avoidance maneuver and skidding
Other Combination		Others

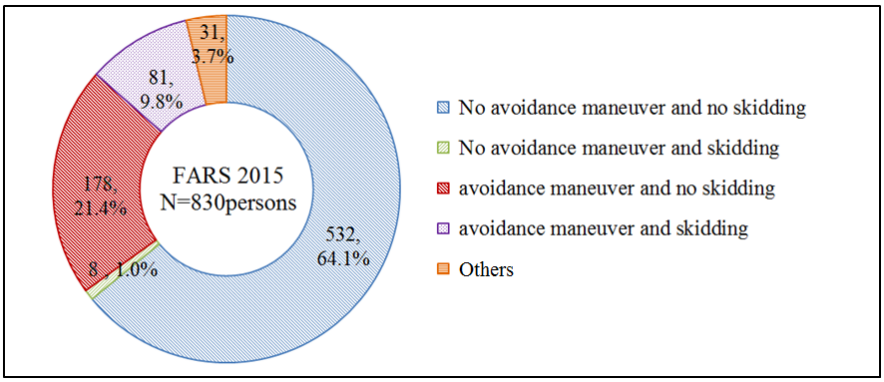

Figure 13. Proportion of KSI by pre-event in near side VTV collisions (FARS 2015).

In the same way, German In-Depth Accident Study (GIDAS) data from 2016 was used to estimate the AEB system activation rate. The GIDAS 2016 data was filtered as shown in Table 4, and data pertaining to 226 people was obtained. As shown in Table 5, the data was categorized in accordance with the presence of avoidance maneuvers by the driver and vehicle stability immediately before the collision. The results are shown in Fig. 14. This figure indicates that the driver performed no avoidance maneuvers and that the vehicle was stable in 40.7% of accidents. Therefore, the AEB system activation rate in Germany was set to 41%.

Table 4.

Filtering Code of Near Side VTV Collisions (GIDAS 2016)

PVERL	4,5	seriously injured,killed
FART	3,4,5,6	passenger cars,HGV,bus,agricultural tractor
Ego's VDI2	1	Front
Opposite's VDI2	2,4	Left or Right
ANZBETFZ	2+	VTV
REAKTGAS	0,1,2,3,4,8	No Avoidance Maneuver,Accelerating,Other Actions
REAKTBR	0,1,2,8	No Avoidance Maneuver,Braking,Other Actions
REAKTLE	0,1,2,3,4,8	No Avoidance Maneuver,Steering,Other Actions

Table 5.

Classification Code for Pre-Event Driver Maneuvers and Vehicle Stability (GIDAS 2016)

REAKTLE	REAKTBR	REAKTGAS	SCHLEU	
2	2	2	2	No avoidance maneuver and no skidding
2	2	2	1	No avoidance maneuver and skidding
1,3,4	1	1,3,4	2	avoidance maneuver and no skidding
1,3,4	1	1,3,4	1	avoidance maneuver and skidding
Other Combination				Others

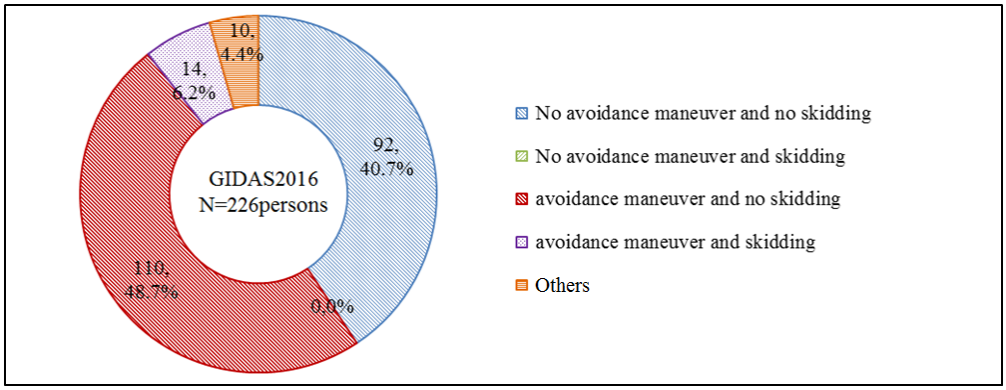

Figure 14. Proportion of KSI by pre-event in near side VTV collisions (GIDAS 2016).

Figure 15 shows the distribution of severe injuries and fatalities at each vehicle speed when the crossing scenario AEB system activated. This distribution uses the relationship between the change in collision velocity and severe injury risk shown in Fig. 11. After comparing the results in Figs. 6 and 15 with the speed of the driver's vehicle (i.e., the vehicle damaged at the front) on the horizontal axis, Fig. 16 shows the potential severe injury reduction effect. This figure indicates that the number of KSI caused by crossing scenario accidents fell after the application of the AEB system. Specifically, the number of KSIs in the U.S. fell by 2,394 people out of a total of 6,944, and in Germany by 873 people out of a total of 3,561.

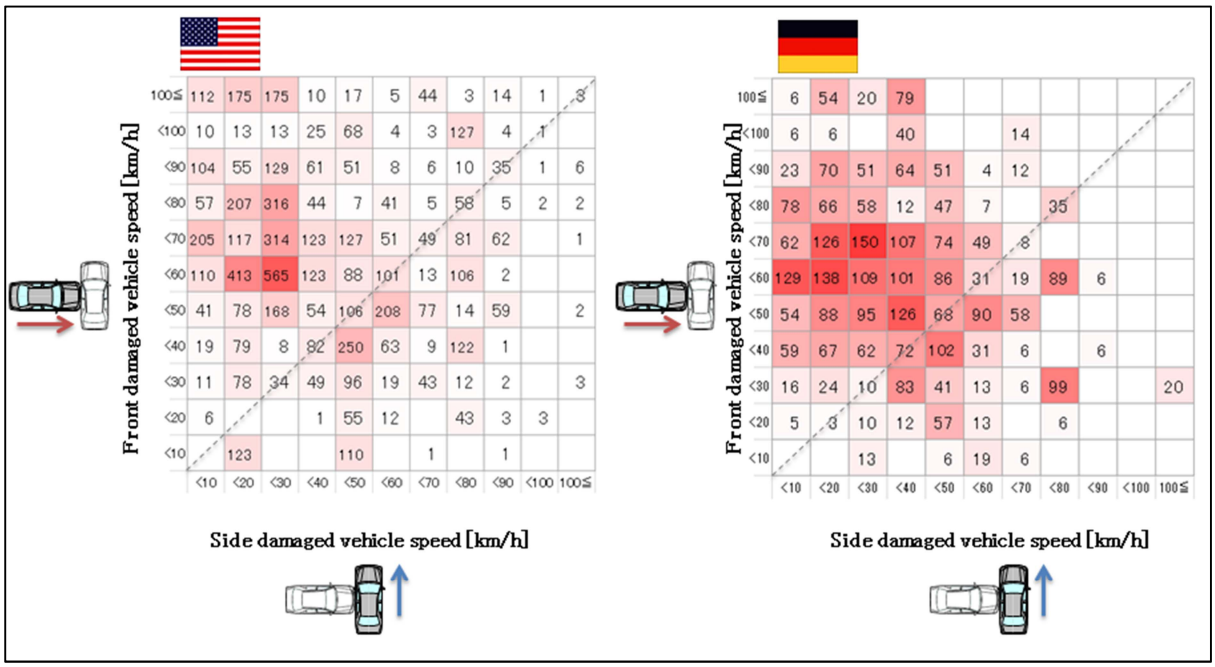

Figure 15. Speed distribution of crossing accidents before and after application of AEB system.

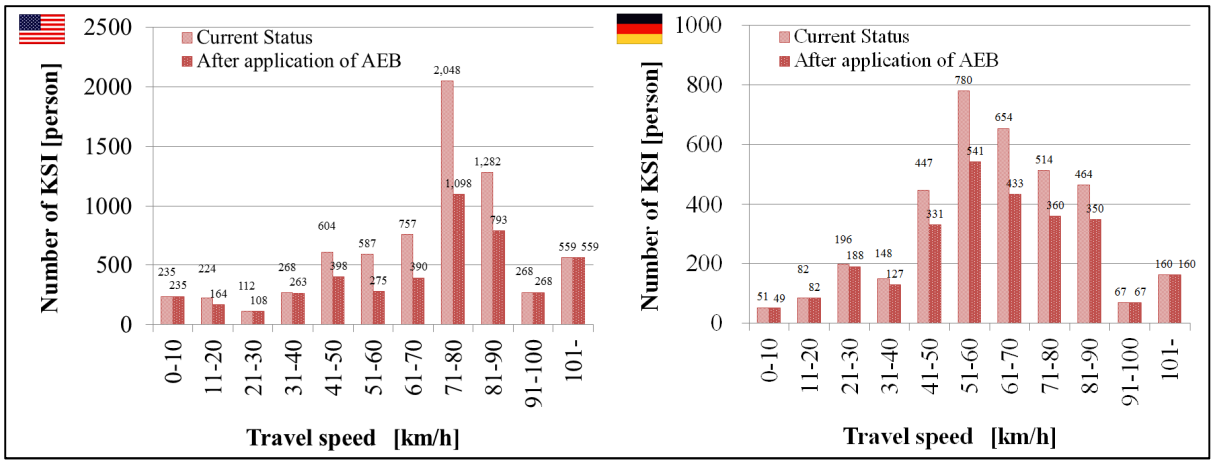

Figure 16. Comparison of number of KSIs before and after application of AEB system.

CONSIDERATIONS

According to Fig. 16, the AEB system has the potential to reduce the number of severe injuries by 2,394 people (34.5%) in the U.S. and by 873 people (24.5%) in Germany. Since the system only has the potential capability to avoid a collision at 30 km/h or less, the potential severe injury reduction rate is limited compared to the total number of severe injuries. However, since it is capable of reducing the collision velocity when the vehicle is traveling between 60 and 90 km/h (i.e., a speed range that covers a large proportion of accidents), this system may be regarded as potentially effective.

According to Fig. 14, the driver performed avoidance maneuvers and the vehicle remained stable (i.e., skidding did not occur) in 48.7% of accidents. In many of these cases, the vehicle was already braking (90.9% or 100/110 cases). Since the driver was already braking the vehicle, a braking assist system that speeds up the AEB activation timing may have an even greater effect.

LIMITATIONS

This paper showed the potential effect of a crossing scenario AEB system. However, any reduction in the number of severe injuries depends greatly on the braking activation timing and activation characteristics, the activation rate of the AEB system, the surrounding environment, and other factors. Additionally, the estimations in this paper are based on a number of assumptions described above. More detailed estimations would require the definition of specific sensor specifications and judgment logic through future AEB system development. As a result, it is entirely possible that the estimated effect described in this paper may change.

Although these estimations were carried out based on accident data, various statistical methodologies were applied. For this reason, there is no guarantee that the estimated system effect would be generated in the case of individual real-world accidents.

CONCLUSIONS

This paper obtained the following conclusions from an analysis of accident databases in various countries and paper estimations of crossing scenario traffic accidents.

Analysis of fatal accident types in these countries found that the proportion of fatal crossing scenario accidents involving cars is approximately 8% in the U.S., higher than in Japan and Germany, in which the proportion is approximately 4%. Furthermore, the rate of crossing scenario accidents involving cars and resulting in a casualty is approximately 12% in Japan, approximately 19% in the U.S., and approximately 10% in Germany.

Analysis of the vehicle speed distribution in crossing scenario accidents resulting in a casualty identified that, in many cases in both the U.S. and Germany, the speed of the vehicle damaged at the front exceeded the speed of the vehicle damaged at the side.

An AEB system was proposed for crossing scenario accidents based on these analysis results. Based on the relationship between the change in collision velocity and severe injury risk, the proposed AEB system is capable of potentially avoiding collisions at low speeds and reducing the collision velocity at medium speeds. The proposed AEB system has the potential to reduce the number of KSIs by 2,394 people (34.5%) in the U.S. and by 873 people (24.5%) in Germany.

REFERENCES

[1] National Agency for Automotive Safety & Victims' Aid (NAVSA): New Car Assessment, http://www.nasva.go.jp/mamoru/about/about.html (retrieved on January 1, 2019)

[2] Gabauer, D.J. and Gabler, H.C. 2006. "Comparison of Delta-V and Occupant Impact Velocity Crash Severity Metrics Using Event Data Recorders." In 50th Annual Proceedings of the Association for the Advancement of Automotive Medicine

[3] Richards, D. and Cuerden, R., 2009. "The Relationship between Speed and Car Driver Injury Severity."

[4] Hasegawa, T. 2017. "Clarification of Priority Factors for Reducing Traffic Accident Fatalities in the U.S. and Benefit Estimation of AEB System for Oncoming Vehicles." 25th ESV, Paper Number 17-0171

A STUDY OF AGE DETECTION SYSTEM FOR APPLICATION TO ELDERLY OCCUPANT PROTECTION

Jun, Shiraishi
Osamu, Ito
Kazuo, Imura
Honda R&D Co., Ltd. Automobile R&D Center
Japan

Nobuhiro, Mochizuki
Yoshiaki, Kikuchi
Fujitsu Connected Technologies Limited
Japan

Paper Number 19-0235

ABSTRACT

Recently, the number of injuries and fatalities in traffic accidents tend to decline. However, the proportion of elderly citizens involved in traffic accidents is tending to increase in Japan and other developed countries. The elderly is known to be less resistant to impacts than younger people due to the deterioration of physical structures, such as bones and muscles. In order to improve safety performance for elderly vehicle occupants, it is necessary to know the age of the drivers in advance. However, actual age of drivers does not always correspond to the representative age because the level of resistance of the elderly has large differences in individuals. It would be necessary to detect not only the driver's age, but also the aging level of the individual differences. In addition, in order to take convenience for the drivers into consideration, it would be necessary to use simply. Therefore, this research focused on the age of the blood vessels which can be measured easily.

The age of the blood vessels expresses the aging level of physical composition, such as the blood vessels and muscle fibers. It is calculated from the acceleration pulse wave of the blood flow. The characteristic points observed in the acceleration pulse wave are classified according to the age. Usually, the blood vessel age is measured by a contact-type photoelectric sensor. This research developed a noncontact measuring method based on an RGB camera. Evaluate accuracy of the blood vessel age with proposed method, moreover examined applicability of the method to onboard use.

In order to verify that the camera device developed in this research, measurements of proposal method were compared with that used the conventional method. The evaluation test was held on in indoor. The test subjects were thirty men aged from 20s to 60s. Proposal method is achieved that accuracy is comparable to that of the conventional method.

It should be considered that the proposed method will apply for a variety of adverse conditions when fitted in a vehicle. For example, use at night, use under backlight conditions, intrusion of the driver's arm operating the steering wheel and movement of the captured area due to vibration. It must be necessary for the method to perform detecting the age of the blood vessels accurately even under these conditions.

This paper has discussed about a noncontact method of detecting a driver's age, focusing on the age of the blood vessels, with the aim of improving safety of the occupant protection system. The experimental testing was verified as the basic concept of a noncontact blood vessel age detection system based on camera images. In order to proceed with research for fitting actual vehicle, it will be necessary to research not only improving system accuracy but also improving its robustness under onboard conditions.

INTRODUCTION

It is tending to decline about fatalities in traffic accidents according to report of traffic accidents in Japan (See Figure 1). Otherwise, population of driver above 75 years old is increasing as background of aging society (See Figure 2). Therefore, it is significant to improve the safety for elderly drivers in recent years.

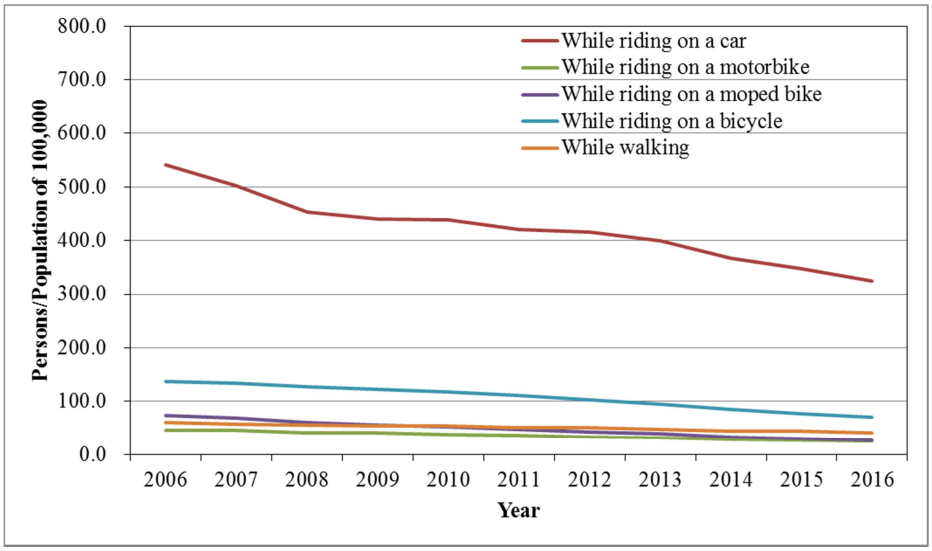

Figure 1. Changes in the number of fatalities in traffic accidents by state per a population of 100,000
WHITE PAPER ON TRAFFIC SAFETY IN JAPAN 2017
(https://www8.cao.go.jp)

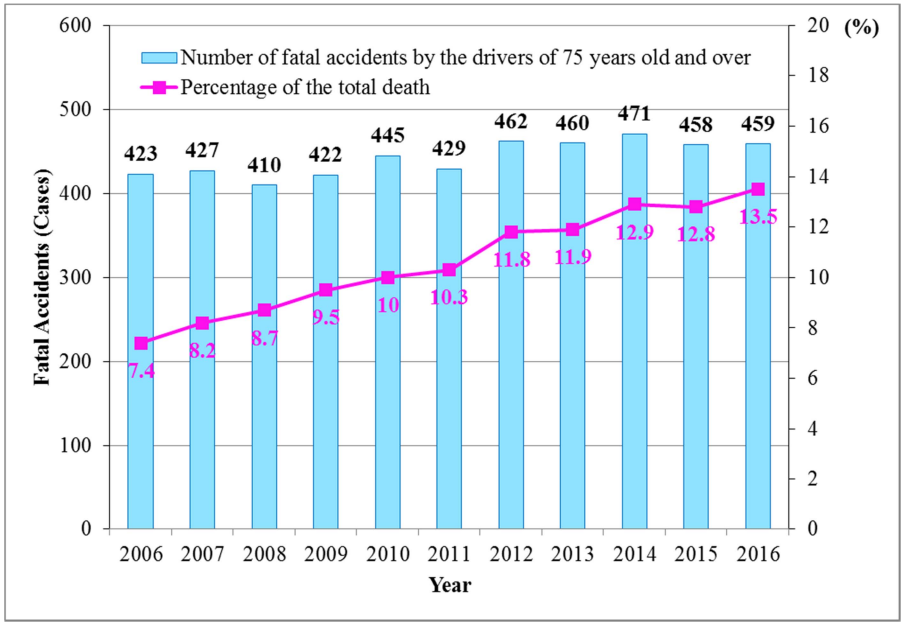

Figure 2. The number and percentage of fatal accidents caused by drivers of 75years and above
WHITE PAPER ON TRAFFIC SAFETY IN JAPAN 2017

Because of this social background, research for the elderly protection has been conducted in the past. Kent et al. [1] reported that changes of the elderly chest characteristics caused by aging. Ito et al. [2] constructed the elderly FE model and proposed an injury evaluation method for the elderly. Gunji et al. [3] studied that restraint device focused on the elderly by the method of Ito et al. According to Gunji et al., it is significant that adjusting restraint force

depending on status of elderly physical resistance to prevent fatality of the elderly. Adults and the elderly are identified with actual age generally. But it is difficult to represent physical resistance with only actual age because of individual difference of physical resistance. For example, there is sturdy elderly person or frail young adult. Therefore, we decided that studying some parameters to represent physical condition and developing a system to recognize the physical parameter.

There are two types of parameters for representing physical condition which are “bone age” and “blood vessel age”. According to Suzuki et al [4], it is difficult to measure the bone age correctly without medical X-ray apparatus. Due to this reason, the authors judged that the bone age is inappropriate parameter for measuring in a vehicle. On the other hand, the blood vessel age can be measured easily using portable measuring system (See Figure 3). There is a possibility that the blood vessel age measuring system can be mounted on a vehicle. Therefore, this research focused on the blood vessel age to recognize driver’s physical aging level.

Figure 3. Portable blood vessel age measuring system (U-medica Artett2 PDU-M200)

METHODOLOGY

This study proposed non-contact measuring system to measure the blood vessel age of driver. This paper reports that accuracy of proposed method with evaluation test.

Algorithm of Proposed Method

Figure 4 shows the algorithm flow of our proposed method. According to Nakaya et al. [5], a parameter as some kind of age is required to calculate a vascular age. The authors used the facial age and the actual age for the input parameter. Firstly, the method detects facial area of a driver from an image recorded by driver camera. Next, the method predicts a facial age by deep learning from the facial image. This deep leering architecture was implemented by “Azure” cloud service provided by Microsoft Corporation. And then, proposed algorithm measures a blood pulse wave from facial color fluctuation. The algorithm was created by Uchida et al [7]. A status of blood vessel age is calculated from blood pulse wave. This calculation method was proposed by Nakaya et al [5]. Finally, blood vessel age is estimated from both statuses of blood vessel and age parameters. This paper proposed two kinds of blood vessel age “Proposed_A” and “Proposed_F”. “Proposed_A” was based on actual age. “Proposed_F” was based on facial age.

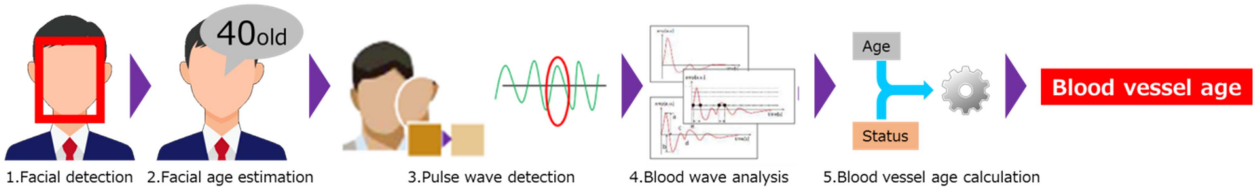

Figure 4. System flow of the proposed algorithm

Accuracy Evaluation of Proposed Method

In order to confirm the accuracy of proposed method, we prepared the reference age which is calculated by the conventional contact type sensor. The target correlation coefficient was set to 0.8 or more and the vessel age error was set within 10 years old. Evaluation test was carried out with the condition of Table 1.

Table 1.
Conditions for evaluation

Environment	Indoor
Illuminance	640 [lx]
Ambient temperature	25 [°C]
Number of subjects	30 persons
Sexuality	Male
Body temperature	From 26.0 to 27.3[°C]

Proposed system was developed as a smart phone application with portable devices (See Figure 5). Reference value of vessel age was measured with conventional measuring system (See Figure 6). Measuring equipment of each value was show in below (See Table 2). Each blood vessel age was evaluated by an average value calculated from values measured three times.

Table 2.
Equipment for each value

Measurement value	Equipment
Blood vessel age (Proposed_F)	Proposed system
Blood vessel age (Proposed_A)	Proposed system
Blood vessel age (Reference)	PDU-M200
Facial age	Proposed system
Body temperature	CISE 01 TE

Figure 5. Components for proposed system

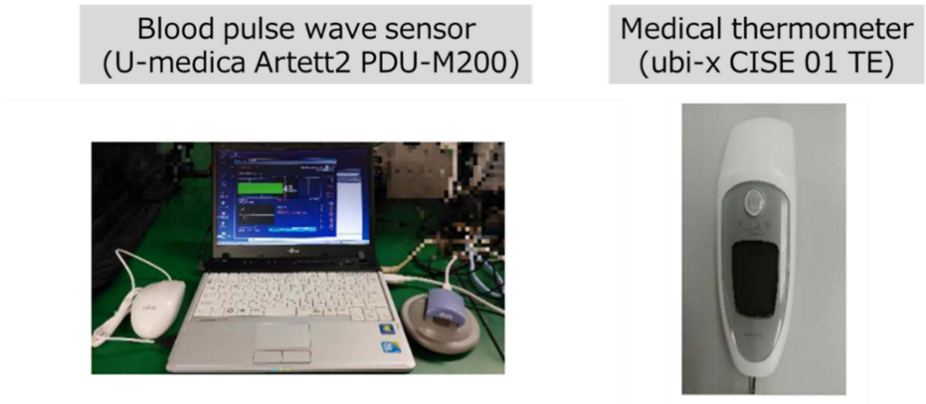

Figure 6. Equipment for reference data

RESULTS

The mean error of Proposed_A was 4.1 years old and Proposed_F was 7.6 years old. The maximum error was Proposed_A of 18.0 years old and Proposed_F of 28.0 years old. The plot (See Figure 7) was relation of the blood vessel age between proposed method and conventional method. The correlation factor of "Proposed_A" was 0.87, "Proposed_F" was 0.63.

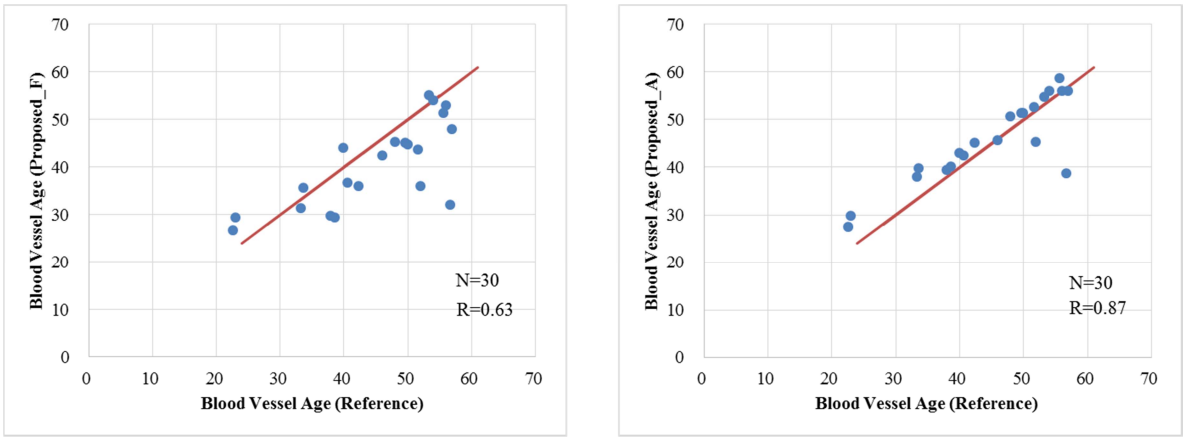

Figure 7. Relation of blood vessel age between proposed and reference

Figure 8 shows the plot between the actual age and the facial age. The correlation factor was 0.86. Mean error was 7.5 years old. Maximum error was 28.0 years old. There were 28 subjects with a facial age lower than the actual age. 2 subjects showed a higher age than the actual age. All values were shown in Table 3.

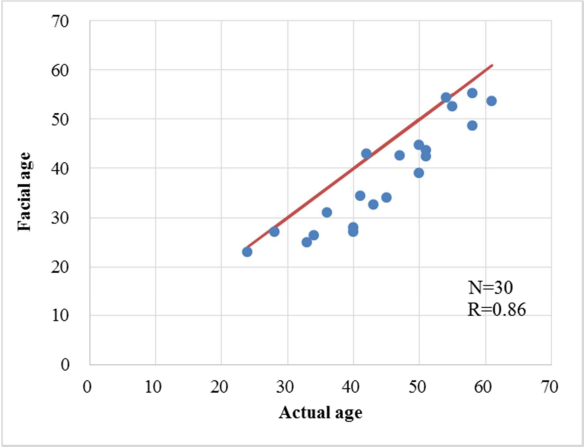

Figure 8. Relation between Actual age and Facial age

Table 3.
Blood vessel ages measured in evaluation test

ID	Age	Facial Age	Reference Age	Proposed_F		Proposed_A	
				Average	Difference from reference	Average	Difference from reference
1	28	27.0	23.0	29.3	6.3	29.7	6.7
2	51	43.7	49.7	45.0	4.7	51.3	1.7
3	40	12.0	44.3	16.3	28.0	42.0	2.3
4	40	28.0	38.0	29.7	8.3	39.3	1.3
5	40	32.3	36.7	35.0	1.7	41.3	4.7
6	60	56.0	63.3	57.0	6.3	60.3	3.0
7	54	54.3	53.3	55.0	1.7	54.7	1.3
8	42	36.3	36.3	38.3	2.0	42.7	6.3
9	36	31.0	33.7	35.7	2.0	39.7	6.0

10	58	55.3	56.0	53.0	3.0	56.0	0.0
11	47	42.7	46.0	42.3	3.7	45.7	0.3
12	41	34.3	40.7	36.7	4.0	42.3	1.7
13	58	48.7	57.0	48.0	9.0	56.0	1.0
14	45	42.7	50.3	43.3	7.0	45.0	5.3
15	61	53.7	55.7	51.3	4.3	58.7	3.0
16	43	32.7	42.3	36.0	6.3	45.0	2.7
17	50	44.7	48.0	45.3	2.7	50.7	2.7
18	40	27.0	38.7	29.3	9.3	40.0	1.3
19	44	28.3	58.0	30.3	27.7	44.0	14.0
20	50	39.0	51.7	43.7	8.0	52.7	1.0
21	33	25.0	33.3	31.3	2.0	38.0	4.7
22	42	43.0	40.0	44.0	4.0	43.0	3.0
23	43	25.0	49.7	30.3	19.3	45.7	4.0
24	34	26.3	56.7	32.0	24.7	38.7	18.0
25	24	23.0	22.7	26.7	4.0	27.3	4.7
26	25	19.0	27.3	29.0	1.7	33.7	6.3
27	45	34.0	52.0	36.0	16.0	45.3	6.7
28	29	28.0	24.0	30.0	6.0	31.0	7.0
29	55	52.7	54.0	54.0	0.0	56.0	2.0
30	51	42.3	50.0	44.7	5.3	51.3	1.3

DISCUSSION

From the evaluation test, the correlation coefficient of the Proposed_F was 0.63. It is considered that the facial age used when calculating the vessel age contains an error. From Figure 8 as well, we can see that the facial age tends to be lower than the actual age. By improving the estimation accuracy of the facial age, Proposed_F can be detected with high accuracy.

As for Proposed_A, the correlation coefficient with the vessel age of the reference machine exceeds the target value by 0.87. The authors confirmed that the proposed method is effective as a noncontact method that can replace contact type blood vessel age measuring instrument. However, looking at the experimental results, there were two subjects who exceeded the target error of 10 years old. For ID No. 19, since the measurement results at the reference machine were 69, 45 and 60 years old, there were many variations in measurements and there is a possibility that the accurate blood vessel age cannot be measured with the reference machine, so further investigation is necessary. Next, we consider subjects with ID 24. His vessel age measured by the reference machine was 56.7 years for the actual age of 34 years. There was a large difference between vessel age and actual age. There is possibility that the proposed method is not able to measure vessel age which is different from actual age largely. Therefore, it is necessary to improve the method so that we can respond to subjects who's the vessel age is remarkably high (low) in the future. We were concerned that these two measurements are unreliable. The correlation coefficient was 0.90 except these two subjects.

LIMITATION

Proposed_A method requires input procedure of actual age and it cannot be said that it is a perfect noncontact method. In the future, in order to replace the actual age with the face age, it is necessary to improve further the estimation accuracy of the facial age. Subjects in this paper were limited to healthy Japanese men from 20s to 60s. In order to make this method available to people all over the world, it is necessary to evaluate accuracy over 60

years old, accuracy for women, and correspondence to races other than Japanese. In the proposed method, the target is limited to drivers, therefore this method is assumed to use a driver camera. Considering that the elderly also sits on seats other than driver's seat, it is necessary to apply this method to all the seats in the future. In that case, a sensor has to be able to detect the entire interior of the passenger compartment.

CONCLUSIONS

In this research, the authors examined the age detection method necessary for improving the safety of elderly drivers at the time of a vehicle crash accident.

The authors proposed the blood vessel age as an index to measure the aging level of the driver. In addition, a noncontact measurement method replacing the conventional contact type was newly constructed and the accuracy was validated.

In order to make the proposed method completely noncontact, it is necessary to reduce the error from actual age to within 1 year by improving accuracy of the facial age detection algorithm.

REFERENCES

[1] Kent, R., Lee, S., Darvish, K., Wang, S. et al. 2005. “Structural and Material Changes in the Aging Thorax and Their Role in Crash Protection for Older Occupants.” SAE Technical Paper 2005-22-0011

[2] Ito, O., Dokko, Y., and Ohashi, K. 2009. “Development of Adult and Elderly FE Thorax Skeletal Models.” SAE Technical Paper 2009-01-0381

[3] Gunji Y., Aoki,T., Okamura, K., and Ito, Y. 2019. “Investigation of Restraint Characteristics for Elderly Occupant Chest Injury Reduction.” ESV conference 2019 to be submitted

[4] Suzuki, T. et al. 1996. “Comparison of Bone Mineral Levels in Healthy Japanese Perimenopausal Women Measured by Dual Energy X-ray Absorptiometry and Ultrasound Methods.” Japanese journal of public health 43-1 Page16-27

[5] Nakaya, K. et al. 2017. “Analyzing the Relationship between Contour-Line-Based Feature and Blood Pressure.” The transactions of the Institute of Electrical Engineers of Japan. C, Vol.137 No.4

[6] Microsoft Corporation, Microsoft Azure Cloud Computing Platform, https://azure.microsoft.com/ja-jp/(accessed 2018-OCT-15)

[7] Uchida, D. et al. 2017. “Continuous Real-Time Measurement Method for Heart Rate Monitoring Using Face Images.” the Communications in Computer and Information Science, Springer, CCIS, Vol. 690

UPDATED CHEST INJURY CRITERION FOR THE THOR DUMMY

Trosseille Xavier
LAB PSA Renault
France

Baudrit Pascal
CEESAR
France

Paper Number 19-0236

ABSTRACT

Anthropomorphic crash test dummies are designed to predict the risks of injury in automotive crash conditions. These dummies must therefore measure parameters that make it possible to calculate a metric related to injury mechanisms. This metric must evaluate the risk of injury whatever the solicitation, in a range covering all the solicitations arising in a crash. More specifically for a frontal impact, the risk of chest injury associated with this criterion must be the same, whatever the contributions of the belt or the airbag load paths. The objective of this paper is to develop such a criterion for the chest.

Several thoracic criteria were proposed by Poplin in 2017 for the THOR dummy, based on the measurement of the 4 3D deflections of the thorax. Unfortunately, for the sample studied, these criteria did not predict the risk of rib fractures better than the central deflection measured on an Hybrid III. The in-depth analysis of the sample showed that the sample configurations were too similar and that the deflection range was too small. Additional tests were added to the Poplin sample, which diversified the types of restraint systems and increased the extent of deflections. A new analysis was performed on this sample.

A new criterion was proposed. This criterion is a linear combination of the maximum value of the 4 chest resultant deflections and the absolute value of the difference of the upper right and left deflections. A risk curve was then constructed based on this criterion and age.

The consistency of the results of the new tests performed with the THOR dummy was assessed against the identical tests performed on the Hybrid III dummy. Similarly, the consistency of the injury assessments between the new tests and those of the initial sample was carefully studied. The results of these analyses confirmed the relevance of the added data. If the statistical methods used have shown the best performance of the new criterion, it has been optimized on the sample used and must be validated on external data. This could be verified on some data from the bibliography and further tests are planned to confirm it.

The use of an expanded test sample allowed to successfully develop a new thoracic criterion for the THOR dummy. It better predicts the risk of rib fractures, while being more consistent with crash investigation findings related to the age effect and the balance between the seat belt and the airbag. This paper brings new experimental data and analysis to improve the ability of the THOR to better predict the risk of rib fractures as a function of age.

INTRODUCTION

Petitjean et al. [1] showed that the deflection measured on the Hybrid III dummy was not sufficient to differentiate between the risks from the belt and the airbag. Her conclusions were the same for THOR. Moreover, Mertz et al. [2] proposed different risk curves for different loads. Petitjean et al. [1] proposed a criterion based on deflection and upper shoulder belt force. But the introduction of a measurement external to the dummy (the belt force) was a limiting factor for the acceptance of this criterion.

Davidsson et al. [3] proposed a criterion combining the maximum deflection along the X-axis with the low and high differential deflections. This criterion made it possible to better take into account the effects of the belt and airbag, but it introduced threshold values defined empirically.

In 2017, Poplin et al. [4] proposed a criterion based on a PCA (Principal Component Analysis). The dependent variable was the total number of fractured ribs, including cartilage fractures (NFR). The explanatory variables were the maximum of the sum of the upper resultant deflections (UPtot), the maximum of the sum of the lower resultant deflections (LOWtot), the maximum of the difference of the upper deflections (UPdif) and the maximum of the difference of the lower deflections (LOWdif). Unfortunately, based on the experimental sample used, this criterion was not better at predicting the injury risk than the resultant maximum deflection (Rmax), and above all, the prediction made with THOR was not better than with HIII (Dmax). An analysis of the sample showed that the THOR data set was highly correlated with the HIII data set (Figure 1) and that, except for a configuration without a shoulder harness, the variables used in the analysis by Poplin et al. [4] were highly correlated with each other (e.g. UPdif versus Rmax in Figure 2).

It then seemed appropriate to enlarge the sample by introducing other tests duplicated with THOR of the same definition as Poplin's (Mod-kit with SD-3).

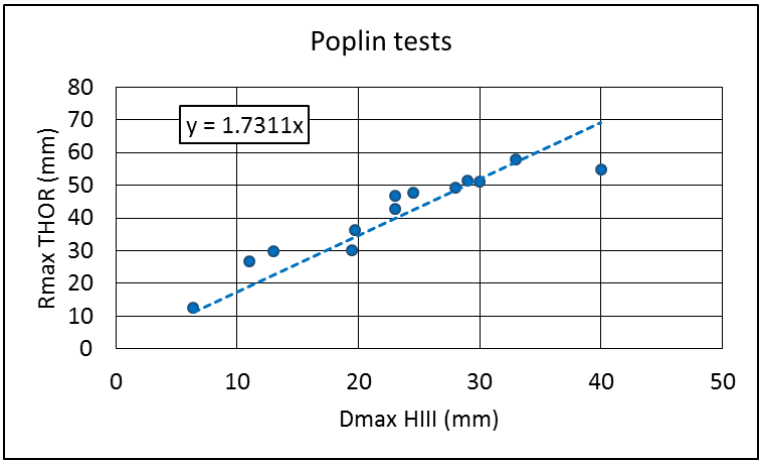

Figure 1. THOR versus HIII deflections for paired tests of Poplin et al. [4]

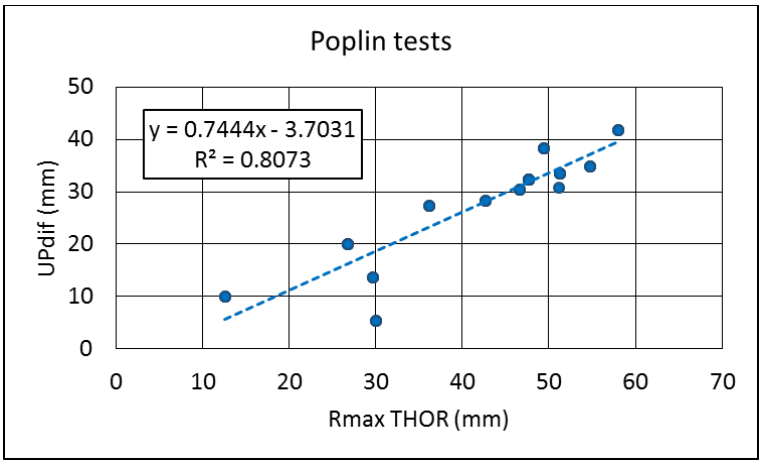

Figure 2. Upper chest deflection difference (UPdif) as a function of maximum resultant deflection (Rmax) for THOR tests of Poplin et al. [4]

METHODS

The first step was to collect PMHS data and check the consistency between data sources. Next, the corresponding THOR and HIII tests had to be found, and then the relationships between the explanatory variables and the number of rib fractures had to be investigated, in order to identify the most relevant criterion. Finally, the injury risk curves had to be constructed.

Experimental dataset

The data from Poplin et al. [4] were used as the starting point and the results of the corresponding HIII tests were collected from the NHTSA database. PMHS sled tests data published in Luet et al. [5], Uriot et al. [6] and Uriot et al. [7] were then collected to expand the range of deflections. In addition, data from Lebarbe et al. [8], Trosseille et al. [9], as well as new data with an airbag loading were added to diversify the types of restraints and increase airbag-type loading. All these tests were duplicated with HIII and THOR Mod-kit with SD-3.

The number of fractured ribs (NFR) included the costal cartilage fractures, as indicated in the definition of the 2008 version of the Abbreviated Injury Scale (AIS) cited by Poplin et al. [4]. In addition, the number of separated fractured ribs (NSFR) was collected when available. This variable was considered by Trosseille et al. [9] to be more representative of the clinical count of rib fractures, since non separated rib fractures cannot be detected on X-Rays.

The chest deflections selected were, as for Poplin et al. [4], the four resultant deflections measured on the THOR dummy.

Poplin sled tests: These are sled tests, in a "Gold Standard" configuration or on a 2004 Ford Taurus seat. The restraints were mainly 3-point belts only (35/45). The remaining restraints were 3-point belts with airbags (7/45) or lap belts with airbags (3/45).

LAB sled tests: These tests were carried out as part of submarining studies: Luet et al. [5] on rigid seat, Uriot et al. [6] on real seat and Uriot et al. [7] on semi-rigid seat. The restraint consisted of a 3-point belt or separated lap and shoulder belts. There were no airbags or knee bolsters in these tests.

LAB airbag tests: The Lebarbe et al. [8] and Trosseille et al. [9] tests consisted of the deployment of unfolded airbags, carried out in such a way as to generate only a membrane effect close to the loading of a subject in a crash test. Additional tests in similar configurations, but with a cold gas generator (CGS) were added too. The test setup was the same as in Trosseille et al. [9], but the power of the generator and the distance between the chest and the airbag were different. The volume of the airbag was 60 liters, except in the SEB 210 test where the airbag was only 45 liters.

LAB sled tests and LAB airbag tests will be defined as "LAB tests" in the rest of the document.

Statistical analysis

Linear regressions were performed between several explanatory variables and the number of fractured ribs (NFR) or the number of separated fractured ribs (NSFR), in order to define the most relevant metric to explain the injuries.

The data were then corrected with respect to the linear regression results corresponding to the selected metrics, and survival analyses were performed to obtain injury risk curves.

RESULTS

Experiments

The analysis of the data from Poplin et al. [4] showed that there was no very clear relationship between the number of fractured ribs and the maximum deflection, although the introduction of morphometric parameters such as the subject mass and size improved the regression. The best correlation coefficient obtained was R^2=0.36, the age being not significant, which is problematic according to the bibliography (Kent et al. [10]).

The addition of the sled tests of Luet et al. [5], Uriot et al. [6] et Uriot et al. [7] did not significantly changed the relationship between the deflection measured on the Hybrid III and the THOR dummies (Figure 3). Same observation

with the addition of the airbag tests of Trosseille et al. [8], even if they deviate slightly from the regression curve (Figure 4).

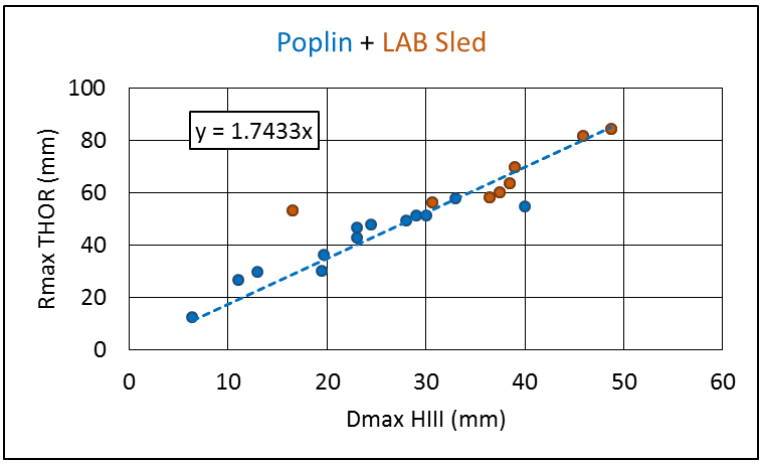

Figure 3. THOR versus HIII deflections for paired tests of Poplin et al. [4], Luet et al. [5] and Uriot et al. [6, 7]

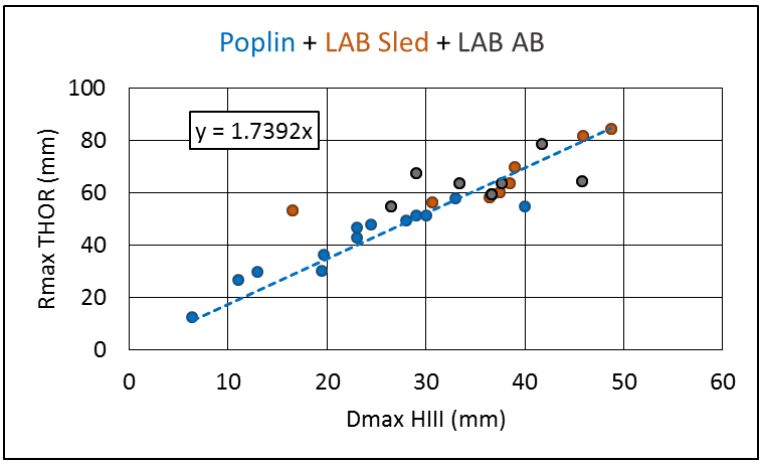

Figure 4. THOR versus HIII deflections for paired tests of Poplin et al. [4], Luet et al. [5], Uriot et al. [6, 7], Lebarbé et al. [8] and Trosseille et al. [9]

With regard to the relationship between the upper differential deflection (UPdif) and the maximum deflection (Rmax), the added sled tests remain in the same trend as the tests of Poplin et al. [4], while the airbag tests deviate from them (Figure 5).

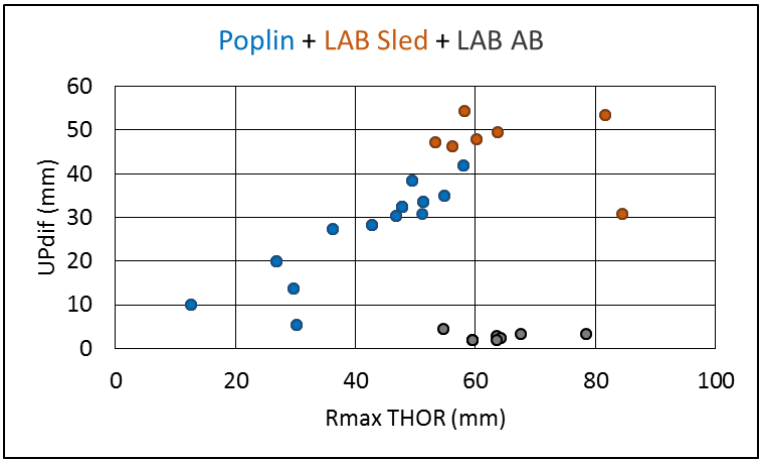

Figure 5. Upper chest deflection difference (UPdif) as a function of maximum deflection (Rmax) for THOR tests of Poplin et al. [4], Luet et al. [5], Uriot et al. [6, 7], Lebarbé et al. [8] and Trosseille et al. [9]

Statistics

A linear regression between the number of fractured ribs (NFR) and the explanatory variables showed that Rmax, the upper differential deflection (UPdif), the age and size of the subjects were all significant factors at 5%. The correlation coefficient was $R^2 = 0.588$, while the best correlation obtained with Rmax was $R^2 = 0.43$ where only the age had a significant effect. The relationship was as follows:

$$NFR = 12.79 + 0.117\ Rmax + 0.194\ UpDif + 0.138\ Age - 0.146\ Height \quad \text{(Equation 1)}$$

$$NFR(45\ y/o\ ;\ 175\ cm) = -6.5 + 0.117\ Rmax + 0.194\ UpDif \quad \text{(Equation 2)}$$

The other explanatory variables were not significant.

The same exercise was done with the number of separated fractured ribs (NSFR). The result was as follows:

$$NSFR = -19.17 + 0.0744\ Rmax + 0.227\ UpDif + 0.213\ Age, \text{ with } R^2 = 0.61 \quad \text{(Equation 3)}$$

Injury risk curves

The risk curves are binomial. There is therefore a significant loss of information for censored data, as the notion of the number of fractures disappears in favor of a binomial variable. It is therefore irrelevant to introduce the variables whose effects were defined by linear regressions (age or height) into these binomial regressions. Similarly, it is not relevant to introduce the two variables Rmax and UPdif separately. Instead, it was decided to calculate a new criterion (TIC for Thoracic Injury Criterion) for each subject, correct it for a given age and size, and then calculate the risk curves associated with that age and size. The new criterion was defined as follows:

$$TIC_NFR = Rmax + 1.66\ UpDif \quad \text{(Equation 4)}$$

$$TIC_NSFR = Rmax + 3\ UpDif \quad \text{(Equation 5)}$$

For a 50th male subject M50 (size 175 cm) of Y years old, the TIC should be corrected by the following formulas:

$$TIC_NFR(M50@Y\ y/o) = TIC_NFR(subject) - 1.25 * (Height - 175) + 1.18 * (Age - Y) \quad \text{(Equation 6)}$$

$$TIC_NSFR(M50@Y\ y/o) = TIC_NSFR(subject) + 2.86 * (Age - Y) \quad \text{(Equation 7)}$$

Risk curves were then constructed for several ages and injury levels. Figure 6 shows the risk curves for 3+ and 7+ fractured ribs (NFR3+ and NFR7+), for 45 and 65 years.

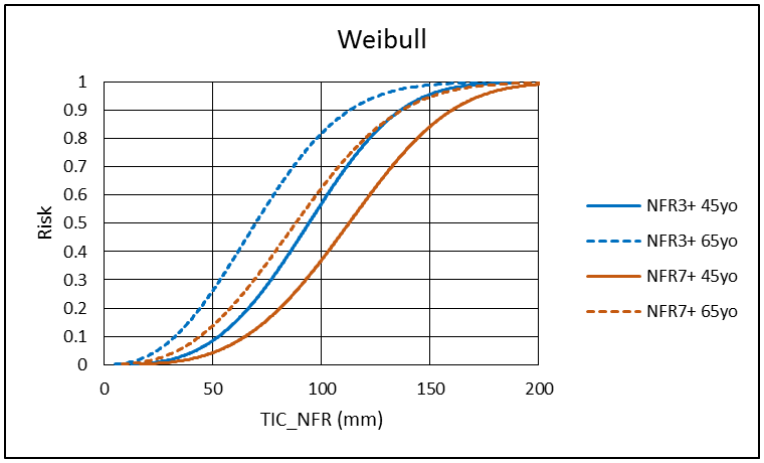

Figure 6. Injury Risk Curves for the total number of fractured ribs (NFR)

Figure 7 shows the risk curves for 3+ displaced fractured ribs (NSFR3+), for 45 and 65 years.

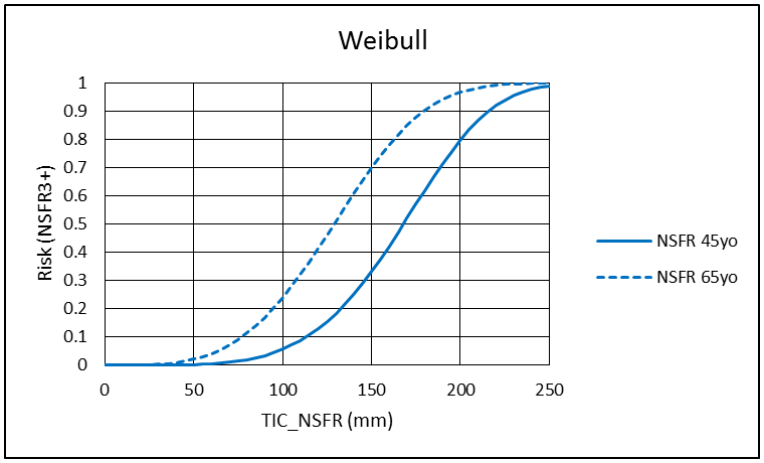

Figure 7. Injury Risk Curves for the number of separated fractured ribs (NSFR)

DISCUSSION

Consistency of THOR/HIII sled tests

The ratios between the maximum deflections measured on the THOR and the Hybrid III in the additional sled tests and in the Poplin et al. [4] sled tests are identical. Since most of the restraint in all these tests is carried out by the belt, this is not surprising. On the other hand, this indicates that the THOR responses in the LAB tests and in the tests of

Poplin et al. [4] are similar. They correspond to the definition of the 2013 mod-kit dummy with SD-3. The test results are therefore consistent and can be aggregated.

Consistency of THOR/HIII airbag tests

If the results of the airbag tests of the LAB remain on the same line as the sled tests on a graph Rmax(THOR) versus Dmax(HIII), the trend is however less clear, the deflections of the THOR seem to be on a plateau. The varying parameters in these tests were further investigated. Only tests performed with the same airbag volume were considered for this purpose.

For the THOR, Dmax is a function of the maximum force and distance between the airbag and the chest (dist):

$$Rmax = 30.2 + 4.1\ Fmax\ (kN) - 0.078\ dist\ (mm) \text{ with } R^2 = 0.94 \qquad \text{(Equation 8)}$$

For the HIII, Dmax is a function only of the maximum force, regardless of the distance whose effect is not significant:

$$Rmax = 8 + 2.8\ Fmax\ (kN) \text{ with } R^2 = 0.85 \qquad \text{(Equation 9)}$$

It is therefore consistent that there is no linear relationship between the HIII and THOR measurements. These tests were performed with the same THOR as in the sled tests. There is therefore no reason to question the results. This only means that the THOR is more sensitive than the Hybrid III to the application surface of the airbag forces.

Definition AIS3 threshold using NSFR

Should the number of fractured ribs be targeted at 3, as in the AIS3 definition, or 7 to take into account the difference between the number of fractures detected on a living subject and a PMHS? Or should the number of fractured ribs displaced be used, so that only the fractures detectable during a clinical examination are counted?

The number of separated fractured ribs (NSFR) is strongly correlated to the total number of fractured ribs found at autopsy (NFR), as shown in Figure 8. According to the regression, a total of 9 fractures are required to observe 3 separated fractures.

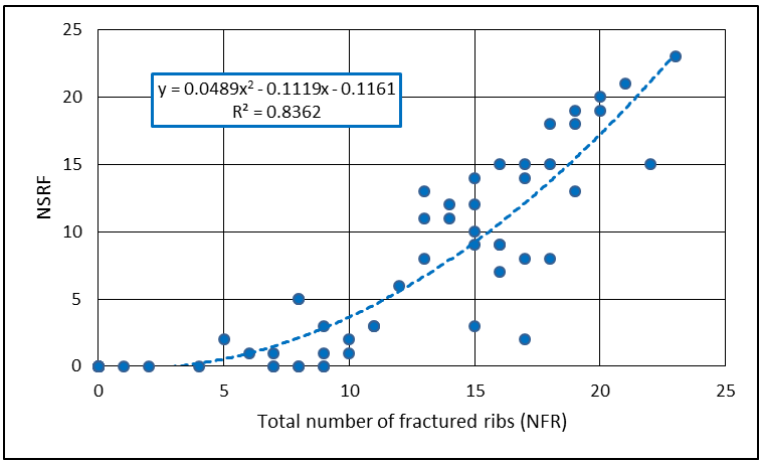

Figure 8. Number of separated fractured ribs (NSFR) as a function of the total number of fractured ribs (NFR)

Crandall et al. [11] compared the number of fractures detected at the autopsy and on X-rays. He found that 44% of fractures were detected on X-Rays for predominantly belt restraints and 24% for AB restraints. Comparing the number of fractures detected on X-Rays with the total number of fractures detected at autopsy (Figure 9), gives almost the same relationship as with the number of separated fractured ribs detected at autopsy.

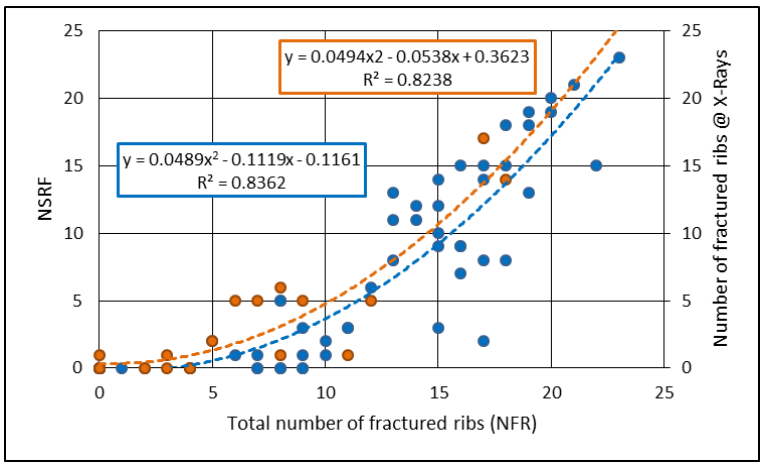

Figure 9. Number of fractured ribs detected on medical imaging as a function of total number of fractured ribs (NFR)

This therefore justifies using the number of separated fractures detected at autopsy to determine the level of AIS, which is clinically determined by the observation of medical imaging. Nota: the direct comparison of the number of fractures detected on X-Rays and the number of separated fractured ribs detected at autopsy could not be performed because there are too few subjects for whom both information are available.

Risk comparison by metrics

For all the dummy tests, the risks calculated from Rmax with the risk curve from Poplin et al. [4] were compared to the risks calculated from TIC_NFR for 3 fractured ribs (Figure 10). The risk calculated from the TIC_NFR and the risk calculated from Rmax for the sled tests (in blue) are similar. On the other hand, the risk calculated from TIC_NFR is much lower than the risk calculated from Rmax for airbag tests.

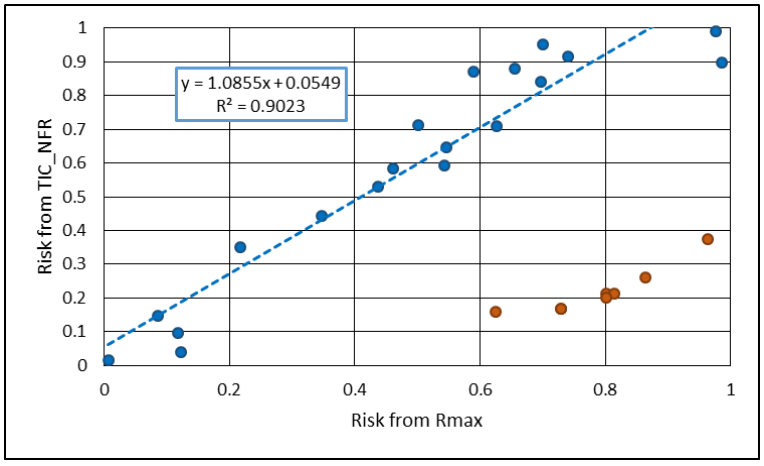

Figure 10. Comparison of risks calculated from Rmax and TIC_NFR for 3 fractured ribs

Perspectives

Simple statistics were used to define the best regression models. Linear regressions may be questionable for count data and other distributions will be investigated to account for the non-normal distribution of the sample. Large differences were also found between airbag like and belt-like restraints, which could bias the statistics. Intermediate restraints would be necessary to fill the gap between the two kinds of restraints and secure the analysis.

Sled tests in configurations with various ratio of belt force to airbag force were undertaken to validate the criterion. They include one configuration where the restraint consisted of a belt with a 3.5kN force limiter with an airbag and

one configuration where the restraint consisted of a belt with a 5kN force limiter and a less inflated airbag. Different combinations of Rmax and TIC values are expected, which will allow for the discrimination between the criteria.

SUMMARY AND CONCLUSIONS

The use of an expanded test sample allowed to successfully develop a new thoracic criterion for the THOR dummy. It is better able to predict the risk of rib fractures, while being more consistent with crash investigation findings related to the age effect and the balance between the seat belt and the airbag.

REFERENCES

[1] Petitjean, A., Baudrit, P., Trosseille, X. (2003) Thoracic Injury Criterion for Frontal Crash Applicable to All Restraint Systems. Stapp Car Crash Journal 47: 323-348

[2] Mertz, H.J., Irwin, A.L., Prasad, P. (2003) Biomechanical and Scaling Bases for Frontal and Side Impact Injury Assessment Reference Values. Stapp Car Crash Journal 47: 155-188

[3] Davidsson J., Carroll J., Hynd D., Lecuyer E., Song E., Trosseille X., Eggers A., Sunnevang C., Praxl N., Martinez L., Lemmen P., Been B. (2014) Development of injury risk functions for use with the THORAX Demonstrator; an updated THOR. Proceedings of IRCOBI Conference, 2014, Berlin, Germany

[4] Poplin, G.S., McMurry, T.L., Forman, J.L., Ash, J., Parent, D.P., Craig, M.J., Song, E., Kent, R., Shaw, G., Crandall, J. (2017), Development of thoracic injury risk functions for the THOR ATD. Accident Analysis and Prevention 106 (2017) 122–130

[5] Luet, C., Trosseille, X., Drazétic, P., Potier, P., Vallancien, G. (2012) Kinematics and Dynamics of the Pelvis in the Process of Submarining using PMHS Sled Tests. Stapp Car Crash Journal 56: 411-442

[6] Uriot, J., Potier, P., Baudrit, P., Trosseille, X., Richard, O., Douard, R. (2015) Comparison of HII, HIII and THOR dummy responses with respect to PMHS sled tests. Proceedings of IRCOBI Conference, 2015, Lyon

[7] Uriot J., Potier P., Baudrit P., Trosseille X., Petit P., Richard O., Compigne S., Masuda M., Douard R. (2015) Reference PMHS sled test to assess submarining. Stapp Car Crash Journal 59: 203-223

[8] Lebarbe M., Potier, P., Baudrit, P., Petit, P., Trosseille, X., Vallancien, G. (2005) Thoracic Injury Investigation Using PMHS in Frontal Airbag Out-of-Position Situations. Stapp Car Crash Journal 49: 323-342

[9] Trosseille, X., Baudrit, P., Leport, T., Vallancien, G. (2008) Rib Cage Strain Pattern as a Function of Chest Loading Configuration. Stapp Car Crash Journal 52, pp. 205-231

[10] Kent, R., Lee, S., Darvish, K., Wang, S., Poster, C., Lange, A., Brede, C., Lange, D., and Matsuoka, F. (2005) Structural and material changes in the aging thorax and their role in crash protection for older occupant. Stapp Car Crash Journal 49: 231-249

[11] Crandall J., Kent R., Patrie J., Fertile J., Martin P. Rib fracture patterns and radiologic detection – a restraint-based comparison. Annu Proc Assoc Adv Automot Med. 2000; 44:235–259

APPENDIX

Ref. #	Ref.	Test#	Cad ID#	Age	Sex	Height	Mass	BMI	NFR	NSFR	NFR X-Ray	UL	UR	LL	LR	Rmax	UP dif	LOW dif	HIII Defl
10	Lopez-Valdes 2010	1397	393	59	F	167	80	28.7	0	0	NA	3.6	12.6	3	6.6	12.6	10	4.8	6.4
		1404	422	60	M	191	81	22.2	0	0	NA	3.6	12.6	3	6.6	12.6	10	4.8	6.4
		1401	462	69	M	178	84	26.5	0	0	NA	3.6	12.6	3	6.6	12.6	10	4.8	6.4
11	Lopez-Valdes 2010	1398	393	59	F	167	80	28.7	11	NA	NA	14	49.4	12.8	31	49.4	38.3	28.5	28
		1405	422	60	M	191	81	22.2	5	NA	NA	14	49.4	12.8	31	49.4	38.3	28.5	28
		1402	462	69	M	178	84	26.5	13	NA	NA	14	49.4	12.8	31	49.4	38.3	28.5	28
8	Shaw 2009	1295	403	47	M	177	68	21.7	17	8	17	47.7	16.1	47.4	14.7	47.7	32.3	35.6	24.5
		1294	411	76	M	178	70	22.1	6	1	5	47.7	16.1	47.4	14.7	47.7	32.3	35.6	24.5
		1358	425	54	M	177	79	25.2	10	NA	NA	47.7	16.1	47.4	14.7	47.7	32.3	35.6	24.5
		1359	426	49	M	184	76	22.4	8	NA	NA	47.7	16.1	47.4	14.7	47.7	32.3	35.6	24.5
		1360	428	57	M	175	64	20.9	5	NA	NA	47.7	16.1	47.4	14.7	47.7	32.3	35.6	24.5
		1379	433	40	M	179	88	27.5	8	0	6	47.7	16.1	47.4	14.7	47.7	32.3	35.6	24.5
		1380	441	37	M	180	78	24.1	2	0	0	47.7	16.1	47.4	14.7	47.7	32.3	35.6	24.5
		1378	443	72	M	184	81	23.9	8	5	1	47.7	16.1	47.4	14.7	47.7	32.3	35.6	24.5
13	NA	S0029	492	66	M	179	70	21.8	0	0	NA	26.8	13.4	19.4	14.7	26.8	20	13.9	11
		S0028	494	59	M	178	68	21.5	0	0	NA	26.8	13.4	19.4	14.7	26.8	20	13.9	11
		S0302	674	67	M	178	72	22.6	4	0	0	26.8	13.4	19.4	14.7	26.8	20	13.9	11
		S0303	736	67	M	170	70	24.2	7	1	5	26.8	13.4	19.4	14.7	26.8	20	13.9	11
		S0304	695	74	M	178	73	22.9	0	0	NA	26.8	13.4	19.4	14.7	26.8	20	13.9	11
14	NA	S0313	362	69	M	173	69	23.1	7	0	NA	35.8	9.4	36.2	17.5	36.2	27.3	19.3	19.7
		S0314	750	66	M	172	76	25.8	5	2	2	35.8	9.4	36.2	17.5	36.2	27.3	19.3	19.7
		S0315	767	67	M	177	64	20.5	0	0	NA	35.8	9.4	36.2	17.5	36.2	27.3	19.3	19.7
2	Kent 2001	580	105	57	M	177	57	18.2	0	0	NA	51.3	23.9	39.4	13.5	51.3	33.5	36.8	29
		579	106	72	F	156	59	24.3	11	NA	1	51.3	23.9	39.4	13.5	51.3	33.5	36.8	29
		578	107	69	F	155	53	21.7	4	NA	0	51.3	23.9	39.4	13.5	51.3	33.5	36.8	29
		577	111	57	M	174	70	23.1	0	0	0	51.3	23.9	39.4	13.5	51.3	33.5	36.8	29

Ref. #	Ref.	Test#	Cad ID#	Age	Sex	Height	Mass	BMI	NFR	NSFR	NFR X-Ray	UL	UR	LL	LR	Rmax	UP dif	LOW dif	HIII Defl
3	NA	652	118	46	M	175	74	24.1	0	0	1	27.2	30.1	19	16.9	30.1	5.4	7.2	19.5
		651	121	70	M	176	70	22.6	0	0	0	27.2	30.1	19	16.9	30.1	5.4	7.2	19.5
		650	124	40	M	150	47	20.9	4	NA	0	27.2	30.1	19	16.9	30.1	5.4	7.2	19.5
4	Kent 2001	665	112	55	M	176	85	27.5	3	NA	0	54.8	22.7	45.7	20	54.8	34.9	37.2	40
		666	115	69	M	176	84	27.1	3	NA	1	54.8	22.7	45.7	20	54.8	34.9	37.2	40
		667	120	59	F	161	79	30.5	12	NA	5	54.8	22.7	45.7	20	54.8	34.9	37.2	40
5	Forman 2006	1094	322	49	M	178	58	18.3	0	0	NA	42.7	15.9	36.2	17.1	42.7	28.2	28.1	23
		1095	323	44	M	172	77	26.1	0	0	NA	42.7	15.9	36.2	17.1	42.7	28.2	28.1	23
		1096	327	39	M	184	79	23.5	0	0	NA	42.7	15.9	36.2	17.1	42.7	28.2	28.1	23
6	Forman 2006	1110	323	44	M	172	77	26.1	0	0	NA	51.2	21.7	46.6	17.7	51.2	30.7	36.8	30
7	Forman 2009	1262	362	51	M	175	55	17.9	9	0	5	58	28.3	43	14.5	58	41.8	40.7	33
		1264	367	57	M	179	59	18.4	9	0	NA	58	28.3	43	14.5	58	41.8	40.7	33
		1263	394	57	F	165	109	40	18	8	14	58	28.3	43	14.5	58	41.8	40.7	33
9	Forman 2009	1386	429	67	M	175	71	23.2	8	NA	NA	46.7	29	35.2	13.8	46.7	30.3	32.3	23
		1387	444	69	M	171	60	20.5	1	NA	NA	46.7	29	35.2	13.8	46.7	30.3	32.3	23
		1389	457	72	M	175	73	23.8	10	NA	NA	46.7	29	35.2	13.8	46.7	30.3	32.3	23
12	Kent 2011	1428	461	69	M	175	69	22.7	0	0		25.4	29.7	20.8	13.6	29.7	13.6	11.5	13
		1427	481	72	M	173	88	29.2	7	NA	NA	25.4	29.7	20.8	13.6	29.7	13.6	11.5	13
		1429	482	40	M	186	83	24	2	NA	NA	25.4	29.7	20.8	13.6	29.7	13.6	11.5	13
LAB1	Uriot 2015 [7]	SubBIO22	683	55	M	177	92	29.4	16	15	NA	32.2	81.7	36.2	52.1	81.7	53.3	30	45.9
		SubBIO23	679	86	M	168	67	23.7	17	15	NA	32.2	81.7	36.2	52.1	81.7	53.3	30	45.9
		SubBIO24	681	87	M	175	77	25.1	15	12	NA	32.2	81.7	36.2	52.1	81.7	53.3	30	45.9
		SubBIO25	682	87	M	171	64	21.9	17	14	NA	32.2	81.7	36.2	52.1	81.7	53.3	30	45.9
LAB2	Uriot 2015 [7]	SubBIO26	678	85	M	165	79	29.0	20	19	NA	33.7	63.9	30.5	84.5	84.5	30.9	58.01	48.7
		SubBIO27	677	84	M	170	57	19.7	13	8	NA	33.7	63.9	30.5	84.5	84.5	30.9	58.01	48.7
		SubBIO28	676	84	M	170	64	22.1	13	11	NA	33.7	63.9	30.5	84.5	84.5	30.9	58.01	48.7
		SubBIO29	680	89	M	175	77	25.1	18	18	NA	33.7	63.9	30.5	84.5	84.5	30.9	58.01	48.7

Ref. #	Ref.	Test#	Cad ID#	Age	Sex	Height	Mass	BMI	NFR	NSFR	NFR X-Ray	UL	UR	LL	LR	Rmax	UP dif	LOW dif	HIII Defl
LAB3	Luet 2012 [5]	IRIS09	631	67	M	171	59.5	20.3	15	3	NA	25.5	53.2	14.7	51.9	53.2	47.2	38.3	16.5
		IRIS10	632	85	M	167	69.5	24.9	23	23	NA	25.5	53.2	14.7	51.9	53.2	47.2	38.3	16.5
		IRIS11	633	76	M	163	54	20.3	10	2	NA	25.5	53.2	14.7	51.9	53.2	47.2	38.3	16.5
LAB4	Luet 2012 [5]	IRIS12	636	77	M	171	61.5	21.0	15	9	NA	26.8	63.7	NA	55.8	63.7	49.5	NA	38.5
		IRIS13	635	56	F	161	57	22.0	19	13	NA	26.8	63.7	NA	56.8	63.7	50.5	NA	39.5
		IRIS14	634	68	M	170	79	27.3	15	10	NA	26.8	63.7	NA	57.8	63.7	51.5	NA	40.5
LAB5	Luet 2012 [5]	IRIS15	639	90	M	162	71	27.1	21	21	NA	29.9	56.1	21.9	48.6	56.1	46.3	41.9	30.7
		IRIS16	638	67	M	170	58	20.1	16	9	NA	29.9	56.1	21.9	48.6	56.1	46.3	41.9	30.7
		IRIS17	637	79	M	161	57	22.0	22	15	NA	29.9	56.1	21.9	48.6	56.1	46.3	41.9	30.7
LAB6	Uriot 2015 [6]	IRIS39	659	70	M	167	54	19.4	12	6	NA	NA	69.7	17.4	54.2	69.7	NA	41.4	38.9
		IRIS40	657	88	M	178	90.5	28.6	14	12	NA	NA	69.7	17.4	54.2	69.7	NA	41.4	38.9
		IRIS41	658	64	M	179	69	21.5	14	11	NA	NA	69.7	17.4	54.2	69.7	NA	41.4	38.9
LAB7	Uriot 2015 [6]	IRIS29	653	75	M	168	57.5	20.4	19	18	NA	20.0	58.2	41.2	47.7	58.2	54.4	39.3	36.4
		IRIS30	652	63	M	180	70	21.6	19	19	NA	20.0	58.2	41.2	47.7	58.2	54.4	39.3	36.4
		IRIS31	651	68	M	176	80.5	26.0	20	20	NA	20.0	58.2	41.2	47.7	58.2	54.4	39.3	36.4
LAB8	Uriot 2015 [6]	IRIS32	649	80	M	178	81.5	25.7	15	14	NA	31.5	60.2	27.9	55.9	60.2	47.9	31.8	37.4
		IRIS33	650	60	M	176	68.5	22.1	11	3	NA	31.5	60.2	27.9	55.9	60.2	47.9	31.8	37.4
		IRIS34	648	76	M	174	73	24.1	13	13	NA	31.5	60.2	27.9	55.9	60.2	47.9	31.8	37.4
LAB9	New data	SEB206	656	83	M	174	76	25.1	9	1	NA	54.5	55.9	78.5	68.6	78.5	3.21	10.9	41.7
		SEB207	660	89	M	164	65	24.2	1	0	NA	45.2	44.8	67.6	60.6	67.6	3.31	10.6	29
		SEB210	672	83	M	167	67	24.0	7	0	NA	39.6	37.4	54.7	52.8	54.7	4.35	6.36	26.5
		SEB220	674	81	M	165	79	29.0	8	5	NA	44.7	42.5	63.5	56.6	63.5	2.85	8.22	37.7
		SEB221	675	91	M	150	54	24.0	16	9	NA	49.7	50.2	64.3	61.8	64.3	2.41	3.77	45.8
LAB10	Trosseille 2008 [9]	SEB144	594	78	M	169	65	22.8	8	0	NA	37.0	37.1	59	59.6	59.6	1.93	5.43	36.6
	Lebarbe 2005 [8]	PCH1624	559	73	M	174	67	22.1	11	3	NA	37.0	37.1	59	59.6	59.6	1.93	5.43	36.6
		PCH1658	561	72	M	173	83	27.7	0	0	NA	37.0	37.1	59	59.6	59.6	1.93	5.43	36.6
LAB11	New data	SEB159	607	84	M	175	56	18.3	18	15	NA	34.7	35.3	63.5	60.0	63.5	2.00	4.70	33.4

NEW APPROACHES IN MODELING BELT-FLESH-PELVIS INTERACTION USING OBESE GHBMC MODELS

Zhaonan Sun
Bronislaw Gepner
Jason Kerrigan

University of Virginia Center for Applied Biomechanics
United States of America

Paper Number 19-0241

ABSTRACT

Obesity is associated with higher fatality risk and altered distribution of occupant injuries in automotive collisions partially because of the increased depth of abdominal soft tissue, which results in limited and/or delayed engagement of the lap belt with the pelvis and increases the risk of pelvis "submarining" under the lap belt exposing occupant's abdomen to belt loading. Previous modeling studies have shown that pelvis submarining could not be replicated using existing human body models. The goal of this study is to perform model modifications and investigate whether they could lead to model submarining. By detaching the connections between the pelvis and surrounding flesh, submarining like belt kinematics were observed. By remeshing the flesh parts of the model, similar belt kinematics was observed but the pelvic wings were fractured. Finally, large shear deformation on the flesh together with submarining like kinematics were observed in the model with its flesh modelled using the meshless Smooth Particle Galerkin Method (SPG) method. The results of this study showed that SPG method has potential to simulate large deformations in soft tissue which may be necessary to improve the biofidelity of belt/pelvis interaction.

INTRODUCTION

Obesity is associated with increased fatality risk and altered distribution of occupant injuries relative to lower BMI occupants in automotive collisions [1-4]. This is partially because of the substantial effect that obesity has on occupant-restraint interaction. Restraining obese occupants is a challenge due to increased body mass, unfavorable belt placement [5], and increased forward excursion within the occupant compartment [6-7]. An increased depth of abdominal soft tissue, results in delayed and limited engagement of the lap belt with the pelvis and increases the risk of pelvis submarining under lap belt, exposing occupant's abdomen to belt loading [7].

Several experimental studies have been performed to study the challenges obesity poses on restraint system during motor vehicle collisions (MVC). Forman et al. and Kent et al. [9-10] performed rear-seat sled tests on both obese male post mortem human surrogates (PMHSs) and 50th percentile PMHS. It was found that obese occupants exhibited backward torso rotation (pelvis forward of shoulders) at the time of maximum forward excursion, whereas non□obese occupants did not. Kent et al. [10] pointed out that obese PMHS in frontal-impact sled tests exhibited submarining behavior, which is defined as the properly-placed belt translated superiorly until it passed over the iliac crests and loaded the abdomen without engaging, or after disengaging, the pelvis [8]. The authors suggested that submarining resulted in increased forward excursion and decreased forward torso pitch, which may be related to increased risk of lower extremity and thoracic injuries in obese occupants.

HBMs with varied stature, age and BMI levels were generated using University of Michigan Transportation Institute's (UMTRI's) rapid mesh morphing tools based on statistical models of external body contour and ribcage geometry. Obese version of both Total Human Model for Safety (THUMS) [11-12], and Global Human Body Models Consortium (GHBMC) [13] were generated. While these HBMs are available to study occupant submarining, simulations illustrating HBM responses similar to PMHS kinematics are not available in the literature. A series of obese THUMS simulation were performed in [14]. Greater forward excursion was observed in frontal impact simulation, but no submarining was observed. Similar efforts have been carried out by Gepner et al. [8] with

the obese GHBMC models. In the belt pull test simulations, the model did not exhibit submarining behavior as observed in the PMHS test [19]. Also, the lap belt pull simulations failed to reproduce the belt/abdomen interaction seen in the PMHS. It was also found that the material model used to represent the human body model flesh was found to be approximately one order of magnitude stiffer than human abdominal subcutaneous adipose tissue. This study shows that improved modeling of the belt-flesh-pelvis interaction should be required to obtain biofidelic response.

Experiments have suggested that adipose tissue is able to undergo substantially large shear deformations [15]. Such large deformations challenge lagrangian finite element approaches to modeling since such large deformations can result in instabilities and collapsing elements. Previous work has shown the potential to model these large deformations using meshfree methods, which offer advantages in simulating large deformation over conventional finite element methods [18]. The earliest developed meshfree method is the smoothed particle hydrodynamics (SPH) method [17]. However, this method suffers from tension instability, lack of consistency and other numerical artifacts if it is applied to solid analyses directly [16,17]. Recently, a robust and accurate meshfree method was developed by LSTC, referred to as Smoothed Particle Galerkin (SPG) method. The formulation is derived based on a smoothed displacement field within the meshfree Galerkin variational framework. It could provide stable and accurate solution for solid mechanics problems [17]. This method has been applied to manufacturing problems including drilling and metal milling. However, no previous study using this method for biological material can be found.

Since improved modeling of belt-flesh-pelvis interaction in existing HBMs are needed, and previous works showed potential in new method for large deformation modelling, the goal of this study is to apply new approaches to model belt-flesh-pelvis interaction to the obese HBMs and evaluate their ability to replicate submarining in the belt pull test.

METHODS

The obese GHBMC models, developed by Hu et al. [13] were used as the baseline model for evaluation and modifications. Model responses were compared with the obese PMHS in a series of tabletop belt pull tests previously performed at the UVA-CAB [19]. Specifically, the PMHS with a BMI of 31 kg/m2, height of 1650 mm and weight of 84.4 kg was chosen for comparison with the GHBMC obese model with a height of 1750 mm and a BMI of 30 kg/m2. FE model of the test fixtures used in the belt pull tests previously developed using 3D drawings of the original test fixture were used in this study Gepner et al. [8]. The baseline belt position, prescribed force time history was adapted from Gepner et al. [8], which was based on the experiment. Three independent methods for model modification were applied. First, the connection between the pelvis and surrounding tissue was removed, enabling relative motion between pelvis and flesh. Second, spatial discretization of the abdominal flesh was improved to obtain better resolution and sensitivity study on material stiffness were performed on the remeshed model. Third, SPG method was introduced to model the outer flesh to enable large deformation.

Contact modification

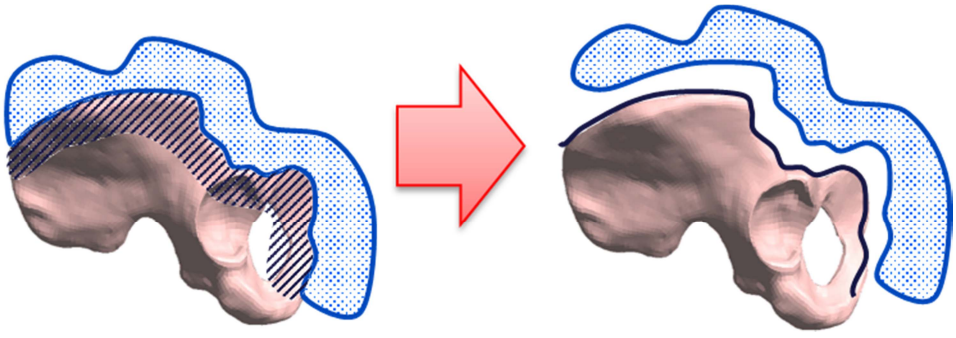

Figure 1 Schematic of detaching the surrounding soft tissue from the pelvis

In the obese GHBMC models, the pelvic wings are connected to surrounding tissue through tied contact and shared nodes (Figure 2). This could potentially prevent the large shear motion within the elements of surrounding soft tissue since some element always have to be connected to the bony pelvis. Since we theorized that the key to

submarining is the large shear motion on the flesh, we released the constraints between the pelvis and the surrounding flesh and explore whether this would enable large shear motion. The schematic of this detachment can be seen in Figure 1. Specifically, we released the tied contacts and shared nodes relation between the parts and ran the belt pull test simulation with three different input pulses. The first pulse is the baseline pulse fitted from the PMHS test. The second pulse was obtained by increasing the peak force to compensate for difference in anthropometry between the HBM and PMHS. Finally, by increasing the holding time of the peak force, the overall energy input was increased to obtain the third pulse.

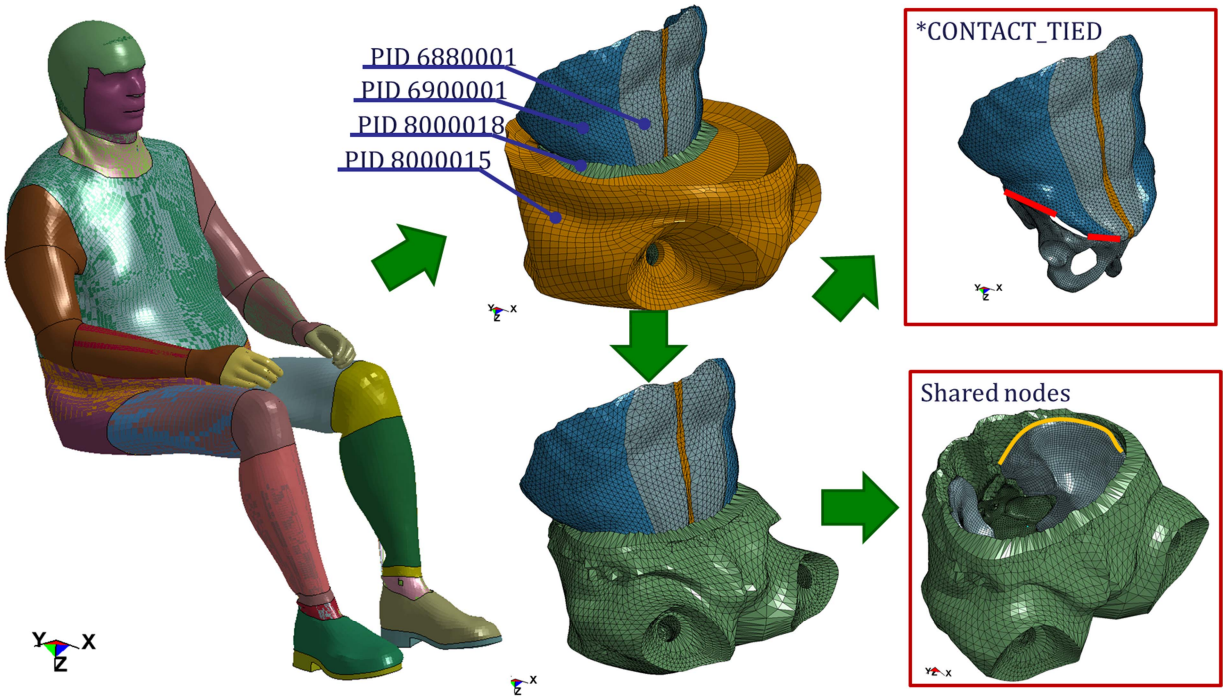

Figure 2 Connections between the pelvis and surrounding tissue in the obese GHBMC model

Model Remeshing

The obese GHBMC models were generated with rapid mesh morphing tools based on statistical models of external body contour and ribcage geometry. During this process, only nodal coordinates changed. Contact definition, material properties and element definition remained unchanged. To account for differences in external body contour of an obese occupant, abdominal and thoracic flesh layer were thickened by stretching the elements in the morphing process. As shown in Figure 8, the obese GHBMC only used three elements across the abdominal front wall. Since these elements were directly stretched from elements in the 50th percentile GHBMC model, they all have suboptimal aspect ratios. To improve mesh quality, remeshing was performed on two solid and two shell parts. Both solid parts were meshed with constant density tetrahedral elements. The number of elements increased by around 50,000 after the remeshing. A baseline simulation was first performed, followed by a three times baseline simulation. Then, pelvic wing yielding criteria was turned off and a three times baseline simulation was performed. Finally, material property was adjusted, and a baseline simulation was performed.

Figure 3 Remeshing the abdominal and thoracic flesh (Complete models with head, upper and lower extremities hidden)

SPG implementation

Although SPG is a meshless method by nature, the creation of SPG particle is mesh based. After creating the mesh, LS-DYNA solver turns each node in the selected SPG section into one smooth particle and discard the solid element connection between the particles. Since the method of SPG performs well with at least 3 layers of smoothed particles in between the lagrangian boundaries and particle needs to be distributed as evenly as possible, the remeshed model nodal coordinates were used to turn the outer thoracic and abdominal flesh nodes into smoothed particles while the skin and inner flesh remained in lagrangian formulation. More than 10 layers of SPG particles were generated at every nodal position in between the lagrangian boundaries of the remeshed model but the nodal connectivity within the flesh parts were neglected in the computation. In this study, two simulations were performed with three times of baseline input. One of them has pelvic wing yielding criteria turned off while the other has it remained on. Another simulation was performed with 1.5 times baseline input and with a less stiff flesh material model.

Figure 4 SPG particles generated from remeshed flesh parts

RESULTS

For all belt pull simulations, graphs showing the comparison of belt trajectories obtained from the experiment and the simulation, as well as time histories of belt pulling force and belt displacement are presented in the results session. For the belt trajectories, the time histories for points on the belt directly anterior to ASISL and ASISR were extracted and plotted in green dots over the experimental results in blue dots.

Detached pelvis to flesh

When the detached model was pulled with the baseline force that fitted to the time history from the experiment, no submarining was observed (Figure 5). The blue dots showed that in the experiment, the belt started moving towards

the ASIS and then changed direction to load the abdomen. The green dots showed that, in the simulation, the belt went straight towards the pelvis without showing trend for direction change.

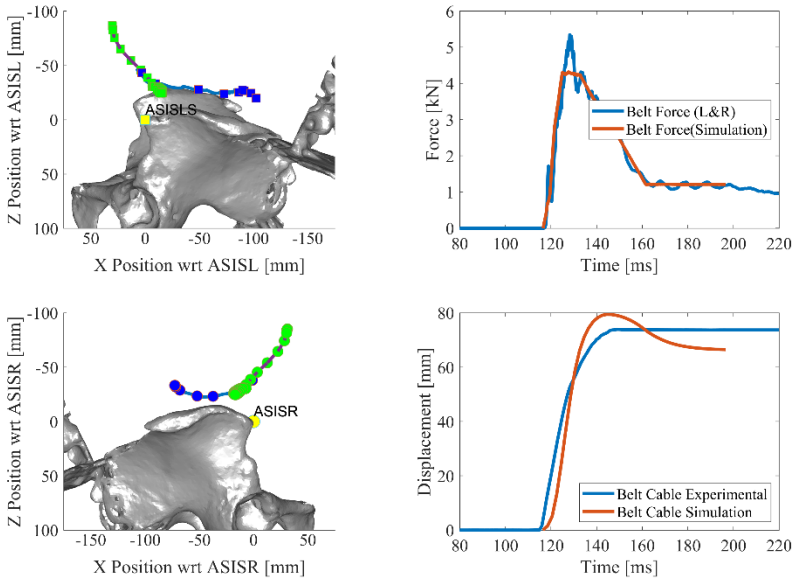

Figure 5 Detached pelvis with a fit-to-experiment input pulse

When the amount of energy input to the system was increased by both increasing the peak force and its holding time before release, highly matched belt trajectory with the experiment was observed (Figure 6). The belt first compressed the abdomen towards the pelvis, then under the influence of the reaction force from the pelvic wings, changed its direction and moved in to compress the abdominal cavity.

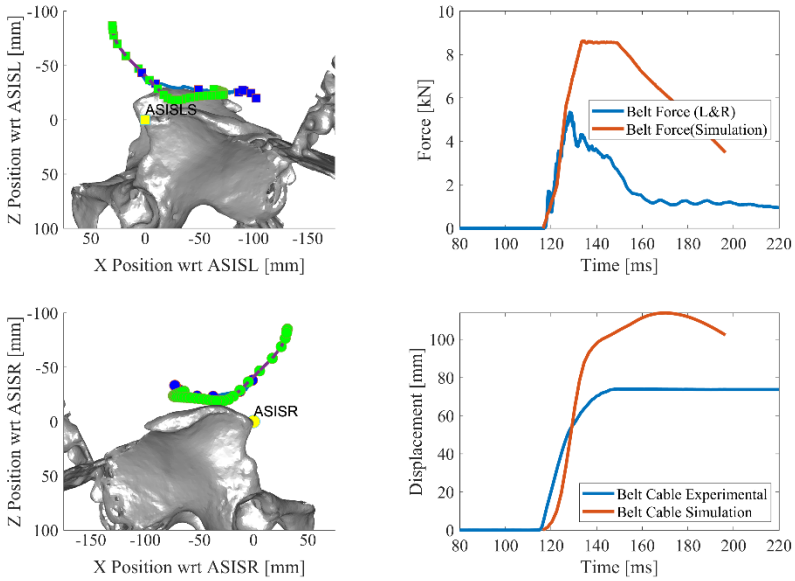

Figure 6 Detached pelvis with added energy double peak input

Remeshed abdomen and thorax

Under baseline loading conditions, the model could not submarine due to lack of energy (Figure 7). When peak force was increased to three times of baseline, the model submarined (Figure 8). However, the pelvic wing elements reached their yielding point and started to fail. By turning off the failure criteria on the

pelvic wings, the same input condition led to a negative volume problem in the flesh and no submarining was observed (Figure 9).

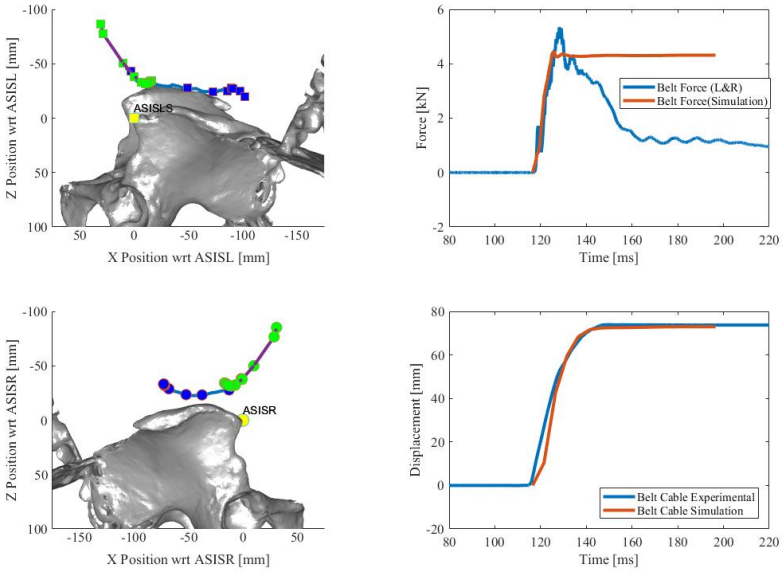

Figure 7 Baseline flat input simulation in lagrangian formulation with complete boundary condition

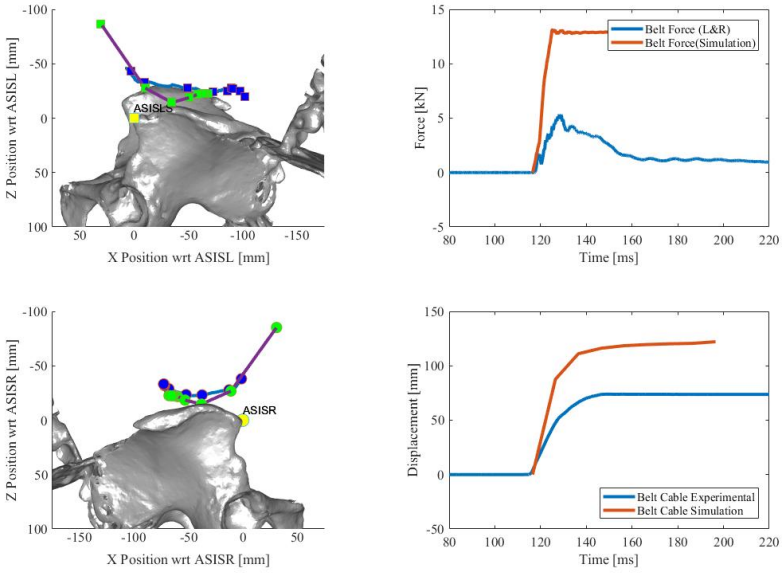

Figure 8 Three times peak force and rate flat input simulation in lagrangian formulation with complete boundary condition

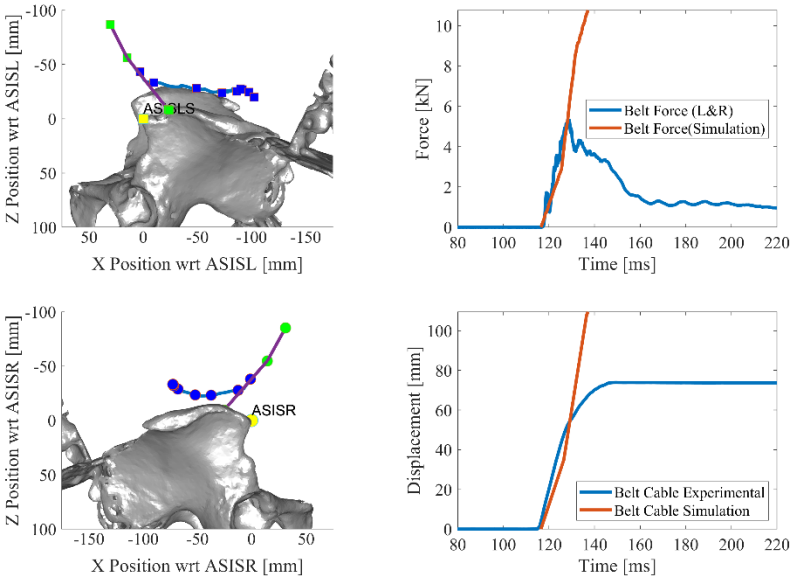

Figure 9 Three times peak force and rate flat input simulation in lagrangian formulation with pelvis failure turned off

SPG abdomen and thorax

Similar to the remeshed lagrangian model, under baseline loading conditions, the SPG model did not submarine possibly due to lack of energy. With a three times baseline force input, the model submarined but the pelvic wing elements were failed when the pelvis failure criteria was on. When turning off the pelvic failure criteria, the belt managed to load the abdomen into large shear without running into negative volume problem as encountered in the lagrangian model. A comparison revealed that lap belt found a different path to load the abdomen, avoiding loading the pelvic wings to failure (Figure 10).

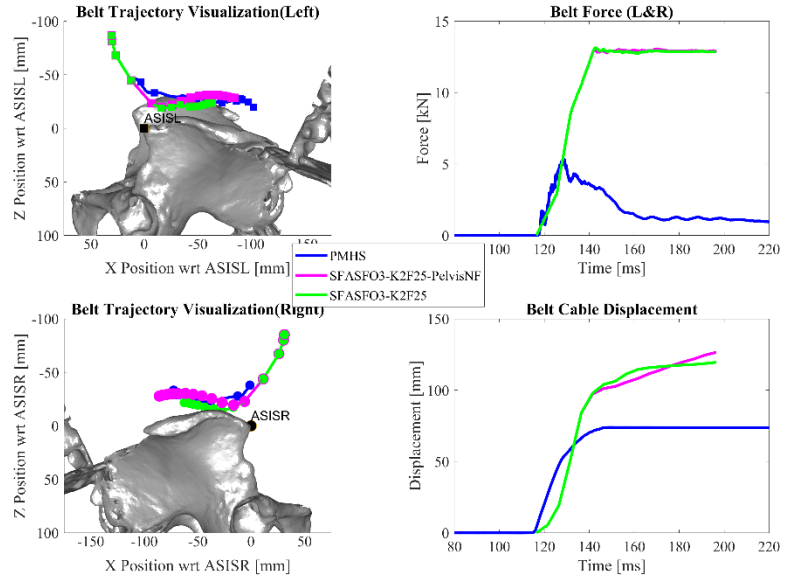

Figure 10 Comparison between both three times peak force and baseline rate flat input simulation in SPG formulation with (in green) or without pelvis failure (in pink)

DISCUSSIONS

Detached pelvis to flesh

When pulling the detached pelvis model with the baseline force, the model did not submarine due to insufficient energy. First, the peak force was hold for less than 20ms, leaving not enough time for belt movement. Second, the obese GHBMC in the simulation is an overall larger person than the PMHS, therefore requiring more energy to achieve the same amount of deformation. Third, [8] we concluded that abdominal flesh in the Obese GHBMC appeared to be orders of magnitude stiffer in shear compared to subcutaneous adipose tissue. These three reasons would affect the pulling force required to reach desired deformation, therefore lead to the non-submarining results.

When the input force was scaled to two times the baseline and held longer, the global belt kinematics matched with the belt pull test well. We concluded this type of simulation as the type I submarining. However, type I submarining is not what happens in human body since surrounding muscles are attached to the pelvic wings. Computationally, the original boundary condition of the belt pull test was broken actively by detaching surrounding tissue from the pelvis. As a result, this method should not be used to modify the current obese GHBMC models for further simulations.

Remeshed abdomen and thorax

The remeshed model submarined since pelvic wing being sheared off to failure broke the original boundary conditions. We define this as the type II submarining, also the pseudo submarining. Turning off the pelvic wing failure criteria would prevent pseudo submarining from happening. This can be achieved in two ways. The first method is to increase the yielding point to make it almost not reachable in the current simulation setting. The second method is to turn off the yielding criteria directly. Both methods gave the same response. After turning off the failure criteria on pelvic wings using either method, negative volume in flesh happened. This showed that by keeping the boundary condition intact, the remeshed model could not submarine.

SPG abdomen and thorax

To the best of authors' knowledge, this is the first simulation study using SPG to model soft tissue in HBMs. This new modeling approach resulted in model submarining in the belt pull test simulation. Gepner et al. [8] theorized that, in the belt pull test, the belt is initially pulled towards the pelvis and then encounters the bony pelvis, which provides a reaction force to guide the belt over the iliac crest and into the abdomen. In this study, when the abdominal flesh is modelled with SPG, tissue compression first happened. Then, under the guidance of the reaction force from pelvic wings, the lap belt changed its direction and went over the iliac wings. By applying proper parameters for the SPG particles, it was found that belt displacement over the pelvic wings can be controlled. Also, by turning off the pelvic wing failure parameter, the belt managed to navigate a different path to submarining, which appears to be superior to the one with pelvic wing failure parameter. This difference in trajectory showed that turning off the pelvic wing failure criteria did change the overall kinematics of the belt.

It is worth noting that this is not a model validation study since the HBM in this study has different anthropometry from the PMHS being compared. However, this study showed that three types of model modifications can make the model reach desired kinematics. Specifically, this study supported the theorized mechanism of submarining by Gepner et. al [8] by showing promising results in the SPG models. However, potential contact and stability issues still exists and need to be further evaluated.

CONCLUSIONS

The following conclusions can be drawn from this study:

1. Submarining could happen due to breaking of boundary condition or large shear deformation in flesh.

2. Detaching the connection between the pelvis and surrounding flesh could break the boundary condition and therefore lead to submarining.

3. Pulling hard with a denser mesh in the flesh could break the boundary condition and therefore lead to submarining.

4. Large shear deformation can be realized through using SPG particle to particle bond failure criteria.

5. Tuned SPG parameters worked well in the belt pull test simulation, recreating similar kinematics in the Obese GHBMC model to the PMHS

REFERENCES

[1] Mock, C. N., Grossman, D. C., Kaufman, R. P., Mack, C. D., & Rivara, F. P. The relationship between body weight and risk of death and serious injury in motor vehicle crashes. Accident Analysis & Prevention, 2002, 34(2), 221-228.

[2] Zhu, S., Layde, P. M., Guse, C. E., Laud, P. W., Pintar, F., Nirula, R., & Hargarten, S. Obesity and risk for death due to motor vehicle crashes. American journal of public health, 2006, 96(4), 734-739.

[3] Viano, D. C., Parenteau, C. S., & Edwards, M. L. Crash injury risks for obese occupants using a matched-pair analysis. Traffic injury prevention, 2008, 9(1), 59-64.

[4] Jehle, D., Gemme, S., & Jehle, C. Influence of obesity on mortality of drivers in severe motor vehicle crashes. The American journal of emergency medicine, 2012, 30(1), 191-195.

[5] Reed, M. P., Ebert-Hamilton, S. M., & Rupp, J. D. Effects of obesity on seat belt fit. Traffic injury prevention, 2012, 13(4), 364-372.

[6] Forman, J., Lopez-Valdes, F. J., Lessley, D., Kindig, M., Kent, R., & Bostrom, O. The effect of obesity on the restraint of automobile occupants. In Annals of Advances in Automotive Medicine/Annual Scientific Conference, 2009, (Vol. 53, p. 25). Association for the Advancement of Automotive Medicine.

[7] Kent, R. W., Forman, J. L., & Bostrom, O. Is there really a “cushion effect”?: a biomechanical investigation of crash injury mechanisms in the obese. Obesity, 2010, 18(4), 749-753.

[8] Gepner, B. D., Joodaki, H., Sun, Z., Jayathirtha, M., Kim, T., Forman, J. L., & Kerrigan, J. R. Performance of the Obese GHBMC Models in the Sled and Belt Pull Test Conditions. In IRCOBI Conference Proceedings, 2018

[9] Forman, J., Lopez-Valdes, F. J., Lessley, D., Kindig, M., Kent, R., & Bostrom, O. The effect of obesity on the restraint of automobile occupants. In Annals of Advances in Automotive Medicine/Annual Scientific Conference, 2009, (Vol. 53, p. 25). Association for the Advancement of Automotive Medicine.

[10] Kent, R. W., Forman, J. L., & Bostrom, O. Is there really a “cushion effect”?: a biomechanical investigation of crash injury mechanisms in the obese. Obesity, 2010, 18(4), 749-753.

[11] Shi, X., Cao, L., Reed, M. P., Rupp, J. D., & Hu, J. Effects of obesity on occupant responses in frontal crashes: a simulation analysis using human body models. Computer methods in biomechanics and biomedical engineering, 2015, 18(12), 1280-1292.

[12] Wang, Y., Bai, Z., Cao, L., Reed, M. P., Fischer, K., Adler, A., & Hu, J. A simulation study on the efficacy of advanced belt restraints to mitigate the effects of obesity for rear-seat occupant protection in frontal crashes. Traffic injury prevention, 2015, 16(sup1), S75-S83.

[13] Hu, J., Fanta, A., Neal, M. O., Reed, M. P., Wang, Y. Vehicle crash simulations with morphed GHBMC human models of different stature, BMI, and age. Proceedings, 4th International Digital Human Modeling Conference. 2016, Montreal, Canada.

[14] Kitagawa, Y., Hayashi, S. and Yasuki, T. Comparison of Impact Kinematics between Non□obese and Obese Occupants in Frontal and Lateral Impacts. In IRCOBI Conference Proceedings, 2017.

[15] Sommer, G., Eder, M., Kovacs, L., Pathak, H., Bonitz, L., Mueller, C., Regitnig, P. and Holzapfel, G.A. Multiaxial mechanical properties and constitutive modeling of human adipose tissue: a basis for preoperative simulations in plastic and reconstructive surgery. Acta biomaterialia, 2013, 9(11), pp.9036-9048.

[16] Libersky, Larry D., et al. "High strain Lagrangian hydrodynamics: a three-dimensional SPH code for dynamic material response." Journal of computational physics 109.1 (1993): 67-75.

[17] Wu, C. T., Y. Guo, and W. Hu. "An introduction to the LS-DYNA smoothed particle Galerkin method for severe deformation and failure analysis in solids." 13th international LS-DYNA users conference, Detroit, MI. 2014.

[18] Li, Shaofan, and Wing Kam Liu. "Meshfree and particle methods and their applications." Applied Mechanics Reviews55.1 (2002): 1-34.

[19] Kim, T., Park, G., Montesinos, S., Subit, D., Bolton, J., Overby, B., ... & Kim, H. Abdominal Characterization Test Under Lap Belt Loading. In24th International Technical Conference on the Enhanced Safety of Vehicles (ESV), 2015, (No. 15-0312).

TEST METHODOLOGY FOR EVALUATING THE RECLINED SEATING ENVIRONMENT WITH HUMAN SURROGATES

Rachel Richardson
John Paul Donlon
Kalle Chastain
Greg Shaw
Jason Forman
Sara Sochor
Mohan Jayathirtha
Kevin Kopp
Brian Overby
Bronislaw Gepner
Jason Kerrigan
University of Virginia Center for Applied Biomechanics
U.S.A.

Martin Ostling
Krystoffer Mroz
Bengt Pipkorn
Autoliv Research
Sweden

Paper Number 19-0243

ABSTRACT

Automated vehicles introduce the potential for non-traditional seating postures, including various degrees of recline. To date, there have been no human surrogate studies in the literature describing reclined occupant response in frontal or other crashes, which suggests that new biofidelity reference targets are needed to evaluate anthropomorphic test device (ATD) and human body model (HBM) predictions. The goal of this study was to develop and demonstrate a methodology for performing biofidelity reference tests for reclined occupants that incorporate methods for capturing these complex kinematics and kinetics. The test methodology developed here is demonstrated with a frontal impact sled test performed with one post mortem human surrogate (PMHS). A simplified, generic, semi-rigid seat pan and minimal back support (at 50 degrees reclined with the vertical) was used to support the occupants as they underwent a 50 km/h crash pulse while restrained with a three pretensioner force-limited seat-integrated belt restraint. Occupant kinematics, seat deflections, belt spool-in and spool-out, and buck motion were collected with an optoelectronic motion tracking system and lumbar spine and pelvic load timing were collected with additional instrumentation. Boundary conditions are critical for finite element (FE) model validation. The forces beneath the seat pan, toe pan and buckle were measured in 6 degrees of freedom (DOF). Additionally, the forces at the lap belt and shoulder belt were measured.

This is the first effort in the field to develop and evaluate a methodology for reclined occupant biofidelity reference testing, which can (and will) be used for: i) additional PMHS testing to generate biofidelity reference targets for assessing the performance of occupant models in reclined postures; and can also be extended to: ii) generate reference data for other reclined configurations and iii) to assess the performance of new and novel restraint system designs.

INTRODUCTION

Highly automated vehicles (HAVs) may bring the potential for alternative seating postures, as the driver may be able to hand over control to the vehicle for extended periods of time. One of these potential postures is reclined seating– while this posture is achievable in current vehicles, the prevalence of occupants seated in recline is

expected to grow as HAVs are introduced. In one CIREN study, reclined seating postures are linked to a higher degree of mortality in motor vehicle collisions, with a high rate of spinal compression and flexion injuries for fatal and nonfatal cases [2]. Limited studies have been performed to assess occupant kinematics and restraint interactions in reclined seating postures; those that exist are predominantly computational studies [3] [4] [5].

Current efforts to model and predict injury risk for reclined occupants are hampered by a lack of fundamental reference data with which to assess model biofidelity. Of particular concern are motion of the pelvis and the lumbar spine. Due to the initial rearward-rotated orientation of the pelvis and the upper body, reclined occupants may be more likely to submarine, with the lap belt translating over the pelvis and into the abdomen [4]. This type of submarining behavior, combined with a greater excursion of the upper body as it pitches forward from recline, may result in substantial flexion in the lumbar spine [5]. Thus, efforts to develop restraint solutions for reclined occupants will require occupant models (physical or computational) that can replicate the interaction of the pelvis with the lap belt and seat, and the kinematics of the spine. Thus, refining and evaluating such models requires detailed reference information (e.g., from tests with post mortem human surrogates, PMHS) describing lumbar spine and pelvis motion (among other factors) in a well-defined test environment instrumented to capture kinetic and kinematic information at all loading boundaries.

Such testing presents unique challenges for reclined occupants. First, to preserve lines of sight for 3D motion tracking of the spine and pelvis, the tests should be performed without a seatback. This requires developing a methodology to suspend a PMHS in a reclined posture (on a sled) without a seatback, in a manner that will not interfere with motion during a test. Second, given the importance of the lumbar spine to kinematics and injury risk for reclined occupants, it is pertinent to quantify motion of the lumbar spine in greater detail (e.g., at more locations) than has typically been performed in past testing [12]. This requires new strategies for instrumentation and motion capture for tracking the spine kinematics. Third, the goal of any fundamental biofidelity reference study should be to utilize a testing environment that can be readily defined, described, and replicated in future modeling or biofidelity assessment experiments. Thus, components such as the seat, toe pan, and belt system anchors should be generic, simplified, rigidized, and well-defined, yet should be representative enough of a typical vehicle environment as to retain significance of the results. These components should also be instrumented to the extent possible to capture all boundary forces applied to the occupant, as well as recording detailed kinematics of any boundary components that move.

The goal of this study was to develop a methodology for performing frontal-impact biofidelity reference sled tests for reclined occupants that incorporate methods to address the concerns described above. All necessary information to perform detailed computational simulations of the test, as well as to make detailed comparisons to dummy response, was captured. This methodology was then demonstrated with the first in a series of sled tests with a 50th percentile male PMHS.

METHODS

The PMHS was obtained and treated in accordance with the ethical guidelines established by the Human Usage Review Panel of the National Highway Traffic Safety Administration, and all testing and handling procedures were reviewed and approved by the Center for Applied Biomechanics and an institutional review board at the University of Virginia (Charlottesville, VA, USA). The subject (age: 66, height: 177.8 cm, weight: 74.4 kg) was seated on a semi-rigid seat and reclined to a 50-degree angle with the vertical using three tethers that were routed through overhead bars on the buck (see Figure 1). The minimal profile and placement of these tethers allowed for full visibility of posterior instrumentation. At time 0, the tethers released via a drop-release mechanism. A net was placed behind the seat to catch the subject on rebound. The subject's feet were placed on a toe pan and fully constrained. To aid in subject positioning, straps were tied around the shins and attached to a support fixture at the front of the buck. The subject's arms were placed in an initial position that allowed for full visibility of the lap belt. As boundary conditions are critical for HBM validation, the forces at the boundary of the occupant, i.e. beneath the seat pan, toe pan, buckle, and at the lap belt and shoulder belt, were measured.

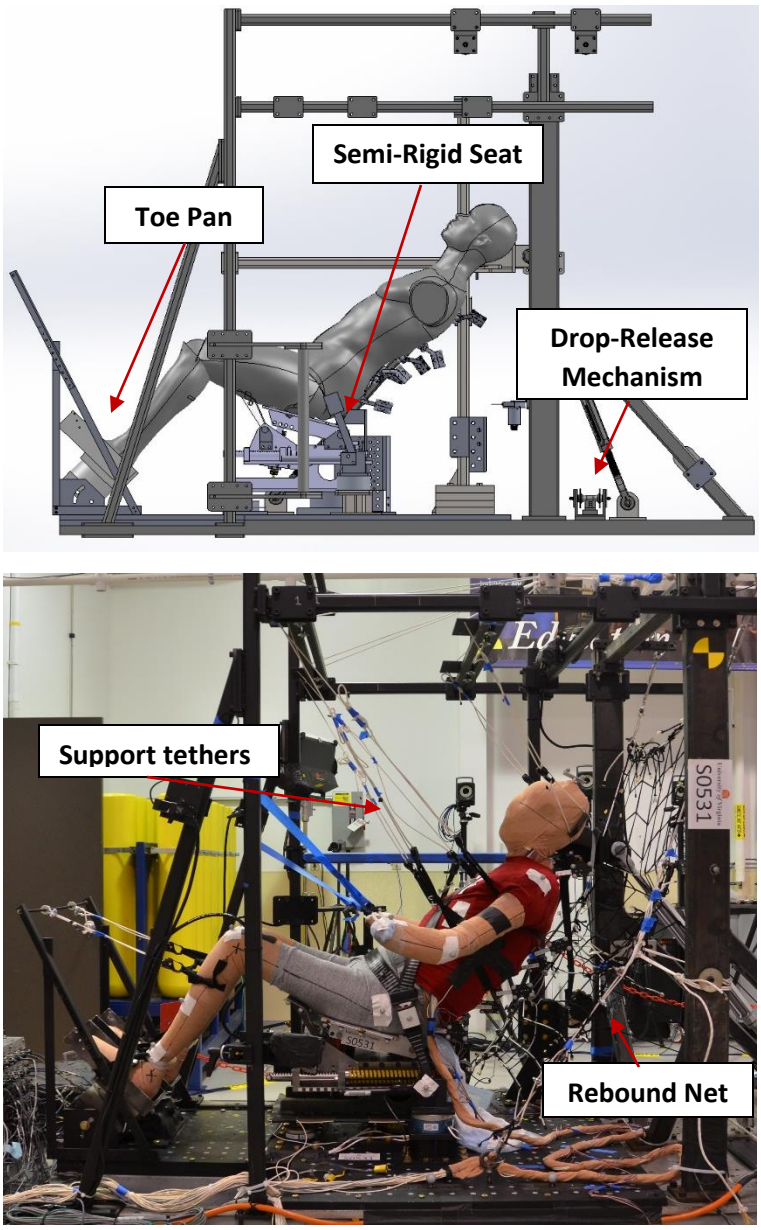

Figure 1. The CAD design of buck setup (top). The experimental setup (bottom).

Test Environment

Semi-rigid seat: The subject was seated on a semi-rigid seat (see Figure 2). The semi-rigid seat used in this test was based on a design developed by [14] to perform biofidelity sled reference tests with PMHS [10] [13]. The seat, consisting of two articulated rigid aluminum plates (see Figure 3), has been designed to reproduce the behavior of a real seat [10] [14]. The angular stiffness of each aluminum plate is generated by means of springs. The stiffness of the springs represents a front seat configuration for this test. This seat pan is angled at approximately 15° from the horizontal. The second articulated aluminum plate, positioned in front of the seat pan, represents an anti-submarining ramp angled at approximately 30° from the horizontal. Upon deflection of the seat pan and anti-submarining pan, an anti-rebound locking mechanism maintains the springs in a compressed state and thereby reduce the level of elastic energy returned into the subject by the seat on rebound.

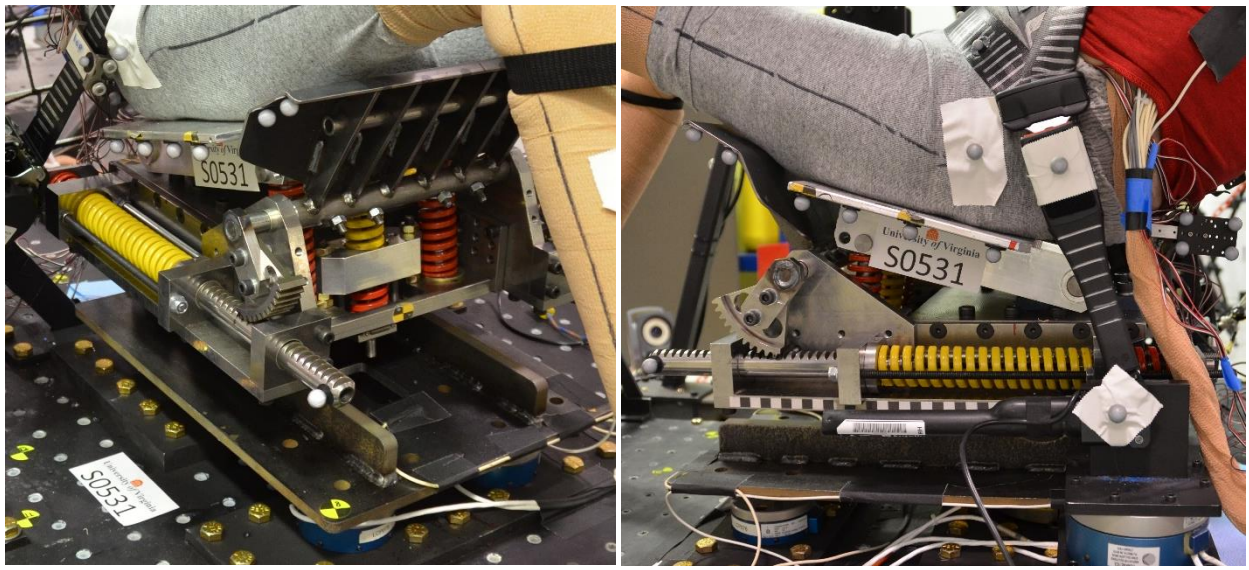

Figure 2. Oblique view of the semi-rigid seat in the experimental test setup (left). Lateral view of the semi-rigid seat (right).

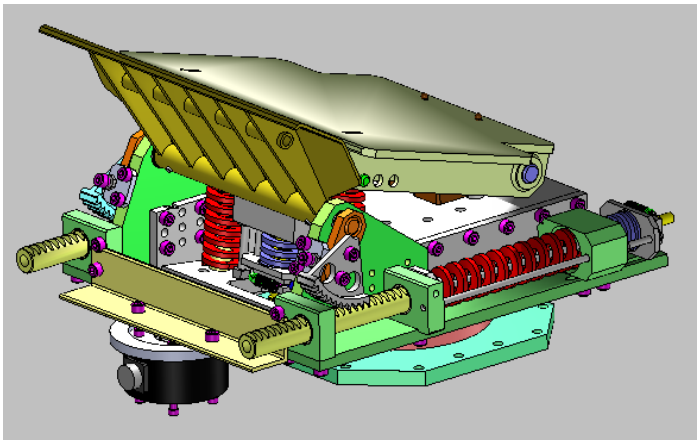

Figure 3. CAD model of the semi-rigid seat.

Belt: The belt system used in this study was designed to increase engagement of the pelvis, reducing the risk of submarining for reclined occupants. This consisted of a 3-point belt equipped with dual lap-belt pretensioners and a shoulder-belt pretensioner. Additionally, the belt system included a crash locking tongue that obstructed webbing transport from shoulder-belt to lap-belt and a shoulder-belt load limiter of approximately 3 kN. The D-ring was positioned to simulate the approximate position of a seatback-integrated D-ring, with an angle of approximately 12° as the belt leaves the shoulder. The shoulder belt crossed the shoulder at approximately mid-clavicle.

Pulse: These tests were performed on a Seattle Safety Systems 1.2 MN ServoSled acceleration sled system. The pulse (see Figure 6) used in this test was developed by [14] and has been used in previous sled tests to assess PMHS submarining [10] [13]. The Delta-v for this pulse is 51 kph.

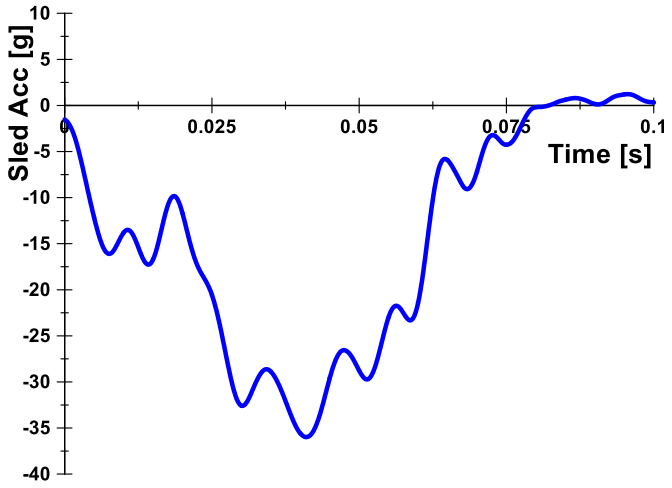

Figure 4. Sled acceleration pulse (CFC 60).

Positioning

The occupant was positioned in a 50-degree recline (measured as the angle the line connecting the H-point to the acromion made in the sagittal plane) with respect to the vertical, using three support straps for the upper- and mid-torso, and head (see Figure 1). Due to the sensitivity of the pelvis position's effect on submarining, the pelvis angle was measured based on targets developed from data on volunteers in 23, 33, 43, and 53 degrees of recline [9]. The methods used by [9] included digitizing the subject's ASIS and PSIS landmark locations, estimating the subject-specific pelvis geometry using an estimate flesh margin at the ASIS based on the adjustment for BMI [8] and utilizing and optimization method described in [7] to find the pelvis position and rotation around the lateral axis that best matches the subject's lumbar and thigh segment lengths. These methods produced pelvis angles measured from the ASIS to the pubic symphysis in the sagittal plane for each degree of recline, each with a set degree of standard deviation. Interpolating the measured pelvis angle between the 43- and 53-degree seatback recline angles resulted in a target of 61.35 degrees with respect to the vertical, with a standard deviation of approximately 15 degrees.

The positioning support straps were routed through overhead bars and attached to a drop-release located at the rear of the buck (see Figure 1). Two straps were routed behind the torso of the subject for both lumbar and thoracic support and positioning (see Figure 5, right). These straps allowed for fine tuning adjustability, individually at the lumbar and thoracic regions, to reach the appropriate torso angle. Similarly, a separate head support strap was used to adjust head angle. The drop release incorporated redundant mechanisms (one electromechanical and one pyrotechnic) with independent triggering pathways to minimize risk of failure and ensure proper release. The support straps were released at time 0. Following the test, during the deceleration phase of the sled, the subject's motion was arrested by a catch net mounted on the sled behind the initial position of the subject.

Three-Dimensional Kinematic Motion Tracking

Spine and pelvis motion tracking: A reclined seating posture introduces a higher likelihood of lap-belt submarining, a phenomenon where the belt is properly placed across the anterior superior iliac spines (ASIS) initially, but then, as a result of interaction with the soft tissue in the area, the belt becomes disengaged from the bony pelvis allowing it to move vertically upward relative to the occupant to load the abdomen [6]. As a result, tracking the motion of the spine and pelvis throughout the full excursion is of importance for this test mode. Kinematic data were collected at 1000Hz using an optoelectronic motion capture system consisting of 20 cameras (Vicon MX^{TM}, VICON, Centennial, CO, USA) that tracked the position of retro reflective spherical markers in a calibrated 3D space lying within the cameras' collective field of view. Four-marker clusters were secured to selected anatomical locations including the head, spine, sternum, and pelvis to facilitate the determination of the position and

orientation of the corresponding bone using rigid body mechanics and coordinate transformations at each time step. This method has been used in previous sled test studies [12].

For sled tests with occupants seated in traditional upright postures, posterior reflective marker cluster hardware are mounted at T1, T8, L2, and the sacrum (see Figure 5, left). In such studies, marker arrays for spine tracking have been oriented to be visible from the posterior of the subject. With a reclined position however, the visibility of the posterior aspect of the subject is limited and is not conducive for rear-facing marker arrays. Additionally, a thorough examination of spine kinematics requires the installation of mounts at more vertebrae locations than has been traditionally studied. Accounting for both the limited space and obscured view posterior of the subject along the spine, novel marker cluster hardware for the vertebrae and pelvis were developed for this test (see Figure 5, right).

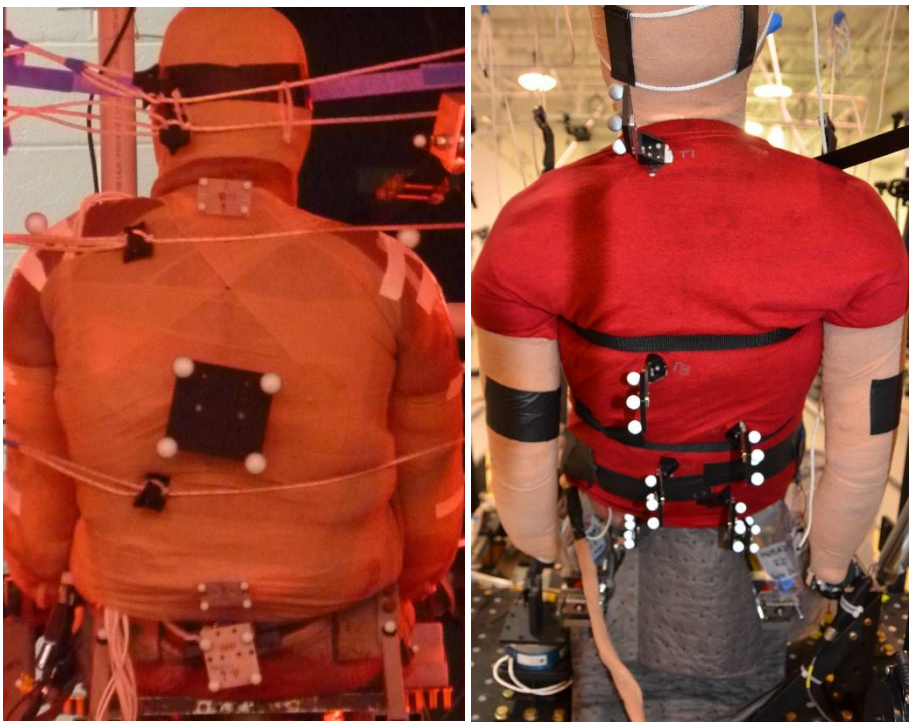

Figure 5. Traditional posterior motion-tracking instrumentation, located at T1, T8, L2, and the sacrum (left) [1]. Novel posterior motion-tracking instrumentation, located at T1, T8, T11, L1, L3, and the pelvis (right).

The main component of the spinal hardware consisted of an aluminum "horseshoe" shaped mount that was flushed against the spinous process of each chosen vertebrae location and drilled in posteriorly with 2 ¾" screws. Spine mounts were mounted at the T1, T8, T11, L1 and L3 locations (see Figure 6). This instrumentation was installed under X-Ray guidance to ensure that the screws did not bridge adjacent vertebrae. On the side of the "horseshoe" mount, a 6 D.O.F. cube was installed to track acceleration and angular rate local to each chosen vertebra. Superior to this, a 3D-printed carbon fiber L-bracket was installed, attaching an aluminum pivot arm to allow for longitudinal adjustability. The marker clusters were arranged on flat 3D-printed carbon plates, adding minimal weight to each chosen vertebra. This hardware allowed visibility of the reflective spherical markers in the lateral plane (see Figure 7). To maximize the available longitudinal space, the plates were staggered facing the left and right lateral planes.

Figure 6. CT Scan of spinal hardware installed on PMHS (head and pelvis hardware also visible).

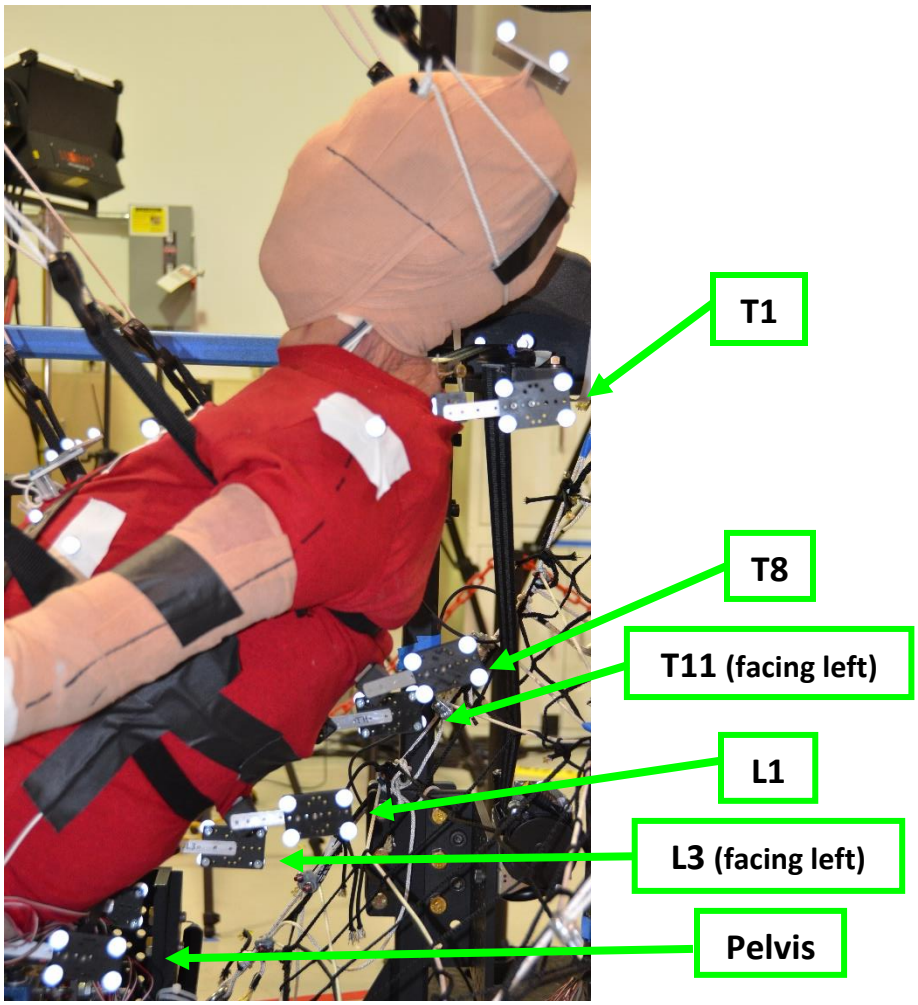

Figure 7. Posterior 3D Motion Tracking Instrumentation.

The pelvis mount included a lateral aluminum bar bilaterally into the posterior superior iliac spine (PSIS) using 1" screws (Figure 11). Upon installation, the screws were angled outward from the pelvis to avoid either fusing the iliac wings to the sacrum or drilling through the iliac wings. The pelvis mount consisted of two Vicon clusters, each facing outward from the center of the subject.

Other motion tracking: Vicon marker arrays were also attached to the skull and sternum (Shaw et al. 2009), and surface markers were placed at various locations on the chest, and extremities. Markers were also attached to track motion of the belt, seat pan, and buck.

Other Instrumentation

6 D.O.F. Cubes: Inertial measurement sensor packages consisting of sets of three mutually perpendicular linear accelerometers and three mutually perpendicular angular rate sensors (6 D.O.F. cubes) were attached to the vertebral mounts, pelvis mount and head mount to track acceleration and angular rate local to the anatomical locations. The sternum acceleration was tracked with a uniaxial accelerometer in the X-direction.

Disc Pressure Transducers: For this test, Model 060S pressure sensors (Precision Measurement Company, Ann Arbor, MI) were inserted in the intervertebral discs at three locations: T12/L1, L2/L3, L4/L5. This sensor, designed for medical applications, is the smallest pressure sensor commercially available today (3 mm L x 1.5 mm W, thickness 0.3 mm). The pressure transducers were inserted into the intervertebral disc posteriorly with a bore

needle gauge apparatus. The end of the bore needle gauge was inserted into the center of the nucleus. After this location was confirmed using X-ray (both posteroanteriorly and laterally), the needle was removed, leaving the pressure sensor in place.

Pelvis Strain Gauges: Two strain gauge rosettes were installed on each iliac wing at the exterior portion of the ilium, between the ASIS and AIIS locations (see Figure 8). The central axes of these gauges were aligned with the anterior portion of the pelvis to measure strain directly resulting from the lap belt load.

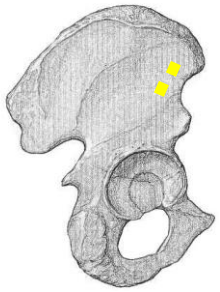

Figure 8. Pelvis strain gauge locations.

Belt Force Sensors: Belt gauges were placed on both the lap belt at the outer anchorage location, as well as on the shoulder belt between the occupant's shoulder and the integrated seatback "d-ring" location. The load was also measured beneath the buckle with a 6-axis load cell.

Seat and Toe Pan Load Cells: Loads were measured beneath the seat using an array of three load cells: a 6-axis load cell in the rear and two 3-axis load cells in the front.

RESULTS

Spine Kinematics: The novel Vicon instrumentation installed to track both spine and pelvis kinematics was proven to be fully visible throughout the occupant's full excursion (see Appendix I). The torso began to accelerate forward at 40 ms. At approximately 70 ms, the torso center-of-gravity was directly over the pelvis. Peak torso excursion occurred at 117 ms.

Pelvis Kinematics: The pelvis first began to slide forward at 26 ms, reaching peak excursion at 70 ms (see Appendix I). The seat pan deformed as a result of this forward excursion, however the anti-submarining pan deflected only slightly, without enough deflection to activate the anti-rebound device for this pan.

Pressure Transducer Signals: Initial testing of the pressure transducers indicated that the magnitude of the load signal was highly sensitive to the positioned location of the gage, and as a result, the magnitude of the recorded pressures did not seem to correlate with pressure readings at other levels. However, the sensors accurately captured loading timing including maximum loading timing.
The pressure transducer located at the T12/L1 disc recorded a maximum pressure at 64 ms (see Figure 16, top). The L2/L3 pressure transducer recorded a maximum pressure at approximately the same time, 63 ms. The pressure transducer installed at the L4/L5 disc failed prior testing.

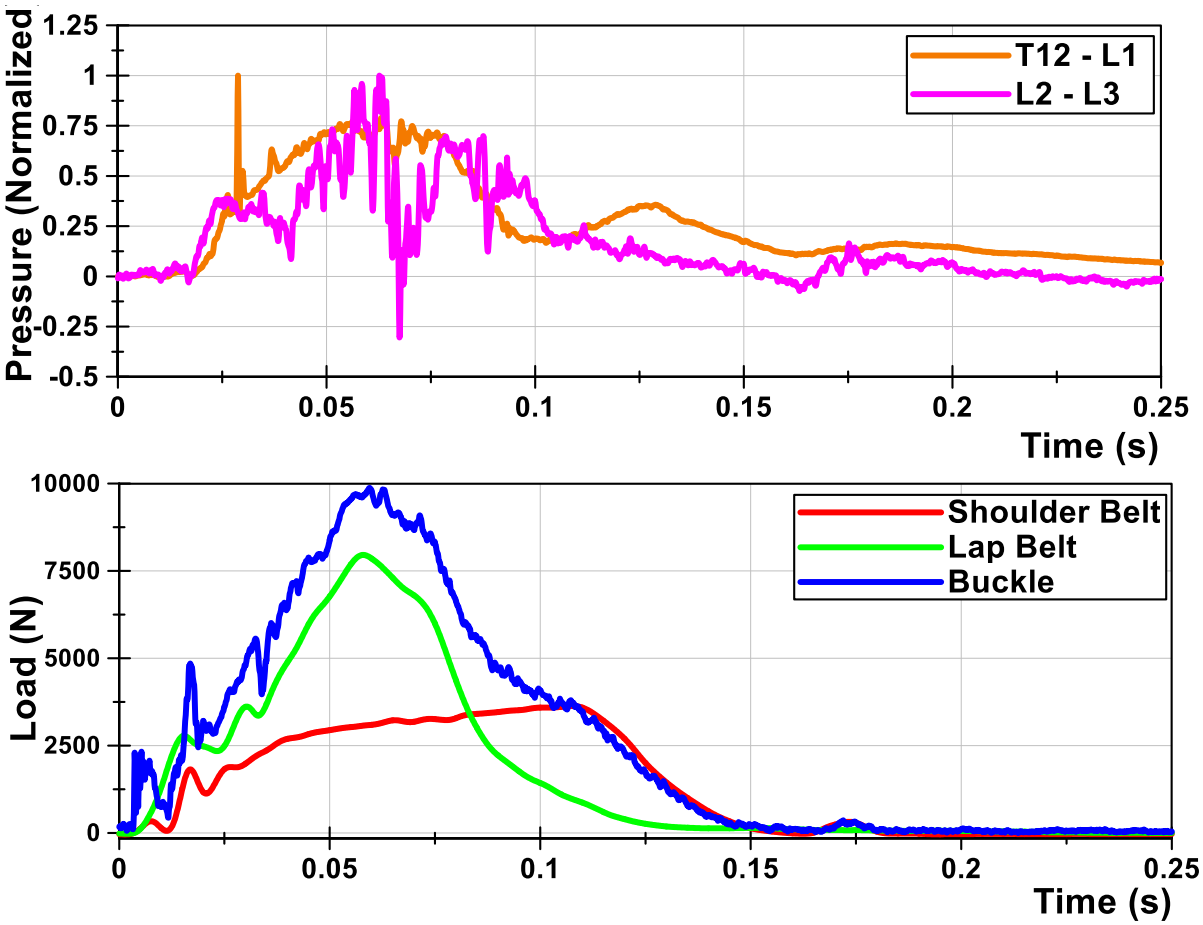

Figure 9. Lumbar pressure transducer signals (top): Normalized signals, filtered at CFC 1000. Belt Forces (bottom): Shoulder belt and lap belt forces filtered at CFC 60; Buckle resultant filtered at CFC 1000.

Belt Forces: The buckle force (resultant) recorded a peak force of 9.88 kN at 59.5 ms (Figure 9, bottom). The lap belt recorded a peak force of 7.96 kN at 58 ms. The shoulder belt recorded a peak force of 3.63 kN at 107.5 ms. The signals from the strain gauges on the pelvis correlated with peaks in lap belt and buckle loads, peaking at 63 ms for the gauges on the right iliac.

DISCUSSION

This setup is the first of its kind to test PMHS in a reclined seating configuration. The novel Vicon mounts have been proven to successfully track the spine and pelvis, whose kinematics play a critical role in the likelihood of submarining-related injuries. At approximately 70 ms, the torso's center-of-gravity was directly over the pelvis. This is estimated to be the time in which the lumbar spine was in its highest degree of compression prior to the forward pitch of the torso, where the lumbar spine is loaded under combined compression and bending (seen at 86 ms). At approximately 70 ms, a peak in intervertebral disc pressure is measured by the T12/L1 pressure sensor (64 ms) and the L2/L3 pressure sensor (63 ms).

These peaks in disc pressure occur shortly after the peak lap belt force, measured via both the lap belt and the buckle resultant force (Figure 9). The peak lap belt forces measured by the belt gauge and buckle load cell are 8 kN and 9.9 kN respectively and occur at approximately 60 ms. The peak shoulder belt load was 3.6 kN and occurred at 108 ms. The pressure at the T12/L1 location again increased following the peak shoulder belt load, with a local maximum of 219 psi occurring at 129 ms.

The pressure transducer signals indicate peak pressure occurs at the stage of maximum spinal compression, before going into bending. Since the pressure transducer is in the center of the intervertebral disc at the nucleus, it does not account for the pressure due at the most anterior landmark of the disc, wherein a high level of pressure is likely seen during flexion. Therefore, a diagnosis of when injury is most likely to occur during frontal impact in a reclined seating posture cannot necessarily be taken from the pressure transducer signal. From the overall kinematics, the spine goes into a high degree of flexion. Future studies should be conducted to determine injury thresholds of the spine in combined compression and bending.

At 70 ms, the pelvis reaches full excursion, however the anti-submarining pan is not deflected enough to engage the anti-rebound device. From the video, it appears that this is not a function of the stiffness of the anti-submarining pan, but rather it is due to the amount of tissue on the subject's femurs. This subject did not have enough soft tissue to engage the anti-submarining pan in order to allow it to articulate about its axis.

The lap-belt maintained contact with the pelvis during the full test and the subject did not appear to submarine (Figure 10). During the pelvis excursion, the pelvis was seen to rotate forward.

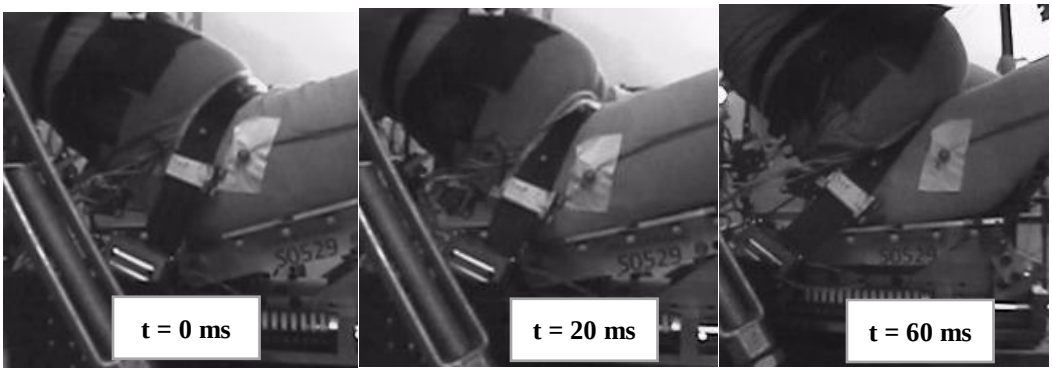

Figure 10. Pelvis excursion time stills from onboard camera view.

The double lap belt pretensioner combined with a shoulder belt pretensioner places a high amount of load on the subject's pelvis. Fractures and soft tissue injuries for this test will be thoroughly investigated.

While the visible tracking of the lap belt is lost due to the abdomen covering the pelvis during forward torso excursion, the data from the belt loads and the pelvis strain gauges clarify that the belt remains engaged with the ASIS AIIS area throughout the test. Therefore, no submarining occurred; however, to prove this restraint configuration is successful in restraining the pelvis, it must be validated through the testing of more subjects. This test setup has proven to be successful in testing a PMHS in a reclined seating configuration, with a high success rate of entirely novel sensors. This methodology will be used for at least 3 additional PMHS tests in this condition. The resulting data from these tests can be used to validate HBM simulations in reclined seating postures. To further validate the restraint configuration, and to further investigate reclined occupant kinematics, this test setup can be used to explore a variety of pulses, degrees of recline, and anthropometries in the future.

CONCLUSIONS

A methodology was developed to test occupants in a reclined seating configuration in frontal impact scenarios, and an example test was performed. A reclined seating posture introduces the likelihood of submarining and combined compression and flexion loading in the lumbar spine, therefore lumbar spine and pelvis kinematics are of great interest. This methodology allows for the visibility of pelvis and spine kinematics in this posture, a strain time history of the pelvic iliac wings, and the timing and severity of lumbar loading. This data will be used to perform detailed computational simulations of the test, as well as to make detailed comparisons to dummy response.

REFERENCES

[1] Acosta, S. M., Ash, J. H., Lessley, D. J., Shaw, C. G., Heltzel, S. B., & Crandall, J. R. (2016). Comparison of Whole Body Response in Oblique and Full Frontal Sled Tests. In *Proceedings of IRCOBI Conference*.

[2] Dissanaike, S., Kaufman, R., Mack, C. D., Mock, C., & Bulger, E. (2008). The effect of reclined seats on mortality in motor vehicle collisions. *Journal of Trauma and Acute Care Surgery*, *64*(3), 614-619.

[3] Forman, J., Lin, H., Gepner, B., Wu, T., Panzer, M. (2018) Occupant safety in automated vehicles: effect of seatback recline on occupant restraint. Japan Society of Automotive Engineers.

[4] Ji, P., Huang, Y., & Zhou, Q. (2017). Mechanisms of using knee bolster to control kinematical motion of occupant in reclined posture for lowering injury risk. *International journal of crashworthiness*, *22*(4), 415-424.

[5] Kitagawa, Y., Hayashi, S., Yamada, K., & Gotoh, M. (2017). Occupant Kinematics in Simulated Autonomous Driving Vehicle Collisions: Influence of Seating Position, Direction and Angle (No. 2017-22-0005). SAE Technical Paper.

[6] Luet, C., Trosseille, X., Drazétic, P., Potier, P., & Vallancien, G. (2012). *Kinematics and Dynamics of the Pelvis in the Process of Submarining using PMHS Sled Tests* (No. 2012-22-0011). SAE Technical Paper.

[7] Park, J., Ebert, S. M., Reed, M. P., & Hallman, J. J. (2015). Development of an optimization method for locating the pelvis in an automobile seat. *Procedia Manufacturing*, *3*, 3738-3744.

[8] Reed, M. P., Ebert, S. M., & Hallman, J. J. (2013). *Effects of driver characteristics on seat belt fit* (No. 2013-22-0002). SAE Technical Paper.

[9] Reed, M. P. (2018). *Effects of Recline on Passenger Posture and Belt Fit*. University of Michigan, Ann Arbor, Transportation Research Institute.

[10] Richard, O., Uriot, J., Trosseille, X., & Sokolowski, M. (2015). Occupant restraint optimisation in frontal crash to mitigate the risk of submarining in out-of-position situation. In *Proceedings of IRCOBI Conference*.

[11] Shaw G, Parent D, Purtsezov S, Lessley D, Crandall J, Kent R, Guillemot H, Ridella SA, Takhounts E, Martin P (2009). Impact response of restrained PMHS in frontal sled tests: Skeletal deformation patterns under seat belt loading. Stapp 53:1-48.

[12] Trosseille, X., Petit, P., Uriot, J., Potier, P., Baudrit, P., Richard, O., ... & Douard, R. (2018). Reference PMHS Sled Tests to Assess Submarining of the Small Female. *Stapp car crash journal*, *62*, 93-118.

[13] Uriot, J., Potier, P., Baudrit, P., Trosseille, X., Richard, O., & Douard, R. (2015). Comparison of HII, HIII and THOR dummy responses with respect to PMHS sled tests. In *Proceedings of IRCOBI Conference*.

[14] Uriot, J., Potier, P., Baudrit, P., Trosseille, X., Petit, P., Richard, O., ... & Douard, R. (2015). *Reference PMHS Sled Tests to Assess Submarining* (No. 2015-22-0008). SAE Technical Paper.

APPENDIX I

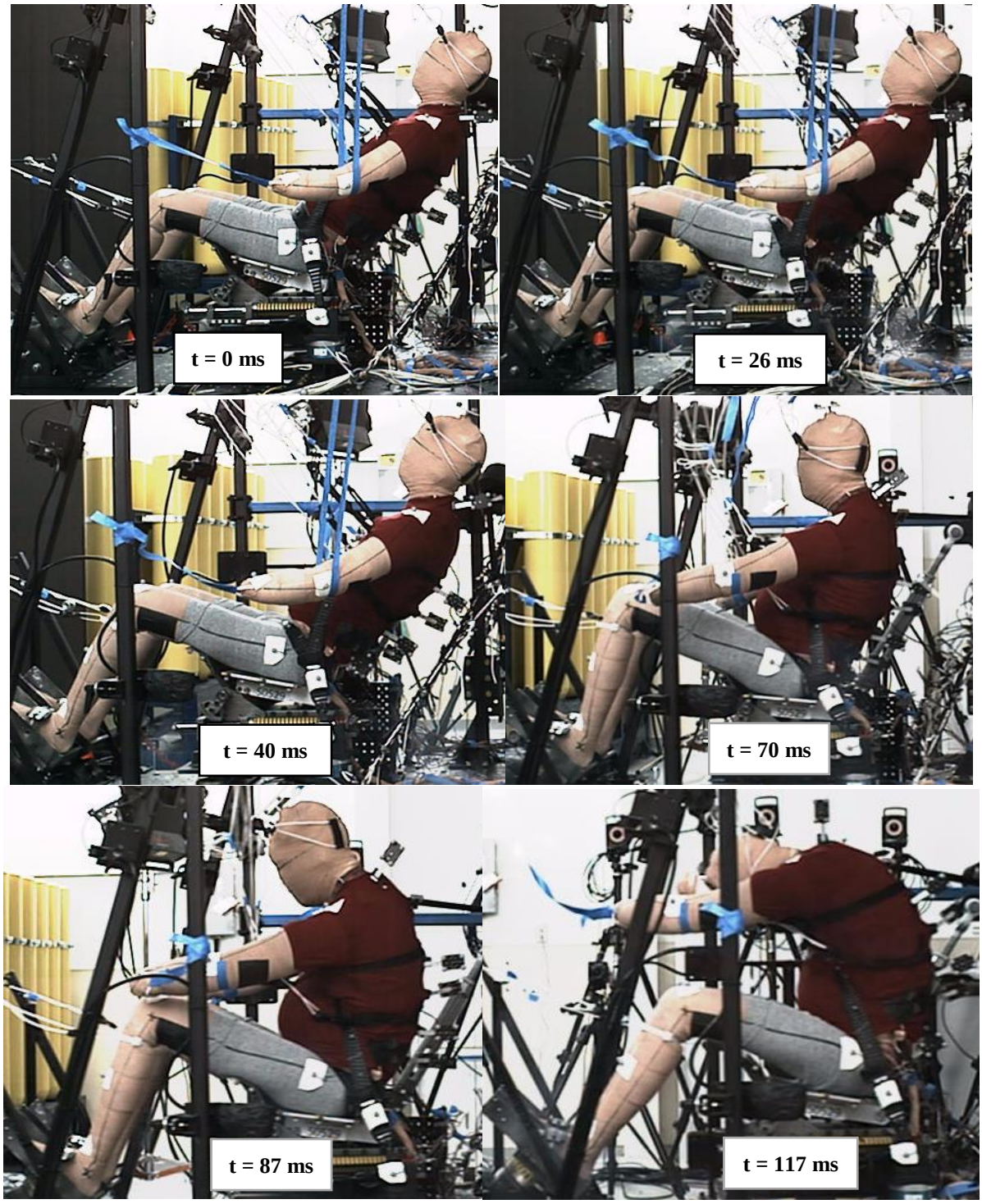

Figure 8. Video stills from sled test.

THE INFLUENCE OF A GAZE DIRECTION BASED ATTENTION REQUEST TO MAINTAIN MODE AWARENESS

Dr. Christina Kurpiers
BMW AG
Germany

David Lechner
BMW AG
Germany

Dr. Florian Raisch
BMW AG
Germany

Paper Number 19-0245

ABSTRACT

Future vehicles will combine different levels of driving automation characterized by varying responsibilities for users. This development will intensify system complexity which poses the risk of confusing the driver. We hypothesize that the users' mode awareness suffers especially when changing from Level 3 "Conditional Automation" to Level 2 "Partial Automation". Therefore, automated systems need to be designed in a way that minimizes confusion with regard to the automation mode. The article describes the influence of a gaze direction based Attention Request (ATR) to avoid mode confusion with the aim of contributing to the reliable operation of different levels of automation in one vehicle.

Two similar studies were conducted. One took place in a dynamic driving simulator with 40 participants. Every participant drove for 10 minutes with a partially automated driving (PAD) (SAE level 2) system and conditionally automated driving (CAD) (SAE level 3) system in the order PAD/CAD/PAD. The second study was conducted on a German highway in a Wizard-of-Oz car. All 40 test persons drove in each PAD and CAD phase 8 minutes in the order of PAD/CAD/PAD/CAD/PAD/CAD. The CAD-system was in both studies a high performing Hands-Off Level 2 system that required no input of the driver. To promote the same mental model for all participants as it is a requirement to measure the differences in mode awareness, all persons became a detailed description of the Level 2 and 3 systems presented by video and text.

Both studies used a between-subject-design to measure the influence of an ATR. The ATR was based on the gaze direction of the driver and initiated by the investigator when the drivers gaze was not in the street AOI for longer than 4 seconds. Mode awareness was operationalized by the visual attention towards driving-relevant areas, a qualitative analysis of a questionnaire and followed by an interview.

The ATR was proven to be an effective action to maintain the mode awareness by using a level 2 and 3 system within one car. Specifically, the visual attention did not decrease by an intermitted CAD drive during PAD. Moreover, the visual attention to the road scene increased for the group with an ATR during PAD. This was indicated by the measurement of a significant interaction effect for the development of the visual attention to the road scene for the groups with and without ATR. Thus, the gaze direction based ATR was proven to be an effective measure to maintain mode awareness, if different levels of automation are combined in one vehicle. This result helps to take the next step for realizing such combined multilevel systems with tailored HMIs for advanced driver assistance systems.

Moreover, it has to be considered, that the studies put the emphasis on the first glance of the drivers, during their first contact with partly and conditionally automated systems. Further studies should investigate the long term effect of an ATR.

INTRODUCTION

Technical advances in recent years lead to the presence of automated vehicles in road traffic within the next few years. As a result of progressive development towards full driving automation, future vehicles will combine different levels of driving automation modes. This development of combining different levels of automation in one car will intensify system complexity which poses the risk of confusing the driver [1, 2] as different levels of driving automation are characterized by varying responsibilities for their users.

The Society of Automotive Engineers (SAE) provides a taxonomy for motor vehicle driving automation systems that perform part or all of the dynamic driving task on a sustained basis and that range in level from no driving automation (level 0) to full driving automation (level 5) [3].

Recently released driving automation systems in production vehicles can be classified as Level 2 "Partial Automated Driving" (PAD). In Level 2, the automation performs both lateral and longitudinal vehicle guidance [3]. However, due to system limits and at system failures where the systems cannot cope, the user is considered to be the fallback level at all times and has to continuously monitor the vehicle behavior for fast and correct intervention. Common current limitations include restrictions in operating speed ranges; how much steering, braking and acceleration the system can apply; and limitations in lane and object detection. Thus, the driver has to supervise both, ongoing automation performance and detection of precrash conditions.

The next step is to temporarily release the driver from all driving-related responsibilities. On Level 3, "Conditional Automated Driving" (CAD), the system comprises the entire range of dynamic driving tasks when it is available, and thus the user can engage in non-driving-related task (NDRT). CAD recognizes its system limits and timely requests the driver to intervene if it becomes necessary [3]. With CAD, the user is considered to be the fallback level, which means he/she is expected to be receptive to the system's requests to intervene and to timely respond accordingly.

Thus, the main difference between Level 2 to Level 3 is that the driver has to continuously monitor the automation during PAD, whereas during CAD he/she is allowed to engage in NDRT.

Trust in automation

Trust in automation is commonly described as an important factor for system use and acceptance. If drivers do not trust, thus undertrust the systems, they will not activate them. However, if drivers overtrust the functionalities, this may certainly lead to unsafe situations.

Lee and See [4] define trust as an "attitude that an agent will help achieve an individual's goals in a situation characterized by uncertainty and vulnerability" [4], p. 54. In this definition, an agent can be automation or another person that actively interacts with the environment on behalf of the person. Lee and See [4] specified calibration of trust as one of three components of appropriate trust and described calibration of trust as having accurate knowledge of the system's capabilities. Calibration is needed for a driver to know when human action is required. However, there is more to trust calibration than just avoiding overtrust and undertrust. Trust may be perfectly calibrated with a system that is very unreliable. In that case there is a very low level of trust, but well calibrated. One could even argue that undertrust is good for traffic safety since the driver will have a high level of attention and a high readiness to take back control. So although trust calibration is an important issue in automated driving, a minimum level of trust seems to be required to have comfort and safety benefits for the user [4]. Lee and See [4] conclude that overtrust is more dangerous than undertrust as drivers ignore a high level of attention and a high readiness to take back control.

Thus, the ability of people to effectively supervise automation is also clearly related to difficulties in achieving calibrated trust, in which the user's trust matches the automation capabilities [4, 5]. Higher levels of trust are associated with less eyes-on-road time and less monitoring [6]. Hancock et al. [7] determined in their meta-analysis that robot performance and attributes were found to be the most important influences of trust development. Therefore, a very reliable Level 2 system can lead to the risk of overtrust in Level 2 automation.

To conclude, overtrust is a very crucial factor for the usage and Human-Machine Interaction of automated systems that can lead to low situation awareness that will be explained in the next paragraph.

Situation Awareness and Mode Awareness

It is first necessary to distinguish the term situation awareness, as a state of knowledge, from the processes used to achieve that state. Situation awareness is defined as the "perception of the elements in the environment within a volume of time and space, the comprehension of their meaning, and the projection of their status in the near future." 8, p. 36. Thus, a person's situation awareness is formed by the perception of the relevant elements in the environment, as determined from system displays or directly by the senses.

Automation effects from aviation [1, 8–10] show that situation and mode awareness are vital criteria for take-over scenarios. The driver has to be aware of the surrounding scenery, traffic constellations, and the system mode at all times.

Mode awareness is defined as "the ability of a supervisor to track and anticipate the behavior of automated systems" [1], p. 7. A user can achieve mode awareness for a system, when he or she perceives system information, interprets the information correctly to have an understanding of the current state of the system and is able to project the future status of the system [1, 11, 12].

Sarter and Woods [1] stated that more complex automated systems might pose the risk of confusing drivers and therefore provoke erroneous behavior. Such incorrect driver behavior occurs when the driver is not aware of the currently activated automation mode and its functional capability or assumes that a different mode is currently activated [1], thus, if there is mode confusion. Bredereke and Lankenau [13] state that mode confusion occurs when the observed behavior of a technical system is out of sync with the behavior of the user's mental model of it.

By implementing different levels of automation modes into one vehicle that increases the complexity of the system, the automotive domain is facing challenges concerning mode awareness. In each automation mode, drivers have to be aware of the current state of the system and the environment and to keep in mind which tasks are taken over by the system and which they have to remain responsible for. While driving in PAD, the driver must monitor the system at all times, meaning that he/she has to verify that the vehicle is behaving as it is supposed to depending on the given situation.

Therefore, mode confusion and lack of mode awareness can be identified as risk factors for the safe operation of automated vehicles and need to be further examined [14].

Kolbig and Müller [11] showed in their model (see Figure 1) the connection of mode and situation awareness within the key components of driver, vehicle and environment. While the scope of information in mode awareness is limited to the system, situation awareness also includes all information about the current situation in which the system and the user are located [11].

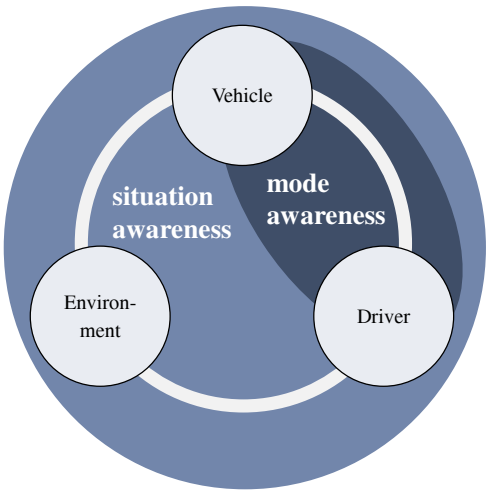

Figure 1. Scope of information for situation and mode awareness (referring to 11, p. 3)

Mental Model

According to Norman [15] mental models are naturally evolving models. Through interaction with a target system, people formulate mental models of that system. Humans use mental models when they interact with technical systems in general, and with automated systems in particular. A person, through interaction with the system, will continue to modify the mental model in order to get to a workable result [15]. Mental models will be constrained by such things as the user's technical background, previous experiences with similar systems, and the structure of the human information processing system. Thus, a mental model represents the user's knowledge about a technical system and it consists of a naive theory of the system's behavior.

Humans often have gaps and misconceptions in their mental models of automated systems due to their complexity. Consequently, operators are often surprised by the automation and they do not understand why it behaves in a certain manner or what it will do next [16]. It is necessary that a correct mental model of the system, along with the associated required driver behavior, is clearly described. Thus, it is very important to communicate system limitations, for example in level 2 automation, to avoid mental model misconceptions and consequently a lack of mode awareness. Therefore, central problems to address in further research are potential gaps and misconceptions in drivers' mental models and transparency of automated systems.

Kolbig and Müller [11] built by following the main findings from Endsley [8] and Norman [15] a model to address the development process of a mental model (see Figure 2). Thus, the development of a mental model is dependent on system knowledge or previous experience, system feedback and relevant system information in the environment.

For the correct execution of supervision during the usage of a level 2 system of automation a detailed mental model of the driver is necessary as this is a precondition for the mode awareness [11]. According to Kolbig and Müller [11] a mental model can mainly be formed by the system feedback. Thus, it can be assumed that in order to achieve mode awareness with increasing automation, an increasing scope of feedback is required. Figure 2 also shows the influence of an attention request as system feedback on the adjustment of the mental model in the case of misconduct of the driver.

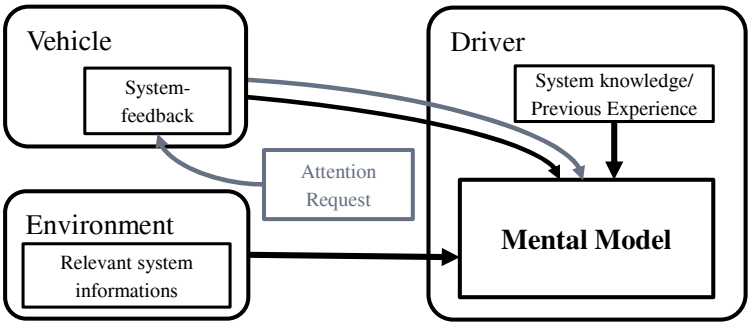

Figure 2. Developing process of mental models according to 11 [11]

Aim of the paper

Studies showed that humans tend to reduce their monitoring of highly reliable automation because of its ability to function properly for an extended period [16, 17]. Therefore, the question comes up how to prompt operators to pay attention to the roadway in level 2 driving and how to contribute to the reliable operation of different levels of automation in one vehicle.

Therefore, a paradigm of vehicle guidance has to be found in which both the automation system and the human can collaborate and mutually compensate the insufficiencies and failures of the other. With such a cooperative manner of vehicle driving the driver shall be kept active and in the loop of the shared driving task.

A review of several incidents and even accidents in the aviation sector caused by a lack of mode awareness revealed that the main reasons for the occurrence of mode confusion and the resulting erroneous behavior were poor system feedback, high complexity of the automated system, and insufficient mental models on the part of the pilots [1]. Thus, automated systems need to be designed in a way that minimizes confusion with regard to the automation

mode. Moreover, an adequate human-machine interface (HMI) is needed to ensure that the user is aware of the activated mode.
To contribute to the reliable operation of different levels of automation in one vehicle, the aim of this paper was to understand how to secure driver supervision engagement, thus how to influence the gaze behavior of the driver that he or she maintains the eyes on the road even though the mental model might not be exhaustive enough from beginning on or might be neglected over time due to arising overtrust.
Therefore, the influence of a gaze direction based Attention Request (ATR) during PAD was investigated to develop and adjust a correct mental model for the levels of automation, to maintain drivers' mode awareness and to avoid encouraging overtrust. The ATR should bring the drivers gaze back to the road scene ahead, if he/she stops monitoring the driving task or starts engaging in a NDRT during PAD.
The ATR was designed as a 3 step warning cascade with increasing urgency and is described in more detail below. The first stage of the ATR-cascade appeared after a continuous eyes-off time of 4 seconds and starts with a message in the instrument cluster behind the steering wheel for reminding them to supervise driving.

METHODS

Measure of mode awareness

To measure mode awareness and compare it between different drivers, it is necessary, that every driver has a comparable knowledge about the used levels of automation (compare Figure 2). The reason is, that the mental model is an underlying construct of mode awareness and is affected by the users' knowledge and previous experience with the used levels of automation [15]. Consequently, every participant was instructed with a detailed description of the different levels of automation by video and text. This description gave an overview of level 2 and 3, their system limits and put emphasis on the monitoring task of the driver during level 2. Moreover, it described that the driver is allowed to engage in non-driving-related-tasks (NDRT) during level 3. To ensure the correct understanding, the instructor controlled the participants' knowledge about the levels of automation. Therefore, they had to repeat the overview of the system functions and limits as well as their tasks. If a participant had an incorrect understanding, he or she had to read again the instruction until he or she achieved a correct and comparable knowledge about the automation levels experienced during the study. This step of a correct understanding is very important to measure the impact of different system designs on the drivers' mode awareness and his/her underlying mental model.
A level 2 and level 3 system can be designed in different ways. The system design of the automated system is an important influence factor for the users' mode awareness [1] and the worst-case scenario to achieve a sufficient mode awareness are two very similar systems as it is very difficult for the driver to distinguish between similar systems. Thus, a level 2 and a level 3 system, that are designed very similar make it more difficult for the user to have enough mode awareness and to behave correct during the use of each system. Therefore, a very similar PAD and CAD system were implemented in the two studies presented in this paper as this seems to be the most suitable method to investigate the impact of different system designs on the drivers' mode awareness. Both were Hands-Off systems and had the same functionality, meaning that the car automatically executed the lateral and longitudinal guidance, independently overtook slower cars and drove up to 130 km/h (80 mph). The driver was able to differentiate between PAD and CAD by the different visual design in the instrument cluster and by the color of the LED bars (see Figure 3). During PAD the LED bars lighted green and during CAD they lighted blue. Additionally, there was a simulated environmental model in the instrument cluster during CAD. Moreover, the user had to activate the systems and confirm the mode change from CAD to PAD by pressing a button. Consequently, the driver could differentiate between PAD and CAD even though the systems felt very similar due to their functionality. The characteristics of the PAD and CAD systems were exemplary systems.

	Instrument cluster	LED-bars
CAD	Blue indication of CAD-state Model of the driving environment	Blue
PAD	Green indication of PAD-state	Green
Manual	Basic instrument cluster	Off

LED-bars to display the system state (surrounded with a white circle and in blue as an example)

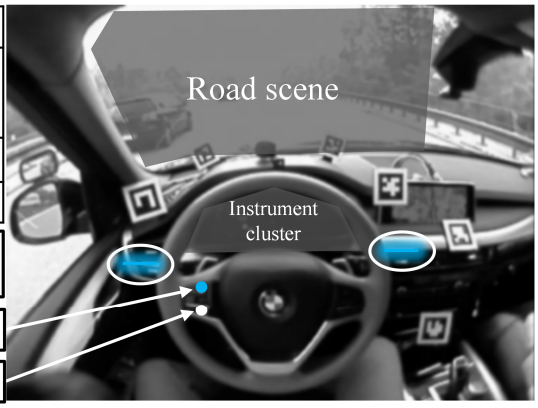

Figure 3. Visual design of the human-machine-interface (field of view of the participant in the Wizard-of-Oz study) and area of interest "Road scene"

Feldhütter et al. [2] showed, that changing between PAD and CAD impairs the drivers' monitoring behavior in PAD. Thus, the order of the PAD- and CAD-sequences is also important for measuring the mode awareness of the participants. Hence, the study started with a PAD-sequence as a baseline for the monitoring behavior during PAD and then alternated between PAD and CAD. To compare the monitoring behavior during PAD and CAD with the monitoring behavior during manual driving, a manual baseline was conducted before the first PAD-sequence.
To ensure a naturalistic behavior of the driver the NDRT should not have an additional extrinsic motivation. Therefore, the participants were instructed to engage in the NDRT, if it is allowed in their opinion and in relation to the actual driving situation. To generate a comparable intrinsic motivation, the drivers could choose between the usage of their own smartphone or of a study smartphone on which a quiz-game was installed. The drivers were allowed to run any application on their own smartphone only the voice-interaction or making a phone call was restricted to ensure a visual engagement in the NDRT.
To operationalize mode awareness and the underlying mental model of the participants with objective measures the definition of the driver behavior according to SAE International [3] was used. Thus, the driver is expected to monitor the driving environment while using a level 2 system, whereas the driver must stay receptive for alerts in level 3. The monitoring behavior of the participants was assessed by using the Dikablis Essentials head-mounted eye-tracking system (by Ergoneers GmbH), with a sampling frequency of 50 Hz. Consequently, the monitoring behavior was operationalized by the visual attention to the road scene ahead (see Figure 3). The attention ratio is representing the percentage of time that a participants' gaze direction is in the area of interest (AOI) in relation to the total duration of each driving phase [18]. The trust into the automated systems was operationalized by a questionnaire from Pöhler et al. (2016) and was therefore measured subjectively. For a more detailed view on the participants' mental model a questionnaire for the system understanding was used after the studies.

Attention Request to correct the mental model

The corrective measure to increase the mode awareness and the underlying mental model of the participants is the gaze direction based attention request during PAD. The ATR should bring the drivers gaze back to the road scene ahead, if he/she stops monitoring the driving task or starts engaging in NDRTs. According to Klauer, Dingus, Neale, Sudweeks, and Ramsey [19] a safety-based time duration to allow the driver to take his or her eyes off the road is two seconds, as they showed that an eyes-off time from the road scene longer than two seconds increases the probability of an accident during manual driving [19]. An earlier investigation of an attention prompt during PAD showed, that an allowed eyes-off time of two seconds leads to habituation-effects and the participants start to ignore the prompts [20]. In accordance to the findings of Groves and Thompson [21] concerning habituation of warnings a trade-off between short eyes-off times with frequent warnings and extended eyes-off times with high acceptance of the driver is necessary. Therefore, the first stage of the ATR-cascade was executed after a continuous eyes-off time of 4 seconds to minimize the risk of ignoring the ATR. In the first stage the driver was requested to look back at the driving scene by an indication sound, green flashing LED-bars and a pop-up message in the instrument cluster. The ATR consisted of three stages and the urgency of the warning increased by changing from green to red color and

using an alert-sound after stage 1. The detailed description of the ATR-cascade is shown in Figure 4. The cascade started to count after the driver took his/her eyes off of the defined AOI road scene (see Figure 3). The driver was then classified as "inattentive" by the investigator, who tracked the gaze direction of the participant during the simulator study on a computer in the control center and during the Wizard-of-Oz study on a tablet at the passenger's seat. The driver was classified as "attentive" again and the ATR-cascade stopped in stage 1 and stage 2, when he/she looked back at the road scene ahead. In stage 3 the driver had to make an active intervention of the vehicle guidance to stop the cascade.

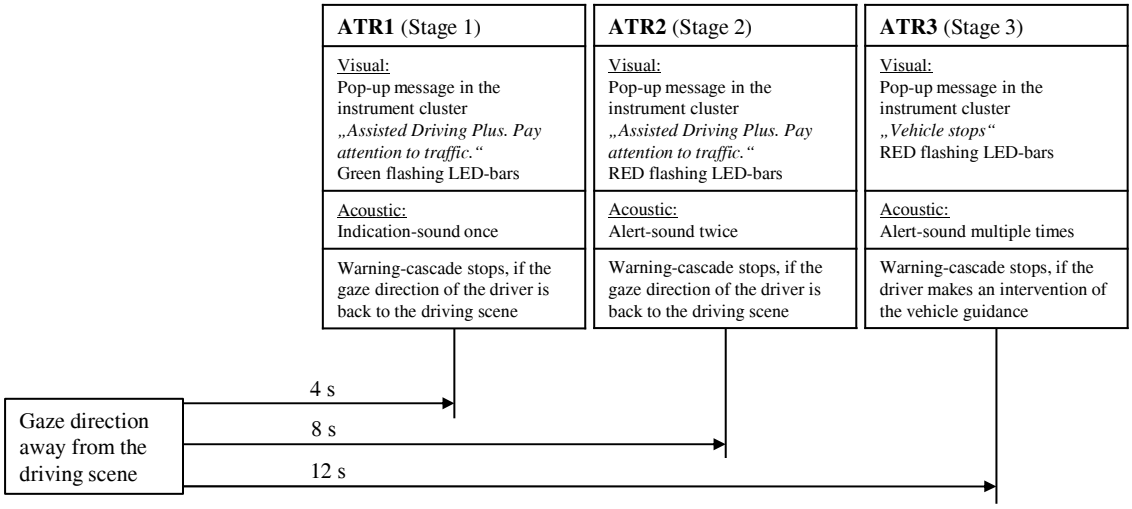

Figure 4. ATR-cascade

Experimental design of the two studies

To investigate the effect of an ATR during PAD two similar studies were conducted. The first took place in a dynamic driving simulator and the second on a public highway in Germany with a Wizard-of-Oz car. The method Wizard-of-Oz is described in the section of Study 2 below. Both studies had a similar design. The independent variable was PAD with and without an ATR and a between-subject-design was used to measure the influence of the ATR. Consequently, half of the participants became an ATR during PAD and the second half of the participants did not became an ATR during PAD. The level auf automation was varied in a within-subject, meaning that every participant experienced PAD and CAD. The two studies shared a similar general methodology according to the explanations for measuring mode awareness as stated above and are explained in detail below.

Study 1 - Dynamic driving simulator The first study was conducted in a dynamic driving simulator at the BMW Research and Innovation Center. A complete 5-series mock-up was mounted in the dome on a hexapod system for motion simulation. The visual simulation in the dome is accomplished with projectors and generates a 360 degrees field of view for the participant. The engine sound, driving and ambient noises are also simulated with the help of speakers in the dome. The dynamic driving simulator was additionally equipped with active steering. The automation modes PAD and CAD were implemented as described above. The virtual driving scenario was a standard three-lane highway with surrounding traffic. In both PAD phases, the test track and the surrounding traffic were designed in such a way that overtaking maneuvers were not necessary. The procedure of the first study and the duration of each phase is shown in Figure 5. The durations of continuous monitoring as it is required during PAD were chosen to be shorter than 15 minutes, to avoid vigilance effects on the monitoring behavior [12, 22]. The duration of 10 minutes should be long enough to develop enough trust in CAD and measure a realistic behavior of the participants. At the beginning of each study, participants became a detailed description of the automation modes presented by video and text. Afterwards they were familiarized with the simulator and the use of the level 2 and level 3 automated systems. The group with ATR neither became any instructions regarding the ATR, nor experienced an ATR during the familiarization-phase. As baseline for the monitoring behavior of the participants, the test drive started with a manual drive. During that baseline drive participants got the instruction not to exceed 130 km/h (80 mph) for a better comparison with the following PAD and CAD-phases, because the maximum speed

of the automated systems also was 130 km/h (80 mph). Afterwards, the participants started with the first PAD-phase (PAD1). During that level 2 phase, people in the "ATR group" became an ATR, if they took their eyes off the road longer than 4 seconds. The mode change from PAD to CAD and back to PAD was not interrupted by a manual drive; the only action from the participants was to activate CAD by pressing the CAD-button (white) and to confirm the mode change to PAD by pressing the PAD-button (blue) another button. The study concluded with a questionnaire and an interview at the end of the study. To obey the ethical guidelines people were debriefed after the study.

Figure 5. Procedure of the driving simulator study

Study 2 - Wizard-of-Oz study on public highway The second study was conducted on a public highway in Germany to investigate the monitoring behavior and the influence of a gaze direction based ATR in real traffic. The BMW AG modified a BMW X5 xDrive50i to allow a Wizard-of-Oz configuration that was used for this study as test vehicle. The Wizard-of-Oz method allows to imitate a complex automated system by a human driver and the participant believes to interact with the automated system [23]. In this study, the wizard imitated both the PAD and CAD system with an additional steering wheel and pedals. The participant did not see the wizard during the whole study and believed to interact with an automated system. This method was chosen to allow us to investigate our research-questions in a safe study in a real traffic environment and to avoid risk for the participant when he or she is not monitoring the systems correctly. The study was conducted on the German highway A92, which is a two-lane, limited access highway. It took place during off-peak hours (late morning and early afternoon) to ensure middle traffic density. The procedure of the second study and the duration of each phase is shown in Figure 6. At the beginning of each study, participants became the same description of the automation modes presented by video and text as in the simulator study. Afterwards, they were familiarized with the test vehicle and the study started due to the environmental conditions with a manual baseline. This was also used as baseline for the participants' monitoring behavior and once again it was not allowed to exceed 130 km/h (80 mph) for a better comparison with the following PAD and CAD-phases because the maximum speed of the automated systems was also 130 km/h (80 mph). The instructor was sitting on the passenger seat during the test drive and the participants were told not to talk with him to create a more realistic scenario. The manual baseline was followed by a familiarization-phase for getting used to the use of the level 2 and level 3 automated systems. The group with ATR neither became any instructions regarding the ATR, nor experienced an ATR during the familiarization-phase. The test drive started with the first PAD-phase and the participants in the "ATR group" became an ATR, if they took their eyes off the road longer than 4 seconds during PAD. The participants had to active PAD by pressing the PAD-button and confirmed the mode change from CAD to PAD by pressing the CAD-button. The mode changes were not interrupted by a manual drive, except the change from PAD2 to CAD2 due to a necessary change of the driving direction and a consequently intermittent manual drive. The participants had to confirm the mode change from CAD to PAD by pressing the CAD-button. In this study, an additional trust questionnaire was conducted before and after the test drive, because the results of the simulator study indicated an influence of the ATR on trust of automation. The study concluded with a questionnaire and an interview at the end of the study. To obey the ethical guidelines people were debriefed after the study and the Wizard-of-Oz method was explained to them.

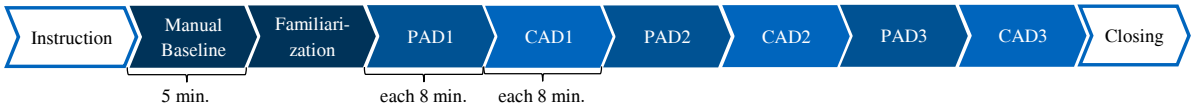

Figure 6. Procedure of the Wizard-of-Oz study

RESULTS

The results of the dynamic driving simulator and the Wizard-of-Oz study will be explained separately and in a chronological order below.

Study 1 - Dynamic driving simulator

38 participants were recruited in cooperation with a market research institute and received an appropriate monetary incentive. The participants did not work in the automotive industry and did not participate in an autonomous driving study 12 month prior to the study. $N = 5$ participants were excluded from the analysis due to a low understanding of the system. The low system understanding was determined in the questionnaire and the interview after the study and it was decided to exclude these participants due to defined requirement of a comparable mental model. Another $n = 3$ participants were excluded from the analysis because they refused to engage in the NDRT and consequently the visual attention to the road scene was not an appropriate objective measure for them. This resulted in a sample size of 30 participants. The 21 male and 9 female participants that were considered for the analysis were between the ages of 28 and 67 ($M = 46.27$ years, $SD = 11.38$). The participants were split into two groups, one without ATR ($n_{None\ ATR} = 16$) and the second with ATR during PAD ($n_{ATR} = 14$).

The monitoring behavior was assessed by the visual attention towards the road scene ahead in the different driving phases (BASELINE, PAD1, CAD and PAD2) and for the different PAD conditions with and without ATR. The left side displays with a boxplot diagram the mean values of the drivers' attention ratio to the road scene during the different driving phases. The mean value of the attention ratio to the road scene ahead is in PAD1 compared to the manual BASELINE for the group without ATR about 24.28 % and for the group with ATR about 31.82 % lower. In PAD1 no major effect of the ATR is visible, but the group with ATR shows a higher interquartile range (IQR) and the Median is lower than the 1st Quartile of the group without ATR. The monitoring behavior between PAD1 and CAD is distinguishable for both groups. The IQR increases for both groups from PAD1 to PAD2. The 1st Quartile for the group without ATR decreases from PAD1 (48.44 %) to PAD2 (36.68 %). This shows a decreasing monitoring behavior of the participants without ATR. Contrarily to this, the 3rd Quartile of the participants with ATR increases from PAD1 (60.46 %) to PAD2 (71.23 %) and represents an increasing monitoring behavior.

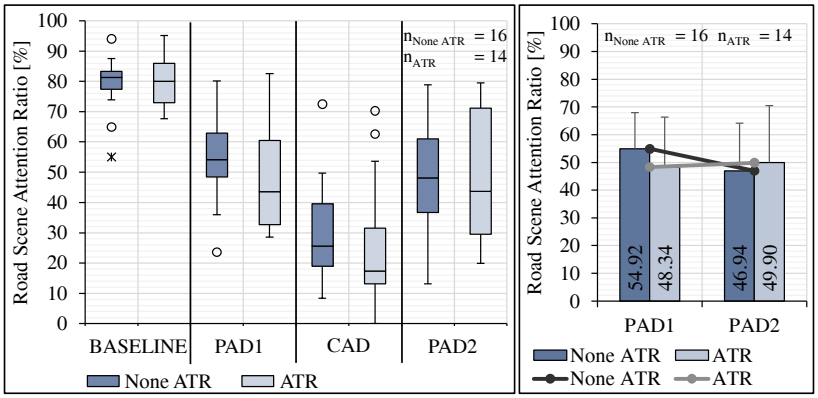

Figure 7. Boxplots for the percentage of glance time at the road scene ahead separated by condition for the simulator study. Whiskers represent upper/lower hinges ± 1.5*IQR. 1st Quartile represents, that 25 % of the values are lower. 3rd Quartile represents, that 75 % of the values are lower. Right: Development of the percentage of glance time at the road scene separated by condition for the simulator study.

The influence of the ATR on the visual attention to the road scene was also statistically analyzed. The two groups for PAD with and without ATR were the between-subject-factor and the measuring points PAD1 and PAD2 were the within-subject-factors, leading to a 2 x 2 analysis of variance. The development of the averages for both groups from PAD1 to PAD2 is shown in Figure 7 on the right side. The interaction effect for group and time of measure is significant ($F(1, 28) = 4.67$, $p = .039$). According to the development of the averages from PAD1 to PAD2 for both groups in the right diagram of Figure 7, this significant interaction effect shows, that the visual attention towards the road scene developed significantly different in dependence of the PAD-design with or without an ATR. The

averages also show that the visual attention for the group with ATR increases from PAD1 to PAD2 and decreases from PAD1 to PAD2 for the group without ATR.

Study 2 - Wizard-of-Oz study on public highway

49 participants were recruited in cooperation with a market research institute and received an appropriate monetary incentive. The participants did not work in the automotive industry and did not participate in an autonomous driving study 12 month prior to the study. $N = 7$ participants had to be excluded from the analysis due to technical problems with Dikablis. Another $n = 3$ participants were excluded from the analysis because variations of the surrounding traffic influenced the trust and the behavior of the participants essential, like for example cars that pass very close to the test vehicle. This resulted in a sample size of 39. The 21 male and 18 female participants considered for analysis were between the ages of 28 and 60 ($M = 45.15$ years, $SD = 9.30$). On average, they owned a driver's license for 26.74 years (SD = 9.32). The participants were split into two groups, one without ATR ($n_{None\ ATR} = 19$) and the second one with ATR during PAD ($n_{ATR} = 20$).

The monitoring behavior was assessed by the visual attention towards the road scene ahead in the different driving phases and for the different PAD conditions with and without ATR. The left side of Figure 8 displays with a boxplot diagram the mean values of the drivers' attention ratio to the road scene during the different driving phases. The mean values in PAD1 are for both groups approximately 9 % lower compared with the manual BASELINE. In PAD1 no major effect of the ATR is visible, however the group without ATR shows two outliers with very low attention ratio during PAD1. The IQR is increasing for the group without ATR from PAD1 (16.56) to PAD3 (29.64), also the minimum decreases to PAD3 (9.97 %). Contrary, the IQR for the group with ATR decreases from PAD1 (18.05) to PAD3 (12.64) and the minimum increases to PAD3 (59.97). The increase of the IQR for the participants without ATR shows a different monitoring behavior of the participants, due to some participants that monitored as good as the participants with ATR. However, in PAD3 at least 25 % of the participants without ATR showed a lower visual attention to the road scene than the minimum of the group with an ATR. The small IQR and absentee of outliers in PAD3 for the group with ATR shows, that there is a low variation in the monitoring behavior of the participants with an ATR. The monitoring behavior for both groups between PAD1 and CAD1 can be distinguished visually. Contrary to this is the difference between PAD3 and CAD3. For the group with ATR it can be clearly distinguished between the monitoring behavior for PAD3 and CAD3, due to no overlaps of the displayed boxplots. The participants without ATR show more similarities in the monitoring behavior for PAD3 and CAD3.

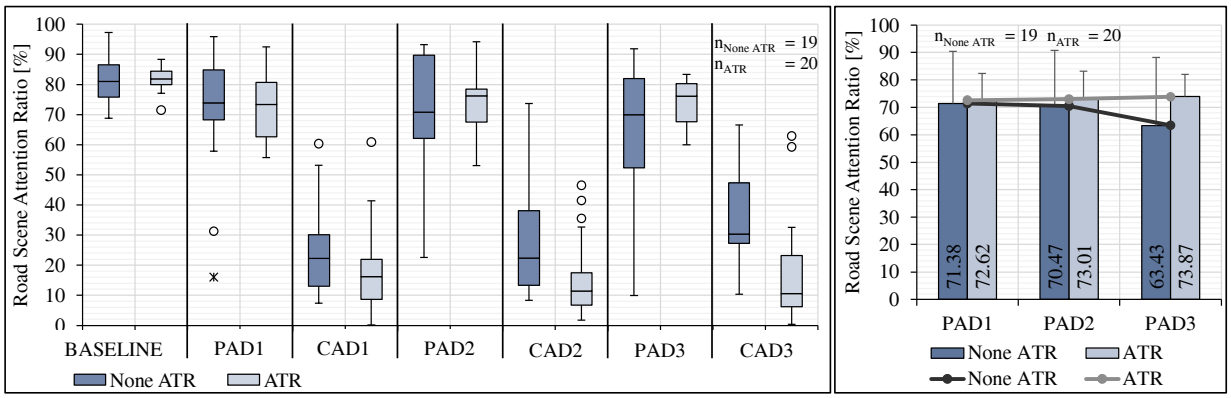

Figure 8. Boxplots for the percentage of glance time at the road scene ahead separated by condition for the Wizard of Oz study. Whiskers represent upper/lower hinges ± 1.5*IQR. 1st Quartile represents, that 25 % of the values are lower. 3rd Quartile represents, that 75 % of the values are lower. Right: Development of the percentage of glance time at the road scene separated by condition for the Wizard of Oz study.

The influence of the ATR on the visual attention to the road scene was also analyzed statistically. The two groups for PAD with and without ATR were the between-subject-factor and the measuring points PAD1, PAD2 and PAD3 were the within-subject-factors, that leads to a 2 x 3 analysis of variance. The development of the averages for both groups from PAD1 to PAD3 is shown in Figure 8 on the right side. The interaction effect for group and time of measure is significant ($F(1.47, 54.33) = 3.91$, $p = .038$). Mauchly's test indicated a violation of sphericity and a

Greenhouse-Geisser correction was applied. According to the development of the averages from PAD1 to PAD3 for both groups in the right diagram of Figure 8, this significant interaction effect shows, that the visual attention towards the road scene developed significantly different in dependence of the PAD-design with or without an ATR. The averages also show, that the visual attention to the rad scene increases for the group with ATR from PAD1 to PAD3 and decreases from PAD1 to PAD3 for the group without ATR.

The trust of the participants was assessed with a questionnaire (5-point-likert scale) prior to and after the test drive for each automation level with nine items from the standardized trust-questionnaire from Pöhler, Heine, and Deml [24]. Two participants from the group with ATR became no ATR during PAD, because they never took their eyes off the road for longer than 4 seconds during PAD. Consequently, for the evaluation of trust they are considered in the group without ATR, because the effect of the ATR should be investigated and they did not experience an ATR. The data was not normal distributed and therefore, statistically analyzed with a Mann-Whitney-U-Test for independent samples. There was no significant difference of trust in PAD prior to the test drive between the groups with and without ATR (z = -0.28, p = .777). After the test drive, the difference was investigated with a one-sided test as the hypothesis was directed. A significant different trust-level in PAD was found between the groups with and without ATR (z = -1.66, p = .049). According to the average values for the trust-level in Table 1, the participants with ATR had after the test drive a significant lower trust level in PAD than the participants without ATR.

Table 1.
Trust in automation: 5-point-likert scale from -2 (no trust) to 2 (high trust) questionnaire from Pöhler et al. (2016).

		Trust in automation			
		M	*SD*	*α*	*N*
Prior to the test drive	$PAD_{None\ ATR}$	0.99	0.55	.936	21
	PAD_{ATR}	0.98	0.41	.721	18
	$CAD_{None\ ATR}$	1.12	0.52	.815	21
	CAD_{ATR}	0.97	0.54	.815	18
Following the test drive	$PAD_{None\ ATR}$	1.66	0.40	.936	21
	PAD_{ATR}	1.49	0.35	.931	18
	$CAD_{None\ ATR}$	1.68	0.55	.911	21
	CAD_{ATR}	1.70	0.29	.849	18

Note. Average (*M*); Standard Deviation (*SD*); Cronbachs Alpha (*α*); Participants (*N*)

DISCUSSION

To contribute to the reliable operation of level 2 and 3 automation in one vehicle, the aim of this paper was to understand how to secure driver supervision engagement during PAD, while intermittent CAD-phases. The question was how to influence the gaze behavior of the driver that he or she maintains the eyes on the road and that the supervision task will not be neglected over time due to for example arising overtrust. During PAD it is necessary that the driver has to unmistakably understand that it is an assistance system that needs an active driver to lead and share control. Therefore, we investigated the question how to prompt operators of a car with different levels of automation to pay attention to the roadway during PAD if they neglect their supervision task and how to differentiate between different levels of automation in one vehicle.

In a dynamic driving simulator study and a Wizard-of-Oz study in real traffic the influence of a gaze direction based ATR during PAD was investigated to develop and adjust a correct mental model for the levels of automation, to maintain drivers' mode awareness and to avoid arising overtrust. The ATR should bring the drivers gaze back to the road scene ahead, if he/she stops monitoring the driving task or starts engaging in a NDRT during PAD.

In both studies a worst-case approach concerning the two different levels of automation was used meaning that PAD and CAD were both Hands-Off systems and had the same functionality. This worst-case approach is most suitable to investigate differences in mode awareness from a safety in use perspective as in that case it is very difficult for the driver to distinguish between similar levels of automation.
As we wanted to measure mode awareness and compare it between different drivers, it is necessary, that every driver has a comparable knowledge about the used levels of automation due to the fact that the mental model is an underlying construct of mode awareness and is affected by the users' knowledge and previous experience with the used levels of automation [15]. Consequently, in both studies every participant was instructed with a detailed description of the different levels of automation by video and text and the participants' knowledge about the levels of automation was controlled by the investigator.
We investigated the influence of the ATR on the visual attention to the road scene during PAD, on the change of the visual attention during the course of alternating PAD and CAD and on the trust in automation.

The results of the simulator study showed that the ATR can reduce the negative influence of an intermediating CAD phase and can help the driver to develop a more correct monitoring behavior during PAD. However, in PAD 1 no major effect of ATR was measured. We found that the group without ATR during PAD1 showed a slightly higher, but not significantly relevant visual attention to the road scene, compared to the group with ATR. This difference in PAD1 can have various reasons. One reason might be the individual driving-related risk-taking of the participants. One can conclude that the random classification of the participants in the groups with and without ATR is a worst-case approach, because it looks like that there are more people with higher driving-related risk-taking or a faster increasing overtrust in PAD in the group with ATR than in the group without ATR, hampering to find significant results.
However, the visual attention increased for the group with ATR from PAD1 to PAD2 and decreased for the group without ATR. The significant interaction effect shows that the ATR increased the visual attention to the road scene from PAD1 to PAD2 in spite of an intermittent CAD-phase.
Also in the Wizard-of-Oz study for the development of the visual attention to the road scene from PAD1 to PAD3 a significant interaction effect of the ATR was measured. Thus, the supervision behavior for the group with ATR increased whereas for the group without ATR it decreased. Consequently, the ATR influenced the development of the monitoring behavior during PAD and was improving it. The visual attention towards the road scene was similar in PAD1 for both groups, except of two outliers in the group without an ATR that showed a very low monitoring behavior during PAD1. From PAD1 to PAD3 more participants in the group without ATR showed a very low monitoring behavior, consequently the lower whiskers of the boxplot (1.5*IQR) included the outliers in PAD2 and PAD3. Contrary to this, there were no outliers during the PAD-phases for the group with ATR and the minimal visual attention to the road scene ahead was 59.97 % in PAD3, whereas the minimal attention ratio for the group without ATR was 9.97 %. For the group without ATR more than 25 % of the participants showed a low monitoring behavior during PAD3, whereas for the group with ATR the drivers showed a very high monitoring behavior in PAD3.
This shows, that also in the Wizard-of-Oz study the ATR helped to prompt drivers not to neglect their monitoring task. Moreover, the group without ATR showed an increasing IQR from PAD1 to PAD3 whereas the group without ATR had a decreasing IQR. Consequently, the ATR was able to counterbalance the negative influence of intermittent CAD-phases.
Furthermore, both studies showed that the ATR helped the drivers to distinguish between level 2 and level 3. The visual attention to the road scene showed that drivers with ATR could better distinguish between level 2 where they had to monitor the driving task and level 3 where they were allowed to engage in NDRT and where it was therefore not necessary to apply a high monitoring behavior. Especially, in the Wizard-of-Oz study in which drivers had due to the design of the study more frequent changes from PAD to CAD the effect of distinctiveness it can be clearly seen.
The monitoring behavior for the group with and without ATR between PAD1 and CAD1 can be distinguished visually. Contrary to this is the difference between PAD3 and CAD3. For the group with ATR it can clearly be distinguished between the monitoring behavior for PAD3 and CAD3, due to no overlaps of the displayed boxplots. The participants without ATR showed more similarities in the monitoring behavior for PAD3 and CAD3 as for them the borders became blurred. The results show that over time it became more and more difficult for the drivers do

distinguish between level 2 and 3 without any feedback of the system when they didn`t behave correctly. Whereas, for the drivers with ATR even after a while of driving in level 2 and level 3 automation mode PAD3 and CAD3 were still clearly distinguishable.
Thus, the ATR can help drivers to establish distinctiveness between level 2 and 3. The ATR can bring the drivers gaze back to the road scene ahead, if he/she stops monitoring the driving task or starts engaging in a NDRT during level 2.
Even though the mental model might not be exhaustive enough from beginning on or might be neglected over time the ATR can help the driver to develop and adjust a correct mental model for the levels of automation, to maintain drivers' mode awareness and to avoid arising overtrust.
Moreover, in the Wizard-of-Oz study participants' trust into the automated systems was conducted before and after the test drive by a questionnaire from Pöhler et al. (2016). The trust level in PAD and CAD before the test drive was similar for the group with and without ATR. By experiencing the PAD- and CAD-system during the test drive the trust level increased for both groups in PAD and in CAD. However, the participants that were in the group with ATR had a significant lower trust level in PAD after the test drive compared to the group without ATR. Thus, the ATR can help to calibrate an adequate trust level in PAD like it is required for the safe use of automated systems [4].

Conclusion

In two different study environments (dynamic driving simulator and real traffic) the gaze direction based ATR was proven to be an effective measure that can calibrate an adequate trust level and maintain mode awareness, if SAE level 2 systems (PAD) and SAE level 3 systems (CAD) are combined in one vehicle.
Hereby, the development of the visual attention towards the road scene during PAD increased in both studies for the group with ATR after an intermittent CAD-phase and decreased for the group without ATR. This difference in the development of the visual attention between the groups with and without ATR was significant.
This result helps to take the next step in the implementation of such combined multilevel systems for advanced driver assistance.

Limitations and Implications for Further Research

Despite the promising results, it has to be considered that the studies are only a first glance on the behaviors of the drivers, during their first contact with level 2 and level 3 systems. Further studies should investigate the long term effect of an ATR to evaluate whether it is effective in the long run.
Moreover, further research concerning the characteristics of the ATR is necessary. It might be for example helpful to introduce a stage before the investigated first stage of the ATR where a pop-up message appears in the instrument cluster, the LED-bars start to flash green and the indication sound chimes to increase the visual attention during level 2. One solution might be an additional silent announcement in the instrument cluster for example after 2 seconds eyes-off time that can encourage drivers to continuously monitor a level 2 automation system and helps to bring the drivers gaze more quickly back to the road scene. Furthermore, the ATR is based on purely visual distraction. However, another key component of driver engagement that should be investigated is the cognitive distraction. Attention and understanding are often implicitly mixed together in descriptions of monitoring. However, it might for example be possible that the driver looks at the road scene but can't act as he or she is cognitively distracted.
Moreover, in both studies every participant was instructed with a detailed description of the level 2 and 3 systems by video and text and the correct understanding was controlled by the instructor. This approach was necessary as we wanted that every driver has a comparable mental model about the used levels of automation to measure mode awareness and compare it between different drivers. But, further studies are necessary that investigate the effectiveness of the ATR without such a detailed instruction of the system.
Furthermore, in both studies PAD was implemented with a high reliability that was close to ideal and there were no situations during the PAD phases that would have reminded the drivers about their monitoring task. This worst case was chosen to investigate participants' behavior in full width, but it could also have caused the development of overreliance. Therefore, future studies should investigate whether overreliance also occurs in a more realistic system design.

ACKNOWLEDGEMENT
We thank Anna Feldhütter from the Chair of Ergonomics of the Technical University of Munich for the scientific support and the helpful amendments concerning the Wizard of Oz study that was conducted within a Master's thesis.

REFERENCES

[1] Sarter, N.B. and Woods, D.D. 1995. “How in the World Did We Ever Get into That Mode? Mode Error and Awareness in Supervisory Control.” Human factors, Vol. 37, No. 1, 5–19
[2] Feldhütter, A., Segler, C. and Bengler, K. 2018. “Does Shifting Between Conditionally and Partially Automated Driving Lead to a Loss of Mode Awareness?” In Advances in Human Aspects of Transportation: Proceedings of the AHFE 2017 International Conference on Human Factors in Transportation, (Los Angeles, California, July 17-21, 2017). 730–741
[3] Society of Automotive Engineers. 2016. "Taxonomy and Definitions for Terms Related to Driving Automation Systems for On-Road Motor Vehicles." SAE International, Warrensdale, PA
[4] Lee, J.D. and See, K.A. 2004. “Trust in automation: Designing for appropriate reliance.” Human Factors, Vol. 46, No. 1, 50–80
[5] Hoff, K.A. and Bashir, M. 2015. “Trust in automation: Integrating empirical evidence on factors that influence trust.” Human factors, Vol. 57, No. 3, 407–434
[6] Hergeth, S., Lorenz, L., Vilimek, R. and Krems, J.F. 2016. “Keep Your Scanners Peeled: Gaze Behavior as a Measure of Automation Trust During Highly Automated Driving.” Human factors, Vol. 58, No. 3, 509–519
[7] Hancock, P.A., Billings, D. R., Schaefer, K. E., Chen, J. Y., De Visser, E. J., and Parasuraman, R. 2011. “A meta-analysis of factors affecting trust in human-robot interaction.” Human factors, Vol. 53, No. 5, 517–527
[8] Endsley, M.R. 1995. “Toward a Theory of Situation Awareness in Dynamic Systems.” Human factors, Vol. 37, No. 1, 32–64
[9] Endsley, M.R. and Kiris, E.O. 1995. “The Out-of-the-Loop Performance Problem and Level of Control in Automation.” Human factors, Vol. 37, No. 2, 381–394
[10] Bainbridge, L. 1983. “Ironies of automation.” Automatica, Vol. 19, No. 6, 775–779
[11] Kolbig, M. and Müller, S., 2013. “Mode Awareness im Fahrkontext: Eine theoretische Betrachtung.” Grundlagen und Anwendungen der Mensch-Maschine-Interaktion, 1–8
[12] Othersen, I. 2016. “Vom Fahrer zum Denker und Teilzeitlenker: Einflussfaktoren und Gestaltungsmerkmale nutzerorientierter Interaktionskonzepte für die Überwachungsaufgabe des Fahrers im teilautomatisierten Modus.” AutoUni - Schriftenreihe, Volkswagen Aktiengesellschaft, Vol. 90, Ed.: Springer
[13] Bredereke, J. and Lankenau, A. 2005. “Safety-relevant mode confusions—modelling and reducing them.” Reliability Engineering & System Safety, Vol. 88, No. 3, 229–245
[14] Martens, M.H. and van den Beukel, A.P. 2013. “The road to automated driving: Dual mode and human factors considerations.” In 16th International IEEE Conference on Intelligent Transportation Systems (ITSC) (The Hague, The Netherlands, Oct. 6-9), 2262–2267
[15] Norman, D.A. 1983. “Some Observations on Mental Models.” In Mental Models, D. Gentner and A. L. Stevens, Eds., 7–14
[16] Parasuraman, R., Sheridan, T.B. and Wickens, C.D. 2008. “Situation Awareness, Mental Workload, and Trust in Automation: Viable, Empirically Supported Cognitive Engineering Constructs.” Journal of Cognitive Engineering and Decision Making, Vol. 2, No. 2, 140–160
[17] Parasuraman, R. and Manzey, D.H. 2010. “Complacency and bias in human use of automation: An attentional integration.” Human factors, Vol. 52, No. 3, 381–410
[18] ISO 15007-1:2015-03. 2015. "Straßenfahrzeuge – Messung des Blickverhaltens von Fahrern bei Fahrzeugen mit Fahrerinformations- und -assistenzsystemen."

[19] Klauer, S. G., Dingus, T. A., Neale, V. L., Sudweeks, J. D., and Ramsey, D. J. 2006. "The Impact of Driver Inattention on Near-Crash/Crash Risk: An Analysis Using the 100-Car Naturalistic Driving Study Data." National Highway Traffic Safety Administration, Ed.

[20] Blanco, M., Atwood, J., Vasquez, H. M., Trimble, T. E., Fitchett, V. L., Radlbeck, J. et al. 2015. "Human Factors Evaluation of Level 2 and Level 3 Automated Driving Concepts." Washington, DC, DOT HS 812 182

[21] Groves, P.M. and Thompson, R.F. 1970. "Habituation: A dual-process theory." Psychological Review, Vol. 77, No. 5, 419–450

[22] Körber, M., Cingel, A., Zimmermann, M. and Bengler, K. 2015. "Vigilance Decrement and Passive Fatigue Caused by Monotony in Automated Driving." Procedia Manufacturing, Vol. 3, 2403–2409

[23] Dahlbäck, N.Jönsson, A.and Ahrenberg, L. 1993. "WIZARD OF OZ STUDIES - WHY AND HOW." Knowledge-Based Systems, Vol. 6, No. 4, 258-266

[24] Pöhler, G., Heine, T. and Deml, B. 2016. "Itemanalyse und Faktorstruktur eines Fragebogens zur Messung von Vertrauen im Umgang mit automatischen Systemen." Zeitschrift für Arbeitswissenschaft, Vol. 70, No. 3, 151–160

COLLISION DETECTION USING ADAS SENSOR AND ITS EFFECT ON OCCUPANT INJURY

Kenyu, Okamura Hajime, Ohya Shinsuke, Odai
Honda R&D Co., Ltd. Automobile R&D Center
Japan

Paper Number 19-0248

ABSTRACT

In real world, Collisions which are faster than NCAP speed are occurring and fatality rate is high in such collisions. In order to solve such the high-speed collisions, it is important to increase the energy absorption amount of the occupant restraint devise. In order to increase the amount of energy absorption, it is necessary to detect the collision early and for the occupant to be restrained at an early timing

We focused on the integrated system using the advanced driver assistance systems (ADAS) sensor as a method to achieve the early airbag deployment timing. And we research whether the collision detection timing can become earlier and the occupant injury can be reduced.

A collision is predicted using the ADAS sensor, and the threshold of an airbag deployment is lowered just before the collision. Furthermore, by lowering the threshold only at the collision speed where an airbag deployment is required, it will prevent an airbag deployment at slight collisions. Also, the threshold is lowered until the rough road toughness can be secured. So the toughness of rough road traveling is equivalent to the conventional one.

For confirming the effect of this sensing system, we conducted simulation using LS-DYNA and the actual vehicle test. The airbag deployment timing was calculated by the simulation results.

In order to calculate the effect on the occupant injury, sled test was also conducted. The input data of floor G and the airbag deployment timing is the results of simulation.

From these results, it was found that the collision would be detected earlier than the conventional one. And we also confirmed the effect of reducing occupant injury.

INTRODUCTION

Front collisions occurring in real world have various collision modes, and the collision speed is various. Regarding the collision speed, the collision that exceed the crash speed of NCAP or regulations such as frontal 56 km/h and offset deformable barrier(ODB) 64 km/h have also occurred. [1][2]

Even if the speed of the own vehicle is low, if the opponent of the collision is a heavy vehicle, it will be a collision with a high ΔV collision. In this case, there is a severe collision similar to the case where own vehicle collides with rigid barrier at the high speed.

Even in such a high ΔV collision, reducing further occupant injury is a challenging point.

According to the results of analysis of the occupant injury factor at head-on collisions, it suggested that there are still many people who were injured by the vehicle body intrusion factor and the occupant restraint factor. [3]

Talking about the body intrusion factor, the body toughness has been improved by the progress of NCAP. Although the energy absorption of the device has also been improved in accordance with the progress of NCAP, further improvement of the energy absorption of the device is required for the occupant protection.

As a method of increasing the energy absorption of the device, there is a method of performing the occupant restraint from the early timing of the collision. One way to achieve that is to make the collision detection earlier.

In this paper, we devised the integrated system using the ADAS sensor. We call it ADAS integrated system. By predicting a collision using this ADAS sensor, we have studied realization of the collision detection at an earlier timing. We also confirmed the effect on the occupant protection performance due to the earlier collision detection.

In this paper, we call that the ignition timing of an airbag is TTF and the TTF of the ADAS integrated system is the early TTF.

METHODS

Conventional System

Generally, the conventional collision detection system uses several G sensors. Figure1 shows as an example. Honda also detects the collision with this method.

As a sensing system for frontal collisions, the SRSUnit is located at the center of the vehicle and satellite sensors are located in the frontal structural members of the vehicle. When the SRSunit detects floor G and it exceeds the collision determination threshold, it is determined that the airbag deployment is needed.

As a method of achieving TTF earlier using the conventional system, it is to lower the collision determination threshold.

In the conventional system, it is acquired three types of the data for setting the collision determination threshold. The first is the data of collision that needs the airbag deployment. We call it airbag ON collision. The second is the data where the airbag deployment is unnecessary. We call it airbag OFF collision. The third is the rough road traveling data. Figure.2 shows the schematic illustration of these waveforms.

These data are large in the following order, airbag ON collision, airbag OFF collision, rough road traveling. In the conventional system, the threshold is determined in the air bag OFF collision. If the threshold can change to low, it will be possible to achieve an earlier TTF than the conventional system.

However, if the threshold changes to low, the airbag deploy in the airbag OFF collision. Therefore, we devised the ADAS integrated system that predicts a collision with the ADAS sensor and the SRS sensor system in order to lower the threshold just before the collision that needs the airbag deployment.

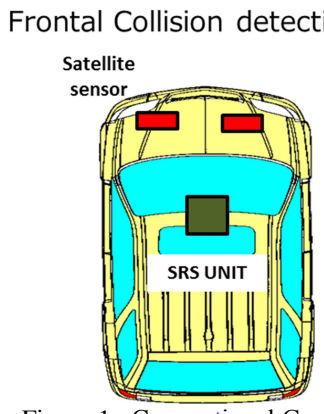

Figure 1. Conventional G sensor system

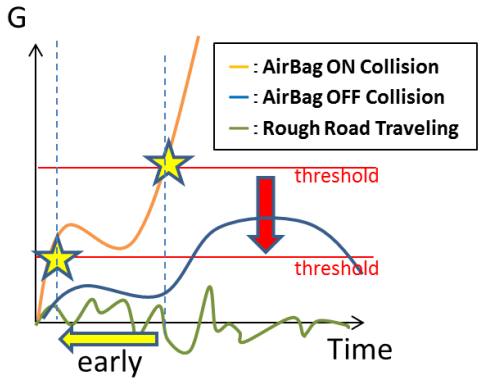

Figure 2. An image of the waveform necessary for the threshold setting

ADAS Integrated System

The overview is shown in Figure 3. The ADAS integrated system has the one radar and the one monocular camera. And it also uses its own vehicle information such as the vehicle speed.

In the prediction method, the ADAS sensor will recognize the kind of object, the relative distance and the relative speed of the opponent. Assuming that the relative speed will continue until the collision, the timing at which the vehicle will pass by the relative distance and the relative speed in the longitudinal direction of the vehicle will be calculated. Furthermore, the amount of the overlap at which the vehicle passes from the relative distance and the relative speed in the vehicle lateral direction will be calculated.

If there is overlap amount with own vehicle, since there is a possibility of collision, the collision prediction flag is set to ON. This flag is always sent in the CAN cycle, and the reliability of the data is checked by continuity of the flag. If it is determined that the flag is highly reliable information and it is determined that the flag is the last flag before the collision, the collision prediction decision flag is set. We call the flag Pre-CDS (Pre-Collision Detection Signal). The SRS sensor system always checks the Pre-CDS and the SRS sensor system immediately lower the threshold when it detects the Pre-CDS.

In addition, as activating condition of the ADAS integrated system, it is added that the own vehicle speed is 40 km/h or more in the mode of the collision to object and the relative speed is 80 km/h or more in the CarToCar collision.

If this system does activate when the own vehicle speed is low, there is a possibility that the airbag may deploy even with a slight collision which does not require the airbag deployment. In order to prevent this situation, the ADAS integrated system has this activating condition.

In this paper, the collision determination threshold is lowered to the level at which the airbag OFF is secured in the rough road traveling.

Although it is the system that lower the threshold immediately just before a collision, considering the CAN cycle and measurement error, it is conceivable that the threshold is lowered for several 100 msec before the collision.

For this time, even if the vehicle passes through pothole, curbstone or like these object, the ADAS integrated system is kept to ensure the airbag OFF. As a result, the real world toughness is equivalent to the conventional system.

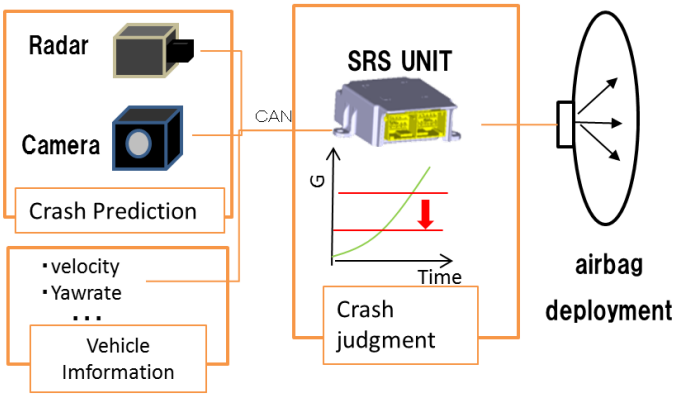

Figure 3. Overview of the ADAS integrated system

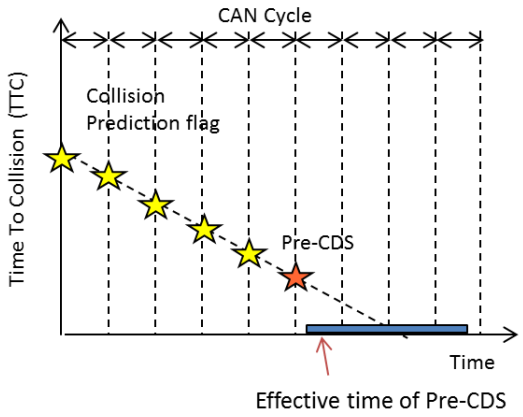

Figure 4. Image of the CAN cycle and the Pre-CDS flag

Performance of Recognition of ADAS Sensor

The point is whether the radar and the camera can recognize the object until just before the collision. This is the reason why the collision threshold is lowered just before the collision. We confirmed the recognition performance of an oncoming vehicle using mass production radar. The radar is located on the end of the cart. The cart passed through the side of the actual vehicle at 50km/h. Figure 5 shows the radar test condition and the data of this test.

It corresponds to the situation when a vehicle whose the radar is located in the center of the vehicle collided with 50% overlap. Figure 5 shows the radar data. The horizontal axis shows the true time until passing and the vertical axis is the passing time calculated by the radar.

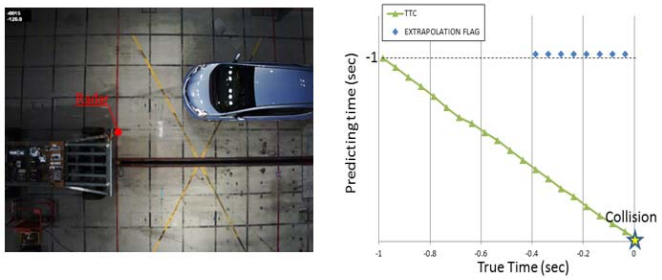

Figure 5. Radar test condition and the data of this test

The main focus point of this data is whether the vehicle can be recognized or not just before the collision. According to the data, extrapolation occurs just before the collision. Therefore, as reliable data, the information about 400 msec before the collision is the last information of the radar. From this fact, it may be impossible to detect the object for 400 msec before collision, but the travel distance during this time of period is only about 5 meter. So it is sufficient as the recognition performance before the collision, because it is considered that the situation does not change while traveling the distance of about 5meter. For the recognition performance of the camera, we also tested on the image processing software where the machine learning was conducted. The right side of Figure 6 is the recognition result assuming just before the collision. Although the vehicle is large relative to the whole image, it was found that recognition is possible.

Figure 6. Camera recognition test the right picture is assumed just before the collision

Calculation of TTF Using ADAS Integrated System

The threshold at the time of receiving the Pre-CDS is lowered to the airbag OFF during the rough road traveling. Therefore, when calculating the early TTF of the ADAS integrated system, it is an important that how much threshold is lower than the conventional threshold.

We used the rough road traveling data acquired by the actual vehicle test. It was assumed that the rough road data was the same as the pothole and curbstone modes. The test speed was selected to meet the conditions that the alignment of the vehicle change and the tire burst occurs.

The collision data for calculating the TTF was obtained from the simulation data with LS-DYNA and some actual vehicle test data.

In addition, in order to verify whether the ADAS integrated system is widely effective, the study was carried out on two models.

RESULTS

Results of Small Size Sedan

Figure 7 shows the rough road data acquired by the actual vehicle test. The conventional threshold is the red line. The value was decided by the airbag off collision.

In the ADAS integrated system, the airbag off is a target in rough road traveling. Therefore, it becomes the blue line. This is the 44% threshold lower than the conventional threshold.

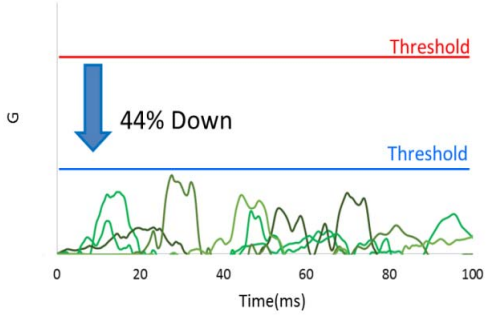

Figure 7. The data on rough road traveling and the threshold

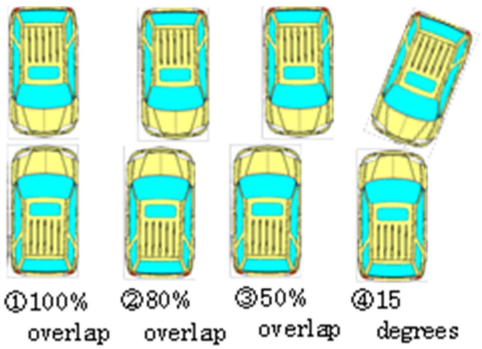

Figure 8. Collision modes and mode No. of the simulation

In order to confirm the effect on the TTF, simulation was conducted in the modes 1 to 4 shown in Figure 8. The collision speed was 60 km/h.

As the mode 5, we confirmed the effect of the TTF in the actual vehicle CarToCar test with 50% overlap and collision speed of 50 km/h. In this collision, the opponent vehicle selected a heavier vehicle. As the result, this actual vehicle test has ΔV which is equivalent to the simulation of 60 km/h CarToCar. In these modes, the calculation results of the TTF are shown in Figure 9.

Depending on the collision mode, there was the change of about 7 msec to 13 msec earlier.

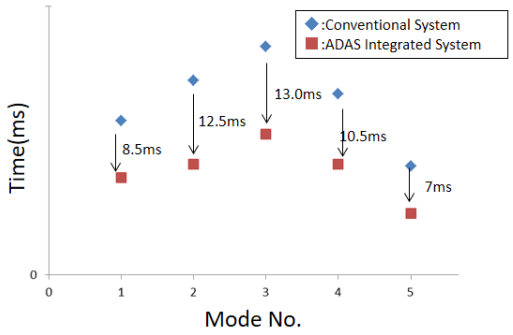

Figure 9. Difference between the TTF of the ADAS integrated system and the conventional TTF

Results of Middle Size Sedan

The test data of the rough road traveling in this vehicle is shown in Figure 10. The red line is the conventional threshold, and the blue line is set based on the rough road traveling data. In this vehicle, the threshold was lowered by 64%.

In order to confirm the effect on the TTF, the simulation was conducted in the CarToCar and the mode in which the vehicle collided with a fixed object. Figure 11 shows these simulation modes. The collision speed was 40 km/h, 50 km/h, 60 km/h and 70 km/h.

By using the ADAS integrated system, Table 1 shows the amount of TTF earlier than the conventional system. Depending on the mode, at the collision speed of 50 km/h or more, it is about 7 to 15 msec earlier. At the collision speed of 40 km/h, it was earlier than 50 km/h.

Compared to the small size sedan, the middle size sedan had similar results. From this, it is considered that the ADAS integrated system can be widely effective.

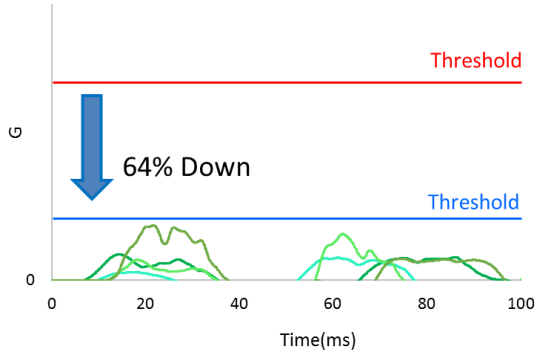

Figure 10. The data on rough road traveling and the threshold

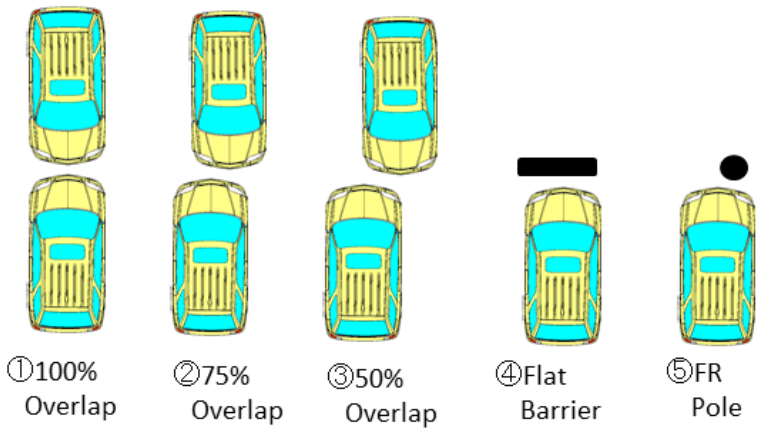

Figure 11. Collision modes and mode No. of the simulation

Table 1. Difference between TTF of ADAS integrated system and conventional one

Unit: msec.

mode No	40km/h	50km/h	60km/h	70km/h
CarToCar100% OverLap	21.5	13.2	11.6	7.1
CarToCar75% OverLap	19.6	14.8	13.1	11.6
CarToCar50% OverLap	19.4	13.2	11.2	9.2
Flat Barrier	19.4	13.1	11.3	7.1
FR Pole	34.6	15.9	13.3	11.6

Effect on Occupant Injury

By achieving the early TTF, it was confirmed that whether the initial constrained could be increased and the occupant injury could be reduced by the sled test. It was confirmed by conducting the sled test.

In the sled test, the floor G of mode 2 in Figure 8 was used. In this study, the large amount of overlap collision was selected because it was severe collision. On the other hand, considering the real world, the number of accidents with 100% overlap is small. Therefore, 80% overlap collision was selected. The occupant injury was compared in this test using the TTF of the conventional system and the ADAS integrated system.

Since the effect on the head injury was expected by the early TTF, we focused on the head injury. The sled test and the head G-Strokes(S) are shown in Figure 12. When comparing the head G-S, the head G decreased. Calculating the HIC, it decreased by 27%. In addition, the head restraint was made from the initial timing of the collision, so that the head stroke decreased because the energy absorption of the device increased.

From this, the ADAS integrated system is effective for the occupant protection performance.

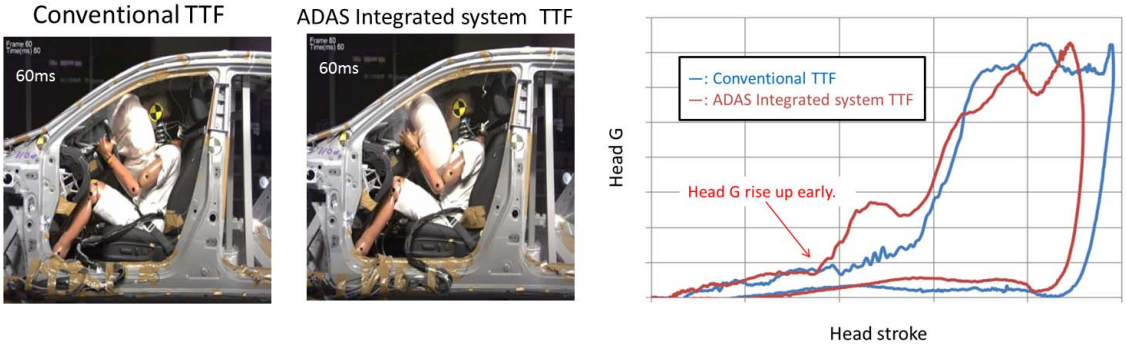

Figure 12. Sled test at 60ms and the results of the head G-S

DISCUSSION

According to the evolution of ADAS in the future, if the rough road can be detected, there is a possibility that the threshold may further be lowered because it is not necessary to secure the rough road toughness. If a sensor for ADAS alone can detect a frontal collision with high reliability, it may be possible to deploy an airbag before collision.

There is the mass production system which detect a side impact before the impact and deploy an airbag. [4]

We investigated whether there is an effect on occupant injury by achieving further early TTF. We made a comparison by simulation using MADYMO. The simulation was conducted in the mode 3 in Figure8.

Figure 13 shows the simulation results. The HIC in the TTF of the conventional system is set to 1. The results indicated that the HIC also can decrease, as the TTF gets earlier.

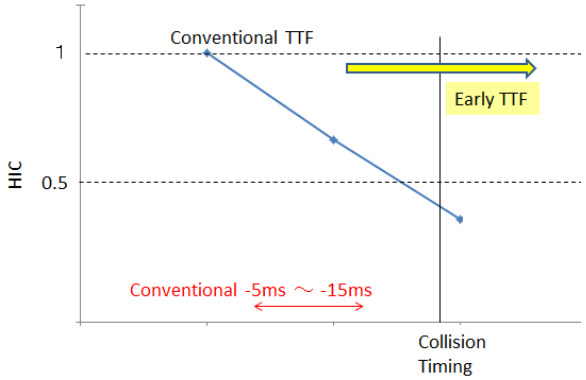

Figure 13. The early amount of the TTF and reduction of the HIC

CONCLUSIONS

By using the ADAS integrated system, it was found that the collision detection was possible at the earlier timing than the conventional system. Although it depends on the collision modes, the TTF can be made form about 7 msec to 16 msec earlier than the conventional TTF in the mode of the collision of 50 km/h or more. In addition, it is considered to be widely effective system because it was confirmed in two car models and it had the similar effect.

As the results of the early TTF, we can also confirm reduction of occupant injury due to increase of the initial constraint and increase of the energy absorption amount of the device.

REFERENCES

[1] The features such as fatal traffic accidents in 2018. Retrieve March 6,2019 from http://www.npa.go.jp/publications/statistics/koutsuu/jiko/H30sibou_tokucyo.pdf

[2] Institute for Traffic Accident Research and Data Analysis. (2010). Collision accident to fixed object of automobile, ITARDA information.No82.

[3] Matthew, L. B., & David, S. Z. (2009). IMPACT AND INJURY PATTERNS IN FRONTAL CRASHES OF VEHICLES WITH GOOD RATINGS, *21th International Technical Conference on the Enhanced Safety of Vehicles (ESV),* Paper No. 09-0257

[4] Rodolfo et al. (2017).Effectiveness Potential of PRE-SAFE Impulse Using the Scenario of a Major Accident at an Intersection as an Example. *25th International Technical Conference on the Enhanced Safety of Vehicles (ESV),* Paper Number 17-0252

INFLUENCE OF SEATING POSITION ON OCCUPANT'S INJURY CRITERIA

Tatsuya Asai, Shinsuke Odai, Hiroyuki Ito, Osamu Kanno
Honda R&D Co., Ltd. Automobile R&D Center
Japan

Paper Number 19-0249

ABSTRACT

The number of fatalities in traffic accidents has been reduced continuously. One of the factors for such reduction may be improvement of safety devices. However, though total number of deaths has been reduced, many lives are still lost in traffic accidents. Nearly half of the deaths while driving automobile is in frontal crash. On the other hand, driver seating position is variable and the distance between the occupant and occupant restraint system becomes longer in rearmost position (RM) than mid position (MP) of seat slide, resulting in a delay of occupant restraint onset. Because of the delay of occupant restraint, pelvis restraint is also delayed and pelvis displacement increases. At that time, the motion of pelvis increases the tension of lap belt and it is transferred to the inboard shoulder belt through the thorough tongue. Tension in inboard shoulder belt increases the loading to the lower rib cage and may increase the risk of chest injury. This research examined the influence of seating in RM position to the occupant's lower thorax injury and the influence on lower thorax injury by controlling pelvis behaviors in RM position. In this study, finite element (FE) simulations of the sled test in flat56km/h were conducted in MP and RM seat positions. Firstly, it was confirmed that the tension of the lap belt caused by pelvis motion transferred to the inboard shoulder belt and it compressed lower rib cage. Especially it seemed to occur in RM. Secondly, simulation was conducted by changing constraint conditions on pelvis translation and lateral axis rotation to confirm the effect on injury criteria in RM. Since the distance between the instrument panel and the occupant became longer in RM, knees were not constrained by instrument panel(IN-PNE), therefore chest deflection increased. It is confirmed that the lap belt tension was increased with the pelvis forward motion caused by reduction of restraint force, and the tension transferred to the shoulder belt, and consequently the deflection of the lower rib cage was increased. By constraining pelvis translation or rotation, or both of them, the constraint of the pelvis was improved and the chest deflection decreased in each condition. In case of fixing translation and rotation, there was an increase in acceleration of the pelvis and acceleration of T12 also increased through the lumbar spine. Therefore, chest deflection was reduced. In terms of the effect to the tension of seat-belt, there was not transferring of the tension to the shoulder belt from the lap belt. Since the tension of the shoulder belt decreased after 80ms, it was seen that loading to the chest from shoulder belt decreased. It was found that in order to reduce chest deflection in lower right side, it is effective not only reducing the load from inboard shoulder belt but also increasing a degree of constraint on the lumbar spine. Loading to the chest from the inboard shoulder belt was able to be reduced by suppressing pelvis rotation and it was effective to reduce chest deflection further.

INTRODUCTION

Regulation or assessment for vehicle safety has been revised in each country or region and evaluation standard has become strict. OEMs or suppliers have continuously improved the safety performance of their products to adapt to such standards or to obtain good ratings in assessment, which has been resulting in a certain decrease of fatal accidents. National Police Agency [1] published the total number of deaths in traffic accident in 2018 was the least as far as the statistics in Japan, while they addressed further effort should be necessary to save more lives from significant accident. Traffic Statistics [2] showed nearly half of the deaths in car drivers is in frontal crash.

On the other hand, in many cases, the seats in the first row of automobile have a mechanism of seat-slide for adjusting the seat position from front-most (FM) to rearmost (RM). Since this mechanism allows occupants a wide range of seating position, car driver's seating position becomes variable. When the driver sits on the seat at the RM position, a driver airbag (DAB) and an instrument panel (IN-PNE) becomes farther than the mid- point (MP) of the seat-slide. According to the sled tests conducted by Yaguchi et al. [3] in FMVSS208 and UMTRI seating position, the femoral forces in the case of UMTRI position that was 49mm rearward from MP arose later. Moreover, since it affects the restraint to the pelvis to increases its forward displacement, it could be considered that the tension of the lap belt increases. Then the tension is transferred to the inboard shoulder belt and it compresses the lower rib cage. It was considered that this tendency appeared strongly in the case of RM. Kemper et al. [4] performed dynamic belt loading on PMHS thoraces and confirmed fractures occurred on the inboard side of lower rib cage where the shoulder belt passed first. Shimamura et al. [5] analyzed the detailed data on traffic accidents and reported that the locations of rib fracture were observed more in the lower parts of the thorax. Kent et al. [6] reported that the presence of rib fractures was associated with a significant increase fatality risk, and chest injury was a serious issue. This research examined the influence of seating in RM position to the occupant's lower thorax injury and the influence on lower thorax injury by controlling pelvis behaviors in RM seating position.

METHODS

In this study, finite element (FE) simulations of sled test were conducted in order to confirm that the tension of the lap belt caused by the increase of pelvis displacement was transferred to the inboard shoulder belt and compressed the lower rib cage. Moreover, how the occupant changed by this effect was also investigated. THOR-Metric finite element (FE) Mode v1.4 developed by Humanetics Innovative Solutions, Inc were used on LS-DYNA R6.1.2 FE code. A collision pulse of a middle size sedan in flat barrier 56km/h test was used for a sled pulse. DAB, seat-belt, IN-PNE and other interior parts were also the same as that vehicle. Firstly, the dummy model was settled on MP or RM of the seat slide range and each calculated result was compared. The seat back angle was set to 22 deg. and the seat height was set to the lower-most position of the adjustable range. Figure 1. shows the seating postures of the dummy models in MP and RM. Accelerometers at the thoracic spine and pelvis, an angular velocity sensor was used to see occupant behaviors. These measurement locations in the dummy structure are shown in Figure 2. For polarity of pelvis angle, the posterior inclination side was defined as positive and the anterior inclination side was defined as negative as shown in Figure 3. Moreover, IR-TRACC

in the lower right side thorax installed in THOR dummy was used for evaluating injury criteria of lower rib cage in case of MP and RM. In order to see the interaction between the lap and shoulder belts due to the pelvis behavior, the tensions of the lap and inboard shoulder belts were used.

Secondly, simulation was conducted by changing pelvis constraint conditions of translation and rotation around the lateral axis to see the tendency of injury criteria reduction due to pelvis constraint in RM seating position. Table.1 shows the simulation matrix. Three constraint conditions of the pelvis were defined. First the translational motion of the hip point (H.P) relative to the center of the seat back recliner was fixed, defined as 'slide fixed' (SF), and second, the rotation around the lateral axis at H.P. was fixed, defined as 'rotation fixed' (RF). Final, both of them were fixed, defined as 'slide and rotation fixed' (SRF).

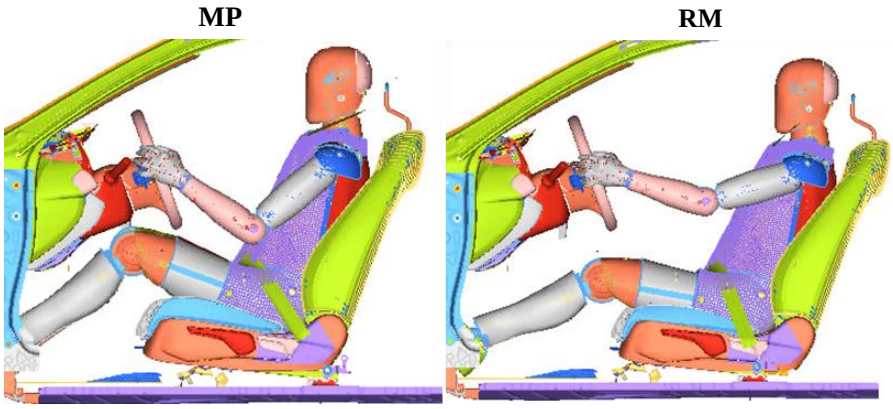

Figure 1. Setups of sled simulation in MP and RM seat positions

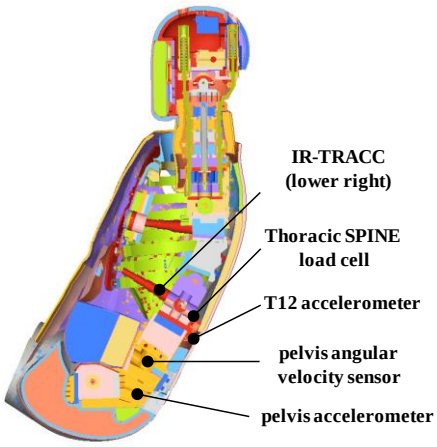

Figure 2. Measurement location in THOR dummy structure

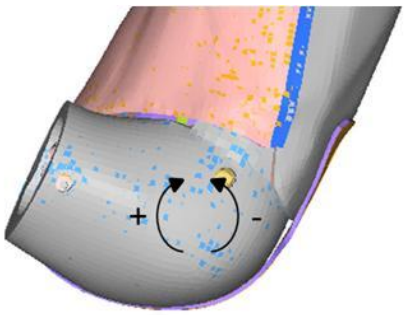

Figure 3. Polarity of pelvis angle

Table 1. Sled simulation condition

	Slide fixed	Rotation fixed
Base CAE (RM)	–	–
CAE No.1 slide fixed (SF)	○	–
CAE No.2 rotation fixed (RF)	–	○
CAE No.3 slide & rotation fixed SRF)	○	○

RESULT

Comparing of MP and RM

The restraint conditions at the time when the dummy was restrained by the DAB in MP and RM conditions are shown in Figure 4. Time histories of the acceleration of spine and pelvis, and pelvis angle, chest deflection, shoulder belt tension, and lap belt tension are shown in Figures 5–10. By increasing the distance between the IN-PNE and the occupant in RM seating position, the results show that knees were not constrained by the IN-PNE (Figure 4). In RM seating position, the tension of the lap belt rapidly increased from 60 ms (Figure 9), slightly later than the lap belt, the tension of shoulder belt also increased (Figure 10), the pelvis rotates to the posterior inclination from 40 ms (Figure 8) and acceleration of the pelvis increased greatly from 60 ms (Figure 6). With T12 as well, acceleration of T12 increased greatly from 60 ms (Figure 5), and chest deflection also increased (Figure 7).

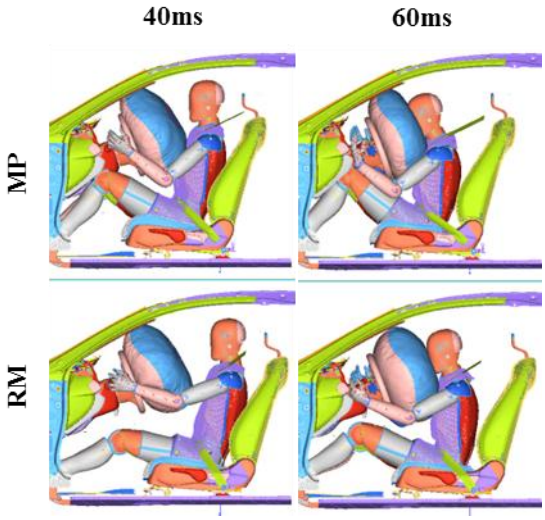

Figure 4. Restraint condition at the time when the dummy was restrained by the DAB in MP and RM

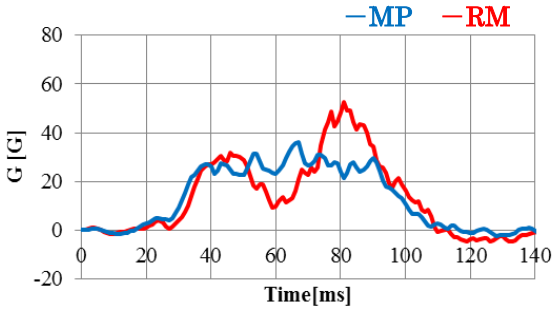

Figure 5. Time histories of T12 accelerometer (X direction) in MP and RM

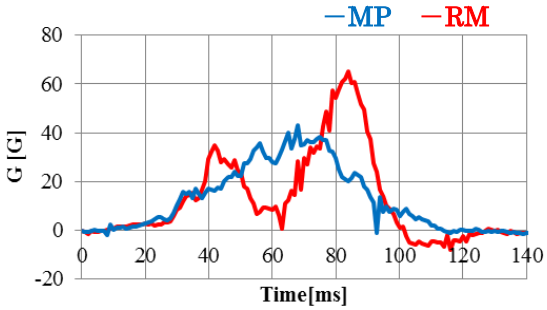

Figure 6. Time histories of pelvis accelerometer (X direction) in MP and RM

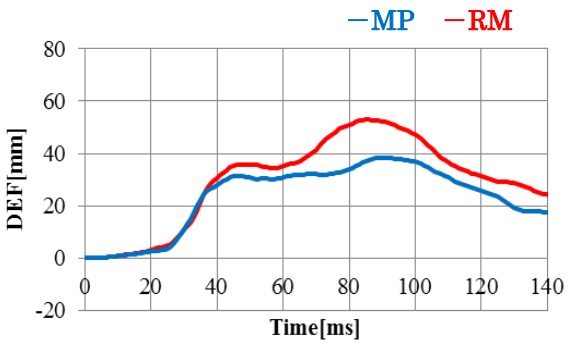

Figure 7. Time histories of chest deflection (lower right) in MP and RM

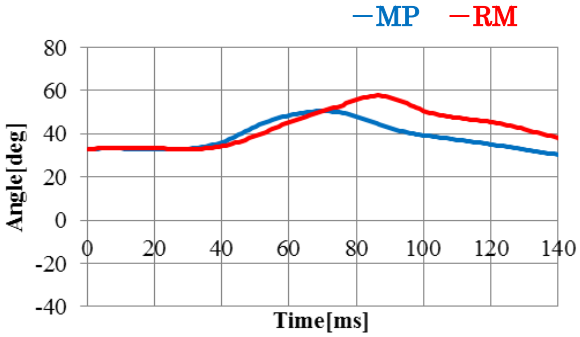

Figure 8. Time histories of pelvis angle in MP and RM

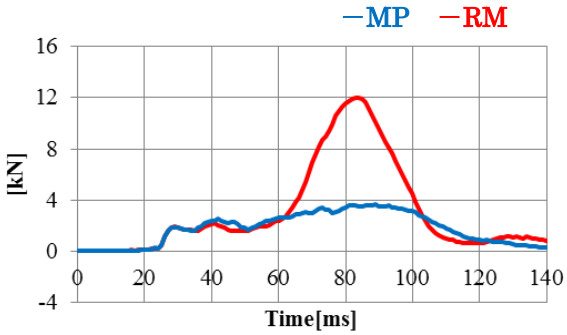

Figure 9. Time histories of the lap belt forces in MP and RM

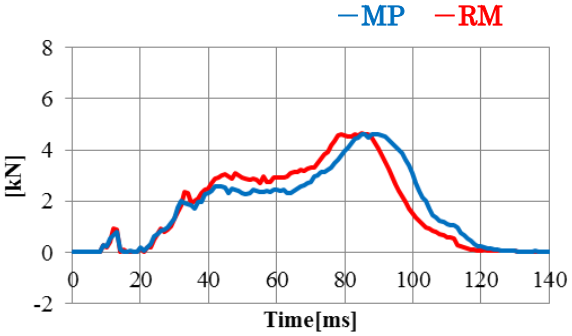

Figure 10. Time histories of the inboard shoulder belt forces in MP and RM

Investigation of the reduction effect on injury criteria by restraining the pelvis.

The effect on chest deflection by changing constraint conditions of the pelvis in RM seating position was investigated.

CAE No.1 slide fixed (SF): Figure 11 shows the restraint conditions at the time when the Pelvis started to rotate and at the time of maximum chest deflection value in RM and SF. Figures 12–15 show the time histories of the acceleration of spine and pelvis, the pelvis angle and chest deflection. Because the translation motion of the pelvis was fixed in SF, acceleration of pelvis increased at 10–30 ms and decreased at 80 ms compared to RM (Figure 13). In SF condition, the pelvis started to rotate to the anterior inclination from about 30 ms together with the seat deformation and got larger from 60 ms (Figure 15), it was confirmed that acceleration of T12 increased at 10–30 ms (Figure 12). Chest deflection greatly decreased at 40–60 ms and the peak value also decreased (Figure 14).

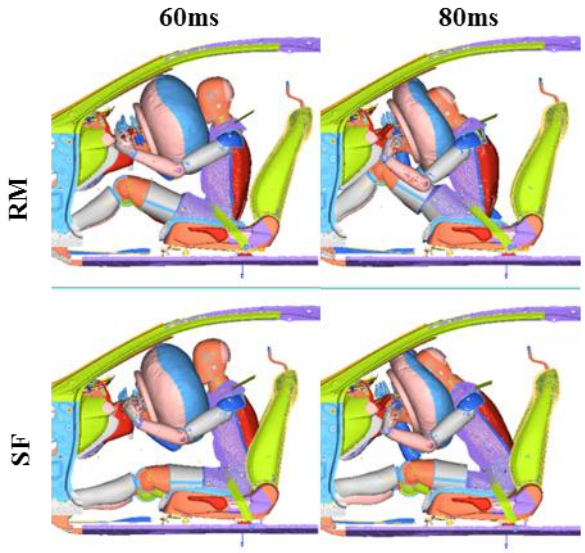

Figure 11. Restraint conditions at the time when the pelvis started to rotate and at the time of maximum chest deflection value in RM and SF.

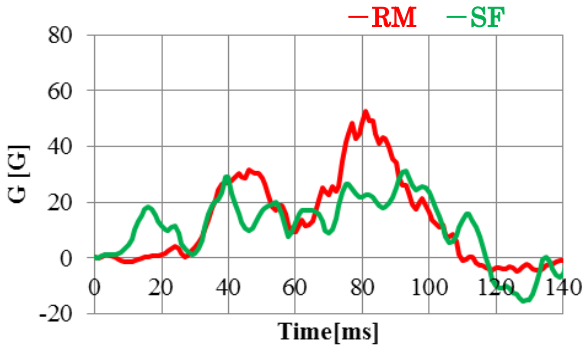

Figure 12. Time histories of T12 accelerometer (X direction) in RM and SF

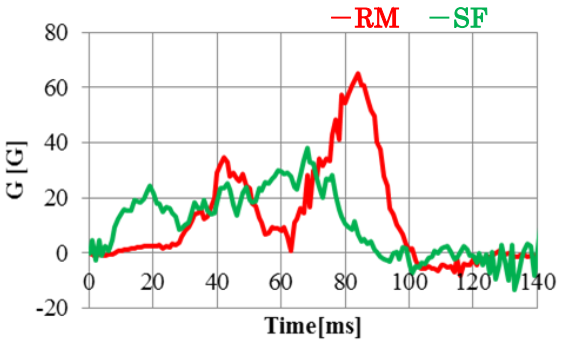

Figure 13. Time histories of pelvis accelerometer (X direction) in RM and SF

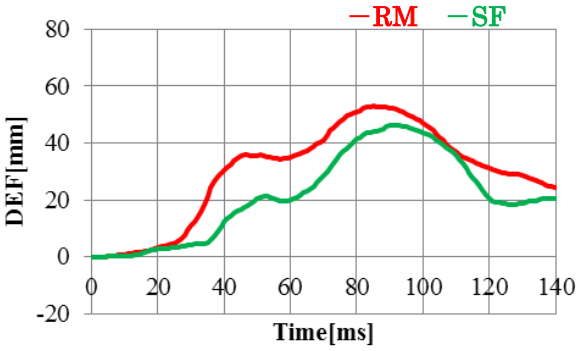

Figure 14. Time histories of chest deflection (lower right) in RM and SF

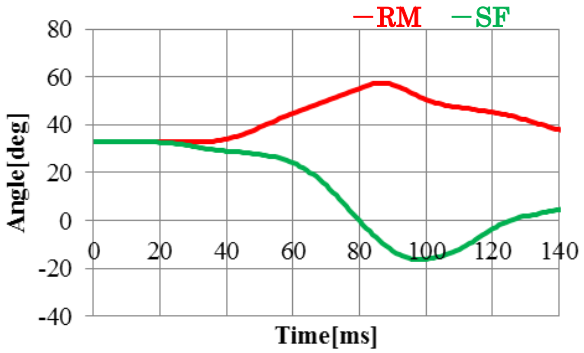

Figure 15. Time histories of pelvis angle in RM and SF

CAE No.2 rotation fixed(RF): Figure 16 shows the restraint conditions at the time when the pelvis started to rotate and at the time of maximum chest deflection in RM and RF. Figures 17-20 show time histories of spine and pelvis acceleration, the pelvis angle and chest deflection. Because the rotation motion of the pelvis was fixed in RF, acceleration of pelvis increased at 50ms (Figure 18). The pelvis rotated to the anterior side in RF relative to RM (Figure 20). In RF condition, acceleration of T12 decreased at around 40ms (Figure 17) and chest deflection slightly increased at around 40ms（Figure 19) compared to RM.

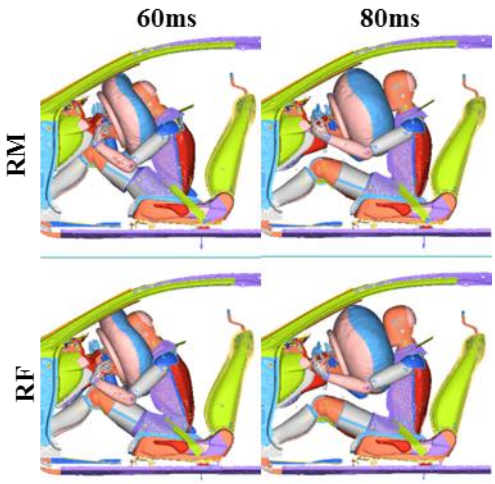

Figure 16. Restraint conditions at the time when the pelvis started to rotate and at the time of maximum chest deflection value in RM and RF.

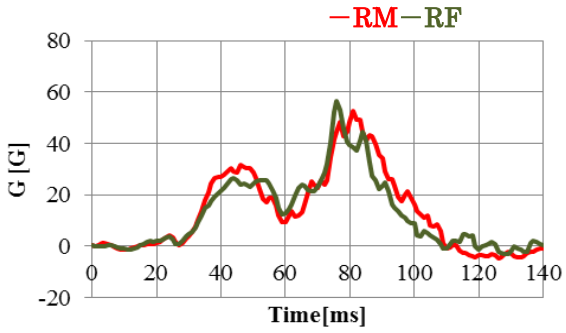

Figure 17. Time histories of T12 accelerometer (X direction) in RM and RF

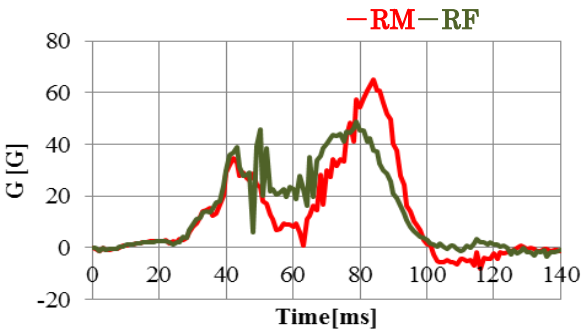

Figure 18. Time histories of pelvis accelerometer (X direction) in RM and RF

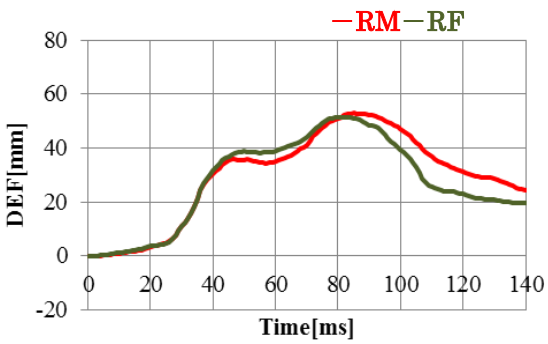

Figure 19. Time histories of chest deflection (lower right) in RM and RF

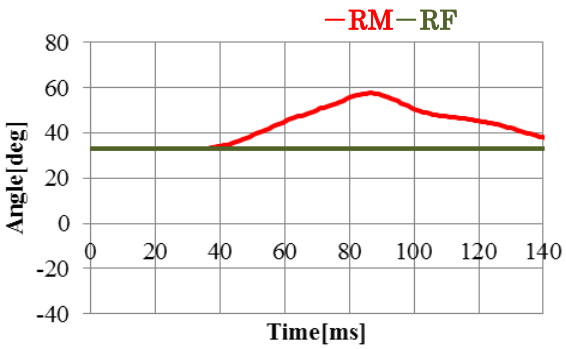

Figure 20. Time histories of pelvis angle in RM and RF

CAE No.3 slide and rotation fixed (SRF): Figure 21 shows the restraint conditions at the time when pelvis started to rotate and at the time of maximum chest deflection in RM and SRF. Figures 22- 25 show time histories of spine and pelvis acceleration, the pelvis angle and chest deflection. Because the translation and rotation motion of pelvis were fixed in SRF, acceleration of pelvis increased at 10-30ms and decreased at 80ms compared to RM (Figure 23). In SRF condition, the pelvis started to rotate to the anterior inclination from about 20 ms together with the seat deformation (Figure 25), acceleration of T12 increased at 10–30 ms (Figure 22). Increase of chest deflection from 60ms did not appear in RSF while it appeared in RM (Figure 24).

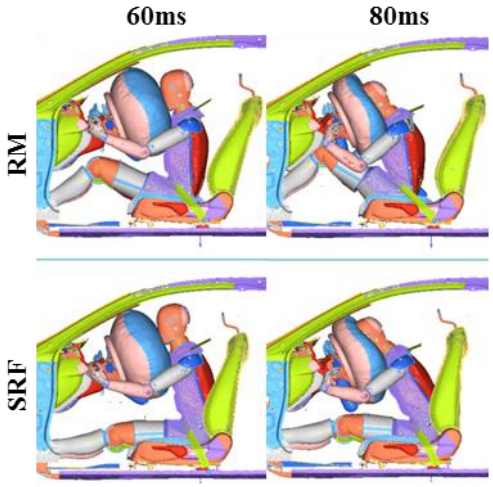

Figure 21. Restraint conditions at the time when pelvis started to rotate and at the time of maximum chest deflection in RM and SRF

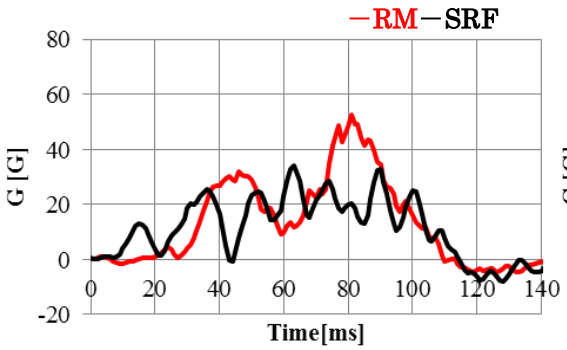

Figure 22. Time histories of T12 accelerometer(X direction) in RM and SRF

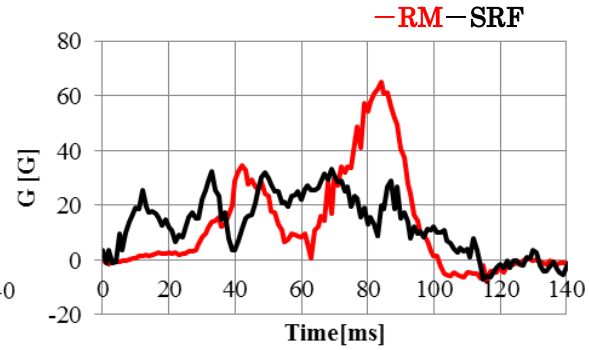

Figure 23. Time histories of pelvis accelerometer(X direction) in RM and SRF

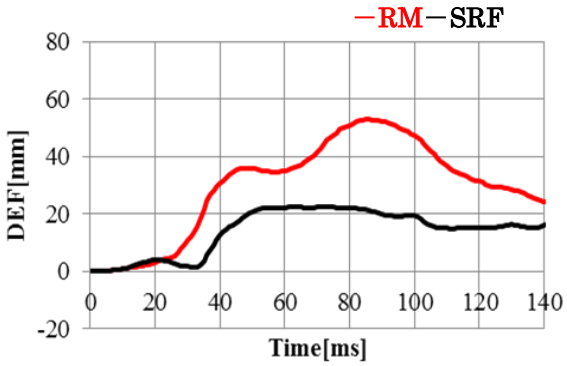

Figure 24. Time histories of chest deflection (lower right) in RM and SRF

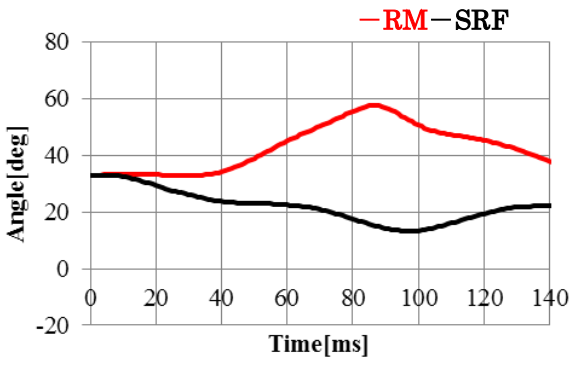

Figure 25. Time histories of pelvis angle in RM and SRF

DISCUSSION

It was discussed that how the difference of seating position and pelvis constrained condition effected to upper body. Comparing MP and RM, because the knees were not restrained by IN-PNE, the lap belt restrained the pelvis in RM (Figure 4, 9). As the RM results showed, it was confirmed that because the pelvis was not restrained and it started forward displacement at initial timing, the lap belt tension increased. Then the tension was transferred to the shoulder belt through the through tongue (Figure 9, 10), and as a result, chest deflection was increased. On the other hand, the increase in chest deflection before 60 ms was caused by decreasing acceleration of T12, which was result from the delay in restraining of the pelvis (Figure 5, 6). To check the effect of the pelvis rotation on the upper body, thoracic load cell shown in Figure 2 was used. The polarity is shown in Fig.26. Although the pelvis rotated to the posterior inclination, the force toward the back of the spine worked together with the rotation of the pelvis as shown in Figure 27, there appeared to be an effect of suppressing the displacement of the upper body. Particularly in RM, the knees were not restrained by the IN-PNE, so the pelvis rotated more to the posterior inclination than in the case of MP, and the effect of suppressing displacement of the upper body was also greater (Figure 8, 27). This made it clear that the delay in pelvis restraint and the behavior resulting from pelvis rotation had an effect on T12 and chest deflection through the lumbar spine.

Therefore the effect of controlling pelvis behavior to T12 and chest deflection thorough lumbar spine was focused on.

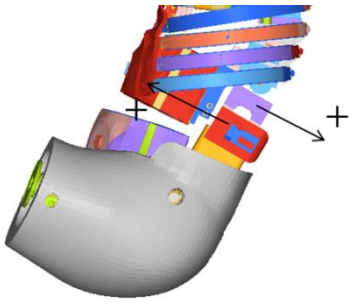

Figure 26. Polarity of spine Load Cell

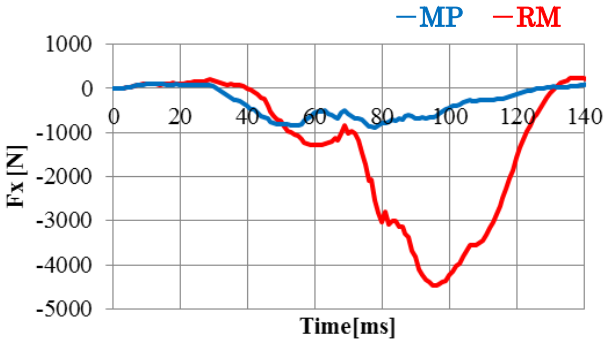

Figure 27. Time histories of spine load cell (X direction) in MP and RM

Comparing RM and SF, the effect by fixing the translation motion of the pelvis was confirmed. Because the translation motion of the pelvis was fixed, there was acceleration of the pelvis before 30 ms (Figure 13), and acceleration of T12 also increased through the lumbar spine (Figure 12), and chest deflection was reduced at 40-60ms by its effect (Figure 14). The pelvis started to rotate greatly to the anterior inclination from 60ms, and along with that, the effect of suppressing displacement of the upper body was decreased (Figure 28). The anterior inclination of the pelvis caused the decrease of T12 acceleration and it increased chest deflection, but early restraint of the pelvis was very effective and maximum chest deflection was reduced finally.

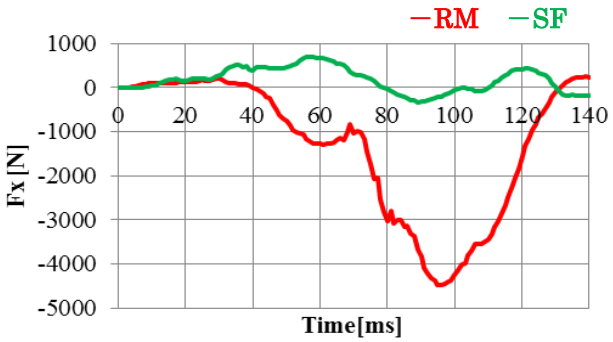

Figure 28. Time histories of spine load cell (X direction) in RM and SF

Comparing RM and RF, the effect by fixing the rotation motion of the pelvis was confirmed. Fixing the rotation of the pelvis means there was no rotational behavior of the pelvis, but in RF, the pelvis inclination was more anterior side relative to in RM (Figure 20). The difference in pelvis rotation started to occur from 40ms and the effect of suppressing displacement of the upper body before 60ms was decreased in RM (Figure 29). As a result, there was a decrease in T12 acceleration at 40–60 ms (Figure 17), therefore chest deflection increased (Figure 19). On the other hand, acceleration of the pelvis increased at close to 60–80 ms and it caused a slight increase in T12 acceleration through the lumbar spine (Figures17, 18). Initially, the relatively anterior inclination of the pelvis causes T12 acceleration to reduce and chest deflection to increase, however, after that, acceleration of the pelvis increased, thus the effect of increasing acceleration of T12 and suppressing upper body displacement was about the same as with RM, and maximum chest deflection was also about the same.

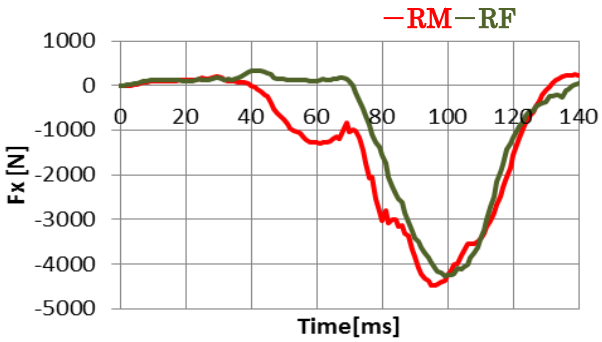

Figure 29. Time histories of spine load cell (X direction) in RM and RF

In preceding part, the influence in case of fixing either translation or rotation of pelvis individually was confirmed. The effect of fixing both translation and rotation of pelvis was confirmed. Because the translation of the pelvis was fixed, there was an increase in acceleration of the pelvis before 30 ms (Figure 23), the same as with SF, and acceleration of T12 also increased through the lumbar spine (Figure 22). This effect could be seen up to about 70ms compared to in RM.

As previously mentioned, the effect of pelvis behavior control on chest deflection was confirmed. Next, this section confirmed the effect on shoulder belt tension when both the translation and rotation of pelvis were fixed. The time histories of the shoulder belt and lap belt tensions in SRF are shown in Figure 30, 31. Fixing the translation and rotation of the pelvis increased pelvis acceleration, and for that reason, the lap belt tension did

not increase (Figure 30). Therefore, there was not transferring of the tension to the shoulder belt from the lap belt, and the shoulder belt tension also could be reduced after 80 ms, (Figure 31), thus it was seen that the loading from the shoulder belt to chest was reduced.

This research confirmed that with sled test in flat 56 km/h, reducing the pelvis translation and rotation motion were effective for reducing chest injury criteria. Moreover, lateral behavior of the vehicle affects the occupantin case of angled collision, the extent of these benefits also needs to be determined for these cases to see if controlling pelvis behavior is effective in reducing chest injury criteria in these situations as well.

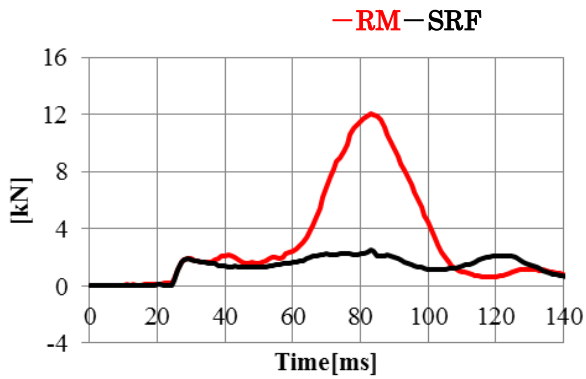

Figure 30. Time histories of the lap belt forces in RM and SRF

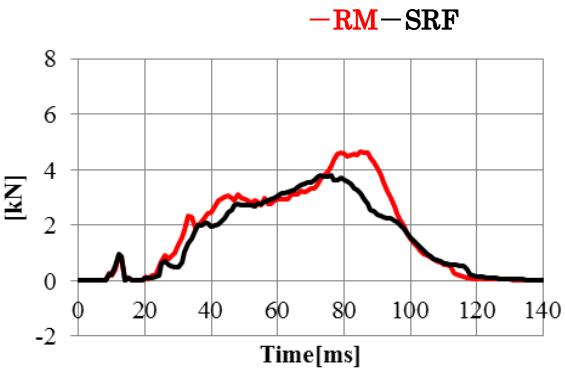

Figure 31. Time histories of the inboard shoulder belt forces in RM and SRF

CONCLUSION

Sled simulation for MP and RM occupant seating positions by using THOR FE model was conducted in this study. In addition, a parametric study which changed the pelvis constrained condition in RM seating position was conducted. As a result, the following were found

・In order to reduce chest deflection in lower right side, it is effective not only reducing the load from inboard shoulder belt but also increasing a degree of constraint on the lumbar spine.

・To improve the constraint on the spine, it is important to constrain the pelvis in early timing to reduce the translation of the pelvis.

・Loading to the chest from the inboard shoulder belt was able to be reduced by suppressing pelvis rotation and it was effective to reduce chest deflection further.

REFERENCES

[1] National Police Agency, 2018; Occurrence situation of traffic accident in 2018 [Published in Japanese]

[2] ITARDA, 2017; Statistical data.

[3] Yaguchi, M., Ono, K., Masuda, M., Fukushima, T., SENSITIVITY TO DIFFERENT SEATING POSITIONS OF THOR-NT AND HYBEID Ⅲ IN SLED TESTING. ESV 13-0333

[4] Kemper ,A. R., Kennedy ,E.A., Mcnally ,C., Manoogian, S.J., Stitzel , J.D., Duma, S.M., Reducing Chest Injuries in Automobile Collisions:Rib Fracture Timing and Implications for Thoracic Injury Criteria. Annuals of Biomedical Engineering. 2011; 39: 2141-2151

[5] Shimamura M.,Ohhashi H.,Yamazaki M., The effects of occupant age on patterns of rib fractures to belt-restrained drivers and front passengers in crashes in Japan. Stapp Car Crash J. 2003; 47:349-65

[6] Kent R., Woods W., Bostrom O., Fatality Risk and the Presence of RIB Fractures. Ann Adv Automot Med. 2008; 52: 73-84

ANCAP CHILD OCCUPANT PROTECTION ASSESSMENT – PERFORMANCE OF AUSTRALASIAN CHILD RESTRAINTS IN FULL SCALE CRASH TESTS

Mark Terrell
ANCAP Australasia
AUSTRALIA

Julie Brown
Neuroscience Research Australia
AUSTRALIA

Thomas Belcher
Australian Government Department of Infrastructure, Regional Development and Cities
AUSTRALIA

Donal McGrane, Jason Smith
ANCAP Australasia
AUSTRALIA

Paper Number 19-0250

ABSTRACT

From the start of 2018 ANCAP's testing and assessment protocols are substantially common with those of Euro NCAP. One key area of difference is assessment and rating of Child Occupant Protection (COP). While alignment of protocols is maintained where possible, differences in products and in vehicle installations require a unique assessment.

The differences arise from a mandatory product standard regulating Child Restraint Systems (CRS) in the Australasian market (AS/NZS 1754). The requirements of the standard mean that all booster seats sold in Australia are high back boosters, while prohibiting of the use of ISOFIX attachments for booster seats. Australian law also mandates use of booster seats by age (up to 7 years).

The 2018 protocols see the first opportunity for assessment of the performance of Australasian booster seats in full scale frontal and side impact crash testing. Typical vehicle accelerations recorded in ANCAP frontal offset tests are above those specified by existing regulatory or consumer CRS testing, and some parties expressed concerns regarding performance of Australasian CRS in comparison with European specification restraints, in particular those CRS recommended by vehicle manufacturers and used in Euro NCAP dynamic COP testing.

The paper provides an overview of early results, considerations for vehicle manufacturers and areas for future consideration in relation to child booster seats in the context of consumer ratings.

INTRODUCTION

From the start of 2018, ANCAP's testing and assessment protocols are substantially common with those of Euro NCAP. However, one key area of difference is assessment and rating of Child Occupant Protection (COP).

The regulatory and usage environment for child occupants in Australia is significantly different to that of Europe, and while alignment of protocols is maintained where possible, differences in products and in vehicle installations are such that a unique assessment is required.

In particular, the differences in product and vehicle installations arise due to unique requirements contained in a mandatory product standard governing the design and performance of child restraints sold on the Australian market (AS/NZS 1754 [1]). Of most relevance are performance requirements within this standard that effectively ensure that all booster seats sold in Australia are high back boosters, while prohibiting of the use of ISOFIX attachments for booster seats. Australian law also mandates use of booster seats by age for occupants of up to 7 years, although best practice guidelines recommend use based on the match between the child's size and rear seat and seat belt geometry.

The 2018 protocols see the first opportunity for assessment of the performance of Australian booster seats in full scale frontal and side impact crash testing. Typical vehicle accelerations recorded in ANCAP frontal offset tests are above those specified by existing regulatory or consumer CRS testing, and some parties expressed concerns regarding performance of Australian CRS in comparison with equivalent testing using European specification restraints.

ANCAP's requirements for Child Occupant Protection from the start of 2018 are contained in two protocols:

- ANCAP ASSESSMENT PROTOCOL - Child Occupant Protection [2]; and
- ANCAP TEST PROTOCOL - Child Occupant Protection [3].

While child restraints and instrumented dummies have been included in ANCAP frontal offset and side impact tests for many years, the 2018 protocols are the first occasion where protection of child occupants forms part of the assessment of the vehicle.

In addition, the 2018 protocols assess children of a different age range to those used in previous ANCAP testing, with 1.5 year old and 3 year old occupants in CRS with integrated harness being replaced with 6 year old and 10 year old occupants in (generally) high-back booster seats.

The 2018 protocols therefore present a new challenge to vehicle manufacturers, particularly for those with vehicle types that have not previously been subject to Euro NCAP assessment. During the lead-up to implementation of the new protocols, ANCAP received representations from a number of vehicle manufacturers suggesting that in-house testing had shown difficulty achieving comparable performance in vehicles fitted with Australian CRS when compared with vehicles of the same specification tested using European specification restraints.

With a range of vehicles of different types having now been tested to the new ANCAP protocols, there is an opportunity to examine performance against the COP dynamic testing and assessment protocols, and to further examine similarities and differences between the performance of the different restraint types.

In this paper, restraints that have been manufactured and certified to the Australian / New Zealand Standard (AS/NZS 1754) and supplied in Australia are referred to as AU. Restraints supplied and used in Europe (meeting UN Regulation 129) are referred to as EU.

BACKGROUND

Child Restraint Requirements in Australia

In Australia, the road rules require vehicle drivers to secure children aged up to 7 years old in an approved child restraint system. For infants up to 6 months of age this must be a rearward-facing CRS with an in-built harness. For children who are 6 months or older, but less than 4 years, this must either be a rearward-facing or a forward-facing CRS with an in-built harness. For children who are 4 years or older, but less than 7 years, this must be a forward-facing CRS with an in-built harness or a booster seat. Children who are 7 years or older, but less than 16 years, must be secured using a child restraint (CRS with in-built harness or booster seat) or by a seatbelt only.

Australian road rules also prohibit children under 4 years old from travelling in the front row of a vehicle with 2 or more rows of seats. Further, children who are 4 years or older but less than 7 years, are prohibited from travelling in the front row of a vehicle with 2 or more rows of seats, unless all seats in the rear rows are occupied by children who are also less than 7 years old. These requirements are to minimise the risks associated with young children travelling in the front seat, including in particular (but not limited to) the risk associated with the installation of a rearward-facing child restraint in a seating position with an active airbag.

Australian /New Zealand Standard AS/NZS 1754 is a mandatory product safety standard and has historically included a number of significant differences in comparison to European product standards. The standard requires that all dedicated child restraint systems, including booster seats, prevent contact between the test dummy's head and a static side door structure in a simulated 90 degree impact. This requirement effectively removes backless booster seats (other than those sold as part of the vehicle i.e. integrated boosters) from the Australian market.

AS/NZS 1754 includes requirements for materials (e.g. webbing, coated metal parts, plastics), general design and construction, dynamic performance, labelling, instructions, marking and packaging.

To meet AS/NZS 1754 a child restraint must satisfy the requirements for at least one designated restraint type. Convertible restraints must meet the requirements set out for the applicable combination of types (e.g. A2/B, A4/B, B/E, B/F etc.). Table 1 summarises each designated restraint type defined by this standard (excluding the Type C harness and the Type H converter). Shoulder height markers are required on all CRS (other than type C and H), providing guidance on when a child should transition to the next designated type, and are prescribed in such a way as to encourage transitions to be as late as possible.

Currently there are two types of booster specified in AS/NZS 1754; Type E boosters which are designated as suitable for use by children approximately 4 years to 8 years, and Type F boosters designated as being suitable for children aged approximately 4 to 10 years. All Type E and F boosters available in Australia are high back boosters.

AS/NSZ 1754 also designates an alternative form of restraint for children aged between 4 and 8 years. This is known as a Type G restraint, which is a forward-facing child seat designed to accommodate a larger child than the traditional Type B forward facing seat. The Type G seat incorporates an integral harness, and is anchored to the vehicle by the three point belt and a top tether strap.

Table 1.
Designated restraint types under AS/NZS 1754

Type Designation	**Description**	**Seated Shoulder Height**	**Approximate Age Range**
A1	Rearward-facing child restraint with in-built harness	Birth up to 290--320 mm	Birth to 6 months
A2	Rearward-facing child restraint with in-built harness	Birth up to 320--350 mm	Birth to 12 months
A3	Side-facing child restraint with in-built harness or other restraint means	Birth up to 290--320 mm	Birth to 6 months
A4	Rearward-facing child restraint with in-built harness	Birth up to 360--390 mm	Birth to 30 months
B	Forward-facing child restraint with in-built harness	From 290 mm up to 405--435 mm	6 months to 4 years
D	Rearward-facing child restraint with in-built harness	From 290 mm up to 405--435 mm	6 months to 4 years
E	Booster seat (child <128cm)	From 385 mm up to at least 475 mm	4 years to 8 years
F	Booster seat (child <138cm)	From 385 mm up to at least 530 mm	4 years to 10 years
G	Forward-facing child restraint with in-built harness	From 290 mm up to 490-510 mm	6 months to 8 years

Generally, AS/NZS 1754 requires child restraints to accommodate specified dummies representative of the smallest child (in summer weight clothing) and the largest child (in winter weight clothing) that the restraint type designation is intended to cover. This is to ensure that the large majority of children will fit properly within restraints of a given designated type, for at least the minimum period required by the road rules.

All restraint types except for booster seats and converters must include provision for attachment to the vehicle using a seatbelt in combination with a top tether. Booster seats greater than 2 kg in mass must also be fitted with a top tether. Rigid ISOFIX connectors or flexible lower anchorage straps/connectors are optional for restraints of Type A, B and D; and are prohibited for all other restraint types. Table 2 summarises the anchoring and attachment system requirements for each designated restraint type.

Finally, while AS/NZS 1754 does include some size requirements, in particular for Type F restraints, it does not include any reference to the European i-Size systems.

Table 2.
AS/NZS CRS Anchoring and Attachment Requirements

Type Designation	Anchoring and Attachment System				
	Anti-rotation Device		Seatbelt Anchorage	ISOfix Connector (Lower)	
	Top Tether	Foot prop (Support Leg)		Rigid	Flexible
A1, A2, A3, A4	✓	✕	✓	✓	✓
B	✓	✕	✓	✓	✓
D	✓	✕	✓	✓	✓
E, F	✓ CRS > 2kg	✕	✓	✕	✕
G	✓	✕	✓	✕	✕

✓ Mandatory ✓ Optional ✕ Prohibited

The dynamic tests required by AS/NZS 1754 include frontal impact, side impact with door, side impact without door, rear impact and inverted tests. For the frontal impact tests, the velocity change must be at least 49 km/h with a negative acceleration of between 24g and 34g for at least 20ms. For the side and rear impact tests, the velocity change must be at least 32 km/h with an acceleration of between 14g and 20g for at least 20ms.

The CRS must meet a range of general structural integrity related requirements for each prescribed test, including retention of the dummy in the restraint on the test rig. For the frontal impact tests, there are also maximum head acceleration limits for Type A and D restraints, head excursion limits for Type A, B, D and G restraints and requirements to limit both movement of the sash belt from the shoulder and submarining for Type E and F booster seats. For the side impact tests there are requirements to avoid head contact with the side door, while in the rear impact tests there are head excursion limits for Type A and D restraints.

Child Restraint Requirements in Europe

In Europe, children under 135 cm in height must, when travelling in light vehicles, be restrained in a United Nations (UN) Regulation No. 44 (R44) or a UN Regulation No. 129 (R129) approved child restraint, which is appropriate for their size and weight. Rearward-facing child restraints are permitted to be used in the front passenger seat, provided the airbag is deactivated. There is no restriction on the use of forward-facing child restraints or booster seats in the front seat.

All child restraints sold in Europe must be approved to either UN R44 or UN R129. Child restraints manufactured and approved to UN R44 are classified into five groups, based on child mass, and the child mass group (i.e. mass range) is indicated on the approval label affixed to the restraint. Child restraints manufactured and approved to UN R129 are classified according to the child height range for which the restraint is suitable, which is also indicated on the approval label affixed to the restraint. Further, maximum child mass is also included on the UN R129 approval label for CRS types with an integrated restraint system.

Under UN R129, child restraints are categorised as either i-Size restraints or specific vehicle restraints. i-Size restraints must meet a range of geometrical requirements to ensure they properly fit i-Size seating positions in vehicles. The requirements for i-Size seating positions are set out in UN Regulation No. 14. Specific vehicle restraints are approved for a specific vehicle type (i.e. model).

The dynamic tests required by UN R129 include frontal impact, side impact (with intruding door) and rear impact. For the frontal and rear impact tests, the requirements include general structural integrity related provisions for the CRS, dummy injury assessment criteria limits and head excursion limits.

In the lateral (side) impact tests, there are requirements for general structural integrity (of the CRS), dummy injury assessment criteria and head containment.

Differences between ANCAP and Euro NCAP

While ANCAP's COP testing and assessment protocols are closely aligned with those of Euro NCAP, there are a number of differences that reflect the nature of CRS available in Australasia, and the way in which they are used. The majority of the changes relate to the CRS Installation and Vehicle Based Assessment sections of the protocol and will not be discussed in this paper. The key differences that relate to the performance in the Dynamic Assessment sections are:

	Euro NCAP	ANCAP
CRS Type	Q6 seated in Booster Seat (High back). Q10 seated on Booster Cushion (no back)	Q6 - An "appropriate" forward facing CRS for a 6 year old child. This may be a Type E or Type F booster seat (with back and sides), or a Type G CRS with integrated harness. Q10 – a Type E or Type F forward facing booster seat. (If selected by the OEM).
CRS Selection	CRS as Recommended by OEM. If no recommendation is made, CRS is selected from "Top Pick List"	CRS may be selected by the OEM (no requirement for 'Recommendation') If no selection is made by the OEM, CRS is from ANCAP CRS list for Q6 and Q10 is placed on the vehicle seat (no CRS).
CRS Head Restraint		CRS head restraint is positioned as specified by vehicle manufacturer. Where no specification is made, CRS manufacturer installation directions are followed.
Fitting the CRS	ISOFIX permitted.	Type E and Type F CRS are installed using the adult belt and top tether. AS/NZS 1754 prohibits the use of ISOFIX attachments on booster seats.
Integrated CRS	Integrated CRS will be used even if they are optional equipment.	Where the integrated CRS is optional equipment, ANCAP will determine whether the optional CRS are to be fitted.

Dummy specifications, test set up (including seating locations), and performance criteria are common between the ANCAP and Euro NCAP COP testing and assessment protocols. Where integrated booster cushions are fitted to the test vehicle and suitable for either the Q6 or Q10 dummy the booster seat they are used for these occupants under both ANCAP and Euro NCAP, however the application for optional integrated seats is different between the two programs (to date ANCAP has not tested any vehicle with an integrated booster seat/cushion).

ANCAP CRS Selection List

As with Euro NCAP, ANCAP's COP protocols include an assessment of installation of a range of child restraints in each vehicle that is rated. However, a key difference is that ANCAP's "CRS Selection List" is intended as a selection of typical, readily available child restraints covering each of the applicable CRS types in the Australian / New Zealand standard, with no relative assessment of the performance of each CRS against other available products (and therefore is not a 'Top Pick' list). The CRSs were chosen, where applicable, to include ISOFIX attachments in addition to the mandatory belt installation, allowing assessment of installation in both modes.

There is no requirement that the CRS selected by vehicle manufacturers for the dynamic tests be chosen from the CRS Selection List, and manufacturers can and do select from the full range of CRSs of the specified types.

COP scoring matrix and considerations

The scoring distribution under COP for ANCAP is the same as the Euro NCAP COP protocol, though ANCAP awards default points for a subset of the static CRS installations. ANCAP also rewards the provision of ISOFIX seating positions, rather than i-Size, which is not applicable under the Australian / New Zealand standard for CRS.

Table 3.
COP Scoring for ANCAP and Euro NCAP

	Euro NCAP (49)	ANCAP (49)
Dynamic Assessment	(24)	(24)
Frontal Impact	16	16
Side Impact	8	8
Vehicle Based Assessments	(13)	(13)
Gabarit Installation on all Passenger Seats	2	2
i-Size and TopTether Marking	3	-
ISOFix Availability	-	3
Two or more ISO/R3 Positions	1	1
Passenger Airbag Warning Marking and Disabling	4	4 (Default 2)
Integrated CRS	3	3
Installation of Child Restraints	(12)	(12)
Universal seats	4	4
Belted with top tether seats		
ISOFIX seats	2	2
i-Size seats	4	Default 4
Recommended seats	2	Default 2

As is the case with Euro NCAP, most vehicles score 8 or fewer points out of 13 for the Vehicle Based Assessment. As a result, the Dynamic Assessment becomes critical for the COP score and ultimate star rating for a vehicle. The minimum score for a 5 star rating in 2018 is 39.2 points, and therefore a vehicle with a Dynamic score lower than approximately 20 is unlikely to be eligible for the highest star rating.

Chest Injury Metrics

At the start of 2018 a change to the chest injury metric for the Q6 dummy has been applied. Under Euro NCAP protocols up to the end of 2017 the chest injury score was calculated from chest (thoracic spine) acceleration, with the higher performance threshold being set at 41g. From 2018 (version 7.2 of the protocol) and for all ANCAP COP assessments, the chest score is calculated from chest deflection, with a higher performance threshold of 30mm. In order to enable comparison of 2017 and 2018 results, both metrics are recorded and presented in this paper. Chest deflection is also presented for the Q10 dummy, which is fitted with upper and lower deflection sensors (IR-TRACCs) – no performance criterion has been specified for the Q10. For normalisation an arbitrary value of 30mm has been applied in this analysis.

Table 4.
Frontal impact criteria, limits and available points per body region for Q6, Q10

	CRITERION	Performance limits			Available points
		Higher	**Lower**	**Capping**	
Head Score	HIC15 (with hard contact)	500	700	800	4 points
	Resultant 3ms acceleration	60g	80g	80g	
	Head excursion modifier Q6 Q10	 450mm	 550mm 550mm	 NA NA	
Upper Neck	Tension Fz	1.7kN	2.62kN	NA (monitoring)	2 points
	Extension My (with head to interior contact) Q6 Q10	 NA NA	 36Nm 49Nm	 NA NA	
Chest (T4)	Resultant 3ms acceleration* Q6 Q10	 41g** 41g	 55g** 55g	 NA 55g	 NA 2 points
	Deflection Q6 Q10	 30mm (monitoring)	 42mm (monitoring)	 NA NA	 2 points NA
TOTAL					**8 points/dummy**

** 2017 limit values

METHODS

The analysis draws on three separate sets of data from full scale crash tests. All results are from frontal crash tests into an Offset Deformable Barrier at 64 km/h in accordance with the "ANCAP Test Protocol – Frontal Impact Offset Deformable Barrier" (v7.1.2) [4]. The test requirements of this protocol are the same as in the Euro NCAP "Offset Deformable Barrier Frontal Impact Test Protocol" (v7.1.2).

AU/EU Comparison Tests

Data were available for two vehicle models that were tested separately by Euro NCAP and ANCAP, allowing comparisons of the COP performance between AU and EU CRS. In some cases, the ANCAP tests formed part of the laboratory commissioning process for the 2018 protocols and were not part of official rating programs. Data were available for two vehicle models, one a small SUV and one a medium SUV. The performance of both models for adult occupant protection is good, and both models carried 5 star ratings under ANCAP and Euro NCAP. It is worth noting, however, that vehicles tested in Australia were right-hand-drive, while the vehicles tested by Euro NCAP were left-hand-drive. This has some effect on the vehicle crash pulse measured at the B-Pillar.

ANCAP Ratings

Complete COP data are available for five vehicle models that have been tested and rated by ANCAP in 2018. These represent a cross section of vehicle types including small and medium family cars, medium and large SUVs. None of the rated vehicle models had been previously tested by ANCAP or Euro NCAP. The CRS used in each case were selected by the vehicle manufacturer. The CRS selections included Type E and Type F booster seats, with both types being applied for Q6 and Q10 occupants.

The Q6 and Q10 dummies were fitted with all instrumentation specified in the ANCAP (and Euro NCAP) COP test protocols.

Comparison Test with Q10 on Adult Seat

An ODB test was conducted on one further vehicle model as part of a separate ANCAP program. The opportunity was taken to place a Q10 dummy on the (passenger side) rear seat, in order to assess performance with no booster seat (or booster cushion). A Euro NCAP test result was available for a variant of the same model for comparison, with the Q10 in the EU vehicle being installed on a booster cushion and restrained by the adult belt. In this case there were some differences in the drivetrain between the EU and AU vehicle, which in combination with a change from left-hand-drive to right-hand-drive resulted in a more severe crash pulse for the AU vehicle on the struck side, however the B-Pillar acceleration on the non-struck side (more relevant for the Q10) was not recorded in the Euro NCAP test and therefore is not presented in this study.

RESULTS

General

There was no hard contact observed between the child dummies and the CRS or vehicle interior in any of the tests. HIC_{15} and Neck Extension Moment are therefore not considered for point-score or rating, but are presented for information. With the changes in chest injury criteria, both deflection and acceleration values are reported. The metrics that are not applicable under 2018 protocols are shaded in charts below for clarity.

Injury metrics presented are normalised against the "Higher Performance" threshold of ANCAP and Euro NCAP protocols. As previously noted, an arbitrary value of 30mm is applied for normalisation of Q10 chest deflections. For the Q10, the values displayed are from the Upper IR-TRACC, which in all cases recorded greater deflection than the lower sensor.

Comparison of results – Australian vs European CRS

Comparison of accelerations at the driver's side B-Pillar shows comparable load cases for the EU and AU CRS, though there is some variation in the peak recorded acceleration. As an additional indicator, the *Occupant Load Criterion* (OLC) [5][6] was calculated using the driver's side B-pillar acceleration for each vehicle. Calculated OLC values are listed in Table 5. For the medium SUV the calculated OLCs were very close. For the small SUV, the EU vehicle showed a slightly higher OLC.

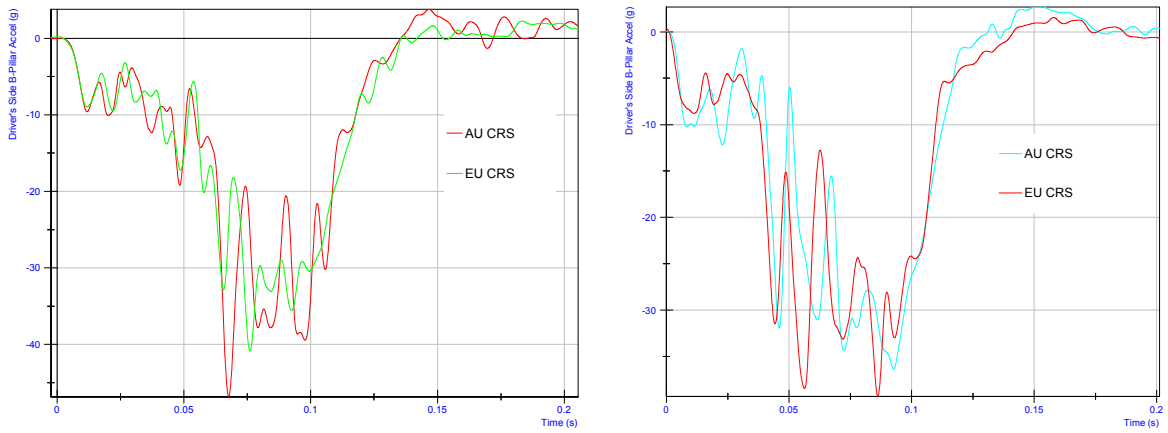

Figure 1 - B-Pillar Acceleration Comparison - Medium SUV (left) and Small SUV (right).

Table 5.
Occupant Load Criterion Comparison - AU and EU CRS

Occupant Load Criterion	Medium SUV	Small SUV
AU (ANCAP)	25.83	26.33
EU (Euro NCAP)	25.38	28.88

Figure 2 shows the injury metrics from the comparison tests. In both cases there is good correlation between the injury metrics of the ANCAP and Euro NCAP test vehicles.

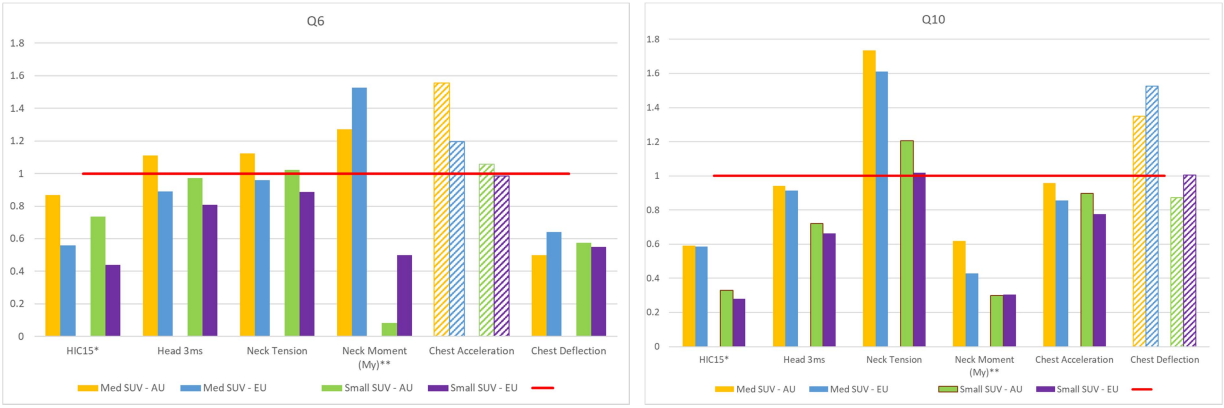

Figure 2 - Comparison of Injury Metrics for Q6 and Q10 with EU and AU CRS.

Results from 2018 ANCAP Ratings Testing

In tests conducted to date, there have been consistently good overall results shown in ANCAP testing for dynamic child occupant protection. While in some cases there were injury metrics that exceeded the higher performance thresholds, there was only one result exceeding the lower performance threshold. The results are shown in Figure 3.

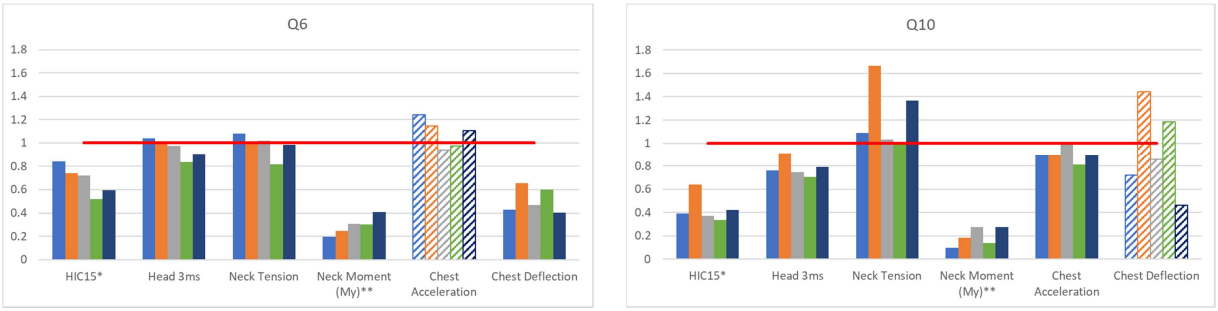

Figure 3 - Normalised results from ANCAP ratings

All vehicles rated during 2018 achieved the COP points score threshold necessary for a 5 star rating. The COP point scores for the five vehicles are shown in Figure 4, identifying the contributions of each of the areas of assessment.

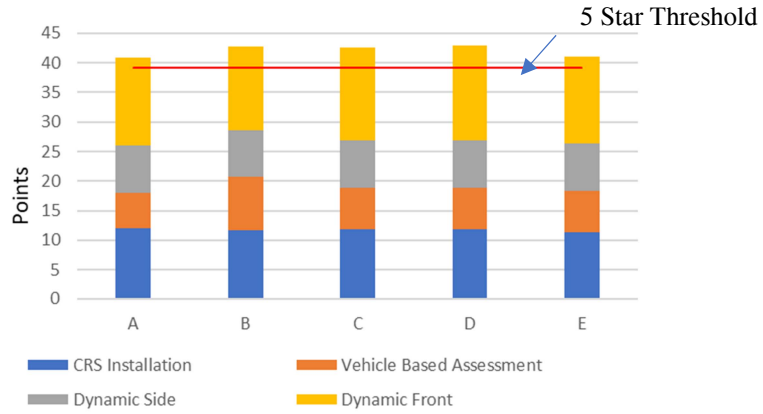

Figure 4 - Comparison of COP point scores for 2018 ANCAP ratings

Results from Comparison Test with Q10 on Adult Seat

Injury metrics for the Q10 were very similar between the two tests (Figure 5) however, where the Q10 was seated on the adult seat without any booster cushion, submarining of the dummy was observed, with the lap belt slipping upwards off the dummy's pelvis and into the abdomen (Figure 6). Submarining was not observed in the test with the Q10 on the booster cushion. Under the ANCAP assessment protocol, a capping modifier is applied to the score where submarining occurs and zero points are scored for that occupant.

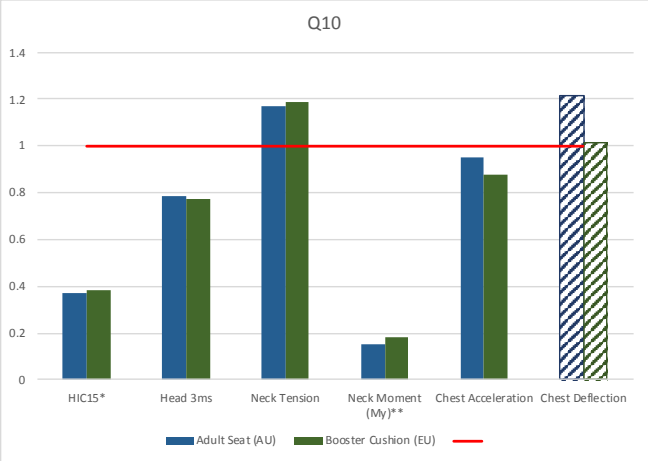

Figure 5 - Comparison of Q10 Injury Metrics on Adult Seat with Booster Cushion.

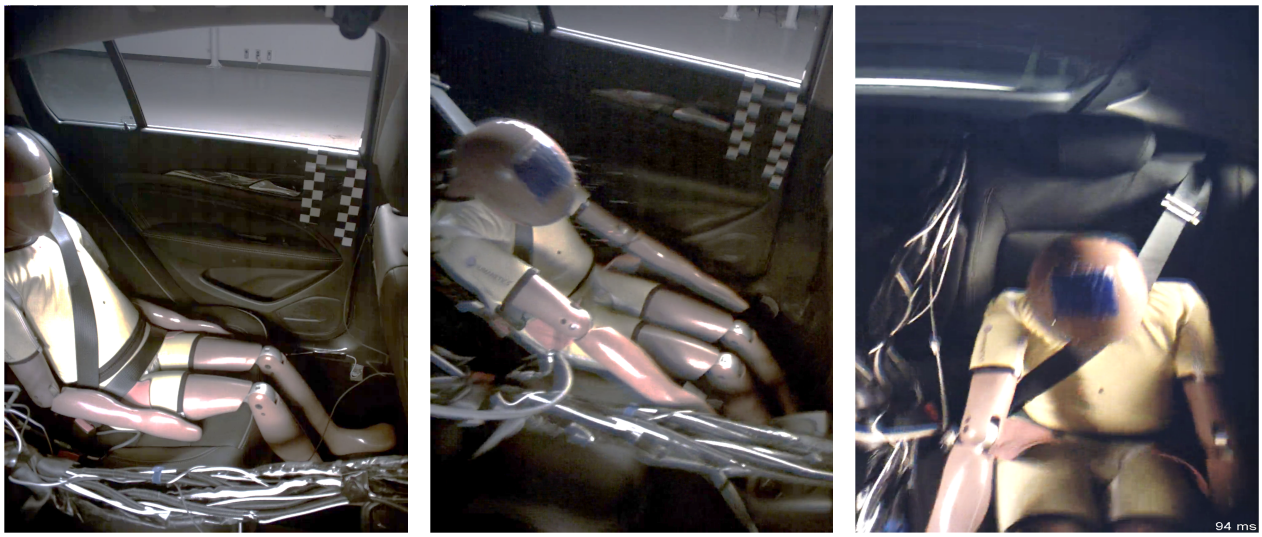

Figure 6 - Submarining of the Q10 on the Adult Seat - Pre-impact (Left) and During the impact.

DISCUSSION

Seat-belt Path

One factor that may result in variations in test performance of AU child restraints appears to be the path of the seatbelt through the CRS belt guide. All of the booster seats have a belt guide that sets the position of the belt over the dummy's shoulder, but that can also introduce friction to the belt. This seems to be most significant where there is a large deviation in belt path due to the belt guide, resulting in a 'z-shaped' belt path (see examples in Figure 7). It appears possible, though not investigated in depth at this time, that friction from the belt guide may inhibit effectiveness of the pre-tensioner, and result in sub-optimal injury metrics. Location of the belt guide also affects the position of the belt across the dummy chest, which may influence chest deflection results.

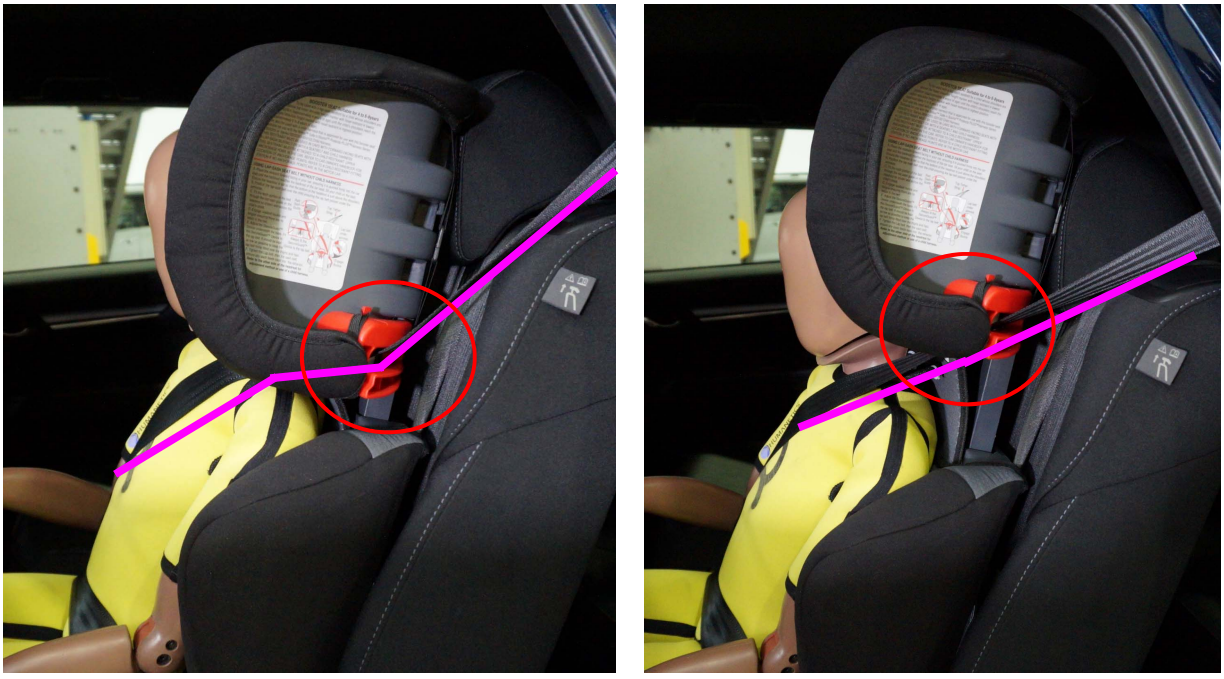

Figure 7 - Examples of Seat Belt Path with CRS in lowest (left) and upper-mid (right) positions

The ANCAP COP testing protocol allows the vehicle manufacturer to specify the position of the head restraint of the selected CRS, which in most cases will result in a CRS head restraint that is higher than the position specified by the CRS manufacturer (which is generally the lowest position for which the shoulder height marker is above the shoulder) and results in a straighter belt path through the CRS belt guide.

The general behaviour of belt guides in high severity crash tests of vehicles with advanced seat belts is an area that warrants some further research.

Chest deflection of Q10 – Type F CRS

For both the Q6 and Q10 child dummies, the ANCAP protocol allows the manufacturer to select either Type E or Type F booster seats – and both types have been applied for both occupant sizes in the tests that have been conducted.

As noted in a study by Adalian and Bendjellal [7], a lower chest deflection was recorded with an AU booster than the EU booster for the same selection of vehicles. It is noted that the AU Type F booster seat, as used in that analysis, has no armrest or belt guide at the buckle. This is a consequence of width requirements for the Type F booster that are included in the Australian / New Zealand Standard.

In ANCAP tests with AU restraints the same trend was noted, with generally lower chest deflections recorded in Type F CRS than in tests using European specification booster seats or using AU Type E seats (noting that the sample size is small at this point).

With no lower belt guide, the belt takes a more rearward position at the hip, allowing the upper part of the belt to sit higher on the dummy thorax, which may influence the deflection measurement.

CONCLUSIONS

From the testing conducted to date the following conclusions have been drawn:

- Good dynamic performance can be achieved in the 64 km/h Offset Deformable Barrier crash test when using Australian / New Zealand Standard child restraints.
- It is realistic for current vehicles to consistently meet 5 star performance requirements under the COP Pillar of current ANCAP protocols.
- Child Occupant Protection performance can be expected to be similar when comparing tests of the same vehicle model using AU and EU child restraints.
- Neck tension was the most common exceedance of the ANCAP higher performance limits.
- Consideration of the CRS selected for dynamic testing, and specifying the applicable CRS head restraint position are likely to contribute to higher overall scores.

REFERENCES

[1] Standards Australia Joint Technical Committee CS-085, “Australian / New Zealand Standard 1754:2013 – Child restraint systems for use in motor vehicles” Amendment 1, 2016, Standards Australia Limited.

[2] Australasian New Car Assessment Program, “Assessment Protocol – Child Occupant Protection”, version 7.2.1, 2018., ancap.com.au/protocols

[3] Australasian New Car Assessment Program, “Testing Protocol – Child Occupant Protection”, version 7.2.1, 2018., ancap.com.au/protocols

[4] Australasian New Car Assessment Program, “Testing Protocol – Frontal Impact Offset Deformable Barrier”, version 7.1.2, 2017., ancap.com.au/protocols

[5] Meyer, E. 2016. “Understanding Injury Mechanisms from Real World Accidents.” Master’s Thesis, Chalmers University of Technology, Göteborg Sweden

[6] Euro NCAP, “Technical Bulletin TB027 - Compatibility Assessment” version 1.0, November 2018., euroncap.com

[7] Adalian, C. and Bendjellal, F. 2018., “Comparison of ANCAP and Euro NCAP Child Occupant Protection Assessments”, 16th Protection of Children in Cars conference proceedings, December 2018, Munich, Germany.

RESEARCH OF BICYCLIST DETECTION BY ENHANCED PEDESTRIAN DETECTION SYSTEM WITH ADAS

Masaki, Umezawa Kenyu, Okamura Hidetoshi, Nakamura Hiroyuki, Asanuma Hyejin, Bae

Honda R&D Co., Ltd. Automobile R&D Center

Japan

Paper Number 19-0251

ABSTRACT

Recent years have seen growing concern with bicyclists in terms of protection for vulnerable road users (VRU) [1]. One instance of this is the establishing of bicyclists to the Euro NCAP protocols for Automatic Emergency Braking (AEB) assessment.

In a real-world environment, however, even if AEB operates, there is still a possibility that the vehicle will not slow down sufficiently because of the timing of that operation, the vehicle environment, or the road surface environment. In this case, impact between the vehicle and the bicyclist may occur.

Consequently, there remains a necessity for technology to detect impact with bicyclists.

For this paper, the investigation was carried out with a focus on the detection of bicyclist impact in two modes. They are run-out mode and rear-end impact mode, in which detection is assumed to present a challenge because the bicyclist and the vehicle bumper do not come into contact.

As a method for detecting impact with a bicyclist in the above modes, a detection system was devised that integrates a conventional pedestrian detection system, deformation sensors mounted around the bumper surface periphery, and ADAS information. This will be referred to as the integrated impact detection system.

Bumper surface deformation sensors are used to detect minute deformations of the bumper surface caused by a bicycle. ADAS information is used to control the threshold for impact judgment. The conventional pedestrian detection system is used mainly to detect the impact of a bicyclist near the central portion of the vehicle.

We conducted CBU tests and simulations on the integrated impact detection system we invented this time and confirmed and investigated the bicyclist impact detection performance.

As a result, it was found that minute inputs to the bumper surface caused by a bicycle can be effectively detected by the deformation sensors. The deformation sensors alone are sensitive to inputs to the bumper surface. However, the reliability of impact detection can be maintained by using ADAS information to control the deformation sensor threshold when operation of the vulnerable road user protection device is required. Incorporating the conventional pedestrian detection system into this system also maintains reliability.

It was determined from these results that the combination of the conventional pedestrian detection system, deformation sensors, and ADAS information in an integrated impact detection system presented possibilities for detection of impact with bicyclists in run-out and rear-end impact modes.

INTRODUCTION

Bicyclist protection has been established to the Euro NCAP protocols for AEB assessment. However, AEB functionality is determined by the vehicle environment, the road surface environment, weather conditions, and other such factors. Some possibility remains, therefore, that even if the AEB operates, it will not slow the vehicle sufficiently and that impact of the vehicle with a bicyclist could occur. Consequently, there is still a necessity for technology to detect impact with bicyclists.

For this paper, therefore, the detection of bicyclist impact was investigated with a focus on impact detection in rear-end impact mode and in run-out mode, when detection is considered to be a challenge because bicyclists themselves do not contact with the vehicle bumper.

As a method of VRU impact detection, it is well known that is used acceleration sensor or pressure sensor located around bumper beam for pedestrian impact detection [2][3]. The purpose of these sensors is to detect the input to the bumper beam caused by pedestrian impact. This presupposes that the impacting object penetrates up to the bumper beam.

When the input to pedestrian detection system sensors is small, the system will determine that the situation does not necessitate operation of a pop-up hood (PUH [4]) or other such pedestrian protection device. That is, the system will determine that no pedestrian impact has occurred or that impact was in a speed range that does not require a device. In other words, when the impacting object does not penetrate up to the bumper beam, the sensors will not detect and pedestrian protection devices will not operate.

In the case of run-out mode or rear-end impact mode, only the front wheel or rear wheel of the bicycle contacts the bumper. Since the bicyclists themselves do not contact the bumper, penetration up to the bumper beam does not occur.

However, bicyclists move at higher initial speeds than pedestrians. When impact occurs, therefore, there may be impact with the vehicle body due to the inertia of the bicyclist, as in Fig. 1, even if the input to the bumper beam is insufficient. It is therefore necessary to have impact detection that will cause protective devices (in this case, e.g., the A pillar airbag) to operate.

Because of the reason mentioned above, the investigation was carried out with a view to detecting impact and causing protective devices to operate even when penetration by bicyclists does not reach up to the bumper beam.

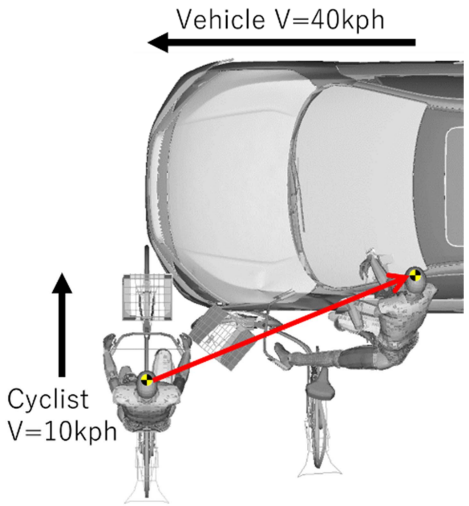

Figure 1. Post-impact behavior of run-out bicyclists

PURPOSE

The purpose is to enhance performance of the conventional pedestrian detection system so that the system will detect the bicyclist in the case of bicyclist impact that does not penetrate up to the bumper beam.

ACHIEVEMENT METHOD

Method of detecting bicyclists

Bicyclists themselves do not contact with the vehicle bumper in run-out mode or rear-end impact mode, but minute deformations of the bumper surface are caused by the bicycle. Consequently, the approach here will be based on configuration of G sensors (hereafter surface-G sensors) on the rear side of the bumper surface as deformation sensors, and these surface-G sensors are added to the pedestrian detection system.

The use of surface-G sensors makes it possible to react to low-input impact modes that only contact with the bicycle front wheel or rear wheel. On the other hand, it is possible that VRU protection devices would operate when impact with something other than a person (such as a road pylon) occurs.

Therefore, we devised integrated safety system using ADAS radar and camera, the ego-vehicle speed, and the relative speed with bicycle, angle. This is used to judge whether impact with a bicyclist is unavoidable, and only when it is judged unavoidable will the impact judgment threshold of the surface-G sensor be lowered to make the system reach an impact judgment. In the case where the impact is escaped by the avoidance behavior of the bicyclist or the vehicle, the threshold is restored to the normal time.

With regard to impact with the central portion of the vehicle when the bicyclist and the vehicle bumper contact, we decided to have the conventional pedestrian detection system make the impact judgment.

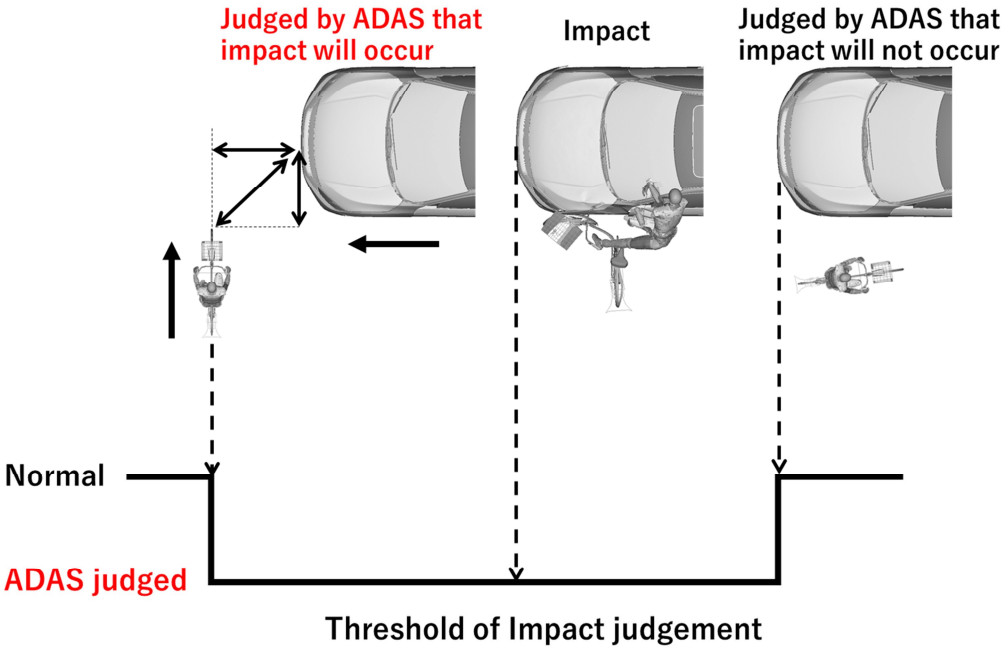

Figure 2. Threshold control by ADAS coordination

Detection algorithm

Only bicyclists are defined as objects that should be detected by means of ADAS. If the system were set to detect objects other than bicyclists and treat them as integrated detection system control objects, the number of such objects would become very large and reliability would be reduced. It was therefore decided to lower the surface-G sensor threshold only when impact with bicyclists is anticipated.

The surface-G sensor threshold is basically set, as the pedestrian detection threshold is set, as shown in Fig. 3, so that the reaction to impact with objects other than bicyclists and the misuse mode about driving on rough roads and other such conditions will both be turned OFF. However, we decided that when the integrated detection system uses ADAS information to control the threshold, the threshold level will be lowered to where the above misuse mode is turned OFF.

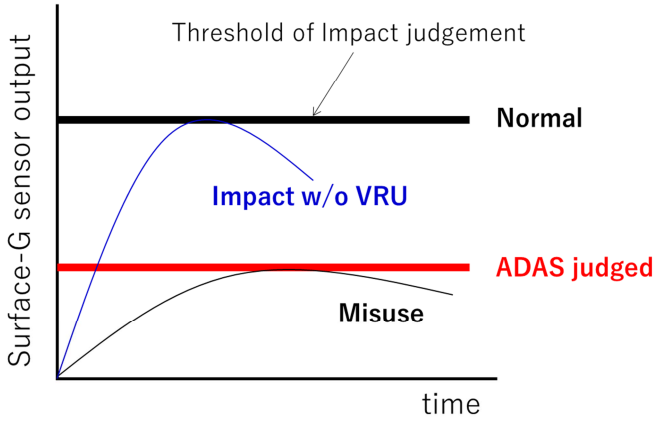

Figure 3. Conceptual approach to setting the threshold

One or two surface-G sensors each are mounted at the left and right sides of the bumper surface. Surface-G sensors on the left side react to impacts on the left side, and surface-G sensors on the right side react to impacts on the right side. As shown in Fig. 4, a VRU protection device will be deployed when judgment is made by pedestrian detection system sensors or by the integrated impact detection system.

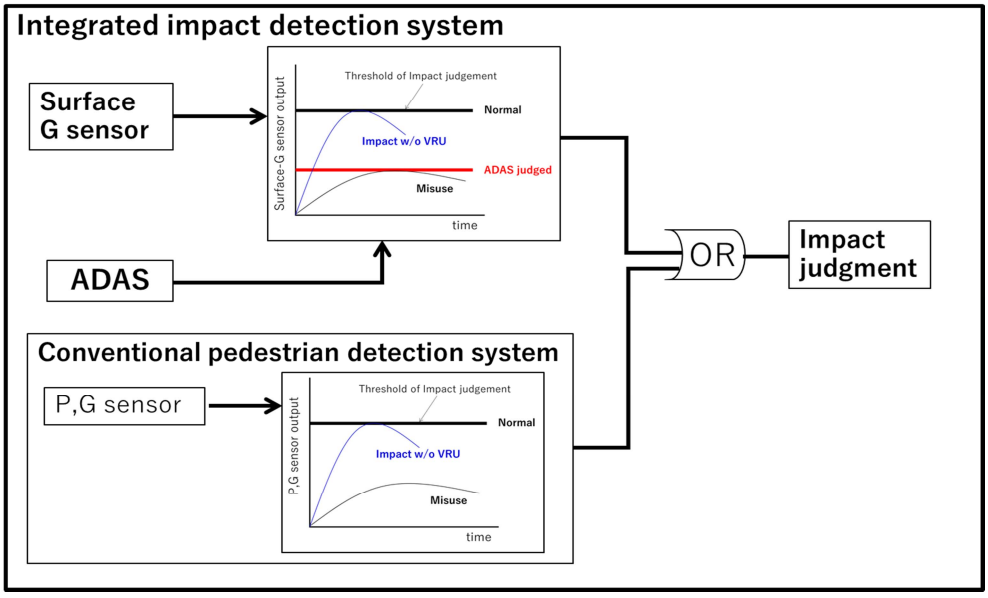

Figure 4. Bicyclist impact detection algorithm

VERIFICATION METHOD

We verified the performance about cyclist detection using Surface-G sensor of integrated impact detection system by CBU impact test and simulation. CBU test and simulation configuration will be described here.

The vehicle was middle class sedan, the bicycle was Citybike-type and the cyclist was POLAR2 dummy [5] which was a pedestrian dummy developed by Honda. The vehicle speed was set at 25 km/h. Vehicle speed at 25 km/h is same as lower limit speed to deploy the PUH. This is based on the thinking that the impact upper limit speed at which pedestrian's HIC become to or below the regulatory standard value when PUH does not deploy is about 25 km/h.

Figure 5 shows a result of simulation in the bicyclist impact with vehicle speed at 25 km/h. Since even in the bicyclist, the head contact with the hood at an impact with a vehicle speed at 25 km / h, we predicted that HIC would be equivalent to pedestrians. Therefore, we decided to proceed with the performance verification with the impact detection lower limit speed for bicyclist detection set at 25 km/h. As for the run-out mode, as shown in Fig. 1, since The bicyclist contacts with the vehicle at a vehicle speed at 40 km/h, we predicted that it will occur even at 25 km/h.

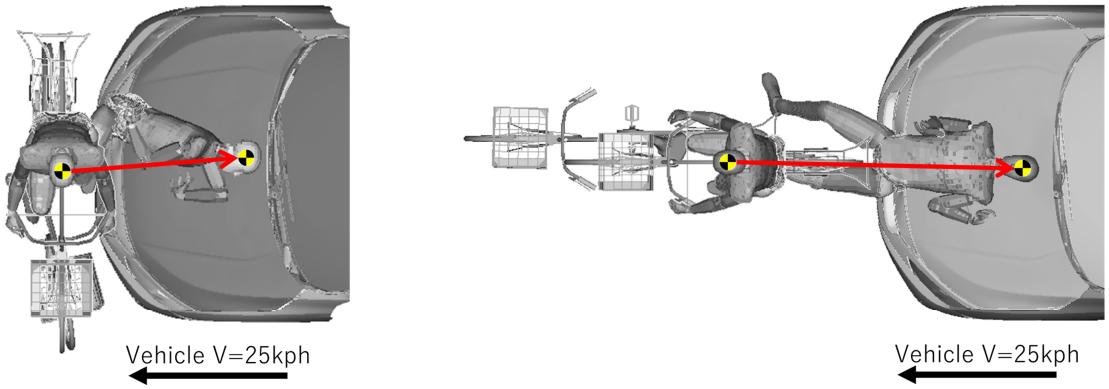

Figure 5. Post-impact behavior of bicyclists at 25 km/h

Test was also carried out in run-out mode with a stationary bicyclist. Because both pedestrian sensors and surface-G sensors primarily detect input in the direction of the vehicle's forward movement (the x axis), and it has little influence on the performance of detection as to whether or not there is input in the direction of the bicyclist's movement (the y axis), and in order to keep the CBU test simple and to heighten reproducibility during continuing investigation.

The vehicle was configured with pressure sensors on the front of the bumper beam as a conventional pedestrian detection system. For the integrated detection system, surface-G sensors were mounted at 100-mm interval length from the vehicle center on the back of the bumper surface.

Impact Mode

The impact modes for verification were configured as the run-out impact mode, rear-end impact mode, and vehicle center impact mode.

Run-out impact mode (impact at end of vehicle): The collision location in run-out impact mode was defined as shown in Fig. 6, as the mode where the vehicle and bicycle overlap by 450 mm. When impact occurs with the vehicle speed at 25 km/h and bicycle speed at 10 km/h, the lower limit for the overlap length where the bicyclist

impacts the vehicle is 450 mm (simulation result). When the overlap length is lower than this, the effectiveness of the VRU protection device will be diminished. Therefore, 450 mm was set as the lower limit for overlap length at which impact detection becomes necessary.

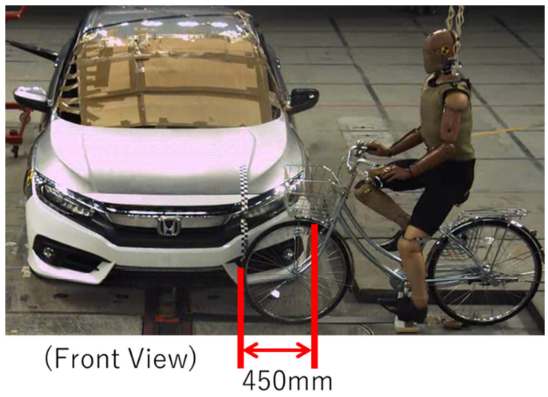

Figure 6. Setting of overlap length of run-out bicyclist and vehicle

Rear-end impact mode: In rear-end impact mode, the behavior will be the same no matter where along the lateral direction of the vehicle is contact. Bicyclists will move toward the vehicle and contact with the vehicle no matter where they contact the vehicle. In light of the above, we decided the IP in rear-end impact mode was set as the vehicle center, as shown in Fig. 7. Furthermore, the contact with the bumper is only for the thickness of the bicycle rear wheel. Therefore, input will occur along a narrower range in the lateral direction than in run-out mode. So the area at which rear-end impact detection becomes necessary becomes almost the whole area in the vehicle width direction. Emplacement of multiple surface-G sensors would enable reaction to any collision location, however this would increase the cost.

In other words, the length in the lateral direction over which a single surface-G sensor is capable of detection is a key point for rear-end impact detection. Verification was therefore carried out from that perspective.

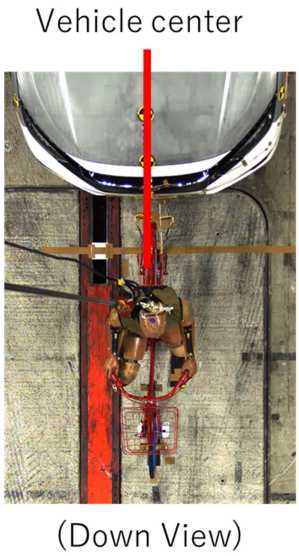

Figure 7. Rear-end impact mode

Impact mode for the central portion of the vehicle: For impact mode for the central portion of the vehicle in which the bicyclist and the vehicle contact, it is envisioned that impact detection will be implemented by the conventional pedestrian detection system. In order for impact judgment to be made from pedestrian sensors, an object of sufficient mass should penetrate to the front of the bumper beam so that input is applied to the sensors. Impact is typically detected from the leg mass of a pedestrian. Consequently, the key point for detection of bicyclists using the pedestrian sensors is relationship of overlap length of the bumper beam and the leg.

When impact occurs between a pedestrian and a vehicle, ordinarily two legs contact with the vehicle at bumper beam height. This applies input to sensors at the front of the bumper beam.

On the other hand, when bicyclists pedal a bicycle, their legs move in up and down strokes. Depending on the position of the pedals, therefore, it is possible that only the mass equivalent to one leg will actually provide input to the sensors.

That state was considered to be the worst case in terms of impact detection. The present CBU testing was therefore carried out with the mode in which the pedal is at the topmost position (this will be termed top-dead-center mode) and the mode in which the pedal is at the bottommost position (this will be termed bottom-dead-center mode) taken as the worst-case conditions.

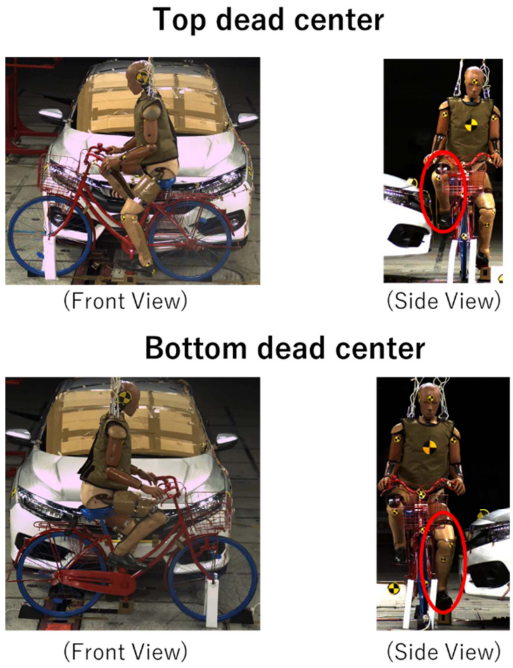

Figure8. Top-dead-center mode and bottom-dead-center mode

RESULTS

Run-out impact mode (impact at end of vehicle)

Figure 9 shows a map of surface-G sensor output in an impact with 450mm overlap. We plotted the impact without VRU (hereafter Light weight object) and the misuse-mode without Light weight object (hereafter Misuse) as the mode in which thresholds intended to keep OFF, and configured two thresholds.

The black line is the threshold at which the judgment by ADAS predicting impact will be OFF. This was configured so that both Light weight object and Misuse would be OFF.

The red line is the threshold at which the judgment by ADAS predicting impact will be ON. This was configured to turn Misuse OFF. This is based on the basic concept that the system should turn Misuse OFF even if the integrated detection system lowers the threshold according to ADAS information.

The vertical axis of the map shows the definite integral value (km/h) of the surface-G sensor. The horizontal axis shows the stroke of the surface-G sensor. The impact causes G to be generated in a short time, while the Misuse like rough road-mode tend to generate G over a long time. Therefore, mapping it enables a grasp of the distinctive characteristics of an impact.

According to the map, run-out bicyclist reaches the threshold ADAS judged, but it largely does not reach the normal threshold.

When compared between impact phenomena, it can be a challenge to differentiate those that are in OFF mode (IP is directly above the sensor) that have high-level sensor outputs and run-out bicyclists that have low-level sensor outputs. This further clarifies the necessity for using ADAS information so that the surface-G sensor threshold can be lowered.

It was apparent from these results that in run-out impact mode, it is effective to use the method of controlling the threshold of surface-G sensors located on the bumper surface by means of ADAS information so that they will be turned ON.

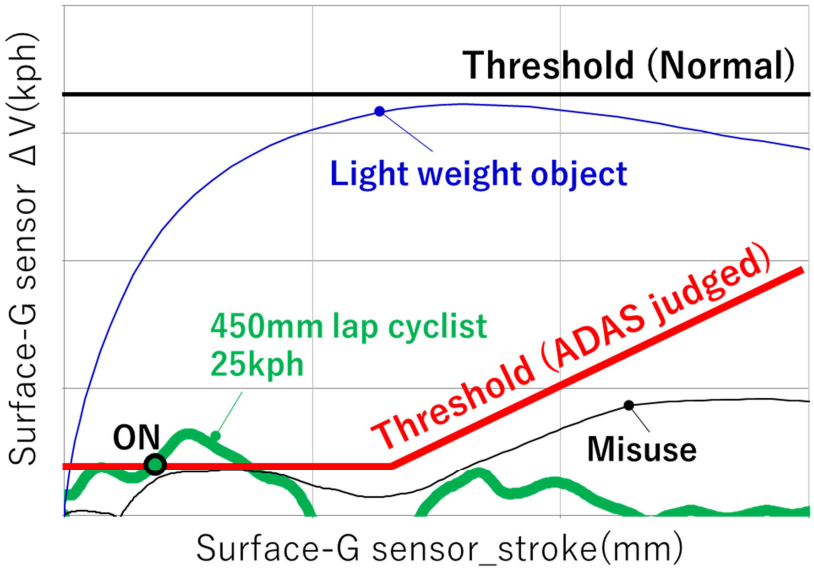

Figure 9. Detection of bicyclist by surface-G sensor (Run-out mode impact)

Rear-end impact mode

Figure 10 shows the results for outputs from surface-G sensors placed at 100mm intervals on the back of the bumper surface, with rear-end impact at the vehicle center when the vehicle speed is 25 km/h.

The largest output comes from the central sensor. The sensitivity decreases as the distance from the center increases, and it was found that outputs at levels exceeding the threshold for turning misuse OFF were obtained from sensors located up to 400 mm away from the center.

However, since the tendency toward lower outputs increased between 300 mm and 400 mm, we considered appropriate to define the location of the surface-G sensor ±300 mm as the area where detection is certain.

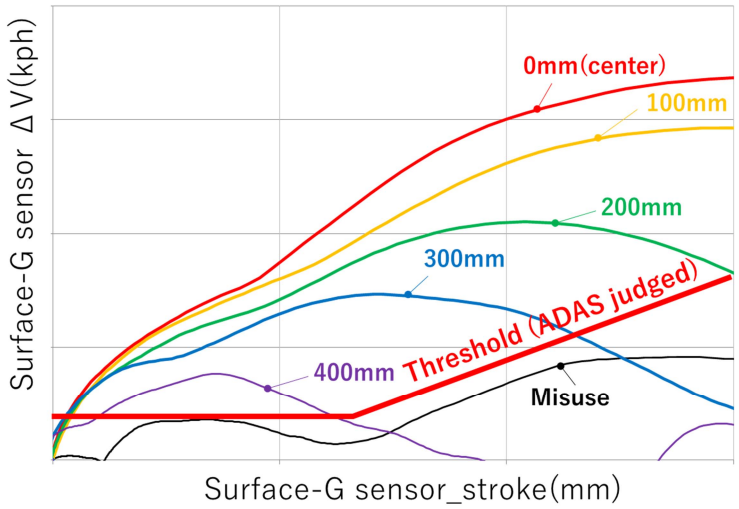

Figure 10. Surface-G sensor sensitivity in rear-end impact detection

Impact mode for the central portion of the vehicle

Figure 11 shows pedestrian sensor outputs at top-dead-center and bottom-dead-center.

At the initial time of impact (up to around 20 ms), sensor outputs are generated due to inputs from the leg on the impact side. However, they are not able to exceed the threshold level since almost all of the bicyclist's weight is on the bicycle saddle and the leg is in a state close to free flight, so that the input to the bumper beam is small.

From around 30 ms, there is additional input generated by the bicycle itself. With inputs from the leg on the impact side together with the bicycle, sensor outputs are generated at a level exceeding the threshold. It is apparent that from around 40 ms, input from the leg on the non-impact side is causing a further increase in sensor output.

It was found from these results that with impact at the central portion of the vehicle, the conventional pedestrian detection system is effective.

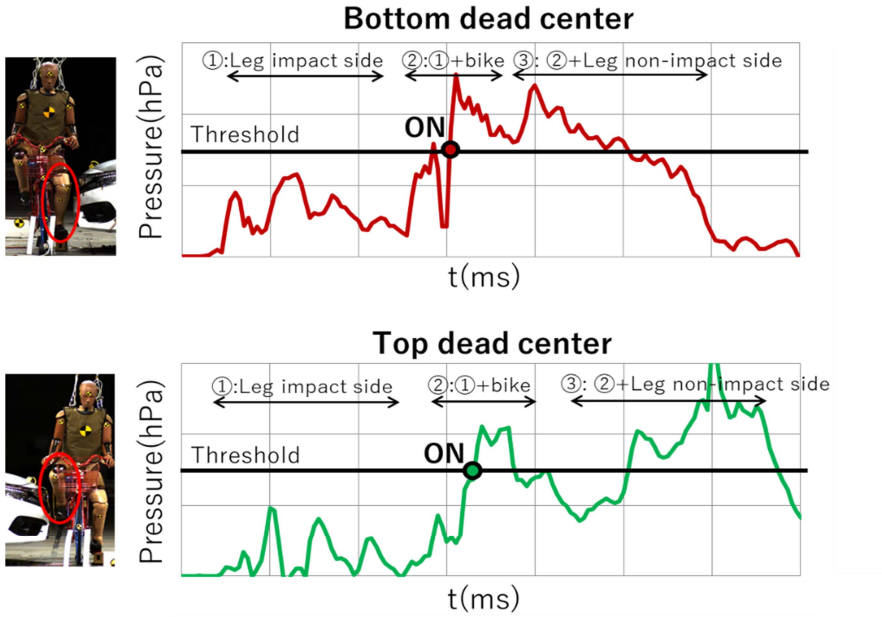

Figure 11. Bicyclist detection by pedestrian sensor (Impact at central portion of the vehicle)

DISCUSSION

Verification of number of surface-G sensors

Figure 12 shows run-out mode (simulation) results for every overlap length. Red portions of the contour indicate the regions where the integrated detection system can detect. Detection is most demanding at 450 mm, the bottom limit for overlap length at which device operation is required. That is because the front wheel that makes initial contact and the bumper are in a mode close to point contact due to the styling camber curve. As the overlap length increases, the front wheel and bumper approach surface-to-surface contact so that inputs to the surface-G sensors also increase, making detection easier. When the overlap reaches or exceeds 1050 mm, the system becomes able to react with the surface-G sensor on the bicyclist's leg or its opposite side (in the case of left side run-out, on the right side).

It was apparent from these results that run-out mode, including 450-mm overlap mode where detection is most challenging, could be fully covered when surface-G sensors are placed at locations near the center with each one for right and left.

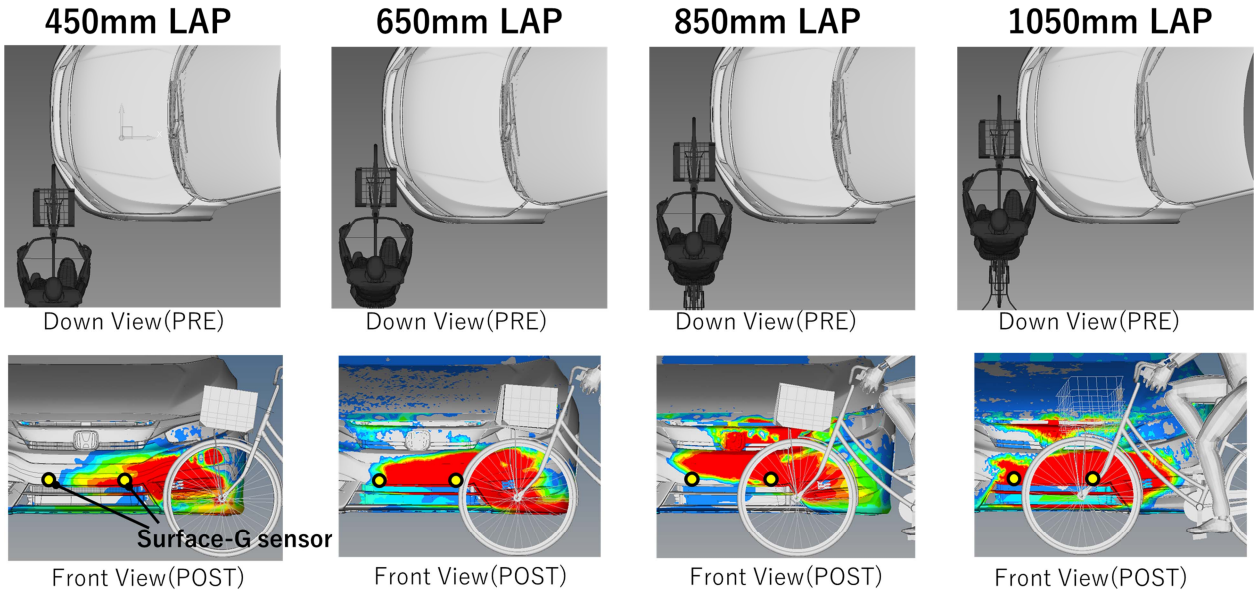

Figure 12. Inputs to surface-G sensors at different overlap length (simulation)

In the rear-end impact mode described above, the detection sensitivity of the surface-G sensor was ±300 mm. It is difficult to detect the Rear end impact of vehicle outside end using surface-G sensor for Run out mode.

Therefore, in order to detect both modes, it was found that multiple sensors were necessary in consideration of sensitivity as shown in Fig.13.

This paper describes results of investigation using a middle class sedan. If the styling design of the vehicle changes, then the input to the surface-G sensors will also change. In the case of styling design that involves a larger camber angle, in particular, and if the impact overlap is small, then it is possible that the bumper input from the bicycle front wheel will not reach all the way to the surface-G sensors.

In that case, we are thinking that is to enhance detection performance either by configuring G-transmission components behind the bumper surface in order to increase the rigidity around the surface-G sensors or by adding more surface-G sensors.

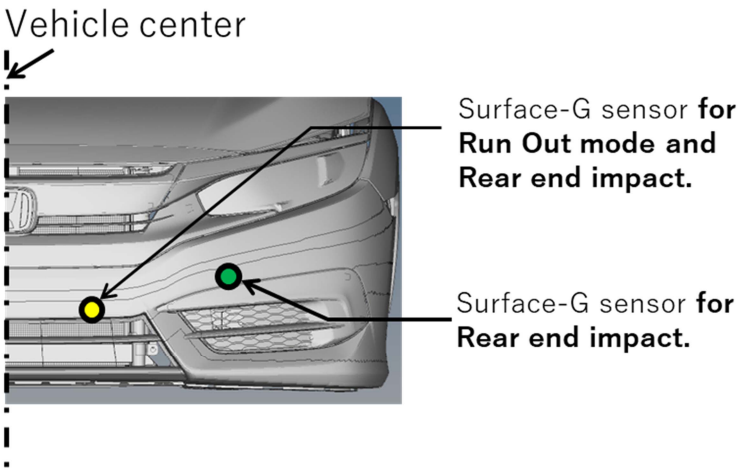

Figure 13. Surface-G sensor arrangement concept

CONCLUSIONS

In this paper, we devised the system for impact detection in bicyclist run-out and rear-end impact modes, which generate very small inputs, by adding surface-G sensors to a conventional pedestrian detection system and verified the performance of the resulting system by CBU impact test and simulation.

It was confirmed that bicyclists could be detected in run-out and rear-end impact modes by controlling surface-G sensor thresholds by means of coordination with ADAS. It was also confirmed that the conventional pedestrian detection system was effective for impacts with the central portion of the vehicle.

It was determined that an integrated impact detection system using a conventional pedestrian detection system with enhanced performance has possibilities for detection of bicyclist impact.

REFERENCES

[1] P. Seiniger, et al., 2017. "NEXT-GENERATION Active Safety and Testing: The Horizon 2020 Project PROSPECT." 25th ESV Paper No. 17-0254

[2] K. Nagatomi. 2013. "Pedestrian protection technology of vehicle." JSAE Motor Ring, No.36

[3] H. Takahashi, et al. 2013. “Development of pop-up hood system for pedestrian protection.” 23rd ESV, Paper No. 13-0262

[4] K. Nagatomi. 2005. "Development and Full-Scale Dummy Tests of a Pop-Up Hood System for Pedestrian Protection." 19th ESV, Paper No. 05-0113

[5] A. Akiyama, et al., 2001. "Development and application of the new pedestrian dummy." 17th ESV, Paper No. 17-0463

TITLE: OBJECTIFYING AND PREDICTING MOTORCYCLE ACCIDENT RISK THROUGH RIDING DYNAMICS

Andreas Hula
Austrian Institute of Technology – Center for Mobility Systems
Giefinggasse 4, 1210 Vienna,
Austria

Klemens Schwieger
Austrian Institute of Technology – Center for Mobility Systems
Giefinggasse 4, 1210 Vienna,
Austria

Peter Saleh
Austrian Institute of Technology – Center for Mobility Systems
Giefinggasse 4, 1210 Vienna,
Austria

Manfred Neumann
TU Wien - Institute of Mechanics and Mechatronics, E325
Getreidemarkt 9, 1060 Vienna,
Austria

Horst Ecker
TU Wien - Institute of Mechanics and Mechatronics, E325
Getreidemarkt 9, 1060 Vienna,
Austria

ABSTRACT

The danger of motorcycle accidents is ubiquitous during the otherwise relaxing and enjoyable activity of riding a motorcycle. The consequences can be severe and the economic burden, both on the individual and the state, is high. Yet, when wanting to prevent such accidents, it can be seen that they are hard to predict, due to the high complexity of individual factors playing a role in each single accident.

To tackle this issue and extract generalizable characteristica of driving dynamics, the authors present the findings of “viaMotorrad”, a project to obtain motorcycle dynamics data on selected roads in Austria and determine the risk of an accident at given road sections. This is a collaborative project by the Austrian Road Safety fund, between the partners Austrian Institute of Technology, TU Wien and KTM.

Through the use of supervised machine learning techniques we demonstrate that there are indeed generalizable factors in the driving dynamics at previous accident sites and use these factors to determine further critical road sections. These results are a first step towards an objectification of motorcycle driving risk and semiautomated risk assessment of roads for motorcycle riders. The method offers the possibility of identifying critical road sections through analysis of a small number of test drives.

INTRODUCTION

Within Europe, among road transport fatalities, a staggering one sixth are motorcycle riders or pillion passengers on a motorcycle. Our special focus, Austria, demonstrates an even higher number: the last 20 years have seen about 1850 motorcycle fatalities and about 66.500 injuries occurred nationally. The number of fatal accidents among motorcycle riders and passengers compared with the total number of traffic accident victims is also alarming: In 1992, the percentage of all fatalities was only 5.7%, while in 2017 a percentage of 20.0% set a new tragic record [1].

We identify two factors which evidently contributed to this outcome: Firstly, motorcycle safety had not been a primary concern compared to more common vehicles and improvements in the more general traffic environment (road layout, road conditions). Secondly, motorcycle use has increased substantially over the last couple of years (with both more registrations and more active use of motorcycles). While the total amount of motorcycle accidents is roughly constant [1], it appears that without specific measures for the safety of motorcycle riders, the otherwise declining number of accidents and fatalities for other vehicle categories will not be observed for motorcycle accidents, at least in Austria. This supports the need for a focus on the scientific study of motorcycle

accidents, since there is a multitude of possible causes in motorcycle accidents and these must be understood further reduce the risks that motorcycle riders face.

Illustrative results as well as the scope of the traffic safety project “viaMotorrad” will be presented in this paper. The underlying initiative aims to improve the safety of motorcycle drivers by collecting riding dynamics data. Following a study of previous accident data, combined with data of potentially critical locations based on the assessment by motorcyclists and focusing on frequently driven motorcyclists’ routes in Austria, road sections were clustered and selected for a unique investigation performed with the newly introduced motorcycle probe vehicle, MoProVe [2]. The goal of the project was to identify high accident-risk spots within the road network, utilizing data collected by MoProVe. The method developed in this project offers a means to locate critical sections within the road network, in order to carry out safety measures to reduce motorcycle accidents and injuries.

Ultimately, the intended outcome is to provide a hazard map of motorcycling dynamics for the selected roads. This map will be part of a general effort to objectify the potential safety impact for motorcyclists on the track. The hazard map could then be prepared for far more extensive road networks in the future. This could yield a priority ranking of road sections in terms of driver safety/risk and necessary steps to be taken to increase road safety for bikers.

The selection of the type of tracks and the individual motorcycle riders who helped to obtain training data for our method introduce natural limits of generalizability. However, an expansion of the data base to more drivers and yet more diverse tracks will be a means to reduce a potential bias in the future. Our result is that generalizable features in the driving dynamics around the locations of previous accidents can be learned by a supervised machine learning algorithm. This is a first step towards objective assessment of motorcycle accident risk locations through driving dynamics of multiple bikers on the same track.

MATERIALS AND METHODS

The project team was kindly provided with a motorcycle by KTM Sportmotorcycle GmbH (KTM) [3] and this motorcycle was equipped with special measurement systems by the TU Wien (TUW) and the Austrian Institute of Technology (AIT). The measurement systems gather all available driving dynamics data for the purpose of later analysis. The vehicle has a normal road approval, so that measurements can be undertaken under normal traffic conditions.

For the purposes of the project, the measurement vehicle had to fulfill a number of criteria: It should be equipped with modern on-board measurement systems, to provide an extension of the data collection of the externally added systems. Furthermore, it had to be user-friendly and provide access to the internal hardware and software features.

The KTM 1290 Super Adventure (see Figure 1) fulfilled all requirements. The motorcycle is powered by a 1300cc V-twin engine, mustering 160 HP (horse power) and a maximum torque of 108 Nm (Newton meter). Its dry weight is 222 kg. This machine provides a multitude of onboard systems such as Motorcycle Traction Control (MTC), Motorcycle Stability Control (MSC), Combined-ABS (C-ABS), Motor Slip Regulation (MSR) and a semi-active suspension system (SCU). These are dependent on numerous sensors, such as several brake pressure gauges, wheel speed sensors, a throttle position sensor and many more. System data is obtained via the vehicle CAN-bus, in addition to being collected and processed by separate data recording systems. Another advantage of this machine is the option to activate or deactivate assistance systems (i.e. the motorcycle offers to select different riding modes). This would make it possibly to imitate a more basic motorcycle, without additional features.

Figure 1. KTM 1290 Super Adventure equipped and instrumented as a Motorcycle Probe Vehicle (MoProVe).

Measurement systems

We illustrate the two main measurement systems that are available in the test motorcycle. Both systems contain a data logger, IMUs (Inertial Measurement Unit), additional sensors and interfaces to the vehicle's CAN-bus. There was some redundancy between the data acquisition by the independent IMUs.

Below, we present the two systems separately and compare the quality of their output within the experiment.

System B (Blue): The blue system is comprised of hard- and software by RACELOGIC [4], with the main component being a VBOX 3i dual-antenna data-logger. This VB3iSL is depicted in Figure 2 (a) besides a functional block diagram of its components in Figure 2 (b).

(a) (b)

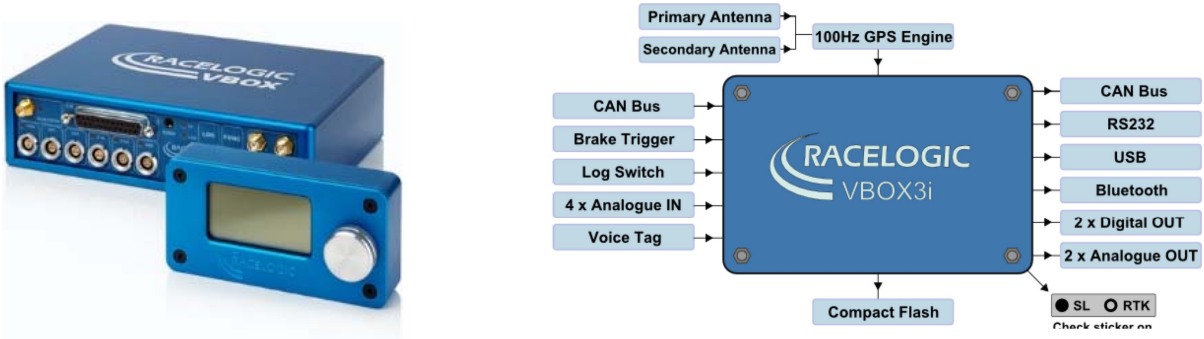

Figure 2. Picture of RACELOGIC data-logger VB3iSL with display unit; (b) Block diagram of Input and Output signals for data-logger VB3iSL (VBOX automotive, 2017).

A high-performance GPS engine employing twin antennas capable of providing a 100 Hz (Hertz) signal update rate for all GPS / GLONASS parameters is available on the VB3iSL. From the Doppler Shift in the GPS carrier signal both heading and velocity can be calculated with high accuracy. Additionally, the VB3iSL tracks the Russian GLONASS range of satellites. This benefits the system in that there are nearly twice as many satellites in range and thus the system maintains a stable satellite lock in places where GPS-only reception can lead to failures in data acquisition. With two GPS / GLONASS antennas simultaneously in use, measurements of signals such as slip angle, pitch or roll angle, yaw rate, true heading, lateral velocity and longitudinal velocity are feasible.

The quality of the system output is improved by two additional features. A DGNSS (Differential Global Navigation Satellite System) Base Station was included to further enhance the accuracy of positional measurements of the VBOX unit, through the use of differential correction data. Utilizing the additional signals from a Base Station, with a known fixed position, the difference between this known position and a position received via GPS/GLONASS can be accurately monitored. This correction signal can then be used to significantly improve the accuracy of the absolute position. While the 95% CEP (Circular Error Probable) is 3 meters for standard position measurements, the DGNSS-station allows a radius of 80 cm (centimeters) to be achieved.

Although the relative position accuracy is higher than the absolute position accuracy, it is yet further improved by an Inertial Measurement Unit (IMU, see Figure 3): The sensor on the MoProVe is a 3-axes accelerometer with additional 3-axes measurement of the angular rate. Through numerical integration of the measured signals, linear velocities and distances as well as roll, pitch- and yaw-angles can be calculated. Combining these postprocessed IMU-signals with the information provided by the GPS-antennas, numerical algorithms implemented in the system software can optimize the system output and return highly accurate position and velocity signals. This enables the system to continue its measurements at locations with weak (or no) GPS/ GLONASS satellite signals, e.g. in tunnels, as the system can rely on the IMU data.

(a) (b)

Figure 3. a) Picture of RACELOGIC Full HD camera system; (b) Inertial Measurement Unit (IMU) to measure 3-axes accelerations and 3-axes angular rates (VBOX automotive, 2017).

System R (Red): The other data acquisition system implemented on MoProVe is a measurement system specifically designed for motorcycle applications, while System B has been developed with a focus on application in automotive engineering. System R is called the 2D ([5], Debus and Diebold) system and it is a popular system with motorcycle racing teams worldwide. On MoProVe, it provides a supplement data source to the other system as the focus and features of this system are different from System B.

System R provides a data logger with dashboard display unit, a single GPS-antenna and two 6-axes IMUs, allowing it to be used as a stand-alone system in principle. With respect to these components, there is a functional redundancy provided by both systems. However, system R is more reliable and capable when it comes to the measurement of vehicle parameters. The logger of the 2D-system can record on up to 200 channels, with the sampling rate being as high as 3.2 kHz. The system provides 2x8 analog input channels with 16 bit (high-resolution) ADC (Analog to Digital Converter) available, several dedicated wheel speed input channels and two independent CAN-lines with full CAN routing [5]. Moreover, the logger and components are small in size, low in weight and robust, with low power consumption.

Comparison of Systems B and R: System R provides more flexibility than system B, since the sampling rate of system R is higher and therefore more accurate data is obtained. Also, more channels are available in system R. In addition to that, access to the motorcycle's CAN-bus system is easier with this system and many CAN signals can be recorded. To add to the already high number of sensors and signals accessible on the KTM bike, a separate steering angle sensor was also installed and its signal was sampled. Examples of measurable signals are Wheel speed signals, brake fluid pressure, throttle position, engine speed, gear position and brake operation.

For the purpose of measuring acceleration signals and angular rates, system R is superior to system B since two lightweight 6-axes IMUs provide data and the sampling rate can be set as high as 3200 Hz. Therefore, it can be seen that in-plane dynamics of the motorcycle, as well as stability and detection of unstable behavior, steering maneuvers, etc. are best studied by using system R.

The technical elements of system R are placed in a side case on the right hand side of the bike, while another side case on the left hand side is used for system B. Positioned at the very end of the luggage bridge, an aluminum "sensor bar" was placed, to hold all 3 GPS-antennas and the IMU of system B. Below the seat, the IMU of system R could be found, in the form of a tiny red box. The additional IMU of system R was contained in the GPS-antenna mounted on the sensor bar.

Measurements

The measurements were performed by experienced but not professional or trained test riders. We could not include new/amateur drivers as the measurement runs and tasks would have been very hard on a novice and we also could not risk the MoProVe being damaged. The authors acknowledge that the quality of the results also hinges on the number of test drivers and diversity of the observed driving dynamics. For this project, the stated aim was to investigate the feasibility and the possible quality of revealing motorcycle accident risk from driving dynamics. Thus, it would be essential that the method would yield instructive results without needing a huge amount of measurement data from many riders and that it could be applied even on a small statistical base of the sampled data.

Data was obtained on all selected road sections by each rider, several times. This turned out to be a crucial feature towards stable results, in that an "average ride" for each rider could be calculated and single events could be removed from the classification of the elements of the road section. Test rides took place during normal traffic hours and in a considerable number of rides it was necessary to eliminate events such as an overtaking maneuver or a hold-up behind an agricultural vehicle.

Six tracks in lower Austria and Styria were included in our study. We got access to single driver and frontal collision accident site data for all tracks dating from the year 2012 to the year 2015.

We used the smoothed (via a rolling average with a window of 60m) data of 9 dynamic variables (including X-, Y- and Z- accelerations, Yaw-, Roll- and Pitch-Rates) and their approximate derivates to set up our model.

Model

In a first step the obtained time-based data of the dynamic variables was transformed into location-based data for the 6 tracks under consideration (see [6] for details).

Our model (patent pending) itself is based on 3 core steps:

1. Determining "default" dynamics (common and/or averaged values) and extracting dynamics at known accident sites [7]. We smooth the location-based dynamics data by computing a rolling average of neighboring values, rather than the raw dynamics data.
2. Calculating a separation between the normal dynamics and the dynamics at accident sites [8], then using this difference to assign a value to each meter and using values at the accident sites to determine a limit value for each driver, [9][10].
3. Creating an overlay across all test drives, of transgressions of the limit values and determining the local maxima of a smoothed version of the resulting "warning surface" along the track.

We then consider the obtained local maxima as warning points along the studied tracks and assign to each of them a range of 100m in either direction (based on an assumed speed of about 70 km/h, and then assuming the "run up" and consequences of an accident may account for several (5) seconds of "influence" on the dynamics of

the recorded accident site), in which we consider driving dynamics to being potentially related to the observed maximum (dubbed the “Warning Area” around a maximum).

See Figure 4 for a schematic representation.

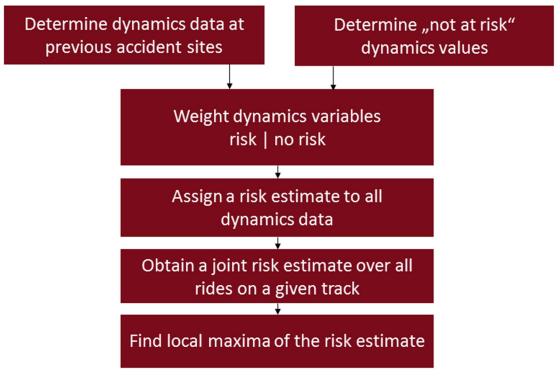

Figure 4. Summarized steps of the algorithm (from top to bottom).

An accident site is then considered to be “included”, if it is within the 100m area of a local maximum.

RESULTS

We fit our model according to the accident site data and driving dynamics of the 6 included tracks. We illustrate the outcome on the “Kalte Kuchl” track in Austria (Figures 5 and 6 below).

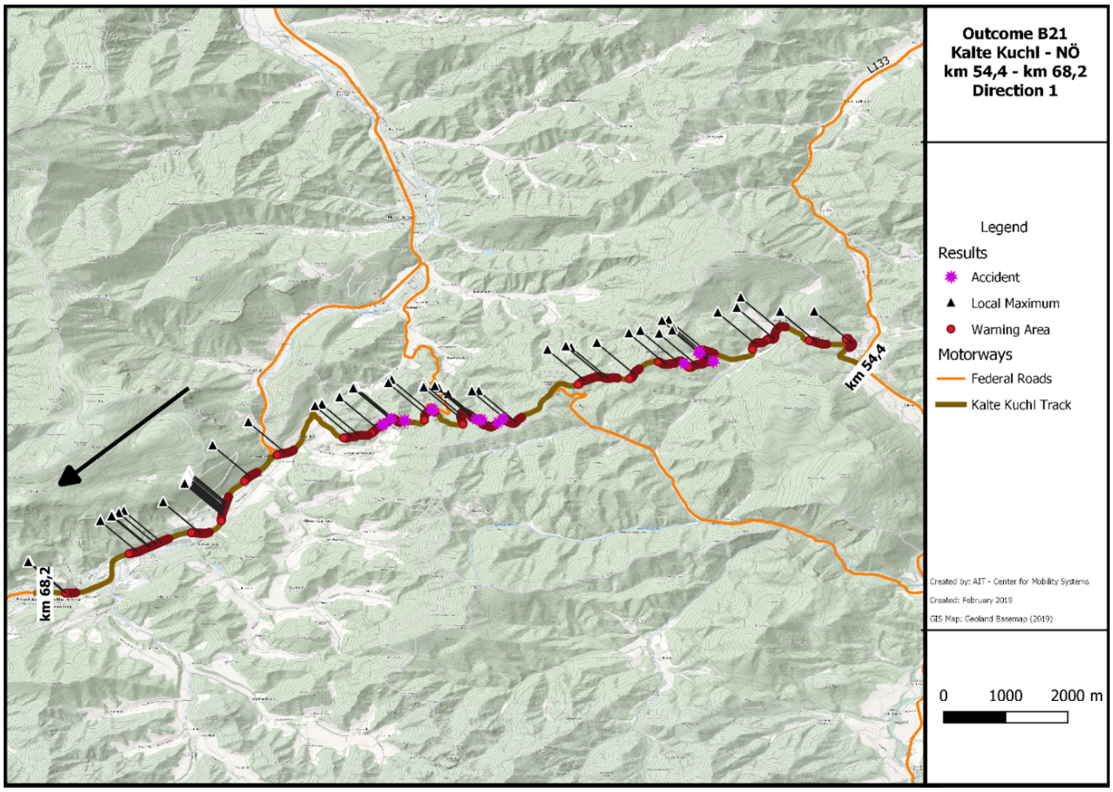

Figure 5. Kalte Kuchl track in Austria. Accidents (black stars), local extrema (tags) and extrema surrounding areas (red). Map created in QGIS 3.4. Driving direction is E to W, note arrow on the map.

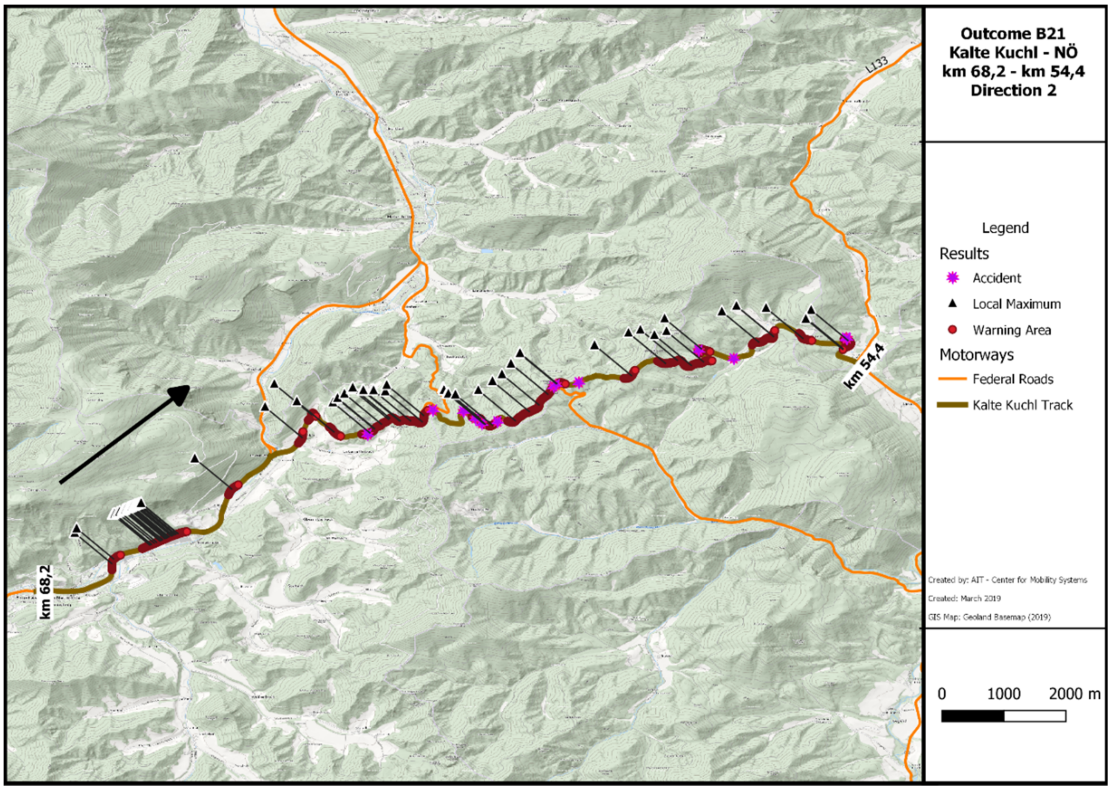

Figure 6. Kalte Kuchl track in Austria. Accidents (black stars), local extrema (tags) and extrema surrounding areas (red). Map created in QGIS 3.4. Driving direction is W to E, note arrow on the map.

Our solution hits 60% of actual accident sites, in a domain that is 35% of the total track length. The overall quality of our solution can be seen in Table 1.

Table 1.

Percentage of Accidents found and Total Area Covered

	Kalte Kuchl	All Tracks
Percentage Covered	45%	35%
Included Accidents	31	90
Percentage Accidents Included	74.2%	60%

Overall, we manage to include a substantial part of the known accident sites, while "covering" 35% of all tracks lengths. The Kalte Kuchl track specifically shows a high percentage of accident sites found, but also a larger proportion of covered areas. This is largely due to the high amount of serpentine shaped parts on the Kalte Kuchl track.

CONCLUSIONS

We present a model capable of identifying locations of locally heightened accident risk, by comparing test driver dynamics data to driving dynamics of the same drivers at given accident sites and overlaying the results of multiple drivers along the given track.

Given the primary locations of our local maxima (serpentine shapes and sharp curves), we conclude that the found locations are not random and the model manages to generalize hidden properties of at least a major portion of these accident sites.

We note that there are a number of maxima in the left area of Figures 5 and 6, even though no accidents have occurred there so far. Currently the method does not differentiate between "high level" local maxima (for instance local maxima with more than 50% of testdrives showing a limit value transgression) and "low level" local maxima (for instance local maxima with less than 20% of testdrives showing a limit value transgression).

We note that the local maxima in the left (western) part of the track would all be of the “low” type i.e. arising from only a small percentage of limit value transgressions. Making a difference between these two types of local maxima should further improve the quality of the predictions made by the method.

We are able to identify at least one potential spot of dangerous dynamics: The sharp-tipped curve that separates the left low-risk domain from the right high-risk domain. No accidents occurred there in recent years, but the observed dynamics are similar to the known accident sites used to fit the model.

We treat single person accidents and frontal collisions in this example. We used the dynamics and accident sites of a popular motorcycle track as basis to fit our model. The outcome of 60% accidents hit in 35% of the tracks covered suggests that there are objectifiable similarities in the driving dynamics occurring in at least a sizeable subset of observed accident sites.

Our results show, that the driving dynamics of multiple drivers provide a feasible means of objective identification of points of motorcycle accident risk, since we are able to include a considerable proportion of accident sites across 6 different tracks.

Limitations include the need to extend the available data and validate our findings more generally on tracks not currently related to the model. We note the need to provide a diverse and representative sample of motorcycle tracks and possibly driver types, in order to extract more robust and generalizable results. We also do by no means claim, that *all* motorcycle accidents, or even just single person motorcycle accidents, would be related *exclusively* to driving dynamics. Rather, we wish to contribute a certain level of predictability and generalizability to the difficult problem of identifying risky or dynamically demanding motorcycling locations.

Possible future applications include the identification of road infrastructure needs for motorcycle safety, based on the locations revealed by our algorithm.

Acknowledgements

This research was partly funded by the VSF Austrian Road Safety Fund [11]. The authors are grateful for the financial support.

KTM Austria [3] generously provided the motorcycle used in these studies.

The authors would like to thank (in alphabetic order) Matthias Hahn, Till J. Kniffka, Johann Schindele and Peter Unterkreuter for their significant support in instrumenting, adapting and riding MoProVe. We would also like to thank Stephan Wittman and Alexander Genser for the creation of QGIS templates and the preparation of geospatial data, used in the project.

References

[1] Statistik Austria 2017

[2] Ecker, H. and Saleh, P. 2016. "MoProVe - A Probe Vehicle for Traffic Accident Research", EVU Proceedings 25th Annual Congress, EDIS - Editing Centre of University of Zilina, ISBN: 978-80-554-1260-3; S. 29 – 41

[3] KTM Sportmotorcycle GmbH

[4] VBOX automotive, VBOX 3i Dual Antenna | 100Hz Vehicle Dynamics Measurement

[5] 2d-datarecording, 2D Debus & Diebold Messsysteme

[6] Schwieger K., Saleh P., Hula A.; Ecker H. and Neumann M.,2018. “viaMotorrad – Can motorcycle safety be measured?” ,12th International Motorcycle Conference Cologne

[7] McLachlan, G.J. 1988, "Mixture Models: inference and applications to clustering", Statistics: Textbooks and Monographs, Dekker

[8] Duda, R.O., Hart, P.E. and Stork, D.G. 2001. "Pattern Classification", Wiley, New York

[9] Draper, N.R. and Smith, H. 1998“Applied Regression Analysis”, Wiley, New York

[10] Seber, G. A. F. and Wild, C. J. 1989 „Nonlinear Regression", John Wiley and Sons, New York

[11] VSF Austrian Road Safety Fund

GVTR: A GENERIC VEHICLE TEST RIG REPRESENTATIVE OF THE CONTEMPORARY EUROPEAN VEHICLE FLEET

Florian Feist, Nisha Sharma, Corina Klug
Graz University of Technology
Austria

Franz Roth
Audi AG
Germany

Stefan Schinke, Alexander Besch
Volkswagen AG
Germany

Florian Dornbusch
Bertrandt AG
Germany

ABSTRACT

In the ACEA funded project ProPose a generic vehicle model was developed: (1) It was specifically developed for replicating the leg-loads in pedestrian accidents. (2) It is representative of the contemporary European sedans meeting FlexPLI requirements. (3) It is available in numerical and experimental environment. (4) It is intended for investigating the performance of aPLI, for validating numerical models of advanced legform impactors like aPLI and for the comparison of kinematics and responses of different HBM lower limbs.
The structural impact response of vehicle front ends was captured with impactors: A rigid cylinder was equipped with 20 contact force transducers along its axis. The impactor's motion was prescribed, such that an intrusion of (up to) 120mm was consistently achieved. Tests were conducted at four levels along the vehicle height (spoiler through bonnet leading edge) and at six positions along the lateral axis of the vehicle. The contact forces of individual force transducers were assigned to the four contact regions (spoiler, bumper, grill and bonnet leading edge). Impactor tests were conducted against nine sedans, eight SUVs and three sportscars. For each vehicle category median force-penetration characteristics were established. The geometry of the CoHerent models was adopted (and cross-checked against the median reference lines established in the study ProPose).
In the numerical environment the GVTR was tested in impacts with full human body models, an isolated leg with an upper body mass and a beta-release of aPLI. In the experimental environment the GVTR was tested with aPLI and FlexPLI. Body loads in GVTR-vs-HBM and a selected vehicle-vs-HBM match very well. The same applies when comparing full HBM and isolated leg loads.
The study included vehicles provided by German, Czech and French manufacturers. The GVTR's structure and geometry is very simplistic for the sake of repeatability, robustness, testing costs and avoidance of error sources in the numerical model of GVTR.

MOTIVATION

In current pedestrian protection testing a flexible pedestrian legform impactor (FlexPLI) is applied, which has a significantly higher biofidelity compared to the EEVC pedestrian legform impactor [1]. Still, both (FlexPLI and EEVC WG17 legform) consider the lower limb only. Such FlexPLI fails in robustly replicating the bending loads in all vehicles (low and high bumper vehicles), particularly in the femur, due to the lack of the upper body [1,2]. In order to further improve the biofidelity of flexible legform impactors, in various attempts an upper body mass was added, eventually leading to impactors like aPLI, which development was largely based on the extensive numerical studies with Human Body models (HBM).
Generally, research and development in the area of pedestrian protection largely relies on numerical simulation methods. Such not only representations of the human body (through HBM), or antropometric test devices (like aPLI) in numerical codes are needed, but also of the vehicle. Ideally, a vehicle model for the development of new pedestrian impactors shall replicate the shape and the structural behaviour of the contemporary vehicle fleet, while not being just the numerical representation of a specific vehicle-make or -model. While providing realistic structural response upon impact loading, the vehicle model should be very simple (almost over-simplistic) in terms of number of materials used, boundary conditions and contact interactions.

INTRODUCTION

The project ProPose is funded by ACEA, the European Automobile Manufacturers' Association. The first phase of the project ProPose investigated injuries to the upper femur and pelvis using the 'Generic Parameterisable Vehicle' (GPV), that was established in LS-Dyna for that purpose [3]. GPV allows to distinguish between the injury risk induced by the structural impact response and the vehicle shape. In the second phase of ProPose also injuries to the lower leg were considered. To close the gap between the numerical and experimental world, a generic vehicle test rig (GVTR) was required, allowing a side-by-side comparison of the purely numerical human body models (HBM) and anthropometric test devices (ATD).
This paper summarizes the development of GVTR v0 and v1, as well as the application of v0 in testing of FlexPLI and aPLI. The GVTR shall provide an optimal framework for validation of ATDs. Hence there are a number of requirements, that arise. The GVTR shall

- provide good repeatability and reproducibility,
- provide realistic and representative structural response upon impact,
- rely on well validated and generally available material models,
- be robust against fabrication and manufacturing tolerances,
- provide simple and time-efficient test-setup,
- provide separated load-paths, not influencing the others,
- be suitable for oblique testing,
- be representative in terms of shape of the contemporary European vehicle fleet.

METHOD

In the following sub-chapters the methods for the creation of GVTRv0 and v1 are summarized: (1) establishing the shape, (2) establishing the structural impact response and (3) designing and manufacturing – each seperated for GVTR v0 and v1.

Establishing the Shape

GVTR v0

GVTRv0's shape is based on the mid-section contour of the generic CoHerent family car, which was developed for EuroNCAP [4]. The interrelations between GPV, GV, GVTRv0 and GVTRv1 are outlined in the chapter 'Discussion'.
The outer contour of 19 contemporary and frequently sold vehicles (market introduction: 2009-2015) were provided by ACEA members, covering four vehicle categories. Only vehicles that were categorized as Sedan (n=6) were considered for GVTR v0. The mid-section contour of each vehicle was approximated with eight bezier-curve segments, each governed through six parameters (due to tangency conditions, the total number of parameter reduces to 29). Then the median of each parameter was established, leading to the CoHerent GV sedan mid-section contour [4]. For the GVTR v0, though, the centreline contour was approximated through four straight lines, by connecting SP1 with BP1 and BP2 with BP3 to form spoiler and bumper, respectively (Figure 1). For BLE a 120mm plane was placed centrally on BL1 at an angel of 50° relative to the horizontal. GRL connects the bumper's upper edge with the BLE leading edge.

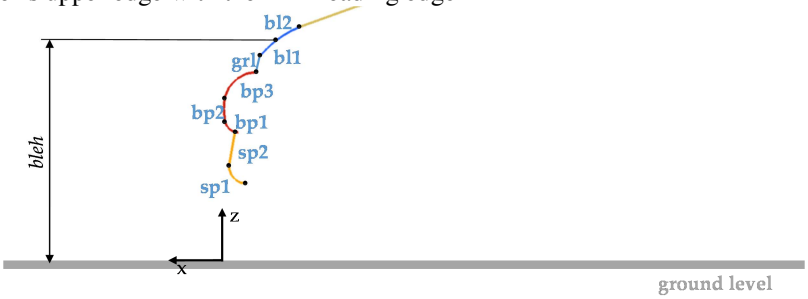

Figure 1: CoHerent GV mid-section curve (exemplary depiction of the approach – shape is made up)

GVTR v1

ACEA members provided the reference lines (spoiler, bumper and BLE reference lines) of 20 Flex-PLI compliant vehicles, covering three vehicle categories: sedan, SUV and sportscar. Further, the OEMs provided ground offsets, i.e. an z-offset which is common for the respective vehicle model. Reference lines were discretized in 50mm steps (y-coordinate). Z-coordinates were offset with the provided ground offset. The x-coordinates were adjusted such that the most forward point (of SPL or BMP reference line) is zero. Then for each discrete y-position (0, 50, 100, …) the median x- and z-coordinate were established. Doing so the median

reference lines for each vehicle category were established. Figure 2 shows the median reference lines in red – and the individual lines in light grey.
GVTR v1's shape was established in the following way:

- BLE segment: A 120mm line placed centrally on the mid-section BLE point and inclined by 50° relative to the vertical. The 120mm are based on the assumption, that the area lying 60mm ahead and behind (measured along a tangent to the BLE-point) are considered the contact area 'BLE'. At the same time this distance covers 6 of the 20 contact force transducers on the impactor (see sub-chapter 'Establishing the Structural Impact Response').
- GRL segment: An oblique line going from the uppermost BMP point to the leading BLE point, leaving a gap of 25mm to the BMP and BLE segment. The 25mm distance between the panels are considered sufficient to prevent any trapping of the ATD.
- BMP segment: Based on impactor testing (described later), the height above ground of the maximum force at an intrusion of 80mm was established for each vehicle. Then the median height of these maximum force levels was established, resulting in a height of 465mm above ground. For the BMP segment a vertical line was placed centrally on that point (x=0, z=465). The length of the line is adjusted such that the GRL segment goes through the mid-section bumper reference line (leading to a BMP line length of 145mm, a SPL line length of 145mm and a GRL line length of 120mm)
- SPL segment: A vertical line going from mid-section SPL point to a point lying 25mm below the lowermost BMP line. Again the 25mm are based on the consideration, that trapping of ATD parts between the deformed panels shall be prevented.

Just like in GVTRv0, the origin of the vehicle coordinate system is such that the x-y-plane coincides with the ground. The x-axis is pointing forward, the y-axis to the left and the origin of the x-axis coincides with the vehicles leading point.

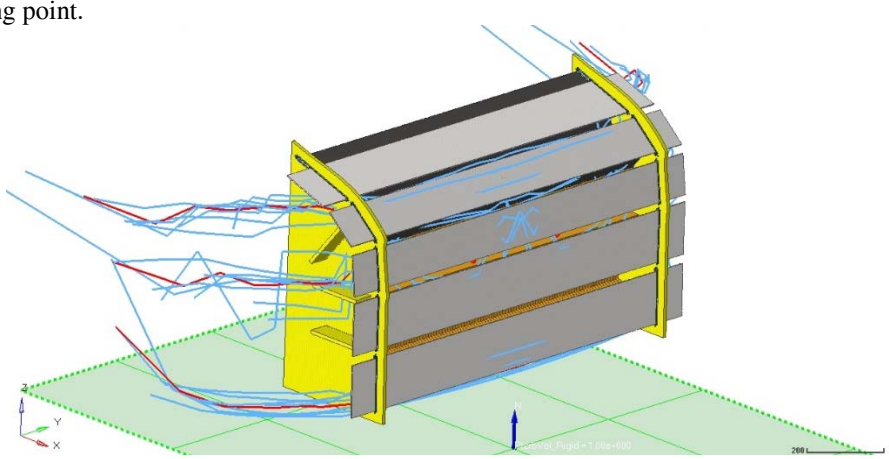

Figure 2: GVTR v1 load path segments (light grey) overlayed with median reference lines (red) and individual reference lines (light blue)

Establishing the Structural Impact Response

GVTR v0

The force-penetration corridors for GVTRv0's are based on the corridors established in the EuroNCAP funded project CoHerent [4]: A rigid cylindrical impactor (length=400 mm, radius= 60 mm, mass= 6 kg) was propelled at 11.1 m/s (i.e. 370 Joule) against the spoiler, the bumper, the bonnet leading edge and the bonnet of the 19 sample vehicles. The tests were conducted to the vehicle's centreline and to a lateral offset position. The simulations were run until the impactor returned to the initial position in the unloading phase. The contact force and the impactor-displacement were used to derive force-deflection curves for each impact location.

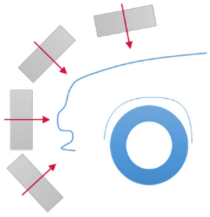

Figure 3: Impactor Testing – GVTRv0: Oblique spoiler test (SPV), horizontal bumper test (BMP), oblique BLE test and oblique bonnet test (BNT)

The number of vehicles per category was limited. Therefore it was decided [5] that the median, maximum and minimum force-deflection characteristics are established based on all vehicles in the study. This seemed feasible

(see Figure 4) since median curves showed comparable behaviour and differences within a category were found higher than differences between the categories.

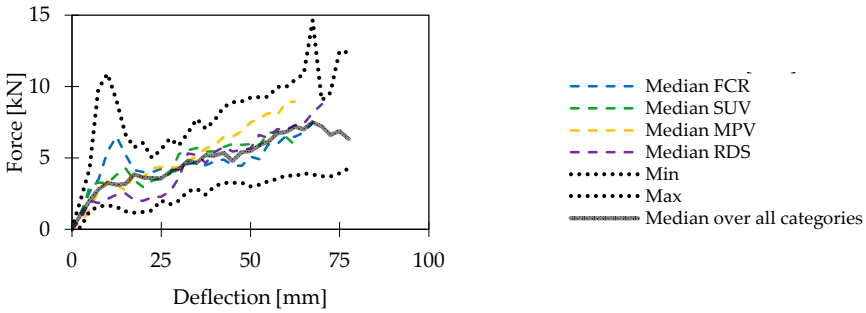

Figure 4: Median force-deflection characteristics at bumper centreline, for different vehicle categories [5]

GVTR v1

A rigid impactor with the same dimensions as in GVTRv0 was used. The following modifications were introduced:

- The impactor's motion was pre-scribed such to gain a consistent intrusion of 120mm.
- The impactor's face was covered with 20 force transducer, to distinguish between contact forces generated by the respective contact area or by the adjacent contact area.
- A horizontal spoiler test was introduced.
- The bonnet impact test was dismissed.
- The vehicle was tested at the centre line and at five lateral offset-positions.
- Vehicle sample was reduced to Flex-PLI compliant vehicles. Further the category 'MPV' was dismissed.

Test Areas or impact points along z-axis (height) were established in the following way – see Figure 5):

- Spoiler impact, horizontal (SPH): Upper edge of impactor aligns with horizontal line 100mm above spoiler reference line (SPR). The SPR is established just like the LBR but with a 45° contact line)
- Spoiler impact, oblique (SPV): Impactor centre is aligned with SPR
- Bumper impact, horizontal (BMP): Impactor centre is aligned with a point 50mm below upper bumper reference line (UBR)
- Bonnet leading egde impact, oblique (BLE): Impactor centre is aligned with BLE

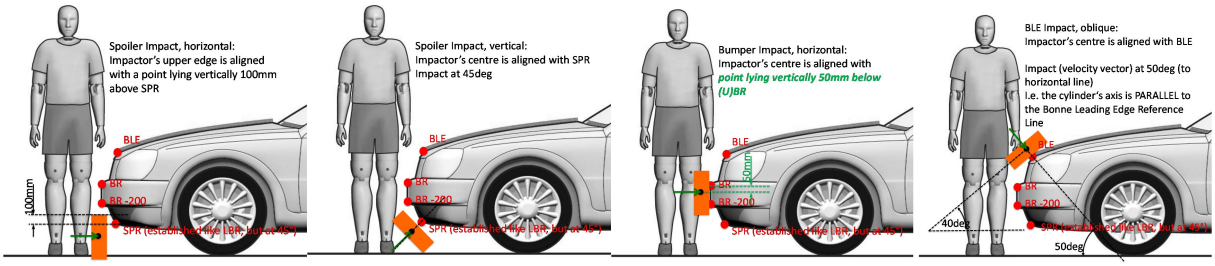

Figure 5: Impactor Testing – GVTR v1 (SPH, SPV, BMP and BLE Test) (Picture of Vehicle: EuroNCAP)

Tests at each z-location are conducted six times, i.e. at centerline, and five offset positons. The two outer impact points are tested at 15 and 30 deg (angle between displacement vector and vehicle's x-z-plane) – see Figure 5.

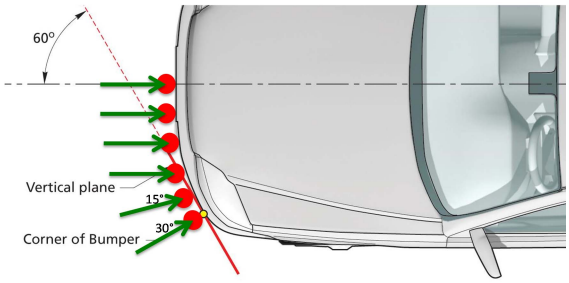

Figure 6: Impactor Testing – GVTR v1 (lateral offset positions) (Picture of Vehicle: EuroNCAP)

The impactor may contact multiple contact areas at a time. To distinguish the effect of adjacent contact areas on the overall contact force, the contact between impactor and vehicle is established through multiple sub-contacts

(contact rings). Contact forces per contact areas are summarized by adding the sub-contact forces. I.e. Contact forces established between impactor and grill in the BLE test are assigned to the contact interface "grill" – see Figure 7. The contact force established over the entire length of cylindrical impactor is denoted as e.g. "BLE all" (=green, orange and magenta in Figure 7). The contact force that can be attributed to the BLE only (=orange) is denoted as 'BLE only'.

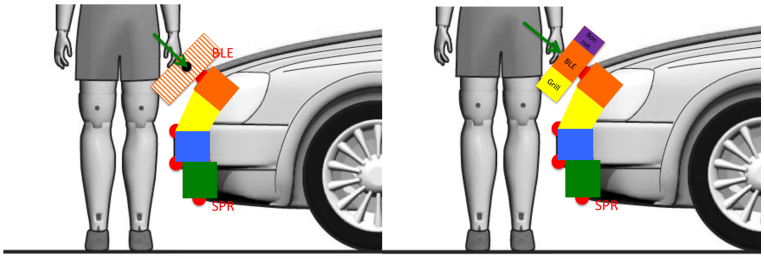

Figure 7: Impactor Testing – GVTR v1 (contact force transducers) – example BLE test (Picture of Vehicle: EuroNCAP)

For each impact area (SPH, SPV, BMP, BLE) and lateral impact location (Loc #1 through #6) 10, 50 and 90 quantile curves were calculated based on the test curves of each vehicle (after offsetting and discretizing the abscissa values at 1mm stepwidth) – see Figure 8. These loading and unloading curves were established for sedan, SUV and sportscar. Further it was distinguished between 'only' (contact force associated with a specific contact area) and 'all' (total contact force, possibly including the contributions of adjacent contact areas).

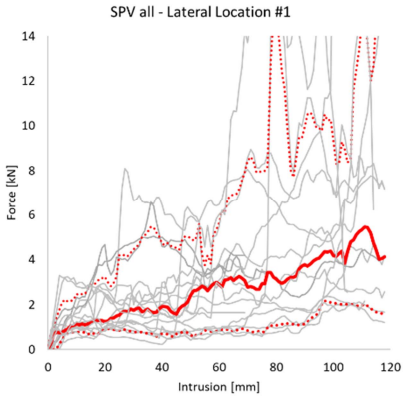

Figure 8: Example for loading curves established in the oblique spoiler impact at vehicle centreline. Solid red line: median curve, dotted red lines: 10 and 90th percentile, grey curves: individual vehicle test results, Sedan only

Results for two vehicle categories (SUV and sedan) are shown in Figure 9 ('all'). The red solid curve is showing the median force penetration curve, established from the median of each lateral impact location (denoted as LOC1 through LOC6).
In general, the structural responses are surprisingly different in the individual vehicles (see Figure 8). The median curves, however, clearly show different structural responses between load paths: i.e. a compliant spoiler, a bumper with increasing load levels starting at 70mm, and a BLE which offers substantial crush space at forces less than 10kN.
Please refer to the Appendix for a complete set of median loading and unloading curves for the vehicle category sedan (Figure 20 and Figure 21).

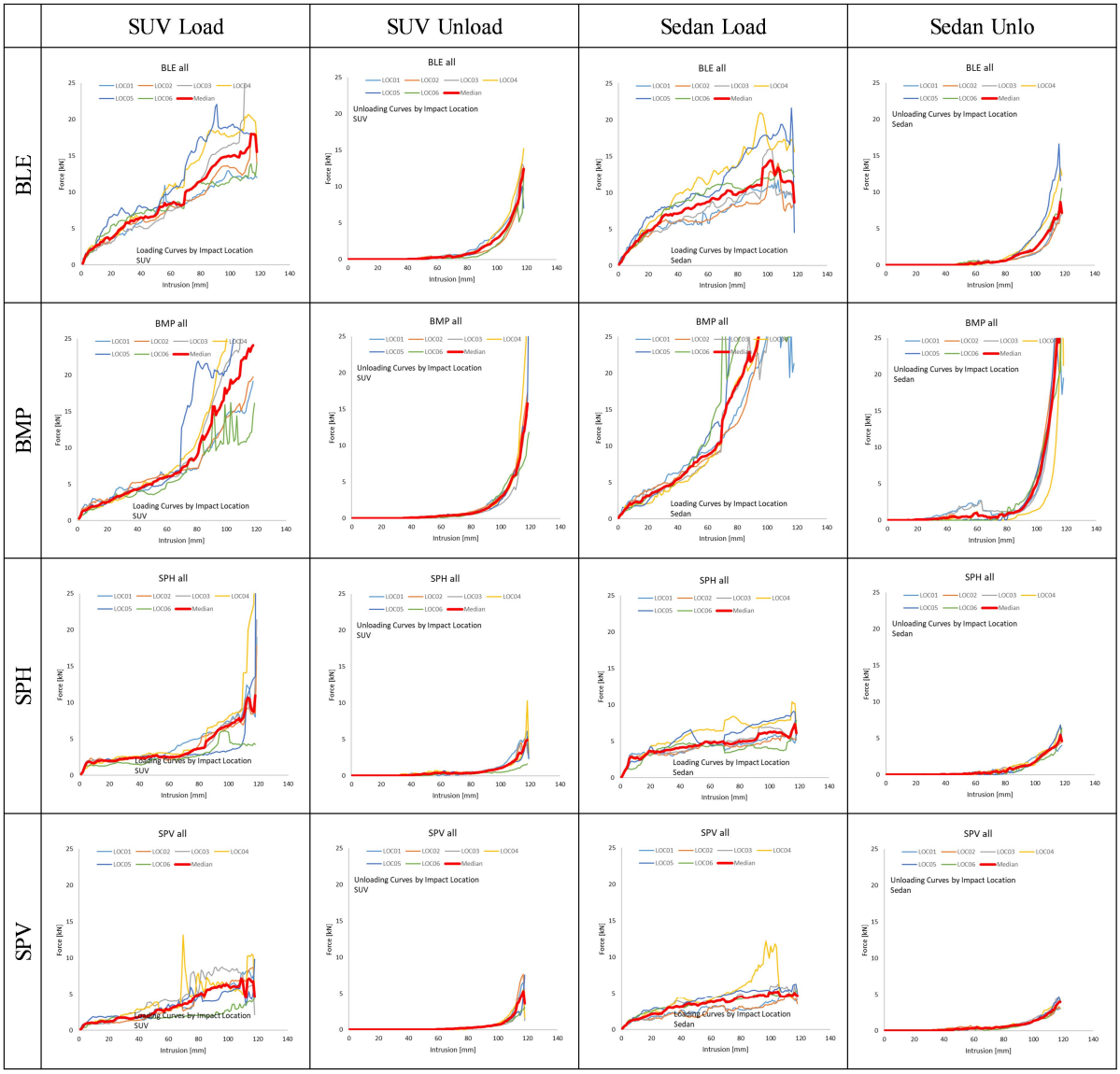

Figure 9: Median force loading and unloading curves by contact area and vehicle category (Sedan and SUV).

As indicated the impactor test regime was changed in the development of GVTRv1. The approach for establishing the median curves was modified, too:

- The CoHerent GV study median curves shown in Figure 13 and Figure 10 are based on centerline impacts only, while the ProPose GVTRv1 study median curves are based on centerline and five lateral offset impacts. This appeared sensible since the GVTR shall be representative in terms of the structural impact response over the entire width of the vehicle.
- The CoHerent GV study median curves are based on all vehicles, while the ProPose GVTRv1 study median curves are based on sedans only (for SUV and Sportscar separate median curves were established)

Given these differences the median curves of the CoHerent GV study (dotted curves) and the ProPose GVTRv1 study (dashed curves) still are quite similar –see Figure 10.

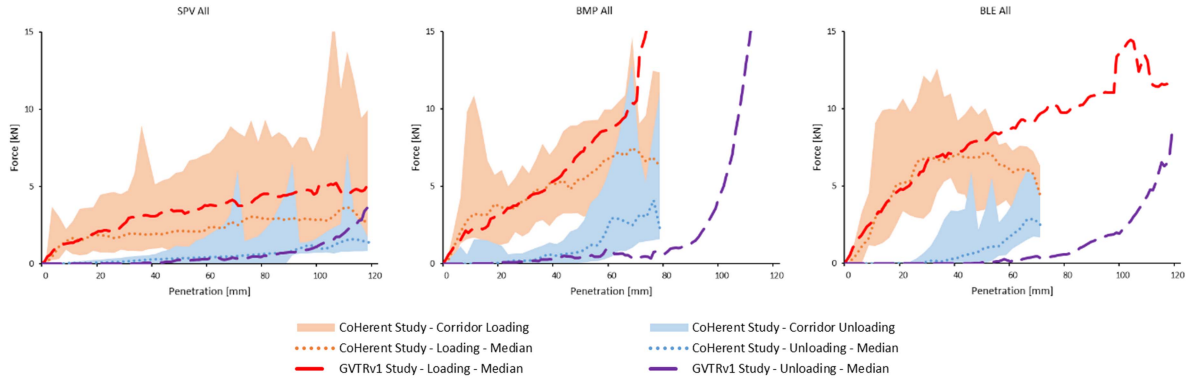

Figure 10: Comparing median curves of CoHerent GV study(dotted) and ProPose GVTRv1 study (dashed)

Designing and Manufacturing of GVTR v0

As mentioned in the introduction, the model shall be simple, to prevent any disparities between the virtual and physical model. Such, any machining, shape forming and joining (e.g. adhesive) shall be kept to a minimum. Ideally panels shall not be moulded or heat-formed, to ensure homogenous cross-sections and prevent any initial strains. The foam materials shall be extracted from the core of large EPP blocks, and all outer faces shall be machined consistently, to provide homogenous densities and interfaces properties (friction). Cavities in the EPP blocks shall be prevented.

The fasciae of real vehicle front ends are mostly made of polypropylene, being 2 to 3mm thick. The energy absorbers in bumpers are mostly made of expanded polypropylene (EPP) with densities between 30 and 60g/l. Hence it seemed reasonable to rely on these two materials only. Clearly there are other materials that might have been used for the purpose of energy absorption (i.e. tubes or honeycombs). The advantages of EPP (rebound characteristics, costs, robustness against dimensional tolerances, isotropy) are outweighing its drawbacks (weak dimensional accuracy, prone to fractures, …) by far.

The two components have distinct duties (see Figure 11):

- The EPP blocks shall replicate the structural impact response, i.e. the loading and unloading behaviour.
- The PP panels shall distribute forces and provide realisitic fricitional properties and a smooth contact interface.

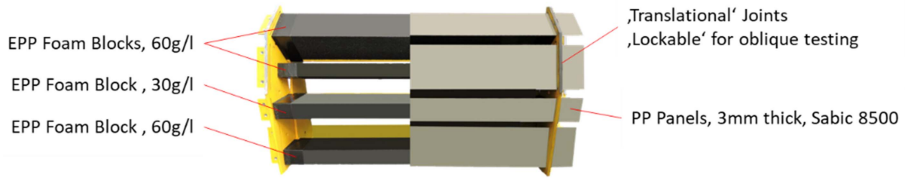

Figure 11: Design of GVTR v0

Both, in GVTR v0 and v1 the panels are floating in the lateral direction. Attempts to fully constrain the panels at the outer edges revealed that a considerable amount of internal energy builds up in the PP panels. In that case not only the EPP but also the PP would contribute to the structural impact behaviour. From a standpoint of numerical modelling this is undesired: It would require that two accurate and fidelic material models are available. Further fully constrained panels distribute intrusions over a wider area in lateral direction. This in turn would require very slim EPP block cross-sections, that tend to buckle or break. Hence the panels were kept unconstrained in y-direction. To allow for oblique testing (i.e. the rig is rotated about its vertical axis), the panels can be locked at one side (see Figure 11).

To minimize the influence of density deviation within one foam block, the deformation elements are milled from the same defined positions each time (see Figure 12). Additionally, reference cubes are being made for material samples. Dimensional accuracy and weight of each block are documented by the manufacturer for quality check and validation.

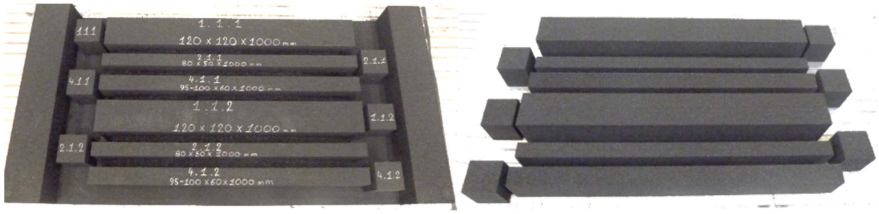

Figure 12: Milling of foam blocks

RESULTS

In the following sub-chapters the results with GVTRv0 and v1 are summarized: (1) impactor testing (for GVTRv0 and v1), (2) study with aPLI and isolated leg (GVTRv0 only) and (3) repeatability (GVTRv0 only).

Impactor Testing

GVTR v0

For GVTR v0 the same corridors as those for the GV [5,6] were applied. Figure 13 shows the corridors for SPL (left), BMP (middle) and BLE (right). The brownish shaded areas show the loading-corridors (minimum to maximum). The light bluish shaded areas show the unloading corridors. Median loading and unloading curves are shown by brownish and bluish dotted lines, respectively. The green solid curve is showing the structural response of the current CoHerent GV. The red solid curve is showing the structural impact response of the GVTRv0.

While CoHerent GV is meeting the median force-penetration curve quite well, it is apparent that GVTRv0 is rather meeting the upper, the maximum corridor. This is by purpose: The numerical study indicated that the median corridors can be met quite well when using lower density foam blocks (EPP 30g/l). For the sake of robustness (to prevent failure or fracture in the BLE and SPL foam blocks) ACEA members opted for higher density foams. In case of the SPL loading ACEA members argued that the oblique loading of the spoiler (load case abbreviated with SPV) might overestimate the compliance (underestimate stiffness). Hence it was decided to employ higher density foams and to rather fit GVTRv0's structural impact response to the maximum corridors.

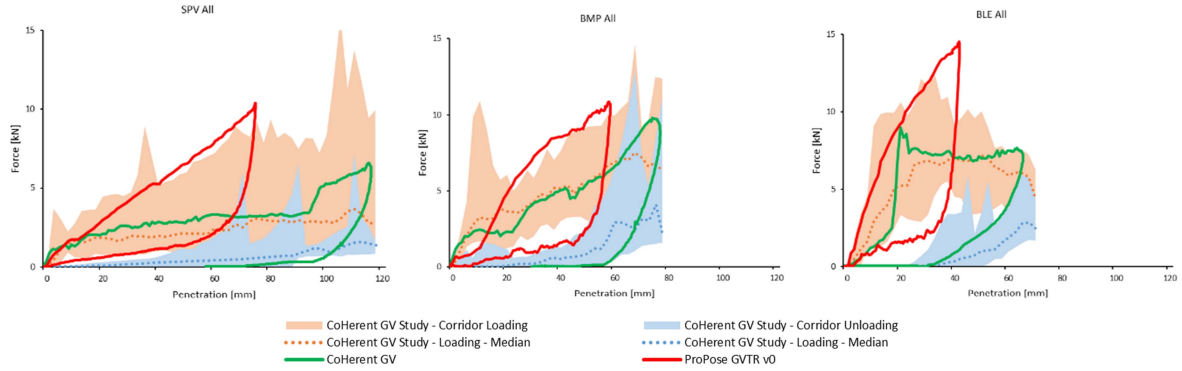

Figure 13: Corridors for GVTR v0 and comparison of CoHerentGV and GVTRv0 force penetration behaviour [4]

GVTR v1

The numerical model of the GVTR v1 meets the target curves (median loading and unloading curves) fairly well – see Figure 14. For the sake of robustness (e.g. to prevent failure of the foam-blocks due to shear stresses or to prevent global buckling of the foam blocks), the maximum penetration was limited to 80mm for BLE and BMP, and to 100mm for the SPL.

These assumptions were based on a numerical study with the "ideal" GVTRv1, which met the median force-deflection curve up to 120mm (but which appeared critical in terms of foam failure in a real, physical test rig). It was found, that the maximum intrusions in simulations with HBM and aPLI (at 40kph impact velocity) against that 'ideal' GVTRv1 reached roughly 40mm in the BLE, 60mm in the grill area, 55 in the BMP and 65mm in the SPL area. Some additional crush space is provided for cases where tests are performed at higher impact velocities.

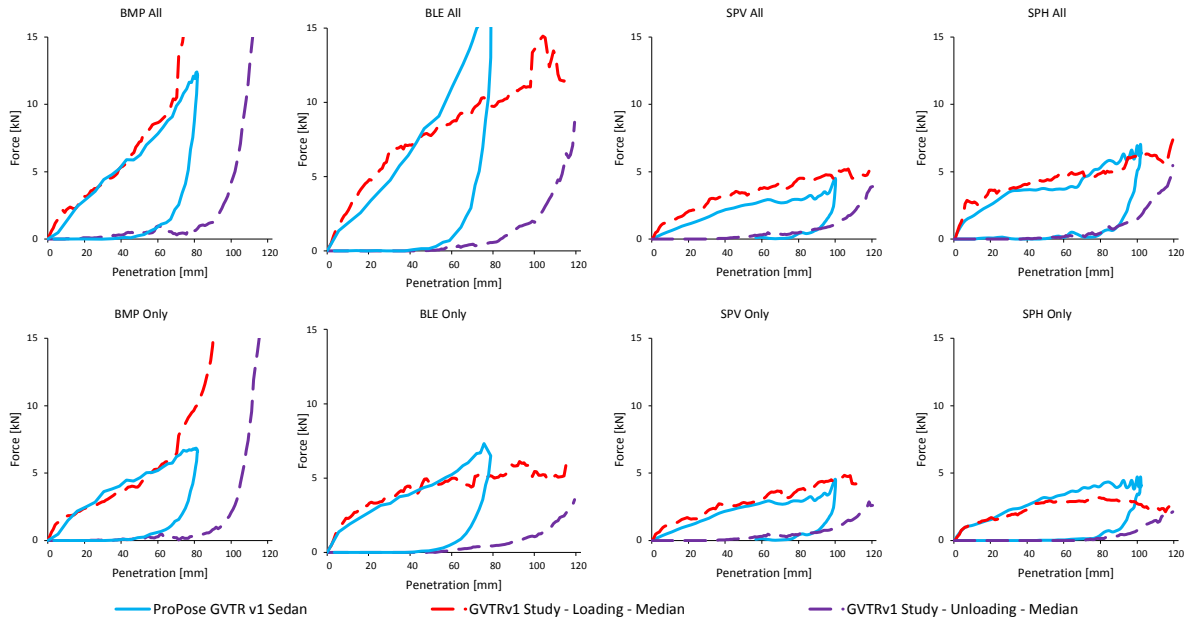

Figure 14: Behaviour of numerical GVTR v1 (solid) versus median loading and unloading curves (dashed)

Study with aPLI and isolated THUMS leg

GVTRv0

The GVTRv0 allows comparing the response, the measurements and kinematics of various impactors and models side-by-side. The following models and impactors were employed in a first study (see Figure 15):

- aPLI model generously provided by ATD-MODELS as a pre-release beta (atd-aPLI-d00.11) [7],
- THUMS v4.02 positioned in gait posture according to EuroNCAP Technical Bulletin TB024 [6], i.e. the struck side leg trailing.
- THUMS isolated leg with upper body mass resembling the upper body mass of aPLI (leg posture consistent with THUMS in gait posture)
- aPLI physical legform impactor. Tests were conducted by Bertrandt.
- flexPLI physical legform impactor. Tests were conducted by Bertrandt.

aPLI and THUMS isolated leg are not identical in terms of length, mass and mass-distribution. Therefore various approaches were investigated (like scaling of the length and/or mass, alignment of hip, knee or sole, …), to allow for a side-by-side comparison with aPLI and flexPLI. Results of that comprehensive study will be published elsewhere. Here only two approaches will be shown: (1) The knee of THUMS isolated leg aligned (abbreviated as “knalgnd”) with the aPLI knee and (2) the ground aligned THUMS (assuming a sole-thickness of 25mm), abbreviated as “grnd”.

Figure 15 shows a comparison in terms of kinematics: In simulations with HBM we find that the knee rotates about the local x-axis first. Starting with 40ms the femur starts to rotate (about the long bone’s axis, i.e. the local y-axis), allowing for some flexion (local z-axis). In the isolated leg simulations, the rotation about the femur’s long bone axis induces a rotation of the upper body mass. Seemingly more rotation about vertical axis is induced in the ground aligned isolated leg test. In THUMS the rotation about the height axis is to the opposite direction and generally smaller.

In gVTRs numerical model we find more bending of the BMP panel in the unloading phase – possibly induced by the lateral translational joint. Based on these observations the height of the bumper panels in GVTRv1 was increased (as this did not occur in the other, higher panels).

Figure 15: Kinematics in experiments and numerical simulations against GVTRv0

To allow for a comparison in terms of x-moments about femur and tibia cross-sectional force/moment transducers were included (10 along tibia and femur, each). At each cross-section a local coordinate system, that is re-adjusted at each time-step, was introduced, with the y-axis pointing towards the knee and the z-axis

pointing towards the struck side. For a comparison with aPLI those cross-sections, that were closest in ground-aligned THUMS in gait-posture to that of aPLI were selected. The sections at a height above ground of 812, 732 and 652mm were selected to resemble the Femur 3, 2 and 1 transducers in aPLI, respectively. For Tibia 1,2,3 and 4 the sections at a height of 383, 303, 223 and 143mm above ground were selected. In the knee aligned simulations, the selected cross-sections along tibia and femur in THUMS remained unchanged. In other words: The z-positions of the moment transducers in aPLI and in the ground-aligned THUMS ('grnd') are about the same. This is not the case in the knee-aligned THUMS ('knalgnd').

To measure the elongations of ligaments in THUMS, discrete elements along the ligaments' edges were introduced. The total elongation was determined by averaging the elongation of the 4-5 ligament edges, which are calculated by adding up the elongations of each single discrete element along the edge. Clearly, there might be other reasonable approaches to that, but this seemed the most straight forward and reproducible approach.

It was found that the numerical model of aPLI , though being a beta version (atd-aPLI-d00.11), matches tremendously well in terms of moments measured in femur and tibia (curves not shown). Further it was found, that the femur moments determined in the THUMS isolated leg are matching very well in terms of peak-values (curves not shown). This is not the case in the tibia. Results will be published later.

When comparing the results of full THUMS (purple curve) and THUMS isolated leg (orange curve), it appears, that moments in the femur are higher in the isolated leg. The same is in the elongation of MCL.

When comparing the knee-aligned (grey) and the ground aligned (orange), it appears that the femur moments in the knee aligned are smaller, in particular next to the knee joint (Femur1). In tibia hardly any difference can be seen.

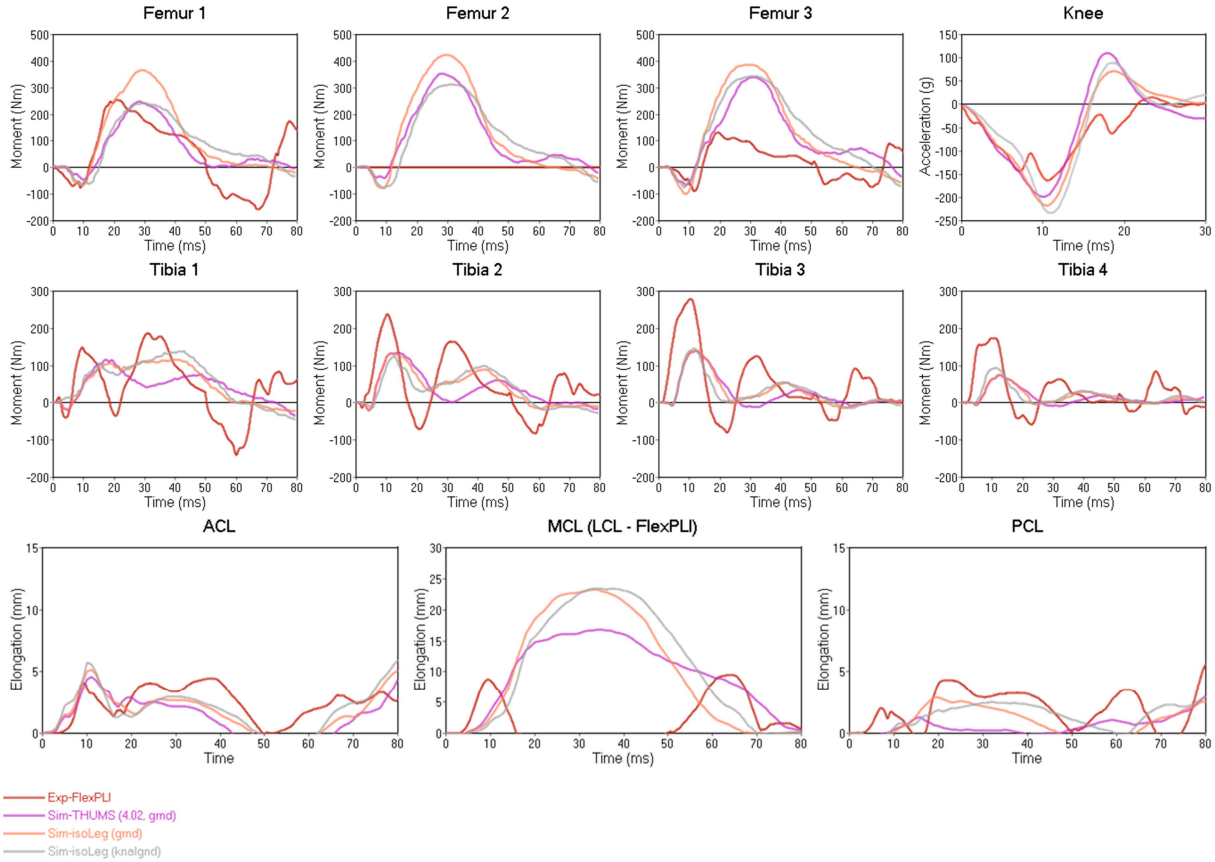

Figure 16: Body Loads in experiments and numerical simulations against GVTRv0

Repeatability of GVTR v0

GVTR v0 was used in tests with aPLI and FlexPLI. Results of three test repetitions (with FlexPLI) are shown in Figure 17. Moments in the tibia and femur as well as knee accelerations are practically identical up to approx. 60ms (that's the time when FlexPLI hits the test-propulsion system's gate during rebound). Repeatability appears excellent. In ligaments, though, differences in terms of elongation in the range of +/-10% can be found. It remains unclear, whether these are induced by GVTR's design or arise from FlexPLI.

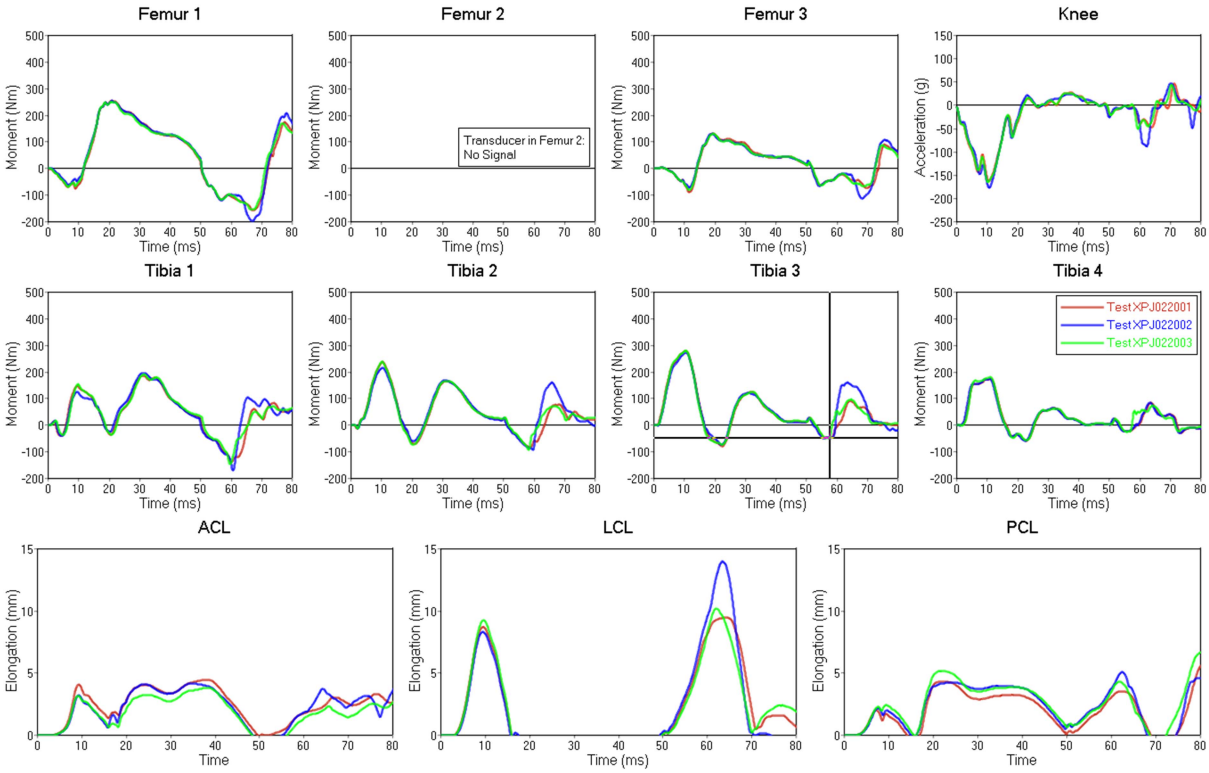

Figure 17: Repeatability of tests against GVTRv0, emloying FlexPLI – 3 test repetitions

DISCUSSION

In the ACEA funded project ProPose and the EuroNCAP funded project CoHerent [4,8,9] multiple generic vehicles were established that allow to study the first phase of pedestrian and bicycle accidents. It seems worthwhile to briefly outline each of these models by chronological order, to understand their interrelation and purpose (see Table 1).

The first model was called “Generic Parameterisable Vehicle”, short GPV . The GPV’s shape as well as its structural impact response model (SIRM) is fully governed by parameters. In the GPV simple modelling techniques are employed, which feature high robustness and stability. The generic vehicle is separated into a number of contact areas (acronyms in brackets): Spoiler (SPL), Bumper (BMP), Grill (GRL), Bonnet Lead (BLE), Bonnet (BNT) and Windshield (WSH). The shape of each contact area (spoiler, bumper, a.s.o.) is governed by three Bezier-curves, approximating the shape of leading, trailing and centreline contour. The aim of GPV was to study the effect of shape and structural impact response characteristics on pelvic and upper femur loading [3].

The second model was called “Generic Vehicle”, short GV, and was developed for EuroNCAP [6]. The aim of the GV was to provide a vehicle fleet that can be used to compare Human Body Models in terms of head-trajectory and head contact timing (and such it was not developed to study leg loading). Bezier-curve parameters were fitted to replicate the median shape of a sample of European vehicles, covering four vehicle categories (SUV, family car, MPV and sportscar). The major difference between GPV and GV lies in the provision of modelling techniques available in all major explicit FEM codes (LS-Dyna, Radioss, VPS and Abaqus). Therefore the large-penetration contact was dismissed in favour of generic foams, with loading and unloading curves fitted to the median force-penetration behaviour of a sample of European vehicles.

The third model is called “Generic Vehicle Test Rig”, version 0. The aim of GVTR v0 was to provide a generic vehicle not only in numerical but also in physical environment for the validation of ATDs, like aPLI. By contrast to the aforementioned GPV and GV, the vehicle’s contour is not approximated through smooth Bezier controlled surfaces, but through simple planar surface segments. Further, the GVTR disregards the vehicle’s curvature in lateral direction. For the sake of robustness and repeatability concessions were made in terms of structural behaviour. Such, GVTR v0’s behaviour is on the “stiffer side”, providing a structural impact response stiffer than the median.

For version 1 of GVTR the structural impact response curves were re-established with a revised impactor testing regime, considering only FlexPLI compliant vehicles. Also vehicle shapes were re-established by determining the median BLE, BMP and SPL reference line for each vehicle category. More emphasis was laid on a close replication of median force-penetration behaviour. Additionally the load-path ‘bonnet’ was included. Furthermore, the experiences from the experiments with FlexPLI and aPLI against GVTRv0 have been

incorporated into the development (e.g. no gap between grill panel and grill EPP block, panel height for bumper increased).

Table 1.
Characteristics of the Generic Vehicles established in ProPose and CoHerent [3,4]

Model	**Generic Parameterisable Vehicle**	**Generic Vehicle**	**Generic Vehicle Test Rig v0**	**Generic Vehicle Test Rig v1**
Acronym	GPV	(CoHerent) GV	GVTR v0	GVTR v1
Project	ProPose	CoHerent	ProPose	ProPose
Funding	ACEA	EuroNCAP/ACEA	ACEA	ACEA
Environment	Numerical	Numerical	Numerical + Physical	Numerical + Physicall
FE-Codes (as of now)	LS-Dyna	LS-Dyna, Radioss, VPS, Abaqus	LS-Dyna, VPS	LS-Dyna, VPS
Aim	Study loading on pelvis (and upper femur)	Comparison of head trajectories and head impact time	Study loading on lower and upper leg	Study loading on lower and upper leg
Shape	Parameterisable. 5 seed vehicles: Family Car (FCR), Old FC, MPV, SUV, Roadster	19 seed vehicles: Sedan (n=6), SUV (n=6), MPV (n=5) and Sportscar (n=2).	Sedan based on 6 seed vehicles	20 Flex-PLI compliant seed vehicles: sedan (n=9), SUV (n=8) and sportscar (n=3).
Structure	Rigid. Parameterisable force-penetration contact 2 seed vehicles: MPV and FCR	Deformable. Generic foam with load/unloading function fitted to median of 19 vehicles	EPP foam, 30-60g/l, Response lying between median and max CoHerent corridors	EPP foam, 30g/l Replicating median of 20 Flex-PLI compliant vehicles
Force-Penetration Corridors	Rigid Cylindrical Impactor against SPL (oblique), BMP, BLE and BNT – at centerline and one lateral offset position			Rigid cyl. impactor with 20 force transducers against SPL (oblique and horizontal), BMP, BLE – at centerline and 5 offset positions
Contact Areas	SPL, BMP, GRL, BLE, BNT, WSH, Remainder	SPL, BMP, GRL, BLE, BNT, WSH, Remainder	SPL, BMP, GRL, BLE	SPL, BMP, GRL, BLE, BNT
Design			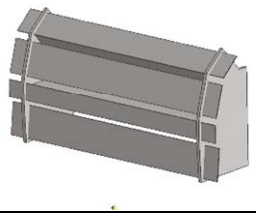	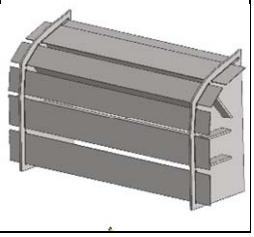

Comparison of Vehicle Test Rigs
Generic Vehicle Test Rigs are not a novelty: Over the past 25 years researchers around the world, mostly for the purpose of PMHS testing, developed a considerable number of GVTRs [10–19]. Hence it appears worthwhile to compare the ProPose GVTR v0 and v1 with other test bucks used in research and development. Figure 18 shows a comparison of recent vehicle test rigs.

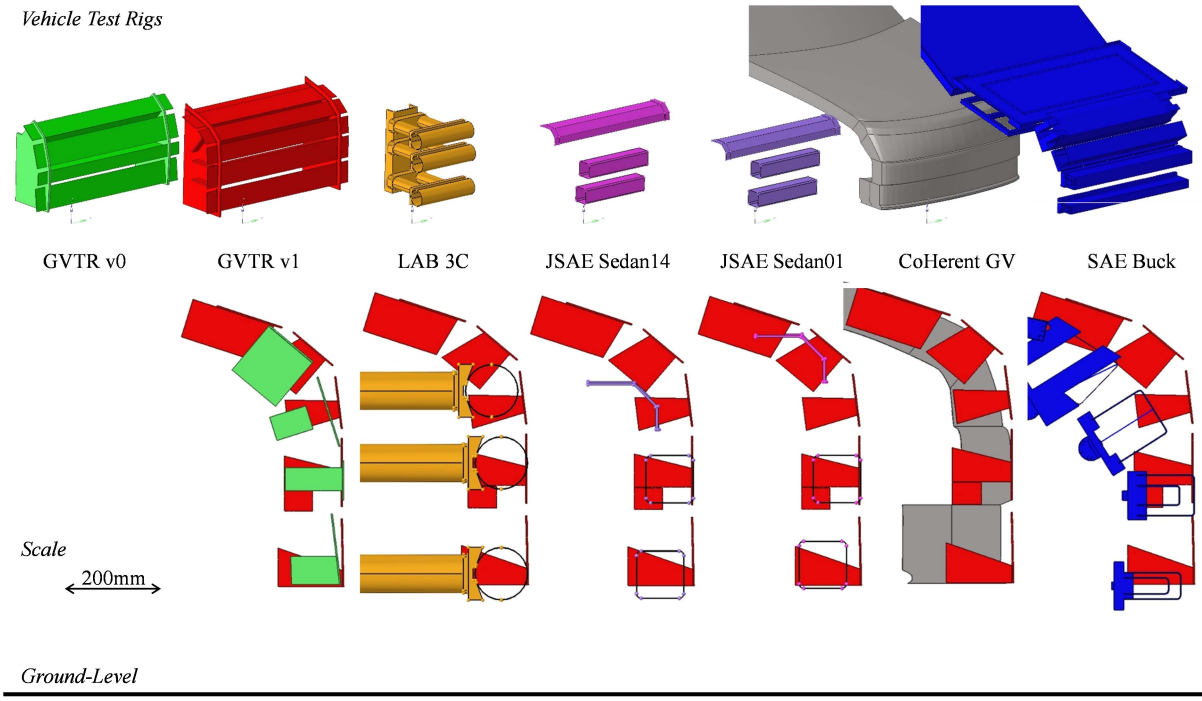

Figure 18. Comparison of Test Bucks with GVTRv1 in terms of geometry. [4,16,18,19]

The structural response of test rigs can not be directly compared, as the characteristics were established differently. Still, in an attempt to do so, Figure 19 shows the curves and corridors of various studies and test rigs in comparison with the GVTRv1 study. In the bumper region, the behaviour is similar to the Large Sedan buck. In the spoiler region the behaviour is similar to the JSAE buck's characteristic 'A'. In the BLE region, the only similar behaviour was established by the CoHerent study.

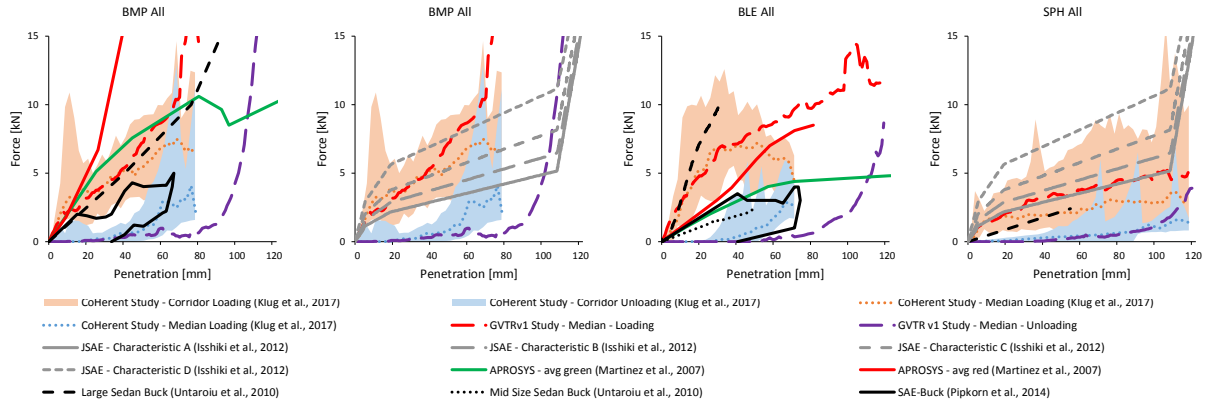

Figure 19: Comparison of other Test Bucks with GVTRv1 in terms of structural response [4,11,18–21]

CONCLUSIONS

GVTRv0 is a test-rig that proved to be a very robust, highly repeatable, fidelic, simple, easy-to-use and low cost tool for the validation of ATDs, while still providing a realistic loading of the pedestrian. It closes the gap between numerical and experimental world.

GVTRv1 features improvements over the GVTRv0:

- The additional loadpath bonnet was included,
- two additional vehicle categories are covered,
- the structural impact response is replicating the latest Flex-PLI compliant vehicles,
- the structural impact response is replicating the median instead of the maximum force-penetration behaviour.

As for now GVTRv1 sedan is available only in numerical environment. It will be available in summer 2019 for experiments. Two other vehicle categories will be introduced: SUV and sportscar.

ACKNOWLEDGEMENT

The project ProPose is funded by ACEA, the European Automobile Manufacturers' Association. The GVTR v0 was manufactured by Bertrandt AG. Tests with legform impactors were conducted by Bertrandt AG. A beta release of the numerical model of aPLI ('atd-aPLI-d00.11') was provided free of charge by ATD-MODELS GmbH.
The authors would like to acknowledge the use of HPC resources provided by the ZID at Graz University of Technology, Austria. The authors acknowledge that Toyota Motor Corporation and Toyota Central R&D labs, Inc., are the owners of the licensed Total Human Body Model for Safety.

REFERENCES

[1] Isshiki T., Konosu A., Takahashi Y., 2016. Development and Evaluation of the Advanced Pedestrian Legform Impactor Prototype which can be Applicable to All Types of Vehicles Regardless of Bumper Height - Part 1: Finite Element Model. In: International Research Council on the Biomechanics of Injury, editor. 2016 IRCOBI Conference Proceedings. IRCOBI, p. 770–785.
[2] Isshiki T., Konosu A., Takahashi Y., 2016. Development and Evaluation of the Advanced Pedestrian Legform Impactor Prototype which can be Applicable to All Types of Vehicles Regardless of Bumper Height -Part 2: Actual Test Tool. In: International Research Council on the Biomechanics of Injury, editor. 2016 IRCOBI Conference Proceedings. IRCOBI, p. 786–799.
[3] Feist F., Klug C., 2017. Verletzungen des Beckens und der Oberschenkel in Fußgängerunfällen mit PKWs. In: CARHS, editor. SafetyUpDate Graz Proceedings.
[4] Klug C., Feist F., Raffler M., Sinz W., Petit P., Ellway J. et al., 2017. Development of a Procedure to Compare Kinematics of Human Body Models for Pedestrian Simulations. In: International Research Council on the Biomechanics of Injury, editor. 2017 IRCOBI Conference Proceedings. IRCOBI, p. 509–530.
[5] Klug C., 2018. Assessment of Passive Vulnerable Road User Protection with Human Body Models [Doctoral Thesis]. Graz: Graz University of Technology.
[6] Euro NCAP, December 2017. Pedestrian Human Model Certification. 1st ed.(TB 024); Available from: https://cdn.euroncap.com/media/34544/tb-024-pedestrian-human-model-certification-v101.pdf.
[7] Blauth D., Droigk P., Schuster P., 2019. ATD-aPLI: Beta release. Schleife-Rohne, Germany: ATD-MODELS GmbH.
[8] Klug C., Feist F., Raffler M., Sinz W., van Ratingen M., 2016. Methodology for kinematic comparison of human body models for pedestrian simulations. In: CARHS, editor. 6th International Symposium: Human Modeling and Simulation in Automotive Engineering.
[9] Klug C., Feist F., Sinz W., Ellway J., van Ratingen M., 2018. A procedure to compare kinematics of Human Body Models for pedestrian assessments. In: SAE International, editor. SAE Government Industry Meeting 2018.
[10] Forman J.L., Joodaki H., Forghani A., Riley P.O., Bollapragada V., Lessley D.J. et al., 2015. Whole-body Response for Pedestrian Impact with a Generic Sedan Buck. Stapp Car Crash J 59:401–44.
[11] Untaroiu C.D., Shin J., Crandall J.R., Fredriksson R., Bostrom O., Takahashi Y. et al., 2010. Development and validation of pedestrian sedan bucks using finite-element simulations: A numerical investigation of the influence of vehicle automatic braking on the kinematics of the pedestrian involved in vehicle collisions. INT J CRASHWORTHINES 15(5):491–503. https://doi.org/10.1080/13588265.2010.484189.
[12] Forman J., Joodaki H., Forghani A., O Riley P., Bollapragada V., Lessley D. et al., 2015. Biofidelity Corridors for Whole□Body Pedestrian Impact with a Generic Buck. In: International Research Council on the Biomechanics of Injury, editor. 2015 IRCOBI Conference Proceedings. IRCOBI, p. 356–372.
[13] Wu T., Kim T., Bollapragada V., Poulard D., Chen H., Panzer M.B. et al., 2017. Evaluation of biofidelity of THUMS pedestrian model under a whole-body impact conditions with a generic sedan buck. Traffic Inj Prev 18(1):148-154. https://doi.org/10.1080/15389588.2017.1318435.
[14] Untaroiu C.D., Shin J., Crandall J.R., Fredriksson R., Bostrom O., Takahashi Y. et al., 2010. Development and validation of pedestrian sedan bucks using finite-element simulations: A numerical investigation of the influence of vehicle automatic braking on the kinematics of the pedestrian involved in vehicle collisions. International Journal of Crashworthiness 15(5):491–503. https://doi.org/10.1080/13588265.2010.484189.
[15] Davidsson, J., Carroll J., Hynd, D., Lecuyee E. et al. Set of injury risk curves for different sizes and ages.
[16] Song E., Uriot J., Potier P., Dubois D., Petit P., Trosseille X. et al., 2017. Reference PMHS Tests to Assess Whole□Body Pedestrian Impact Using a Simplified Generic Vehicle Front□End. In: International Research Council on the Biomechanics of Injury, editor. 2017 IRCOBI Conference Proceedings. IRCOBI, p. 133–150.

[17] Song E., Petit P., Trosseille X., Uriot J., Potier P., Dubois D. et al., 2017. New Reference PMHS Tests to Assess Whole-Body Pedestrian Impact Using a Simplified Generic Vehicle Front-End. Stapp Car Crash J 61:299–354.
[18] Isshiki T., Konosu A., Takahashi Y., 2014. Development of an Appropriate Pedestrian Legform Impact Test Method which can be used for all Types of Vehicles including High Bumper Vehicles: Development of a Simplified Upper Body Part (SUBP) FE Model. In: International Research Council on the Biomechanics of Injury, editor. 2014 IRCOBI Conference Proceedings. IRCOBI, p. 759–784.
[19] Pipkorn B., Forsberg C., Takahashi Y., Ikeda M., Fredriksson R., Svensson C. et al., 2014. Development and component validation of a generic vehicle front buck for pedestrian impact evaluation. In: International Research Council on the Biomechanics of Injury, editor. 2014 IRCOBI Conference Proceedings. IRCOBI, p. 718–729.
[20] Isshiki T., Antona-Makoshi J., Konosu A., 2017. Optimal specifications for the Advanced Pedestrian Legform Impactor. Stapp Car Crash J 61:1–24.
[21] Martinez L., Guerra L.J., Ferichola G., Garcia A., Yang J., 2007. Stiffness corridors of the European fleet for pedestrian simulation. In: NHTSA, editor. The 20th ESV Conference Proceedings. NHTSA.

APPENDIX

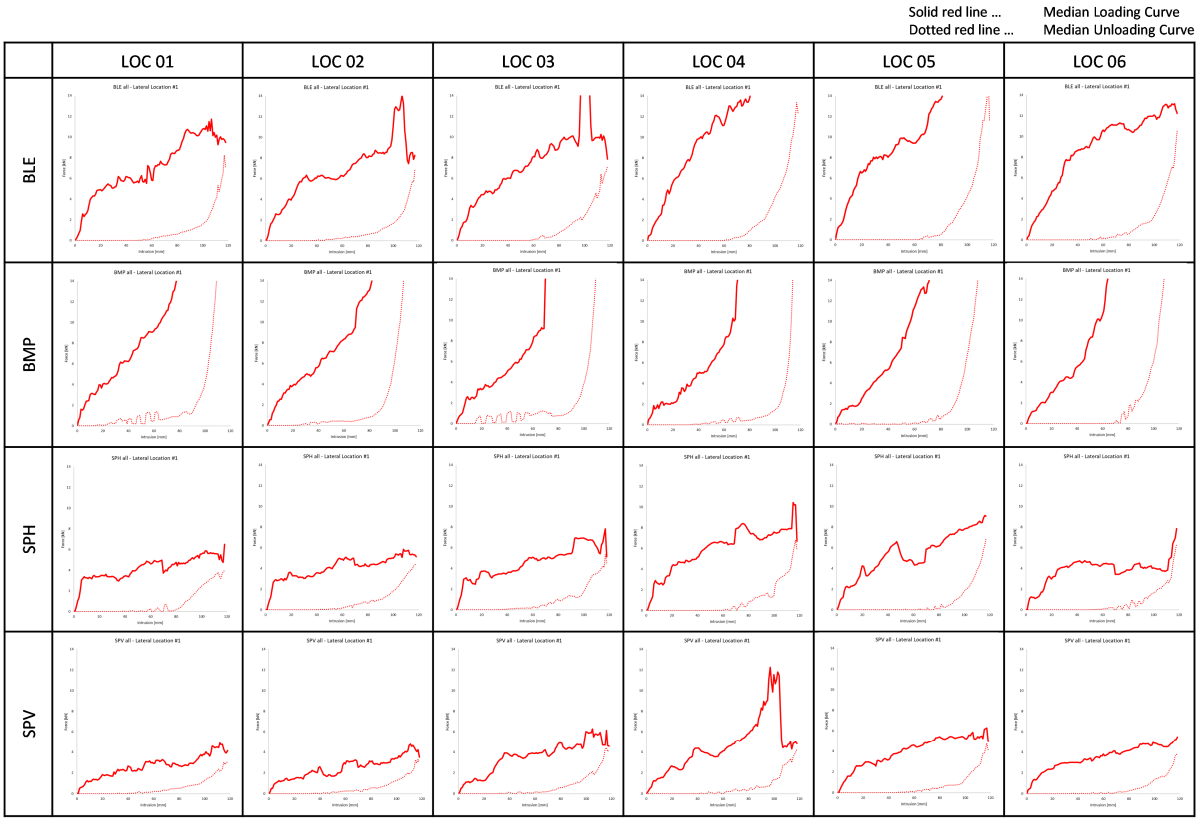

Figure 20: Median loading and unloading by horizontal and vertical (LOC1..6) impact location for Sedan. Areas 'All'

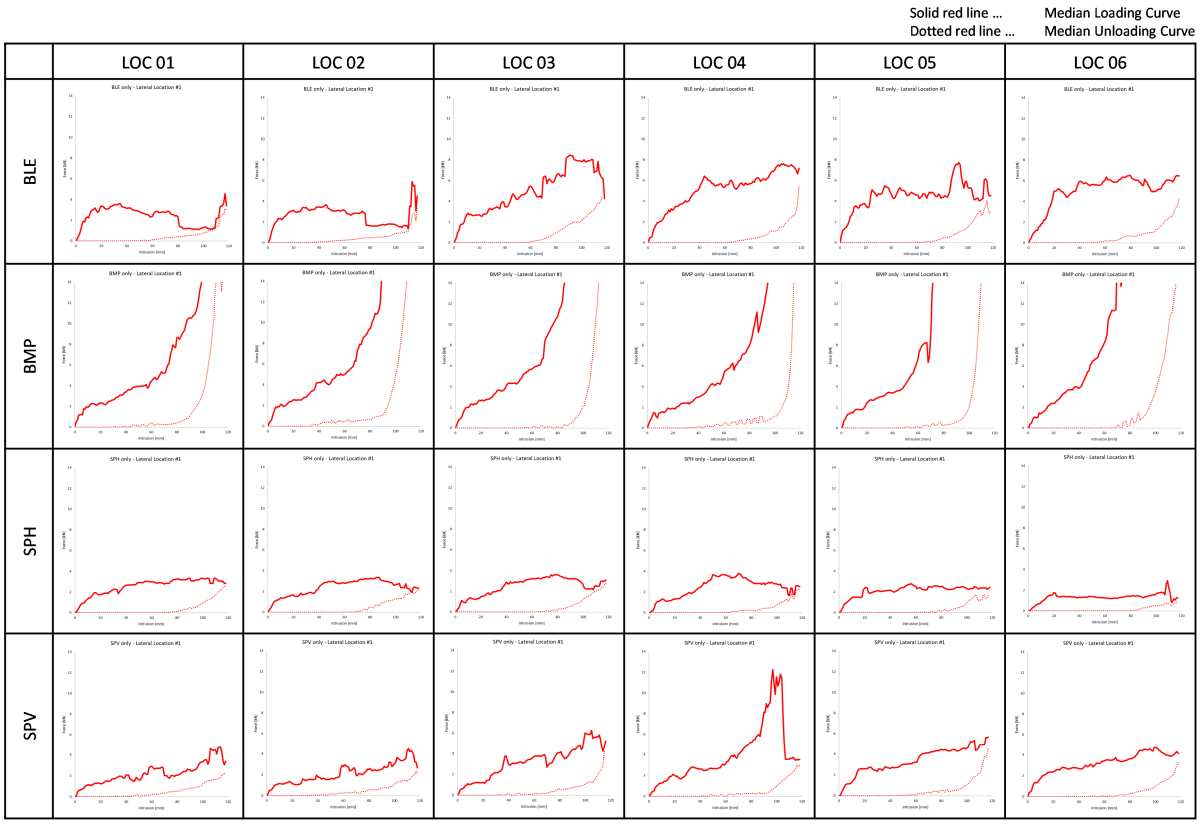

Figure 21: Median loading and unloading by horizontal and vertical (LOC1..6) impact location for Sedan. Areas 'Only'

AUTOMATIC IDENTIFICATION OF CRITICAL SCENARIOS IN A

PUBLIC DATASET OF 6000 KM OF PUBLIC-ROAD DRIVING

Jan-Pieter Paardekooper
TNO department of Integrated Vehicle Safety
The Netherlands

Radboud University, department of Artificial Intelligence
The Netherlands

Sjef van Montfort,
Jeroen Manders,
Jorrit Goos,
Erwin de Gelder,
Olaf Op den Camp
TNO department of Integrated Vehicle Safety
The Netherlands

Annie Bracquemond,
Gildas Thiolon
VEDECOM
France

Paper Number 19-0255

ABSTRACT

An increasing number of driving tasks in vehicles is being taken over by automation as automated driving technology is developed. An important aspect in this development is the safety assessment of new functions and systems. Scenario-based assessment is a promising tool, but it relies heavily on the availability of realistic scenarios for generating test cases.

Traditional methods take analyses from in-depth accident databases as a starting point to describe accident scenarios. In TNO's StreetWise methodology, the list of critical scenarios resulting from accidentology is expanded with scenarios that are identified from normal every day driving dat. In this paper we describe a machine learning approach of automatic scenario identification in a dataset of public-road driving. The dataset together with the results will be made public to serve as a benchmark.

TNO will publish a dataset containing 6000 kilometers of driving on the public road, containing information on the ego vehicle CAN; the GPS position; information on the objects around the ego vehicle from radar and camera; and road lanes and lines. Furthermore, we propose a framework for automatic scenario extraction from real-world microscopic driving data, including measures of safety criticality.

Scenarios that are similar form a scenario class, currently we distinguish approximately 60 of such classes. Each instance of a scenario is described by a set of parameters that is specific for the scenario class. By analyzing large amounts of driving data, not only scenarios to fit in different classes are identified, but also the parameter values for each scenario instance are determined. This results in the frequency of occurrence of scenarios and the probability density function (PDF) for each of the scenario parameters. Metrics for safety criticality are defined based on time-to-collision, time-headway, post-encroachment time, etc. For each case, the safety criticality is evaluated based on the proposed metrics.

We have automatically identified two scenarios in the data: 1. Gap closing; 2. Cut-in of a vehicle in front of the ego vehicle. From the identified PDFs the nominal scenarios are identified as well as corner cases with parameter values

in the tail of the PDF. By changing parameter values within a realistic range around the corner cases, a check is made regarding their criticality.

The two scenarios that are identified describe only a small part of the total number of kilometers driven. However, the bottom up approach to scenario mining described here can be extended to more scenarios in a relatively straightforward way, with the goal of describing the entire dataset with scenarios.

Automatic scenario mining from driving data is an essential step towards safety validation of AD functionalities. TNO publishes a dataset with 6000 kilometers of public-road driving, for which we show that it is possible to identify critical scenarios, in addition to nominal scenarios, even if in these kind of studies critical situations are rare.

INTRODUCTION

Automated driving (AD) functions are considered an important tool for increasing road safety and comfort, reducing emissions and improving traffic flow. The increase in automation requires a different protocol for quality and performance assessment of vehicles than traditionally done [1][2][3]. For this, a scenario-based approach has been proposed [4][5]. The collection of scenarios used for defining test cases should represent and cover the entire range of real-world traffic situations that might be encountered by the AD system under test. In the TNO StreetWise methodology, scenarios are extracted from real-world microscopic traffic data, and are used to build a database suitable for testing and validation of automated driving functions [6]. The use of real-world scenarios for testing purposes requires accurate scenario extraction methods from driving data, to ensure representativeness of the scenario database. In order to facilitate a comparison between different scenario-mining methods, a public benchmark dataset would be a valuable tool.

Several public public-road driving datasets already exist. The Oxford robotcar dataset contains data of 100 repetitions of the same route in Oxford, UK [7]. The sensors that were used on the recording vehicle include multiple cameras, LIDAR and GPS, but no sensor fusion has been performed on the raw data. Hence, no object level data is available from this dataset. For the Next Generation Simulation (NGSIM) program[1], data was collected at several US highways with a network of synchronized digital video cameras, from which vehicle trajectory data was extracted. This provides a bird's eye view of specific portions of road. The Apollo obstacle trajectory prediction dataset[2] contains data collected with LIDAR, cameras and GPS. The data has been turned into features that can be used to train a Machine Learning algorithm on the provided labels on the intention of the other road users.

In this work we present a dataset of public-road driving for benchmarking scenario-mining algorithms. This dataset is available at www.tno.nl/streetwise. Unlike the previously mentioned public datasets, this dataset contains object-level data from an in-car perspective that can be directly used to identify scenarios in the data. As a first benchmark, we present the results of a scalable approach to scenario mining, based on fundamental building blocks describing the trajectories of all road users. Two scenarios are shown as example, 'gap closing' and 'cut in'. As scenario-mining algorithms are continuously improved, progress can be measured on this public dataset. Finally, we show how a scenario database of driving data can be used to assess the safety criticality of the scenarios found in the data.

METHOD

Real-world data logging

TNO recorded data from 20 different drivers between 25-60 years old, all of whom had their driving license for more than 5 years and are driving more than 5000 km per year. They drove together about 6000 km in mixed traffic, of which approximately half in manual mode and half in ACC mode. All driving was performed during the day time (from 8:30 to 17:00) under dry weather conditions.

A dedicated specially prepared vehicle (Toyota Prius) was used for the tests. The vehicle records information from the following sensors:

[1] https://data.transportation.gov/

[2] http://data.apollo.auto/

- Vehicle CAN (velocity / accelerations / yaw rate / steering wheel angle / wheel speeds)
- Mobileye camera (object / lane information)
- Continental-30x radar front centre, rear left, rear right
- U-blox GPS
- Ibeo LIDAR

The position and viewing angle of the sensors is depicted in Figure 1. Besides these sensors also an additional forward-facing camera was used to record reference footage. The LIDAR has not been used in the analysis of the data.

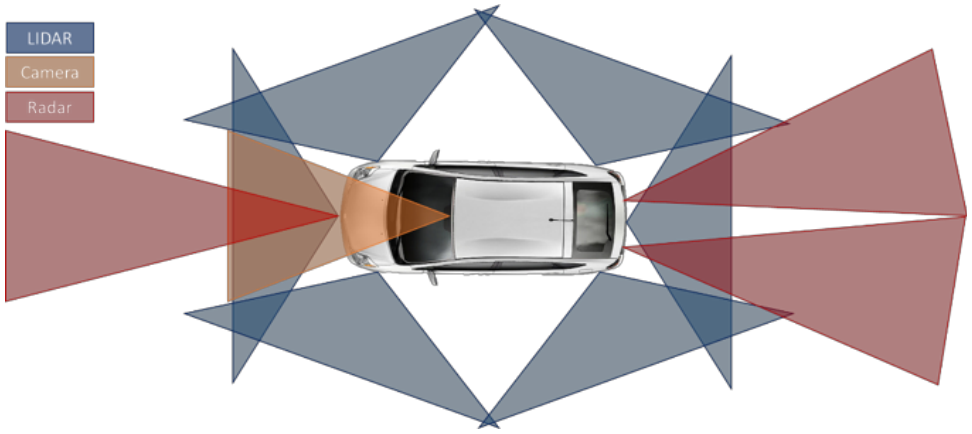

Figure 1: Field of view of the external sensors of the recording vehicle. Orange: front-looking MobilEye camera. Red: Continental-30x radar, front centre, rear left, rear right. Blue: Ibeo LIDAR.

Data pre-processing

The recorded data is converted to a uniform representation (the so-called world model) of the static and dynamic environment around the ego vehicle. In this dataset the static environment is only represented by the road markings of the ego lane. The lateral position of all road users is considered relative to these lanes. The output of the Mobileye camera is used for the road markings. This contains the type of lane marking and predicted position of the marking with certain confidence level.

The dynamic traffic is modelled with a multi-target tracker that has been developed by TNO [8]. The multi-target tracker uses the sensor output of the Mobileye camera and the 3 Continental radars (front center, rear left and rear right radar). The test vehicles were also equipped with Ibeo LIDARs, but those were not used. The multi-target tracker fuses the sensor data and provides the position and motion of detected objects. The targets are represented as points. The distance between the ego vehicle and a target in front of ego vehicle is the distance between target vehicle rear bumper center and ego vehicle front bumper center. For the distance between the ego vehicle and a target behind the ego vehicle the distance between target vehicle front bumper center and ego vehicle rear bumper center is used. For lateral position the center of the vehicle (both ego and target) is used as reference point.

The test drivers drove a fixed route in the region of Amersfoort in the Netherlands. The route has a length of approx. 46 km and takes about 50 minutes driving without delays. About 55% of the distance is highway, 40% is rural and the remaining 5% is urban area. About 55% of the route are multi-lane uni-directional roads. The route and driving direction are shown in Figure 2. Every test person drove the route 6 times, 3 times with ACC and 3 times without.

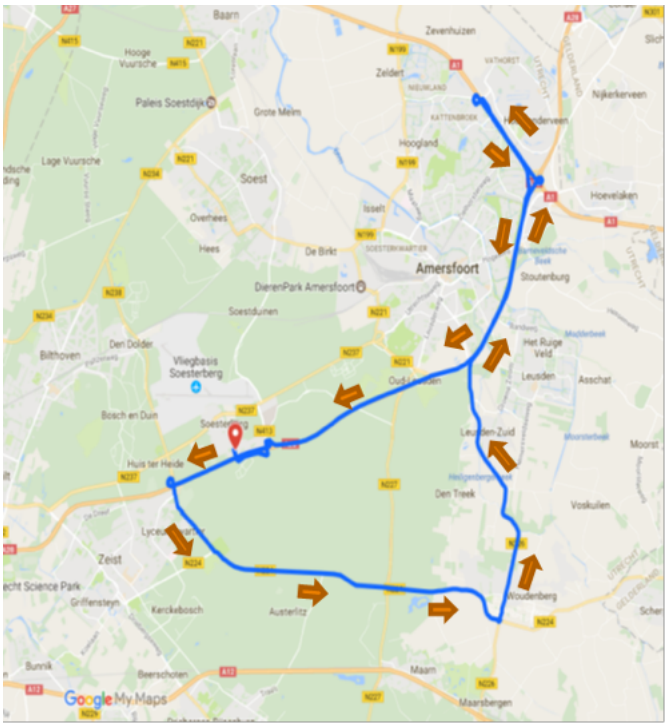

Figure 2: The route, including driving direction, that was driven by the test drivers.

Identification of scenarios

In the StreetWise methodology traffic is interpreted as a sequence of scenarios, meaning that every instance of the data is assigned to a scenario [6]. These scenarios need to be defined by a consensus among experts in order to make them as useful as possible for testing. In this work we focus on two relatively straightforward scenarios: one scenario that is centered on longitudinal interaction between two vehicles, and one centered on lateral interaction. The first scenario is the 'gap-closing' scenario. It consists of a target vehicle in front of the ego vehicle that is in the same lane as the ego and decelerates. This scenario ends when the distance between the two vehicles no longer decreases. The second scenario is the 'cut-in' scenario. In this scenario a target vehicle moves from an adjacent lane to the ego lane in front of the ego vehicle, such that the target becomes the lead vehicle of the ego vehicle. Figure 3 shows a graphical representation of the two scenarios.

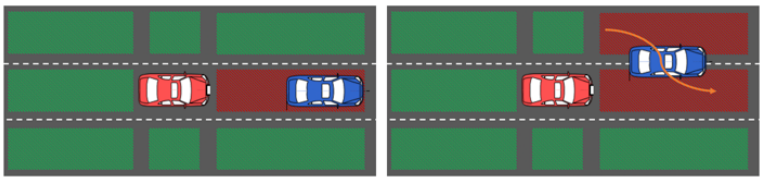

Figure 3: *Left*: Gap-closing scenario. *Right*: Cut-in scenario.

As described in [6], we define activities as building blocks and construct scenarios by combining activities of different road users. Activities can fall into two categories: longitudinal and lateral. Longitudinal activities can be either acceleration, cruising or deceleration. Lateral activities are defined with respect to the lane and can be either lane following, turn (or lane change) left or turn (or lane change) right. These 6 activities cover all the allowed movement of a vehicle on the road and are sufficient to describe any possible trajectory. The activities are identified in the data for the ego and all the targets that are detected around the ego. The trajectory of a road user is described by at least two (i.e. longitudinal and lateral) activities at all times.

Scenarios are found by combining activities with the relative position and speed of every target. We use template matching on a graphical network to efficiently find the scenarios in the dataset. In this bottom-up approach, given

the right template to search for, any scenario can be detected straightforwardly without the need to write a separate algorithm for every scenario. The activity detection and scenario mining algorithms will be detailed in a forthcoming publication.

Identification of critical scenarios
For all scenarios the minimal set of parameters needed to describe the activities and the scenarios is stored. This includes a full description of the time evolution of every activity of the ego and every target, the relative positions of the targets with respect to the ego, the relative speeds of the targets with respect to the ego, and the absolute position of the ego. This set of parameters can be used to determine the safety criticality of the scenarios found in the data. Many possible safety indicators have been proposed [9][10]. As an example, we consider in this work the following safety criticality indicators:

- Start longitudinal distance [m]: the longitudinal distance between the ego and the target at the start of the scenario.
- Maximal deceleration during the scenario [m/s^2].
- Minimal Time-To-Collision (TTC) [s]: the time to collision is the time it takes for the rear vehicle to cover current longitudinal distance between rear and front vehicle, also taking into account the possible distance covered by front vehicle. The TTC is computed in the following way:
  TTC [s] = inter-vehicle-distance [m] / (rear vehicle velocity – front vehicle velocity) [m/s].
- Maximal lateral speed during the scenario [m/s].

RESULTS

We have applied the scenario identification algorithms to the 6000 km of public-road driving. In this section we describe the results and give an example of the analysis of criticality of a scenario based on the safety criticality indicators described in the previous section.

Braking in front
We have identified 1460 braking in front scenarios in the data. An example of the relevant signals for this scenario is shown in Figure 4. The target vehicle has initially a higher speed than the ego, before it starts decelerating. About 1 second after the longitudinal distance starts the decrease, the ego vehicle decelerates until the distance between the vehicles is 8 meters, at which point the target accelerates again.

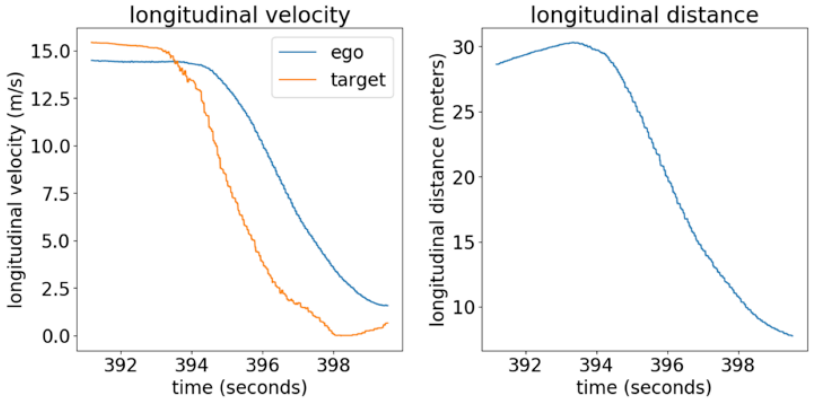

Figure 4: *Left*: Longitudinal speed as function of time for the ego and the target. *Right*: Inter-vehicle distance as function of time.

By comparing the safety criticality parameters of this scenario with the probability density functions (PDF) of these parameters constructed from all scenarios in the data, the relative safety criticality of this scenario can be assessed.

In Figure 5 the longitudinal distance at the start of the scenario, the maximal deceleration of the target and the minimal TTC are shown.

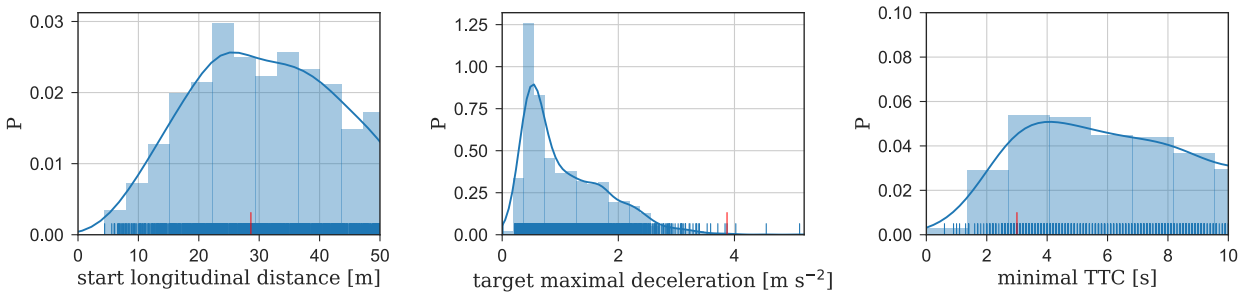

Figure 5: Probability densities of safety indicators for the braking-in-front scenario. Solid line is a univariate non-parametric fit of the histogram with Kernel Density Estimation using a Gaussian kernel. Vertical lines on the x-axis denote the data points. The red vertical line indicates the example shown in Figure 4. *Left*: Longitudinal distance at the start of the scenario. *Centre*: Maximal deceleration of the target during the scenario. *Right*: Minimal time to collision during the scenario.

The maximal deceleration of the target is among the highest found in the dataset. However, due to the relatively high inter-vehicle distance at the start of the scenario, this does not result in a safety critical scenario. This is reflected in the minimal TTC that is above 2 seconds. The drawback of only using the TTC for safety analysis is that it is not always defined, even in cases where the target might still be dangerously close to the ego [9]. This analysis shows that it is not sufficient to rely on a single parameter to judge the safety criticality of a scenario.

Cut in

We have identified 403 cut-ins in the dataset. An example of a cut-in scenario with the relevant signals is shown in Figure 6. The lateral speed of the target increases at the start of the scenario indicating the lane change. Although the longitudinal speed of the target is initially much lower than that of the ego, the target quickly accelerates and as a result the longitudinal distance is never less than 17 meters during the scenario.

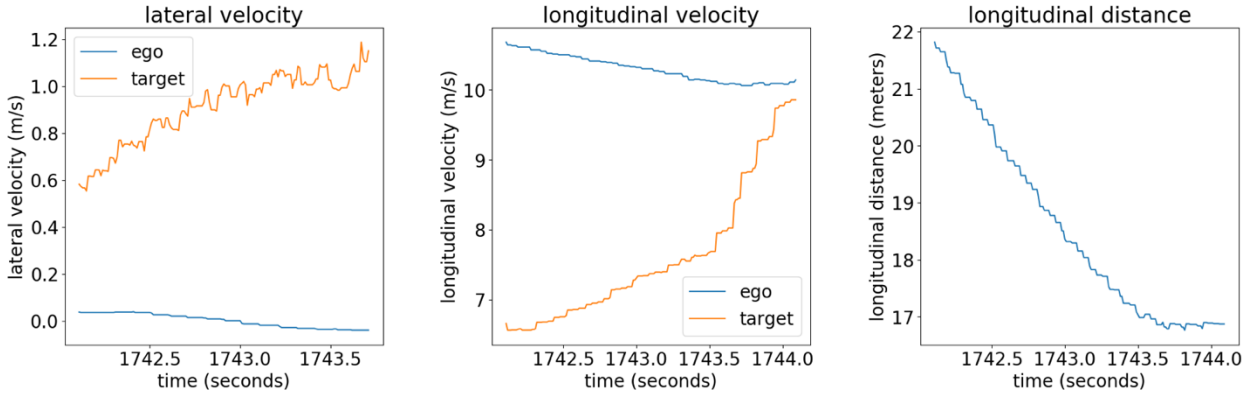

Figure 6: *Left*: Lateral speed as function of time for the ego and the target. *Centre*: Longitudinal speed for the ego and the target. *Right*: Inter-vehicle distance as function of time.

To determine the safety criticality of this example, in Figure 7 we show the PDFs of 3 safety indicators. These indicators show that even though the lateral speed of the target was relatively high and the longitudinal distance at the start of the scenario was below average, this example is not safety critical, as the minimal TTC of more than 5 seconds shows. However, as noted earlier, relying only on TTC for defining safety criticality has severe drawbacks.

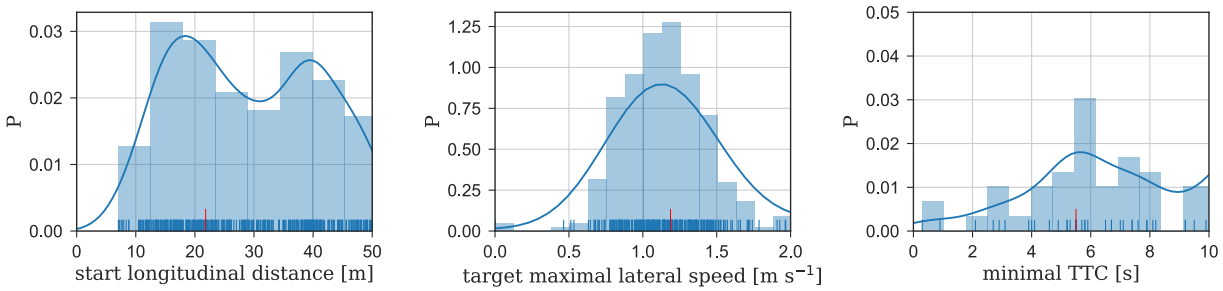

Figure 7: Probability densities of safety indicators for the cut-in scenario. Solid line is a univariate non-parametric fit of the histogram with Kernel Density Estimation using a Gaussian kernel. Vertical lines on the x-axis denote the data points. The red line indicates the example shown in Figure 6. *Left*: longitudinal distance at the start of the scenario. *Centre*: Maximal lateral speed of the target during the scenario. *Right*: Minimal TTC during the scenario.

CONCLUSIONS AND DISCUSSION

We have presented a dataset of driving on the public road that consists of 6000 kilometers of a mix of highway (55%), rural (50%) and urban (5%) driving and contains information on the ego vehicle CAN; the GPS position; information on the objects around the ego vehicle from radar and camera; and road lanes and lines. The dataset will be made publicly available at www.tno.nl/streetwise.

In addition, we have presented the results of a bottom-up approach to scenario mining in this dataset. By first detecting activities in the data that serve as building blocks, scenarios can be identified in the data in a scalable manner. With the input of experts about what a certain scenario entails, a template of the scenario can be defined that can immediately be used in the scenario mining algorithm to extend the scenario catalogue. The two scenarios described in this work only describe a very small portion of the data, but we expect to add more scenarios in the near future, working towards the goal of assigning every instance of data to at least one scenario.

Finally, we have presented a method for determining the safety criticality of scenarios based on the probability density functions of a set of safety indicators. By comparing where different safety indicators are in the distributions of all scenarios, the safety criticality of the scenario can be quantified. The dataset presented in this paper is too small for a thorough statistical analysis and does not contain any critical scenarios, we plan to extend the analysis with more data in the future.

REFERENCES

[1] International Organization for Standardization (ISO), “ISO 26262: Road vehicles – functional safety”.

[2] Knapp, A., Neumann, M., Brockmann, M., and Winkle, T. 2009 “Code of practice for the design and evaluations of ADAS”, RESPONSE III: a PReVENT Project

[3] Wachenfeld, W. and Winner, H. 2016. “The release of autonomous vehicles.” In Autonomous Driving, Spring, pp. 425-449

[4] Pütz, A., Zlocki, A., Bock, J., and Eckstein, L. 2017. “System validation of highly automated vehicles with a database of relevant traffic scenarios.” In 12th ITS European Congress, pp. 1-8

[5] Roesener, C., Fahrenkrog, F., Uhlig, A. and Eckstein, L. 2016. “A scenario-based assessment approach for automated driving by using time series classification of human-driving behavior.” In IEEE 19th International Conference on Intelligent Transportation Systems (ITSC), pp. 1360-1365

[6] Elrofai, H., Paardekooper, J.-P., De Gelder, E., Kalisvaart, S., and Op den Camp, O. 2018. “Scenario-Based Safety Validation of Connected and Automated Driving”. Tech. rep. Netherlands Organization for Applied Scientific Research, TNO. www.tno.nl/streetwise

[7] Maddern, W., Pascoe, G., Linegar, C. and Newman, P. 2017. "1 Year, 1000km: The Oxford RobotCar Dataset", The International Journal of Robotics Research (IJRR) 36, No. 1, 3-15

[8] Elfring, J., Appeldoorn, R. P. W., van den Dries, S., & Kwakkernaat, M. R. J. A. E. 2016. Effective world modeling: multisensor data fusion methodology for automated driving. Sensors, 16(10), 1668. DOI: 10.3390/s16101668

[9] Laureshyn, A. (2010). Application of automated video analysis to road user behavior, PhD thesis, Lund University

[10] Mahmud, S., Ferreira, L., Hoque, S., Tavassoli, A. 2017. “Application of proximal surrogate indicators for safety evaluation: A review of recent developments and research needs”, IATSS Research 41, 153-163

HYDROPLANING AVOIDANCE – A HOLISTIC SYSTEM APPROACH

Bernd Hartmann
Anton Klöster
Dr. Matthias Kretschmann
Dr. Thomas Raste
Continental AG
Germany
Paper Number 19-0256

ABSTRACT

Accidents in severe weather mainly arise due to a drastic loss of friction between the tires and the road surface unexpected by the driver. Beside all kinds of slippery winter conditions hydroplaning situations are even more dangerous not just for manually driven vehicles but also for automated vehicles when cruising at speeds above 80 to 100 km/h. This paper describes the Continental approach for a cascaded holistic safety system in imminent hydroplaning situations independent of the degree of automation. First, to reduce the overall hydroplaning risk a continuous tire tread depth monitoring function is integrated to trigger a timely replacement of worn-out tires. Second, a surround view camera and new tire-sensor-based early hydroplaning risk recognition allows an in-time driver warning or a system-initiated speed adaptation in case of automated vehicles. Especially for Automated Driving (AD) vehicles it is of major importance to avoid hydroplaning before it happens. Third, this information is send to the cloud-based eHorizon service so that also other traffic participants can be informed before entering a hydroplaning risk area. In case hydroplaning cannot be avoided a control system is designed and tested to evaluate an innovative assistance strategy in hydroplaning situations. The test cases demonstrate the suitability of this assistance concept.

1. INTRODUCTION

Heavy rain and bad weather conditions involving reduced traction because of wet, snowy and icy surfaces have been major contributory factors to traffic accidents in general. Extreme weather conditions are responsible for 39% of all accidents in Germany, [2]. One of the most dangerous driving situations is hydroplaning, which is difficult to predict and almost impossible to manage for the driver but also for automated vehicles. The hydroplaning situation depends on both vehicle and tire conditions as well as on environmental parameters such as water film thickness on the road. During hydroplane steering generally is not possible, because tire-road friction is completely lost at the front axle and therefore any transfer of lateral and longitudinal forces is not possible by the front tires anymore. Today's measures to avoid the risk of hydroplaning are almost exclusively infrastructure-based such as roadway draining and/or speed limits.
The Continental AG is developing a cross-divisional bundle of vehicle-based solutions proposing a cascaded holistic approach. This holistic approach is based on the four following cornerstones:

- Avoid
- Predict
- Warn
- Assist

Beside the proposal to analyze vehicle dynamics and controllability in hydroplaning situations and sketch an active safety system to assist the driver safely through this dangerous situation the main scope of this paper is to avoid the hydroplaning danger by a continuous tire tread depth monitoring system and the integration of two complimentary sensor-based systems to detect the imminent hydroplaning risk in an early pre-hydroplane phase before hydroplaning occurs. This information is used to warn the driver or to actively control the speed of an automated vehicle in imminent hydroplaning risk situations. Additionally, in such cases the potential risk to other vehicles on the road can be mitigated by an early communication via V2X technology and eHorizon, facilitating

a network of solidarity where one vehicle acts as a safety sensor for all other vehicles and not just those in its direct vicinity. eHorizon can provide this information to vehicles that could potentially be affected, so they are able to adjust their routing and driving functions to the risky weather conditions.

2. HYDROPLANING THEORY

A hydroplaning imminent situation can be explained by the following three-phase tire zone model concept in figure 1.

Exemplarily at a vehicle speed of 100 km/h a discrete element of the tire tread (P1) has a total contact duration with the surface and its top water layer of only 5 msec, where the three phases as displayed in the figure are passed through. In phase 1 the tread element is touching the water surface and displacing the water into the void volume of the tire's tread pattern. In phase 2, when the void is filled with water, the tire is analogously acting as a slick tire and more water cannot be absorbed by the void volume any more. This is the reason why the excessive water must be displaced to the front and to the sides underneath the tire.

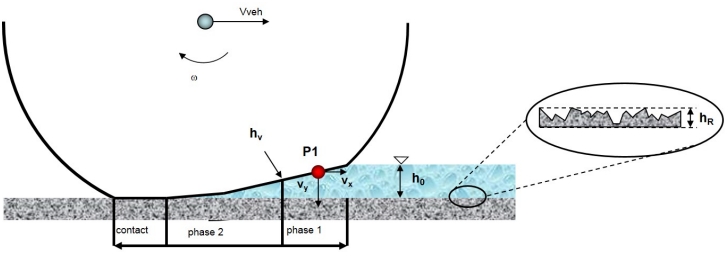

Figure 1. Three-Zone model concept for hydroplaning: separation zone (phase1), intermediate zone (phase2) and contact zone

As long as the tire's inside pressure is higher than the water pressure generated by the water wedge in front of the tire, the tire is successful in displacing the water to keep its road surface contact in the runout of the footprint. Just if the pressure relation changes and

the pressure of the water wedge in front gets higher than the tire's inside pressure the tire will swim up. This water displacement phase before it comes to hydroplaning is used to be detected by the systems for an early hydroplaning warning. This physics are the reason why there is a reasonable good chance to warn the driver up-front before the tires will completely hydroplane.

The critical vehicle speed is calculated as the averaged footprint length (L_m) divided by the touch down time (t_A) for a discrete tread element (P1), where the touch down time depends on the water height (h_0), the surface roughness (h_R) and the radius (R) for a circular tread bar, [1].

$$v_{krit} = \frac{L_m}{t_A} \qquad \text{(Equation 1)}$$

$$t_A = \frac{R/2}{2\sqrt{\frac{p_m}{\rho}}} \cdot \ln \frac{1+\sqrt{1-h_R/h_0}}{1-\sqrt{1-h_R/h_0}} \qquad \text{(Equation 2)}$$

With a mean support pressure (p_m) of 0,3 MPa, a density (ρ) for water of 1000 kg/m^3, a water height (h_0) of 8mm and a surface roughness (h_R) of 1mm the characteristic squeeze-out velocity for the water is approximately 35 m/sec. This results in considerably splash and spray water as a physical principal effect before it comes to hydroplaning. This splash water effect together with the oscillation caused by the water wedge in front of the tire's footprint is used by the system to detect the hydroplane risk in the pre-hydroplane phase.

3. TIRE TREAD DEPTH MONITORING

A critical factor in the context of hydroplaning is the residual tread depth of each tire. While periodic checks are sometimes done when changing from summer to winter tires (and back), there is no permanent monitoring of the tread depth. When using all season

tires, or in regions where the local climate does not require a seasonal change of the tires, the only tread depth monitoring relies on the user. Continental's TreadDepthMonitoring function continuously estimates the tread depth of each tire and can provide a timely recommendation for a tire change. Based on the tire mounted sensor eTIS (electronic Tire Information System) which was launched for the European tire pressure monitoring aftermarket in 2014, the system can now access not only the tire Pressure P and temperature T, but also the acceleration of the tire itself – not only the RIM. This allows for several new features (see also the direct indication of hydroplaning in chapter 5.2). It is clear, that by means of the tire acceleration, it is possible to measure the footprint length, which combined with the tire pressure provides the tire load L. Similarly, it is possible to accurately measure the impact factors influencing the dynamical tire radius R_{Dyn}. The dynamical tire radius itself can accurately be obtained by utilizing the wheel speed sensors ω in context with a GPS reference velocity V^{GPS} (see fig. 2) and state of the art methods dealing with the geometric impact of curves and situations that produce slip. Given that the tread of a tire is a rather slowly varying parameter, unsuitable situation (e.g. high tire slip) can be discarded and the remaining measurements can be filtered appropriately to deal with remaining measurement noise and effects like tire belt expansion in the beginning of a tire life.

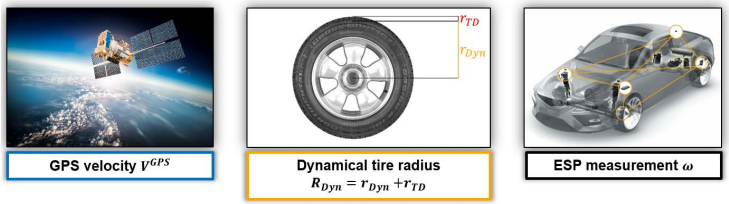

Figure 2. Dynamical tire radius R_{Dyn} separated into two contributions 1) Dynamical tire radius up to the tread r_{Dyn} and 2) Dynamical tire radius from tread r_{TD}

This accurately determined dynamical tire radius is impacted by the tire velocity V, tire pressure P, tire load L, tire temperature T and finally the tire tread depth r_{TD}.

$$V^{GPS} = R_{Dyn} \times \omega = [r_{Dyn}(P, T, V, L) + r_{TD}] \times \omega \quad \text{(Equation 3)}$$

Common to all the impact factors is that their impact depends on measurable noise factors. Here eTIS is an integral component for the tire pressure, load, and temperature, while the velocity V can be obtained from ω. After compensating for the noise factors and employing state of the art learning techniques to deal with manufacturing tolerances, the remaining impact on the tires dynamical radius is its tread depth which can be extracted by proper algorithms from r_{TD}. Based on this tread depth the following information (see figure 3) can be communicated to the driver in context with a specific tire type (e.g. summer vs. winter tire):

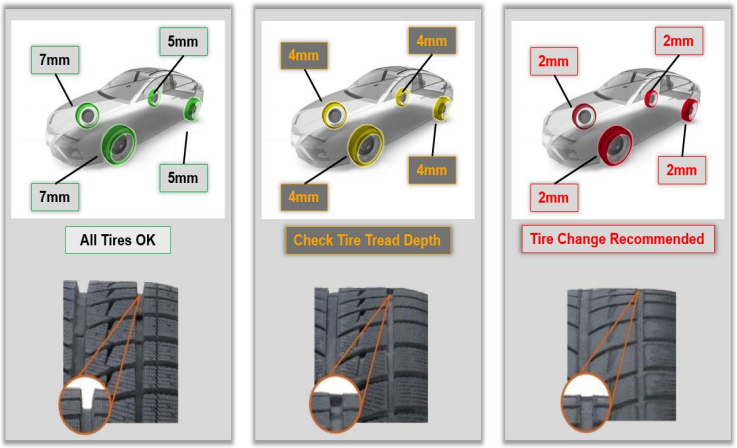

Figure 3. Information strategy for timely tire replacement

This provides ample time for an upcoming necessary tire replacement. Additionally, suboptimal tread depth levels (like the ones indicated in orange and red can be treated by the vehicle in context with the current velocity and information from the other

systems presented in this paper. This can then lead to a speed warning to the driver or a direct reduction of velocity via autonomous driving systems. In the following figure results are shown where the system was installed after some 8.000km into tires which were subsequently driven for another 40.000km on the front axle before they needed replacement, while the tires on the rear axle lasted a total of 60.000km. The vehicle has a front wheel drive architecture. The green lines indicate reference measurements together with min / max values (indicated by the bars). The black line is the output of the systems algorithm, while the red lines indicate the algorithms own error estimation. After carrying out several fleet campaigns with different vehicles and mission profiles, the overall accuracy of the algorithm was found to be +/-1mm, which is clearly achieved for the specific tire life on the vehicle in figure 3.

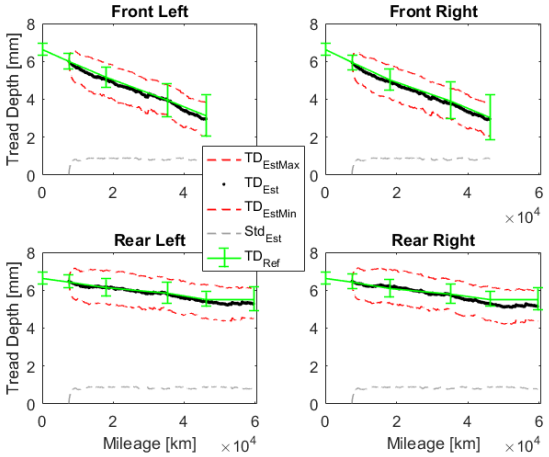

Figure 4. Results of TreadDepthMonitoring for the 4 tires of a front wheel drive vehicle driving a total of 60.000km

The front tires have been replaced after some 47.000km. The solid black line is the output of the algorithm with the red dashed lines being an error estimation. The green lines are reference measurements with corresponding uncertainties (bars).

4. LEVERAGING eHORIZON SERVICES

Weather has a strong impact on the road friction and thus the driver safety. For instance, after a long period without rain, a lot of particles and oils percolate through the road surface. Thus, at the beginning of rainfall, those oils ascend on the top of the road, resulting in a reduced friction potential.

Precisely predicting rainfall and especially friction related weather conditions is a major requirement for the future of Automated Driving solutions. This precision must not only boil down to temporal and spatial but to a strong reflection of the weather phenomena.

Nevertheless, forecasts delivered by the Weather Forecast Providers (WFP) are not sufficient in both spatial and temporal resolution. Actually, those forecasts might be sufficient at the city level (1 km square grid and hourly update) but not for Automated Driving (A.D.) and Advanced Driver Assistance Systems (A.D.A.S.) purposes: for which less than 100 meters of precision and below 5 minutes of frequency update are required. Figure 5 shows 4 weather cells near Frankfurt-City, WFP weather cell size is 1/100 of degree (in both longitude and latitude).

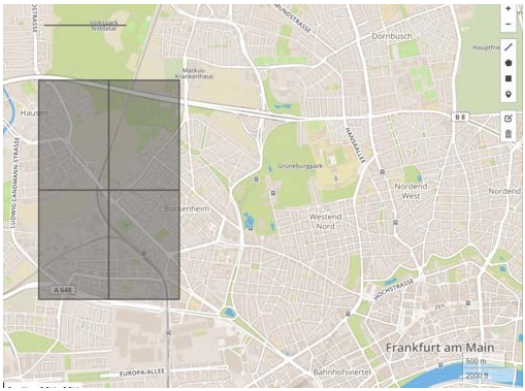

Figure 5. Example of weather cells in Frankfurt a. M.

Relying on vehicles as IoT weather stations, is a way to overcome this precision drawback. Vehicles are constantly collecting a large amount of weather related data and producing real-time weather-related observation system (*i.e.* activation of wiper, lights, and user or automated actuators as well as the information from temperature, hygrometry and pressure sensors). At a local level, vehicle data can be used to enhance weather forecast data. For instance, when a driver encounters a rainfall, either he activates the wipers, or the rain sensor is enabled. Those events are uploaded to the cloud where they are used to update short term weather forecasts. Wiper activation at the vehicle level increases the probability of precipitation at the cell level and thus each car contributes to changing the probability of the weather phenomenon. Figure 6 illustrates this behaviour. Thus, from local information, *eHorizon* produces a high accuracy map from both WFP and vehicle data.

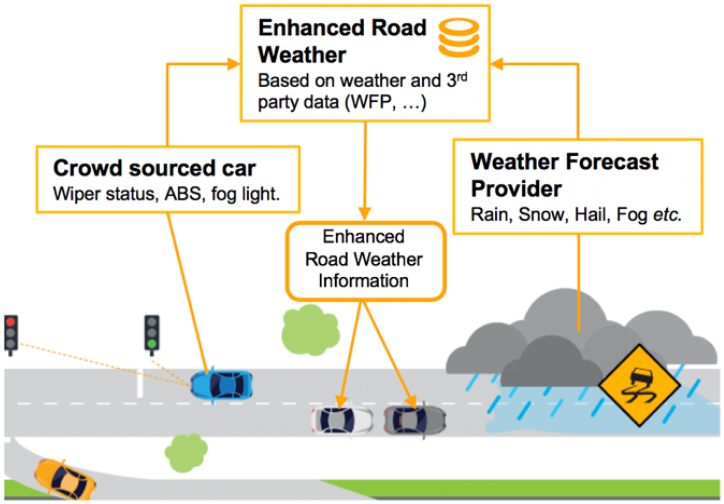

Figure 6. Road Weather Enhancement using vehicle data

The confusion matrix below compares results on rain detection for a Weather Forecast Provider (WPF) and our Road Weather (RW) service for a trip of 20 minutes with rain by only one vehicle. As the

matrix shows, the WFP does not predict rain for the whole trip (only 69%). RW, with only one vehicle, increases the precision by 30% (90% of good classifications).

Table 1.
Confusion Matrix for rain weather

	% False Predictions	% True Predictions
Rain : WFP	31%	69%
Rain : RW	10%	90%

With eHorizon Road Surface Condition services as an extension of eHorizon Road Weather it becomes possible to predict weather related situations and their impact on the road conditions and tire/road friction for the road ahead. Machine Learning approaches facilitate training of personalized road models to detect friction related hazardous weather situations such as hydroplaning or black ice. This method allows an accurate and fast prediction for a single road segment. eHorizon supports driving functions by delivering required information along the vehicle path in advance, before sensors can detect dangerous situations in immediate surroundings.

Adverse weather with heavy rain and exceptionally when first vehicles have already experienced and detected pre-hydroplane or even (full) hydroplane the information about the potential hydroplane risk for a specific weather cell is send to eHorizon. eHorizon services again will provide this information to other vehicles that could potentially be affected, so that they are able to adjust their driving functions to the risky weather conditions.

5. PREDICTIVE HYDROPLANING RISK RECOGNITION

5.1. Water Spray Recognition by surround view cameras

The approach to integrate surrounding sensors for early hydroplaning risk detection is because emerging of hydroplaning goes along with increasing water pressure between the tire's

footprint and the road surface which generates the above-mentioned splash water and spray in all directions (see chapter 2). The physical effect of the squeezed-out water is used to be detected and classified by an intelligent surround view camera system.

Figure 7. Water spray detected by surround view cameras for vehicle near field sensing

Surround view systems are based on four miniaturized wide-angle cameras, one front, one rear and two side cameras integrated in the base of the two exterior mirrors. These systems provide a 360° panorama view as well as single images from all four cameras in the near-field of the vehicle's environment. Additionally, to the sole imaging functionalities a bundle of different functionalities based on computer vision algorithms can be offered to the customer. Main use cases are parking functionalities with scalable level of automation.

The main goal of the surround view camera approach for this application is to use computer vision and machine learning methods to discriminate between different road conditions and to detect the imminent risk of hydroplaning. Figure 8 shows an example image of

the right-side mirror-integrated camera for the hydroplane risk recognition and the relevant region of interest (ROI) in red to be evaluated.

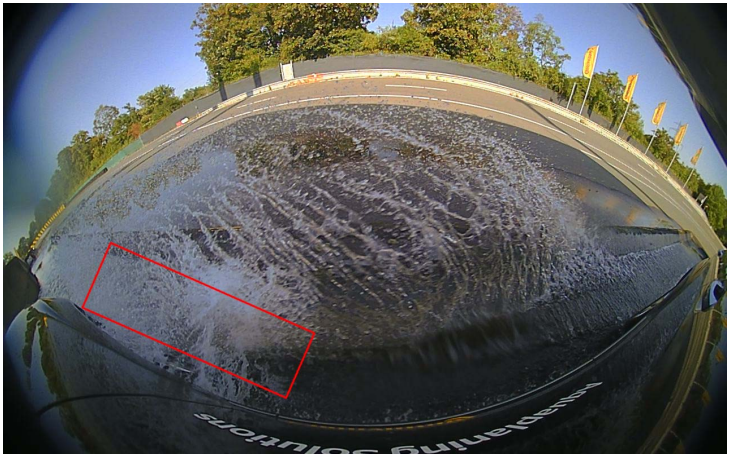

Figure 8. An example of the ROI for the Hydroplane (risk) class

To automatically distinguish between different road conditions, a classification framework based on Fisher Vector Encoding [14], which has become the state-of-the-art approach for a variety of image classification tasks, is proposed. In a pre-processing step, a Region Of Interest (ROI) is extracted from the original surround view image (see figure 9). The determination of its location, shape, and size is a crucial aspect for robust classification. On the one hand, the ROI must provide sufficient information to allow for the separation of the different classes. On the other hand, however, the ROI should only cover as few as possible information of the environment, since characteristics, which are not related to the actual road condition, might cause overfitting, especially in the case of limited training data. Once an appropriate ROI is defined, a compact and generic representation of the image is computed.

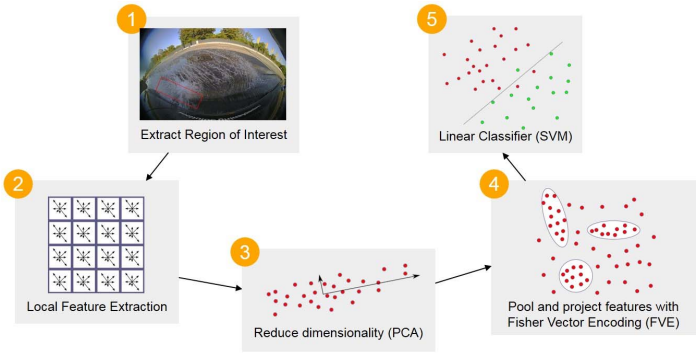

Figure 9. Typical pipeline for digital image processing

For this purpose, a set of local image features are extracted on a regular dense grid. For instance, the frequently used Histograms of Oriented Gradients (HOG) [12] feature descriptors can be applied to obtain a compact feature vector for each grid cell by computing a histogram of occurrences of image gradient orientations. In a further step, it is possible to reduce the dimensionality of the feature space by applying Principal Component Analysis (PCA) [13] and discarding the dimensions that contain the least information. Finally, the set of feature vectors are embedded into one global representation per image using Fisher Vector Encoding (FVE) [14]. In the training phase, a Gaussian mixture model is fitted to the training data. During encoding, the gradient of the log-likelihood with respect to the model parameters are determined based on the soft assignments of every local descriptor to each Gaussian distribution of the mixture model. Those gradients can be understood as adjustments to the parameters of the trained model with respect to a given image which results in a generic and unique representation. The gradients of individual model parameters are finally concatenated into a single global feature vector for each image. In the last step of the proposed framework, a classifier is trained to obtain a mapping from global feature vectors to road condition classes. As suggested by the authors of FVE [14], a linear Support Vector Machine (SVM) [15] is applied, where the feature

space is separated by a hyperplane which is determined during training. Thereby, the hyperplane is defined by a small set of training examples located at the class boundaries which are referred to as support vectors. Furthermore, a probabilistic output can be achieved by applying logistic regression.

The avoidance of overfitting poses a challenge in the particular case of hydroplane. Overfitting means the memorization of the training data, rather than understanding the concepts of the classes. As it is extremely dangerous to drive in hydroplaning situations in "real-world situations" on public roads the training data for this class can only be generated in a safe proving ground environment. The state-of-the-art test site of Continental is called "Contidrom". Here are different water basins for tire tests available that can be filled up to a specified water depth to create different reproducible hydroplaning situations in a safe vehicle test environment. So far there are no examples of hydroplaning from real world situations available for training. Therefore, special precautions must be taken to learn the typical characteristics of hydroplane. In this paper, the results of two different basic experiments are presented. For the experiment "only Contidrom", the system is trained and tested on images for all three classes (dry, wet & hydroplane risk) generated just at the safe proving ground environment. In the experiment "all Data" the system is trained and tested on images from the "Contidrom" proving ground (all three classes) as well as from "real-world situations" on public roads for dry and wet conditions only. Furthermore, hydroplaning situations only from the "Contidrom" are provided, as no real-world data can be generated safely for this class. In both experiments 50% of the data is used for training and the remaining 50% for testing, then the sets are switched in a second run.

Table 2 shows the first results of the experiments for both cases. The Overall Recognition Rate (ORR) describes the ratio of correct classifications to the number of samples, whereas Average Recognition Rate (ARR) calculates this ratio per class, averaged over classes. The "Contidrom" tests form the baseline for the experiments, as no real-world influences are present. Hydroplaning risk is detected correctly in 97.4% of the cases.

Table 2.
Results of the experiments: ORR (Overall Recognition Rate; ARR (Average Recognition Rate) per class

Experiment	ORR	ARR	Dry	Wet	Hydroplane
only „Contidrom“	95.6%	95.0%	93.3 %	94.4 %	**97.4%**
all Data	**98.5%**	**96.0%**	**99.0 %**	**100 %**	89.2%

The experiment “all Data” shows, that the system can learn the real-world situation well and even exceeds the “Contidrom” results for both ORR and ARR. However, a decreasing detection rate for hydroplaning is apparent in this setting. This suggests that the system has not only learned hydroplaning features but has also taken features of the test site environment into account. Since there is a much higher variability in the road characteristics for “real-world”, the classification of hydroplaning is a much more difficult task.
More experiments were carried out, where the system was only trained on “Contidrom” data and tested on a mixture of “Contidrom” and “real-world” data. In these settings, system performance decreased for wet and dry roads. This shows that the classifier trained only on the “Contidrom” data is prone to overfitting on the training environment and is not able to generalize very well.

Since no large data set of real-world hydroplaning data can be generated safely, potential overfitting on the test site environment has to be prevented in a different way. The biggest improvements can be achieved by generating more data for the case of hydroplaning by a wide variation of surrounding influences, e.g., different road surfaces, perturbations, and illumination situations. Additionally, methods of data augmentation to artificially generate more variability in the training data can be applied.

The first experiments clearly show that the discrimination between the different road conditions by surround view cameras is possible and on a good way. In particular, also the combination with feature

detection by a front camera and the enhancement by Deep Learning algorithms shows to be very promising.

5.2. Water Pressure Recognition by new Tire Sensors

Beside the usage of the eTIS Sensor for tire tread depth estimation, information about the interaction between the tire footprint region and the road when water is present is specifically of high interest. A model is outlined that explains a unique signature of hydroplaning in the radial acceleration that is measured by the sensors inbuilt accelerometer. The intended target is the detection of the very first manifestations of hydroplaning before the tire has lost a substantial amount of grip. Such an approach allows an early warning at vehicle speeds lower than the speed that ultimately results in full hydroplaning. With such an approach many of the driving situations that gradually lead to hydroplaning can be detected and by means of a driver warning or a more direct velocity reduction full hydroplaning can be avoided altogether.

For a constant water film covering a road, it is well known [11] that increasing the vehicle velocity when driving on a wet road causes the tire road interaction to change through different stages. At low velocities, where the water can fully be absorbed by the tire's void volume of the tread, the tire road interaction is characterized by its "normal" wet grip behavior. When increasing the velocity, at some point the tire's tread is not able any longer to fully absorb the water (ref. also Chapter 2). There will be a water wedge build-up in front of the tire, which partially penetrates underneath the forward-facing section of the footprint region, while the rest of the footprint region still has full & partly wet grip on the road. Consequently, the tire has lost only a fraction of its contact area and still enables vehicle control for most practical purposes. This state is of special interest for the detection with the eTIS sensor. When increasing the vehicle velocity even more, at some point the water wedge will fully penetrate between the footprint of the tire and the road. At this point, the tire has lost its contact to the road and there is no more grip at all. This state can be labelled as full hydroplaning.

5.2.1. Model for radial acceleration measured by eTIS

A model is presented explaining the radial accelerations seen by the eTIS sensor during the three different stages (wet grip, pre-hydroplaning, full hydroplaning). It explains how the concept introduced in Chapter 2 (ref. also Fig. 1) is sensed by the accelerometer in the eTIS Module.

In Fig. 10d) the radial acceleration a_R measured by eTIS as a function of the rotation angle ϕ is plotted. This acceleration data is based on an interpolation between different acceleration values derived from the corresponding curvature experienced on the path that eTIS moves along. Assuming that the longitudinal velocity V is constant along the circumference of the tire, the radial acceleration at a given rotation angle ϕ is given by,

$$a_R = V^2 / r(\phi) \qquad \text{(Equation 4)}$$

where $r(\phi)$ is the radius of the circle locally converging to the path of the eTIS. The left part (Figs. 8a and 8d) shows the case of wet grip. At 0° the radial acceleration is defined by the radius of curvature of the tire r_0, i.e. by V^2 / r_0. When the sensor enters the footprint region, the radius of curvature decreases to smaller values. The largest acceleration corresponds to the smallest radius r_1, i.e. V^2 / r_1. Inside the footprint area the path is nearly flat, i.e. the corresponding radius of curvature is very large which produces a measured acceleration of roughly 0. When leaving the footprint, the acceleration overshoot is approximately the same as when entering, i.e. V^2 / r_1. Finally, eTIS experiences the radial acceleration corresponding to the radius r_0, i.e. V^2 / r_0 at 360°.

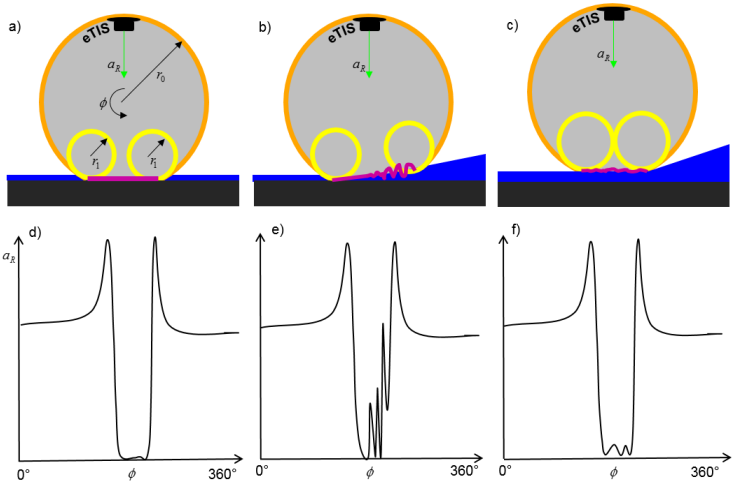

Figure 10. eTIS radial Acceleration as a function of the tire rotation angle. a), d): wet grip. b), e): pre-hydroplaning. c), f): full hydroplaning. a), b), c): Radius of curvature corresponding to top position (orange), entering/leaving the footprint (yellow), inside the footprint (magenta). d), e), f): Radial acceleration model output for eTIS position

In the case of pre-hydroplaning (Fig. 10b and 10e), this picture changes uniquely in the footprint region. Due to the penetration of the water wedge at the leading footprint edge, the small radius r_1 does not directly go to large values but shows oscillations during this transition phase. These oscillations originate from the expulsion of the water at the leading footprint edge. They are much less present at the trailing edge. Consequently, a unique asymmetry between trailing and leading edge in the case of pre-hydroplaning can be expected.

In the case of full hydroplaning (Fig. 10c and 10f) the tire slides virtually friction less over the water. In this case, the oscillations are expected to be of much smaller amplitude since the contact to the road is completely lost.

5.2.2. Hydroplaning tests with eTIS

To test the model, a vehicle was equipped with eTIS samples that specifically focus on measuring the radial acceleration around and in the footprint region. This vehicle has been driven on a test track into a water basin with approximately 10-20 mm of water. The vehicle was fitted with new "Continental Viking Contact 205/55R16" tires with full tread depth. In a first test run the vehicle was driven with 60km/h over a wet road. In this case, the shape of the measurement resembles the expectation for the wet grip case (Fig. 10d).
In a second test run attention towards the radial acceleration when driving with 60km/h inside the water basin was payed, where the full hydroplaning threshold was ~75km/h. This pre-hydroplaning situation was analyzed in the time domain and also by means of a spectrogram in the following figure:

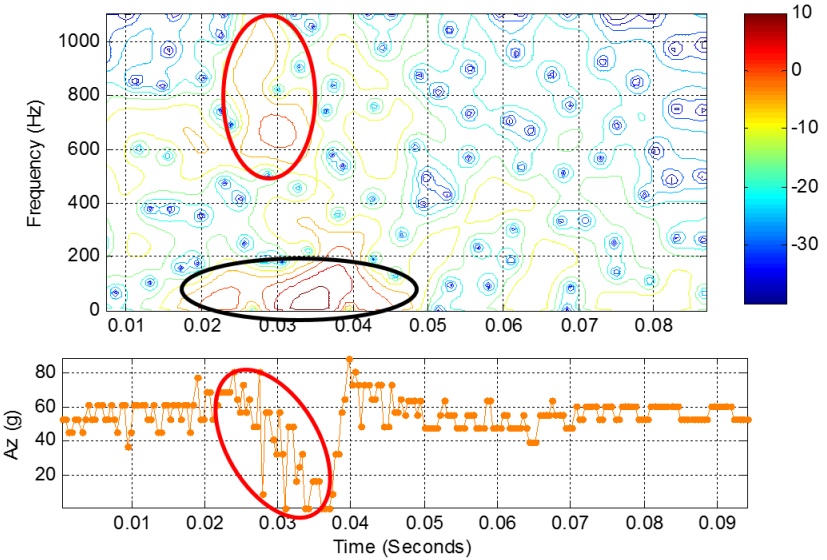

Figure 11. eTIS radial acceleration and spectral density

At the bottom of the figure, the eTIS radial acceleration signal as a function of time for this typical pre-hydroplaning situation is

plotted. It is important to note that when plotting against the time, the leading edge occurs before the trailing edge. In Fig. 10, the acceleration curve was plotted as a function of the counterclockwise defined rotation angle ϕ. The leading edge displayed exactly the oscillations expected from the expulsion of the water (red diagonal oval). These oscillations are not visible at the trailing edge. Consequently, the expected strong asymmetry was fully visible in the time-domain.

At the top of the figure, the spectral density (color coded) as a function of the same time axis and also the frequency (y-axis) is displayed. One can clearly see an increased spectral density of rather low frequencies (0…200Hz) that is distributed somewhat symmetrically over the entire footprint area (indicated by a black oval). Additionally, an increased spectral density is also clearly visible at higher frequencies (500-1100Hz), but only around the leading edge (indicated by red oval). This analysis reveals an asymmetry between the leading and the trailing edge of the footprint. The spectrogram confirms the higher frequency oscillations associated with the leading edge of the footprint, visible on the time signal, while also evaluating quantitatively the frequency range of the oscillations - roughly 500 Hz to 1100 Hz.

Theory and measurements show promising potential for the detection of pre-hydroplaning. A unique asymmetric signature in the radial acceleration measurement has been identified. The corresponding eTIS based detection is able to trigger the prevention of full hydroplaning.

6. HYDROPLANING ASSISTANCE BY BRAKE INTERVENTION AT THE REAR AXLE

6.1. Active Safety Assistance

In a hydroplaning situation the driver needs assistance in two distinct ways: firstly, to stabilize the vehicle in case of disturbances and secondly, to guide the vehicle safely along the course of the road. For control design a linear single-track model is used, in which

the front tire forces are neglected due to the hydroplaning behavior. The state vector **x** contains yaw rate and side slip angle as state variables. Control input **u** is the rear axle longitudinal force difference. This control action can be provided e.g. by torque vectoring based on rear wheel individual braking. The disturbance input **s** is an unknown yaw torque M_z. caused e.g. by not homogeneous water film thickness at the front left and right wheels.

The assistance is triggered by evaluating wheel slip and other signals provided by a standard ESC (Electronic Stability Control) system. The controller is designed as a state feedback in combination with feed-forward of the driver steering input **w** and disturbance compensation, i.e. the control law is given by

$$\boldsymbol{u = -K_x x - K_s \hat{x}_s + K_w w} \qquad \text{(Equation 5)}$$

The control structure is further extended by an inner-loop longitudinal slip control described in [4] to access the full control potential whilst ensuring that the rear axle will not be destabilized during the intervention. The sign of the control variable **u** determines which rear wheel is in slip control mode. The overall control structure of the hydroplaning active safety assistance is shown in Figure 12. Details of the design of the controller are given in [3].

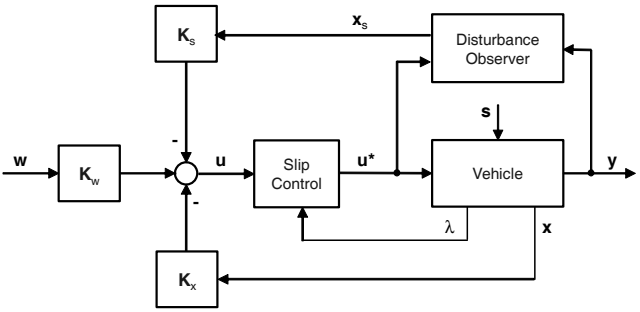

Figure 12. Control structure of the hydroplaning active safety assistance system with inner-loop slip control and outer-loop yaw rate control

6.2. Vehicle test results

Figure 13 illustrates the hydroplaning tests with a rear-drive vehicle at the “Contidrom” proving ground. The hydroplaning basin is 100 m long and 6 m wide. The water film thickness is approx..10 – 20 mm.

Figure 13. Hydroplaning assistance vehicle test at the “Contidrom” proving ground with front wheels floating. The vehicle is controllable by rear wheel brake torque vectoring

The following figure illustrates the assistance principal as well as typical vehicle dynamics signals.

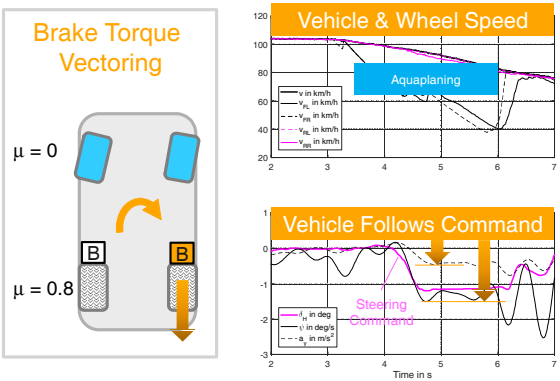

Figure 14. Hydroplaning vehicle tests at the “Contidrom” proving ground. (Left): Assistance principle: vehicle is controllable by torque vectoring at the rear axle. (Right):

Vehicle dynamics showing that vehicle is following driver steering command during hydroplaning phase

Figure 14 illustrates the performance of the hydroplaning assistance. The driver initiated a steering wheel angle ramp-step during floating phase of the front wheels. With the assistance system active the vehicle is controllable and follows the driver commands by building up sufficient yaw rate and lateral acceleration. Without assistance the vehicle is moving uncontrollable in straight direction despite driver steering command.

7. CONCLUSIONS

The integration of the eTIS-based TreadDepthMonitoring function is intended to avoid driving with too low tire tread depth during heavy rain and adverse weather situations in the first place. A surround view camera and tire sensor (eTIS) based system for early hydroplaning risk detection has been proposed to recognize the imminent hydroplane risk and to warn the driver or to intervene in the case for an automated vehicle in an early phase before (full) hydroplaning occurs. Based on outdoor vehicle tests in real hydroplaning situations feasibility studies have been carried out where both systems demonstrate the potential and ability for a proof of concept and further base development.
After adverse weather and pre-hydroplane events have been detected the cloud-based eHorizon services will be updated and provides services to inform other vehicles that could be affected before entering the hydroplane risk area.
Further-on a simulation environment has been designed to study an active safety system with the purpose to assist within the physical limits when the vehicle already hydroplanes (full). An extended tire model reproduces the effect of the surface water leading to a complete loss of grip at the front wheels. The proposed assistance strategy is based on a state feedback and feed-forward control torque vectoring actuating the rear brakes. The system enables an adequate amount of yaw damping as well as a minimum guidance capability. Vehicle tests have shown significant benefit of the assistance.

The hydroplaning assistance as proposed in this paper is the next

step to strongly support Continental's long-term strategy "Vision Zero" leading to zero traffic-related fatalities, injuries and road accidents in future.

8. References

1] Bathelt, H.: Analytische Behandlung der Strömung in der Aufstandsfläche schnell rollender Reifen auf nasser Fahrbahn ("Aquaplaning"). *PhD Thesis*, *Technische Hochschule,* Wien, 1971.

[2] Ditze, M.; Golatowski, F.; Laum, N.; Varhelyi, A.; Gustafsson, S.; Geramani, K.: A Survey on Intelligent Vehicle Safety Systems for Adverse Weather Conditions. In, *Proc. of FISITA World Automotive Congress*, Budapest, 2010.

[3] Frerichs, D.: Design and Simulation of Vehicle Dynamics Control to Improve Stability during Aquaplaning. *Master Thesis, Technical University,* Darmstadt (in German), 2015.

[4] Gengenbach, W.: The Behavior of Passenger Car Tires on Dry and Wet Roads. *PhD Thesis, Technical University,* Karlsruhe (in German), 1967.

[5] Görich, H.-J.: System That Detects the Current Friction Potential of a Passenger Car During Driving. *PhD Thesis*, VDI-Verlag, Düsseldorf (in German), 1993.

[6] Herrmann, S.R.: Simulation Model of Water Drainage and Aquaplaning on Road Surfaces. *PhD Thesis,* Stuttgart (in German), 2008.

[7] Müller, P.C. & Lückel, J.: Disturbance Rejection Control in Linear Multivariable Systems. In *Regelungstechnik,* Heft 2, pp. 54-59 (in German), 1977.

[8] Orend, R.: Modelling and Control of a Vehicle with Single-Wheel Chassis Actuators. In *Proc. of IFAC World Congress*, Prague, 2005.

[9] Raste, T., Frerichs, D.: Study on Active Safety for Aquaplaning Assistance. In *Proc. of AVEC International Symposium*, Munich, 2016.

[10] Semmler, S., Isermann, R.; Schwarz, R.; Rieth, P.: Wheel Slip Control for Antilock Braking Systems Using Brake-By-Wire Actuators. In *Proc. of SAE World Congress*, Detroit, 2002.

[11] Tuononen A., Niskanen A., Xiong Y., Mahboob-Kanafi M.: Advanced Tire Sensing for wet grip and rolling resistance improvements. *Intelligent Tire Technology,* 2013

[12] Dalal, N. and Triggs, B.: Histograms of Oriented Gradients for Human Detection, In: IEEE Computer Society Conference on Computer Vision and Pattern Recognition, 2005

[13] Pearson, K. F.R.S.: On lines and planes of closest fit to systems of points in space, In: The London, Edinburgh, and Dublin Philosophical Magazine and Journal of Science, Pages 559-572, 1901

[14] Sánchez J., Perronnin, F., Mensink T., Verbeek, J.: Image Classification with the Fisher Vector: Theory and Practice, In: International Journal of Computer Vision Vol 105 Issue 3, Pages 222-245, December 2013

[15] Cortes, C. Vapnik, V.: Support-Vector Networks, In: Machine Learning, Pages 273-297, 1995

A STEP TOWARDS INTEGRATED SAFETY SIMULATION THROUGH PRE-CRASH TO IN-CRASH DATA TRANSFER

Abdulkadir Öztürk
Christian Mayer
Daimler AG
Germany

Hemanth Kumar G
Pronoy Ghosh
Atul Mishra
Ravi Kiran Chitteti
Mercedes-Benz Research and Development India Pvt. Ltd
India

Dirk Fressmann
DYNAmore GmbH
Germany

Paper Number 19-0257

ABSTRACT

Occupant simulation methods in the area of passive safety address usually the investigation and prediction of crash dummy behavior after the time of collision. The development and optimization of active and also pre-triggered passive safety systems [1] require new simulation methodology including improved occupant models [2][3] and data transfer possibility between pre-crash and crash phase of a crash event. Prediction of occupant behavior in the pre-crash phase is one important enabler for such a new occupant simulation methodology dealing with optimization of integrated safety systems.

In this work, a semi-automated method is developed for posture and velocity data transfer between pre-crash Active Human Body Model (AHBM) and in-crash Human Body Model (HBM) or dummies. In one use case the application of the developed method is shown.

INTRODUCTION

Two questions are becoming more and more important to be answered with the increasing market penetration and number of functions from PRE-SAFE® and driver assist systems. The first one is how to capture the occupant kinematics and predict it in a pre-crash phase and the second one is how to evaluate its influence on a crash result. A PRE-SAFE®[1] system in general serves for pre-conditioning of the vehicle occupant and partly also of the car in a critical driving situation. Driver assist systems can perform driving maneuvers to mitigate a critical driving condition, e.g. undertaking a braking or steering action to avoid a suddenly appearing obstacle. During such PRE-SAFE® or/and assist system actions the occupant position may change depending on the occurring low-g loading condition.

The classical occupant simulation method deals with the occupant behavior in crash phase. However, it is becoming considerably important to predict the occupant behavior prior to a crash event because most countermeasures performed on a vehicle or/and occupant are prior to this event. These countermeasures may influence the occupant initial position at the start of an unavoidable crash phase. Therefore, coupling the pre-crash phase with crash phase would capture the vehicle and occupant dynamics in the crash simulation. Such a procedure enables the evaluation of the influence of e.g. PRE-SAFE® parameters like triggering times and belt force levels and further optimizations of those parameters.

[1] PRE-SAFE® activates e.g. the reversible belt pretensioner, inflatable multi-contour seat bolsters for side support, seat movement as pre-conditioning (for passenger)

METHOD

Method overview

The simulation process chain consists of three main steps (cf. Figure 1). In the first one a reduced pre-crash model is created to provide a robust and fast base to simulate the pre-crash phase. The second step contains the pre-crash data processing and data creation for the in-crash phase. In the last step a crash model with the inputs from the previous step is created containing the pre-crash dynamics and geometric requirements.

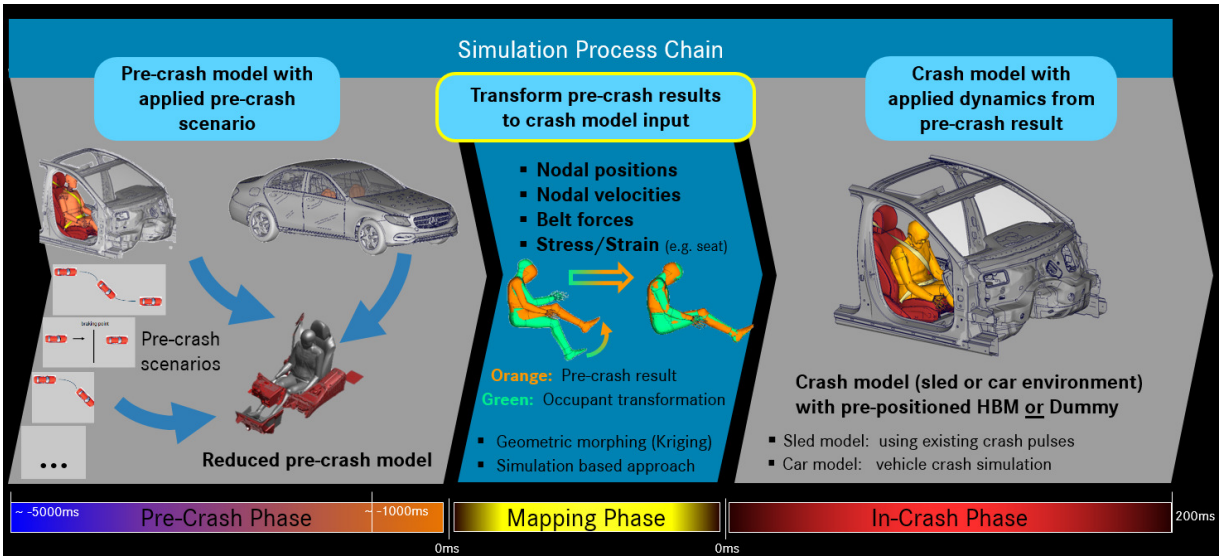

Figure 1: Overview of the Simulation Process Chain.

Due to the fact that simulation is not running in just one shot from pre-crash until the end of crash phase, it is possible to use different, optimized or suitable occupant models in each phase and also set up the crash configuration in a flexible way. That means by using the same pre-crash input it is possible to run different crash configurations.

Model setup of the pre-crash model

The pre-crash vehicle model is reduced as much as possible containing only the important surroundings of the occupant. Depending on the interaction possibility, parts having only slight contact with the occupant model are also switched to rigid material.

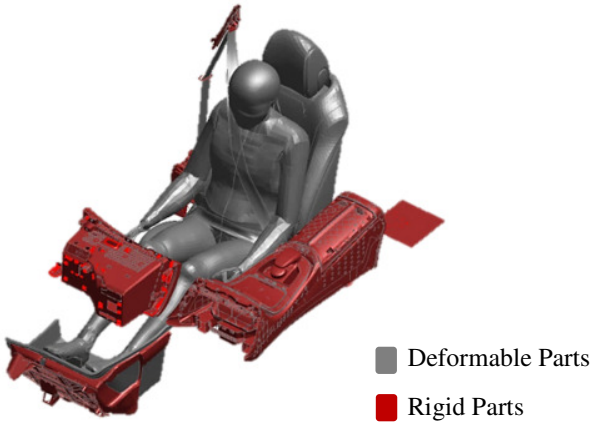

Figure 2: Pre-crash model set-up

The model contains mainly the seat, footwell area, parts of the instrument panel, center console & belt system. If needed the door trim could also be integrated. As occupant model the A-THUMS-D [4] model with active muscles is included.

The boundary conditions representing the pre-crash maneuver could be derived from vehicle test data or from simulation data (e.g. accident reconstruction, vehicle dynamics simulation, etc.). This data could be imposed as acceleration, velocity or displacement boundary condition on the pre-crash model.

The main focus by setting up the pre-crash model is to reduce the CPU time and ensure the robustness since the required time frame is much longer (up to 5sec.) than the common used time duration for crash simulation. Due to long simulation time usage of the double precision version of the FE solver could be necessary.

Occupant Models for crash and pre-crash phase
For each phase a different version of the THUMS-D occupant model is used.

THUMS-D Human Body Model The HBM used in this study is the THUMS-D 50th percentile occupant model. The THUMS-D model represents a mid-size adult male occupant model, whose height and weight are 175 cm and 73.5 kg, respectively. The model is derived from THUMS® [5] classical version 1 & 3. This model was previously modified for in-house Daimler AG usage. The modifications conducted on this model involved mesh refinement in several body regions, connections in lower extremities and implementation of a new shoulder model. This model is henceforth, in the study is referred as THUMS-D as it was developed for the crash phase ("in-crash"). Figure 3 (a) below illustrates the THUMS-D model.

Active THUMS-D Human Body Model The *Active THUMS-D* human body model is developed based on "relaxed" THUMS-D which is derived from the THUMS-D explained above. Initial investigations made obvious that available HBM models and therefore also THUMD-D validated under high g loading conditions, are not applicable under low g conditions. There general behavior is too stiff and muscle control cannot be implemented directly. The details of relaxed THUMS-D model development are discussed in our research conducted previously [6]. Relaxed THUMS-D is then integrated with active muscles [4] to create *Active THUMS-D*. Figure 3(b) below illustrates the *Active THUMS-D* model ("A-THUMS-D").

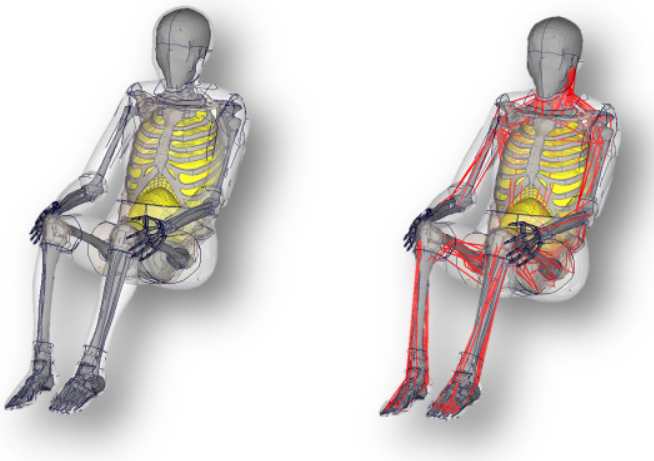

(a) THUMS-D (b) Active THUMS-D

Figure 3: In-crash & Active pre-crash Human Body Models

Data Transfer

As described in the previous sections, the pre-crash simulations are performed using a modified THUMS model that involves also active muscles to reflect the physical behavior of the human body during the low-g pre-crash phase and which also has been validated accordingly. On the other side, the in-crash phase requires a (mostly passive) model, which has been validated against in-crash (high-g) load cases. For the most general case, the pre-crash and in-crash models could be totally different in terms of meshing, materials and geometry, e.g. Active THUMS-D model for pre-crash and dummy model for the in-crash phase. Thus, no direct (one-to-one) relation between the two model meshes is available.

At the end of the pre-crash phase, the model's posture is obviously different from the initial standard posture (actual nodal positions) and also is in motion (actual nodal velocities), according to the pre-crash situation, e.g. lane change and/or braking maneuver. This requires a transfer of the nodal positions and velocities from the pre-crash to the in-crash phase. The latter is necessary to reflect the initial motion at the start of the in-crash phase. At the same time, a decent mesh quality has to be ensured to enable a stable simulation process of the in-crash phase and aspects of automation also have to be considered to include the data transfer method into a process chain with as little user interaction as possible.

AdaPT3 - Adjustment and Positioning Tool for Human Models To achieve this, a generic software tool is being developed by the authors to simplify and automate positioning and scaling processes with special applications to human body models (cf. Figure 4). Multiple geometric transformation procedures, like e.g. translations or rotations of model regions, are implemented, which are solely based on nodal relocations. The mesh smoothing of interfacial parts can be realized by simulations or interpolation methods like for instance the kriging or radial basis function methods.

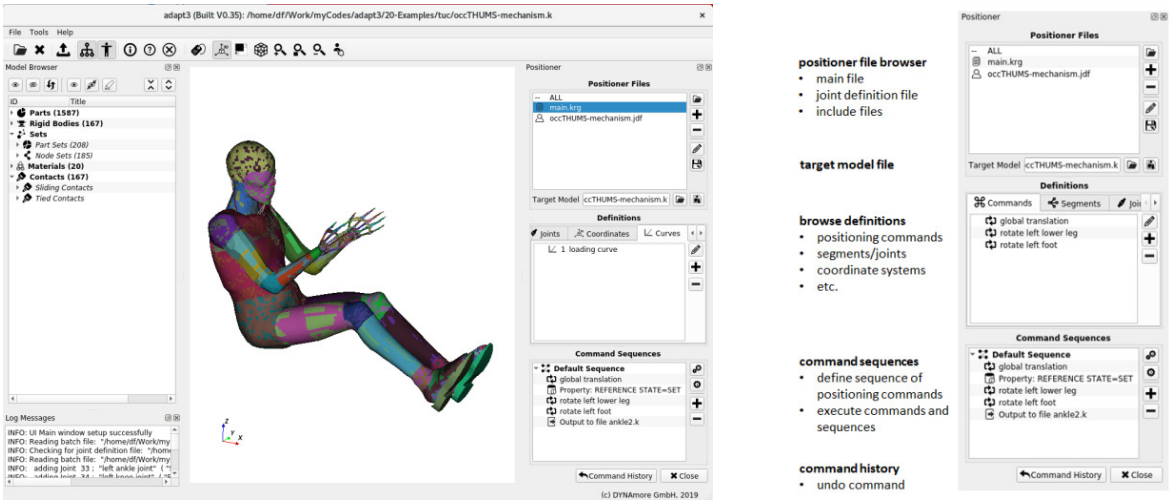

Figure 4: Main GUI of AdaPT3 showing the THUMS human model (left) and the positioner widget (right)

The tool is a generic tool which is not bound to a specific human model. The model dependency is rather realized by positioning and configuration files. Here model-specific definitions are given in terms of body segments (cf. Figure 5), joints, local coordinate systems or curves and task-specific definitions in terms of rotations, translations or scaling commands are specified to achieve a specific positioning task. These commands can be organized in positioning sequences and automatically run in a batch mode or interactively in the graphical user interface (GUI). Other features of the tool are for instance a browser for the positioning files, a command overview and history (UNDO) widget, a special-purpose positioner file editor, import/export capabilities and the possibility to interactively position the model or generate simulation decks.

Furthermore, functionalities have been implemented into *AdaPT3* to realize the posture transfer and the velocity mapping from the pre-crash to the in-crash models.

Data Transfer Approach In the following, the pre-crash model is also denoted as the source model, while the in-crash model will be referred to as the target model. Since in the most general case, no direct relations are present between the source and target occupant models, both models are divided into segments which will act as basic common properties. The segmentation might be realized as depicted in Figure 5 and includes the left foot, left lower leg, left patella, left upper leg, pelvis, etc.

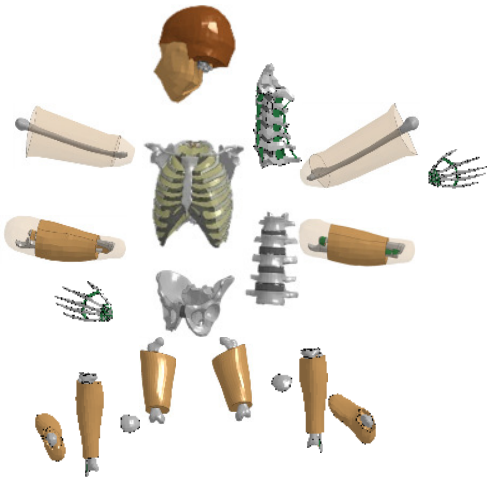

Figure 5: THUMS Model Segmentation

Based on this segmentation, the general mapping approach can roughly be defined using the following three steps

1. averaging of quantities within segments of the source model (pre-crash model)
2. transfer of averaged values between the models
3. distribution of averaged values to mesh of the target model (in-crash model)

The special implementations for the posture transfer and the velocity mapping are described in the following.

Posture Transfer

For the posture transfer, nodal positions have to be transferred from the source to the target models. Since no direct link is available between both meshes, the body segments of the target model are aligned to the segments of the source model. Therefore, local coordinate systems are defined on the body segments in the source and in the target model. To ensure a good model integrity and decent joint connections, the location and orientation of these local coordinate systems have to match the main features and the direction of the body segments. To perform the posture transfer, the local system of the target model is aligned with the local system of the source model and the nodes of the corresponding segment are updated accordingly. This implies that possible deformations of the segments are ignored which is acceptable since the segment deformations in low-g acceleration cases are mostly small in the pre-crash phase.

Please note that this step only repositions the body segments and the deformation of the joints and interfacial parts (e.g. knee flesh and ligaments, pelvis flesh) is entirely ignored. To adapt these interfacial parts, a model smoothing step is also required. This step can be based on geometric transformations or on simulations.

Simulation based positioning The most straightforward and mostly used approach is based on simulations (cf. Figure 6). A simulation deck is generated by the *AdaPT3* tool to move the body segments of the target model into the position of the source model. This is usually realized using the *string-pulling* or *marionette* technique, where string and damper elements pull the body parts towards the target position. The main advantage is that the physics, i.e. the material stiffness distribution and also contact interactions is accounted for during the simulation. However since current human models are still simplified in terms of representing real human anatomy and flexiblity, and this might lead to unphysiological motions also to unacceptable mesh quality. Another problem is that simulations can be very time consuming and postprocessing in terms of mesh smoothing and corrections might still be necessary.

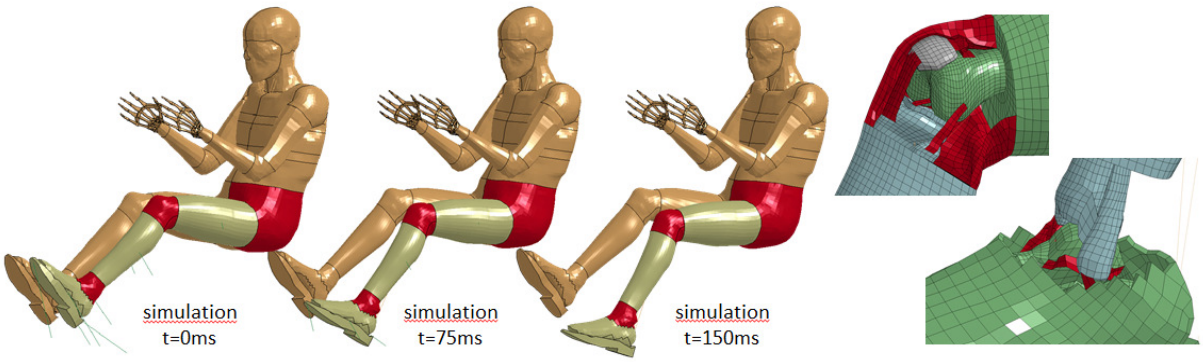

Figure 6: Posture adaptation using simulations

Positioning via geometric transformations Another approach is based on purely geometric mesh transformations using a kriging or radial basis function approach . Here the kriging method [7] is used to smooth the interfacial joint parts, e.g. the knee flesh or ligaments (cf. Figure 7). This requires the definition and decent choice of control points which define the basis for the interpolation approach. These control points are derived from the connected and prepositioned parts, like the upper and lower legs or the patella. The most important advantage of this method is the very fast execution time which is only a few seconds or minutes, depending on the number of control points. The mesh quality is also often better compared to the simulation results. However this method does not account for the physics of the model and might lead to problems in case of large posture changes. Thus the method should be restricted to small or moderate motions.

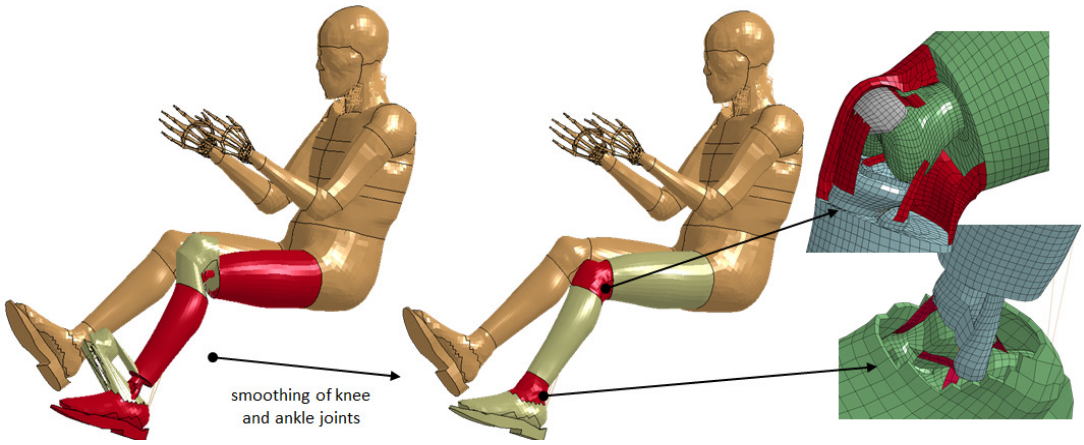

Figure 7: Smoothing of the prepositioned leg using the kriging method

Velocity Transfer

For the velocity transfer, again no direct link is available between the source and target models. Therefore the velocity mapping is again done on the body segment level where for each segment a representative set of nodes is selected. The nodal positions and velocities at the end of the pre-crash simulation are evaluated from the simulation result files. To compute the segment translational and rotational velocity, the nodal translational velocities are averaged over the source segment, the rotation center and the rotational velocities w.r.t. to the rotation center have to be computed on the source segment first. These quantities are then transferred to the target model and distributed to the nodes of the target segments using appropriate FE solver keyword cards. Finally, the simulation can be started using the initial segment velocities

Model setup of the crash model

The crash model setup comprises of standard decks either a sled model or a full vehicle model. The selection of the type of simulation deck depends on type of the load case. The methodology discussed above ensures the transfer of both the vehicle/sled model. Moreover, the flexibility offered by the tool chain is that it enables transfer of occupant data from pre-crash phase from Active HBM-to-HBM or Active HBM-to-Dummy.

APPLICATION IN COMBINED MANEUVER SCENARIO

The semi-automated methodology discussed above has been used for evaluating integrated safety – pre-crash and in-crash as a continuous event.

Pre-Crash maneuver

The present use case represents a simple conflict scenario. The ego vehicle is assumed to be travelling at 50kmph into another road, as shown in Figure 8a, having green traffic lights. The opponent vehicle e.g. ignores its red traffic light and, therefore, hits the ego vehicle from the side driving with a speed of 50kmph. The driver in the ego vehicle starts emergency breaking after becoming aware of the opponent car and decelerates from 50kmh to 31kmph at the time of impact.

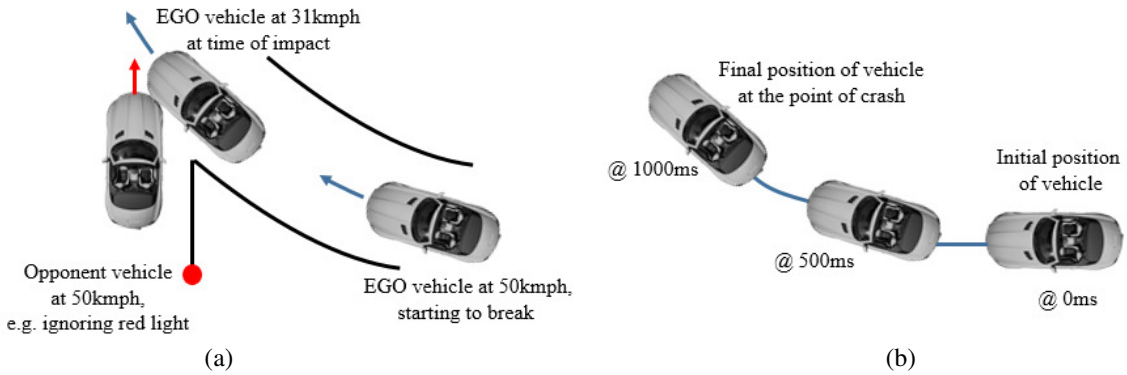

Figure 8: (a) Conflict scenario combined maneuver setup and (b) Vehicle trajectory during combined maneuver

Figure 9 illustrates the combined maneuver vehicle dynamic profile which was used to simulate pre-crash maneuver is based on the work conducted in OM4IS2 project [9].

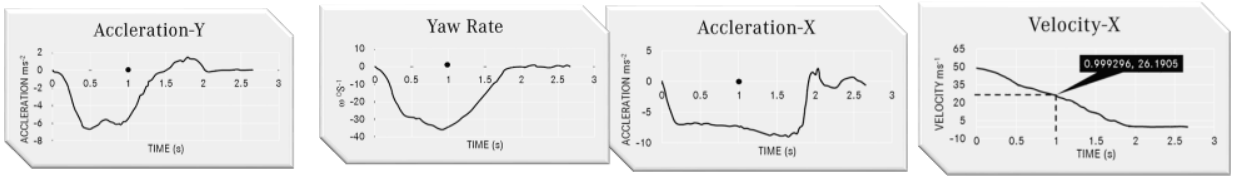

Figure 9: OM4IS2 combined maneuver dynamic profile [9]

The time duration of the pre-crash maneuver considered in this study is 1000ms. Figure 8b illustrates the vehicle trajectory and orientation at the end of pre-crash phase. The occupant under investigation is the passenger.

In-crash pulse generation

The crash pulse for conducting this study was generated from a vehicle to barrier impact (MDB-to-vehicle). The simulation was performed with position and velocity inputs from pre-crash end state. Figure 10 shows the full vehicle model and MDB configuration used for pulse generation. The vehicle FE model includes detailed BIW parts, engine compartment, doors, wheels and the suspension assembly etc.

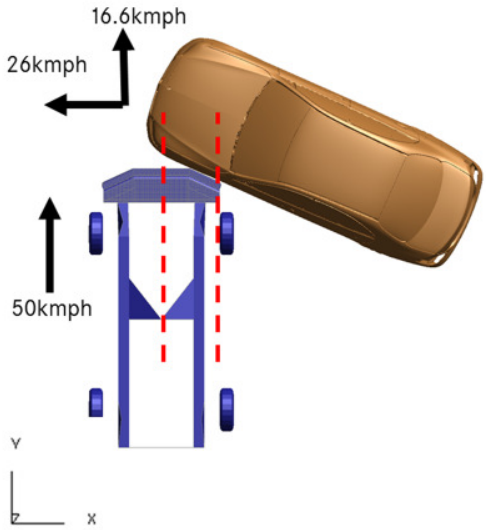

Figure 10: Final position of models for the full vehicle simulation

The motion pulse was generated based on vehicle kinematics using three nodes were minimal deformation was observed in structure. The displacement data from these three nodes were extracted and applied to the respective nodes in the sled to impart motion to the sled model. The sled simulation was overlaid over full vehicle simulation as illustrated in Figure 11 to verify transfer of displacement data which were now used in the FE sled model.

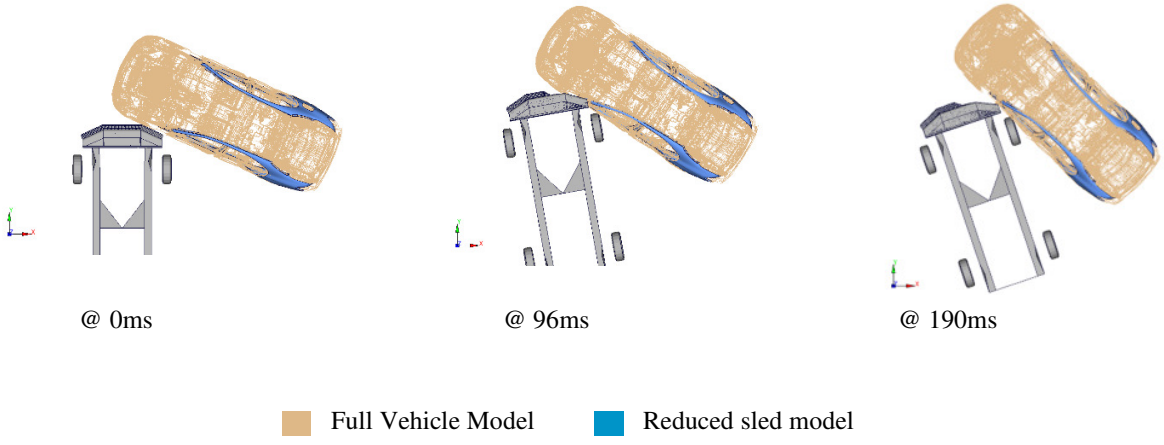

Figure 11: Sled model simulation overlaid over full vehicle simulation for extraction of motion pulse

Dynamic Occupant Data Transfer

The dynamic data at the end of the pre-crash phase was then transferred to in-crash phase model using the methodology above. The data transfer involved posture and velocity data transfer for the occupant. The in-crash HBM posture was generated using simulation approach (ref. Method section). Figure 12 shows the comparison of initial and final posture of the in-crash THUMS-D. The quality of the generated posture was evaluated by overlaying the initial state of in-crash and final state posture of pre-crash model as illustrated in Figure 12(b). The velocity data was transferred for individual body segments by estimating the average velocity of individual body region.

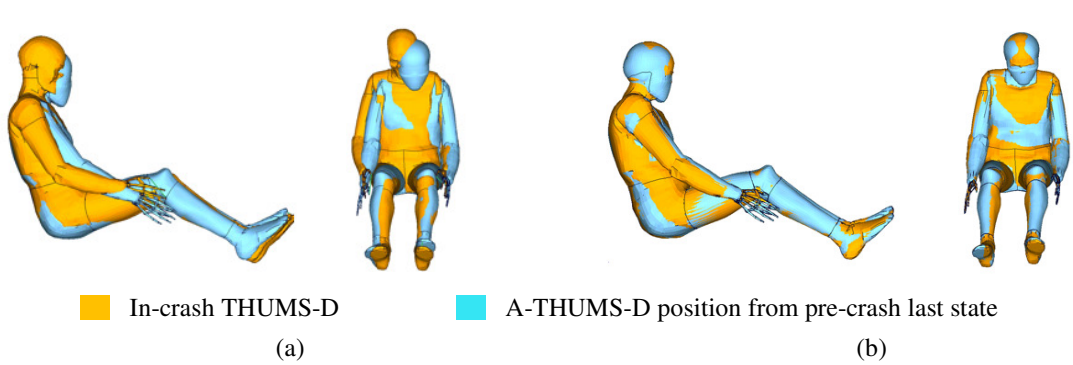

(a) (b)

Figure 12: (a) Initial position of the in-crash occupant (b) Final position of the in-crash occupant after pre-simulation

In-crash simulation carried out in sled model

The pre-crash vehicle response alters the occupant kinematics inside the vehicle. The occupant inside the vehicle starts reacting to the situation which is accomplised using A-THUMS-D for studying the effect of pre-safe system.

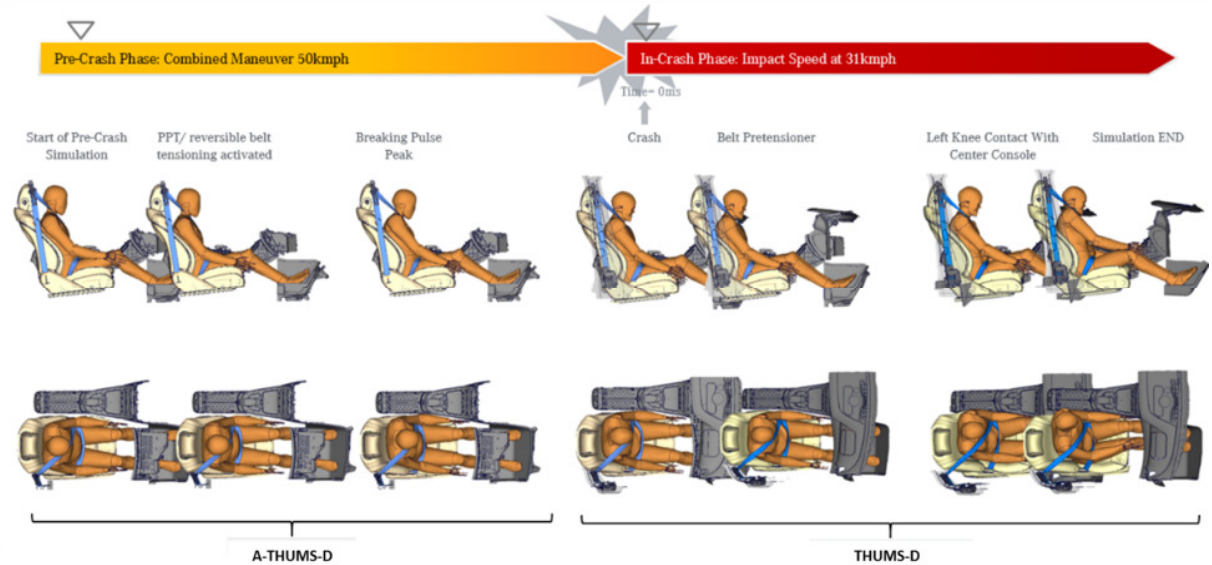

Figure 13: Occupant kinematics in pre-crash and in-crash scenario

In the current study, at 1000ms prior to impact brake assistant system is activated to avoid crash. The crash reversible pretensioner is activated to hold the occupant in seat at a given time point prior to crash. The influence of pre-crash vehicle dynamics moves the occupant closer to center console and instrument panel at the time of impact. The last state of pre-crash is the input for in-crash phase. In addition to the dynamic occupant data stresses in the seat were

also transferred to the in-crash environment. The passenger airbag is not triggered and only the belt pre-tensioner is activated. Complete occupant kinematics from pre-crash to in-crash is illustrated in Figure 13.

DISCUSSION AND LIMITATIONS

The two methods developed for posture data transfer have their own strengths and limitations. The 'geometric method' is fast but is suitable only for small changes in posture while the simulation approach though relatively more time consuming can be used for cases with large posture difference commonly observed when doing pre-crash to in-crash data transfer. Local deformations on the pre-crash occupant are currently not considered in the posture creation for the crash occupant, since those are in generall small.

Velocity data is currently transferred through averaging for body regions where small velocity gradients cannot be captured.

CONCLUSIONS

Integrated safety evaluation for the vehicle occupants in the simulation environment raises the demand to cover and couple the pre- and in-crash phases with a suitable simulation methodology. The presented tool chain offers the use of optimized occupant and vehicle models for each phase and the transfer of the needed pre-crash dynamics as initial condition for the in-crash model. Since both phases running separately in the simulation, it is possible to run different crash configurations with the same pre-crash phase and vice versa. The required posture for the occupant in the crash model can be achieved by using the simulation approach or the faster geometric transformation with automatic smoothing steps.

The presented simulation method is a step towards the development of a seamless integrated safety tool chain.

REFERENCES

[1] Hartlieb,M., Mayer, C., Richert, J., Öztürk, A., Mayer, F., Pal, S., Chitteti, R., „Implementation of new rib material model to a FE-Human Body Model for evaluation of the PRE-SAFE® Impulse Side Restraint System for side impact protection", *ESV Conference 2015*, Gothenburg

[2] Ghosh, P., Andersson, M., Mendoza Vazquez, M., Svensson, M., Mayer, C., Wismans, J. 2015. "A proposal for integrating pre-crash vehicle dynamics into occupant injury protection evaluation of small electric vehicles". *Proceedings of IRCOBI conference*, IRCOBI Conference, IRC-15-88, France.

[3] Teibinger, A., Krzysztof, M., Andersson, M., Wismans, J., Mayer, C., Ghosh, P., Luttenberger, P., D'Addetta, G. 2014. Report on definitions of requirements for a consistent safety analysis for occupant protection (including compatibility). *Reports of SafeEV Project, Grant Agreement No. 314265*, Austria.

[4] Martynenko, O., Neininger, F., Schmitt, S. 2019. "Development of a hybrid muscle controller in LSDYNA for an active Finite Element Human Body Model capable of occupant kinematics prediction in frontal and lateral maneuvers". *Proceeedings of ESV Conference,* Netherlands.

[5] Iwamoto, M., Kisanuki, Y., Watanabe, I., Furusu. K., Miki, K., Hasegawa, J. 2002. "Development of a finite element model of the total human model for safety (THUMS) and application to injury reconstruction". *Proceedings of IRCOBI conference*, IRCOBI Conference, Germany.

[6] Shelat, C., Ghosh, P., Chitteti, R., Mayer, C. 2016. "Relaxed HBM – an Enabler to Pre-Crash Safety System. Evaluation." *Proceedings of IRCOBI conference*, IRCOBI Conference, IRC-16-34, Spain.

[7] Trochu, F. A contouring Program based on Dual Kriging Interpolation", *Engineering with Computers, 9, 160-177*, 1993.

[8] Desai, C., Sharma, G., Shah, P., Ageorges, C., Mayer, C., Fressmann, D. 2012. "A generic Positioning Tool for Human Body FE Models", *Proceedings of IRCOBI Conference,* IRCOBI Conference, Ireland.

[9] Huber, P., Kirschbichler, S., Prüggler, A., Steidl T. 2015. "Passenger kinematics in braking, lane change and oblique driving maneuvers." *Proceedings of IRCOBI Conference*, IRCOBI Conference, IRC-15-89 France.

APPROACH FOR DERIVING SCENARIOS FOR SAFETY OF THE INTENDED FUNCTIONALITY

Paul Rau
National Highway Traffic Safety Administration
United States

Christopher Becker
John Brewer
Volpe National Transportation Systems Center, USA

Paper Number 19-0258

ABSTRACT

Safety of the Intended Functionality (SOTIF) is a safety process in the automotive industry that addresses unintended system behaviors in the absence of electronic faults. Electronic system malfunctions are addressed through industry's functional safety process, ISO 26262. SOTIF on the other hand helps mitigate hazards that may arise when the driving conditions exceed the technology limitations of one or more system components or from certain human factor considerations, such as foreseeable system misuse or mode confusion.

The current approach applies a combination of analysis, simulation, test track, and on-road testing to identify unknown and potentially unsafe scenarios. This study supports the analytical part of this approach by developing a structured framework for deriving scenarios necessary for a SOTIF analysis. The scenarios derived through this framework could then be used to inform simulation and testing.

This paper provides a brief overview of the SOTIF process, describes the development of a framework for deriving scenarios, and presents preliminary results from applying this framework to a highly automated chauffeur system. The framework described in this paper could evolve over time as additional SOTIF-relevant parameters are identified.

INTRODUCTION

Driving automation systems and other advanced electronic and electrical (E/E) systems have the potential to transform the transportation landscape. Safety assurance of E/E systems introduced into the vehicle fleet is a primary consideration for industry and regulators. Recognizing the unique safety challenges presented by E/E systems, such as heavy reliance on software and complex system interactions, the International Organization for Standardization (ISO) published ISO 26262 (Functional Safety – Road Vehicles). ISO 26262 represents the current approach in the automotive industry with respect to the functional safety of E/E systems [1].

Functional safety deals primarily with electronic faults in E/E systems and is one component of the overall evaluation of system safety. In 2019, ISO published Publically Available Specification (PAS) 21448 (Safety of the Intended Functionality; SOTIF). SOTIF is a complementary process to functional safety that addresses the identification and mitigation of hazardous events that may occur in the absence of electronic faults. One aspect of the SOTIF approach focuses on identifying scenarios that may exceed the technology and performance limitations of the system, or increase the potential for system misuse by human operators. This paper describes a framework and approach for deriving scenarios that could be used in a SOTIF analysis.

SOTIF OVERVIEW

Figure 1 shows key steps in the SOTIF process as described in PAS 21448. This section describes relevant SOTIF concepts and the reader is referred to PAS 21448 [2] for a more detailed description of the overall SOTIF process.

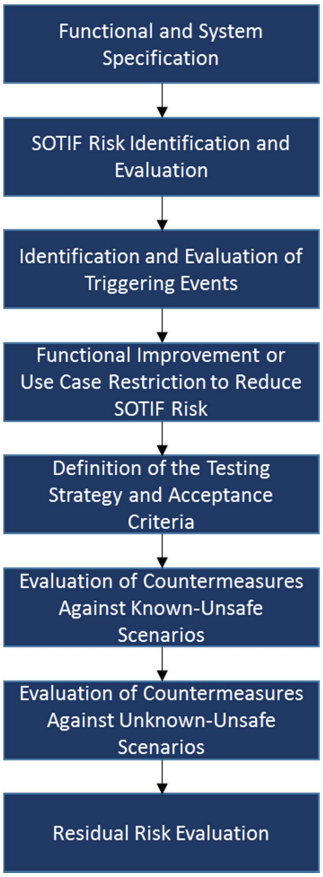

***Figure 1*. Key steps in the SOTIF process [2].**

The SOTIF risk identification and evaluation step determines if credible harm may result from hazardous events. PAS 21448 defines hazardous events as a combination of a potential system hazard and a particular operating situation [2]. Operating situations are defined in ISO 26262 as scenarios[1] that can occur during a vehicle's life [3]. PAS 21448 provides the following example of a hazardous event:

- Hazard: Unintended automatic emergency brake activation at x m/s^2 for y s;
- Operation situation: Operating on a highway [2].

After identifying hazardous events, the SOTIF process then focuses on identifying triggering events that may lead to unintended system behavior and ultimately one or more of the identified hazardous events. PAS 21448 defines triggering events, which include foreseeable misuse scenarios, as *driving scenarios with specific conditions that serves as an initiator for a subsequent system reaction* [2]. The analysis of triggering events attempts to identify system weaknesses as well as the related scenarios that could lead to an identified hazardous event [2].

Triggering events can be divided into two classifications.

- The first category contains events that exceed the performance limitations of the system and components. This paper defines triggering events in this category as SOTIF Type I events. This category includes both sensor limitations as well as limitations in algorithms, such as machine learning and neural net algorithms For example, a highly automated chauffeur system may be operating within its intended operating domain (e.g., highway, good weather) but then encounters a roadway configuration with glare conditions. The resulting lighting conditions may exceed the performance limitations of a front-facing camera.

- The second category contains human factor limitations, particularly in relation to the driver-vehicle interface. This paper defines triggering events in this category as SOTIF Type II events. This area broadly covers several human factors issues, such as the driver failing to keep their hands on the steering wheel; the driver's understanding of the system capabilities and limitations, and the driver's responsibilities; and the driver's ability to understand and respond to warnings and alerts. Under SOTIF, human factor limitations do not extend to intentional abuse of the system, such as intentionally ignoring driver takeover requests or purposely using products intended to override the system limitations.

The scenarios in which triggering events occur are defined in PAS 21448 as a sequence of scenes (i.e., snapshots of the environment) beginning with an initial scene and evolving through a series of events and actions (e.g., triggering events and system responses) [2]. A scene has several characteristics, including dynamic elements, scenery, and self-representations of actors and observers.

According to PAS 21448, scenarios may be classified as known-safe or known-unsafe depending on whether the mitigation strategies sufficiently reduce the SOTIF risk [2]. A third category, unknown-unsafe, represents those scenarios that are not known at the time of system design and are identified through long-term vehicle tests,

[1] Note that ISO 26262 does not define the term "scenario" as rigorously as PAS 21448.

simulations, random input testing, and other measures.[2] The approach in this study attempts to improve the initial identification of known-unsafe scenarios through use of a more comprehensive analysis.

APPROACH

Techniques for developing scenarios for SOTIF continues to be a challenge. Some guidance is provided in Annex F of PAS 21448. The approach described in this paper further develops an existing taxonomy to produce a hierarchical framework of variables that could be used to derive scenarios for SOTIF systematically. The intent is to enable a more comprehensive analysis and development of countermeasures by increasing the number of known-unsafe scenarios identified at the outset of the system design. Some elements of a scenario are not covered by the framework, such as system capabilities or programmed system goals and values [2]. The framework is intended to help identify the aspects of a scenario external to the vehicle.

Thorne et al. developed a top-level taxonomy for the operational design domain. The taxonomy identifies 6 top-level categories and 22 immediate subcategories, as shown in Table 1 [4].

Table 1.
Thorne et al. ODD Taxonomy Categories

Top-Level Category	Immediate Subcategory
Physical Infrastructure	Roadway Types
	Roadway Surface
	Roadway Edges
	Roadway Geometry
Operational Constraints	Speed Limit
	Traffic Conditions
Objects	Signage
	Roadway Users
	Non-Roadway User/Obstacles/Objects
Connectivity	Vehicles
	Traffic Density Information
	Remote Fleet Management System
	Infrastructure Sensors and Communications
Environmental Conditions	Weather
	Weather-Induced Roadway Conditions
	Particulate Matter
	Illumination
Zones	Geofencing
	Traffic Management Zones
	School/Construction Zones
	Regions/States
	Interference Zones

This study used the Thorne et al. taxonomy to categorize scenario factors presented in Annex F of PAS 21448 and relevant parameters from the Fatality Analysis Reporting System (FARS).[3] The FARS database provides coded variables based on decades of analyzing historical causes of fatal crashes. While FARS does not differentiate between human drivers and driving automation systems, the FARS variables still provide general insight into known challenging roadway conditions and behaviors that driving automation systems may need to navigate.

This study further expanded the Thorne et al. taxonomy as a list of 200 variables categorized into 41 detailed

[2] SOTIF is an iterative process and unknown-unsafe scenarios, once identified, become known-unsafe scenarios that can be mitigated through modifications of the system design.
[3] The FARS database contains information on all crashes on public roadways in the United States resulting in at least one fatality within 30 days of the crash [4].

subcategories, a feature of the SOTIF framework. For some variables and situations, analysts may need to consider the appropriate "negative case" when applying the framework. For example, one variable is "pedestrians, pedal-cyclists, other non-motorist permitted in road." The corresponding "negative case" is that non-motorists are prohibited from using the roadway. Negative cases are not explicitly included in the framework.

Table 2 provides an example of the expanded framework using roadway type variables from FARS. Attachment A provides the full framework. The scenario variables in Attachment A also include some variables from the Thorne et al. study that were not included in the FARS database [4] and PAS 21448 Annex F [2].

Table 2.
Example Expanded Taxonomy based on FARS and PAS 21448 Parameters

Top-Level Category	Immediate Subcategory	Detailed Subcategory	Scenario Variable
Physical Infrastructure	Roadway Type	Functional Class	Interstate
			Principal Arterial (Other Freeways/Expressways)
			Principal Arterial – Other
			Minor Arterial
			Major Collector
			Minor Collector
			Local
			Other
		Trafficway	Two-way, Divided, Unprotected
			Two-way, Divided, Positive Median Barrier
			Two-way, Not Divided
			Two-way, Not Divided, Continuous Left Turn Lane
			One-way Trafficway
			Non-trafficway or Driveway Access
…	…	…	…

In order to organize the variables from FARS and PAS 21448 further and into a structure amenable to scenario construction, this study categorized each variable as either permanent-regional, permanent-local, a compounding event or condition, or a potential threat.

- **Permanent-Regional –** These variables are characteristics of the ODD and form the backdrop of scenarios. Permanent-regional variables do not change over time or over significant spatial portions of the trip. Examples of permanent-regional variables include roadway functional class, lane type, and permitted types of non-vehicle uses. Permanent-regional variables may be most amenable to geocoding because of their persistent and pervasive nature. This study identified 31 scenario variables in the permanent-regional category.

- **Permanent-Local –** These variables persist over time, but are localized spatially. From a mobile frame of reference (e.g., a vehicle), permanent-local variables may only be encountered for brief portions of a trip.[4] A vehicle may encounter multiple permanent-local variables over the course of a trip. Each combination of permanent-local variables may represent different variations of the backdrop defined by permanent-regional variables. Examples of permanent-local variables include curves, hills, bridges, and intersections. Since permanent-local variables are temporally persistent, they could be geocoded—for instance, to inform vehicles of approaching intersections, tunnels, or other similar features. This study identified 44 scenario variables in the permanent-local category.

- **Compounding Event or Condition –** These variables are temporary events and conditions that may occur within the scenery defined by permanent-regional and permanent-local variables. For a fixed point in space,

[4] From a fixed frame of reference (e.g., vehicle-to-infrastructure sensors), permanent-local variables may not be appreciably distinct from permanent-regional variables.

compounding events or conditions are those aspects of the initial scene that can change. While a compounding event or condition may persist through an entire trip (e.g., rain), it is also possible for the same compounding event or condition to persist for only a portion of a trip (e.g., a short rain shower) or to change between trips (e.g., the weather may be clear one day and rainy the next). This study further defines compounding events or conditions as variables that are aspects of normal driving. This study identified 75 compounding event or condition variables.

- **Threats –** These variables are temporary events or conditions that relate to specific roadway threats to which the system may need to respond. Unlike compounding events/conditions, threats represent unexpected behaviors or deviations from normal driving situations—for example, other vehicles disobeying signs or traffic controls or pedestrians darting out into the roadway. Threats may be static (e.g., a stalled or disabled vehicle) or dynamic (e.g., an aggressive driver). This study identified 50 threat variables.

Together, the persistent regional, persistent local, compounding events or conditions, and threats define key aspects of the initial scene. Figure 2 shows the relationship of categories assigned to the FARS and PAS 21448 variables incorporated into the taxonomy.

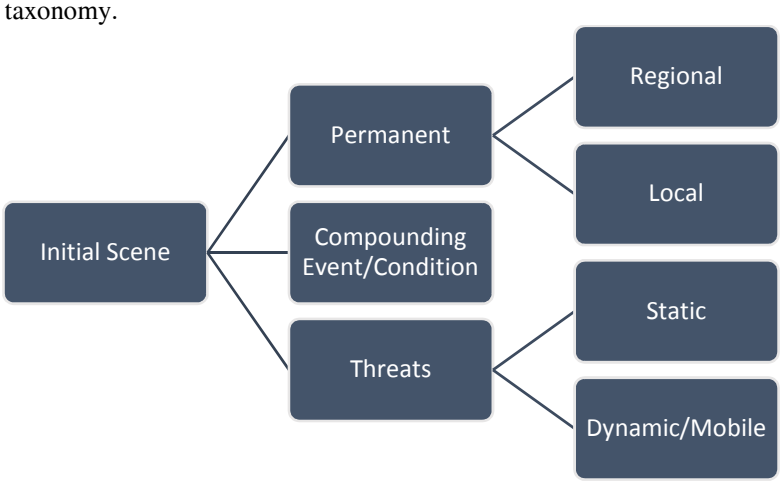

Figure 2. **Categorization schema for variables in the taxonomy.**

PAS 21448 does not differentiate between temporary and permanent elements of the scene. For instance, PAS 21448 includes "environment conditions" as part of the scenery element [2]. However, the framework presented in this study categorizes environmental conditions (e.g., weather, lighting) under compounding events or conditions that are more akin to other dynamic elements, such as traffic, objects, and pedestrians. Separating out the permanent variables can help identify elements of the scenario that a system could predict with greater confidence. This could be particularly important for systems that rely on transitioning control back to the driver. These variables may be more amenable to geocoding or mapping in order to transfer control to the driver with sufficient time for the driver to regain situational awareness.

This study derived triggering events through analysis of the physical limitations of sensors and probabilistic nature of algorithms (Type I SOTIF events). Analysis techniques such as Systems Theoretic Process Analysis (STPA) were used to derive potential driver misuse scenarios (Type II SOTIF events). For each triggering event, initial scenes were constructed that linked the triggering event to a potential hazardous event to create a SOTIF scenario.

EXAMPLE SCENARIO DERIVATION

This study uses hazardous events and triggering events to constrain the development of scenarios. Note that other approaches to develop scenarios exist and this paper presents only one possible way through which scenarios could be derived. To illustrate this process used in this study, this paper presents examples related to the lane centering maneuver of highly automated chauffeur system. This maneuver attempts to keep the vehicle centered in the travel lane. A prior study by Brewer, et al., identified hazards for a generic lane centering system [5]. A relevant hazard

identified in that prior study is "lane/roadway departure while the system is engaged."[5]

This study begins developing scenarios by identifying hazardous events. This corresponds to the second step in the SOTIF process shown in Figure 1. The study applied the permanent-regional variables to develop the operating situation for the hazardous event. One example hazardous event derived through this process is:

- Hazard: Lane/roadway departure while the highly automated chauffeur system is engaged
- Operating situation: Operating in a shoulder lane on a two-way divided interstate or freeway/expressway (i.e., restricted access)
- Potential crash type: Sideswipe (same direction of travel)

Permanent-regional variables are the most consistent with the examples of operating scenarios provided in PAS 21448. Permanent-regional variables define the general context of a trip and may be the only variables that persist throughout the segment of the trip in which the system is engaged. Worst-case assumptions can be made about other conditions when assessing the hazardous event at this level.

In developing operating situations, some variable categories may not be relevant to the particular situation. For instance, in the example above, the shoulder type (paved/gravel versus dirt) does not matter. The omission of a variable means that all relevant cases considered are included as subsets of the stated operating situation.

Triggering events were developed independent of the hazardous events, based on system limitations and potential driver misuse. This corresponds to the third step in the SOTIF process shown in Figure 1. Note that in this paper only SOTIF Type I triggering events are considered. Example triggering events developed for highly automated chauffeur system include:

- The lane model algorithm[6] incorrectly establishes the lane lines.
- The road model algorithm[7] incorrectly establishes the road model in the absence of clear lane markings.
- The camera fails to detect landmarks because of inadequate contrast between the landmarks and the environment.

At this point in the SOTIF process, system designers may consider functional improvements to mitigate triggering events (Step 4 in Figure 1) and establish testing and acceptance criteria (Step 5 in Figure 1). The next step in the SOTIF process relevant to scenario development is to identify known-unsafe scenarios (Step 6 in Figure 1).

The operating situation used for this hazardous event imposes restrictions on the types of variables to consider in constructing the scenario. For example, since the operating situation is specific to interstate or freeway/expressway (i.e., restricted access) roadways, only certain intersection types need to be considered during development of the initial scene—tollbooth/tollgate and entrance/exit ramp.[8]

The triggering events may also impose restrictions on the types of variables to consider in constructing the scenario. For example, to develop scenarios related to the first triggering event listed above, this study only considers variables and combinations of variables that could affect detection of the lane markings. Similarly, to develop scenarios for the third triggering event, this study considered variables that affect the contrast of lane markings and pavement.

This paper provides three examples of scenarios developed within the constraints of the example hazardous event

---

[5] Brewer et al. considered two variations of this hazard based on whether a system fault resulted in excessive or insufficient steering [5]. However, SOTIF presumes that the underlying system is free from faults and therefore this study did not identify a need to differentiate between the two variations of the hazard.

[6] The lane model algorithm is responsible for identifying the lane boundaries and road edge.

[7] The road model algorithm establishes a lane for the vehicle based on landmarks in the absence of lane markings or a lead vehicle to follow.

[8] According to the Federal Highway Administration Highway Functional Classification Concepts [8], some freeways/expressways could have a limited number of at-grade intersections. However, this study assumes that freeways/expressways roadways are more akin to interstates and have restricted access; a possible SOTIF mitigation measure may be to restrict use of the system on freeways/expressways with at-grade intersections.

and triggering events, using the variables presented in the framework.

Table 3.
First Example SOTIF Scenario

Operating Situation	Operating in a shoulder lane on a two-way divided interstate or freeway/expressway (i.e., restricted access)	
Triggering Event	The lane model algorithm incorrectly establishes the lane lines, and the vehicle drifts into the adjacent lane.	
Permanent-Local Variables	*Physical Infrastructure → Roadway/Lane Edges → Lane Characteristic*	Narrow lanes
Compounding Event or Condition	*Operational Constraint → Traffic Conditions → Standard Traffic*	Traffic backup due to regular congestion
Threat	*Objects → Local Traffic Control Missing*	Inadequate warning of exits, narrowing lanes, traffic controls, etc.
Scenario	In heavy traffic, certain roads allow travel on the shoulder lane. However, the shoulder lane might narrow without adequate advance warning that would allow the system to merge out of the shoulder lane. If the vehicle enters a narrower shoulder lane, the lane model algorithm may not be able to determine the appropriate lane width. The system could cross over into the adjacent lane.	

Table 4.
Second Example SOTIF Scenario

Operating Situation	Operating in a shoulder lane on a two-way divided interstate or freeway/expressway (i.e., restricted access)	
Triggering Event	The road model algorithm incorrectly establishes the road model and causes the vehicle to drift into the adjacent lane in the absence of clear lane markings.	
Permanent-Local Variables	*Physical Infrastructure → Roadway/Lane Edges → Road Edge Type/Quality*	Guard rails
Compounding Event or Condition	*Environmental Condition → Weather → Precipitation*	Snow
Threat	*Physical Infrastructure → Roadway/Lane Edges → Lane Marking Type/Quality*	No markings or obscured lane markings
Scenario	Snow may cover the lane markings, making it difficult for the lane model algorithm to track the lane boundaries. Heavy snow may also stick to radars, preventing detection of other landmarks to support the road model algorithm, such as guardrails. Without an appropriate road model, the vehicle may drift out of the shoulder and into the adjacent lane.	

Table 5.
Third Example SOTIF Scenario

Operating Situation	Operating in a shoulder lane on a two-way divided interstate or freeway/expressway (i.e., restricted access)	
Triggering Event	The camera fails to detect landmarks because of inadequate contrast between the landmarks and the environment.	
Permanent-Local Variables	*Physical Infrastructure → Roadway Geometry → Alignment*	Curve Right
Compounding Event or Condition	*Environmental Condition → Light Conditions → Ambient Light*	Dark (unlighted)
Threat	*Physical Infrastructure → Roadway/Lane Edges → Lane Marking Type/Quality*	No markings or obscured lane markings
Scenario	The vehicle is operating on the shoulder at night on an unlit road, and encounters a region without lane markings. A roadway curving to the right may reduce illumination of roadside features by the vehicle's headlights, which may result in inadequate contrast between the landmarks and the environment. The vehicle may drift out of the shoulder lane and into an adjacent lane.	

APPLICATION BEYOND SOTIF

The framework presented in this study could extend beyond SOTIF to provide a general classification of challenging scenarios for driving automation systems. In particular, by separating permanent-regional and permanent-local variables depending on the frame of reference, this framework in this study could help characterize scenarios for vehicle to infrastructure (V2I) and improved GPS mapping (e.g., for geofencing).

Use of a common framework for defining scenarios both in the development of driving automation systems as well as supporting infrastructure could provide consistency between analyses (e.g., types of situations where vehicle-based systems may rely more heavily on V2I). For example, SOTIF scenarios developed using the framework could translate into scenarios where V2I may improve vehicle operation.

CONCLUSIONS

This study established a framework to help develop SOTIF scenarios. The framework combines variables derived from three sources (Thorne et al., PAS 21448, and FARS) into a common typology proposed by Thorne et al. This paper also presents a categorization schema for the variables in the framework to facilitate development of SOTIF scenarios. Certain variables were classified as permanent, with permanence depending on the frame-of-reference (i.e., regional or local features). Non-permanent variables were classified as either compounding events/conditions or threats, based on whether the variable could be anticipated as part of normal driving.

The permanent-regional and permanent-local variables tend not to change over long periods, and can be geocoded with reasonable confidence. If the SOTIF mitigation strategy includes restricting the ODD to avoid certain hazardous events related to permanent-regional or permanent-local variables (e.g., branching or merging lanes), it may be possible to begin alerting the driver with sufficient lead-time through use of detailed maps and GPS. This could increase the probability that the driver will safely resume control of the vehicle. Compounding events or conditions and threats are less predictable and therefore less amenable to geocoding. For instance, a compounding event or condition, or threat may emerge suddenly, necessitating a quick transfer of control to the driver.

The variables presented in this expanded framework can be combined to develop scenarios to support the SOTIF analysis. Three such examples are presented in this paper. Considering a more expanded set of variables and scenarios during the analysis at the outset of the SOTIF process could help reduce the amount of on-road testing and simulation required to identify unknown-unsafe scenarios.

It is important to note that the framework in Attachment A is not intended to be a complete set of *all* relevant variables. Rather, it represents an extension of the taxonomy in Thorne et al. as an effort to progress the state-of-the-art in SOTIF scenario development. The framework presented in this paper could be enhanced by adding additional

factors, such as those observed during real world road tests of driving automation systems. A more complete framework would improve the overall comprehensiveness of the SOTIF analysis.

REFERENCES

[1] H. Martin, K. Tschabuschnig, O. Bridal and D. Watzenig, "Functional Safety of Automated Driving Systems: Does ISO 26262 Meet the Challenges?," in *Automated Driving: Safer and More Efficient Future Driving*, Springer International Publishing, 2017, pp. 387-416.

[2] International Organization for Standardization, *PAS 21448: Road vehicles—Safety of the intended functionality,* Geneva: [Author], 2019.

[3] International Organization for Standardization, *ISO 26262: Road Vehicles—Functional Safety,* Geneva: [Author], 2018.

[4] E. Thorn, S. Kimmel and M. Chaka, "A Framework for Automated Driving System Testable Cases and Scenarios," NHTSA, Washington, D.C., 2018.

[5] J. Brewer, C. Becker, L. Yount and J. Pollard, "Functional Safety Assessment of a Generic Automated Lane Centering (ALC) System and Related Foundational Vehicle Systems," National Highway Traffic Safety Administration, Washington, D.C., 2018.

[6] National Center for Statistics and Analysis, "2012 Fatality Analysis Reporting System (FARS) and National Automotive Sampling System (NASS) General Estimates System (GES) Coding and Validation Manual," DOT HS 811 854, U.S. Department of Transportation, National Highway Traffic Safety Administration, November 2013.

[7] Federal Highway Administration, "Highway Functional Classification Concepts, Criteria and Procedures," [Author], Washington, DC, 2013.

APPENDIX A: SOTIF SCENARIO FRAMEWORK

Table 6.
Permanent-Regional Variables

Top-Level Category	Immediate Subcategory	Detailed Subcategory	Scenario Variable
Physical Infrastructure	Roadway Type	Functional Class	Interstate
			Principal Arterial (Other Freeways/Expressways)
			Principal Arterial – Other
			Minor Arterial
			Major Collector
			Minor Collector
			Local
			Other
		Trafficway	Two-way, Divided, Unprotected
			Two-way, Divided, Positive Median Barrier
			Two-way, Not Divided
			Two-way, Not Divided, Continuous Left Turn Lane
			One-way Trafficway
			Non-trafficway or Driveway Access
	Roadway Surface and Features	Lane Type	Single Lane
			Multi-lane
			Reversible Lane
			Shoulder Lane
			Managed Lane (HOV, etc.)
		Surface Type	Concrete
			Blacktop, Bituminous, or Asphalt
			Brick or Block (Including Cobblestone/Belgian Brick)
			Slag, Gravel, or Stone
			Dirt
	Roadway/Lane Edges	Shoulder Type	Paved/Gravel
			Unpaved
Objects	Roadway Users	Other Non-Vehicle Users Permitted on Roadway	Pedestrian, Pedal-cyclist, Other Non-motorist Permitted in Road (e.g., Restricted versus Unrestricted)
	Non-Roadway Users	Pedestrian Crosswalks/ Intersections	Crosswalks/Intersections Present in Roadway Type (e.g., Restricted versus Unrestricted)
		Other Users on Side of Roadway	Non-motorists Permitted Along Roadway
Zones	Regions/States	Regional Traffic Laws	Special Regional Traffic Laws and Norms
		State Traffic Laws	Special State Traffic Laws and Norms

Table 7.
Permanent-Local Variables

Top-Level Category	Immediate Subcategory	Detailed Subcategory	Scenario Variable
Physical Infrastructure	Roadway Surface and Features	Intersection	Median Crossover Road
			Tollbooth/Tollgate
			Entrance/Exit Ramp
			Four-way Intersection
			T-intersection
			Y-intersection
			Traffic Circle
			Roundabout
			Five-point or More
			L-intersection
		Surface Type	Local Change in Surface (e.g., Concrete Bridge)
			Step Difference/Uneven
		Roadway Condition	Manhole Cover
	Roadway/Lane Edges	Lane Marking Type/Quality	Bott's Dots or Cat's Eye
			Other Non-Traditional Markings
		Lane Type	Narrow Lane
			Wide Lane
			Merging
			Branching
		Road Edge Type/Quality	Median
			Curb
			Concrete Barrier
			Guardrails
			Grating
			Telephone Poles
	Roadway Geometry	Alignment	Straight
			Curve Right
			Curve Left
		Grade	Level
			Grade, Unknown Slope
			Hillcrest
			Sag (Bottom)
			Uphill
			Downhill
			Banked
Operational Constrain	Speed Limit	Speed Limit Signage	Posted Speed Limit
Zones	Traffic Management Zone	Variable Speed Zone	Variable Speed Zone
		Loading/Unloading Zone	Loading/Unloading Zone
	School/ Construction Zone	School Zone	Within Designated School Zone
	Interference Zones	Structures	Tunnels
			Bridges (Double-deck, Covered, Viaduct, etc.)
			Tall Buildings (e.g., Urban Canyon)
			Parking Garage
		Natural Conditions	Geologic Formations (e.g., Canyons, Overhang)

Table 8.
Compounding Event or Condition Variables

Top-Level Category	Immediate Subcategory	Detailed Subcategory	Scenario Variable
Physical Infrastructure	Roadway Surface and Features	Roadway Condition	Ruts, Holes, Bumps in Road
			Other Maintenance or Construction-Related Condition
			Shoulder Related (Design or Condition)
			Inadequate Construction or Poor Design of Roadway, Bridge, etc.
	Roadway/Lane Edges	Road Edge Type/Quality	Cones
Operational Constraints	Speed Limit	Operating Speed	Posted Maximum Limit Below Minimum System Operating Speed
			Posted Minimum Limit Above Maximum System Operating Speed
			Relative Speed Above Surrounding Traffic
			Relative Speed Below Surrounding Traffic
			Speed Inappropriate for Conditions (e.g., Surface, Geometry)
		Speed Limit Signage	None (Inferred Speed Limit)
	Traffic Conditions	Standard Traffic	Light or No Traffic
			Backup Due to Prior Non-Recurring Incident
			Backup Due to Prior Crash
			Backup Due to Regular Congestion
		Altered Traffic Flow	Tollbooth/Plaza Related
Objects	Signals and Signage	Local Traffic Control Type	No Control or Uncontrolled
			Flashing Traffic Control Signal
			Traffic Signal with or without Pedestrian Crossing Signal
			Regulatory Sign
			Warning/Information/Temporary Sign
			Railroad Crossing Device/Gate
			Traffic Officer/Flag Person/Hand Signs
	Roadway Users	Standard Vehicles	Standard Vehicles in Roadway
		Non-Standard Vehicles	Special Cargo Body Type (e.g., Garbage, Gravel, Flatbed, Auto Transporter)
			Large Vehicle Configuration (e.g., Bus, Tractor-Trailer, Single Unit Truck, Etc.)
			Towed Vehicle (Fixed or Non-Fixed Linkage)
			Multiple Trailing Units
			Wide-Load Vehicle
		Other Non-Vehicle Users Permitted on Roadway	Pedestrian, Bicyclist, Other Cyclist or Person on Personal Conveyances in Travel Lane
			Pedestrian, Bicyclist, Other Cyclist or Person on Personal Conveyances on Paved Shoulder/Bicycle Lane/Parking Lane
			Pedestrian Jogging/Running in Roadway

Top-Level Category	Immediate Subcategory	Detailed Subcategory	Scenario Variable
Objects (cont.)	Non-Roadway Users	Pedestrians	Pedestrian, Bicyclist, Other Cyclist, or Person on Personal Conveyances in Intersection Area
			Pedestrian, Bicyclist, Other Cyclist, or Person on Personal Conveyances in Crosswalk Area
			Pedestrian, Bicyclist, Other Cyclist, or Person on Personal Conveyances in Median/Crossing Island
			Pedestrian, Bicyclist, Other Cyclist, or Person on Personal Conveyances Waiting to Cross Roadway
		Other Users on Side of Roadway	Pedestrian, Bicyclist, Other Cyclist, or Person on Personal Conveyances on Sidewalk/Shared-Use Path/Driveway Access
			Pedestrian, Bicyclist, Other Cyclist, or Person on Personal Conveyances in Unpaved Right-of-Way
			Pedestrian, Bicyclist, Other Cyclist, or Person on Personal Conveyances in Non-trafficway (Driveway)
			Pedestrian, Bicyclist, Other Cyclist, or Person on Personal Conveyances in Non-trafficway (Parking Lot/Other)
			Pedestrian, Bicyclist, Other Cyclist, or Person on Personal Conveyances Adjacent to Roadway (e.g., Shoulder, Median)
			Pedestrian Jogging/Running Adjacent to Roadway
Environmental Conditions	Weather	Wind	Severe Crosswind
			Wind from Passing Truck
		Precipitation	Clear/Cloudy
			Rain
			Sleet/Hail
			Snow
			Blowing Snow
			Freezing Rain or Drizzle
		Particulate Matter	Fog, Smog, Smoke
			Blowing Sand, Soil, Dirt
	Weather-Induced Roadway Condition	Roadway Obscured	Surface Under Water
			Splash or Spray from Another Vehicle
		Surface Condition (Including Low-μ)	Wet
			Snow
			Ice/Frost
			Sand
			Water (Standing or Moving)
			Mud, Dirt, Gravel
			Slush
			Surface Washed Out (e.g., Cave-in, Road Slippage)
			Loose or Slippery Surface (Mud, Gravel, Sand, Wet Leaves)
	Light Conditions	Ambient Light	Daylight
			Dark (Lighted)
			Dark (Unlighted)
			Dawn
			Dusk
		External Lighting	Reflected Glare, Bright Sunlight, Headlights

Top-Level Category	Immediate Subcategory	Detailed Subcategory	Scenario Variable
Zones	Special Zone	Special Zone	Special Zone
	School/ Construction Zone	School Zone	Pedestrian, Bicyclist, Other Cyclist, or Person on Personal Conveyances Going To or From School (K-12)
		Construction Zone	Construction
			Utility Work
			Maintenance
	Interference Zone	Natural Conditions	Dense Foliage

Table 9.
Threat Variables

Top-Level Category	Immediate Subcategory	Detailed Subcategory	Scenario Variable
Physical Infrastructure	Roadway/Lane Edges	Lane Marking Type/Quality	No Markings or Obscured Lane Markings
Operational Constraints	Traffic Conditions	Altered Traffic Flow	Recent Previous Crash Scene Nearby
			Police Pursuit
			Stalled/Disabled Vehicle or Vehicle Fire
Objects	Signals and Signage	Local Traffic Control Missing	Inadequate Warning of Exits, Narrowing Lanes, Traffic Controls, Etc.
			Traffic Controls Not Functioning Properly
	Roadway Users	Standard Vehicles	[Other Vehicle] Aggressive Behavior by Non-Contact Vehicle Owner
			[Other Vehicle] Overloading or Improper Loading of Vehicle with Passengers or Cargo
			[Other Vehicle] Following Improperly
			[Other Vehicle] Travelling on Prohibited Trafficways
			[Other Vehicle] Passing Through or Around Barrier
			[Other Vehicle] Failure to Observe Warnings or Instructions on Vehicles Displaying them
			[Other Vehicle] Failure to Signal Intentions
			[Other Vehicle] Driving Wrong Way or On Wrong Side
			[Other Vehicle] Other Bad Driving
			[Other Vehicle] Disobeying Signs or Traffic Controls
			[Other Vehicle] Other Driving in the Wrong Place (e.g., Bike Lane)
			[Other Vehicle] Other Misbehavior – Moving (e.g., Not Dimming Headlights)
			[Other Vehicle] Other Misbehavior – Fixed (e.g., Open Door into Trafficway)
			Jackknife of Articulated Vehicle
			Nearby Trailer (Swerving, Swaying, or Fishtailing)
			[Vision Obscured by] In-Transport Motor Vehicle (including load)
		Other Non-Vehicle Users Permitted on Roadway	Non-Occupant Struck Vehicle
			Non-Motorist Inattentive, Careless, Distracted
			Non-Motorist Failure to Yield Right-of-Way
Objects (cont.)	Roadway	Other Non-Vehicle	Non-Motorist Failure to Obey Traffic Signs, Signals, or

Top-Level Category	Immediate Subcategory	Detailed Subcategory	Scenario Variable
	Users (cont.)	Users Permitted on Roadway (cont.)	Officer
			Non-Motorist Improper or Erratic Lane Changing
			Non-Motorist Failure to Keep in Proper Lane or Running Off Road
			Non-Motorist Passing with Insufficient Distance or Inadequate Visibility, or Failing to Yield to Overtaking Vehicle
			Non-Motorist Making Improper Entry To or Exit From Trafficway
			Non-Motorist Making Improper Turn or Merge
			Non-Motorist Improper Passing
			Non-Motorist Not Visible (Dark Clothing, No Lighting, etc.) or Failing to Have Lights On When Required
			Non-Motorist Operating without Required Equipment
			Non-Motorist in Roadway Improperly (Standing, Lying, Working, Playing)
			Non-Motorist Wrong-way Riding or Walking
			Non-Motorist Working in Roadway (Incident Response)
			Non-Motorist Entering/Exiting Parked or Stopped Vehicle
			Disabled Vehicle Related (Working On, Pushing, Leaving/Approaching)
	Non-Roadway Users	Stationary Object	Debris or Objects in Road
			[Vision Obscured by] Curve, Hill, or Other Roadway Design Features
			[Vision Obscured by] Building, Billboard, etc.
			[Vision Obscured by] Trees, Crops, Vegetation
			[Vision Obscured by] Not-in-Transport Motor Vehicle (Parked, Working)
		Dynamic Object	Struck by Falling Cargo or Something that was Set in Motion by Vehicle
			Non-Occupant Struck by Cargo/Debris
			Animal in Road
		Pedestrian	Pedestrian, Bicyclist, Other Cyclist, or Person on Personal Conveyances Dart-out
			Pedestrian, Bicyclist, Other Cyclist, or Person on Personal Conveyances Improper Crossing of Roadway or Intersection (Jaywalking)
			Pedestrian, Bicyclist, Other Cyclist, or Person on Personal Conveyances Crossing Expressway

DRIVER ALCOHOL DETECTION SYSTEM FOR SAFETY (DADSS) – A NON-REGULATORY APPROACH IN THE RESEARCH AND DEVELOPMENT OF VEHICLE SAFETY TECHNOLOGY TO REDUCE ALCOHOL-IMPAIRED DRIVING – A STATUS UPDATE.

Abdullatif K. Zaouk
Michael Willis
KEA Technologies, Inc.
U.S.A.

Eric Traube
National Highway Traffic Safety Administration
U.S.A.

Robert Strassburger
Automotive Coalition for Traffic Safety
U.S.A.

Paper Number 19-0260

ABSTRACT

Alcohol-impaired driving continues to exact a significant toll among road users both in the United States and around the world. In 2017, in the U.S. alone, alcohol-impaired motor vehicle fatalities totaled almost 11,000 – a number that has seen very little change since 2009. To better address this ongoing problem, in 2008 the National Highway Traffic Safety Administration (NHTSA) and the Automotive Coalition for Traffic Safety (ACTS) formed a cooperative research partnership to explore the feasibility, the potential benefits of, and the public policy challenges associated with the widespread use of non-invasive technology to prevent alcohol-impaired driving. This partnership, known as the Driver Alcohol Detection System for Safety (DADSS) Program has made great strides forward in the development of in-vehicle technologies that will measure blood or breath alcohol and prevent alcohol-impaired drivers from driving their vehicles. Exploratory research in Phases I and II established the feasibility of two sensor approaches, breath- and touch-based, for in-vehicle use. In Phase III, the sensors have become increasingly refined, in terms of both hardware and software, as the program strives to meet the very high standards required for unobtrusive and reliable alcohol measurement. Numerous parallel research programs are currently underway including sensor development, development of calibration processes, materials and instrumentation that will verify the technologies are meeting these elevated standards, human subject testing in conditions that replicate those likely to be experienced in the real world, and real-world pilot field operational trials in diverse settings. At the completion of this effort a determination will be made as to whether the DADSS technologies can ultimately be commercialized. This paper will outline the technological approaches and the status of the various DADSS research programs.

INTRODUCTION

Alcohol-impaired driving (defined as driving at or above the legal limit of 0.08 g/dL or 0.08 percent in all US States except in Utah where the limit is 0.05 g/dl) is one of the primary causes of motor vehicle fatalities on U.S. roads every year (IIHS, 2018). In 2017 alone, crashes involving at least one driver with a blood alcohol concentration (BAC) of 0.08 g/dl resulted in 10,874

deaths of U.S. road users (NHTSA, 2018). Although strong laws and enforcement have led to fewer alcohol-impaired deaths on the roadways (Ferguson, 2012), to effectively reduce or eliminate the problem it will be necessary to prevent alcohol-impaired drivers from driving in the first place. In 2008, the National Highway Traffic Safety Administration (NHTSA) and the Automotive Coalition for Traffic Safety (ACTS)[1] began research to develop in-vehicle solutions to the problem of alcohol-impaired driving. The alcohol sensors under development are required to be seamless with the driving task, that is, accurate, fast, reliable, durable, and require little or no maintenance. Ultimately, the vehicle will not be able to be driven when the device registers that the driver's blood alcohol concentration (BAC) exceeds

[1] Members of ACTS comprise motor vehicle manufacturers representing approximately 99 percent of light vehicle sales in the U.S.

0.08 g/dl (%), although other limits could be programmable. This cooperative research partnership, known as the Driver Alcohol Detection System for Safety (DADSS) Program, has been developing both breath-based and touch-based non-invasive technologies that will be able to prevent alcohol-impaired driving, (Ferguson et al., 2009, Ferguson et al., 2010, Ferguson et al., 2011, Zaouk et al., 2015, Zaouk et al., 2017).

To effectively measure blood and breath alcohol in real time with negligible misclassification errors, stringent performance specifications have been developed that provide a template to guide the overall research effort. The ability to calibrate the performance of each generation of sensor prototypes is a critical component of the development process. These elevated standards, especially those for accuracy and precision, have necessitated the development of innovative approaches that will enable measurement of the technologies' performance on an ongoing basis. Specifically, calibration processes, materials, methodologies and instrumentation have been the subject of extensive cutting-edge research to enable the requisite testing.

Research vehicles have been readied for Field Operational Testing (FOT) and the latest versions of the sensors are being seamlessly integrated within the vehicle interiors. Instrumentation packages also have been developed that will provide a myriad of data on sensor performance under challenging real-world driving conditions. Along with determining whether the DADSS sensors are working as anticipated, the FOT data collection effort will allow the identification of areas for system improvement.

A comprehensive program of human subject research is being carried out, starting with the laboratory environment where better control of conditions can be exerted, and in the vehicle where the sensors can be tested in the environment in which they will be used. This research aims to establish that alcohol measurements made with diluted breath as well as capilary blood (in the tissue of the finger) are comparable to the well-accepted standards of venous blood and deep-lung air widely used in traffic law enforcement.

At the same time, media coverage and consumer sentiments are being monitored in anticipation of a future launch of the technology. These efforts will be ramped up once the technology is available for public scrutiny because the driving public must be onboard with the DADSS technology if it has any chance of being widely implemented.

The purpose of this paper is to provide a status update on the following key DADSS program areas:

- Touch-based DADSS subsystem research
- Breath-based DADSS subsystem research
- Field Operational Testing
- Standard Calibration Devices
- Human Subject Testing

PROGRAM PROGRESS

DADSS Sensor Development

Senseair breath–based subsystem The sensor technology under development by Senseair and its partners uses infrared (IR) spectroscopy, which is stable over the full product lifetime, eliminating the need for recurrent calibrations. The challenge in measuring breath alcohol within the vehicle cabin is that the breath is diluted with the cabin air. The breath-based approach uses sensors to measure the concentration of alcohol and carbon dioxide (CO_2) in diluted breath simultaneously. The use of CO_2 in human breath as a tracer chemical allows it to be used as an indicator for the degree of breath dilution, and thus the dilution of the alcohol concentration in the expired breath. A fan draws diluted breath into a chamber where a detector measures the interaction with the alcohol and CO_2 in the sample (Hök et al., 2006). Breath alcohol concentration is then quickly and accurately calculated (see Figure 1).

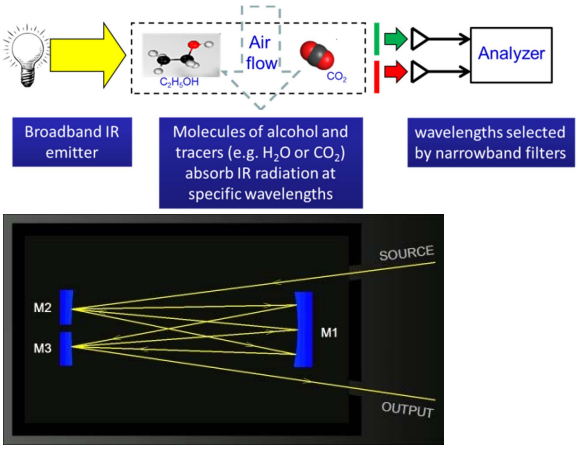

Figure 1. Breath-based sensor block diagram

The goal of the DADSS sensors is to passively measure breath alcohol within the vehicle cabin without directed input from the driver. The challenge is to meet the stringent performance requirements while measuring highly diluted breath. Thus, a significant component of the research is focused on understanding the behavior and flow patterns of the expired breath plume within the vehicle cabin and identifying effective locations for the sensors.

The breath-based sensor has been updated in Phase III with the goal of improving the ability to accurately detect breath alcohol passively. The latest, 3rd Generation version (Gen 3), underwent a complete re-design to increase sensitivity for measurements of passive samples through improvements in the overall signal-to-noise ratio (SNR), reduce the overall size, and improve performance over the full temperature range of -40°C to +85°C as specified by the DADSS Performance Specifications (Biondo et. al. 2017). A major improvement of the Gen 3 sensor is the optical module configuration. Ethanol detection takes place over the full length of the cavity, whereas CO_2 is detected cross-wise to eliminate systematic timing differences between the two signals. This enables the possibility of passive in-vehicle sensing (Ljungblad, 2017). See Figure 2 for a graphic representation of the Gen 3 sensor evolution, key performance metrics and planned Gen 4.

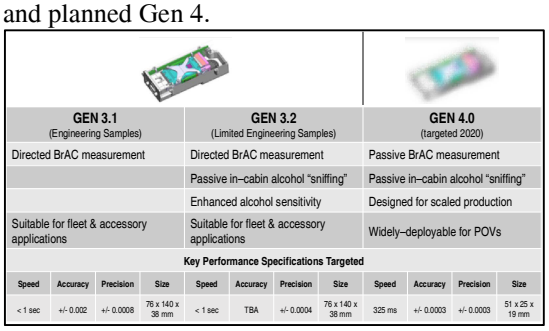

GEN 3.1 (Engineering Samples)	GEN 3.2 (Limited Engineering Samples)	GEN 4.0 (targeted 2020)
Directed BrAC measurement	Directed BrAC measurement	Passive BrAC measurement
	Passive in–cabin alcohol "sniffing"	Passive in–cabin alcohol "sniffing"
	Enhanced alcohol sensitivity	Designed for scaled production
Suitable for fleet & accessory applications	Suitable for fleet & accessory applications	Widely–deployable for POVs

Key Performance Specifications Targeted

Speed	Accuracy	Precision	Size	Speed	Accuracy	Precision	Size	Speed	Accuracy	Precision	Size
< 1 sec	+/- 0.002	+/- 0.0008	76 x 140 x 38 mm	< 1 sec	TBA	+/- 0.0004	76 x 140 x 38 mm	325 ms	+/- 0.0003	+/- 0.0003	51 x 25 x 19 mm

Figure 2. Evolution of Breath-based DADSS Sensor

Recently, significant improvements have been made. The detector and sensor fan were modified to allow more homogeneous airflow through the system. This resulted in improved SNR and increased peak gas levels when measuring breath exhalations at the same distance. See Figure 3 for a graphic representation of the SNR improvements. This is a critical step for passive breath measurement. Software algorithms for passive detection of breath alcohol also have been enhanced, whereby several consecutive signal features can be accumulated to provide sufficient data for reliable measurement.

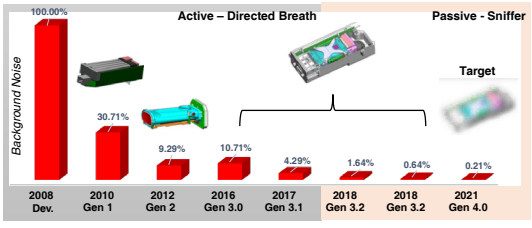

Figure 3. Breath-based DADSS sensor SNR improvements

Further investigations of critical components, including detectors, emitters and mirrors, have shown noteworthy options for more production friendly choices which may be integrated in the future. Sensor calibration procedures have been upgraded in laboratories in Sweden and are now in-line with those used in the United States. These additions have increased the calibration accuracy over the entire concentration span. The latest generation 3.2 sensors have undergone rigorous environmental testing aimed to simulate a sensor life time of fifteen years.

As a result of all these advances, the Gen 3.2 breath sensors now are sufficiently advanced to undergo on-the-road testing. In preparation for fitment of the new Gen 3.2 sensors in the FOT vehicles, the outer housing remained unchanged from the Gen 3.1 version to facilitate rapid exchange of in-vehicle installed sensors. Also, to facilitate exchangeability, a connector printed circuit board (PCB) was developed to avoid the removal of the HMI board with every disassembly/reassembly.

TruTouch touch-based subsystem The touch-based subsystem, developed by TruTouch Technologies, uses near-infrared (NIR) spectrometry - a noninvasive approach that utilizes the near infrared region of the electromagnetic spectrum (from about 0.7 µm to 2.5 µm) to measure substances of interest in bodily tissue (Ferguson et. al., 2010, Ridder et al., 2005). TruTouch has determined that the 1.25-2.5 µm portion of the spectrum provides the highest sensitivity and selectivity for alcohol measurement because the alcohol signal is hundreds of times stronger than the signal in the 0.7-1.25 µm part of the NIR.

The measurement begins by illuminating the user's skin with NIR light (similar to a low power flashlight). The light propagates into the tissue (the skin has to be in contact with the device) and a portion of it is diffusely reflected back to the skin's surface where it is collected by an optical touch pad. The light contains information on the unique chemical information and tissue structure of the user. This light is analyzed to determine the alcohol concentration and, when applicable, verify the identity of the user. The challenge is to measure the concentration of alcohol (sensitivity) while ignoring all the other interfering analytes or signals within the skin (selectivity).

The shift from the Gen 1 prototype, which used a traditional Michelson interferometer that utilizes moving parts, to a solid-state laser spectrometer (which is better suited to the automotive environment) has required extensive hardware and software research (Ver Steeg et al., 2017). The key to enabling such innovation is the ability to define an optimized subset of optical wavelengths which will

provide the high quality non-invasive alcohol measurement in humans that is needed (see Figure 4 for a schematic representation of this approach). It was determined that the new spectrometer requires the use of modulated laser diodes to generate 40 unique wavelengths of light that are physically configured for optimal alcohol measurements. The laser diode specifications were derived from the comparison and analysis of human subject data and comparative reference data.

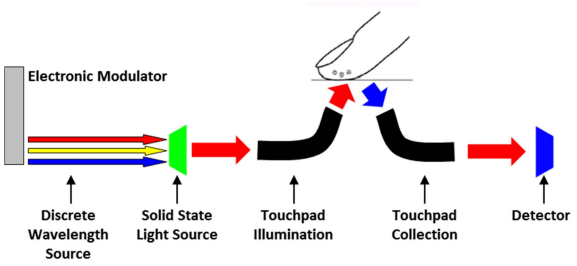

Figure 4. Touch-based subsystem solid-state laser spectrometer approach

The highest risk technical element of the touch-based system is the fabrication of the laser device in order to meet target specifications. Extensive, cutting-edge research has been undertaken to develop the requisite lasers, many of which have not been manufactured before, and assembling them in a multi-laser butterfly package.

The Gen 2 prototype included the first implementation of the 4 multi-laser butterfly packages that interrogate the 40 wavelengths required. Each multi-laser butterfly package, as shown in *Figure 5*, includes 10 laser diodes at 10 unique wavelengths.

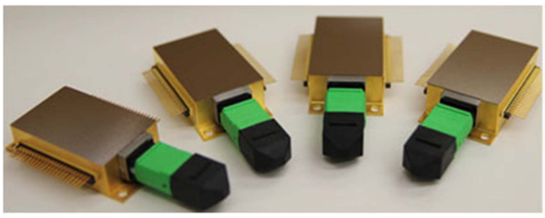

Figure 5. Gen 2 multi-laser butterfly packages

The combined light source is generated by the laser packages and routed onto the touchpad. This light then illuminates the finger and is reflected back to the detector where alcohol measurements are made. After initial work to develop the laser diodes and packaging, Nanoplus, a new supplier, with greater expertise in these areas, was selected. Each stage of the development process has required painstaking research which has been the subject of multiple patent applications.

As with any new technology development, complications have been experienced along the way. For example, research on the Gen 2 touch-based system revealed a problem with laser intensity fluctuations resulting in unreliable tissue alcohol measurements.

In 2017, laser fluctuations were discovered, the source of which was pinpointed to the reference channel. Research has been undertaken to correct for that through redesign of the optical subsystems. Multiple optical laser mixing and delivery systems were evaluated via simulations and modelling and four of the best candidates were fabricated and bench tested. The best performing combinations were incorporated into the Gen. 3 system, shown in Figure 6.

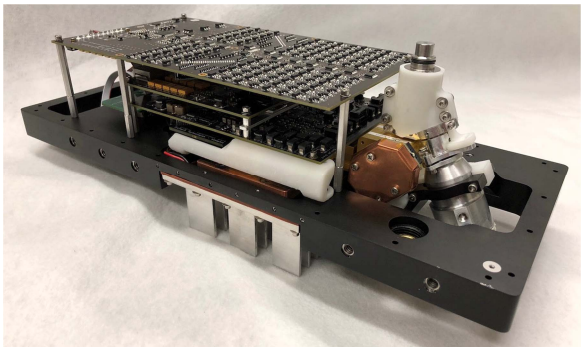

Figure 6. Touch-based Gen 3 prototype

The Gen 3 prototype includes the first implementation of a single package, Stingray, that interrogates all 40 wavelength. The package, as show in Figure 7, includes 20 chips with each chip able to interrogate 2 wavelength, thus reducing the number of chips from 40 to 20 while maintaining the ability to interrogate the required 40 wavelength.

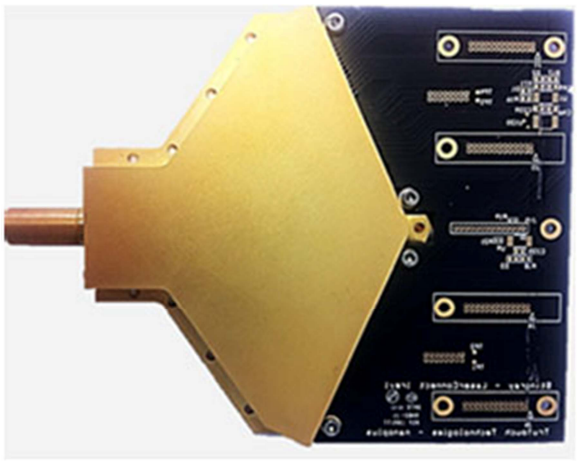

Figure 7. Gen 3 single Stingray lasers package

In anticipation of delivery of functioning stingray laser packages, mechanical enclosures and electronic subsystems were designed, fabricated and tested. Firmware and software that oversee and control the touch system operation were updated. A custom, automated laser calibration system also was built to test the power and wavelengths of the incoming laser packages.

The Gen. 3 laser packages were incorporated into the Gen. 3 touch-based system and underwent in vitro (bench) testing. These tests identified an elevated error rate due to laser dynamic behavior and optical system throughput. Improvements to the optical subsystem mixing and delivery are underway to address this shortcoming.

DADSS Pilot Field Operational Trials

Now in Phase III of development, the breath-based technology is ready for real-world testing. (The touch-based sensors will be integrated once they are ready for installation). Currently, two different research programs are underway to evaluate the DADSS sensors in naturalistic on-road settings in pilot and field operational trials (PFOTs, FOTs). The first PFOTs are currently taking place in Virginia, U.S.A (Fournier et al., 2019). The second set of initial PFOTs are taking place in Massachusetts (Willis et al., 2019).

The Driven to Protect, Powered by DASS initiative, a partnership with the Virginia Department of Motor Vehicles, Highway Safety Office and ACTS, has partnered with James River Transportation (JRT), a transportation company with offices in Richmond and Norfolk, VA, to conduct the first in-vehicle, on-road naturalistic test trials with prototype breath-based alcohol sensors in their vehicles.

KEA Technologies has instrumented and deployed a small fleet of demonstration vehicles to determine if a) the system is generally accepted by drivers, b) there are any technical modifications required to significantly improve the system, and c) the system is ready for wider implementation in fleet, privately-owned, commercial, or other vehicles.

Four 2015 Ford Flex “For Hire” commercial livery service vehicles (see Figure 8) have been instrumented with the latest in-vehicle breath-based alcohol detection systems including supporting data collection and transmission systems (Fournier et al., 2019). The goal is to collect approximately 15,000 data points from the sensors. It is not anticipated that the transportation company drivers will have measurable alcohol on their breath but directed breath measurements are taken at the start and end of each day, and passively throughout the day. Lessons learned will be used to refine the performance specifications, sensor technology as well as data acquisition systems for future on-road vehicle testing.

Figure 8. James River Transportation Ford Flex Driven to Protect Vehicle

Each vehicle is equipped with two Gen 3.1 prototype sensors, one data acquisition system (DAS), two data transmission technology systems (i.e., WIFI and 4G), and one video system including two cameras and a digital video recorder. Breath samples are collected by the sensors both in “directed” mode, where drivers direct their breath toward each of the sensors, and in “sniffer” mode to capture breath alcohol present in the ambient air. The sensors were adapted for installation in the DADSS research vehicles in two different positions: the top of the steering column clamshell, directly in front of the driver’s face and in the driver’s door panel (see Figure 9). These positions improved analysis of the impact of cabin air flow and the driver’s position on alcohol measurements and optimized performance.

The DAS is the central processing system or “brain” of the DADSS system (see Figures 10 and 11). The DAS obtains power from the vehicle battery and

distributes to the other system components. It powers the reference sensor and collects acquired serial data. The DAS relays power to the two SenseAir breath sensors and receives the Control Area Network (CAN) data coming from those sensors. Objective data collected consists of numerical and video data that capture host vehicle states and maneuvers, surrounding traffic, system operation, and driver behavior. All these data are stored by the DAS. Subjective data collected includes driver background information before participation in the FOT and at the conclusion of each day.

Figure 9. DADSS Breath-based sensors; Steering column (top) and driver-side door (bottom)

Figure 10. Data Acquisition System (DAS)

Figure 11. Location of Data Acquisition System (DAS) in Ford Flex vehicle

The second series of PFOTs are utilizing Chevy Malibus donated by General Motors. Forty vehicles are being fitted with the latest breath-based alcohol sensors and comprehensive DAS at the KEA Technology laboratory in Marlborough, MA (see Willis et al., 2019 for more details). The Chevrolet Malibus have been prepared to gather sensor validity, reliability, and durability data as well as to assess the real-world use of the sensors with vehicle passengers who have been drinking. The sensors will be tested in extreme real-world environmental conditions, including high heat, cold, varying humidity, corrosive environments, etc. to ensure that they will be operational for the harshest real-world conditions that they are likely to encounter.

As with the Virginia PFOTs, DADSS breath sensors (Gen 3.2) and a reference sensor are being installed along with the DAS, video cameras and DVR, and wireless modem (see Figure 12 for sensor locations).

The initial 10 DADSS vehicles will be equipped with two Gen 3.2 breath sensors and thereafter the vehicles will include four Gen 3.2 breath sensors; two on the driver side and two on the passenger side.

The majority of the hardware for the DADSS system is mounted onto a plate that resides in the trunk of the Chevrolet Malibu (see Figure 13). From left to right the systems are: DAS, Network switch (MP70E), and DVR (Axis).

Figure 12. Breath sensors; Driver-side door (top)Steering wheel (bottom)

Figure 13. From left to right, the DAS, WiFi LTE, and DVR located in the vehicle's trunk

The PFOT/FOT program will be conducted in three phases, each involving five integrated Chevrolet Malibu vehicles. Phases 1 and 2 will include only drivers and Phase 3 will also include passengers who will be dosed with alcohol.

Prior to the PFOT, the vehicles are undergoing a "shakedown" stage, in which DADSS Program researchers are driving five fully-equipped test Chevrolet Malibu vehicles to and from work, to ensure that the sensors, DAS, cameras, and communications systems etc. are fully operational. These initial tests will provide a detailed insight into the necessary requirements of the PFOT test site set up and will be used to complete the development of the PFOT Test Plan (test routes, number of starts/stops, number of samples required, etc.).

These data will be critical in determining the effectiveness (accuracy, precision) of the DADSS sensors in diverse real-world driving environments. They will also be used to evaluate the effects of repeated use and vehicle mileage on sensor function, analyze driver behavior and user acceptance, analyze and assess the impact of the DADSS sensors using real-world data, improve awareness of in-vehicle alcohol detection systems and assess potential impact of the sensors on alcohol-impaired driving.

Standard Calibration Devices (SCD)

As each new generation of the breath-and touch-based sensors are developed, researchers need to evaluate the sensors' performance. Instrument and/or sensor calibration is one of the primary processes used to confirm and maintain a sensor's accuracy and precision. An important component of the calibration process is to develop a qualification and verification process that is able to illustrate in a traceable manner that the breath-based and tissue surrogates meet the requisite performance specifications. The calibration process involves using reference or calibration standards (SRMs or CRMs), that is, samples of known value. The calibration standard in the U.S is normally traceable to a national standard held by the National Institute of Standards and Technology (NIST). Using the NIST procedures allows calibration materials to be certified that they conform to the stated concentrations.

Considering that the accuracy and precision requirements for DADSS alcohol sensors exceed those established for commercially available alcohol measurement devices, it has not been possible to find NIST certified sources of gas and liquid with the requisite accuracy and precision from which to produce the surrogate samples. Existing NIST reference materials have been used to measure accuracy and precision, but going forward, reference materials for the specified levels of accuracy and precision are being developed by the DADSS team. The SRMs, when combined with the delivery systems are considered to be the SCD.

A multi-pronged program of research and development is underway to address the various aspects of the calibration process. The initial efforts focused on the development of breath and tissue surrogates that could meet the DADSS accuracy and

precision requirements. This ongoing research is conducted in-house at the DADSS laboratory and in concert with outside providers of relevant materials. Once developed, the materials' composition, accuracy, and precision has to be confirmed at these elevated specifications. The instrumentation necessary for such verification has to exceed the DADSS performance requirements by a significant order of magnitude.

Initially, components of the breath and tissue SCD were measured with a Gas Chromatograph (GC) using a Flame Ionization Detector (FID). The GC-FID system underwent numerous tests and incremental improvements to reduce the variability of the gas delivery system for the breath-based SCDs (see *Figure 14*).

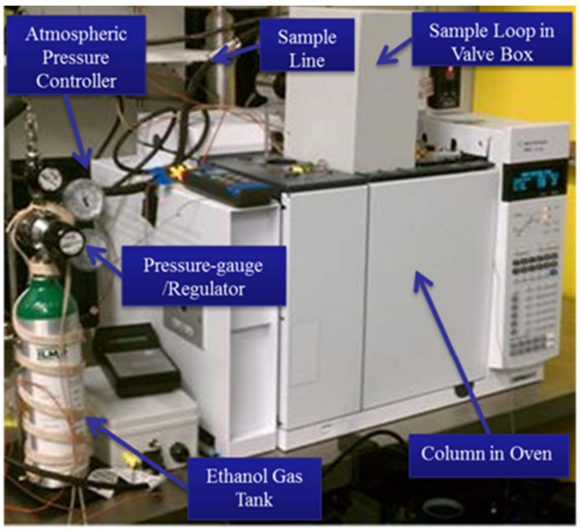

Figure 14. GC system used to measure ethanol gas

The GC-FID system was optimized for dry gas. However, introducing humidified gas revealed unexpected weaknesses in the system. The water in the gas stream increased measurement variability due to the nature of the GC-FID's ability to separate water. This initiated a comprehensive study of the state-of-the-art technologies currently available from over a dozen manufacturers across the globe using different chemical properties to quantitate and identify the components in the breath and tissue SCDs.

As research progressed, it became clear that two different measurement technologies would be required for sample and sensor calibration: one for the breath-based SCD and another for the tissue-based SCD. Various instruments using methods such as gas chromatography, liquid chromatography, and infrared spectroscopy were evaluated. The chosen instrumentation must quantify the chemical components within the samples with better precision and accuracy than the touch and breath-based surrogates. The specified accuracy and precision of the DADSS sensors is 0.0003% at a BAC of 0.08%. This requires the surrogates to be measured with instrumentation that can meet a precision and accuracy target of 0.000075%. Another requirement is that the instruments not only quantify accuracy and precision but also identify substances in the tissue and breath samples.

Breath-based SCD verification An MKS MultiGas™ 2030 FTIR Continuous Gas Analzyer, specifically designed for gases, was selected over other technologies due to its ability to identify and measure ethanol, CO_2, and H_2O in the breath-based SCDs (see *Figure 15*). This ability to identify materials in the sample has enabled detection of contaminants in the breath SCDs. Initial measurements of dry gas cylinders and humidified gases yielded significant precision improvements. The standard deviation for 105 measurements was 0.00006 %BrAC - well below the DADSS Performance Specification.

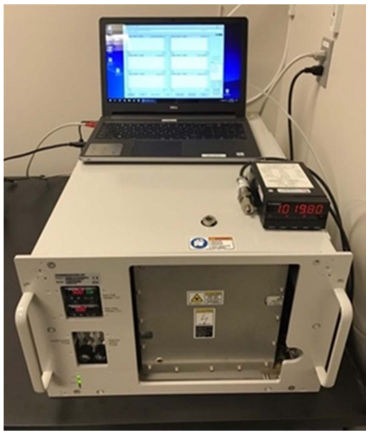

Figure 15. FTIR used for verification of the breath-based SCDs

Sensor testing is implemented in two different settings; a) in the ambient air of the laboratory (at about +22°C), and b) using an environmental chamber where temperature and humidity can be controlled. Sensor performance has been measured at temperatures of: -40°C, +22°C, and +85°C and at alcohol concentrations of (0.000, 0.020, 0.050, 0.080, and 0.100) % BrAC. The overlapping tests at +22°C allows estimation of the effects of the environmental chamber.

Improvements were made to the gas delivery systems by creating the humidified gasses as steady flow and diverting them into the sensors in a pulsed fashion for maximum performance. This procedure improves

control of the gas delivery to the breath-based alcohol sensor and allows for simultaneous testing of multiple breath-based alcohol sensors to improve testing efficiency.

New testing procedures have been developed to understand what the DADSS breath sensor is measuring in real time by drawing on a flow through approach to sample measurement. In the laboratory environment, the MKS FTIR is run in-line with the WGBAS and sensors to allow effluent from the WGBAS to confirm the precision of the gas sample before entering the sensor. (see Fratto et al., 2015, in press, Verma et al., 2016, Katz et al., 2016). In the future, the MKS also will be utilized for the environmental chamber testing to study the atmospheric effects on the SCD.

Recent updates to the SCD gas sources have been investigated as well. Researchers at KEA Technologies, Inc. have developed an Automated Breath-Based SCD (ABBS) whereby independent gas sources are combined to generate the SCD rather than blended gas cylinders manufactured by a gas supplier. By keeping the gases independent it is possible to better control the concentrations of all the gases. An added advantage of the ABBS is that it facilitates testing of multiple sensors at a time.

As FOTs ramp up, there is a need to increase the throughput of sensor testing and characterize multiple sensors simultaneously. A new manifold has been developed in the KEA chemistry laboratory to test eight sensors at once both in the ambient conditions of the laboratory and the environmental chamber (see Figure 16).

Figure 16. Concurrent testing of multiple breath sensors

Efforts are underway to identify additional sources of traceable gases that can be NIST certified or produced by another country's national laboratory as a CRM. Additionally, the use of a Liquid Ethanol Gas Generation System (LEGGS) has been researched and implemented where applicable. This device is capable of creating a highly accurate and precise alcohol dry gas in real-time.

With the start of in-vehicle testing, work has begun on a device that permits controlled and uniform gas delivery to the breath sensors outside of the controlled laboratory conditions. The initial concept for the portable SCD delivers dry compressed gas from a gas cylinder at a defined pressure and with a controlled flow rate and pulse duration. Initial versions utilize mixed gas ILMO tanks of ethanol with CO_2, O_2, and N_2 (see Figure 17). At his stage of development, the precision and accuracy of the device is limited by the gas cylinder's accuracy and precision.

Figure 17. Portable Gas SCD

Tissue-based calibration An Ultra Performance Liquid Chromatography (UPLC) with three detectors was chosen for characterization of the tissue-based SCD. The Refractive Index (RI) detector quantitates ethanol, the Photo Diode Array (PDA) quantitates non-ethanol reagents, and a mass spectrometer is used for identification of the non-ethanol reagents. Identification of the liquid ethanol in the tissue SCD is performed by a benchtop ThermoFisher Scientific Nicolet FTIR. Figure 18 shows the Waters Acquity UPLC and ThermoFisher Scientific Nicolet FTIR. The RI detector has demonstrated its ability to precisely quantitate NIST certified ethanol in water at the DADSS performance specification.

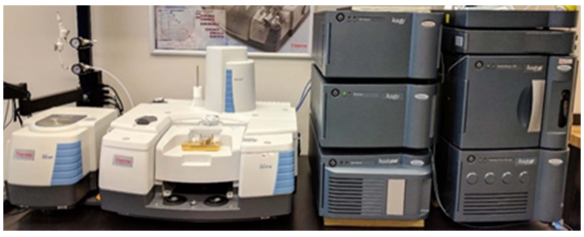

Figure 18. FTIR and UPLC used for verification of the tissue-based SCDs

The initial tissue-based SCDs included ethanol, saline, creatinine, urea, glucose, triton and polymeric beads. However, more recently the formula has been changed to exclude the organic components (glucose, creatinine, and urea). The simplification of the tissue-based SCD was done to remove the potential for cross-reactivity of the components and potential bacterial contamination, resulting in an improved shelf life. The initial version of the tissue-based SCD proved to be unstable, with a fermentation or polymerization process evident from residue noted in the bottom of the vials. Moreover, there was an issue with potential volatility of the ethanol in the solution that needs to be addressed.

Going forward, the goal is to map the new tissue SCD, referred to as the Liquid Alcohol Test SCD (LATS), to determine which individual components are responsible for different parts of the spectra. Such mapping techniques have been used previously to understand many complex chemical systems and develop methods for tuning the specific output concentrations (Privman et al., 2013). The SCD solutions will be created using highly accurate scales, along with a densitometer that will provide accurate ethanol concentration measurements in water solutions. The aim is to build a library of the individual components to determine how they react with one another. With this understanding it will be possible to further tailor the SCD to either include or exclude components that interfere with the long-term storage, accuracy, precision of the standard.

Human Subject Testing

Human subject testing is a critical part of understanding how the DADSS sensors will perform in the real world when confronted with large individual variations in the absorption, distribution, and elimination of alcohol in the various compartments within the human body (blood, breath, tissue) over the myriad factors that can affect BAC. There has been extensive research to understand these relationships with respect to venous (blood) alcohol and breath alcohol when samples of deep lung air are used. However, the new measurement methods being researched as part of the DADSS program that determine alcohol levels from diluted breath samples and within human tissue are not well understood. In particular, the rate of distribution of alcohol throughout the various compartments of the body under a variety of scenarios requires further study.

The purpose of human subject testing is:

- To quantify the rate of distribution of alcohol throughout the various compartments of the body (blood, breath, tissue) under a variety of scenarios.
- To quantify alcohol absorption and elimination curves among a wide cross section of individuals of different ages, body mass index (BMI), race/ethnicity, and sex using a wide range of scenarios.

Significant progress has been achieved in conducting human subject testing at the DADSS Satellite Lab at McLean Hospital in Belmont, MA (See Figure 18). The initial scenarios explore a variety of conditions that are designed to mimic real-life situations (see Lukas et al., 2019 for further details). They include the lag time of the appearance of alcohol in bodily compartments (blood, breath or tissue) after subjects consume alcohol, social drinking while snacking, social drinking with a full meal, last call, where drinkers have a last drink before the bar closes, and dancing and drinking.

Figure 19. Human Subject Testing at DADSS Satellite Lab at McLean Hospital in Belmont MA using the breath- and tissue-based sensors

Significant progress has been made in a number of critical areas, including method development and human subject testing. Many insights have been gained regarding the alcohol absorption and elimination curves and maximum BAC/BrACs reached by the subjects in the scenarios outlined above. In addition, human subject research has begun on new scenarios identified as potentially important in breath and touch alcohol measurement, including the effects of smoking on breath alcohol

measurements and the effects of hand sanitizer gel and skin temperature on tissue alcohol measurement.

Across the range of scenarios, a solid linear relationship between blood, breath-based and tissue-based BAC/BrACs has been established. These results indicate that the measurements produced by the various generations of breath-based and touch-based (tissue-based) prototypes is consistent, reproducible, and correlates very well with the "gold-standard" method of measuring alcohol in the body, which is accomplished by measuring blood via gas chromatography. Moreover, the breath and touch sensors responded to the various environmental conditions in the same way that blood alcohol did, providing justification that they serve as a valid alternative for BAC and BrAC measurements.

TECHNOLOGY & MANUFACTURING READINESS LEVELS

The DADSS Program adopted a set of automotive metrics derived from the methodology used by the Department of Defense to quantify a technology's commercial feasibility. The Technology Readiness Level (TRL) provides an objective measure for assessing the maturity of a particular technology. TRL metrics facilitate informed decisions regarding investment and risk associated with technology development and transition to commercialization. Similarly, the Manufacturing Readiness Level (MRL) assesses the maturity of manufacturing readiness. These two sets of readiness levels assist all those engaging with the automotive sector, by providing specific, identifiable stages of maturity, from early stages of research all the way through to supply chain entry. Both the TRL and the MRL are comprised of 9 levels, 1 – 9, although the MRL is offset (delayed) from the TRL. Transfer to the private sector for applied research and development leading potentially to commercialization and mass production is targeted to occur at a TRL equal to eight (8) and an MRL equal to seven (7). Figure 20 shows the DADSS technology and manufacturing readiness levels.

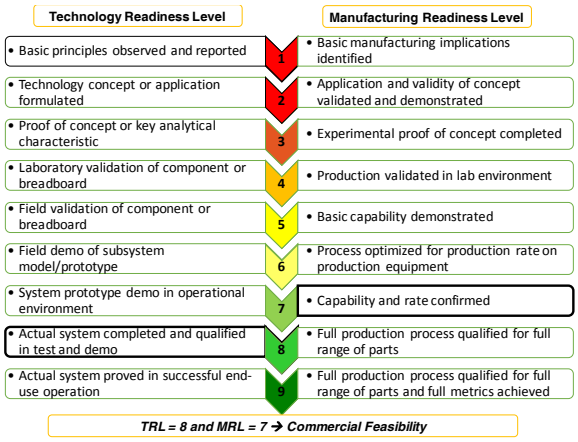

Figure 20. TRL/MRL Demonstrated Commercial Feasibility

Figure 21 summarizes a preliminary evaluation of the "readiness" of the breath–based and touch–based technologies determined by the DADSS team.

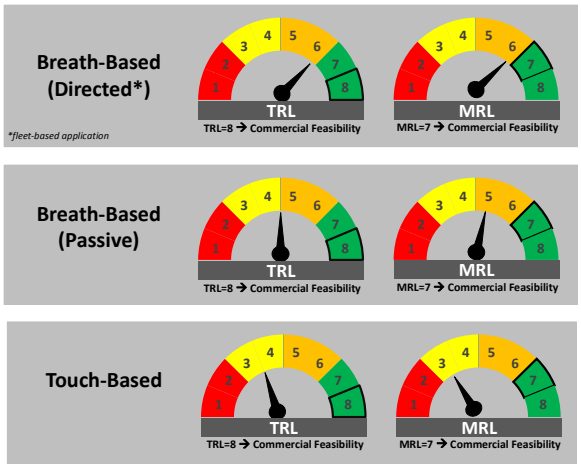

Figure 21. Technology and Manufacturing Readiness Levels by Technology Type

These rating indicate that the breath–based technology research is ahead, but the touch–based technology lags expectations due to challenges with the development of the laser diodes and its associated supply chain, which are in the process of being resolved.

CONCLUSIONS

Since its inception in 2008, the DADSS Program has made tremendous progress in the development of in-vehicle technologies that will prevent impaired drivers from driving their vehicles. The breath- and touch-based sensors have become increasingly refined, both in terms of hardware and software, as headway is made in meeting the high standards required for unobtrusive and reliable alcohol measurement. At the same time, additional research

and development is paralleling the sensors' development to allow the characterization of sensor performance in the laboratory, on the road, and among human subjects.

Significant progress has been made in the development of breath and touch-based calibration processes, materials and methodologies making the testing of multiple sensors at a time a reality. Moreover, instrumentation has been identified that can enable the requisite testing across the range of specified environmental conditions.

As sensor development has progressed, research vehicles have been readied for Field Operational Testing (FOT) with the latest versions of the breath sensors seamlessly integrated within the vehicle interiors. Vehicle instrumentation packages have been developed and installed and pilot testing trials now are beginning to provide data on sensor performance under real-world driving conditions. The accumulated data from an extended program of FOTs under diverse conditions will determine whether the DADSS sensors are working as anticipated and allow the identification of areas for system improvement.

Also, a comprehensive program of human subject research also is well underway, starting with the laboratory environment where better control of conditions can be exerted, and continuing in the vehicle where the sensors can be tested in the environment in which they will be used. This research has quantified alcohol absorption and elimination across a wide range of conditions that are anticipated to affect BAC and BrAC as well as some new scenarios specific to the breath and touch-based approaches. Testing showed that the data collected from the various generations of breath-based and touch-based prototypes was consistent, reproducible, and correlates very well with the "gold-standard" method of measuring alcohol in the body, which is accomplished by measuring blood via gas chromatography.

In summary, great progress has been made on a number of fronts to develop in-vehicle sensors that will seamlessly measure driver's blood and breath alcohol and prevent them from driving while impaired. Moreover, additional research is ongoing to continue the progress toward meeting the exacting performance specifications to ensure acceptance and longevity in the vehicle environment.

REFERENCES

Ferguson, S. A. 2012. Alcohol-impaired driving in the United States: Contributors to the problem and effective countermeasures. Traffic Injury Prevention, 13, 427-441.

Ferguson, S.A., Traube, E, Zaouk, A, Strassburger, R. 2009. Driver Alcohol Detection System For Safety (DADSS) – A non-regulatory approach in the development and deployment of vehicle safety technology to reduce alcohol-impaired driving. Paper Number 09-0464. Proceedings of the 21st International Technical Conference on the Enhanced Safety of Vehicles.

Ferguson, S.A., Zaouk, A., Strohl, C. 2010. Driver Alcohol Detection System for Safety (DADSS). Background and Rationale for Technology Approaches. Society for Automotive Engineers Technical Paper, Paper No. 2010-01-1580, Warrendale, PA: Society of Automotive Engineers.

Ferguson, S.A.; Traube, E; Zaouk, A; Strassburger, R. 2011. Driver Alcohol Detection System For Safety (DADSS) – Phase I Prototype Testing And Finding. Paper Number 11-0230. Proceedings of the 22nd International Technical Conference on the Enhanced Safety of Vehicles.

Fournier, R, Zaouk, A.K., Willis, M., Strassburger, R. 2019. Assessing system implementation readiness of the Driver Alcohol Detection System for Safety (DADSS) to reduce alcohol-impaired driving in a real-world driving pilot deployment project. Paper Number 19-0263. Proceedings of the 26th International Technical Conference on the Enhanced Safety of Vehicles.

Fratto, B.E. & Katz, E. Utilization of a fluidic infrastructure for the realization of enzyme-based Boolean logic operations. *Int. J. Parallel Emergent Distrib. Syst.* In Press. (DOI: 10.1080/17445760.2016.1213250.

Fratto, B.E. & Katz, E. Reversible Logic Gates Based on Enzyme-Biocatalyzed Reactions and Realized in Flow Cells: A modular Approach. *ChemPhysChem.,* 2015, 16, 1405 –1415 DOI: 10.1002/cphc.201500042

Hök, B., Pettersson, H., Andersson, G. 2006. Contactless measurement of breath alcohol. Proceedings of the Micro Structure Workshop. May, 2006, Västerås, Sweden.

Jones, A.W. 2008 Biochemical and Physiological Research on the Disposition and Fate of Ethanol in the Body. Garriott's Medicological Aspects of Alcohol (Fifth Edition), 47.

Katz, E. & Fratto, B.E. Enzyme-based reversible logic gates operated in flow cells. In: *Advances in*

Unconventional Computing, A. Adamatzky (ED.), Springer, 2016, Volume 2, Chapter 2, pp 29-59.

Lindberg, L., Brauer, S, Wollmer, P., Goldberg, L., Jones, A.W., Olsson, S.G. 2007. Breath alcohol concentration determined with a new analyzer using free exhalation predicts almost precisely the arterial blood concentration. Forensic Science International. 168: 200-207.

Ljungblad, J., Hök, B., Allalou, A., Pettersson, H. 2017. Passive in-vehicle driver breath alcohol detection using advanced sensor signal acquisition and fusion. Traffic Injury Prevention, Vol 18, 31-36.

Lukas, S.E., Ryan, E., McNeil, J., Shepherd, J., Bingham, L.,Davis, K., Ozdemir, K., Dalal, N., Pirooz, K., Willis, M., Zaouk, A. K. 2019. Driver Alcohol Detection System for Safety (DADSS) – Human Testing of Two Passive Methods of Detecting Alcohol in Tissue and Breath Compared to Venous Blood. Paper Number 19-0268. Proceedings of the 26th International Technical Conference on the Enhanced Safety of Vehicles.

Privman, V., Fratto, B.E., Zavalov, O., Halámek, J., Katz, E. Enzymatic AND Logic Gate with Sigmoid Response Induced by Photochemically Controlled Oxidation of the Output. *J. Phys. Chem. B*, 2013, *117* (25), pp 7559–7568

Ridder, T.D., Hendee, S.P., Brown, C.D. 2005. Noninvasive alcohol testing using diffuse reflectance near-infrared spectroscopy. Applied Spectroscopy, 59, 181-189.

Verma, A., Fratto, B.E., Privman, V., Katz, E. Design of Flow Systems for Improved Networking and Reduced Noise in Biomolecular Signal Processing in Biocomputing and Biosensing Applications. *Sensors (MDPI)* 2016, 16, 1042; doi: 10.3390/s16071042

Willis, M., Zaouk, A.K., Bowers, K., Chaggaris, C., Spicer, R., Bahouth, G., Strassburger, R., Traube, E. Driver Alcohol Detection System for Safety (DADSS) – pilot Field Operational Tests (PFOT) vehicle instrumentation and integration of DADSS technology. Paper Number 19-0262 Proceedings of the 26th International Technical Conference on the Enhanced Safety of Vehicles.

Zaouk AK, Willis M, Traube E, & Strassburger R. 2015. Driver Alcohol Detection System for Safety (DADSS) – A Status Update. Paper Number 15-0276. Proceedings of the 24th International Technical Conference on the Enhanced Safety of Vehicles.

Zaouk A. K, Willis, M., Dalal, N., Traube, E., Strassburger, R. 2017. Driver Alcohol Detection System for Safety (DADSS) – A Status Update. Paper Number 17-0271. Proceedings of the 25th International Technical Conference on the Enhanced Safety of Vehicles.

Biondo, W., Zaouk A. K, Sundararajan, S. 2017. Driver Alcohol Detection System for Safety (DADSS) – Development of the Sybsystem Performance Specifications. Paper Number 17-0301. Proceedings of the 25th International Technical Conference on the Enhanced Safety of Vehicles.

ASSESSMENT, EVALUATION, AND APPROACHES TO TECHNICAL TRANSLATIONS OF FMVSS AND TEST PROCEDURES THAT MAY IMPACT COMPLIANCE OF INNOVATIVE NEW VEHICLE DESIGNS ASSOCIATED WITH AUTOMATED DRIVING SYSTEMS

Myra, Blanco
Michelle, Chaka
Clay, Gabler
Loren, Stowe
Warren, Hardy
Joshua, McNeil
Vikki, Fitchett
Virginia Tech Transportation Institute
United States

Ellen, Lee
National Highway Traffic Safety Administration
United States

Paper Number 19-0261

ABSTRACT

The project described in this paper provides research findings in terms of options regarding technical translations of select Federal motor vehicle safety standards (FMVSS) and related Office of Vehicle Safety Compliance (OVSC) test procedures. The research findings are based on potential regulatory barriers identified for self-certification and compliance verification of innovative new vehicle designs that may appear in vehicles equipped with Automated Driving Systems (ADSs). This paper documents the framework used to evaluate the regulatory text and OVSC test procedures with the goal of identifying possible options to remove regulatory barriers for the self-certification and compliance verification of ADS-Dedicated Vehicles (ADS-DVs) that lack manually operated driving controls. It also describes the research activities for 15 crash avoidance standards (100-series) and 15 crashworthiness/occupant protection standards (200-series). This research effort incorporates feedback obtained from stakeholders and subject matter experts (SMEs).

RESEARCH QUESTION/OBJECTIVES

The goal of this project was to provide research findings in terms of options regarding technical translations of select Federal motor vehicle safety standards (FMVSS) and related Office of Vehicle Safety Compliance (OVSC) test procedures based on potential regulatory barriers identified for self-certification and compliance verification of innovative new vehicle designs that may appear in vehicles equipped with Automated Driving Systems (ADSs). A technical translation is a modification that would allow regulatory text and/or test procedures that are identified as potential barriers to be carried out with the same basic engineering performance without manual control-specific restrictions. Technical translations developed under this effort present options for the regulatory text (i.e., performance requirements and test procedures) and related OVSC test procedures when a regulatory barrier is present. This paper describes the option development process used to address the technical translations and the testing procedures for 30 select FMVSS, such that the identified potential regulatory barriers could be removed for vehicles operated exclusively by an ADS that do not have the traditional controls used by human drivers. These 30 FMVSS represent a mix of standards where potential straightforward translations are presented (e.g., FMVSS No. 125, “Warning devices”) and other standards that could yield findings near-term that could be utilized for mid-term and long-term research (e.g., FMVSS No. 126, “Electronic stability control systems for light vehicles”). An initial set of 12 FMVSS was selected by NHTSA and the research team selected the remaining 18 FMVSS with a focus on how they could contribute to long-term research. Technical translations were used to either present potential modifications to the existing regulatory text or, alternatively, to create new regulatory language that would be capable of accommodating an ADS’s functionalities. The FMVSS of focus for this study are illustrated in Figure 1 below.

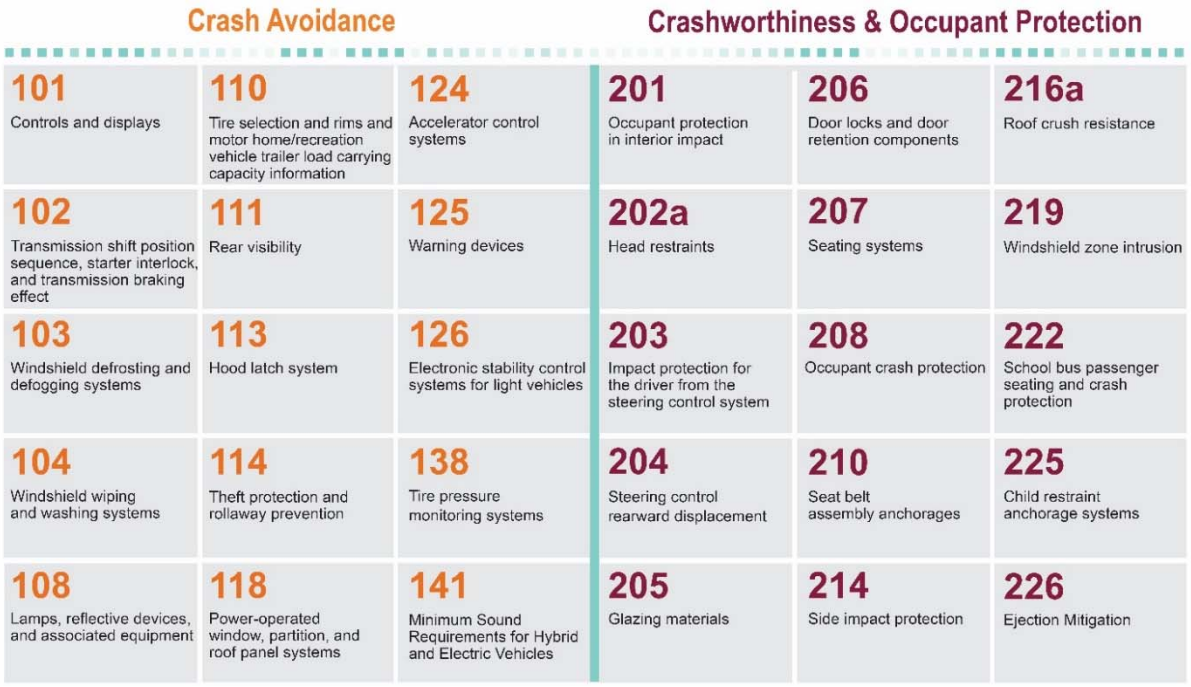

Figure 1. 100-series and 200-series FMVSS of focus

DATA SOURCES

NHTSA recognizes that advanced-concept vehicle designs are on the horizon and may not be addressed throughout the current FMVSS. The findings from this project help identify potential regulatory barriers to self-certification and compliance verification of some of these advanced-concept vehicles that are equipped with ADSs. SAE International's (SAE's) Recommended Practice *J3016 Taxonomy and Definitions for Terms Related to Driving Automation Systems for On-Road Motor Vehicles* [1] defines an ADS as "The hardware and software that are collectively capable of performing the entire DDT [Dynamic Driving Task] on a sustained basis, regardless of whether it is limited to a specific operational design domain (ODD); this term is used specifically to describe a level 3, 4, or 5 driving automation system." The same Recommended Practice defines Automated Driving System-Dedicated Vehicle (ADS-DV) in this way: "A vehicle designed to be operated exclusively by a level 4 or level 5 ADS for all trips within its given ODD limitations (if any)" but goes on to say that level 3 systems could possibly be included under this term in the future [1]. However, this project's development of FMVSS technical translation options focused on a particular type of ADS-DV; i.e., vehicles designed to be operated exclusively by an SAE level 4 or level 5 ADS for all trips, and which are not equipped with manually operated driving controls. Thus, level 3 ADS-equipped vehicles (i.e., vehicles equipped with a user interface that permits operation by a human driver) were outside of the scope of this project, even if they could be categorized as ADS-DVs under the SAE definition.

A report prepared by the United States Department of Transportation (USDOT) Volpe National Transportation Systems Center entitled *Review of Federal Motor Vehicle Safety Standards (FMVSS) for Automated Vehicles: Identifying Potential Barriers and Challenges for the Certification of Automated Vehicles using Existing FMVSS* [2]—referred to hereafter as the "Volpe Report"—included two reviews of the FMVSS: 1) a review to identify standards that include an explicit or implicit reference to a human driver, and 2) a review to identify standards that might pose a barrier for compliance verification of a wide range of concept vehicles that may be equipped with an ADS. From this review, 13 automated vehicle concepts were defined to reflect the identified barriers and potential future applications of automated vehicle technology. The 13 concepts differed in their design convention and speed classification. Design convention considered differences in the application of advanced features that take full advantage of automation (e.g., removing steering wheel). Speed classification regarded low-speed (e.g., speed restricted to 40 kmph/25 mph) and high-speed (i.e., no speed restriction).

The ADS-FMVSS project presented herein focused on design concepts similar to three design concepts from the Volpe Report [2] which do not have vehicle controls for human drivers. Those concepts are:

- *Highly Automated Vehicle with Advanced Vehicle Design*
- *Highly Automated Vehicle with Novel Design*
- *Low Speed Highly Automated Vehicle with Advanced Design*

The Volpe Report categorized certain types of regulatory barriers for ADS-equipped vehicles and linked them to corresponding standards and concepts [2; Appendix B]. It identified several regulatory barriers, highlighting uncertainty about how vehicles with innovative designs would execute some FMVSS test procedures and, therefore, how these vehicles would be tested to verify compliance with the standards. The Volpe Report was used during the current project to develop a framework to describe ADS-DV features. The vehicle features for each of the three concepts noted above were grouped into cohesive categories in the framework development process. These categories identified the main areas where ADS-DV concept designs could potentially need very specific terminology and specifications relating to FMVSS regulatory barriers (i.e., technical translation options). The framework focused on concepts that are impacted by the technical translations, concepts that helped the research effort anticipate how an ADS may perform the entire DDT without user intervention, and any safety-related aspects of interest. In addition, the work included expanding the features of interest to include features not described in the Volpe Report that may be necessary for the implementation of advanced and novel designs (Figure 2).

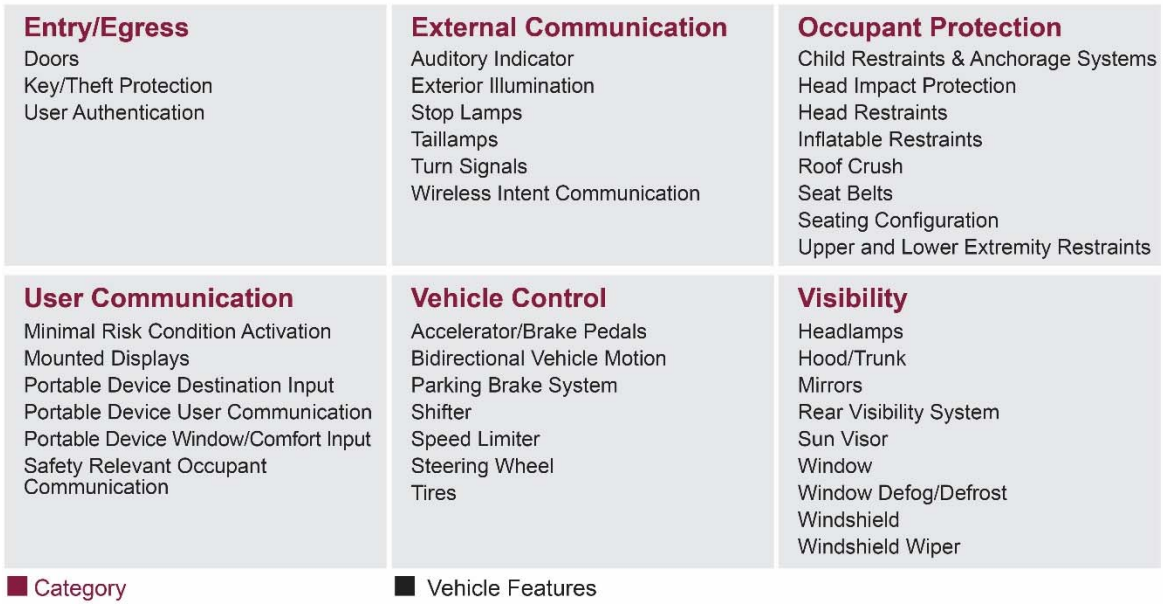

Figure 2. Categories and features of interest

METHODS

The translation process that was used entailed analyzing the language of select 100-series (crash avoidance) and 200-series (crashworthiness/occupant protection) FMVSS for key terms or descriptions that might present regulatory barriers to vehicle compliance, in order to then develop options as to how the language could be altered. Crosscutting analyses were developed to drive consistency in the translation options and clarify when individual standards required unique options or approaches. Each FMVSS evaluation produced a set of options that NHTSA may consider for translating the FMVSS for ADS-DVs.

Potential ADS-DV barriers indicating a possible need for translations were analyzed at two levels: 1) regulatory language, and 2) implementation of test procedures. Several parts of the regulatory language include standards that are incorporated by reference (e.g., American National Standards Institute [ANSI], ASTM International [ASTM], International Organization for Standardization [ISO], SAE). The standards incorporated by reference are part of the

FMVSS regulatory language and were analyzed in the same way as the rest of the regulatory text. A taxonomy was then developed for completing and capturing the translation analysis.

Documents incorporated into the FMVSS by reference (49 CFR § 571.5 [3]) posed a unique challenge for translation, since they were issued by organizations outside of NHTSA (e.g., ASTM, SAE) and then became part of the regulatory text when incorporated by reference in the FMVSS. Through rulemaking, NHTSA can change its incorporation by reference of those documents, and can decide to no longer incorporate them, adopt them in part, or incorporate a different document provided by the external organization.

The process for developing the technical translation options for the FMVSS of focus is outlined in the steps below:

1) Transfer the standard and related test procedure(s) into a spreadsheet designed for this effort.
2) Identify relevant information and documents.
3) Obtain relevant incorporated references by external organizations (e.g., SAE, ANSI standards) and evaluate potential barriers to ADS-DV self-certification or compliance verification.
4) Evaluate the language of both the standard and the test procedure to identify references to the driver, driver-oriented displays, designated seating positions, bidirectionality, manual controls, or other language that could pose a barrier for ADS-DV self-certification or compliance verification.
5) Coding the translation type as 0, 1, or 2 (as shown in Figure 3 below).
6) Suggest potential translations of the standard text and test procedures for ADS-DVs, including investigating options for new testing methods.
7) Identify FMVSS requirements where a technical translation was evaluated but not performed. When not clearly evident why a translation was not performed, document the reasoning for which a translation either cannot occur (based on current knowledge of ADS-DVs) or was deemed unnecessary.
8) Document specific barriers in translating the standard/test procedure language to ADS-DVs.

Reason		Technical Translation Type Description
0	Not performed	Translation evaluated but not performed.
1	Translation is straightforward	The translation performed is straightforward.
2	Limited research may be beneficial	Can translate standards or provisions of standards, maintaining current performance levels, with some limited amount of research for NHTSA to conduct compliance verification for both conventional vehicle designs and new vehicle designs associated with Automated Driving System - Dedicated Vehicles (ADS-DVs).

Figure 3. Technical translation taxonomy

Every section within the FMVSS of focus was coded from the choices shown in Figure 3. The reasons and descriptions were based on the best forecast of what might need to be addressed during the course of the project. Those categorized as *0-Not performed* were deemed as non-problematic for ADS-DVs within the scope of this project. The code of *1-Translation is straightforward* is self-explanatory; i.e., the determination was made that the translation options provided allowed for a straightforward translation to be performed for ADS-DVs. Any translations of standards coded as *2-Limited research may be beneficial* may require additional testing and/or research to develop the appropriate translations.

By way of example, the spreadsheet for FMVSS No. 102 is shown in Figure 4. Translation options are included in the spreadsheet in red text. Note that driver definitions 1 and 2, referenced in Figure 4 below, are potential translation options provided for the driver definition in 49 CFR § 571.3. These definition options were created as the word “driver” is used throughout various FMVSS.

S3.1.4.2 Identification of shift positions and of shift position sequence			
Standard Text	**Translation Options**		**Potential Considerations**
Except as specified in S3.1.4.3, if the transmission shift position sequence does not include a park position, identification of shift positions, including the positions in relation to each other and the position selected, shall be displayed in view of the driver whenever the ignition is in a position in which the engine is capable of operation.	**Option 1**	...shall be communicated to the driver …	Uses driver definition 1. Eliminates the dependency on a display. Opens the possibility of other communication means to human drivers (e.g., auditory). May need to provide conditional language such as "via visual or electronic means." May need a means to confirm operation for ADS.
	Option 2	Except as specified in S3.1.4.3, if the transmission position sequence does not include a park position, identification of positions, including the positions in relation to each other and the position selected, shall be displayed in view of the driver in a vehicle with a transmission shift mechanism intended for operation by a human driver, and shall be communicated to the ADS driver in a vehicle equipped with such a system, whenever...	Uses driver definition 2. Separates the human and ADS. If taken out of context, exclusion of "shift" could be ambiguous. "Shift" could be kept as currently stated while keeping the distinction between human and ADS.
	Option 3	...shall be displayed in view of the human driver whenever the ignition is in a position in which the engine is capable of operation.	Use driver definition 2. Only display information for vehicle operated by a human driver.

Figure 4. FMVSS No. 102: Transmission Shift Position Sequence, Starter Interlock, and Transmission Braking Effect

Work on the 100-series standards focused on addressing some of the fundamental aspects that cut across many of the FMVSS, such as definitions for driver and seating position, service brake application, and gear position/selection, as well as on developing initial considerations for translating requirements for telltales and addressing bidirectional vehicles. Work on the 200-series standards focused on occupant protection for ADS-DVs with conventional seating.

Stakeholder Engagement

The involvement of stakeholders and subject matter expert (SME) reviewers was a critical component of the translation process. Stakeholders included companies, organizations, and advocacy groups that were invited to be involved in this project in the early stages based on their experience with FMVSS and ADS-DVs. Additional stakeholder entities were later added; in some cases, organizations asked to be involved and in other cases a need was identified for additional expert feedback. The SME reviewers were a subset of the larger stakeholder group; these were individuals with demonstrated expertise in and knowledge of a particular FMVSS and/or laboratory test procedure along with how potential FMVSS barriers to innovative vehicle designs may be addressed. The SME reviewers for each FMVSS of focus were involved in providing input to the technical translation options developed;

as such, they were able to review the translation development work and provide feedback. In addition, several industry and research entities were engaged as collaborators on this project in order to obtain input and feedback, and produce prototype technology for testing and evaluation. Figure 5 illustrates the various organizations that participated in this project.

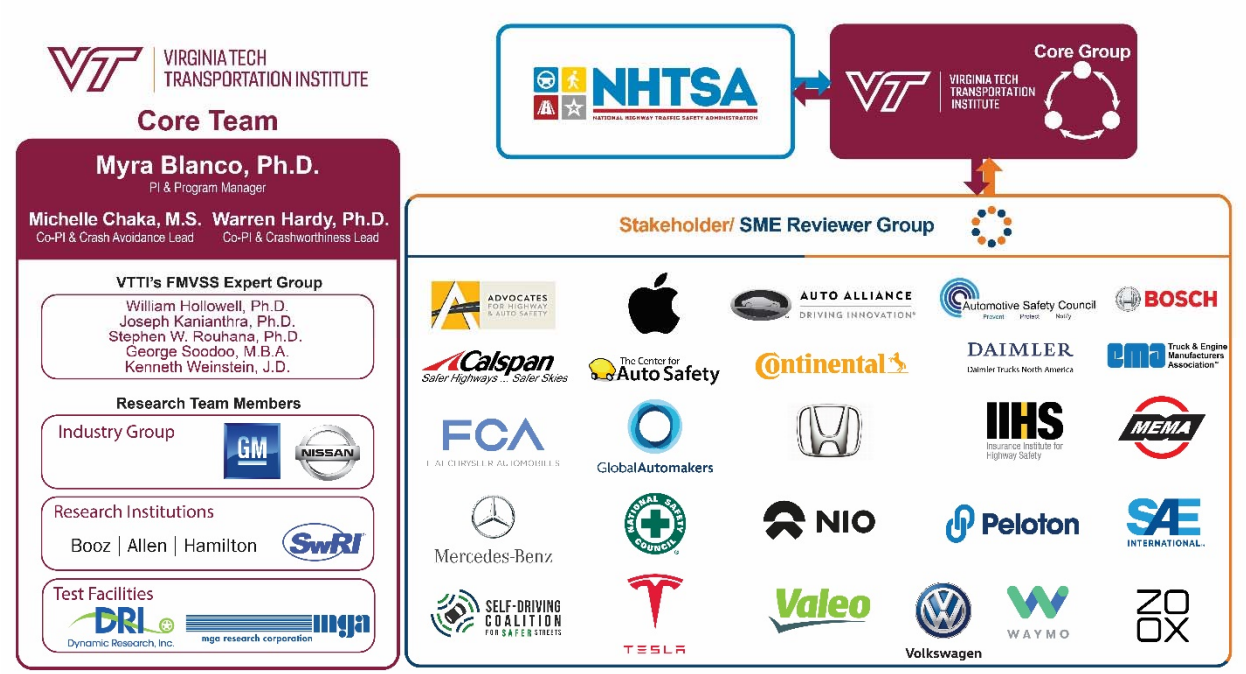

Figure 5. The project team, stakeholders, and SME reviewers

The SMEs were divided into working groups based on their expertise with a particular FMVSS and/or OVSC test procedure. The working group members assisted with the review process once technical translation options were developed or feedback was needed for the test methods. The purpose of the SME review process was to ensure that the options being developed did not produce more far-reaching or different regulatory barriers. The SMEs also provided feedback on alternative methods evaluated for test procedures of interest. In addition, stakeholders participated in open project meetings and provided input regarding this project during those events.

Test Procedures

The goal was to identify the equipment and/or procedures that may help NHTSA perform compliance verification on ADS-DVs not equipped with manual controls. Similar to the regulation text translation assessment analysis, the same taxonomy was used to determine appropriate translation options or modifications to data sheet checklists. As an addition to the regulation text translation assessment framework, the test procedure analysis expanded the focus to vehicle functionalities. Developing and evaluating test methods to exercise the required vehicle functionalities may require one or more categories of functionalities. The functionalities, which are also shown in their respective categories later on in this paper, are: steering control, speed control (vehicle/engine), service brake application, parking brake, gear selection, telltales/warnings/indicators, key insertion/removal, ignition start/stop, accessory mode, door open/close, non-driving controls, and visibility.

The following steps illustrate the approach taken as part of the crash avoidance test procedure analysis:

1. Classification of standards
2. Selection of standards for inclusion
3. Implementation and execution
4. Evaluation of test methods
5. Select functionalities needed to verify compliance, if applicable

6. Iteration of testing and evaluation of results as necessary
7. Validation of test platform and execution

The implementation, execution, and evaluation of the testing was first applied to standards containing functionalities with less-demanding requirements to verify the test platform and test methods. The expectation was that this approach would provide a sufficient set of test cases to allow the selection of an appropriate test method that could be applicable for any requirements and associated test procedures.

Five potential methods were identified for verifying compliance; these fall into two general categories that are outlined below. Some are more appropriate for some standards than for others. The methods are:

Vehicle-based

Human control: Testing is performed using a controller console, connected either physically or through a wireless link (which could include teleoperation), to provide manual driving control.

Programmed control:

- Scripted control – A standard set of commands (e.g., "start engine," "apply parking brake," "speed = *x*") are used to define the actions the ADS is required to take to execute the test.
- Pre-programmed routine – The steps for executing the test are predefined and compiled into a script that can be run but not modified in the field.

ADS normal operation: The normal operation of the ADS is used to perform some or all of the test procedure.

Non-vehicle-based

Simulation: Simulation, either solely software-based or including a hardware-in-the-loop solution, is used to execute the test procedure.

Technical design documentation: Vehicle-specific technical design and/or build documentation which provides sufficient information and detail (e.g., a wiring diagram showing that a sensor signal is connected to an ADS electronic control unit) to show the system in question was designed to be in compliance with part or all of a particular standard. It should be noted that this is different than the Test Specification Forms that are provided to NHTSA when a vehicle is selected for potential verification testing. Instead, it is technical design documentation used by the manufacturer in the design, construction, and validation of the vehicle.

While the OVSC test procedures are not requirements, they do capture functionalities that are often implied by the regulatory text (e.g., to test the requirements of the backup camera the vehicle must be started and backed up) and which NHTSA currently uses to verify compliance. Bidirectionality provided a unique challenge for functionalities as they do not follow a standard rear vs. front direction determination of the vehicle. Further research is needed to translate test procedures for bidirectional vehicles; thus, this will be performed as part of long-term research.

Figure 6 shows the 15 crash avoidance FMVSS under study and the associated functionality requirements that are either specified in the FMVSS or that are necessary to execute the associated test procedures. These are organized into categories shown in the first column. The first four categories apply to vehicle operation and the last category (Environment Awareness) addresses items that allow the driver to perceive the environment outside of the vehicle. Within the categories, the functionalities are grouped (e.g., vehicle position control, braking) and ordered by use and occurrence within the standards.

Category	Functionality	101	102	103	104	108	110	111	113	114	118	124	125	126	138	141
Driving Tasks	Steering control						●	●		●				●	●	●
	Speed control (vehicle/engine)			●	●		●	●		●		●		●	●	●
	Service brake application						●	●		●				●	●	●
	Parking brake							●		●						●
	Gear selection		●	●	●		●	●		●				●	●	●
Vehicle Communications	Telltales/warnings/indicators	●	●			●				●		●		●	●	
Key/Ignition Function	Key insertion/removal									●						
	Iginition start/stop		●	●	●		●	●		●	●	●		●	●	
	Accessory mode									●	●					
	Door open/close									●	●					
Non-driving Tasks	Non-driving controls			●	●	●		●			●					
Environment Awareness	Visibility	●		●	●			●	●							

Figure 6. Functionalities identified in standards and test procedures for the 15 crash avoidance FMVSS under study

Test procedures from FMVSS No. 114, Theft protection and rollaway prevention and No. 138, “Tire pressure monitoring systems," were selected first for testing as they capture many of the functionalities shown in Figure 6 above. These FMVSS also have less-demanding requirements than others (e.g., FMVSS No. 126, “Electronic stability control systems for light vehicles”) and, as such, allowed early verification of the test platform and test methods. Following the testing of FMVSS Nos. 114 and 138, more demanding standards—such as FMVSS No. 126—will be tested, and the test methods will be refined as appropriate.

CONCLUSIONS

This paper describes the work conducted to create technical translation options for FMVSS and OVSC test procedures for innovative new vehicle designs. These options may assist with the self-certification and compliance verification of automated vehicles without manual controls with regard to existing FMVSS, and note where the existing standards may need to be modified. The test procedure portion of the project focused on the test methods used to exercise the required vehicle functionality (e.g., start/stop ignition, gear selection) for executing the test procedures. A range of test means was considered which included human control, programmed, normal ADS operation, simulation, and technical documentation methods. Multiple criteria were assessed; for example: ease of execution, test time, scalability, and standardization. For each FMVSS of focus during this research, the effort developed one or more potential options for NHTSA to verify compliance with FMVSS requirements for vehicles without manual controls.

With regard to the 100-series (crash avoidance) standards, the effort addressed some of the fundamental aspects that cut across many of the FMVSS and developed initial approaches to translating requirements for telltales, indicators, and alerts in addition to addressing bidirectional vehicles. Vehicle functionalities such as steering, transmission control, and service brake application were identified that are explicitly referenced in FMVSS and OVSC test procedures, and options were developed for potential alternatives that could be used in compliance verification.

Work on the 200-series (crashworthiness) standards focused on occupant protection for ADS-DVs with conventional seating. This included ADS-DVs with forward-facing seating, but without manually operated driving controls (e.g., steering wheel). For ADS-DVs without manually operated driving controls, researchers applied the test procedures that have been developed for the passenger seating positions to the left front outboard seating position, given that the main difference between the two front outboard seating positions in conventional vehicles is the presence or absence of these controls. Subsequent research as part of this effort will focus on knowledge gaps in several areas that could be beneficial since passenger seating preferences (e.g., rear seat) as well as translation considerations for unconventional seating configurations may begin to vary with different concept vehicles.

Limitations

This research was built on current information, which is subject to change. In this complex regulatory and technological landscape, ADSs may continue to evolve and FMVSS may need to evolve along with them. It should also be noted that NHTSA may determine that the options that resulted from this project may be unworkable for legal or policy reasons.

REFERENCES

[1] SAE International (2018). J3016 *Taxonomy and Definitions for Terms Related to Driving Automation Systems for On-Road Motor Vehicles*. Accessed on June 25, 2018.

[2] Kim, A., Bogard, D., Perlman, D., & Harrington, R. (2016). *Review of Federal Motor Vehicle Safety Standards (FMVSS) for Automated Vehicles: Identifying potential barriers and challenges for the certification of automated vehicles using existing FMVSS*. Preliminary Report DOT-VNTSC-OSTR-16-03. Washington, DC: U.S. Department of Transportation.

[3] 49 CFR § 571. Retrieved from https://www.ecfr.gov/cgi-bin/ECFR?mc=true&page=browse

DRIVER ALCOHOL DETECTION SYSTEM FOR SAFETY (DADSS) – PILOT FIELD OPERATIONAL TESTS (PFOT) VEHICLE INSTRUMENTATION AND INTEGRATION OF DADSS TECHNOLOGY

Michael Willis
Abdullatif K. Zaouk
Kyle Bowers
Chris Chaggaris
KEA Technologies, Inc.
U.S.A.

Rebecca Spicer
George Bahouth
Impact Research
U.S.A.

Robert Strassburger
Automotive Coalition for Traffic Safety
U.S.A.

Eric Traube
National Highway Traffic Safety Administration
U.S.A.

Paper Number 19-0262

ABSTRACT

The Driver Alcohol Detection System for Safety Program – a joint effort between the National Highway Traffic Safety Administration and the Automotive Coalition for Traffic Safety since 2008 - has been developing unique, in-vehicle breath-and touch-based alcohol detection systems to address the problem of alcohol-impaired driving. The sensors under development are intended to be passive, seamless with the driving task, non-intrusive, accurate, fast, reliable, durable, and requiring little or no maintenance. When installed in vehicles, the technology is intended to prevent alcohol-impaired driving when the driver's blood alcohol concentration is at or above 0.08 %. Sensor technology, now in Phase III of development, is undergoing more extensive testing in real-world driving environments. Research vehicles are being fitted with breath-based alcohol sensors and comprehensive Data Acquisition Systems (touch-based sensors will be integrated once they have completed the requisite test protocols). Pilot Field Operational Trials have recently begun, and data are being collected. In this paper, an overview is provided of the instrumentation and integration of the test vehicles in readiness for field trials. Data is being collected from the DADSS alcohol sensors as well as from breath-alcohol reference sensors. Instrumentation also has been installed to track environmental conditions, vehicle system data, and test participant video. The data are uploaded via 4G and WIFI and stored in the cloud. These data will be critical in determining the effectiveness (accuracy, precision) of the DADSS sensors in real-world driving environments and when compared with breath alcohol reference sensors. They will also be used to evaluate the effects of repeated use and vehicle mileage on sensor function and in diverse environments, analyze driver behavior and user acceptance, analyze and assess the impact of the DADSS sensors using real-world data, improve awareness of in-vehicle alcohol detection systems and assess potential impact of the sensors on alcohol-impaired driving. The findings will be used to refine the DADSS Performance Specifications and ultimately for modifying the systems designs and enhance product development. The DADSS technology, if proven to be reliable and reproducible under diverse environmental and biological conditions, would represent a significant technological breakthrough in crash avoidance and a significant advance in driver monitoring technologies in vehicles.

INTRODUCTION

Alcohol-impaired driving (defined in almost all U.S. states as driving at or above the legal limit of 0.08 g/dL or 0.08 percent blood alcohol concentration (BAC), 0.05 g/dL in Utah) is one of the primary causes of motor vehicle fatalities on U.S. roads every year. In 2017 alone, crashes involving at least one driver with a blood alcohol concentration (BAC) of 0.08 g/dl resulted in 10,874 deaths of U.S. road users (NHTSA, 2018).

Although strong laws and enforcement have led to fewer alcohol-impaired deaths on the roadways (Ferguson, 2012), there are still large numbers of such deaths every year in the United States and around the world. To effectively reduce or eliminate the problem it will be necessary to prevent alcohol-impaired drivers from driving in the first place. In 2008, the National Highway Traffic Safety Administration (NHTSA) and the Automotive Coalition for Traffic Safety (ACTS)[1] began research to develop potential in-vehicle solutions to the problem of alcohol-impaired driving. The alcohol sensors under development are required to be seamless with the driving task, non-intrusive, accurate, fast, reliable, durable, and require little or no maintenance. Ultimately, the vehicle will not be able to be driven when the device registers that the driver's blood alcohol concentration (BAC) exceeds 0.08 g/dl (%), although other limits potentially are programmable. This cooperative research partnership, known as the Driver Alcohol Detection System for Safety (DADSS) Program, has identified feasible non-invasive technologies to prevent alcohol-impaired driving, both breath-based and touch-based (Ferguson et al., 2009, Ferguson et al., 2010, Ferguson et al., 2011, Zaouk et al., 2015, Zaouk et al., 2017).

Now in Phase III of the research and development effort, the breath-based sensors have undergone extensive laboratory and human subject testing (Lukas et al., 2017, Zaouk, et al., 2017). The latest generation sensors (Gen 3.2) are ready for pilot testing (PFOTs) in real-world driving environments (touch-based sensors will be incorporated at a later stage when they have completed the requisite test protocols). After completion of the PFOTs, more extensive and comprehensive Field Operational Trials (FOTs) will be conducted. Results from these tests will be critical in determining the effectiveness of the DADSS sensors in a wide range of environments including the impact of environmental factors on sensor function over time, the impact of repeated use and vehicle mileage on sensor function, and user interactions with prototype devices in a vehicle environment, including driver behavior and user acceptance. The DADSS Program has submitted FOT test plans for review and is awaiting official approval to proceed.

[1] Members of ACTS comprise motor vehicle manufacturers representing approximately 99 percent of light vehicle sales in the U.S.

SENSOR TECHNOLOGY

SenseAir Breath–Based Sensor technology

The breath-based approach uses sensors to measure the concentrations of alcohol and carbon dioxide (CO_2) in the breath simultaneously. The known quantity of CO_2 in the human breath is an indicator of the degree of dilution of the alcohol concentration in expired air. Diluted breath is drawn into the sensor by a fan, which directs infrared light beams on the breath sample and analyzes the wavelengths returned for both alcohol and CO_2. Breath alcohol concentration is then quickly and accurately calculated (Hök et al., 2006). See Figure 1 for the breath sensor block diagram.

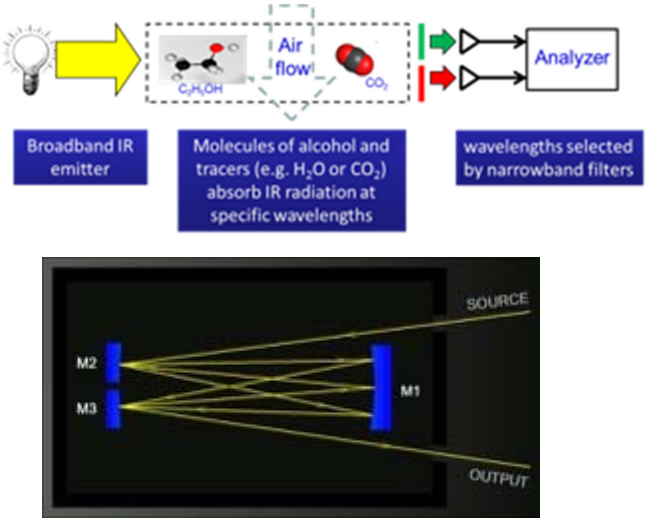

Figure 1. Breath-based sensor block diagram

The ultimate goal of the DADSS sensors is to measure breath alcohol within the vehicle cabin without direct input from the driver, that is, passively. The challenge with the breath-based system is to meet the performance requirements while measuring highly diluted breath. Thus, a significant component

of the research is focused on understanding expired breath aerodynamics within the vehicle cabin and identifying effective locations for the sensors. After comprehensive research that investigated optimal sensor placement in numerous locations within the vehicle, the sensor was adapted for installation in the DADSS research vehicles in four different positions: above the steering column, above the glove box, in the passenger's door panel and in the driver's door panel. These positions improved analysis of the impact of cabin air flow and the driver's position on alcohol measurements as well as optimized performance. It also allows a sober driver to operate the vehicle while a dosed passenger can provide samples for analysis.

The breath-based sensor has been updated in Phase III with the goal of improving this capability (see Figure 2 for evolution of sensor development). The latest, third Generation sensor (Gen 3), underwent a complete re-design to increase resolution for passive sensing, reduce the overall size, and obtain improved performance over the full temperature range of -40°C to +85°C as specified by the DADSS Performance Specifications. A major improvement of the Gen 3 sensor was the optical module configuration in which ethanol detection takes place over the full length of the chamber, whereas CO_2 is detected cross-wise. With this configuration there is no systematic timing difference between the two signals, thus enabling the possibility of passive in-vehicle sensing (Ljungblad et al., 2017).

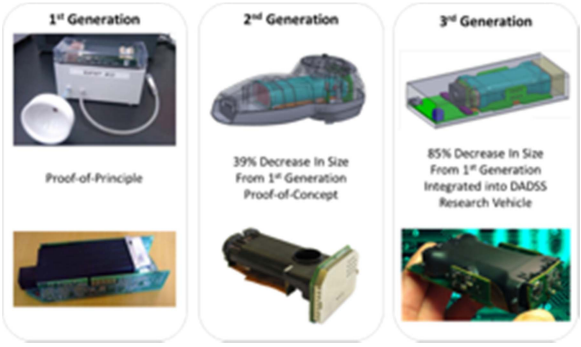

Figure 2. Evolution of Breath-based DADSS Sensor

TruTouch Touch-Based Subsystem

The tissue-based approach analyzes alcohol found in the driver's fingertip tissue (or more specifically, the blood alcohol concentration detected in the capillaries). The driver touches an optical module and a near infrared light shines on the driver's skin, similar to a low power flashlight, which propagates into the tissue. A portion of the light is reflected back to the skin's surface, where it is collected by the touch pad. This light transmits information on the skin's unique chemical properties, including the concentration of alcohol (Ridder et al., 2005).

The shift from the Phase I prototype, which used a bulky spectrometer engine with moving parts, to a fully solid-state laser spectrometer (which better suited the automotive environment) has required extensive hardware and software research (Ver Steeg et al., 2017). The key enabling innovation is the ability to define an optimized subset of optical wavelengths which provide a high quality non-invasive alcohol measurement in humans (see Figure 3 for schematic representation). It was determined that the new approach required the use of modulated laser diodes to generate 40 unique wavelengths of light for optimal alcohol measurement. The necessary laser diode target specifications were derived from an analysis of the human subject system data with accurate comparative reference data.

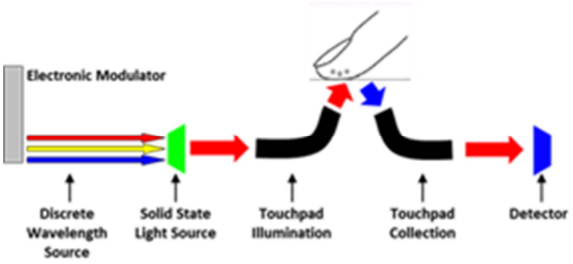

Figure 3. Touch-based solid-state laser spectrometer approach

The highest risk technical element of the touch-based system is the laser device fabrication which needs to meets target specifications. Extensive, cutting-edge research has been undertaken to develop the requisite lasers and to assemble them in initially multi-laser butterfly packages and most recently in a "stingray" shaped package. Many of these laser wavelengths had not been manufactured before. The combined light source generated by the laser packages in a touchpad, then has to illuminate the finger and is reflected back to the detector where alcohol measurements are made. After initial work to develop the laser diodes and packaging, a new supplier, Nanoplus, was selected with greater expertise in these areas. Each stage of the development process has required painstaking research which has been the subject of multiple patent applications. As with any new technology development, complications have been experienced along the way. For example, research on the fourth generation (see Figure 4), revealed a problem with laser intensity fluctuations resulting in unreliable tissue alcohol measurements. Once the various technical issues have been resolved,

a touch-based sensor will be incorporated into each of the DADSS research vehicles.

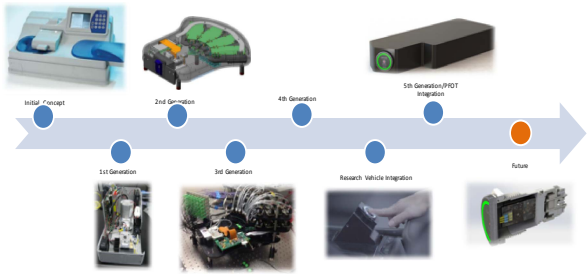

Figure 4. Evolution of touch-based DADSS Sensor

PILOT AND FIELD OPERATIONAL TRIALS

Study Design

The breath-based alcohol Gen 3 sensors have undergone significant laboratory testing and human subject testing. The next phase will be to evaluate them in extreme real-world environmental conditions, heat, cold, varying humidity, etc. to ensure that they will be operational for the harshest real-world conditions that they are likely to encounter. Research vehicles have been developed for use in PFOTs, and later in more extensive FOTs, to gather sensor validity, reliability, and durability data as well as to assess the real-world use of the sensors with human participants in varying environmental conditions.

Prior to the PFOT, the vehicles have undergone a "shakedown" stage, in which DADSS Program researchers are driving five fully-equipped test Chevrolet Malibu vehicles on a daily basis, to and from work, to ensure that the sensors, Data Acquisition Systems (DAS), cameras, and communications systems etc. are fully operational. These initial tests will provide a detailed insight into the necessary requirements of the PFOT test site set up and will be used to complete the development of the PFOT Test Plan (test routes, number of starts/stops, number of samples required, etc.). These initial vehicle tests are being conducted in Marlborough, MA, and Sterling, VA. Once approval has been given from OMB to move forward the FOT will commence.

The PFOT will be conducted in two phases. PFOT 1 and 2 will be comprised of vehicles equipped with four Gen 3.2 breath sensors – two on driver side (driver door and steering column), and two on the passenger side (above the glove box and passenger door). A touch-based sensor can be added once it is ready for field testing (for more details see PFOT Vehicle Integration Layout and Systems, next section).

The FOT will utilize fully-equipped Chevrolet Malibu vehicles, donated by General Motors. These vehicles currently are going through vehicle fit out at the KEA Technology laboratory in Marlborough, MA.

Required climatic conditions for FOT:

- Site 1 Low Humid, Low Temp
- Site 2 High Temp, Low Humidity
- Site 3 High Temp, High Humidity
- Site 4 High Elevation, Low Temp
- Site 5 Corrosive, Low Temp (High salt)

PFOT 1 and 2 will involve drivers and passengers in Marlborough, MA, and Sterling, VA. The ensuing FOT will involve both drivers and passengers at sites that cover the above required climatic conditions. Drivers will not be permitted to consume alcohol and only alcohol-free measurements will be obtained from the driver side sensors. Passengers will be asked to consume two different amounts of alcohol, approaching a breath alcohol concentration (BrAC) of 0.02-0.03% and 0.04-0.05%, respectively. It was found during human subject testing that once subjects' reached BACs in excess of 0.05% they experienced some difficulty in properly using the sensors. Thus, the design of the passenger user interface was designed to accommodate the perceptual and information processing limitations associated with a BrAC at the maximum dosage (0.05%). In that way, errors in user interface issues due to alcohol consumption will be mitigated. It will also help to provide a safer environment for the driver.

Assignment of the passenger roles will be alternated so that no given participant will be required to consume alcohol every test day. Moreover, the test protocol will ensure that adequate time elapses between the end of a test day and the beginning of the next test day, so that a drinking passenger's BrAC returns to zero BAC.

When a passenger is included, each dosed passenger will provide a minimum of 3 breath samples every 10 minutes or 18 per hour. This will result in a minimum of 72 samples per day per vehicle. For two vehicles over 40 days this will result in a minimum 5,760 samples. Each breath sample to the SenseAir breath sensors will be directed, but the sensors will also be operating in sniffer mode throughout the day.

The initial trials involving passengers will be conducted in the winter in the North East to test the sensors in a cold climate. Each of the daily drives

will last 4 hours and will follow a different route each day.

Participant Details

Adult male and female volunteers (age 21-55 years) will be recruited in the Boston Metropolitan area via web sites, newspaper ads and flyers. Participants must not meet DSM-IV criteria for any psychiatric disorder or substance dependence. Reasons for exclusion include: unstable or uncontrolled medical illness, serious central nervous system disease (e.g. multiple sclerosis or cerebral vascular accident), major depression, bipolar disorder or a family history of bipolar disorder, schizophrenia, psychosis, or organic mental disorder. Participants will also be excluded if they take any regularly prescribed prescription medications, have a history of head trauma, seizure disorder, or other intracerebral pathology or have a pacemaker, metallic surgical hardware or other metal in his/her body. Women of childbearing potential must be using a method of birth control throughout the study. Participants will be screened prior to participating for drug use and pregnancy.

FOT Vehicle Integration

The DADSS vehicles will be equipped with four Gen 3.2 breath sensors. Prior to installation, all of the sensors are put through a detailed characterization regimen in the KEA Technology laboratory. Standard calibration testing is conducted at temperatures of +40°C, ambient (approx 22 ^{o}C, and +85°C using breath samples at concnetrations of 0.0, 0.05, 0.08, and 0.10 % BrAC. In addition to the SenseAir breath sensors, the vehicles are equipped with a breath-alcohol Reference sensor, two video cameras, a Web interface, the DAS, Data and video storage, and the ability to accommodate one touch sensor (when available). The vehicles with four breath sensors will also have a user interface for use by the passengers.

The first DADSS breath sensor on the driver's side is mounted into the steering column clamshell, directly in front of the driver's face. The second sensor is mounted on the driver's side door (see Figure 5 for driver-side sensor placement).

Figure 5. Driver-side Breath sensors; driver-side door (top) steering wheel (bottom)

On the passenger side, sensors will be located above the passenger glove box and the passenger-side door.

The "reference" handheld breath sensor that the driver and passenger are required to blow into to obtain an accurate BrAC reading is situated on the left side of the center stack (see Figure 6).

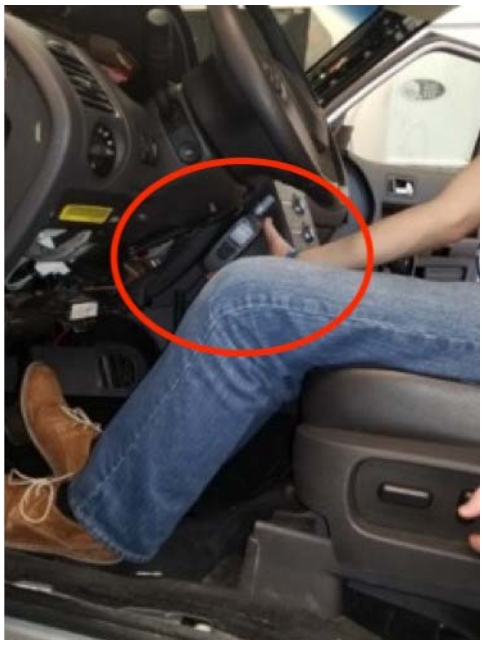

Figure 6. Smart Start Reference sensor

In addition, each vehicle is equipped with an automatic data collection system, (DAS). The DAS is the central brain of the DADSS system. It takes in power from the vehicle battery, and distributes this

power to all other components of the system. Utilizing a wake signal from the 12V inverter in the car, the DAS will activate upon the turn of the key. The DAS powers the reference sensor as well as collects the serial data it captures. The DAS also relays power to the SenseAir breath sensors, as well as receives the Control Area Network (CAN) data coming from the sensors. Along with the sensors, the DAS provides power to the router and the DVR, for network and video capabilities. All these data are stored by the DAS. In sum, the DAS will record sensor, vehicle and participant data without requiring any input from the participants and will automatically transmit data to the research team. Objective data collected will consist of numerical and video data that capture host vehicle states and maneuvers, surrounding traffic, system operation, and driver behavior. Subjective data collected will include driver background information before participation in the FOT and at the conclusion of each FOT day.

The majority of the hardware for the DADSS system is mounted onto a plate that resides in the trunk of the Chevrolet Malibu (see Figures 7 and 8). The three antennae are located on the rear deck (see Figure 9).

Figure 7. Location of DAS, Network Switch, and DVR in trunk

Figure 8. From left to right, DAS, WIFI LTE, network switch, and DVR

Figure 9. Rear deck view of the 3 antennae with seats down

The research vehicles also are equipped with video recording systems. The video data will be used for a number of different purposes. The study requires physical verification of the participant's three-dimensional position in the vehicle interior space so that their position may be correlated with sensor data from the breath-based sensors as well as height and weight data collected from the demographic interview. Video verification also can be used to correlate touch-based sensor interaction with the data collected from those sensors in the event that there are data artifacts and/or anomalies. Each video system is comprised of two cameras, a digital video recorder, a DAS, and two data transmission technology systems (i.e., WIFI and 4G). The two camera locations are shown in Figure 10, and the camera angles in Figures 11 and 12.

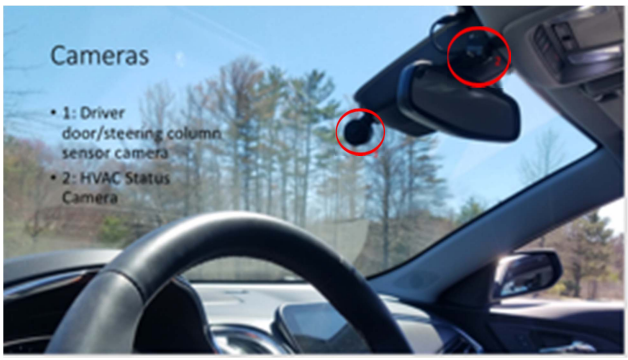

Figure 10. Video cameras to record driver interaction with the sensors.

Figure 11. Camera 1 view

Figure 12. Camera 2 view

CONCLUSIONS

Significant progress has been made in the development of DADSS in-vehicle alcohol sensors. Two specific approaches are under development; breath-based and touch-based sensors. Now in Phase III of the research and development effort, the SenseAir breath-based sensors have undergone extensive laboratory and human subject testing to ensure that they are approaching or meeting the stringent performance specifications (accuracy, reliability, durability) outlined in the DADSS Performance Specifications. The critical next stage is to test how they function when installed in vehicles in a diverse range of real-world driving environments (hot, cold, dry, humid, corrosive etc.).

Research vehicles have been fitted with the latest generation, Gen 3.2, breath sensors in both the driver and passenger positions (touch-based sensors will be incorporated at a later stage when they have undergone the requisite testing protocols). Pilot Field Operational Trials are underway and comprehensive DAS including a video recording system are collecting data from the alcohol sensors as well as from instrumentation designed to track environmental conditions, vehicle system data, test participant video, and breath-alcohol reference sensors. The PFOTs and subsequent FOTs will be key in determining the effectiveness of the DADSS sensors in a wide range of real-world driving environments including the effects of repeated use and vehicle mileage on sensor function. Of equal importance, driver behavior when interacting with the sensors and user acceptance will be evaluated with the potential to assess future impact of the sensors on alcohol-impaired driving. The findings will be used to refine the DADSS Performance Specifications and ultimately to modify the systems design and enhance product development. The DADSS technology, if proven to be reliable and reproducible under diverse environmental and biological conditions, would represent a significant technological breakthrough in crash avoidance and a significant advance in driver monitoring technologies in vehicles.

REFERENCES

Ferguson, S. A. 2012. Alcohol-impaired driving in the United States: Contributors to the problem and effective countermeasures. Traffic Injury Prevention, 13, 427-441.

Ferguson, S.A., Traube, E, Zaouk, A, Strassburger, R. 2009. Driver Alcohol Detection System For Safety (DADSS) – A non-regulatory approach in the development and deployment of vehicle safety technology to reduce alcohol-impaired driving. Paper Number 09-0464. Proceedings of the 21st International Technical Conference on the Enhanced Safety of Vehicles.

Ferguson, S.A., Zaouk, A., Strohl, C. 2010. Driver Alcohol Detection System for Safety (DADSS). Background and Rationale for Technology Approaches. Society for Automotive Engineers Technical Paper, Paper No. 2010-01-1580, Warrendale, PA: Society of Automotive Engineers.

Ferguson, S.A.; Traube, E, Zaouk, A, Strassburger, R. 2011. Driver Alcohol Detection System For Safety (DADSS) – Phase I Prototype Testing And Finding. Paper Number 11-0230. Proceedings of the 22nd International Technical Conference on the Enhanced Safety of Vehicles.

Hök, B., Pettersson, H., Andersson, G. 2006. Contactless measurement of breath alcohol. Proceedings of the Micro Structure Workshop. May, 2006, Västerås, Sweden.

Ljungblad, J., Hök, B., Allalou, A., Pettersson, H. 2017. Passive in-vehicle driver breath alcohol detection using advanced sensor signal acquisition and fusion. Proceedings of the 25th International Technical Conference on the Enhanced Safety of Vehicles.

Lukas, S, Zaouk, A., Ryan, E., McNeil, J., Shepherd, J., Willis, M., Dalal, N., Schwartz, K. 2017. Driver alcohol detection system for safety (DADSS) – preliminary human testing results. Paper Number 17-0304. Proceedings of the 25th International Technical Conference on the Enhanced Safety of Vehicles.

National Highway Traffic Administration (NHTSA). 2018. DOT HS 812 630 Alcohol-impaired driving. Traffic Safety Facts. Washington DC.

Ridder, T.D., Hendee, S.P., Brown, C.D. 2005. Noninvasive alcohol testing using diffuse reflectance near-infrared spectroscopy. Applied Spectroscopy, 59, 181-189.

Ver Steeg, B., Treese, T., Adelante, R., Kraintz, A, Laaksonen, B., Ridder, T., Legge, M., Koslowski, N., Zeller, S., Hildebrandt, L., Koeth, J., Cech, L., Rumps, D., Nagolu, M., Cox, D. 2017. Development of a solid state, non-invasive, human touch-based blood alcohol sensor. Paper Number 17-0036. Proceedings of the 25th International Technical Conference on the Enhanced Safety of Vehicles.

Zaouk A. K., Willis M., Traube E., Strassburger R. 2015. Driver Alcohol Detection System for Safety (DADSS) – A Status Update. Paper Number 15-0276. Proceedings of the 24th International Technical Conference on the Enhanced Safety of Vehicles.

Zaouk A. K, Willis, M., Dalal, N., Traube, E., Strassburger, R. 2017. Driver Alcohol Detection System for Safety (DADSS) – A Status Update. Paper Number 17-0271. Proceedings of the 25th International Technical Conference on the Enhanced Safety of Vehicles.

ASSESSING SYSTEM IMPLEMENTATION READINESS OF THE DRIVER ALCOHOL DETECTION SYSTEM FOR SAFETY (DADSS) TO REDUCE ALCOHOL-IMPAIRED DRIVING IN A REAL-WORLD DRIVING PILOT DEPLOYMENT PROJECT

Remi Fournier
Abdullatif K. Zaouk
Michael Wills
KEA Technologies, Inc.
U.S.A.

Robert Strassburger
Automotive Coalition for Traffic Safety
U.S.A.

Rebecca Spicer
Impact Research, LLC
U.S.A.

Paper Number 19-0263

ABSTRACT

The Driver Alcohol Detection System for Safety Program – a joint effort of the National Highway Traffic Safety Administration and the Automotive Coalition for Traffic Safety - has been developing unique, in-vehicle alcohol detection systems to more effectively address the problem of alcohol-impaired driving. These technologies, both breath-and touch-based, are intended to be seamless with the driving task, non-intrusive, accurate, fast, reliable, durable, and require little or no maintenance. Now in Phase III of development, the breath-based technology is ready for real-world road testing in a naturalistic setting in the State of Virginia, U.S.A. The Driven to Protect Powered by DADSS initiative, is a partnership with the Virginia Department of Motor Vehicles Highway Safety Office and the Automotive Coalition for Traffic Safety. As the technical and program management lead, KEA Technologies, Inc. has instrumented and deployed a small fleet of pilot test vehicles to examine the data from breath-based prototype sensors under various environmental, driver/user interaction, and user demographics conditions. The alcohol detection system is known to be accurate, precise, reliable, and maintainable based on laboratory and controlled test results. This pilot program seeks to obtain data from naturalistic, uncontrolled test conditions. The pilot program will determine if: a) the system is generally accepted by drivers, b) there are any technical modifications required to significantly improve the system, and c) the system is ready for wider implementation in fleet, privately-owned, commercial, or other vehicles. Four 2015 Ford Flex "For Hire" commercial livery service vehicles have been instrumented with in-vehicle breath-based alcohol detection sensors including supporting data collection and transmission systems. The Pilot Deployment Project is ongoing with a goal of collecting at least 15,000 data points from the sensors. Lessons learned will be used to refine the performance specifications, sensor technology, and data acquisition systems for future on-road vehicle testing.

INTRODUCTION

Alcohol-impaired driving - defined as driving at or above the legal limit of 0.08 g/dl or 0.08 percent in all U.S. States except where the limit is 0.05 g/dl in Utah - is one of the primary causes of motor vehicle fatalities on U.S. roads every year. In the U.S. in 2017, 10,874 people were killed in alcohol-impaired driving crashes (NHTSA, 2018). And specifically as it relates to this Pilot Deployment project, in 2017, 248 people were killed and 4,430 injured on Virginia's roadways due to alcohol-impaired crashes.

There are a variety of countermeasures that have been effective in reducing this excessive toll, many of which center around strong laws and visible enforcement (Ferguson, 2012). However, to drastically reduce these deaths it will be necessary to prevent alcohol-impaired drivers from driving in the first place. To that end, the National Highway Traffic Safety Administration (NHTSA) and the Automotive Coalition for Traffic Safety (ACTS) began research in February 2008 aimed at identifying potential in-vehicle approaches to identifying and preventing alcohol-impaired driving as it happens. ACTS members are comprised of motor vehicle

manufacturers representing approximately 99 percent of light vehicle sales in the U.S. This cooperative research partnership, known as the Driver Alcohol Detection System for Safety (DADSS) Program, has identified feasible non-invasive technologies aimed at preventing alcohol-impaired driving (Ferguson et al., 2009, 2010, Zaouk et al., 2015, 2017). These technologies are designed to be seamless with the driving task, they are non-intrusive, accurate, fast, reliable, durable, and require little or no maintenance. The vehicle cannot be driven when the device registers that the driver's blood alcohol concentration (BAC) meets or exceeds 0.08 g/dl.

The breath-based prototype sensors have been installed and integratred into vehicles for pilot testing in real-world driving conditions. Results from these tests will help to determine whether the system is generally accepted by drivers, if there are any technical modifications required to significantly improve the system, and whether or not the system is ready for wider implementation in fleet, privately-owned, commercial, or other vehicles.

SENSOR TECHNOLOGY

Breath–Based Sensor technology

The breath-based approach uses sensors to measure the concentrations of alcohol and carbon dioxide (CO_2) in the breath simultaneously. The known quantity of CO_2 in the human breath is an indicator of the degree of dilution of the alcohol concentration in exhaled air. Diluted breath is drawn into the sensor by a fan, which directs infrared light beams on the breath sample and analyzes the wavelengths returned for both alcohol and CO_2. Breath alcohol concentration is then quickly and accurately determined. (Hök et al., 2006, see Figure 1).

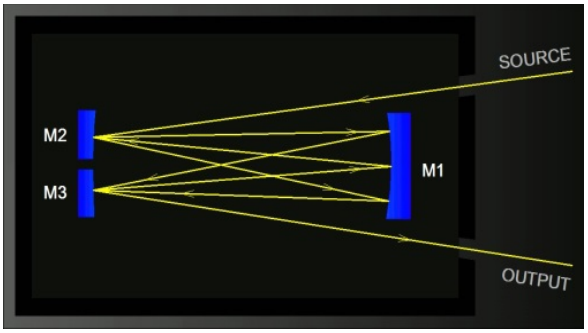

Figure 1. Breath-based sensor block diagram

The ultimate goal of the DADSS sensors is to passively measure breath alcohol within the vehicle cabin - without direct input from the driver. The challenge with the breath-based system is to meet the stringent performance requirements while measuring highly diluted breath. Thus, a significant component of the research is focused on understanding expired breath aerodynamics within the vehicle cabin and identifying effective locations for the sensors.

The breath-based sensor has been updated in Phase III with the goal of improving this capability. The latest, 3rd Generation version (Gen. 3), underwent a complete re-design to increase resolution for passive sensing, reduce the overall size, and obtain improved performance over the full temperature range of -40°C to +85°C as defined in the DADSS Performance Specifications. A major improvement of the Gen. 3 sensor over previous versions was the optical module configuration in which ethanol detection takes place over the full length of the device where CO_2 is detected cross-wise. With this configuration there is no systematic timing difference between the two signals, enabling the possibility of passive in-vehicle sensing (Ljungblad et al., 2017). See Figure 2 for a graphic representation of the sensor evolution.

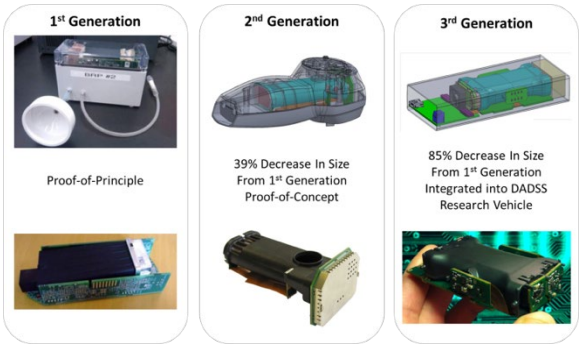

Figure 2. Evolution of Breath-based DADSS Sensor

NATURALISTIC DRIVING TRIALS – JRT Pilot Deployment Project

Overview

Driven to Protect, Powered by DADSS, has partnered with James River Transportation (JRT), a transportation company with offices in Richmond and Norfolk, VA, to conduct the first in-vehicle, on-road naturalistic test trials with prototype breath-based alcohol sensors in their vehicles. In August 2018, the first Ford Flex vehicles in the JRT commercial fleet started operating from Richmond International Airport (RIC) and Norfolk International Airport (ORF), conveying clients to local destinations. The breath-based prototypes were seamlessly integrated into these fleet vehicles and are collecting real-world operational data throughout the ride. The feedback and data collected from drivers

will be invaluable in modifying the technology as it is prepared for widespread commercialization. Through mid-January 2019, the JRT vehicles have travelled nearly 40,000 miles in 149 days, and the sensors have been in operation more than 4,000 hours and collected over 16,000 data points.

Vehicle Layout and Systems

Four 2015 Ford Flex vehicles (similar to that shown in Figure 3), initially two at RIC and two at ORF, have been instrumented with two Gen 3.1 breath-based sensors and one "reference" breath-alcohol sensor. Prior to installation, groups of sensors were characterized at the KEA Technology Laboratory in Marlborough, MA U.S.A. Characterization typically includes the use of a climate chamber where sensors are tested at -40ºC, +22ºC (representing ambient), and +85ºC, and at controlled ethanol concentrations of 0.000%, 0.020%, 0.040%, 0.060%, 0.080%, and 0.100% Breath Alcohol Content (BrAC).

Each vehicle is equipped with two prototype sensors, one "reference" breath alcohol sensor, one data acquisition system (DAS), two data transmission technology systems (i.e., WIFI and 4G), and one video system including two cameras and digital video recorder.

Figure 3. James River Transportation Ford Flex Driven to Protect Vehicle (Platform car shown)

The two breath-based prototype sensors are collecting samples both in directed mode, where drivers direct their breath toward each of the sensors, and in "sniffer" mode to capture breath alcohol present in the ambient air. After comprehensive research that investigated optimal sensor placement in numerous locations within the vehicle, the sensor was adapted for installation in the JRT Pilot Deployment vehicles in two different positions: above the steering column and in the driver's door panel. These positions improved analysis of the impact of cabin air flow and the driver's position on alcohol measurements as well as optimized performance. One breath sensor is mounted into the top of the steering column clamshell, directly in front of the driver's face. A second sensor is mounted on the driver's side door in the upper trim panel just forward of the driver's left shoulder (see Figure 4).

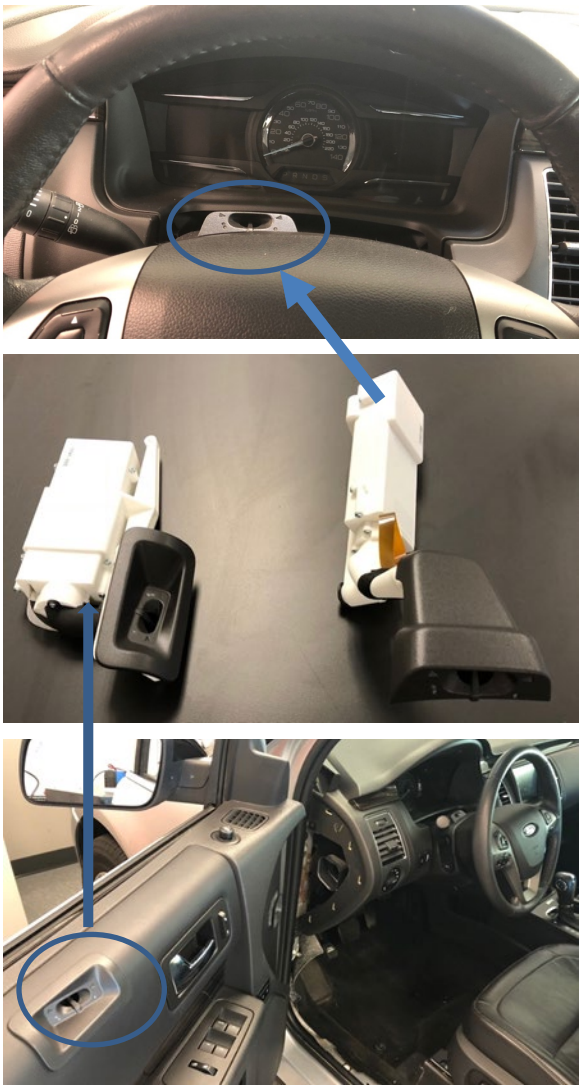

Figure 4. DADSS Breath-based sensors; Steering column (top) and driver-side door (bottom)

A "reference" handheld breath sensor is situated on the left side of the center stack and infotainment center. This sensor has been previously validated. As a part of the Test Plan, the drivers are required to blow into the reference sensor to provide "control" data for comparison against the prototype sensor data. Under 49CFR Part 40 alcohol conformance tests, this reference device has been recognized by NHTSA as an approved *evidential breath testing (EBT)* unit (see Figure 5).

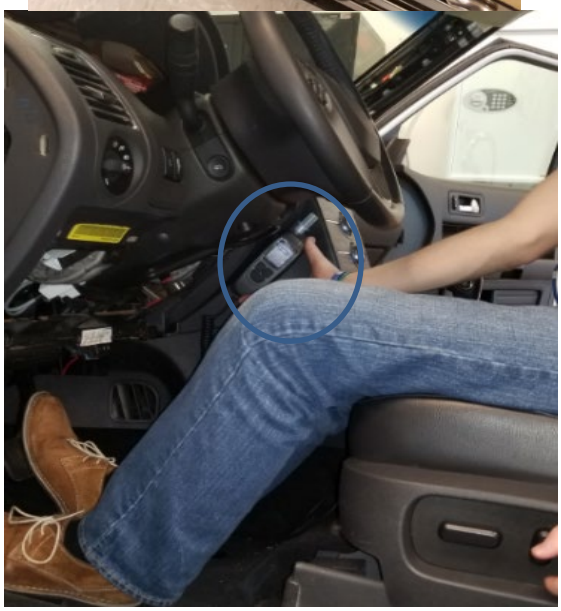

Figure 5. Reference sensor

Two cameras record the drivers interaction with the sensors (see Figure 6) and video data are stored in an Axis DVR.

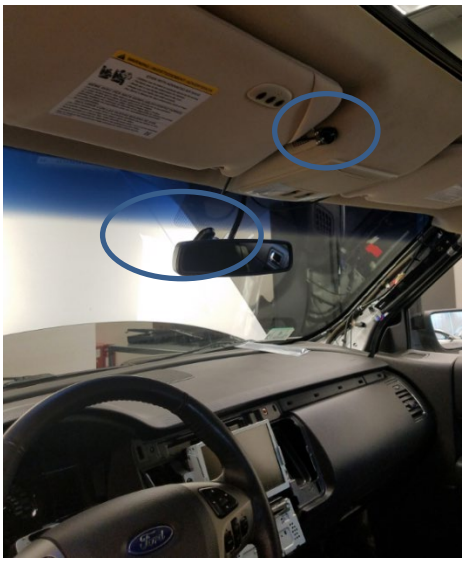

Figure 6. Locations of video cameras

The DAS is the central processing system – the "brain" of the DADSS system (see Figure 7). The DAS obtains power from the vehicle battery and distributes it to the other system components. Utilizing a wake signal from the 12V inverter in the car, the DAS activates once the vehicle power is activated through accessory or fully powered on. It powers the reference sensor and collects acquired serial data. The DAS relays power to the two prototype breath sensors and receives the Control Area Network (CAN) data coming from those sensors.

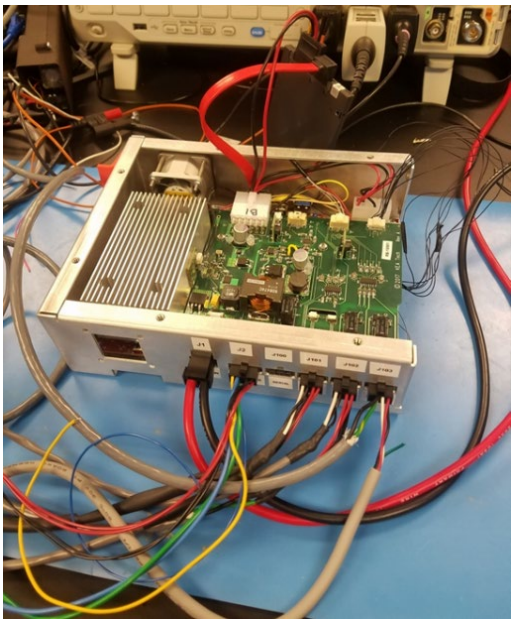

Figure 7. Data Acquisition System (DAS), internal and external views

In the JRT Pilot Deployment project, the DAS is mounted in the rear right quarter panel of each 2015 Ford Flex vehicles (see Figure 8).

Figure 8. Location of Data Acquisition System (DAS) in Ford Flex vehicle

One configurable vehicle-grade router with 3 antennas is the hub for Wi-Fi, 4G and GPS capabilities. Positive alcohol alerts and critical system information is sent from the DAS via 4G, while raw sensor and video camera data is sent via Wi-Fi when the vehicle is within range of the access point antenna and transmission equipment (see Figure 9). The router is mounted in the same rear quarter panel next to the DAS.

Figure 9. Vehicle-grade Router location

The GPS antenna is mounted inside the trim in the front right "A pillar" of the Flex. The Wi-Fi and 4G antennas are mounted in the front and rear of the cargo area window frame, respectively.

Driver Protocols

Nineteen JRT-employed drivers have been using the sensor-equipped vehicles for their regular work shifts. Drivers were given training and orientation prior to the beginning of the pilot project with a focus on testing-related activities: when, where, and how to give "directed" breath samples. The protocol includes obtaining breath samples from drivers at the beginning and the end of each shift, and each time after a passenger is dropped off (i.e., when no passengers are present). No other changes were made to their regular work/drive routine.

At the beginning of the shift, using a phone app, drivers are asked to fill out a short survey including questions such as when they last consumed alcohol and how much, medical ailments, use of over-the-counter medications that might yield a false-positive (e.g. cold medications), and whether they have used mouth wash or hand sanitizer which may affect prototype sensor readings. When the driver starts the vehicle, the DADSS system (including DAS, sensors, and video system) turns on automatically, with no driver action required. At the beginning of the shift, the driver provides a "set" of samples: one directed breath sample into each of the prototype sensors (steering column and driver-side door). Next, the driver provides a deep-lung breath sample to the reference sensor by blowing into the disposable

plastic tube. This "set" of samples is repeated a second time to indicate the beginning of a shift. If there is a positive reference sensor reading (≥ 0.02% BrAC), an alert will be sent wirelessly to JRT Management personnel for action, and to KEA for informational purposes. If the second sample using the reference sensor also reads ≥ 0.02%, then JRT will execute their standard operating procedure relating to suspicion of impairment and try to determine the cause of the reading. In the event of an invalid reference sensor reading, the driver will be prompted to give another sample. In addition to these active Driver test conditions, throughout the day the breath sensors are also operating in "sniffer" mode, passively testing the ambient air around the driver. All of the data from these "directed" and "sniffer" breath samples are captured and recorded in an on-line Data Viewer available only to specific authorized program personnel.

DATA COLLECTION AND ANALYSIS

Data Collection

The data analysis plan includes exploration of sensor measurements and troubleshooting sensor performance on a daily basis, as well as longer-term analysis of sensor performance. Data collection includes both qualitative feedback from drivers and quantitative breath alcohol measures during driving shifts. Because the drivers of the fleet vehicles are expected to be free of alcohol in their breath (< 0.02 BrAC), the focus of the project is sensor performance with zero or low levels of breath alcohol. The goal to collect a total of 15,000 breath sensor measurements was reached after five months of deployment.

Quantitative data collection involves pre- and post-shift driver surveys that gather feedback on driver experience with the sensors but also inform any troubleshooting of anomalous readings or problems with the sensors and data acquisition system. Driver factors include last reported alcohol use and medication use (e.g. cold medicine) or use of other products that could trigger a positive sensor reading (e.g. mouth wash, hand sanitizer). Drivers also report on presence of intoxicated passengers in the vehicle and any challenges in providing breath samples. Continuous video surveillance adds information on driver interaction with the sensor and visual cues the sensor provides during use. In addition, two small focus groups were conducted to gain an understanding of driver receptiveness to the technology, preferences for sensor prompts, other interactions with the sensors, and feedback on the program training and driver test plan.

Quantitative sensor data are collected continuously by the in-vehicle DAS. Data elements include the measured BrAC (g/210L) from both "directed" and "sniffer" breath prototype sensor samples in addition to the corresponding sensor firmware status, time from start up, breath dilution levels, and the breath-alcohol reference sensor measurement reading.

Data Analyses

The objectives of the data analysis include assessment of driver receptiveness of the technology, case studies of false-positive prototype sensor readings (BrAC≥0.02%), gathering data that inform technical modifications to improve sensor performance, surveilling the exposure of the sensors to in-vehicle use and troubleshooting issues that arise in this first field deployment. Lessons learned will be used to refine the sensor performance specifications, sensor technology and data acquisition systems for future on-road vehicle testing.

In the first approximately five months of the deployment, the prototype sensors have been present in vehicles driven nearly 40,000 miles during approximately 4,000 hours of driving time. During these shifts the prototype sensors measured BrAC from over 16,000 directed or "sniffed" breath samples. Pre- and post-drive surveys have been completed by a total of 19 drivers for over 200 shifts.

During this time, the reference sensor registered a positive BrAC (≥0.02%) in 4 events. Immediate follow-up to these events involved contacting the driver and asking about possible medication, mouthwash or other product use that would trigger a positive BrAC. Requested follow-on breath samples using the reference sensor showed a sharp decline to BrAC<0.02% within twenty minutes. The conclusion in these 4 investigations is that mouthwash was likely the cause of the initial positive BrAC. Pre-drive surveys, in particular the questions regarding last alcohol use and use of medications and mouthwash, were critical in concluding that the positive breath samples were due to short-term, residual mouth alcohol from the over-the-counter products and not due to positive blood alcohol levels.

Driver feedback shows an initial learning and acclimation period in use of the prototype sensors. Around a quarter of post-drive feedback in the first two months indicated a problem with the sensors (21% and 25%, respectively). Reported problems during the shift then declined to 11% in the third months, 5% in the fourth months, and 0% in the fifth month. Feedback in the focus groups indicated that

there was a “small” learning curve in providing a breath sample to the sensors, but after “a short time” they “got the hang of it.” The focus groups provided feedback on driver-sensor interactions. Drivers expressed annoyance with the beeping from the reference sensor and the data acquisition fan. With respect to the prototype sensors, the drivers noted that the orange and green lights were informative/useful and not annoying. The drivers did not feel the prototype sensors were distracting.

The post-drive surveys were important for feedback on the functioning of the sensors and DAS. Several drivers reported problems with interference with in-vehicle GPS, radio, and keyless entry. This real-time reporting allowed quick technical modifications to be made to limit this interference.

As discussed above, the measured quantity of CO_2 in a breath is an indicator of the degree of dilution in the breath in ambient air. This degree of dilution is represented by a “dilution factor” (DF), computed based on the measured CO_2 compared to the expected exhaled CO_2 in human breath. For the purposes of this project, the data acquisition system reports all breath samples that resulted in a BrAC measure, regardless of DF.

Assuming all drivers were BAC negative, sensor readings above BrAC 0.02% were considered high erroneous readings. An interim analysis of the prototype data found that a quarter of the measures were above BrAC≥0.02%. DFs ranged from 0 to 149. This analysis further found an association of erroneous high BrAC readings with a high DF (i.e. highly diluted breath samples). The lower the dilution factor, the lower the percent of erroneous readings.

To inform future filtering of the sensor readings by a given DF threshold in order to minimize erroneous readings, the project examined the trade-off between reducing erroneous readings without eliminating correct readings. The analysis suggests DF=30 as the cut-off because it hits a "sweet spot": a reduction in the number of high/erroneous readings (1.8% of readings remain that are BrAC≥0.02%) without deleting too many correct readings. In comparing readings at DF=30 to DF=25 and DF=20, we observed that lowering the dilution factor below 30 only eliminated correct measures (BrAC<0.02%).

In this ongoing project, sensors continue to be monitored to ensure they are performing as expected on a daily basis in order to identify immediate solutions and understand erroneous BrAC readings. Further analyses include examination of the agreement of breath sensors with the reference sensor and with each other; examining factors that affect this agreement; and variations in sensor function over time and as a function of continued use.

CONCLUSIONS

Significant progress has been made in the identification and development of DADSS sensor technologies that have the potential to be used on a more widespread basis in passenger vehicles. While the testing from this project and the data obtained are very important, analysis suggests that additional testing under other conditions is warranted. A near-term future project is planned to continue the on-road testing of the prototype sensors. This next stage in the development effort is the evaluation of the performance of the next generation (Gen 3.2) of prototype sensors in vehicles under real-world driving conditions including alcohol-positive samples obtained from dosed passengers under strict test conditions. The Driven to Protect, Powered by DASS initiative, is a partnership between the Virginia Department of Motor Vehicles, Highway Safety Office and the Automotive Coalition for Traffic Safety. This is the first state partnership with a private company to conduct in-vehicle, on-road test trials of the DADSS technology. KEA Technologies has installed the latest generation 3.1 prototype breath-based sensors into four vehicles in the James River Transportation commercial fleet. Results from this JRT pilot testing will be invaluable in finalizing the technology as it is prepared for widespread commercialization.

REFERENCES

Ferguson, S. A. 2012. Alcohol-impaired driving in the United States: Contributors to the problem and effective countermeasures. Traffic Injury Prevention, 13, 427-441.

Ferguson, S.A., Traube, E, Zaouk, A, Strassburger, R. 2009. Driver Alcohol Detection System For Safety (DADSS) – A non-regulatory approach in the development and deployment of vehicle safety technology to reduce alcohol-impaired driving. Paper Number 09-0464. Proceedings of the 21st International Technical Conference on the Enhanced Safety of Vehicles.

Ferguson, S.A., Zaouk, A., Strohl, C. 2010. Driver Alcohol Detection System for Safety (DADSS). Background and Rationale for Technology Approaches. Society for Automotive Engineers Technical Paper, Paper No. 2010-01-1580, Warrendale, PA: Society of Automotive Engineers.

Ferguson, S.A.; Traube, E; Zaouk, A; Strassburger, R. 2011. Driver Alcohol Detection System For Safety (DADSS) – Phase I Prototype Testing And Finding. Paper Number 11-0230. Proceedings of the 22nd International Technical Conference on the Enhanced Safety of Vehicles.

Hök, B., Pettersson, H., Andersson, G. 2006. Contactless measurement of breath alcohol. Proceedings of the Micro Structure Workshop. May, 2006, Västerås, Sweden.

Ljungblad, J., Hök, B., Allalou, A., Pettersson, H. 2017. Passive in-vehicle driver breath alcohol detection using advanced sensor signal acquisition and fusion. Proceedings of the 25th International Technical Conference on the Enhanced Safety of Vehicles.

National Highway Traffic Administration (NHTSA). 2018. DOT HS 812 630 Alcohol-impaired driving. Traffic Safety Facts. Washington DC.

Zaouk A.K., Willis, M., Traube, E, Strassburger, R. 2015. Driver Alcohol Detection System for Safety (DADSS) – A Status Update. Paper Number 15-0276. Proceedings of the 24th International Technical Conference on the Enhanced Safety of Vehicles.

Zaouk A. K, Willis, M., Dalal, N., Traube, E., Strassburger, R. 2017. Driver Alcohol Detection System for Safety (DADSS) – A Status Update. Paper Number 17-0271. Proceedings of the 25th International Technical Conference on the Enhanced Safety of Vehicles.

EFFECT OF SUBARU EYESIGHT ON PEDESTRIAN-RELATED BODILY INJURY LIABILITY CLAIM FREQUENCIES

Kay Wakeman[1]
Matt Moore[1]
David Zuby[1,2]
Laurie Hellinga[1]
[1]Highway Loss Data Institute, [2]Insurance Institute for Highway Safety (IIHS)
United States of America

Paper Number 19-0265

ABSTRACT

Research Question/Objective
Subaru's EyeSight is a camera-based driver assistance system that includes the ability to brake automatically when it detects a crash-imminent situation involving a pedestrian. The objective of this study was to evaluate whether Eyesight was preventing vehicles from striking pedestrians. Insurance claims under bodily injury (BI) liability coverage without associated first-party (collision) or third-party (property damage liability [PDL]) claims for vehicle damage were used as a surrogate measure of pedestrian crashes.

Methods and Data Sources
EyeSight is an option on various 2013–17 Subaru series. The presence or absence of EyeSight is discernible from information encoded in the vehicle identification numbers (VINs). The number of BI-only claims per insured vehicle year was compared for Subaru vehicles with and without EyeSight, using regression analysis to account for other factors also known to affect insurance claim frequency. A Poisson distribution was used to model claim frequency. Covariates included calendar year, garaging state, vehicle density, age group, gender, marital status, risk classification, and vehicle model year and series. Twenty percent of the insured-vehicle-year exposure came from vehicles equipped with EyeSight. Prior investigation has shown that injury-only BI claims are consistent with pedestrian or other nonoccupant injuries. Even so, these may include some nonpedestrian crashes, and some pedestrian crashes that were severe enough to also cause vehicle damage may be excluded. This study was based on vehicles with overlapping BI liability, collision, and PDL insurance in U.S. states with traditional tort liability insurance laws.

Results
When all series were combined, Subaru vehicles with EyeSight showed a statistically significant 35% reduction in BI-only claim frequency. When the Subaru Forester, Legacy, and Outback were separated by generation, results also showed statistically significant reductions of 33% for the first generation and 41% for the second generation. When the vehicle series were modeled individually, claim frequency reductions ranged from 18 to 57%, although only the Legacy (57%) and Outback (34%) results were statistically significant.

Discussion and Limitations
Claim frequency reductions for the EyeSight generations are similar, but it is promising that the second generation is showing a larger reduction. There are limitations to the data used in this analysis. Covariates describing driver characteristics are generally those of the primary driver of each vehicle and not necessarily the driver involved in the crash claim. Likewise, geographic covariates describe where the owner of the insured vehicle lives and not necessarily where crashes occurred. Nevertheless, these variables are consistently predictive in explainable ways.

Conclusions and Relevance to Session Submitted
Subaru's Eyesight system is associated with a lower BI-only claim frequency than the same Subaru vehicles without EyeSight. In 2016, there were nearly 6,000 pedestrian fatalities in the United States, up 9% from 2015, and an 11% increase in bicyclist deaths. Pedestrian detection systems like Subaru EyeSight have the potential to effectively reduce these numbers, and efforts to promote similar systems will help protect vulnerable road users.

INTRODUCTION

In 2017, there were 5,977 pedestrians and 783 bicyclists killed in traffic crashes in the United States. This is slightly less than in 2016, when there were 6,080 pedestrian fatalities and 852 bicyclist fatalities [1]. However, 2016 pedestrian fatalities were 9% higher than 2015 [2]. In addition, in 2015, an estimated 70,000 pedestrians were injured in traffic crashes [3]. Along with the growth of the number of pedestrian fatalities in recent years, there has also been an increase in the number of pedestrian deaths as a proportion of total motor vehicle crash deaths. Pedestrian deaths represented 11% of motor vehicle crash deaths in 2007 and 16% of motor vehicle crash deaths in 2016 [4].

From 2009 to 2016, the largest increases in pedestrian deaths occurred under these conditions: in urban areas (a 54% increase from 2009 to 2016); on arterials (a 67% increase); at nonintersections (a 50% increase); and in dark conditions (a 56% increase) [5]. Pedestrian detection systems, like the Subaru EyeSight system, have the potential to effectively reduce the number of crashes involving pedestrians by as much as 39,000, which includes 2,932 fatal crashes [6].

Previous Highway Loss Data Institute (HLDI) studies have examined the effectiveness of the Subaru EyeSight system at reducing collision, property damage liability (PDL), and bodily injury (BI) liability claim frequencies [7–11]. In the most recent study, EyeSight showed a 1.1% reduction in collision claim frequency, a 14.8% reduction in PDL claim frequency, and a 28.3% reduction in BI liability claim frequency. However, information about the types of crashes in those studies is unavailable.

The current study evaluates whether the EyeSight system is preventing vehicles from striking pedestrians. Insurance claims under BI liability coverage without associated first-party (collision) or third-party (PDL) claims for vehicle damage were used as a surrogate measure of pedestrian crashes for 2013–17 Subaru vehicles with and without the EyeSight system.

METHODS

Vehicle Data

Subaru's EyeSight is a camera-based driver assistance system that includes the ability to brake automatically when it detects a crash-imminent situation involving a pedestrian. The system detects pedestrians from their size, shape, and movement. The system detects a pedestrian when the contour of the head and shoulders are clear.

EyeSight's Pre-Collision Braking function can respond to pedestrians in the vehicle's path or about to cross the vehicle's path. When the system determines that a collision with a pedestrian is imminent, it will activate braking to mitigate or avoid the collision. Because it is camera based, Eyesight cannot detect pedestrians in all conditions, especially those characterized by low visibility.

EyeSight is an option on various 2013–17 Subaru series. The presence or absence of EyeSight is discernible from the information encoded in the vehicle identification numbers (VINs).

Insurance Data

Automobile insurance covers damages to vehicles and property, as well as injuries to people involved in crashes. Different insurance coverages pay for vehicle damage versus injuries, and different coverages may apply depending on who is at fault. The current study is based on BI liability coverage, collision coverage, and PDL coverage. Collision coverage insures against vehicle damage to an at-fault driver's vehicle sustained in a crash. PDL coverage insures against vehicle damage that at-fault drivers cause to other people's vehicle and property in crashes. BI liability coverage insures against medical, hospital, and other expenses for injuries that at-fault drivers inflict on occupants of other vehicles or others on the road.

HLDI has data on the individual vehicles insured by its member companies, including the length of time those vehicles were insured and any claims filed for those vehicles under BI liability, collision, or PDL coverage. Using this information, HLDI calculates BI liability, collision, and PDL claim frequency as the number of claims divided by exposure, where exposure is defined as the number of insured vehicle years. One insured vehicle year can

represent one vehicle insured for one year, two vehicles insured for six months, etc. Vehicles in the HLDI database are identified by full 17-digit VINs.

This study was based on vehicles with overlapping BI liability, collision, and PDL insurance in U.S. states with traditional tort liability laws. In forming the data for this study, exposure and claim data for BI liability coverage were joined with those for collision and PDL coverages at the VIN level, so that during the overlapped exposure period, the association between claims could be explored to identify whether a BI claim occurs in an injury-only crash that has no associated vehicle damage. Only BI liability claims with no same-day collision or PDL claims are included in this study. Prior investigation has shown that injury-only BI claims are consistent with pedestrian- or cyclist-related claims. Hereafter, these claims will be referred to as BI-only or pedestrian-related claims.

Analysis Methods

Regression analysis was used to quantify the effect of EyeSight while controlling for other covariates. The covariates included calendar year, garaging state, vehicle density (number of registered vehicles per square mile), rated driver age group, rated driver gender, rated driver marital status, deductible range, risk, and vehicle series. Based on the model year and vehicle series, a single variable called *vehicle model year and series* was created for inclusion in the regression model. Effectively, this variable controlled for the variation caused by vehicle design changes that occur from model year to model year. EyeSight was included as a binary variable, indicating whether this safety feature was present or not. Claim frequency was modeled using a Poisson distribution with a logarithmic link function.

RESULTS

Figure 1 shows the estimated change in BI-only claim frequency for EyeSight vehicles versus non-EyeSight vehicles. All the series combined show a 35% reduction in claim frequency. When the vehicle series are modeled individually, all the series show reductions, although only the results for the Legacy (57%) and Outback (34%) are statistically significant. The reductions in claim frequency range from 18 to 57%. Two generations of the EyeSight system were fitted to Forester, Legacy, and Outback vehicles depending on model year. When the results for these models are separated by generation, the results also show significant reductions of 33% for the first generation and 41% for the second.

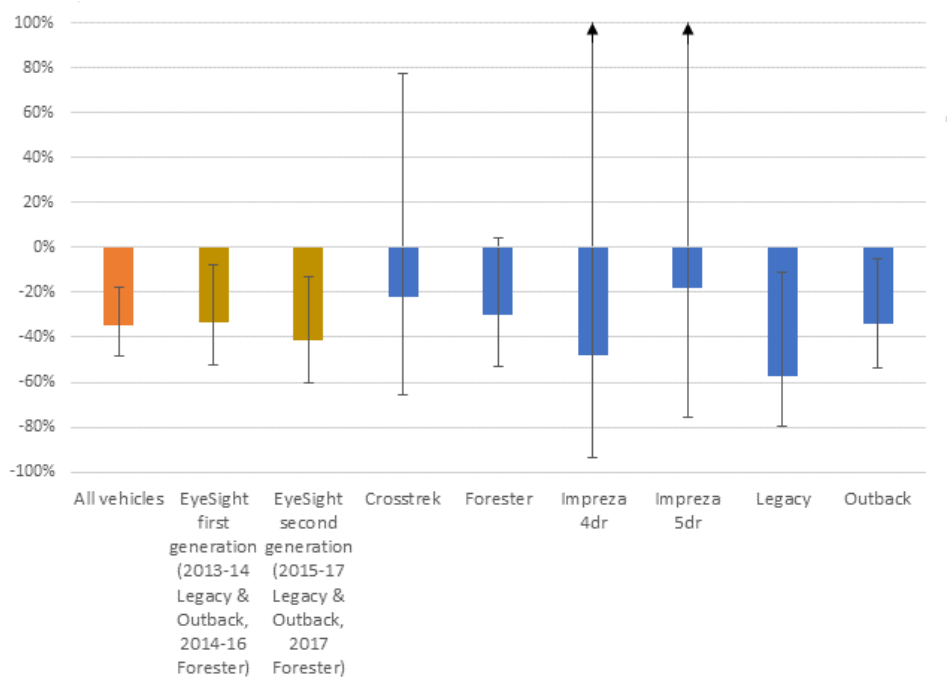

Figure 1. Estimated change in BI-only claim frequency for EyeSight vehicles versus non-EyeSight vehicles

DISCUSSION

Subaru vehicles with EyeSight, which includes pedestrian detection, show a statistically significant 35% reduction in pedestrian-related claim frequency. Reductions were observed for every Subaru model on which Eyesight is available, although at the individual vehicle level, only results for the Legacy and Outback were statistically significant. The lack of statistical significance for the other models is not surprising given their much lower exposure in the HLDI data. In any case, these results provide strong evidence that Eyesight is helping Subaru drivers avoid collisions with pedestrians.

Two generations of the EyeSight system were represented in the data for this study. The first generation was available as an option on 2013–14 Subaru Legacy and Outback vehicles and the 2014–16 Forester. In model year 2015, Subaru introduced a second generation of the EyeSight system on the Legacy and Outback. It also appeared for the first time on the Crosstrek and Impreza four-door and five-door in 2015. The second generation was introduced on the Forester in model year 2017.

The first generation utilized dual black-and-white cameras. The second generation shifted to color cameras along with longer and wider detection ranges, an increased ability to handle the speed differential with leading vehicles, and brake light detection. Claim frequency reductions for the EyeSight generations are similar, with a 33% reduction in the first generation and a 41% reduction in the second generation. Both reductions were statistically significant. While the different reductions are not significantly different from one another, the larger reduction for the newer generation may indicate an increase in effectiveness over the original EyeSight.

Based partly on the apparent efficacy of Subaru's pedestrian detection system, in February 2019 the Insurance Institute for Highway Safety launched a consumer information program to promote and rate pedestrian-detecting automatic emergency braking (AEB) systems. The ratings – no credit, basic, advanced and superior – are based on measured AEB speed reductions in three different simulated pedestrian crash scenarios, each at two different speeds. The Subaru Eyesight system is the benchmark for a superior rating. Systems providing lower speed reductions in fewer tests are rated advanced, basic, or no credit. In a test series covering 11 small sport utility vehicles, four including the 2019 Subaru Forester were rated superior, five were rated advanced, one was rated basic, and one received no credit because it did not provide meaningful speed reductions in any of the tests [12].

IIHS is not the first to recognize the potential for pedestrian-detecting AEB to address the problem of collisions between vehicles and pedestrians. The European New Car Assessment Program (EuroNCAP) has been rating these systems since 2016. Already, two thirds of front crash prevention systems available in the U.S. in 2019 include a pedestrian detection feature [12]. The United Nations Economic Commission for Europe (UNECE) in February 2019 adopted a draft regulation that would specify AEB performance including pedestrian detection and would go into force in 2020 [13].

These results suggest great promise for pedestrian-detecting AEB for preventing or mitigating collisions between vehicles and pedestrians. However, other HLDI research [14] suggests it will take 35 years or more for 95% of vehicles on U.S. roads to be equipped with AEB, and not all AEB systems on the road have pedestrian detection functionality. Consequently, it will require other efforts such as separating pedestrians from vehicles by time or space, making pedestrians easier to spot, and reducing vehicle speeds [15]. Recent moves by cities to lower speed limits in areas where pedestrians are present have been shown as an effective way to reduce vehicle speeds, which gives drivers more time to react to an encroaching pedestrian as well as mitigate the consequences of the collisions that do occur [16].

CONCLUSION

Vehicles with Subaru's Eyesight system are associated with a lower BI-only claim frequency than the same Subaru vehicles without EyeSight. In 2016, there were nearly 6,000 pedestrian fatalities in the United States, up 9% from 2015, and an 11% increase in bicyclist deaths [2]. Pedestrian detection systems like Subaru EyeSight have the potential to effectively reduce these numbers, and efforts to promote similar systems will help protect vulnerable road users.

LIMITATIONS

There are limitations to the data used in this analysis. Although injury-only BI claims are consistent with pedestrian or other nonoccupant injuries, our data do not allow us to know definitively if a crash involved a pedestrian. However, prior checks on this assumption verify that injury-only BI claims in fact involve nonoccupants. Even so, there may be some crashes included that are not pedestrian-related. Likewise, some pedestrian crashes may have been excluded unintentionally. For example, a crash in which a person was struck that resulted in a BI liability claim and also damaged the vehicle would have been excluded, because a collision claim would have been filed for the same day for the damaged vehicle.

Additionally, the data supplied to HLDI do not include detailed crash information such as point of impact or transmission status. The EyeSight system studied for this report targets certain crash types. For example, EyeSight is not expected to mitigate pedestrian crashes that occur when the vehicle is backing up. All crashes, regardless of the ability of a feature to prevent or mitigate them, are included in the analysis.

The EyeSight system is optional and associated with increased costs. The type of person who selects EyeSight may be different from the person who declines it. While the analysis controls for several driver characteristics, there may be other uncontrolled attributes among people who selected EyeSight.

REFERENCES

[1] National Highway Traffic Safety Administration, National Center for Statistics and Analysis. (2018). *2017 Fatal motor vehicle crashes: Overview* (Traffic Safety Facts Research Note. Report No. DOT HS 812 603). Washington, DC. Retrieved from https://crashstats.nhtsa.dot.gov/Api/Public/ViewPublication/812603

[2] National Highway Traffic Safety Administration, National Center for Statistics and Analysis. (2017). *2016 Fatal motor vehicle crashes: Overview* (Traffic Safety Facts Research Note. Report No. DOT HS 812 456). Washington, DC. Retrieved from https://crashstats.nhtsa.dot.gov/Api/Public/ViewPublication/812456

[3] National Highway Traffic Safety Administration, National Center for Statistics and Analysis. (2017). *Pedestrians: 2015 data* (Traffic Safety Facts. Report No. DOT HS 812 375). Washington, DC. Retrieved from https://crashstats.nhtsa.dot.gov/Api/Public/ViewPublication/812375

[4] Retting, R. (2018). *Pedestrian traffic fatalities by state, 2017 preliminary data*. Washington, DC: Governors Highway Safety Association.

[5] Hu, W., & Cicchino, J.B. (2018). An examination of the increases in pedestrian motor-vehicle crash fatalities during 2009–2016. *Journal of Safety Research, 68*, 37–44. doi:/10.1016/j.jsr.2018.09.009

[6] Jermakian, J.S., Zuby, D.S. (2011). *Primary pedestrian crash scenarios: factors relevant to the design of pedestrian detection systems*. Arlington, VA: Insurance Institute for Highway Safety.

[7] Highway Loss Data Institute. (2014). Subaru collision avoidance features: initial results. *Loss Bulletin, 31*(24). Arlington, VA.

[8] Highway Loss Data Institute. (2015). Subaru collision avoidance features: an update. *Loss Bulletin, 32*(8). Arlington, VA.

[9] Highway Loss Data Institute. (2016). 2013–15 Subaru collision avoidance features. *Loss Bulletin, 33*(6). Arlington, VA.

[10] Highway Loss Data Institute. (2017). 2013–16 Subaru collision avoidance features. *Loss Bulletin, 34*(10). Arlington, VA.

[11] Highway Loss Data Institute. (2018). 2013–17 Subaru collision avoidance features. *Loss Bulletin, 35*(2). Arlington, VA.

[12] Insurance Institute for Highway Safety. (2019). Safe passage: New ratings address pedestrian crashes. *Status Report, 54*(2). Retrieved from https://www.iihs.org/iihs/sr/statusreport/article/54/2/1

[13] United Nations Economic Commission for Europe. (2019, February 12). *UN regulation on advanced emergency braking systems for cars to significantly reduce crashes* [Press release]. Retrieved from http://www.unece.org/?id=51189

[14] Highway Loss Data Institute. (2018). Predicted availability and fitment of safety features on registered vehicles — a 2018 update. *Loss Bulletin, 35*(27). Arlington, VA.

[15] Retting, R.A., Ferguson, S.A., & McCartt, A.T. (2003). A review of evidence-based traffic engineering measures to reduce pedestrian-motor vehicle crashes. *American Journal of Public Health, 93*(9), 1456–1463. doi: 10.2105/AJPH.93.9.1456

[16] Hu, W., & Cicchino, J.B. (2019). Lowering the speed limit from 30 to 25 mph in Boston: effects on vehicle speeds. *Injury Prevention* (published online, 13 January 2019). doi: 10.1136/injuryprev-2018-043025

APPLICATION OF MULTIPLE RIB GAGES TO IMPROVE CHEST INJURY MEASUREMENTS

Kennerly Digges
Automotive Safety Research Institute
USA

Dainius Dalmotas
D.J. Dalmotas Consulting. Inc
Canada

Priya Prasad
Prasad Engineering, Inc.
USA

Paper Number 19-0266

ABSTRACT

In 2011 the National Highway Traffic Safety Administration (NHTSA) made changes to the new car assessment program (NCAP) frontal full-width test rating that introduced a chest deflection metric. The dummy seating protocol did not specify routing procedures that consistently control shoulder belt positioning on the dummy. Thus, most NCAP tests were conducted with the D-ring in the full up position, placing the shoulder belt far above the center chest potentiometer, thereby loading the dummy's chest asymmetrically.

Previous research conducted with a Dodge Caliber, showed that differences in chest deflection measurement caused by variations in belt routing are not trivial. The NHTSA NCAP test produced a chest deflection of 11.8 mm, corresponding to a risk of serious chest injury for older females of 0.6%. A crash test conducted by the Insurance Institute for Highway Safety (IIHS) under the same conditions but with the belt routed across the deflection potentiometer produced a chest deflection of 34.5 mm, corresponding to a risk of serious chest injury for older females of 44.7%. This indicated a need for a better belt positioning procedure to replace the vehicle body-based D-ring procedure. This improved positioning would ensure that the belt location relative to the chest deflection potentiometer could be more carefully specified and controlled.

The objective of this study is to investigate the use of supplementary chest deformation sensors, such as RibEye and IR-TRACCs for identifying belt fitment procedures which provide accurate chest readings by ensuring that the shoulder belt is routed near the dummy's center chest gage.

The present study examines in detail the chest deflections observed in the initial series of sled and full vehicle tests with the Dodge Caliber. In addition, the study examines the chest deflections observed in NHTSA and Transport Canada (TC) full frontal tests with dummies containing supplemental chest deformation sensors. The supplementary data took the form of Hybrid III 5th female dummies outfitted with either RibEye sensors or IR-TRACCs and Hybrid III 50th male dummies outfitted with IR-TRACCs.

The results indicate greater disparity between the center chest gage measurements and the supplemental RibEye or IR-TRACC readings when the belt routes higher on the dummy's neck, associated with the upper anchorage D-ring in the full up position. Effects of the D-ring positioning are lessened as the seat track is moved from full forward to midtrack for the 5th female dummy. Since the belt routes closer to the center gage, both the center gage and maximum RibEye measurements indicate more deflection than at the full-forward position. Other factors also contribute to these higher peak measurements.

For both the 50th male and 5th female right front passenger dummies, when the belt was routed closer to the dummy's design intention at the center gage, the center gage and left side supplemental (RibEye or IR-TRACC) measurements were similar. Additionally, when the belt was placed across the center of the dummy's chest, the supplemental sensors deflected quite uniformly across the chest.

Despite the promising test results of these supplemental chest measurement devices, currently, there is no US federal basis for calibrating or interpreting RibEye or IR-TRACC measurements in Hybrid III dummies, so using these devices to relate to injury risk remains problematic.

RibEye and IR-TRACC supplemental chest deflection technologies have the potential to better identify belt routings consistent with the design characteristics of the dummy chest and deflection sensor. This knowledge could be used to develop testing and belt placement protocols which support more meaningful and consistent estimates of chest injury risk. This, in turn, would greatly enhance the utility of NCAP programs to drive restraint system changes to further reduce real-world chest injuries.

BACKGROUND

Beginning with Model Year 2011, NHTSA introduced a wide variety of changes to the nature and structure of the NCAP rating program [Federal Register 2008]. The more significant changes, as they apply to the measurement of chest injury risk in the portion of the program involving frontal crash protection, included:

- Substituting chest compression in place of chest acceleration to assess chest injury risk;
- Including new chest injury risk functions for chest compression;
- Substituting a Hybrid III 5th percentile female dummy for the 50th male dummy in the front right seating position;
- Positioning the seat for the 5th percentile female right front passenger dummy in the full-forward position; and,
- Permitting the manufacturer to specify the shoulder belt anchorage height position for both dummies.

The variation of the chest deflection measurement according to belt position on the chest, relative to the chest deflection gage, has been noted by several researchers. In a 1991 paper, Horsch tested a restrained Hybrid III dummy and reported a 34% reduction in chest compression when the belt placed against the neck was compared with a similar test except with the belt placed 50 mm laterally away from the neck [Horsch 1991]. Other researchers have observed similar measured chest deflection reductions when the shoulder belt was moved away from the deflection gage [Tylko 2006, Yamanski 2011, Tylko 2012]. A 2017 study by Digges et al., demonstrated that in an US NCAP full width test of a Dodge Caliber, risk of serious chest injury increased from 0.6% to 15% based on the 64 mm difference in shoulder belt routing across the dummy's chest between the D-ring positioned at full-down and full-up. When considering an elderly risk curve, these differences magnify from a 0.6% risk with the belt routed at D-ring full up to 44.7% with the belt routed at D-ring full-down. This study concluded that a dummy landmark-based belt positioning procedure should be developed to replace the vehicle body-based D-ring procedure. Such a change would ensure that belt location relative to the chest deflection potentiometer could be more carefully specified and controlled.

Trends in test location of the driver and right front passenger upper anchorage D-ring changed significantly in the US after the introduction of the 2011 test protocol. Prior to 2011, NCAP full width tests were conducted with the 50th male, typically with the D-ring in the mid position. From 2011 onwards, the majority of vehicles have been tested with the D-ring positioned at full up position, both for the driver and passenger. This had the effect of routing the shoulder belt higher than the dummy's center chest gage. In Canada, closer harmonization of CVMSS 208 to FMVSS 208 did not occur until 2013. As a consequence, compliance tests prior to 2014 continued to be conducted with the 50th male at 48 km/h, typically with the D-ring in the mid-position. Historically, research tests with the 5th female were conducted typically at one of three speeds: 40 km/h, 48 km/h and 56 km/h, typically with D-ring in the full down position. Consequently, comparing chest deflections observed in Canadian and US tests, provides an opportunity to gain an appreciation of the influence of D-ring location on chest deflections measured by center chest gage.

Subsequent to the introduction of the 2011 NCAP, Digges et al. [2013] proposed an NCAP rating system for seniors, subsequently known as a "Silver Rating." The suggested rating used chest injury risk functions based on the higher vulnerability of seniors to chest injuries and the higher risk of death associated with these injuries.

When exposed to frontal crashes, the injury risks for the elderly population differ from those of younger people in terms of both tolerance to impact and the body region most susceptible to life-threatening injuries. Numerous studies have shown that the chest region is much more vulnerable to life-threatening injuries for the older population [Augenstein et al. 2005, Kent et al. 2005, Ridella et al. 2012]. Augenstein et al. [2007] noted that elderly occupants in the right front seating position have fatality rates that are 42% higher than those of elderly occupants in the driver seat. Age dependent injury tolerances of the chest have been proposed by several researchers [Zhou et al. 1996, Laituri et al. 2005 and Prasad et al. 2010].

OBJECTIVE

The objective of this study is to investigate the use of supplementary chest deformation sensors, such as RibEye and IR-TRACCs for identifying belt fitment procedures which provide accurate chest readings by ensuring that the shoulder belt is routed near the dummy's center chest gage.

METHODS AND DATA COLLECTION

The Dodge Caliber platform was selected for the sled tests and full-scale crash vehicle. This selection was based on a previous analysis of the effect of belt positioning, in which it was observed that NCAP and FMVSS 208 had differences in the specifications for the D-ring position that greatly affected the resulting chest deflection output in tests of the Caliber. [Haight et al., 2013]

Haight et al. compared the results of an FMVSS 208 test of a Caliber at 48 km/h, with that of an NCAP crash test at 56 km/h. In the FMVSS 208 test the D-ring was positioned in the mid position, while in the NCAP test the D-ring was positioned in the uppermost position. Higher chest deflection was observed in the lower speed FMVSS 208 test. Since the crash speeds were different, the test results were not directly comparable but pointed to the need to study belt geometry effects on chest deflections. The effect of belt geometry on chest deflections was studied in the 2017 paper by Digges et al. using a 5th percentile female dummy in the right front passenger seat in the 56 km/h NCAP condition.

For this study, a Dodge Caliber buck was created by PMG Technologies and a series of sled tests were conducted using a crash pulse representing a 56 km/h full-frontal rigid barrier test. A matrix of tests is shown in Table 1. The time to fire airbags and seatbelt pretensions was matched to the official NCAP times. All dummies were positioned in the right front seat position and consumable vehicle components, such as airbags, were replaced after each test. Dummies were marked with a grid of targets to observe the differences in belt routing and measure distance from the belt to the center chest potentiometer, which at rest is located at the lowest center target. The belt routings relative to these target locations are shown in Figures 1 and 2. For the Hybrid III 5th female dummy, the chest instrumentation included both the center chest potentiometer, as used in the NCAP tests, and the RibEye. [Tylko et al., 2007]. Twelve RibEyes were positioned in accordance with the TC methodology described in the above paper. For the Hybrid III 50th male dummy, the chest instrumentation included both the center chest potentiometer and IR-TRACCs. The four IR-TRACCs are located at the left upper (LU), right upper (RU), left lower (LL) and right lower (RL) regions of the chest.

Table 1.
Sled Test Matrix

Seat track position	**D-ring position**	**Hybrid III 50th male**	**Hybrid III 5th female**
Full forward	*Full-up*		X
	Full-down		X
Midtrack	*Full-up*	X	X
	Full-down	X	X

In addition to the data obtained from the sled tests, additional RibEye and IR-TRACC data were obtained from TC and US full width vehicle tests. The additional data included:

- Five vehicle models (six tests) tested in NCAP-like 56 km/h rigid wall tests with a 5th female right front passenger fitted with RibEyes seated at midtrack (Keon, 2016);
- Four 56 km/h full width CMVSS 208 compliance tests with a 5th female right front passenger with RibEyes seated at full forward with D-ring full-down; and,
- Three 48 km/h full width CMVSS 208 compliance tests, each with two 5th female dummies, one with RibEyes, one with IR-TRACCs, seated in the rear outboard positions.

RESULTS

Sled Tests: Hybrid III 5th Female with RibEyes

Static comparisons of shoulder belt routing for the Hybrid III 5th female dummy sled test configurations are shown in Figures 1 and 2. The full forward seat track with D-ring full up condition, shown in Figure 1 (right), closely matches the NCAP test configuration, which places the top of the belt 116 mm above the center chest gage. Both moving the D-ring lower and moving the seat track rearward were effective at routing the shoulder belt closer to the center chest gage. In addition to the targets placed on the dummy's chest, 5th female dummies are constructed with two chest jacket holes that have the potential to help better orient belt routing relative to the dummy's design intention at the center chest gage.

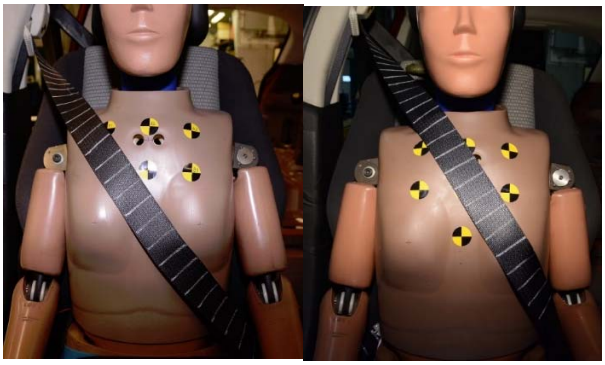

Figure 1. Forward Seat Position D-Ring Full-down (left) and Full-up (right)

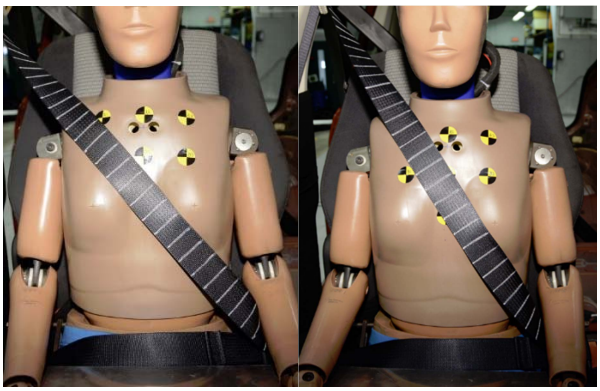

Figure 2. Mid Seat Position D-Ring Full-down (left) and Full-up (right)

The peak deflections recorded from the standard center gage and supplemental RibEye sensors for the sled test series with the 5th female dummy are shown in Table 2. Only x-direction data was compared to the center gage. The readings from the right RibEye number 6 were frequently lost and so were not reported in the Table. In the case of the test with the mid seat position D-ring full down, the left maximum RibEye readings occurred later than the center gage reading. However, the difference between measurement at the time of maximum center pot reading and

the time of maximum RibEye readings was small. The spread between the maximum and minimum RibEye readings was also relatively small. Figures 3 to 6 show the chest deflection histories of the center chest potentiometer and individual RibEye deflections for each of the sled test conditions. For both the forwardmost and midtrack seat positions, when the belt is routed closer to the center potentiometer (D-ring full down), the RibEye sensors are better aligned with the measurement from the center potentiometer, while in the tests where the belt is routed further away (D-ring full-up), the peak RibEye measurements are greater than the center potentiometer and more dispersed.

Table 2.
Chest Deflection Measurements from Sled Tests of 5th Female with Varying Seat and D-ring Positions

	Seat track	**Full forward**		**Mid track**	
	D-ring	**Full-up**	**Full-down**	**Full-up**	**Full-down**
Central Pot		-20.4	-29.8	-33.8	-36.8
Max RibEye		*-30.2*	*-30.4*	*-37.2*	*-36.9*
RibEye Left	*Rib 1*	*-30.2*	*-30.4*	*-37.2*	*-36.4*
	Rib 2	*-28.9*	*-29.6*	*-37.0*	*-35.7*
	Rib 3	*-27.7*	*-29.4*	*-36.6*	*-36.1*
	Rib 4	*-25.6*	*-28.8*	*-36.3*	*-36.4*
	Rib 5	*-23.9*	*-28.4*	*-36.0*	*-36.8*
	Rib 6	*-22.2*	*-27.6*	*-35.1*	*-36.9*
RibEye Right	*Rib 1*	*-14.4*	*-26.5*	*-25.9*	*-31.4*
	Rib 2	*-12.7*	*-24.2*	*-23.8*	*-29.2*
	Rib 3	*-11.1*	*-22.4*	*-21.8*	*-27.2*
	Rib 4	*-9.6*	*-21.4*	*-21.0*	*-26.8*
	Rib 5	*-8.1*	*-19.7*	*-19.8*	*-25.8*

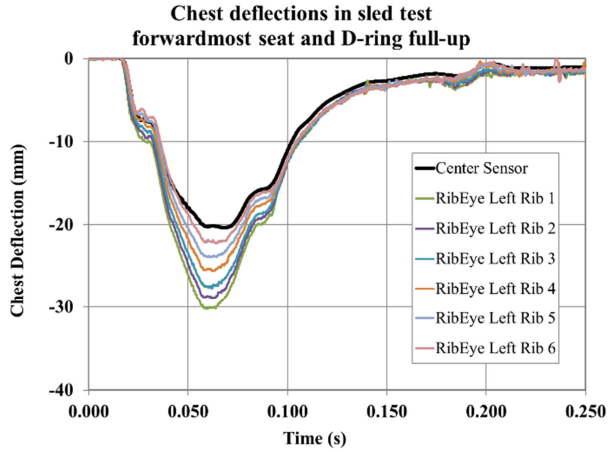

Figure 3. Chest deflection comparison for sled test: forwardmost seat position and D-ring full-up

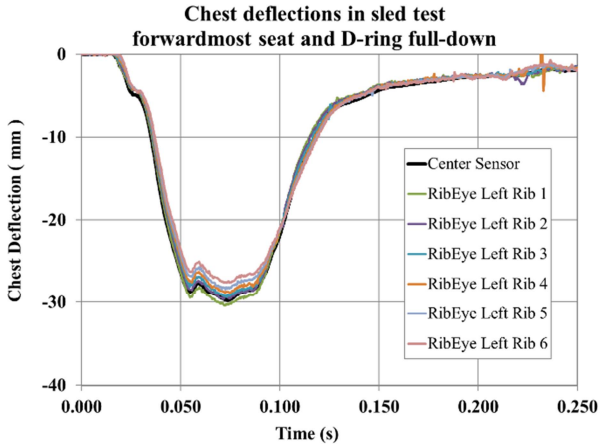

Figure 4. Chest deflection comparison for sled test: forwardmost seat position and D-ring full-down

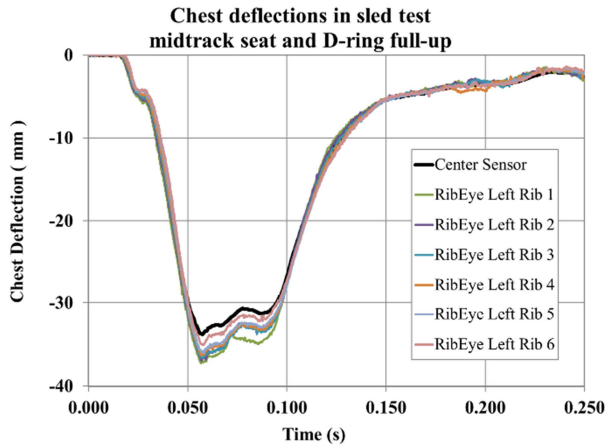

Figure 5. Chest deflection comparison for sled test: midtrack seat position and D-ring full-up

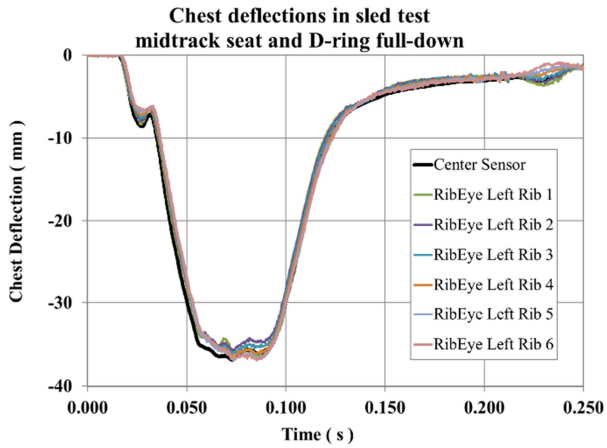

Figure 6. Chest deflection comparison for sled test: midtrack seat position and D-ring full-down

Sled Tests: Hybrid III 50th Male with IR-TRACCs

Static comparisons of shoulder belt routing for the Hybrid III 50th male dummy sled test configurations are shown in Figure 7. The midtrack seat position with D-ring full up condition, shown in Figure 7 (right), places the top of the belt well above the center chest gage. Moving the D-ring lower was effective at routing the shoulder belt overlapping the center chest gage.

Figure 7. Belt Routing 50th Male Dummy D-ring Down (Left) and D-ring Up (Right) – Dodge Caliber

Peak deflections recorded from the standard center gage and supplemental IR-TRACC sensors for the sled test series with the 50th male dummy are shown in Table 3. Figures 8 and 9 show the chest deflection histories of the center chest potentiometer and individual IR-TRACC deflections for each of the sled test conditions. In the sled test with the D-ring full down, which routes the shoulder belt closest to the center chest gage, the center gage measured the maximum peak deflection and the 4 IR-TRACCs measured very similar peak values, ranging from 27.5 to 32.4 mm. These close readings indicate the chest is being loaded symmetrically, focused on the center sternum. In contrast, the sled test with the D-ring full-up and the belt routed significantly higher than the center gage showed the greatest peak deflection at the left upper IR-TRACC location, with a wide range of peak values from each sensor location, ranging from 8.7 to 29.9 mm.

Table 3.
Chest Deflection Measurements from Sled Tests of 50th Male with Varying D-ring Positions

	Seat track	Mid track	
	D-ring	**Full-up**	**Full-down**
Central Pot		27.1	42.6
IR-TRACC Left	*Upper*	29.9	32.4
	Lower	26.9	34.5
IR-TRACC Right	*Upper*	13.2	32.4
	Lower	8.7	27.5
Difference between upper locations		16.7	0
Difference Left upper to lower		3.0	-2.1

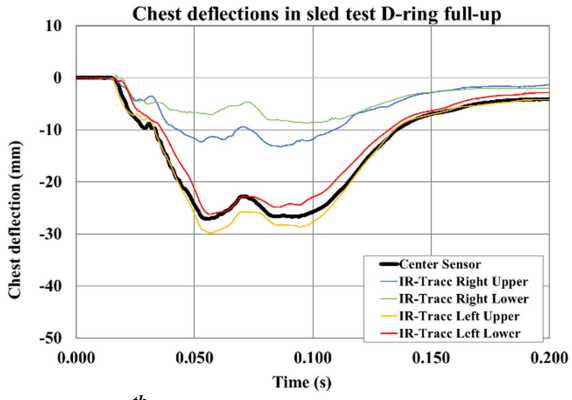

Figure 8. 50th Male Dummy IR TRACC Measurements for NCAP Sled Test with Mid-position Seat and D-ring Up (Dodge Caliber)

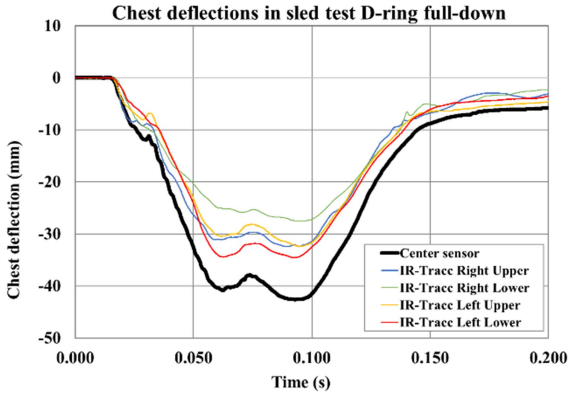

Figure 9. 50th Male Dummy IR TRACC Measurements for NCAP Sled Test with Mid-position Seat and D-ring Down (Dodge Caliber)

Comparison to Other Frontal Crash Test Data

Full scale crash test data from NHTSA in a 56 km/h full width test condition were examined for the effect of seat position on the peak chest deflections for the right front passenger 5th female dummy (Table 4). In the research tests, the dummy's seat track was moved to midtrack, but all other aspects of the seating remained the same, including the D-ring at full up position. Moving the seat track from full forward to midtrack resulted in the shoulder belt routing 5 to 45 mm closer to the center chest gage, based on PBU standard clearance measurements. The seating change produced chest deflections that were 5 to 13 mm greater. Numerous other factors may have contributed to these deflection differences, as the change in seat position would also results in different interactions with airbags, seatbelts and knee bolsters.

The PBU measurement is the vertical distance between a horizontal reference plate in the dummy lap and the upper edge of the belt, measured at the centerline [NHTSA 2012]. Since the measurement does not rely directly on dummy landmarks, it is subject to variations with dummy positions. As can be observed in Table 4, while chest

deflection increases between NCAP and Research tests were observed as the PBU values decreased, no clear relationship between the magnitude of the change in the PBU measurement and the change in chest deflection was observed. The increases in chest deflection associated with moving the seat from full forward to mid-track position ranged from 45% to 162%. However, the largest deflection increase was associated with one of the lowest changes in PBU.

Figures 10 and 11 show the RibEye and center gage traces for the 5th female dummies in the Malibu #1 research test. The traces in Figure 10 are from the right front passenger dummy, seat in midposition and D-ring full-up. The traces in Figure 11 are for the rear seat dummy. For this dummy, the D-ring is fixed and belt force limiting is not present. The traces in Figure 11 display a close spread of the RibEye reading suggesting symmetric loading of the chest and improved belt routing relative to the center pot.

The traces in Figure 10 have a wider spread of readings, suggesting less symmetric chest loading than observed for the rear dummy. However, the chest load distribution for this right front passenger is better than that observed in the Caliber sled test with the dummy seated full forward and the D-ring full up ((Figure 3), showing closer, but not as good as, the agreement than observed with the seat mid-track and the D-Ring full up (Figure 5).

Table 4.
Chest Deflection and Shoulder Belt Measurements Research and NCAP of 5th Females in Right Front Seat

	PBU Belt to Reference (mm)			Chest Deflection (mm)		
Vehicle	**NCAP**	**Research**	**Change**	**NCAP**	**Research**	**%Change**
Chevrolet Malibu #1	320	305	-15	9.0	13.9	54%
Chevrolet Malibu #2	320	285	-35	9.0	17.6	96%
Toyota Highlander	325	280	-45	9.2	22.6	146%
Ford F-150	310	295	-15	7.9	20.7	162%
Mazda3	335	300	-35	12.2	17.7	45%
Honda Fit	300	295	-5	14.5	24.4	68%

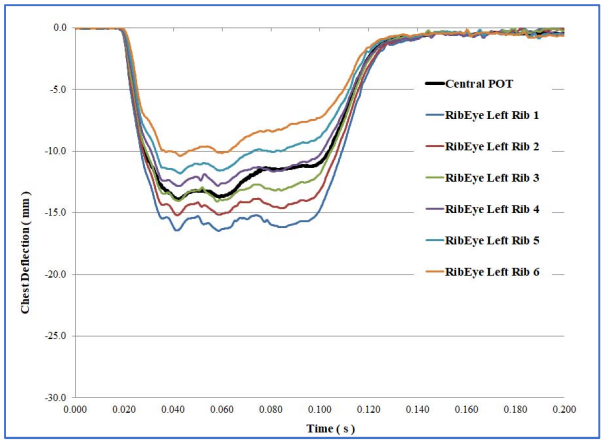

Figure 10. Right Front Passenger Chest Deflections Observed in NHTSA Test of Chevrolet Malibu #1 (9332): Mid-Seat / D-Ring: Full-Up

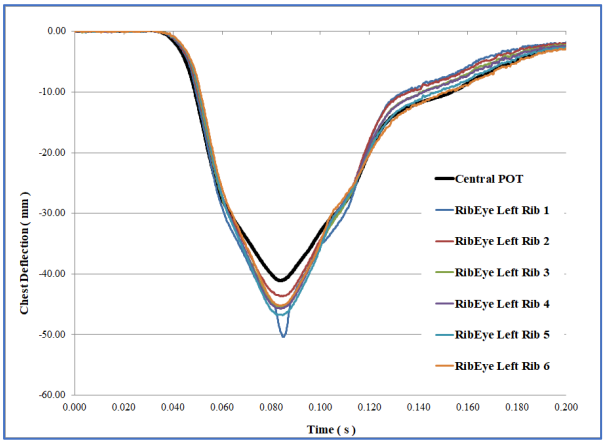

Figure 11. Right Rear Passenger Chest Deflections Observed in NHTSA Test of Chevrolet Malibu #1 (9332)

An improved understanding of how the position of the D-ring is influencing quantification of chest injury risk, at the fleet level, can be achieved by comparing the deflections observed in TC compliance tests at 56 km/h with those observed in NCAP tests of the same vehicle platform for the subset of TC tests run with the RibEye. A direct platform comparison of the 5th female dummy deflections observed on the right front passenger side in TC tests with the D-ring in the full down position with those observed in NCAP tests with the D-ring in the full up position is possible for four TC tests with the RibEye. A detailed comparison of the responses observed in these four platform tests is provided in Table 5. A comparison of the chest deflections observed is depicted in Figure 12.

From the results presented in Table 5, it can be seen that the NCAP deflections were consistently lower than those observed in the TC tests. In the case of Platform 1, the reduction was of the order of 60%, similar to the reduction in the deflection value observed in the Caliber car and sled tests when the D-ring was moved from the full down position to the full up position, the typical NCAP setting. We can also observe that the TC chest pot values consistently show close agreement with maximum Ribeye values measured on the left side of the dummy. These results suggest the belt routing provided by the lower D-ring more consistently places the belt close to the chest sensor.

Table 5 also includes a calculated metric which has the potential of highlighting belt routings above the chest sensor, the "implied chest stiffness" value. This value is calculated by dividing the maximum shoulder belt force value by the maximum chest pot value. As the D-ring is moved from the full down position, shoulder belt routing moves away from the chest sensor, reducing the magnitude of the measured pot deflection, but not the applied belt force. All four of the NHTSA NCAP tests produced implied chest stiffness values above 200, while all four of the TC tests produced values below 175.

Table 5.
Response Comparisons - Front Right Passenger (5th Female) / 56 km/h Full Frontal
TC (D-Ring Lowermost) vs NHTSA (D-Ring Uppermost)

Vehicle Model	Test		Center chest gage (mm)		RibEye (mm)	Shoulder Belt Force (N)		Chest Implied Stiffness N/mm	
	TC 208	*NHTSA*	*TC 208*	*NCAP*	*TC 208*	*TC 208*	*NCAP*	*TC 208*	*NCAP*
Platform #1	17-110	9157	22.5	9.0	24.9	2,357.80	3,272.10	104.8	363.6
Platform #2	17-108	7564	14.2	7.4	16.4	2,453.70	2,453.70	172.8	331.6
Platform #3	17-172	9296	16.0	11.8	17.4	2,621.90	3,029.00	163.9	256.7
Platform #4	16-146	9552	22.9	20.5	28.5	3,725.90	4,323.90	162.7	210.9

It may be observed that Platform 1 and 2 both show large differences between the center chest pot readings from the two D-ring conditions (Figure 12). In the TC tests, the max RibEyes deflections are slightly higher than the D-ring down center pot deflections. Platform 3 shows similar trends, but the difference between the center pots is less. For Platform 4, the difference between center pots is less and the differences between the center pot and the RibEye is greater. The observations suggest that the range of D-ring adjustment makes less difference on Platform 4 and, to some extent, on Platform 3. The high RibEye reading for Platform 4 indicates that, even with the D-ring full down, the belt is not over the center pot and the chest is loaded asymmetrically. A review of the picture of dummy placement confirmed that the shoulder belt remained close to the neck in the D-ring full down test.

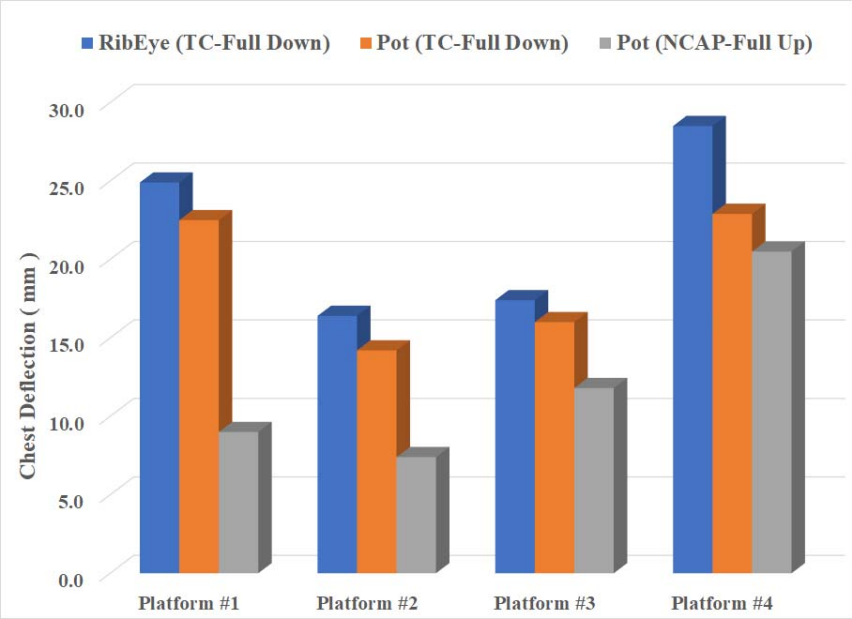

Figure 12. Right Front Passenger (5th Female) Chest Deflections as a Function of Vehicle Platform, D-Ring Location and Monitoring Technology

Included among the 48 km/h TC CMVSS 208 compliance tests reviewed were three tests in which a rear seated 5th female fitted with IR-TRACCs was accompanied by a rear seated 5th female fitted with RibEyes. These tests provide a convenient environment for the comparison of chest deflection pattern, as quantified by the IR-TRACC with that quantified by the RibEye. To facilitate the comparisons in terms of mirror images, the deflections from ribs 1 and 2 of the Ribeye were averaged to produce an upper quadrant value and the deflections from ribs 5 and 6 were averaged to produce a lower quadrant value. This was possible for left side quadrant values. In the case of the right side of the Ribeye, rib 6 values were typically lost. As such, the lower right quadrant values simply reflect right rib 5 values. For completeness, the average deflections of RibEye ribs 3 and 4 were also computed. The IR-TRACC data, the computed quadrant data and the central pot data from this series of tests are summarized in Table 6. All measurements are in millimeters.

From the results presented in Table 6, it can be observed that there was generally agreement in the quadrant deflections between the IR-TRACC and the RibEye. This was particularly true when one compared the left side quadrant values of the rear left dummy (IR-TRACC) and the right side quadrant values of the rear right dummy (RibEye). Here the maximum difference was only 3.2 mm. The differences in the central pot deflection values were more pronounced and consistently higher with 8.3 mm in test TC08-135. The source of the difference was not readily evident. The peak shoulder belt forces and the peak lap belt forces measured in the two rear seating positions differed less than 100 N in this test. However, the implied chest stiffness values of the RibEye chest ranged from 160 to 169 in this test series, while the corresponding values for the IR-TRACC ranged from 190 to 207. So the more elevated chest pot values observed with the Ribeye may simply have been an attribute of a slightly more compliant chest assembly. It may also have been associated with a difference in belt routing.

Table 7 summarizes the differences between the max gage readings. The first row, top-center, shows the difference between the top IR-TRACC or RibEye and the center gage for the three TC tests in Table 6. The second row substitutes the bottom IR-TRACC or RibEye for the top ones. The third row is the difference between the two top sensors. An examination of differences in readings of these four gages provides insight into the uniformity of loading of the chest. Large differences between the upper gages suggest the belt is close to the neck. Large differences between the upper and lower gages suggest asymmetric chest loading. This data suggests that the belt on the RibEye Test 139 dummy was positioned closest to the center gage. For this dummy, the difference between the RibEye gages and the center gage was small and the difference between the upper gages was much smaller than for

the other dummies. The upper gage reading was slightly lower than the center gage and the lower gage was slightly higher. These characteristics were observed in the Caliber sled tests when the D-ring was full down and the belt routing was optimum.

The TC data indicates that either the RibEye or the IR-TRAC would be useful in determining the degree to which the belt passes over the center gage.

Table 6.
RibEye, IR-TRACC and Center Gage Measurements from TC Tests of 5th Females in Rear Seat

		Rear Left Dummy			**Rear Right Dummy**		
		IR-TRACC			**RibEye**		
	Sensor location	*Right Side*	*Center*	*Left Side*	*Right Side*	*Center*	*Left Side*
TC08-135	*Upper*	49.7	39.5	29.9	28.1	47.8	49.7
	Center				26.3		49.7
	Lower	46.0		22.8	22.6*		54.5
TC08-139	*Upper*	40.1	30.6	24.5	23.4	35.0	33.4
	Center				20.7		33.7
	Lower	34.8		16.0	19.2*		36.0
TC08-140	*Upper*	38.2	27.9	21.9	19.2	29.8	35.5
	Center				15.8		34.0
	Lower	31.9		13.3	13.0*		32.6

* Excludes rib #6.

Table 7.
Difference in Measurements for RibEye, IR-TRACC and Center Gage, TC Tests of 5th Females in Rear Seat

Gage Locations	IR-TRACC Test 135	RibEye Test 135	IR-TRACC Test 139	RibEye Test 139	IR-TRACC Test 140	RibEye Test 140
Top-Center	10.2	1.9	9.5	-1.6	10.3	5.7
Bottom-Center	6.5	6.7	4.2	1.0	4.0	2.8
Upper Right-Left	19.8	21.6	15.6	10	16.3	16.3

DISCUSSION

Static measurements of dummy position and belt routing across the 5th female and 50th male dummies' chests indicate that a relatively small adjustment of the upper anchorage D-ring location can have a significant effect on shoulder belt location across the dummy's chest. The worst-case scenario is the 5th female dummy with the seat track full forward, where the adjustment of the D-ring in a Dodge Caliber exemplar vehicle can create variation in shoulder belt location of up to 64 mm. This study found that moving the seat track to midtrack lessened the effect of the D-ring adjustment variation but did not completely solve it. The 50th male dummy showed less dramatic differences than the 5th female in belt routing, but observations were large enough to suggest dynamic performance could be affected.

Both chest sensor measures at the standard center gage and supplemental RibEye and IR-TRACC devices detected variation in symmetry/asymmetry of the belt routing across the dummy's chest. The 2017 Digges et al. study showed that the center gage measured an additional 23 mm of deflection when the belt was adjusted closer to the sensor in a pair of full vehicle tests. Similar observations were made through this sled test series, where the 50th male dummy measured an additional 16 mm of deflection with the belt positioned across the center chest rather than above. The 5th female dummy measured an additional 8 mm of deflection with the belt positioned across the center chest with seat track at full forward. For the 5th female, the effect was less at the midtrack seat position, with the variation in D-ring position only accounting for a difference of 3 mm of center chest deflection.

The variations in chest deflections observed in this study have much to do with dummy design. As with any measuring instrument, a dummy needs to be used within the confines of its calibration and intended use. The Hybrid III dummy calibration procedure involves a 15.25 cm (6") diameter cylinder impacting the dummy chest centered upon the chest deflection potentiometer. This calibration test was based on a similar test that established the compression response corridors for the human chest, and was the basis for the dummy chest design [Kroll 1974]. Although real-world occupants may position their belts so they cross the chest in a variety of locations, a dummy, with only a central deflection sensor, produces an excessively wide range of measurements when an equivalent latitude of belt positioning is permitted, as in the NCAP test.

The RibEye and IR-TRACC deflection measurements provide an evaluation of asymmetry in loading of the chest by the restraint system. For configurations in which the belt is routed farther away from the center potentiometer (D-ring full up conditions), there is a large difference in the peak center sensor and peak RibEye sensors. For example, in the forwardmost seat D-ring full-up condition, the maximum center chest deflection was 20 mm and the highest RibEye deflection was 30 mm, with peak deflections ranging from 22 to 30 mm for the remaining locations. This trend was also true for the midtrack seat D-ring full-up condition but less pronounced, (peak differences of 35 mm vs. 37 mm), likely because the belt was routed more closely in this condition. In contrast, when the belt is routed closer to the center sensor (D-ring full down condition), the center sensor and RibEye deflection sensors were similar in magnitude, with a maximum of approximately 30 mm in the forwardmost seat track condition and 37 mm for the midtrack seat condition. This suggests highly symmetric loading of the chest by the restraint.

Currently, supplemental deflection measuring devices like RibEye and IR-TRACCs offer advantages for evaluating chest injury. Their use appears to be a positive addition to evaluating symmetry of chest loading, especially when used in a way that reflects the dummy's chest compression calibration procedure and intended use. However, the devices have their limitations. The evaluation of chest injury risk measurements in locations away from the center deflection sensor may be problematic, due to limitations of biomechanical data about the human chest response under similar loading.

Results from these sled tests suggest that for both the 5th female and 50th male dummies, positioning the seat at midtrack and lowering the D-ring height to the lowest setting achieved the best belt routing over the dummy's center chest potentiometer, producing symmetric loading across the chest. This configuration creates belt routing that more closely corresponds to the dummy calibration procedure for chest compression response and intended use [NHTSA 2008].

Additionally, the 5th female dummy measured greater chest deflections at midtrack compared to full forward in this study's sled tests and other NHTSA and TC observations, suggesting that vehicles are not optimized for this condition. The dummy's position, farther away from the frontal airbags and knee bolsters, places more reliance on the belt system to absorb crash energy. Testing at midtrack position covers a larger segment of the population and is expected to advance protection for right front passengers.

This study suggests a vehicle's NCAP chest rating is highly dependent on shoulder-belt routing. Better control of belt routing is necessary for future comparative evaluations of chest injury to be meaningful. If the future NCAP seating protocol includes a seat track change from forwardmost to midtrack as proposed, belt routing may improve. However, neither the current nor the proposed future NCAP seating procedures specify D-ring position. A dummy landmark-based belt positioning procedure should be developed to replace the vehicle body-based D-ring procedure. This would ensure that belt location relative to the chest deflection potentiometer can be more carefully specified and controlled.

CONCLUSIONS AND RECOMMENDATIONS

Proposed changes to future US NCAP, such as testing the right front passenger 5th female dummy at midtrack seat position, have the potential to reduce some of the shoulder belt routing variation observed in tests of the dummy at full forward. More consistent belt routing near the center chest gage would ensure more repeatable and accurate evaluations of chest injury risk.

Supplemental chest measurement devices, IR-TRACCs and RibEyes, were able to detect that when the shoulder belt was routed close to the center sensor, the dummy's chest was loaded symmetrically and when the shoulder belt was routed higher up on the neck, the dummy's chest was loaded asymmetrically. In conditions where the belt was routed close to the center sensor, the peak measure from the supplemental sensor was similar to the center chest pot, while in conditions where the belt was routed higher than the sensor, the peak measures from the standard and supplemental devices were disparate and the supplemental sensor locations measured a wide range of results.

The implied chest stiffness metric, calculated from shoulder belt loads and center gage chest deflections, may be useful in future evaluations of symmetry of belt routing. High implied chest stiffness values were associated with the high D-ring test condition in NHTSA NCAP tests.

Supplemental chest deflection measuring devices should be investigated further because they appear effective at identifying asymmetric belt loading conditions. More research must be devoted to understanding their biomechanical relationship to human injury tolerance.

This study suggests a vehicle's NCAP chest deflection measurement used for rating is highly dependent on seat position and shoulder-belt routing. Better control of belt routing is necessary for future comparative evaluations of chest injury to be meaningful. At the least, future NCAP seating procedures should specify the D-ring position at full down for tests with the 5th female.

A dummy landmark-based belt positioning procedure should be developed to replace the vehicle body-based D-ring procedure that would ensure that belt location relative to the chest deflection potentiometer can be more carefully specified and controlled. For example, a minimum distance between the belt edge and the dummy chest holes should be established.

Additional studies are needed of how RibEye and IR TRACC perform in tests involving restraint systems with a variety of technical advancements. Involvement of ISO Working Group 5 and the HBSS of the SAE for further evaluation of these technologies is encouraged.

ACKNOWLEDGEMENTS

The authors would like to express their appreciation to the staff of Motor Vehicle Regulation Enforcement at Transport Canada for their efforts in responding to our requests for test data and test reports. Thanks also to the Insurance Institute for Highway Safety and Becky Mueller for supporting dummy measurement setup and the preceeding high speed tests related to the current research objectives.

REFERENCES

Digges K, Dalmotas D, Prasad P and Mueller B; The need to control belt routing for silver NCAP ratings, Proceedings of the 25th ESV Conference, Paper Number 17-0403, 2017

Digges, K., Dalmotas, D., and Prasad, P; An NCAP star rating system for older occupants, Proceedings of the 23rd ESV Conference, Paper No. 13-0064, 2013

Eggers A. Eikhoff B, Dobberstein J, Zellmer H, and Adolph T; Effects od Variations in Belt Geometry , Double Pretensionig and Adaptive Load Limiting on Advanced Chest Measurements of THOR and Hybrid III, IRC 14-40, 2014 IRCOBI Conference

Federal Register, Vol. 73, No. 134/Friday, Notices, July 11, pp. 40016-40050, 2008.

Haight, S, Biss, D. and Samaha, R.; Analysis of seat belt positioning in recent NCAP crash tests; SAE Technical Paper No. 2013-01-0460, 2013.

Horsch, J., Melvin, J., Viano, D., and Mertz, H.; Thoracic injury assessment of belt restraint systems based on Hybrid III chest compression; SAE Technical Paper No. 912895; 1991.

Kent, R., Henary, B., and Matsuoka, F.; On the fatal crash experience of older drivers; Proceedings of the 49th Conference of the Association for the Advancement of Automotive Medicine, pp. 371-389, September 2005. 2016-01-1540

Koen, T.; Alternative approaches to occupant response evaluation in frontal impact crash testing, SAE 2016-01-1540

Kroll, C., and Schneider, L.; Impact tolerance and response of the human thorax II; SAE Technical Paper No. 741187; 1974.

Laituri, T., Prasad, P., Sullivan, K., Frankstein, M. and Thomas R.; Derivation and evaluation of a provisional, age-dependent, AIS>=3 thoracic risk curve for belted adults in frontal impacts; SAE Technical Paper No. 2005-01-0297, 2005.

NHTSA; U.S. Department Of Transportation National Highway Traffic Safety Administration, Laboratory Test Procedure; Appendix B Part 572, Subpart O (5th Female) Dummy Performance Calibration Test Procedure; NHTSA Office of Vehicle Safety Compliance Report; TP208-14; April, 2008.

NHTSA; U.S. Department Of Transportation National Highway Traffic Safety Administration, Laboratory Test procedure for new car assessment program frontal impact testing, Appendix N, Data Sheet 5, September 2012.

Prasad, P., Mertz, H., Dalmotas, D., Augenstein, J. and Digges, K.; Evaluation of the field relevance of several injury risk functions; Stapp Car Crash Journal; Vol. 54, 2010.

Ridella, S., Rupp, J., and Poland, K.; Age-related differences in AIS 3+ crash injury risk, types, causations and mechanisms, Proceedings of the IRCOBI Conference 2012, pp. 43-60, 2012.

Tylko, S., Higuchi, K., St. Lawrence, S., Bussières, A., Fiore, J.; A Comparison of Hybrid III 5th Female Dummy Chest Responses In Controlled Sled Trials. Society of Automotive Engineering World Congress, Detroit, MI, 2006. 2006-01-0455

Tylko, S. and Bussières, A.; Responses of Hybrid III 5th female and 10-year-old ATD seated in the rear seats of passenger vehicles in frontal crash tests; Proceedings of the IRCOBI Conference, pp. 565-579, 2012 .

Tylko, S., Charlebois, D. and Bussières, A.; Comparison of kinematic and thoracic response of the 5th percentile Hybrid III in 40, 48 and 56 km/h rigid barrier tests; Proceedings of the 20th ESV Conference Paper No. 07-0506

Yamasaki, T., Uesaka, K.; Rear occupant protection JNCAP test – test results and findings; Proceedings of the 22nd ESV Conference, Paper No. 11-0445, 2011.

Zhou, Q. Rouhana, S. and Melvin, J.; Age effects on thoracic injury tolerance; SAE Paper No. 962421, 1996.

DRIVER ALCOHOL DETECTION SYSTEM FOR SAFETY (DADSS) – HUMAN TESTING OF TWO PASSIVE METHODS OF DETECTING ALCOHOL IN TISSUE AND BREATH COMPARED TO VENOUS BLOOD

Scott E. Lukas, Ph.D.
Elizabeth Ryan, Ph.D.
Jane McNeil, M.S.
Justin Shepherd, M.S.
Lucy Bingham, B.A.
Katharine Davis, B.A.
Behavioral Psychopharmacology Research Laboratory (BPRL), McLean Imaging Center, McLean Hospital
McLean Hospital, Belmont, MA, 02478, USA

Kelly Ozdemir, Ph.D.
Neeraj Dalal, B.S.
Kianna Pirooz, B.A.
Michael Willis, B.S.
Abdullatif Zaouk, Ph.D.
KEA Technologies, Inc., Marlborough, MA 01752, USA

Paper Number 19-0268

ABSTRACT

Alcohol-related traffic crashes and deaths remain a major problem in the United States as data indicate that there are approximately 37,000 traffic fatalities yearly, with 30% (~11,000) of them alcohol related. The Automotive Coalition for Traffic Safety (ACTS) and the National Highway Traffic Safety Administration (NHTSA) entered into a Cooperative Research Agreement to explore the feasibility of using passive technologies as an in-vehicle alcohol detection system that is less intrusive than ignition interlocks, but still able to reduce the incidence of drunk driving. Two passive technologies (TruTouch™ and Senseair™) were tested against breath (Alco-Sensor-FST™) and venous blood under a number of environmental scenarios in which individuals engage every day.

A total of 92 healthy male and female volunteers (age 22-38) signed an IRB-approved informed consent and participated in experiments in which they consumed 0.9 g/kg of alcohol under a variety of drinking regimens and scenarios that mimicked real-life situations. The volunteers then provided passive breath and tissue (finger touch) samples and had their blood drawn at 5 min intervals for quantification of alcohol via gas chromatography. Lag time of appearance of alcohol, peak concentration, time to peak, and elimination rate were the primary dependent variables. The overall aim of the experiments was to test whether the alcohol concentrations measured by the two prototype devices correlated with venous blood under the following scenarios: lag time, eating a snack, eating a full meal, exercising, and "last call." Each scenario was simulated in the experimental laboratory.

The lag time experiment revealed that the order of alcohol appearance after drinking was (from first to last): breath, blood, and tissue, although early breath samples were contaminated by mouth alcohol. However, with over 4,000 matched points, the concentration-time curves for both prototypes paralleled that of blood with correlation coefficients of 0.7876 and 0.819 for touch- and breath-based technologies, respectively. Similar profiles were observed in the "last call" experiment with a "surge" of alcohol being observed after an extra drink was consumed during the distribution phase. The exercise scenario revealed similar profiles, and finally, the two eating scenarios indicated that blood alcohol concentrations (BAC) were lower after consuming a meal compared to a snack; the breath and tissue samples paralleled this profile.

The data not only support the proof-of-concept that two different passive technologies (breath and tissue) can detect alcohol fast enough to be useful in a motor vehicle environment, but extend the parameters by demonstrating that the measurement of alcohol in the human body is not affected by many of the common scenarios that are known to alter blood alcohol concentrations. The passive devices each tracked the time course of BAC regardless of the situation demonstrating that these two compartments provide a high degree of accuracy while at the same time minimizing the disruption to the driver.

These two devices, if proven to be reliable and with reproducible results under additional environmental and biological conditions, represent a significant technological breakthrough in strategies to reduce alcohol-impaired individuals from driving a vehicle and causing injuries and/or deaths.

INTRODUCTION

Excessive alcohol consumption is responsible for approximately 88,000 deaths and 2.5 million years of potential life lost (YPLL) in the United States each year (CDC, 2013). Binge drinking (consuming 4 or more drinks per occasion for women; 5 or more drinks per occasion for men) is responsible for more than half of the deaths and two-thirds of the YPLL due to excessive drinking (Stahre *et al*., 2004) and is associated with many health and social problems, including alcohol-impaired driving, interpersonal violence, risky sexual activity, and unintended pregnancy (Naimi *et al.,* 2003). Most people under age 21 who drink, report binge drinking 2-3 times per week (Miller *et al.,* 2006).

According to the 2016 National Survey on Drug Use and Health (NSDUH), in 2016, 20.7 million people aged 16 or older drove under the influence of alcohol in the past year and 11.8 million drove under the influence of illicit drugs (SAMHSA, 2017). Alcohol-related traffic accidents and deaths remain a major problem in the United States as recent data indicate that there were 37,133 traffic fatalities in 2017, 10,874 of them related to alcohol (DOT, 2018). This report also revealed that every day, almost 30 people in the United States die in motor vehicle crashes that involve an alcohol-impaired driver. This translates to one death every 51.5 minutes. The annual cost of alcohol-related crashes totals more than $59 billion (Blincoe *et al.,* 2015). And while the focus is often on the number of deaths attributed to alcohol-impaired driving, the number of injuries and destruction to personal and public property is staggering:

1. Alcohol-related fatalities on the highway by state ranged from 19% in Utah to 52% in the District of Columbia (DOT 2018).
2. Of the traffic fatalities among children under the age of 14 years and younger from 2001 - 2010, 20% involved an alcohol-impaired driver (Quinlan *et al*., 2014).
3. Drunk driving costs the United States $199 billion a year (NHTSA, 2015).
4. In 2010, over 1.4 million drivers were arrested for driving under the influence of alcohol or narcotics (DOT, 2011). This only represents 1% of the 112 million self-reported episodes of alcohol-impaired driving among U.S. adults each year (Bergen *et al*., 2011).
5. Drugs other than alcohol (e.g., marijuana, cocaine) are involved in approximately 18% of motor vehicle driver deaths. These other drugs are often used in combination with alcohol (Jones *et al*., 2003).

What makes these data even more important is the fact that alcohol-related deaths on the highway are vastly underreported (Castle *et al*., 2014) because many states do not require blood alcohol testing on all fatalities. Laboratory and on-road research shows that the vast majority of drivers, even experienced drivers, are significantly impaired at the blood alcohol concentration (BAC) of 0.08% with regard to critical driving tasks such as braking, steering, lane changing, judgment and divided attention. Decrements in performance for drivers at a BAC of 0.08% are on the order of 40 - 60% worse than when they are at a BAC of 0.00%. Research findings suggest that the most crucial aspect of impairment is the reduction in the ability to handle

several tasks at once. This skill is precisely what driving a motor vehicle requires.

Case studies reveal that an elevated relative risk of crashing begins at 0.05 – 0.06% BACs with an accelerating increase in risk at BACs greater than 0.10% (Blomberg *et al*., 2005) and the impact of alcohol is much greater than other drugs (Romano *et al.,* 2013). Drivers with a BAC of 0.08% or higher involved in fatal crashes were seven times more likely to have a prior conviction for driving while intoxicated (DWI) than were drivers with no alcohol in their system (7% and 1%, respectively) (DOT, 2014). There is overwhelming evidence that ethyl alcohol adversely affects driving performance by impairing skills that are critical to properly operating a motor vehicle. These include judgment, visuospatial recognition, reaction time and time estimation. In the aggregate, the effects of alcohol significantly interfere with an individual's ability to divide his or her attention to the many rapidly changing elements that occur while driving. There are three fundamentally different types of individuals who drive while under the influence of alcohol (Hedlund, 1994):

1. "normal" drivers who are social drinkers. Such drivers may miscalculate the effects of alcohol on their performance. Alcohol increases their crash risk and their crash rates would decrease substantially if they did not drive after drinking.
2. "high-risk" drivers. These are frequent drinkers, for whom alcohol abuse "may be just another manifestation of risk-taking behavior or may enable this behavior by removing what inhibitions they have." Abstaining may not have as much of an impact on reducing their crash rates.
3. "alcoholics," for whom alcohol abuse is an integral part of life and abstaining would require a complete lifestyle change. If they abstained, their crash rates should drop significantly.

A passive alcohol detection system could easily help all three of the above types of drinkers. The challenge presented to law enforcement and the medical community is to minimize the impact that alcohol has on driving performance. Treatment for alcohol abuse or dependence is desirable, but that might not be realistic because it if often sought only after a significant event has happened. Thus, it is deemed far more desirable to *prevent* the disease or disorder than to have to deal with the consequences. The prevention model is significantly favorable to the treatment model when you consider the burden to health and well-being as well as the substantial financial impact of alcohol use disorders. As an analogy, every dollar invested in school-based substance abuse prevention programs has the potential to save up to $18 in costs related to substance use disorders (Miller and Hendrie, 2009), which translates into saving $7 in future costs for every $1 spent on prevention measures.

This valuable epidemiological data from over three decades of research in the drug abuse field is now being applied to contend with the issue of the alcohol-impaired driver. The historical perspective of both regulatory (i.e., interlock systems) and voluntary methods to reduce the impact of driving while intoxicated has been well documented (Ferguson *et al*., 2009). The focus is on developing a passive system that requires little or no action by the driver in order to quickly and accurately assess BAC in order to render the vehicle inoperable if the reading is above the legal limit. The fundamental aims and goals of the Driver Alcohol Detection System for Safety (DADSS) program have been articulated and punctuated with successful initial Phase I testing completed (Ferguson *et al*., 2011).

The Challenge to In-Vehicle Technology—DADSS

The Driver Alcohol Detection System for Safety (DADSS) Program is a cooperative research partnership that was initially signed in 2008 and renewed in 2013 between the National Highway Traffic Safety Administration (NHTSA) and the Automotive Coalition for Traffic Safety (ACTS) that was formed to conduct research on the feasibility of using in-vehicle, noninvasive, passive technology to reduce and/or prevent alcohol-impaired driving. The DADSS website can be found at http://www.dadss.org. Members of ACTS comprise motor vehicle manufacturers representing approximately 99 percent of light vehicle sales in the U.S (BMW, Fiat Chrysler Automobiles, Ford, General Motors, Honda,

Hyundai, Jaguar/Land Rover, Kia, Mazda, Mercedes Benz, Mitsubishi Motors, Nissan, Porsche, Subaru, Toyota, Volkswagen, and Volvo). The success of this program will depend upon driver acceptability (many do not drink alcohol), which means that the system must be reliable as well as unobtrusive and not interfere with driving. Furthermore, the system must be durable and require little or no maintenance. The cooperative agreement's first task was to select the technologies on which to base the program, and then determine if they are consistent with concurrent blood alcohol concentrations (BAC). The coalition elected to pursue both a breath-based (BrAC) and a tissue-based (TiAC) system and support the development and testing of two prototypes that could be installed in vehicles. A more extensive review and update of the program is provided by Zaouk *et al*., (2015).

The fundamental challenge is to ensure that the levels of alcohol that are detected by the passive technology incorporated into the DADSS system do, in fact, reflect the concentration that is in venous blood, which is the gold standard of measurement. However, it is important to note that many of the factors identified below will also affect any standard method of measuring BAC that would be used by law enforcement. What is critical to this examination is to identify factors that could have a *differential effect* on the BAC measured by passive alcohol detection devices from levels measured via blood or breath using conventional methods. The next step is to design and carry out experiments that will improve their precision and reliability under a wide number of conditions.

One of the major goals of the DADSS system is to avoid a false negative (that is, allow an individual whose BAC is above the legal limit of 0.08% to drive the vehicle). This defeats the underlying purpose of the program. However, a false positive (that is, preventing the vehicle from being driven when the driver's BAC is below the legal limit of 0.08%), will undoubtedly raise concern and may deter public support for the program.

In order to assess the reliability, reproducibility, precision, and accuracy of these technologies, they must be tested under different "scenarios" in which the public is likely to engage. Samples from the prototypes were compared to a blood sample that is processed using gas chromatography with a Flame Ionization detector (Lex *et al.,* 1988; Lukas *et al.,* 1986, 1992; Penetar *et al.,* 2008). We incorporated the serial sampling technique developed over the past three decades to test the performance of these prototype devices under real-life conditions.

Blood Alcohol Concentration (BAC) Standards

BAC remains the standard for documenting the amount of alcohol in the body (Tiscione *et al*., 2011) because alcohol is ubiquitous with water and so alcohol concentrations equilibrate throughout the body and brain very quickly once absorbed. Because of this direct relationship, BACs parallel changes in psychomotor performance and subjective reports of intoxication (Grant *et al.,* 2000; Tagawa *et al*., 2000; Lukas *et al.,* 1986, 1989a, b).

While blood is the standard biological sample, it is not the most convenient to collect. For many years forced breath samples have been an accepted surrogate for BAC, though breath is more closely related to arterial than venous blood (Martin *et al.,* 1984). This is because the air in the lungs exchanges with the alveoli capillaries that are an extension of the pulmonary arteries. Forced breath sampling is the basis behind a wide range of hand-held breathalyzers, evidentiary breath, and Breath Alcohol Ignition Interlock Devices (BAIID). A driving while intoxicated (DWI) offender is required to use a BAIID by either a court or by state law administered by the state licensing agency. While the method used to quantify alcohol concentrations in breath samples differ, these devices share one common element—the subject must exhale forcibly into a mouthpiece for a specified amount of time to obtain a valid reading. These devices lack the appeal of measuring alcohol passively and therefore limit their utility in a continuous drunk driving deterrent system.

Historically, wearable biosensors for alcohol have been developed to sample sweat (e.g., Swift, 1993). However, sweat is not a dynamic matrix as it is a glandular product and as such there are significant deviations in the maximum and concentrations over time. This makes correlating the readings with BAC quite challenging (Sakai *et al*., 2006). Transdermal sampling has been used in various

devices in law enforcement, but it is important to note that it reflects alcohol vapor that evaporates from the skin surface and so is not temporally linked to blood. In contrast, tissue measurements that use an optical probe to direct near infrared (NIR) radiation into the dermal layer of the tissue and collect the radiation that is diffusely reflected to the tissue surface directly interrogates the aqueous alcohol present in the interstitial fluid of the dermis (Ridder *et al.,* 2005, 2009, 2011). The critical distinction between transdermal and tissue alcohol measurements is that the latter is more dynamically related to the rapidly changing BAC while the former is more sluggish and therefore cannot be equated to alcohol-induced impairment.

The Technologies

In an attempt to provide a comprehensive coverage to increase accuracy, two different technologies were selected to be integrated. The first is a passive breath-based system and the second is a touch-based system that detects tissue alcohol concentration.

Breath-Based Technology

Breath-based systems use an approach similar to tissue spectrometry, in that they utilize the mid infrared (MIR) region of the electromagnetic spectrum (2.5 - 25 μm), but no skin contact is required. The approach under development aims to remotely analyze alcohol in breath within the vehicle cabin without the driver having to specifically provide a deep-lung breath sample. The working principle of the sensor is to use measurements of expired carbon dioxide (CO_2) as an indication of the degree of dilution of the alcohol in expired air. Normal concentration of CO_2 in ambient air is close to zero. Furthermore, CO_2 concentration in alveolar air is both known and predictable, and remarkably constant. Thus, by simultaneously measuring CO_2 and alcohol, the degree of dilution can be compensated for using a mathematical algorithm. According to Hök (2006), the ratio between the measured concentrations of CO_2 and alcohol, together with the known value of CO_2 in alveolar air, can provide the alveolar air alcohol concentration. The breath sensor technology under development uses MIR spectroscopy for both alcohol and CO_2 and is manufactured by Senseair (Sweden). The MIR-based sensors can be stable over the full product lifetime, eliminating the need for recurrent calibrations (**Figure 1**).

Figure 1. Passive breath detector currently being tested (Senseair).

For in-vehicle use, the system could employ multiple sensors placed strategically around the cabin of the vehicle close to the driver. The challenge is to determine the number and placement of sensors needed to measure alcohol quickly and accurately given the dynamics of the cabin air, and to ensure that there is no potential bias introduced as a result of passengers who may have been drinking.

Touch-Based Technology

Tissue spectrometry systems, also known as near infrared (NIR) spectrometry, this is a noninvasive approach that utilizes the near infrared region of the electromagnetic spectrum (from about 0.7 to 2.5 μm) to measure substances of interest in bodily tissue. The measurement begins by illuminating the user's skin with NIR light which propagates into the tissue (the skin must be in contact with the device). The beam of light can penetrate tissue at depths of up to 5 mm to reach the dermal layer where alcohol that is dissolved in water resides. A portion of the light is diffusely reflected back to the skin's surface and collected by an optical touch pad. The light contains information on the unique chemical information and tissue structure of the user. This light is analyzed to determine the alcohol concentration and, when applicable, verify the identity of the user. Because of the complex nature of tissue composition, the challenge is to measure the concentration of alcohol (sensitivity) while ignoring all the other interfering analytes or signals (selectivity).

Although the entire NIR spectrum spans the wavelengths from 0.7 - 2.5 μm, the device currently under study (TruTouch Inc., Riverside, CA) uses the 1.25 - 2.5 μm region because of its high sensitivity and selectivity for alcohol. The 0.7 -

1.25 µm region of the NIR spectrum is limited by the presence of skin pigments such as melanin that can create large differences among people, particularly of different ethnicities. In contrast, the longer wavelength portion of the NIR, from 1.25 - 2.5 µm, is virtually unaffected by skin pigmentation (Anderson *et al.,* 1981). One other advantage of using this region of the spectrum is that the alcohol signal in the 1.25 - 2.5 µm region is hundreds of times stronger than the signal in the 0.7 - 1.25 µm part of the NIR.

The TruTouch prototype system is based on a proprietary Fourier transform spectrometer coupled with a compact, fiber optic touchpad with which the user interfaces. To conduct a test, the user places an intermediate phalange of the index finger onto the fiber optic touchpad (**Figure 2**). The prototype automatically detects the presence of the finger and initiates an alcohol test. Once the spectral data have been collected, automated quality control metrics ensure that the test sample is a valid human finger and that all test parameters are within acceptable limits. An alcohol test result then is calculated and displayed on-screen.

The prototype system is a stand-alone test unit with the sensor, data processing unit, and operating software fully contained inside the unit. For operation in benchmark testing, a PC-based application is run on an external computer and communicates with the prototype via a wired Ethernet connection. This setup allows for flexible configuration and data logging requirements for this phase of testing. All data collection, quality control screening, and measurement calculations are performed within the prototype itself.

Figure 2. The Touch-based device currently being studied (TruTouch).

METHODS

Participants

A total of 92 healthy adult male and female volunteers between the ages of 22-38 were recruited via online advertisements to participate in the studies, for which they were compensated. Most individuals participated in more than one experiment, providing within-subject comparisons. All participants were well matched by age, sex, ethnicity, body mass index (BMI), and current alcohol consumption (**Table 1**). The protocol and informed consents were approved by the Partners Healthcare Institutional Review Board (IRB). Individuals received a full physical and psychiatric evaluation before being enrolled in the study. On each test day, they received a breath alcohol test, a urine toxicology screen, and urine pregnancy test (women) – all had to be negative before the study could proceed.

Table 1. Demographic profile of participants in each of the drinking scenarios

Scenario	N (male)	Age (years)	BMI (kg/m^2)	Drinks/wk (#)	Regular Drinker (# years)
Lag Time	18 (11)	28.0 ± 3.4	23.8 ± 3.9	7.1 ± 3.9	7.9 ± 4.1
Lag Time (low)	15 (9)	28.5 ± 4.0	23.9 ± 3.4	7.1 ± 4.4	9.1 ± 4.9
Social Snacking	13 (9)	27.8 ± 4.8	25.1 ± 3.8	8.0 ± 4.6	8.5 ± 4.7
Full Meal	14 (10)	27.1 ± 4.8	24.8 ± 3.5	8.0 ± 4.7	7.6 ± 4.5
Exercise	16 (10)	28.5 ± 3.9	23.4 ± 3.2	7.2 ± 4.3	8.4 ± 4.4
Last Call	16 (11)	27.7 ± 3.9	23.8 ± 3.8	7.1 ± 4.1	8.2 ± 4.3

Participants were not permitted to drive to the laboratory but were instead required to take a taxicab. Participants were required to remain in the laboratory until their BAC dropped to below 0.04% and they were able to pass a field sobriety test.

General Procedure

Figure 3 shows the layout of the experimental and control rooms in the BPRL. Each of the scenarios involved inserting an indwelling intravenous catheter (Dakmed-Kowarski Thrombo-Resistant Catheter) into participants' arms that was then attached to an exfusion pump and set to draw blood at a rate of 1 mL/min. Participants were seating in a comfortable recliner chair (except for the exercise scenario) while they had their blood sampled, breathed into the Senseair and reference breath device, and placed the back of their index finger (first intermediate phalange) on the TruTouch device's touchpad.

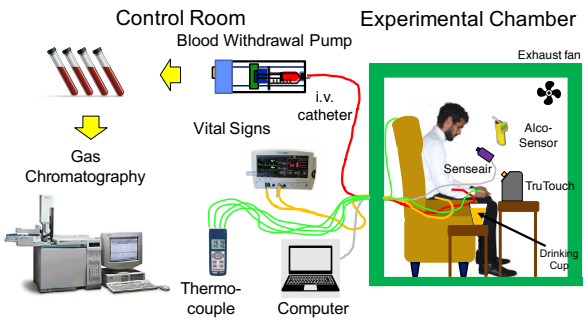

Figure 3. Laboratory layout for the alcohol challenge experiments depicting the various devices and collection of blood samples that are then subjected to gas chromatography.

Blood Alcohol Concentrations

Blood alcohol levels were analyzed in our laboratory (Penetar *et al.,* 2008). Briefly, each sample was collected at either 2 or 5 minute intervals, transferred to a gray top blood collection tube (containing EDTA to prevent the blood from clotting), and then inverted 10 times to ensure proper mixing of the anticoagulant to ensure that a blood sample remained intact. Whole blood is extracted with an internal standard prepared in acid in the presence of sodium tungstate to precipitate out the proteins (Berkman *et al.,* 1954). After centrifugation, the clear supernatant is transferred to vials, injected onto a gas chromatograph (GC) (Model 7890A, Agilent Technologies) and analyzed with the use of capillary chromatography and flame ionization detection (FID) (Folin and Wu, 1919). Intra-assay CVs were 1.61% and inter-assay CVs were 2.43%

TruTouch Tissue Measurements

At designated time intervals (approximately every 2 or 5 minutes), participants were instructed to place their index finger (using the limb that did not have the intravenous catheter inserted) on the touch pad and keep it there for approximately 30 - 60 sec.

Senseair Breath Measurements

At the designated times (approximately every 2 or 5 minutes), participants were instructed to exhale towards the Auto-Liv collection funnel, capturing a "relatively" passive breath sample since they do not have to physically blow into a tube.

Reference Breath Samples

As an added control, breath samples were also collected via a hand-held research-grade device (Alco-Sensor FST®, Intoximeter Corp., St. Louis, MO) at the same time intervals as the other measures. Participants were required to breath directly into the mouthpiece at a steady force for at least 8 seconds.

Alcohol Dosing

All participants were dosed on the basis of their body weight (0.9 g/kg). Drinks were prepared fresh immediately prior to the experiments and included 40% vodka that was either taken as straight shots or mixed with orange juice to maintain a total volume of 400 mL. As the drinking scenarios differed slightly, participants were provided specific instructions for the rate and volume of the beverage that was consumed (either as a large bolus dose or as three drinks spread out over the course of 90 minutes.

Scenario #1—Lag Time

Participants consumed the entire 0.9 g/kg dose in a rapid manner such that all alcohol was ingested by 90 seconds. Because of the artificial elevations in breath alcohol concentration due to buccal absorption, participants were provided with a plain water rinse before the first breath sample was taken. Furthermore, only the first sample after two minutes had passed was recorded. We also conducted a parallel study using a lower dose of alcohol (Lag Time-Low) in which individuals consumed a dose of 0.3 g/kg.

Scenario #2—Social Snacking

Participants consumed the alcohol in three different episodes over a 90-minute period. During each drinking episode (that lasted 20 minutes), participants consumed 1/3 of the total dose and they were asked to snack on pretzels and Goldfish® crackers (for a total of 220 calories) while drinking.

Scenario #3—Full Meal

This protocol was similar to the social snacking except that the first 1/3 of the alcohol dose was consumed on an empty stomach. The next 1/3 of the total dose was consumed along with a first course of a typical breakfast (275 calories) consisting of an English muffin with butter and a cup of fruit. The last 1/3 dose was consumed along

with the second course of the breakfast and consisted of an omelet with vegetables and cheese accompanied by a side order of two chicken sausages (375 calories for women, 500 calories for men).

Scenario #4—Exercise (Simulated Dancing)
This protocol involved having the participants consume the entire drink in a single bolus and then immediately engage in three bouts of exercise during which they maintained a steady energy expenditure of 450 kcal/hr by operating a recumbent elliptical machine. The first exercise episode lasted eight minutes, followed by a four-minute break to collect breath and tissue samples, followed by two additional four-minute exercise episodes with a four-minute break to collect samples. After the participant completed the exercise, they were moved to a comfortable chair where they remained for the duration of the study; blood, breath and tissue samples were sampled as before.

Scenario #5—Last Call
This scenario was conducted by having the participants consume 2/3 of the total drink as a bolus beverage, and then wait for 70 minutes at which time the last 1/3 of the dose was consumed, also as a bolus. This last drink simulated a "last call" drink that would be consumed just before the individual would leave a bar and drive home.

RESULTS

General Results
Alcohol concentration data points were averaged by compartment (i.e., blood, the two different breath devices, and tissue) across all participants and then were plotted over time.

Scenario #1 Lag Time Results
This experiment was conducted to determine in which of the compartments (blood, breath, or tissue) the alcohol would first appear after consuming a bolus dose of alcohol. However, because of the difficulties with breath sampling (due to buccal or mouth absorption), the accuracy of the lag time in breath was difficult to determine. As can be seen in **Figure 4**, the first appearance of alcohol in the breath was difficult to establish due to the very rapid rise in breath concentration immediately after consumption. Alcohol appeared in the blood within 6 minutes, but did not show up in tissue until 14 minutes had passed.

Peak alcohol concentrations in blood and breath samples were attained between 1.25 and 1.5 hours after consumption, while the peak alcohol concentration in tissue occurred 15 to 20 minutes later. These differences were not significant. **Figure 5** depicts a similar relationship among the various compartments except that the maximum BAC was lower due to the lower dose. In addition, there is a greater separation due to the initial buccal absorption of alcohol on the two breath based devices.

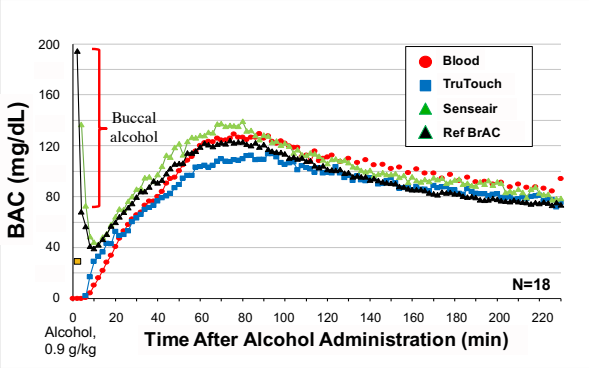

Figure 4. Lag Time. Alcohol concentration/time curves in blood, breath and tissue after a bolus dose of 0.9 g/kg of alcohol.

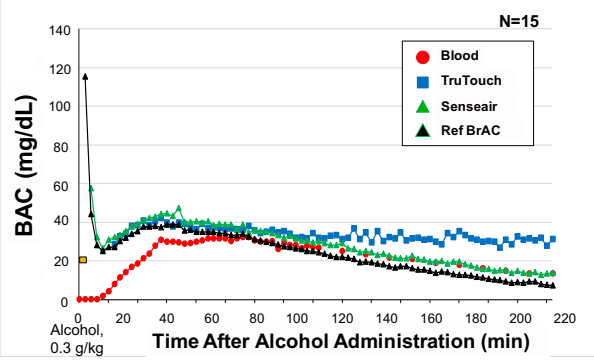

Figure 5. Lag Time-Low. Alcohol concentration/time curves in blood, breath and tissue after a bolus dose of 0.3 g/kg of alcohol.

Scenario #2 Social Snacking Results

This experiment was conducted to determine if alcohol concentrations are different in blood, breath, or tissue after consuming a small snack over an extended period of time. In addition, the participants were required to remain sedentary, which is designed to simulate drinking alcohol while sitting at a bar. **Figure 6** depicts the alcohol concentration by time curves for each of the compartments. Note that because of the continuous snacking and drinking protocol, it was impossible to obtain accurate measures of breath and tissue, so only the blood alcohol concentrations were obtained throughout the snacking period. Breath and tissue samples were obtained between the two breaks from snacking; all samples were collected once the third epoch had finished.

The rate of alcohol absorption during the social snacking scenario was significantly slower than the bolus drinking, but it must be remembered that the alcohol was consumed more slowly over a longer time interval. Even though the tissue sample at the 30-minute time point was higher than the other compartments, all achieved the same peak alcohol concentration within 10 to 15 minutes after the third epoch of drinking and snacking.

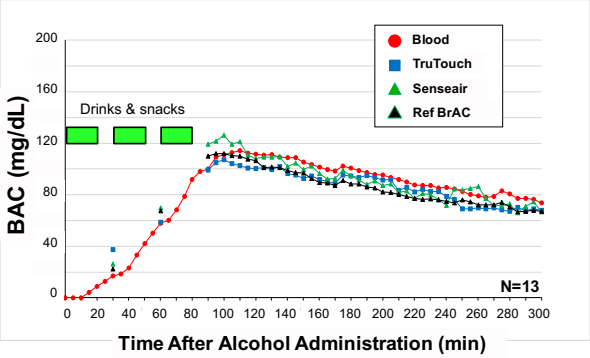

Figure 6. Social Snacking. Alcohol concentration/ time curves in blood, breath and tissue during snacking and drinking a total dose of 0.9 g/kg of alcohol, distributed over three epochs.

Scenario #3 Full Meal Results

This experiment was conducted to determine if alcohol concentrations in each of the three compartments are altered after consuming alcohol along with a full meal. As with the social snacking, the alcohol dose was divided into thirds, but in this scenario, they consumed the first 1/3 dose on an empty stomach. After a short break, they started to eat the first course of the meal while consuming 1/3 of the alcohol dose. Finally, after a second short break, they consumed the second course while simultaneously consuming the last third of the 0.9 g/kg dose of alcohol. Breath and tissue samples were collected during the breaks while blood samples were collected throughout the meal period.

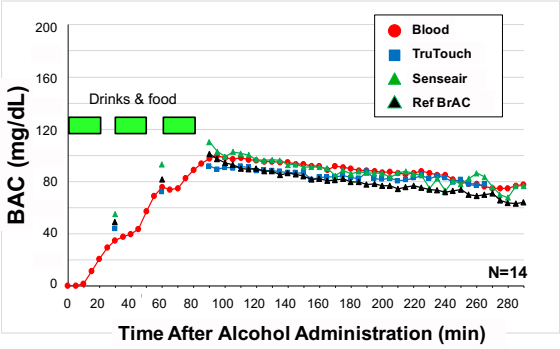

Figure 7. Full Meal. Alcohol concentration/time curves in blood, breath and tissue during a full meal and drinking a total dose of 0.9 g/kg of alcohol, spaced over three epochs.

Figure 7 shows the concentration/time curve for all compartments. The absorption rates were similar to those during the social snacking scenario, but the peak alcohol concentration after the full meal was lower than when the participants snacked.

Scenario #4 Exercise Results

This experiment was conducted to determine if alcohol concentrations in each compartment was affected by exercise. The use of a recumbent elliptical machine was selected for both safety and to simulate dancing with both arm and leg motion. Participants were given a bolus dose of alcohol to consume (as in the Lag Time experiment) and then engaged in three epochs of exercise. Participants were given two short breaks between exercising in order to permit collecting breath and tissue samples for alcohol determination.

Figure 8 depicts the effects of exercise on alcohol concentrations in each of the compartments. The rate of alcohol absorption during exercising is steeper than the lag time control rate. In addition, the rate appears to accelerate as soon as the participants cease exercising. Peak alcohol concentrations were attained at about the same time

after drinking (approximately 60-75 minutes) and the actual peak concentrations did not differ among the compartments.

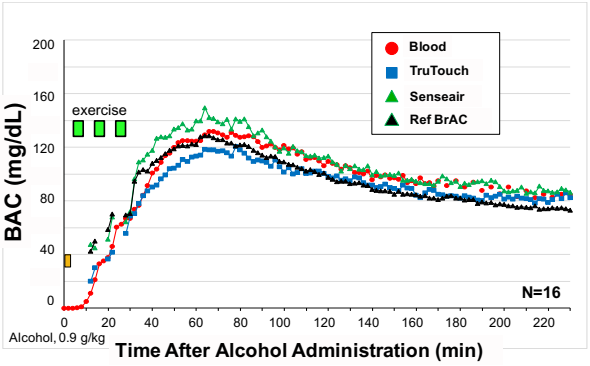

Figure 8. Exercise. Alcohol concentration/time curves in blood, breath and tissue after exercising and drinking a bolus dose of 0.9 g/kg of alcohol.

Scenario #5 Last Call Results

This experiment was conducted to determine the pharmacokinetic profile of drinking a last alcoholic beverage after peak alcohol concentrations had been attained from drinking earlier. Participants consumed 2/3 of the total dose as a bolus and then the last 1/3 (i.e., "last call") when the distribution phase had been attained, approximately 70 minutes after the initial drink.

The two breath-based devices recorded the artificially high concentrations right after drinking, but then returned to concentrations that were detected in blood and tissue (**Figure 9**). Consuming the last drink caused an immediate rise in alcohol concentration in all compartments.

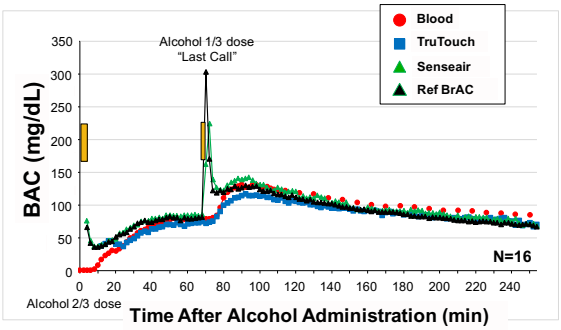

Figure 9. Last Call. Alcohol concentration/time curves in blood, breath and tissue after in a simulated "Last call" scenario in which 1/3 of the dose was consumed 70 minutes after consuming 2/3 of the total dose of 0.9 g/kg of alcohol.

Correlations Between Alcohol as Measured via the Prototypic Devices and BAC

Because each participant had multiple blood, breath and tissue samples collected during each experiment, we have amassed a significant number of pairings of alcohol concentration measures. Regression analyses of blood and breath as well as blood and tissue revealed that both prototypic devices provided excellent correlations with blood. **Figure 10** shows the relationship between blood and Senseair breath samples. Note that we have many more samples in the 80 - 125 mg/dL range because the dose of alcohol was high enough to produce an extended "distribution" phase. In addition, alcohol is absorbed rather quickly, so the amount of time that participants spent with lower BAC was less than when their BAC were higher.

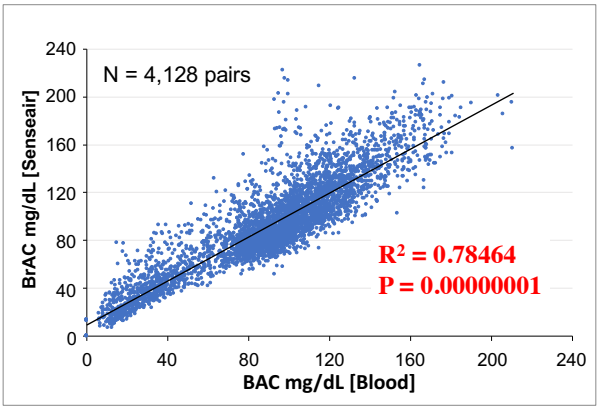

Figure 10. Regression analyses revealing strong correlations between alcohol as measured via the Senseair breath device and blood. Data are from 4,128 pairs of samples that were collected at the same time.

Figure 11 depicts the same regression analysis for TruTouch and blood, but with 4,265 pairs of samples that were collected at the same time.

Subjective Reports of Intoxication

During the experiments, participants filled out a self-report Visual Analog Scale questionnaire in which they rated themselves on a scale of 0 - 10 (zero meant "none" while 10 meant "most ever") to the following questions: "How HIGH Are You Right Now?" and "How DRUNK Are You Right Now?" In addition, they rated themselves on whether they would drive a vehicle right now.

Figures 12 - 14 show the results of these assessments.

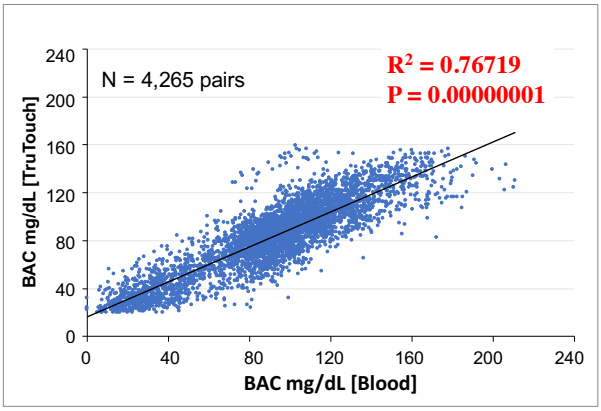

Figure 11. Regression analyses revealing strong correlations between alcohol as measured via the TruTouch tissue device and blood. Data are from 4,265 pairs of samples that were collected at the same time.

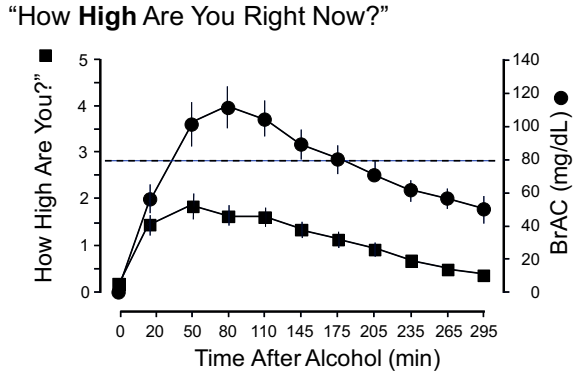

Figure 12. Subjective reports of intoxication reflecting how "high" participants felt at the time. The BrAC concentrations are plotted to provide a comparison of subjective effects and alcohol concentration.

Note that the subjective effects of alcohol parallel the rise and fall of alcohol in the breath. This is a unique aspect of alcohol that is not shared by other drugs that impair driving performance.

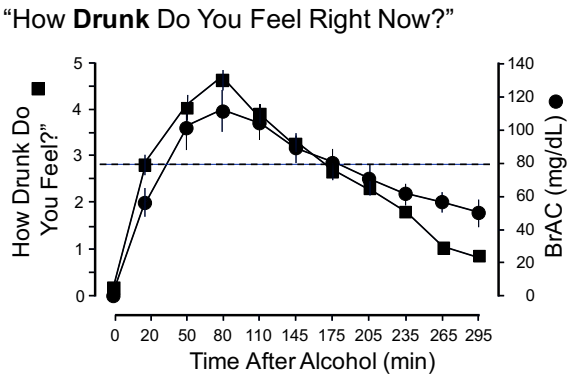

Figure 13. Subjective reports of intoxication reflecting how "drunk" participants felt at the time. The BrAC concentrations are plotted to provide a comparison of subjective effects and alcohol concentration.

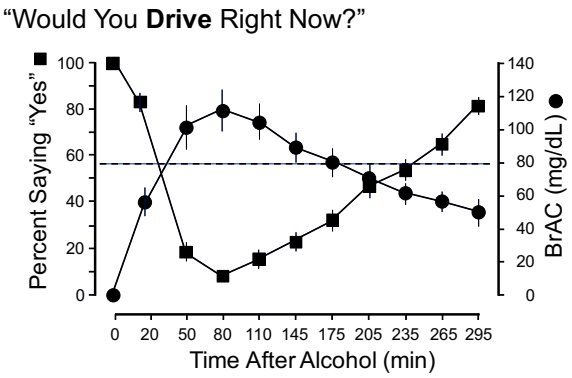

Figure 14. Subjective reports of whether a participant would feel comfortable driving a vehicle at the time. The BrAC concentrations are plotted to provide a comparison of subjective effects and alcohol concentration.

CONCLUSIONS

The data clearly support the proof-of-concept that two different passive technologies (breath and touch) can detect alcohol concentrations very quickly and are not affected by many of the common scenarios that are known to alter blood alcohol concentrations. While the alcohol pharmacokinetic profile was altered by the various real-life scenarios in the present series of experiments, the most important observation is that the alcohol concentrations measured via the different devices (that reflect different biological compartments) paralleled one another. The two prototypes performed very well against blood and

"forced" breath referential alcohol concentrations. The absolute concentrations differed, but they deviated in a predictable and linear manner such that recalibrations of the instruments will result in excellent direct correlations with blood concentrations. This relationship is of utmost importance because if these devices are going to be useful in curbing drunk driving, then the measured concentrations from these devices must accurately track BAC as that is the gold standard that documents driving while under the influence.

The present series of experiments fulfilled many key target aims: 1) we demonstrated the feasibility of passive, unobtrusive breath- and touch-based alcohol detection systems that could eventually be placed in vehicles; 2) as the design of these prototype devices was based on infrared spectroscopy, the data collected was consistent and reproducible; 3) the data from the two prototype devices were very well correlated with the gold-standard method of measuring alcohol in the body— gas chromatography of blood samples; 4) the prototypes recorded the alcohol concentrations relatively quickly and tracked the changes observed in blood, regardless of the type of scenario that was involved; 5) because of the excellent correlation between breath and blood and tissue and blood, there is no need to adjust the algorithm for converting the alcohol concentrations measured by the prototypic devices.

The addition of subjective reports of intoxication in the present study yielded very interesting findings. While the parallel in degrees of "high" and "drunk" and BrAC was not surprising, the fact that the participants' confidence in their driving ability declined as their breath alcohol concentration increased was not universal. Case studies reveal that an elevated relative risk of crashing begins at 50 - 60 mg/dL BACs with an accelerating increase in risk at BACs greater than 100 mg/dL. It is interesting to note that in the present study, we discovered that 50% of the participants reported that they would still drive even though their BrAC was at the legal limit of 80 mg/dL and 20% of them would still drive at a BrAC of 100 mg/dL. It is this finding that validates the need for the DADSS system—to intercept individuals who are above the legal limit for alcohol in the blood, are clearly aware that they are drunk and yet still feel confident in getting behind the wheel of an automobile.

The caveat of the findings, and thus a focus of the next phase of the research program is that the present prototypes required between 20–30 sec for the alcohol concentrations to be recorded. Both engineering teams are working on the acquisition time intervals and the current devices can now detect alcohol more quickly, especially the Senseair. The target will be to have the detection time reduced to 0.5 sec so that the devices can easily function in an automobile environment. The two prototype devices have entered the next level of testing by being placed in test vehicles that are running in different parts of the country. If this phase of testing demonstrates similar reliability and precision in a vehicle as was measured in a laboratory setting, then the approach taken by DADSS represents a significant technological breakthrough in strategies to reduce alcohol-impaired individuals from driving a vehicle and causing injuries and/or death.

REFERENCES

1. Anderson RR & Parrish JA (1981) The Optics of Human Skin. *The Journal of Investigative Dermatology, 77*, 13-19.

2. Blomberg RD, Peck RC, Moskowitz H, Marcelline Burns M, & Fiorentino D (2005) Crash Risk of Alcohol Involved Driving: A Case-Control Study. Technical Report Contract DTNH22-94-C-05001, U.S. Department of Transportation, National Highway Traffic Safety Administration (NHTSA) and Dunlap and Associates, Inc.

3. Bergen G, Shults RA, & Rudd RA (2011) Vital Signs: Alcohol-Impaired Driving Among Adults – United States, 2010. *Morbidity and Mortality Weekly Report, 60*, 39:1351.

4. Berkman S, Henry RJ, Golub OJ, & Segalove M (1954) Tungstic acid precipitation of blood proteins. *Journal of Biological Chemistry, 206*, 937–943.

5. Blincoe L, Miller TA, Zaloshnja E, &

Lawrence BA (2015, May) The Economic Impact of Motor Vehicle Crashes, 2010 (*Revised*). (Report No. DOT HS 812 013). Washington (DC): National Highway Traffic Safety Administration. 1-299.

6. Castle IJ, Yi HY, Hingson RW, & White AM (2014) State variation in underreporting of alcohol involvement on death certificates: motor vehicle traffic crash fatalities as an example. *Journal of Studies on Alcohol and Drugs, 75,* 299-312.

7. Centers for Disease Control and Prevention (2013) Alcohol Related Disease Impact (ARDI) application. Available at www.cdc.gov/ARDI.

8. Department of Transportation (US), Federal Bureau of Investigation (FBI) (2011) Crime in the United States 2010: Uniform Crime Reports. Washington (DC): FBI. [cited Sept 29 2012]. Available at URL: http://www.fbi.gov/about-us/cjis/ucr/crime-in-the-u.s/2010/crime-in-the-u.s.-2010/summary

9. Department of Transportation (US), National Highway Traffic Safety Administration (NHTSA). (2015) Traffic Safety Facts 2014 Data: Alcohol-Impaired Driving. Washington (DC): NHTSA. Available at URL: https://crashstats.nhtsa.dot.gov/Api/Public/ViewPublication/812231

10. Department of Transportation (US), National Highway Traffic Safety Administration (NHTSA) (2018) 2017 Fatal Motor Vehicle Crashes: Overview. Washington (DC): NHTSA. Available at URL: https://crashstats.nhtsa.dot.gov/Api/Public/ViewPublication/812603.

11. Ferguson SA, Traube E, Zaouk A, & Strassburger R (2009) Driver Alcohol Detection System for Safety (DADSS) – A non-regulatory approach in the development and deployment of vehicle safety technology to reduce alcohol-impaired driving. In Proceedings of the 21st International Technical Conference on the Enhanced Safety of Vehicles (Stuttgart, Germany), pp. 09–0464.

12. Ferguson SA, Zaouk A, Dalal N, Strohl C, Traube, E, & Strassburger R (2011) Driver Alcohol Detection System for Safety (DADSS) – Phase I Prototype testing and findings. In Proceedings of the 22rd International Technical Conference on the Enhanced Safety of Vehicles, (Washington, DC), paper Number 11–0230.

13. Folin O & Wu H (1919) A system of blood analysis. *Journal of Biological Chemistry, 38*, 81–87.

14. Grant SA, Millar K, & Kenny GN (2000) Blood alcohol concentration and psychomotor effects. *British Journal of Anaesthiology*, 85, 401-416.

15. Hök B, Pettersson H, & Andersson G (2006) Contactless measurement of breath alcohol. In Proceedings of the Micro Structure Workshop, Västerås, Sweden.

16. Hedlund JH (1994) If they didn't drink, would they crash anyway? – The role of alcohol in traffic crashes. *Alcohol Drugs Driving, 110*, 115-125.

17. Jones AW & Andersson L (2003) Comparison of ethanol concentrations in venous blood and end-expired breath during a controlled drinking study. *Forensic Science International, 132*,18-25.

18. Lex BW, Greenwald N, Lukas SE, Slater J, & Mendelson JH (1988) Blood ethanol levels, self-rated ethanol effects, and cognitive-perceptual tasks. *Pharmacology Biochemistry and Behavior, 29,* 509-515.

19. Lukas SE, Benedikt R, Mendelson JH, Kouri E, Sholar M, & Amass L (1992) Marihuana attenuates the rise in plasma ethanol levels in human subjects. *Neuropsychopharmacology, 7,* 77-81.

20. Lukas SE, Lex BW, Slater J, Greenwald N, & Mendelson JH (1989a) A microanalysis of

ethanol-induced disruption of body sway and psychomotor performance in women. *Psychopharmacology*, 98, 169-175.

21. Lukas SE, Mendelson JH, Woods BT, Mello NK, & Teoh SK (1989b) Topographic distribution of EEG alpha activity during ethanol-induced intoxication in women. *Journal of Studies of Alcohol*, 50, 176-185.

22. Lukas SE, Mendelson JH, Benedikt RA, & Jones B (1986) EEG alpha activity increases during transient episodes of ethanol-induced euphoria. *Pharmacology, Biochemistry & Behavior*, 25:889-895.

23. Lukas SE, Mendelson JH, & Benedikt RA (1986) Instrumental analysis of ethanol-induced intoxication in human males. *Psychopharmacology, 89,* 8-13.

24. Martin E, Moll W, Schmid P, & Dettli L (1984) The pharmacokinetics of alcohol in human breath, venous and arterial blood after oral ingestion. *European Journal of Clinical Pharmacology*, 26, 619-626.

25. Miller TR & Hendrie D (2009) Substance abuse prevention dollars and cents: A cost-benefit analysis. Substance Abuse and Mental Health Services Administration, Center for Substance Abuse Prevention. Rockville, MD: DHHS. Pub.No (SMA) 07-4298.

26. Miller JW, Naimi TS, Brewer RD, & Jones SE (2006) Binge drinking and associated health risk behaviors among high school students. *Pediatrics, 119*, 76-85.

27. Naimi TS, Brewer RB, Mokdad A, Denny C, Serdula MK, & Marks JS (2003) Binge drinking among U.S. Adults. *Journal of American Medical Association, 289,* 70–75.

28. National Highway Traffic Safety Administration (2015) "The Economic and Societal Impact of Motor Vehicle Crashes, 2010 (Revised)." National Highway Traffic Safety Administration, DOT HS 812 013. http://www-nrd.nhtsa.dot.gov/Pubs/812013.pdf.

29. Penetar DM, McNeil JF, Ryan ET, & Lukas SE (2008) Comparison among plasma, serum, and whole blood ethanol concentrations: impact of storage conditions and collection tubes. *Journal of Analytical Toxicology, 32,* 505-10.

30. Quinlan K, Shults RA, Rudd RA.(2014) Child passenger deaths involving alcohol-impaired drivers. Pediatrics 133:966-972 .

31. Ridder TD, Hendee SP, & Brown CD (2005) Noninvasive alcohol testing using diffuse reflectance near-infrared spectroscopy. *Applied Spectroscopy,* 59, 181-189.

32. Ridder TD, Hull EL, Ver Steeg BJ, & Laaksonen BD (2011) Comparison of spectroscopically measured finger and forearm tissue ethanol concentration to blood and breath ethanol measurements. *Journal of Biomedical Optics*, 16, 028003.

33. Ridder TD, Ver Steeg BJ, & Laaksonen BD (2009) Comparison of spectroscopically measured tissue alcohol concentration to blood and breath alcohol measurements. *Journal of Biomedical Optics*, 14, 054039-1 – 11.

34. Romano E, Torres-Saavedra P, Voas RB, & Lacey JH (2014) Drugs and alcohol: their relative crash risk. *Journal of Studies of Alcohol and Drugs*, 75, 56-64.

35. Sakai JT, Mikulich-Gilbertson SK, Long RJ, Crowley TJ. Validity of transdermal alcohol monitoring: fixed and self-regulated dosing. Alcohol Clin Exp Res 30:26-33, 2006.

36. Center for Behavioral Health Statistics and Quality. *Results from the 2016 National Survey on Drug Use and Health: Detailed Tables*. Rockville (MD): SAMHSA; 2017. https://www.samhsa.gov/data/sites/default/files/NSDUH-DetTabs-2016/NSDUH-DetTabs-2016.pdf.

37. Stahre M, Brewer R, Naimi T, & Miller J (2004) Alcohol-Attributable Deaths and Years of Potential Life Lost due to Excessive

Alcohol Use in the U.S. *Morbidity and Mortality Weekly Report, 53,* 866-870.

38. Swift R (2000) Transdermal alcohol measurement for estimation of blood alcohol concentration. *Alcoholism Clinical & Experimental Research*, 24, 422–423.

39. Tagawa M, Kano M, Okamura N, Itoh M, Sakurai E, Watanabe T, & Yanai K (2000) Relationship Between Effects of Alcohol on Psychomotor Performances and Blood Alcohol Concentrations. *Japanese Journal of Pharmacology*, 83, 253-260.

40. Tiscione NB, Alford I, Yeatman DT, & Xiaoqin Shan X (2011) Ethanol Analysis by Headspace Gas Chromatography with Simultaneous Flame-Ionization and Mass Spectrometry Detection. *Journal of Analytical Toxicology*, 35, 501-511.

41. Zaouk AK, Willis M, Traube E, & Strassburger R (2015) Driver Alcohol Detection System for Safety (DADSS) – A Status Update. *Presented to ESV 2015 Conference.*

CHANGES IN CRASH PROTECTION WITH VEHICLE MODEL YEAR

Kennerly Digges
Automotive Safety Research Institute
USA

George Bahouth
Amin Vahabaghaie
Impact Research, LLC
USA

Paper Number 19-0269

ABSTRACT

NASS 1993-2015 was queried for frequency of exposed vehicles with belted driver injuries separated by injury severity and vehicle model year. Vehicle model-years were aggregated by 3 model year groupings – 1985 -1994; 1995-2000; 2001-2015. These percentages of the crash exposed populations for the 3 groups were: 27%, 34% and 39%. The total exposed population was 27,347,705. The total and Mean AIS 3+ HARM for each model year grouping was calculated for each crash mode – frontal, near-side, far-side, rear and rollover. Changes in total AIS 3+ HARM distribution and Mean AIS 3+ HARM by crash mode and model year grouping were reported.

The largest source of AIS 3+ HARM to belted drivers in the 2001-2015 NASS population remains the frontal crash mode. Near-side and rollover injury rates have dramatically decreased in recent model years. Frontal and far-side crash mode injury rates have decreased slightly and rear has remained relatively constant, but at a low injury rate.

The data suggests that for light trucks, the near-side Mean AIS 3+ HARM has increased during the 2001-2015 model years. However, the level remains below that of passenger cars which have experienced dramatic reductions in near-side Mean AIS 3+ HARM during the same period.

BACKGROUND

The analysis to follow examines vehicle safety trends based on changes to the HARM that was present in groupings of motor vehicles from three successive time periods. The concept of HARM was introduced in a landmark paper by key NHTSA staff [Malliaris, 1982]. A frequent alternative to the use of HARM is to categorize all severe injuries greater than AIS 3 in a single group labeled AIS3+ injuries. An issue with this categorization is that the AIS 3+ population is overwhelmed by AIS 3 injuries and the AIS 4+ population is not given increased priority. Alternatively, the HARM weighting scheme is applied to injuries of different severity based on the average cost of the injury. This injury weighting system has the advantage of increasing the priority for preventing the most severe injuries.

The mean HARM is defined as the total HARM for a grouping divided by the exposure for that grouping. The mean HARM is a measure of the combined injury risk and has been widely used to conduct benefits analyses. The mean HARM is a weighted injury risk and is useful for determine how the safety has changed. HARM and mean HARM were used extensively at NHTSA and elsewhere in the 80's and 90's to assess priorities for safety systems. GM Australia used HARM calculations in designing the first air bag introduced in Australia and the Australian Ministry of Transport used HARM to establish frontal and side impact regulations [Fildes, 1992].

The analysis in this paper follows the methodology of an earlier analysis by Eigen [Eigen, 2007]. However, the Eigen analysis examined HARM to injured body regions and, therefore, considered all of the multiple injuries that were coded for each individual. The present analysis uses the Malliaris methodology and considers only the most severe injury to each occupant.

.

In 2012, NHTSA stopped doing reconstructions for NASS/CDS included vehicles 10 years old and older at the time of the crash. For that reason, even though the vehicles would be stored in the dataset, the general area of damage (GAD) and principal direction of force (PDOF) were not computed for these vehicles. These components of the collision deformation classification (CDC) were used in this analysis to categorize cases into crash modes. Consequently some of the very oldest vehicles were excluded from the counts by crash mode for crashes occurring in 2012 and later.

Another limitation of this longitudinal HARM analysis is that it assumes that the mean crash severity has not changed with model year.

METHODS AND DATA SOURCES

The source for exposure and injury data was the NASS/CDS (National Automotive Sampling System/Crashworthiness Data System) years 1993 to 2015. NASS/CDS is a weighted estimate of tow-away crashes occurring in the United States. The NASS/CDS weighted data contains approximately 59 million drivers of passenger cars, SUV's, passenger vans or light trucks (pickups) who were exposed to crashes. NASS/CDS data were disaggregated by vehicle model year and crash mode. Since this study focused on the safety changes for belted drivers, only vehicles with belted drivers were included. The resulting exposed population of belted drivers including those with unknown injury was 27,347,705.

The resulting data permitted the assessment of changes in injury distributions and rates by model year, crash mode and body region for belted drivers. The front, side and rear crash mode categories excluded all rollovers. The rollover crash mode contains all rollovers including those with planar impacts as an earlier or later event.

The HARM calculations applies a weighting factor to each AIS 3+ injury in the database. The weighting factor is proportional to the cost of the occupant's most serious injury. In general, minor and moderate injuries (AIS 1 and 2) are high frequency, events that tend to cloud the analysis of serious injury reduction by safety systems. For this reason, AIS 1 and 2 injuries were excluded from the AIS 3+ HARM calculations. The AIS 3+ HARM, measured in equivalent fatalities, was based on NHTSA's data on average cost of injuries. The equivalent fatality measurement is obtained by normalizing the average cost of a given injury by the cost of a fatality. The average cost of each injury severity was obtained from a Table E-1 in the 1995-1997 NASS/CDS Summary [NHTSA 2001]. The injury cost values are: MAIS 3, $98,011; MAIS 4, $221,494; MAIS 5, $697,533; and MAIS 6, $822,328.

In order to examine how the HARM content has changed with model year, it is necessary to examine how the injury rate or some equivalent factor has changed. The rate of AIS 3+ injuries is a commonly used injury risk factor. For the 1985 to 2015 population of interest the distribution of AIS 3, 4, 5 and 6 was 74%, 18%, 8% and 2%, respectively. When HARM weights are applied, the distributions become: 40%, 22%, 29% and 9%. By applying HARM weighting, the influence of AIS 3 injuries is reduced and the more severe injuries are given added priority. The Mean AIS 3+ HARM per exposed occupant provides an injury rate similar to the AIS 3+ rate but with more priority on the AIS 4+ injuries.

The Mean HARM for each category of interest was calculated by dividing the HARM suffered by drivers by the number of drivers exposed to that category. The Mean HARM results were multiplied by 100 to simplify the presentation.

The total and mean AIS3+ HARM for each model year grouping was calculated for each crash mode – frontal, near-side, far-side rear and rollover. The data was further disaggregated by vehicle class – passenger cars (PC), sport utility vehicles (SUV), light trucks (LT) and minivans (MV). The distribution of belted drivers by vehicle class was: PC-66%; SUV-16%; LT-11% and MV-7%. Since the entire populations of LT, SUV and MV constituted about one third of the vehicle population and they were combined in a single group. Changes in total AIS 3+ HARM distribution and Mean HARM by crash mode, model year grouping and vehicle class were computed and reported.

RESULTS

Vehicle model-years were aggregated by 3 model year groupings – 1985-1994; 1995-2000; 2001-2015. The NASS/CDS was queried for all injuries by AIS including AIS 0 (no injury) and unknown injury. This total population was 27,347,699. The total AIS 3+ HARM for the three model year groupings were 27%, 34% and 39%. The total AIS 3+ HARM for each model year grouping was calculated for each crash mode – frontal, near-side, far-side, rear and rollover. Changes in total AIS 3+ HARM distribution and Mean AIS 3+ HARM by crash mode and model year grouping were reported.

Figure 1 shows the total AIs3+ HARM distribution by crash mode and how it has changed with the model year groupings. The percentages for each model year grouping add to 100%, consequently the Figure shows the distribution for each model year grouping but not the total content for that group.

The changes in Mean AIS 3+ HARM by Crash Mode and Model Year Groupings are displayed in Figure 2.

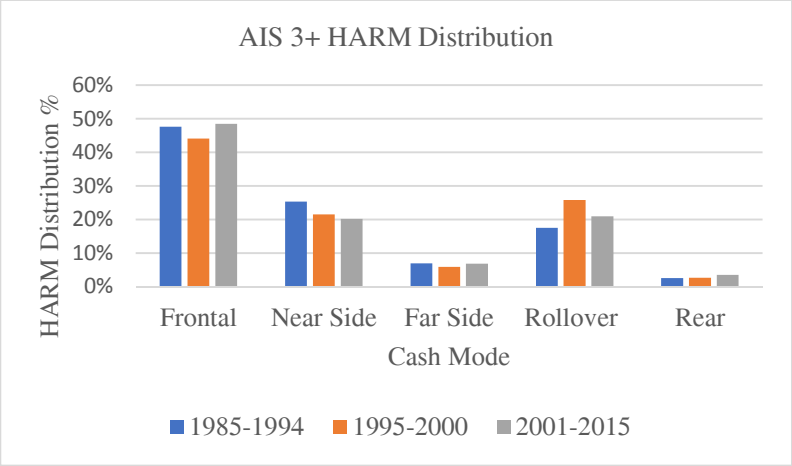

Figure 1. Distribution of Restrained Driver AIS 3+ HARM by Crash Mode and Vehicle Model Years

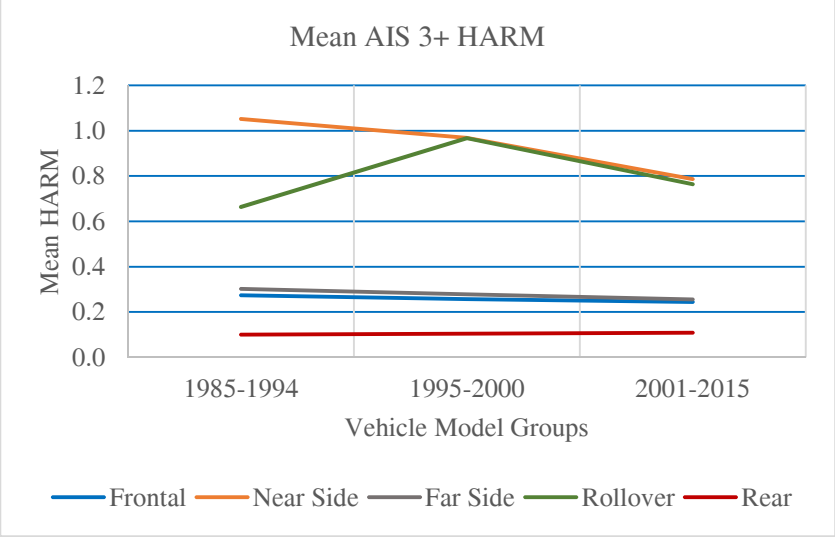

Figure 2. Distribution of Restrained Driver Mean AIS 3+ HARM by Crash Mode and Vehicle Model Years

Table 1 shows how the distribution AIS 3+ HARM has varied among vehicle types for the three vehicle model year groupings.

Table 1.
Distribution of Belted Drivers and AIS 3+ HARM by Vehicle Classes and Model Year Groups

	Pass Car		Lt Truck, SUV, Van	
Model Years	Drivers	HARM	Drivers	HARM
1985-1994	67.1%	71.7%	32.9%	28.3%
1995-2000	68.0%	71.1%	32.0%	28.9%
2001-2015	63.7%	67.2%	36.3%	32.8%

Table 2 shows how the distribution mean HARM has varied among vehicle types for the three vehicle model year groupings.

Table 2.
Belted Driver Mean AIS 3+ HARM by Crash Mode and Model Year Groups for Passenger Car and Light Truck, SUV and Van Groupings

Lt Truck, SUV, Van					
Model Year	**Frontal**	**Near Side**	**Far Side**	**Rollover**	**Rear**
1985-1994	0.275	0.413	0.241	0.445	0.065
1995-2000	0.242	0.407	0.245	0.720	0.026
2001-2015	0.208	0.749	0.192	0.701	0.050
Average	0.236	0.547	0.220	0.647	0.047
Pass Car					
Model Year	**Frontal**	**Near Side**	**Far Side**	**Rollover**	**Rear**
1985-1994	0.272	1.377	0.319	0.958	0.111
1995-2000	0.263	1.154	0.288	1.204	0.126
2001-2015	0.265	0.804	0.281	0.971	0.135
Average	0.266	1.081	0.294	1.058	0.126

DISCUSSION

Figure 1 shows that the largest source of AIS 3+ HARM to belted drivers in the 2001 and later NASS population remains the frontal crash mode. Figure 2 indicates that the reduction in Mean AIS 3+ HARM has been relatively small for frontal crashes. Table 2 shows that for frontal crashes, most of the reductions in Mean AIS 3+ HARM have been in vehicles other than passenger cars.

Figure 2 shows that near-side and rollover injury rates have dramatically decreased for recent vehicle model years. Frontal and far-side crash mode injury rates have decreased slightly and rear has remained relatively constant, but at a low injury rate.

Table 1 permits the comparison of belted driver exposure and total AIS 3+ HARM distributions by crash mode for the three model year groupings. Each row adds to 100%, so the extent of safety improvements cannot be determined

from this table. It may be noted that passenger cars still comprise the largest fraction of vehicles in the NASS/CDS – 63.7% in the 2001-2015 model year grouping. They also account for 67.2% of the total AIS 3+ HARM.

Safety initiatives that may have influenced the side crash mode improvements include the IIHS side impact rating, the NHTSA FMVSS 214 upgrade, and widespread incorporation of air curtains. The changes to comply with standards may have been more extensive for cars than for light trucks. The reason for the increase in near-side Mean AIS 3+ HARM for the non-passenger car category cannot be explained from the data in this paper. However, the near-side Mean AIS 3+ HARM for the combined group of light truck, SUV and van was lower than the passenger car near-side Mean AIS 3+ HARM.

For rollovers, the large reduction in Mean AIS 3+ HARM occurred in both vehicle groupings. Safety initiatives that may have influenced rollover improvements include the roof strength rating by IIHS, FMVSS 216 upgrade, voluntary incorporation of air curtains that function in rollover and widespread introduction of electronic stability controls.

REFERENCES

Eigen A, and Digges K, (2013) Safety changes in the us vehicle fleet by vehicle model year 2013 ESV Conference, Paper Number 13-0062, 2013

Fildes B, et. al. (1992) Feasibility of occupant protection meassures, Monash University Report to Federal Office of Road Safety, Australia, CR100, June 1992.

Malliaris A, Hitchcock R, Hedlund J, (1982) A search for priorities in crash protection.SAE International paper #820242. Society of Automotive Engineers, Warrendale, PA.

National Highway Traffic Safety Administration (2001) National Automotive Sampling System Crashworthiness Data System 1993 – 1997, DOT HS 809 203, page 152, February 2001.

National Highway Traffic Safety Administration, National Automotive Sampling System Crashworthiness Data System Data Set, 1995 – 2015, Washington, DC.

TRENDS IN PEDESTRIAN PROTECTION FOR VEHICLES RATED BY AUSTRALASIAN NCAP

Michael Paine

David Paine

Vehicle Design and Research, Australia

Andrew van den Berg

Giulio Ponte

Centre for Automotive Safety Research, Australia

Paper Number 19-0270

ABSTRACT

Analysis of scores in pedestrian protection tests conducted by ANCAP between 2001 and 2017 indicates that the average score has improved from 7.5 to 25. This has been achieved by steady improvement in the design of relevant vehicle components. Many of these improvements are unlikely to have significant adverse effects on costs or vehicle appearance, provided that good design for pedestrian protection is taken into account early in the design phases for the vehicle.

Based on several real-world crash studies, it is estimated that the improvement of 17.5 points is associated with a 21% reduction in the risk of serious injury for pedestrians.

The improvement was likely driven by NCAP programs in Europe, Australia and Japan, the introduction of GTR9/UN127 in most developed nations (but not Australia) and, more recently, fleet demand for 5-star rated vehicles.

INTRODUCTION

In 2000 the Australasian New Car Assessment Program (ANCAP) commenced rating pedestrian protection using the same protocol as Euro NCAP. This has enabled some Euro NCAP results to be used for ANCAP ratings. Between 2000 and 2017 ANCAP rated more than 600 vehicles, with about half of these ratings based on tests carried out by Euro NCAP. Almost one third of the pedestrian tests were carried out by the Centre for Automotive Safety Research (CASR) in Adelaide, South Australia.

This paper sets out the results of an analysis of the trends with pedestrian protection ratings during the period 2001-2017. An estimate is made of the road trauma savings due to improvements in pedestrian protection.

BACKGROUND

The role of the design of the front of the vehicle in the risk of serious injury to pedestrians has been recognised for many years. Fisher and Hall (1972) looked at the influence of frontal design and speed of impact. Harris (1976) developed early test procedures using the sub-system approach where separate impacts are conducted using headforms and legforms to simulate a collision between pedestrian and vehicle. The European Enhanced Vehicle Safety Committee (EEVC) developed a draft protocol in the late 1980s. This became the basis of the first Euro NCAP protocol for pedestrian protection, which was implemented in 1997 (Lawrence & Hardy 1998).

ANCAP implemented the same pedestrian protection protocol as Euro NCAP in 1999, as part of a package to align with Euro NCAP test and assessment protocols. The first ANCAP results were published in 2000 (Paine & Coxon 2000). Since then CASR has conducted testing for ANCAP and contributed to the development and interpretation of the Euro NCAP protocols.

Test protocol

The test protocol requires three sets of sub-system tests. Impactors used for these tests represent an adult head and a child head striking the bonnet and windscreen areas, an upper legform striking the leading edge of the bonnet and a lower legform striking the bumper fascia. Scores are allocated on the basis of the head injury criterion (HIC) when using the head impactors (maximum 12 points each for the child and adult head impactors respectively), bending moment and forces in the case of the upper legform (maximum 6 points) and for the lower leg impactor shear displacement, knee bend angle and tibia acceleration were measured giving a maximum 6 points.

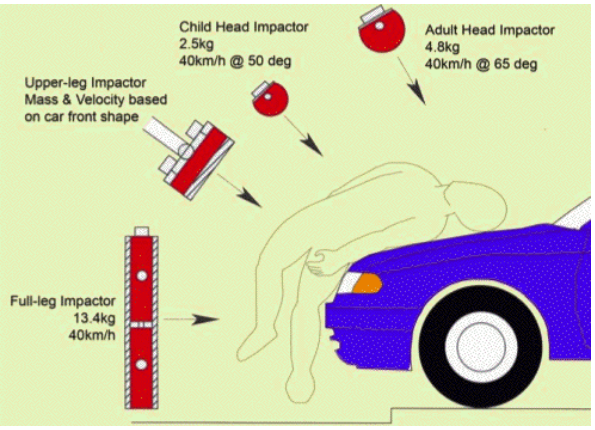

Figure 1. Sub-system tests for pedestrian protection (circa 2008)

An overall score is derived by summing the subsystem scores. Over the period of analysis the maximum available overall score has remained at 36. Between 2000 and 2010 the results were presented as star ratings and as a descriptive rating from 2011:

Table 1 ANCAP Pedestrian Protection Ratings

Score	2000-2010	2011+
27.5 or more	4 stars	Good
18.5 to 27.49	3 stars	Acceptable
9.5 to 18.49	2 stars	Marginal
0.5 to 9.49	1 Star	Poor
Less than 0.5	Zero stars	Poor

There were minor changes to the protocol in 2002 (discussed in Ponte et al., 2004) and significant changes in 2010. The 2010 change generally resulted in lower scores (Ponte et al., 2013).

In 2012 ANCAP introduced the "grid method" where the vehicle manufacturer submits detailed head impact test results for every 100x100 mm grid location and the ANCAP laboratory conducts verification tests on a sample of grid locations. An adjustment is made to the final manufacturer expected score if there is a discrepancy between the submitted and verification test results. These changes also influenced the pedestrian protection scores, but to a lesser extent than the change in 2010.

In 2015 ANCAP replaced the "TRL" lower legform with the "FlexPLI" legform and also made significant changes to the location, energies and performance criteria for the upper leg impactor.

No adjustment for these effects has been made in the following analysis but, generally, the observed improvements will be conservative (vehicles rated to the newer protocols will have slightly better pedestrian protection than the scores suggest).

Other influences on vehicle design

In 2009 Global Technical Regulation 9 (GTR9/UN Regulation 127) "Pedestrian Safety" was published by the United Nations. In 2011 the Australian Department of Infrastructure and Transport issued a Regulation Impact Statement (RIS) recommending that the GTR be implemented as an Australian Design Rule (Department of Infrastructure and Transport, 2011). However, the RIS was withdrawn and the initiative did not go ahead (King, 2011). The latest WHO report on the Global Status of Road Safety notes that "Australia has signed the UN127 for Pedestrian Protection as a Contracting Party but is not enforcing it." (WHO 2018).

Although Australia has not implemented GTR9/R127 it is likely that most cars marketed in Australia have been designed to meet the requirements since they are usually also sold in Europe or Japan. Exceptions are where the extra features such as a pop-up bonnet are standard in Europe/Japan but not in Australia or where additional (e.g. aftermarket bullbars) structures are fitted to the front of the vehicle .

In 2012, under its new Road Map, ANCAP set a minimum pedestrian protection performance threshold as part of an assessed vehicle's overall star rating, (ANCAP 2011). This provided much stronger incentive for manufacturers to do well in the pedestrian impact tests. The Road Map requirements became progressively more stringent between 2012 and 2017. For example, to earn an overall rating of 5 stars in 2012 a vehicle needed at least a "marginal" pedestrian protection rating (minimum of 9.5 points). This increased to a requirement of an "acceptable" rating (minimum 18.5 points) in 2014.

The 2011 ANCAP Road Map set lower pedestrian safety performance requirements for high-seat vehicles (some SUVs, 4WDs, utilities and vans) in recognition of industry claims about the challenges faced in designing these vehicles to perform well in pedestrian protection tests. For example, a pedestrian protection rating of "acceptable" (18.5 or more) was not required for an overall 5 star rating of high-seat vehicles until 2017. However, soon after ANCAP published its 2011 Road Map, Euro NCAP awarded the Australian-designed Ford Ranger pickup the highest score for pedestrian protection of any vehicle tested (at the time), bringing into question the claims about high-seat vehicles.

In 2012 BHP introduced an NCAP 5-star requirement for company light vehicle purchases and for contractors using BHP worksites (Jenkins 2012). Because Euro NCAP and ANCAP included pedestrian protection in the assessment this likely

resulted in improved pedestrian protection for vehicles typically purchased by mining companies.

Figure 2. Ford Ranger - a high-seat vehicle that provides good pedestrian protection

SOURCES OF DATA

A database of ANCAP safety ratings from 2000, maintained by one of the authors, was analysed to determine trends in pedestrian protection scores. Only overall scores were analysed.

The trends in pedestrian protection scores were compared with a recent analysis of trends in pedestrian injury in road crashes in Australia and New Zealand (Keall et al., 2018).

RESULTS

Figure 3 illustrates the results of the analysis. A linear trend line for all vehicle types indicates that the average pedestrian protection score improved from 7.5 in 2001/2 to 25 in 2017, a threefold improvement.

Note that the values are based on the number of ANCAP ratings for each vehicle type and the year in which the tested model was released. The method does not account for annual sales. Vehicle types with small sample sizes are not shown in the chart but are included in the overall values ("All"). Appendix B has a table with all data.

RISK OF INJURY

Paine and Coxon (2000) describe Transport Research Laboratory estimates that 8% of all pedestrian fatalities and 21% of all pedestrian serious injuries in the Europe could be prevented through improved vehicle design. The research was associated with Euro NCAP introducing pedestrian protection tests in 1997 (Lawrence 1998).

There have been several studies looking for a correlation between NCAP pedestrian protection scores/ratings and real-world injury to pedestrians. For the purpose of comparison, in the following analysis we translate the estimated injury savings to a percentage reduction for a 10-point improvement in ANCAP/Euro NCAP pedestrian protection score.

Lawrence and others (2006) estimated that introducing the GTR for pedestrian protection in Europe would result in a 4% reduction in fatalities and a 12% reduction in serious injuries. It should be noted that vehicles which score well in NCAP testing are likely to pose a lower risk of pedestrian injury than vehicles which just meet the minimum

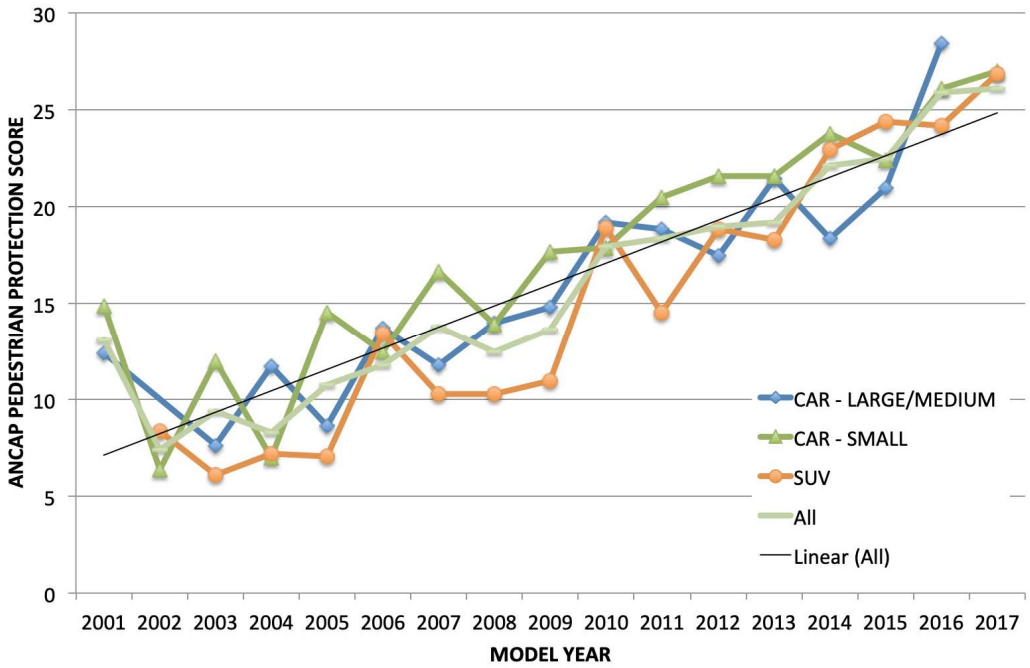

Figure 3. Average ANCAP Pedestrian Protection Scores

requirements of the GTR and so benefits of a high NCAP score will be greater. Based on this, it is estimated that the benefit from a 10-point improvement in NCAP score is at least a 12% reduction in serious injuries.

The Australian RIS that attempted to introduce GTR9 in 2011 used Lawrence's estimates in the benefit-cost analysis (Department of Infrastructure and Transport, 2011).

Strandroth et al., (2011) analysed 609 Swedish crashes where a Euro NCAP-rated vehicle collided with a pedestrian. They grouped the vehicles into 1 and 2 star pedestrian ratings (there were insufficient cases of 3 stars or better). The average score was 6.24 for 1-star vehicles and 13.84 for 2-star vehicles. It was found that injury severity was lower for 2-star cars compared to 1-star cars, with the relative difference in serious injuries (AIS2+) being 17% lower with 2-star cars and severe injuries (AIS3+) were 28% lower, compared to 1-star cars.

This is equivalent to a 22% reduction in serious injury risk for a 10-point improvement in NCAP score.

Pastor (2013) analysed the German National Accident Records and, from 7,576 relevant records, found that the risk of a fatality is reduced by 35% for a vehicle scoring 22 for pedestrian protection, compared with a vehicle scoring 5. The risk of serious injury was reduced by 16%. This is equivalent to a 9.4% reduction in serious injury risk for a 10-point improvement in score.

Keall and others (2018) analysed data on police-reported road crashes in Australia and New Zealand and calculated the risk of serious injury to pedestrians by vehicle type and year of manufacture. Based on that analysis the average risk for vehicles manufactured between 1997 and 2001 was 39.4% compared with 33.6% for vehicles manufactured between 2007 and 2012. This is a 15% reduction in risk.

Over the period 2001 to 2012 the average ANCAP pedestrian protection scores improved from 7.5 to 17. The Keall study did not look specifically at ANCAP pedestrian scores and there are numerous confounding factors but over the period when ANCAP scores improved by 10 point there was an observed 15% reduction in the risk of serious injury to pedestrians.

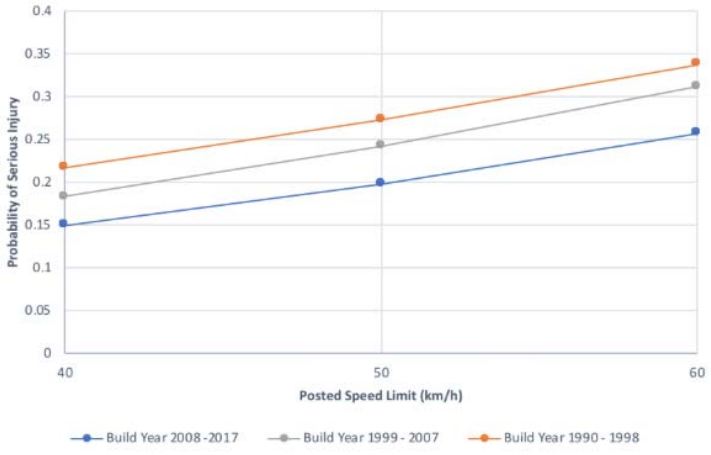

Figure 4. Probability of serious/fatal injury for pedestrians struck by a car in South Australia (1990-2016)

One of the present authors recently examined South Australian pedestrian crash data from 1990 to 2016. A total of 1,118 serious injury crashes were analysed using a logistic regression model to predict the probability of a fatality or hospital admission. Figure 4 presents the key results of the analysis for posted speed limits of 40, 50 and 60 km/h. The probability of serious injury for vehicles built between 2008 and 2016 was around 19% less than those built between 1999 and 2007. The average ANCAP pedestrian scores for these two build date ranges were 11 and 19 respectively.

Figure 5 shows the derived values for the five studies. Overall it is estimated that a 10 point improvement in NCAP score is associated with a 16% reduction in serious injuries to pedestrians.

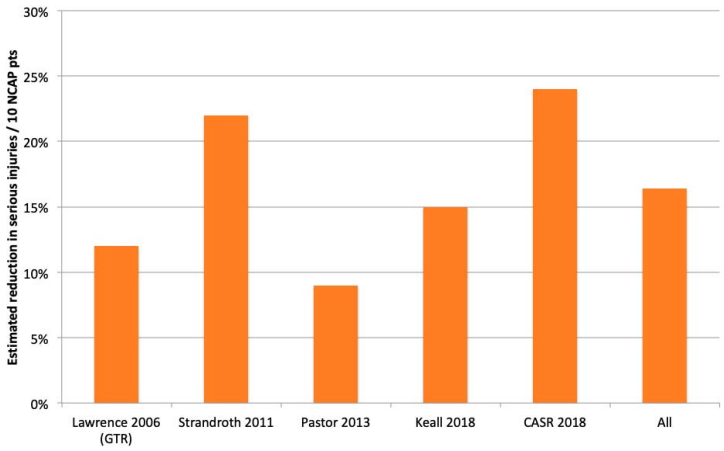

Figure 5. Derived reduction in serious injuries to pedestrians due to a 10 point improvement in NCAP score

Therefore, assuming a linear relationship, the observed 17.5 point improvement in average ANCAP pedestrian scores between 2001 and 2017 equates to a 29% reduction in serious injuries over this period.

IMPROVEMENTS TO VEHICLE DESIGN

Several of the papers referred to above contain observations and information about vehicle design to improve pedestrian protection.

Lawrence (1998) notes that that relatively simple changes to detail in the early design stages of a new model can lead to major improvements in pedestrian protection. Suggested improvements include front bumper fascia re-design (deeper profile, with localised compliance and energy absorption), headlamps (plastic better than glass), bonnet leading edge (locate bonnet latch further rearwards, relocate transverse stiffeners) and bonnet/fender tops (design for crush, increase under-bonnet clearances).

The Australian RIS (Department of Infrastructure and Transport, 2011) quotes the head of a vehicle insurance research organisation that is an ANCAP stakeholder and also conducts evaluations of the cost of repairs in low speed collisions: "...this proves that manufacturers can design vehicles that can perform well in both pedestrian safety and vehicle protection".

The RIS also referred to UK research (Lawrence, 2006) that estimated the cost of design changes to meet the GTR requirements ranged from 27 Euro for a small family car to 47 Euro for a large SUV. However, it was noted that executive cars and sports cars might need relatively expensive active safety such as pop-up bonnets (subsequent Euro NCAP ratings effectively show that this is not essential for meeting the GTR).

Two of our authors have conducted pedestrian protection test for ANCAP over many years. They have observed a change in attitude of vehicle manufacturers towards these tests. In particular, many manufacturers have appointed engineers who specialise in design for pedestrian protection and these engineers have frequently attended the ANCAP testing.

Most of the improvements in head protection are the result of optimising the deformation characteristics of the vehicle's hood, to help 'cushion' the head in a pedestrian head impact. Additionally, allowing adequate space between the under-surface of the optimised vehicle hood and any hard structures underneath it has also been undertaken by most manufacturers to ensure the protective design of the hood is not undone by a rigid structure within the deformations zone (see Hutchinson et al., 2011). This has been observed during testing, as manufacturers are genuinely considering the height and placement of rigid structures such as suspension towers, batteries and engine intakes so deformation space is provided during an impact. Traditionally rigid hood support areas have also been addressed to improve head protection. Examples include moving the top of the firewall lower and rearward and placing a collapsible plastic plenum to create the seal between the rear of the hood and the firewall (a traditionally stiff hood support area). Similarly, the structures of the sidewall supports of the engine bay have been lowered, and collapsible brackets have been used to position wheel guard panels so head impacts in these areas are also less severe.

For vehicles with restrictions on available under bonnet space, active safety systems such as deployable or "pop-up" hoods are being used to create space and give clearance between rigid structures beneath the hood, during a head impact.

Improvements for lower leg protection include the addition of energy absorbers (foam or crush cans) and lower stiffening rails to keep a pedestrian's leg from bending under the front of the vehicle.

Improvements to the upper leg area have involved moving the radiator support and the bonnet latch rearward and creating space between the latch and outer bonnet surface. Headlights with plastic lenses (instead of glass) with breakaway mounting tabs also improve pedestrian protection.

Appendix A contains examples of the changes observed by CASR personnel.

DISCUSSION

The importance of good vehicle design in preventing serious and fatal injuries to pedestrians was recognised in the 1970s at a time when regulations were introducing substantial improvements to vehicle occupant protection (e.g. seat belts). However, the development of suitable test methods for assessing pedestrian protection did not make good progress until the late 1980s, mainly through the work of EEVC.

Euro NCAP introduced pedestrian protection ratings in 1997 as part of its new vehicle safety program. NCAPs in Australia and Japan introduced pedestrian protection ratings a few years later. These consumer programs found that most vehicles of the day had woeful designs for pedestrian protection, although a few vehicles demonstrated that good design was possible without compromising style and functionality.

The first international regulation for pedestrian protection (GTR9/UN127) was published in 2009. Around this time Euro NCAP began to require

reasonable performance in pedestrian tests as part of its overall rating. These two developments likely focussed vehicle manufacturer attention on improving vehicle designs for pedestrian protection.

In 2011, the Australian government halted the process to implement GTR9/UN127 but it is likely that the Australian vehicle fleet still improved in terms of pedestrian safety, due to overseas developments (since most vehicles sold in Australia are built overseas). This would have been boosted by ANCAP adding pedestrian protection to its overall rating requirements from 2012.

ANCAP ratings show that there has been a steady improvement in pedestrian protection scores between 2011 (18) and 2017 (25). Noting that just passing the GTR is equivalent to an ANCAP score of 18 (Anderson et al., 2008), it is considered that most of the improvement can be attributed to NCAP programs in Europe, Japan and Australia.

In summary we agree with this statement: "In the absence of any pedestrian regulation in Australia, the incorporation of the pedestrian assessment as part of the ANCAP star rating is by far the most important mechanism for compelling manufacturers to think 'outside the car' and incorporate pedestrian safety in vehicle design." (Ponte et al., 2013)

LIMITATIONS

It took several years for ANCAP to assign ratings to a large proportion of all models for sale in Australia and New Zealand. During the period 2001 to 2004 the ratings were dominated by models tested by Euro NCAP. These tended to be luxury models in Australia and this may have influenced the trends in early years.

Protocol changes described above will have influenced the scores and this has not been taken into account in the analysis of results in this paper.

ANCAP pedestrian protection ratings have not been the sole influence on pedestrian injury during the study period. Europe implemented GTR 9 in 2009 and many cars entering the Australian market since then are likely to have been designed to that regulation.

In 2003, most Australian states reduced residential speed limits from 60k/h to 50km/h. This had a substantial effect on pedestrian fatalities on these roads (Woolley, 2005). Additionally, there was also a reduction in pedestrian casualty crashes (and mean speeds on various roads) as a result of the speed limit changes (Kloeden et al., 2007). The speed limit changes perhaps brought many more car/pedestrian collisions into the 40 km/h impact range, where improved frontal design can be more effective.

Some variation between real-world and laboratory results is understandable because the ANCAP tests simulate a collision at 40km/h and collisions between cars and pedestrians occur over a much wider range of speeds. Design improvements that mitigate a 40km/h collision are unlikely to be as effective at 50km/h or higher speeds (Strandroth et al., 2011). In this regard, the data used for the CASR analysis was confined to posted speed limits from 40 to 60km/h.

The assumption of a linear relationship between NCAP score and risk of serious injury has not be verified but it is considered that over a small range of scores this assumption is reasonable.

CONCLUSIONS

ANCAP pedestrian protection testing between 2001 and 2017 indicates a steady improvement in vehicle design over this period, with the average score improving from 7.5 to 25. Based on several real-world crash studies, it is estimated that this improvement is associated with a 29% reduction in the risk of serious injury for pedestrians.

The improvement was likely driven by NCAP programs in Europe. Japan and Australia, the introduction of GTR9/UN127 in most developed nations (but not Australia) and, more recently, fleet demand for 5-star rated vehicles.

REFERENCES

ANCAP (2011) *ANCAP Rating Road Map 2011-2017*,

Anderson R, Ponte G and Searson D (2008) Benefits for Australia of the introduction of an ADR on pedestrian protection, Report CASR048, Centre for Automotive Safety Research Adelaide

Department of Infrastructure and Transport (2010) Regulation Impact Statement for Pedestrian Safety, Report DIT VSS 01/2011, January 2011, Canberra

Fisher A and Hall R (1972) The Influence of Car Front Design on Pedestrian Accident Trauma *Accident Analysis and Prevention* 4, pp47-58.

Hutchinson T, Searson D, Anderson R, Dutschke J, Ponte G, Van Den Berg A (2011) 'Protection of the unhelmeted head against blunt impact: The pedestrian and the car bonnet', 2011 Australasian Road Safety Research, Policing and Education Conference, Perth, 6-9 November 2011.

Jenkins D (2012) 'Light Vehicle Fleet Selection and NCAP', Presentation to SAE-Australasia Seminar on Fleet Safety, September 2012.

Kloeden C , Woolley, J, & McLean, J (2007). A follow-up evaluation of the 50km/h default urban speed limit in South Australia. 2007 Road Safety Research, Education and Policing Conference, Melbourne, Australia, 17-19 October 2007.

King C (2011) Pedestrian Safety and Bull Bars, media release CK006/2011, Parliamentary Secretary for Infrastructure and Transport, Canberra

Lawrence G and Hardy B (1998) Pedestrian safety testing using the EEVC pedestrian impactors, *Proceedings of 16th International Conference on the Enhanced Safety of Vehicles (ESV)*, Windsor

Lawrence G, Hardy B, Carroll J, Donaldson W, Visvikis C and Peel D (2006). A study on the feasibility of measures relating to the protection of pedestrians and other vulnerable road users. European Commission, EC Contract No. FIF.20030937

Paine M and Coxon C (2000) Assessment of Pedestrian Protection Afforded by Vehicles in Australia*, Impact Biomechanics & Neck Injury 2000*. Institution of Engineers Australia, Sydney

Pastor C (2013) Correlation between pedestrian injury severity in real-life crashes and Euro NCAP pedestrian test results, *Proceedings of 23rd International Conference on the Enhanced Safety of Vehicles (ESV)*, Seoul

Ponte G, van den Berg A, Streeter L and Anderson R (2004) Pedestrian protection and vehicle impacts; further results from the Australian New Car Assessment Program, *Proceedings of Australasian Road Safety Research, Policing and Education Conference*, Perth

Ponte G, van den Berg A, Anderson R and Linke B (2013) The Pedestrian Protection in Vehicle Impacts: Demystifying Pedestrian Testing Procedures and Assessment, *Proceedings of Australasian College of Road Safety Conference*, Adelaide

Strandroth J, Rizzi M, Sternlund S, Lie A and Tingvell C (2011) The correlation between pedestrian injury severity in real-life crashes and Euro NCAP pedestrian test results, *Proceedings of 22nd International Conference on the Enhanced Safety of Vehicles (ESV)*, Washington

WHO (2018) Global Status Report on Road Safety, World Health Organisation, Geneva

Woolley J (2005) Recent advantages of lower speed limits in Australia, *Journal of the Eastern Asia Society for Transportation Studies*, Vol. 6, pp. 3562 - 3573

APPENDIX A - EXAMPLES OF IMPROVEMENTS TO VEHICLE DESIGN (CASR)

Under-bonnet components

Mid-1980s: Stiff firewall and sides of engine bay supporting edge of bonnet. Minimal clearance between suspension tower/air cleaner and bonnet.

Early 2000s: Stiff firewall and sides of engine bay supporting edge of bonnet. Minimal clearance between suspension tower/engine cover and bonnet.

Recent: Firewall and sides of engine bay lowered with bonnet supported by collapsible elements. Suitable clearance is provided between suspension tower/other under bonnet structures and bonnet.

Top edge of fender

Traditional design: Wheel guard supported directly by stiff structure.

Recent design: Wheel guard supported by collapsible element.

Bumper design

Lower support in position to keep leg from bending under car and energy absorbing foam to protect the knee.

Leading edge of bonnet

Bonnet latch moved rearwards and radiator support moved rearward and lowered (recent model)

APPENDIX B - DATA

The following table includes the data presented in Figure 3.

Average ANCAP score for pedestrian protection [number of rated models]

YEAR MODEL RELEASED	CAR LARGE /MEDIUM	CAR SMALL /LIGHT	SUV	ALL
2001	12.4 [7]	14.9 [6]	-	13.1 [15]
2002	-	6.3 [3]	8.4 [9]	7.4 [13]
2003	7.6 [8]	12 [8]	6.1 [7]	9.4 [29]
2004	11.7 [8]	7 [8]	7.2 [4]	8.3 [25]
2005	8.6 [6]	14.5 [13]	7 [4]	10.8 [27]
2006	13.7 [11]	12.5 [6]	13.4 [11]	11.8 [38]
2007	11.8 [7]	16.6 [17]	10.3 [7]	13.8 [39]
2008	13.9 [10]	13.9 [23]	10.2 [7]	12.4 [47]
2009	14.8 [8]	17.7 [18]	10.9 [7]	13.7 [39]
2010	19.2 [5]	17.9 [18]	18.9 [8]	17.9 [33]
2011	18.8 [9]	20.5 [16]	14.5 [9]	18.4 [42]
2012	17.4 [13]	21.5 [10]	18.8 [11]	19 [43]
2013	21.4 [15]	21.6 [12]	18.3 [14]	19.2 [50]
2014	18.4 [3]	23.8 [11]	22.9 [6]	22.1 [30]
2015	20.9 [9]	22.4 [4]	24.4 [18]	22.5 [47]
2016	28.4 [6]	26.1 [13]	24.2 [9]	25.9 [29]
2017	-	27 [3]	26.9 [6]	26.1 [11]

Notes

"ALL" include other types of vehicles with small sample sizes

2001 data were mostly Euro NCAP ratings of "prestige" vehicles, as sold in Australia

TYPICAL PRE-CRASH SCENARIOS RECONSTRUCTION FOR TWO-WHEELERS AND PASSENGER VEHICLES AND ITS APPLICATION IN PARAMETER OPTIMIZATION OF AEB SYSTEM BASED ON NAIS DATABASE

Yi Cao
School of Transportation & Automotive, Xihua University
China

Lingyun Xiao
Corresponding author: xiaoly@dpac.gov.cn
SAMR Defective Product Administrative Center
China

Honglei Dong, Yan Wang
SAMR Defective Product Administrative Center
China

Xiaobo Wu
China National Institute of Standardization
China

Pingfei Li
School of Transportation & Automotive, Xihua University
China

Yuanchao Qiu
Shanghai University of Engineering Science
China

Paper Number 19-0272

ABSTRACT

The crash between two-wheelers and passenger vehicle causes a higher fatality rate and many casualties for the two-wheelers riders. Both two-wheelers and pedestrians are considered as VRU. Compared to pedestrians, two-wheelers are featured with fast moving speed and uncertain driving route, which poses a challenge to the optimal control for the autonomous emergency braking (AEB) system. This paper firstly screened 216 cases of frontal collision accidents between passenger vehicles and two-wheelers from the database of National Automobile Accident In-depth Investigation System (NAIS) in China, extracted the static and dynamic variables related to the pre-crash scenarios reconstruction in each case. This paper extracted four typical pre-crash scenarios between two-wheelers and passenger vehicles from 216 accident scenarios through clustering analysis and chi-square test, reconstructed and simulated typical pre-crash scenarios by using PreScan software and completed matching, optimization and analysis on the field of view (FoV), braking trigger width (w), time to collision (TTC) of AEB system to obtain the boundary parameter conditions of the AEB system to avoid crash or greatly reduce the collision speed, providing a reference for the development of AEB systems applicable to China's road traffic scenarios. The research method used in this paper is applicable to the reconstruction and simulation analysis of pre-crash scenarios for passenger vehicles and pedestrians as well as the parameter optimization of other ADAS. In addition, the research method used in this paper also provide a technical solution for the design, test and evaluation of the automatic driving function based on typical scenarios.

Key Words: two-wheelers; pre-crash scenario; accident in-depth investigation; clustering analysis; autonomous emergency braking system; advanced driving assistance system

INTRODUCTION

The vision for development of autonomous vehicle is to achieve “zero casualty, zero accident”. Advanced driving assistance systems (ADAS) have been put into the market as an important part of autonomous vehicles. However, in complex and diverse traffic scenarios, ADAS is still facing major challenges in the accuracy of scenario recognition and rationality of decision algorithms. At present, the test and evaluation on ADAS is mainly based on limited field operational test (FOT). But in real traffic scenarios, ADAS faces more complex and special traffic scenario elements, especially in different countries and regions with the particularity of traffic scenarios. Therefore, the evaluation method based on the limited field operational test has certain limitations and the test methods based on natural driving scenarios and dangerous scenarios gradually attracting great attention in the industry [1].

Both two-wheelers and pedestrians are vulnerable road users (VRU) in traffic scenarios. Two-wheelers riders and pedestrians are often vulnerable groups in road traffic accidents. Compared with pedestrians, two-wheelers are featured with fast moving speed and uncertain driving route, so the two-wheelers are more likely to cause casualties. According to the 2015 statistical report of the World Health Organization (WHO), cyclists and motorcyclists of powered two or three wheelers accounting for 27% of fatality rate in road traffic [2]. The number of two-wheelers is huge in China, in recent years, especially after the promotion of green travel and shared bicycle travel in large and medium-sized cities in China, the number of riders and passengers of two-wheelers has increased significantly. At the same time, the number of fatality and injury of riders and passengers of two-wheelers in traffic accidents are also increasing. According to statistics, from 2004 to 2010 the number of fatality in road traffic accidents decreased from 107,077 to 65,225, but the number of fatality from powered two-wheelers (PTW) in road traffic accidents increased from 589 to 4,029 in China [3] [4]. In the Advanced Driving Assistance System (ADAS), the AEB system is the most popular type and has a great effect on improving the safety of vehicle in collisions. According to the research data providing by the Insurance Institute for Highway Safety (IIHS), AEB can reduce 27 % of traffic accidents [5]. The Federal Highway Research Institute (BASt) study shows that 70% of serious traffic accidents can be avoided by ADAS [6]. However, AEB still needs further research and evaluation on the accurate identification and reasonable decision-making of VRU, especially two-wheelers. With the gradual increase in the fatality rate of two-wheelers in recent years, global attention has been paid to the two-wheelers collision accidents. Some institutions have added or are ready for adding the collision avoidance assessment indicators for the two-wheelers in the relevant collision evaluation procedures. At present, Europe New Car Assessment Program (Euro-NCAP) [7] has added the AEB safety test for the protection of users of two-wheelers in the protection of VRU in 2018 and will add the AEB safety test for PTW in 2020. But now China New Car Assessment Program [8] (C-NCAP 2018 version) have not included the safety requirements for the AEB system aiming at two-wheelers.

At present, the AEB system as a key ADAS, has been installed and used in some vehicles and has been gradually launched in the market. However, the AEB system has caused a defective car recall case due to its false identification and mis-operation in complex road traffic scenarios. Therefore, the accuracy of the AEB system for scenario identification still requires in-depth research and test, especially the accuracy of identifying VRU. But currently, there are limited research literature about the safety tests of the AEB for VRU and the research literature mainly focuses on the safety tests of the AEB for pedestrians, so there are fewer literature about the safety tests of the AEB for two-wheelers. Based on the typical pedestrian dangerous condition on the roads in Shanghai, Liu Ying et al. [9] obtained five typical hazard scenarios by using clustering analysis and simulation analysis of AEB-pedestrian, but this study did not analyze the matching and optimization of AEB parameters. Su Jiangping et al. [10] made the analysis based on the pedestrian dangerous condition stored in the natural driving data of five cities in China and obtained four typical pedestrian traffic conflict scenarios. Chen Qiang et al. [11] analyzed three typical pedestrian use scenarios based on accident data and obtained the result that AEB system can reduce by 20% of pedestrian collision accidents, but this study also did not analyze the matching between pedestrian dangerous scenarios and AEB parameters. James Lenard et al. [12] conducted an analysis on pedestrian risk scenarios based on the UK OTS and STATS19 accident databases and constructed an AEB test scenario based on parameter deduction. Huang and Yang et al. [13] analyzed the typical pedestrian use scenarios based on the STRADA database and expertise, established a mathematical model and analyzed the field of view (FoV) parameter selected of the AEB sensor, but this study did not involve other parameters of the AEB system. Erik Rosen et al. [14] analyzed the correlation between the selection of FoV parameters of the AEB system and reduction of pedestrian collision

accidents based on German GIDAS data. David Good et al. [15] analyzed the collision speed distribution between pedestrians and vehicles based on the US GES and FARS accident data and designed the pre-crash system test scenario.

The extraction of pedestrian risk scenarios and the analysis on the parameters of AEB system based on natural driving data and accident data provide reference for the extraction of two-wheelers risk scenarios with optimization and design of corresponding parameter of AEB system. Liers [16] analyzed the accident pattern of PTW and the typical accident scenarios based on the German GIDAS data, concluded that the proportion of collisions of PTW crossing the road and intersection is high and analyzed the main cause of PTW accident, but this study did not consider the design of the AEB two-wheelers test scenario. Based on the typical risk use cases of two-wheelers on the roads in Shanghai, Li Lin et al. [17] obtained seven typical risk scenarios by using clustering analysis and chi-square test and conducted simulation analysis by using simulation software, but the matching and optimization of the AEB parameters were not studied here. Sui and Zhou et al. [18] analyzed the basic situation of crush accident between two-wheelers and automobiles based on Chinese road traffic accident data and concluded that the main scenarios of crush between two-wheelers and automobiles is that the car going straight at the speed of 60km/h or above has a vertical collision with the PTW going straight at an intersection in the day and recommended as a typical scenario for the AEB two-wheelers test, but this study did not perform scenario reconstruction and simulation analysis. Based on traffic accident data, Hu Lin et al. [19] extracted 11 typical car and two-wheelers collision accident scenarios by using clustering analysis and respectively obtained the AEB test scenarios of cars-electric powered two wheelers, cars-motorcycles and cars-bikes collision, but this study did not perform scene reconstruction and parameter optimization analysis. Compared with pedestrians, two-wheelers, especially PTW, have the characteristics of fast driving speed and uncertain driving route. They pose great challenge to sensor selection, parameter optimization and performance evaluation of AEB system and they need to be solved urgently.

In view of two-wheelers safety test by the AEB system, this paper firstly screened the frontal collision accident between passenger cars and two-wheelers based on the NAIS accident in-depth survey data, extracted the static and dynamic variables of the accident cases, extracted the typical pre-crash scenarios of two-wheelers and passenger cars by clustering analysis and chi-square test and performed reconstruction and simulation of typical pre-crash scenarios by using PreScan software. Then, the main control parameters of the AEB system were matched and optimized to obtain the boundary parameter conditions for the AEB system to avoid collision or greatly reduce the collision speed.

DATA SOURCES

The basic data studied in this paper is derived from the vehicle accident in-depth data collected by the National Automobile Accident In-depth Investigation System (NAIS). NAIS mainly collects the data about serious road traffic accidents in China. In such accident case, one or more fatality exists or accident participant injury value is AIS≥3. Each accident case includes about 2,200 parameters, including people, vehicles, roads and environmental information. NAIS was established by the State Administration for Market Regulation Defective Product Administrative Center together with universities and research institutions, as shown in Figure 1. The purpose of establishing NAIS is to collect in-depth data with the characteristics of road traffic accidents in China and establish a basic database for active and passive safety research of vehicles. The accident areas include plain areas, mountainous areas, plateau areas and coastal areas etc. In addition, the data about urban road accidents, highway accidents and rural road accidents are also collected. The accident data is representative. The NAIS database includes coded data, accident photos, police data, accident scene videos (if available), PC-Crash accident reconstruction files, CAD accident scene maps and accident analysis reports.

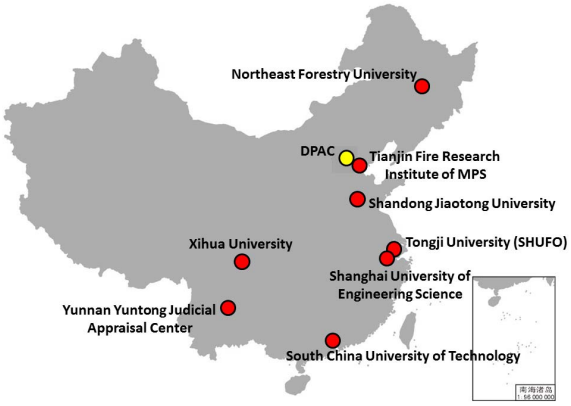

Figure 1. Map of NAIS sites

This paper selected and analyzed 2,203 motor vehicle collision accident cases (by the end of 2017) from the NAIS accident database. There were 406 accidents involving motor vehicles and two/three-wheelers, accounting for 18% of all accidents, as shown in Figure 2. According to the number of accidents, it can be seen that the proportion of collisions between motor vehicles and two/three-wheelers is high in China and the proportion of such accident will continue to increase with the increasing number of Chinese two-wheelers, especially bicycles. At present, two-wheelers are widely used in China, they are popular in large and medium cities and rural areas. And there are many violations of traffic regulations by two-wheelers riders. Meanwhile, the routes and rules of two-wheelers in the traffic scene are more complicated. Therefore, it is more difficult for ADAS especially the AEB system to identify. And it is necessary to carry out in-depth research and analysis.

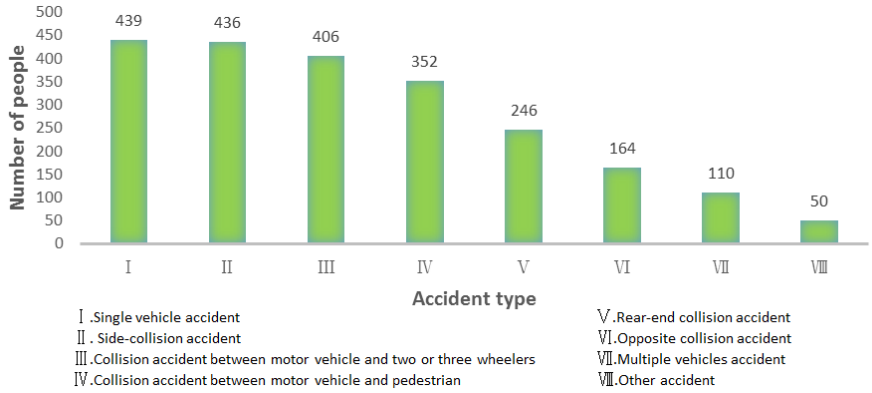

Figure 2. Classification of NAIS accident data (by accident pattern)

In the analysis of NAIS data about 2203 accidents, it is found that the number of fatality in the collision accident between motor vehicles and two or three wheelers is 362 people, where the most fatality occurred. Meanwhile, it is also found that its accident fatality rate is second only to the collision accident between motor vehicle and pedestrian, up to 33%, as shown in Figure 3. Therefore, both the riders of two or three wheelers and pedestrians are VRU, which should be given more attention to study during the development of ADAS and automated driving functions. Because the AEB system is mainly used to reduce vehicle frontal collision accidents and it is considered that three-wheelers are seldom used in other parts of the world, this paper selected 216 frontal collision accidents between passenger car and two-wheelers to explore and extract the static and dynamic information about pre-crash scenarios.

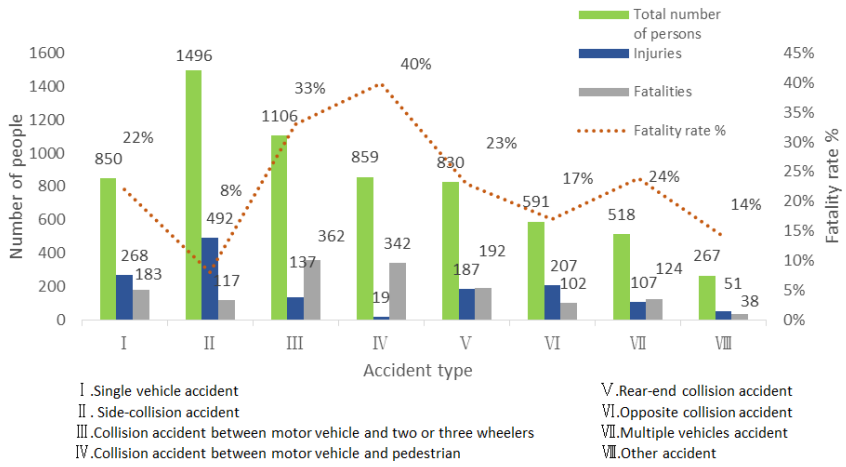

Figure 3. Classification of NAIS accident data (by casualty)

EXTRACTION OF TYPICAL SCENARIOS BASED ON CLUSTERING ANALYSIS AND CHI-SQUARE TEST

Variables Selection and Definition

The main purpose of this paper is to extract the typical scenarios from the in-depth accident data to conduct simulation analysis on the parameters of the AEB system. It is necessary to select the parameter variables that are highly compatible with the AEB system function and sensor environment and are easy to reproduce in the field operational test for clustering analysis. The parameter variables include environment variables, road variables, traffic participants variables and dynamic variables. The in-depth accident data involves more than 2,200 parameter variables. After analysis and screening, seven parameter variables are selected and defined as follows:

(1)Section: It refers to the type of road and it is divided into straight road and intersection;

(2)Light: It means whether the light is good when the accident occurs. It is divided into daytime, light at night and no light at night.

(3)Motion of passenger vehicle: It refers to the motion pattern of passenger vehicle. It is divided into “go straight, turn left and turn right”, as shown in Figure 4.

(4)Motion of two-wheelers: It refers to the motion pattern of two-wheelers. It is divided into “go straight, turn left and turn right”, as shown in Figure 4.

(5)Relative motion zones: It is determined by the angle α formed by the speed direction of passenger vehicle v_v and two-wheelers v_t. If both passenger vehicle and two-wheelers have a turn, the speed direction before the turn is taken as the direction, the direction v_v is 0° and the counterclockwise direction is positive. Based on the different range of α value, it is divided into Zone 1, Zone 2, Zone 3 and Zone 4, as shown in Figure 5. The relative motion relationship between passenger vehicle and two-wheelers can be uniquely determined by the relative motion zones and the motion pattern of both passenger vehicle and two-wheelers.

(6)Type of two-wheelers: It includes bicycles, electric two-wheelers and motorcycles. Because electric two-wheelers and motorcycles are faster than bicycles, they are deemed as PTW in this paper. That is to say, two-wheelers are divided into bicycles and PTW.

(7)Speed of passenger vehicle: It refers to the vehicle speed during collision, which can be accessed through accident site trace calculation, accident reconstruction simulation analysis and accident calculation by video.

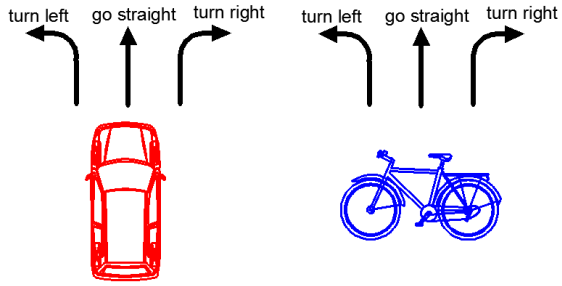

Figure 4. Motion of passenger vehicle and two-wheelers

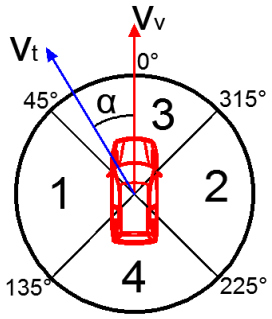

Figure 5. Relative motion zones

The selected variables are shown in Table 1.

Table 1.
Type and Value of Variables

Name	Type	Value	Numeric Representation
Section	Nominal	Intersection	1
		Straight road	2
Light	Nominal	Daytime	1
		Light at night	2
		No light at night	3
Motion of passenger vehicle	Nominal	Go straight	1
		Turn left	2
		Turn right	3
Motion of two-wheelers	Nominal	Go straight	1
		Turn left	2
		Turn right	3
Relative motion zones	Nominal	Zone 1	1
		Zone 2	2
		Zone 3	3
		Zone 4	4
Type of two-wheelers	Nominal	Bicycle	1
		PTW	2
Speed of passenger vehicle (km/h)	Scale	2 (Minimum speed)	0
		102 (Maximum speed)	1

Clustering analysis and chi-square test

The clustering analysis is used to collect the data with similar features. Then the chi-square test is used to extract the parameters with significant features, so as to obtain typical pre-crash scenarios. This method can reduce the influence on subjective scenario classification by human factors and is repeatable [17, 19].

The variables should be pre-processed before clustering. Variables are divided into interval scale variables (such as speed of passenger vehicle) and nominal scale variables (such as light, type of two-wheelers etc.). For interval scale variables, the distance between variables takes the absolute value of the difference between the values of the variable, which should be subject to normalization. For example, for the variable "speed of passenger vehicle" after normalization, the maximum value of the distance is 1 and the minimum value of the distance is 0. The calculation formula is $v' = \frac{v_v - v_{min}}{v_{max} - v_{min}}$, where: v' is the speed value after normalization, v_v is the speed value of the sample, $v_{max}$and $v_{min}$are the maximum and minimum values of the sample. For nominal scale variables, the distance is 0 when the values of the variable are same, while the distance is 1 when the values of the variable are different. However, when the nominal scale variable is greater than or equal to 3, such as the variable "motion of passenger vehicle" includes "go straight", "turn left" and "turn right", the distance between any two of the three variable values is 1. However, based on the values of the variables showed in Table 1, "go straight" and "turn left" are represented

by "1" and "3" and the absolute value of the difference is 2, which is logically inconsistent with the distance 1 between the two variables. Therefore, in order to ensure that the distance between the two variables is 1, the variable value is represented by three values, as shown in Table 2. Similarly, when the variable value is represented by four values, it can also be processed by this method.

Table 2.
Conversion of Variable Parameter Values

Motion of passenger vehicle	**Before conversion**	**After conversion**		
Go straight	1	0	0.5	0.5
Turn left	2	0.5	0	0.5
Turn right	3	0.5	0.5	0

Take 216 accident cases as 216 samples, calculate the distance between different samples, merge the two nearest samples into a new group, then calculate the distance between the new group and other groups, continue to merge two groups in the nearest distance. In this way, cut a group each time, until the number of groups ultimately required is obtained. The distance between samples are calculated by using the City Block, while the distance between groups are calculated by using the Average Linkage Method. After clustering analysis, multiple samples with higher similarity are clustered into one group.

Obtain significant results by using chi-square test, identify the typical eigenvalues of each type of scenario and construct a typical scenario. The degree of confidence is 90% and the chi-square value χ^2 obtained by comparison with the standard. If the chi-square value χ^2 is greater than the standard value, it indicates that the variable value is significant and it can be used as a parameter of the typical scenario.

Analysis and extraction of typical scenario

Firstly, the "inconsistent" formula in MATLAB is used to calculate the inconsistency coefficient. Found the inconsistency coefficient is greatly improved after 208 clusters and the first four groups account for 88.4% of the total samples. Therefore, all samples are clustered into nine groups [12].

Secondly, the nominal variables in nine groups of scenarios and their sample size, variable value ratio and calculated chi-square value are listed in Table 3.The first four groups with most sample size are taken as the research object. For the variables with significance, the typical values are selected by the proportional value of the variable values; for the variables without significance, the value of variable with the largest number of absolute values is selected as the typical value. Therefore, a typical scenario in the four classes of clustered samples is extracted. During the analysis, it is found that the variable “motion of two-wheelers” in the fourth group of sample is significant, but the scenario composed of the value “turn right” and the remaining variable values does not belong to the logical category of the motion pattern of the accident sample. So, the variable value selected based on the absolute number. In addition, the interval scale variable (speed of passenger vehicle) is represented by a box diagram, as shown in Figure 6.

Table 3.
Results of Clustering

Variable			**group**					**Total**
			1	2	3	4	5-9	
Section	Number (proportion)	Intersection	78 (55.7%)	1 (0.7%)	27 (19.3%)	16 (11.4%)	18 (12.9%)	140
		Straight road	1 (1.3%)	43 (56.6%)	15 (19.7%)	10 (13.2%)	7 (9.2%)	76
	Chi-square value		39.86	75.47	0.01	0.12		
Light	Number (proportion)	Daytime	48 (40.7%)	18 (15.3%)	30 (25.4%)	10 (8.5%)	12 (10.2%)	118
		Light at night	23 (34.3%)	23 (34.3%)	6 (9%)	12 (17.9%)	3 (4.5%)	67
		No light at night	8 (25.8%)	3 (9.7%)	6 (19.4%)	4 (12.9%)	10 (32.3%)	31

	Chi-square value		1.62	9.66	5.96	3.18		
Motion of passenger vehicle	Number (proportion)	Go straight	78 (43.1%)	44 (24.3%)	42 (23.2%)	0 (0%)	17 (9.4%)	181
		Turn left	0 (0%)	0 (0%)	0 (0%)	25 (100%)	0 (0%)	25
		Turn right	1 (10%)	0 (0%)	0 (0%)	1 (10%)	8 (80%)	10
	Chi-square value		13.18	8.51	8.12	182.52		
Motion of two-wheelers	Number (proportion)	Go straight	78 (52%)	40 (26.7%)	0 (0%)	22 (14.7%)	10 (6.7%)	150
		Turn left	0 (0%)	3 (5.8%)	41 (78.8%)	0 (0%)	8 (15.4%)	52
		Turn right	1 (7.1%)	1 (7.1%)	1 (7.1%)	4 (28.6%)	7 (50%)	14
	Chi-square value		32.09	9.56	124.62	10.30		
Relative motion zones	Number (proportion)	Zone 1	51 (72.9%)	8 (11.4%)	5 (7.1%)	4 (5.7%)	2 (2.9%)	70
		Zone 2	27 (67.5%)	7 (17.5%)	3 (7.5%)	0 (0%)	3 (7.5%)	40
		Zone 3	1 (1.7%)	21 (35%)	17 (28.3%)	5 (8.3%)	16 (26.7%)	60
		Zone 4	0 (0%)	8 (17.4%)	17 (37%)	17 (37%)	4 (8.7%)	46
	Chi-square value		72.47	9.41	18.08	31.55		
Type of two-wheelers	Number (proportion)	Bicycle	17 (45.9%)	8 (21.6%)	3 (8.1%)	1 (2.7%)	8 (21.6%)	37
		PTW	62 (34.6%)	36 (20.1%)	39 (21.8%)	25 (14%)	17 (9.5%)	179
	Chi-square value		1.07	0.03	2.95	3.23		
Total	Number (proportion)		79 (36.6%)	44 (20.4%)	42 (19.4%)	26 (12%)	25 (11.6%)	216

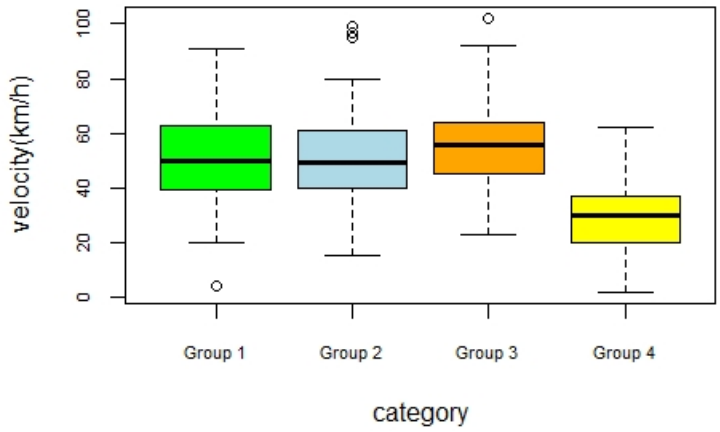

Figure 6. Box diagram of different groups in speed

Finally, the variable values with outstanding features in the four groups of scenarios are extracted and integrated. The speed of passenger vehicle uses the 25th to 75th percentile of each group as the upper and lower bounds. PTW is extracted from the variable "type of two-wheelers" as a typical value, indicating the typicality of PTW among two-wheelers under Chinese road traffic conditions - PTW speed is generally higher than the bicycle. The typical pre-crash scenarios for four types of collision between two-wheelers and passenger vehicle are formed, as shown in Table 4. Typical scenarios 1 and 2 are similar with the test scenarios of E-NCAP, but they do not involve relatively complex conditions such as turning; typical scenarios 3 and 4 involve turning, which accounts a high proportion in real accidents, so these scenarios are the focus of the analysis. The extraction of typical risk scenarios can provide a reference for the design of simulation test scenarios and field test scenarios.

Table 4.
Typical Pre-crash Scenarios

Variable	Typical Pre-crash Scenarios			
	1	2	3	4
Section	Intersection	Straight road	Intersection	Intersection
Light	Daytime	Light at night	Daytime	light at night
Motion of passenger vehicle	Go straight	Go straight	Go straight	Turn left
Motion of two-wheelers	Go straight	Go straight	Turn left	Go straight
Relative motion zones	Zone 1	Zone 3	Zone 4	Zone 4
Type of two-wheelers	PTW	PTW	PTW	PTW
Speed of passenger vehicle (km/h)	39.5-63	40-60.58	45.75-63.75	20-36.75
Diagram	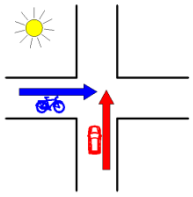	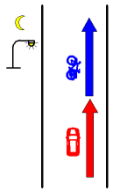	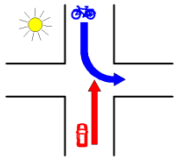	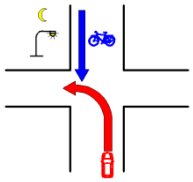

PARAMETER MATCHING AND OPTIMIZATION OF THE AEB SYSTEM BASED ON RECONSTRUCTED SCENARIOS

Reconstruction and simulation analysis of typical scenarios

Based on the above four typical pre-crash scenarios, the simulation test scenarios for collision between two-wheelers and passenger vehicle are constructed through the given key parameters such as road environment, participants and sensors. The road selected is two-way four-lane road, where bicycle lanes are set on both sides and street lamps are installed to adjust the lighting conditions. The velocity of passenger vehicle is set with reference to the upper and lower limits of the velocity in each type of scenario, rounding to the times of 10. The velocity gradient is 10km/h. The PTW velocity is set to 10km/h, 20km/h and 30km/h. When AEB is not triggered, the collision point is the front center point of passenger vehicle and the front/rear wheel center points of PTW. PreScan and MATLAB/Simulink software are used for simulation analysis. The selected sensor in the simulation is medium and short range millimeter-wave radar and the AEB control strategy used is full brake. The trigger distance w refers to the maximum lateral distance between two-wheelers and the side of the passenger vehicle when the two-wheelers is recognized as a dangerous obstacle and the AEB system is triggered. TTC_{max} refers to the maximum predicted time to collision, for an unbraked passenger vehicle, when the brake decision is triggered. Referring to the research [20,21], the main parameters used in the construction of simulation test scenarios are shown in Table 5.

Table 5.

Main parameters used in the construction of the simulation test scenarios

Category	Parameter	Value
Environment	Number of driveways (pcs)	4
	Width of driveway (m)	3.5
	Width of bicycle lane (m)	2
Participant	Velocity of passenger vehicle (km/h)	40/50/60 (Scenario 1 & Scenario 2) 50/60 (Scenario 3) 20/30/40 (Scenario 4)
	PTW velocity (km/h)	10/20/30
	Maximum braking deceleration (g)	0.9
Sensor	FoV (°)	60
	Trigger width w (m)	0.75
	Detection range (m)	40
	TTC_{max} (s)	0.9

The simulation test results of four typical pre-crash scenarios are shown in Figure 7. Specifically, collision occurred in the first and third classes of scenarios, while collision was avoided by using the AEB system in the second and fourth classes of scenarios. The velocity of passenger vehicle during the collision in the first and third classes of scenarios are shown in Table 6. It can be found that the higher the velocity of passenger vehicle or two-wheelers is, the higher the velocity is at the time of collision. When the velocity of two-wheelers is same in these two classes of scenarios, it is more dangerous in the first class of scenario than the third class of scenario. In the first and third scenarios, even if the vehicle is equipped with an AEB system, collision cannot be avoided under certain conditions. Therefore, it is necessary to optimize the parameter matching of the AEB system in the first and third classes of scenarios.

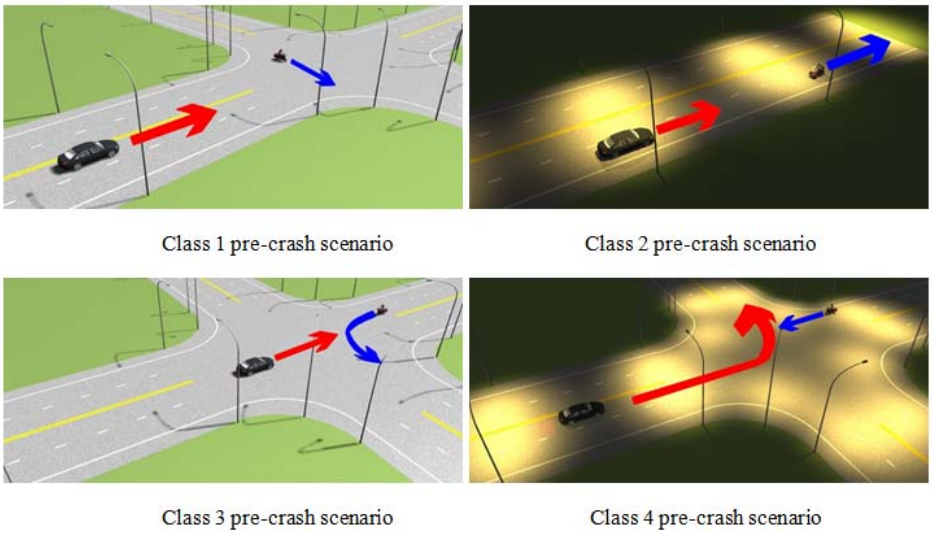

Figure 7. Simulation tests

Table 6.

Simulation results of Scenario 1 and Scenario 3

Scenario Number	Velocity of passenger vehicle (km/h)	PTW velocity (km/h)		
		10	20	30

		Velocity of passenger vehicle during collision (km/h)		
1	40	18	30	40
	50	31	40	50
	60	44	49	54
3	50	10	38	44
	60	25	47	54

Parameter matching and optimization of the AEB system

Take the front sensor of the passenger vehicle as the origin, build a coordinate system, mark the target position points of the object sensed by the sensor at different times before collision on the coordinate system, connect all position points in a line and obtain the approximate motion trail of the two-wheelers on the coordinate system. As time goes on, the two-wheelers continues to approach the passenger vehicle along the motion trail. When there is no AEB function and the velocity of the passenger vehicle is set as 50km/h, the motion trail of the two-wheelers at three different speeds in the motion coordinate system is shown in Figure 8. $a = \frac{v_v}{v_t}$ where: v_v and v_t respectively represent the velocity of passenger vehicle and the two-wheelers.

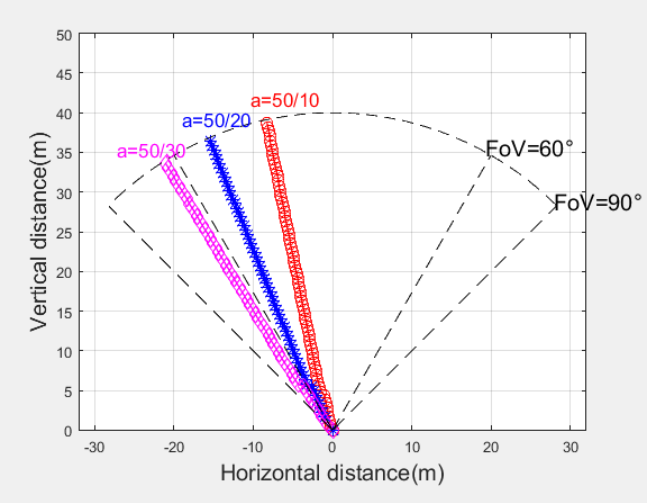

Figure 8. Motion trail of two-wheelers on the motion coordinate system

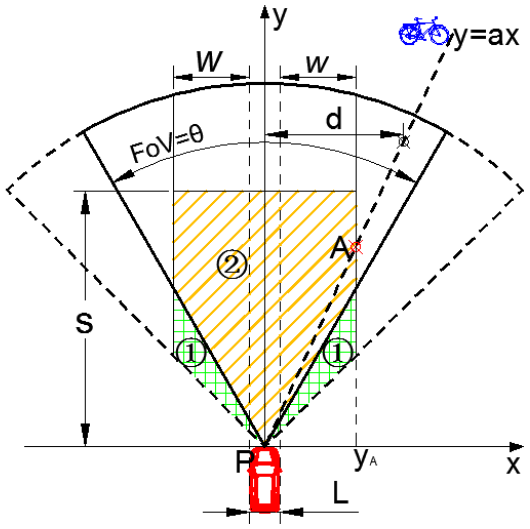

Figure 9. AEB-based collision avoidance mode on the motion coordinate system

It is found from the above figure that the motion trail of the two-wheelers on the coordinate system is almost straight. If the two-wheelers is regarded as a mass point, its motion can be regarded as being continuously approached to the passenger vehicle along a straight line $y = ax$, as shown in Figure 9. Two conditions are required for the two-wheelers to trigger the AEB system: one is the lateral distance $d \leq (w + \frac{L}{2})$, where L is the width of the vehicle (its value is 2m in the simulation model); another one is $TTC \leq TTC_{max}$. To trigger AEB, the longitudinal distance between vehicle and two-wheelers must below the maximum longitudinal distance s. And $s = v_v \times TTC_{max}$. Therefore, when the motion trail of the two-wheelers is in the Zone ②, the AEB system is triggered to take full-force braking. The AEB system trigger area can be extended to Zone ① by increasing the FoV.

As shown in Figure 9, the critical point of the two-wheelers triggering the AEB system is the boundary point between the straight line $y = ax$ and Zone ②. Assumed that the intersection of the straight line $y = ax$ and the straight line $x = \left(w + \frac{L}{2}\right)$ is A, the longitudinal distance between Point A and the passenger vehicle is $y_A = a \times (\frac{L}{2} + w)$. If $s > y_A$, i.e. $TTC_{max} > (\frac{L}{2v_t} + \frac{w}{v_t})$, the triggering boundary is on a straight line $x = (w + \frac{L}{2})$. It means that TTC_{max} is large enough now and there is no influence on improving collision avoidance of the AEB system by increasing TTC_{max}. In this case, it is required to continue to adjust w value to improve collision avoidance.

Similarly, in case of $w > \frac{2v_t TTC_{max} - L}{2}$, the increase in w value has no effect on improving collision avoidance. As shown in Figure 6, when the velocity of passenger vehicle is 50km/h, it is closest to the 50th percentile of the velocity in the first scenario. Therefore, 50km/h is used as the object for analysis in the subsequent simulation analysis.

(1) Optimization of FoV

Assumed that the FoV value is a, if $a < \cot\frac{\theta}{2}$, it indicates that the target two-wheelers is beyond the sensor detection range. The AEB system is useful only under the premise that the target object is within the detectable range. When FoV is 60°, $\cot\frac{\theta}{2}$=1.73, if a is less than 1.73, the sensor will fail to detect and the simulation showed that the collision velocity was equal to the initial velocity. In most cases, v_v is greater than v_t, thus the FoV of the sensor increases to 90° from 60°. The optimized results are shown in Figure 10. Increase in FoV value may improve collision avoidance when the PTW velocity is high, while it has no significant effect when the PTW velocity is low.

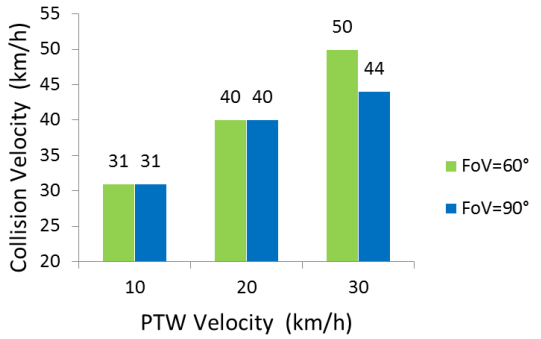

Figure10. Result of FoV parameter matching and optimization

(2) Optimization of TTC

The sensor FoV is fixed at 90°. TTC_{max} is optimized on this basis. The simulation results under different values are shown in Figure 11. With the increase in TTC_{max}, in the same v_t, the collision velocity is gradually reduced until it is stable. Combined with the above analysis, when w is 0.75m and v_t is 10km/h, 20km/h and 30km/h, the critical value TTC_{max} respectively is 0.45s, 0.225s and 0.15s. TTC_{max} corresponding to the inflection point of the collision velocity obtained by simulation is close to the critical value of TTC_{max} calculated theoretically, which proves that the theoretical reasoning is reasonable. Therefore, during the parameter optimization process, it is not better when TTC_{max} is larger. When other parameters are unchanged, if TTC_{max} exceeds its threshold value, there is no improvement in collision avoidance.

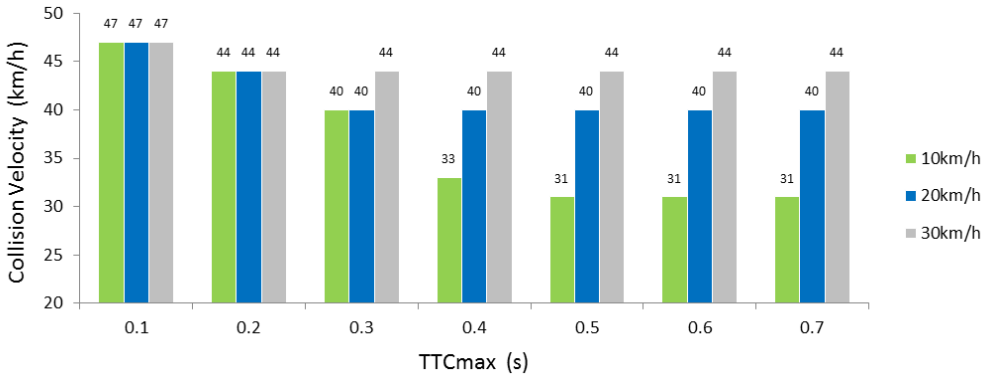

Figure 11. TTC optimization result

(3) Optimization of w

The sensor FoV is fixed at 90°, TTC_{max} is fixed at 0.5s and v_t is set as 10km/h, 20km/h and 30km/h. The simulation results under different w values are shown in Figure 12. Where v_t is 10km/h and 20km/h, it can be seen that the collision velocity firstly decreases and then stabilizes with the increase of w. When v_t is 30 km/h, the collision velocity is gradually reduced. Theoretically, the critical point of the w value respectively is 0.89m, 2.28m and 3.67m, when TTC_{max} =0.5s and v_t is 10 km/h, 20 km/h and 30 km/h. When v_t is 10km/h and 20km/h, the w value corresponding to the inflection point of the collision velocity obtained by simulation is close to the critical value of w value calculated theoretically, which proves that the theoretical reasoning is reasonable. Similarly, it can be inferred that the collision velocity tends to a stable value with the increase in the w value when v_t is 30 km/h.

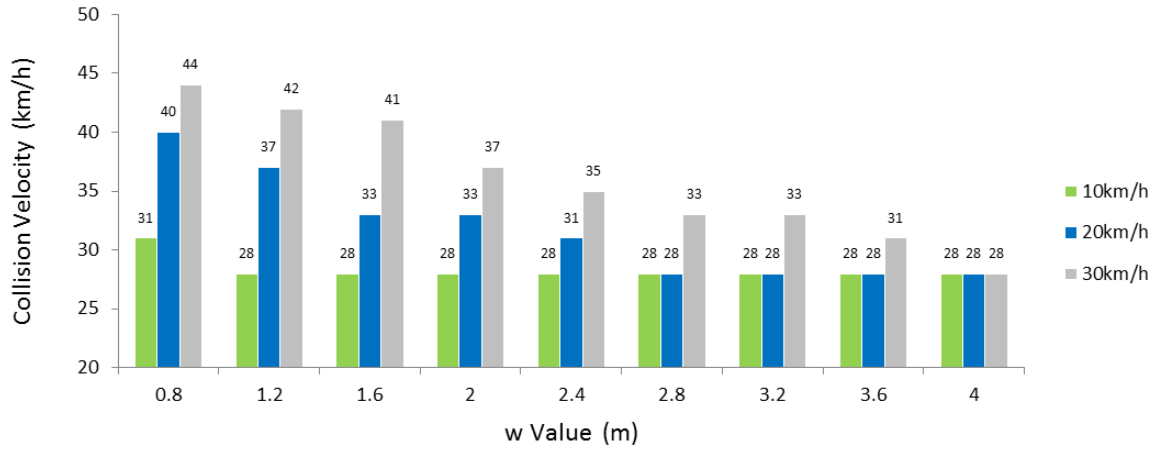

Figure 12. w value optimization result

In summary, in the pre-crash scenario 1, when $TTC_{max} > (\frac{L}{2v_t} + \frac{w}{v_t})$, the increase in TTC_{max} value is not helpful to improve collision avoidance performance; when $w > \frac{2v_t TTC_{max} - L}{2}$, the increase in the w value is also not helpful to improve collision avoidance performance. Therefore, the AEB parameter optimization needs to consider the mutual constraint relationship among the parameters. Only when the optimal parameters are achieved at the same time, it can guarantee the safety to the greatest extent. v_t is a key variable used in the theoretical derivation formula. The larger value range of this variable has a greater impact on the AEB parameter setting and it is also a challenge that has to be faced in the identification by sensors in the scenarios involving two-wheelers.

DISCUSSION AND CONCLUSIONS

"How safe is safe enough" has become an unavoidable scientific and engineering challenge for the test validation of automated driving functions and advanced driving assistant system (ADAS). This paper proposes an autonomous emergency braking (AEB) system parameter optimizing method based on typical risk scenarios, which can speed up the development and verification of the AEB system and lay the foundation for field operational test and actual road test. This paper analyzed the data of collision accidents between passenger car and two-wheelers stored in the NAIS database, extracted the typical scenarios by using clustering analysis and chi-square test and then reconstructed and simulated typical pre-crash scenarios and analyzed the matching of AEB system parameters applying PreScan software. The main conclusions are as follows:

1. Under normal circumstances, it is difficult to obtain more urgent emergencies in natural driving scenarios and the acquired scenario data has little effect on the development of the AEB system. However, it is a more effective engineering method for the development, verification and evaluation of AEB system by extracting representative typical pre-crash scenarios based on the accident-related big data and applying them in system parameter matching design and function test.

2. This paper extracted four typical pre-crash scenarios between passenger car and two-wheelers, which cover 88.4% of the sample and are representative. Especially, the first and second scenarios in the four typical scenarios are similar to the AEB test scenarios of cyclist crossing and cyclist along the roadside introduced by Euro-NCAP 2018, but the first and second scenarios in this paper are more complicated. In addition, the third and fourth scenarios extracted in this paper occur at the intersection, indicating that the AEB system needs to focus on the identification and collision avoidance of the two-wheelers at the intersection in the process of development, test and evaluation.

3. Since the speed of two-wheelers is higher than that of pedestrian and the route is more complicated, the AEB system is facing great challenges to detecting two-wheelers riders in both hardware and software. The simulation analysis reveals the larger the sensor FoV is, the larger the identification field of two-wheelers is and the better the performance of the AEB system in avoiding collision or mitigating collision speed. This shows that the AEB system should select a sensor with a larger detection angle to effectively identify the fast-moving two-wheelers and make correct decision.

4. During the simulation, it is found that the collision avoidance problem cannot be completely solved by merely increasing the angle of FoV. It is necessary to comprehensively adjust the braking trigger width, brake trigger time to avoid vehicle collision. In the simulation analysis of the first scenarios, the AEB can avoid the occurrence of collision accidents or greatly mitigate the speed of the collision by comprehensively adjusting the above key parameters.

The research of this paper still has certain limitations. At present, the number of collision accidents used for scenario clustering analysis is limited and the pre-crash scenarios that may be extracted cannot completely represent the typical collision scenarios between passenger car and two-wheelers in China. But, the method studied in this paper is a good reference for the development of the AEB system. And AEB system can be improved with more accident data of NAIS in the future. In addition, the simulation specified in this paper does not consider the specific shape parameters and the variability in the movement of two-wheelers. In the subsequent research, it is considered to establish a unified bicycle and PTW model for the simulation, test and evaluation of the AEB system.

ACKNOWLEDGMENT

This work was financially support by National Fund for Fundamental Research: Research on Key Technologies for Construction of Automatic Driving Critical Scenarios Based on NAIS Accident In-depth Investigation Data.

REFERENCES

[1] Ding Zhao, et al. 2017. “Accelerated evaluation of automated vehicles safety in lane-change scenarios based on importance sampling techniques.” IEEE Trans. Intell. Transp. Syst., vol. 18, no. 3, pp. 595–607, Mar. 2017.

[2] World Health Organization. 2016 “Global status report on road safety”.

[3] The Ministry of Public Security of the People's Republic of China. 2004. “The People's Republic of China Road Traffic Accident Annual Statistic Report (2004)”.

[4] The Ministry of Public Security of the People's Republic of China. 2010. “The People's Republic of China Road Traffic Accident Annual Statistic Report (2010)”.

[5] Dr. Ing, Alois Seewald. “Active Passive Safety Integration [R/OL]. (2011-06-09).” https://www.researchgate.net/

[6] Vollrath M, Briest S, Schieβl C, et al. 2006 “Ableitung von Anforderungen an fahrerassistenzsysteme aus Sicht der Verkehrssicherheit.” Bergisch Gladbach:BAST.

[7] Euro-NCAP. https://www.euroncap.com/en/for-engineers/protocols/vulnerable-road-user-vru-protection/

[8] C-NCAP. http://www.c-ncap.org/

[9] Ying Liu, Jinpeng He, Weiguo Liu, et al. 2014. “Research on Test Scenarios for AEB Pedestrian System.” Automobile Technology, 2014(03):35-39.

[10] Jiangping Su, Junyi Chen, Hongyan Wang, et al. 2017. “Establishment and Analysis on Typical Road Traffic Near-Crash Scenarios Related to Pedestrian in China.” Traffic & Transportation, 2017(01):209-214.

[11] Chen Qiang, Lin Miao, Bai Bing, et al.2015. “Typical pedestrian accident scenarios in China and crash severity mitigation by autonomous emergency braking systems.” SAE Technical Papers, 2015-01-1464.

[12] Lenard J., Badea-Romero A., Danton R.. 2014. “Typical pedestrian accident scenarios for the development of autonomous emergency braking test protocols.” Accid Anal Prev, 2014, 73(73):73-80.

[13] Huang S., Yang J. 2006. “Analysis of Car-Pedestrian Impact Scenarios for the Evaluation of a Pedestrian Sensor System Based on Accident Data from Sweden.” Expert Symposium on Accident Research, 2006: 136-143.

[14] Erik Rosén, Källhammer J E , Eriksson D , et al. 2010. “Pedestrian injury mitigation by autonomous braking.” Accident Analysis & Prevention, 2010, 42(6):1949-1957.

[15] David Good and Rachel Abrahams. 2014. “Vehicle Speeds for Pedestrian Pre-Crash System Test Scenarios Based on US Data.” IEEE International Conference on Intelligent Transportation Systems. 2014: 1632-1637.

[16] Liers, H.. 2013. “Analysis of the accident scenario of powered two-wheelers on the basis of real-world accidents.” Proceedings of Expert Symposium on Accident Research, 2013.

[17] Li Lin, Zhu Xichan, et al. 2014 “Typical Traffic Risk Scenarios Related to Pedal Cyclists.” Journal of Tongji University (Natural Science), 2014,42(07):1082-1087.

[18] Bo Sui, Shengqi Zhou, Xiaohua Zhao, Nils Lubbe. 2017. “An Overview of Car-To-Two-Wheeler Accidents in China: Guidance for AEB Assessment.” International Technical Conference on the Enhanced Safety of Vehicles. Paper No.:17-0204.

[19] Hu Lin, Yi Ping, et al. 2018. “A Research on Test Scenes of Two-wheeled Vehicles for Automatic Emergency Braking System Based on Real Accident Cases” Automotive Engineering, 2018, 40(12):1435-1446.

[20] Erik Rosén. 2013. “Autonomous Emergency Braking for Vulnerable Road Users.” IRCOBI Conference. 2013: 618-627.

[21] Liu Jianping, Zheng Wangxiao, et al. 2018. “Research on Relevance of AEB System Performance and TTC.” Automobile Technology. 2018, 515(08):54-56.

COMPARING RESTRAINT SYSTEM SENSITIVITY BETWEEN THE THOR AND THE HYBRID III, AND POTENTIAL IMPLICATIONS IN RESTRAINT OPTIMIZATION

Jason Forman, Salvador Montesinos Acosta,Varun Bollapragada, Bronislaw Gepner
University of Virginia Center for Applied Biomechanics
U.S.A.

Philipp Wernicke
BMW
Germany

Paper Number 19-0274

ABSTRACT

Restraint system optimization is affected by the sensitivity of dummies to relative loading between the seatbelt and airbag. Differences in design between the THOR and Hybrid III dummies may affect the mechanisms of interaction with the various restraint system components, and the factors that influence compression measured in the dummy's chest. Previous studies have compared dummy responses in sled tests representing select specific configurations. The goal of this study was to compare the mechanisms of chest compression in the THOR and Hybrid III, and sensitivity to loading by various restraint system components, in full vehicle crash tests.

The NHTSA full-vehicle crash test database was queried to find cases of matched tests with the THOR and the Hybrid III. Four cases of matched tests were found - one with a sub-compact hatchback, one with a compact sedan, one with a mid-sized sedan, and one with a full-sized pickup. All were 56 km/h frontal-impact, rigid barrier tests, with the dummy seated in the driver position. The vehicles were matched based on make, model, model base year, and restraint system characteristics (e.g., observed belt force limit). Shoulder belt forces, chest deflection time histories, and frame-by-frame videos were examined to restraint system interaction and factors influencing compression measured in the chest.

In all four cases the shoulder belt force time histories were similar between the THOR and the Hybrid III. In one case the chest compression in the Hybrid III appeared to be predominantly dependent on force limiting in the shoulder belt, while the THOR exhibited a greater sensitivity to combined loading by the belt and airbag. In two cases the results were mixed, with both the dummies exhibiting some sensitivity to both belt and airbag loading (though the airbag appeared to contribute to a greater degree with the THOR). The nature of chest compression appeared most similar in a case of an apparent digressive force limiter, with both dummies exhibiting a plateau associated with a transition to airbag loading with a drop belt force limit.

These results suggest that the relative sensitivity to belt and airbag loading can vary between the THOR and the Hybrid III, depending on the specific characteristics of the restraint system and vehicle being studied. The THOR is more flexible, tends to experience greater forward excursion into the airbag, rides up higher on the airbag, and is capable of measuring deflection in the upper chest where a majority of the airbag loading occurs in some cases. As a result, in some cases the THOR appears to be more sensitive to loading by the airbag than the Hybrid III. Sensitivity to loading by the various restraint system components will likely affect optimization of the restraint systems, affecting the perceived optimal apportionment of load between the belt and the airbag. These results suggest that the two dummies may lead to different strategies for restraint system optimization in some cases, and that the relation of restraint system interaction between the THOR and Hybrid III may vary in the fleet.

INTRODUCTION

Restraint design relies on evaluation in full vehicle crash tests with anthropomorphic test devices (ATDs, dummies) serving as surrogates for the vehicle occupants. These crash tests challenge the restraint system to provide a balance between applying sufficient force to halt the motion of the occupant, while applying said restraining force in a manner that minimizes risk of injury from loading by the restraints. The risk of injury is commonly assessed through measurements taken from specific internal sensors of the dummy (e.g., force, acceleration, deformation), compared to injury assessment reference values (IARVs) or injury risk functions.

One of the drivers of restraint system optimization for frontal impacts is chest compression (used to estimate chest injury risk), measured by internal sensors arranged to observe the displacement of the ribcage relative to the spine [1-5]. Dummy chest compression may be affected by factors such as position of the shoulder belt, force limiting in the shoulder belt, forward excursion and forward pitch of the torso, and engagement with the airbag and steering wheel [3,6]. Most formalized vehicle crashworthiness evaluation programs utilize dummy chest compression in their frontal impact safety assessments in some manner [7]. Designing restraint systems to address the performance requirements of those programs requires understanding the factors that contribute to chest compression in the dummy, including the mechanisms of engagement with the restraint system components and how they affect compression measurements in the chest.

The Hybrid III 50th percentile male dummy (H3) is currently the primary dummy for frontal impact, belted driver safety assessment for formalized crashworthiness test programs worldwide [8]. Recent efforts have considered a shift towards evaluation with the THOR dummy [9,10]. There are several differences between the two dummies that may result in differences in the manner in which they engage with restraint systems, potentially affecting the factors that influence chest compression measurement. The THOR has a more flexible spine than the H3 [11], potentially affecting the stiffness of coupling between the upper and lower body. This may affect forward excursion of the torso, and the nature in which restraint of the lower body (e.g., via the lap belt) contributes to restraint of the upper body [12-15]. The THOR chest is also more compliant [16], and less coupled [17] than the H3, resulting in more chest compression for a given amount of concentrated load. The THOR includes a shoulder structure with a clavicle, affecting the manner in which shoulder belt engagement translates into compression of the chest [18,19]. The THOR also includes multi-point compression measurement on the chest (compared to single-point measurement in the H3), potentially affecting the observation of chest compression under various patterns of loading [1,14]. Understanding how the dummies will affect restraint system design requires understanding how their differences will affect interactions with the restraint system components, and the factors that influence chest compression measurement (as well as other injury prediction measures).

THOR and H3 responses have been compared previously in sled testing. For example, Kent et al. [1,3] and Petitjean et al. [4] each compared THOR and H3 responses in frontal impact sled tests with various types of airbag and seatbelt systems (e.g., comparing non-force limiting to force-limiting 3-point belts). Others have compared responses in more simplified sled environments designed specifically for biofidelity evaluation under 3-point belt loading [13]. More recently, Albert et al. [20,21] compared THOR and H3 responses to post mortem human surrogates (PMHS) in sled tests with a modern belt and driver airbag system, and with a simulated representation of a knee airbag. While these types of studies provide valuable information in controlled testing environments, they are limited in that they evaluate a single specific scenario (or a small number of scenarios) from among the wide variety of restraint designs and vehicle interior geometries that are present in the fleet. To understand how the dummies will affect restraint design in real crashworthiness testing, comparison should not be limited to a small number of sled tests, but should include evaluation among vehicles with different restraint and interior designs. This may be accomplished by comparing responses in full-vehicle crash tests utilizing the THOR and H3 dummies.

The goal of this study was to compare restraint interactions and mechanisms of chest compression between the THOR and Hybrid III in matched full vehicle crash tests. This was accomplished through a detailed examination of publicly-available frontal crash tests from the NHTSA Vehicle Test Database. Outcomes of interest included chest compression measured by the dummies, and their relation to engagement by various components of the vehicle's restraint system.

METHODS

NHTSA's publicly-available crash test database was first queried for full vehicle crash tests that included the THOR 50th percentile male crash test dummy as either the driver or the right front passenger. At the time of the search this returned 122 crash tests with the THOR dummy, 116 of which were oblique moving deformable barrier tests and six of which were NCAP-style rigid full frontal barrier tests. These were then cross-referenced with a search for tests with the Hybrid III 50th percentile male dummy, seeking to match on test condition, seating position (e.g., driver vs. passenger), and vehicle make, model, and model base year. As this required matching based on vehicle information, cases that did not include such information were excluded. This cross-reference returned just five cases of tests with the Hybrid III that potentially matched tests with the THOR dummy, all of which were 56 km/h NCAP-style rigid frontal barrier tests. Data from each of the potential matches were then qualitatively examined to ensure that the vehicle responses (via the vehicle acceleration pulse) and restraint system design (via the upper shoulder belt force time history) were comparable. This resulted in exclusion of one of the potential matches, based on differences in the shoulder belt force limit (and thus potentially differences in restraint design version) between the Hybrid III and THOR tests.

Thus, at the time of the query and evaluation there were four cases of vehicles with matched crash tests with both the Hybrid III and THOR 50th percentile male dummies (publicly available from NHTSA). One was a sub-compact hatchback, one was a compact sedan, one a mid-sized sedan, and one a full-sized pickup (Table 1). Each of these included the THOR and Hybrid III in the driver position.

These tests were each examined to observe and compare the restraint interaction factors that contributed to the chest compression measured in the dummies. This included examining the time history of chest compression compared to shoulder belt force, cross-referenced with the high-speed video to identify the engagement with the restraint components at various time points of interest. The THOR is capable of measuring compression at four locations on the chest (upper right and left, lower right and left), compared to one location for the Hybrid III (mid-sternum). The time history of maximum chest compression measured with the THOR (of the four possible measurement locations) was compared to the mid-sternum compression measured with the Hybrid III. Focus was placed not necessarily on comparing the magnitude of chest compression, but instead on comparing the shape of the time history of chest compression and how it relates to the timing of engagement with the restraint system components. Kinematics of the dummies relative to the restraint system components were compared via examination of the high-speed video to elucidate any differences in restraint engagement and mechanisms of chest compression.

Table 1.

Matrix of matched THOR and Hybrid III tests selected from the NHTSA crash test database.*

Make, Model	Type	Model Year	Dummy (driver)	NHTSA Test No.	Real Speed (kph)	Notes
Honda Fit	Subcompact hatchback	2015	HIII	9033	56.55	--
		2015	THOR	9337	56.27	
Mazda 3	Compact sedan	2014	HIII	8539	56.39	--
		2015	THOR	9336	56.61	
Chevrolet Malibu	Mid-sized sedan	2015	THOR	9332	56.63	Includes Knee Airbag
		2016	HIII	7856	56.30	
Ford F-150	Full-sized pickup	2015	HIII	9097	56.40	--
		2015	THOR	9335	56.15	

* All full-width rigid frontal barrier tests. Matched tests checked for common base year.

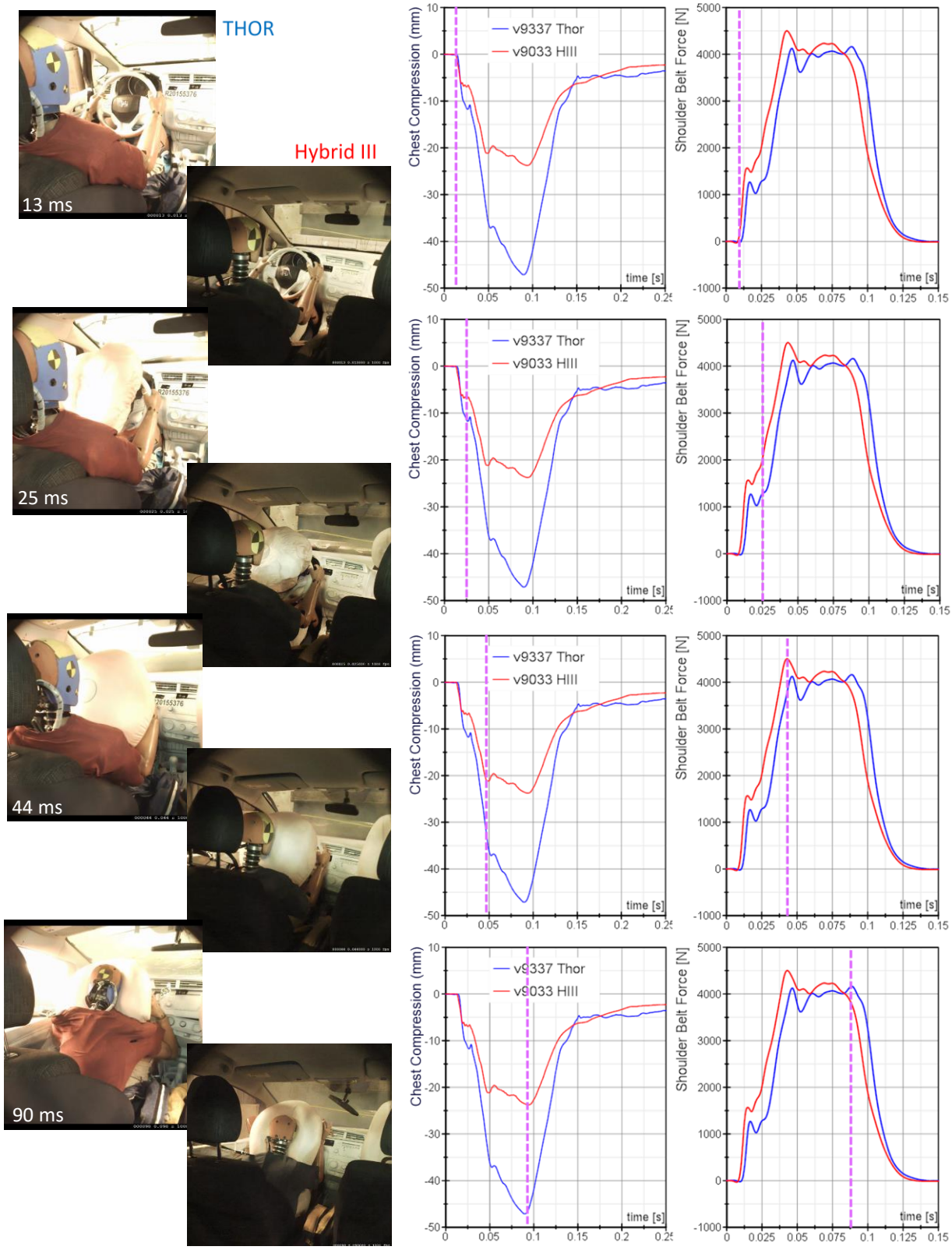

Figure 1: Video stills, chest compression, and shoulder belt force in the subcompact hatchback comparing the THOR to the Hybrid III. 56 km/h frontal rigid barrier. Chest compression is shown at the peak location for THOR (upper right) and the sternum slider for H3. Pink dashed line - time shown in the video captures.

RESULTS

In all four cases, the peak chest compression in the THOR occurred at the upper right (inboard) measurement location. Figure 1 shows the chest compression and upper shoulder belt force time histories for one pair of matched crash tests (subcompact hatchback), along with high-speed video images at particular timepoints of interest. At approximately 13 ms both dummies begin to move forward and engage the shoulder belt. At 25 ms the airbag has begun to deploy, and force has begun to build in the shoulder belt. At approximately 44 ms the dummies have moved forward enough to begin to engage with the airbag. At this point in time, the belt force has also risen to the point at which the belt force limited begins to yield. As the belt force plateaus the chest compression in the Hybrid III also plateaus, with minimal increase as the dummy moves forward into the airbag. In contrast, the chest compression in the THOR continues to increase as the dummy moves forward into the airbag. In both cases the peak chest compression occurs at the time of peak forward excursion, however the increase in chest compression resulting from forward motion into the airbag was greater with the THOR than the Hybrid III.

Figure 2 shows expanded views of the high speed video images at the approximate time of peak chest compression (90 ms) from the tests discussed above. The approximate locations of peak chest compression measurement are also shown for illustration (upper right for the THOR, compared to the mid-sternum measurement site for the Hybrid III). As can be seen in these images, the THOR appears to ride up higher on the airbag than the Hybrid III (note the location of the top of the top of the head relative to the top edge of the airbag; the location of the shoulders on the airbag; and the angle of the shoulder belt as it leaves the shoulder). This, in combination with the higher measurement location afforded by the upper chest IR-TRACCS, may place the measurement site of peak compression in a position where it can be affected more by engagement with the airbag compared to the Hybrid III.

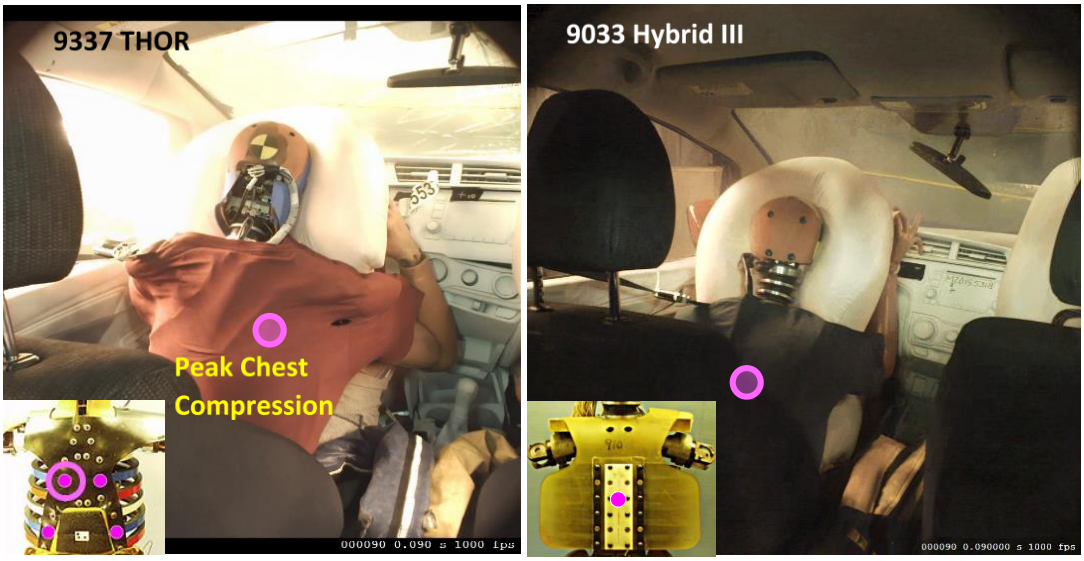

Figure 2: Screen captures at the time of peak chest compression, illustrating the approximate location of peak chest compression measurement in the THOR, compared to the Hybrid III.

Figure 3 shows the chest compression and belt force time histories for two of the other pairs of matched tests (the compact sedan and the mid-sized sedan), as well as high speed video stills at the approximate time of peak chest compression measured in the THOR. As with the tests above, the chest compression measured in the THOR continues to rise after the belt force limiter yields, increasing as the dummy moves forward into the airbag. The chest compression in the Hybrid III also continues to increase after the time at which the belt force limiter begins to yield, but plateaus at a time prior to when the peak chest compression was observed with the THOR. Though the video views are not as directly as comparable as with the test above, it appears that the THOR rides up higher on the airbag than the Hybrid III in these tests as well (for example, based on the height of the shoulders relative to the airbag at the time of peak chest compression).

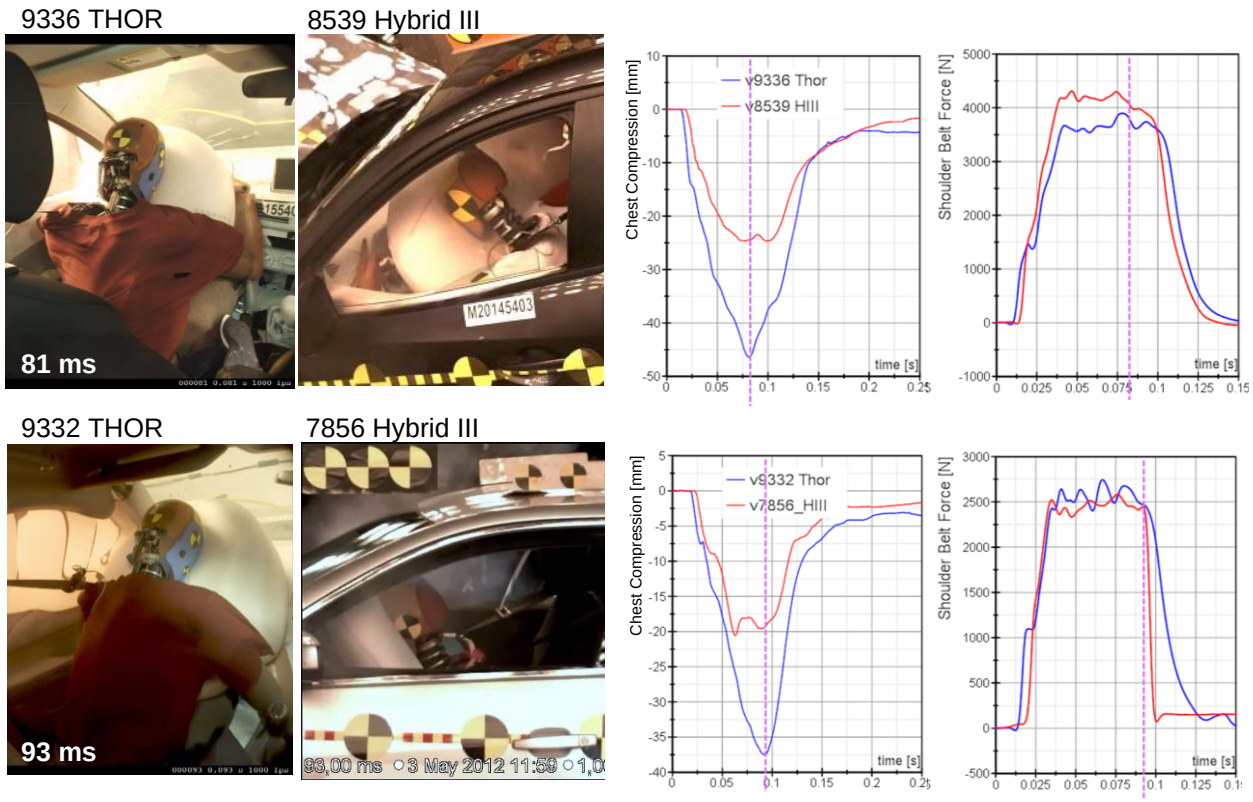

Figure 3: Chest compression, shoulder belt force, and video stills at the time of peak chest compression in the compact and mid-sized sedans. 56 km/h frontal rigid barrier. Chest compression is shown at the peak location for THOR (upper right) and the sternum slider for H3. Pink dashed line - time shown in the video captures.

Figure 4 shows the results for the full-sized pickup, with video stills from two timepoints of interest. Unlike the other tests, in this case the THOR chest compression exhibits a plateau similar in nature to that observed with the Hybrid III. This plateauing response occurs in conjunction with a drop in upper shoulder belt force from what appears to be a digressive force limiter. As can be seen from the video stills, the drop in shoulder belt force occurs approximately at the time at which the chest begins to engage with the airbag. There is a brief dip in chest compression in the THOR coinciding with the drop in belt force. This may be attributable to a brief offloading of the chest as the belt force drops, transitioning to increased loading by the airbag as the dummy moves forward. This plateauing behavior is also observed in the Hybrid III.

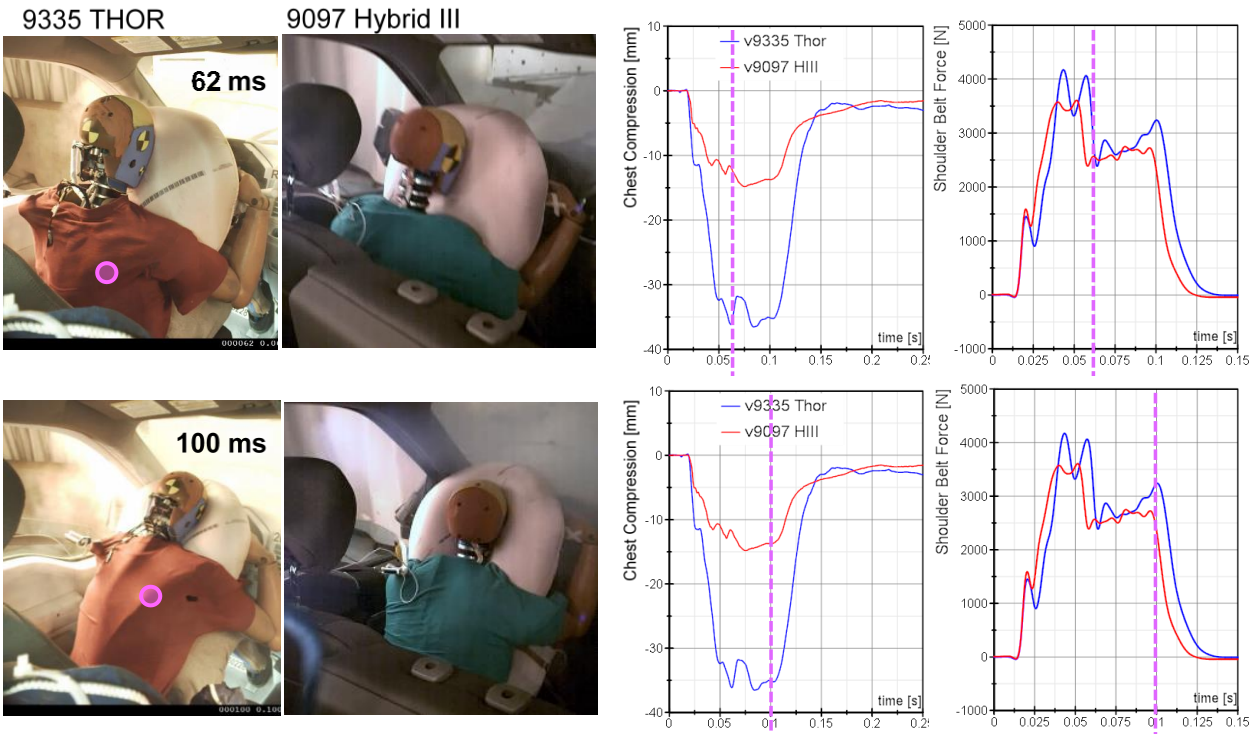

Figure 4: Chest compression, shoulder belt force, and video stills for the full-sized pickup. 56 km/h frontal rigid barrier. Chest compression is shown at the peak location for THOR (upper right) and the sternum slider for H3. Pink dashed line - time shown in the video captures - showing the time at which the secondary digressive force limits engages, followed by the time of peak forward excursion.

DISCUSSION

These results suggest that in full-vehicle crash tests, the THOR dummy may exhibit sensitivity to combined belt and airbag loading in a manner that is different than the Hybrid III. The differences in sensitivity to airbag loading appear to vary among the fleet, likely dependent on factors such as proximity to the airbag, shape of the airbag, and characteristics of the belt force limiter.

In the case of the subcompact sedan shown here, the chest compression observed in the Hybrid III appears to be almost entirely dependent on the belt force limiter, exhibiting a distinct plateau in chest compression following the yielding of the belt force limiter. In contrast, with the THOR the chest compression continues to increase as the dummy moves into the airbag after the force limiter yields. In the cases of the compact sedan and the mid-sized sedan, the sensitivity appears airbag loading more mixed – the Hybrid III appears to exhibit some increase in chest compression after the force limiter yields, however this is still abbreviated compared to what was observed in the THOR. The THOR and the Hybrid III responses appear to be most similar (in nature) in the case of the full-sized pickup truck with a digressive force limiter. In that case it appears that as the belt force limit drops, engagement with the airbag increases, resulting in a net plateau in chest compression with both dummies.

The differences observed in the contribution of airbag loading to chest compression are not necessarily reflective of differences in sensitivity to airbag loading itself (though that may also be a factor). Instead, this likely represents the combined effects of multiple differences in the construction and response of the dummies that culminates in a difference in how the dummy engages the airbag. With its two flex joints, the spine of the THOR tends to be more flexible than the spine of the Hybrid III [11,13-15]. The chest of the THOR is also more compliant and less structurally-coupled than the Hybrid III [17], and the shoulder allows for degrees-of-freedom not present in the Hybrid III [15]. With these factors combined, the THOR tends to exhibit greater forward excursion compared to the

Hybrid III. In the crash tests examined here, this resulted in the THOR moving forward and riding up on the airbag higher than the Hybrid III, resulting in engagement with the airbag around the region of the upper chest compression measurement locations. Thus, a chain of multiple differences in the design and response of the dummies manifest as context-specific differences in engagement with the restraint system, and differences in sensitivity to loading by the various restraint system components.

The relative sensitivity to belt and airbag loading likely has a direct effect on restraint system optimization. In cases where the Hybrid III response is dominated by sensitivity to the belt force limit, the dummy may suggest that the optimal design would be one where the belt force limit is very low [22]. In contrast, in cases where both the belt and airbag loading contribute comparably to chest compression (such as the THOR in the sub-compact), there likely exists an optimal belt force limit where chest compression is minimized by balancing engagement contributions from the belt and the airbag. Thus, in cases where the sensitivity to loading by the various restraint system components is different between the two dummies, the Hybrid III and the THOR may result in different optimization strategies when designing restraints for that vehicle.

The observation that the relative belt/airbag sensitivity is different across vehicles suggests that it will be difficult to infer if (and how) a transition to THOR would affect systematic trends in restraint optimization and design philosophy. The implications of using one dummy over the other will likely be dependent on the specific characteristics of the vehicle and the restraint systems being studied, with limitations in generalizability.

These results also highlight the importance of evaluating the biofidelity and injury prediction ability of dummies from the context of sensitivity to changes in restraint system design. Dummy biofidelity is most often evaluated by comparing against reference data (e.g., tests with post-mortem human surrogates, PMHS) in a few select testing conditions. The dummy responses in a particular test mode are typically compared to reference results in that test mode, and judged as acceptable or not. This has been codified in recent years by the advent of objective ratings schemes that can aggregate multiple individual test mode comparisons into a single biofidelity score [23-25].

To be useful as a tool to guide restraint design and optimization, however, a dummy must be able to accurately predict how a change in loading condition will affect changes in engagement and injury risk for a human occupant. Existing objective ratings schemes lack a means to incorporate sensitivity to changes in loading condition, and a dummy's sensitivity to changes in restraint is rarely considered in biofidelity evaluations [3,26]. These results suggest that in some cases the Hybrid III and the THOR exhibit differences in engagement with restraint system components that may result in differences in sensitivity to changes in restraint system design. It is currently unknown which more accurately reflects the sensitivity that would be exhibited by a human occupant. Evaluating dummy biofidelity from the standpoint of sensitivity to changes in loading requires substantially more data than is typically available from PMHS-based experimental datasets. Instead, such an evaluation may require novel means to generate reference targets spanning a wide range of loading conditions using parametric human body modeling, anchored with a select set of physical experiments to spot-check the accuracy of the resulting response surface.

CONCLUSIONS

This study sought to compare factors that influence chest compression between the THOR and Hybrid III dummies in matched full vehicle tests publicly available in NHTSA's Vehicle Crash Test database. Four sets of matched tests were found, and examined for chest compression timing and the relation to engagement with the various components of the restraint system. The observations may be summarized as follows:

- In at least one case, the chest compression in the Hybrid III appeared to be related to predominantly to loading by the shoulder belt, with chest compression plateauing in-phase with yielding of the shoulder belt force limiter. In contrast, the chest compression in the THOR appeared to be affected by a combination of loading by the belt and the airbag, with an increase in chest compression as the dummy moved forward into the airbag. This is likely due to the combined effects of differences in shape and compliance of the shoulder and chest, differences in chest compression measurement location, and differences in the flexibility of the spine (allowing the THOR to move forward, and ride up onto the airbag to a greater degree than the Hybrid III in this case).

- In other cases, the relative sensitivity appeared more mixed, with both dummies exhibiting some chest compression related to both belt and airbag loading. However, in these cases the airbag-related chest compression in the Hybrid III still appeared abbreviated compared to the THOR. The Hybrid III chest compression exhibited a plateauing behavior at some time after belt force limiter yielding, while the THOR chest compression continued to build towards a peak occurring near the time of maximum forward excursion.
- The two dummies exhibited the most similar phasing of chest compression in a case of a vehicle with an apparent digressive belt force limiter. In both dummies the chest compression remained steady as the dummy moved forward into the airbag, after the drop in belt force associated with the digressive limiter.

These results suggest that the mechanisms of chest compression in the two dummies, and the relative sensitivity of the two dummies to differences in restraint design, may be variable dependent on the specific characteristics of the vehicles and restraint systems being evaluated. Thus, in some cases optimized restraint designs may be different for the two dummies, dependent on the specific characteristics of the vehicle and the restraints. These results also highlight the importance of including sensitivity evaluation in biofidelity assessment, evaluating a dummy's (or human body model's) ability to replicate sensitivity to changes in restraint system interaction in a manner reflective of what would occur in a real occupant.

ACKNOWLEDGEMENTS
This work was supported in part by a grant from the Partnership for Dummy Technology and Biomechanics. The opinions presented here are those solely of the authors.

REFERENCES

[1] Kent, RW, Shaw, CG, Lessley, D, Crandall, JR. (2003) Comparison of Belted Hybrid III, Thor, and Cadaver Thoracic Responses in Oblique Frontal and Full Frontal Sled Tests. SAE Transactions: Journal of Passenger Cars - Mechanical Systems, 112(2003-01-0160): 71-84.

[2] Kent, RW, Patrie, J, Benson, N. (2003) The Hybrid III Dummy as a Discriminator of Injurious and Non-Injurious Restraint Loading. Annual Proceedings/Association for the Advancement of Automotive Medicine (AAAM), 47: 51-75.

[3] Kent, RW, Lessley, DJ, Shaw, CG. (2003) The Utility of Hybrid III and THOR Chest Deflection for Discriminating between Standard and Force-Limiting Belt Systems. Stapp Car Crash Journal, 47(2003-22-0013): 267-297.

[4] Petitjean A; Lebarbe M; Potier P; Trosseille X; Lassau JP; (2002) Laboratory Reconstructions of Real World Frontal Crash Configurations Using the Hybrid III and THOR Dummies and PMHS. Stapp Car Crash Journal, 46(2002-22-0002): 27-54.

[5] Rangarajan N; Shams T; McDonald J; White R; (1998) Response of THOR in Frontal Sled Testing in Different Restraint Conditions. Proceedings of the International Research Council on the Biomechanics of Impact (IRCOBI). 513-526. Goteborg, Sweden, September 16-18.

[6] Butcher, JT, Shaw, CG, Bass, CR, Kent, RW. (2001) Displacement Measurements in the Hybrid III Chest. SAE International Journal of Passenger Cars - Mechanical Systems, 110(2001-01-0118): 26-31.

[7] Prasad, P. (2015) Injury criteria and motor vehicle regulations. In Accidental Injury – Biomechanics and Prevention, 3rd Edition. Ed. Yoganandan, N., Nahum, A.M., Melvin, J.W.. Springer, New York.

[8] Mertz, H.J., Irwin, A.L. (2015) Anthropomorphic test devices and injury risk assessments. In Accidental Injury – Biomechanics and Prevention, 3rd Edition. Ed. Yoganandan, N., Nahum, A.M., Melvin, J.W.. Springer, New York.

[9] Saunders J; Parent D; Ames E; (2015) NHTSA Oblique Crash Test Results: Vehicle Performance and Occupant Injury Risk Assessment in Vehicles with Small Overlap Countermeasures. International Technical Conference on the Enhanced Safety of Vehicles (ESV). 24. Goteborg, Sweden, June 8-11.

[10] Sander, V., Ellway, J., van Ratingen, M. (2017) Euro NCAP frontal impact working group report. Proc. Conference on the Enhanced Safety of Vehicles (ESV), Paper No. 17-0205.

[11] White RPJ; Rangarajan N; Haffner MP; (1996) Development of the THOR advanced frontal crash test dummy. SAFE Association Annual Symposium, 122-135.

[12] Shaw, CG, Crandall, JR, Butcher, J. (2002) Comparative Evaluation of the THOR Advanced Frontal Crash Test Dummy. International Journal of Crashworthiness, 7(3): 239-253.

[13] Shaw, CG, Lessley, DJ, Ash, JH, Crandall, JR, Parent, DP, (2013) Response Comparison for the Hybrid III, THOR Mod Kit with SD-3 Shoulder, and PMHS in a Simulated Frontal Crash. International Technical Conference on the Enhanced Safety of Vehicles (ESV). Paper 13-0130. 23. Seoul, South Korea, May 27-30.

[14] Rangarajan N; Fournier E; Dalmotas D; Rhule D; Pritz H; Eppinger R; Haffner MP; Fullerton J; Beach D; Shams T; White R; (1998) Design and Performance of the THOR Advanced Frontal Crash Test Dummy Thorax and Abdomen Assemblies. International Technical Conference on the Enhanced Safety of Vehicles (ESV). 16. Windsor, Ontario, May 31-June 4.

[15] Tornvall, F, K Holmqvist, J Davidsson, M Svensson, J Gugler, H Steffan, TU-Graz, Y Haland, (2008) Evaluation of Dummy Shoulder Kinematics in Oblique Frontal Collisions. Proceedings of the International Research Council on the Biomechanics of Impact (IRCOBI). 195-210. Bern, Switzerland, September 17-19.

[16] Parent D;Craig M;Moorhouse K; (2017) Biofidelity Evaluation of the THOR and Hybrid III 50(th) Percentile Male Frontal Impact Anthropomorphic Test Devices. Stapp Car Crash Journal, 61: 227-276.

[17] Shaw, CG, Lessley, DJ, Kent, RW, Crandall, JR. (2005) Dummy Torso Response to Anterior Quasi-Static Loading. International Technical Conference on the Enhanced Safety of Vehicles (ESV). Paper 05-0371-W. 19. Washington, DC, June 6-9.

[18] Rouhana SW; Bedewi PG; Kankanala SV; Prasad P; Zwolinski JJ; Meduvsky AG; Rupp JD; Jeffreys TA; Schneider LW; (2003) Biomechanics of 4-Point Seat Belt Systems in Frontal Impacts. Stapp Car Crash Journal, 47(2003-22-0017): 367-399.

[19] Forman, JL, Kent, RW, Ali, T, Crandall, JR, Bostrom, O, Haland, Y. (2005) Biomechanical Considerations for the Optimization of an Advanced Restraint System: Assessing the Benefit of a Second Shoulder Belt. Proceedings of the International Research Council on the Biomechanics of Impact (IRCOBI). 337-354. Prague, Czech Republic, September 20-22.

[20] Albert DL;Beeman SM;Kemper AR; (2018) Occupant kinematics of the Hybrid III, THOR-M, and postmortem human surrogates under various restraint conditions in full-scale frontal sled tests. Traffic Injury Prevention, 19: S50-S58.

[21] Albert, D. L., Beeman, S. M., & Kemper, A. R. (2018). Assessment of Thoracic Response and Injury Risk Using the Hybrid III, THOR-M, and Post-Mortem Human Surrogates under Various Restraint Conditions in Full-Scale Frontal Sled Tests. Stapp car crash journal, 62, 1-65.

[22] Mertz, H, Williamson, J, Vander Lugt, D. (1995) The Effect of Limiting Shoulder Belt Load with Air Bag Restraint. SAE International Congress and Exposition. Paper 950886. Detroit, MI.

[23] Gehre, C., Gades, H. and Wernicke, P. (2009) Objective rating of signals using test and simulation responses. 21st International Technical Conference on the Enhanced Safety of Vehicles, Stuttgart, Germany.

[24] Rhule H, Donnelly B, Moorhouse K, Kang Y; (2013) A Methodology for Generating Objective Targets for Quantitatively Assessing the Biofidelity of Crash Test Dummies. Paper 13-0138, International Technical Conference on the Enhanced Safety of Vehicles (ESV), 23. Seoul, Korea.

[25] Rhule H, Maltese MR, Donnelly BR, Eppinger RH, Brunner JK, Bolte JH; (2002) Development of a New Biofidelity Ranking System for Anthropomorphic Devices. Stapp Car Crash Journal, 46: 477-512.

[26] Perez-Rapela, D., Markusic, C., Whitcomb, B., Pipkorn, B., Forman, J.L., Donlon, J.-P., Montesinos Acosta, S., Crandall, J.R. (2018) Comparison of WorldSID to PMHS in far-side impact. Proc. International Research Council on the Biomechanics of Impact.

INVESTIGATION OF RESTRAINT CHARACTERISTICS FOR ELDERLY OCCUPANT CHEST INJURY REDUCTION

Yasuaki Gunji, Takashi Aoki, Kenyu Okamura, Yuichi Ito
Honda R&D Co., Ltd. Automobile R&D Center
Japan

Paper Number 19-0275

ABSTRACT

Objective
In recent years, the increase in the number of traffic accident fatalities of elderly in Japan is one of the urgent tasks for future traffic accident countermeasures.
Moreover, from the trend of a global aging society, in the future it is expected that the number of traffic fatalities involving the elderly and the importance of correspondence will also increase. In this research, in order to cope with the reduction of elderly traffic accident fatalities, chest injuries are focused on as one of the factors of elderly occupant fatalities, measures to reduce chest impact of elderly occupants at the time of a frontal collision are examined and then, the direction of the corresponding technology required for realization was considered.

Methods
In this study, using a human body FE model with different physiques to reproduce the bone characteristics and skeletal shape of both adults and elderly people, frontal collision simulations within different collision speed ranges were performed. Comparison of chest injuries was undertaken of elderly occupants, which can occur in the middle and low speed range, to adults. Examination of optimum occupant restraint characteristics by seat belts enabled chest injuries of elderly occupants to be reduced to the same level of adults. Then, the effect of reducing elderly occupant's chest injuries in each physique was confirmed.

Results
The occupant restraint characteristic by the seat belt calculated was able to confirm the chest injury reduction effect of an elderly occupant in each physique in the front collision in the medium to low speed range. In addition, this restraint characteristic combines the restraint characteristics for reduction of chest injuries of elderly occupants with different physiques, and secondary collision damage reduction.

Discussion and Limitations
In this research, focus was on medium and low speed and frontal collision. In order to realize this occupant restraint characteristic, it was necessary to be compatible with occupant protection performance in the collision mode of each regulation. For this purpose, achieving sensing technology to determine the severity of car body deformation at the time of a collision, occupant protection system technology that can change occupant restraint characteristics according to the situation is essential. In order to further reduce the number of deaths, it is necessary to investigate occupant restraint characteristics that can reduce injuries, and look at other measures for reducing chest injuries in the high speed region for each type of collision.

Conclusion
In this study, we used a human body FE model with different physiques to calculate the occupant restraint characteristics necessary for a reduction of chest injuries of elderly occupants and reduction of secondary collision damage in frontal collisions in the medium and low speed range, and confirm the effect. In order to further reduce elderly occupant injuries, as a type of integrated safety technology with more damage mitigation effects, collision prediction technology by evolution of ADAS's external detection technology uses identification of an occupant's physique, posture, and age judgment technology It is necessary to evolve protection device technology, which can vary occupant restraining force and time according to situation and occupant.

INTRODUCTION

According to Japanese traffic accident statistics [1], the percentage of elderly people 65YO and over traffic accident fatalities (within 24hours) has recently been increasing. Measures to address traffic accidents involving the elderly is one of the urgent issues faced as part of Japan's efforts to reduce traffic accident fatalities. Statistical data from the Institute for Traffic Accident Research and Data Analysis (ITARDA) [2] on fatalities and injuries in automobile accidents that occur while riding in passenger cars, limited to drivers wearing seatbelts, was aggregated by age group and most severe injury. According to the results, a comparison between those 64YO and under and those 65YO and over by most severe injury body region shows that the percentage of fatalities due to chest injuries among adults 64YO and under was 27%, while the percentage among the elderly 65YO and over was 51%, and same trend in severe injury of AIS3+ (Figure 1). The percentage of fatalities due to chest injuries was conspicuously high compared to other injury body regions.

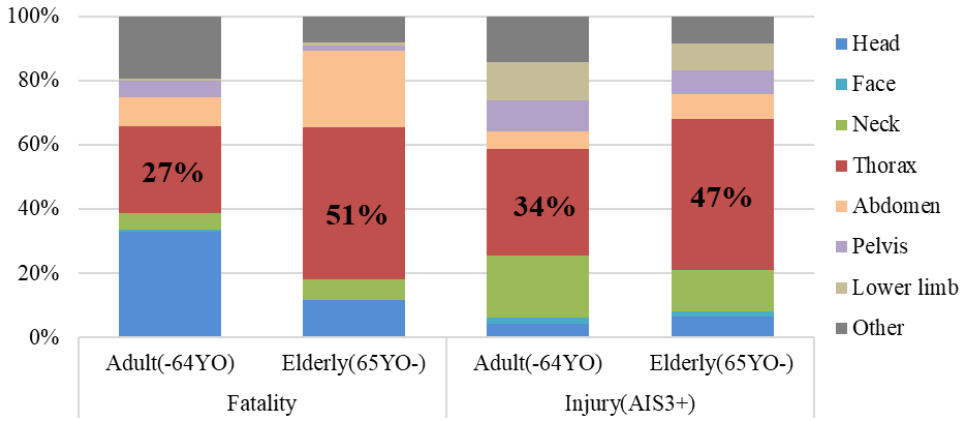

Figure 1. Injured body region on passenger car occupant by age groups (Driver)

Research by Kent et al. [3] suggests the significant differences between adults and the elderly in their skeletal structures, bone strengths, skeletal shapes, and bone structures, which are already known to medical science. Therefore, elderly seem to have a higher possibility of injury at medium and low speed. World population statistics [4] also point to a global trend toward the aging of societies so that the number of traffic accident fatalities among the elderly is projected to increase, and measures to counter that increase are considered a matter of growing importance. The present research seeks to support the reduction of traffic accident fatalities among the elderly by concentrating on the reduction of chest injuries, which are one of the causal factors in the death of elderly occupants in motor vehicles. Measures to reduce the thoracic load on elderly occupants during frontal collisions were investigated and approaches for the technology needed in order to realize such measures were considered.

METHODS

Human Body Model and Vehicle Model

In the present research, simulation used the FE models of adult and elderly vehicle occupants [5] [6] [7] that employs the explicit dynamics code of PAM-CRASH™ to reproduce the bone characteristics and skeletal shape of adults and elderly people. These human body FE models were used for three different physique types in the United States, namely the AF05, corresponding to a small female physique, the AM50, corresponding to a standard male physique, and the AM95, corresponding to a large male physique. As in the research by Sugaya et al. [8], these types were prepared through simple geometry scaling by body height and mass ratios. Figure 2 shows the front view of the models scaled to three physiques and Table 1 shows the scale factors for each physique.

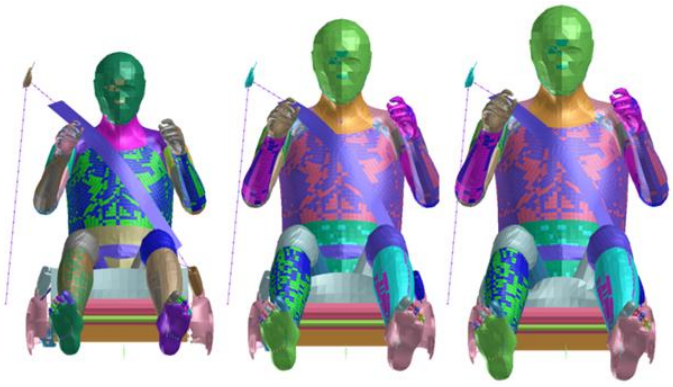

Figure 2. Human FE Models of Three Physiques (Left Side AF05, Center AM50, Right Side AM95)

Table 1. Scaling factors for each physique

Physique	Height	Mass
AF05	0.862	0.612
AM50	1.0	1.0
AM95	1.066	1.323

In the present research, a vehicle body FE model of a typical mid-sized sedan was used to reproduce the steering wheel and steering column, and the driver's seat, driver airbag, and seatbelt with three-point seatbelt with pretension (equivalent to mass produced products). Each collision simulations were performed with human body FE models for each physique in place.

Figure 3 shows the vehicle body model with a settled occupant model. The AF05 was seated at front-most, the AM50 at neutral, and the AF95 at rear-most positions in the seat slide range.

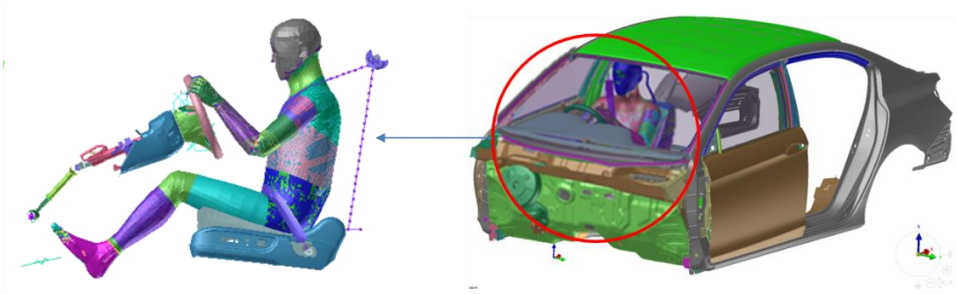

Figure 3. Vehicle FE model and occupant seating condition (AM50)

Parametric Studies for Rib Fracture (Rib Fx) Mitigation

Sled simulation of full-overlap frontal collisions was performed using the vehicle body decelerations that corresponded to 26 km/h and every 4 km/h increments up to 50 km/h. The airbag deployment timing and seatbelt pretensioner onset timing were varied according to the vehicle deceleration at the time of collision. The chest injuries that can occur to adult and elderly occupants under those conditions were evaluated by the thoracic deflections expressed by the relative deflection between the middle of the sternum and the T8 interbody as shown in Figure 4, and by the number of rib fractures expressed by the 'element elimination' when the strain of an element of rib cortical bone exceed a specified critical value as shown in Figure 5.

Next an examination was made of the optimal occupant restraint characteristics of seatbelts. The seatbelt load limiter characteristic was taken as a parameter and the load was varied by 0.25 kN increments between 2.25 kN and 3.0 kN as shown in Figure 6. The state of the chest injuries that occurred were confirmed for each of the elderly

occupant's physiques. A comparison was made of the results obtained at that time for occurrence of thoracic deflections and rib fractures by physique and by seatbelt load limiter characteristics, and the seatbelt lower limit load characteristics for rib fractures that occurred with each physique were derived. The results obtained by the above parametric study were used to determine the optimal occupant restraint characteristics for seatbelts that could reduce elderly occupant chest injuries to the same level as adult chest injuries. The chest injury reduction effects for the elderly occupants of each physique were confirmed.

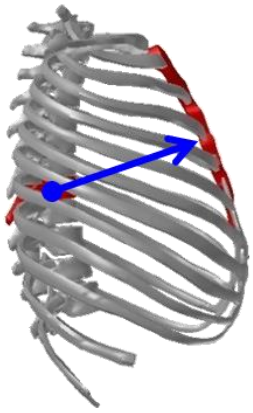

No.8 Thoracic Vertebra(T8)-Sternum Relative deflection

Figure 4. Measurement location of thoracic deflection

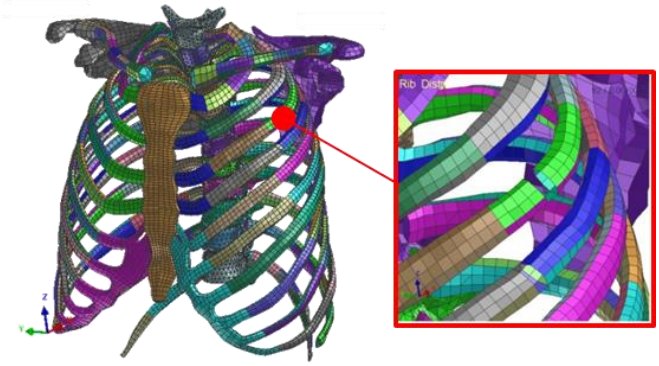

Figure 5. Rib fracture condition using element elimination option

Table 2. Parametric study for comparison of rib fracture condition

Vehicle Type	Mid-Size Sedan
Floor G Condition	26kph～50kph Full lap
Restraint Devices	Load limiter (3kN Constant) with Pretensioner, Airbag
Human FE Model of Occupant	Adult / Elderly
Physique	AM50

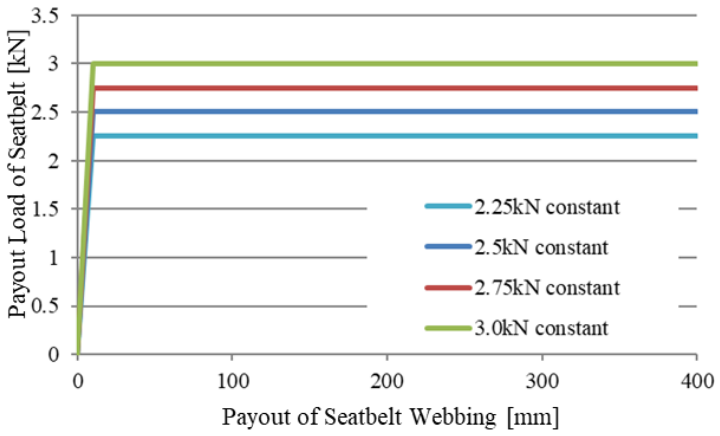

Figure 6. Seatbelt payload characteristic for parametric study

RESULT

Comparison of Rib Fracture between Adult and Elderly and Setting of Target Collision Speed

As a baseline examination, a comparison was made of differences in occurrence of chest injuries in adult/elderly occupants in frontal collision simulations at different collision speed ranges using the AM50 model. The number of rib fractures in the elderly model were compared with the number of rib fractures and resulting thoracic deflections in the adult model. The comparison results showed that one rib fracture occurred in the adult in a collision with speed equivalent to 40 kph, and as defined in AIS2005, this was AIS1, while at the same collision speed, it was found that four rib fractures occurred in the elderly, for a code of AIS3 as shown in Figure 7. However, the AIS code for rib cage injuries varies according to whether or not hemo/pneumothorax occurs. This cannot be evaluated with the present model, so the AIS was evaluated solely by the number of rib fractures. Based on these results, the target was defined as achieving the same or lower level of injury from chest injuries in elderly occupants in a medium-speed collision at a speed of about 40 kph as occur in adults as maked in Figure 7.

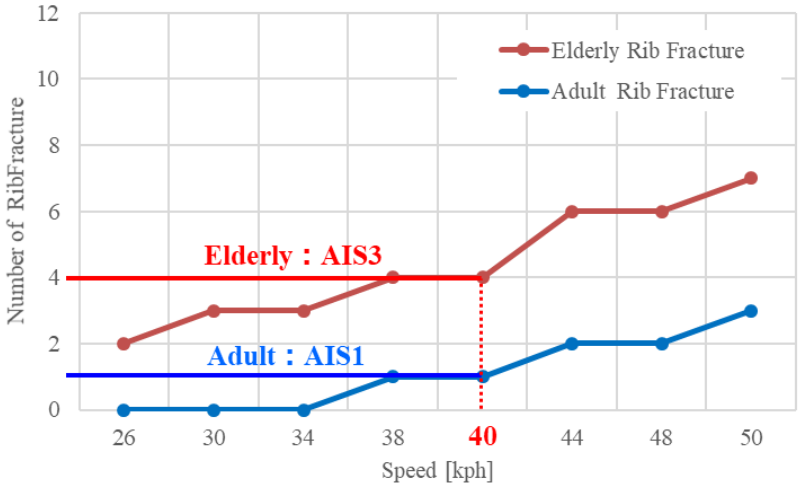

Figure 7. Rib fracture comparison between adult and elderly and target collision speed

Examination of Seatbelt Payout Load Characteristic for Each Physique for Elderly Rib Fracture Reduction

The optimal occupant restraint characteristics for seatbelts were examined. This involved taking the seatbelt load limiter characteristic as a parameter and confirming the circumstances of chest injury occurrence among elderly occupants with AF05, AM50, and AM95 physiques. The results for the circumstances of thoracic deflection and rib fracture occurrence in collisions at 40 kph by physique and by seatbelt load limiter characteristics were compared in terms of the circumstances of thoracic deflection and rib fracture in each physique model as shown in Table 3. The seatbelt lower limit load characteristics were derived for those rib fractures coded as AIS1 or above that occurred in each physique. The results were 2.5 kN for AF05, 3.0 kN for AM50, and 2.5 kN for AM95 as shown in Figure 8. However, even though the thoracic deflections in AM95 were smaller than in the other physiques, fractures did occur with a seatbelt payout load of 2.5 kN.

Table 3. Result of elderly rib fracture and chest deflection at each seatbelt payout load at 40kph (AM50)

Payout Load [kN]	2.5	2.75	3.0
Max Def. [mm]	46.3	49.0	51.1
Max Def. Time [ms]	67.8	66.8	64.8
Number of Rib Fractures	0	0	2
Part of Rib Fractures			
Rib Fracture Location			R3, L10

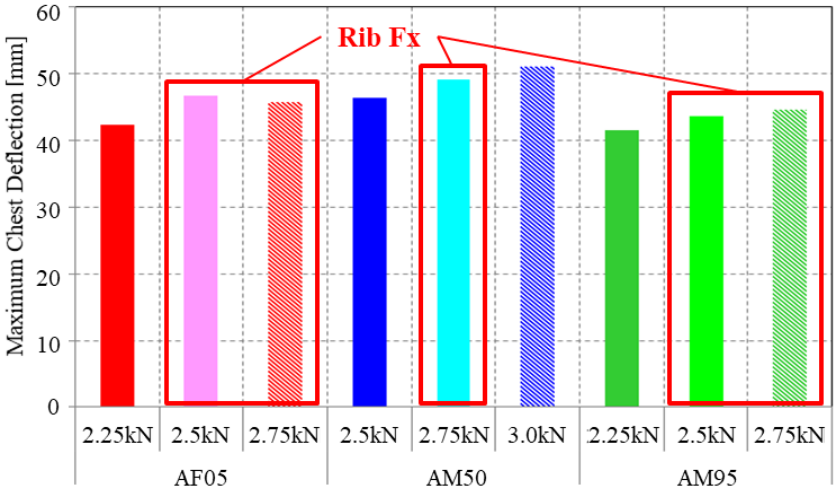

Figure 8. Result of rib fracture and chest deflection of each physique and seatbelt payout load

Target Setting for Secondary Collision Avoidance

The results, including occupant movement, were examined in detail for AM95. It was found that due to the low restraint load, contact with the steering wheel (STRG) occurred at every seatbelt payout load as shown in Figure 9 and Figure 10.

.

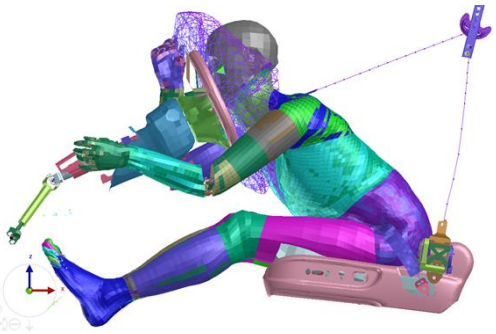

Figure 9. Secondary Collision of AM95 with STRG at 40kph

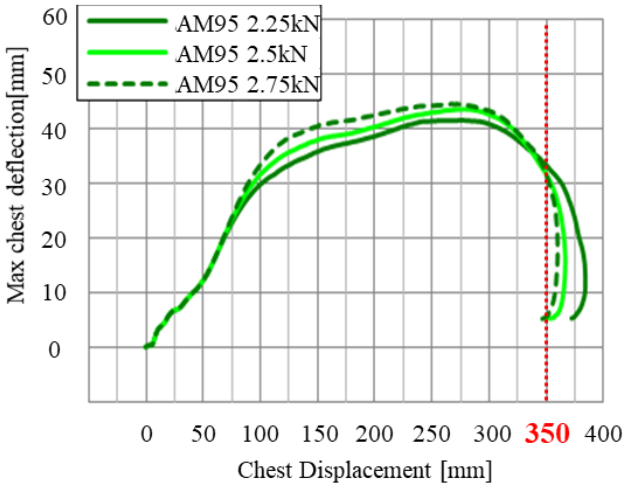

Figure 10. Chest displacement of AM95 for each payout load at 40kph

Consequently, the absence of contact with STRG was added to the target performance for the purpose of avoiding secondary collision in AF05 and AM95. An examination was made of the combination of seatbelt load limiter characteristics and collision speed that would enable avoidance of rib fractures and of contact with STRG in AF05 and AM95.

The seatbelt limit load and limit speed that could achieve the status of non-rib fracture and non-contact with STRG was calculated while lowering the collision speed to 34 kph that reduced the occupant's initial energy. The result was that the limit load for non-rib fractures in AF05 was 2.25 kN or lower, and the limit speed for non-contact with STRG and none rib fracture in AM95 was 36 kph.

Based on the above results, the relationship between the upper limit seatbelt payout load of seatbelt for none rib fractures and the maximum seatbelt payout needed to restrain the occupant at that point was put into an organized form. As shown in Table 4 and Table 5, the result was that the speed range enabling reduction of chest injuries and avoidance of secondary collision injuries, and the seatbelt payout load needed to restrain the occupant, differed for each of the AF05, AM50, and AM95 physiques.

Table 4. Result of elderly rib fracture for each seatbelt payout load at 34/36/40kph (AF05)

Physique	AF05					
Payout Load [kN]	2.25			2.5		
Speed [kph]	34	36	40	34	36	40
Max Def. [mm]	37.5	37.0	42.2	38.7	40.1	46.7
Max Def. Time [ms]	65.0	65.3	61.8	68.3	68.5	61.5
Number of Rib Fractures	0	0	0	1	1	1
Part of Rib Fractures	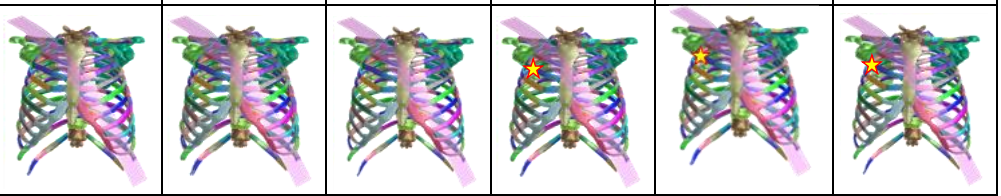					
Rib Fracture Location				R3	R3	R3
Chest Def. [mm]	105.5	112.9	114.2	99.7	109.8	93.4

Table 5. Result of elderly rib fracture for each seatbelt payout load at 34/36/40kph (AM95)

Physique	AM95					
Payout Load [kN]	2.25			2.5		
Speed [kph]	34	36	40	34	36	40
Max Def. [mm]	38.0	40.2	41.6	39.4	40.2	43.6
Max Def. Time [ms]	83.5	82.5	83.3	85.8	85.3	84.5
Number of Rib Fractures	0	0	0	0	0	2
Part of Rib Fractures	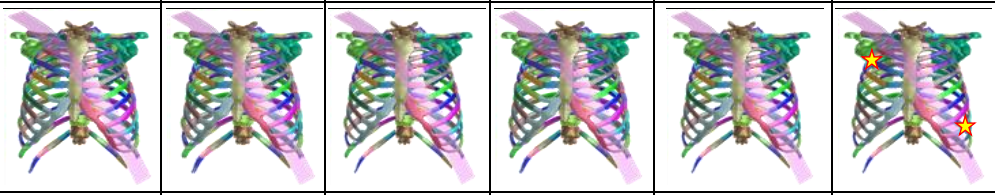					
Rib Fracture Location						R3,L8
Chest Def. [mm]	336.6	353.0	384.2	318.4	336.0	366.6

Comparison of Adult and Elderly Rib Fracture

The next step was to ascertain the seatbelt restraint characteristics that could maximize the injury reduction effect for elderly occupants of AF05, AM50, and AM95 physiques regardless of physique differences. This was done by fixing the collision speed at 35 kph, with reference to the limit speed for STRG contact by AM95, and setting the lower limit seatbelt payout load at 2 kN. Then a parametric study was carried out with the seatbelt load limiter characteristic set to increase gradually and consistently in conjunction with the seatbelt webbing payout, keeping it inclusive of the fracture limit load for each of the AF05, AM50, and AM95 physiques as shown in Figure 11.

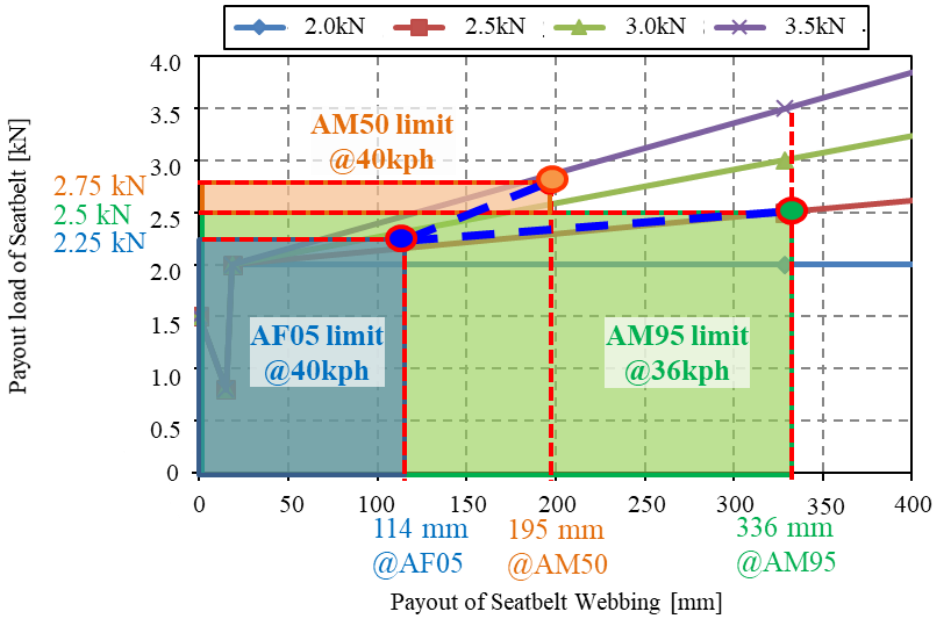

Figure 11. Relation of rib fracture and seatbelt payout load characteristic

Simulation using three physiques and four seatbelt restraint loads obtained the results for locations and numbers of rib fracture, for the fracture timing, and for the seatbelt webbing payout at the point where the upper body of the occupant moved farthest forward as shown in Table 6. These results were put in order and the seatbelt force limiter characteristic capable of realizing zero rib fractures while avoiding bottoming out against the STRG even for AM95 was successfully verified within the parametric study.

Table 6. Result of elderly rib fracture each seatbelt payout load at 35kph (AF05/ AM50/ AM95)

Physique	Payout Load @330mm	Max.Chest Def. [mm]	Chest Def.@Fx [mm]	Fx or No Fx	Time [ms]	Rib Fx location
AF05	2.0	72	-	No Fx	-	-
	2.5	66	65	Fx	87	R1
	3.0	66	37	Fx	66	R2
	3.5	66	35	Fx	63	R2
AM50	2.0	189	-	No Fx	-	-
	2.5	176	-	No Fx	-	-
	3.0	169	111	Fx	74	R3
	3.5	158	98	Fx	72	R3,4
AM95	2.0	338	-	No Fx	-	-
	2.5	314	-	No Fx	-	-
	3.0	291	-	No Fx	-	-
	3.5	289	255	Fx	97	R3

With seatbelt payout load on the vertical axis and seatbelt webbing payout on the horizontal axis, the above results for seatbelt payout and occurrence or non-occurrence of fractures were put in order and plotted by physique and seatbelt payout load in Figure 12. When the seatbelt load limiter characteristic was traced against the boundary for occurrence or non-occurrence of fractures with each physique, the result was a payout load characteristic that trended steadily upward. The restraint load characteristic obtained through this parametric study that enables mitigation of chest injuries and damage from secondary collision regardless of physique, and that has an energy

absorption (EA) load that also increases together with the increase in payout of seatbelt webbing, will hereafter be referred to as Progressive EA.

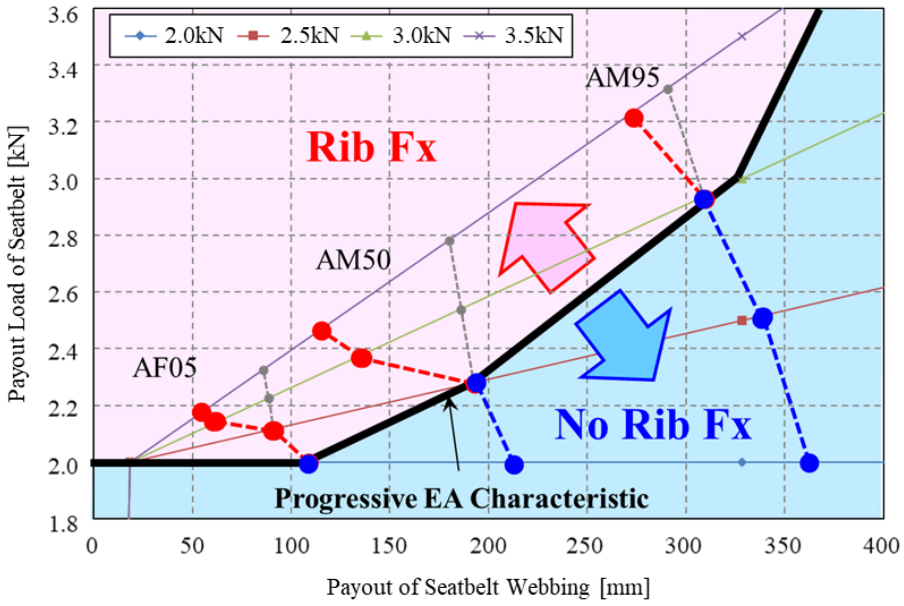

Figure 12. Relation of rib fracture and seatbelt characteristic (Progressive EA) at 35kph

DISCUSSION

The characteristics obtained through the present research are the simulation results for frontal collisions at low to medium speed. In order to confirm the collision angle and speed range covered by the characteristics obtained, a model that reproduces the interior and door trim of a mid-size sedan was used. For comparison of confirmed effectiveness, simulations were carried out with the seatbelt payout load fixed at 3 kN and with the Progressive EA seatbelt payout load varied from 2 kN to 3 kN, with the angle of collision with the barrier varied by 15° increments from 15° to 45°, and with the collision speed varied by 4 kph increments from 28 kph to 60 kph.

The changes in the number of rib fractures under the respective seatbelt payout loads were scrutinized. As shown in Figure 13, even with the seatbelt payout load fixed at 3 kN, which served as the base for comparison, the number of rib fractures was one or fewer under every collision angle as long as the collision speed was 28 kph. By contrast, although simulation with the Progressive EA characteristic successfully held down rib fractures under every collision angle up to a collision speed of around 36 kph, it was found that the number of fractures gradually increased as the collision speed. In some cases, this is because fracture occurs from collision with the center console or the door trim due to the collision angle and the rising speed. In the case of rib fractures occurred close to 40 kph, however, fracturing of the lower ribs was observed due to compression of the lower rib cage by the webbing on the shoulder belt side close to the seatbelt buckle as shown in Figure 14.

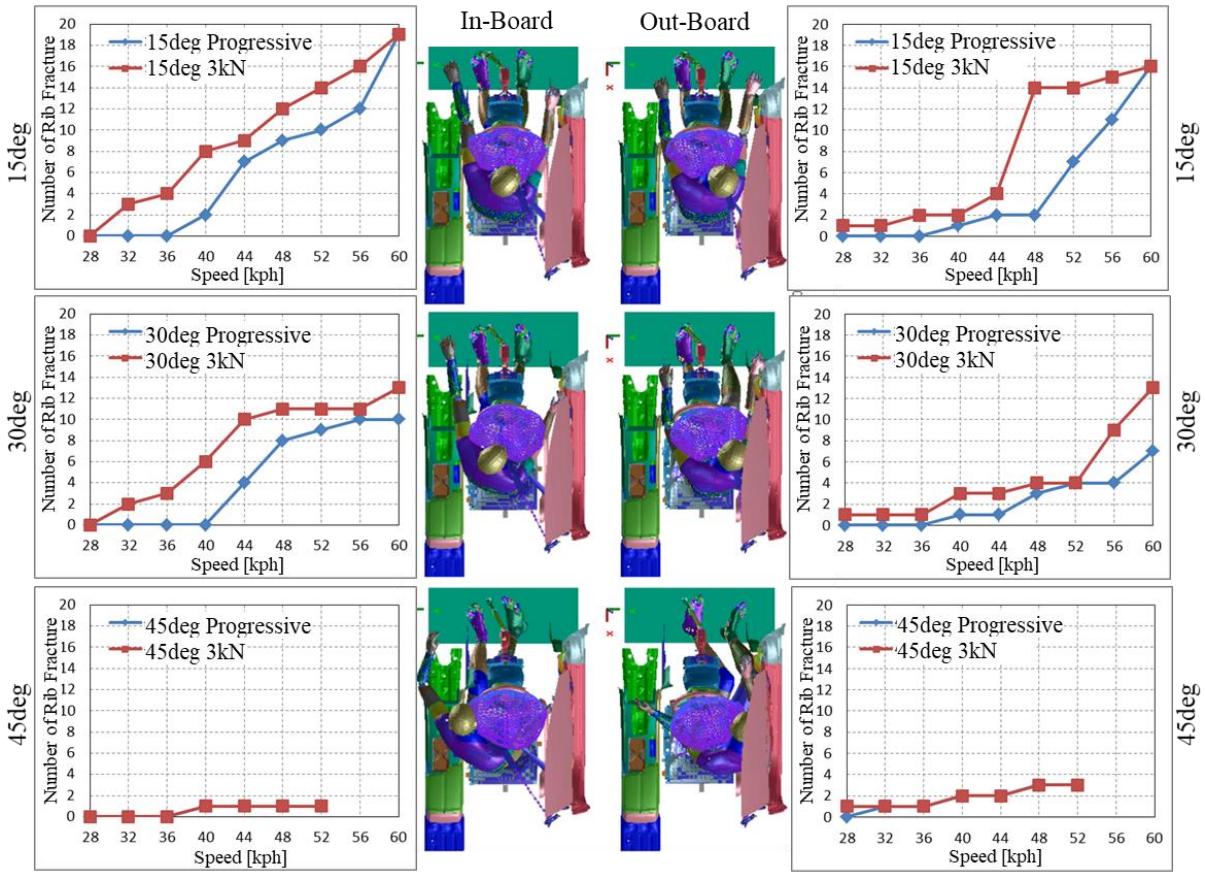

Fig. 13. Comparison of amount of rib fracture by collision direction / velocity (75YO)

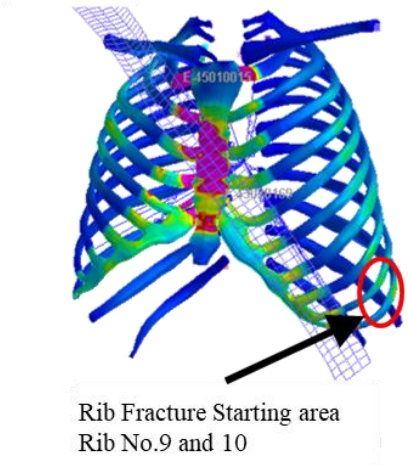

Fig. 14. Occurring rib fracture in oblique collision (75YO)

As to methods used in the present investigation for directly confirming rib fractures, evaluation of the fractures themselves is possible. However, evaluation of fractures in the lower ribs is not possible using another indicator, which is the measurement of chest deflection at representative points. In order to further reduce chest injuries in elderly occupants, the issues to be addressed include achieving a balance of necessary occupant protection performance in the collision modes specified in regulations and statutes for the purpose of realizing these occupant

restraint characteristics. At the same time, they also include expanding the range of collision speed and collision angle supported by the device while formulating indicators allowing for appropriate evaluation of the effectiveness of injury reduction in the lower ribs. The chest deflections and chest deflection reduction amounts achieved by the present simulation under the various seatbelt payout loads in the vicinity of 40 kph were compared in terms of the relative displacement between the sternum and T8, which were adopted as representative points for the present investigation, and the relative deflection between ribs 9 and 10 and T8 as shown in Figure 15, which are starting points for fractures of the ribs. Table 7 shows comparison of chest deflection reduction rate difference of measurement point.

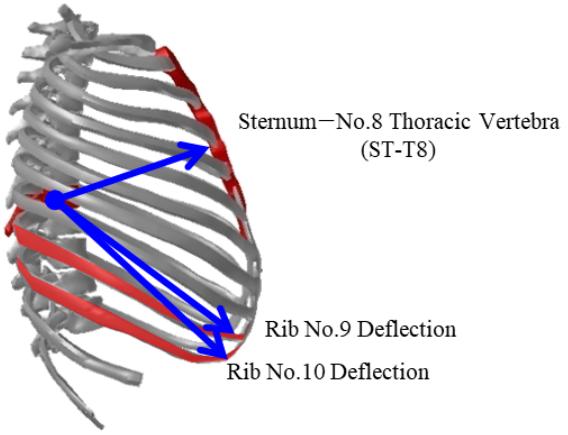

Figure 15. Comparison of chest deflection reduction effective measurement by collision direction

Table 7. Comparison of chest deflection reduction rate difference of measurement point

Payout Load	ST-T8 [mm]	Def. Reduction [mm]	Reduction Rate [%]	Rib Def. [mm]	Def. Reduction [mm]	Reduction Rate [%]
3kN	50.9	–	–	L9:23.4	–	–
				L10:15.0	–	–
2kN-3kN	44.0	6.9	**13.6**	L9:12.9	10.5	**45.0**
				L10:6.7	8.4	**55.7**

Where there was relative deflection between the sternum and T8, the reduction in chest deflection amounted to 6.9 mm, which was a reduction rate of 13.6%. By contrast, the reduction in displacement of ribs 9 and 10 was from 8 mm to 10 mm. Although very small, this reduction achieved the significant reduction effect of around 45-55.7%, and it will be necessary to devise an index that enables appropriate evaluation of this reduction effect for use in future investigation of devices supporting the protection of elderly occupants.

In Figure 16, one example can be seen when these simulation results are plotted by the number of fractures on the vertical axis and by the consequent chest deflection at representative points on the horizontal axis. Inspection of the correlation between rib cage displacement and the number of fractures shows large variations. No distinct correlation can be seen. This suggests that the evaluation of rib fracture injuries by representative points on the rib cage is inadequate as an indicator. For future investigation of chest injury reduction taking the real world accidents into consideration, it will no doubt be necessary to create an appropriate injury evaluation method that can be used to evaluate the rib fracture reduction effect in the ribs as a whole, such as suggested in the research of Kawabuchi et al. [9]. This needs to be in addition to injury evaluation by measurement of rib cage displacement at four points using a recent THOR dummy equipped with IR-TRACC.

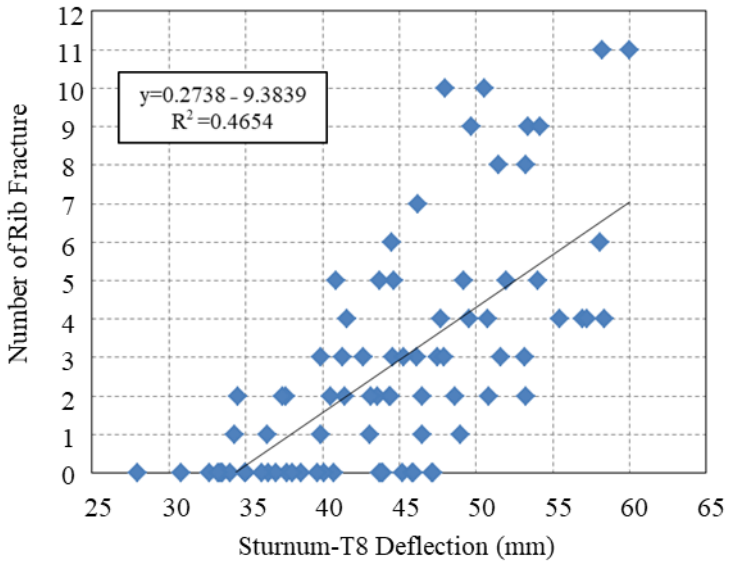

Figure 16. Correlation of human chest deflection and rib fracture

In addition, in order to further reduce fatalities among elderly occupants, it will also be essential to have technology for occupant protection systems capable of varying occupant restraint load and timing continuously, according to collision pattern and occupant variation. And, as an integrated safety technology that has greater damage reduction effectiveness, sensing technology needs to determine the severity of vehicle body deformation during a collision in combination with technology for collision prediction using evolved Advanced Driving Assistance System (ADAS) technology for sensing the external environment, and also for identifying occupant physique and posture and for determining age. It is also considered necessary to investigate occupant restraint characteristics capable of injury reduction, and measures capable of reducing chest injuries at high speeds, for collision patterns other than frontal collision. The results of this study, combined with these integrated safety technologies, will be able to reduce injuries not only elderly people but also various vehicle occupants.

CONCLUSION

In the present research, further reduction of fatalities, we were examined by focusing on chest injuries, which are one of the causal factors in the fatal of elderly people while riding as occupants in automobiles. Measures to reduce the thoracic load on elderly occupants during frontal collisions were investigated and approaches for the technology needed in order to realize such measures were considered. As a result, Progressive EA characteristics that are a seatbelt load limiter characteristic capable of reducing damage from chest injuries and secondary collision regardless of the elderly occupant's physique were obtained through simulation using a human model.

Issues that remain for the future include the creation of appropriate injury evaluation methods capable of evaluating effectiveness in reducing rib fractures in the ribs as a whole in the course of investigating chest injury reduction that takes real world accidents into consideration further chest injury reductions.

In addition to this, it will be necessary to create occupant restraint technology that is capable of covering an expanded range of collision speeds, collision angles, and adjust to each occupant in various situations, by using ADAS sensing information and varying occupant restraint load and timing.

REFERENCES

[1] Institute for Traffic Accident Research and Data Analysis (ITARDA), Annual Traffic Accident Report 2017 (in Japanese)

[2] Institute for Traffic Accident Research and Data Analysis (ITARDA), http://www.itarda.or.jp/

[3] Kent, R.W. Lee, S. Darvish, K. Wang, S. Poster, C.S. Lange, A.W. Brede, C. Lange, D. Matsuoka, F. 2005. "Strucural and Material Changes in the Aging Thorax and Their Role in Crash Protection for Older Occupants." Stapp Car Crash Journal, vol.49, pp. 231-249

[4] United Nations, World Population Prospects the 2017 Revision

[5] Ito, O. Dokko, Y. Ohashi, K. 2009. "Development of adult and elderly FE thorax skeletal models." SAE Technical Paper 2009-01-0381

[6] Ito, O. Ito, Y. Dokko, Y. Mori, F. Ohhashi, K. 2010. "Successive development of adult and elderly FE thorax models (Japanese)." Paper presented at: Society of Automotive Engineers of Japan (JSAE), paper #20105713

[7] Ito,Y 2011." Kinematics Validation of Age-Specific Restrained 50th Percentile Occupant FE Model in Frontal Impact" SAE Technical Paper 12B-0105

[8] Sugaya, H. Takahashi, Y. Gunji, Y. Dokko, Y. Ayyagari, M. Whitcomb, B. Markusic, C. Agnew, A. Kang, Y.S. Bolte, J., 2019." Development of a Human FE Model for Elderly Female Occupants in Side Crashes" ESV 26th Paper Number 19-0052

[9] Kawabuchi, T. Dokko, Y. 2019. "Evaluation of Thoracic Deflection Criteria in Frontal Collision using Thoracic Impactor Simulation with Human Body FE Model" ESV 26th Paper Number 19-0068

APPENDIX A

Table A1. Result of elderly rib fracture and chest deflection at each seatbelt payout load at 40kph (AF05)

Payout Load [kN]	2.5	2.75	3.0
Max Def. [mm]	42.2	46.7	45.8
Max Def. Time [ms]	61.8	61.5	61.5
Number of Rib Fractures	0	1	9
Part of Rib Fractures	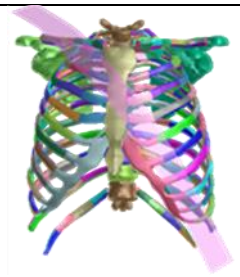		
Rib Fracture Location		R3	R2-3, L4-10

Table A2. Result of elderly rib fracture and chest deflection at each seatbelt payout load at 40kph (AM95)

Payout Load [kN]	2.5	2.75	3.0
Max Def. [mm]	41.6	43.6	44.5
Max Def. Time [ms]	83.3	84.5	84.3
Number of Rib Fractures	0	2	4
Part of Rib Fractures			
Rib Fracture Location		R3, L8	R3, L7-9

IMPROVEMENTS TO ASEAN NCAP CRASH TEST RATING SANS A PLATFORM CHANGE

Khairil Anwar Abu Kassim
Muhammad Shafiq Ahmad Laili
Yahaya Ahmad
Mohd Hafiz Johari
Siti Zaharah Ishak
ASEAN NCAP
Malaysia

Paper Number 19-0276

ABSTRACT

Besides other reasons, car manufacturers often develop new cars with the aim to improve on their ASEAN NCAP crash safety performance rating. Apart from car safety assist, such ratings depend on the degree of adult occupant protection (AOP) and child occupant protection (COP) measured via the seriousness of injuries to dummies. This study shall explain how car manufacturers can improve their crash performance rating without changing the platform structure of a new car. The move shall be more cost effective as platform structure development is expensive; and less time consuming to enable a product to be launched in time (Al-zaher & Elmaraghy, 2014; Al-zaher & Elmaraghy, 2014). Two ASEAN NCAP crash tests have been conducted on 2 car brands on two different occasions, with the more recent result showing improvement from 3-Star to 4-Star rating. This proves that without a platform structure change, a high rating can still be achieved. Such a situation will help manufacturers save cost and reduce time to develop a new car by using the same platform structure but with better safety performance.

INTRODUCTION

An important element of any car is the body structure or platform [1]. The platform connects all the different components; whereby it houses the drive train and more importantly carries and protects passengers and cargo. The body structure needs to be rigid to support weight and stress and to securely tie all the components [2]. Furthermore, it must resist and soften the impact of a crash to safely protect the occupants. Thus, most automobile manufacturers seek to design better automobile structure to ensure passenger safety as well as reduce the automobile mass [3].

ASEAN NCAP Safety Star Rating *vis-a-vis* or pertaining to a car body structure focuses more on passive safety whereby tests are carried out to assess frontal and side impacts. Nonetheless, the regulations in regard to these assessments have become more stringent in the past decade. Many automobile industries are therefore aiming to design better platform structure for passenger safety as well as to reduce platform mass [4]. Better platform structure will hopefully enhance passive safety and a good body structure base will possibly result in better crash performance. It is important to note that a good crash performance is achieved by way of impact energy absorption [2]. In other words, how impact energy is absorbed will affect the severity of passenger physical injuries as well as damage to the car interior [5]. The less injury a passenger dummy suffers, the higher the structure performance is rated.

All passenger cars are built on platforms or architectures defining the core engineering of a vehicle. Traditionally, automotive OEMs have shared this engineering across products. For example, under the hood, Skoda Fabia and Volkswagen Polo use the same engineering structure. As platform development accounts for nearly half of the product development cost borne by Original Equipment Manufacturers (OEMs), the strategy of using common engineering across vehicle models have enabled them to cut cost as well as save time [6]. If the industry can create one good platform to enhance crash performance and use this method of sharing, there will be an increase of safer cars on the market and more lives can be saved as a consequence of a reduced passenger injury. This paper shall highlight that with some enhancements made to new car *sans* or without a platform change, it is possible to improve their ASEAN NCAP rating from 3-Star to 4-Star.

PLATFORM STRUCTURE

A vehicle frame, which is also called chassis, is the main supporting structure of a motor vehicle to which all other components are attached. Most car models and even car types share a set of common design, engineering, production efforts, as well as major components [7]. This practice is a norm in the automotive industry to reduce the cost associated with product development by basing several products on a smaller number of platforms [8]. This further allows companies to create distinct models from a similar design perspective.

As mentioned earlier, ASEAN NCAP Star Rating for platform structure is conducted via the frontal crash and side impact barrier crash tests. The detail calculation is based on (i) injuries suffered by a dummy's head, chest, knees, tibia, and foot during a crash test and (ii) the car body structure (also known as modifiers). For the frontal impact against offset deformable barrier (ODB) with 40 % overlap at 64 km/h, the structure rating will divided into two parts, namely the upper occupant compartment and lower occupant compartment. In addition, for side impact mobile deformable barrier (MDB) at 50 km/h, scores will only be calculated for rating purposes.

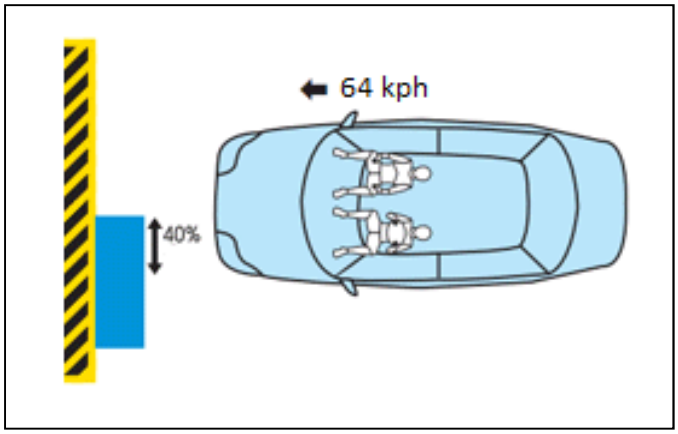

Figure 1. Example of frontal impact 40% ODB

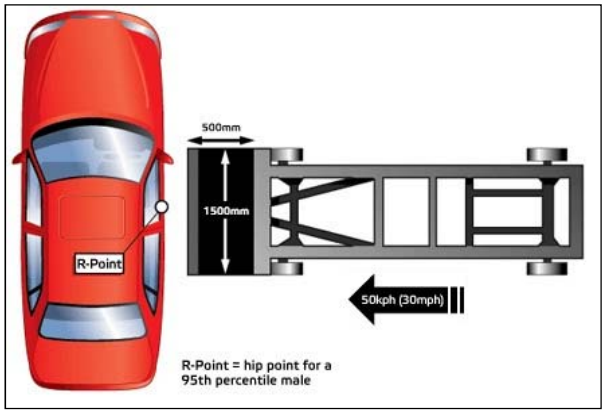

Figure 2. Example of side impact MDB

CASE STUDY

ASEAN NCAP rating calculation is divided into three categories, which are AOP, COP and safety assist. Each category has different calculations and will affect the overall Star Rating [9]. Table 1 below shows AOP rating and COP rating from 5-Star to 0-Star based on ASEAN NCAP protocol 2012-2016.

Table 1.
Rating protocol based on protocol 2012-2016

Adult occupant protection (AOP) Rating	Child occupant protection (COP) Rating
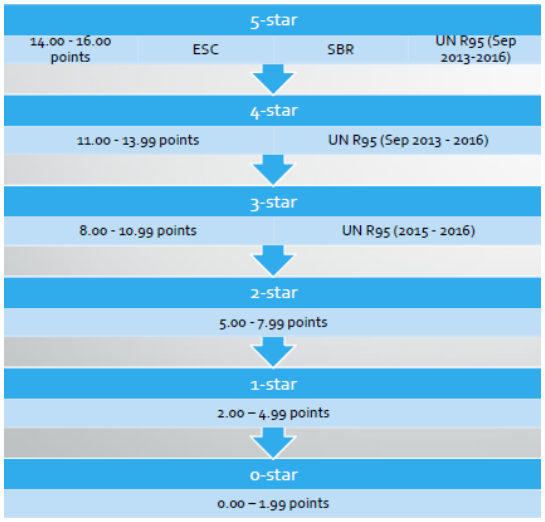	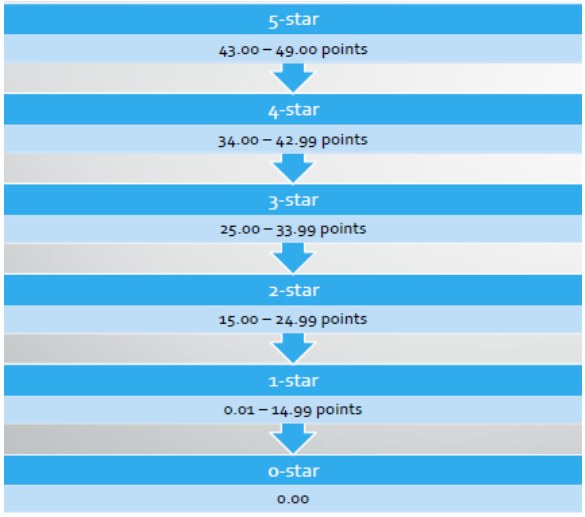

The entire Star Rating is based on the frontal crash and side impact crash tests. Both crashes use P1.5 and P3 dummies to represent children and hybrid III 50% dummies for adults. In the frontal crash, a car will impact the 40% OBD (Offset-Deformable Barrier) at a travelling speed of 64 km/h. As for the side impact test, a car occupied by ES-2 dummy will be impacted with MDB EEVC (Mobile deformable barrier European Enhanced Vehicle-safety committee) (900kg) at a travelling speed of 50km/h. For AOP assessment, results of the frontal crash impact will be calculated in terms of the injury suffered by the dummies and the car structure modifier. Figure 3 shows the division of points for AOP dummy injury. Further, COP also looks at inclusion of CRS (child restrain seat), as well as vehicle-based test and dynamic test to obtain the highest score of 49.00 points.

This testifies that the main contributor to the points in determining ASEAN NCAP Star Rating is the injury to the dummies. The less the injury to the dummies, the higher Star Rating shall be awarded. Further, crash test impact is conducted to determine the level of strength and impact energy absorption of a vehicle [10]. In order to reduce injury of the dummies upon impact, automotive manufacturers need to improve passive safety technology which shall in turn elevate their ASEAN NCAP rating. To enhance passive safety capability, it is not necessary to change the platform structure because in the past, ASEAN NCAP has seen two car brands which had successfully upgraded their rating without changing their original platform structure [11]. Such a feat was achieved by adding strength to the platform structure and upgrading some components in both cars.

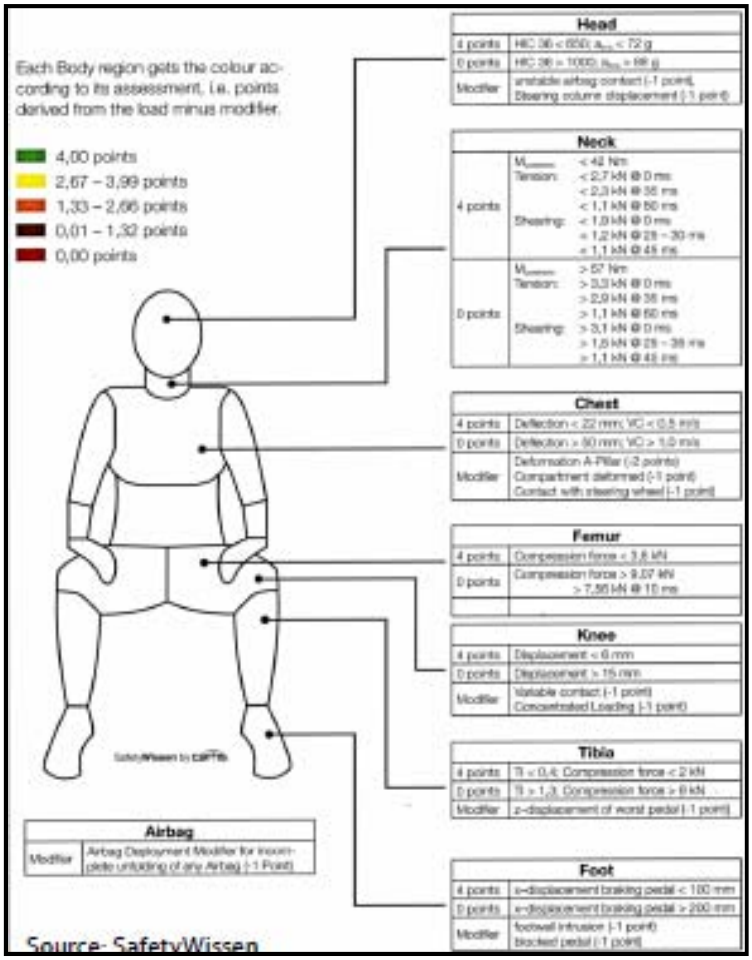

Figure 3. Example AOP Calculation Point

HISTORY OF ASEAN NCAP RATING UPGRADE

Vehicle brand 1

As per its background, Vehicle 1 is categorized as a 4-door sedan of the same variant and platform but with different engine capacity and kerb mass. In order for the manufacturer to use the platform for a new car but with better safety, some upgrading works had to be done. The result of the first crash test was 3-Star, but following some upgrading to the body structure, the rating improved to 4-Star upon being re-crashed. The gap between both crash tests was 3 years. The upgrading carried out is as shown below:

<u>Body structure improvements</u>

- Improved Bumper beam area
- Improved Mounting engine
- At driver and passenger area of leg to knee - changed from UHSS to advance HSS side sill
- Strut bar added
- Improved seatbelt system
- Adding of patch car floor

<u>Component structure system upgrading</u>

- Improved the ‘collapsible’ steering shaft
- Upgraded steering wheel
- Enlarged size of vent DAB and PAB
- ACU position changed to more strategic location

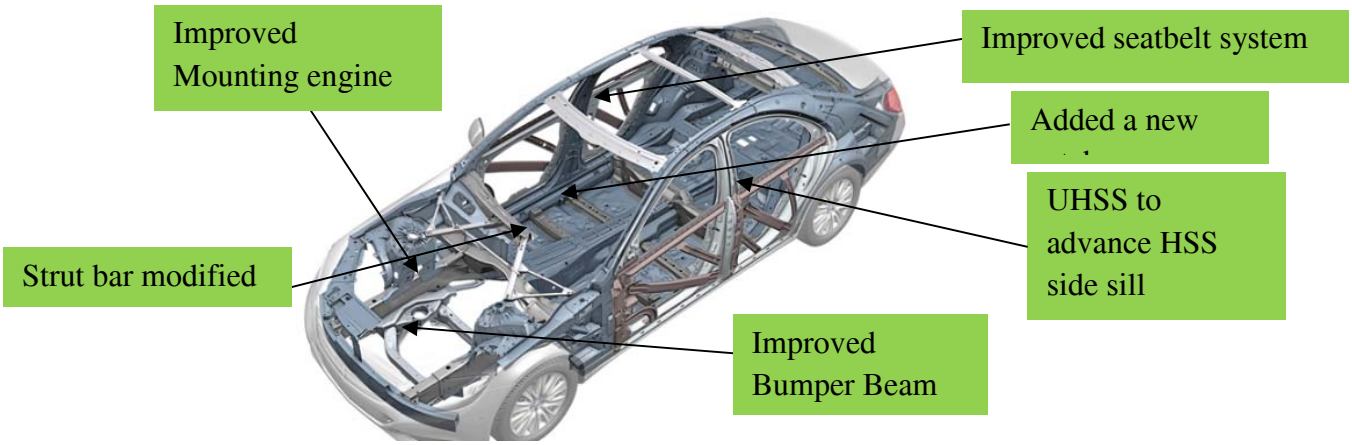

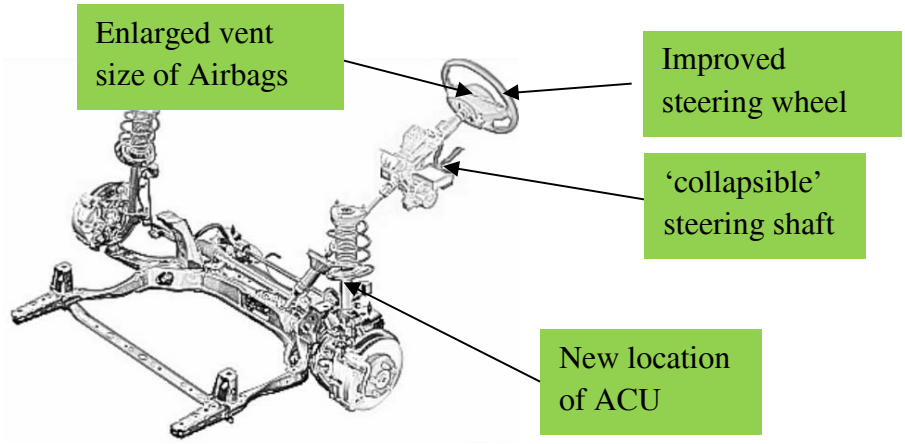

The first crash test was in 2013, and following a lot of changes and upgrading, the second crash test for Vehicle 1 registered an improvement in terms of its safety features where it achieved 13.33 over 16.00 points in the AOP, thus placing it in the 4-Star category. Compared to the previous test, Vehicle 1 was awarded 10.23 points with 3-Star rating for its AOP.

As for the COP, Vehicle 1 recorded a commendable achievement by obtaining 71% compliance, which was within 4-Star rating. Vehicle 1 comes with standard dual airbags and Seatbelt Reminder System (SBR) for driver only. Furthermore, Vehicle 1 is equipped with standard ISOFIX and top tether. However, Anti-lock Braking System (ABS) is not available in all variants while Electronic Stability Control (ESC) can only be found in the premium variant.

Vehicle brand 2

As per the background, Vehicle 2 is categorized as a 5-door hatchback of the same variant with the same platform and engine capacity but different kerb mass. In order for the manufacturer to use the same platform structure for a new car with better safety, some upgrading works had to be done. In the first crash test, Vehicle 2 was awarded 3-Star, but upon improvements to the body structure, it was awarded 4-Star after being re-crashed. The gap between the first and second crash tests was 2 years. The upgrading carried out is as shown below:

Body structure (improved to prevent cabin and body deformation)

- Door beam
- A pillar
- Side sills
- Centre brace

- Front-end cross member

Passenger restraint

- Improved quality of airbag
- Improved material of seatbelt
- Additional Knee bolster
- Additional bracket P-P member
- Changed front seat driver
- Changed inflator driver airbag
- Changed passenger airbag

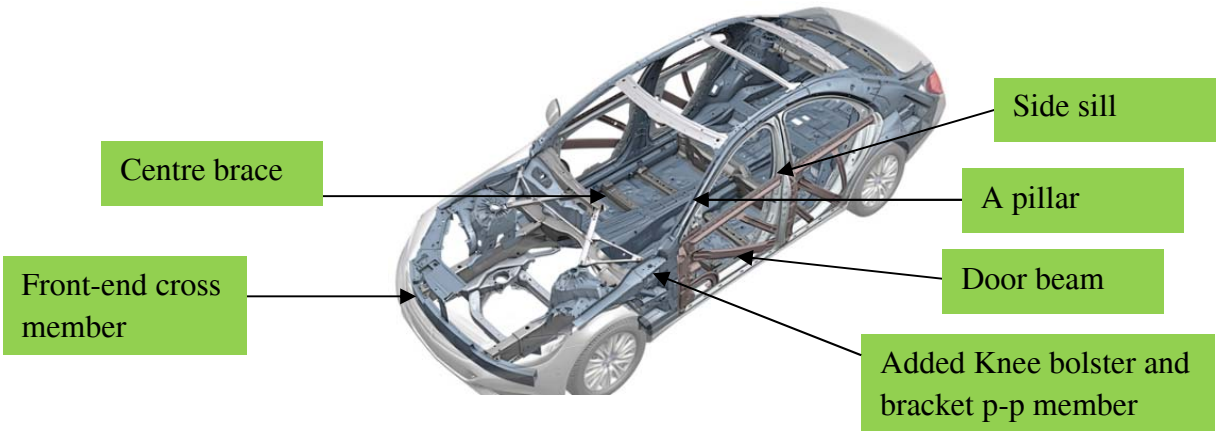

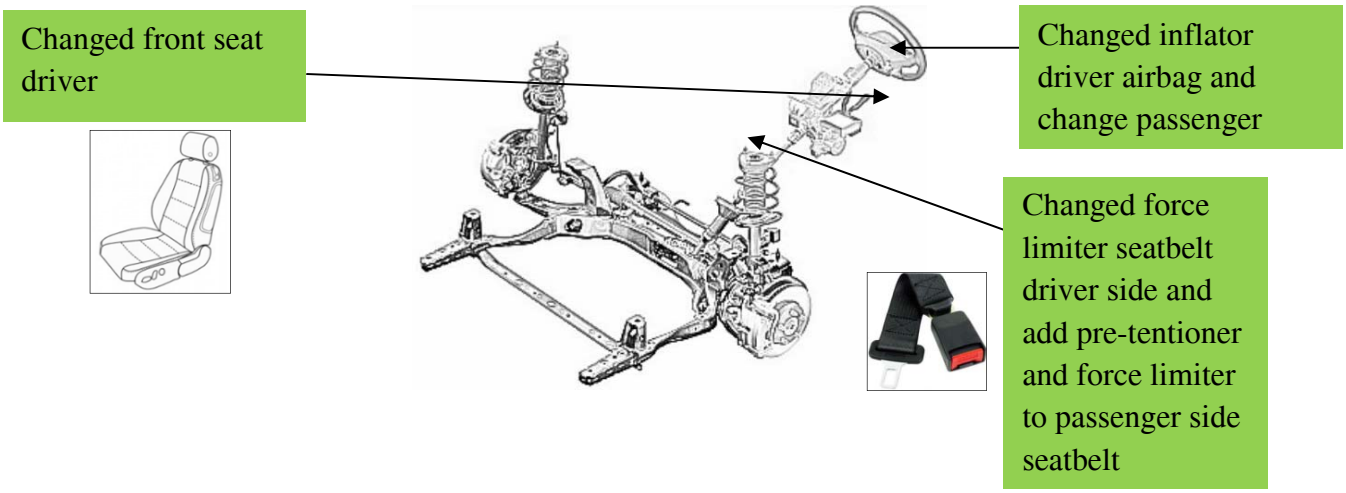

Upon making some changes to the body structure and passenger restraint, Vehicle 2 latest version (crash tested in 2015) obtained 4-Star in AOP with 11.55 points. In comparison, it was awarded 3-Star AOP with 8.71 points in 2013. Vehicle 2, which is the all time best selling model in Malaysia has also improved its score in COP with 71 % compared to 54% in the first crash test. It is therefore rated 4-Star. As per the child restraint system, ISOFIX & top tether are available as standard fitment. The stability control system (ESC) is, nevertheless, only offered in higher variants.

CONCLUSION

Car manufacturers have always competed by coming up with newer cars in a bid to become the market leader. Of late, with the launch of each new model, they will make sure that aside from the aesthetic features and fuel efficiency, the safety aspects will also be taken into account. Such safety aspects are translated into high Star Rating awarded by NCAPs across the globe. At the same time, car makers must also find the most viable solution to come up with competitive products at lower costs and increased profits [12]. This study has

elucidated that in order to improve crash safety performance, a manufacturer does not necessarily need to change the platform structure for a new car. ASEAN NCAP's crash test results involving Vehicle brand 1 and Vehicle brand 2 provided a clear example that a car safety performance rating can be improved without changing the platform structure. What was needed were merely several changes to the passenger restraint system, component system as well as the body structure. Furthermore, better crash performance is indicated by lower injury levels to passenger which in return raises interest among potential car buyers. Collaboration between brands to share the platform structure with good crash performance result could, at the same time, reduce the cost of producing safer new cars. But more importantly, such a practice will ensure more safer cars on the market and thereby result in safer roads.

REFERENCE

[1] Gonçalves, A., & Ferreira, N. (n.d.). Automobile Front-End Structure: Modularity and Product Platform, (2), 1–21.

[2] Lee, Y., Ahn, J., & Park, G. (2015). Crash Optimization of Automobile Frontal and Side Structures Using Equivalent Static Loads, (June), 1–5.

[3] Ferguson, S., & Kasprzak, E. M. (2005). Design and Optimization of Reconfigurable Vehicle Platforms, 1–17.

[4] Korta, J., Ricerche, C., & Fiat, S. C. (2014). Multi-Objective Optimization of a Car Body Structure, 1143–1152. https://doi.org/10.4271/2012-01-1555

[5] Droste, A., & Röttger, J. (2007). Crash Performance Increase with Structural BETAFOAM. *6. LS-DYNA Anwenderforum, Frankenthal 2007*, 37–44.

[6] Michael Brylawski, O. N. A. (1999). UNCOMMON KNOWLEDGE :, (1), 27–29.

[7] Suh, E. S., Weck, O. L. De, & Chang, D. (2005). Flexible Product Platforms : Framework and Case Study, (October).

[8] Kuys, B., Gutowski, M., Li, S., Gutowski, W. V. S., & Cerra, A. (2016). MODULAR DESIGN AND ASSEMBLY OF AUTOMOTIVE AND ARCHITECTURAL STRUCTURES : PRODUCT INTEGRATION THROUGH ADHESIVE BONDING facilitate communication between inter-connected product sub-systems . into individual modules which can be readily re-arranged into diff, *40*(3). https://doi.org/10.2478/amst-2016-0013

[9] Asean ncap, (2018). The rating explanation – Our Test, http://www.aseancap.org/v2/?page_id =3087, ASEANNCAP.org, 125-135, Jalan TKS 1, Taman Kajang Sentral, 43000 Kajang, Selangor. (Accessed: 29 Jun 2018).

[10] Zellner, J. W. (2006). Physics in the crumple zone demonstrate how less stiff materials, like plastic, can help prevent injury and save lives. Retrieved from http://www.k12.nf.ca/gc/Science/Physics3204/Projects2003/SlotA/ProjectA2/link20.htm%5Cnhttp://www.k12.nf.ca/gc/Science/Physics3204/Projects2003/SlotA/ProjectA2/link20.htm%5Cnhttp://www.k12.nf.ca/gc/Science/Physics3204/Projects2003/SlotA/ProjectA2/link20.h

[11] Asean ncap, (2018). Result, http://www.aseancap.org/v2/?page_id =3087, ASEANNCAP.org, 125-135, Jalan TKS 1, Taman Kajang Sentral, 43000 Kajang, Selangor. (Accessed: 29 Jun 2018).

[12] Al-zaher, A., & Elmaraghy, W. (2014). Design Method of Under-Body Platform Automotive Framing Systems. *Procedia CIRP*, *17*, 380–385. https://doi.org/10.1016/j.procir.2014.03.116

IMPROVING THE EFFECTIVENESS OF ACTIVE SAFTY SYSTEMS TO SIGNIFICANTLY REDUCE ACCIDENTS WITH VULNERABLE ROAD USERS - THE PROJECT PROSPECT (PROACTIVE SAFETY FOR PEDESTRIANS AND CYCLISTS).

Ilona Cieślik
Advanced Driver Assistance Systems, IDIADA Automotive Technology
Santa Oliva 473710, Spain

Jordanka Kovaceva
Vehicle Safety, Chalmers University of Technology
SE-412 96 Gothenburg, Sweden

Marie-Pierre Bruyas
Cognitive Psychology, Institut Français des Sciences et Technologies des Transports, de l'Aménagement et des Réseaux (IFSTTAR)
F-69675 Bron Cedex, France

David R. Large
Human Factors Research Group, University of Nottingham
NG7 2RD Nottingham, UK

Martin Kunert
Advanced Engineering Sensor Systems, Robert Bosch GmbH
71226 Leonberg, Germany

Sebastian Krebs
Environment Perception, Daimler AG
Ulm D-89081, Germany

Maxim Arbitmann
Enhanced ADAS & Tire Interactions, Continental Teves
60488 Frankfurt/Main, Germany

Paper Number 19-0277

ABSTRACT

Accidents involving Vulnerable Road Users (VRU) are still a very significant issue for road safety. ´PROactive Safety for PEdestrians and CyclisTs´ is a collaborative research project funded by the European Commission. The objective of PROSPECT was to improve significantly the effectiveness of active VRU safety systems compared to those currently on the market by: (i) expanding the scope of urban scenarios addressed (ii) improving the overall Autonomous Emergency Braking (AEB) and Autonomous Emergency Steering (AES) system performance (iii) proposing extensive validation methodologies for consumer testing, simulation and acceptance studies with tools for testing. Concepts for sensors and control systems were shown in three vehicle demonstrators and a mobile driving simulator and tested with novel VRU dummy specimen. Those systems address the well-known barriers of current AEB systems such as limited sensors field-of-view, fuzzy path prediction, unreliable intent recognition and slow reaction times for the actuation. User acceptance tests with the participation of drivers were also crucial in PROSPECT for the success of all active safety systems. Driving simulator studies were then used in a controlled and repeatable environment for the collection of data regarding the interaction between the driver and the safety function. Finally, project consortium implemented a novel benefit estimation methodology that includes an assessment of the combined effect of active and passive safety measures of PROSPECT-like systems.

Keywords: Active safety; Advanced Driver Assistance Systems (ADAS); Vulnerable Road Users (VRU); Autonomous Emergency Braking (AEB); video and radar technology.

1. INTRODUCTION AND MOTIVATION FOR PROSPECT PROJECT

Considering the countries in the European Union (EU) and the latest year of data availability for 2017, according to the accident data published by the EU [1], about 1.3 million people die each year on the world's roads, of which 25.300 lost their lives in the EU. In 2017, vulnerable road users (VRU) accounted for almost half of the road victims, where 21% of all people killed on roads were pedestrians and 8% were cyclists. These percentages show the magnitude of the problem and the need to take action in order to reduce these figures (see Fig. 1).

The White Paper (Roadmap to a Single European Transport Area – Towards a Competitive and Resource Efficient Transport System) contains European Union goals on the area of traffic safety [2]: *„By 2050, move close to zero fatalities in road transport. In line with this goal the EU aims at halving road casualties by 2020."*

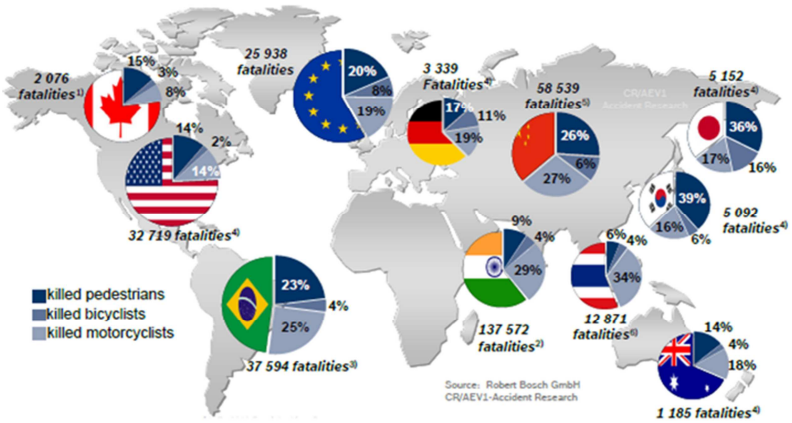

Figure 1. Road traffic deaths by type of road user in Europe and world (Source: Robert Bosch, 2015)

Nowadays, Advanced Driver Assistance Systems (ADAS) are the basis for the development of automated cars. The last decade has seen significant progress on active safety, as a result of advances in video and radar technology. Nevertheless there is still high potential for improvement in this field.

In particular, a study by Euro NCAP and NCAP concluded in 2015 (Author's Note: the independent safety bodies for Europe and Australasia) confirms high effectiveness of Autonomous Emergency Braking systems (AEB) which lead to a 38% reduction in real-world rear-end crashes at low speeds [3]. Further on, according to estimates by the European Commission, AEBs could save more than 1,000 lives every year within the EU only [4].

At this stage AEBs are already available for some car models in the EU countries, but up to date there were no standard technical requirements guaranteeing the effective performance of such systems. What is already under way, the introduction of AEB functions will be a must for vehicles sold in the United States and in the European Union by 2020-2022, since AEB Systems have the potential to increase safety for drivers as well as for VRU.

Currently around 40 countries have agreed on a draft United Nations Regulation for Advanced Emergency Braking Systems for cars. The draft of the United Nations Regulation, adopted at United Nations Economic Commission for Europe (UNECE), will lay down the technical requirements for the approval of vehicle-to-pedestrian and vehicle-to-vehicle AEBs fitted on cars. The new Regulation sets out test requirements for the deployment of AEBs at a range of different speeds, from 0-60 km/h. When this Regulation will enter in force, most of existing systems fitted into cars will have to be updated to meet stricter requirements. This would finally mean that over 15 million new cars in the EU would be equipped with the lifesaving AEBs technology every year [5].

To improve the effectiveness of active safety systems fitted into cars, the consortium of 17 partners: top automotive manufacturers, suppliers and test labs proposed the ´PROactive Safety for PEdestrians and CyclisTs´ (PROSPECT project). The main objective was to significantly reduce accidents with Vulnerable Road users (VRU).

PROSPECT is a collaborative research project funded by the European Commission. The project pursues an integrated approach comprising in-depth and multiple European accident studies involving VRUs, combined with results from urban naturalistic observation. A vast variety of data collected at European level, where vehicles and VRU interact in real traffic situations, helped to understand critical situations, identify factors that lead to conflicts and better anticipate possible accidents. As the output, the Accident Scenarios were identified for pedestrians and cyclists with a special focus on urban environments, where indeed the majority of accidents involving VRU occur. Further on, the most important Use Cases were derived as basis for the development of Test Scenarios for the ADAS systems. Proposed test cases are more detailed than the defined use cases - they are a description of how to reproduce a specific use case on test tracks.

Finally, this accident analysis represented a key input for the system specifications, integration and demonstration to the public in three project prototype vehicles. These demo-vehicles were extensively tested in realistic scenarios. Proposed by the PROSPECT team a broad testing methodology went beyond what has currently been used: VRU intention detection (dummies with additional degrees-of-freedom), intersection driving style (natural driving style using robots by analysis of human driving) and transferability to real life (testing in realistic traffic scenarios, user acceptance tests).

What is novel is that the project consortium implemented the benefit estimation methodology that includes an assessment of the combined effect of active and passive safety measures (i.e. integrated safety). The results from this analysis depended strongly on testing activities within the project and were extrapolated to the EU-28 level. Finally, the expected fleet penetration rates for 2020-2025 were analysed. The PROSPECT project technical approach is presented herein below (see Fig. 2).

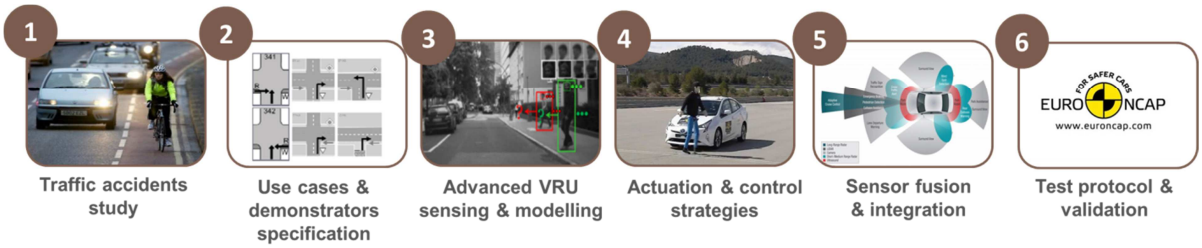

Figure 2. The PROSPECT project technical approach

In PROSPECT, just like other functions implemented in automated driving, vehicle-based sensors (i.e. video, radar) survey the vehicle surroundings, advanced algorithms enable safety related decision-making, and the system acts actively when necessary. Being active safety solutions focused on VRU, the systems developed in PROSPECT take action when a critical situation with a VRU occurs. Moreover, each of the demonstrators completed within the project has its unique focus:

- I demonstrator is equipped with stereo vision camera and high resolution radars, featuring a high dynamic brake system combined with a power assisted steering actuator.
- II demonstrator features improvements in earlier, accurate and more robust detection of VRUs where sensor fusion with radar / lidar technologies is planned to extract VRU intention-related features.
- III demonstrator integrates enlarged FOV radar sensors including side and rear coverage and avoids critical situations or collisions by steering and/or braking in complex urban scenarios.

- Additionally, one driving simulator included advanced warning/HMI and control strategies to evaluate interaction between the driver and the vehicle inside PROSPECT.
- Advanced realistic pedestrian and cyclist dummies including a platform propulsion system improves realistic testing by extending dummy trajectories, organic materials, kinematics and physical behaviour.

AEB Systems have the high-potential to improve VRU safety. The findings within PROSPECT contributed not only to the generation of state-of-the-art knowledge of VRU-vehicle behaviour but as well to technical innovations i.e. assessment methodologies and tools for testing of next generation VRU active safety systems. Besides, in terms of the impact, the introduction of a new generation safety system in the market will enhance VRU road safety in the 2020-2025 timeframe, contributing to the 'Vision Zero' objective of no fatalities or serious injuries in road traffic set out in the Transport White Paper. Test methodologies and tools shall be considered as well for 2022-2024 Euro NCAP road-maps [6].

2. ACCIDENT ANALYSIS: ACCIDENT SCENARIOS, USE CASES AND TEST CASES

The first stage of the project included macro statistical and in-depth accident studies involving VRUs, performed in Europe and focused mainly in pedestrians and cyclists. An overview and an in-depth understanding of the characteristics of road traffic crashes involving vehicles (focus on passenger cars) and VRUs (i.e. pedestrians, cyclists, riders of mopeds, e-bikes or scooters) was provided for different European countries.

The in-depth understanding of the crashes includes the identification of the most relevant road traffic "accident scenarios" and levels of injury severity sustained, as well as the transport modes that represent a higher risk for VRUs. Besides extensive literature studies, comprehensive data analyses have been performed including information from recent years.

Several crash databases have been analysed: CARE database (Europe), the German, Swedish and Hungarian national road traffic statistics as well as the in-depth databases IGLAD (Europe), GIDAS (Germany), from Central Statistical Office (Központi Statisztikai Hivatal – KSH) and the Volvo Cars Cyclist Accident Database (Sweden).

Accident type	UTYP Pictogram	PROSPECT pictogram (basic version)
(I) Car straight on, cyclist from near-side	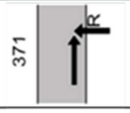	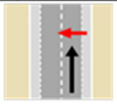
(II) Car straight on, cyclist from far-side		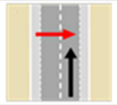
(III) Car turns	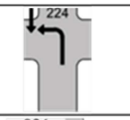	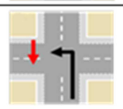
(IV) Car and cyclist in longitudinal traffic	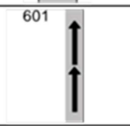	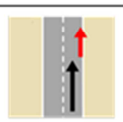
(V) Others		

Figure 3. Most relevant car-to-cyclist scenarios

PROSPECT_UC_PD_x (x=1...8)	Pictogram	in %	Description
PROSPECT_UC_PD_1 PROSPECT_UC_PD_2		23% 22%	Crossing a straight road from near-side / off-side; No obstruction
PROSPECT_UC_PD_3a PROSPECT_UC_PD_3b		5,5% 5,5%	Crossing at a junction from the near-side / off-side; vehicle turning across traffic
PROSPECT_UC_PD_4a		4%	Crossing at a junction from the near-side / off-side; vehicle not turning across traffic
PROSPECT_UC_PD_5 PROSPECT_UC_PD_6	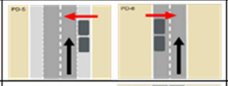	10% 7%	Crossing a straight road from near-side / off-side;With obstruction
PROSPECT_UC_PD_7a PROSPECT_UC_PD_7b		3%	Along the carriageway on a straight road away from vehicle / towards vehicle; No Obstruction
PROSPECT_UC_PD_8	No Pictogram	6%	Driving Backwards
Others		14%	Others

Figure 4. Pedestrian accident scenarios

The focus of the project was on crashes with two participants. Regarding the injury severity of the vulnerable road users two groups were considered: first “slightly, seriously injured and killed (SSK) VRU” and second “killed and seriously injured (KSI) VRU”. Early investigations have shown that the crashes between passenger cars and pedestrians or cyclists are from highest relevance for Europe. Fig. 3 shows a summary of the most relevant accident scenarios related to car-to-cyclist crashes were generated from this study.

From the most relevant accident scenarios, detailed car-to-cyclist crash analyses have been performed focusing on the causation of crashes: car-to-cyclist accidents have been analysed from the car driver’s point of view. With this approach deeper insight can be gained about the situations faced by the drivers especially why they sometimes failed to manage these crash situations [7].

In the analysis of car-to-pedestrian accidents, the Accident Scenarios introduced in the European project AsPeCSS [8] were considered as basis. Regarding crashes between cars and pedestrians, all databases confirmed that the Accident Scenario 1 “Crossing a straight road from nearside; no obstruction” was ranked highest regarding killed or seriously injured pedestrians, and the Accident Scenario 2 “Crossing a straight road from the offside; no obstruction” was ranked highest regarding all pedestrian injury severities. An additional Accident Scenario “Driving backwards” has been considered. The car-to-pedestrian accident scenarios can be seen in Fig. 4.

The ‘Accident Scenarios’ obtained from the studies describe the type of road users involved in the accident, their motions (e.g., the motion of the cyclist or pedestrian relative to the vehicle) expressed as ‘accident types’ and further contextual factors like the course of the road, light conditions, weather conditions and view obstruction. More information is available on the project deliverable “Accident Analysis, Naturalistic Driving Studies and Project Implications” [9]. The most relevant accident scenarios have been clustered in “Use Cases” or “target scenarios” addressed by the project.

The final goal was to define representative ‘Test Scenarios’ from available Use Cases, taking into account relevant parameters and representative values for the selected parameters based on accident potential and system analysis. Constraints taken into account are a limited and feasible number of test runs, durability (e.g. maximum impact speed) and the feasibility of the test tools (Fig. 5).

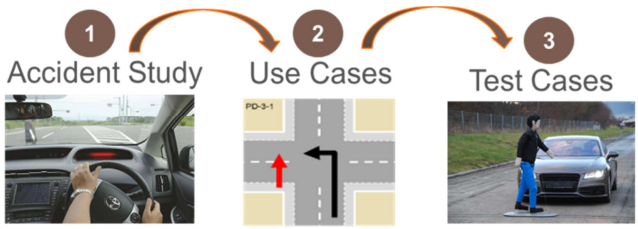

Figure 5. From accident analysis to test cases

Complementary to accident studies which have derived the most relevant use cases to study, naturalistic observations have been carried out to provide information that cannot be inferred from accident data bases, since these usually do not contain detailed information about the time before the accident happened (the so-called “pre-crash phase”). The first goal has been to acquire data about indicators of VRU’s behaviours that sign their intent in the near future. Naturalistic observations were also used to look for correctly managed situations by the road users that could have led to false alarms for an active safety system.

As seen in Fig. 6, two types of naturalistic observations were carried out in four countries. A first data set (France and Hungary) was collected from on-site observations by infrastructure-mounted cameras. A second data set was collected by cars equipped with sensors and cameras (Hungary and Spain) to observe interactions with surrounding VRUs. The additional study was performed in the final stage of the project in city of Leuven (Belgium) to annotate data samples and to validate final Vehicle under Test (VUT) trajectories for testing.

a b

Figure 6. Two types of naturalistic observations carried out in PROSPECT: (a) View from infrastructure-mounted cameras, (b) Video data from in-vehicle camera

3. HUMAN FACTORS AND HUMAN MACHINE INTERFACE (HMI) STUDIES

Human Factors (HF) as a discipline is concerned with understanding the characteristics and capabilities of people, and their interactions with technology and systems, to ensure safe, effective and engaging performance. HF has therefore been applicable at each stage of the PROSPECT project and across multiple partners, activities and work-packages.

In the context of PROSPECT, HF activities have included literature reviews, focus groups, expert evaluations, simulator studies, text track evaluations and video analyses. These have been used to help understand and specify user needs and requirements, inform the design of the PROSPECT system, evaluate HMI and control strategies, assess drivers' reactions and responses, and determine acceptance (i.e. likely uptake) of the final product.

At the start of the project, focus groups involving cyclists and car drivers were conducted by the University of Nottingham, in collaboration with TNO, in the UK and Netherlands. The focus groups aimed to uncover the cues (e.g. hand signals, head movements) that indicate a cyclist's future path and the characteristics of the environment/contextual variables that may affect their choice, to inform the design of the system. Cues and characteristics were identified and categorised into themes: cyclists' appearance, communications and signalling, movement and position of bicycle, and environment and conditions. Results indicated consistency between groups of cyclists and drivers, but were tempered by a cultural perspective, reflecting the higher social status afforded to cyclists in the Netherlands [10].

Functional requirements were also explored by investigating the relationship between false alarms and driver acceptance during a medium-fidelity driving simulator study conducted at the University of Nottingham. By varying urgency ('when') based on the time-to-collision (TTC) at which the warning was presented, and modality ('how') by presenting warnings using audio-only and audio combined with visual alerts presented on a head-up display (HUD), the study explored the effect of false-alarms and HMI modality. False-positive alarms (the system warned, when no hazard was present) corresponded with TTC, in so far as a higher proportion of false alarms occurred at longer TTCs, although there were no false negatives, or 'misses'. Overall, the study indicated a greater margin of safety associated with the provision of earlier warnings, with no apparent detriment to acceptance, despite relatively high false alarm rates at longer TTCs. It was also evident that drivers felt more confident with a warning system present, especially when it incorporated auditory and visual elements, even though the visual cue did not necessarily improve hazard localisation or driving performance beyond the advantages offered by auditory alerts alone [11].

In addition, PROSPECT partners TME and Chalmers University and associated partner Autoliv collaborated to explore and identify driver comfort boundaries. Experienced drivers negotiated an urban scenario in which they approached a road intersection. As they approached the intersection, a pedestrian appeared and then crossed the road ahead. The drivers were instructed to drive as normal as they would have done in the same situation in real life, to gain an understanding of where the driver would naturally ('comfortably') brake. Results indicated that car speed,

pedestrian size, crossing entry and lane width had a significant effect on TTC at brake onset for all drivers – increased car speed was associated with shorter TTC at brake onset, whereas as longer TTC were associated with adult compared to child pedestrians, and wider lane width. There was also evidence of learning and adaptation effects for frequent drivers [12].

To support initial HMI choice by car manufacturers for the PROSPECT demonstrator vehicles, the University of Nottingham in collaboration with IFSTTAR developed HMI taxonomy. The taxonomy was based on the literature review and expert analysis from HFs experts in consortium. It provided a novel framework for the assignment of appropriate feedback modes to different actions of an active safety system. Elements included a classification of possible HMI feedback modes, an identification of active safety system actions at different levels of automation, a set of heuristics to guide HMI design, and taxonomy of action-mode assignment supported by examples.

A number of HF activities were also conducted as part of the acceptance testing later in the project. Partners Toyota and Audi conducted simulator studies that aimed to identify and tune user acceptance of the PROSPECT functions. The 'comfort boundaries' model developed at the start of the PROSPECT project was used to select warning times for a forward collision warning (FCW) system, with the expectation that the system would react in a more 'natural' way if it were based on what an attentive human driver would do (i.e. their 'comfort boundary'). Using a 'vehicle-in-the-loop' simulator, whereby participants drove around a test track in a real vehicle while wearing a VR headset to provide the visual stimuli, warnings were provided either inside or outside the identified comfort limits based on the responses of 95% of the population in a between-subjects design. In addition to exploring issues associated with acceptance (to validate the models), the study also investigated when people actually decided to brake following the warning, with the aim of providing an indication of how the PROSPECT system should behave. Audi also conducted experiments to investigate the interaction of the driver, system and VRU in critical situations in a real-car environment using its mobile driving demonstrator. The aim of this study was to examine the role of sensory conspicuity of cyclists within the drivers' detection of cyclists in specific scenarios.

Finally, Volvo and VTI conducted test track and simulator studies to assess drivers' reactions to warnings and automatic steering interventions in critical longitudinal VRU scenarios. The studies aimed to evaluate ADAS performance with a forward collision warning (FCW), both with and without intervention while the driver was distracted (engaged in a secondary task on a touchscreen). In a novel approach, the same study was conducted by VTI in their driving simulator, and by Volvo on the test track, thereby also allowing issues of simulator validity to be explored. The FCW HMI included auditory (alarm), visual (blinking LED) and haptic (brake pulse) elements, in conjunction with an automatic steering intervention.

4. SYSTEM SPECIFICATION AND DEMONSTRATORS - CHALLENGES AND GENERAL METHODOLOGY FOR ADDRESSING BARRIERS OF CURRENT ADAS SYSTEMS

Based on the derived Use Cases, the sensor specification was achieved including hardware characteristics (e.g. stereo vision base line, image resolution, microwave radar sensitivity/accuracy, field of views) and items that relate to the sensor processing e.g. VRU detection area, correct vs. false recognition rates, localization accuracy, and computational latencies.

PROSPECT focuses on active safety solutions, where the vehicle surveys surroundings based on video and radar sensing. The developed sensors intend to support a larger coverage of accident scenarios by means of an extended sensor field of view (e.g. frontal stereo vision coverage increased to about 90°, radar coverage increased up to 270° covering vehicle front and one side), high-resolution and sensitive microwave radar sensors with enhanced micro-Doppler capabilities for a better radar-based VRU classification. For automated driving however, the system should not only detect VRUs, but also predict their trajectories to anticipate and avoid potentially dangerous situations. In

this case, advanced algorithms enable safety related decision-making and the systems developed within PROSPECT take action in case of a critical situation with a VRU, increasing the effectiveness of current active safety systems.

Improved VRU sensing and situational analysis functions (enlarged sensor coverage; earlier and more robust VRU detection and classification; sophisticated path prediction and reliable intent recognition) were shown in three vehicle demonstrators at the final project event at IDIADA proving ground (Spain) in October 2018. All vehicles are able to automatically steer and / or brake to avoid accidents. Special emphasis is placed on balancing system performance in critical scenarios and avoiding undesired system activations. Information about the demonstrators developed in the project is available in the related PROSPECT deliverables [13]. This section provides an overview of the applied methodology pursued in this project in relation to PROSPECT car demonstrators.

Demonstrator car I

Demonstrator car I is able to quickly detect and classify VRU from -90° to 90° with respect to the vehicle center line with three RADAR sensors, additionally detect the lane markings with a lane camera. There are actuators for the steering and the brake. Especially the brake actuator can increase brake force much quicker than current production brake systems (approx. 150 ms from start of braking to fully cycling ABS). Due to shorter reaction time a prediction horizon can be reduced and the prediction error is lower. The reduction of false activations improves overall driver acceptance and usability. Fig. 7 shows the addressed use cases and utilized sensors of the demonstrator.

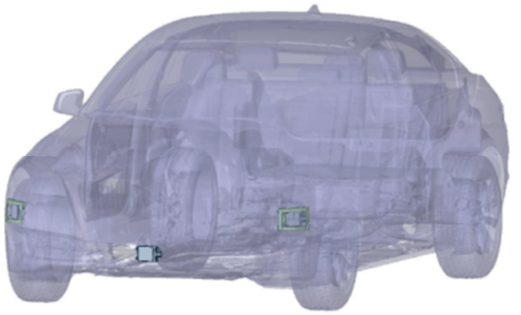

a b

VRU	Illustration	Median velocities at hit point (from D3.1)	Type
Cyclist		$v_{EGO@HP}$ ≈ 40 km/h $v_{VRU@HP}$ ≈ 22 km/h	Longitudinal
		$v_{EGO@HP}$ ≈ 15 km/h $v_{VRU@HP}$ ≈ 15 km/h	Crossing
		$v_{EGO@HP}$ ≈ 15 km/h $v_{VRU@HP}$ ≈ 18 km/h	
		$v_{EGO@HP}$ ≈ 40 km/h $v_{VRU@HP}$ ≈ 15 km/h	Longitudinal
Pedestrian		$v_{VRU@HP}$ ≈ 3 km/h	Crossing
		$v_{VRU@HP}$ ≈ 3 km/h	Longitudinal

c

Figure 7. The Demonstrator car I - vehicle with functional setup and addressed use cases: (a) Sensors integration site RADARS, (b) Overview Radar sensor setup, (c) Use Case selection

Demonstrator car II

To handle the defined use cases (e.g. car moving straight with VRU crossing/moving straight, car turning right/left with VRU crossing) the II demo-car is equipped with a front facing stereo camera and two side-mounted cameras. By this camera setup a horizontal FOV of approx. 210° is covered, which is suitable for most of proposed use cases (see Fig. 8 with the sensor setup). In the near range (longitudinal distance up to ~ 40 m) a more detailed analysis of the VRUs will be executed. Based on this detailed information intention recognition can be performed. The correct estimation of VRU's intention helps to increase the possible prediction time horizon, allowing much earlier warnings and interventions without increasing the false-positive rate.

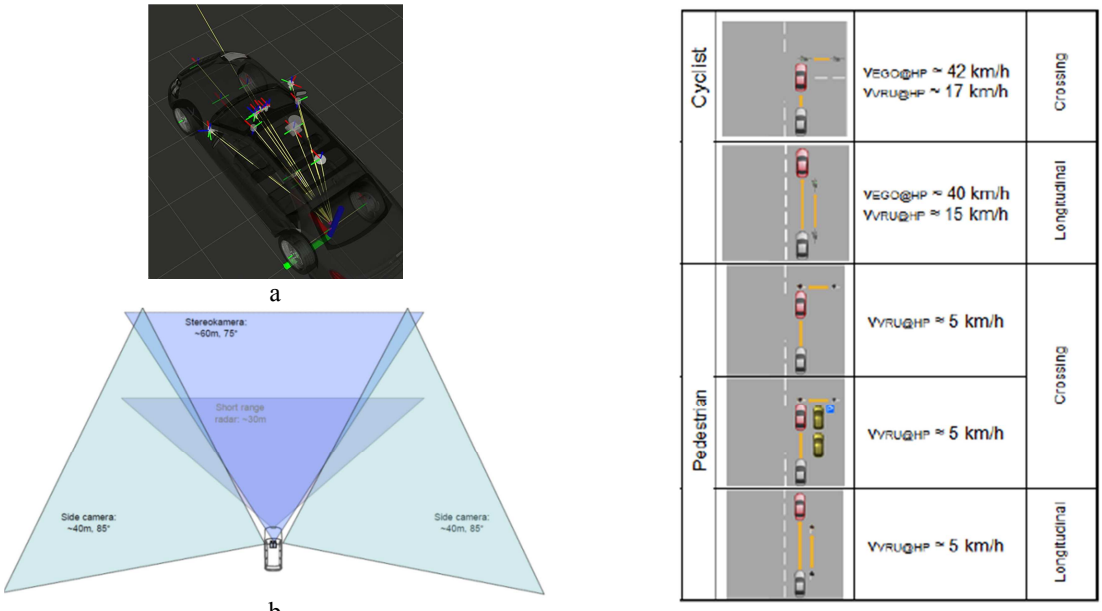

Figure 8. Demonstrator car II - calibrated and synchronized stereo camera and lidar system and addressed use cases: (a) Calibrated and synchronized stereo camera and lidar system, (b) Sensor setup consisting of one front facing stereo camera and two side-oriented cameras, (c) The addressed use cases

Demonstrator car III

Demonstrator car III focuses on high resolution RADAR sensors with a coverage of the regions in the front, rear and at least at one side of the vehicle: especially accidents with crossing or rewards approaching, quick-running bicycles in combination with a relatively slow or stopped car require a sufficient large field-of-view zone for a sound detection and appropriate vehicle action (e.g. for a stopped car in a parking lot and an approaching cyclist from the rear a warning or even the blocking of the door is needed to avoid an accident). See Figure 9 for more details.

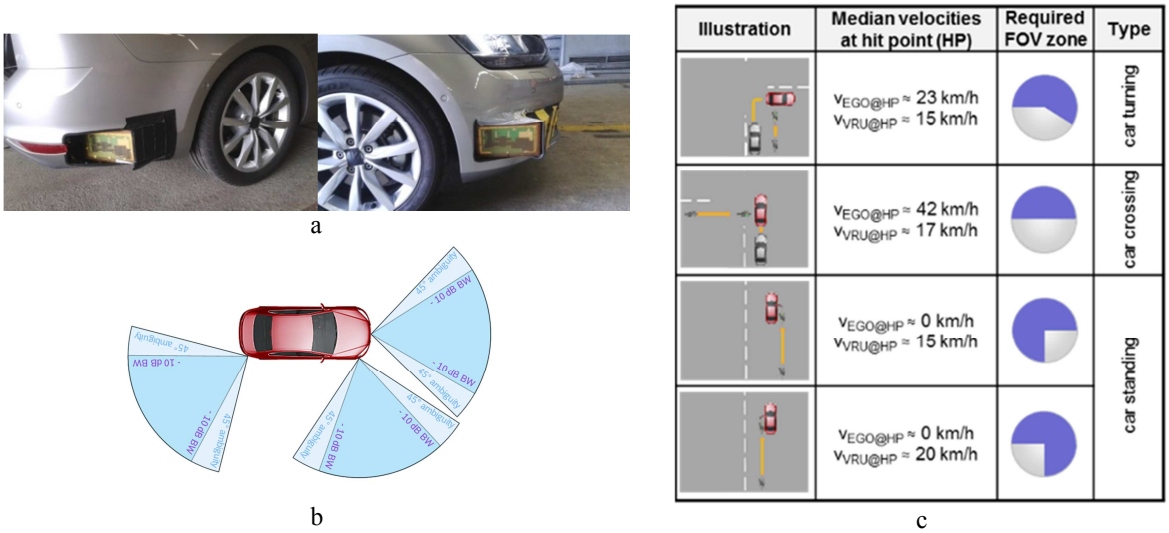

Figure 9. Demonstrator car III - high resolution radar sensors and addressed use cases: (a) The demo-car equipped with radar sensor, (b) Radar sensor mounting positions and FOV, (c) The addressed use cases

5. NEXT GENERATION TESTING

A sound benefit assessment of the prototype vehicle's functionality required a broad testing methodology which goes beyond what has currently been used. A collection of 'test scenarios', representative for all accident scenarios, was required to be defined and specified within the project, resulting in a test protocol **¡Error! No se encuentra el origen de la referencia.**. A key aspect of the test methodology was the provision of naturalistic driven trajectories on the test track with driving robots. For this task, data from real driving studies with subjects in a suburb of Munich, Germany; Leuven, Belgium and from Barcelona, Spain were used.

Test methodologies and assessment protocols

Apart from technology demonstrators that will help to maintain and extend the leadership of European car manufacturers in intelligent vehicles and for autonomous driving, PROSPECT took a step forward in defining test and assessment methods for Euro NCAP consumer testing AEB VRU systems. Euro NCAP assessment programmes provide truthful, accurate and independent comparative safety information on vehicles. This programme encourages manufacturers to exceed the minimum legal requirements and promote safety innovation.

Euro NCAP directly benefited from the project's findings and results, especially by being supplied with deliverables including test protocol as a proposal for consumer testing, the dummies prototypes and verification testing. Since Euro NCAP is the leading NCAP in the world regarding active vehicle safety, this helps to keep the European automotive industry in the pole position of active safety.

At this stage, Euro NCAP has published a roadmap document that outlines the strategy for the timeframe 2020 to 2022, which announces several requirements for e.g. steering intervention and cross-junction AEB systems that need specifically conditioned VRUs. PROSPECT results were an early input for the definition of all these requirements (see Fig. 10).

PROSPECT testing results gave deep insight not only in breaking but especially for steering strategies. In PROSPECT radar perception was conducted on feature level with static and dynamic grid-maps. Moreover, free space detection and critical objects monitoring for evasive path planning task was performed by developed systems. Evasive steering opens many more possibilities with respect to VRU collision avoidance, but provokes also new challenges and the need of innovative, advanced control and perception performance. In final PROSPECT protocol, evaluation of the improvements and benefits of additional steering for Euro NCAP AEB systems is elaborated.

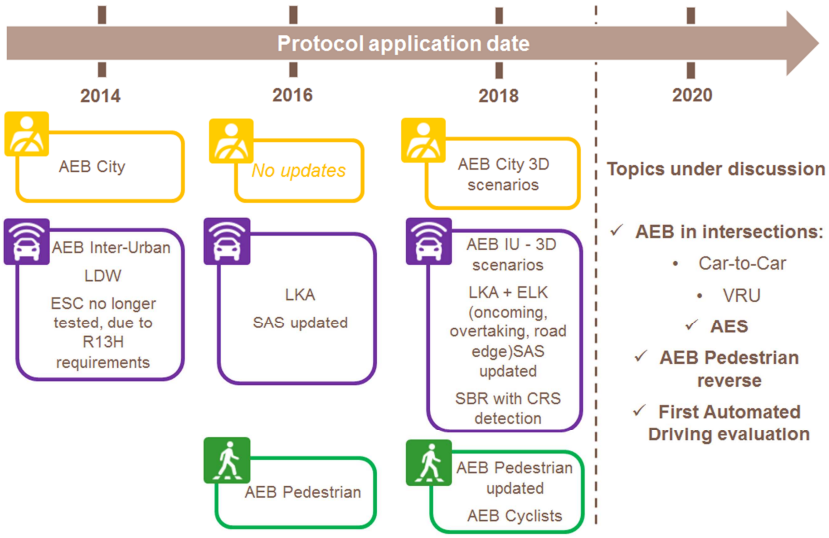

Figure 10. Euro NCAP roadmap for active safety (Source: Euro NCAP, 2018)

Testing tools

PROSPECT focuses on functions that avoid collisions with vulnerable road users, so at least one other traffic participant was a part of the test. Active safety functions might or might not be able to avoid a collision, so the "other" traffic participant needs to be an impactable dummy, a surrogate either for a bicycle or a pedestrian. Both objects (Vehicle-Under-Test (VUT) impact partner) are moved on a predefined track and with predefined speeds so that a critical situation develops. Active safety functions in the VUT might intervene and avoid the collision.

In the context of testing tools development, advanced articulated dummies - pedestrian and cyclist - prototypes were completed by partner 4activeSystems to obtain higher degrees of freedom (head rotation, torso angle, pedaling, side leaning, etc.) and an improved behaviour during the acceleration- and stopping-phase (see Fig. 11). The demonstrator vehicles made use of novel realistic VRU dummy specimen features for a better object classification and prediction of intended VRU movements. The dummies were mounted on fully self-driving platforms to take into account even complex test scenarios with different arbitrary movements.

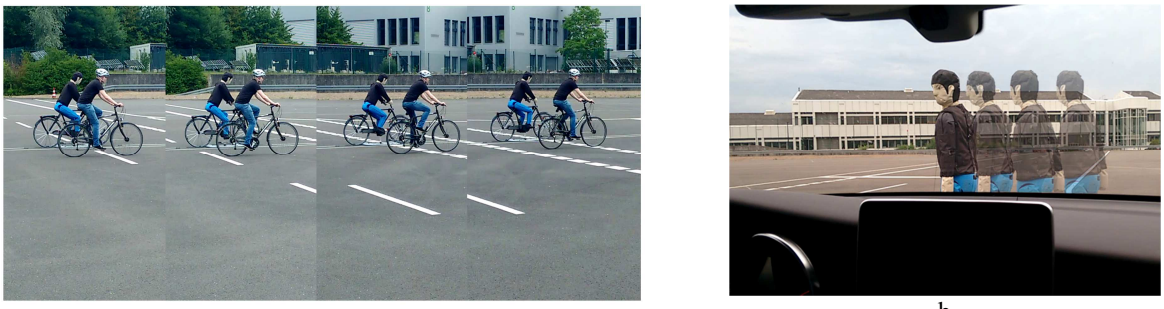

a b

Figure 11. Examples of advanced dummy features: (a) Pedaling cyclist dummy with rotating wheels, (b) Pedestrian dummy full stop and rotate head towards approaching car

Further elements of the PROSPECT test methodology were a standard intersection marking to be implemented on the test track which allows the efficient testing of all PROSPECT test cases and a concept for tests in realistic surroundings. The proposed intersection is in compliance with the German recommendations for road construction for urban intersections (see ERA, 2010 for bicycle lanes, EFA, 2002, for pedestrian crossing definition, and in General RASt, 2016 for street design in cities). It was adopted for the purpose of PROSPECT test cases on the IDIADA and BASt test tracks.

Since the exactly same test tools were used on a test track and in realistic surroundings by BASt and IDIADA, all tests were repeatable (test results measured in the same condition are comparable) and test results from a test track were reproducible (test results from different test tracks, but same vehicle and test setup are comparable). Test results on real city streets however are not reproducible (they cannot be reproduced on another intersection, in another city etc.). The Deliverable D7.1 shows the defined test cases. Speed ranges and behaviors have been selected according to what has been found within the use case generation [15].

Proving ground test results

What was completed within PROSPECT test campaigns, were the baseline tests according to the PROSPECT test methodology that started in September 2017 with four most advanced production vehicles from the market. These tests represent the baseline for the state-of-the-art of AEB/AES systems and focus on testing dummy-vehicle interactions. The other objectives of testing production vehicles against the first PROSPECT draft test program were to generate not only baseline data but as well to refine the test procedures. In the final stage of the project, these results were compared with the prototype performance. The hypothesis that was deeply studied was that current vehicles from the market are able to address only a limited number of PROSPECT scenarios. The final tests of the three prototype vehicles developed within PROSPECT were conducted in the first half-year of 2018; in

surroundings and conditions as realistic as possible to real urban roads. The results from consumer testing are summarized in the deliverable D7.1 ´Report on vehicle-based functional tests´ [15] and show great improvements on the car safety when PROSPECT-like AEBs systems are fitted on cars.

Acceptance testing
Acceptance testing was an important part of the project since it provides knowledge on the user perception of the proactive systems that were developed, and an indication of their likelihood to purchase such systems. Fundamentally, it is crucial for the success of active safety systems that they are acceptable for the drivers (e.g. useful and trusted). If not, they could be permanently turned off and would then have no effect on traffic safety. Moreover, interventions of active systems being rare, they may lead to unpredictable reactions from non-aware drivers being potentially frightened or startled when activated.

In this context, a specific acceptance methodology was developed based on existing questionnaires [16], [17], [18]. It integrates acceptance of false positive (warnings and/or interventions occurring at inappropriate times) and false negatives (no warning or activation when needed) and evaluates their influence on the drivers' acceptance. By using common questionnaires, this work enabled an overall evaluation of the acceptance of the developed functions. Collecting them in such a way ensured data being acquired in the same format and thus be easily be compared. The questionnaires were chosen with the objective to make acceptance evaluation not too invasive during the tests, and to disturb the test participants as little as possible.

Results show a high likelihood of acceptance of PROSPECT systems, whatever the experimental conditions or the system investigated (UoN, IFSTTAR, VTI). However, ISFTTAR experiment showed that the more participants are aware of the risks associated with VRUs the more they give high acceptability values, which substantiates Choi and Ji (2015) findings on the influence of the perceived risk on acceptability.

The participants also expressed high confidence in the systems (UoN, IFSTTAR). Indeed, trust in the systems increased after having experienced situations where PROSPECT functionalities could help to avoid accidents. An interesting point from IFSTTAR experiment was the influence of drivers' attitude towards in-car technologies in their confidence in the systems. As a result, drivers ready to drive highly automated car would rely more on PROSPECT systems.

Participants were most positive towards the warning function, but nevertheless they indicated also a high likelihood of using the braking and steering functions (UoN, IFSTTAR, VTI). It is interesting to note the influence of the driving environment. The participants declared to be more ready to use all functionalities in urban areas. Regarding highway and express road, only warnings seem to be acceptable, since braking and steering functionalities obtain quite low values of intention of use.

Willingness to buy was influenced by various factors, such as: the situation experienced (VTI: dummy versus bike), and the time at which the warning occurred (TME). Participants' willingness to buy increased after they were presented with 'critical' situations (IFSTTAR). A significant correlation was also found between the willingness to buy a car equipped with a PROSPECT system and acceptability and trust in the systems. Participants who expressed a high level of acceptability were those who declared being the more inclined to buy such systems, which is consistent with acceptability models.

These studies, that were complementary to testing activities at the proving ground, show improvement of PROSPECT technologies compering to the current state of the art and their benefits/challenges. Results of both, simulator and acceptance studies are included in Deliverable D7.3 [19].

6. SAFETY BENEFIT ASSESSMENT

The test results were used for benefit estimation of the PROSPECT systems. An important aspect of the project was to estimate the real-world benefit of the developed systems, i.e. the improvement for traffic safety in terms of saved

lives or serious injuries and the resulting overall benefit - not only the system performance measured in terms of detection rate or speed reduction.

A new methodology has been proposed for safety benefit assessment of real-world benefit of the Advanced Driver Assistance Systems (ADAS) in terms of saved lives and prevented injuries as well as the resulting monetary benefit for society (Fig. 12) . This methodology was demonstrated and applied to PROSPECT systems that address potential crashes of passenger cars with vulnerable road users (VRUs) such as pedestrians and cyclists [20].

Pre-crash kinematics data from crashes between passenger cars and VRUs from the Pre-Crash Matrices (PCM) based on the German In-Depth Accident Study (GIDAS) have been analysed with respect to twelve use cases [21]. Counterfactual simulations using relevant models for PROSPECT sensors and algorithms have been performed on car-to-cyclist and car-to-pedestrian crashes corresponding to the use cases. The counterfactual simulation is a method that has been used to analyse crashes amenable to the technology and assess what the crash outcome would have been had the vehicle been equipped with the investigated technology [22], [23]. Four algorithms of the PROSPECT systems have been modelled and implemented in the counterfactual simulation tool.

The simulation results were updated with the results from vehicle-based testing on closed test tracks for each use case. A key aspect in the benefit methodology was the combination of results from different sources concerning the effectiveness of the PROSPECT systems in different use cases, e.g. simulation results and test results. For this purpose, Bayesian statistical methods [24], [25] were proposed as an appropriate mathematical framework.

Injury Risk Functions (IRF) for all cyclist use cases as well as for all pedestrian use cases per severity were developed based on the police coded injury severity and the collision speed. The computation of the local safety benefit of the PROSPECT systems was based on a combination of models for crash avoidance probability and collision speed in case of a crash (resulting from the Bayesian analysis combining simulation results and test results) with the developed IRFs, using a variant of the dose-response model.

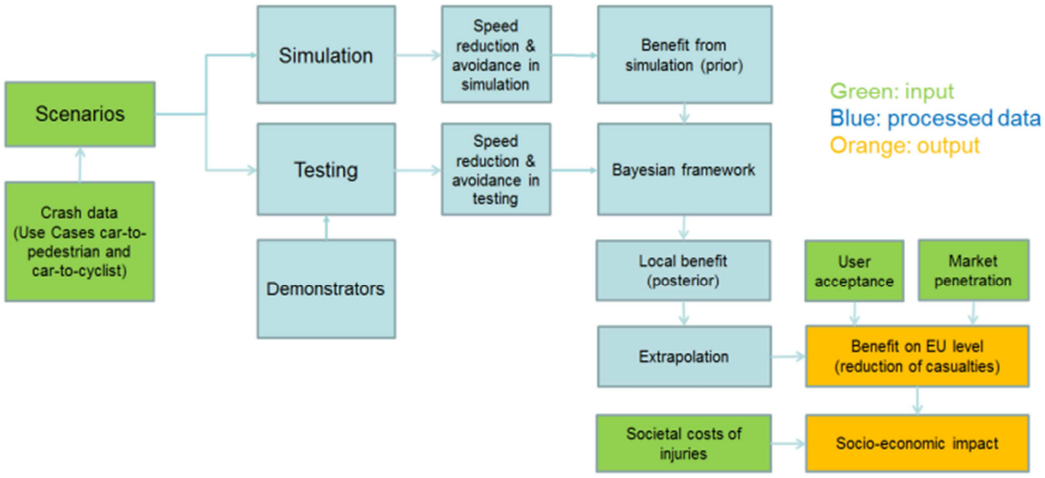

Figure 12. PROSPECT Assessment framework

The local benefit regarding fatalities, serious and slight injuries showed 55%-98% benefit of the algorithms, depending on the use case. The system gives a somewhat greater overall fatality reduction (82-86%) for all cyclist use cases combined than for pedestrian use cases combined (69-76%, depending on the algorithm). These use cases are addressing 86% of car-to-cyclist fatalities and 39% of car-to-pedestrian fatalities in GIDAS PCM data, hence the reductions within the use cases correspond to an overall estimated local reduction of 70-74% within car-to-cyclist fatalities and 27-30% within car-to-pedestrian fatalities.

The reduction for serious injuries is somewhat lower than for fatalities, especially for pedestrians. The results are in the range of 53-93% for cyclists and 23%-58% for pedestrians depending on the use case and yielding an overall reduction of 71-76% for cyclists and 36-44% for pedestrians within the use cases for the different algorithms. This corresponds to an overall reduction of 53-56% for seriously injured within car-to-cyclist and a 19-23% decrease of seriously injured within car-to-pedestrian crashes. The reduction of slight injuries is generally smaller than the reduction for serious or fatal injuries, especially for pedestrians.

This local benefit was extrapolated to EU-28 by using the community database on road accidents (CARE - European centralised database on road accidents which result in death or injury across the EU) and a decision tree method [26], [27], [28]. It was assumed that market penetration and user acceptance of the PROSPECT systems gradually increase, from 5.8% and 84.5% in 2025 to 20% and 87% in 2030. Due to the assumed increasing market penetration and user acceptance, the annual number of lives saved in EU-28 increases from an estimate of 79-95 in 2025 to 280-336 in 2030, while the corresponding estimates for the reduction of seriously injured are 439-697 in 2025 and 1558-2474 in 2030. Accordingly, the socio-economic benefit of PROSPECT systems increases from 203-296 million euros in 2025 to monetary values exceeding 878-1280 million euros from 2030 on. The results have potential implications for policies and regulations in understanding the real-world benefit of new ADAS.

7. CONCLUSIONS

The proliferation and performance of ADAS systems has increased in recent years. PROSPECT's primary goal was the development of novel active safety features to prevent accidents with VRUs such as pedestrians and cyclists in intersections. The know-how obtained in the accident analysis and the derivation of the PROSPECT use cases enable the development of improved VRU sensing, modelling and path prediction capabilities. These facilitate novel anticipatory driver warning and vehicle control strategies, which will significantly increase system effectiveness without increasing the false alarm/activation rate.

Multiple PROSPECT demonstrators (three vehicles, one mobile simulator, dummy specimen) integrated the different technologies including sensor setup position and orientation, sensor fusion, environment information evaluation and processing, actuators and HMI required covering the selected relevant use cases. Disruptive AEB/AES systems were finally demonstrated to the public in prototype vehicles with the use of realistic dummy specimen during the final PROSPECT event in 2018 at IDIADA testing tracks, Spain.

Full motion driving simulators were used for the collection of data regarding the interaction between the driver and the safety function. The driving simulator studies aimed specifically to evaluate HMI/warning in combination with automatic intervention by braking and/or steering with the driver in the loop. Finally, simulator studies helped to evaluate acceptance of PROSPECT-like systems - if the systems are unacceptable for the drivers (e.g. annoying), they could be permanently turned off and would then have no effect on traffic safety. Moreover, interventions of active systems being rare, they may lead to unpredictable reactions from non-aware drivers i.e. being potentially frightened.

What is known is that the European New Car Assessment Program (Euro NCAP) will include the testing of Cyclist-AEB systems from 2018 onwards in their safety assessment [29]. With respect to PROSPECT, more complex car-to-cyclist scenarios were implemented in demonstrators and assessed through testing activities. The test methodologies generated in this project were proposed to Euro NCAP for standardization on a regular basis.

Acknowledgments
PROSPECT is a collaborative research project funded by the EC under Grant Agreement nº 634149. The authors would like to thank partners of PROSPECT who contributed to the work described in this paper: Applus IDIADA, BASt, Audi, BMW, Bosch, Continental, Volvo, TNO, VTI, University of Nottingham, University of Budapest, University of Amsterdam, IFSTTAR, 4activeSystems, TME, Daimler, and Chalmers.

8. REFERENCES

[1] The European Commission 2018: “Road safety in the European Union.”, Trends, statistics and main challenges

[2] The European Commission 2011: Vision Zero “White Paper on Transport.”

[3] Euro NCAP 2015: “Study Confirms High Effectiveness of Low Speed Autonomous Emergency Braking (AEB).”

[4] The European Commission staff working document 2018: “Impact Assessment - Proposal for a Regulation of the European Parliament and of the Council on type-approval requirements for motor vehicles and their trailers, and systems, components and separate technical units intended for such vehicles, as regards their general safety and the protection of vehicle occupants and vulnerable road users.”

[5] UNECE 2019: “UN Regulation on Advanced Emergency Braking Systems for cars to significantly reduce crashes.”

[6] European New Car Assessment Programme Euro NCAP 2019: “AEB VRU Test Protocol v2.0.4.”

[7] Gohl, A. Schneider, J. Stoll, M. Wisch, V. Nitsch 2016: “Car-to-cyclist accidents from the car driver’s point of view.”, International Cycling Safety Conference (ICSC)

[8] M. Wisch, P. Seiniger, M. Edwards, T. Schaller, M. Pla, A. Aparicio, S. Geronimi and N. Lubbe 2013: “European project AsPeCSS - Development of test scenarios based on identified accident scenarios.”, 23rd ESV Conference, Seoul, Paper Number 13-0405

[9] PROSPECT Deliverable D2.1 2016: “Accident Analysis, Naturalistic Observations and Project Implications.”

[10] Large, D.R., Harvey, C., Burnett, G., de Hair-Buijssen, S. 2016: “Understanding the cues and characteristics which indicate and affect a cyclist’s future path.” International Cycling Safety Conference

[11] Large, D. R., Kim, H., Merenda, C., Leong, S., Harvey, C., Burnett, G., Gabbard, J. 2018: “Investigating the Effect of Urgency and Modality of Pedestrian Alert Warnings on Driver Acceptance and Performance.” Transportation Research Part F: Traffic Psychology and Behaviour, 60, pp 11–24

[12] Jaber, L., Thalya, P. 2016: “Driver Interaction with Vulnerable Road Users.” Department of Applied Mechanics, Chalmers University of Technology

[13] PROSPECT Deliverable D3.2 2016: “Specification of the PROSPECT demonstrators.”

[14] PROSPECT Deliverable D7.5 2017: “Update of test protocol as a proposal for consumer testing.”

[15] PROSPECT Deliverable D7.1 2018: “Report on vehicle-based functional tests.”

[16] Van Der Laan, J.D., Heino, A. and De Waard, D., 1997: “A simple procedure for the assessment of acceptance of advanced transport telematics.” Part C, Emerging technologies, 5(1), pp.1-10

[17] Jian, J.Y., Bisantz, A.M. and Drury, C.G., 2000: “Foundations for an empirically determined scale of trust in automated systems.” International Journal of Cognitive Ergonomics, 4(1), pp.53-71

[18] Bellet, T. and Banet, A., 2012: “Towards a conceptual model of motorcyclists.” Risk Awareness: A comparative study of riding experience effect on hazard detection and situational criticality assessment. Accident Analysis & Prevention, 49, pp.154-164

[19] PROSPECT Deliverable D7.3, 2018: “Report on simulator test results and driver acceptance of PROSPECT functions.”

[20] PROSPECT Deliverable D2.3, 2018: “Assessment of the PROSPECT safety systems including socio-economic evaluation.”

[21] Wisch, M., Lerner, M., Kovaceva, J., Bálint, A., Gohl, I., Schneider, A., . . . Lindman, M, 2017: “Car-to-cyclist crashes in Europe and derivation of use cases as basis for test scenarios of next generation advanced driver assistance systems.” Enhanced Safety of Vehicles. Detroit

[22] Bärgman, J., Lisovskaja, V., Victor, T., Flannagan, C., & Dozza, M., 2015: “How does glance behavior influence crash and injury risk?” Transportation Research Part F: Traffic Psychology and Behaviour

[23] Bärgman, J., Boda, C., & Dozza, M., 2017: “Counterfactual simulations applied to SHRP2 crashes: The effect ofdriver behavior models on safety benefit estimations of intelligent safety systems.” Accident Analysis and Prevention 102, 165–180. doi:10.1016/j.aap.2017.03.003

[24] Hoff, P. D., 2009: “A First course in Bayesian statistical methods. Springer.”

[25] Kruschke, J. K., 2015: “Doing Bayesian Data Analysis: A Tutorial with R.”, JAGS and Stan, ed. 2. Elsevier

[26] Broughton, J., & al, e., 2010: “Estimation of the real number of road casualties in Europe.” Safety Science, 48(3), 365-371. doi:https://doi.org/10.1016/j.ssci.2009.09.012

[27] Ferreira, S. F., 2’15: “The quality of the injury severity classification by the police: An important step for a reliable assessment.”, Safety Science, 79, 88-93. doi:https://doi.org/10.1016/j.ssci.2015.05.013

[28] Kreiss, J.-P., Feng, G., Krampe, J., Meyer, M., Niebuhr, T., Pastor, C., & Dobberstein, J., 2015: “Extrapolation of GIDAS accident data to Europe.” ESV. Gothenburg, Sweden: NHTSAm

[29] Euro NCAP, 2018: “2020 ROADMAP.”, https://www.euroncap.com/en/about-euro-ncap/timeline/, accessed 17 February 2019

THE DEVELOPMENT OF A EURO NCAP FAR SIDE OCCUPANT TEST AND ASSESSMENT PROCEDURE

James Ellway
European New Car Assessment Programme
Belgium

Karsten Hallbauer
Joyson Safety Systems / CLEPA
Germany

Torsten Kerz
Opel Automobile GmbH – Groupe PSA / ACEA
Germany

On behalf of the Euro NCAP Side Impact Working Group

Paper Number 19-0278

ABSTRACT

The European New Car Assessment Programme (Euro NCAP) has been evaluating side impact protection since 1997. The original side impact test procedure utilised the EuroSID anthropometric test device (ATD) and Multi 2000 barrier face. In the year 2000, the side impact assessment was expanded to incorporate the perpendicular pole impact test. Both procedures were upgraded in 2003 to use the ES-2 ATD and Advanced 2000 barrier face in the side barrier impact. The most recent update to the side impact test procedures saw the adoption of the WorldSID 50th male ATD and the Advanced European Mobile Deformable Barrier face (AE-MDB) along with the oblique pole impact in 2015. To date, the adult side impact assessments have focussed on struck-side impact protection with the use of a driver dummy only and two child occupants in the rear.

A number of European research projects have interrogated accident databases to establish the nature and magnitude of the risks to far-side occupants. In 2015, the Euro NCAP Board of Directors agreed that the level of side impact protection offered to drivers and front seat passengers should be improved and the Euro NCAP Side Impact Working Group (SIWG) was tasked with addressing far-side occupant protection. The group was asked to draft an updated far-side impact procedure that could be incorporated into the existing assessment regime without significantly increasing the test burden. The focus of the new procedure is on passengers seated in the front row and will evaluate excursion and contact injury risk. The new assessment is sled based rather than being a full-scale test, allowing for a wider coverage of real-world scenarios and offering a method for the development of countermeasures in the most effective and efficient way.

This paper details the group's work in the development of a far-side occupant test procedure. The outcome of real-world accident analyses from numerous European databases has been summarised along with a review of existing work already undertaken for far-side occupants. This data allowed for boundary conditions to be established, which were evaluated by the group with the use of physical and CAE testing. The outcome of this research has been used to develop a Euro NCAP assessment procedure for non-struck side front seat occupants.

BACKGROUND

In 2009, Euro NCAP identified that the side impact test procedures should be more reflective of the high number of deaths and seriously injured occupants that are seen on the road [1]. Euro NCAP subsequently updated the front and side impact test procedures in 2015. The changes were aimed at promoting restraint systems that were more advanced and more robust for the driver and all passengers. Further updates to the front and side impact procedures will also be applied in 2020 as front and side crashes will continue to dominate traffic accidents in terms of the killed and seriously injured [2]. Advanced avoidance technologies are emerging that can mitigate typical head-on and crossing scenarios, but the requirements are technically very challenging. Crash protection remains essential and Euro NCAP continues to promote excellent structural and restraint system performance, even where advanced driver assistance systems are offered.

Euro NCAP's overall goal is to incrementally improve the assessment of crash protection so that it can continue to reward those vehicles that provide the best possible protection against serious and fatal injuries. An in-depth analysis of crashes in Europe performed by ADAC for Euro NCAP highlighted several areas where vehicle manufacturers might improve general vehicle design. One key area was the protection of car occupants in far-side crashes. In 2016, Euro NCAP created a group dedicated to developing a far-side test and assessment procedure. The membership of the group consists of Euro NCAP members, official test laboratories and industry representatives from ACEA and CLEPA.

PREVIOUS RESEARCH

The first step taken by the group was to review existing data on far-side impacts. There have been a number of studies published over the years on far-side occupants, yet side impact test procedures and the resulting protection offered by vehicles still focus on the struck-side occupants.

A study performed by Fields et al identified the high risk to far-side occupants from head contacts with vehicle structures on the struck-side [3]. In 2006, the European 6th framework project for Advanced Protection Systems (APROSYS) published a methodology to address non-struck side injuries [4]. This project reviewed real-world far-side crashes that were contained in several accident databases including CCIS, GIDAS and ZEDATU. The accident data indicated that the head and torso suffered AIS3+ injuries three times more frequently than any other body region. As with the study from Fields et al, the side structure, belt/buckle and adjacent occupants were the most injurious hazards. An examination of the impact characteristics indicated that, in most cases, the direction of force was perpendicular to the vehicle centreline. Regarding velocity, in order to address 50% of all non-struck side occupants with MAIS2+ injuries, a delta V of 41km/h would be required. In 2008, the European Enhanced Vehicle-safety Committee (EEVC) Working groups 13 and 21 produced an overview of side impacts using data from the United Kingdom, France, Germany and Sweden [5]. Of all the occupants in single side impacts analysed, 55% of occupants were on the far-side, leaving 45% on the non-struck side. A study of NASS data examined the characteristics of belted occupants with MAIS3+ injuries from far-side impacts [6]. The analysis found that 79% of drivers sustained MAIS3+ injuries with the head and chest being the most commonly injured body regions. The mean impact severity was a lateral delta V of 36km/h. The most frequent impact direction was found to be between 60 and 90 degrees.

ACCIDENT DATA REVIEW

In addition to the accident data in published literature, the group undertook additional analyses of accident data in 2016. The databases used were NASS, GIDAS, Volvo, BAAC, LAB, CCIS and ADAC. Further details of the accident data samples are contained in Appendix I. The databases contained differing injury severity levels, for example, the LAB data was known to contain higher severity impacts compared to GIDAS due a smaller vehicle fleet. As a result, the data was combined to establish general trends rather than specific conditions.

The databases were interrogated for occupants that met the following criteria:
Belted drivers and front seat passengers above the age of 10 years that suffered at least MAIS2+ and MAIS3+ injuries.

Impact conditions

The data showed that for MAIS2+ injuries the impact opponent was another vehicle in 70-86% of cases. Narrow object (pole) impacts were also represented in all databases and this condition was subsequently considered by the group. Figure 1 shows the impact opponent distribution average across all databases.

Although vehicle to vehicle impacts were more prevalent, data from EEVC Working Group 21 report indicated that the significance of pole impacts increases for MAIS3+ injuries and fatalities [5].

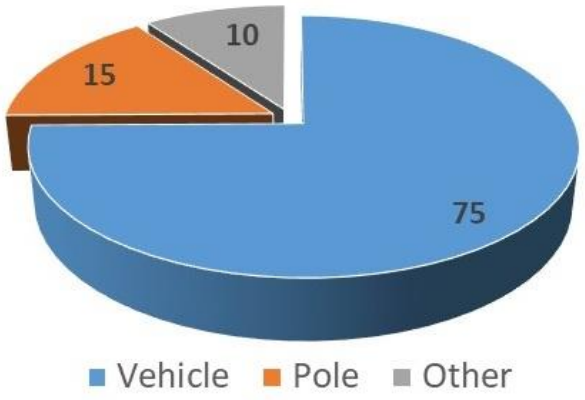

Figure 1: Impact Opponent - MAIS2+ injuries %

The impact location on the target vehicle was mostly on the occupant compartment i.e. the structures rearward of the A-pillar and forward of the C-pillar. This was the case in 64-70% of the impacts across the databases and is shown in Figure 2.

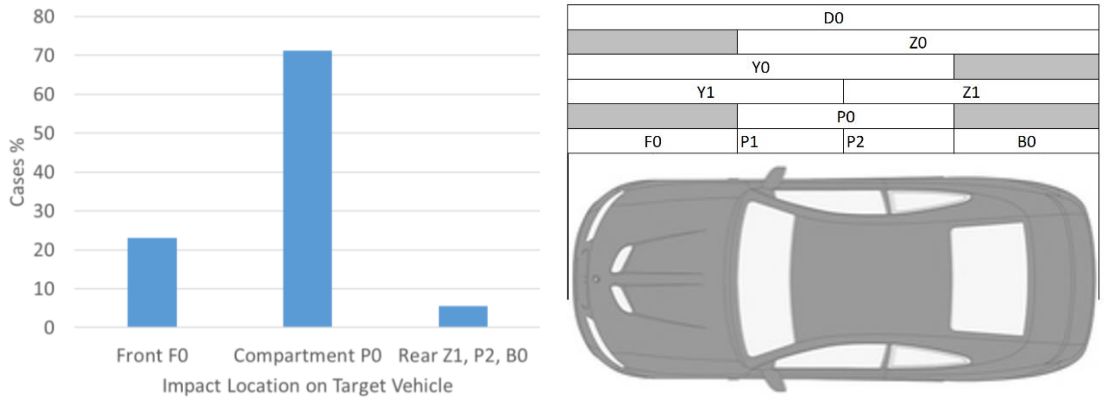

Figure 2: Impact location – MAIS2+ injuries %

Using the clock notation method, impact directions of 5 to 7 o'clock and 11 to 1 o'clock were not considered as side impacts and subsequently excluded. Of the remaining data, the mean impact angles ranged from 71 to 85 degrees. This data was similar to that reported by APROSYS (83 degrees) [2]. The impact angles should be treated with caution due to limits in the accuracy of defining impact angles. The distribution is shown in Figure 3.

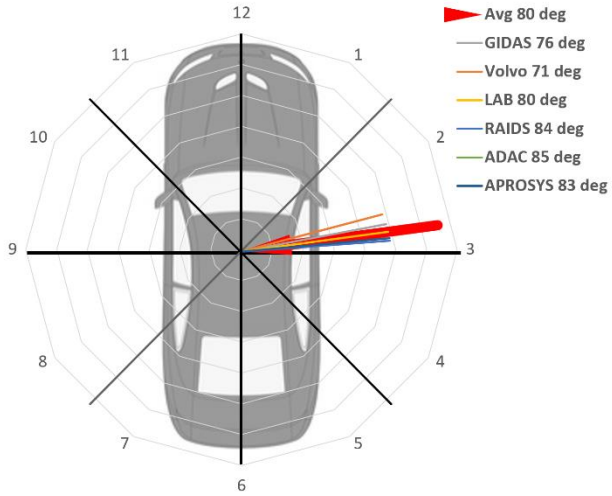

Figure 3: Impact angle

Intrusion levels showed a median level of 190mm for MAIS2+ injuries and 450mm for MAIS3+. As mentioned previously, LAB data contains more severe impacts and smaller vehicles resulting in higher intrusion levels compared to GIDAS data, see Figure 4. ADAC and NASS data indicated similar findings where the intrusion, recorded as a Collision Deformation Classification (CDC) of 3.5, covered between 50-75% MAIS2+ injuries.

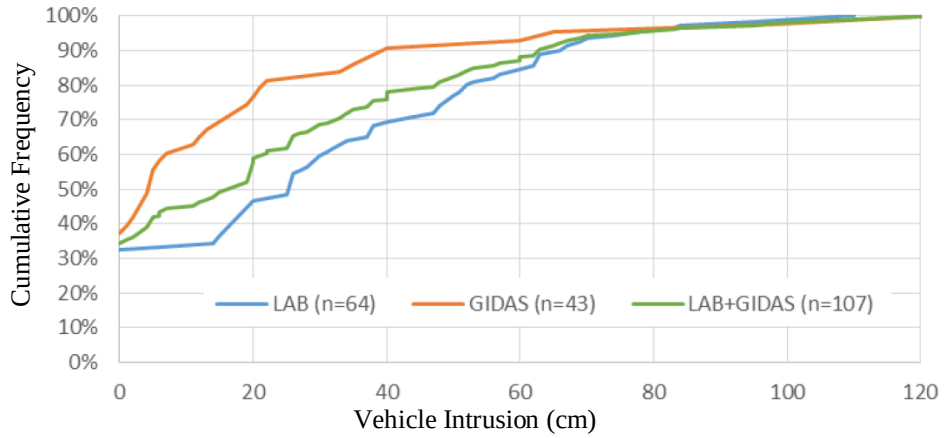

Figure 4: Occupant compartment intrusion MAIS2+

Velocity
There were some discrepancies in delta V between data sets. The accident studies reported a median equivalent energy speed (EES) for MAIS2+ of 37km/h, approximating this to a delta V of 41km/h would cover 37% of LAB data, 84% of GIDAS data and 54% of RAID-CCIS data. As there were eight databases contained in the APROSYS analysis, the report indicated that a delta V of 41km/h would address 40 to 75% of MAIS2+ injuries.

Injuries
Far-side occupants were involved in almost half of the accident cases, the data was broken down further as follows:

Far-Side: Driver, single occupancy
The injured body regions in decreasing frequency were the head, thorax and abdomen. Head injuries were mainly caused by the struck side interior and roof; the thoracic and abdominal injuries were generally caused by the seat belt system and struck side interior.

Far-Side: Driver and front seat passenger occupants
The injured body regions in decreasing frequency were the thorax followed by the head and then the abdomen, a different order to single occupancy. Head injuries were mainly caused by the struck side interior and the other occupant. As with a driver only, the thoracic injuries were caused by the seat belt system and adjacent seat.

It should be noted that the incidences of two front seat occupants were lower than those of single occupant impacts. However, the data did show that when occupant to occupant contact did occur, it was potentially life threatening. A study of NASS-CDS data indicated that in 35% of cases, head injuries were caused as a result of contact with the adjacent occupant, Thomas et al [7]. This research also conducted a sled test with two occupants (ES2-re & Bio-SID) showing that the passenger dummy recorded values multiple times higher than the established head injury criteria as a result of the far-side dummy head impacting the driver's shoulder. Further testing also showed that the head injury risk could be greatly reduced with an airbag that deployed between the occupants.

BOUNDARY CONDITIONS

The findings of the accident analyses were used to establish a set of boundary conditions upon which a test procedure could be based. Two aspects of far-side protection were identified as necessary assessments: head excursion and occupant loading. A sled-based test was chosen over a full-scale test as this offered greater flexibility in the scenarios that could be assessed along with a more cost-efficient means of doing so. Euro NCAP already requires four vehicles to be tested destructively and adding an additional full-scale test would increase the test burden beyond what could reasonably be expected. Adoption of a sled procedure would allow for testing of multiple impact scenarios at an early stage in the vehicle development process.

Angle
As the accident data suggested a range of impact angles, it was decided that, in order to simplify the test set-up, an angle of 75 degrees would be appropriate for both pulses. It is worth noting that although the AE-MDB test is perpendicular, the barrier face design was intended to represent the most frequent impact angle observed in moving car to moving car side impact accidents [13].

Intrusion
Occupant excursion beyond the seat centreline towards the intrusion line represents a significant risk of injury. ADAC estimated that, based on a size study of 291 vehicles in seven size groups, a CDC of 3 is around 450mm of intrusion and in the area of the seat centreline. CDC was considered as an assessment measure, but it was decided that the actual vehicle intrusion recorded in the AE-MDB and pole tests would be used.

Pulse
A delta V of 41km/h would cover the majority of MAIS 2+ cases. Much consideration was given to the shape of pulse, both in terms of the accident situation and relevance in a simplified test/assessment scenario. The initial intention was to use a single generic pulse for the assessment, for example the APROSYS pulse or a combination of AE-MDB and pole impact pulses. After taking into account the variation between the AE-MDB and pole test pulses, it was decided that two vehicle specific pulses would be necessary to account for the range of vehicle masses. The group acknowledged that, depending on the vehicle size or weight, the worst-case scenario could be either the AE-MDB pulse or the pole pulse.

A simple analysis of the vehicles tested by Euro NCAP in 2015 showed that for heavier vehicles, the difference in delta V between the AE-MDB and pole impact pulses is greater than that for smaller vehicles, Figure 5. In general, heavier vehicles have a pole impact pulse that is more severe than that of the AE-MDB impact. For smaller vehicles, this difference is not so marked.

In 2020, the Euro NCAP AE-MDB test speed will increase from 50km/h to 60km/h with a trolley mass increase from 1300kg to 1400kg. An analysis of GIDAS data by BASt indicated that the current AE-MDB test speed of 50km/h only covers 20% of MAIS3+ injuries.

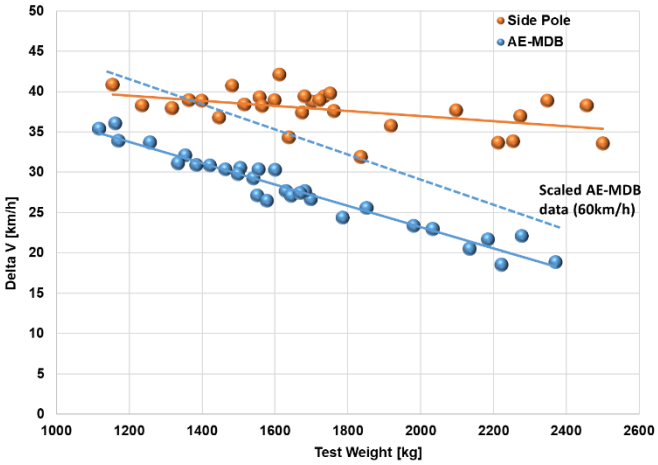

Figure 5: Delta V for vehicles tested in 2015

A speed of 60km/h would be appropriate to cover 50% of MAIS3+ injuries. The trolley mass was increased by only a small amount to be more reflective of the vehicles that Euro NCAP has tested in recent years. ACEA established, with the use of numerical simulations, that to achieve a minimum delta V of 41km/h, the AE-MDB pulse must be scaled up by a factor of 1.255 for small vehicles and 2.096 for large vehicles. For small vehicles, the scaling results in a delta V slightly above that of the pole impact but also closer to the target of 41km/h identified in the accident data. No combination of worst-case factors (e.g. AE-MDB pulse and pole intrusion) would reflect the worst-case for all vehicle sizes. Adoption of a single generic pulse test would require too many compromises that would have questionable relevance to the real-world situation. This made it necessary to consider both the AE-MDB and pole impact pulses for use in the procedure.

The AE-MDB (60km/h) and oblique pole test pulses were chosen for the procedure, Figure 6. Note, the AE-MDB pulse shown is at 50km/h. A scaling factor of 1.035 is applied to both pulses to translate to the 75 degree angle of the sled. It was acknowledged that the shape of the pole impact pulse has less relevance to real-world data compared to the AE-MDB test, but in addition to the pulse and delta V, the intrusion of the target vehicle was identified as an important factor. Higher levels of intrusion were observed in narrow object impacts when compared to vehicle to vehicle impacts. The intrusion from each impact scenario would be applied to the respective test.

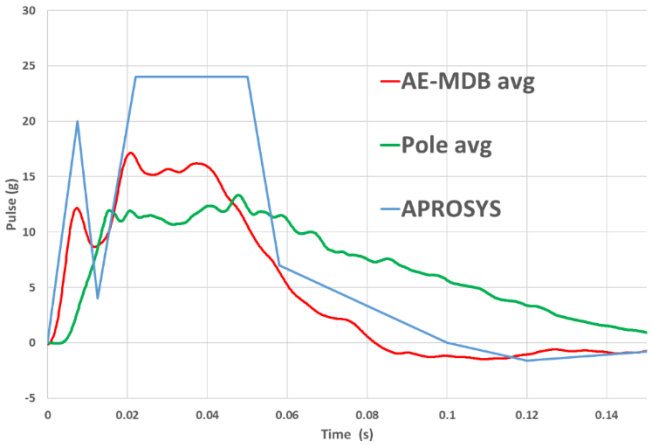

Figure 6: 2015 Average pulses and APROSYS pulse

Occupancy

A greater proportion of single occupants were injured compared to those with an adjacent occupant, 60% to 40%. To limit the complexity of the test setup, a single occupant was chosen for the test. A comparison of five different side impact dummies and post mortem human subjects (PMHS) performed by Fields et al indicated that although all of the dummies had limitations in far-side impacts, the WorldSID 50th male ATD seemed to offer improved performance compared to the others [3]. The work of the SIWG was conducted when availability of the WorldSID 5th female was very limited. The adoption of the WorldSID 50th male by Euro NCAP in 2015 and its availability across the official laboratories meant that this ATD was an obvious choice for the far-side procedure. All further references to WorldSID in this report are to the 50th male stature.

PRELIMINARY SIMULATIONS

In order to gain a basic understanding of the loading and excursion the WorldSID would be subjected to under the conditions identified by the group, a series of generic sled tests and equivalent simulations were performed. Simulation work began with the sled tests to validate the CAE model. Details of the set-up are contained in Figure

7 and Appendix II. Apart from a small amount of additional excursion in the CAE model compared to the dummy, the simulation of the WorldSID gave an adequate representation of the dummy kinematics. A further series of ten simulations was performed with a combination of the three pulses detailed in Figure 8, two impact angles and different centre consoles (rigid and none) were also used. The configurations used were as follows:

Pulse	**Angle**	**Centre console structure**
APROSYS pulse	90 deg & 80 deg	Rigid & none
Average AE-MDB 2015	90 deg & 80 deg	Rigid & none
Average Pole pulse 2015	75 deg	Rigid & none

The belt pretensioners were fired in all simulations

Figure 7: Sled and CAE

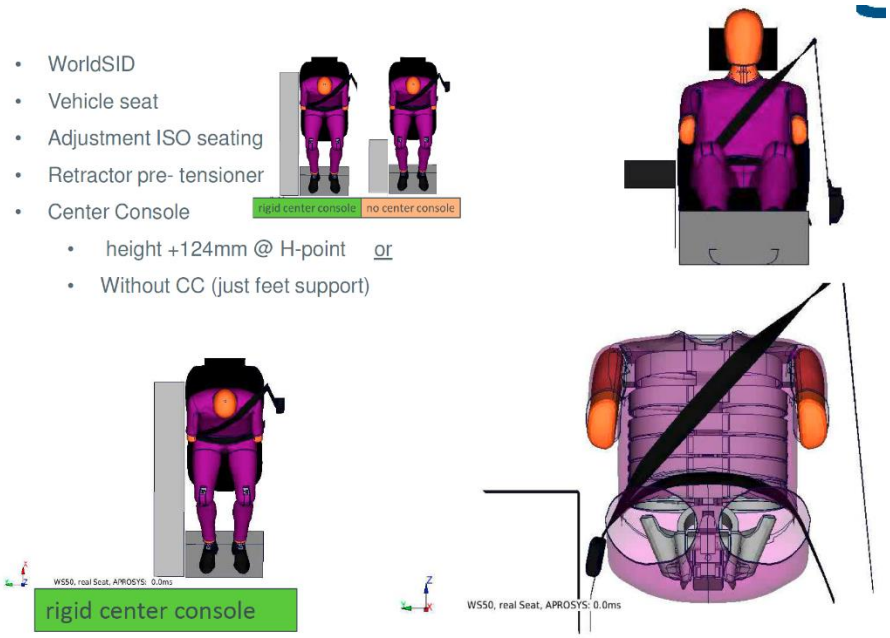

Figure 8: Simulation set-up

As this work was only intended to provide a basic level of information of how the WorldSID performed under the aforementioned conditions, the results were limited to the influence of a centre console and an analysis of head excursion. Only a limited amount of information is available in this paper regarding dummy outputs. The APROSYS and pole impact pulses generally have a higher delta V than the AE-MDB at 50km/h, even for smaller vehicles. Where there was no centre console, the head excursion increased in the lateral and downwards directions compared to when a centre console was present. The thorax and abdominal rib deflections were highest with the centre console and higher delta V. However, they were well below the Euro NCAP higher performance limits (28mm and 47mm respectively) and not at a level shown in the accident analyses. Pure belt loading was observed in the cases without a centre console but with low values (<6mm), again well below what was seen in the accident analyses. The impact angle only had a slight influence on the rib deflections.

The evaluations with the generic sled were extended to the human model developed by the Global Human Body Model Consortium (GHBMC). The simulations were limited to the APROSYS pulse only. Results of this work are available in Appendix III and further details can be found in the work of Hallbauer et al [12].

Pulse	Angle	Centre console structure
APROSYS pulse	90 deg & 75 deg	Rigid & none

The belt pretensioners were fired in all simulations

Where the centre console was present the lateral travel of the head, T4 and pelvis was reduced in both the 90 and 75 degree impacts when compared to no centre console. The reductions were small for the head (5-14%) and approximately 31-34% for the pelvis. As was the case for the WorldSID simulations, there was little difference in excursion between the two impact angles. A comparison of the kinematics between the GHBMC and WorldSID models indicated that the dummy model gave slightly more lateral and forwards excursion compared to the human body model. This lower excursion (70mm) can be explained by the stiffer spine in the WorldSID.

One final comparison made between the HBM and WorldSID models was the influence on the kinematics of the outboard elbow joint 'hooking' around the diagonal belt. The WorldSID was modelled with the standard half arm assembly only, whereas the HBM had full arms. Where the steering wheel was not modelled, the HBM showed there was hooking on the belt. The HBM simulation was repeated to allow the elbow to pass through the diagonal belt, which gave no difference in the lateral displacement of the head, T4 and pelvis when compared to when the elbow engaged with the belt. This aspect was highlighted as something that should be verified with the use of the WorldSID dummy.

PHYSICAL TESTING

Having established the boundary conditions with the use of accident data, it was then necessary to perform a series of tests to evaluate the feasibility of a sled based approach and to check the correlation between the physical tests and simulations. A supermini was chosen for the series. The vehicle had a low centre console and no far-side protection countermeasures. As the arm to belt interaction was highlighted as an area that should be examined during the physical testing, Transport Canada kindly provided Euro NCAP with the WorldSID full arm. The physical testing performed by the group consisted of two full-scale pole impacts and fourteen sled tests.

Full-scale pole tests

Two full-scale oblique pole tests were performed to establish the delta V for the vehicle and provide a comparison with the APROSYS pulse. The dummy positioning was in line with the Euro NCAP pole impact protocol, i.e. with a WorldSID on the driver's seat, but the pole impacted the passenger's side of the vehicle. The standard test speed of 32km/h resulted in a delta V of 38.8km/h. As this was below the target of 41km/h a second oblique pole test was performed at 36km/h giving a delta V of 42.4km/h. A higher test speed was not considered feasible due to the risk of structural failures in the vehicle body.

A comparison of the pulses from the chosen supermini are shown in Figure 9. The data provided is from the 32km/h and 36km/h tests along with APROSYS and the official Euro NCAP pulses recorded in the AE-MDB and oblique pole impacts.

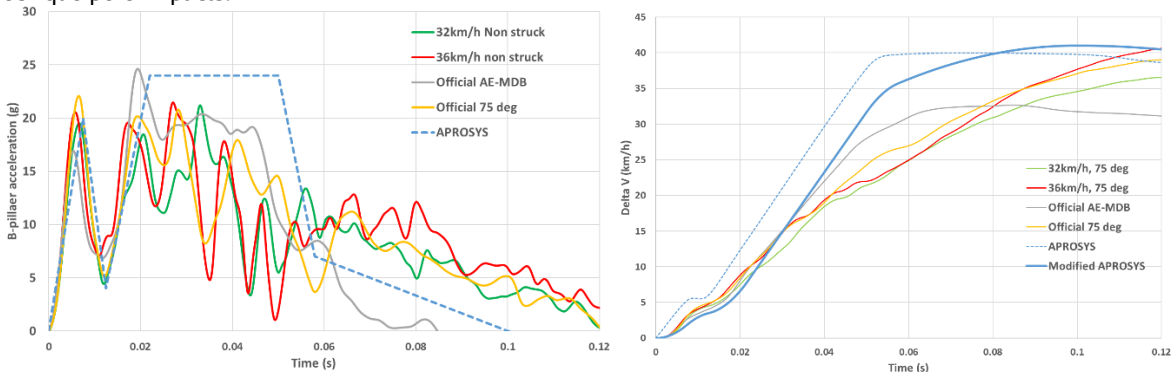

Figure 9: Supermini test vehicle pulses and delta V

The data from the 32km/h test showed all dummy outputs to be well below the WorldSID higher performance thresholds used in the Euro NCAP rating scheme. There was also no contact between the head and vehicle interior. In the 36km/h test, there were no structural issues with the bodyshell but there was a head contact with the far-side door (HIC3305), all other dummy outputs were below the higher performance thresholds, see Figure 10. The reason for the low torso outputs was a high level of rotation preventing the thoracic and abdominal ribs from being loaded in the expected manner. The rotation induced high loading in the neck and lumbar spine (forces and moments). This highlighted the need for both a kinematic and numerical assessment.

Figure 10: Oblique pole impact - 36km/h

Sled tests

Following the full-scale tests, two series of sled tests were performed. The sled tests were to be performed with the APROSYS pulse, which was chosen instead of the vehicle pulse because the intention was to examine the feasibility of the test procedure and not to perform an assessment of the vehicle. However, upon closer examination of the APROSYS pulse, it was discovered that the pulse did not have a delta V of 41km/h, the calculated value being 42.7km/h. As a result, the pulse was modified to match the target delta V of 41km/h. The initial peak of the pulse at 10ms was reduced from 20g to 14g to be more representative of the average peak seen in recent Euro NCAP AE-MDB tests on superminis. The plateau of the peak was also reduced from 24.0g to 23.8g to achieve the target delta V of 41km/h. For the purposes of this paper, this new pulse is termed the 'modified APROSYS' pulse and was used in the sled testing along with the 32km/h and 36km/h pulses.

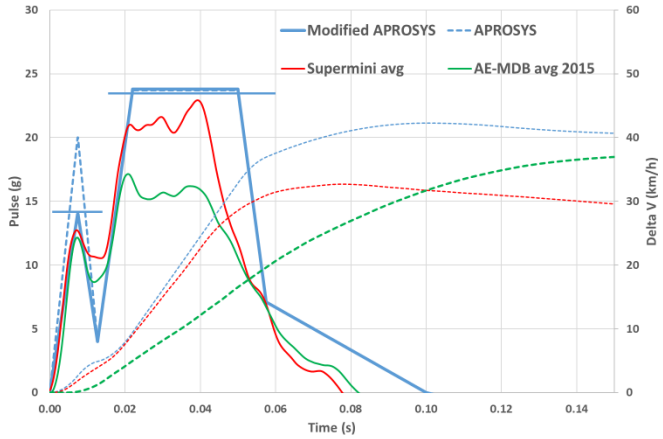

A comparison of pulse and delta V from APROSYS, six superminis in AE-MDB impacts and the average fleet of vehicles assessed by Euro NCAP in 2015 is shown in Figure 11. The pulse is shown on the primary y-axis and delta V on the secondary y-axis.

Figure 11: Pulse and delta V comparison

Test set-up for series 1

Based on the findings of the of the aforementioned publications and discussion of the various practical considerations with sled-based testing, a simplified setup was chosen for the sled tests as follows:

- Vehicle body in white
- No representation of struck-side intruding structures. Simulations showed that peak intrusion occurred before peak head excursion and a static marking would be sufficient.

- Body in white mounted at 75 degrees
- Modified APROSYS pulse & vehicle specific pulses
- One WorldSID 50th male driver, sleeved suit, in the standard pole impact seating position
- Full standard facia assembly including centre tunnel trim
- All first row seats
- The belt pretensioner was not fired in any of the tests as this would not occur in a far-side impact on the road with the vehicle chosen

Lines were marked on the buck to offer a comparison of head excursion. The blue line was placed on the vehicle centreline, yellow line on the struck-side seat centreline and the red line was marked at the location of the maximum static intrusion of the interior trim observed in the 32km/h pole or AE-MDB impact, see Figure 12.

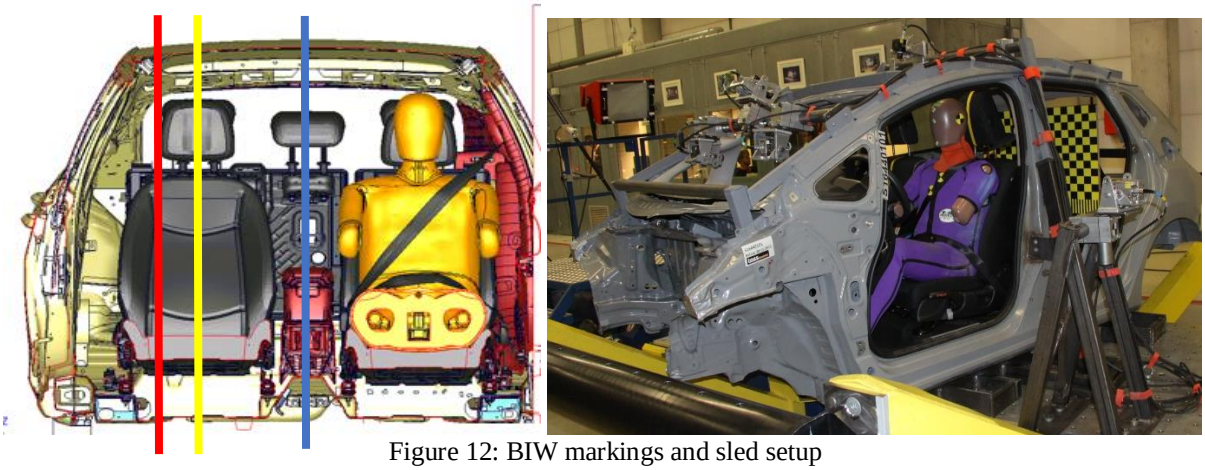

Figure 12: BIW markings and sled setup

Sled test series 1
Repeatability tests
The test matrix detailing the test numbers referenced in this report can be found in Appendix IV. Please note that the test numbers in the images differ from those in the test matrix. The first three sled tests were aimed at establishing repeatability of the sled and dummy setup, tests #1, #2 and #3. The struck-side airbags were fired only in the first test to identify any interaction with the dummy. As no interaction was observed, these airbags were not fired for the remaining sled tests. However, there was a difference observed in the seat kinematics due to the deployment of the side airbag in the first test filling the gap between the seat and vehicle structure.

The peak head excursion in the first test was approximately 50mm lower than of the other two tests and approximately 9ms earlier. This was caused by interaction between the WorldSID shoulder/jacket (with sleeves) and seatbelt, see Figure 13 and Figure 14. The belt slid into the gap between the shoulder and arm for a longer amount of time in the first test and subsequently increased the level of restraint up to the point where the belt began to slide down the dummy arm. It was found that the shoulder pad was incorrectly positioned in the shoulder rib prior to test. However, this interaction occurred in a number of the tests to a greater or lesser extent and was not considered top have influenced the results. In the third test, the interaction was such that the zip on the jacket was pulled open.

It was thought that the interaction would be reduced with the use of the sleeveless WorldSID suit and triggering of the seat belt pretensioner. The sleeveless suit was already implemented in the Euro NCAP AE-MDB and pole tests.

The full table of dummy outputs can be found in Appendix V. The dummy head and shoulder values were comparable and below the existing AE-MDB higher performance limits (HPL). In test #1, where the belt interaction was greatest, the thoracic rib deflections (TR) were all relatively low. In test #2 and #3, only one rib was close to the higher performance limit. In test #2, this was TR2 and in test #3 TR3, the difference being

dependent on how the dummy was aligned with the loading structures (belt and/or centre console). All other dummy parameters were comparable and well below the HPL.

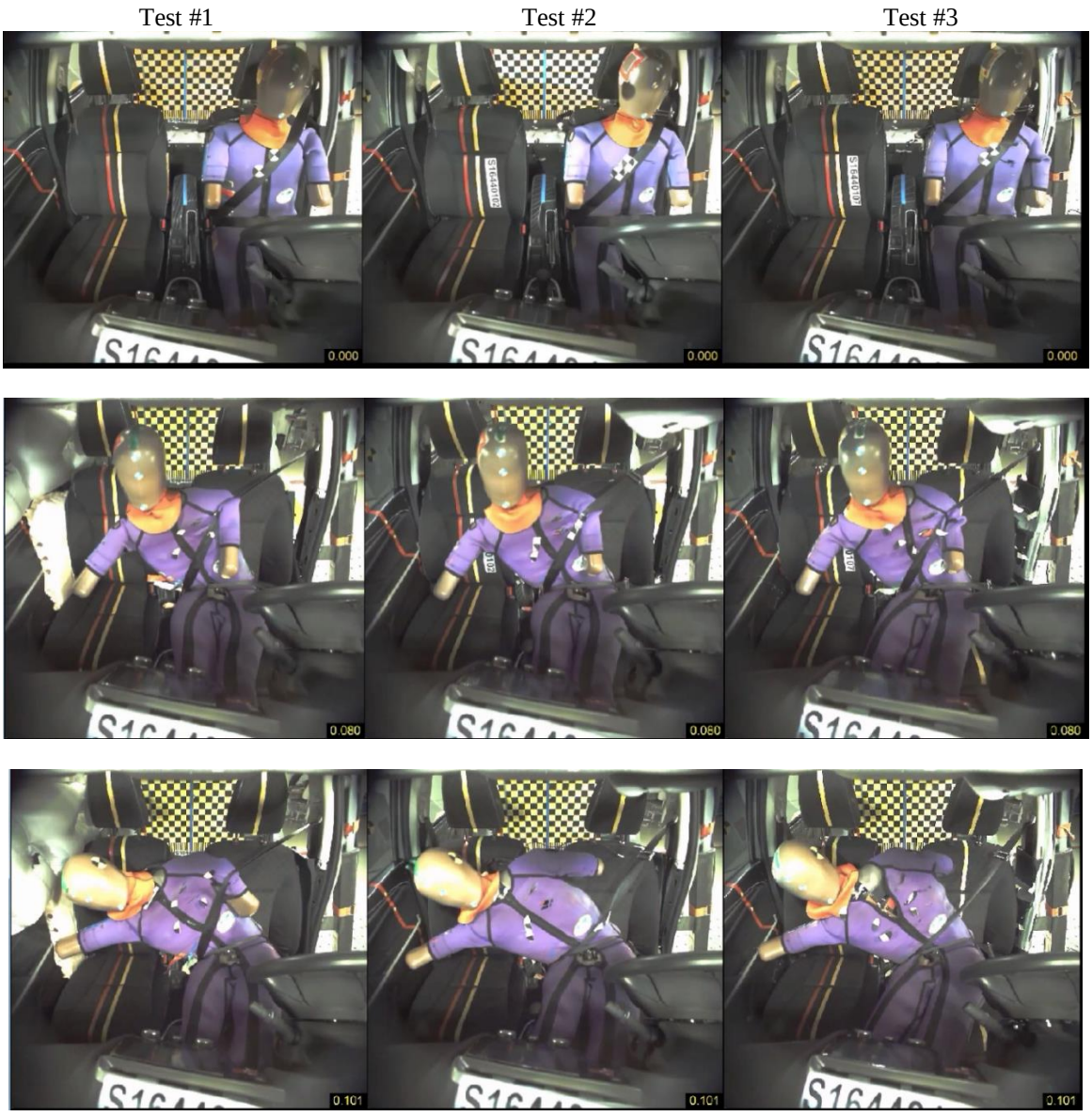

Figure 13: Repeatability test - belt interaction

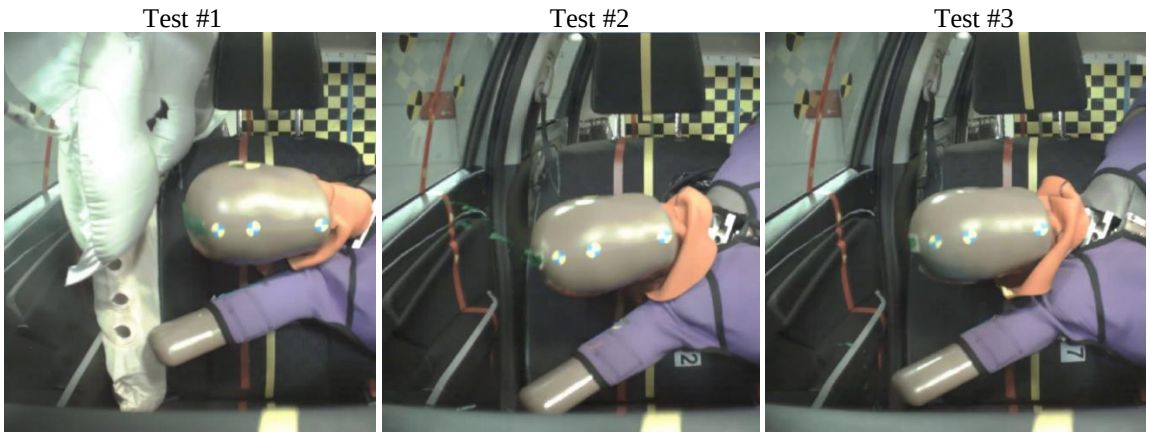

Figure 14: Repeatability test - max head excursion

WorldSID full arm, test #4

The second of the repeatability tests (#2) was chosen as the best baseline scenario for comparison with other tests due to the least amount of shoulder/belt interaction. A test was performed with the prototype full arm assembly attached to the driver's outboard arm, #4. It was used to provide a comparison with the HBM simulations that suggested the elbow hooking on the diagonal belt would not have a significant influence on the results. Having observed the shoulder to belt interaction in the first tests, the full arm tests were subsequently performed with a modified shoulder pad from the THOR dummy to limit the likelihood of the belt sliding into the shoulder gap. The full arm assembly and shoulder pad are shown in Figure 15.

Although the addition of the shoulder pad prevented the belt from interacting with the shoulder, the belt was caught by the top of the bicep resulting in a higher level of restraint than occurred with the half arm assembly. The bicep of the full arm has a flat upper surface and is of a different shape to that of the half arm assembly. This led to approximately 40mm less excursion with the full arm, see Figure 16. The torso and pelvis were unaffected by the different engagement. It was suspected that the arm hooked on the shoulder belt but a direct comparison of the kinematics with the HBM simulations could not be made due to the different belt interaction. Given the status and availability of the full arm, implementation into a test protocol was not realistic. The full arm was subsequently given no further consideration for use the test protocol. The dummy outputs are detailed Appendix V, but this part of the work focussed on the kinematic differences observed with the full arm.

Figure 15: WorldSID full arm and THOR shoulder pad

Test #2 Test #4

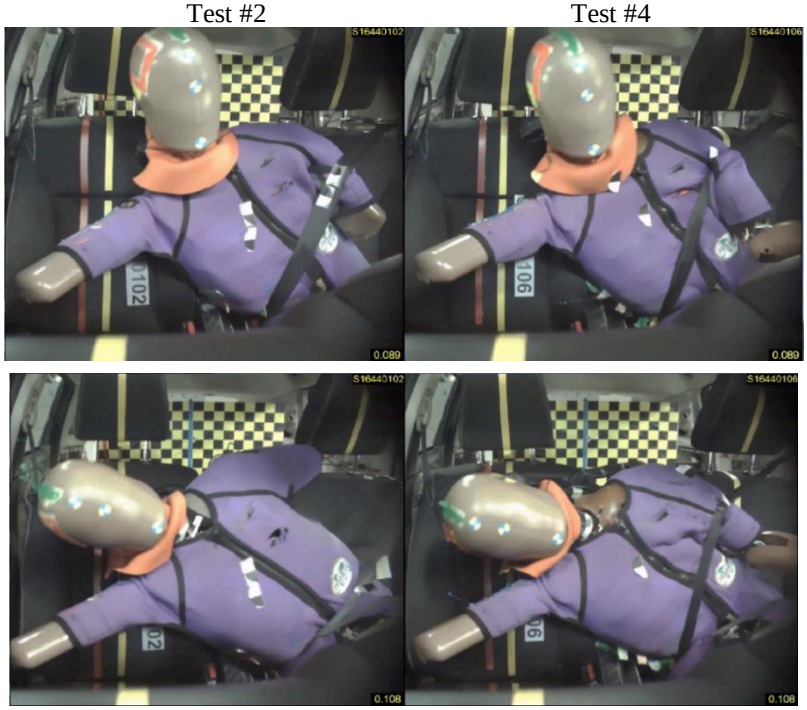

Figure 16: Half arm and full arm belt interaction - max excursion

Large centre console, test #5

Previous research indicated that the WorldSID might be suitable for use in far-side impacts [1]. A test was performed with a high centre console to see how well the dummy could detect the presence of such structures. A structure was fabricated out of stiff foam covered with sheet metal that was 180mm above the dummy H-point and approximately 60mm taller than the standard console. As expected, the presence of the large center console reduced the lateral head excursion by approximately 115mm, but also resulted in 42% greater neck My loading. The additional neck loading was caused by further rotation of the head. The outboard arm rotated rearwards around its fixing and contacted the head after the time of peak excursion. Although this was not detrimental to the kinematics or dummy outputs, the performance was not biofidelic. The torso loading was focused on the abdominal ribs (AR): AR 1, 46mm and AR2, 31mm, posing an additional risk of abdominal injury. The test with the standard console had maximum loading in the thoracic ribs, (TR): TR2 28mm and TR3 14mm. See Figure 17.

Test #2 Test #5

Figure 17: With and without centre console max excursion

Vehicle pulse tests #6 & #7

Two sled tests were performed with vehicle specific pulses (#6 & #7) obtained from the two full-scale pole tests at 36km/h and 32km/h. Tests #6 and #7 were compared with the modified APROSYS pulse (#2). The characteristics of the pulses and delta V is shown in Figure 9. Although the delta V of the 36km/h test was similar to that of the modified APROSYS pulse (41km/h), the profile was different.

When comparing the 36km/h pulse (#6) with the modified APROSYS pulse (#2), the more severe modified pulse between 25ms and 120ms led to an earlier max head excursion (118ms vs 135ms). However, the maximum excursion was approximately 20mm greater with the vehicle pulse. The thoracic rib loading was higher in the 36km/h pulse compared to the modified pulse, whereas the abdominal ribs were higher in the modified pulse. However, the only limit that was exceeded was TR3 in the 36km/h pulse, being 128% of the HPL. See Figure 18.

The pulse characteristic of the modified APROSYS pulse (#2) was significantly different to that of the 32km/h vehicle pulse (#7), with a delta V of 41km/h vs 38km/h. As mentioned above, the initial phase of the test influenced the dummy kinematics in a similar way. Due to the lower severity, the head excursion in the 32km/h tests was 20mm below that of the modified pulse. None of the HPL were exceeded in the 32km/h test.

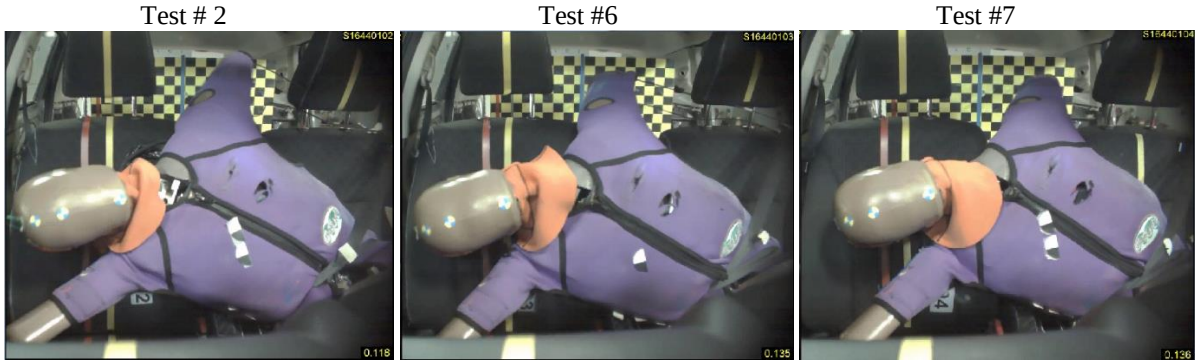

Figure 18: Modified APROSYS pulse vs 36km/h pulse vs 32km/h pulse - max head excursion

Comparing the tests using the two vehicle specific pulses (#6 & #7) shows a higher head excursion in the 36km/h pulse of approximately 40mm. This was to be expected given the higher delta V. The dummy thoracic loading showed a slight difference between these tests; in test #7 TR2 was highest, whereas in test #6, TR3 was highest. There was visibly more bending of the torso in test #6. Only the compression from TR3 in test #6 exceeded the HPL (128%). The abdominal loadings were all below 33% of the HPL. It is worth reaffirming that the intrusion line in both of these tests was based on the 32km/h test; in a 36km/h impact there would be approximately 70mm of additional intrusion.

The final comparison made was between the two vehicle specific sled pulses and the respective full-scale pole test. Unfortunately, the onboard cameras on the 32km/h full-scale pole tests failed so no detailed comparison of the dummy kinematics could be made. As there was no intrusion simulated in the sled tests, the kinematics differed to those of the full-scale test after the head contacted the intruding door in the full-scale test at 36km/h, see Figure 19. The head acceleration trace shows that although the curtain airbag deployed in the full-scale tests, it was not able to prevent the head from contacting the top of the door panel at approximately 115ms. Up to that point, there were only slight kinematic differences found in the head rotation between the full-scale and sled tests. There was no head contact with the intruding door in the 32km/h test. Replication of the pole intrusion was out of the test scope for this first series of testing. As the intention was to evaluate the feasibility of a sled procedure, reproducing intrusion was considered an unnecessary complication.

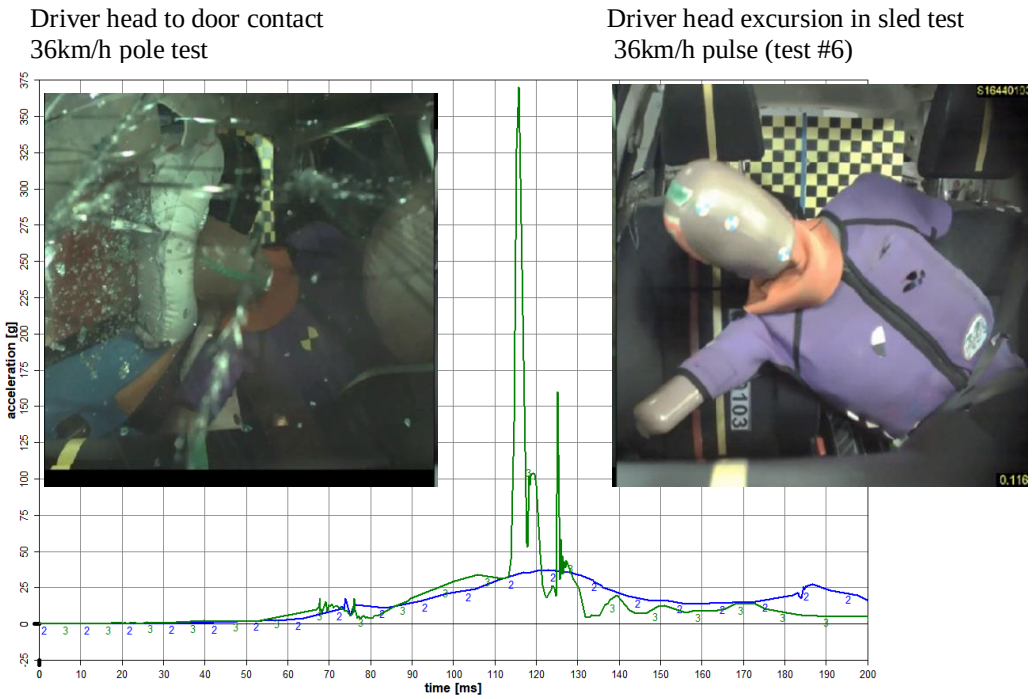

Figure 19: Driver head resultant accelerations - sled and full-scale test comparison

Summary of sled test series 1

In the full-scale tests the deploying struck-side airbag bridged the gap between the seat and intruding vehicle structure. This bridging effect was not replicated in the first series of tests, but it was thought that supporting the seat with foam spacers would offer a simplified way of simulating the presence of the airbag.

The influence of the full arm was not considered significant enough to require the full arm to be used in all sled tests. The THOR shoulder pad could not prevent belt interaction with the upper arm and a subsequent reduction in head excursion. Unfortunately, the effect of the elbow hooking on the diagonal belt could not be fully established or compared directly with the HBM data due to an incorrect test setup.

The baseline tests (#1, #2 & #3) were all influenced by shoulder to belt interaction. The greater the interaction, the smaller the excursion and the spread of max head excursion was approximately 80mm across the three tests. It was thought that this interaction could be reduced with the use of the sleeveless suit and the deployment of the belt pretensioner.

The fabrication of a large centre console resulted in head to arm contact and increased neck loading. The arm kinematics were not representative of a human. The large centre console did reduce lateral excursion by approximately 115mm, although it introduced an additional risk of abdominal injury. However, none of the HPL were exceeded.

Three different pulses were used in the first test series: 32km/h and 36km/h vehicle specific pole impact pulses and the generic modified APROSYS pulse. The 36km/h pulse and modified pulse had a similar delta V of approximately 41km/h and the 32km/h pulse had a delta V of approximately 37km/h. Delta V was not the only factor influencing occupant kinematics, the shape and duration of the pulses also having a significant effect.

Almost all of the dummy outputs resulted in readings below the established higher performance limits. The head excursion in all tests was beyond the (red) intrusion line and the seat centreline.

Sled test series 2

The outcome of the first seven sled tests was used to plan the second series of seven sled test series. Again, the modified APROSYS pulse was used along with the vehicle specific pulses. The test matrix detailing the variables is in Appendix VI and a table of dummy outputs can be found in Appendix VII. It should be noted that the camera locations differ slightly between the two series of tests and the lines superimposed on the images differ from the seat centreline due to movement of the seat during the tests.

The considerations for the second series tests were:

- Sleeveless suit (all series 2 tests)
- Belt pretensioning
- Near-side seat support
- Large centre console
- Spacers between seat and vehicle structure

Sleeveless suit, test #8

The first test performed in series 2 (test #8) was a repetition of the repeatability tests with the use of the sleeveless WorldSID suit, test #1. There was no interaction between the belt and sleeveless suit, the more close fitting sleeveless suit had less material which prevented the bunching of material that was observed with the sleeved suit, see Figure 20. The maximum head excursion was approximately 80mm greater with the sleeveless suit.

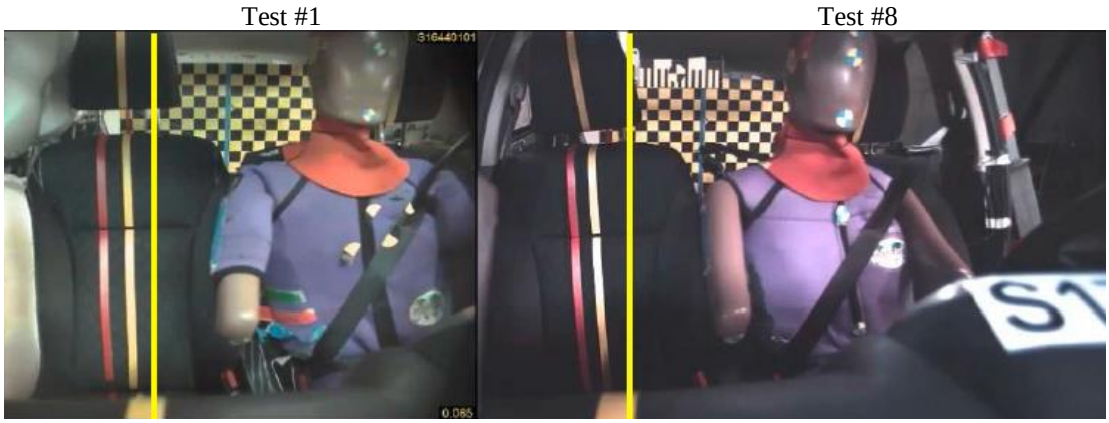

Figure 20: Sleeved vs sleeveless WorldSID suit – belt to shoulder interaction

Pretensioners, test #9

Test #9 was similar to that of test #8 but the belt pretensioner was fired. Unfortunately, the analysis of the pre-tensioner effects was hindered by a different arm adjustment and a different upper belt anchorage position prior to test. In test #9, the arms were set closer to the torso and the belt anchorage lower than in test #8. The lower anchorage increased the shoulder rearward movement up to 50ms and resulted in less interaction with the arm below the shoulder joint, see Figure 21. The pretensioning limited the rotation of the torso and pelvis, leading to a shift from the even TR2/TR3 load distribution of test #8 to a higher load on TR2.

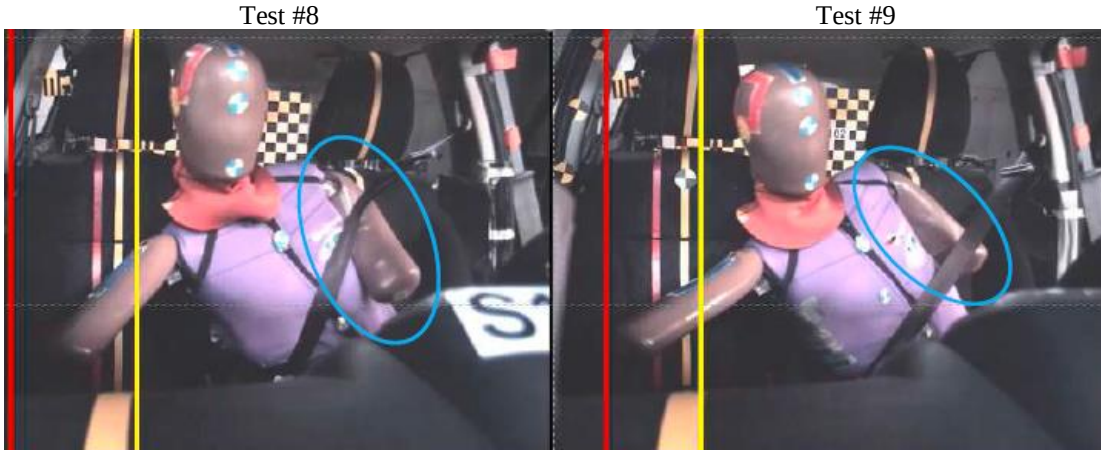

Figure 21: With and without pretensioning – belt to arm interaction

Spacers, test #10

The movement of the seats due to airbag deployment and, in the real-world, intrusion was identified in series 1. The seat was seen to move inboard, bridging the gap to the centre console. In order to replicate this, a test (#10) was performed with stiff foam spacers bridging the gaps on both sides of the unoccupied seat. The belt pretensioner was fired meaning a comparison with test #9 was necessary. Bearing in mind the incorrect setting of the dummy arms and belt anchorage in test #9, a comparison was made of tests with and without spacers. There was slightly more torso rotation without the spacers (with higher belt anchorage position) but only a small difference in max head excursion (20mm). The neck loading was uninfluenced but there were slightly higher lumbar moments (Mx) and lower torso rotation. It was thought that the spacers supported the centre console as it was loaded by the dummy.

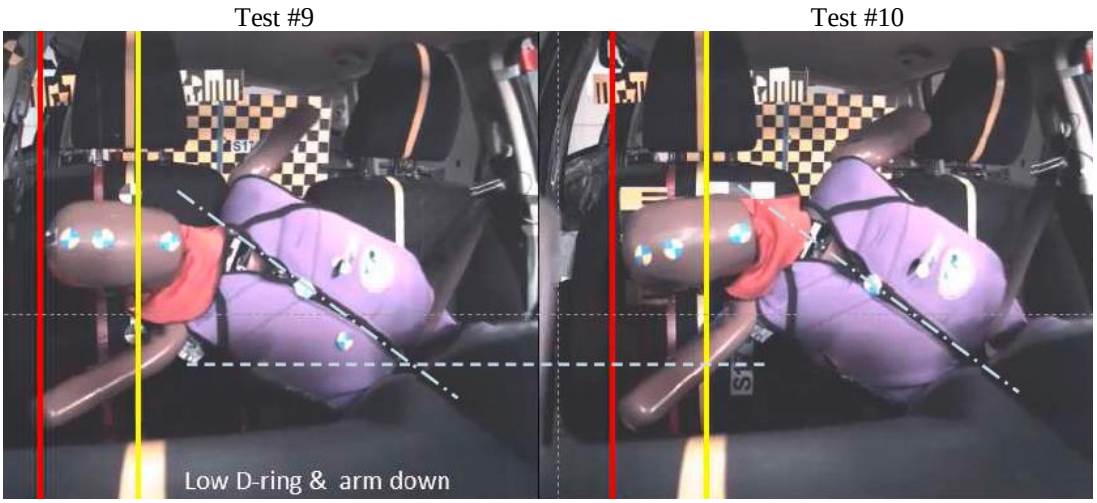

Figure 22: With and without spacers – max head excursion

Pretensioning and spacers, test #8 & #10

A comparison of test #8 and #10 was made to examine the influence of pretensioning and spacers. Without the spacers the centre console was seen to move laterally from about 42ms. With pretensioning and the addition of the spacers the max head excursion was reduced by approximately 20mm. The rib loading shifted from TR2 and TR3, to TR3 with AR2 loading significantly reduced, lumbar My increased by about 44%.

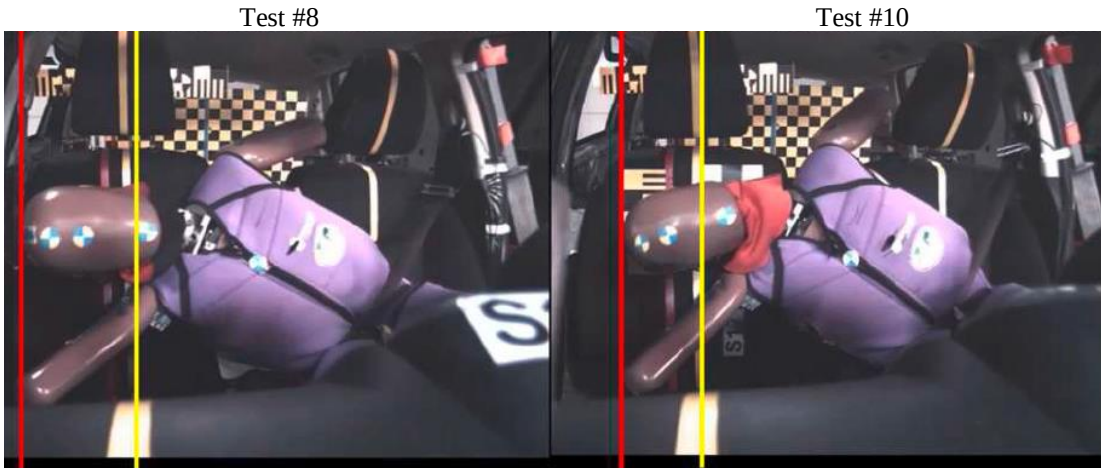

Figure 23: With and without pretension and spacers – max head excursion

Large centre console, test #11

As was the case in series 1, the presence of a large centre console was examined. The outcome was similar to that of the first series where the lateral head excursion was reduced and the abdominal rib loading increased, but still below the higher performance criteria, See Figure 24.

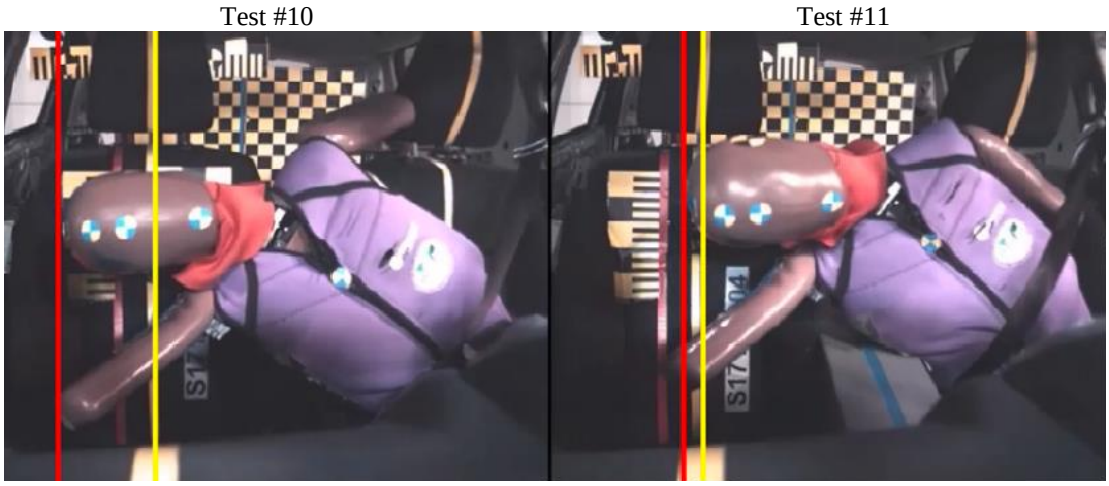

Figure 24: With and without large console – max head excursion

The presence of the centre console was compared between the test from series 1 (no pretensioning and sleeved suit) and series 2 (with pretensioning and spacers). The dummy outputs were very similar as was the max head excursion. See Figure 25.

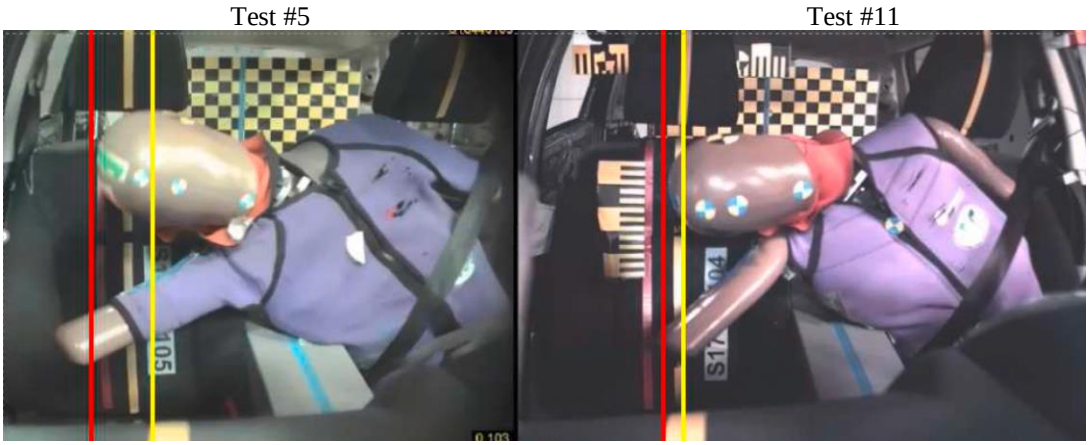

Figure 25: With and without sleeveless suit pretension and spacers – max head excursion

Pretensioning, spacers and jacket

The pretensioning, spacer and jacket effects were compared using the vehicle specific pulses at 32km/h (Figure 26) and 36km/h (Figure 27). These comparisons gave similar results to those above (#8 and #10) with the modified APROSYS pulse. There was slightly lower lateral head excursion and some Z axis rotation in the test with pretensioning, spacers and sleeveless suit. There was no significant influence on the dummy outputs. The greatest head excursion and dummy outputs were seen in the 36km/h tests followed by the modified APROSYS pulse and then the 32km/h pulse.

Test #7 Test #12

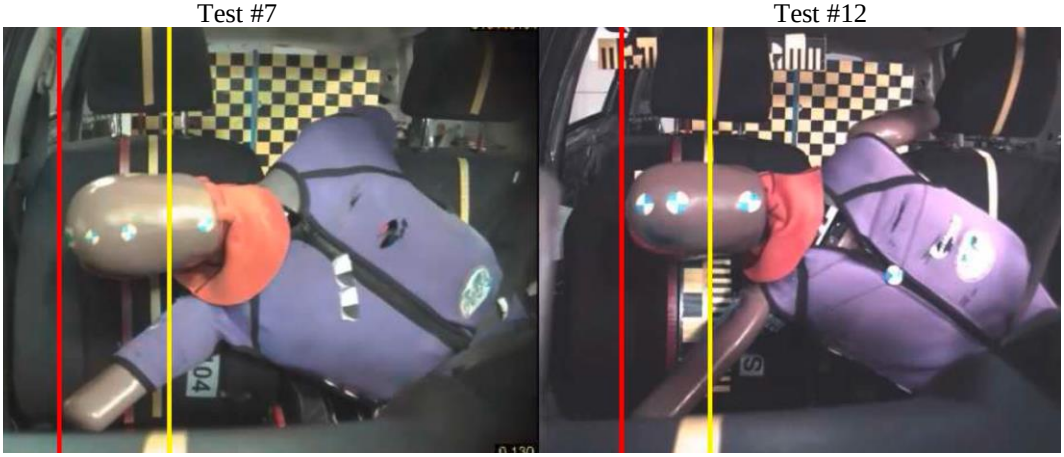

Figure 26: With and without sleeveless suit pretension and spacers – max head excursion

Test #6 Test #14

Figure 27: With and without sleeveless suit pretension and spacers – max head excursion

Vehicle specific pulses, #12, #13 & #14

The presence of the large centre console was evaluated with the vehicle specific 32km/h pulse. The findings of this comparison were similar to those of the previous comparison with tests #10 and #11 that used the modified APROSYS pulse, see Figure 28.

The final comparison was between the two vehicle specific pulses at 32km/h and 36km/h. As expected, the higher pulse gave more lateral head excursion (50mm) and a shift of loading from the TR2 to TR3. The other dummy outputs were comparable.

Test #12 Test #13 Test #14

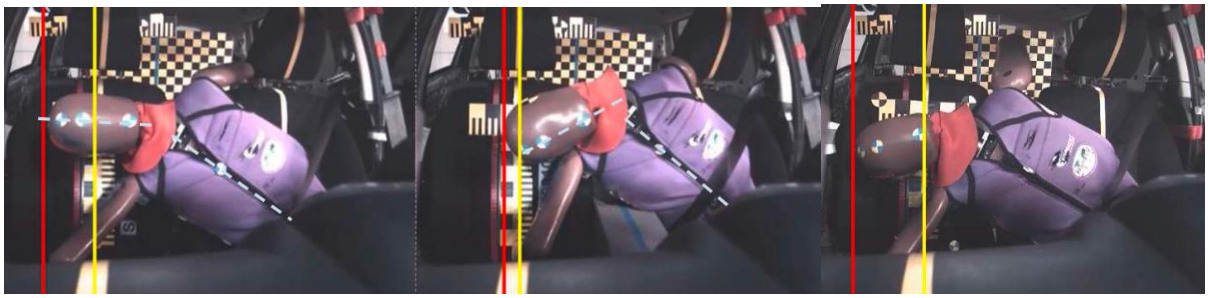

Figure 28: With and without large console

Summary of series 2

One of the major issues highlighted in series 1 was the interaction between the shoulder belt and sleeved WorldSID dummy jacket. This interaction was successfully reduced by the adoption of the sleeveless jacket and pretensioning of the belt. There were no instances of shoulder to belt interaction observed in series 2.

The effect of 'spacers' between the B-pillar, seat and centre console was examined. Spacers were added to replicate the effects of intrusion during an impact that closes the gap between the vehicle and seat. This was achieved in the undeformed sled setup, albeit in a simplified manner, by fitting rigid foam blocks to support the seat frame with the surrounding structures. The dummy outputs were seen to increase slightly in the neck and lumbar body regions, but it was thought that the effect of deformation must be represented in vehicle between the struck-side seat and BIW. The spacers also help to limit the movement of the centre console. It was not necessary to trigger seat mounted side airbags as their influence on bridging the gap between the vehicle and seat would be represented by the spacers. In the event that there is a far-side occupant countermeasure, e.g. larger side airbags, then this can be accommodated by the test procedure.

The modified APROSYS pulse and 36km/h pole impact pulses had similar delta Vs, both higher than that of the 32km/h pulse. However, it was not just a higher delta V that resulted in greater head excursion and dummy readings. The shape of the pulse can also determine the amount of dummy loading. The dummy readings from the modified APROSYS test were higher than both of the vehicle specific pulses, for which the results were similar.

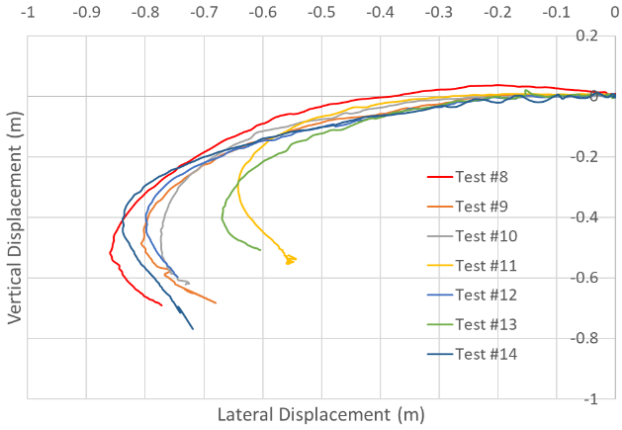

Figure 29: Series 2 head top film tracking

The greatest influence on the lateral head (top) excursion was due to the presence of the large centre console, which was present in tests #11 & #13. This reduced the excursion in these two tests to approximately 0.65m, whereas the excursion in all other tests (with standard centre console) was 0.77m to 0.86m. See Figure 29.

DUMMY DURABILITY ISSUES

One of the first issues highlighted in the sled tests was the WorldSID jacket being cut above the outboard abdominal ribs. As the dummy moved inboard and slid beneath the seatbelt, the upper edge of the first thoracic rib cut through the suit. The damage to the jacket did not influence results in any of the sled tests. Solutions to this damage were discussed with a dummy manufacturer. Enlarged and reinforced Kevlar patches on the inside and outside of the jacket were thought capable of preventing such suit damage.

Under certain conditions, the sternum plate holes have been known to tear at the shoulder rib connection. It is assumed that this component was originally designed for compression loading only (near-side testing) and the far-side testing subjects it to tensile loading. The holes for the shoulder rib, the only area where damage has been found, were closer to the material edge than the other ribs, increasing the likelihood of failure. A modified sternum plate has been developed with additional material outboard of the holes along with a fabric overlay, either as additional strengthening or an interim solution, that strengthens the sternum plate holes under tensile loading but has no influence on the compressive stiffness. It is believed that this issue has been presented to the ISO group. See Figure 30.

Figure 30: Sternum modifications

The WorldSID arm kinematics observed in some of the tests was not biofidelic. The use of the full arm was not thought necessary and, given the prototype status, cannot be implemented in the far-side procedure in the foreseeable future. It was necessary to continue drafting the procedure with the half arm assembly, even though its biofidelity is limited. Care should also be taken to ensure that ATDs with umbilicals have their cables routed in a way that does not influence the movement of the dummy and limits interaction between the cables and vehicle interior.

The far-side testing appears to be applying greater loads to the WorldSID lumbar spine than the near-side testing. An investigation by JAMA highlighted an incidence where the lumbar spine mount contacted the abdominal rib, resulting in a spike in the lumbar traces. The abdominal rib has also been known to contact the pelvis flesh. It should be noted that no such occurrences were identified in the SIWG tests or the 2018 assessments from Euro NCAP. The lumbar rubber is not a certified component and may not lend itself to a reliable certification test. At

this stage, it is questionable as to how much of an influence this may have on the head excursion, particularly where a vehicle offers good control of the dummy kinematics by limiting the inboard movement. The relevance and need for a test will be examined in the future along with how such a corridor might be established.

ASSESSMENT CRITERIA

Euro NCAP has highlighted the protection of far-side occupants as an area of vehicle design that should be improved. The objective of the assessment is to reward vehicles that offer control of occupant kinematics, thus limiting head and torso excursion and reducing the risk of contacts with the struck-side interior and other occupants. Euro NCAP would like to encourage countermeasures that have been specifically designed for far-side impact scenarios which would prevent occupant to occupant contact while also ensuring that there are no additional risks presented to the occupants. The assessment of far-side protection focuses on two areas, dummy head excursion and evaluation of the dummy outputs. The accident data indicated that reduced lateral excursion of the occupant potentially reduces interaction with the vehicle and subsequently reduces the risk of injury not just to the head, but also the torso [8] [9].

Excursion lines were established at the location of peak vehicle intrusion and the seat centreline. The position of the intrusion line would be based upon that seen in the official Euro NCAP test, or an equivalent in-house test if testing is performed early in the vehicle development. Where an in-house test is used, the pulses and intrusion will be cross checked with the official Euro NCAP tests. The intrusion is measured at the most inboard point of the vehicle interior. As mentioned previously, peak intrusion occurs before the maximum head excursion, so there was no need to reproduce the dynamic intrusion in the test procedure, see Table 1.

An occupant to occupant interaction limit was specified at the inboard edge of the far-side seat. This area of interaction was identified in a series of numerical simulations performed by ACEA, AE-MDB tests with two occupants showed head to shoulder contact in this region. The simulation showed there was significantly more rebound of the driver in the pole impact scenario compared to the AE-MDB.

The simulations were performed with the WorldSID model and were based on a number of the vehicles tested by Euro NCAP in 2015. The head contacts were mostly on the door trim (armrest) and therefore too low to be covered by the curtain airbag.

- 2 Small family cars
- 1 Supermini
- 1 Large Family Car
- 2 Small MPVs

Table 1: Vehicle simulations

Vehicle	Vehicle width [mm] without mirrors	Max. B-pillar velocity non-struck side [kph]	Max. Intrusion door trim 100mm above sill [mm] @time		Max. Intrusion door trim 100mm below side window aperture [mm] @time		Max. Head Excursion Y [mm]	Max. Head Excursion Z [mm]	Max. Spine T4 Excursion Y [mm]	Max. Mid Sternum Excursion Y [mm]	Max. Pelvis Excursion Y [mm]
Average AE-MDB Baseline	1788	28	148	55	159	57	587	304	378	223	100
Average AE-MDB Variation 1	1788	28	154	55	151	55	567	282	353	212	101
Average AE-MDB Variation 2	1788	44	307	58	324	61	691	274	489	315	113
Average AE-MDB Variation 3.1	1788	23	90	49	96	53	518	244	335	181	100
Average AE-MDB Variation 3.2	1788	27	101	49	116	50	545	307	364	201	106
Average AE-MDB Variation 3.3	1788	28	139	51	138	54	555	303	363	203	100
Average Pole Baseline	1788	38	331	95	352	99	635	348	448	258	67
Average Pole Variation 1	1788	38	327	97	379	101	646	291	438	269	64
Average Pole Variation 2	1788	39	301	103	325	104	620	334	423	247	72

The other part of the far-side assessment is dummy criteria. Existing criteria were adopted where possible, e.g. the head, rib compression, pubic symphysis etc, but additional criteria were also included. Some criteria for brain injury risk are also being monitored for possible future adoption. The thoracic rib compression limit of 28mm is based on the skeletal risk, whereas abdominal rib compression (47mm) is based on the soft tissue risk. Nevertheless, even with the presence of a large, 'rigid' centre console the maximum abdominal rib compression in the two series of tests was 45mm.

The accident data showed cases of cervical spine injury, Forman et al [10]. GIDAS data also showed that impacts with a lower delta V (16 & 34km/h) than the target of 41km/h can result in C2 vertebrae fractures (AIS 3). Unfortunately, biomechanical criteria for the neck and lumbar regions is limited, so the decision was taken to specify pragmatic limits that prevent unreasonably high values. As there is no WorldSID transfer function for neck tension (Fz) and little reliable data for moments, the limits were adopted as pass/fail criteria only. This was also the case for the lumbar, where data showed disc breaking in the region of 2.84kN [11].

A rating was developed based upon three body regions with four points being awarded to each body region, a maximum of 12 points is available for each impact scenario, see Table 2. A penalty is applied to the overall score of a test where the lumbar loads exceed the prescribed limit. The head excursion assessment is then applied to the dummy score of each scenario. Where the head passes the seat centreline, zero points are awarded for the head, and if it passes the intrusion line, no points will be awarded for that scenario. Finally, where the occupant interaction line is passed, the score for that scenario will be halved. The scores for each scenario are then combined and scaled down from 24 points to four.

Further details of the assessment are contained in the Euro NCAP Far-Side Test and Assessment Protocol v1.1.

Table 2: Assessment criteria

	Criteria	**Performance limits**			**Points**
		Higher	**Lower**	**Capping**	
Head	HIC_{15} (with hard contact)	500	700	700	4 points
	Resultant 3ms acceleration	72g	80g	80g	
	SUFEHM/BrIC	monitoring			
Neck	Tension Fz		3.74kN		4 points
	Lateral flexion MxOC		50Nm		
	Extension negative MyOC		50Nm		
Chest & Abdomen	Chest lateral compression	28mm	50mm	50mm	4 points
	Abdomen lateral compression	47mm	65mm	65mm	
Pelvis & Lumbar	Pubic symphysis	2.8kN			-4 points
	Lumbar Fy	2.0kN			
	Lumbar Fz	2.84kN			
	Lumbar Mx	100Nm			

2018 RESULTS

It was initially planned for the far-side assessment to be implemented in 2018. However, as the development of the procedure took longer than anticipated this was delayed until 2020. A draft protocol was made available in 2017, with 2018 and 2019 designated as a period of monitoring and protocol 'fine tuning'. During the monitoring phase, far-side data was required by Euro NCAP but not considered in the vehicle rating.

In 2018, a total of 20 vehicles were assessed by Euro NCAP and it is worth noting that none of these vehicles were superminis. Vehicle manufacturers provided sled data with vehicle specific pulses for AE-MDB (60km/h) and oblique pole impacts. Two vehicles were not equipped with side curtain airbags and were not subjected to the pole tests, so no far-side data was provided for these vehicles.

In all cases, the peak head excursion was beyond the occupant interaction limit. In four cases, the head exceeded the seat centreline; in a further three cases the head excursion exceeded the intrusion line. Head excursion was higher in the pole impact for 13 of the cars, and in the AE-MDB for three. In the remaining cases the excursion was so similar an accurate determination could not be made. In many cases, although the excursion was deemed highest in the pole test, there was not a large difference compared to that observed in the AE-MDB test. There were no hard contacts with any part of the vehicle interior or any notable interaction with the far-side seat, as was to be expected given that intrusion was not replicated.

In three of the tests the thoracic rib higher performance limit (28mm) was exceeded, all on the lower rib. One of these tests was the AE-MDB pulse and the remaining two were pole pulses, the largest value recorded being

31mm. The soft tissue abdominal rib HPL (47mm) was not exceeded in any of the tests. Application of the skeletal risk limit (28mm) would result in only three tests above this limit (max 31mm).

The neck Mx limit was exceeded in 12 tests; the My limit was exceeded in one test only. The lumbar Fz limit was exceeded in one test, Fz and Mz were exceeded in five and four of the tests respectively. As mentioned previously, biomechanical criteria for the neck and lumbar regions is limited, so pragmatic limits were set to prevent unreasonably high values. There was no correlation between exceeding the neck limits and head excursion, the lumbar Mx limit was only exceeded in cases where the head excursion approached the seat centreline.

Given the frequency of far-side injuries in accident data and the results of the monitoring phase, it appeared that the WorldSID may not be predicting thoracic or abdominal injury risk as originally anticipated. The assessment of head excursion would seem to offer the best evaluation of far-side occupant protection as the kinematics of the dummy are sufficiently representative of those of a human. Further consideration of the assessment limits will be made by the group in the future.

FUTURE WORK

Due to the limited capabilities of the WorldSID, the focus of the assessment must be on excursion of the head and torso. The working group is discussing ways to be more discriminative of the vehicles assessed and to ensure that the procedure encourages the fitment of countermeasures that reduce excursion and offer protection against occupant to occupant contact. At the time of writing, the details of this assessment are still to be finalised, but one possible option is with the use of an additional excursion line, see Figure 31. Proof of sufficient protection for vehicles with an occupant to occupant countermeasure is also under discussion. The current proposal is for a second WorldSID to be included in the official oblique pole impact to enable a demonstration of the efficacy of such countermeasures. The feasibility of such a test is still under consideration by the group.

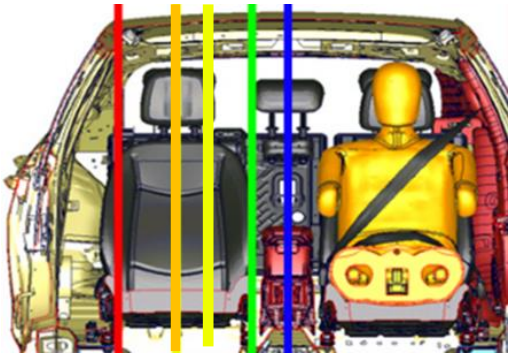

Figure 31: Draft assessment update

CONCLUSION

The development of the Euro NCAP far-side procedure began with accident data analyses. Previous accident research was combined with new analyses to establish the parameters that could be applied to a sled-based test procedure. In additional to the accident research, various numerical simulation studies were performed along with fourteen sled tests to investigate the factors affecting far-side protection.

The procedure aims to encourage vehicles to limit occupant excursion and mitigation of occupant to occupant interaction. A single ‘generic’ pulse was considered but this was found to be too limited given the variation in mass of the vehicle fleet and the increasing prevalence of electric vehicles. Two impact scenarios are therefore used to evaluate each vehicle model: a barrier to car impact and a pole impact, and both tests use vehicle-specific pulses. The sled setup is a simplified body in white that does not replicate struck-side intrusion as this was considered an unnecessary complication.

Results from the 2018 monitoring phase show that the WorldSID dummy has limited capability in predicting thoracic and abdominal injury risk. None of the dummy outputs exceeded the established injury criteria. However, in a number of cases the pragmatic neck and lumbar spine limits were exceeded. The kinematic assessment is appropriate and a simple method for assessing the head excursion has been adopted. This method is still under discussion and subject to change in favour of a more discriminating method. The far-side assessment will become part of the Euro NCAP rating from 2020. At the time of writing, the latest version of the procedure is version 1.1, November 2018 and is available at www.euroncap.com.

REFERENCES

1. Euro NCAP. Moving Forward, 2010 – 2015 Strategic Roadmap, December 2009.

2. Euro NCAP. In Persuit of Vision Zero, 2025 Roadmap, September 2017.

3. B Fields, L Sparke, O Bostrom, F Pintar, N Yoganandan, A Morris. Suitability of Current Side Impact Test Dummies in Far-Side Impacts. Munich IRCOBI 2002.

4. F Feist, J Gugler, R Curden. Methodology to Address Non Struck Side Injuries. APROSYS deliverable, AP-SP11-D115A, 2006.

5. EEVC Working Group 21 Report, Side Impact Analysis May 2008, WP1 Overview of Side Impacts.

6. G Bahouth, D Murakhovskiy, K Digges, H Rist, R Wiik. Opportunities for Reducing Far Side Casualties. 24th ESV Conference, paper number 0444, 2015.

7. S Thomas, R Wiik, J Brown. The Front Centre Airbag. SAE International, 2013-01-1156.

8. F Pintar, J Moore, N Yoganandan, B Stemper, K Digges, O Bostrom, S Rouhana, B Fields. ARC Far Side Impact Collaborative Research Program, task 2 final report.

9. B Fields, M Fitzharris, H Gabler, K Digges, S Smith. Chest and Abdominal Injuries to Occupants in Far Side Crashes. 20th ESV Conference, paper number 0384, 2007.

10. J Forman, F Lopez-Valdes, D Lessley, P Riley, M Sochor, S Heltzel, J Ash, R Perz, R Kent, T Seacrist, K Arbogast, H Tanji, K Higuchi. Occupant Kinematics and Shoulder Belt Retention in Far-Side Lateral and Oblique Collisions: A Parametric Study.

11. G Nyquist, J Melvin, K Weber. Review of Biomechanical Impact response and Injury in the Automotive Environment, Task B Final report, 1985.

12. K Hallbauer, U Dierks, I Kalliske, A Riedel. Investigation of new Euro NCAP Far Side Impact Requirements. 14th Internation Symposium on Sophisticated Car Safety Systems, 2018.

13. J Ellway. The Development of an Advanced European Mobile Deformable Barrier Face. 19th ESV Conference, paper number 05-0239, 2005.

ACKNOWLEDGEMENTS

The working group and authors would like to thank F Ochiai from Honda for his technical contributions and S Tylko from Transport Canada for the use of the WorldSID full arm.

Members of the Side Impact Working Group

J Ellway, Euro NCAP (Chairman)
A Thompson, Thatcham (Secretary)
C Adalian, IDIADA
H Ammerlaan, RDW
L Baroncelli, CSI
K Hallbauer, Joyson Safety Systems on behalf of CLEPA
C Kerkling, Honda
T Kerz, Opel on behalf of ACEA
T Langner, BASt
J P Lepretre, UTAC
M Ribo, Magna
S van Montfort, TNO
V Sandner, ADAC
C Weimer, HKMC
P Wernicke, BMW

Appendix I
Accident data summary

	GIDAS	Volvo Cars Traffic Accident Database	BAAC French National Database	LAB (weighted data)	ADAC	RAIDS-CCIS	APROSYS
Accidents	2005 – 2014 Germany Injured accidents No P or 2W	2002 – 2013 Sweden High repair costs	2010-2013 France Injured+ accidents (under reporting) No P or 2W	2005 – 2014 France Injured+ accidents No P or 2W	2005 – 2014 NO P OR 2W	1998 - 2010	ZEDATU CCIS PENDANT HIT GIDAS TNO DIANA BASC-CCIS
Impacts	Lateral						
Vehicles	Cars Reg. 2000+	Volvo cars MY 98+	Cars Reg. 2000+	Cars Reg. 2000+	Cars Reg. 2000+	1998-2010	1995+
Occupants	Belted drivers and front seat passengers						
Ages	10+	14+	10+	10+	10+	12+	
Sample	1,719 (804/915)	2,852 (1,295/1,557)	14,775 (6,801/7,974)	432 (199/233)	899 (374/525)	2108 (962/1146)	
MAIS 2+	99 (43/56)	41 (14/27)		172 (64/108)	538 (211/327)	585 (219/366)	
MAIS 3+	34 (9/27)	10 (1/9)		89 (34/55)	191 (74/117)	391 (141/250)	
Fatal & Seriously Injured			3,433 (1,391/2,042)				

Appendix II
Generic Sled setup

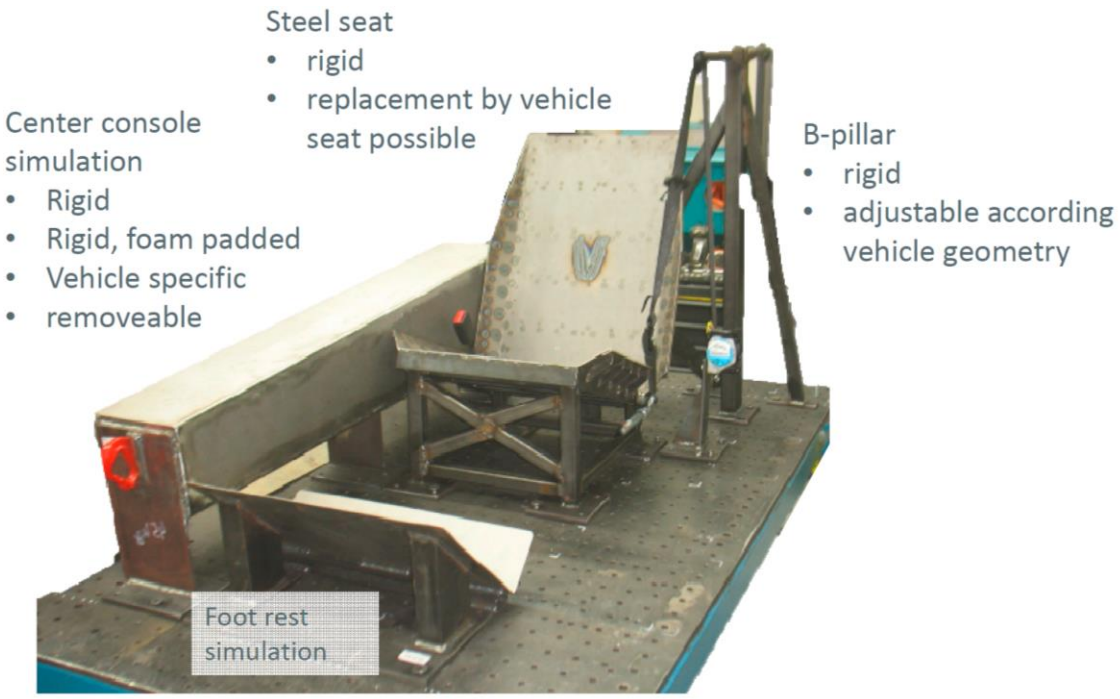

Sled and CAE comparison

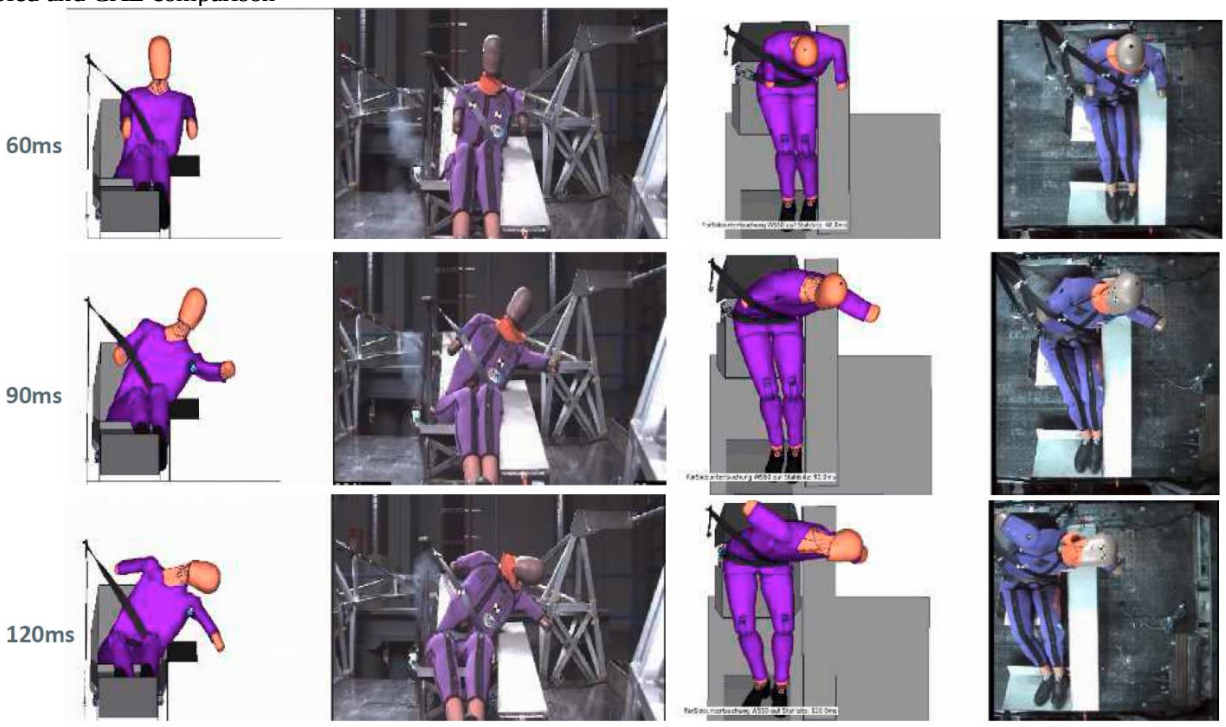

HBM SIMULATIONS

Comparison AROSYS pulse 75° without center console HBM and WorldSID

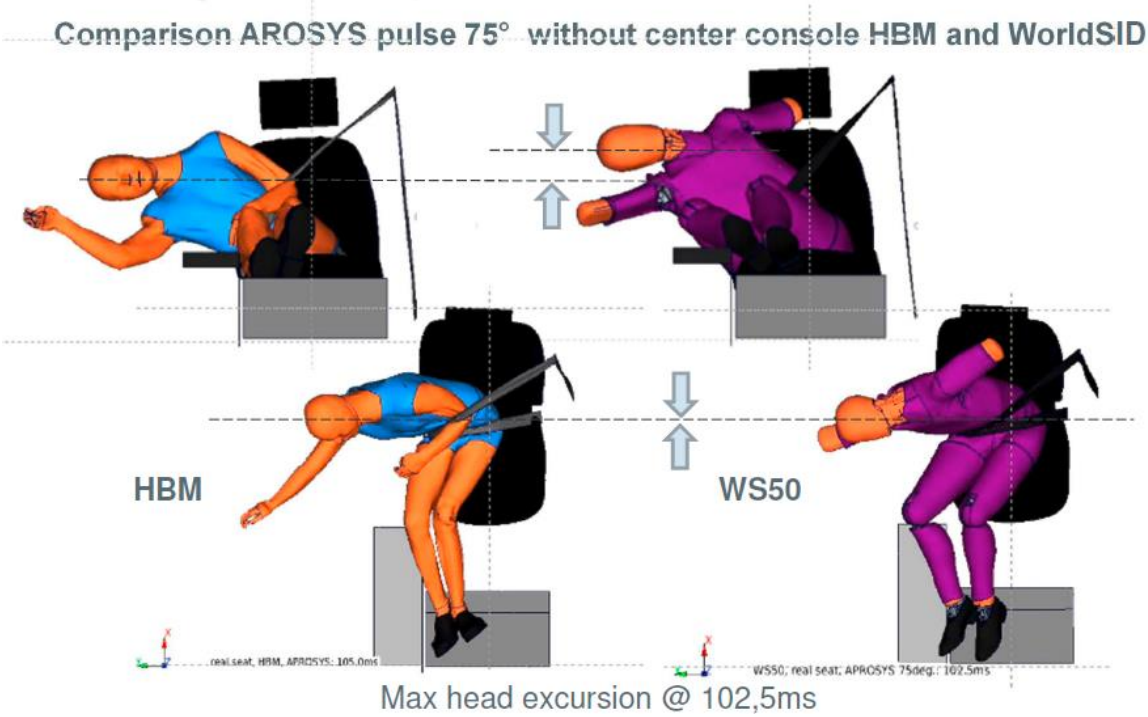

Max head excursion @ 102,5ms

HBM SIMULATIONS

Comparison AROSYS pulse 75° without center console HBM and WorldSID

HEAD

appr. 70mm more lateral Head CoG travel of HBM

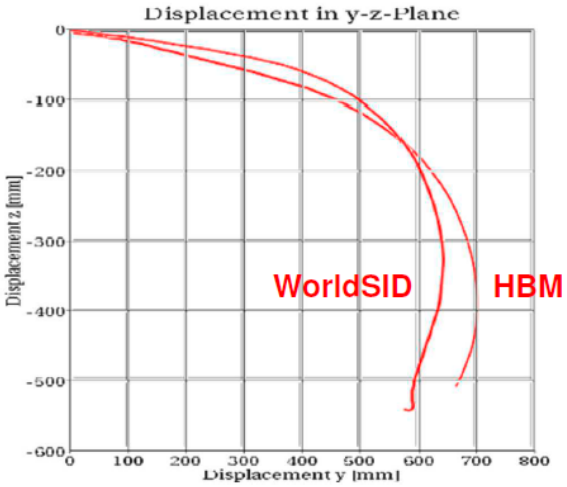

Appendix IV
Sled test series 1

Test No.	1	2	3	4	5	6	7
Loadcase	AE-MDB					Pole	
Delta V	41km/h					42.4km/h	38.8km/h
Pulse	Generic modified Aprosys pulse					36 kph-75° Pole F164609	32 kph-75° Pole F164302
Angle of Impact				75°			
Occupant (Driver)	WorldSID half arm			WorldSID full arm	WorldSID half arm	WorldSID half arm	
Centre console present above H-point	Standard (119mm above H-point)				Large & strong foam block with 2mm tin layer (185mm above H-point)	Standard (119mm above H-point)	
Deploy struckside curtain airbag	yes (5,5ms) side glazing closed	No, if no head interaction in first test				No	
Deploy struckside airbag	yes (5,5ms)	No, if no arm/torso interaction in first test				No	
Deploy driver pretensioner				No			
Seat & dummy position				Euro NCAP			
Remark	Baseline	Repeatability		Full arm influence		Baseline	

Appendix V
Series 1 results summary table

Test-Nr.				1	2	3	4	5	6	7
Loadcase				AE-MDB					Pole	
Velocity (Km/hr) / Pulse				41 / Generic Modified Aprosys Pulse					36 / 75° Pole F164609	32 75° Pole F164302
Angle of Impact				75°	75°	75°	75°	75°	75°	75°
Occupant (Driver) WorldSID50				w/o Full Arm			With Full Arm	w/o Full Arm	w/o Full Arm	
Centre console (Xmm above H-point)				Standard (119)				"Big CC" (185)	Standard (119)	
Deploy of struckside SIAB & CAB (TTF, ms)				Yes (5,5)	No					
Deployment of Driver Retractor PT				No*						
Seat & Dummy Position				EuroNCAP						
Head	HIC15	500	700	310.29	227.62	187.92	344.33	501.70	114.51	84.67
	Accn. Res. (g)	72	80	58.20	50.30	46.45	59.61	74.01	37.03	33.40
Neck Forces - Max; Min	Fx (kN)			0.19; -0.24	0.31; -0.24	0.30; -0.21	0.23; -0.27	0.08; -0.36	0.15; -0.18	0.15; -0.19
	Fy (kN)			0.14; -0.50	0.16; -0.41	0.09; -0.38	0.10; -0.50	0.16; -0.68	0.10; -0.39	0.11; -0.39
	Fz (kN)		3.74	2.21	1.96	1.80	2.29	2.88	1.45	1.30
Neck Moments - Max; Min	Mx (Nm)		-50	-60.21	-51.80	-47.65	-57.07	-66.52	-33.84	-36.19
	My (Nm)		-50	-33.83	-38.79	-40.48	-38.57	-26.96	-33.93	-34.64
	Mz (Nm)			14.28; -16.75	15.43; -13.07	19.37; -16.18	13.94; -17.63	0.82; -11.82	13.84; -13.50	13.89; -13.77
Neck NIC	Fx +; - (%)			6.3; 7.8	14.1; 7.9	14.8; 8.8	7.4; 7.0	2.5; 12.7	6.6; 5.7	7.5; 6.1
	Fz +; - (%)			67.0; 0.1	62.5; 0.1	75.2; 0.1	87.5; 0.1	87.4; 0.1	51.4; 0.1	54.5; 0.1
Chest - Shoulder Force	Res. Max (kN)			1.38	1.69	1.55	1.45	1.84	1.44	1.11
	Fy Max (kN)			1.25	1.31	1.34	1.25	1.69	0.85	0.74
Thorax Rib Deflection (mm)	1	-28	50	-13.21	-7.83	-5.05	-4.37	-7.94	-1.06	-3.08
	2	-28	50	-14.21	-27.75	-6.89	-14.65	-10.74	-9.03	-23.06
	3	-28	50	-2.38	-13.90	-29.97	-6.09	-19.93	-35.75	-16.30
Abdomen Rib Deflection (mm)	1	-47	65	-1.76	-2.73	-8.86	-7.63	-45.65	-15.33	-1.97
	2	-47	65	-19.07	-21.29	-17.28	-25.07	-31.40	-2.48	-5.41
Pelvis	Pubic ForceY (kN)		2.8	-0.92	-0.90	-0.73	-0.68	-1.06	-0.70	-0.63
Lumbar	Fy (kN)		2							
Lumbar	Fz (kN)		2.84							
Lumbar	Mx (Nm)		100							
Remarks				with infl. Restraints shoulder belt trapped in sh joint (sh pad concern)	no top view camera in prel data no lower retractor fixation buckle opend	zipper opened by interaction suit w/ sh belt				

Appendix VI
Sled test series 2

Test No.	8	9	10	11	12	13	14
Loadcase	AE-MDB				Pole		
Main Evaluation Priority							
Delta V	41km/h				38.8km/h	38.8km/h	42.4km/h
Pulse	Generic modified Aprosys pulse				32 kph-75° Pole F164302	32 kph-75° Pole F164302	36 kph-75° Pole F164609
Angle of Impact				75°			
Occupant (Driver)	WorldSID half arm and sleeveless suit						
Centre console present above H-point	*Standard (119mm above H-point)*	*Standard (119mm above H-point)*	*Standard (119mm above H-point)*	*High console*	*Standard (119mm above H-point)*	*High console*	*Standard (119mm above H-point)*
Deploy of struckside curtain airbag	No	No	No	No	No	No	No
Deploy of struckside airbag	No	No	No, with spacer	No, with spacer	No, with spacer	No, with spacer	No, with spacer
Deploy driver pretensioner	No*	Yes;	Yes	Yes	Yes; 10ms	Yes; 10ms	Yes; 10ms
Seat & dummy position	Honda Jazz EuroNCAP	Honda Jazz EuroNCAP	Honda Jazz EuroNCAP	Honda Jazz EuroNCAP	Honda Jazz EuroNCAP	Honda Jazz EuroNCAP	Honda Jazz EuroNCAP
Remark	Record T1 and T4 acceleration Markers for	If pretensioning causes interaction with	Support B-pillar to PASSseat AND PASSseat to	Support B-pillar to PASSseat AND PASSseat to	Support B-pillar to PASSseat AND PASSseat to	Support B-pillar to PASSseat AND PASSseat to	Support B-pillar to PASSseat AND PASSseat to

Appendix VII
Series 2 results summary table

Far Side Occupant Protection - Sled Test Matrix													Crash	
Test No.				S17120101	S17120102	S17120103	S17120104	S17120105	S17120106	S17120107			F164609	F164302
Test No.				1	2	3	4	5	6	7			Pole	
Loadcase				AE-MDB				Pole					Pole	
Velocity (Km/hr) / Pulse				41 / Generic Modified Aprosys Pulse				32 75° Pole F164302		36 / 75° Pole F164609			36 / 75° Pole F164609	32 75° Pole F164302
Angle of Impact				75°	75°	75°	75°	75°	75°	75°				
Occupant (Driver) WorldSID50				WS50 w/o full arm - WITH sleeveless suit									w/o Full Arm - WITH sleeved suit	
Centre console (Xmm above H-point)				Standard (119)			"Big CC" (185)	Standard (119)	"Big CC" (185)	Standard (119)			Standard (119)	
Deploy of struckside CAB - Yes / No (TTF, ms)				No									Yes (5,5)	
Deploy of struckside SIAB - Yes (TTF, ms)				No		No - Support B-pillar to PASS seat AND PASS seat to centre console								
Deployment of Driver Retractor PT				No*	Yes; 7ms			Yes; 10ms					No	
Seat & Dummy Position				EuroNCAP									EuroNCAP	
Head	HIC15	500	700	192.00	225.20	210.60	501.90	93.80	133.70	101.60			3305.41	253.77
	Accn. Res. (g)	72	80	47.00	51.60	51.00	70.50	36.00	39.20	39.10			370.98	72.84
Neck Forces - Max; Min	Fx (kN)			0.25 -0.27	0.37; -0.30	0.17; -0.24	0.07; -0.42	0.16; -0.18	0.05; -0.24	0.15; -0.25			0.05; -1.55	0.10; -0.24
	Fy (kN)			0.11; -0.47	0.15; -0.45	0.08; -0.51	0.15; -0.68	0.03; -0.48	0.09; -0.57	0.03; -0.40			0.31; -0.80	0.20; -0.60
	Fz (kN)		3.74	1.83	2.03	2.03	2.77	1.40	1.54	1.43			1.45	1.26
Neck Moments - Max; Min	Mx (Nm)		-50	-46.39	-44.64	-47.85	-56.59	-31.52	-44.52	-28.87			-16.31	-48.67
	My (Nm)		-50	-36.33	-48.19	-37.94	-23.41	-46.02	-32.70	-47.01			-60.28	-37.51
	Mz (Nm)			16.00; -17.83	19.79; -18.79	14.81; -15.84	3.34; -11.54	17.76; -19.22	4.63; -14.52	18.61; -19.41			4.67; -47.07	11.08; -23.93
Neck NIC	Fx +; - (%)			9.3; 8.6	14.4; 9.6	6.2; 7.9	5.8; 14.4	5.3; 10.0	1.8; 8.3	5.0; 14.0			1.5; 50.2	9.3; 7.8
	Fz +; - (%)			58.3; 0.1	61.6; 0.1	66.4; 0.1	84.0; 0.1	47.1; 0.1	46.6; 0.1	49.5; 0.1			44.1; 154.2	38.3; 66.5
Chest - Shoulder Force	Res. Max (kN)			1.68	1.55	1.58	1.78	0.97	1.19	0.95			1.35	0.92
	Fy Max (kN)			1.46	1.38	1.43	1.64	0.84	1.07	0.83			0.80	0.79
Thorax Rib Deflection Max (mm)	1	-28	50	-4.6	-7.1	-3.4	-6	-5.1	-4.1	-3.9			0	-0.04
	2	-28	50	-22.4	-26.1	-4.9	-9.5	-19.4	-6.9	-8			0	-0.17
	3	-28	50	-23.1	-10.2	-18.7	-21.6	-19.7	-21.3	-32.3			3.22	-1.59
Abdomen Rib Deflection Max (mm)	1	-47	65	-7.9	-3.1	-11.2	-40.7	-7	-26.1	-14.2			-2.66	-4.26
	2	-47	65	-24.8	-1.9	14.4	-30.5	-5.6	-16.2	-2.6			-5.57	-6.93
Pelvis	Pubic ForceY (kN)		2.8	-0.78	-0.82	-0.77	-1.01	-0.77	-0.7	-0.75			-0.66	-0.69
			2											
			2.84											
			100											
Remark				Cut in new sleveless suit; no belt interaction with dummy shoulder / jacket	Belt height adjuster in lowest posn. +1 notch instead of up; no belt interaction with dummy shoulder / jacket									

CONSUMER INITIATIVES TO IMPROVE CHILD SAFETY IN EUROPE

Michiel van Ratingen
European New Car Assessment Programme (Euro NCAP)
Belgium

Ronald Vroman
International Consumer Testing and Research (ICRT)
United Kingdom

Andreas Ratzek
Allgemeiner Deutscher Automobil Club (ADAC e.V.)
Germany

Paper Number 19-0279

ABSTRACT

Safe transport of children in cars is the joint responsibility of parents, child restraint suppliers and vehicle manufacturers. Responsible parents and caregivers must ensure that children are properly restrained in a correctly installed child restraint system (CRS) that is appropriate for the size and weight of the child. Child restraint suppliers make certain their products meet local regulations, offer adequate protection and can be fitted easily and correctly in all cars. Finally, it is the vehicle manufacturers' obligation to guarantee that children are as well protected as adults in the event of crash and that special any provisions needed for children are offered as standard. In practice, this joint responsibility leads to a set of complex interactions and a patchwork of solutions that make it difficult for average consumers to know how their child is carried in the best and most safe way.

In Europe, two independent consumer-oriented programmes work cooperatively to help consumers find the best answer for their unique situation. Child restraint testing is carried out by European consumer groups under the umbrella of International Consumer Testing and Research (ICRT) and the Automobile Clubs. The program publishes ratings based on standardised dynamic sled tests and an ease-of-use assessment, amongst other items. The European New Car Assessment (Euro NCAP) rates vehicle performance and equipment availability for new cars on the market. Its Child Occupant Protection assessment includes full-scale crash tests with child test dummies in child restraints and evaluates the availability and functionality of attachments and provisions for safe transport of children. Collectively, these programmes address one of the most pertinent and persistent challenges in child safety: the risk of misuse and incorrect installation of a child restraint system in a vehicle.

Child restraint testing is based on body-in-white setup applying standardised pulses. This set up only broadly approximates real life use in actual cars. In-vehicle testing comes closer to actual crash circumstances, but the result only applies to the combination of car model and CRS type. Both approaches are complementary, and both are needed to improve child safety in cars.

INTRODUCTION

Since May 2006, it has been compulsory to use safety belts and United Nations Regulation No. 44 type-approved child restraint systems in all vehicles in Europe [1]. It is also mandatory to use child car seats within the EU for children up to the heights of 1.35m or 1.5m - depending upon the country. Thanks to these laws and increased consumer awareness and compliance, child deaths in motor vehicle crashes have steadily declined over the last decades [2] (Figure 1).

Child Restraint Systems

The European Test Standard for Child Restraints [3] was introduced in 1982. From this time onwards, only seats displaying the European Standard orange label, indicating approval to UN Regulation No. 44, may be used or sold. Child restraint systems approved under R.44 are classified into five mass groups. For children up to 9kg they must be side- or rearward facing. Most common are rearward facing infant carriers up to 13kg. For the groups up to 18kg these child restraint systems have an integrated harness or shield system. The groups for heavier children up to 36kg mostly use the vehicle's safety belt for restraining. Approvals are based on several criteria, the foremost of which is the child restraint's performance in a simplified dynamic sled test, representing a frontal impact.

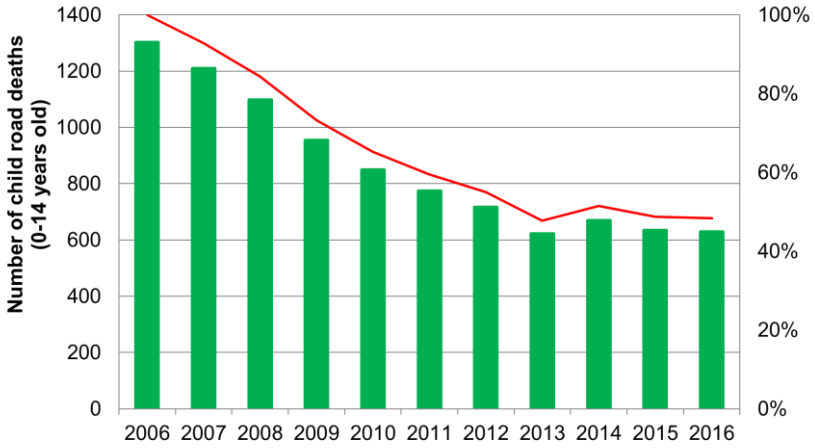

Figure 1. Development in the number of child road deaths in 27 EU countries over the period 2006-2016 (ETSC, [2])

UN Regulation No. 44 has been amended and updated many times since the 1980s. To facilitate correct installation of child restraints, the ISOFIX [4] standard for attachment points and connectors for child safety seats in passenger cars was introduced in 1997. ISOFIX became a standard in 2004, but only became mandatory in the EU for all new models launched from November 2012, and in all vehicles manufactured after November 2014 [5]. ISOFIX child seats can be either "Universal", approved for use in all vehicles that meet UN Regulation No. 14[1] [6] and No. 16 [7], or "Semi-Universal" or "Vehicle Specific" for use in specified vehicles.
The Reg.44 standard for child restraints can appear complicated from a consumer point of view. It covers belted, ISOFIX, Universal, Semi-Universal & Vehicle Specific approvals as well as having confusing overlaps in the weight groups. This has led to a kaleidoscopic of product offerings on the market that can easily cause parents to make the wrong choice for their child. Despite the availability of ISOFIX, there still are many mistakes made when installing a child restraint in the car or the child in the seat [8]. Furthermore, the standard allows forward facing transport as of 9 kg and does not encourage rearward facing transport of toddlers (>13kg), nor does it require child restraints to offer adequate protection in side crashes. These concerns, amongst others, have been addressed by the new UN Regulation No. 129 that came into effect in 2013 [9]. Even though i-Size clearly delivers superior child seats, UN Regulation No. 44 (currently R44.04) and UN Regulation No. 129 (currently R129/03) have been allowed to run side by side, at least for the time being. For the consumer, the situation on the ground therefore remains very confusing.

For more than 50 years, consumer groups under the umbrella of International Consumer Research and Testing (ICRT) and Automobile Clubs have been testing child restraint systems in order to guide consumers into buying the best seat for their child. Initially run as separate programs in various countries, they joined forces in 2003 by forming the European Testing Consortium (informally referred to as "ETC"). The main partners are ADAC (D), ÖAMTC (AT) and TCS (CH) on behalf of the automobile clubs and Stiftung Warentest (D), Which (UK), Consumentenbond (NL), Test Achats (B) and Que Choisir (F). The program is fully independent and funded by partners. Test results are published by more than 30 organisations across Europe (and beyond) in different presentation formats (Table 1). Twice a year a batch of new CRS models is tested, and the results are published by the end of May and October. On average some 50 models are published each year. Benchmarking testing has become a powerful tool to drive improvements in CRS design, as a good ETC rating is a must for child seat manufacturers to be successful in the market.

Passenger Cars
In Europe a type approval is applied by national authorities to certify that a vehicle meets all EU safety, environmental and conformity of production requirements before authorising it to be placed on the EU market. As the EU is a Contracting Party to the 1958 Agreement of the World Forum for Harmonization of Vehicle Regulations, it generally applies the technical requirements of the UN ECE to verify compliance with safety rules. This is also the case for child occupant protection, which is ensured directly via production requirements on seat-belts, ISOFIX anchorages and top-tethers in Regulation No. 14/145 and No. 16, and indirectly (as testing does not involve child dummies) through the application of mandatory crash front and side impact crash tests for the whole vehicle.

[1] In 2017, ISOFIX and child restraint system anchorage provisions were separated from UN Regulation No. 14 and included in Regulation No. 145.

Table 1.
Publishing partners distributing ETC test results in European countries (2018)

Country	Partner	Country	Partner
Austria	ÖAMTC, VKI	Luxembourg	ACL
Belgium	Test Achats/Test Aankoop	Netherlands	ANWB; Consumentenbond
Bosnia & Herzegovina	BIHAMK	Norway	Forbrukerrådet
Croatia	HAK	Poland	Świat Konsumenta
Czech Republic	dTest	Portugal	ACP; DECO Pro Teste
Denmark	FDM; Forbrukerrådet	Romania	APC Romania
Finland	Autoliitto; Kuluttaja	Slovenia	AMZS; ZPS
France	Que Choisir	Spain	RACC; RACE;
Germany	ADAC; Stiftung Warentest		Oficina de Co. Universitaria
Hungary	Kosár; Magyar	Sweden	Råd & Rön; Motormännen
Italy	Altroconsumo	Switzerland	TCS
Lithuania	LNVF	United Kingdom	Which?

Since 1997, Europe's type approval system is complemented with the new car assessment programme Euro NCAP, which provides motoring consumers with a realistic and objective assessment of the safety performance of the most popular cars sold in Europe [10]. Euro NCAP encourages manufacturers to exceed the legal requirements by applying more stringent and/or additional test conditions and by extending the assessment to new areas of vehicle safety. At present the organisation has 12 members representing the citizens and consumers in the whole of Europe. These include the Member State governments of the United Kingdom, Germany, France, Sweden, the Netherlands, Luxemburg and the regional government of Catalonia; the International Automobile Federation FIA; motoring clubs ADAC and ACI; International Consumers Research and Testing; and the Motor Insurance Centre Thatcham Research. In the 22 years of its existence, Euro NCAP has published ratings on over 700 different vehicles, including superminis, family cars and MPVs, roadsters, SUVs, pick-up trucks, hybrids and full electric vehicles.

From 2003, Euro NCAP has specifically addressed the protection of children in the event of a crash. The child occupant protection star rating aims to help consumers choose the best car for their family, to motivate all car manufacturers to deliver improved child protection and to facilitate a better dialogue between car manufacturers and child restraint suppliers. In 2009, the Child Occupant Protection rating became part of the overall safety rating, making a good child protection score a prerequisite for 5 stars [11].

METHODS

Consumer test programmes such as ETC and Euro NCAP give consumers the ability to hold manufacturers to account, by giving them more control over the product which they need. They make sure that markets work properly so that competition between manufacturers drives down prices and sparks innovation from which consumers benefit. Central to their mission is to provide data and tools to inform, educate and, if necessary, support consumers when they must make difficult choices, such as buying a child seat for their firstborn, or the safest car for the family.

Both consumer programmes have a wide scope, covering more aspects than what is legally considered, to reveal hidden product properties and to promote best practice. They share an underlying philosophy that children should benefit from at least the same level of protection as adults/their parents. Despite their complex technical assessment, ETC and Euro NCAP have adopted a simple communication language to explain the results, using "stars" or easy to understand labels. Their test methodologies are regularly reviewed and updated considering regulatory and market changes. In the case of ETC, industry is consulted in hearings at Stiftung Warentest (the so-called "Fachbeirat"), whereas Euro NCAP has invited vehicle manufacturers and seat suppliers to its working group on child safety.

Child Restraint System Test Methodology (ETC)

The main aim of the ETC test is to inform parents of the best solution to transport their child: the child seat that offers the best protection, is easy to handle, comfortable for the child and is free from hazardous substances. For this purpose, ETC has developed its own test methodology that assesses (1) dynamic performance, (2) ease-of-use, (3) ergonomics and (4) the presence of hazardous materials (Figure 2). Seats from all five mass groups (0, 0+, I, II, III) in UN Regulation No 44 and all size ranges in UN Regulation No. 129 are tested. If a seat covers

several mass groups, a wide size range or different installation modes, all modes are tested and rated. The test results are combined into one overall rating per product. Where there are several installation modes, the overall rating will be based on the worst-case performance of the product. However, because it is expected that ISOFIX products will usually be used in ISOFIX mode, ISOFIX results will be prioritised over belted results. A well-known example of this "worst-case performance" policy is that booster seats with detachable backrests are unable to score well owing to their lack of side impact protection when used as cushion only.

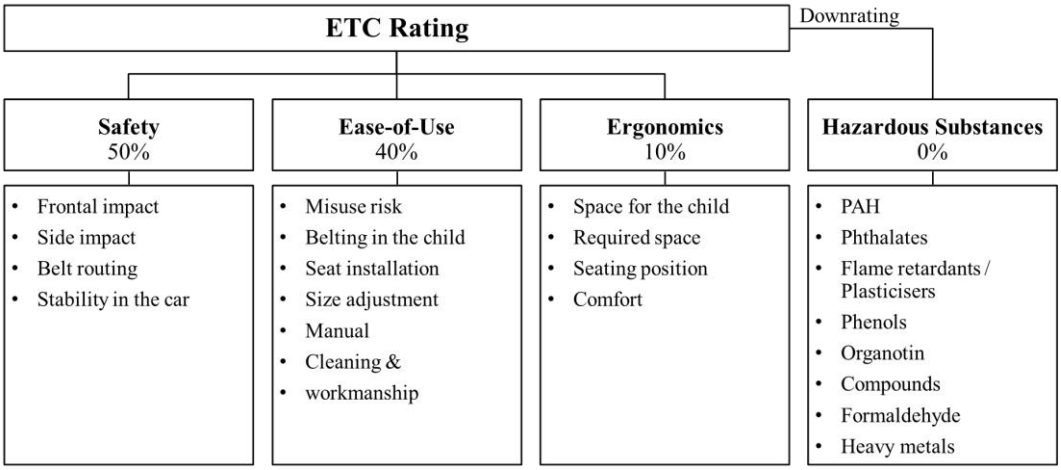

Figure 2. ETC Test overview (2018)

To ensure that results are representative, test samples are exclusively procured in retail point of sales, without the prior knowledge of the child seat supplier. From time to time, the testing procedure and the assessment are adapted based on the latest findings. For example, in 2007, the P-series dummies (except P10) were replaced by Q-series dummies; in 2011, the test of hazardous substances was implemented; and, in 2015, a side impact test with an intruding door, the Q10 dummy and Q3 abdominal load sensors were introduced.

Dynamic tests The latest dynamic test matrix includes fontal impact tests on Body-in-White (BIW), side impact tests on a test bench derived from Regulation No. 129, and an assessment of belt routing and seat stability in the car (Figure 3). A summary of tests is given in Table 2.

Table 2.
Summary of ETC Child Restraint Dynamic Tests & Assessment (2018)

Load Case	Test Parameters	Assessment
Frontal impact	• VW Golf VII BIW – child seats on rear seat • VW Golf VII ODB B-pillar pulse (Euro NCAP) • All available installation and adjustment possibilities and child sizes (5 tests on average)	• Q-dummies • Head, neck, chest and abdominal loads (Q3) • Belt routing • Seat stability
Side Impact	• Regulation No. 129 bench, 80° impact angle • VW Golf VII AE-MDB barrier pulse (Euro NCAP) • Intrusion depending on installation and adjustment possibilities and child sizes (3 tests on average)	• Q-dummies • Head, neck and chest loads

The dynamic tests are more demanding than legally required, thereby highlighting the extra protection the seat offers. The crash severity is comparable to Euro NCAP full scale tests, which nowadays are survivable types of crashes. All products tested are measured to the same yardstick irrespective to their (Regulation No. 44 or No. 129) approval. Dynamic tests are carried out at ADAC Technical Centre and the result contributes to the overall score with a weight of 50%.

Ease-of-use test In the ease-of-use tests, several handling aspects are assessed. These include misuse risk, the ease of strapping the child in the seat, ease of seat installation (by experts and laymen) and size adjustment, clarity of the user's manual and cleaning & workmanship aspects. In the latest version, three car models are used: Opel Adam 3-door, Golf VII 5-door and Ford C-Max. Ease of use assessments are carried out at ÖAMTC (Vienna) and the result has a weight of 40% in the overall score.

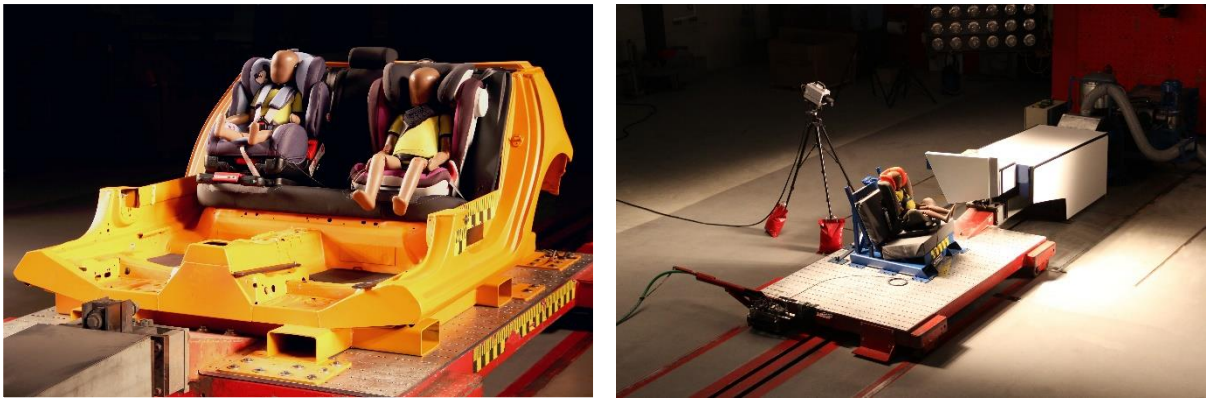

Figure 3. ETC front (left) and side (right) impact test © 2018 ADAC

Ergonomics test Expert and layman tests are carried out to verify the space available for the child, the required space inside the vehicle for installation, the resulting seating position, and comfort. The Opel Adam 3-door, Golf VII 5-door and Ford C-Max are used for these assessments as well handling dummies and actual children. Ergonomics checks are carried out at ÖAMTC and TCS and the result has a weight of 10% in the overall score.

Hazardous substances test Finally, all parts of the seat that are in contact with the child are screened for the presence of the following substances: Polycyclic aromatic hydrocarbons (PAH, based on the AfPS GS 2014:01 PAK document), Phthalates (based on Regulation EC No. 2005/84, Directive 76/769/EEC, Oeko-Tex Standard 100, and RAL-UZ textile toys), Flame retardants (based on Oeko-Tex Standard 100, EN 71-9 and Directive 2014/79/EU), Phenols (based on Oeko-Tex Standard 100), Organotin compounds (based on Oeko-Tex Standard 100), Formaldehyde (based on EN ISO 14184-1 and EN 71-9), and Heavy metals (based on EN 71-3). The findings do not contribute directly to the overall score but may be used to downgrade the overall score in case of pollution.

Child Occupant Protection Assessment Methodology (Euro NCAP)

Up until the nineties, car manufacturers relied on the makers of child restraints to provide protection for children in cars. Very few offered child restraints through their dealerships or provided any recommendation to their customers, and there were almost no special provisions in the vehicle, over and beyond the basic requirements in Regulation No. 14/145 and No. 16, for the safe transport of children. It has become clear, however, that there are many aspects of child protection which cannot be influenced by the child restraint manufacturer alone and which require action on the part of the car manufacturer as well. For this reason, Euro NCAP developed a specific assessment of the vehicle's ability to safely transport children.

From the beginning, the Euro NCAP Child Occupant Protection (COP) rating focused on three main elements: (1) the protection offered in front and side crash tests, (2) the interface between vehicle and child seat and (3) the special provisions for children in cars (Figure 4). The test results are converted into item scores, which are summed to form the COP score. Up until 2008, this score was communicated as a separate star rating. From 2009, the COP score, along with the Adult Occupant, Pedestrian Protection and Safety Assist scores, has been used to calculate the overall safety rating of the vehicle. Euro NCAP most commonly follows a VIN selection method [12] to source test vehicles, while child seats for testing are provided by either supplier or manufacturer.

Dynamic tests The frontal off-set deformable barrier and the side mobile deformable barrier test have formed the backbone of Euro NCAP's crashworthiness assessment since the start of the programme in 1997. Initially, the 3-year old and 18 months old P-series dummies were used to check dynamic performance. As test results improved over time, the focus shifted to the protection of older children. Since the latest revision (2016), the more biofidelic 10-year old and 6-year old Q-series dummies are placed on the rear seat (Q10 behind the passenger in the frontal impact test, behind the driver in the side impact test). The Q6 dummy is seated on booster seat appropriate for its mass or stature and recommended by the vehicle manufacturer. The Q10 dummy is placed on a booster cushion from a list of preselected products, even if a high back booster is recommended by the vehicle manufacturer in the user manual. The reason for this somewhat unusual set-up is the low use rate of high back boosters in real-life for children of 8 years and up. The use of the booster cushion will verify if adequate protection is offered by the vehicle's restraint systems alone.

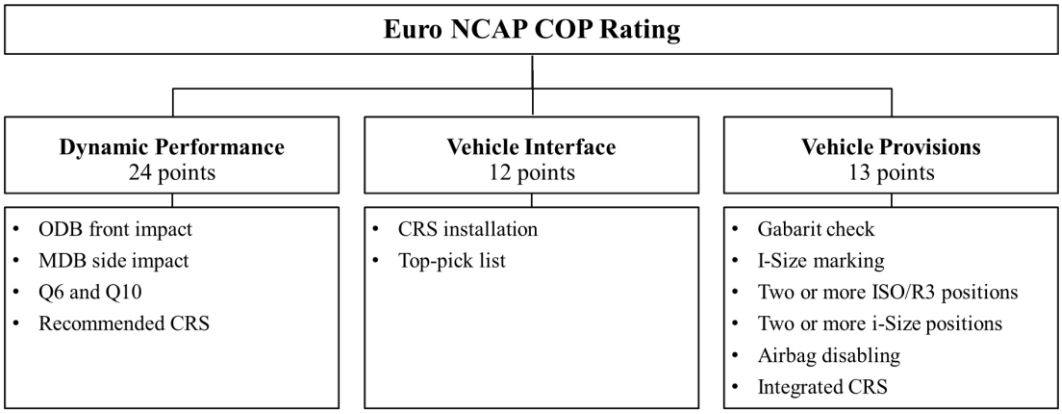

Figure 4. Euro NCAP Child Occupant Protection overview (2018)

Overall, for a good dynamic score in Euro NCAP's tests, vehicle manufacturers must ensure children are well protected by providing, amongst other things, robust seat attachments, good belt geometry and head protection. They also must correctly inform parents about the best child seat to use for all ages and ensure that these seats are available on the market.

A summary of the Euro NCAP dynamic tests & assessments is given in Table 3.

Table 3.
Summary of Euro NCAP Dynamic Tests & Assessment (2018)

Load Case	Test Parameters	Assessment
Frontal impact (ODB, 64 km/h)	• Instrumented Q6 in recommended booster seat (ISO 13499, position 4) • Instrumented Q10 on booster cushion from top-pick list (ISO 13499, position 6)	• Q6 and Q10 dummies • Head, neck, chest* • Contact, excursion, ejection
Side Impact (AE-MDB, 50 km/h)	• Instrumented Q6 in recommended booster seat (ISO 13499, position 6) • Instrumented Q10 on booster cushion from top-pick list (ISO 13499, position 4)	• Q6 and Q10 dummies • Head, neck and chest* • Contact, excursion, ejection

** Criteria and limits are included in Table 7 and 8.*

Vehicle interface assessment The original vehicle marking and vehicle interface requirements - such as clear vehicle handbook instructions, belt length and correct marking of ISOFIX attachment points – were replaced in 2013 by a Child Seat Installation Check, in which a selection of popular products is used to assess the vehicle's ability to safely and correctly accommodate child seats.

The so-called top pick list contains a sample of widely available, well performing (i.e. ETC rated "good") child seats that represent most common types of products available on the European market. The list is checked annually and updated if seats are no longer available on the market. The installation procedure focusses on typical and known incompatibilities that often lead to misuse in the real world, such as insufficient seat belt length for rearward facing seats; instability caused by child seat contact with head restraint, C-pillar or roof; inaccessible ISOFIX anchorages; and insufficient floor strength for a support leg. Seating positions where, for any reason, child restraints cannot be safely installed should be clearly identified by the manufacturers in the user's manual.

Vehicle based assessment Not all cars offer the same provisions especially when more than one child seat is required. Euro NCAP rewards vehicle manufactures that have clearly designed the vehicle with families in mind and apply best practice solutions. To be eligible for scoring, the information provided in the user's manual should clearly state what is and what is not possible in terms of installing child restraint systems on the different seating positions in the vehicle.

Additional points are available for extra seat belt length, meeting extended i-Size marking requirements, the availability of two or more ISO/R3 positions and offering two or more i-Size seating positions in the vehicle. Similarly, points can be rewarded for automatic and manual Passenger Airbag disabling switches with correct warning marking, and for the installation of one or more integrated child seats as standard.

RESULTS

Trends in Child Restraint System Performance

Since 2003 more than 700 different child seat models have been tested and rated by ETC. Currently about 75% of the tested products are rated “very good”, “good” or “satisfactory”. All of them far exceed the legal requirements. An overview of the overall ratings of all tested seats since 2003 is displayed in Figure 5. From the figure it can be observed that the number of good performing seats has increased over the last years. It is especially encouraging that two thirds of the tested products achieve a “very good” or “good” safety score even though the ETC frontal impact test energy exceeds the approval test by 50% and side impact testing is mandatory only for products that are approved to Regulation No. 129. This means that most of the seat manufacturers respect the requirements of the consumer test for the development of their products.

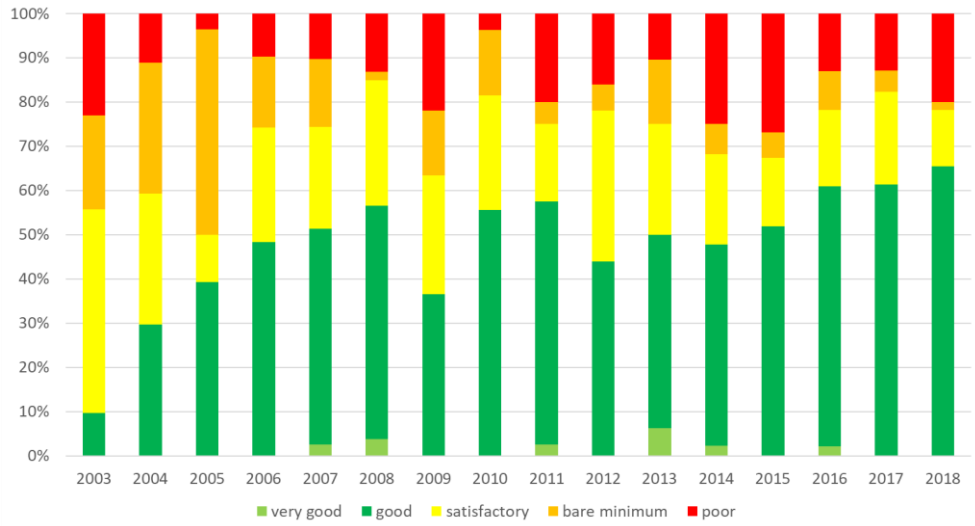

Figure 5. ETC Overall Child Seat Rating results since 2003

Unfortunately, every year there are a few seats tested that fail the tests and cannot be recommended to the consumer. The detailed reasons for the poor safety ratings are listed in Table 4 below.

Table 4.
Problems found in ETC Safety Tests (2015-2018)

Rating year	Total number of seats	Seats with one or more safety critical problem	Description of the problem
2015	52	1 (2%)	• The seat shell partially detached from its base in frontal impact test
2016	46	4 (9%)	• In two of the seats the dummy loadings indicated an increased high injury risk in case of a side impact and the head was not properly contained within the seat • One seat shell partially detached, and a second seat fully detached from its base in frontal impact test
2017	62	6 (10%)	• In two of the seats the lap portion of the seatbelt heavily cut into the abdomen of the dummy during the frontal impact test • In one seat the smallest dummy was ejected during the frontal impact test • One seat shell fully detached from its base in frontal impact test • On one seat one ISOFIX attachment opened within the frontal impact test • One seat was rated poor due to the lack of side impact protection
2018	55	3 (5%)	• In two of the seats the lap portion of the seatbelt heavily cut into the abdomen of the dummy during the frontal impact test • In one seat the smallest dummy was ejected during the frontal impact test • One seat shell fully detached from its base in frontal impact test

Side impact performance was improving long before the side impact sled test became mandatory in legislation (first introduced for Regulation No. 129-approved products in 2013; the share of Reg. 129-approved products tested by ETC test can be found in Table 5). Since 2015, only three of the 215 tested models were rated poor because of the high injury risk during the side impact test. An overview of the safety ratings of all tested seats since 2003 can be found in Figure 6, with an overview of the side impact ratings in Figure 7.

Table 5.
Share of products approved under "i-Size" Regulation No. 129 (2013-2018)

Rating year	Total number of seats	Number (share) of i-Size seats
2013	48	0 (0%)
2014	44	1 (2%)
2015	52	6 (12%)
2016	46	13 (28%)
2017	52	18 (29%)
2018	55	28 (51%)

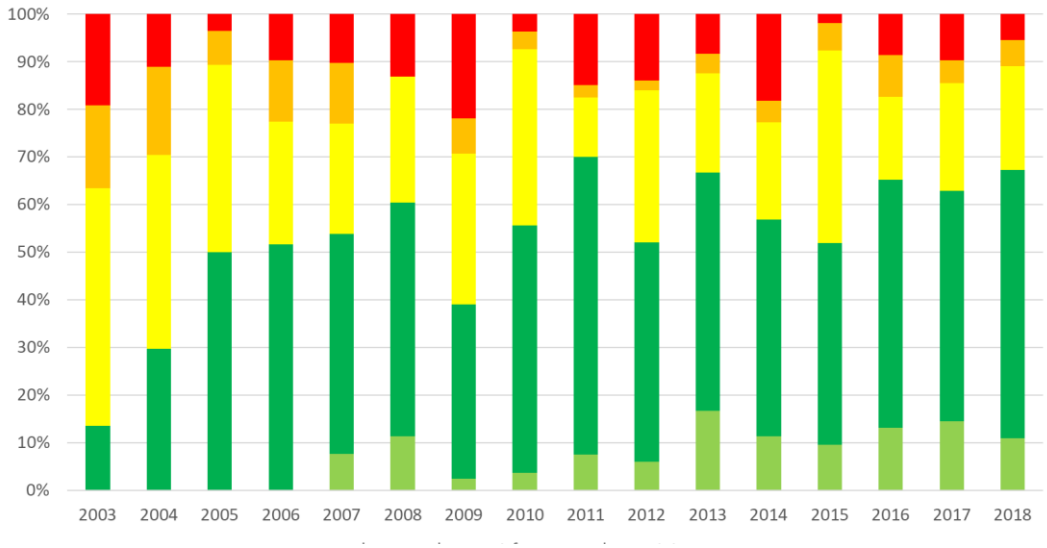

Figure 6. ETC Safety ratings of all tested seats since 2003

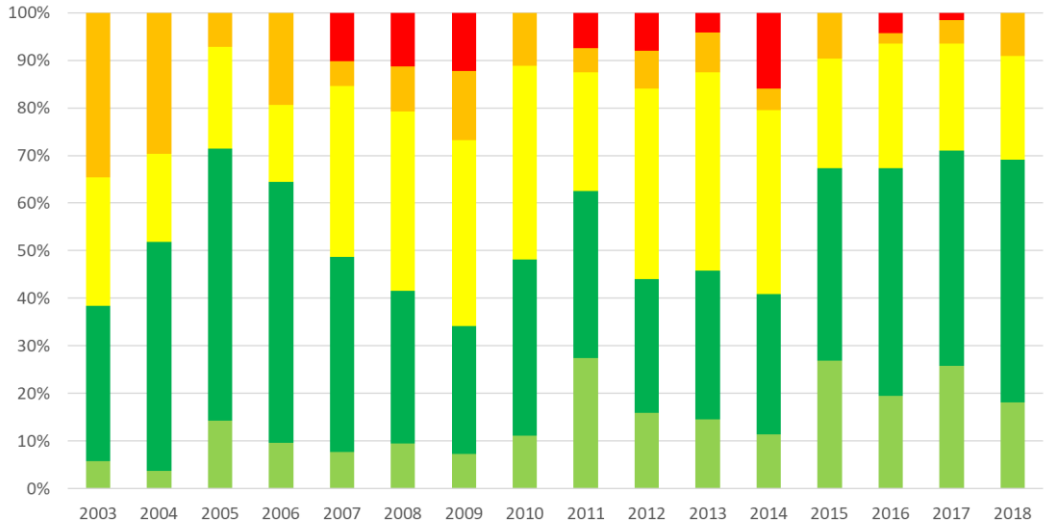

Figure 7. ETC Side impact scores of all tested seats since 2003

Although a rare occurrence, in 2016 the overall rating of one seat was downgraded because of a poor ease of use score. Tightening the integral harness took excessive force and several separate accessories were required to adapt the seat to the child's correct weight. Both facts would result in a high risk of misuse and due to this there is a

high potential risk of an inadequate protection in case of a crash. Beside this outlier, the ease of use ratings of most of the seats were favourable. The ease of use ratings of all tested seats since 2003 can be found in Figure 8.

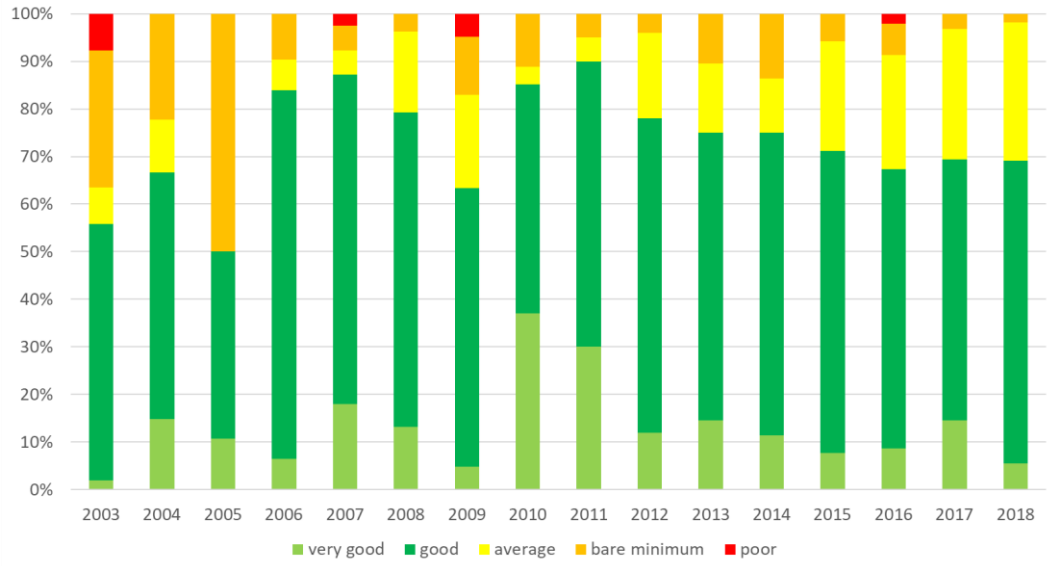

Figure 8. ETC Ease of use ratings of all tested seats since 2003

Since 2011 all fabrics of the CRS that are in direct contact with the child are screened for hazardous substances. If the rating of this criterion is "average" or better, it does not influence the overall rating. A "bare minimum" rating leads to a gradual downgrading of the overall result, and a "poor" rating will downgrade the overall rating to poor. Figure 9 summarises the hazardous substances ratings of all tested seats. After the "safety" rating, the hazardous substances rating is the second most common reason for a poor recommendation for a child seat.

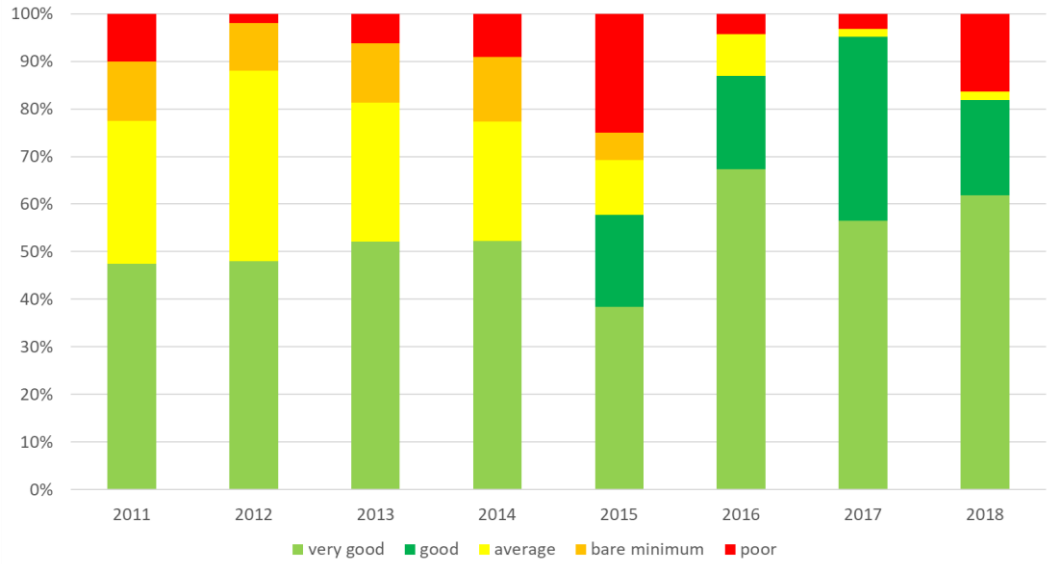

Figure 9. ETC hazardous substances ratings since the introduction in 2011

Trends in Child Occupant Protection

The start of Euro NCAP in 1997 coincided with the introduction of European whole vehicle type approval crash tests, leading to fast improvement of vehicle crashworthiness in the market. Euro NCAP's first COP test protocol strongly emphasised the availability of ISOFIX attachment points - accessible and clearly marked. This served as a market catalyst until ISOFIX lower anchorages and top tether attachments finally became mandatory for all vehicles in 2014 (Figure 10).

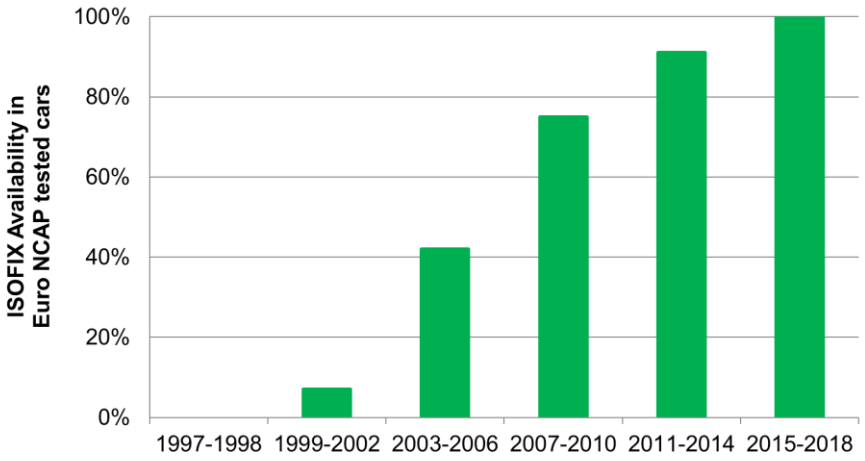

Figure 10. Share of Euro NCAP rated cars, standard equipped with ISOFIX. From 1997 until 2003, Euro NCAP evaluated but not rated child seat performance.

The most challenging part of the early protocol were the dynamic crash tests. To mitigate any risk, manufacturers settled on a handful of recommended child seats, such as the Britax-Römer Baby Safe and Duo Plus, that were known to meet Euro NCAP's labelling requirements and had few test issues. Other requirements such as the availability of integrated child seats and automatic airbag disabling switches were mostly ignored. Overall, however, significant progress was made over the first decade after the introduction in 2003 (Figure 11).

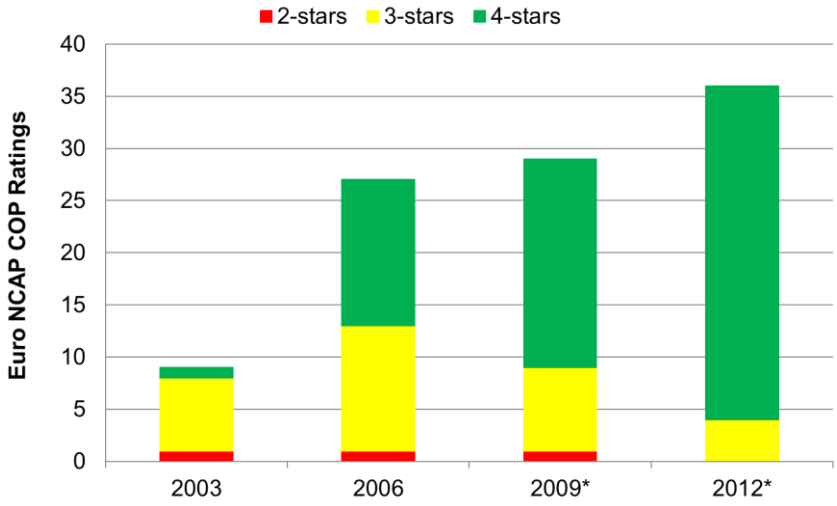

Figure 11. COP Ratings over the years. *For 2009 and 2013, COP percentage scores (used to compute the overall rating) were converted to COP stars using the original thresholds.

From 2013, the assessment of child occupant protection in Euro NCAP has taken a different direction. The objectives of the revision were twofold: firstly, to better address child seat misuse and handling issues through CRS installation checks and the promotion of i-Size; and secondly, to enhance the test relevance to real-world by including more biofidelic dummies and addressing more child ages.

Euro NCAP collaborated with ETC to select common installation seats with different characteristics: belt mounted, belt mounted with base & support leg, ISOFIX mounted with base & support leg rearward facing, ISOFIX with Top-tether mounted, ISOFIX mounted forward facing as well as i-Size variants [13]. Each car model has been assessed by installing each seat (in different modes if applicable) on all eligible seating positions in the vehicle.

Table 6 shows the number of vehicles in which one or more critical safety problems were found during the CRS installation check in recent years. A "safety critical problem" points towards an incompatibility between the CRS and the seating position in the vehicle, which could lead to incorrect installation or misuse. Overall, installation problems were found predominantly with universal, belt mounted child restraints, specifically on the front passenger and rear centre seating positions (Figure 12).

Table 6.
CRS Installation Check Results (2013-2018)

Rating year	Total number of cars*	Cars with one or more safety critical problem	Affected seating positions
2013	32	7 (22%)	Front, 2nd row centre and 2nd row outboard
2014	41	7 (17%)	Front, 2nd row centre and 2nd row outboard
2015	42	6 (14%)	Front, 2nd row centre and 2nd row outboard
2016	17	6 (35%)	Front, 2nd row centre and 3rd row
2017	59	20 (34%)	Front, 2nd row centre, outboard and 3rd row
2018	20	3 (15%)	Front, 2nd row outboard and 3rd row

**Excluding twins, partners, dual ratings and re-assessments.*

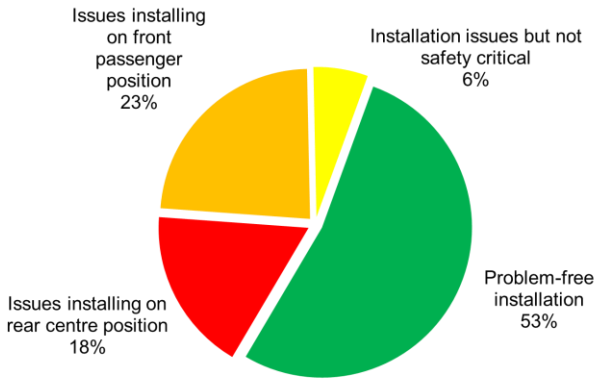

Figure 12. Issues encountered during installation of Universal CRS in Euro NCAP rated cars (N=17, 2016)

The decision to reward vehicle manufacturers for offering two or more i-Size positions has had a profound impact on the availability of the voluntary standard in new cars (Figure 13) in recent years. Within two years of the coming into force of Regulation 129 Phase 1 in July 2013, most cars tested offered two outboard i-Size compatible positions and, increasingly, the front or centre rear seats are also covered.

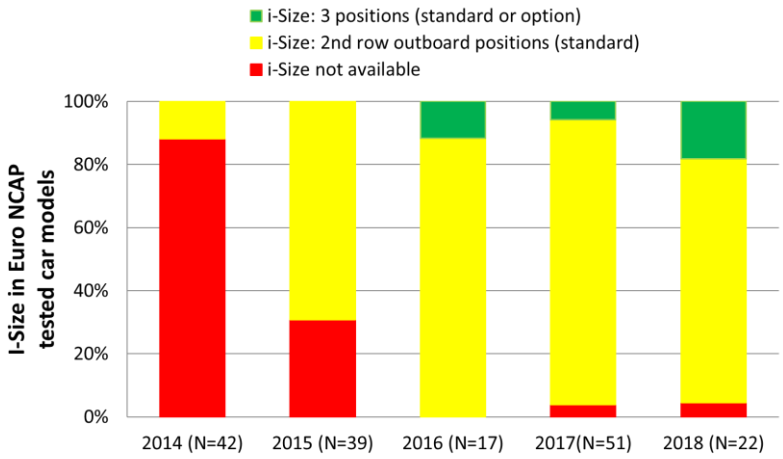

Figure 13. i-Size positions in Euro NCAP tested cars, from 2014 to 2018

If, for any reason children are obliged to travel in the front passenger seat in their child restraint system, it is important (and required by law) that the airbag is disabled. Euro NCAP also encourages automatic disabling of passenger airbag in case a child is detected. However, over the years most vehicle manufacturers have offered either a manual switch or a dealer-disconnect option instead. From 2016 onwards, several cars have been evaluated that offer automatic switches based on pressure-sensing technology in the passenger seat (Figure 14). Euro NCAP

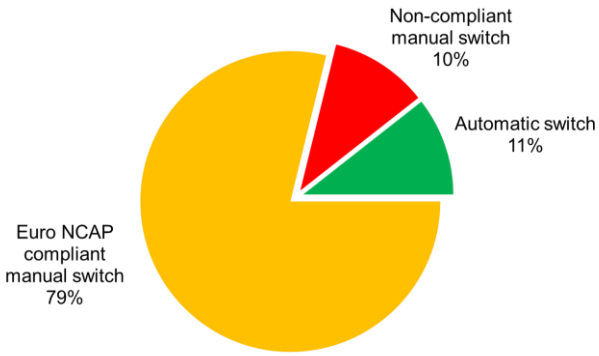

Figure 14. Airbag disabling switches in Euro NCAP tested cars (2016-2018, N=104)

has recognised the need to introduce a standard method of assessment for automatic passenger airbag disabling systems and introduced a laboratory test to check if the following requirements are met:

- Airbag is OFF when using a Rearward Facing CRS.
- Airbag is ON for a 5th percentile (female) occupant and above.

The responsibility for the remaining cases (forward facing CRS or child alone) is for the OEM, and different strategies are allowed. The requirements and test matrix covering a variety of possible occupant sizes and installation modes are listed in Euro NCAP Technical Bulletin 23 [14].

The availability of integrated seats as an option, let alone as standard, remains poor, despite the incentive that Euro NCAP has put in its test protocol. Primarily, large Volvo cars, including the S90/V90 and XC90, were equipped but only as optional equipment. Costs and conflicting design requirements are often cited as the main causes why integrated seats are not more common.

Finally, the new dynamic assessment using the Q6 in a booster seat and, in particular, the Q10 seated on a cushion has brought some new challenges for vehicle and CRS manufacturers [15]. Of the 114 models rated between the start of 2016 and the end of 2018, in 102 cases (89%) the Q6 was placed in a Britax-Römer supplied seat, most cases the KIDFIX XP (SICT) original or manufacturer branded. The seat had a reliable performance in both front and side impact crash tests, which explains its popularity amongst vehicle manufacturers. In general, Q6 results in Euro NCAP crash tests are good (Table 7), demonstrating that a child properly restrained in a CRS rated good by ETC and mounted correctly in the car with ISOFix/i-Size attachment points, is delivering a safe solution. In frontal impact, there were no instances recorded of hard contact with the vehicle interior, ejection or seat failures, and only in one case the Q6 submarined due to large forward rotation of the seat. In side impact, a few cases of hard contact where observed but only in one case did this result in the HIC value grossly exceeding the limit.

Table 7.
Euro NCAP COP Dynamic Test Results for Q6 Dummy (2016-2018)

Criterion	Performance Limits		Dummy Values		
	Higher	Lower	Average	Min	Max
Frontal impact (average B-pillar deceleration, 39g)					
HIC_{15} (with hard contact)	500	700	372	148	913
Head Resultant 3ms Acceleration (g)	60	80	59	40	91
Head Excursion (mm)	-	550	197	51	549
Neck Tension Fz (kN)	1.7	2.62	1.8	0.7	3.0
Neck Extension My with contact (Nm)		36	14	6	36
Chest T4 Acceleration (g)	-	-	47	35	61
Chest Deflection (mm)	30	42	20	13	26
Side impact (average B-pillar acceleration, 29g)					
HIC_{15} (with hard contact)	500	700	136	1	4675
Head Resultant 3ms Acceleration (g)	60	80	35	15	85
Neck Resultant Force (kN)		2.4	0.9	0.3	2.2
Chest T4 Acceleration (g)		67	32	13	54

The Q10 dummy more often caused issues during testing, revealing shortcomings in the rear seat restraint design for taller children. The dummy is placed on a booster cushion using the adult belt. The purpose of the cushion is to raise the seating position and improve the belt fit; the specific design of the cushion is less relevant however. For this reason, the cushion is most often selected from a list of available products.

In frontal impact, poor belt geometry may cause the belt to slide off the shoulder or towards the neck. In some cases, this has led to the dummy becoming unrestrained during the crash or to the dummy submarining, both of which incur a penalty. The Q10 dummy shoulder and barrel-like chest design is partly to blame for this behaviour and Euro NCAP has adopted suggested modifications to the dummy hardware to address this [16].

In side impact, both head contact with the C-pillar and head curtain bottoming out has been observed with high resulting HIC and Head Resultant Accelerations. An overview of Q10 dummy results can be found in Table 8.

Table 8.
Euro NCAP COP Dynamic Test Results for Q10 Dummy (2016-2018)

Criterion	Performance Limits		Dummy Values		
	Higher	Lower	Average	Min	Max
Frontal impact (average B-pillar deceleration, 39g)					
HIC_{15} (with hard contact)	500	700	254	111	908
Head Resultant 3ms Acceleration (g)	60	80	50	36	94
Head Excursion (mm)	450	550	184	40	551
Neck Tension Fz (kN)	1.7	2.62	2.1	1.5	4.1
Neck Extension My with contact (Nm)	-	49	13	5	34
Chest T4 Acceleration (g)	41	55	37	27	53
Chest Deflection (mm)	-	-			
Side impact (average B-pillar acceleration, 29g)					
HIC_{15} (with hard contact)	500	700	211	2	2245
Head Resultant 3ms Acceleration (g)	60	80	49	14	109
Neck Resultant Force (kN)	-	2.2	0.7	0.4	2.32
Chest T4 Acceleration (g)	-	67	50	17	88

DISCUSSION

Nowadays the ETC rating can make or break a product's success on the market. A good rating can boost child seat sales, whereas products that have failed in the test have been recalled or even withdrawn from the market in the past. For this reason, a good ETC child seat rating is a design aim for many seat manufacturers. The impact of the ETC programme can be explained by its huge outreach to European consumers, but also because the tests are more realistic, more complete and more demanding than the basic regulatory tests. The consortium stands by its decision to withhold the exact details regarding the way that the rating is calculated to ensure that products are not optimised for the test. In other aspects, such as test procedure, supplier meetings, Fachbeirat, etc., ETC is committed to an open and transparent process.

In many cases ETC tests have revealed shortcomings in the regulatory tests and its finding have contributed to enhancements in type approval requirements. A good example is side impact protection, that has been addressed in the ETC test for many years. Consequently, most products on the market provided adequate side protection well before side impact test specifications and requirements were introduced in UN Regulation No. 129. More recently, the consumer groups have raised concerns about the absence of limits on neck tension force in Regulation No. 129, especially for babies in lie-flat infant carriers [17]. Likewise, they have observed inconsistencies with the abdominal load sensor specified in Regulation No. 129 which at present seems to be unable to distinguish between well and poorly designed child seats.

On the downside, ETC has been criticised for its favourable position regarding so-called booster shield systems, that do not require a belt harness to restrain the child. Many international experts do not consider booster shield systems appropriate crash protection for children, as crash investigations have documented ejections, excessive excursions, and shield-contact injuries in rollover, side and frontal crashes. ETC has adopted the abdominal load sensor in its recent tests to improve its assessment of injury risk in the abdominal region, but many still believe that shield systems should not be given the benefit of the doubt, even if laboratory test results indicate good performance. This situation is in stark contrast with the consortium's red line on booster seats with removable backrest, that are always penalised for the perceived lack of side impact protection.

Euro NCAP is one of a limited number of NCAPs around the world that test child restraint systems in full-scale vehicle test conditions. Whereas the focus of ETC is on improving CRS performance, Euro NCAP addresses the car design, equipment and the interface with child restraint systems. A strong link between the programs has been forged to improve the situation on misuse of child restraints, where Euro NCAP verifies the problem-free installation of popular, well rated child restraints. Incentives for vehicle provisions such as ISOFIX and airbag disabling switches have been effective and their availability as standard has increased significantly as a result. But child occupant protection is only one of four pillars in the Euro NCAP star rating and underperforming in this area can lead to a lower overall rating or jeopardize investments in the other areas of safety. For this reason, Euro NCAP makes its test and assessment protocols public, including the criteria and their limits, generally with a short but adequate lead-time.

A key principle behind the COP assessment is that vehicle manufacturers should take responsibility for safe transport of adults and children alike. Among other things, this means that manufacturers must recommend the best child seats for their car for testing. In practice, this leads to a bias amongst the tested child restraint systems towards high-end products that are usually available Europe-wide and stable in the market. Normally, they only represent a small share of the sales and the dynamic results may be less useful to buyers of child restraints for that reason.

The shift in focus from toddlers to taller children in Euro NCAP testing was aimed at improving car restraints for the "forgotten age" of children. Many European countries require children to be in appropriate child restraints up to 12 years old or 150cm stature. Despite this, the use of CRS and particularly high-back boosters over the age of 8 years old is not widespread, leaving many children exposed to unnecessary risks. Euro NCAP's opinion is that adequate side impact protection may be more achievable with a booster cushion and well-performing vehicle restraint systems than through the enforcement of high-back booster use in the real world. This, however, puts Euro NCAP at odds with ETC.

CONCLUSIONS

Safe transport of children is the joint responsibility of consumers, and child restraint and vehicle manufacturers. The approaches presented in this paper are complementary and both are needed to improve child safety in cars. Both ETC and Euro NCAP can look back at many years of testing which has had a real impact on the situation in the market place. They share many principles, viewpoints and objectives, but they also have different opinions on some points.

In general, both programs will continue to evolve and be updated according to relevant technical developments (such as the availability of new test methods, dummies, sensors and criteria), be guided by societal and market changes and stay aligned with type approval.

As mobility continues to grow and is radically transformed by digitisation, decarbonisation and automation, the opportunities to further improve safety must be seized. This is also true for the safety of children in transport. For instance, child presence detection technology that can sense infants left in cars, are entering the market: built into the CRS, built into the car, or as loose accessories. Many them come with a smartphone app. ETC is exploring if and how this can be implemented in the program, while Euro NCAP will include this technology in the 2022 COP protocol [18].

We can expect that, in the future, communication protocols will allow the CRS and the car to exchange information, such as crash direction and severity, that features built into the CRS can detect [19]. The effectiveness of such technology may also be considered in one or both programmes, as it becomes available.

REFERENCES

[1] European Commission. 2003. "Directive 2003/20/EC of the European Parliament and of the Council of 8 April 2003 Relating to Compulsory Use of Safety Belts in Vehicles of Less than 3,5 Tonnes." Date of Compliance 9 May 2006.

[2] European Transport Safety Council. 2018. "Reducing Child Deaths on European Roads." PIN Flash Report 34.

[3] United Nations. 1982. "Uniform Provisions Concerning the Approval of Restraining Devices for Child Occupants of Power-driven Vehicles ("Child Restraint Systems")." Regulation No. 44.

[4] International Standards Organisation. 2004. "ISOFIX child seats for cars." ISO 13216.

[5] European Union. 2009. "Regulation (EC) No 661/2009 of the European Parliament and of the Council of 13 July 2009 Concerning Type-Approval Requirements for the General Safety of Motor Vehicles, their Trailers and

Systems, Components and Separate Technical Units Intended Therefor." Official Journal of the European Union.

[6] United Nations. 2009. "Uniform provisions concerning the approval of vehicles with regard to safety-belt anchorages, ISOFIX anchorages systems, ISOFIX top tether anchorages and i-Size seating positions." Regulation No. 14.07.

[7] United Nations. 2009. "Uniform provisions concerning the approval of: I. Safety-belts, restraint systems, child restraint systems and ISOFIX child restraint systems for occupants of power-driven vehicles — II. Vehicles equipped with safety-belts, safety-belt reminder, restraint systems, child restraint systems and ISOFIX child restraint systems." Regulation No. 16.06.

[8] Lesire P., Cuny S., Alonzo F., Cataldi M. 2007. "Misuse of Child Restraint Systems in Crash Situations - Danger and Possible Consequences.", In Proceedings of the Association for the Advancement of Automotive Medicine, 51: 207–222.

[9] United Nations. 2013. "Uniform provisions concerning the approval of enhanced Child Restraint Systems used on board of motor vehicles (ECRS)." Regulation No. 129.

[10] Hobbs C., McDonough P. J. 1998, "Development of the European New Car Assessment Programme (EuroNCAP)" In Proceedings of the 16th Technical Conference on the Enhanced Safety of Vehicles (ESV), Windsor.

[11] Van Ratingen M., 2008. "The Changing Outlook of Euro NCAP" In Proceedings of the 9th International Symposium & Exhibition on Sophisticated Car Occupant Safety Systems, Karlsruhe.

[12] Euro NCAP. 2019. "Vehicle Specification, Sponsorship, Testing and Retesting Protocol." v7.2.

[13] Euro NCAP. 2013. "Child Restraint Systems for Installation Checks." Euro NCAP Technical bulletin 012.

[14] Euro NCAP. 2016. "Assessment of Automatic Passenger Airbag Disabling Systems." Euro NCAP Technical bulletin 023.

[15] Bendjellal F., Frank R. Haas M., 2017 "Child Occupant Protection in Rear Seats: An Example Of CRS Development With Respect to Euro NCAP 2016 Protocol Requirements.")" In Proceedings of the 25th Technical Conference on the Enhanced Safety of Vehicles (ESV), Detroit.

[16] Lemmen, P., Dudley A., Gonzalez J., Schnottale B., Ott J. 2018. "Q10 Update Kit – hardware design and evaluation using Human Body Model simulations" In proceedings of the Children in Cars Conference, Munich.

[17] Ratzek, A. 2018. "Is there a gap in UN Reg 129?", In proceedings of the 16th Protection of Children in Cars Conference, Munich.

[18] Euro NCAP. 2017. "Euro NCAP Roadmap 2025: In Pursuit of Vision Zero."

[19] Visvikis C. 2018. "ISOFIX at 20 years: the past, present and future.", In proceedings of the 16th Children in Cars Conference, Munich.

Assessment of Technical Requirements for Level 3 and Beyond Automated Driving Systems Based on Naturalistic Driving and Accident Data Analysis

Feig, Philip
Schatz, Julian
Labenski, Volker
Dr. Leonhardt, Thorsten
AUDI AG
Germany

Paper Number 19-0280

ABSTRACT

Automated driving systems of SAE Level 3 and beyond allow transferring the driving task and responsibility to the vehicle and its automation systems. A crucial challenge for development and real-world performance is the balance between functionality, availability and safety, as a human driver only needs to be available as a fallback after sufficient lead-time. Consequently, automated driving requires enhanced capabilities of sensors, algorithms and actuators. This paper focuses on improved safety and driving comfort of automated vehicles and upcoming technical requirements compared to driver-only or assisted driving. It uses and adapts the state-of-the-art prospective effectiveness assessment method of ADAS to estimate accident avoidance potentials of automated driving systems. The data sources for this analysis are the Strategic Highway Research Program 2 (SHRP2) and the German In-Depth Accident Database (GIDAS). Exemplary automated driving functionalities for highways are prospectively evaluated and the impact on both traffic safety and driving comfort are presented using crash, near-crash and baseline data. Furthermore, relevant technical requirements for corresponding automated driving systems are derived. For an exemplary use-case, possible impacts on system functionality, availability and safety are presented. Additionally, safety potentials of installing high-performance sensors for automated systems of Level 3 and beyond when driving manually are discussed.

INTRODUCTION

In literature, there are different approaches to define automation levels. Internationally, SAE J3016 [Sae18] is among the most prevalent, and thus used in the following analysis. SAE J3016 outlines six automation levels starting from Level 0 (No Driving Automation) to Level 5 (Full Driving Automation). In this paper, system automation is defined from Level 3 (Conditional Automation) where the Automated Driving System (ADS) performs the entire Dynamic Driving Task (DDT) within the Operational Design Domain (ODD). In Level 3, the ADS sends a transition demand to a fallback-ready user to take over the DDT in the event of a system error or approaching the ODD boundary. In case the driver does not respond appropriately, the ADS might engage a failure mitigation strategy. Automated driving systems in higher automation levels (Levels 4 and 5) incorporate a system response to perform the DDT fallback.

When developing Level 0-2 systems, there are no minimum system requirements due to the instant availability of the driver as a system fallback. Thus, a bottom-up approach can be pursued. The accident prevention potential of active safety systems for manual driving is developed step-by-step addressing more complex scenarios. In contrast, for a Level 3+ automated driving system, the driver/user is not readily available as an instant fallback maneuver. Therefore, a bottom-up approach is not suitable. Using a top-down approach, a corresponding system effectiveness can be determined by restricting the ODD according to system functionalities. For this purpose, the respective system requirements must be derived from different application cases. Hence, a new development process has to be established that is not only based on crash data but also on critical situations (near-crashes) and normal driving situations (baseline).

This paper is structured as follows: to begin with, related work regarding accident prevention potential of ADS and technical requirements are discussed. In the subsequent section, a critical review of literature and research questions of this paper are presented. Section *Methods and Data Sources* introduces the applied methodology to analyze comfort and safety gain based on naturalistic driving and accident data. Section *Results* presents the impact on safety, availability and functionality for different capabilities of ADS. Finally, results and corresponding limitations are discussed and an outlook is offered.

RELATED WORK AND LITERATURE REVIEW

Enhanced safety measurements like improved passive safety and infrastructure have led to reductions in bodily injuries in high-income countries during the previous decades [Who15]. Furthermore, active safety systems such as autonomous emergency braking are increasingly being required by consumer protection, insurance organizations and regulation [Eur19], [Gdv18], [UNa14]. These kinds of systems show significant reductions in accident frequency, bodily injuries and overall losses [Doy15, Fil15, Rat15, Hld11-Hld15b].

Current safety systems, e.g. autonomous emergency braking, are contrived following a bottom-up development process (Figure 1). In this approach, the system functionality and the corresponding real-world accident prevention potential are continuously improved from rear-end vehicle-to-vehicle collision scenarios to current and upcoming functionalities like emergency braking for pedestrians, cyclists and powered two-wheelers, including junction and crossing scenarios. In order to develop automated driving systems (corresponding to Levels 3 to 5) this kind of process is no longer suitable, as the driver is not promptly available as a fallback solution. In this paper, a new approach is developed to evaluate automated driving systems of Level 3 and beyond using a top-down development process. Such a process offers an adjustment of system availability in accordance with previously established technical system requirements of certain driving scenarios.

The typical approach to define technical requirements for future safety systems includes the following steps [Wis13, Wis13a, Edw14, Sei14]:

- Accident analysis of critical real-world collisions
- Clustering and weighting of accident data to scenarios
- Deriving a test scenario and procedure based on clustered accident scenarios
- Developing, testing and real-world validation of a specific function

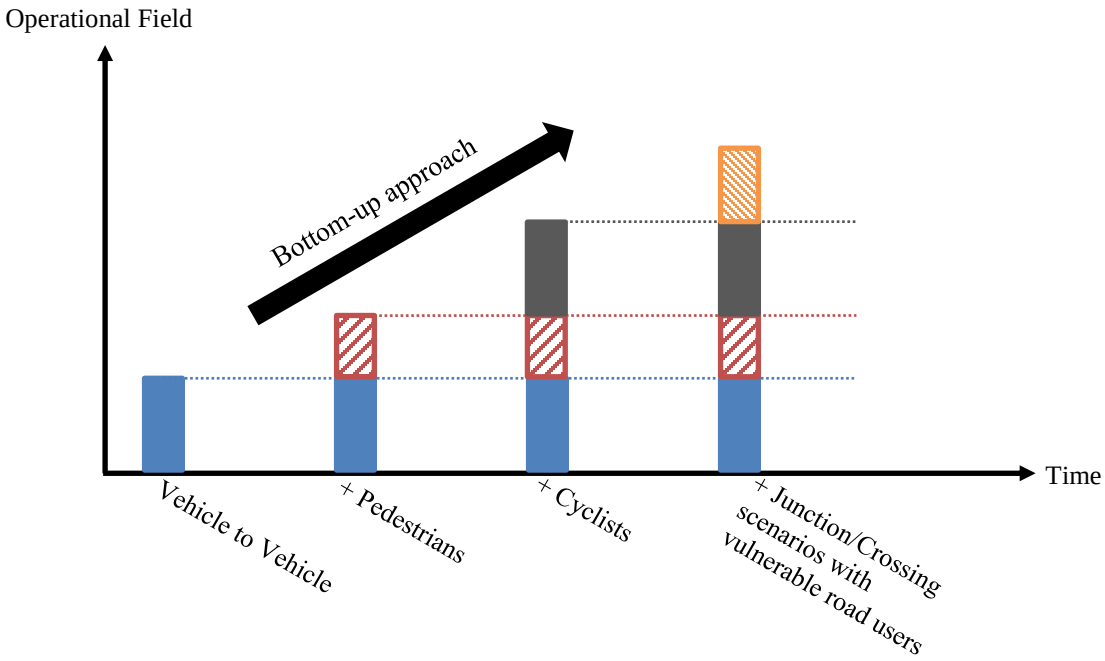

Figure 1. Schematic bottom-up approach for active safety or assistance functions

The German Insurance Association conducted an analysis regarding the impact of automated driving functions on the expected claim expenditure until 2035 [GDV17]. For that study, the monetary reduction of corresponding systems was calculated from system relevance, system efficiency, utilization rate and market penetration rate. The system relevance was determined using accident data and describes the number of crashes a system would be able to address. As not every addressable accident will be a preventable, system efficiency was defined. To take into account that the system might not be active in every driving condition and not present in every vehicle, a utilization rate and a market penetration rate was introduced. Different system functionalities and corresponding requirements (e.g. driving in unfavorable weather condition, performing a lane change etc.) can be addressed by adapting the system efficiency. However, using the method presented, a system efficiency highly depends on expert estimates. To evaluate system requirements regarding the system availability, an analysis of normal driving situation (baseline) has to be conducted as well.

With respect to system requirements of L3+ systems only generic approaches are presented in literature, for example in [Udv18]. Unfallforschung der Versicherer [Udv18] introduces universal requirements for automated driving. However, these do not permit to address the impact on system functionality, system safety and system availability.

AIMS AND OBJECTIVES

Current assessment methods for Level 3+ automation systems have a number of limitations. State-of-the-art effectiveness assessments are based on crash data. Another aspect that should be considered is the additional comfort a driver can gain from using such an automated driving system by transferring the driving task to the system. Thus, drivers' workload may be reduced. Further safety benefit is also to be expected by resolving near-crash situations. A large proportion of near-crashes would show that humans can adequately handle critical situations. These must also be addressed by a Level 3+ automation system. In order to answer these research questions, driving data is needed for baseline events in addition to crash data. As currently used databases only include crash data, an alternative database setup needs to be investigated.

Previous analyses consisted of potential assessments of generic systems without establishing system requirements. An assessment of Level 3+ systems requires a detailed analysis of system requirements for functionality, safety and availability.

This raises the following research questions:

- What is the accident prevention potential of different automated driving functionalities?
- How can the driver comfort be assessed?
- How do various functionalities affect driver comfort?

METHODS AND DATA SOURCES

The data source for our analysis is the Strategic Highway Research Program (SHRP) 2 naturalistic driving database. This data source includes 4,300 years of accumulated driving data, approximately 3,400 participants and 3,300 participant vehicles [Han16]. The study took place in six different cities within the USA. The installed data measurement system stored various time series data, like velocity or steering angle [Vtt16]. Furthermore, manually coded event data and videos of scenarios are available. In total, within the data set 1,465 crashes, 2,710 near-crashes and 20,000 balanced-sample baselines exist.

In the first step, different circumstances, such as locality, crash severity or pre-incident maneuver, are analyzed based on the available NDS SHRP2 data. In this analysis, we focus on automated driving functions for interstates/bypasses/divided highways. Streets with no separated driving directions and traffic signals are hence excluded. An accident prevention potential for a generic highway pilot is determined based on the crash and near-crash events within the SHRP2.

The next steps describe the influence of different technical requirements, their specifications and boundary conditions regarding the impact on functionality, availability and safety. As a human driver is not promptly available for redundancy, a new approach is needed and proposed in this paper. A top-down methodology is applied to determine the influence of different boundary conditions and corresponding technical requirements on the availability of an automated system (Figure 2). In each step, the top-down approach describes the influence of technical requirements on the operational design domain. As not all boundary conditions are manageable, an actual implementation will not cover the operational design domain of a generic highway pilot. Exemplary boundary conditions include:

- weather and surface conditions
- locality, e.g. highway with separated driving directions and no traffic signals
- driving velocity
- use cases, e.g. lane changes, overtaking
- traffic control, e.g. toll gates or police officers

Considering the data from SHRP2 as a baseline, an analysis can be performed whether a specific technical implementation would cover a specific scenario from the database. This allows to judge the comfort advantage of an automated driving function – "how many driving events can be covered by specific functionalities under various boundary conditions?" A similar approach can be taken to analyze the proportion of crashes and near-crashes to establish the accident prevention potential of a specific automated driving system. Thus, the balance between availability and safety has to be considered for different functionalities of a highway pilot – e.g. lane changes, entering/exiting highway or driving under unfavorable weather conditions.

If a current technical solution is not able to handle the baseline scenarios or manage existing crashes/near-crashes, the operational design domain of an automated driving system has to be successively reduced until an acceptable status has been achieved. The influence of various boundary conditions on comfort advantage or safety benefit will be shown for different system specifications of a highway pilot based on SHRP2 data.

To compare SHRP2 data with German accident data the German-In-Depth-Accident-Study (GIDAS) [Erbs08] was used to analyze accidents on German highways. The GIDAS teams have been analyzing and reconstructing approx. 2,000 accidents per year since 1999 in the vicinity of Hanover and Dresden. The advantage of this database is the availability of information about every person involved in the accident. Therefore, an analysis was conducted and required data was extracted for all passenger vehicles involved, meeting specific filter criteria. The GIDAS dataset from June 2018 was used and only reconstructed and fully coded accidents were included.

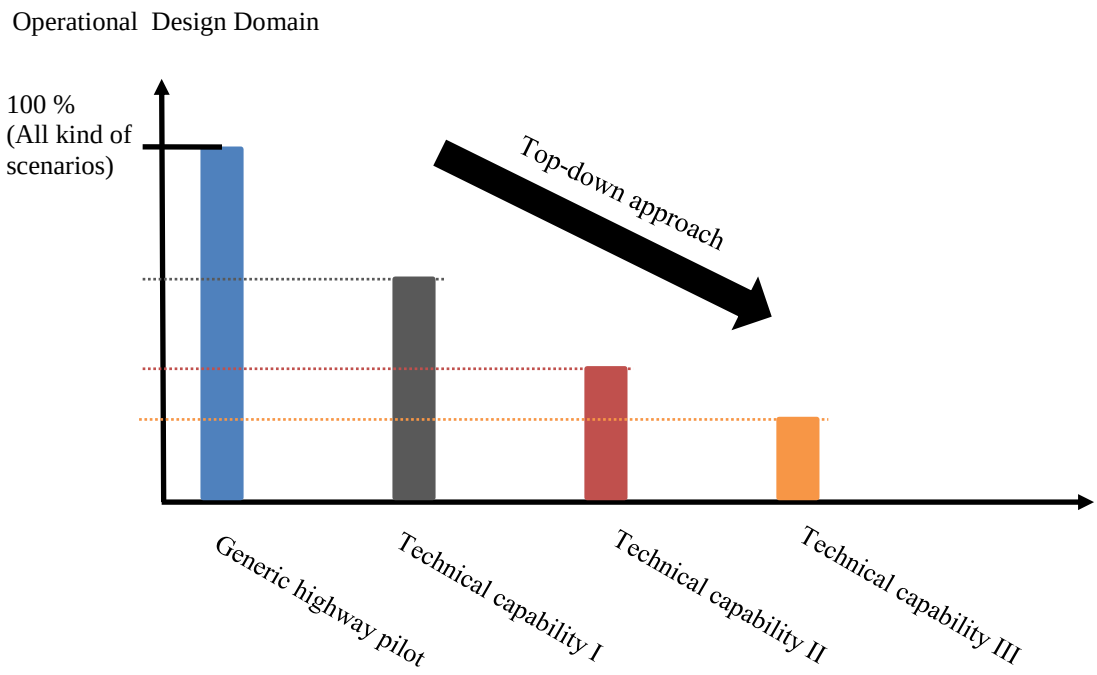

Figure 2. Top-down approach demonstrating the influence of technical requirements on the operational design domain and comfort advantage of an automated driving function

RESULTS

Within the SHRP2 naturalistic driving study, 1,465 accidents, 2,710 near-crashes and 20,000 baseline events are available. Figure 3 a) shows the relative distributions thereof for the respective localities. In this figure, localities are ordered by descending number of crashes. Nearly 48 % of all collisions (including low-risk tire strikes) occurred within business and industrial areas. However, participants only drove within these localities for 32 % of the time. In contrast, only 5 % of all collisions occurred at interstates/bypasses/divided highways with no traffic signals, where a large amount of all near-crashes (21 %) and especially baseline events (27 %) took place. Within this street type fewer collisions occurred, but a large amount of critical near-crash events were mitigated successfully by the human drivers. In addition, a high proportion of baseline events occurred on streets with separated traffic directions and no traffic signals. Consequently, a high comfort advantage may be provided with a highway pilot.
Figure 3 b) illustrates the relative proportion of crash severity under the influence of locality. More severe and police-reportable crashes occurred on interstates/bypasses/divided highways. On streets with no traffic signals but divided driving directions 26 % of crashes were severe and 25 % were police-reportable, while most accidents occurred on business/industrial streets where 12 % were severe and 17 % police-reportable.

In conclusion, on interstates/bypasses/divided highways with no traffic signals fewer accidents occur compared to localities such as business/industrial, residential or school. This result is similar to existing research for a potential safety benefit of a generic highway pilot [Gdv17]. In contrast, this NDS analysis shows that a relatively high proportion of near-crashes occurred on streets with divided traffic directions and no traffic signals. These critical events were handled well by human drivers, thus an automated system needs to perform equally well in these scenarios by avoiding such near-crashes or by predictive driving. Furthermore, collision avoidance for highways/interstates would particularly reduce severe collisions. In general, a large positive influence on critical events, on crash severity, and on accident reduction potential can be established for a generic highway pilot. For the further analyses in this paper we focus on automated driving functions for interstates/bypasses/divided highways use cases excluding streets with no separated driving directions and traffic signals.

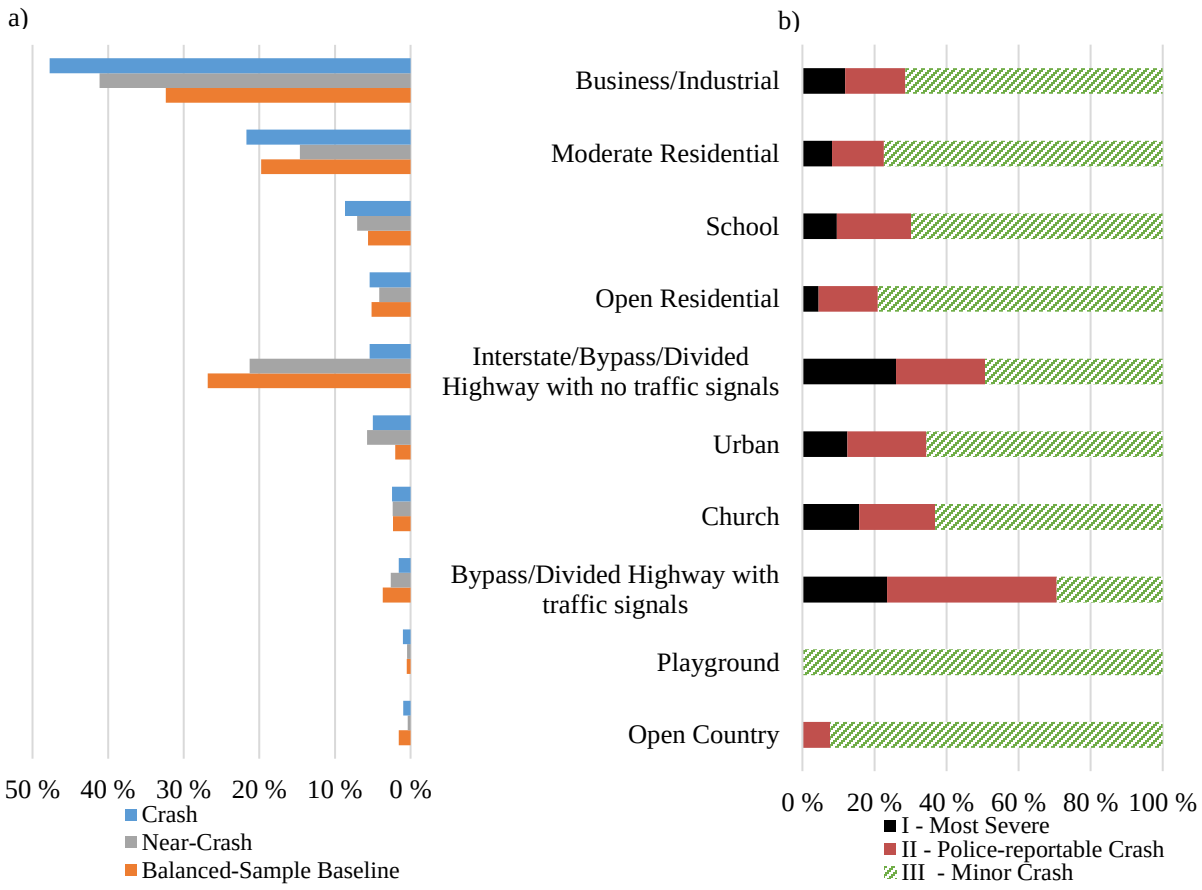

Figure 3. a) Relative proportion of crashes, near-crashes and baseline events depending on locality b) Relative proportion of crash severity depending on locality

In the next step, we concentrate on pre-incident maneuvers on interstates/bypasses/divided highways with no traffic signals. This variable describes the type of action or driving maneuver just prior or at the time of the event [Vtt16]. Within this category, 79 crashes (5.4 %), 577 near-crashes (21.3 %) and 5,367 (26.8 %) baseline events are included in our data set. Figure 4 depicts the relative proportion of pre-incident maneuvers within crashes, near-crashes and baseline events. 66 % of the time subjects went straight with constant speed. Fewer crashes (43 %) and near-crashes (42 %) occur within this type of scenario. Critical scenarios for human drivers are: going straight while accelerating, decelerating in traffic lane, changing lanes (intentionally and unintentionally), and merging. Therein, the relative proportion of crashes and near-crashes is higher than existing baseline events.

Furthermore, the pre-incident maneuver *decelerating in traffic lane* shows an interesting correlation: in this scenario more near-crashes (19 %) occur relatively compared to crashes (11 %). This may be explained by drivers avoiding an accident through an appropriate evasive maneuver.

Based on the available times series data, the initial velocity of each event is analyzed. Figure 5 shows the velocity distribution under the influence of different event types on interstates/bypasses/divided highways with no traffic signals. Within all baseline events, the velocity was below 60 km/h for 5.7 % of the time, below 100 km/h for 36.8 % of the time, and below 130 km/h for 97.9 % of the time. This analysis includes entering and exit ramps. Thus, if a L3+ system is able to handle all boundary conditions – e.g. unfavorable weather, toll gates, ramps – up to a velocity of 130 km/h, 97.9 % of baseline driving time may be covered. Between 50 to 110 km/h, more near-crashes and crashes occurred compared to the baseline events. This corresponds to the analysis of the pre-incident maneuver (Figure 4): a high proportion of crashes and near-crashes occurred while accelerating, decelerating or negotiating a curve.

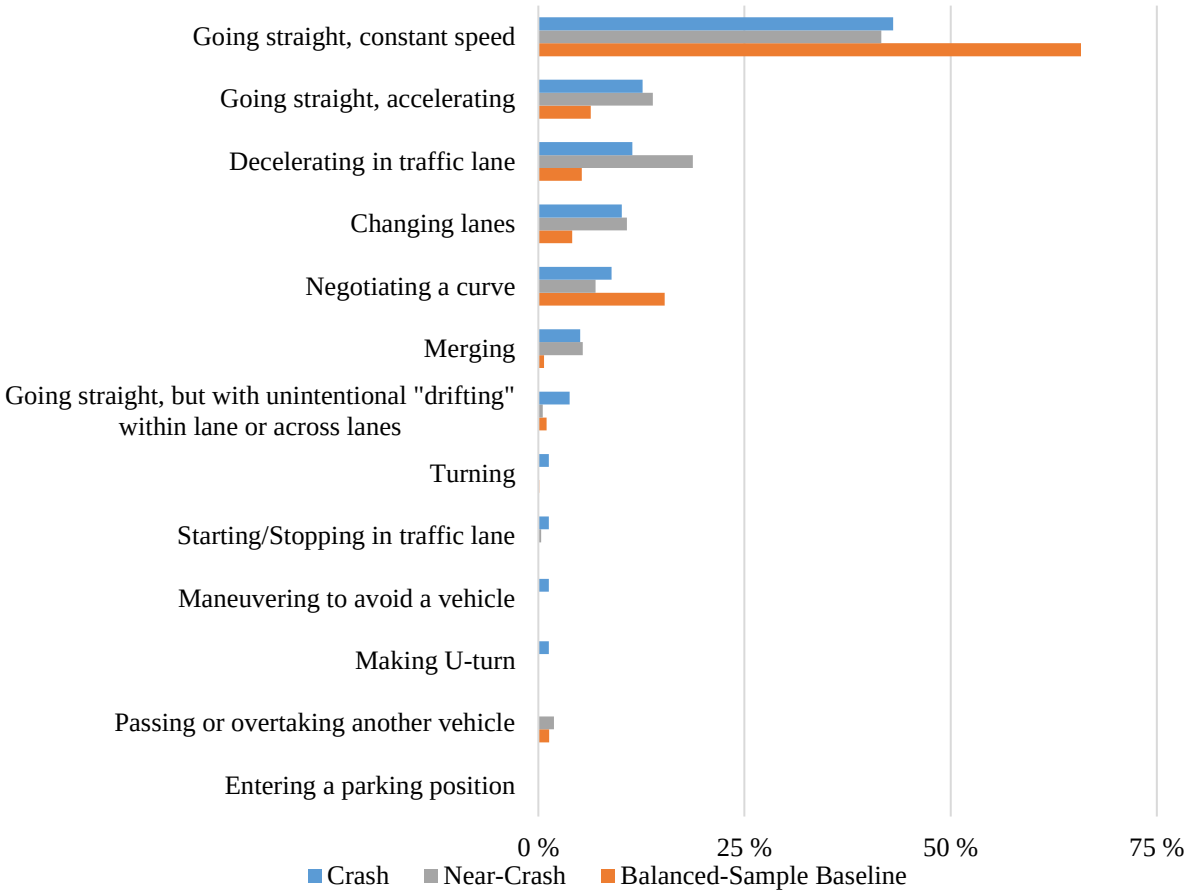

Figure 4. Relative proportion of pre-incident maneuvers for interstates/bypasses/divided highways with no traffic signals

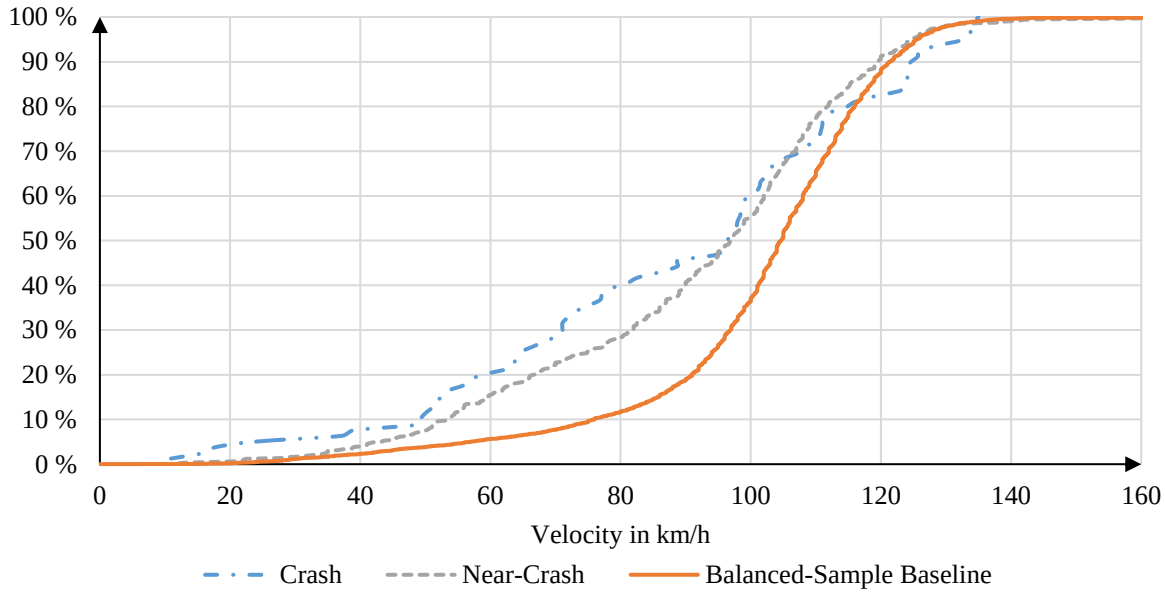

Figure 5. Velocity distribution for interstates/bypasses/divided highways with no traffic signals

Figure 6 shows the availability for different functionalities of a highway pilot and the influence of boundary conditions and technical requirements. Therefore, the baseline events are evaluated starting with a generic highway pilot (=100 %

- all trips within the SHRP2 NDS on interstates/bypasses/divided highways with no traffic signals may be covered by the highway pilot). Accordingly, all kinds of events and circumstances must be handled by a corresponding Level 3+ system, as a human driver cannot be expected to be promptly available as a fallback.

In the following steps, different boundary conditions and technical requirements are analyzed with respect to their influence on availability. Thus the cascade of boundary conditions/technical requirements and the influence on substituting manual driving by an automated system may be analyzed. If a system is not capable to handle situations with a watchman, officers or traffic controls such as toll gates 99.7 % of naturalistic driving time may still be covered. In addition, if the operational design domain is limited by unfavorable weather conditions, the availability is reduced from 99.7 % to 98.5 %. Boundary conditions/technical requirements such as automated driving on exit or entrance ramps, lane changes (detection of rear or side traffic) and construction zones (different/narrow drive paths) show higher influence on a customers' comfort advantage. If these scenarios cannot be managed by the automated system, the comfort advantage due to the automation is still 82.6 % of driving time. If the maximum speed is additionally limited to 130 km/h, the availability reduces to 80.8 %. A further speed reduction to 100 km/h results in a high decrease of availability (27.3 %). A maximum speed of 60 km/h and presence of a leading vehicle – here defined as traffic jam – results in an availability of 3.9 %.

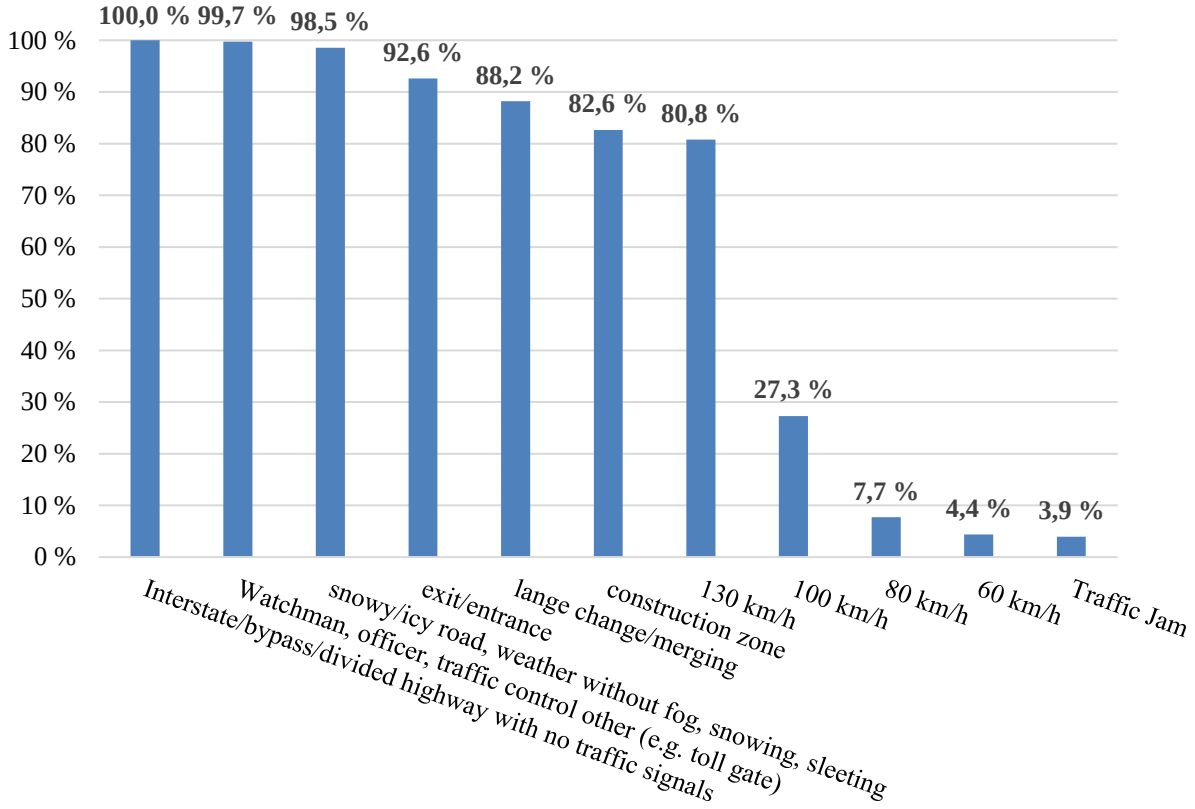

Figure 6. Top-down evaluation of availability for different functionalities of a highway pilot under the influence of boundary conditions and technical requirements

Beyond that, an automated driving function has a potential safety benefit due to avoiding or reducing criticality of (near-)crashes. On interstates/bypasses/divided highways with no traffic signals 79 crashes (5.4 %), 577 near-crashes (21.3 %) and 5,367 (26.8 %) baseline events occurred. For a generic highway pilot, it is assumed that these crashes and near-crashes can be avoided. The impact on safety and availability for different types of the operational design domain are analyzed in Figure 7. This analysis shows that boundary conditions such as weather, exit/entrance or construction zones have a high influence on the safety benefit of an automated driving function. The safety potential drops to 63 % of addressable crashes and 65 % of near-crashes if these cannot be addressed. Compared to the baseline events (83 % of availability) more critical events occurred under such conditions. Furthermore, low velocity automated driving functions (traffic jam, 60 and 80 km/h) have a higher safety potential compared to baseline events. A

traffic jam highway pilot is able to address 9 % of crashes and 8 % of near-crashes while this function will only be offered in 3.9 % of baseline events. Thus, even a generic traffic jam feature has a higher impact on traffic safety compared to availability.

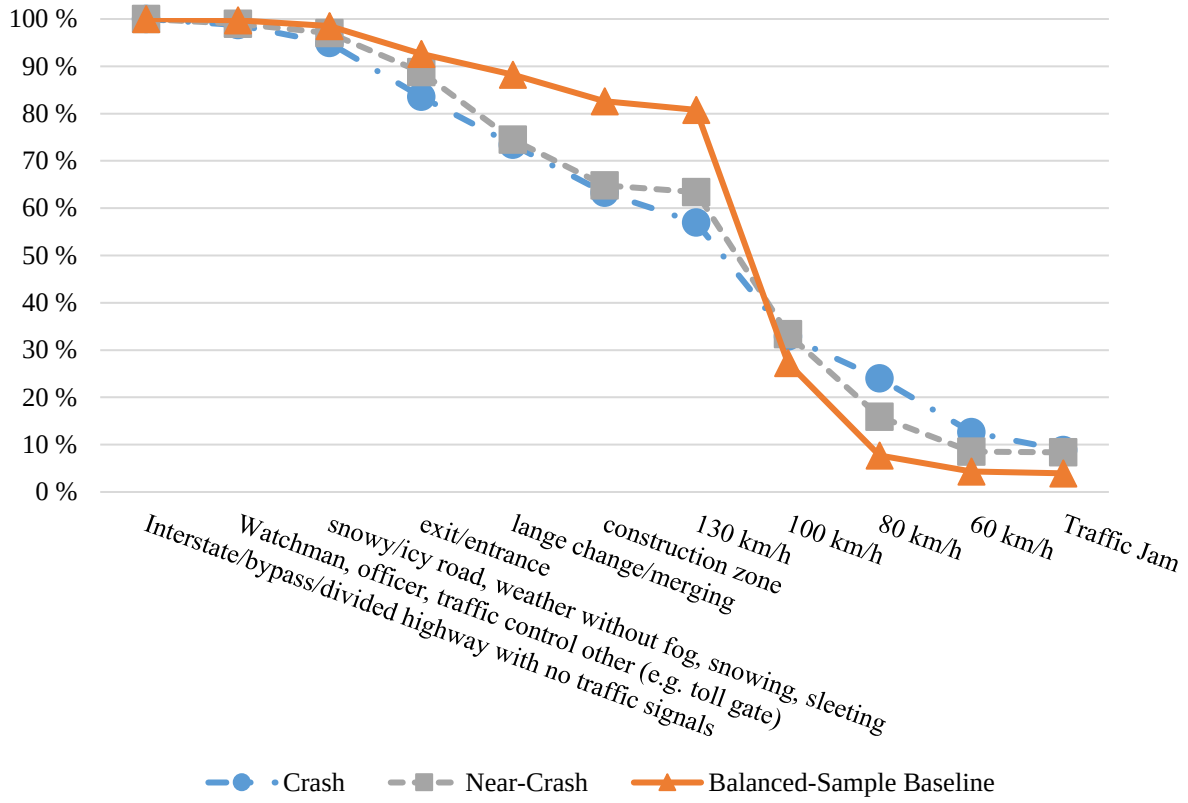

Figure 7. Top-down evaluation of safety potential for different functionalities of a highway pilot

To analyze the impact on collision avoidance, an investigation on GIDAS data has been conducted as well. In total 3,052 passenger vehicles on highways or similar (separated roadways without intersections and traffics lights) were included in our study. The set of all vehicles constitutes 100 % safety potential of a system for highways and comparable roadways. The top-down methodology of different boundary conditions and technical requirements were analyzed with respect to the influence on the safety potential as before. There was no relevant information in the database with respect to situations with a watchman, officer or traffic control such as toll gates. Consequently, there is no reduction in accident prevention potential. Without unfavorable weather conditions, the safety potential is reduced to 94 %. In the next step, vehicles driving on exit/entrance ramps, performing lane changes, merging maneuvers, or passing construction zones were excluded. Hence, the system benefit is reduced to 83 %. When the vehicle's speed prior to the situation becoming critical is below 130 km/h, the gain is 68 %. In traffic jams, with other vehicles present and a system's operating envelope of at most 60 km/h, the associated benefit is at about 9 %. All applied steps are displayed in Figure 8. In contrast to the NDS dataset, for GIDAS all vehicles on the respective type of road are analyzed. This leads to a vehicle-based focus.

DISCUSSION AND LIMITATIONS

The previous section has shown the potential safety benefit of automated driving functions. Additionally, the avoidance of accidents by human errors (e.g. impairment, inattention) during manual driving results in increased safety and comfort.

The high performance sensors installed for Level 3+ functionalities could additionally be used to improve active safety systems for manual or assisted driving. Within the NDS, comparable collisions also occurred on interstates/bypasses/divided highways with traffic signals. Thus, the operational field and performance of state-of-the-art active safety systems could be increased by harnessing these sensors.

By using the NDS's data, some limitations of our analysis need to be considered. On the one hand, only the time series data of the participants' vehicle is known. In contrast, in GIDAS the accident is reconstructed for everyone involved.

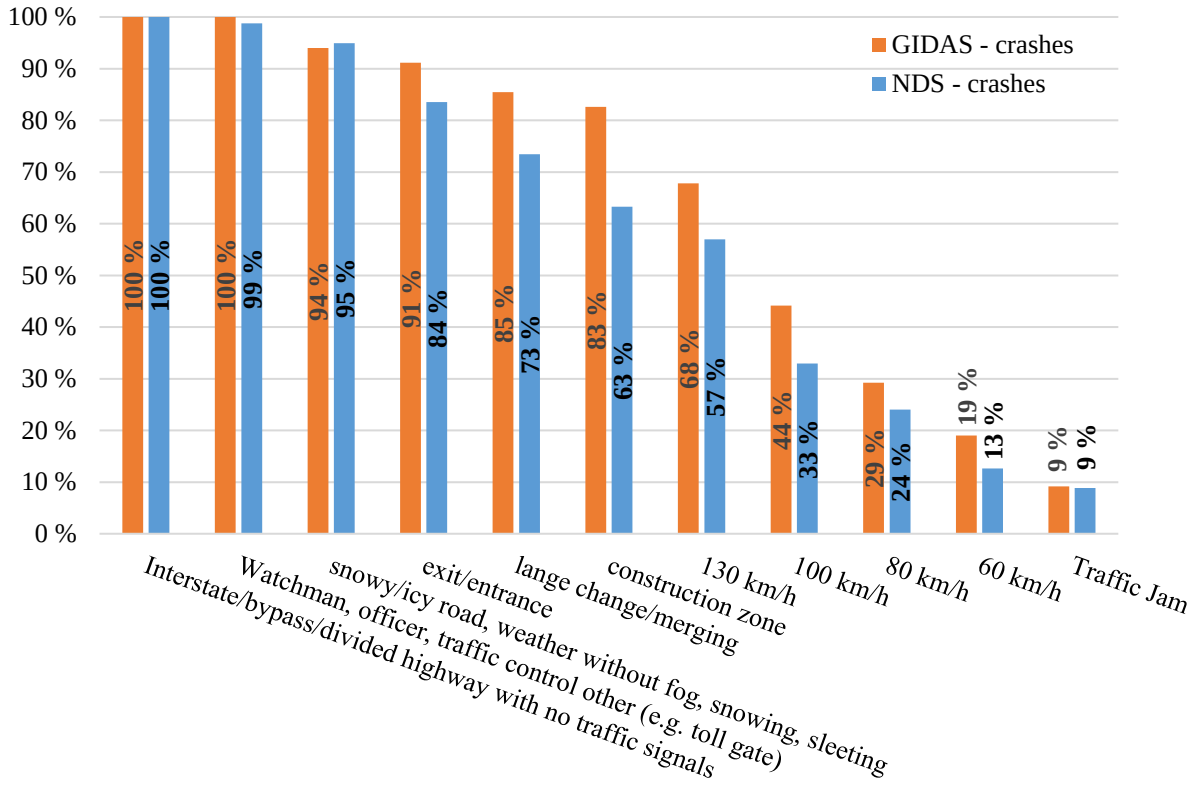

Figure 8. Top-down evaluation of safety potential for different functionalities of a highway pilot under the influence of boundary conditions and technical requirements

On the other hand, for some events specific time series data (e.g. velocity) was not included. In this analysis, events with missing data were excluded.
To investigate safety and comfort gain, it has been assumed that the automated driving function can consider crashes, near-crashes and baseline events. Furthermore, the NDS database is fairly limited with respect to crashes on interstates/bypasses/divided highways with no traffic signals (n=79).
Beyond that, misbehavior of other traffic participants has not been included in our analysis. An example could be a collision during a lane change that is caused by the speeding of the approaching vehicle.

CONCLUSION AND OUTLOOK

For automated driving systems, the balance of functionality, availability and safety is a crucial real-world deployment challenge. Consequently, this paper presents a prospective effectiveness assessment based on naturalistic driving data. For a top-down development process of Level 3 and beyond systems, an evaluation of technical requirements for upcoming automated driving functions is essential.

In this paper, a new method to assess and quantify this impact has been presented. The conducted analysis shows that a generic highway pilot can significantly improve driver comfort, since 26.8 % of the analyzed baseline events are highway driving. Especially the prevention of severe highway crashes leads to a high safety potential. Furthermore, a high proportion of near-crashes on the highway indicate a rather demanding driving task even for human drivers. An analysis of crashes in the GIDAS database shows comparable results and allows to create a range of safety benefits of highway pilots.

In conclusion, the conducted analysis enables a differentiation of various operational design domains on customers' comfort and reduced criticality due to avoided crashes or near-crashes.

ACKNOWLEDGMENT

The findings and conclusions of this paper are those of the authors and do not necessarily represent the views of the VTTI, SHRP 2, the Transportation Research Board, or the National Academies.

REFERENCES

[Doy15] Doyle, M.; Edwards, A.; Avery, M., "AEB REAL WORLD VALIDATION USING UK MOTOR INSURANCE CLAIMS DATA", 24th International Technical Conference on the Enhanced Safety of Vehicles (ESV), Gothenburg, Sweden, 2015, https://www-esv.nhtsa.dot.gov/proceedings/24/files/24ESV-000058.PDF. Accessed on: Feb. 27 2019.

[Edw14] Edwards, M; Nathanson, A.; Wisch, M.: "Benefit estimate and assessment methodologies for pre-crash braking part of forward-looking integrated pedestrian safety systems". AsPeCSS D1.3, 2014, http://www.aspecss-project.eu/userdata/file/Public%20deliverables/ASPECSS-D1.3-FINAL-Benefit%20assessment%20methodologies-2014.04.30.pdf. Accessed on: Jan. 16 2019.

[Erbs08] Erbsmehl, C. and Hannawald, L., "Simulation realer Unfalleinlaufszenarien der German In-Depth Accident Study (GIDAS)". Erstellung und Nutzen von "pre crash scatter plots". ISSN: 0083-5560. 2008. p. 91-103.

[Eur19] Euro NCAP, "Timeline", https://www.euroncap.com/en/about-euro-ncap/timeline/. Accessed on: Jan. 15 2019.

[Fil15] Fildes, B. et al., "Effectiveness of low speed autonomous emergency braking in real-world rear-end crashes," (eng), Accident Analysis and Prevention, vol. 81, pp. 24–29, http://dx.doi.org/10.1016/j.aap.2015.03.029, 2015.

[Gdv17] Gesamtverband der Deutschen Versicherungswirtschaft e. V. (GDV), „Automatisiertes Fahren - Auswirkungen auf den Schadenaufwand bis 2035," Berlin, 2017. https://www.gdv.de/resource/blob/8282/c3877649604eaf9ac4483464abf5305d/download-der-studie-data.pdf. Accessed on: Feb. 11 2019.

[Gdv18] Gesamtverband der Deutschen Versicherungswirtschaft e.V., "The Type Class System applied in the German Vehicle Insurance Industry", 2018, http://www.rcar.org/Papers/Procedures/German_Rating_System_02_2018_V1.pdf. Accessed on Jan. 15 2019.

[Han16] Hankey, J. M.; Perez, M. A. and McClafferty, J. A., "Description of the SHRP2 Naturalistic Database and the Crash, Near-Crash, and Baseline Data Sets: Task Report," Blacksburg, 2016. https://vtechworks.lib.vt.edu/bitstream/handle/10919/70850/SHRP_2_CrashNearCrashBaselineReport_4-25-16.pdf?sequence=1&isAllowed=y. Accessed on: Nov. 04 2016.

[Hld11] Highway Loss Data Institute, "Buick collision avoidance features: ini-tial results, Vol. 28, No. 22," 2011. www.iihs.org/media/cc9c4b27-7a86-4299-b2d4-10e61eb6b6f5/-322649981/HLDI%20Research/Collisions%20avoidance%20features/28.22-Buick.pdf. Accessed on: Apr. 12 2016.

[Hld12] Highway Loss Data Institute, "Mercedes-Benz collision avoidance fea-tures: initial results, Vol. 29, No. 7," 2012. www.iihs.org/media/e368e3e5-ff90-4db7-86d1-e7daecc4afc8/-1481340172/HLDI%20Research/Collisions%20avoidance%20fea-tures/29.7-Mercedes.pdf. Accessed on: Apr. 12 2016.

[Hld15] Highway Loss Data Institute, "Honda Accord collision avoidance fea-tures, Vol.32, No. 33," 2015. www.iihs.org/media/98e59e28-6667-478c-8fb2-5dd51865fa60/794581164/HLDI%20Research/Bulletins/hldi_bulle-tin_32.33.pdf. Accessed on: Apr. 12 2016.

[Hld15a] Highway Loss Data Institute, "Mazda collision avoidance features, Vol. 32, No. 22," 2015. www.iihs.org/me-dia/7d84f7ba-b0d1-4ed9-a4d5-e5b82a460787/1592277885/HLDI%20Research/Bulletins/hldi_bul-letin_32_22.pdf. Accessed on: Apr. 12 2016.

[Hld15b] Highway Loss Data Institute, "Subaru collision avoidance features: an update, Vol. 32, No. 8," 2015. www.iihs.org/media/8941f012-991d-49e0-992c-8bb853b6e829/-995536910/HLDI%20Research/Bulletins/hldi_bulletin_32.8.pdf. Accessed on: Apr. 12 2016.

[Rat15] Ratingen, M. van; Fildes, B.; Lie, A.; Keall, M. and Tingvall C., "Validating Vehicle Safety Using Meta-Analysis: A New Approach to Evaluating New Vehicle Safety Technologies," in 24th International Technical Conference on the Enhanced Safety of Vehicles (ESV), Göteborg, 2015.

[Sae18] SAE International, „Taxonomy and Definitions for Terms Related to Driving Automation Systems for On-Road Motor VehiclesVehicles," SAE Standard J 3016, revised version of September 2016, June 2018. https://saemobilus.sae.org/content/J3016_201806/. Accessed on: Feb. 11 2019.

[Sei14] Seiniger, P.; Bartels, O.; Kunert, M.; Schaller, T.: "Test procedure including test target and misuse tests, based on test results". AsPeCSS D2.5, 2014, http://www.aspecss-project.eu/userdata/file/Public%20deliverables/ASPECSS-D2.5-FINAL-Active%20Safety%20Results-BASt-2014-06-12.pdf. Accessed on: Jan. 16 2019.

[Udv18] Unfallforschung der Versicherer (UDV), „Does automated driving improve safety?," Berlin, 2018. https://udv.de/download/file/fid/11111. Accessed on: Feb. 11 2019.

[UNa14] United Nations, "ECE R131 Uniform provisions concerning the approval of motor vehicles with regard to the Advanced Emergency Braking Systems (AEBS)", 2014, https://www.unece.org/fileadmin/DAM/trans/main/wp29/wp29regs/2015/R131r1e.pdf. Accessed on Jan. 15 2019.

[Vtt16] Virginia Tech Transportation Institute, Dataset. http://ezid.cdlib.org/id/doi:10.15787/VTT1W88Z. Accessed on: Dec. 28 2016.

[Who15] World Health Organization, "Global status report on road safety 2015: Supporting a decade of action". Geneva, Switzerland: WHO, 2015.

[Wis13] Wisch, M.; Seiniger, P.; Edwards, M.; Schaller, T.; Pla, M.; Aparicio A.; Geronimi, S.; Lubbe, N.: "European project AsPeCSS - interim result: Development of Test Scenarios based on identified Accident Scenarios", 22nd International Technical Conference on the Enhanced Safety of Vehicles (ESV), Wahington D. C., 2013, https://www-esv.nhtsa.dot.gov/Proceedings/23/files/23ESV-000405.PDF. Accessed on: Jan. 16 2019.

[Wis13a] Wisch, M.; Seiniger, P.; Pastor, C.; Edwards, M.; Visvikis, C.; Reeves, C.: “Scenarios and weighting factors for pre-crash assessment of integrated pedestrian safety systems”. AsPeCSS D1.1, 2013, http://www.aspecss-project.eu/userdata/file/Public%20deliverables/ASPECSS-D1.1-FINAL-Scenariosweighting-BASt-2013-02-17-PUBLIC.pdf. Accessed on: Jan. 16 2019.

OCCUPANT PROTECTION FOR AD CARS – THE PARADIGM SHIFT IN CRASH SAFETY?

Lotta Jakobsson
Katarina Bohman
Bo Svanberg
Trent Victor

Volvo Cars
Sweden

Paper Number 19-0281

ABSTRACT

When moving towards unsupervised autonomous driving (AD) and the customer expectations of those vehicles, the approach, tools and methods used today in occupant protection assessment are likely not sufficient. Single sitting postures, limited sizes of occupants and crash test set-ups used today will not cover the situations arising. Fundamental changes in evaluation approach and underlying assumptions are foreseen, similar to a paradigm shift.

The objective of this paper is to elaborate on and concretize the research needed, specifically targeting the question: How do we assess the protection of the heterogeneous passenger population in future vehicle crashes enabling occupant protection in unsupervised AD, providing the extended customer benefits of those cars? This paper summarizes relevant state-of-art research in the area and identifies topics for further research focusing on methods and tools for occupant protection assessment.

Future unsupervised AD cars, in addition to future manually driven cars, are likely to be exposed to crashes. Hence, the occupants' need to be protected is obvious, as today. The paradigm shift is driven by and relates to the mindset on car usage and occupant requests. It calls for new ways of addressing crashworthiness evaluation, emphasizing the large effort in research and knowledge creation needed, as well as a new setup in procedures and responsibilities of stakeholders involved. It likely requires addressing expanded crash set-ups, taking the whole event into account (including pre-crash maneuvers), in addition to a larger population of occupants, and a larger range of seat positions, seating configurations and sitting postures. A human-centric approach is proposed as the way forward. Being an alternative to a technology-driven approach (e.g. the SAE levels of automation), the human-centric approach sets the human needs and abilities in focus, and designs technology around them.

Substantial data on sitting postures and behavior in cars today needs to be collected and analyzed, to enhance the interpretation of existing real world data and to form the knowledge foundation towards the future challenges. Furthermore, user studies of future expectations are desired, especially in the light of changes in mobility trends. Simplified crash test dummy designs will not be sufficient. There is a need of continuous development of today's human body models facilitating the expansion in sitting postures and sizes, enhanced injury predictability and capable of simulating pre-crash kinematics. This includes generation of validation data and biomechanics research on injury mechanisms as well as material data such as adipose tissues. Pediatric occupant tools need special attention, in addition to investigating and cooperating around the protection of children in future cars.

In order not to be a stopper for enabling the customer benefits in the development of autonomous drive, the occupant protection challenges need to be addressed. This paper discusses some different aspects of this, however being a paradigm shift, a common discussion and cooperation among stakeholders is needed to cover the whole spectra of aspects.

INTRODUCTION

Passenger car occupant protection today is evaluated through a limited number of crash tests. Although extensive, a limited number of situations are evaluated through the safety standards, such as the FMVSS and UN ECE. In most cases, the standard specifies a certain crash scenario using a single specific occupant size, in one sitting posture. Child restraints are mainly considered add-on devices, certified using a generic rig. In addition, the consumer test programs (eg. performed by IIHS and EuroNCAP) add to the tests for which most cars are evaluated in. In addition, some additional real-world situations form the platform for occupant protection. However, when difficult to protect, the passengers will be informed and/or restricted in usage, through the user manual or similar. Examples of this are compulsory seat belt use, and information on limitations in protection if the seat is substantially reclined.

When moving towards unsupervised autonomous driving (AD) and the customer expectations with those self-driving cars, the approach, tools and methods used today are likely not sufficient. Single sitting postures, limited sizes of occupants and crash test set-ups used today will not cover the situations arising for occupant protection evaluations.

The objective of this paper is to elaborate on and concretize the research needed, specifically targeting the question: How do we assess the protection of the heterogeneous passenger population in future vehicle crashes enabling occupant protection in unsupervised AD, providing the extended customer benefits of those cars?

THE PARADIGM SHIFT IN CRASH SAFETY?

As shown in several studies, the extended customer benefits of future cars include other activities and seating configurations as of today. Extended ways of using the car are foreseen. A qualitative study in Sweden, Jorlöv et al. (2017) showed user expectations of seating configuration facing each other, when travelling together with friends and families for a longer trip. In the shorter trip scenario, the users were less in desire to rotate the seat, but instead aspiring to recline the seat into a more relaxed position enabling relax, sleep, surf the internet, work, or read. Similar findings were found when the study was repeated in Shanghai, China (Östling and Larsson, 2019).

Using online survey with 1,000 respondents in Germany, Fraedrich et al. (2016) investigated use-case-oriented mindsets on several topics for different types of automated concepts, For trips in the city and with shopping and luggage haulage, ‘Parking Pilot’ was seen as helpful while ‘Highway Pilot’ was deemed most positive on longer trips and journeys. Both of these allow a driver to disengage from the driving task, but the driver needs to be prepared to take over whenever requested. While, among the steering-wheel free concepts, the so called ‘Fully Automated Vehicle’ was perceived as being more useful than the ‘Vehicle on Demand’ (e.g. “robotaxi”), likely related to that a larger share of the respondents could not really picture what that concept was. Long distance trips, longer journeys and cross country trips were the trip types most stated as being helpful for the so called ‘Fully Automated Vehicle’.

Hence, new ways of using the cars could include long trips, where the car replaces the train or even the plane. Examples of this was shown with this business model of using the car as a comfortable experience for replacing short-haul flights, such as the Volvo 360c concept (Volvo Cars, 2018). This concept can transform from a comfortable seat, possible to recline in different degrees, into a sleeping compartment, providing an alternative to the flight. The concept is capable of taking you to the meeting in the other city during the night, from door to door; arriving more relaxed than after a flight travel. Some other variants of interior concept models were shown within the Volvo 360c concept. One of them being a business case of an office on wheels, e.g. replacing the need for an expensive office in an attractive city location, enabling use of pick-up time, in addition to use the parked car as the meeting place. The set-up of such a car would include face-to-face seating, table and devices needed for meetings. When addressing the user’s demands in these examples, occupant protection challenges includes activities and a range of sitting postures, including lying down.

The other end of new ways of using the cars is exemplified by the ‘robotaxi’/’robocab’, enabling transportation of passengers during shorter trips. On one hand, the sitting postures and activities might not deviate substantially from today’s cars, with the addition of increasing degree of rearward facing. On the other hand, those vehicles will likely pick-up new passengers frequently, and there will be protection challenges accommodating the variety of passengers, including children, in addition to the lack of dedicated on-board human support and supervision.

Introducing new types of vehicles will add to the variations in traffic. It will likely be a combination of mixed traffic, including AD, driver assistance and manually driven cars, and fully autonomous traffic, both having their challenges. Simply, it will provide a larger variety of cars that need to be addressed from a crashworthiness perspective, on top of adding the complexity in the rules/ guidelines on responsibility set-up.

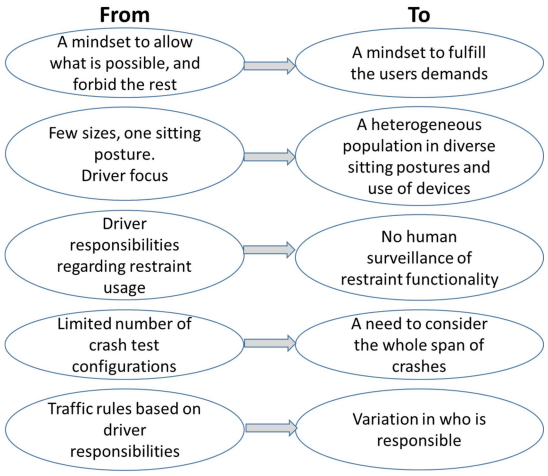

Figure 1. Examples of aspects in the paradigm shift

As illustrated in Figure 1, we need to move towards a mindset of addressing the demands of the user, from a reality today of allowing what is possible, and to forbid the rest. An example of this is when reclining the seatback to get a more relaxed position. Although it is possible to recline most front seats today, it is requested in most cars' user manuals to have the seat in an upright position, according to the certified position.

Applying such mindset of addressing customer demands, also includes that everyone should be equally protected, in their chosen sitting posture and activity. Today, the capabilities of the occupant tools are limited, restricting the inclusion in a regulative perspective. There is a need for increased focus on passengers of all sizes and ages, expanding the scope of today with few occupant sizes, one sitting posture and a driver focus.

Today, there is a driver having an overall responsibility (or at least a possibility to have) to ensure usage of restraints. It could be the seat belt or child restraints usage, or simply ensure that the passengers are seated within dedicated space. In the future non-driver environment, this is a challenge that needs to be taken care of.

The limited number of crash test set-ups that the vehicles are certified for today, will likely not be sufficient in the context of tomorrow. As a result of the advancements in occupant protection over the years, more unique cases are needed to be addressed. In addition, the rapid implementation of collision mitigation technologies is seen. Hence, an important topic is the need to handle the large span of crashes, in addition to that the crash will be dependent by the collision mitigation technology, or the autonomous drive systems. Today, the influence of an autonomous pre-crash intervention (e.g. braking or steering) is usually not taken into consideration in the crash testing for evaluating crashworthiness, while they in real world situations could contribute to the occupant protection by reducing speed. From a real-world perspective, today as well as in the future, enabling the automated pre-crash maneuvers to be a part of the design of the crashworthiness evaluation is desired.

As also listed in Figure 1, the role of the driver today to obey the traffic rules plays an important part of the traffic system. In future cars without dedicated drivers, the aspects of this role need to be included in the context as well.

Summing this up, fundamental changes in evaluation approach and underlying assumptions are foreseen, similar to a paradigm shift.

The paradigm shift can be summarized by the following main points:

- The mindset
- The population
- New seating configurations, seat positions and sitting postures
- Responsibilities; who takes over the driver's role in occupant protection?
- The span of crashes and whole crash events to understand and handle

In order not to be a stopper for enabling the customer benefits in the development of autonomous drive, the occupant protection challenges need to be addressed. This paper discusses some different aspects of this, however being a paradigm shift, a common discussion and cooperation among stakeholders is needed to cover the whole spectra of aspects.

HUMAN-CENTRIC SAFETY

The development towards autonomous drive has been ongoing for more than a decade, starting with driver support systems in car-following situations, followed by autobrake functionality including when turning in front of an oncoming vehicle in intersections (Ljung Aust et al., 2015). Assisting the driver when inattentive or distracted, the auto brake and/or auto steer functionalities will add to the proportion of crashes which are preceded by a maneuver. Hence, moving towards higher degree of automation, a large share of the crashes that occur are likely to have exerted the occupants to a pre-crash kinematics exposure (e.g. from deceleration), caused either by the driver or the technology.

From an occupant protection point of view, it does not make much difference whether a human driver is driving the car, or the machine. Except, for the driver for whom the steering wheel would be included in the protection systems, and the differences in his/her pre-crash kinematics. What really influences the occupant protection needs are the business cases for which the vehicles are designed for (e.g. those described in the 360c concept above); adding customer values influencing the use of the car, including possible sitting postures and seating configurations.

From a human-centric point of view, the SAE levels of automation (SAE J3016) do not provide a relevant framework. This is quite obvious with respect to occupant protection. In addition, even from a driver's role perspective it does not provide sufficient structure. A human-centric approach calls for a need to clarify the driver's role, reducing the confusion on whether the automation is driver assistance which requires driver engagement and responsibility or whether the automation is designed for the operator to safely do something else while relieved from the driving task (unsupervised AD). Driver assistance systems only partly support the driving task (e.g. headway control with some degree of steering assistance), and the driver is still required to supervise the driving and intervene at sensing or actuation limits (e.g. conflict situations). In contrast, unsupervised AD enables either (1) periods of drive-free time where the driver assumes a temporary role of a passenger for a period of time or (2) full trips where the user delegates full control and responsibility to the vehicle (e.g. 'robotaxis'). Until unsupervised AD exists and the driver can switch roles to become a passenger, automation is assistance and the driver is not free to disengage from the driving task to freely do non-driving related activities. The driver must clearly understand when automation provides a role switching from a driver role to a passenger/operator role.

Thus, different types of automation are associated with and designed for different expectations on the driver or passengers. For example systems could be designed to allow all occupants to sleep, or could be designed to expect a driver to monitor and act when automation encounters its limitations. Clearly, knowledge regarding human limitations is key to setting constraints. Safe, human-centric automation sets the human needs and abilities in focus, and designs technology around this. Safe, human-centric types of automation is to be seen as an alternative to the technology-driven approach, which the SAE levels of automation represents.

Human-centric safety relies on three parts, as illustrated in Figure 2. The three parts are based on areas in which human limitations can help create a platform of knowledge and implementation. 'Human cognitive abilities, skills and behavior' and 'Safe user experience' are the two complements to the more established 'Human injury tolerances'. The latter will be further addressed in this paper.

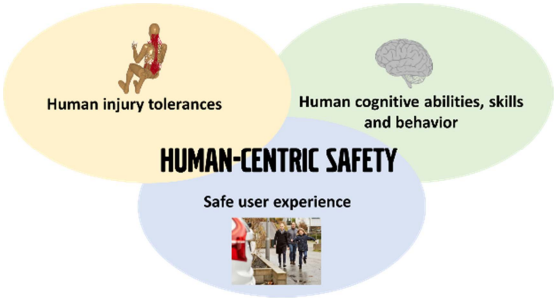

Figure 2. Human-centric safety at Volvo Cars

Human injury tolerances are the foundation in occupant protection. Biomechanics and fundamental principles of protection are the guiding essentials and the paradigm aspects (as presented in prior chapter) and type of automation is a crucial context.

FOCUS AREAS FOR HUMAN INJURY TOLERANCES

Future unsupervised AD cars, in addition to future manually driven cars, are likely to be exposed to crashes. Hence, the occupants' need to be protected is obvious, as today. As described in previous chapter, the current situation for occupant protection calls for fundamental changes in evaluation approach, underlying assumptions and role of different

stakeholders. This includes new research and application of this research.

Following a summary of *Biomechanical Principles*, this chapter provides a description of the major challenges within knowledge needed to encompass the wide spectra of future cars. The challenges include the *Complete Crash Event*, *Occupant Sitting Postures at Impact* and *Occupant Protection Principles* described in a human-centric perspective.

Biomechanical Principles

The fundamental biomechanical principles for impact trauma apply. The most important are summarized as follows:

- Restrain strong body parts
- Early coupling
- Distribute load
- Minimize relative motion between body parts
- Reduce contact forces to interior

Strong body parts are pelvis, shoulder, thorax and femur, including axial direction through the lower extremities, including the feet. Protection should be achieved by adapting the force distribution over various body regions by controlling and adapting kinematics and restraint forces. The three-point seat belt is an example of interaction with strong body regions, see Figure 3.

Figure 3. Example of interacting with strong body parts. The three point seat belt should be positioned over the pelvis and across the chest and shoulder.

As emphasized by (Kent and Forman, 2015), early coupling of the occupant is beneficial. This means achieving occupant deceleration similar to the vehicle deceleration, in contrary to an unrestrained occupant that does not benefit from the vehicle deceleration and will thus experience higher forces when contacting. This occupant/vehicle coupling can be referred to as "ride down of the vehicle deceleration". By the use of the whole time of the crash and to distribute the load during the whole event, the internal loadings will be less. The distance include both interior space and vehicle crush zone, in addition to the contribution of crash mitigation time. It is essential to maintain the coupling during the complete crash event (also including a pre-crash maneuver), to ensure control of the occupant kinematics and force control.

Distributed loads are essential to minimize deformation to the body tissues and reduce loads between body parts. As an example, the spine is sensitive to shear forces if applied locally, but can withstand high forces if distributed over a larger area (Crandall et al., 1997, Kent et al., 2001). By distributing the load over e.g. the whole ribcage, or by supporting the head and torso together, as for astronauts when launched in space, or the principles of a rearward facing child seat (Aldman, 1964, Figure 4), needed protection is achieved.

Figure 4. A child in a rearward facing seat, illustrating the protection principle of distributed loads, in case of a frontal impact.

The principle of minimizing relative motion between body parts is essential. Unbalanced head and neck kinematics may result in neck injuries, including whiplash injuries (Siegmund et al., 2009). Unbalanced pelvis and upper torso kinematics may contribute to submarining (Adomeit and Heger, 1975). It is vital to control kinematics and restraint forces to manage the relative motion between body parts.

If the distances are not enough for a smooth "ride down of the vehicle deceleration", the forces when the occupant impacts the interior surface should be controlled. Padding and airbags are means to control the stiffness of interior surfaces. The challenge is higher when short distance between the occupant and the interior, such as for an occupant today in a side impact. To control contacts include means to help protect the occupant, e.g. knee contact with the

interior, assisting in the early coupling. Car body strength is an enabler to help keep the intruding structure (magnitude and velocity) into the vehicle compartment low, and thereby the loading to the occupant.

Complete Crash Event

In most of the crashes, the AD car will likely perform a maneuver prior to the crash targeting avoidance or mitigation. Already today, occupants are exposed to braking and steering prior to a crash, and technology influencing the crash configuration is available. However, in the standardized crash testing today, the cars are not exposed to pre-crash maneuvers, and the crash test dummies used are limited in their capabilities. As example, the crash test dummies designed for frontal impact tests are not capable of capturing biofidelic kinematics nor injury mechanisms in side impacts. None of them are designed for biofidelic kinematics in braking or steering movements.

There are two main concerns in this area. Firstly, it is relevant to include the influence of pre-crash kinematics into the occupant protection evaluation. In that way, the collision mitigation technology can be evaluated as part of the occupant protection. A simple example is how an autobrake in car-following situations can serve the purpose of reducing the occupant impact exposure in the same way as a well-designed energy absorption of the front structure. Occupant tools are needed that are capable of humanlike kinematics throughout a complete crash event, including the preceding event. Secondly, it is relevant to develop methods and tools that are omnidirectional in kinematics and injury prediction capabilities, i.e. possible to use independent of direction of impact. This will enable the possibility to design collision mitigation technologies that influence the crash configuration as a part of the occupant protection. An example of this is that for an intersection autobrake system, the activation algorithms can be further developed together with the interior restraint systems and car body design.

Today, the most capable tools to address these concerns are human body models (HBM). As compared to crash test dummies, HBMs have biofidelic sensitivity to different loading directions and differences in acceleration levels and can represent different occupant sizes, gender, and anthropometry. In addition, if muscle tonus is implemented in the models, so called Active HBMs, they have the potential to predict the occupant response in pre-crash and emergency events (Östh et al. 2015). An example of an active HBM capable of occupant simulation comprising a maneuver and crash event was used in studies on braking and/or lane-change followed by frontal impacts (Östmann and Jakobsson, 2016, Saito et al, 2016, Pipkorn and Wass, 2017, Östh, 2018). Figure 5 is an illustration of the model and the sequences, taken from the study by Östmann and Jakobsson (2016).

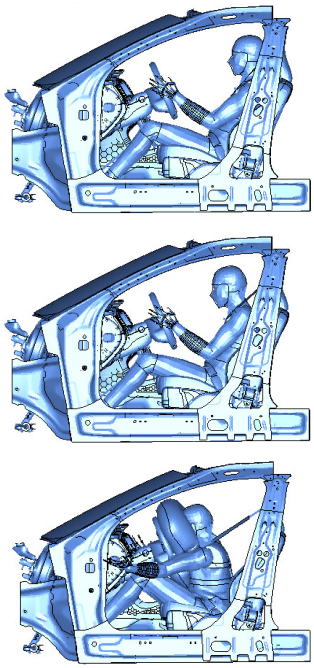

Figure 5. Illustration of an active HBM capable of simulating a brake event prior to a crash event. Top: initial position, Middle: at time of impact, Bottom: at most forward head position

Methods to evaluate complete crash events need to be in focus for future occupant protection assessment. The methods and tools should be capable of including maneuvers and simulating occupant movements prior to the crash, in addition to being capable of injury prediction, independent of direction of impact.

Occupant Sitting Postures at Impact

In real world crashes, the occupants' sitting postures at impact are influenced by the selected sitting posture and the sitting posture as a result of the vehicle motion prior to the crash. This was described by Stockman (2016) and Jakobsson et al. (2017), focusing children in the rear seat. Driving studies with children showed that children choose a range of common user positions, which includes upright sitting posture, as well as forward leaning positions, including bending their necks forward when using

e.g. electronic hand-held devices (Osvalder et al., 2013, Andersson et al., 2010, Jakobsson et al., 2011, Arbogast et al., 2016, Cross et al., 2017). This is referred to as voluntary sitting postures, driven by comfort and the activities they engage into. Studies with children exposed to steering and braking maneuvers illustrate examples of non-voluntary sitting postures, moving the occupants forward or sidewise, even moving out of the shoulder belt (Stockman et al., 2013, Bohman et al., 2011b, Baker et al., 2017, Baker et al., 2018). It was hypothesized that the influence of the sitting posture at time of impact could explain why children sustained head impact related injuries, although they were correctly restrained according to the dataset analyzed (Bohman et al., 2011a). Based on this work, Jakobsson et al. (2017) emphasized that it is essential to monitor occupant postures and kinematics for enhanced understanding of protection needs at time of impact.

There is limited knowledge on voluntary sitting postures of front seat adult passengers, with only a few studies available on the topic. Zhang et al. (2004) made a survey with 560 participants. They identified 29 sitting postures for adult passengers and estimated the frequency of those. Upright selected posture was the most common (45%), followed by leaning inboards (8%) and leaning outboards towards b-pillar (8%). In an observational study by Bingley et al. (2005), front seat occupants were observed from the outside of the car. Passenger head centerline to vehicle centerline was collected, in addition to use of seatbelts, hand positions and activities.

Studies on front seat passenger kinematics in evasive maneuvers have been performed with the primary purpose of creating validation corridors for active human body models (Ólafsdottir et al., 2013, Ghaffari et al., 2018). The studies provide evidence on non-voluntary movements in braking and lane-change maneuvers. Although not comparable in set-up, the adult front seat passengers seemed more restricted in sidewise movements, as compared to the child rear seat passengers, likely due to more side support by the seat in the front seat, and probably more likely to support themselves with the feet than the children were .

Sitting posture influences injury outcome in case of a crash, in vehicles today. McMurry et al. (2018) analyzed data from CIREN and NASS-CDS, and found an elevated injury risk for occupants registered in the data as in an out-of-positions, e.g. reclined position, as compared to the occupants registered as in-position. Real world case studies have shown the limitations of protection in reclined sitting postures in existing cars, causing submarining resulting in injuries to the abdomen as well as cervical spine (Jeffery and Cook 1991, Rehm and Goldman 2001, Dissanaike et al. 2008). Investigating thoraco-lumbar spine injury mechanisms, it was seen that a forward bended occupant posture, due to kinematics in run-off road events, influenced the occurrence of spine injuries at the sudden stop (Jakobsson et al., 2006).

Using multibody human body models, Bose et al. (2010) investigated influence of sitting posture on injury outcome in frontal impacts, as one of four occupant parameters. They found several of the eight sitting postures evaluated to increase the risk of injury. Another study, using finite element human body models, showed that reclined sitting postures with state-of-art restraint system increase the risk of submarining (Lin et al. 2018).

Substantial data on sitting postures and behavior in cars today needs to be collected and analyzed, to form the knowledge foundation for the future challenges. Furthermore, user studies of future needs and expectations should be conducted, especially in the light of changes in mobility trends

Occupant Protection Principles

Traditionally, occupant protection principles have been related to principle direction of force (PDOF) of the crash and with the seats facing forward of the direction of travel. In future seating configuration, we may see seats rotated in various degrees, taking any direction up to turned rearward facing relative to the travel direction. Hence, it is more logical and constructive to relate the protection principles to the direction of force for which the occupant will be exposed to. This means taking into account both PDOF of the vehicle and the seating configuration. Therefore, we will refer to e.g. “forward”, “rearward”, “lateral”, “oblique” movement of the occupant, irrespectively what direction the occupant and the seat is facing in the car. This is an example of human-centric approach, referring to the human instead of the car or crash.

No matter direction of occupant movement, the protection should to be designed around the occupant, e.g. both the seat belt as well as the seat itself. Future technical solutions are likely different from today’s in order to work in new seating configuration. New seating configurations may include other direction of travel than today, as well as traditional support surfaces such as the instrument panels may not be available. The purpose of the description of the occupant protection principles in this chapter is to describe and exemplify the human-

centric approach, which should be valid, irrespectively of the boundary conditions.

Restraining the occupant in a pure forward movement (sagittal-anterior, such as a forward facing occupant in a frontal impact), the hipbone (pelvis) is essential to catch – allowing for controlled forward motion of the upper body. The conventional three point seat belts work in line with these principles. An essential part is the lap belt anchorage placement below the hips, as stated already when introduced in 1959 (Bohlin, 1964 and 1981). The seat structure is also a fundamental part of the protection. Airbags could be used to reduce relative motions between body parts and to distribute the load, but they may be designed differently than in today's vehicles. Load paths using the knees or feet could be effective means, especially when the occupant is reclined, helping to restrain the forward motion of the pelvis. It will be more challenging when using conventional restraints since it is more difficult to restrain a pelvis when it is rotated rearwards from its initial position. The real world case studies reported on injures passengers exposed to frontal impacts when substantially reclined confirm the challenges of today's technologies (Jeffery and Cook, 1991, Rehm and Goldman, 2001, Dissanaike et al. 2008).

Restraining the occupant in a pure rearward movement, has been a successful way of reducing injuries to the youngest children. By distributing the load of upper torso, neck and head over the whole the seat back (Figure 4), risk of injury is reduced. It is essential that the occupant remains supported by the seat back and head restraint during the whole crash, and does not slip off the seat back or head restraint, in order to control the relative motion between the head and torso.

Protecting the occupant in a pure lateral movement and all oblique combinations follows the fundamental biomechanical principles, as presented above. However, depending on the seating configuration and the surrounding interior structure, it will be more or less challenging. Likely, these situations are driving the most challenging needs of developments of tools, methods and new restraint strategies.

Studies have already provided insights into the challenge of maintaining the occupant in its protection as the occupant movement becomes oblique (Kitagawa et al. 2017). Already in today's vehicles, oblique frontal impacts, as well as far-side side impacts, for forward facing occupants are demanding in terms of controlling the kinematics of the upper torso and head. The way forward is to base the protection on the biomechanical principles, including an early coupling of the occupant, restraining the strong body parts and distribute the loads. Likely, this means that the seat belt plays the fundamental role of protection but may need to be supported by other technical solutions in order to control the loading to the occupant and the kinematics of the occupant.

Specific concerns for children: Two major areas of concerns are special for children, otherwise the basic principles of occupant protection are valid, and independent of size and age. The two areas are neck vulnerability for the infants and toddlers, and pelvic bone size and shape for children up to puberty.

The infants and toddlers are especially vulnerable for relative motion between the head and the upper body. The special concern for this group is due to a combination of relatively large head size/weight (see Figure 6) and an immature neck with more horizontal vertebra which grow stronger when bone is replacing cartilage. It is therefore essential that the forces are distributed over a larger part of body, which can be achieved by riding in a seat with the back towards the travel direction (illustrated in Figure 4), also having side supports close to the body for lateral support.

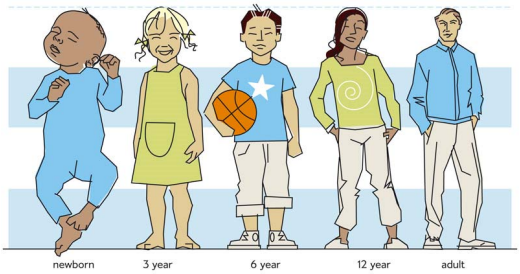

Figure 6. Body proportions for different ages

For children with relatively smaller pelvic body, using an adult designed seat belt, usually need to be adjusted in height to benefit from the same principles in the forward movement as explained above. However, from a principle perspective there are no major difference, although the shorter limbs and body regions call for comfort adjustments to accommodate a comfortable ride in the protected mode. As an example, if the seat cushion is too long for the child's legs to be comfortably bended, he/she will likely slouch forward whereby the intended interaction with the seat belt is missed.

DISCUSSION

The paper suggests that fundamental changes in evaluation approach and underlying assumptions are foreseen, similar to a paradigm shift. The paradigm shift is driven by and relates to the mindset on car

usage and occupant requests. It calls for new ways of addressing crashworthiness evaluation, emphasizing the huge effort in research and knowledge creation needed, as well as a new set-ups in procedures and responsibilities of stakeholders involved. It likely requires addressing expanded crash test set-ups, taking the whole event into account, in addition to a larger population of occupants, and a larger range of seat positions and sitting postures.

This is not the first time the crashworthiness challenges in unsupervised AD are addressed. In 2016, NHTSA published a Federal Automated Vehicles Policy as agency guidance to speed the delivery of an initial regulatory framework and best practices to guide manufacturers and other entities in the safe design, development, testing, and deployment of highly automated vehicles (NHTSA, 2016). Occupant protection, as part of crashworthiness, was addressed as one of 15 safety assessment topics. They stated that manufactures and other entities should exercise and demonstrate due care to provide countermeasures that will fully protect all occupants given any planned seating or interior configurations, and the tools to be used need not be limited to physical testing but also could include virtual tests with vehicle and human body models.

In Europe the focus on AD challenges is also high. Thatcham states that the rapid development of AD may force regulators to consider alternative and faster regulatory approaches than today, highlighting the need of fully redundant systems for robust automated driving solutions and how to prevent systems sold as 'Automated' when they require driver intervention to be safe (Thatcham, 2017). Euro NCAP describes in their road map 2025 a focus on the assessment of automated driving systems and driver/vehicle interaction (Euro NCAP, 2017). However, at this point neither Thatcham nor EuroNCAP address how occupant protection in AD cars should be assessed.

Safe Kids Worldwide organized a Blue Ribbon panel on children in autonomous vehicles, since they identified there is a great focus on adults and autonomous vehicles but there is lack of understanding the unique needs of children in this context. (Safe Kids Worldwide, 2018). They summarize five areas of actions encompassing safety standards, usability testing, inclusive design, appropriate supervision and marketed standards, emphasizing that children should be included in all phases. The report concludes that it is time to act straightaway, as it is necessary to build the knowledge of the needs of the children and the families now, enabling them to be addressed in the ongoing rapid development of the technology.

Future unsupervised AD cars are likely to be exposed to crashes. The AD cars will be mixed with human-driven cars. Hence, the occupants' need to be protected is obvious. This paper suggests a human-centric approach as the way forward to address fundamental changes in evaluation approach, underlying assumptions and role of different stakeholders. This includes new research and application of this research. A human-centric approach applied to occupant protection is based on human injury thresholds. It addresses the needs of the occupants based on who they are, how they are sitting and what forces they are exerted to, according to the human reference system. It is also about a mindset, of changing from e.g. forward facing occupant in frontal impact; to understanding the occupant's sitting posture at impact, as a result of the whole crash event, and referring the protection principles to the human instead of the interior setting of the car or the impact type.

Based on the state-of-art tools and methods today, substantial knowledge gaps are evident, which we need to address through collective research in several areas. This paper highlights three main areas important for occupant protection assessments; the whole crash event, the sitting postures at impact and challenges regarding protection principles applied for relevant real world situations.

Occupant protection in cars is continuously improving. The large steps in injury reduction taken in the past, exemplified by introduction of e.g. seat belts, airbags, advanced front vehicle structures and side impact protection structure, are likely to be less frequent in the future. Instead, as result of the efficient work, the remaining priorities are more unique cases, in which tools and methods replicating a larger variety of crash and occupant characteristic are necessary. In addition, the rapid implementation of collision mitigation technologies calls for methods and tools including the pre-crash phase into the evaluation. Hence, methods and tools to evaluate complete crash events need to be in focus, considering maneuvers and occupant kinematics prior to the crash, in addition to all directions of impact.

Today, passenger cars are mainly designed to protect upright sitting occupants, who are centralized in their seat. At least, this is the way the crash test dummies are designed to be used. To change this and to form the knowledge foundation towards the future challenges, research in this area is needed both to interpret the real world data today, i.e. what are the

ranges of postures that are reflected by the data in the databases, as well as to understand future priorities.

Different activities will result in different sitting postures, for example a comfortable resting position will be different from a working position. It should be acknowledged, that changing sitting posture is part of our natural way of gaining comfort. To enable protection, the different postures need to be understood, and if not possible to protect based on available technology, ways of guiding the occupant into a preferred posture based on comfort should be in focus. Hence, data on sitting postures are also essential to understand the preferences of humans and how to address their preferences with respect to protection in the best way.

Substantial data, especially on passengers, needs to be collected during standard car drives, in addition to evasive maneuvers, quantifying differences between individuals as well as situations. Manual analysis of naturalistic driving studies is time consuming. Development of more automatic analysis methods has recently been initiated (Reed et al., 2018), and should be further enhanced capturing details on sitting postures as well as restraint positions.

Furthermore, user studies of future needs and expectations should be conducted, especially in the light of changes in mobility trends. Staged studies investigating seating configurations and sitting postures in relation to future perceived needs when moving towards higher degree of automation will help guide the development of functionalities not available in traffic today. Jorlöv et al. (2017) and Östling and Larsson (2019) are examples of such studies on seating configurations and activities.

Being the most capable tools to address the whole crash event and inherently designed with human properties, HMBs including muscle activation are today the most promising tools. Already today it can be used for combination of pre-crash events and impacts in different directions. This is needed when moving towards including the crash mitigation technologies being a part of the occupant protection. Just as important as being capable of recreating human kinematics in different types of maneuvers, is the ability to compare injury prediction responses resulting from different directions and contact points of a body region, resulting from a change in impact configuration due to the collision mitigation technology. Further, there is a need to include similar research for child occupant tools and to develop relevant physical tools (crash test dummies) as complement enabling hardware validation.

Substantial research is required to support the development of the occupant tools needed in the future. The research includes foundation for validation, development of relevant injury prediction, in addition to understand and take into account individual differences of all aspects.

New morphing techniques of HBM opens up the possibility of developing the families of HBM that can represent the population to a much wider extent, than the limited sizes of crash test dummies and HBMs currently available. There is need of research to determine what that population should look like, and if different families are needed for the difference in crashes and seating configuration. Knowledge is needed to understand who is vulnerable in the specific situation, but also to complement with other representatives of the population to ensure the wide range of occupants will be protected. The families include children as well. The biofidelic validation of existing pediatric tools (crash test dummies and HBMs) is lagging behind the work ongoing for adult tools, due to lack of data.

The morphed family needs to be validated, since it is not enough to morph the occupant to a relevant shape and size. The need of validation data include kinematics and muscle responses in maneuvers in addition to biomechanical data providing validation corridors for occupant movement directions and interactions. Especially there is a lack of validation data for occupants in a non-upright seat position.

NHTSA recently started a research program, including generation of validation data in reclined seat positions. Pure forward occupant movements and pure rearward occupant movements (simulating rear facing occupant in a frontal impact) are within the scope (Reed, 2019). In addition to the reclined postures, the inclusion of high severity rearward occupant movement is new. The latter providing a good complement to the available extensive rear-end impact research at lower severity. In addition, and just as important, validation data in lateral and oblique directions is urgently needed.

Applying the protection principles on new seating configurations and seat positions is challenging and it will require more advanced tools. In the development of new types of restraints, the tools are needed to help predict occupant interaction in a variety of sitting postures and occupant sizes. Hence, detailed models and biomechanical data is required, especially for the load bearing body parts. Restraint interaction with the pelvis is essential as this is a basic structure to use as load path. Interaction with the shoulder will likely continue to be an essential part of the protection system, ensuring the occupant remains restrained,

especially in oblique occupant movements. The load to lumbar spine may be increasing depending on how the load path in reclined sitting positions can be solved, and it is essential to have tools that can predict loads to the spine. Another challenge is valid representation of soft tissues, which today is very limited in any of the tools used for occupant protection. One example is the importance of adipose tissues influencing the position of the restraints, as well as the time of restraint interaction to the skeleton. Reed et al. (2012 and 2013) showed how the lap belt will be positioned more forward of the pelvis bones if the occupant has high body mass index (BMI) compared to occupants with normal BMI.

For children, smart adaption of protection is a focus area with increasing importance in the future. Today the children's needs are addressed by adding child restraint systems into the vehicle. The majority of these solutions are aftermarket solutions, while only a few cars offer built-in solutions, such as booster seats (Jakobsson et al., 2007). In line with the increased shared mobility, it is essential that the solutions for child occupant protection are convenient, easy to use and provide adequate safety in case of a crash. Jakobsson et al. (2017) summarized that from a real-world safety perspective, the vehicle and child restraint should be designed together targeting a range of acceptable common user positions; sitting postures preferably guided by comfort and positive means. Such designs will ensure robust function of the protection systems for these young occupants, and advance the development of countermeasures that protect children in real-world crashes, also including dynamic events prior to a crash. Again, a human-centric approach understanding the users' specific needs, is likely the most successful way.

We foresee a paradigm shift in occupant protection. It is partly driven by the unsupervised AD, especially concerning change in mindset of enabling an expanded user request, exemplified by sitting postures and activities in the cars. It is also driven by the fact that less people are injured in cars today, and therefore improved methods and tools are needed to address the remaining cases. The paradigm shift will impact the assessment tools and underlying knowledge for occupant protection, as elaborated on in this study. It will require synchronized cooperation among stakeholders to collect and create the needed real world data, validation data and tools. In addition we need to raise our view and perspective in the area. Specifically, it requires a consensus that we together need to take this step on development of assessment methods, as well as taking on the discussion of the whole picture, exemplified by issues like who will take care of the occupant protection relevant tasks as the driver has today.

REFERENCES

Adomeit D, Heger A., Motion sequence criteria and design proposals for restraint devices in order to avoid unfavorable biomechanic conditions and submarining, *19th Stapp Car Crash Conf*, SAE-751146, 1975:3150--9

Andersson M, Bohman K, Osvalder A-L. Effect of booster seat design on children's choice of seating positions during naturalistic riding. *54th AAAM Annual Conference, Annals of Adv in Automot Med*, 54, 2010:171-80

Aldman B. A protective seat for children – Experiments with a safety seat for children between one and six, *8th Stapp Car Crash Conf*., SAE-640855, 1964:320-328

Arbogast KB, Kim J, Loeb H, Kuo Johnny, Koppel S, Bohman K, Charlton J, Naturalistic driving study of rear seat child occupants: Quantification of head position using a Kinect™ sensor. *Traffic Inj. Prev*. 17(1), 2016: 168-74

Baker G, Stockman I, Bohman K, Jakobsson L, Svensson M, Osvalder A-L, Wimmerstedt M. Kinematics and shoulder belt engagement of children on belt-positioning boosters during emergency braking events. *IRCOBI Conference*, Antwerp, Belgium, 2017

Baker G, Stockman I, Bohman K, Jakobsson L, Osvalder A-L, Svensson M, Wimmerstedt M. Kinematics and shoulder belt engagement of children on belt-position boosters during evasive steering maneuvers. *Traffic Inj. Prev*. 19:sup1, 2018

Bingley L, Richard M, Gabrielle C. Determination of real world occupant postures by photo studies to aid smart restraint development. *19th Int. Tech. Conf. Enhanced Safety Vehicle, ESV,* Paper No. 2005-0319, Washington DC, USA, 2005

Bohlin NI. Studies of three-point restraint harness systems in full-scale barrier crashes and sled runs. *8th Stapp Car Crash Conf*, SAE-640854, 1964:258-319

Bohlin NI. Refinements of restraint system design – A primary contribution to seat belt effectiveness in Sweden, *International Symposium on Occupant Restraint, AAAM,* Toronto, Ontario, Canada, June 1-3, 1981

Bohman K, Arbogast K, Boström O. Head injury causation scenarios for belted, rear-seated children in frontal impact, *Traffic Inj. Prev*. 12(1), 2011a:62-70

Bohman K, Stockman I, Jakobsson L, Osvalder AL, Bostrom O, Arbogast KB. Kinematics and shoulder belt position of child rear seat passengers during vehicle maneuvers. *55th AAAM Annual Conference, Annals of Adv in Automot Med, 55,* 2011b:15-26.

Bose D, Crandall JR, Untaroiu CD, Maslen EH. Influence of pre-collision occupant parameters on injury outcome in a frontal collision. *Accid. Anal. Prev*. 42, 2010

Crandall J, Bass CR, Pikey WD, Miller HJ , Sikorski J, Wilkins M. Thoracic response and injury with belt, driver side airbag and force limited belt restraint systems, *Int J Crashworthiness*, 2(1) 1997:119-32

Cross S, Charlton J, Koppel S. How do child occupants really behave during motor vehicle travel, *15th International Conference on Protection of Children in Cars*, Munich, Germany, 2017

Dissanaike S, Kaufman R, Mack CD, Mock C. The effect of reclined seats on mortality in motor vehicle collisions, *J Trauma*, 64(3), 2008

Euro NCAP, EuroNCAP 2025 Roadmap, EuroNCAP, June 2017. https://cdn.euroncap.com/media/30700/euroncap-roadmap-2025-v4.pdf (Downloaded 20190219)

Fraedrich E, Cyganski R, Wolf I, Lenz B. User perspectives on autonomous driving. A Use-Case-Driven Study in Germany. *Arbeitsberichte, Heft 187, Geographisches Institut, Humboldt-Universität zu Berlin, Germany*, ISSN 0947 – 0360, 2016

Ghaffari G, Brolin K, Bråse D, Pipkorn B, Svanberg B, Jakobsson L, Davidsson J. Passenger kinematics in lane change and lane change with braking manoeuvres using two belt configurations: standard and reversible pre-pretensioner. *IRCOBI Conference*, IRC-18-80, Athens, Greece, 2018

Jakobsson L, Bergman T, Johansson L. Identifying thoracic and lumbar spinal injuries in car accidents. *IRCOBI Conference*, Madrid, Spain, 2006

Jakobsson L, Wiberg H, Isaksson-Hellman I, Gustafsson J. Rear seat safety for the growing child – A new 2-stage integrated booster cushion. *20th Int. Tech. Conf. Enhanced Safety Vehicle, ESV,* Paper No. 07-0322, Lyon, France, 2007

Jakobsson L, Bohman K, Stockman I, Andersson M, Osvalder AL. Older Children's Sitting Postures when Riding in the Rear Seat. *IRCOBI, Conference*, Krakow, Poland, 2011

Jakobsson L, Bohman K, Svensson M, Wimmerstedt M. Rear seat safety for children aged 4-12: Identifying the real-world needs towards development of countermeasures, *25th Int. Tech. Conf. Enhanced Safety Vehicle, ESV,* Paper no. 17-0088, Detroit, USA, 2017

Jeffery RS, Cook PL. Seat belts and reclining seats, *Injury: the British Journal of Accident Surgery* 22(5), 1991

Jorlöv S, Bohman K, Larsson A. Seating positions and activities in highly automated cars – A qualitative study of future automated driving scenarios. *IRCOBI Conference*, Antwerp, Belgium, 2017

Kent R, Forman J. Restraint biomechanics, *In: Yoganandan N. Accidental Injury, Springer,* 2015:116-118

Kent RW, Crandall JR, Bolton J, Prasad P, Nusholtz G, Mertz H. The influence of superficial soft tissues and restraint condition on thoracic skeletal injury prediction. *Stapp Car Crash Journal*, 45, SAE-2001-22-008, 2001

Kitagawa Y, Hayashi S, Yamada K, Gotoh M. Occupant kinematics in simulated autonomous driving vehicle collisions: Influence of seating position, direction and angle, *Stapp Car Crash Journal*, 61, 2017:101-155

Lin H, Gepner B, Wu T, Forman J. Panzer M. Effect of Seatback recline on occupant model response in frontal crashes, *IRCOBI Conference*, Athens, Greece, 2018

Ljung Aust M. Jakobsson L, Lindman M, Coelingh E. Collision avoidance systems - Advancements and efficiency, *SAE World Congress*, SAE- 2015-01-1406, 2015

NHTSA. Federal Automated Vehicles Policy: Accelerating the Next Revolution in Roadway Safety, *NHTSA, U.S. Department of Transportation (DOT)*, USA, 2016 https://www.transportation.gov/AV/federal-automated-vehicles-policy-september-2016/ (downloaded 2019-03-03)

McMurry TL, Poplin GS, Shaw G, Panzer MB. Crash safety concerns for out-of-position occupant postures: A look toward safety in highly automated vehicles. *Traffic Inj. Prev.,* 19(6), 2018:582--7.

Ólafsdóttir JM, Östh J, Davidsson J, Brolin K. Passenger kinematics and muscle responses in autonomous braking events with standard and reversible pre-tensioned restraints, *IRCOBI Conference*, Sweden, 2013

Osvalder AL, Hansson I, Stockman I, Carlsson A, Bohman K, Jakobsson L. Older children's sitting postures, behaviour and comfort experience during ride – A comparison between an integrated booster cushion and a high-back booster, *IRCOBI Conference*, Gothenburg, Sweden, 2013

Pipkorn B, Wass J (2017). Pre-crash triggered pretensioning of the seat belt for improved safety. *25th Int. Tech. Conf. Enhanced Safety Vehicle, ESV,* Paper no. 17-0104, Detroit, USA, 2017

Reed M, Ebert-Hamilton S, Rupp J. Effects of obesity on seat belt fit. *Traffic Inj. Prev.,* 13(4), 2012:364-72.

Reed MP, Ebert SM, Hallman JJ. Effects of driver characteristics on seat belt fit. *Stapp Car Crash Journal*, 57, 2013:43-57.

Reed MP, Park B-K, Ebert S, Hallman JJ, Sherony R. Marker-less tracking of head motion in abrupt vehicle maneuvers, *IRCOBI Conference*, Athens, Greece, 2018

Reed M. Personal communication, March 5, 2019

Rehm CG, Goldman K, Seat belt and car seat in a reclined position: A dangerous combination*, J Trauma*, 51(6), 2001

Safe Kids Worldwide. Children in Autonomous vehicles, Blue Ribbon Panel. *Safe Kids Worldwide*, USA, 2018. https://www.safekids.org/sites/default/files/children_in_av-brp-report-2018.pdf (Downloaded 20190219)

Saito H, Matsushita T, Pipkorn B, Boström O Evaluation of frontal impact restraint system in integrated safety scenario using Human Body Model with PID controlled active muscles, *IRCOBI Conference*, IRC-16-35, Malaga, Spain, 2016

Siegmund GP, Winkelstein BA, Ivancic PC, Svensson MY, Vasavada A. The anatomy and biomechanics of acute and chronic whiplash injury. *Traffic Inj. Prev*. 10(2), 2009

Stockman I, Bohman K, Jakobsson L, Brolin K. Kinematics of child volunteers and child anthropomorphic test devices during emergency braking events in real car environment, *Traffic Inj. Prev.,* 14(1), 2013: 92-102

Stockman I. Safety for children in cars – Focus on three point seatbelts in emergency events. *Doctoral Thesis*, Department of Applied Mechanics, Chalmers University of Technology, ISBN: 978-91-7597-468-2, 2016

Thatcham, Regulating Automated Driving, *Thatcham Research*, https://news.thatcham.org/documents/regulating-automated-driving-a-uk-insurer-view-69167, UK, Aug 2017

Volvo Cars, Volvo Cars' new 360c autonomous concept: reimagining the work-life balance and the future of cities, *Press Release by Volvo Car Group*, 2018 https://www.media.volvocars.com/global/en-gb/media/pressreleases/237020/volvo-cars-new-360c-autonomous-concept-reimagining-the-work-life-balance-and-the-future-of-cities (Downloaded 20190219)

Zhang L, Chen L, Vertiz A, Balci R. Survey of front passenger posture usage in passenger vehicles. *SAE 2004 World Congress & Exhibition,* SAE-2004-01-0845, Detroit, USA, 2004

Östh J, Marín Ólafsdóttir J, Brolin K, Davidsson J, Pipkorn B, Jakobsson L, Törnvall F, Lindkvist M. Muscle Activation Strategies in Human body Models for the Development of integrated Safety, *24th Int. Tech. Conf. Enhanced Safety Vehicle, ESV,* Paper no. 15-0345, Gothenburg, Sweden, 2015

Östh J. Implementation and Application of Human Body Models for Vehicle Development. *7th International Symposium: Human Modeling and Simulation in Automotive Engineering, carhs,* Berlin, Germany, Oct. 18 - 19, 2018

Östling M, Larsson A. Occupant activities and sitting positions in automated vehicles in China and Sweden, *26th Int. Tech. Conf. Enhanced Safety Vehicle, ESV,* Paper no. 19-0083, Eindhoven, Belgium, 2019

Östmann M, Jakobsson L. An Examination of Pre-crash Braking Influence on Occupant Crash Response using an Active Human Body Model; *IRCOBI Conference,* IRC-16-37, Malaga, Spain, 2016

INVESTIGATION ON RESTRAINT APPROACH: REDUCE THORACIC INJURY BY DISTRIBUTING HIGH RESTRAINT FORCES IN OBLIQUE CRASHES

Takayuki Kawabuchi, Takashi Saso, Takayuki Shimizu, Hiroyuki Ito, Osamu Kanno
Honda R&D Co., Ltd. Automobile R&D Center
Japan

Paper Number 19-0284

ABSTRACT

The number of traffic fatalities is decreasing due to improvements of vehicle crash safety performance, which is promoted by crash safety regulations and consumer information assessments such as the New Car Assessment Program (NCAP). On the other hand, according to Japanese accident statistics, the reduction of fatality rates of those involved in oblique impact crashes is less than those in frontal and side impact crashes. This is considered because the risk of secondary impacts with interior structures increases as the seat belt slips, or occupants do not properly interact with the airbag due to lateral occupant motion induced by oblique vehicle movement. If restraint force is increased, thereby reducing the amount of occupant movement, it is possible to increase the injury risk of vulnerable people, such as the elderly. Therefore, applying high restraint force while distributing such loading to mitigate occupant injury should be the focus. The objective of this study is to develop restraint approaches that achieve effective occupant restraint and a reduction of injury risks by restraining body regions that have relatively high stiffness.

The stiffness sensitivity of a rib cage was investigated by using the thoracic impactor simulation with the Human Body Model (HBM) and it was found that the stiffness of the shoulder region, which includes upper rib cage and clavicle, has relatively higher stiffness than other thoracic regions. Therefore, it was determined to restrain around the shoulders.

Subsequently, the influences of restraint around the shoulders with respect to occupant kinematics and injury reduction were compared with those of conventional restraint systems under oblique impact simulation with the Test device for Human Occupant Restraint Anthropometric Test Dummy (THOR ATD). In addition, the influences of each restraint system on the number of fractured ribs caused by thoracic loading were investigated with the HBM under the same loading conditions as the THOR ATD simulation.

When the shoulder region was restrained, THOR ATD movement and chest deflection were reduced compared to the conventional restraint systems. The HBM results indicated that shoulder restraint reduces the chest deflection, similar to the THOR ATD, and the number of fractured ribs also reduced.

It was found that the load generated by the shoulder restraints was broadly distributed on the whole thorax, compared to loads of the conventional restraint systems. The restraint force was higher than that of conventional restraint systems and it reduced amount of occupant movement however the concentrated force on the thorax decreased. Based on these findings, an investigation of the mechanisms of load distribution is necessary considering the structural differences between the THOR ATD and the HBM.

This study described an approach to reduce thoracic injury while distributing loads over the whole thorax and keeping high restraint forces by restraining the shoulders, which have a relatively higher stiffness than other thoracic regions. In order to reduce the number of traffic fatalities, it is desirable to develop restraint systems based on the approach in this study.

INTRODUCTION

Bean et al. studied the influence of seatbelts and airbags on fatality reduction in traffic accidents and described that they reduced by 61% [1]. In other words, despite an increased in number of seat belt and airbag usage, a zero fatality rate was still not accomplished. The factor that fatality rate was not reduced by 100% was affected by Corner and/or Oblique crash, according to statistical analysis using the National Automotive Sampling System- Crashworthiness

Data System (NASS-CDS) and Bean et al. indicated that severity of Corner and/or Oblique crash was the second highest risk following high velocity collisions. Oblique crash was defined as “Oblique crashes engaged one of the main longitudinal members and caused the occupant to move in an oblique manner” according to National Highway Traffic Safety Administration (NHTSA) [2]. The occupants in oblique movement do not interact properly with the deploying airbag and that results in reduction in energy absorption, which causes injury rate increase. Iraeus et al. described that a small overlap crash was also a sort of oblique crash, because the small overlap crash causes oblique occupant movement, and studied a mechanism of thoracic injury caused by occupant oblique movement. Asymmetrical seatbelt loading induces outward deformation on the thorax and then door structure impact on the thoracic side might cause rib fractures. In addition, it was shown that the 1st rib to the 3rd rib was fractured by the seat belt loading itself [3]. Rudd et al. showed that oblique occupant movement causes door interaction and it increases the Abbreviate Injury Risk (AIS) 3+ compared to Co-linear crash [4]. Furthermore, Lindquist [5] and Brumbelow [6] showed an increase of fractures on the thoracic side and bilateral contusion under crash mode which causes the occupant to move in oblique manner.

As such, the function of the restraint system does not work properly and reduces energy absorption under an oblique crash, which causes thoracic injury by interior structures. Therefore, it is required to restrain occupant movement in an oblique manner with high restraint forces. However, since loading on the thorax is directly associated with thoracic injury, an increase in input loading on the thorax is a concern. Vulnerable occupants, such as elderly people, have a high possibility of the thoracic injury due to the loading from restraint systems.

The aim of this paper was focused on the approach to reduce both the amount of occupant movement and thoracic injury by distributing restraint forces considering the stiffness in the body regions using simulation.

METHOD

Restraint approach on occupant upper body

Three types of restraint surfaces were constructed to reduce the amount of lateral movement of the occupant. The restraint surfaces are shown in Figure 1. Each surface restricts the upper body movement in longitudinal-only direction (Front Plate), in lateral-only direction (Side Plate), and in both directions (Front + Side Plate), respectively. Each plate model was connected to the seat back frame by a beam element with rigid constraint. The Front Plate had a degree of freedom on perpendicular rotation around the connection point between the beam element and seat frame. The Side Plate had no degree of freedom on rotation. The effects of the three types of surfaces were evaluated by the change on the amount of occupant movement and injury criteria. The surfaces were restrained around the clavicle or shoulders, which have relatively high stiffness among the thoracic region according to Maehara [7].

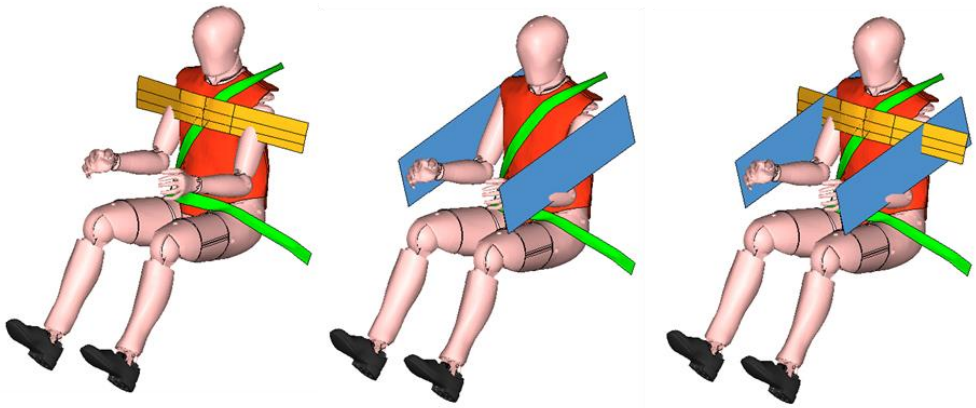

Figure 1. Three types of restraint surfaces

Simulation Model Construction

The evaluations of restraint surfaces were conducted by the Test device for Human Occupant Restraint 50th percentile model (THOR-50th) Metric Version 1.4.1 [8] with LS-DYNA (ver.971 R6.1.2. LSTC, Livermore, CA, USA). THOR model set on the driver seat at mid track in a small sized sedan. The vehicle model was equipped with a seatbelt with a pretensioner and 2 kN load limiter, driver air bag, and collapsible steering column. These conventional restraint systems were defined as baseline restraint systems. The interior structures in the model included a door structure and a center console.

As a secondary evaluation of restraint surfaces, simulations using a Human Body Model (HBM) were conducted and assessed reduction in the injury severity by restraint on the upper region of the thorax. HBM was developed by Dokko et al. [9] and Ito et al. [10] based on the characteristics of a 35 years old and adapted with finite element capable software, LS-DYNA (ver. R7.1 LSTC, Livermore, CA, USA). Thoracic geometry was constructed based on CT scan data from the database of medical CT scan imagery at the University of Michigan Program for Injury Research and Education. The thorax model was validated against thoracic impact tests conducted by Lessley et al. [11] and Shaw et al. [12]. Rib fractures were predicted by element deletion, which occurs when strain on the cortical bone shell exceeds the threshold.

Boundary conditions of collision simulation

Car-to-Car collision simulation was conducted; given the same vehicle class. Delta Velocity was determined as 55 km/h, which covers 90% of traffic accidents according to NASS-CDS. The inclusion criteria were following: case years 2000 to 2013, model year 2000 or later, front right- and left-side seat position, frontal crash condition, belted occupants, and AIS 3+ injury. The collision vehicle interacted with the main frame structure of its counterpart in order to increase the amount of occupant movement since the aim of this research was focusing on the influence of occupant movement on the thoracic injury. The collision angle was determined as 30 degrees, which occupant head did not properly interact with the airbag and the thorax hit the door trim.

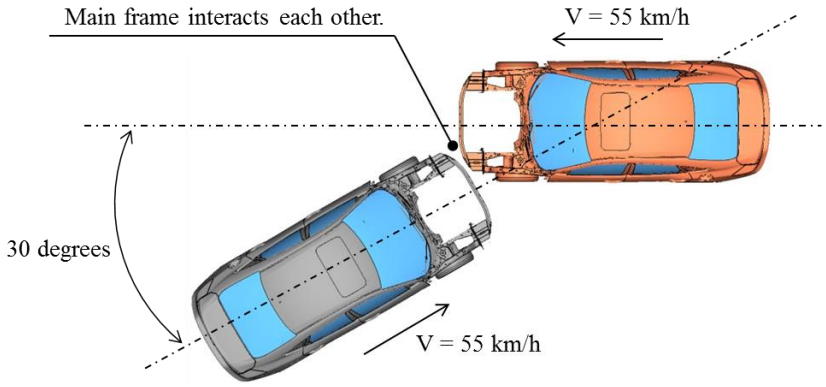

Figure 2. Boundary condition of Car-to-Car collision simulation

Evaluation items

The performance of restraint surfaces on the injury were evaluated by the amount of occupant movement, generated restraint force, and injury criteria. The THOR dummy movements against the vehicle were measured at Head, T1, T4, T12, and Pelvis, which were the locations of the accelerometers. The restraint forces on the dummy were measured seat belt tensile force, contact force of airbag, and the restraint surfaces. Seatbelt tensile forces were measured at two locations, on the upper location of the shoulder (Seatbelt Upper) and directly over the seat belt tongue (Seatbelt Lower). Thoracic injury was evaluated by the chest deflections measured by four 3D IR-TRACCs (Infra-Red Telescoping Rod for the Assessment of Chest Compression) in four quadrants, which was indicated as upper left and upper right, lower left and lower right. Measurement deflection data in the x, y, and z directions in the local spine coordinate were processed in resultant deflection. Input loading around the clavicle and shoulder was measured by a medial clavicle load cell.

HBM evaluated restraint surface by similar method as the THOR dummy. The amount of occupant movement was measured at the Head, T1, T9, L2, and Pelvis, which were close to the THOR dummy sensor locations as shown in Figure 3. Loading forces were measured at the same locations as THOR; seat belt force, airbag contact force, and restraint surfaces. Thoracic deflection was measured at the 4th and the 8th ribs as injury criteria, which were geometrically close in location to THOR IR-TRACCs. Rib deflection was measured between the tip of rib and costovertebral joint of the 4th and the 8th ribs. The resultant of x, y, and z directional deflections were calculated. As a specific injury criterion of HBM, rib fracture was defined as injury criteria. Rib fracture was expressed by rib element deletion. Loading around the clavicle and shoulder was measured at the medial clavicle section.

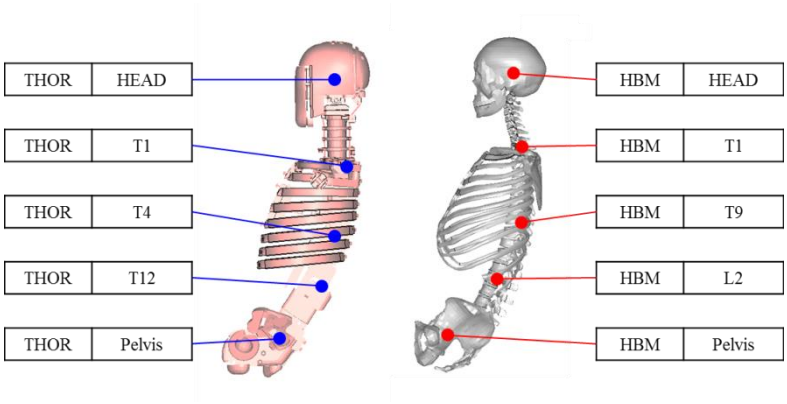

Figure 3. Measurement location of THOR and HBM

RESULTS

Simulation results by THOR

Seatbelt tensile force and contact forces on THOR were shown in Table 1 and 2, respectively. Seatbelt Upper force was not different among each restraint system by the function of load limiter. On the other hand, Seatbelt Lower forces under restraint surface decreased against baseline restraint systems. Total contact force increased by the effects of restraint surfaces, although airbag contact force was reduced.

Clavicle forces were shown in Table 3. Front Plate and Front + Side Plate increased clavicle force, however Side Plate did not increase loading on the clavicle. As mentioned in the methodology, the purpose of the restraint surface was restraint around the shoulders, thus Front Plate and Front + Side Plate could increase the load on the region.

Longitudinal and lateral direction movement of each measurement point from overhead view was shown in Figure 4. Longitudinal and lateral direction were defined as X and Y direction, respectively. Restraint force increased by surfaces reduced occupant upper body movement. Occupant movement reduction was considered to result in the decrease in Seatbelt Lower tensile force against baseline restraint as shown in Table 1. Figure 5 shows that the THOR dummy interacted with the door structure under the baseline restraint system, which was a similar incident as indicated in the previous paper [3]. Interaction with the door structure did not occur with every restraint surface.

Table 1.
Maximum seatbelt force on THOR

	Shoulder Upper [N]	Ratio to baseline	Shoulder Lower [N]	Ratio to baseline
Baseline	4,058	-	4,260	-
Front Plate	4,038	1.00	3,507	0.82
Side Plate	4,148	1.02	3,826	0.90
Front + Side Plate	4,025	0.99	3,459	0.81

Table 2.
Maximum contact force on THOR

	Air Bag [N]	Front Plate [N]	Side Plate [N]	Total Contact Force [N]	Ratio to baseline
Baseline	5,098	-	-	5,098	-
Front Plate	2,303	7,696	-	9,999	1.96
Side Plate	3,040	-	10,290	13,330	2.61
Front + Side Plate	2,351	5,586	2,898	10,835	2.13

Table 3.
Maximum force on the clavicles of THOR

	Clavicle R [N]	Ratio to baseline	Clavicle L [N]	Ratio to baseline
Baseline	550	-	773	-
Front Plate	782	1.42	3,068	3.97
Side Plate	332	0.60	663	0.86
Front + Side Plate	828	1.51	1,536	1.99

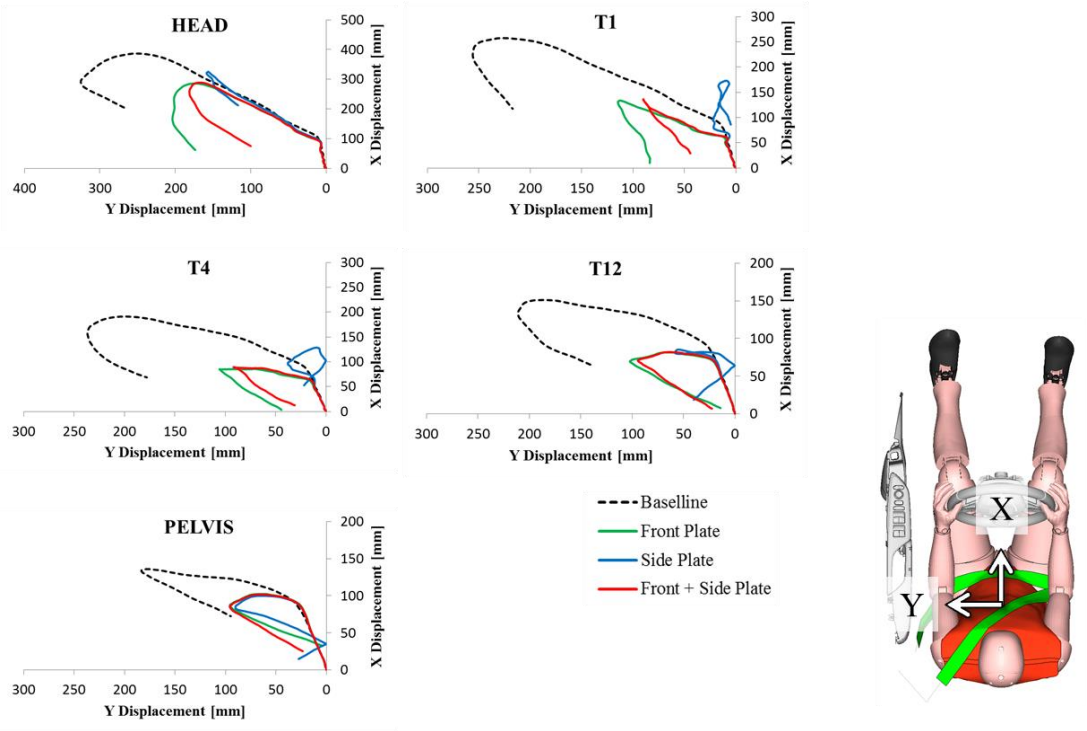

Figure 4. THOR Trajectory on XY plane

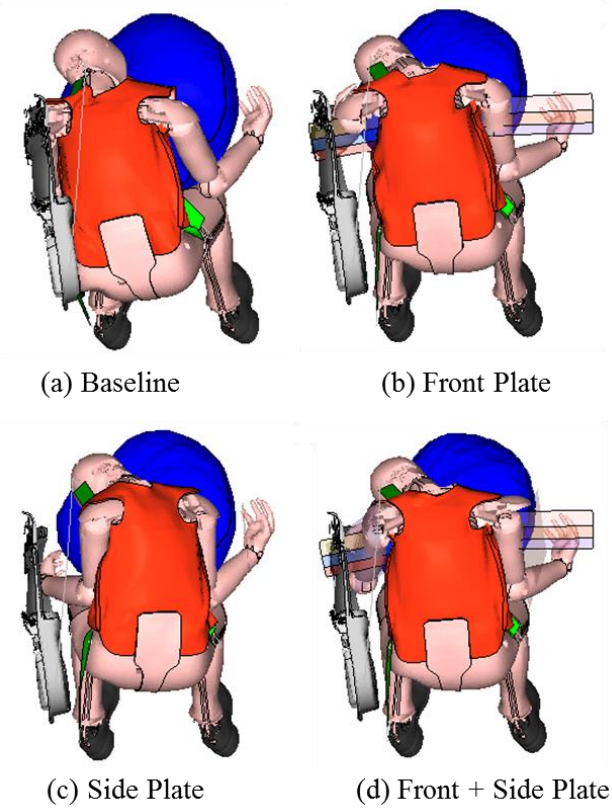

Figure 5. Comparison of the back view of THOR at maximum displacement

Thoracic maximum deflections measured by IR-TRACCs were shown in Figure 6. Front Plate and Front + Side Plate reduced thoracic deflection, although restraint loading on the thorax increased roughly twice as much as the baseline restraint system. Side Plate increased thoracic deflection on lower right side and showed different trends from other restraint surfaces.

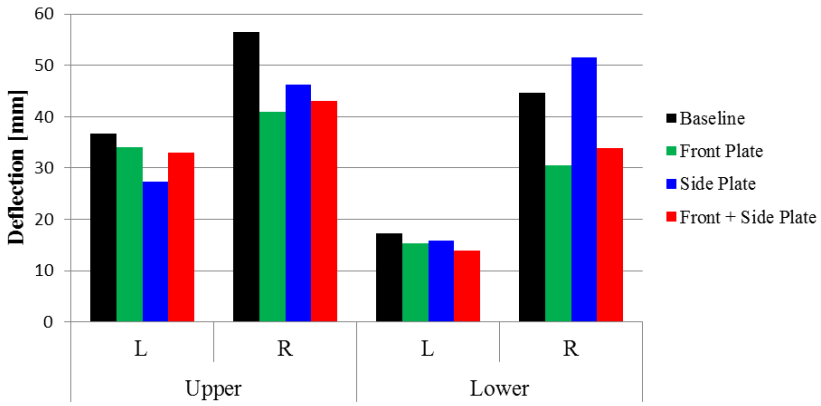

Figure 6. Comparison of IR-TRACCs between each restraint

Simulation results by HBM

Seatbelt tensile force and contact forces on HBM were shown in Table 4 and 5, respectively. HBM also showed Seatbelt Lower force reduction under restraint surfaces. Seatbelt Upper force was not different among each restraint system due to the function of load limiter. Total restraint force increased from the baseline. This result showed similar trend as THOR.

The clavicle section force was shown in Table 6. Front Plate and Front + Side Plate increased loading on the clavicle against baseline.

The amount of HBM movement was reduced by restraint surfaces, as shown in Figure 7, and the door structure interaction did not occur, as shown in Figure 8.

Table 4.
Maximum seatbelt force on HBM

	Shoulder Upper [N]	Ratio to baseline	Shoulder Lower [N]	Ratio to baseline
Baseline	3,706	-	4,488	-
Front Plate	3,782	1.02	3,679	0.82
Side Plate	3,770	1.02	3,709	0.83
Front + Side Plate	3,792	1.02	3,554	0.79

Table 5.
Maximum contact force on HBM

	Air Bag [N]	Front Plate [N]	Side Plate [N]	Total Contact Force [N]	Ratio to baseline
Baseline	2,011	-	-	2,011	-
Front Plate	1,216	8,686	-	9,902	4.92
Side Plate	1,838	-	9,702	11,540	5.74
Front + Side Plate	1,266	5,519	3,173	9,958	4.95

Table 6.
Maximum force on the clavicles of HBM

	Clavicle R [N]	Ratio to baseline	Clavicle L [N]	Ratio to baseline
Baseline	377	-	376	-
Front Plate	673	1.78	343	0.91
Side Plate	143	0.38	583	1.55
Front + Side Plate	593	1.57	377	1.00

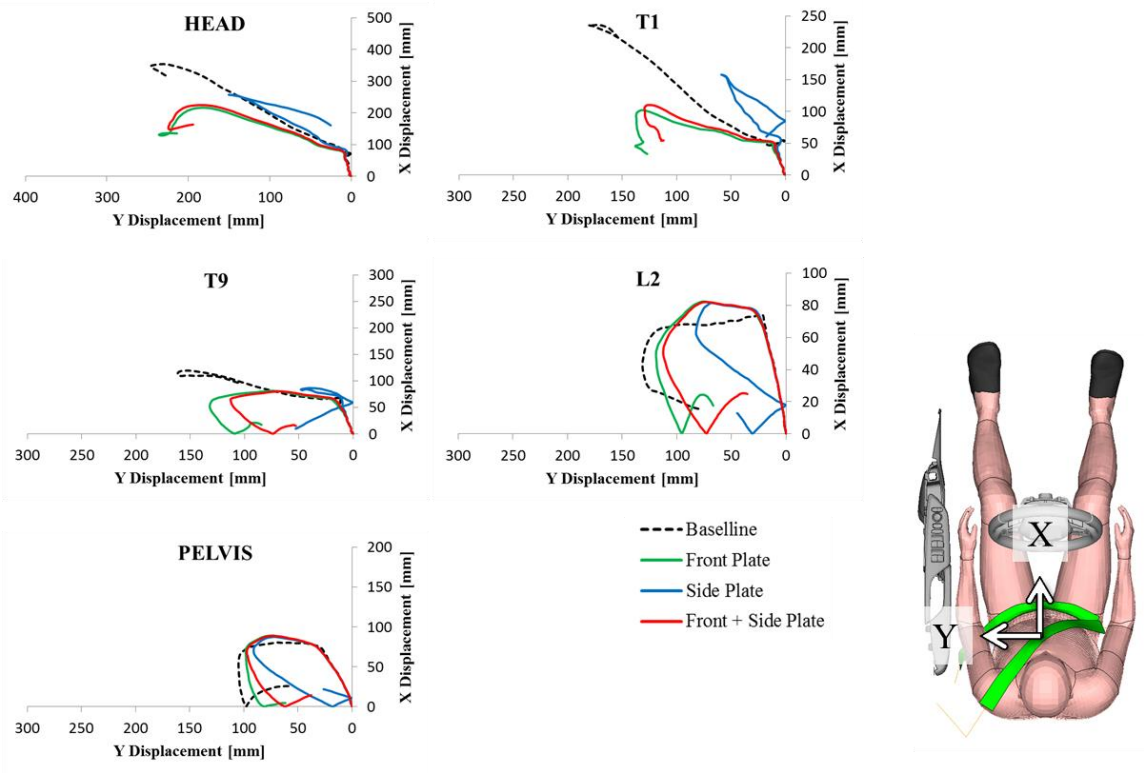

Figure 7. HBM Trajectory on XY plane

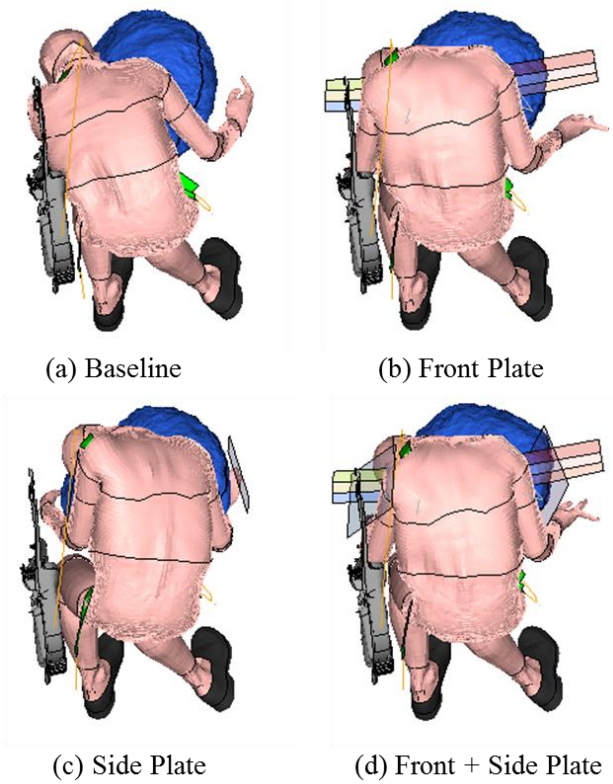

Figure 8. Comparison of the back view of HBM at maximum displacement

Maximum rib deflections at the 4th and the 8th ribs were shown in Figure 9. The amount of reduction in rib deflection was not as much as those of THOR. Front + Side Plate reduced rib deflections more than Front Plate. Side Plate did not reduce rib deflections; on the contrary, deflection on the lower part increased.

The location of rib fracture was shown in Figure 10. Rib fracture occurred on upper left side rib under baseline restraint. Front + Side Plate did not exhibit fractures on the region. On the other hand, fractures occurred on the 1st and the 2nd rib on the right side. Front Plate exhibited rib fracture on the same right side region as baseline restraint, and the other fracture occurred on the right side. Side Plate exhibited fractures on the 3rd to the 9th ribs on the left side. This was caused by the left arm which was stacked between the thorax and Side Plate.

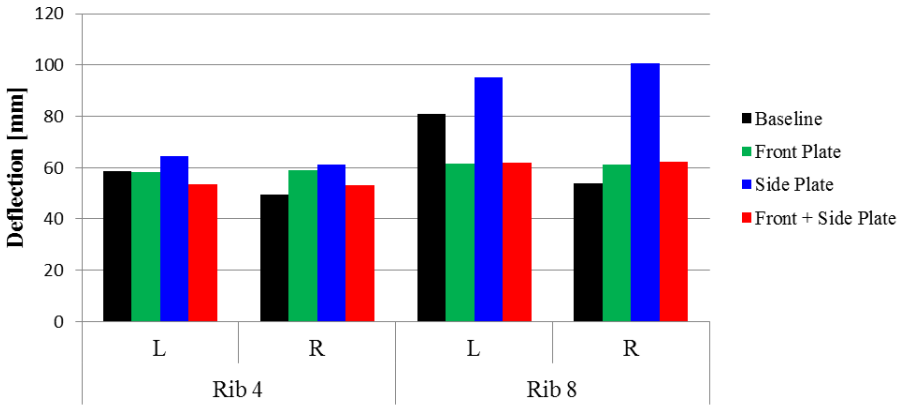

Figure 9. Comparison of rib deflection between each restraint

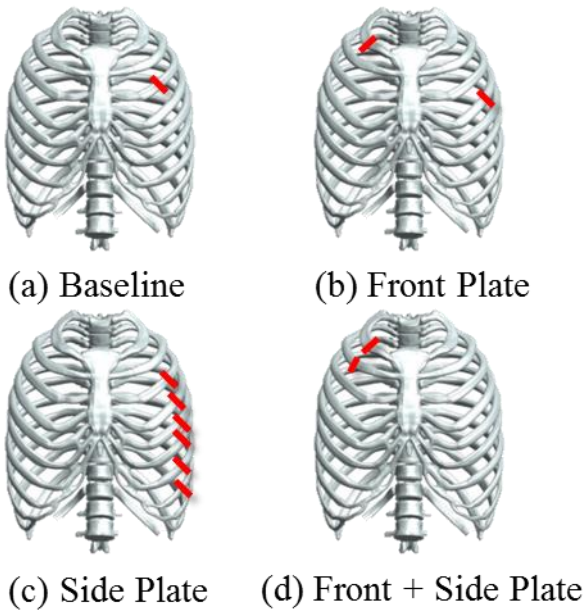

Figure 10. Comparison of rib fractures by each restraint

DISCUSSION

Simulation by THOR and HBM showed that restraint plates increased loading on the upper body. It reduced the amount of movement by half and prevented interaction with the door structure. Moreover, the simulation result indicated that the restraint on the region around clavicles and shoulders by surfaces has the possibility of reduction in thoracic injury, although high restraint force was loaded on the thorax.

This result was considered to have originated from distributing restraint force on the upper region of the thorax by Front Plate without increasing the force on the rib cage. Front Plate increased both the clavicle loads of THOR and HBM as shown in Table 3 and 6, respectively. The clavicle force of HBM showed an increase only on the right side, however, the total force on the right and left clavicle was increased. On the contrary, the clavicle load was not increased by Side Plate, although the largest contact force was generated among each four simulations of THOR and HBM. Small load distribution under Side Plate restraint was considered to result in small reduction in thoracic deflection. This result indicates that it is a highly efficient approach to distribute the restraint load on the upper thoracic region, which has a relatively high stiffness than that of other parts.

Side Plate constraint showed different occupant kinematics from other boundary conditions. Right shoulder of occupants moved forward and upper body counterclockwise rotation occurred under Side Plate, as shown in Figure 11. The rotation occurred by a combination of oblique occupant movement limited by Side Plate and seatbelt. The center of rotation is located at seatbelt interaction point. The seat belt slipped to the center of the body due to oblique occupant movement; on the other hand, Side Plate restricts sideward movement of the upper body, thus the shoulder belt location stayed on the outside of the left clavicle. In addition, left shoulder lateral movement was restricted by Side Plate, nevertheless the occupant still moves forward due to inertia force. In consequence, a counterclockwise rotation around the belt interaction point was more apt to occur and seatbelt contact force concentrates on the thorax, which was supported only by the seatbelt. The effect of belt force concentration was also implied by an increase in the lower right thoracic deflection with Side Plate on both THOR and HBM. Upper body rotation was considered to result in thoracic deflection. The effect of Front Plate was not only load distributing, but also to prevent seatbelt force concentration by upper body rotation.

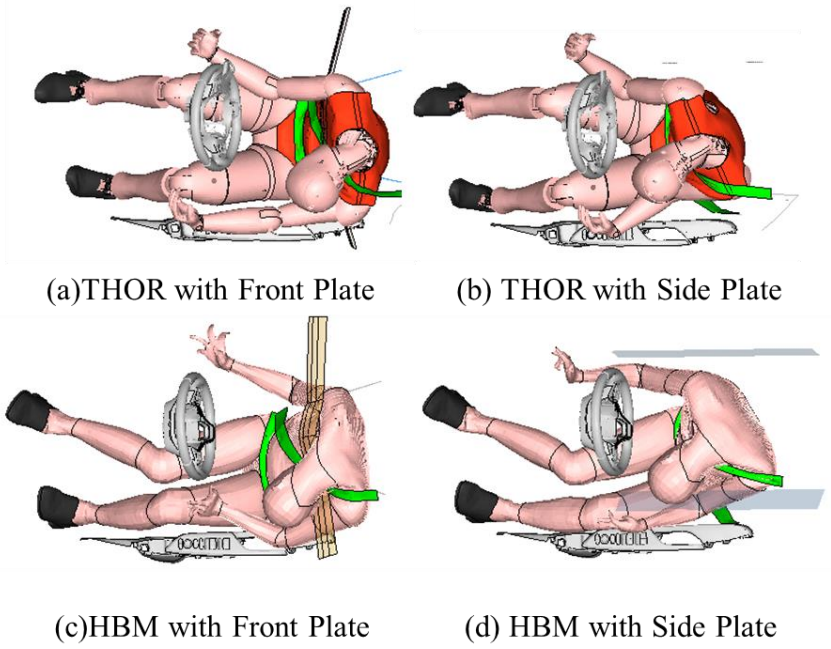

Figure 11. Counterclockwise kinematics caused by Side Plate

Meanwhile, comparing HBM and THOR simulation results, they have differences on the degree of rise in clavicle force and reduction in thoracic deflections.

Firstly, an increase in clavicle force was lower on HBM than THOR. This is considered to be ascribed to the difference of their shoulder structure. The THOR metric mimics human shoulder structure and it can straighten the shoulder, which is defined as shoulder retraction. The limit of the amount of THOR shoulder retraction was determined by the structure interactions. On the other hand, the human shoulder has more a flexible structure than THOR because the shoulder consists of bones and soft tissue such as muscles. Thus, the THOR shoulder generates a larger reaction force than that of the HBM. The small reduction in upper thoracic deflection on HBM was considered to be the result of low force distribution on the clavicles due to the difference of shoulder structure.

Secondly, the effect of Front and Front + Side Plate on HBM thoracic deflection reduction was smaller than that of THOR. This difference between THOR and HBM was considered to be ascribed to the difference of structural stiffness. Rib cage lateral stiffness of the human body is lower than longitudinal stiffness. On the contrary, lateral stiffness of the THOR rib cage is higher than longitudinal stiffness according to Maehara [7]. Since the upper body moves in an oblique direction, Front Plate generates force in both longitudinal and lateral directions. Front + Side Plate restricts directory from the side thus the lateral force on the thorax was obviously smaller than that of Front Plate. The difference in amount of the lateral direction force results in the difference in the amount of lateral thoracic deflection between Front Plate and Front + Side Plate. HBM thorax is more apt to deform by the lateral force than THOR because of the difference of lateral rib cage stiffness. As considering human body structure, this restraint approach would be preferable to combine front and side surface to restrict both upper body rotation and sideward movement. In addition, this result implied the biofidelity concerns on THOR.

Front + Side Plate occurred a rib fracture on the upper right side of the thorax despite the fracture on the upper left side region in baseline. In addition, rib fracture occurred on the side thorax through an arm by Side Plate. Since the restraint surface was connected by rigid constraint, excess load was generated on the body. In order to practically apply this restraint approach to a real vehicle as a restraint device, sort of load limiter is required.

CONCLUSIONS

This study suggested the approach which increases restraint force on the thorax to reduce the amount of upper body movement, with thoracic injury decreasing. It was confirmed that the approach has similar effects not only on the dummy but also on the human body. However, sort of load limiter is required for practical application. It was not enough to restrict only lateral movement under oblique crashes because upper body rotation had a possibility to increase thoracic injury. In addition, lateral movement generated lateral force on the thorax and induced transverse thoracic deformation. Based on these results, this restraint surface was preferable combining front and side surfaces when considering human body structure.

REFERENCES

[1] Bean, J.D., Kahane, C.J., Mynatt, M. et al., 2009. “Fatalities in Frontal Crashes Despite Seat Belts and Air Bags – Review of All CDS Cases – Model and Calendar Years 2000-2007 – 122 Fatalities.” NHTSA Technical Report: DOT HS 811 202, National Highway Traffic Safety Administration, US Department of Transportation, Washington, DC

[2] NHTSA, 2013. “Crashworthiness. Online Database.” Available at http://www.nhtsa.gov/Research/Crashworthiness

[3] Iraeus, J., Lindquist, M., Wistrand, S., Sibgård, E., Pipkorn, B., 2013. “Evaluation of Chest Injury Mechanisms in Nearside Oblique Frontal Impacts.” 57th AAAM, Annual Conference September 22-25

[4] Rudd, R.W., Scarboro, M., Saunders, J., 2011. “Injury Analysis of Real-World Small Overlap and Oblique Frontal Crashes.” Proc. Int. Tech. Conf. Enhanced Safety Vehicles 2011

[5] Lindquist, M.O., Hall, A.R., Björnstig, U.L., 2006. “Kinematics of Belted Fatalities in Frontal Collisions: A New Approach in Deep Studies of Injury Mechanisms.” Journal of Trauma; 61: p.p. 1506-1516

[6] Brumbelow, M.L., Farmer, C.M., 2013. “Real-world injury patterns associated with hybrid III sternal deflections in frontal crash tests.” Traffic Injury Prevention, vol. 14, issue 8a

[7] Maehara, K., Hikida, K., Shibata, S., Mikami, H., Dokko, Y., Ohhashi, K., 2018. “A Study on the Biofidelity of the Thorax Response of the Next-generation Frontal Crash Test Dummy THOR. (Japanese)” Journal of Society of Automotive Engineers of Japan (JSAE), vol. 49, 6, p.p. 1261-1266

[8] HUMANETICS Innovative Solutions, 2016, “THOR-50th Metric V 1.4.1 LS-DYNA Model Technical Report User’s Manual”

[9] Ito, O., Dokko, Y., Ohashi, K., 2009. “Development of adult and elderly FE thorax skeletal models.” SAE Technical Paper 2009-01-0381

[10] Ito, Y., Dokko, Y., Motozawa, Y., Mori, F., Ohashi, K., 2012. “Kinematics Validation of Age-Specific Restrained 50th Percentile Occupant FE Model in Frontal Impact.” SAE Technical Paper 2012-01-0565

[11] Lessley, D.J., Salzar, R., Crandall, J., Kent, R., Bolton, J.R., Bass, C.R., Guillemot, H., Forma, J.L., 2010. “Kinematics of the Thorax under Dynamic Belt Loading Conditions.” International Journal of Crashworthiness, vol15 No.2, p.p. 175-190

[12] Shaw, G., Parent, D., Purtsezov, S., Kerrigan, J., Shin, J., Crandall, J., Zama, Y., Ejima, S., Kamiji, K., Yasuki, T., 2009. “Frontal Impact PMHS Sled Tests for FE Torso Model Development.” Proceedings of IRCOBI Conference (York, United Kingdome, Sep. 9-11)

RESEARCH OF PEDESTRIAN INJURY REDUCTION MECHANISM BETWEEN THE BEGINNING OF THE COLLISION AND FALL OF THE GROUND

Hidetoshi, Nakamura Kenyu, Okamura Masaki, Umezawa Osamu, Ito Hiroyuki, Asanuma
Honda R&D Co., Ltd. Automobile R&D Center
Japan

Masato, Sasaki
Honda R&D America, Inc.,
United States

Paper Number 19-0285

ABSTRACT

Recently, safety standards for pedestrian protection in third party evaluation typified by NCAP have been increased, and safety performance of vehicles is improving. Among them, the safety performance of the bonnet hood has been particularly enhanced in terms of injury index represented by HIC from the viewpoint of head protection. However, according to the accident statistics, pedestrian fatalities have remained high, and the causes of death include not only the vehicle injury but also the ground injury. Therefore, it is necessary that pedestrian protection technology includes not only vehicle but also ground. In order to reduce the number of pedestrian fatalities, this research focused on the control of the pedestrian's behavior after accidents and studied methods that can reduce head injuries caused by various factors.

In many pedestrian accidents, the speed difference between the vehicle and the pedestrian is large. The pedestrian is accelerated to the speed of the vehicle due to force input from the vehicle. Therefore, if pedestrians can be gently accelerated, the action is expected to be effective in reducing various injuries. For this purpose, it is important to restrain the pelvis close to the center of gravity at the beginning of a collision. As for the ground, by controlling behavior so that a pedestrian can fall from their leg to the ground, head injury can be greatly reduced. For this purpose, it is important to reduce local input to the legs and suppress the swinging up of the legs. In this research, the effect of early pedestrian pelvis restraint was verified using a pedestrian dummy (POLAR) and modified vehicle model. Head injury was evaluated by using Convolution of Impulse Response for Brain Injury Criterion (CIBIC). For verification, a sedan type vehicle with a small initial input to the pedestrian's pelvis was used, and the collision speed was limited to 40 km/h. Then, based on the vehicle model, which can change the input part and the load characteristics, the relationship between the behavior of the pedestrian and the injury value was studied.

In this research, it was confirmed that the angular velocity of the upper body around the center of gravity is reduced by the early input to the pedestrian pelvis, and it is effective for various injury values of the head. It was also confirmed that the swinging up of the leg can be suppressed by controlling the input to the pedestrian leg.

Although collision speed and physique are limited in this research, it is necessary to consider the influence of the difference in physique and speed. Furthermore, it is important to integrate with external sensing technology in order to deploy the pelvis restraint device in front of the vehicle before a collision.

In this research, it was confirmed that a pedestrian behavior control device may be effective for reduction of generalized injury by vehicle crush and secondary damage by the ground as one solution for further reduction of the number of pedestrian fatalities.

INTRODUCTION

Traffic accident fatalities in Japan are trending downward, going from 6,415 fatalities in 2006 to 3,694 in 2017[1]. However, Pedestrian fatalities accounted for about 36% of overall fatalities and traffic accident, and the ratio is the highest among the fatality group. In terms of pedestrian safety performance, evaluation using a subsystem impactor

is performed, and head injury is evaluated by HIC. Accidents in the real world include brain damage due to the influence of head rotation at the time of a collision and injuries on the ground. As current sub-system impactors are incapable of evaluating injury caused by head rotation and impact with the ground, a method is needed to evaluate the whole body behavior of the pedestrian throughout the series of events in a pedestrian accident. In many pedestrian accidents, the speed difference between the vehicle and the pedestrian is large. The Pedestrian is accelerated to the speed of the vehicle due to force input from the vehicle, and the upper body rotates toward the vehicle. The pedestrian's head rotates along with the behavior of the upper body, hitting the vehicle. Next, the pedestrian is thrown to the ground by the speed difference with the vehicle and sustains injury. The head injury received on the ground depends on the falling behavior, and allowing the legs to land on the ground could reduce the risk of head injury. (Figure 1) With a focus on the fact that these injuries occur at each step along the series of behavior in pedestrian accidents, in this study, the effect of controlling pedestrian behavior from the point of vehicle impact until ground contact was verified.

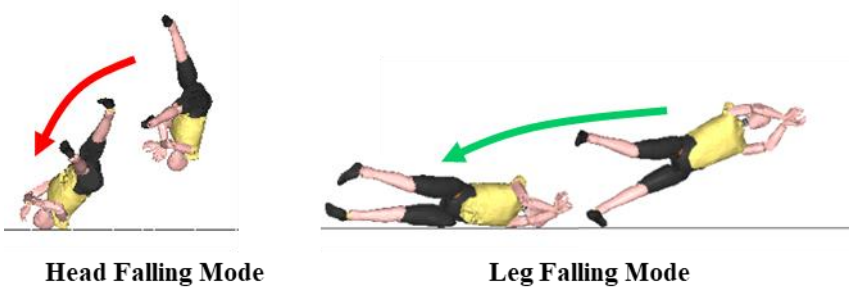

Figure 1. Falling mode from the vehicle

METHODS

Verification of effects from early pelvis restraint

In this study, pedestrian FE model was used POLAR [2]. This model simulates POLAR which was developed as a dummy for pedestrian injury measurement, and enables the verification by actual vehicle test in the course of study. As pedestrian behavior is thought to depend on how the center of gravity is restrained, the vehicle used for verification was a sedan model, which exerts little force on the pelvis close to center of gravity. To verify the effect of early pelvis restraint, a pelvis restraining surface was added to a standard sedan model vehicle. The restraining surface and vehicle were connected by a spring element with load-displacement properties. A single input model to the legs was also prepared for comparative verification, applying the same load-displacement properties as were applied to the pelvis. (Figure 2) (Table 1) The added spring element was determined by the contact load and vehicle side displacement when the pedestrian model was struck. Vehicle models with different restraint characteristics were crashed into the pedestrian model at 40 km/h.

Evaluation criteria

As the pedestrian model response, longitudinal velocity at the pelvis and the angular velocity around the pedestrian's center of gravity were confirmed. Brain injury of Pre-Impact phase was evaluated using Convolution of Impulse Response for Brain Injury Criterion (CIBIC) from the research of Takahashi et al. [3] The trajectory of the head to the vehicle was measured to verify the behavior of the pedestrian dummy model.

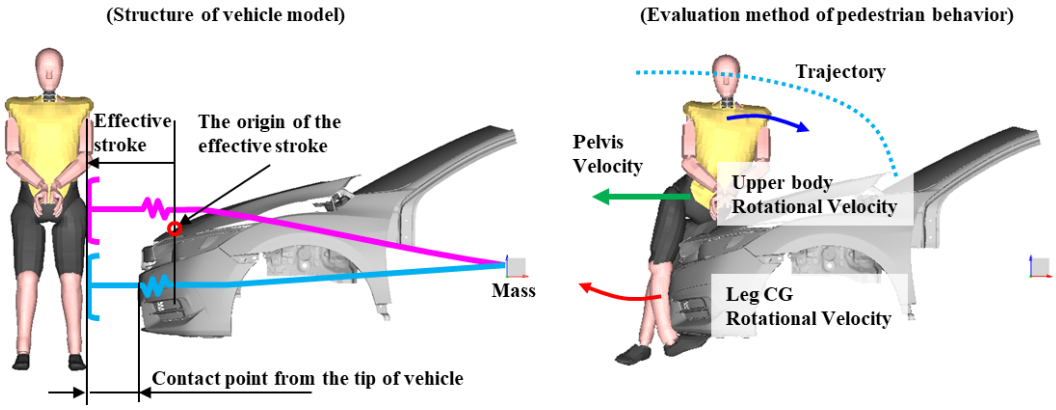

Figure 2. Structure of vehicle model and evaluation method of pedestrian behavior

Table 1.
Restraint characteristics

	Contact point from vehicle (mm)	Spring characteristic for Pelvis			Spring characteristic for Leg		
		Force (N)	Effective Stroke (mm)	Energy (J)	Force (N)	Effective Stroke (mm)	Energy (J)
Original	N/A	N/A	N/A	N/A	N/A	N/A	N/A
Case (a)	260	4.0	420	840	N/A	N/A	N/A
Case (b)	230	4.0	390	840	N/A	N/A	N/A
Case (c)	150	4.0	310	620	N/A	N/A	N/A
Case (d)	100	4.0	260	520	N/A	N/A	N/A
Case (e)	50	4.0	210	420	N/A	N/A	N/A
Case (f)	0	4.0	160	320	N/A	N/A	N/A
Case (g)	-50	4.0	110	220	N/A	N/A	N/A
Case (h)	260	N/A	N/A	N/A	4.0	420	840
Case (I)	230	N/A	N/A	N/A	4.0	390	840
Case (j)	150	N/A	N/A	N/A	4.0	310	620
Case (k)	100	N/A	N/A	N/A	4.0	260	520
Case (l)	50	N/A	N/A	N/A	4.0	210	420

RESULTS

Comparisons of movement

The pelvis longitudinal velocity, angular velocities of the upper body and legs around the center of gravity, cranial velocity perpendicular to the vehicle, and head trajectory, all taken when the restraint characteristic vehicle models and the pedestrian dummy models collided, are given in Figures 3-7, respectively. As the collision progresses, input force from the vehicle body clearly accelerates the pedestrian, with the upper body being wrapped onto the vehicle by a rotational motion and the lower body swinging up. In Figure 3 and Figure 7, the pelvis velocity of original case occurs slowly due to no direct input to the center of gravity and it is confirmed to be large head displacement. In the pelvis restraint model, change in the upper body angular velocity and head collision velocity is dependent on the restraint characteristics. In Case (a), the pelvis slowly accelerates from the start, and the center of gravity is restrained properly. Meanwhile, while the upper body angular velocity for the leg restraint model exhibits the same tendencies as with the pelvis restraint model, the leg restraint model showed no change in head collision velocity, and head trajectory was equal. In terms of head behavior, Case (a) in the pelvis restraint model collided most forward. In terms of leg swing-up, while both the pelvis restraint model and leg restraint model reduced the initial generated angular velocity, neither were very effective overall.

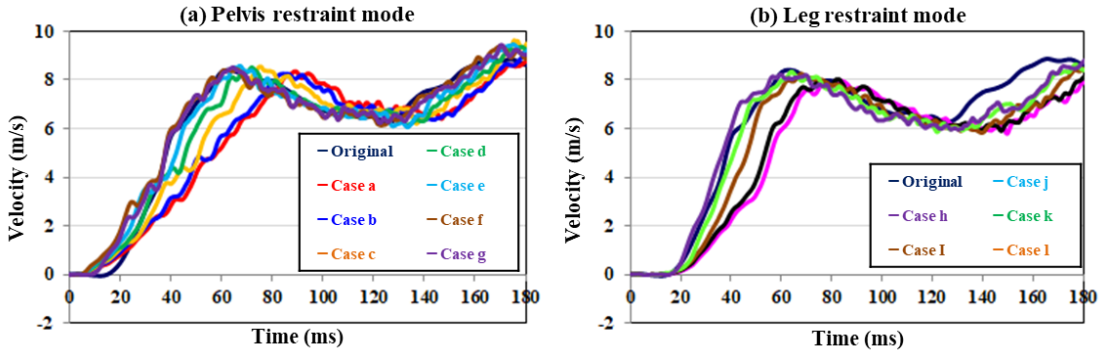

Figure 3. Time history of Pelvis Longitudinal Velocity

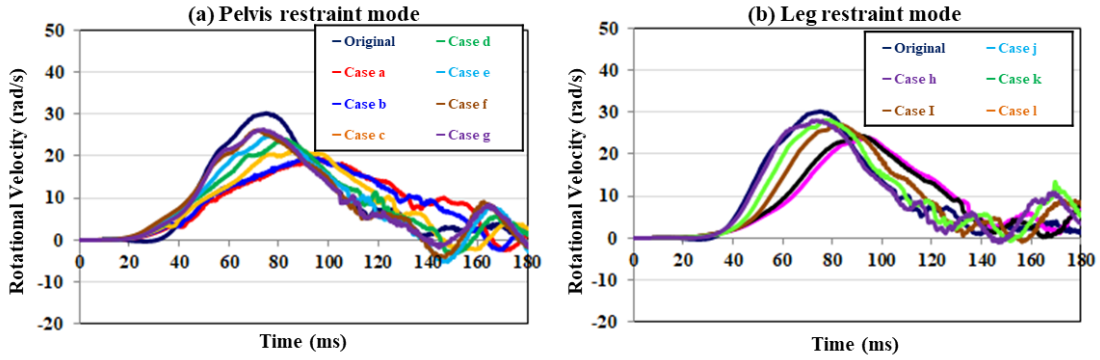

Figure 4. Time history of Upper Body Rotational Velocity

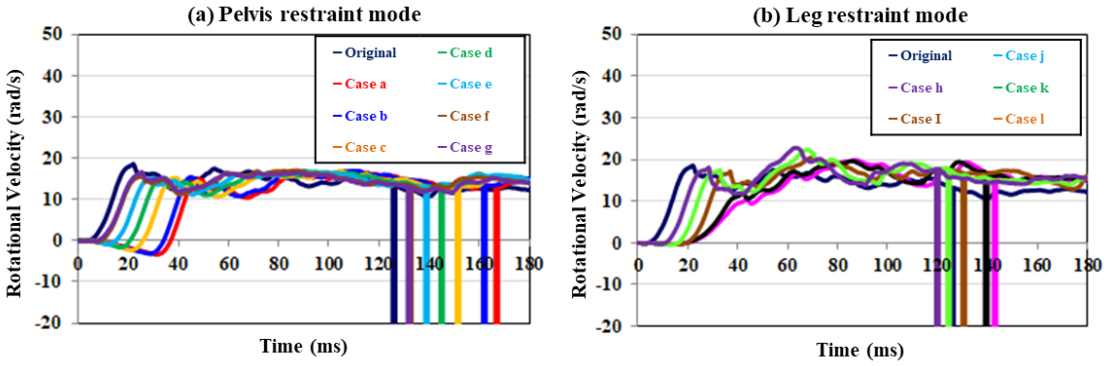

Figure 5. Time history of Leg CG Rotational Velocity

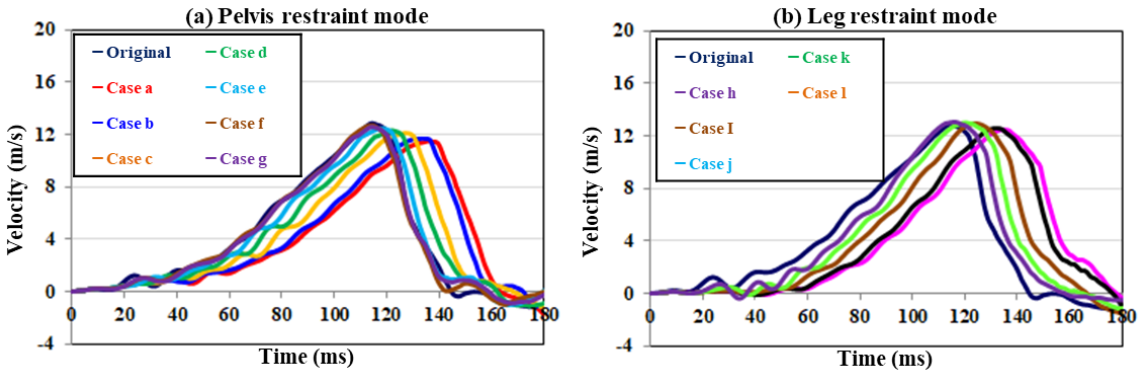

Figure 6. Time history of Pelvis Longitudinal Velocity

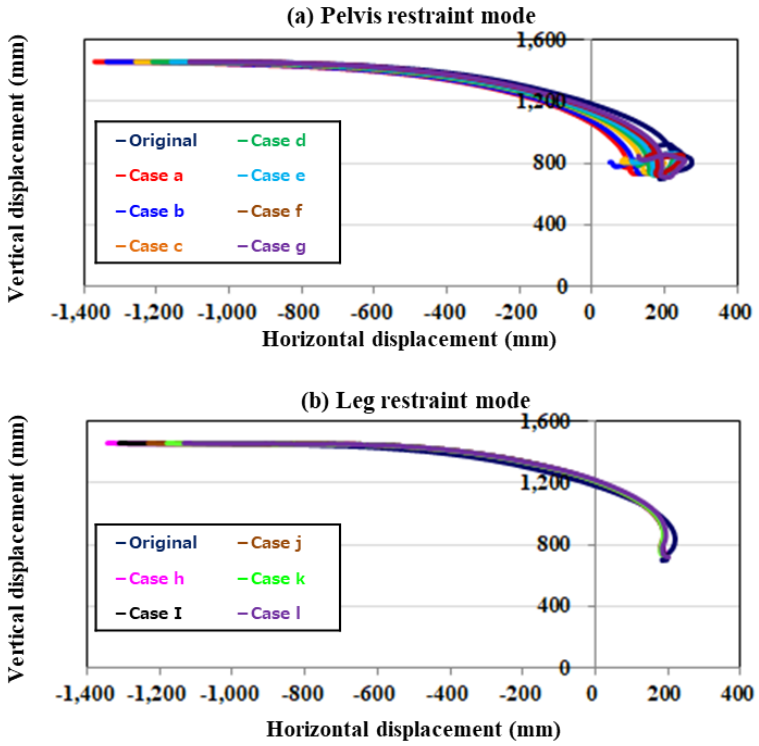

Figure 7. Trajectories

Comparison of injury levels

In this study, brain injury was evaluated in the time region before head collision. Based on the original case, CIBIC of each parameter study case is represented by ratio. (Figure 8) Case (a) of the pelvic restraint model reduced CIBIC during rotation of upper body, and it was found that it is effective to restrain the pelvis close to the center of gravity of the human body to reduce brain injury.

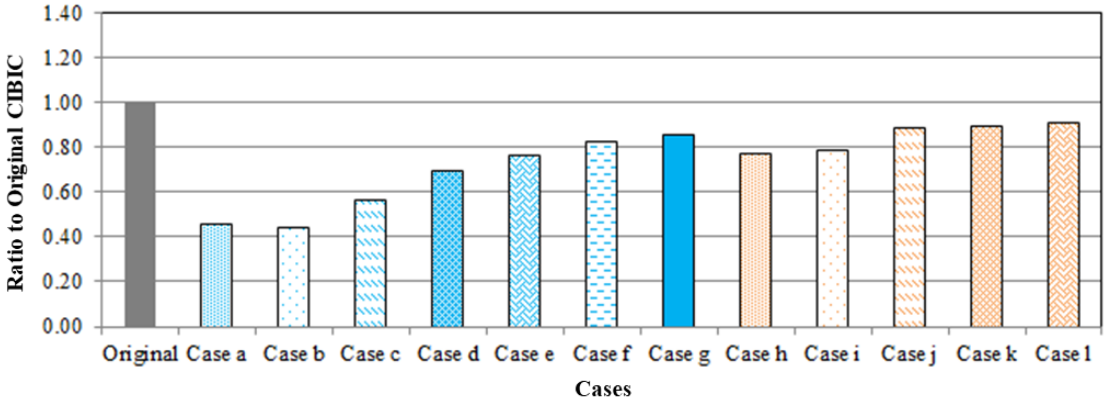

Figure 8. Injury value ratio to original during of upper body rotation

DISCUSSION

Mechanisms for reducing injury

Internal force of the pedestrian dummy was analyzed to understand the brain injury reduction mechanism by the pelvis early restraint. (Figure 9)

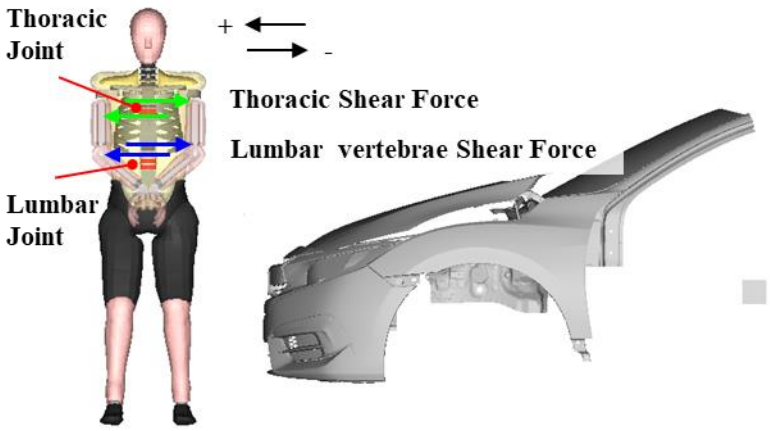

Figure 9. Dummy internal force analysis

The intracranial strain waveform and pedestrian dummy behavior generated by head rotation in the Original case is shown in Figure 10 and Figure11. As shown Figures 10 to 11, CIBIC before head collision is generated 120 ms prior to collision between the vehicle and head. Yanaoka mentioned that pedestrian CIBIC showed multiple peaks from in pre-impact to impact phase [4]. The result of this study showed the same tendency. Thus, internal force was analyzed within the range of 0-120 ms.

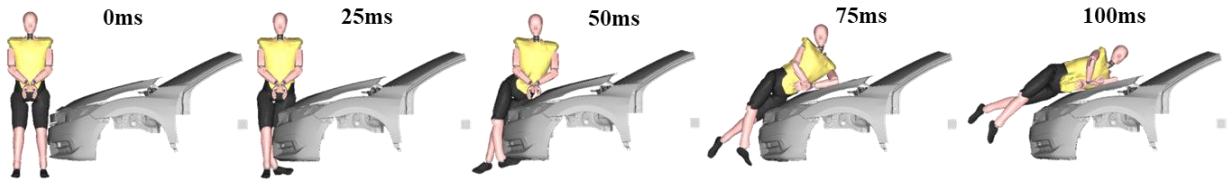

Figure 10. Pedestrian dummy behavior in original case

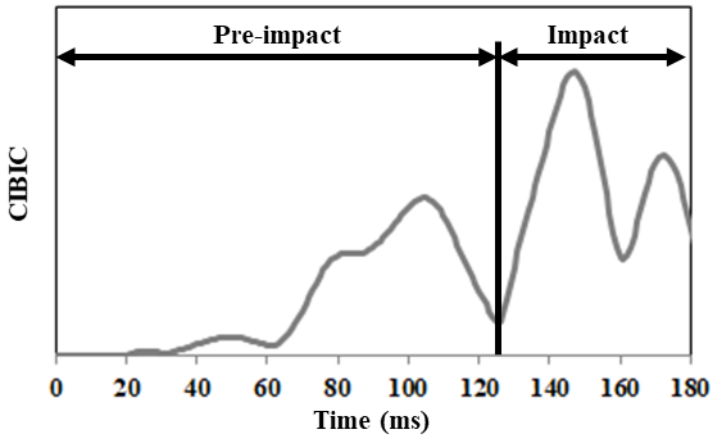

Figure 11. CIBIC waveform of the original case

In the pelvis restraint model and leg restraint model, shear force generated in the thoracic and lumbar vertebrae were measured to verify the impact to head rotational behavior. (Figure 12, Figure 13) For Case (a), the shear force of thoracic was the closest to 0 and the shear force of lumbar vertebrae was the smallest. This result shows that the dummy rotation behavior has changed depending on the restraint characteristics.

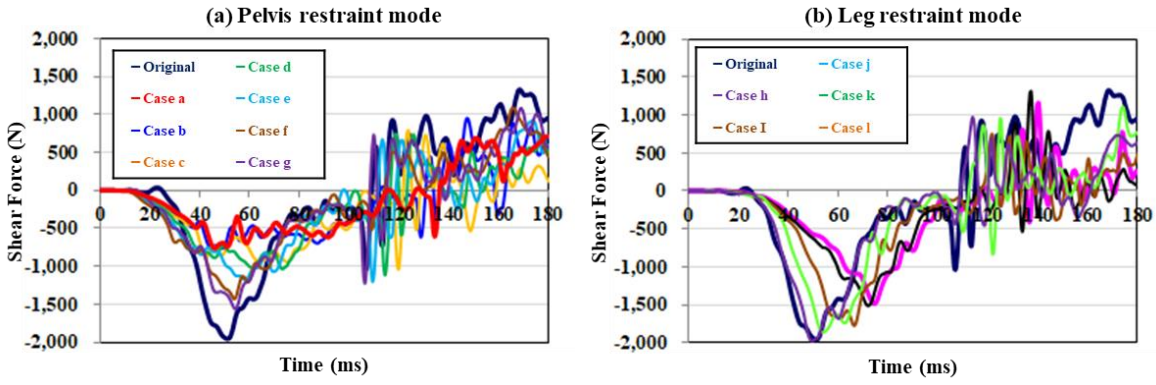

Figure 12. Time history of Thoracic shear force

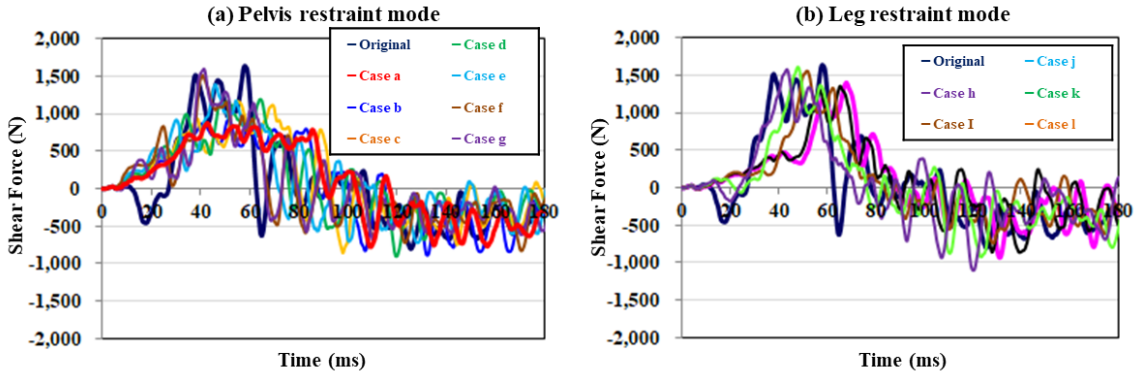

Figure 13. Time history of lumbar vertebrae shear force

The relation between the CIBIC levels of each restraint characteristic with the Original level being 1 and the thoracic shear force peak values up to 120 ms is shown in Figure 14. In Figure 14, there is a clear correlation between CIBIC levels and thoracic shear force. As head rotation is generated by upper body rotation and inertia of the head, reduction the upper body rotation through this interaction within the pedestrian dummy reduced the brain injury. Next, the relation between thoracic and lumbar vertebrae shear force is illustrated in Figure 15. In Figure 15, there is a clear correlation between thoracic and lumbar vertebrae shear force, softly restraining the dummy with its center of gravity have efficacy for brain injury reduction.

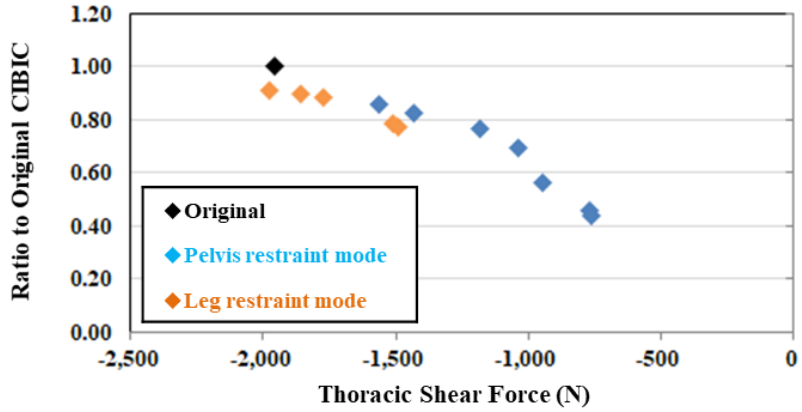

Figure 14. Relationship between Raito to original CIBIC and Thoracic Shear Force

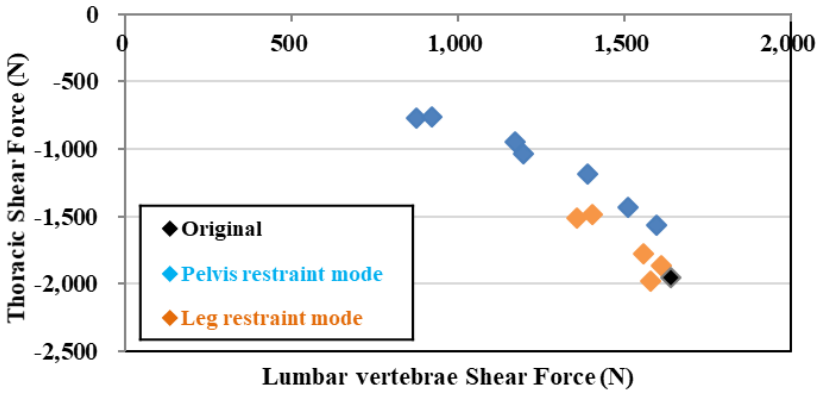

Figure 15. Relationship between Thoracic Shear Force and Lumbar Vertebrae Shear Force

LIMITATION

In this study, pedestrian dummy models were used for verification. The cervical characteristics affecting head rotation need to be compared with human body characteristics. This study focused on an AM50% model at a collision velocity of 40 km/h, leaving the impacts at different physiques and velocities as outstanding issues for future studies to consider. More study is also needed on how to reduce CIBIC when head and vehicle collide. This will require tests using actual pedestrian dummy to confirm the mechanism for reducing injury criteria value.

CONCLUSIONS

In this study, the effect of reducing injury by controlling the behavior of pedestrians between the beginning of collision and the fall of the ground was verified. In order to control the behavior of pedestrian, it is important to softly restraining of the center of gravity close to the pelvis, and as a result, it was confirmed that it is effective in reducing the brain injury due to head rotation. Although it was effective to reduce the leg angular velocity with respect to the ground influence and suppress the swinging up of the leg, it was confirmed that the effect was small with only the pelvis restraint alone.

REFERENCES

[1] Institute for Traffic Accident Research and Data Analysis, “2017 Traffic Accident Statistics” (in Japanese).

[2] Akiyama, A., Okamoto, M., Kanayama, Y., Takahashi, Y., “Full-scale Validation of a New Pedestrian Dummy” JSAE Spring Congress Proceedings, No. 39-10, Paper Number 20105321, 2010 (in Japanese).

[3] Takahashi, Y., Yanaoka, T. 2017. "A study of injury criteria for brain injuries in traffic accidents." Paper presented at: 25th ESV conference, Paper Number: 17-0040.

[4] Yanaoka, T. and Takahashi, Y. and Sugaya, H. and Kawabuchi, T. 2019. “INVESTIGATION OF STRAIN-INDUCED BRAIN INJURY MECHANISM IN SIMULATED CAR ACCIDENTS.” 26th ESV conference, Paper Number: 19-0070

DEVELOPMENT OF A SAFETY ASSURANCE PROCESS FOR AUTONOMOUS VEHICLES IN JAPAN

Jacobo, Antona-Makoshi
Nobuyuki, Uchida
Kunio, Yamazaki
Japan Automobile Research Institute (JARI)
Japan

Koichiro, Ozawa
Honda R&D Co. and Japan Automobile Manufacturers Association, Inc. (JAMA)
Japan

Eiichi, Kitahara
Nissan Motor Co. and JAMA
Japan

Satoshi, Taniguchi
Toyota Motor Co. and JAMA
Japan

Paper Number 19-0000

ASBTRACT

In order to introduce autonomous driving systems into the market, socially acceptable and technically sound safety assurance methodologies need to be agreed. In Japan, vehicle manufacturers and traffic safety experts have gathered regularly under the auspice of the Ministry of Economy, Trade and Industry, in a coordinated initiative to harmonize the required collaborative research, methodology development and standardization activities. Within this initiative, a comprehensive safety assurance process is to be agreed and made publicly available. The process shall be driven by top safety goals defined by authorities, shall consider the systems' performance limitations, and must be supported by state-of-the-art methodologies and real-world data. At this point, consensus on the overall safety assurance process for SAE Level 3+ autonomy in motorways as well as on the methodology to develop testing scenarios has been achieved and the results are hereby reported. The process and methodology are directly applicable to support the development of systems towards a safer autonomous driving society.

INTRODUCTION

Socially acceptable and technically feasible safety assurance methodologies and criteria need to be established as state-of-the-art global standards for a safe deployment of Autonomous Driving (AD) vehicles into the market. In order to guide this deployment in different regions, corresponding authorities such as the US National Highway Traffic Safety Administration, the UN Economic Commission for Europe, and the Ministry of Land Infrastructure, Transportation and Tourism of Japan have released their own safety guidelines [1, 2].

Product failures and design errors can be covered by an existing functional safety standard ISO26262:2011 [3]. This standard is used to evaluate if a process conforms and hence can be considered safe. In particular, the Safety of the Intended Functionality (SOTIF) process contained within the standardad provides coverage of SAE Level 2 AD systems. However, a specific safety assurance process for non-failure conditions that considers SAE Level 3 and higher (3+) AD systems and their performance limitations has not been established yet.

Traditional proving ground and field operation testing are insufficient to proof safety for vehicles with highly autonomous vehicles [4], and the incorporation of complementary virtual testing methodologies is essential. To support the development of these methodologies, joint efforts between industry and authorities are required.

In Japan, vehicle safety and AD experts have gathered regularly supported by the Ministry of Economy, Trade and Industry under the umbrella of the JAMA AD safety assurance working group, in a coordinated initiative to harmonize the required collaborative research, methodology development and standardization activities. A first scope for application of the developed methodologies has been set to SAE level 3+ AD systems on motorways [1].

Within this initiative and scope, our aim is to propose an AD system safety assurance engineering process for non-failure conditions that considers the system's performance limitations. A summary of the overall process is provided, followed by detailed description of the methodology to define virtual test scenarios and related criteria required to assure AD systems safety.

ENGINEERING FRAMEWORK FOR AD VEHICLE TEST SCENARIOS

A schematic of the overall safety assurance process developed is shown in Figure 1. The schematic is based on the project management V-model typically applied to develop connected vehicles, advanced driver assistance systems (ADAS) and AD systems [5]. The process covers all the product development stages from planning, design, implementation, evaluation (verification and validation), to release. Descriptions of each of these steps are provided below.

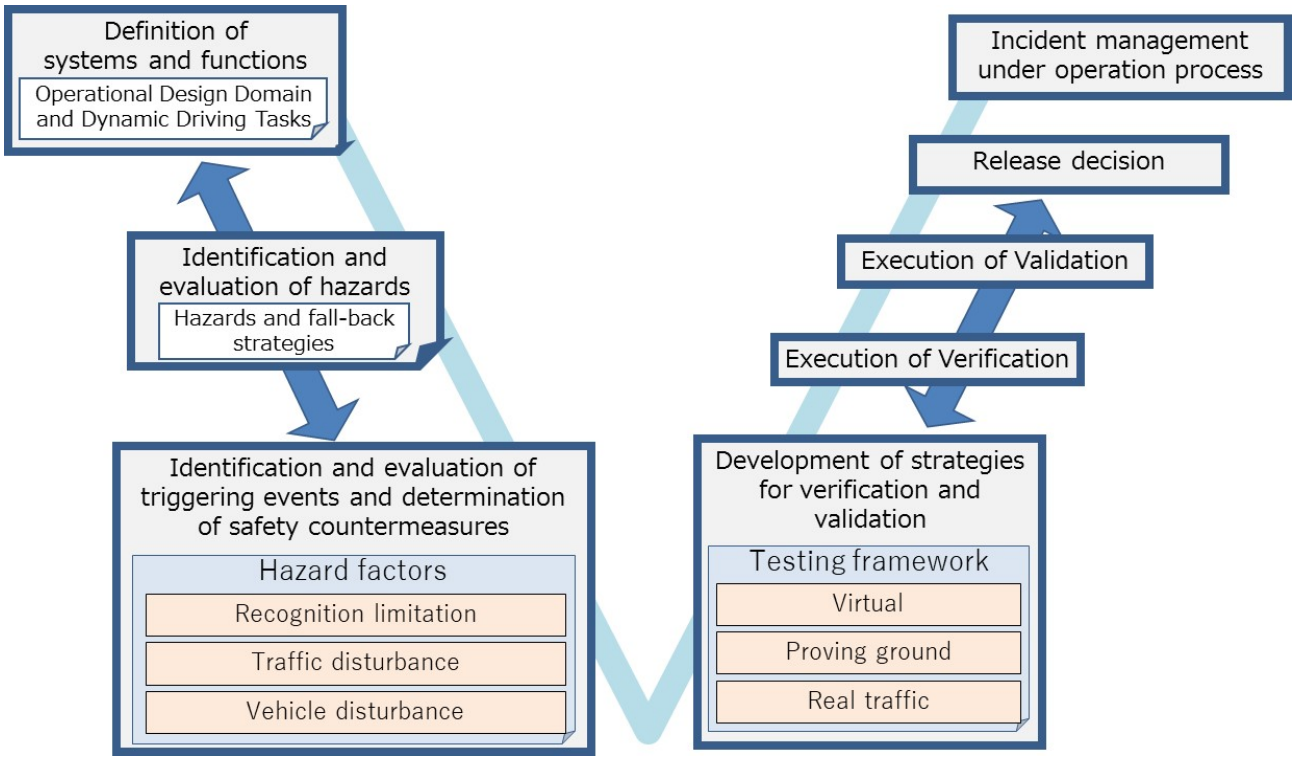

Figure 1 Overall scheme of the safety assurance process

Definition of systems and functions: Operational Design Domain and Dynamic Driving Tasks

The complete safety assurance process is to be conducted within well-defined and pre-determined operational and responsibility share boundaries. Therefore, upon the collection of existing information concerning the purpose and specification of different AD systems and functions, the Operational Design Domain (ODD), defined as the boundaries within the system is intented to operate, is described at the initial stage. ODD contents shall include at least information on roadway types, location within the road, vehicle speed ranges, and environmental conditions. The ODD definition needs to be structurized in a way that the user can understand and operate the AD system safely. On the other hand, the test scenarios that will be developed shall consider the ODD in a technically comprehensive way based on the physics of the system. For example, when rainy conditions are included in the ODD, the term 'rain' may be enough to communicate with the user, but the scenario might consider the effect of rain from different physical viewpoints such as the possible influence of raindrops on sensor performance, or the influence of rain on vehicle dynamics due to a decrease of the friction coefficient between the tires and the wet road surface. In order to organize all the ODD related information concerning the vehicle and its surroundings in a systematic manner, the Goal Structuring Notation methodology is applied [6]. This methodology is a standardized graphical argumentation technique widely applied to document and present safety goals and arguments in a clearer format than plain text [6].

The Dynamic Driving Tasks (DDT) and the responsibility share between the system and the driver are also defined at this point. It is noted that clarifying the responsibility share in accidents involving other vehicles that committed traffic rule violations or emergency rescue operations is particularly challenging, and solutions beyond vehicle development

engineering may be required (e.g. crashes involving roads with potholes due to lack of road maintenance; crashes involving vehicles running in the wrong direction; or recognition limitations to take appropriate interventions in crashes involving emergency vehicles such as ambulances or police cars).

Identification and evaluation of hazards

Hazards, defined as potential sources of harm [2], are identified and evaluated at this point. Since hazards can be expressed at the vehicle behavior level, the ISO 26262 framework may be applied and the standardized hazard and risk assessment results may be diverted for the current purpose. If the hazards identified are judged unacceptable, a validation target shall then be specified for further analysis in the validation process. In addition, actuation strategies can be implemented at this stage to ensure safety for all traffic participants for the cases that fall within the ODD ranges but face hazards that the system is not designed to cope with (eg. when the system detects that the accuracy of a sensor measurement is lower than specified), or for cases that fall outside the ODD range (eg. when the vehicle enters a road type in which the system is not intended to work).

Triggering events and determination of safety countermeasures

Triggering events, defined as events that cause a risk to take place, are accounted for in this step. For hazards that have been judged unacceptable, the triggering events are analyzed under vehicle control categories, including traffic disturbance, recognition limitations, and vehicle disturbance sub-categories.

Traffic disturbance relates to traffic scenarios that may lead to a hazard as a combination of "road geometry", "ego-vehicle behaviour", and "surrounding vehicle location and motion". In order to handle a large amount of possible traffic disturbances, a well structured catalogue of foreseeable scenarios is jointly built by AD vehicle developers and traffic safety experts. The following sections in this paper ellaborate in detail on the construction of such catalogues.

Recognition limitations refer to conditions in which the sensor system fails to correctly recognize hazard factors. Examples include part mounting conditions (e.g. unsteadiness related to sensor mounting or manufacturing variability), environmental conditions (e.g. sensor cloudiness, dirt, light, etc), or vehicle conditions (e.g. vehicle inclination due to uneven loading that modifies sensor orientation, or vehicle state due to sensor shielding with external attachments such as bicycle racks).

Vehicle disturbance relates to situations in which, recognition and vehicle control command works correctly, but the vehicle fails to follow the control command. These may include vehicle conditions (e.g. total weight, weight distribution, mechanical functions) and driving environment including aspects that may affect vehicle dynamics (e.g. road surface irregularities and inclination, road friction, wind).

The safety countermeasures that will be applied and the systems and features that will intervene to avoid or mitigate the identified risk need to be decided for the triggering events that have been judged to require intervention. In addition, after

confirming that the intervention is valid for the triggering event, the necessary functions may be either improved or newly developed according to the definition of systems and functions, and the system shall be updated accordingly.

Strategies for verification and validation

The strategies to validate and verify the system and to secure its safety are defined at this point. These strategies combine intensive virtual testing, with comparatively limited amount of physical tests in proving grounds and real-traffic environments.

The verification sub-process shall check the mathematical and physical correctness of the systems and functions developed and the safety countermeasures applied. It shall also confirm that all the safety specifications and requirements from the perspective of sufficiency of sensor-, algorithm- and actuator-related countermeasures are fulfilled.

The validation sub-process confirms that the systems and components including the safety countermeasures applied do not lead to an unreasonable risk for the traffic participants, and that the validation target previously defined is achieved, therefore demonstrating safety of the AD System.

Release decision

The release decision sub-process confirms that the safety of the AD system can be explained and that the remaining risk (if any) falls within an acceptable tolerance by reviewing whether adequate actions were implemented according to the results of the safety assurance process. Finally, based on the review results, it is decided whether the release of the system is acceptable or not.

Social contextualization of the engineering framework

The corresponding authorities in different regions are releasing safety guidelines. For example, the Japanese government recently released a technical safety guideline for AD systems, which reads ‘Automated vehicle systems, under their Operational Design Domain (ODD), shall not cause any traffic accidents resulting in injury or death, that are rationally foreseeable and preventable’ [1]. By contextualizing the AD systems safety assurance engineering framework proposed (Figure 1) with respect to governmental safety guidelines proposed by authorities, it is possible to develop engineering workframe that covers both social acceptance and technical aspects of the AD vehicles.

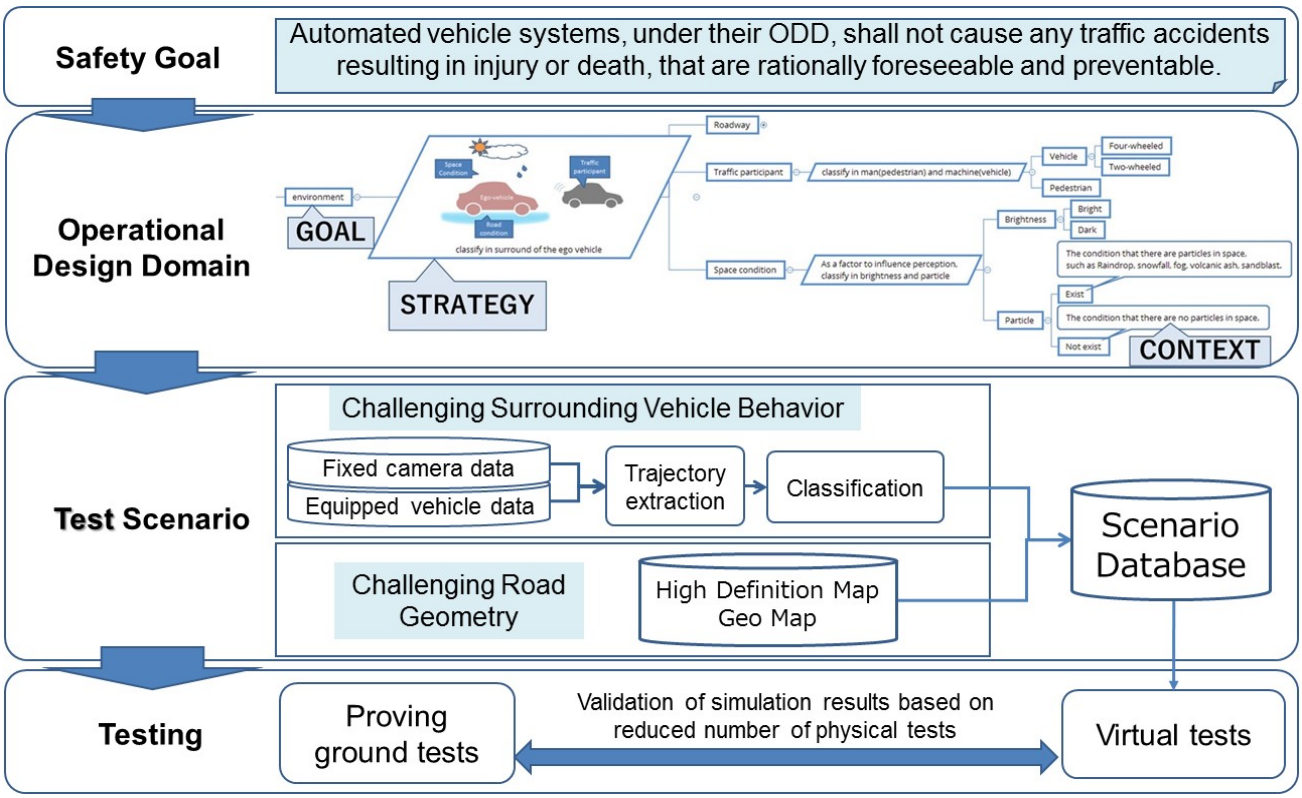

Figure 2 Top-down approach for social contextualization of the engineering framework for AD safety assurance

A scheme that illustrates such contextualization is shown in Figure 2. The scheme follows a top-down approach in which the ODD is defined considering the top safety goal, and test scenarios and validation strategies are developed under the same framework based on real-world data.

In order for AD test scenarios to be able to address the safety gudelines by the Japanese government, technical definitions for foreseeability and preventability becomes necessary. Foreseeable conditions are described as technically possible scenarios with quantitative parameter ranges. Preventable conditions are described as avoidable scenarios by means of technical intervention. The inter-relation between forseeability and preventability is illustrated in Figure 3. The focus of the scenario catalogue development in the current paper focuses on foreseeable and preventable scenarios according to the figure. It is noted at this point that preventing crashes in situations that involved other vehicles that committed traffic rule violations or extreme maneuvers is particularly challenging, and strategies complementary to vehicle engineering may be required (e.g. crashes involving vehicles running in the wrong direction at very high speeds).

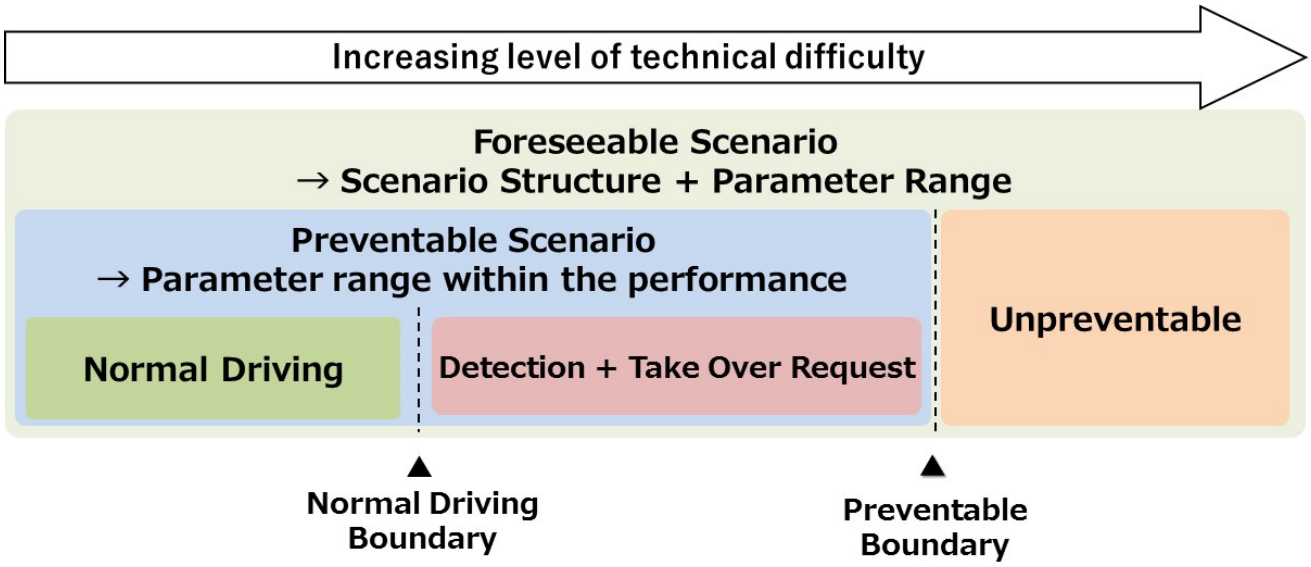

Figure 3. Forseeable and preventable scenarios and their inter-relations

Approach to AD safety test scenarios

Figure 4 summarizes the technical approach to develop test scenarios including quantified parameter ranges for AD vehicle safety assurance. First, scenarios are structured in order to cover holistic root causes from the point of view of the physics of the AD systems.

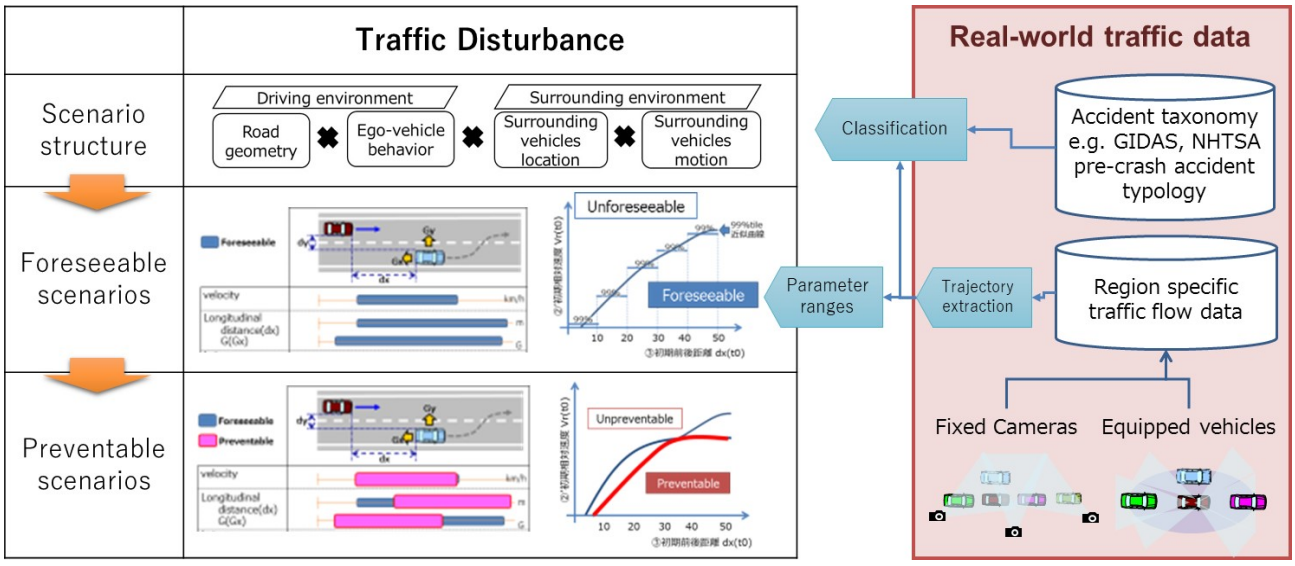

Figure 4 Approach to test scenarios for AD safety assurance

For each structured scenario, parameters and their ranges for foreseeable conditions are defined based on real-world traffic monitoring data. Among the foreseeable conditions, the ranges are narrowed down to those that correspond with

preventable conditions. Both the evaluation of the completenesss of the structured scenarios as well as the steps to define ranges for foreseeable and preventable conditions are developed based on real-world traffic monitoring and accident data. The completeness of the structured scenarios is conducted based on accident data that contains information on pre-crash conditions. Traffic monitoring data is utilized to define the parameter ranges representative of foreseeable scenarios. Detailed descriptions of the methodologies to structurize and to generate test scenarios for AD safety assurance purposes follow.

STRUCTURE OF AD VEHICLE TEST SCENARIOS FOR SAFETY ASSURANCE

This chapter provides a description and practical guidance on the development of test scenario structure for AD safety assurance purposes. The scenario structure aims to cover all foreseeable root causes of traffic accidents that may possibly caused by AD vehicles. The applicability of the methodology proposed is limited, at this moment, to motorways.

Traffic scenario structure systematization

A scheme of the traffic scenario structure developed is presented in Figure 5. By analyzing and classifying traffic disturbances systematically and considering the driving environment and the surrounding environment, lists of traffic scenarios can be developed. Driving environment comprises Road geometry and Ego-vehicle behavior. Surrounding environment comprises surrounding vehicles location, and surrounding vehicles motion.

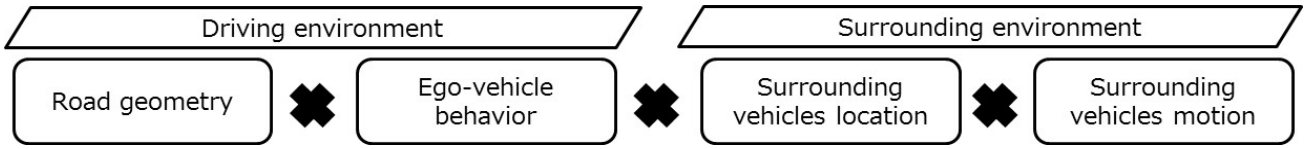

Figure 5. Structure for traffic scenarios

Road geometry classification and parameterization: Basic road geometry structure is defined according to the Japanese road structure ordinance [7], which provides technical standards for the development of roads in the country. In addition to road geometry related information such as cross sections, horizontal sections, sight distances, or speed changes, the ordinance includes parameters to ensure traffic safety and traffic flow smoothness.

Using the ordinance as a basis, road geometry sectors are categorized into Main road, Merging lane, Departure lane, and Ramp (Figure 6). Following this basic scheme, the corresponding critical road parameters for each of these components and for each scenario are defined based on expertise. As a result, critical parameters for traffic disturbances including the number of lanes, lane width, speed change lane and vertical gradients are proposed. Although the ordinance is generic, minor adaptations of the road structure may be required to become applicable to regions outside Japan.

Ego-vehicle behavior classification and parameterization: A lane change maneuver from a contiguous line or from a merging lane may differ in road geometry category, but share the ego-vehicle behavior. The same holds for lane keeping. Therefore, possible ego-vehicle behaviors are categorized in Lane Keep and Lane Change categories. This simple categorization of vehicle behaviours, in combination with the road geometry information provided previously, lead to a number of combinations (Figure 6).

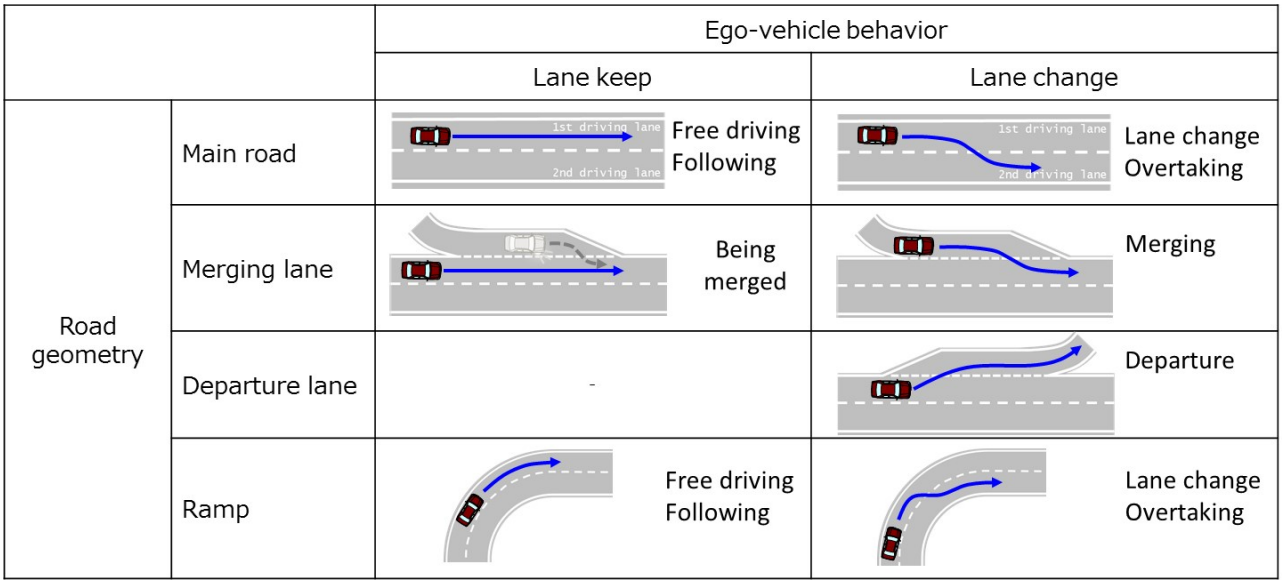

Figure 6. Road geometry and ego-vehicle behaviour parameters

Surrounding vehicle location classification and parameterization: The location of surrounding vehicles to be considered in the safety evaluation is defined according to adjacent locations in eight directions around the ego-vehicle, as these may invade the ego-vehicle's trajectory. In addition, when there is a large speed difference between the leading vehicle and the vehicle ahead of the leading vehicle, the former may cut out to avoid a collision. If this cut out occurs suddenly, the oncoming ego-vehicle may also need to intervene for crash avoidance. To account for this possible scenarios, the location of the vehicles ahead of the leading vehicle is also considered and is noted as '+1' (Figure 7, left).

Surrounding vehicle motion classification and parameterization: Possible motion of the surrounding vehicles is categorized in five groups: cut-in, cut-out, acceleration, deceleration, and synchronization. From the perspective of safety evaluation, it is possible to minimize the number of evaluation tests by focusing on the motion of the target participants that may obstruct the ego-vehicle's behavior (Figure 7, right chart).

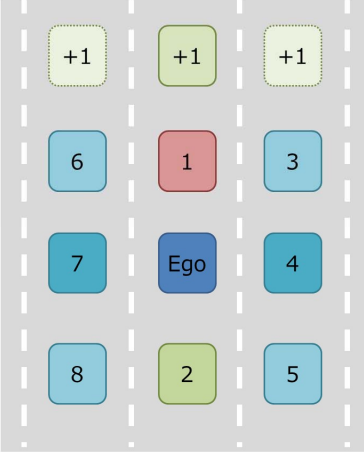

	Surrounding vehicle motion				
Surrounding vehicle location	Cut in	Cut out	Accel.	Decel.	Sync
1.Lead		○		○	
2.Follow			○		
3.Parallel	○			○	
4. Parallel	○				○
EGO vehicle					
5. Parallel	○		○		
6. Parallel	○			○	
7. Parallel	○				○
8. Parallel	○		○		

'○' indicates a combination of surrounding vehicle location and motion that may become obstructive to the ego-vehicle

Figure 7. Surrounding vehicles locations (left) and cases that may become obstructive to the ego-vehicle (right)

Resulting structure for Autonomous Driving vehicle scenario

As a result of the systematization process described, a methodology to structure scenarios as a combination of road geometry, ego-vehicle behavior, and surrounding vehicles location and motion is proposed. Following this structure, a matrix containing 32 test scenarios was developed based on expert discussions (Figure 8). The completeness of this matrix may be evaluated based on comparative accident taxonomy. The critical parameters and ranges for each of the scenarios can be defined and quantified based on traffic monitoring data.

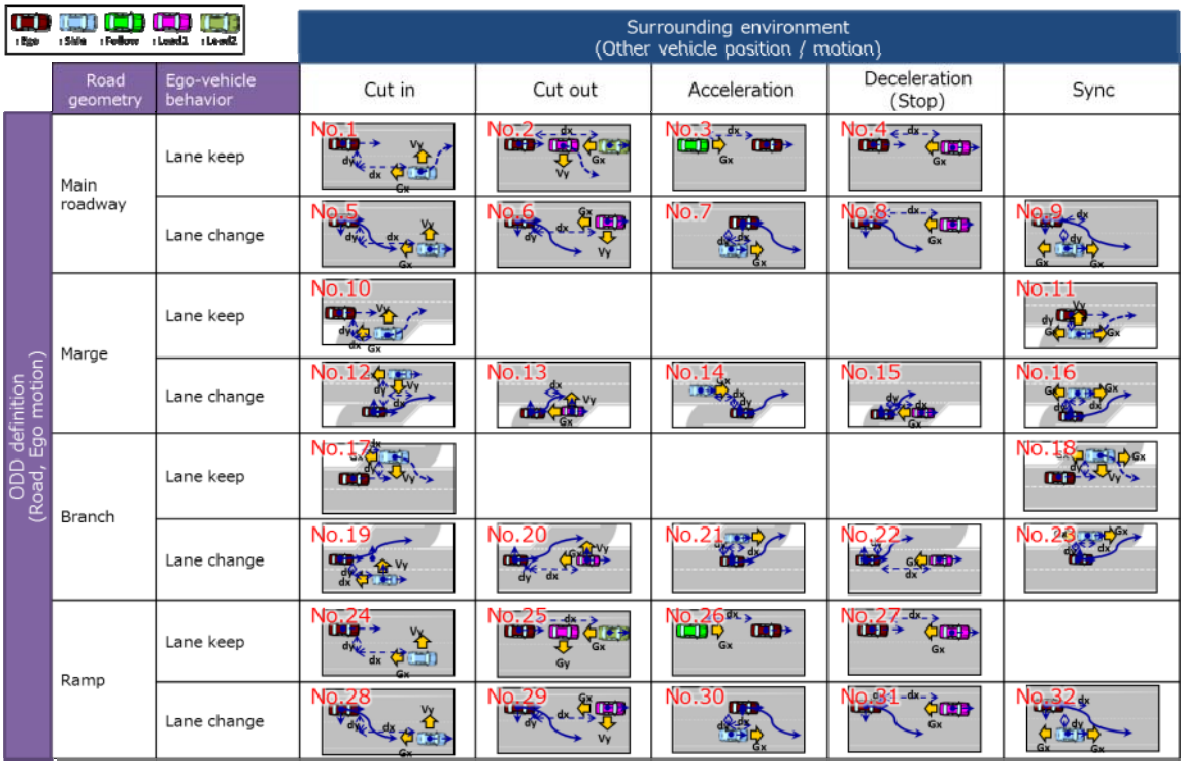

Figure 8. Traffic scenario matrix and corresponding parameters

Scenario matrix completeness evaluation based on accident data

The completeness of the scenario matrix proposed (Figure 8) may be evaluated by comparing its ability to cover accidents as reported in, for example, German in-depth accident study (GIDAS) database [8]. The underlying assumption of such comparison is that the accidents contained and classified in GIDAS represent all foreseeable scenarios in the German traffic environment.

GIDAS classifies traffic accidents according to predefined codes related to crash characteristics. Through a comparative taxonomy analysis between the GIDAS codes and the matrix of scenarios proposed (Figure 8), a relationship is established.

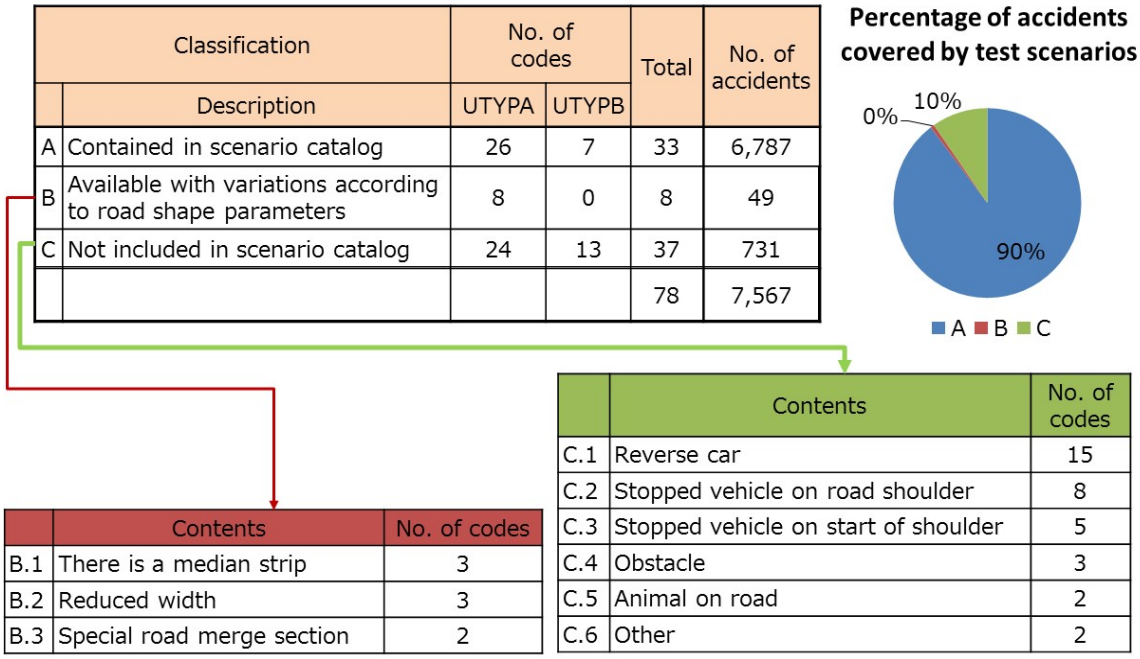

Classification		No. of codes		Total	No. of accidents
	Description	UTYPA	UTYPB		
A	Contained in scenario catalog	26	7	33	6,787
B	Available with variations according to road shape parameters	8	0	8	49
C	Not included in scenario catalog	24	13	37	731
				78	7,567

	Contents	No. of codes
B.1	There is a median strip	3
B.2	Reduced width	3
B.3	Special road merge section	2

	Contents	No. of codes
C.1	Reverse car	15
C.2	Stopped vehicle on road shoulder	8
C.3	Stopped vehicle on start of shoulder	5
C.4	Obstacle	3
C.5	Animal on road	2
C.6	Other	2

Figure 9. Scenario matrix evaluation based on GIDAS accident taxonomy

The upper left table in Figure 9 shows GIDAS accident code counts categorized based on the comparative taxonomy analysis. Categories A, B and C represent together 78 codes and 7,567 accidents in motoroways contained in the dataset analyzed. From these accidents, the comparative analysis shows that 33 codes and 6,787 accidents can be analyzed under the proposed matrix of scenarios (Figure 8), suggesting that the proposed matrix may potentially address nearly 90% of the motorway accidents reported in German motorways.

Category B comprises a total of 8 codes and 49 accidents (0.006% of all motorway accidents) that are related with road characteristics not covered by the matrix of scenarios. It is noted that the road geometry data applied to develop the list of scenarios was based on the Japan road structure ordinance [7], which may not cover some characteristics of German motorways. In order to provide coverage of the 8 remaining codes, adaptations of the proposed methodology to the German road characteristics may be required.

Category C comprises 37 codes and 731 accidents (10% of the total) that are not covered by the safety methodology proposed. Further analysis of the codes reveals that three code sub-categories (adding up to 28 codes) involved illegal maneuvers such as reversing in the motorway or illegal parking on the motorway shoulder (C1 to C3). The remaining 7 codes include obstacles or animals on the road and other unknowns (C4 to C6). The preventability of the crashes in this category (C) remains challenging for AD engineering intervention and call for complementary approaches that also involve, for example, rule enforcement.

GENERATION AND FORMATION OF AD VEHICLE TEST SCENARIOS FOR SAFETY ASSURANCE

This chapter provides a description and practical guidance on the process to generate test scenarios for AD vehicle safety evaluation by means of application of real-traffic data. The tests scenario structure is based on the previously proposed and the focus is on defining foreseeable scenarios including quantitative critical parameter ranges.

Road geometry parameter settings based real-world map data

To determine road geometry parameters, baseline road geometry critical parameters were assigned the most demanding values based on the Japan road structure ordinance, according to

Table 1.

Table 1. Baseline road geometry parameters from the road structure ordinance of Japan

Road parameters				Demanding value	
Cross section	Number of lanes			3	
	Width (m)			3.25	
	Center zone	Median (m)		1.25	
		Shoulder (m)		0.25	
	Side strip (m)			1.25	
	Linear gradient (%)			2.5	
Linear	Velocity (km/h)			120	100
	Horizontal alignment	Curve section	Radius (m)	570	380
			Transition section (m)	100	85
			Superelevation (%)	10	
		Speed change lane	Type	Direct	Parallel
			Direction	Deceleration	Acceleration
			Taper length (m)	70	60
			Pre-determined length (m)	110	220
	Vertical Alignment	Vertical Curve	Radius curve convex (m)	11000	6500
			Radius curve concave (m)	4000	3000
			Length (m)	100	85
		Vertical gradient (%)		5	6
Sight distance	Velocity (km/h)			120	100
	Sight distance (m)			210	160

In practice, real road geometries may not strictly comply with the road structure ordinance due to different reasons (e.g. merging lane length may be shorter than stipulated by the road ordinance due to limited construction space in crowded cities). Therefore, the previously defined baseline values for road geometry parameters need to be updated to reflect the actual strict road geometry conditions. With this purpose, dynamic map data are incorporated into the process. For example, a search of motorway characteristics in the region of Tokyo for “legal speed limit of 100 km/h” and “minimum curve section radius lower than 100 m” (Figure 10, left) shows numerous locations (resulting blue spots on the right of Figure 10). This exemplary search indicates that the baseline parameter values for road geometry (

Table 1) need to be updated from 380 m to no more than 100 m, to better reflect the actual road demanding parameter for curve radius in the region of Tokyo.

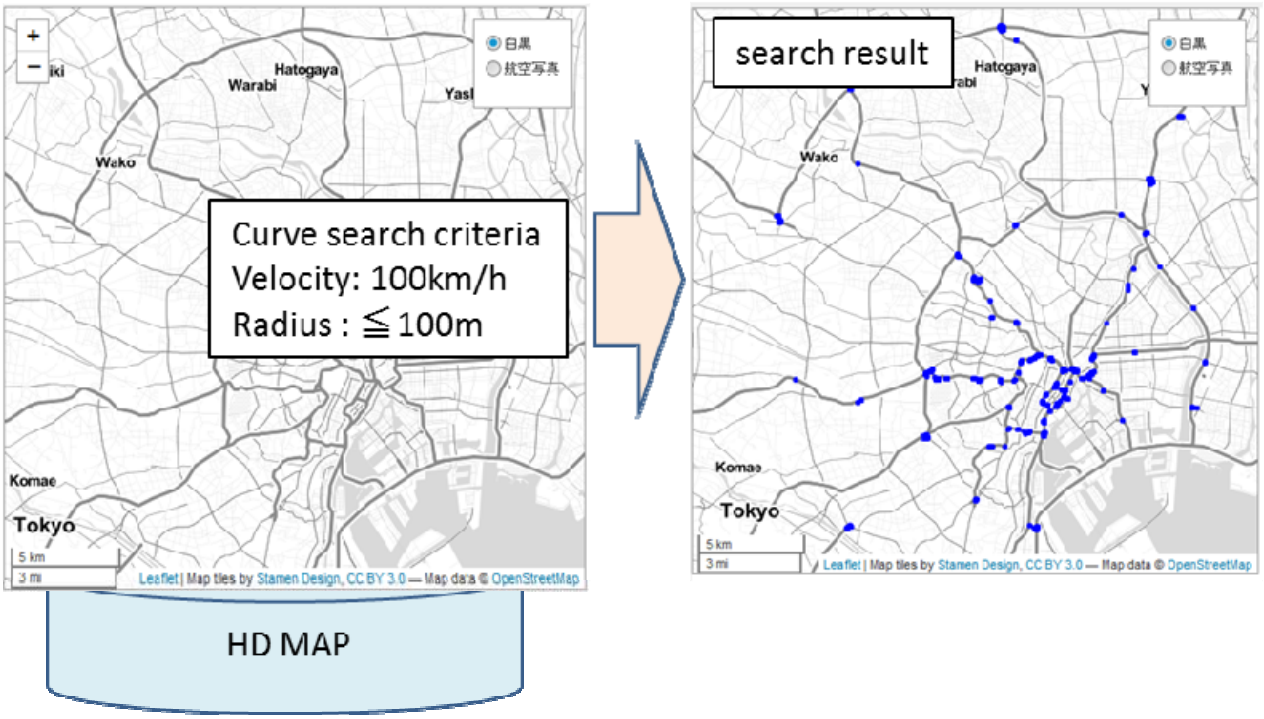

Figure 10. Data extraction utilizing dynamic map data

Surrounding vehicle foreseeable parameter ranges based on real-world traffic data

The process to derive critical parameter ranges in a cut-in test scenario (No.1 in Figure 8) is described in Figure 11. The basic idea is to define a list of surrounding vehicle motion critical parameters, and a simplistic model of the evolution of these parameters in time. In parallel, collection of real traffic data with stationary cameras and vehicles equipped with data collection devices is conducted, and correlation analysis between the simple surrounding vehicle behavior model and the corresponding field data measurements is conducted. Thereafter, parametric simulation studies are conducted to develop statistical distributions of a wide range of possible combinations of parameters. Based on these distributions, the parameter ranges that correspond with foreseeable scenarios are defined.

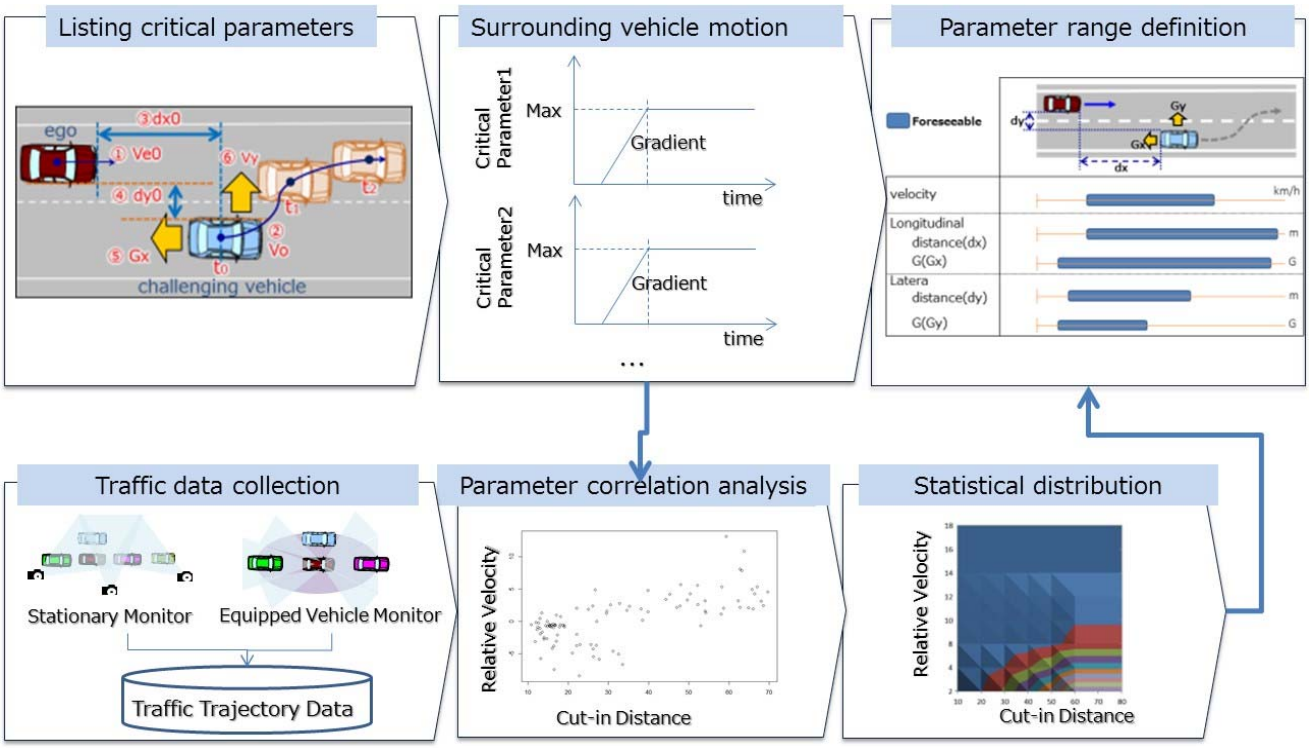

Figure 11. Process to extract surrounding vehicles motion to determine foreseeable scenario parameter ranges

Critical parameters and ranges: The same cut-in scenario is used to further ellaborate on the process to define critical parameter ranges. Similar processes are applied to extract the critical parameters for other scenario.

Two main aspects regarding the process to define critical parameter ranges are considered. The first one concerns the definition of the start and end time for the test scenario based on trajectory data (Figure 12, left). In this example, the start time of the scenario is defined by first identifying the lateral velocity of the challenging vehicle (Vy) at the timing (t1) in which the relative lateral distance between both vehicles (dy) becomes zero, and then by tracking back the lateral velocity (Vy) until the point in which it becomes zero. The end time is defined as the time in which the difference between the longitudinal velocities of the challenging and the ego-vehicle (Vo-Ve) becomes zero.

The second aspect regarding the process concerns to the definition of critical parameter ranges from the recorded trajectories. These ranges are defined by extracting cumulative ratios for large amounts of data cases (Figure 12, right). In the example, the cumulative ratio of lateral velocity (Vy) is obtained for different initial longitudinal distances (dx).

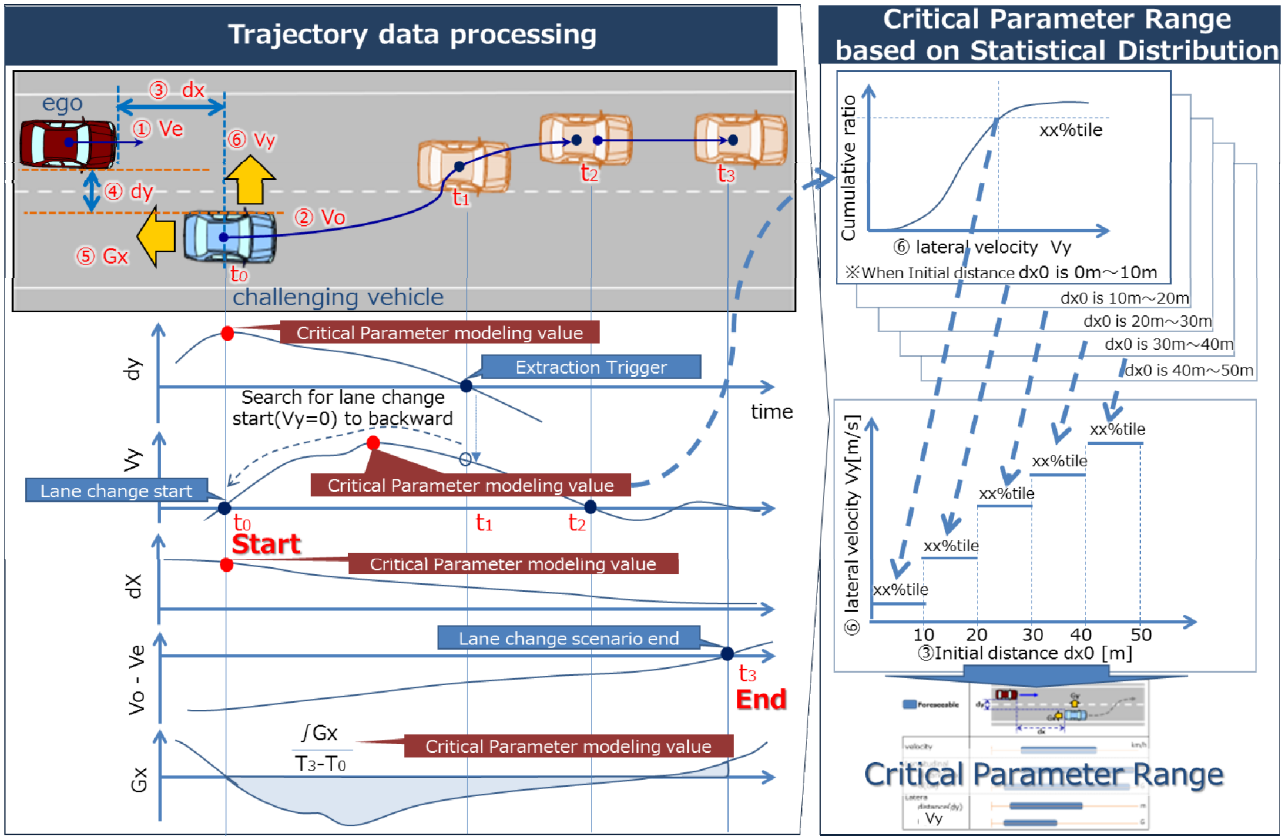

Figure 12. Definition of scenario start and end based on trajectory data processing (left) and critical paremeter ranges definition based on cumulative ratios (right)

Catalogue of functional scenarios: By applying the same methodology to each of the scenarios in Figure 8, sets of scenario-dependent foreseeable parameter ranges are developed. This provides a complete catalogue of functional scenarios that can be applied for AD safety evaluation. The format of these scenarios is similar to those in the matrix in Figure 8, but includes lists of critical parameter and corresponding quantified ranges for each of the scenarios proposed.

Scenario database

The outcome of the overall process is envisioned as a database that provides the outcome of tests, but that also enables bidirectional traceability of the entire between the raw traffic monitoring data and the critical parameter ranges that define foreseeable conditions (Figure 13). Efforts to harmonize the development, maintenance, and accessibility to such database could lead to a common international database to support the a safe and global deployment of AD vehicles.

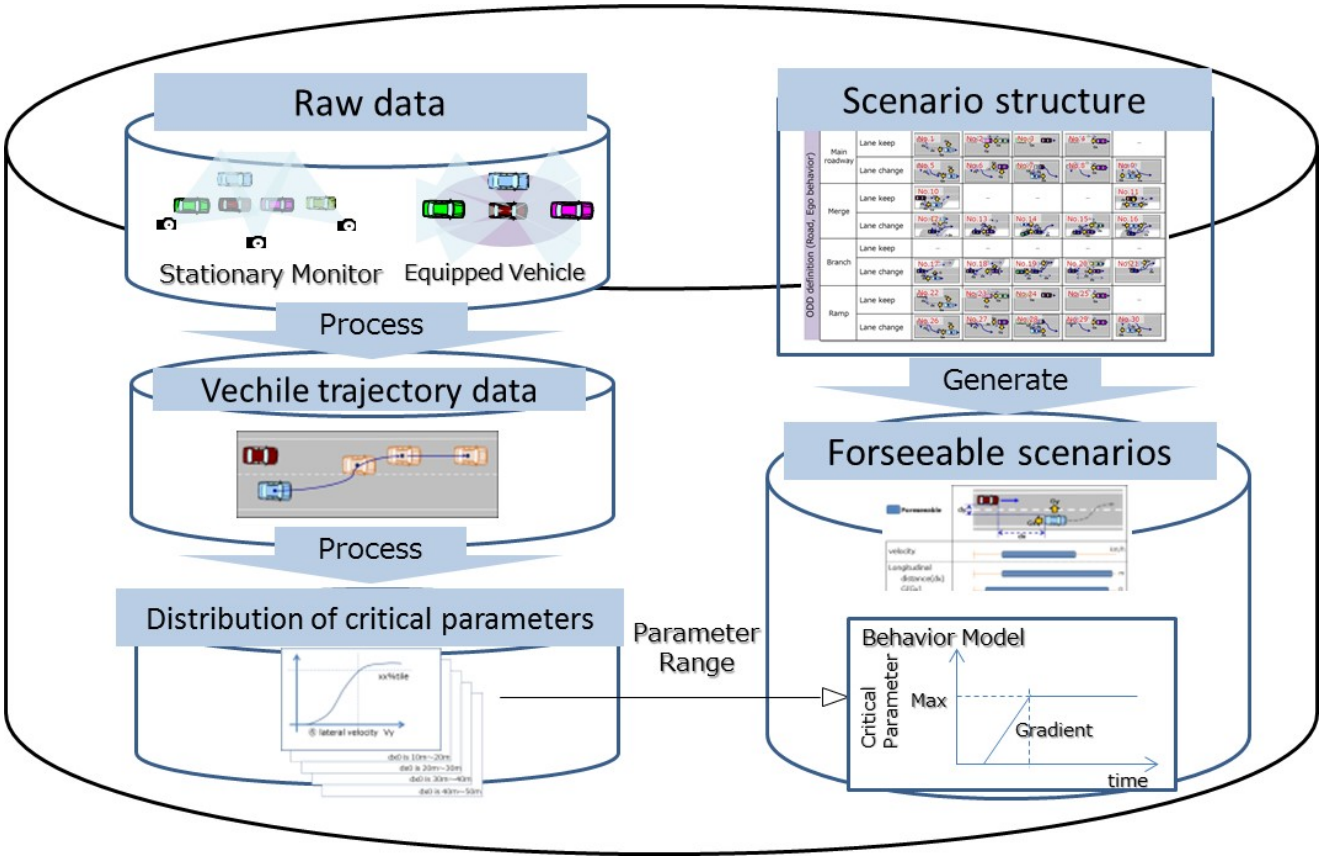

Figure 13 Database scheme with tracability from raw data to critical parameter Range

CONCLUSION

A safety assurance process for AD vehicles has been developed by JAMA and JARI under the auspice of the Japanese government and is hereby proposed. The proposal provides guidance on the overall safety assurance engineering process for Level 3+ AD systems under non-failure conditions on motorways, and on the methodologies to develop test scenarios and related criteria from real traffic monitoring data.

ACKNOWLEDGMENT

The results from a project financed by the Ministry of Economy, Trade and Industry of Japan have been utilized in this paper.

REFERENCES

1. Japan Traffic Agency of the Ministry of Land Infrastructure and Transportation. Guideline regarding safety technology for Automated Vehicles in Japan. September; 2018. Available from: https://www.unece.org/fileadmin/DAM/trans/doc/2018/wp29grva/GRVA-01-34.pdf.

2. NHTSA. Automated Driving Systems 2.0: A Vision for Safety. September; 2017. Available from: https://www.nhtsa.gov/sites/nhtsa.dot.gov/files/documents/13069a-ads2.0_090617_v9a_tag.pdf.

3. ISO. 26262: Road vehicles-Functional safety. Geneva, Switzerland: International Organization for Standardization; 2018.

4. Wachenfeld W, Winner H. The release of autonomous vehicles. Autonomous Driving: Springer; 2016. p. 425-49.

5. Themann P, Raudszus D, Zlocki A, Eckstein L. Holistic Assessment of Connected Mobility and Automated Driving. ATZ worldwide. 2016;118(1):26-31.

6. Kelly T, Weaver R, editors. The goal structuring notation–a safety argument notation. Proceedings of the dependable systems and networks 2004 workshop on assurance cases; 2004: Citeseer.

7. Association JR. Explanation and application of road structure ordinance. Maruzen; 2004.

8. Otte D, Krettek C, Brunner H, Zwipp H, editors. Scientific approach and methodology of a new in-depth investigation study in germany called gidas. Proceedings: International Technical Conference on the Enhanced Safety of Vehicles; 2003: National Highway Traffic Safety Administration.

THE ROLE OF VEHICLE AGE IN ROAD FATALITIES AND THE COMMUNITY AWARENESS ACTIVITIES EMPLOYED TO ENCOURAGE FLEET RENEWAL AND REDUCE ROAD TRAUMA

James Goodwin, Jason Smith, Rhianne Robson
ANCAP Safety
Australia

Paper Number 19-0287

ABSTRACT

Following a period of steady decline in national road tolls in Australia and New Zealand, recent consecutive increases in annual road fatalities have caused community concern, with policy makers and road safety organisations working to ascertain reasons for this trend reversal.

It is well established that newer vehicles generally offer higher levels of safety when compared to older vehicles, due to technology developments and the inclusion of specific safety features, with studies based on real-world data supporting this [1,2]. Statistical studies of real world crashes often report on factors such as driver age, crash type and posted speed limit, however the involvement of vehicle age in fatal crashes is less understood.

To build a greater understanding of the age of vehicles involved in crashes occurring in Australia and New Zealand, ANCAP began monitoring the age of light passenger and sports utility vehicles involved in fatal crashes, with the findings used to inform road safety policies and community education and awareness activities.

In 2018, ANCAP developed a national community awareness campaign targeting community consideration of vehicle age with the objective of encouraging fleet renewal.

This paper sets out the research findings over the analysed five-year period from 2012-2016 and the effectiveness of the subsequent national community awareness campaign.

BACKGROUND

The Australasian New Car Assessment Program (ANCAP Safety) provides consumers with transparent advice and information on the level of occupant and pedestrian protection provided by different vehicle models in the most common types of crashes, as well as their ability - through technology - to avoid a crash. The program influences the design of new vehicles, encouraging vehicle manufacturers to offer a level of safety above that required by regulation and to continue to increase safety performance as technology develops.

CRASH DATA ANALYSIS

Method

Vehicle occupants represent the largest road user group in road fatalities each year, accounting for 66% of Australian road fatalities over the period 2012-2016 and 71% in New Zealand [3,4]. Specifically, occupants of light passenger vehicles and sports utility vehicles (SUVs) represent approximately 49% and 56% of road fatalities in Australia and New Zealand respectively over the period, while these vehicle types represent 75% and 78% of the respective vehicle fleets [5,6].

The analysis focusses on road fatalities where an occupant of a passenger car or SUV was fatally injured and compares the age distribution of those vehicles involved against the age distribution of the passenger car and SUV fleet. Other road user groups and vehicle types have not been included. Australia and New Zealand have been analysed separately due to fleet profile differences and to provide information specific to each country.

To perform the analyses, two key datasets were required:

1. Road fatality data identifying the fatality type, vehicle type and year of manufacture; and
2. Fleet data identifying the type and age of vehicles within the registered (AUS) / licensed (NZ) fleet.

Datasets for occupant fatalities occurring in light passenger vehicles and SUVs range from 500 to 700 fatalities each year in Australia and 120 to180 fatalities in New Zealand. Organising this data into groups by vehicle year of manufacture matching the information reported by the fleet statistical data allowed age comparisons to be made between vehicles involved in occupant fatalities and vehicles within the respective fleets.

Data sources

Australian fleet information was sourced from the *Motor Vehicle Census, Australia* reports published by the Australian Bureau of Statistics (ABS) [5,7-10], while New Zealand fleet information was sourced from the *New Zealand Vehicle Fleet Status* reports published by the New Zealand Ministry of Transport [11-14].

For Australia, Motor Vehicle Census reports are based on the fleet at 31 January of the report year. For the purpose of this analysis, fleet information at 31 January is considered a good representation of the fleet at the end of the previous year.

Vehicle age amongst the Australian passenger car and SUV fleet is reported in four groups based on year of manufacture. Three of these groups span five years each while the remaining group includes vehicles that are fifteen years or older. These groups roll over based on the year in which the motor vehicle census is conducted.

For New Zealand, the fleet status data is reported at 31 December. Vehicle year of manufacture is generally reported in six groups, each spanning 10 years, however these groups do not rollover and remain consistent each year. As a result, the newest group identifying vehicles built between '2010-current' continues to grow with each status report as more new vehicles are added to the fleet.

Australian road fatality data identifying the fatality type, vehicle type and year of manufacture was sourced from the Bureau of Infrastructure, Transport and Regional Economics (BITRE) National Crash Database [16]. Corresponding New Zealand data has been provided by the New Zealand Ministry of Transport and the New Zealand Transport Agency [17].

Results

Tables 1 and 2 show the age distribution amongst passenger vehicles and SUVs involved in occupant fatalities over the period 2012 to 2016. Vehicle age shown is based on the age in the year in which the crash occurred. Occupant fatalities where the vehicle year of manufacture is unknown represent 11% of the Australian dataset and less than 1% of the New Zealand dataset.

Vehicles aged 24 years or less were involved in the majority of occupant fatalities, with older vehicles, particularly those aged 30 years or more, involved in relatively few occupant fatalities. The average age of light passenger vehicles involved in occupant fatalities during the five-year period was found to 12.7 years in Australia and 16.1 years in New Zealand.

Table 1.
Occupant fatalities by vehicle age at the time of crash (2012 to 2016)

Vehicle age (years)	Occupant fatalities in Australia	Percentage	Occupant fatalities in New Zealand	Percentage
0-4	361	12%	42	6%
5-9	554	18%	79	10%
10-14	745	25%	162	22%
15-19	638	21%	259	34%
20-24	297	10%	155	21%
25-29	62	2%	44	6%
30-34	25	1%	3	0%
35-39	4	0%	3	0%
40-44	3	0%	0	0%
45-49	5	0%	2	0%
50-54	1	0%	0	0%
55-59	1	0%	0	0%
60-64	2	0%	0	0%
65-69	0	0%	0	0%
70-74	0	0%	0	0%
75-79	0	0%	2	0%
80-84	1	0%	1	0%
Unknown	334	11%	1	0%
Total	3033	100%	753	100%

Table 2.
Occupant fatality data key statistics (2012 to 2016)

	Average age (years)	Mode	Minimum age (years)	Maximum age (years)
Australia	12.7	14	0	83
New Zealand	16.1	18	0	83

The results comparing the age of vehicles involved in occupant fatalities and the age of vehicles within the fleet are shown separately for each year in Australia and New Zealand in Figures 1 and 2 below.

Australia

The results found that in Australia during 2016, vehicles built in 2012 or later represented the largest portion of registered vehicles at 31%, and were involved in the fewest occupant fatalities at 12%. Vehicles built between 2007 and 2011 represented 27% of registered vehicles and were involved in 13% of occupant fatalities. Vehicles built between 2002 and 2006 represented 22% of registered vehicles and were involved in 21% of occupant fatalities. The oldest group, those built in 2001 or earlier, represented the smallest portion of registered vehicles at 20% and held the largest share of occupant fatalities at 36%.

On average over the five-year period analysed, the newest vehicles aged up to four years (at the time of crash) represented 31% of registered vehicles in Australia and were involved in 12% of occupant fatalities. The oldest age

group, those vehicles aged 15 years or older, represented 20% of registered vehicles on average and were involved in 34% of occupant fatalities.

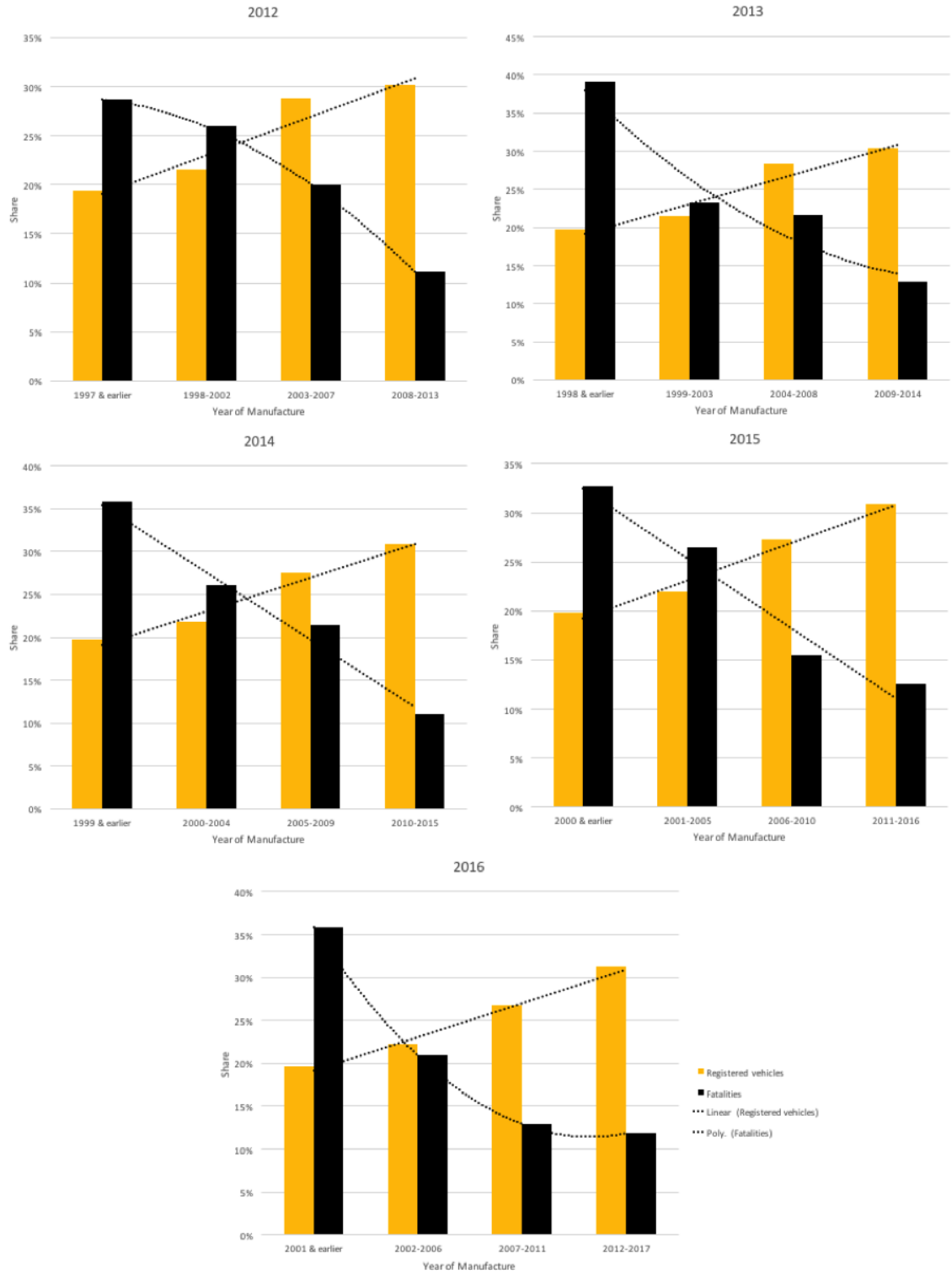

Figure 1 Age of vehicles involved in occupant fatalities vs age of registered vehicles (light passenger vehicles and SUVs) in Australia

New Zealand

The results found that in New Zealand for 2016, the newest vehicles built in 2010 or later represented 22% of licensed vehicles and were involved in 6% of occupant fatalities. Vehicles built between 2000 and 2009 represented 50% of licensed vehicles and were involved in 44% of occupant fatalities. Vehicles built from 1990 to 1999 represented 25% of licensed vehicles and were involved 45% of fatalities. Vehicles built prior to 1990 collectively represented 3% of licensed vehicles and were involved in 5% of occupant fatalities.

The New Zealand analysis shows relative consistency over the five-year period for vehicles built between 1990 and 2009. On average over the period, vehicles built between 1990 and 1999 represented 35% of licensed vehicles and were involved in 56% of occupant fatalities, while vehicles built between 2000 and 2009 represented 47% of licensed vehicles and were involved in 33% of occupant fatalities.

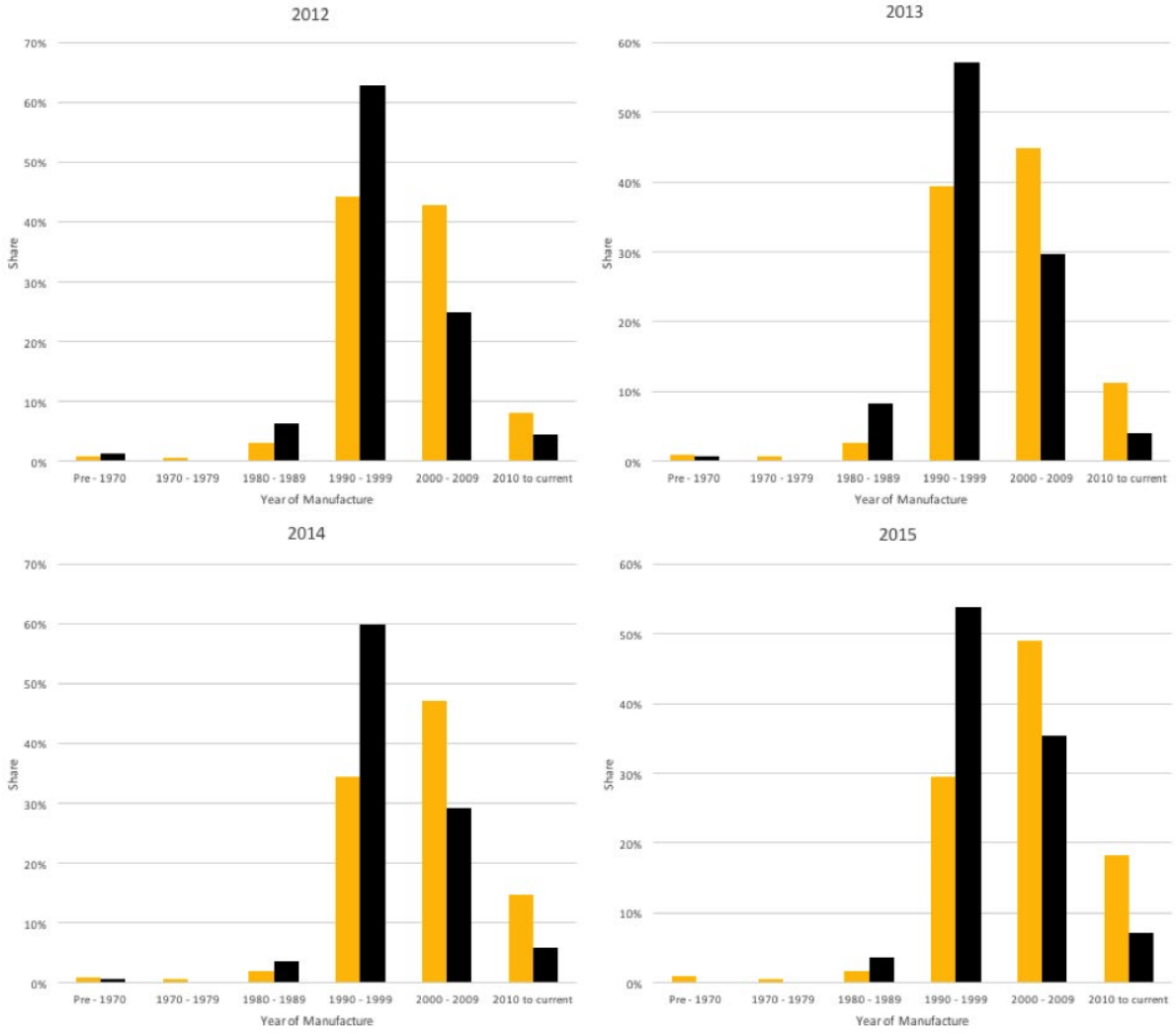

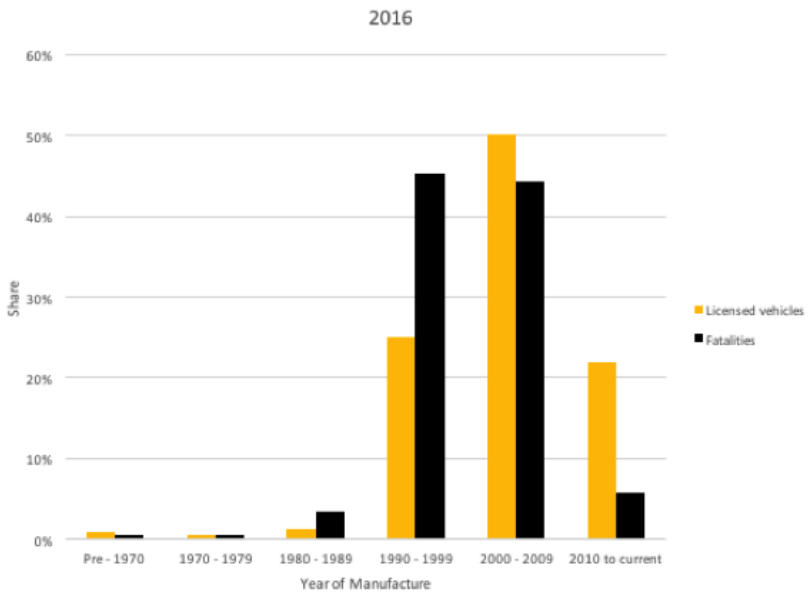

Figure 2. Age of vehicles involved in occupant fatalities vs age of licensed vehicles (light passenger vehicles and SUVs) in New Zealand.

The differing age groupings reported by Australia and New Zealand, due to the differing reporting methods of the respective fleet statistics, make comparisons between the two datasets difficult. However, limited statistical datasets of the New Zealand fleet were available [6] allowing for some comparison to be made between the results. Figure 3 shows the age of vehicles involved in occupant fatalities in New Zealand during 2016 grouped into age groups common with the corresponding Australian results.

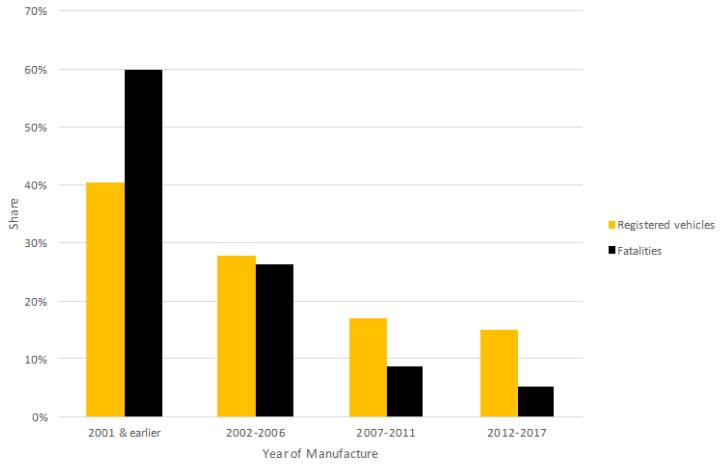

Figure 3. Age of vehicles involved in occupant fatalities vs age of licensed vehicles (passenger vehicles and SUVs) in New Zealand (2016).

Figure 3 shows that in New Zealand during 2016, the oldest vehicles, built in 2001 or earlier, represented 40% of licensed vehicles and were involved in 60% of occupant fatalities. In contrast, the newest vehicles built in 2012 or later represented 15% of licensed vehicles and were involved in 5% of occupant fatalities.

Table 3
Average age of vehicles involved in occupant fatalities

	2012	2013	2014	2015	2016	2012-2016
Australia						
Fatalities	12.2 years	12.8 years	12.5 years	12.9 years	13.1 years	12.7 years
Registered vehicles	9.8 years	9.8 years	9.8 years	9.8 years	9.8 years	9.8 years
New Zealand						
Fatalities	15.7 years	16.4 years	15.6 years	15.9 years	16.8 years	16.1 years
Licensed vehicles	14.0 years	14.2 years	14.2 years	14.3 years	14.4 years	14.2 years

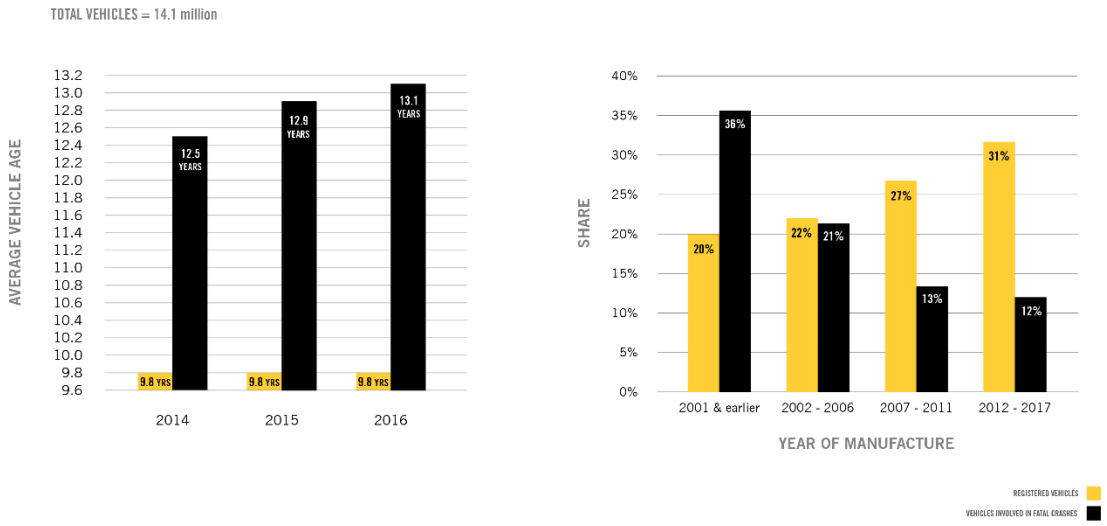

Figure 4. Fatalities vs. Registered Vehicles, Australian Light Vehicle Fleet (passenger cars & SUVs)

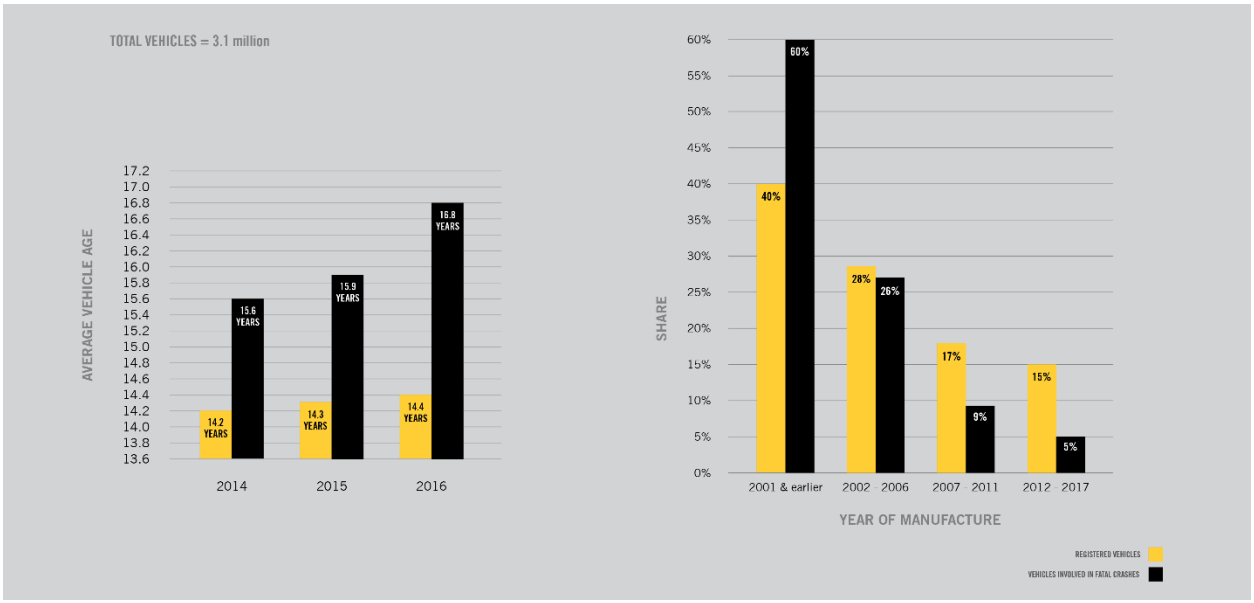

Figure 5. Fatalities vs. Registered Vehicles, Australian Light Vehicle Fleet (passenger cars & SUVs)

Analysis Discussion

The results of the analysis show that older vehicles were consistently over-represented in occupant fatalities in both Australia and New Zealand over the period 2012 to 2016. Australian Motor Vehicle Census data consistently shows a relatively linear relationship between vehicle age and the share of the registered vehicle fleet over the five-year period, with fleet share decreasing with vehicle age. In contrast, the results suggest the relationship between vehicle age and involvement in occupant fatalities is the reverse, with crash involvement increasing with vehicle age. This relationship however is limited, as shown in Table 1, where vehicles aged 25 years and older were involved in much fewer occupant fatality crashes.

Over the five-year period, the Australian results consistently show that the oldest group of vehicles reported in the Motor Vehicle Census data represented the smallest portion of registered vehicles, yet were involved in the most occupant fatalities. Contrast to this, the newest vehicles represented the largest portion of registered vehicles and were involved in the smallest portion of occupant fatalities.

The New Zealand results comparing the age distribution of vehicles involved in occupant fatalities and licensed vehicles in the fleet presents differently due to the vehicle age groups provided in the source fleet statistics datasets. Vehicles built between 1990 and 1999 were consistently over-represented in occupant fatalities while vehicles built between 2000 and 2009 were consistently shown to be involved in less fatalities yet represented more of the licensed fleet. The portion of registered vehicles built in 2010 or later increased over time as expected, however the involvement of those vehicles in occupant fatalities remained relatively constant.

In comparing the results between Australia and New Zealand, Figure 3 suggests a differing relationship between vehicle age and share of the licensed vehicle fleet in New Zealand, with newer vehicles representing less of the fleet than older vehicles. However, the relationship between vehicle age and involvement in occupant fatalities does appear similar, increasing with age.

This observed difference between the Australian and New Zealand distribution of vehicle age amongst the fleet reflects significantly differences in fleet profiles. Notably in New Zealand, used imports represent roughly 50% of the passenger vehicle and SUV fleet [15].

Over the five-year period, the average age of vehicles involved in occupant fatalities was found to be consistently older than the average age of vehicles in the respective fleet for both Australia and New Zealand, supporting the notion that older vehicles are over-represented in occupant fatality crashes.

The average age results shown in Table 3 also suggest a potential trend where the average age of vehicles involved in occupant fatalities is increasing. It is plausible that as newer vehicles become safer, and therefore are involved in fewer serious crashes, the share of serious crashes which older vehicles are involved in may increase. This does, however, imply that overall road fatality numbers will reduce. Further work is needed to establish whether a trend indeed exists or is emerging.

COMMUNITY AWARENESS ACTIVITIES

The findings of the analysis of the Australian and New Zealand registered light vehicle fleet highlighted the need for a redoubling of efforts across all *Safe Systems* pillars, and provided added impetus for ANCAP to enhance community awareness of the importance of newer, safer vehicles beyond the routine publication of ANCAP safety ratings for new market entrants.

New Car Assessment Programs such as ANCAP have the ability to drive improvements in vehicle safety through non-regulatory, consumer information and advocacy activities and this was leveraged through a series of interlinked community awareness activities.

Car-to-Car Advocacy Test

The first of these activities was the conduct of a car-to-car crash test - undertaken to visually communicate the research findings to the general community. The advocacy test was conducted between a 1998 Toyota Corolla hatch

and a 2015 Toyota Corolla hatch using similar test parameters as ANCAP's offset deformable barrier (frontal offset) crash test at 64 kilometres per hour with a 40 per cent offset on the driver's side.

The older vehicle sustained catastrophic structural failure with dummy readings showing a high risk of serious head, chest and leg injury to the driver. The 1998 model achieved a score of 0.40 out of 16.00 points which would fall within the parameters for a zero star ANCAP safety rating. In contrast, the 2015 model performed well, scoring 12.93 out of 16.00 points – within five star parameters. Test results and imagery were distributed widely with unprecedented global public interest.

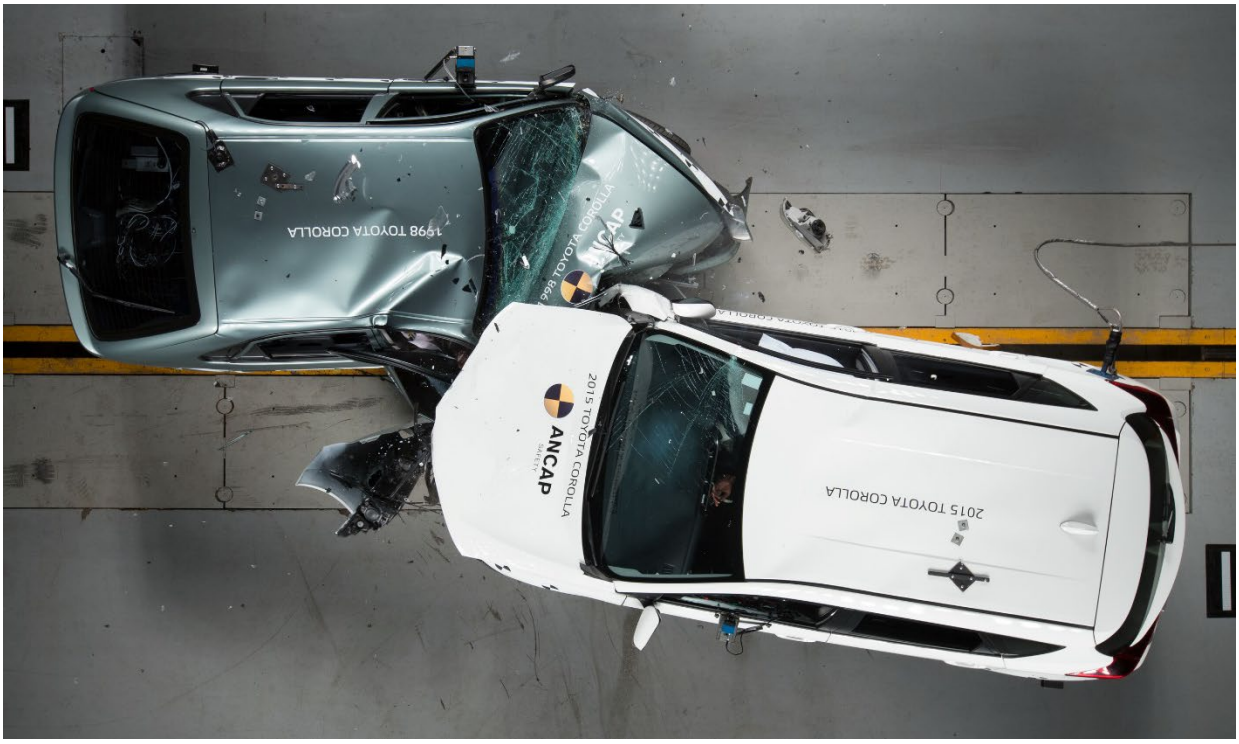

Figure 6. ANCAP car-to-car advocacy test between 1998 Toyota Corolla and 2015 Toyota Corolla (2017).

National Community Awareness Campaign

Drawing upon the public success of the car-to-car test, a national community awareness campaign was derived, titled '*Safer Vehicle Choices Save Lives*'[18]. The primary element of the campaign was the production and national screening of two parallel television commercials (TVC) with the premise to highlight the different crash outcomes between occupants of older vehicles and occupants of more contemporary vehicles. The commercials were produced to evoke consumer awareness and active consideration of vehicle age as a key contributing factor in road fatalities, and the effect safer vehicle choices can have on reducing road trauma.

Vision of the car-to-car advocacy test was incorporated into the commercials with the viewer left to consider the fate, or survivability, of each driver based on the safety performance of the two vehicle models. The call-to-action used in the commercials was, "*Find out who survives*".

This was the first national road safety campaign released in Australia which highlighted the *vehicle* as the determining factor in crash survivability.

Campaign execution

The campaign commenced national rollout from July 2018 in collaboration with all 23 ANCAP member organisations. While nationally-executed, campaign materials were produced for carriage across all Australian states and territories through the use of tailored branding and inclusion of local vehicle registration plates to reinforce jurisdictional relevance to the viewer.

By August 2018, over two thirds of Australia's total population, or 78 per cent of its car driving population, had been exposed to the campaign achieving an audience reach figure of 15.26 million [19] through a moderate investment of AUD$225,000.

Campaign effectiveness

Formal evaluation of the effectiveness of the campaign - including recall, messaging and behavioural impacts - was undertaken half way through the execution of the campaign. 1,041 respondents across all Australian state and territories – regional and metropolitan – were surveyed to explore unprompted and prompted recall and cut-through. In order to provide a nationally representative sample the survey targeted respondents from a mix of genders, age ranges (18-65 years), and driving status (drivers and non-drivers) [20].

The survey revealed a very high level of consumer impact, and attitudinal and behaviour change. As a result of seeing the campaign, respondents were compelled to think, discuss and act. It prompted 29 per cent of respondents to *consider* and 27 per cent to *check* the safety of their current vehicle(s). For one in five (21 per cent), this meant visiting the ANCAP website. This correlated to a 15.2 per cent increase in visitors to the ANCAP website when compared against the same period the year prior. Seventy (70) per cent of respondents stated they would check the ANCAP safety rating before buying their next car.

More serious reflections such as considering purchasing a new car (13 per cent) or actually committing to purchase a safer car (12 per cent) were also reported. One in three (34 per cent) reported feeling compelled to discuss car safety with others. Eighty (80) per cent of respondents stated the campaign message was '*Very / Quite Good*'.

Message recall was also strong with 72 per cent of respondents stating the campaign related to the importance of newer, safer vehicles.

LIMITATIONS

A key limitation to the research findings is that the study does not investigate crash causation and factors contributing to the involvement of vehicles of various ages in fatal crashes. Driver demographics are considered a significant factor contributing to older vehicle involvement in serious crashes with many older vehicles being driven by more at-risk drivers, such as the young and inexperienced, and the elderly and frail [21].

The size of the dataset and statistical significance of the results, particularly New Zealand, also presents a limitation in the reliability of the analysis findings.

CONCLUSIONS

Investigating the involvement of vehicle age in fatal crashes and comparing the age distribution to that of the registered / licensed fleet over the period 2012 to 2016, found that older vehicles aged between 15 and 25 years old were consistently over-represented in road fatalities where the occupant of a passenger vehicle or SUV was fatally injured. Significantly older vehicles aged 30 years or more were not found to be significantly involved in occupant fatality crashes.

The average age of vehicles involved in occupant fatality crashes each year over the analysed period suggests a potential trend towards an increasing over-representation of older vehicles involved in occupant fatalities, which may be influenced by a reduced involvement of newer vehicles in occupant fatalities.

Equal in importance to understanding road safety challenges is to undertake independent testing to prove it, and then activate change through public communication and advocacy. Non-regulatory, consumer-focused communications activities can have a positive impact on consumer behaviour and vehicle choice. The '*Safer Vehicle Choices Save Lives*' campaign, while activated through a modest investment, has achieved strong consumer cut-through and resultant behavioural change.

Active consideration of vehicle safety among the general community can be bolstered through the conversion of scientific testing into compelling and effective consumer-facing materials screened through mainstream and social

media. This can be leveraged further by partnering with credible organisations which are relevant and resonate with the viewer. Public advocacy activities such as this can and should be applied globally to assist in reducing the age of registered vehicles and subsequently drive down road trauma.

REFERENCES

[1] T.P Hutchinson, R.W.G. Anderson (2011), *New Cars: Much Safer,* Paper presented to the Australasian Transport Research Forum 2011 Proceedings, Adelaide, Australia.

[2] S. Newstead, L. Watson & M. Cameron (2011), *Vehicle Safety Ratings Estimated from Police Reported Crash Data: 2011 Update,* Report No. 304, Monash University Accident Research Centre.

[3] Bureau of Infrastructure, Transport and Regional Economics (2018), *Australian Road Deaths Database,* Canberra, Australia. BITRE

[4] New Zealand Ministry of Transport (2017), *Motor vehicle crashes in New Zealand 2016, Section 1 Historical data,* Wellington, New Zealand.

[5] Australian Bureau of Statistics, (2017). *Motor Vehicle Census, Australia, 31 January 2017,* cat. No. 9309.0, Canberra, Australia, ABS

[6] New Zealand Ministry of Transport (2018), *2016 New Zealand Vehicle Fleet Annual Statistics Annual Spreadsheet,* Wellington, New Zealand.

[7] Australian Bureau of Statistics, (2016). *Motor Vehicle Census, Australia, 31 January 2016,* cat. No. 9309.0, Canberra, Australia, ABS

[8] Australian Bureau of Statistics, (2015). *Motor Vehicle Census, Australia, 31 January 2015,* cat. No. 9309.0, Canberra, Australia, ABS

[9] Australian Bureau of Statistics, (2014). *Motor Vehicle Census, Australia, 31 January 2014,* cat. No. 9309.0, Canberra, Australia, ABS

[10] Australian Bureau of Statistics, (2013). *Motor Vehicle Census, Australia, 31 January 2013,* cat. No. 9309.0, Canberra, Australia, ABS

[11] New Zealand Transport Agency (2013), *New Zealand Vehicle Fleet Status as at December 31 2012,* Wellington, New Zealand

[12] New Zealand Transport Agency (2014), *New Zealand Vehicle Fleet Status as at December 31 2013,* Wellington, New Zealand

[13] New Zealand Transport Agency (2015), *New Zealand Vehicle Fleet Status as at December 31 2014,* Wellington, New Zealand

[14] New Zealand Transport Agency (2016), *New Zealand Vehicle Fleet Status as at December 31 2015,* Wellington, New Zealand

[15] New Zealand Ministry of Transport, 2017, *Annual Fleet Statistics 2016,* Wellington, New Zealand.

[16] Bureau of Infrastructure, Transport and Regional Economics (2017), *National Crash Database,* unpublished dataset, BITRE.

[17] New Zealand Transport Agency (2017), *Crash Analysis System,* unpublished dataset.

[18] ANCAP Safety, (2018-19), '*Safer Vehicle Choices Save Lives*' national community awareness campaign, www.ancap.com.au/WhoSurvives

[19] ANCAP Safety, (2018-19), '*Safer Vehicle Choices Save Lives*' campaign reach analysis

[20] ANCAP Safety, (2018-19), '*Safer Vehicle Choices Save Lives*' Campaign Evaluation Report, Torchlight Research, February 2019

[21] Transport for New South Wales, (2017), Centre for Road Safety, *Young Driver Trauma Trends report,* Sydney, Australia.

SEAT BELT USE AND EFFECTIVENESS OF SEAT BELT REMINDERS AMONG CHILDREN AND YOUNG ADULTS IN REAL-WORLD CRASHES

Amanda Axelsson
Folksam Research
Sweden

Anders Kullgren
Folksam Research and Chalmers University of Technology
Sweden

Paper Number 19-0289

ABSTRACT

The seat belt is one of the most effective ways to protect occupants in car crashes. Unfortunately, the average seat belt use in Europe (2018) was 83% for drivers and 81% for front seat passengers, where teenagers often have the lowest rate. The study aimed to use real-world car crashes to analyze the seat belt use among 0 to 18 year old children and teenagers as occupants and 18 to 20 year old drivers in Sweden 2011-2018. An additional aim was to analyze the effectiveness of seat belt reminders for both the front and the rear seats for the same age groups.

The Swedish Traffic Accident Data Acquisition was used, which is the Swedish national system for road traffic injury data collection. The data included 26 270 car crashes involving 30 447 car occupants in passenger cars. Regarding passengers, 5% were children aged 0 to 18 years and 12% of the drivers were aged 18 to 20 years.

Occupants aged 14 to 18 years had a lowest seat belt usage rate (89%), where the rate was even lower when these passengers had a young driver, 86% if the driver was aged 18 to 20 years and 93% if the driver was aged 30 years or above. And male passengers had a higher seat belt usage rate if they had a female driver, 94% if they had a female driver and 87% if they had a male driver. In the rear seat, children and teenagers aged 12 to 18 had a lowest seat belt usage rate and 18 year olds had the lowest (79%). The usage rate was lower when the passengers were sitting in the rear seat and when the driver was young.

For children above 8 years, seat belt use was higher in cars with an SBR. This was also the case for adults (over 30 years). There was a clear difference for the rear seat, especially for teenagers 14 to 18 years, among whom 100% used the seat belt in a seat with an SBR.

Young drivers had a higher risk to be involved in a road traffic accident compared to other age groups. Unfortunately, teenage passengers to these young drivers also have the lowest seat belt usage rate in the data. And there was indications that male teenage passengers have lower seat belt usage rate if their drivers also were male. One conclusion may be that the seat belt usage for a teenage passenger can depend on the driver. Therefore, it is important to put extra focus on this age group of drivers to increase seat belt use for their passengers

The present study clearly shows the need of actions aimed to increasing the seat belt use for rear seat passengers. The seat belt use in the rear seat is lower compared to the front seat, especially when the driver is young. The SBR has been shown to be effective in the front seat, and should therefore have the same specifications in the rear seat.

BACKGROUND

It is well known that seat belt usage is one of the most effective ways to protect occupants in car crashes. A modern seat belt reduces the risk of death of approximately 50% [1]. Combined with airbag the protective effect is approximately 65% [2]. In 2018, average seat belt use in Europe was 83% for drivers and 81% for front seat passengers [1]. Unfortunately, seat belt use in the rear seat is still much lower, where the average usage rate is 60%. It is a global pattern that the seat belt usage rate in the rear seat is lower than in the front seat.

In Sweden, as in 104 other countries, there is a seat belt law. Furthermore, the driver has full responsibility for seat belt usage for all passengers of age 15 or younger [3].

Studies around the world have shown that teenagers have the lowest seat belt wearing rate [4-6]. A study from the U.S., based on self-reported seat belt use, showed that only 51% of high school students always wore a seat belt when riding as passengers [7]. In Britain, young drivers and passengers (aged 17-34) have the lowest seat belt usage rate, as compared to other age groups, combined with the highest accident rate [8]. Furthermore, drivers aged 16-19 years are three times more often involved in a crash than older drivers, and young males are more often involved in crashes than young females [9]. The seat belt use is lower in crashes, and in fatal accidents only 40% uses the seat belt [10].

Seat Belt Reminders (SBR) have been shown to be very effective in increasing seat belt wearing rates, where SBRs increase the seat belt use from 90% to 98% [11] for the driver. The same study also presented observational studies regarding seat belt use all over Europe. In Brussels, Belgium, for example, the seat belt use was 93% in cars with SBR systems compared to only 70% in cars without SBR.

The European New Car Assessment Program (Euro NCAP) gives points for an SBR since 2004 for both front and rear seats [12]. However, the requirements for front and rear seats differ. The requirements for front seats are considerably higher [13]. For example, there is a requirement for occupant detections for the front seats but not for the rear seats. There is also a difference regarding an audible signal between the front and the rear seats, and where the driver can choose to switch off the reminder for the rear seats but not for the front seats.

The study aimed at using real-world car crashes to analyze the seat belt use among 0 to 18 year old children and teenagers as occupants and 18 to 20 year old drivers in Sweden. An additional aim was to analyze the effectiveness of seat belt reminders for both the front and the rear seats for the same age groups.

MATERIAL AND METHOD

The Swedish Traffic Accident Data Acquisition (STRADA) was used, which is the Swedish national system for road traffic injury data collection, containing police reported crashes and injury data from emergency care centers. The analyzed data included all car occupants who had been involved in a road traffic accident between 2011 and 2018, and who had received medical treatment at emergency departments of Swedish hospitals. In total, 26 270 car crashes with 30 447 car occupants were included. Occupants with unknown seat belt use were excluded (9%).

Three subgroups of passengers were defined: 0-8, 9-13 and 14-18 years of age, and three groups of drivers: 18-20, 21-30 and 30+ years of age. In 87% of the accidents, detailed information about the vehicle was known. This information was used to identify types of SBRs, and the Euro NCAP point scores.

Table 1.
Euro NCAPs point score for SBR

SBR, only the driver's seat	1 point
SBR, only the front seats	2 points
SBR for all seats	3 points

To analyze the effectiveness of an SBR, only cars from 1999 or later were included (73%), because the number of cars with SBR started to increase at this time in Sweden. The points given by Euro NCAP were used together with information about seating position (driver seat, front passenger seat, rear passenger seat and unknown). When positions were unknown (3%), the accidents were excluded in the analyses comparing front and rear seat and analyses including the SBR. To analyze the effectiveness of the SBR a standard binomial hypothesis test was conducted.

The seat belt use for all 0 to 18 year old passengers was analyzed as well as comparisons between males and females. It was also analyzed if the age of the driver affects the seat belt use for the passengers of ages 0 to 18.

Comparisons were also made between young drivers in ages 18 to 20 and older drivers (> 20 years). The effectiveness of the SBR for these age groups was also analyzed.

RESULTS

The data included 26 270 car crashes involving 30 447 car occupants in passenger cars. In total 81% were drivers, 12% were front seat passenger, 4% were rear seat passenger, and 3% were unknown. Of the passengers, 1 486 (5%) were children aged 0 to 18 years (15% below 8 years, 20% were 8 to 13 years, 65% were 14 to 18 years). In total, 2910 (12%) of the drivers were aged 18 to 20 years.

Including all data, males was more often involved in crashes (54% males and 46% females). Regarding drivers, males were more common for all age groups (See Figure 1). However, the greatest proportion (58%) was found for young males (aged 18 to 20 years).

Regarding passengers, females were more common as passengers aged 35 years and older, 72% of these passengers were females (See Figure 1). For passengers aged 0 to 18 years, the distribution between males and females was similar, except for passengers aged 15 to 16 years where females were more common (68% of these passengers were females).

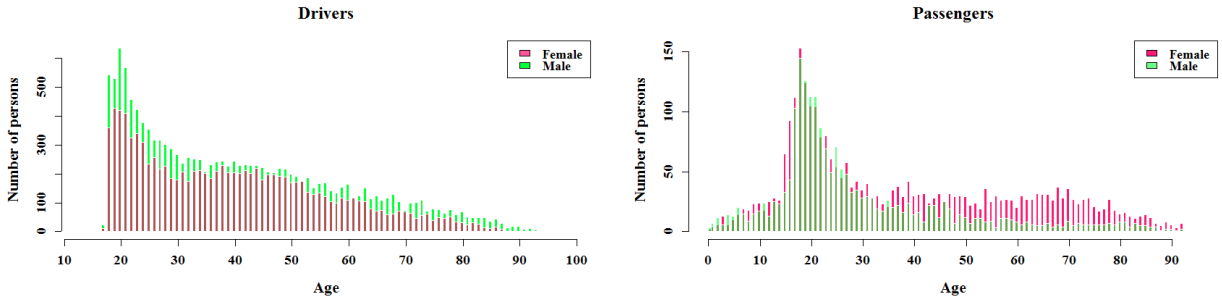

Figure 1 Age distribution for women and men in car crashes related to drivers and passengers

The average seat belt usage rate for all ages was 96%, but for older children and teenagers the seat belt usage rate decreased, (See Figure 2). Occupants aged 14 to 18 years had a low seat belt usage rate (89%), and 16 year olds' showed the lowest rate (83%).

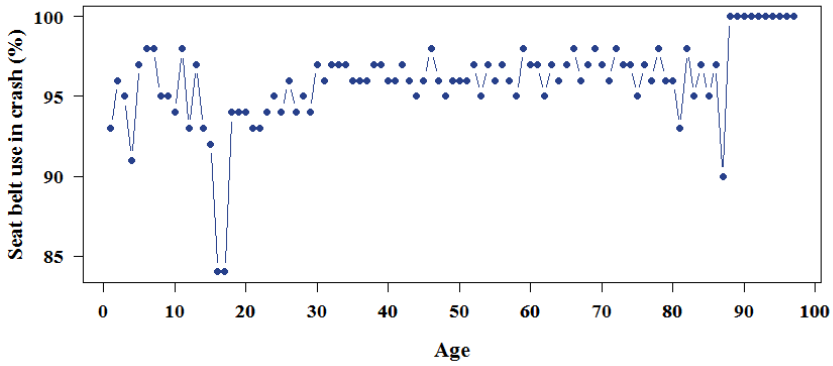

Figure 2. Seat belt usage rate in car crashes as related to age

There was a small difference in seat belt use between males and females, especially for 15-17 year old occupants, 84% usage rate for boys and 88% for girls (See Figure 3).

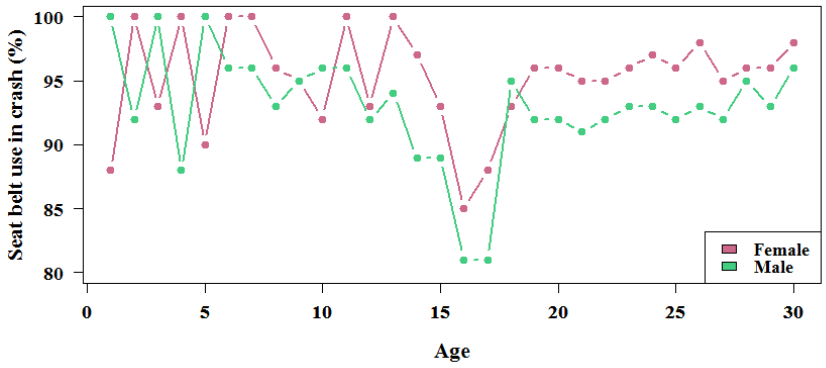

Figure 3. Seat belt usage rate in car crashes as related to age (0 to 30 years) for females and males

There was a notable difference in the seat belt usage rate for male passengers aged 14 to 18 years related to their driver's gender (See Figure 4). If they had a female driver the seat belt usage rate was 94%, compared to 87% if they had a male driver. This was also a seen for male passengers in all other ages. This large difference could not be found for females passengers in any age group.

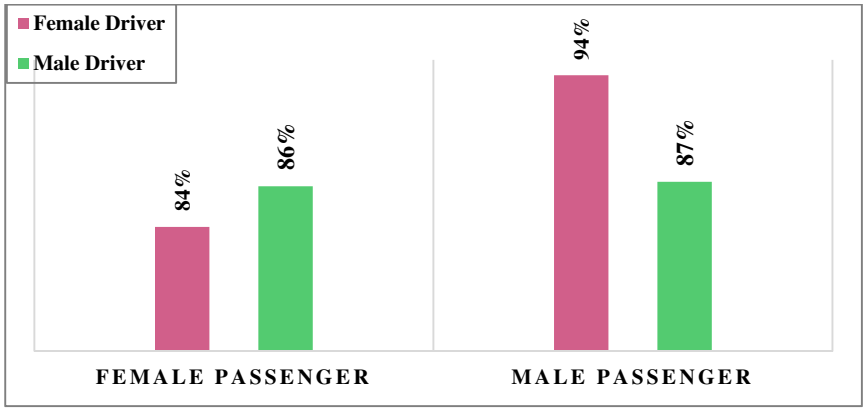

Figure 4. Seat belt usage rate for female and male passengers (aged 14 to 18 years) related to gender of the driver

The seat belt usage rate was lower in the rear seat, as compared to the front seat for all ages (94% in the front seat and 86% in the rear seat). Children and teenagers aged 12 to 18 had a low usage rate (See Table 1), and 18 year old rear seat passengers had the lowest, only 79%.

Table 1.
Seat belt usage rate among passengers in the front and the rear seat

Age group	Front seat	Rear seat
Under 8 years	100%	93%
9 to 13 years	96%	94%
14 to 18 years	92%	81%

Teenagers traveling with young drivers

The seat belt usage rate was lower when the passengers had a young driver, especially for passengers in the age interval 12 to 18 years. If these passengers had a driver between 18 and 20 years age, the seat belt usage rate was 86%. This can be compared to a 93% seat belt usage rate when the drivers were 30 years and above.

For passengers aged 15 years or younger, the driver has the responsibility of their seat belt use. In cases where the driver was 18 to 20 years, seat belt usage among the passengers was 85%.

The seat belt usage rate was lower when the passengers were sitting in the rear seat and when the driver was young, especially for passengers aged 14 to 18 years (See Table 2). If the driver was aged 18 to 20 years, seat belt use in the rear seat was lower than if the driver was 30 and above (79% and 88%, respectively). Eighteen year old passengers had the lowest seat belt usage rate (76%).

Table 2.
Seat belt use for passengers aged 14 to 18 years, in the rear seat as related to the age of the driver

Age (years)	With a driver 18 to 20 years		With a driver 30+ years	
	n	(%)	n	(%)
14	6	83%	22	91%
15	11	64%	13	92%
16	27	81%	23	91%
17	39	85%	23	87%
18	56	80%	21	76%

Seat belt reminders

The model year of the car was 1998 or later in 19 287 of the evaluated crashes (73%). Of these, 45% were not fitted with an SBR, 4% had an SBR for the driver seat only, 19% for both front seats, 12% for all seats, and in 21% the information regarding SBR was unknown.

The seat belt usage rate for children under 8 years in the front passenger seat was 100% irrespective if the seat had an SBR or not, (see Table 3). For children above 8 years, seat belt use was higher in cars with an SBR. This was also the case for adults (over 30 years). There was a clear difference for the rear seat, especially for teenagers 14 to 18 years, among whom 100% used the seat belt in a seat with an SBR. For children under 8 years, 89% were using a seat belt if the car had an SBR for the front seat. Note, however that this subgroup only included 9 children.

Table 3. Seat belt usage rate in cars with and without SBR related to age

	Driver's seat		Passenger in front seat		Passenger in rear seat	
Age groups	**With SBR**	**Without SBR**	**With SBR**	**Without SBR**	**With SBR**	**Without SBR**
Over 30 years (n = 17 583)	98%	95%	98%	93%	93%	85%
14 to 18 years (n = 1 885)	98%	95%	99%	90%	100%	78%
8 to 13 years (n = 300)	n/a	n/a	100%	93%	100%	93%
Under 8 years (n = 220)	n/a	n/a	100%	100%	89%	97%

The estimated probability of seat belt use in the front seat was 92% if the car had an SBR for the front seat, based on cars involved in crashes. The null-hypothesis that the probability to use a seat belt in the rear seat if the car had an SBR was the same as the front seat could be rejected at the 99%-level. In other words, the likelihood is lower that a car occupant uses a seat belt in the rear seat than in the front seat.

DISCUSSION

The present study showed that children under 8 years often used a seat belt (95%). Unfortunately, the seat belt usage decreases with age, and teenagers (aged 12 to 18 years) had the lowest seat belt usage rate in the data (89%). This is in line with other studies in Sweden, Europe and in the U.S. [4-7]. Despite the seat belt law in Sweden, occupants sometimes chose not use a seat belt. The legal consequences of not wearing the seat belt may be too low. Other countries in Europe are using tools such as safety cameras to detect seat belt usages in cars on certain high-risk sites [14].

There was an indication that the seat belt usage rate among teenagers aged 14 to 18 was affected by the age of their drivers. The seat belt use for these passengers was much lower when the driver was aged 18 to 20 years. And there was an indication that the seat belt usage rate among male passengers was affected by their driver's gender. Male passengers had a much higher seat belt usage rate if they had a female driver (94%). This is higher compared to the average seat belt usage rate for the same age group (89%). One conclusion is probably that female drivers have a larger impact on the passenger seat belt use compared to male drivers. One way to influence the low seat bel use among teenage passengers may be to make the law stricter so that the driver is responsible for seat belt use for passengers up to age 18 years, not only for children below 15.

Young drivers are more often involved in car crashes compared to older drivers. It is therefore important to put extra focus on this age group, also to increase seat belt use for their passengers. Above all, they need to understand the importance of seat belts, and the consequences for those choosing not wear them. One way to target this may be through road safety campaigns. The Campaigns and Awareness-Raising Strategies in Traffic Safety (CAST) project was aimed to improve road safety with more efficient campaigns, supported by the European Commission [15]. The CAST-project developed tools for design, implementation and evaluation of the campaigns. However, campaigns should primarily be based on knowledge from real-world accident findings. Knowledge about how to reach out to the right target groups, together with research from real-world crashes and observations can change underlying factors known to affect road user behavior among young car occupants and their attitude to seat belts. However, other studies showing the effect of similar campaigns are rare.

The present study showed that seat belt use is much lower in the rear seat for all ages in Sweden (94% in the front seat and 86% in the rear seat). This is in line with other studies all over Europe [1, 5] and U.S. [4, 7]. The present study clearly shows the need for actions to increase seat belt use for rear seated passengers. SBR was shown to be very effective. However, the results indicate that there are big differences between the SBR for the front seat compared to SBR for the rear seat. Therefore, Euro NCAP should have similar requirements for SBR also in the rear seat, as studies have shown a high effectiveness of SBR for the front seat [11]. As mentioned, rear seats currently do not need to have occupant detections [13]. This means that the system will not detect when a rear passenger are seated and therefore the SBR will not be able to warn in the same way. But it should be emphasized that Euro NCAP has upgraded their point scoring involving occupant detections from November 2015 [16]. Manufacturers may now have the possibility for 0.5 extra points per rear seat position with occupant detection [13].

Unfortunately, there is a safety risk when occupants choose to disconnect the SBR due to annoyance, for example when the SBR is warning for a seat that no one is using. Fortunately, there are car maker's that invest in cameras inside the car, today to identify the driver's status (such as fatigue). In the future, these cameras may identify which seats that are used by a passenger but also if this passenger is unbelted.

CONCLUSIONS

Young drivers have a higher risk to be involved in a road traffic accident compared to other age groups. Unfortunately, teenage passengers to these young drivers also have the lowest seat belt usage rate in the data. Also, there was indications that male teenage passengers have a much lower seat belt usage rate if their driver was male, compared to if their driver was female. One conclusion may be that the seat belt usage for a teenage passenger can depend on the driver. Therefore, it is important to put extra focus on this age group of drivers to increase seat belt use for their passengers

The present study clearly shows the need of actions aimed to increasing the seat belt use for rear seat passengers. The seat belt use in the rear seat is lower compared to the front seat, especially when the driver is young. The SBR has been shown to be effective in the front seat, and should therefore have the same specifications in the rear seat.

REFERENCES

[1] WHO. 2018. "Global Report on Road Safety 2018. (Geneva: World Health Organization)

[2] Bjurlin, M. et al. 2014. "The Impact of Seat belts and Airbags on High Grade Renal Injuries and Nephrectomy Rates in Motor Vehicle Collisions". p. 13

[3] Transportstyrelsen, S.T.A. 2019. "Belt Control (In Swedish: Bältesregler)". Available from: https://www.transportstyrelsen.se/sv/vagtrafik/Trafikregler/I-fordonet/Baltesregler/

[4] (CDC), C.f.D.C.a.P. 2011. "Adult Seat Belt Use". Available from: https://www.cdc.gov/vitalsigns/seatbeltuse/index.html#problem

[5] Trafikverket. 2017. "In Swedish: Bilbältesanvändning i Sverige 1988–2016". Borlänge

[6] Mousel, T. K. Ueda. M. Takahashi. 2014. "Advanced Seat Belt Reminder System for Rear Seat Passengers". ESV Conference

[7] Shults, R.A. et al. 2016. "Teens and seat belt use: What makes them click?*". J Safety Res. p. 18

[8] "THINK!". 2019. "Road safety laws - Seat belts". The THINK! campaign is run by the Department for Transport. Available from: https://www.think.gov.uk/road-safety-laws/#seat-belts

[9] Lloyd, D. et al. 2015. "Reported Road Casualties Great Britain, Annual Report". Department for Transport: London. p. 414

[10] Tingvall, C. et al. 2010. "The properties of Safety Performance Indicators in target setting, projections and safety design of the road transport system". Accid Anal Prev, **42**(2): p. 372-6

[11] Lie, A. et al. 2007. "Intelligent seat belt reminders: Do they Change seat belt use in Europe. in 20th International Conference on the Enhanced Safety Vehicles (ESV)". Lyon, Frankrike

[12] Van Ratingen, M. et al. 2015. "The European New Car Assessment Programme: A historical review"

[13] NCAP, E. 2018. "Assessment Protocol - Safety Assist Version 8.0.4". p. 26

[14] Council, E.-E.T.S. 2017. "New Spanish safety cameras to detect seat belt use". Available from: https://etsc.eu/new-spanish-safety-cameras-to-detect-seat-belt-use/

[15] VTI. 2010. "Communication campagins for traffic safety (In Swedish: Kommunikationskampanjer för trafiksäkerhet)". Luxemburg. p. 20

[16] NCAP, E. 2015. "Assessment Protocol - Safety Assist Version 7.0". p. 16

GUIDELINE FOR A VEHICLE PURCHASE POLICY AIMING AT A SAFE AND SUSTAINABLE VEHICLE FLEET

Anders Ydenius
Folksam Insurance Group
Anders Kullgren
Folksam Insurance Group and Chalmers University of Technology
Sweden

Paper Number 19-0290

ABSTRACT

Vehicle safety and emissions are addressed in the UN Sustainable development goals 3.6, road traffic safety, and 13, reduced climate impact. In Sweden, a large proportion of new passenger vehicles (62%, 236 546 vehicles) were purchased by legal entities in 2017. Those vehicles are driven for 18 years in average. Therefore, well-reasoned company car policies in terms of safety and emissions are imperative to meet the global goals.

The objective was to show how a company car policy that includes requirements regarding safety and CO_2 emissions can be a tool to reach global safety and environmental goals. The paper describes the development of a vehicle purchase policy that was introduced by Folksam Insurance Group in 1998. The criteria of the policy have been revised on a yearly basis to meet developments of vehicle safety and environmental technology, as well as environmental goals.

The vehicle data consists of new passenger vehicles available on the Swedish market. Data regarding crash tests, safety equipment and CO_2 emissions are listed for every vehicle model and version. The safety requirements cover crashworthiness, performance in whiplash tests, and availability of selected safety systems. The environmental criteria are adapted to meet global goals regarding CO_2 emissions. The goal is zero carbon emissions from new vehicles in 2030. A general goal is that approximately 15 % of the new vehicles on the Swedish market should fulfill the requirements in the policy.

It is shown in this study that safety and environmental criteria have changed rapidly during the last two decades. Furthermore, it is shown that safety and emission policies are important tools to guide fleet procurement managers as well as private consumers. A comparison of vehicles for sale and with those that are actually sold shows a higher rate of safety assist system in sold models compared to models for sale. The CO_2 emission requirement has been halved during the two decades the policy has been active, indicating that the vehicle fleet has made large progress in reducing their CO_2 emissions as the proportion of vehicles fulfilling the requirements has been approximately 15% during the two decades.

It is important to guide vehicle fleet buyers of vehicles for private use to choose the safest and most environmentally friendly vehicles since those vehicles will be used for many years. Company car policies are important tools in this process. A vehicle purchase policy will indirectly influence car manufactures to offer vehicles that fulfil the requirements in the policy.

An important recommendation is that a vehicle purchase policy should be revised annually to follow rapid changes in available safety technology and emission standards in order to substantially influence the vehicle fleet. A vehicle purchase policy is an important tool to guide vehicle consumers towards the safest and most sustainable vehicles. It is recommended that a vehicle purchase policy should consist of requirements regarding crashworthiness, fitment of important safety systems, CO_2 emissions. Preferably, it should be complemented with a vehicle list for tangible and feasible advice to consumers.

BACKGROUND

In Sweden 4 845 609 passenger vehicles were registered in 2017 and 379 315 new vehicles were purchased [1], of which 236 546 (62%) were purchased by legal entities. Private cars are large contributors to CO_2 emissions [2, 3]. Crashworthiness and crash avoiding techniques for personal vehicles are crucial interventions to reduce accidents with serious or fatal outcome [4-6].

New vehicles have environmental and safety performances that will influence the number of road casualties and the environment for many years ahead, in average18 years in Sweden [7]. Although vehicle safety is generally a high priority for private buyers and fleet managers in Sweden compared to e.g. Spain [8], vehicle safety is not the most prioritized factor. On the other hand, consumers who focus on safety may need some guidance among all safety systems that may appear in new vehicles. A well founded vehicle safety policy may guide consumers

to choose the safest vehicle, even if safety is prioritized by the consumer. Investigations show that there is a need to continuously improve understanding of what safety means to consumers and policy makers [9].

Consumer test programs such as Euro NCAP are important in the way that they put focus on the best practice in vehicle safety. However, the fitment of specific safety equipment varies between countries. A policy with detailed safety criteria is therefore important in order to guide vehicle buyers to a specific model version with desirable safety equipment.

Governmental incentives provide one way for long-term guidance towards vehicles with less CO_2 emissions [10]. However, a buyer needs to find the specific vehicles that are affected by the incentives. A vehicle policy with continuously updated emission criteria also helps to guide towards long-term emission targets and to point out the specific vehicle models with high occupant safety and low emissions.

Vehicle purchase policies used by large fleet purchasers such as companies and local authorities are important to guide towards safe and low emission vehicles [11, 12]. There is however a risk that those policies will quickly become inadequate due to rapid changes both regarding vehicle safety and emission standards. This paper illustrates the speed at which new safety systems are introduced and how difficult it is to predict. The speed of vehicle industry capability to reduce CO_2 has also been difficult to predict. Many CO_2 emission policies in Sweden has until recently used a definition of an environmentally friendly vehicle based on a state definition from 2013. This definition classified vehicles with CO_2 emissions below 120g/km as environmentally friendly. From 2018 this definition does no longer exist and there is a confusion within companies and local authorities how to define future CO_2 emission policies.

The paper aimed to show the development of the Folksam company car policy since the introduction 20 years ago and to describe the outcome of the 2019 year policy.

THE FOLKSAM VEHICLE PURCHASE POLICY

In 1997 the Folksam Group took a decision to adapt a company car policy consisting of vehicle safety and environmental requirements for vehicle transports within the company. The policy should contain tough requirements both regarding vehicle safety and CO_2 emissions. The policy criteria should be continuously improved with an annual revision regarding long-term goals but also to mirror continuous improvements in safety and emissions of the vehicle models for sale. The policy should also be supplemented with a vehicle list.

This decision also led to a guideline for rental cars used in the claims handling process at Folksam. In 2001 the policy was complemented with a vehicle list of models fulfilling the policy requirements.

Vehicles must fulfill criteria with respect to vehicle crashworthiness, fitment of safety assist systems and CO_2 emissions. An overall goal with the policy requirements was to select approximately 15% of the models for sale (in at least one version). The CO_2 emission requirement should at least be adapted to the European environmental goals [13].

The requirements in the Folksam company car policy have continuously been adapted to the developments in vehicle safety and CO_2 emissions since the introduction of the policy in 1998. In the beginning of 1998 the safety criteria consisted of crashworthiness requirements, limitations of curb weight, fitment of airbag, seat belt pretension, three point belt and head rest. The crashworthiness requirements were based on the Euro NCAP ratings and on the Folksam car model safety ratings (“How safe is your car?”) based on real-world crash data [14]. The use of Euro NCAP as a predictor of performance in real-world crashes has been verified in several studies, see for example [15-17].

The environmental criteria was initially covering fuel consumption based on vehicle size (the vehicle size was defined by a classification of exterior measures [9]) and diesel fuel was initially not approved due to high levels of NO_x and PM.

DEVELOPMENTS OF THE POLICY SINCE 1998

Two different databases have been used during the years containing data from new vehicles during the period 1998-2019. Between 1998-2013 data were used from a Swedish vehicle database “Bilfakta-Bisnode” and since 2014 the vehicle data has been provided by Jato Dynamics Ltd [18]. The vehicle data cover the current status of all new vehicle models for sale in Sweden. Every six months the vehicle list is updated with new models.

Developments of safety requirements

In 1998 the requirements regarding crash safety was that the vehicle should have least a three stars in the Euro NCAP rating or shown to be at least 20% better than average in the Folksam car model safety ratings. The requirements have been continuously harder during the years, see Table 1. In recent years top results in either Euro NCAP or Folksam ratings are required. In the late 1990s whiplash research [19, 20] led to additional criteria regarding whiplash protection. The whiplash protection has been shown by Folksam, IIWPG or Euro NCAP results. During the period 2005-2016, when IIWPG whiplash rating were used, 22(16 %) of 134 tested vehicle models in 2005 were "good" compared to 79 (75%) in 2016. Table 1 shows how the various safety criteria have been gradually changed in the policy since 1998.

Table 1.
Safety criteria 1998-2019

	Crashworthiness						Seat belt			Whiplash						Safety assist				
Policy Year	How Safe is your Car	NCAP Star	NCAP Adult pt.	NCAP Pedestr pt.	Curb weight kg	Airbag driver	Pret front	3-p belt	Seat belt reminder	Head rest	Active head rest	Folksam test	IIWPG rating	NCAP rating	IIHS Dynamic rating	ESC	AEB City	AEB Urban	AEB pedestrian	LDW
1998	≥20%	≥3			1000-1600	Std	Std	Std		Std										
1999	≥20%	≥3			1000-1600	Std	Std	Std		Std										
2000	≥20%	≥3			1000-1600	Std	Std	Std		Std	Std									
2001	≥20%	≥3			1000-	Std	Std	Std		Std	Std									
2002	≥20%	≥3			1000-	Std	Std	Std		Std	Std									
2003	≥20%	≥4				Std	Std	Std		Std	Std									
2004	≥20%	≥4				Std	Std	Std		Std	Std									
2005	≥20%	≥4				Std	Std	Std		Std	Std	≤7,4p	A/G							
2006	≥20%	5				Std	Std	Std	≥1p	Std	Std	≤7,4p	A/G			Std				
2007	≥20%	5			-1900	Std	Std	Std	≥1p	Std	Std	Yellow/Green	A/G			Std				
2008	≥20%	5			-1900	Std	Std	Std	≥1p	Std	Std	Yellow/Green	A/G			Std				
2009	≥20%	5			-1900				≥1p		Std	Yellow/Green	A/G			Std				
2010	≥20%	5			-1900				≥1p		Std	Green	G	≥3p		Std				
2011	≥30%		≥88%	≥40%	-1900				≥2p			Green	G	≥3p		Std				
2012	≥30%		≥88%	≥40%	-1900				≥2p			Green	G	≥3p		Std				
2013	≥40%		≥88%	≥40%	-1900				≥2p				G	≥3p		Std				
2014	≥40%		≥88%	≥40%	-1900				≥2p				G	≥3p		Std				
2015	≥40%		≥88%	≥40%	-1900				≥2p				G	≥3p		Std				
2016	≥40%	5							≥2p				G	≥3p		Std	Std/opt			
2017	≥40%	5							≥2p				-	≥3p		Std	Std/opt			
2018	≥40%	5							≥2p				-	≥3p		Std	Std	Std		
2019	≥40%	5							≥2p				-	≥3p/G	G	Std	Std	Std	Std/opt	Std/opt

The crashworthiness of the vast majority of new vehicles has during the years been verified by Euro NCAP results. Rating results from real-world crash data has only been available for a smaller number of vehicles. Figure 1 shows the distribution of Euro NCAP stars for all new vehicles in Sweden 2019. 157 (58%) of 270 new vehicles available of model year 2019, have a five-star rating. 66 (24%) were either not tested or tested prior to 2012. In 2001, when the vehicle policy was complemented with a vehicle list, Euro NCAP data from 89 new vehicle were evaluated of which only one model received five stars and 42 (47%) received four stars. In 2001 the requirements for superminis and small family cars was that they should have at least four stars and for large family cars and executive cars that they should have at least three stars in Euro NCAP.

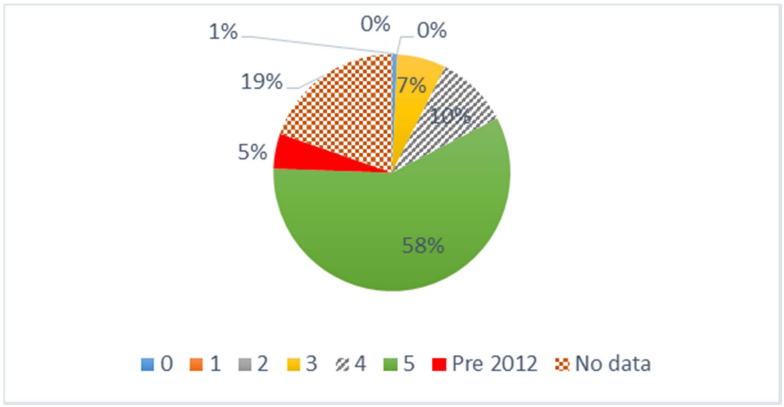

Figure 1. Euro NCAP star 1997-2019

Safety systems

Requirements regarding fitment of new effective safety technologies have been introduced continuously, see Table 1. In 2006 fitment of Electronic Stability Control (ESC) was introduced as a requirement (Table 1) and 82(32%) vehicle models have had ESC as standard on all versions and reached 80% in 2009 and 100% in 2017.

In 2016 fitment of Autonomous Emergency Braking (AEB) was introduced as a requirement (see Table 1). In 2016, AEB City (all versions with 100% fitment) was available in 24% of vehicle models (see Table 2). In comparison 59% of sold models have had AEB City 2016 (see Table 2). It is shown in Table 2 that 76% of vehicle models in 2016 have had AEB city as standard, option or not available, depending on the model version. A higher rate of safety assist systems in sold models compared to models for sale can be seen in Table 2-4. The implementation of AEB interurban, and AEB with detection of vulnerable road users (VRU) is not as fast as for the AEB city. For AEB interurban, 26% of all models with standard fitment was reached in 2017 (see Table 3). Standard fitment of AEB with VRU detection reached 22% in 2017 (see Table 4). In 2018 the proportion of vehicle models with standard fitment of AEB Interurban was 42% and for AEB VRU it was 37%, which was lower than for AEB city (59%). The number of sold vehicle models with standard fitment of AEB of all types, has increased more rapidly than the fitment rate in the models for sale. The rate of sold vehicle models 2017 with standard fitted AEB with VRU detection was 45% lower than for AEB city.

In 2019 also AEB with detection of VRU was introduced as a requirement (see Table 1). This is a result of real-world results indicating a good safety performance [21] [22] together with the rapid implementation of this system since 2014 (see Table 4).

Standard fitment of Lane departure warning (LDW) is not as common as AEB city/interurban, neither for vehicle models for sale or for sold vehicles. In 2018 29% of vehicle models had LDW as standard fitment (see Table 5). LDW was introduced as a requirement in 2019 (see Table 1) as a consequence of studies indicating good safety performance [6, 23].

Table 2.
City AEB – fitment/sold models

		2012	**2013**	**2014**	**2015**	**2016**	**2017**	**2018**
100% Std	Fitment	5,0%	5,0%	8,0%	15,9%	23,6%	38,0%	58,7%
	Sold	18,0%	26,0%	30,0%	50,8%	58,6%	69,0%	No data
Std/Opt/Not available	Fitment	6,0%	5,0%	5,0%	10,5%	11,1%	14,8%	4,2%
	Sold	5,0%	2,0%	7,0%	3,6%	19,8%	12,0%	No data
100% Option	Fitment	12,0%	15,0%	21,0%	13,2%	13,2%	11,8%	12,5%
	Sold	20,0%	25,0%	23,0%	15,2%	9,6%	9,0%	No data
100% Not available t	Fitment	77,0%	75,0%	66,0%	60,3%	52,0%	35,4%	24,7%
	Sold	57,0%	47,0%	40,0%	30,4%	12,0%	10,0%	No data

Table 3.
Interurban AEB – fitment/sold models

		2012	**2013**	**2014**	**2015**	**2016**	**2017**	**2018**
100% Std	Fitment	0,0%	0,0%	3,0%	8,5%	11,6%	25,5%	42,4%
	Sold	0,0%	0,0%	7,0%	17,8%	24,4%	59,0%	No data
Std/Opt/ Not available	Fitment	5,0%	5,0%	7,0%	8,8%	13,3%	10,3%	2,8%
	Sold	10,0%	9,0%	15,0%	12,3%	23,2%	9,0%	No data
100% Option	Fitment	5,0%	8,0%	12,0%	12,2%	12,3%	10,7%	12,5%
	Sold	10,0%	13,0%	25,0%	20,7%	19,1%	12,0%	No data
100% Not available	Fitment	90,0%	85,0%	78,0%	70,5%	62,8%	53,5%	42,4%
	Sold	80,0%	78,0%	53,0%	47,9%	33,4%	20,0%	No data

Table 4.
AEB VRU detection – fitment/sold models

		2012	2013	2014	2015	2016	2017	2018
100% Std	Fitment	0,0%	0,0%	2,0%	5,0%	12,0%	22,1%	36,8%
	Sold	0,0%	0,0%	4,0%	12,0%	20,0%	38,0%	No data
Std/Opt/ Not available	Fitment	0,0%	0,0%	1,0%	3,0%	5,0%	1,5%	1,7%
	Sold	0,0%	0,0%	4,0%	6,0%	10,0%	17,0%	No data
100% Option	Fitment	3,0%	3,0%	5,0%	6,0%	7,0%	8,1%	10,4%
	Sold	6,0%	6,0%	10,0%	12,0%	14,0%	11,0%	No data
100% Not available	Fitment	97,0%	97,3%	92,0%	86,0%	76,0%	68,3%	51,0%
	Sold	94,0%	94,0%	82,0%	70,0%	56,0%	34,0%	No data

Table 5.
LDW fitment models

Fitment	2016	2017	2018
100%Std	7,1%	20,7%	28,8%
Std/Option/ Not available	29,2%	25,4%	25,7%
100% Option	18,6%	17,3%	17,7%
100% Not available	45,2%	36,6%	27,8%
Sum	100,0%	100,0%	100,0%

Emission criteria

The CO_2 emission requirements in 1998-2012 were divided for various vehicle size groups. From 2013-2019 this criterion was changed to emission level by curb weight. To be able to present the emission figures from 1998-2019 with respect to vehicle size in this paper, the average curb weight was calculated for each vehicle size and model year and associated emission figures are presented (see Table 5-8).

During 1998-2002 vehicles with diesel engines were not allowed in the policy. In 2003-2012 diesel engines needed to have a 20% lower fuel consumption than petrol to fulfill the emission criteria. Since 2013 the CO_2 emission criteria were equal for diesel and petrol.

The CO_2 emission requirements have been tightened during 1998-2019. Table 5 presents the CO_2 limits for petrol vehicles in the vehicle policy, showing a reduction in emission level of 47-50% between 1998 and 2019.

Table 5.
CO_2 emission limit petrol 1998-2019

Policy year	CO_2 g/km Super mini	CO_2 g/km Small family car	CO_2 g/km Large family car	CO_2 g/km Executive car
1998	186	186	205	231
1999	182	182	201	227
2000	151	177	196	222
2001	149	175	194	219
2002	146	172	191	215
2003	144	168	186	210
2004	139	163	182	205
2005	139	163	182	205
2006	139	158	179	201
2007	137	156	175	196
2008	132	153	170	191
2009	130	151	168	189
2010	127	149	165	184
2011	125	146	158	177
2012	123	142	151	170
2013	112	120	126	139
2014	105	105	113	126
2015	105	105	109	120

2016	105	105	110	120
2017	104	104	109	118
2018	99	99	108	116
2019	99	99	108	115
Change (%)	-46,9	-46,9	-47,6	-50,1

Table 7 shows the reduction of CO_2 emission limit during 16 years. For smaller family cars a 36% reduction can be seen and for large vehicles a 39% reduction.

Table 7.
CO_2 emission limit diesel 2003-2019

Policy year	CO_2 g/km Super mini	CO_2 g/km Small family car	CO_2 g/km Large family car	CO_2 g/km Executive car
2003	131	152	168	189
2004	125	147	165	187
2005	125	147	165	187
2006	125	144	163	181
2007	123	144	160	179
2008	120	141	157	173
2009	120	139	155	171
2010	120	136	152	168
2011	123	133	149	163
2012	123	133	147	157
2013	112	120	126	139
2014	96	105	113	126
2015	88	101	109	120
2016	90	102	110	120
2017	88	101	109	118
2018	89	99	108	116
2019	90	98	108	115
Change (%) 2003-2019	31,3	35,5	35,7	39,1

THE FOLKSAM VEHICLE PURCHASE POLICY 2019

Safety criteria

The vehicle crash worthiness was verified either from the Folksam car model safety ratings [24] or from vehicle safety ratings from Euro NCAP results. The car must be at least 40% better than average in the Folksam ratings or receiving a five star rating in Euro NCAP. Since the Euro NCAP test protocol continuously undergoes changes, older test results than 2012 was not accepted in the 2019 years requirements of the policy.

To reach top score in Euro NCAP, specific safety equipment needs to be available on the test vehicle. Since the availability varies for different markets, it was a need to have additional requirements for important safety systems. The safety systems required in the policy are shown in Table 1.

Table 1. Required safety systems in Folksam vehicle policy

Safety system	Availability
AEB (Autonomous Emergency Braking)	Standard
AEB VRU (AEB with detection of vulnerable road user)	Standard or option
LDW (Lane Departure Warning)	Standard or option
ESC (Electronic Stability Control)	Standard

The level of whiplash protection was also included in the safety requirements verified through whiplash rear impact score in Euro NCAP. The whiplash score for the front seats had to be “Green”. As an alternative, the dynamic rating in “Head restraint & seats” published by IIHS was used [25]. The dynamic rating score had to be “Good”.

Emission criteria

The current emission criteria for 2019, was adapted to reach the European targets of CO_2 emission [13]. However, the long-term goal is to reach net zero emission of new vehicles by 2030 [26].

The 2019 year revision of the policy consists of two levels of CO_2-emissions. Until 2019 the assessed CO_2 emissions have been based on the driving cycle NEDC (New European Driving Cycle). Since September 1st 2017, a new driving cycle, WLTP (Worldwide Harmonized Light Vehicle Test Procedure) was introduced and became mandatory for vehicles launched September 1st 2018 and onwards. During 2019 two CO_2 emissions figures will appear for new vehicles, NEDC values or NEDC corr values. NEDC corr was used as a transition to WLTP and was calculated from the WLTP value. From 2020 only WLTP will be used.

The emission criteria are illustrated in Figure 3. The CO_2 emission value are related to the vehicle curb weight. NEDC emission limits start at 99 g/km and ends at 110 g/km. NEDC corr emission limits is higher to correspond to the differences between NEDC and NEDC corr values. The limit starts at 108 g/km and ends at 121g/km.

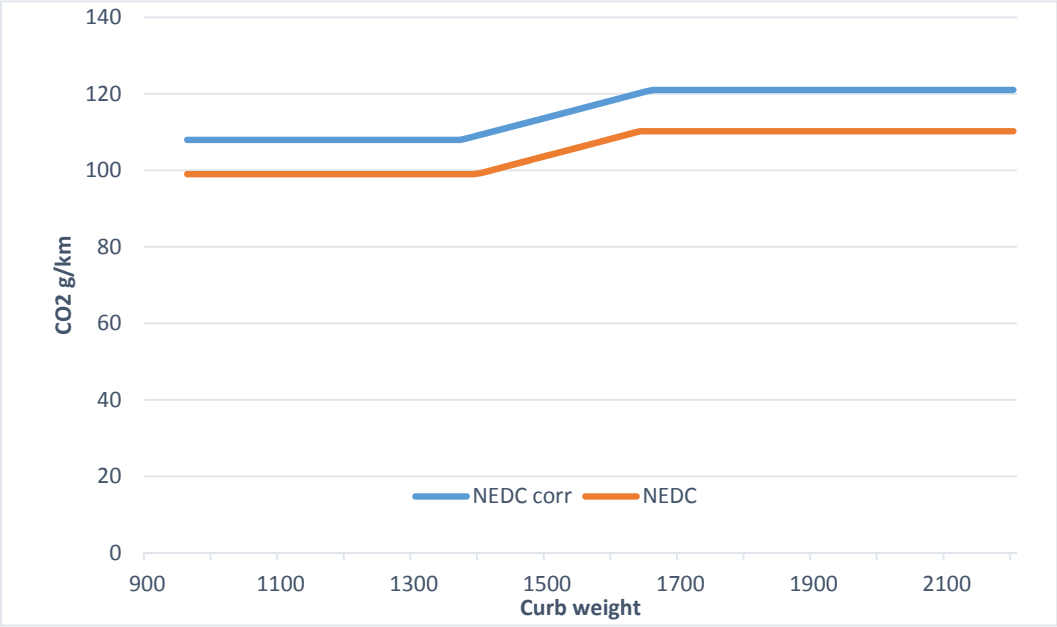

Figure 2. Emission criteria

The difference of emission values between NEDC and NEDC corr were evaluated from an analysis of 1253 vehicle model versions with model year 2017, identical to current versions (see Figure 3). The analysis shows that 75% of the observed versions had an increase of CO_2 from NEDC to NEDC corr of 0-20 g/km. The difference in emission between NEDC and NEDC corr was also shown to be larger for larger vehicles in general. This is the reason for the difference of 9-11 grams between NEDC and NEDC corr CO_2 limits (see Figure 2).

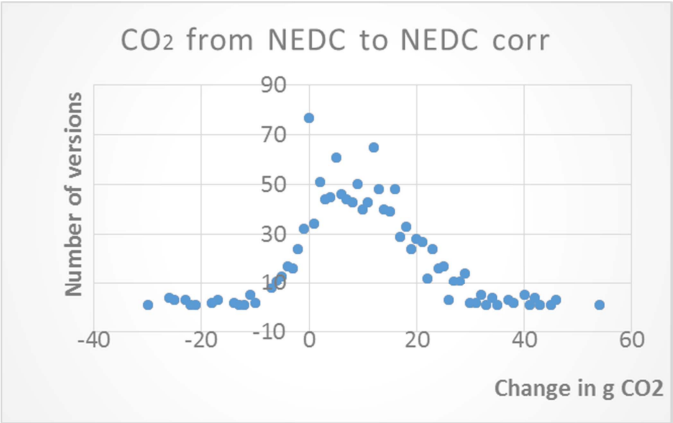

Figure 3. Number of model versions with changed CO_2 emission values from NEDC to NEDC corr

Out of 270 new vehicle models of model year 2019, 44 models (16%) fulfilled the requirements in the policy. In total 44 out of the 270 available models fulfilled the requirements of the 2019 revision of the policy (see Table 9). The listed models have at least one version that fulfills the policy requirements. In total 206 versions of these models fulfilled the requirements (see Table 10). Only a few superminis, large MPVs and Large SUVs can be seen in Table 9 and 10, showing that these size categories have lower specifications regarding safety and/or higher CO_2 emissions.

Table 9.
Number of models with at least one approved version vs. models without any approved version

Size	Models fulfilling the requirements	Models without any version approved	Total
Super mini	1	32	33
Small family car	8	52	60
Large family car	13	24	37
Executive car	8	26	34
Small MPV	5	8	13
Large MPV	0	12	12
Small SUV	8	35	43
Large SUV	1	37	38
Total	44	226	270

Table 10.
Number of model versions approved/failed

Size	Versions approved	Versions failed	Total
Super mini	10	207	217
Small family car	27	517	544
Large family car	90	584	674
Executive car	40	603	643
Small MPV	6	78	84
Large MPV	0	135	135
Small SUV	28	468	496
Large SUV	5	462	467
Total	206	3054	3260

The vast majority of the vehicle models fulfilling the criteria (23) are models with diesel engines. Only three models have pure petrol engines. Nine models have at least one electric hybrid version. Thirteen models have at least one plug-in hybrid version. Six pure electrical vehicle models are among the ones fulfilling the policy requirements. Two models with CNG (Compressed Natural Gas) and one model with fuel cell also fulfill the policy requirements 2019.

DISCUSSIONS

It is important to guide vehicle fleet buyers of personal vehicles to choose the most safe and environmentally friendly vehicles since those vehicles will be used for many years. It is also important that the requirements follow the developments in vehicle safety and that they are in line with the global emission targets.

One of the purposes with a vehicle purchase policy is to speed up the implementation rate of important safety technologies. One example of a fast implementation in Sweden is the introduction of ESC [27]. ESC only had 15% market penetration in the 2003, but after five years the fitment rate was above 90%. Since 2009 the increase has been slow, but in 2017 the fitment rate of ESC in Sweden was 100%. ESC has been included in the Folksam policy since 2006. However, in the 2020 revision of the policy it might be excluded.

Other safety technologies that have been introduced and that have increased their implementation rate is various kinds of AEB and LDW. Many of these technologies have a more than 50% fitment rate of sold cars in 2019. In Table 2, 76% of the vehicle models have AEB City as standard, option or not depending on model version. The vehicle policy guides the consumer to find vehicle models fitted with those safety systems, but it also influence the vehicle manufacturers to make the important safety systems as standard fitment. This is important because fleet purchasers or private consumers often have difficulties to identify which of the safety features that are of importance for safety. An example is ABS, that has been shown to be less effective [28, 29] in contrast to for example AEB or lane departure system that have been shown to be effective[4, 6].

Table 2-4 show differences in fitment rates between vehicle models for sale and sold models. There are probably several reasons for this. In Sweden there is a lot of communications towards vehicle consumers that e.g. AEB is an important feature so customers are aware of its importance. Several car fleet purchasers also include safety requirements in their purchase policies. It is not surprising that sold vehicles have a higher safety standard compared to the models for sale.

During the last two decades limitations in curb weight have been included in the requirements. Studies of vehicle compatibility shows that there is a need to limit the large variation in curb weight [5, 30-32]. The upper limitation of 1900kg was previously included in the Folksam policy as a result of this knowledge[33]. There is however a development towards a larger spread in curb weight. Small vehicles becomes heavier but new smaller vehicle segments appear. It is still 11 new vehicle models of model year 2019 in the database, which has a curb weight below 1000kg. At the same time there are 45 vehicle models with curb weight over 2000kg in the database. 16 of those heavier vehicle models are supported by electrical motors. In conclusion there will be a need for a curb weight limitation in the policy criteria that does not exclude new environmentally friendly engine techniques.

The list of model presented in Table 9 shows that only a few models of the vehicle categories superminis, large MPVs and Large SUVs fulfill the requirements. The main reason for the superminis to fail is the absence of AEB with pedestrian detection. The large MPVs most commonly fail due to large emissions but also lack of AEB with pedestrian detection. MPVs are not usually fitted with alternative fuels such as batteries. The large SUVs fail most often due to large emissions.

The emission requirement contains only limits regarding CO_2. The emission of CO_2 is crucial for the climate change and historically diesel engines has had lower CO_2 emissions compared to petrol engines. However emission of NOx, especially from diesel engines, is also a health problem, especially in dense cities [34]. There is a need to control the NOx emission as well since investigation of real emissions is shown to be extensively higher than the emission level defined by Euro 6. In the transition period to alternative fuels, diesel and petrol will be used. The RDE (Real Driving Emission) which is included in the WLTP test cycle from 2017, measures NOx emitted by the vehicles while driven on the road [35]. This will probably control the NOx emission and will mean that requirements for NO_x emission does not need to be included in the policy.

There is an increasing interest of more fuel saving vehicles and vehicles that can be driven fossil free. Fuel economy is one of top three purchase criteria which makes PHEV vehicles and electrical cars of special interest for car buyers [36]. The number of plug-in hybrids for sale is increasing. However, there are relatively few plug-in hybrids in the policy list 2019. One reason is the change from the emission driving cycle NEDC to WLTP. A large number of plug-in hybrids has not been tested according to WLTP and will therefore need to wait until the WLTP test is done.

CONCLUSIONS

It is important to guide vehicle fleet buyers of vehicles for private use to choose the safest and most environmentally friendly vehicles since those vehicles will be used for many years. Company car policies are important tools in this process. A vehicle purchase policy will indirectly influence car manufactures to offer vehicles that fulfil the requirements in the policy.

An important recommendation is that a vehicle purchase policy should be revised annually to follow rapid changes in available safety technology and emission standards in order to substantially influence the vehicle fleet. A vehicle purchase policy is an important tool to guide vehicle consumers towards the safest and most sustainable vehicles. It is recommended that a vehicle purchase policy should consist of requirements regarding crashworthiness, fitment of important safety systems, CO_2 emissions. Preferably, it should be complemented with a vehicle list for tangible and feasible advice to consumers

REFERENCES

1. BilSweden. 2017. "Automotive holdings". Available from: http://www.bilsweden.se/statistik/fordonsbestand#.
2. Fuglestvedt, J., et al., 2008. "Climate forcing from the transport sectors". Proceedings of the National Academy of Sciences, 105(2): p. 454-458.
3. Rockström, J., et al., 2017. "A roadmap for rapid decarbonization". Science, 355(6331): p. 1269-1271.
4. Rizzi, M., A. Kullgren, and C. Tingvall. 2014. "Injury crash reduction of low-speed Autonomous Emergency Braking (AEB) on passenger cars". in International Research Council on the Biomechanics of Injury Conference, IRCOBI 2014 Berlin; Germany.
5. Huang, H., S. Hu, and M. Abdel-Aty, 2014. "Indexing crash worthiness and crash aggressivity by major car brands". Safety Science, 62: p. 339-347.
6. Sternlund, S., et al., 2016. "The effectiveness of lane departure warning systems – a reduction in real-world passenger car injury crashes". Traffic Injury Prevention: p. 00-00.
7. Trafikanalys, 2016. "Statistik över fordonsflottans utveckling – delredovisning av regeringsuppdrag": Stockholm. p. 52.
8. Koppel, S., et al., 2005. "How important is 'vehicle safety' in the new vehicle purchase process? ", in Report of sub-task 4.1 SARAC II Project, EU Commission.
9. Langwieder, K., B. Fildes, and T. Ernvall. 2003. "SARAC - Safety Rating Based on Real-World Crashes for Supplementation of new Car Assessment Programs".
10. Mersky, A.C., et al., 2016. "Effectiveness of incentives on electric vehicle adoption in Norway". Transportation Research Part D: Transport and Environment, 46: p. 56-68.
11. Zhang, X., et al., 2014. "Policy Incentives for the Adoption of Electric Vehicles across Countries". Sustainability, 6(11): p. 8056.
12. Lutsey, N., 2015. "Transition to a global zero-emission vehicle fleet: a collaborative agenda for governments": Washington DC. p. 40.
13. EuropeanCouncil, 2014. "2030 climate & energy framework": Brussels.
14. Hägg, A., et al., 2001. "Folksam Car Model Safety Ratings 2001". Folksam Research: Stockholm, Sweden.
15. Lie, A. and C. Tingvall, 2002. "How Do Euro NCAP Results Correlate with Real-Life Injury Risks? A Paired Comparison Study of Car-to-Car Crashes ". Traffic Inj Prev, 3(4): p. 288-293.
16. Kullgren, A., A. Lie, and C. Tingvall, 2010. "Comparison Between Euro NCAP Test Results and Real-World Crash Data". Traffic Inj Prev, 11(6): p. 587 - 593.
17. Kullgren, A., et al. 2019. "Developments in Car Crash Safety and Comparisons Between Results From Euro NCAP Tests and Real-World Crashes". in 26th ESV Conference. Eindhoven.
18. JATO, 1984. "JATO Dynamis Limited": Uxbridge, UK.
19. Krafft, M., et al., 2000. "How crash severity in rear impacts influences short- and long-term consequences to the neck". Accident Analysis and Prevention, 32(2): p. 187-95.
20. Bostrom, O., et al., 2000. "Comparison of car seats in low speed rear-end impacts using the BioRID dummy and the new neck injury criterion (NIC)". Accident Analysis and Prevention, 32(2): p. 321-8.
21. Cicchino, C., 2016. "Effectiveness of Forward Collision Warning Systems with and without Autonomous Emergency Braking in Reducing Police-Reported Crash Rates", IIHS, Editor.

22. Isaksson-Hellman, I. and M. Lindman. 2015. "Evaluation of Rear-End Collision Avoidance Technologies based on Real World Crash Data". in Proc. 3rd International Symposium on Future Active Safety Technology towards zero traffic accidents. Gothenburg.

23. Sternlund, S., 2017. "The safety potential of lane departure warning systems—A descriptive real-world study of fatal lane departure passenger car crashes in Sweden". Traffic Injury Prevention, 18(sup1): p. S18-S23.
24. Folksam. 2005. "How safe is your car?". [cited 2005; Available from: http://www.folksam.se/engelsk/trafik_eng/sakrabilar2005.pdf.
25. IIHS/HLDI. 2019. Available from: https://m.iihs.org/mobile/ratings.
26. TheHagaInitiative, 2017. "Greenhouse Gas Emissions Disclosure 2017".
27. Krafft, M., et al. 2009. "From 15 % to 90 % ESC Penetration in New Cars in 48 Months - The Swedish Experience". in 21th International Conference on the Enhanced Safety Vehicles (ESV). Stuttgart.
28. HLDI, H.L.D.I., 1994. "Collision and property damage liability losses of passenger cars with and without Antilock Brakes.", H.L.D. Institute, Editor: Arlington, VA.
29. Kullgren, A., A. Lie, and C. Tingvall. 1994. "The Effectiveness of ABS in Real-Life Accidents". in 14th International Conference on the Enhanced Safety Vehicles (ESV). München.
30. Acierno, S., et al., 2004. "Vehicle mismatch: injury patterns and severity". Accid Anal Prev, 36(5): p. 761-72.
31. Kullgren, A., et al. 1990. "The Problem of Compatibility in Car-to-car Collisions. Invited commentary to paper by C Thomas et al. published at IRCOBI 1990". in Int. IRCOBI Conf. of the Biomechanics of Injury: IRCOBI, Inrets, France.
32. Teoh, E.R. and J.M. Nolan, 2012. "Is Passenger Vehicle Incompatibility Still a Problem?". Traffic Injury Prevention, 13(6): p. 585-591.
33. Greenwell, N.K., 2012. "Evaluation of the Enhancing Vehicle-to-Vehicle Crash Compatibility Agreement: Effectiveness of the Primary and Secondary Energy-Absorbing Structures on Pickup Trucks and SUVs": Washington DC.
34. Sjödin, Å., et al., 2017. "On-Road Emission Performance of Late Model Diesel and Gasoline Vehicles as Measured by Remote Sensing". IVL: Stockholm.
35. Merkisz, J., et al. 2016. "Analysis of Emission Factors in RDE Tests As Well as in NEDC and WLTC Chassis Dynamometer Tests": SAE International.

36. Musti, S. and K.M. Kockelman, 2011. "Evolution of the household vehicle fleet: Anticipating fleet composition, PHEV adoption and GHG emissions in Austin, Texas". Transportation Research Part A: Policy and Practice, 45(8): p. 707-720.

DEVELOPMENTS IN CAR CRASH SAFETY AND COMPARISONS BETWEEN RESULTS FROM EURO NCAP TESTS AND REAL-WORLD CRASHES

Anders Kullgren
Folksam Insurance Group and Chalmers University of Technology
Sweden
Amanda Axelsson
Folksam Insurance Group
Sweden
Helena Stigson
Folksam Insurance Group and Karolinska Institutet
Sweden
Anders Ydenius
Folksam Insurance Group
Sweden

Paper Number 19-0291

ABSTRACT

Developments in car crash safety is preferably demonstrated by analyzing results from real-world crashes. Also results from crash tests can be used to show improvements in crash performance. Previous research has shown a positive development regarding safety performance. Studies from the early 2000 have shown that the European New Car Assessment Programme (Euro NCAP) consumer tests seem to predict the outcome in real-world crashes, although they consider only a part of all accident scenarios. In 2009 Euro NCAP added rear-end crash tests to the test protocol and since 2012 Euro NCAP has gradually further revised the rating protocol. It is therefore important to study developments in crash safety, and to evaluate how Euro NCAP test results correlate with real-world performance.

This study aimed to show developments in car crash safety in cars launched since the 1980s based on real-world data, and to present how Euro NCAP crash test results predict the outcome in real-world crashes.

Two-car crashes reported by the police (n=202 360) and occupant injuries reported by emergency care centers (n=57 863) to the Swedish Traffic Accident Data Acquisition database (STRADA) were analyzed. The cars were categorized in 5-year periods, according to the year of introduction. Developments were studied in terms of risk of any injury, risk of serious injury, risk of fatality, and risk of permanent medical impairment (PMI). Correlations with Euro NCAP test results were evaluated based on star levels for all categories of injury severity.

It was found that vehicle crashworthiness has improved steadily over the years studied. The proportion of serious injuries was found to be reduced, as well as the injury risk for all injury severities studied. In a comparison of car models launched 1980-1984 with those launched 2015-2018 the proportion of AIS 3+ injuries was 67% lower. Furthermore, the risk for serious and fatal injury was 58% (+/-17%) lower, the risk for fatal injury was 88% (+/-57%) lower, and the risk for PMI was 73% (+/-14%) lower. It was also shown that Euro NCAP crash test ratings mirror real world injury outcomes for all injury severities studied. Comparing 5-star with 2-star rated cars, the proportion of AIS 3+ injuries was 34% lower. Furthermore, the risk for serious and fatal injury was 22% (+/-4%) lower, the risk for fatal injury was 40% (+/-16%) lower, and the risk for PMI was 42% (+/-4%) lower.

Large improvement in crash safety was found, especially regarding the risk for fatal injuries and injuries leading to PMI. Euro NCAP star ratings were found to well mirror the risk for fatal injuries and injuries leading to PMI.

Consumer crash tests play an important role for the development in car safety. It is however important to continuously study how well these consumer tests predict the outcome in real-world crashes. Especially considering rating systems that reward the overall safety of a vehicle, such as the Euro NCAP.

INTRODUCTION

Studies have shown improvements in vehicle crashworthiness over time [1,2,3,4,5]. The improvements have been shown with crash test results and real-world crash data analyses. There are several crash test programs like European New Car Assessment Programme (Euro NCAP) that evaluate the safety level of new cars using laboratory crash tests (e.g.,: USNCAP, ANCAP, JNCAP, IIHS Tests). By the end of 2018, Euro NCAP had tested approximately 600 of the most popular car models in Europe since 1994. Details of the tests and the results are available at Euro NCAP's web site http://www.euroncap.com.

The Euro NCAP star rating is based on point scores from front and side impacts, as well as rear sled tests that evaluate the car seats (added 2009 to evaluate the risk of whiplash injury). Since 2012 the protocol has been revised regarding, e.g., point score and weighting. The intention of these scores is not necessarily to predict the real-world outcome (although this is inferred from the test results), but to indicate what is the best practice (benchmarking) for an individual car model and the fleet generally. However, it is clearly of interest to continuously evaluate how the crash test results correlate with real-world outcome.

Due to test limitations, laboratory crash tests can only provide a relatively limited evaluation of the overall safety level of a specific car model. Real-world performance gives a more comprehensive picture of the overall safety level, as it covers a variety of real-world crash configurations. Over the years, a number of international institutions have conducted retrospective statistical vehicle safety ratings using real-world crash databases, such as Transport Road Research Laboratories in the United Kingdom, Highway Loss Data Institute in the USA, Used Car Safety Ratings in Australia, VALT in Finland, and the Folksam Insurance Group (Folksam) in Sweden. Folksam has regularly published car safety ratings since the 1983. The Folksam system rates the relative risk that a driver sustains an injury that leads to fatality or permanent medical impairment (PMI), across all impact directions and locations [3].

Previous studies have presented the correlation between Euro NCAP results and injury risk based on real-world crashes [6,7,8]. In these studies, police assessments of injury outcome (killed, seriously injured, minor injuries or uninjured) were used as the injury descriptors. In Kullgren at al. [8] the risk for injuries leading to permanent medical impairment (PMI) was additionally shown. The study by Lie and Tingvall [7] showed a strong and consistent correlation when the risk for a fatal or serious injury was the dependent variable, although no correlation was found for minor injuries. A significant correlation between Euro NCAP scores and Folksam car model safety ratings was shown in 2001 [6], where 4-star rated Euro NCAP cars had a lower risk of serious injury than 2- and 3-star rated cars. The study by Kullgren et al. [8] showed that 5-star rated cars had a 27% lower risk of injuries leading to PMI compared to 2-star rated cars. The corresponding figure for fatal injury was 68%.

In Swedish road safety strategies fatal injuries and injuries leading to PMI are in focus. In 1997, the Swedish parliament decided on the Vision Zero strategy with the long-term vision of no fatal or serious injuries within the road transport system [9]. The definition of a serious injury is an injury leading to PMI. It is, therefore, important to follow the improvements in the passenger car fleet with respect to injury outcome in terms of both fatality and injuries leading to PMI.

The aim of this study was to evaluate developments in crash safety in cars launched since the 1980s based on real-world injury outcomes, and to evaluate how Euro NCAP crash test results predict the outcome in real-world crashes. Various severities of injury outcome were analyzed; the risk of any injury, serious and fatal injury, fatal injury, and the risk for injuries leading to PMI, as used in the Folksam car model safety ratings.

MATERIAL AND METHODS

The Swedish Traffic Accident Data Acquisition database (STRADA) was used that covers two data sets: car crashes reported by the police, and occupant injury data from emergency care centers [10]. Relative injury risk was calculated using paired comparisons from 202 360 two-car crashes with at least one injured front-seat occupant reported by the police. In these collisions the police classified the injuries as minor, serious or fatal. The accident

years were 1994 to 2018. The risk for PMI was calculated from 57 863 injured front-seat occupants in car crashes between 2000 and 2018.

Two sets of analyses were made using the same method, one covering developments in crash safety since the early 80s, and the other evaluating the correlation between Euro NCAP star ratings and outcomes in real-world crashes. To mirror the developments in crash safety, the car models were categorized in 5-year periods according to year of introduction, beginning in 1980-84 and ending in 2014-2018. The year of introduction was chosen as a way to describe the year of design. The correlation between Euro NCAP crash test scores and real-world injury outcomes was made based on the star level. For both analyses four different injury levels were studied: any injury, serious and fatal injury, fatal injury and injury leading to PMI. The following sections describe how the relative risk using paired comparisons and the risk for PMI were calculated.

Calculating the Relative Injury Risk using Police Data

Relative injury risks were calculated using the paired comparison technique for two-car crashes. The method was initially developed by Evans [11], but has been further refined by Folksam for car-to-car collisions [12,13,8]. By studying two-car crashes in which both cars were involved in the same impact, the paired comparison method controls for variation in impact severity apart from the influence of car mass. The relative injury risk for a specific group of vehicles was calculated by comparing the injury outcome for that group with the injury outcome for the vehicles they collide with. In two-car crashes, mass differences can influence the relative injury risk, as they alter the impact severity distribution between the groups. This can be taken into account in the model and the influence of mass on the relative injury risk can be controlled for.

Another factor potentially influencing the results is aggressivity. Aggressivity is defined as the properties of a vehicle other than the mass that can influence the risk of injuries to the occupants of other vehicles (its structure and stiffness for instance can have such an effect). However, the influence of aggressivity on injury risk in paired comparisons has been shown to be much smaller than the influence of mass [12,14], thus aggressivity was not adjusted for in this analysis. All car-to-car crashes were included irrespective of crash type. It was assumed that the injuries among occupants in one car are independent from the injuries among occupants in the other car, given a particular impact severity.

Using the paired comparison method, crash outcomes in two-car crashes were grouped in four groups (see Table 1), where x_1 is the number of crashes causing injuries among occupants in both cars, x_2 is the number of crashes causing injuries in the case car only (but not in the other vehicle), x_3 is the number of injuries among occupants in the colliding vehicle only (but not in the case vehicle), x_4 reflects the situation that no one is injured in the crash (often little data are available here). In calculating the relative risk, x_4 is not used, as it does not add any important information.

Table 1.
Number of impacts with different combinations of injured drivers in Car 1 and Car 2

		Driver of Car 2		Total
		driver injured	driver not injured	
Driver of Car 1	driver injured	x_1	x_2	$x_1+ x_2$
	driver not injured	x_3	x_4	
Total		$x_1+ x_3$		

The unadjusted relative risk between the studied car or group of cars and its collision partners is calculated as the ratio between injuries in the studied car compared with the injuries in its collision partners (Equation 1). The collision partners are considered to be a sample of the whole car population, and therefore they provide the exposure basis that allows for comparisons across all case vehicles.

$$R=(x_1+x_2)/(x_1+x_3) \quad \text{(Equation 1)}$$

Compensation for Mass Differences

The influence of mass on injury outcome described by power model functions has been described extensively by Elvik et al. [15] and Krafft et al. [16]. If there are mass differences between the case vehicles and the vehicles that they collide with, both groups will be exposed to an impact severity different to that from when the two groups of vehicles have the same mass. If the case vehicle group is lighter than the other vehicle group, it will experience a higher impact severity compared to its collision partners (Impact Energy = mass * velocity^2). At the same time, the other heavier vehicles will experience a lower impact severity. The mass differential will therefore result in a benefit for one vehicle and a disadvantage for the other vehicle in a two-car crash. In order to allow for accurate comparisons and take into account the importance of mass for the case vehicles, the altered impact severity distribution for the cars they collide with must be compensated for. The adjusted relative injury risk is therefore expressed as in Equation 2. The power '*y*' in Equation 2 varies depending on the severity of the injury studied. Three mass adjustments were used depending on the injury severity; all injuries *y*=0.5, fatal and serious injury *y*=1.8, fatal injury *y*=3.5. The more severe the injury, the higher power '*y*', resulting in a steeper slope of the risk curve.

$$R_{\text{mass adjusted}} = (x_1+x_2)/(x_1+x_3) * M^y \qquad \text{(Equation 2)}$$

where M = (average case vehicle mass)/(average other vehicle mass)

Crash testing into a fixed barrier is equivalent to a crash into a car of the same mass, while the real-world outcome integrates mass as a factor that influences impact severity. In order to have a relevant comparison between crash test results and real-world performance, the influence of mass has to be fully adjusted for, considering both the case vehicle group and the group of cars that it collides with. The effect in the calculations will be that the power '*y*' in Equation 2 has to be doubled in the evaluation of Euro NCAP star ratings so that the pure safety design benefit can be isolated.

Compensation for the Year of the Crash

It has previously been found that the average safety level of vehicles in the fleet increases every year [13]. When using the paired comparison method with an accident sample including accidents that occurred several years back in time, the comparison between car models launched in different years will be influenced by this difference. By using the paired comparison method, it is possible to calculate the average decrease in injury risk of the whole car fleet. In [13,8] the average decrease in risk was found to be 1,5% per accident year as a linear relationship. For example, a car model involved in collisions 10 years back experienced an average collision partner that was 15% less safe than the average level today. This means that the rating result for that model will be 15% better than the "true" result if compared with the average safety level of models existing today. Therefore, based on these results, compensations have been made to adjust for the year of impact according to Equation 3.

$$x_{i,\text{ adjusted}} = \sum_{j=1}^{m} [x_{i,j} * (1 + f*(\text{Year}_{\text{actual}} - \text{Year}_j))] \qquad \text{(Equation 3)}$$

$f = 0.015$ (1.5% per year)

$\text{Year}_{\text{actual}}$ = latest accident year in the sample

Year_j = accident year for the particular crash

The accident year compensation was made for each crash with a factor linked to the accident year. The adjusted relative injury risk was calculated based on the ratio between the adjusted x_1+x_2 in the nominator and the unadjusted x_1+x_3 in the denominator, Equation 4.

$$R_{\text{year adjusted}} = (x_{1,\text{ adjusted}}+x_{2,\text{ adjusted}})/(x_1+x_3) \qquad \text{(Equation 4)}$$

The final formula used to calculate the relative injury risk from the police data would therefore be:

$$R_{\text{adjusted}} = (x_{1,\text{ adjusted}}+x_{2,\text{ adjusted}})/(x_1+x_3) * M^y \qquad \text{(Equation 5)}$$

95% confidence intervals (CI) were calculated for each risk value. The variance of the relative injury risk, R, was based on Gauss' approximation of variance for ratios.

Calculation of risk of permanent medical impairment

The risk of permanent medical impairment (RPMI) was used to measure the risk of long-term consequences [17]. The risk of sustaining a PMI of at least 10% according to the procedures used by Swedish insurance companies [18] was chosen (see Table 2). All injuries were classified according to the 2005 revision of the Abbreviated Injury Scale, AIS [19]. RPMI was based on the AIS scale, where an impairment risk has been calculated for each AIS level and body region [17].

Table 2.
Risk of permanent medical impairment in percent (from Malm et al. 2005).

Body region	**1**	**2**	**3**	**4**	**5**
Head	2.5	8	35	75	100
Cervical Spine	2.5	10	30	100	100
Face	0.4	6	60	60	n.a.
Upper Extremity	0.3	3	15	100	n.a.
Lower Extremity and Pelvis	0.0	3	10	40	100
Thorax	0.0	0	0	15	15
Thoracic Spine	0.0	7	20	100	100
Abdomen	0.0	0.0	5	5	5
Lumbar Spine	0.1	6	6	100	100
External (Skin) and Thermal Injuries	0.03	0.03	50	50	100

Table 3 shows the probabilities for permanent medical impairment for different body regions and AIS levels.

The RPMI for an occupant is calculated by multiplying the individual risks for each injury diagnose with the highest AIS level in each body region according to Equation 6, where p_i is the risk of sustaining a permanent medical impairment as a result of an injury of a certain AIS level to body region *i*. The body regions can be seen in Table 2.

$$RPMI = (1-\prod[1 - p_i])) \qquad \text{(Equation 6)}$$

Based on all reported injuries for a specific group of cars an average risk that an injury would lead to a permanent medical impairment was calculated.

Calculation of Relative Risk of Permanent Medical Impairment

The overall relative risk of receiving an injury leading to fatality or permanent medical impairment is then obtained by combining the relative injury risk and injury severity measures (Equation 7). The method has been used in Folksam's car model safety ratings since the 1990s. The latest description of the rating procedure was published by [13]. For the relative risk of PMI the 95% confidence intervals (CI) were calculated using monte carlo iterations.

$$\text{Relative RPMI} = R_{adjusted} * RPMI \qquad \text{(Equation 7)}$$

RESULTS

The proportion of serious injuries was found be reduced in modern cars. Comparing car models launched 1980-1984 with those launched 2015-2018 the proportion of AIS2+ injuries (AIS2 and more severe) was 41% lower, the proportion of AIS3+ injuries (AIS3 and more severe) was 67% lower and the proportion of AIS4+ injuries (AIS4 and more severe) was 81% lower (see Table 3).

The higher number of stars in Euro NCAP, the lower proportion of serious injuries. Comparing 5-star rated cars with 2-star rated ones, the proportion of AIS2+ injuries was 24% lower, the proportion of AIS 3+ injuries was 34% lower and the proportion of AIS4+ injuries was 66% lower (see Table 3).

Table 3.
Proportions of injuries with different AIS levels at different years of introduction and for car models with various Euro NCAP stars.

	AIS Level						
Year of launch	**1**	**2**	**3**	**4**	**5**	**6**	**Tot**
1980-1984	76,7%	13,6%	6,45%	1,71%	1,17%	0,45%	100%
1985-1989	75,9%	15,3%	5,84%	1,08%	1,32%	0,59%	100%
1990-1994	80,6%	12,8%	4,19%	1,25%	0,96%	0,14%	100%
1995-1999	82,2%	12,4%	3,66%	0,88%	0,61%	0,17%	100%
2000-2004	84,3%	11,1%	3,57%	0,58%	0,37%	0,10%	100%
2005-2009	85,9%	10,4%	3,00%	0,40%	0,25%	0,08%	100%
2010-2014	84,8%	11,3%	3,19%	0,22%	0,43%	0,14%	100%
2015-2018	86,1%	10,6%	2,58%	0,65%	0,00%	0,00%	100%
Euro NCAP stars	**1**	**2**	**3**	**4**	**5**	**6**	**Tot**
2	80,76%	13,24%	3,88%	1,05%	0,91%	0,17%	100%
3	82,31%	11,98%	4,10%	0,82%	0,69%	0,11%	100%
4	83,57%	11,74%	3,35%	0,72%	0,52%	0,11%	100%
5	85,36%	10,68%	3,22%	0,38%	0,27%	0,08%	100%
Total	83,74%	11,56%	3,45%	0,65%	0,49%	0,11%	100%

Comparing car models introduced in 1980-1984 with models introduced in 2015-2018, it was found that the risk of any injury was reduced by 40% (+/-4.5%), the risk of serious and fatal injury by 58% (+/-17%), the risk of fatal injury by 88% (+/-57%) and the risk of PMI was reduced by 73% (+/-14%) (see Table 4). Regarding the risk of fatality, the number of crashes was relatively low for the two later 5-year periods. When comparing cars introduced 1980-1984 with those introduced 2010-2014 the fatality risk was reduced by 69% (+/-15%).

Comparing 5-star with 2-star rated cars in Euro NCAP, it was found that the risk of any injury was reduced by 18% (+/-1%), the risk of serious and fatal injury by 22% (+/-4%), the risk of fatal injury by 40% (+/-16%) and the risk of PMI was reduced with 42% (+/-4%) (see Table 5).

Table 4.
Relative risk of any injury, fatal and serious injury, fatal injury and injury leading to PMI (grey column).

	Year of launch	n	mass case	mass other	x_1	x_2	x_3	R	R_{adj}	95% CI
All injuries	**1980-1984**	21018	1205	1326	8132	10274	5748	1,326	1,17	0,0108
	1985-1989	18209	1262	1341	6791	8503	5157	1,280	1,14	0,0119
	1990-1994	24980	1363	1383	8936	10294	7508	1,169	1,04	0,0108
	1995-1999	43318	1406	1424	14085	16217	13675	1,092	0,94	0,0087
	2000-2004	27290	1511	1464	7978	9278	9291	0,999	0,86	0,0115
	2005-2009	21271	1574	1498	5643	7004	7598	0,955	0,82	0,0133
	2010-2014	8340	1519	1524	2094	2732	2986	0,950	0,78	0,0216
	2015-2019	1297	1711	1557	323	367	525	0,814	0,70	0,0554
	Total	202360	1407	1409	64500	82204	64195	1,140	1,00	0,0039
Fatal and serious injuries	**1980-1984**	21018	1205	1326	998	1863	863	1,537	1,16	0,0293
	1985-1989	18209	1262	1341	812	1432	752	1,435	1,14	0,0322
	1990-1994	24980	1363	1383	890	1509	1161	1,169	0,98	0,0310
	1995-1999	43318	1406	1424	1214	2240	1969	1,085	0,89	0,0259
	2000-2004	27290	1511	1464	566	989	1236	0,863	0,75	0,0373
	2005-2009	21271	1574	1498	337	616	968	0,730	0,65	0,0462
	2010-2014	8340	1519	1524	151	264	347	0,833	0,66	0,0718
	2015-2019	1297	1711	1557	17	28	71	0,515	0,49	0,1941
	Total	202360	1407	1409	6207	11773	9100	1,175	1,00	0,0113
Fatal injuries	**1980-1984**	21018	1205	1326	24	295	96	2,655	1,56	0,0986
	1985-1989	18209	1262	1341	26	176	104	1,553	1,03	0,1169
	1990-1994	24980	1363	1383	24	170	136	1,211	0,93	0,1121
	1995-1999	43318	1406	1424	26	230	205	1,109	0,85	0,0966
	2000-2004	27290	1511	1464	11	81	134	0,635	0,56	0,1435
	2005-2009	21271	1574	1498	1	35	108	0,333	0,31	0,1858
	2010-2014	8340	1519	1524	4	25	44	0,614	0,48	0,2451
	2015-2019	1297	1711	1557	0	1	6	0,169	0,18	0,8879
	Total	202360	1407	1409	149	1361	1060	1,249	1,00	0,0396
	Year of launch	**n**	**mass case**	**mass other**	**R**	**R_{adj}**	**n RPMI**	**RPMI**	**Rel RPMI**	**95% CI**
Injuries leading to PMI	**1980-1984**	21018	1205	1326	1,326	1,17	3332	0,0489	0,054	0,0042
	1985-1989	18209	1262	1341	1,280	1,14	3701	0,0523	0,058	0,0040
	1990-1994	24980	1363	1383	1,169	1,04	8347	0,0401	0,041	0,0025
	1995-1999	43318	1406	1424	1,092	0,94	18229	0,0343	0,032	0,0016
	2000-2004	27290	1511	1464	0,999	0,86	11569	0,0299	0,026	0,0017
	2005-2009	21271	1574	1498	0,955	0,82	8524	0,0260	0,022	0,0020
	2010-2014	8340	1519	1524	0,950	0,78	2761	0,0275	0,021	0,0034
	2015-2019	1297	1711	1557	0,814	0,70	310	0,0221	0,016	0,0080
	Total	202360	1407	1409	1,140	1,00	57863	0,0378	0,038	0,0009

Table 5.
Relative risk of any injury, fatal and serious injury, fatal injury and injury leading to PMI (grey column).

	Euro NCAP stars	n	mass case	mass other	x_1	x_2	x_3	R	R adj	95% CI
All injuries	2	10450	1313	1381	3737	4464	3014	1,21	1,03	0,01659
	3	13437	1348	1425	4241	5337	4099	1,15	0,95	0,01558
	4	43160	1432	1445	13323	15464	13967	1,05	0,90	0,00894
	5	35419	1565	1492	9531	11801	12439	0,97	0,85	0,01029
	Total	102466	1455	1452	30832	37066	33519	1,00	0,91	0,00582
Fatal+serious	2	10450	1313	1381	393	691	441	1,30	0,96	0,04700
	3	13437	1348	1425	357	779	562	1,24	0,87	0,04653
	4	43160	1432	1445	991	1858	1921	0,98	0,80	0,02827
	5	35419	1565	1492	640	1074	1603	0,76	0,75	0,03476
	Total	102466	1455	1452	2381	4402	4527	1,00	0,84	0,01829
Fatal injuries	2	10450	1313	1381	14	79	52	1,41	0,84	0,16910
	3	13437	1348	1425	5	71	57	1,23	0,69	0,18366
	4	43160	1432	1445	24	182	203	0,91	0,70	0,10381
	5	35419	1565	1492	7	75	181	0,44	0,50	0,13640
	Total	102466	1455	1452	50	407	493	1,00	0,70	0,06857
Injuries with PMI	**Year of launch**	**n**	**mass case**	**mass other**	**R**	**R adj**	**n RPMI**	**rpmi**	**Rel RPMI**	**95% CI**
	2	10450	1313	1381	1,21	1,03	3534	0,0374	0,0386	0,00358
	3	13437	1348	1425	1,15	0,95	5392	0,0334	0,0316	0,00292
	4	43160	1432	1445	1,05	0,90	18590	0,0323	0,0290	0,00150
	5	35419	1565	1492	0,97	0,85	13152	0,0266	0,0226	0,00148
	Total	102466	1455	1452	1,00	0,91	40668	0,0310	0,0281	0,00101

DISCUSSION

These results clearly show that vehicle crashworthiness has improved since the early 80s. Such results have also been found in other studies [1,2,3,4,5]. They also show that the improvements are larger for more severe injuries. The largest improvement was found for fatal injuries, but a large improvement was also found for injuries leading to permanent medical impairment. In Sweden, which has adopted the Vision Zero approach, this is very positive, because the vision includes both fatal and serious injuries, and serious injury is in Sweden defined as an injury leading to any kind of permanent medical impairment.

The study also demonstrated that 5-star rated cars offer superior safety performance over 2-star rated cars for all types of injury severity studied. A consistent and positive correlation was found between real-world injury outcomes and Euro NCAP test results. Similar results have been seen in other parts of the world and in other studies [20,6,7,21,8]. The findings reported here though controlled for differences in vehicle mass and the year of impact using the two-car paired comparison method. Furthermore, of the previous studies only Kullgren et al. [8] was able to contrast differences in injury outcome in terms of relative risk of permanent medical impairment.

It should be stressed that as the cars were grouped by their star level, and that these results say nothing about the potential correlation for an individual car model. It is instead an evaluation of the Euro NCAP assessment principles with statistical findings from real-world crash data. While not shown here, though, a car with generally good

performance in Euro NCAP was found to perform well in real-world crashes, in coherence with what has been reported previously.

The estimates in this study are based on star bands. It is important to stress that the average point performance (basis for star rating) is not necessarily in the center of the star band [7]. Furthermore the Euro NCAP test protocol has been revised in 2009 to also mirror vehicle seat performance in rear-end crashes. Whiplash injuries are very important in terms of the risk of permanent medical impairment. Swedish evidence shows that they constitute the vast majority of injuries leading to permanent medical impairment [22]. Furthermore, since 2013 it has been revised every year to also include driver assistant technologies, for example. It is important to conduct further studies to evaluate how these revisions of the test protocol correlates with real-world outcome. The Euro NCAP procedure does not try to predict the relative real-world injury risks. Instead the program is aimed at promoting the best practice in a more general way. Despite this, it is reassuring that there is good correlation between the crash test results and real-world performance, confirming Euro NCAP's relevance to vehicle crashworthiness.

It is important, however, for other studies to confirm the correlation between consumer crash test results and performance in real-world crashes to ensure that the outcome and interpretation of consumer crash tests are relevant to vehicle safety. Sweden is a small country and these findings are only possible with long exposure times before reliable data are available. A pan European co-operation using police accident records from a number of different countries would allow faster comparisons in just a few years. Studies that examine ways of undertaking such analyses would be extremely useful.

While not central to this analysis, a good score of a particular car model can be achieved in the paired comparison by being aggressive to its collision partner. While an earlier study by Kullgren et al. [14] showed that aggressivity was less important than vehicle mass, it would nevertheless be beneficial if aggressivity could be controlled for in the way that mass and age were in the current study. This would further enhance similarities between real world crash ratings and Euro NCAP scores.

The risk figures may also be influenced by systematic differences in seatbelt use and accident type. However, these factors seem not to be likely sources of error in this study, although high rated cars that normally have seat belt reminders might have a slightly higher seat belt use. This should, on the other hand, be included in modern cars to improve safety for the occupants.

It is important to stress that while the weight of new cars have gone up substantially in recent years, the results of this study confirm that improved crashworthiness has been the primary factor in enhanced vehicle safety, rather than the increase in mass. For an individual consumer though, the benefit of choosing a new car with greater mass might be larger than for the overall population, as would choosing a car with a higher Euro NCAP score or superior result in the Folksam car model safety rating.

CONCLUSIONS

It was found that vehicle crashworthiness has steadily improved over the vehicle years studied. The proportion of serious injuries was found to be reduced and also the injury risk for all injury severities studied. When comparing car models launched 1980-1984 with those launched 2015-2018, the proportion of AIS 3+ injuries was 67% lower. Furthermore, the risk of serious and fatal injury was found to be 58% (+/-17%) lower, the risk of fatal injury 88% (+/-57%) lower, and the risk of PMI was 73% (+/-14%) lower.

It was also shown that Euro NCAP crash test ratings mirror real-world injury outcomes for all injury severities studied. Comparing 5-star rated cars with 2-star rated ones, the proportion of AIS 3+ injuries was 34% lower. Furthermore, the risk of serious and fatal injury was 22% (+/-4%) lower, the risk of fatal injury was 40% (+/-16%) lower, and the risk of PMI was 42% (+/-4%) lower.

REFERENCES

[1] Lie A, Tingvall C, Larsson P. 1996. The crash safety of new car models – a comparative accident study of new versus old car models. Proc. of the ESV Conference in Melbourne 1996, Paper no. 96-S9-O-13, Vol. 2, pp 1441-1443

[2] Kullgren A, Krafft M, Ydenius A, Lie A, Tingvall C. 2002. Developments in Car Safety with Respect to Disability - Injury Distributions for Car Occupants in Cars from the 80s and 90s. Proc. of the 2002 IRCOBI Conf. on the Biomechanics of Injury, München, pp 145-154

[3] Folksam. 2017. "How safe is your car?". Folksam. SE-10660 Stockholm, Sweden, or www.folksam.se. Accessed 2019-02-28

[4] Anderson RW, Searson DJ. Use of age-period-cohort models to estimate effects of vehicle age, year of crash and year of vehicle manufacture on driver injury and fatality rates in single vehicle crashes in New South Wales, 2003-2010. *Accid. Anal. Prev.* Feb 2015;75:202-210

[5] Hoye A. Vehicle registration year, age, and weight - Untangling the effects on crash risk. *Accid. Anal. Prev.* Feb 2019;123:1-11

[6] Lie A, Kullgren A, Tingvall C. 2001. Comparison of Euro NCAP Test Results with Folksam Car Model Safety Ratings. Proc. of the 17th techn. conf. on ESV, Paper No. 277, Amsterdam

[7] Lie A, Tingvall C. 2002. How Do Euro NCAP Results Correlate with Real-Life Injury Risks? A Paired Comparison Study of Car-to-Car Crashes. Traffic Injury Prevention. 3:288–293, 2002, pp288 293.

[8] Kullgren A., Lie A., and Tingvall C. 2010. Comparison Between Euro NCAP Test Results and Real-World Crash Data. *Traffic Inj Prev* 11(6): 587 - 593

[9] Tingvall C. 1997. The "Vision Zero" - a Road Transport System Free from Health Losses. In Transportation, Traffic Safety and Health: the New Mobility. Editors: von Holst H, Nygren Å, Thord

[10] SwedishTransportAgency. 2013. STRADA – Swedish Traffic Accident Data Acquisition. Available from: http://www.transportstyrelsen.se/en/road/STRADA/

[11] Evans L. 1986. Double paired comparison – a new method to determine how occupant characteristics affect fatality risk in traffic crashes. Accident Analysis and Prevention. Vol. 18 No. 3. pp 217-227

[12] Hägg A, v Koch M, Kullgren A, Lie A, Nygren Å, Tingvall C. 1992. Folksam Car Model Safety Rating 1991-92, Folksam Research 106 60, Stockholm, Sweden

[13] Hägg A, Krafft M, Kullgren A, Lie A, Malm S, Tingvall C, Ydenius A. 2001. Folksam Car Model Safety Ratings 2001, Folksam Research 106 60, Stockholm, Sweden.

[14] Kullgren A, Lie A, Tingvall C. 2001. Mass Data Evaluation of the Importance of Structural and Mass Related Aggressivity. Proc. of the ESV conf.

[15] Elvik. R, Christensen P, Amundsen A. 2004. Speed and road accidents. An evaluation of the Power model. TÖI. Oslo. ISBN 82-480-0451-1

[16] Krafft M, Kullgren A, Lie A, Strandroth J and Tingvall C. 2009. The effects of automatic emergency braking on fatal and serious injuries. Proc. of the ESV Conference 2009, Stuttgart, Paper number 09:0419

[17] Malm S, Krafft M, Kullgren A, Ydenius A, Tingvall C. 2008. Risk of Permanent Medical Impairment (RPMI) in Road Traffic Crashes. Annu Proc Assoc Adv Automot Med. Oct;52:93-100

[18] Sveriges Försäkringsförbund. 2004. Medicinsk invaliditet. Gradering av medicinsk invaliditet (in Swedish)

[19] American Association for Automotive Medicine. 2005. “The Abbreviated Injury Scale 2005 Revision” (AAAM) Des Plaines IL

[20] Newstead S, Cameron M (1998) Updated correlation of results from the Australian New Car Assessment Program with real crash data from 1987 to 1996. Monash University Accident Research Centre (MUARC) Report, Melbourne, Australia

[21] Langwieder C, Fildes B Ernvall T, Cameron M. 2003. SARAC – Safety Rating Based On Real-World Crashes for Supplementation of New Car Assessment Programs. Proc. of the 18th ESV conf. in Nagoya, Japan, paper No. O-175

[22] Krafft M (1998) Non-fatal injuries to car occupants. Injury assessment and analysis of impacts causing short- and long-term consequences with special reference to neck injuries, PhD thesis. Folksam Research, 10660 Stockholm, Sweden

EURO NCAP'S FIRST STEP TO ASSESS AUTOMATED DRIVING SYSTEMS

Richard Schram
European New Car Assessment Programme
Belgium

on behalf of the Euro NCAP Working Group on Automated Driving

Paper Number 19-0292

ABSTRACT

Technology is evolving quickly and more and more of the driving function is being handed to the vehicle. Given that a significant portion of road accidents are attributable to "driver error", the potential safety benefits of increased automation are clear, if the automation is at least as competent as the driver in complex traffic situations. It is therefore in Euro NCAP's interests to raise awareness of the technologies that exists and to promote their introduction in such a way that these safety benefits are realised.

Based on the Euro NCAP's existing active safety testing protocols, extended test scenarios were derived that cover the Operational Design Domain of currently available SAE Level 2 systems. These systems are designed for use on motorways where speeds up to 130 km/h are most typical on European roads. With the first round of evaluating Assisted Driving technologies, Euro NCAP is entering a whole new area of safety and safety assessments where public expectations are high yet understanding may be low. Euro NCAP is striving to promote automated driving technologies while at the same time raise awareness of their safety benefits and moreover their limitations.

BACKGROUND

More than 70% of car drivers believe that it is already possible to purchase a car that can drive itself, according to a consumer survey commissioned by Euro NCAP, Global NCAP and Thatcham Research in 2018. The findings of the survey, which coincided with Euro NCAP's first assessment of automated driving technology, are in stark contrast to the current capabilities of such systems and highlight the significant confusion that exists amongst motoring consumers when it comes to the reality of automated or autonomous driving.

On the question: "Which of the following brands currently sell cars with technology that enables the car to drive itself, without the driver having to do anything?", 1107 respondents from Europe (France, Germany, Italy, Spain and UK), US and China believed that this type of technology is currently available, depending on the vehicle brand 10-40%. Only 11% of the respondents clearly stated that this is not offered in any of these brands. This underlines the need for better and more objective information for consumers on state of advanced driving technology.

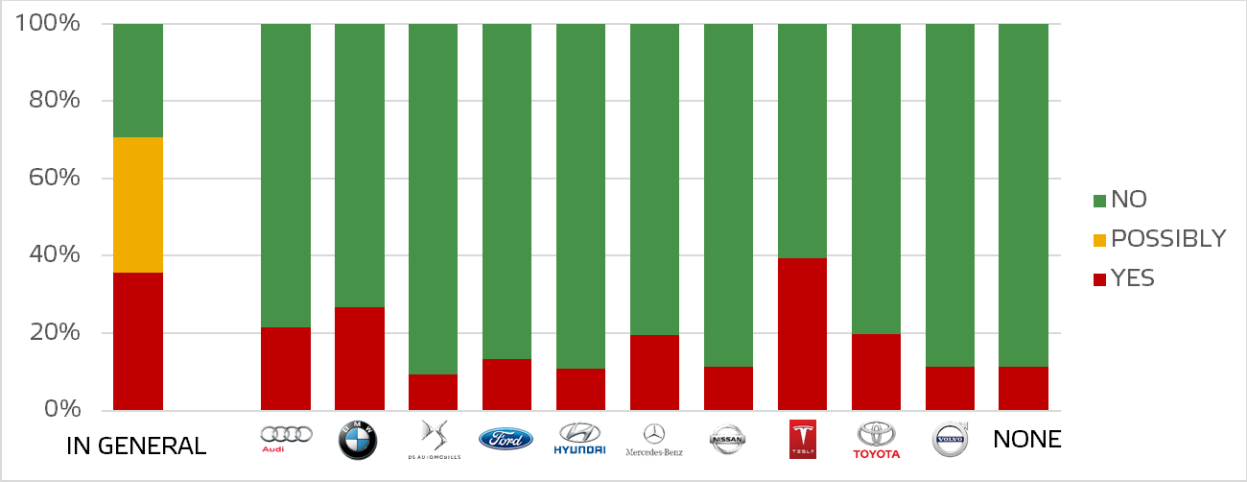

Figure 1. Survey results on the consumers perception on the availability of self-driving technology

As part of its ongoing commitment to independently assess the benefits of new vehicle safety technologies, Euro NCAP has tested the comparative performance of so-called Highway Assist systems in ten cars: the Audi A6, BMW 5 Series, DS 7 Crossback, Ford Focus, Hyundai NEXO, Mercedes-Benz C Class, Nissan LEAF, Tesla Model S, Toyota Corolla and the Volvo V60. The Highway Assist tested combine Adaptive Cruise Control, Lane Centering and Speed Assist Systems to support the driver in driving situations on motorways.

Dedicated test and assessment procedures were developed to grade different driver assistance systems that are currently available by a Working Group consisting of Euro NCAP members, labs and supported by car manufacturers and suppliers.

LEVELS OF AUTOMATION

It is difficult enough for engineers to understand the different levels of automation as defined by Society of Automotive Engineers in SAE J3016 [1], let alone for the typical consumer. For that reason, it was decided to develop a simpler and easier to understand definition around the possible levels of Automation in a car.

SAE J3016 Levels of Driving Automation

The latest update of the SAE J3016 Levels of Driving Automation already provide a clear distinction of driver support and automated driving, but Euro NCAP believes that further simplification is needed for the general public to understand the limitations and proper use of the systems they may have available on their vehicle.

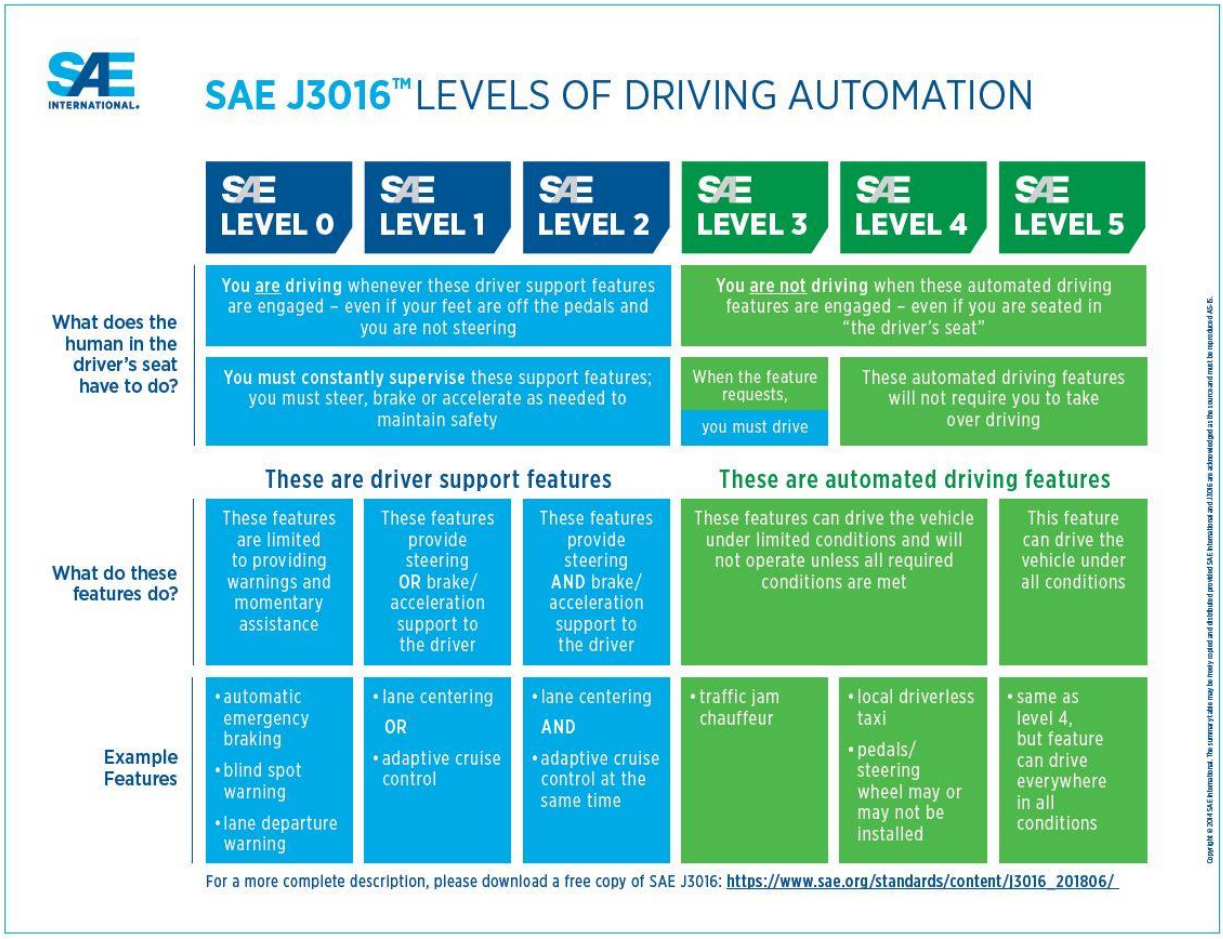

Figure 2. SAE J3016 Levels of Driving Automation

Euro NCAP Driving Modes

The clear separation between driver support and automated driving which is now part of SAE J3016 is supported by Euro NCAP, but a clear understanding of the Operational Design Domain is still missing as this may be different per system and per OEM. Therefore, Euro NCAP decided to define the Levels of Automation as Driving Modes and combine this with defined Operational Domains.

Three Driving Modes exist for Euro NCAP; Assistance, Automation and Autonomous, where the difference between the Automated Driving Mode and the Autonomous Driving Mode is subtle.

Table 1.
Euro NCAP Driving Modes

DRIVING MODE	
Assisted	1. Driver retains full responsibility and shares control with the Vehicle 2. Vehicle & Driver share Object and Event Detection and Response (OEDR) 3. Driver may not perform secondary tasks over and above those permitted during normal driving
Automated	1. Vehicle has full responsibility for control in Operational Design Domain (ODD) defined by the OEM 2. Vehicle performs OEDR 3. Driver may perform certain other non-driving tasks 4. Driver needs to be available for safe transition of control
Autonomous	1. Vehicle has full responsibility for control in Operational Design Domain (ODD) defined by the OEM 2. Vehicle performs OEDR 3. Driver is effectively a passenger 4. Driver has no ability to control (apart from switching to another mode)

In the Assisted Driving Mode, the driver is fully responsible but shares control with the vehicle. The Object and Event Detection and Response (OEDR) is performed by the both vehicle and driver, where the driver is not allowed to perform any secondary task over and above those permitted during normal driving. In short this means that the driver is driving and the vehicle provides support where it can.

The Automated Driving Mode gives full responsibility to the vehicle and the vehicle will have full control. As the driver is allowed to perform certain other non-driving tasks, the vehicle has to perform the OEDR, but the driver needs to remain available for a safe transition of control.

Vehicles function which take away the ability of the driver to take control of the vehicle are called Autonomous Driving modes. In this mode pedals and steering wheels may be retracted, which effectively will change the driver to a passenger in this specific driving mode.

These driving modes are combined with Operational Domains that are understandable by a consumer and moreover give Euro NCAP a defined range of assessment of different systems that the car manufacturers may offer to their costumers. The Operational Domains considered are: Parking, City, Inter-Urban and Highway. Combining Driving Modes and Operational Domains result in a matrix of possible systems, e.g. Assisted Highway systems or Automated City systems.

Table 2.
Euro NCAP Automated Driving Matrix

AUTOMATED DRIVING	Parking	City	Inter-Urban	Highway
Assisted				
Automated				
Autonomous				

The Euro NCAP Working Group on Automated Driving is detailing the test and assessment procedures for each cell in the matrix for Euro NCAP to be able to comparatively provide consumer information on the different driver assist or automated systems offered by the car manufacturers.

HIGHWAY ASSIST SYSTEMS

A first set of evaluations of Highway Assist systems was published with the goal to highlight the current level of performance and limitations of Highway Assist systems in the area of longitudinal, lateral and speed control. Highway Assist systems are supposed to support the driver in monotonous driving situations on motorways and adapt to the traffic conditions. The first publications investigated three different aspects of these assist systems; Human-Machine-Interaction (HMI), Adaptive Cruise Control (ACC) and Lane Centering (LC). For both ACC and LC, the Euro NCAP Working Group developed test scenarios where the limitations of the systems would be highlighted.

Table 3.
Automated Driving test vehicles with their Highway Assist system names

AUTOMATED DRIVING	
Audi A6	Adaptive Cruise Assist
BMW 5-series	Active Driving Assistant Plus
DS 7 Crossback	Connected Pilot
Ford Focus	Co-Pilot360 (ACC,LC & SAS)
Hyundai Nexo	Smart Cruise Control with Lane Following Assist
Mercedes-Benz C-Class	Active Distance Assist DISTRONIC with Active Steering Assist
Nissan Leaf	ProPILOT
Tesla Model S	Autopilot
Toyota Corolla	Toyota Safety Sense (ACC & LTA)
Volvo V60	Pilot Assist

Human-Machine-Interaction

In addition to physical testing, Euro NCAP reviewed the system names, official media from the car manufacturers as well as the vehicle handbooks to verify how the consumers are informed about these Highway Assist systems in the areas of marketing and technical details. For information purposes, additional features available in the different systems were published but not verified, like automatic speed adaptation. Finally, the vehicle response in case of no driver input (hands-off) was monitored.

Adaptive Cruise Control Tests

The ACC tests use the Autonomous Emergency Braking tests as a basis because these procedures are well known and represent the typical situations that ACC systems have to cope with on Highways. The speed ranges that are currently used for AEB were extended to cover the typical driving speeds on European Highways.

In addition to the stationary, slower moving and braking vehicles ahead, a so-called cut-in and cut-out scenario were added which were aimed to cover realistic driving situations and were knowingly ACC systems are responding well.

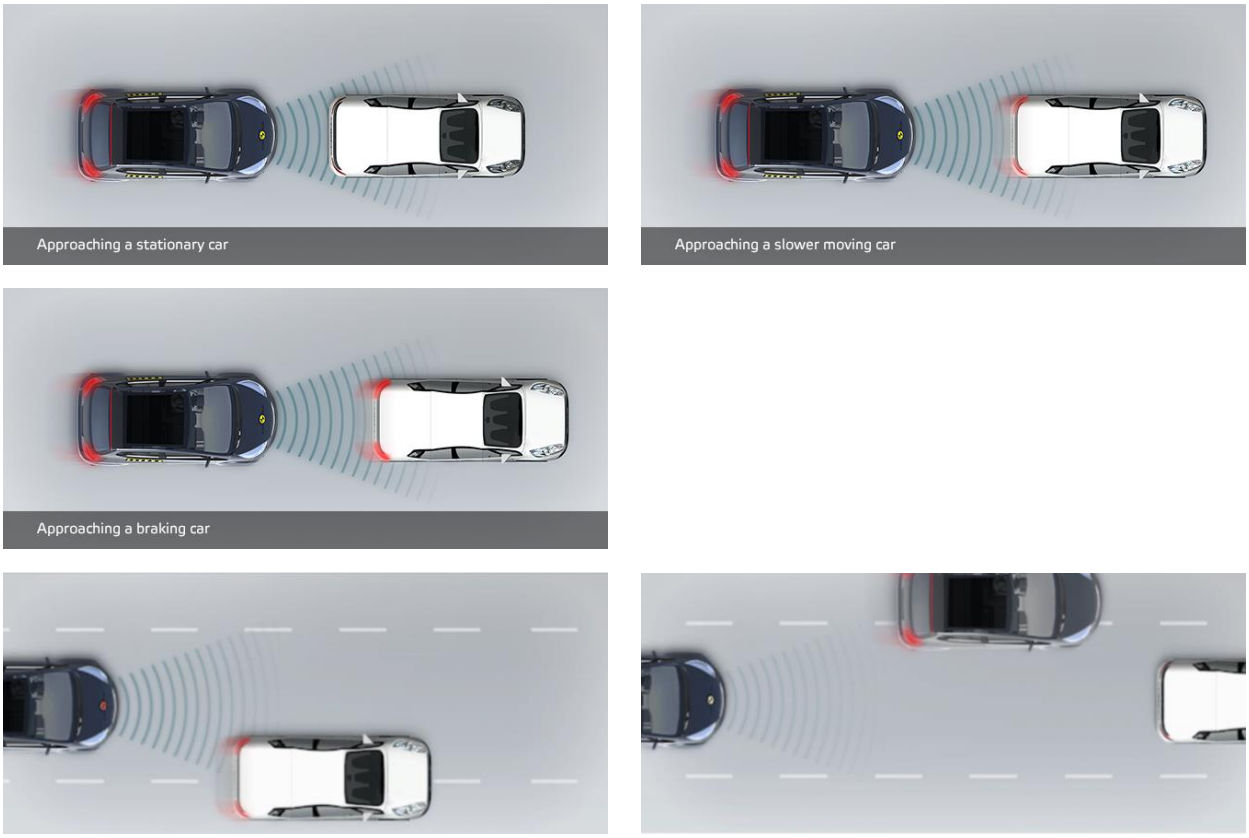

Figure 3. Highway Assist test scenarios for Adaptive Cruise Control (Left top: Approaching a stationary car, Right top: Approaching a slower moving car, Middle left: Approaching a braking car, Left bottom: Other car cuts-in into your lane, Right Bottom: Car in front changes lane to avoid a stationary car)

Lane Centering

Steering Support systems were evaluated in two very simple tests where the level of steering support was evaluated by hands-off driving through an S-curve and a second test where the driver steered the car away from the middle of the lane to avoid a small obstacle to identify the interaction between car and driver.

Figure 4. Highway Assist test scenarios for Lane Centering (Left: Steering in a S-curve, Right: Steering to avoid an obstacle)

RESULTS

The main goal of the first series of tests was to highlight that all Highway Assist systems currently offered have a limited performance and they all need a vigilant driver to avoid the vehicle ending up in a critical situation. A vehicle which can comfortably, by ACC level braking, avoid all of the situation is not per se seen as a safe vehicle as the risk of overreliance is prominent. A balanced result where the role of the driver is clear, and where the vehicle merely provides support is what is expected of these systems. This paper will not go into the detailed test results of all vehicles separately but will provide the general observations and main conclusions from Euro NCAP's first Automated Driving publication.

Detailed results can be found on the Euro NCAP Automated Driving campaign website.[2]

Human-Machine-Interaction

Often system names will instantly give the consumer the wrong idea about the system's capabilities as they do not clearly state whether the system is an assist system or not. Names like "Pilot" will give a false impression that the system is able to drive by itself, without the need of a driver. Of the ten systems verified, only three system names contained the word "Assist"; Adaptive Cruise Assist on the Audi A6, Active Driving Assistant Plus on the BMW 5-series and Pilot Assist on the Volvo V60. Hyundai, Mercedes and Toyota have non-specific for the their Highway Assist systems and simply combine the separate functions. Four system names however, were perceived as misleading as they all contained the word "Pilot" without adding the word "Assist"; Connected Pilot in the DS 7 Crossback, Co-Pilot360 in the Ford Focus, ProPilot in the Nissan Leaf and Autopilot in the Tesla Model S.

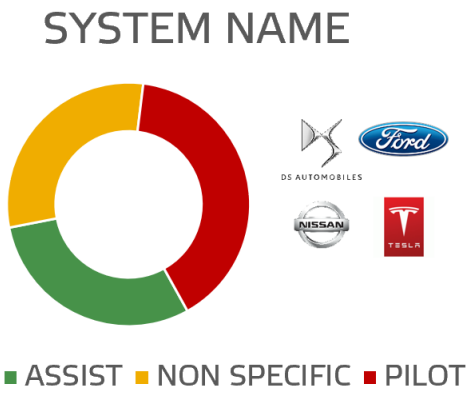

Figure 5. Highway Assist system name assessment

In general terms it was found that user manuals were extremely conservative and cautious regarding the role of the driver stating that the driver always has full responsibility. Contrary to this, marketing videos that were provided to Euro NCAP were seen as misleading for both the BMW and the Tesla where the drivers were shown to take their hands off the steering wheel and hand over control to the vehicle.

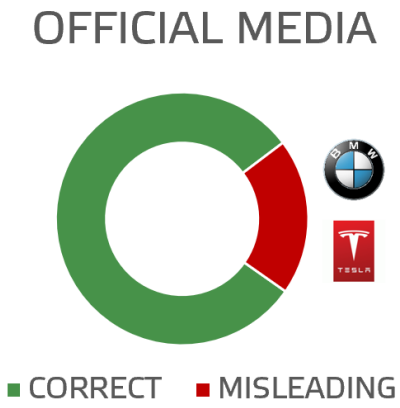

Figure 6. Highway Assist system official media assessment

UNECE Regulation 79 requires all vehicles to have a monitor driver input on the steering wheel and warn the driver when the system detects that the driver is not in the loop. Two main strategies were applied by the vehicle manufacturers tested. In case the driver does not take back control after a certain warning sequence, half of the vehicles simply switched off their lane support and ACC, leaving the vehicle in principle uncontrolled. In case of sudden sickness or a driver falling asleep, this may have catastrophic results. The other half of the vehicles would bring the vehicle to a controlled stop within the lane, which was perceived as safer solution than simply cancelling the vehicle support functions.

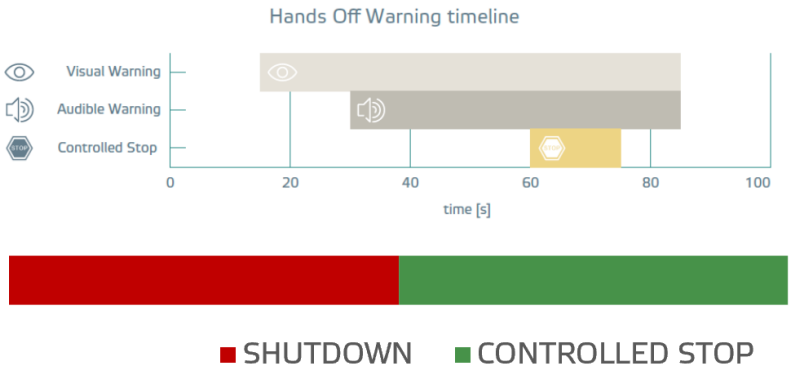

Figure 7. Highway Assist system Hands Off Warnings

Adaptive Cruise Control Tests

The performance in the ACC test scenarios revealed the strategies implemented by the different manufacturers, but also clearly shows that these systems are designed to work best in the slower moving scenarios.

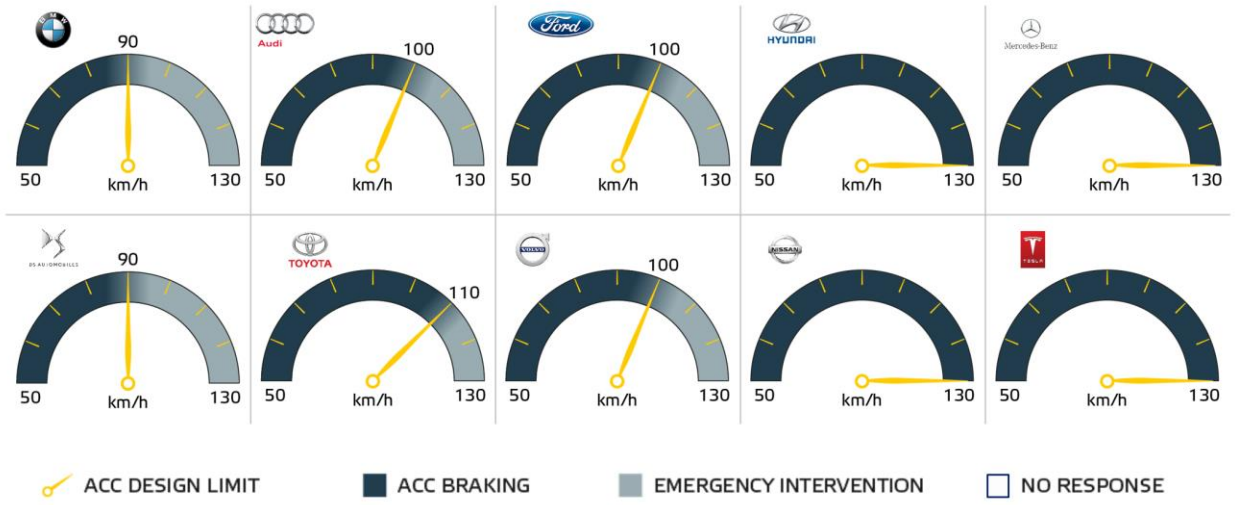

Figure 8. Results of the Aproaching a slower moving car scenario

In the stationary car in front scenario, most systems were very conservative and provide ACC level braking only upto 60 km/h to safely avoid the collision. DS, BMW, Audi and Nissan provided emergency support (FCW and/or AEB) only upto a speed of 80 to 90 km/h, where Toyota, Volvo, Hyundai, Mercedes, Ford provided emergency support over the whole speed range. Tesla however provided ACC level braking over the full speed range in this scenario which may lead to a consumer perceiving the system as full automation, with a high risk of the driver over relying on the system. Assist systems offering such a high level are expected to have a direct driver monitoring system to ensure the driver is in the loop but this was not the case for this vehicle.

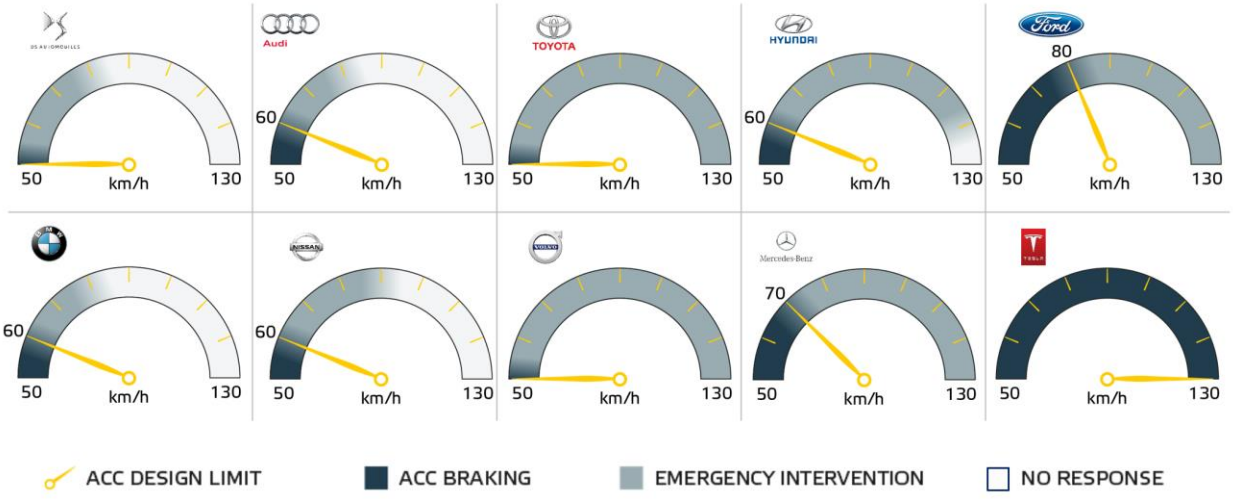

Figure 9. Results of the Aproaching a stationary car scenario

In the most challenging scenarios, the cut-in and cut-out of a vehicle in front, all vehicles highlighted limitations showing that a driver is always needed to respond to the situation before the vehicle does to avoid a collision.

Lane Centering

The steering tests showed that all manufacturers apart from one, apply the same strategy where the driver keeps control of the lateral control and where the vehicle offers lane centering. This strategy is what one would expect from an assist system to avoid the driver thinking he is not required which can ultimately result in overreliance.

Tesla's Autopilot is not designed to work together with the driver and will not allow any driver input. As soon as the test driver steered around the obstacle in the lane, the system disengaged and stopped the steering support.

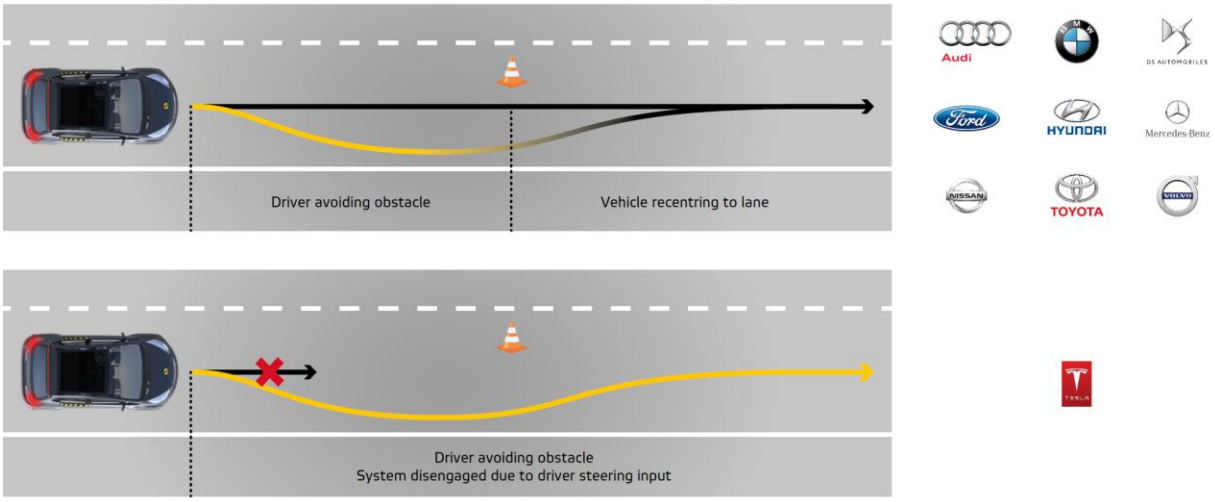

Figure 10. Results of the Steering to avoid an obstacle scenario

Summary of results

In general terms all vehicles, apart from Tesla, behaved very similar with different levels of steering support and ACC performance. Overall, both BMW and DS were judged to be too conservative, where a consumer may not see the added value of the support function. On the other extreme, Tesla was seen as providing too much support for a Highway Assist system which results in the risk of a driver over relying on the system. The Highway Assist systems of the other seven manufacturers provided different levels of support but were all seen as balanced systems where the driver will clearly understand its role while the function is engaged.

Figure 11. Overall Highway Assist system results

DISCUSSION

The different scenarios for testing the ACC performance are extended AEB scenarios but there is only an intuitive link to accident data or potential risk at crashes at the moment. More research is needed on the relevance of certain scenarios within the ODD of the systems assessed.

Clear and objective criteria need to be developed that can quantify and/or assess over-reliance so that car manufacturers can take this into account while developing these systems. Over the next years, when more automation is expected to penetrate the market, requirements need to be reviewed and updated to incentivise better, safer and more intuitive assist systems that support the driver in normal driving conditions.

CONCLUSION

With the first round of evaluating Assisted Driving technologies, Euro NCAP is entering a whole new area of safety and safety assessments where public expectations are high, although understanding may be low. Euro NCAP is striving to promote automated driving technologies while at the same time raise awareness of their safety benefits and moreover their limitations.

For future assessments a clear and understandable definition to classify different driving modes so that consumers will have no problems understanding the capabilities of these systems and what the role of the driver is once the system is engaged. By combining these Driving Modes with well-defined Operational Domains, a solid foundation is available for Euro NCAP to develop specific test and assessment procedures for different levels of automation.

REFERENCES

[1] Society of Automotive Engineers, 2014 - Taxonomy and Definitions for Terms Related to On-Road Motor Vehicle Automated Driving Systems J3016

[2] Euro NCAP Automated Driving campaign website, www.euroncap.com/en/vehicle-safety/safety-campaigns/2018-automated-driving-tests

ANALYSIS OF SERIOUS INJURY IN CAR TO CAR ACCIDENTS TO IMPROVE OF CRASH TEST PROTOCOLS IN KNCAP

Siwoo KIM
Korea Automobile Testing & Research Institute (KATRI)
Korea, Republic of

Yohan PARK, Seungki KIM
Samsung Traffic Safety Research Institute
Korea, Republic of

Paper Number 19-0293

ABSTRACT
All over the world, there are many institutional programs used to enhance the safety of vehicles. The NCAP is a program that assesses the safety of vehicles sold by manufacturers in order to provide consumers with information on vehicle safety and to induce them to produce vehicles with enough safety. In Korea, the KNCAP has been carried out continuously since 1999. However, the fatal rate from traffic accidents per 100,000 population in 2017 is 8.1, which is above the OECD average. Therefore, it is necessary to improve various systems, but it is also necessary to improve the crash assessment protocols reflecting the actual accident. The purpose of this paper is to improve the crash test protocols of KNCAP by analyzing the status of the serious injury in case of an accident in Korea. Accident data were used for the latest three years(2015-2017) in car to car accident of domestic insurers. Raw data shows that 9,399 cases occurred due to accidents involving more than MAIS3 + of occupants' injuries. Of these, 279 cases were analyzed. In the collision type, the full width impact was the largest at 68.5%, and the small overlap and moderate at 28.3%. The low severity with 0 failure depth was 2% and the center impact was 2%. Impact angle was 51.1% for co-linear, 33.3% for left oblique angle and 15.6% for right oblique angle. In case of overlap, moderate overlap was about 47.9% and small overlap was about 17.5%. In the case of full width, crash extent3 + was 80.6%, while moderate overlap and small overlap were 36.8% and 24.3%, respectively. The collision type and impact angle compared to other country.

1. Introduction

There are many systems used to enhance the safety of motor vehicles around the world. Among them, the new car assessment program which is not legally binding is the most effective system under which the safety of motor vehicles is improved voluntarily by the vehicle manufacturers. This system is being employed in countries such as USA, Europe, Japan, China, and Korea. Recently, it has been introduced in India, ASEAN and countries in South America. The motor vehicle safety assessment system tests and evaluates the safety of motor vehicles sold by manufacturers. The system also makes the information on the motor vehicle safety public to encourage manufacturers to make safer motor vehicles. Korea has implemented the KNCAP since 1999. However, the fatalities from traffic accidents in every 100,000 people in 2017 years is 8.1, which is still higher than that of OECD average. The safety of motor vehicles has been improved, but more effective measures to reduce casualties shall be devised. For example, some safety devices may not function as intended under the accident conditions other than the test conditions. It is necessary to reflect the accident conditions in real world on the test methods. Internationally the traffic accidents pattern has been reflected on the test methods.
Euro-NCAP will replace the existing offset deformable barrier frontal impact method (40% Overlap) with a ca-to-car test method(a moving barrier, 50% overlap) for moderate overlap assessment under Roadmap 2020. In NCAP US NHTSA also announced the introduction of a car-to-car frontal oblique test using OMDB (Oblique Moving Deformable Barrier) based on NHTSA's 2015 RFC (Request for

Comments). However, in the Korean NCAP unlike those in Europe and the United States researches for the specific assessment details, protocols, and timeline have not been carried out yet for car-to-car collisions. The current domestic vehicle safety assessment is carried out under the test conditions simulating vehicle-to-fixed objects collisions and vehicle-to-pedestrian collisions among real world accidents.

Since the introduction of KNCAP the safety of vehicles in the domestic market has been continuously improved so that vehicles with high safety ratings have the effect of reducing the injury severities and fatalities. However, it is suspected that the safety performance may not be not fully realized due to the failure of some safety devices in the real accident conditions other than the assessment conditions, These discrepancies between assessment ratings and real world performances are posing a potential threat to the credibility of the safety ratings.

Therefore, it is necessary to take a careful consideration and improvement measures for vehicle safety in case of car-to-car accidents with high frequency in addition to car-to-pedestrians accidents and single vehicle accidents among real world vehicle accidents. In particular, considering the fact that car-to-car accidents are more frequent than single vehicle accidents from casualties' point of view among the victims of traffic accidents, it is necessary to investigate that the occupant protection in car-to-car accidents is equivalent to that in single vehicle accidents through the current assessment program. In this study, based on the analysis of the main accident type and injury characteristics of fatalities and severe injuries excerpted from vehicle accidents database, the improvement of motor vehicle assessment program will be proposed through feasibility study on car-to-car crash tests.

2. Contents and Methods of Investigation

For the in-depth analysis of the injury characteristics of severely injured occupants from car-to-car accidents, the injury characteristics were analyzed based on accident data from insurance companies database between from 2015 and 2017(3 years) met the following conditions. Among frontal collisions and side impacts involving only two vehicles were selected and the ones with more than two vehicles involved were excluded. In the cases investigated, the accidents resulted in fatal or injured occupants with AIS 3 or higher, who had fastened their safety belts at the time of accidents. In addition, damage on vehicles due to collision has to be identifiable in the accidents involving only passenger vehicles. Analysis data were in the following Table 1.

Table 1. Overview of Analysis Data

Category	Item	Explanatory Note
Scope	·Collision Type	·Frontal collision
	·Occupant	·Severely Injured Occupants with AIS 3 or higher
	·Vehicle Classification	·Passenger vehicle-to-Passenger vehicle
Period	·Reported Period	·1. 1. 2015 ~ 31. 12. 2017
Contents	·Analysis of Frequent Accident Types → Vehicle Deformation → Collision Angle and Degree of Overlap	· 279 cases in Frontal collision
	·Characteristics of Severely Injured Occupants → Distribution of Severe Injury Areas → Injury Types in Severe Injury Areas	· 311 severely injured occupants in frontal collision

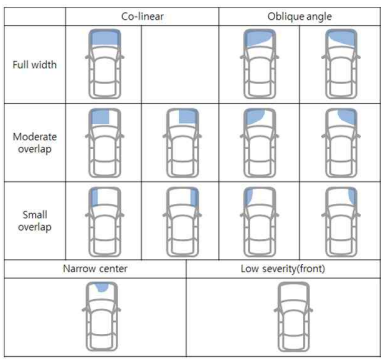

Figure 1. Collision Deformation Classification

The types of damage and the angles of collisions were classified by the Collision Deformation Classification (CDC) as the Figure 1, and the types of collisions and the angles of collisions were categorized based on detailed damaged areas and extent of damage.

The types of damage from frontal collision were classified into 5 types as Figure 2. A full frontal collision case is the case when both left and right side member structures, including the center, of a vehicle were destroyed. A moderate overlap frontal collision case is the case when either left or right

side member of a vehicle was damaged and also the center of a vehicle was damaged. A small overlap frontal collision case is the case when only either left or right side member of a vehicle was damaged, but the center of a vehicle was not damaged. A narrow center frontal collision case is the case when both left and right side member structures of a vehicle were not destroyed, but the center of a vehicle was destroyed. A frontal collision case with low severity is the case where the extent of damage is zero regardless of the location of damage.
The degree of overlap in a partial frontal collision was defined by the step of 20% overlap after the front part of a damaged vehicle was divided into 5 parts vertically and laterally. The degree of overlap in the partial frontal collision was set as follows according to the point of the damaged part.

20% Overlap : point 2~3 or 4~5 damaged
40% Overlap : point 1~3, 2~4, 3~5 or 4~6 damaged
60% Overlap : point 1~4 or 3~6 damaged

the degree of small overlap was defined as follows.
10% Overlap: only point 1 or 6 damaged
20% Overlap: only point 1~2 or 5~6 damaged

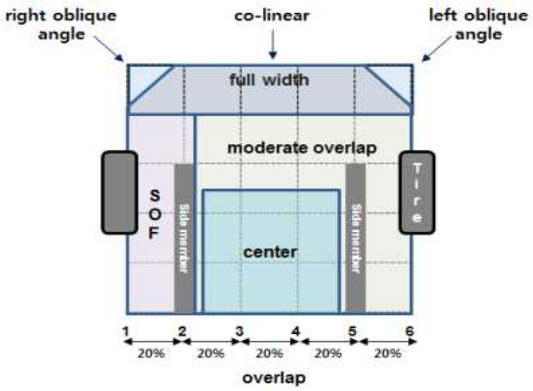

Figure 2. Types of Frontal Collision and Definition of Overlap

The injury characteristics analysis of severely injured occupants was carried out by the gender and occupied seat of an occupant according to the type of deformation, collision angle and degree of overlap of an accident vehicle as follows. The type of deformation, collision angle and degree of overlap was examined according to the criteria described previously. During the analysis, severely injured occupants resulted from a narrow center frontal collision and a frontal collision case with low severity were excluded from the analysis. For injury area analysis, multiple injuries in various areas of single severely injured occupant were repeatedly counted in consideration of multiple compound injuries. For example, if one severely injured occupant sustained two injuries in the head, two injuries were counted as two.

3. Results of Analysis

3-1. Analysis of Deformation Characteristics of Accident Vehicles with High Frequency and Severely Injured Occupants

The type of full frontal damage(Full width) accounted for 68.5% and the type of partial frontal damage(Moderate overlap + Small overlap) accounted for 28.3% as Table 2. In the type of partial frontal damage, a similar share was observed between two sub categories.

Table 2. Types of Deformation in case of Frontal Collisions with High Frequency (unit: No. of vehicles, %)

Types of Deformation		Frequency(%)
Full Frontal (Full width)		191 (68.5)
Partial Frontal	Moderate overlap	38 (13.6)
	Small overlap	41 (14.7)
Narrow Center Frontal Collision		4 (1.4)
Frontal Collision with Low Severity		5 (1.8)
Total		279 (100.0)

In terms of collision angles, as Table 3, the type of frontal collision in the perpendicular direction accounted for 51%, the type of frontal collisions in the left oblique direction accounted for 33% and the type of frontal collisions in the right oblique direction accounted for 16%.

Out of frontal collisions in the perpendicular direction, the type of full frontal collisions accounted for 64.5%, the type of partial frontal collisions accounted for 15.2%, and the type of small overlap frontal collisions accounted for 20.2%. For the type of frontal collisions in the left oblique direction, the type of full frontal collisions accounted for 78.9%, the type of partial frontal collisions accounted for 12.2%, and the type of small overlap frontal collisions accounted for 8.9%. For the type of frontal collisions in the right oblique direction, the type of full frontal collisions accounted for 73.8%, the type of partial frontal collisions accounted for 14.3%, and the type of small overlap frontal collisions accounted for 11.9%.

Table 3. Collision Angles in case of Frontal Collisions with High Frequency (unit: No. of vehicles, %)

Collision Angle	Deformation Type	Damage Area	Frequency(%)	Total
Co-liner Direction	Full width	Full with	89(64.5)	138 (51.1)
	Moderate	Left side	14(10.1)	
		Right side	7(5.1)	
	Small overlap	Left side	14(10.1)	
		Right side	14(10.1)	
Sum			138(100.0)	
Left oblique Direction	Full width	Left side	71(78.9)	90 (33.3)
	Moderate	Left side	11(12.2)	
	Small overlap	Left side	8(8.9)	
Sum			90(100.0)	
Right oblique Direction	Full width	Right side	31(73.8)	42 (15.6)
	Moderate	Right side	6(14.3)	
	Small overlap	Right side	5(11.9)	
Sum			42(100.0)	
Total				270(100.0)

Note) Total No. is not included the Narrow center and Low severity cases

As comparison of the degrees of overlap in partial frontal collisions shown in the Table 4, the average degree of overlap in the partial frontal collisions(moderate overlap) was 47.9%, and the portions of 40% overlap and 60% overlap were similar to each other. The average degree of in the partial frontal collisions(small overlap) was 17.5%, and 20% overlap accounted for the largest portion of 75.6%.

Table 4. Degree of Overlap in case of Partial Frontal Collisions with High Frequency (unit: No. of vehicles, %)

Degree of Overlap		Frequency(%)	Average Degree of Overlap
Moderate overlap	20% overlap	3(7.9)	47.9%
	40% overlap	17(44.7)	
	60% overlap	18(47.4)	
	Sum	38(100.0)	
Small overlap	10% overlap	10(24.4)	17.5%
	20% overlap	31(75.6)	
	Sum	41(100.0)	

Table 5. shows the results of comparison and analysis of the extent of damage according to the types of damage. Most full frontal collisions resulted in Extent of Damage 3 or higher, and most partial frontal collisions resulted in Extent of Damage 3 or less. In case of full frontal collisions, Extent of Damage 3 or higher accounted for 80.6%, while in case of partial frontal collisions Extent of Damage 3 or less accounted for the majority.

Table 5. Types of Deformation in case of Frontal Collisions with High Frequency(units : No. of vehicles, %)

Types of Deformation		Extent of Damage					Total
		1	2	3	4	5	
Full width		7 (3.7)	30 (15.7)	82 (42.9)	66 (34.6)	6 (3.1)	191 (100)
Partial	Moderate overlap	12 (31.6)	12 (31.6)	10 (26.3)	3 (7.9)	1 (2.6)	38 (100)
	Small overlap	20 (48.8)	11 (26.8)	5 (12.2)	5 (12.2)	0 (0)	41 (100)
Narrow center		0 (0)	3 (75.0)	1 (25.0)	0 (0)	0 (0)	4 (100)

Note) frontal collision with low severity : EXTENT 0 = 5 units

3-2 Injury Analysis of Severely Injured Occupants

The analysis of distribution of severely injured occupants according to the gender and seat of occupant showed that the majority of male were drivers and the majority of female were passengers. In the case of severely injured male occupants, 74% of occupants in the driver's seat and 14% in the passenger seats account for 91.7% of the occupants in the first row seats (driver's seat + passenger's seat). In the case of severely injured female occupants, 78.2% of severely injured female occupants were seated in the first row seat (driver's seat + passenger's seat), but the occupancy rate of severely injured female occupants in the second row seat (18.3%) was higher than that of the male. (See the Table 6.)

Table 6. Distribution of Severely Injured Occupants according to the Seat/Gender in case of Frontal Collisions with High Frequency(units : No. of injuries, %)

Gender	1st row Seat		2nd row Seat			Total
	Driver'	Passenger'	behind Driver	Center	behind Passenger	
Male	125 (74.0)	30 (17.8)	1 (0.6)	1 (0.6)	10 (5.9)	169 (100.0)
Female	63 (44.4)	48 (33.8)	10 (7.0)	1 (0.7)	15 (10.6)	142 (100.0)
Total	188 (60.5)	78 (25.1)	11 (3.5)	2 (0.6)	25 (8.0)	311 (100.0)

Table 7. shows the analysis of distribution of severely injured occupants according to the age of occupant. Severely injured adult occupants were drivers who accounted for 76.9%. Severely injured

adult female drivers accounted for 50.9%, while severely injured adult female passengers accounted for 46.6%. There is little difference. For elderly people, the majority of injured occupants were male drivers, while the majority of old female occupants were seated in the passenger seat in the 1st and 2nd rows. For elderly female occupants, passengers next to the driver accounted for 31.8%. Female occupants in the passenger seat in the 1st and 2nd rows accounted for 40.9%.

Table 7. Distribution of Severely Injured Occupants according to the Seat/Age of Occupant in case of Frontal Collisions with High Frequency(units : No. of injuries, %)

Age		1st row Seat		2nd row Seat			Total
		Driver'	Passenger'	behind Driver	Center	behind Passenger‘	
Male	Child	0 (0.0)	1 (33.3)	0 (0.0)	0 (0.0)	2 (66.7)	3 (100.0)
	Adult	110 (76.9)	22 (15.4)	1 (0.7)	1 (0.7)	7 (4.9)	143 (100.0)
	Elderly	15 (65.2)	7 (30.4)	0 (0.0)	0 (0.0)	1 (4.3)	23 (100.0)
Female	Child	0 (0.0)	1 (25.0)	1 (25.0)	1 (25.0)	1 (25.0)	4 (100.0)
	Adult	59 (50.9)	40 (34.5)	5 (4.3)	0 (0.0)	9 (7.8)	116 (100.0)
	Elderly	4 (18.2)	7 (31.8)	4 (18.2)	0 (0.0)	5 (22.7)	22 (100.0)
Total		188 (60.5)	78 (25.1)	11 (3.5)	2 (0.6)	25 (8.0)	311 (100.0)

Table 8. shows the analysis of distribution of severely injured occupants according to types of deformation in frontal collisions. In case of a full frontal collision, chest injuries were most frequent, followed by low extremity injuries and head injuries. In case of a moderate frontal collision, low extremity injuries were most frequent, followed by chest injuries and upper extremity injuries. In case of a small overlap frontal collision, upper extremity injuries were most frequent, follwed by low extremity injuries and chest injuries. As the area of the damaged part if an accident vehicle changes, the behavior of occupants may also change. Due to the different behavior frequently injured areas in occupants shows different tendency. The chest injuries became less and less frequent from full frontal collision to partial frontal collision, which is considered to be correlated with the reduction in damaged area. In case of upper/lower extremities, the rate of injury increased in a full frontal collision compared with a partial frontal collision because the safety belt could not effectively restrain an occupant due to yawing in a frontal collision.

Table 8. Severely Injured Area according to Types of Deformation in case of Frontal Collisions with High Frequency(units : No. of injuries, %)

Deformation Type	head	neck	back-spine	chest	abdominal	upper extremity	lower extremity	full body	Total
Full width	43 (14.4)	39 (13.1)	5 (1.7)	115 (38.6)	2 (0.7)	30 (10.1)	63 (21.1)	1 (0.3)	298 (100.0)
Moderate overlap	6 (8.8)	8 (11.8)	0 (0.0)	19 (27.9)	0 (0.0)	11 (16.2)	22 (32.4)	2 (2.9)	68 (100.0)
Small overlap	4 (7.0)	10 (17.5)	2 (3.5)	11 (19.3)	0 (0.0)	17 (29.8)	13 (22.8)	0 (0.0)	57 (100.0)

The analysis of distribution of severely injured area of occupants according to the collision angle in frontal collisions shows that in case of a full frontal collision, the differences among the shares of

injured areas were little regardless of collision angles, while the shares of injured areas tend to differ greatly depending on collision angles in case of a partial frontal collision as Table 9.
In case of a moderate overlap frontal collision, lower extremity injuries in frontal collisions in the left oblique direction decreased by 12% compared with that in frontal collisions in the perpendicular direction; chest injuries increased by 13%; head injuries increased by 8%.
In case of a small overlap frontal collision, lower extremity injuries in frontal collisions in the left oblique direction decreased by 11% compared with that in frontal collisions in the perpendicular direction; chest injuries increased by 10%; head injuries increased by 5%.

Table 9. Distribution of Severely Injured Area of Occupants according to the Collision Angle in case of Frontal Collisions with High Frequency(units : No. of injuries, %)

Collision Angle		head	neck	back-spine	chest	abdominal	upper extremity	lower extremity	full body	Total
Full width	perpendicular	22 (15.9)	17 (12.3)	1 (0.7)	49 (35.5)	0 (0.0)	15 (10.9)	33 (23.9)	1 (0.7)	138 (100.0)
	oblique	21 (13.1)	22 (13.8)	4 (2.5)	66 (41.3)	2 (1.3)	15 (9.4)	30 (18.8)	0 (0.0)	160 (100.0)
Moderate overlap	perpendicular	2 (5.4)	5 (13.5)	0 (0.0)	8 (21.6)	0 (0.0)	6 (16.2)	14 (37.8)	2 (5.4)	37 (100.0)
	oblique	4 (12.9)	3 (9.7)	0 (0.0)	11 (35.5)	0 (0.0)	5 (16.1)	8 (25.8)	0 (0.0)	31 (100.0)
Small overlap	perpendicular	2 (5.3)	7 (18.4)	1 (2.6)	6 (15.8)	0 (0.0)	11 (28.9)	11 (28.9)	0 (0.0)	38 (100.0)
	oblique	2 (10.5)	3 (15.8)	1 (5.3)	5 (26.3)	0 (0.0)	6 (31.6)	2 (10.5)	0 (0.0)	19 (100.0)

The analysis of distribution of severely injured area of occupants according to the degree of overlap in frontal collisions shows that upper/lower extremity injuries increased as the degree of overlap decreased.(See the Table 10) In case of a moderate overlap frontal collision, neck injuries decreased and upper extremity injuries increased from 6.3% to 29.0% as the degree of overlap decreased. In case of a small overlap frontal collision, neck injuries decreased from 22% to 6% and lower extremity injuries increased from 12% to 50% as the degree of overlap decreased.

Table 10. Distribution of severely Injured Area of Occupants according to the Degree of Overlap in case of Frontal Collisions with High Frequency(units : No. of injuries, %)

Degree of Overlap		head	neck	back-spine	chest	abdominal	upper extremity	lower extremity	full body	Total
Moderate overlap	20%	0 (0.0)	0 (0.0)	0 (0.0)	0 (0.0)	0 (0.0)	0 (0.0)	5 (100.0)	0 (0.0)	5 (100.0)
	40%	4 (12.9)	1 (3.2)	0 (0.0)	9 (29.0)	0 (0.0)	9 (29.0)	8 (25.8)	0 (0.0)	31 (100.0)
	60%	2 (6.3)	7 (21.9)	0 (0.0)	10 (31.3)	0 (0.0)	2 (6.3)	9 (28.1)	2 (6.3)	32 (100.0)
Small overlap	10%	1 (6.3)	1 (6.3)	0 (0.0)	2 (12.5)	0 (0.0)	4 (25.0)	8 (50.0)	0 (0.0)	16 (100.0)
	20%	3 (7.3)	9 (22.0)	2 (4.9)	9 (22.0)	0 (0.0)	13 (31.7)	5 (12.2)	0 (0.0)	41 (100.0)

As Table 11, the analysis of distribution of severely injured area of occupants according to the seat/gender in frontal collisions shows that chest injuries were most frequent in the occupants in the 1st row seats while head injuries were most frequent in the occupants in the 2nd row seats. In case of drivers, the distribution of severely injured areas in male and female drivers were similar to each other. Chest injuries were most frequent, followed by lower extremity injuries and neck injuries. Head

injuries were least frequent. For male drivers, chest injuries(37.4%) were most frequent, followed by lower extremity injuries(23.6%) and neck injuries(17.1%). Head injuries(13.0%) were least frequent. For female drivers, chest injuries(39.3%) were most frequent, followed by lower extremity injuries(19.6%) and neck injuries(14.3%). Head injuries(12.5%) were least frequent. In case of passengers next to drivers, chest injuries were most frequent in male and female passengers. For male passengers, head injuries were the next most frequent, while for female passengers, lower extremity injuries were the next most frequent. For male passengers, chest injuries(46.5%) were most frequent, followed by head injuries(18.2%) and upper/lower extremity injuries(15.2). For female passengers, chest injuries(45%) were most frequent, followed by lower extremity injuries(24%), upper extremity injuries(21%) and head injuries(4%). Head injuries were least frequent. In case of occupants in the 2nd row, head injuries were most frequent in male and female passengers. Chest injuries for male passengers and lower extremity injuries for female passengers were next highest. For male passengers, head(35.7%) and chest injuries(35.7%) were most frequent, followed by neck injuries(21.4%). For female passengers, head injuries(31.8%) and lower extremity injuries(31.8%) were most frequent, followed by chest injuries(22.7%).

Table 11. Distribution of Severely Injured Area of Occupants according to the Occupied Seat in case of Full Frontal Collisions(Full Width) with High Frequency(units : No. of injuries, %)

Occupied Seat		head	neck	back-spine	chest	abdominal	upper extremity	lower extremity	full body	Total
Male	Driver's	16 (13.0)	21 (17.1)	2 (1.6)	46 (37.4)	1 (0.8)	8 (6.5)	29 (23.6)	0 (0.0)	123 (100.0)
	Passenger's	6 (18.2)	2 (6.1)	0 (0.0)	15 (45.5)	0 (0.0)	5 (15.2)	5 (15.2)	0 (0.0)	33 (100.0)
	2nd Row	5 (35.7)	3 (21.4)	1 (7.1)	5 (35.7)	0 (0.0)	0 (0.0)	0 (0.0)	0 (0.0)	14 (100.0)
Female	Driver's	7 (12.5)	8 (14.3)	1 (1.8)	22 (39.3)	0 (0.0)	6 (10.7)	11 (19.6)	1 (1.8)	56 (100.0)
	Passenger's	2 (4.3)	3 (6.4)	0 (0.0)	21 (44.7)	0 (0.0)	10 (21.3)	11 (23.4)	0 (0.0)	47 (100.0)
	2nd Row	7 (31.8)	2 (9.1)	0 (0.0)	5 (22.7)	1 (4.5)	0 (0.0)	7 (31.8)	0 (0.0)	22 (100.0)

Table 12. Distribution of Severely Injured Area of Occupants according to the Occupied Seat in case of Moderate Frontal Collisions with High Frequency (units : No. of injuries, %)

Occupied Seat		head	neck	back-spine	chest	abdominal	upper extremity	lower extremity	full body	Total
Male	Driver's	1 (3.6)	3 (10.7)	0 (0.0)	8 (28.6)	0 (0.0)	3 (10.7)	11 (39.3)	2 (7.1)	28 (100.0)
	Passenger's	1 (25.0)	0 (0.0)	0 (0.0)	0 (0.0)	0 (0.0)	0 (0.0)	3 (75.0)	0 (0.0)	4 (100.0)
	2nd Row	0 (0.0)	0 (0.0)	0 (0.0)	1 (100.0)	0 (0.0)	0 (0.0)	0 (0.0)	0 (0.0)	1 (100.0)
Female	Driver's	1 (9.1)	1 (9.1)	0 (0.0)	3 (27.3)	0 (0.0)	3 (27.3)	3 (27.3)	0 (0.0)	11 (100.0)
	Passenger's	1 (12.5)	2 (25.0)	0 (0.0)	2 (25.0)	0 (0.0)	2 (25.0)	1 (12.5)	0 (0.0)	8 (100.0)
	2nd Row	1 (8.3)	1 (8.3)	0 (0.0)	4 (33.3)	0 (0.0)	2 (16.7)	4 (33.3)	0 (0.0)	12 (100.0)

The distribution of severely injured area of occupants according to the seat/gender in moderate overlap frontal collisions was analyzed. For the occupants in the 1st row seats, lower extremity injuries for male passengers

and chest and upper extremity injuries for female passengers were most frequent. For female occupants in the 2nd row seats, chest injuries and lower extremity injuries were most frequent. (See the Table 12)
Lower extremity injuries were most frequent for both male and female drivers. For passengers next to drivers, lower extremity injuries were most frequent for male passengers and chest injuries, neck injuries and upper extremity injuries for female passengers were most frequent.
Table 13 shows that the analysis of distribution of severely injured area of occupants according to the seat/gender in small overlap frontal collisions were that upper extremity injuries for male passengers and lower extremity injuries for female passengers were most frequent among the occupants in the 1st row seats.
In case of male drivers, upper extremity injuries were most frequent, followed by lower extremity injuries and chest injuries. In case of female drivers, neck injuries were most frequent, followed by lower extremity injuries and chest injuries.

Table 13. Distribution of Severely Injured Area of Occupants according to the Occupied Seat in case of Small Overlap Frontal Collisions(Full Width) with High Frequency(units : No. of injuries, %)

Occupied Seat		head	neck	back-spine	chest	abdominal	upper extremity	lower extremity	full body	Total
Male	Driver's	2 (8.3)	3 (12.5)	1 (4.2)	4 (16.7)	0 (0.0)	9 (37.5)	5 (20.8)	0 (0.0)	24 (100.0)
	Passenger's	0 (0.0)	1 (25.0)	0 (0.0)	1 (25.0)	0 (0.0)	2 (50.0)	0 (0.0)	0 (0.0)	4 (100.0)
	2nd Row	0 (0.0)	0 (0.0)	0 (0.0)	2 (100.0)	0 (0.0)	0 (0.0)	0 (0.0)	0 (0.0)	2 (100.0)
Female	Driver's	1 (6.3)	5 (31.3)	1 (6.3)	3 (18.8)	0 (0.0)	2 (12.5)	4 (25.0)	0 (0.0)	16 (100.0)
	Passenger's	0 (0.0)	1 (14.3)	0 (0.0)	1 (14.3)	0 (0.0)	1 (14.3)	4 (57.1)	0 (0.0)	7 (100.0)
	2nd Row	1 (33.3)	0 (0.0)	0 (0.0)	0 (0.0)	0 (0.0)	2 (66.7)	0 (0.0)	0 (0.0)	3 (100.0)

4. Discussion

It is time for a new car assessment program on which multiple vehicle accidents patterns are reflected to encourage manufacturer to improve vehicle safety through assessing vehicle safety in the car-to-car accidents which account for the majority among traffic accidents. It is expected that vehicle safety will be assessed in the event of car-to-car collisions under both Euro-NCAP and US NCAP. It is required to develop measures to strengthen the competitiveness of domestic automobile industry, in addition to enhance the domestic traffic safety index.
In consideration of the high fatality and severe injury rate in partial frontal collisions, the damage area/collision angle/speed of an assessed vehicle should be reviewed when developing a scenario for a new car assessment program on which the characteristics of real world vehicle accidents in Korea will be reflected. Specially the high severe injury rate in partial frontal collisions should be noted even though the extent of damage in a partial frontal collisions is lower than that of a full frontal collision. Because fatalities and severely injured occupants in the same occupied seat are quite different in the genders, various type of test dummies and occupied seats may be considered in a new car assessment program on which the characteristics of real world vehicle accidents in Korea will be reflected.
In addition, in consideration of major injured areas and injury types of severely injured occupants resulted from car-to-car accidents were chest fractures and upper/lower extremity fractures, It is deem to be necessary to establish the evaluation criteria to reduce these kinds of injuries in assessing impacts to the parts of a test dummy corresponding to the frequently injured areas of occupants. It is possible to minimize the discrepancy between the assessment and the actual accident injury reduction

effect by supplementing the additional parts in addition to the parts of a test dummy used in the current new car assessment program in consideration of the injury characteristics of severely injured occupants resulted from real world car-to-car accidents.

5. Conclusion

The following conclusions were drawn from the analysis of characteristics of the severely injured occupants based on the database of domestic insurance companies.
Partial frontal collisions and side impacts resulted in severely injured occupants even though the extent of damage was low. For partial frontal collisions, the type of 60% off-set collision co-linearly on the left(driver side) was most frequent. In this type of collisions male drivers and female passengers were severely injured with high frequency regardless of age. Chest injuries were most frequent in the severely injured occupants.
Based on the results of the analysis of the car-to-car accidents in Korea, it is necessary to further study the standardization of the collision assessment technology which the real world accidents patterns can be reflected in order to secure the collision safety additionally in the new car assessment program.

REFERENCES

[1] Injury distribution, The Guarantee of Automobile Accident Compensation Act in KOREA,

[2] Traffic Accident Analysis System Datebase, 2008~2017, http://tass.korad.or.kr

[3] ANDERS LIE, CLAES TINGVALL, How Do Euro NCAP Results Correlate with Real-Life Injury Risks? A Paired Comparison Study of Car-to-Car Crashes, Traffic Injury Prevention, 3:288-293, 2002

[4] Kullgren A, Lie A , Tingvall C.Comparison Between Euro NCAP Test Results and Real-World Crash Data. Traffic Injury Prevention, 11:587-593, 2010

[5] Dennis R. Durbin, Jessica S.Jermakian, Michael J Kallan, Anne T. McCartt, Kristy B.Arbogast, Mark R.Zonfrillo, Rachel K. Myers, Rear seat safety: variation in protection by occupant, crash and vehicle characteristics, IIHS, 2015

[6] Hampton Gabler, Kennerly Digges, Brian N. Filders, Laurie Sparke, Side impact injury risk for belted far side passenger vehicle occupants(Hampton et al., 2005)

[7] Sandner et al, EURO NCAP FRONTAL IMPACT WORKING GROUP REPORT, 25th ESV conference proceedings, paper number 17-0205

[8] Saeed Barbat et al, ANALYSIS OF THE PROPOSED FRONTAL OBLIQUE CRASH TEST, 25th ESV conference proceedings, paper number 17-0130

[9] Matthew L. B., David S. Z., IMPACT AND INJURY PATTERNS IN FRONTAL CRASHES OF VEHICLES WITH GOOD RATINGS FOR FRONTAL CRASH PROTECTION, 21th ESV conference proceedings, paper number 09-0257

[10] National Highway Traffic Safety Administration, Federal Register, Vol. 80, No. 241, 2015

[11] National Highway Traffic Safety Administration, NASS Analysis in Support Of NHTSA's Frontal Small Overlap Program, DOT HS 811 522, 2015

EURO NCAP CHILD OCCUPANT PROTECTION – HOW THE 2016 PROTOCOL IMPROVED CARS AND CRS COMPATIBILITY AND DYNAMIC INTERACTION

Farid Bendjellal[1], Mark Pitcher[2]

Britax Childcare Group, Germany[1], UK[2]

Paper Number 19-0294

ABSTRACT

In 2015 Euro NCAP updated its test protocols and in 2016 Euro NCAP updated its assessment protocol. The aim of this was to advance the vehicle restraint systems in the second seat row for both small adults and children. This included the introduction of a full width frontal test and modification to the existing offset frontal and side impact tests.

The update to the protocols aimed to enhance the vehicle restraint systems towards a more efficient one, including belt load limiters and belt pretensioners. As far as child occupant protection is concerned the objective of Euro NCAP was to seek a combined restraint strategy allowing both the vehicle restraint system and the child restraint system (CRS) to work together. The child restraint systems used for the crash testing are a highback booster for the Q6 and a booster cushion for the Q10.

The aim of this study was to investigate the performance of the vehicles tested with regards to the three key areas covered by the protocol: i.e. CRS installation checks, safety provisions in the vehicle and crash performance. The test results from 97 vehicles tested by Euro NCAP between January 2016 and December 2018 were analysed. Where possible the reasons for differences between the best and worst performers for each assessment were investigated.

BACKGROUND

The aim of Euro NCAP's 2015 and 2016 updates to the testing and assessment protocols was to advance the restraint systems in vehicles' second seat row for both small adults and children. Amongst the features of this protocol were two key new features:

- Full width frontal impact including a 5th percentile adult dummy occupant sat in the rear of the vehicle introduced since 2015
- Using larger child dummies, Q6 and Q10 in frontal offset and side impact tests introduced since 2016

The introduction of a full width crash test, using the 5th percentile Hybrid III dummy in the rear seat of a vehicle, with its associated performance criteria was a way to enhance the vehicle restraint system towards a more efficient one, including belt load limiters and belt pretensioners.

The test conditions of the pre-existing frontal offset deformable barrier (ODB) and side mobile deformable barrier (MDB) tests remained unchanged. However, as far as child occupant protection (COP) is concerned the objective of Euro NCAP was to seek a combined restraint strategy allowing both vehicle restraint system and the child restraint system (CRS) to work together.

For this purpose, the protocol was changed from the previously used Q1.5 and Q3 child dummies, to assessing the ability of the vehicle to protect older children. Therefore, Q6 and Q10 dummies representing older children were used. The child restraints used to protect these older children where therefore also updated to a highback booster for the Q6 and a booster cushion for the Q10.

OBJECTIVE

This study investigated all the vehicles tested by Euro NCAP between January 2016 and December 2018. In addition, data collected at the Euro NCAP manufacturers viewings sessions was used. Where possible video footage was used to understand the performance of the vehicle seat belt restraint in frontal impact and the curtain airbag interaction with the Q10 dummy in side impact.

The aim of this study was to investigate the performance of the vehicles tested with regards to the three key areas covered by Euro NCAP's child occupant protection (COP) assessment protocol [1]:

- CRS installation checks
  Assessing the vehicle's ability to accommodate a large range of different designs of child restraints
- Safety provisions in the vehicle
  Provisions of 3-point seat belts, i-Size positions and markings, top tether markings, passenger airbag warning label and deactivation information and ability to install large rearward facing ISOFIX CRSs
- Crash performance
  Q6 and Q10 dummy responses in frontal offset deformable barrier (ODB) impact test and side mobile deformable barrier (MDB) impact test

The relationship between the vehicle overall star rating and the size of the vehicle was also investigated to see if any trends could be identified.

Euro NCAP CHILD OCCUPANT PROTECTION PROTOCOL

The following sections describe how the child occupant protection protocol assesses vehicles in each of the three key areas.

CRS installation checks

Child restraints are designed to protect the occupant in the event of an impact. However, if the child restraint cannot be installed correctly in a vehicle, it can diminish the ability of that child restraint to protect the occupant. Euro NCAP attempts to reduce the likelihood of a mismatch between the child restraint and the vehicle by installation checks for each seating position in the vehicle.

Child restraints, representing different designs and installation methods available on the market, are installed in the vehicle to assess the ease of installation. Euro NCAP publish a "Top Pick List" [2] of child restraints that are used for the installation checks (Figure 1). The top pick list contains child restraints with at least a good rating in consumer testing.

Figure 1. Euro NCAP child restraint top picks (2016-2018)

The installation checks of the different child restraints mean a number of different vehicle characteristics are assessed including: seat belt length, belt buckle location, ISOFIX anchorage accessibility and CRS stability. The top picks list also includes large rearward facing child restraints to encourage vehicles to provide space for these types of child restraint.

The vehicle is rewarded if the child restraints on the top pick list can be installed correctly and easily on all suitable seating positions in the vehicle. The vehicle handbook should clearly mention the seating positions where a CRS cannot be installed. If a certain child restraint cannot be installed in a position it loses points. If the CRS cannot be installed easily or there are vehicle interference problems the points score is reduced.

Safety provisions in the vehicle

All child restraints must be tested and Type Approved to either UN Regulation 44 (R44) or UN Regulation 129 (R129) before they can go on sale in Europe. R129 was introduced in July 2013 and it introduces the concept of i-Size child restraints compatible with i-Size vehicle seating positions. Current vehicle regulations do not mandate the requirement to have i-Size ready seating positions in the vehicle, it is optional for the vehicle manufacturer.

However, the Euro NCAP assessment encourages the availability of i-Size ready seating positions in the vehicle. The vehicle is also rewarded for providing important features such as ISOFIX anchorages, a top tether anchorage and a strong vehicle floor for each seating positions. Points are also awarded for clear i-Size labelling, a front seat airbag-disabling switch with clear user instructions and integrated vehicle child restraints as a standard option.

Points are awarded if the following criteria are fulfilled:

- Seat belt length (Gabarit installation) on all passenger seats
- Ability to install large size “ISO/R3” CRS in two or more seating positions
- Integrated child restraints in one position
- More points are awarded if there are integrated child restraints in two or more positions
- i-Size and top tether markings (conspicuous design, permanent labels) for each i-Size seating position
- At least two i-Size seating position available
- More points are awarded if there are three or more i-Size seating positions
- Passenger airbag disabling for the front passenger seat(s)

Crash performance

Four different impact tests are conducted as part of the Euro NCAP assessment. However only the frontal offset deformable barrier (ODB) impact test [3] and the side mobile deformable barrier (MDB) impact test [4] have child dummies installed in the rear of the vehicle.

Frontal offset deformable barrier (ODB) impact test The vehicle is tested with child dummies representing a 6 year-old child (Q6) and a 10 year-old child (Q10). The Q6 is seated in a highback booster recommended by the vehicle manufacturer and the Q10 is seated on a booster cushion (either recommended by the manufacturer or from the Euro NCAP list). The Q6 is placed behind the driver in the vehicle (Figure 2).

During the frontal impact test the assessed vehicle is propelled at 64 km/h into a deformable barrier. There is a 40% overlap between the vehicle and the barrier.

Head displacement, head acceleration, upper neck force and chest accelerations are the main dummy criteria measured during the tests. The vehicle is rewarded if test criteria remain below defined limits and if neither dummy was ejected from its seat or made any hard contact with the vehicle interior during the impact. This ensures that the child remains correctly restrained during the crash event.

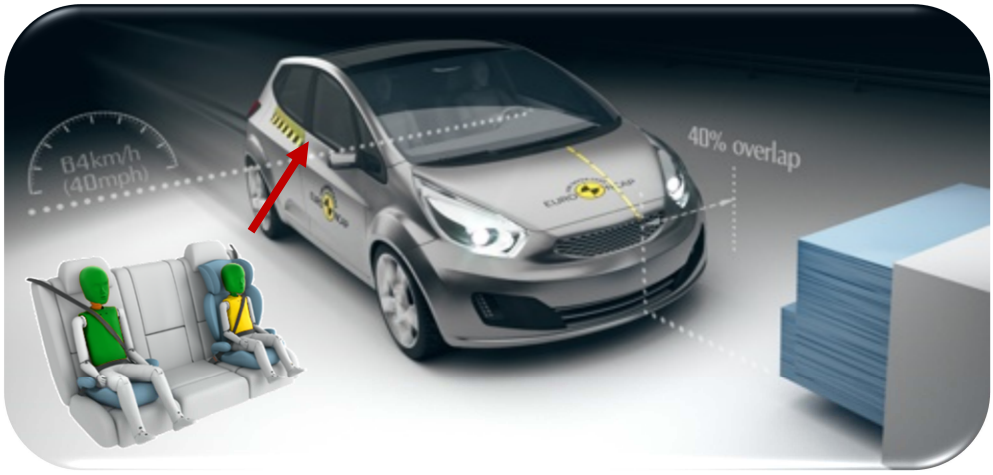

Figure 2. Frontal impact offset deformable barrier (ODB) test [5]

Side mobile deformable barrier (MDB) impact test The vehicle is tested with the same child dummies and child restraints as the frontal impact test. The Q10 is placed on the stuck side of the vehicle (Figure 3).

During the side impact test the assessed vehicle is struck at 50 km/h by a mobile deformable barrier.

Head acceleration, upper neck force and chest accelerations are the main dummy criteria measured during the tests. The vehicle is rewarded if test criteria remain below defined limits and there is no hard contact with the vehicle interior during the impact.

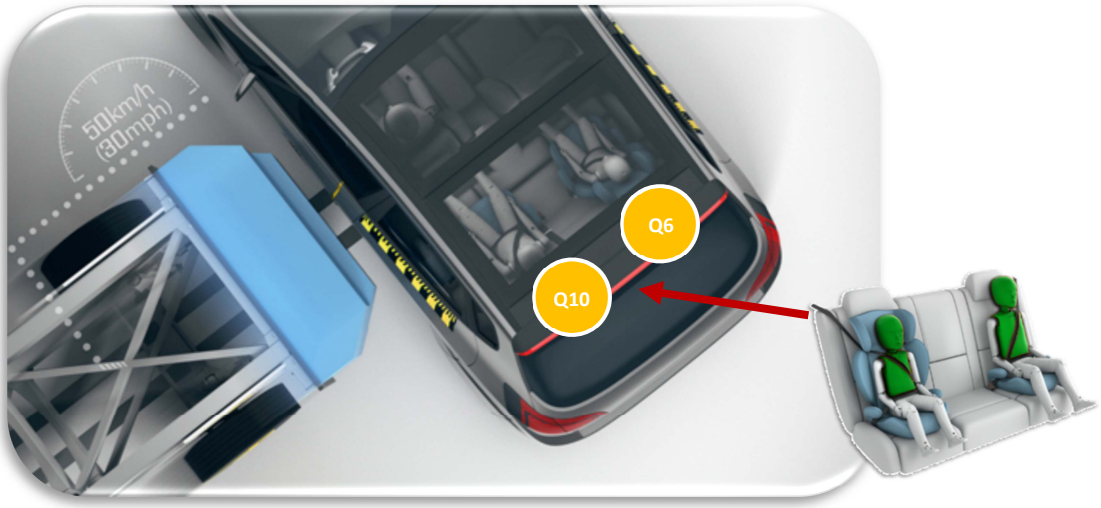

Figure 3. Side impact mobile deformable barrier (MDB) test [6]

Overall Rating

A vehicle can score a total of 49 points for the child occupant protection (COP) score. The COP score accounts for 20% of the final overall rating of the vehicle [7].

However there are also balance limits that means for a vehicle to score 5 stars overall it needed to score at least 75% COP score when tested between 2016 and 2017. From 2018 vehicles needed to score 80% COP score to achieve 5 stars overall. Similar balance limits exist for adult (80%), pedestrian (60%) and safety assist (50%) assessments. This is to ensure the vehicle provides all round protection.

RESULTS ANALYSIS

Analysis of the Euro NCAP Child Occupant Protection (COP) test results from vehicles assessed between 2016 and 2018 has been carried out. The results only from the standard versions of each vehicle was analysed. If a reassessment had been carried out, only the reassessment has been included in the analysis. In total, the results from 97 different vehicles tested by Euro NCAP have been analysed.

COP Score

Figure 4 shows the comparison of overall vehicle star rating with child occupant protection score. Figure 4 shows that some 3 star vehicles were able to provide a high level of child occupant protection (>80%).

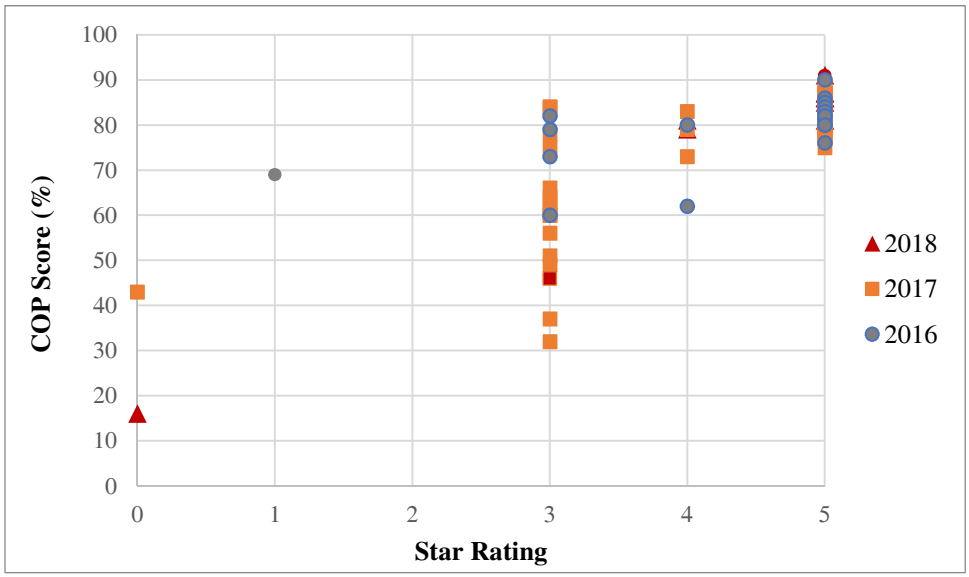

Figure 4. Overall star rating vs child occupant protection score (COP)

Table 1 shows the average score per assessment category for each class of vehicle. This shows that for installation checks and safety provisions in the vehicle, Executive and Large Family vehicles are on average the highest scoring vehicles. On average the lowest scorers in these categories are Small MPVs. Therefore, these categories were analysed in greater detail to identify the reasons for the scoring differences.

Executive vehicles are also amongst the highest scoring in the dynamic tests, whereas Superminis are on average the lowest scoring.

Pick-up and Roadster vehicles were not considered for the analysis due to the low number of vehicles tested.

Table 1. Euro NCAP child occupant protection average score per category

Class	No. vehicles	Installation Checks /12	Safety provisions in the vehicle /13	Dynamic Test /24	Total /49
Large Family	8	11.7	7.0	22.9	41.6
Executive	8	12.0	7.0	22.4	41.4
Small Off-road	21	11.5	6.8	22.5	40.8
Large Off-road	13	11.4	6.9	22.1	40.5
Small Family	19	10.9	6.1	20.2	37.3
Small MPV	8	9.4	5.3	22.0	36.6
Supermini	17	10.8	5.4	17.2	33.4
Pick-up	2	11.2	8.5	22.0	41.7
Roadster	1	2.2	0.0	13.6	15.8

CRS installation checks
This assessment is scored out of 12 points. The score is calculated based on whether it is possible to fit each of the different child restraints from the Top Pick list in each available vehicle seating position. If a certain child restraint cannot be installed in a position it loses points. If the CRS cannot be installed easily or without problems the points score is reduced.

Figure 5 shows the comparison of the CRS installation checks results for the Small MPV and Executive vehicle classes. This shows that all Executive vehicles scored full points for this assessment. However, for Small MPVs there is a wide range of scores between 2.5 points and 12 points.

It is common for points to be lost for seating positions which could not accommodate large rearward facing child restraints. In addition, vehicles with 3 rows often have seat belt length that are not suitable for rearward facing child restraints. The lowest scoring vehicle lost points because it was not possible to fit any ISOFIX or i--Size child restraints in the vehicle.

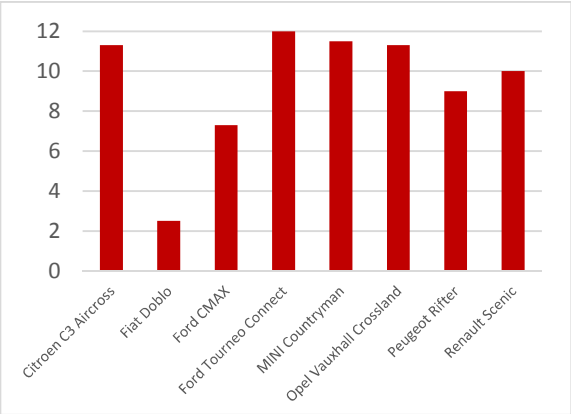

Small MPV vehicles (2016-2018)

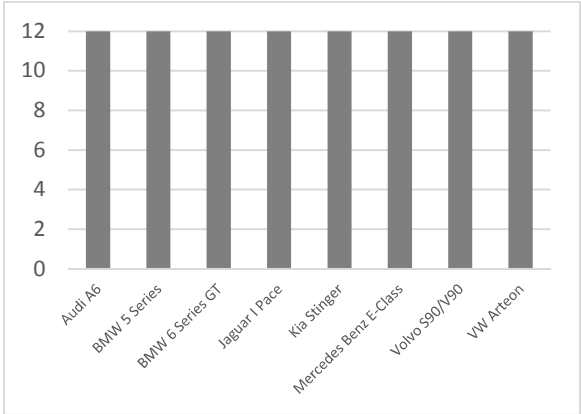

Executive vehicles (2016-2018)

Figure 5. CRS installation checks results

Safety provisions in the vehicle
This assessment is scored out of 13 points. Points are awarded based on the assessment described previously.

Figure 6 shows the comparison of the safety provisions in the vehicle results for the Small MPV and Executive vehicle classes. This shows that none of the vehicles score the full 13 points. 9 points is the joint highest score for this assessment for all the vehicles assessed between 2016 and 2018 (7 vehicles). As shown in Table 1, 7 points is typically the best average score for vehicles.

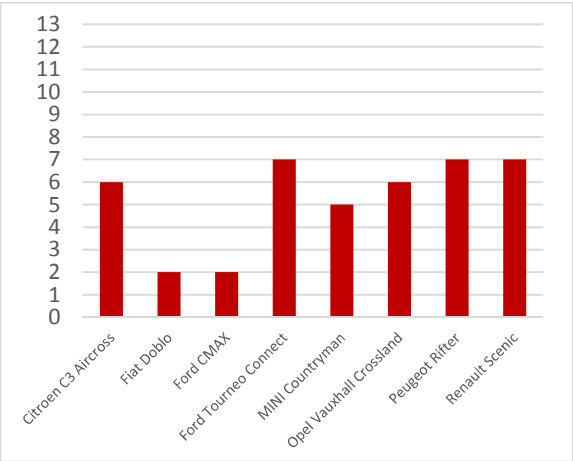

Small MPV Vehicles (2016-2018)

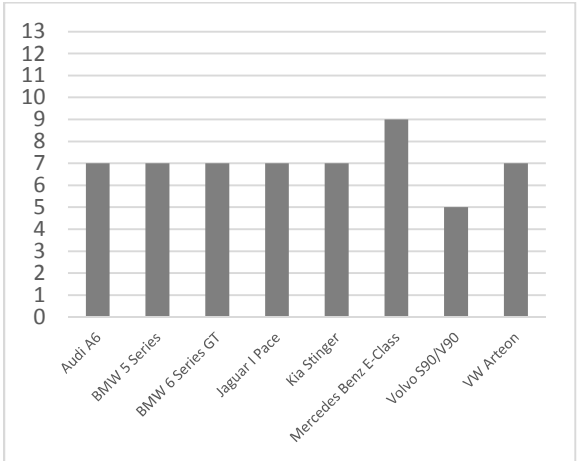

Executive Vehicles (2016-2018)

Figure 6. Safety provisions in the vehicle results

The reasons vehicles don't score full marks for this assessment is that they don't have at least two integrated child restraints fitted in the vehicle as a standard option (3 points) and that they are not equipped with three i-Size positions (1 point). Vehicles without an automatically disabling front airbag also miss out on a further 2 points. Meaning for most vehicles 7 points is the maximum points they can score.

Figure 6 shows that the majority of Executive vehicles scored 7 points for this assessment. However, for Small MPVs there is a wide range of scores between 2 points and 7 points.

The reasons vehicles don't score 7 points is due to poor labelling of the i-Size position, accessibility of the ISOFIX and poor labelling of the top tether. Some examples of good and poor i-Size execution are shown in Figure 7. The poor examples require the user to move the cushion to find the ISOFIX anchorages. Whereas for the good examples, the anchorage locations are clearly labelled and easy to access.

Good Examples *Poor Examples*

Figure 7. Examples of good and poor i-Size execution

Figure 8 shows a good example of a clearly labelled top tether anchorage and a top tether anchorage, although labelled, the anchorage itself is hidden within the seat back.

Good Example *Poor Example*

Figure 8. Examples of good and poor top tether execution

For the lowest scoring vehicles either it was not possible to deactivate the front passenger airbag or it was not clear to the user when the airbag was deactivated.

Figure 9 shows that over the last three years that the majority of vehicles tested now have at least two i-Size positions in the vehicle. This is positive trend as it means that vehicle/CRS compatibility is increasing.

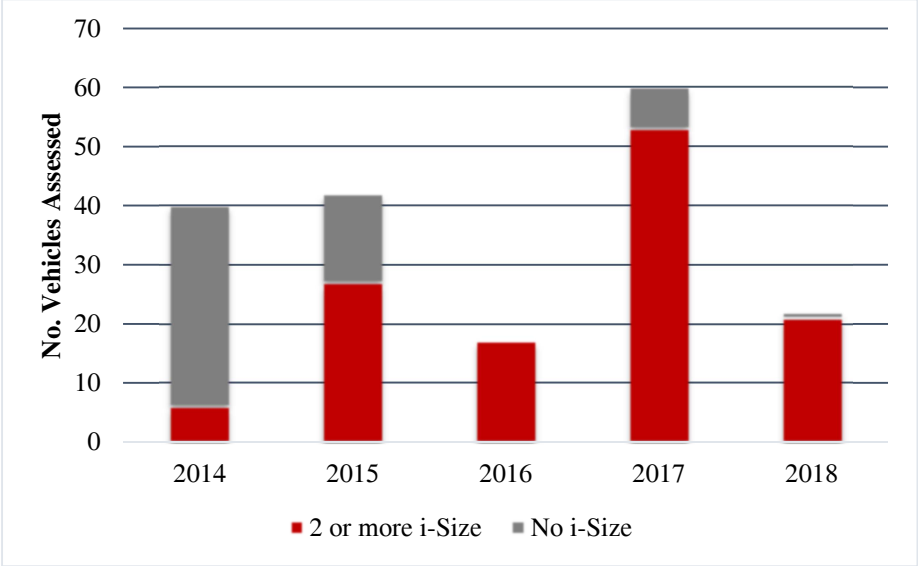

Figure 9. i-Size penetration

Crash performance

A total of 24 points can be scored for crash performance. For frontal impact each dummy receives a score out of 8 points. For side impact each dummy is scored out of 4 points.

The responses of the Q6 and Q10 dummy have been analysed in the frontal offset barrier and side impact tests. The dummy readings from each of the scored body regions have been analysed to identify any trends.

Frontal impact – Head displacement A check of the dummy's horizontal movement is made from the video footage to verify the head has not exceeded a certain limit. However, an exact excursion measurement is not necessarily recorded. Therefore, a comparison of head displacement is not possible.

Frontal impact – Head acceleration Figure 10 shows that prior to 2018 that only one vehicle failed to score full points for head resultant acceleration. This is likely to be one of the reasons why the points limits were adjusted to a lower threshold. For the vehicles tested in 2018, two vehicles failed to score full points for the Q6 and two vehicles failed to score full points for Q10.

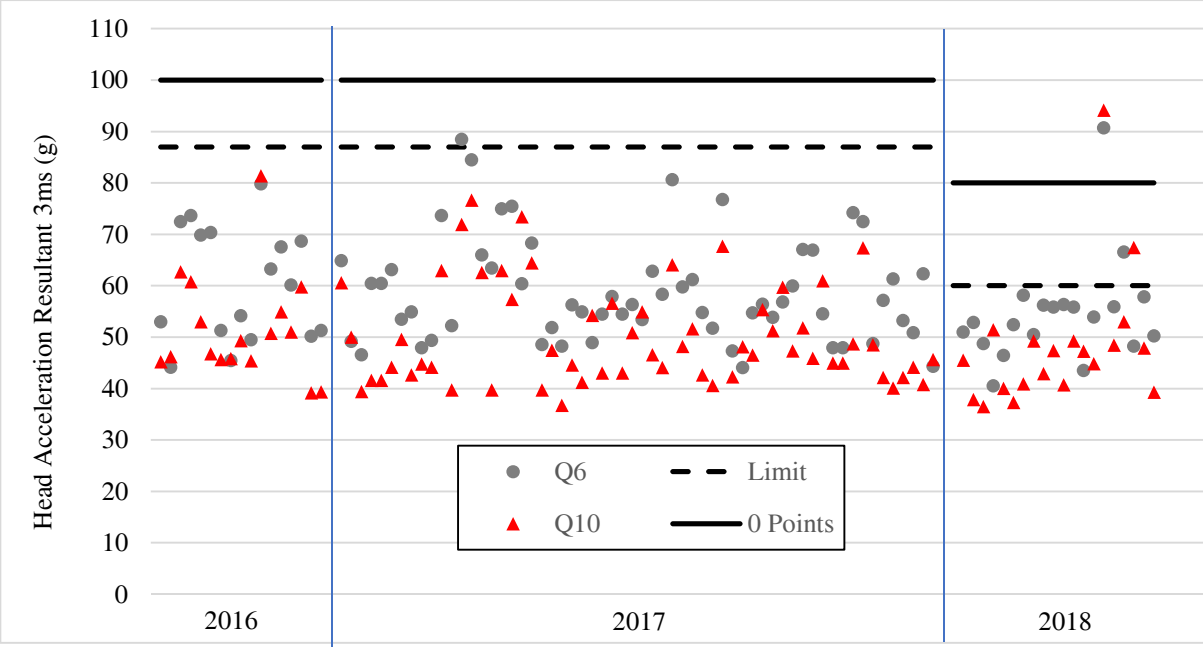

Figure 10. Q6 & Q10 head accelerations frontal ODB impact tests

Frontal impact – Upper neck force Figure 11 shows that only a small number of vehicles have scored full points for the Q6 and Q10 upper neck force. There does not seem to be a trend relating to vehicle size.

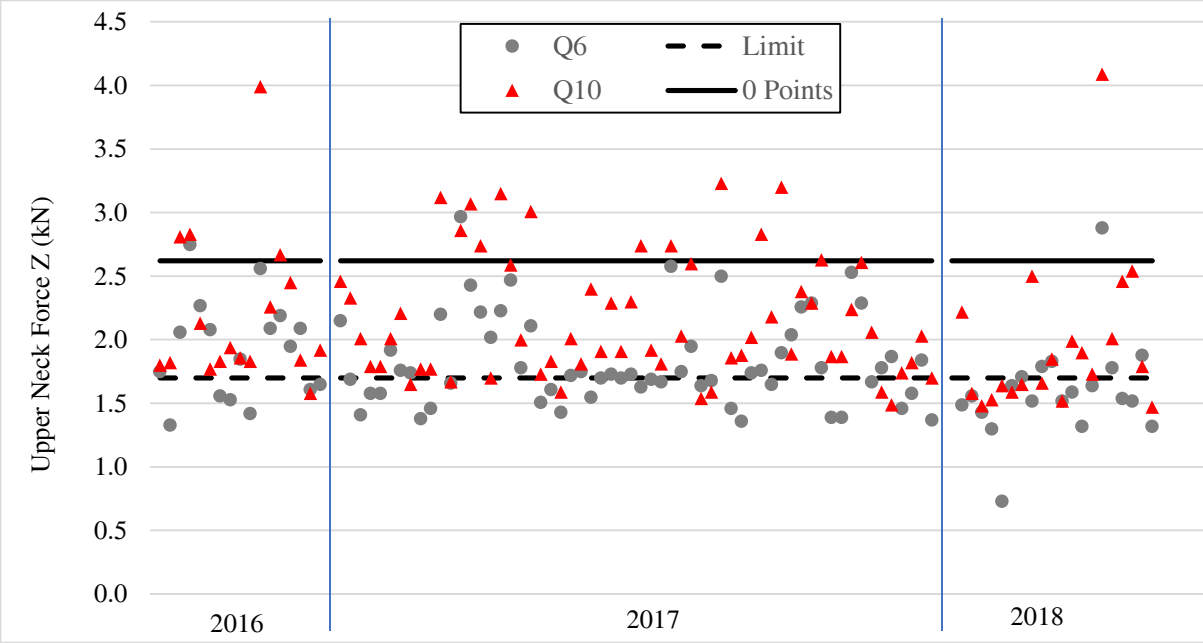

Figure 11. Q6 & Q10 upper neck forces frontal ODB impact tests

Frontal impact – Chest Acceleration Figure 12 shows that the majority of vehicles score full points for the Q10. However only a small number of vehicles have scored full points for the Q6 chest resultant acceleration. Though, from 2018 chest acceleration was no longer scored for the Q6. Instead chest deflection was measured and scored for the Q6.

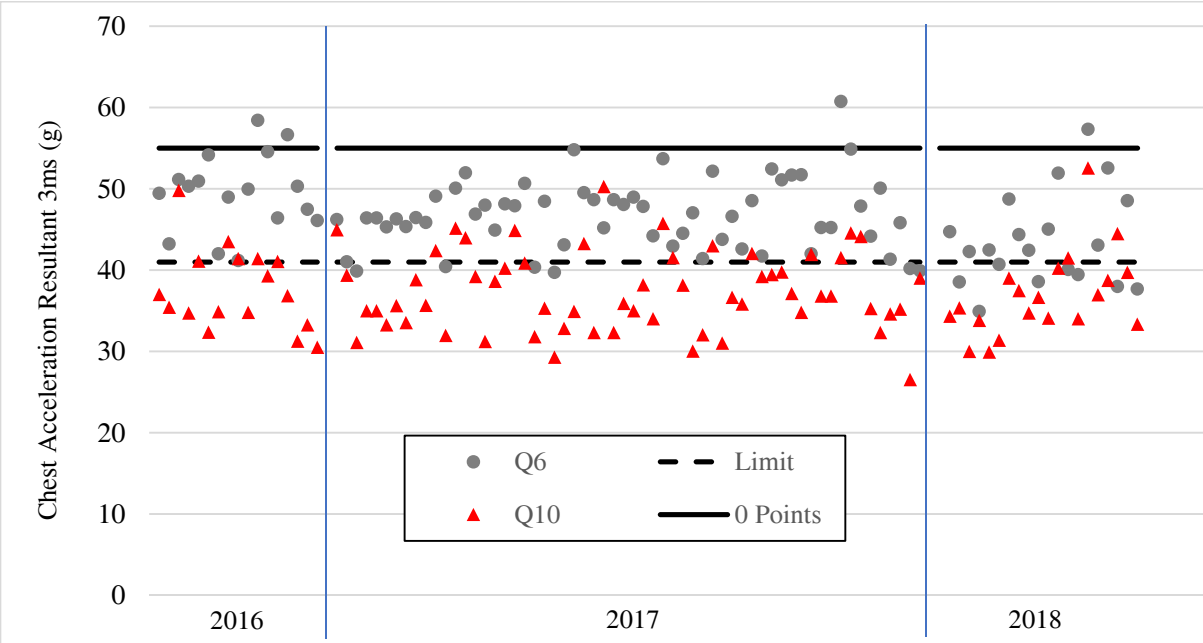

Figure 12. Q6 & Q10 chest accelerations frontal ODB impact tests

Frontal impact – Chest Deflection Figure 13 shows that measured chest deflection for Q6 and Q10 for vehicles tested in 2018. Though only the Q6 chest deflection is scored. Prior to 2018 the chest deflection results were not necessarily recorded. This shows that all the vehicles scored full points for the Q6 deflection.

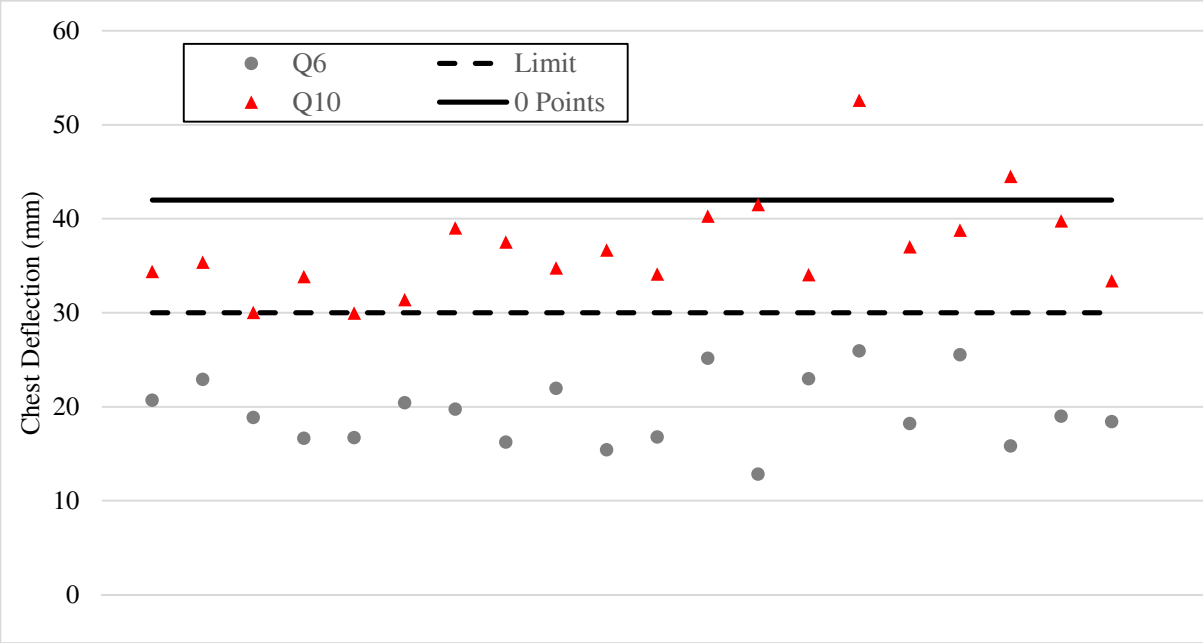

Figure 13. Q6 & Q10 chest deflections frontal ODB impact tests (2018 vehicles)

Frontal impact – Modifiers For frontal impact testing a score modifier is apply if one of the following occurs:

- Diagonal belt slips off the shoulder
- Submarining
- Dummy ejection
- Failure of restraint system components

The position of the diagonal belt on the shoulder of the dummy is assessed from the in-vehicle video footage. A sliding points scale is applied depending on the position of the diagonal belt during the impact (Figure 14). If the belt remains on the shoulder of the dummy no modifier is applied. If however the belt slips towards the arm and gets caught in the arm-shoulder gap then a -4 point modifier is applied. If the belt slips of the shoulder completely then a -8 point modifier is applied, meaning that the dummy scores zero points in the frontal test.

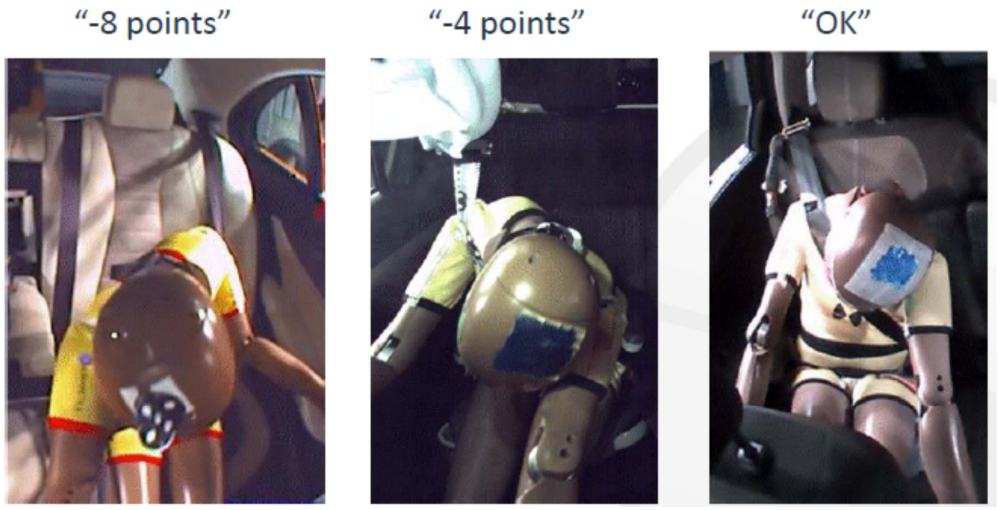

Figure 14. Diagonal belt position modifier assessment

If submarining of the dummy under the lap belt occurs (Figure 15) during the frontal test a modifier is applied. This occurred for one vehicle in 2016.

Figure 15. Diagonal belt position modifier

Side impact – Head acceleration Figure 16 shows only one vehicle failed to score full points for head resultant acceleration for the Q6. In this vehicle a head to head contact occurred between the Q6 and Q10 dummies, resulting in high accelerations measured by both dummies.

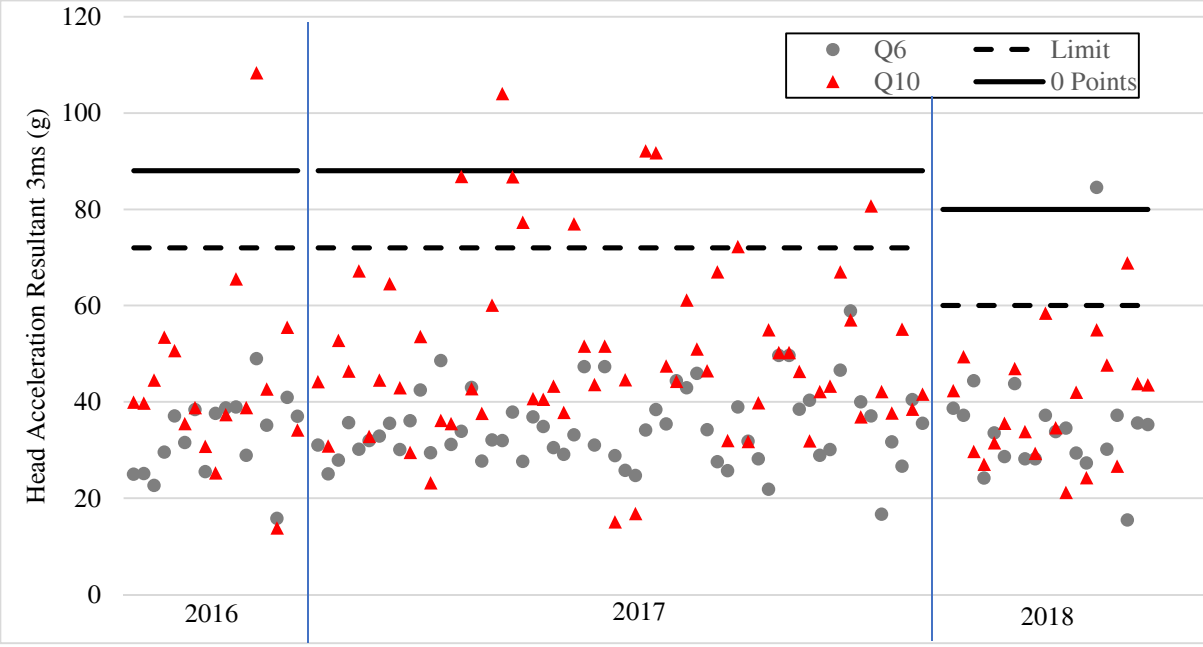

Figure 16. Q6 & Q10 head accelerations side MDB impact tests

Prior to 2018, before the points limits were adjusted to a lower threshold, only a few vehicles exceeded the head acceleration limit with the Q10. The reasons for the Q10 recording high head accelerations was typically either the head missed or bottomed out the curtain airbag. This can result in head contact with the vehicle c-pillar (Figure 17). Only a few of vehicles (4) were not fitted with curtain airbags in the rear of the vehicle. This resulted in the Q10's head contacting the vehicle structure and recording high head accelerations.

Curtain bottoming out *Head contact with c-Pillar*

Figure 17. Curtain airbag performance

Side impact – Upper neck force Figure 18 shows that only one vehicle exceeded the limit for the Q10 upper neck force. This vehicle also had the high Q6 upper neck force. This is the same vehicle where the head to head contact occurred.

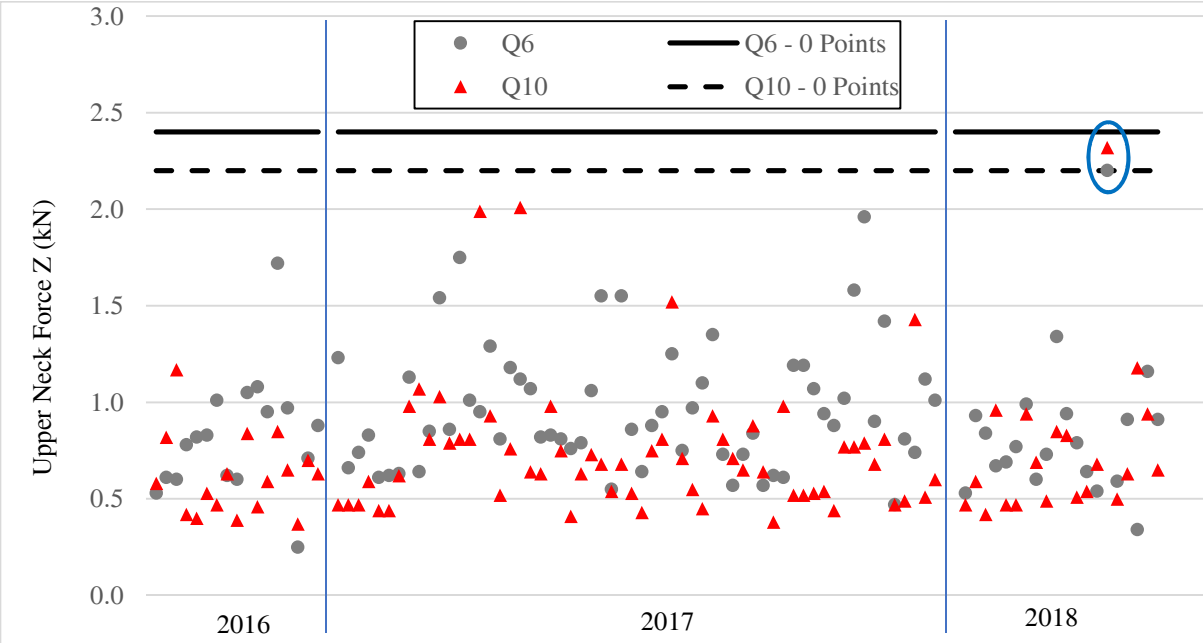

Figure 18. Q6 & Q10 upper neck forces side MDB impact tests

Side impact – Chest Acceleration Figure 19 shows that all vehicles scored full points for the Q6 chest acceleration. The majority of vehicles scored full points for the Q10. Only a small number of vehicles exceeded the chest resultant acceleration limit for the Q10. These vehicles are mostly Supermini vehicles.

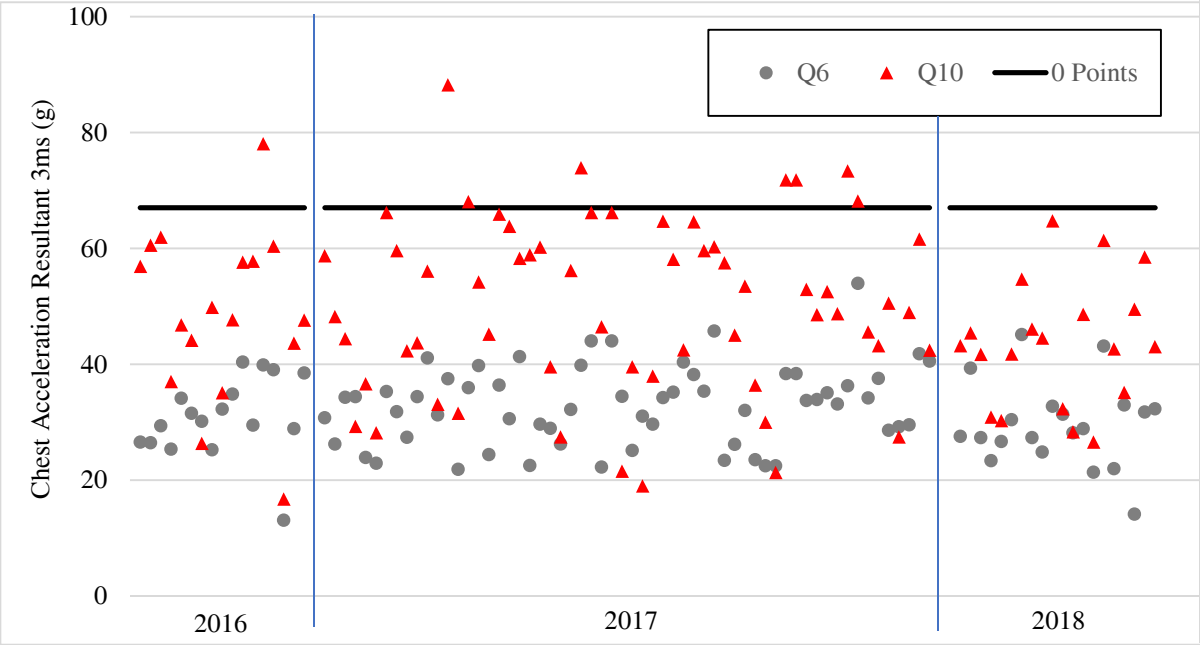

Figure 19. Q6 & Q10 chest accelerations side MDB impact tests

Vehicle restraint observations

From analysis of the test video footage and information provided by the Euro NCAP website [8] the following trends can be observed:

Curtain airbags Rear row curtain airbags are not mandated by vehicles regulations. However 93 of the 97 vehicles tested by Euro NCAP between 2016 and 2018 were fitted with a curtain airbag. Some vehicles have also started to introduce rear row side and pelvis airbags, but these are usually an optional extra.

Pretensioners and load limiters The introduction of the full width barrier test in 2015 and the change to the assessment protocol to evaluate the protection of older children in the rear of vehicles in 2016 has resulted in an increase in the number of pretensioners and load limiters equipped in the rear row of vehicles as a standard option. Figure 20 shows that before 2015 only 40% of vehicles tested were fitted with a load limiter or a pretensioner and load limiter. However, since 2015 over 85% of tested vehicles have at least a load limiter.

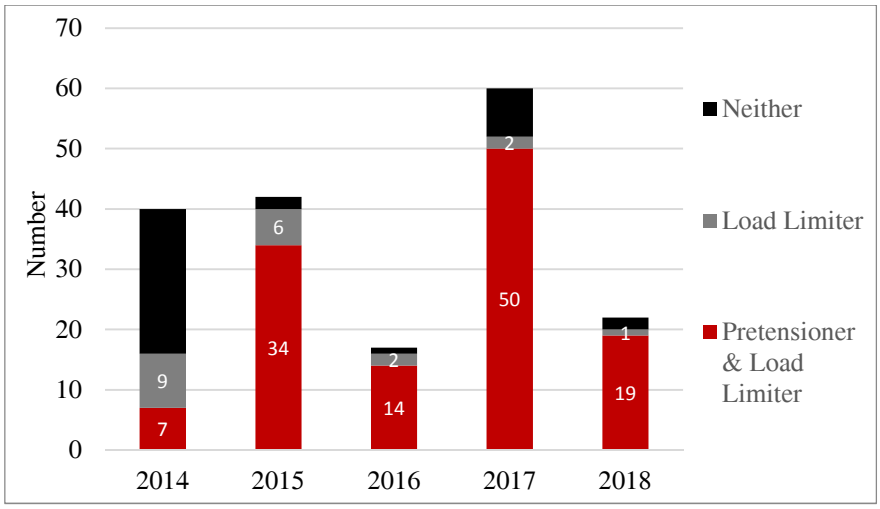

Figure 20. Pretensioners and load limiters fitted to tested vehicles

CONCLUSIONS

The aim of Euro NCAP's 2015 and 2016 updates to the testing and assessment protocols were to advance the restraint systems in vehicles' second seat row for both small adults and children.

In terms of child occupant protection (COP) the new requirements seem to have the following effects:

- Requiring a COP of at least 75/80% to achieve an overall 5 star rating has required vehicle manufacturers to provide an improved level of protection for older child occupants
- The percentage of vehicles with at least two i-Size positions has increased (>88%)
- The majority of vehicles score good crash performance (20+ points)

Crash test requirements and performance limits have had the effect of:

- Presence of seat belt pretensioners and load limiters in the rear of vehicles is increasing (>85%) as a result of the introduction of the frontal full barrier test
- Seat belt geometry improvement to ensure correct shoulder belt position for older children
- Curtain airbags to protect older children in side impact. 96% of vehicles tested provided a curtain airbag
- Head accelerations have reduced in 2018 compared to 2016-2017, in both frontal and side impacts

Overall, most vehicles score around 20 points for crash performance. However, there is still some improvements to be made for some vehicles as far as ISOFIX visibility, accessibility and marking. The compatibility of some vehicles with some designs of child restraint could also be improved.

THE FUTURE

Euro NCAP is already planning to update the testing and assessment protocols to improve the performance of vehicles in 2020. These changes increase the severity of the frontal and side impact tests. This is likely to result in the need for an improved combined restraint strategy from the vehicle restraint systems and the child restraint system.

The main update changes that will affect child occupant protection in 2020 will be:

Frontal impact mobile progressive deformable barrier (MPDB)

Instead of the vehicle striking a static impact barrier, the vehicle is now impacted into a mobile progressive deformable barrier. Both the vehicle and the mobile barrier will have an impact speed of 50 km/h (Figure 21).

The vehicle is still tested with child dummies representing 6 year-old child (Q6) seated in a highback booster and 10 year-old child (Q10) seated on a booster cushion. However, the Q10 will have a new upgrade kit that is designed to improve the interaction with the vehicle seat belt.

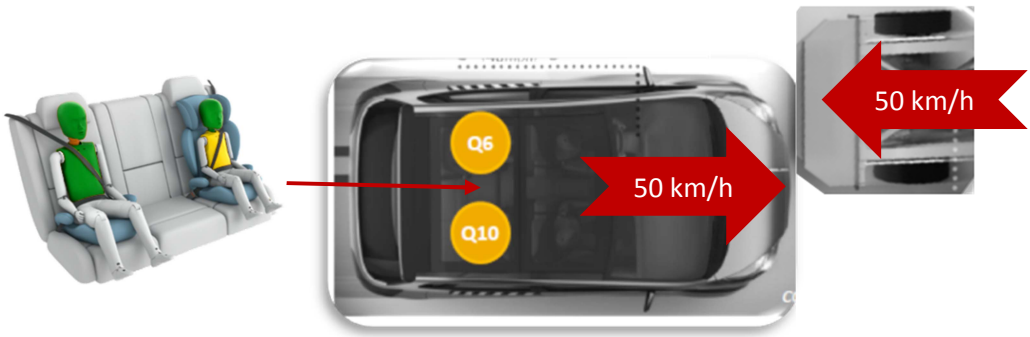

Figure 21. Frontal impact offset deformable barrier (ODB) test

Side impact mobile deformable barrier (MDB)

The main change for this test is that the impact speed of the barrier has been increased. The vehicle is now struck by a mobile deformable barrier travelling at 60 km/h (Figure 22).

The vehicle is still tested with child dummies representing 6 year-old child (Q6) seated in a highback booster recommended by the vehicle manufacturer and 10 year-old child (Q10) seated on a booster cushion.

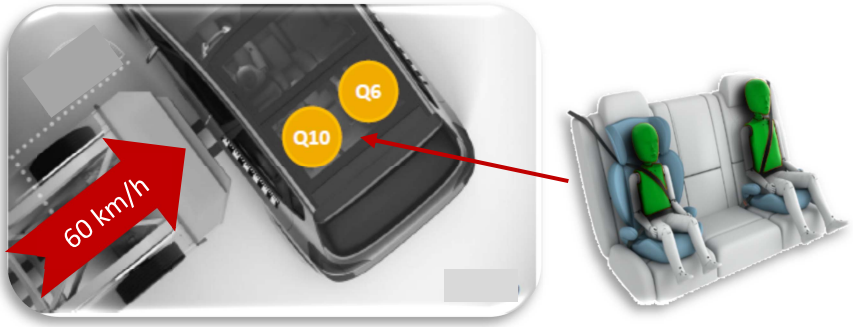

Figure 22. Side impact mobile deformable barrier (MDB) test

ACKNOWLEDGMENT

Britax would like to acknowledgment Euro NCAP for providing the test data to allow this analysis to be conducted.

REFERENCES

[1] Euro NCAP. 2017. "ASSESSMENT PROTOCOL – CHILD OCCUPANT PROTECTION" https://cdn.euroncap.com/media/32281/euro-ncap-assessment-protocol-cop-v721.pdf

[2] Euro NCAP. 2017. "Technical Bulletin 12 – Child Restraint Systems for Installation Checks" https://cdn.euroncap.com/media/32295/tb-012-child-restraint-systems-for-installation-checks-v23.pdf

[3] Euro NCAP. 2015. "OFFSET DEFORMABLE BARRIER FRONTAL IMPACT TESTING PROTOCOL" https://cdn.euroncap.com/media/20870/offset-deformable-barrier-frontal-impact-test-protocol-v711.pdf

[4] Euro NCAP. 2015. "SIDE IMPACT MOBILE DEFORMABLE BARRIER TESTING PROTOCOL" https://cdn.euroncap.com/media/20873/side-impact-mobile-deformable-barrier-test-protocol-v711.pdf

[5] Euro NCAP. 2019. "Offset-Deformable Barrier – ODB" https://www.euroncap.com/en/vehicle-safety/the-ratings-explained/adult-occupant-protection/offset-deformable-barrier/

[6] Euro NCAP. 2019. "CRS Performance" https://www.euroncap.com/en/vehicle-safety/the-ratings-explained/child-occupant-protection/crs-performance/

[7] Euro NCAP. 2016. "ASSESSMENT PROTOCOL – OVERALL RATING" https://cdn.euroncap.com/media/22107/euro-ncap-assessment-protocol-overall-rating-v701.pdf

[8] Euro NCAP. 2019. "LATEST SAFETY RATINGS" https://www.euroncap.com/en/ratings-rewards/

Q10 EURO NCAP 2020 UPDATE DUMMIES COMPARED TO CURRENT Q10 IN FRONTAL AND SIDE IMPACT SLED TESTS

Katarina Bohman
Isabelle Stockman
Lotta Jakobsson
Maria Wimmerstedt
Volvo Cars
SAFER, Vehicle and Traffic Safety Centre at Chalmers

Dion Kruse
Autoliv Research

Håkan Sundmark
Autoliv Sweden

Sweden

Paper Number 19-0295

ABSTRACT

There is a need of improving the current Q10 (Q10original) due to unstable seatbelt interaction with the shoulder. Several design changes to shoulders and torso have resulted in a prototype Q10 (Q10update). Some design changes were removed which resulted in a second prototype Q10 (Q10light). The aim was to compare kinematics, shoulder belt interaction and dummy responses of the Q10update and Q10light with the current Q10original in frontal impacts. Q10original and Q10update were also compared and evaluated in side impacts.

Q10original, Q10update and Q10light were compared in frontal sled tests in a midsize SUV, for two different crash pulses. Three different belt geometries were evaluated. Dummy kinematics and loadings were analysed. The dummies were positioned on booster cushions and restrained by seatbelt with pretensioner and load limiter.

Q10original and Q10update were included in eleven side impact sled tests simulating a Euro NCAP 2020 Side AE-MDB impact, using a midsize passenger car. The dummies were positioned on booster cushions and restrained by seatbelt and combinations of thorax side airbag (SAB) and inflatable curtain (IC), in addition to a reference test without SAB and IC. All tests included a retractor with pretensioner and load limiter. Two arm positions were evaluated in one restraint configuration.

In the frontal sled tests, the Q10update was less sensitive to initial shoulder belt position far out on the shoulder than the Q10original. The shoulder belt had a tendency to move inboard on the Q10update during the crash, even if the shoulder belt was initially positioned far out on the shoulder, possibly influenced by the soft tissue at upper chest and forward shift of the shoulder joint compared to Q10original. The Q10light had a similar shoulder belt interaction as the Q10original. Both update dummies showed a greater forward excursion of the head and a larger tilt of the upper torso than the Q10original, potentially due to the mass redistribution from pelvis to upper body. The increased excursion is considered an improvement, since the mass redistribution is more biofidelic compared to Q10orginal. Both update dummies had higher chest deflection, lower chest acceleration and lower neck tension compared to the Q10original.

The differences in dummy responses in the side impact sled tests were mainly due to mass redistribution. Especially in tests without SAB, lower chest acceleration, but higher chest deflection was obtained for the Q10update compared to Q10original. Furthermore, the shoulder force was higher for Q10update compared to Q10original for the three restraint combinations, while in the reference test head impact to the vehicle interior occurred. Angled arm position resulted in both reduced shoulder force and reduced chest deflection, compared to aligned arm position.

Due to its improved kinematics and sensitivity to changes in seatbelt geometry, the Q10light was preferred of the three tested dummies for frontal impact testing. Q10light was not evaluated for side impact loading. For side impact testing, this study provides no firm recommendation on the Q10update, acknowledging that a biofidelity evaluation needs to be made. Further dummy refinements and lateral validation and certification tests are encouraged.

BACKGROUND

Children younger than age 13 accounted for a significant proportion of the serious injuries (35.7%) and deaths (42.9%) to restrained rear row occupants, highlighting the challenges vehicle and restraint system manufacturers have in providing optimal protection to a wide range of rear occupants according to Durbin et al. (2015). Hence, there is a need of adequate tools, from children to adults, to develop the rear seat occupant protection.

During the 90s, the development of the Q dummies was initiated in to replace the P dummies (EEVC, Wismans et al. 2008). The Q10 crash test dummy was developed in the European project EPOCh (Enabling Protection for Older Children). In 2015, Euro NCAP revised the protocol for rear seat evaluation, by replacing the Q1.5 and Q3 dummies with the Q6 and the Q10, in both frontal Offset Deformable Barrier (ODB) and side impact test. The Q10 was positioned behind the passenger in the ODB, resulting in an inboard movement during the crash. In the side impact test, the Q10 was positioned behind the driver, meaning the near side.

The Q10 has been criticized for an unstable shoulder belt interaction in frontal impacts, but also of a pronounced shoulder belt slippage towards the neck. Bohman and Sunnevang (2011) showed that the chest deflection of the Q10 was more sensitive to belt geometry than to any other countermeasure. Arbogast et al (2013) compared shoulder belt interaction of child volunteers with the HIII10 year-old crash test dummy and Q10 in low speed sled tests. They found that the shoulder belt moved to greater extent towards the neck on the Q10 compared with the child volunteers, resulting in an underestimate of chest deflection in the Q10.

In order to improve the Q10 behaviour in frontal impacts, Humanetics updated the dummy to a second version, referred to as Q10update in this paper. Five changes were implemented including shoulder joint movement of 20mm forward, head and neck shifted 20mm forward and 5.3° nose up, soft tissues representation at nipples, continuous shoulder liner and mass redistribution change, by moving 1.7 kg from the pelvis to the torso (Waagmeester et al. 2017). In a CAE comparison of Q10originial, Q10update and Thums v4 10 year-old Human Body Model (HBM), it was found that the Q10update was not sensitive to an outboard shoulder belt geometry; the shoulder belt stayed on the shoulder while the other two dummies showed shoulder belt slipping off (Schnottale et al. 2017). In order to make the Q10update a bit more sensitive to various shoulder belt geometries, only three of the changes from the Humanetics Q10 was included in a third version of Q10, referred to in this study as Q10light. This version included the following design changes; the head and neck shift 20mm forward and 5.3° nose up, continuous shoulder liner and mass redistribution change, by moving 1.4 kg from the pelvis to the torso. This Q10light update kit was supplied by Cellbond. Recently, Euro NCAP has decided to include the Q10light in the rating program in 2020. Ipek (2018) compared the Q10light with Q10originial and concluded that Q10light had a more realistic shoulder geometry and a more realistic head position. The shoulder liner included in the Q10light also provide a clear understanding of shoulder belt slippage, since the belt can no longer get stuck in the gap between the shoulder and the arm.

In the current Euro NCAP protocol, the Q10 is positioned with the arms along the side of the torso. However, since children can choose a wide range of sitting postures, for example playing on their electronic devices with forward angled upper arms, it is of interest to understand if the arm position has any effect on the dummy responses in a side impact crash.

The aim of this study is firstly, in frontal impacts, to compare kinematics, shoulder belt interaction and dummy responses of the Q10update and Q10light with the current Q10original in different belt geometries. Secondly, in side impact, the study aims to compare the dummy responses of the Q10update with the Q10original for varying side airbag configuration and also highlighting the responses of the Q10 update for alternative arm position and booster cushion.

METHOD

This study includes both frontal and side impact sled testing. Three versions of the Q10 child crash test dummy are compared: Humanetics Q10original, Humanetics Q10update with full update kit including five updates and Humanetics Q10 with update kit light from Cellbond, Q10light, including three updates. The details on the update is shown in Table 1.

In the frontal impact tests, all three versions of the Q10 dummy were tested. In the side impact tests, the Q10original and Q10update were tested, while instrumented with the original side impact kit (EEVC WG, Wismans et al. 2015). When a Q10 dummy is rebuilt with a side impact kit, the scapula and arms are changed from front to side impact versions, and the sensors are moved to enable measurement of lateral chest deflection. The kit also includes shoulder force sensor. Hip shields were used in all frontal tests and for the Q10original in side impact tests while the hip liner was used for the Q10update in side impact tests.

Table 1. Q10 versions and details on included updates.

Dummy	Supplier dummy	Supplier update kit	Shoulder joint shift	Head and neck shift	Soft tissue at upper chest	Cont. shoulder liner	Mass re-distribution
Q10 original	Humanetics	N/A	N/A	N/A	N/A	N/A	N/A
Q10 update	Humanetics	Humanetics	X	X	X	X	X
Q10 light	Humanetics	Cellbond		X		X	X

Frontal Impacts

A series of frontal sled tests were performed in a reinforced sled body of a midsize SUV mounted using an acceleration sled, at Volvo Cars Safety Centre, Sweden. Two different crash test pulses were simulated (Figure 1) replicating; a typical 35mph full frontal crash and a typical 64km/h Euro NCAP ODB (offset deformable barrier) crash, with the sled body rotated 18 degrees.

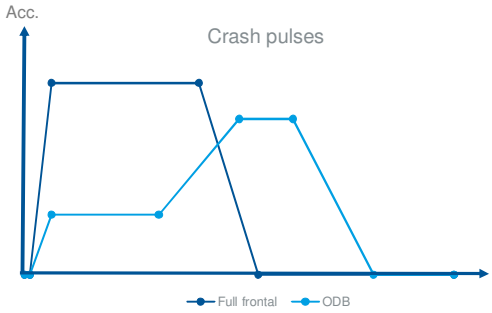

Figure 1. Frontal impact crash test pulses used in the study; a full frontal pulse and an ODB pulse.

The crash test dummies were restrained with a three point seatbelt with pretensioner and load limiter, and seated on a Volvo Booster Cushion (BC) without backrest. In all tests except two, the booster cushion was positioned centralised in the seat and the dummy was centred on the booster cushion. The spacer behind lumbar spine were used when positioning the dummy according to Euro NCAP's current testing protocol (2019). Load cells were placed on the diagonal belt above the dummy shoulder level and on the outer part of the lap belt. Three different belt geometries were tested, as illustrated in Figure 2. The left and mid belt geometries were achieved by routing the diagonal belt above and under the inner guiding loop of the BC, resulting in belt geometries closer to the neck and further out on the shoulder, respectively. These two geometries were tested in both full frontal and ODB. The third belt geometry, shown to the right in Figure 2, resembling a belt position far out on the shoulder, was achieved by routing the diagonal belt under the inner guiding loop of the BC and move the dummy and BC 15mm inboard. This geometry was tested in one full frontal test and in one ODB.

Diagonal belt above inboard guiding loop of booster cushion

Diagonal belt under inboard guiding loop of booster cushion

Diagonal belt under inboard guiding loop, and dummy/booster cushion moved 15mm inboard

Figure 2. The three seatbelt geometries included in test setup.

In the full frontal sled tests, the Q10original and Q10update were tested simultaneously, Q10original seated on the left hand side (LHS) of the rear seat and Q10update seated on the right hand side (RHS). In the ODB tests, the Q10original, Q10update and Q10light were tested in separate tests, all on the RHS, resulting in an inboard motion of the dummy relative to the sled body during the test. The test matrix is presented in Table 2. As can be seen, all three dummy versions were run in two comparable configurations with the ODB pulse, while the Q10original and the Q10update, only, were run in the three comparable configurations with the full frontal pulse and one configuration with the ODB pulse.

Table 2. Test matrix with overview of pulse, dummy and belt geometries.

Test number	Pulse	LHS	RHS	Belt geometry
1	full frontal	Q10 original	Q10 update	Diagonal belt above guiding loop
2	full frontal	Q10 original	Q10 update	Diagonal belt above guiding loop
3	full frontal	Q10 original	Q10 update	Diagonal belt under guiding loop
4	full frontal	Q10 original	Q10 update	Diag. belt under guiding loop, BC moved 15mm inboard
5	ODB		Q10 original	Diagonal belt above guiding loop
6	ODB		Q10 original	Diagonal belt above guiding loop
7	ODB		Q10 update	Diagonal belt above guiding loop
8	ODB		Q10 light	Diagonal belt above guiding loop
9	ODB		Q10 original	Diagonal belt under guiding loop
10	ODB		Q10 original	Diagonal belt under guiding loop
11	ODB		Q10 update	Diagonal belt under guiding loop
12	ODB		Q10 update	Diagonal belt under guiding loop
13	ODB		Q10 light	Diagonal belt under guiding loop
14	ODB		Q10 update	Diag. belt under guiding loop, BC moved 15mm inboard

High speed cameras captured a front view, LHS and RHS views and a top view of the dummy. Dummy kinematics responses and seatbelt-to-body interactions during the forward motion of the dummy were analysed and compared. Head accelerations (CFC1000), neck forces (CFC1000), chest accelerations (CFC600), chest deflections (CFC600) and diagonal belt (CFC60) and lap belt forces (CFC60) were captured and used in the analysis. The position of the shoulder belt during the event was categorised as on the shoulder, moved outboard on the shoulder from initial position during the event, and off the shoulder. For the Q10original in which the continuous shoulder liner is not included, shoulder belt slip-off was defined as shoulder belt in the gap between the torso and the arm.

Side Impacts

A series of side impact simulations was performed in a deceleration sled system at Autoliv Research, Sweden. A generic pulse replication of the Euro NCAP 2020 side Advanced European Mobile Deformable Barrier (AE-MDB) test for a midsize passenger vehicle was used, as shown in Figure 3. The 2020 side AE-MDB test method includes a barrier weight of 1400kg and barrier speed of 60km/h. The sled system comprises three sleds; one vehicle sled carrying the rear seat, a rigid-door-side sled where the interior (pre-tilted door and trim panel) are mounted and a load carrier sled. The vehicle and door sleds are accelerated by the load carrier sled to mimic a door sled intrusion velocity (peak approximately at 10m/s) and a vehicle sled response velocity. A feed-back system provides a realistic drop of the door sled intrusion velocity to meet the vehicle sled velocity at an almost unified velocity level (approximately 8m/s) before final braking. The initial position of the door interior in relation to the child dummy was replicated from an estimated average door intrusion. This was obtained from several tested midsized cars, based on accelerometer signals at different heights using a pre-tilted door (approximately 10 degrees, lower inboards) at a mid-point door position. The door panel is cut just above the seat bench, in order not to deform the seat bench. The side structure rear of the door panel on the door sled is simulated by a foam block to support the side airbag when deployed and preventing the arm to slide off the door panel.

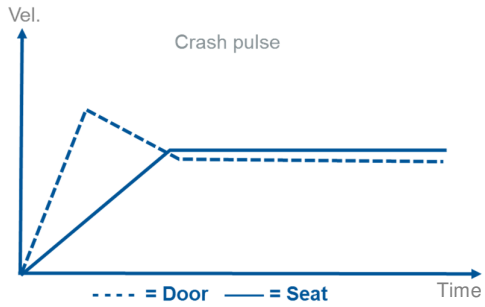

Figure 3. Door and seat velocities during side impact.

Six different test setups were used, see Table 3, combining inflatable curtain (IC) and thorax side airbag (SAB), in addition to arm position and a comparison between two types of boosters. The five first test setups were conducted for both the Q10original and Q10update enabling comparison between the two dummy models. Test setup 6 (IC/SAB/IBC) was conducted for the Q10update only, hence enabling evaluation of the capabilities of the Q10update to differentiate between two different types of boosters, when comparing to Q10update in test setup 4 (IC/SAB/BC). In addition, test setup 5 (IC/SAB/45) enabled evaluation of influence of arm position, when comparing to test setup 4 (IC/SAB), for both dummies.

In test setups 1-5, the child dummy was positioned on the BC without backrest (as in the frontal test series), while a Volvo integrated booster cushion (IBC) was used in test setup 6. The booster cushions and some of the test setups are shown in Figure 4. In each test, the child dummy was restrained with a three-point seatbelt including both a retractor load limiter function and a retractor pretensioner. The pretensioner was activated at 7ms after the pulse started. The diagonal belt was routed, as recommended by the manufacturer, above the inboard guiding loop of the booster cushion (as shown in Figure 4). A combination of SAB and IC was used, as shown in Table 3. The IC was inflated with pressurized air to a representative static pressure (appr.40kPa), while the SAB was dynamical inflated with a standard inflator. None of the restraint components were tuned prior to the tests for this load case. In test setup 5 (IC/SAB/45) the arm was angled 45 degrees forward, as an alternative to the standard arm position, which is aligned with the body, see Figure 4.

*Table 3. Side impact test matrix for both dummies, Q10original and Q10update, except for IC/SAB/IBC, *)Q10 update only.*

No.	Test Setup	Seatbelt	Inflatable Curtain	Side Airbag	Arm +45°	Booster Cushion
1	Reference	Yes	No	No	No	Yes
2	IC	Yes	Yes	No	No	Yes
3	SAB	Yes	No	Yes	No	Yes
4	IC/SAB	Yes	Yes	Yes	No	Yes
5	IC/SAB/45	Yes	Yes	Yes	Yes	Yes
6	IC/SAB/IBC*	Yes	Yes	Yes	No	No

Figure 4. Side impact test set-up, Reference test (Q10original left), IC/SAB/45 test (Q10original mid) and IC/SAB/IBC (Q10update right).

High speed cameras captured front, side, top and oblique views. The following measurements were captured and analysed in the tests: x, y, z acceleration of the head (CFC1000, 3ms clip), chest (CFC180, 3ms clip) and pelvis (CFC600, 3ms clip), upper neck forces (CFC1000), upper and lower chest deflection (CFC600), left shoulder forces (CFC600), pubic force (CFC600), accelerations (CFC60) of door and seat sled.

RESULTS

Frontal Impacts

In total 14 sled tests were performed; four full frontal impacts and 10 ODB impacts. The Q10original and Q10update, only, were compared in the full frontal tests, while all the three dummy versions were compared in the ODB tests. Two pair of repetitions of tests were run for each of the Q10original and Q10update; tests 1 and 2; 5 and 6; 9 and 10; 11 and 12 (see Table 2). The responses showed repeatable dummy behaviour. In repeated tests, the difference in response varied in a range from 1% to 10%, with an average difference in responses of 4%.

Dummy responses: Overall, the dummy responses were affected by the dummies' kinematics and their seatbelt-to-body interaction. The dynamic interaction with the seatbelt was greatly influenced by the initial seatbelt geometry and by the dummy designs. When the seatbelt was initially positioned close to the neck by routing the diagonal belt above the inboard guiding loop, a more similar seatbelt-to-body interaction between the dummy designs were seen. However, when the seatbelt was routed under the inboard guiding loop resulting in an initial position further out on the shoulder, belt slip-off occurred more frequently in the Q10original and Q10light compared to the Q10update (Table 4).

Figure 5 provides a summary of the head, neck, chest and seat belt responses in all the frontal tests. In the full frontal (FF) tests, the Q10original showed decreased head acceleration, neck tension, chest acceleration and lap belt force as the initial seatbelt position was moved outboard on the dummy's shoulder. The chest deflection increased, while the diagonal belt force remained the same. The Q10update showed a small increase in the head and chest accelerations and the chest deflection as the initial seatbelt position on shoulder was moved outboard, while the neck tension and lap belt force decreased and the diagonal belt force remained the same (Figure 5). When the initial seatbelt geometry was close to the neck, higher upper neck tension and chest acceleration were

seen in the Q10original compared to the Q10update, while the Q10update showed higher upper chest deflection. When the initial seatbelt geometry was further out on the shoulder, the neck tensions and upper chest deflections were similar to both dummies, while Q10update had higher chest acceleration compared to Q10original. In the full frontal tests, the lap belt forces were always higher in the Q10original, while the diagonal belt forces were similar between the dummies. When comparing the full frontal tests with the ODB tests, higher pulse peak accelerations were obtained in the full frontal tests, which likely correspond to the relatively higher crash severity of the full frontal test. In general, this resulted in increased dummy neck tension, and head and chest accelerations in the full frontal tests, regardless of dummy.

In the ODB tests a wider spread in dummy-to-seatbelt-interaction between the three Q10 versions was seen. This influenced the dummies' responses to a greater extent, as compared to full front tests (Figure 5). With the seatbelt initially positioned close to the neck similar seatbelt-to-body interactions were seen between the dummy designs. When comparing the results, the Q10original showed higher neck tension and lap belt force as compared to the update dummies, while the chest deflection was lower.

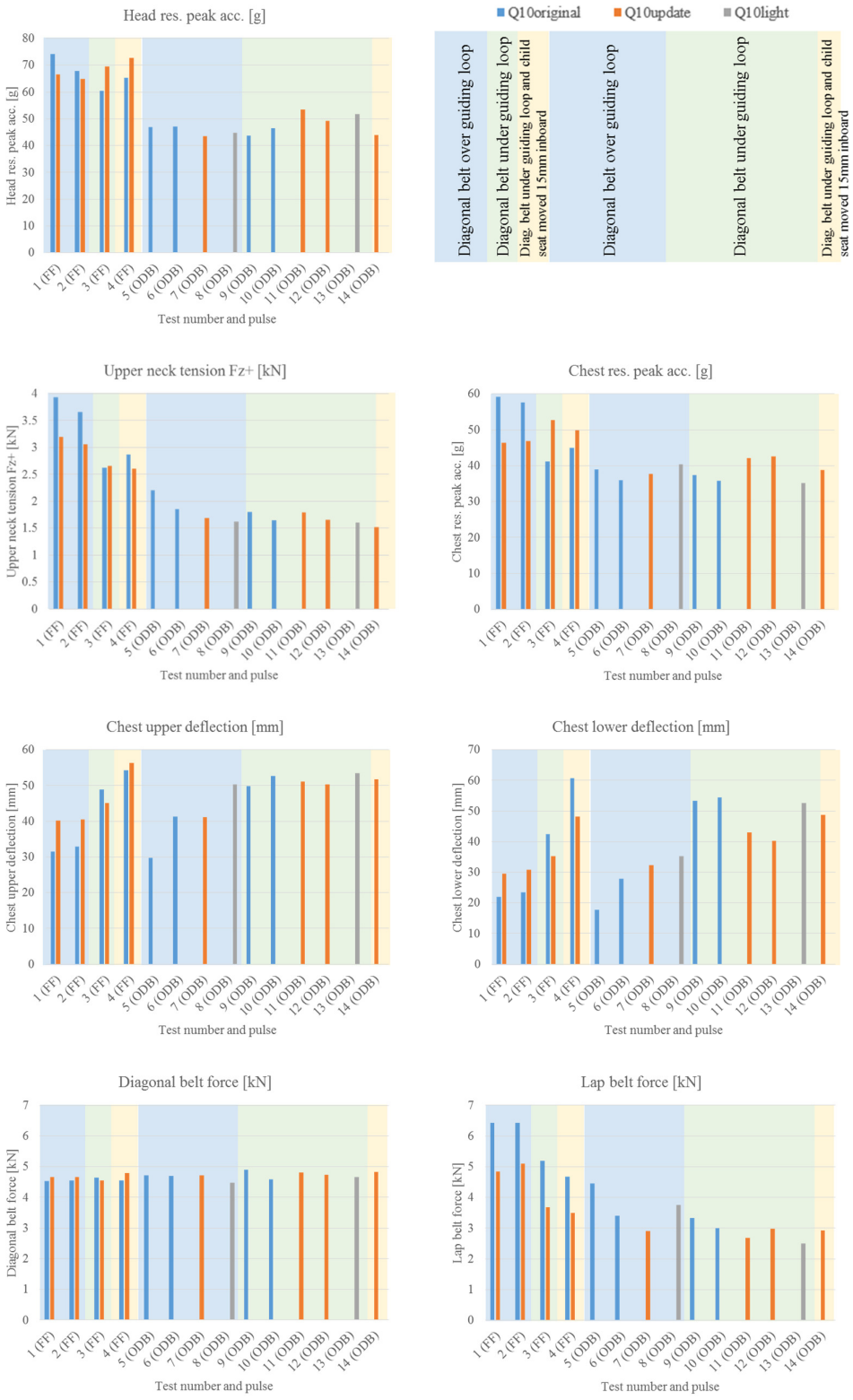

Figure 5. Head, neck, chest and seat belt maximum responses for the three dummies. The shoulder belt geometries are shown by the background colour of the graph, see figure at the top right for colour coding.

Kinematics: The initial position of the dummies differed due to the changes made to the Q10update and Q10light compared with the Q10original. The initial head positions of the Q10update and the Q10light were more perpendicular to the horizontal plane, compared to the Q10original, where the head had a greater forward rotation.

In the full frontal tests, the Q10update showed greater head excursion and upper body tilt, as well as more pronounced shoulder excursion as compared to the Q10original, regardless of initial seatbelt geometry. The pelvis excursion of the Q10update showed less forward excursion as compared to the Q10original, see Figure 6.

In the ODB tests with the diagonal belt guided above the inboard guiding loop of the booster cushion, the seatbelt remained on the shoulder for all three dummy versions. The Q10update and Q10light had more head excursion and upper body tilt compared to the Q10original. The Q10update was the one with the most forward excursion of the head, followed by the Q10light and the Q10original, see Figure 7.

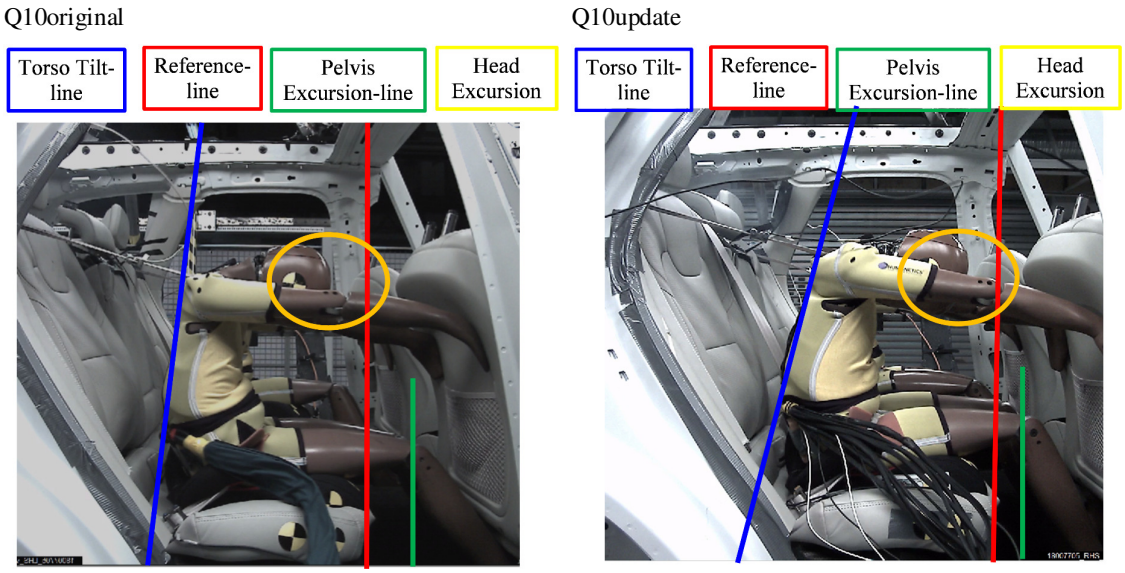

Figure 6. The kinematics of the Q10original and the Q10update in full frontal test at the time of max head excursion.

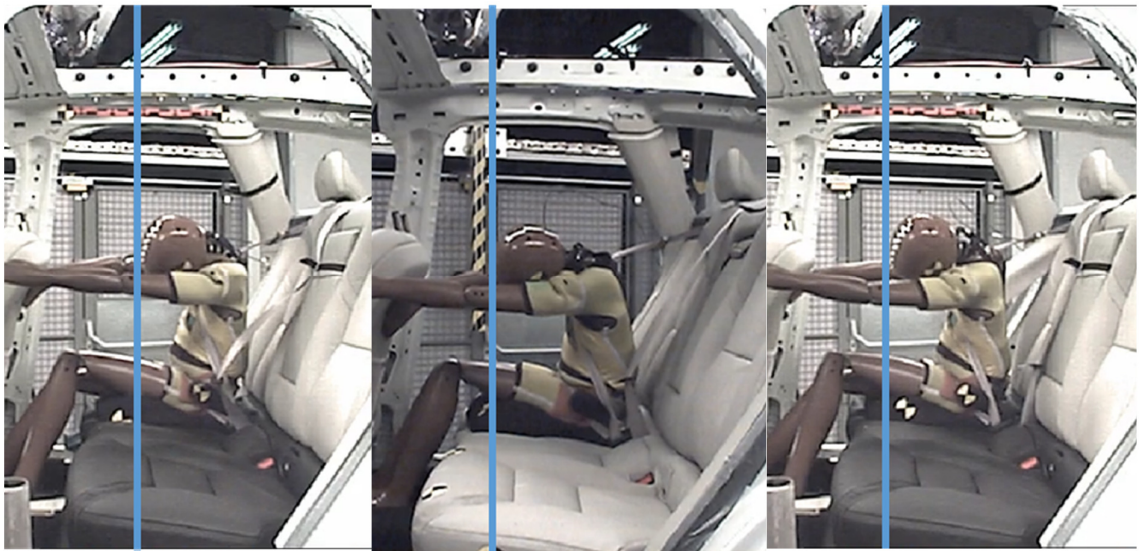

Figure 7. The kinematics of the Q10original (left), the Q10update (mid) and the Q10light (right) in the ODB test at time of maximum head excursion (vertical line).

Seatbelt-to-body interaction:

An overall summary of the diagonal belt position relative to the shoulder, for each dummy and test condition, is shown in Table 4. In the full frontal test with diagonal belt under the guiding loop and BC moved 15 mm inboards, the diagonal belt slipped off the shoulder for the Q10original, while for the Q10update the diagonal belt moved further out on the shoulder but it did not slip off (see Table 4 and Figure 8).

Table 4. The diagonal belt position relative the shoulder at maximum head excursion of the dummy in the various seat belt geometries for the three dummies.

	Full front			ODB		
Dummy	**Diagonal belt above guiding loop**	**Diagonal belt under guiding loop**	**Diag. belt under guiding loop BC moved inboard**	**Diagonal belt above guiding loop**	**Diagonal belt under guiding loop**	**Diag. belt under guiding loop BC moved inboard**
Q10 original	on shoulder	outboard motion	off shoulder	on shoulder	off shoulder	
Q10 update	on shoulder	on shoulder	outboard motion	on shoulder	outboard motion	off shoulder
Q10 light				on shoulder	off shoulder	

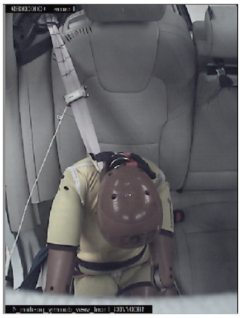

Q10original: Diagonal belt above inboard guiding loop

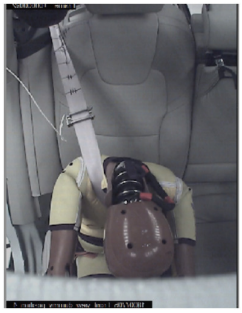

Q10original: Diagonal belt under inboard guiding loop

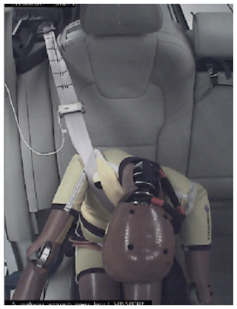

Q10original: Diagonal belt under inboard guiding loop, BC moved 15mm inboard

Q10update: Diagonal belt above inboard guiding loop

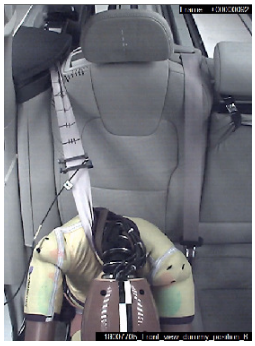

Q10update: Diagonal belt under inboard guiding loop

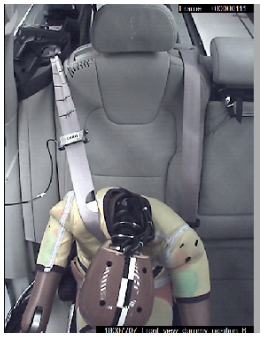

Q10update: Diagonal belt under inboard guiding loop, BC moved 15mm inboard

Figure 8. Full frontal tests, comparing Q10original (top) and Q10update (bottom), at time of maximum head excursion.

Figure 9 shows the maximum forward head excursion in the ODB tests, comparing the three dummy versions and the three different belt geometries. For all the three dummies, the diagonal belt stayed on the shoulder when the diagonal belt was routed above the guiding loop. This also corresponded to when the starting position was closer

to the neck. In the tests with the diagonal belt routed under the guiding loop, the diagonal belt slipped of the shoulder for both the Q10original and the Q10light, while it stayed on the shoulder for the Q10update. In the single test with the BC moved 15mm inboards (and shoulder belt under the loop), the diagonal belt slipped off the shoulder on the Q10update as well (see Figure 9).

For the Q10original, the diagonal belt got stuck in the gap between the arm and the shoulder, as the belt slips of the shoulder. The shoulder liner in the Q10update and Q10light prevents this, as can be seen in Figures 7 and 8.

Q10original: Diagonal belt above inboard guiding loop

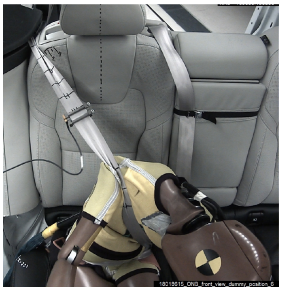

Q10original: Diagonal belt under inboard guiding loop

N/A

Q10update: Diagonal belt above inboard guiding loop

Q10update: Diagonal belt under inboard guiding loop

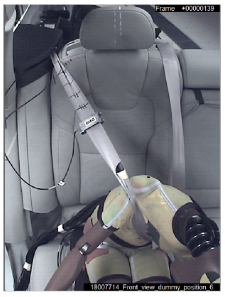

Q10update: Diagonal belt under inboard guiding loop, BC moved 15mm inboard

Q10light: Diagonal belt above inboard guiding loop

Q10light: Diagonal belt under inboard guiding loop

N/A

Figure 9. ODB tests, comparing Q10original (top), Q10update (mid) and Q10light (bottom) at time of maximum head excursion.

Side Impacts

In total 11 tests were performed. The two dummy versions were compared for four different combinations of side impact protection systems (including a reference test) and when varying the arm position in the combination of SAB and IC. In addition, a comparison was made between the BC and the integrated booster cushion (IBC) together with SAB and IC using the Q10update only.

Different side impact protection systems: Figure 10 displays a comparison of the maximum responses of head acceleration, neck resultant force, shoulder resultant force, chest and pelvis accelerations for the Q10original and the Q10updated in all the tests, as listed in Table 3.

Figure 10. Head, neck, chest, shoulder and pelvis maximum responses for the Q10original and Q10update in the side impact tests.

In the reference test, a head-to-door contact occurred at 50ms for the Q10update but not for the Q10original (see Figure 11). In the test with the IC only, no head-to-door contact occurred for any of the two dummies. For the Q10update, lower head acceleration and upper neck force were obtained, while the chest acceleration increased, as compared to the reference test (Figure 10). In the test with SAB only, no clear head-to-door contact was observed. Compared to the reference tests, both dummies measured lower chest acceleration, pelvis acceleration and pubic force, while the head acceleration increased slightly if not considering the head-to-door contact reference test case (Figure 10).

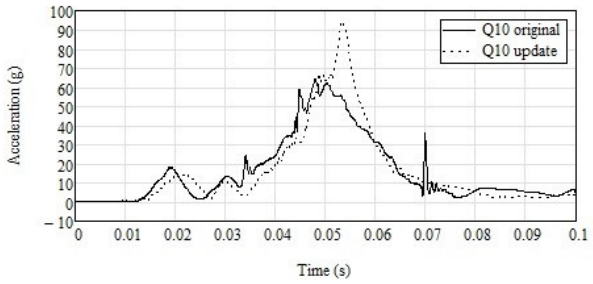

Figure 11. Head accelerations Q10original (solid) and Q10update (dotted) in reference tests.

Compared to the reference tests, both the dummies measured a relative decrease of all responses, except the upper chest deflection, for the combination of IC and SAB, se Figure 10. A comparison of head, chest and pelvis responses for the Q10update and the Q10original, in the test with the combination of IC and SAB and the reference test is shown in Table 5. The relative difference of the Q10 update compared to the Q10original is higher head accelerations (9-26%) and pelvis accelerations (35-46%), while lower chest accelerations (7-22%), for the reference and the IC/SAB setups. Higher chest deflections were seen in the Q10update (5-21%) in both the test configurations.

Table 6 presents the results from the tests with the IC and SAB and arm angled 45 degrees forward. The difference between the Q10update and the Q10original results are similar to the IC/SAB situation with the arm in in-line with the torso; however more pronounced in the chest area, and only a marginal difference between the dummies in head acceleration (Table 5). The difference in chest deflections were more within the same range as the dummy comparisons in the reference test.

Table 5. Comparison between Q10update and Q10original in the reference and IC/SAB tests.

Test	Head acc.	Chest acc.	Pelvis acc.	Chest def. up	Chest def. low.
Reference test					
Q10original	58.4	69.1	70.2	20.2	28.2
Q10update	73,1*	54.1	102.3	24.5	31.5
Update vs. Original	[26%]	-22%	46%	21%	12%
IC/SAB test					
Q10original	54.3	40.1	45	21	26.8
Q10update	59.1	37.3	60.8	22.1	28.5
Update vs. Original	9%	-7%	35%	5%	6%

*) Head-to-door contact

Table 6. Comparison between Q10update and Q10original in IC/SAB/45 tests.

Test	Head acc.	Chest acc.	Pelvis acc.	Chest def. up	Chest def. low.
IC/SAB/45 test					
Q10original	53.1	41.3	45.1	16.4	20.6
Q10update	52.3	38.8	58.5	20.2	22.8
Update vs. Original	-2%	-6%	30%	23%	11%

Different arm positions: Tables 7a and 7b summarize a comparison of the different arm positions (IC/SAB/45 versus IC/SAB) for the same dummy (Q10update and Q10original respectively). It can be seen that the 45 degrees angled arm position mainly resulted in a decrease in shoulder resultant force and chest deflection and to some extent head acceleration, while chest and pelvis accelerations were less influenced. The IC/SAB/45 lower chest deflection showed the lowest chest deflection of all performed tests.

Table 7a. Comparison between IC/SAB/45 and IC/SAB tests for the Q10update.

Test	Head acc.	Chest acc.	Pelvis acc.	Chest def. up	Chest def. low.	Shoulder res. force
Q10update						
IC/SAB	59.1	37.3	60.8	22.1	28.5	1453
IC/SAB/45	52.3	38.8	58.5	20.2	22.8	793
+45° vs. Std. Pos.	-12%	4%	-4%	-9%	-20%	-45%

Table 7b. Comparison between IC/SAB/45 and IC/SAB tests for the Q10original.

Test	Head acc.	Chest acc.	Pelvis acc.	Chest def. up	Chest def. low.	Shoulder res. force
Q10original						
IC/SAB	54.3	40.1	45	21	26.8	1142
IC/SAB/45	53.1	41.3	45.1	16.4	20.6	846
+45° vs. Std. Pos.	-2%	3%	0%	-22%	-23%	-26%

The influence on shoulder resultant force for the Q10update, was also seen for the Q10original. Figure 12 displays shoulder resultant force plots for the two dummies in the two different arm positions. Although some differences in amplitude, the two dummies follows the same load pattern for each of the test setups. In the test with the raised arm (IC/SAB/45), the "twin peak" characteristics is seen for both dummies.

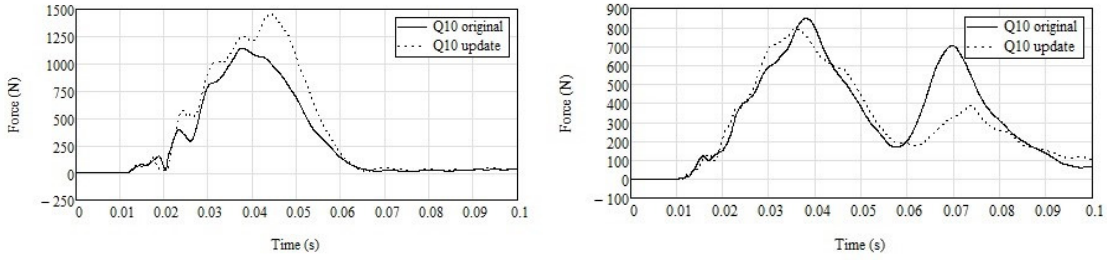

Figure 12. Shoulder resultant force Q10original (solid) and Q10update (dotted) in IC/SAB (left) and IC/SAB/45 (right) tests.

Different booster cushions: Table 8 summarizes the responses from the Q10update tests with the two booster types in a test setup including both SAB and IC. For these tests, there is no comparison to the Q10original. All responses were lower when using the IBC as compared to the BC. This was most pronounced for the pelvis acceleration and shoulder resultant force. A plot of the pelvis acceleration is displayed in Figure 13, showing a flattening out for the IBC at 30ms, while the BC continues to increase. This is due to differences in contact time and the difference in stiffness between the direct contact of the belt guiding loop and the side airbag that results in a difference of pelvis displacements.

Table 8. Comparison between IC/SAB/IBC and IC/SAB tests for the Q10update.

Test	Head acc.	Chest acc.	Pelvis acc.	Chest def. up	Chest def. low.	Shoulder res. force
Q10update						
IC/SAB	59.1	37.3	60.8	22.1	28.5	1453
IC/SAB/IBC	54	37	41.6	19.4	25.3	1172
IBC vs. BC	-9%	-1%	-32%	-12%	-11%	-19%

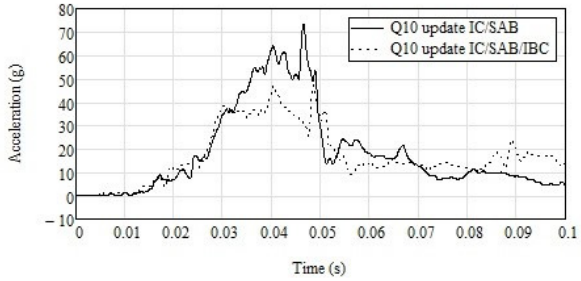

Figure 13. Pelvis accelerations IC/SAB (solid) and IC/SAB/IBC (dotted) using the Q10update.

DISCUSSION

The Q10 dummy was introduced in consumer rating procedures and regulatory tests at Euro NCAP, UNECE 129 and ETC (ADAC) and is used in both frontal and side impact tests. An update of the Q10 was initiated for the introduction of Euro NCAP 2020. The experience gained so far has initiated a request for an update, primarily in frontal but also in side impact load cases. Regarding the Q10 performance at side impact the priority has been lowered in favour for the frontal impact performance. This study provides feedback on the comparison of the updated version in a variety of test configurations in frontal and side impacts. The study does not include any comparisons performance according to biofidelity corridors.

Frontal impacts

Overall, both update-dummies showed a difference in kinematics compared with the Q10original dummy. Especially the Q10update showed difference in dummy responses compared to the Q10orginal.

The Q10update showed more head excursion and torso tilt compared to the Q10original in full frontal tests regardless of initial shoulder belt position, even though the Q10original had the diagonal belt further out on the shoulder during the event allowing a more forward motion. The increased mass of the upper body contributed to this change in kinematics. Furthermore, the shoulder joint shifted 20mm forward allowing more forward motion of arms that are clearly stretched forward, which also contribute to the forward motion of thorax. Schnottale et al. (2017) showed that the Q10update dummy's kinematics included an increased upper torso tilt, which was more like the kinematic pattern of the Thums v4 10 year-old HBM than to the Q10original.

In the ODB tests performed in this study, the Q10light and Q10update showed more head excursion and torso tilt as compared to the Q10original. Comparing the Q10light and the Q10update, the Q10light had slightly less head

excursion and torso tilt than the Q10update. The Q10light only had a mass distribution change of 1.4kg compared to 1.7kg, also, the shoulder joint shift of 20mm was not included in the Q10light. This difference in update design features explains the difference in kinematics of the two dummies. The change in mass distribution is more biofidelic (Waagmeester et al. 2017), and therefore, the changes in kinematics due to this design change is viewed as improvements of the dummy.

The differences in dummy response between the Q10original and the Q10update were mainly seen in reduced neck tension and increased chest deflection in the Q10update. The increased mass to upper torso contributed to increased chest deflection in the updated versions of the dummy in tests when the seatbelt remained on the shoulder. Small differences between the Q10original and the Q10light in dummy responses were seen. They included mainly differences in upper neck tension (greater in the Q10original) and in chest deflection results in the ODB tests with diagonal belt guided above the inboard guiding loop resulting in greater chest deflection in the Q10light. In the ODB tests with guiding loop under the inboard guiding loop, the shoulder belt slipped off the shoulder for both Q10original and Q10light and no distinct difference in dummy responses was seen.

The Q10update showed limited sensitivity to seatbelt geometries when the initial seatbelt position was far out on the shoulder, as compared to the two other dummies. This is potentially due to the combination of design changes in the Q10update resulting in a shoulder belt motion towards the neck rather than off the shoulder. The shoulder belt interaction with the shoulder in the Q10update was influenced by the soft composition of shoulder liner contributing in stabilising the belt over the jacket. In addition, the shoulder rubber design together with the shoulder joint shifted 20mm forward contributed in holding the shoulder belt in position. The Q10light and the Q10original showed similar sensitivity to various seatbelt geometries. However, if the diagonal belt slipped off the shoulder, the belt slipped completely off the shoulder due to the shoulder liner on the Q10light, while the belt slipped into the gap between the arm and the torso on the Q10original.

The Q10update was repeatable in both loading and kinematics. There were no repeated tests conducted for the Q10light, so it was not possible to evaluate this. This may be an issue, since this has been one of the drawbacks of the Q10original (Bohman and Sunnevang, 2012).

In all three dummies, the lap belt was intruding into the gap of the thighs and the pelvis, despite the hip shields. In the final Q10light version, Cellbond has modified the femurs such that the intruding of the lap belt into the pelvis/thigh gap will not occur.

Side Impacts

This study also compared the Q10update to the Q10original in side impact tests including standard arm position and positioned on the booster cushion. The Q10update showed a lower chest acceleration by 22% compared to the Q10original in the reference test and the reduction can be explained by the mass redistribution of 1.7 kg from the pelvis to the chest. A lower chest acceleration for the Q10update compared to the Q10original was also noticed in the IC and IC/SAB tests but not in the SAB only test. The consequence of reduced chest acceleration in similar test setups results in reduced displacement of the chest (actual in spine) which will cause a lower neck and head displacement as well. This behaviour reduced the distance between the head and intruding side structure, potentially leading to higher head loadings, which could also result in a head-to-side structure impact. This was the case in the Q10update reference test in which the head contacted the side structure and the acceleration was increased by 26% compared to the Q10original where no contact was observed. In the IC/SAB tests the head accelerations were increased by 9% for the Q10update, consequence of mass redistribution was also noticed in the response of the pelvis acceleration. The pelvis accelerations increased with 46% and 35% for the reference and the IC/SAB tests respectively. The proposed mass redistribution for the Q10update was referred to a more biofidelic mass distribution (Waagmeester et al. 2017) and is thereby more relevant to consider although the sensitivity of mass distribution was less in the tests including the side impact protection systems, such as inflatable curtains and thorax side airbags, compared to the reference tests. A possible explanation to less sensitivity of mass distribution when using inflatable curtains and thorax side airbags is the fact that the contact time is earlier and the duration time of load transfer is longer resulting in lower acceleration level compared to the reference test without any airbags.

The load paths in a side impact are mainly covered by the pelvis, chest and shoulder interaction with the intruding door or side structure of the car for a near-side impact rear-seated passenger. All these three load paths are possible to control and measure in the tested Q10update and Q10original. The pelvis (pubic) and shoulder are equipped with load cells, the spine (in the chest area) is equipped with an accelerometer and the chest is equipped with rib

deflection measurements. The Q10 dummies have a side impact kit, including a short arm and the shoulder force load cell mentioned above, for side impact testing. The arm is positioned vertically aligned to the thorax according to the Euro NCAP's current testing protocol (2018).

Wismans et al. (2015) presented an evaluation of the Q10 reporting that the responses in the biofidelity assessment pendulum tests were not within the required corridors of force, and that the chest could be considered as too stiff. Discussions are ongoing regarding the side impact kit and the certification test of the thorax. Wismans et al. (2015) did not include the Q10update versions. The side impact load paths and dummy response need to be further investigated, before any conclusions can be drawn regarding which of the dummy versions tested in this study is to be preferred. From a usability perspective, in case of an approved update of the Q10 dummy in lateral and side impact Euro NCAP rating tests it would be desirable to harmonize the dummy development and version implementation with the UN Regulation No 129 to avoid confusion and not use different dummy versions. At this stage, the conclusions are that both are sensitive to different side impact protection configurations, which is a good starting point for developing restraint system in order to reduce child injuries in side impacts.

The test with the Integrated Booster Cushion (IBC) provided the possibility to evaluate the Q10update sensitivity for differences in door-to-pelvis contact time. This was achieved due to the different designs of the boosters. The increased door-to-pelvis contact time resulted in substantial differences in pelvis acceleration, as shown in Figure 9. A later contact time between door and pelvis could have a preventative effect of body rotation towards to door, in combination with the relative earlier engagement of the side airbags, resulting in lower levels of shoulder resultant force. The Q10update's sensitivity to differences in booster design, is valuable when developing restraint systems. However, the Q10original was not tested using the IBC, whereby no conclusions regarding the differences between the two dummy version regarding this can be made.

Arm positioning influenced the dummy responses substantially. Gierczycka et al. (2015) studied a detailed representation of the thorax using a human body model and an ES-2re dummy model in a midsized sedan vehicle and investigated occupant response from a moving deformable barrier in side impact. The human body model demonstrated significant sensitivity, relative to the dummy, to different arm positions with lesser sensitivity to the door interior properties. This implies that the arm aligned with the body can act as a source of load transmission to the thorax for the HBM, increasing the potential for injury. This load transmission is not sufficiently reflected by dummies. Although different in setups, the tests with the angled arm in the present study have some similarities with the study by Gierczycka et al. (2015). The tests with the Q10update, using a thoracic airbag and an inflatable curtain and forward angled arm, showed reduced lower and upper chest deflections by 20% and 9% respectively and a reduced shoulder resultant force by 45%. The interference of the side impact arm kit was not only causing chest deflections to increase but was also "bridging" loads from the arm area into the shoulder in standard arm position. The influence of this alternative load path did not influence the pubic force, pelvis or chest accelerations but could be noticed in neck resultant forces and a slightly reduction of head accelerations. If chest deflection-based criteria were to be used or evaluated in the future, then the performance of the ribcage and the arm in combination with a new mass redistribution would need to be evaluated further.

The "twin peak" shoulder resultant force characteristic (Figure 12) is related to the loading of the arm and the inward bending of the forward angled arm, creating a y-directional compression force in the initial phase of the impact and causing a tension force in the later part of the impact when the arm is moving back towards the initial position. This behaviour could strictly be related to the choice of the initial position of the arm not neglecting the difference of chest deflection influence of the arm position. A thorax stiffness based biofidelity corridor and a potential shoulder-force criteria should be considering the influence of the arm position during impact.

An alternative side impact dummy, the WorldSID 5th percentile, was evaluated in comparison to the Q10 by EEVC WG12 (Wismans et al. 2015) and had a better compliance than the Q10 to specified requirements regarding biofidelity corridors in the thorax area. Awaiting a next generation of Q10update, we suggest that the WorldSID 5th percentile could be used as a complement to the Q10 in side impact testing and simulation. In addition, Brolin et al. (2015) concluded and presented in their review a need for enhanced tools, such as child human body models, to take into account the requirements of children of different ages and sizes in the development of countermeasures.

Limitations

After the tests in this study was conducted, additional changes to the Q10light was added, which were decided to be included in proposed Euro NCAP 2020 protocol. These changes include feet shortened by 30 mm and the

thighs are produced of material properties from Cellbond, which are different to those of Humanetics that was used in this study.

Side impact tests were not repeated in the same condition, hence repeatability and reproducibility cannot be commented upon. The observed differences in dummy responses must be interpreted with caution and with consideration of expected repeatability.

CONLUSIONS

In the frontal tests, the Q10update was less sensitive to seatbelt geometry far out on shoulder compared to the Q10original and Q10light. For the Q10update, the seatbelt moved inboard towards the neck regardless of initial belt geometry. Both updated dummies, showed increased head excursion and upper torso tilt, which is considered as a more biofidelic behaviour compared to Q10original, due to the biofidelic mass redistribution. Due to its improved kinematics and sensitivity to seat belt geometry, the Q10light was preferred of the three tested dummies, for the frontal load cases.

In the side impact tests, the Q10update showed lower chest acceleration compared to the Q10original but also led to head-to-structure contact in one test and increased pelvis acceleration. The chest deflections were overall higher for the Q10update compared to the Q10original. The standard arm position increase chest deflection and influence the loads path into the shoulder compared to a forward angled arm. The proposed mass redistribution is considered as more biofidelic and that effect will shift focus from chest acceleration to chest deflection, pelvis acceleration and head acceleration criteria. This study provides no firm recommendation on the Q10update, acknowledging that a biofidelity evaluation needs to be made. Further dummy refinements, lateral validation and certification tests are encouraged.

ACKNOWLEDGEMENT

The authors would like to acknowledge Humanetics and Cellbond for lending the tested update dummies.

REFERENCES

Arbogast KB, Locey C, Seacrist T, Bohman K. (2013*). Relative kinematics of the shoulder belt and the torso: Comparison of the Q10 ATD and Pediatric Human Volunteers*. Proceedings of IRCOBI conference, Gothenburg, Sweden.

Bohman K, Sunnevang C (2012). *Q10 child dummy performance in side and frontal sled tests*, 10th International Conference Protection of Children in Cars, Munich, Germany.

Brolin K. et al. (2015), *Safety of children in cars: A review of biomechanical aspects and human body models*. IATSS Research 38 (2015) 92-105.

Durbin D.R. et al. (2015), *Rear seat safety: Variation in protection by occupant, crash and vehicle characteristics*, Accident analysis and prevention, 80, 185-192.

Euro NCAP's Testing protocol, (2019, September), *Child occupant protection*, Version 7.2.2.

Gierczycka D, Watson B, Cronin D, (2015), *Investigation of occupant arm position and door properties on thorax kinematics in side impact crash scenarios - comparison of ATD and human models . International journal of crashworthiness* 20:3, 242-269, DOI: 10.1080/13588265.2014.998000.

Ipek H. (2018, December). *Comparisons of Q10 original and different Q10 Euro NCAP 2020 update dummies in frontal and side impact sled tests,* 16th International Conference Protection of Children in Cars, Munich, Germany.

Schnottale B, Ott J, Eggers E, Lorenz B. (2017, December). *Comparative study regarding the effect of the Q10 update in simulation*, 15th International Conference Protection of Children in Cars, Munich, Germany.

Waagmeester K, Lakshminarayana A, Burleigh M, Lemmen P, (2017, December). *Q10 Update Hardware and Validation*, Protection of Children in Cars, 15th International conference, Munich, Germany.

Wismans J. et al. (2008), *Advancement of Child Dummies and Injury Criteria for frontal impact*. EEVC WG 12 and 18 Report, Document No 514.

Wismans J. et al. (2015), *Q10 dummy in lateral impact - Advanced child dummies and injury criteria for lateral impacts*, EEVC WG 12 Report document no 646.

VEHICLE INTEGRATED NON-DISPERSIVE INFRARED SENSOR SYSTEM FOR PASSIVE BREATH ALCOHOL DETERMINATION

Jonas Ljungblad
Bertil Hök
Martin Åhlenius
Gabriel Eriksson
Senseair Alcohol Sensing AB, Flottiljgatan 49, SE-721 31 Västerås, Sweden

Paper Number 19-0296

ABSTRACT

The objective of the present investigation performed within the Driver Alcohol Detection System for Safety (DADSS) program is to demonstrate the effect of further recent improvements of the breath-based nondispersive infrared sensor technology in realistic settings. More specifically, sensor systems installed in vehicles have been tested by: a) exposing them to a controlled, realistic breathing pattern from artificially generated gas pulses mimicking that of an intoxicated driver and b) human subjects entering a test vehicle and performing a simulated drive while under the influence of alcohol. The tests with artificial gas pulses correspond to human directed forced exhalation from positions up 70 cm from the sensor. The tests provide experimental evidence that in-vehicle, driver breath alcohol determination is feasible with a single sensor positioned at the top of the steering column. The human subject study was designed to test both active and passive detection modes. Good correlation to the breath alcohol reference instrument was found in both cases over the full range of alcohol intoxication exceeding 0.08 percent (the legal limit in most U.S. states). Time to detection is a remaining challenge of the passive mode but is manageable by requesting an active breath in the absence of reliable data. The results illustrate the feasibility of using breath-based NDIR based sensors in different operational modes. In the active mode, a simple exhalation directed towards the sensor is enough for a test to be approved and the alcohol content quantified. In the passive mode, the operator does not actively interact with the sensor. In a real-world scenario, sensors set to a passive mode could be used for driver monitoring and to assist the driver to choose a smarter option when alcohol is detected. The overall conclusion from the present investigation is that in-vehicle breath-based alcohol determination is feasible with the current state of the art sensor technology.

INTRODUCTION

Driving under the influence of alcohol increases the likelihood of being involved in a car crash, and the risk increases dramatically with increasing blood alcohol concentration (BAC) [1]. Statistics from the U.S. National Highway Traffic Safety Administration (NHTSA) indicates that almost 11,000 people were killed in the US in 2017 alone due to drunk driving [2]. The Driver Alcohol Detection System for Safety (DADSS) program is addressing the challenge of preventing drunk driving by means of non-intrusive sensors installed in vehicles [3]. The ideal DADSS system would prevent the vehicle from being driven when alcohol at or above 0.08 percent is detected in the driver's breath. On the other hand, it would not inconvenience the sober driver in any way.

A principle for contactless determination of breath alcohol concentration (BrAC) using simultaneous measurement of alcohol and carbon dioxide (CO_2) at one point in the vicinity of the test subject has been demonstrated [4] and validated [5]. The CO_2 signal is used for detection of a breath and to compensate for the dilution of the breath sample. A prototype sensor system based on this principle using non-dispersive infrared (NDIR) sensor technology was reported [6]. Improvement of system performance and usefulness for in-vehicle contactless and even passive breath alcohol detection have been demonstrated [7, 8].

The objective of the present investigation is to demonstrate the effect of further improvement of the NDIR sensor technology in realistic settings. More specifically, sensor systems installed in vehicles have been tested by exposing them to: a) controlled 'breathing pattern' from artificially generated gas pulses mimicking that of an intoxicated driver b) human subjects entering a test vehicle and performing a simulated drive while under the influence of alcohol.

METHODS AND TECHNOLOGY

The sensor system is based on an infrared measurement cell, simultaneously measuring CO_2

and ethanol. The CO_2 measurement is used as an indicator of an exhalation and to account for the dilution of the breath sample. Details of the sensor technology and vehicle integration have been reported earlier [7, 8]. A major issue with earlier implementations was the resolution of the alcohol sensor. The present investigation has been performed using alcohol sensors with significantly improved resolution.

A test of the alcohol sensor resolution was performed by recording sensor signals with zero input during an extended period of time. The resulting plot of the calibrated output root mean square (RMS) signal as a function of the time window, called the Allan deviation, is a useful characterization of the noise behind the observed resolution [9].

The test equipment for generating artificial breathing patterns includes gas cylinders containing air and CO_2, valves to control the gas flow bubbling through tanks with water and ethyl alcohol at accurately controlled concentration heated to body temperature. Exterior and interior views of the equipment are shown in Figure 1 and 2. More technical details of the equipment can be found in previous reports [7, 8]. The distance between the orifice generating the gas pulses and the sensor located at the top of the steering column was varied between 10 and 70 cm. Four alcohol concentrations were tested: 0.0, 0.1, 0.25 and 0.4 mg/L (0.4 mg/L corresponds to the legal limit in most U.S. states of 0.08% BAC). Each one of the three liquid tanks shown in Figure 1 generated gas pulses with one of these alcohol concentrations. The volume of each gas pulse was 1.5 L corresponding to a forced human exhalation.

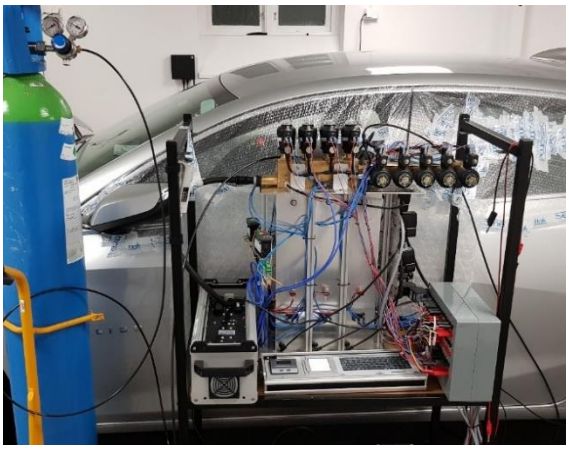

Figure 1: Exterior view of the experimental setup used for tests with artificially generated breathing pattern. The sensor is positioned on top of the steering column.

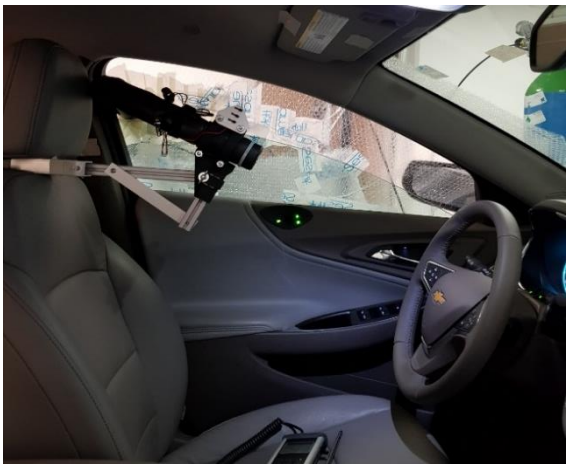

Figure 2: Interior view of the experimental setup used for tests with artificially generated breathing pattern. The sensor is positioned on top of the steering column.

Also shown in Figure 1 is the reference instrument (Evidenzer, Nanopuls AB, Sweden) used for verification of the gas pulse concentration. The hosing carrying the gas to the orifice outlet shown in Figure 2 was heated to above body temperature to avoid water condensation. The orifice position shown in the right-hand photograph was at a measuring distance of 50 cm to the sensor.

The human subject study was performed with ten subjects recruited from outside the project team. In Table 1 some characteristics of the population and the study format are summarized. The study was approved by the Regional Swedish Human Ethics Board in Uppsala (ID 2018/148).

Table 1: Population characteristics and study format of human subject's study. In total 10 subjects were recruited, including 6 males and 4 females.

	Min	Max	Mean	Median
Age	25	71	46	53
Height (cm)	162	187	176	178
Weight (kg)	48	140	86	87
Session (h)	6	10	7.5	7.5

The study protocol involved an initial inquiry about the subject's present health condition. Initial breath tests were performed first with the reference instrument (Evidenzer, Nanopuls AB, Sweden) then within the test vehicle while performing a simulated driving task lasting approximately ten minutes. The in-vehicle breath tests included both active breath tests directed towards the sensor and passive tests without active involvement of the subject. The subject then consumed alcohol 0.8 g / kg body weight with the objective of peaking above 0.08

percent. After thirty-five minutes, breath testing was resumed while the subject was performing a simulated driving task. The procedure was repeated every 45 minutes until the subject's reference BrAC was below 0.03 mg/L). Figure 3 and 4 shows a subject demonstrating active directed breath while leaning forward (Figure 3) and from a relaxed position (Figure 4).

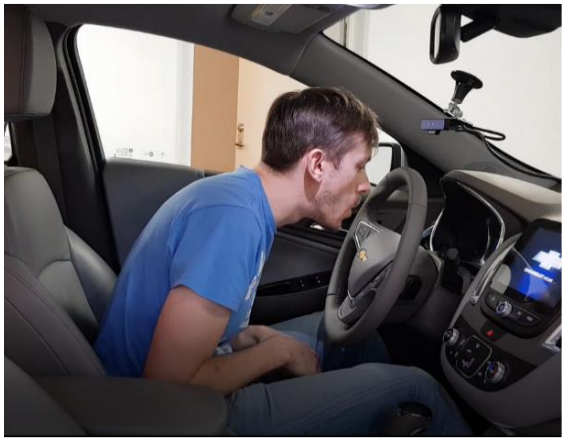

Figure 3: Human subject demonstrating active modes of detection while leaning forward.

Figure 4: Human subject demonstrating active modes of detection while in a relaxed position.

RESULTS

In this section, the experimental results of the present investigation will be summarized. Figure 5 shows the resolution of the present implementation of the NDIR sensor technology. The graph shows a logarithmic plot of the Allan deviation as a function of the time window τ(s) [9], and the curve exhibits the characteristic V-shape. The resolution at τ(s)=1 second of $3.5*10^{-4}$mg/L is representative for a single breath. It is an improvement by a factor of 2.9 between the present and previous implementation [10]. The minimum value $8.5*10^{-4}$ mg/L occurring at a time window of 53 seconds represents the ultimate resolution of the current implementation.

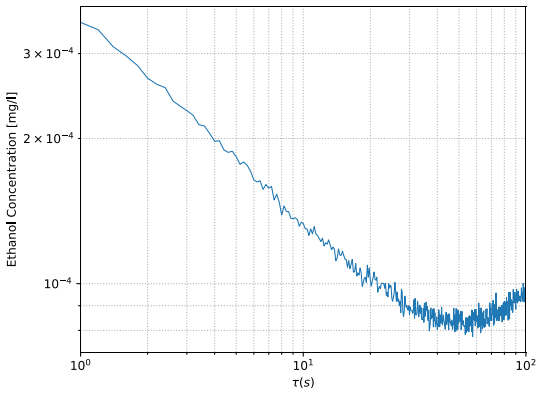

Figure 5: Allan plot of the sensor resolution according to the present NDIR implementation.

The results of the tests with artificial breathing are summarized in Figure 6. The four graphs show BrAC determined by the sensor after dilution compensation at three nominal concentrations, 0.0, 0.1, 0.25, and 0.4 mg/L as a function of the distance between the source of the gas pulse and the sensor. The calculated BrAC values range from a distance of 10 to 70 cm for each concentration. At all distances, the sensor output result is close to the nominal concentration of the gas pulse with a standard deviation of less than 0.01mg/L in each group.

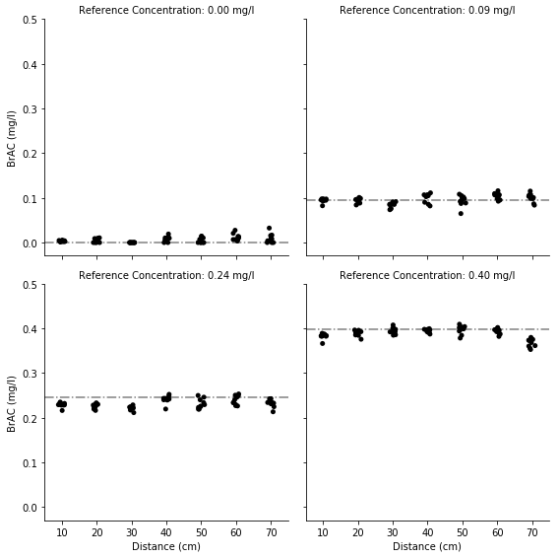

Figure 6: Test results of artificially generated breathing patterns at four nominal breath alcohol concentrations.

The results of the human subject study are summarized in Figures 7 to 10. The graphs depict 'true' BrACs determined by the reference instrument at the abscissa, and BrAC determined

by the sensor system with various types of breath tests. Figure 7 and 8 shows BrAC determined after directed breaths from a leaned-forward position (Figure 7) and from a relaxed position (Figure 8). Both graphs show good correlation between the reference and sensor system BrACs over the full range of 0-0.6 mg/L. The error band is relatively straight over the concentration range in Figure 8 with a standard deviation of approximately 0.05 mg/L. In the lean-forward mode (Figure 7) the error band is smaller at low concentrations and somewhat diverging.

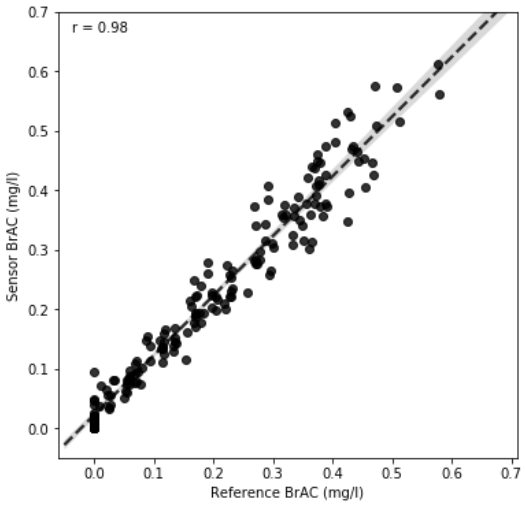

Figure 7: Results from the human subject study with active breathing leaning towards the sensor.

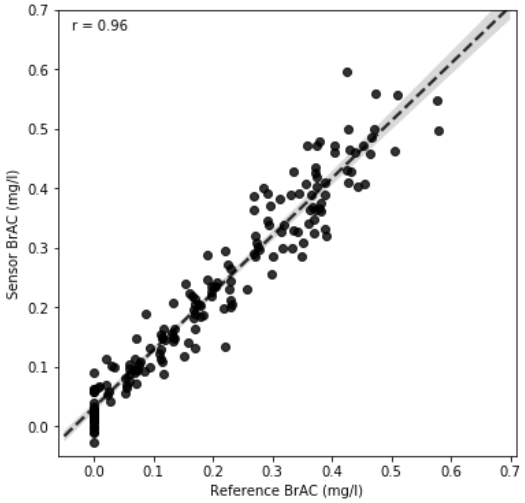

Figure 8: Results from the human subject study with active breathing at a relaxed position.

The results of the passive BrAC determinations in Figure 9 and 10 show a pattern similar to the active breath tests in Figure 7 and 8. The graph in Figure 9 shows the results of the first classified breath sample during the session, and Figure 10 shows the accumulated values of the whole session. In five of the ten subjects, the first breath classification occurred after less than one minute from stepping into the vehicle. The correlation between 'true' and test system BrAC was good. The error bandwidth of the accumulated BrAC values (Figure 9) is reduced from 0.05 mg/L (1σ) for the corresponding first detection values (Figure 10) to 0.04 mg/L.

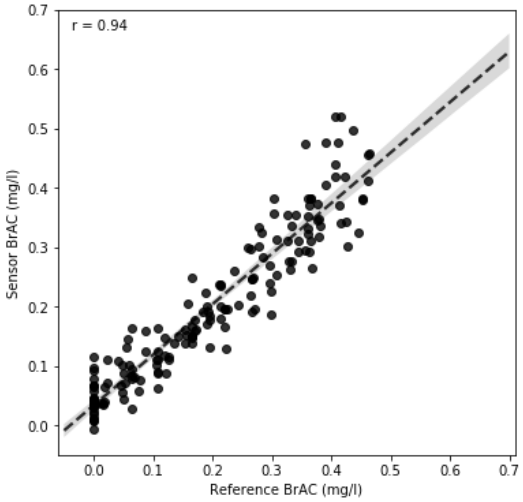

Figure 9: Results from the human subject study with passive breathing after first detection.

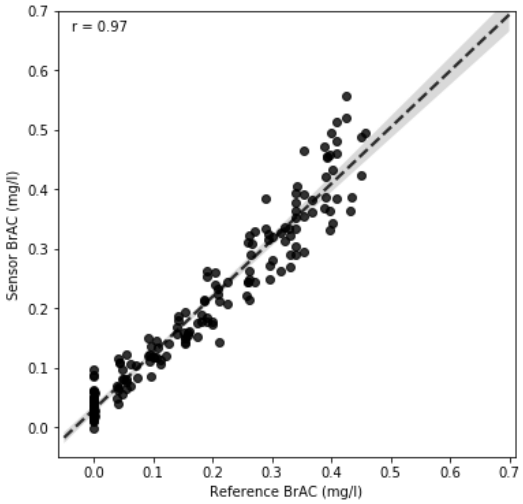

Figure 10: Results from the human subject study with passive breathing showing accumulated results of the current driving session.

The field operational test provided vital information of sensor functionality in a real-world scenario but at the time of writing the data has not yet been analyzed.

DISCUSSION

The Allan plot in Figure 5 shows that the resolution of the present sensor system has been

improved by a factor of 2.9 compared to the previous sensor implementation. The downslope at small values of the time window indicates that the noise in this region is stochastic. The minimum indicates the ultimate resolution of the specific implementation, reachable by time averaging over several measurement cycles. The positive slope at large values of the time window is an effect of slow offset signal variations which could be either circumstantial or due to some inherent cause. The results represent good progress based on the best components available today. Further progress can be expected due to the current rapid rate of technology development.

The tests with artificial gas pulses correspond to human directed forced exhalation from positions as large as 70 cm from the sensor. The tests provide experimental evidence that in-vehicle, driver breath alcohol determination is feasible with a single sensor positioned either at the steering column or the door rim. The reduced accuracy at very large distance is manageable by requesting another breath sample at a shorter distance.

The human subject study was designed to test both active and passive detection modes. Good correlation to the reference instrument was found in both testing conditions when alcohol intoxication exceeded 0.08 percent. The lean-forward case (Figure 7), with a moderate sample dilution, exhibits a slightly diverging error band indicating heteroscedasticity, as reported earlier [11]. In the other three graphs from the human subjects' studies (Figure 8, 9 and 10) there is no clear concentration dependence of the total error bandwidth, which amounts to approximately 0.08 percent. In the passive mode, only spurious exhalations directed towards the sensor will be detected. Therefore, it may take some time before sufficient data has been accumulated to enable a useful BrAC estimation. This issue is manageable by requesting an active exhalation from the driver.

In the near future, field tests with sensor systems installed in vehicles will be performed. Scenarios including varying climate conditions and human behavior aspects of both drivers and passengers will be targeted.

CONCLUSIONS

The results of the performed investigations clearly illustrate the feasibility of using NDIR based sensors in both active and passive operational modes. In the active mode, a simple exhalation directed towards the sensor is enough for a test to be approved and the alcohol content quantified. In the passive mode, the operator does not actively interact with the sensor. However, sensor signals need to be collected over a period of time before the alcohol content of the drivers' breath can be classified. In a real-world scenario, sensors set to a passive mode could be used for driver monitoring and to assist the driver to choose a smarter option when alcohol is detected. The overall conclusion from the present investigation is that in-vehicle breath-based alcohol determination is feasible with the current state of the art technology.

ACKNOWLEDGEMENTS

This work is financially supported by NHTSA (National Highway Traffic Safety Administration and ACTS (Automotive Coalition for Traffic Safety) through the DADSS program.

REFERENCES

[1] Blomberg RD, Peck RC, Fiorentino D, Crash risk of alcohol involved driving: A case-control study. Stamford, CT: Dunlap & Associates, 2005.

[2] National Highway Traffic Safety Administration. 2018. Traffic Safety Facts. Alcohol-Impaired Driving. DOT HS 8124450. Washington DC.

[3] Zaouk, A. Driver alcohol detection system for safety, Paper presented at Transportation Research Board 90th Annual Meeting, January 25, 2011; Washington, DC.

[4] Hök B, Pettersson H, Andersson G, Contactless measurement of breath alcohol. Paper presented at the Micro Structure Workshop 2006, MSW2006; May 9-10, 2006, Västerås, Sweden.

[5] Kaisdotter Andersson A, Improved breath alcohol analysis with use of carbon dioxide as the tracer gas, PhD Thesis No. 83, 2010, Mälardalen University, Västerås, Sweden.

[6] Hök B, Pettersson H, Kaisdotter Andersson A, Haasl S, Åkerlund P, Breath analyzer for alcolocks and screening devices, IEEE Sensors J. 2010; 10:10-15.

[7] Ljungblad J, Hök B, Allalou A, Pettersson H, Passive in-vehicle driver breath alcohol detection using advanced sensor signal acquisition and fusion, Traffic Injury Prevention, vol. 18, 2017, No. S1, S31-S36.

[8] Ljungblad, High performance breath alcohol analysis, PhD Thesis No 240, 2018, Mälardalen University, Västerås, Sweden.

[9] Allan D, Statistics of atomic frequency standards, Proc. IEEE 54, 1966, 221-230.

[10] Ljungblad J, Hök B, Ekström M, Critical performance of a new breath alcohol analyzer for screening applications, 2014 IEEE Ninth International Conference on Intelligent Sensors, Sensor Networks and Information Processing (ISSNIP), Singapore, April, 2014.
[11] Hök B, Ljungblad J, Kaisdotter Andersson A, Ekström M, Enlund M, Unobtrusive and highly accurate breath alcohol analysis enabled by improved methodology and technology, J Forensic Investigation, vol 2, 2014, Issue 4, 8-16.

REAL-WORLD EVALUATION OF DRIVER ASSISTANCE SYSTEMS FOR VULNERABLE ROAD USERS BASED ON INSURANCE CRASH DATA IN SWEDEN

Irene Isaksson-Hellman
If P&C Insurance
Sweden

Magdalena Lindman
Volvo Car Corporation
Sweden

Paper Number 19-0300

ABSTRACT

In 2010 Volvo cars introduced advanced driver assistance systems (ADAS) designed to detect vulnerable road users (VRUs) in specific conflict situations. The aim of this study was to evaluate the first generation of the optionally mounted Pedestrian ADAS, which covers car-to-pedestrian collisions, and Cyclist ADAS, which covers car-to-cyclist collisions.
Data from collisions in Sweden between passenger cars and pedestrians or cyclists were collected from 2015-2017. Crashes involving Volvo cars with third-party liability insurance at If P&C Insurance/Volvia were included in the dataset, and cars with these ADAS were compared to crashes involving cars without the systems. A total exposure of 490,000 insured vehicle years was used in the evaluation.
Overall, the number of collisions for cars with the Pedestrian ADAS system was 21% less than the number for cars without it. When studying straight crossing path crashes only, which accounted for more than half of all car-to-pedestrian collisions in Sweden, these were reduced by 36%. However, the results are not statistically significant due to the low number of crashes. For the ADAS, which covers car-to-cyclist collisions, an overview of data available for retrospective performance evaluation is discussed.
One clear restriction in the evaluation of VRU ADAS at this point in time is the relatively low number of cars equipped with the system together with the low rates of car-to-cyclist collisions (≈ 0.0002 per insured vehicle year) and car-to-pedestrian collisions (≈ 0.0001 per insured vehicle year).
This study is the first real-world evaluation of the initial generation of VRU ADAS targeting traffic situations relevant for these technologies. ADAS for avoiding collisions with pedestrians and cyclists have a high traffic-safety potential; recent and future generations of these systems, cover more conflict situations and are thus expected to provide increasing safety benefits.

INTRODUCTION

Globally, pedestrians and cyclists represent 26% of all road traffic deaths [1]. There is a big variation in death rates across regions and countries, with low- and middle-income countries the worst affected. In EU countries, pedestrians and cyclists comprised around 21% and 8% of all road traffic deaths, respectively, in 2015 [2]; in the US the corresponding numbers were 16% and 2.2%, in 2016, [3]. In Sweden, in 2017, 15% of the road fatalities were pedestrians and 8% were cyclists [4, 5]. In many countries, roads still lack separate lanes for cyclists and adequate pedestrian crossings—and motor vehicle speeds are too high [1].
Infrastructure measures, such as the physical separation of motor-vehicle and VRU paths, have proven to be effective in preventing VRU crashes. The expansion of walking and cycling paths in Sweden is a good example: fatal pedestrian and cyclist crashes have decreased from one third of the total road-traffic fatalities in the 1970s to just over one fifth today [4]. Still, VRUs often share the road with motor vehicles, and crashes occur frequently—most commonly in urban areas where walking and cycling are common modes of transport [6].
For car-to-VRU collisions, the distribution of conflict situations in crash databases are used to identify frequent or severe situations to address with traffic safety measures. The majority of crashes are Straight Crossing Path (SCP) situations, i.e. the car is moving straight forward, and the car and the VRU are crossing each other's paths.

Situations in longitudinal traffic, when the car and the VRU are traveling in the same or opposite direction while sharing the same roadway are not as frequent, but often with more severe injuries for the VRU. Specific situations for car-to-pedestrians are collisons where the car is reversing hitting a pedestrian, and for car-to-cyclists; the cyclist riding into a car door that was being opened by the car driver or a passenger, hereafter called dooring [7-11].
As unprotected road users, pedestrians and cyclists are particularly vulnerable to severe or fatal injuries in case of a crash. One important way to reduce the consequences of a crash is to lower the impact speed [12-14]. To improve the situation where vulnerable road users and motor vehicles share the road, speed limits have been reduced in Swedish cities over the last decade (where appropriate) [15]. Additional speed-reducing measures, such as speed bumps and raised crosswalks and chicanes, have been implemented to achieve better speed compliance [16]. In the work with the Vision Zero initiative, a key indicator measuring the share of safe walking, bike, and moped passages was introduced [17, 18].
In the last decade, vehicle manufacturers have developed countermeasures to reduce the consequences of an impact with VRUs. These involve redesign of the bumper area [19], the hood, windshield, and pillar [20], and introduction of pedestrian airbags [21], and pop-up bonnets [22].
One of the most promising countermeasures presented by the automotive industry is advanced driver assistance systems (ADAS) specifically for pedestrian and cyclist situations. One example is the collision warning with full autobrake and pedestrian and cyclist detection implemented in Volvo car models [23]. Real-world evaluations have shown that autobrake systems are very effective in avoiding (as well as mitigating) car-to-car crashes in rear-end situations [24-33], and test institutes and predictive studies estimate that including pedestrian and cyclist detection will greatly reduce crashes with VRUs [34-38]. In December 2017, HLDI examined pedestrian-related collisions which showed a reduction in the frequency of bodily injury (BI) liability claims, as a result of analyzing an ADAS with a pedestrian detection feature. [39].
The aim of this study was to evaluate the first generation of driver support systems which are intended to detect VRUs, covering car-to-pedestrian- as well as car-to-cyclist collisions, by investigating real-world crashes collected from traffic situations relevant for these technologies.

DATA & METHOD

In this study we used insurance claims data from car-to-pedestrian collisions involving Volvo models with and without Pedestrian ADAS (collision warning with full autobrake and pedestrian detection). Also, car-to-cyclist collisions involving Volvo models with and without Cyclist ADAS (collision warning with full autobrake and cyclist detection) was studied.
To calculate the exposure, information covering all cars registered in Sweden with third-party liability insurance at If P&C insurance/Volvia was used. The analysis was performed using accident and exposure data for the years 2015-2017.

Data collection

Data including both car-to-pedestrian collisions and car-to-cyclist collisions in Sweden are continuously coded and collected in two databases. For cars with third-party liability insurance at If P&C insurance/Volvia, all crashes involving cyclists and pedestrians were coded using information from the claims. This means that a representative set of data, ranging from very low-severity crashes to fatal crashes, is available. These data include crashes sometimes not collected in, e.g. the national crash databases, because they are lower in severity or simply not included in the collection criteria; however, even these situations can result in injuries for VRUs. Two examples illustrate this point: the dooring situation, (defined as a single accident in police-reported accidents in Sweden) and the frequent situation; car reversing hitting a pedestrian, that is not considered at all in official statistics.
In most cases, information about the crash situation was available for both the pre-crash and crash events between car and pedestrian/cyclist. The pre-crash event was described by the conflict situation classification, if available, the driver's estimate of the car's speed just before the accident; and whether the driver's view was restricted. The crash event was described by the point of impact and the impact direction for both the pedestrian/cyclist and the car during the collision. This information was obtained from the claims form and descriptions by the driver and the pedestrian/cyclist. To more fully describe each situation, environmental conditions (light and weather conditions and road status), when (time of day) and where the collision occurred (urban or rural area), and demographics about the driver and the pedestrian/cyclist were recorded. Personal injuries were coded using the Abbreviated Injury Scale (AIS) [40].

Exposure data
Exposure data were calculated for the Volvo car models included in the study, by summing up the number of insured vehicle years (IVY): one car insured for one year is one insured vehicle year, two cars insured for half a year each is equal to one insured vehicle year, etc. Crashes involving cars with the optionally mounted VRU ADAS were identified and compared to crashes involving cars without the systems. For the Pedestrian ADAS detection system, the total exposure was 490,000 vehicle years and for the Cyclist ADAS detection system it was 420,000 vehicle years. For detailed information about the number of selected cases, see Tables 1 & 2.

System description: Pedestrian ADAS
The pedestrian detection technology (consisting of collision warning and autobrake system) was included in the third generation of Volvo Cars' collision avoidance system, available from 2010 (MY 2011) as an option in the Volvo models S/V60. From MY 2012 it has been available in the V/XC70 and S80 models, and from MY 2013 in the V40. Models introduced from 2015 on, starting with the new XC90, are equipped with the next generation of collision warning and autobrake system as standard. The system uses a combination of a long-range radar and a forward-sensing wide-angle camera that continuously monitors the area in front of the vehicle. For best performance, the pedestrian detection needs a clear view of the person's head, arms, shoulders, legs, and the upper and lower parts of the body—and the person should be moving normally; Figure 1. If large parts of the pedestrian's body are not visible, the system cannot detect it. In the first version of the system, representing all cases included in the study, the capacity for detecting a pedestrian in darkness was limited, but the version introduced in 2015 represents a great improvement. However, some contrast between the pedestrian's silhouette and the background is still needed for detection.

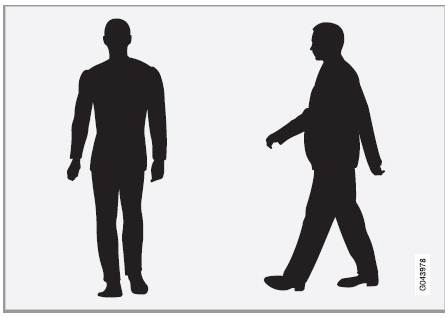

Figure 1. Examples of the clear body contours that the system regards as pedestrians, adapted from [41]

The pedestrian detection system will provide a warning and brake support in some of the situations when there is a credible risk of an accident. If the driver does not intervene after the warning, and the collision threat becomes imminent, intervention braking may automatically be applied to help slow down the car. Up to a speed of 80 km/h, the system may autobrake for a pedestrian, and up to approximately 35 km/h the collision may be avoided completely. In the most recent version, the system is able to reduce speed in up to 45 km/h in some car-to-pedestrian critical situations.

System description: Cyclist ADAS
Cyclist ADAS was an available option in Volvo's collision avoidance system starting in 2012 (MY 2013) in the S/V60, V/XC70, XC60, S80, and V40 models. Like the pedestrian ADAS, this system has been a standard feature in models introduced in 2015 and later, starting with the new XC90.

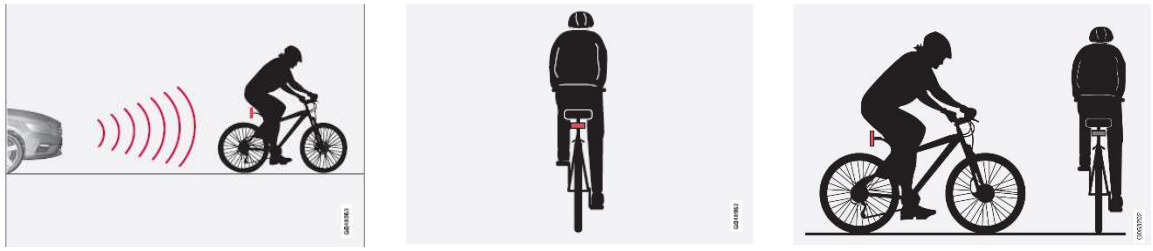

a) *b)* *c)*

Figure 2. Examples of clear body and bicycle outlines that the system regards as cyclists, adapted from [41-42]

For Cyclist ADAS, the technology is similar to the Pedestrian ADAS. To be able to recognize a cyclist, the system will optimally be able to detect clear, distinct body and bicycle outlines; Figure 2. The first version of the system was able to detect cyclists traveling in the same direction from behind; Figures 2.a & b. In the second generation of the system, introduced in 2015, cyclists can also be recognized from a side view; Figure 2c.

Crash data

Volvo car models V40, S/V/XC60, V/XC70, S80 and S/V/XC90 were selected from the car-to-pedestrian and car-to-cyclist crash databases, starting with the date Pedestrian ADAS and cyclist ADAS respectively were available for these models.

Car-to-pedestrian crash data The car-to-pedestrian crash data contain 12 Pedestrian ADAS cars and 37 non-Pedestrian ADAS cars, collected in Sweden between 2015 to 2017; Table 1.

Of the 12 car-to-pedestrian collisions in which the car was equipped with the Pedestrian ADAS system, six were SCP situations (the pedestrian was crossing the road in front of the car, going straight). The other cases represent a variety of situations: the car turned right as the pedestrian was crossing the road, a young boy was playing beside the road and rolled out onto the road as the car approached, the car was going straight and the pedestrian was standing still beside the road, and the pedestrian ran into the side of the car; in two cases, the car drove over the pedestrian's foot (one in a parking lot and one in a petrol station). In one case the car was reversing.
For cases with information of pre-crash factors, six occurred in daylight and four in darkness. In nine cases the weather was clear, nine cases happened in urban areas and two in non-urban areas. There were two seriously injured pedestrians, the remaining ten have moderate or minor injuries.

Of the 37 collisions with non-Pedestrian ADAS cars, 23 were SCP situations, in four cases the car was turning before the collision with a pedestrian crossing the road. In one case the car hit a pedestrian standing still beside the road. In two cases the car was moving forward in a parking lot when hitting the pedestrian, in one case the car skidded before hitting two pedestrians. One case occurred on a motorway in the night. In four cases the car was reversing.
Of the known pre-crash factors 19 of the cases occurred in daylight, 15 in darkness. It was clear weather in 24 of the cases, in two it was raining. The main part, 33 of the collisions, occurred in urban areas. Four of these pedestrian crashes were fatal, one pedestrian had a serious injury, in 11 of the cases the pedestrian had a moderate injury and the rest have only minor injuries.

Car-to-cyclist crash data The car-to-cyclist crash data contains 27 cars with Cyclist ADAS and 56 cars without the system (non-Cyclist ADAS) collected in Sweden between 2015 to 2017, Table2. Of the 27 cars with Cyclist ADAS, only four cars had the updated version of the system where cyclists can also be recognized from a side view.

Of the 27 collisions involving cars with the Cyclist ADAS system, there were one case where the car and the cyclist travelled in the same direction: the handlebar of the bicycle and the side of the car made contact. Of the remaining cases, 19 were SCP situations (the car was going straight when the cyclist crossed the road in front, from either the left or the right). Two of these cases occurred in a roundabout. In six cases, the car was turning right, and in one case the car was turning left, and collided with a cyclist crossing the road.

The majority of the cases occurred in urban areas, during daylight and in clear weather. None of the cyclists were seriously injured.

Of the 56 collisions with non-Cyclist ADAS cars, three cases were same direction situations. Of these three cases two occurred in a roundabout; in one case the car was overtaking the cyclist the handlebar of the bicycle touched the side of the car, in the other case the car was running into the cyclist, diagonally when the cyclist was leaving the roundabout. 31 of the collisions were SCP situations, 13 were situations where the car turned left or right before colliding with a cyclist crossing the road. In eight cases, the car was not moving forward, in three of these cases the car was reversing and five cases were dooring situations. The majority of these 56 crashes occurred in urban areas, during daylight and in clear weather without seriously injured cyclists.

Statistical methods

The rate of car-to-pedestrian collisions was compared per 10,000 IVYs for cars with and without the Pedestrian ADAS system.

The rate of car-to-pedestrian collisions for Pedestrian ADAS cars is defined as

$$\text{Rate}_{\text{Pedestrian ADAS}} = (n_{\text{Pedestrian ADAS}} / \text{IVY}_{\text{Pedestrian ADAS}}) \qquad (1)$$

where n is the number of car-to-pedestrian collisions. The number of claims can be considered using a Poisson distribution. Exact 95% Poisson confidence limits for the estimated rate were calculated as

$$\text{LCL} = \frac{\chi^2_{2n,\ \alpha/2}}{2}\ , \qquad \text{UCL} = \frac{\chi^2_{2(n+1),\ 1-\alpha/2}}{2} \qquad (2)$$

The rate and confidence interval of pedestrian and car crashes for non-Pedestrian ADAS cars were defined comparably.

To evaluate the effectiveness of the Pedestrian ADAS technology, Poisson regression was used to compare the car-to-pedestrian collision rates per IVY for Pedestrian ADAS and non-Pedestrian ADAS cars. The calculations were performed with PROC GENMOD (SAS Institute) [42], using a model with a logarithmic link function. Regression models were constructed for the total number of pedestrian and car collisions. Rate ratios (RRs) were provided from the output, together with 95% confidence limits. The system's effectiveness (the reduction in crashes as a percentage) was calculated as $(1 - \text{RR}) * 100$.

RESULTS

Car-to-pedestrian collisions:

The crash database contained 12 car-to-pedestrian cases involving Pedestrian ADAS cars and 37 cases with cars without the system. Six of these cases where car-to-pedestrian straight crossing path (SCP) situations with Pedestrian ADAS cars, and 23 where cars in SCPs without the system; Table 1.

Table 1.
Number of car-to-pedestrian collisions and insured vehicle years for cars with and without the pedestrian detection system Pedestrian ADAS.

	Number of collisions all	Number of collisions SCP	Insured vehicle years
Pedestrian ADAS	12	6	142,627
non-Pedestrian ADAS	37	23	347,661

The crash rate for car-to-pedestrian collisions per 10,000 IVYs, all conflict situations included, was 0.84 (95% confidence interval [CI], 0.43, 1.47) for Pedestrian ADAS cars and 1.06 (95% CI, 0.75,1.47) for non-Pedestrian ADAS cars. The rate was 21% lower (nonsignificant) for the Pedestrian ADAS cars (RR = 0.79, 95% CI, 0.41–1.51).
When only SCPs were selected, the rate per 10,000 IVYs was 0.42 (95% CI, 0.15, 0.92) for Pedestrian ADAS cars and 0.66 (95% CI, 0.42, 0.99) for non- Pedestrian ADAS cars. The SCP crash rate was 36% lower (nonsignificant) for the Pedestrian ADAS cars (RR=0.64, 95% CI, 0.26–1.57).

Car-to-cyclist collisions:
For car models XC90, S/V90 and S/V60 (introduced in 2015 and after), the system is now standard mounted with the second generation of the system that is able to recognize cyclists in several conflict situations, see Figure 2. The crash data contain 27 car-to-cyclist collisions involving Cyclist ADAS cars, of which only four have the second generation of the system, and 56 collisions involving non-Cyclist ADAS cars; Table 2.

Table 2.
Number of car-to-cyclist collisions and insured vehicle years for cars with and without the cyclist detection system Cyclist ADAS.

	Number of collisions all	**Number of collisions same-direction**	**Insured vehicle years**
Cyclist ADAS	27	1	133,916
non-Cyclist ADAS	56	1	285,012

The rate for all car-to-cyclist collision situations per 10,000 IVYs was 1.98 (95% CI, 1.58, 2.46).

Given that the same-direction conflict situation, targeted by the first generation of the Cyclist ADAS, accounted for only 3 % of all car-to-cyclist crashes [10], no difference could be identified for this type of crash when cars with and without the Cyclist ADAS system were compared.

DISCUSSION

Predictions based on virtual simulations as well as physical testing in specific test scenarios have promised traffic safety improvements from VRU ADAS technologies [34-38]. The present study describes real-world follow-up results in car-to-pedestrian collisions, providing preliminary confirmation of these predictions.
These results, although not significant, indicate that cars equipped with Pedestrian ADAS system reduced car-to-pedestrian collisions by 21% when all types of conflict situations in the data were considered—and by 36% for the SCP situation specifically. This is in line with a predictive estimation of the system's performance made in 2010 that suggested that 30% of the pedestrian crashes could be avoided, and that fatal crashes when the pedestrian is struck by the front of a passenger car could be reduced by 24% [34]. A similar study predicted a reduction in fatally and severely injured pedestrians of 40% and 27%, respectively, for a conceptual AEB system [35].
The performance of Cyclist ADAS in car-to-cyclist collisions was not investigated, since the dataset available mainly covered the first generation of the system only targeting same-direction situations, (Figure 2a-b). This conflict situation was not frequent in the dataset analyzed, nonetheless, the Cyclist ADAS illustrates one small, but important, step towards car-to-cyclist crash avoidance functionalities. In the second generation of the Cyclist ADAS introduced in Volvo car models in 2015, cyclists can also be identified from a side view (Figure 2c). Since more than 40% of all car-to-cyclist collisions in Swedish data [10] are SCP situations, this second generation is expected to perform substantially better.
This study is based on insurance data, covering all levels of crash severity and including situations – that are not always covered in other crash databases with other selection criteria [8]. In general, results from performance estimations depend on the methodology that was applied; how the analysis is implemented, which situations are considered, and the representativeness of the input data. Thus, specific numbers need to be carefully interpreted. For example, in this study, only situations where the car was driving forward are relevant and expected to be reduced.

This is exemplified by the two results presented for Pedestrian ADAS. The overall car-to-pedestrian crash potential consider all types of conflict situations also including crashes where the car was reversing, and taking this total sample into account, 21 % of car-to pedestrian collisions were reduced. On the other hand, a specific evaluation of the SCP situation, one of the target situations of the system, reveals a greater effect (36%), from the Pedestrian ADAS.

Some limitations in this study should be mentioned. It was not possible to find any significant safety benefits attributable to the ADAS systems in this study. The number of cars in traffic equipped with this functionality was low in the first years after its introduction. Further, the accident rates of pedestrian and bicycle crashes with cars are relatively low in Sweden, so it takes time before there are enough data available to study. As a comparison, approximately 50 rear-end-frontal collisions occur per 10,000 IVYs—compared to one car-to-pedestrian and two car-to-cyclist collisions for the same exposure. This was obvious when the collision warning and autobrake systems were evaluated in 2016; there was only one crash for the cars equipped with the pedestrian detection feature, and no crashes for the cars equipped with cyclist detection [32]. The possibility of achieving reliable performance estimations will increase, since the systems are now standard features in all new Volvo models. Given the higher frequency of VRU crashes in other regions of the world [1], it is suggested that research on the effectiveness of advanced driver assistance systems also be performed in other countries.

This study did not evaluate a mitigation effect, i.e. when the system was activated and the speed (and thus the crash severity) was reduced, but the crash was not completely avoided. In car-to-VRU crashes even slight reductions in impact speeds have a large effect on the injury outcome for pedestrians and cyclists [12], so it is therefore suggested that crash mitigation be included in future studies.

In this study, we found a clear indication that the first generation of Pedestrian ADAS is effective in reducing car-to-VRU crashes, and it was suggested that more recent generations of both Pedestrian- and Cyclist ADAS will be even more efficient in terms of traffic safety improvements for VRUs. Other countermeasures to reduce or mitigate car-to-VRU injuries have been implemented, including: infrastructure measures [15, 44], consumer rating tests on vehicles [36, 37], protective gear for cyclists [45], and motor-vehicle measures [19-23]. All of these initiatives should be considered in order to maximize a long-term decrease in VRU injury rates.

CONCLUSIONS

To our knowledge, this is the first study to analyze real-world crash data in relevant situations to evaluate ADAS systems targeting car-to-pedestrian and –cyclist collisions. Car-to pedestrian collisions were reduced by 21% when all conflict situations were considered, and by 36% in the specific straight-crossing path conflict situation, for cars equipped with Pedestrian ADAS. For Cyclist ADAS, the target situation in the first generation of the system only cover a low share of car-to-cyclist collisions, and no performance estimation was made. Our results, albeit nonsignificant, indicate that as more data become available, further improvements are foreseen in crash reduction and mitigation for the vulnerable road users that share the road with motor vehicles.

ACKNOWLEDGEMENTS

The authors are very thankful to Kristina Mayberry for language revisions.

REFERENCES

[1] GLOBAL STATUS REPORT ON ROAD SAFETY 2018, WHO Available at: https://www.who.int/violence_injury_prevention/road_safety_status/2018/en/ Downloaded 20190123.

[2] Annual Accident Report 2017, European Road Safety Observatory: Available at: https://ec.europa.eu/transport/road_safety/specialist/observatory/statistics/annual_accident_report_en Downloaded 20190123.

[3] Traffic Safety Facts, 2016; Report DOT HS 812 554. NHTSA, U.S. Department of Transportation; May 2018.

[4] Vägtrafikskador, 2017: Available at https://www.trafa.se/vagtrafik/vagtrafikskador/ Downloaded 20190123.

[5] IRTAD, International Transport Forum. Road Safety Annual Report 2018. Available at: https://www.itf-oecd.org/road-safety-annual-report-2018. Downloaded 20190215.

[6] Pedestrian and Cyclists 2015, European Road Safety Observatory: Available at: https://ec.europa.eu/transport/road_safety/sites/roadsafety/files/ersosynthesis2015-pedestrianscyclists25_en.pdf Downloaded 20190123.

[7] Isaksson-Hellman, I. 2012. A study of bicycle and passenger car collisions based on insurance claims data. In: Proceedings of the Ann. Adv. Automot. Med., vol. 56, pp.3-12.

[8] Isaksson-Hellman I and Werneke J. 2017. Detailed description of bicycle and passenger car collisions based on insurance claims. Safety Science. 92:330-337.

[9] Lindman, M., Jakobsson, L., Jonsson, S. 2011. Pedestrians interacting with a passenger car; a study of real world accidents. IRCOBI Conference Proceedings. No. IRC-11-61.

[10] Lindman, M., Jonsson, S., Jakobsson, L., Karlsson, T., Gustafson, D., Fredriksson, A. 2015. Cyclists interacting with passenger cars; a study of real world crashes. IRCOBI Conference Proceedings. No. IRC-15-10.

[11] Op den Camp, O., Ranjbar, A., Uittenbogaard, J., Rosén, E., Fredriksson, R. and de Hair, S. 2014. Overview of main accident scenarios in car-to-cyclist accidents for use in AEB-system test protocol. Proceedings of: International Cycling Safety Conference, Gothenburg, 2014.

[12] Rosén, E., Sander, U., 2009. Pedestrian fatality risk as a function of car impact speed. Accid. Anal. Prev. 41, 536-542.

[13] Kim, J.-K., Kim, S., Ulfarsson, G.F., Porello, L.A. 2007. Bicyclist injury severities in bicycle-motor vehicle accidents. Accid. Anal. Prev. 39, 238–251.

[14] Bíl, M., Bílová, M., Müller, I. 2010. Critical factors in fatal collisions of adult cyclists with automobiles. Accid. Anal. Prev. 42, 1632A–1636A.

[15] Isaksson-Hellman I. and Töreki J. 2018. The effect of speed limit reductions in urban areas on cyclists' injuries in collisions with cars. Presented on International Cycling Safety Conference ICSC Barcelona.

[16] Gustafsson, S., Jägerbrand, A., Grumert, E. Hastighetsdämpande åtgärder, En litteraturstudie med fokus på nya trafikmiljöåtgärder och ITS-orienterade lösningar. 2011. VTI 17-2011. Available at: www.vti.se/publikationer. Downloaded 20190215.

[17] Swedish transport administration, Trafikverket This is vision zero. Available at: https://www.trafikverket.se/en/startpage/operations/Operations-road/vision-zero-academy/Vision-Zero-and-ways-to-work/. Downloaded 20190220.

[18] Swedish transport administration, Trafikverket. Trafiksäkerhetsmål och indikatorer. Available at: https://www.trafikverket.se/for-dig-i-branschen/samarbete-med-branschen/Samarbeten-for-trafiksakerhet/tillsammans-for-nollvisionen/mal-och-indikatorer/. Downloaded 20190220.

[19] Ahmed, S., Patil, G. 2013. Bumper Shape Optimization for Pedestrian Safety. International Journal of Engineering Research and Applications (IJERA) ISSN: 2248-9622 www.ijera.com Vol. 3, Issue 1, January - February 2013, pp.1724-1732.

[20] Hu, J., Klinich, K. D. 2012. Toward designing pedestrian-friendly vehicles. Int. J. Veh. Saf. 2012, 8, 102873.

[21] Jakobsson, L., Broberg, T., Karlsson, H., Fredriksson, A., Gråberg, N., Gullander, C., Lindman, M. 2013. Pedestrian airbag technology – a production system. 23rd ESV Conference; 2013; Soeul, Korea. Paper No. 13-0447.

[22] Lee, K. B., Jung, H. J., Bae, H. I. 2007. The study on developing active hood lift system for decreasing pedestrian head injury. 20th ESV Conference; 2007; Lyon, France. Paper Number 07-0198.

[23] Coelingh, E., Eidehall, A., Bengtsson M. 2010. "Collision Warning with Full Auto Brake and Pedestrian Detection - a practical example of Automatic Emergency Braking" 13th International IEEE Annual Conference on Intelligent Transportation Systems Madeira Island, Portugal.

[24] Isaksson-Hellman I, LindmanM. 2012. The effect of a low-speed automatic brake system estimated from real life data. In: Proceedings of the Ann. Adv. Automot. Med. vol; 56: pp. 231–240.

[25] Rizzi, M., Kullgren, A., Tingvall, C. The injury crash reduction of low-speed autonomous emergency braking (AEB) on passenger cars. 2014. IRCOBI Conference Proceedings. No IRC-14-23.

[26] Highway Loss Data Institute. 2015. Volvo city safety loss experience—a long-term update. HLDI Bull. 2015;32(1):1–24.

[27] Doyle, M., Edwards, A., Avery, M. 2015. AEB real world validation using UK motor insurance claims data. Paper presented at: 24th ESV Conference; 2015; Gothenburg, Sweden. Paper Number 13-0058.

[28] Isaksson-Hellman I, Lindman M. 2015. Real-world performance of city safety based on Swedish insurance data. Paper presented at: 24th ESV Conference; 2015; Gothenburg, Sweden. Paper Number 15-0121.

[29] Fildes, B., Keall, M., Bos, N., et al. 2015. Effectiveness of low speed autonomous emergency braking in real-world rear-end crashes. Accid Anal Prev. 2015; 81:24–29.

[30] Isaksson-Hellman, I. and Lindman M. 2015. "Evaluation of rear-end collision avoidance technologies based on real world crash data. Paper presented at: 3rd International Symposium on Future Active Safety Technology Towards Zero Traffic Accidents; Gothenburg, Sweden.

[31] Isaksson-Hellman, I. and Lindman, M. 2016. Evaluation of the crash mitigation effect of low-speed automated emergency braking systems based on insurance claims data, Traffic Inj. Prev. 2016; 17:sup1, 42-47.

[32] Isaksson-Hellman, I. and Lindman, M. 2016. "Using insurance claims data to evaluate the collision avoidance and crash-mitigating effect of CWB+ACC." Paper presented at IEEE, IV'16; 2016; Gothenburg, Sweden.

[33] Cicchino, J. 2016. Effectiveness of Volvo's City Safety Low-Speed Autonomous Emergency Braking System in Reducing Police-Reported Crash Rates. Insurance Institute for Highway Safety.

[34] Lindman, M., Ödblom, A., Bergwall, E., Eidehall, A., Svanberg, B. and Lukaszewicz, T. 2010. "Benefit Estimation Model for Pedestrian Auto Brake Functionality". ESAR, Hanover, Germany.

[35] Rosén, E., Källhammer, J.E., Eriksson, D., Nentwich, M., Fredriksson, R. and Smith, K., "Pedestrian injury mitigation by autonomous braking". 2009. Paper presented at: 21st ESV Conference; Stuttgart, Germany, 2009. Paper Number 09-0132.

[36] Euro NCAP TEST PROTOCOL – AEB VRU systems. Version 2.0.2. November 2017

[37] IIHS Pedestrian Autonomous Emergency Braking Test Protocol (Version 1). December 2018.

[38] Kovaceva, J.,Balint, A., Schindler, R., Schneider A., Stoll, J., Breunig, S., Bräutigam, J.,Jaussein, M., Bruyas, M-P., Puente guillen, P., large, D., Perlet, K., Petersson, M., Esquer, A. Prospect, proactive safety for pedestrians and cyclists. 2018. European Commission Eighth Framework Programme Horizon 2020 GA No. 634149. Assessment of the PROSPECT safety systems including socioeconomic evaluation, D2.3.

[39] HLDI. 2017. Effect of Subaru EyeSight on pedestrian-related bodily injury liability claim frequencies. Bulletin Vol. 34, No. 39.

[40] AAAM (Association of the Advancement of Automotive Medicine), 2005. The Abbreviated Injury Scale (AIS), 2005 Revision. AAAM, Des Plaines, IL, USA.

[41] V70/XC70 owner's manual. Available at: https://carmanuals2.com/get/volvo-v70-2016-agarmanual-61589. Downloaded 20190123.

[42] XC90 owner's manual. Available at: https://carmanuals2.com/get/volvo-xc90-201x-agarmanual-52988. Downloaded 20190123.

[43] SAS Institute. PROC GENMOD. SAS: Statistical Software [computerprogram]. Version 9.4. Cary, NC: SAS Institute Inc. Available at:https://support.sas.com/documentation/cdl/en/statug/63033/HTML/ default/viewer.htm#genmod_toc.htm.

[44] Lu, M. 2006. Modelling the effects of road traffic safety measures. Accid. Anal. Prev. 38, 507-517.

[45] Høye, A. 2018. Bicycle helmets – To wear or not to wear? A meta-analyses of the effects of bicycle helmets on injuries. Accid. Anal. Prev. 117, 85-97.

A FRAMEWORK FOR AUTOMATED DRIVING SYSTEM TESTABLE CASES AND SCENARIOS

Paul Rau
National Highway Traffic Safety Administration
United States

Eric Thorn
Southwest Research Institute
United States

Paper 19-0301

ABSTRACT

Automated Driving Systems (ADS) are being developed to perform the primary functions of the dynamic driving task (DDT). These technologies hold great promise to improve safety and mobility for transportation. Test scenarios are critical for assessing the safety assurance of ADS in a range of operational environments and roadway conditions. The development of testing scenarios for ADS is proving to be an important challenge for the development of safety assurance requirements, certification and licensing frameworks, testbed services, standards, and international harmonization.

This paper summarizes foundational research undertaken to identify a sample preliminary, objective testing and evaluation approach for ADS. The paper considers technologies of interest that fall within Level 3 through Level 5 of the SAE International levels of driving automation and identifies a cross-section of prototype and conceptual ADS that are then categorized into seven generic ADS features.

This research also takes the first steps to partition the ADS performance space by identifying and assessing the primary variables that comprise an ADS test scenario. Those primary variables are described in detail, and include:

- Tactical and Operational Maneuvers
- Operational Design Domain (ODD)
- Object and Event Detection and Responses (OEDR)
- Failure Mode Behaviors

Tactical and operational maneuver capabilities largely focus on the control-related elements of the DDT (i.e., lateral and longitudinal control) that enable an ADS to navigate to reach its destination (e.g., lane centering / following, turning). A working list of these capabilities is presented. The ODD represents the operating conditions under which an ADS is designed to function (e.g., roadway types, weather conditions, etc.). A notional hierarchical ODD taxonomy is presented and described. OEDR capabilities include the elements of the DDT that involve monitoring the driving environment and implementing appropriate responses to relevant objects and events. A working list of OEDR capabilities is presented. Failure mode behaviors include fail-safe (FS) and fail-operational (FO) strategies that will allow an ADS to respond to a variety of failures, including DDT performance-relevant system failures that require the ADS or a DDT fallback-ready user to achieve a minimal risk condition.

The paper also considers the implementation of the proposed evaluation framework using existing test methods, including modeling and simulation (M&S), closed track testing, and open road testing. It further seeks to examine how each of the testing methods can be logically used to minimize the complexity of comprehensive safety assessments of ADS by leveraging each method's strengths to maximize the knowledge gained from each test. It also includes extensive discussion of challenges associated with testing ADS, including challenges related to the technology itself as well as challenges associated with test execution. This paper is based on research completed by NHTSA and its contractors, and is more fully documented in NHTSA Report DOT HS 812 623, "A Framework for Automated Driving System and Testable Cases and Scenarios"; September 2018.

INTRODUCTION

Since 1975, the first year that the Fatality Analysis Reporting System began collecting data, the rate of traffic fatalities per 100 million miles traveled in the United States has decreased by 66 percent, according to the National

Highway Traffic Safety Administration's (NHTSA's) Traffic Safety Facts 2015 data (NHTSA, 2017b). Advancements in motor vehicle safety have been made through continuous engineering innovation, public education, industry agreements, safety regulations, and safety rating programs. There is, however, significant room for continued focus on motor vehicle traffic safety. In October 2017, NHTSA reported that traffic fatalities increased by 5.4 percent from 2015 to 2016 (35,485 to 37,461) for the United States (NHTSA, 2017c), which follows an 8.4 percent increase from 2014 to 2015 (32,744 to 35,485) (NHTSA, 2017b).

Many forces are at work in the automotive industry to advance safety technology. The worldwide automotive industry has recognized driver performance (e.g., error and choice) as a key factor that impacts safety and has begun to introduce systems that complement the driver in terms of enhanced perception with 360-degree vehicle views and rear video systems. Advanced Driver Assistance Systems that monitor the operational environment and enhance driver detection and response, such as Forward Collision Warning (FCW) and Lane Keeping Assist (LKA), are increasingly common in newer model vehicles. Additionally, 20 automakers have committed to making Automatic Emergency Braking (AEB) a standard feature in new vehicles by 2022 (IIHS, 2016).

Recently, research activities by several companies to develop ADS that can perform certain driving functions automatically have captured the nation's attention. ADS have been the subject of multiple congressional hearings and the public has provided numerous responses to NHTSA's Federal Automated Vehicles Policy (NHTSA, 2016b), including over 1,100 responses from industry participants, state and municipal transportation agencies, policy groups, and citizens (Kyrouz, 2017). The United States Department of Transportation (USDOT) and NHTSA recently released an update to their federal guidance for ADS that focused on their development and safe deployment and operation. NHTSA also continues to advance its ADS research. The research summarized in this paper sought to analyze aspects of ADS testing and develop examples of tests and evaluation methods for specific ADS features. A sample testing framework was developed that could further support the goals of improving safety for all users of the transportation network.

OBJECTIVE

The purpose of this study was to analyze aspects of ADS testing to create a framework for developing test cases and test scenarios for ADS. Consideration was given to keeping the framework flexible and extensible such that it could be applied with different test approaches and methods. The ultimate goal of this framework is to support the safe deployment of ADS in the broader transportation system.

AUTOMATED DRIVING SYSTEM FEATURES

As an initial step to develop this framework, sample concept ADS features that have been proposed for deployment were identified. This analysis focused on SAE International Levels 3-5 ADS (SAE International, 2018), such as Google's (Waymo's) self-driving car project and others like it that focus on next-generation automation. This step is critical because the sample concept ADS features are used to identify ODDs and OEDRs, develop preliminary tests and/or evaluation methods, and assess FS and FO mechanisms, which form a foundation to begin considering validation and verification approaches for ADS.

A four-stage approach was followed to identify ADS features: 1) review the literature, 2) define a framework for discussing ADS features, 3) define features and behaviors, and 4) categorize the features. To guide later analysis, priority ADS features on which to focus were identified. Over 50 literature sources were reviewed, including original equipment manufacturer (OEM) websites, press releases of vehicles being tested in specific domains, NHTSA pre-crash scenario analysis (NHTSA, 2007), NHTSA's Fiscal Year 2017 budget request (NHTSA, 2016c), NHTSA L2 and L3 Human Factors Concepts (NHTSA, 2015), Federal Highway Administration (FHWA) managed lane use cases (FHWA, 2008), and technical and international publications, including proceedings of the 2015 and 2016 Automated Vehicles Symposiums and United Nations Economic Commission for Europe (UNECE) World Forum for Harmonization of Vehicle Regulations (WP.29) Automatically Commanded Steering Function working group, among others. Research sponsored by USDOT, such as the Crash Avoidance Metrics Partnership Automated Vehicle Research for Enhanced Safety (Christensen, et al., 2015; NHTSA, 2016d), which details functional descriptions for on-road driving automation levels, was also used.

Twenty-three concept ADS features were identified:

1. Audi Traffic Jam Pilot

2. Audi Highway Pilot
3. Auro Self Driving Shuttle
4. Baidu Automated TNC[1] Bosch Valet Parking
5. CityMobil2 Automated Shuttle
6. Bosch Highway Pilot
7. EZ10 Self Driving Shuttle
8. Ford Automated TNC
9. GM Cruise Automation TNC
10. Google Car
11. Honda Automated Drive
12. Mercedes Highway Pilot Truck
13. Navya Arma Shuttle
14. Nissan Autonomous Drive
15. Olli Local Motors Shuttle
16. Otto Trucking
17. Tesla Self-Drive
18. Toyota Chauffeur
19. Toyota Guardian
20. Uber Automated TNC
21. Varden Labs Self Driving Shuttles
22. Volkswagen I.D. Pilot
23. Volvo IntelliSafe Auto Pilot

These 23 features were categorized into the following seven generic categories:

1. L3 Conditional Automated Traffic Jam Drive
2. L3 Conditional Automated Highway Drive
3. L4 Highly Automated Low Speed Shuttle
4. L4 Highly Automated Valet Parking
5. L4 Highly Automated Emergency Take-Over
6. L4 Highly Automated Highway Drive
7. L4 Highly Automated Vehicle / TNC

Through the literature review and analysis, a working list of tactical and operational maneuvers related to ADS driving control was created. Some examples of these tactical and operational maneuvers included: parking, maintaining speed, lane centering, low-speed merge, right-of-way decision, following driving laws, and U-turns, among others.

Each of the identified generic ADS features was then described in terms of tactical maneuver behaviors, estimated commercial availability, and estimated level of automation. Figure 1 shows a sample analysis for the L4 Highly Automated Vehicle / TNC Feature. It should be noted that these commercial ADS features were identified several years ago and the list has changed quite significantly. It should also be noted that the estimates for commercial availability, level of driving automation, and tactical maneuver demonstration were deduced from the information available, which was limited, and as such should be considered notional.

[1] TNC: Transportation Network Company

ADS Features and Tactical Maneuvers (X = demonstrated, ? = speculated)	**Commercially Available? (Y/N)**	**Level of Automation (SAE 1-5)**	Parking	Maintain Speed	Car Following	Lane Centering	Lane Switching/Overtaking	Enhancing Conspicuity	Merge	Navigate On/Off Ramps	Follow Driving Laws	Navigate Roundabouts	Navigate Intersection	Navigate Crosswalk	Navigate Work Zone	N-Point Turn	U-Turn	Route Planning
Waymo Automated TNC	N	4	X	X	X	X	X	X	X	X	X	X	X	X	X	X	X	X
Tesla Self-Drive	N	4	X	X	X	X	X	X	X	X	X	X	X	X	X	X	X	X
Volkswagen I.D. Pilot	N	4?	X	X	X	X	X	X	X	X	X	X	X	X	X	X	X	X
Volvo IntelliSafe Auto Pilot	N	4	X	X	X	X	X	X	X	X	X	X	X	X	X	X	X	X
Nissan Autonomous Drive *(2020)*	N	4?	X	X	X	X	X	X	X	X	X	X	X	X	X	X	X	X
GM Cruise Automation	N	4	X	X	X	X	X	X	X	X	X	X	X	X	X	X	X	X
Uber Automated TNC	N	4	X	X	X	X	X	X	X	X	X	X	X	X	X	X	X	X
Honda Automated Drive *(2020)*	N	4	X	X	X	X	X	X	X	X	X	X	X	X	X	X	X	X
Ford Automated TNC *(2022)*	N	4	X	X	X	X	X	X	X	X	X	X	X	X	X	X	X	X
Baidu Automated TNC	N	4	X	X	X	X	X	X	X	X	X	X	X	X	X	X	X	X
Toyota Chauffeur	N	4	X	X	X	X	X	X	X	X	X	X	X	X	X	X	X	X

Figure 1. L4 Highly Automated Vehicle / TNC Features.

OPERATIONAL DESIGN DOMAIN

An operational design domain (ODD) describes the specific operating domain(s) in which an ADS feature is designed to function with respect to roadway types, speed range, lighting conditions (day and/or night), weather conditions, and other operations constraints. ODD will likely vary for each ADS feature, even if there is more than one ADS feature on a vehicle. The testing framework presented in this paper considers the potential range of ODDs and how ODDs factor into developing potential test cases.

A three-stage approach was taken to define the ODDs:

1. Review the literature, including popular media, press releases, technical journals, and conference proceedings to identify key concepts, enumerate potential ODD characteristics, and examine approaches to ODD in other industries.
2. Define and categorize ODD into a sample taxonomy that can be used by departments of transportation (DOTs) and industry to discuss ADS.
3. Describe ODDs in which concept ADS features may operate based on literature review and engineering judgment.

Over 50 literature sources were reviewed, including OEM websites, press releases, USDOT documents, including NHTSA pre-crash scenario analysis and FHWA managed lane use case, as well as technical and international publications, including proceedings of the 2015 and 2016 Automated Vehicles Symposiums. Additionally, the NHTSA Fiscal Year 2017 Budget Request to Congressional Appropriations Committees (NHTSA, 2016c) identifies several ADS use cases that were considered when defining the ODD for this analysis. It should be noted that given the emerging and highly competitive nature of ADS technology, it is inherently difficult to obtain explicit and complete information about the intended ODD of an ADS feature. In the absence of information about an ODD,

engineering judgement was used at times to define the ODD taxonomy and identify the ODD for concept ADS features.

While the literature provided many examples of ODD elements, no classification framework was identified. This work takes an initial step towards developing a taxonomy to organize the many ODD elements identified in research. This sample ODD taxonomy takes the form of a hierarchy of categories and subcategories, each with definitions and, where appropriate, gradations. This taxonomy is meant to be descriptive, not normative, as it is envisioned that these elements may be organized into several different groupings. The taxonomy offers a structured approach to organize and identify various ODDs for ADS features, especially when there are several different possible combinations. Figure 2**Error! Reference source not found.** shows the broad range of top-level categories and immediate subcategories. It should again be noted that this sample taxonomy was derived using available information at the time the research was conducted and should be considered notional.

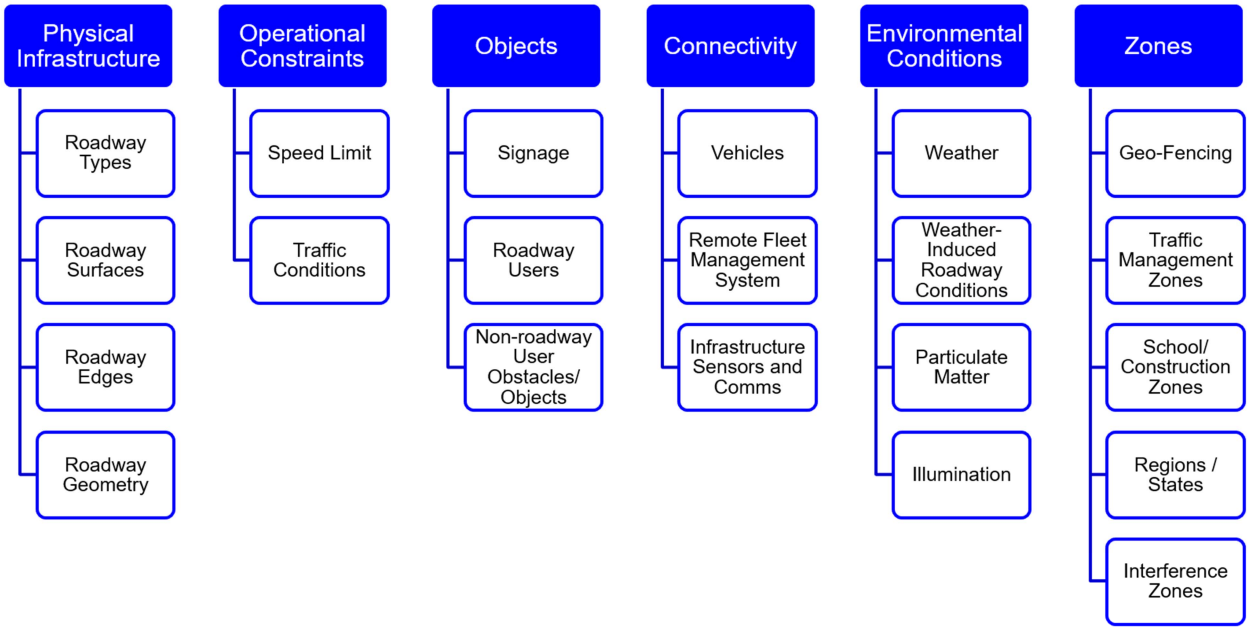

Figure 2. ODD Classification Framework with Top-Level Categories and Immediate Subcategories.

The hierarchy extends into multiple sublevels. For example, **Error! Reference source not found.** shows that the "Environmental Conditions" category was divided into four subcategories: weather, illumination, particulate matter, and road weather. Weather is further subdivided into rain, temperature, wind, and snow. For this research, it was helpful to further subdivide rain into gradations to capture the data that were collected on ADS features. For example, some ADS features had been tested in light rain, while others had been tested in heavy rain. Although the application of this sample taxonomy has been useful in the context of this research, further research and stakeholder engagement would be beneficial in refining and objectively quantifying the categories and gradations.

The sample ODD taxonomy lends itself to serving as a checklist for identifying the ODD of an ADS feature. A comprehensive ODD checklist was generated based on the ODD taxonomy described above. To demonstrate a potential application of the checklist, the checklist was filled out for three theoretical ADS features. It should be noted that the manufacturer determines the ODD for a feature, and the ODD may vary for similar ADS features. The theoretical features presented here are purely demonstrative, not representative of any commercially marketed ADS feature.

To test a vehicle's ability to operate safely, ODD is considered in test development and execution. Scenarios consider a combination of ODD elements that can be used to describe conditions for test cases and scenarios; for example, a highway with a concrete surface with a light mist. Test facilities are limited in their ability to re-create certain ODDs (e.g., urban environments, hill crests) and may need to be upgraded with new infrastructure to support

testing. Some ODD elements are difficult to quantify and re-create (e.g., weather), though it is possible they could be addressed through functional safety design practices and on-road testing.

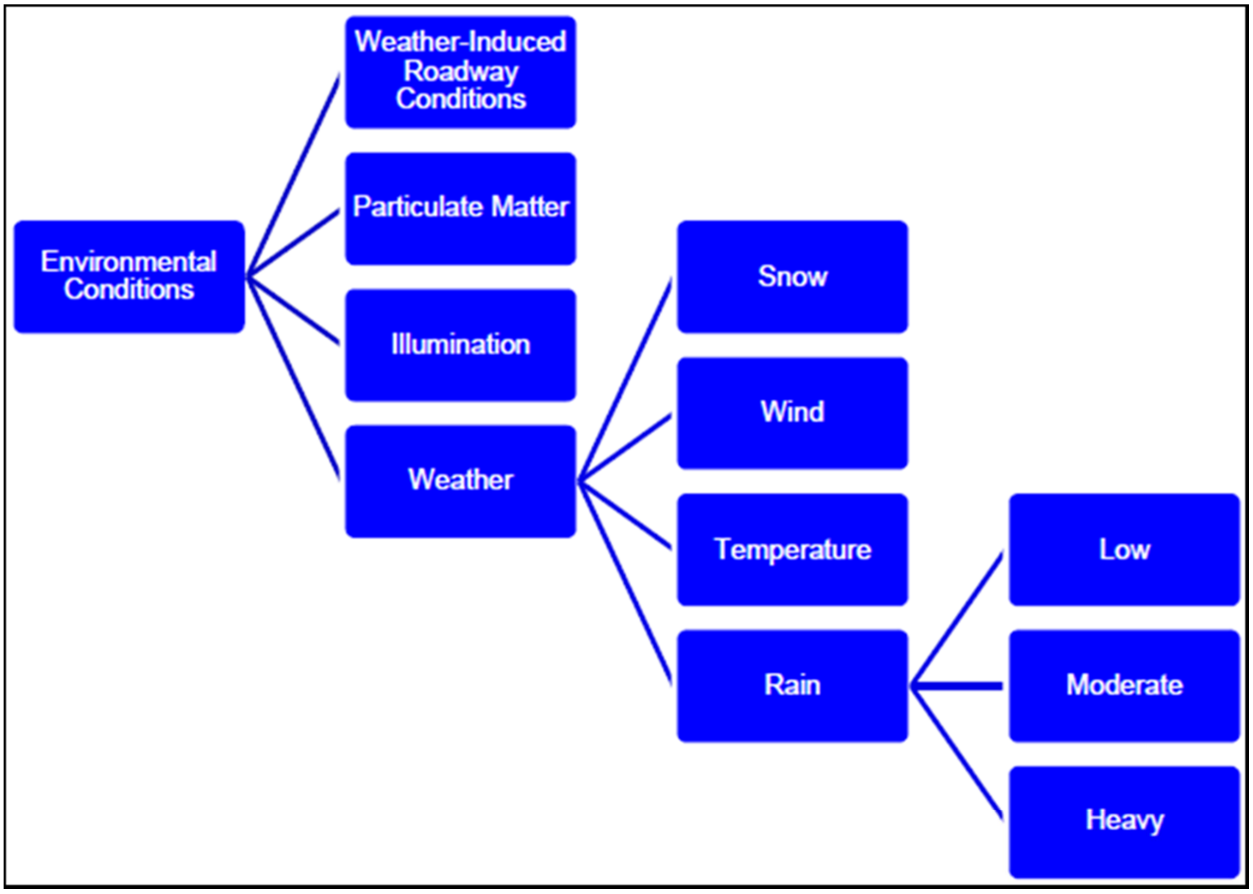

Figure 3. Example of Hierarchy Levels within the Environmental Conditions Category.

OBJECT AND EVENT DETECTION AND RESPONSE

While performing tactical maneuver behaviors described previously, ADS will inevitably interact with a variety of static and dynamic physical objects that may alter how these behaviors are executed. SAE J3016 identifies the following real-time functions as elements of the DDT related to addressing these interactions with objects:

- Object and event detection, recognition, and classification
- Object and event response

These functions can be generalized under the term Object and Event Detection and Response (OEDR). OEDR represents the ability of the ADS feature to detect any circumstance that is immediately relevant to the driving task and implement an appropriate response. One of the factors that determines the level of driving automation of an ADS is whether the human driver or ADS is responsible for monitoring the driving environment. ADS, which were the focus of this research, range from SAE International L3 through L5, which means that the ADS feature is completing all aspects of monitoring the driving environment.

The elements of an ADS functional architecture that are specifically relevant to OEDR generally include hardware and software components that support:

- Sensing (e.g., radar, laser scanners, cameras, etc.)
- Perception (e.g., road feature classification, object segmentation and classification, etc.)

- World modeling (e.g., persistent data mapping, dynamic obstacle tracking, and prediction, etc.)
- Navigation and planning (e.g., path planning and motion control commands to implement responses)

The sensing and perception elements of the architecture specifically support detection of relevant objects. World modeling supports the aggregation of perception and other information to identify and understand events that may occur through interactions with those objects. Navigation and planning support determination of the appropriate response to those events and interactions, and the generation of control commands to implement that response.

Three of the generic ADS features were selected for an OEDR analysis (L3 Conditional Automated Traffic Jam Drive, L3 Conditional Automated Highway Drive, and L4 Highly Automated Vehicle / TNC). This allowed for an evaluation of a cross-section of operating environments and conditions, as well as driving scenarios. Following the evaluation of the operational needs of the selected ADS features, a focusing exercise established baseline ODDs for each feature to further refine the analysis to identify OEDR capabilities for the three selected features. This exercise served to frame the OEDR analysis to account for the potential variability of certain ODD elements, as well as the substantial number of combinations and permutations of ODD elements. It is reasonable to expect that different organizations developing similar ADS features will generate unique designs and implementations, and thus will ultimately define different ODDs for their respective systems. With the ODD baselines established for each feature, a survey and analysis of the driving scenarios resulting from the operations descriptions led to the identification of relevant objects and interactions that the ADS could encounter. These objects and events are derived from an evaluation of normal driving scenarios for a given ADS feature operating in its ODD.

The developed baseline ODDs were used to identify important objects and events that ADS could feasibly encounter within those ODDs. Aggregated OEDR behavior capabilities are shown in Table 1.

Table 1. Summary of OEDR Behavior Capabilities.

Detect & Respond to Speed Limit Changes	Detect & Respond to Relevant School Buses
Detect & Respond to Encroaching, Oncoming Vehicles	Detect & Respond to Relevant Emergency Vehicles
Perform Vehicle Following	Detect & Respond to Relevant Pedestrians
Detect & Respond to Relevant Stopped Vehicles	Detect & Respond to Relevant Pedalcyclists
Detect & Respond to Relevant Lane Changes / Cut-ins	Detect & Respond to Relevant Animals
Detect & Respond to Relevant Static Obstacles in Lane	Detect & Respond to Relevant Vehicle Cut-out / Reveal
Detect & Navigate Work Zones	Detect & Respond to Relevant Vehicle Roadway Entry
Detect & Respond to Relevant Safety Officials	Detect & Respond to Relevant Adjacent Vehicles
Detect & Respond to Relevant Access Restrictions	Detect & Respond to ODD Boundary Transition
Detect & Respond to Relevant Dynamic Traffic Signs	

FAILURE MODE BEHAVIOR

ADS will utilize FO and FS mechanisms when the system does not function as intended. These mechanisms are intended to cause the ADS to attain a minimal risk condition (MRC) that removes the vehicle and its occupants from harm's way, to the best extent possible. Defining, testing, and validating FO and FS strategies for achieving an MRC are important steps in promoting the safe operation and deployment of ADS.

The appropriate failure mitigation strategy and resulting MRC for a given ADS is largely dependent on the type and nature of failures the ADS experiences. To this end, an understanding of potential ADS failure modes is necessary. As such, a high-level failure analysis was performed. The results of this analysis informed the assessment of FO and FS mechanisms. A variety of failure and hazard analysis techniques exist, including fault tree analysis (FTA), system failure mode and effects analysis (FMEA), failure modes, effects, and criticality analysis (FMECA), system-theoretic process analysis, and hazard and operability analysis (HazOp). System FMEA was identified and selected

as an initial approach to develop the high-level analysis needed to identify potential failures in each subsystem of the representative functional architecture, as well as their causes and impacts.

Existing reports and literature on ADS failures, including from the Defense Advanced Research Projects Agency (DARPA) Grand and Urban Challenges (DARPA, 2008), as well as engineering judgments and prior experience in ADS development and testing were leveraged and considered. It was assumed that a detailed failure analysis employing a range of techniques noted above has been performed on the base vehicle platform, and therefore efforts were focused on components specifically related to the ADS. This allowed for a deeper dive into a representative ADS functional architecture. Furthermore, failures that could have safety implications, as opposed to failures that are merely an inconvenience, were prioritized. The FMEA was broken down by architecture subsystems to identify potential key failures at each step through the ADS "pipeline":

- Sensing and communication
- Perception
- Navigation and control
- Human Machine Interface (HMI)

In general, many of the ADS failure modes described above could be attributed to some kind of failures by the ADS to obtain information needed to perform the DDT. These were summarized into three primary categories as failures attributed to:

- No data – Information is absent altogether
- Inadequate quality data – Information is of poor or degraded quality
- Latent data – Information is delayed or old

After completing the FMEA for the ADS architecture, the various failure modes and effects were summarized and mapped to the relevant tactical maneuver and OEDR behaviors for the three down-sampled ADS features (L3 Traffic Jam Drive, L3 Highway Drive, and L4 Highly Automated Vehicle/TNC). This notionally provides a mapping from the specific failures identified in the FMEA, to the generalized failures summarized in the previous section, to the behaviors implemented by various ADS features.

Based on the general failure modes identified, potential failure mode responses and strategies were identified. This effort focused on FS strategies for cases where the ADS cannot continue to operate due to a significant failure, and FO strategies for cases where the ADS could continue to operate even in the face of a failure. It should be noted that these potential FS and FO strategies were determined from engineering judgements and available literature, and as such should be considered notional.

The primary goal of an FS strategy is to rapidly achieve an MRC where the vehicle and occupants are safe. Three candidate FS mechanisms were considered for further evaluation:

- Transition vehicle control to fallback-ready user
- Safely stop in lane of travel
- Safely move out of travel lane and stop

FO strategies allow the ADS to continue to function, even in the event of one or more failures. It is important to note that this operation may only be supported for a limited duration, or potentially with a reduced set of capabilities. Three primary FO mechanisms were considered for further analysis:

- Hardware/software redundancy
- Adaptive compensation (e.g., ignore data coming from failed sensor or component and weight inputs from other sensors or components more heavily)
- Degraded operation(s)
    - Reduced top speed
    - Reduced level of automation
    - Reduced ODD
    - Reduced maneuver capabilities
    - Reduced OEDR capabilities

PRELIMINARY TEST AND EVALUTION METHODS

After evaluating prototype ADS features, potential ODDs, potential OEDR capabilities, and potential failure mode strategies, a sample evaluation framework was developed to support the assessment of ADS for safe deployment. Sample test procedures were also developed using engineering judgements, previous test procedure development experience, and use cases. The test framework and procedures developed gave special consideration to achieving repeatability, reliability, and practicality. Lastly, many challenges associated with testing ADS and further research needed to help address these challenges were identified. Challenges included those related to the technology itself as well as test execution.

To identify appropriate methods to evaluate ADS, a review and assessment of existing testing methods and tools was performed. This evaluation served to develop an understanding of how testing is currently being executed for vehicles capable of various levels of automation. It also served to identify potential gaps in this existing testing framework, which led to the identification of additional and modified tools and methods to fill those gaps and helped create a testing framework. This assessment included a meeting with crash avoidance test engineers at NHTSA's Vehicle Research and Testing Center (VRTC) in Ohio to discuss their current testing of vehicles capable of SAE International L1 and L2 driving automation. Findings from the previous analyses were presented and initial thoughts on the steps to develop a useful set of test methods and actual tests were provided.

A common test scenario framework that could be used broadly across the various testing methods and tools was then established. This framework built upon the findings of the previous tasks to include the principal elements of ADS operation (tactical maneuver, ODD, OEDR, and failure behaviors) that are thought to have a direct impact on their overall safety. Each of these elements can be viewed as an input or integrated component in the overall test scenario. The framework was developed in such a way that it could be used for both black-box and white-box testing. Each of the core scenario components can be applied similarly for both black-box and white-box analyses; the differences come in the ability to inject inputs and take output measurements at various levels within the system under test. As part of this analysis, key interfaces where this injection and measurement could take place were identified.

Available literature and reports on current ADS testing activities conducted by both government and industry were reviewed. The review identified three ways that these tests are primarily being conducted:

- Modeling and simulation (M&S)
- Closed-track testing
- Open-road testing

These three techniques offer a multifaceted testing architecture with varying degrees of test control, and varying degrees of fidelity in the test environment. In many cases, two or more of these techniques can be used in parallel or in an iterative fashion to progressively evaluate a complex system such as an ADS.

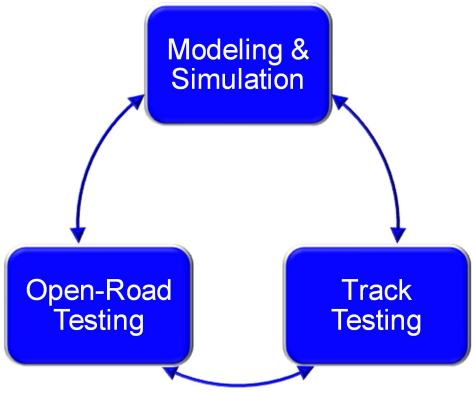

Figure 4. Primary Testing Methods.

Simulation testing provides several advantages:

- Controllability – Simulation affords an unmatched ability to control many aspects of a test.
- Predictability – Simulation is designed to run as specified, so there is little uncertainty as to how the test will run.
- Repeatability – Simulation allows a test to be run many times in the same fashion, with the same inputs and initial conditions.
- Scalability – Simulation allows for generation of a large number and type of scenarios.
- Efficiency – Simulation includes a temporal component, which allows it to be sped up faster than real time so that many tests can be run in a relatively short amount of time.

The following components were identified as collectively making up the core aspects of a common ADS test scenario:

- Tactical maneuver behaviors
- ODD elements
- OEDR capabilities
- Failure mode behaviors

Tactical maneuver behaviors relate to the immediate control-related task(s) the ADS is executing as part of the test (e.g., lane following, lane change, turning). The relevant ODD elements generally define the operating environment in which the ADS is navigating during the test (e.g., roadway type, traffic conditions, or environmental conditions). OEDR capabilities relate directly to the objects and events the ADS encounters during the test (e.g., vehicles, pedestrians, traffic signals). Finally, some tests may include injection or simulation of errors or faults that induce failures at various stages within the ADS's functional architecture.

Test scenarios can be composed of one or more elements of each of these core components, visualized as the individual dimensions of the multidimensional test matrix in Figure 5. Each of these components may be included in a checklist identifying the aspects of each category that are incorporated in a given test.

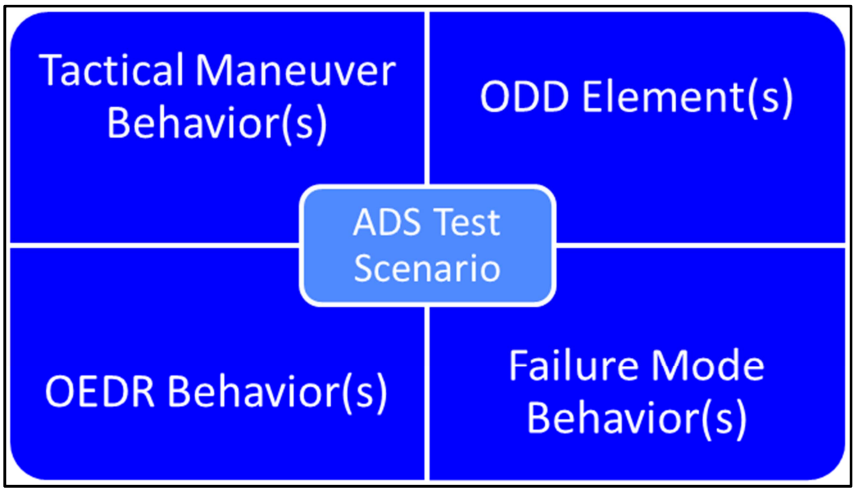

Figure 5. ADS Test Scenario Matrix.

CONCLUSIONS

This paper describes an example of a testing architecture and a scenario-based test framework to support the safe deployment of ADS and evaluate and assess their performance. Efforts focused on the testing of ADS (SAE International L3–L5), where the ADS is fully capable of all aspects of the DDT. To facilitate the identification of the testing architecture and framework, common and relevant operational components for ADS were identified and evaluated, specifically:

- ADS features
- ODD
- OEDR
- FO and FS strategies

The primary contribution of this research is the conceptual development of a test scenario framework that incorporates elements of each of these operational components. The framework uses a checklist-type approach to identify high-level scenario tests by specifying relevant tactical maneuvers, ODD, OEDR, and potential failures.

Each of these components are then further specified to develop a comprehensive set of procedures for a given scenario test. The scenario framework lends itself well to being applied across the three testing techniques identified for the testing architecture (M&S, closed-track testing, and open-road testing), although specific test procedures and implementations will vary, depending on the technique and tools used. This test scenario framework and the sample test procedures developed can provide a launching point to more comprehensive ADS test development and ultimately, test execution. Figure 6 shows a sample ADS test scenario visualization, with the principal elements notionally specified. (In this figure, SV stands for subject vehicle; POV stands for principal other vehicle.)

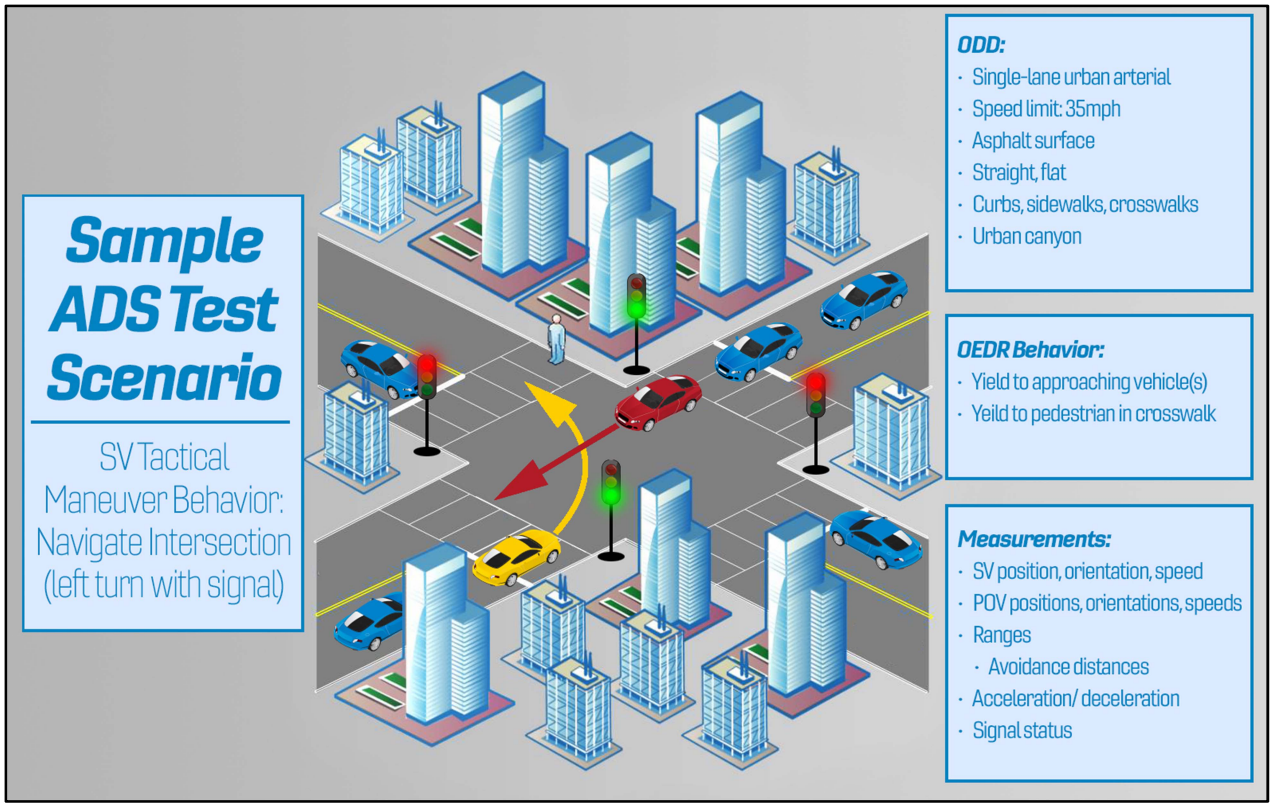

Figure 6. Sample ADS Test Scenario

The expansiveness of conceivable ODD, OEDR, and failure conditions presents a significant challenge to achieving comprehensive testing, even considering the test scenario framework identified during this research and described in this paper. The concept of risk associated with driving scenarios, notionally based on probability and severity of occurrence, has helped focus the analyses of ODD, OEDR, and failure modes to identify an appropriate testing process. A "reasonable worst case" approach may prove sufficient for general safety assessments; however, it is necessary to extend testing beyond the reasonable cases to understand the performance boundaries and limitations of ADS. This paper also identifies M&S capabilities and tools as a potential approach to addressing the expansiveness of these test components, as well as their potential combinations.

REFERENCES

Christensen, A., Cunningham, A., Engelman, J., Green, C., Kawashima, C., Kiger, S., . . . Barickman, F. (2015). Key Considerations in the Development of Driving Automation Systems. *Enhanced Safety Vehicles Conference*. Gothenberg, Sweden: NHTSA .

DARPA. (2008). *Urban Challenge*. Retrieved from DARPA: http://archive.darpa.mil/grandchallenge/

FHWA. (2008). *Managed Lanes: A Primer*.

IIHS. (2016, March). *Automakers agree to standard AEB by 2022*. Retrieved from IIHS HLDI: http://www.iihs.org/iihs/news/desktopnews/u-s-dot-and-iihs-announce-historic-commitment-of-20-automakers-to-make-automatic-emergency-braking-standard-on-new-vehicles

Kyrouz, M. (2017). *Medium*. Retrieved from https://medium.com/smart-cars-a-podcast-about-autonomous-vehicles/industry-comments-to-nhtsas-federal-automated-vehicles-policy-436e7e24911a

NHTSA. (2007). *Pre-Crash Scenario Typology for Crash Avoidance Research.* NHTSA.

NHTSA. (2015). *Human Factors Evaluation of Level 2 and Level 3 Automated Driving Concepts.* NHTSA.

NHTSA. (2016b). *Federal Automated Vehicles Policy.*

NHTSA. (2016c). *Budget Estimates - Fiscal Year 2017.* NHTSA.

NHTSA. (2016d). *Automated Vehicle Research for Enhanced Safety - Final Report.* NHTSA.

NHTSA. (2017b). *Traffic Safety Facts 2015.* NHTSA.

NHTSA. (2017c). *Traffic Safety Facts - 2016 Fatal Motor Vehicle Crashes Overview.* NHTSA.

SAE International. (2018). *J3016: Taxonomy and Definitions for Terms Related to Driving Automation Systems for On-Road Motor Vehicles.* SAE International.

POWER REQUIREMENTS FOR A REDUNDANT AUTOMATED STEERING SYSTEM FOR TRUCKS

Herold, Maximilian
Liebler, Maximilian
Winner, Hermann
Institute of Automotive Engineering, Technische Universität Darmstadt, Otto-Berndt-Str. 2, 64287 Darmstadt Germany

Paper Number 19-0302

ABSTRACT

For automated driven vehicles with a driving automation level above two, the driver is not available immediately as fallback when the automated driving system fails. Therefore, a redundant design for each automated driving system (e.g. the automated steering system) is a central safety requirement. The grade of redundancy, i.e. if it has to be fully fail operational or just a certain level of fail degraded, depends on the definition of the safe state in case of a failure and on the way how to reach it. The safe state itself depends on the driving situation respectively the type of road, where the automated vehicle is driving. The goal of this article is to determine the amount of steering power and energy required in different use cases and road types to reach the safe state.
Therefore, a definition of the safe state for automated driving trucks is determined using the ISO 26262 and existing definitions. With the help of German national road construction guidelines for highways, rural roads and urban roads, the safe state and the necessary driving maneuvers to reach it are determined for different defined road types. A 12-t two-axle truck has been equipped with measurement equipment as test vehicle. The determined driving maneuvers to reach the safe state are driven with the test vehicle and the required steering power and steering energy are measured.
The results of this investigation are the minimum required steering torque, power and energy for each tested driving maneuver. The minimum redundancy requirements to the automated steering system for a specific use case of automated driving, such as fully automated highway driving, are determined considering all driving maneuvers to reach the safe state in the worst case. Depending on the intended use cases for the automated vehicle, different fallback requirements are determined for the redundant automated steering system. Although the achieved results of this contribution are only representative for the used test vehicle, they are still helpful to get an impression and some real data for the required fallback steering torque, power and energy. It has to be considered that the required steering power and steering energy are highly influenced by the front axle load and thus by the load of the vehicle and by the steering and axle geometry of the vehicle as well. However, based on the findings of this article, the fallback concepts of future redundant active steering systems for highly and fully automated driven trucks can be developed according to the intended use cases.
The requirements for the mentioned exemplary use case of fully automated driving on highways with hard shoulders are very low, thus it should be possible to realize the steering redundancy with low effort. However, for other use cases the redundancy requirements are much higher.

INTRODUCTION

Automated driving is a key topic of development not only in the passenger car industry, but also in the commercial vehicle industry. The increase of safety, the reduction of emissions and the cost saving are the main motivation for such development actions. Whereas there are no technical hurdles for partial automated driving of trucks, e.g. Adaptive Cruise Control (ACC) with Lane Keeping Support (LKS), there are still a lot of open questions, before highly automated driving can be introduced on public roads. Exemplary systems with higher levels of automation are “exit-to-exit highway automation”, “traffic jam assist” or “automated trailer backing” [1].
One of those challenges is to ensure a safe operation during highly automated driving in all possible situations, which also includes a malfunction of one of the systems, which are necessary for the automated driving. [2] categorizes the levels of driving automations, whereby partially automated driving is listed as level 2 (AD2) and highly automated driving is listed as level 3 or higher (AD3+). The driver is not available anymore as immediate fallback level for AD3+. Hence, the automated system has to be redundant and has to provide its own fallback level for the case of a malfunction. This redundancy can be realized inside one system or outside by an additional system. In case of an automated steering system, the steering system can be redundant by itself, but a steering function can also be realized by the brake system using differential braking to steer the vehicle. Although it is possible to steer a truck with the brake system, [3] proofs that it is not feasible for all relevant driving maneuvers of a truck. Additionally [4] argues that the dynamic and the precision of brake steering is not sufficient for the use as steering redundancy. Thus, a redundant automated steering system is mandatory for AD3+.

This article covers the question, how much steering torque, steering power and steering energy is required for the fallback level of a redundant automated steering system for trucks. Therefore, the used research methods are described first and the different results of the investigation are shown and explained afterwards. The article ends with the conclusion of the obtained test results and their discussion.

METHODOLOGY

For the determination of the demanded fallback steering requirements, it is necessary to derive the requirements for a safe state of a truck. Different safe states are defined for different Road Classes using these requirements and German guidelines for road construction. With this definitions, it is possible to determine the different relevant maneuvers, which are necessary to reach the defined safe state. With the help of a test vehicle equipped with measurement equipment for steering torque and angle, the steering power and the steering energy required for each relevant driving maneuver are recorded. The steering redundancy requirements are derived from the measured test data and the determined relevant maneuvers to reach the safe state.

Definition of a Safe State

Since an automated driven vehicle contains a lot of E/E systems (electric/electronic), the definition of its safe state bases on the ISO 26262 on functional safety of E/E systems of vehicles. According to [5] the safe state is defined as an "operating mode of (a vehicle) without an unreasonable level of risk", whereas the risk is defined as the "combination of the probability of occurrence of harm and the severity of that harm" and the harm is the "physical injury or damage to the health of persons". In the context of automated driving [6] describes the safe state as an operating mode, where no unreasonable risk occurs for all persons involved in road traffic. Thus, the internal system state as well as the environment of the vehicle are important for the safe state.
Based on the definitions from the ISO 26262, eight requirements of the safe state are determined here (See Table 1). The first requirement is the most important and a high-level requirement. All the other requirements serve to fulfill this superior requirement. The requirements no. 2 to no. 6 are the important requirements for this investigation. The safe state in each specific driving situation depends on those five requirements. Therefore, we separate the safe state for city roads, country roads, and highways.

Table 1.
Requirements to the Safe State of an Automated Driven Vehicle

No.	Requirement
1	No hazard for passengers, other road users, pedestrians or for the environment
2	Vehicle stands still
3	Visibility to other road users bigger than required stopping visibility
4	Relative velocity to other road users less than 70 km/h
5	No blocking of rescue routes
6	No blocking of bridges, tunnels, intersections or roundabouts
7	Protection of the stopping place and warning of other road users
8	Emergency call (if necessary)

To define a safe state for each different type of road, it is important to know all the specific properties of each type, especially according to the possibilities for a safe stop of the vehicle. The German guideline for the construction of city roads [7], the guideline for the construction of country roads [8] and the guideline for the construction of highways [9] describes the properties of the roads and are used to define three different Road Classes according to the possibility for a safe stop.
The different types of roads are characterized into three Road Classes (see Table 2). The number of lanes, counting both directions, the availability of a hard shoulder or an emergency stopping bay, the speed limit, the minimum curve radius and the maximum required stopping visibility are used for the classification. The first Road Class contains the roads with a permanent hard shoulder, i.e. highways except urban highways. The second Road Class describes the roads with emergency stopping bays instead of a permanent hard shoulder, i.e. urban highways and big country roads with two lanes at least in one direction. The last Road Class, which requires steering maneuvers to get to a safe state, contains the roads without a hard shoulder and without any emergency stopping bays. City roads are not part of these three classes, because according to [7] there are always speed limits below 70 km/h. A relative velocity to other road users of more than 70 km/h is not possible. Hence, the transition to the safe state is

always an immediate braking maneuver and no steering is required for this classes. The claim is, that the automated vehicle knows what the safe states and the maximum distances between the single safe states are and how it gets there, depending on the Road Class.

Table 2.
Characterization of Road Classes according to [7], [8], [9]

Class	**1**	**2**	**3**
Number of lanes (both directions)	≥ 4	≥ 3	2
Hard shoulder available?	yes	partially	none
Emergency stopping bay available?	-	at least every 1000 m	none
Speed limit	none	≥ 100 km/h	≤ 100 km/h
Minimum curve radius	470 m	280 m	200 m
Maximum required stopping visibility	250 m	190 m	160 m

The safe state of the class with a hard shoulder is the stand still on the hard shoulder. Usually, no other road user drives on the hard shoulder, thus there is no relative velocity to others. In addition, the stopping visibility has no influence on this safe state and no bridge, tunnel or rescue route is blocked here. The relevant maneuvers to reach the safe state depends on the amount of lanes of the road and on which road the vehicle drives currently, when a failure occurs and the transition to the safe state is required. If the vehicle is not on the lane next to the hard shoulder, one or more lane changes and the change to the hard shoulder are the relevant maneuvers to reach the safe state. Because in areas of highway accesses or exits are no hard shoulders, a change to the hard shoulder could be temporarily not possible. In that case, the vehicle needs to drive on for a defined distance until the hard shoulder is available again.
Driving into and stopping inside an emergency stopping bay is the safe state of the second Road Class, where such a stopping bay intended to be every 1000 m. The emergency stopping bays are at least 84 m long and 3 m wide according to [8]. Because the emergency stopping bay is no continuous lane, no other road user is able to drive on it, whereby the risk seems to be lower standing inside an emergency stopping bay as standing on a hard shoulder. The relevant maneuvers to reach the safe state inside a stopping bay contain one or more lane changes as well, the drive and stopping maneuver into the stooping bay and the required drive on to the next available stopping bay. It is also possible, that there are temporarily hard shoulders available on this Road Class, but for the design requirements of the steering system, the highest fallback requirements are used, which occur for the drive into an emergency stopping bay for this Road Class.
Because of the missing hard shoulders and the missing emergency stopping bays, the safe state of the third class is not obvious. A safe stop at the side of the road is usually not possible due to a relative velocity to the other road users above 70 km/h. However, in practice there are frequently junctions appearing on this class of roads, whereby a turn-off to a side road with a speed limit lower than 70 km/h or to a road with a hard shoulder or emergency stopping bays is possible. A safe stop on such a side road, e.g. a city road, represents the safe state in this Road Class. Hence, the relevant maneuvers are the drive on until the next turn-off to a side road and the turn-off maneuver itself. Of course, it is possible, that there is a stopping bay or a parking lot at this Road Class as well, but this is an exception and the fallback requirements of the steering system are higher for the turn-off maneuver thus these are the crucial design requirements.

Driving Maneuvers
Based on the previous defined safe states for the three different Road Classes, the different relevant driving maneuvers (see Table 3) are performed with a 12-t truck meanwhile the required steering torque, steering power and steering energy are recorded.
Besides the previous mentioned relevant driving maneuvers, the avoidance maneuver is also considered as relevant, because it is possible at any time and at any Road Class, that an avoidance maneuver becomes necessary. The different types of maneuvers are driven several times on several roads, i.e. different routes of country roads, different highways and different city routes were tested. For each type of maneuver, the biggest occurring values for torque, power and energy are used to determine the fallback requirements. With this approach, it is supposed to cover the worst case of each type of maneuver. The measured data of the several maneuvers are combined according to the definition of the safe state in the previous chapter to determine the final fallback requirements for each Road Class. Hereby, the most critical moment for the failure of the steering system is assumed. However, a complete cover of all possible situations is not guaranteed of course.

Table 3.
Relevant Driving Maneuvers driven by 12-t Truck

Maneuver type	$v_{\max}$ in $\frac{\mathrm{m}}{\mathrm{s}}$	$a_{y,\max}$ in $\frac{\mathrm{m}}{\mathrm{s}^2}$	$R_{\min}$ in m
Turn-off to side road (out of city)	-	5,00	70
Lane change (slow)	17	1,37	-
Lane change (fast)	25	2,16	-
Avoidance maneuver	17	5,00	-
(Big) Emergency stopping bay [8]	25	1,96	-
(Small) Emergency stopping bay [8]	17	1,57	-
Highway access/exit	-	3,14	150
Highway interchange	25	3,14	400
Road Class 1	25	2,45	470
Road Class 2	25	3,43	280
Road Class 3	20	3,43	140
Mountain pass	17	3,53	45
City driving	14	3,24	50

Test Equipment
For the test drives, a fully loaded 12-t truck is used with a measured front axle load of 42.6 kN (vehicle data see Table 6 in Appendix). A measurement steering wheel records the torque and the steering angle at the steering wheel. Strain gauges are applied at the pitman arm to measure the output steering torque of the steering system. In addition, the acceleration in all three directions, the velocity and the GPS position of the truck are recorded as well.
The steering angle velocity of the pitman arm is derived from the measured steering wheel angle and the known ratio of the steering gear. The measured output steering torque is integrated over the steering angle at the pitman arm and thus determines the overall steering energy, which itself determines the steering power by derivation over time. Exemplary for the data recording, the measured steering torque at the pitman arm, the measured angular velocity at the pitman arm, the calculated steering energy and power as well as the particular maximum values are shown in Figure 3 (see Appendix) for the maneuver highway exit.

Requirements for a Redundant Automated Steering System
The feature of a redundant automated steering system is the fail operational fallback level integrated inside the steering system. Hence, in case of a partial failure of the steering system, it is still able to steer the vehicle safely without the need of a take-over by the driver. It is required, that the fallback level of the steering system is able to transfer the vehicle into a defined safe state at any time. Therefore, the fallback steering system has not to fulfill the requirements for the failure-free steering system, but the reduced fallback requirements. This reduced performance is called fail degraded.
The maximum required steering torque and steering power determines the minimum steering torque and power the steering system has to produce at least to pass the relevant driving maneuvers in the fail degraded mode. The minimum required steering energy determines the steering system has to provide to reach the safe state even in case of a failure of the power supply.

RESULTS

The maximum occurring steering torque at the pitman arm and the maximum occurring angular velocity at the pitman arm during the different maneuvers are described first. Both parameters are used later to calculate the maximum required steering power and steering energy for each maneuver.

Steering Torque
Figure 1 shows the maximum steering torque and the maximum angular velocity occurring at the pitman arm during the different maneuver. The illustrated values of maximum pitman arm torque and maximum angular velocity of the pitman arm not always occur simultaneously during a maneuver, which is why the product of those two maximum values could be higher than the actual required maximum steering power (see Figure 2).
The maneuver types can be classified into three groups according to their required maximum steering torque. Group A considers the maneuvers requiring less than 600 Nm of torque at the pitman arm. With those maneuvers,

regular driving on the Road Classes 1 and 2 is possible including lane changes, interchanges as well as the driving into a stopping bay. Group B with required steering torques between 600 Nm and 1000 Nm contains the Road Class 3 driving without turning maneuvers, the maneuvers for leaving a highway as well as an avoidance maneuver. The most advanced steering torque requirements between 1000 Nm and 1500 Nm arise for Group C during mountain pass driving, city driving and turning maneuvers.

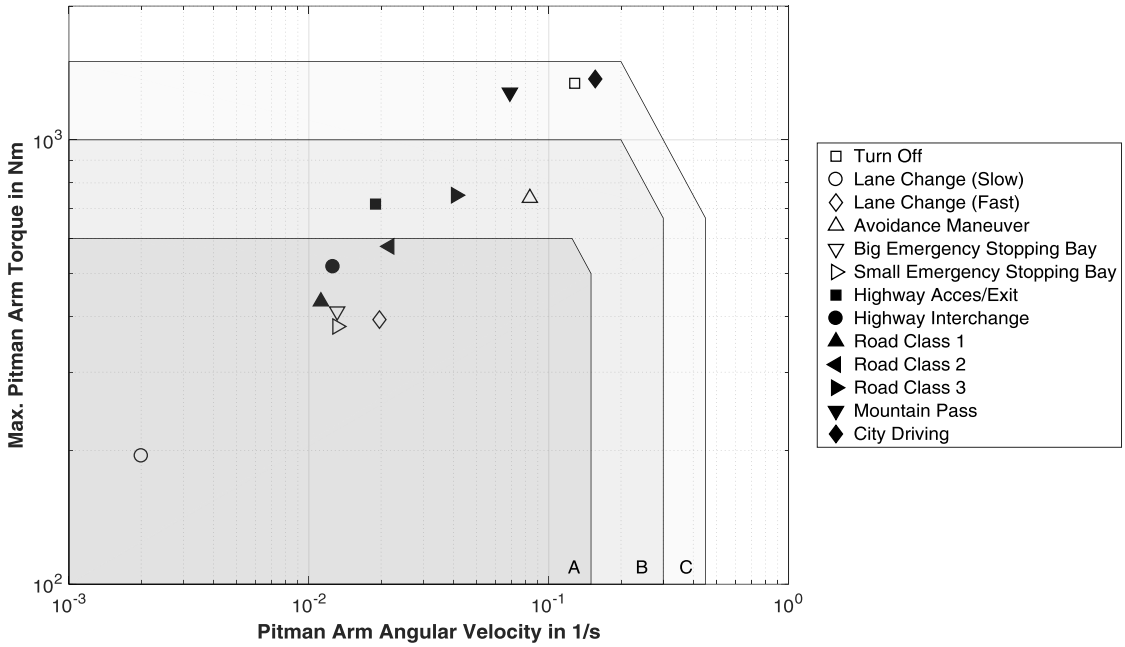

Figure 1. Maximum Occurring Steering Torque T_{Pitman} and Angular Velocity at Pitman Arm $\dot{\delta}_{\text{Pitman}}$

Steering Energy

The energy required for steering during the different driving maneuvers is the measured steering torque at the pitman arm T_{Pitman} integrated over the steering angle at the pitman arm δ_{Pitman} as described in Equation 1:

$$E_{\text{Steering}} = \int T_{\text{Pitman}}\, d\delta_{\text{Pitman}} \qquad \text{(Equation 1)}$$

The maneuvers highway driving, country road, mountain pass and city driving are special cases here, since the required energy depends on the driven distance of course. However, to get an indication for the required steering energy during these maneuvers the maximum demanded steering energy on a driving distance of 1 km is used and illustrated with the required steering energy during the other maneuvers in Figure 2.

The classification into the three Groups of driving maneuvers is also feasible for the steering energy. Group A has again the lowest requirements with a required steering energy of less maximum 100 J for the drive of a single maneuver. Between 100 J and 500 J are required by the maneuvers of Group B. Group C requires with between 500 J and 1000 J by far the most steering energy.

Steering Power

The steering power at the pitman arm of the truck occurring during the different driving maneuvers is the derivation of the steering energy E_{Steering} as described in Equation 2:

$$P_{\text{Steering}} = \frac{dE_{\text{Steering}}}{dt} \qquad \text{(Equation 2)}$$

Figure 2 shows the maximum steering power required during each maneuver type. The maneuver types are classified into three Groups according to the maximum required steering power, similar to the classification in the previous chapters. Group A with the lowest power requirement of maximum 75 W contains the Road Classes 1 and 2, highway interchanges, lane changes and the driving into emergency stopping bays. The highway exit, the avoidance maneuver and the Road Class 3 driving form Group B with a maximum required steering power between 75 W and 150 W. The maneuvers turn-off, mountain pass and city driving requires between 150 W and 300 W of steering power and thus are classified to Group C.

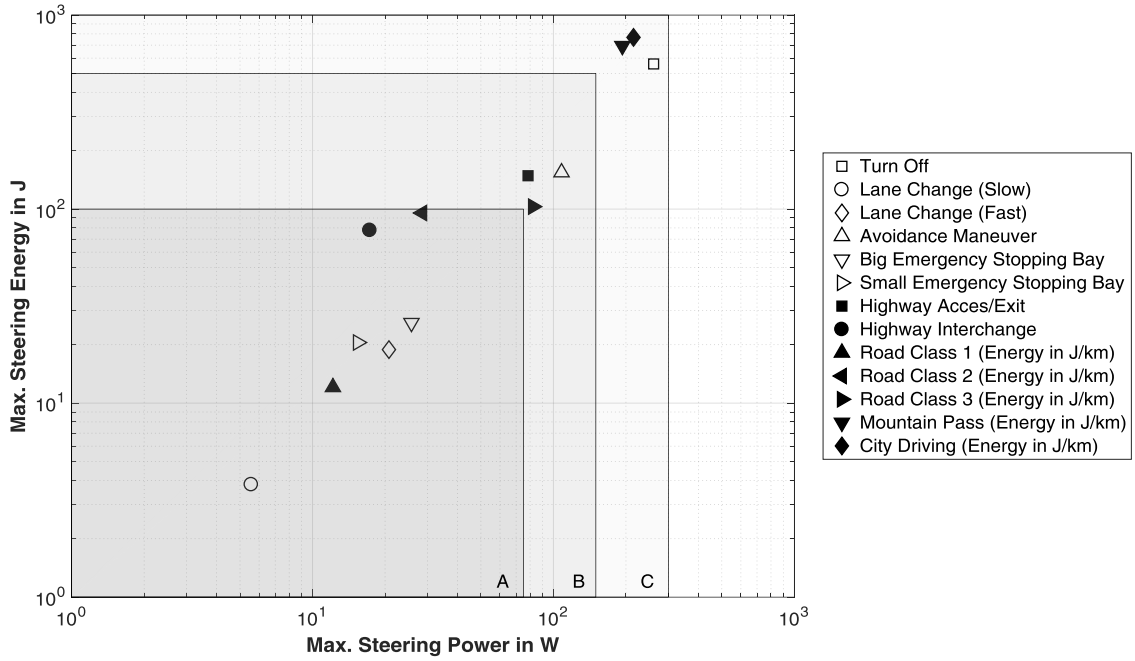

Figure 2. Maximum Steering Power and Maximum Steering Energy

The results from the performed test runs considering the required steering torque, power and energy during the defined relevant maneuvers as well as the classification of these maneuvers into three Groups according their requirements are listed in Table 4. The maneuvers are separated into the three Groups without any overlapping.

Table 4.
Steering Requirement Groups

Group	Maneuver type	$T_{\text{Pitman,max}}$	$P_{\text{Steering,max}}$	$E_{\text{Steering,max}}$
A	Lane change (slow)	< 600 Nm	< 75 W	< 100 J
	Lane change (fast)			
	(Big) Emergency stopping bay			
	(Small) Emergency stopping bay			
	Highway interchange			
	Road Class 1			
	Road Class 2			
B	Avoidance maneuver	600 – 1000 Nm	75 – 150 W	100 J – 500 J
	Highway access/exit			
	Road Class 3			
C	Turn-off to side road (rural roads)	1000 - 1500 Nm	150 - 300 W	500 - 1000 J
	Mountain pass			
	City driving			

Redundancy Requirements

The determined requirements for the different Groups (see Table 3) are used to develop exemplary redundancy requirements for the three different Road Classes and the available 12-t truck. For each Road Class an exemplary combination of maneuvers out of the three different requirement Groups is set up, which are necessary to reach the defined safe state (see Table 4). The exemplary cases are set up according to the worst-case situations for the occurrence of a malfunction, which were found by analysis the roads in the surrounding area of Darmstadt. The torque and power requirements are independent of the amount of necessary maneuvers to reach the safe state. Of course, the required steering energy increase with an increasing amount of necessary maneuvers and with an increasing necessary driving distance.

For the Road Class 1 with a permanent hard shoulder, a worst-case scenario of a failure is, if the malfunction occurs when the truck is on the third lane from the hard shoulder, thus to reach the safe state, three lane changes

are required to stop on the hard shoulder. Because lane changes are not always possible immediately, 1000 m of Road Class 1 driving are considered as well for determining the redundancy requirements. If an avoidance maneuver is necessary as well, the requirements are much higher for this Road Class (see Table 4). The Road Class 2 with emergency stopping bays is quite similar to the Road Class 1, but the difference is, that a safe stop is not possible at any time. A safe stop is only possible at an emergency stopping bay instead, which are only available at a distance of 1000 m. Therefore, to reach a safe state of this Road Class in the worst-case, 2000 m of Road Class 2 driving, two lane changes and the drive into an emergency stopping bay are necessary. The requirements for this class are also much higher, if an avoidance maneuver or another maneuver from Group B is necessary (see Table 4). The Road Class 3 differs from the other two, because there is no safe stop possible at the side of the road. In contrast, a turn-off maneuver is necessary to get to a road where a stop at the side of the road is possible or where the speed limit is below 70 km/h and thus a safe stop in the road is possible. Since a turn to such a road is not possible within a short distance in any case, a 5000 m Road Class 3 drive and a subsequent turn to a side road are considered as relevant to reach a safe state of this class. These maneuvers causes the highest steering redundancy requirements (see Table 5).

Table 5.
Redundancy Requirements

Road Class	**Exemplary Maneuvers to reach Safe State**	$T_{\text{Pitman,max}}$	$P_{\text{Steering,max}}$	$E_{\text{Steering,max}}$
1	4x Group 1 (add. avoidance maneuver: 1x Group 2)	600 Nm (1000 Nm)	75 W (150 W)	400 J (900 J)
2	5x Group 1 (add. avoidance maneuver: 1x Group 2)	600 Nm (1000 Nm)	75 W (150 W)	500 J (1.00 kJ)
3	5x Group 2 1x Group 3	1500 Nm	300 W	3.50 kJ

CONCLUSION

This paper investigates the redundancy requirements exemplary for a 12-t truck. Therefore, the requirements for a safe state of an automated vehicle are developed with the help of the definitions from the ISO 262626 [5] and [6] (see Table 1). According to German road construction guidelines three different Road Classes are defined according to their different safe states. Several driving maneuvers are determined, which are necessary to reach the different defined safe states (see Table 3).
With the help of driving tests with an available 12-t truck equipped with appropriate measurement equipment, the steering requirements for each of these defined relevant driving maneuvers are recorded and the maneuvers are classified into three groups according their requirements (see Table 4). By combining some of these maneuvers to reach a safe state in an exemplary scenario, the redundancy requirements are calculated for each Road Class (see Table 5).
Although the determined requirements are only exemplary for the used test vehicle and the combinations of maneuvers to reach the safe state are only exemplary as well, it is significant, that the requirements for the Road Class without a hard shoulder or stopping bays are much higher compared to the requirements of the other two Road Classes. Hence, it is concluded that the redundancy requirements for steering systems are much lower, if the automated driven truck only drives on roads with hard shoulders or emergency stopping bays. The fully automated highway driving is such a use case. According to the definition of the safe state in this paper, there are no steering redundancy requirements for inner city automated driving, since an immediate safe stop is possible here at any time. If the truck should be able to drive automated on all types of roads, including on roads with an operation speed above 70 km/h and without hard shoulder or stopping bays, such as country roads, the highest steering fallback steering torque, steering power and steering energy are required.
To determine feasible values for the steering redundancy requirements, an exact definition of the intended use case is necessary to be able to determine the relevant maneuvers to reach the safe state at any time. With this information, the steering requirements necessary for these maneuvers can be used to determine the final steering requirements for this defined use case.
With the help of a simulation model of a truck steering system, including the geometry of the truck's front axle and its tire properties and the trajectory of the described driving tests as an input, it is possible to simulate the required steering torque, power and energy. Such a model is adaptable to calculate the redundancy requirements for other trucks, for example with higher steering axle loads. Of course, not only the axle load, but also the axle geometry and the tire properties has to be adapted to other trucks.

REFERENCES

[1] Engström, J. et al. 2019. "Deployment of Automated Trucking: Challenges and Opportunities.“ In Road vehicle automation 5. Springer, Cham, Switzerland, 149–162

[2] Society of Automotive Engineers. 2016. "Taxonomy and definitions for terms related to on-road motor vehicle automated driving systems." J3016. SAE International

[3] Herold, M.,Said, O. and Winner, H. 2018. "Simulative Assessment of Differential Braking for Steering Redundancy in Automated Driven Trucks.“ In SIMVEC*:* Simulation und Erprobung in der Fahrzeugentwicklung, Baden Baden

[4] Michael Reichenbach. "Interview with Alexander Gaedke: Mit 1000 Parametern für das Lenkgefühl können wir richtig Gas geben.“ *ATZ Automobiltech Z*, Nr. 6, 22–242017.

[5] International Organization for Standardization. 2011. "Road vehicles - Functional safety - Vocabulary." ISO 26262-1. Schweiz

[6] Reschka, A. 2017. "Fertigkeiten-und Fähigkeitengraphen als Grundlage des sicheren Betriebs von automatisierten Fahrzeugen im öffentlichen Straßenverkehr in städtischer Umgebung." TU Braunschweig

[7] Forschungsgesellschaft für Straßen- und Verkehrswesen. 2006. "Richtlinie für die Anlage von Stadtstraßen." RASt 06. FGSV Verlag GmbH, Köln

[8] Forschungsgesellschaft für Straßen- und Verkehrswesen. 2012. "Richtlinie für die Anlage von Landstraßen." RAL. FGSV Verlag GmbH, Köln

[9] Forschungsgesellschaft für Straßen- und Verkehrswesen. 2008. "Richtlinie für die Anlage von Autobahnen." RAA. FGSV Verlag GmbH, Köln

APPENDIX

Table 6.
Vehicle Data

Parameter	Value
Total mass	11900 kg
Front axle mass	4340 kg
Wheel base	3.25 m
Track width front axle	1.94 m
Track width rear axle	1.79 m
Tire dimension	245/75 R17.5 134/132 L
Tire pressure	8 bar
$\dot{\delta}_{\mathbf{SteeringWheel}}/\dot{\delta}_{\mathbf{Pitman}}$	16.4 – 18.9
$\dot{\delta}_{\mathbf{SteeringWheel}}/\dot{\delta}_{\mathbf{FrontWheel}}$	12.0 – 20.0

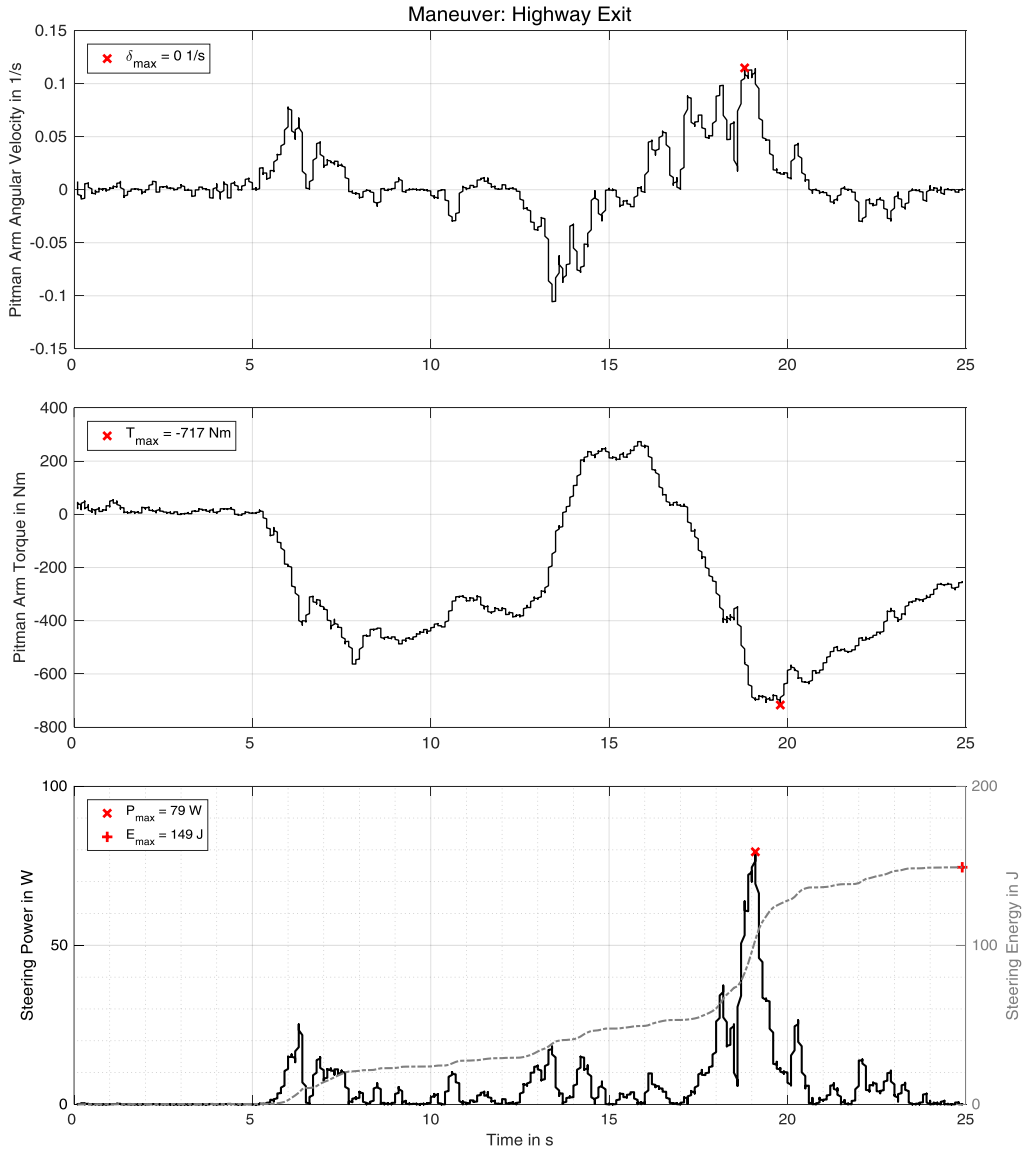

Figure 3. Pitman Arm Angular Velocity, Pitman Arm Torque, Steering Power and Steering Energy exemplary for the Maneuver Highway Exit

NATURALISTIC STUDY OF LEVEL 2 DRIVING AUTOMATION FUNCTIONS

Paul Rau
National Highway Traffic Safety Administration
United States

Sheldon Russell
Myra Blanco
Vikki Fitchett
Jon Atwood
Virginia Tech Transportation Institute
United States

Paper Number 19-0303

ABSTRACT

Currently, there are commercially available vehicles that include features capable of providing Level 2, Partial Driving Automation as defined by SAE International. Research on the use and performance of the systems that these vehicles employ in natural settings is needed to help clarify the systems' potential benefits. The *Naturalistic Study of Level 2 Driving Automation Functions* (L2 NDS) project described herein has generated practical data to support the understanding of the use of automated lateral and longitudinal control functionality by evaluating a subset of currently available advanced technologies as drivers experience them during daily use.

The objective of the L2 NDS project was to investigate, through a naturalistic driving study, real-world driver interaction with commercially available driving automation systems. Ten vehicles equipped with both lateral and longitudinal automated features were instrumented and loaned to participants for a 4-week period. A total of 120 drivers were recruited over a 14-month data collection period. Each study vehicle was equipped with Virginia Tech Transportation Institute's NextGen Data Acquisition System, which continuously records video of the both the driver and the roadway, as well as vehicle data and automated lateral and longitudinal control activations. These data were used to analyze driving automation system use and driver performance during the study.

Focus area 1 investigated *System Performance*, including overall use of the features. Participants drove 216,585 miles, with 70,384 miles driven with both lateral and longitudinal control features active. Focus area 2 investigated *Driver-System Interaction* and involved a review of driver behaviors during driving automation system use, specifically the prevalence of non-driving tasks. Drivers were observed engaging in non-driving tasks, but these were not related to feature use. Focus area 3 investigated *Driver Performance*, which was measured by drivers' responses to Request to Intervene (RTI) alerts generated by the driving automation systems. Driver behavior was consistent with active driving/supervision of the automated features; drivers were receptive to RTI alerts. No RTIs were associated with any safety-critical events (i.e., crashes and near-crashes). In total, 5 minor crashes (no injury or visible damage) and 66 near-crashes were observed across the entire data set. No statistical relationship was observed between safety-critical event rates and feature activation level. Focus area 4 investigated *Driver Engagement*, which includes subjective feedback obtained from participants. Participants reported that they were generally comfortable and felt safe using the features, with self-reported trust increasing over the course of the study.

INTRODUCTION

The objective of the *Naturalistic Study of Level 2 Driving Automation Functions* (L2 NDS) project was to investigate, through a naturalistic driving study (NDS), real-world driver interaction with commercially available vehicles that could sustain lateral and longitudinal motion control. The study objectives were to observe and evaluate how drivers operated vehicles equipped with lateral and longitudinal driving automation features intended for operation in mixed traffic under a variety of roadway types, driving conditions, and speeds. This study was also intended to support the identification and/or refinement of human factors-related needs to help encourage the safe operation of vehicles with driving automation features.

Currently, there are several commercially available vehicle models offering optional features that automate at least some portion of lateral and longitudinal vehicle control. Depending on the make of the vehicle, different terms are used to name and describe these automated lateral and longitudinal control features. For example, the lateral control feature may be referred to as steering assist, lane keep assist, or lane centering, while the longitudinal control feature is often termed adaptive cruise control, intelligent cruise control, or advanced cruise control. In some cases, these systems activate together, while other implementations require two separate feature activations. When automated lateral and longitudinal control features are combined, the overall driving automation systems can be considered Level 2 (L2), Partial Driving Automation [1]. SAE describes the roles of the driving automation system and the driver during L2 driving automation in standard J3016, originally published in 2016:

> The Driving Automation System (while engaged): 1) Performs part of the dynamic driving task (DDT) by executing both the lateral and longitudinal vehicle motion control subtasks, and 2) Disengages immediately upon driver request.
>
> The Driver (at all times): 1) Performs the remainder of the DDT not performed by the driving automation system, 2) Supervises the driving automation system and intervenes as necessary to maintain safe operation of the vehicle, and 3) Determines whether/when engagement and disengagement of the driving automation system is appropriate, and immediately performs the entire DDT whenever required or desired. (p. 19)

The research team notes that there is ongoing discussion regarding classification and definitions of driving automation systems and features. Although the report title includes the term “Level 2,” the goal of this research project was not to classify features as Level 2, but rather to determine how drivers interact with a range of driving automation features. Given the myriad of terms used to name or brand these types of automation, the general terms “automated lateral control features” and “automated longitudinal control features” are used in this paper.

The project was designed to address four main focus areas, with specific research questions assigned to each. Focus area 1 investigated ***System Performance***. Sampled and reduced data were used to provide insight into the systems’ performance. Focus area 2 investigated ***Driver-System Interaction*** and involved a review of driver behaviors during driving automation system use, specifically the prevalence of non-driving tasks. Focus area 3 investigated ***Driver Performance***. Driver performance was measured by drivers’ responses to Request to Intervene (RTI) alerts generated by the driving automation systems. Focus area 4 investigated ***Driver Engagement***, which includes subjective feedback obtained from participants. The project also included a Longer Drive Sub-Study focused specifically on drives longer than 2 hours.

METHODS

Two each of the following vehicles were leased for the duration of the study. Each of the selected models allowed drivers to simultaneously activate longitudinal and lateral automation features (relevant packages required are listed). As part of the lateral automation feature, all vehicles generated RTIs informing the driver to return hands to the steering wheel or otherwise administer lateral control input.

- 2017 Audi Q7 Premium Plus 3.0 TFSI Quattro with Driver Assistance Package
- 2015 Infiniti Q50 3.7 AWD Premium with Technology, Navigation, and Deluxe Touring Package
- 2016 Mercedes-Benz E350 Sedan with Premium Package, Driver Assistance Package

- 2015 Tesla Model S P90D AWD with Autopilot Convenience (software version 8.0)
- 2016 Volvo XC90 T6 AWD R with Design and Convenience Packages

Each vehicle was equipped with Virginia Tech Transportation Institute's (VTTI's) NextGen Data Acquisition System (DAS). As shown in Figure 1, the DAS continuously recorded video of the forward roadway, the driver's face, an over-the-shoulder view of the driver's hands and lap area, a view of the footwell, and a rear view. The DAS also recorded vehicle data, including speed, accelerator pedal position, brake application, acceleration, lane position, turn signal activation, and GPS coordinates.

Figure 1. Example of video views collected by the DAS

For each driving automation system, the general operational envelope was ascertained in various driving environments. The longitudinal control features utilized a forward-looking set of sensors (typically radar-based; for some vehicles, forward camera data was also included). None of the longitudinal control features directly responded to traffic ahead in adjacent lanes. Following distance could be adjusted by the driver, with following distance settings having an approximately 2–3-second headway.

Lateral control features varied in their overall capability. In some cases, the lateral control feature would initiate steering as the study vehicle approached a lane marking, while in others the system operated more akin to a "lane centering" feature, with active steering from the feature. Lateral control features utilized a forward-looking camera with a vehicle-specific machine vision algorithm to track lane markings.

Regardless of overall capability, all features required active monitoring from the driver and frequent intervention. For all vehicles, the intended use of the lateral control features required the driver's hands on the wheel to engage it, and drivers were warned not to use the driving automation systems in poor visibility conditions, weather related or otherwise. As noted, the vehicles varied somewhat in feature availability and activation; in some cases, the lateral control feature was only available if the longitudinal control feature was already engaged, or the two features engaged simultaneously. For most of the vehicles, the following feature generalizations are most relevant for the current paper:

- Driving automation systems were intended for use in highway driving environments with clear weather
- Lateral control features were generally available at speeds above 40 mph with visible lane markings
- Lateral control features were based on a vehicle-specific machine vision system to track lane markings
- Additional sensors (e.g., ultrasonic) may have been used for lateral safety systems such as blind spot warning
- Longitudinal control features were available above 20 mph
- Longitudinal control features were forward-radar based

- No vehicles included corner or side-facing radar units
- RTIs were all generated as part of the lateral driving automation feature
- Timing was based on the lack of detected steering inputs from the driver and/or crossing a detected lane marking
- RTIs were multi-modal, including both a visual and auditory component (no RTIs included a haptic component)

Although some vehicles tested included a "low speed" version of driving automation (i.e., traffic jam assist, pilot assist, autopilot), baseline epochs for this effort were sampled from the speeds outlined above for lateral and longitudinal control features. However, RTIs and safety-critical events (SCEs; i.e., crashes and near-crashes) were included from all speeds.

PARTICIPANTS

A total of 120 participants were recruited—12 participants for each of the 10 selected study vehicles. All participants were recruited from the Washington, DC region, which included both northern Virginia and Maryland suburbs. Participants were balanced across age and gender and were recruited from two age groups: 25 to 39 years old, and 40 to 54 years old, which were the age groups used in previous test track research [2]. For each set of 12 participants, six were from the younger age group (three male and three female) and six were from the older age group (three male and three female).

Drivers were compensated up to $500 as follows: 1) up to $360 if their total mileage was under or equal to 1,200 miles; or 2) $500 if they exceeded 1,200 miles. They were also lent a transponder that gave them free access to the high-occupancy toll lanes managed by Transurban.

APPROACH

Each driver was assigned to one vehicle for the duration of their 4-week participation time in the study. Drivers received training on the vehicles designed to mimic what they would receive at a dealership if purchasing a new car. Training consisted of a static orientation and a two-part test drive. The static orientation included instruction on all of the driving automation system features. During the first part of the test drive, the onsite researcher drove the study vehicle and demonstrated the driving automation features. Once the researcher completed the demonstration of the features, the participant took over driving the vehicle. The participant was then able to experience features and ask the researcher any remaining questions. After completing training, participants drove the study vehicle instead of their own vehicle during the 4-week participation period.

Participant data was saved to a secure server and analyzed once driving periods were complete. Continuously recorded data were then sampled for further annotation and analysis. Trained data reductionists reviewed the sampled recorded video, audio, and parametric data to annotate the driver, vehicle, and environmental factors that were present during each of the sample types (driving automation system use, RTI alerts, and SCEs).

DATA SAMPLING AND REDUCTION

NDSs provide continuous data recording while participants are driving. The focus of this section is to describe the approach to sampling, reducing, and analyzing continuously recorded data. Established kinematic algorithms (e.g., hard decelerations, lane departures, high yaw rates) were used to identify potential SCEs. Trained data reductionists (see below) then inspected the videos associated with these events to verify the occurrence of an SCE. For baseline driving samples, 15-second epochs were sampled from the continuously recorded data. The 15 seconds were divided into 10 seconds prior to and 5 seconds after the time of interest. Samples were taken during instances in which both the lateral and longitudinal driving automation features were engaged, during instances in which the driving automation system was available but not engaged, and during instances in which both features of the driving automation system were available but only one was engaged. Instances in which an RTI was issued were also sampled. Driving automation was available when the vehicle was traveling above the speed required for activation on a road with visible lane markings. The sampling approach was as follows:

- All periods in which the driving automation system was available for use and also active were identified using a VTTI-developed machine-vision algorithm combined with available vehicle network information.
- Up to twelve 15-second epochs per driver were randomly sampled from the periods in which the driving automation system was active (samples were stratified by each week of participation). It was determined that 12 samples per driver were needed to provide a reliable statistical estimate of driver performance, and 15-second samples allowed for the assessment of drivers' visual behavior and engagement in non-driving-related tasks; this sampling method was adapted from a previous NDS [3].
- Up to 12 epochs per driver of instances in which the driving automation system was available, but only one feature (either lateral or longitudinal) was active, were sampled. These were instances where only lateral or only longitudinal control was automated, but vehicle speed was above 40 mph and data reductionist-verified lane markings were present.
- Up to 12 epochs per driver of instances in which both functions of the driving automation system were available, but neither lateral nor longitudinal control automation was active, were sampled. These were instances where the vehicle speed was above 40 mph and data reductionist-verified lane markings were present.
- Up to 12 RTI epochs per driver per week were sampled. These were instances where an RTI was issued by the vehicle's human-machine interface.
- All SCEs that were observed in the dataset were analyzed. See the Results section below for details regarding the total number and type of SCEs (crashes and near-crashes) observed during data collection.

This sampling strategy was implemented to allow comparisons of driver behavior and roadway scenarios between levels of driving automation system engagement (when such activation was available). As noted, for each epoch type, 12 epochs per driver week were planned. In practice, 12 epochs were not observed in all cases for all vehicles; Table 2 shows the number of samples collected. In cases where there were fewer than 12 samples for a week, all instances of that activation were reduced.

Table 1.
Total epochs samples and average samples per driver

Epoch	Total	Average Samples per Driver	Average Samples per Week
Both Features Engaged	1,295	11	3
No Features Engaged, Both Features Available	1,052	9	2
One Feature Engaged, Both Features Available	1,083	9	2
RTIs	449	4	1
SCEs	71		

RESULTS AND KEY FINDINGS

The L2 NDS was intended to produce an initial understanding of commercially available driving automation systems. This project is the first study sponsored by the National Highway Traffic Safety Administration to review driver interaction with vehicles that include lateral and longitudinal automated features in real world settings. This research effort was intended to provide insight into four focus areas: System Performance (during unscripted, on-

road driving), Driver System Interaction, Driver Performance, and Driver Engagement. Key findings for each focus area are summarized below.

System Performance
Across all 120 participants, a total of 216,585 miles were driven (1,805 average per participant), with 53,360 miles driven below 40 mph. The remaining 163,225 miles were driven at speeds at or above 40 mph—of these, 70,384 miles were driven with both lateral and longitudinal driving automation active, 50,454 with one feature active, and 42,431 with no features active.

The analysis of environmental factors observed indicated that, in most cases, participants were operating the driving automation system-equipped vehicles in a manner consistent with manufacturers' intended use. When operating the vehicles at speeds above 40 mph, drivers typically drove with both features active. Drivers were less likely to activate the systems in heavy traffic, on non-interstate roads, and in rainy weather conditions.

Driver System Interaction
Non-driving task prevalence was observed to be similar across all activation levels; there was no increase in non-driving tasks when both lateral and longitudinal control features were active. The most common non-driving tasks observed were interacting with a passenger and monitoring the instrument panel. Furthermore, the types of tasks performed and eyes-off-road time were also similar across activation levels. The observed prevalence of non-driving tasks was high, but it should be noted that the current study used a 15-second reduction window to assess non-driving tasks. Previous estimates of secondary tasks performed as part of the Second Strategic Highway Research Project (SHRP 2) were based on a 6-second reduction window [3]. Additionally, drivers were observed to be monitoring and/or interacting with the instrument panel (center dashboard console and instrument cluster) in about 10% of sampled cases; this is consistent with supervisory behaviors as feature activation level (e.g., on or off), settings (e.g., following distance setting), or other system status (e.g., lane marking tracking) were presented in the instrument panel.

Driver Performance
In total, there were 71 SCEs observed in the data set. Five SCEs were crashes, and 66 were near-crashes. All crashes were low severity, rated as Level 3 or Level 4 based on previously adapted SHRP 2 definitions [4] (Virginia Tech Transportation Institute, 2015). No statistical relationships were observed between SCE rates and feature activation level. No RTIs were observed in the context of any SCE. The one observed crash with both features active was a single vehicle crash in which the driver struck a toll lane access gate at low speed (the driver attempted to enter a buses-only entrance). Although both features were active at some point during the reduction window, the driver pressed the brake prior to impact, overriding the driving automation features. The driver was not distracted and had at least one hand on the wheel throughout the event. No damage to the gate or vehicle was observed in this instance.

A total of 449 RTIs were sampled; in 118 of these, drivers were observed to have hands off the wheel. Analysis of reaction times for the RTIs in which drivers had hands off the wheel showed that the average reaction time of 0.94 seconds was within an expected range based on the results of previous research (e.g., [2]). However, there were some cases that showed longer response times or no intervention from the driver. Examination of these cases revealed that drivers were exploring the boundary conditions associated with the driving automation systems (e.g., intentionally keeping hands off wheel to test RTI duration and lateral control feature capabilities). Drivers were often observed explaining system functionality to passengers in these events, which all occurred when traffic was generally free flowing, weather was clear, and drivers were looking forward and attentive.

Driver Engagement
Overall, drivers appeared to trust the driving automation systems, and were comfortable using them. Driver interviews and trust ratings gathered at specific intervals during the 4-week participation period suggested that there was little change in trust in the lateral systems, although summarized comments also indicated that there were situations reported where the lateral systems did not function as expected. Again, these limitations are consistent with how the vehicles were characterized, and it is likely that even after the features were demonstrated, participants still had a higher than realistic expectation of function. Trust in the longitudinal system did increase over time; subjective feedback suggested that drivers learned the limitations of the longitudinal system and were able to use it more effectively after understanding its limitations.

REFERENCES

[1] SAE International (2016). Surface Vehicle Recommended Practice J3016: Taxonomy and Definitions for Terms Related to Driving Automation Systems for On-Road Motor Vehicles.

[2] Blanco, M., Atwood, J., Vasquez, H. M., Trimble, T. E., Fitchett, V. L., Radlbeck, J., … & Morgan, J. F. (2015, August). *Human factors evaluation of level 2 and level 3 automated driving concepts*. (Report No. DOT HS 812 182). Washington, DC: National Highway Traffic Safety Administration.

[3] Dingus, T. A., Hankey, J. M., Antin, J. F., Lee, S. E., Eichelberger, L., Stulce, K., … & Stowe, L. (2015). *Naturalistic driving study: Technical coordination and quality control*. (SHRP 2 Report S2-S06-RW-1). Washington, DC: Transportation Research Board. Retrieved from http://onlinepubs.trb.org/onlinepubs/shrp2/SHRP2_S2-S06-RW-1.pdf

[4] Virginia Tech Transportation Institute (2015). SHRP 2 Researcher Dictionary for Video Reduction Data Version 4.1. Blacksburg, VA.

INFORMED TRUST – AN EXTERNAL USER INTERFACE FOR HIGHLY AUTOMATED VEHICLES

Alexander Mankowsky
Stephan Mücke
Daimler AG
Germany

Paper Number 19-000304

ABSTRACT

Traffic research so far was focused on accidents and accident prevention. With the introduction of automated or semi-automated cars into the public realm however, the question is, how automated cars must be designed to blend in.

The presentation is based on the approach of traffic seen as a cooperative activity, where people are implicitly collaborating in the frame of given traffic rules. The Perception Action Model (PAM, Stephanie Preston 2007) in short suggests that perception and action are inseparable - people perceive actions of others and act immediately. This process is mutual and draws on empathy to predict the activities of the others. “Mind-Reading” (Eric Kandel, 2012) enables to read mood, energy, intention out of the other traffic participants.

Today it seems sufficient to perceive the way other drivers move their vehicle to trigger the Mind Reading process and enable predictive behavior. In case of automated vehicles, human perception has to be triggered properly to avoid misinterpretation or just wrong results of the empathic process.

Based on this approach the presentation introduces an experimental external user interface for highly or fully automated vehicles to address the underlying functionality of traffic. It includes the following features

- Indication of highly automated mode according to and exceeding the SAE recommendation
- Signaling of cooperative behavior
- Communication especially with vulnerable road users.

The system is demonstrated in various everyday driving situations on highways and city roads, such as merging traffic or a stop for pedestrians at a cross walk. Especially the aspects of an intuitive and intercultural understanding are discussed.

In addition, the external user interface can be used to share the vehicle’s knowledge about impending dangerous situations with its immediate surroundings – thus helping others to avoid potential accidents.

The presentation aims to demonstrate and discuss how an intuitively designed external user interface can help build informed trust in highly automated vehicles as a major factor of success and even give back to society by sharing its situation awareness.

Informed Trust is a major factor of success for Real-Word Deployment of Automated Driving Systems.

Most of the time our movement through the public realm is simply uneventful, and it is so because humans are cooperating with one another to make it so [1].

Traffic research has so far focused on accidents and accident prevention. With the introduction of automated or semi-automated cars into the public realm, however, the focus changes to understanding the magic of normal traffic and asking the following questions: how do we manage to avoid bumping into each other all the time? What will happen when automated cars are mixed into the magic? Automated cars must be designed to blend into this process; otherwise, known types of accidents will only be replaced by new types of accidents.

We have developed a conceptual framework, building on Social Sciences and Neuroscience, to understand the behavior of the involved actors in mobility. *Informed Trust* is our approach to designing self-driving cars in such a way that allows all actors to achieve agency. The overarching goal is to enable all actors in mobility to *produce a successful and harmonious mobility*, with fewer accidents than in today's traffic.

CONCEPTUAL FRAMEWORK

What is Mobility?

We are walking in crowded places, driving in crowded streets, and usually nothing bad happens – we manage. For the eye, it is mostly just a flow of people, cars, cycles and other means of mobility. "*The sociologist Lyn Lofland argues persuasively that the ordinary flow of movement on big - city sidewalks should be regarded as a collaborative production — a hard - won achievement in "cooperative motility" that requires the most sensitive attention to the subtle signals other pedestrians issue as to their intended course and speed.*" Lyn Lofland and others [2] are comparing our movement with a dance: we assume the movements of the others, as they do our own, and adapt continuously. As a result of the cooperative mass behavior, a rhythm emerges. Many cities are producing their own rhythm on a daily basis – you have to adapt, when switching from slow motion Charlotte, North Carolina to busy and dense NYC. For our topic, it is important to notice that walking, driving, riding a bike or a scooter is, from the standpoint of cooperation, the same. Somehow, we manage to predict the behavior of the others and adapt immediately. With self-driving cars, we introduce robots into the collective dance. Since we have not yet experienced robotic behavior in the public realm, the smooth collective dance may not happen.
Practically speaking, will their behavior provoke dangerous situations? What can we do to avoid this?

Mobility is a cooperative activity par excellence

The Role of Empathy in Mobility

Our approach is based on traffic seen as a cooperative activity, where people are implicitly collaborating in the frame of given traffic rules. Normally, we do not have to think while moving. We avoid accidents automatically. It is a subconscious process. One model from Neuroscience to explain our capabilities is the Perception Action Model, from Stephanie Preston and Frans de Waal [3]. In short, it suggests that perception and action are inseparable - people perceive actions of others and act immediately. This process is mutual, and draws on empathy to predict the activities of the others.

The need for empathy as a basic function of life is simple: individually, we have to find out about the intentions of other actors in our environment, and decide to run, approach, or simply freeze[1]. Therefore our perception scans our environment for signs of life – most importantly, for eyes watching us.

You can test it for yourself: you will be aware of the first raindrops at the window, but soon they will be not interesting anymore – they do not show signs of intention. They are not *alive*. However, if a fly approaches the same window, your perception will give you notice. Our eyes are moving more than a 100.000 times a day to achieve this, without giving us any awareness that they do so. Our perception-action mechanism runs on its own.

A hypothesis on empathy is that we incorporate the movement of other living beings. While doing so, a feeling emerges in us as we wonder how the other living being might feel and what it is up to. Neuroscientists like Erik

[1] Freezing in the face of danger implies that we are not able to drive accident free without assistance systems

Kandel [4] call this process 'Mind Reading'. It works well with living beings showing a direction when moving, like all mammals do.

Applied to traffic, it enables us to read the mood, energy, and intentions of the other traffic participants.

Today it seems sufficient to perceive the way other drivers move their vehicles to trigger the Mind Reading process and initiate predictive behavior. If empathy is impaired, like in people who suffer from autism, driving can become quite exhausting, which underscores the importance of empathy as a basic functionality for fluid cooperation in traffic.

With self-driving cars however, empathy will fail, unless measures are taken design wise.

Non-deterministic automation in Self-Driving Cars

Self-driving cars are complicated constructs based on Machine Learning (ML) for the interpretation of the traffic scene. ML is basically a statistical process. Training data are fed into the system, until the systems can label their environment sufficiently. Since the training data and the real environment are never the same, the labeling cannot be deterministic and proven 100% right. ML based systems are therefore non-deterministic systems. Possible errors are falling into three categories: mismatch in given categories, like a mismatch between a pedestrian and a cyclist, or a total failure like labeling a golf players portrait as a golf ball, caused by golf balls visibility in too many pictures used for training the ML system. Therefore, the non-deterministic ML systems must always be framed by a classical deterministic system as a backstop. In self-driving cars, for example, a simple radar system, which overrides the ML system and stops the car, when something is sensed on the road that contradicts the traffic scene created by the ML program.

The resulting behavior of a self-driving vehicle can be weird [5] for us, because our prediction skills fail against non-deterministic automation.

To enable our predictive capabilities, the car needs to provide hints for our perception, so that we can 'feel' it the way we can feel other participants in traffic.

Design Approach - Informed Trust

Informed Trust is opposed to blind trust: the goal of *Informed Trust* is to enable all the participants in a traffic scene to act: in short, to foster agency. Without agency, some actors in traffic will end up as victims by design, others as villains, also by design[2] [6].

To enable agency when dealing with self-driving cars, we have to prepare design elements working as handles for empathy, design elements functioning as enablers for learning, and finally, define procedures for when the systems degrade.

Informed Trust: Empathy and insight

Empathy: Feel the car

- Has it seen me? Is it friendly? Is it coming?
- Which direction is it heading? Is it relaxed or strained?
- Shall I help? Is it helping? I miss it already!
- Is it aware of me?

Insight: Learning process

- Display the mode of the car: is it in self-driving mode or not

[2] Compare 'Moral Machines' from MIT, Iyad Rahwan, Jean-Francois Bonnefon, Azim Shariff. Once you enter the game-like traffic situation, you end up as a executioner by design. http://moralmachine.mit.edu/

- Avoid misinterpretation of the role of a person sitting in the driver's seat
- Predictability of the car in different situations
- Offer simple conceptual models of the technical functions

Lessons: Graceful degradation

- Clear functional steps in case of break down
- Universally understandable warning signs to driver and traffic
- Standard procedure in case of accident detection

Empathy is based on functions of our perception. Our perception is scanning our environment continuously for body-movement and eyes. Once we encounter life, the prediction process starts. For a self-driving car, the communication of intention and state through movement can be implemented in several ways. The body of the car itself can be set in motion, parts of the cars body can be used, the way it is moving ahead, creeping, accelerating, decelerating and so on. The body of the car can be equipped to simulate muscle movement or wrinkles.
We experimented successfully with a wake-up motion of the car similar to an animal[3] [7]. The result was awareness on the side of pedestrians in front of the car when it 'awakes' in the parking lot, without any alarmism. The effect triggered a reaction which was felt by test participants as quite natural.

The importance of eye contact is paramount for informed trust. It can be implemented through various means, such as an LED pointing at people within a critical distance. These LEDs can be programmed to follow somebody, communicating to them a 'Hey it's you'. A short blink is similar to what we are doing regularly when walking the street. We also used a virtual shadow on the surface of the concept-car Vision URBANETIC, which is more complicated to implement, but very natural. Once we get used to such a shadow, we get alarmed when it is missing, and are so able to avoid a possible accident. Moreover, directed sounds are helpful to underscore urgency to make contact, especially for the visually impaired.

To ensure the empathic effect, the tools should work together organically. Our perception is watching for signs of life, so we should strive for a 'half-life' approach, as we know it from animated objects.

Insight needs simple and dependable signaling on the side of the self-driving car. In traffic school for children, it should be as easy as possible to teach them how to interact with such a car.

Teaching example for children:

'Is the car in self-driving mode?	- Watch for the signaling lights
'Has it seen you?'	- Check signs of eye contact
'No signs of eye contact?	- Go away

To achieve this scenario, the car must show its state as self-driving in 360 degrees around the car. The signaling should be arranged in such a way that the signal is applied in direction of the driver's seat, as it is the ritualized direction of the short gaze. The mode signaling has to be standardized. Standardization here is seen as the single most important success factor for the application of the technology.

Lessons have to be prepared for the case of a system failure. When the system is failing, it has to use a standard procedure, also known as Graceful Degradation in automation. To know this procedure will be most important for

[3] Clifford Nass, Psychology of Automated Vehicles, Stanford, 2013.
Nass suggests to compare self-driving cars with domesticated animals and design the interaction-narrative accordingly. https://www.youtube.com/watch?v=hrxf7lG-j9c

people inside and outside of the car. Graceful Degradation is fundamental to the debate on ethics and automation. From the perspective of the program running a self-driving car, an accident is always a failure out of missing or incorrect data, with failed prediction as the outcome. The concept of Graceful Degradation can be helpful here, defining the standard procedure in such a case. Straight emergency braking will give the other actors in the accident scene the opportunity to act meaningfully, once they know for sure that all self-driving cars will behave in exactly this way.

INTRODUCING AN EXTERNAL USER INTERFACE FOR AUTOMATED VEHICLES

Sensor setup, high-definition maps and digital integration

The environmental perception system of automated vehicles consists of sensors and perception algorithms. Their customized sensor setup uses various sensor types like radars, lidars, cameras and ultrasonic sensors as well as microphones. It provides a robust 360-degree field-of-view around the vehicle to enable the vehicle to handle all relevant use cases and maneuvers [1].

Deep Learning algorithms allow an object classification. The example in figure 1 illustrates different object classes by color-coding: vehicles are shown in blue, pedestrians in red, the road in purple, and traffic signs in yellow. It even includes objects partially blocked from the automated vehicle's perception system, such as pedestrians partially hidden by other vehicles.

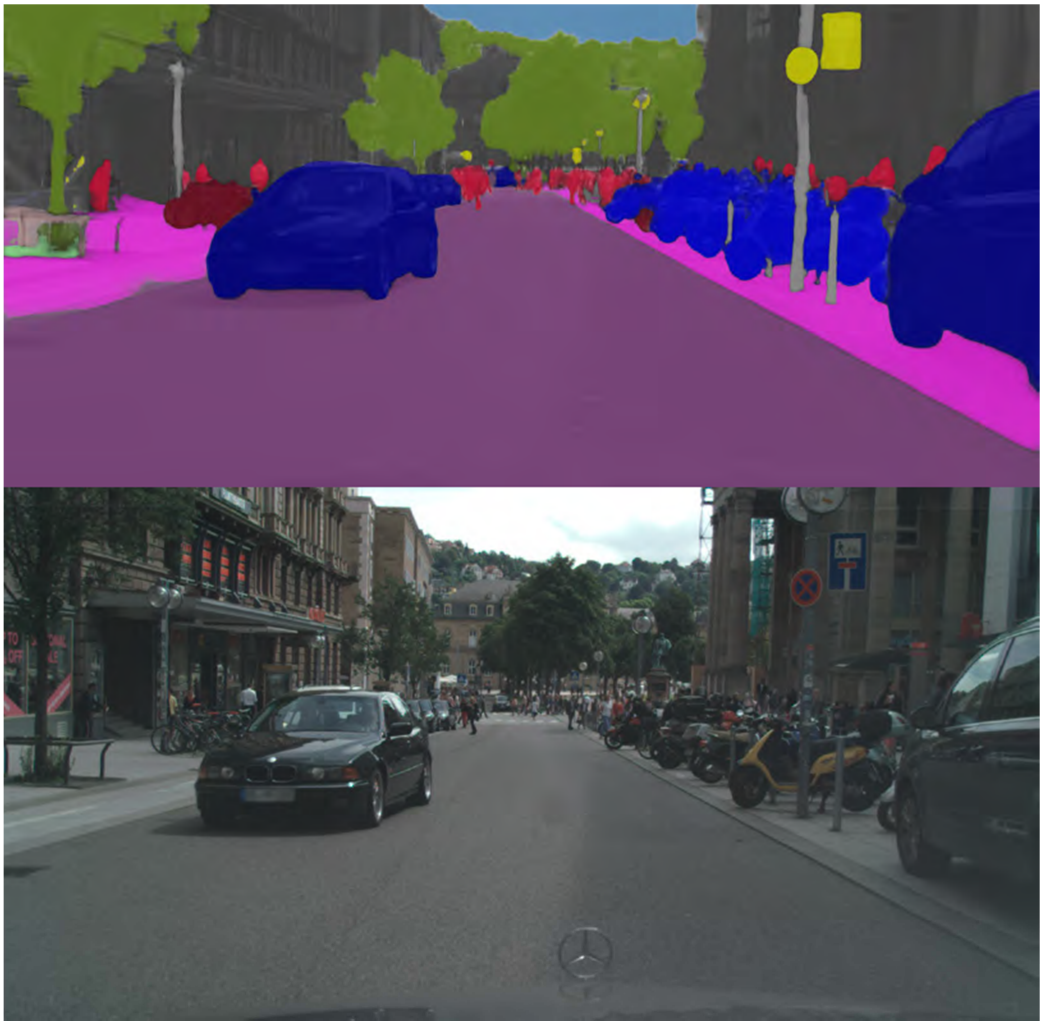

Figure 1. Object classification based on camera images [8]

A high-definition digital map defines the operational design domain and allows locating the automated vehicle and surrounding vehicles, pedestrians and objects. Environment modeling anticipates and predicts what other objects on the roadway might do.

Automated vehicles will be integrated within a digital infrastructure, which is capable of connecting to a Fleet Operations Center, data sources from public agencies (e.g. traffic signal data from local road authorities) and data from other vehicles. It also has an interface to the cloud where information such as status reports, relevant traffic, weather, incident and construction zones can be accessed.

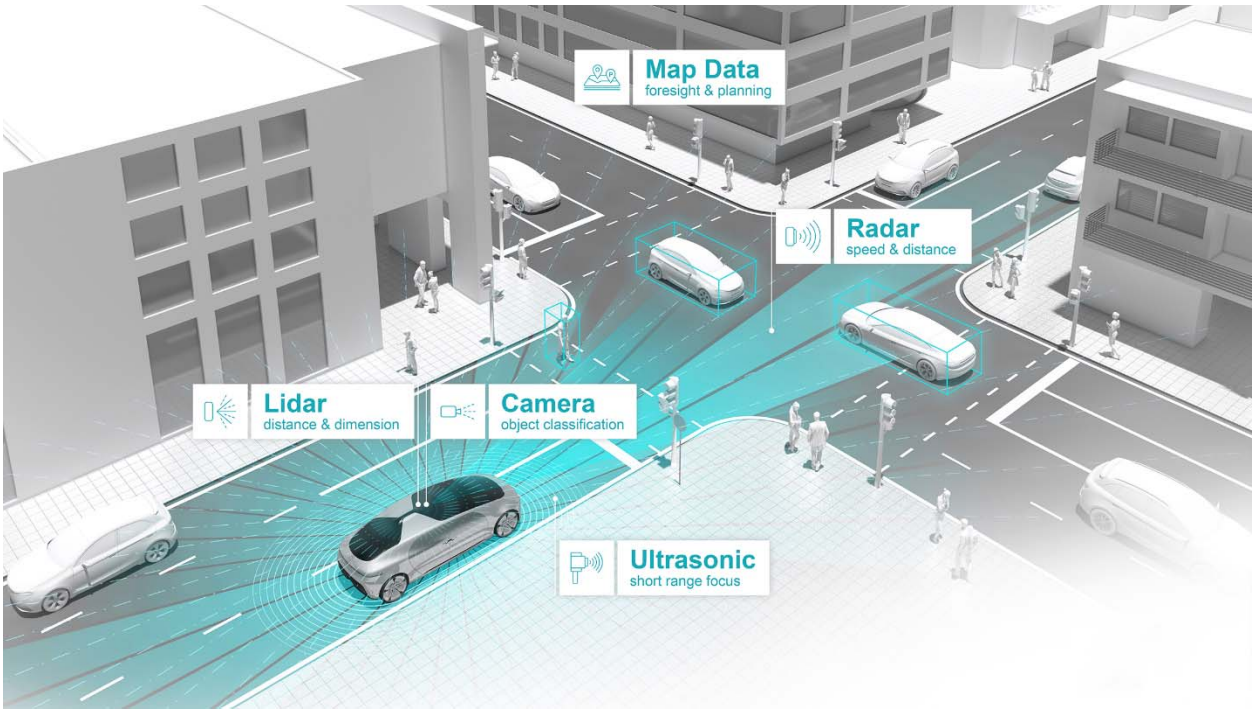

Figure 2. Sensor setup of an automated vehicle

External User Interface

Indication of automated driving mode

As mentioned in the context of interaction with pedestrians, the indication of automated driving mode is essential for the acceptance of automated vehicles. It allows pedestrians and other road users to identify automated vehicles, learn to read their intentions and thus build the aforementioned “informed” trust.

In 2018, Mercedes-Benz and Bosch started an Automated Valet Parking Service as a pilot project in Stuttgart [9]. Figure 4 shows a first realization to indicate the automated driving mode using turquoise illumination of already existing lights in the exterior mirrors and the third brake light.

Figure 3. Automated Valet Parking: Indication of automated driving mode [9]

Turquoise was chosen as indication of automated driving mode because it is unique, event peripherally visible and not used for any other exterior vehicle lighting. An internal Mercedes-Benz study with pedestrians revealed that a majority of the participants preferred turquoise and all of them voted for the 360° indication. Mercedes-Benz is supporting activities of the SAE, to develop an exterior lighting concept for automated vehicles.

Intuitive communication with other road users

In many situations road users, especially pedestrians should know instantaneously and reliably what an automated vehicle will do next.

Figure 4. Communication with a pedestrian wanting to cross the road [10]

Signaling cooperative behavior
An important goal for automated vehicles is to reduce the likelihood of accidents and to mitigate risks for passengers and other road users by operating like a defensive and attentive driver who consistently monitors the driving environment and responds appropriately and safely to changing conditions. However, trust in automated vehicles doesn't only require their cooperative behavior. They also must inform their immediate surroundings about their intentions in a way that can be understood intuitively.

Again, the combination of an indication of autonomous driving mode and an intuitively understandable message help other drivers to learn the behavior of automated vehicles and to build “informed” trust.

Warnings
In addition, the external user interface is used to share the automated vehicle’s knowledge about impending dangerous situations with its immediate surroundings – thus helping others to avoid potential accidents.

Especially vulnerable road users like pedestrians and bicyclist who are easily missed or obscured and do not have their own assistance systems may profit from this feature.

Local Hazard warnings**:** Driving safely and smoothly in complex environments requires detailed and ongoing awareness of the real-time traffic situation, coupled with the ability to forecast future traffic developments.

CONCLUSIONS

The presentation aims to demonstrate and discuss how an intuitively designed external user interface can help to build informed trust in automated vehicles and to create an additional safety benefit for others by sharing its situation awareness. The Mercedes-Benz Experimental Safety Vehicle 2019 (**E**xperimentales **S**icherheits**f**ahrzeug ESF 2019) will show how these considerations can be implemented in future vehicles.

REFERENCES

[1] Lofland, Lyn H. The Public Realm, p. 29. Taylor and Franci, 1998. Kindle Edition.

[2] Greenfield, Adam. Radical Technologies: The Design of Everyday Life. Verso, 2017. Kindle Edition, Location 1296

[3] Preston, Stephanie D. and de Waal, Frans B.M. (2001) Empathy: Its ultimate and proximate bases. https://greatergood.berkeley.edu/images/uploads/Preston_dewaal2002.pdf

[4] Kandel , Eric: Age of Insight, 2012. The hypothesis may explain why some people are afraid when encountering spiders or snakes. We cannot replay their behavior, and therefore not predict what they are about to do. Could be similar when encountering robots and self-driving cars

[5] The State of Self-Driving Cars in 2018, https://www.youtube.com/watch?v=1Jf1ZM-ho4o

[6] Rahwan , Iyad; Bonnefon, Jean-Francois and Shariff, Azim: Moral Machines. MIT. http://moralmachine.mit.edu/

[7] Nass, Clifford: Psychology of Automated Vehicles, Stanford, 2013.

[8] "Reinventing Safety: A Joint Approach to Automated Driving Systems", Mercedes Benz in cooperation with BOSCH, VSSA, 2018 Mercedes-Benz Research & Development North America, Inc. and Robert Bosch LLC. https://www.daimler.com/dokumente/innovation/sonstiges/vssa-mercedes-benz-and-bosch.pdf

[9] Future insight: https://media.daimler.com/marsMediaSite/de/instance/ko/Mercedes-Benz-FutureInsight-Human-first-Empathie-als-Anker-in-der-digitalen-Transformation.xhtml?oid=41918249

[10] Automated Valet Parking: https://media.daimler.com/marsMediaSite/de/instance/ko.xhtml?oid=23076118&ls=L3NlYXJjaHJlc3VsdC9zZWFyY2hyZXN1bHQueGh0bWw_c2VhcmNoU3RyaW5nPXZhbGV0K3Bhcmtpbmcmc2VhcmNoSWQ9MCZzZWFyY2hUeXBlPWRldGFpbGVkJmJvcmRlcnM9dHJ1ZSZyZXN1bHRJbmZvVHlwZUlkPTQwNjI2JnZpZXdUeXBlPWxpc3Qmc29ydERlZmluaXRpb249UFVCTElTSEVEX0FULTImdGh1bWJTY2FsZUluZGV4PTAmcm93Q291bnRzSW5kZXg9NQ!!&rs=1

MEASURING STATES' ALIGNMENT TO THE MODEL MINIMUM UNIFORM CRASH CRITERIA (MMUCC) 5TH EDITION

Sarah Weissman Pascual
John Siegler,
National Highway Traffic Safety Administration
United States of America
Paper Number 19-0305

ABSTRACT

In 1998, the National Highway Traffic Safety Administration (NHTSA) and the Governors Highway Safety Association (GHSA) developed the Model Minimum Uniform Crash Criteria (MMUCC), a voluntary guideline to encourage greater crash data uniformity by identifying a minimum set of motor vehicle crash data elements and attributes that States should collect and include in their State crash data system. NHTSA relies on State crash data for the Fatality Analysis Reporting System (FARS). FARS is a nationwide census providing NHTSA, Congress, and the American public yearly data regarding fatal injuries suffered in motor vehicle traffic crashes. States have implemented MMUCC differently, often combining or deleting attributes, which causes problems with data uniformity when attempting to aggregate data across States. The purpose of this paper is to describe methods used to measure States' alignment to MMUCC 5th Edition, examine the variance of States' crash data to MMUCC data elements, and describe how NHTSA will use the results of this analysis to inform future editions of MMUCC with the goal of improving the quality of FARS data.

INTRODUCTION

In 1998, NHTSA published the MMUCC, a voluntary guideline to collect data on motor vehicle crashes that can generate the information necessary to improve highway safety within each State and nationally. Early editions of MMUCC lacked guidance on implementation, which led to each of the 50 States, the District of Columbia (DC), and the U.S. Territories enacting MMUCC differently. Between the 4th and 5th Editions, NHTSA created a methodology to measure States' alignment to MMUCC, which was later updated and incorporated into the MMUCC 5th Edition. In 2018, NHTSA mapped the crash data elements and attributes from all States, DC, and Puerto Rico to the MMUCC 5th Edition and established the first baseline measurement of alignment to MMUCC. The results of this mapping exercise provide NHTSA a framework for offering States and territories technical assistance and training to increase their alignment to MMUCC, and will inform future changes to NHTSA's crash data publications, from MMUCC to the Fatality Analysis Reporting System (FARS) / Crash Report Sampling System (CRSS) Coding and Validation Manual.

BACKGROUND

NHTSA uses police-reported motor vehicle traffic crash data to conduct research, analyze traffic crash trends, support safety programs, and make data-driven decisions daily. Understanding States' crash data capabilities are reporting is critical to ensuring accuracy for all data-driven programs. Historically, each State developed their own methods for collecting, managing, and analyzing data on motor vehicle crashes. Consequently, crash data varied substantially between States. The lack of uniform data elements and attributes made it challenging to understand national crash trends. In 1975, NHTSA began collecting a census of fatal crashes using the FARS to provide an overall measure of highway safety. NHTSA trained analysts in each of the 50 States, DC, and Puerto Rico to convert the State data sources into FARS data codes.

Similarly, in 1988, NHTSA began the National Automotive Sampling System General Estimates System (NASS GES), a program to collect a nationally representative sample of police-reported motor vehicle crashes of all severities (fatal, injury, property-damage-only) to identify traffic safety problem areas, provide a basis for regulatory and consumer initiatives, and form the basis for cost and benefit analyses of traffic safety initiatives. The NASS GES and its replacement the Crash Reporting Sampling System (CRSS), requires analysts to recode the crash data collected from different States into a standard format. Early on, it was apparent that the substantial variability in State crash data made it costly and challenging to produce national crash datasets.

In 1998, NHTSA and GHSA published the first MMUCC. This provided States voluntary guidance on the minimal set of standardized data elements and attributes necessary to describe the characteristics the vehicles, the persons, and the environment involved in motor vehicle crashes,. NHTSA and GHSA encouraged States to adopt MMUCC to increase crash data uniformity. Greater standardization of crash data enables State highway safety agencies to more efficiently and cost-effectively share data with other agencies in their State (such as public safety), compare their crash data with other States, and, exchange crash data with federal data systems. Since the initial release of the MMUCC Guideline in 1998, NHTSA and GHSA have revised MMUCC four times in response to technological changes and evolving traffic safety needs. Early editions of the MMUCC Guideline did not provide States with implementation guidance, resulting in each State adopting MMUCC differently. As States developed their own data collection guidelines regarding what crash data to collect, what is a reportable crash, and what data to maintain on their Crash Databases, the variance between States' crash data increased. As a result, States often use different formats and names for data elements and attributes or they may combine (or split) elements and attributes.

In 2014, NHTSA and GHSA recognized the need to develop a methodology for measuring the alignment of the crash data States collected on their Police accident reports (PAR) and the data entered and maintained on Crash Databases to the data elements and attributes in the MMUCC Guideline. Through extensive consultation with the State stakeholders at the Association of Traffic Records Information Professionals (ATSIP) International Traffic Records Forum, NHTSA and GHSA developed a methodology to map the data elements and attributes from States PARs and their crash databases to MMUCC. This process recognized that while State data systems often use different terminology and formatting, different data sets can often be mapped to the MMUCC data elements and attributes. Thus, if an element or attribute on a State PAR or in its Crash Database did not match a MMUCC element or attribute verbatim, but is essentially the same, it is considered "mapped" to MMUCC. In 2015, NHTSA published *"Mapping to MMUCC: A Process for Comparing Police Crash Reports and State Crash Databases to the Model Minimum Uniform Crash Criteria,"* [1] a set of rules to assist States in evaluating their alignment to MMUCC.

In 2017, NHTSA and GHSA published the 5th Edition of MMUCC [2], which included updated mapping rules to address significant changes to the MMUCC content and format. In addition, the MMUCC 5th Edition no longer designated elements to be "collected at the scene," "derived," or "linked." Instead, MMUCC encouraged States to collect data elements based on the States' capabilities. States that have integrated traffic records datasets collect less data for their crash reports at the scene of a crash because they can instead link or derive data elements from other sources, such as the roadway, driver, and vehicle file. As a result, comparing a State's crash database to MMUCC is more useful than comparing a State PAR to MMUCC.

Following the publication of the 5th Edition of MMUCC, NHTSA collected crash data documentation (data dictionary, police instruction manual, database schema, and crash report forms) for all 50 States, DC, and Puerto Rico to measure how each States' crash database structure aligns to MMUCC. The objectives for this project included establishing a baseline for understanding the States' crash data capabilities, identifying the data elements and attributes that are problematic for States, providing States a measure of how they align to MMUCC and detail opportunities for improvement, and to inform future editions of MMUCC by understanding potential impacts changes might have on the States.

METHODS

Measuring the alignment of a State's crash data to MMUCC involves several steps to compare the data elements and attributes within the State crash database (the source) to the data elements and attributes in the target). Figure 1 provides a brief overview of this process. The first step involves gathering the relevant documentation, which includes the most recent version of MMUCC and documentation on the State's crash data system. Typically, a State's crash database is comprised of the corresponding data collected on police crash reports, derived from data collected on crash reports, and obtained from other data sources (e.g., a roadway database). Ideally, the State's crash data elements and attributes should contain all 115 MMUCC data elements and their attributes. If the data dictionary for the State Crash Database does not list all data elements and element attributes used in the crash database, then analysts examine the State's PAR and police instruction manual for all relevant terms and definitions needed to map to the MMUCC.

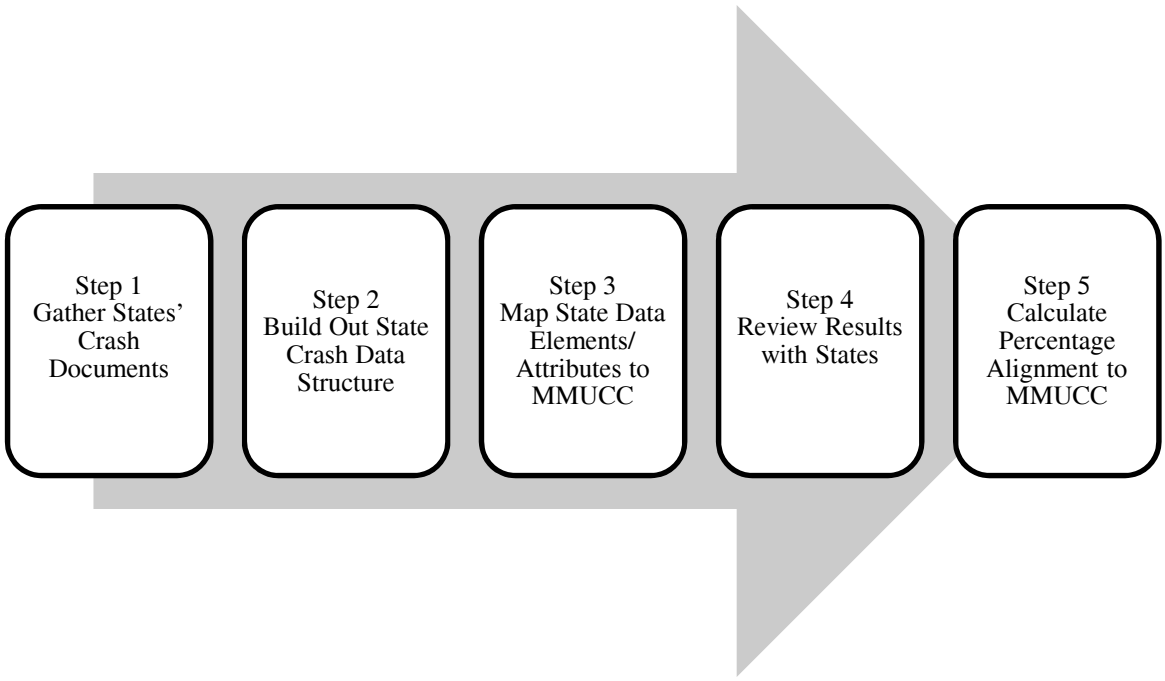

Figure 1: The MMUCC Mapping Process

The second step for measuring a State's alignment to MMUCC involves building out the target MMUCC data structure and the source State data structure to compare and evaluate the similarity of the State's data elements and attributes to those of the MMUCC. Table 1 is an example of the table used to map a State's data element and attributes for "Weather" to the MMUCC date element and attributes for "C11. Weather conditions". Since the MMUCC Guideline allows two attribute selections for "C11. Weather Conditions" the table is set up to include both subfields. Initially, analysts used an Excel spreadsheet to facilitate side-by-side comparisons of the data elements and attributes, which was cumbersome. NHTSA developed an IT application for analysts to build and update the source and target data structures, record the analyst's comments and mapping decisions, and export a final report. The application can maintain the mappings when either the target MMUCC data structure or the source State data structure are updated, which will facilitate future efforts to re-map a State's data to MMUCC when either change. This application also included many safeguards to ensure the integrity of the mapping results (i.e. color-coded mapping status notations and preventing attributes from being coded twice).

The third step involves determining how consistent the States crash data structure is with MMUCC by identifying which of the State's crash data elements and attributes can map to each MMUCC data element and attributes. Analysts apply mapping rules published in the MMUCC 5th Edition to determine if a State data attribute can be mapped, or matches MMUCC. All mapping decisions are binary at the attribute level where analysts decide whether the State's data matches MMUCC or not. The mapping process is a "top-down mapping" approach that starts with the data elements and works down to attributes. Individual elements with zero attributes (i.e., VIN) either will map to a corresponding MMUCC element/attribute or will not. While there is no partial mapping for data elements with no attributes, data elements with multiple attributes can partially map, if at least one State attribute matches an attribute for that MMUCC element. Many States collect more data elements than what MMUCC prescribes. The MMUCC mapping process is only concerned with the 115 MMUCC data elements and their associated attributes. The mapping rules include two primary sets of rules: The general rules, such as the many-to-one rule, where two State data attributes can match to one MMUCC data attribute, and the one to many rules that prohibits one State data attribute from mapping to two MMUCC data attributes. Another set of rules covers specific data elements that have unique characteristics requiring additional explanation and interpretation.

Table 1.
Mapping State Data Element "Weather" to the MMUCC "C11. Weather Conditions"

Target: **MMUCC Data Element "C11. Weather Conditions" Selection 1**	**Ability to Map? (1 = Yes, 0 = No)**	***Source:*** **State Data Element "Weather"**	***Target:*** **MMUCC Data Element "C11. Weather Conditions" Selection 2**	**Ability to Map? (1 = Yes, 0 = No)**	***Source:*** **State Data Element "Weather"**
Blowing Sand, Soil, Dirt	0	(9) Blowing Sand, Soil, Dirt, or Snow *cannot be split.*	Blowing Sand, Soil, Dirt	0	*N/A*
Blowing Snow	0		Blowing Snow	0	*N/A*
Clear	0	(1) No Adverse Conditions (Clear, Cloudy) *cannot be split*	Clear	0	*N/A*
Cloudy	0		Cloudy	0	*N/A*
Fog, Smog, Smoke	1	(2) Fog (7) Smoke/Dust *includes Dust*	Fog, Smog, Smoke	0	*N/A*
Freezing Rain or Freezing Drizzle	0	*N/A*	Freezing Rain or Freezing Drizzle	0	*N/A*
Rain	1	(4) Rain	Rain	0	*N/A*
Severe Crosswinds	1	(10) Severe Crosswinds	Severe Crosswinds	0	*N/A*
Sleet or Hail	1	(6) Sleet/Hail	Sleet or Hail	0	*N/A*
Snow	1	(5) Snow	Snow	0	*N/A*
Other	0	*N/A*	Other	0	*N/A*
Unknown	0	*N/A*	Unknown	0	*N/A*

Table 1 identifies the State's data attributes that can map to the MMUCC attributes and the rules that apply. Specifically, the State's attribute *'(1) No Adverse Condition (Clear, Cloudy)'* cannot map to the MMUCC attributes '*Clear'* or '*Cloudy'* because the State combines two MMUCC attributes '*Clear'* and '*Cloudy.'* Likewise, the State attribute '*(9) Blowing Sand, Soil, Dirt, or Snow*' cannot map to the MMUCC attributes '*Blowing Snow'* or *'Blowing Sand, Soil, Dirt.'* However, the State attributes *'(2) Fog'*, and *'(7) Smoke/Dust'* can map to the MMUCC attribute '*Fog, Smog, Smoke'* without a loss in data integrity. Four attributes from the State were mapped one-to-one to a MMUCC attribute ('*Rain,' 'Sleet or Hail,' 'Snow,'* and '*Severe Crosswinds'*). According to the general mapping rules, the State attribute '*Other*' cannot map to the MMUCC *'Other'* because the State did not possess all other C11 attributes. The State did not have an attribute to map to the MMUCC attribute *'Unknown.'* Finally, the State only allows for one attribute, while the MMUCC guideline suggests States should choose up to two attributes. However, C11 provides two attribute selections, which means that any State must provide 24 total attributes (12 C11 attributes, selected twice). Therefore, this State element has five attributes that map to the 24 possible attributes in MMUCC.

After analysts completed the mappings for each State's crash data, NHTSA encouraged each State to participate in a debriefing to provide that State an opportunity to learn which of their crash data elements and attributes did not map to MMUCC. States could also use the debriefing to provide additional documentation about their crash data, which often led to revised results. NHTSA encourages States considering updating their PAR or crash database to review their MMUCC mapping report to identify opportunities to increase alignment with MMUCC.

Finally, the MMUCC mapping method results in standardized scores that measure the percentage of alignment to MMUCC at the element level, system level, and overall total. Each MMUCC data element was scored by dividing the number of attributes that the State could map to MMUCC by the total number of MMUCC attributes for that element.

$$\text{MMUCC Element Mapping Score (\%)} = \frac{\text{Number of State Attributes that Map to the MMUCC Data Element}}{\text{Total Number of Attributes for the MMUCC Data Element}^{*}}$$

In Table1, there are 24 attributes for the for MMUCC element "C11 Weather Conditions" (12 attributes, selected twice). Of these 24 attributes, the State can map five attributes. The score for this data element is calculated as follows:

$$\text{MMUCC Element Mapping Score (\%)} = \frac{5}{24} = 20.8\%$$

The score for each of the eight data sections of MMUCC were calculated by summing the scores for all the data elements in each section and dividing by the number of data elements in each section. Table 2 shows the distribution of MMUCC data elements by section

$$\text{MMUCC Section Mapping Score (\%)} = \frac{\sum \text{MMUCC Element Mapping Scores in the Section}}{\text{Number of MMUCC Elements in the Section}}$$

Table 2.
MMUCC Data Elements by Section

Section	Data Elements
Crash Section	27
Vehicle Section	24
Person Section	27
Roadway Section	16
Fatal Section	3
Large Vehicle and Hazardous Materials Section	11
Non- Motorist Section	6
Dynamic Data Element Section	1
Total	115

The score for each State's alignment to MMUCC is the sum of each element mapping score divided by the total number of MMUCC data elements. The result is the overall State mapping percentage:

$$\text{Overall State to MMUCC Mapping Score (\%)} = \frac{\sum \text{MMUCC Element Mapping Score}}{115}$$

RESULTS

Overall, States' alignment to MMUCC is low and varies greatly. More than half the States aligned to less than 50% of the 115 MMUCC data elements. The mean percentage of States' alignment to MMUCC is 45.9%, with alignment ranging from a low of 9.4% to a high of 84.8% and a standard deviation of 13.66. As Figure 2 shows, a little less than half the States (46.2%) scored between 39.6% and 54.7%.

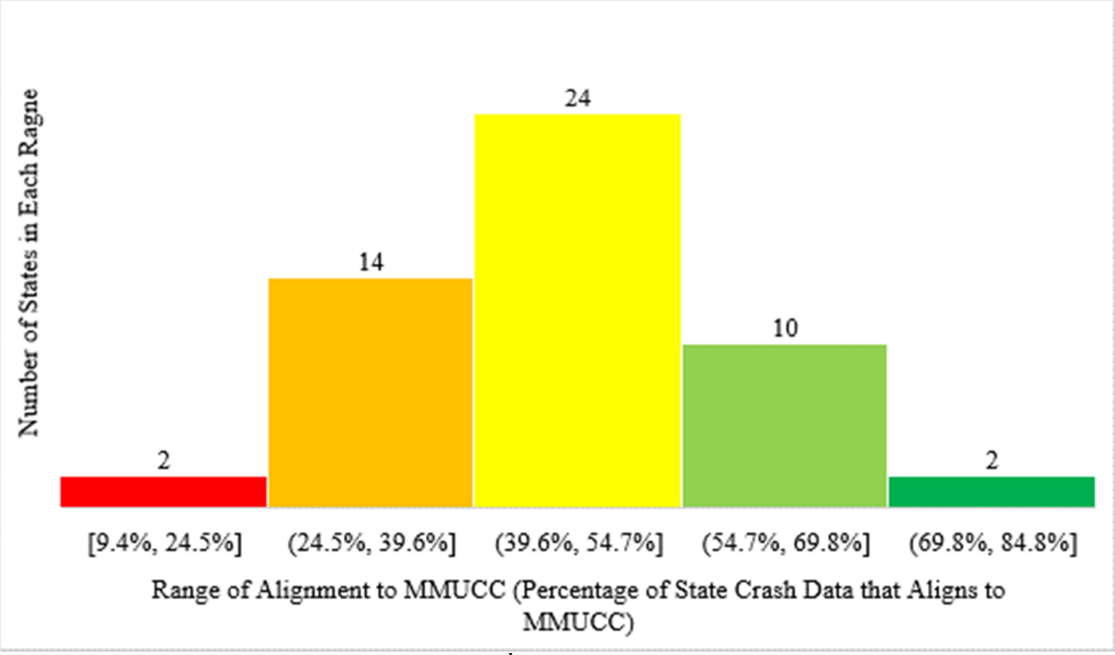

Figure 2. States' Alignment to the MMUCC 5th Edition

The MMUCC guideline includes eight sections that focus on a different type of data. As **Error! Reference source not found.**Table 3 shows, States alignment to MMUCC varies according to the different types States. States had the greatest alignment to MMUCC's crash data elements with a mean score of 70.5% ranging from a low of 32.8% to a high of 96.4%. States had the lowest alignment to the dynamic data element, which is the most recent addition to MMUCC and measures *Motor Vehicle Automated Driving System(s)*. Only one State's data was aligned 100%, and 46 States had zero alignment to this data element, resulting in a mean score of 3.4%.

Table 3.
States' Alignment to 115 MMUCC Data Elements

MMUCC Data Elements	Mean Score (%)	Median Score (%)	Lowest Score (%)	Highest Score (%)	Standard Deviation
Crash (N=27)	70.5	72.1	32.8	96.4	13.88
Vehicle (N=24)	56.7	58.3	6.7	95.4	17.61
Person (N=27	46.5	44.2	1.5	91.7	17.21
Roadway (N=16)	12.0	0.0	0.0	85.9	17.55
Fatal (N=3)	20.3	16.3	0.0	100.0	22.40
Large Vehicles and Hazardous Materials (N=11)	30.4	24.9	0.0	87.9	25.87
Non-Motorist (N=6)	28.0	26	0.0	96. 7	22.48
Dynamic Data Element (N=1)	3.4	0.0	0.0	100.0	14.56
Total (N=115)	45. 9	44.4	9.4	84.8	13.66

Collecting national data on alcohol-related crashes is central to NHTSA's work to understand risky driving behavior. Approximately one-third of all traffic crash fatalities in the United States involve drunk drivers (with blood alcohol content of .08 grams per deciliter (g/dL) or higher). MMUCC includes several data elements to capture data on alcohol-related crashes. Table 4 summarizes States alignment to MMUCC alcohol-related data elements and attributes. MMUCC data element "C25. Alcohol Involvement" is the most uniformly adopted alcohol-related element by States with a mean national alignment of 74.4% that includes 28 States that are in complete alignment with this data element, seven States with no alignment to this data element, and 17 States that can map to

some of this data element's attributes. In contrast, the lowest level of alignment was for "F2. Alcohol Test Type and Results", which had a mean national score of 27.9% that includes only one State in complete alignment and 11 States with no alignment to this data element.

Table 4.
States Alignment to MMUCC Alcohol-Related Data Elements and Attributes

MMUCC Alcohol-Related Data Elements and Attributes	Mean Score (%)	Median Score (%)	N States with 0.0% Alignment	N States with 100.0% Alignment	Standard Deviation
"C25. Alcohol Involvement"	74. 4	100.0	7	28	34.35
"P19. Condition at Time of the Crash" Attribute 5, 'Under the Influence of Medications/Drugs/Alcohol'	34.0	34.4	16	2	30.21
"P20. Law Enforcement Suspects Alcohol Use"	66. 7	66.7	8	20	34.59
"P21. Alcohol Test"	55.0	65.4	11	5	35.36
"F2. Alcohol Test Type and Results"	27.9	22.2	11	1	25.94

NHTSA collects data on other risky driving behaviors, including drowsy driving, drugged driving, speeding, and distracted driving. Table 5 identifies the MMUCC data elements and attributes that relate to each risky behavior.

Table 5.
Risky Driving Behavior captured in MMUCC

Issues	MMUCC Data Elements and Attributes
Drowsy Driving	"P19. Condition at Time of the Crash" 1.1 and 1.2 *Asleep or Fatigued*
Drugged Driving	"C26. Drug Involvement", "P19. Condition at Time of the Crash Subfield 1.1 *Under the Influence of Medications/ Drugs/ Alcohol* Subfield 1.2 *Under the Influence of Medications/ Drugs/ Alcohol*, "P22. Law Enforcement Suspects Drug Use", "P23. Drug Test", "F3. Drug Test Type and Results".
Speeding	"P13. Speeding Related"
Distracted Driving	"P18. Distracted By"

As Table 6 show, States alignment to the MMUCC data elements related to risky driving behavior varies greatly with standard deviations ranging from 19.24 to 42.43. States had the greatest alignment to the MMUCC data elements related to drowsy driving (41. 4%). Data elements that States were in complete alignment to MMUCC was limited to 15 States collecting data on drowsy driving, nine States collecting data on speeding, and one State collecting data on distracted driving . No States collected data on drugged driving that aligned completely to MMUCC.

Table 6.
States Alignment to MMUCC Data Elements for Risky Driving Behavior

MMUCC Data Elements for Risky Driving Behavior	Mean Score (%)	Median Score (%)	N States with 0.0% Alignment	N States with 100.0% Alignment	Standard Deviation
Drowsy Driving	41.4	50.0	24	15	42.43
Drugged Driving	32.5	26.3	5	0	28.67
Speeding	30.4	0	28	9	39.12
Distracted Driving	6.3	0	42	1	19.24

NHTSA promotes road safety through grants to States and countermeasures programs, which focus on school bus safety, seat belts, teen driving, child passenger safety, non- motorist safety, and motorcycle safety. Table 7 identifies the MMUCC data elements and attributes that relate to each safety countermeasure program. Collecting this data helps States and NHTSA understand the effectiveness of safety countermeasure programs.

Table 7.
Critical Safety Issues Captured in MMUCC

Issues	MMUCC Data Elements and Attributes
School Bus Safety	"V10. Special Function of Motor Vehicle in Transport" Attribute 01 *'Bus – School (Public or Private)'*; "P12. Driver License Number, Class, CDL and Endorsements" Attribute 04 *'School'*.
Seat Belt Safety	"P8. Restraint Systems/Motorcycle Helmet Use" Attributes 05 *'Lap Belt Only Used'*, 06 *'None Used – Motor Vehicle Occupant'*, 07 *'Restraint Used – Type Unknown'*, *08 'Shoulder and Lap Belt Used'*, 09 *'Shoulder Belt Only Used'*, and Subfield 2 'Any Indication of Improper Use?'
Teen Driving Safety	"P16. Driver License Restrictions" Attributes 08 *'Intermediate License Restrictions'*, 09 *'Learner's Permit Restrictions'*; "P17. Driver License Status" Attribute 02 *'Non-CDL Restricted Driver license (Learner's permit, Temporary/ Limited, Graduated)'*.
Child Passenger Safety	"P8. Restraint Systems/Motorcycle Helmet Use" Attributes 01 *'Booster Seat'*, 02. *'Child Restraint System – Forward Facing'*, 03 *'Child Restraint System – Rear Facing'*, 04 *'Child Restraint – Type Unknown'* ; and Subfield 2 'Any Indication of Improper Use?'
Non Motorist Safety	"C22. Number of Non-Motorists" "P4. Person Type" Attributes 04 *'Bicyclist'*, 05 *'Other Cyclist'*, 06. *'Pedestrian'*, 07 *'Other Pedestrian (wheelchair, person in a building, skater, personal convey.)'*, 08 *'Occupant of a Non-Motor Vehicle Transportation Device'*, 09 *'Unknown Type of Non-Motorist'*, and 99 *'Unknown'*.
Motorcycle Safety	"P8. Restraint Systems/Motorcycle Helmet Use" Attributes 12 *'DOT-Compliant Motorcycle Helmet'*, 13 *'Not DOT-Compliant Motorcycle Helmet'*, 14 *'Unknown If DOT-Compliant Motorcycle Helmet'*, 15 *'No Helmet'*, 97 *'Not Applicable'*, 98 *'Other'*, 99 *'Unknown'*; and Subfield 2 'Any Indication of Improper Use?'

As Table 8 show, States' crash data alignment to the MMUCC data elements related to critical traffic safety issues was low and varies greatly. States had the greatest alignment to those MMUCC data elements related to school bus safety (56.4%) and seat belt safety (56.0%). In contrast, motorcycle safety ("P8. Restraint Systems/Motorcycle Helmet Use" per **Error! Reference source not found.**) has the least alignment by States with an average of 30. 6% alignment including nine States that cannot map anything to this data element. Of note also are the 16 States that do not map anything to the MMUCC child passesnger safety data elements.

Table 8.
States Alignment to MMUCC data Elements for Critical Traffic Safety Issues

	Mean Score (%)	Median Score (%)	N States with 0.0% Alignment	N States with 100.0% Alignment	Standard Deviation
School Bus Safety	56.4	58.3	4	12	34.15
Seat-Belt Safety	56.0	57.1	5	4	24.72
Teen Driving Safety	43.1	41.7	2	2	23.78
Child Passenger Safety	43.0	50	16	3	32.25
Non-Motorist Safety	37.9	31.4	2	0	24.66
Motorcycle Safety	30. 6	22.2	9	1	24.35

DISCUSSION

The most common issue NHTSA encountered during this MMUCC mapping project was outdated, incomplete or missing documentation, especially related to States' crash data dictionary. However, as a result of this project, many States updated or created documentation because the initial measurement of their database alignment to MMUCC was not reflective of their crash data capabilities. After receiving the new documentation, analysts updated the mapping scores to accurately reflect the contents of the primary production database. While some States took steps to improve or create documentation, several States still lack documentation about the external data systems linked to their crash database, and specifically those States lack definitions for data elements with established time-lapsed linkages with other traffic records data system, such as roadway, driver, and vehicle data systems. Conversely, States that have robust interfaces (live linkages) all had documentation in some form, and most had documentation that was fully updated and reflective of their existing system

Another common issue NHTSA encountered was discrepancies between the States' crash report form (or forms) and their database. In one instance, the mapping uncovered that a State had updated their statewide crash report form, but had failed to plan for or update their State crash database. In this case, the database could not save the new crash data elements that law enforcement collected. As a result, NHTSA finds that States may benefit from conducting regular data mappings and other data quality assessments and adjustments to keep their crash data system accurate and operational.

Lastly, some jurisdictions collected elements at different levels than suggested in MMUCC (e.g., States collected vehicle or person-level elements at the overall crash level instead). The primary problem with collecting elements at higher levels than suggested is the loss in specific data about the people, vehicles or roadways involved. For example, the State might collect "Sequence of Events" for the entire crash, which yields a single value as opposed to collecting this for each vehicle involved. Conversely, States that opt to collect elements at lower levels than suggested collect more granular data than MMUCC. This provides more detailed data for State analysts and can still be rolled up into a MMUCC aligned mapping.

Each State can use their MMUCC alignment score to develop an action plan for updating their crash report (or reporting software) and crash database. Since it may not be possible or desirable to update everything all at once, States can prioritize the elements to revise. NHTSA encourages States to establish an action plan and include the priority for change, rationale, deadline, and the person or agency responsible for each element for which they are considering a change.

CONCLUSION

The results of this mapping exercise provide NHTSA with the first nationwide understanding of State crash data capabilities, from which several initiatives are planned. First, the results form a baseline of capabilities that NHTSA plans to use to design and implement appropriate technical assistance and training to increase State alignment with MMUCC and improve data quality. Second, NHTSA plans to use the results to inform future changes to both the

MMUCC Guidelines and FARS Coding and Validation Manual. By understanding where the States' capabilities currently reside, NHTSA can make better-informed decisions regarding additions, deletions, and changes to the existing data publications that will serve to enhance alignment between the States' crash data systems and NHTSA's MMUCC Guidelines and FARS Manual simultaneously. Thirdly, NHTSA plans to repeat this exercise on a regularly recurring basis to provide consistent, relevant information to all crash data stakeholders. This will result in NHTSA having the means and opportunity to conduct research and analysis on State crash data capability changes and trends over time, leading to further enhancements of all the programs listed herein.

REFERENCES

[1] National Highway Traffic Safety Administration. (2015, July). *Mapping to MMUCC: A Process for Comparing Police Crash Reports and State Crash Databases to the Model Minimum Uniform Crash Criteria.* (Report No. DOT HS 812 184). Washington, DC: National Highway Traffic Safety Administration.

[2] National Highway Traffic Safety Administration. (2017, July). *MMUCC Guideline: Model Minimum Uniform Crash Criteria Fifth Edition (2017).* (Report No. DOT HS 812 433). Washington, DC: National Highway Traffic Safety Administration

DYNAMIC EVALUATION OF CLOUD-BASED ACTIVE SAFETY SYSTEMS

Gropengießer, Uwe

Maier, Christina

Kallweit, Dr. Roland

IAV GmbH

Germany

Paper Number 19-0306

ABSTRACT

The field of driver assistance systems faces new technologies like vehicle-to-x (V2X) communication [1] and cloud services to improve safety on the streets. These upcoming functions carry new possibilities and new challenges as well. Thanks to scaling-up techniques, it is already possible to gather and manage huge amounts of data in the cloud with less time consumption compared to standard systems. This data is suitable to be used for statistics and pattern recognition based functions with time-critical demands.

But beside the development of these functions there is always a need for evaluation to assure correct functionality. Therefore, IAV created a concept to dynamically evaluate cloud-based active safety systems like the wrong-way driver detection function developed by IAV, which is conceived to warn oncoming vehicles on motorways. This goal is achieved with cloud and V2X techniques.

The wrong-way driver warning is a service running on the cloud, which receives V2X messages from vehicles including their positioning data, heading and other information to reference their traces via map matching [2] algorithms. An underlying database compares the data with continuously calculated thresholds to recognize wrong-way drivers and warn others in the surrounding areas via V2X against them. As changing infrastructures like construction sites have an effect on the false-positive rate of the classification, it needs to be dynamically tested if the function is able to react appropriately.

For this reason we propose an approach for an evaluation process based on an integrated self-controlling module. This module notices changes in trajectories which can be caused by changed traffic guidance and adapts the detection parameters. As a result, the following detection should classify the vehicles correctly based on the changed conditions.

The discussed process of the introduced wrong-way driver warning shows an example how a specific cloud-based function can be dynamically evaluated without dependence on the functional logic. Especially functions whose results strongly depend on ever-changing input data need solutions to test their behavior in critical situations. This approach delivers also a possible answer how to implement additional methods to create more flexible and long-term reliable cloud-based active safety systems.

INTRODUCTION

With the possibilities offered by V2X communication and the opportunity to calculate models in the cloud, the field of predictive safety functions has experienced kind of a revolution. This is also a necessary development to fire progression towards autonomous driving. Therefore, research is driven to V2X and cloud-based functions to evaluate their potentials and limits [3]. There are also functions that dynamically adapt their algorithm parameters to changing inputs. These methods offer advantages and disadvantages, e.g. reacting to intraday situations but also learning algorithms incorrectly. One example of such a function is IAV's wrong-way driver warning which uses different information like vehicle positioning to detect wrong-way drivers on motorway junctions and warn endangered drivers nearby (Figure 1).

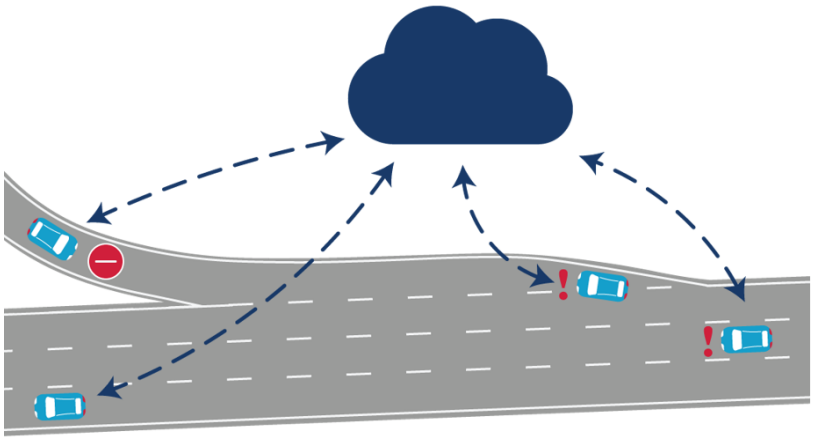

Figure 1. **IAV´s wrong-way driver warning function.** In this figure you can see a possible scenario for the detection of a wrong-way driver and the need for the warning of the endangered drivers nearby.

According to given example, we present an algorithm that contains two different modes. The first mode is the training mode. In the first phase, data is collected to evaluate a motorway junction not yet trained by the algorithm. Among other things, the position data of the vehicles will be used to perform a map matching. A threshold value is searched, which indicates how far an object may move away from a map matched position, in order to avoid false-positives.

In the second phase, which is called “live” phase, the system allows to activate the detection of wrong-way driver for a given motorway or exit. In this phase every vehicle that drives this way will be evaluated. Whenever a vehicle exceeds the way specific threshold, the function warns the endangered drivers nearby.

This approach leads to the situation of handling position offsets regarding to e.g. daytime construction sites. Such scenarios can lead to the situation that the algorithm is not able to map match a vehicle or much worse to result in false-positives. In this paper we provide a method to calculate new thresholds while the live phase. The main goal is to avoid false-positives in any situation.

GPS BASED WRONG-WAY DRIVER DETECTION

Statistically speaking, the most validated incidents of wrong-way driving in Germany are caused by taking wrong entries at motorway junctions [4]. Therefore, we decided to observe the junctions regarding to the ramps and exits of the motorway. From this idea, we started to use the GPS tracking which is basically concentrated on such areas. To have a starting point we use a junction next to Ingolstadt. As you can see in Figure 2 there are four different ways to drive on this junction. Visualized GPS trajectories show their different traceable ways, which will be related to mapped roads.

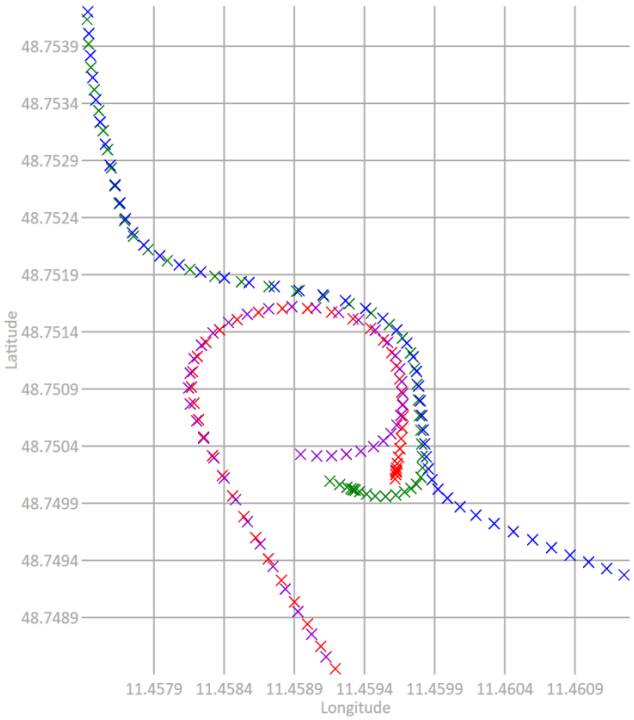

Figure 2. **Measured GPS trajectories over time, based on real vehicle bus signals.** As an example, this image illustrates four different GPS trajectories that describe the four different ways a vehicle can take on a motorway junction in Ingolstadt, Germany. This includes two motorway ramps (blue, green) and two motorway exits (red, purple).

Matching these trajectories on a map is needed to calculate thresholds for our wrong-way driver detection. This leads to the problem of map matching the vehicle to the correct road. The map matching process has to be done carefully, because GPS accuracy may vary and incorrect matches may influence the detection quality in a considerable way. To ensure that there is no false-positive, each motorway junction has a learning phase. Therefore, there is a need of doing different steps. Generally it is necessary to match each vehicle to the regarding road it takes. This is needed for the detection as well as for the warning part. This leads to the problem of map matching algorithms. In particular the algorithm has to handle the accuracy of GPS which has a potentially high variance. This can lead to incorrect matches. Therefore, the algorithm needs to calculate a threshold for each motorway junction and has to update the model in cycles. The thresholds are stored together with the map information like ways and prescribed driving direction in a database within the cloud. As descripted above, after the phase of learning the algorithm determines a threshold which is suitable for a given motorway junction and this way gets active for detecting wrong-way drivers.

When the live phase is released, the detection algorithm is running and warning endangered drivers (Figure 3). The detection is done by calculating probabilities. This probabilities are dependent on the positions over time, which are matched on the map information. The algorithm makes use of data from the database including the prescribed driving direction and compares them to the real vehicle driving direction, traceably by its GPS trajectory. If the probability is steadily increasing and moving into a danger area, a wrong-way driver will be detected and all endangered drivers nearby, as well as the wrong-way driver itself, will be warned via V2X messages. During the process of detection, the thresholds are still changing based on the input data from vehicles in order to provide flexibility to adapt to changing circumstances.

As mentioned in the introduction, daytime construction sites can lead to changed traffic guidance and sometimes lanes are closed or redirected over opposite lanes. This can result in false-positive detections, therefore

validation checked input data and a solution for handling changing infrastructures is advised. Otherwise the quality, robustness and durability of the function cannot be guaranteed.

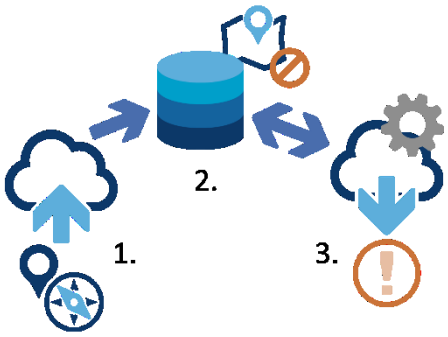

Figure 3. **Productive wrong-way driver warning with dynamic adaption of detection parameters.** In this illustration you see the processing steps of learning and warning of the wrong-way driver detection. In the first step the data is collected from the objects and sent to the cloud database. In the next step the data is map matched and compared with entries in the database for the detection algorithm. If a wrong-way driver is detected, the endangered drivers nearby and the wrong-way driver itself will be warned in step three.

This problem is not appearing exclusively at the described IAV wrong-way driver detection, but is also applicable to several other functions with dynamic behavior. To handle this problem, this paper introduces a solution concept and discusses the challenges and possible adaption to other functions.

IMPROVING THE APPROACH: DETECTING ALTERNATIVE WAYS AND RATE WAY VALIDITY

The already introduced wrong-way driver detection function uses map matching algorithms to relate the vehicle´s trajectory to the map. The role of the used map database is essential, the function uses this as reference for the calculated thresholds as well as during map matching in the detection phase. But this dependency can have bad effects, like obsolete map data or temporary construction sites that is not considered nor recognized by the algorithm. This could lead either to false-positive detections or to no possible map matching, which in turn effects the productivity of the function. This lack of efficiency and reliability is not desirable for a safety function.

For this reason, solution concepts need to be developed to prevent from this effects. A conceivable approach for a self-controlling module could be the following described alternative way detection method.

This method takes up the theory that the way information could be extended by an expiration date attribute. This attribute could be used to register the actuality and validity of each section of way from the map. Usually a motorway junction is used several times per day. This means that map matching should happen on each way or section of way regularly. Exceptions from this assumption are closed or redirected lanes using opposite lanes or temporary roads (Figure 4). Respecting this scenarios during detection, an algorithm to indicate possible new ways and register no longer used ways is considered.

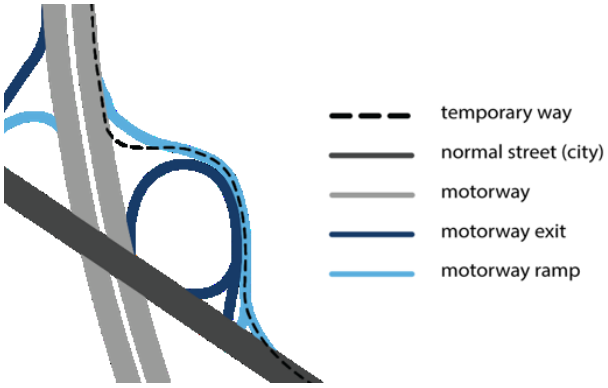

Figure 4. **Example A for a temporary road due to construction site.** The alternative way is following the motorway ramp excluding a specific section that leads to the motorway.

To detect such scenarios we need to classify each road within the database. The classification will have four different categories. We assume that the validation of the category increases with the usage of the road over time. Therefore, every way is classified by the categories seen in Figure 5.

If a way is indicated as used regularly, this is marked with the related expiration attribute and updated every time of map matching. Not regularly used ways and expired, not used ways can be detected by specific indicator rules or statistical calculations. During designing this indicators, it is important to consider seasons of the day and the amount of map matches over time. This is important, because overnight traffic volume is lower than during the day.

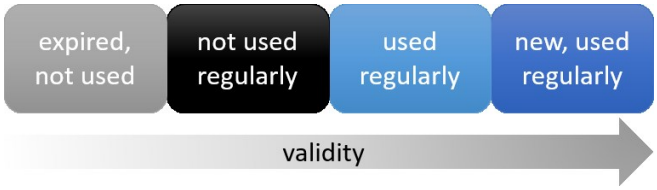

Figure 5. **Classification scheme based on the validity of used ways.** We provide a categorization of a way with four possible states. Expired means not used for a specific time, not used regularly has not been used for a specific time, used regularly is a normal used way and new, regularly used way is a validated alternative way.

Taking into account that already expired ways could also increase invalidity because of recently mapped trajectories, this ways are still stored in the database. From this point on they can also gain importance and be reactivated. Especially in scenarios of short-term closed or redirected routes this is a potential method to update the database without information loss.

Furthermore alternative ways, which are pretended as temporary roads, can have different characteristics. Basically they can be divided into three different types.

A. Ways that have common sections with already known ways

By their nature, there are different challenges in detecting sections as a potential new way. Caused by already known points, ways that have sections in common with ways in the database can be detected more precisely in general than completely unknown ways (Figure 4). It must be noted here that this statement is also dependent on how many sections or points are in common with already saved ways from database. In principle, the more points are common, the more certain is a successful and contemporary detection of an alternative branching way. This is based on the fact that already known sections are interpreted as validated and therefore they are weighted as more likely than unknown sections. Sections which are not known are not saved in the database and will be accepted with lower probability of existence. If trajectories are mapped to already known sections of ways and also describe new unknown ways, they are saved as possible alternative way, but not immediately as new and regularly used way. Only if this alternative way can be map matched frequently to appearing trajectories, thresholds are calculated and it will be marked as a new way.

B. Ways that have same start- and/or endpoints in common with already known ways

In cases of ways, which only have a common start- or endpoint (Figure 6) it is essential to know the covered way of a vehicle trajectory to get an indication of an alternative way. This means not only tracking motorway junctions but also trajectories before and after a known motorway junction. If the trajectories can be mapped to already known ways that are connected to a motorway junction, every successfully map matched point of the GPS position increases the probability of a plausible alternative way. This requires correct and reliable map matching without jumps in mapped ways, which means that the mapping process must not result in a variety of different possible ways. Otherwise map matching is unsteady and alternative way creation should be waived to prevent from erroneously applied ways and resulting false-positive detections of the wrong-way driver function. This suggested method requires information from additional ways that are connected to motorway junction and also need to be persisted in a database. To provide thresholds for map matching trajectories to additional ways, it is possible to use calculated average values from directly connected ways around, or they will be trained like the motorway junction way. If the alternative way is frequently map matched, the probability of a plausible alternative way increases every time of matching until it can be marked as new, regularly used way.

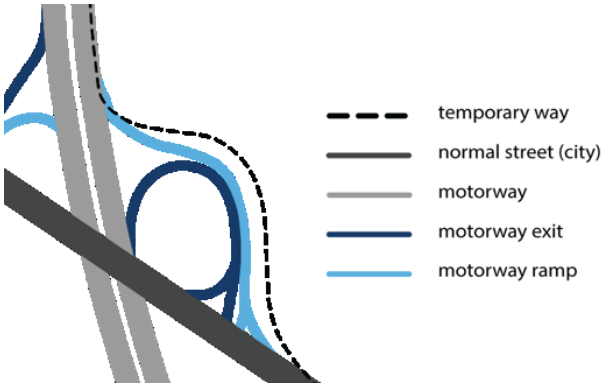

Figure 6. **Example B for a temporary road due to construction site.** The alternative way is next to the motorway ramp but ends up in the same point as the motorway ramp.

C. Completely new ways without common sections

Ways that have no point in common with any way from database only can be indicated by collecting trajectory information over a period of time (Figure 7). This also includes trajectories before and after motorway junction to detect where a way branches to another way that is not persisted in database. Indications are increased incidences of no further mapped positions at a specific position on the way. Every point of the unknown trajectory from the vehicle is insecure at the first time, so the probability of a plausible alternative way is low and increasing with every additional map matched trajectory from other vehicles. The required thresholds for map matching to the alternative way can be transferred from other known ways for the first times until they can be calculated individually. If an alternative way is considered, it must be handled with care, because the information about the correct driving direction is not validated by already known sections at this point. Therefore, only frequently occurrence of trajectories from vehicles in a certain time can be assumed as plausible and their driving direction interpreted as the correct driving direction. Every time of successful map matching to the alternative way increases the probability of plausibility, until the level is reached and specified as a new way in database.

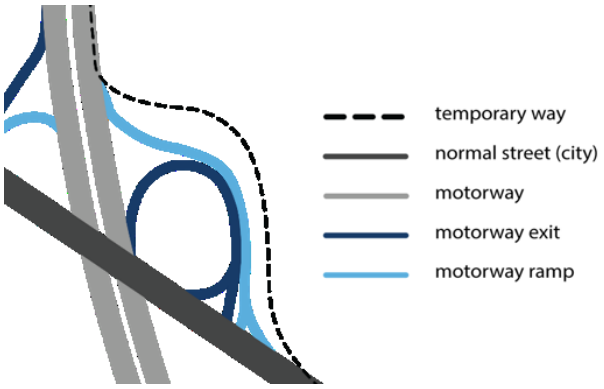

Figure 7. **Example C for a temporary road due to construction site.** The alternative way is next to the motorway ramp and has no point in common with it.

The described methods for detecting new ways on basis of already known ways require different additional information and have their limits. To get a first idea, if the described method is an applicable solution approach for the mentioned problem, exemplary tests were carried out.

EXEMPLARY TESTS

To prove the general functionality of the method, a first test set is used. This set includes an exemplary database with ways and thresholds for a simple motorway ramp (Figure 4). For each type of alternative way (A, B, C) a manually created artificial trajectory is used for testing. Therefore, a test trajectory is created which has no point in common with the motorway ramp (C), one that has the same startpoint and no other common sections (B), and another that has a section in common and a section apart from the motorway ramp (A). It is necessary that the section apart from the motorway ramp is not included in any threshold from the database, to prevent from map matching to existing ways. In this test environment the following mentioned values are assumptions and variably adaptable.

Because of the need for a frequently occurrence of the trajectories, each of the artificial trajectories is taken as basis to create 10 additional trajectories with a randomized deviation for each point respecting a maximum deviation of $5 \cdot 10^{-6}$ degrees in longitude and latitude. These trajectories serve as a test set to analyze the behavior of the algorithm to detect new ways.

Each point of the trajectory that is map matched to an existing way is rated with a percentage of 5%. This value is added to the general probability of existence of the alternative way. The expiring of ways is not considered in the test environment. Trajectories with GPS points that could not be map matched to existing ways, will be reserved as potential alternative way to compare them with new incoming trajectories. The next time a trajectory can be map matched to the potential alternative way, each GPS point is rated with a percentage of 0.5%, if it happens in less than a minute, the probability of existence assumes to be higher and the percentage is rated with 1%. In this test environment we suppose day time, so usually ways should be taken frequently.

If a potential alternative way is rated with at least a percentage of 90% it is considered as a new, regularly used way. If a way is not used, the percentage decreases every five minutes about 5%. The wrong-way driver detection algorithm only uses validated categories of ways (Figure 5) and no potential alternative ways.

With this parameterization the test environment is operated. For each categorized artificial trajectory every 30 seconds one of the randomized trajectories serves as input for the wrong-way driver detection function. After that, one of the trajectories is inverted to simulate a wrong-way driver and proof, if this is correctly detected. This procedure is repeated for each trajectory, so that for each category and each generated trajectory one inverted trajectory has been processed by the wrong-way driver detection.

RESULTS

During the tests we discovered that the process of map matching the changed traffic guidance to the already stored ways has to be done consciously. Failures during this steps can lead to bad influences on the detection algorithm, therefore a high specificity is required. In general, trajectories of category B and C could not constantly be detected as new ways caused by the problem of map matching and parametrization. Depending on the different categorized trajectories, the trajectories of type (A) has been detected earlier than for type B or C. This is an expected result, because of the common section to already existing ways in the database. The percentage of 0.5% or 1% for points that cannot be map matched to existing ways has been too low to reach the 90% level in some cases. When new ways have been identified correctly, and the map matching of the points to the new ways succeeded, the inverted trajectories have been detected successfully as wrong-way driver. The same applies to not inverted trajectories, which have been detected as driving in the correct direction.

Generally speaking, the regulation which defines the way when and how strong the changed conditions affect the database has to be defined by the amount and time intervals of their occurrence. Under these conditions we achieved higher quality rates than without the self-controlling module. When the map matching failed, the amount of false positives increases in some cases.

LIMITATIONS

The described evaluation process is limited to handling changed traffic guidance which is temporary not considered in the map. Depending on the parametrization of map matching the results of the evaluation process vary in both directions. In general this process enables to react automatically to changing street conditions and test the resulting behavior of the detection algorithm. But there are limitations.

Changed infrastructure directly on motorways is not considered. Furthermore, to build up a reliable self-controlling module it is advised and partly necessary to extend the database with connected ways around motorway junction ways, especially for completely new ways, which correspond to a new motorway junction. It is also necessary to respect the fact that motorway junction ways can have various forms, which are not further discussed in this paper, nor tested.

The introduced approach is mainly tailored to IAV´s wrong-way driver detection, but also has adaptable aspects. For example, going one step back and gather additional information to indicate changes to react appropriately can also be adapted to other functions. Also the discussed classification scheme of ways is build up dynamically and not determined for a special defined function. The concept behind is extendable and open for changes.

CONCLUSIONS

The discussed process of the introduced wrong-way driver warning shows an example how a specific cloud-based function can be dynamically evaluated without dependence on the functional logic. Especially functions whose results strongly depend on ever-changing input data need solutions to test their behavior in critical situations. This approach delivers also a possible answer how to implement additional methods to create more flexible and long-term reliable cloud-based active safety systems.

REFERENCES

[1] (in german). Fuchs, H., Hofmann, F., Löhr, H., & Schaaf, G. (2015). Car-2-X. In Handbuch Fahrerassistenzsysteme (pp. 525-540). Springer Vieweg, Wiesbaden.

[2] (in german). Kartengestützte Ortung. Retrieved February 28, 2019 from https://www.iigs.uni-stuttgart.de/forschung/projekte/mapmatching/

[3] Ress, C., & Wiecker, M. (2016). Evaluating the Potential of V2X Communication for Road Safety and Efficiency. ATZ worldwide, 118(1), 16-21.

[4] (in german). Gerlach, J. Univ.-Prof. Dr.-Ing., Seipel, S. Dipl.-Ing., & Leven, J. (2012). Falschfahrten auf Autobahnen – Langfassung [PDF file]. 52. Retrieved February 28, 2019 from https://www.bast.de/BASt_2017/DE/Verkehrstechnik/Publikationen/Download-Publikationen/Unterseiten/V-falschfahrten.html

Real World Accident Analysis of Car-to-Car Intersection Near-Side Impacts: Focus on Pelvis Injury

Chinmoy, Pal
Shigeru, Hirayama
Shinichi, Hayashi
Nissan Motor Company Ltd,
Japan

Manoharan, Jeyabharath
Vimalathithan, Kulothungan
Renault Nissan Technology Business Centre India,
India

Paper Number 19-0090

ABSTRACT

Near-side impacts are one of the severe crash modes of all the impacts. Even though 90% of vehicles have achieved "Good" in IIHS rating, there is hardly any sign of decreasing trend in side impact fatalities for last few years. IIHS is planning to introduce a new test protocol because even the cars with “Good Rating” in IIHS tests can still have AIS3+ injuries. In side impacts, a higher number of severe injuries were found in thorax, head and then followed by pelvic region. Though many researchers addressed the mechanism of thorax and head injuries, there are a few in-detail accident analysis of pelvis injuries. Pelvis injury often leads to significant medical expense and impacts the long-term quality of life. This study is focused to find out (i) the relation between pelvis injury with structural deformation (ii) the frequency and the type of pelvis injuries (iii) the type of target of population to considered (size: small/large, gender: male/female) with the help of accident data and simulation results. C2C intersection accidents were selected from NASS-CDS (CY2004-15, n=913 cases) to identify the influential parameters by logistic regression. From the accident analysis it is found that a)pelvic ring fracture is one of the most frequent injuries, b)10 o’clock impact caused the highest number of injuries, c) pelvis injury frequency is more in female than male, and d) risk of pelvis injury increases when the maximum intrusion of B-pillar and surrounding door structure exceeds a certain level. Logistic regression indicates that angle of impact, location of impact and initial velocity of the struck car are also important parameters. To gain more benefit in real-world accidents by introducing future side impact protocols, a rational approach is necessary to focus more on evaluating the most frequent pelvic ring fracture by introducing more bio-fidelic dummy (say World-SID) in future protocol tests.

INTRODUCTION

Near-side (lateral impact location on driver side) impacts are one of the most severe crash modes with high frequency in real traffic accidents, commonly resulting in serious injuries (Randa, 2003[4], Matthew, 2015[5], Helena, 2011[2]). In SINCAP tests, at the time of impact, the barrier is moving at 62kph and "crabbed" 27 degrees toward the rear of the test vehicle to keep the front of the barrier parallel to the side of the test vehicle. The resulting change in velocity can vary within a range of 22 to 32kph, depending on the mass of the struck vehicle. Insurance Institute for Highway Safety (IIHS) side-impact crash tests consist of a stationary test vehicle struck on the driver's side by a moving trolley fitted with a deformable honeycomb barrier for perpendicular impact. The leading end of the barrier is shaped to simulate the typical front end of a pickup or Sports Utility Vehicle (SUV). The 1,500kg moving deformable barrier strikes the vehicle on the driver's side at a velocity of 50kph. Vehicles with high-hood front-end profile caused more head injuries in passenger vehicles in real world accidents and it could not be assessed with the FMVSS 214 barrier. As a result, the IIHS started its side test program in 2003 with a barrier designed to represent the front end of a typical SUV and pickup. Later, in the FMVSS No. 214, the oblique pole test was introduced. To simulate the real world accidents, the vehicle to be tested is propelled sideways into a rigid pole at an angle of 75 degrees with a speed of 32kph. Three different C2C related side impact protocols were given in Figure 1. For detail information of different NCAP test conditions and regulations of different countries refer to the Safety Companion [24] compiled by CARHS.

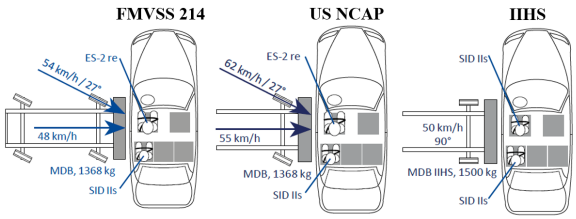

Figure 1. C2C related side impact protocols

Statistics showed that car-to-car(C2C) near side impacts account for more than 60-70% of side impact crashes resulting in serious-to-fatal injuries (Pal 2017[12]). Due to limited survival space on the struck side, near-side occupants, adjacent to the side of the vehicle subjected to major impact, frequently sustain severe injuries than far-side occupants. Occupant injury can be significantly affected by a different set of crash characteristics and the effects of a crash configuration such as impact direction, impact angle, and change in delta-V need to be studied in detail with real world accident data. Xinghua Lai et al., (2012[9]) investigated the effects of specific impact direction and impact regions on serious-to-fatal injuries of driver occupants involved in near-side collisions using data gathered from National Automotive Sampling System Crashworthiness Data System NASS-CDS (CY1995–2005, [1]) and found that the risk of serious injury was higher for side center (P) and side front distribution (Y) than the side front (F) or rear end (B) locations.

Even though 90% of vehicles have achieved "Good" in IIHS rating, there is hardly any sign of decreasing trend in side impact fatalities for last few years. IIHS is planning to introduce new tests because even the cars with "Good Rating" in IIHS tests can still have AIS3+ injuries. In side impacts, a higher number of severe injuries were found in thorax, head and then followed by pelvic region. Though many researchers addressed the mechanism of thorax and head injuries, [6,7,8], there are a few in-detail accident analysis of pelvis injuries. Pelvis injury often leads to significant medical expense and impacts the long-term quality of life. In order to improve occupant safety in C2C side impact intersection crashes, the objectives of this paper are to find out (i) the relation between pelvis injury with structural deformation (ii) the frequency and type of pelvis injuries and (iii) the type of target of population to considered (size: small/large, gender: male/female, BMI) with help of accident data, and simulation.

DATA & METHODS

This study used accident data from the National Automotive Sampling System Crashworthiness Data System (NASS-CDS) for the calendar year 2004 to 2015. Table 1 shows the assumptions used to prepare the accident data set for this study. The accident samples are limited to C2C intersection side imact planar collisions (i.e., excluded crashes with the primary general area of damage as top or bottom and rollovers). Values with unknowns have been omitted. In total, 913 vehicles were extracted to perform the accident analysis and logistic regression analysis [13]. Details of those analyses are described in later sections. Table 2 shows the final data set extracted from NASS-CDS CY 2004-15 using the criteria mentioned in Table1. In total, 913 occupants with 4195 injuries involved in near side impacts were

selected with six collision deformation codes (F, P, Y, Z, D, B) and with three main impact angles (8-10 o'clock, driver side) as shown in Figure 2.

Table 1.
List of criteria for input dataset

General Area Damage1=Left
The direction of Force DOF=8−10 o'clock
Impact Location=F, P, Y, B, D, Z
Body Type PV (1-9,17)
Model Year>=2000
Driver Role=1, (Seat Position=11)
Age16+
V2V OBJCTD<=30
Towed Away Vehicles
No Ejection
No Rollover
No Fire Occurrence
Excluded AIS7 injury

Table 2.
List of dataset

	Raw data		Weighted	
	Total no	With pelvis-injury	Total no	With pelvis-injury
Drivers	913	203 (22.2%)	639280	131436 (20.5%)
Injuries	4195	291 (7.0%)	3359148	191858 (5.7%)

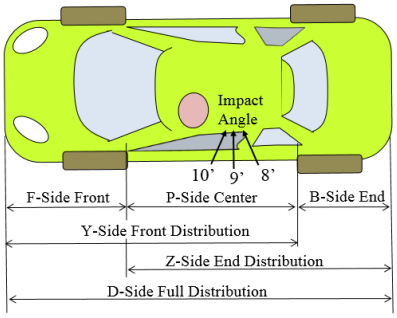

Figure 2. NASS-CDS collision deformation code (8, 9, 10 o'clock impact angles)

There were 203 cases on driver side impact involving pelvis injuries which account for 22.2% of overall side impact injury cases (Table 2).

RESULTS

The pelvis injury pattern of occupants involved in C2C near side collisions is discussed in this section. The order of explanation is: a) first, an overview of pelvis region and distribution of injuries, the effect of b) impact angle, c) gender, and d) intrusion magnitude w.r.t pelvis injury. Logistic regression is performed to check the probability of pelvis AIS3+ and AIS2+ injuries occurrence using different factors such as lateral delta-V, gender, the angle of impact, BMI etc. Results were calculated using XLSTAT software[10, 11]. A separate sensitivity analysis was also performed, to see the effect of lateral delta-V and angle of impact and finally, the pelvis injury results were verified using human body simulations. In this study, all the logsitic regression models developed using weighted data.

Overview of side impact injuries

Figure 3 shows the number of injuires in different body regions for three AIS level of severity in nearside impacts. Pelvis AIS1+, AIS2+, and AIS3+ injuries account for 7%, 17%, and 10%, respectively of overall near side impact injuries. The percentage of head and thorax injuries are increasing as the AIS level increases.

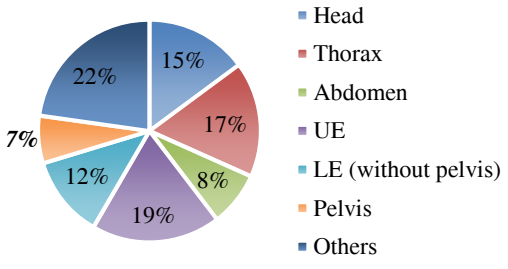

a) AIS1+ injuries

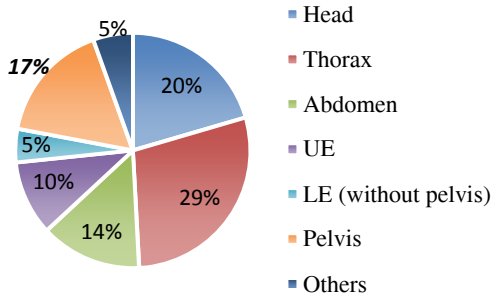

b) AIS2+ injuries

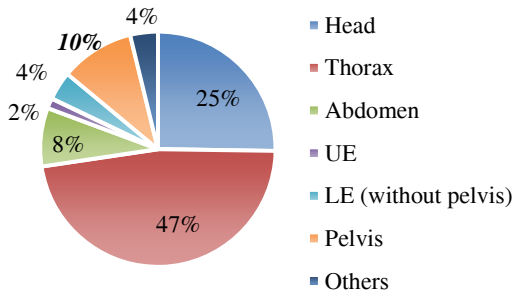

c) AIS3+ injuries

Figure 3(a, b, c). Number of AIS injuries in different body regions of near side impacts

Overview of pelvic region and related injuries

Figure A1 shows the important parts associated with the pelvis and they are lumbar spine (cord, disc), sciatic nerve, pelvis ring, acetabulum, sympysis pubis, hip joint, and sacroilliac. Table A1 shows the count of AIS1+, AIS2+ and AIS3+ injuries of each individual sub-parts. AIS2+ and AIS3+ injuries constitute 16.5% (233) and 10.2% (72) of overall side impact injuries. It is interesting to find that, when one plots (refer Figure 4) the percenatge of pelvis related AIS injuries as mentioned in Figure A1 and Table A1, AIS2+ was highest. 75% of those AIS2+ injuries were pelvis ring fracture(refer Figure 5). Hence, together with AIS3+, AIS2+ pelvis injuries need some attention in the future. Note that the percenatge is calculated with respect to different AIS levels among the injuries of different body regions when pelvis injury occurred.

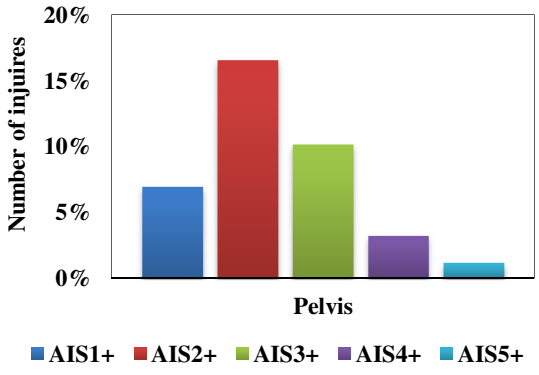

Figure 4. Percentages of pelvis injury across different AIS levels within the injuries of various body regions, when pelvis injury occurred.

Figure 5 shows the distribution of different injuries in each part of the pelvis region. It is found that the pelvic ring fracture (60%) is the most frequent compared to all the injuires and then followed by lumber spine (cord+disc, 31%) injuries. Symphysis pubis fracture is also one of the common injuries wihtin the pelvis region.

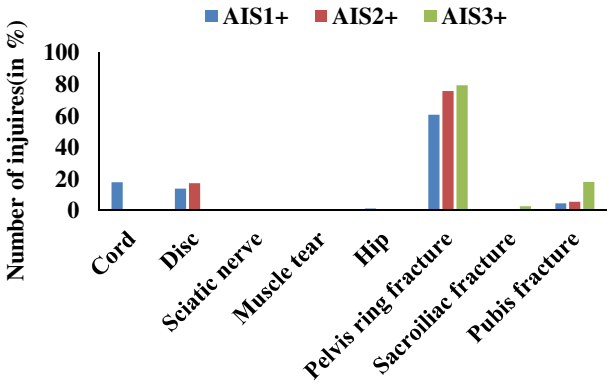

Figure 5. Distribution of pelvis injuries

Effect of angle of impact

Figure 6 shows the effect of angle of impact on the pelvis injuires for different AIS injury levels. It is observed that the oblique 10 o'clock impact angle caused the maximum no. of injuries when compared with those of 9 o'clock and 8 o'clock impacts.

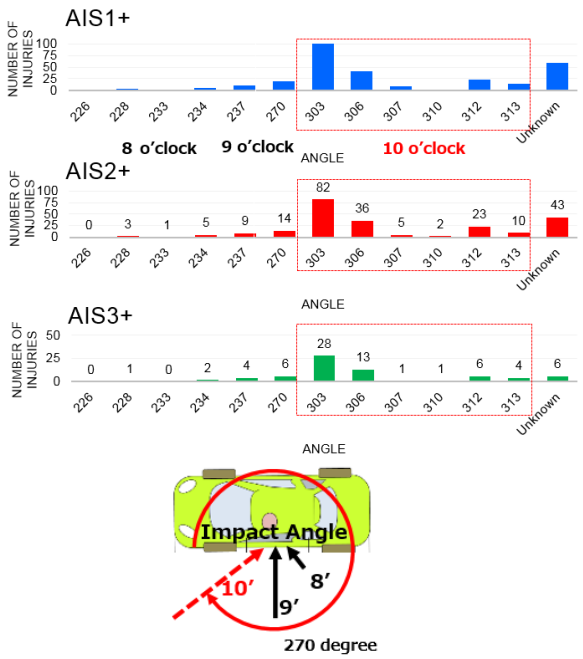

Figure 6. Variation of pelvis injury w.r.t angle of impact. (255~285 deg. corresponds to 9 o'clock)

This shows that most of the real world side injuries are due to oblique impact but not caused by perpendicular impact. The angle of impact of each case is verified by the ratio of delta-V (longitudinal and lateral components) as mentioned in the accident

report. The present real accident data clearly indicates that in future test protocol, proper consideration has to be given about the angle of impact during the loading phase of the pelvis in dummies to capture the real world phenomena.

Effect of gender

Figure 7 shows the effect of gender on the pelvis injury. It is observed that female were having more number of injuires than male. This shows that female were most likely to have higher pelvis injuries than male. Some of the possible reasons may be that (i) the females sit further forward towards the steering wheel than males who are usually taller in height than females (refer Figure A6) and (ii) the shape and strength of pelvis are different. It is to be noted that the pelvis injury is influenced by trochanteric soft tissue thickness and BMD of female occupants [15].

Logistic models: lateral delta-V, gender, and angle of impact

Logistic regression is peformed to check the probability of pelvis AIS3 and AIS2+ injury occurance using different factors such as lateral delta-V, gender, and angle of impact.

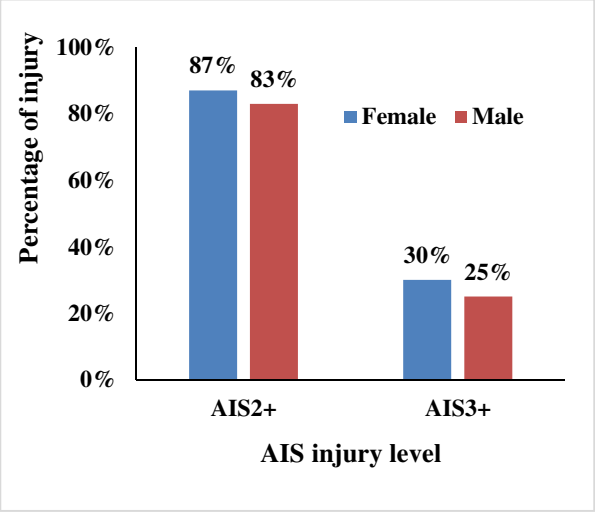

Figure 7. Variation of injuries w.r.t gender

Results of logistc regression were mentioned in Table 3 and Table 5 with AIS3+ and AIS2+ pelvis injury as dependent variables. All the probability values are calculated by varying the lateral delta-V for two 9 o'clock and 10 o'clock impact angles. As shown in Figures 8 and 10, it is clearly evident that the probability curve for 10 o'clock impact is above the 9 o'clock impact curve for both AIS3+ and AIS2+ injuries. The probability of AIS3+ injury is higher for 10 o'clock impact than 9 o'clock impact. Table 4 and 6 show the typical examples of the change in probability values for 10 and 9 o'clock impacts with respect to lateral delta-V changes. At 25kph (equiv. to 50kph barrier impact) and 30kph (equiv. to 60kph barrier impact) lateral delta-V, the probability values changes from 5.5% to 17.38% (3.16 times) and 8.87% to 26.04% (2.93 times) for inclined 10 o'clock and perpendicular 9 o'clock impacts, respectively.

Table 3.
Logistic Model when predicting pelvis AIS3+

n=221, Pelvis AIS3+(0:158,1:63)	Value	Pr. > Chi²	Odds ratio
Intercept	-11.911	< 0.0001	
Ln(Lateral delta-V)	2.826	< 0.0001	16.88
Gender Male: 0	0.000		
Gender Female: 1	-0.030	0.945	0.970
Angle 9 o'clock: 0	0.000		
Angle 10 o'clock: 1	1.286	0.007	3.617

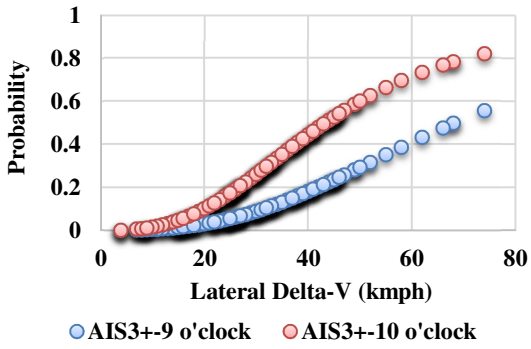

Figure 8 Comparison of probability of AIS3+ for 10 and 9 o'clock impacts with respect to lateral delta-V.

Table 4.
Example of the probabilities of AIS3+ of 10 and 9 o'clock impacts with respect to change in lateral delta-V from 25kph to 30kph

Lateral delta-V (kph)	9 o' clock impacts	10 o' clock impacts	Ratio of 10→9 o'clock impacts
25	5.50%	17.38%	**3.16**
30	8.87%	26.04%	**2.93**
Probability ratio of 30→25kph change in delta-V	**1.61**	**1.50**	Effect of angle is more than 5kph delta-V increase

Table 5.
Logistic Model when predicting pelvis AIS2+

n=221, Pelvis AIS2+(0:41,1:180)	Value	Pr. > Chi²	Odds ratio
Intercept	-19.137	< 0.0001	
Ln(Lateral delta-V)	6.481	< 0.0001	652.5
Gender Male: 0	0.000		
Female: 1	-2.912	< 0.0001	0.054
Angle 9 o'clock: 0	0.000		
10 o'clock: 1	2.466	< 0.0001	11.777

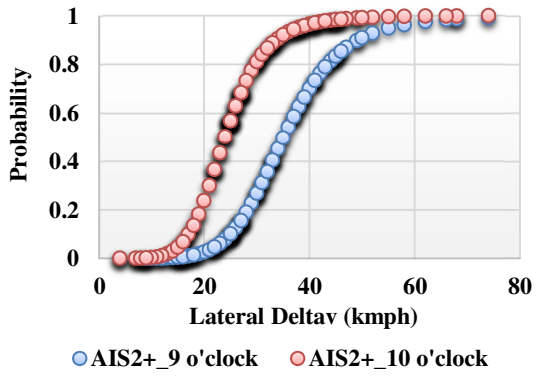

Figure 9. Comparison of probability of AIS2+ for 10 and 9 o'clock impacts with respect to lateral delta-V.

Table 6.
Example of the probabilities of AIS3+ of 10 and 9 o'clock impacts with respect to change in lateral delta-V from 25kph to 30kph

Lateral delta-V (kph)	9 o' clock impacts	10 o' clock impacts	Ratio of 10→9 o'clock impacts
25	10.08%	56.91%	**5.64**
30	26.76%	81.15%	**3.03**
Probability ratio of 30→25kph change in delta-V	**2.65**	**1.43**	Effect of angle is more than 5kph delta-V increase

Similar results were observed when predicted with AIS2+ injury level (refer to Table 5, 6 and Figure 9).

Effect of impact location (CDC code)

Figure 10(a,b,c) shows the number of pelvis injuries with respect to the location of impact. Y region had the highest number (for AIS1+: 40%, AIS2+: 43%, AIS3+: 39%) of injuries compared to other locations and then followed by P and Z locations. Combined Y and P locations cover more than 2/3rd of all injuries from AIS1-3.

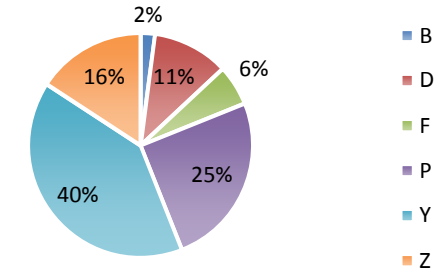

a) AIS1+ pelvis injuries

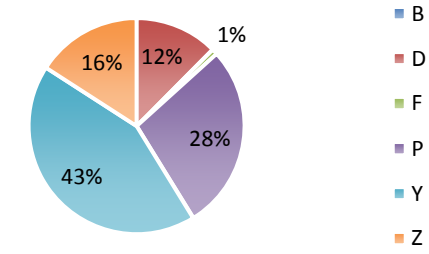

b) AIS2+ pelvis injuries

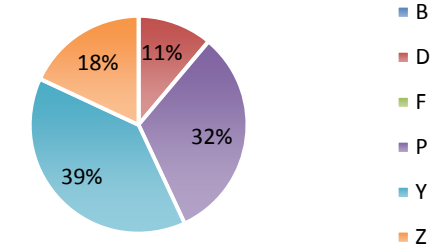

c) AIS3+ pelvis injuries

Figure 10 (a, b, c). Number of AIS injuries with respect to the location of impact (based on CDC code)

Effect of impact location (from crash pictures)

In order to estimate more accurately the effect of impact location, BMI and intrusion magnitude, the number of cases were increased from 203 (driver alone) to 265 by adding pelvis injury of right side passengers cases also(Figure 11). By detail inspection of damage pictures of each case in the

NASS-CDS database, one could identify the location of impact from B pillar accurately. This will help one to estimate the changes of injury pattern with respect to the impact location of maximum external deformation.

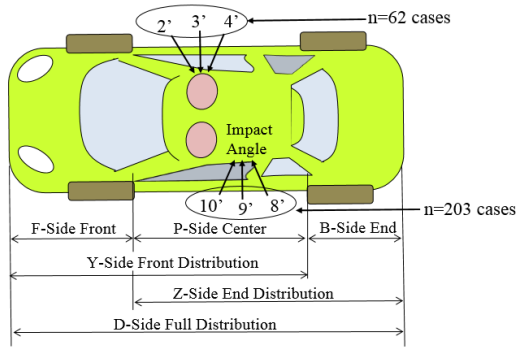

Figure 11. Driver plus passenger cases selection criteria

In order to observe the overall picture of impact location on pelvis injuries, the distribution of AIS2+ (Figure 12) and AIS3+(Figure 13) injuries (based on binary count Yes=1 and No=0) was plotted with respect to the location of maximum external deformation. It is observed that AIS2+ and AIS3+ injuries are more when imapct location is close to B pillar. It is also observed that 80% of serious AIS3+ injuries are coming between -50cm to +50cm. which means more pelvis serious injuries in this region.

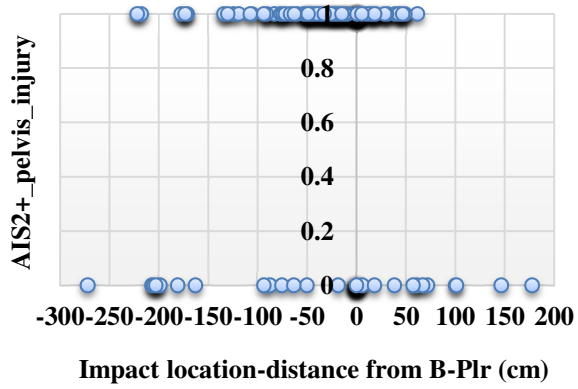

Figure 12. Distribution of AIS2+ injury (binary cases: serious: 1, minor: 0) with respect to impact location-distance from B pillar (cm).

Figure 14 shows the distribution of AIS2+ and AIS3+ injuries with the location of imapct as a continuous variable. It is observed that as the maximum deformation of impact location moves away from B pillar to either left or right of the vehicle, the percentage of injuries were decreasing. The peak values were observed near to B pillar (around driver sitting postion). There was a high chance (AIS2+: 96%, AIS3+:60%) of injury when the imapct location was very close to the driving position near B-pillar.

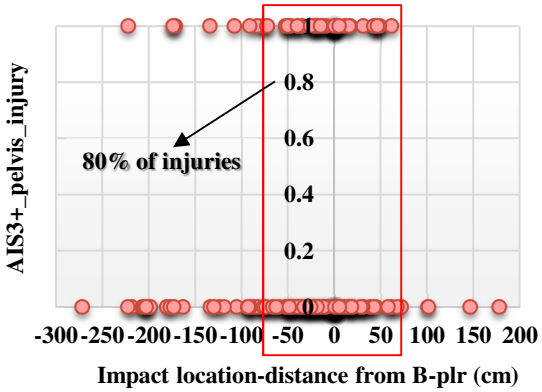

Figure 13. Distribution of AIS3+ injury (binary cases: serious: 1, minor: 0) with respect to impact location-distance from B pillar (cm).

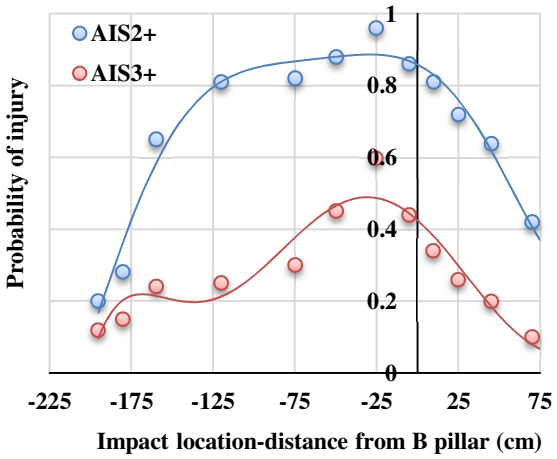

Figure 14. Comparison of probabilities of AIS2+ and AIS3+ injury with respect to impact location-distance from B-pillar (cm) of maximum deformation.

Real world accident data

Figure 15 shows the variation of pelvis injury with respect to various compartment (door inner) intrusion magnitudes 0-8cm, 8-15cm, 15-30cm, and > 30cm.

The X-axis shows different injury levels and Y-axis shows the number of cases considered. All the injury levels are labeled in different categories of intrusion magnitude. It is observed that the risk of pelvis injury increases if the magnitude of intrusion increases beyond a certain level to cause more serious AIS3+ injuries as indicted by two circled portions (①,②).

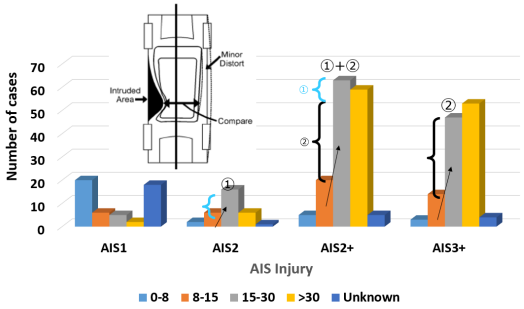

Figure 15. Variation of number of cases (AIS levels) w.r.t compartment intrusion magnitude

Figure 16 shows the probabilities of AIS2+ and AIS3+ injury with respect to intrusion magnitude. As the intrusion magnitude was increasing the probability of both the injuries were increasing. Hence, the magnitude of intrusion is a useful parameter in identfying the injury classification. Figure 17 shows the average intrusion magnitude (AIS2+ and AIS3+) with respect to impact location. It is observed that even though the intrusion magnitude was low near the B-pilllar, AIS2+ and AIS3+ injuries are likely to occur. As the impact location moves further away from B-pillar, either forward or rear side of the vehicle, the average of maximum intrsuion magnitude was increasing in order to cause the same AIS level of injuries.

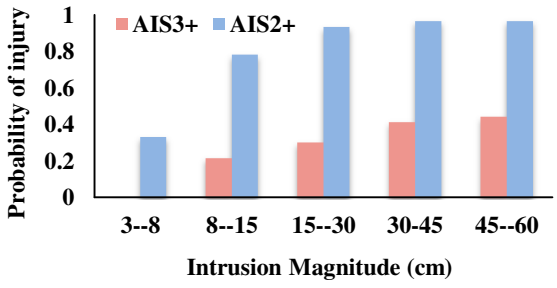

Figure 16. Comparison of probabilities of AIS2+ and AIS3+ injury with respect to intrusion magnitude (cm).

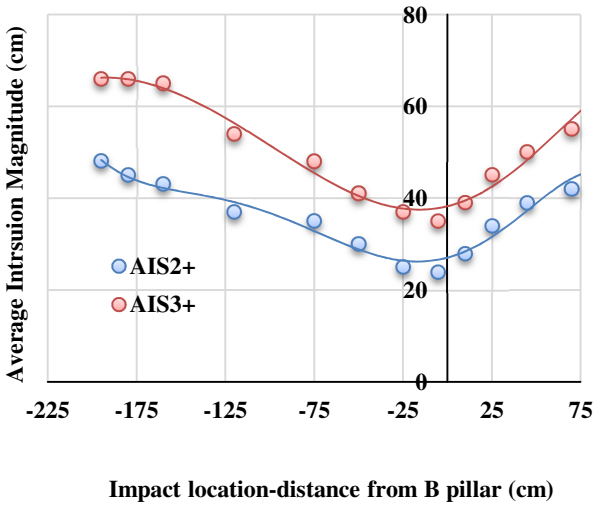

Figure 17 Comparison of average intrusion magnitude for AIS2+ and AIS3+ injury with respect to impact location-distance from B pillar (cm) at maximum external deformation.

Effect of BMI

.

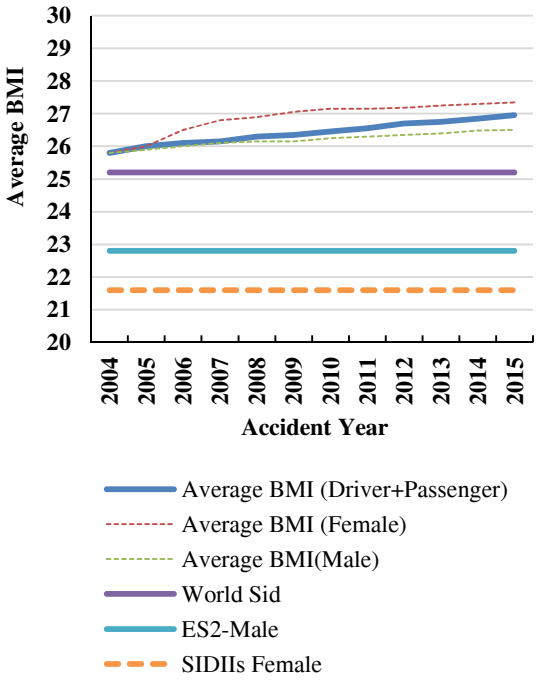

Figure 18 Comparison of Average BMI variation with respect to year of the accident

In order to estimate the effect of BMI on pelvis injuries in a side impact, average BMI was calculated

using 11 years of accident data. Figure 18 shows the variation of average BMI of US driving population with respect to the accident year. BMI values of World SID, ES2 Male and SID-IIs female also plotted in the same graph. It clearly captures the increasing trend of average BMI values (average is around 26). In general, the average BMI values of females were greater than that of the male. Hence, BMI can be an infulencial factor for identifying the injury classification. Figure 19 shows the percentage of injuires for below and above the average value of BMI=26.

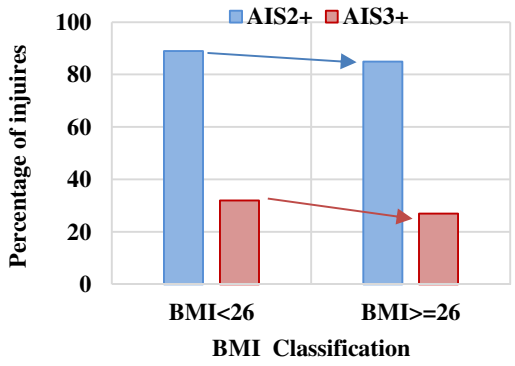

Figure 19 Comparison of AIS2+ and AIS3+ injuries for BMI classification (Average 26)

It is found that the percentage of injuries for <26 was more than >26 which indicates that as the BMI is incresing the percentage of injuries were decreasing. This is may be due to the fact that the relatively shorter and more obese occupants were getting fewer injuires than less obese occupants. As the amount of accumulated fat in pelvis and abdomen region is increasing, there may be less chance of injury in the pelvis region.

Logistic Models (BMI and intrusion magnitude)

In order to find out the effect of BMI and intrusion magnitude, logistc regression models (Table 7 and 8) were developed for both AIS2+ and AIS3+ pelvis injury prediction using the variables such as belt usage (not used:0, used:1) and age (Age<65: 0, Age>=65: 1). In these logistic regression models, total delta-V was splitted into two components as longitudinal and lateral delta-V as continuous variables.

Table 7.
Logistic Model when predicting pelvis AIS3+ injuries when all the variables were considered

n=209 AIS3+: 64, AIS3-: 145 ROC: 0.65	Value	Pr > Chi²	Odds ratio
Intercept	-4.19	0.00	
Longitudinal delta-V	-0.06	***0.04***	0.95
Lateral delta-V	0.02	***0.03***	1.02
Belt not used: 0	0.00		
Belt used: 1	-1.55	***0.00***	0.21
BMI<26-0	0.00		
BMI>=26: 1	-0.85	***0.05***	0.43
Age<65: 0	0.00		
Age>=65: 1	0.91	***0.05***	2.48
Intrusion<15cm: 0	0.00		
Intrusion>=15cm: 1	3.17	***0.01***	23.7

Table 8.
Logistic Model when predicting pelvis AIS2+ injuries when all the variables were considered

n=209 AIS2+: 184, AIS2-: 25 ROC: 0.83	Value	Pr> Chi²	Odds ratio
Intercept	0.29	0.61	
Longitudinal delta-V	-0.10	***0.00***	0.90
Lateral delta-V	0.02	***0.02***	1.02
Belt not used: 0	0.00		
Belt used: 1	-1.58	***0.00***	0.21
BMI<26: 0	0.00		
BMI>=26: 1	-0.43	0.21	0.65
Age<65: 0	0.00		
Age>=65: 1	-0.74	***0.05***	0.48
Intrusion<15cm: 0	0.00		
Intrusion>=15cm: 1	1.21	***0.01***	3.35

As the average BMI is around 26, BMI was categorized into a binary variable (BMI<26: 0, BMI>=26: 1) and the percentage of AIS3+ injury was more than 20% around 15cm of compartment intrusion, the intrusion level was splitted in to a binary variable (Intrusion<15: 0, Intrusion>=15: 1). It is observed from the Table 7 that when predicting the AIS3+ pelvis injury, longitudinal component delta-V,

lateral component of delta-V, belt-usage, BMI, age and intrusion variables were significant ($p<0.05$). However, when predicting AIS2+ injuries (Table 8) all the variables were significant except BMI ($p=0.21$). In both AIS3+ and AIS2+ predictions, BMI coefficient was negative (-0.85, -0.43) which indicates that as the BMI is increasing, the injury level may be less for occupants of higher obesity. Total delta-V was splitted into two to verify the effect of each individual component. It is observed from both the logistic prediction models that the lateral component is more significant than the longitudinal one. However, they also indicate that in side imapct accident cases, the longitudinal component is also an influential parameter. As ROC value(0.65) is not high for AIS3+ logistic regression (Table7), it needs further investigation. Hence, a non-linear SOM clustering analysis is carried out to verify the results of the above linear logistic cluster analysis and it is discussed briefly in the discussion section. SOM stands for Self Organization Map. It is a neural network based classification technique which can be used efficiently in accident analysis to find out the inherent relationship of complex phenomena (Pal 2017, [17]).

Human body model simulation

To understand the influence of BMI on pelvis injury, human body model (HBM) based impactor simulation was carried out. Based on prior studies (Petit P, 2018, [18] & Matthieu Lebarbé, 2016 [19]) a simple rigid rectangular impactor of size: 400mm x 200mm, mass: 23.4kg & speed: 11.2m/s is used to impact the HBM near pelvis region as shown in Figure 20.

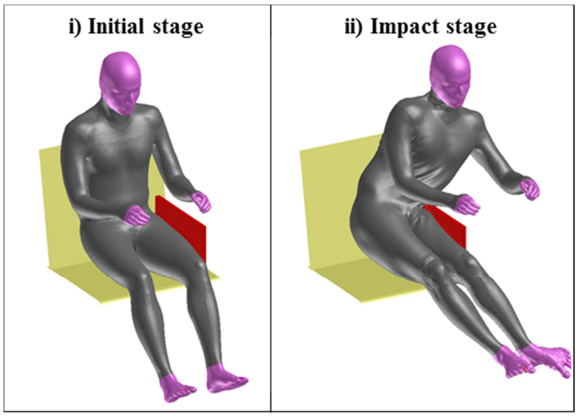

Figure 20 Simple sled impactor test near pelvis region with latest GHMBC Human Body Model.

People with high BMI, have more fat/ flesh content in the hip region as explained in the introduction section. To understand its influence on pelvis injury, an additional layer of flesh is added in the hip region of human body model as shown in Figure 21 to represent occupants of slightly higher BMI=30 based on the information of the reference paper [15].

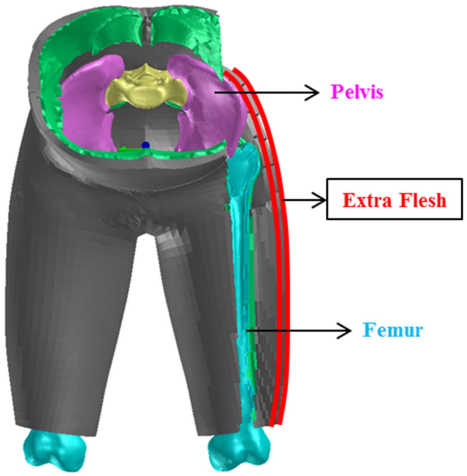

Figure 21 Extra layer of flesh added to hip region of HBM to simulate increased BMI occupant.

Higher BMI human body model with extra outer layer of flesh was impacted against the impactor and the pelvis injury values are compared with the base GHBMC human model. Pelvis bone injury was measured using volume ratio of region which crossed the plastic limit threshold (T*) and the region which do not cross threshold limit. (Note: Threshold T* = one-tenth of GHBMC reference value for fracture). Additional flesh content near the hip region act as a cushion layer to reduce pelvis injury as shown in Figure 22 and Figure A7. Higher BMI is one of the causes of less pelvis ring fracture injury.

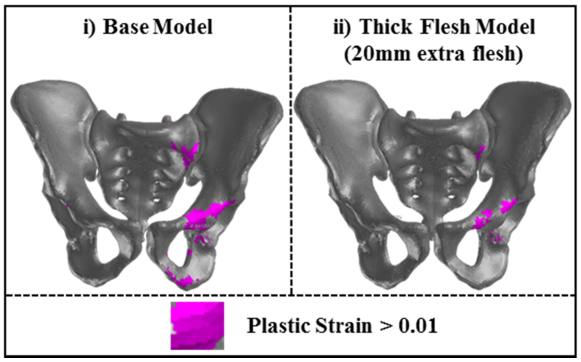

Figure 22 Comparison of pelvis bone injury patterns for base and high BMI thick flesh HBMs

DISCUSSION

The results, as discussed above, suggest that in order to properly evaluate the crash worthiness and occupant performances of different types and sizes of vehicles, it is worth thinking about more rational approach with respect to types and location of structural deformation on the vehicle to identify the actual benefits of existing and future protocols. Collecting more detail intrusion data at relevant different locations near the occupant will be very helpful. Modern camera based image analysis can be one of the possible ways to measure that. In addition to that, EDR data before the crash will add more useful (dimension and depth) of information as future vehicles will be fitted with various sensors.

As the bio-fidelity of the pelvis of SID-2s is low, World-SID is one of the better choices [16]. It is necessary to focus more on evaluating the most frequent pelvic ring fracture by introducing more bio-fidelic dummies equipped with advanced sensors in future protocol tests (refer to Figure A2 and A3). It is also true from the change in BMI trend of US driving population as shown in Figure 18.

To verify the relation between BMI and AIS injury, Self-Organizing-Maps(SOM) based non-linear analysis results were plotted using the pelvis injury input data(refer Figure A4 and A5) related to Tables 7,8. SOM reduces the n-dimensional feature information into 2-dimensional space. The objects (each individual accident case) which are of similar characteristics are placed side by side. The accident cases which are dissimilar are placed further away. A few regions were highlighted using thick black lines to illustrate the effect of BMI on AIS3+ and AIS2+ injury levels in Figures A4 and A5. There are as many numbers of feature based SOM maps as the number of independent input variables of the above mentioned logistic regressions of Tables 7, 8 together with corresponding AIS2+ and AIS3+ injury levels as a dependent variable.

As shown in Figure A4, there were few AIS3+ injuries for BMI>30 within the area surrounded by a thick black line. It indicates that the level of pelvis injury (corresponding to the blue area) will be reduced for obese occupants of older (>65yrs) and younger (<65yrs) occupants. However, there are some small patches of red regions with AIS3+ injury within this thick black line where either the amount of compartment intrusion or the age of the occupants is extremely high. On the other hand, outside the thick black line where AIS3+ SOM map indicates the occurrence of AIS3+ injury (red color), BMI is not that high. These visual clustered results of SOM analysis match well with those of linear logistic regression analysis of Table7.

As shown in Figure A5, the SOM map of AIS2+ injury is clearly clustered in red(AIS2+: 1, yes) and blue(AIS2+: 0, no) regions separated by a thick black closed boundary line marked by ‘a’. The blue part contains a wider range of variations of BMI values and compartment intrusion levels of different accident cases with mixed similarity and dissimilarity patterns. It suggests that BMI (a measure of obesity) is not a definite influential factor for the occurrence of AIS2+ pelvis injury. These visual results of SOM analysis match well with those of logistic regression of Table8. However, one should also note that in the rectangular region as indicated by ‘b’ having AIS+2 injury, there are relatively slim occupants with less BMI (<19), higher compartment intrusion and sitting position very close to B-pillar. This is opposite to the trend of higher BMI obese occupants group as mentioned above. In linear logistic regression analysis, it is difficult to identify correctly such non-linear change in the trend of AIS2+injuries with respect to the change of BMI.

LIMITATIONS

A limited number of cases were studied in this research work. However, considering all possible accident scenarios, more detailed verifications are needed by using various combinations of physical C2C experiments and simulations using different dummies and types of vehicles in order to make any generalized statement as stated above. It is also necessary to do a similar accident analysis for

other countries having good accident database for further verification.

CONCLUSION

This paper discussed the sensitivity of the pelvis injury patterns of C2C side impact accidents at the intersection for PV vehicles using NASS-CDS CY 2004-2015 data. From the accident analysis it was revealed that a) pelvic ring fracture is one of the most frequent injuries, b) 10 o'clock impact caused the highest number of injuries, c) pelvis injury frequency is higher in female than male, d) risk of pelvis injury increases when the maximum intrusion of B-pillar and surrounding door structure exceeds a centain level.
It is also verified using HBM simulation that higher BMI>30 obese occupants will probably have less chance of AIS+3 injury when compared with those of normal occupants with BMI<26 in similar severity of C2C intersection impact. Non-linear SOM cluster analysis supports the effect of BMI on pelvis injury.

REFERENCES

[1] National Highway Traffic Safety Administration (NHTSA), National Automotive Sampling System (NASS) Crashworthiness Data System Analytical User's Manual 2014, National Centre for Statistics and Analysis, U.S. Dept. of Transportation, Washington, DC.

[2] Helena, S., et al, 2011. "Effect of Side Impact Protection in Reducing Injuries" 22th ESV, Paper Number 11-0319 (2011).

[3] Tomiji, S., et al, 2011. "Study on Car-To-Car Side Impact" 22th ESV, Paper Number 289 (2011).

[4] Randa, R.S., et al, 2003. "NHTSA Side Impact Research: Motivation for Upgraded Test Procedures" ESV, Paper Number 492 (2003).

[5] Matthew, L. 2015. "Occurrence of Serious Injury in Real-World Side Impacts of Vehicles with Good Side-Impact Protection Ratings" IIHS, Ruckersville, Virginia. Traffic Injury Prevention 16.S125-S132, (2015).

[6] Narayan, Y., et al, 2008. "Chest Deflections and Injuries in Oblique Lateral Impacts" Traffic Injury Prevention (2008) 9:162-167, 2008.

[7] Pintar, F.A., et al, 2009. "Test program to define oblique chest loading in side impact" Paper presented at Experimental Safety of Vehicles; June 6–11, 2009; Washington, DC.

[8] Shaw, J.M., et al, 2006. "Oblique and lateral impact response of the PMHS thorax" Stapp Car Crash J. (2006), 50:147–167.

[9] Xinghua, L. 2012. "Impact direction effect on serious-to-fatal injuries among drivers in near-side collisions according to impact location: focus on thoracic injuries" Accident Analysis Prevention 48, page 442-450, (2012).

[10] David G. Kleinbaum Mitchel Klein, 2010. "Logistic Regression, A Self Learning Text" Third Edition. ISBN: 978-1-4419-1741-6 (2010).

[11] XLSTAT User's Guide, version, 2015.1.1(2015).

[12] Safety Companion 2016, CARHS publications

[13] Chinmoy Pal, et al. 2017. "Improvement of injury severity prediction (ISP) of AACN during on-site triage using vehicle deformation pattern for Car to Car side impact", short communication, AAAM 2017.

[14] Chinmoy Pal, et al. 2015. "Development of High Efficiency Load Path Structure to Enhance Side Impact Safety Performance", ESV2015 Paper Number 15-0363.

[15] Sven A. Holcombe, Stewart C. Wang. "Subcutaneous Fat Distribution in the Human Torso", IRCOBI Conference 2014 IRC-14-43.

[16] Taewung Kim, et al, 2016. "Biofidelity evaluation of WorldSID and ES-2re under side impact conditions with and without airbag", Accident Analysis and Prevention 90 (2016) 140–151

[17] Chinmoy Pal, et al, 2017, "An insight of World Health Organization (WHO) accident database by cluster analysis with self-organizing map (SOM)" , Traffic Injury Prevention, Vol. 19, 2018. https://doi.org/10.1080/15389588.2017.1370089

[18] Petit, P., et al., "Update of the WorldSID 50th Male Pelvic Injury Criterion and Risk

Curve," SAE Technical Paper 2018-01-0539, 2018, doi:10.4271/2018-01-0539.

[19] Matthieu Lebarbé et al., "Investigation of Pelvic Injuries on Eighteen Post Mortem Human Subjects Submitted to Oblique Lateral Impacts", Stapp Car Crash Journal, Vol. 60 (November 2016), pp. 89-134

NOMENCLATURE:

AF05: 5th percentile American female
AIS: Abbreviated Injury Scale (1998 version)
AM50: 50th percentile American male
C2C: Car to Car
BMD: Bone mineral density, the mass of mineral per volume of bone
BMI: Body Mass Index, the measure of body fat based on height and weight
IIHS: International Institute of Highway Safety
NCAP: New Car Assessment Program
NASS-CDS: National Automotive Sampling System Crashworthiness Data System
PV: Passenger Vehicle
SOM: Self Organization Map
SUV: Sports Utility Vehicle

APPENDIX A.

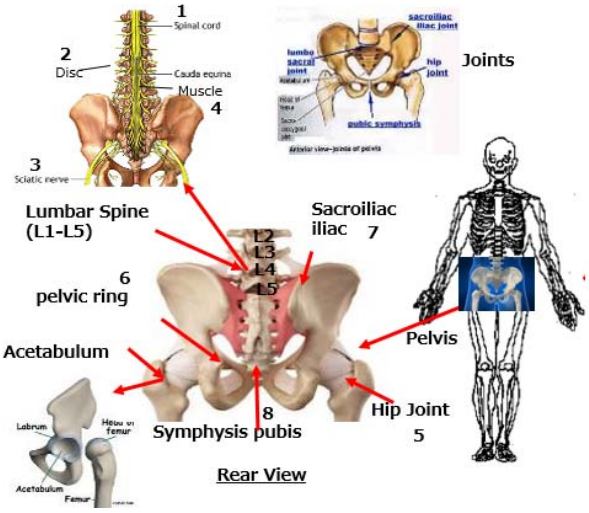

Figure A1. Schematic view of the pelvis region

Table A1.
Distribution of injuries in each part of the pelvic body structure

		AIS1+	AIS2+	AIS3+
All body region (AIS98 code)	***Injury code***	4195	1408	709
Lumbar spine				
1.Cord	640601	52	0	0
2.Disc	650699	40	40	0
Lower extremity				
3.Sciatic nerve	830476	2	2	0
4.Muscle tear	840604	2	0	0

5.Hip (Acetabulum; femur head)	850699	4	0	0
6.pelvic ring fracture	852602	176	176	57
7.Pelvis Sacroiliac fracture	852800	2	2	2
8.Symphysis pubis fracture	853000	13	13	13
Lumbar spine + Lower extremity related pelvis injury		***291 (7.1%)***	***233 (16.5%)***	***72 (10.2%)***

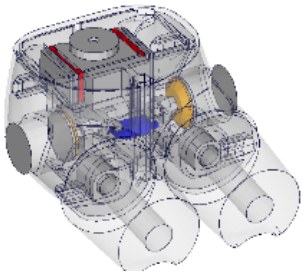

Figure A2. Schematic view of SID-IIs pelvis

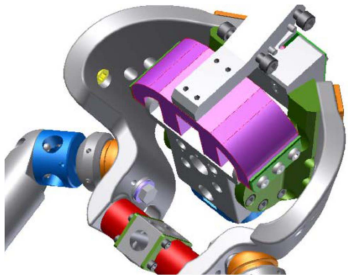

Figure A3. Schematic view of World-SID pelvis

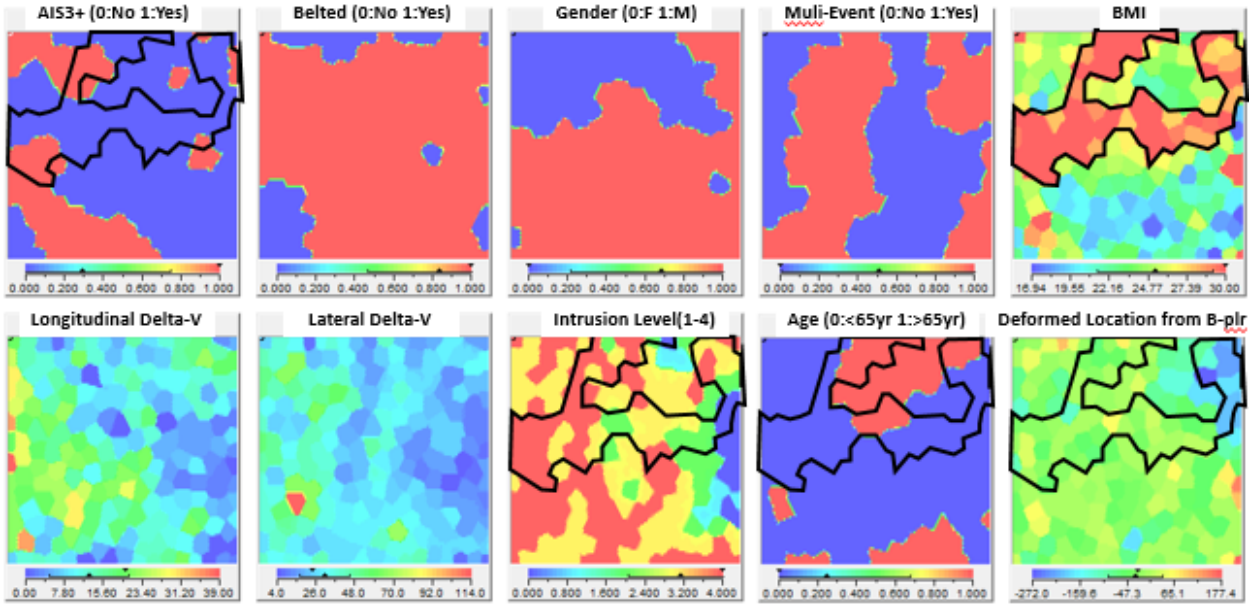

Figure A4. Self-Organizing-Maps (SOMs) of AIS3+ pelvis injury (10 attributes with 10 maps) to visualize the nonlinear relationship of the variables of the linear logistic regression analysis of Table 7. At the bottom of each SOM map, the red and blue scale bars indicate the corresponding highest and lowest values of corresponding variables.

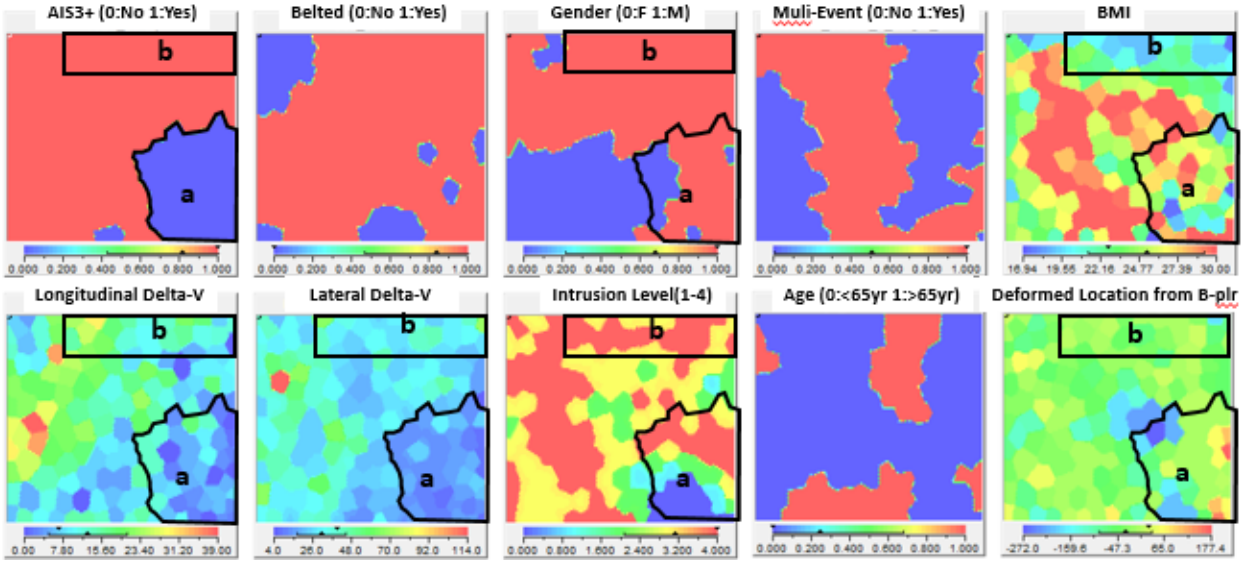

Figure A5. Self-Organizing-Maps (SOMs) of AIS2+ pelvis injury database (10 attributes with 10 maps) to visualize the nonlinear relationship of the variables of the linear logistic regression analysis of Table 8. At the bottom of each SOM map, the red and blue scale bars indicate the corresponding highest and lowest values of corresponding variables.

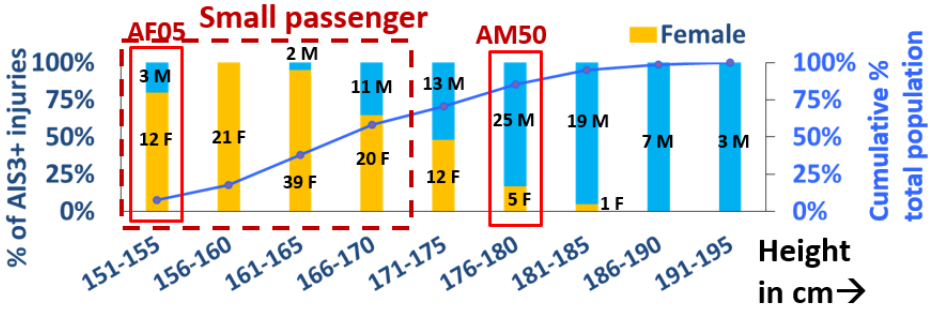

Figure A6. Distribution of occupant height in cm

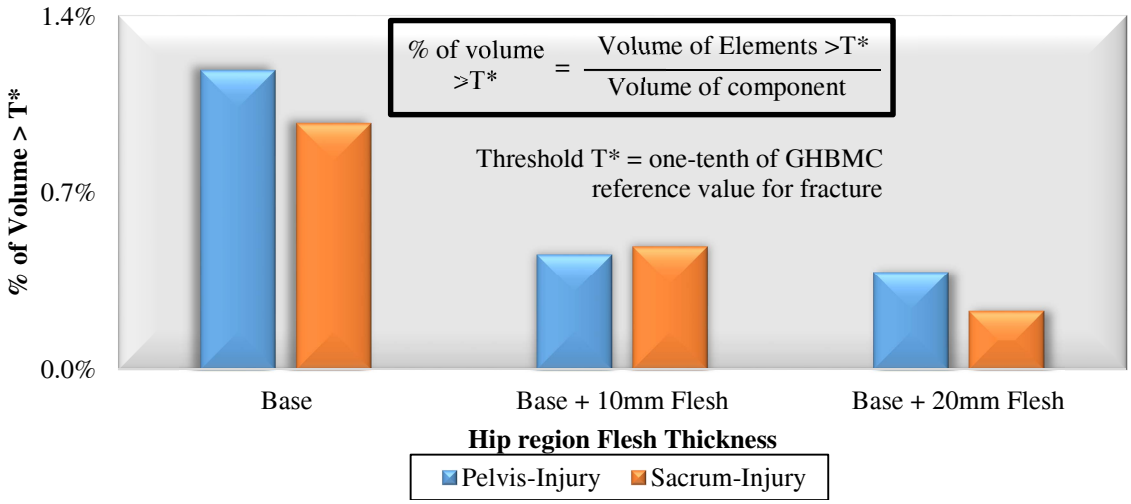

Figure A7. Influence of hip region flesh thickness on pelvis injury

Improved Thoracic Injury Risk Functions for the THOR-M-50 developed in a new simulation-based Approach

Andre Eggers, Marcus Wisch, Matthias Schießler
Federal Highway Research Institute (BASt)
Germany

Bengt Pipkorn, Krystoffer Mroz
Autoliv Research
Sweden

David Hynd
TRL
United Kingdom

Paper Number 19-0187

ABSTRACT

To assess occupant safety in a crash test, criteria associating the measurements made with a crash test dummy to injury risk are necessary. To enable better protection of elderly car occupants the objective of this study was to develop improved thoracic injury criteria for the THOR average male dummy. The development of these criteria is usually based on matched dummy and Post Mortem Human Surrogate (PMHS) tests by relating the obtained PMHS injuries to dummy measurements. This approach is limited, since only a few tests in relevant loading conditions are available and any new test series requires high efforts to be performed due to their complexity and costs. To overcome these limitations and to extend the dataset for the development of THOR dummy chest injury risk functions a simulation-based approach was applied within the EC funded project SENIORS (Safety Enhanced Innovations For older Road Users - www.seniors-project.eu).

Within this study frontal impact sled simulations with an FE model representing a THOR average male dummy and matched simulations with a human body model (HBM) representing an elderly car occupant were carried out. The HBM used for this study was the THUMS TUC with modified rib cage, which was developed in SENIORS. The modifications included material and geometry changes aiming to represent an elderly car occupant.

The rib fracture risk was predicted with a deterministic approach whereby a rib was considered broken when the strain exceeded an age-dependent threshold. Furthermore, a probabilistic method was applied to predict the probability of sustaining a certain number of fractured ribs by comparing local strain values to the distribution of cortical rib ultimate strain. By relating the output from the HBM simulations to a multi-point dummy injury criterion, injury risk curves were calculated by statistical methods.

The wide range of loading conditions resulted in the desired range of injuries and THOR ATD output. The number of fractured ribs predicted by the HBM based on the deterministic prediction method was between 0 and 15. Furthermore, the probabilistic risk for the number of rib fractures equal or greater than two, three or four was calculated for each load case. The THOR rib deflection criterion R_{max} was between 18 and 56 mm, while the PC Score was in the range of 2.5 to 7.2.

Based on these outputs new risk curves for the predicted deterministic (AIS2+/3+) and probabilistic injury risk were calculated. The new curves show reasonable shapes and significance that provide trust in their application. The new risk curves are compared to risk curves obtained by traditional methods. The results were found similar to previous injury risk functions based on physical tests, which gives a high level of confidence in the chosen approach.

The simulation-based approach of matched ATD model vs. HBM simulation was successfully applied. R_{max} curves show a slightly better quality than the injury criterion PC Score.

INTRODUCTION

The THOR-M is the most advanced frontal impact dummy to be used for assessment of thoracic risk in upcoming test procedures. The dummy provides chest deflection measurement at multiple locations. To use the measurement for injury risk assessment and design of occupant restraint systems, criteria relating the measurements made with a crash test dummy to injury risk are needed. One objective of the EC funded project SENIORS (Safety Enhanced Innovations For older Road Users - www.seniors-project.eu) was to improve THOR dummy based thoracic injury metrics and risk functions to assess and enhance the protection of elderly car occupants in relevant loading conditions.

For the THOR different injury criteria and risk functions to assess the risk of thorax injury have been proposed previously (Crandall et al. 2013; Poplin et al. 2017; Davidsson et al. 2014). These criteria and risk functions are based on the approach of matched pair testing using ATD and Post Mortem Human Subject (PMHS) tests. Due to the matched test results the injury level from PMHS tests is related to different injury predictors or criteria derived from multi-point ATD deflection. In order to achieve the goal of improved thoracic injury criteria and risk functions, an extended dataset of PMHS and dummy test results was needed.

However, several limitations with this approach were identified. One the one hand, only a few matched PMHS and dummy tests are available that represent loading conditions of interest. Furthermore, the available tests were too severe in terms of loading and not representative of contemporary vehicles. They mainly consisted of fixed three-point belt loading, while only a few tests with distributed (airbag) or combined belt and airbag loading were available.

Some matching THOR dummy tests, including sled tests with combined belt airbag loading to improve thoracic injury criteria, were performed in the EC funded project THORAX (Davidsson et al. 2014). However, the dummy version used is now considered outdated. Thus, to work with this data set of load cases it would be necessary to repeat matched tests with the current ATD version. This led to another limitation, which is the availability of components for hardware testing, especially restraint components (belts, airbag) and vehicle seats. Based on this experience it would be necessary to perform a large number of new tests including PMHS and matching tests with the latest THOR dummy version to obtain a sufficient representative data set that would fulfil the requirements for improving chest injury criteria and risk functions. This was not possible within the limited time frame and resources of the project.

To overcome these limitations a new computer model simulation-based approach was proposed within the SENIORS project. The idea was to extend the data by performing matched frontal impact sled computer simulations with a model representing the latest THOR-M ATD version and matching simulations with a human body model (HBM) representing an elderly car occupant. This covers a wider range of loading conditions and generates an extended dataset of matched HBM and ATD test. More test conditions (restraint system, impact angle, velocity) could be included, especially addressing the less severe chest loading in modern vehicles.

Preliminary results were shown by Eggers et al. (2018c). Meanwhile the methods of this approach were refined and updated. The objective of this paper is to provide an updated detailed description of this simulation-based approach, the methods used, and to present the updated injury risk curves.

METHODS

The method of the simulation-based approach that was developed and applied within the EC funded project SENIORS is shown in Figure 1.

Simulation Matrix

The approach starts with the definition of the simulation matrix. This is crucial since the simulation space should cover the loading conditions which are identified to be relevant based on collision data analysis and representative of the loading condition in current and possibly also future vehicle occupant restraint systems. It should preferably be inhomogeneous in terms of chest loading to avoid a correlation of possible injury criteria to specific single loading conditions. It was decided to include only frontal and oblique (+/-30°) sled load cases in this study.

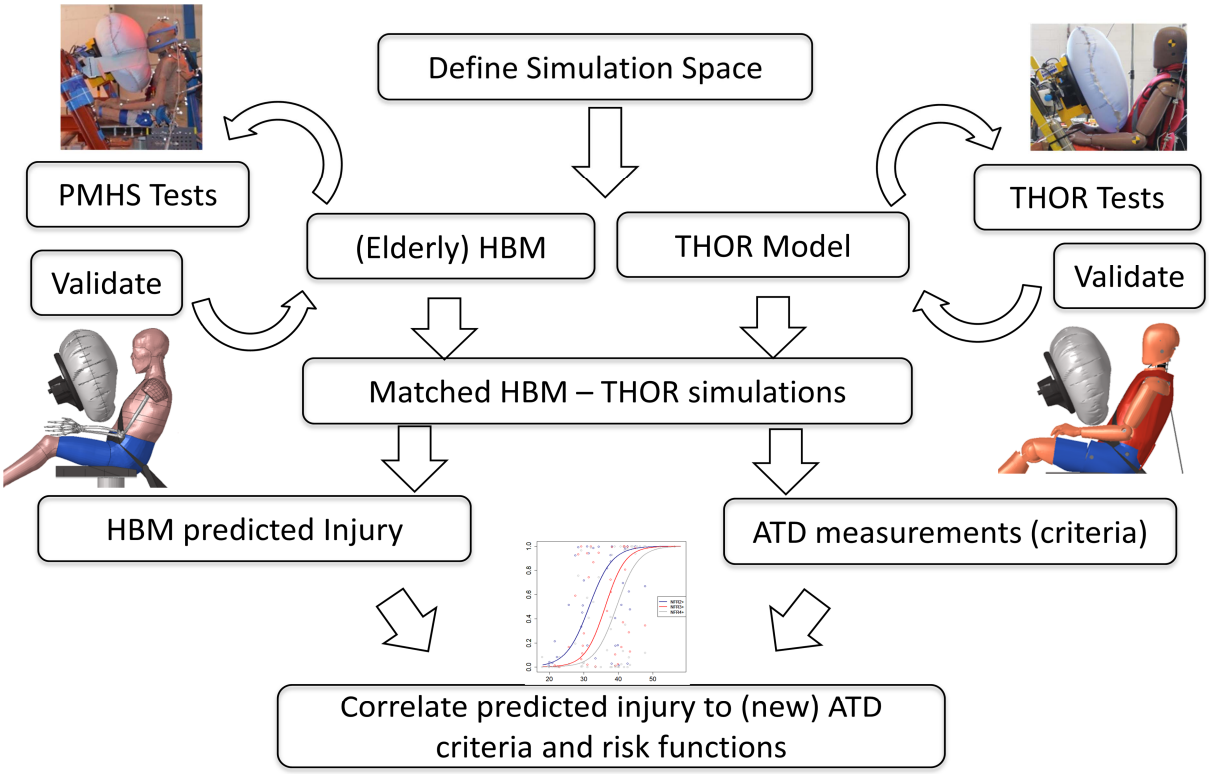

Figure 1. SENIORS simulation-based approach for improved occupant thoracic injury criteria and risk functions

Appendix 1 shows the simulation matrix consisting of 58 load cases that was used for this study. The variation of some key parameters in this simulation matrix is listed below:

- Impact velocities between 25 km/h and 56 km/h
- Impact directions: frontal (0°), near-side (+30°) and far-side (-30°)
- Different belt load limiter levels (no load limiter, 2 kN to 6 kN)
- Without pretensioner / with single and multiple pretensioning
- Without airbag / with airbag
- Different 3-point belt routing (variation of upper D-ring and buckle position)
- Load cases with alternative restraints (four-point belt system, split buckle)
- Different seat friction coefficients (standard/high)

In order to be able to reproduce these tests and simulations in the future (e.g. with another or new occupant model), for most load cases generic components were used. The main part of the simulation matrix is based on a simple generic test setup, which was developed within the SENIORS project (Eggers et al., 2017) using a three-point belt system (L01 to L16). For some load cases a generic load limiter and a pre-inflated driver airbag were used. The basis of this set-up including seat pan and generic bag was used for further load cases (A17 to A45) with advanced restraint systems like four-point belts, split buckle and multiple pretensioning. Details of theses alternative belt systems are described by Mroz et al. (2018). Furthermore some load cases were based on the 'Gold Standard' test set-up (Shaw et al. 2009, Crandall et al. (2015a, 2015b)) including a generic load limiter and oblique conditions (A01 to A08).

The gold standard test conditions were also used for biofidelity evaluation of the HBM simulations. Results can be found in the SENIORS report D2.5a (Eggers et al., 2018b). To assess the validation of the THOR dummy model and the components of sled environment, THOR dummy tests of some of these load cases were performed. Detailed descriptions of the loading configurations and validation results are provided in D2.5a. (Eggers et al., 2018b). Based on the results the validation status of the HBM, dummy and sled models were found to be sufficiently validated to be used in this simulation-based study.

Occupant models and output definition

THOR dummy model

THOR dummy simulations were done with the LS-DYNA version 1.3.2 of the Humanetics THOR adult average male model. This FE-model represents the US NCAP Version of THOR-M SBL-A with THOR-LX legs.

The output from the dummy model simulations that is used for injury criteria and risk curve development are the four resultant IR-Tracc measurements. From the measurements two candidate injury criteria that are currently discussed to be used for vehicle safety assessment tests (PC Score according to Poplin et al. (2017) and R_{max}) were calculated.

Human body model

For this study, a modified version of the THUMS TUC v3.01 was used. Age-related modifications focused on representing the rib cage of a 65+ year-old car occupant. Therefore, the rib cage was geometrically morphed and the corresponding properties were adapted to account for age-related changes to the biomechanical characteristics of the thorax. Age- related material properties were taken from literature. Thereby, the cortical bone thickness decreases with age and was consequently set to 0.63 mm while the Young's modulus of the costal cartilage was increased to 69.38 MPa (calcification). Details of the age-related rib cage morphing and adjustments to the material properties are described in the SENIORS deliverable D2.4 (Eggers et al., 2018b). Figure 2 (left) shows the rib cage of the original THUMS model while Figure 2 (right) shows the 65+ year-old morphed rib cage that was used for this study.

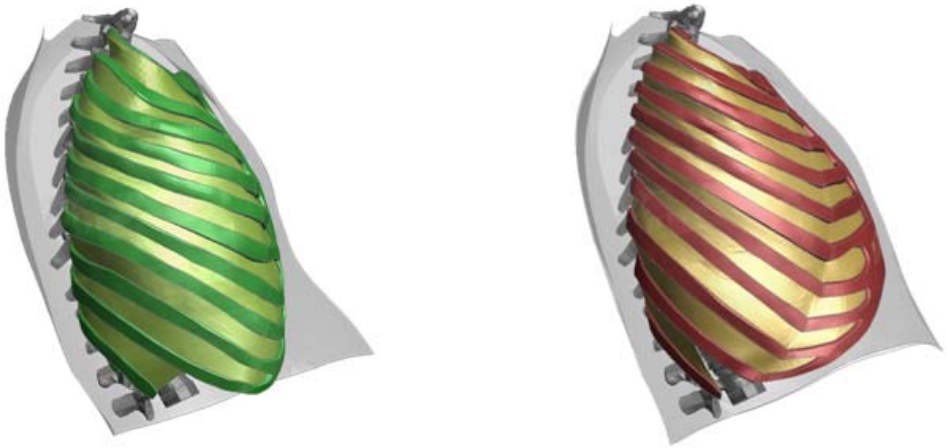

Figure 2. Chest of original THUMS TUC 3.0.1(left) and THUMS TUC 65+ years-old morphed chest (right)

While reviewing the results of the SENIORS project, some questionable interactions of the rib cage and seat-belt with a presumably too stiff pelvic region were observed. For verification, the pelvic region was compared against abdominal impact response corridors defined by Hardy et al. (2001). The abdominal impact response of the original model in the free-back rigid bar tests, as well as for the seatbelt loading test was overall too stiff, while a model with adjusted pelvic soft tissue material properties (bulk modulus reduced by a factor of 10^3) showed good conformity with these biofidelity targets (Figures 3 and 4).

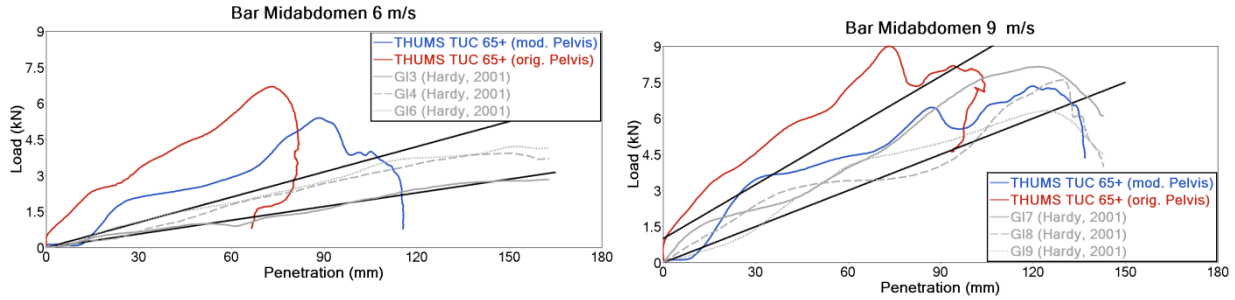

Figure 3. Abdominal impact response to free-back rigid bar tests with v = 6 m/s (left) and v = 9 m/s (right) for the original pelvic material (red) and with adjusted material properties (blue)

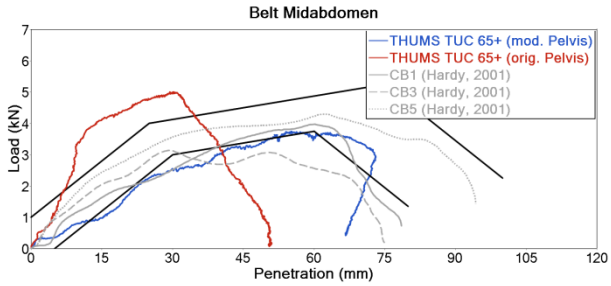

Figure 4. Abdominal impact response to seat belt loading for the morphed THUMS TUC with original pelvic material (red) and with adjusted material properties (blue)

Since adjusting the pelvic soft tissue material showed good conformity with the biofidelity targets, these changes were adopted for this study.

Rib fracture injury risk assessment based on HBM simulations

To assess the thoracic injury risk, deterministic and probabilistic approaches were used. For both approaches the peak strain of the cortical bone in each rib was obtained by using a post-processing script, which calculates the extrapolated surface strains with the first principal strain at the outermost and innermost integration point of the strain tensor:

$$\varepsilon_{\text{extrapolated surface}} := \left| \varepsilon_{\text{IP,outer}} + \frac{1 - d_{\text{NIP}}}{2 \cdot d_{\text{NIP}}} \cdot \text{diff}\left(\varepsilon_{\text{IP,inner}}, \varepsilon_{\text{IP,outer}}\right) \right|_{\text{max}} \qquad \text{(Equation 1)}$$

The distance from the outermost integration point to the actual surface is dependent on the number of integration points. Within this study, the cortical bone of each rib was modelled with five integration points; therefore, d_{NIP} is equal to 0.9062. For the deterministic approach the peak strain in each rib was compared to the assumed ultimate failure strain threshold of a 65 year old occupant based on Kemper at al. (2007). Thereby each individual rib, which peak strain exceeded 1.9%, was considered to have fractured. For each load case the number of fractured ribs was counted and then translated to the AIS thoracic injury coding using the 2008 update of the 2005 version of the Abbreviated Injury Scale (AAAM, 2008). Consequently, load cases with three or more fractured ribs were classified as an AIS3+ rib cage injury, while two or more fractured ribs resulted in an AIS2+ rib cage injury.

Additionally, a probabilistic approach suggested by Forman et al. (2012) was used to determine the severity of each load case. Thereby, with the peak strain in each rib and using a statistical distribution, the risk of fractures to the whole rib cage can be predicted. The method provides a risk percentage value for exactly two, three or four broken ribs as well as risk percentage values for at least two, three or four broken ribs.

Matching occupant positioning and belt fitting to the ATD and HBM Model

The results of the HBM and ATD simulations are later matched. Therefore, high effort went into positioning the models in matching postures and to obtain a comparable belt path and distance to the airbag. To position the occupant models the focus was to align the H-point and the chest surface in the mid-sternum area between the HBM and the THOR ATD model (see Figure 5). Since there are no directly comparable landmarks on the chest of the occupant models, the chin-to-belt distance was chosen as a reference measure to define a comparable belt path. Additionally, the distance between the belt and the sternum notch was used as an additional measurement to check the matching positions of the belt.

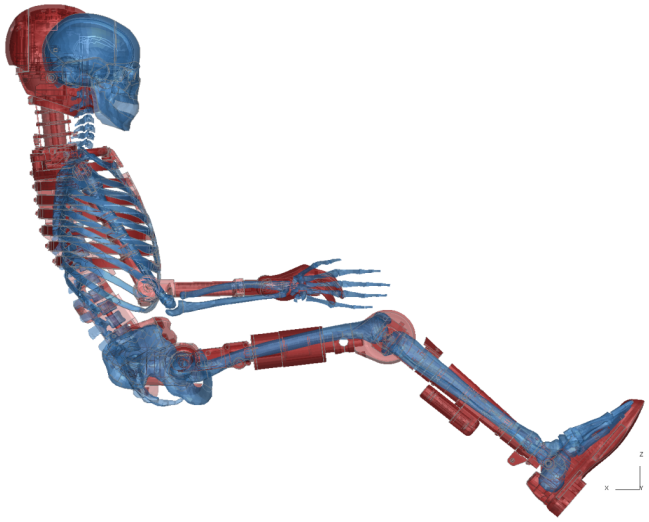

Figure 5. Comparison of the matching seating position of THUMS TUC (blue) and THOR-M-50 model (red).

Statistical methods for new risk curves

Two approaches were used to update injury risk curves establishing a relationship between rib fracture risk and multi-point measurement based THOR dummy chest injury criteria. Details of the statistical models are provided in SENIORS Deliverable 2.5a (Eggers et al., 2018a). A short summary is provided below.

Deterministic models

A Weibull model, commonly used for survival analysis, has been applied to the matching simulation data to determine the relationship between the probability of thorax injury in terms of AIS2+/3+ chest injury risk (based on number of fractured ribs) from HBM rib strain output and the injury prediction based on R_{max} and PC Score (Poplin et al., 2017) from the THOR simulations.

Probabilistic model using linear regression model

To determine the relationship between the probability of a certain injury severity, here expressed as the risk to sustain a certain number of fractured ribs NFR (Forman et al., 2012), and an injury predictor provided by the THOR dummy simulations (R_{max} and PC Score), a probabilistic approach using a linear regression model was used.

In more detail a dose response relationship (logit, Generalized Linear Model) between the PC Score and the response in terms of "x" fractured ribs was assumed for which reason a logit transformation was applied to the given probabilities. Assuming a generalized linear model, a linear relationship shall exist between the logit transformed values and the dose parameter (PC Score values). The coefficients are computed by means of a linear regression. Finally, the intercept and the slope of the linear regression model were used for the inverse logit transformation to calculate the estimators for the probabilities, see also SENIORS D2.5a (Eggers et al., 2018a).

RESULTS

In total 58 matching sled simulations as defined according to the simulation matrix (Appendix 1) have been performed with the THOR ATD model and the THUMS elderly human model respectively.

Distribution of dummy and HBM output

IR-Tracc outputs (resultant multi-point deflections) and belt loads from THOR simulations are provided in Appendix 2. Chest injury predictors determined from IR-Tracc output (R_{max} and PC Score) are also provided.

The table in Appendix 3 shows the corresponding HBM output for each load case. The injury output from the HBM simulations includes the probabilistic risk to sustain exactly or more than two, three or four fractured ribs based on the method proposed by Forman et al. (2012), the number of fractured ribs determined by the deterministic approach and the corresponding AIS2+ and AIS3+ chest injury level.

The objective was to cover a wide range of injury severities and loading conditions. The output shows that this resulted in a wide distribution of IR-Tracc deflection peak values as well as the injury predictors indicating a broad distribution of chest loading severity, which was the intention of the extend loading condition matrix. The belt loads in THOR simulations ranged between 1 and 6 kN. R_{max} values were in the range between 18 and 56 mm. The PC Score (Poplin et al. 2017) values ranged between 2.5 and 7.2.

Also the distribution of the number of fractured ribs showed a good variation in a range between zero and 15 fractured ribs (see

Figure 6). The probabilistic injury risk prediction also showed a good distribution having a zero injury risk for several load cases through to load cases with 100% risk.

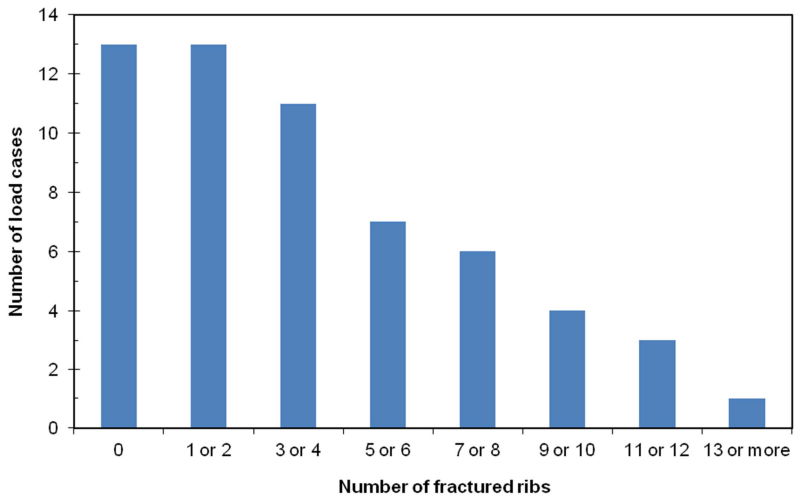

Figure 6. Frequency distribution for the number of fractured ribs in the 58 load cases (determined in HBM simulation based on extrapolated rib surface strain exceeding 1.9%)

New injury risk curves

The matched simulation outputs of the THOR (injury predictors) and HBM (injury in terms predicted rib injury) were used to develop new THOR dummy chest injury risk functions.

Deterministic Injury Risk Functions

The following plots show the injury risk functions relating a rib injury severity in terms of AIS2+ or AIS3+ based on deterministic rib fracture prediction from HBM simulation, and injury criteria from THOR dummy simulations (R_{max} and PC Score, respectively). The new injury risk functions are shown in Figure 7 to Figure 10. Table 1 shows the p-values of the generated injury risk function models.

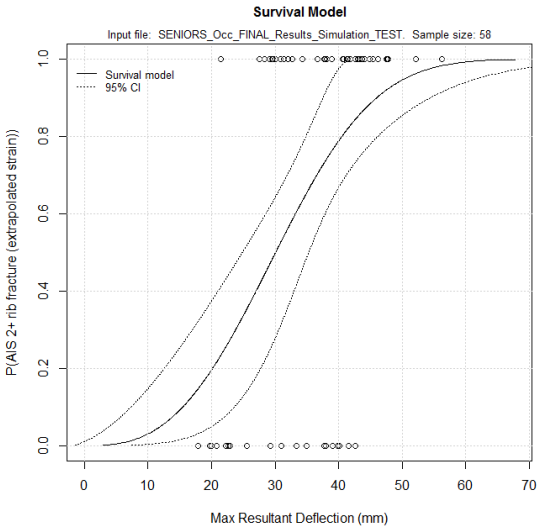

Figure 7. AIS2+ rib injury vs. R_{max}

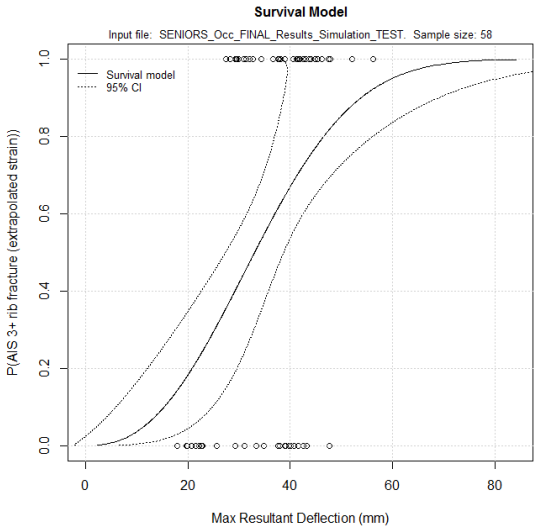

Figure 8. AIS3+ rib injury vs. R_{max}

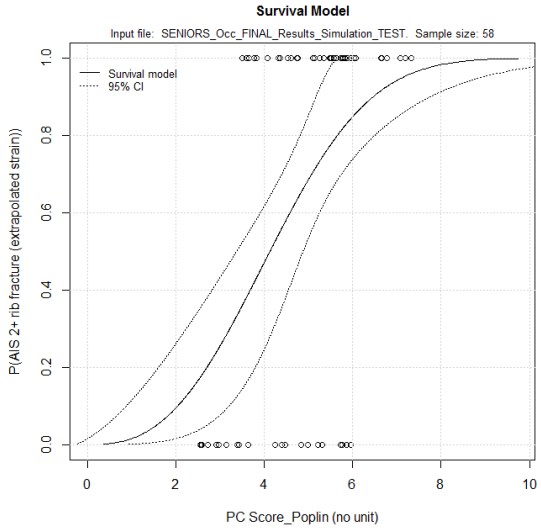

Figure 9. AIS2+ rib injury vs. PC Score

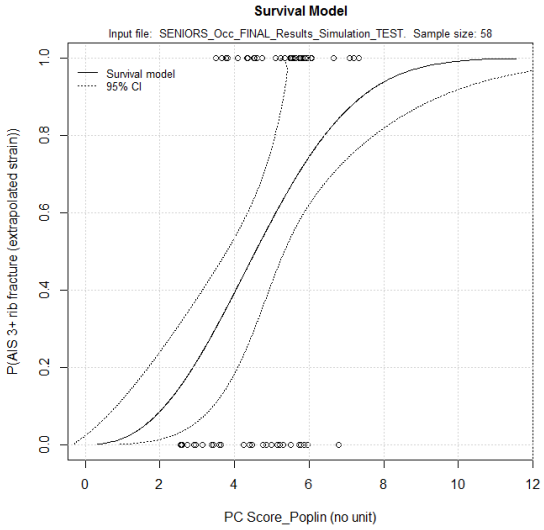

Figure 10. AIS3+ rib injury vs. PC Score

Table 1. P-values received processing the survival model based on deterministic HBM injury output

	AIS2+	AIS3+
R_{max}	5.35E-04	7.84E-03
PC Score	1.54E-03	7.70E-03

The p-values indicate that all risk curves are statistically significant. For the AIS2+ risk the curves that are based on the injury criterion R_{max} shows better results in terms of p-values compared to the risk curves based on PC Score. Regarding AIS3+ injury risk curves based on R_{max} and PC Score show very similar results in terms of statistical significance. In general, the p-values were slightly better for R_{max} injury risk functions at a given AIS than for PC Score.

Probabilistic Injury Risk Functions

The relationship between the probability of a certain number of fractured ribs (NFR) predicted by HBM simulation, and injury criteria (R_{max} and PC Score) using the output from the THOR dummy simulations, was determined by processing a probabilistic model using a generalized linear regression model. The resulting injury risk functions are shown in Figure 11 and Figure 12. Table 2 shows the observed p-values of the generated injury risk function models. It can be observed that all curves are statistically significant (<5%).

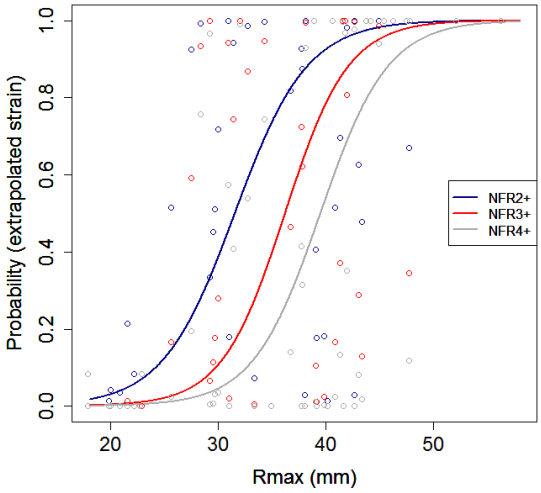

Figure 11. Probability of sustaining two or more (2+), three or more (3+) or four or more (4+) fractured ribs vs. R_{max}

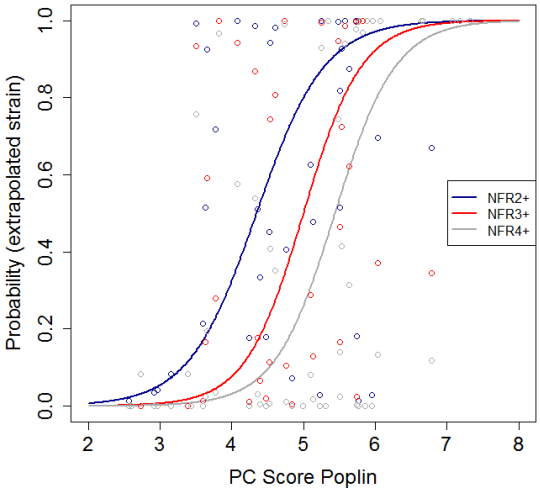

Figure 12. Probability of sustaining two or more (2+), three or more (3+) or four or more (4+) fractured ribs vs. PC Score

Table 2. P-values received processing the probabilistic model using a linear regression model

	NFR2+	NFR3+	NFR4+
Rmax	4,26E-06	8.79E-07	2.24E-06
PC Score	1.46E-05	1.89E-06	2.35E-06

Overall, the injury risk functions presented here show reasonable shapes and excellent p-values of the regression models. In addition, it can be generally confirmed that a higher injury criterion (R_{max} or PC Score) corresponds with a higher probability of injury which was a prerequisite of the applied statistical model.

DISCUSSION AND LIMITATIONS

The main purpose of the simulation-based approach was to address one major limitation of the traditional experimental testing based approach, which is the limited size of the data set that is not sufficiently representing relevant loading conditions. The new dataset is more representative for occupant loading in modern vehicles, including a broader range of chest ATD loading patterns in terms of peak and differential deflections.

New risk curves relating the injury criteria to AIS thorax injury and to a probabilistic risk for a certain number of rib fractures were developed. The results regarding new risk curves look very promising. Compared to the preliminary curves provided before (Eggers et al., 2018a) the curves show improvement in terms of statistical significance. This might be related to improvements to the HBM used for this study giving more consistent injury output.

The deterministic risk curves developed in this simulation based approach can be directly compared to risk curves developed by the traditional approach using PMHS and ATD tests. The AIS3+ risk curves shown by Poplin et al.

(2017) are very similar in terms of shape, which gives confidence in this new approach. A more detailed comparison shows differences in the level predicted injury risk, which should be further investigated. For example the PC Score based AIS3+ risk is slightly higher based on the risk curves developed by the simulation based approach. This is similar for the R_{max} based risk. In a next step it would also be possible to combine the data from test and simulation to develop curves based on a further extended data set.

The risk curves that were developed based on the probabilistic approach cannot be directly compared to previously published curves that were based on PMHS test. However, a comparison of curves obtained by the deterministic approach within this study is possible. Comparing for example the deterministic AIS3+ risk based on R_{max} to the probabilistic NRF3+ shows a slightly higher risk. For the PC Score a respective comparison of the risk curves indicates much lower risk values based on the probabilistic method compared to the deterministic AIS3+ risk. The probabilistic approach by Forman et al. (2012) might need some further discussion and improvement itself to be used for this kind of applications. Furthermore, some limitation related to the applied statistics to generate the risk curves should be considered.

The application of the logistic regression model in the probabilistic approach has some limitations. By default, the logistic model is used for binary outcome variables. However, considering the theoretical backgrounds (e.g. considering a rather linear relationship between the PC Score and the NFR), it was assumed that the logistic model could also be applied to the given injury probabilities. Further, the results are based on a small number of simulated probabilities and show high variations; therefore, the linear relationship between the log odds and the injury criteria cannot be shown clearly. This shows that the ability of the injury criteria (e.g., PC Score) in describing the injury outcome is limited. Therefore it is recommended establishing further work and validation on this method.

The comparison of risk curves based on R_{max} and PC Score do not show a clear advantage of the PC Score for improved differentiation of injury risk. This would suggest applying R_{max} for further restraint system evaluation based on statistical significance. However, a further improved multi-component version of the PC Score taking into account for example more principal components, taking full advantage of the extended data set, might lead to different findings.

A further limitation that was already mentioned in previous publications related to this work (Eggers et al., 2018a) is related to the validity and quality of the occupant models. The HBM as well as the ATD model are constantly being improved. Some improvements regarding robustness and biofidelity of the HBM injury have been taking into account for this study. However, further improvements might be necessary, which consequently could lead to more reliable results.

Another limitation resulting from the use of only one HBM in this simulation based approach is related to the missing human biomechanical variation, e.g. in terms of anthropometry. In PMHS test this human variation is introduced by the use of several test subjects for each load case. However, the number of subjects per test condition is usually very limited and thus far away for being statistically representative of the population. A possible solution to address this variation in a simulation based approach could be the use of several HBMs for each loading condition, with variations representing for example an elderly occupant by varying the anthropometry and/or material properties.

CONCLUSIONS AND RECOMMENDATIONS

A simulation-based approach was used to develop multi-point deflection chest injury risk functions for the frontal impact dummy THOR applicable to low-to-moderate severity collisions. This application range of the new risk curves is especially relevant for elderly car occupant protection. This approach allowed to extend matched-pair data, to include lower severity and more representative loading. It also allowed the use of restraint systems being more representative of those fitted to modern cars, which apply lower forces to the thorax than the older-style restraints used in most of the physical PMHS and ATD test data in the literature.

An advantage of the simulation-based approach is the possibility to easily re-evaluate the results and thus consider modification or updates to the ATD. The changes to the ATD hardware and certifications requirements could be easily integrated into the ATD simulation model, which could be used to repeat the whole ATD simulation part of the simulation matrix. In an experimental testing based approach, the effort required to generate the data to update injury risk functions for new dummy updates would be significantly higher.

Previous studies by Eggers et al. (2018a) suggested a repetition of the HBM simulations with an improved human body model, since the validity of the applied simulations and the rib fracture prediction approach was questioned. Within this study the pelvic region of the HBM was updated, which improved the biofidelity of the lower abdomen and furthermore improved the risk curves in terms of statistical significance. However, further improvement to the HBM and strain based injury prediction approach are recommended.

Regarding the work on improved multi-point criteria, it is recommended to develop and evaluate a higher order version of the PC Score to take further advantage of the extended data set. The currently applied version of PC Score (Poplin et al., 2017) uses only the first principal component to relate the four primary deflection parameters (UP_{tot}, LOW_{tot}, UP_{dif}, LOW_{dif}) to calculate the PC Score. The reason is that based on the data used by Poplin et al. (2017) they found sufficient explanation of the variance in the deflection patterns by using only the first component. However, with the extended dataset covering a broad range of loading conditions the influence of the second or even third component to the explained variance should be considered as it is assumed that these components will show a higher importance. This could provide an improved new version of PC Score, which might be able to better assess the injury protection effect of load distributing advanced restraint systems. This work could also require adding even more relevant load cases to the simulation matrix. Using a simulation-based approach allows doing this with significantly less effort and in a more reliable way compared to the traditional experimental approach.

The whole approach including occupant simulation models and the load cases including models of the generic sled environment in a simulation version as well as hardware version for validation test of added load case are well described and documented within SENIORS project reports and publications. Based on these findings it will be possible to continue the work taking into account the proposed steps to improve the results and extent the dataset.

REFERENCES

AAAM, 2008. The Abbreviated Injury Scale 2005, Update 2008. Association for Advancement of Automatic Medicine, Barrington, IL. Campbell, J.Q., Tannous, R.E., Takhounts, E.G., Martin, P.,

Crandall, J. (2013) ATD Thoracic Response: Effect Of Shoulder Configuration On Thoracic Deflection Thor Mod Kit Advanced Frontal Crash Test Dummy Frontal Sled Tests UVAS0001-6, 10-15, 19-24. National Highway Traffic Safety Administration (NHTSA), USA.

Crandall, J. (2015a) ATD Thoracic Response Test Development, Gold Standard Buck Condition 2: Force Limited Belt, 30 km/h Frontal, Tests UVAS00302, UVAS00303, UVAS00304. National Highway Traffic Safety Administration (NHTSA), USA.

Crandall, J. (2015b) ATD Thoracic Response Test Development, Gold Standard Buck Condition 3: Force Limited Belt, 30 km/h 30 Degree Oblique Frontal, Tests UVAS0313-315. National Highway Traffic Safety Administration (NHTSA), USA.

Davidsson, Johan; Carroll, Jolyon; Hynd, David; Lecuyer, Erwan; Song, Eric; Trosseille, Xavier; Eggers, Andre; Sunnevang, Cecilia; Praxl, Norbert; Martinez, Luis; Lemmen Paul and Been, Bernard (2014). Development of injury risk functions for use with the THORAX Demonstrator; an updated THOR. Proceedings of IRCOBI Conference, 2014, Berlin, Germany.

Eggers A, Ott J, Pipkorn B, Bråse D, Mroz K, López Valdés F and Hynd D (2017). A generic sled test set-up for frontal occupant evaluation developed within the EU‐project SENIORS.Proceedings of the 25th Enhanced Safety of Vehicles (ESV) Conference, 5-8 June, Detroit, USA.

Eggers, A., Wisch, M., Wagner, A., Mühlbauer J., Fuchs, T., Peldschus, S., Pipkorn, B., Mroz, K., Jaber, L., Fiorentino, A., (2018a). Deliverable 2.4 - Updated Human Body Models representing elderly occupants and pedestrians (incl. overweight/obese). SENIORS, H2020 European Commission, GA No. 636136.

Eggers, A., Wisch, M., Mroz, K., Pipkorn, B., Hynd, D., Peldschus, S., Piqueras, A., Lorente, A., Maza, M., López Valdés, F., (2018b). Deliverable 2.5a - Updated injury criteria for the THOR. SENIORS, H2020 European Commission, GA No. 636136.

Eggers, Andre; Wisch, Marcus; Hynd, David; Pipkorn, Bengt; Mroz, Krystoffer. (2018c). A Simulation-based Approach for Improved Thorax Injury Risk Function for the THOR ATD. IRC-18-94, IRCOBI conference 2018, Athens, Greece.

Forman JL., Kent RW, Mroz K, Pipkorn B, Bostrom O (2012). Predicting Rib Fracture Risk With Whole-Body Finite Element Models; Development and Preliminary Evaluation of a Probabilistic Analytical Framework. Vol 56, AAAM.

Hardy, W.N., Schneider, L., Rouhana, S. (2001) Abdominal Impact Response to Rigid-Bar, Seatbelt, and Airbag Loading. Stapp Car Crash Journal, 2001, 45: pp. 375-408.

Hynd, David; Hylands, Nicola; Wagner, Anja; Zander, Oliver; Eggers, Andre; Ott, Julian; Wisch, Marcus; Pipkorn, Bengt (2016). D2.1 - Biofidelity Requirements for Older and Obese Car Occupants and External Road User Surrogates. SENIORS, H2020 European Commission, GA No. 636136.

Kemper AR, McNally C, a Pullins C, Freeman LJ, Duma SM, and Rouhana SM (2007). The biomechanics of human ribs: material and structural properties from dynamic tension and bending tests. Stapp Car Crash J., vol. 51, pp. 235–273.Mroz, Krystoffer; Pipkorn, Bengt; Sunnevång, Cecilia; Eggers, Andre; Bråse, Dan (2018). Evaluation of Adaptive Belt Restraint Systems for the Protection of Elderly Occupants in Frontal Impacts. IRC-18-15, IRCOBI conference 2018, Athens, Greece.

Poplin, Gerald S., McMurry, Timothy L., Forman, Jason L., Ash, Joseph, Parent, Daniel P., Craig, Matthew J., Song, Eric, Kent, Richard, Shaw, Greg, Crandall, Jeff (2017). Development of thoracic injury risk functions for the THOR ATD. Accident Analysis and Prevention 106 (2017) 122–130

Saunders, James; Parent, Dan; Ames, Eva (2015) NHTSA Oblique Crash Test Results: Vehicle Performance and Occupant Injury Risk Assessment in Vehicles with Small Overlap Countermeasures. Proceedings of the 24th International Technical Conference on the Enhanced Safety of Vehicles, Gothenborg, Sweden.

Shaw, Greg; Parent, Dan; Purtsezov, Sergey; Lessley, David; Crandall, Jeff; Kent, Richard; Guillemot, Herve; Ridella, Stephen; Takhounts, Erik; Martin, Peter (2009). Impact response of restrained PMHS in frontal sled tests: skeletal deformation patterns under seat belt loading. Stapp Car Crash J, 53(2009-22-0001), 1-48.

APPENDIX 1

	Load Case	Velocity (km/h)	Angle (deg)	Pulse	Belt Type	Load limiter setting	Airbag	D-Ring	Seat Friction
L01	SENIORS Generic set-up	25	0	SENIORS 25km/h	3p, no PT	No	No	D1	Standard
L02	SENIORS Generic set-up	35	0	SENIORS 35km/h	3p, no PT	No	No	D1	Standard
L03	SENIORS Generic set-up	25	0	SENIORS 25km/h	3p, no PT	medium	No	D1	Standard
L04	SENIORS Generic set-up	35	0	SENIORS 35km/h	3p, no PT	medium	No	D1	Standard
L05	SENIORS Generic set-up	35	0	SENIORS 35km/h	3p, no PT	medium	No	D2	Standard
L06	SENIORS Generic set-up	25	0	SENIORS 25km/h	3p, no PT	medium	No	D2	Standard
L07	SENIORS Generic set-up	35	0	SENIORS 35km/h	3p, no PT	medium	Yes	D3	Standard
L08	SENIORS Generic set-up	35	0	SENIORS 35km/h	3p, no PT	low	Yes	D3	Standard
L09	SENIORS Generic set-up	35	0	SENIORS 35km/h	3p, no PT	medium	No	D3	Standard
L10	SENIORS Generic set-up	35	0	SENIORS 35km/h	3p, no PT	low	No	D3	Standard
L11	SENIORS Generic set-up	35	0	SENIORS 35km/h	3p, no PT	medium	Yes	D1	Standard
L12	SENIORS Generic set-up	35	0	SENIORS 35km/h	3p, no PT	medium	Yes	D2	Standard
L13	SENIORS Generic set-up	35	0	SENIORS 35km/h	3p, no PT	medium	No	D3	High
L14	SENIORS Generic set-up	35	0	SENIORS 35km/h	3p, no PT	medium	Yes	D3	High
L15	SENIORS Generic set-up	45	0	SENIORS 45km/h (scaled)	3p, no PT	low	Yes	D3	Standard
L16	SENIORS Generic set-up	45	0	SENIORS 45km/h (scaled)	3p, no PT	medium	Yes	D3	Standard
A01	Gold Standard 1	25	0	SENIORS 25km/h	3p, no PT	No LL	No	GS	Standard
A02	Gold Standard 1	40	0	GS 40km/h	3p, no PT	No LL	No	GS	Standard
A03	Gold Standard 2	30	0	GS 30km/h	3p, no PT	2,7	No	GS	Standard
A04	Gold Standard 2	45	0	SENIORS 45km/h (scaled)	3p, no PT	2,7	No	GS	Standard
A05	GS3 30deg farside	25	30	SENIORS 25km/h	3p, no PT	2,7	No	GS	Standard
A06	GS3 30deg farside	30	30	GS 30km/h	3p, no PT	2,7	No	GS	Standard
A07	GS3 30deg farside	35	30	SENIORS 35km/h	3p, no PT	2,7	No	GS	Standard
A08	GS3 30deg farside	45	30	SENIORS 45km/h (scaled)	3p, no PT	2,7	No	GS	Standard
A09	SENIORS alt restr	25	0	SENIORS 25km/h	3-point, double PT	4,0	Yes	D2	Standard
A10	SENIORS alt restr	35	0	SENIORS 35km/h	3-point, double PT	4,0	Yes	D2	Standard
A11	SENIORS alt restr	45	0	SENIORS 45km/h (scaled)	3-point, double PT	4,0	Yes	D2	Standard
A12	SENIORS alt restr	56	0	SENIORS 56km/h	3-point, double PT	4,0	Yes	D2	Standard
A13	SENIORS alt restr	25	0	SENIORS 25km/h	3p 2-retr, double PT	2,0	Yes	D2	Standard
A14	SENIORS alt restr	35	0	SENIORS 35km/h	3p 2-retr, double PT	2,0	Yes	D2	Standard
A15	SENIORS alt restr	45	0	SENIORS 45km/h (scaled)	3p 2-retr, double PT	5,0-2,0	Yes	D2	Standard
A16	SENIORS alt restr	56	0	SENIORS 56km/h	3p 2-retr, double PT	5,0-2,0	Yes	D2	Standard
A17	SENIORS alt restr	25	0	SENIORS 25km/h	Criss-cross 2-retr, triple PT	1,0+1,0	Yes	D2	Standard
A18	SENIORS alt restr	35	0	SENIORS 35km/h	Criss-cross 2-retr, triple PT	1,0+1,0	Yes	D2	Standard
A19	SENIORS alt restr	45	0	SENIORS 45km/h (scaled)	Criss-cross 2-retr, triple PT	2,0+2,0	Yes	D2	Standard
A20	SENIORS alt restr	56	0	SENIORS 56km/h	Criss-cross 2-retr, triple PT	2,0+2,0	Yes	D2	Standard
A21	SENIORS alt restr	25	0	SENIORS 25km/h	split buckle, triple PT	6,0	Yes	D2	Standard
A22	SENIORS alt restr	35	0	SENIORS 35km/h	split buckle, triple PT	6,0	Yes	D2	Standard
A23	SENIORS alt restr	45	0	SENIORS 45km/h (scaled)	split buckle, triple PT	6,0	Yes	D2	Standard
A24	SENIORS alt restr	56	0	SENIORS 56km/h	split buckle, triple PT	6,0	Yes	D2	Standard
A25	SENIORS alt restr	25	30 nearside	SENIORS 25km/h	3-point, double PT	4,0	Yes	D2	Standard
A26	SENIORS alt restr	35	30 nearside	SENIORS 35km/h	3-point, double PT	4,0	Yes	D2	Standard
A27	SENIORS alt restr	45	30 nearside	SENIORS 45km/h (scaled)	3-point, double PT	4,0	Yes	D2	Standard
A28	SENIORS alt restr	25	30 nearside	SENIORS 25km/h	3p 2-retr, double PT	2,0	Yes	D2	Standard
A29	SENIORS alt restr	35	30 nearside	SENIORS 35km/h	3p 2-retr, double PT	2,0	Yes	D2	Standard
A30	SENIORS alt restr	45	30 nearside	SENIORS 45km/h (scaled)	3p 2-retr, double PT	5,0-2,0	Yes	D2	Standard
A31	SENIORS alt restr	25	30 nearside	SENIORS 25km/h	Criss-cross 2-retr, triple PT	1,0+1,0	Yes	D2	Standard
A32	SENIORS alt restr	35	30 nearside	SENIORS 35km/h	Criss-cross 2-retr, triple PT	1,0+1,0	Yes	D2	Standard
A33	SENIORS alt restr	45	30 nearside	SENIORS 45km/h (scaled)	Criss-cross 2-retr, triple PT	2,0+2,0	Yes	D2	Standard
A34	SENIORS alt restr	25	30 nearside	SENIORS 25km/h	split buckle, triple PT	6,0	Yes	D2	Standard
A35	SENIORS alt restr	35	30 nearside	SENIORS 35km/h	split buckle, triple PT	6,0	Yes	D2	Standard
A36	SENIORS alt restr	45	30 nearside	SENIORS 45km/h (scaled)	split buckle, triple PT	6,0	Yes	D2	Standard
A37	SENIORS alt restr	25	30 farside	SENIORS 25km/h	3-point, double PT	4,0	Yes	D2	Standard
A40	SENIORS alt restr	25	30 farside	SENIORS 25km/h	3p 2-retr, double PT	2,0	Yes	D2	Standard
A41	SENIORS alt restr	35	30 farside	SENIORS 35km/h	3p 2-retr, double PT	2,0	Yes	D2	Standard
A43	SENIORS alt restr	25	30 farside	SENIORS 25km/h	Criss-cross 2-retr, triple PT	1,0+1,0	Yes	D2	Standard
A44	SENIORS alt restr	35	30 farside	SENIORS 35km/h	Criss-cross 2-retr, triple PT	1,0+1,0	Yes	D2	Standard
A45	SENIORS alt restr	45	30 farside	SENIORS 45km/h (scaled)	Criss-cross 2-retr, triple PT	2,0+2,0	Yes	D2	Standard

APPENDIX 2

	UL Res	UR Res	LL Res	LR Res	PC Score	Rmax	DcTHOR	Dmax	shoulder (B3)	diagonal belt at buckle (B4)	lap (B6)
L01	38,9	13,2	33,6	20,1	5,89	38,9	34,00	36,2	3,88	7,82	4,53
L02	46,2	18,3	38,5	24,0	7,08	46,2	46,16	42,8	5,37	10,28	6,22
L03	29,2	14,4	27,4	16,4	4,40	29,2	14,04	23,6	2,51	5,83	4,47
L04	34,3	20,4	31,9	19,3	5,48	34,3	17,04	29,0	3,09	7,48	6,15
L05	37,7	26,0	37,5	15,6	5,53	37,7	37,70	34,7	3,39	8,01	6,26
L06	32,7	22,8	33,3	15,9	4,84	33,3	28,01	29,7	2,94	6,69	4,94
L07	27,7	42,6	39,6	16,7	5,95	42,6	38,74	40,4	3,47	8,93	7,00
L08	24,7	38,0	32,8	15,3	5,22	38,0	29,99	35,5	2,56	7,06	6,52
L09	24,7	41,6	38,2	15,4	5,86	41,6	39,70	39,1	3,50	8,77	6,64
L10	20,0	34,9	31,9	12,0	4,99	34,9	28,15	32,4	2,62	7,15	6,43
L11	37,8	21,3	34,6	21,7	5,64	37,8	26,10	34,1	3,15	7,48	6,06
L12	39,8	32,9	39,8	19,0	5,74	39,8	40,42	37,2	3,37	8,01	6,37
L13	23,4	37,7	35,3	14,5	5,30	37,7	32,70	35,1	3,44	7,22	3,97
L14	36,7	40,1	38,2	15,8	5,77	40,1	39,30	38,1	3,42	7,27	3,99
L15	35,4	41,3	38,6	19,4	6,04	41,3	38,74	38,9	2,76	7,82	7,88
L16	33,7	47,7	44,9	20,4	6,78	47,7	49,32	45,6	3,53	9,46	7,59
A01	36,7	12,9	35,4	24,7	5,50	36,7	27,30	34,7	4,39	3,19	0,51
A02	39,0	13,0	40,6	25,5	5,96	40,6	35,81	37,2	6,04	4,48	0,53
A03	31,0	11,3	24,0	16,3	4,48	31,0	13,96	26,7	2,80	3,32	0,60
A04	32,7	14,0	21,4	13,0	4,33	32,7	16,90	26,7	2,81	3,55	1,12
A05	29,7	9,8	26,8	19,8	4,35	29,7	16,96	26,1	2,80	3,33	0,71
A06	29,5	9,3	27,9	20,4	4,53	29,5	14,70	25,5	2,80	3,46	0,54
A07	31,4	11,4	27,3	18,6	4,54	31,4	18,51	27,0	2,81	3,60	0,82
A08	32,0	14,5	28,8	22,7	4,73	32,0	15,39	27,3	2,82	4,47	1,19
A09	37,4	26,7	38,1	15,1	5,25	38,1	33,65	36,1	3,92	2,97	2,54
A10	41,5	29,4	41,4	14,0	5,77	41,5	39,91	40,6	4,21	3,28	3,49
A11	43,7	30,6	43,3	13,2	6,06	43,7	44,97	43,0	4,26	4,02	5,65
A12	48,0	37,7	56,2	16,4	7,32	56,2	66,49	55,3	4,35	5,83	9,80
A13	21,9	20,1	22,7	12,5	3,43	22,7	16,44	20,7	2,03	1,96	2,93
A14	25,6	21,9	24,2	12,7	3,64	25,6	19,12	24,2	2,05	2,22	3,91
A15	37,6	31,0	40,8	12,4	5,50	40,8	41,74	39,1	4,26	3,98	5,81
A16	40,5	31,8	42,6	15,4	5,73	42,6	45,33	41,0	4,30	4,38	10,70
A17	17,1	19,8	15,5	15,4	2,56	19,8	12,27	13,7	1,05	1,20	2,97
A18	17,1	19,8	15,5	15,6	2,57	19,8	12,38	13,7	1,05	1,19	4,22
A19	21,2	21,5	22,2	21,6	3,15	22,2	18,94	19,1	2,11	1,85	5,41
A20	27,9	28,3	21,5	23,1	3,51	28,3	23,51	27,9	2,14	2,31	11,12
A21	31,2	39,1	21,2	18,4	4,25	39,1	20,00	31,6	4,52	3,62	3,20
A22	34,6	43,3	29,7	17,0	5,14	43,3	27,07	38,5	5,22	3,91	3,62
A23	36,4	43,0	27,8	16,2	5,09	43,0	26,04	38,7	5,35	3,84	6,57
A24	42,3	44,9	31,8	19,9	5,58	44,9	35,11	42,1	5,44	3,85	11,08
A25	38,8	28,9	41,8	19,3	5,82	41,8	38,85	39,2	3,70	4,02	2,48
A26	45,4	33,0	44,6	19,3	6,65	45,4	45,96	42,7	4,24	4,76	3,14
A27	47,3	35,0	47,5	22,7	7,19	47,5	50,46	45,7	4,30	5,29	4,94
A28	21,2	20,1	30,0	15,9	3,78	30,0	18,55	27,0	2,03	2,75	2,94
A29	23,8	20,8	30,9	17,2	4,08	30,9	20,25	27,3	2,07	3,06	2,95
A30	39,6	34,6	44,1	18,8	6,66	44,1	44,80	41,9	4,23	4,87	4,16
A31	16,5	17,9	17,2	13,0	2,60	17,9	11,68	12,4	1,02	1,23	2,93
A32	18,5	18,0	20,8	15,4	2,92	20,8	12,03	12,5	1,04	1,49	2,92
A33	20,7	19,6	29,2	27,3	3,82	29,2	19,83	24,5	2,19	2,66	4,30
A34	31,4	41,9	23,1	18,7	4,60	41,9	19,36	32,5	4,74	5,22	3,18
A35	36,5	47,8	26,5	21,7	5,34	47,8	22,88	37,8	5,45	5,77	3,24
A36	39,5	52,1	28,7	25,1	5,78	52,1	26,66	41,3	5,51	6,01	4,40
A37	28,7	26,7	39,0	18,1	4,75	39,0	31,95	36,1	3,78	2,61	2,65
A40	18,2	20,1	22,9	13,9	3,39	22,9	15,33	20,5	2,02	1,62	2,97
A41	20,7	20,8	21,5	18,9	3,60	21,5	15,35	19,4	2,04	1,85	5,86
A43	16,6	17,9	14,8	17,8	2,73	17,9	11,92	12,6	1,06	1,19	2,94
A44	16,7	17,9	18,9	20,0	2,97	20,0	12,19	13,1	1,06	1,20	5,69
A45	19,6	20,6	26,2	27,5	3,65	27,5	19,59	22,4	2,08	1,58	7,38

APPENDIX 3

	Probabilistic Risk (%)			Probabilistic Risk (%)			Belt Loads	
	NFR 2+ 65+	NFR 3+ 65+	NFR 4+ 65+	NFR peak strain > 1,9% (65+)	AIS3+ (yes/no)	AIS2+ (yes/no)	Shoulder Belt Force (B3) / kN	Lap belt force (B6) / kN
L01	100,0%	100,0%	100,0%	8	1	1	4,3	3,2
L02	100,0%	100,0%	100,0%	11	1	1	5,8	4,9
L03	33,3%	6,7%	0,4%	1	0	0	2,5	3,1
L04	99,6%	94,6%	74,3%	6	1	1	3,1	4,6
L05	92,8%	72,5%	41,4%	5	1	1	3,3	4,6
L06	7,2%	0,5%	0,0%	0	0	0	2,9	3,1
L07	2,8%	0,0%	0,0%	0	0	0	3,5	4,8
L08	2,8%	0,0%	0,0%	0	0	0	2,5	4,8
L09	0,0%	0,0%	0,0%	1	0	0	3,5	4,9
L10	0,0%	0,0%	0,0%	1	0	0	2,5	4,8
L11	87,4%	62,2%	31,5%	5	1	1	3,1	4,7
L12	18,1%	2,5%	0,2%	1	0	0	3,3	4,5
L13	0,0%	0,0%	0,0%	0	0	0	3,5	3,5
L14	1,4%	0,0%	0,0%	0	0	0	3,5	3,4
L15	69,6%	37,2%	13,3%	3	1	1	2,5	6,0
L16	67,0%	34,5%	11,9%	2	0	1	3,7	6,1
A01	81,9%	46,4%	13,9%	4	1	1	5,2	0,7
A02	100,0%	100,0%	100,0%	9	1	1	6,9	0,7
A03	18,0%	2,0%	0,1%	1	0	0	2,8	0,5
A04	98,5%	86,8%	53,9%	4	1	1	2,8	1,7
A05	51,0%	17,7%	3,2%	3	1	1	2,8	0,8
A06	45,1%	11,4%	0,7%	3	1	1	2,8	0,7
A07	94,3%	74,4%	40,8%	4	1	1	2,8	1,1
A08	100,0%	99,9%	99,0%	9	1	1	2,8	1,6
A09	100,0%	99,4%	93,0%	7	1	1	4,0	2,6
A10	100,0%	100,0%	99,6%	8	1	1	4,2	3,7
A11	100,0%	100,0%	100,0%	9	1	1	4,3	4,9
A12	100,0%	100,0%	100,0%	15	1	1	4,4	10,1
A13	0,0%	0,0%	0,0%	0	0	0	2,4	3,6
A14	51,5%	16,6%	2,5%	0	0	0	2,4	3,6
A15	51,5%	16,6%	2,5%	2	0	1	4,2	5,2
A16	100,0%	99,7%	97,8%	11	1	1	4,3	10,5
A17	0,0%	0,0%	0,0%	0	0	0	1,8	3,5
A18	1,4%	0,0%	0,0%	0	0	0	1,8	3,5
A19	8,3%	0,0%	0,0%	0	0	0	2,1	4,6
A20	99,3%	93,4%	75,7%	5	1	1	2,1	10,4
A21	17,8%	1,2%	0,0%	1	0	0	5,1	3,5
A22	47,7%	12,9%	1,7%	2	0	1	5,3	3,5
A23	62,6%	28,9%	8,2%	3	1	1	5,4	5,6
A24	99,8%	98,6%	94,1%	11	1	1	5,4	11,1
A25	100,0%	100,0%	96,8%	6	1	1	3,8	2,6
A26	100,0%	100,0%	100,0%	7	1	1	4,3	3,1
A27	100,0%	100,0%	100,0%	10	1	1	4,4	4,3
A28	71,8%	27,9%	3,6%	3	1	1	2,4	3,5
A29	100,0%	94,3%	57,5%	4	1	1	2,4	3,5
A30	100,0%	100,0%	100,0%	7	1	1	4,2	4,4
A31	0,0%	0,0%	0,0%	0	0	0	1,8	3,5
A32	3,5%	0,0%	0,0%	1	0	0	1,8	3,5
A33	100,0%	100,0%	96,7%	5	1	1	2,1	3,7
A34	98,1%	80,7%	35,2%	4	1	1	5,0	3,5
A35	100,0%	100,0%	100,0%	5	1	1	5,4	3,5
A36	100,0%	100,0%	100,0%	8	1	1	5,5	4,2
A37	40,7%	10,5%	1,1%	2	0	1	3,9	2,9
A40	0,0%	0,0%	8,3%	0	0	0	2,4	3,6
A41	21,4%	1,4%	0,0%	2	0	1	2,4	5,5
A43	0,0%	0,0%	8,3%	0	0	0	1,8	3,6
A44	4,2%	0,0%	0,0%	1	0	0	1,8	4,6
A45	92,6%	59,1%	19,5%	3	1	1	2,1	6,4

STUDY OF CHEST INJURY RISK PROBABILITY WITHIN THE SENIORS PROJECT FOR 45- AND 65- YEAR OLD CAR OCCUPANTS USING CURRENT AND ADVANCED RESTRAINT SYSTEMS IN SLED TEST WITH THOR DUMMY

Alba Fornells, Maria Odriozola, Genís Mensa
IDIADA Automotive Technology
Spain

Krystoffer Mroz
Autoliv Research
Sweden

Andre Eggers
Federal Highway Research Institute (BASt)
Germany

Paper Number 19-0309

ABSTRACT

From European accident data the proportion of fatal and severe crashes suffered by over 65 year old road users is increasing. In response to this, the SENIORS project [1] aims to improve the safety of elderly road users by determining appropriate requirements towards passive safety systems. The objective of this paper is to present the results obtained in frontal deceleration sled tests with the THOR (Test Device for Human Occupant Restraint) dummy using different restraint systems to compare the chest deflection for each of them. The frontal sled tests were performed at two speeds 56km/h and 35km/h with the THOR dummy as driver and co-driver following the test procedures defined in the SENIORS project. The different safety systems were used one by one at the low-speed deceleration to understand the effect on the dummy deceleration and chest deflection. The standard restraint systems – frontal airbag and seatbelts – were combined with advanced restraint systems for the driver – Knee airbag (KnAB), Pelvis restraint cushion (PRC) and the Driver Load Limiter Adaptive seatbelt (DLLA) – and for the co-driver position – Pelvis Restraint Cushion (PRC) and the Load Limiter Adaptive seatbelt (LLA). Then, at the higher speed deceleration pulse the basic restraint systems and the chosen combination of advanced safety systems were performed. It is aimed at comparing the chest deflection with the injury risk AIS3+ that is calculated from Rmax and PCA (Injury criteria) for a 45- and 65- year old person. The results observed showed that all the advanced restraint systems reduce the thorax injury risk for both ages 45 and 65 years old, however not always reducing all the IR-TRACC displacement but reducing the Rmax and the PCA calculations. It could also be observed that the most effective restraint system to reduce the thorax high injury for people over 65 years old is Load Limiter Adaptive seatbelt. In this study it can be concluded that with the current standard or advanced restraint systems the chest injury risk for elderly people over 65 years old is very high in high deceleration tests but is also important at lower decelerations. Moreover, the differences in position P1 and P3 are compared in this paper.

INTRODUCTION

Previous projects on accident research, such as DaCoTa project [2], found that the risk of being killed in a crash was higher for the elderly than for the middle aged person in most EU countries. Based on crash data from 2010 [3] (J. Broughton, 2012), and that older occupants received more often thoracic injuries than younger ones [4] (T. Adolph, 2009). Also, according to [5] (J. Carrol and al., 2009), older occupants (over 52 years of age) were 3.7 times more likely to receive an AIS2+, and 2.8 times more likely to receive an AIS3+ torso injury than younger occupants (12-52 years). Within the SENIORS project a new analysis of the collated European and high-level national crash datasets was carried out (using the in-depth accident datasets from Germany (GIDAS) and the UK (RAIDS)), which confirmed the findings from literature. The data consistently demonstrated a higher risk of serious and fatal injury for older car occupants and the thorax was also identified as the most critical body region for car occupants, which showed the highest share of AIS3+ injuries of all body regions. As explained in [6] and [7], the older occupants of passenger cars – car vehicles manufactured in 2005 or later – have a higher likelihood of suffering from MAIS2+ injuries in frontal car collisions than for middle-aged ones. Moreover, it was seen that the probability of a thorax MAIS2+ injury increases noticeably more by higher delta-v values for older than for mid-aged car occupants.

For example, for a delta-v of 60 km/h the probability of a thorax AIS2+ injury was found as being around 35 percentage points higher for older compared to mid-aged car occupants. According to this conclusion, an injury risk curve for MAIS0+, MAIS1+ and MAIS2+ regarding the delta-v for younger and older car occupants was calculated (Figure 1). Besides this, in SENIORS research it could be observed that the majority of accidents with severe injuries were found in frontal collisions.

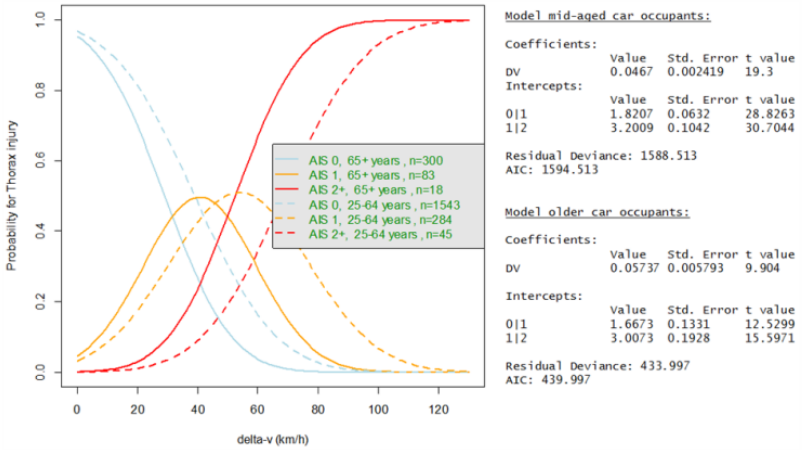

Figure 1: Probability of thorax injury severity (MAIS) over delta-v for mid-aged and older car occupants in frontal collisions, GIDAS, cars manufactured in 2005 or later

Based on the observed facts, the SENIORS project aimed to improve the safety of elderly road users by updating the test procedures and improving the assessments as described in D4.1a SENIORS [8] which determined appropriate requirements towards passive safety systems that better solve senior car users' biomechanical issues. Within the project, specific test characteristics were used to assess elderly safety - such as frontal decelerations at lower levels which were representative with the senior occupant injury.

Also, new multi-point chest injury criteria and risk functions applicable to low deceleration collisions, which considered the age-related characteristics were calculated for the frontal impact THOR 50th male dummy, described in D2.5a SENIORS [9] (Eggers, et al., 2018). Moreover, some advanced safety systems were investigated in the SENIORS project, some of which were presented [10]. To prove the efficacy of the proposed solutions the focus was on thorax injuries. Sled tests were chosen as a widely non-destroyable environment. A total of 14 tests were performed at low deceleration pulse and 4 were performed with a higher deceleration pulse with the THOR dummy in the driver and co-driver position also using different safety systems. Finally, the results were compared and presented regarding young and elderly injury risk.

TEST DESCRIPTION

Test environment

The test environment was a compact car BiW (Body in White) which was cut-off behind the b-pillar and mounted in driving direction on the sled platform to simulate a full-frontal crash. In addition, the BiW was reinforced to avoid any unintentional deformation. The occupant compartment was equipped with an instrument panel, steering wheel, and a driver and a passenger seat from the series production. These parts have not been replaced after each test, but were modified to ensure their full integrity to dismiss any damage, except for the seats which were changed anyway 3 and 2 times for driver and passenger position respectively.

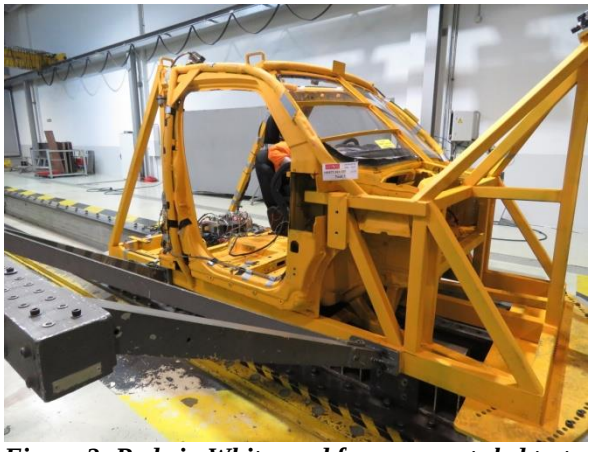

Figure 2: Body in White used for occupant sled tests with the THOR dummy

Deceleration test pulse

Two different pulses were used for this sled testing. The first pulse reflects a moderate speed of 35 km/h, whereas the second pulse represents a higher speed of 56 km/h. The low crash pulse was selected because its severity represented well the expectations for moderate speed test which included a reliable basis for comparisons of the performance of the same restraint systems in frontal and oblique impacts. Moreover, literature was reviewed, and it was seen in [11] (Gabler, 2005) a description of the total struck-vehicle delta-v of tow-away far-side impact collisions in the US (NASS-CDS 1993-2002).

Other studies such as the one by Forman [12] used a similar crash pulse for PMHS sled tests in far-side oblique impacts. The high-speed pulse used is representative of mid-sized sedan vehicles and in the range of current test speed. Using a generic pulse at 56km/h, validated with pulses of the NHTSA's vehicle being representative of European and current vehicles.

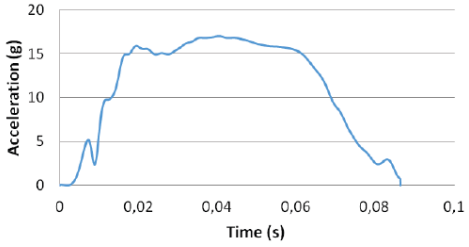

Figure 3: SENIORS generic moderate speed sled test pulse

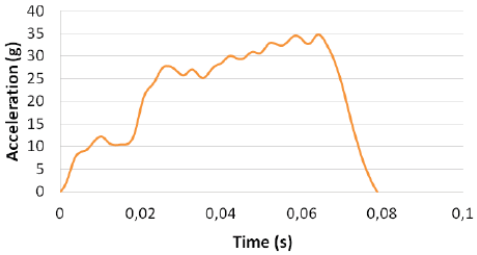

Figure 4: SENIORS generic high-speed sled test pulse

Test tool, ATD

The ATD (anthropomorphic test device) used as test tool was the THOR 50th, which shows superior biofidelity compared to the dummy Hybrid III [13]. For the updated version of this dummy, new thoracic injury risk functions were proposed [14, 15, 16] and the dummy version THOR-M SBL-A is specified by the European New Car Assessment Programme (EuroNCAP) [17] for use in Euro NCAP testing protocols.

Assessment injury risk curve

The injury probability used for the assessment based on the THOR IR-Tracc chest deflection was the PCA score (Figure 5) and the Rmax values calculated by Crandall [15], which have age variation parameters and show the AIS3+ injury risk for a 45-year-old with respect to a 65-year-old. This makes it possible to evaluate the chest injury risk of old or young car occupants according to the IR-TRACC displacement.

Multi-point Thoracic Injury Criterion – Peak Resultant Deflection [Crandall, 2013]	$R_{max} = max(UL_{max}, UR_{max}, LL_{max}, LR_{max})$ where $[U/L\|R/L]_{max} = max\left(\sqrt{[L/R]X^2_{[U/L]S} + [L/R]Y^2_{[U/L]S} + [L/R]Z^2_{[U/L]S}}\right)$	R_{max}	Overall peak resultant deflection in mm	$P(AIS \geq 3\| age, R_{max}) = 1 - exp\left(-\left[\frac{R_{max}}{exp(4.4853 - 0.0113age)}\right]^{3.03896}\right)$
		$[U/L\|R/L]_{max}$	Peak resultant deflection of the [upper/lower | left/right] quadrant in mm	
		$[L/R][X/Y/Z]^2_{[U/L]S}$	Time-history of the [left/right] chest deflection along the [X/Y/Z] axis relative to the [upper/lower] spine segment in mm	
Multi-point Thoracic Injury Criterion – PC	$PCA\ Score = 0.485\left(\frac{up_{tot}}{17.509}\right) + 0.499\left(\frac{low_{tot}}{15.526}\right)$	up_{tot}	total upper chest resultant deflection, independent of time	$P(AIS3+\| age, PCA\ Score) = 1$

Figure 5: Thorax injury prediction formula of THOR-M

Test restraint systems

The standard restraint systems – frontal airbag and seatbelts – were combined with advanced restraint systems for the driver – Knee airbag (KnAB), Pelvis restraint cushion (PRC) and the Driver Load Limiter Adaptive seatbelt (DLLA) – and for the co-driver position – Pelvis Restraint Cushion (PRC) and the Load Limiter Adaptive seatbelt (LLA).

The knee airbag module is mounted in the lower instrument panel. The airbag is initially folded in a container and inflated during the crash using a pyrotechnical inflator (Figure 6). The knee airbag usually has a thickness of 150 mm and covers the potential impact area of the knees with the instrument panel. In a crash, the working pressure is approx. 80kPa. With the knee airbag, increased restraining of the pelvis is obtained by means of the upper legs which have the potential to improve the chest-to-steering wheel clearance and reduce the loading to the chest. The pelvis restraint cushion (PRC) is made of an air tight textile material and is installed on the seat pan and below the seat cushion foam (Figure). The PRC is initially folded and inflated in a crash using a pyrotechnical inflator to a thickness of approx. 100mm. The working pressure of the PRC is approx. 30-40 kPa and its response controlled using a venting hole in the cushion. With the PRC, increased restraining of the pelvis is achieved by means of improved coupling to the seat. With improved coupling, the PRC has the potential to reduce pelvis excursion, pelvis accelerations and chest loading. The PRC has also proven to be effective in the prevention of submarining.

The shoulder belt retractors for all belt systems are equipped with two-level load limiting. In the project, the level of the load limiting was adapted to the impact severity using a pre-defined switch time. The switch time was used to activate the use of the upper or lower or even a combination of both load limiting levels (Figure 7***: Pelvis restraint cushion in a front seat.***). In a vehicle installation, the frontal crash sensors are used to decide the load limiting setting. The load limiting level can also be adapted to other sensor information, such as occupant weight, size, position etc.

Figure 6: Inflated knee airbag in a frontal sled test.

Figure 7: Pelvis restraint cushion in a front seat.

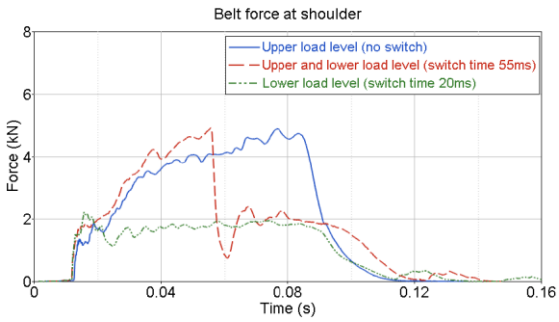

Figure 8: Belt force at the shoulder for three different setting of the adaptive load limiting

Test plan

At moderate speed pulses the advanced restraint systems were introduced one by one to see the effect on the dummy resultant signals, also two different restraint system combinations (Mix) were selected. At higher speed pulses, only two tests were conducted with the standard restraint system and the best performing restraint system combination from the moderate speed tests. The sled tests were organized as shown in Table 1.

Table 1: Test lists

Position	Pulse	nº	Description	Frontal airbag	Seatbelt	Pelvis Restraint Cushion	Adaptative Load Limiter	Knee airbag	Collapsible steering column
Driver	35 km/h	1	Safety system std for SENIORS	V	V				
		2	Safety system std for SENIORS + PRC	V	V	V			
		3	Safety system std for SENIORS + LLA (t12ms)	V	V		V (12ms)		
		4	Safety system std for SENIORS + LLA (t27ms)	V	V		V (27ms)		
		5	Safety system std for SENIORS + KAB	V	V			V	
		6	Safety system std. for SENIORS + collapsible steering column	V	V				V
		7	Mix 1 (DLLA 12ms + KAB 12ms)	V	V		V (12ms)	V	
		8	Mix 2 (DLLA 12ms + PRC 12ms)	V	V	V	V (12ms)		
	56km/h	9	Actual safety restraints system	V	V				
		10	Mix (DLLA 12ms + KAB 12ms)	V	V		V (12ms)	V	
Co-driver	35 km/h	12	Actual safety restraint system	V	V				
		13	Actual safety restraint system + PRC	V	V	V			
		14	Actual safety restraint system + LLA	V	V		V (12ms)		
		15	Actual safety restraint system + LLA different time to fire	V	V		V (27ms)		
		16	Actual safety restraint system + MIX 1 (LLA t12ms+PRC)	V	V	V	V (12ms)		
		17	Actual safety restraint system + MIX 2 (LLA t27ms+PRC)	V	V	V	V (27ms)		
	56 km/h	18	Actual safety restraint system (no double pretension)	V	V				
		19	Actual safety restraint system + LLA t 27ms	V	V		V (27ms)		

RESULTS

The plots in Figure 7 and Figure 8 show the resultant deceleration from different dummy body parts of the low deceleration tests of the THOR dummy in the driver and co-driver positions. The black curve stands for the reference test at low speed with only the standard restraint systems and the other curves are tests where different advanced restraint systems were added. In consequence, different dummy behaviour for each of the tests could be observed.

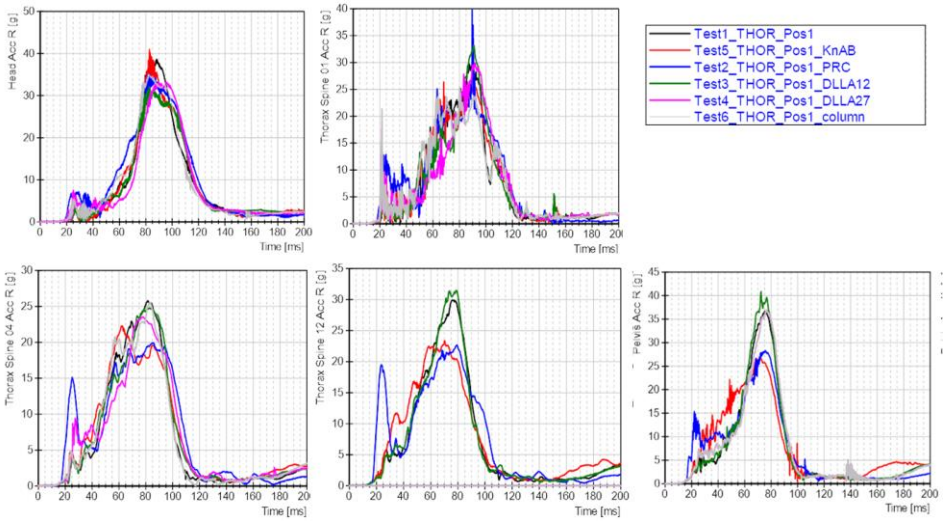

Figure 7:Deceleration results of different THOR body regions as driver in the sled tests at low speed

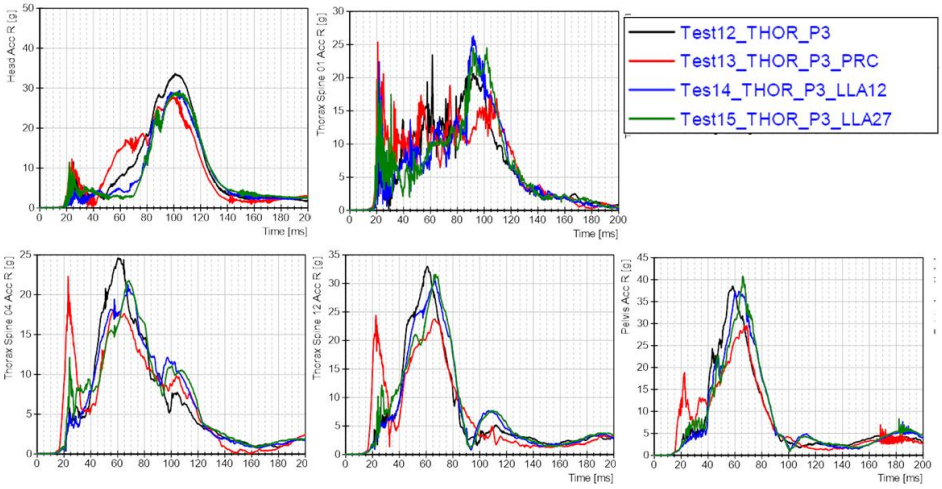

Figure 8: Deceleration results of different THOR body regions as co-driver in the sled tests at low speed

Focusing on the chest results, which are the most critical body regions, the chest IR-TRACC displacements were analysed. Table 2 and Figure 1 show a summary of the maximum chest IR-TRACC displacements for each test and the current assessment values Rmax and the PCA for the THOR in the driver position.

Driver chest test results

The RIUP (upper right IR-TRACC) displacement was always the highest due to the seatbelt position. This was reduced, by 10-15%, in the third and fourth test where the DLLA – load limiter fired at 12 and 27 ms respectively - was used. This reduction comes together with the slight reduction and increment of the other IR-TRACC displacements. The two red bars in Figure 9 show the results obtained in the Mix 1 and Mix 2 tests with the combination of different restraint systems: Mix 1 with the frontal airbag, the DLLA and KnAB fired at 12 ms; Mix 2 with the frontal airbag, the DLLA and the PRC fired at 12 ms. It can be observed that in both cases the IR-TRACC deflection reductions were nearly similar, with a higher deflection on lower IR-TRACC applied in the Mix 1 test.

Table 2: Maximum IR-TRACC displacements, Rmax and PCA of the THOR chest in tests 1-10

	Test 1	Test 2	Test 3	Test 4	Test 5	Test 6	Test 7	Test 8	Test 9	Test 10
	35km/h	35km/h	35km/h	35km/h	35km/h	35km/h	35km/h	35km/h	56km/h	56km/h
	Standard rest. syst.	str. + PRC	str + DLLA 12	str + DLLA 27	str + KnAB	str + collaps. column	Mix 1: Str+DLLA 12+ KnAB	Mix 2: Str+DLLA 12 + PRC	Str. rest. Syst.	Mix: str.+DLA 12 +KnAB
Upper Left IR-TRACC (mm)	33,94	24,59	26,86	23,97	22,4	22,34	23,86	23,81	33,07	57,81
Upper Right IR-TRACC (mm)	40,88	40,13	36,75	34,55	41,51	39,38	36,81	32,89	56,4	52,78
Lower Left IR-TRACC (mm)	8,52	18,53	9,79	12,92	9,75	11,3	6,18	15,73	12,69	23,27
Lower Right IR-TRACC (mm)	33,92	39,81	29,55	34,08	26,12	32,05	20,92	32,82	42,37	29,75
PCA	5,10	5,38	4,54	4,60	4,86	4,84	4,07	4,47	7,04	6,23
Rmax (mm)	40,88	40,13	36,75	34,55	41,51	39,38	36,81	32,89	56,4	57,81

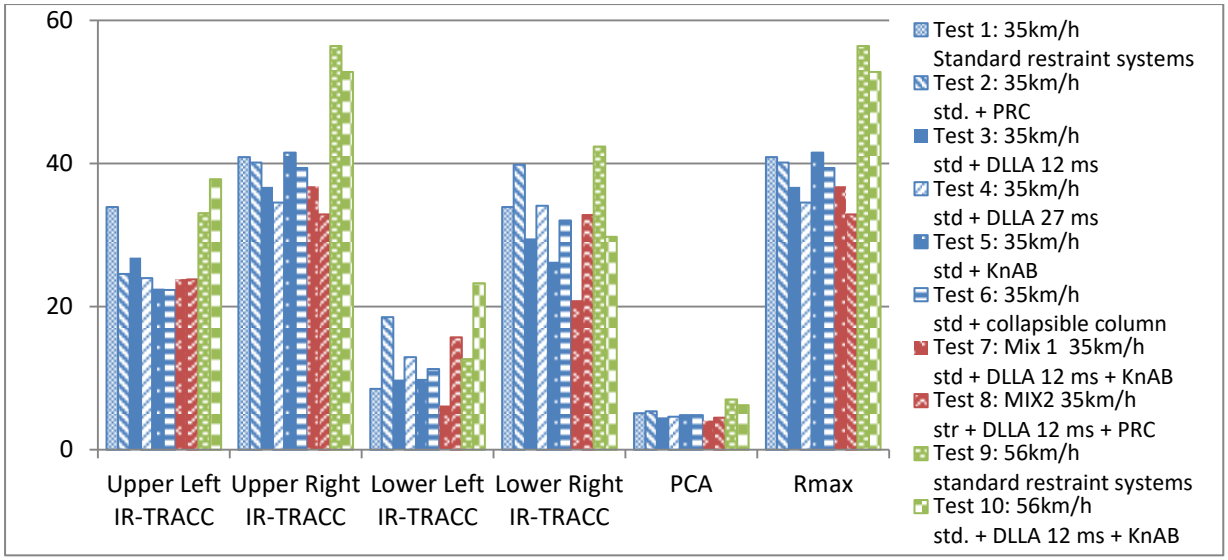

Figure 9: Maximum chest IR-TRACC displacements, Rmax and PCA values for each THOR dummy in driver position tests

Comparing the first test with the ninth one both were reference tests where only the standard restraint systems were used – it is clear that at 56km/h the chest deflection is higher mainly for the RIUP chest part. When applying the chosen restraint system combination (Mix 1) to the high speed tests a slight reduction - 6% - of the RIUP IR-TRACC could be observed, but the lower left IR-TRACC showed a highly increased deflection.

According to these observations, the safety system with a higher effect on thorax displacement reduction is the DLLA. It is interesting to evaluate the differences between test 3 and 4 in more depth where the DLLA was activated at 12 and 27ms respectively. Figure 10 shows the forces of the seatbelt at B3 and the belt displacement. The B3 force of the DLLA seatbelt fired at 12ms (green line) which had a lower load limit and a lower seatbelt displacement than the standard seatbelt. However, the B3 force of the DLLA fired at 27 ms (pink line) which had the same lower load limit and a higher belt displacement, but it starts the restraint before all the other seatbelts tested. The lower load limit of the DLLA seatbelts achieved a reduction in the thorax deceleration peak. Also, it maintained the seatbelt force of the DLLA which fired at 27 ms, the seatbelt stay in the correct position on the chest and the chest force was then better distributed between the different IR-TRACCs. Overall, a higher homogeneity of chest IR-TRACC deflections reduced the IR-TRACC peak values and therefore the Rmax value, but did not influence the PCA. Test 6 had the collapsible steering column, however due to the low severity deceleration pulse, it did not collapse. In the videos a small steering wheel displacement was observed in test 6 but also in the other tests. This could be explained by the displacement of the steering wheel position due to the impact. Moreover, there is nearly no difference between test 6 and the reference test 1. The steering wheel used in high-speed tests was also reinforced to become non-collapsible as seen in the previous tests. This fact may be one of the reasons why the chest deflection is so high.

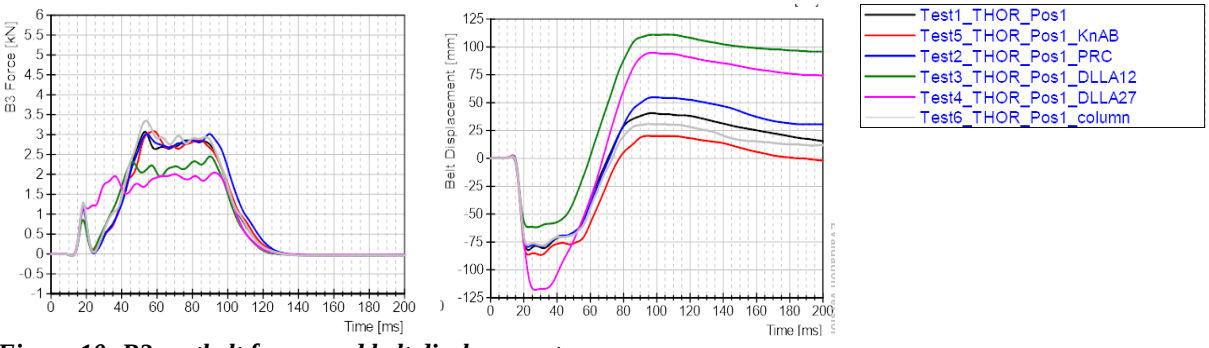

Figure 10: B3 seatbelt forces and belt displacements

Besides this, the injury risk was calculated regarding the PCA and the Rmax according to the NHTSA protocol [15] and can be observed in the following Figure 11. At moderate speed it can be seen that the injury risk calculated with the Rmax is lower using the Mix 2 of the available restraint systems – DLLA fired at 12 ms and the KnAB; however, using the PCA it was lower with the Mix 1 of the safety systems - DLLA 12 ms and the

PRC (Pelvis Restraint Cushion). At higher speed tests, the injury risk was in all cases lower using a mix of safety restraint systems – DLLA 12 ms and PRC - and following the same logic as before, this reduction is higher when it is calculated with the PCA value. Nonetheless, it should be said that the injury risk in any case was very high. Also, differences could be observed between injury risks for the 45- and 65-year-old population. This is much higher for elderly car occupants who reached 98% or 95% of injury risk using the Rmax the PCA value and were reduced to 95% and 77% respectively.

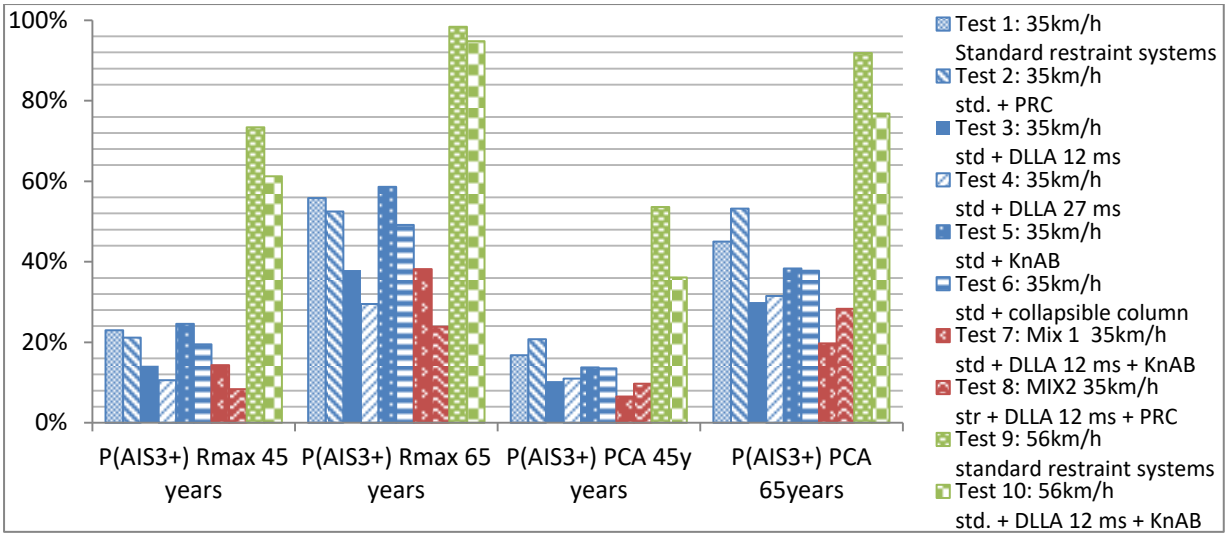

Figure 11: Injury risks for each test according with PCA and Rmax values for 45 years old occupants and 65 years old occupants

Co-driver chest test results

Regarding the co-driver position, similar analyses were performed. Analysing the chest IR-TRACC displacement, summarized in Table 3 and Figure 13, it can be seen that the most affected IR-TRACCs are the upper left and lower left. The best results observed are in tests 14 and 15 where the DLLA was used, firing the load limiter at 12 and 27 ms. Even though the Left Upper IR-TRACC was not so much reduced, the other IR-TRACC was reduced achieving a lower and more homogenous chest deflection. The PRC achieves an important reduction in LeLO (lower left) IR-TRACC which is interesting due to the higher values observed in the standard test.

Table 3: Maximum IR-TRACC displacements, Rmax and PCA of the THOR chest in tests 12-19

	Test 12: 35km/h	Test 13: 35km/h	Test 14: 35km/h	Test 15: 35km/h	Test 16: 35km/h	Test 17: 35km/h	Test 18: 56km/h	Test 19: 56km/h
	Standard restraint systems	str. + PRC	str. + LLA 12ms	str. + 27 ms	MIX 1: str. + LLA 12ms + PRC	MIX 2: str. + LLA 27ms + PRC	standard restraint systems	str. + LLA 27ms
Upper Left IR-TRACC (mm)	31,08	35,74	33,66	30,82	26,05	24,8	45,45	41,61
Upper Right IR-TRACC (mm)	24,99	18,21	16,48	17,05	18,4	15,37	25,88	19,37
Lower Left IR-TRACC (mm)	37,06	32,44	21,61	23,42	27,55		35,55	32,14
Lower Right IR-TRACC (mm)	12,42	11,89	10,46	11,1	11,25	11,56	13,28	16,81
PCA	5,04	4,87	4,26	4,14	4,09	3,78	6,26	5,57
Rmax (mm)	37,06	35,74	33,66	30,82	27,55	26,63	45,45	41,61

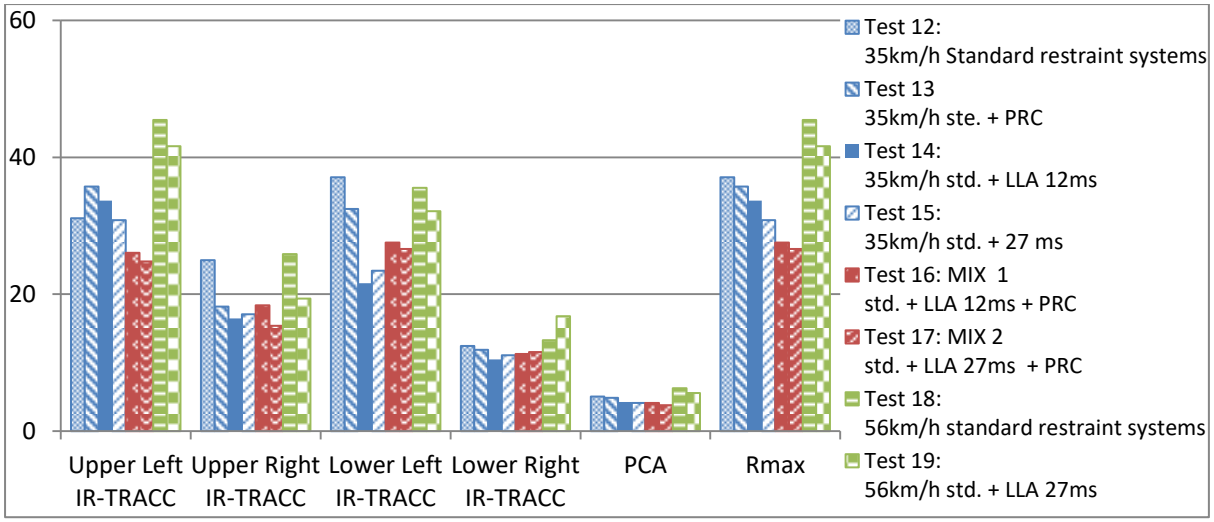

Figure 12: Maximum chest IR-TRACC displacements, Rmax and PCA values for each THOR dummy in co-driver position tests

Mix 1 and Mix 2 tests – Test 16 and 17- were a combination of safety systems used to achieve better results than in the other tests. Both tests were performed with the PRC and the DLLA, at 12 and 27 ms. A slightly lower chest deflection was achieved within the Mix 2 test, firing the DLLA at 27 ms, and therefore this combination was used in the second high-speed pulse test. The green columns in the chart are the high-speed pulse tests and as was expected the IR-TRACC displacements are higher. However, the difference between test 12 and test 18 – THOR in P3 position - both with standard restraint systems, is lower than the difference between test 1 and test 9 – with the THOR in the P1 position.

As previously mentioned, it is interesting to analyse the differences between the use of the DLLA firing at 12 or at 27 ms – tests 14 and 15. In the following graphs, the B3 seatbelt force of the DLLA fired at 12 ms – blue line – shows a lower load limiter, which should reduce the thorax deceleration. However, the B3 force of the DLLA fired at 27ms – green line – shows the same lower load limit and a higher belt displacement, but it also starts the restraint before all the other seatbelts tested. The lower limiter of the DLLA seatbelts achieves a reduction in the thorax deceleration peak and maintains the seatbelt force of the DLLA at 27 ms makes the seatbelt stay in the correct position on the chest and the chest force is better distributed between the different IR-TRACC.

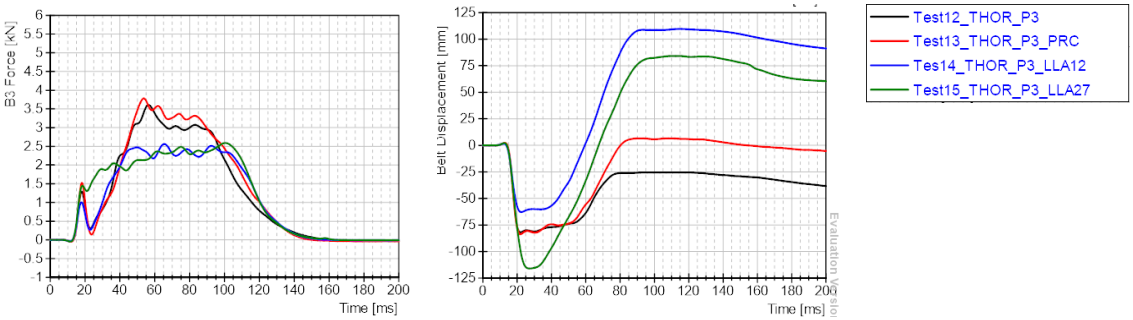

Figure 13: B3 seatbelt forces and belt displacements in the co-driver position

Besides this, the injury risk was calculated regarding the PCA and the Rmax according to the NHTSA protocol [15] and can be seen in Figure 14. The injury risk was reduced in all cases with the Mix 2 of safety restraint systems. The injury risk was significantly reduced for 45 year-olds as well as for 65 year-olds achieving 59% of injury AIS 3 or more for elderly people using both the Rmax and the PCA formula. In comparison with the driver results observed – the injury probability is between 61% and 73% the safety systems used for the passenger are significantly better.

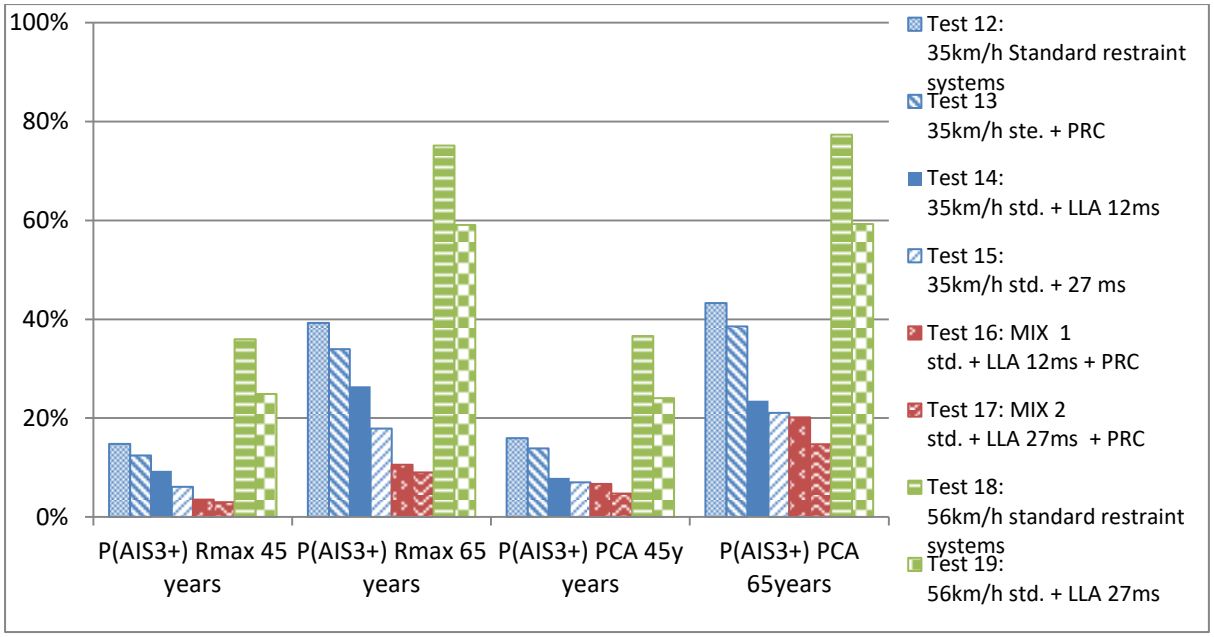

Figure 14: Injury risk for each test according with PCA and Rmax values for 45 years old occupants and 65 years old occupants

LIMITATIONS

The limitations of the current study are the limited number of tests performed. Only one test for each advanced restraint system was performed and therefore it was not possible to adjust or optimize the system's effect. Moreover, the effect of each of the advanced restraint systems could not be studied at a higher deceleration and it could not be studied if they have the same response at both decelerations. Only the chest deflection and chest injury risks were studied, since is the most critical body region for the elderly. However, other body regions should be studied.

CONCLUSIONS

With the aim of understanding and improving the safety of the elderly as car occupants some sled tests were performed; comparing the thorax injury risks calculated for occupants aged 45 and 65, to see the effect of the different vehicle safety systems at low and high decelerations.

The results obtained throughout this work support the data observed in literature and within the SENIORS project regarding the high risk of severe injuries for senior car occupants in road accidents. It was seen that the injury risk reaches 95% for the 65-year-old driver population. This work also showed that the driver injury risk is always higher than for the passenger, especially in high speed test. These results can be explained by the use of a non-collapsible steering column during the testing.

Furthermore, the testing activities performed also identified the thorax as the main injured body region in these scenarios. The chest deflection results and the corresponding injury risks are relatively high for older car occupants whose chest injury risk is not only increasing in high deceleration tests but also important at lower deceleration ones as well.

Finally, the combination of several standard and advanced restraint systems improved the results of the thorax injury calculations in all cases. Focusing on chest deflection resulting data the best restraint system combination is using the standard restraint systems (regular seatbelts and frontal airbags) with the Load Limiter Adaptive seatbelt for both driver and passenger positions. Although, the results showed that the Pelvis restraint cushion (PRC) was also very effective preventing severe thorax injury.

ACKNOWLEDGEMENTS

The research leading to the results of this work has received funding from the European Union's Horizon 2020 research and innovation programme under grant agreement No 636136.

REFERENCES:

[1] - SENIORS Project (2018): http://www.seniors-project.eu/

[2] - Dimitris Margaritis, Angelos Bekiaris, Julian Hill, Helen Fagerlind, Gabriele Giustiniani, Michael Jaensch, Pierre van Elslande, Thierry Hermitte, Ragnhild Davidse, Heike Martensen (2013) “Pan-European In-depth Road Accident Database” Road Safety on Four Continents Conference (RS4C). Beijing.

[3] - J. Broughton, a. (2012) Traffic Safety Basic Facts 2012 "The elderly". Project DaCoTA, Loughborough (UK)

[4] - T. Adolph, A. E. (2009) Deliverable D5 “Matrix of serious thorax injuries by occupant characteristics, impact conditions and restraint types and identification of the important injury mechanisms to be considered in THORAX and THOMO”. C DG RTD, FP7, SST.2007.4.1.2, COVER, GA No. 218740

[5] - J. Carrol and al. (2009) “A comparison between crash test results and real-world accident outcomes in terms of.” Brussels. European Commission

[6] - WISCH, M. e. (2017) “Road traffic crashes in Europe involving older car occupants, older pedestrians or cyclists in crashes with passenger cars–Results from SENIORS” Proceedings of the 25th International Technical Conference on the Enhanced Safety of Vehicles (ESV)

[7] - Wisch, M. L. (2017) “Injury patterns of older car occupants, older pedestrians or cyclists in road traffic crashes with passenger cars in Europe” IRCOBI

[8] - Fornells, A., Huster, D., Wisch, M., Hynd, D., Barlog, T., Mroz, K., Melloncelli, (2018) “D 4.1a Draft Test and assessment procedure for current and advanced passive safety Systems”. SENIORS project

[9] - Eggers, A., Hynd, D., Mühlbauer, J., Fuchs, T., Peldschus, S., Pipkorn, B., & Mroz, K. (2018) “D2.5a Updated injury criteria for the THOR”. SENIORS project

[10] - Mroz, Krystoffer, Pipkorn, Bengt, et al. (2018) “Evaluation of Adaptive Belt Restraint Systems for the Protection of Elderly Occupants in Frontal Impacts” IRCOBI Conference, Athens, Greece.

[11] - Gabler, H. F. (2005) “Far side impact injury risk for belted occupants in Australia and the United States” Proceedings of the International Technical Conference on the Enhanced Safety of Vehicles (p. Paper No. 05-0420)

[12] - Forman, J. L.-V. (2013) “Occupant Kinematics and Shoulder Belt Retention in Far Side Lateral and Oblique Collisions: A Parametric Study” Proceedings of the 57th Stapp Car Crash Conference

[13] - Ridella, S. P. (2011) “Modifications to improve the durability, usability and biofidelity of the THOR-NT dummy” International Technical Conference on the Enhanced Safety of Vehicles (p. Paper No. 11-0312.)

[14] - Davidsson, J. C. (2014) “Development of injury risk functions for use with the THORAX Demonstrator; an updated THOR” Proceedings from the International Research Council on Biomechanics of Injury (IRCOBI)

[15] - Crandall, J. (2013) “ATD Thoracic Response: Effect Of Shoulder Configuration On Thoracic Deflection Thor Mod Kit Advanced Frontal Crash Test Dummy Frontal Sled Tests” National Highway Traffic Safety Administration (NHTSA), 10-15, 19-24

[16] - Poplin, G. S. (2017) “Development of thoracic injury risk functions for the THOR ATD” Accident Analysis and Prevention *106*, (p. 122–130)

[17] - EuroNCAP. (November / 2017) “Full width frontal impact testing protocol 2018” p. Version 1.0.4

DEVELOPMENT OF A CERTIFICATION PROCEDURE FOR NUMERICAL PEDESTRIAN MODELS

Corina Klug, Florian Feist, Bernd Schneider, Wolfgang Sinz
Graz University of Technology
Austria

James Ellway, Michiel van Ratingen
Euro NCAP
Belgium

Paper Number 19-0310

ABSTRACT

In the Euro NCAP testing of deployable pedestrian protection systems (i.e. active bonnets and airbags), head impact time (HIT), wrap around distance and bonnet deflection due to body loading are assessed by means of simulations with numerical pedestrian models. The aim of this study was to define requirements for numerical pedestrian models and simulation setups to ensure comparable performance of models and simulation results. These requirements were summarized in a certification procedure which focuses on the pedestrian's kinematics that are important for the Euro NCAP assessment. Twelve different institutions (academia and industry) applied a harmonised pedestrian simulation protocol, which was established within a previous study. Numerical pedestrian models in the stature of the 50th percentile male (all applicable for the assessment of deployable systems until 2017) were impacted with four differently shaped generic vehicle models at three different collision speeds according to the protocol. Trajectories, contact forces and HITs were evaluated. Finally, 18 full data sets including the 12 load cases were available covering different Human Body Models and Humanoid Multibody Models in four different FE codes. Reference values, corridors and tolerances for the certification procedure were derived, based on identified consistent results. Comparable behaviour was observed for the majority of pedestrian models. However, a small number of simulations showed clearly outlying behaviour in terms of HITs, trajectories and contact forces. The consistent models were within a range of +3.5% and -7% throughout all load cases. Corridors for the z- and x- trajectories as a function of time were developed for the head centre of gravity, T12 and the centre of acetabuli for each load case. Furthermore, corridors for the contact forces between pedestrian model and generic vehicle model were established. The developed certification procedure ensures that a specific pedestrian model within a specific environment, solver version and specific simulation settings gives comparable kinematic results relevant for the assessment of deployable systems. Inconsistent pedestrian models, incompatibilities with control settings and user errors can be identified and sorted out. The procedure was implemented in the Euro NCAP Technical Bulletin 24 and has been in force since January 2018.

INTRODUCTION

The Euro NCAP (European New Car Assessment Programme) assessment of deployable systems (i.e. active bonnets) represents the first application of Human Body Models within a consumer information safety rating. The timing and the impact location of the head are essential information for the assessment of deployable systems such as active pop-up bonnets. The system must detect the pedestrian and deploy rapidly enough before the head contacts the bonnet. Furthermore, evidence must be provided showing that the bonnet and the support structures are sufficiently stiff to ensure that the additional clearance has not already been significantly compromised due to the body load prior to the head impact.
These parameters cannot be assessed using the conventional subsystem impactors. Therefore, input from simulations is needed: A hybrid approach has been adopted by Euro NCAP for the assessment of deployable systems, which covers virtual simulations with pedestrian models, and physical tests with pedestrian subsystem impactors. The simulations with the pedestrian models are carried out to derive inputs for the subsequent physical tests with headform impactors. The virtual tests cover multiple collision speeds and pedestrian statures: Firstly, the head impact location (*WAD*) and Head Impact Time (*HIT*) for several pedestrian sizes are determined to assess whether the system can be fully deployed by the time of head impact for the most critical pedestrian stature. Secondly, the pedestrian size that is hardest for the sensor system to detect can be determined by means of performing simulations as an alternative to physical tests and to select appropriate test tools, which is in almost all cases the 6yo stature. Finally, the bonnet deflection due to the bonnet loading is derived from the

simulations with pedestrian models to prove that the head protection is not compromised by a collapse of the bonnet. Based on the simulation results, physical tests are performed when the active bonnet is deployed, undeployed, or deploying. Conventional headform impactors are used, and the measured linear accelerations are applied to derive the Head Injury Criterion (*HIC*) values upon which the final scores are based. [1]
The virtual pedestrian simulations described above must be carried out at varying collision speeds with several sizes of the pedestrian models (6yo, 5th, 50th, 95th) but Euro NCAP does not specify the type of Human Body Model [1]. Ensuring comparability of simulation results for this application, however, is of great importance as differences between simulated HIT values and the total response times (TRT= sensing time + deployment time) of the active bonnets are often very close. This is shown in Figure 1, where results submitted to Euro NCAP are shown, which were used for the assessment of deployable systems. The HIT values of the simulations with different pedestrian statures are overlaid and compared with the TRT values. HIT values are only provided for the statures where head contact with the bonnet occurred, which is why there are fewer values for the 95th model (green bars), than values representing the other statures. The 6yo model was not contacting the bonnet in only two of the 47 analysed dossiers. In six cases the TRT was higher than the TRT of the smallest pedestrian model that impacts the bonnet. The average relative positive deviation between the HIT of the smallest stature that was impacting the bonnet and the TRT was 15.6% and the median relative deviation was 11.7% (for the 41 results in which the HIT was ≤TRT). In five of the dossiers the HIT value of the 6yo model was even equal to the TRT.

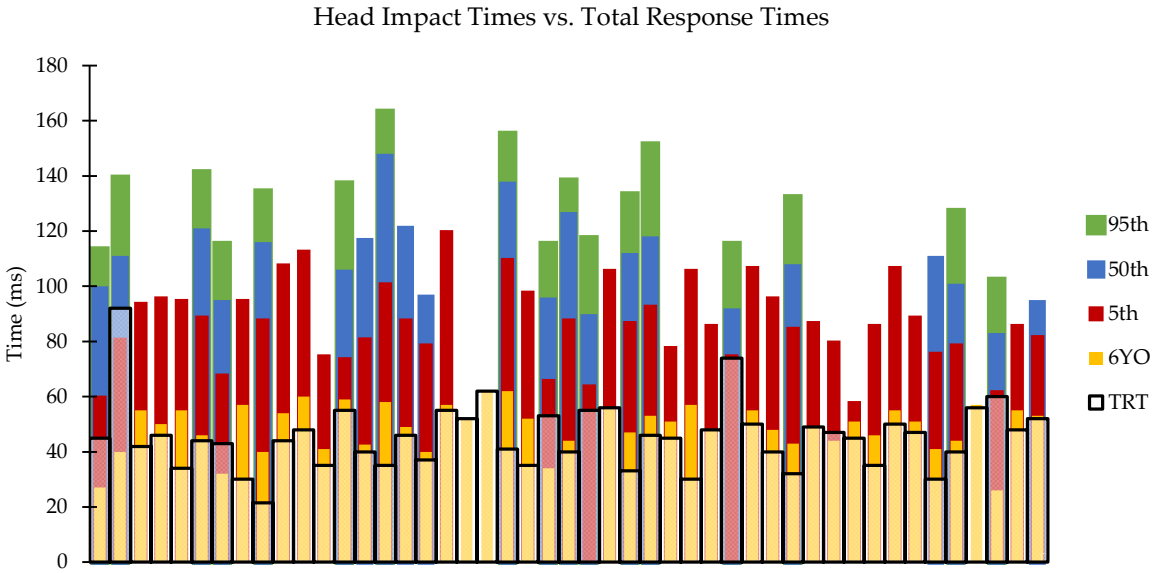

Figure 1: Head Impact Times of different pedestrian sizes overlaid and compared to Total Response Times of active bonnets based on results submitted to Euro NCAP from 2010-2018 (n=47).

Prior to 2018, all pedestrian models listed in Technical Bulletin 13 [2] could be applied for the virtual part of the assessment [1]. The list of models did not cover the effects of altering simulation settings and was difficult to maintain, because HBMs are continuously revised. Furthermore, the protocol did not include all details for the HBM simulations (e.g. open arm and torso posture, open contact settings), although these boundary conditions have been shown to have an effect in several studies [3–9].
As an alternative to a list of models, a certification procedure for virtual pedestrian models was established within the current study. The idea of the certification procedure is that simulations performed by a specific user with a specific HBM using a specific FE solver and specific control settings can be compared to a set of reference simulations. This will help to ensure comparability of the simulation results. For the final assessment simulations only the vehicle model is exchanged (using the detailed serial FE vehicle model to be assessed instead of the generic vehicle model), while anything else (solver, control settings, pedestrian model, contact settings) remains unchanged.
The aim of the study was to define corridors and tolerances for a certification procedure based on consistent reference results from state-of-the-art HBMs.

METHOD

Simulation setups

Generic vehicle (GV) models were applied as impact structures. The GV models were defined such that were easily transferrable to other codes and were thus applicable for comparison of HBMs in different codes (LS-

Dyna, VPS, Radioss and Abaqus). The model structure and geometry is explained in detail in [10]. Four different shapes of the models were established, representing the geometry of an FCR (family car), an MPV (Multipurpose Vehicle), an RDS (roadster) and an SUV (sport utility vehicle). The LS-DYNA version of the GV models was translated into the other FE codes by the FE code houses (ESI Group, Altair and Dassault Systèmes). The simulation protocol was developed with THUMS v4.02 and the simplified GHBMC pedestrian model in LS-DYNA and was published previously [10,11]. Twelve load cases were defined, in which the pedestrian is impacted with the four GV models at three different collision speeds (30, 40 and 50 km/h) in a specified reference posture [10] mimicking a natural walking position.

Analysed outputs

Sensors were implemented in the HBMs at selected reference points for the evaluation of trajectories:

- the head centre of gravity (HC)
- the centre (average of all nodal coordinates) of the vertebral body of C7 and T12
- the midpoint of the left and right centre of the acetabulum (AC)

A detailed description of the reference point sensor locations can be found in the Appendix (Table 2), allowing different users to position comparable sensor positioning in multiple HBMs. The sensors were connected with the structure using the keyword *CONSTRAINED_INTERPOLATE in LS-DYNA. In the other FE software packages, keywords with the same algorithm were identified and are provided in Table 3 in the Appendix.

For the evaluation of the trajectories, the x-displacement of the vehicle was subtracted from the x coordinates of the sensors (stationary vehicle view in local vehicle coordinate system) according to Figure 7. Contact forces and node histories were outputted every 0.1 ms. Unfiltered curves were used.

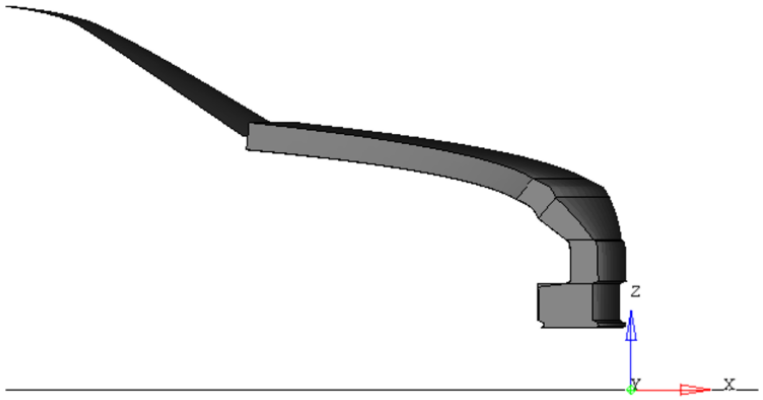

Figure 2: Coordinate system of the vehicle as applied in this study (x=0 at foremost point on vehicle front).

The kinematic assessment placed a focus on the head, as this is most relevant for the assessment of active bonnets.

The *HIT* was defined as the time from the first increase in the bumper contact force (*C*) until the first increase in the contact force between the head and vehicle (*H*), as shown in Figure 3 and described in Equation 1.

$$HIT\ [ms] = H - C \qquad \text{(Equation 1)}$$

The acceleration measured within the head CoG was also used to double-check the result, as shown in Figure 3. To determine *C,* only the contact between the lower extremities and bumper was considered (as this is also used as a trigger for active bonnets). A first contact between upper extremities and bumper was ignored.

The contact forces were separated by body region and contact surface. For the comparison between the models, the resultant total contact force between HBM and GV was used. The times of all contact forces were offset with the value C (time of first contact = 0).

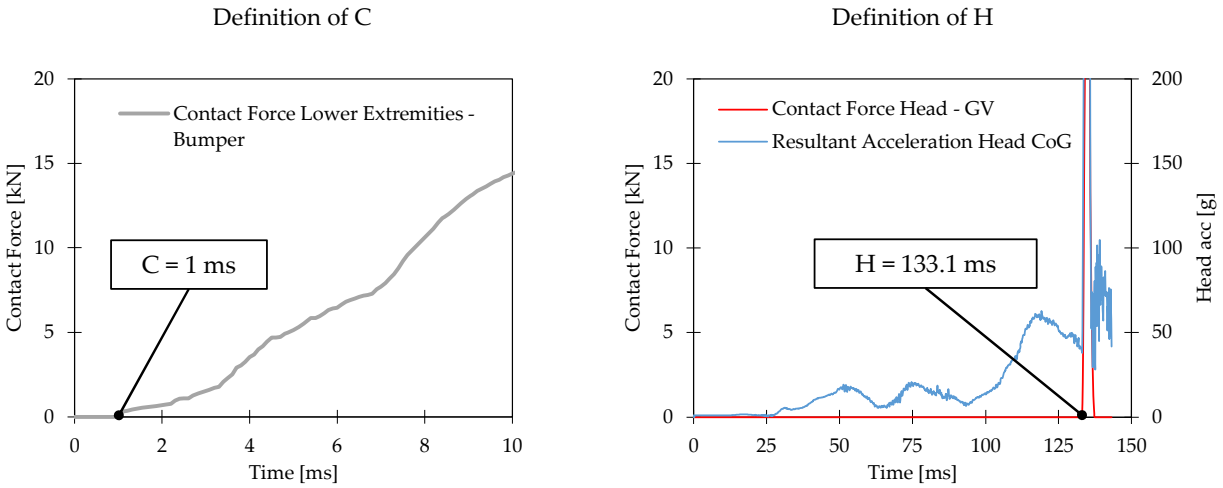

Figure 3: Example for the calculation of HIT based on H and C.

Dataset

A number of institutions from around the world run simulations according to the protocol [10] using the GV models and have provided their results. These are Audi AG, BMW Group, Daimler AG, ESI Group, HongIk University, Jaguar Land Rover, Honda R&D, Japan Automobile Manufacturers Association (JAMA) and Japan Automobile Research Institute (JARI), Nissan Motor Company, Siemens Industry Software and Services B.V. (formerly known as Tass International), Subaru Corporation and Wake Forest University. The results from the following pedestrian models (HBMs and multibody humanoid models) were included in the final dataset (random order):

- GHBMC simplified pedestrian model:
  - VPS version without fracture mode (two different institutions)
  - RADIOSS version without fracture mode
  - LS-DYNA with fracture mode (v1.4.5 and v1.4.3)
- THUMS:
  - THUMS v4.02 in LS-DYNA without fracture mode (two different institutions)
  - THUMS v4 in VPS without fracture mode
  - THUMS TUC in LS-DYNA without fracture mode
  - THUMS-D in LS-DYNA without fracture mode
  - THUMS v3 in Abaqus without fracture mode
- JAMA Pedestrian Model (HBM) in VPS with and without fracture mode
- Honda HBM in VPS without fracture mode
- Simcenter Madymo™ pedestrian models (multibody humanoid model) coupled with LS-DYNA (two different institutions)
- JLR humanoid FE model in LS-DYNA
- ESI PED 50 humanoid FE model in VPS

The results were anonymised and named as Model 01 to Model 18. All of the above listed models were included in the list of Euro NCAP TB013 and were, therefore, applicable for Euro NCAP assessment of deployable systems until December 2017.

The results from different models at different institutions and in different FE software packages were grouped into “consistent” and “inconsistent” results based on qualitative comparisons of the curves and the results of the statistical analyses.

Boxplots were used to identify outliers and to compare the HITs. Outliers were defined as points beyond the 1.5 interquartile ranges ($IQR = Q3 - Q1$) from the median value (shown as a whisker in the diagrams). Reference values and tolerances for head impact times were derived.

Corridors were derived for trajectories for the locations of HC, T12 and AC based on the consistent results. The median, minimum and maximum values for each coordinate were derived from all consistent results every 0.1 ms.

Additionally, corridors for the total resultant contact force between HBM and GV were defined based on the minimum and maximum value of the consistent results (again every 0.1 ms).

RESULTS

Eighteen different dossiers of results were available for the subsequent analysis, again using the names Model 01 to Model 18. In the case of Model 5, no results of the impacts with 30 km/h were provided. The dossier was complete for all other models and included all twelve load cases. In the first step, outliers were identified and removed from the dataset. Corridors for the trajectories, displacements and contact forces were specified based on consistent results. Furthermore, reference values and tolerances for *HIT*s were defined for the final certification procedure.

Head Impact Time

The head impact times resulting from the eighteen different pedestrian simulations with varying pedestrian models in four different codes are shown in Figure 4. Boxplots were created to identify outliers in the datasets. The boxes show the 1st quartile (*Q1*), median value and 3rd quartile (*Q3*). The whiskers represent the highest or lowest value within the 1.5 *IQR*. The cross indicates the mean value for each load case. As the distributions were not symmetric, the median values together with quartiles were found to be more useful than the mean values with standard deviation.

Six outlying results were identified and are shown as circles in the figure: Results from Pedestrian Models 2, 5, 6, 11, 12 and 15 did not fall within the 1.5 *IQR* for at least one load case.

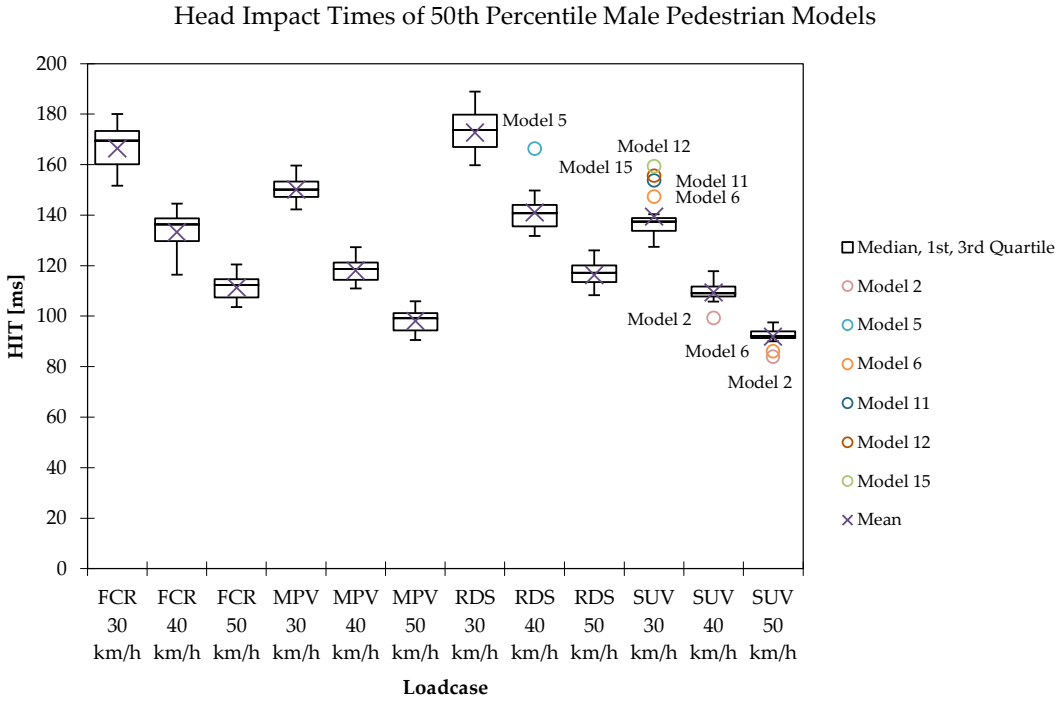

Figure 4: Boxplots of HITs from eighteen different pedestrian simulations for impacts with FCR, MPV, RDS and SUV at 30, 40 and 50 km/h with outliers marked with circles.

In the next step, the outliers were excluded from the dataset that was used to define the tolerances and corridors. The median value from the remaining data was calculated as a reference value. The relative deviation of each result from the reference value per load case was calculated as a percentage and plotted in Figure 5. All datasets with outlying behaviour were marked as unfilled circles and the remaining, consistent datasets that were also used to derive the median / reference value are shown as filled circles. A maximum span of 24% variation of *HIT* compared to the reference value in one loadcase (SUV 30 km/h) was observed in the dataset for all the results provided. Pedestrian Model 2 showed smaller *HIT*s than the consistent models in most of the load cases. For the other outlier models, no clear trend could be detected. While they tended to have smaller *HIT*s for family cars, higher *HIT*s were observed for the SUV impacts at 30 and 40 km/h.

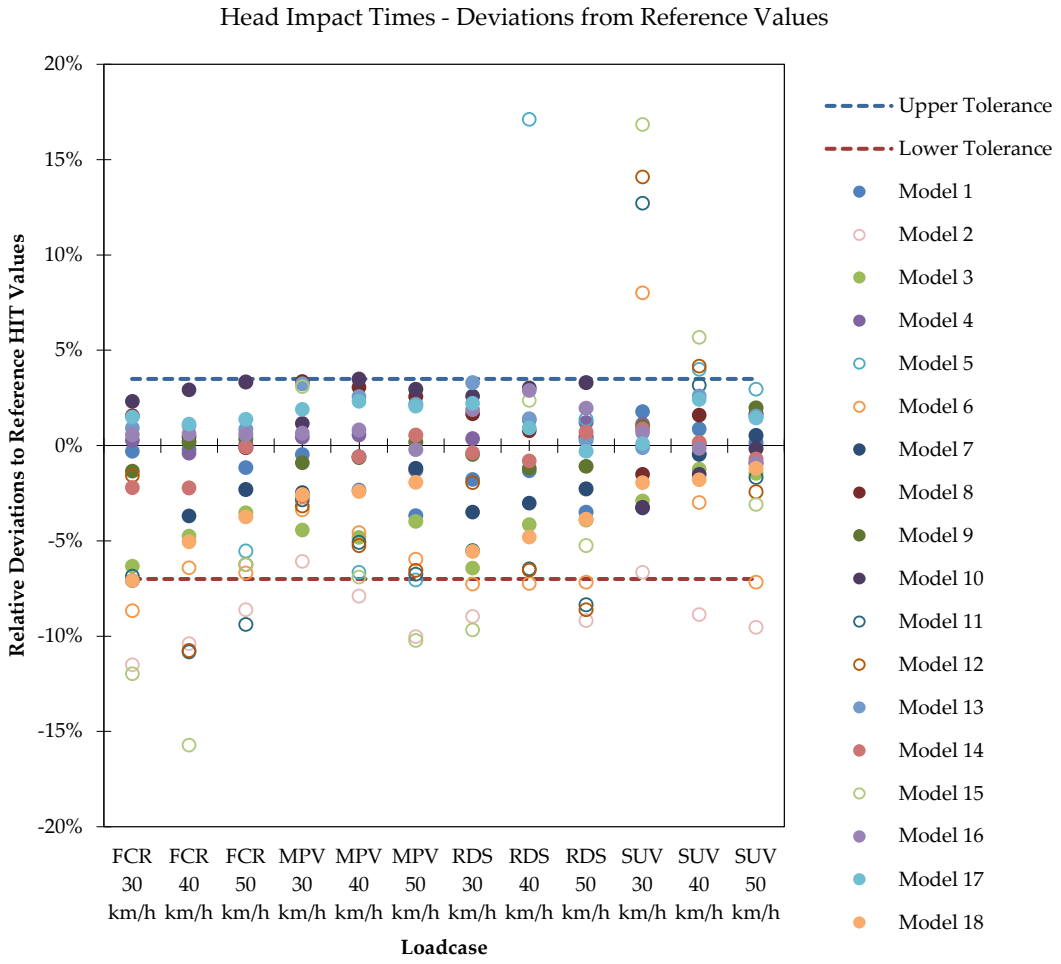

Figure 5: Deviation from reference HIT values of the eighteen different datasets in percent for all twelve load cases (FCR, MPV, SUV, RDS at 30, 40 and 50 km/h).

The maximum and minimum relative deviations within the consistent datasets from the reference value were +3.5% (Model 10 for impact with MPV at 40 km/h) and -7% (Model 18 for impact with FCR at 30 km/h), respectively. These values were chosen as upper and lower allowed tolerance values for the current certification procedure [12]. The reference values together with the derived upper and lower boundaries for the certification procedure are summarised in Table 1.

Table 1.
Reference HIT values and upper and lower boundaries for the certification procedure.

HIT [ms]	**FCR**			**MPV**			**RDS**			**SUV**		
v [km/h]	30	40	50	30	40	50	30	40	50	30	40	50
Reference value	172.3	138.1	114.3	151.5	120.4	100.8	176.9	142.1	119.3	136.5	109.0	92.9
Maximum value (+3.5%)	178.4	143.0	118.4	156.9	124.7	104.4	183.1	147.1	123.5	141.3	112.9	96.2
Minimum value (-7%)	160.2	128.4	106.2	140.8	111.9	93.7	164.5	132.1	110.9	126.9	101.3	86.3

Trajectories

When analysing the trajectories, it was observed that Models 2 and 15 were also outliers in terms of the initial location of the head CoG. They are shown in red in Figure 16 and Figure 6. The initial posture of the head CoG was significantly lower than that of the other models (1635 mm and 1638 mm, respectively, while the median value was 1680 mm and 1.5 *IQR* was 10 mm). They were even beyond the 95% interval of the mean value ± 2 times the standard deviation (1644-1714 mm).

The head CoG of Model 14 was initially located at 1714 mm and, therefore, higher than the median value ±1.5 *IQR*, but fell within the 95% interval. It was maintained in the data sample, since it showed no outlying behaviour in terms of its *HIT*, i.

The minimum and maximum values for each time step were derived in the x and z-directions ($x_{min/max}$ *and* $z_{min/max}$). All models that displayed outlying behaviour in terms of their *HIT*s were excluded prior to creating the corridor. The corridors shown in Figure 6 are exemplary for the 40 km/h impact with the FCR and were derived by connecting the coordinates $[x_{min}(t_n) \quad z_{min}(t_n)]$ for the ascending trajectories (HC, T12) and $[x_{min}(t_n) \quad z_{max}(t_n)]$ for the descending trajectories (AC), as shown in Figure 7. The thick black line in Figure 6 shows the corresponding corridor that was created. Each colour represents the results of one pedestrian model.

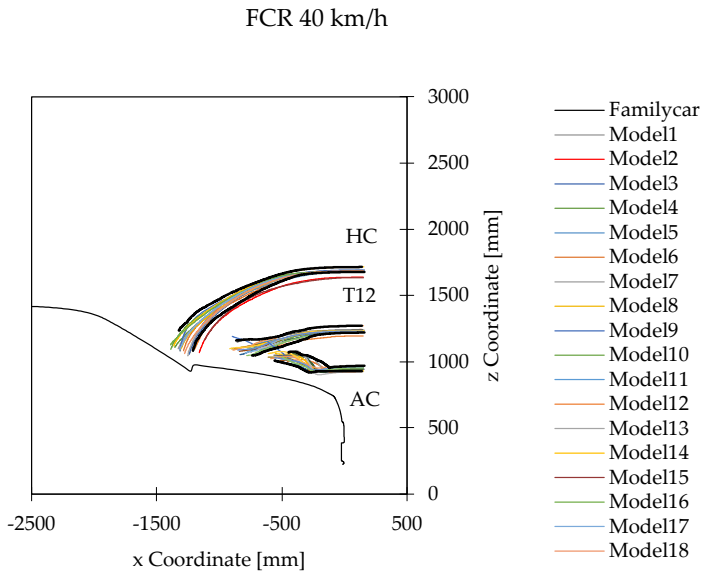

Figure 6: Corridors (black line) for trajectories for z as a function of the x trajectory relative to the vehicle coordinate system for the FCR impact at 40 km/h.

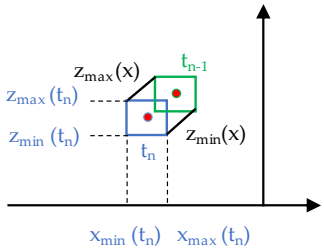

Figure 7: Relationship between time-dependent and x-trajectory-dependent corridors.

As timing is essential for the assessment of the deployable systems, a time dependent approach was finally chosen. This means the coordinate of the analysed reference point (shown as a red point in Figure 7) must lie within a box extending from x_{min} to x_{max} and z_{min} to z_{max} (shown as blue and green boxes in Figure 7 for two different time steps) at each time step. The resulting corridors for z and x as a function of time are shown in Figure 8-Figure 13 as black dashed lines.

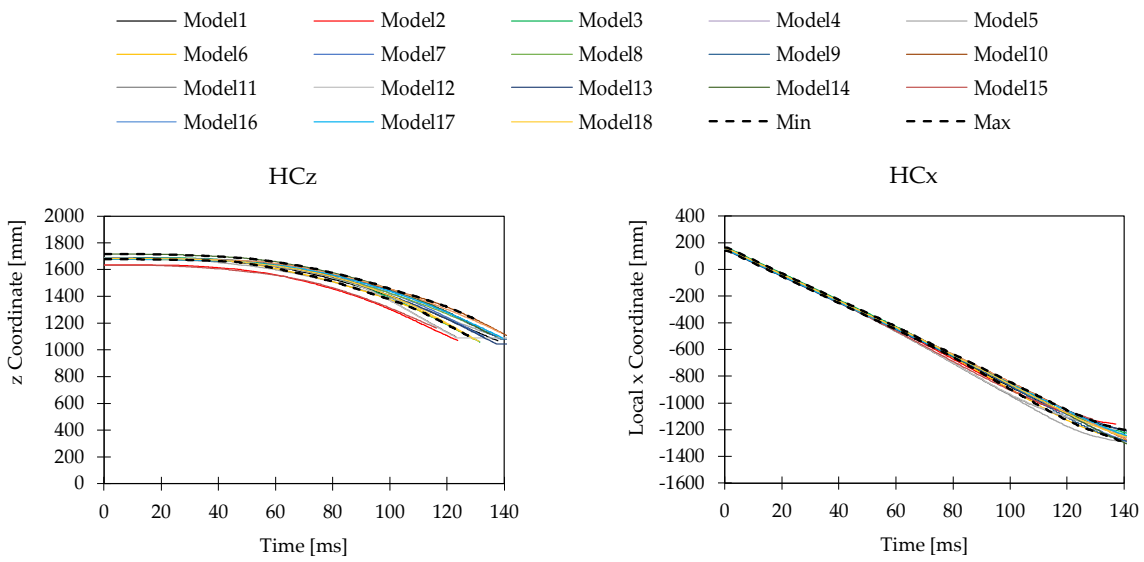

Figure 8: Corridor for the z trajectory as a function of time (black dashed line) for Head CoG for FCR 40 km/h load case.

Figure 9: Corridor for the x trajectory as a function of time (black dashed line) for Head CoG for FCR 40 km/h load case.

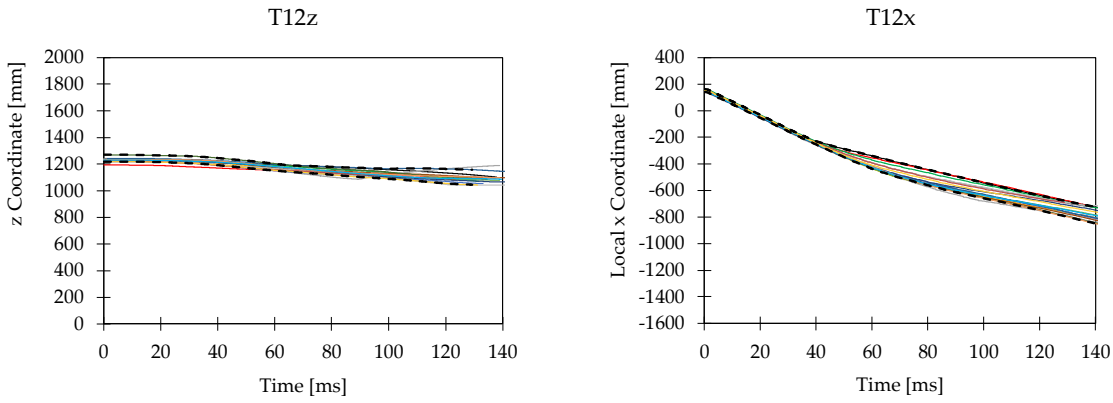

Figure 10: Corridor for the z trajectory as a function of time (black dashed line) for T12 for FCR 40 km/h load case.

Figure 11: Corridor for the x trajectory as a function of time (black dashed line) for T12 for FCR 40 km/h load case.

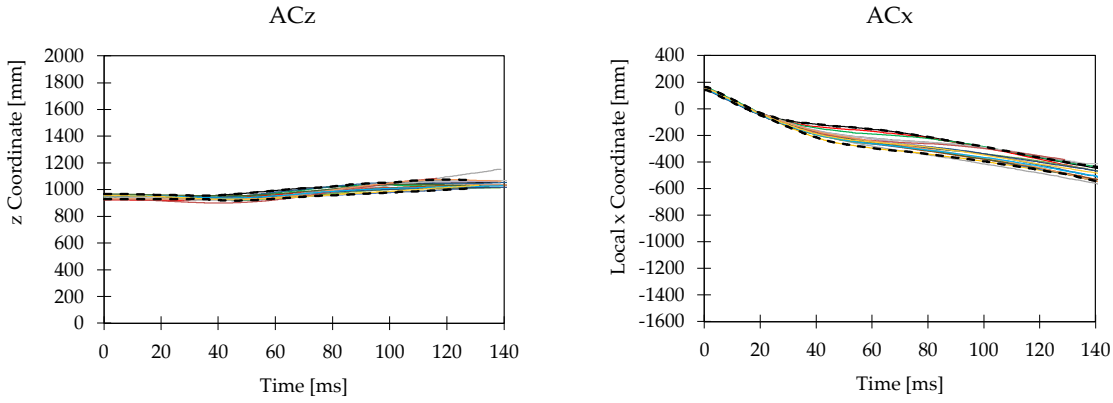

Figure 12: Corridor for the z trajectory as a function of time (black dashed line) for centre of acetabuli for FCR 40 km/h load case.

Figure 13: Corridor for the x trajectory as a function of time (black dashed line) for centre of acetabuli for FCR 40 km/h load case.

As shown in Figure 8, Models 11 and 12 (already defined as outliers because of their *HIT*s – shown in grey) fell outside the z corridor towards the end of the simulation. The responses of the other fourteen pedestrian models remained inside the corridors. The corridors for all the load cases can be found in the Appendix.

Contact Forces

Figure 14 shows the resultant total contact force (unfiltered) observed between the pedestrian and GV using the varying HBMs and varying codes, for the 40 km/h impact with the generic FCR model. At around 130 ms the head is impacting the rigid windshield, which is why the forces are increasing drastically. All results for which *HIT*s or trajectories showed outlying *HIT* behaviour are shown in grey. Additionally, the red and orange lines (Models 1 and 3) were also removed, as they showed significantly higher first peaks compared to those in the other models. The corridors, shown as black dashed lines, represent the minimum and maximum values of the contact forces of the remaining consistent models as derived at each time step.

The final corridors for all load cases are shown in the Appendix. Code-specific issues were identified when analysing the contact forces, which is why the contact force corridors are used for monitoring purposes only at the current stage.

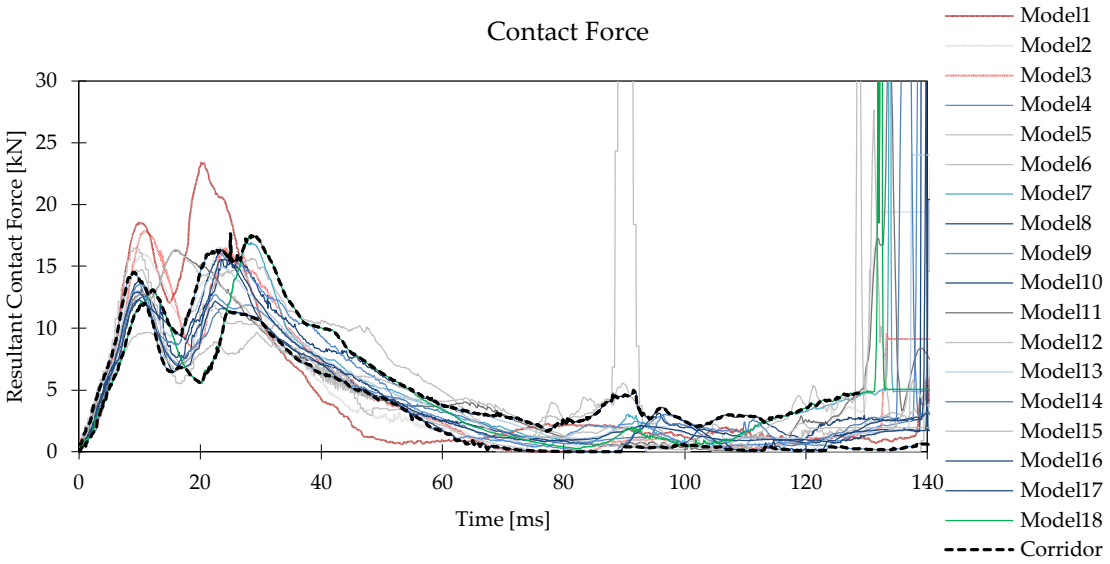

Figure 14: Total resultant contact forces between vehicle and pedestrian models for all submitted results and the derived corridors for a 40 km/h impact with an FCR.

DISCUSSION

Analysed output

A cross-check with the head acceleration in the resultant and global z-directions was performed to see if the time of the head impact had been determined correctly. Whenever the maximum resultant head acceleration was observed before the derived time *H* of head contact, a manual check was performed by examining the animated results. In some cases, this discrepancy was caused by the fact that a direct contact between the head and GV was avoided, as the arm was located between head and GV, leading to high accelerations in the head, but no measured contact force between the head and GV. In these cases, the applied definition led either to no identifiable, or a very high *HIT*.

Three approaches could be applied to deal with this issue:

1. The time *H* could be defined as the time when the head contacts the arms and at the same time the arms contact the vehicle
2. The time *H* could be defined as the time of maximum head acceleration
3. The contact between arms and head could be disabled in such cases.

Approach 1 leads to significantly lower *HIT*s compared to those obtained in simulations with no contact between arms and head and, therefore, leads to less comparable results. Approach 2 can lead to misleading results, as multiple peaks in the head accelerations were observed in some simulations. When the head of the HBM

contacts the shoulder, this can lead to even higher acceleration than if it contacts the bonnet. For these reasons, approach 3 was chosen as it allowed an automatic analysis of *HIT* to be performed and the most readily comparable results to be obtained.
To cover the body kinematics that were relevant for the chosen assessment focus, the trajectories for the head CoG (HC), centre of T12 and the centre of *acetabuli* (AC) were considered as the final reference points and corridors were defined for these: The location of the head is obviously important for the assessment of deployable system because the wrap-around distance and HIT are important outputs for the assessment simulations. AC and T12 enable an analysis of the hip and the torso kinematics, which are important for the evaluation of the deflection due to the body load and for avoiding implausible full-body kinematics. The reference point AC tends to be close to the CoG of the full-body, and the CoG of the torso is located between AC and T12.
Furthermore, T12 and AC together were shown to be indicators that could effectively be used to identify the time when the curvature of the spine started to change its direction. The spine kinematics could be separated into two phases as shown in Figure 15. In the first phase, the pelvis moved away from the head and the upper torso as it was accelerated by the vehicle impact, while the upper torso and head remained in place due to their inertia. The spine posture at 66 ms showed the maximum spine curvature for this load case (FCR impact at 40 km/h) as the pedestrian wrapped around the vehicle. The head and upper torso then were pulled downwards and the spine was straightened, before its curvature changed into the other direction prior to the head impact at 140 ms. This is clearly visible when examining the figures that had fixed pelvises on the bottom of Figure 15 showing the skeleton of THUMS v4.02 in simulations with the GV FCR model in LS-DYNA: In phase 1, T12 is located on the left side of AC, while it is located on the right side in phase 2. The observed kinematics are in accordance with movement patterns seen in PMHS tests [13].

Phase 1 **Phase 2** **Head Impact**

Full-body kinematics (initial position in the background) in the global coordinate system.

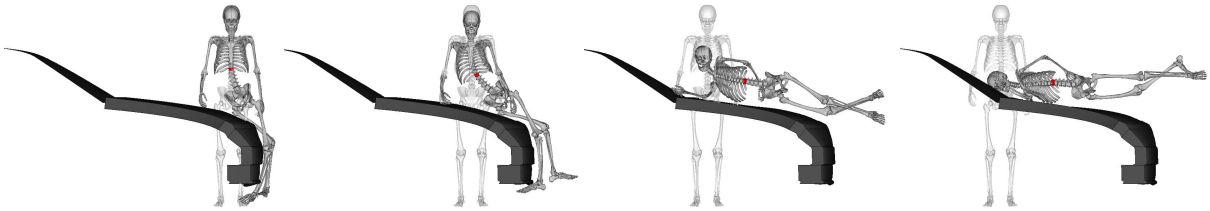

Spine kinematics relative to fixed pelvis coordinate system.

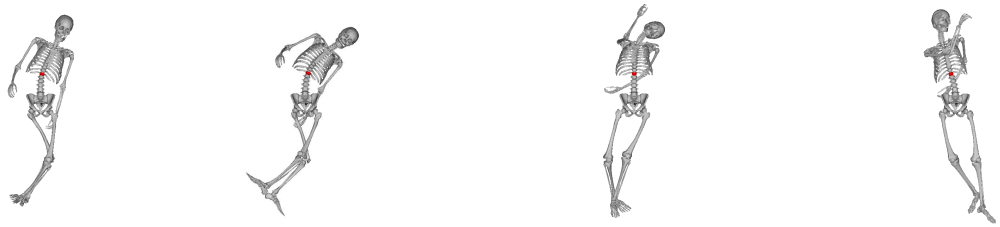

42 ms 66ms 118 ms 140 ms

Figure 15: Kinematics of the spine for an impact with the generic FCR model at 40 km/h relative to the global and a local pelvis coordinate system (T12 shown in red).

The trajectories of the lower extremities were not relevant for the assessment of active bonnets and, therefore, were not included.

Alternative corridor definitions

To define the corridors for the certification procedure, several approaches were taken into account. As a first approach, the method described in the SAE norm J2868 [14] was applied, defining the corridor as a percentage of the path length based median reference trajectories. In this approach, the path length at each time step is derived from the median x and z coordinates for each reference point as a first step. A tolerance of +10% and -5% of the path length is added to the median trajectory, resulting in the corridors shown in Figure 16. As the corridor for the head trajectory was much wider than the spread observed in the analysed data, the method was rejected.

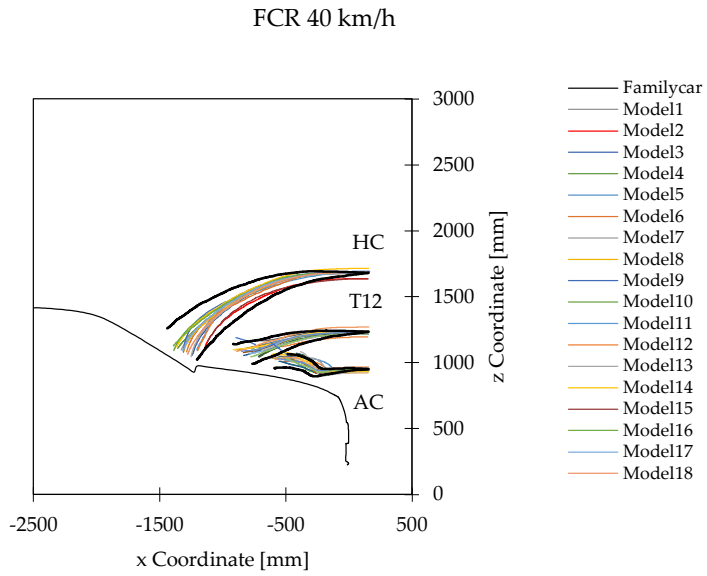

Figure 16: Corridors derived with SAE J2868 approach based on path length for z as a function of the x trajectory relative to the vehicle coordinate system for the FCR impact at 40 km/h.

The corridors introduced in the current paper are based on minimum and maximum values at each timestep. After receiving the first ten certification dossiers, it was realised that even the models used to create the corridors can fall out of the corridor for a short duration (a few milliseconds) and for a few millimetres. Numeric effects can lead to such small deviations, which can be crucial for models that are defining the upper and lower boundary of the corridors. Therefore, an appropriate tolerance was defined for the introductory period. The reference points are allowed to have a maximum deviation of 50 mm to the reference corridors in x- and z-direction. This reference was chosen, as it represents the half the size of the grid used for the head impactor tests. However, at the beginning of the corridor the differences between the models tend to be very small and therefore the additional tolerance tends to be higher in that time period than the maximum differences observed in the simulations.

As a next step, new corridors will be established that are based on another alternative method to avoid this issue, where the mean location at each time step and a corridor based on standard deviations (SD) are derived.

The locations of the reference points in the local vehicle coordinate system (x_i and z_i summarized as c_i) are paired with the time (t_i) as sequences.

$$(t_i, c_i) \text{ for } i = 1, \dots, n. \qquad \text{(Equation 2)}$$

Since multiple datasets are available, there are m sequences of measured values

$$(t_i^r, c_i^r) \text{ for } r = 1, \dots, m \text{ and } i = 1, \dots n_r \qquad \text{(Equation 3)}$$

where a mean of c over r is of interest at each t_i. Subsequently, only sequences are considered which have the same time resolution, but they might stop at different lengths, so n_r can be different for each r. To simplify notation, it is further assumed that the sequences are ordered by their length i.e. $n_1 \geq n_2 \geq \cdots \geq n_m$. The number of sequences that have values for an index i will be denoted as m_i. So m_i equals m for $i \leq n_m$ but it might be smaller than m for $i > n_m$. Let $\bar{n}$ be the longest sequence length for which all sequences have values i.e. $m_i = m$ for $i \leq \bar{n}$ and $m_i < m$ for $i > \bar{n}$. If all sequences have the same length, the mean can be calculated by simply taking the mean over all y-values for each x-value, that is

$$c_i^{mean} = \frac{1}{m}\sum_{r=1}^{m} c_i^r. \quad \text{(Equation 4)}$$

If the sequences have different lengths, this approach can be modified to

$$c_i^{mean} = \frac{1}{m_i}\sum_{r=1}^{m_i} c_i^r. \quad \text{(Equation 5)}$$

However, this will lead to "jumps" when a sequence ends. In the following, a method will be outlined to calculate a mean that avoids these "jumps". As long as there is data for all sequences, the usual mean will be used i.e.

$$c_i^{mean} = \frac{1}{m}\sum_{r=1}^{m} c_i^r \text{ for } i \leq \bar{n}. \quad \text{(Equation 6)}$$

To calculate the mean for $i > \bar{n}$, a mean of the changes of the c is used. Let $\Delta c_i^r = c_{i+1}^r - c_i^r$ be the difference between two consecutive c in the rth sequence. The mean of these differences can be calculated by a similar formula as the mean of c, as

$$\Delta c_i^{mean} = \frac{1}{m_{i+1}}\sum_{r=1}^{m_{i+1}} \Delta c_i^r. \quad \text{(Equation 7)}$$

To calculate the mean for $i > \bar{n}$ the previous mean value is updated with this mean difference i.e.

$$c_i^{mean} = c_{i-1}^{mean} + \Delta c_{i-1}^{mean} \text{ for } i > \bar{n}. \quad \text{(Equation 8)}$$

Casually speaking, the mean moves in the direction of the mean slope. If all sequences have the same length, this approach would lead to the ordinary mean even if $\bar{n}$ would be artificially set to 1.

The upper and lower boundaries of the corridors are then defined at each time step as:

$$c_i^{corridor} = c_i^{mean} \mp 2 * SD_i \quad \text{(Equation 9)}$$

If $i > \bar{n}$, SD_i is no longer updated and is set to $SD_{\bar{n}}$. The corridors according to this new method (SD based) are compared to the corridors introduced in this paper (Min/Max based corridors) in Figure 17. The advantage of the SD based method is also that the whole dataset can be used and outliers do not have to be sorted out necessarily to define the corridor (however, they will affect the standard deviation). The grey area in the figure shows the additional 50 mm tolerance that is allowed in the current version of technical bulletin. The SD-based corridor lay between this additional tolerance (grey shaded area) and the min/max based corridors and would therefore appear to be a good solution to solve the issues described above. If a higher tolerance is needed for an introduction period, the corridor width can be increased to $\mp 3 * SD$.

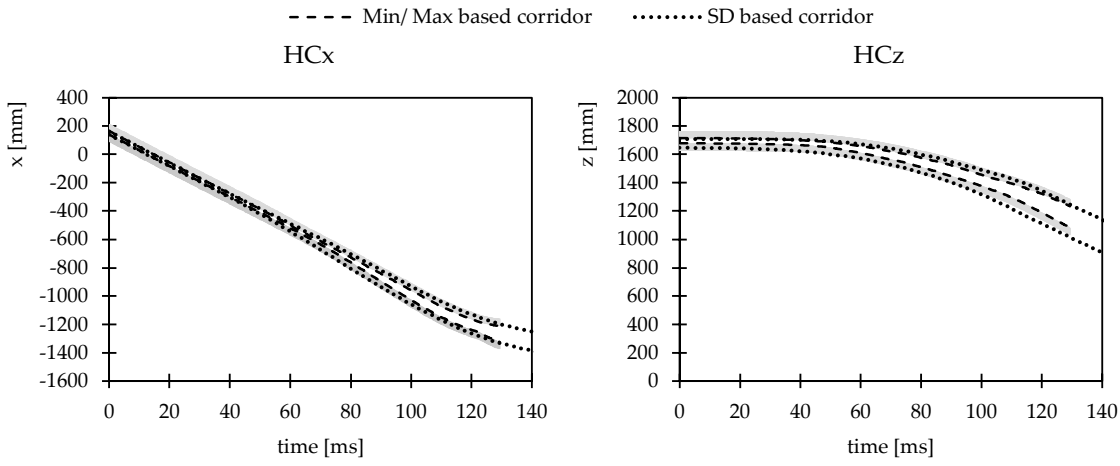

Figure 17: Comparison of time dependent corridors for HCx and HCz.

Comparability of results from HBM simulations

Although GHBMC PS and THUMS AM50 pedestrian models are validated using differing PMHS tests and do not have the exact same anthropometry, the kinematic responses seen were very similar. This was not true for some of the other pedestrian models. It was possible to identify outliers with inconsistent behaviour compared to the majority of results, and these will have to be revised to pass the certification.

Models that showed outlying behaviour for *HIT* also showed outlying behaviour for the trajectories, indicating that the chosen approach, which began with the identification of outliers based on *HIT*s, was appropriate. Two additional outliers were identified for the contact forces that showed comparable behaviour to the other results in the previous analyses. When examining the details, it was observed that discrepancies seem to come from specific output definitions of the contact forces in one FE software package. In the current certification procedure described in TB024 [12] the contact forces are only monitored, which means that the model response does not have to fall within the corridors. The attempt should be made, however, to harmonise the contact force outputs more, with the intention of being able to add this as an additional requirement in the future.

The presented certification procedure does not replace the validation of the HBM in terms of biofidelity. The certification proceeds the validation and allows an HBM in a specific environment to be used as a "virtual test device" for a specific assessment focus (in this case, the kinematic-based assessment of deployable systems). When performing any revisions of the Human Body Models, validations also have to be repeated. While the HBM has to be morphed to the anthropometry of the PMHS to perform a proper validation, reference anthropometries are needed for assessment purposes.

Certification procedures are important prerequisites for virtual testing, as they enable users to determine whether the response of a specific virtual test device in a specific environment answers a specific question and provides a comparable response. Within the certification procedure the response of the model is compared to reference simulations using the harmonized setup, target posture and harmonized anthropometry that should be also used for the final assessment simulations.

The certification procedure has been developed to provide evidence that the pedestrian model leads to comparable results within specified tolerance levels when it is applied in a harmonised setup (this is very similar to the setup that is used for the subsequent assessment). This is required to ensure that the variations in the results fall within an acceptable range. An alternative approach could also be taken to solve this issue: A virtual testing lab performs assessment simulations with the same pedestrian model in the same code for all kinds of cars. Still, once more than one test lab is performing the simulations, or more than one code is used, comparability would be unknown without a certification procedure.

The developed procedure allows users and evaluators to identify user errors when setting up the simulations and to find compatibility problems with FE solver versions. Furthermore, the certification can be used to check the sensitivity of the HBM when control settings have to be changed to comply with the full FE vehicles. The certification procedure can help to increase awareness of the fact that small changes can imply significant effects on the HBM simulation results and that precautions are needed as a result. It can be also used by HBM developers to check the robustness of their models.

The introduced certification procedure is only applicable to kinematic-based assessments. The comparability of injury metrics, and especially strain-based injury metrics, is not addressed. First of all, the kinematics and validations have to be harmonised. Once this has been achieved, similar methods could be applied to compare other metrics for varying models with different setups and codes.

The corridors and tolerances were defined using current state-of-the-art HBMs. No active pedestrian models were covered. The corridors and tolerances are based on biofidelic models, but should not be understood as biofidelity corridors. The corridors will need to be revised when significant changes in the state of the art of HBMs occur and biofidelity significantly improves compared to the current status (e.g. due to newly available test data).

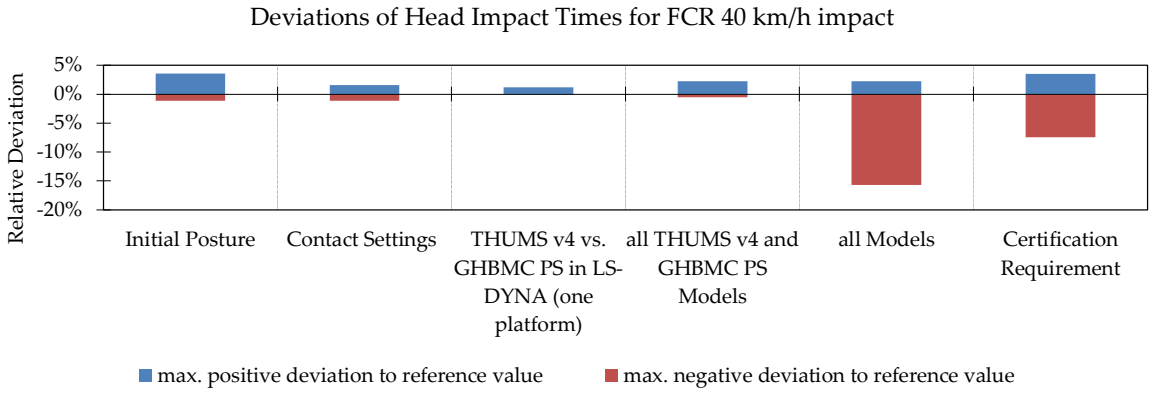

Figure 18 shows the deviations among the *HIT* resulting from different variations for one exemplary load case, the family car impact at 40 km/h, as this is the only load case where results for all variations were available: Due to the harmonised simulation protocol that was introduced in [10], it was possible to narrow down the differences between two models in one FE code and on one platform in terms of *HIT* from 4.7% to 1.2% for this load case. A total variation of 2.75% was observed from the results received with the two models THUMS v4 and GHBMC PS when including the external simulations performed in different codes by different institution.
Without a certification procedure, the models that were listed within TB013 were showing a variation of up to 18% within the FCR 40 km/h load case. Using the current version of the certification procedure results in a decrease in these differences by allowing a maximum of 10.5% variation.
Asymmetric tolerances for the HIT values were defined: A greater amount of negative deviation was accepted, because it represents the worst case for the assessment of the deployable system, while a too high *HIT* was unacceptable. The aim for the future should be to find a way of narrowing down the corridors in when harmonisation in the HBMs is progressing.

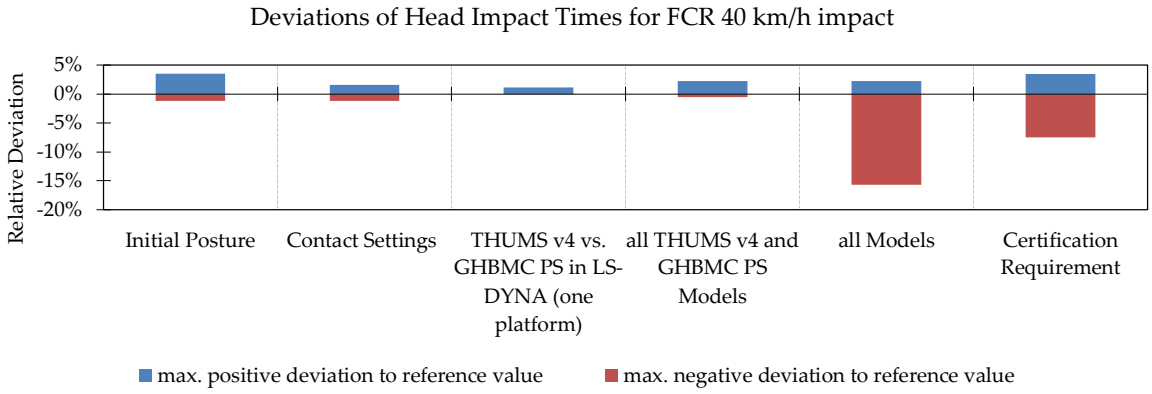

Figure 18: Relative deviations of HITs to reference HIT (138.1 ms) for the 40 km/h impact with generic FCR models.

The benefit of the certification procedure becomes even more obvious when examining the maximum differences observed throughout all load cases and all eighteen sets of analysed results. As shown in Figure 19, the sum of the absolute maximum deviations observed throughout all simulations made up a total of 33% (maximum of 24% within one load case). Due to the certification requirements, this is more than halved to a maximum of 10.5%. The critical positive deviation compared to the reference value, which led to higher *HIT*s, decreased from 17% to 3.5%. The results of the THUMS and GHBMC PS models – in all codes – did not need the full tolerance. Their results fell within a 6.5% range throughout all load cases.

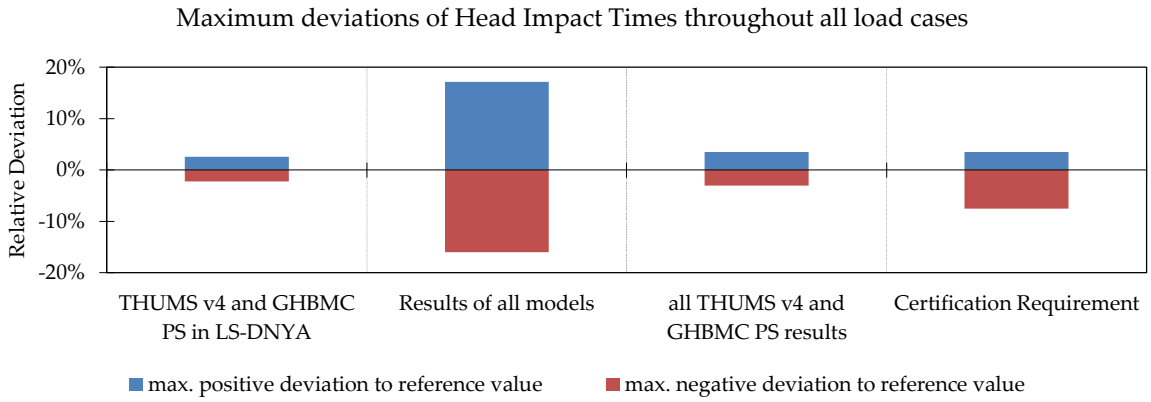

Figure 19: Relative deviations of HITs to reference HITs throughout all twelve load cases.

Outlook

As the 6yo child tends to be the most critical size when it comes to the evaluation of HIT, the response of those models was analysed as a next step. Some additional challenges for the child models were identified compared to the adult models: No full-scale PMHS tests are available with children. Furthermore, there are different kinds of child models available. While the adult models tend to differ only in terms of geometry, there are child models available that have been developed from scratch, such as the PIPER models [15], or some child models that belong to a family, but have been significantly adapted (e.g. material models), to better replicate a child, such as the GHBMC child model [16]. Another challenge is that the anthropometries among the child models differ more than the AM50 models.

The results of simulations with different child models have again been collected, to address those challenges by aiming to establish a second set of reference corridors for the pedestrian models in the size of the 6yo.

The work is still in progress, which is why the results are not included in the current paper. In contrast to the AM50 models, no clear outliers were identified. The preliminary results based on different GHBMC models, THUMS models, PIPER models and one Simcenter Madymo™ model are shown in Figure 20. Summarising all twelve load cases, the maximum spread of HIT values was -12% and +10% and the average spread -7.2% and +6.7% to the mean value derived for each load case, with the same methodology as for the AM50 model. The aim for the future should be to find a way of narrowing down these spreads.

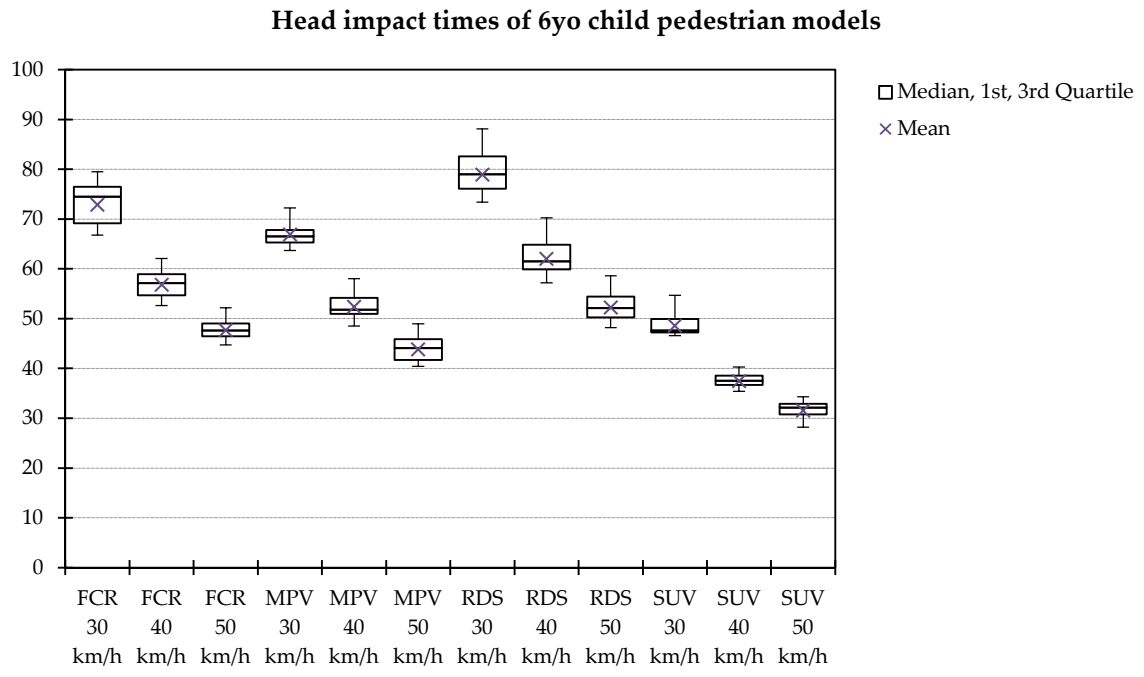

Figure 20: Preliminary HIT values for simulations with 6yo child pedestrian models shown as boxplots.

CONCLUSION

The paper describes the first certification procedure that enables an objective standardised comparison of the kinematic response of various numerical pedestrian models in multiple codes. The procedure was adopted by Euro NCAP and published as Technical Bulletin 024 in January 2018.
When eighteen different results for the twelve reference load cases – performed by different institutions with different HBMs in different FE software packages – were obtained according to the protocol, outliers were identified. The relative amount of deviation among the kinematic-based assessment results was drastically reduced when these were eliminated.
The newly developed certification procedure for HBMs limits the amount of variation allowed for the simulations in the reference load cases to the amount of variation that was observed within the consistent reference simulations (without outliers). The comparability of kinematic-based assessment was, therefore, drastically improved. While, for example, the head impact times in the initial data set varied by up to 24%, the procedure limits the variation to a maximum of 10.5%. This means that the relative deviation of results was more than halved for this output, which is essential for the Euro NCAP assessment of deployable systems.
Certification procedures for numerical models are an important prerequisite to enable virtual testing with numeric pedestrian models for the assessment of safety features. The developed certification procedure provides confirmation that a specific pedestrian model within a specific environment, solver version and specific simulation settings leads to comparable kinematic results relevant for the assessment of deployable systems. Inconsistent pedestrian models, incompatibilities with control settings and user errors can be identified and addressed.

ACKNOWLEDGEMENT

The study is part of the CoHerent Project funded mainly by Euro NCAP. The authors would also like to thank ACEA TF□P for financial support.
The authors would like to thank all the experts who took part in the CoHerent meetings for their inputs and especially all the participants who provided their results for developing the corridors. All the contents of the presented work, except the data from the data providers, are made solely at the own discretion of the authors.
The authors also gratefully acknowledge the use of HPC resources provided by the ZID at Graz University of Technology, Austria.

REFERENCES

[1] Euro NCAP, December 2016. Euro NCAP Pedestrian Testing Protocol(8.3); Available from: http://euroncap.blob.core.windows.net/media/25840/euro-ncap-pedestrian-testing-protocol-v83-december-2016.pdf. [February 22, 2017].
[2] Euro NCAP, November 2015. Pedestrian CAE Models & Codes. 1st ed.(13); Available from: http://euroncap.blob.core.windows.net/media/21510/tb-013-pedestrian-cae-models-v15.pdf.
[3] Tang J., Zhou Q., Nie B., Yasuki T., Kitagawa Y., 2016. Influence of Pre-impact Pedestrian Posture on Lower Extremity Kinematics in Vehicle Collisions. SAE Int. J. Trans. Safety 4(2):278–88. https://doi.org/10.4271/2016-01-1507.
[4] Chen H., Poulard D., Crandall J.R., Panzer M.B., 2015. Pedestrian Response with Different Initial Positions During Impact with a Mid-Sized Sedan. In: NHTSA, editor. The 24th ESV Conference Proceedings. NHTSA, p. 1–12.
[5] Paas R., Östh J., Davidsson J., 2015. Which Pragmatic Finite Element Human Body Model Scaling Technique Can Most Accurately Predict Head Impact Conditions in Pedestrian-Car Crashes? In: International Research Council on the Biomechanics of Injury, editor. 2015 IRCOBI Conference Proceedings. IRCOBI, p. 546–576.
[6] Watanabe R., Miyazaki H., Kitagawa Y., Yasuki T., 2011. Research of the Relationship of Pedestrian Injury to Collision Speed, Car-type, Impact Location and Pedestrian Sizes Using Human FE Model (THUMS Version 4). In: NHTSA, editor. The 22nd ESV Conference Proceedings. NHTSA, p. 1–13.
[7] Kam C.Y., Kerrigan J., Meissner M., Drinkwater C., Murphy D., Bolton J. et al., 2005. Design of a Full-Scale Impact System for Analysis of Vehicle Pedestrian Collisions. In: SAE, editor. SAE 2005 World Congress & Exhibition. SAE International.
[8] Elliott J.R., Simms C.K., Wood D.P., 2012. Pedestrian head translation, rotation and impact velocity: The influence of vehicle speed, pedestrian speed and pedestrian gait. Accid Anal Prev 45(0):342–53. https://doi.org/10.1016/j.aap.2011.07.022.

[9] Kerrigan J., Arregui C., Crandall J., 2009. Pedestrian Head Impact Dynamics: Comparison of Dummy and PMHS in Small Sedan and large SUV Impacts. In: NHTSA, editor. The 21st ESV Conference Proceedings. NHTSA, p. 1–15.
[10] Klug C., Feist F., Raffler M., Sinz W., Petit P., Ellway J. et al., 2017. Development of a Procedure to Compare Kinematics of Human Body Models for Pedestrian Simulations. In: International Research Council on the Biomechanics of Injury, editor. 2017 IRCOBI Conference Proceedings. IRCOBI, p. 509–530.
[11] Klug C., Feist F., Sinz W., Ellway J., van Ratingen M., 2018. A procedure to compare kinematics of Human Body Models for pedestrian assessments. In: SAE International, editor. SAE Government Industry Meeting 2018.
[12] Euro NCAP, November 2017. Pedestrian Human Model Certification. 1st ed.(TB 024):TB 024, 1-35; Available from: https://cdn.euroncap.com/media/32277/tb-024-pedestrian-human-model-certification-v10.pdf.
[13] Subit D., Kerrigan J., Crandall J., Fukuyama K., Yamazaki K., Kamiji K. et al., 2008. Pedestrian-vehicle interaction: Kinematics and injury analysis of four full-scale tests. In: International Research Council on the Biomechanics of Injury, editor. 2008 IRCOBI Conference Proceedings. IRCOBI, p. 275–294.
[14] SAE International, 14.10.2010. Pedestrian Dummy Full Scale Test Results and Resource Materials. 201010th ed.(J2868). USA.
[15] Peres J., 2018. A Pedestrian Version of the Piper 6 Year Old Child Model. In: International Research Council on the Biomechanics of Injury, editor. 2018 IRCOBI Conference Proceedings. IRCOBI, p. 247–248.
[16] Meng Y., Pak W., Guleyupoglu B., Koya B., Gayzik F.S., Untaroiu C.D., 2017. A finite element model of a six-year-old child for simulating pedestrian accidents. Accid Anal Prev 98:206–13. https://doi.org/10.1016/j.aap.2016.10.002.

APPENDIX

Table 2.
Reference Points

Abbreviation	Long Name	Definition
HC	Head centre of gravity	CoG of all parts of skull, scalp, face, brain, intracranial space, scalp) connected to all nodes of inner cranium (at least 100 nodes)
T12	Centre of twelfth thoracic vertebrae	Centre* of all nodes of vertebral body (as defined in Figure 21) T12; connected to all nodes of vertebral body of T12
ACr	Centre of the right acetabulum	Centre* of all nodes within the concave surface of the right acetabulum as shown in Figure 22, connected with all nodes inside. The sharp edge where the bone changes curvature is selected as boundary, and all nodes inside are picked
ACl	Centre of the left acetabulum	As ACr, but for the right acetabulum
AC	midpoint of the right and left acetabulum centres	The midpoint of the left and right acetabulum centres (ACr and ACl) connected to all nodes of the right and left acetabulum.

* Centre always refers to the node with the averaged coordinates of the nodes that were selected to derive the centre as described in Equation (10).

$$x_c = \sum_{i=1}^{n} \frac{x_i}{n} \qquad y_c = \sum_{i=1}^{n} \frac{y_i}{n} \qquad z_c = \sum_{i=1}^{n} \frac{z_i}{n} \tag{10}$$

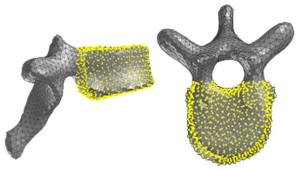

Figure 21. Definition of vertebral body

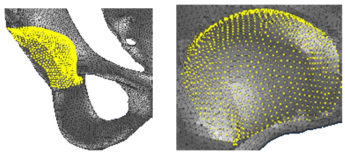

Figure 22. Nodes to derive centre of acetabulum

Table 3.
Keywords for connection of sensor nodes to surrounding structure

Code	Keyword	Recommended Parameters
LS-DYNA	*CONSTRAINED_INTERPOLATE	DDOF = 123456, CIDD = 0, ITYP = 1, IDOF = 123, TWGHTi = RWHGTi = 0
VPS	OTMCO_/	DOFCOD = 111000, IMETH = 0, IELM = 1, ITYP = 0, RADIUS = 0, WTFAC = 1
RADIOSS	/RBE3	I_MODIF = 2 or 3, WTi = 1, TRAROT_REFi = 111111, TRAROT_Mi = 111000
ABAQUS	*MPC	BEAM, NSET1, NSET2

FCR 30 km/h

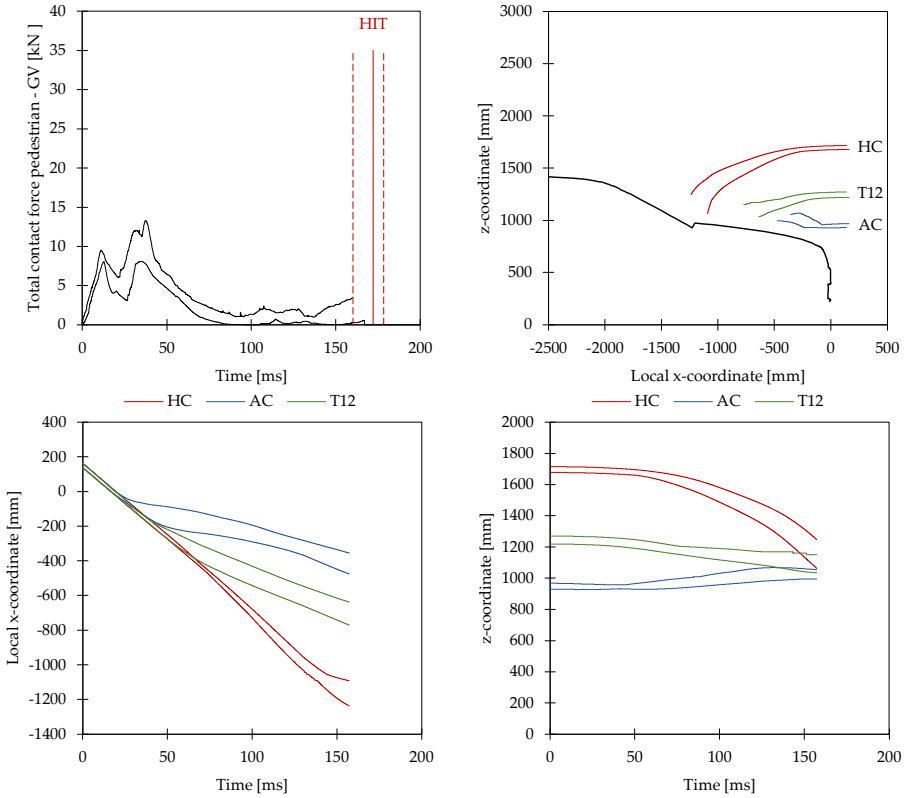

Figure 23. Corridors for impact with generic FCR model at 30 km/h – Reference* HIT = *172.3 ms.

FCR 40 km/h

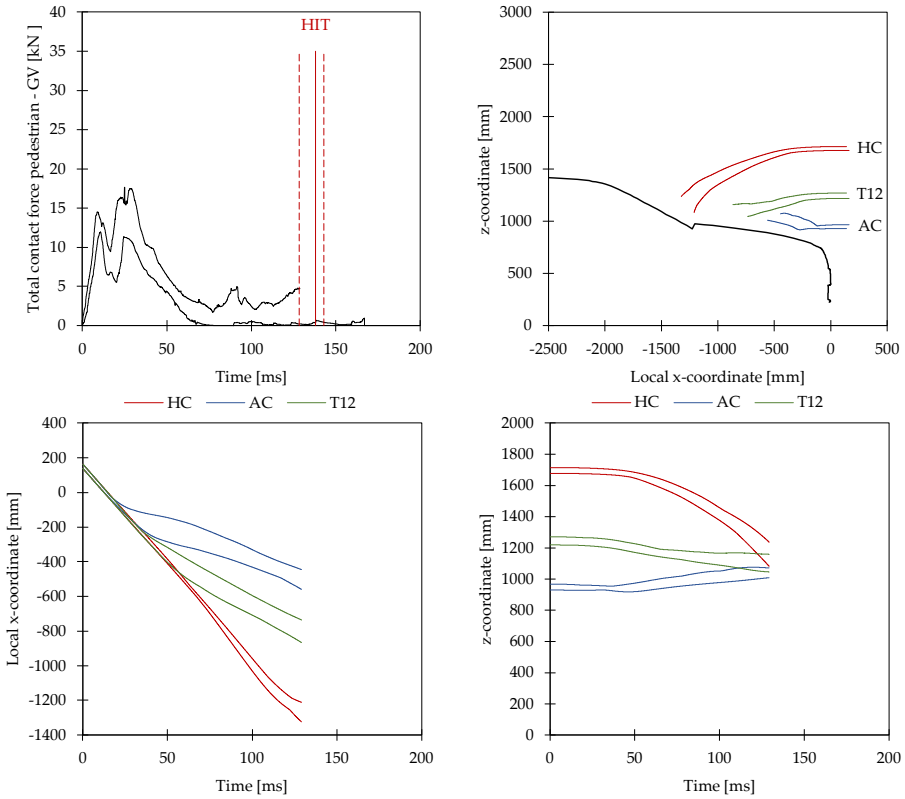

Figure 24. Corridors for impact with generic FCR model at 40 km/h – Reference* HIT = *138.1 ms.

FCR 50 km/h

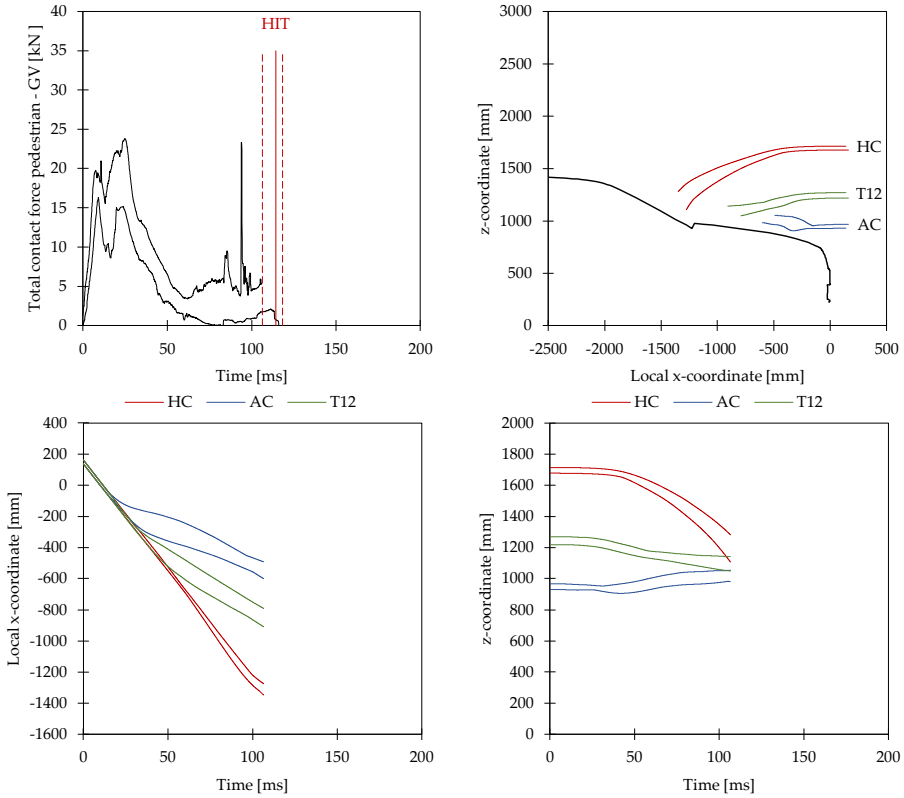

Figure 25. Corridors for impact with generic FCR model at 50 km/h – Reference* HIT = *114.3 ms.

MPV 30 km/h

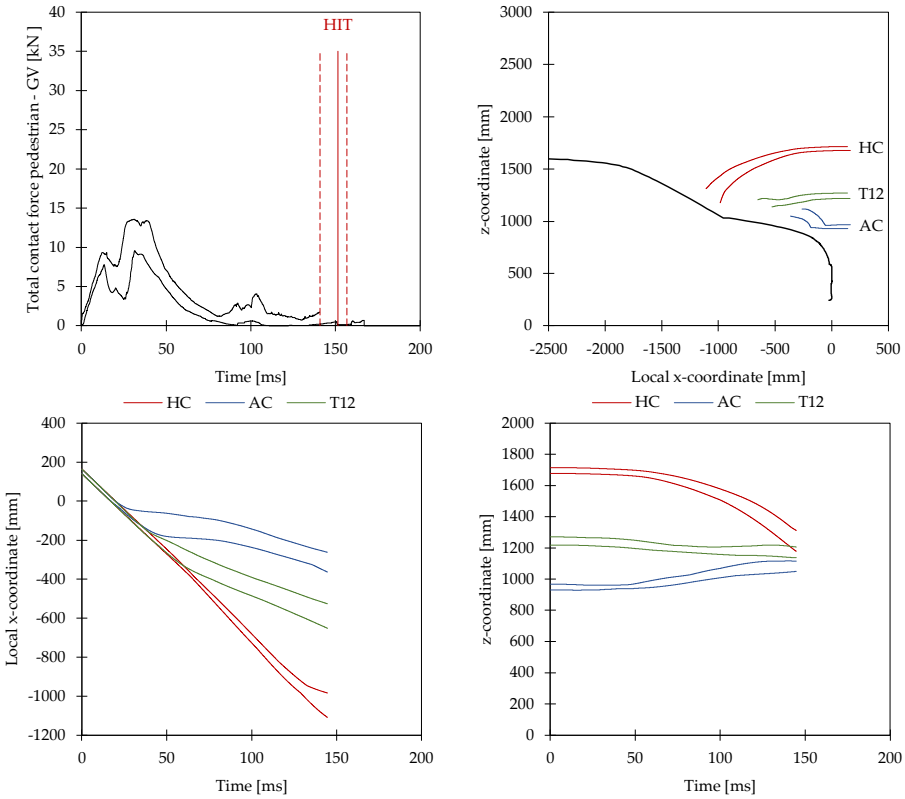

Figure 26. Corridors for impact with generic MPV model at 30 km/h – Reference* HIT = *151.5 ms.

MPV 40 km/h

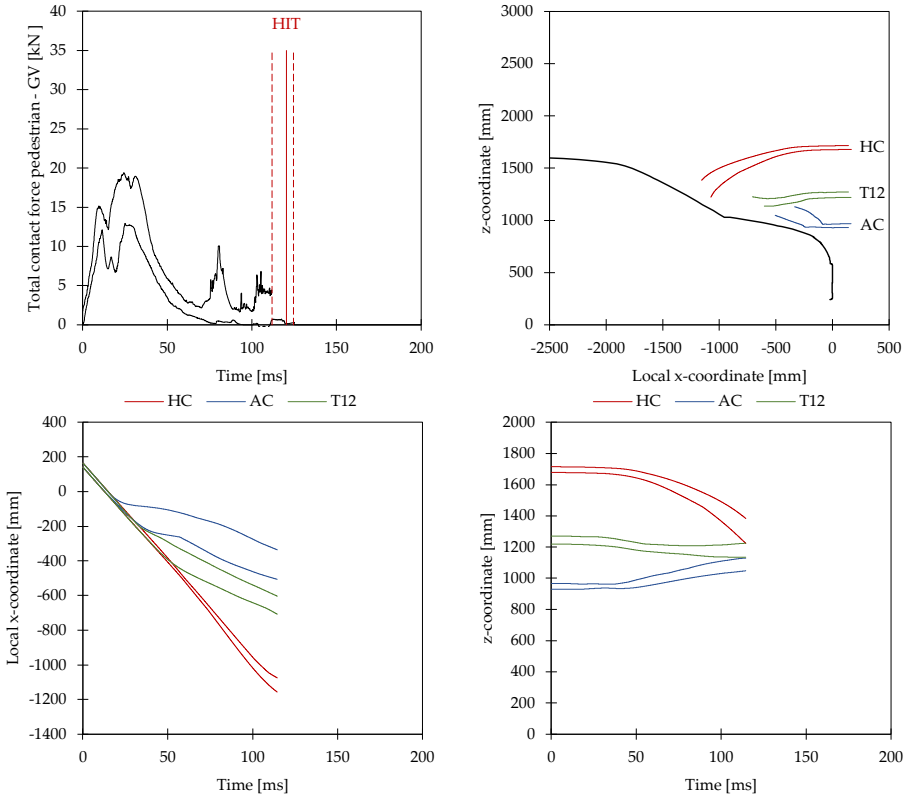

Figure 27. Corridors for impact with generic MPV model at 40 km/h – Reference* HIT = *120.4 ms.

MPV 50 km/h

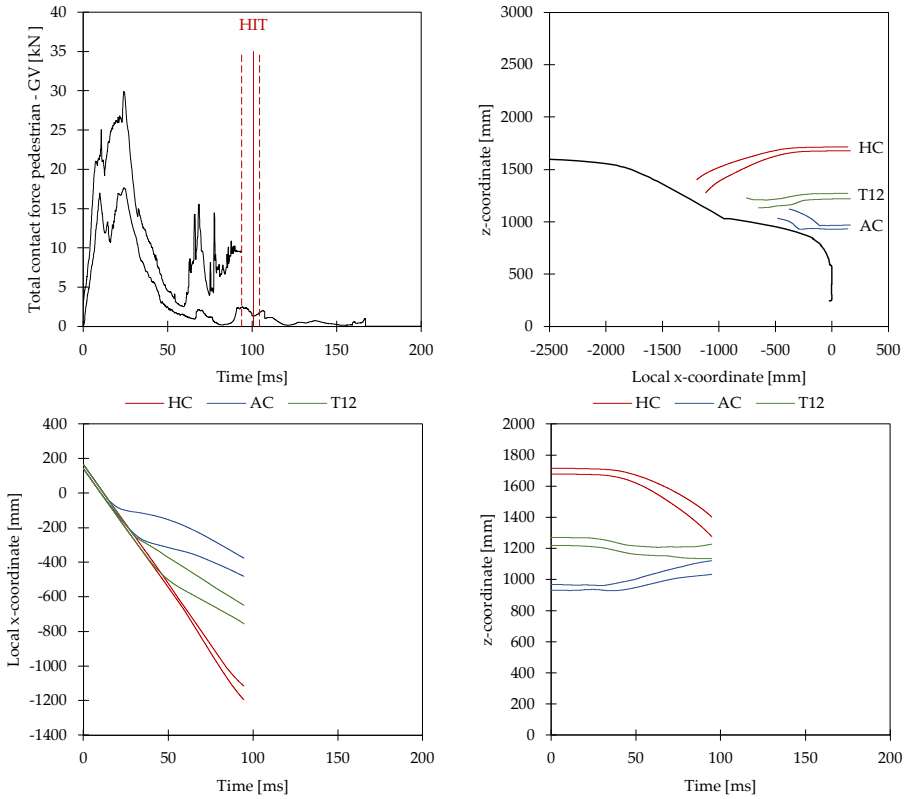

Figure 28. Corridors for impact with generic MPV model at 50 km/h – Reference* HIT = *100.8 ms

RDS 30 km/h

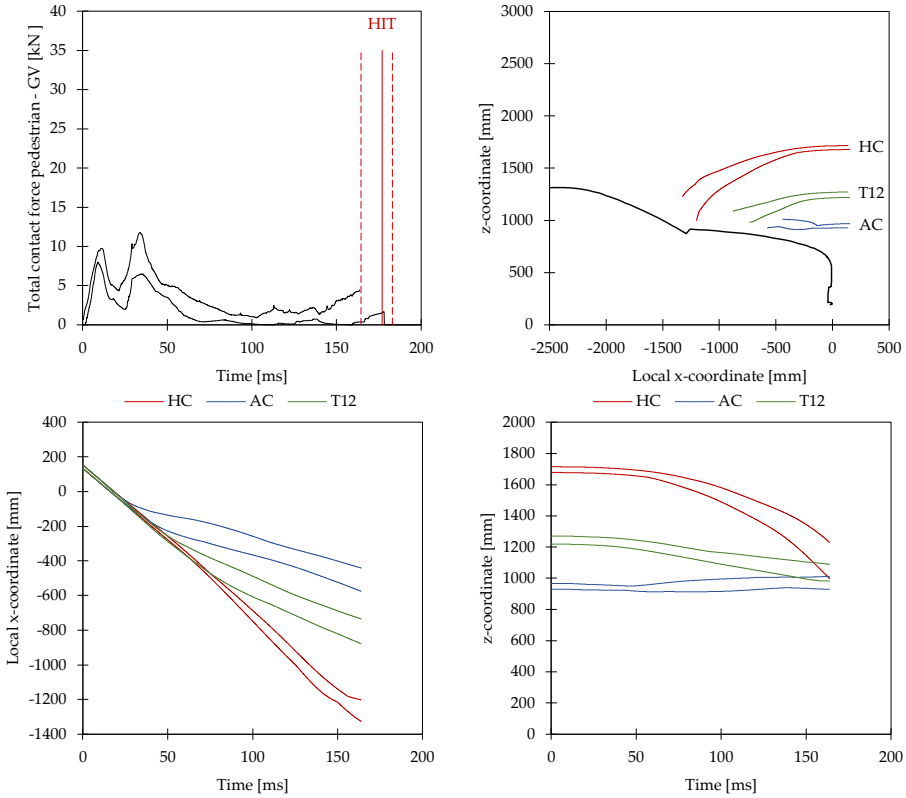

Figure 29. Corridors for impact with generic RDS model at 30 km/h – Reference* HIT = *176.9 ms.

RDS 40 km/h

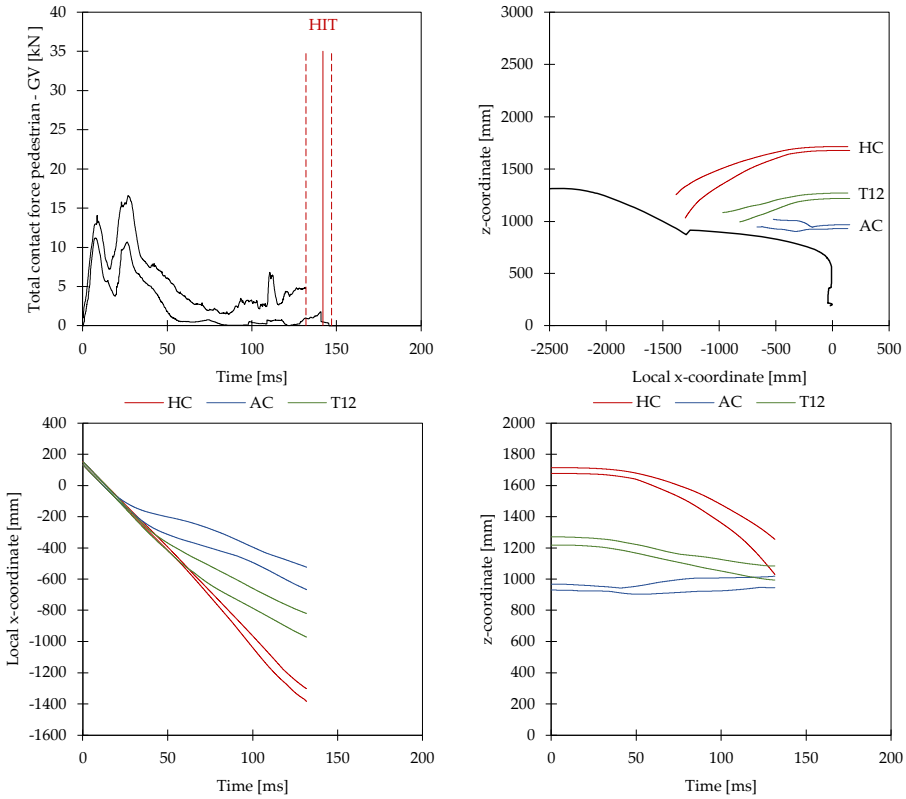

Figure 30. Corridors for impact with generic RDS model at 40 km/h – Reference* HIT = *142.1 ms.

RDS 50 km/h

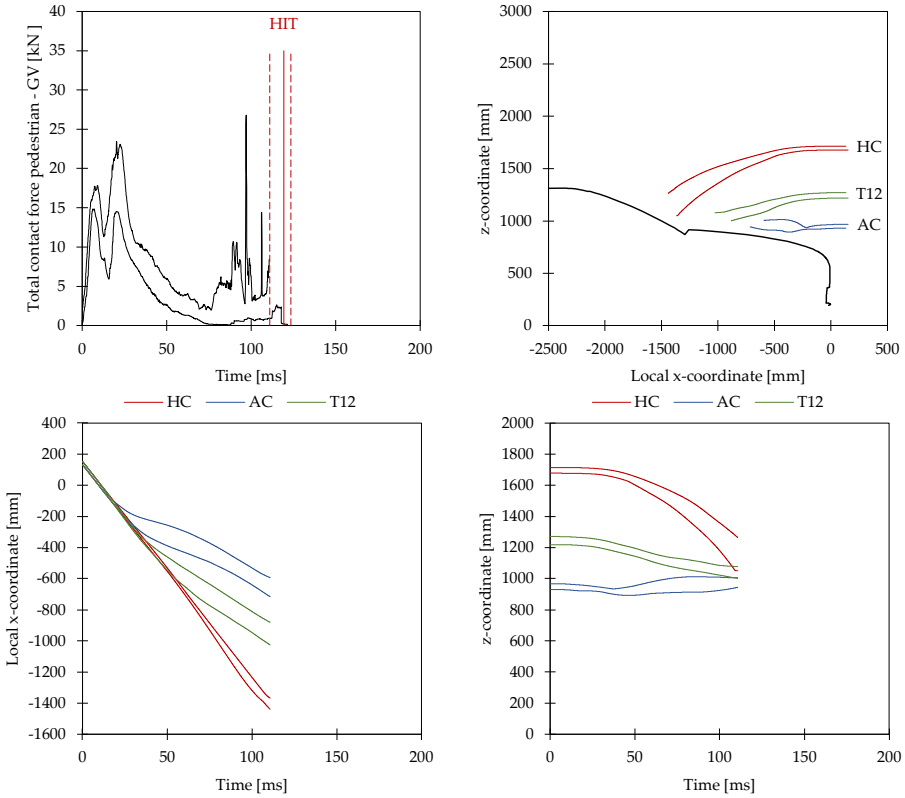

Figure 31. Corridors for impact with generic RDS model at 50 km/h – Reference* HIT = *119.3 ms.

SUV 30 km/h

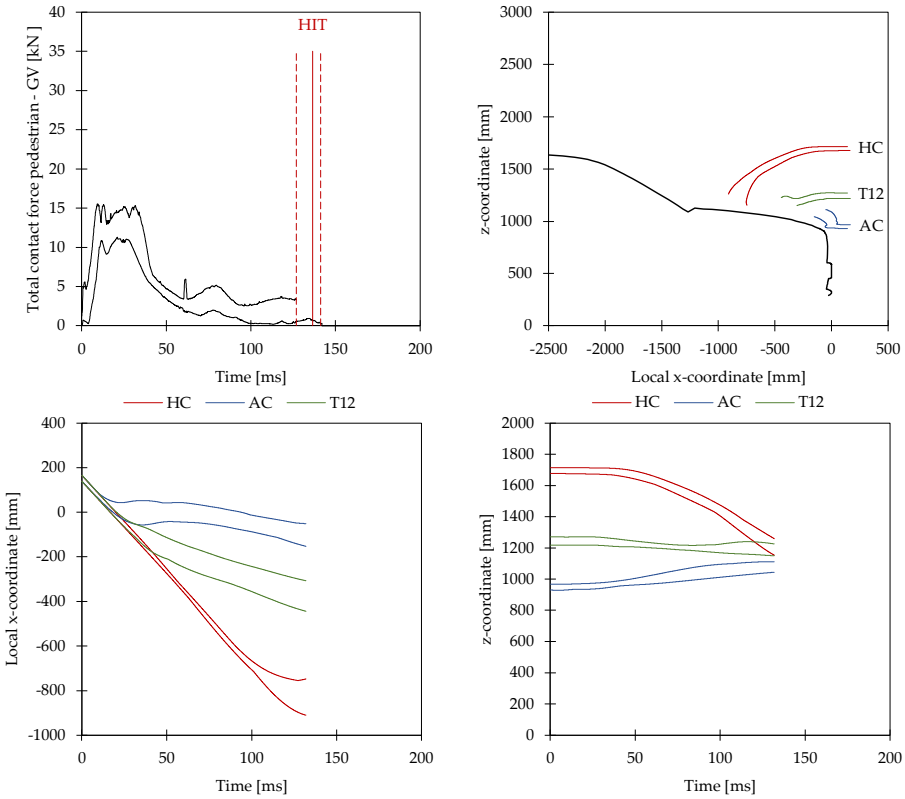

Figure 32. Corridors for impact with generic SUV model at 30 km/h – Reference* HIT = *136.5 ms.

SUV 40 km/h

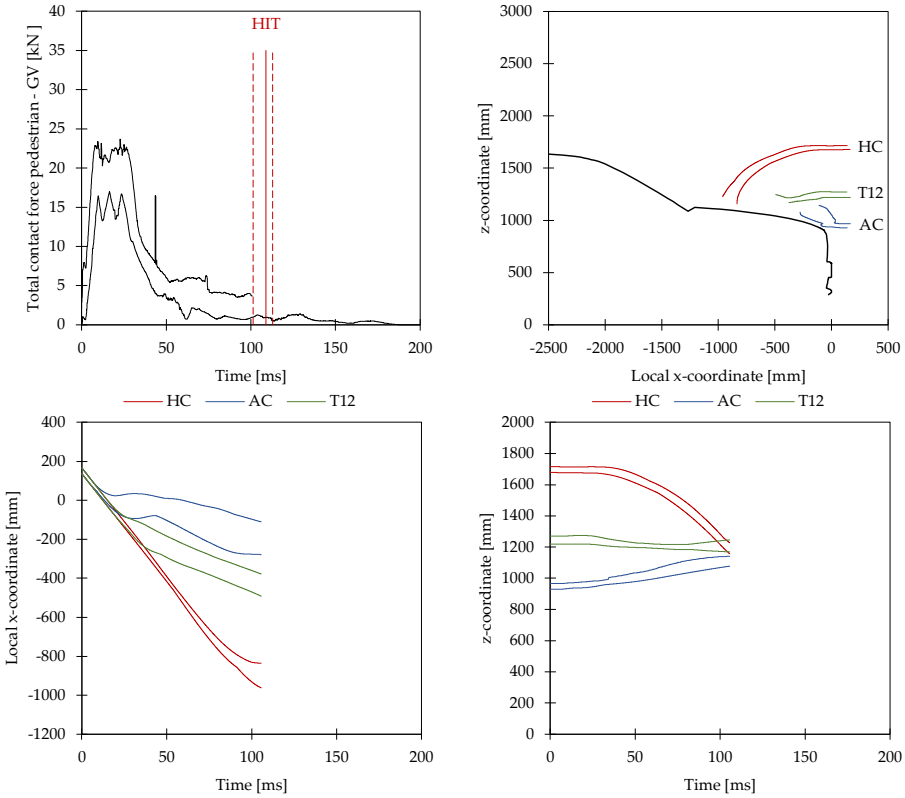

***Figure 33. Corridors for impact with generic SUV model at 40 km/h – Reference* HIT = *109.0 ms* .**

SUV 50 km/h

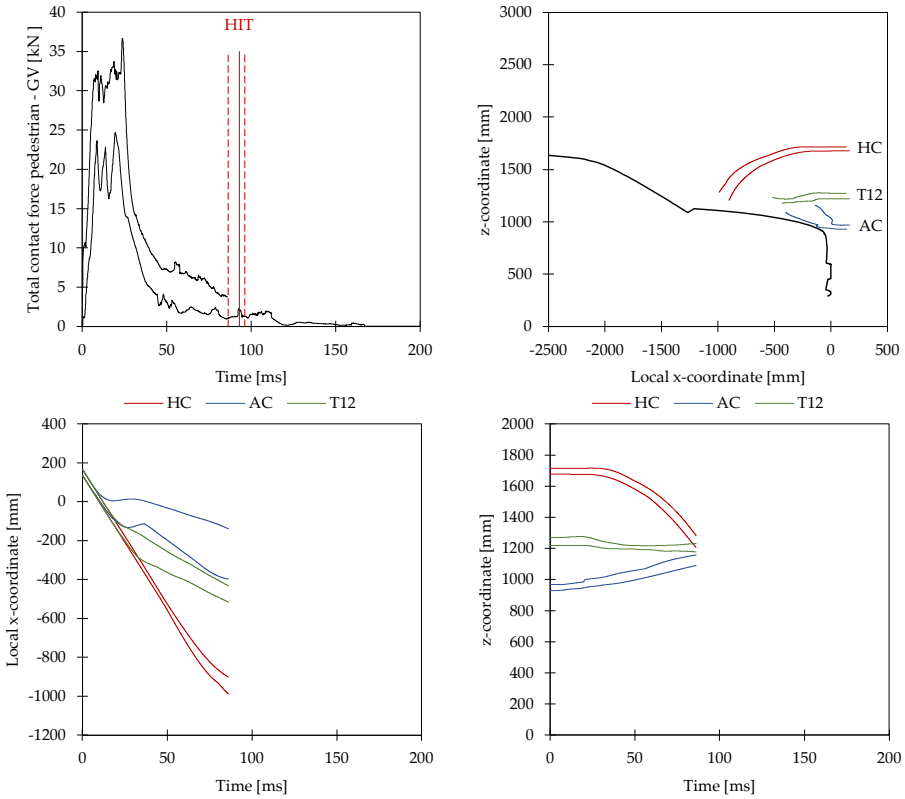

Figure 34. Corridors for impact with generic SUV model at 50 km/h – Reference* HIT = *92.9 ms

AN ASSESSEMENT APPROACH TO ASSISTED DRIVING SYSTEMS

Colin Grover
Matthew Avery
Dominic Tough
Thatcham Research
United Kingdom

Paper Number 19-0313

ABSTRACT

An increasing number of vehicles on the global market provide Assisted Driving technology, also referred to as SAE Level 2 partial automation, providing the opportunity for increased driver and road safety. It is the next step towards automated vehicles. To ensure its safety benefits consumers need to be aware and informed about the capabilities of these systems. With these systems being at the cutting edge of modern vehicle technology only limited vehicles currently have these systems fitted, although they are slowly being installed into lower priced mass-produced vehicles, and therefore few consumers have experience or know of the capability of these systems.

This paper investigates a way of assessing the driver support capabilities and HMI of vehicles with Assisted Driving systems to provide information of how the systems cope in different everyday scenarios which they may encounter. This paper outlines the development process of these assessments through both desk-based literature considerations and on track testing methods. Ten different vehicles where put through the assessment process to prove out the test method and offer information on the abilities of various systems. The vehicles are all produced by different manufactures and range from cheaper less capable to higher end advanced systems with the purpose of showing that within Assisted Driving systems there is vast difference in the performance outcome in both everyday driving and safety critical situations. The assessment of the systems will allow for a basis which will be expanded on for greater in-depth evaluation into the overall safety of the systems and ultimately the assessment of automated vehicles.

The assessment protocol has been developed in agreement with Euro NCAP for the evaluation of ten production vehicles available to buy late 2018, looking into developing the protocol for future testing and grading of new vehicles to be released with Assisted Driving technology.

INTRODUCTION

Latest advances in Advanced Driver Assistance System (ADAS) technology implemented on modern vehicles has seen the introduction of Assisted Driving technology, also referred to as SAE Level 2 partial automation. Assisted Driving provides braking and acceleration control in combination with a steering support function that assists with keeping the vehicle in the driving lane. To achieve this systems use a combination of radar, lidar and camera sensors fitted variously at the front, rear, sides, corners and windscreen of the vehicle to monitor the driving environment and immediate traffic. These functions allow for simultaneous longitudinal and lateral control support, facilitating potentially reduced driver workload and an associated road safety benefit.

Currently no defined assessment protocols exist for Assisted Driving systems and systems developed to date have evolved with notable differences between the technical solutions implemented by various vehicle manufacturers. This has caused differing functionality, performance and Human Machine Interaction (HMI) designs for vehicles fitted with Assisted Driving systems, with the potential to confuse drivers. If a vehicle equipped with Assisted Driving technology is used correctly and the driver works in collaboration with the system, then there is the potential for improved vehicle and road safety. However, if the consumer is uninformed regarding the capability of the system that their vehicle is equipped with then those safety benefits maybe lost in over reliance on the system by the driver, or the driver not having the confidence in using the system and never activating it.

Assisted Driving system functionality that is anticipated to be of benefit to road safety given the effects in regular driving include:

1) Headway maintenance: Adaptive Cruise Control (ACC) operates to maintain speed or a set headway to traffic ahead, the shortest setting of which is typically greater than maintained by drivers in regular driving.
2) Lane guidance: helps maintain the vehicle within the lane, reducing the possibility of drifting into oncoming or overtaking traffic or running off the road.
3) Reduced driver workload: assistance with controlling the vehicle has the potential to reduce driver fatigue through supporting the actions required.

For safe and effective Assisted Driving there is the need to strike a balance regarding the level of assistance provided to deliver a perceivable benefit whilst ensuring the driver remains engaged with the driving task, and not relying on driver monitoring systems to force the driver to pay attention. Studies show that if the system effectively performs fully effective Object and Event Detection and Response (OEDR) drivers can develop over-trust in its capability and fall out-of-the-loop [3]. As a result, if the vehicle enters a situation the system is unable to manage, and the driver is not attentive to identify the developing situation, there is an increased risk of collision. This also works in the opposite way in that if the system is not very capable the driver is less likely to use the system and not gain the additional safety benefits. **Error! Reference source not found.** represents this 'irony of automation' in graphical form.

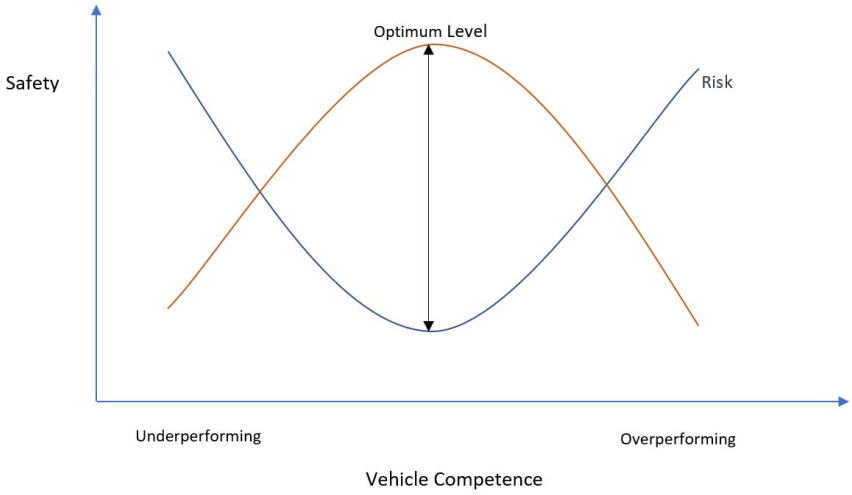

Figure 1. Assisted Driving – safety against vehicle competency

AIM

The aim of this research is to develop an assessment protocol for evaluating Assisted Driving technology that provides a means of considering the system naming and associated literature and testing the system for safety in an objective and repeatable format. It will provide the consumer with information describing the system capability, performance and limitations in typical real world driving scenarios and emergency situations, helping the consumer to understand the system and use it effectively and responsibly to the benefit of road safety. Ultimately the assessment protocol will develop into a consumer grading scheme for Assisted Driving safety.

METHOD

In the absence of any proposals or formalised procedures for assessing Assisted Driving systems the 'Assisted and Automated Driving Technical Assessment1' [1] was used as a basis to create initial assessment criteria. Within the literature the criteria for Assisted Driving is outlined under ten headings of:

1) Naming
2) Law abiding
3) Design domain
4) Status
5) Capability
6) Driver monitoring
7) Safe stop
8) Crash intervention
9) Back-up systems
10) Accident data

For developing the assessment, the criteria were regrouped because of the nature of their complementary content to desk-based literature review and track-based testing.

Literature Review

The literature associated with a vehicle's Assisted Driving system, such as online promotional material, operational tutorials and the vehicle handbook etc. can influence a driver's anticipation of the capabilities of the system, how it will perform and what their role and responsibilities are whilst using the system [4]. Assessment commences by reviewing the literature accompanying the vehicle describing the system to gather information on the functionality, performance, limitations and driver responsibility. The information therefore needs to be clear and accurate. The following is assessed:

- The naming of the system: it should not specify or suggest automation. The source material should not imply self-driving or automation.
- Capability and limitations: a description of how the driver can expect the system to function and any situations in which the system is limited or unable to perform.
- Operational environment: whether functions are generally available or limited to specified design domains e.g. highways.
- Initial operation: whether a quick start operational guide is provided to explain the system.

Track Testing

To assess the safety aspect of the Assisted Driving system it must be presented with typical the real-world driving situations that can be readily expected to be encountered on the public road. However, to ensure a safe environment and achieve repeatable testing this activity must be performed within the confines of a controlled test track. Vehicles are assessed in the following scenarios.

Longitudinal testing The current Euro NCAP AEB test protocol scenarios were used as a basis for testing the longitudinal capabilities of the ACC system replicating the case where a lead vehicle is directly ahead in lane on a straight section of road. Speeds were increased to those typically encountered on highways (130km/h) because this is the environment in which current systems are recommended for operation.

ACC Test Scenarios:
CCRs: 50 to 130km/h (10km/h increments)

CCRm: VUT 80 to 130km/h
Target 20km/h & 60km/h

CCRb @ -4m/s²: VUT 55km/h
Target 50km/h

In addition to these in-line traffic scenarios additional lane changing tests based on a typical highway manoeuvres were included. The first is where a slower moving vehicle cuts in ahead from an adjacent lane. A second is a vehicle in front changes lanes into an adjacent lane revealing a stationary vehicle ahead in lane. These two tests were named as cut-in & cut-out scenarios as shown in Figure 2 & Figure 3.

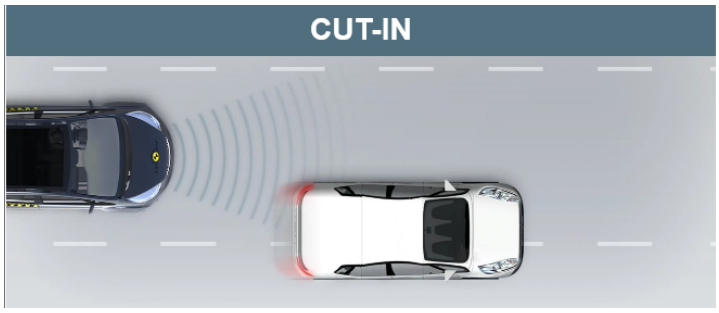

Figure 2. Cut-in test scenario

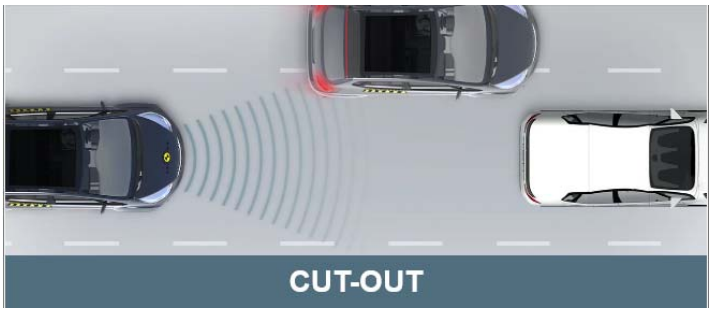

Figure 3. Cut-out test scenario

Cut-in @ TTC -1.5: VUT 50km/h
Target 10km/h
Cut-in @ TTC 0.5: VUT 130km/h
Target 80km/h

Cut-out @ TTC 2.0: VUT 70km/h
Target 50km/h
Cut-out @ TTC 2.0: VUT 90km/h
Target 80km/h

All tests are performed with the ACC set to the nearest following setting.

The test target specified for use is the Global Vehicle Target (GVT) impactable 3D car target according to ISO 19602 Part 1 (see Figure 4). This document specifies the properties of an omni-directional multipurpose vehicle target that will allow it to represent a passenger vehicle in terms of size, shape and sensor attributes for testing purposes.

Figure 4. Global Vehicle Target (GVT) according to ISO 19602 Part 1

Lateral testing Testing the lateral control of an Assisted Driving system involves testing the lane guidance system relative to a marked lane and the interactivity of the steering system in response to driver steering inputs.

The capability of the steering system is evaluated by driving along a straight section of lane markings that transition into a curve to the left immediately followed by a curve to the right, a so-called 's bend' (**Error! Reference source not found.**5). This configuration was selected because it investigated not only the ability of the system to steer into a curve, but also transition between curves in alternate directions as often encountered on the public road.

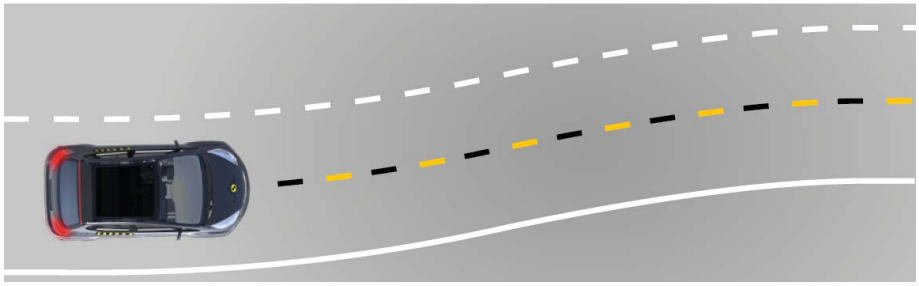

Figure 5. S-Bend test scenario

S-Bend dimensions:
- Left turn radius 900m at 6° angle
- Right turn radius 500m at 6° angle

The S-bend test is performed at increasing speeds from 40mph up to 75mph in 5mph increments.

The test is used to identify the overall level of assistance the vehicle provides driving through the layout. It is considered appropriate that an Assisted Driving system should support the steering through the curves acknowledging necessary directional changes but not necessarily perform complete guidance centering the vehicle in lane throughout the entire manoeuvre. Such authority would infer more automated-like control leaving little for the driver to contribute, potentially affecting perception of the system and ultimately their engagement with the driving

Assessing the driver interactivity with the steering system is performed by investigating the change steering effort required to alter the position of the vehicle within the lane sideways by 0.5m during normal manual driving compared to when the Assisted Driving system activated. The response of the Assisted Driving system to driver inputs is also monitored i.e. does the system shut down or will it tolerate driver inputs and continue to operate. An example of this manoeuvre is avoiding an object, such as a pot hole, within a lane, as shown in Figure 6 below.

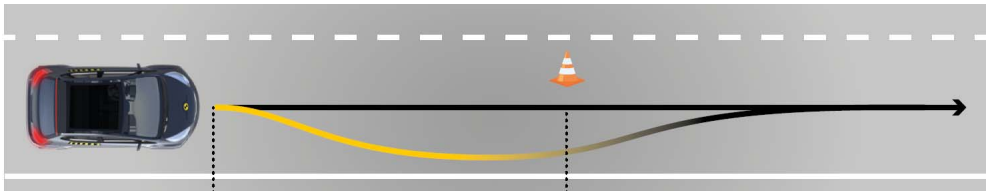

Figure 6. Driver interactivity test scenario

This test is performed with a driving robot following a defined path and investigating the steering torque required for each testing configuration. The baseline reference measurement is then compared with the Assisted Driving measurement to identify the change in steering torque profile throughout the manoeuvre.

Driver inactivity escalation By law Assisted Driving systems must incorporate a means of providing a timely audio-visual warning escalation and ultimately cease assistance in case continuous driver inactivity is detected. However what action to take when ceasing assistance if the driver fails to respond is not specified. Testing is undertaken to investigate the various strategies implemented.

TEST FLEET

A range of ten vehicles equipped with Assisted Driving systems from different manufacturer were assessed. These include:

1) Audi A6
2) BMW 5 Series
3) DS7 Crossback
4) Ford Focus
5) Hyundai NEXO
6) Mercedes-Benz C-Class
7) Nissan Leaf
8) Tesla Model S (v8.1 software)
9) Toyota Corolla
10) Volvo V60

RESULTS

Assessing a broad range of state-of-the-art production systems identified the breadth of Assisted Driving capability currently available on the market. A summary of the results of all ten vehicles tested was published in October 2018 on the Euro NCAP website [2]. A subset of key results identifying differences between the vehicles tested is presented.

Literature Review

The literature review of promotional material identified that the vehicle manufacturer Assisted Driving system naming conventions were split with five incorporating appropriate ‘assist’ terminology (Audi, BMW, Hyundai, Mercedes-Benz and Volvo), four using inappropriate ‘pilot’ terminology suggesting automation (DS, Ford, Nissan and Tesla), otherwise non-descript terms were used (Toyota). Only two cases of notably inappropriate promotional material were identified from Tesla and BMW, promoting full self-driving capability with respect to future developments and showing hands-off driving respectively.

All the vehicle handbooks included information advising that the Assisted Driving system was a driver support function and that the driver retained full responsibility for the safe driving of the vehicle. The majority identified that the Assisted Driving system was intended for use on highways and all listed various performance and operational limitations regarding the road and traffic situations.

Track Testing

Longitudinal control The Tesla Model S stands out by stopping for the stationary target in lane ahead deploying comfort braking by ACC system throughout the entire speed range tested up to 130km/h. Whereas, for example, in the same test the Audi A6 test avoids up to 70km/h using the ACC system, 70 to 100km/h

avoids using emergency intervention by AEB or FCW, and mitigates the collision speed between 100 to 130km/h.

Generally, the longitudinal control in all vehicles tested performed more effectively at higher speeds when approaching the slow-moving vehicle compared to when approaching the stationary vehicle. It is understood that is because of the confidence of identifying and classifying a moving vehicle compared to a static vehicle.

The highly dynamic cut-in and cut-out scenarios challenged all vehicles. In the cut-in scenario four vehicles issued a late collision warning that was insufficient to respond to for avoiding the collision. In the cut-out scenario one vehicle managed to avoid a collision by emergency intervention, six provided a late collision warning and three did not respond at all.

Lateral control The capability of the steering systems also showed demonstrable differences in performance driving through the 's bend'. For example, Tesla Model S navigates the curves remaining centred in the lane throughout the entire manoeuvre at all speeds tested, whereas the Volvo V60 would steer in lane through the initial left turn and attempt to turn in the opposite direction to the right but start to drift out of lane in the transition to the right turn, especially at higher speeds. This is shown in Figure 7 & Figure 8 below.

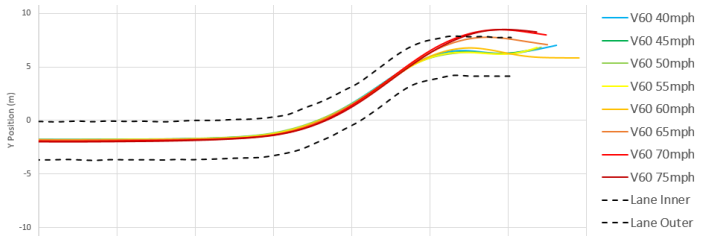

Figure 7. Volvo V60 S-Bend results

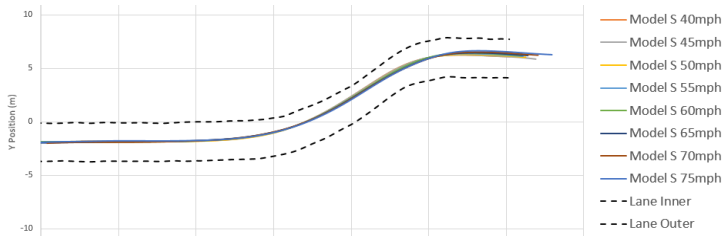

Figure 8. Tesla Model S S-Bend results

The Tesla Model S demonstrated a high degree of steering authority navigating the 's-bend', and this is also identified in the steering interactivity test. The Tesla has the greatest peak proportional increase in steering torque of all ten test vehicles, as shown in Figure 9.

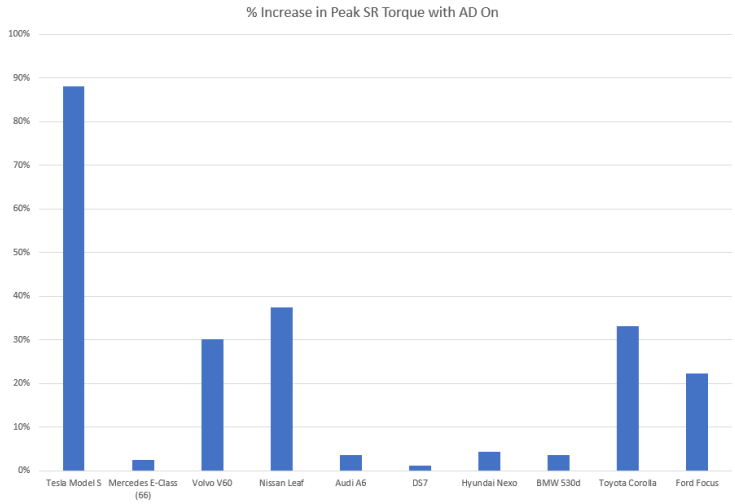

Figure 9. Percentage of steering torque increase during driver interactions test

With the Assisted Driving system active the peak steering torque required to alter the vehicle position within the lane almost doubled compared to that during normal driving. Comparatively the Mercedes, Audi, DS, Hyundai and BMW vehicles demonstrated only modest increases in peak steering torque of less than five per cent. Additionally, the Tesla was the only steering assistance system to completely disengage in response to the driver input with no further operation until the driver reactivates the system. All other systems either continued to provide lane guidance support throughout the manoeuvre or were suspended whilst the steering input was applied and then automatically resumed shortly after the vehicle returned to the centre of the lane.

Driver inactivity escalation Various solutions have been implemented in current production vehicles regarding the action taken if the driver fails to respond to an inactivity warning. This ranges from simply ceasing to provide steering support whilst maintaining ACC speed control, to maintaining steering support and bringing the vehicle to a controlled stop in lane, activating the hazard warning lights and initiating an emergency eCall.

The testing identified that five of the vehicles ceased to provide steering assistance and five came to a controlled stop in lane. Figure 10 is an example of the Nissan Leaf escalating the warnings before beginning a controlled stop after 30 seconds of driver inactivity.

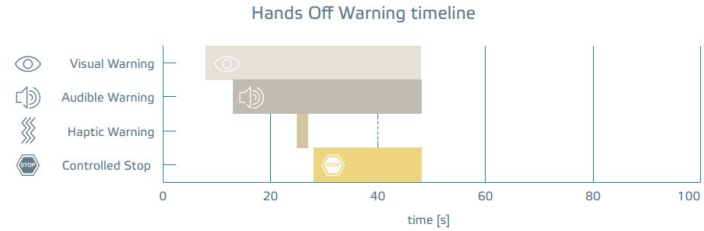

Figure 10. Example of driver disengagement procedure on Nissan Leaf

LIMITATIONS

The tests presented are a first step in assessing Assisted Driving systems and as such are limited to a handful of simplistic, repeatable track tests. However, on the public road drivers, and therefore Assisted Driving systems, encounter a wide variety of road and traffic situations on every journey, not to mentioned changes in lighting and weather conditions etc. Therefore, to develop a meaningful grading scheme a wider range of assessment must be undertaken to inform drivers on the relative merits of the various systems. It would also serve to inform drivers on the limitations of systems thus reinforcing the requirement for them to always remain engaged and vigilant and be prepared to take full manual control of the vehicle. Some examples are discussed below.

Road Environment

Assisted Driving systems have demonstrated a level of competency at manging interactions with other traffic straight ahead in the assessments presented. It has been identified that in a similar traffic situation on a curve system performance can deteriorate substantially with apparently minor changes in the boundary conditions from the driving point of view. To assess this the CCRm & CCRs tests can be performed around the s-bend, at the same speeds, as show in Figure 11.

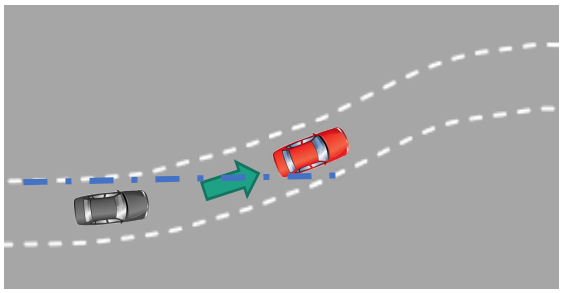

Figure 11. Target vehicle placed within a bend scenario

Vulnerable Road Users

Vulnerable Road Users (VRUs), such as pedestrians and cyclist, frequent roads in which Assisted Driving systems are available to use. The assessments presented are focussed towards highway driving using the GVT to represent other vehicular traffic, however VRUs may also be present if, for example, a traffic queue assist function was used in an urban area. The current AEB VRU test scenarios could be implemented for pedestrians crossing between stop-start queueing vehicles or for cyclists riding in line with the traffic to demonstrate performance or limitations.

Figure 12. Example of ACC longitudinal VRU test scenario

Weather and Lighting

The tests presented are all performed under good testing conditions to achieve repeatability, namely daylight, clear visibility, no precipitation falling etc. Real world experience has highlighted that Assisted Driving system performance can deteriorate in less optimal conditions such as darkness or poor weather conditions. Testing could be considered under these conditions to illustrate the effects to drivers.

Sensor Issues

The sensors used to enable Assisted Driving technology are necessarily positioned towards the perimeter of the vehicle structure to provide a clear view of the surroundings. However, this also makes them susceptible to fouling and damage. Exploratory testing has identified that whilst some systems advise of the need for maintenance almost immediately in case of a sensor blocking issue, others continue to apparently operate for extended periods of time without the driver being advised of a degradation in their functionality and system performance e.g. ACC reverting to normal cruise control.

CONCLUSIONS

Assisted Driving systems are already available in a wide range of vehicles and are rapidly being introduced into mass market affordable vehicles. The combination of lateral and longitudinal assistance, when used responsibly by the driver, could benefit road safety through improved headway, lane positioning and reduced driver fatigue through being supported with the driving task.

The literature review of promotional material identified that the vehicle manufacturer Assisted Driving system naming conventions were split between appropriate and inappropriate terms and only two cases of notably inappropriate promotional material were identified. All the vehicle handbooks included information advising that the Assisted Driving system was a driver support function and that the driver retained full responsibility for the safe driving of the vehicle.

The track tests developed for assessing Assisted Driving systems evaluating longitudinal control, lateral support and driver interactivity proved effective at identifying differences in functionality and performance between vehicles. However, it is acknowledged that the tests themselves are a simplistic representation of typical scenarios encountered in real world driving. A future grading scheme would require a broader range of scenarios to be considered to achieve a more representative grading and illustration of system functionality and limitations. Similarly, the testing was performed under a limited set of controlled conditions necessary to

achieve repeatability. Real-world driving conditions vary substantially, and a more representative assessment could be achieved by considering additional factors e.g. driving in darkness.

This initial assessment of ten production vehicles has identified that there is a range of functionality and performance differences between Assisted Driving systems. Some systems portray a high degree of driving competence in response to the lane geometry and interactions with other traffic whilst others offer more modest performance. For example, the Tesla Model S stood out in CCRs test by coming to a halt behind the stationary target at all speeds up to 130km/h using comfort braking only whereas all other vehicles tested either failed to acknowledge the stationary vehicle at higher speeds or only achieved collision mitigation by emergency response.

The Tesla was also the only vehicle to navigate the ‘s bend’ curves remaining centred in the lane throughout the entire manoeuvre at all speeds tested, however it also demonstrated the highest proportional increase in peak steering effort in the driver interactivity tests and subsequently steering support was disengaged whereas all other systems continued to operate after returning to the central lane position. The highly dynamic cut-in and cut-out scenarios challenged all vehicles and little meaningful intervention was identified except for in one vehicle.

Various solutions have been implemented in current production vehicles regarding the action if the driver fails to respond to an inactivity warning ranging from simply ceasing to provide steering support whilst maintaining ACC speed control, to maintaining steering support and bringing the vehicle to a controlled stop in lane.

For safe and effective Assisted Driving there is the need to strike a balance regarding the level of assistance provided to deliver a perceivable benefit whilst ensuring the driver remains engaged with the driving task, and not relying on driver monitoring systems to force the driver to pay attention. The next step is to develop the testing and an associated grading scheme to enable the evaluation of system performance and drive best practice to achieve the road safety benefits associated with Assisted Driving technology maintaining headway, improving lane guidance and reducing driver workload and associated fatigue.

References

1) Thatcham Reseach & ABI, 2018. *Assisted and Automated Driving Technical Assessment.* Thatcham: Thatcham Research.

2) Euro NCAP, 2018. *2018 Automated Driving Test.* [Online]
Available at: https://www.euroncap.com/en/vehicle-safety/safety-campaigns/2018-automated-driving-tests/

3) Draper, D. M., 2018. Automation expectation mismatch: Incorrect prediction despite eyes on threat and hands on wheeel. *Human Factors: The Journal of the Human Factors and Ergonomics Society,* 1(1).

4) Abraham, H., Seppelt, B. D., Reimer, B. & Mehler, B., 2017. *What's in a Name: Vehicle Technology Branding & Consumer Expectations for Automation,* s.l.: s.n.

ASSESSING THE CASE FOR REQUIRING AEB ON CITY BUSES AND DEVELOPING TECHNICAL REQUIREMENTS AND TEST PROCEDURES

Iain Knight, Martin Dodd,
Apollo Vehicle Safety Limited
UK

Alix Edwards
TRL Limited
UK

Paper Number 19-0315

ABSTRACT

In London, around two-thirds of those killed in collisions involving a bus are pedestrians and most of these are killed crossing the road. The time between the pedestrian first being recognisable as a threat and the moment of impact is usually less than 2 seconds. Human drivers have very limited opportunity to avoid the collision. Automated Emergency Braking (AEB) has been developed to avoid such collisions and is becoming widespread on passenger cars. However, city buses pose a unique additional challenge. Bus operations already generate a significant quantity of non-collision injuries because passengers fall during normal operation. This includes when standing, or seated but unrestrained, passengers fall under braking. Automated brake applications where deceleration exceeds what a human driver would have applied increases this existing injury risk.

The research was sponsored by Transport for London (TfL) and aimed to quantify this balance of opportunity versus risk, and generate technical requirements allowing them to encourage or mandate AEB on their London bus fleet. The work involved:

- Traditional collision data analysis
- Case by case review of both collision and non-collision incidents recorded by CCTV systems provided by a London bus operator
- A road trial involving an AEB-equipped bus
- AEB Performance tests on a closed test track.

Up to around 25% of bus-pedestrian fatalities could be prevented. In true positive situations, any additional risk to bus occupants was small. Human drivers rarely failed to brake in collisions with pedestrians, they just braked too late to avoid collision. Earlier intervention would mean that in some cases AEB could achieve avoidance with lower deceleration than the driver actually applied. In others, only a small increase was required.

False positives always create additional risks. The extent of the risk was strongly related to the level of deceleration and increased very substantially at 6 m/s^2 or above in the modelling. The net balance was a likely increase in slightly injured casualties but a substantial decrease in deaths and serious injuries.

Technical requirements were developed based on adaptations of the Euro NCAP standards with two false positive tests added to discourage systems that were inadequately tuned.

The analysis is strongly dependent on the rate of brake applications in service at different deceleration levels, the number of bus occupant injuries that occur at those levels and the decelerations achieved during an AEB false positive event, which is often of very short duration. Larger scale in-service trials would help to quantify these parameters more robustly.

Despite some risks, overall AEB would have strong safety potential on city buses and can be encouraged through TfL's bus safety standard in co-operation with manufacturers and researchers to mitigate risks as far as possible.

INTRODUCTION

In London, around two-thirds of those killed in collisions involving a bus are pedestrians and most of these are killed crossing the road. In these fatal cases, the time between the pedestrian first being recognisable as a threat and the moment of impact is usually less than 2 seconds. Human drivers have very limited opportunity to avoid the collision.

Advanced Emergency Braking (AEB) is a system that uses forward looking sensors such as Lidar, Radar, Camera, or combinations of more than one sensor, to identify a risk of an imminent collision. It will typically first warn the driver of the risk and, if the driver does not act, then it will apply braking automatically to avoid the collision or to reduce the collision speed and therefore the potential for injury.

AEB systems have been developed to avoid certain types of car, pedestrian and cyclist collisions and is becoming widespread on passenger cars. However, city buses pose a unique additional challenge. Bus operations already generate a significant quantity of non-collision injuries because passengers fall or sway during normal operation. This includes when standing, or seated but unrestrained, passengers fall under heavy braking. Automated brake applications where deceleration exceeds what a human driver would have applied will, therefore, create additional injury risk.

The research was sponsored by Transport for London (TfL) and aimed to quantify this balance of opportunity for the prevention of serious injury, particularly to pedestrians, versus the risk of an increased incidence of falls among bus occupants. The research was also intended to develop technical requirements allowing TfL to specify the fitment of appropriate AEB on their London bus fleet.

DATA SOURCES

Collision Data Analysis

A sample of 48 police fatal collision reports where London buses were involved, previously compiled by (Edwards, et al., 2017), were analysed to provide detailed information about the circumstances of fatalities arising from collisions with a bus.

Additionally, Transport for London's Incident Reporting and Investigation System (IRIS) database was analysed to identify collision incidents, in which someone on board the bus had been injured, and non-collision incidents where injuries had been caused by a slip, trip or fall during normal operation.

These data were supplemented by a sample of mainly lower severity incidents obtained from a review of the CCTV incident records of one bus operator. The CCTV footage included an overlay of some telematics data allowing the timing and magnitude of any driver or passenger actions to be identified (e.g. brake pedal application and x/y acceleration). The ability of the CCTV data to define the moment the pedestrian became recognisable as a threat, the moment the driver braked, and the amount of braking applied, was a major advantage over many other studies that have relied only on approximations and judgement from traditional collision reconstruction.

Track Tests

Two sets of track tests were completed. Firstly, the authors were not aware of any production AEB system fitted to a city bus and only one production AEB system fitted to an HGV that was sensitive to collisions involving pedestrians. It was known from the development of pedestrian AEB for passenger cars that the ability to apply the brakes hard and quickly was important to the potential casualty savings. It is well documented that commercial vehicle air brakes combined with commercial tyres could lead to slower brake build up times and lower peak acceleration potential than for passenger cars. Given this lack of existing information about the likely performance of AEB fitted to buses, independent testing of a system was considered necessary to establish the potential. At the time, Alexander Dennis buses was part-way through the development of an AEB system sensitive to front to rear, pedestrian and cyclists and agreed to provide a prototype vehicle for the test work and to provide technical support, allowing the project team some insight into the details of what the sensor system saw and reacted to.

The Euro NCAP AEB VRU 2018 protocol was selected as the basis for the evaluation testing because it provided the greatest coverage of the relevant test conditions required for a city bus, e.g. pedestrian and cyclist manoeuvres.

Later in the project additional track tests were also undertaken to evaluate two false positive scenarios that were under consideration for inclusion in the final technical requirements based on the false positive scenarios identified during the road trial, and to validate the test protocol defined for true positive testing.

Road Trial

The main objective of the road trial was to characterise the type of false activations that occur during normal driving to support the development of suitable false positive tests within the technical requirements. It should be noted that the prototype system had not, at that stage of development, undergone any tuning to eliminate false positives. It was, therefore, expected that substantial numbers of false positives would occur, and the system cannot be considered representative of what is expected of the fully developed system. However, it could be considered representative of an under-developed system that any technical specification should aim to prevent entering service. A secondary objective was to gather data on the frequency and magnitude of typical brake activations during normal service.

A single decker bus of similar type and construction to that which is typically used in London was used for the road trial. The vehicle was equipped with the prototype AEB system that was set-up to operate in an open loop or "Shadow Mode" – whereby it was actively monitoring the road environment, processing data and making decisions on warning and brake action, but the output signals were not connected to the normal bus controls so that no automated braking could take place. Thus, the control of the vehicle remained fully with the driver. The manufacturer recorded data from the AEB sensors/systems and, within commercial constraints, non-sensitive data was shared with the project team. In addition to this, independent data was recorded and overlaid onto a video that was synchronised to four cameras, as shown in Figure 1, below.

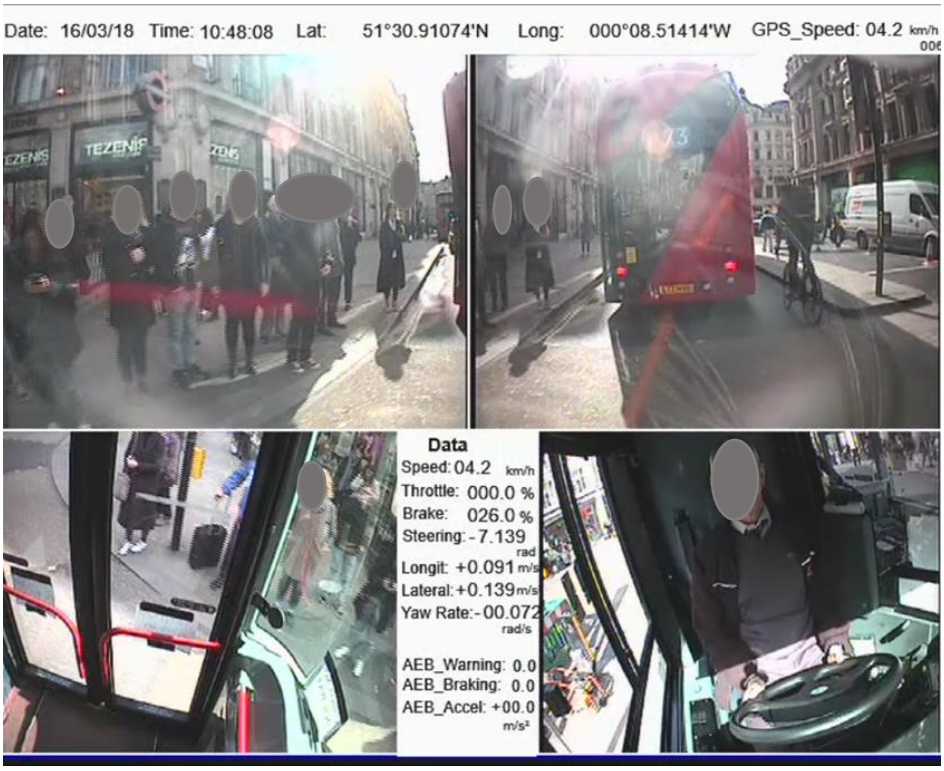

Figure 1: Example of video and data collection during the road trial

Although the bus was not in service during the trial, official London bus routes were followed, driven by drivers from the bus companies operating those routes and familiar with them, and the drivers were instructed to pull into bus stops and bring the vehicle to a stop as they would under normal operation.

Six different drivers drove the vehicle a total of 399km during a one-week road trial, covering five different routes. The routes selected included the wide range of bus driving environments likely to be encountered in service in London, while still being broadly representative of the most common routes and situations. They had been chosen partly based on including routes with both high and low casualty rates per km, as well as practical constraints in terms of ensuring support from the operators of those routes.

METHODOLOGY

The analysis was structured to consider the effects of true positive and false positive activations, as illustrated by Figure 2. For True Positive scenarios, AEB could potentially activate in different types of collision; offering a casualty saving by avoiding or mitigating the severity of a collision but also potentially risking an increase in the frequency or severity of injury to bus occupants due to falls. The STATS19 database, the bus fatal database and CCTV footage from a bus operator were used alongside data compiled within the system verification and road trial parts of this project to estimate the likely effects on casualty numbers as a result of fitting AEB.

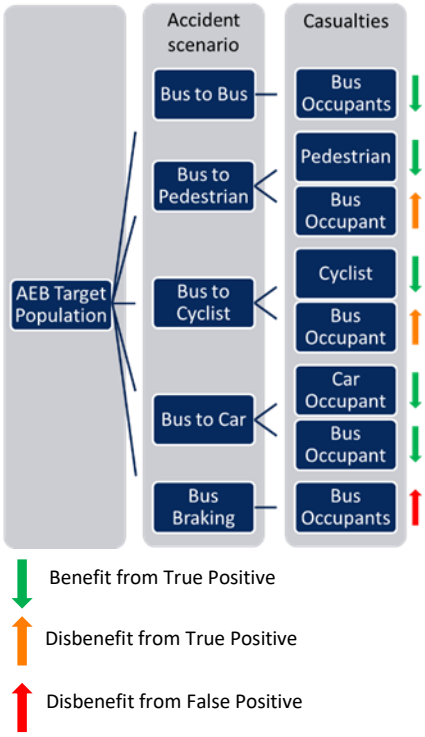

False Positive incidents represent cases in which the AEB system activates when it should not have done so. The effect of such incidents was estimated by analysing the typical bus occupant injury outcome of non-collision incidents caused by vehicle braking (road trial, IRIS data and operator CCTV data) and the magnitude of acceleration applied in false positive activations (road and track trials).

The true positive benefit of the system was evaluated on a case by case basis across the samples of police fatal and operator CCTV data available, using reconstruction, calculations and engineering judgments to assess whether the system was likely to have avoided the collision or reduced the impact speed. It was assumed that the above samples were broadly representative of Britain's official Road Accident Statistics (STATS19) data set within the Greater London Area. Therefore, the estimated effect identified in those samples was applied to a similar data set from STATS19 to estimate the casualty savings that could be expected within London each year.

Figure 2: True positive and false positive analysis

True Positive Analysis

For car occupant, pedestrian and cyclist casualties completely avoiding the accident or reducing the impact speed was expected to reduce the number and/or severity of casualties since the magnitude of deceleration experienced during the impact was likely to be greater than that experienced during braking. For bus occupants injured in collision with cars and other vehicles then collision avoidance or a reduction in collision speed would also be expected to substantially reduce the acceleration they experience and, hence, the probabilities of falls or other injuries which may otherwise be likely because of the fact they are standing or seated but unrestrained. However, when a bus hits a pedestrian or cyclist, the acceleration caused to the bus by the impact is negligible. So, the benefit to the bus occupant of avoiding or mitigating the collision is also negligible. An AEB system can brake no harder than the best human driver, so in the best case, there is no difference to the level of risk from braking. However, it is well documented, for example (Perron, et al., 2001) (Dodd & Knight, 2007) that many human drivers do not fully exploit the maximum braking performance available to them and may brake less sharply than the best human driver. Therefore, in some circumstances, an AEB system could brake harder than the average human driver which could increase the frequency or severity of injuries on board the bus.

Of course, emergency braking does take place in bus to pedestrian collisions where AEB is not fitted. Thus, the number of bus occupants injured in single vehicle collisions with pedestrians was taken as a baseline. Data on the

distribution of on-board injuries in relation to peak deceleration, taken from the study of bus operator CCTV incident records, was combined with data on the average occupancy of buses to estimate how this baseline number might change if AEB were fitted to all vehicles.

False Positive Analysis

In a genuinely false positive situation, automated braking always creates a risk of injury to bus occupants that would not have existed if AEB was not fitted. However, it is worth noting that, true and false positives are not as binary as the name implies. There are many situations where whether an activation should be considered false is open to significant interpretation and several studies have considered additional categories of 'premature' positive, near miss, or even desirable false positive, e.g. Lubbe (2014). These are activations that occur where there is a clearly recognisable hazard that prompts the activation but where the activation occurs at a time where the driver considers themselves aware of the risk and able to avoid it themselves without assistance. In addition to this, a false positive does not necessarily mean the brakes are applied until the vehicle comes to a complete stop. The sensing, detection and decision system may 'make a mistake' and activate the brakes but may also 'realise it's error' only a short time later and subsequently release the brakes. Thus, false positives could potentially be of much shorter duration than true positives (i.e. a lower change in velocity).

At the time of the project no published information was identified to confirm the typical false positive rate experienced by comparable AEB systems in production, the proportion of those that were completely false or just premature, or the proportion that were momentary blips of the brakes compared to full emergency stops.

RESULTS

The two main questions that this research was aiming to answer were:

1. Does the fitment of AEB on buses produce a net safety benefit?
2. If so, develop a test procedure and rating system that can be used to encourage the most effective systems

Does the fitment of AEB on buses produce a net safety benefit?

True Positive Collision Situations. Collision data for London shows that in terms of fatalities from collisions with buses, by far the largest group is pedestrians. AEB was expected to be of benefit where the bus was travelling at normal traffic speeds and the pedestrian crossed the road in front of them or was walking along the road in the same direction as the bus. AEB was not expected to be of benefit where the bus was turning into or out of a side road at the time of collision or where the vehicle was just moving off from rest. A total of 21 relevant fatalities (with sufficient information for the reconstruction) were identified in the Police data and a total of 27 relevant non-fatal casualties were identified in the operator CCTV data. All cases in the sample were crossing scenarios.

For the fatalities, the travel speeds of the buses involved was between 5 and 36 mile/h with an average of 20 mile/h. This is likely to reflect the prevailing speed limits and traffic collisions typically resulting in low travel speeds in London. It was found that in all cases, there was less than 2 seconds available between the pedestrian becoming recognisable as a collision threat and the moment of impact, with an average time of just 0.76 seconds. Given typical human reaction times of between 0.75 and 1.5 seconds, e.g. (Olson & Farber, 2003), then avoiding collisions would be very challenging for human drivers. The study found evidence to show that 45% of the drivers involved did manage to react before impact but even in these cases the action was insufficient to avoid collision and the average impact speed was in fact only 1 mile/h less than the average travel speed before reaction.

For the non-fatal casualties, identified in the operator CCTV data, the bus travel speeds were very similar, ranging from 11 to 30 mile/h with an average of 17 mile/h. However, in these cases, the time between the pedestrian first becoming recognisable as a possible collision threat and the moment of impact tended to be greater, with a range from 0.7 seconds to 4.1 seconds, and an average of 2 seconds (1.24s longer than in the fatal cases). This translated to a higher proportion of drivers reacting before collision (87%) and a greater reduction in speed at the moment of impact, with impact speeds ranging from 7 to 15 mile/h, with an average of 11 mile/h (8 mile/h less than the average in the fatal cases). In the CCTV data it was also possible to calculate the amount of time that passed between the

pedestrian first becoming recognisable as a collision threat and the moment the driver first took avoiding action. This was found to range between 0.7s and 3.9 seconds, with an average reaction time of 1.9 seconds, slower than might be expected based on the body of laboratory and test evidence, e.g. (Olson & Farber, 2003) (Coley, et al., 2008), typically used in collision reconstruction. However, the case involving the 3.9 seconds was a bit of an outlier in an unusual case where the moment the pedestrian became a threat was open to interpretation. Ignoring this case changes the reaction times to between 0.7 and 2.5 seconds with an average of 1.7.

The peak accelerations achieved during braking were available and ranged between -1.4 m/s^2 -8.7m/s^2, with an average of 4.3m/s^2. Mean accelerations over the course of the stop were considerably lower with an average of 2.9 m/s^2. This is likely to reflect the well documented fact (Perron, et al., 2001) (Dodd & Knight, 2007) that drivers often do not exploit the maximum braking available to them. Some stakeholders have suggested this may be exacerbated for bus drivers by the training they are given to brake gently during normal driving to help prevent passenger falls.

In each case, the potential benefit of AEB was assessed by replacing the actual driver reaction, with an AEB reaction. The AEB applied braking was assumed to commence at the lesser of the time to collision (TTC) at which the pedestrian became recognisable as a threat minus a system reaction time, or a range of TTC at which the AEB in the prototype bus actually commenced braking in the true positive track tests. The acceleration applied was the lower of the level required to avoid impact or the maximum that the system could achieve. A new impact speed was then calculated based on the initial travel speed, the moment of AEB activation and the level of deceleration applied.

The maximum deceleration that could be applied by an AEB system on a bus was initially based on the levels observed in track tests of the prototype system. However, the debate between maximising protection to collision partners and minimising risks to bus occupants meant that it was conceivable maximum deceleration should be capped. Thus, three 'nominal' systems were defined based on maximising deceleration (9 m/s^2 peak) or capping peak deceleration at either 7 or 5 m/s^2.

Across all the variations, it was found that between 10% and 48% of the fatal sample and between 48% to 89% of the non-fatal sample could potentially have been avoided by fitting AEB. In addition to this, the results suggested that 14% to 43% of the fatal sample could have had at least some mitigation of impact speed and 4% to 41% of the non-fatal sample. It should be noted that the uncertainty in some parameters meant that ranges were used and thus there is overlap in the populations for avoidance and mitigation. That is, where a case would definitely have been avoided it will not appear in the mitigation figures. Where a case definitely cannot be avoided it may appear in neither figure or the mitigation only. Where there is some chance of avoidance but, if not avoided, a better chance of mitigation, then it appears in both sets of figures.

It was found that a large proportion of the benefits obtained above, were obtained due to an earlier braking intervention than provided by the driver. However, it was also found that on average, the AEB would have applied greater deceleration than the population of real drivers did, even though in some individual cases the AEB had to apply less deceleration to avoid the collision than the driver eventually applied later in failing to avoid collision. On average, the AEB systems increased the mean braking deceleration from 2.9 m/s^2 to between 3.0 and 5.5 m/s^2, depending on the system characteristics assumed.

Analysis of the CCTV data highlighted that for different ranges of peak deceleration, the proportion of passengers that sustained slight or moderate injuries increased with increasing deceleration (Figure 3). The difference between the proportion of occupants injured from AEB braking to the proportion of occupants injured during driver-applied deceleration represents an additional risk to bus occupants. By applying the change in acceleration from driver-controlled to AEB-controlled to all bus occupants on board at the time of the pedestrian incidents, the total number of bus occupant injuries was estimated. It was assumed that all buses involved in collisions with pedestrians had the average number of passengers on board (19.3)[1].

[1] Source: DfT Bus Statistics Table BUS0304 data for London in 2016/17. Note that the equivalent figure for England excluding London is 9.5 suggesting any risk to occupants would be substantially lower outside of London

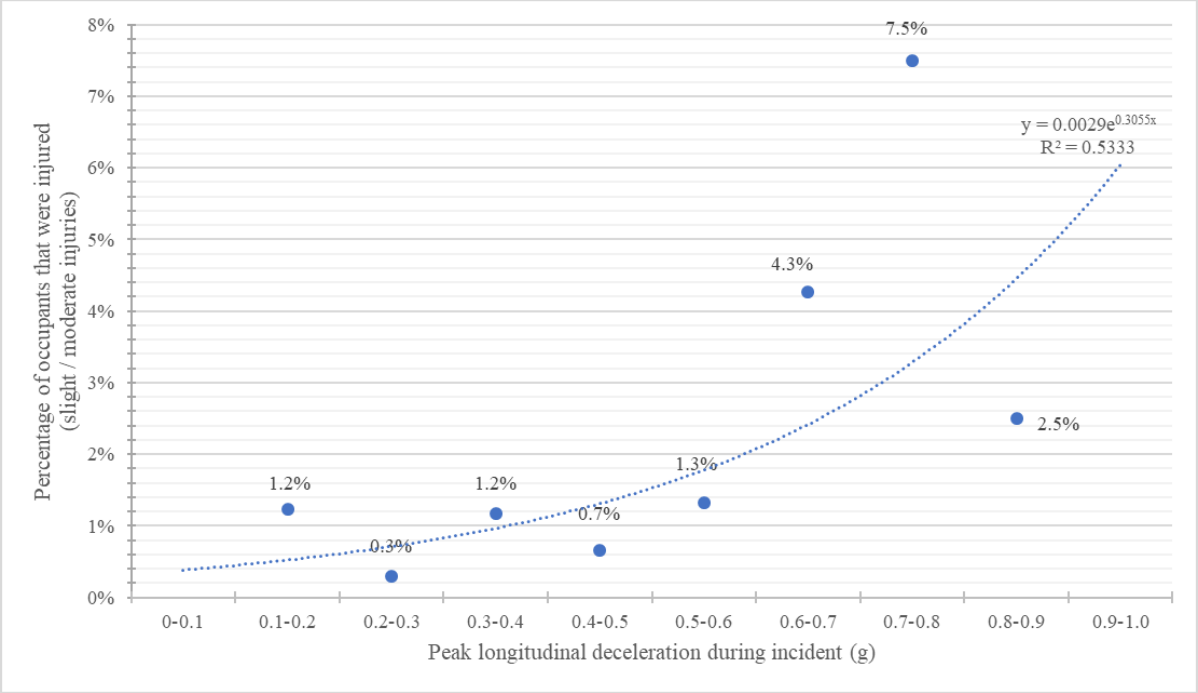

Figure 3: Proportion of occupants on board the bus that were injured during braking events, by magnitude of peak deceleration. Source: Sample of operator CCTV collision records.

This form of analysis was repeated for collisions with cars, other buses, and cyclists. The percentage effectiveness figures were combined with total casualty populations derived from the UK national accident database (STATS19) restricted to London only and the total net casualty effects in true positive situations was calculated.

False Positive Situations. If the AEB system were to apply braking in a situation where most careful competent and alert human drivers would not have applied braking, it can be considered a false positive. In this situation, the braking creates a risk of injury to bus occupants, and potentially other road users though they should still be travelling at a distance to be able to avoid collision with the braking bus. A subtle but important distinction is that this is different from a situation where the system applies braking in response to a recognisable threat of collision but that this is applied a little too early. Such interventions can annoy the driver but are much less likely to cause a direct injury risk because there was a genuine need for braking, whether human or system applied. With a prototype vehicle that had not yet undergone tuning to eliminate false positive brake applications, 17 false system activations were logged during the road trial where braking would have occurred if the system was fully operational. In seven cases, the system demand would have been limited to a deceleration 4m/s² and in the remaining 10 cases it would have peaked at a demand of between 8.0m/s² – 9.8m/s²).

What the brake system would actually have delivered in response to these braking demands depends on the duration for which they were demanded and the initial speed because air brake systems are relatively slow to react and build up compared with hydraulic systems. To estimate this lag, information from the vehicle manufacturer and data from the true positive test programme was used. Firstly, the manufacturer indicated that it would take approximately 0.15 seconds for the AEB demand signal to be delivered to the braking system. In addition, the results from the true positive tests then showed that it would take a further 0.05 seconds before the deceleration began to significantly ramp up (Figure 4).

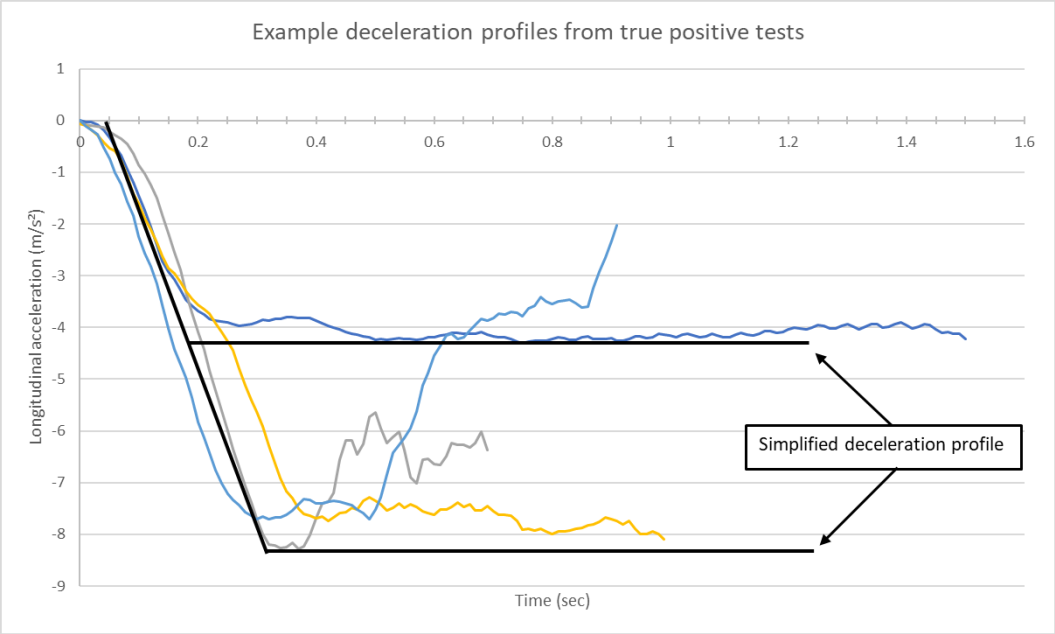

Figure 4: Example deceleration profiles from true positive test

Based on this information, a simplified deceleration profile of the actual level of braking that occurred during each false positive event was calculated, as illustrated by the example in Figure 5.

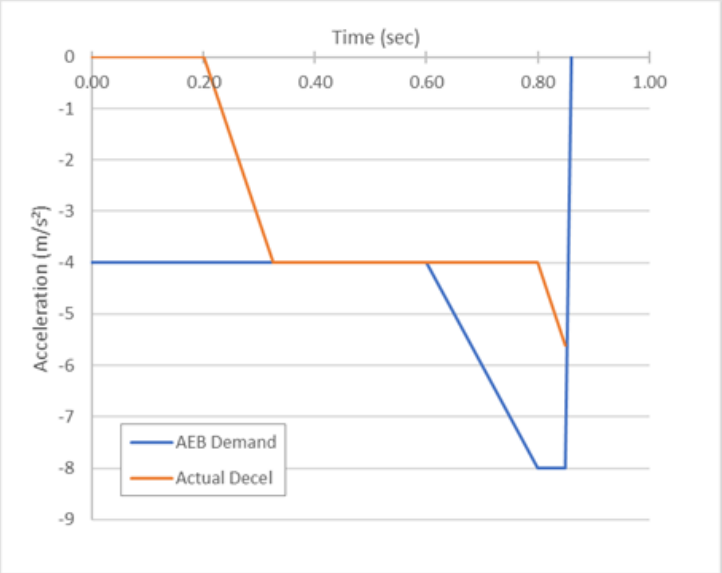

Figure 5: Comparison of braking demand and actual estimated braking

The estimated response of the braking system was applied to the level of deceleration demanded by the system and the actual peak deceleration calculated. Figure 6 shows that in some cases, the actual peak deceleration of the bus was lower than the peak demand, and in four of the 17 false positive events (24%) the duration of the demand would have been too short for there to be any deceleration at all.

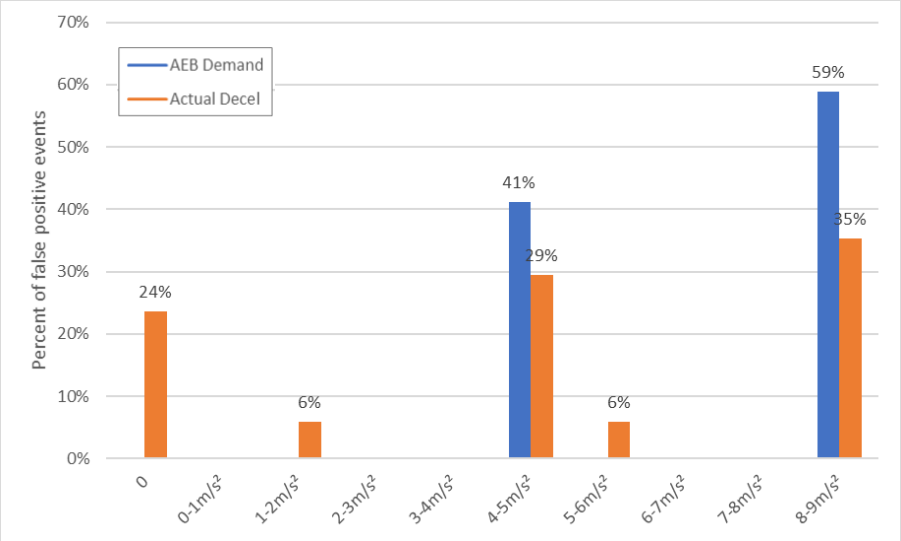

Figure 6: Comparison of AEB demand and actual deceleration for false positive events (road trial)

The false positive events that produced the greatest peak deceleration were all cases in which the level of deceleration ramped up over the duration of the event. Feedback from the manufacturer indicated that this was a result of running the AEB system in an "open loop" mode such that no actual braking took place. For example, Figure 7 shows one event where the AEB system initially demanded a deceleration of 4m/s². The system will check in the next instant and detect that no actual braking had occurred and that the vehicle was now closer to the hazard such that a higher level of deceleration is required to avoid a collision. In reality, a production system would have responded to the initial demand so the ramp up of acceleration may not have occurred or may have been smaller.

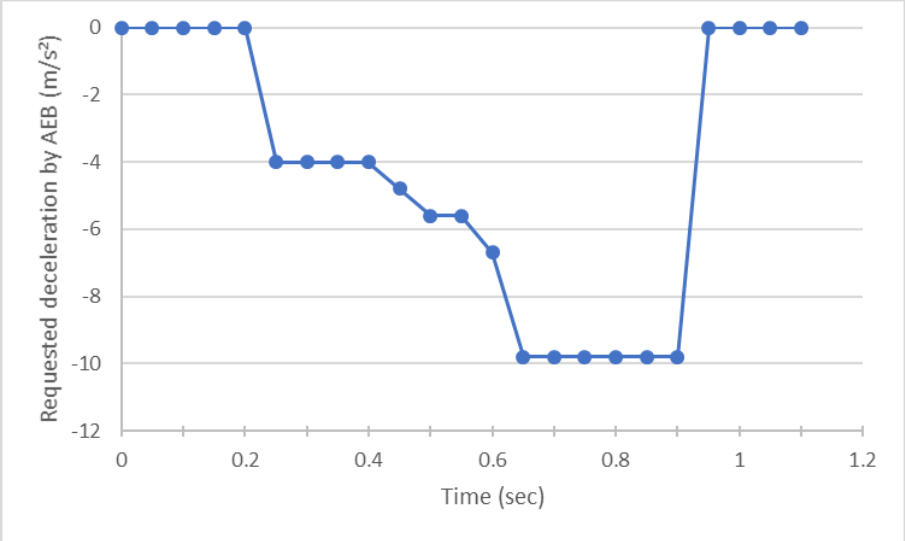

Figure 7: Example of increasing AEB brake demand during open-loop operation

The peak value of deceleration that would have been requested during normal "closed-loop" operation is unknown, but it is reasonable to expect that it would be somewhere between the initial requested deceleration of 4m/s² and the peak deceleration of 7.5m/s² observed during the track tests involving false positive scenarios.

In order to translate information on the deceleration achieved during false positive brake applications to their potential for casualties it was necessary to understand how many falls and injuries occur as a result of braking acceleration more generally. A range of laboratory experimentation has attempted to assess thresholds below which

standing occupants would not fall. For example, (De Graaf & Van Weperen, 1997) found that even very low accelerations (<1/5 m/s2) could make a standing occupant fall. They also showed that the rate of change of acceleration (or brake jerk) could be a significant factor in making people fall. The effect of acceleration on the frequency of falls can also be quantified from existing real-world data about buses not equipped with AEB.

The average number of driver-applied brake events per km was recorded during the 400km road trial and divided by peak deceleration. In the relatively short road trial no emergency brake activations were required, so the results were extrapolated to estimate the potential frequency of higher deceleration events (Figure 8). Applying these figures to the total number of bus vehicle km travelled in London each year (490million[2]) gave an estimate of the number of deceleration events that occur in London each year by peak deceleration.

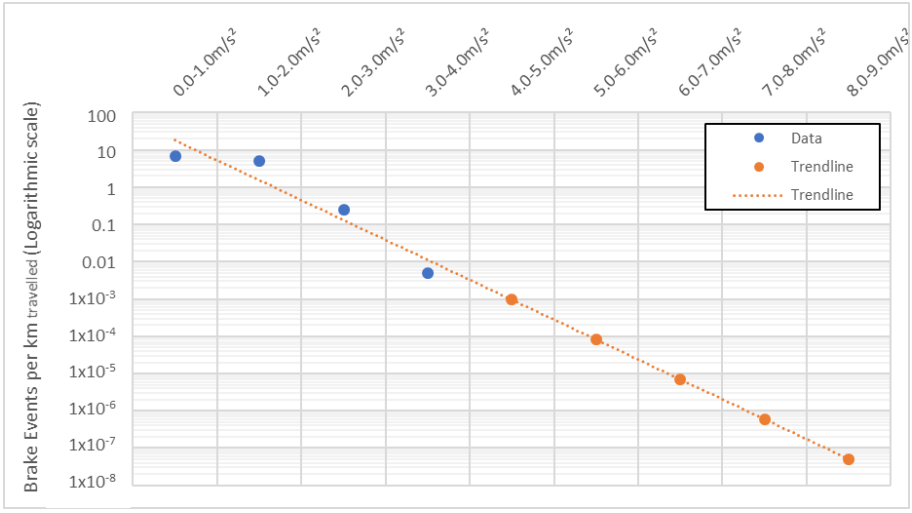

Figure 8: The frequency of brake applications in normal London bus service, by level of peak deceleration.

Data from the CCTV analysis (Figure 9) shows the proportion of casualties that occur at each acceleration level.

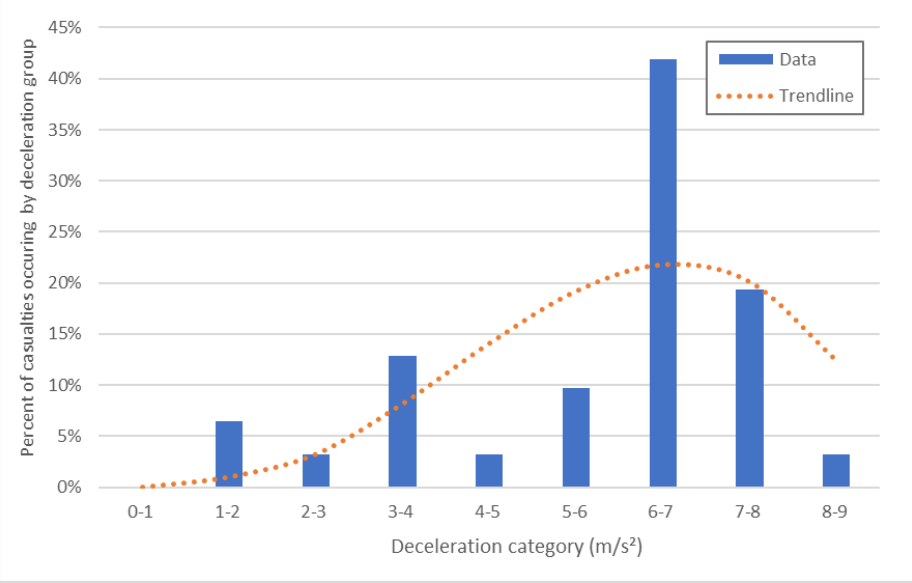

Figure 9: Proportion of bus occupant casualties that fell under braking by peak deceleration.

[2] Source: DfT Bus Statistics Table BUS0203b. Note TfL data suggests a total of 492.3 million bus km for 2016/17

Analysis of the IRIS database identified an average of 974 casualties per year that resulted from non-collision incidents in which braking was coded as the cause of the injuries. Combining this total with the proportions in Figure 9 produced an estimate of the annual average number of London bus occupant casualties that occur at each braking level. Combining this with the frequency of brake events by deceleration allows an estimate the number of casualties per braking event at each acceleration level. The results are shown in Table 1, below.

Table 1: Estimated number of casualties per braking event by deceleration level

Deceleration (m/s^2)	Brake events/year in london buses (number)	Bus occupant casualties per deceleration event (rate)
0.0-1.0m/s^2	3,277,342,050	0.00
1.0-2.0m/s^2	2,420,568,735	0.000000026
2.0-3.0m/s^2	119,064,478	0.00000026
3.0-4.0m/s^2	2,454,938	0.000051
4.0-5.0m/s^2	468,428	0.000067
5.0-6.0m/s^2	40,020	0.0024
6.0-7.0m/s^2	3,419	0.12
7.0-8.0m/s^2	292	0.65
8.0-9.0m/s^2	25	1.26

This analysis shows that the laboratory experiments on balance and falling cannot be taken to directly map to a probability of falls. It certainly does happen that standing passengers fall at accelerations of 1.5 m/s^2 as expected by (De Graaf & Van Weperen, 1997). However, in real service with more than 2 billion brake applications in London each year reaching that sort of level, then if a fall was anything but extremely rare in light braking, then the total number of casualties from falls under braking would be huge. The empirical evidence (974) suggests that this is not the case. Based on the CCTV study, the proportion of those at less than 2 m/s^2 is small. Overall, the probability of injury as a result of that level of acceleration is tiny. The probability of injury rises very sharply at accelerations of around 5 or 6 m/s^2.

Net effect of true and false positive situations. Given the information above, and knowledge of how many false positives brake applications would be likely to occur in service, it was possible to estimate the total number of bus occupant casualties that would occur as a consequence of false positives. The casualties were divided by severity based upon the observed distribution in bus occupant falls resulting from normal bus driving. However, at this stage of the research, and of the development of the prototype system that has been studied, the eventual false positive rate of a production London bus system is fundamentally unknown. The rate observed during the road trial with the early prototype vehicle is in no way indicative of expectations of the final production version. No published information has been identified that can confirm the typical false positive rate experienced by comparable systems already in production. Thus, results have been expressed in terms of the effect on casualties given different assumptions about the distribution of decelerations in false positive events and different frequencies of events (Figures 10 and 11).

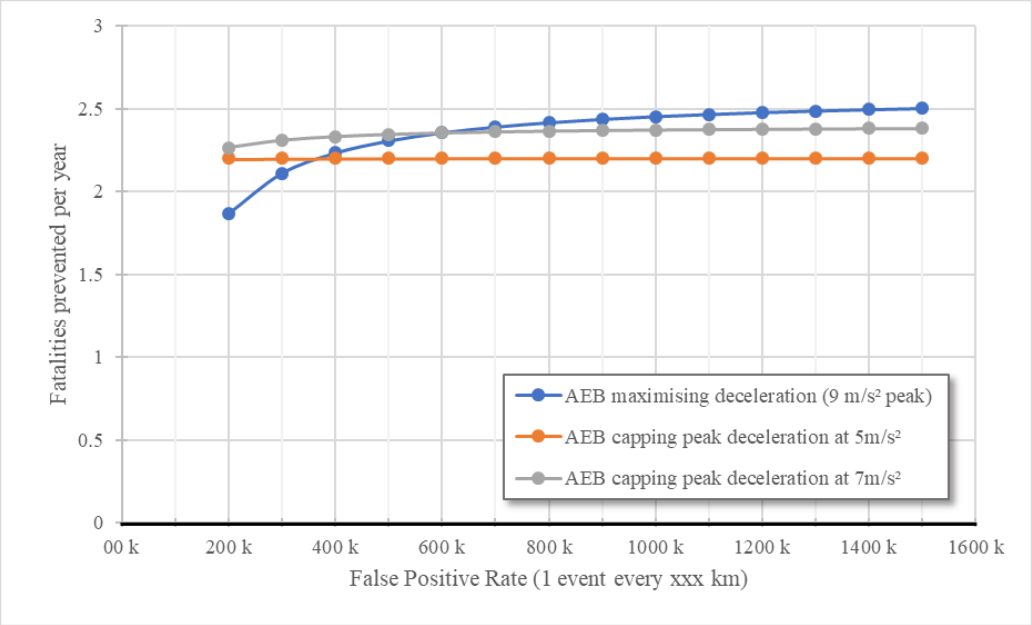

Figure 10: Central prediction of AEB effect on fatalities by false positive rate

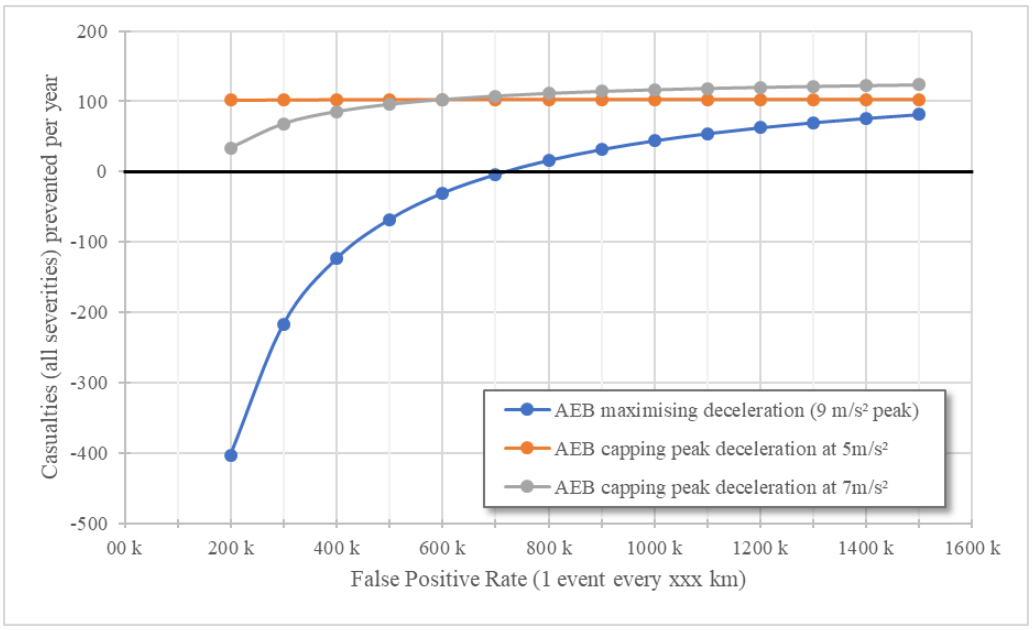

Figure 11: Central prediction of AEB effect on casualties of all severities by interval between false positives

It can be seen that the smaller the distance travelled between false positives, the less the benefit is. At intervals between false positives of greater than 700,000km, all of the AEB braking strategies considered offer a net benefit in terms of the total number of casualties prevented. For fatalities, the most effective system is that with the highest deceleration provided a good false positive rate is achieved. However, this is the least beneficial system if all casualties are considered, because of the effect of false positives on bus occupants falling under braking, which predominantly result in slight injuries. In order to balance these considerations, the casualties were monetised according to standard valuations provided by the UK Department for Transport and the results are as shown in Figure 12, below.

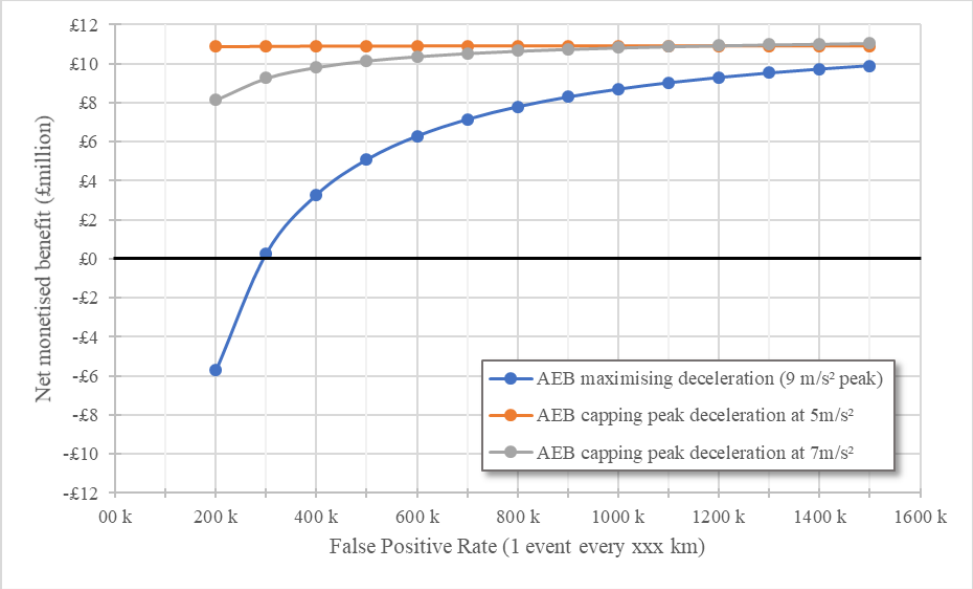

Figure 12: Central prediction of AEB effect on net monetised benefit of casualty prevention, by interval between false positives

Development of test procedures and rating scheme

Test Scenarios. The approach of this project was to base decisions on the inclusion of different test scenarios, and the weighting of each variable within an overall test score, based on the risk to casualties defined using casualty data extracted from the STATS19 database. On this basis, the following test scenarios were selected for inclusion in the Bus AEB test protocol (equivalent EuroNCAP test code shown in brackets):

- Pedestrian crossing.
    - Adult walking from nearside (CPNA-25 & CPNA-75)
    - Adult running from farside (CPFA-50)
    - Child walking from nearside - obstructed by car (CPNC-50)
    - Longitudinal cyclist - 25% and 50% overlap (CBLA-25 & CBLA-50)
- Bus to stationary car (CCRs)

The adult walking from nearside test is to be repeated in night-time conditions because the collision statistics show that performance at night in street lit conditions will be an important feature of an effective system.

Longitudinal pedestrian tests were not included because the collision data highlighted that, over a 10-year period, there were no pedestrian fatalities with a bus when the pedestrian had been walking along in the road. Cyclist crossing tests were also excluded because the prototype vehicle that was used for testing in the project was unable to achieve significant performance in this configuration.

In addition to the above tests, an aborted crossing test was also added to assess the false positive performance of a system. It has the same test geometry as the true positive test that assesses an adult walking from the nearside. However, instead of crossing into the path of the bus, the VRU dummy stops at varying lateral distances from the path of the bus. An effective system will need to activate before the pedestrian enters the path and the scoring is set such that it is acceptable to activate s small distance outside the path but where activations occur while the pedestrian is still at greater distances, the score is penalised to disincentivise this.

A 'bus stop' scenario was also added based on some of the false positives observed during the road trial (Figure 13). For this false positive test, the vehicle follows an s-bend path driving past a stationary pedestrian positioned to the

nearside of the vehicle. At all times in this test the VRU is easily avoidable by steering and, therefore, the AEB should not intervene. Thus, passing this test is considered a pre-requisite that all vehicles must achieve. However, a concern was flagged that the easy way to achieve this would be to switch off AEB whenever steering angle was applied, which would be undesirable. To ensure that this does not happen, a true positive version of this scenario was also included. For the true positive case, test geometry is the same as for the false positive test except that the pedestrian movement is configured such that it is on a collision course with the centre of the front of the bus.

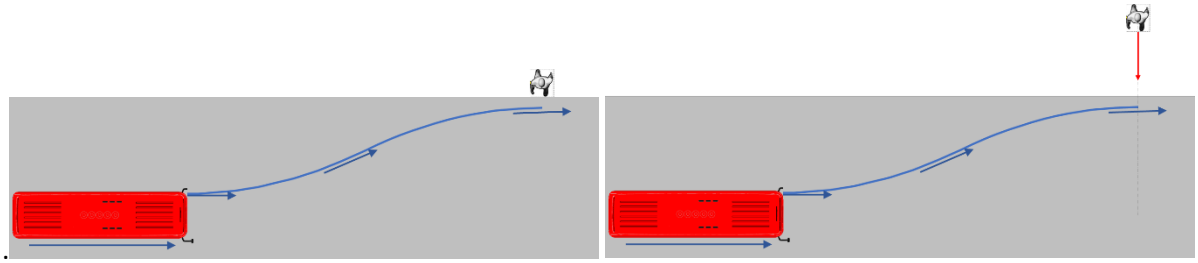

Figure 13: Bus- stop tests. False positive test (left), true positive test (right)

DISCUSSION

Strong potential benefits of fitting AEB to city buses exist in true positive situations, in particular for preventing pedestrian fatalities. Up to around 25% of pedestrian fatalities caused in collision with a bus could be prevented. In addition to this, there are significant benefits in reducing more minor collisions with other vehicles, particularly cars and buses. This will have little effect on fatality statistics but should benefit bus operators in terms of reducing high frequency damage and low severity injury claims, reducing operating costs and downtime.

The risk that AEB causes injury to unrestrained or standing bus occupants in true positive situations exists but is very low due to low numbers of true positive events, potentially earlier brake intervention and only small increases in required decelerations compared to those recorded in driver applied situations.

The risk to bus occupants as a consequence of falls during false positive events is substantial and a good false positive rate is very important to minimise this risk. The level of deceleration applied in false positive events will also be very important.

Permitting an AEB system that maximises the braking performance of the bus (AEBmax) has the potential to save the most fatalities, provided that false activations occur less than once every 600,000 vehicle-km on average. However, capping peak deceleration to a maximum of 7 m/s^2 has the potential for the largest reduction in monetised casualty benefit. This is because the analysis shows that the reduced deceleration substantially reduces the risk of large numbers of slight injuries to bus occupants as a consequence of false positive activation while reducing the monetised benefits to fatalities by less.

However, this analysis will only hold true if the correlation between the risk of injuries to standing and seated but unrestrained occupants is with peak deceleration only. Experimental data suggests that the rate of change of deceleration (brake jerk) is also an important factor in the risk of injury. The empirical analysis could not account for that factor and with a capped deceleration there would be an incentive to increase the brake jerk to improve true positive performance. Thus, there is a risk capping deceleration could fail to achieve the benefits expected by the analysis or even reverse them.

The analysis of benefits versus disbenefits is also very strongly dependent on two key input parameters that are weakly based (due to small sample sizes): the frequency with which heavy brake applications ($5m/s^2+$) occur in real service and the frequency with which bus occupant casualties occur under different levels of braking acceleration. This is particularly true when considering an AEB system that can apply peak braking of 9 m/s^2. Further research is proposed to increase the sample size available for these elements with a view to increasing confidence in the results.

Requirements have been developed for AEB that effectively define a minimum standard that must be achieved in terms of true and false positive performance to be considered an AEB system suitable for a London bus. In addition to this, the tests then measure and rate additional performance in excess of this standard. Thus, if implemented in an appropriate purchasing specification in this form, the market would be free to choose how to implement AEB in terms of deceleration levels, brake jerk etc.

The test track assessments developed are based on the Euro NCAP tests for cars, with adaptations to account for different collision patterns observed with London buses. The assessments contain two novel false positive tests because of the degree to which false positive rate is considered critical to the net benefit of the system. However, the track test assessments merely ensure to the extent possible that the systems are well designed and will work in the real world. There are an almost infinite range of circumstances that can be encountered in the real world and not all can be tested on a test track. It is, therefore, very important that industry design for real world use and not just test track performance. This is of particular concern in relation to false activations. The inclusion in any resulting specification of a requirement for industry to demonstrate to TfL how they have satisfied themselves that they will achieve a defined false positive rate in the real world, would add additional reassurance of proper design diligence.

CONCLUSIONS

AEB on city buses offers clear potential benefits in true positive situations, particularly in collisions involving pedestrians, preventing up to around 25% of pedestrian fatalities based on the analytical modelling presented in this paper.

False positive activations clearly risk significant increases in typically lower severity injuries to bus occupants who are standing or seated but unrestrained. The frequency with which false positives occur, and the deceleration achieved in false positive events will be critical to the success of any implementation.

Analysis suggests that if, in service in a busy city, the average interval between false positives is more than 600,000km, then substantial net benefits would be achieved.

The analysis is particularly sensitive to two results derived from small sample sizes and additional research is planned to improve the robustness of the data.

REFERENCES

[1] Coley, G., Wesley, A., Reed, N. & Parry, I., 2008. *Driver reaction time to familiar but unexpected events,* Crowthorne: TRL Published Project Report PPR313.

[2] De Graaf, B. & Van Weperen, W., 1997. The retention of balance: An exploratory study into the limits of acceleration the human body can withstand without losing equilibrium. *Human Factors,* pp. 111-118.

[3] Dodd, M. & Knight, I., 2007. *Technical Assistance and Economic Analysis in the Field of Legislation Pertinent to Automotive Safety: provision of information and services on the subject of brake assist systems,* Brussels: European Commission.

[4] Edwards, A. et al., 2017. *Analysis of bus collisions and identification of countermeasures,* Crowthorne: TRL Project Report PPR819.

[5] Lubbe, N., 2014. *Integrated pedestrian safety assessment methodology,* Gothenburg: Chalmers University of Technology.

[6] Olson, P. & Farber, E., 2003. Forensic aspects of driver perception and response. *Lawyers and Judges,* pp. 313-357.

[7] Perron, T., Kassaagi, M. & Brissart, G., 2001. *Active Safety Experiments with common drivers for the specification of active safet systems,* Amsterdam: Proceedings of the 17th international technical conference on the enhances safety of vehicles, US DOT.

AMOK SAFETY LOCK (ASL)

DEVELOPMENT AND DEMONSTRATION OF A NEW FUNCTION FOR THE PREVENTION OF INTENTIONAL VEHICLE MISUSE AGAINST PEDESTRIANS

João Graciano, Miso Kvesic, Thorsten Scheibe, Dr.-Ing. Dominik Kufer, Dr. Roland Kallweit

IAV GmbH Ingenieurgesellschaft Auto und Verkehr
Carnotstraße 1
10587 Berlin
Germany

Paper Number 19-0317

ABSTRACT

Most fatalities and serious injuries in traffic result from accidents caused by human error. Today, a series of driver assistance functions exist to help avoid or reduce the severity of such accidents (e.g. Autonomous Emergency Braking), while still allowing the driver to interrupt the function at any time. This overriding behavior – mandated by the Wiener convention [1] – is particularly important in the case of an incorrect function activation on the part of the vehicle's system. Due to this built-in override functionality, driver assistance functions – which typically support the driver in de-escalating a critical situation – cannot help preventing cases where drivers actively target pedestrians with the vehicle (as in recent vehicle ramming attacks). This makes clear the need for active safety functions able to prevent the driver from (intentionally or unintentionally) causing harm to other traffic elements. The function Amok Safety Lock (ASL) was developed as a prototype function to research the possibility of increasing the safety of pedestrians in the case of vehicle misuse. The function ASL looks at the driver's driving behavior, the predicted vehicle's motion and the relative positions and motions of pedestrians in the vicinity of the vehicle to identify an imminent collision. If the driver does not act to de-escalate the situation, the function initiates an emergency braking maneuver without the possibility of overriding. Simultaneously, warning signals (horn, front and turn lights) are emitted to alarm the pedestrians nearby. This behavior was confirmed in both simulations and vehicle tests using IAV's Vehicle-in-the-Loop approach. Due to its unilateral behavior, changes in the legal framework are necessary before such a function can be deployed.

INTRODUCTION

Motivation

Advanced Driver Assistance Systems (ADAS) are a key feature of modern vehicles and have contributed to a significant reduction in traffic accidents and traffic-related deaths [2]. One such function is the Autonomous Emergency Braking (AEB), nowadays available for most light and heavy vehicles: it uses environment information gathered by sensors to identify an immediate collision with another traffic element and, if the driver is unresponsive, activates an emergency braking maneuver and relevant safety systems (e.g. safety belt). Due to regulations put in place at both international [1] and national level [3], all ADAS functions are required to allow an override by the driver at any time. Due to this override capability, ADAS-functions are incapable of preventing drivers from causing injuries to other traffic elements (of which pedestrians are the most vulnerable), as demonstrated by the numerous terrorist attacks which saw drivers intentionally targeting pedestrians with vehicles [4]. To prevent such cases a function is necessary that takes control *away* from the driver, a requirement that clashes directly with the need for the permanent possibility of an override.

To bridge these two conflicting requirements and at the same time contribute to the discussion over regulations for advanced driver assistance functions, a new active safety function Amok Safety Lock (ASL) was developed at IAV GmbH, which can unilaterally trigger an emergency maneuver if the driver intention is recognized as nefarious.

Scenarios

The recent cases of terrorist ramming attacks [4, 9] provide some hints for defining the functional range of the ASL function and therefore to identify the relevant scenarios. Approximately 86% of the fatalities happened in public streets or public gatherings [9]; in all situations, the driver intentionally accelerated while steering to target pedestrians; and it continued to do so even after a first collision (that is, it was not a one-off situation). With these characteristics in mind, a representative scenario was developed and used as reference for the demonstration of the ASL functionality (see Figure 1. The reference scenario for the Amok Safety Lock function: the vehicle leaves the road and targets pedestrians). In this scenario, the driver steers the vehicle outside of the road and targets pedestrians. Taking this scenario as reference, several scenario variations were developed to validate the function's behavior. In these scenarios, the following characteristics were varied and combined:

- On-road vs. off-road
- Driver steering and acceleration/braking behavior
- Avoiding vs. targeting behavior
- Parking speed vs. attack speed
- Relative position of other pedestrians (avoidance maneuver available vs. not available)
- Prediction of pedestrian motion (static vs. dynamic)

Figure 1. The reference scenario for the Amok Safety Lock function: the vehicle leaves the road and targets pedestrians

FUNCTIONAL ARCHITECTURE

The functional range of the ASL function was initially divided into four high-level requirements:

a) The driver intention shall be estimated;

b) Potential collisions with pedestrians shall be predicted;

c) Potential collision avoidance maneuvers shall be identified;

d) If the driver's intention is estimated as nefarious (no de-escalation of the situation) and an unavoidable collision with at least one pedestrian is identified (i.e. no collision avoidance maneuvers available), the ASL function shall bring the vehicle into a safe state and trigger warnings to the immediate surroundings, without the possibility of an override by the driver.

The functional architecture of the ASL function closely follows this breakdown and was implemented as illustrated in Figure 2. System overview and main functional blocks of the ASL function. All the functional blocks are executed in real-time such that, should the conditions change, the function can immediately react.

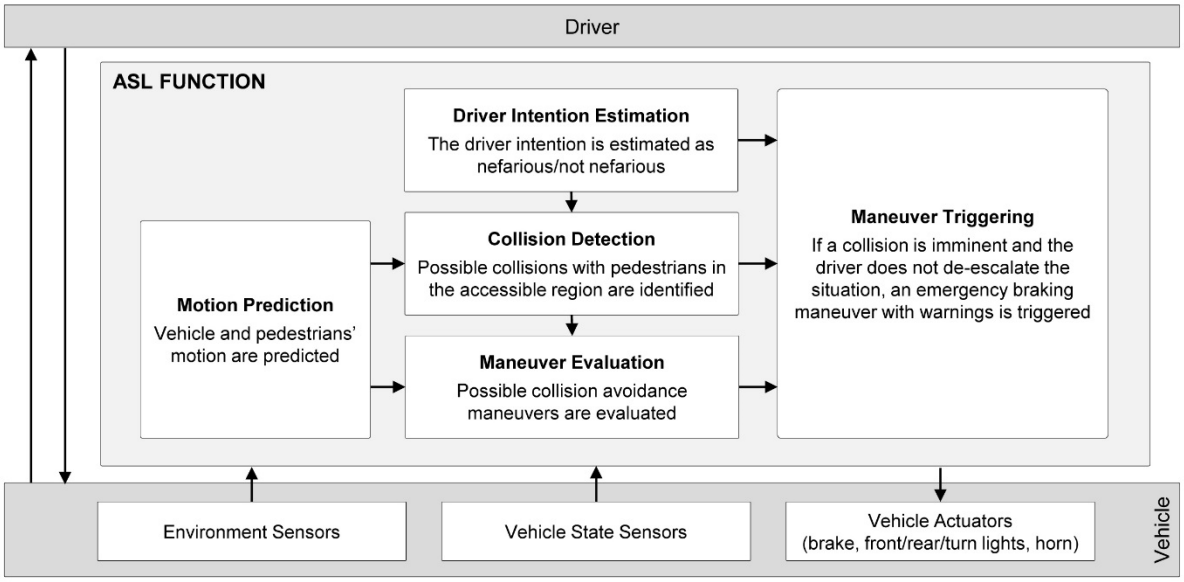

Figure 2. System overview and main functional blocks of the ASL function

Estimation of driver intention

A driver typically de-escalates a dangerous collision situation by braking and/or steering the vehicle away from the collision. To estimate the driver's intention ('requirement a' above), the ASL function monitors the gas and brake pedals, and the steering wheel. The driver's intention is classified as "nefarious" if the driver does not steer the vehicle away from pedestrians and/or does not reduce speed (i.e. does not press the brake pedal). If the driver does act to avoid the collision, no triggering of the emergency braking maneuver takes place, even if his actions are evaluated as insufficient to completely avoid the collision.

To further support the estimation of the driver's intention and minimize the probability of an unjustified ASL triggering (particularly important considering the significant impairment the ASL causes to the driver), two additional criteria are taken into account:

- Information about the road limits (road marks, curb, high-precision positioning) is used to determine if the vehicle is driving *on* or *outside* the road. The ASL function is allowed to trigger a collision avoidance maneuver only after the vehicle leaves the road (vehicle state changes from in- to off-road);
- The vehicle's speed is used to limit the ASL activation: an emergency maneuver can be triggered only if the speed is within a given range (currently 10 km/h – 80 km/h). This helps eliminating cases where the vehicle moves very slowly and accidentally touches a pedestrian (e.g. vehicle driving slowly through a crowd) and general cases where damages are expected to be minor.

Motion prediction

For the prediction of the pedestrians' motion, and due to the relatively short time-scales involved in typical collision-scenarios (milliseconds to a few seconds), a relatively simple motion model assuming constant speed was used (more complex models are possible [8]). To predict the vehicle's motion the ASL function uses a clothoid-based approach which takes into account vehicle-specific dynamical characteristics to generate a realistic dynamical motion for the particular vehicle [5].

The prediction calculation identifies three relevant regions in the environment around the vehicle (Figure 3. The vehicle's surrounding region is divided into three regions with different criticality.):

- Region 1 – The »most critical« region, which will be driven through with certainty, independently of changes made to the vehicle dynamics;
- Region 2 – The »critical« region, which will be driven through with certainty if the vehicle holds its current state;
- Region 3 – The »latent critical« region, which could be reached if the vehicle changes its current motion.

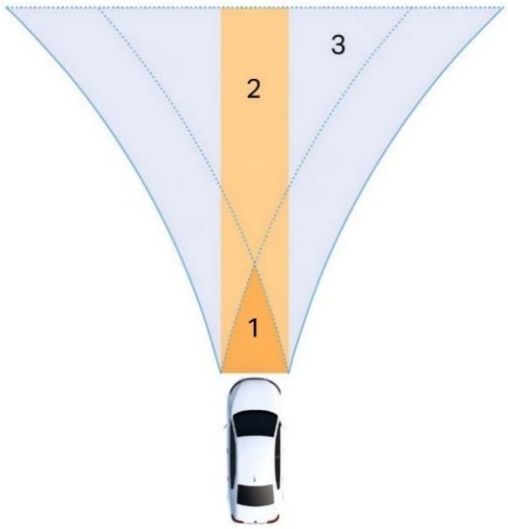

Figure 3. The vehicle's surrounding region is divided into three regions with different criticality.

Region 3 is used to identify all relevant pedestrians - pedestrians which are detected by the sensors outside this region are not considered. Region 2 is used to estimate potential collisions if the driver does not change the current vehicle's motion. Region 1 is used to trigger the emergency braking maneuver: the limits of this region represent the last possible moment at which a collision avoidance maneuver can be successfully undertaken by the driver.

Collision detection

The identification of a collision with pedestrians (‘requirement b’) is performed by calculating the intersection of the area swiped by the vehicle during its predicted motion with the area covered by the pedestrian during its predicted motion. Additionally, a distinction is made between an individual pedestrian and a group of pedestrians: if the distance between pedestrians is less than a given threshold (taken as the approximate width of the vehicle), they are considered to be a “group”. This group classification is then used in the next step to identify possible collision avoidance trajectories for the vehicle (i.e. trajectories which lead the vehicle between groups).

Maneuver evaluation

After identifying all possible collisions with pedestrians, the ASL function searches for maneuvers which can avoid the predicted collision (requirement c). To identify an unavoidable collision, the function executes sequentially the following steps (Figure 4. The steps for identification of a collision-free vehicle path (for simplicity the motion of pedestrians is not represented). From left to right: a pedestrian is identified in the vehicle’s path; other pedestrians are identified in the accessible region; a collision-avoidance path between groups of pedestrians is determined.):

1. The function determines the predicted presence of at least one pedestrian in the »critical« area (zone 2 in Figure 3). If there are several pedestrians in the critical area, the one closest to the vehicle is taken as reference;
2. The function detects other pedestrians in the »latent critical« area (zone 3 in Figure 3) and separates all pedestrians into groups with at least one pedestrian;
3. The function verifies the existence of trajectories capable of leading the vehicle between the groups of pedestrians without colliding with any of them. Any other objects detected in the vicinity of the vehicle are also considered in this step.

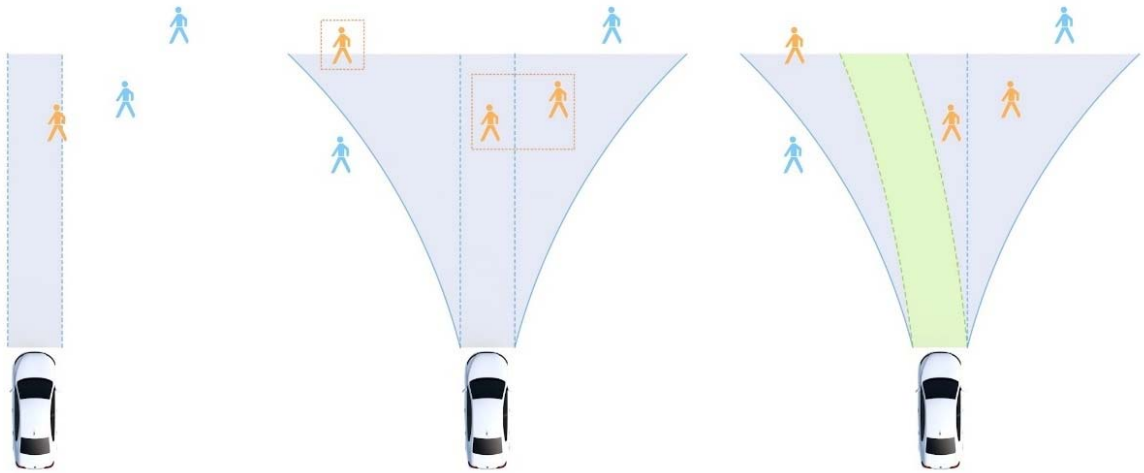

Figure 4. The steps for identification of a collision-free vehicle path (for simplicity the motion of pedestrians is not represented). From left to right: a pedestrian is identified in the vehicle’s path; other pedestrians are identified in the accessible region; a collision-avoidance path between groups of pedestrians is determined.

If no collision-free maneuver exists at end of step 3, the collision is classified as unavoidable (more exactly: the collision becomes classified as unavoidable shortly before it becomes unavoidable, as to provide sufficient reaction time for the system). As long as no pedestrian is predicted to be in the critical area (step 1) or at least one collision-free maneuver exists (step 3), the function will not perform any action and will not trigger an emergency braking.

Maneuver triggering

If a collision with a pedestrian is imminent (i.e. the vehicle is about to enter a state where no collision avoidance maneuver is feasible) and the driver does not de-escalate the situation (i.e. does not brake or steer away from collision), the function ASL triggers an emergency braking maneuver without the possibility of driver intervention, effectively bringing the vehicle to a standstill ('requirement d'). Additionally, acoustic (horn) and optical (front, rear and turn lights) warnings are triggered to warn the immediate surroundings about the dangerous driver's behavior.

VALIDATION

The ASL function was validated concurrently using computer simulations and vehicle tests. While simulations allowed for the exact verification of the function's logic, the validation in a real vehicle allowed the function to achieve a high degree of maturity in a relatively short period of time. This was possible by using IAV's Vehicle-in-the-Loop test approach [6, 7]. In this test method, a real vehicle is fed with virtual traffic objects (in this case pedestrians and roads); virtual sensors then detect the (also virtual) objects and pass this information to the ASL function which, if necessary, commands the (real) actuators to act. The function itself does not run on the vehicle's target hardware but on a standard laptop computer while the tester can observe the scene as seen from the driver's point-of-view in a display fixed to the windscreen (see Figure 5. Inside IAV's Vehicle-in-the-Loop: the test scenario is visualized in a display showing the (real) environment and the (virtual) pedestrians.). The use of this setup allowed to test the ASL function in all developed scenario variations using relatively little resources and without endangering any pedestrians.

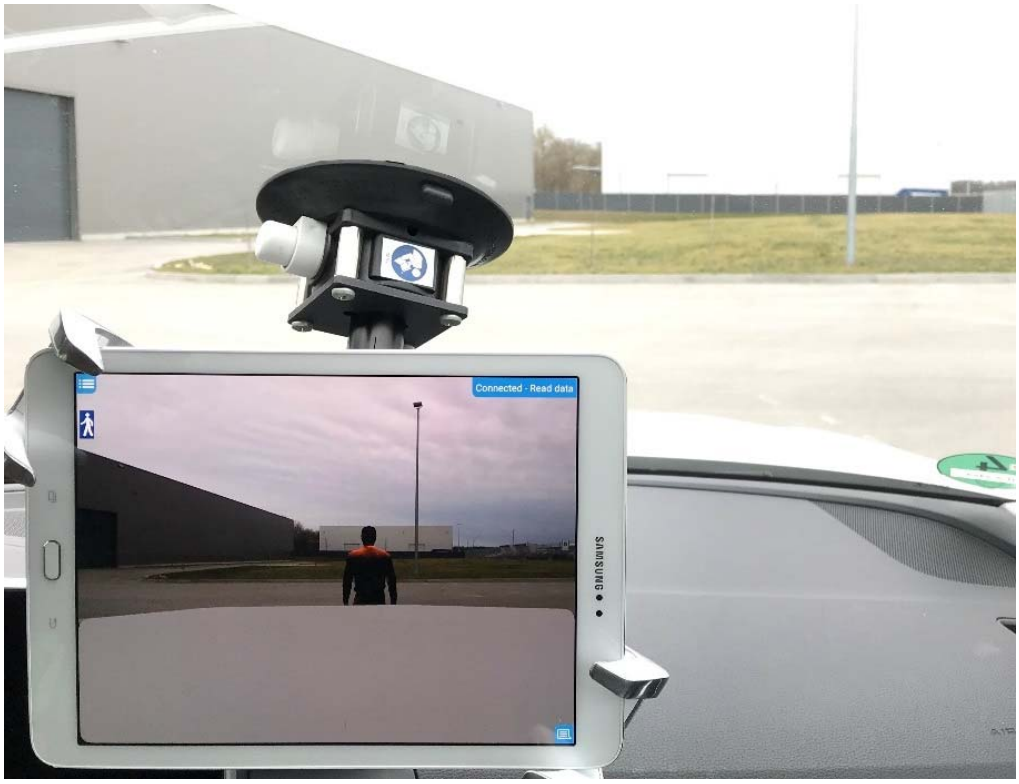

Figure 5. Inside IAV's Vehicle-in-the-Loop: the test scenario is visualized in a display showing the (real) environment and the (virtual) pedestrians.

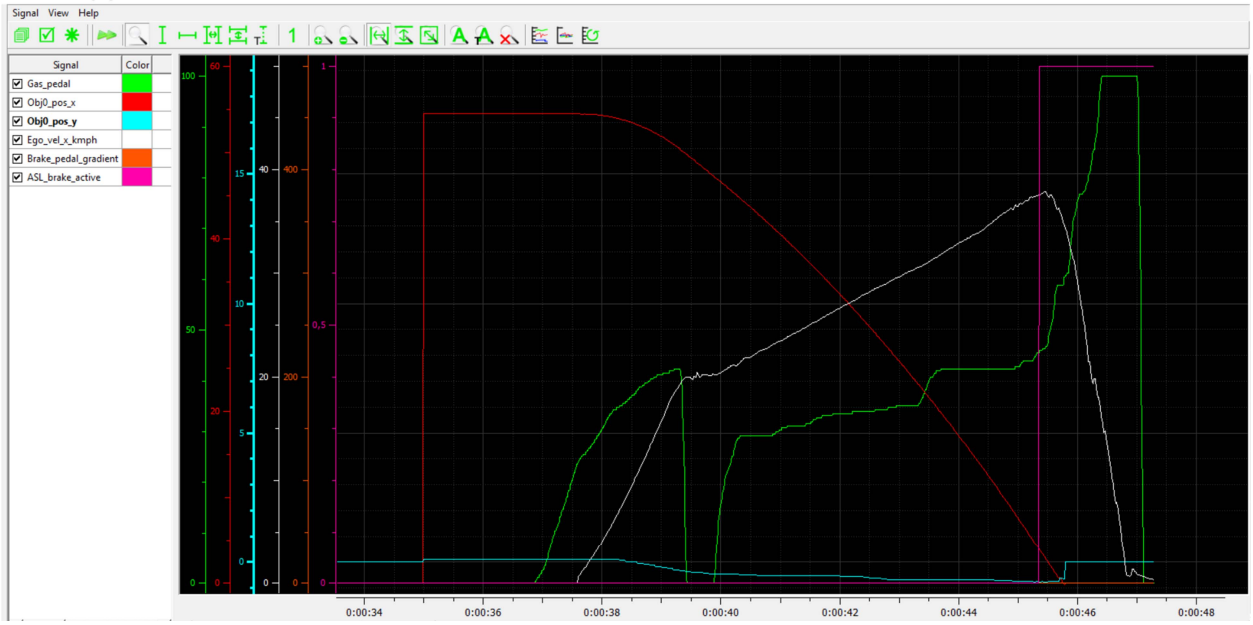

Figure 6. Validation of the ASL function using IAV's Vehicle-in-the-Loop approach: the vehicle breaks until standstill (left) and simultaneously activates lights and horn (right) even if the driver tries to accelerate.

A particular important part of the validation was the verification of the function's full authority, i.e. the demonstration that control over the acceleration of the vehicle was taken *away* from the driver. In Figure 6. Validation of the ASL function using IAV's Vehicle-in-the-Loop approach: the vehicle breaks until standstill (left) and simultaneously activates lights and horn (right) even if the driver tries to accelerate. are shown the results of such a test case. At first, the driver accelerates (signal "Gas_pedal") and continuously reduces the distance to the pedestrian (signals "Obj0_pos_x" and "Obj0_pos_y"). Once the collision becomes imminent, the ASL function requests a braking maneuver (signal "ASL_brake_active"). Despite the driver accelerating (note that the brake pedal is not pressed, see signal "Brake_pedal_gradient"), the vehicle slows down to standstill (consequently the engine stalls and shuts down).

CONCLUSIONS

There have been approximately 78 terrorism-motivated vehicle ramming attacks between 1973 and 2018, from which resulted 281 deaths and approximately 1200 injuries [9]. Even if the number of casualties is not comparable with the casualties due to other causes, the psychological effects on the society at large are significant. The possibility to actively influence the motion of a vehicle opens up possibilities for increasing the safety of pedestrians in addition to the safety of the vehicle's occupants. Particularly in the case of an intentional misuse of a vehicle it is important to have functionalities capable of avoiding or at least minimise the harm to pedestrians, i.e. some kind of "driver prevention" functionality.

The ASL function monitors the driver's behavior (steering wheel, brake and acceleration pedals) and the environment. If an imminent collision with a pedestrian is identified and the driver does not maneuver to avoid the collision, the function commands an emergency braking maneuver until the vehicle is brought to a standstill and activates optical (front and turn lights) and acoustical (horn) warnings to the surroundings. Once the emergency braking is activated, the function cannot be overridden by the driver: the vehicle is brought to standstill and warnings are emitted, even if the driver tries to accelerate or maneuver. Tests using IAV's Vehicle-in-the-Loop approach have demonstrated the correct functioning of the ASL: in the case of an imminent collision, the function

activates and brings a real vehicle to standstill even if the driver accelerates, while activating the acoustic and optical warnings. Furthermore, the use of simulations and Vehicle-in-the-Loop testing back-to-back allowed the function to reach a high maturity level in a short timeframe: while simulations confirmed the correct logic of the function, Vehicle-in-the-Loop tests demonstrated its robustness vis-à-vis the inputs from the vehicle, i.e. the real vehicle dynamics. Because of the nature of the test approach, issues specific to sensors and sensor measurements (e.g. faulty sensor data) were largely not addressed but need to be before such functions can be deployed. With the objective of increasing the ASL function's robustness, several new approaches are currently being evaluated, including new motion models [8] and new methods for determining the vehicle's position relative to the road (e.g. artificial intelligence for curb recognition).

The function ASL is not meant as substitute to existing Autonomous Emergency Braking functions, but as an extension thereof; and while its functionality clearly goes against current vehicle regulations [1, 3], it is also a case in point on how to increase function autonomy while contributing to further reduce the number of casualties caused by (intentional or unintentional) human action. However, changes in regulations are needed before such functionalities are implemented.

Currently, every ADAS function is required to allow an overriding [10]. While this is intended to allow the driver to perform his duties according to road traffic legislation, it does nothing to prevent the driver from going against that same legislation. Legislation is currently being drafted to allow autonomous systems to drive but not to let them *prevent* the human from driving. To effectively give control of a vehicle to the machine instead the human sitting in the driver's seat, both the circumstances in which this can happen as well as the actions allowed to happen have to be very clearly defined. With that in mind, the following regulatory changes could help the deployment of this functionality:

- Definition of the range of vehicle states. Only when the vehicle is in a specific state should any function be allowed to have full authority over any aspect of the vehicle control. The most immediate one is the state where all the necessary sensors are operational. But other ones are possible (e.g. only when no trailer is present), and these should be explicitly laid out;
- Definition of the range of actions. Any function preventing a human user from exerting control over the vehicle shall be allowed to have full authority over only very specific dynamic tasks. In a first step, this influence could extend to longitudinal control and more specifically to deceleration; in a further step, the function could be allowed to also perform lateral control;
- Definition of the range of circumstances. As implemented into the ASL function, full authority over the vehicle (even if just a specific action) should be allowed only in very strict circumstances. These circumstances should be highly critical and explicitly connected with danger to human life in the immediate vicinity of the vehicle.

Apart from these regulatory changes, technical developments are also necessary, especially what concern the certification mechanism for such functions. As it is currently being discussed in the framework of autonomous driving, the current test process should be updated for dealing with the extreme requirements of such a function. Once the test process is accepted at the regulatory and legal level, the question of liability is automatically addressed.

We thank Paul Prescher, Steve Haselbach, Anton Egger and Matthias Butenuth for their support and motivation.

REFERENCES

[1] (1968) Article 8, 19th Convention on Road Traffic, United Nations, Vienna, 8 November

[2] J. Cicchino (2017) “Effectiveness of Forward Collision Warning Systems with and without Autonomous Emergency Braking in Reducing Police-Reported Crash Rates”, Insurance Institute for Highway Safety, January

[3] (in german) Straßenverkehrsgesetz (2019) “§1a Kraftfahrzeuge mit hoch- oder vollautomatisierter Fahrfunktion”

[4] (2019) “Vehicles as Weapons of Terror”, Counter Extremism Project, January (available online at https://www.counterextremism.com/sites/default/files/Vehicles%20as%20Weapons%20of%20Terror_010819.pdf)

[5] (in german) M. Kvesic (2018) “Trajektorienplanung für hochdynamisches autonomes Fahren”, Master Thesis, Hochschule für angewandte Wissenschaften München

[6] M. Butenuth, R. Kallweit and P. Prescher (2017) „Vehicle-in-the-Loop – Combining real vehicle tests with virtual scenes“, in ATZ - Automobiltechnische Zeitschrift, 09

[7] R. Kallweit, P. Prescher, and M. Butenuth (2017) „Vehicle-in-the-loop: augmenting real-world driving tests with virtual scenarios in order to enhance validation of active safety systems“, in Proceedings of the 25th International Technical Conference on the Enhanced Safety of Vehicles

[8] (in german) F. Pinsker, K. Krumbiegel and J. Graciano (2019) “Analytisches und numerisches Verfahren zur Prädiktion eines beweglichen Verkehrsteilnehmers” (patent pending)

[9] B. Jenkins and B. Butterworth (2018) “An Analysis of Vehicle Ramming as a Terrorist Tactic”, MINETA Transportation Institute, May (available online at transweb.sjsu.edu/sites/default/files/SP0518%20Vehicle%20Ramming%20Terrorism.pdf)

[10] (2008) “Regulation No 79 of the Economic Commission for Europe of the United Nations (UN/ECE) - Uniform provisions concerning the approval of vehicles with regard to steering equipment”, Addendum 78: Regulation No 79, Revision 2, 27.05 (available online at eur-lex.europa.eu/legal-content/en/ALL/?uri=CELEX%3A42008X0527%2801%29)

EVALUATION OF THE PROTECTIVE PERFORMANCE OF A NOVEL RESTRAINT SYSTEM FOR HIGHLY AUTOMATED VEHICLES (HAV)

Tetsuya Matsushita
Hiro Saito
Autoliv Japan Ltd.
Japan

Cecilia Sunnevång
Martin Östling
Autoliv Research
Sweden

Abhiroop Vishwanatha
Avinash Tabhane
Autoliv India Pvt. Ltd.
India

Paper number 19-0321

ABSTRACT

As automated driving further penetrates the market, opportunities continue to arise for new vehicle interior designs, and new seating positions might be allowed. Flexible seating with a wider range of positions will require new restraint systems, independent of the steering wheel or instrument panel. The aim of this study was to evaluate a novel seat-integrated restraint system created for future potential seating position, compared to the current conventional restraint system in forward-facing seat condition.
The seat-integrated restraint system was evaluated using a virtual simulation model correlated to physical sled tests. The CAE model included a generic seat, the seat integrated belt system with a 2kN load limiter, and the new Dual Shoulder Airbag system (DSA). The DSA was mounted to the seat back on both sides of the seat. The DSA was also connected below the seat pan to raise the occupant's pelvis-thigh area during a crash, to avoid submarining in the reclined position. For reference, a standard system (3-point 4 kN load limiter belt and driver airbag) was used. Occupant injury assessment reference values (IARV) were evaluated using the AM50_THOR, AF05_Hybrid III, and AM95_Hybrid III models and compared to IARVs from the current and new proposed New Car Assessment program in the U.S (US NCAP). The IARVs compared were HIC15, BrIC, Nij and Chest deflection. The load cases evaluated were full rigid-barrier frontal crash (FRB) and NHTSA Oblique Impact (NOI), with crash pulses representing a mid-size sedan. The occupant protection was evaluated for the standard seating position (23 degrees from vertical) as well as for a reclined position (45 degrees from vertical).
The new restraint system resulted in lower IARVs than the reference system in every case except HIC15 and Nij in the NOI condition.
A comparison of the standard and reclined positions revealed that every IARV was increased in the latter.
No submarining occurred for any of the restraint systems.
The new proposed airbag system has the potential to offer equivalent or lower IARVs compared to the reference system in frontal crash mode (forward-facing seat condition).

INTRODUCTION

Over the last decade, highly automated vehicles (HAV) have been a focus of future mobility innovations for many players—like automobile manufacturers, automotive suppliers, IT professionals, mobility-service providers, and governments. They are also working to develop related technology enabling more flexible seat layout, as there will no longer be a need for someone to drive the vehicle. This trend has been summarized by Filatov et al. (2019) [1]. Mercedes introduced the "F015 Luxury in Motion" research vehicle [2], equipped with four rotating seats which allow occupants to select their orientation according to their preference. Volvo introduced "Concept 26" [3], which allows the driver's seat to be repositioned away from the steering wheel and instrument panel when the car is in automated driving mode. Volkswagen's "ID BUZZ electric minivan" [4] also employs the rotated-seats concept. Several component manufacturers have introduced similar concepts. Some representative seat-layout images of these trends (seats that are deeply reclined, far from the steering wheel, and

rotated) are shown in Figure 1. In fact, many people have realized that one of the benefits of HAV technology is that the vehicle interior can transform from a cabin just for driving and riding into a living space, where many daily activities like reading, working, and relaxing can be performed. Jorlöv et al. (2017) [5] and Östling et al. (2019) [6] investigated which seat layout consumers prefer in automated driving mode in static conditions using normal chairs. They found that consumers' preference depended on the situation, but they generally preferred seats that could rotate and recline. Thus the developers of HAV technology and consumers both seem to want the same thing: that the technology of flexible seating be developed further. The ensuing challenge is to make flexible seating as safe as the seating in current vehicles.

Current occupant restraint systems comprising seatbelts and airbags are designed to protect passengers in traditional seating positions from either frontal or side impacts. The occupants are moved by the inertia force produced by crash deceleration, and the airbags are located in line with the forces, in order to prevent occupant contact with the vehicle interior (i.e., they are located at the steering wheel, the instrument panel, the side window, and between the seat and the door's inner panel). Seatbelts are normally anchored through the upper part of the B-pillar, although some vehicles place the thru-anchor on the top of the seatback.

Given the future possible sitting positions (Figure 1) and the current airbag layout (Figure 2), it should be pointed out that the current conventional system might need adjustments. The occupants in the rotated seats have no airbags directly in front, and a seatbelt anchored onto the B-pillar cannot be routed to restrain them in their initial position. Further, the reclined posture is related to increased likelihood of submarining, as described in Östling et al. (2017) [7].

A novel concept has been created in response to these challenges that has the potential to protect the occupant in any type of crash event, independent of seat position. This concept was evaluated in this study, using the current and upcoming New Car Assessment program in the U.S (US NCAP) as a reference for both loading conditions and injury assessment reference values (IARVs). The target was to achieve IARVs equivalent or below to that of the current conventional restraint system in a frontal 56 km/h crash [8]. To make the comparisons with the current conventional system as valid as possible, the new-concept model maintained the knee bolster and instrument panel, and only the forward-facing seat condition was applied. Every evaluation was performed by numerical simulation.

In this study the main objective is to compare the proposed new system to the current standard system. As a result, although the most representative future seat position would be rotated, as in Figure 1, only the traditional forward-facing seating position has been evaluated. In addition to rotated seats, reclined posture is anticipated in future vehicles, so both the reclined posture and the standard one have been evaluated. The effect of occupant size has also been evaluated. Three crash test dummies were selected: AF05_HybridIII (small female), AM50_THOR (average male), and AM95_HybridIII (large male).

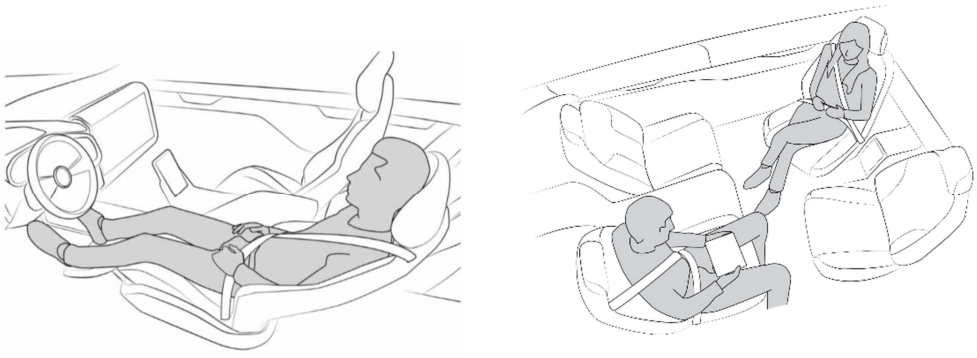

Figure 1. Examples of future flexible seat layouts

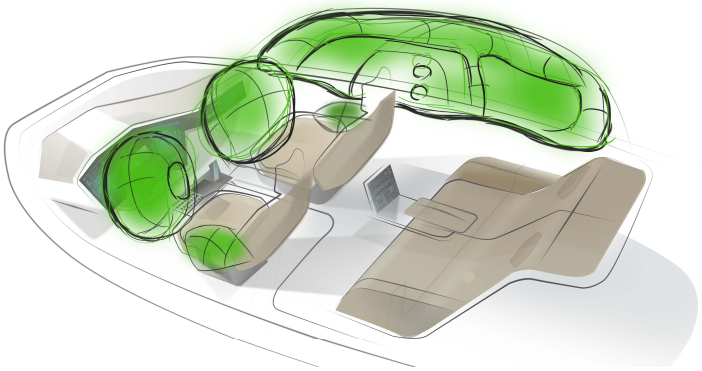

Figure 2. Diagram of current airbag layout

METHOD

The novel system, with seat-integrated restraints, was evaluated to determine whether it could achieve target IARVs for occupants seated in the potential seat positions in the two most frequent load cases of frontal crashes. The conditions are explained in more detail in the "Evaluation condition" section.

To evaluate restraint performance, the IARVs for HIC15, BrIC, Nij, and Chest deflection, developed for the head, brain, neck, and chest regions, respectively, were used.

HIC15 has been authorized and applied to many regulations and assessment programs for a long time. Nij has also been authorized for a long time. AF05_HybridIII applied Nij as is, and AM50_THOR applied the same formula with updated reference values of Fzc: +4200N (tension), -6400N (compression); Myc, +88.1Nm (flection), -117Nm (extension). These values were proposed in the NHTSA US NCAP upgrade protocol's second request for comments (RFC) in 2017 [9]. (The first RFC in 2015 proposed different values, based on Nightingale et al. (2009) [10], which were then updated to the second version.) BrIC is a new criterion, continuously being developed; in this study the one proposed by Takhounts et al. (2013) [11] was used. For Chest deflection, AM50_THOR has four measuring points that quantify displacement in the x, y and z directions. The maximum of the four resultant peak deflections (Rmax) was applied to quantify Chest deflection. The HybridIII dummies have a single point located at the center of the sternum quantifying displacement only in the x direction. For this reason, Chest deflection cannot be directly compared between the crash dummies.

Since the IARVs for BrIC, Nij, and Rmax (for THOR only) are still under discussion, they, too, were used for comparison purposes—not for the actual injury assessment.
Every evaluation was obtained by numerical simulation using LS-DYNA software V971 R7.1.2 (Livermore Software Technology Corporation, Mich., U.S.A.). The conditions are explained below.

Numerical models

The applied vehicle environment geometry was a generic vehicle interior, representing a mid-size sedan (MY 2010). For occupants, THOR v1.3 US NCAP model as average size for male, Hybrid III AF05 v7.0.6 as a small female size, both are produced by Humanetics Innovative Solutions, Inc. and AM95 v3.03 which is produced by LSTC as a large-size male, have been used. The models were positioned according to the seating protocol designated in US NCAP. The vehicle model's seat had a deformable seat pan and rigid seatback; the dimensions were obtained from the same vehicle used for the interior geometry setting. In addition, the knee bolster, steering wheel (SW) column, and toe board were all assigned simple force deflection properties which reflected physical testing data. Each property is shown in Figure 3.

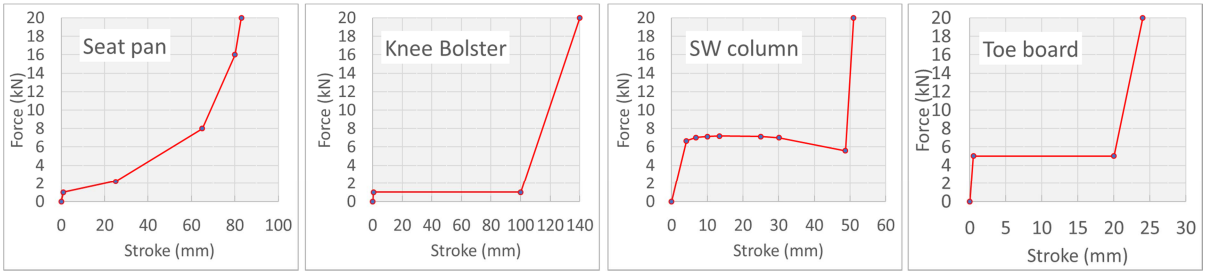

Figure 3. Vehicle interior force deflection properties

The numerical model was validated using measured forces from the belt system as well as head acceleration from the dummy. Accordingly, B3 force (seatbelt force at shoulder), B6 force (seatbelt force at lap anchor), head acceleration on interaction with the driver airbag, and left and right femur forces on interaction with the knee bolster are compared with physical test results (Figure 4).

Figure 4. Comparison between CAE results and physical test results

The Reference restraint system

The conventional restraint system (hereinafter called “Reference system”) was set up with the vehicle conditions which achieved a 5-star rating in current US NCAP protocol. The system was developed to meet the current US NCAP requirements with HybridIII. It comprises a conventional 3-point seatbelt installed in the B-pillar, with a pre-tensioner activated 10 ms after the crash start (TTF 10 ms), a load limiter of 4 kN (at shoulder), a 60-liter driver airbag with a peak pressure of 55 kPa (left in Figure 5) and a 30mm-diameter vent hole. The airbag, activated at the same time as the pre-tensioner, is supported by a steering wheel with a collapsible steering column, which allows the steering wheel to collapse approximately 50 mm. Further, the driver airbag has an adaptive function: an additional vent hole can be activated when a softer airbag is desired. This function is typically used for the small female crash dummy.

Concept description for novel restraint system

Seat-centric One of the features of HAV interiors is the more relaxed sitting position, with a deeply reclined seat back, more legroom, and rotating seat arrangement. The relative positioning of an occupant and the interior parts—except the actual seat—can be changed according to occupant preference. Because the occupants are always seated, the relative position of the seat is always constant, unlike other interior parts such as the steering wheel or instrument panel.

In principle, the in-crash protection system comprising seatbelts and airbags is affected by the relative position of the occupant, as its function is to absorb the kinetic energy from the occupant, who either strikes the airbag or

pulls out the seatbelt. To keep this relative position between the restraint system and the occupant, it is natural that the novel protection system be fitted into the seat, a so-called seat-centric restraint system.

System composition The proposed concept (hereinafter called "New system") is shown to the right in Figure 5. The New system comprises a 3-point belt with the same function as the Reference system, but installed in the back of the seat (the so-called Belt-in-Seat: BiS). The BiS also has a pre-tensioner (TTF10 ms) and a load limiter, but the latter's force is only 2kN (at shoulder). Further, the new system is equipped with a novel type of airbag, the Dual-Shoulder-Airbag (DSA), which deploys from the seatback and goes around both sides of the occupant's shoulders; see Figure 5. Each DSA has a volume of 45 liters and a peak pressure of 50 kPa with no vent holes. The DSAs are triggered at the same time as the BiS pre-tensioner. Each DSA is supported by a virtual vertical reaction plane (VRP); their size and locations are indicated in Figure 6. These VRP represents some fabric membrane to be deployed with DSA in real vehicles and were introduced to simplify simulations. The distance between the two planes (670mm) is twice the distance from the dummy's center to the door's inner panel. The plane is rigid and the friction coefficient with the DSA is zero. The DSAs are connected to the seat pan through an Engage belt (EnB); see Figure 5. Through this connection, the seat pan is pulled up by the EnB when the DSAs are triggered, pulling the femurs up.
The main factor to be evaluated is the effect of the DSA. The methods to retain them could vary, because although one side of the door inner panel can be the one, for the other side there is no part to retain it, so some new device or structure must be developed in future. Hence, generic VRPs are used at this time.

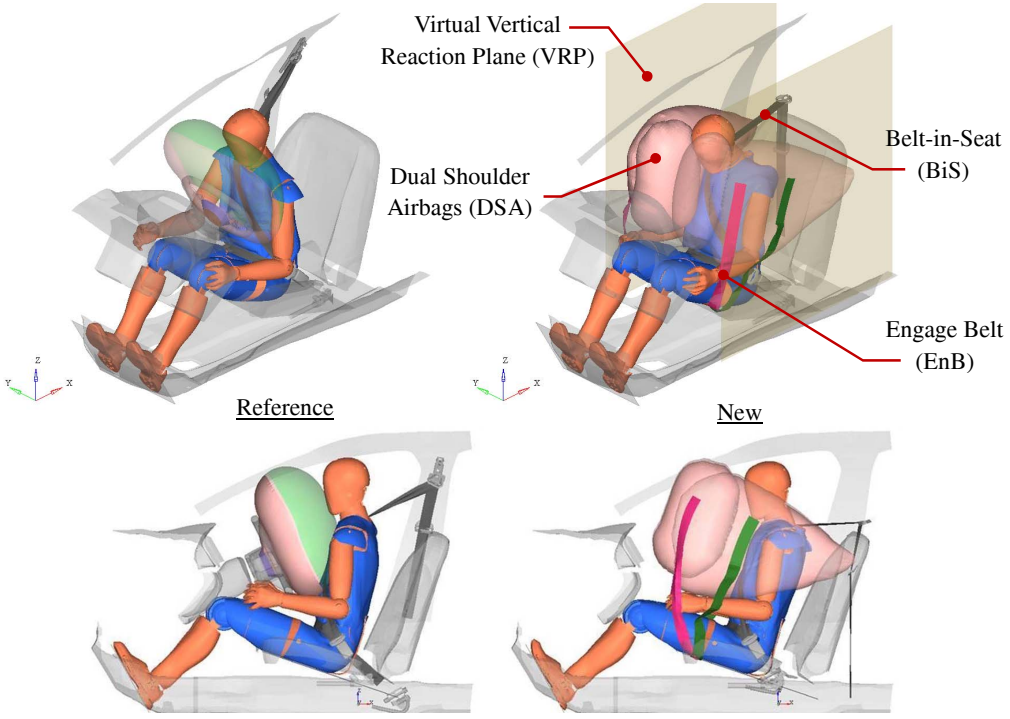

Figure 5. Restraint system comparison
Left: Reference system, Right: New system

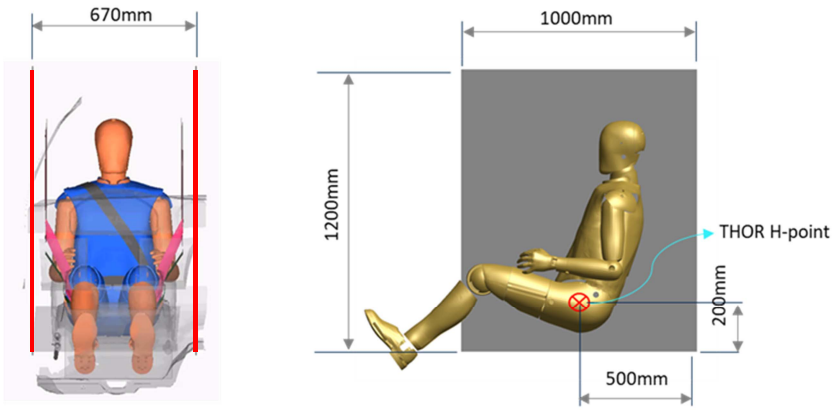

Figure 6. Virtual vertical reaction plane (VRP) setting

How it works In a direct or oblique frontal crash, the BiS enables the seatbelt to fit an occupant with the same relative positioning regardless of seat arrangement, and the DSA provides a more distributed loading in order to stop upper body excursion. Distributed loading has been shown to reduce injury risk [12][13]. Therefore it is proposed that the New system is more protective in more severe crashes, because there is less localized loading of the chest and more distributed loading across the chest, including of the shoulders.

The DSA would play a main role in stopping the upper body in a crash, reducing the localized seatbelt force on the chest to less than that of the Reference system. To restrain the head and neck sufficiently, each DSA also has a sub-chamber located at the front. The sub-chamber restrains the head and neck less stiffly compared to the main chamber. This is an important design feature, since the mass of the head is lower than the mass of the chest.

The seat pan is pulled up by the DSA via the EnB, pulling the femurs up. This action, which complements the lap part of the seatbelt, would also be effective in a reclined position, avoiding or reducing the probability of submarining. Submarining, which occurs when the lap belt passes over the pelvis and penetrates the abdominal area, can cause serious injuries (further explained in Luet et al. (2012) [14]).

The DSA can adapt to differences in occupant size. It is retained by the VRP, which is always in the same location relative to the seat, independent of occupant size. The DSA inflates in the gap between the occupant and the VRP, so the gap changes depending on the occupant size: the bigger the occupant, the smaller the gap; the smaller the occupant, the bigger the gap. If the inflator output level is the same, then with a bigger occupant (and a smaller gap) the DSA's inner pressure would be higher when it makes contact, resulting in a stronger restraint force—and the opposite would hold for a smaller occupant. The DSA connects to the seat pan via the EnB; the pulling force at the seat pan is changed by the inertial force of the occupant's femur. The bigger occupant generates more EnB tension to pull the DSA closer, while the smaller occupant generates less tension. Hence, the DSA could achieve occupant adaptivity with a single inflator setting and airbag design. We have named it the "self-adaptive function". Figure 7 illustrates the concept.

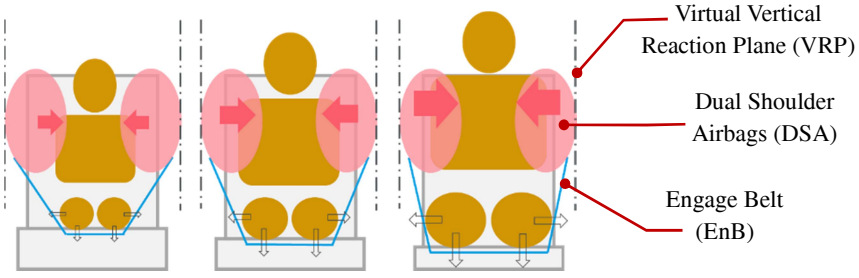

Figure 7. Image: Self-adaptive function reacting to occupant size

Evaluation condition

Test Matrix Table 1 shows the test matrix with ten simulations to evaluate the potential of the New system compared to the Reference system. The parameters are System type (Reference/New), Load case (FRB/NOI), Occupant posture (Standard/Reclined), and Occupant size (AF05/AM50/AM95).
Note that for the four simulations with NOI and/or the reclined seat back, only the AM50_THOR was used, because the Hybrid dummies are too stiff to capture the dynamics accurately.

Table 1.
Simulated configurations of load case, occupant posture, and occupant size

ID#	System	Load case	Occupant Posture	Occupant Size
1	Reference	FRB	Standard	AM50_THOR
2				AF05_Hybrid-Ⅲ
3				AM95_Hybrid-Ⅲ
4			Reclined	AM50_THOR
5		NOI	Standard	AM50_THOR
6	New	FRB	Standard	AM50_THOR
7				AF05_Hybrid-Ⅲ
8				AM95_Hybrid-Ⅲ
9			Reclined	AM50_THOR
10		NOI	Standard	AM50_THOR

FRB: Full-Rigid-Barrier frontal crash, NOI: NHTSA-Oblique-Impact

Parameters The settings of the system model are described in Table 2. The detailed deformation properties of the vehicle interior are shown in the "Numerical model" section. Significant factors that differ between the systems are airbag type, seatbelt load limiter level, and the fact that no steering wheel was used when evaluating the New system.

Table 2.
Parameter descriptions: System

		Reference system	New system
Vehicle interior	Knee bolster	Common (deformable)	
	Toe board	Common (hardly deformable)	
	Seatback	Common (rigid, no rotation)	
	Seatpan	Common (deformable)	
	Steering wheel	Yes	N/A
	Steering column	with (deformable)	N/A
Restraint devices	Driver airbag	Yes	N/A
	Seatbelt	3points thru B-pillar	3points belt (BiS)
	Load limiter at shoulder	4 kN	2 kN
	Shoulder airbags	N/A	Yes

	Engage Belt (EnB)	N/A	Yes

The Load case parameter is the kind of frontal crash (FRB or NOI); they are both expected to apply to the next, upgraded US NCAP test protocol [15]. In an FRB the vehicle impacts a full-width rigid barrier directly in front at 56km/h. In an NOI the vehicle is impacted by a moving deformable barrier (MDB) traveling at 90km/h, angled at 15 degrees with respect to the vehicle. The overlap ratio between the MDB and the struck vehicle's front end is 35%. The Oblique MDB (OMDB) used in this study weighs 2486kg. The impact pulses of each load case were simulated by the same mid-size sedan. The setup is illustrated in Figure 8. We applied a RH driver and a LH struck side (the farside NHTSA Oblique impact). The reason for this choice is that this type of impact does not involve the side-curtain airbag, which is becoming standard equipment. If a nearside impact were evaluated, the side-curtain airbag would be involved (if present) and it could create some noise in the analysis. However, since this study is evaluating a frontal crash protection system, the farside impact was selected.

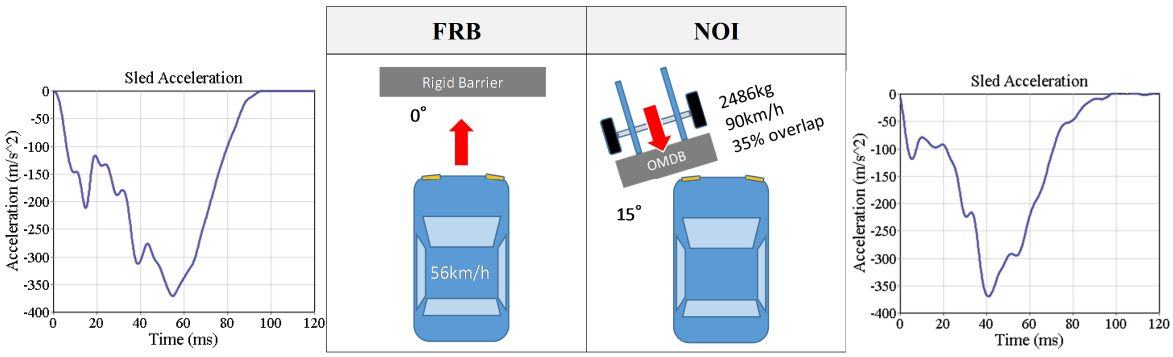

Figure 8. Parameter description: Load case

The parameter for the Occupant posture can be either Standard (23 degrees from vertical), or Reclined (45 degrees from vertical) (See Figure 9).

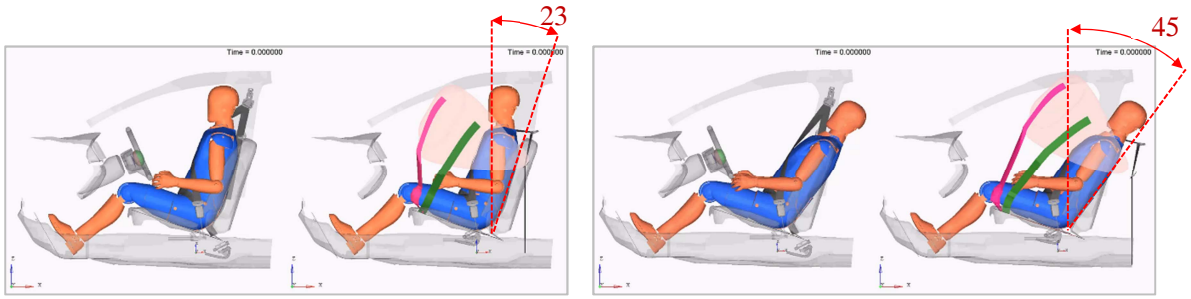

Figure 9. Parameter description: Occupant posture

The parameter for Occupant size is either a small female, an average male, or a big male. The AF05_HybridIII, representing a small female, has been used for a long time in regulation and assessment all over the world (e.g., US NCAP and Euro NCAP). The AM50_THOR represents an average size male; THOR is a newly developed dummy with higher biofidelic properties than the HybridIII series. The AM95_HybridIII represents a big male. The three types are shown in Figure 10.

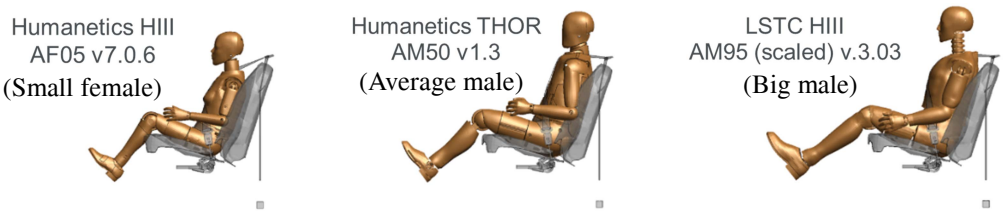

Figure 10. Occupant size of each type

RESULTS

Comparison based on Occupant size

For configurations 1, 2, 3, 6, 7, and 8 (see Table 1), the three occupants were compared in the standard posture (see Figure 11).
The New system resulted in lower IARVs than the Reference system in every case.
The Chest deflection graph shows that the New system has lower IARVs, and the range of values between the different occupant sizes is narrow. It is assumed that the distributed loading including shoulder and low seatbelt tension at chest contributed to these values.
The Reference system resulted in higher IARVs, which may be due to the THOR dummy's differences from HybridIII.

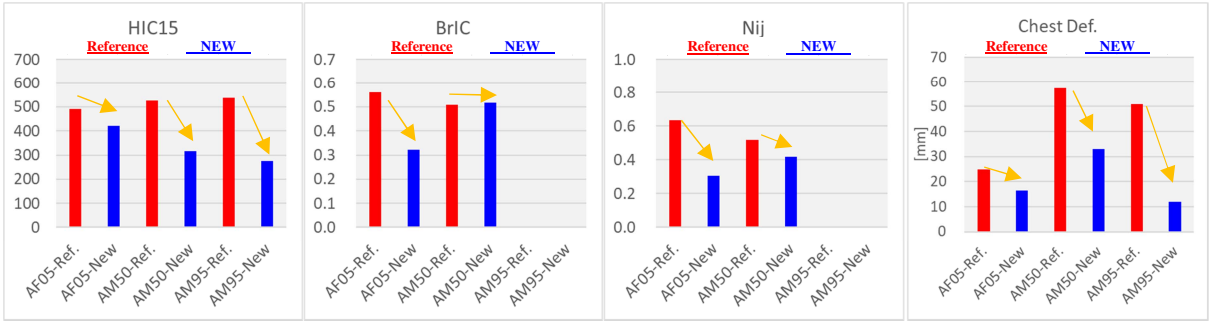

Figure 11. IARVs comparison based on Occupant size

Comparison based on Occupant posture

For configurations 1, 4, 6 and 9 (see Table 1), the two types of posture (Standard and Reclined) were compared for the FRB load case (see Figure 12).
Both systems produced higher IARVs in the Reclined posture than in the Standard posture in every case except Chest deflection in the Reference system. The head and neck region in particular showed a substantial difference.
The New system resulted in lower IARVs than the Reference system in every case.
For Chest deflection Rmax, the New system showed lower IARVs and a narrower range of values between postures. As in the previous chapter, these results can be explained by the shoulder restraint scheme and the low level of seatbelt tension at the chest. However, it must be stated that the THOR_AM50 is not validated for the reclined sitting posture so the values should be interpreted with caution.
The velocity of the head region deceleration started later with the Reference system (i.e., the free-flight motion continued longer), because the relative distance between the head and the driver airbag in the Reclined posture is much greater than in the Standard posture. The New system creates equivalent relative distances between the head and the DSA in both Standard and Reclined postures, while the performance gap at HIC15 is much smaller than that of the Reference system.
As a side note, there is currently no regulation and assessment program to evaluate the risk of reclined posture.

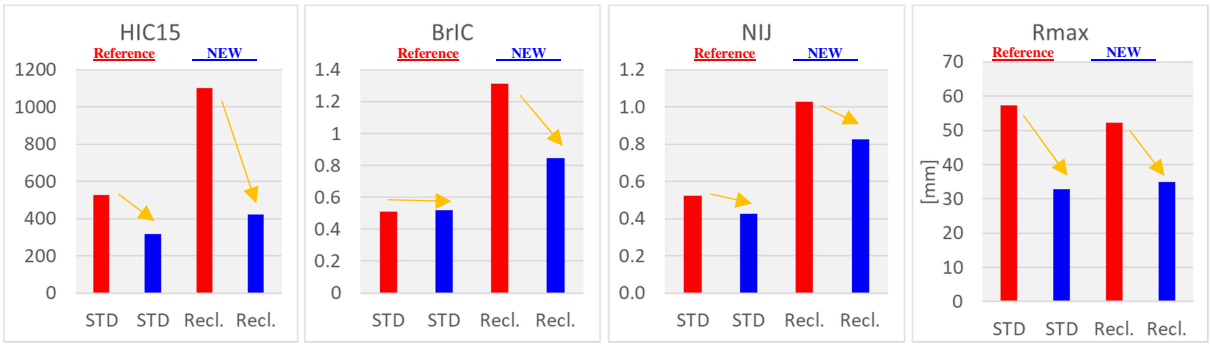

Figure 12. IARVs comparison based on Occupant posture

Comparison based on Load case

For configurations 1, 5, 6 and 10 (see Table 1), the two load cases of FRB and NOI in standard posture are compared (Figure 14).
The New system did not show substantial decrease of IARVs compared to the Reference system. HIC15 and Nij were higher for the New system, although Chest deflection and BrIC resulted in lower IARVs. For BrIC, the New system had a lower value than the Reference system, but a higher magnitude.
The Reference system in this study was not equipped with any unique feature designed specifically for the NOI load case; the head rotated clockwise around the Z axis after contacting the airbag. Although the New system caught the head in the valley between the sub- and main chambers of the DSA as intended, the head rotated counterclockwise around the Z axis (See Figure 15).

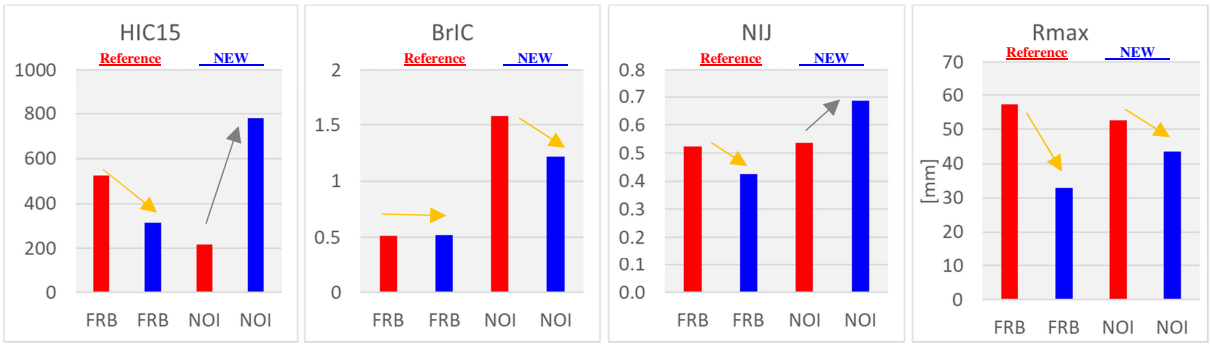

Figure 14. IARVs comparison based on Load case

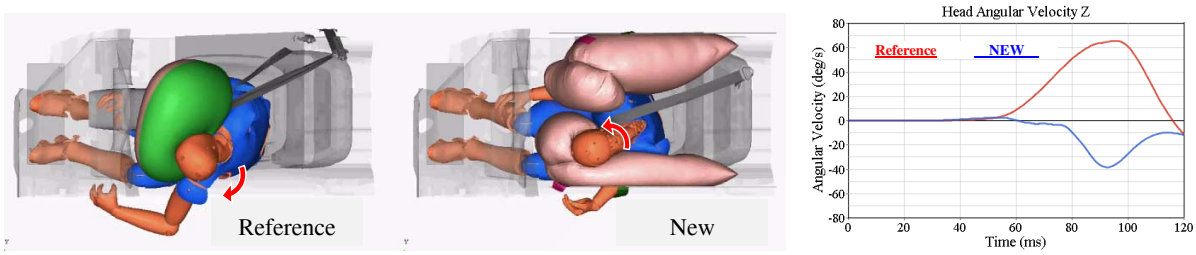

Figure 15. Occupant motion behavior comparison and Head angular velocity Z

Comparison focusing on rib deflection

As mentioned, AM50_THOR has four measuring points for Chest deflection (Figure 16). Figure 17 shows the result of the Chest deflection at each point: Upper-Right (UR), Upper-Left (UL), Lower-Right (LR), and Lower-Left (LL). The graphs on the left illustrate the Reference system, the graphs on the right illustrate the New system. The upper two graphs permit a comparison of the two Occupant postures in the FRB condition. The lower two graphs permit a comparison of the two load cases for Standard posture. The Reference system produced higher IARVs at UL and LL, corresponding to the seatbelt route across the chest, while the LR, far from the seatbelt route, has a very lower IARV. These results mean that there was a local rib cage deformation at the chest. For the New system, there was less local deformation, indicating that loading at the chest was more broadly distributed.

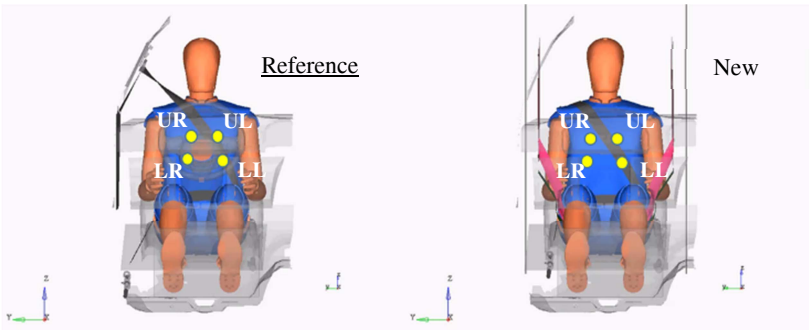

Figure 16. Seatbelt route w.r.t. Chest deflection measuring points (yellow dots)

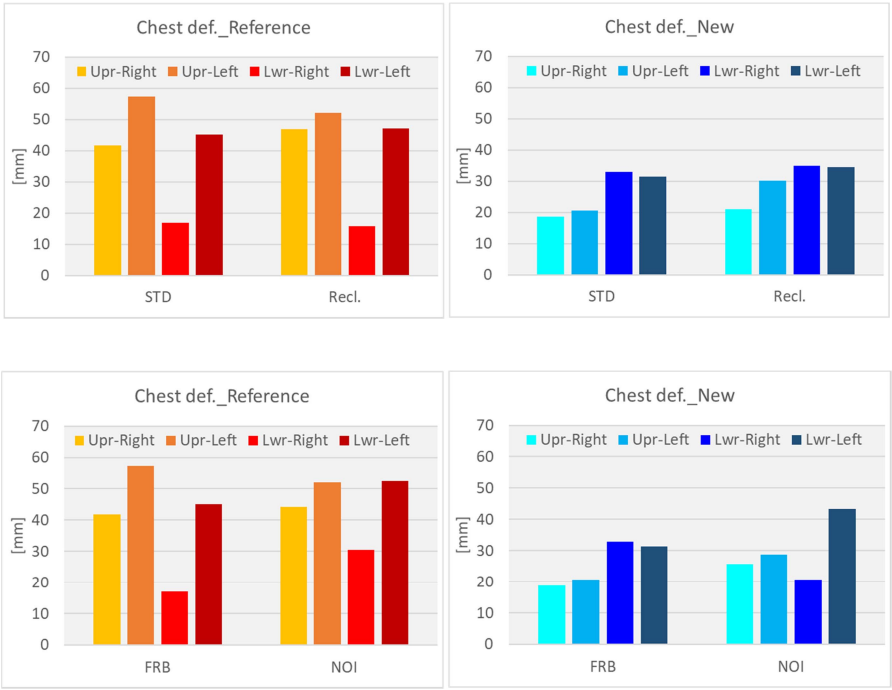

Figure 17. Chest deflection results from three cases (Left: Reference system, Right: New system)

Contact force measurement

Figure 18 shows the contact forces between occupants and restraint devices in the Reclined posture. The Chest contact force (between the DSA and the occupant) shows that restraint starts earlier with the New system compared to the Reference system; the seatbelt contact forces for both chest and pelvis are lower in the New system than in the Reference system, due to the low load-limiting force on the seatbelt. In spite of the lower

seatbelt-to-pelvis force of the New system (Figure 18, lower right), the higher seat pan force (Figure 18, lower left) was indicated; it is a key feature of the New restraint system.

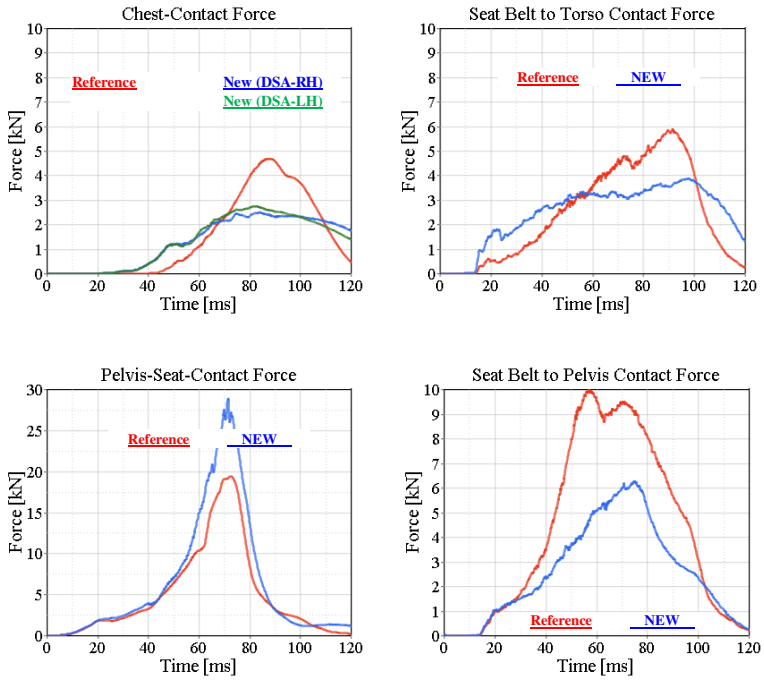

Figure 18. Contact forces between the restraint system and the occupant in reclined
Upper left: Chest Contact Force, Upper Right: Seat Belt to Torso Contact Force,
Lower left: Pelvis-Seat Contact Force, Lower right: Seatbelt to Pelvis Contact Force

Submarining check

When the submarine phenomenon occurs, the force exerted by the lap part of the seatbelt tension drops suddenly as it slips over the ASIS, the top-front part of the iliac wing, into the abdomen. (This acute force decrease is one of the assessment criteria proposed in Euro NCAP [16]). The ASIS has a dented shape where the lap belt fits, transferring the restraint force from the seatbelt to the pelvis. Accordingly, the lap belt force was checked in configurations 1–10, and the ASIS load was checked for AM50_THOR. Like the lap belt force, if the ASIS load shows a sudden drop, it means that submarining has occurred. None of the configurations showed submarining. Representative graphs of the Reclined condition are shown in Figure 19.

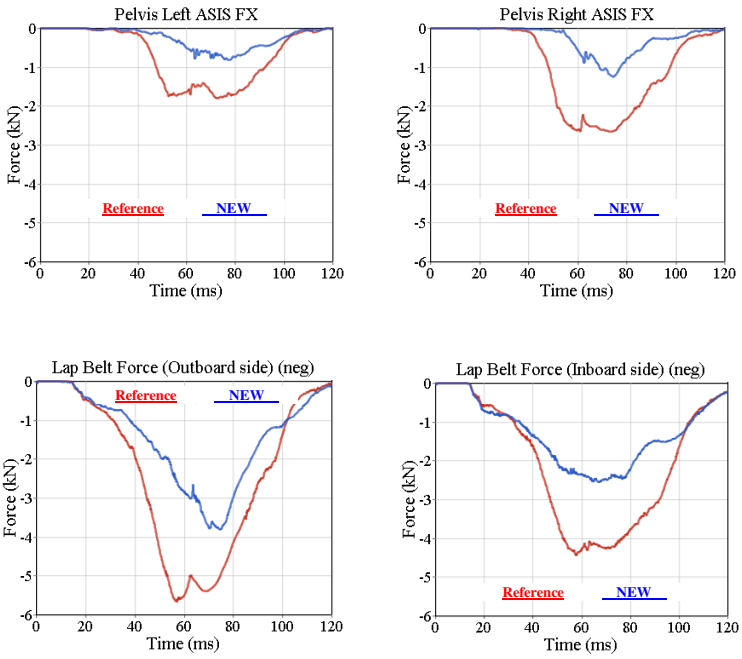

Figure 19. ASIS load and Lapbelt Force in Reclined posture

DISCUSSION

The New system had lower IARVs than the Reference system in almost all cases. However, it had higher IARVs for the head, as determined by the HIC15 and Nij results in the NOI condition. The main element of Nij is NTE (tension-extension), which means the head has been rotated back in a bouncing motion; a softer airbag could lower the Nij value. In fact, the HIC15 value could also be lowered with a softer airbag.

For BrIC in the NOI condition, the New system resulted in a lower value than the Reference system. In the New system, the VRP is a rigid wall, which may cause a high-reaction lateral force against the head, resulting in rotation around the z axis and a high BrIC value. In this study we used a virtual VRP, but for the next step a VRP made of real material could be used to support the DSA. If the VRP could retain the DSA while allowing some deformation, it could create a softer head impact with the DSA, improving head-protection performance.

Considering the evaluation of the New system, we would like to make the following two points.

First, the New system's distributed loading including the shoulder provides a great advantage over the Reference system. The DSA restrains the chest more broadly, including the shoulders, and thereby loads the chest less localized. Thanks to this decrease, the seatbelt load-limiting force can be reduced (it was 2kN in this study). This design contributed to lower Chest deflection values in every case. For the AF05 and AM95_HybridIII dummies, the DSA did not impact any measuring point directly at all. The AM50_THOR, with four points to be measured, permits a more realistic evaluation of how chest loading is distributed: the results show that chest loading is more broadly distributed in the New system. The main contributor to the restraint is not the seatbelt; it is the DSA. The findings of Knobloch et al. (2016) [17], who used an accident database to make comparisons between several restraint systems, indicate that a restraint system designed to provide distributed loading reduces rib fracture risk. Thus this New system, by distributing the loading across the chest more effectively, could contribute to reducing risk in real-world accidents.

Second, in the reclined posture, the New system can restrain the occupant earlier than the Reference system does, due to DSA which equipped seat, the early restraint to chest; it is to reduce more amount of potential kinetic energy of upper body before head contacting to airbag, can reduce the velocity of head contact to airbag, head injury risk could be reduced. The New system generated a high contact force from the seat pan; it is assumed that the DSA pushes shoulders down. At the same time, the contact force from the lapbelt to the pelvis was low due to the low load limit. The combination of high seat pan contact force and low lapbelt force may help us achieve sufficient pelvis-stopping force while reducing abdominal injuries.

LIMITATIONS

This study shows the potential of the New system. The system was, however, only evaluated by numerical simulations of mechanical crash dummies and not verified by mechanical tests. The DSA needs to be validated with real physical material in order to develop it into a manufactured system. It should also be validated using more complex Human Body Models.
The only seat condition evaluated was forward-facing, which involves the knee bolster and toe board, which help restrain the lower body. If these parts were removed (for example, in the case of a rotated rear facing-seat), it would be more difficult to restrain the lower body.
The New system uses a unique restraint concept, which deploys from left and right sides of an occupant instead of from the front, thereby providing more distributed loading, also including the shoulders. The existing crash dummies and its model in this study has been developed and verified with the conventional restraint system and airbag, both of which restrain the chest from the front. As pointed out by Shaw et al. (2009) [18], rib cage deformation (as commonly defined by relative uniaxial displacement toward the spine) is insufficient to characterize the observed multiaxial deformation patterns.
In addition, it is possible that early restraint, even in the reclined posture, might increase the axial spine force and leading to spine compression. In another study of the effect of reclined posture, Valevan et al. (2018) [19] described three types of challenges through their CAE simulation with a crash dummy model: 1) high head acceleration, 2) submarining, and 3) increased spine force. The New system could be a countermeasure against 1) due to its early restraint start. It could also address the challenge 2); the DSA could pull femurs up via EnB to stop the pelvis with shorter displacement. However, we have not measured the spine force, so we cannot evaluate the third challenge. Further, spine flexibility greatly affects the load level, and even the state-of-the-art dummy THOR may not be the proper tool since it has not yet been evaluated in terms of spine force.

CONCLUSION

The New system was confirmed to have the potential for equivalent or lower IARVs compared to the Reference system in frontal crash mode in the forward-facing seat condition.
In the Full-Rigid-Barrier (FRB) load case, the IARVs of AF05/AM95_HybridIII and AM50_THOR with standard posture were compared; the New system provided lower chest IARVs through the combination of distributed restraint by the DSA and the low seatbelt load.
Using AM50_THOR, the effect of occupant posture in the FRB case was evaluated. It was confirmed that the New system has advantages in reclined-occupant protection by early restraint start of the seat-centric concept. In addition, the robust performance for chest protection was indicated also in this parameter of occupant posture.
AM50_THOR was also used to evaluate the effect of load case on restraint system performance.

REFERENCES

[1] Filatov, et al. “Effects of Innovation in Automated Vehicles on Occupant Compartment Designs, Evaluation, and Safety: A Review of Public Marketing, Literature, and Standards” presented at WCX SAE World Congress Experience, SAE International, issn: 0148-7191, 2019

[2] The Mercedes-Benz F 015 Luxury in Motion. - Mercedes-Benz, https://www.mercedes-benz.com/en/mercedes-benz/innovation/research-vehicle-f-015-luxury-in-motion/, Oct. 2018.

[3] Volvo - Concept 26, https://www.futureofdriving.com/concept26.html, Oct. 2018.

[4] Volkswagen I.D. Buzz EV Concept Photos and Info | News | Car and Driver, https://www.caranddriver.com/news/volkswagen-id-buzz-ev-concept-photos-and-info-news, Oct. 2018.

[5] Jorlöv S., Bohman K., and Larsson A., 2017. “Seating Positions and Activities in Highly Automated Cars–A Qualitative Study of Future Automated Driving Scenarios.” In Proceedings of IRCOBI conference. Antwerp, Belgium

[6] Östling M., and Larsson A., 2019. “Occupant activities and sitting positions in automated vehicles in China and Sweden. “ Proceedings of 26th International Technical Conference on the Enhanced Safety of Vehicles (ESV), Eindhoven, Netherlands.

[7] Östling M., Sunnevång C., Svensson C., and Kock H.O., 2017. “Potential future seating positions and the impact on injury risks in a Learning Intelligent Vehicle.” 11. VDI-Tagung Fahrzeugsicherheit, 29th of November 2017, Berlin, Germany.

[8] National Highway Traffic Safety Administration. 2012. “Laboratory Test Procedure For New Car Assessment Program Frontal Impact Testing.

[9] National Highway Traffic Safety Administration (2017) New Car Assessment Program; Request for comments; [Docket No. NHTSA-2015-0119].

[10] Nightingale R., et al. “THOR Head and Neck IARVs,” SAE THOR Evaluation Task Group, 2009

[11] Tackhounts E., et al. “Development of Brain Injury Criteria (BrIC)” Stapp Car Crash Journal, vol. 57 (November 2013), pp. 243-266

[12] Forman J., et al. “Biomechanical Considerations for The Optimization of an Advanced Restraint System: Assessing The Benefit of a Second Shoulder Belt” IRCOBI Conference - Prague (Czech Republic) - September 2005

[13] Bostrom O., et al. “Mechanism of Reducing Thoracic Deflections and Rib Strains Using Supplemental Shoulder Belts During Frontal Impacts” The 23rd International Technical Conference on the Enhanced Safety of Vehicles (ESV) Seoul, Republic of Korea, May 27-30, 2013.

[14] Luet C., Trosseille X., Drazetic P., Potier P., Vallancien G.: Kinematics and dynamics of the pelvis in the process of submarining using PMHS sled tests. Stapp Car Crash Journal, 2012, Vol. 56: pp. 411 - 442

[15] National Highway Traffic Safety Administration (2015) New Car Assessment Program; Request for comments; Docket No. NHTSA–2015–0119.

[16] European New Car Assessment Program (Euro NCAP) Assessment protocol – Adult Occupant Protection, Version 8.0.3, October 2018. https://cdn.euroncap.com/media/41746/euro-ncap-assessment-protocol-aop-v803.201811061520101516.pdf

[17] Knobloch K., et al. “Sternal Fractures Occur Most Often in Old Cars to Seat-Belted Drivers Without Any Airbag Often With Concomitant Spinal Injuries: Clinical Findings and Technical Collision Variables Among 42,055 Crash Victims”, The Annals of Thoracic Surgery, 82(2): 444-450

[18] Shaw G., et al. “Impact Response of Restrained PMHS in Frontal Sled Tests: Skeletal Deformation Patterns Under Seat Belt Loading” Stapp Car Crash Journal, vol. 53 (November 2009), pp.1-48

[19] Valevan S., et al. “Development of occupant restraint system for future seating positions in fully or semi autonomous vehicles”, FISITA World Automotive Congress, Paper No. F2018-APS-056

NEW PASSENGER RESTRAINTS WITH ADAPTIVITY TO OCCUPANT SIZE, SEATING POSITIONS AND CRASH SCENARIOS THROUGH PAIRED ATD-HM STUDY

Jay Zhao
Pareed Kumar Jakkamsetti
Maika Katagiri
Sungwoo Lee
Joyson Safety Systems
United States,

Paper Number 19-0322

ABSTRACT

This study was undertaken to develop new passenger side Advanced Adaptive Restraint Systems to better protect automobile passenger occupants from serious injuries in frontal and oblique motor vehicle crashes.

New concept designs of a passenger airbag and a knee airbag, each with controllable dual-volume and tunable vents, were developed. A new advanced adaptive restraint system, integrated with such developed passenger airbag, knee airbag and an updated seatbelt system consisting of a switchable dual-load limiter retractor with shoulder and lap pretensioners, was optimized to achieve good performance for all the fourteen load cases defined in this study.

The fourteen load cases represent various real-world crash scenarios comprising passengers of three body sizes seated at different seating positions (the small-size female at full-forward, mid-track, and full-rearward, the mid-size and large-size males at mid-track and full-rearward) under a "hard" pulses representing the 35mph full frontal and frontal oblique crashes of a sub-compact passenger car. The system performances were evaluated with the two sets of occupant injury assessment tools: 1) the Anthropomorphic Test Devices (ATDs) of the three body sizes (the Hybrid-III 5th%ile female dummy, the THOR 50th%ile mid-size male dummy and the Hybrid-III 95th%ile large-size male dummy) with the injury risk functions used in current regulatory lab tests, and 2) the full body Human Models (HMs) of the three body sizes (the 5th%ile female model F05-O v3.1, the 50th%ile male model M50-O v4.5 and the 95th%ile male model M95-O v1.2) developed by Global Human Body Model Consortium (GHBMC)) with the published injury risk functions derived from the Postmortem Human Subject (PMHS) tests. For each load case, four passenger side sled system models were developed, paired with the ATD and the HM of the same size, and for the current production restraints (baseline) as well as the new restraint designs. The injury risks of the occupant body regions and combined injury risks (referred to "Occupant Injury Measures") were estimated with both ATDs and HMs.

The new adaptive restraint system design was developed through individualized optimization for all the fourteen cases in multiple iterative steps. Firstly, the new concept designs were made at the component level, evaluated using two validated ATD sled test models simulating the two load cases (5th%ile female at full-forward position and 50th%ile male in full-rearward position). Secondly, the new advanced adaptive restraint system was optimized with the ATDs in seven successive steps, obtained the optimal restraint design parameters set for each load case. And finally, the optimal adaptive restraint configuration for each case was verified with the HMs sled models. Hundreds of the sled simulations were performed in such processes.

The results demonstrated that the new adaptive passenger restraint system design has more versatile adaptivity and improved performances for all the considered load cases than the baseline restraints. The benefits for the occupant injury risks reduction vary case by case, within 12%-79% margin estimated with the ATDs and 8%-66% with the HMs.

INTRODUCTION

Since their introduction, restraint system technologies such as air bags and seat belts have been effective at mitigating injuries and fatalities associated with motor vehicle accidents. Over the past 40 years, there has been a general downward trend in traffic fatalities in the United State. Still, in 2017, there were 37,133 people killed in

motor vehicle traffic crashes in U.S. roadways ("NHTSA Traffic Safety Facts", DOT HS 812 603, October 2018). As such, the industry continues its efforts to improve restraint system effectiveness by adding new field relvant tests and adjusting the injury risk values to achieve higher rating.

In the past, passive restraint devices were designed as "one size fits all"— the restraint system performance in frontal crashes was optimized with one ATD size in one "standard" seating postion in a lab crash test. In the current enhanced regulatetory lab tests, two ATDs (representing 5th%ile female and 50th%ile male) at one seating positon each were deployed for a restraint system design performance evaluation. In the real world, however, occupant crash induced injuries occur to a large and highly variable population [Stewart C. Wang et al., 2016]. The injury severity and patterns are highly affected by occupants' demographic variables such as age, gender and size (height and weight), and morphomic variables such as BMI, body shape geometry, bone mineral density (HU), fat distribution etc. as well as crash variables such as seating position/posture, vehicle crash severity, and crash modes. A earlier study on CIREN & 1995-2005 NASS/CDS filed data [Bulger et al., 2005] concluded that occupants with fully reclined seat positions suffered higher real-world crash induced fatality rate. Other studies found that variability in occupant posture state resulted in maximum statistical dispersion in overall injury [Bose, et al., 2008], [Gaewsky J., 2015]. Therefore, improving occupant protection requires that the effectiveness of restraint devices be consistent across a wide range of these variables. Adaptive restraint systems will be needed to optimally protect an increasingly vulnerable occupant population in various real-world crashes.

To quantify the potential benefits of the "Adaptive Restraint Systems", the National Highway Traffic Safety Administration (NHTSA) sponsored the Advanced Adaptive Restraints Program (AARP) during 2014-2016, in which we investigated the opportunity to reduce injury to the driver and front right occupants by adapting the restraint system to three occupant sizes (5th%ile female represented by the Hybrid-III 5F dummy, 50th%ile male by the THOR-50M, and 95th%ile male by the Hybrid-III 95M dummy), four seating positions (full-forward, mid-track, rear, full-rear) and four postures (nominal, forward, outboard, inboard leaning), and two crash types (frontal & 15° oblique) at two crash severities (35mph "hard" pulse and "soft" pulse) using a fully-functional prototype Advanced Adaptive Restraint System (referred to ARS1 in this study) [Cyliax et al. 2015]. The considered seating positions could be classified as two kinds: "In-Position (IP)" for the Federal Motor Vehicle Safety Standards (FMVSS) 208 defined or nominal positions, and "Out-Of-Position" (OOP) for those non-nominal or not defined in FMVSS 208. A sled evaluation matrix consisting of thirteen In-Position seated ATD sled tests and eleven Out-Of-Position tests was performed. For each load case, the restraint system performance was quantified by calculating the Occupant Injury Measure (OIM), which predicts the risk of injury as estimated by the Abbreviated Injury Scale (AIS) 3+. The OIM was calculated using the measures of head injury (Head Injury Criterion (HIC15)) and Brain Injury Criterion (BrIC)), neck injury (Neck Injury Criterion (NIJ)), chest injury (Chest Deflection (ChD)), and lower extremity injury (femur force) either measured or calculated for each test. Effectiveness of the tested adaptive restraint system over the baseline (current production restraints) was estimated from the study [Cyliax et al. 2015]. It showed that for the thirteen In-Position load cases, a reduced injury risk was achieved eleven of the front right passenger side load cases (ranging from 11% to 52% improvement). For the eleven Out-Of-Position load cases, however, a reduced risk of injury was achieved only in four of the front right passenger side load cases (1% to 20% improvement). Futher improvement of the ARS1 performance was desired especially for those Out-Of-Position seated occupants.

Our analysis of the AARP sled test data [Zhao et al., 2017] indicated that the injury risks for the occupants in some Out-of-Positions cases could be higher than those seated in the nominal position. In other words, the nominal seating positions defined in FMVSS 208 could not be the worst cases. The identified worst cases from the AARP study were: 1) the full-rearward seated mid-size and large-size males with higher injury risks of the body regions of chest, knee-thigh-hip and lower extremities; 2) The full-forward seated small-size female with higher injuries of the head and lower extremities; and 3) the small-size female or a mid-size male in the mid-track position at inboard leaning posture with higher injury risks of the head, neck and thorax under the left oblique crash. Another observation from the AARP study was that the Hybrid-III 95th%ile dummy had lower OIMs than the THOR 50th%ile male dummy across all the load cases. However, our analysis with the GHBMC human body models showed that a large size male could suffer higher injury risks than the mid-sized male at same position. It indicated that biofidelty of the Hybrid-III 95th%ile dummy is questionable. Evaluation of effectiveness of adaptive restraints requires more reliable biofidelic tools and evaluation methods than those used in current regulatory lab tests, especially for the larger-size occupants.

In the past decades new technologies of human body modeling have advanced. With NHTSA's support, GHBMC has been developing a series of human occupant models including detailed and simplified 5th%ile female, 50th%ile and 95th%ile males occupant models. These models have been validated at some extent at tissue, component and full body levels. These human models have high potential to be used as a virtual test tools representing real-world human occupants to assess the crash-induced injury risks. Evalution of the restraint performance could be made for both ATDs and HMs. Injury measures could be verifiable experimentally with ATDs; and the occupant injury risks could be estimated more realistically, especially for a large-size heavy occupant group, with HMs. In this study we deployed the detailed human models as supplemental injury assessment tools.

Considering all the facts and thoughts explained above, we were motivated to develop a new approach to design, evaluate and optimize adaptive restraints performance with paired ATD and HM sled test simulation models.

The objectives of this study were:

1) to develop new concept designs of adaptive restraints with good adaptivity and effectiveness for multiple load cases considering variations of the occupant sizes (height and weight), the seating positions and the crash modes at the severe ("hard") AARP 35mph crash pulse,
2) to develop a new methodology to evaluate and optimize the restraint system performance using both ATDs and HMs of three body sizes (5th%ile female, 50th%ile male and 95th%ile male),
3) to identify potential benefits of the new passenger adaptive restraint system.

METHODS

In this study, we focused on the passenger or right hand side occupants of vehicle first row. The development of new concept designs of adaptive restraints was executed in the multiple steps explained below.

ATD Sled System Models Validation

This computational study requires well validated sled test system models as good bases. For the model validation, we used a set of experimental data from the ATD sled tests performed in AARP. As listed in Table 1, thirteen sled tests were modeled, including the three sizes of ATDs (Hybrid-III 5th%ile female dummy, the 50th%ile Metric THOR dummy, and the Hybrid-III 95th%ile male dummy), the three seating positions (most Out-of-Position), and with both tested baseline and adaptive restraints.

Table 1.
The validation matrix for the passenger ATD sled models and the model correlation quality assessment summary

ATD	Case No	Pulse	Posture	Seat Position	Restraints	Kinematics Rating score	CORA Rating score	IR Rating Score
HB3-F05	1A	Hard 0°	Nominal	Full forward	Baseline	Good	0.64	0.02
	1C	Hard 0°	Nominal	Full forward	ARS1	Good	0.68	0.04
	2A	Hard15°	Nominal	Full forward	Baseline	Good	0.71	-0.01
	2C	Hard15°	Nominal	Full forward	ARS1	Good	0.70	-0.03
	5A	Hard 0°	Nominal	Full rear	Baseline	Good	0.60	0.10
	5C	Hard 0°	Nominal	Full rear	ARS1	Good	0.67	0.07
THOR-M50	7A	Hard 0°	Nominal	Mid-track	Baseline	Good	0.63	-0.09
	7C	Hard 0°	Nominal	Mid-track	ARS1	Good	0.71	0.02

	8A	Hard15	Nominal	Mid-track	Baseline	Good	0.66	-0.10
	9A	Hard 0°	Nominal	Full rear	Baseline	Good	0.66	0.05
	9C	Hard 0°	Nominal	Full rear	ARS1	Good	0.64	-0.06
HB3-M95	15A	Soft 0°	Forward	Mid-Track	Baseline	Good	0.56	0.02
	16A	Hard15	Nominal	Rear	Baseline	Fair	0.61	0.02

For each case in Table 1, correlation of the ATD sled test model with the test data was performed. The model correlation quality was assessed with the following method.

Three criteria or rating scores were calculated for each case in Table 1: 1) Kinematics Correlation Rating Score (from 1 to 5) by comparing snapshots the simulation and the test video at every 5msec during 0-120 msec; 2) CORA Rating Score for correlating the simulation and the test of the fifteen time-history curves essential for the ATD injury measures calculation; 3) Injury Risk Correlation Rating Score defined as the difference of the injury risks between the model predicted and the test, i.e., $IR = OIM_{model} - OIM_{test}$).

Table 1 summarizes the three rating scores for all the validation cases. A detailed model correlation for the injury risks between the calculated from the model and the test was shown in Figure A-1 in Appendix-A. Overall, good correlations were achieved for all the cases.

Load Cases and ATD-HM Paired Sled Models

Fourteen load cases as shown in Table 2 were defined for design and evaluation of new adaptive restraint systems. The conditions in each case varied with the occupant sizes, the seating positions, and the crash modes (represneted by the two sled angles). The "hard pulse", as shown in Figure B-1 in Appendix-B, represented a 35mph crash of a sub-compact car. The 0 degree sled represents the full frontal crashes, and the left 15 degree angled sled test simulates the oblique crashes.

Table 2.
Load cases for design and evaluation of new adaptive restraint systems

Occu. Size \Seating Position	Full-Forward (FF)	Mid-Track Position (MP)	Full-Rearwad (FR)
AF05	Case 1--0 deg "hard" pulse	Case 3--0 deg "hard" pulse	Case 5--0 deg "hard" pulse
	Case 2--15 deg "hard" pulse	Case 4--15 deg "hard" pulse	Case 6--15 deg "hard" pulse
AM50	NA	Case 7--0 deg "hard" pulse	Case 9--0 deg "hard" pulse
		Case 8--15 deg "hard" pulse	Case 10--15 deg "hard" pulse
AM95	NA	Case 11--0 deg "hard" pulse	Case 13--0 deg "hard" pulse
		Case 12--15 deg "hard" pulse	Case 14--15 deg "hard" pulse

For each case in Table 2, we built four sled models classified as A—ATD with the baseline restraints, B—human model (HM) with the baseline restraints, E— ATD with the new adaptive restraints, and F—HM with the new adaptive restraints. A complete list of all the sled test models is in Table B-1 in Appendix B.

Among the A- class sled models, the five model cases (1A, 2A, 5A, 7A, 9A) were the same validated cases in Table 1. For the other small-size female and mid-size male cases, each case model was built based on the validated case with similar conditions by only updating one system variable (such as the seating position or the pulse). For the large-size male cases, the case models were built from the validated cases 16A.

Each E- class sled model was built based on its partner of A- model by only replacing the baseline with the new designed adaptive restraints explained in the next section.

The class B- or F- class sled models were re-constructed from its ATD partner model by replacing it with the HM. The seatbelt route and seat cushion profiles were then adjusted to fit the HM body. It was noticed that even for the same body size the HM has somewhat different body shape and height than his/her partner of the ATD. To position the HM to the ATD as close as possible, the key body positioning measures, such as the HIP CG coordinates, the body reclined angle, the angles of upper and lower extremities, were kept as similar to partner ATD.

In total, fifty-six sled models were created for the fourteen load cases.

New Adaptive Restraints Design

New concept designs of adaptive restraints were developed based on the main requirement to make the system performances for all the load cases defined in Table 2 better than the baseline restraint. In addition, consideration for the components production feasibility was also kept in mind.

The component design of a new adaptive passenger airbag (PAB) was based on new concepts of adaptivity having adjustable dual-volume (large and small) and vents (discrete vents plus an active vent). Several PAB cushion designs with different shapes having such adaptivity were modeled. An inflator was selected and evaluated to fill the PAB cushion to the targeted volumes. The larger volume cushion coverage, stiffness and performance was evaluated with the load Case 9 (the 50th%ile THOR dummy at full-rearward position at 0 deg hard pulse), while the smaller volume cushion coverage, stiffness and performance was evaluated with the load Case 1 (the 5th%ile female dummy at full-rearward position at 0 deg hard pulse). Dozens of the ATD sled simulations for Case 1 and Case 9 were performed. The "best" performed PAB cushion was selected from this process for next design parameters optimization at system level.

New knee airbag (KAB) cushion designs were made with the similar idea for adaptivity as the PAB. Change of the deployed cushion volume was realized by changing the depth while keeping the coverage area about the same. An active vent was also introduced to make the cushion stiffness adjustable. A new design of KAB module with such adaptivity features was also evaluated with the simulations of Case 1 and Case 9. The "best" performer of the KAB concept design was identified for next design parameters optimization at system level.

The seatbelt system was upgraded from the system used in AARP. The same shoulder retractor with the switchable dual-load limiter and the pretensioner was used. Such a seatbelt model was further validated in the five sled cases in Table 1 (1C, 2C, 5C, 7C, 9C). Then a validated lap pretensioner model was added. Thus, the integrated new seatbelt system consists of the dual-pretensioner (shoulder and lap) and the dual-load limiter retractor with switchable loads.

The new passenger adaptive restraint system integrated the newly designed PAB, KAB and seatbelt components. The next step was to determine optimal set of restraint system design parameters for each load case through the optimization process at the system level as explained below.

System Performance Optimization

The system performance optimization was to determine a unique set of restraint system parameters for each load case such that the adaptive restraints enable optimal functionality for reducing the occupant injury risks for all the considered crash conditions.

Table C-1 summarizes the adaptive restraint system design parameters and the classification. As shown, there are eighteen design parameters, which can be classified into two types: non-programmable and programmable in the circuit board control units. The non-programmable or non-controllable parameters were those fixed in the restraint device design (such as a vent size), while the programmable parameters were those controllable inputs for the squibs (such as a time-to-fire).

Since a full scale optimization considering the seventeen design variables and the fourteen load cases is practically not doable, we developed a simplified process performing individualized optimization case by case iteratively. The work flow chart of such an optimization process is shown in Figure 1.

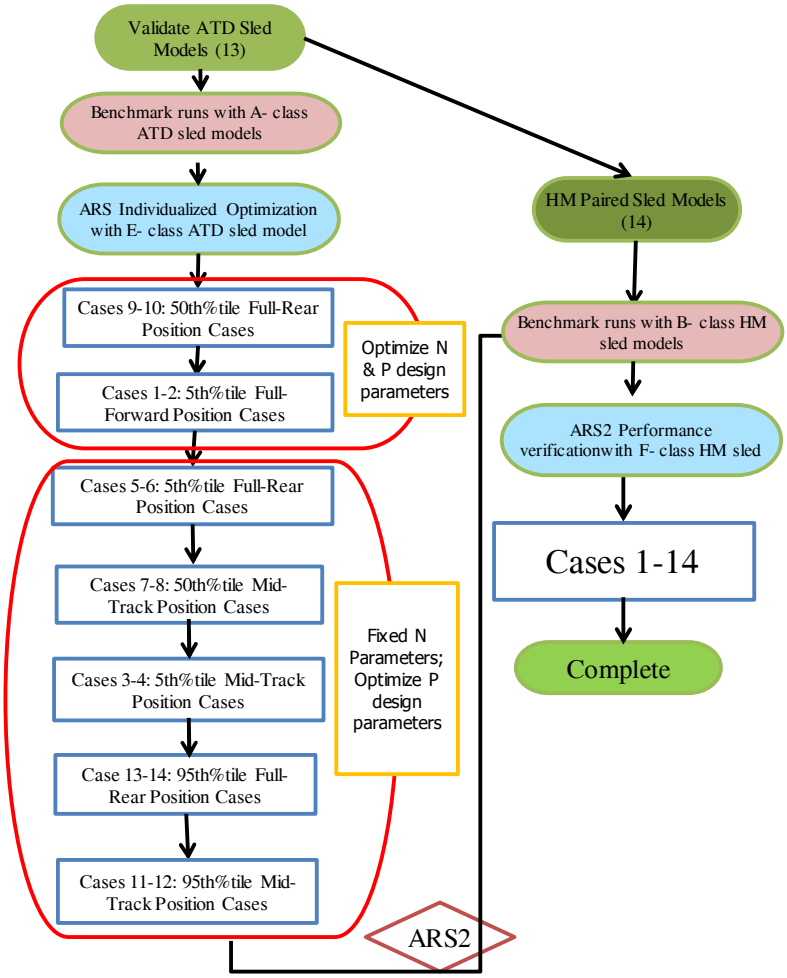

***Figure 1*. The work flow chart of the adaptive restraint optimization process**

The optimization for the new adaptive restraint systems was performed in two cycles: ATDs and HMs. The ATDs cycle was performing the individualized optimization for all the fourteen load cases with the E- class ATD sled models. The adaptive restraint systems with optimal system parameters for each load case were obtained from this cycle (referred to "ARS2" in this paper). The HMs cycle verified the ARS2 system performance using the F- class HM sled models with the injury risks assessment based on the OIMs outputted from the HMs.

In the ATDs cycle, the individualized optimization was executed at seven successive steps for all the load cases in the order shown in Figure 1. At each step, we run iteratively the DOE (Design-of-Experiment) matrices until an optimal set of the system design parameters were found out. In the first two steps for Cases 9-10 ad 1-2, the non-programmable and programmable design parameters were optimized simultaneously, and at the end those optimal non-programmable parameters were determined. While in the last five steps, only those programmable system design parameters were included in the DOE matrices for the optimization. In this way, the total number of DOE iterations was reduced significantly. The ARS2 system configuration with optimal design parameters for each load case was defined in this cycle.

In the HMs cycle, the same ARS2 system configuration from the ATD optimization was implemented into the F- class HM sled model for each load case. The ARS2 benefits were assessed with the HMs explained below.

Injury Risks Calculation and Benefit Assessment

The Occupant Injury Measure (OIM_{AIS3+}^{ATD}) for the AIS 3+ injury risk estimated from the ATDs was calculated by (1)

$$OIM_{AIS3+}^{ATD} = 1 - (1 - P_{HIC}) * (1 - P_{BrIC}) * \left(1 - Max(P_{NIJ}, P_{NeckFz+}, P_{NeckFz-})\right) * (1 - P_{ChCD}) * (1 - P_{FemurF})$$

(Equation 1)

where P_{HIC}, P_{BrIC}, $P_{NIJ}, P_{NeckFz+}, P_{NeckFz-}$, P_{ChCD}, P_{FemurF} are the AIS 3+ injury probabilities calculated with the measures of Head Injury Criterion (HIC15) and Brain Injury Criterion (BrIC), Neck Injury Criterion (NIJ) and Neck Extension and Compression Forces, Chest Deflections, and Femur Force, respectively. Table D-1 in Appendix-D summarizes the formulas for these probabilities and references for the three ATD sizes: the Hybrid-III 5th%ile small-size female dummy, the 50th%ile mid-size male THOR and the Hybrid-III 95th%ile large size male dummy.

The Occupant Injury Measure (OIM_{AIS3+}^{HM}) for the AIS 3+ injury risk estimated from the HMs was calculated by (2)

$$OIM_{AIS3+}^{HM} = 1 - (1 - p_{HIC}) * (1 - p_{BrIC}) * \left(1 - Max(p_{NeckFz+}, p_{NeckFz-})\right) * (1 - p_{ChCD}) * (1 - p_{FemurF})$$

(Equation 2)

where p_{HIC}, p_{BrIC}, $p_{NeckFz+}, p_{NeckFz-}$, p_{ChCD}, p_{FemurF} are the AIS 3+ injury probabilities calculated with the measures of Head Injury Criterion (HIC15) and Brain Injury Criterion (BrIC), Neck Extension and Compression Forces, Chest Deflections, and Femur Force, respectively. Table D-2 in Appendix-D summarizes the formulas for these probabilities and references for the three HM sizes: the 5th%ile small-size female HM, the 50th%ile mid-size male HM and the 95th%ile large size male HM. It is noted that the chest deflections were defined and outputted at the five locations at the thorax: the center of the sternum, and the upper left and right, and the lower left and right. The last four locations are same as the THOR dummy for comparison. The chest deflection at the sternum center was used for calculating the injury risk of the thorax region.

The benefit of new adaptive restraints was estimated by the percentage of reduction of the OIM from the ARS2 over the OIM from the baseline restraints.

To establish a benchmark for comparison, the ATD sled simulations for the baseline restraints (with A- class models) were performed and the results were processed. Also, the HM sled simulations for the baseline restraints (with E- class models) were performed.

RESULTS

Occupant Injury Measures from ATDs

Figure 2 compares the Occupant Injury Measures for the AIS 3+ injury risks between the optimal adaptive restraints (ARS2) and the baseline restraints for the fourteen load cases. The calculations were based on the body injury measures outputted from the ATDs as listed in Table E-1 in Appendix E. The ATD study showed that the ARS2 had the lower OIMs than the baseline across all the load cases. The percentages of the AIS 3+ injury measure reduction over the baseline were in the range of 12%-79%. For all the fourteen load cases, there were no case with the baseline restraints in which the OIM was less than 20%. The adaptive restraint system brought down the OIMs of two cases below 20%.

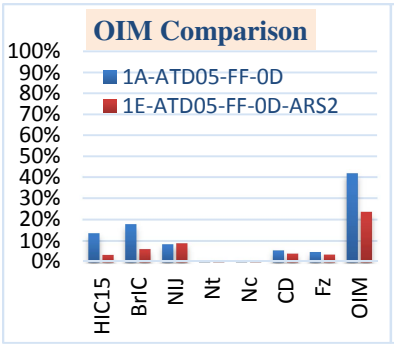

(i) Case 1E vs. 1A

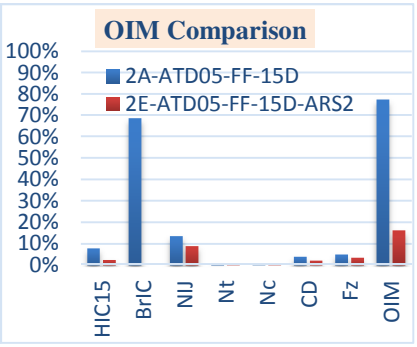

(ii) Case 2E vs. 2A

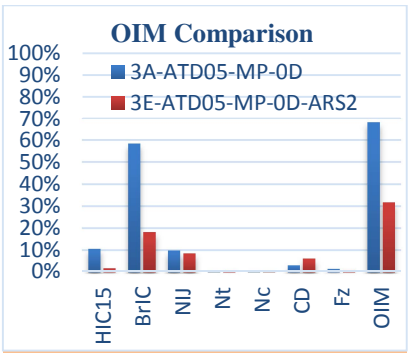

(iii) Case 3E vs. 3A

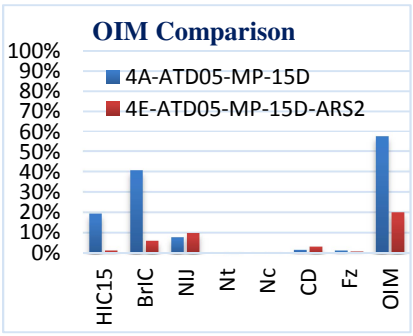

(i) Case 4E vs. 4A

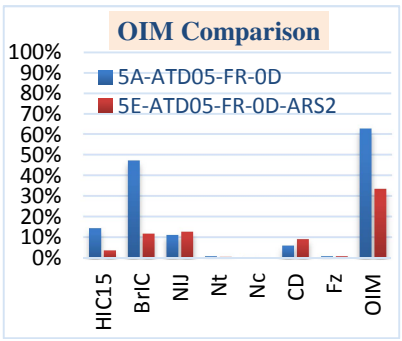

(ii) Case 5E vs. 5A

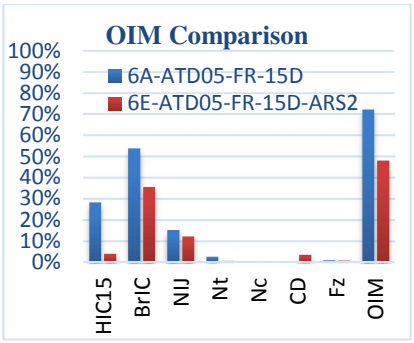

(iii) Case 6E vs. 6A

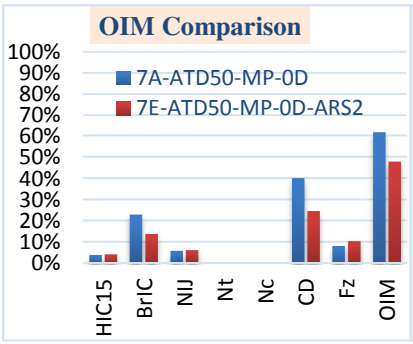

(i) Case 7E vs. 7A

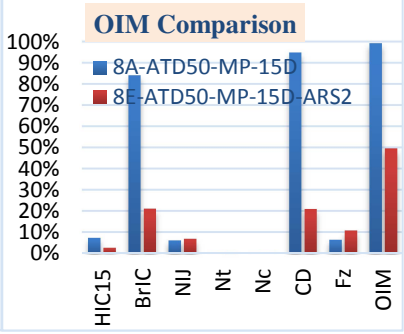

(ii) Case 8E vs. 8A

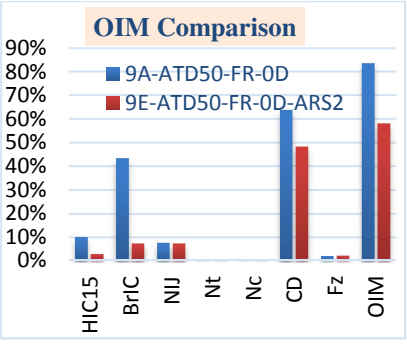

(iii) Case 9E vs. 9A

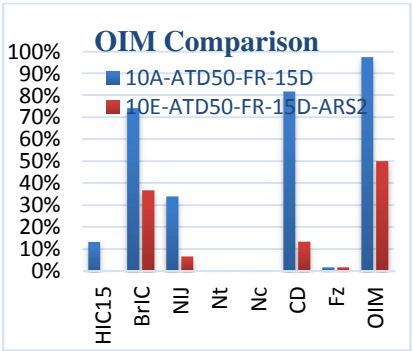

(i) Case 10E vs. 10A

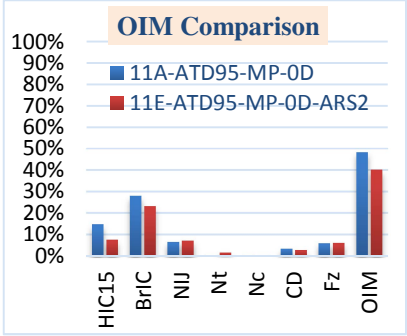

(ii) Case 11E vs. 11A

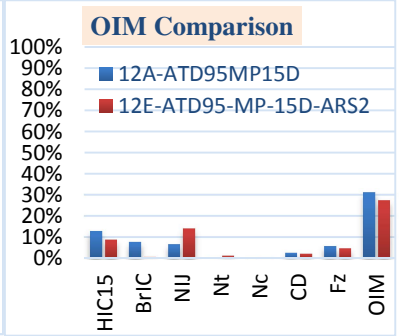

(iii) Case 12E vs. 12A

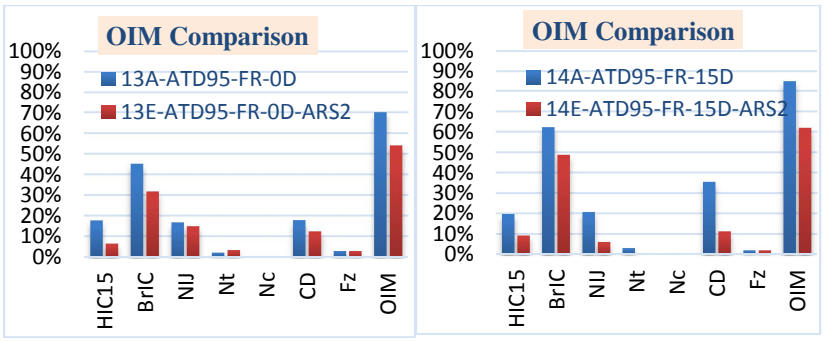

(i) Case 13E vs. 13A (ii) Case 14E vs. 14A

Figure 2. Comparison of the ATD estimated Occupant Injury Measures for the AIS 3+ injury risks between the adaptive restraints (ARS2) and the baseline restraints for the fourteen load cases. Blue bars—the baseline; red bars—the ARS2.

Occupant Injury Measures from HMs

Figure 3 compares the HMs estimated Occupant Injury Measures for the AIS 3+ injury risks between the ARS2 and the baseline restraints for the fourteen load cases. The human body injury measures outputted from the HMs are listed in Table E-2 in Appendix E. For the thirteen out of the fourteen load cases, the human models predicted that the ARS2, obtained from the optimization ATDs cycles, generated the lower OIMs than the baseline restraints. The percentages of the injury measure reduction over the baseline were in the range of 8%-66%. For all the fourteen load cases, there were no case with the baseline restraints, in which the OIM was less than 20%. With the adaptive restraint system, less than 20% of the OIMs estimated from the HMs were observed from five cases.

However, there was one exceptional case (Case 11F: the 95th%ile male human model at the mid-track position at the 0° hard pulse), in which the OIM from the ARS2 was higher than that from the baseline mainly caused by the spike of the HIC number due to the airbag bottoming out. In this case, the "optimized" set of design parameters from the Hybrid-III 95th%ile dummy lead to the soft passenger airbag deployment.

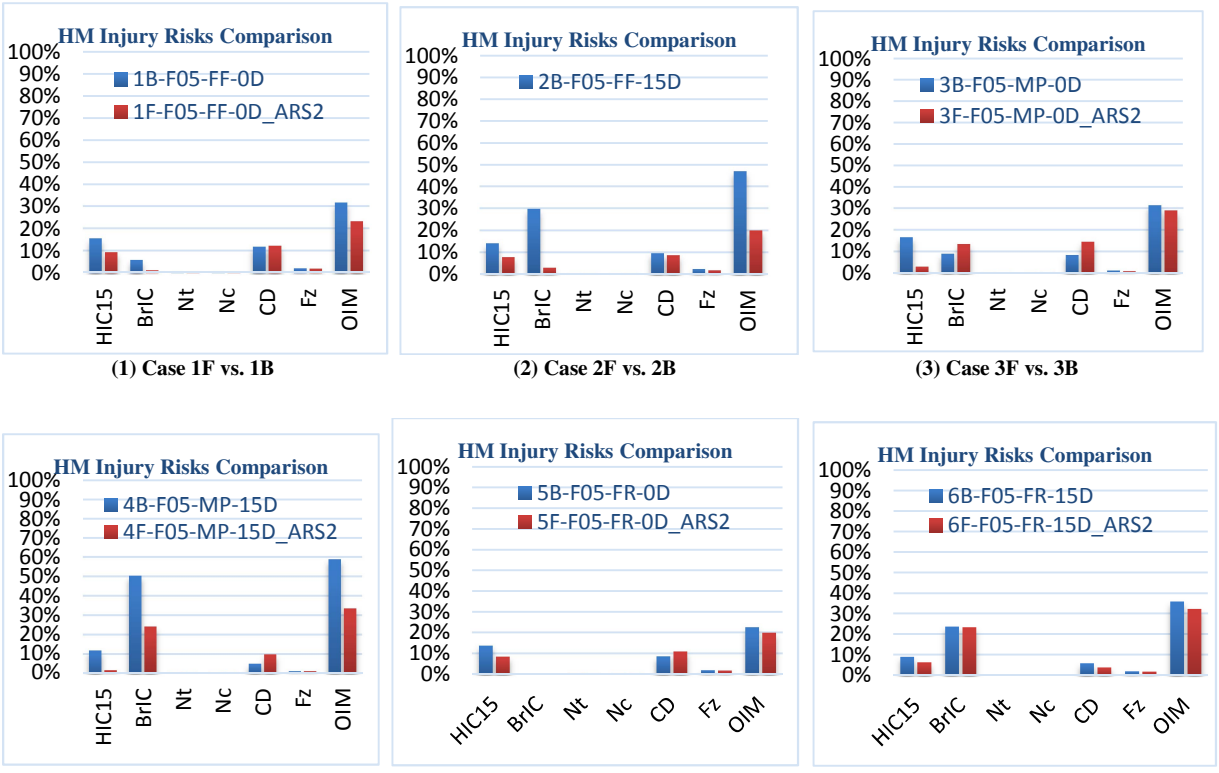

(1) Case 1F vs. 1B (2) Case 2F vs. 2B (3) Case 3F vs. 3B

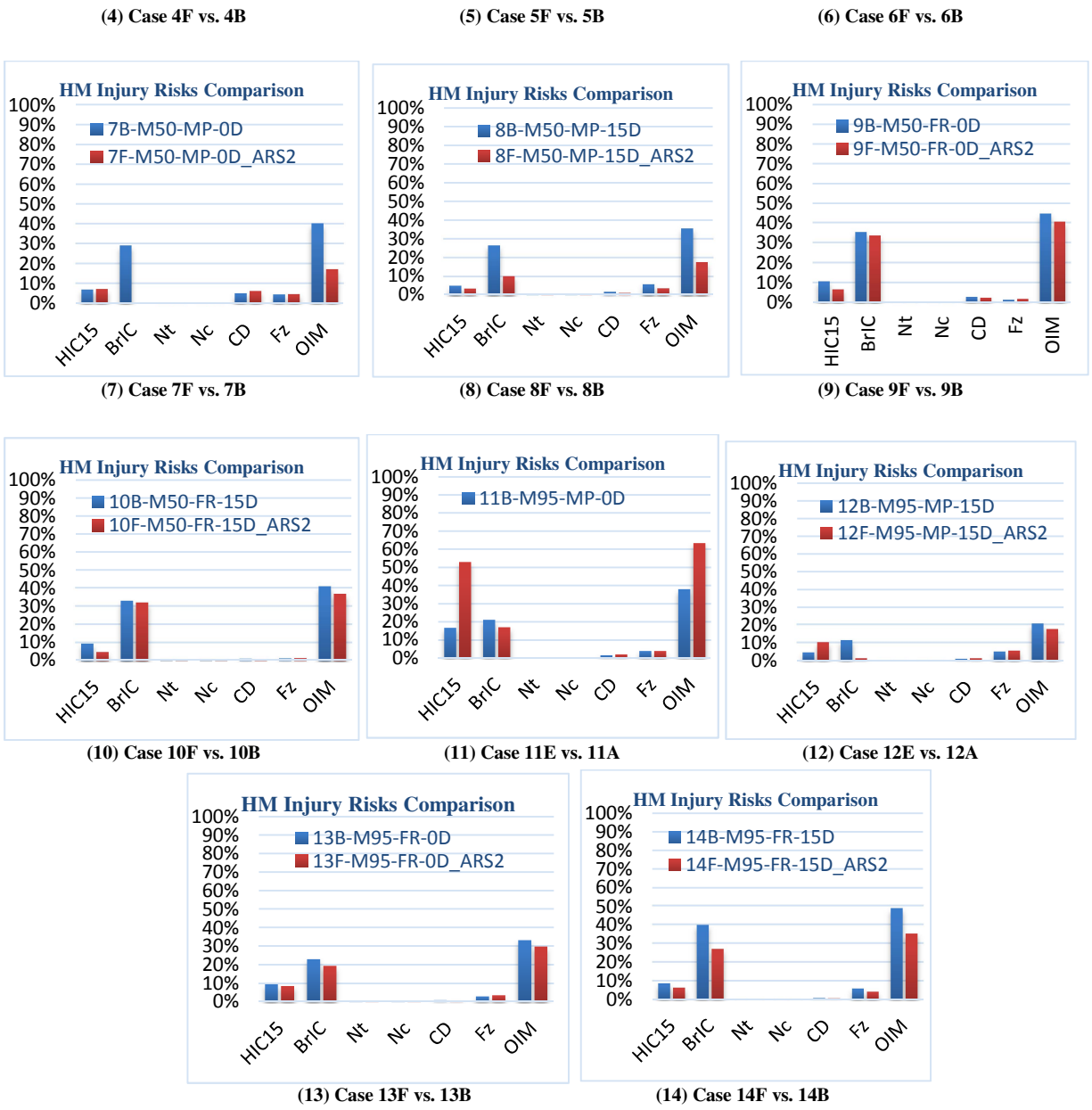

Figure 3. Comparison of the HM predicted Occupant Injury Measures for the AIS 3+ injury risks between the adaptive restraints (ARS2) and the baseline restraints for the fourteen load cases. Blue bars—the baseline; red bars—the ARS2.

It was seen from Figure 3 that the neck injury risk values were very low for all the cases. As shown in Table E-2, there were no outputs of the neck tension and compression forces in some cases for the 5th%ile female dummy, which had zero risk values for these cases. For the rest of cases with the neck forces outputs, however, the neck forces were so low such that the calculated maximum neck injury risk value was only 1.3%. The accuracy of the HM neck occipital forces outputs needs to be further evaluated.

DISCUSSIONS

Differences of the Estimated Occupant Injury Risks: ATDs. vs. HMs

An overview across Figure 2 and 3, we observed differences of the occupant injury risks between those estimated from the ATD and from the HM even at same load case conditions. One observation was that the

ATDs generally estimated higher BrIC based injury risks than the HMs. For some cases, the ATD estimated BrIC based injury risk probabilities were very high (exceeding 80%), while the maximum HM estimated BrIC based injury risk probabilities were less than 50%.

To understand more about the main body regions risks, we compared the predicted OIMs by HMs with the ones estimated by ATDs for the six load cases of the three occupant sizes and seating positions, as depicted in Figure 4. In this analysis, the neck injury risk values were excluded. It was seen that overall the HMs predicted the smaller OIMs than the ATDs. Further review of the four body region injury measures, we observed the lower chest injury risks (CD) estimated from the mid-size and large-size occupant HMs compared to those from the ATDs.

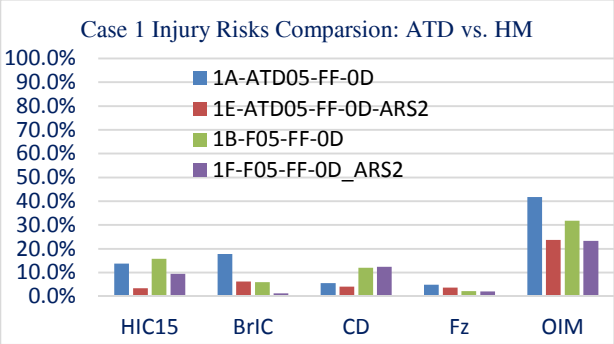

Case 1: the 5th %ile female at full-forward position

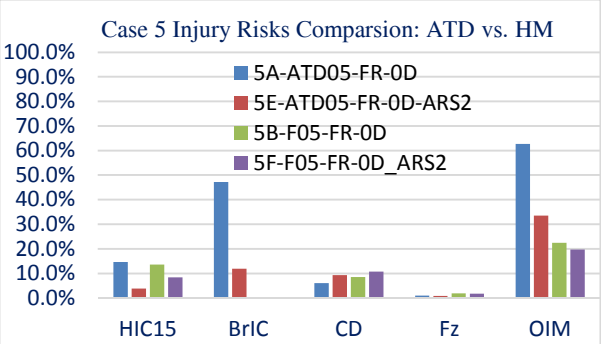

Case 5: the 5th %ile female at full-rearward position

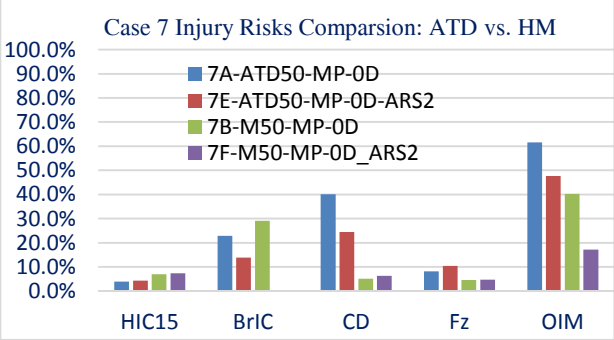

Case 7: the 50th %ile male at mid-track position

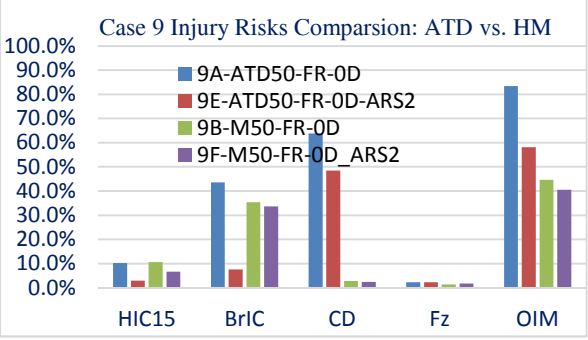

Case 9: the 50th %ile male at full-rearward position

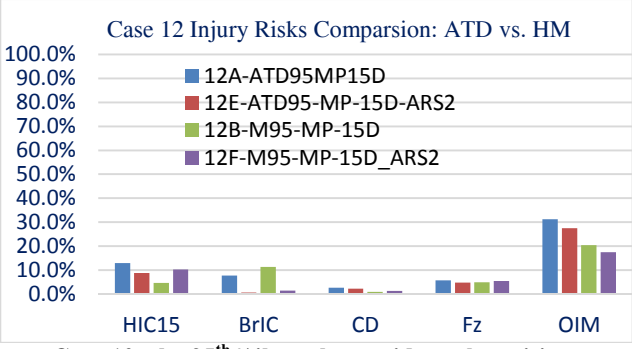

Case 12: the 95th %ile male at mid-track position

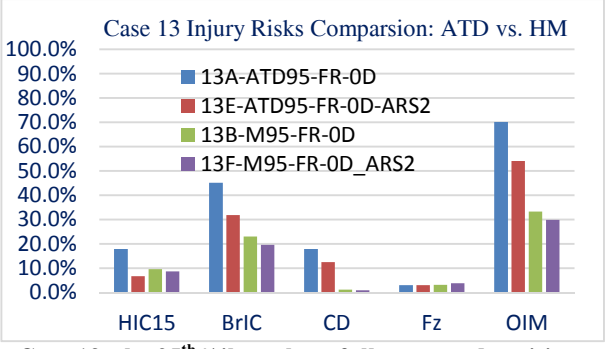

Case 13: the 95th %ile male at full-rearward position

Figure 4. Comparison of the HM predicted Occupant Injury Measures with the ATD estimated ones for the six load cases

Occupant Body Size Effect

We also analyzed the data to better understand the effects of the occupant body sizes and the injury assessment tools. Figure 5 shows the trends of OIMs varying with the occupant sizes, the seating positions (focused on the

Mid-Track and Full-rearward positions), and the crash modes. The data were obtained from the simulations with ATDs and the HMs for the baseline restraints. It was seen that the mid-size and large size males suffered relatively higher OIMs at the left 15° angled hard pulse in general. Another observation was that regardless of the seating positions and the pulse modes the Hybrid-III large sized male dummy generated the lower OIMs than the mid-size THOR dummy, which was confirmed from the ATD sled tests in the AARP. While the large-size male HM predicted the higher OIMs than the mid-sized male at the same full-rearward position at 15° angled hard pulse.

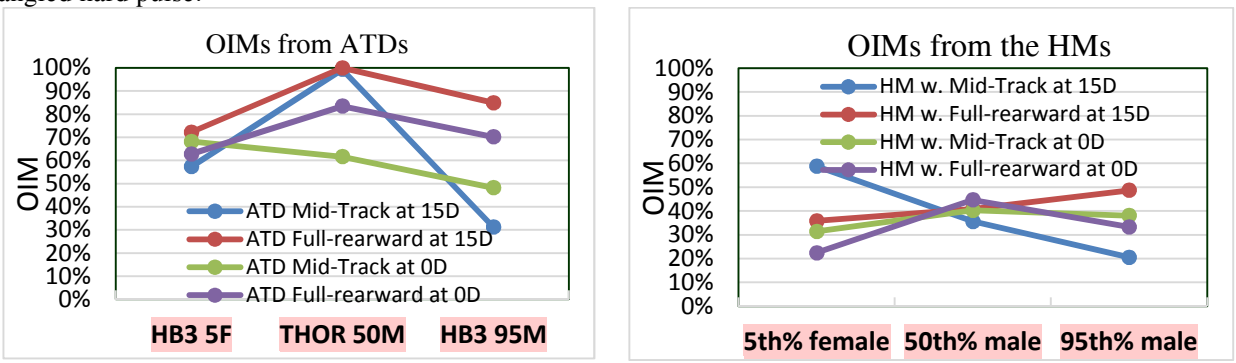

(1) the OIMs estimated from the ATDs **(1) the OIMs estimated from the HMs**

Figure 5. Comparison of the trends of OIMs varying with the occupant sizes, the seating positions, and the crash modes: the ATDs vs. the HMs. All the plotted data related to the baseline restraints.

Limitations of this Study

This study generated a large set of data from hundreds of the sled test simulations using the fifty-six sled system models. Although a portion of the ATD sled test models were directly validated with the real sled tests, the rest of the sled models with ATD or GHBMC Human Body Models were not directly validated since such experimental data does not exist. Nevertheless, this study was performed in multiple steps at large scale to evaluate potential benefits of the new concept design of the adaptive restraint system. The benefits were strictly assessed on the relative basis.

For the first time we deployed three sizes of GHBMC detailed human occupant models in the sled system simulations for evaluation of the adaptive restraint performances. Only those global injury measures that are the same as the ATD injury measures used in the regulation were analyzed in this paper. The other global injury measures for other body regions like the abdomen and lower extremities were processed from the human models, but the data were not included in this analysis. More analysis for those missed body region injuries are in working progress.

As shown in the results section, the outputted neck occipital joint forces were relatively low, for which further validation of the outputs is suggested for the occupant models.

The human models could generate a lot of data for assessing possible tissue level injuries of the occupants. In this paper such data analysis is not included. Considering that the GHBMC human models have been under continuous development, more detailed analysis on the tissue level injuries will be included in the next step studies once the update versions of the GHBMC models with more validations are available.

CONCLUSIONS

The new passenger adaptive restraint system developed from this study showed good benefits of reducing occupant injury risks over the current production restraints for the fourteen load cases considering the three body size occupants at the three seating positions under the two severe frontal crash modes. The occupant injury risks reduction percentages, varying case by case, are 12%-79% estimated with the ATDs and 8%-66% with the HMs.

New methods for evaluation and optimization of the adaptive restraint system designs were exercised using both the ATDs and the HMs of three body sizes. This new restraint evaluation protocol, with further

enhancement for the tools and processes, could be standardized for assessment of future adaptive restraint system designs.

Emerging occupant classification and monitoring systems offer the potential for protection improvement by calibrating the advanced restraint systems to optimize the level of protection for every occupant in the vehicle at different seating position. The future of occupant protection would be a dynamic, situational, intelligent personalized system based on the occupant data collected during normal vehicle usage. A combination of human body modeling tools and advanced occupant sensing would drive reduction in serious injuries caused by motor vehicle crashes.

ACKNOWLEDGEMENTS

Mike Scavnicky, Bernd Cyliax, Ingo Mueller, Torsten Steiner at Joyson Safety Systems made great contributions to AARP activities, from which the selected sled tests data were used for this study. The AARP project was funded by NHTSA Contract #DTNH22-12-C-00266. The authors greatly appreciate the support from NHTSA, especially James Saunders, Stephen Summers, and Dan Parent,

REFERENCES

Cyliax, B., Scavnicky, M., Mueller, I., Zhao, J., and Aoki, H. 2015. "Advanced Adaptive Restraints Program Individualization of Occupant Safety Systems", SAE 2015 Government/Industry Meeting, Washington, DC.

Bose, D., Crandall, J., Untaroiu, C., Maslen, E., "Influence of Pre-collision Occupant Properties on the Injury Response During Frontal Collisions", IRCOBI paper, September 2008.

Bugler, et al., Seattle CIREN Team (Bulger, Dissanaike, Kaufman, Mack), University of Washington, Harborview Injury Prevention and Research Center, " The Effects of Seatback Reclined Positions of Occupants in Motor Vehicles Collisions", CIREN Meeting 2007.

Eppinger, R., et al., 1999, "Development of Improved Injury Criteria for the Assessment of Advanced Automotive Restraint Systems - II", NHTSA

Eppinger, R., et al., 2000, "Supplement: Development of Improved Injury Criteria for the Assessment of Advanced Automotive Restraint Systems - II", NHTSA.

Gaewsky J., "Driver Injury Metric and Risk Variability as a Function of Occupant Position in Real World Motor Vehicle Crashes", Traffic Injury Prevention 16(sup2):S124-S131 · October 2015

Kent, R., Forman, J., et al., 2006, "Whole-body Kinematic and Dynamic Response of Restrained PMHS in Frontal Sled Tests", Stapp Car Crash Journal 50: 299-336.

Kuppa, S., et al., 2001, "Lowe Extremity Injuries and Associated Injury Criteria", 24th ESV Conference, Paper No. 457.

Laituri, T., et al., 2005, "Derivation and Evaluation of a Provisional, Age-Dependent, AIS3+ Thoracic Risk Curve for Belted Adults in Frontal Impacts", SAE World Congress, 2005-01-0297.

Parent, D. et al., 2015, "NHTSA THOR Update", THOR Public Meeting, Washington, DC.

Wang, S. C., et al., " Reference Analytic Morphomics Population (RAMP): A Reference to Measure Occupant Variability for Crash Injury Analysis", *IRC-16-80,* IRCOBI Conference 2016

Takhounts, E., Craig, JC., Moorhouse, K., and McFadden, J., 2013, "Development of Brain injury Criteria (BrIC)", Stapp Car Crash Journal 57: 343-266.

Zhao, J., Katagiri, M., "GHBMC Model Simulations in Frontal and Oblique Sled Tests for Different Body Sizes and Seating Positions", VDI Conference on Human Body Modelling in Automotive Safety, November 28-29, 2017, Waldorf Astoria Berlin, Germany.

Zhao, J., Zhang, N., and Hu J. 2015. "Implementation of THOR FE Model in AARP Project", NHTSA Public Meeting Concerning Test Device for Human Occupant Restraint, Washington, DC.

Appendix-A: The ATD Sled Test Models Correlation

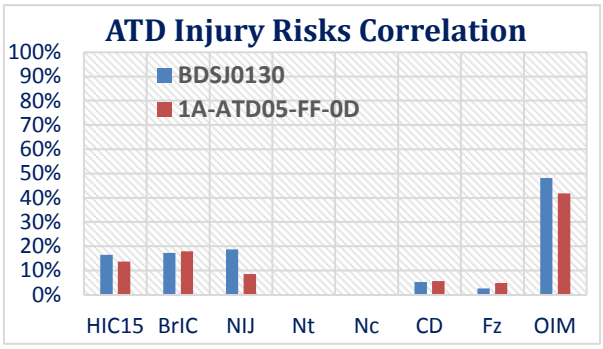

(a) Case 1A-ATD05-FF-0D

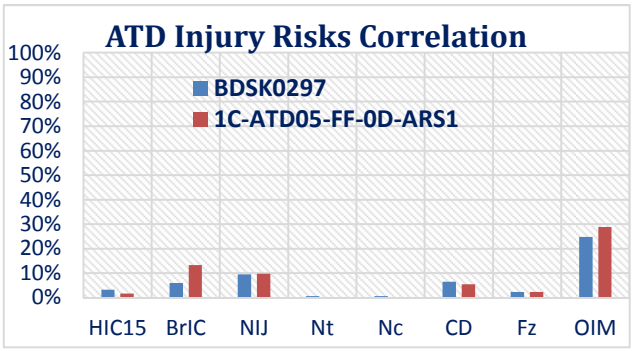

(b) Case 1C-ATD05-FF-0D-ARS1

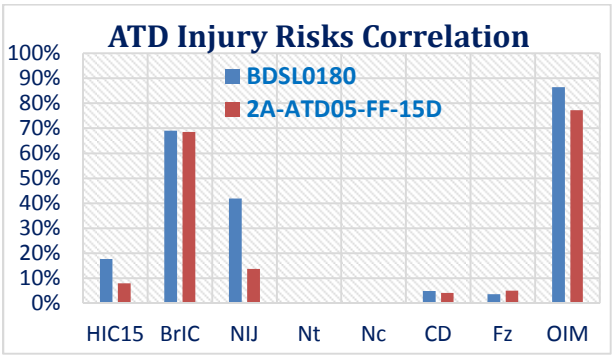

(a) Case 2A-ATD05-FF-15D

(b)

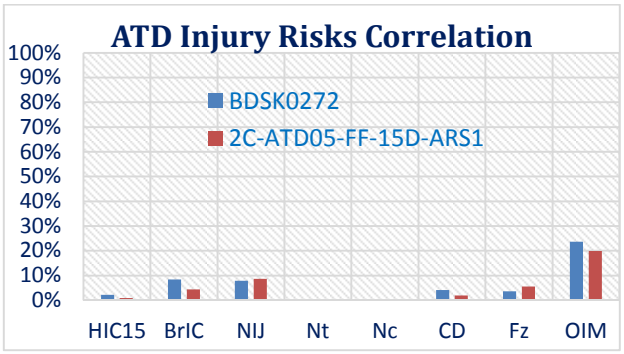

(b) Case 2C-ATD05-FF-15D-ARS1

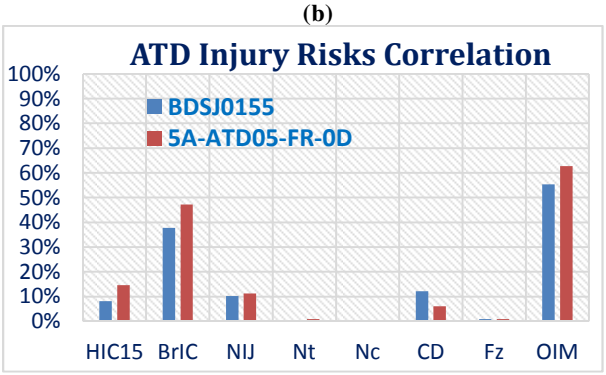

(a) Case 5A-ATD05-FR-0D-B

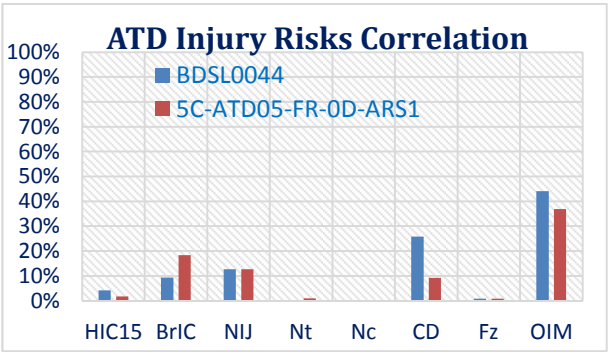

(b) Case 5C-ATD05-FR-0D -ARS1

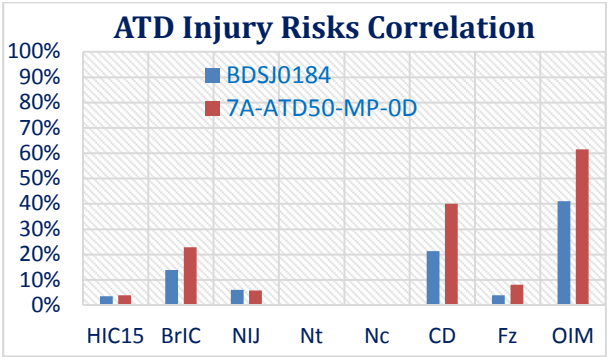

(a) Case 7A-ATD50-FR-0D

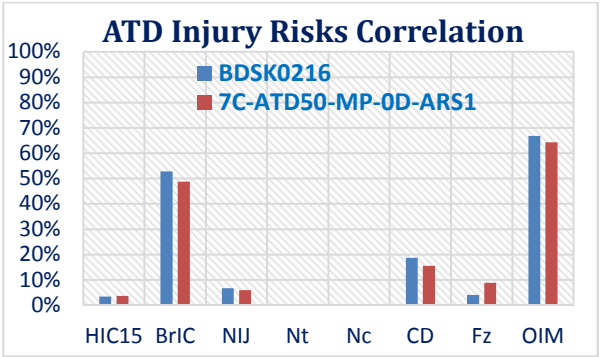

(b) Case 7C-ATD50-FR-0D-ARS1

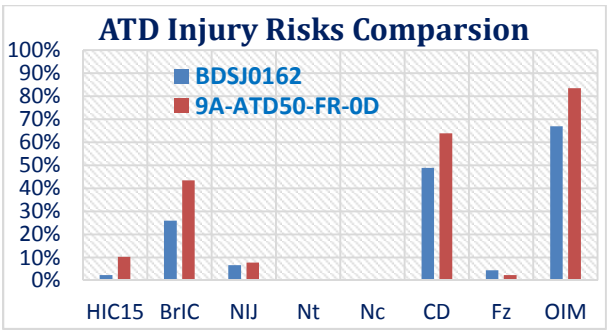

(a) Case 9A-ATD50-FR-0D

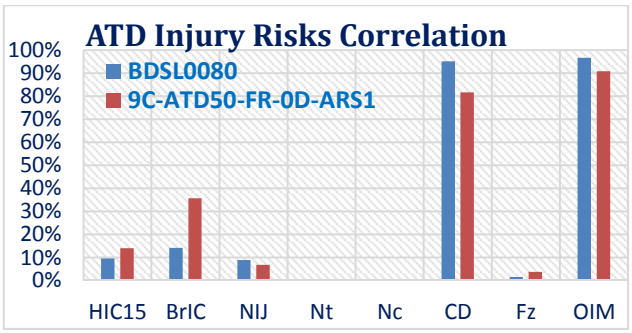

(b) Case 9C-ATD50-FR-0D-ARS1

Figure A-1. Correlation of the injury risks between the predicted from the sled simulations (red) and the calculated from the test measurement data (Blue)

Appendix-B: Additional Technical Info on The Load Case Definitions

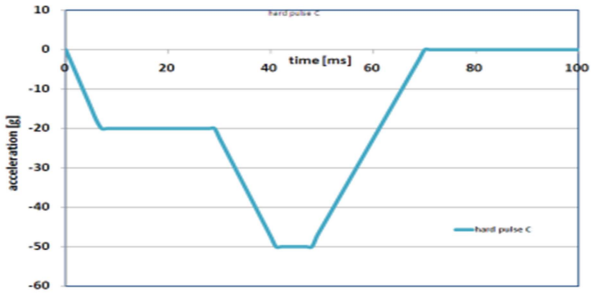

(a) 35mph Hard Pulse 0°

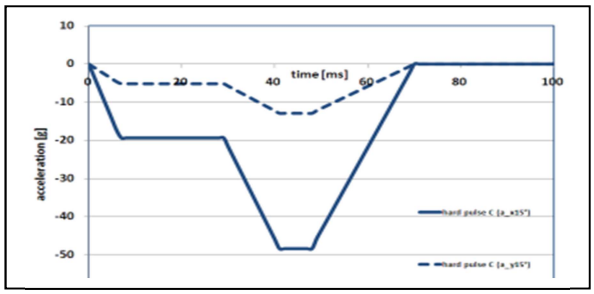

(b) 35mph Hard pulse 15°

Figure B-1. The AARP hard pulses represented a 35mph crash of a sub-compact car used in this study

Table B-1.
The sled test models developed from this study

Seq #	Case No	Case Name	Occ. Model	Pulse Angle	Occ. Size	Seat Position	Restraints
1	1A	ATDF05_FF_0D	HB3-05	0°	5%	Full Forward	Baseline
2	2A	ATDF05_FF_15D	HB3-05	LT-15°	5%	Full Forward	Baseline
3	3A	ATDF05_MP_0D	HB3-05	0°	5%	Mid-Track	Baseline
4	4A	ATDF05_MP_15D	HB3-05	LT-15°	5%	Mid-Track	Baseline
5	5A	ATDF05_FR_0D	HB3-05	0°	5%	Full Rear	Baseline
6	6A	ATDF05_FR_15D	HB3-05	LT-15°	5%	Full Rear	Baseline
7	7A	ATDM50_MP_0D	THOR-50M	0°	50%	Mid-Track	Baseline
8	8A	ATDM50_MP_15D	THOR-50M	LT-15°	50%	Mid-Track	Baseline
9	9A	ATDM50_FR_0D	THOR-50M	0°	50%	Full Rear	Baseline
10	10A	ATDM50_FR_15D	THOR-50M	LT-15°	50%	Full Rear	Baseline
11	11A	ATDM95_MP_0D	HB3-95	0°	95%	Mid-Track	Baseline
12	12A	ATDM95_MP_15D	HB3-95	LT-15°	95%	Mid-Track	Baseline
13	13A	ATDM95_FR_0D	HB3-95	0°	95%	Full Rear	Baseline
14	14A	ATDM95_FR_15D	HB3-95	LT-15°	95%	Full Rear	Baseline
15	1B	F05_FF_0D	GHBMC F05-O 3.1	0°	5%	Full Forward	Baseline

16	2B	F05_FF_15D	GHBMC F05-O 3.1	LT-15°	5%	Full Forward	Baseline
17	3B	F05_MP_0D	GHBMC F05-O 3.1	0°	5%	Mid-Track	Baseline
18	4B	F05_MP_15D	GHBMC F05-O 3.1	LT-15°	5%	Mid-Track	Baseline
19	5B	F05_FR_0D	GHBMC F05-O 3.1	0°	5%	Full Rear	Baseline
20	6B	F05_FR_15D	GHBMC F05-O 3.1	LT-15°	5%	Full Rear	Baseline
21	7B	M50_MP_0D	GHBMC M50-O v4.5	0°	50%	Mid-Track	Baseline
22	8B	M50_MP_15D	GHBMC M50-O v4.5	LT-15°	50%	Mid-Track	Baseline
23	9B	M50_FR_0D	GHBMC M50-O v4.5	0°	50%	Full Rear	Baseline
24	10B	M50_FR_15D	GHBMC M50-O v4.5	LT-15°	50%	Full Rear	Baseline
25	11B	M95_MP_0D	GHBMC M95-O v1.3	0°	95%	Mid-Track	Baseline
26	12B	M95_MP_15D	GHBMC M95-O v1.3	LT-15°	95%	Mid-Track	Baseline
27	13B	M95_FR_0D	GHBMC M95-O v1.3	0°	95%	Full Rear	Baseline
28	14B	M95_FR_15D	GHBMC M95-O v1.3	LT-15°	95%	Full Rear	Baseline
29	1E	ATDF05_FF_0D	HB3-05	0°	5%	Full Forward	ARS2
30	2E	ATDF05_FF_15D	HB3-05	LT-15°	5%	Full Forward	ARS2
31	3E	ATDF05_MP_0D	HB3-05	0°	5%	Mid-Track	ARS2
32	4E	ATDF05_MP_15D	HB3-05	LT-15°	5%	Mid-Track	ARS2
33	5E	ATDF05_FR_0D	HB3-05	0°	5%	Full Rear	ARS2
34	6E	ATDF05_FR_15D	HB3-05	LT-15°	5%	Full Rear	ARS2
35	7E	ATDM50_MP_0D	THOR-50M	0°	50%	Mid-Track	ARS2
36	8E	ATDM50_MP_15D	THOR-50M	LT-15°	50%	Mid-Track	ARS2
37	9E	ATDM50_FR_0D	THOR-50M	0°	50%	Full Rear	ARS2
38	10E	ATDM50_FR_15D	THOR-50M	LT-15°	50%	Full Rear	ARS2
39	11E	ATDM95_MP_0D	HB3-95	0°	95%	Mid-Track	ARS2
40	12E	ATDM95_MP_15D	HB3-95	LT-15°	95%	Mid-Track	ARS2
41	13E	ATDM95_FR_0D	HB3-95	0°	95%	Full Rear	ARS2
42	14E	ATDM95_FR_15D	HB3-95	LT-15°	95%	Full Rear	ARS2
43	1F	F05_FF_0D	GHBMC F05-O 3.1	0°	5%	Full Forward	ARS2
44	2F	F05_FF_15D	GHBMC F05-O 3.1	LT-15°	5%	Full Forward	ARS2
45	3F	F05_MP_0D	GHBMC F05-O 3.1	0°	5%	Mid-Track	ARS2
46	4F	F05_MP_15D	GHBMC F05-O 3.1	LT-15°	5%	Mid-Track	ARS2
47	5F	F05_FR_0D	GHBMC F05-O 3.1	0°	5%	Full Rear	ARS2
48	6F	F05_FR_15D	GHBMC F05-O 3.1	LT-15°	5%	Full Rear	ARS2
49	7F	M50_MP_0D	GHBMC M50-O v4.5	0°	50%	Mid-Track	ARS2
50	8F	M50_MP_15D	GHBMC M50-O v4.5	LT-15°	50%	Mid-Track	ARS2
51	9F	M50_FR_0D	GHBMC M50-O v4.5	0°	50%	Full Rear	ARS2
52	10F	M50_FR_15D	GHBMC M50-O v4.5	LT-15°	50%	Full Rear	ARS2
53	11F	M95_MP_0D	GHBMC M95-O v1.3	0°	95%	Mid-Track	ARS2
54	12F	M95_MP_15D	GHBMC M95-O v1.3	LT-15°	95%	Mid-Track	ARS2
55	13F	M95_FR_0D	GHBMC M95-O v1.3	0°	95%	Full Rear	ARS2
56	14F	M95_FR_15D	GHBMC M95-O v1.3	LT-15°	95%	Full Rear	ARS2

Appendix-C: The ARS2 Restraint System Parameters

Table C-1.
ARS2 system components and design parameters defined in this study

Component	NO.	Parameter	Classification
Passenger Airbag (PAB)	1	Inflator TTF (ms)	P
	2	Fixed Vent size (mm)	N
	3	Tether Length	N
	4	Active Vent (AV) size (mm)	N
	5	AV Opening Time (ms)	P
	6	Volume Switch Time (ms)	P
Knee Airbag (KAB)	7	Inflator TTF (ms)	P
	8	Tether Length	N
	9	AV Size (mm)	N
	10	AV Opening Time (ms)	P
	11	Volume Swtich Time (ms)	P
Seatbelt (SB)	12	Retractor & Sho PT TTFs (ms)	P
	13	1st Load Limiter (KN)	N
	14	2nd Load Limiter (KN)	N
	15	Load Limiter Switch Time (ms)	P
	16	Lap PT TTF (ms)	P
RH Curtain Airbag (CAB)	17	Inflator TTF (ms)	P

- P—Programmable; N—Non-programmable

Appendix-D: Injury Risk Functions for the ATDs and HMs

The risk injury functions for each measure as well as a combined injury probability for the whole body were same as those defined in new US NCAP NPRM [US NCAP NPRM, 2016], summarized in Table E-1. The function of Nt and Nc for Hybrid III 95th%ile male was scaled from that for 50th%ile male based on the scaling factor reported in Eppinger et al., 1999. The injury risk functions for the human models were summarized in Table E-2.

Table D-1.
The injury risk functions for the ATDs

	Hybrid III 5th%ile female	THOR 50th%ile male	Hybrid III 95th%ile male	Function	Reference
HIC	✓	✓	✓	$P(AIS\,3+) = \emptyset\left[\frac{\ln(HIC) - 7.45231}{0.73998}\right]$	US NCAP
BrIC	✓	✓	✓	$P(AIS\,3+) = 1 - e^{-\left(\frac{BrIC-0.523}{0.531}\right)^{1.8}}$	US NCAP

Nij	✓	✓	✓	$P(AIS\,3+) = \frac{1}{1+e^{(3.227-1.969*Nij)}}$	US NCAP
Nt, Nc	✓			$P(AIS\,3+) = \frac{1}{1+e^{(10.958-3.77*Nt\ or\ Nc)}}$	US NCAP
		✓		$P(AIS\,3+) = \frac{1}{1+e^{(10.975-2.375*Nt\ or\ Nc)}}$	US NCAP
			✓	$P(AIS\,3+) = \frac{1}{1+e^{(10.975-1.966*Nt\ or\ Nc)}}$	US NCAP*
CD	✓			$P(AIS\,3+) = \frac{1}{1+e^{(10.5456-1.7212*CD^{0.4612})}}$	US NCAP
		✓		$P(AIS\,3+) = 1-e^{-\left(\frac{CD}{e^{4.4853-0.0113}}\right)^{5.03896}}$	US NCAP
			✓	$P(AIS\,3+) = \frac{1}{1+e^{(10.5456-1.4956*CD^{0.4612})}}$	FMVSS 208
Femur Fz	✓			$P(AIS\,3+) = \frac{1}{1+e^{(4.9795-0.478*Fz)}}$	US NCAP
		✓		$P(AIS\,3+) = \frac{1}{1+e^{(4.9795-0.326*Fz)}}$	US NCAP
			✓	$P(AIS\,3+) = \frac{1}{1+e^{(4.9795-0.257*Fz)}}$	FMVSS 208

Table D-2.
The injury risk functions for the HMs

	HM 5th%ile female	HM 50th%ile male	HM 95th%ile male	Function	Reference
HIC	✓	✓	✓	$P(AIS\,3+) = \emptyset\left[\frac{\ln(HIC)-7.45231}{0.73998}\right]$	Eppinger, 2000
BrIC	✓	✓	✓	$P(AIS\,3+) = 1-e^{-\left(\frac{BrIC-0.523}{0.531}\right)^{1.8}}$	Takhounts, 2013
Nt, Nc	✓			$P(AIS\,3+) = \frac{1}{1+e^{(10.958-3.77*Nt\ or\ Nc)}}$	Eppinger, 1999
		✓		$P(AIS\,3+) = \frac{1}{1+e^{(10.975-2.375*Nt\ or\ Nc)}}$	
			✓	$P(AIS\,3+) = \frac{1}{1+e^{(10.975-1.966*Nt\ or\ Nc)}}$	
CD	✓	✓	✓	$P(AIS\,3+) = \frac{1}{1+e^{(12.957-0.05861*65YO-26.9*CD\%)}}$	Laituri, 2005
Femur Fz	✓			$P(AIS\,3+) = \frac{1}{1+e^{(4.9795-0.478*Fz)}}$	Kuppa, 2001
		✓		$P(AIS\,3+) = \frac{1}{1+e^{(4.9795-0.326*Fz)}}$	
			✓	$P(AIS\,3+) = \frac{1}{1+e^{(4.9795-0.257*Fz)}}$	

Appendix-E: Injury Measures from the ATDs

Table E-1.
The injury measures from the baseline restraints A- class ATD sled test models and the ARS2 E- class ATD sled models

Body Region	Head		Neck			Thorax					KTH	
Injury Measure /Case	HIC 15	BrIC	NIJ	Neck Tension (kN)	Neck Compression (kN)	Chest G 3ms (G)	Chest Def. UR (mm)	Chest Def. UL (mm)	Chest Def. LR (mm)	Chest Def. LL (mm)	Femur Load - Right (kN)	Femur Load - Left (kN)
1A-ATD05-FF-0D	767.5	0.785	0.44	1.028	0.331	58.3	25.9	25.9	25.9	25.9	3.480	4.197
1E-ATD05-FF-0D-ARS2	446.6	0.664	0.46	1.143	0.379	44.1	23.5	23.5	23.5	23.5	3.350	3.560
2A-ATD05-FF-15D	608.6	1.225	0.70	1.409	0.103	60.5	23.5	23.5	23.5	23.5	3.213	4.276

2E-ATD05-FF-15D-ARS2	403.9	0.482	0.46	1.224	0.080	44.0	19.6	19.6	19.6	19.6	2.756	3.498
3A-ATD05-MP-0D	685.9	1.126	0.51	0.768	0.201	56.6	21.7	21.7	21.7	21.7	1.690	1.257
3E-ATD05-MP-0D-ARS2	365.9	0.789	0.43	1.610	0.128	46.7	26.8	26.8	26.8	26.8	0.558	0.551
4A-ATD05-MP-15D	912.1	0.974	0.39	0.707	0.461	58.8	17.7	17.7	17.7	17.7	1.332	1.218
4E-ATD05-MP-15D-ARS2	331.6	0.663	0.52	1.391	0.136	42.2	22.1	22.1	22.1	22.1	0.458	0.560
5A-ATD05-FR-0D	790.0	1.027	0.59	1.656	0.848	46.5	26.5	26.5	26.5	26.5	0.619	0.399
5E-ATD05-FR-0D-ARS2	463.0	0.728	0.66	1.597	0.544	40.1	30.0	30.0	30.0	30.0	0.398	0.558
6A-ATD05-FR-15D	1129.1	1.083	0.77	1.946	0.306	72.1	0.3	0.3	0.3	0.3	0.920	0.579
6E-ATD05-FR-15D-ARS2	470.8	0.933	0.64	1.613	0.115	44.2	22.5	22.5	22.5	22.5	0.216	0.559
7A-ATD50-MP-0D_B	470.5	0.829	0.23	1.385	0.415	45.8	34.8	38.0	9.2	46.7	6.937	7.826
7E-ATD50-MP-0D-ARS2	481.9	0.747	0.27	1.411	0.595	50.8	0.8	35.6	8.6	41.5	8.685	7.419
8A-ATD50-MP-15D-B	589.8	1.433	0.25	1.489	0.911	52.1	30.6	6.5	30.6	66.3	5.811	7.036
8E-ATD50-MP-15D-ARS2	412.5	0.814	0.32	1.980	0.306	47.2	0.5	35.6	6.9	40.0	8.778	6.559
9A-ATD50-FR-0D-B	674.9	0.997	0.38	1.764	0.201	90.3	1.2	30.0	12.8	53.5	3.218	3.669
9E-ATD50-FR-0D-ARS2	426.2	0.680	0.36	1.635	0.030	51.1	1.1	28.5	14.5	49.1	2.640	3.799
10A-ATD50-FR-15D-B	756.5	1.288	1.30	1.219	1.461	67.6	49.8	11.9	49.8	59.3	3.028	2.025
10E-ATD50-FR-15D-ARS2	253.8	0.942	0.30	1.678	0.029	45.2	1.2	18.0	12.0	36.3	2.884	2.453
11A-ATD95-MP-0D	797.9	0.872	0.30	2.062	1.390	49.5	30.4	30.4	30.4	30.4	8.705	7.283
11E-ATD95-MP-0D-ARS2	598.5	0.832	0.34	3.538	1.219	41.9	28.5	28.5	28.5	28.5	8.808	8.310
12A-ATD95MP15D	746.4	0.683	0.30	2.242	1.296	57.8	27.8	27.8	27.8	27.8	8.525	7.304
12E-ATD95-MP-15D-ARS2	633.5	0.561	0.72	3.353	1.436	56.5	26.3	26.3	26.3	26.3	7.433	7.699
13A-ATD95-FR-0D	870.9	1.010	0.83	3.666	1.743	66.4	49.2	49.2	49.2	49.2	4.120	5.861
13E-ATD95-FR-0D-ARS2	566.5	0.903	0.76	3.894	1.891	51.1	44.4	44.4	44.4	44.4	3.704	5.774
14A-ATD95-FR-15D	918.4	1.162	0.96	3.821	0.545	67.8	60.9	60.9	60.9	60.9	4.203	3.871
14E-ATD95-FR-15D-ARS2	646.3	1.040	0.25	1.287	0.035	68.7	43.2	43.2	43.2	43.2	4.299	4.242

Table E-2.
The injury measures from the baseline restraints B- class HM sled test models and the ARS2 F- class HM sled models

Body Region	Head		Neck		Thorax						KTH	
Injury Measure	HIC 15	BrIC	Neck Tension (kN)	Neck Compression (kN)	Chest G 3ms (G)	Chest Def. UR (mm)	Chest Def. UL (mm)	Chest Def. LR (mm)	Chest Def. LL (mm)	Chest Def-Sternum (mm)	Femur Load - Right/kN (FzR)	Femur Load - Left/kN (FzL)
1B-F05-FF-0D	818.9	0.66	0.36	0.023	83.1	57.6	57.8	56.4	53.4	53.0	2.510	2.175

1F-F05-FF-0D_ARS2	652.0	0.58	0.30	0.037	66.5	54.8	54.5	63.2	49.3	53.3	2.385	2.323
2B-F05-FF-15D	779.3	0.89	NA	NA	80.6	54.9	53.6	11.1	33.7	51.1	2.731	2.164
2F-F05-FF-15D_ARS2	551.3	0.67	0.048	0.052	72.4	51.5	50.9	50.9	44.9	50.4	2.078	2.024
3B-F05-MP-0D	842.8	0.70	NA	NA	64.5	51.9	48.6	70.7	55.4	50.0	1.233	0.809
3F-F05-MP-0D_ARS2	432.0	0.75	NA	NA	56.0	56.3	49.5	55.6	42.3	54.8	0.574	0.744
4B-F05-MP-15D	715.9	1.05	NA	NA	79.5	46.6	41.2	46.4	28.3	45.5	0.987	0.918
4F-F05-MP-15D_ARS2	352.4	0.84	NA	NA	65.2	52.8	46.5	41.0	24.4	51.3	1.165	0.906
5B-F05-FR-0D	764.5	0.52	NA	NA	70.3	55.7	46.6	24.0	39.1	50.0	2.128	1.508
5F-F05-FR-0D_ARS2	599.7	0.40	0.132	0.039	57.8	58.2	47.7	11.9	39.6	52.1	2.040	1.401
6B-F05-FR-15D	638.0	0.84	NA	NA	242.8	52.2	44.9	27.8	37.5	47.0	2.232	1.434
6F-F05-FR-15D_ARS2	556.7	0.83	NA	NA	254.4	48.2	40.9	24.5	34.4	43.4	2.112	1.393
7B-M50-MP-0D	575.7	0.88	0.56	0.012	68.7	50.6	56.7	40.2	48.3	48.5	5.924	5.388
7F-M50-MP-0D_ARS2	588.1	0.51	0.91	0.090	65.5	51.2	59.1	36.5	50.7	50.4	6.029	5.039
7B-M50OS-MP-0D	397.7	0.79	15.00	3.292	68.8	45.3	61.4	9.8	57.2	54.9	5.239	4.992
7F-M50OS-MP-0D_ARS2	394.3	0.98	15.44	34.074	69.4	40.6	63.3	9.7	59.9	54.9	5.061	3.877
8B-M50-MP-15D	511.1	0.86	0.70	0.035	65.6	42.1	46.7	21.9	39.5	40.2	3.997	6.761
8F-M50-MP-15D_ARS2	452.9	0.71	0.87	0.024	84.3	36.8	44.0	29.3	35.1	37.0	5.286	4.980
9B-M50-FR-0D	685.6	0.93	1.11	0.002	165.4	45.1	58.7	20.1	69.4	43.5	1.646	2.028
9F-M50-FR-0D_ARS2	565.4	0.92	1.32	0.001	158.6	41.9	56.0	24.8	69.2	42.1	2.928	2.471
10B-M50-FR-15D	652.4	0.91	1.19	0.002	87.5	42.3	48.4	40.4	63.1	37.0	1.709	2.253
10F-M50-FR-15D_ARS2	508.1	0.90	1.11	0.199	160.1	34.3	41.8	14.3	54.7	31.5	2.433	1.570
11B-M95-MP-0D	845.7	0.81	0.82	0.065	74.0	63.0	52.1	17.7	54.7	41.0	6.285	7.030
11F-M95-MP-0D_ARS2	1823.9	0.778	1.004	0.057	79.0	63.7	50.6	9.5	55.3	42.9	5.536	6.928
12B-M95-MP-15D	495.4	0.72	0.823	0.069	67.5	55.5	44.3	13.2	47.8	36.6	5.500	7.908
12F-M95-MP-15D_ARS2	674.4	0.584	0.931	0.059	82.9	57.2	44.1	29.1	49.9	39.0	5.134	8.314
13B-M95-FR-0D	656.7	0.83	1.33	0.028	79.9	64.5	55.7	9.6	80.0	37.7	4.200	5.906
13F-M95-FR-0D_ARS2	628.9	0.80	1.27	0.018	79.8	61.8	52.3	38.3	73.2	35.8	2.904	6.735
14B-M95-FR-15D	631.2	0.97	1.29	0.025	127.3	57.1	47.5	55.0	68.9	34.8	2.995	8.641
14F-M95-FR-15D_ARS2	560.1	0.86	1.16	0.015	91.6	53.0	43.4	60.4	60.2	34.0	2.425	7.250

DRIVER WORKLOAD ESTIMATION BASED ON REALISTIC IN-VEHICLE SENSORS

Florian Ripper
Ardit Dvorani
Christoph Hemprich
Koshan Mahdi
Lukas Scholz
Joyson Safety Systems (JSS)
Germany

Leonard Cech
Joyson Safety Systems (JSS)
USA

Paper Number 19-0325

ABSTRACT

The introduction of automated driving motivates the need for driver state detection, prediction and monitoring. The first introduced systems for automation (SAE level 2 or 3) rely on the ability of the driver to resume the driving task, both manually (steering control) and visually. The automation system monitors the presence of the driver's hand(s) on the steering wheel and some systems monitor the driver's visual attention as well. This is necessary to ensure that the driver monitors the automated drive and responds manually and/or visually to HMI cues from the automation system.

Considering higher levels of automated driving (SAE level 3 or 4), several challenges and opportunities arise. First, as driver confidence in the performance of automation grows, they will switch attention to secondary tasks increasing their cognitive workload. The driver may be busy doing other tasks and a system which estimates cognitive workload can indicate that a longer take-over period is necessary, or, in the extreme, a human driver take-over may not be safe or even feasible. Secondly, the driver may be visually, manually or mentally overloaded (or a combination of these) during manual control and the automation system might encourage or intervene automation modes to enhance safety. These two use cases can be improved using accurate real-time prediction of the driver's mental workload using one or more in-vehicle sensors.

In this paper a robust method for estimating driver workload based on real in-vehicle sensors is presented. Sensors in the seatbelt and at the steering wheel rim derive heart rate metrics which are used to estimate cognitive workload. Furthermore, an analysis is conducted to determine if additional metrics derived from vehicle dynamics data have an impact on the calculation accuracy. Comparing individual-based driver classification approaches versus a generalized driver algorithm is also part of this investigation. A driving simulator study with n-back task induced workload is used to validate the driver cognitive workload estimation method accuracy.

INTRODUCTION

The introduction of automated driving motivates the need for driver state detection, prediction and monitoring. The first introduced systems for automation (SAE level 2 or 3) rely on the ability of the driver to resume the driving task, both manually (steering control) and visually. The automation system monitors the presence of the driver's hand(s) on the steering wheel and some systems monitor the driver's visual attention as well. This is necessary to ensure that the driver monitors the automated drive and responds manually and/or visually to HMI cues from the automation system.

As higher levels of automated driving (SAE level 3 or 4) are introduced, several challenges and opportunities arise. First, as drivers gain confidence in the performance of automation, switching to secondary tasks (for example, reading, talking, cellphone manipulation, playing games, etc.) will re-direct and/or increase cognitive workload. In these situations, a system which continuously estimates cognitive workload can indicate that a longer take-over period is necessary, or a human driver take-over may not be safe or even feasible [1]. Secondly, the driver may be visually, manually or mentally overloaded during manual control and the automation system might encourage or intervene automation modes to enhance safety. These two use cases require accurate real-time prediction of the driver's mental workload based on one or more in-vehicle sensors.

Societal and technology changes such as cellular phone proliferation, adoption of advanced driver assistance systems and the nearly continuous availability of virtual social engagement are also contributing factors which drive ongoing research in this field coupled with increased attention by safety regulatory agencies. As an example, EuroNCAP has acknowledged the importance of advanced driver monitoring measures by putting a special emphasis on this topic in their 2025 Roadmap [2].

STRESS, MENTAL WORKLOAD, & DISTRACTION

Stress, fatigue and proclivity for risk-taking behaviors are some examples of human factors that limit effective driver performance. Cognitive workload, defined synonymously as mental workload represents the measure of effort applied towards cognition (e.g. thinking, understanding, perception, reasoning, learning ...). Therefore, it can be expected that driver mental workload is affected in all these situations. Mental workload is a volatile concept which must be interpreted carefully in each situation. Simultaneous secondary tasks to the primary driving task increase mental workload and decrease the driving performance efficiency [3]. Furthermore, increased mental workload can occur in situations with monotonous traffic environment and is dependent on driver experience or presence of circumstantial contexts like fatigue or sickness [3]. Mental workload can be conceptualized in terms of information processing capability and demand. Information processing includes cognitive as well as motivational and emotional aspects. Each individual person will evaluate the demands which they have to cope with and self-regulate their cognitive effort for processing these demands [4].

Several papers have shown that predicting mental workload in an automobile environment can be achieved by deriving and combining vehicle performance measures, video based (behavioral) measures and driver physiological measures [5]. When a secondary task involves visual cues in the cockpit, for example glances to the center stack display or other locations within the vehicle, behavior detection by means of a driver monitoring camera is very efficient. Measuring the percentage of gaze time directed towards the forward road center, as described in the NHTSA distraction guidelines [6], provides a good way to track visual attention to secondary tasks. This paper is based on a study design which concentrates on mental workload apart from visual distraction and investigates physiological measures for further analysis. In this study, periods of high mental workload are induced through a graded mental secondary task (n-back) [7].

While a variety of physiological measures have been studied in the context of mental workload estimation; electrocardiogram (ECG) is one of the most widely utilized measures. Metrics derived through the ECG signal, specifically heart rate (HR) or inter-beat-interval (IBI) directly reflect activity of the autonomous nervous system (ANS). Several past studies indicate a relation between the ECG signal and mental workload in a driving environment. For example, Mehler et al (2009), Rodriguez-Ibanez et al (2012), and Fallahi et al. (2016) all indicate a decrease in mean IBI with increased cognitive workload and an increase in mean IBI with increased drowsiness [5, 7, 11, 12] for drivers in these studies.

Another promising data source for estimating mental workload is the dynamic response of the vehicle itself. The effects of cognitive workload on a driver can be measured indirectly through data obtained from the vehicle dynamics data, for example, vehicle average speed or steering wheel rotation angle [5].

HYPOTHESIS

In this paper examination of vehicle dynamics data and physiological data is carried out in order to establish a classifier-system for driving with varying cognitive load. A related literature search indicates, that there are few studies with repeating subject measures (e.g. same subject over several days) in a driving environment with varying cognitive load. Repeated trials include effects of circumstantial contexts and may reveal differences in driving performance over time. Previous studies have indicated that the ANS reacts sensitively to different cognitive load conditions in comparison to a baseline for between subject comparisons [5]. A premise for this study was to include repeated trials to derive a classifier system for mental workload which includes physiological data depending on the (initial) state of the ANS for each individual driving subject. The following hypotheses are proposed in this paper:

- Driver ANS will react sensitively to cognitive load conditions between and within subjects (increasing HR)
- Vehicle dynamics performance data and driver physiological (e.g. ECG) data show complementary trends during cognitive load conditions
- Accuracy of a feature-based classification is higher when applied to an individual subjects' dataset (repeated measures) than when used across multiple subjects
- Physiological and driving performance data is affected by time of day (difference between morning and evening trials)

DRIVING SIMULATOR STUDY

For this study a small fixed-base driving simulator was used, consisting of a dashboard with cockpit display and touch screen center console, a steering wheel and a seat from a mid-sized vehicle. SILAB Version 5 by WIVW is used as the driving simulation software. The simulation is displayed on a 55-inch TV.

Five test subjects participated in a repeated measure driving study. The test subjects were randomly selected from JSS Berlin, Germany staff and consisted of four male and one female test subject aged 25 to 50. The test drives for each subject were spread over a period of five consecutive days with one trial in the morning and one trial in the evening; resulting in 10 trials in total. At the beginning of the experiment the subjects were asked to complete a 20-minute test drive to become familiar with the secondary cognitive tasks and characteristics of the driving simulator. None of the subjects was affected by simulator sickness (assessed with a simulator sickness questionnaire) [14]. The subjects were directed to focus on the primary driving task and to follow local traffic laws.

Each trial was designed to emulate a commute from home to work (morning) or work to home (evening). The trial consisted of a 30 min drive mainly through rural roads, separated into five 6-minute-sections each followed by a questionnaire presented on the center stack touch screen display. The first and the last 6-minute sections were baselines with no secondary cognitive tasks. The three middle sections included an audible n-back task presented with one of three difficulty levels to raise the total cognitive task demand on the driver. These audible secondary tasks do not conflict with the manual control or visual processing demands of the primary driving task [7]. The presented n-back tasks were 0-back, 1-back and 2-back in pseudo random order with the evening drive consisting of the exact same order as the morning drive. The driver section profile and secondary task structure are shown in Figure 1.

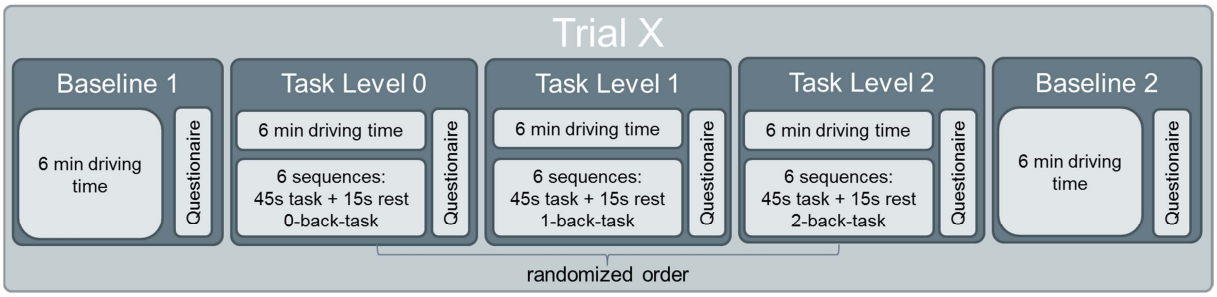

Figure 1. Test procedure per trial.

An ECG reference sensor was used to validate the heart rate measurements of the in-vehicle sensors. The reference sensor is an internal development of JSS and was previously validated against an industry/university

standard reference equipment. The JSS reference is portable and uses gel electrodes placed on the bare chest of the test subject. It records a 24-bit ECG with 1 kHz sample rate and calculates the IBI (Interbeat Interval) with an accuracy of ±2mn.

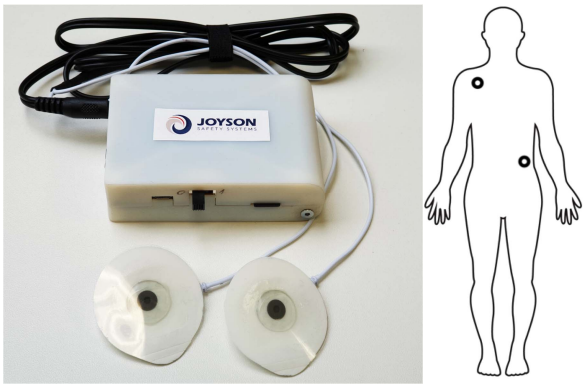

Figure 2. JSS Vital Recorder and electrode position.

VITAL SIGN SENSORS FOR IN-VEHICLE APPLICATIONS

JSS is a leading supplier of steering wheels, including several production wheels which include hands-on-wheel detection and classification sensors. JSS also developed one of the first production driver monitoring cameras which supports automated driving (SAE Level 2+) in passenger vehicles through facial head pose, eyelid closure and eye gaze tracking. As the importance of vital sign sensing for advanced driver state detection continues to evolve, JSS has extended its portfolio to deliver steering wheels capable of sensing driver physiological (vital) signals such as ECG. This steering wheel is designated the Vital Sign Steering Wheel and was used in this study.

The steering wheel incorporates two electrode zones on the sides of the steering wheel rim surface and senses a 2-lead electrocardiograph (ECG) of the driver's heart activity. The inter-beat-interval (IBI) derived from the ECG has an accuracy typically in the range of ±4ms. This signal can be used to derive typical measures of heart rate variability such as the Root Mean Square of Successive Interbeat Interval Differences (RMSSD) or the number of successive IBIs that differ by more than 50ms (NN50). Both measures have been used in literature as a metric for estimating mental workload. Figure 3 shows an example of the raw ECG output of the Vital Sign Steering Wheel and the derived IBI signal. Figure 4 shows a higher resolution example of the steering wheel ECG signal for several heart beat cycles which highlight the signal deflections characteristic of the QRS complex.

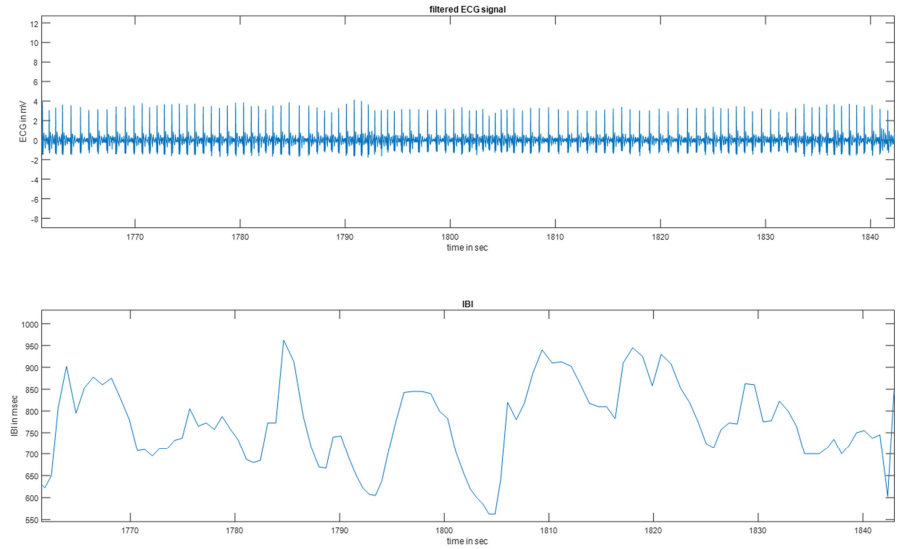

Figure 3. Vital Sign Steering Wheel ECG signal (top) and derived IBI time series (bottom).

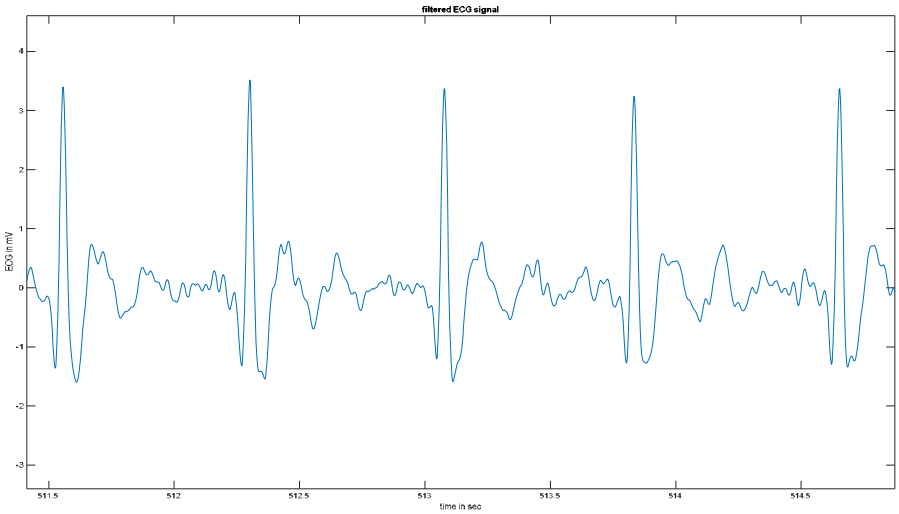

Figure 4. Zoom into the output signal of the Vital Sign Steering Wheel showing the QRS peaks.

In this study, a prototype Vital Sensing Seatbelt was included to complement the vital sensing steering wheel. This seatbelt uses a very thin sensor inlay embedded into the thorax section of the 3-point seatbelt and is capable to sense the heartbeat signal for a stationary occupant. As automated driving evolves, vital sensing in the seatbelt is essential as the hands of the driver are no longer on the steering wheel. This system can provide status assessment for drivers (or occupants) during periods of automation and can provide information to support intelligent driver/automation take-over.

Based on the sensing principle, the prototype outputs a mean heart rate (HR) estimate over a sliding 30 second window but cannot be used to derive an accurate IBI signal. As automation evolves, there will be a need to assess driver cognitive state when the hands are not placed on the steering wheel. The Vital Sensing Seatbelt can provide driver HR during these periods of fully automated control and improve feature estimates if used in combination with the Vital Sign Steering Wheel when the driver is in control.

It is important to note that in real world driving conditions, the signal of the Vital Sensing Seatbelt also includes noise induced by the road/wheel vibration and occupant movement. Accordingly, an accurate HR estimate is not always available. Real world driving studies conducted by JSS indicate, that in a typical road mix, using the current prototype, the signal availability is between 70 and 80% of driving time.

APPROACH

The study design enabled a widespread set of potential variables that could be used to derive features for a 2-level-classifier model. Considered variables were narrowed down selecting the most widely used data and their extracted features from ECG and vehicle dynamic data [5]. The objective of this paper is to maximize classifying accuracy with a small set of features to facilitate a low complex and comprehensible classifying system. The extracted features of the ECG signal were mean heart rate (HR) and heart rate variability (RMSSD). Selected features of the vehicle dynamic data were steering wheel reversal rate (SWRR) and standard deviation from center of lane (SDCL).

The recorded signals from the different sensors (reference ECG sensor, vital sensing steering wheel, vital sensing seatbelt) were synchronized using timestamps recorded with each data set. All signals were resampled to 40 Hz to allow synchronous processing of the recorded data. Features were calculated within a time window of 60 seconds which was repeatedly shifted by 5 seconds. The data was subsequently normalized using the minimum value of the first baseline section and the maximum value of the 2-back-task period to eliminate the day-to-day baseline fluctuation and improve the classification performance.

As a first attempt at classifying the workload level, a decision tree was created both for each individual subject and all subjects together using different combinations of the derived features. After analysis, only three of four features turned out to be meaningful and were taken into further consideration. The fourth feature, steering wheel reversal rate, did not show a measurable effect between the different task periods and the baseline.

RESULTS OF THE SIMULATOR STUDY

The verbal answers to the n-back-tasks of each trial were recorded with an automated voice recognition (Microsoft Speech API) and compared to the list of correct answers. Seven trials were left out of the analysis, because the subjects did not manage to complete individual n-back tasks. Overall 143 out of 150 observations were analyzed (3 per trial for each subject).

Mean performance in the easiest task condition (0-back) was nearly perfect and below 1% error rate in both daytime conditions (Figure 5). As the level of cognitive challenge rises the error rate rises also. The mean 1-back error rates in the morning were 3.3%, and, in the evening 2.5%. The mean 2-back error rates in the morning were 10.2%, and, in the evening 11.2%. The observed error rates show that mental workload increased across the task periods independently from daytime. The mean error rates were on a comparable level both in the morning and evening. Wilcoxon tests were carried out in between each task period and show a significant difference in mean values.

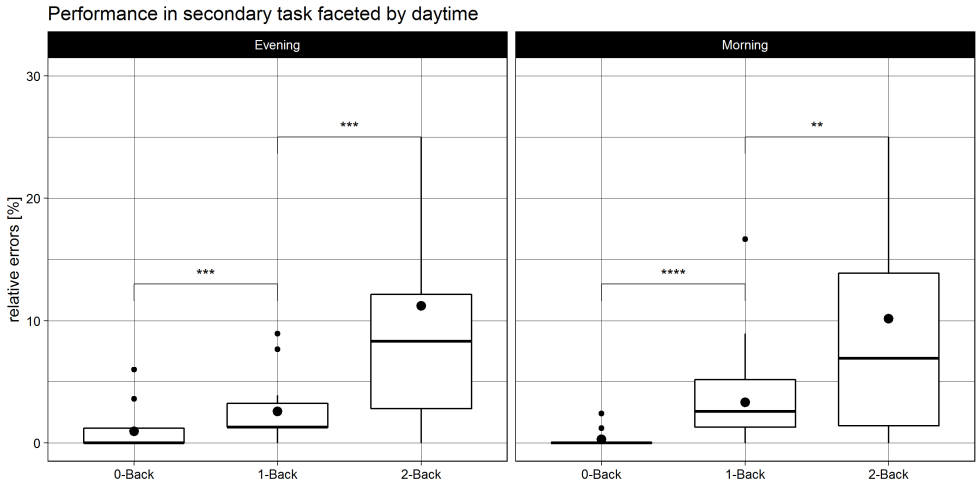

Figure 5. Mean error rates in different n-back-task difficulties sorted by daytime (**: p <= 0.01, ***: p <= 0.001, ****: p <= 0.0001).

The subjective rating of mental workload was assessed with NASA-TLX questionnaire, 248 of 250 observations were analyzed (5 per trial for each subject). Two samples had to be omitted due to loss of data. Wilcoxon tests were carried out in between each task period. Both diagrams in Figure 6 show a significant difference in means of each task period. As an exception the 0-back task condition in the evening does not differ significantly from the baseline. Overall the diagrams show that the subjects experience differences in workload between the task periods in both morning and evening.

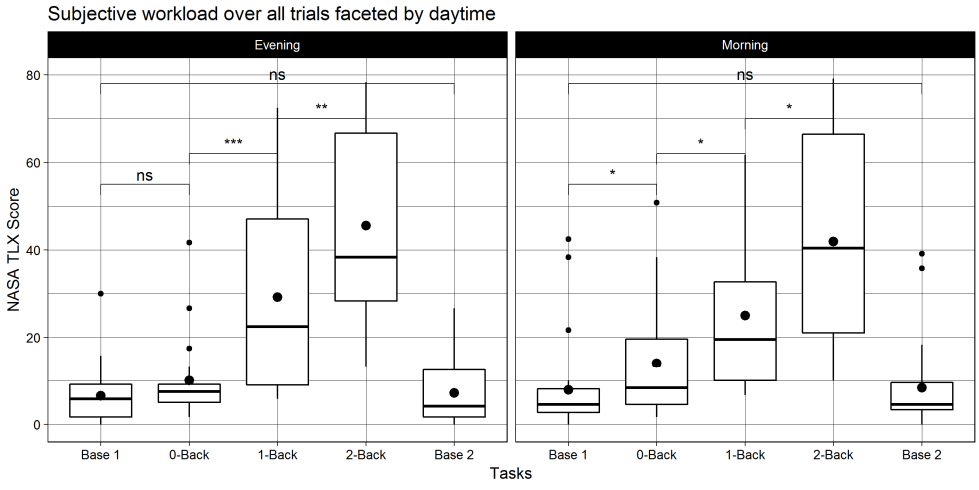

Figure 6. Boxplot of subjective multidimensional workload rating (ns: >0.05, *: p <=0.05, **: p <= 0.01, ***: p <= 0.001).

To identify the cognitive workload using sensors available in vehicles, two features derived from vital data (mean HR, RMSSD) and two features derived from vehicle data (SWRR, SDCL) were analyzed:

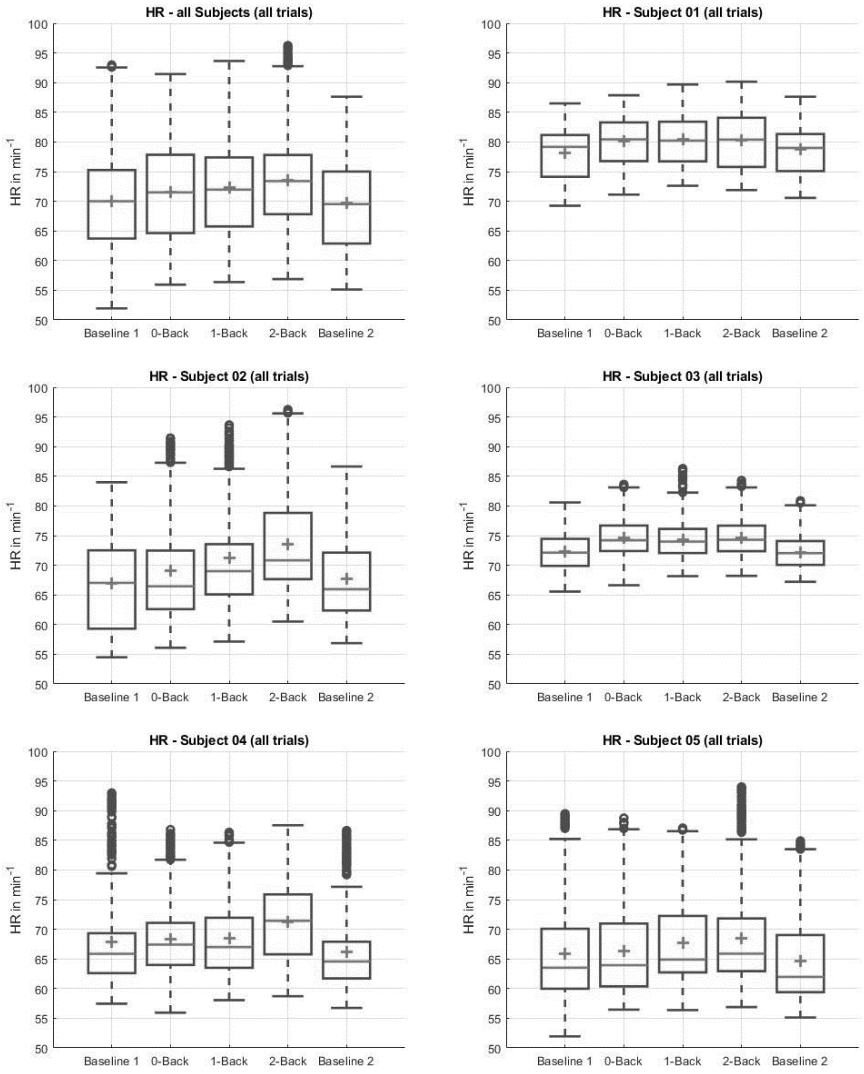

Figure 7. Distribution of HR.

Figure 7 supports the hypothesis that cognitive workload activates the ANS: The mean heart rate of all subjects rises with the increasing difficulty of the secondary task. Over all subjects, this feature increases by 5% from the first baseline to the 2-Back task. However, finding a classifier that identifies workload based on this data is difficult since the distributions are widely spread and overlap each other to a high degree. Two reasons for this observation were identified. First, the typical HR range varies from subject to subject, which distorts the boxplot over all subjects resulting in a wider spread of distributions. Second, a fluctuation of HR baseline from trial to trial was observed with a comparable magnitude to task difficulty variation.

To minimize these two influences for classification, the features were normalized using the minimum value of the first baseline section and the maximum value of the 2-back period of each trial. This normalization reduced the spread of the distributions (see Figure 8) and improved the results of the classification.

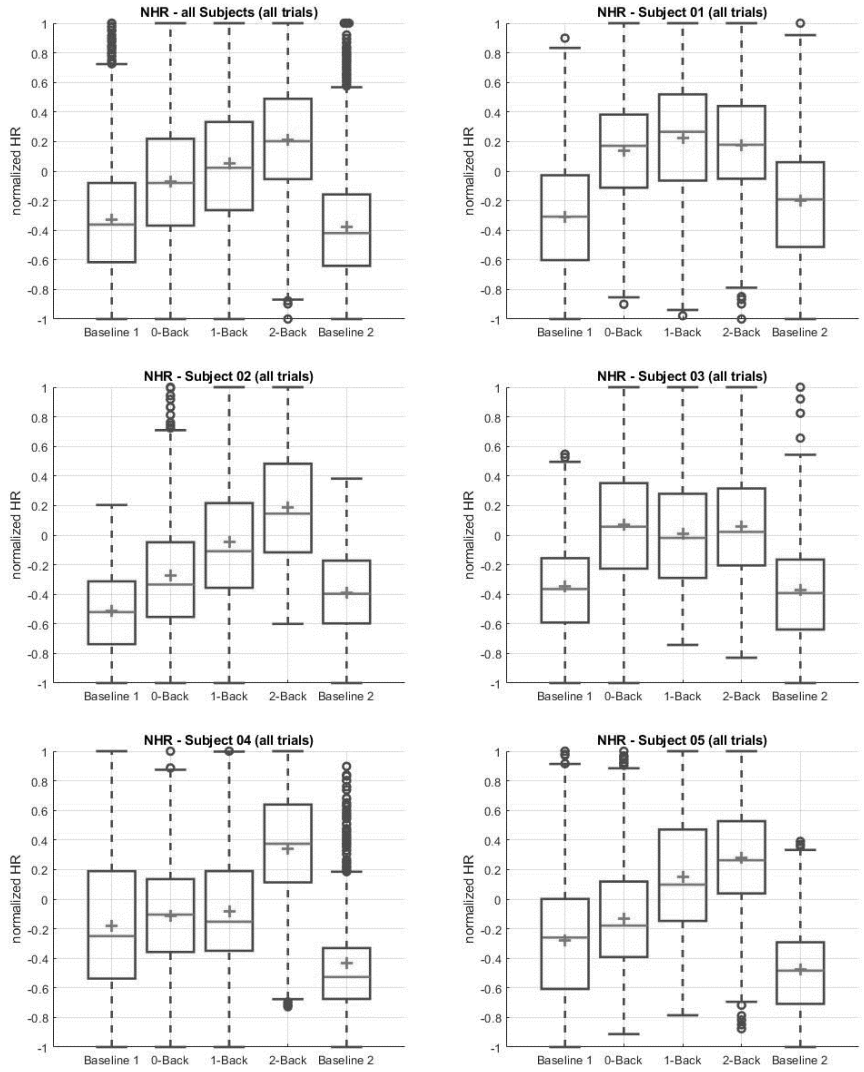

Figure 8: Distribution of normalized HR.

Figure 9 shows the distribution of mean HR over all subjects divided into morning and evening trials. The increase in mean HR is almost identical, but the baseline level of mean HR is, as hypothesized, different during the two times of day. The morning HR is 7.1 bpm higher on average.

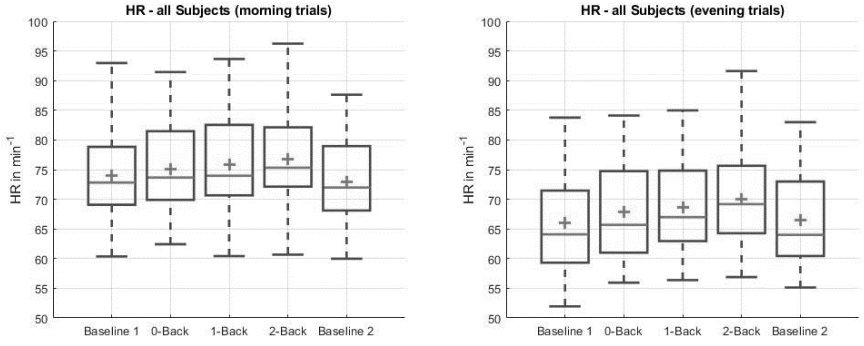

Figure 9. Distribution of HR during morning and evening trials.

The second vital data feature examined was the RMSSD. The boxplots in Figure 10 show that the RMSSD has a similar correlation to the applied task demands as the HR. The mean values of the distributions show a similar, but inverse response to task demand. The RMSSD decreases as the difficulty of the secondary task increases. However, the overlap of the distributions is even higher in relation to the difference of the mean values when compared to the HR. Both the range differences between the subjects and the fluctuations between the trials can also be observed in the RMSSD.

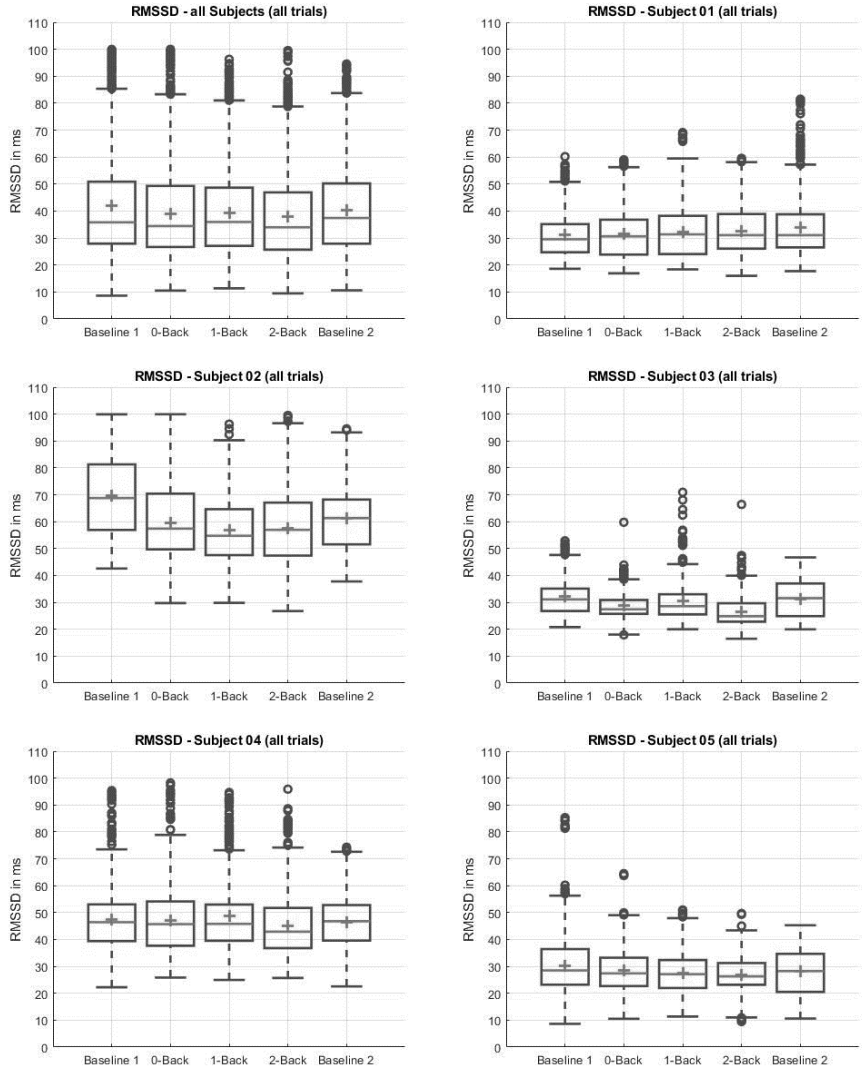

Figure 10: Distribution of RMSSD.

In addition to the features derived from vital data, the features from vehicle dynamics, standard deviation from center of lane (SDCL) and steering wheel reversal rate (SWRR) were analyzed to assess their value as an identifier for periods of high cognitive workload.

In this study, analysis shows the SDCL reacts to cognitive workload like the RMSSD. The mean of the distributions decreases as the task difficulty increases, but the distributions overlap each other as shown in Figure 11. In contrast to the HR and the RMSSD we observed less fluctuations between the individual trials and subjects. Accordingly, applying normalization brings less benefit to the classification.

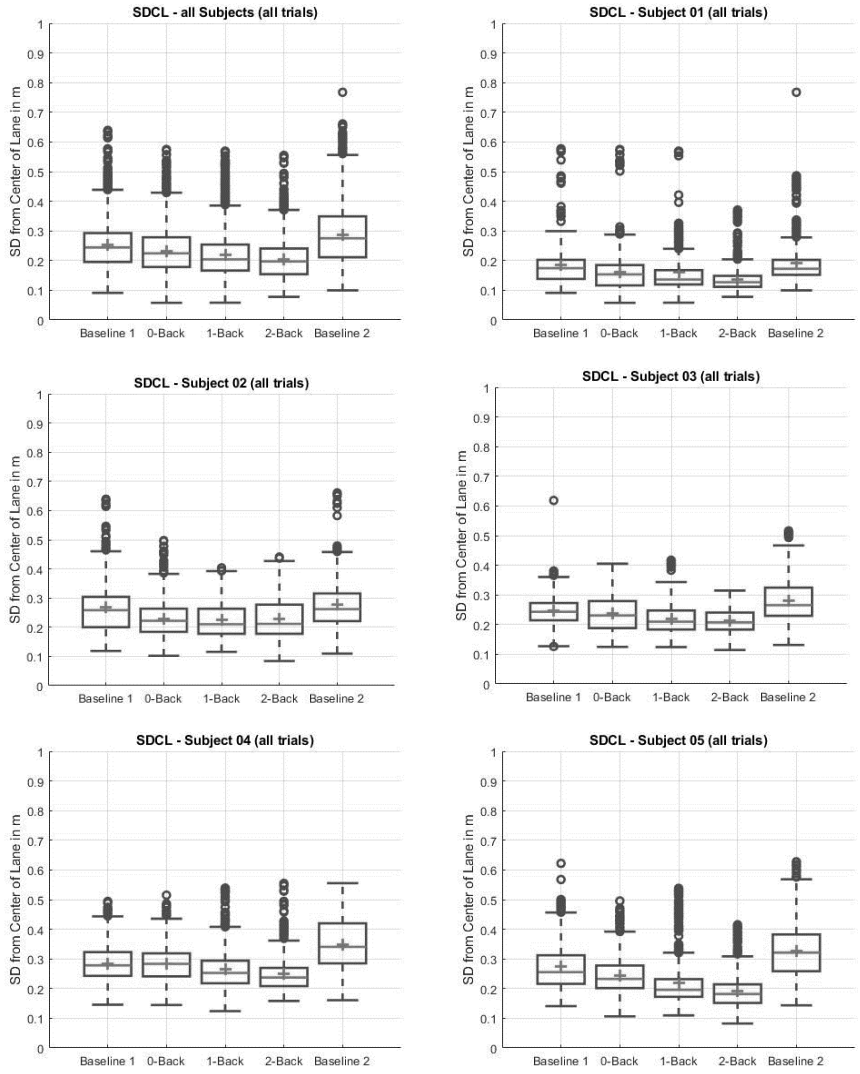

Figure 11: Distribution of SDCL.

Despite being used as a measure for stress recognition in several relevant papers [8, 9] the SWRR in this study, shows no evident connection to the difficulty of the secondary task. Figure 12 shows that the distributions of the first baseline and the 2-back task are almost identical. Even when analyzing the individual trials, no relation of the SWRR to the task difficulty was observed.

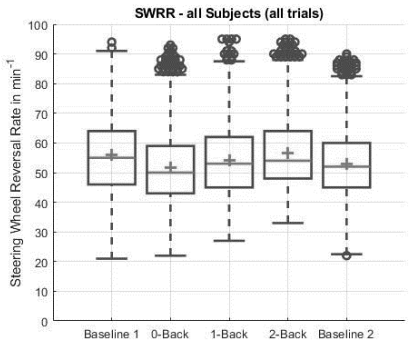

Figure 12: Distribution of SWRR.

To build a workload estimation model, a decision tree was applied to the features HR, RMSSD, and SDCL. This model could correctly separate baseline and 2-back task with an accuracy of 79.2 %. For single subjects, classification accuracies up to 88.4 % were shown.

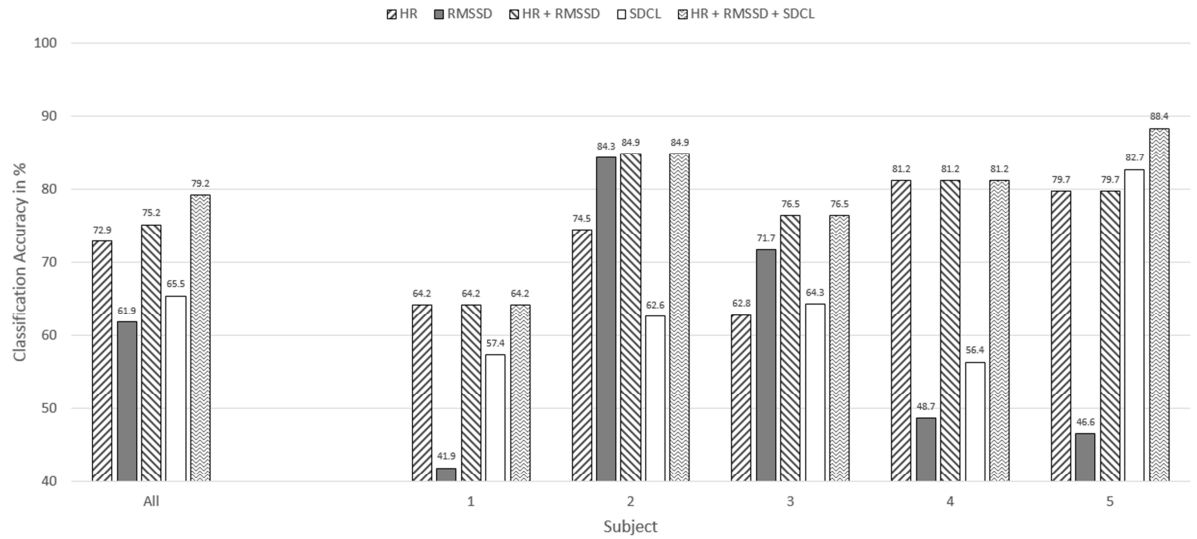

Figure 13: Classification results for different feature combinations.

Analyzing the classification results shown in Figure 13 leads to the following observations. When training a generalized classifier, each added feature improves the accuracy. In general, the HR seems to be the most reliable of the examined features. In most subjects using only the HR is good enough for estimating mental workload while the RMSSD and SDCL improve the accuracy of the prediction in some cases. A decision tree is one method to determine the impact of each feature, but more complex classification models like Support Vector Machines or Artificial Neural Networks have the potential to achieve even better results.

CONCLUSIONS

The results of this study support the proposed hypotheses and lead to several conclusions regarding the approach for implementing an estimation algorithm for mental workload:

Based on this study, the results of the classification using a simple decision tree, classification on individual subjects appears to be the superior approach. The response of the different features to mental workload differs strongly from subject to subject. With such individually optimized classification an accuracy of more than 80% was shown. In order to achieve these results, it was necessary to determine a baseline for each single drive since the features vary strongly depending on the time of the day and the driver's current condition.

For a vehicle application it will be beneficial (and may be necessary) to combine a workload detection system based on physiological data with a driver monitoring camera system. These systems can reliably detect distraction-based workload as described in the NHTSA distraction guidelines [6]. Recent research also indicates that eye gaze features, such as the range of pupil movement can be good indicators for mental workload [13].

While the results from this study were promising, the authors recommend that they be verified with a larger database containing more subjects and more conditions such as different levels of mental workload and different types of workload induction. Considering the strong effect of the time of day on the heart rate shown in this small study, it is also clear, that a deeper investigation of the effect of drowsiness, circadian rhythm, and possibly other contributing factors which could affect mental workload is necessary.

REFERENCES

[1] National Transportation Safety Board. 2017. „Collision Between a Car Operating with Automated Vehicle Control System and a Tractor-Semitrailer Truck Near Williston, Florida, May 7, 2016“Highway Accident Report NTSB/HAR-17/02

[2] EuroNCAP. 2017. “EuroNCAP Roadmap 2025”. Revision 4. Brussels

[3] da Silva, F.P. 2014. “Mental Workload, Task Demand and Driving Performance: What Relation? “Procedia - Social and Behavioural Sciences

[4] Hacker, W., 2018. “Definitions of Mental Workload Psychology Essay.”. Retrieved from https://www.ukessays.com/essays/psychology/definitions-of-mental-workload-psychology-essay.php?vref=1. Essays UK

[5] Rastgoo, Naim & Nakisa, Bahareh & Rakotonirainy, A & Chandran, V & Tjondronegoro, Dian. 2018. “A Critical Review of Proactive Detection of Driver Stress Levels Based on Multimodal Measurements.” ACM Computing Surveys. 51. 88:1:35. 10.1145/3186585.

[6] Garrett, R. 2012. “Visual-Manual NHTSA Driver Distraction Guidelines for In-Vehicle Electronic Devices” (No. NHTSA-2010-0053) (p. 177). Washington, DC, USA: National Highway Traffic Safety Administration (NHTSA)

[7] Mehler, B., Reimer, B., Coughlin, J. F., & Dusek, J. A. 2009. “Impact of Incremental Increases in Cognitive Workload on Physiological Arousal and Performance in Young Adult Drivers.” Transportation Research Record, 2138(1), 6–12. https://doi.org/10.3141/2138-02

[8] Lanatà, Antonio, et al. 2015. "How the autonomic nervous system and driving style change with incremental stressing conditions during simulated driving." IEEE Transactions on Intelligent Transportation Systems 16.3 (2015): 1505-1517.

[9] Bořil, Hynek, Pinar Boyraz, and John HL Hansen. 2012. "Towards multimodal driver’s stress detection." Digital signal processing for in-vehicle systems and safety. Springer, New York, NY, 2012. 3-19.

[10] De Waard, D. 2002. Mental workload. In R. Fuller and J. A. Santos (Eds.) Human Factors for Highway Engineers. (pp. 161-175). Netherlands: Pergamon Press

[11] Rodrigues, João & Kaiseler, Mariana & Aguiar, Ana & Cunha, João Paulo & Barros, Joao. 2015. “A Mobile Sensing Approach to Stress Detection and Memory Activation for Public Bus Drivers.” IEEE Transactions on Intelligent Transportation Systems.

[12] Fallahi, Majid et al. 2016. "Effects of mental workload on physiological and subjective responses during traffic density monitoring: a field study." Applied ergonomics 52 (2016): 95-103.

[13] Fridman, L., Reimer, B., Mehler, B., Freeman W. 2018. “Cognitive Load Estimation in the Wild.” Proceedings of the 2018 CHI Conference on Human Factors in Computing Systems, Paper No. 652. http://dx.doi.org/10.1145/3173574.3174226

[14] Kennedy, R. S., Lane, N. E., Berbaum, K. S., & Lilienthal, M. G. (1993). Simulator sickness questionnaire: An enhanced method for quantifying simulator sickness. *The international journal of aviation psychology*, *3*(3), 203-220.

ESTABLISHING AND COMMUNICATING RULES FOR AUTOMATED DRIVING VEHICLES

Matthew Avery, Dave Baldwin, Colin Grover
Thatcham Research
United Kingdom

Paper Number 19-0328

ABSTRACT

There has been considerable confusion in the interpretation of the SAE Levels of Automation J3016, in particular when defining whether a vehicle can be classed as automated. This is particularly relevant for insurers where there is a question of liability over who was in control of a vehicle when an accident has occurred. To clarify this a set of Requirements for Automated Vehicles has been developed to give a common benchmark for consumers, manufacturers, insurers and regulators.

The approach to developing the rules has been iterative. Initially they were formulated from an insurer paper focussed on the emerging Regulation 79 UNECE steering function rules and the requirements for partial automation. The challenge of driver disengagement and driver as back-up from Level 3 automation highlighted the issue of classifying these vehicles as automated.

To address this, Thatcham Research defined vehicles as Automated or Assisted based on whether they can meet ten specific criteria for automation. The criteria are based on road safety experience, anticipated vehicle capability, consideration of other road users and the fundamental requirement that these vehicles will generate less accidents. Experience using ADAS and Assisted Vehicles helped to give practical experience of some of the challenges that needed to be addressed.

These ten requirements have now been through insurer, regulator and manufacturer challenge and review in a number of different international territories. The rules have been strongly welcomed by manufacturers and regulators who had not seen any clear guidance when the rules were first issued. They have been used in a number of European countries for insurers to lobby government for safe and insurable vehicles. At the same time the marketing and communication of the rules combined with differentiating Assisted and Automated Driving have been key to disseminating the message to the wider public. Campaigns promoted wider understanding of the differences between the new technologies and the driver's responsibility in Assisted Vehicles.

The Classification of Automated Vehicles will be a key challenge for international regulators over the next five years making the development of the rules and framework essential at this time.

BACKGROUND

The SAE J3016 Taxonomy for Automated Vehicles introduced five levels of Automated Driving Systems (ADS) which are frequently referred to in media and consumer communications. Whilst the levels allow for an evolution of automation up to fully autonomous systems, there is also a need for more clarity on when an ADS can be classified as safe to drive in an automated mode.

The levels of automation transition from Assisted Driving, where the driver is in control, through to Automated Driving where, for specific conditions, the ADS can drive without human intervention. A clear area of concern is Level 3, Conditional Automation, where the ADS is capable of driving but requires the human driver to act as a monitor and intervene as a back up.

Highly capable automated driving systems (Level 4+) will reduce the risk of accidents and present a significant future societal benefit both in terms of safety and mobility. Thatcham Research and the UK's Automated Driving Insurer Group (ADIG) recognized that an approach was needed to address the lack of clarity over safe automation to

reduce the risk of an ADS being misused or misunderstood resulting in potentially catastrophic incidents. Such an incident would not only reduce the attractiveness of these vehicles for insurers but also impact the adoption and acceptance of ADS by consumers and regulators.

At the time of developing this work, no clear guidelines on the requirements for safe automated driving systems were available to regulators or OEMs. The communications developed an evolving framework for safe Automated and Assisted driving systems.

METHOD AND DEVELOPMENT

The UNECE WP29 ACSF sub-group was developing changes to Regulation 79 to address increasingly automated steering regulations. This work formed the basis of an initial technical paper 'Regulating Automated Driving' to highlight the issues of safe automation.

Starting from the assumption that a driver will want to undertake secondary tasks while the ADS is activated, it was necessary to consider under what circumstances the system could become unsafe and where clear rules and guidelines would be needed to ensure that the system would remain safe.

The adoption and influence of these rules and guidelines could only be effective if widely shared during their development - thus open sharing with OEM safety teams, regulators, insurance bodies and insurers allowed suitable challenge to the approach, framework and recommendations presented. The 'Regulating Automated Driving' document provided a technical baseline to the market on the issues recognized at that time.

Addressing Autonomous Ambiguity

A core challenge for the approach was that the SAE Levels, OEM marketing of systems and lack of consumer and media understanding created **Autonomous Ambiguity** leading to driver confusion as to the vehicle's capability and the driver's responsibility. This was summarised as vehicles needing to be either classed as **Assisted**, where the driver is always responsible, or **Automated**, where the vehicle can take over the driving task for some or all of a journey. In the UK, personal vehicle insurance policies make this critical since until a vehicle is classed as automated, traditional vehicle insurance policies apply. At the time there was no provision for insuring vehicles when driving in an automated mode.

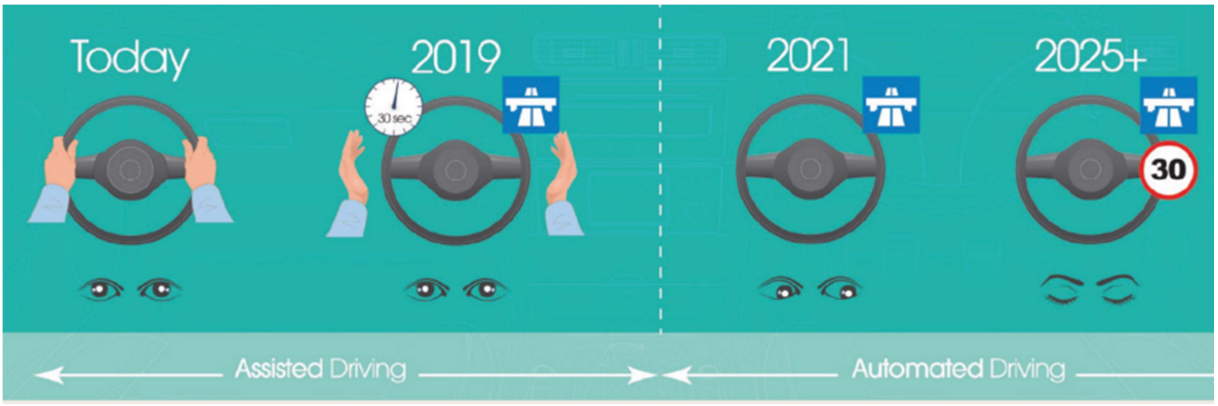

Figure 1. Assisted vs Automated Vehicles

Communication of this concept needed a simple infographic (See Figure 1) demonstrating Assisted driving with eyes on the road ahead, systems operating in a highway environment with limited hands off wheel time. Level 4 shows a disengaged driver in a single domain for level 4 awake to come back into the loop at the end of the ODD whereas Level 5 allows the driver to switch off entirely in all ODDs.

At this time international media reports of highly assisted Level 2 vehicles being misused as 'self-driving' demonstrated the combination of over-reliance on the system and confusion over the system capabilities reinforcing the need for clarity.

Establishing and Communicating Rules for Automation

Having established a clear break between Assisted and Automated vehicles, it was necessary to determine the criteria for what constituted an Automated vehicle. 'Clarity in an Uncertain World – A Model for Automated Driving' brought together the main elements of automated driving to allow common understanding of the issues positioned at a level which could be more widely used beyond regulatory and technical audiences.

The framework rules were built around the assumption that an Automated Vehicle will allow the driver to disengage and do secondary tasks.

If the driver can disengage from the driving task then the vehicle must be capable of driving safely in its operational design domain (ODD), a basic requirement. The system should similarly not be able to operate outside its operational design domain – so it must be geo-fenced. If it is to drive safely, it must be law abiding. Allowing a vehicle to break the law makes little sense in promoting safe automation. To ensure no confusion, the system should be named and marketed appropriately when describing its functionality. Thus Auto Pilot may be fine for Automated Vehicles but not for an Assisted Vehicle as this is misleading.

It is unlikely that the ODD will apply for every part of a journey, so there needs to be a controlled and managed timely hand-over and hand-back process between human driver and ADS. It is essential that the driver is clear whether or not they are in control of the driving task. At the same time, if the driver is needed to re-engage then the system cannot simply hand back control without warning. The vehicle needs to be capable of identifying when the ODD is coming to an end. This may happen based on location, but also where weather or road conditions end the ODD. The ADS will therefore need to manage a controlled hand-over even when the situation could not be anticipated at the start of the journey. If the driver does not take control back from the ADS, the ADS will need continue and stop safely (Safe Harbour), not presenting a hazard to other traffic, and without relying on the driver.

The need for the vehicle to be highly capable, manage handovers and be able to find safe harbour requires a sufficient level of system redundancy to be built in.

Not every event can be anticipated within systems testing. Some events will require emergency intervention. In this case the ADS should be able to carry out a minimal risk manoeuvre to attempt to mitigate or avoid a crash (in the same manner a human driver may do).

In addition to the above requirements, insurers identified the need to have sufficient data in the event of a crash to establish who was driving. Availability of near real time incident event information will be more widely needed. For example, a fault introduced through an over the air (OTA) software update could potentially affect all ADS operating the software and may need an immediate response.

The rules for automation were summarized in an infographic (See Figure 2) for easier communication to non-experts and wider dissemination to media, safety and consumer groups as well as regulatory and industry stakeholders.

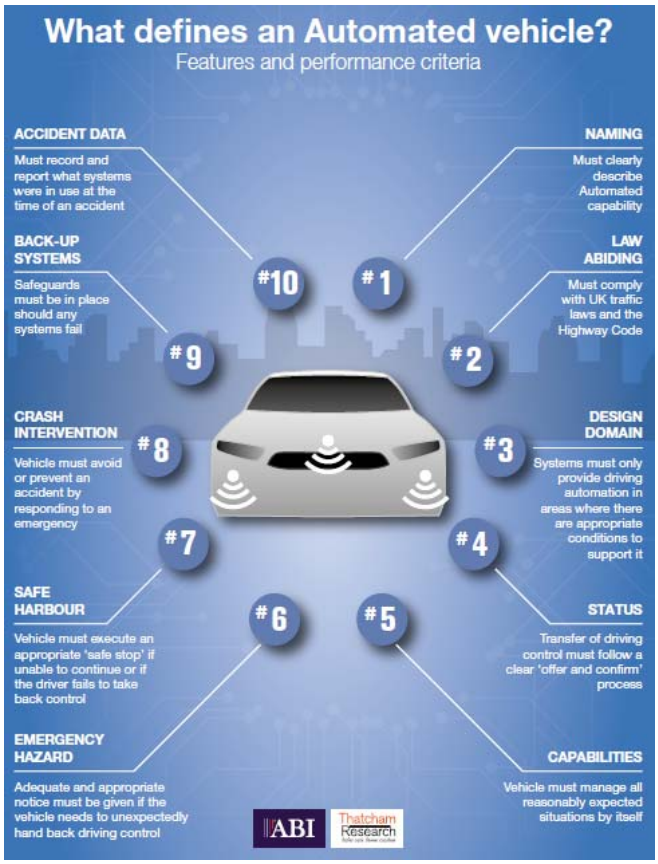

Figure 2. What defines an Automated Vehicle

Whilst the rules are useful in building a high-level framework, more detailed technical descriptions of the ten requirements outlined above were needed to support technical users. These descriptions were initially developed in a series of brainstorming sessions followed by a number of external stakeholder review iterations to ensure broad agreement with the concepts (See Table 1).

Table 1.
Detailed Criteria for Automated Vehicles

	Automated Vehicle Criteria
Naming	*The naming of the system must clearly specify automated driving.* The description of the system must be unambiguous and clearly describe the automated system functionality, limitations and driver responsibility.
Law Abiding	*Systems must abide by local traffic law including seat belt use, speed and driving behaviour. The system must abide by Road Traffic Laws and follow the Highway code including limiting speed to posted speed limits.* Some exceptions may be permissible to avoid a collision or to deal with a developing emergency situation. Such exceptions and anticipated vehicle behaviour must be recorded in manufacturer documentation.

	Automated Vehicle Criteria
Design Domain	*Systems must only provide driving automation in areas where there are appropriate conditions to support driving automation. Systems must indicate to the driver where automation is available.* The system must be able to determine in what circumstances it is able to offer its driver an Automated Mode of operation taking into account, for example: the environment in which it is operating (type of road, car park, private drive etc); Traffic conditions, road pavement conditions etc.; weather; connectivity; and speed limit and/or average traffic speed
Status	*Hand over and hand back must follow a clear 'offer and confirm' process between driver and vehicle with appropriate notice.* The Automated Mode is only engaged after the vehicle has understood the planned journey and/or parking manoeuvre and confirmed it is safe to operate in the Automated Mode for all or part of that journey. When Automated mode becomes available there must be a clear offer and confirm process from vehicle to driver. Similarly, the reverse must be true when the vehicle hands control back to the driver. Hand back from Automated Mode to manual driving must take place at a predetermined point in the journey (e.g. motorway off-ramp) with warnings given to the driver and a countdown timer from a minimum of 60 seconds. Driver monitoring must be in place to establish the level of driver engagement to ensure and appropriate hand over is achieved. Should the driver fail to respond to a hand back request the vehicle must execute a '**safe harbour**' manoeuvre, as described below
Capabilities	*The system must provide driving automation which safely controls the vehicle in all reasonably foreseeable driving situations within the design domain environment.* The vehicle must be able to deal with any obstruction or incident that may appear in its path and not require involvement from, or monitoring by, the driver for any part of the journey where it is in an Automated Mode.
Emerging Hazard	*If the Automated Vehicle becomes aware of a situation which was unknown at the start of automation (e.g. poor weather) and which requires a hand over to the driver earlier than planned, adequate and appropriate notice must be given.* Where such a situation arises, the vehicle must provide at a minimum a 60 second warning to the driver. The procedure must then follow that outlined for hand back under **Status** above, with the vehicle performing a '**safe harbour**' manoeuvre should the driver fail to respond.
Safe Harbour	*If the driver fails to respond to a hand back request, the vehicle must execute a 'safe harbour' manoeuvre and navigate to a safe harbour appropriate to the design domain and traffic conditions* Safe Harbour will generally be in a position away from the main carriageways In heavy traffic. In certain circumstances Safe Harbour may be to stop in lane but this will vary depending on Design Domain, traffic conditions and road speed.
Crash Intervention	*If the vehicle senses an immediate unforeseen dangerous situation the system must initiate the minimum risk manoeuvre to avoid or mitigate a collision* The vehicle must be able to use its available functionality to avoid or mitigate any collision to the best of its ability. Decisioning should be based on 'doing least harm'. It should not be expected to make ethical choices in life threatening circumstances

	Automated Vehicle Criteria
Back-Up Systems	*The system must be fault tolerant so that in the event of a fault the vehicle can continue in its Automated Mode or provide a planned system hand over to the driver.* Sufficient redundancy must be included within the vehicle systems to allow the Automated Mode to 'fail operational', that is to continue normally and safely with its journey whilst notifying the driver that an issue exists and its nature. As a minimum there must be sufficient redundancy for the vehicle to complete the planned journey in a reduced speed 'limp home' mode or to complete a controlled Offer and Confirm hand back to the driver**.** The system must have a self-diagnostic capability to detect faults and the functionality to communicate these to the driver. The system must also be capable of over the air (OTA) updates to its software or firmware and any such update deemed safety-critical must be applied automatically without any requirement for intervention or interference by the vehicle owner, operator or user.
Accident Data	*Data must be recorded in the event of a collision and made available to both manufacturer and insurer to quickly and impartially assess the status of automated systems and extent of driver input leading up to the accident.* In the event of a collision, the vehicle must be able to record, and preferably transmit the minimum dataset, described in the Clarity on Driver Status: Shared Accident Data section below, via a suitable intermediary (or 'neutral server'). For the UK it is also proposed that the that most suitable intermediary would be the Motor Insurers Bureau.

The requirements for accident data are already being progressed through the DSSAv event data proposed by UNECE. The communication documents propose that insurers have access to sufficient data to establish whether the ADS or the human driver was in control leading up to the crash. This data will only be used to confirm who or what was in control of the Automated Vehicle and not the liability between different vehicles.

The limited data request is:

- GPS-event time stamp
- GPS-event location
- Automated Status – on or off
- Automated Mode - Parking or Driving
- Automated Transition time stamp
- Record of Driver Intervention of steering or braking, throttle or indicator
- Time since last driver interaction
- Driver Seat Occupancy
- Driver Belt Latch

It is recognized that there will also be a challenge in determining accident trigger rules to generate a data event which is not currently captured in the evolving communications to date.

Extending the Framework for Assisted Vehicles

Whilst the framework rules developed had provided rules to define safe automation and a simple message for all stakeholders, requests were received to extend these to lower level Assistance, specifically Level 2 vehicles. These requests came from industry bodies seeking to bridge the gap between today's production vehicles and the future Automated systems. Since the rules for automation defined a set of features to determine whether a vehicle is automated, the assisted features allowed the team to start establishing a framework for the features of good assistance systems.

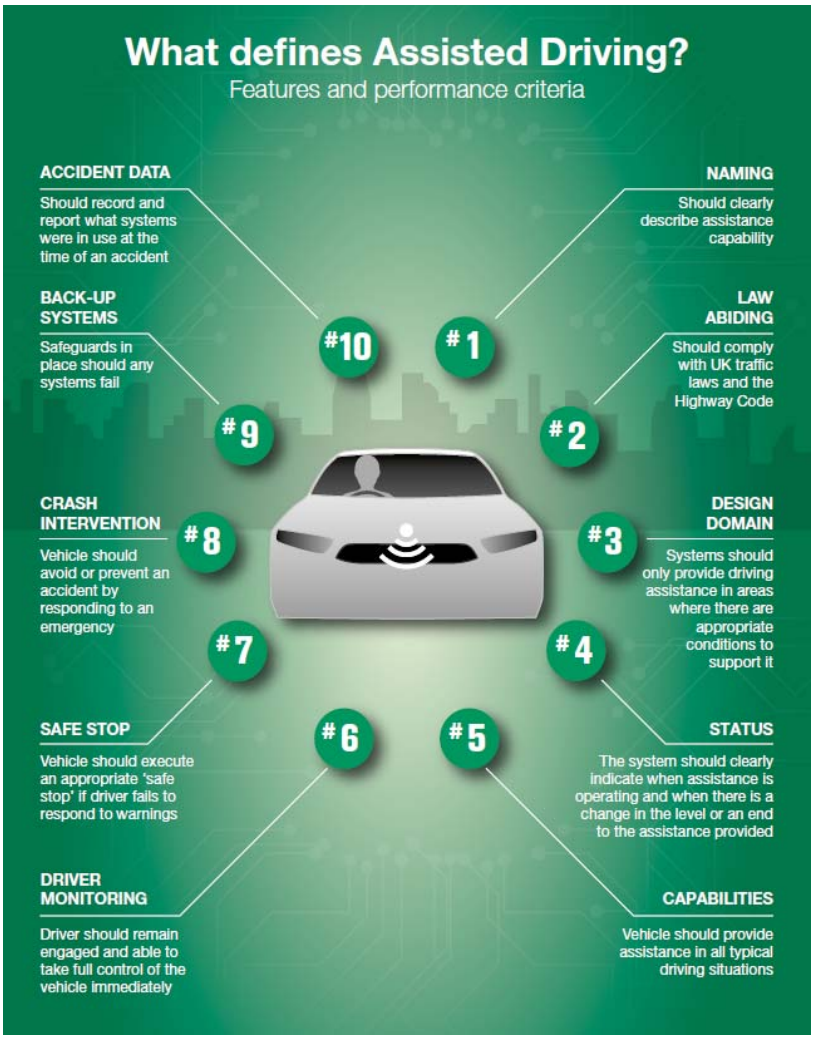

Figure 3. Features and Performance Criteria for Assisted Driving

Once again ten features were selected (See Figure 3). There were two subtle differences to reflect the lower level of capability in these systems. Firstly, the change from Safe Harbour to Safe Stop reflects the need for the system to be able to execute a safe stop if the driver does not respond to 'hands on wheel' warnings but also that the ADS may not have lane change capability. Secondly, the replacement of Emerging Hazard (for managed Hand-Back) by Driver Monitoring where drivers' engagement levels can be monitored and action taken if a driver starts to disengage. Driver monitoring is of value for all systems providing increasing levels of driver support whether assisted or automated – as the driver's workload decreases they are more likely to start disengaging from the driving task creating a less safe system overall.

Once again the Technical Assessment document gave lower level detail for specialists and provided contrast to the automated rules. Note the language is framed as systems 'should' rather than the 'will' language used in the Automated rules. (See Table 2)

Table 2.
Detailed Criteria for Assisted Vehicles

	Assisted Driving Criteria
Naming	*The naming of the system should not specify, suggest or indicate automation.* The description of the system should be unambiguous and clearly describe the assistance system functionality, limitations and driver responsibility.
Law Abiding	*Systems should only provide driving assistance when driving in accordance with local traffic laws relevant to seat belt use, speed and driving behaviour.* The system should default to the speed limit on activation or current speed if lower, provide Intelligent Speed Adaptation (ISA) and overspeed warnings. A clear warning should be displayed to the driver if driving with Assistance while contravening local traffic law.
Design Domain	*Systems should only provide driving assistance in areas where there are appropriate conditions to support driving assistance.* The vehicle should not operate in areas determined as inappropriate by the manufacturer. This will be supported by clear and robust manufacturer documentation. The system should be geo-fenced to those roads and/or locations where it is deemed safe to operate.
Status	*The system should clearly indicate when assistance is operating and when there is a change in the level or an end to the assistance provided.* There should be a clear, commonly used display of Continuous Assistance statuses. Required statuses include: Enabled, Available, Engaged, Disengaged, Driver Intervention Required
Capabilities	*The system should provide driving assistance which assists with the safe control of the vehicle in all typical driving situations within each Design Domain* The system should provide driving assistance that delivers safe lateral and longitudinal support to guide the vehicle along the road taking into account other road users. If a situation is encountered that it is unable to cope with, then a clear and timely warning should be given and ideally the hand over completed in a controlled manner.
Driver Monitoring	*Driver monitoring should ensure that the driver remains engaged in the driving task and able to take full control of the vehicle immediately. Ignoring warnings should lead to system deactivation.* While system is engaged the driver should be monitored to ensure that they remain present and able to control the vehicle. Driver inactivity or inattention should require an escalating cascade of warnings to re-engage the driver
Safe Stop	*If the driver fails to respond to the escalating cascade of engagement warnings, the vehicle should execute a safe stop.* Safe stop should vary with the design domain and traffic conditions. The system should provide appropriate warnings to other drivers to minimize the risk of stopping (e.g. hazard warning lights). An eCall event must be triggered
Crash Intervention	*The vehicle should be equipped with collision avoidance systems capable of preventing or mitigating an emergency situation likely to result in a crash.* The vehicle should be able to react to any such situation, using its available functionality to avoid or mitigate a collision to the best of its ability. Technology to address collisions with other vehicles and vulnerable road users includes, for example, AEB and lane support systems for lateral control.
Back-Up Systems	*The assistance system should clearly indicate to the driver a reduction in assistance as a result of vehicle sensor or system failure.* System should provide sufficient warnings if the system becomes unavailable and should be capable of a controlled hand back to the driver
Accident Data	*Limited data set should be provided in the event of an accident.* Where data can be made available, this should be provided in line with DSSAV specifications.

Communication Timeline and Media Coverage

The communication timeline for publications and associated media activity to date is summarized below .

July 2017 – **Regulating Automated Driving** [1] - R79 Strategy Document – laying out issues – fed into the UK Automated and Electric Vehicle Bill (AEVB) to ensure Insurance needs addressed.

November 2017 – **Clarity in an Uncertain World** [2]– first iteration of 10 Rules of Automation Framework

May 2018 - Publication of **Assisted and Automated Definition** [3] – Framework doc defining both insurance issues and ten criteria for Automated and Assisted vehicles. This formed the basis of defining a test procedure for Insurers and Euro NCAP as well as wider adoption by International Insurers – GDV FFA IBC

June 2018 – Presentation '**Assisted and Automated Driving – International Insurance Views**' by Matthew Avery to UN ECE WP29[4]

The Assisted and Automated Definition launch attracted significant media attention worldwide with 250 pieces of coverage in the week following launch with a reach of more than 550 million. Pre-launch interviews/demos were conducted with BBC News[5], WIRED, The Guardian, Insurance Times and Press Association. Key broadcast coverage included BBC Breakfast, Radio 4 Today programme, BBC national and regional news updates, plus BBC Online. Worldwide the launch was covered in more than 20 countries, across national and technology media, especially within US. Social media generated over 320k video views on YouTube and social channel plus tens of thousands of social posts/commentary. Overarching sentiment across all media was that terminology used needed to change.

DISCUSSION AND LIMITATIONS:

The development and communication of the Assisted and Automated Driving rules has been very successful in breaking some of the public misunderstanding of both the vehicles and the media messaging. The rules are intended to be a benchmark which will continue to grow and evolve as the technologies come closer to publicly available vehicles and approval standards.

There is an ongoing challenge to build consumer understanding that will need to be reinforced as we move towards the first Automated Vehicles in particular providing sufficient education and support in promoting safe system usage.

This work continues to be built on. The next iteration will be a further level of technical detail to produce a Definition of Safe Automated Vehicles with a more regulatory level of detail. It is likely that this document will lay out detailed criteria to establish what threshold a Level 3 vehicle would need to reach to be classed as Safely Automated.

CONCLUSION

Although the communications outlined in this paper have evolved with the fast pace of technology, there is still considerable work to do to ensure the development and adoption of safe automation is achieved. The 10 rules of automation have provided the basis for a framework for regulators, OEMs and safety test development. This will need to continually evolve as AD systems come closer to market and regulation of ADS moves forward.

We recognize that there is also considerable work to do to build understanding within the general population who do not have a sufficient understanding of the likely benefits and limitations of Automated Vehicles. However, we also need to recognize that the work already undertaken has helped to build a common baseline for regulators, OEMS insurers and other stakeholders to work from.

REFERENCES

[1] Thatcham Research, ABI : Regulating Automated Driving https://www.abi.org.uk/globalassets/files/publications/public/motor/2017/07/regulating-automated-driving/

[2] Thatcham Research, ABI : Clarity in an Uncertain World https://www.abi.org.uk/globalassets/files/publications/public/motor/2017/11/clarity-in-an-uncertain-world---final-version.pdf

[3] Thatcham Research, ABI : Assisted and Automated Definition Summary https://news.thatcham.org/documents/assisted-and-automated-definition-and-assessment-summary-79399

[4] Matthew Avery : Assisted and. Automated Driving –. International Insurance Views https://wiki.unece.org/download/attachments/60364189/%28ITS_AD-15-05b%29%20UN%20Deck%20June.pdf?api=v2

[5] BBC Technology : Car insurers warn on 'autonomous' vehicles https://www.bbc.co.uk/news/technology-44439523

ASSESSMENT OF NEW ACTIVE SAFETY SYSTEMS ADDRESSING URBAN INTERSECTION SCENARIOS INCLUDING VULNERABLE ROAD USERS

Julia Bräutigam
Federal Highway research institute (BASt), Brüderstraße 53, 51427 Bergisch Gladbach, Germany

Alvaro Esquer
Applus+ IDIADA, Santa Oliva, 43710, L'Albornar, Tarragona, Spain

Paper Number 19-0329

ABSTRACT

Bicyclists and pedestrians belong to the most endangered groups in urban traffic. The EU-funded collaborative research project PROSPECT ('PROactive Safety for PEdestrians and CyclisTs´) aims to significantly improve safety of those unprotected traffic participants by expanding the scope of scenarios covered by future active safety systems in passenger cars. Concepts for sensor control systems are built into three prototypes covering emergency interventions such as Autonomous Emergency Braking (AEB) as well as Autonomous Emergency Steering (AES). These systems tackle the well-known challenges of currently available systems including limited field-of-view by sensors, fuzzy path prediction, unreliable intent reaction times and slow reaction times. These highly innovative functions call for extensive validation methodologies based on already established consumer testing procedures. Since these functions are developed towards the prevention of intersection accidents in urban areas, a key aspect of the advanced testing methodology is the valid approximation of naturalistic trajectories using driving robots. Eventually, several simulator studies complemented a user acceptance and benefit analysis to evaluate the expected overall impact of the PROSPECT systems.
The results achieved within the PROSPECT project are highly relevant for upcoming test protocols regarding the most critical situations with Vulnerable Road Users (VRU). With introducing the new methods in Euro NCAP (European New Car Assessment Programme) a significant increase in road safety is expected.

INTRODUCTION

Accidents involving bicyclists and pedestrians remain a significant issue for road safety, accounting for more than 25% of road fatalities in the European Union [1]. This value stresses the importance to take measures aimed to reduce the number of occurring fatalities with vulnerable road users (VRU) significantly. The corresponding intention of the European Union planning to move close to zero fatalities in road transport by 2050 is already stated in the white paper (Roadmap to a Single European Transport Area – Towards a competitive and resource efficient transport systems), which was published in 2011[2].

To meet these ambitious goals, Advanced Driver Assistance Systems (ADAS) are a promising option to focus on active safety systems addressing VRU safety. Autonomous Emergency Braking systems (AEB) are already established in state-of-the-art consumer testing [3]. Consumer test organizations such as Euro NCAP (European New Car Assessment Programme) have a high impact on vehicle safety by introducing transparent safety requirements and accompanying test procedures. Consumer testing is considered to be an important part of vehicle safety, therefore PROSPECT ('PROactive Safety for PEdestrians and CyclisTs´) will supply test procedure proposals to Euro NCAP (the dominant vehicle consumer testing organization in the EU-28) starting in 2020.

PROSPECT is a collaborative research project funded by the European Commission. The project pursues an integrated approach comprising in-depth and multiple European accidents studies involving VRUs, combined with results from urban naturalistic observation. Real intersections throughout Europe were monitored to understand critical situations that occur between vehicles and VRUs. The gained knowledge from these observations is used to identify crucial factors leading to conflict situations and to better anticipate accidents. As the output, the most relevant accident scenarios are identified for pedestrians and cyclists focusing on urban environments, where the majority of accidents involving VRU occur. Further on, generic use cases were derived as basis for the development of test scenarios for the ADAS systems. Proposed test cases derived from the accident data as well provide a description of how to reproduce a specific use case on closed test tracks.

The accident analysis represents a key input for the system specifications for development of the three project prototype vehicles. These demo-vehicles are extensively tested in more realistic scenarios. PROSPECTs broad testing methodology goes beyond what is currently used in consumer testing, such as turning in intersection scenarios based on naturalistic driving observations in real traffic throughout Europe. The concept for more realistic testing includes intersection markings which allow the efficient testing of all test cases, mobile and light obstruction elements and realistic surroundings like traffic signs or lights. Eventually, the testing results from

the prototype evaluation as well as several simulator studies build the basis for an over benefit analysis assessing the socio-economic benefit of the developed functions. The PROSPECT methodical approach is presented below in *Figure 1*.

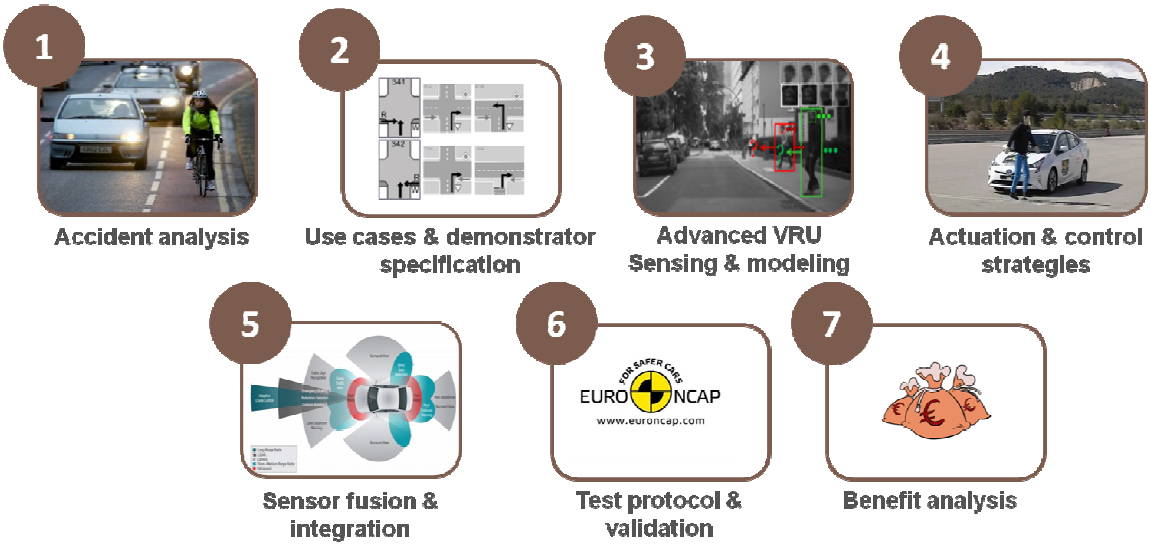

Figure 1: PROSPECT methodology

The findings within PROSPECT contribute not only to the state-of-the-art knowledge of VRU-vehicle behavior, but to technical innovations, i.e. assessment methodologies and tools for testing of next generation VRU active safety systems, as well. In terms of the estimated impact, the introduction of a new level of safety systems in the market will enhance VRU road safety in the 2020-2025 timeframe, contributing to the 'vision zero' objective of no fatalities or serious injuries in road traffic set out in the Transport White paper. Test methodologies and tools are considered for 2022-2024 Euro NCAP road-maps.

This paper will focus on the test protocol and prototype evaluation that was conducted within the PROSPECT project. Initially, the derivation of test cases based on the accidentology is explained followed test protocol development. Eventually, the assessment of the prototype is exemplarily explained. In the discussion section, the findings and limitations are summarized and an outlook is given.

From Accident Analysis over use cases to test cases

The first stage of the project included macro statistical and in-depth accident studies targeting VRU accidents in urban traffic. The studies were performed in Europe focused specifically on pedestrians and cyclists. An overview and an in-depth understanding of the characteristics of road traffic crashes involving vehicles and VRUs (i.e. pedestrians, cyclists, riders of motorcycles, e-bikes and scooters) was provided for different European countries. Early investigations have shown that the crashes between passenger cars and pedestrians or cyclists are the most relevant in Europe. *Figure 2* shows a summary of the most relevant accident scenarios related to car-to-cyclist crashes that were extracted from this study.

The in-depth understanding of the crashes includes the identification of the most relevant road traffic accident scenarios and levels of injury severity sustained, as well as the transport modes that represent a higher risk for VRUs. Besides extensive literature studies, comprehensive data analyses have been performed featuring information from recent years. From the most relevant accident scenarios, detailed car-to-cyclist crash analyses have been performed focusing on the causation of crashes: car-to-cyclist accidents have been analyzed from the car driver's point of view. With this approach deeper insight can be gained about situations faced by the drivers especially why they sometimes failed to manage these crash situations [4].

Accident type	UTYP Pictogram	PROSPECT pictogram (basic version)
(I) Car straight on, cyclist from near-side	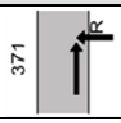	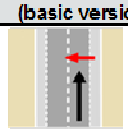
(II) Car straight on, cyclist from far-side	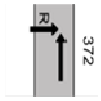	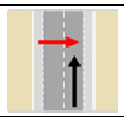
(III) Car turns	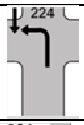	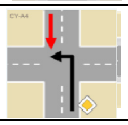
(IV) Car and cyclist in longitudinal traffic	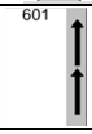	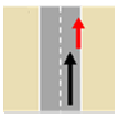
(V) Others		

Figure 2: Overview of most relevant accident scenarios between passenger cars and bicyclists.

The accident scenarios obtained from the studies describe the type of road users involved in the accident, their motions (e.g., the motion of the cyclist or pedestrian relative to the vehicle) expressed as accident types and further contextual factors, like the course of the road, light conditions, weather condition and view obstruction. More information is available on the project deliverable "Accident analysis, Naturalistic Driving studies and Project implications" [5].

The most relevant accident scenarios have been clustered in use case or target scenarios addressed by the project. These use cases contain less detailed information and are used to derive the sensor specifications of the prototypes including information, such as stereo vision base line, image resolutions, microwave radar sensitivity/accuracy or the necessary field of view of the corresponding sensor. Additionally, issues related to sensor processing required by the chosen scenarios including VRU detection areas, correct vs. false recognition rates, localization accuracy and computational latencies had to be taken into account. Since the safety systems developed within PROSPECT are relying on video and radar based technology constantly surveying the surroundings of the vehicle by an extended field of view, more complex scenarios can be addressed than currently state-of-the-art systems are capable of. Specific information on the configured and evaluated prototypes is available in the related PROSPECT deliverable [6].

The final goal was to define representative Test cases from available Use Cases, taking into account relevant parameters and representative values for the selected parameters based on accident potential and system analysis. Constraints taken into account are a limited and feasible number of test runs, durability (e.g. maximum impact speed) and the feasibility of the test tools (see *Figure 3*).

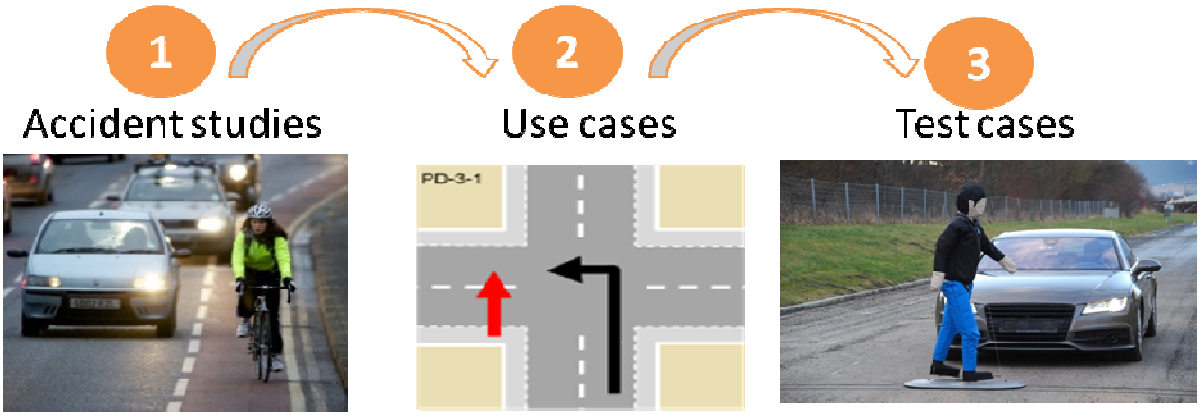

Figure 3: From accident analysis to test cases - scheme

TEST PROTOCOLS

For the benefit assessment of the prototype vehicle's functionality a testing methodology is required that goes beyond what has currently been used in European consumer testing (Euro NCAP). While under evaluation, the Vehicle Under Test (VUT) has to be equipped with driving robots, including a steering and pedal system as well as a DGPS measurement system, to keep each individual test repeatable and comparable between vehicles. This equipment ensures a reproducible path for the VUT with a lateral tolerance of less than 5 centimeters (see *Figure 4*, left). In PROSPECT the crash opponent is a VRU dummy on a self driving platform which is time-synchronized with the VUT. In *Figure 4* the test tools are displayed. In various accidents that had been analyzed for the use case definition, the VRU was significantly often hidden by obstructive element. Bringing a solid obstruction element into consumer testing, the test are becoming more and more advanced for the safety systems to fully avoid impacts (see *Figure 4*, left below).

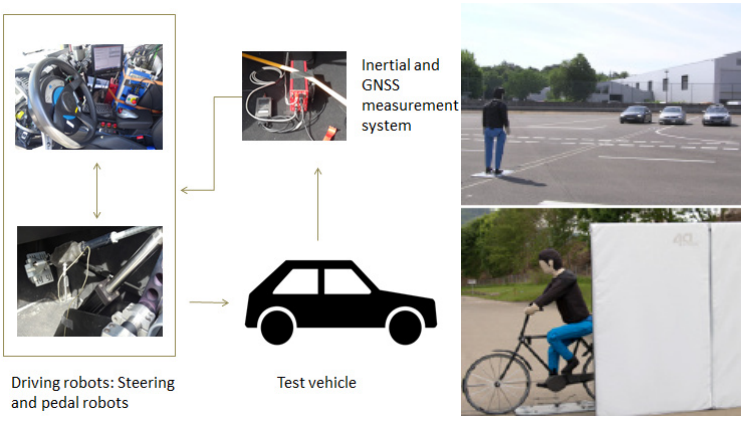

Figure 4: VUT testing equipment (left); Pedestrian and bicycle dummy with obstruction (right)

In the following the main two adaptations regarding the introduction of a basic intersection layout and the use of naturalistic trajectories reproduced by using driving robots are explained.

Intersection design

Intersections and the possibilities for different drivers to turn in these intersections are various. Defining a specific layout where all addressed scenarios could be tested is the initial step to limit the options for turning scenarios on the one hand and on the other hand, it already prepares the testing procedure for more advanced technologies that would be able to take the intersection boundaries into account for the decision on their behavior. The proposed intersection in PROSPECT (see *Figure 5*) is based on German recommendations for road construction for urban environmental intersections [7]. The intersection layout allows a cornering radius ranging from 8 – 15 meters. Aligning this with the information from the detailed accident analyses that measure the impact speeds in urban intersection accident scenario in a range from 10 to 25 kph will result in estimated lateral accelerations below 3 m/s².

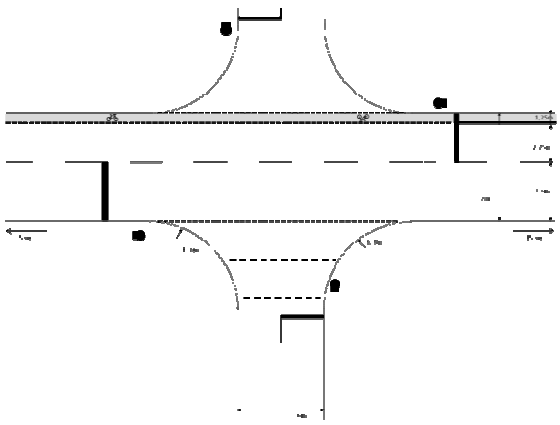

Figure 5: Intersection layout proposed by PROSPECT

The advantage of that simple intersection design is that depending on the future test cases at hand and the intention of the potential test, the suggested intersection layout can be easily adapted to a bigger size. PROSPECT proposed a small intersection as a start for future VRU test cases, but depending on increased driving speed and the desired trajectory it might be of interest to set up a medium to large intersection. In *Figure 6* the idea for designing custom intersections for oncoming scenarios is shown.

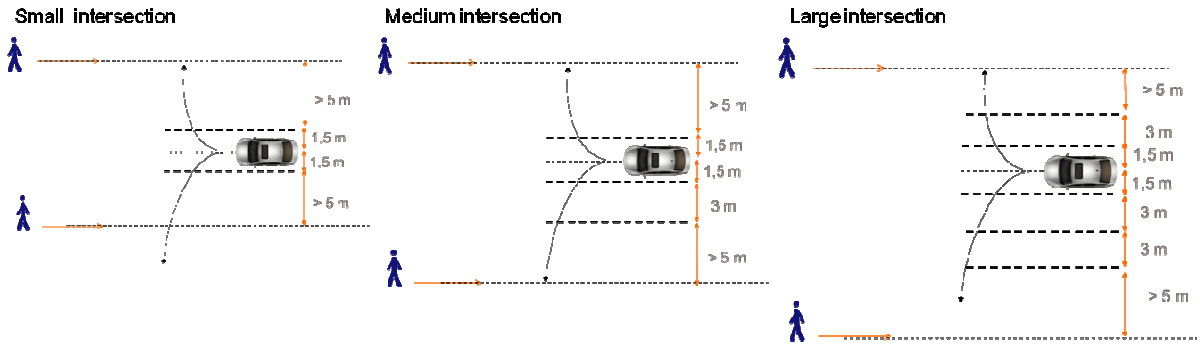

Figure 6: Different intersection sizes depending on the test design.

Trajectories

For the analysis of realistic driving behaviour, naturalistic driving studies (NDS) were conducted to observe the behaviour of different driver in different countries throughout Europe. Unfortunately, real intersection layouts highly vary regarding basic parameters such as lane width and the angle between the two crossing streets. Of course, strong variations can be found in other characteristics, especially regarding the environmental features. In urban areas buildings, parked cars or trees often block the free view over the approaching street arm. Additionally, surrounding traffic, for example oncoming cars, alters the chosen trajectory and speed profiles to a not negligible extent. As a result, the collected data shows a wide range of possibilities how to negotiate many variants of different intersections.

As mentioned above, consumer testing scenarios require a high repeatability ensuring a sufficient comparability of the results. Moreover, any additional test scenario is under strong boundaries regarding a reasonable time and money frame for the executing test laboratories. Therefore, the aim for generating feasible trajectories on closed test tracks is to simplify out of the whole range of possible real turning scenarios into one or a few signature trajectories representing the data found in the naturalistic driving studies and accident analyses as best as possible. As can be seen in *Figure 7*, restricting the intersection geometry stills leads to various possible trajectories.

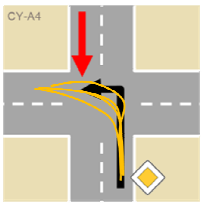

Figure 7: Possible trajectories for a given intersection layout depending on various factors, including obstructions, traffic, and driver condition.

Nevertheless, a detailed analysis of the available data shows that despite the differences in highest curvature, start and end position of the vehicle, the overall process of negotiation a turn is similar almost every time and can be split into three sections (see *Figure 8*) consisting of two clothoids and a constant radius.

- Section 1 Linear increase of the curvature, corresponding to curve entry
- Section 2 Constant radius cornering
- Section 3 Linear decrease of the curvature, corresponding to the curve exit

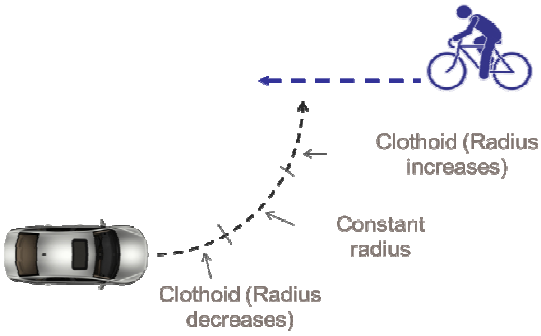

Figure 8: schematic description of the cornering sections

There is a tendency for the last section to be longer than the prior sections in the data from the naturalistic driving studies. This turned out to be of difficulty for the testing equipment on the test track. To be able to ensure tight tolerances over a wide variety of Vehicles under Test (VUT), the sections were split equally with a length distribution of 1/3 each. In *Figure 9* the derived trajectory based on the naturalistic driving data, accident analysis and testing experience is shown in *Figure 9* (solid line). The dashed lines represent selected trajectories from the naturalistic driving studies for one specific intersection close to the layout chosen in the project.

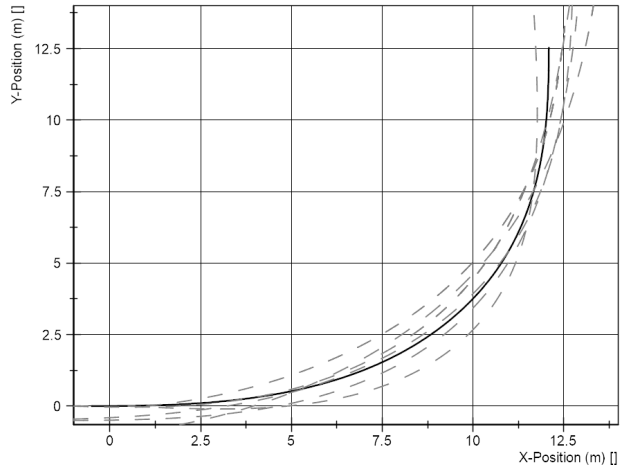

Figure 9: PROSPECT trajectory (solid) overlaid with selected naturalistic driving trajectories

The selected trajectory is a compromise between manifold possibilities provided by human driver behaviour and a repeatable and easy-to-use trajectory on the test track.

EVALUATION OF PROTOTYPES

The vehicle-based functional tests have been carried out in 2017 and 2018. Initially some of the PROSPECT use cases were reproduced in proving grounds with four production vehicles equipped with state-of-the-art active safety systems respecting VRU protection. These baseline systems are able to identify pedestrians and bicyclists and if necessary react in dangerous situations. With respect to current consumer test programmes these reference cars have achieved the highest qualification. These preliminary tests allowed obtaining the baseline performance of current AEB systems applied to VRU. The vehicles were treated anonymously when releasing the results, because only the average performance of market vehicles is of interest. Moreover, the reference testing helped to define the methodology and test procedures that were later used to evaluate the three prototype functions developed in the project.

Scenarios involving bicyclists are generally more challenging for the safety systems as they travel faster than pedestrians. Functions need to process and identify hazard situations as quick as possible to activate the automatic braking or steering application and avoid the crash. Therefore, only the longitudinal test case (bottom right in *Figure 10*) is additionally conducted with a pedestrian dummy. The velocity of the bicyclist is 15 km/h, for the pedestrian the velocity is set to 5 km/h. All scheduled test cases are displayed in *Figure 10*.

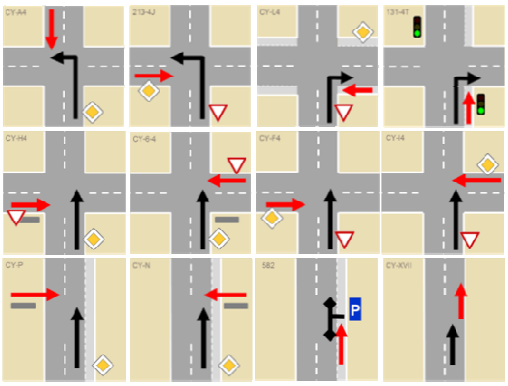

Figure 10: Assigned prototype test cases

The top row of the figure contains all intersection scenarios where a turning trajectory is required. In the middle row and the two left cases of the bottom row of the figure, crossing scenarios are shown. The second to last scenario describes a parking test case. The VUT is parked and the bicycle dummy is coming from the back. The test engineer opens the door when the dummy is close to the vehicle. The last scenario on the bottom right of the figure is the longitudinal test case. This scenario was conducted with more than one prototype and with different parameters regarding the placement of the VRU-dummy and the autonomous vehicle intervention. The basic setup of this scenario was conducted with 25% and 50% offset between VRU und VUT. For higher speeds ranging from 50 to 60 km/h, one prototype showed an ESP-induced emergency steering manoeuvre, while another prototype vehicle applied some torque on the steering wheel for the evasive manoeuvre. The dummy was placed to the very right side of the lane for this specific case.

The Euro NCAP 'Test Protocol AEB-VRU systems' [3] is the reference document mainly used to reproduce the crossing and longitudinal scenarios. The document provides the test tolerances for test velocities, lateral deviations and steering wheel velocities among others that are strictly followed by test laboratories for the evaluation of AEB VRU systems. Both stationary and turning scenarios are not yet part of Euro NCAP test protocols and therefore a PROSPECT test protocol had to be developed. The challenges regarding the derivation of naturalistic trajectories were described above.

Results

In the following exemplary final test procedures and test results are shown and explained. Since the PROSPECT project was focused on urban intersection scenarios with VRU participation, these scenarios are described in this paper. All results will be publicly available in the corresponding Deliverable later in 2019. As expected, the baseline performance was negligible in the newly addressed scenarios, whereas the prototype systems have shown the improvement towards a reaction in complicated urban accident scenarios impressively.

In Figure 11 the right turn scenario with the bicyclist is coming from behind is shown. This scenario is particularly challenging regarding the available field of view. The prototype vehicle had radar sensor to the back to be able to react properly and in time to this critical situation. The graph in the right of the figure provides an example of one of the right turns at 15 kph with AEB activation at 1.25 s before the collision. The programmed right turning trajectory for the test vehicle is represented by the dashed black line. The trajectory travelled by the Vehicle Under Test (VUT) is represented in red. The green dashed line represents the activation point of the AEB system. Only shortly after triggering the intervention the vehicle come to a complete stop, indicated by the end of the red solid line. The blue line is representing the trajectory of the bicycle dummy, which is displaced 3.5 m to the right of the VUT in this scenario. Both, the vehicle and the dummy, are time synchronized to meet at the calculated impact point and the right front of the vehicle where both trajectories cross. The front wheel of the bicyclist would collide with the front right corner of the vehicle. In the given representation, the solid lines (test vehicle and dummy) are referring to the corresponding GPS measurement point, which is the geometric centre of both bodies. The dotted red line represents the right edge of the vehicle's body whereas the blue dotted line one is the left edge of the bicyclist dummy. The minimum distance between the vehicle and dummy at the end of the test is 0.82 m. The green X indicates the bicycle position at the moment of the AEB activation. The vehicle cornering speed was varied between 10 and 15 kph, whereas the bicyclist was constantly travelling at 15 kph. The warnings were issued in a range from 1.41 -1.58 s TTC (Time To Collision) and the following AEB intervention was triggered between 1.16 s and 1.32 s TTC.

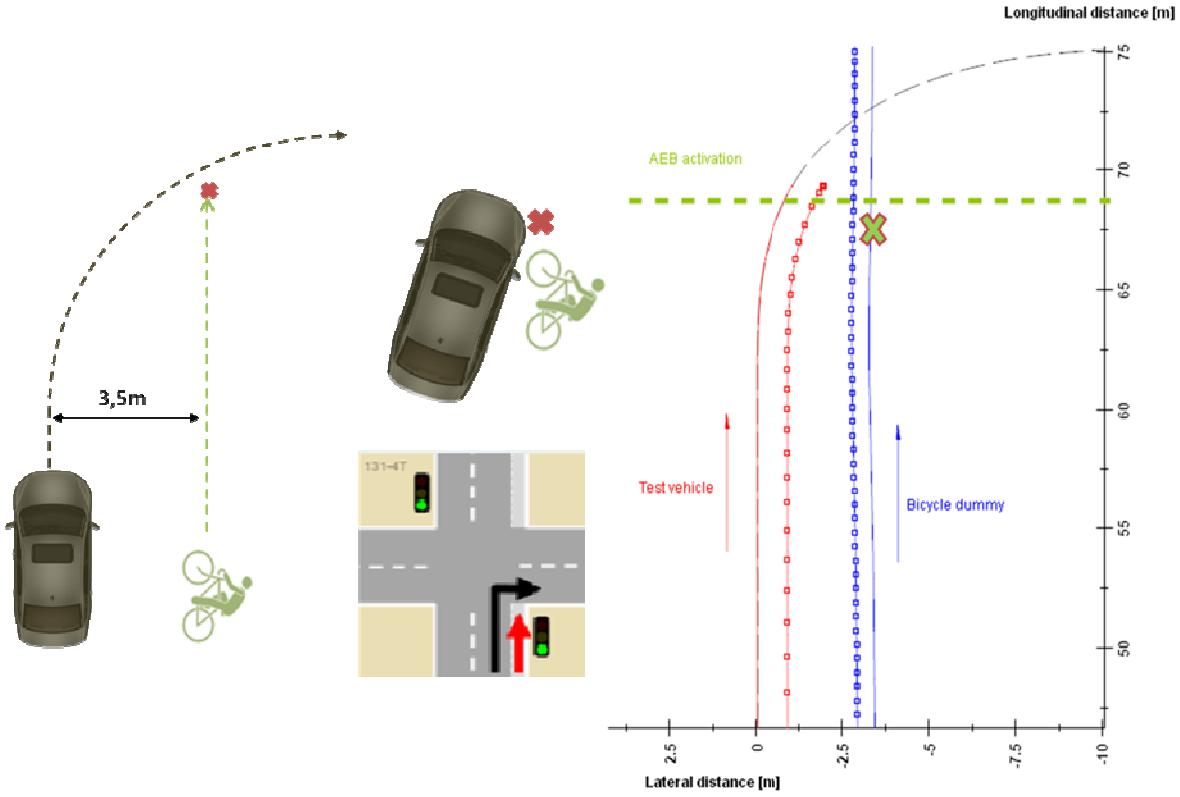

Figure 11: Right turning with bicyclist coming from behind.

In *Figure 12* the right turn scenario with the bicyclist is coming from the far side is shown. For this scenario braking before the turn was introduced. The VUT travels at 30 kph and before turning it decelerates to 20, 15 or 10 kph. The graph in the right of the figure provides an example of one of the right turns at 10 kph with AEB activation at 0.75 s before the collision. The bicyclist is coming from the right side riding next to the road three meters away from the targeted trajectory for the VUT (see *Figure 12*). The impact point for this scenario is the front wheel of the bicycle colliding with the centre of the front bumper of the VUT (50%). The bicyclist was constantly travelling at 15 kph. The AEB intervention was triggered between 0.72 s TTC for lower speeds and a maximum TTC of 2.3 s for higher cornering speed with avoiding all crashes.

In *Figure 13* the left turn scenario with the bicyclist is coming from the near side is shown. The VUT initially travels at 30 kph and before turning it decelerates to 20, 15 or 10 kph. The graph in the right of the figure provides an example of one of the right turns at 10 kph with AEB activation at 0.76 s before the collision. The bicyclist is coming from the left side riding at the road four meters away from the targeted trajectory for the VUT (see *Figure 13*). The impact point for this scenario is the front wheel of the bicycle colliding with the centre of the front bumper of the VUT (50%). The bicyclist was constantly travelling at 15 kph. The AEB intervention was triggered between 0.76 s and 1.06 s TTC avoiding all crashes.

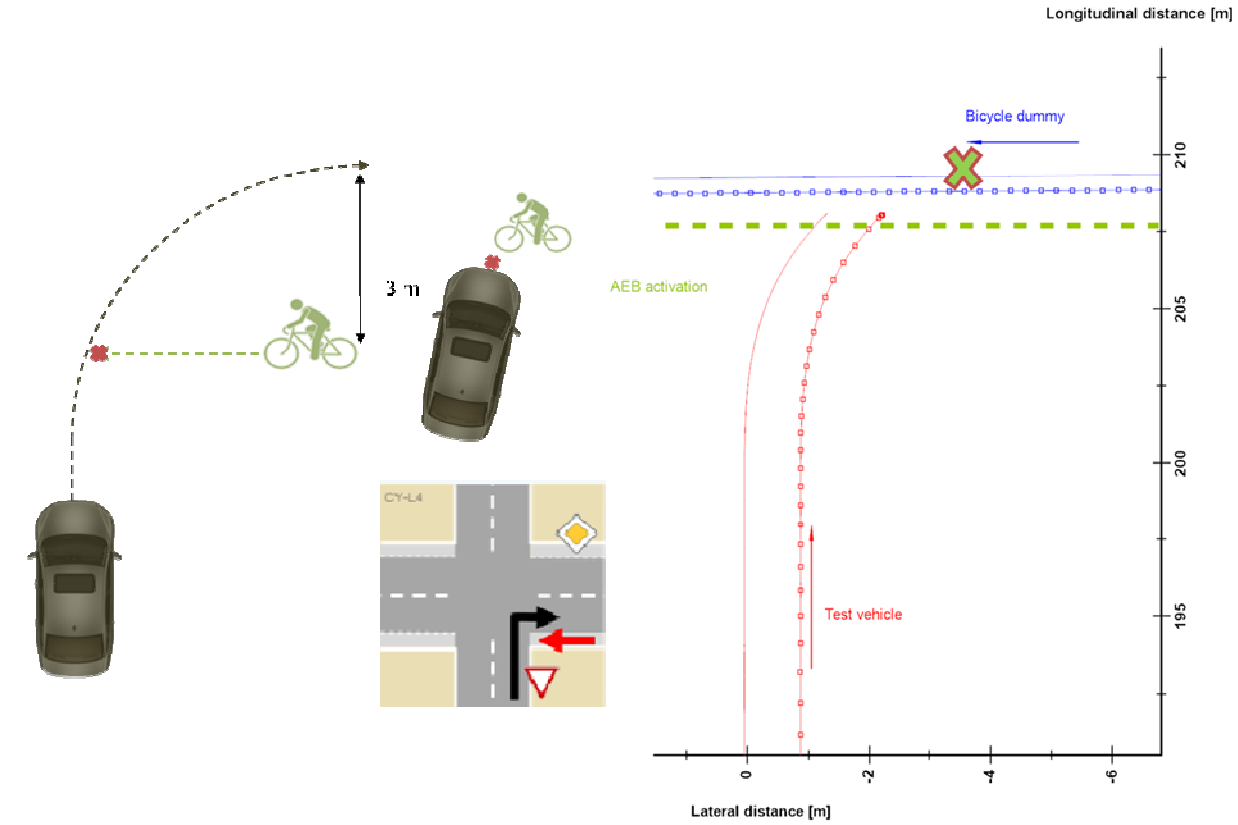

Figure 12: Right turning with bicyclist crossing from the near side.

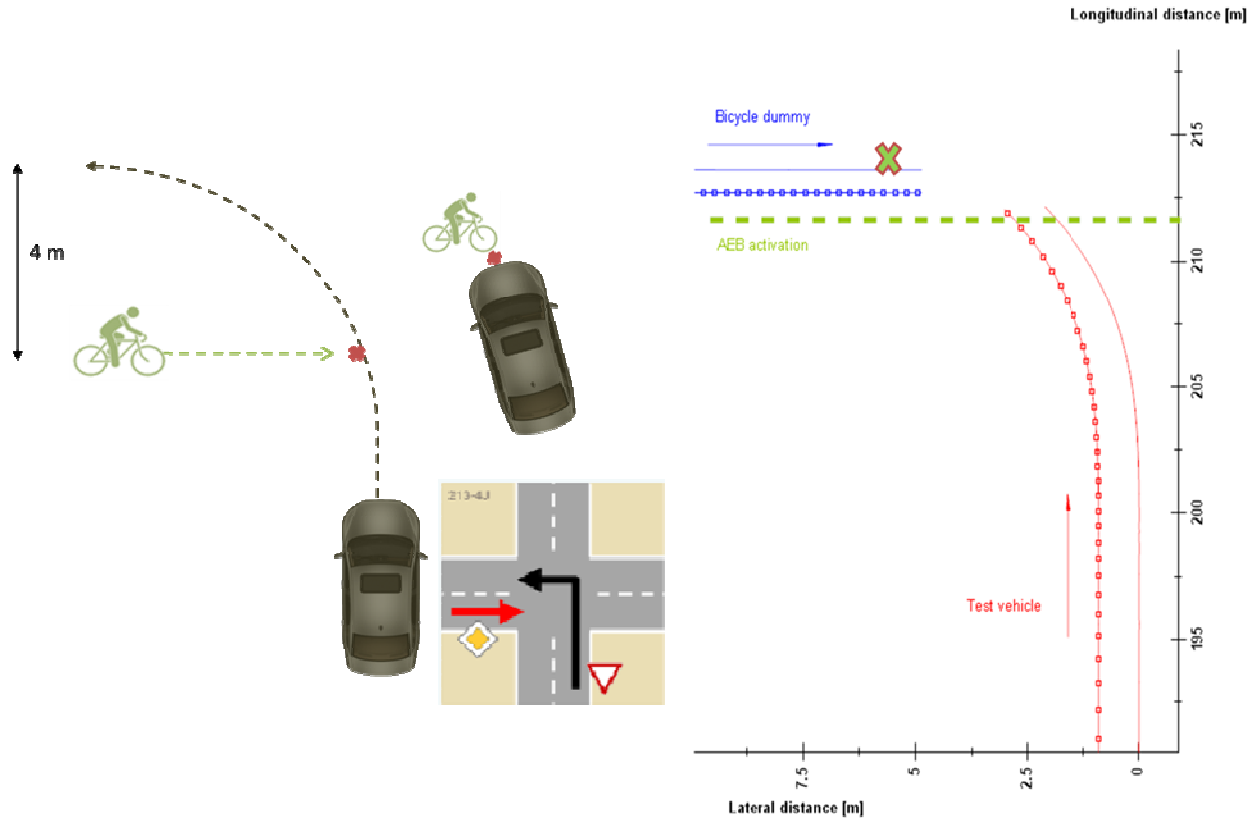

Figure 13: Left turning with bicyclist coming from the far side.

CONCLUSION

The testing activities have been carried out successfully and have met with the initially described objectives to improving current and developing novel active safety features to prevent accidents involving VRUs like pedestrians and bicyclists. The developed prototypes have performed according to expectations on their assigned test cases avoiding any kind of impact in all the tests. This achievement is mainly due to their advanced processing technology that allows identifying and assessing critical situations involving pedestrians more quickly.

In the roadmap of the European consumer testing agency Euro NCAP 2020 [8] intersection scenarios are planned to become a part of the future protocols. The research in the European funded project PROSPECT provides a first step towards addressing such scenarios in the near future. The findings and the proposed trajectories for negotiating a left and right turn are a solid basis for further research.

Potential is seen in control strategies for driving robots currently used for conducting those test cases. Since this has not been part of the scope yet, control strategies could be optimized for more detailed trajectories beyond the proposed three sections in this paper. In addition to that, the tuning for those driving tasks has to become more sophisticated. The project was focused on slow urban scenarios with a rather tight radius. In the future, interurban scenarios with higher curvatures and speeds might become a research focus. In this case, the trajectories need to be adapted in dependence of the desired speed profile. Apart from naturalistic driving studies in the field, specific studies on the test track could support a deeper insight in how trajectories are chosen depending on the circumstances and surroundings, e.g. obstructed views or the traffic situation.

ACKNOWLEDGEMENTS
PROSPECT is a collaborative research project funded by the EC under Grant Agreement n°634149. The authors would like to thank partners of PROSPECT who contributed to the work described in this paper: Applus IDIADA, BASt, Audi, BMW, Bosch, Continental, Volvo, TNO, VTI, University of Nottingham, University of Budapest, University of Amsterdam, IFSTTAR, 4activeSystems, TME, Daimler and Chalmers.

REFERENCES

[1] WHO, 'Global status report on road safety', World Health Organization, 2018
[2] Vision Zero European Commission, 'White Paper on Transport', The European Comission, 2011
[3] European New Car Assessment Programme (Euro NCAP): 'Test Protocol AEB-VRU systems', Version 2.0.3, November 2018
[4] I. Gohl, A. Schneider, J. Stoll, M. Wisch, V. Nitsch, 'Car-to-cyclist accidents, from the car driver's point of view', International Cycling Safety Conference (ICSC), 2016
[5] PROSPECT Deliverable D2.1 'Accident Analysis, Naturalistic Observations and Project Implications', 2016
[6] PROSPECT Deliverable D3.2 'Specification of the PROSPECT demonstrators', 2016
[7] FGSV, Richtlinien für die Anlage von Stadtstraßen (RASt), Köln, 2007
[8] European New Car Assessment Programm (Euro NCAP): 'Euro NCAP. 2020 Roadmap'

REPEATABILITY OF THE CAROUSEL DYNAMIC STABILITY AND ROLLOVER TEST DEVICE

Garrett Mattos
Keith Friedman
Safety Research Institute
USA

Kennerly Digges
Carl Nash
Automotive Safety Research Institute
USA

Acen Jordan
Jordan & Co
USA

Paper Number 19-0330

ABSTRACT

A novel test device (Carousel) for measuring the dynamic rollover stability of vehicles and initiating a full-scale dynamic rollover test has been installed and evaluated for repeatability and reliability. This work describes the test device function and presents results from preliminary repeatability testing. Both the test device and the test article were evaluated to objectively identify the repeatability between tests using correlation analysis. The results demonstrate that the fixture is capable of producing highly repeatable responses.

INTRODUCTION

Rollovers of passenger cars, vans, and light trucks not equipped with electronic stability systems in the U.S. are typically single-vehicle events (82.5%) initiated by a yaw followed by tripping (>80%) such as a furrowing, and gouging [1]. Vehicle rollover resistance ratings in the U.S. are determined by the National Highway Traffic Safety Administration (NHTSA) New Car Assessment Program (NCAP) using two methods; a static measurement of vehicle dimensions and a dynamic handling test. The static measurement method uses a vehicle's track width (T) and center of gravity (CG) height (H) to calculate a *static stability factor* (SSF) (Eq. 1). The vehicle's CG height is generally measured dynamically on a vehicle inertia measuring machine. A lower SSF indicates a higher risk of rollover [2], however more stable vehicles (higher SSF) have been shown to have higher injury risk during rollovers likely due to the increased speeds required to initiate a rollover [3]. The relationship between SSF and rollover risk has been shown to extend to smaller vehicles such as quad bikes [4] and larger vehicles such as heavy trucks [5].

$$SSF = \frac{T}{2H} \qquad \text{Eq. 1}$$

While the SSF does not account for the effects of tire design, suspension characteristics, wheelbase, effects of braking, or electronic stability control these parameters are considered during dynamic tests [2]. Depending on the scenario dynamic tests generally fall into two categories: closed-loop and open-loop maneuvers. Closed-loop maneuvers, such as the ISO 3888 double lane change, require all vehicles to follow a given path and are generally described as evaluations of vehicle maneuverability, not rollover resistance. Open-loop testing, such as the J-turn or fishhook maneuver, provides the same steering input for all vehicles and more frequently produces tip-up. While automated steering controllers are used to improve steering input repeatability, the complexity of the dynamic tests provide challenges in repeatability and reproducibility due to variations in environmental factors (e.g. temperature, humidity), road surface friction and finish, effects of safety outriggers, electronic stability control (ESC), and suspension age. Dynamic maneuver testing is much more expensive, time consuming, and potentially dangerous to drivers than static testing.

Centrifuge-style test methods were considered as an improvement to SSF in a NHTSA notice of proposed rulemaking that was generated in response to the Transportation Recall, Enhancement, Accountability and

Documentation (TREAD) Act of November 2000 [6]. Tests using this method are similar to the tilt-table and side-pull ratio tests and have been promoted for replicating rollover events initiated by both tripped or turn-over mechanisms [7]. The major drawbacks to a rollover rating system that solely used a centrifuge method include the potential for rewarding undesirable suspension characteristics (e.g. oversteer, roll stiffness distribution), lack of sufficient "dynamic" loading, and the fact that ESC would provide no benefit. Coupling a centrifuge test with a dynamic maneuver test would solve this issue. It is worthwhile to note that many manufacturers suggested that ESC be switched off for dynamic testing so that it couldn't be used to mask poor rollover resistance. The benefits of a centrifuge test include simple test setup, small test area, quick turnaround times, reliable tripping mechanism, insensitivity to pavement friction, and low cost of operation. The centrifuge test results would be expected to have a high correlation with SSF while improving the rating due to more realistic evaluation of the test article response by including vehicle load transfer and tire and suspension deflections. Concept tests conducted by the NHTSA at NASA's High Capacity Centrifuge facility demonstrated consistent liftoff values that were in agreement with expected lateral acceleration for rollover initiation.

The objective of this research was to evaluate and quantify the repeatability of a centrifuge-style test fixture (Carousel) with regard to both test fixture and test article response. While the device concept was born out of an interest related to vehicle rollover stability testing it can be applied to many other aspects of physical testing. The Carousel is simply a circular sled that could potentially be used in the same manner as traditional linear sleds following some modifications and/or additions such as a decelerator or test buck stand. The simplicity and compact nature of the device coupled with its high level of repeatability support its use in a wide range of applications.

METHODS

Two Series of tests without test article release were conducted; a Series of four (4) low-speed tests with no tip-up and a Series of four (4) high-speed tests with tip-up.

The test device, shown in Figure 1, consists of a stationary pivot at the center of a 5.4 m radius (approximate test article center) concrete circular track. A steel-framed wood-topped platform rotates about the stationary pivot and rolls on six (6) pairs of 20 cm wheels. The platform designed to accommodate a test article up to 2500 kg with track width and wheelbase not to exceed 1.7 m and 4.4 m, respectively. The device is powered pneumatically with on-board air stored in twin 0.227 m3 (60 gallon) pressurized tanks at a maximum pressure of 1240 kPa. The pressurized air is used to force two (2) pistons down parallel cylinders. The angular acceleration is controlled by the amount of air pressure. Each piston is attached to a steel wire rope that is wound around a central sheave which is rigidly attached to the stationary pivot. As the pistons are forced down the cylinders a torque is developed between the sheave and the platform which accelerates the platform around the track as the wire ropes unwind from the central sheave. The ratio of the central sheave circumference to wire rope length provides approximately 340 deg of angular acceleration. After the platform reaches a displacement of 340 degrees it coasts to a stop unless otherwise decelerated.

Figure 1 Test fixture with test article at start position

The test article was a 2000 Ford Ranger two-door super cab pickup with the dimensions and inertial properties summarized in Table 1. The test article is positioned on the platform with the transmission in 'park' and the parking brake engaged. Square aluminum tubes are positioned in front of and behind each tire and clamped to the platform to prevent fore-aft motion during the test. The outside faces of the outside tires are positioned in contact with trip bars. The trip bars consist of aluminum plates that pivot as they are loaded by the tires and the vehicle rotates over them as shown in Figure 2. Inside tire lift-off height is controlled with the used of chains affixed to the platform.

Table 1 Test article dimensions

Parameter	Value
Test weight / Distribution	1610 kg / 59 % front
Roll moment of inertia	638 kg m^2
Yaw moment of inertia	2661 kg m^2
Pitch moment of inertia	2628 kg m^2
Wheelbase	3.2 m
Track Width front/rear	1.5 m / 1.45 m
CG height	0.625 m
SSF	1.18
Tires	BF Goodrich All-Terrain 31x10.50R15 100s

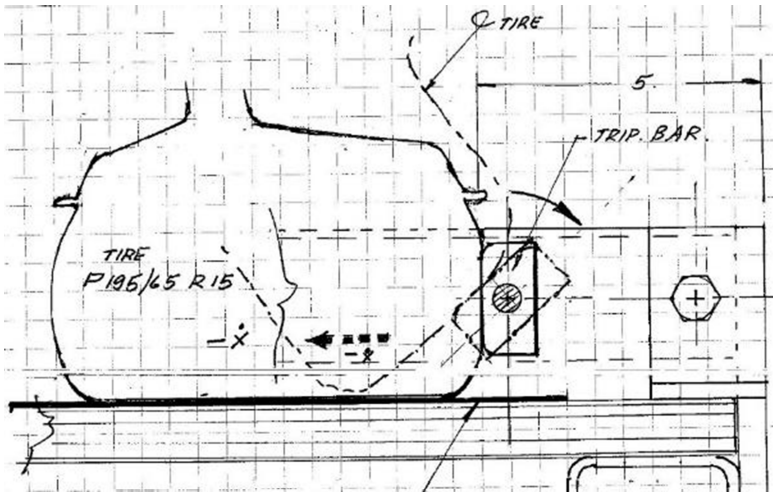

Figure 2 Cross-section view of tire and trip bar

A dual-output rotary potentiometer (Novotechnik RSC2832) was used to measure platform angular displacement. String potentiometers (Space Age Control 301432) were placed between the platform and the inside frame rail at the front and rear of the test article to measure the displacement of the test article during three of the Series 2 tests (Figure 3). The string potentiometer data in the fourth Series 2 test was erroneous and is not included below. Onboard real-time cameras were used to record each tire response and off-board cameras recorded the event from multiple angles.

Figure 3 Front (left) and rear (right) string potentiometer placement

The first Series of four (4) tests was selected to replicate a non-tip-up event. A test pressure of 689 kPa (100 psi) was expected to produce a test article lateral acceleration of approximately 0.6 g. The goal of the second test Series was to provide enough lateral acceleration to initiate a rollover. The second test Series comprised four (4) tests and used a tank pressure of 1034 kPa (150 psi). In all tests the inside tires of the test article was restrained to allow for a maximum lift of approximately 75 mm. A summary of the test conditions is provided in Table 2.

Table 2 Test summary

Test Series	Test parameters	Goal values
1	Tank pressure	689 kPa (100 psi)
	Test article lateral acceleration	0.6 g
	Peak platform velocity	60 deg/s
	Number of tests	4
2	Tank pressure	1034 kPa (150 psi)
	Test article lateral acceleration	1.1 g
	Peak platform velocity	80 deg/s
	Number of tests	4

The tests were conducted over a two-day period from 10 am to 6 pm each day. The weather was stable with temperatures ranging from 25 to 37° C (77 to 99° F) and humidity ranging from 84 to 35 % between the morning and afternoon. Multiple warmup and practice runs were performed prior to conducting the test Series to ensure that the moving parts of the test fixture and test article had loosened up. After the initial setup and practice runs were complete the test runs in each test Series was completed consecutively within 90 minutes from start to finish.

Correlation analysis (CORA) was utilized to objectively compare the platform angular displacement and the test article displacement in each test to the average values for a given test Series. CORAplus version 4.04 with

recommended global settings was used to calculate the scores using the cross correlation method. Curves were filtered according to J211 recommended protocol.

RESULTS

At test initiation the accelerating platform produced a slight rearward pitching motion of the test article which can be seen in the initial negative displacement of the rear string pot data. As the platform angular velocity increased the vehicle began to roll outboard. None of the tires lifted off of the platform in the Series 1 tests. The goal test conditions were achieved in all tests.

The platform angular displacement time history matched very well between tests in a given series as shown in Figures 4 and 5. The average maximum angular velocity for each test series was 60.1 deg/s and 79.25 deg/s. On average, the platform reached 340 deg of displacement (end of angular acceleration) in 9.7 seconds and 7.6 seconds in test series 1 and 2, respectively.

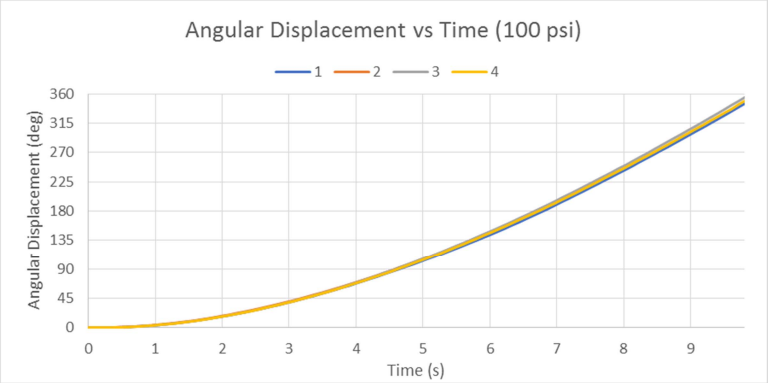

Figure 4 Platform angular displacement time-history (Test Series 1)

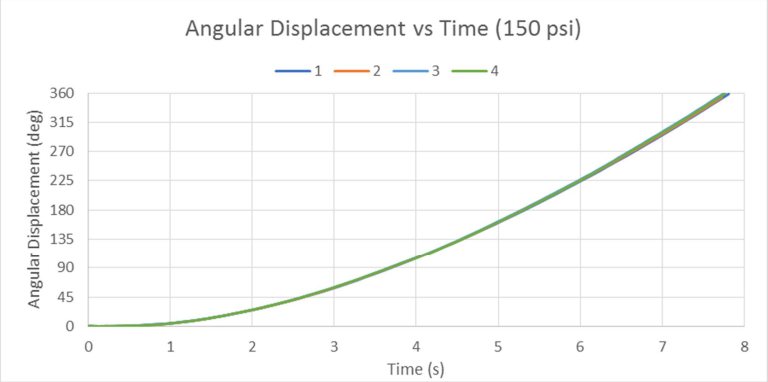

Figure 5 Platform angular displacement time-history (Test Series 2)

Test article displacement was consistent between tests as shown in Figures 6 and 7. String potentiometer data from the fourth Series 2 test was erroneous is not included here. The average maximum displacement at the front and rear string potentiometer locations was approximately 31 mm and 47 mm, respectively. The values correspond to the maximum displacement allowed by the tie-down chains. In the Series 2 tests the front and rear tires lifted off at approximately 4.5 and 7.7 seconds, respectively. The video footage indicates that a difference in chain response in Test 2 is likely the reason for the relatively large difference in displacement for that test.

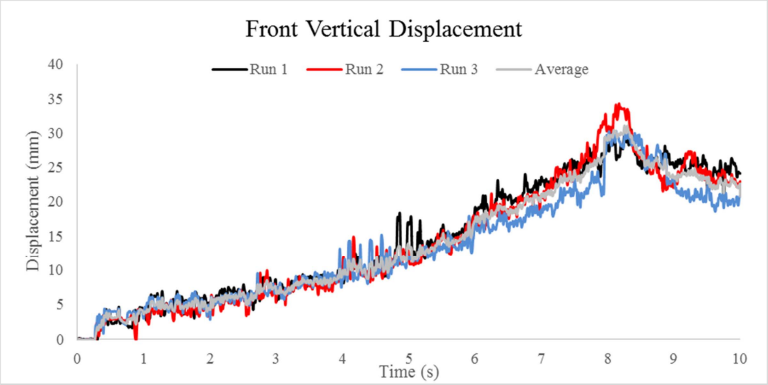

Figure 6 Test article displacement time-history (front; Test Series 2)

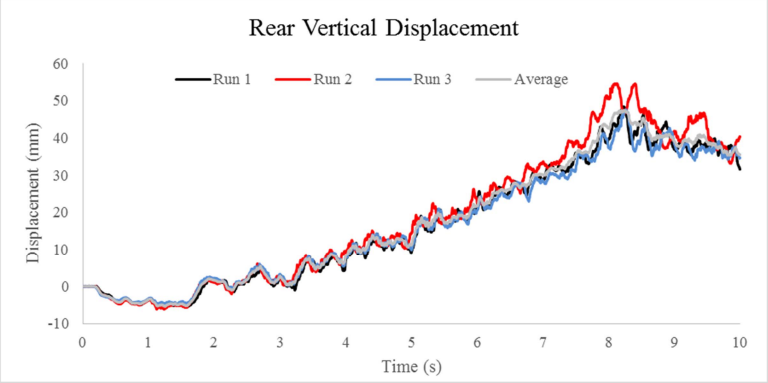

Figure 7 Test article displacement time-history (rear; Test Series 2)

The results of the CORA analysis are summarized in Table 3. Values above 8.6 are considered to indicate excellent repeatability.

Table 3 CORA results summary

Test Series	Measurement	Test	Cross correlation rating – per test				Total Series rating
			Cross correlation	Size	Phase shift	Total	
1	Platform displacement	1	1.0	0.966	1.0	0.992	0.995
		2	1.0	0.984	1.0	0.996	
		3	1.0	0.974	1.0	0.993	
		4	1.0	0.993	1.0	0.998	
2	Platform displacement	1	1.0	0.997	1.0	0.999	0.998
		2	1.0	0.978	1.0	0.994	
		3	1.0	0.987	1.0	0.997	
		4	1.0	0.999	1.0	1.0	
2	Test article displacement (rear)	1	0.994	0.937	1.0	0.981	0.968
		2	0.990	0.845	1.0	0.956	
		3	0.993	0.884	1.0	0.968	
2	Test article displacement (front)	1	0.987	0.939	1.0	0.978	0.975
		2	0.986	0.946	1.0	0.980	
		3	0.984	0.90	1.0	0.967	

DISCUSSION

The test fixture and test article demonstrated excellent repeatability for the two test series evaluated above. After initial test setup, tests could be performed with two technicians and 45 minute turnaround times. The greatest time-cost between tests included re-pressurizing the system and downloading the data. During test setup it was observed that initial 'warm-up' runs would be required to exercise both the fixture and the test article such that all joints and suspensions were loosed up and would perform consistently.

The lowest levels of repeatability were related to test article performance, though the repeatability was still considered excellent. This was expected as the test article introduced many additional characteristics that could affect response such as suspension and tire properties that could vary with changes in temperature or use. One proposed method to limit the effects of tire characteristics is to define a standardized tire or tire surrogate that would be used for all vehicles and provide a consistent interface between the tire and the trip-bar.

Some lateral motion of the test article was expected based on the results of a similar test series conducted by the NHTSA at National Aeronautics and Space Administration's High Capacity Centrifuge [8], however no custom mechanisms were created to account for this with regard to the string pot measurements. It is anticipated that future rollover stability testing will require the use of custom-designed load cell mounts that move laterally with each tire. The lateral motion of the vehicle during initial warm-up testing and subsequent calibration testing presents a challenge in identifying the initial position of the vehicle for a test. Differences in the initial lateral position of the vehicle, specifically regarding pre-loading against the trip-bar, could potentially alter the performance. Lateral positioning of the vehicle during initial setup proved challenging and pre-loading the outside tires against the trip-bar was not possible. A pre-load could be applied by conducting one or more low-speed tests, however variations in the suspension spring back were observed after the platform came to rest.

While this paper has focused on using the Carousel to evaluate the dynamic rollover resistance of a passenger vehicle it could easily be extended to evaluating all-terrain vehicles (ATVs) and side-by-side vehicles. The device has the potential to evaluate restrain performance under varying yaw and roll rates in a repeatable, safety, and non-destructive manner. The platform can be modified with addition of a deformable barrier face to apply impact loads to stationary test articles. Various high- and low-rate deceleration mechanisms have been proposed that would allow the Carousel to perform as a traditional non-destructive deceleration sled.

CONCLUSIONS

A centrifuge-style test device (Carousel) was described. The performance of the Carousel and the response of a test article were evaluated to quantify their repeatability under low and high-speed test conditions. The Carousel and the test article both demonstrated excellent repeatability according to cross-correlation analysis using the CORA methods. The results demonstrate that the device is a suitable candidate for performing repeatable dynamic stability tests.

REFERENCES

[1] Bose, D., et al., Planar impacts in rollover crashes: significance, distribution and injury epidemiology. Ann Adv Automot Med, 2011. **55**: p. 243-52.

[2] Boyd, P.L. NHTSA's NCAP rollover resistance rating system. in The 19th International Technical Conference on the Enhanced Safety of Vehicles. 2005. Washington DC: NHTSA.

[3] Brumbelow, M.L. and E.R. Teoh, Roof strength and injury risk in rollover crashes of passenger cars. Traffic Inj. Prev., 2009. **10**(6): p. 584-592.

[4] Grzebieta, R., et al., Final Project Summary Report: Quad Bike Performance Project Test Results, Conclusions, and Recommendations. 2015, UNSW: Transport and Road Safety Research.

[5] Mengert, P., et al., Statistical Estimation of Rollover Risk. 1989, Research and Special Programs Administration: NHTSA, US DOT, Washington D.C.

[6] NHTSA, 49 CFR Part 575: Consumer Information Regulations; Federal Motor Vehicle Safety Standards; Rollover Resistance, in Notice of proposed rulemaking. 2001.

[7] Patel, B. and P. Atkinson, Towards A Definition of A Test Methodology for Rollover Resistance and Rollover Performance. 2004.

[8] Chambers, W.V., SUV Rollover Test, in 23rd IEST-NASA/ASTM/AIAA/CSA Space Simulation Conference. 2004, NASA; AIAA; ASTM; CSA: Annapolis, MD; USA.

PAIRED COMPARISON OF ATD RESPONSES FOR THE CMVSS 213 BENCH AND PROPOSED FMVSS 213 BENCH

Suzanne Tylko
Transport Canada
Canada

Kathy Tang, Alain Bussières, Amanda Starr
PMG Technologies
Canada

Paper Number 19-0331

ABSTRACT

A controlled matched pair comparison of child ATD responses, installed in different models of child restraints was conducted to investigate differences between the current CMVSS 213 bench and the proposed FMVSS 213 bench. The effect of acceleration and deceleration pulses on ATD responses were also examined.

The CRABI 12-month-old and the Hybrid III 6-year-old were placed in rear facing and forward-facing child restraints installed on the current CMVSS 213 bench and the proposed FMVSS 213 bench. Repeatability of installation was verified with a 3D Faro measurement system. A total of 114 tests were conducted on the Seattle Safety acceleration sled and on the Messring HydroBrake deceleration sled.

Head, chest and pelvis acceleration responses were compared for pairs matched as a function of ATD, seat type, and installation method. Maximum head excursion, maximum knee excursion, and seat excursion at the time of maximum head excursion were estimated using video recordings.

Downward displacement of rear facing seats was reduced on the proposed bench when compared to the current CMVSS 213 bench. The Hybrid III 6-year-old head, chest, and pelvis responses on the two benches were similar (difference of $\leq$ 5g). One forward facing seat exhibited a higher chest response on the proposed bench. Maximum head excursions relative to both the bench and the seat tended to be greater on the proposed bench for all seats regardless of installation method. Paired responses on the acceleration and deceleration sleds were similar. Differences in paired responses were found to be more strongly linked to product design characteristics than to test bench characteristics or sled type.

The study contributes to an understanding of the influence of test configuration and is pertinent to the development of child restraint regulations or consumer evaluation programs.

INTRODUCTION

The Canadian Motor Vehicle Safety Standard 213 and Federal Motor Vehicle Safety Standard 213 (C/FMVSS 213) are two very similar standards in place in Canada and the United States specifying performance requirements for child restraint systems (CRS). Both standards require dynamic testing on an acceleration or deceleration sled. The geometry and cushion stiffness of the test bench were originally based on the front seat of a 1974 Chevrolet Impala [1]. In 2003, the National Highway Traffic Safety Administration (NHTSA) introduced a new drawing package for the seat assembly which included changes to the seat bottom and seat back cushion angles, lap belt anchorage locations, and seat back rigidity [2], [3]. Changes to the seat cushion stiffness were not included in this revision [4].

In 2015, a new version of the bench was proposed by the NHTSA to replace the bench used in the FMVSS 213 standard [5], [6]. As part of a review of this proposal, Transport Canada fabricated the proposed bench and began a paired comparative study to quantify differences in the evaluation of seat performance attributable to the new seat assembly. Since the study was conducted between 2016 and 2018, the evaluation was based on the drawings that were shared by the NHTSA at that onset of the study, to ensure constancy. The intent of this paper is to present the results of paired comparisons of ATD responses obtained with the current CMVSS 213 bench and the proposed NHTSA bench. The principal objective is to provide a comparison of the regulatory measures used to determine compliance of bench belt-positioning booster seats, forward-facing CRS (FFCRS), and rear-facing CRS (RFCRS) in North America. Numerous ATD measures are included for the sake of completeness and for future analysis.

METHODS

Sled Testing

Sled tests were run in three different conditions: (1) using the proposed NHTSA bench on the acceleration sled (Fig. 1A); (2) using the CMVSS 213 bench on the acceleration sled (Fig. 1B); and (3) using the proposed bench on the deceleration sled (Fig. 1C). To assess CRS performance on the two benches or the two sleds, tests in condition (1) were respectively compared to those in condition (2) or (3).

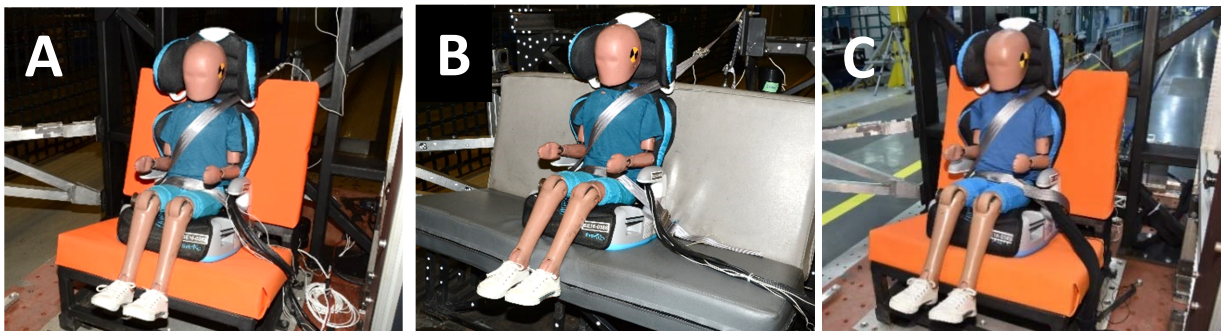

Figure 1. The Hybrid III 6-year-old installed in a high-back booster seat on (A) the proposed FMVSS bench + accel sled, (B) the CMVSS bench + acceleration sled, and (C) the proposed FMVSS bench + deceleration sled.

For each condition, child seats were installed in up to eight different configurations (Table 1), with each configuration varying by seat type (FFCRS, booster seat, or RFCRS with or without base) and attachment method (Type 2 belt or universal anchorage system (UAS)). FFCRS and booster seats were installed with the Hybrid III 6-year-old ATD, and RFCRS were installed with the CRABI 12-month-old. All tests with FFCRS included the use of a harness and the top tether. For each RFCRS, two targets were placed on the RFCRS shell to estimate RFCRS rotation.

A few minor changes, detailed in the Appendix were made to the proposed bench to increase durability. The sleds included a Seattle Safety 2 MN servo controlled pneumatic acceleration sled (Seattle Safety, Kent, WA, USA) and a MESSRING HydroBrake deceleration sled (MESSRING GmbH, Krailling, Germany). Figure 2 presents the pulses obtained. The pulses corresponding to the acceleration sled are shown in red while the deceleration pulses are presented in green.

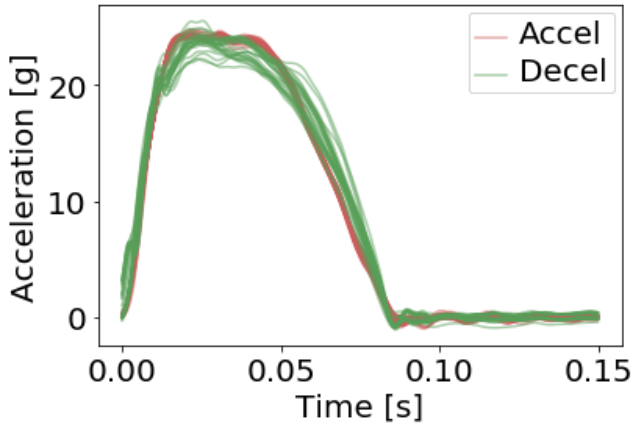

Figure 2. Time-acceleration traces of the sled pulse on the acceleration (red) and deceleration (green) sleds.

Installations of the child restraints and booster seats were carried out as per manufacturer instructions. The same Hybrid III 6-year-old and 12-month CRABI ATDs were used throughout the study. A FaroArm 3D metrology system (FARO, Lake Mary, Florida, USA) was used to precisely record placement and to reproduce the positioning of the ATDs between matched tests. Front, left, right, and top views of the tests were recorded using NAC high-

speed cameras (NAC Image Technology, Simi Valley, CA, USA), Integrated Design Tools (IDT, Pasadena, CA, USA) at a rate of 1000 frames per second.

Table 1.
Test matrix.

Model	Configuration	ATD	Proposed FMVSS + accel sled	CMVSS + accel sled	Proposed FMVSS + decel sled
A	FF + Belt + tether	Hybrid II 6YO	3	3	0
B	FF + Belt+ tether		2	2	0
	FF + UAS+ tether		2	2	0
	HB		1	1	1
C	FF + Belt+ tether		1	1	0
D	FF + Belt+ tether		3	4	0
	FF + UAS+ tether		1	1	0
	Conv. RF + Belt	CRABI 12MO	1	1	1
E	HB	Hybrid II 6YO	1	1	1
F	HB		3	1	3
G	HB		2	2	1
	LB		3	3	1
H	HB		1	1	1
	LB		1	1	1
I	LB		4	4	2
J	Conv. RF + Belt	CRABI 12MO	1	1	2
K	RF + Belt		1	1	1
	RF + Base + Belt		2	2	2
	RF + Base + UAS		3	1	3
L	RF + Belt		1	1	1
	RF + Base + Belt		1	1	1
	RF + Base + UAS		1	1	1
M	RF + Base + Belt		1	1	1
N	RF + Base + Belt		1	2	1
	RF + Base + UAS		1	1	1
O	RF + Base + UAS		1	1	0
P	RF + Base + Belt		1	1	1

FF = forward-facing, HB = high-back booster, LB = low-back booster, RF = rear-facing, UAS = universal anchorage system

Data Analysis

High-speed videos were used to visually compare ATD and CRS movements. The vertical displacements, rotations and excursions of the two targets on each RFCRS were tracked using TEMA 3.5 (Image Systems Motion Analysis, Linköping, Sweden). RFCRS rotation was calculated as the angle from the vertical (12 o'clock) of the line drawn between the two targets, measured in degrees. The absolute values of the x, y, and z accelerations were determined at the time of peak resultant acceleration.

To compare ATD responses on the two benches or the two sleds, linear mixed effects models were constructed for each comparison. This allowed us to compute configuration-specific differences in mean responses and test for their significance while accounting for the variation in responses resulting from differences between specific child seat models. Linear mixed effects models were favoured over paired tests because they allowed for the inclusion of replicate tests. For each comparison, linear mixed effects models were constructed as

$$X = \beta_0 + \beta_1 + \gamma + \epsilon \qquad \text{Equation (1)}$$

where

X: Response (e.g. maximum head excursion) observed for either condition (2) or (3), depending on the comparison of interest

β_0: Response observed for condition (1)

β_1: Difference between the responses in the two conditions

γ: Random effect describing variance attributed to differences between CRS models; follows a normal distribution with mean 0

ϵ: Residual term; follows a normal distribution with mean 0

The difference between the responses either on the two benches or on the two sleds is thus given by β_1. To test for the significance of this difference, Eq. (1) was tested against a model which assumed no difference in responses under the two different conditions, i.e. β_1=0 and $X = \beta_0 + \gamma + \epsilon$. Significance testing was conducted using p-values determined by the likelihood ratio test (implementation using the anova function in R) and a 5% significance level. Linear mixed effects models were constructed in R using the lme4 package [7].

RESULTS

Comparison of FFCRS and Booster Seats Between Benches Using the Hybrid III 6-Year-Old

Aggregate comparisons of the Hybrid III 6-year-old response on the two benches In a number of tests with the FF + belt configuration, the path of the shoulder belt was altered by contact with the seat back foam on the proposed FMVSS bench (Fig. 3A). The shoulder belt path was straighter on the CMVSS bench (Fig. 3B).

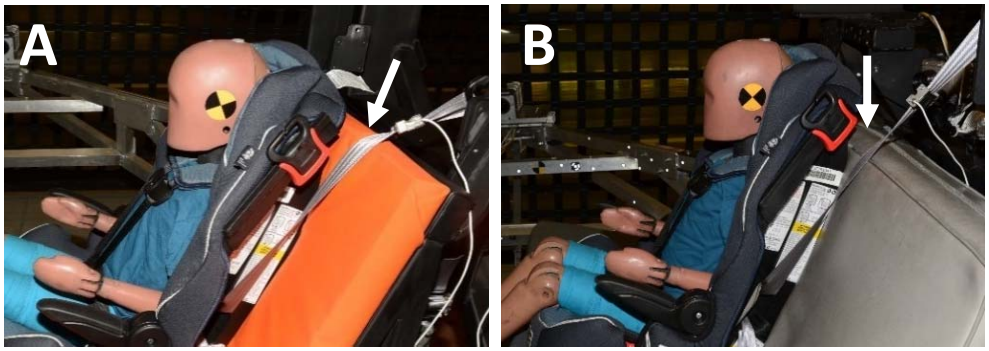

Figure 3. Example of a FFCRS installed with the Type 2 belt on (A) the proposed bench and (B) the CMVSS bench. White arrows indicate the point on the shoulder belt where differences in contact with the bench were observed.

Figure 4 compares the means and standard deviations of ATD responses on the two benches for each configuration, and Table A1 specifies the differences in mean response (i.e. β_1 in Eq. (1)) and p-values for each comparison. While all excursions were well below the compliance limits, head excursions tended to be slightly greater on the proposed bench. The difference was statistically significant for only the FF + belt and LB configurations (Fig. 4A). Knee excursions were significantly greater on the proposed bench for all configurations (Fig. 4B). Head and chest 3ms clips were not significantly different on the two benches (Fig. 4C-D). The difference between mean peak chest deflections was only significant for the FF + UAS (Fig. 4E).

Statistically significant differences in the responses on the two benches were found for peak shoulder belt loads, upper neck axial loads, and lumbar spine moments about z. Shoulder belt loads were significantly greater on the CMVSS bench than on the proposed bench for all configurations using a Type 2 belt (Fig. 4F). For tests with booster seats, upper neck loads tended to be greater on the proposed bench, although the difference was statistically significant for only high-back boosters. Conversely, peak (maximum) lumbar spine moments about z for booster seats were lower on the proposed bench than on the CMVSS bench.

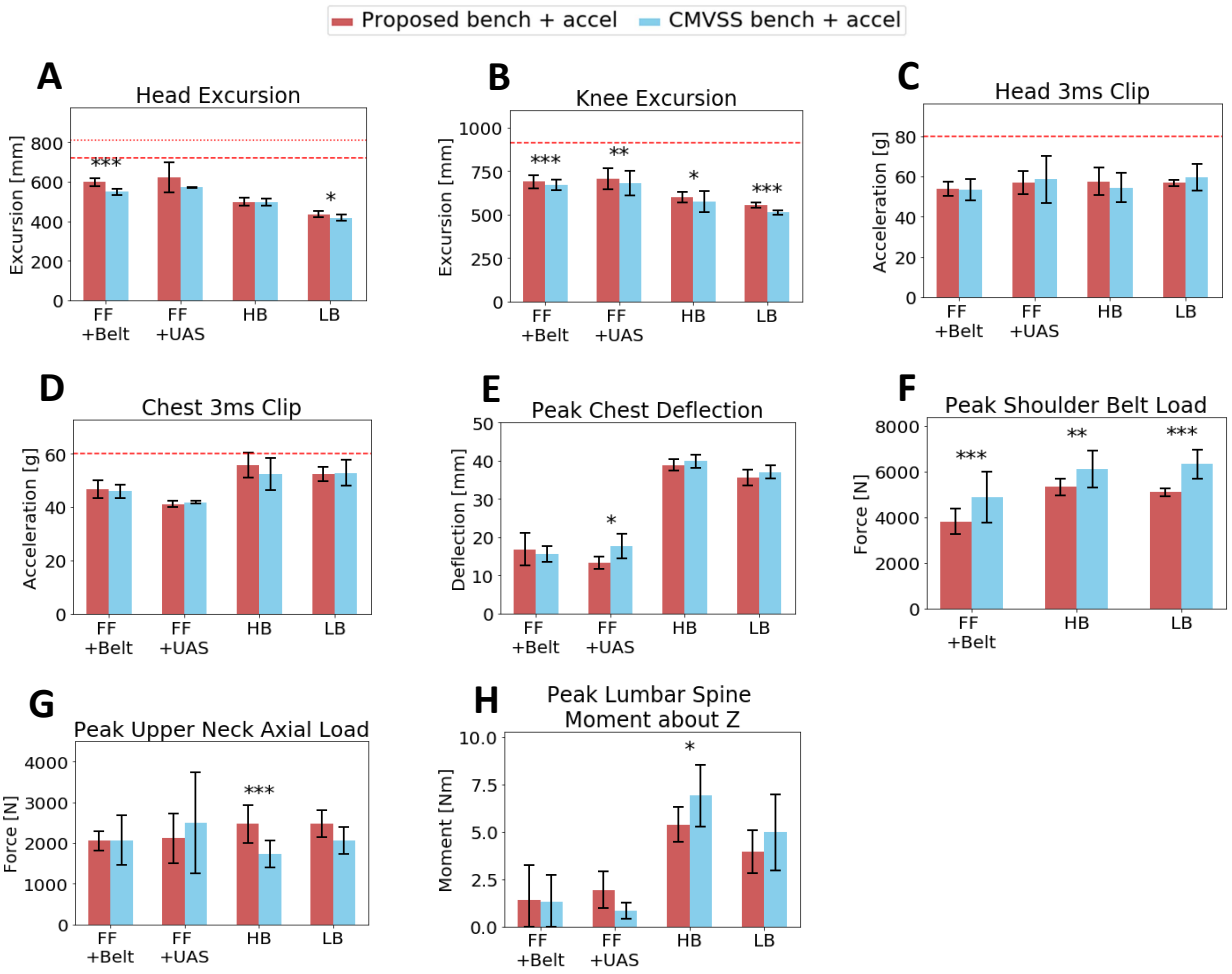

Figure 4. Differences in responses of the 6-year-old on the proposed (red bars) and CMVSS (blue bars) benches for each configuration[1].

Matched comparisons of the Hybrid III 6-year-old response on the two benches Paired tests[2] were carried out to investigate the responses associated with specific CRS models. To this end, we found large differences in head excursion for Model B when installed with the UAS. The mean head excursion in this seat installed on the proposed bench (n=2) exceeded the mean head excursion on the CMVSS bench (n=2) by 92 mm. At peak head excursion, the ATD torso and the CRS backrest appeared to be more upright on the proposed bench compared to the CMVSS bench (Fig. 5). Mean knee excursions were 33 mm greater on the proposed bench than on the CMVSS bench. The differences in mean head and chest 3ms clips, chest deflections, and upper neck axial loads were all relatively small (Table A2).

[1] Bars in all charts represent the mean ± standard deviation of each response. Statistical significance is indicated by the asterisks above pairs of bars (* for $p<0.05$, ** for $p < 0.01$, *** for $p < 0.001$).

[2] Refers to tests matched by model and configuration

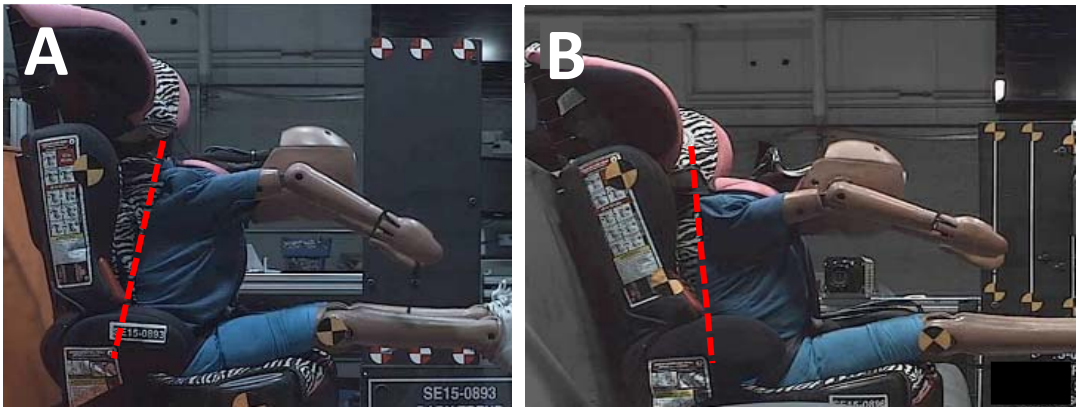

Figure 5. Freeze frames at maximum head excursion of the 6-year-old on Model B FFCRS installed with tether + UAS on the (A) proposed bench and (B) CMVSS bench.

Comparison of FFCRS and Booster Seats Between Sleds Using the Hybrid III 6-Year-Old

Aggregate comparisons of the Hybrid III 6-year-old response on the two sleds Assessments of CRS performance on the acceleration and deceleration sleds using the Hybrid III 6-year-old were limited to comparisons of booster seats only. In general, the responses seen on the two sleds were not significantly different from each other (Fig. 6A-D, F-H). We did observe, slightly greater peak chest deflections (2.7 mm and 2.5 mm for high-back and low-back boosters, respectively) on the acceleration sled compared to the deceleration sled (Fig. 6E).

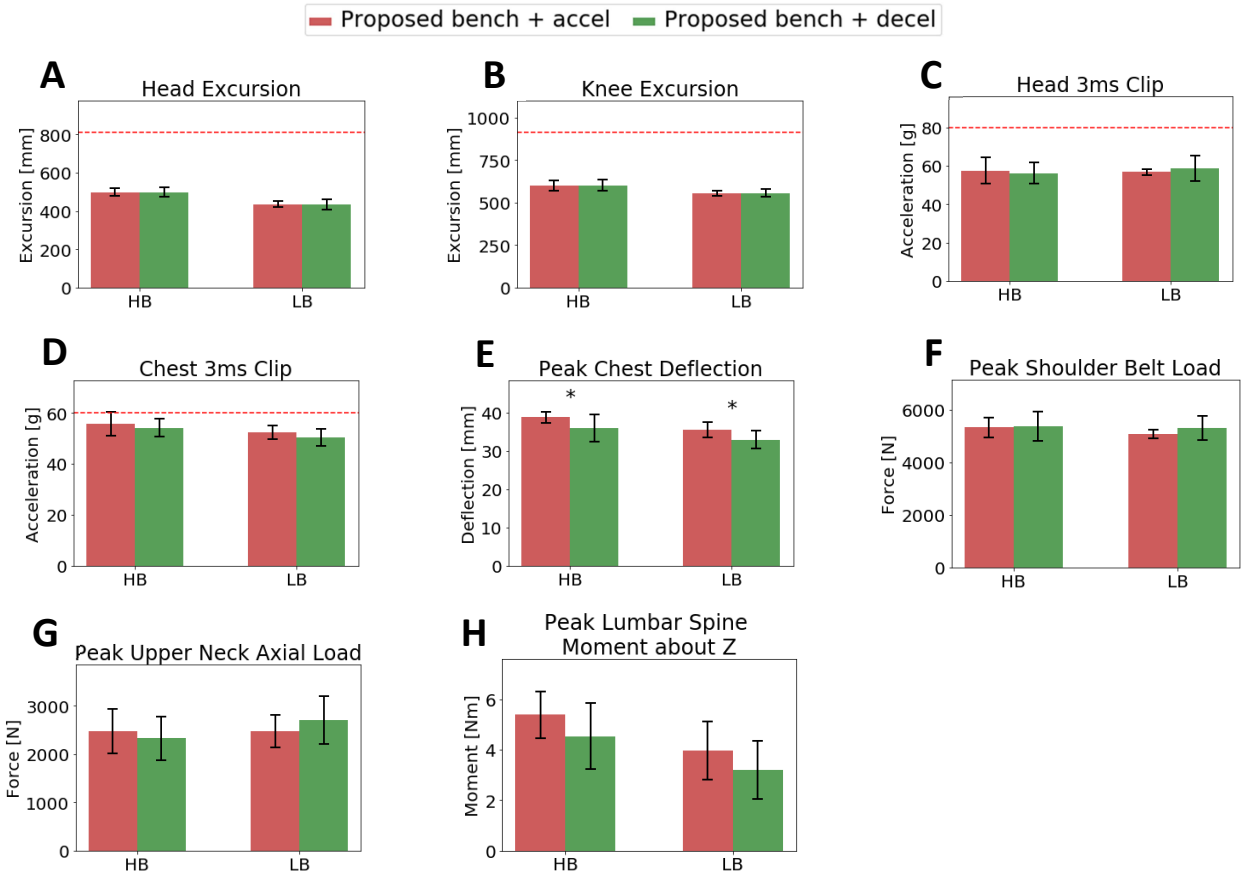

Figure 6. Differences in responses of the 6-year-old on the acceleration (red bars) and deceleration (blue bars) sleds for HB and LB booster seats. Dashed red lines in panels A-D indicate the regulatory limits of each response.

Matched comparisons of the Hybrid III 6-year-old response on the two sleds Comparisons of responses seen for specific booster seat models showed that for tests with Model F, one of the three tests conducted on the acceleration sled resulted in a chest 3ms clip exceeding 60g (Table 2). In the three matched tests conducted on the deceleration sled, all chest 3ms clips were below 60 g.

Table 2.

Chest 3ms clips for six tests with Model F installed on the proposed bench.

Sled	Acceleration			Deceleration		
Test no.	1	2	3	4	5	6
Chest 3ms clip [g]	63.2	58.9	57.5	57.7	56.5	52.9
Mean (Stand dev.)	59.9 ± 3.0			55.7 ± 2.5		

Comparison of RFCRS Performance Between Benches Using the CRABI 12-Month-Old ATD

Aggregate comparisons of the CRABI 12-month-old response on the two benches The CRABI 12-month-old responses were compared for four different configurations. Additionally, tracking of the targets on the RFCRS shell allowed for comparison of RFCRS motions. The differences in mean responses seen on the two benches (i.e. β_1 in Eq. (1)) and their associated p-values are summarized in Table A4.

Visual comparisons of the two benches showed that the path of the shoulder belt was altered by contact with the seat back foam on the proposed NHTSA bench (Fig. 7A, white arrow). The shoulder belt path was straighter on the CMVSS bench (Fig. 7B, white arrow). This difference was consistently seen for all tests where the Type 2 belt was used.

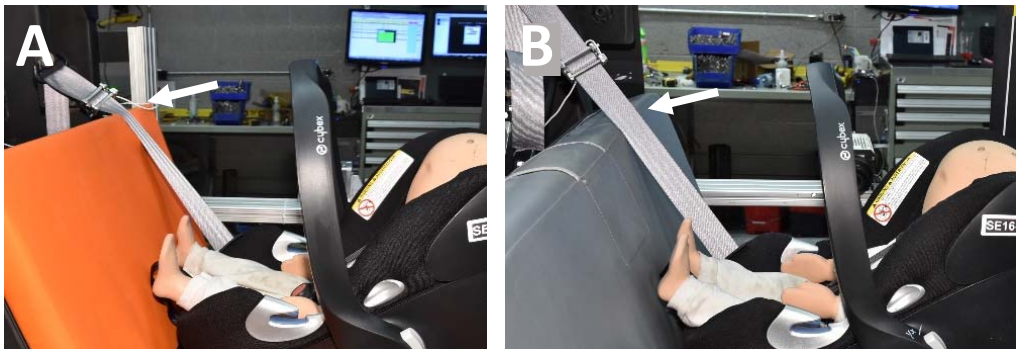

Figure 7. Example of an installation of the RF + base + belt configuration on the (A) proposed bench and (B) CMVSS 213 benches. White arrows indicate the point on the shoulder belt where differences were observed.

Comparisons of RFCRS motions on the two benches showed significantly greater peak angle changes and vertical displacements on the CMVSS bench compared to the proposed bench (Fig. 8A-B). Differences in peak excursion varied by configuration (Fig. 8C). For the non-convertible RF + belt configuration, mean excursion on the proposed bench was slightly greater than the mean excursion on the CMVSS bench. Conversely, for both configurations where the RFCRS was installed with a base, mean excursions were lower on the proposed bench. Peak shoulder belt loads were significantly greater on the CMVSS bench than on the proposed bench (Fig. 8D). Differences in head and chest 3ms clips on the two benches also varied by configuration (Fig. 8E-F). The only significant difference in head 3ms clip occurred for the RF + base + belt configuration, where responses were greater on the proposed bench. The chest 3ms clips were generally slightly greater on the proposed bench for both the convertible RF + belt and RF + base + UAS configurations. In contrast, the chest 3ms clip for the RF + base + belt configuration was less on the proposed bench.

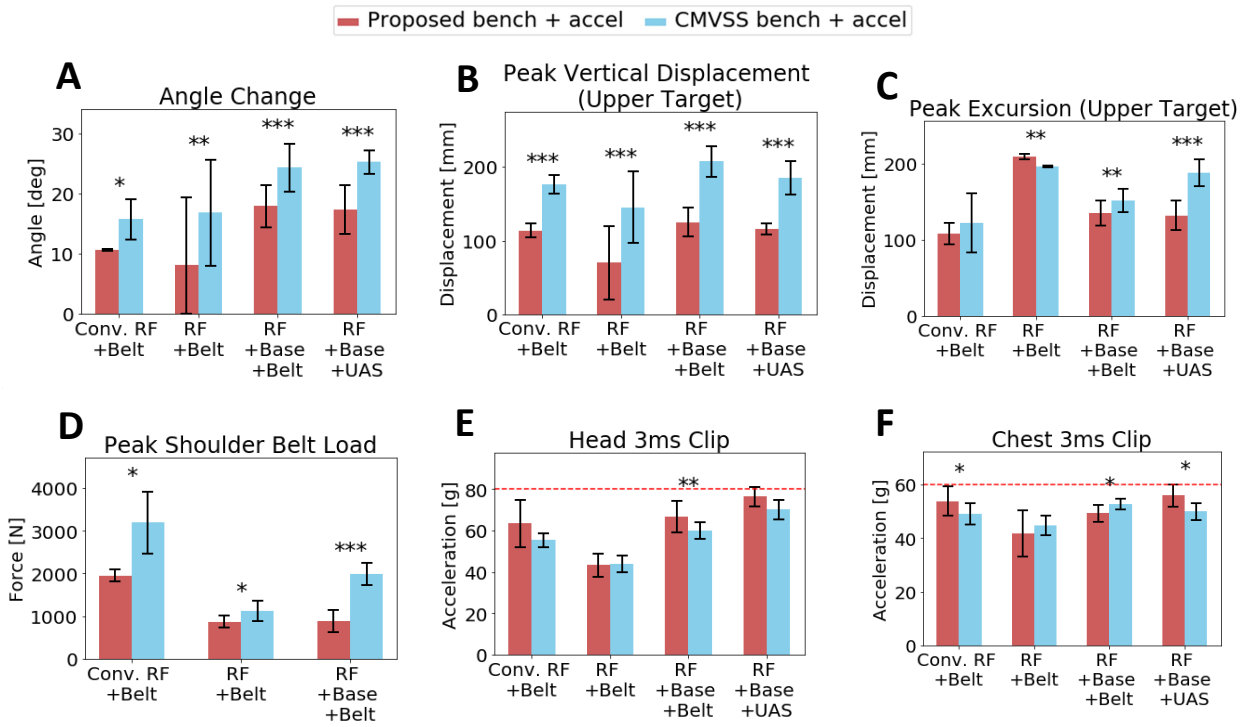

Figure 8. Differences in responses of the 12-month-old on the proposed FMVSS (red bars) and CMVSS (blue bars) benches for each configuration. Thick dashed red lines in panels E-F indicate the regulatory limits of each response.

In order to better understand the chest clip differences, the chest acceleration components were examined. At the time of peak resultant acceleration, the x components in the tests for the two RF + Base configurations were greater in magnitude for the proposed bench (Fig. 9A) compared to the CMVSS bench. The z components in contrast, were much lower in magnitude for the proposed bench compared to the CMVSS bench (Fig. 9B). For these two test configurations, the differences in the z component associated with the proposed bench were comparable (Fig. 9B) but the difference in the magnitude of the x component associated with the proposed bench was smaller and much less significant for the RF + base + belt installation (Fig. 9A).

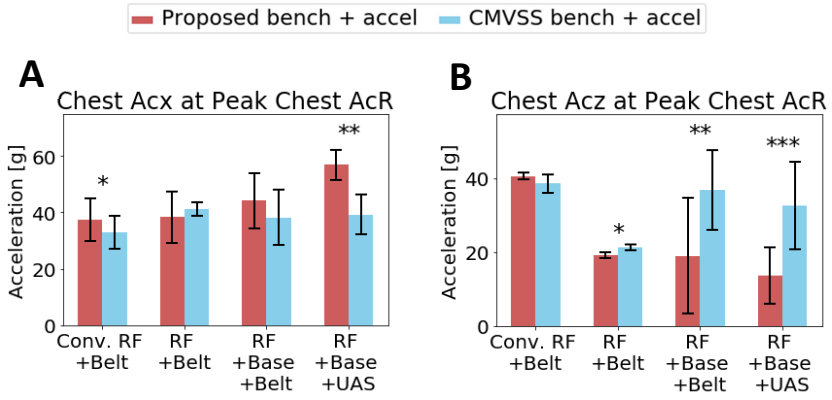

Figure 9. Differences in (A) Chest Acx and (B) Chest Acz at the time of peak chest resultant acceleration on the proposed FMVSS (red bars) and CMVSS (blue bars) benches for each configuration.

In addition to the differences in chest responses shown in Fig. 9, we also found differences in the relationship between the chest 3ms clip and RFCRS motion for the belt and UAS installations. For tests in the RF + base + belt configuration, chest 3ms clips were lower when the peak angle change was reached before the lower visual target on the CRS attained its peak vertical displacement; but the chest 3ms clips were greater when the peak angle change occurred at or after peak vertical displacement was attained (Fig. 10A). On the other hand, for tests with the RF +

base + UAS configuration, the correlation between chest 3ms clip and the timing of peak angle change relative to peak vertical displacement was weak. Instead, tests with this configuration showed a stronger relationship between chest 3ms clip and peak (lower target) excursion, where greater peak excursions were associated with lower chest 3ms clips (Fig. 10B). R values shown are Pearson correlation coefficients.

Multiple linear regression using all of the tests on the proposed bench suggested that both the peak excursion and the timing of peak angle change relative to peak vertical displacement were significant predictors of chest 3ms clip values (Table 3).

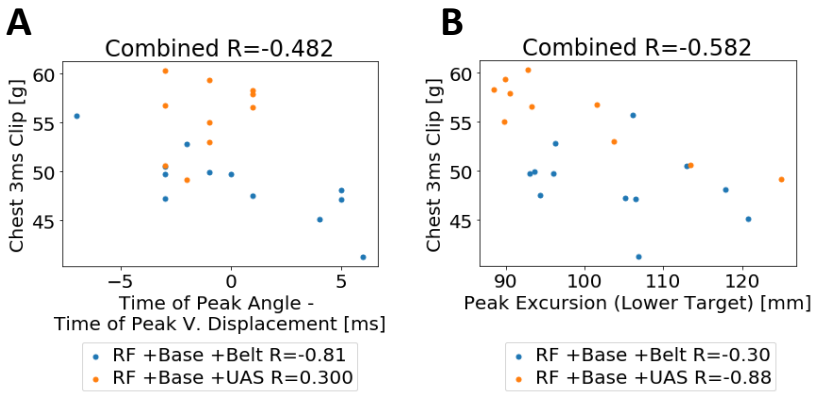

Figure 10. Correlations between chest 3ms clips and (A) the time of peak angle change relative to the time of peak vertical displacement and (B) peak lower target excursion in RFCRS installed in the RF + base + belt (blue points) and RF + base + UAS (orange points) configurations.

Table 3.

Coefficients and associated p-values of each predictor of the multiple regression model.

	Coefficient	p
Intercept	67.0	< 0.001
Time of peak angle change – time of peak vertical displacement	0.2	< 0.001
Peak excursion	-0.7	0.011

Matched comparisons of the CRABI 12-month-old response on the two benches Matched comparisons of responses seen with specific RFCRS models on the two benches revealed that in tests using Model K with a base and UAS, the chest 3ms clips seen on the proposed bench across three tests ranged from 56.6-60.3g. Testing the same RFCRS model on the CMVSS bench yielded a chest 3ms clip of 53.5 g, which was 3.1 g lower than the lower bound of the range obtained on the proposed bench and 1.6 standard deviations lower than the mean.

Comparison of RFCRS Performance Between Sleds Using the CRABI 12-Month-Old ATD

Aggregate comparisons of the CRABI 12-month-old response on the two sleds For all installations except the RF + belt configuration, tests on the two sleds showed no significant differences in RFCRS movement. For the RF + belt configuration, the angle change, peak upper target excursion, and peak upper target vertical displacement were statistically significantly greater on the deceleration sled, although the differences were small (Fig. 11A-C, mean differences of 2°, 4 mm, and 10 mm, respectively). Lower target excursions for tests in this configuration were not significantly different on the two sleds (Fig. A1), suggesting that the differences shown in Fig. 11A-C are related to differences in the peak CRS angle change. Head and chest 3ms clips on the two sleds tended to be similar, except in tests with convertible RF + belt, for which they were greater on the acceleration sled than on the deceleration sled (Fig. 11F).

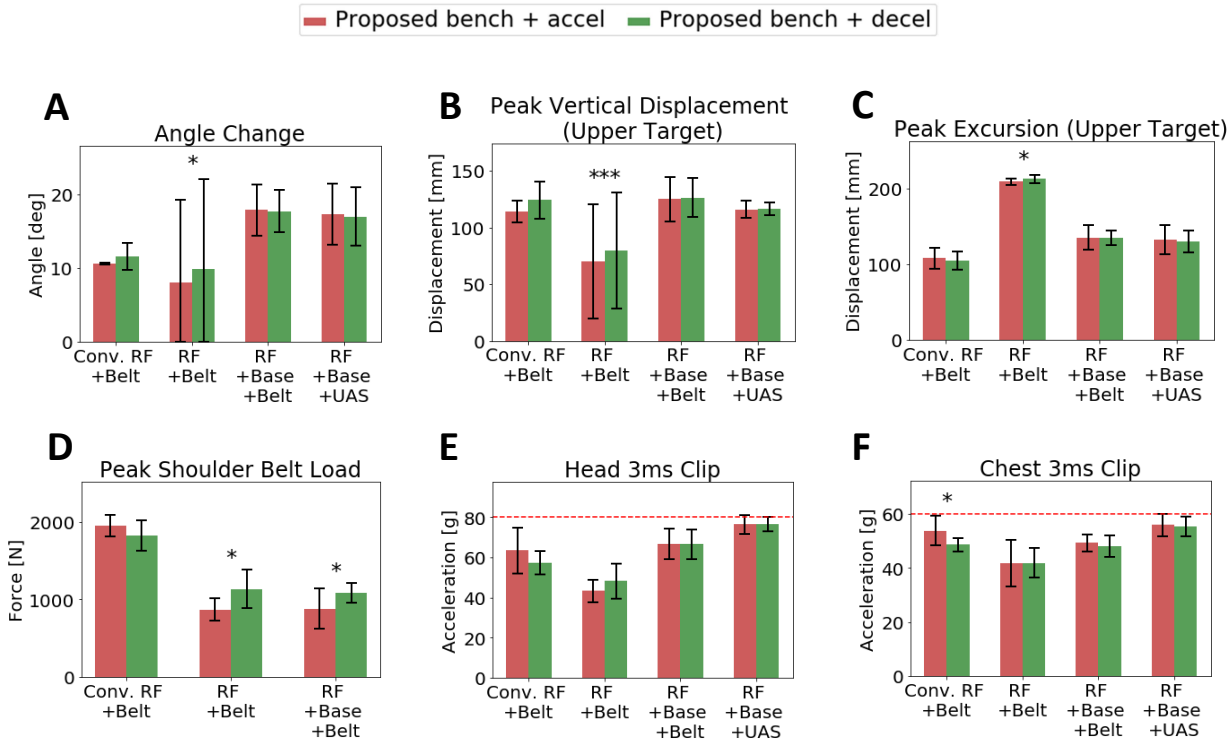

Figure 11. Differences in responses for the 12-month-old on the acceleration (red bars) and deceleration (green bars) benches for each configuration. Dashed red lines in panels E-F indicate the regulatory limits of each response.

Matched comparisons of the CRABI 12-month-old response on the two sleds For both models tested in the convertible RF + belt tested configuration, chest accelerations in x at peak resultant acceleration were higher on the acceleration sled (Fig. 12A) while z was comparable (Fig. 12B). The time of peak angle change on the acceleration sled was within 1ms of that of peak vertical CRS displacement, whereas on the deceleration sled, the peak angle change preceded the peak vertical displacement by up to 4 ms.

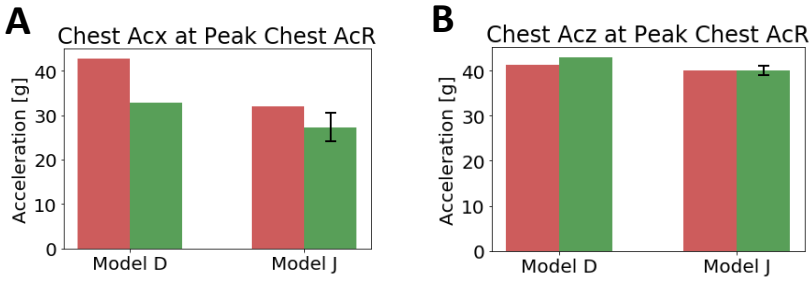

Figure 12. Differences in (A) Chest Acx and (B) Chest Acz at the time of peak chest resultant acceleration on the acceleration (red bars) and deceleration (green bars) sleds for each configuration.

SUMMARY & DISCUSSION

Results from 114 tests that included belt-positioning booster seats, forward-facing CRS (FFCRS), and rear-facing CRS (RFCRS) installed on the proposed NHTSA and current CMVSS benches were presented. In tests with the 6-year-old, differences in responses on the two benches, if any, were minor. Forward facing child restraints and booster seats installed on the proposed bench were associated with slightly greater head and knee excursions for the 6-year-old however, all remained well below the established compliance limits. There was no significant difference in the head and chest acceleration clips. Chest deflections were not significantly different with the exception of the

FF + UAS configuration which resulted in a very small decrease (4.3 mm, $p<0.05$) in chest deflection on the proposed bench. Paired testing of a specific FFCRS installed with the UAS demonstrated that certain CRS designs can produce results that are different from the average response of the sample. In this pair, the upper torso of the ATD was more upright on the proposed bench. This difference in motion is likely the effect of the increased seat cushion stiffness and bench geometry. The influence of the bench characteristics was much more apparent with this CRS model. Previous comparisons of Hybrid III 6-year-old responses in FFCRS showed that head and knee excursions were greater on vehicle seats than on the CMVSS bench, and that CRS rotated forward on vehicle seats and rearward on the CMVSS bench [8]. The differences observed here between the two benches may be indicative that the proposed bench is more representative of modern vehicle seats than the CMVSS bench.

No significant difference in responses were observed for the proposed bench as a function of sled type with the single exception of the chest deflection responses which were approximately 2.5 mm greater on the acceleration sled. Analysis of the matched pair comparison of a specific seat model produced a chest acceleration response that was on average 4 g greater on the acceleration sled. The cause of this difference is being investigated in a separate study.

Comparisons of RFCRS movements on the two benches showed significantly lower mean RFCRS angle changes and vertical displacements on the proposed bench. In a previous study [9] comparing RFCRS performance on the CMVSS bench and on vehicle seats, RFCRS vertical displacements were lower in magnitude on vehicle seats than on the bench. The similarities between the comparisons made in the current study and those made between the CMVSS bench and vehicle seats in [9] suggest that the proposed bench reproduces RFCRS motions as seen on a vehicle seat better than the CMVSS bench.

Head and chest responses of the 12-month-old that were statistically significantly different were higher on the proposed bench. The only exception was the chest 3ms clip for the RF + base + belt configuration. We suspect that this exception is due to a difference in the x and z contributions of the resultant acceleration which are in turn the result of differences in the timing and magnitude of CRS rotations.

Multiple linear regression suggested that the peak excursion and the timing of peak angle change relative to peak vertical displacement were significant predictors of chest 3ms clip values. Contact with the bench frame, which may interrupt RFCRS rotation, was suspected in tests where peak angle change and vertical displacement coincided. The likelihood of contact with the seat frame was reduced if peak angle change occurred much earlier than peak vertical displacement. Contact with the frame may contribute to an increased chest response.

Comparisons of RFCRS performance on the two sleds did not generally show statistically significant differences in RFCRS movement or ATD response. Where statistical significance was identified, the differences were relatively small.

CONCLUSION

Results of paired tests conducted with forward-facing child restraints and booster seats that were installed on the proposed NHTSA and current CMVSS benches suggest that the differences in responses were generally small. Though excursions of the head and knees tended to be greater on the proposed bench these were all well below the regulatory limits. No significant difference in responses were observed for the proposed bench as a function of sled type with the single exception of the chest deflection responses which were greater on the acceleration sled.

Differences in the angle changes and vertical displacements of rear-facing child restraints suggest that the proposed bench may produce a better representation of motions produced on a contemporary vehicle seat than the current CMVSS bench. Small differences in the timing of the CRS motion and small differences in chest acceleration were observed for rear facing installations on the proposed bench as a function of sled type.

Certain differences appeared to be more strongly linked to product design characteristics than to test bench characteristics or sled type and will be investigated in future studies.

LIMITATIONS AND FUTURE WORK

- The sample size of child seats tested in this study allowed for evaluation of aggregate responses as well as statistical testing. For most configurations, at least three tests were conducted in each of the three conditions (proposed NHTSA bench + accel, CMVSS bench + accel, and proposed bench + decel). However, for the FF + UAS and convertible RF + belt configurations, only two tests were conducted in each condition. The low sample size for tests in each of these two configurations limits our knowledge of how well the samples represent the typical behaviours of other child seats in those configurations.
- In 2018, NHTSA published a revised drawing of the proposed bench [10] which included new drawings of the lap belt anchorages, rear locking belt anchor, and D-ring. Given these changes, further testing should be conducted to quantify the differences in ATD responses on the original and revised versions of the proposed bench.
- Although the current CMVSS and FMVSS 213 benches are very similar, differences exist between the two benches, such as the height of the lower anchorages [9]. Differences in the ATD responses as a function of CMVSS/ FMVSS benches were not included in this analysis.
- Qualitative video analysis of the tests was limited by differences between camera positioning, especially in comparisons of the two sleds, where the top and frontal views were not identical.
- A study is currently underway to examine the influence of sled pulse, seat design, belt path, and arm position on the 6-year-old chest response.

DISCLAIMER

This paper shall not be construed as an endorsement, warranty, or guarantee, expressed or implied, on the part of Transport Canada for any evaluated material, product, system or service described herein. Readers should not infer that Transport Canada's evaluation is for any purpose or characteristic other than as stated herein. All information in this document is for information purposes, only and is not intended to provide any specific advice. Any reliance on or use of the information contained in this document is at the user's sole risk and expense.

ACKNOWLEDGMENTS

The authors are grateful to the child seat manufacturers who graciously provided child restraints and booster seats for this study and the excellent sled team at PMG Technologies for conducting the tests.

REFERENCES

[1] Glass, W. 2002 "Technical Report on the FMVSS 213 Crash Pulse and Test Bench Analysis" Naval Air Warfare Center (NAVAIR) Report No. NAWCADPAX/TR-2001/184
[2] 67 FR 21836.
[3] 68 FR 37619.
[4] Wietholter, K., Echemendia, C., Louden, A.E. 2017. "Development of a Representative Seat Assembly for FMVSS No. 213." In Proceedings of the 2017 Enhanced Safety of Vehicles Conference. (Detroit, MI, Jun. 5-8). 17-0431.
[5] NHTSA. 2015. Federal Register Docket Number NHTSA-2013-0055-0002.
[6] NHTSA. 2015. Federal Register Docket Number NHTSA-2013-0055-0008.
[7] Bates, D., Maechler, M., Bolker, B. and Walker, S. 2015. "Fitting Linear Mixed-Effects Models Using lme4." Journal of Statistical Software 67, No. 1, October: 1-48.
[8] Maltese, M.R., Tylko, S., Belwadi, A., et al. 2014. "Comparative Performance of Forward-Facing Child Restraint Systems on the C/FMVSS 213 Bench and Vehicle Seats." Traffic Injury Prevention 15, S103-S110.
[9] Tylko, S., Locey, C. M., Garcia-Espana, J. F., et al. 2013. "Comparative Performance of Rear Facing Child Restraint Systems on the CMVSS 213 Bench and Vehicle Seats." Annals of Advances in Automotive Medicine 57, September 2013: 311-328.
[10] NHTSA. 2018. Federal Register Docket Number NHTSA-2013-0055-0014.

APPENDIX

Modification of the Proposed FMVSS 213 Bench

The proposed FMVSS bench was constructed according to the drawings provided by NHTSA in the Federal Docket (Docket No. NHTSA-2013-0055-0002) with the modifications specified in Docket No. NHTSA-2013-0055-0008 as well as the following modifications to improve durability:

1. Two legs were attached to the back of the bench (Fig. 1A, labeled as 1);
2. Braces were added behind the lower anchorages (Fig. 1A, labeled as 2) and D-ring (Fig. 1B); and
3. The D-ring was secured to a plate attached to the bench (Fig. 1B).

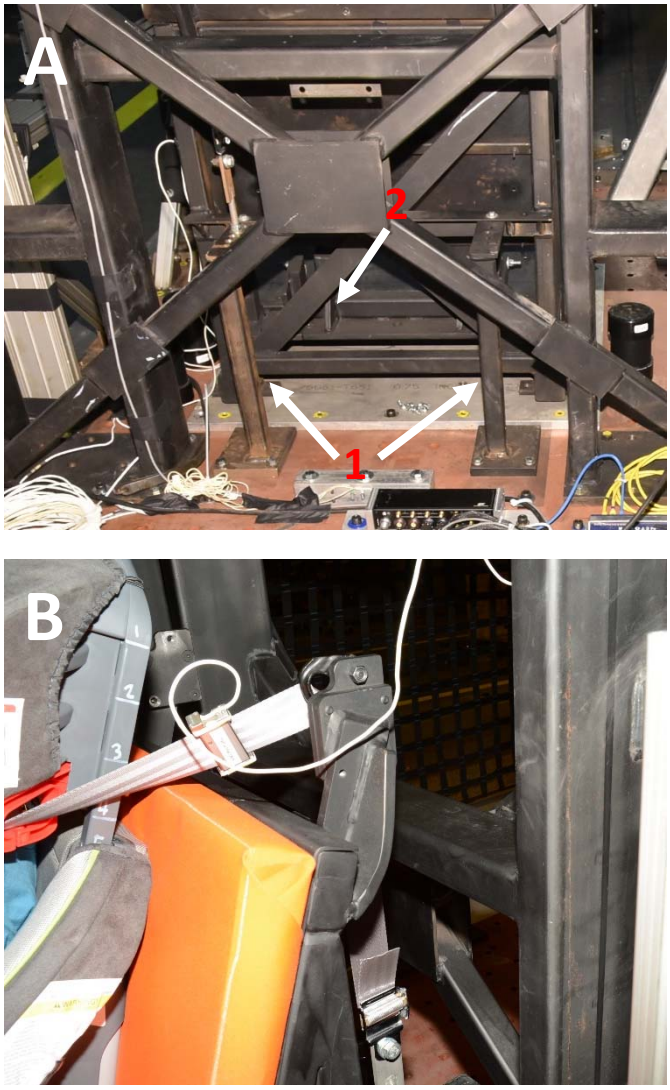

Figure A1. (A) Rear view of the proposed NHTSA bench showing (1) legs added to the back of the bench and (2) braces added behind lower anchorages. (B) D-ring on the proposed NHTSA bench.

Table A1.

Differences in mean responses of the Hybrid III 6-year-old on the two benches in four different configurations and associated p-values. A positive difference indicates that the response on the CMVSS bench was higher. Highlighted cells indicate responses that were statistically significantly different on the two benches.

	FF + Belt		**FF + UAS**		**HB**		**LB**	
	Difference	**p**	**Difference**	**p**	**Difference**	**P**	**Difference**	**P**
Head Excursion	-49 mm	< 0.001	-50 mm	0.154	-2 mm	0.812	-19 mm	0.015
Knee Excursion	-21 mm	< 0.001	-26 mm	0.006	-32 mm	0.011	-43 mm	< 0.001
Head 3ms clip	-1.0 g	0.291	1.5 g	0.671	-0.8 g	0.541	2.9 g	0.183
Chest 3ms clip	-0.9 g	0.463	0.7 g	0.306	-1.9 g	0.171	0.5 g	0.669
Peak chest deflection	-1.2 mm	0.247	4.3 mm	0.023	1.3 mm	0.076	1.4 mm	0.116
Upper neck axial load	-62 N	0.607	375 N	0.206	-696 N	<0.001	-331 N	0.051
Lumbar spine moment about z	0.2 Nm	0.496	-1.1 Nm	0.057	1.4 Nm	0.011	1.1 Nm	0.132
Peak shoulder belt load	971 N	0.001	N/A	N/A	836 N	0.001	1242 N	< 0.001

Table A2.

Mean difference in response of the Hybrid III 6-year-old on the two benches installed with the Baby Trend + harness + tether + UAS.

	Difference (CMVSS-proposed)
Head Excursion	-92 mm
Knee Excursion	-33 mm
Head 3ms clip	-2.5 g
Chest 3ms clip	0.1 g
Chest deflection	3.6 mm
Upper neck axial force	5 N

Table A3.

Differences in mean responses of the Hybrid III 6-year-old on the two sleds in two different configurations and associated p-values. A positive difference indicates that the response on the deceleration sled was higher. Highlighted cells indicate responses that were statistically significantly different on the two benches.

	HB		LB	
	Difference	**P**	**Difference**	**P**
Head Excursion	-1 mm	0.736	-8 mm	0.230
Knee Excursion	-3 mm	0.319	-2 mm	0.746
Head 3ms clip	-2.4 g	0.097	1.9 g	0.351
Chest 3ms clip	-2.2 g	0.082	-2.2 g	0.131
Peak chest deflection	-2.7 mm	0.044	-2.5 mm	0.030
Resultant upper neck load	-220 N	0.135	237	0.291
Lumbar spine moment about z	-0.9 Nm	0.127	-0.8 Nm	0.256
Peak shoulder belt load	9 N	0.927	230 N	0.165

Table A4.

Differences in mean responses of the CRABI 12-month-old on the two benches in four different configurations and associated p-values. A positive difference indicates that the response on the CMVSS bench was higher. Highlighted cells indicate responses that were statistically significantly different on the two benches.

	Conv. RF + belt		RF + belt		RF + base + belt		RF + base + UAS	
	Difference	**p**	**Difference**	**p**	**Difference**	**p**	**Difference**	**p**
Angle Change	5 °	0.030	9 °	0.010	6 °	< 0.001	6 °	< 0.001
Excursion (upper target)	14 mm	0.330	-13 mm	0.002	16 mm	0.009	48 mm	< 0.001
Vertical Displacement (upper target)	63 mm	< 0.001	75 mm	< 0.001	81 mm	< 0.001	73 mm	< 0.001
Excursion (lower target)	9 mm	0.556	-26 mm	0.028	7 mm	0.148	39 mm	< 0.001
Vertical Displacement (lower target)	44 mm	< 0.001	57 mm	< 0.001	66 mm	< 0.001	61 mm	< 0.001
Shoulder Belt Load	1235 N	0.018	254 N	0.019	1112 N	< 0.001	N/A	N/A
Head 3ms clip	-8.1 g	0.137	0.7 g	0.457	-7.1 g	0.003	-6.2 g	0.068
Chest 3ms clip	-4.8 g	0.013	3.0 g	0.304	3.5 g	0.013	-4.8 g	0.017
Chest Acx at peak chest resultant	-4.5 g	0.021	2.8 g	0.437	-6.9 g	0.068	-17.7 g	0.001
Chest Acz at peak chest resultant	-2.0 g	0.087	2.1 g	0.014	19.3 g	0.002	22.9 g	< 0.001

Table A5.

Differences in mean responses of the CRABI 12-month-old on the two sleds in four different configurations and associated p-values. A positive difference indicates that the response on the deceleration sled was higher. Highlighted cells indicate responses that were statistically significantly different on the two benches.

	Conv. RF + belt		**RF + belt**		**RF + base + belt**		**RF + base + UAS**	
	Difference	**p**	**Difference**	**p**	**Difference**	**p**	**Difference**	**p**
Angle Change	1 °	0.378	2 °	0.046	0 °	0.780	0 °	0.457
Excursion (upper target)	0 mm	0.850	4 mm	0.031	0 mm	0.976	-2 mm	0.494
Vertical Displacement (upper target)	7 mm	0.199	10 mm	0.001	1 mm	0.705	0 mm	0.818
Excursion (lower target)	-1 mm	0.625	0 mm	0.763	0 mm	0.919	-1 mm	0.551
Vertical Displacement (lower target)	6 mm	0.066	6 mm	0.007	2 mm	0.357	1 mm	0.215
Shoulder Belt Load	-130 N	0.341	266	0.022	170 N	0.032	N/A	N/A
Head 3ms clip	-4.1 g	0.078	5.0 g	0.060	-1.3 g	0.481	0.2 g	0.938
Chest 3ms clip	-4.5 g	0.030	0.2 g	0.902	-1.2 g	0.258	0.4 g	0.731

ARE WISCONSIN PEDESTRIAN CRASHES REPRESENTATIVE OF NATIONAL TRENDS?

Dale Halloway

Medical College of Wisconsin

United States of America

Paper Number 19-0334

ABSTRACT

Introduction: The question: "Are Wisconsin Pedestrian Crashes Representative of National Trends?" was asked in the context of how to estimate the denominator of pedestrians using public traffic-ways. Data from the Federal Highway Administration, the National Highway Traffic Safety Administration, the United States Census Bureau, the Wisconsin Department of Transportation and other organizations was used to try and answer it.

Method: Comparisons between national and state level data were made relative to: The number of miles of urban and rural roads in Wisconsin relative to the number of miles nationally, the trends in the frequency of fatal pedestrian crashes, the proportion of these crashes in rural and urban areas and factors that may contribute to them. Demographics at the county level were reviewed to assess which counties may be representative of the state.

Results: In all categories of rural roadway classification, Wisconsin is within one standard deviation of the national mean and median. The median number of miles of the total miles of rural roadways nationally is 64,672 miles. In most categories of urban roadway classification, Wisconsin is within one standard deviation of the mean and median for the nation. The median number of miles of the total miles of urban roadways nationally is 17,568 miles. With 23,578 total miles of urban roadways, it is closest to the national average of the total number of miles urban roadways 23,530.

NHTSA analysis of 2015 pedestrian crash data reported 26% of pedestrian fatalities occurred from 6 to 8:59 p.m. In Wisconsin data from 2011 to 2013, 23% of fatal pedestrian crashes occurred 6 to 8:59 p.m. NHTSA reported the split between fatal urban and fatal rural crashes as: 76% in urban areas and 24% in rural areas. In Wisconsin, the split was 64% urban and 36% rural. Per NHTSA data, 19% of fatally injured pedestrians were 55-years-old or older. A query for fatal pedestrian crashes in Wisconsin for 2017 found that the average pedestrian age was 54 and 43.6% of fatally injured pedestrians were 55-years-old or older.

Discussion: U.S. Department of Transportation data collection programs are amenable to using state government documents, which can be transcribed to compile national level data sets. State level traffic crash data can be disaggregated to the county or municipal levels. Both data sets can be linked to U.S. Census Bureau data for each county, down to the level of the census tract, to characterize the relationship of vulnerable populations such as children and older adults and to features in the environment affecting mobility.

Conclusion: What is lacking are actual counts of pedestrians at a weighted sample of locations to base a statistical inference of the denominator of pedestrian using trafficways on. With the appropriate statistical technique and accurate counts, a nationally representative estimate of vulnerable road users is possible. In-depth local studies involving agreements with law enforcement and county road department would be advantageous.

Introduction

In the U.S., traffic fatalities in urban areas increased by 17.4 percent from 2008 to 2017 while rural fatalities declined by 18.0 percent. This corresponds to the 13.1% increase in Vehicle Miles Traveled (VMT) and the 3.7% increase in the urban traffic fatality rate per 100 million VMT, nationally, over the same period. While passenger vehicle occupant fatalities in urban areas have increased by 9 percent since 2008, there has been a 46% increase in fatal traffic crashes involving pedestrians in urban areas. The trend for traffic fatalities in rural areas over the same period has been decreasing. The changes in these two trends is in line with changing US demographics; there was a 12.7% increase in urban population from 2007 to 2016[1].

The Governors Highway Safety Association (GHSA), has accurately predicted recent trends in pedestrian fatalities. Per the GHSA: (1) Pedestrians now account for a larger proportion of traffic fatalities than they have in the past 33 years. (2) The number of states with pedestrian fatality rates at or above 2.0 per 100,000 population has more than

doubled, from seven in 2014 to 15 in 2016. (3) In Wisconsin, a record 63 pedestrians were killed amounting to a 40% increase in the number of traffic related pedestrian fatalities in 2017 over 2016[2].

The reason why traffic frequency of pedestrian fatalities is increasing is currently unknown. To try to address the question in terms of what factors contribute to the risk of injury, an accurate estimate the number of pedestrians using the nations trafficways is needed. The question: "Are Wisconsin pedestrian crashes representative of national trends?" was asked in the context of the need to estimate the denominator of pedestrians using trafficways. Data from the Federal Highway Administration, the National Highway Traffic Safety Administration, the United States Census Bureau, the Wisconsin Department of Transportation and other agencies was used to answer it.

Method

State-wide comparisons were made relative to: Trends in the rates of fatal pedestrian crashes in the United States, the proportion of these crashes in rural and urban areas, how many miles of urban and rural roads Wisconsin has relative to the rest of the nation, and the location of the pedestrian when struck and the time of day a conflict occurs. The National Highway Traffic Safety Administration is the source for data on U.S. national trends. The Governors Highway Safety Association and the Wisconsin Department of Transportation (WISDOT) Bureau of Transportation Safety (BOTS) are the primary sources of published data at the state level. This data is supplemented by the analysis of data obtained from queries of state crash reports available from the Traffic Operations and Safety Laboratory (TOPS) at the University of Wisconsin-Madison.

Data on the estimated number of lane-miles by functional system is taken from the Federal Highway Administration publication, Highway Statistics 2017[3]. The sources of demographic data used are the U.S. Census Bureau and data extrapolated from national survey data by Wisconsin Department of Health Services. Milwaukee, Waukesha and Dane counties were selected for a more detailed examination because these three counties account for the majority of pedestrian and bicycle crashes in Wisconsin.

Results

Comparison of Roads by Roadway Classification

Table 1 below provides descriptive statistics of U.S. roads by roadway classification in rural and urban areas. The median number of miles of the total miles of rural roadways nationally is 64,672 miles. Wisconsin has a total of 91,567 miles of roads in rural areas. This is within the standard deviation (SD) for the total miles of rural roads nationally: SD = 40,033 miles. Figure 1 below, depicts the distribution of all road classification types in rural areas nationally.

Table 1.

US Roads by Roadway Classification and Land Use

Variable	Label	N	N Miss	Minimum	Mean	Median	Maximum	Std Dev
R INTERSTATE	R INTERSTATE	50	3	0	593.5670800	587.2035000	2080.34	376.6118891
R Other Freeways	R Other Freeways	50	3	0	96.8461800	0.2535000	922.7720000	189.9302242
R Principal Arterial	R Principal Arterial	50	3	66.0900000	1808.10	1794.70	7707.71	1284.49
R Minor Arterial	R Minor Arterial	50	3	91.3270000	2656.90	2545.68	10095.64	1974.22
R Major Collector	R Major Collector	50	3	197.0470000	8296.32	7093.88	34888.61	6783.41
R Minor Collector	R Minor Collector	50	3	0	5249.79	4427.09	17431.97	4079.05
R Local	R Local	50	3	859.4580000	40047.99	43755.99	140713.76	27306.13
R Total	R Total	50	3	1363.57	58749.51	64672.30	212918.04	40032.58
U INTERSTATE	U INTERSTATE	50	3	40.2120000	357.6904400	271.1100000	1334.84	310.3636812
U Other Freeways	U Other Freeways	50	3	0	231.7282000	118.9200000	1471.59	314.5254374
U Principal Arterial	U Principal Arterial	50	3	104.5650000	1328.07	991.5465000	7041.80	1369.32
U Minor Arterial	U Minor Arterial	50	3	151.6160000	2217.28	1626.93	11392.56	2173.29
U Major Collector	U Major Collector	50	3	0.6940000	2424.66	1913.57	12833.52	2614.57
U Minor Collector	U Minor Collector	50	3	0	102.2485400	2.7810000	1021.10	209.3700610
U Local	U Local	50	3	920.6190000	16868.02	12195.12	70664.52	16273.96
U Total	U Total	50	3	1452.39	23529.70	17568.47	100309.58	22518.16
R&U Total	R&U Total	50	3	4430.13	82279.21	81022.59	313227.62	54314.40

Figure 1.

Distribution of U.S. Rural Roads All Classifications

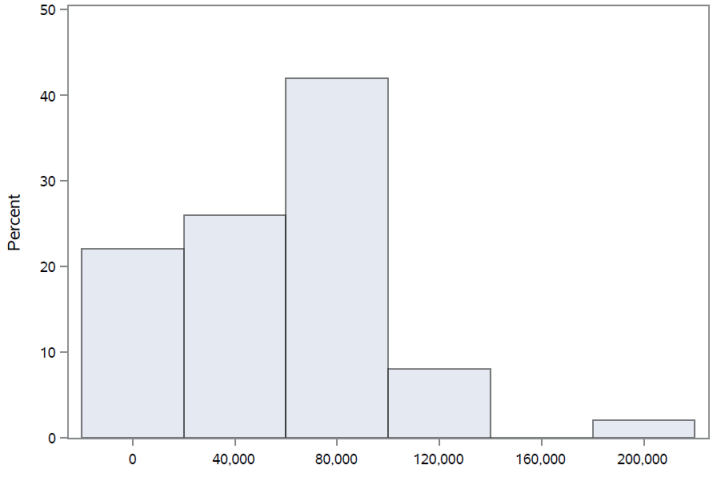

The median number of miles of the total miles of urban roadways nationally is 17,568 miles. Wisconsin has a total of 23,578 miles of roads in urban areas. This is within the standard deviation for total miles of urban roads nationally: SD = 22,518 miles. Figure 2 depicts the distribution of all road classification types in urban areas nationally.

Figure 2.

Distribution of U.S. Urban Roads All Classifications

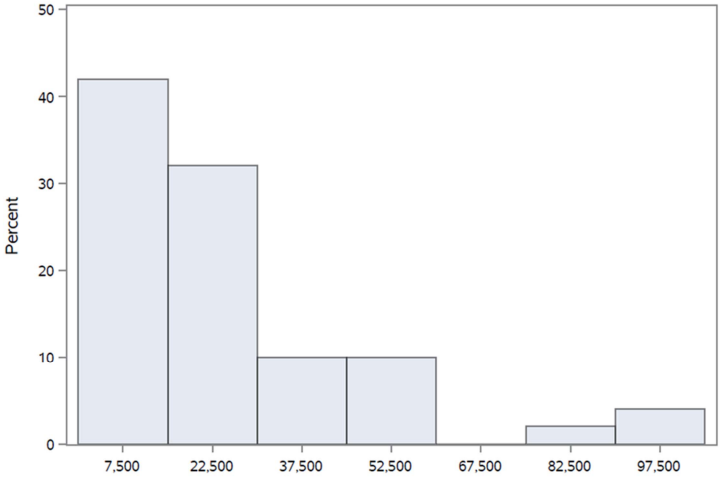

Table 2 provides descriptive statistics of Wisconsin rural roads by roadway classification. In every category of rural roadway classification, Wisconsin is within one standard deviation of the U.S. National mean and median. Nationally, Wisconsin ranks 7th highest with 62,491 total miles of rural roadways.

Table 2.

Miles of Rural Roadway by Classification U.S. Mean and Median VS Wisconsin Total Miles

Roadway Classification	National Mean	National Median	Wisconsin	SD
Rural Interstate	594	587	464	376.6
Rural Freeway	97	.25	189	189.9
Rural Principal Arterial	1808	1795	2926	1284.4
Rural Minor Arterial	2657	2546	4741	1974.2
Rural Major Collector	8296	7094	12134	6783.4
Rural Minor Collector	5250	4427	8621	4079
Rural Local Roads	40048	43756	62491	27306.1
Total All Rural Roadways	58,750	64,672	91567	40,032

Table 3 provides descriptive statistics of Wisconsin urban roads by roadway classification. Except for roadways classified as urban minor collector, Wisconsin is within one standard deviation of the U.S. National mean and median. Nationally, Wisconsin ranks 20th with 23,578 total miles of urban roadways. Minnesota with 22,208 total miles of urban roadways ranks 19th and Missouri with 24,367 total miles of urban roadways ranks 21st. In almost every category of urban roadway classification, Wisconsin closely approximates the U.S. National average.

Table 3.

Miles of Urban Roadway by Classification U.S. Mean and Median VS Wisconsin Total Miles

Roadway Classification	National Mean	National Median	Wisconsin	SD
Urban Interstate	357	271	279	310.3
Urban Freeway	232	119	383	314.5
Urban Principal Arterial	1,328	992	1,976	1369.3
Urban Minor Arterial	2,217	1627	2,665	2173.2
Urban Major Collector	2,425	1914	2,746	2614.5
Urban Minor Collector	102	2.8	0	209.3
Urban l Local Roads	16,868	12195	15,499	16,273.9
Total All Urban Roadways	23,530	17,568	23,578	22,518.1

Comparison by Environmental Characteristics

Per an NHTSA analysis of 2015 data on pedestrian crashes[4], nationally 26% of pedestrian fatalities occurred from 6 to 8:59 p.m. in 2015. An analysis of Wisconsin data from 2011 to 2013[5] found that 23% of fatal pedestrian crashes occurred between 6 to 8:59 p.m. NHTSA analysis of 2015 data found 76% of fatal pedestrian crashes were in urban areas and 24% in rural areas. The analysis of Wisconsin data reported that 64% of fatal pedestrian crashes were in urban areas and 36% in rural areas. NHTSA reported that nationally 72% of fatal crashes were non-intersection related and 18% were intersection related. The Wisconsin data analysis reported that 55% of fatal crashes occurred on a roadway between intersections; defined as more than 15m (50 feet) from the nearest intersection[6].

Per NHTSA data 19% of fatally injured pedestrian were 55-years-old or older. A query for fatal pedestrian crashes in Wisconsin for 2017[7] found that the average pedestrian age was 54 and the 24 of the 55 (43.6%) of fatally injured pedestrian were 55-years-old or older. 16 of the 55 (29%) fatal crashes involved pedestrians 65-years-old or older. The average age of the 55+ cohort was 69.5-years-old.

The three post populous counties in the state are Milwaukee, Dane and Waukesha. Milwaukee County has a land area of 6266 square kilometers. Of this, 24 square kilometers (3.8%) is classified as farmland. There are no roadways classed as rural in Milwaukee County. The WISDOT Milwaukee Urban Area includes approximately

72% of Waukesha county. The includes Milwaukee Urban Area has 6,586 miles of roadways. Waukesha County has a land area of 1,439 square kilometers of this, 397 square kilometers (27.5%) is classified as farmland. There are 203 miles of rural roads in Waukesha county. Dane County Land Area has a land area of 3,113 square kilometers. Of this, 2,084 square kilometers is farmland (67%). There are 2072 miles of rural roads in Dane county. Madison is the largest city in Dane county and has 1,959 miles of urban roads.

In the Wisconsin, over the period 2011 to 2013 there were 134 fatal pedestrian crashes. 55 (41%) of the occurred in Milwaukee, Dane and Waukesha counties. Of these 55 fatal pedestrian crashes, 96% were in urban areas and 4% in rural areas. Table 4 presents US Census Bureau[8] demographic data for Milwaukee, Dane and Waukesha counties.

Table 4.

Milwaukee, Waukesha and Dane Counties VS State and National Indicators

	Dane	**Milwaukee**	**Waukesha**	**Wisconsin**	**U.S.**
Population estimates, July 1, 2016,	531,273	951,448	398,424	5,778,708	323,127,513
Persons under 18 years:	20.9%	24.3%	21.9%	22.3%	22.8%
Persons between 18 and 64 years:	66.3%	63%	60.5%	61.6%	62%
Persons 65 years and over:	12.8%	12.7%	17.6%	16.1%	15.2%
High school graduate or higher, percent of persons age 25 years+, 2012-2016:	95.3%	86.9%	95.9%	91.4%	87%
Bachelor's degree or higher, percent of persons age 25 years+, 2012-2016:	49.0%	29.7%	41.6%	28.4%	30.3%
Mean travel time to work (minutes), workers age 16 years+, 2012-2016	20.9	22.4	24.0	21.9	26.1
Median household income (in 2016 dollars), 2012-2016:	$64,773	$45,263	$78,268	$54,610	$55,322

Median household income (in 2016 dollars) for other states 2012-2016: California: $63,783, New York: $60,741 and Virginia: $66,149

Discussion

As most pedestrian crashes occur in urban areas, relative to the total miles of urban roadways, Wisconsin urban roads seem to represent the center of the national distribution well. In terms of the mean the representation nearly is an exact match of the national average, but the distribution is skewed. Relative to the median value of 17,568 miles the total miles of urban roadways nationally, Wisconsin is within one standard deviation.

In terms of the frequency at which pedestrian crashes happen relative to environmental conditions like land use, time of day and relation to an intersection crashes in Wisconsin are aligned with national trends. Where the trend in the data for Wisconsin markedly differs from what is observed nationally is in the age of pedestrians killed. The Wisconsin (WI) age cohorts for persons between the ages of 18 and 64 and persons 65-years-old or older closely approximate the U.S. population. For the 18 and 64 cohorts: WI 61.6% vs 62% U.S. and for the 65+ cohorts: WI 16.1 vs 15.2% US. In the three counties that account for most pedestrian crashes the average size of the 65+ cohort is 14.4%. On the face of it, the size of the cohort aged 55+ is not expected to explain the difference.

Data extrapolated from national survey data by Wisconsin Department of Health Services[9] may offer some insight to the reason for the disparity. In Wisconsin, 526,744 individuals age 65+ are estimated to have some type of disability.

- 232,274 (44%) are estimated to have a hearing impairment
- 111,326 (21%) are estimated to have a cognitive impairment
- 82,738 (15.7%) are estimated to have a vision impairment
- 317,652 (60%) are estimated to have an ambulatory impairment

Unfortunately, data on traffic crashes does not provide information on any physical impairments people involved in the crash whether a driver or a pedestrian and there is no statistically valid estimate of the number of people with physical impairments using public trafficways.

U.S. Department of Transportation data collection programs are amenable to using state government documents, which can be transcribed to compile national level data sets. State level traffic crash data can be disaggregated to the county or municipal levels. If a valid estimate of the of the number of people using public trafficways could be constructed, both data sets can be linked to census data for each county, down to the level of the census tract, to characterize the relationship of vulnerable populations such as children and older adults to features in the environment affecting mobility.

Conclusion

Except for roadways classified as urban minor collector, the inventory of roads in Wisconsin is representative of the nation. In general, the trends in Wisconsin's fatal pedestrian crashes in reflect those in U.S. national data. The difference in the proportion of fatal pedestrian crashes national (19%) and in Wisconsin (41%) is puzzling. The three counties that might serve as locations to draw a sample of a of pedestrian crashes representative of the state represent an area that is 67% urban and 33% rural. If a valid estimate of the of the number of people using public trafficways could be constructed, it appears only a scheme to collect representative sample of crashes in urban areas could be devised for them. A number of rural counties would need to be selected to devise a scheme to collect a representative sample of all pedestrian crashes.

What is lacking are actual counts of pedestrians at a weighted sample of locations to base a statistical inference of the denominator of pedestrian using trafficways on. With the appropriate statistical technique and accurate counts, a nationally representative estimate of vulnerable road users is possible. In-depth local studies involving agreements with law enforcement and county road department would be advantageous.

REFERENCES

[1] National Highway Traffic Safety Administration Traffic Safety Facts. October 2018, DOT HS 812 603

[2] Pedestrian Traffic Fatalities by State 2017 Preliminary Data. Governors Highway Safety Association, 444 North Capitol Street, Suite 722, Washington, DC 20001. https://www.ghsa.org/resources/spotlight-pedestrians18. Accessed 11/04/2018

[3] Highway Statistics 2017, Table HM-60. U.S. Department of Transportation, Federal Highway Administration, 1200 New Jersey Avenue, SE Washington, DC 20590. https://www.fhwa.dot.gov/policyinformation/statistics.cfm. Accessed 02/24/2018

[4] National Highway Traffic Safety Administration Traffic Safety Facts. February 2017, DOT HS 812 375

[5, 7] Wisconsin Traffic Operations and Safety (TOPS) Laboratory, University of Wisconsin-Madison in the College of Engineering and the Department of Civil and Environmental Engineering. https://transportal.cee.wisc.edu/. Accessed most recently: 03/08/2019

[6] Schneider R, and Stefanich, J 2015. "Wisconsin Pedestrian and Bicycle Crash Analysis: 2011-2013" Wisconsin Department of Transportation (WISDOT) Bureau of Transportation Safety (BOTS). PDF link: https://wisconsindot.gov/Pages/safety/education/pedestrian/default.aspx. Accessed 09/14/2017

[8] US Census Bureau: https://www.census.gov/quickfacts. Accessed: 01/15/2018

[9] Wisconsin Department of Health Services, Demographics of Disability in Wisconsin web page link to: Population Reporting Disability by Age and Sex and by Type of Disability, 2010-14 spread sheet. https://www.dhs.wisconsin.gov/disabilities/physical/demographics.htm. Accessed: 01/15/2018

CHALLENGES FOR OCCUPANT SAFETY IN HIGHLY AUTOMATED VEHICLES ACROSS VARIOUS ANTHROPOMETRIES.

Bronislaw Gepner, Katarzyna Rawska, Rachel Richardson, Shubham Kulkarni, Kalle Chastain, Junjun Zhu, Jason Forman, Jason Kerrigan
University of Virginia, Center for Applied Biomechanics
4040 Lewis and Clark Dr., Charlottesville, VA 22911 USA

Paper Number 19-0335

ABSTRACT

The introduction of automated driving systems (ADS) is likely to change the very nature of personal transportation. Without the need to drive, occupants will have more freedom to engage in other activities, which could result in major changes to vehicle interiors, controls, and seating configurations. Reclined posture seating may be an option that manufacturers consider in the relatively near term. The goal of this study is to evaluate how varying occupant anthropometry, distance to the knee bolster, and seatback angle affect occupant response.

A finite element model of a vehicle occupant compartment with the state-of-the-art seatback integrated restraint system was used, to evaluate three different simplified Global Human Body Model Consortium (GHBMC) occupant models (small female, midsize and large male) in frontal crashes. A full factorial sensitivity study was performed with four different levels of seatback recline (0, 10, 20, 30 deg) and four different distances to the instrument panel knee bolster resulting in total of 40 simulations.

Increasing the seatback recline angle caused the occupants' pelvis to submarine under the lap belt, which, in turn, resulted in poor pelvis-belt engagement and increased occupant excursion. Larger occupants tended to be able to withstand higher seatback recline angles without submarining than smaller occupants. Additionally, across all occupants, increased recline angle resulted in increased lumbar compression and shear force.

The new ADS environment is likely to pose substantial challenges to occupant restraints systems. Increased seatback angle increases the propensity of occupants to submarine, and results in increased lumbar spine load.

INTRODUCTION

The introduction of automated driving systems (ADS) is likely to influence almost every aspect of personal transportation. With Level 3 autonomy, the occupants will no longer be required to constantly interface with the vehicle controls [1-3]. Consequently, they may no longer be constrained to traditional seating postures. They will have more time and freedom to engage in other activities, which could result in major changes to vehicle interiors, controls, and seating configurations. While it will take time to develop the new automated technology, and revolutionize the layout of the occupant compartment, the greatest near-term changes will likely occur with drivers choosing to recline their seats and move them away from the knee bolster (KB) to rest during periods where autonomous modes are engaged. Thus, these seating choices may soon challenge the ability of current vehicle safety systems to adequately protect the occupants.

There are few studies focusing on occupant kinematics and restraint performance in reclined postures [4-7]. Those studies indicate that higher recline angles as well as increased distance to the KB may result in higher risk of submarining. Submarining occurs when the lap belt loads the abdominal area, after passing over the iliac crest of the pelvis to load the abdominal soft tissues without engaging, or after disengaging, the pelvis. This in turn results in series of adverse effects onto occupant-restraint engagement, occupant kinematics and occupant injury risk. These studies identified pelvis motion and lumbar spine loads as areas of particular interest. Additionally, some studies considered the differences between traditional b-pillar-mounted 3-point belt, and seat integrated restraint [4, 7]. While a seat-integrated D-ring resulted in earlier engagement of the torso, and less forward head motion, the b-pillar-mounted belt resulted in lower resultant force and flexion angle in the lumbar spine. However, none of these studies considered the effect of occupant anthropometry on occupant response.

The goal of this study was to evaluate the response for reclined occupants in frontal impacts across variations in occupant anthropometry, recline angle and the KB position. The specific goal of this study was to provide general overview of occupant, and restraint system responses across all varied conditions. This was accomplished using the family of Global Human Body Models Consortium (GHBMC) simplified human body models (HBM): mid-sized male, large male, and small female, subjected to 56 km/h frontal-impact simulations in a finite element model of a generalized vehicle interior.

METHODS

Overview

The simulation environment was developed based on the finite element (FE) model of the prototype vehicle provided by the OEM. Several changes were incorporated into the original model in order to make it suitable for the current study. First, the seatback integrated 3-point seatbelt system was developed. The seatbelt included lap belt pre-tensioner, shoulder retractor pre-tensioner and force limiter. Second, the seatback was reinforced with additional beam elements to provide appropriate structural support for the loads expected from the seatback integrated restraint system. Third, the KB was decoupled from the vehicle interior to facilitate rapid and parametric interior configuration adjustment. All simulations were performed with the occupant seated in the right front passenger seat, with generic passenger airbag, subjected to a USNCAP 56 km/h frontal crash pulse.

A full factorial design of experiments (DOE) was performed with respect to the parameters including, occupant anthropometry, seatback recline and KB position. Three different occupant anthropometries, small female (F05), midsize (M50) and large male (M95) were considered in this study. Seatback recline angle was defined as the angle between the headrest post and vehicle side sill. Four different recline angles were considered: 0, 10, 20 and 30 deg. recline (Figure 1). The distance between the occupant and KB was adjusted by moving the entire KB assembly relative to the vehicle frame (Figure 1). This was done in order to isolate the effect of the KB's position without altering any other restraint components such as belt anchorage position, or the distance to the frontal airbag. Four KB positions were considered, three positions representing a distance to a KB when the seat is placed at forward-track (fIP, +120mm), mid-track (sIP, 0mm) and back-track (bIP, -120mm) position, and one position when the KB is removed from the vehicle (nIP, -450mm). Since midsize and large male did not fit into the seat with the forward KB position, these conditions were removed from the simulation matrix. Consequently, the DOE resulted in total of 40 FE simulations (Table 1).

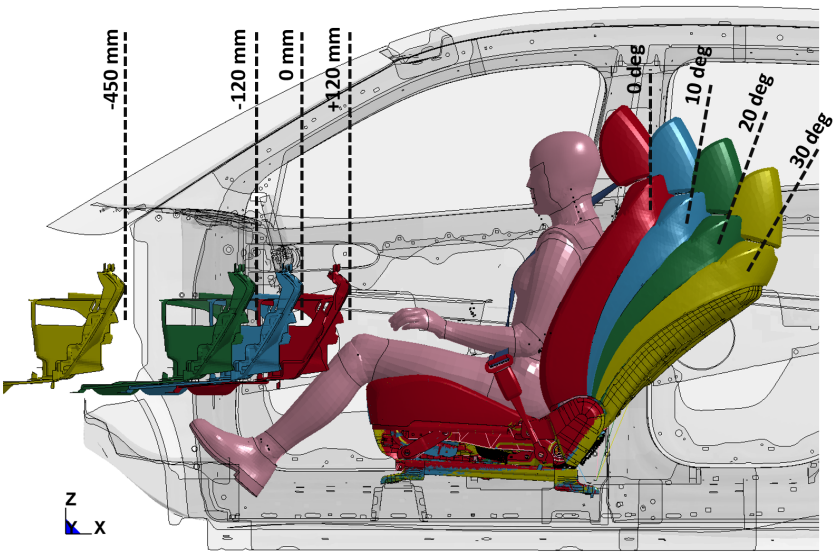

Figure 1. Simulation environment. Investigated seatback recline angles (0, 10, 20, 30 deg.) and knee bolster positions: fIP (+120 mm), sIP (0 mm), bIP (-120 mm), and nIP (-450 mm).

Table 1. Simulation matrix.

	Parameters			
Occupant anthropometry (version)	F05-OS (2.0)	M50-OS (1.8.4.1)	M95-OS (1.2)	
Seat recline angle (deg)	0.9	10.9	20.9	30.9
Knee bolster position (position)	Forward (fIP)*	Standard (sIP)	Backward (bIP)	No knee bolster (nIP)
	(+120 mm)	(baseline)	(-120 mm)	(-450 mm)
TOTAL	40 simulations*			

All of the simulation in this study were performed using LS-Dyna (R9.1.0) explicit finite element (FE) solver and the high performance computational cluster (Intel Xeon E5-2670v2, 2.5 GHz, 20 core). In order to eliminate decomposition performance variability, all jobs were run using two computational nodes.

Simulation setup

All occupant models were positioned in the vehicle seat following the methodology described in [7]. Additionally, care was taken to ensure that occupants' pelvis was positioned as close as possible to the seatback, thus avoiding unnecessary slouching that could lead to unfavorable belt placement and consequently submarining. The HBM and seat stress and strain data was carried through the positioning phase to the final simulations in order to achieve proper boundary conditions and contact initiation. The seat belts were fitted individually for each occupant size and each seat recline angle.

Additionally, throughout the setup process and during initial shakedown simulations several modeling issues/discrepancies were discovered in the utilized HBMs. First, M50 and M95 had several redundant single surface contact definitions, which impacted the overall stability of these models, and forced premature error termination. Second, it was discovered that male models had inverted polarities of the zero length discrete beam definitions in the lumbar spine, affecting the kinematic response as well as polarity of the obtained signal. Third, male models had a misaligned coordinate systems used for measuring forces in the occupant's femurs. Fourth, small female model carried additional attachment between pelvic flesh and pelvis which made it different from the male models. All discovered issued were addressed and the models were modified to unify the modeling approach.

Post-processing

A custom automated post-processing code was developed to analyze the results from all of the performed simulations. The occurrence of submarining was assessed through visual assessment of simulation results. The submarining was identified if the belt passed either of left, right or both iliac wings and moved above the anterior superior iliac spine (ASIS) into the abdomen.

RESULTS

A total of 40 simulations were performed in this study. Since some of the simulations did not proceed through a maximum of 150 ms, and terminated in error, the termination times were evaluated to identify trends with respect to simulation parameters (Table 2). The completion rate declined with the increase of the seatback angle. Forward and standard KB positions had the highest completion rate followed by the back and no KB condition. The M50 model had the highest percentage of normal terminations, followed by the M95 and F05 models.

Table 2. Termination times (out of 150 msec.) for all investigated cases.

HBM	IP Position	Recline Angle				Completion rate (IP)	Completion rate (HBM)
		0	10	20	30		
F05	fIP	150	150	82	90	50%	44%
	sIP	150	150	74	90	50%	
	bIP	150	150	110	78	50%	
	nIP	102	150	118	82	25%	
M50	fIP	N/A	N/A	N/A	N/A		67%
	sIP	150	150	150	84	75%	
	bIP	110	150	150	150	75%	
	nIP	150	150	70	74	50%	
M95	fIP	N/A	N/A	N/A	N/A		50%
	sIP	150	150	150	150	100%	
	bIP	150	88	88	96	25%	
	nIP	150	80	82	86	25%	
Completion rate (Rec.)		80%	80%	30%	20%		

For all occupants, increased occupant recline angle lead to increased posterior tilt of the pelvis. Additionally, with increased angle of recline, the lap belt moved vertically up and away from the ASIS (Figure 2).

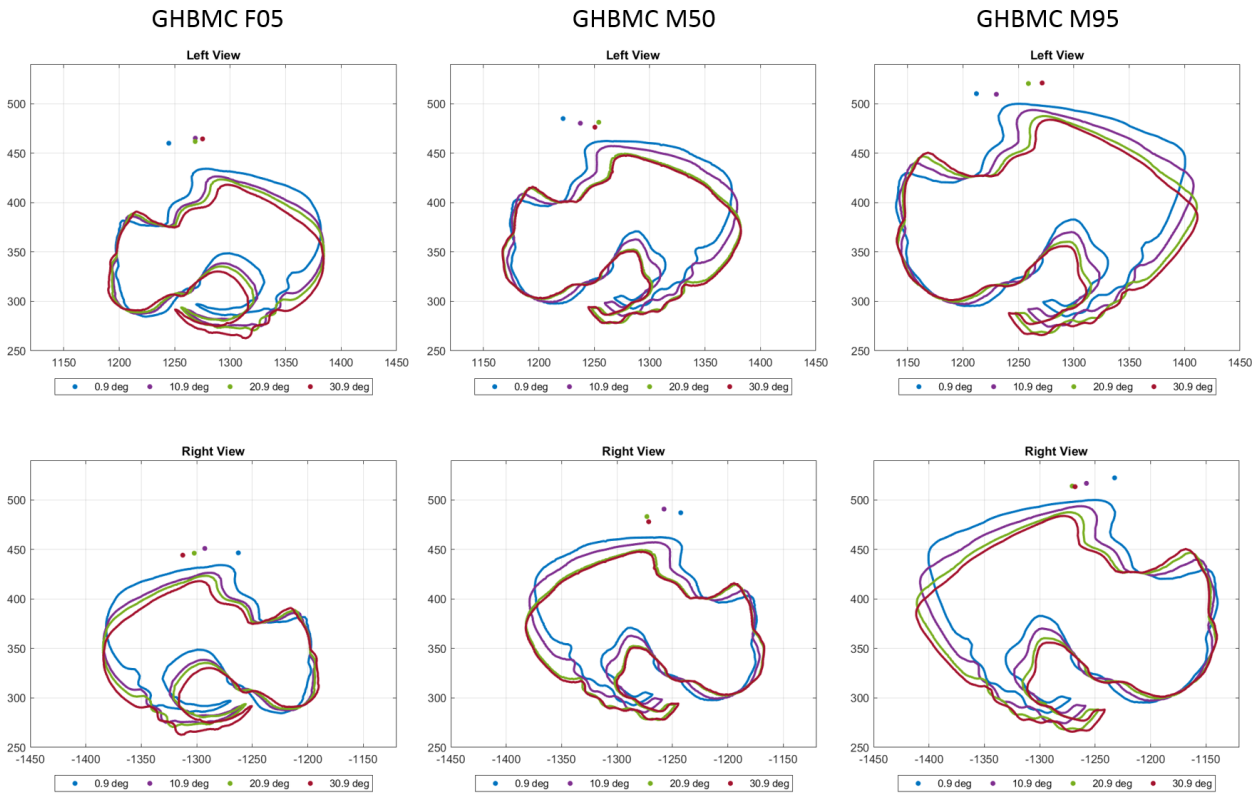

Figure 2. Lateral view of the pelvis with respect to the recline angle along with the top edge of the lap belt relative to the ASIS, shown for all three HBM models.

The occurrence of submarining was evaluated across all 40 of the simulations (Table 3, Table 4, Table 5, and Table 6). In general, submarining was observed more frequently at higher recline angles. The small female model submarined in the most cases, followed by the mid-size, which submarined in fewer cases, and then the large male, which submarined in the fewest cases. The KB distance also played a role in limiting the occurrence of submarining. In several cases where the submarining was observed in the back KB position it was effectively eliminated by moving the KB into the standard position (Table 4 and Table 5).

Table 3. Submarining outcome for the fIP knee bolster position. Cases highlighted with a red/pink background were cases where at least partial submarining occurred.

	0.9 deg	10.9 deg	20.9 deg	30.9 deg
F05	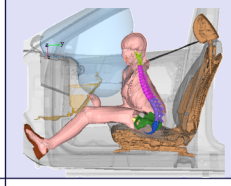	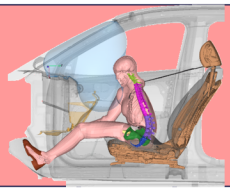	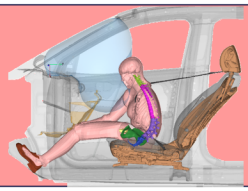	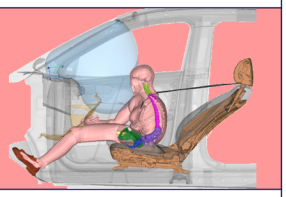
M50	N/A	N/A	N/A	N/A
M95	N/A	N/A	N/A	N/A

No Submarining Submarining

Table 4. Submarining outcome for the sIP knee bolster position. Cases highlighted with a red/pink background were cases where at least partial submarining occurred.

	0.9 deg	10.9 deg	20.9 deg	30.9 deg
F05	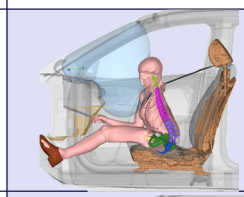	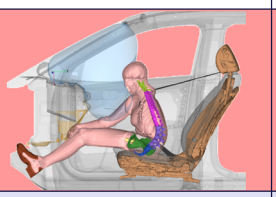	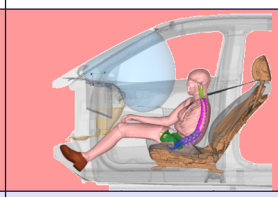	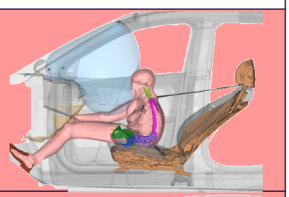
M50	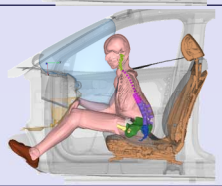	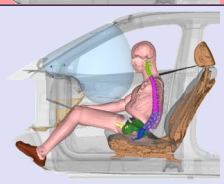	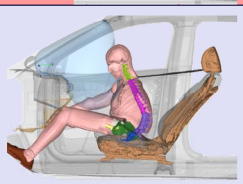	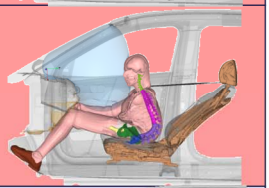
M95	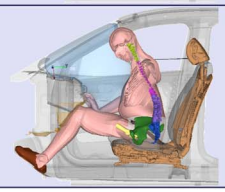	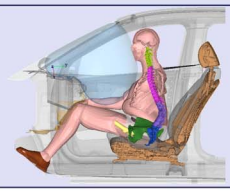	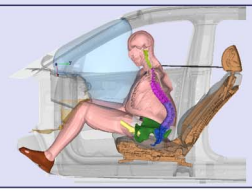	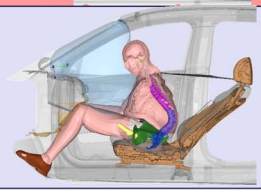

No Submarining Submarining

Table 5. Submarining outcome for the bIP knee bolster position. Cases highlighted with a red/pink background were cases where at least partial submarining occurred.

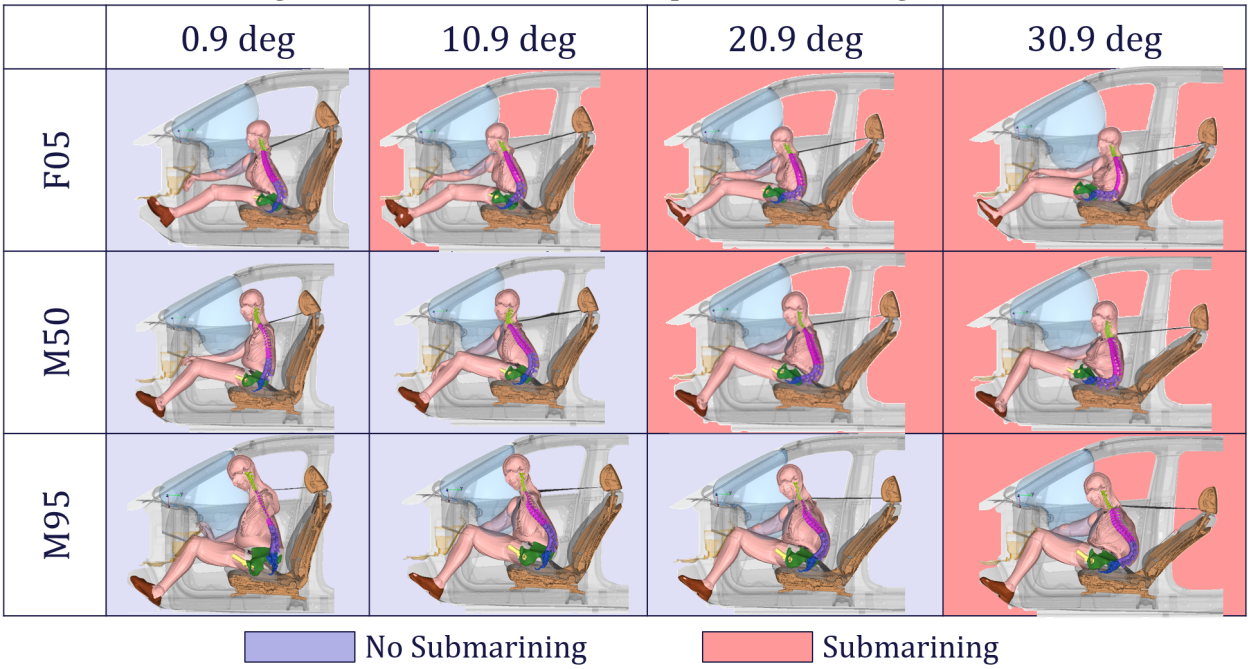

Table 6. Submarining outcome for the nIP knee bolster position.

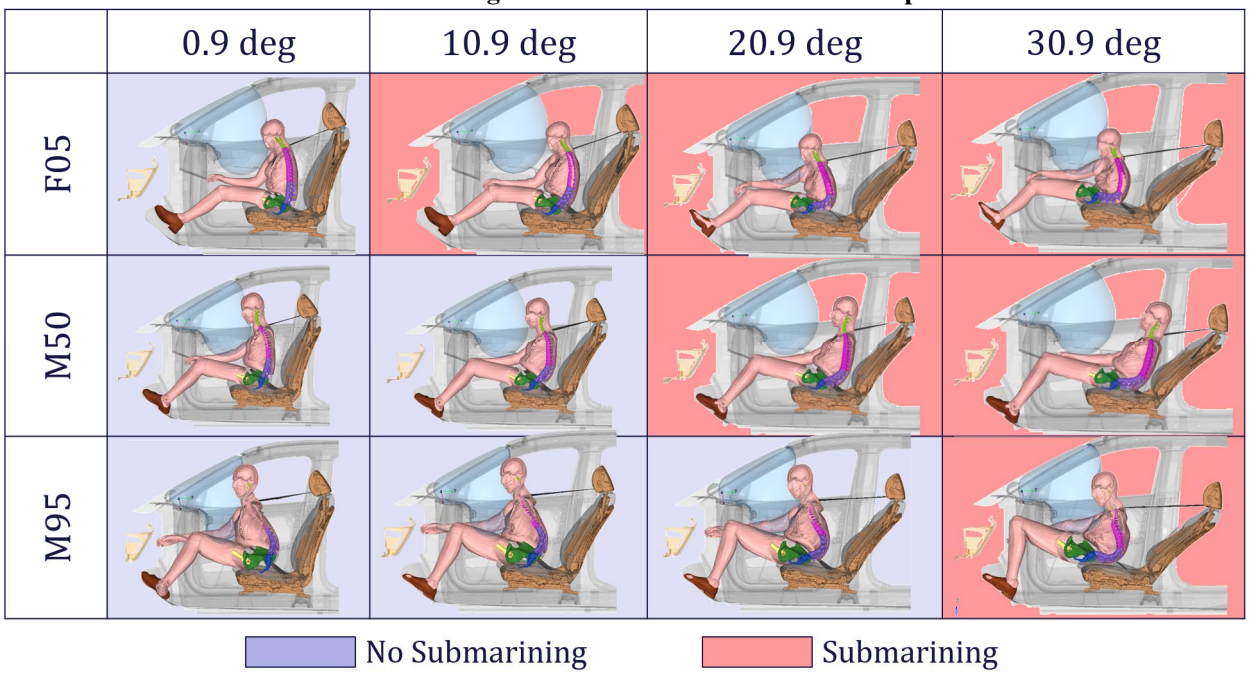

In all cases, pelvis excursion increased with an increase of seatback recline angle and the increase of distance between the occupant and KB. In comparable cases with the KB present (fIP, sIP or bIP) larger occupant experienced smaller forward pelvis excursion (Figure 3).

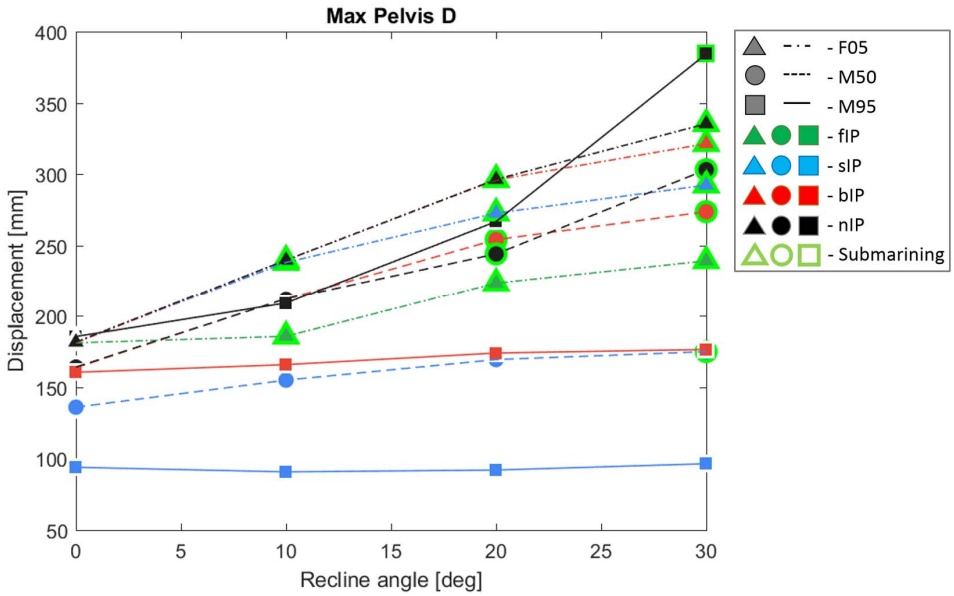

Figure 3. Maximum forward pelvis motion relative to the vehicle across all anthropometries, knee bolster positions, and recline angles.

As expected, the maximum lap belt force (measured at the anchor) increased with the increased size of the occupant. An increase in the lap belt force was observed with the increase distance between the occupant knees and KB. Interestingly the maximum lap belt force showed general decrease with the increased level of seatback recline (Figure 4).

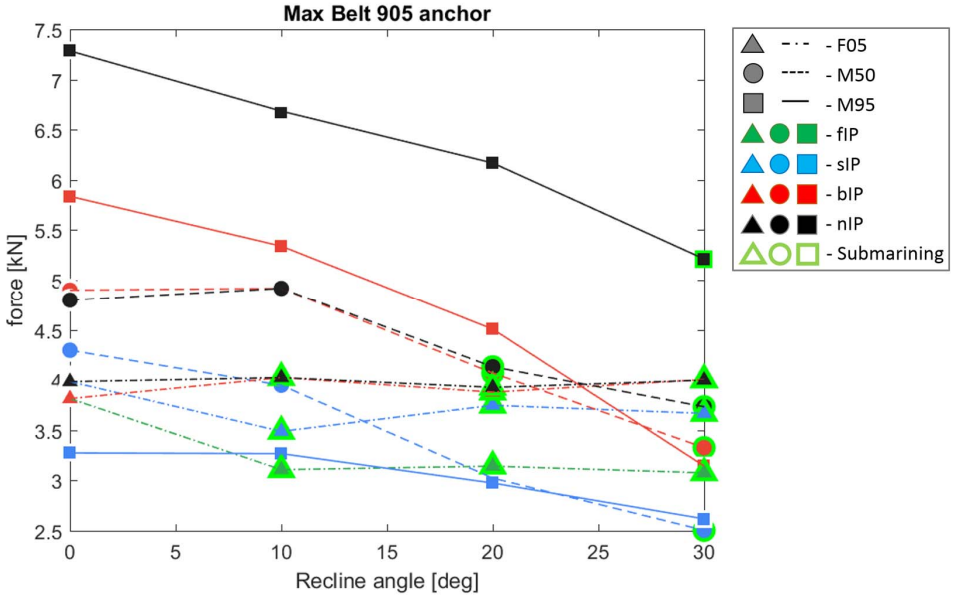

Figure 4. Maximum recorded lap belt force measured at the outboard anchor across all anthropometries, knee bolster positions, and recline angles.

The maximum femur compression force, used as a surrogate for knee to KB contact, showed an increase with the increase of the seatback recline angle. Only F05, sIP, 20 deg. and 30 deg. recline cases showed the opposite trend, however upon in depth review it was discovered that these simulation terminated prematurely, before the maximum femur force was recorded (Table 2). Interestingly the maximum femur compression force didn't show consistent trend with the size of the simulated occupant (Figure 5).

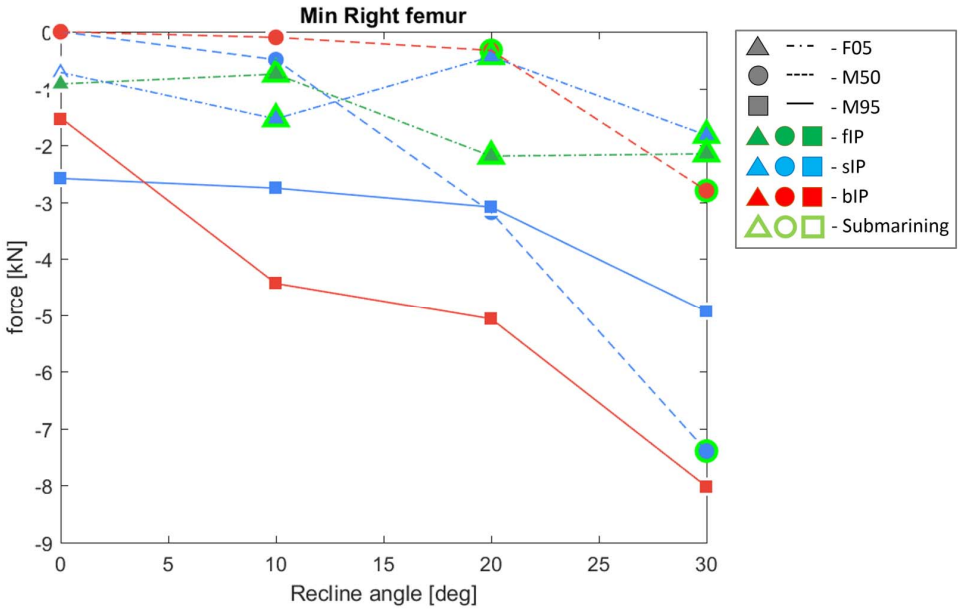

Figure 5. Maximum femur compression force across the cases where knee to knee bolster contact was present. No IP cases (nIP) for all anthropometries, and back IP (bIP) for F05 didn't have knee bolster contact and were removed for brevity.

The maximum lumbar spine forces were obtained by finding a maximum force across all vertebral levels in the lumbar spine. The maximum compression and anterior posterior (AP) shear force in lumbar spine increased with the increase of the recline angle (Figure 6 and Figure 7). Additionally, cases where submarining was observed, showed a substantial increase in a maximum lumbar spine shear force (Figure 7).

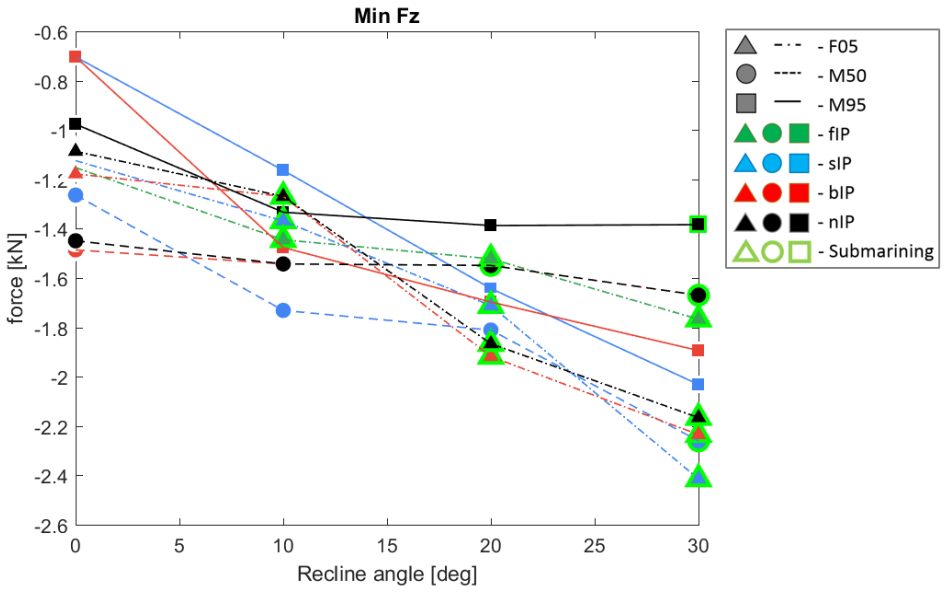

Figure 6. Maximum compression force in the lumbar spine measured for all lumbar vertebral levels (T12-S1), across all anthropometries, knee bolster positions, and recline angles.

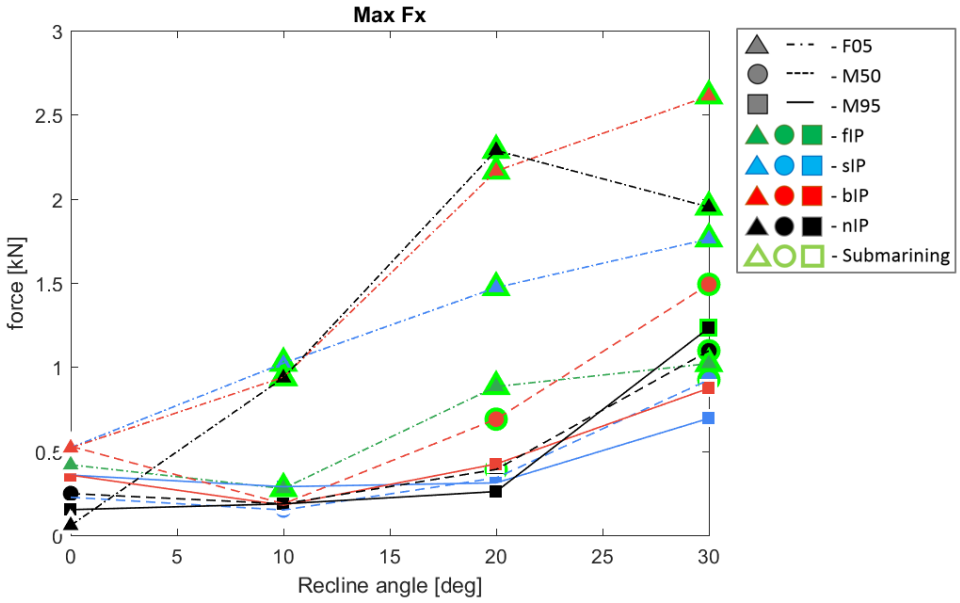

Figure 7. Maximum anterior-posterior shear force in the lumbar spine measured for all lumbar vertebral levels (T12-S1), across all anthropometries, knee bolster positions, and recline angles.

DISCUSSION

This study provides an overview of occupant responses in the environment relevant to the future of personal transportation. The initial results indicate that current state-of-the art restraint systems will require additional research and development to offer an adequate level of occupant protection in the future ADS environment. Additionally, the results of this study show that current numerical tools need additional development, for evaluating occupant safety in nontraditional seating postures. Several modeling errors, which influenced either the stability or the actual response of the model were discovered. These modeling discrepancies have been addressed, and the modified models were used for this study.

The results show that these models perform best in the conditions that cover their development and validation regime, which is based on the current vehicle environment (upright occupant with KB). All models were also more stable in simulations with more upright occupants, and where traditional knee support was present. This is not surprising given that they were developed to be used in such environment [8]. However when used outside the development regime their stability decreases.

The occurrence of submarining was highly related to the setback recline angle and pelvis posterior rotation. All occupants were more likely to submarine with the increase of seatback recline, however each occupant had a different submarining threshold. The smallest occupants were most likely to submarine. When submarining was observed for larger occupants it was at higher seatback recline angles. All non-upright F05 simulations resulted in the model submarining under the lap belt, even in cases when the occupant was in contact with KB. This suggests that the occupant size, and consequently pelvis size and pelvis orientation may play a role in influencing occupant propensity to submarine (Figure 2). This also suggests that the current state-of-the-art restraint systems will be especially challenged by small occupants in recline configurations.

The KB was an effective measure controlling occupant's pelvis motion. The shorter the distance to the KB, the fewer submarining cases were identified. In cases where the occupant interacted with the KB (Figure 5), its pelvis forward motion was limited. Consequently, the pelvis forward excursion remained constant, or increased only slightly for the cases with increased seatback recline angle (Figure 3, F05:fIP, M50:sIP, M95:sIP, bIP). The cases with limited or no KB engagement showed substantial increase in pelvis forward

excursion and increased submarining occurrence with increase of the seatback recline angle (Figure 3, Table 4 and Table 5). This suggests that the KB could be an effective countermeasure for controlling occupant kinematics, and reducing submarining likelihood for reclined occupants in the ADS environments.

The results indicate that reclined positions may lead to the increase in lumbar spine compressive loads (Figure 6). The increase of seatback recline angle aligns the occupant's lumbar spine with the direction of the acceleration pulse, resulting in increased lumbar compressive load from upper body inertia. Establishing lumbar spine biofidelity targets and injury tolerance should be at the center of future research. Especially, given limited development, biofidelity and validation data available for GHBMC's lumbar spine model, which is shared between simplified and detailed models [8, 9]. In author's understanding, the stiffness functions in the current model were calibrated to match a set of whole body PMHS sled tests [10, 11] without using data from component tests. Few studies attempted to address this issue by using available tests data. However, these studies used either data from unidirectional tests on functional spinal units without ligamentous structure [12], or whole spine experiments that had unrealistic boundary conditions and failed to apply and maintain follower load [13, 14].

The maximum lap belt force was dependent on occupant size and KB position (Figure 4). Naturally, larger occupants subject the belt system to higher restraint forces. Additionally, the contact with the KB creates an alternative load path through occupant femurs, further offloading the belt system (Figure 5). Interestingly, the lap belt forces obtained for both male HBMs showed a force reduction with an increase of initial recline angle. This was a consequence of the substantial belt transfer from the shoulder to the lap belt. The increase of seatback recline angle resulted in the increased flexion in the lumbar spine and reduction in seated height during torso forward motion (Table 6, M95:30:nip). The shortened distance between the occupant's shoulder and the buckle facilitated shoulder-lap belt transfer, and reduced the restraint of the pelvis allowing further forward excursion. This effect could be eliminated with the belt locking tongue, however an increase in lumbar spine forces (Figure 6) suggests that aggressive pelvic restraint may lead to increased lumbar spine injuries.

Lumbar spine AP sear force was a good predictor for submarining (Figure 7). In the model, when the belt slips off the ASIS it penetrates the abdomen and load is transferred directly to the lumbar spine. Out of all cases where submarining was observed, only two (F05:10:fIP, M50:20:nIP) did not show a substantial increase in the lumbar shear force. In both of these cases, the lap belt only slipped off one side of the pelvis, but remained hooked on the other (Figure 8), stopping the belt from engaging the lumbar spine. Interestingly, in all cases the buckle side, which was not pre-tensioned, was more prone to disengaging first. This indicates that pre-tensioning on both sides of the lap belt might be an effective countermeasure to ensure lap belt-pelvis engagement.

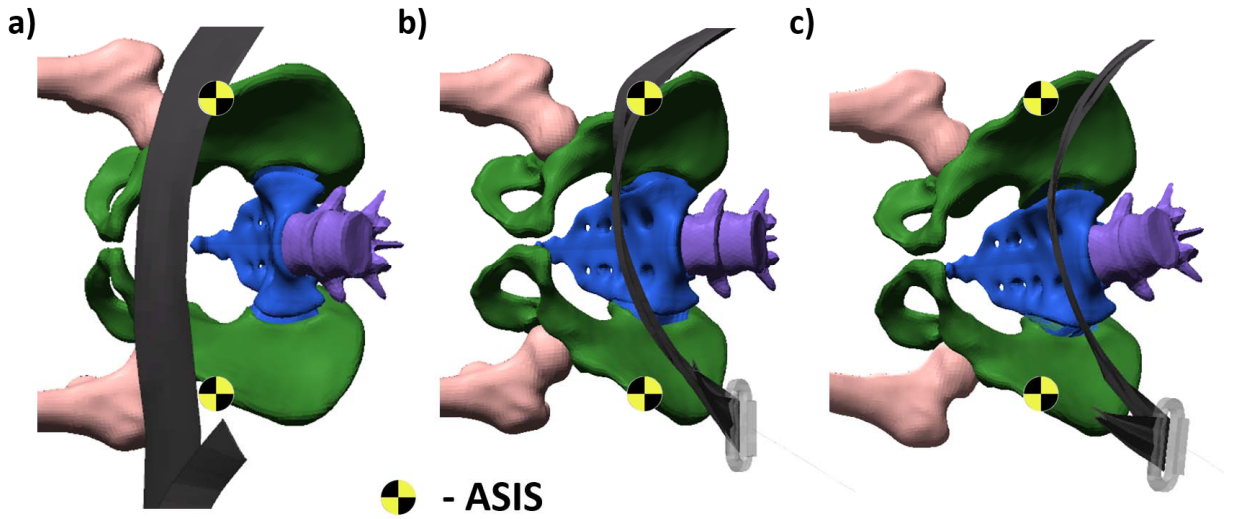

Figure 8. Comparison of different submarining mechanisms. Superior view, a) initial belt placement, b) unilateral submarining, c) bilateral submarining.

CONCLUSIONS

This study provides an overview of occupant responses in non-traditional vehicle environment relevant to the future automated vehicles. It focused on evaluating the occupant response with respect to anthropometry, recline angle and distance to the KB. The results lead to the following conclusions:

1. Current numerical tools need additional development, for evaluating occupant safety in nontraditional seating postures.
2. Reclined postures pose a challenge for the current state-of-the-art restraint systems.
3. Increased recline angles lead to more submarining cases.
4. Smaller occupants may be more prone to submarining.
5. The knee bolster could be an effective countermeasure for controlling occupant kinematics and preventing submarining.
6. Higher recline angle reslults in a high compression force in the lumbar spine
7. Submarining results in large shear force recorded in the lumbar spine.

ACKNOWLEDGEMENT

This study was supported by Hyundai-Kia America Technical Center Inc. (HATCI). Views or opinions expressed or implied are those of the authors and are not necessarily representative of the views or opinions of HATCI.

REFERENCES

[1]. SAE On-Road Automated Vehicle Standards Committee, (2014) Taxonomy and definitions for terms related to on-road motor vehicle automated driving systems. SAE International.

[2]. U.S. Department of Transportation, 2017. Automated Driving Syatems 2.0 - A Vision for Safety. Available at: https://www.nhtsa.gov/sites/nhtsa.dot.gov/files/documents/13069a-ads2.0_090617_v9a_tag.pdf Accessed February 21, 2019.

[3]. U.S. Department of Transportation, 2017. Automated Driving Syatems 3.0 - Preparing for the Future of Transporttation. Available at: https://www.transportation.gov/sites/dot.gov/files/docs/policy-initiatives/automated-vehicles/320711/preparing-future-transportation-automated-vehicle-30.pdf Accessed February 21, 2019.

[4]. Forman, J., Lin, H., Gepner, B., Wu, T., Panzer, M. (2018) Occupant safety in automated vehicles: effect of seatback recline on occupant restraint. Japan Society of Automotive Engineers.

[5]. Ji, P., Huang, Y., & Zhou, Q. (2017). Mechanisms of using knee bolster to control kinematical motion of occupant in reclined posture for lowering injury risk. International journal of crashworthiness, 22(4), 415-424.

[6]. Kitagawa, Y., Hayashi, S., Yamada, K., & Gotoh, M. (2017). Occupant Kinematics in Simulated Autonomous Driving Vehicle Collisions: Influence of Seating Position, Direction and Angle (No. 2017-22-0005). SAE Technical Paper.

[7]. Lin, H., Gepner, B., Wu, T., Forman, J., (2017) Effect of Seatback Recline on Occupant Model Response in Frontal Crashes. 2017. Available at: http://www.ircobi.org/wordpress/downloads/irc18/pdf-files/64.pdf. Accessed February 21, 2019.

[8]. Gayzik, F.S., Moreno, D.P., Vavalle, N.A., Rhyne, A.C. and Stitzel, J.D., 2011. Development of the Global Human Body Models Consortium mid-sized male full body model. In *International Workshop on Human Subjects for Biomechanical Research* (Vol. 39). National Highway Traffic Safety Administration.

[9]. Schwartz, D., Guleyupoglu, B., Koya, B., Stitzel, J.D. and Gayzik, F.S., 2015. Development of a computationally efficient full human body finite element model. *Traffic injury prevention*, *16*(sup1), pp.S49-S56.

[10]. Global Human Body Models Consortium, 2016,User Manual: M50 Detailed Occupant Version 4.5 for LS-DYNA. Document Revision 5.1

[11]. Luet, C., Trosseille, X., Drazétic, P., Potier, P. and Vallancien, G., 2012. *Kinematics and Dynamics of the Pelvis in the Process of Submarining using PMHS Sled Tests* (No. 2012-22-0011). SAE Technical Paper.

[12]. Arun, M.W., Hadagali, P., Driesslein, K., Curry, W., Yoganandan, N. and Pintar, F.A., 2017. *Biomechanics of lumbar motion-segments in dynamic compression* (No. 2017-22-0001). SAE Technical Paper.

[13]. Zheng, J., Tang, L. and Hu, J., 2018. A numerical investigation of risk factors affecting lumbar spine injuries using a detailed lumbar model. *Applied bionics and biomechanics*, *2018*.

[14]. Katagiri, M., Zhao, J., Kerrigan, J., Kent, R. and Forman, J., 2016. Comparison of whole-body kinematic behaviour of the GHBMC occupant model to PMHS in far-side sled tests. In *Proceedings of IRCOBI Conference* (pp. 679-693).

APPENDIX

Table A1: Data extracted from the simulations.

ID	Occupant	Recline Angle	IP location	Submarine (Yes = 1, No =0)	Max. Pelvis X Excursion [mm]	Max belt force (anchor) [kN]	Max femur comp. force [kN]	Max lumbar comp. force [kN]	Max lumbar AP shear force [kN]
1	M50	0	sIP	0	136	4.30	0.00	-1.26	0.23
2	M50	10	sIP	0	155	3.95	-0.49	-1.73	0.15
3	M50	20	sIP	0	169	3.02	-3.18	-1.81	0.34
4	M50	30	sIP	1	175	2.50	-7.40	-2.26	0.92
5	M50	0	bIP	0	164	4.90	0.00	-1.49	0.53
6	M50	10	bIP	0	212	4.92	-0.10	-1.54	0.19
7	M50	20	bIP	1	254	4.07	-0.33	-1.55	0.69
8	M50	30	bIP	1	274	3.33	-2.80	-1.67	1.49
9	M50	0	nIP	0	164	4.80	-	-1.45	0.25
10	M50	10	nIP	0	212	4.92	-	-1.54	0.19
11	M50	20	nIP	1	244	4.13	-	-1.55	0.39
12	M50	30	nIP	1	303	3.73	-	-1.67	1.10
13	M95	0	sIP	0	94	3.27	-2.58	-0.70	0.36
14	M95	10	sIP	0	91	3.27	-2.75	-1.16	0.29
15	M95	20	sIP	0	92	2.97	-3.09	-1.64	0.31
16	M95	30	sIP	0	96	2.62	-4.93	-2.03	0.69
17	M95	0	bIP	0	160	5.84	-1.51	-0.70	0.36
18	M95	10	bIP	0	166	5.34	-4.44	-1.48	0.18
19	M95	20	bIP	0	174	4.51	-5.07	-1.70	0.42
20	M95	30	bIP	0	176	3.14	-8.02	-1.89	0.87
21	M95	0	nIP	0	185	7.29	-	-0.98	0.15
22	M95	10	nIP	0	209	6.69	-	-1.33	0.19
23	M95	20	nIP	0	267	6.17	-	-1.39	0.26
24	M95	30	nIP	1	384	5.21	-	-1.38	1.23
25	F05	0	sIP	0	182	3.98	-0.72	-1.12	0.52
26	F05	10	sIP	1	238	3.49	-1.53	-1.37	1.02
27	F05	20	sIP	1	273	3.75	-0.44	-1.71	1.47
28	F05	30	sIP	1	292	3.67	-1.82	-2.41	1.76
29	F05	0	fIP	0	181	3.81	-0.92	-1.15	0.42
30	F05	10	fIP	1	186	3.11	-0.75	-1.45	0.28
31	F05	20	fIP	1	223	3.14	-2.19	-1.52	0.88
32	F05	30	fIP	1	239	3.08	-2.15	-1.77	1.02
33	F05	0	bIP	0	181	3.81	-	-1.18	0.52
34	F05	10	bIP	1	240	4.02	-	-1.27	0.94
35	F05	20	bIP	1	296	3.88	-	-1.92	2.17
36	F05	30	bIP	1	321	4.00	-	-2.23	2.61
37	F05	0	nIP	0	182	3.98	-	-1.09	0.06
38	F05	10	nIP	1	240	4.02	-	-1.27	0.94
39	F05	20	nIP	1	296	3.93	-	-1.87	2.29
40	F05	30	nIP	1	335	4.00	-	-2.17	1.95

A FRAMEWORK FOR IMPROVING OF HEAVY TRUCK CAB CRASHWORTHINESS UNDER ROLLOVER CONDITIONS

Garrett Mattos
Keith Friedman
John Hutchinson
Khanh Bui
Friedman Research Corporation
USA

Paper Number 19-0336

ABSTRACT

In 2012 the US Congress directed the Federal Motor Carrier Safety Administration (FMCSA) to improve commercial motor vehicle safety through the MAP-21 Act. NHTSA reported to the US Congress in 2015 that heavy truck rollover crashworthiness should be improved. To that end NHTSA sent a letter to the president of SAE asking if improvements in test methods could be suggested that would result in improvement of rollover performance. In this study we review the performance of heavy truck cab structures that meet the requirements of J2422 and suggest a framework for improving rollover crashworthiness for heavy trucks.

INTRODUCTION

Historically, there has been significant work to support the advancement of heavy truck occupant crash protection. However, in many areas of heavy truck crashworthiness the results of these efforts have not been translated into adequate safety standards and/or test procedures. In many cases this can be attributed to the lack of coordination and planning between government, industry, and research stakeholders. This paper will outline a suggested framework for improving evidence-based heavy truck cab safety standards based on the lessons learned from previous efforts. Specific focus will be on the structural integrity of heavy truck cabs in response to rollover conditions.

The foundation for all vehicle safety improvements often lies in crash data. Heavy truck crash data have been collected in the U.S. at a large scale since 1966 [1]. This data has consistently shown that single-vehicle rollover crashes area a significant threat to the safety of heavy truck occupants. The use of a combination of crash data, biomechanical metrics, structural analysis, and highway parameters to develop a comprehensive strategy to minimize vehicle accident death and injury has been the backbone of safety improvements for many decades [2]. Further, coordinated efforts that include all relevant stakeholders such as government, industry, and research communities are generally provide the most beneficial and efficient outcomes. This has been a clear desire of the heavy truck industry for many years as exemplified by the recommendations provided to the National Vehicle Safety Advisory Council by the Motor Truck Manufacturers Division [3]. Coordinated efforts among stakeholders provides an opportunity for the benefit and evaluation of safety standards in conjunction with determining feasibility and the cost-benefit outcome of any proposed rules.

A three-phase cooperative research program managed by the Society of Automotive Engineers (SAE) in the 1990s followed this general framework to develop a set of recommended practices for evaluating truck crashworthiness. Cab-to-ground impact forces ranging from 150 kN to 250 kN and energy absorbed (cab only) of approximately 100,000 Nm were calculated with similar values reported for baseline and reinforced models [4]. A primary goal of the recommended practice for evaluating cab strength was to use two testing phases to reproduce both the lateral and vertical loading scenarios that were observed in 180 deg rollovers as these were lacking in the ECE Regulation 29 and a Swedish standard at the time. The ECE R29 test calls for quasi-static vertical load to be applied to the roof of the cab via a large platen with a peak force requirement of 98 kN. The Swedish standard required a maximum 147 kN vertical load followed by pendulum impacts to the A-pillar and rear cab wall. Both of these standards require a level of survival space to be maintained after loading. In the SAE recommended procedure the two test phases consisted of a dynamic impact (via sled or pendulum) to a cab rolled at 20° followed by a quasi-static roof test similar to the ECE R29 protocol. The energy value selected for the dynamic impact was not based on the amount of

energy absorbed by the cab during the rollover reconstructions, but instead based on minimum roll energy tests which had no foundation in relation to occupant injury. The final energy value used in the recommended practice (J2422) was 17,626 Nm. The authors notes deficiencies in the ability to calculate the energy absorbed during a rollover event were noted as problematic to determining an appropriate test energy.

Subsequent to the large SAE-CRP the International Organization of Motor Vehicle Manufacturers (OICA) put together a working group consisting of heavy truck manufacturers with the goal of harmonizing truck cab standards. In the latest large scale effort related to heavy truck crashworthiness the NHTSA concluded that further work should investigate the potential effectiveness of reducing injury and death and the cost-effectiveness of countermeasures related to increasing the integrity and robustness of cab structures with respect to rollover [5].

This paper describes a framework for developing and/or updating test procedures that can improve the rollover crashworthiness of heavy truck cabs. Many advancements in crash data collection, reconstruction, finite element analysis, manufacturing processes, material specifications and costs, and injury metrics have been made since the development of current heavy truck cab test procedures. These advancements can be leveraged to support improvements in cab design that are feasible and cost-effective.

METHODS

Crashes of heavy trucks that produced serious or fatal injuries were identified with the FRC internal crash database. This database includes fully reconstructed heavy truck crashes with detailed medical records and vehicle information. For each crash the detailed LSYDNA finite element models of the vehicle and terrain, which had been produced previously, were used to simulate the rollover event. The deformation and internal energy of the cab as well as contact forces with the ground were calculated during each run. The orientation of the cab relative to the ground at the time of maximum initial deformation was determined for each case. The time of maximum initial deformation was defined as the first event with the greatest single increase in cab deformation, thus separating the primary roof intrusion event from subsequent loadings. Often a cab will experience the greatest magnitude of roof intrusion when and if it comes to rest on its roof, yet this does not necessarily describe the most injurious event.

A baseline cab structure, modeled in LS-DYNA and validated against the results of a SAE J2422 test, was subjected to select test conditions representative of the impact energy and orientation determined from the reconstructions. The test setup consisted of a flat faced platen on a sled constrained to move in a direction perpendicular to the platen face. The platen impacted a cab that was rigidly constrained at its mounting locations. The total mass of the sled was 5645 kg. The orientation between the cab and plate was defined using the following sequence of rotations and an example of the setup is shown in Figure 1. The cab was initially placed in an upright position with its x-z plane parallel to the face of the platen. The cab was then rotated about its roll axis a predetermined amount. Finally, the cab was rotated about the global z-axis which produced both a yaw and pitch relative to the platen face. Table 1 summarizes the test protocol. The baseline cab was subjected to each of the combinations listed in Table at a 35 kJ impact energy. The modified cab was subjected to the 60 deg roll, 30 deg yaw scenario at both 35 kJ and 80 kJ as this was determined to be the scenario that produced the greatest amount of damage in the baseline cab.

An additional drop test was conducted on the baseline cab fitted to a full tractor to investigate the effect of an unconstrained test on cab response. The cab was oriented relative to the ground at the same 60 deg roll, 30 deg yaw position as utilized in the sled impact scenarios.

Figure 1 Baseline cab setup for 60 deg roll, 30 deg yaw platen impact (proprietary cab purposely distorted)

Table 1 Summary of simulated test protocol

	Yaw				
Roll	**0**	**10**	**20**	**30**	**40**
20	B35	B35	B35	B35	B35
40	B35	B35	B35	B35	B35
60	B35	B35	B35	B35/M35/M80	B35

B35 – Baseline cab, 35 kJ impact energy
M35 – Modified cab, 35 kJ impact energy
M80 – Modified cab, 80 kJ impact energy

The baseline FE cab was modified using manufacturing methods and materials available in the 1990s to improve crashworthiness, increase survival space, and reduce the risk of occupant injury in the reconstructed scenario. The modified cab was then evaluated against select test conditions to assess for comparison.

RESULTS

Due to the low counts of crashes investigated and the preliminary nature of this study some of the results have been normalized. It is not the intent of this work to propose any specific test procedure or energy level, but to demonstrate a methodology using data that was immediately available to the authors.

Three fully reconstructed heavy truck rollover crashes were identified for this preliminary analysis and are summarized in Table 1. The orientation at maximum initial roof deformation had a much greater range in the roll and pitch directions than in the yaw direction. Resultant roof deformation ranged from 408 mm to 793 mm. The amount of roof deformation was reduced from 793 mm to 255 mm with the use of a modified cab. The amount of energy absorbed by the cab varied from 32 to 50 kJ.

Table 2 Summary of reconstructed rollover crash response

Crash ID	**Orientation of cab at maximum initial roof crush (deg)**			**Maximum resultant roof crush (mm)**	**Energy absorbed by cab (kJ)**
	Roll	**Pitch (+ve nose up)**	**Yaw**		
1	131	27.8	50.8	408	43
2	180	6	40	553	50
3	116	-12	46	793	32
MOD3	112	-12	45	255	38

The vast majority of crash energy in typical heavy truck rollover crashes is dissipated through friction as the truck slides across the ground surface and only a relatively small percentage is associated with the damage related to the most harmful event (e.g. cab roof damage) [6]. This is demonstrated in Figure 2 which illustrates the total amount of energy that was dissipated through deformation (i.e. internal and eroded energy) vs the total amount of kinetic energy dissipated throughout the entire event. The total amount of energy associated with damage to the tractor, cab, and trailer was roughly 12 % of the total available energy.

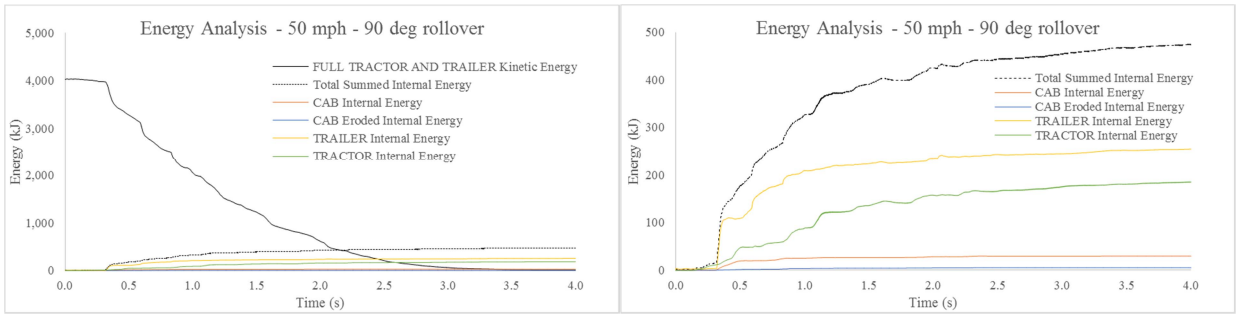

Figure 2 Energy summary for typical 90 deg heavy truck rollover

Platen motion was used to measure maximum cab deformation in the simulated sled tests. Cab deformation was highly dependent on the orientation of the platen relative to the cab as shown in Figure 3. Greater roll angles produced greater deformation. The maximum amount of deformation was achieved at a roll angle of 60 deg combined with a yaw angle of 30 deg. The lowest levels of deformation were 56% of the maximum value.

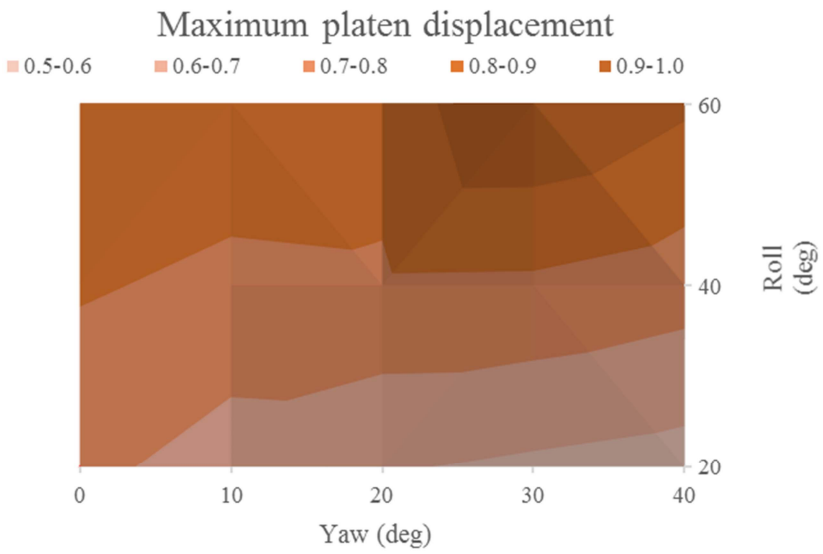

Figure 3 Contour plot of cab deformation vs orientation (data normalized to maximum value)

Platen force was inversely related to the cab deformation as described in Figure 4. The greatest platen force was measured in a 60 deg roll, 40 deg yaw orientation. Though, high force levels were also measured at 20 deg roll angles. It is expected that greater force values would be associated with lower deformations.

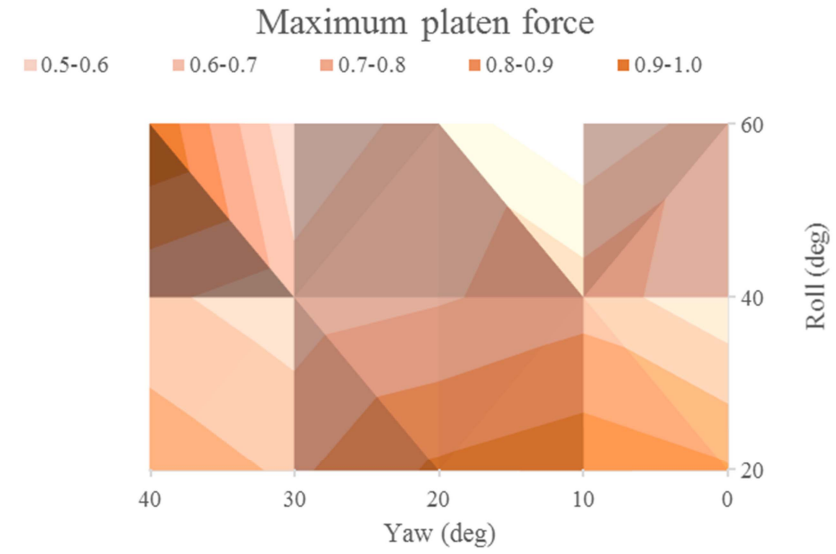

Figure 4 Contour plot of platen force vs orientation (data normalized to maximum value)

The internal energy absorbed by the cab was distributed in a similar pattern as the maximum cab deformation values. Figure 5 shows that the maximum energy was absorbed in the 60 deg roll, 30 deg yaw orientation but that the range in absorbed energy was relatively small. For all orientations the difference in the minimum and maximum internal energy was 10.9 %

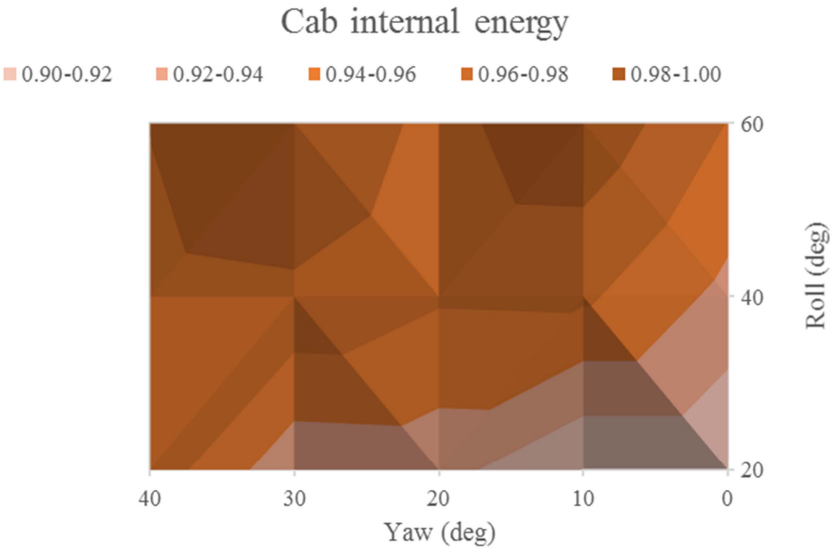

Figure 5 Contour plot of cab internal energy vs orientation (data normalized to maximum value)

The response of the modified cab to the 60 deg roll, 30 deg yaw sled impact demonstrated much less deformation yet similar amounts of internal energy. The cab experienced 60% less deformation and absorbed 4% greater energy. Under the 80 kJ sled impact (also at 60 deg roll, 30 deg yaw) the modified cab suffered 30% less deformation than the baseline did under the 35 kJ condition.

The drop test produced a maximum deformation equal to 81% of that produced in the sled scenario. The cab in the drop test absorbed 87% of the total energy absorbed in the sled test. After the initial impact with the ground in the drop test, which used a FE model of the full tractor and cab, the vehicle pitched rearward until the vehicle was horizontal. The tractor also rolled slightly toward the driver's (left) side.

DISCUSSION

The results of this effort highlight the technical and procedural issues related to developing and improving crash test protocols for heavy trucks. It has also demonstrated, on a small scale, the ability to use reconstructed crash data to develop evidence-based test protocols that could be used to evaluate heavy truck cab crashworthiness in rollovers. Perhaps most importantly, this effort also demonstrated the ability to create a generic cab that could pass a given test. Notably no pass/fail test metrics were provided in this work, yet this is would be an additional step in the process.

The proposed framework includes the creation of a database of reconstructed heavy truck rollovers that produced serious and fatal injuries under reasonable circumstances and in which the cab would have the potential to mitigate those injuries. Existing crash databases would support this effort by providing nationally representative crash data to inform the project on exposure and risk. A range of impact conditions and response metrics would be produced through these reconstructions. A matrix of potential test conditions could then be developed using some threshold (average or 90th percentile) of these values. At this point it will be important to define those injuries and/or crash scenarios that the test protocol will aim to mitigate. This can be supported by parametric finite element analysis.

It will be important that all phases of the effort are coupled with an analysis of injuries and the biomechanical response of occupants. The relationship between the structural response of the cab and the risk of injury to an occupant is the most important feature of a crash test, especially its pass/fail criteria. Finite element modeling ATDs and human body models can be used to evaluate this relationship with respect to testing methods.

Generic cabs and tractors would be created in a virtual environment to parametrically study the effects of select test conditions. The use of a generic cab has advantages. It often invites a greater level of cooperation from industry partners as they are less inclined to be involved in a project that could potentially demonstrate less-than-ideal responses from their vehicles. It can also provide a platform on which to evaluate novel techniques that would otherwise conflict with existing designs. The results above demonstrated the sensitivity of cab deformation and energy absorption to orientation of an impacting platen. Additionally, the effects of various constraint methods for both the cab and the impacting device would have to be investigated to find the right balance between test repeatability and relevance to the real world.

Two primary paths for a new test standard are envisioned. The first, traditional, path would use a limited number of physical tests to evaluate the response of a cab under a very narrow set of conditions. The second path would use a combination of physical and numerical testing to evaluate the response of a cab under a wide range of conditions. The pros and cons of each path will be investigated to determine the potential increase in performance, cost, and desired outcome from a test plan. The advantages of coupling numerical with physical testing includes the ability to conduct full-scale rollovers under a wide variety of conditions in an efficient and cost-effective manner. Numerical testing also assists manufacturers to demonstrate due diligence. Such methods of allowing for some level of certification by analysis are already in use for aircraft seats and roadside hardware.

One key aspect of the test protocol development process will be to demonstrate the feasibility of producing a cab that can pass the test. The modified cab described above is an example of this. This cab was developed using materials and manufacturing processes that were available and in use by passenger vehicle manufacturers in the 1990s. It was demonstrated to successfully mitigate injuries in a reconstructed rollover test as well as improve the response in an example platen impact. By coupling the research of developing a test protocol with the demonstration of practical conceptual designs the chance of success of producing a more stringent test protocol, and therefore better cabs in the future, is improved. A logical next step would involve working with an industry partner to develop and test a physical concept cab that is capable of passing the required test.

Along with demonstrating the feasibility of passing the test method, it will be important to provide estimates of the cost-effectiveness of modified designs as well as appropriate lead times for potential changes in standards. This will require working closely with industry to develop designs that are within the capabilities of existing manufacturing technology. Again the use of injury and crash data will support the cost-benefit analysis and continue to provide an evidence base for all decisions.

CONCLUSIONS

It is clear that much of this framework is not entirely novel or new to crashworthiness test development, however it does apply the recent advancements in finite element analysis to test design which were demonstrated above. The current state of heavy truck cab crashworthiness calls for a review and update of existing recommended practices and crash tests standards. The improvements and advancements in data recording, finite element analysis crash data collection, reconstruction, manufacturing processes, material specifications and costs, and injury metrics should be leveraged at this time to develop a modern rollover crashworthiness test that help heavy truck cabs reach their ultimate safety potential. This research supports the recent efforts of the NHTSA and SAE in improving heavy truck cab rollover crashworthiness. It presents a framework for developing improved testing methods that should include state-of-the-art modeling techniques that are becoming increasingly relevant in the design and evaluation of vehicle safety. This work is directly relevant to the improvement of physical and virtual test methods and identification of enhanced performance measures in support of vehicle safety.

REFERENCES

[1] Ernst & Ernst, *Truck Accident Study; Report of procedures and findings*. 1968, Automobile Manufacturers Association.

[2] Krall, F.L. *Truck, Bus and Multipurpose Vehicle Safety* in *The Williamsburg Conference on Highway Safety Research; a technical conference to develop a plan of needed safety research*. 1972. Williamsburg, Virginia, USA: SAE Vehicle Research Institute.

[3] Motor Truck Manufacturers Division, *Key Issues in Heavy Truck Safety*. 1976, National Motor Vehicle Safety Advisory Council: Motor Vehicle Safety Seminar.

[4] Parnell, T.K., et al., *Heavy truck 180 deg dynamic rollover and static roof crush simulation; Phase II-SAE Heavy Truck Crashworthiness*. 1996, SAE International.

[5] Woodrooffe, J. and D. Blower, *Heavy truck crashworthiness: injury mechanisms and countermeasures to improve occupant safety*. 2015, National Highway Traffic Safety Administration: Washington DC.

[6] Failure Analysis Associates, *Heavy Truck Crashworthiness, Phase I, Task B, Accident Reconstruction*. 1992: SAE International.

STUDY ON IDENTIFICATION OF CHARACTERISTICS OF THORAX OF THOR-M50 (METRIC)

HyunJae Park
AHyun Cho
Taewung Kim
Korea Polytechnic University
Korea

MinGi Cho
TaeHee Lee
SooYul Lee
Wook Jin
Hyundai Motor Group
Korea

Moonkyu Lee
Sogang University
Korea

Paper Number 19-0337

ABSTRACT

The current study aimed to characterize the structural responses of the thorax during compressive loading conditions to aid interpret the behavior of the thorax during more complex loading conditions or validate computational THOR dummy models. A series of quasi-static compression tests were performed for individual ribs and the thorax complex using two types of indenters. For a rib compression test, an indenter with a 10 mm diameter was used to load the end of a rib. This indenter was installed on a linear guide array to minimize the application of shear forces to the dummy. The influence of the thoracic bib was investigated by performing this test with and without the bib. The displacements of the other ribs were measured using a three-dimensional motion tracking system. Another 52 mm by 104 mm indenter was used to apply more belt-like loading to the loading site. From these two series of tests, stiffness was calculated using the applied force at 25.4 mm of compression. In addition, compliances of the four thoracic IR-TRACC sites (rib 3 and 6) were calculated using the applied force at 25.4 mm of compression and deflection of the IR-TRACCs. During the rib compression test without the bib, the 7th rib exhibited the highest stiffness (2.3 N/mm) while the stiffness of other ribs ranged from 0.8 to 1.5 N/mm. During the rib compression test with bib, the 1st rib region demonstrated the highest stiffness (17 N/mm), while the stiffness of other regions ranged from 6.8 to 11.3 N/mm. The bib increased the rib stiffness substantially, and its effect was the highest for the 1st rib region. The compliance results indicated that the IR-TRACC deflection is mainly influenced by the forces applied to the ribs that the IR-TRACC was installed and their adjacent ribs, e.g. rib 2 and 4 for the upper thoracic IR-TRACC, on the same side. The thoracic responses of the THOR-M50 obtained from the current study can be utilized in model validation and interpretation of the response of the thorax during more complicated loading conditions such as crash test.

INTRODUCTION

THOR (Test device for Human Occupant Restraint) dummy is expected to be introduced in the new car assessment program in the US and Europe to assess injury risk of occupants during frontal crash scenarios (Shaw et al., 2004, Yaguchi et al., 2008, Lebarbé et al., 2012, Lemmen et al., 2012). THOR dummy differs from the Hybrid III frontal crash dummy in terms of mechanical structure (Shaw et al., 2005). In addition, the number of measurement locations of the chest deflection has been increased from one to four compared to the Hybrid III dummy. Due to these

differences, THOR and Hybrid III dummies demonstrated different chest deflection during 48 km/h frontal sled tests (Shaw et al., 2000 biofidelity evaluation of the THOR advanced frontal crash test dummy, IRCOBI). During the test, the THOR dummy showed more PMHS-like anterior chest wall movement than did the Hybrid III. Also, THOR showed more PMHS-like interaction with the restraint in terms of the shoulder and lap belt loads. Sunnevång et al. (2014) evaluated the sensitivity of the thoracic regions of THOR and Hybrid III dummies under frontal sled conditions. Chest deflection responses of THOR dummy was more sensitive to the change of the configurations of the restraint systems, which included belt load limiter and driver airbag, than was the Hybrid III. Although the frontal sled test is useful to investigate the sensitivity of the THOR responses to the changes of the restraint systems, it is difficult to deduce mechanisms for the sensitivity due to the dynamic nature of the crash test conditions and complex loading conditions that the dummy experience.

As a first step to understand the interaction between the thoracic region of the THOR dummy and the safety belt system, the current study aimed to characterize the structural responses of the thorax during a series of compression tests under quasi-static loading conditions. The thoracic region of the THOR dummy was mounted to a test fixture through its upper spine structure and loaded using a 10 mm diameter indenter with and without the thoracic bib. Another series of the thorax indentation test was performed by mimicking the test condition from Shaw et al (2005).

METHOD

Dummy Positioning

The THOR dummy without its jacket was mounted to a uniaxial material testing machine through its upper spine structure (See Figure 1). The rib 3, 5, and 7 were used to fix the upper spine to the test fixture. The dummy was positioned so that the levels of the back of the rib 5 and 7 are the same with each other. Its pelvic region was simply supported using a horizontal bar to maintain its seating posture. After the positioning, the inclination of the thoracic surface at the center at the middle of the upper IR-TRACC was 2 degrees, which means the toward the head is downhill. Please note that the rib support was used only for the thorax compression test.

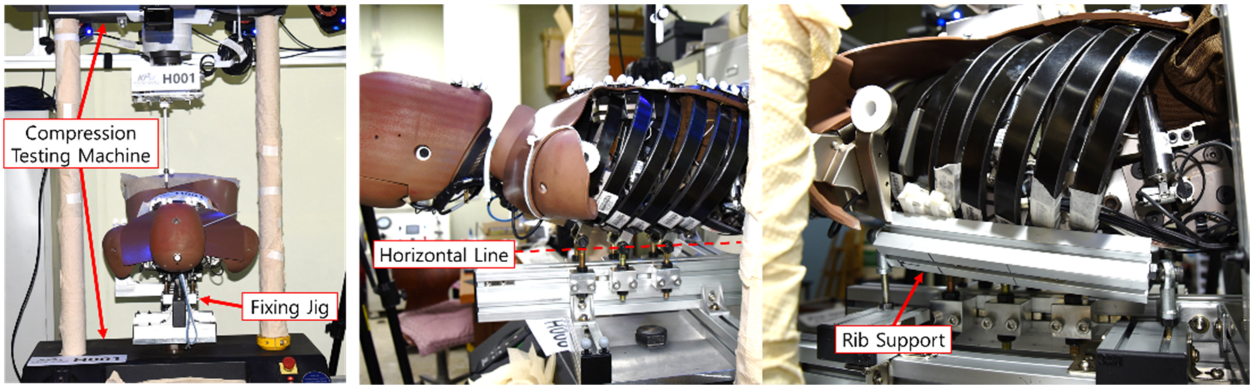

Figure 1 Dummy Positioning

Test Conditions

Rib compression test Rib compression test was performed using 10 mm diameter and 250 mm long indenter with and without the thoracic bib (See Figure 2). The end hole of each rib on the seven levels was loaded by the indenter. The end of the indenter was fabricated so that its surface becomes concave with 9 mm of the radius of curvature. The bolt at the end of the rib was replaced to the cup square neck bolt of which the radius of curvature of the head was 9 mm. The end of the indenter and the head of the bolt behaved like a ball-socket joint during the testing. The mating surface of the indenter and the head of the bolt was lubricated prior to each test. The indenter

holder consisted of two linear guides, which were perpendicular to each other so that the loading site can be translated in shear directions during the test. The loading rate was 1.7 mm/s, and the maximum compression amount ranged from 35 mm to 45 mm depending on the loading site. Each test was performed at least three times to calculate average values.

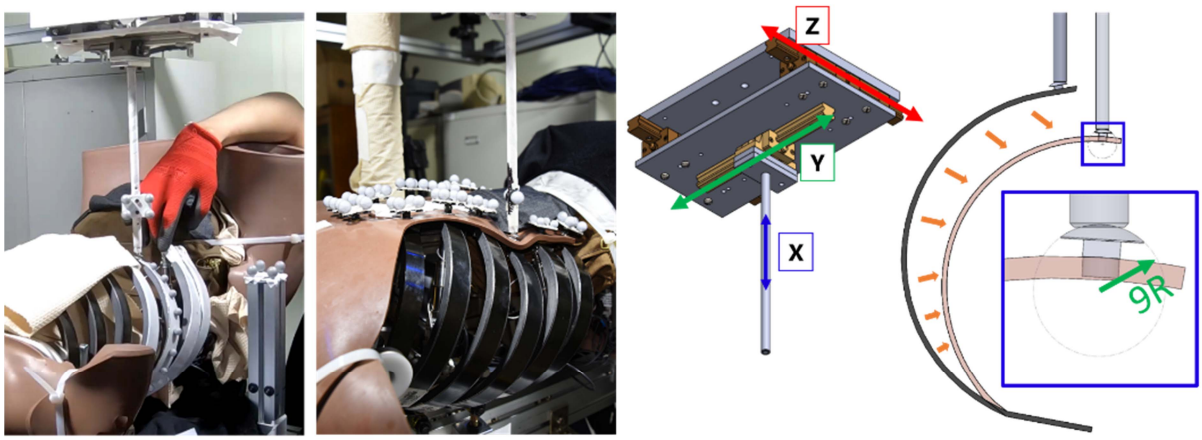

Figure 2 Indentor of rib compression test and indenter holder

Thorax compression test Thorax compression test was performed using an indenter, which the area of the contacting surface was 52 mm by 104 mm (Shaw et al., 2005, Cavanaugh et al., 1988). Following the procedure from Shaw et al. (2005), the indenter was installed to the test fixture through a ball-socket joint, which allowed around 27 degrees of rotation. The distance from the center of the rotation of the joint and the loading surface was 60 mm (See Figure 3). Three locations along the centerline of the thorax and three off centered locations were loaded (Shaw et al., 2005). Six locations, which were right-up, right-mid, right-low, stern-up, stern-mid, stern-low, was loaded with the bib installed. The indenter was rotated 30 degrees from the vertical line for the right-up and right-low tests. Twenty-five newtons of the preload was applied to ensure proper contact between the thorax and the indenter. The test was performed three times for each loading site with 1.7 mm/s of the loading rate and the 40 to 50 mm of the maximum compression amounts.

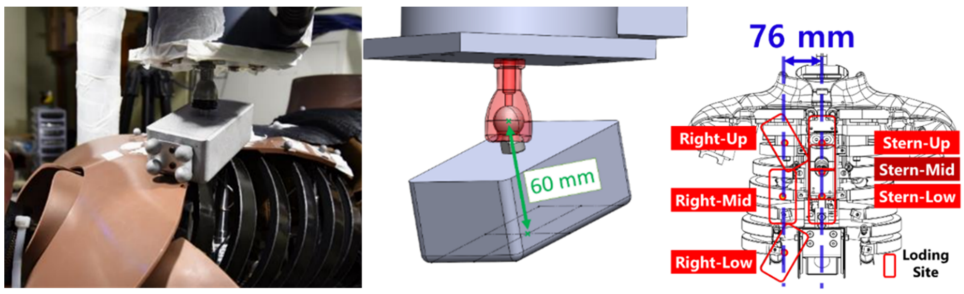

Figure 3 Indenter and indenter holder for the thorax compression test

Data Collection

The compressive force was measured using a uniaxial loadcell. The three-dimensional deformation of the thoracic and abdominal regions was measured using the built-in IR-TRACC sensors. For the rib compression test, the deformation of the other ribs without IR-TRACC installed was measured using a three-dimensional motion capture system (VICON MX^{TM}). The upper thoracic IR-TRACC (UT) and lower thoracic IR-TRACC (LT) were at the rib 3 and rib 6, respectively. For the following analysis, deflection along the direction of the compression, which was X-axis in Figure 1, was considered. The deformation of the unloaded site was calculated using the motion tracking data along the X-axis (See Figure 2). There were differences between the location of the marker and the center of the holes at the end of each rib. The displacement of the center of the hole was estimated based on the four markers attached to the end of the rib through a rigid body transformation scheme.

The stiffness was calculated using the force measured from the uniaxial loadcell at 25.4 mm of the displacement of the test device. For the rib compression test with bib and the thorax compression test, compliance, which is the deflection over the force, was calculated for the rib 3 and rib 6 where the IR-TRACC was installed. As a result, four compliance values were obtained for each test. For example, when right-side rib 2 was compressed 25.4 mm along the X-axis, the force was 0.19 kN and the right upper IR-TRACC indicated 11 mm of compression (See Figure 4). It resulted in 57 mm/kN of the compliance for the loaded-side upper thorax. During the rib compression test with bib, the coupling effect from the bib was evaluated using the displacement along the X-axis of the unloaded sites normalized to that of the loaded site, which was 25.4 mm.

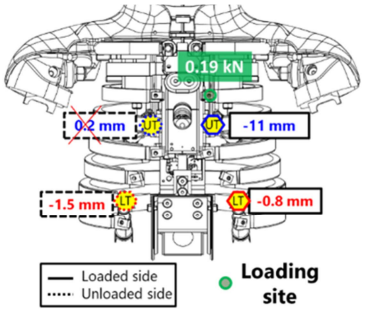

Compliance X-only	Loaded side [mm/kN]	Unloaded side [mm/kN]
UT	**57**	**0**
LT	**7**	**4**

Figure 4 Calculation of the compliance

RESULTS

Stiffness

For the rib compression test, the stiffness of the individual ribs (no bib condition) ranged from 0.8 to 2.3 N/mm (See Figure 5). When the bib was installed, the stiffness of each loading site increased from 5 to 14 times compared to the no bib condition. For the thorax compression test, the stiffness of the central area was higher than that of the corresponding off centered area.

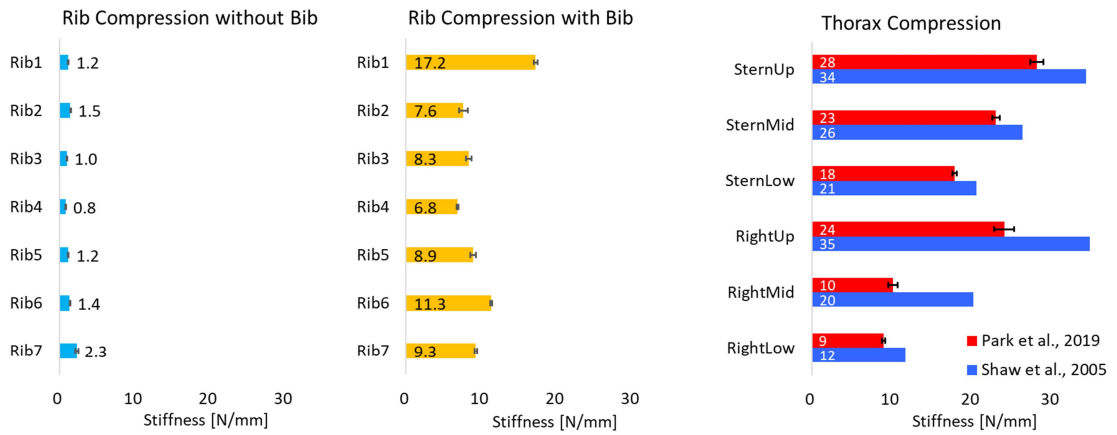

Figure 5 Summary of stiffness at 25.4 mm compression of the loading sites

Deflections of Coupled Ribs

The degrees of coupling between the loaded site and unloaded site varied depending on the loading site (See Figure 6). The coupling effect between upper and lower rib was higher than that of the loaded-side and unloaded-side except for the rib 1.

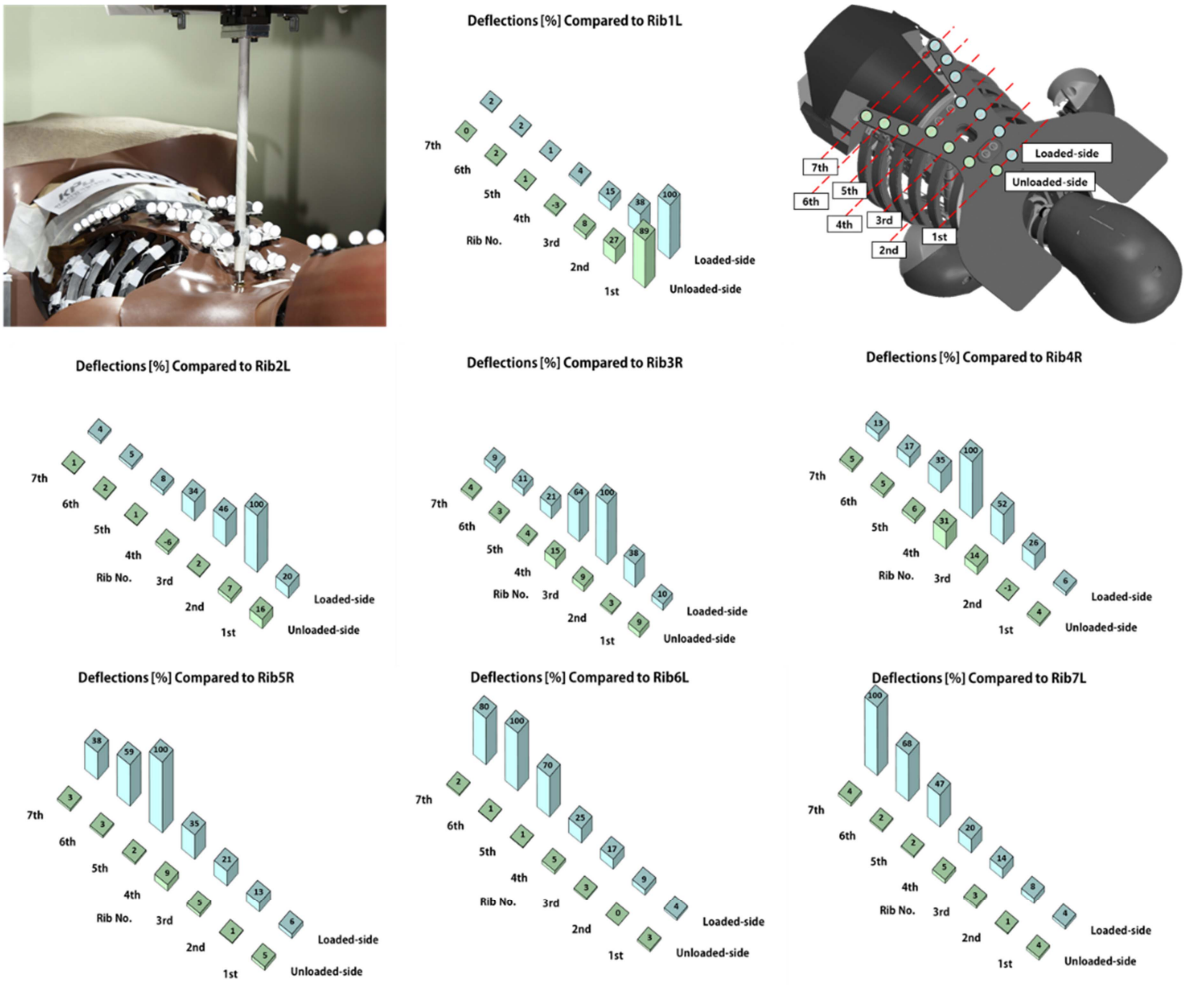

Figure 6 Summary of normalized compression amount during the rib compression tests with bib

Compliance Data

Rib compression test For the loaded side, the compliances of the upper and lower thorax showed maximum value at the rib 3 and rib 6, respectively. The compliance values for the unloaded side was less than 20 mm/kN for all the loading sites.

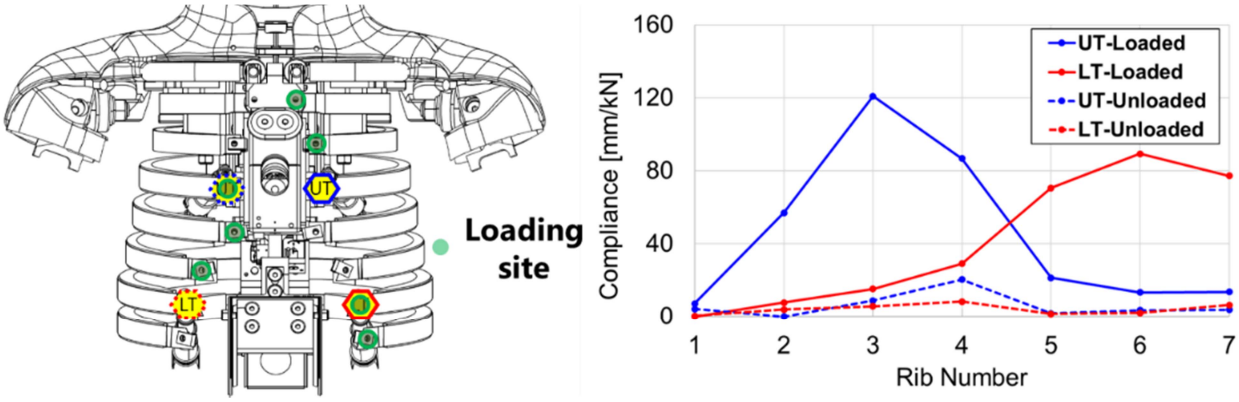

Figure 7 Compliance of four IR-TRACC sensors for each loaded rib

Thorax compression test The thorax compliance map was created by mirroring the right-side data to the left side (See Figure 8).

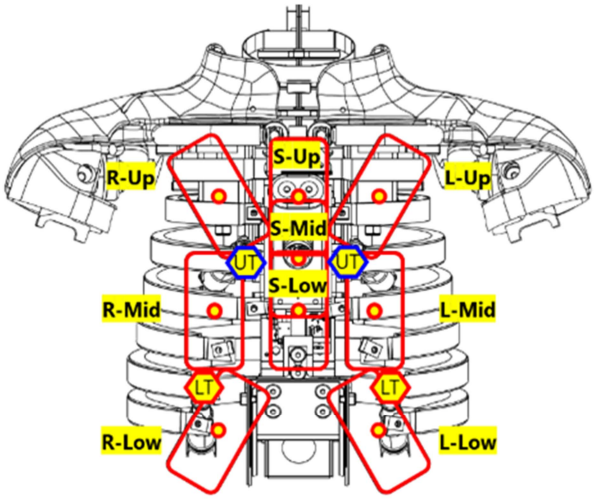

R-Up	Right	Left
UT	33	0
LT	2	1

S-Up	Right	Left
UT	20	20
LT	1	1

L-Up	Right	Left
UT	0	33
LT	1	2

S-Mid	Right	Left
UT	37	37
LT	2	2

R-Mid	Right	Left
UT	74	8
LT	52	0

S-Low	Right	Left
UT	41	41
LT	1	1

L-Mid	Right	Left
UT	8	74
LT	0	52

C=dx/F [mm/kN]
C: compliance

R-Low	Right	Left
UT	2	-4
LT	68	2

L-Low	Right	Left
UT	-4	2
LT	2	68

Figure 8 Compliance of four IR-TRACC sensors for each loaded site

DISCUSSION

A series of the thoracic compression test was performed using the THOR M50 (Metric) dummy under quasi-static loading conditions to characterize its behavior under compressive loading condition. Since the maximum deflection amount of any IR-TRACCs is used for the injury risk assessment, the emphasis was given to the deflection of the IR-TRACCs. Because of the simplified loading and boundary conditions, the test results will be useful for the THOR dummy computational model validation. During the rib compression tests, a pair of linear guides were used no to impose shear force to the rib. While the linear guide was well lubricated and it required less than 10 N to slide

in each direction under the unloaded condition, the shear force applied from the indenter to the rib during the test is unknown. During the thorax compression test, there was 60 mm of offset between the loading surface and the center of the ball-socket. This offset and the rotation of the indenter for the thorax compression test resulted in the shift of the loading sites as the joint rotated. In addition, the joint allowed the rigid body rotation of the indenter so that part of the displacement might have not resulted in the compression of the thorax. For this reason, the compliance of the thoracic IR-TRACC was calculated, which measured internal deformation. While the shear forces from the indenters to the loading sites are unknown from the current tests, the rib compression test results are less limited thanks to the linear guide for the model validation purpose.

During the rib compression test, the thoracic bib increased the stiffness of the loading site by a factor of 5 to 14. The bib created coupling between the loaded rib and unloaded ribs. Although we consider the contribution of the unloaded ribs by multiplying the stiffnesses of the unloaded ribs and compression amount due to the coupling, these amount of increase in the stiffness is not explained entirely. From the separate investigation of the three-dimensional motion tracking data, it was found that the shear displacements of the ribs during compression was decreased. It was estimated that the effects of the coupled deflection along the X-axis of the unloaded ribs contributed about 3 times increase of the stiffness of the loaded site on average. The rest of the increase in the stiffness, which was estimated three times of increase in average, attributed to the soft constraint imposed on the ribs along the shear directions. For the thorax compression test, the stiffness was higher for the superior area of the thorax for both the mid and the off-centered regions.

During the thorax compression test, the stiffness from the current study was lower than that of the Shaw et al. (2005). There are two possible contributors. First, there have been updates from the THOR-alpha to THOR-Metric dummies. Second, the range of motion of the ball joint from the current study was around 27 degrees, while that from the Shaw et al. (2005) was 12 to 15 degrees depending on the direction of the rotation.

The coupling effects due to the bib were greater for the adjacent levels than that between left and right sides except the rib 1 (See Figure 6). The rib 1 is connected to the opposite side rib via a metal part while other levels of ribs did through rubber-like material. While the sternum exists along the rib 2 to 4, it is just an added mass rather than connecting the two ribs at the same level. The thickness of the bib gets thicker for the rib 5, 6, and 7 compared to the above area. The coupling effect between the adjacent levels was the maximum when the rib 6 was loaded.

The compliance was calculated to understand the contribution of the belt forces applied to the ribs to the IR-TRACC deflection. The compliance information from the rib compression test suggested that the deflections of both the upper and lower thoracic IR-TRACCs mainly resulted from the loading applied to itself and adjacent ribs. For example, the upper thoracic IR-TRACC will be deformed mainly by the forces applied to rib 2, 3, and 4 of the same side. In addition, the IR-TRACC deflection would not be influenced by the forces applied to the opposite side due to the weak coupling between the right and left sides (See Figure 6 and Figure 7). Eggers et al. (2014) performed frontal sled tests using THOR-M50 and investigated the effect of the route of a belt on the IR-TRACC deflection of the thoracic region. The authors tried two belt routes which one of the two was lower than the other by 25.4 mm. In both cases, the belt went through the above of the left-side rib 4, and the lower left thoracic IR-TRACC showed no change in its deflection.

CONCLUSIONS

The current study provided the structural responses of the thorax of the THOR-M50 (Metric) dummy. The provided results can be used for the THOR dummy model validation as well as to understand interactions between the thorax of the THOR dummy and the restraint systems during crash test results.

ACKNOWLEDGEMENT

The authors thank Greg Shaw from University of Virginia Center for Applied Biomechanics for his guidance in reproducing the test condition.

REFERENCES

Cavanaugh, J., Jespen, K., & King, A. (1988). Quasi–static frontal loading on the thorax of cadavers and Hybrid III dummy. In Proceedings on the 16th International Workshop on Human Subject for Biomechanical Research, Atlanta (pp. 3-18).

Eggers, A., Eickhoff, B., Dobberstein, J., Zellmer, H., & Adolph, T. (2014). Effects of Variations in Belt Geometry, Double Pretensioning and Adaptive Load Limiting on Advanced Chest Measurements of THOR and Hybrid III. In Proceedings of IRCOBI Conference.

Lebarbé, M., & Petit, P. (2012, September). New biofidelity targets for the thorax of a 50th percentile adult male in frontal impact. In Proceedings of the 2012 IRCOBI Conference.

Lemmen, P., Hynd, D., Carroll, J., Davidsson, J., Been, B., Song, E., & Steeger, B. (2012). Thoracic injury assessment for improved vehicle safety. Procedia-Social and Behavioral Sciences, 48, 1649-1661.

Shaw, G., Crandall, J., & Butcher, J. (2000, September). Biofidelity evaluation of the THOR advanced frontal crash test dummy. In IRCOBI Conference on the Biomechanics of Impact.

Shaw, G., Lessley, D., Bolton, J., & Crandall, J. (2004). Assessment of the THOR and Hybrid III crash dummies: Steering wheel rim impacts to the upper abdomen (No. 2004-01-0310). SAE Technical Paper.

Shaw, G., Lessley, D., Kent, R., & Crandall, J. (2005, June). Dummy Torso Response to Anterior Quasistatic Loading. In 19th ESV Conference, Paper (No. 05-0371).

Sunnevång, C., Hynd, D., Carroll, J., & Dahlgren, M. (2014, September). Comparison of the THORAX Demonstrator and HIII sensitivity to crash severity and occupant restraint variation. In Proceedings of the IRCOBI Conference, Berlin, Germany.

Yaguchi, M., Ono, K., & Masuda, M. (2008). Biofidelic responses of the THOR-NT and Hybrid III based on component tests (No. 2008-01-0520). SAE Technical Paper.

ADAS TESTING IN CANADA: COULD PARTIAL AUTOMATION MAKE OUR ROADS SAFER?

Eric Meloche
Dominique Charlebois
Benoit Anctil
Transport Canada
Canada

Guillaume Pierre
Annie Saleh
PMG Technologies
Canada

Paper Number 19-0339

ABSTRACT

As part of an ongoing effort to further improve the safety of its road transportation system, Transport Canada (TC) has been evaluating Advanced Driver Assistance Systems (ADAS) for a number of years now. The main objective of this paper is to determine the potential of ADAS technology in reducing fatalities and injuries on Canadian roadways while using proven international test protocols and certified test equipment. The findings will be used to provide science-based evidence in support of future regulatory, research and policy development.

Results from this study clearly demonstrated that Automatic Emergency Braking (AEB) and Pedestrian AEB (P-AEB) technologies can provide significant improvements in terms of collision mitigation which can directly result in reduced road fatalities and injuries. These findings are also in line with those of studies based on real-World data predicting significant reductions in rear-end collisions due to AEB deployment.

Nonetheless, this ADAS program also exposed an important number of flaws and performance variability. While the best AEB and P-AEB systems were able to fully avoid collisions with vehicles and pedestrians at speeds up to 60 kilometers per hour (km/h), others were challenged at speeds below 10 km/h. Also, a few P-AEB systems were never able to avoid a collision with a pedestrian despite manufacturers' claims of pedestrian avoidance capabilities. Scenarios replicating AEB activation in moving traffic showed that most systems unnecessarily came to a full stop rather than match the speed of vehicles they detected on their path, potentially generating higher safety concerns than those they were designed to prevent in high density traffic. Finally, due to variability in test results and overall unpredictable system behaviour, it was not possible to gather enough data to confidently assess the potential safety benefits associated with Lane Support Systems (LSS).

AEB, P-AEB and LSS are essential components of automated driving systems which will need to reliably brake and steer at all time to safely avoid other road users. That level of performance is not yet evident from the extensive testing carried out within this project. Substantial progress is therefore needed to reach the level of detection, braking and steering performance that will be required to make commercial automated driving systems a reality.

INTRODUCTION

At the time of writing, Transport Canada (TC) had just released its latest motor vehicle collision statistics report which is generated every year from the National Collision Database (NCDB). The NCDB contains detailed information from all police-reported motor vehicle collisions that occur on Canadian roads. According to this report, fatalities, severe injuries and total injuries were at an all-time low in 2017. TC started collecting these data in the early 70's when fatalities were almost 4 times greater than what they are today despite a much lower count in licensed drivers and registered vehicles. Thankfully, with the advent of effective safety policies and technological advancement, amongst things, Canadian motorists have been witnessing a continued improvement in road safety for nearly five consecutive decades. However, even if statistics showed a downward trend in casualties for 2017, 1,841 people still lost their lives due to traffic-related collisions across the nation while 154,866 suffered injuries [1].

As part of a constant effort to further improve the safety of its road transportation system, TC has been evaluating crash avoidance technologies and Advanced Driver Assistance Systems (ADAS) for several years now. In short, ADAS technologies are the building blocks of full automation and include a wide variety of active safety features that can assist drivers in: applying the brakes automatically if an imminent crash is detected; keeping a vehicle on its traveling lane; detecting vehicles in a blind spot; or keeping a safe distance from vehicles ahead. Some of the World-leading safety experts believe that the greatest gains in highway safety in the coming years will result from a widespread application of crash avoidance technologies [2] [3].

An in-depth analysis of the latest statistics extracted from the NCDB revealed that the most frequent occurrences in which current driver assistance technologies could offer either full or partial mitigation measures was rear-end collisions (25% of collisions with casualties) while those offering the best potential for saving lives correspond to road departures (17% of fatalities) and collisions involving vulnerable road users (17% of fatalities). The latter being composed of pedestrian (15% of fatalities) and cyclists (2% of fatalities). 746 of the collisions involving fatalities (44%) and 85,993 of those involving personal injuries (74%) took place in urban settings while the remainder occurred in rural areas.

While several ADAS technologies are currently being evaluated by TC, this study will specifically focus on the assessment of Automatic Emergency Braking (AEB), Pedestrian AEB (P-AEB) and Lane Support Systems (LSS). These particular technologies were intensively investigated as they were deemed able to offer substantial safety benefits in the high risk areas previously identified. The findings of this study will be used to provide science-based evidence in support of future research, regulatory and policy development.

METHODS

The crash avoidance technologies investigated in this study use sensors such as radars, lidars, ultrasonic or cameras to scan the road ahead or surrounding a vehicle and detect potential conflicting situations. In order to properly evaluate each system, these conflicts need to be reproduced with high repeatability in controlled environments. The following sections will describe the protocols, equipment and methodology used to perform these evaluations.

Systems Tested

AEB and P-AEB systems are designed to prevent crashes or reduce their severity by braking automatically when an imminent collision is detected and the driver fails to react on time, or at all. They are characterized by 3 different functionalities: Forward Collision Warning (FCW) which warns a driver when a conflicting situation is detected; Crash Imminent Braking (CIB) which applies the brakes automatically if a driver fails to respond to the warning on time; and Dynamic Brake Support (DBS) which provides supplemental braking power if a driver does respond to the warning on time but does not brake hard enough.

LSS incorporates a group of technologies designed to assist drivers in keeping their vehicles on their traveling lane. They include Lane Departure Warning (LDW), Lane Keeping Assist (LKA), Lane Centering Systems (LCS), Emergency Lane Keeping (ELK), and others. The current evaluation will focus on LDW and LKA.

Test Vehicles

During the course of this program, approximately 100,000 km of combined on-road and track testing were conducted by TC and its contracting partner PMG Technologies on 36 different ADAS-equipped vehicles. Caution was taken to assemble a test fleet that was as diverse as representative of the real-world Canadian fleet. The vehicles selected ranged from model year (MY) 2012 to 2018 and were sourced from every manufacturers selling light passenger vehicles in Canada under 24 different brands. With the exception of a 2017 Volvo XC90 and a 2016 Tesla Model S, which were graciously lent by Volvo Canada and Environment and Climate Change Canada (ECCC), the test vehicles where acquired by TC. No details about the programs were communicated throughout the procurement process to ensure that the vehicles remained comparable to those available commercially. Table 1 provides the detailed list of vehicles used in this study.

Table 1.
Transport Canada ADAS Test Vehicle Fleet

Manufacturer	Test Vehicles
Ford Motor Company	Ford Focus, Lincoln MKX, Ford Fusion
General Motors	Chevrolet Impala, GMC Acadia
Toyota Motor Corporation	Toyota Prius PHEV (2), Toyota Corolla and Toyota Highlander
FCA	Jeep Grand Cherokee, Chrysler 200, Fiat 500X, Chrysler Pacifica
Honda Motor Company	Honda CRV, Honda Civic
Hyundai Kia Auto Group	Hyundai Genesis, Hyundai Elantra and Kia Sportage
Nissan Motor Co	Infiniti Q50 and Mitsubishi Outlander, Nissan Rogue
Volkswagen Group	Audi A3, Volkswagen Golf
Mazda	Mazda 6
Subaru Corporation	Subaru Legacy, Subaru Outback, Subaru Impreza, Subaru Crosstrek
Daimler	Mercedes-Benz C400, Mercedes-Benz E300
BMW Group	BMW i3
Tesla	Tesla Model S
Jaguar Land Rover	Land Rover Discovery Sport
Volvo	Volvo S60, Volvo XC90, Volvo XC60

Test Procedures and Protocols

For comparison and validation purposes, the work carried out in this study was based primarily on test procedures developed by the National Highway Traffic Safety Administration (NHTSA) [4] [5], the International Organization for Standardization (ISO) [6] [7], the European New Car Assessment Program (Euro NCAP) [8] [9] [10], as well as the Insurance Institute for Highway Safety (IIHS) [11] [12].

Table 2 shows the test scenarios used for both the AEB and P-AEB evaluations. A total of 4 scenarios were used to evaluate the CIB and DBS variants of AEB in static and dynamic modes: a moving car approaching a stopped car (A1) representing a car stopped at a red light, at a stop sign or in traffic; a fast car approaching a slow car (B1 / B2); and an emergency stop where two cars are traveling at the same speed in close proximity and the lead car brakes suddenly (C1). 4 scenarios were also used for P-AEB testing: a running adult crossing the path of a car far-side (CPFA-50) with a theoretical impact point located at 50% of the width of the car (median); a walking adult crossing the path of a car near-side (CPNA-25 / CPNA-75) with a theoretical impact point located at 25% / 75% of the width of the car (passenger side / driver side); and a child running from behind two near-side road-side obstructing vehicles (CPNC-50) with a theoretical impact point on the median. The target and vehicle speeds required for each scenario are provided in Table 2 while more details can be found in the above-mentioned test procedures.

Table 2.
AEB and P-AEB Test Scenarios

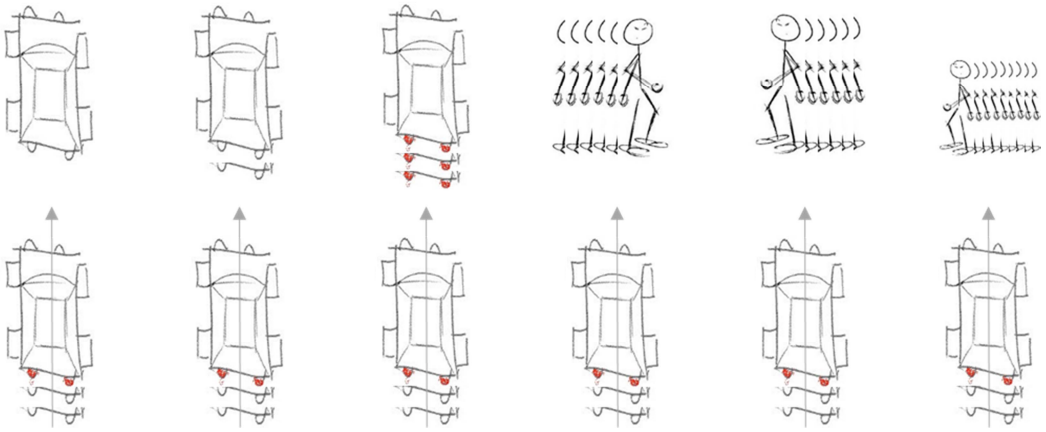

Test Scenario	STATIC A1	DYNAMIC B1 / B2	DYNAMIC C1	PED CPFA-50	PED CPNA-25/75	PED CPNC-50
Target Speed (km/h)	0	16 / 32	56	8	5	5
Vehicle Speed (km/h)	0-50	40 / 72	56	0-50	0-50	0-50

There are over 1 million kilometers (km) of roads in Canada with varied state of maintenance and quality [13]. These include 17,000 km of expressway and a total of 415,600 km of paved roads. A mixture of road segments from TC's Motor Vehicle Test Center (MVTC) which were judged representative of this vast road network were selected for the LSS evaluation. 3 different scenarios were used to evaluate the 10 different systems included in this study. The first was a drifting scenario in a straight line where a vehicle would drift towards a shoulder lane (SSL) or towards a dotted center lane (SDL) [10]. The second scenario was a vehicle entering a 493 meters (m) radius curve towards a dotted center lane (DC) [7]. The third scenario was an S-Curve course that forced the vehicle to react to a left and right lane marking consecutively (based on Scenario #1 and #2). In the Doted S-Curve scenario, the vehicle encounters the dotted line first (DS) while in the Solid S-Curve scenario, it encounters the solid line first (SS). All 3 scenarios are illustrated in Table 3.

The surface type for both Straight Line and the S-Curve scenarios was asphalt with white dotted center lines and solid yellow shoulder lanes. The Curve scenario was performed on a concrete section of a high-speed track with the same paint configuration. The road markings were mapped using an Oxford Technical Solutions (OxTS) RT 4002 system and imported into an RT-Range system to have a 2D representation of the test bed. The outer edges of the vehicles' tires were also measured and digitalized into the system to increase precision. This method allowed testing under various weather condition while always providing vehicle's position with respect to the lane markings.

Table 3.
LSS Scenarios

Scenario #1	Scenario #2	Scenario #3
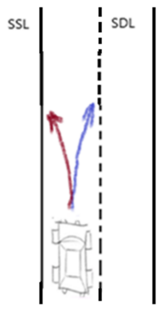	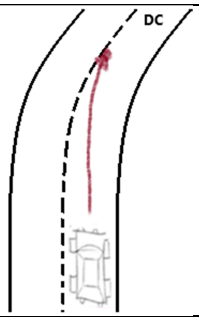	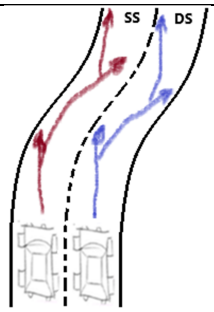
Straight Solid Line (SSL) and Straight Dotted Line (SDL)	Dotted Curve (DC), 493 m radius	Dotted S-Curve (DS) and Solid S-Curve (SS), 1,219 m radius
Entering Gate at 72 km/h		

Test Equipment

The targets used for the AEB evaluation included the Euro NCAP Vehicle Target (EVT), the NHTSA Strikeable Surrogate Vehicle (SSV) and the Euro NCAP Global Vehicle Target (GVT) coupled to the Guided Soft Target (GST) system from Anthony Best Dynamics (ABD). The P-AEB evaluation used the Euro NCAP pedestrian targets (50th percentile adult male (EPTa) and 7-year-old child (EPTc)) paired with the Soft Pedestrian Target (SPT-20) system from ABD. All of these systems were used in accordance with the test protocols previously described. Figure 1 shows the evolution of the test targets used in the Crash Avoidance program. From left to right: TC/PMG's inaugural "pendulum" vehicle surrogate target (not included in analysis), the EVT, the SSV, the EVT in winter testing condition, the GVT and to complete, the full family of pedestrian dummies.

Figure 1: Surrogate Targets used in AEB and P-AEB Evaluation Programs

The test vehicles where instrumented with RT4002 Inertial GPS Navigation Systems and RT-Range from OxTS to measure vehicle position and heading, vehicle speed and angular velocities (yaw, roll, and pitch rate), linear acceleration (longitudinal, lateral and vertical), distance to target and relative velocity. The accuracy of the GPS was augmented through the use of a portable GPS Base Station. To increase accuracy and repeatability of crucial longitudinal test parameters (i.e.: throttle input, braking input, velocity, headway), test and target tow vehicles were fitted with Combined Brake and Accelerator Robots (CBAR) from ABD. All lateral test parameters were controlled by the test drivers.

Test Methodology

The methodology used for the AEB evaluation was based on both the CIB and DBS procedures designed by NHTSA [4] [5] with the only exception that static tests (A1) were performed at speeds within the range of 10 km per hour (km/h) to 50 km/h (to allow comparison with Euro NCAP) rather than only at 40 km/h. In order to reduce the number of tests required to complete each vehicle's assessment and preserve the test equipment's integrity the following strategy was followed: the vehicle was driven at an initial speed of 20 km/h; if there was no impact, the

speed was then increased in increments of 10 km/h up to the maximum speed of 50 km/h; if an impact occurred, the speed was reduced by 5 km/h. A series of tests was considered valid if no impacts were observed in at least 5 out of 7 tests. If 3 impacts occurred before reaching 5 out of 7 tests without impact, the vehicle speed was reduced by 5 km/h. The goal was to determine the maximum avoidance speed of the systems. The test speed chart used for the static AEB scenario and all 4 P-AEB scenarios is shown in Figure 2.

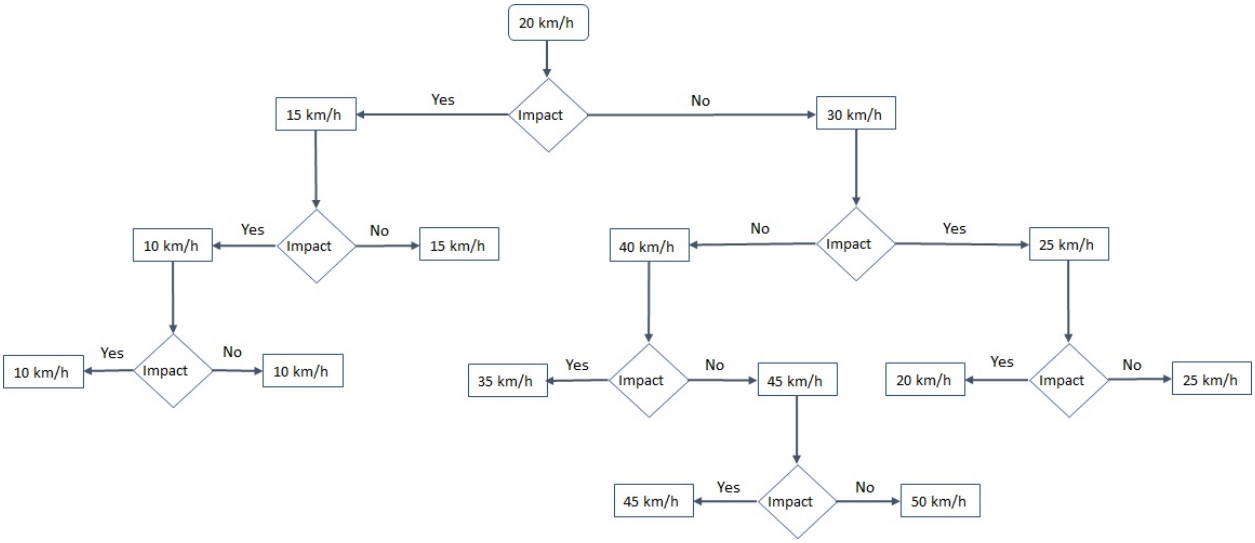

Figure 2: Test Speed Chart for Static AEB and P-AEB Evaluation Programs

The procedure used for the LSS evaluation was based on existing American and European test protocols and was designed to capture the LSS behaviours of 10 vehicles from TC's test fleet. It consisted of 5 repetitions of each test scenario (Table 3) with cruise control "on" and with cruise control "off". If the results with and without cruise control were similar, the tests were only performed 3 times in the "off" configuration. Vehicles were tested with LKA system active and inactive. Haptic signals were collected via an accelerometer on the steering wheel and audio signals via a sound probe.

The data collected during the LSS testing included: environmental conditions; offset from lane marking at warning; distance travelled from the entrance gate at warning; ambient temperature; wind speed; wind direction; the type of warning (visual, audio, haptic); test speed; and state of cruise control (on/off). The warnings were produced visually for most of the vehicles tested.

In the winter of 2019, TC started assessing the performance of LSS on snow covered roads (Figure 3). The method consisted of: creating tire tracks to produce a contrast with the surrounding environment after a snow fall; and try to engage the LSS while driving on this portion of road. 4 vehicles were tested and none of them were able to fully engage and recognize the road path. This type of condition is typical of Canadian roads in winter.

Scenario 2 Segment	Scenario 1 and 3 Segment	Winter conditions

Figure 3: Road Surfaces for LSS Testing

RESULTS

This study includes the comparative analysis of 7,710 individual crash avoidance tests obtained from 36 specimen vehicles equipped with automatic emergency braking, pedestrian automatic emergency braking and lane support systems. Over 100,000 km of combined on-road and track testing were conducted with these vehicles in a wide range of climate conditions replicating the Canadian landscape in the best possible way (standard conditions, direct sun, darkness, rain, fog, ice, and snow).

Automatic Emergency Braking (AEB) Test Results

All AEB systems tested during this evaluation were evaluated for both their CIB and DBS variants. The complete test matrix included 4 test scenarios (A1, B1, B2, C1) to be tested at a potential of up to 5 different speeds in static configuration and at one single speed in each of the dynamic scenarios. All 3 targets (EVT, SSV, GVT) were typically used for standard or rainy conditions when possible. The EVT was the only target used during the winter testing portion of the program and only the static test scenario (A1) was conducted on dry, ice and snow surfaces. The speed reductions and maximum avoidance speed presented in the Tables and Figures below consist of an average of 5 out of 7 tests as previously described.

AEB Maximum Avoidance Speed. Figure 4 shows the maximum avoidance speed achieved by each of the test vehicles in this evaluation. Some of the best systems were able to fully avoid a rear-end collision at speeds in excess of 60 km/h while others were challenged by speeds below 10 km/h. This exercise demonstrated that all systems were not designed equally and that some were not even capable of avoiding a collision at all in static scenarios. 2 of the test vehicles could not avoid a collision at any speed while 6 of them were able to avoid a collision at 50 km/h. In general, the evaluation of the CIB and DBS variant of the systems would produce similar results but for a few specimens, the level of performance measured in the DBS configuration far exceeded the level of performance measured in the CIB configuration (Table 4). For instance, one of the 2 vehicles that could not avoid a rear-end collision at any speed in the CIB configuration was able to avoid a collision at 50 km/h in the DBS configuration.

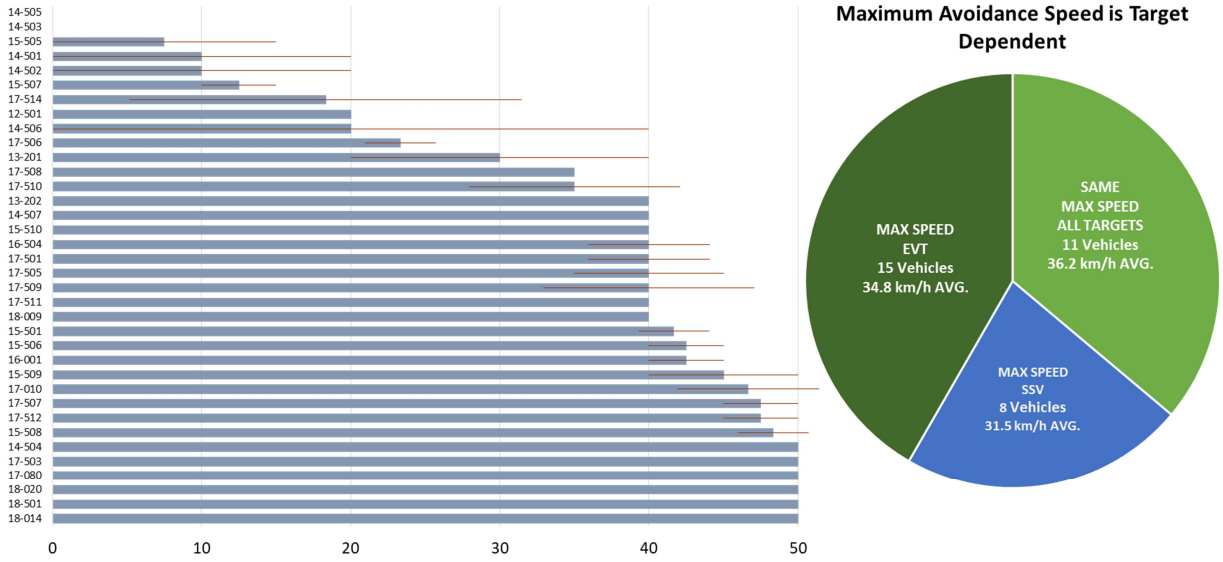

Figure 4: Maximum Avoidance Speed of 36 AEB Systems, CIB Configuration (km/h)

The maximum avoidance speed measured for each of the test vehicles as proven to be target dependent. The maximum avoidance speed was highest when tested with the EVT for 15 vehicles while 8 vehicles reached higher avoidance speeds when tested with the SSV. This could potentially be explained by the fact that a large amount of

manufacturers had indicated that their systems were developed using the EVT. For 11 of the systems tested, the test target had no influence on the maximum avoidance speed and 2 vehicles had similar results with at least 2 out of the 3 targets. The test to test variation is also illustrated by the error bars on the chart of Figure 4.

AEB Maximum Speed Reduction. Table 5 lists the speed reductions achieved by each of the AEB systems in their CIB configuration. The results were organized in a way to provide a good visual representation of the overall test fleet performance. Results are presented in increments of 5 km/h for each target and a scale of green tones was created to rank the level of speed reduction achieved for every target speed. This scale would attribute the color light grey for a speed reduction of 0 km/h (severe impact) or test speeds that were not conducted due to repeated impacts at lower speeds, the color light green for a low speed impact and the color dark green for a full avoidance or 100% of the expected speed reduction. The dark grey zones indicate scenarios that were not conducted. The results were then organized in chromatic order with the darker shades from top to bottom. A simple look at this table provides a good overview of what can generally be expected from AEB technology in terms of speed reduction and associated safety benefits as its deployment in the field is in constant progression. To sum up, the greener, the better.

The overall results suggest that 7 or 8 test samples that found themselves at the bottom of the chart did not seem to perform as well as the average of the rest of the fleet. However, when comparing these results against established performance criteria, 24 out of the 36 AEB systems evaluated achieved a level of performance sufficient to meet all the requirements set forth in NHTSA's CIB test procedure, as shown in Table 6. Concurrently, only 2 of the systems did not meet the minimum performance requirement used for the voluntary memorandum of understanding (MOU) signed between IIHS, NHTSA and the car industry for a commitment to make AEB a standard feature by 2022 in the United States (U.S.). This minimum requirement consists of a subset of NHTSA's requirement for the static test with the option of achieving a speed reduction of 15.8 km/h in either a 20 km/h or 40 km/h test or achieving a speed reduction of 7.9 km/h in both tests. Again, one of these two specimens was found to meet NHTSA's minimal performance requirements when evaluated in the DBS configuration.

As many manufacturers indicated that their system would perform better in scenarios where a target is in motion, it was expected that the level of performance would be greater for the dynamic scenarios. The chromatic scale used in Table 5 demonstrates this quite eloquently as very few areas of the 16-40 (B1), 32-72 (B2) and 56-56 (C1) columns are labelled in light grey. However, amber and red shaded cells do appear in the B1 and B2 columns. As many of the systems did bring the vehicles to a full stop instead of modulating their speed to that of the target they detected on their path, these amber and red shaded areas represent excessive speed reductions or over-braking. For every speed reduction that exceeded 24 km/h in the B1 scenarios or 40 km/h in the B2 scenarios (with a slight tolerance for both cases) a scale of amber to red tones was created. The color amber is associated with mild excessive deceleration and the color red is associated with severe excessive deceleration or a full stop. This representation is not absolutely perfect as it includes cases were vehicles did not produce excessive braking because of their system design but simply because they crashed with a target, or a vehicle if this was to be transposed in the real world. Nevertheless, this demonstrates a scenario where, if in high density traffic, AEB systems could potentially generate safety concerns which are greater than those they can prevent.

Table 4.
Vehicles with better Maximum Avoidance Speed in DBS than CIB (km/h)

Vehicle	EVT (A1)		SSV (A1)	
	CIB	DBS	CIB	DBS
14-505	0	50	0	50
16-504	40	50	30	50
17-506	25	50	20	50

AEB Performance Criteria. Table 6 provides a list of performance requirements used for the assessment of AEB systems. All requirements presented in this table are in accordance with those of NHTSA's CIB test procedure. One additional requirement for the static test scenario (A1) was also included to allow for direct results comparison with the Euro NCAP test protocol [8].

Table 5.
Speed Reductions Provided by 36 AEB Systems, CIB Configuration (km/h)

Test Vehicle	EVT A1							B1	B2	C1	SSV A1							B1	B2	C1	GVT A1							B1	B2	C1
	20	25	30	35	40	45	50	16 40	32 72	56 56	20	25	30	35	40	45	50	16 40	32 72	56 56	20	25	30	35	40	45	50	16 40	32 72	56 56
18-020	19	-	29	-	39	44	48	28	45	55	19	-	29	-	39	-	49	29	47	56	21	-	30	-	39	44	50	34	44	56
17-503	19	-	30	-	40	-	49	36	58	56	20	-	30	-	39	-	49	38	64	55	20	-	30	-	40	-	50	35	55	56
17-504	-	-	29	-	38	-	48	37	48	55	18	-	29	-	38	-	48	37	51	55										
17-507	19	-	29	-	39	-	49	40	48	50	20	-	29	-	39	41	33	34	57	47	-	-	-	-	-	41	-	-	-	-
18-501	-	-	-	-	39	-	49	37	65	46	-	-	-	-	39	-	49	37	48	48	-	-	-	-	-	-	-	37	48	51
18-014	19	-	29	-	39	44	48	39	51	55	19	-	29	-	39	-	49	-	-	-	20	-	30	-	39	-	50	-	-	-
17-010	20	-	30	-	39	44	47	35	48	52	20	-	30	-	40	-	43	39	55	54	20	-	30	-	40	-	-	37	48	53
13-201	20	-	30	-	40	-	50	40	71	48	20	-	30	-	40	-	50	40	72	45										
15-509	-	-	-	-	39	-	49	39	56	55	19	-	29	-	39	45	49	39	63	56	-	-	-	-	-	45	-	-	-	-
15-501	-	-	-	35	34	44	46	20	67	46	-	-	-	-	37	40	38	23	57	46	19	-	-	-	40	40	41	30	49	38
14-504	20	23	27	-	40	-	50	37	64	42	-	-	-	35	40	-	49	35	61	35										
16-504	20	-	30	-	40	44	34	29	41	53	-	-	30	34	34	-	-	30	29	38	19	-	30	35	36	-	-	37	26	33
17-501	-	-	-	-	39	33	41	40	66	56	15	-	30	-	39	43	41	29	40	52	19	-	30	35	38	43	-	30	45	47
17-505	20	-	29	-	40	45	45	38	48	49	13	-	30	33	33	-	-	34	25	40										
15-508	10	-	30	-	40	45	48	40	70	48	19	22	25	33	33	-	48	37	65	48	-	-	30	-	38	-	42	37	45	50
17-512	13	-	30	-	40	45	44	36	61	24	-	25	30	-	40	32	31	36	60	17	-	-	-	-	-	32	-	-	-	-
15-506	-	-	-	-	38	45	43	40	67	33	-	-	28	25	26	16	-	40	72	33										
17-511	20	-	30	-	39	39	30	40	65	29	-	-	30	-	40	39	32	32	45	21	20	-	27	27	39	39	-	40	36	23
14-507	16	17	14	-	32	-	23	25	43	22	14	20	27	35	40	45	24	27	32	27	-	-	-	-	-	45	-	-	-	-
18-009	20	-	30	-	40	18	19	36	32	48	16	-	30	-	40	18	-	39	42	45	10	-	30	-	40	18	17	38	37	48
16-001	19	25	28	35	40	38	-	37	45	53	19	25	-	35	-	44	38	23	37	40	-	-	-	-	-	44	-	-	-	-
17-510	20	25	30	-	36	34	-	19	49	56	-	25	30	32	33	-	-	32	48	49	-	25	19	-	31	-	9	28	37	56
17-509	20	-	30	35	32	-	-	40	70	56	20	-	30	-	40	-	50	39	67	56	-	-	29	33	29	-	-	40	49	46
13-202	20	-	30	35	30	-	-	36	44	35	20	-	30	29	27	-	-	40	40	40										
17-514	20	-	30	17	11	-	-	36	42	51	20	24	21	-	-	-	-	39	67	42	-	-	-	-	-	-	-	40	53	41
15-510	-	-	30	22	21	-	-	40	28	29	-	23	26	20	21	-	-	-	-	-										
14-506	19	25	19	-	16	-	-	32	27	17	-	24	19	-	16	-	-	40	20	18										
17-506	20	23	15	-	-	-	-	22	14	13	20	17	13	-	-	-	-	10	11	13	-	25	17	-	-	-	-	-	-	-
17-508	-	-	-	-	-	-	-	33	17	-	-	-	29	33	26	-	-	18	13	6										
14-501	-	18	-	-	-	-	-	-	-	-	20	-	-	-	-	-	-	-	-	-										
14-502	17	12	11	3	4	-	-	18	31	-	-	-	-	-	-	-	-	31	33	-										
14-503	10	4	9	9	7	-	5	13	8	12	-	-	-	-	-	-	-	30	63	11										
14-505	5	-	-	-	6	-	-	14	16	17	2	-	-	-	-	-	-	11	11	19										
15-505	14	11	11	-	11	-	-	11	6	14	11	-	-	12	12	-	-	10	8	-										
15-507	6	7	17	-	-	-	-	36	26	24	16	24	17	-	-	-	-	24	24	21										
12-501	17	11	-	-	-	-	-	-	-	14	12	8	4	-	-	-	-	40	-	-										

Table 6.
Crash Imminent Braking (CIB) Performance Requirements

Minimum Performance Requirements for CIB Assessment					
Scenario	A1		B1	B2	C1
Target (km/h)	0	0	16	32	56
Vehicle (km/h)	0-50	40	40	72	56
Minimum Speed Reduction Requirement	No Impact At least 5/7 valid test trials	>15.8 km/h At least 5/7 valid test trials	No Impact At least 5/7 valid test trials	>15.8 km/h At least 5/7 valid test trials	>16.9 km/h At least 5/7 valid test trials

Pedestrian Automatic Emergency Braking (P-AEB) Test Results

The P-AEB analysis included a total of 19 systems ranging from MY 2016 to 2018. Similarly to the AEB evaluation, the test matrix included 4 different test scenarios (CPFA-50, CPNA-25, CPNA-75, CPNC-50) to be tested between 10 km/h and 50 km/h. The 50th percentile adult articulated pedestrian dummy was used for the first 3 scenarios mentioned, while the 7-year-old articulated child dummy was used for the CPNC-50. Unlike the AEB evaluation, the systems were not typically tested for both their CIB and DBS variants. However, two specimens which did not perform to expectations in the CIB configuration were re-tested in the DBS configuration and showed significant improvement. The speed reductions and maximum avoidance speed presented in the Tables and Figures below consist of an average of 5 out of 7 tests as previously described.

P-AEB Maximum Avoidance Speed. The maximum avoidance speeds measured during the P-AEB evaluation were seen in the CPNA-75. For this scenario, as the theoretical point of impact was past the median line of the vehicle and that there was no obstruction, it seemed easier for the systems to detect potential conflicts. Similarly to what was experienced during the AEB evaluation, some systems were challenged by speeds below 10 km/h while others were able to fully avoid a collision with a pedestrian at speeds in excess of 60 km/h. 4 of the test vehicles evaluated could not avoid a collision at any speed while 4 of them were able to avoid a collision at 50 km/h. In general, comparing the AEB and P-AEB results showed a good correlation. The top 3 performing test samples of the P-AEB evaluation are the same as the top 3 performers of the AEB evaluation.

An analysis comparing TC's results to those of Euro NCAP showed variability in 3 out of 4 sample vehicles. The speed reductions observed with TC's sample TC17-503 where higher than those measured in the Euro NCAP test for a similar model (one MY older and lower model trim). Samples TC18-020 and TC18-501 showed good correlation except for TC18-501 that could never detect a running adult in the CPFA-50 test. The previous evaluation of a different sample from the same manufacturer (TC15-509) showed the same phenomenon even if both vehicles measured up to expectations in all 3 other P-AEB test scenarios. Finally, sample TC17-512 never detected a pedestrian in any of all 4 test scenarios in TC's tests but performed well in Euro NCAP's tests.

Table 7.
TC/Euro NCAP P-AEB Maximum Avoidance Speed in km/h

	TC17-503		TC17-512		TC18-020		TC18-501	
Scenario	Euro NCAP	TC	Euro NCAP	TC	Euro NCAP	TC	Euro NCAP	TC
CPNC-50	30	40	30	No response	40	45	35	35
CPFA-50	20	50	20	No response	60	50*	50	No response
CPNA-25	40	55	35	No response	60	50*	60	50*
CPNA-75	40	60	40	No response	60	50*	60	50*

* Maximum test speed performed

P-AEB Maximum Speed Reduction. Table 8 lists the speed reductions achieved by each of the P-AEB systems in their CIB configuration. The chromatic scale previously described in the AEB section was also used to present the P-AEB results. While there was good correlation in maximum avoidance speeds between the car-to-car and pedestrian AEB results, a comparison between the two speed reduction tables clearly demonstrates that current AEB systems perform better in car-to-car scenarios then in pedestrian scenarios. This may not necessarily be a surprise as detecting moving pedestrians and predict their position in time and space is a far more complex and challenging task than detecting a larger vehicle in a straight line. Since pedestrian and vulnerable road users represent a large portion of road fatalities, this shows that P-AEB should be identified as a primary area of research were innovation and technological advancement could produce important safety improvements. The chromatic organization of the table demonstrates that the CPNA-75 scenario produced the highest speed reductions while the CPNC-50 scenario with the child dummy and obstruction had proven to be the most challenging of all scenarios. Finally, and of concerning note, the P-AEB program also demonstrated that 4 out of 19 test specimens evaluated did not provide any mitigation in any of the 4 test scenarios despite the manufacturers' claim of pedestrian avoidance capabilities.

Table 8.
Speed Reduction Provided by 19 Pedestrian AEB Systems (km/h)

Test	CPNA-75							CPNA-25							CPFA-50							CPNC-50						
Vehicle	20	25	30	35	40	45	50	20	25	30	35	40	45	50	20	25	30	35	40	45	50	20	25	30	35	40	45	50
18-020	-	-	-	-	-	-	50	20	-	-	-	-	-	50	-	-	30	-	40	-	50	20	-	30	-	40	35	28
17-503	20	-	30	-	40	-	42	17	-	30	-	40	-	49	19	-	30	-	40	41	48	-	-	-	-	38	37	27
17-504	-	-	30	-	40	-	50	20	-	30	-	40	-	50	20	-	30	-	40	-	50	-	-	30	35	24	29	33
18-501	-	-	-	-	-	-	50	20	-	30	-	40	-	50	-	-	-	-	-	-	-	19	-	29	35	13	-	-
15-509	-	-	30	-	-	-	50	10	-	30	-	38	37	-	-	-	-	-	-	-	-	20	12	-	-	-	-	-
17-010	20	-	30	-	40	38	26	19	-	30	32	21	-	-	20	25	30	35	23	26	-	-	25	8	-	-	-	-
17-509	-	-	-	-	36	21	-	20	25	14	-	-	-	-	16	23	17	-	-	-	-	20	-	25	18	-	-	-
15-501	-	-	-	-	-	37	24	1	4	-	-	-	-	-	12	12	9	-	-	-	-	10	-	-	-	-	-	-
17-505	15	-	30	29	19	-	-	7	-	-	-	-	-	-	1	-	-	-	-	-	-	-	-	-	-	-	-	-
17-506	20	-	30	14	-	-	-	13	-	-	-	-	-	-	20	21	30	12	-	-	-	20	18	13	-	-	-	-
17-508	20	21	24	-	-	-	-	11	11	-	-	-	-	-	17	15	24	-	-	-	-	18	9	-	-	-	-	-
17-507	20	25	14	-	-	-	-	5	-	-	-	-	-	-	2	-	-	-	-	-	-	-	-	-	-	-	-	-
18-014	-	-	21	-	15	-	24	-	-	-	-	-	-	-	-	-	-	-	-	-	-	-	-	-	-	-	-	-
17-501	-	-	-	26	11	-	-	8	-	-	-	-	-	-	4	-	-	-	-	-	-	1	-	-	-	-	-	-
16-504	5	-	-	-	-	-	-	13	10	18	-	-	-	-	-	-	-	-	-	-	-	1	-	-	-	-	-	-
16-001	2	-	-	-	-	-	-	-	-	-	-	-	-	-	-	-	-	-	-	-	-	-	-	-	-	-	-	-
17-514	-	-	-	-	-	-	-	-	-	-	-	-	-	-	-	-	-	-	-	-	-	-	-	-	-	-	-	-
18-009	-	-	-	-	-	-	-	-	-	-	-	-	-	-	-	-	-	-	-	-	-	-	-	-	-	-	-	-
15-505	-	-	-	-	-	-	-	-	-	-	-	-	-	-	-	-	-	-	-	-	-	-	-	-	-	-	-	-

Fleet Averaged AEB and P-AEB Test Results. Figure 5 provides a general overview of the averaged speed reduction results observed during this study for all AEB and P-AEB scenarios in the CIB configuration, all targets combined. The intention was to provide a visual representation of the overall potential safety benefits associated with AEB and P-AEB, based on this scientific assessment. The break-down of speed reductions was in the range of: 15 km/h for pedestrian scenarios; 27 km/h for static AEB scenarios; and 43 km/h for dynamic AEB scenarios. The test to test variability is also illustrated by the error bars for each data set. The graph shows fleet average excessive braking in the range of 8-12 km/h and 4-5 km/h in the B1 and B2 scenarios, respectively, depending on the target. The red boxes represent the NHTSA performance requirements while the green box represents the requirements of the MOU between the car industry, IIHS and NHTSA, both described previously. These show that the averaged industry standard currently far exceeds the minimum performance requirements set by these two safety agencies.

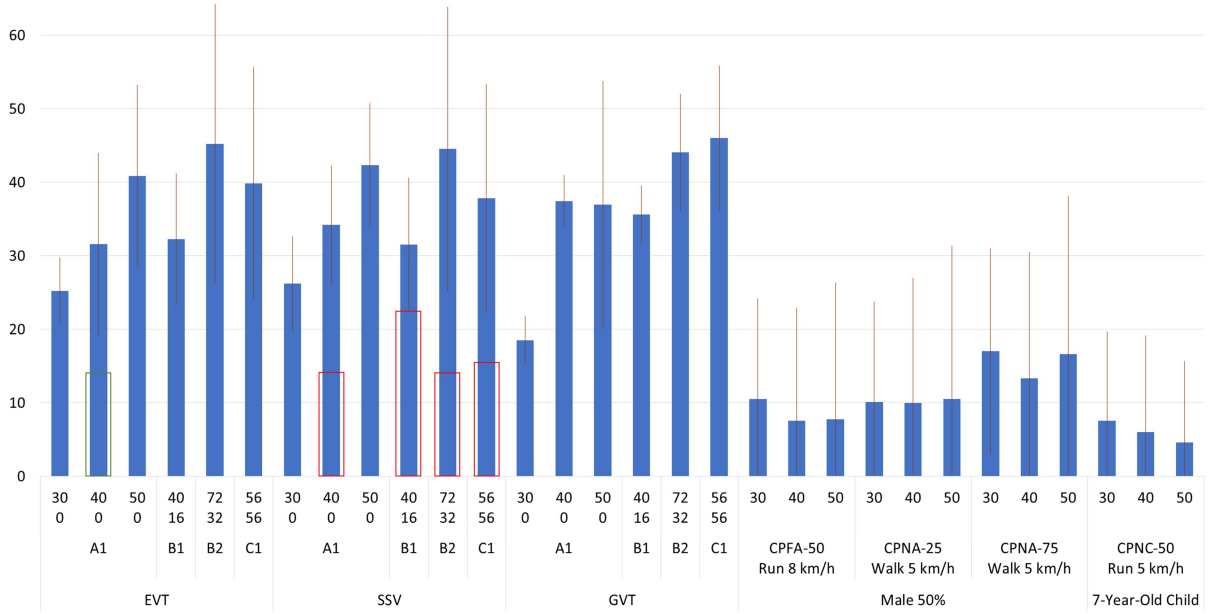

Figure 5: Averaged Speed Reductions of 36 AEB Systems and 19 P-AEB Systems (km/h)

Lane Support System (LSS) Test Results

The procedure used for the LSS evaluation was based on existing U.S. and European test protocols and was designed to capture the LSS behavior of 10 vehicles from TC's test fleet. Results from some of the test samples varied in functionalities and some systems operated differently under similar testing conditions. Some vehicles were equipped with systems that only provided warnings, while others provided warnings and correction or lane-centering capabilities. Other vehicles were equipped with LKA systems that auto-corrected without warning the driver.

Lane Departure Warning (LDW) System. All vehicles were not tested with the lane departure correction system activated. 4 out of 10 were tested in LDW only. The main focus was to evaluate the signals provided to the driver. The procedure was adapted to include the vehicles with lane correction capabilities. 4 vehicles were tested in the LDW mode and the results are presented in Table 9. 5 tests were done with the cruise control "on" in order to activate the LKA and to assist with the speed control. 3 tests were completed without cruise control. Vehicles with only the LDW functions activated resulted in at least a visual signal for all tests.

Table 9.
Lane Departure Warning

		SSL			SDL			DC		
Specimen	Cruise	Visual	Audio	Haptic	Visual	Audio	Haptic	Visual	Audio	Haptic
17-512	On	5/5	1/5	5/5	5/5	0/5	5/5	5/5	0/5	5/5
	Off	3/3	2/3	3/3	3/3	0/3	3/3	3/3	0/3	3/3
17-511	On	5/5	0/5	5/5	3/5	0/5	0/5	3/5	0/5	3/5
	Off	3/3	0/3	3/3	0/3	0/3	0/3	3/3	0/3	3/3
17-010	On	5/5	5/5	0/5	5/5	4/5	0/5	5/5	5/5	0/5
	Off	3/3	3/3	0/3	3/3	3/3	0/3	3/3	3/3	0/3
15-508	On	5/5	0/5	5/5	5/5	0/5	5/5	5/5	0/5	5/5
	Off	3/3	0/3	3/3	3/3	0/3	3/3	3/3	0/3	3/3

Lane Keeping Assist (LKA) System. Using the same tests scenarios to test the LKA functions yielded different results as can be seen in Table 10. 2 out of 8 vehicles tested stayed in their traveling lane during the 3 tests scenarios without generating warnings. This "background" system corrected for the driver to keep the vehicle in the lane and did not generated alerts unless crossing the lane. In our test, the two vehicles drove in the lane and remained between the lane markings. 4 out of 8 vehicles used their LKA system and warned the driver when approaching lane markings by using audio and visual alerts for each test. The vehicles corrected, but always warned the driver. This approach was interesting as the system tried to keep the vehicle on track, but also warned the driver if the vehicle was drifting away from the center lane. Warnings generated by number of tests are presented in the Tables below.

Table 10.
Lane Keeping Assist

		SSL			SDL			DC		
Specimen	Cruise	Visual	Audio	Haptic	Visual	Audio	Haptic	Visual	Audio	Haptic
17-503	On	On	0/5	0/5	0/5	0/5	0/5	0/5	0/5	0/5
	Off	Off	3/3	0/3	3/3	0/3	0/3	3/3	0/3	0/3
17-512	On	On	1/3	0/3	1/3	0/5	0/5	0/5	0/4	0/4
18-009	Off	Off	0/3	0/3	0/3	0/3	0/3	0/3	0/3	0/3
	On	On	5/5	0/5	0/5	5/5	0/5	0/5	5/5	0/5
18-020	Off	Off	3/3	0/3	0/3	3/3	0/3	0/3	3/3	0/3
	On	On	5/5	0/5	0/5	5/5	0/5	0/5	5/5	2/5
17-010	Off	Off	3/3	0/3	0/3	3/3	0/3	0/3	3/3	1/3
	On	On	5/5	6/5	5/5	5/5	4/5	0/5	5/5	3/3
17-503	Off	Off	3/3	3/3	0/3	3/3	2/3	0/3	3/3	3/3
18-501	On	On	2/5	2/5	0/5	5/5	5/5	0/5	3/5	3/5
	Off	Off	0/3	0/3	0/3	3/3	3/3	0/3	2/3	2/3
17-514*	On	On	5/5	0/5	0/5	5/5	0/5	0/5	5/5	5/5
	Off	Off	3/3	0/3	0/3	3/3	0/3	0/3	3/3	3/3
17-501	On	On	5/5	5/5	0/5	4/5	4/5	0/5	1/5	1/5
	Off	Off	3/3	3/3	0/3	3/3	3/3	0/3	0/3	0/3

*LKA does not correct every time, works randomly

The other observation noted for this test is a combination of lane keeping and warning systems. 2 out of 8 vehicles produced warnings and made corrections. It was interesting to see that for consecutive and repeatable test conditions, different results were observed. One of the two vehicles had issues engaging the LKA in certain tests, resulting only in audio warnings. One vehicle did not perform the same during the SSL and SDL which could be related to lane marking quality. It could be attributed to the sensitivity to recognize the "road" like lanes or simply put, a calibration difference for this system.

For scenario #3 (S-Curve) presented in Table 11, the tests were performed starting in the right lane, moving to a dotted line first and again starting in the left lane moving towards the edge of the road first. The goal of this test was to challenge the robustness of the system in having more than 1 signal input, a left input followed by a right input. In the case of pure warning only, the driver made the correction to the steering wheel to follow the path. The length of the course was 800 meters or 40 seconds in duration. The vehicle encountered an S-shaped road with a radius of curvature of 1,219 m. Some LKA systems prompted the driver to touch the steering wheel before the end of the procedure, with the first warning appearing before the end of the course. For 26 out of 40 tests conducted, the LKA helped the driver staying in the lane and 14 out of 40 tests warned of lane departure (LDW).

Looking at all combinations of the two tests, from the right and the left lane, cruise control operational or not as well as LKA system activated, 7 out of 10 vehicles reacted the same way in terms of alerting the driver. With the LKA off, visual alerts in conjunction with a vibratory alert was produced 6 times out of 8. With the LKA on, 2 vehicles

Table 11.
Scenario #3 with LKA "off" – Warning only

		SS			**DS**		
Specimen	Cruise	Visual	Audio	Haptic	Visual	Audio	Haptic
15-508	On	5/5	0/5	5/5	5/5	0/5	5/5
	Off	3/3	0/3	3/3	3/3	0/3	3/3
17-514	On	5/5	0/5	0/5	5/5	0/5	0/5
	Off	3/3	0/3	0/3	3/3	0/3	0/3
17-503	Off	3/3	0/3	3/3	0/3	0/3	3/3
17-512	On	5/5	4/5	5/5	5/5	0/5	5/5
	Off	3/3	3/3	3/3	3/3	0/3	3/3
17-511	On	5/5	0/5	5/5	5/5	0/5	5/5
	Off	3/3	0/3	3/3	3/3	0/3	3/3

Table 12.
Scenario #3 with LKA activated

		SS			**DS**		
Specimen	Cruise	Visual	Audio	Haptic	Visual	Audio	Haptic
17-514	On	0/5	0/5	0/5	5/5	0/5	0/5
	Off	0/3	0/3	0/3	3/3	0/3	0/3
18-501	On	5/5	5/5	0/5	2/5	2/5	0/5
	Off	3/3	3/3	0/3	3/3	3/3	3/3
17-010	On	5/5	5/5	0/5	5/5	5/5	0/5
	Off	3/3	3/3	0/3	3/3	3/3	0/3
17-503	On	0/5	0/5	0/5	4/5	1/5	0/5
17-512	On	0/3	0/3	0/3	0/3	0/3	0/3
	Off	0/2	0/2	0/2	0/3	0/3	0/3
18-009	On	5/5	0/5	0/5	5/5	0/5	0/5
	Off	3/3	0/3	0/3	3/3	0/3	0/3
18-020	On	5/5	0/5	0/5	5/5	0/5	0/5
	Off	3/3	0/3	0/3	3/3	0/3	0/3
17-501	On	5/5	5/5	0/5	3/5	3/5	0/5
	Off	3/3	3/3	0/3	3/3	3/3	0/3

out of 6 warned the driver with both a visual and audible signal. 3 vehicles only warned visually and 1 vehicle did not warn the driver and simply maintained its lane for the duration of the test. Two vehicles were not consistent with their warnings while the LKA was engaged and the number of alerts varied depending on whether the test was performed from a dotted line to a solid lane and vice-versa.

A difference in system reaction was observed during scenario #3, a test that represented real road conditions. It was interesting to capture the limits of the system under more challenging situations. Table 11 showed warning only and Table 12 with LKA activated mode during scenario #3.

DISCUSSION

The specific objectives of this study were as follows: evaluate the performance of ADAS to determine their potential in reducing fatalities and injuries on Canadian roadways; determine the limitations of ADAS to identify potential risks to road safety; provide scientific evidence to help shape future regulatory, research and policy development surrounding automated and connected vehicle technologies; assess and develop test methods and procedures; and evaluate the suitability of surrogate vehicle and pedestrian targets for future research and regulatory programs. To address these objectives, 7,710 individual crash avoidance tests obtained from 36 ADAS-equipped vehicles were conducted at the MVTC. While the effects of all test parameters are included in this discussion, the focus of the study banks on results obtained on-track and in standard conditions. An in-depth analysis of these results follows.

AEB. AEB systems were evaluated for their CIB and DBS variants according to 4 different test scenarios with 3 different targets replicating the characteristics of a real vehicle. The test results suggested that all systems were not designed equally. Important performance variability were observed across the fleet and some systems were not even capable of avoiding collisions in static scenarios. However, when comparing results against established performance criteria set forth by internationally recognized road safety organizations, 24 out of 36 AEB systems achieved a fully satisfactory level of performance. Concurrently, only 2 of the systems did not meet the minimum performance requirement used for the voluntary MOU signed between IIHS, NHTSA and the car industry for a commitment to make AEB a standard feature by 2022 in the U.S.

Overall, the evaluation of the CIB and DBS variant of the systems did produce similar results but for a few specimens, the level of performance measured in the DBS configuration far exceeded the level of performance measured in the CIB configuration. For instance, one of 2 vehicles that could not avoid a rear-end collision at any speed in the CIB configuration was able to avoid a collision at 50 km/h in the DBS configuration. The maximum avoidance speed measured for each of the test vehicles was found to be mostly target dependent. While 11 test specimens produced the same results independently of which target they were evaluated with, 15 vehicles could avoid the target at a higher speeds when tested with the EVT target.

A chromatic scale of the results obtained during the AEB evaluation was developed to provide an overall visual perspective of what can be expected from AEB technology in terms of safety benefits as its deployment in the field is in constant progression. The chart created clearly demonstrates that AEB technology can provide significant improvements in terms of collision mitigation which can directly result in reduced road casualties.

P-AEB. 19 P-AEB systems were evaluated according to 4 different test scenarios simulating some of the most common real-life situation involving collision between vehicle and adult or child pedestrians. The maximum avoidance speeds of the P-AEB evaluation were observed for the CPNA-75 condition. For this scenario, as the theoretical point of impact was past the median line of the vehicle and that there was no obstruction, it seemed easier for the systems to detect potential conflicts. Similarly to what was experienced during the AEB evaluation, some systems were challenged at speeds below 10 km/h while others were able to fully avoid a collision with a pedestrian at speeds in excess of 60 km/h. Overall, the speed reductions observed during the AEB evaluation of the systems were more important than those observed during the P-AEB evaluation. This may not necessarily be a surprise as detecting moving pedestrians and predict their position in time and space is a far more complex and challenging task than detecting a larger vehicle in a straight line.

An analysis comparing TC's results to those of Euro NCAP showed variability in 3 out of 4 sample vehicles. It also showed that one of the sample vehicle never detected a pedestrian in any of all 4 test scenarios in TC's tests while it performed well in the Euro NCAP tests.

Finally, and of concerning note, the P-AEB testing program demonstrated that 4 out of 19 test specimens did not provide any mitigation in any of the 4 test scenarios despite the manufacturers' claim of pedestrian detection capabilities. Since vulnerable road users and more specifically pedestrians account for a large portion of road fatalities, this shows that P-AEB should be identified as a primary area of research were innovation and technological advancement could produce important safety improvements.

LSS. As more advanced LSS testing methods are being developed using steering robots, such as described in the *Euro NCAP Lane Support Systems* test protocol [10], the testing procedure developed for this program demonstrated some limitations. The work presented here consists of an exploratory approach aiming at evaluating the status of commercially available LSS under realistic conditions. The operational limitations of 10 LSS systems were evaluated on a mixture of roads at the MVTC according to 3 different scenarios.

4 out of 4 vehicles tested with LDW produced visual warnings for SSL, SDL and DC. For that same sequence, 1 vehicle constantly produced visual and audio warnings while the others generated a combination of visual and haptic or visual and audio warnings. Only 1 vehicle generated haptic, audio and visual warnings for the SS test only. With LKA activated, 2 out of 8 vehicles stayed on their traveling lane for the SSL, SDL and DC scenarios without generating warnings. The system operated in the background and did not communicate with the driver. 3 out of 8 vehicles generated audio and visual alerts. The SS scenario was more consistent than the DS scenario as only 2 vehicles reacted differently from SS and DS. Scenario #3 was performed only with LKA activated and simulated real-world driving of an S-Curve. Only one vehicle generated a haptic signal during the DS test with the cruise control "off". This test was more challenging as 4 out of 8 vehicles did not reproduce the same warnings going into the SS or DS test. It may be attributed to lane markings as differences with respect to line types were observed in other scenarios. LSS was only constant for visual warnings and not for the enhancement of haptic and audio signals.

While the preferred strategy used to warn drivers of lane crossing for the systems tested during this evaluation was through visual signals, supplemental haptic and audio signals were inconsistent from vehicle to vehicle. At times, test drivers felt bombarded with alarms and signals without exactly knowing how they should be interpreted. System sensitivity to lane markings also seemed to be an issue for a subset of sample test vehicles. Ideally, more data and a comprehensive human factor assessment would be required in order to articulate an accurate estimate of potential safety benefits associated with LSS technologies.

Findings. As the deployment of ADAS is in constant progression, TC will continue to monitor the evolution and performance of new systems introduced on the global markets. As mentioned previously, despite being in its relative infancy, ADAS safety benefits are already recognized by several international consumers, insurance and safety organizations [2] [3]. Results from this study clearly demonstrated that AEB and P-AEB technologies can provide significant improvements in terms of collision mitigation which can directly result in reduction of road fatalities and injuries. An in-depth analysis of these results showed that while driving at speeds typical of an urban environment, the vehicle fleet evaluated in this study could provide average speed reductions of: 15 km/h in pedestrian scenarios; 27 km/h in static scenarios; and 43 km/h in dynamic scenarios. Furthermore, 66% of all tests conducted during the AEB evaluation resulted in a full avoidance. While it is not expected that such a ratio would translate to real-world conditions it seems that the findings of this study are in line with those of other studies that predicted that AEB technology could potentially reduce rear-end collisions by 38% to 50% [14] [15].

Some limitations of AEB and P-AEB systems were also exposed during this evaluation. While most systems demonstrated a satisfactory level of performance when compared against established performance criteria, the overall results suggested important performance variability across the entire fleet. Scenarios replicating AEB activation in moving traffic showed that excessive braking was generated by most systems. While the speed reduction required for the *fast vehicle approaching a slow vehicle* scenarios should ideally match the speed of the vehicle ahead and not crash into it (i.e., 16 km/h and 32 km/h), most of the test specimens rather came to a full stop. This represented speed reductions of 40 km/h and 72 km/h, respectively. This excessive deceleration is concerning as it shows a situation where AEB systems could generate higher safety risks than those they can prevent in high

density traffic. Only a few of the latest, pricier and more technologically advanced specimens behaved appropriately in these tests. Of equally concerning nature, 4 out of 19 vehicles evaluated for P-AEB were never able to avoid a collision with a pedestrian.

While a full analysis on the effects of weather conditions on AEB and P-AEB as not yet been completed due to insufficient data, it is worth mentioning that decreased performance was observed in both rain and winter conditions. More data is also required in order to articulate a comprehensive assessment of LSS technologies and their associated safety benefits due to variability in test results and generalized unpredictable system behavior.

CONCLUSION

The concept of mitigating the severity of a collision or avoiding it altogether being the best possible way to reduce traffic-related fatalities and injuries on motorways is certainly something that resonates well with most motorists. Modern ADAS technologies hold the promise of doing just that. They could potentially, or will, save thousands of lives around the world in years to come while we await a driverless and collision free future. This is assuming that they are used within the scope of their limitations and functionalities, and that it is understood that for the time being, in the vast majority of situations, they are only designed to assist drivers and not replace them.

Since its inception, TC's crash avoidance program has been investigating some of the most prominent ADAS technologies currently available on the market and evaluating how they can benefit Canadians. Results from this study clearly demonstrated that AEB and P-AEB technologies can provide significant improvements in terms of collision mitigation which can directly result in reduced road fatalities and injuries. These findings are also in line with those of studies based on real-World data predicting significant reductions in rear-end collisions due to AEB deployment.

Nonetheless, this research program also exposed an important number of flaws and performance variability. While the best AEB and P-AEB systems were able to fully avoid collisions with vehicles and pedestrians at speeds up to 60 km/h, others were challenged at speeds below 10 km/h. A few P-AEB systems were never able to avoid a collision with a pedestrian despite manufacturers' claims of pedestrian detection capabilities. Scenarios replicating AEB activation in moving traffic showed that most systems unnecessarily came to a full stop rather than match the speed of vehicles they detected on their path, potentially generating higher safety concerns than those they were designed to prevent. Finally, due to variability in test results and general unpredictable system behaviour, it was not possible to gather enough data to confidently assess the potential safety benefits associated with LSS.

AEB, P-AEB and LSS are essential components of automated driving systems which will need to reliably brake and steer at all time to safely avoid other road users. That level of performance is not yet evident from the extensive testing carried out within this project. Substantial progress is therefore needed to reach the level of detection, braking and steering performance that will be required to make commercial automated driving systems a reality.

ACKNOWLEDGMENTS

Motor Vehicle Safety (TC), Human Factors (TC), ecoTECHNOLOGIE for Vehicles (TC), Compliance (TC), Collision Investigations (TC), Defects and Recalls (TC), Transportation Division (ECCC), Emissions Research and Measurements Section (ECCC), PMG Technologies, Volvo Canada

DISCLAIMER

The contents of this report reflect the views and interpretation of the authors, who are responsible for the results, the information, and their accuracies herein. The contents do not necessarily represent, or otherwise reflect, the official opinion, position or policies of Transport Canada or the Government of Canada.

REFERENCES

[1] Transport Canada, "National Collision Database," Transport Canada, Ottawa, 2017.

[2] NHTSA, "New Car Assessment Program," Federal Register, Washington DC, 2015.

[3] Thatcham Research, "What is AEB?," 2019. [Online]. Available: https://www.thatcham.org/what-we-do/car-safety/autonomous-emergency-braking/. [Accessed March 2019].

[4] NHTSA, "Crash Imminent Brake System Performance Evaluation for the New Car Assessment Program," Washington DC, 2015.

[5] NHTSA, "Dynamic Brake Support Performance Evaluation Confirmation for the New Car Assessment Program," Washington DC, 2015.

[6] ISO TC 204/WG14 N309.48, "Intelligent Transport Systems - Forward Vehicle Collision Mitigation Systems - Operation, Performance, and Verification Requirements," 2012.

[7] ISO/FDIS 11270:2014(E) , "Intelligent transport systems lane keeping assistance systems (LKAS) performance requirement and test procedures," 2014.

[8] Euro NCAP, "AEB Systems (Car-to-Car)," 2017.

[9] Euro NCAP, "AEB Systems (Vulnerable Road Users)," 2017.

[10] Euro NCAP, "Lane Support Systems," 2017.

[11] IIHS, "Autonomous Emergency Braking Test Protocol (Version 1)," Insurance Institute for Highway Safety, Ruckersville, VA, 2013.

[12] IIHS, "Pedestrian Autonomous Emergency Braking Test Protocol (Version 1)," Insurance Institute for Highway Safety, Ruckersdale, VA, 2018.

[13] Central Intelligence Agency, "The World Factbook - North America - Canada," [Online]. Available: https://www.cia.gov/library/publications/resources/the-world-factbook/geos/ca.html. [Accessed March 2019].

[14] Fildes, "Effectiveness of low speed autonomous emergency braking in real world rear-end crashes," Accident Analysis and Prevention, Melbourne, 2015.

[15] J. B. Cicchino, "Effectiveness of forward collision warning and autonomous emergency braking systems in reducing front-to-rear crash rates," Accident Analysis and Prevention, 2017.

[16] NHTSA, "Lane Departure Warning System Confirmation Test and Lane Keeping Support Performance Documentation," Washington DC, 2013.

DETECTION OF CYCLIST AND PEDESTRIANS AROUND HEAVY COMMERCIAL VEHICLES

Dominique Charlebois
Eric Meloche
Peter Burns
Transport Canada
Canada

19-0340

ABSTRACT

Large trucks have significant blind spots, and urban settings often bring these vehicles in close proximity to vulnerable road users (VRUs). Over 13% of VRU fatalities in Canada in 2016 involved collisions with heavy commercial vehicles. Transport Canada launched a multi-year field trial, in collaboration with municipal partners, to evaluate the state of VRU detection and warning technologies. The project evaluated cyclist and pedestrian alert systems retrofitted onto different types of heavy-duty commercial vehicles. Prior to the field trial, in-depth assessments were conducted on a test track to identify suitable systems for more extensive long term testing. The equipment had to accurately and reliably alert drivers of an imminent risk of collision, based on a time to collision warning, as well as limiting the number of false positive detections. Five different candidate systems were subjected to a series of simulated "urban environment" scenarios performed on a close track. The results of these tests are presented in this paper. The technologies included, ultrasonic, radar, 360 video cameras, smart cameras, and a combination of these systems. The test scenarios were based on the most common real world VRU-truck collisions identified from collisions investigation reports. Six dynamic and four false positive scenarios were created to test the capabilities of sensors designed to alert the driver of surrounding VRUs. Data were recorded on the timing of audio and visual alerts, the GPS position of the vehicle/VRU, the velocity and environmental conditions. All the detection systems were installed on a single vehicle, traditional cabin dump truck. Three test dummies were used: a 50th percentile male, a 7 year-old-child and an adult cyclist. The results suggested that the current VRU detection and warning technology may not be sufficiently mature to fully address the risks. No single system could successfully warn the driver in time to avoid a collision in all of the test scenarios. The smart camera system performed best overall and was selected for more extensive testing on different vehicles in a multi-city field operational test.

INTRODUCTION

A common challenge for heavy-duty commercial vehicles circulating in urban areas is that they have large blind spots that can easily conceal vulnerable road users (VRUs). These risks are compounded by higher driver workload of having to maneuver large vehicles in heavy mixed urban traffic. Even in a low speed setting, a pedestrian can easily be in harm's way without having a large speed differential with the heavy-duty commercial vehicle. In 2016, 393 VRUs, 21% of all road fatalities [1], lost their lives on Canadian roads. Of these, 52 VRUs or 13.2% of those fatalities were directly attributed to heavy-duty commercial vehicles. The aim of this research was to evaluate the performance of VRU detection and warning systems to address the safety issues surrounding heavy-duty commercial vehicles operating in urban settings.

Discussions on road design, road segregation, signalization and other countermeasures have been brought forward to address the issue [4][5]. In terms of countermeasures, operators might benefit from systems that warn of VRU's close proximity and at risk. Such system used in combination with the mirrors installed on the vehicle can enable the operator to take actions to avoid a collision in a timely fashion. To improve current heavy-duty commercial vehicles, Transport Canada scanned the market for off-the-shelf solutions that could assist the operator in an urban setting [6]. A wide array of technologies were observed and studied for this evaluation: smart camera technologies, radar based alert system, ultrasonic proximity sensors and 360 view camera setup were evaluated.

In order to evaluate the performance of aftermarket solutions, ten urban scenarios were designed from detailed fatal or severe injury collision investigations. The track testing evaluated system performance in these most common hazardous situations.

METHOD

Background

The test scenarios were developed based on one hundred detailed cases analyzed by Transport Canada's collision investigations teams over the last ten years [2]. The cases were investigated due to the high sensitivity of VRUs' fatalities implicating heavy-duty commercial vehicles, as well as the need to better understand the dynamics and parameters leading to these needless events. For this study, the most common scenarios were categorized and reproduced in a closed course environment. Six scenarios were developed for direct conflict and four designed to identify false positive situations.

Equipment

Transport Canada owned a 1988 GMC Brigadier at its test facility. This test specimen represented a heavy-duty commercial vehicle, equipped with a dump box. The test vehicle was instrumented with RT4002 Inertial GPS Navigation Systems and RT-Range from Oxford Technical Solutions (Ox-TS) to measure the vehicle's position, heading, vehicle speed, angular velocities (yaw, roll, and pitch rate), linear acceleration (longitudinal, lateral and vertical) and distance to target. Three 4-Active articulated pedestrian dummies (50th percentile adult male, 7-year old child, 50th percentile adult cyclist as shown in figure 1) paired with the Soft Pedestrian Target (SPT-20) system from Anthony Best Dynamics were used to safely and accurately challenge the detection systems. The dummies were pulled by a track system and synchronized to produce dynamic conflicts between the heavy-duty commercial vehicle and the VRU. Used to evaluate passenger vehicles' ADAS systems (Advanced Driver Assistance Systems), the standardized dummies provided reliable and repeatable test conditions. These pedestrian/cyclist dummies are designed to be impacted by a vehicle. They have a radar signal cross section similar to a human and are articulated to mimic human motions which enable the evaluation of the detection system's safety and accuracy.

50th percentile male

Adult cyclist

7-year-old child

Figure 1. Surrogate dummies

Procedure

The scenarios chosen challenged the aftermarket crash avoidance technologies with a 5 seconds time to collision. The position of the VRU was recorded with respect to the position of the truck to evaluate when/where on that path to collision, the system warned the driver of the presence of the VRU. Audible and visual signals were analyzed. Videos images of the interior and exterior of the vehicle were recorded as well. The system had to provide enough time to direct the driver's attention towards the critical situation.

All systems provided either an audio or a visual signal to warn the driver about the proximity of a VRU. For the six dynamic scenarios, the smart camera technology offered a two stage warning. This extra time enabled up to 1 second of additional heads-up warning for the driver to react in certain scenarios. Radar technology was also very effective at identifying the dummies, but also triggered the alert when passing by inert objects – leading to a greater incidence of false positives. Ultrasonic sensor technology and 360 degrees view cameras only offered the benefits during four stopped scenarios, where it provided a warning of an incoming VRU into the blind spot in very close proximity of the vehicle.

Five systems were acquired and installed on the same vehicle. See Table 1 for details and specifications. All systems were tested independently from each other to ease the signal acquisition. Two systems were installed by the manufacturer's technicians and one was installed by PMG technologies based on the manufacturer's instructions.

Table 1.
Warning Systems

ID	**Provider/ type**	**Location on Truck**	**Range**	**Driver signal**
A	Ultrasonic proximity sensors	4 units along the front bumper of the vehicle 4 units along the bed of the truck on each side	1m – 2m. The testing was performed with the setting at 2 meters detection	**Visual:** LED light (light) **Audio:** Beep **Position in cabin:** A, B Pillar and middle of dashboard
B	360 view camera	3 cameras on the box, located high up: 1 at the back, and 1 on each side. 1 camera was fixed on the edge of the hood All digitally stitched.	The view really is for the close proximity of the vehicle. Approximately 2 meters around the truck.	Live monitor **Position in cabin:** Center Console
C	Radar	The radars were located on each side of the truck and activated with the turn signal. A camera was located on each side of the vehicle from the wheel fender location looking backwards.	The radar has a very narrow scan. Our radar was setup at 15 meters and had a field of view of 30 degrees.	**Visual:** gradual proximity light bar **Audio:** Beep Position in cabin: A, B Pillar
D	Smart Camera	3 smart cameras were located around the vehicle 1 at the front, 1 on each side of the truck pointing forward	To be determined based on VRU movement and direction	**Visual:** various color indicating proximity **Audio:** Beep **Position in cabin:** A, B Pillar and middle of dashboard
E	Smart Camera + Radar	One unit pointed at the back of the vehicle	Close proximity of the vehicle laterally within 2.5 meters.	Audio

Emergency braking procedure. In order to minimize the risk of damaging the dummies, an emergency braking procedure was established. The technician had a screen monitor indicating where to drive on the course and a red warning when to apply the brakes fully to avoid a collision. This sequence of hard braking was calculated to mimic an emergency braking procedure and to stop the heavy-duty commercial vehicle within a meter of the dummy. The time was recorded between the onset of the alert system and the moment the technician starts applying the brakes. Therefore, a negative time results indicated that the warning occurred after the brakes were applied, leaving no time for a reasonable warning period to allow an operator in a real world condition to understand the situation and act accordingly.

Test Protocol

Table 2 below describes the dynamic scenarios, and Table 3 contains the scenarios depicting false positives used for the project. Each scenario was repeated 5 times with each system and test configuration. This enabled repetitive data and ensure that the vehicle and VRU had the same interaction each time.

Table 2.
Collision Scenarios

Scenario #1		Scenario #2	
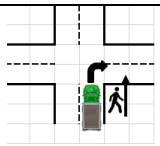	V_{truck} = 10 km/h V_{ped} = 5 km/h Impact zone = 50% front of truck	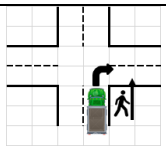	V_{truck} = 10 km/h V_{ped} = 5 km/h Impact zone = right side of truck, behind front wheel
Scenario #3		Scenario #4	
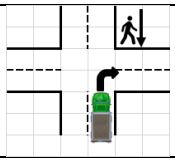	V_{truck} = 10 km/h V_{ped} = 5 km/h Impact zone = 25% front of truck (left corner	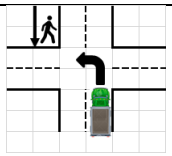	V_{truck} = 10 km/h V_{ped} = 5 km/h Impact zone = 25% front of truck (right front)
Scenario #5		Scenario #9	
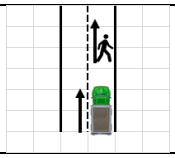	V_{truck} = 20 km/h V_{ped} = 5 km/h Impact zone = 25% front of truck	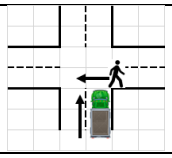	V_{truck} = 20 km/h V_{ped} = 5 km/h Impact zone = 50% front of truck

Table 3.
False Positive Scenarios

Scenario #6		Scenario #7	
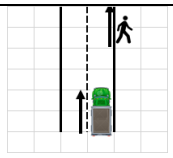	V_{truck} = 20 km/h V_{ped} = 5 km/h Impact zone = 0% front of truck, 1 meter distance between truck and pedestrian	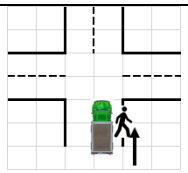	V_{truck} = 0 km/h V_{ped} = 8 km/h Impact zone = none, pedestrian between curb and truck, 1 meter zone
Scenario #8		Scenario #10	
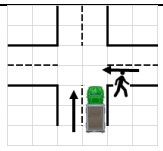	V_{truck} = 20 km/h V_{ped} = 5 km/h Impact zone = none, stops at edge of curb	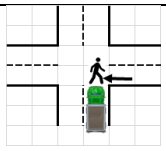	V_{truck} = 0 km/h V_{ped} = 5 km/h Impact zone = none, pedestrian walks in front of truck, 2 meters away from bumper.

The dummy was activated 5 seconds before impact and was triggered by a speed trap. Sound probe was used to trigger the alert provided by the crash avoidance system in order to include a timestamp before impact. A GoPro Camera was filming the inside of the vehicle to capture the visual portion of the alerts, the surrounding of the vehicle and to emphasize the important blind spots from inside the cabin. Two cameras were posted outside to capture the dynamics of the scene. This helped in situating the dummy with respect to the truck and to validate testing in case the dummy did not start, fell or simply behaved differently from test to test.

As testing progressed, not all scenarios were tested with each of the technologies due to limitations of certain system and time constraints. For example, the cyclist dummy was on loan for a limited period of time. Table 4 contains the matrix of the tests performed.

Table 4.
Test Matrix

		Scenarios									
		Dynamic						**False Positive**			
System	Dummy	**1**	**2**	**3**	**4**	**5**	**9**	**6**	**7**	**8**	**10**
A	Adult	X	X	X	X	X		X	X		
B	Adult	X	X	X	X	X	X	X	X	X	X
C	Adult	X	X				X	X	X	X	X
D	Adult	X	X	X	X	X	X	X	X	X	X
	Child	X	X				X				
	Cyclist	X	X		X		X	X	X	X	
E	Cyclist							X	X		

RESULTS

The results collected during this project focused on parameters such as; the type of warning (audio, visual), the time at which the alerts are produced before the emergency braking procedure. The systems were evaluated based on the lead time in the form of an audio or visual alert provided to the operator of the vehicle. Also, the false positive scenarios helped assessing the potential of nuisance during daily operation of a heavy-duty commercial vehicle in an urban environment, where these vehicles are surrounded by hundreds of VRU on a daily basis.

Performance of alert systems
Each system was evaluated individually.

System A. The ultrasonic sensors were located at the front of the vehicle as well as on the left and right side of the vehicle under the dump box. The range of this technology is limited to a 2 meters detection range, which rendered all the testing at speed obsolete. It warned the operator of a potential risk after the emergency braking procedure was engaged. One advantage of the system was demonstrated during the scenario for detection of VRU when the truck was stopped. It warned the operator if the VRU was in close proximity of the vehicle as in scenario #10. At each scenario from #1 to #5, the ultrasonic sensor alerted the driver of close proximity between 0.3 to 1.0 seconds on average after the emergency braking procedure was triggered.

Table 5.
System A warning time [seconds] with regards to emergency braking procedure

Scenarios	**1**	**2**	**3**	**4**	**5**
Time [seconds] at emergency stop (all negative values mean that the truck had initiated the emergency braking)	-0.298	-1.592	-0.905	-1.004	-0.993

In one test scenario, (#10) where the truck is idling at an intersection, the driver was alerted that pedestrians were crossing in close proximity, 2 meters in front of the truck. The ultrasonic sensor saw the pedestrian and generated an audio alert for all 5 tests. This could be a benefit to ensure that the way is clear in a congested area before starting to engage the intersection. The second scenario that could promise an advantage was Scenario #7 where a pedestrian would walk up to the right hand side of a vehicle, directly in the blind spot of our test vehicle. For 3 of the 5 tests, the ultrasonic system alerted the driver that there was activity on the side of the truck. The operator could then confirm the level of attention required by using the mirrors. One note regarding that system, if a large amount of people crossed in front of the vehicle, the level of annoyance could be high since the system would generate an alert for each VRU.

System B. The 360 view camera assisted the operator during tight manoeuvers. The top view camera did not have a field of view large enough to enhance safety in a dynamic situation. In other words, the VRU was in a critical position before he appeared on the monitor and did not provide enough time to react. Having to look at a monitor, could also lead to distraction. Due to the configuration of our test truck, the front camera was at a different height. The blind spots created at the stitching of the video was emphasized. It provided a clear view around the vehicle when stopped, increasing the operator's capacity to see around the vehicle but it could give a false sense of security if objects can't be properly defined through distortion. For our vehicle, the blind spot of the vehicle should not coordinate with the blind spot of the camera. They should be phased out to provide better coverage. Table 6 showed that the time when the VRU was identifiable on the monitor was after the emergency braking procedure was initiated.

Table 6.

Time to emergency braking procedure to appearance of VRU in the System B.

	Dynamic						**False Positive**			
	1	**2**	**3**	**4**	**5**	**9**	**6**	**7**	**8**	**10**
Average (3 tests)	0.075	-0.532	-0.895	-0.956	-1.595	-0.811	-1.695	N/A Note 1	-0.791	N/A Note 2

Note 1: The picture of the dummy deformed while standing in the blind spot. The dummy was positioned in the stitching zone of the video cameras. In this test configuration, the front camera mounted on the fender had the dummy identifiable for 4.16 seconds. System C detected the VRU and stopped warning the operator at the same time that the dummy walked out of the video streaming zone. This indicated that in that configuration, the radar covered the same zone as the camera field of view.

Note 2: For all the test, it was possible to see the dummy, waist down in the camera field of view. We did not performed the test with the child dummy, but in this configuration, the hood would have hidden the dummy from the operator and most of the dummy would have been shown on the screen, based on the height of the dummies.

Figure 2 below shows the dummy on the 360 view camera 0.43 seconds after the braking procedure was initiated. The monitor on the dashboard, right of the steering wheel was used by the technician to maintain a repeatable route and to activate the emergency braking procedure at the right time.

Figure 2. Dummy identifiable 0.43 seconds after emergency braking initiated during Scenario #1

During dynamic scenarios, it was not possible to see the pedestrian on the screen on time for the operator to start the emergency manoeuver. Two tests had 0.03 seconds lead time to the emergency procedure. This was not sufficient for the operator to realize that an action was required. As well, the operator needed to monitor the screen and this might distract from other safety tasks.

System C. The radar units were first installed on each side of the vehicle oriented backwards. This configuration would assist in detecting a VRU coming from behind especially, in combination of the camera view associated from the front fender view looking backwards. This configuration was found however not very practical to detect VRU while turning into an intersection unless they are coming from behind the vehicle. In order to increase the number of test configurations, the radar units were re-positioned frontward and therefore detecting VRU along the side of the road while the vehicle is turning. It was observed that it would increase the potential detection in Scenarios #1, 2, 3 and 4. The rearward configuration was useful in testing Scenario #7. The alert in that configuration was not sustained since the dummy travelled to position itself in the front right corner blind spot, in the opposite direction of the radar.

The radar operating field of view was kept as configured originally. This radar system was also configurable into various depth and width. For the purpose of testing here, we kept the original configuration. Radar results were produced for Scenarios #1, 2, 6, 7, 8 and 9. During Scenario #7, the system alerted 7/7. For Scenario #9, the system detected the pedestrian 4/5 and too late by an average of 0.7 seconds.

System D. The smart camera system warned the driver using two different alerts. The first alert was a visual amber light that assisted the driver in directing its attention where the potential risk was (left, right or in front). Since all our scenarios were in close proximity, the system rarely warned only of an amber alert. As the vehicle and pedestrian intend on crossing paths, the alert turned on visually red and accompanied with an audio signal. There were still blind spots around the vehicle even with this camera system. The concept was to warn the driver before VRU were too close to the vehicle. This was the only system used with the 3 dummies since it had the capability to identify both pedestrians and cyclists. It was decided due to time constraints and a generous loan from NHTSA, to limit the number of scenarios with the cyclist dummy and select the most likely conditions to represent a truck/cyclist conflict. The same configurations were used for all dummies and therefore only the shape of the VRU would be different between the adult, child and cyclist. The edge cases studied in this project were very critical

situations and the system did not always warned on time. Nevertheless, this system warned when necessary as opposed to the other systems studied. For example, the Scenario #7 did not warned the driver that pedestrians were crossing in front, unless the vehicle was starting to move. This type of approach is beneficial to limit the number of nuisance alerts to the operator.

On average, Scenarios #1, 3, 5 and 9 using the adult dummy produced audio alerts that were generated before engaging the emergency braking procedure. The same observations were made using the child dummy and the cyclist dummies as seen in table below. Only Scenario #2 (right turn and impact below the front wheel) was more challenging for this system. In all tests, the alert was generated after the emergency braking procedure was initiated. The system also generated amber warnings, which increased the response time in Scenarios #4, 6, 7, 8 and 9. It was possible to calculate a certain number of time increment using the videos from the cabin. For Scenario #9, the cyclist gained 0.98 second prior to the red warning/audio and the child gained 0.82 second. The adult gained 0.98 second as well. The Scenario #5 produced an amber warning signal that was 2.28 seconds before the red alert. And even if small, the Scenario #10 gained 0.31 second with the amber alert.

System E. The system was ordered from England and installed by PMG Technologies following the instruction provided. The system was a single unit containing the camera and radar and designed to detect cyclists only. Two relevant Scenarios (#6, 7) were tested. This system detected the cyclist using image recognition and decided if the cyclist was in arms way before alerting the driver. The system was not very reliable to detect cyclist, it could have been the speed differential with the truck, the proximity, or other parameters. The company was helpful in troubleshooting the device. Nevertheless, we could not get it to generate an audio alert using our surrogate cyclist dummy. For the purpose of our testing, we had to respect the required height and therefore locate the camera in the middle of the truck, at the front of the dump box. It is important to notice that the system was designed and calibrated to be affixed on a city bus at the A pillar location. The system appeared to work well for very particular situations. More work should be carried with a real cyclist since the manufacturer was not convinced our cyclist dummy could trigger the system as effectively.

Figure 3 shows the path used during the scenario #1. The bullet "truck at warning" was repeatable indicating that the relation between the truck and VRU was constant. On that diagram, it is important to notice that the end of the heavy commercial vehicle's path was not extrapolated to the front bumper, but simply the position of the RT range in the vehicle.

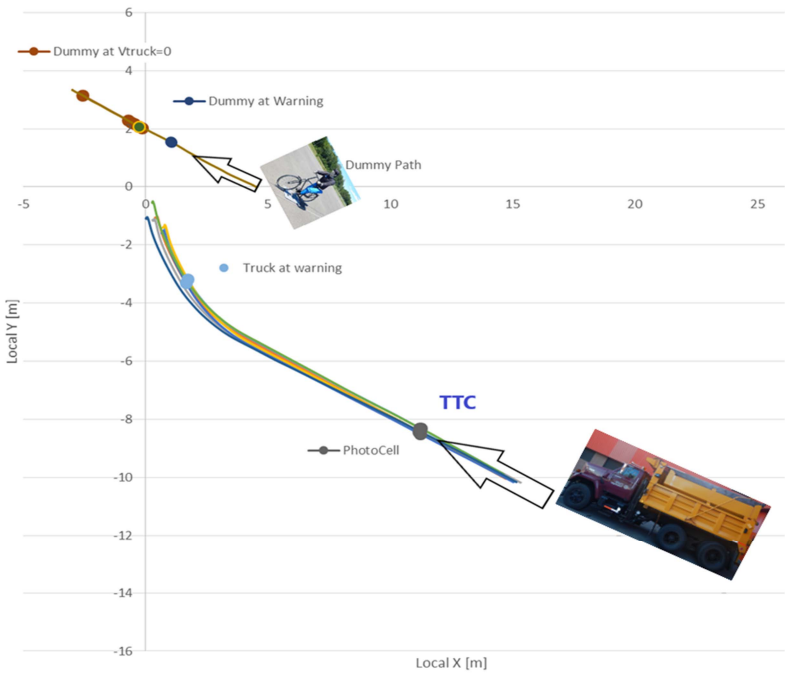

Figure 3. Sample top view Scenario 1 with a cyclist dummy

Table 7 demonstrated the time recorded by the audio warning before the emergency braking procedure took place.

Table 7.
Time to Brake in Seconds [audio warning]

		Scenarios							
		Dynamic						False Positive	
System	**Dummy**	**1**	**2**	**3**	**4**	**5**	**9**	**6**	**8**
C	Adult	n/a	-0.64				-0.78	4.77	3.71
D	Adult	0.57	-0.34	1.55		0.55	0.29		
	Child	0.14	-0.13				-0.15		
	Cyclist	0.19	-0.35		1.46				
A	Adult	-0.55	-1.59	-0.91	-1.00	-0.99		2.14	

The Scenario #2 was a very challenging scenario. It was challenging for the operator of the truck, but ever so challenging for the system to generate a proper alert. This configuration presented very little time for operators to react. It is also described in otter studies as a difficult manoeuver in urban environment [3].

At times, System D generated amber alerts on top of the red and audio alert demonstrated in Table 8 (the audio and red visual alerts were always generated together). Scenarios #5, #9 and #10 provided more time to the driver to react the incremental risk ahead.

Table 8.
Additional warning Time [seconds] by Amber Alert

		Scenarios									
		Dynamic						False Positive			
Technology	Dummy	**1**	**2**	**3**	**4**	**5**	**9**	**6**	**7**	**8**	**10**
D	Adult					2.276	0.978				0.307
	Child						0.823				
	Cyclist						0.984				

In Table 9, System D generated visual amber warnings only at times, alerting the driver that there is a potential risk. This was found to be very useful especially in false positive scenarios where the driver would not be annoyed of a more aggressive alert due to the low level of risk.

Table 9.
Test where only amber alerts were generated

		Scenarios									
		Dynamic						False Positive			
Technology	**Dummy**	**1**	**2**	**3**	**4**	**5**	**9**	**6**	**7**	**8**	**10**
D	Adult				8		1	5			
	Child						2				
	Cyclist				5		4	15	5	5	4

False Positive. Four tests were designed to trigger false positive situations where an alert to the driver might cause more annoyance than benefits. More alerts generated could overload the operator's tasks and cause distraction

or lead to complacency over time. The various scenarios sometimes generated an alert on a portion of the repetition and sometimes no alerts at all. Table 10 below indicates the rate of success or repetition as well as the outcome during the false positive scenarios. At times, more repetitions were conducted to ensure enough valid data were recorded. This should not be associated directly with the limitations of alert system, but more with the capabilities of the data acquisition equipment.

System C generated alerts for each test corresponding to Scenarios #6 and #7. The radar was not activated via the turn signal during the Scenario #8, and therefore did not generated alerts. System D was the least intrusive during all 4 false positive scenarios. Audio and visual alerts were generated for Scenario #10 only when the truck began to move forward into the intersection. When the pedestrian was crossing in front of the vehicle, no alerts (audio or visual) were generated. As soon as the vehicle moved forward, the immediate danger was communicated with a red visual alert and audio.

Table 10.
Number of Alerts Generated by Scenarios

		Scenarios									
		Dynamic						**False Positive**			
Systems	**Status**	**1**	**2**	**3**	**4**	**5**	**9**	**6**	**7**	**8**	**10**
C	Alerts	-	5				5	10	7		
	No Alerts						1			7	
D	Alerts: audio and visual	10	13	5	6	5	13				3
	Alerts: visual				4		7	11	5	9	
	No Alerts	5	4		3		1		5		4
E	No Alerts							5	6		
A	No Alerts		5	3	3	1		5	2		
	Alerts	6		3	2	4		1	3		5

DISCUSSION

During this evaluation, edge cases of urban driving were studied. A child that runs in front of a heavy-duty commercial vehicle is not something that an operator would encounter everyday but a reliable system should assist effectively in mitigating such rare occurrences. The test scenarios do not take into consideration the "real" environment such as trees, poles, other vehicles and other environmental noise. During testing with System C and System A, it was noticed that the systems alerted when passing by the speed trap setup at the beginning of the test or by any structure used to operate our equipment in the vicinity of the pedestrian test setup. The number of false alerts can play a role in diminishing the impact of the urgency of the situation. Such false alert could drive the operator of the vehicle into complacency and reduce the effectiveness of useful alerts.

Relevance of test scenario

The scenarios proved to be challenging for the systems. These edge cases with short distances at tight urban intersections and close proximity to the VRU required quick response to avoid an impact. Scenario #2, which implicated a VRU during a right turn ended up being challenging for all the systems. No system was able to generate an alert early enough to make an emergency braking procedure efficient. A test that would have started more than 5 seconds earlier than the time to collision (TTC) might have given enough time to System D to understand the complexity of the scenario. Also, the system D was installed on a short wheel base vehicle which might reduce the field of view for that particular point of impact. The system A was inefficient for this test. The system E was inappropriate for this configuration and the radar was outside the field of view range for that

configuration. System C would need to be installed lower and further back from the front of the vehicle. More optimization would be required for Scenario 2. It was also observed that systems C and D could warn of danger in a time range adequate for the operator to stop the vehicle.

Two stage warning

Based on the time required to "brake" to avoid a collision, it was calculated that the system D provided extra time to react due to the alert type. This extra time and the capability to limit the number of alerts were desirable qualities for a driver assistance system. Due to the complexity of the scenarios, most of the instances triggered red alerts and audio right away as an indication of the severity of our test scenarios.

System C used the side view camera when the turn signal was "on". It was also an interesting mitigation system as the operator required to manually activate the turn signal to gain access to the imagery. It was difficult to use the scale of the radar from amber to red as the object was approaching in close proximity. It did not provide a large amount of time before turning red due to the speed and configuration of the testing. One particular scenario that was interesting, was with the vehicle stopped at the intersection, the system produces a warning sound when the dummy passed the radar, then appeared in the camera view to end up located in a blind spot. It was interesting to see the amount of information transmitted to the driver. The issue with such a system was that, on top of normal driver workload, the operator also needed to focus on the monitor to assess the risk. Having more than one cyclist, or pedestrian executing that manoeuver at an intersection might cause information overload which could lead to unsafe distraction. More information is needed as such a system might be beneficial on certain vocational vehicles.

Limitations

The tests were performed at the same speed under each configuration. This approach was used to normalize the test method between the different systems. Having different systems under 10 various configurations created a large amount of data. The idea was to observe city speed conflicts. With higher speed, the systems would require to detect the vulnerable road user faster to enable more time to react and stop/avoid a collision. It was found from collision investigation that the majority of fatalities implicating VRU occurred at very low speed.

The equipment was not altered or optimized for the test. The approach was to install the different systems and gain experience with their responses. Sensors were slightly optimized based on manufacturer's installation instructions. But, for this particular application, one could develop the field of view of the radar differently depending on the type of detection desired, the cameras could be oriented a certain way to capture a specific blind spot or the smart camera system could be calibrated with a wider angle due to the fact that it was originally designed for a longer vehicle (City bus).

All tests were conducted up to the point of collision. The brakes were applied at the last second in order to avoid contact with the dummy. The time required to alert the driver was taken from the time our technician applied the brakes before impact. This was performed in order to reduce the impact on our equipment and to provide a repetitive work environment. The hypothesis is that if the technician is alerted before he has to technically perform the emergency brake, the chances of reducing the impact and the collision are greater. The emergency braking procedure was executed manually without the help of a robot or automation. Overlaying the paths travelled during the repetition helped in assessing when similar tests were performed. The speed and acceleration of the various dummies were repeatable and constant within tests.

Each system was tested as received and installed in order to assess the functionalities and responses to a family of surrogate dummies. The vehicle was tested without a load and therefore kinematics in real life could be slightly different. A dump truck with an added loaded cargo such as gravel, dirt or snow would have a different momentum. At the same approach speed, it would require more time and more distance to stop the vehicle due to the kinematics of a loaded truck. A loaded vehicle could also change the height of the vehicle and therefore the angle at which the cameras and radar are originally aimed. Again, this configuration was not explored in this study. The weather conditions for this testing were mostly ideal with no precipitation (snow, rain) or dirt on sensors. Future studies will use new measurement equipment to precisely measure the system sounds and visual alerts.

Candidate for FOT

This study helped us understand the limitations and functionalities of commercially available warning systems for VRU. The system D was selected due to its capabilities to select when or not to warn the operator. This particularity was of interest in the real world application of vocational vehicles. In a following field trial, fourteen vocational vehicles were equipped with this system assisted by telematics to collect valuable field data. This part of the study is currently on-going and will assess the operators' feedback and comments as well as the impact of a year round Canadian weather on the ruggedness of the equipment.

CONCLUSION

The research conducted on the test track corroborated the complexity and short reaction times of real world collision data. The tests revealed a VRU detection and warning system that provided a two-staged alert tended to be more effective. The smart camera warning system helped to increase driver awareness and provided additional time for them to assess the situation and respond. Some scenarios proved too challenging for all of systems tested. The different VRU tests scenarios, created for the purpose of this research, could be used to assess the safety of other systems in the future such as more advanced technologies like automated driving systems. Alerting the operator too frequently, or when it might not be needed, as demonstrated with the false positive scenarios was an important factor when collecting information about a system. Heavy-duty commercial vehicles operate in different environments and some system might be more useful in certain contexts. As a look to the future, a system that works with the operator to identify risk constantly, and in a predictable fashion, may better complement the current mirrors and training provided to the vehicle operators. In terms of the next steps, the performance of the smart camera VRU detection and warning system will be investigated in a field operational test. This research will evaluate the real-world performance of the system over an extended period of time in different cities across Canada. Automatic emergency braking systems may also help to avoid or mitigate collisions between VRUs and heavy vehicles (UNECE VRU Proxi). The results of this research will be used to help inform federal motor vehicle safety policy.

ACKNOWLEDGMENTS

Motor Vehicle Safety (TC), Collision Investigations (TC), Human Factors (TC), PMG Technologies, NHTSA

DISCLAIMER

The contents of this report reflect the views and interpretations of the authors, who are responsible for the results, the information, and their accuracies herein. The contents do not necessarily represent, or otherwise reflect, the official opinion, position or policies of Transport Canada or the Government of Canada.

REFERENCES

[1] Transport Canada, "National Collision Database," Transport Canada, Ottawa, 2017.

[2] Comeau, J.L., Monk, B., Boase, P., Charlebois, D., Burns, P. and German, A. (2019). Commercial Vehicles and Vulnerable Road Users, Canadian Association of Road Safety Professionals Conference (CARSP, 2019). May 26-29, Calgary, Alberta.

[3] Department of Civil, Construction and Environmental Engineering, Sapienza University of Rome, "Safety Problems in Urban Cycling Mobility: A quantitative Risk Analysis at Urban Intersection", Rome Italy, 2019 [Online] https://www.mdpi.com/2313-576X/5/1/6/htm .

[4] CCMTA-CCATM, "Countermeasures to Improve Pedestrian Safety in Canada", 2013 [Online] http://ccmta.ca/images/publications/pdf/CCMTA_Pedestrian_Report_Eng_FINAL.pdf .

[5] Council of Ministers, "Safety Measures for Cyclists and Pedestrians Around Heavy Vehicles", June 2018 [Online] https://comt.ca/reports/safetymeasures.pdf .

[6] Olaf Op den Camp and Al., "CATS Final project summary report TNO 2016 R10921", TNO, The Netherland, 2016.

CERTIFICATION OF HIGHLY AUTOMATED VEHICLES FOR USE ON PUBLIC ROADS

John McDermid
University of York and FiveAI
UK

Phil Koopman
Carnegie-Mellon University
USA

Robert Hierons
Brunel University
UK

Siddartha Khastgir
University of Warwick
UK

John A Clark
University of Sheffield
UK

Michael Fisher
University of Liverpool
UK

Rob Alexander
University of York
UK

Kerstin Eder
University of Bristol
UK

Pete Thomas
University of Loughborough
UK

Geoff Barrett
UK

Philip Torr
University of Oxford and FiveAI
UK

Andrew Blake
FiveAI
UK

Subramanian Ramamoorthy
University of Edinburgh and FiveAI
UK

Paper Number 19-0343

ABSTRACT

Objective: A number of different methods must be combined for the robust certification of highly automated vehicles (HAVs) for deployment in ODDs encompassing public roads. This paper, which is authored by a braintrust of the world's leading academics in validation, verification and certification and affiliated with Europe's largest autonomous vehicle developer FiveAI, proposes a core set of processes.

Methods: The paper discusses in detail: (1) requirements discovery; (2) behaviour requirements; (3) simulation as a tool for verification; (4) useful tools and methods.

Results: We propose a process centred around hyper-scale fuzzed scenario-based testing and the use of coverage driven verification methods in digital twins of the ODD and using generative models representative of each ODD. Testing must cover both full stack testing, which will require photo-realistic and sensor-realistic rendering of scenarios and objects, together with accurate sensor modelling and motion planning stack testing, will require robust beliefs over scenario actor behaviours to test predictive, planning and motion synthesis.

Discussion and Conclusions: The paper poses several questions for policy makers: (1) Could a validation, verification and certification system that incentivizes sharing of scenarios while protecting the value intrinsic to their discovery, improve safety across the industry? Could it be used by an approval body such as a national Certification Agency to establish a high standard for national certification? (2) Can the industry agree on a scenario description language that supports coverage-driven verification and is extensible? (3) What should the specification of an appropriate simulation environment be? (4) Could the specification for a test oracle be made available and could this be based on a formal description of 'good driving'? (5) Is auditable adherence to the IATF16949:2016 quality assurance process sufficient to satisfy 'Conformity of Production'?

Key questions also remain, including: (a) What machine learning methods should be applied to directed random testing in coverage driven verification? (b) Given the high dimensionality of the test space, what coverage measures are meaningful in generative and ODD digital twin verification? (c) Which computer vision methods can we apply to the 3D reconstruction of digital twin worlds from photogrammetry, LIDAR scans and other modalities that mean accurate, up-to-date digital twins are feasible? (d) What hardware acceleration beyond GPUs can we design and apply to enable faster-than-real-time full stack verification of HAVs? (e) How can we apply formal software checking to the complex integrated systems required for autonomous driving to ensure that each build achieves its goals without bugs or gaps? (f) How do we really apply formal mathematical methods to express the Digital Highway Code (DHC), vehicle dynamics and other road user expectations and behaviours to verify the behavioural safety of HAVs? (g) How can we verify HAV systems that comprise of one or more end-to-end neural networks with the requirements to explain failure modes and take corrective actions to improve their performance using human readability and intermediate outputs of modular processes? (h) How might we extrapolate randomized testing, including near collisions, into a measure of probability of collision generally?

INTRODUCTION

The development of Highly Automated Vehicles (HAVs) capable of performing SAE Level 4 autonomous driving (AD) is a huge attractor of intellectual and capital investment across the world today. No single company has developed a complete system of hardware and software that can realistically be deployed in unconstrained urban environments yet, but several teams expect to attain a standard that they consider should be deployable in our cities within 3-5 years, perhaps sooner in simple, wide, well-lit and sparse urban zones.

If we are able to deploy such systems, they have the potential to unlock major economic and societal benefits for city dwellers and our economies as whole: the means to offer low cost universal demand-responsive mobility to every citizen, a tool for unlocking unproductive commuting time and enabling economic engagement for everyone, increased road safety for all road users and materially lower pollution, congestion and resources today wasted in manufacturing, assembling, parking and disposing of personal vehicles. In delivering safe, on-demand, shared end-to-end journeys across a city, including zero occupancy dispatch, the advent of HAVs will presage an inevitable and

dramatic shift away from the car ownership model which has prevailed for over 100 years towards a low cost, shared mobility-as-a-service world which can integrate more successfully with shared public transport services.

Reaching that goal is requiring large teams of computer scientists, mathematicians, engineers, roboticists and manufacturers to work together across disciplines to meet many engineering and implementation challenges. These are highly complex technologies which must be built using commercially feasible hardware and by selecting, hardening and integrating many recent, and still being developed, cutting-edge research breakthroughs from academia. Not only must those teams themselves test and validate the resulting systems to ensure they do not cause injury or death to humans and animals or endanger property, the public as a whole – along with their elected representatives – need the reassurance of a clear and rational means to validate the safety of these systems independently through an appropriate regime of validation and a process of certification.

What is already clear is that the combinatorial effects of different road topologies, road users, appearances, lighting, weather, behaviours, sensors, seasons, velocities, randomness and deliberate actions cannot be adequately experienced in on-road testing alone, even in the constrained operational design domain (ODD)[1] constraints implied by level 4 autonomy. And if they could, it would take billions of highly varied miles of drive testing on each individual build of hardware and software to reach a statistically reliable level of validation that the proposed system could even attain human levels of safety. The stakes are high: even a single bad character in one line of software code can, and has, caused catastrophic failure. Any such failures found in testing would require build change with the potential for regressive effects meaning that the testing process would need to start again. This means that a methodology that rests solely, or mainly, on on-road testing is infeasible.

Although international and national standards exist for the functional safety of individual components and sub-systems (e.g. ISO 26262), no regulatory authority today has a well-defined system for validation of HAVs as a complete system rooted in an understanding of the problem space. For example, measures set out by California's Department for Motor Vehicles (DMV) include the reporting of 'driven miles per disengagement' and this is sometimes presumed as a competitive measure of maturity and safety of proposed systems. Not only can these measures be statistically meaningless[2] – only a tiny fraction of the potential state space has been explored – but they are potentially harmful in encouraging premature and non-representative on-road testing, discouraging interventions and propagating a misleading perspective on safety, leading to loss of life. Our opportunity is to set out a framework and ensure our testing and validation processes are world-leading, thereby ensuring safety for our citizens, gaining economic advantage first and unlocking global business opportunity for our scientific and engineering companies who embrace the regime.

In light of the perceived benefits from HAVs, the UK government has indicated a willingness to provide an exemption from (or modification to) the construction and use regulations so that they can be used on public roads before 2021, with more wide-sweeping legislative reform targeted thereafter.

While nobody should expect these systems to be perfect, we should expect them to reach human driver safety levels and to be progressively tightened to significantly higher safety levels over time. In that quest, it's important that development and testing practices are established, are followed and that developers and regulators can measure the safety performance of each combination of technologies in representative environments to a statistically meaningful standard.

This paper therefore seeks to explore the problem space, propose appropriate practices and contribute to the establishment of a certification regime that will safely unlock the value of HAVs to our citizens.

SAFETY OBJECTIVE

Once human levels of safety have been attained and surpassed, a primary objective for any HAV program should be to reduce the incidence of injury to humans, animals and property.

The UK's Department for Transport reported that in 2016, 327 billion vehicle miles were driven in the UK and there were 137,000 'accidents' reported to the police which are essentially collisions reported to insurance companies. That equates to one reported 'accident' every 2.4 million driven miles, with reported serious injury occurring every

12.6 million driven miles. Not all incidents are police-reported 'accidents' and collisions are likely to be significantly more frequent than the reported statistics indicate. The number of motor insurance claims in 2016 was 4.34 million[3], or one claim every 75,000 driven miles and many accidents are not reported to insurers.

The Institute of Advanced Motorists in their 'Licensed to Skill' report in 2010 estimated that around 94% of these incidents can be traced directly to human error but, in terms of public acceptance, HAVs that cause human injury or death are likely to be held to a higher standard than fellow humans, however irrational that may be. We do not know exactly how much higher these standards will need to be, but it seems likely that in order for the general public to accept the relinquishing of control to these emerging autonomous systems, halving the collision rate would be a minimum target. And that implies an incident rate of around once per 200,000 miles.

If the above were achieved, HAVs could halve serious injury and death on our roads, saving over a thousand lives each year in the UK alone, most in the 15-29 age bracket. The societal benefit is an overwhelming one.

REGULATORY CONTEXT

Regulations governing the standards, testing and certification of product conformity of vehicles on public roads in Europe are governed by European Union (EU) Directives and, by virtue of the fact that the EU is a contracting party to global technical regulations coordinated by the United Nations (UN), are also governed by safety and environmental aspects of UN regulations too. The UN regulations are managed by the World Forum for Harmonization of Vehicle Regulations, a permanent working party of the United Nations Economic Commission for Europe (UNECE). UNECE and EU countries take part in the technical preparatory work of the Forum and UNECE exercises the right to vote in the Forum on behalf of the EU.

Directive 2007/46/EC provides that EU countries share a common legal framework and general technical requirements for the approval of new vehicles and of systems, components and technical units designed for them. It establishes a harmonized framework so as to facilitate the registration, sale and entry into service of new vehicles anywhere in the EU, as well as rules regarding the sale and entry into service of vehicle parts and equipment.

For vehicles to be approved for registration, sale and entry into service, the 'whole vehicle' must pass all applicable approvals and, for this purpose, a single production sample is selected and tested as representative of the type to be approved, hence the term Type Approval. In order to gain whole vehicle Type Approval, each of the various systems, e.g. brakes, emissions, noise, etc., must be tested and meet the standards set out in the relevant EU Directives and UNECE regulations. There are no additional whole vehicle tests; instead the sample vehicle will be considered as a whole by a designated approval body and if the production sample of the complete vehicle can be confirmed to match the specifications contained in all the separate Directive approvals, then on submission of the relevant manufacturer's information documents, it will result in the issue of a European Whole Vehicle Type Approval Certificate (EWVTA).

EU Regulations permit any EU Member State to appoint an Approval Authority to issue those EWVTAs and to appoint a Technical Service to carry out the testing to the EU Directives and Regulations standards. In the UK, both the Approval Authority and Technical Service functions are performed by the Vehicle Certification Agency (VCA).

No technical Directive yet exists for the approval of HAVs. Moreover, existing Directives sometimes conflict with such operation: one example being the UNECE regulation no 79 on steering type approval which places an effective 12km/h limit on HAVs through clause 5.1.6.1 which states that 'Automatically Commanded Steering …. action shall be automatically disabled if the vehicle speed exceeds the set limit of 10 km/h by more than 20 per cent'.

Several working groups have been established to seek consensus on how UNECE and EU Directives should be amended to permit HAV operation.

OBJECTIVE OF THIS PAPER

The objective of this paper is not to identify conflicts within the existing Type Approval process or suggest amendments to the existing Directives – this work is already underway through the various working groups – but to

identify the key components of a validation, verification and certification process for HAVs that could be adopted to ensure their safe introduction on UK and European roads, along with highlighting the open research questions in relation to that process.

Until now, there have been no universally accepted dividing lines between validation (which checks that the required specification is complete and accurate), verification (which is the process used to gain confidence in the correctness of a design or system with respect to its specification) and certification (which is the legal recognition by a certification authority that a product or service complies with the requirements).

This paper therefore proposes the following approach:

- To propose a target general framework, to be achieved over time, which is capable of being applied to the discovery and establishment of adequate specifications for HAVs, which defines a process for validating those specifications (including safety properties) and which establishes a means of verifying that any candidate System under Test (SUT) is robust to all major classes of defects against those validated specifications to a measurable standard. This will permit HAV technology developers to attain and, over time, exceed human levels of driver safety

- To establish that framework as a code of practice that the UK (and by extension, if adopted, the EU) will require HAV technology developers to internally adopt for V&V, if they want to deploy in those regulatory environments

- To require that the UK (and by extension, if adopted, the EU) certification authorities adopt the same framework to independently verify a randomized subset of the design verification

- To require certification authorities (or an approval body) to conduct an audit of the quality assurance (QA) processes of the HAV technology vendor to ensure that the design and test methodology they employ is rigorous

- To require that there is a process whereby HAV technology developer software updates remain robust to regressions and conform to specifications as they are updated

This paper is structured in the above order, first identifying the key attributes of a V&V framework for HAVs and then discussing how this may be applied in the context of certification.

A FRAMEWORK FOR HIGHLY AUTOMATED VEHICLE SAFETY VALIDATION & VERIFICATION

To ensure a HAV validation framework can establish and measure performance against necessary safety standards, it must address at least five types of defects. These are intended to cover all types of potential faults in the system, its environment or its use:

- **Requirements defect**: the system is specified to do the wrong thing (defect) or is not required to do the right thing (gap) or the Operational Design Domain (ODD) description is incomplete (gap) or inaccurate (i.e. a validation defect). These types of defects may manifest as product defects where the system does something unsafe or as process defects, i.e. where there is insufficient evidence of safety

- **Design defect**: the system design fails to meet a specified safety and/or functional requirement or fails to respond properly to violations of the defined ODD

- **Implementation defect**: the implementation of the system does not conform to its design specification

- **Verification plan defect**: the verification plan fails to exercise potential states (e.g. corner cases) in requirements or to identify instances in which the vehicle's interpretation of the external world is incorrect to the degree that safety is impaired

- **Safety or reliability defect**: an invalid input or a corrupted system state causes an unsafe system behaviour or failure (e.g. sensor noise, component fault, software defect) or an excursion beyond the ODD due to external forces

HAV Requirements
A key challenge for the safety assurance of HAVs is in understanding the system requirements and validating that they sufficiently represent the ODD before verification of the system against those requirements can begin.

Vehicle Road Testing for Requirements Discovery Discovering the system requirements for HAVs in a target ODD is a huge and necessarily incomplete task, partly because the real world has high dimensionality and combination possibilities – objects, environment, behaviours, degradations, sensors, occlusions and so on – but also because the process of discovering precisely what is needed is never finished as the real world keeps changing.

Since no digital record exists anywhere that does or could possibly describe all the possible stand-alone and combinatorial possibilities that might exist in anything other than the simplest ODD the HAV could be presented with, any system specification will inevitably still present gaps to the real requirements.

Minimizing those requirement gaps is the primary motivation for on-road vehicle data-gathering and testing operations. These include:

- Detecting novel road hazards
- Detecting lighting, weather, specularities, sensor combinatorial failures in the ODD
- Discovering behaviours that violate normal traffic rules and finding exceptional but possible scenarios
- Learning accepted norms of driving
- Discovering unusual road user configurations, surfaces, aesthetics and behaviours
- Discovering how behaviours vary by time of day, weather, season
- Finding situations where sensing modalities fail, localization exhibits randomness or biases
- Finding and correcting misleading but well-formed map data
- Discovering types of novel road signs and traffic management mechanisms specific to a micro-location or event
- Finding unusual road markings and vandalism, degradations, mistakes
- Learning emergent traffic effects caused by the HAV and learning third-party behaviours due to the presence of the HAV
- Learning malicious third-party behaviours

Once a discovered requirement is identified by vehicle testing in the ODD and validated (distinct from an SUT verification failure against an existing system specification), there should be an update to the system requirements for that ODD, an update to the requirements for the fidelity of the simulation environment, the generation of one or more new test cases or a combination of all three.

The larger the ODD, the longer and more expensive the requirements discovery process will be. It is for this reason, amongst others, that we are a long way away from a true SAE level 5 autonomous driving capability.

Hazard Analysis While real-world discovery of requirements is an essential part of requirements capture, systems engineering methods like STPA (Systems Theoretic Process Analysis developed by MIT) or Functional Hazard Analysis (FHA) should also be adopted to better understand where defects of any kind can lead to hazards. STPA has been used in the aviation industry by Boeing, Embraer and NASA.

Encoding Scenario Requirements Efforts are underway in various countries to document the HAV's requirements as a curated set of vehicle behaviours and scenarios, the largest being the **P**roject for the **E**stablishment of **G**enerally **A**ccepted quality criteria, tools and methods as well as **S**cenarios and **S**ituations for the release of highly-automated driving functions supported by Germany's Federal Ministry for Economic Affairs and Energy (the **Pegasus** project).[4]

The capture and curation of such scenarios and behaviours provides a means not just to specify system performance but to develop and verify functionality that attempts to meet those system specifications. Such scenarios and behaviours can also be used to generate regression tests which can be replayed in simulated worlds to play a part in verifying some aspects of the behaviour of an entire system-under-test (SUT), as well as to provide a baseline from which to randomize variables to discover new failure modes of the SUT.

The Pegasus project, which has gained the broad support of many major participants in the German automotive industry, has the aim of developing procedures for the testing of AD functions, in order to facilitate the rapid implementation of HAVs into practice.

Scenarios are a key element of the Pegasus verification concept in that they are the basis for eliciting whether the HAV under test exhibits appropriately safe system-level behaviours. Scenarios have a functional view (described in free text), a logical view (with a set of ranges for the "interesting variables"), and a concrete view (with all these variables given concrete values).

Pegasus scenarios can be captured in a number of different ways but since the whole project is still at an early stage, today there is just one live capture method, **OpenSCENARIO**. This is an XML-based format proposed by Vires Simulations Technologie GmbH and capable of being interpreted on Virtual Test Drive, a widely-used simulation platform Vires has developed and marketed. OpenSCENARIO is therefore currently being adopted by all participants in Pegasus as a pro tem standard for capturing concrete test cases. Longer-term, the Pegasus project hopes that OpenSCENARIO might evolve to become a cross-platform industry-wide standard for encoding scenarios and behaviours that could be ported to many or all simulation and testing execution platforms (including software-in-the-loop simulators, hardware-in-the-loop simulators and test track setups).

Behaviour Requirements

Encoding such scenarios and confirming the ability of the SUT to perform a manoeuvre that avoids collision in testing against each scenario has limitations unless we can also verify whether the SUT can conform to traffic laws and to driving codes of practice during that testing.

Encoding Traffic Law & Driving Behaviours For that, we need a publicly-available, machine-readable and complete set of those traffic laws and driving codes and conventions, a Digital Highway Code (DHC). That DHC must include exception handling rules, for example: when and how exactly can a vehicle cross a centre dividing line, if present, to avoid a lane obstruction; when would it be acceptable to mount a sidewalk; what should a driver be permitted to do if traffic lights are defective and so on. These conventions should extend to polite behaviour on the road in that jurisdiction, including when a HAV should let other road users merge into its lane, to what extent does the HAV have a responsibility to ensure the most efficient use of the road network, etc.

Simulation as a Tool for Verification

The core of any effective verification program for HAVs will be the use of simulation.

One or more simulators must be developed to be capable of replaying scenarios in which the road, lighting, weather, degradations, objects, road user actions and interactions can be re-generated and used for verifying the SUT. How complete and representative of the real world a simulator needs to be depends on which parts of the SUT stack is being exercised and tested and how much testing is necessary to explore the state space. But at some level, the full SUT stack must be tested, which means that photo-realism, radar and Lidar reflectivity, sensor models, vehicle dynamics, road surface, human actions must be model variables on top of a baseline simulation capability. A critical issue is how good these simulations must be in order to be effective verification tools, when considered in conjunction with other verification methods including lab test, real-world driving, etc.

Components An example of the principal components of a simulation model suitable for HAV verification is shown in figure 1.

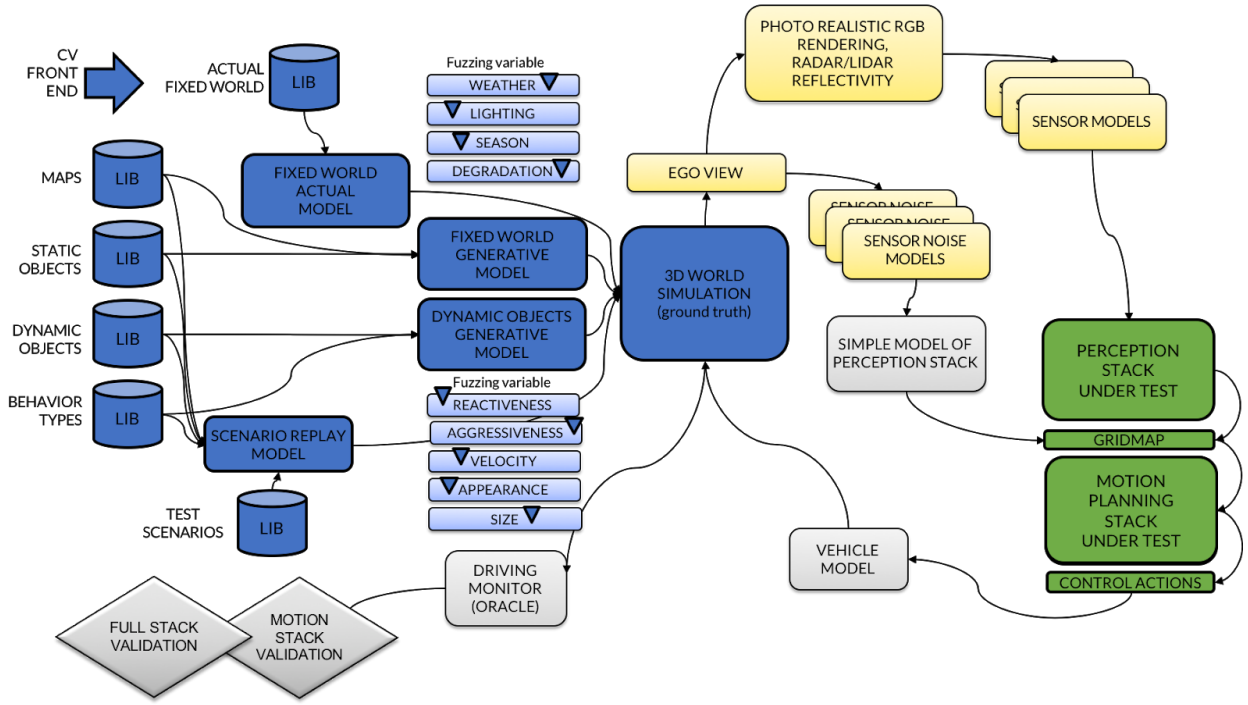

Figure 1: Example simulation model to support HAV verification

Scenario Replay The base point for using a simulator is the interpretation of a scenario and its re-creation in a simulated world, including the instantiation of all recorded dynamic agents and behaviours captured in that scenario. Given a model of road, layout, obstacles, occlusions, road users and behaviours, a simulator can test the predictive capability of the SUT stack, test its ability to plan the HAV motion in the context of road rules and uncertainties, set a trajectory and control the HAV safely, given a model of the HAV vehicle dynamics. A noise model is used to inject perception stack uncertainty into measurements and, at a base level, testing would confirm safe operation given that scenario and noise. Such behavioural tests could run much faster than real-time since the perception layers of the stack would be replaced with noise models. Types of noise as well as scene and user behaviours are varied to discover new failure modes in a process sometimes referred to as 'fuzzing'.

Coverage Driven Verification In addition, simulation models can also be generative in the construction of new scenarios that are theoretically possible but have not yet been captured in road testing or in manual test case generation. Generative models allow the exploration of state space beyond fuzzing, either on a random or directed basis. Several useful techniques exist for exploring and finding new failure modes. These include (i) coverage metrics which then can direct random test generation to broaden that coverage and (ii) using machine learning to reward finding new combinations of layouts, objects, behaviours, velocities, lighting, weather, season etc. that cause the SUT to fail using the proximity of close or actual test failures from random test generation. These types of verification are usually referred to a coverage driven verification. Since the state space being explored for HAVs is extremely large, to all intents and purposes infinite, coverage driven verification using generative modelling would emphasize exploration over density of test coverage which would, by definition, remain sparse.

Randomization & Direction Hand-written tests can be created by focusing on expected corner cases and then automatically 'fuzzing' around them. This involves human generation of very general abstract scenarios which are then instantiated into many different concrete scenarios and coverage is typically clustered around these corner cases.

Another approach, currently favored by the Pegasus project, is to use randomization with expected distributions, often referred to as Monte Carlo simulation. This approach provides sparse coverage but will deliver estimates of the frequency of failures.

But directed or machine-learning randomization is the favored method for defect-finding. These techniques emphasize the capability to reach edge cases, at the expense of overall failure rate estimation and can also be used to support the systematic discovery of defects with respect to adversarial perturbations.[5]

It is important to note that the statistical distribution of test cases has to be driven both by the probability of occurrence and the magnitude of a potential loss (i.e., by risk, not just occurrence). Otherwise a relatively rare scenario that could result in a fatality will be under-represented. In other words, while some testing should concentrate on normal functionality, a substantial portion of testing will need to emphasize infrequent but dangerous situations.

Verification in Digital Twins As well as fuzzed scenario replay and the use of coverage driven verification in generative models, simulation models can also be built that replicate the real world ODD and the likely object types and behaviours in it. Applying coverage driven verification to such digital twins will find additional failure modes which may not be found in fuzzed test scenarios nor easily found in fully-generative models. It can also provide a higher level of coverage that, to some extent, is measurable in relation to the real-world twin the digital model represents. This approach is therefore an extremely useful addition to the first two techniques but requires the creation of a 'digital twin': literally a realistic model of the ODD along with a distribution of dynamic agents and behaviours that are representative, in absolute terms, of that specific ODD.

Full Stack as well as Motion Planning Not only must the predictive, behavioural and control aspects of the HAV stack be tested in simulation (motion planning) but the full stack must be tested too, since many failure modes are possible in the sensors, localization, perception, interpretation, classification and confidence measurement layers of the stack alone, or as they interact with the motion planning layers as a whole.

Full stack testing is a bigger task than behavioural testing, since the simulation model must now render the scene with photorealistic textures, lighting effects, reflections, specularities, shadows, weather and seasons. The same is true for all road users, pedestrians, cyclists and any other objects in the scene, and a library of such objects must be curated and maintained. Sensor outputs need to be modelled based on the placement of the sensors on the HAV and on accurate models of the behaviour of those sensors, including any dynamic range limitations, calibration limitations or errors, quantization, timing delays, race effects, color and lighting sensitivities, blur and other optical perturbations. And it's not just RGB that needs rendering, it's also radar, Lidar and other sensing outputs, given material, density, weather and other conditions. A useful contribution here may also come from the Pegasus project, in the shape of the proposed standard for defining weather, signs, sensor inputs and so on, called Open Simulator Interface (OSI). OSI could be used in the future to connect various simulated artefacts produced by different companies.

Not surprisingly, full stack testing is computationally expensive and may run well below real-time, meaning that attaining meaningful levels of coverage will require substantial datacenter resources to spin up multiple instances of the simulator, sensors and the SUT.

Useful Tools and Methods

A Scenario Language A well-defined language to describe scenarios that can be interpreted by each simulator to re-create essentially the same scenario and behaviours with high fidelity is likely needed. Perhaps OpenSCENARIO is such a language, but if is not suitable a new one will need to be created. One such initiative is being pioneered by Foretellix, an Israeli startup, and they simply call this language Scenario Description Language or SDL. But whether it is OpenSCENARIO, SDL or something different, a cross-industry agreement must be reached.

A Scenario Sharing Library A library of scenario test cases must be developed by or made available to each company building HAV technology. Of course, it needs to be as comprehensive as possible in many dimensions.

A suitable scenario library should:

- Cover cases where collisions are possible and must prove SUT avoidance within the boundaries of the DHC
- Monitor and report behaviour before, during and after collisions or near-collisions
- Pay specific attention to interactions between HAVs and humans and grade for collisions, near collisions, breaches of the DHC and any other behaviours where the SUT adversely affected any virtual passengers, traffic flow or other road users
- Emphasize the verification of inference or deep neural network-based algorithms and find failure cases where interpretability is poor
- Use (i) replayed scenarios (ii) fuzzed replayed scenarios (iii) generative models with directed or machine-learning randomization and (iv) replayed, fuzzed and generative behaviours in a digital twin of representative (or whole) digital twin instantiations of target ODDs
- Look for both “expected” and “unexpected” defects
- Employ configuration files that permit portability from city-to-city through tractable modification of vehicle, sensors, weather files, location, signage, human behaviours, road markings and DHC

These objectives must be met whilst maintaining transparency and maintainability. As the number of test scenarios grows and as they become ever more intricate, this will become a real problem unless tackled from the outset by the industry in initiatives, like the Pegasus project or by the adoption by several key players of a succinct means of encoding those scenarios.

A Motion Language A motion language with qualitative actions (e.g. "follow at a safe distance" or "pull in safely") could add significant value to the validation and verification processes. In the UK, learner drivers are tested on their knowledge of the Highway Code and advanced motorists are encouraged to follow the guidance set out in Roadcraft: The Police Driver’s Handbook.

Codifying what constitutes good driving as described in these manuals, as in the suggested DHC can serve the following uses:

- Engage with the public on target HAV behaviours on UK roads
- Complement scenario-based, coverage driven system testing
- Provide the basis behaviour for a test oracle
- Provide the basis functionality for low complexity monitoring systems to be used by HAVs in run time to improve safety robustness.[6]

Model-checking using a formal method might be used to automatically verify safety properties of the DHC using observation of behaviours from the real world.

Application of Formal Methods Important aspects of hardware design are already amenable to automated proof methods, making formal verification possible to introduce. But the application of these methods to software design is a more complex problem, although a number of mathematical methods do exist for proving a computer program satisfies a formal specification of its behaviour.

As development moves towards higher levels of autonomy then the need for stronger, formal software verification becomes acute. One of the fundamental steps that needs to be taken to understand and analyse HAVs is that we must assess not just what a system will do, but why it chooses to do it.[7] This, together with the need for explainability and responsibility leads towards systems with an identifiable central decision-making software component and, in this case, the formal verification of this software component can ensure that its decision-making is correct and allows us to analyse the decisions an autonomous system makes against the decisions that a human driver should

take. In complementary work, in aerospace[8], it is formally verified that an autonomous (air) vehicle always follows (selected) "Rules of the Air".

In the past 2-3 years, work has also started on how formal verification methods could be applied to making the problem of verifying HAVs easier. For example, by understanding and formalizing specific desired granular driving behaviours and checking by conventional means that any SUT can be verified to satisfy those granular behaviour requirements, the goal would be to eliminate collisions by design. Two notable contributions have come from TU Munich and MobilEye respectively as first attempts at producing a formal mathematical model for acceptable driving behaviour, using a concept of measuring and determining blame in the case of a collision.[9,10]

These are useful contributions to the process of HAV verification but the work so far is insufficient, not least in that proposed formulation for defining blame-free behaviour as set out in the most recent paper (for example in the presence of a child playing near parked cars) would imply a vehicle speed of just 10-15mph, yet humans can and do drive safely at 20-25mph in the same scenarios. Work is needed to consider how those formulations can discover and capture the more complex processes that humans are using for driving, including the social norms, customs and behaviours that are an essential (locally specific) element of the safe driving in mixed human/HAV environments.

COMPONENTS OF A HIGHLY AUTOMATED VEHICLE CERTIFICATION PROCESS

New Type Approval Process

The current Whole Vehicle Type Approval is well-suited to the present model where those component, system and vehicle specifications can be well-defined, stable, recorded, tested and approved.

But this process is clearly inadequate for HAVs, because:

- Many requirements will be highly specific to the ODD
- Requirements will change on a continuous basis as new vehicles, objects, behaviours, signage are emergent in the ODD over the life of the SUT and HAV
- There will always be a gap to the real-world requirements, necessitating a continuous process of requirements discovery through vehicle testing and/or live vehicle logging
- On discovery of a failure, HAV technology developers will be obligated to provide updated software and models to the vehicle and/or upgrade sensors, compute, communications technology or other AD capabilities and this could be very frequent and/or urgent
- Those updates, in improving performance on certain identified failure modes, may cause unexpected regressions or changes in others

The safety risks from AD operation are very different to those being managed in the current Whole Vehicle Type Approval process and a new testing and certification process is required.

To protect the public, improve road safety over time, assure public trust and ensure our economies and citizens reap the benefits of HAVs ahead of other developed economies:

- A new **HAV Type Approval** process must discover and establish a very high safety standard for the verification and certification of any SUT used on public roads in the UK and, if adopted, across the EU
- The certification of HAV Type Approval, at least initially, must be specific to the requirements of a well-defined ODD and a well-defined DHC; those requirements must represent a complete specification, following extensive discovery
- That high standard must be consistently applied to all HAVs seeking certification for any ODD/DHC pair

- Each certification of HAV Type Approval granted for any ODD/DHC pair must carry the obligation of Conformity of Production, meaning that all subsequent hardware and/or software changes must not reduce the overall safety of the design measured against the then current and most complete ODD/DHC requirements specification; the meaning of overall safety in this context will need to be established, likely as a high threshold pass rate of a statistically significant sample of regression and generative test cases in an ODD/DHC pair in full stack and motion planning simulation environments

- Any request for a HAV to operate outside its ODD/DHC pair must be accompanied by a further certification process for the changed ODD or DHC respectively

Practical Aspects of Validation, Verification and Certification

Scenario Sharing As discussed, discovering scenarios that can inform safe system requirements for HAVs is expensive work spanning large scale, multi-fidelity simulation as well as physical testbed and public road testing. Much like the expensive process of drug discovery, no commercial organization could incur the expense and take the commercial risk unless they were assured some preferential use of the resulting outputs, which in the case of drug molecule development and testing, is achieved through patent protection. For the organizations developing HAV technology, requirements discovery is a similarly huge investment but also a source of competitive advantage.

Clearly a balance needs to be struck between sharing discovered requirements for the public good and that commercial imperative, without retreating to a legally enforceable patenting regime.

We propose a model by which HAV technology developers are encouraged to share the scenarios they discover with the UK certification authority (UKCA). Independent test houses would be commissioned by the UKCA and provided with controlled access to the scenarios for the purposes of evaluating HAV performance for both certification and also on behalf of regulated UK insurers, where required:

- Submitted scenarios are evaluated by UKCA for possible acceptance into an ODD certification test catalog, for example on the basis of probability in the target ODD or on the basis of more than one HAV technology developer executing the scenario and passing the test

- HAV technology developers can elect for submitted and accepted scenarios to be made public, but are not obligated to do so

- Any SUT for any target ODD must be tested in simulation by an independent test house against the full test catalog applicable for the ODD certification (whether publicly visible or not)

- A publicly described test oracle will determine whether a test has passed or failed, based on an overall safety threshold set by the UKCA in which the probability of occurrence of each scenario for the target ODD must be evaluated

- Where a SUT fails a private scenario, abstracted feedback would be provided to the HAV technology developer of that SUT, e.g. SUT failed in interaction with a cyclist.

A process along these lines has the following advantages:

- All HAV technology developers are encouraged to submit scenarios for testing in order to raise the bar for competitors seeking certification in an ODD

- Abstracted feedback from failed tests should encourage HAV technology vendors to generally improve their system safety performance rather than ‘gaming’ a solution to a specific scenario. However, the UKCA must ensure that vendors are not prevented from passing certification by being required to pass highly unlikely scenarios for which they are not provided details

- A market is created for non-competing HAV vendors, e.g. component suppliers or others, to find and submit private scenarios which, once accepted by the approval body have in themselves a value which can be licensed to technology vendors seeking system certification

- Independent test houses would not be subject to the same Freedom of Information (FOI) requests as a government body and could thus protect HAV technology vendors from being forced to disclose exhaustive details about their performance in relation to specific scenarios which could result in the disclosure of valuable trade secrets

Scenario Validation Process The validation of submitted scenario candidates into an ODD test catalog that becomes mandatory is a process which must be developed.

Lessons can likely be drawn from other sectors which have successfully tackled similar challenges of competitive technology development which must evolve standards and operate in a shared common environment.

Cellular wireless telecommunications is perhaps a good example, where the establishment of a cross-industry body, the Global Certification Forum (GCF) was established to define the priority of different work items (in their case dependent on Mobile Network Operators' deployment plans) and how to test conformance to relevant Third Generation Partnership Project (3GPP) wireless standards, such as 3G and LTE, so that the standard is met and there is a strong basis for expecting inter-operability between different networks and network equipment. GCF defines work items to prioritize specific test areas, working groups are drawn from industry participants to review those work items and to seek agreement on the ingredients of conformance test cases, pass criteria, parameters for simulation etc. and to be the final determinant of formal adoption of test cases as part of the mandatory program to be certified as GCF compliant by independent test houses. Obligatory test cases for each work item grow as standards are evolved and field failures are identified. In the example of 3G standards, the mandatory test program as a whole escalated quickly from tens of test cases to thousands of increasingly complex test cases over several quarters. In GCF's case, for any new test case to be adopted, it must be shown to be reproducible and repeatable, which normally means that two separate test and measurement organizations must demonstrate the implementation and execution of the same test. Cellular wireless technology development has different market and technology dynamics (global standards, established test and measurement companies, already a highly competitive market, contained functionality, and not safety critical, etc.), so an exact read across to HAVs will not work, but adaptation of some of these ideas for certifying HAVs could be instructive.

Simulation and Test Tool Sharing HAVs will ultimately operate over a wide range of real-world environments, some of which will be extremely complex with enormous possible state spaces and failure conditions to explore and verify. That leads to the conclusion that simulation must play a lead role in any effective testing procedure, in the generation of test conditions, in the parallelization and/or faster than real-time scaling up needed in the measurement of test coverage and in the defect-seeking capabilities of the randomization testing.

Closed course, physical testbed testing is one form of simulation that has a role to play in any meaningful testing regime. It serves an important purpose in that a real HAV's full stack response is measured with hardware in-the-loop within a full physical environment that has been designed to stress known specific risk aspects of the system and can not only identify system defects against those specific scenarios but can also pinpoint simulation modelling defects and gaps to the real world.

However, the dominant focus of any robust certification process should rest on system verification using high-fidelity software simulation at hyper-scale across a vast number of permutations and combinations. Moreover, this process must leverage tools to explore state space and seek defects, such as fuzzing and directed random testing as well as replaying regression suites of curated scenarios.

Engaging private enterprises in developing and contributing to the development and operation of this certification process is a real consideration, particularly in relation to parties who do not themselves plan to be operators of HAVs in the target ODDs, as may be the case for some HAV technology developers. Even in these cases, there may be a preference for reserving tools and models as trade secrets over sharing their utility across the industry as a whole.

Governments therefore may have an important role to play in enabling a market to exist for the licensing of tools or for their commercial use by practising entities. The objective needs to be to ensure that development expenses required for necessary and valuable independent simulation and tools are capable of being leveraged into meaningful

revenue streams by technology developers. One means of achieving this would be for government to signal and enable a market for such tools to be created, for example through the UKCA or to sponsor a cross-industry unit to step up to the important task, one possible candidate being the UK Government's Meridian initiative.

Non-Deterministic Behaviour Verification Process The behaviour of SUT for HAVs will exhibit non-determinism in the sense that if we repeat what is an identical test execution with what we believe to be an identical opening state, we might still get a different system behaviour. This non-determinism may be a result of e.g. random noise injection, race conditions, or some other aspects of operating system performance.

Therefore, in order to build confidence in system performance, an effective verification program may need to run a single test case multiple times. Where possible, that program must eventually reason about the number of test executions necessary to achieve a defined confidence level in the results, using probabilistic arguments.

Where possible, however, the industry should seek to build tools that offer repeatability and possibly even random stability to ensure that defects can be re-found and corrective actions can be proven to have been effective.

Test Oracle A test oracle is a mechanism for determining whether a system has passed or failed a test and usually is comprised of three capabilities:

- A generator, to provide predicted or expected results for each test
- A comparator, to compare predicted and obtained results
- An evaluator, to determine whether the comparison results are sufficiently close to be a pass

Any of the oracle capabilities may be automated and an automated test oracle will be required to generate, compare and evaluate the performance of the SUT across the test scenario catalog, and perhaps in a fully generative model within the ODD constraints, to ultimately determine if the system performed acceptably given the certification criteria.

The generator should make use of the DHC as extended and the comparator should compare the SUT results against the desired DHC and safety outturns. Evaluation is significantly more complex than simply determining if the SUT was involved in a collision since at one extreme bad driving behaviour doesn't always result in a collision and at the other, a collision is the safest choice for a given set of circumstances.

The specification for the test oracle should be made available to HAV technology developers seeking certification.

Conformity of Production (CoP) Audit Conformity of Production (CoP) is a means of evidencing the ability to produce a series of products that exactly match the specification, performance and marking requirements outlined in the type approval documentation.

In the context of HAVs and a new certification process, HAV technology developers will need to provide evidence to the satisfaction of UKCA that the HAV SUT is representative of all of that Type and that the process of developing and deploying design changes is robust. The form of evidence will need to be carefully considered but could follow the lines of a process review.

The International Automotive Task Force (IATF) together with the International Organization for Standardization (ISO) has developed a standard, IATF16949:2016.[11] This defines the quality management system requirements for the design and development, production, installation and service of automotive-related products.

To achieve IATF certification, an automotive supplier has to work according to automotive core tools, such as:

- Advanced Product Quality Planning – a structured approach to the design and development of products and processes
- Production Part Approval Process – formal release by the customer of a supplier's product and process

- Failure Mode Effect Analysis – risk analysis tool in which a supplier analyses the major risks of not fulfilling the required functions in the current design or process
- Measurement System Analysis – evaluation of the reliability of the measurement systems used by a supplier in its process
- Statistical Process Control – a method of quality control which uses statistical methods to monitor and control a process
- 8D Problem Solving – structural approach to analyze problems, including root causes analysis, containment and corrective actions[12]

Since IATF16949:2016 contains all the key elements for a QMS and is already centered on automotive applications, it is a strong candidate to deliver the framework for the CoP audit compliance of HAVs.

PROMISING NEW RESEARCH AREAS

Swiss Cheese Model Recent promising research at TU Darmstadt has centered on applying a technique known as the Swiss Cheese Model to HAV verification for assessing the probability of collision. In essence, each sensing modality, process, behavioural or environmental variable has 'holes' which could permit a failure and when those holes line up, a collision can occur. One of the key unknowns for assessing the safety of HAVs versus human drivers is a strong understanding of the gap between the probability of critical situations arising in driving scenarios and probability that those critical situations do actually result in a collision. In human driven cars, this difference is a representation of the driving skill and attention of the driver themselves. But on replacing the human with the SUT, those human failure modes (which could be inattention, blind spots etc.) are replaced with new failure modes (which could be detection and classification accuracy, prediction failures etc.). The replacement of one set of cheese slices with another can exhibit quite different failures which demands further research.

Quantifying and measuring these impacts has the potential for us to measure the probability of collision and to compare the two in quantifiable ways and deserves further research.[13]

Extreme Value Theory In another initiative, this time from a research team at Volvo Cars, studies into the use of near-collision measurement as a means of estimating the frequency of actual collisions show good promise. Their approach uses a technique called Extreme Value Theory but more importantly highlights the need for further research into capturing and using near collision data for robust collision rate estimation.[14]

These ideas, and many others, should be reviewed and considered for the on-going development of HAV validation, verification and certification processes.

Remaining Research Questions Key research questions remain, and industry participants can and should work together with leading academics in UK and EU to address them, including:

- What machine learning methods should be applied to directed random testing in coverage driven verification?
- Given the high dimensionality of the test space, what coverage measures are meaningful in generative and ODD digital twin verification?
- Which computer vision methods can we apply to the 3D reconstruction and annotation of digital twin worlds from photogrammetry, Lidar scans and other sensing modalities that mean accurate, up-to-date digital twins are feasible?
- What hardware acceleration beyond GPUs can we design and apply to enable real-time and faster-than-real-time full stack verification of HAVs?

- How can we apply formal software checking to the complex integrated systems required for autonomous driving to ensure that each build achieves its goals without bugs or gaps?
- How do we really apply formal mathematical methods to fully express the DHC, vehicle dynamics and other road user expectations and behaviours to allow us to verify the behavioural safety of HAVs?
- How can we verify HAV systems that comprise of one or more end-to-end neural networks with the requirements to explain failure modes and take corrective actions to improve their performance using human readability and intermediate outputs of modular processes?
- How might we extrapolate randomized testing, including near collisions, into a measure of probability of collision generally?

QUESTIONS FOR POLICY MAKERS

This paper makes a number of suggestions that fall into the realm of policy making, including:

- Could a validation, verification and certification system, such as that outlined in this paper, that incentivizes sharing of scenarios while protecting the value intrinsic to their discovery, improve safety across the industry? Could it be used by an approval body such as UKCA to establish a high standard for UK certification?
- Can the industry agree on a scenario description language that supports coverage-driven verification and is extensible? Is Pegasus a suitable basis for extension to meet this?
- What should the specification of an appropriate simulation environment be and would the government request to tender for delivery of such a tool?
- Could the specification for a test oracle be made available and could this be based on a formal description of 'good driving' in accordance with a DHC?
- Is auditable adherence to the IATF16949:2016 quality assurance process sufficient to satisfy 'Conformity of Production'?

CONCLUSIONS

A number of different methods must be combined for the robust certification of HAVs for deployment in ODDs in the United Kingdom and, by extension, other jurisdictions in Europe.

At the centre of this process is hyper-scale fuzzed scenario-based testing and the use of coverage driven verification methods in digital twins of the ODD and using generative models representative of each ODD. Testing must cover both full stack testing, which will require photo-realistic and sensor-realistic rendering of scenarios and objects, together with accurate sensor modelling and motion planning stack testing, which will require robust beliefs over actor behaviours to test predictive, planning and motion synthesis capabilities. A method for sharing scenarios to a UKCA for industry-wide testing will be required and a means of balancing that sharing for the public good with the need to retain economic leverage over the necessary costs of discovering those requirements will need to be devised. A DHC to include good driving behaviours will be needed and a test oracle will be required to evaluate and publish certification performance.

REFERENCES

[1] The specific conditions under which a given driving automation system or feature thereof is designed to function, including, but not limited to, driving modes is known as the ODD, in accordance with SAE J 3016

[2] "Even if the safety of autonomous vehicles is low—hundreds of failures per 100 million miles, which is akin to human-driven injury and crash rates—demonstrating this would take tens or even hundreds of millions of

miles, depending on the desired precision." Kalra, Nidhi and Susan M. Paddock, Driving to Safety: How Many Miles of Driving Would It Take to Demonstrate Autonomous Vehicle Reliability?. Santa Monica, CA: RAND Corporation, 2016. https://www.rand.org/pubs/research_reports/RR1478.html.

[3] Number of motor insurance claims notified in the United Kingdom (UK) from 2010 to 2016 (in millions), Statista 2018

[4] http://www.pegasus-projekt.info/en/

[5] Huang X., Kwiatkowska M., Wang S., Wu M. (2017) Safety Verification of Deep Neural Networks. In: Majumdar R., Kunčak V. (eds) Computer Aided Verification. CAV 2017. Lecture Notes in Computer Science, vol 10426. Springer, Cham

[6] Monitor/actuator pair architectures can be used in-vehicle to separate the most complex autonomy functions from simpler safety functions. The primary AV functions are performed by the high complexity 'actuator' system, and a paired module (the 'monitor') performs an acceptance test / behavioural validation. The low complexity monitor system should be more straightforward to verify and therefore could, potentially, be verified to ISO 26262 ASIL-D

[7] Fisher, Dennis, Webster: Verifying Autonomous Systems. Communications of the ACM 56(9):84-93, 2013. http://doi.acm.org/10.1145/2494558

[8] Webster, Cameron, Fisher, Jump: Generating Certification Evidence for Autonomous Unmanned Aircraft Using Model Checking and Simulation. J. Aerospace Inf. Sys. 11(5):258-279, 2014. https://doi.org/10.2514/1.I010096

[9] Rizaldi, A., & Althoff, M. (2015, September). Formalising traffic rules for accountability of autonomous vehicles. In Intelligent Transportation Systems (ITSC), 2015 IEEE 18th International Conference on (pp. 1658-1665). IEEE.

[10] Shalev-Shwartz, S., Shammah, S., & Shashua, A. (2017). On a Formal Model of Safe and Scalable Self-driving Cars. arXiv preprint arXiv:1708.06374.

[11] http://www.aiag.org/quality/iatf16949/iatf-16949-2016

[12] "Working in the automotive industry" H. Broekman; D. Ekert; M.I. Kollenhof A.E. Riel; H.C. Theisens; R. Winter, 2017

[13] Winner, H., Wachenfeld, W., & Junietz, P. (2018). Validation and Introduction of Automated Driving. In Automotive Systems Engineering II (pp. 177-196). Springer, Cham

[14] Åsljung, D., Nilsson, J., & Fredriksson, J. (2016). Comparing Collision Threat Measures for Verification of Autonomous Vehicles using Extreme Value Theory. IFAC-PapersOnLine, 49(15), 57-62

This document is a place holder for Marion

This document is a place holder for Marion

This document is a place holder for Marion

This document is a place holder for Marion

This document is a place holder for Marion

This document is a place holder for Marion

This document is a place holder for Marion

This document is a place holder for Marion

This document is a place holder for Marion

This document is a place holder for Marion

This document is a place holder for Marion

This document is a place holder for Marion

This document is a place holder for Marion

This document is a place holder for Marion

This document is a place holder for Marion

This document is a place holder for Marion

TIM JOHNSON| NHTSA
United States Department of Transportation

UNITED STATES GOVERNMENT STATUS REPORT

There were 37,133 people killed in motor vehicle traffic crashes on U.S. roadways during 2017, a 1.8-percent decrease from 37,806 people killed in 2016. The 2017 increase followed two yearly consecutive increases in 2015 and 2016.

10.8-percent decrease from 37,806 806 people killed in 2016

TRENDS IN ROADWAY FATALITIES

Over the past 40 years, there has been a general downward trend in traffic fatalities. Safety programs such as those increasing seat belt use and reducing impaired driving have substantially lowered the traffic fatalities over the years. Vehicle improvements such as air bags and electronic stability control have also contributed to the reduction of traffic fatalities.

Beginning in 2015, the long-term decline in fatalities on U.S. roadways began to shift, raising questions about the general decline in deaths and whether a new pattern was emerging. The 37,133 motor vehicle traffic fatalities in 2017 are 673 fewer fatalities than the 37,806 that occurred in 2016. The 1.8-percent decrease compares to the 6.5-percent increase from 2015 to 2016 and the 8.4-percent increase from 2014 to 2015. NHTSA has been closely monitoring the yearly changes in fatality data and the constructs and characteristics of those fatal incidents.

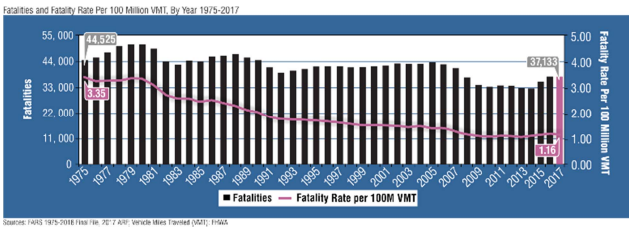

The fatality rate per 100 million vehicle miles travelled (VMT) decreased by 2.5 percent from 1.19 in 2016 to 1.16 in 2017. The 2017 rates are based on VMT estimates from the Federal Highway Administration's (FHWA) May 2018 Traffic Volume Trends (TVT). Overall, 2017 VMT increased by 1.2 percent from 2016 VMT – from 3,174 billion to 3,213 billion. This 2017 VMT increase of 1.2 percent is less than the increase of 2.6 percent from 2015 to 2016.

Looking at a 10-year change in fatalities based on the type of vehicle the occupant was in or if the person was outside a vehicle shows the major shifts over this time. The fatality compositions for 2008 and 2017 are shown in the figure. The biggest change is the proportion of nonoccupant fatalities, which increased from 14 percent to 19 percent from 2008 to 2017. During this same decade, the percentage of passenger car

occupant fatalities decreased from 39 percent of the fatalities to 36 percent. The percentage of light-truck occupant fatalities decreased from 29 percent in 2008 to 27 percent in 2017. The proportion of motorcyclist fatalities stayed the same, at 14 percent.

Fatality Composition, 2008 and 2017

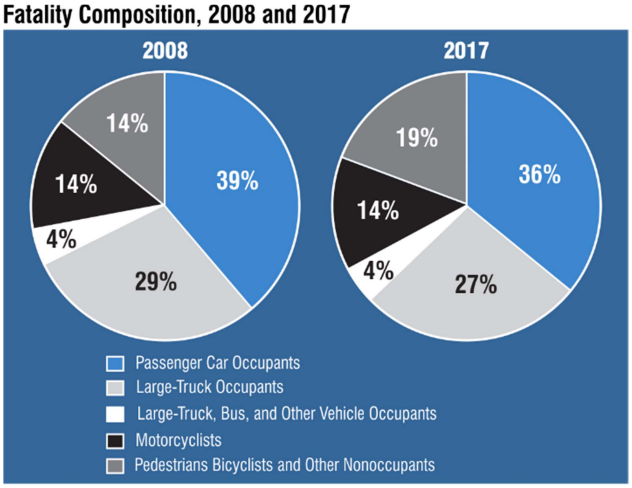

Source: FARS 2008 Final File, 2017 ARF
Note: Sum of individual slices may not add up to 100 percent due to rounding.

Recent Crash-Related Statistics

Certain crash characteristics stand out for the 2017 year.

In 2016 and 2017, urban fatalities have overtaken rural fatalities with an emerging trend towards an increasing divide. The U.S., in general, has seen a resurgence in urban living in recent years which could contribute to this change in fatality location.

Notable in 2017 was that 6,988 nonoccupants were killed in motor vehicle crashes – this includes pedestrians, bicyclists and other nonoccupants. While there was a slight decrease in nonoccupant fatalities, the general trend for this group of individuals has been increasing since 2010.

In 2017, 10,874 people died on U.S. roadways in crashes involving an alcohol-impaired driver. An alcohol-impaired driving fatality is defined as a fatality in a crash involving a driver or motorcycle rider (operator) with a blood alcohol concentration of .08 grams per deciliter (g/dL) or greater. These deaths constitute 29 percent of all fatalities in the year. Most alarming of these fatality figures is the number of large truck drivers involved. Alcohol-impaired drivers of large trucks involved in fatal crashes had the largest percent increase of 61.1 percent from 2016 to 2017, and this is at a .08 g/dL. However, commercial drivers that often drive large trucks, have a lower threshold for legal intoxication than the general public which makes the data striking.

Alcohol-Impaired* Drivers Involved in Fatal Crashes by Vehicle Type, 2016 and 2017

Type	2016	2017	Change	% Change
Passenger Car	4,411	4,297	-114	-2.6%
Light Truck - Van	280	284	+4	+1.4%
Light Truck - Utility	1,632	1,721	+89	+5.5%
Light Truck - Pickup	2,030	1,932	+98	-4.8%
Motorcycle	1,425	1,454	+29	+2.0%
Large Truck	72	116	+44	+61.1%

Source: FARS 2016 Final File, 2017 ARF
*See definition in text.

Restraint use, measured by the National Occupant Protection Use Survey (NOPUS) in a roadside observational survey, in 2017 was 89.7 percent. This contrasts with only 53 percent restraint use for those occupants that died in passenger vehicles in crashes in 2017 as reported through the Fatality Analysis Reporting System.

DATA MODERNIZATION

NHTSA has collected crash data since the early 1970s to support its mission to reduce motor vehicle crashes, injuries, and deaths on our Nation's highways. The Fatality Analysis Reporting

System (FARS) is a census of fatal crashes in the 50 States, the District of Columbia, and Puerto Rico (Puerto Rico is not included in the U.S. totals discussed above). This system has been in place since the 1970s and remains the data collection source for fatalities on U.S. roadways. However, NHTSA's National Center for Statistics and Analysis redesigned the nationally representative sample of police-reported traffic crashes, which enables NHTSA to estimate the number of police-reported injury and property-damage-only crashes in the United States. The new system, called the Crash Report Sampling System (CRSS), replaced National Automotive Sampling System (NASS) General Estimates System (GES) in 2016. The 2016 CRSS data was initially released in March 2018 and rereleased with corrections in May 2018. This is the latest year for which CRSS data is available.

In 2016, there were an estimated 7,277,000 police-reported traffic crashes, in which estimated 3,144,000 people were injured. There were an estimated 5,065,000 property-damage-only crashes in 2016. A direct comparison of the 2016 injury, and property-damage-only crash estimates cannot be made with any previous year, due to the change in data collection practices.

VEHICLE SAFETY RESEARCH

NHTSA's Office of Vehicle Safety Research executes short- and long-term research projects with the goal of providing a scientific basis to help inform future agency decisions. The research covers all phases of the crash scenario – advanced pre-crash and crash-avoidance warnings, technologies, and equipment; occupant protection and vehicle behavior during a crash; and post-crash vehicle integrity, egress, and notifications. Emerging technologies are a constant source of research activities which offer the opportunity to encourage the safety of the technologies, conduct assessments and develop performance criteria and test procedures when necessary.

Advanced Driver Assistance Systems – Current crash avoidance systems rely on sensors such as radar, lidar, camera, ultrasonic, and others to detect potential collisions with other vehicles, pedestrians, or objects and then warn the driver to take appropriate action, as well as technologies that automatically intervene by applying brakes or providing steering inputs to avoid or mitigate a crash if the driver's actions are delayed or insufficient. Advanced driver assistance systems (ADAS) provide the driver with added convenience, safety or functionality during "normal" driving scenarios, but still require the driver to be fully engaged in the driving task. The overall objective of NHTSA's ADAS research program is to provide automotive industry stakeholders with information, analyses, and tools to help evaluate and advance the safe development and deployment of these crash avoidance systems. When appropriate, the program also facilitates (e.g. by developing more technologically neutral performance criteria and test procedures) the removal of unnecessary regulatory barriers that may prevent introduction of these systems.

Automated Driving Systems – Vehicle Safety Research's focus on Automated Driving Systems (ADS) aims to establish a safety assessment framework, contribute to the body of knowledge,

and provide leadership that advances the safe testing and deployment of ADSs such that their benefits are optimized and risks appropriately mitigated. Current and upcoming efforts address the technical challenges associated with safe testing and deployment of SAE automation levels 3 through 5 – conditional, high, and full – driving automation. NHTSA's ADS research follows *Automated Driving Systems 2.0: A Vision for Safety*, the Secretary's strategic goals, *Preparing for the Future of Transportation: Automated Vehicles 3.0*, and involves efforts with stakeholders, other DOT modal administrations, States and other federal agencies. While interests of the different types of stakeholders vary widely, the main goal of the NHTSA ADS research is to support the development of safety criteria, metrics, and assessment methods for ADSs. This is a challenge of considerable breadth and depth that the agency is still in the early stages of addressing.

Crashworthiness – This research program focuses on understanding causes of human injury in motor vehicle crashes and vehicle safety countermeasures that can reduce their severity and frequency of occurrence. This program is responsible for developing and upgrading test procedures for evaluating motor vehicle crash safety and developing associated test tools, such as crash test dummies and injury metrics. Crashworthiness research encompasses new and improved vehicle design, biomechanics and injury causation, field data collection and analysis of serious injury cases, and safety countermeasures and vehicle equipment to enhance safety for all road users. Current and upcoming research includes evaluating the safety of occupants in vehicles with Automated Driving Systems (ADS – SAE International Automation Levels 3-5) due to potential non-traditional occupant compartment designs and seating conditions. Additional research is ongoing related to the safety of alternative fuel vehicles safety including electric and hydrogen vehicles.

Human Factors – The effectiveness of many crash avoidance technologies available on motor vehicles relies in part on the way the (human) driver interfaces with the system – ranging from simply whether (or not) they engage the system (i.e., controls), to how warnings are conveyed (i.e., driver-vehicle interface). Other factors include a driver's ability to regain situational awareness and make and execute a correct decision quickly enough. In addition, more advanced driving automation systems (that are anything short of "fully automated") also rely on the driver's ability to properly understand the capabilities, constraints, and control settings of driving automation – including the circumstances and way the human driver takes-over or "partners" with the automated systems to complete the driving task. Even fully automated systems may need some degree of user engagement to ensure safe operation. Efforts within Vehicle Safety Research aim to: establish a basis for efficient and objective methods for evaluating driver-vehicle interfaces; use such methods to profile effective interface design approaches; understand how driver readiness (or "state") may impact the efficacy of such designs and engagement methods; and, determine if and how drivers may adapt to such technologies, thereby also impacting effectiveness (either positively or negatively).

Vehicle Cybersecurity – Digital electronics that include many new safety, mobility, and efficiency features commonly are included in modern vehicles today. These software-intensive functions, and wired and wireless data exchange interfaces, introduce cybersecurity challenges and potential safety concerns. While cybersecurity is germane to data security, intellectual property, and privacy, NHTSA is primarily focused on the safety implications of vehicle cybersecurity. NHTSA's Research activities include research tracks that identify risks, defensive methods, test tools, and ecosystem factors impacting vehicle security; lifecycle cybersecurity risk management; processes that manage associated safety and security risks; and efforts to identify emerging research opportunities that have the potential to facilitate continuous improvement in the cybersecurity of motor vehicles.

RESEARCH AREA ACTIVITIES

Crashworthiness

The crashworthiness research program is responsible for developing and upgrading test procedures for evaluating motor vehicle safety and developing the test devices and appropriate injury metrics. The purpose of the program is to investigate the problems of vehicle crash safety and associated factors that contribute to serious injuries and fatalities. Ongoing research includes:

- Biomechanics research to develop publicly available data, tools, performance measures, and procedures;
- Work with trauma centers to understand the detailed nature of occupant injuries;
- Completing biofidelity testing and development of associated requirements for tools to be used in the assessment of potential alternative seating arrangements that are forecasted for ADS-equipped vehicles;
- Safety Systems research to utilize the tools developed through Biomechanics and begin development strategies for enhancing occupant safety for alternative seating arrangements;
- Completion of technical documents for the THOR 5th percentile female;
- Evaluation of potential crash interaction between current vehicles and commercial ADS-equipped vehicles designed to carry cargo without occupants.

Crash Avoidance

Given that more than seven million police-reported crashes occur every year in the U.S., NHTSA sees an increased emphasis on crash avoidance and driver assistance technologies. These technologies have the potential to reduce fatalities and injuries by preventing the crash from occurring, or reducing the severity of crashes by providing timely warnings to the driver to take appropriate action. NHTSA's continued research activities in crash avoidance include:

- ADAS research, which includes SAE level 0-2 vehicles, to develop objective test procedures and performance evaluation methods;
- Evaluation of system reliability, unintended consequences, and potential safety benefits of new emerging ADAS technologies;

- Understanding performance characteristics and operational envelope of crash avoidance technology and systems;
- Assisting the agency in developing approaches to addressing potential regulatory barriers for emerging driver assistance systems;
- Human Factors research to help develop the community's understanding around the safety impacts of human-machine interface approaches as well as potential longer term behavioral changes related to ADAS uses and how they might impact safety outcomes.

Alternative Fuel Safety

Recently introduced vehicle engine technologies, including hydrogen and advanced lithium ion battery vehicles, are being introduced to the market at a fast rate. This research will examine the safety issues and promote research to enhance industry best practices. NHTSA will continue to perform research activities such as:

- Continuing fleet safety validation testing of high voltage traction battery systems;
- Conducting thermal propagation testing at the pack- and full-vehicle level to assess test procedure suitability and evaluate performance criteria;
- Assessing battery management system. functionality, including all levels of charging.
- Developing and evaluating lithium ion battery diagnostics that can detect damage prior to battery fire initiation;
- Evaluating the safety of the fiber-wrapped pressure vessels used for storing high pressure hydrogen and compressed natural gas in vehicle systems. Refine, demonstrate, and document safety best practices for laboratory testing.

Vehicle Electronic and Emerging Technology

This program advances NHTSA's expertise in vehicle electronics to address the safety and security of emerging electronics and software technologies, and their implications to the safety of vehicle occupants and other road users. NHTSA will continue to pursue the following activities:

- Perform cybersecurity research to facilitate cyber-resilient vehicle designs that mitigate safety risks. This includes a focus on developing test and validation approaches to vehicle software, application of the NIST framework to automotive architectures, and assessing wireless interface vulnerabilities.
- Expand functional safety research to include emerging subsystems used to support advanced technology vehicle designs including perception/sensor systems and decision-support software.

Automated Driving Systems

Preliminary research indicates that there is the potential for significant safety enhancement associated with Automated Driving Systems (ADS), which includes SAE level 3-5 vehicles. The main goal of the ADS research program is to assure that ADS are being designed, operated, and used safely within their given operational design domain. NHTSA activities include:

- Research to support policy decisions on potential changes to federal safety standards to facilitate continued safe innovation in ADS technologies;

- Perform research with key stakeholders, including the automotive industry, standards setting organizations, academia, and other safety organizations to refine safety principles for ADS, and develop test procedures and performance criteria;
- Complete critical human factors research including research on "takeover-ready driver" attributes and governing factors for SAE L3 systems as well as research on how ADS can communicate their intent with other road users (drivers, pedestrians, and cyclists);
- Initiate new research on the ADS design needs for disabled and vulnerable populations;
- Perform crashworthiness research to develop test tools to support safety testing of future ADS vehicle designs with non-traditional seating (as outlined above in the *crashworthiness* activities area).

GOVERNMENT STATUS REPORT, 2019

Dr. Ir. Peter Striekwold

RDW, special advisor to the director

The Netherlands

Status of Motor Vehicle Crashes/Fatalities/Injuries

The trend of a yearly decrease in road victims was not seen in the last two years. In 2017, there were 613 casualties and 20.800 severely injured. The percentage of casualties with cars equals that for cyclists. Casualties under cyclists are on average above 60 years old. The majority of severely injured persons are caused in accidents with bicycles without a motor vehicle.

Status of Advances in Motor Vehicle and Infrastructure Safety

In order to further decrease casualties and injuries a number developments have taken place. One action is to extend the prohibition to use mobile devices during driving from car drivers to cyclists. Also, a campaign was developed to stimulate people to switch of the mobile devices when driving, e.g. by using apps or others ways which may arrange this automatically. Moreover, a new Strategic Plan Road Safety has been published, with a huge number of different actions to improve road safety. These methods include improved collaboration between stakeholders, introducing risk-based approaches with proper statistical analyses and monitoring the actual effects in order to find out if and where adjustments are appropriate.

Evolving Research/Rulemaking Strategy

With regard to Research and Rulemaking, a number of developments are worthwhile mentioning. The first one it the introduction of the new “Experiments Law”. This law stimulates experiments with fully automated vehicles without a driver on public roads. Several stakeholders for road safety are involved in the preparation of the decision by the Ministry. The second one is the development of a strategy for admittance of innovative vehicles like e-steps. Some of these innovative vehicles do not fit in existing regulation, and safety should not be compromised whereas on the other hand there is a desire to support innovation. Finally, the Ministry started development of a Smart Mobility roadmap. With a 4 year horizon, together with other institutes for road safety, relevant changes in legislation are identified, supporting Safety, Security and Privacy.

Status of Current Key Research Programs

There are three elements in the current research programs. The first one is the development of a Vehicle Safety and Security Framework. This method is developed to assess safety and security for new vehicles, including OEM’s processes. This framework is developed in collaboration with some of our type

approval OEM's and includes elements of UNECE work (Security/Updates/Validation Methods). In addition, the second program is related to the determination of the driving capabilities of automated functions. In order to support the new Experiments Law, we are developing criteria and methods to decide if the automated functions can replace the human driver. The experience from application of this framework might be input for future legislation. The third part in our program is the development of an ADAS covenant to stimulate introduction and above all proper use of automated functions by drivers.

Government Status Report

GSR19'

26th ESV 19 NETHERLANDS

JUNE 2019

Dr. Ir. Peter Striekwold, Special Advisor to the Director RDW | The Netherlands

Safety Overview for the Netherlands

GSR19'

- **Status of Motor Vehicle Crashes/Fatalities/Injuries**
- **Status of Advances in Motor Vehicle and Infrastructure Safety**
- **Evolving Research/Rulemaking Strategy**
- **Status of Current Key Research Programs**

Status of Motor Vehicle Crashes/Fatalities/Injuries

GSR19'

- **Source: Institute for Road Safety Research (SWOV)**
- **2017: 613 casualties, appr. 20.800 severely injured (of which 25% permanent impact)**
  - Casualties: 34% bicycles, 33% passenger cars
    72% of cyclists older than 60; 31% of cyclists older than 80
  - Severely injured: 53% bicycles without motor vehicle, 11% bicycles with motorvehicle, 11% cars, 6 % motorbikes, 13 % scooters
- **The historical improvement seems to cease, figures are a bit worse than 5 years ago**

Status of Motor Vehicle Crashes/Fatalities/Injuries

GSR19'

- **Fatalities: relation transport mode victim and counterpart**

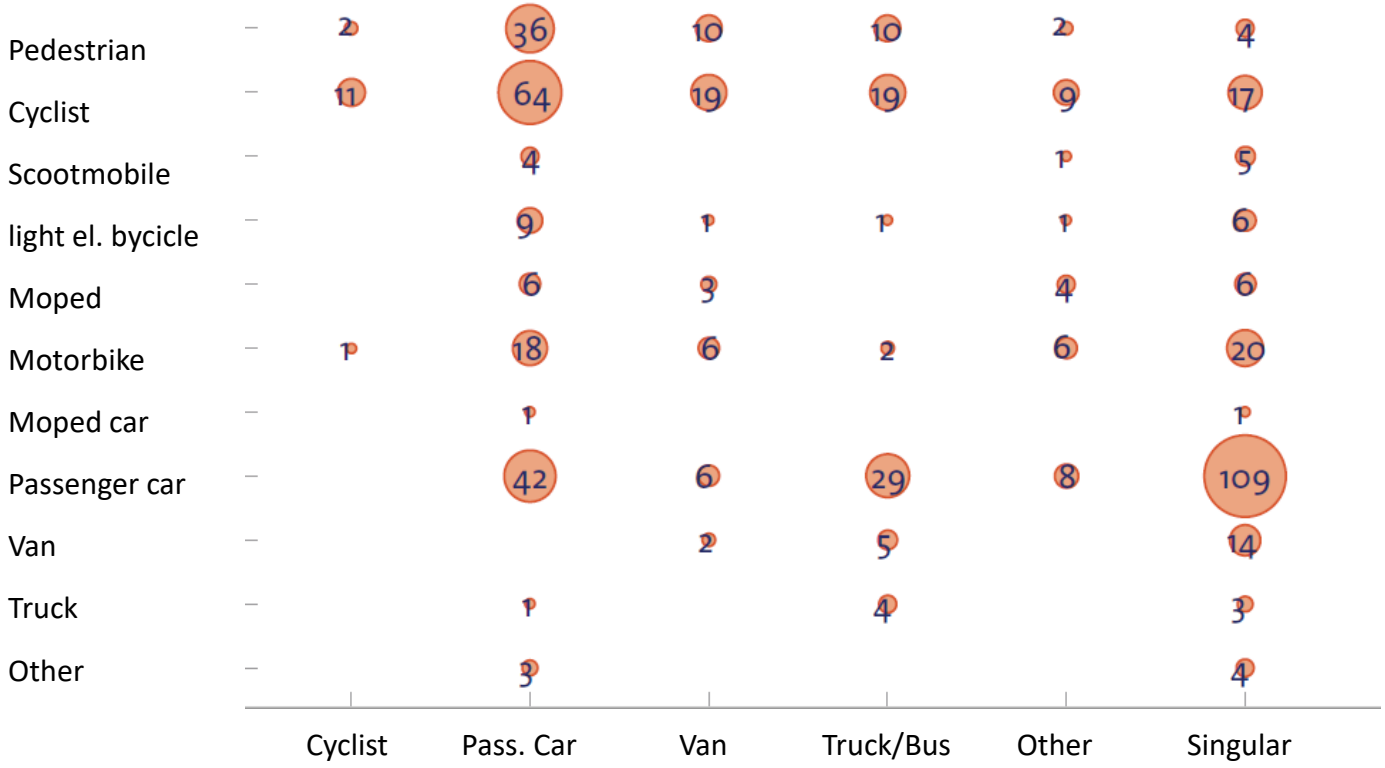

Status of Motor Vehicle Crashes/Fatalities/Injuries

GSR19'

- **Fatalities and severe injuries: percentage related to age**

Fatalities

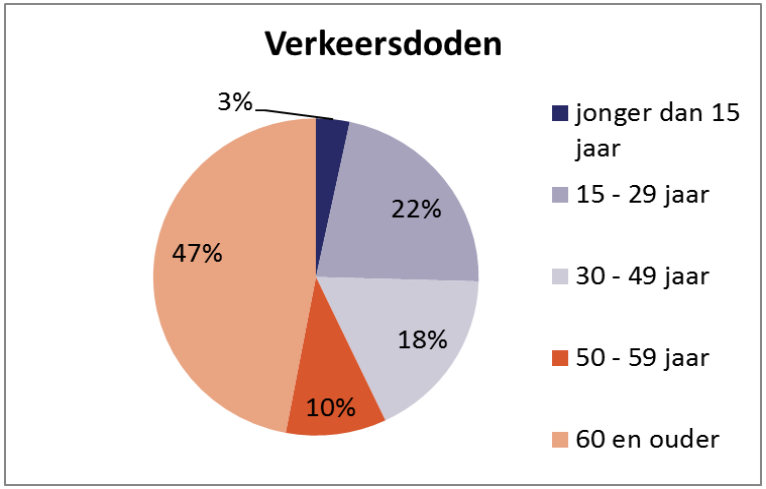

Severe Injuries

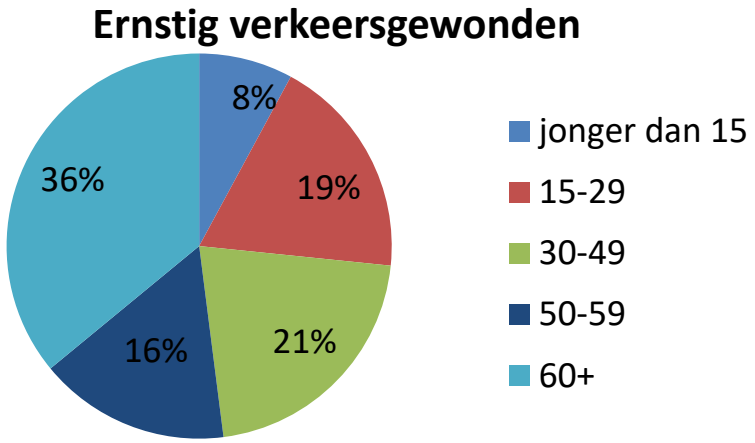

Status of Advances in Motor Vehicle and Infrastructure Safety

GSR19'

- **Extension of the prohibition to use a mobile device from car drivers to cyclists (due 2019)**
- **Campaign to switch off mobile devices while driving ("drive MONO")**
- **Publication of Strategic Plan Road Safety**

  Vision how traffic safety can be improved until 2030

  - Higher priority
  - More and better collaboration between relevant organizations
  - Risk-based approach with proper statistical analysis
  - Integral approach
  - Monitoring the actual effects and adjustments when appropriate

Evolving Research/Rulemaking Strategy

GSR19'

- **2019 introduction of new "Experiments Law"**
  - Stimulating experiments with fully automated vehicles without driver
  - Ministry decides per request
    - RDW coordinates related organizations for the advice to the Ministry
- **Development of a strategy for admittance of innovative vehicles (e.g. e-step)**
  - Supporting innovation without compromising safety
- **Development of a Smart Mobility roadmap**
  - Together with relevant stakeholders (RWS, RDW, CBR, SWOV)
  - Horizon 4 years, including practical consequences
    - Covering safety, security and privacy

Status of Current Key Research Programs

GSR19'

- **National project "Vehicle Safety and Security Framework"**
  - Developing a method to assess safety and security
  - Already used with several OEM's awaiting the UNECE requirements, includes more aspects then the UNECE requirements
- **National project "Vehicle Driving License Framework"**
  - Developing a method to assess the vehicle as driver when in automated mode, used for experiments on public roads
  - Approach is adjusted with other projects (Headstart, …) and results may be used by UNECE working group Validation Method for Automated Driving

Status of Current Key Research Programs

GSR19’

- **Development of ADAS covenant with all Dutch stakeholders to stimulate introduction and use**

Thank you

GOVERNMENT STATUS REPORT, 2019
FEDERAL REPUBLIC OF GERMANY

Stefan Strick, President of Federal Highway Research Institute (BASt)
Germany

26th ESV-Conference

Eindhoven, Netherlands, June 10-13, 2019

1. STATUS AND TRENDS

1.1. Road accidents in Germany

The total number of police registered road accidents has increased by 12 per cent since 2000 – from 2.4 to 2.6 million road accidents in 2017. In the beginning of the century slight increases were offset by slight decreases, resulting in almost the same accident figures in 2011 as in 2000. Since then the number of accidents has started to increase slightly year by year, with yearly increases between 0 and 5 percent. The forecast for 2018 also indicates a further increase in accident figures by about 1 percent.

The number of road accidents with personal injury has decreased by more than 20 % since 2000, resulting in 302,656 road accidents with personal injury in 2017. The decrease has mainly been realized from 2000 to 2009 (- 19 percent). Since then, no further substantial decrease has been noted, the figures have stagnated around 300,000 injury accidents. A slight increase is expected for 2018.

Casualty figures have also decreased since 2000, with lower reductions for slight injuries and higher reductions for severe injuries and fatalities. The total number of casualties has decreased by approximately 23 percent from 511,577 in 2000 to 393,492 in 2017. The stagnating number of injury accidents in the last years is mirrored in the stagnating number of casualties. In 2018 an increase to about 400,000 casualties is expected.

Since 2000, the number of serious injuries has been reduced by about 35 percent to 66,513 seriously injured road users in 2017 and the number of slight injuries has been reduced by more than 19 percent to 323,799 slightly injured road users. Both injury severity groups follow the same pattern: Most of the decrease has been realized until 2009/2010. In the years after, no decrease was noted for slight and serious injuries.

Fatalities have decreased by almost 58 percent from 7,503 fatalities in 2000 to 3,180 fatalities in 2017. Although a deceleration of the decrease can be noticed since 2010 fatality figures are still slowly regressing. For 2018 an increase to approximately 3,230 fatalities has been predicted. This might be the first year with an increase following two consecutive years with decreasing fatality figures.

While many factors concerning e.g. safety behavior or vehicle and infrastructure safety play an important role for the long term development of fatality and crash figures, short-term increases result mainly from changes in mobility and traffic behavior due to different and extreme weather conditions. The year 2018 was characterized by very dry and sunny weather from spring to late autumn, very likely entailing an increase in traffic of certain modes of transport associated with this kind of weather. As a result fatality figures increased especially for cyclists and riders of mopeds. Increases are also expected for children and the elderly.

1.2. Socio-economic costs due to road traffic accidents in Germany

The Federal Highway Research Institute (BASt) calculates the costs of traffic accidents on an annual basis. The costs burden of German national economy caused by traffic accidents includes costs of fatalities, injuries and damage to goods.

The socio-economic accident costs include direct costs (e.g. medical treatment, vehicle repair/replacement), indirect costs (police services, legal system, insurance administration, replacement of employees), lost potential output (including the shadow economy), lost added value of housework and voluntary work, humanitarian costs

and costs of monetised travel time losses due to traffic jams caused by accidents. The mathematical model developed for the purpose of accident costs assessment enables an analysis of slight, severe and severest injuries and the effect of underreporting on total accident costs.

The total traffic accident costs amounted in 2017 to approximately 34.23 billion Euro. The costs of fatalities and injuries reached 13.19 billion Euro whereas the costs of about 21.04 billion Euro were caused by damage to goods. Comparing 2017 data with accident costs occurred 2015 (previous reporting year) we observe an 8% decrease of fatalities costs and injuries costs. However, the increase of damage to goods by 4.5% equalized the above positive effect and the total amount of accident costs was 2017 only 0.5% lower than that of 2015.

The costs per person added up to 1.150 million Euro for a fatality, 116,335 Euro for a severely injured person and 5,138 Euro for a slightly injured person.

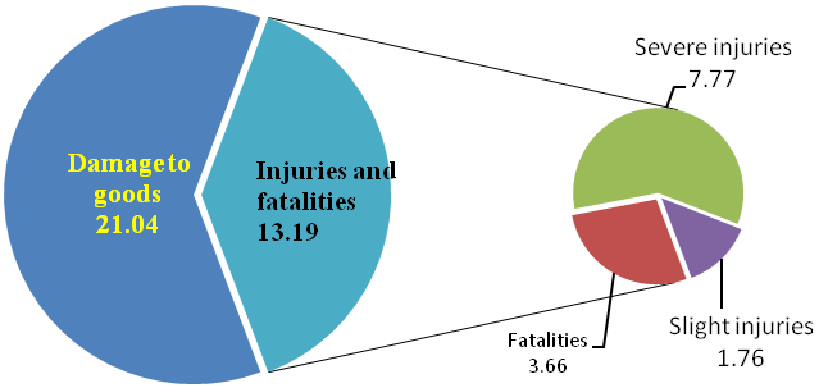

Figure 1: Costs due to road traffic accidents in 2017 (billion Euro)

1.3. German Road Safety Programme

The present German Road Safety Program was launched in autumn 2011 and will be running for ten years until 2020. The principal aim of the program is to enable safe, ecologically sensitive and sustainable mobility for all road users in Germany. It comprises a wide range of road safety measures addressing road users, vehicles and the road infrastructure.

The program addresses new challenges (e.g. demographic change and mobility of elderly) and aims at safeguarding the efficiency of the road network. At the same time, it reflects recent technological developments in vehicles such as driver assistance systems, cooperative vehicle systems or new engine concepts. In these latter areas, the main focus lies on ensuring that the development of vehicle technology induces safety gains rather than safety risks. Activities also focus on rural roads and on reducing not only the number of fatalities, but also the number of serious injuries. Work is currently underway to develop the following German Road Safety Programme.

2. RESEARCH

2.1. Finished projects

2.1.1. Turning Assist Systems for Trucks

Accidents between right turning trucks and straight riding cyclists often show massive consequences. Accident severity is much higher than in other accidents. The situation is critical especially due to the fact that, in spite of the mirrors that are mandatory for ensuring the field of view for the truck drivers, cyclists in some situations cannot be seen or are not seen by the driver. Either the cyclist is overlooked or is in a blind spot area that results from the turning manoeuvre of the truck and its articulation if it is a truck trailer or truck semitrailer combination.

Assistance systems that provide the driver with an information way before a situation becomes control are considered to be a solution. Such systems would generally bear a high potential to avoid accidents of right turning trucks and cyclists no matter if they ride on the road or on a parallel bicycle path.

BASt therefore carried out a research project in order to develop a testing method and elaborate requirements for turning assist systems for trucks. In-depth accident data was evaluated. These findings served to determine characteristic parameters (e.g. boundary conditions, trajectories of truck and cyclist, speeds during the critical situation, impact points). Based on these parameters and technical feasibility by current sensor and actuator technology, representative test scenarios and pass/fail-criteria were defined. This work has led to activities on UN ECE level, namely a working document was submitted to GRSG early 2017, which was send to an informal group for further optimization. Finally, the 115th GRSG in October 2018 adopted a proposal for a new regulation for blind spot information systems for heavy vehicles and sent it to WP.29 for further consideration in its March 2019 meeting.

2.1.2. Handbook „Accessibility in long-distance bus transport“

Accessible travel is becoming increasingly important, considering demographic change and the increasing demand for mobility by older passengers and those with restricted mobility. Since the liberalisation of bus transport in Germany, travel on long-distance buses has increased greatly. A new regulation (the passenger transport law, PBefG) came into effect on 1 January 2013. Under an agreement in the coalition contract for the 18th legislature period, the production of a handbook “Accessibility in long-distance bus transport” was foreseen, including an accessible electronic version. The intention was to prepare the handbook as an easily understandable, succinct brochure with examples of best practice for the implementation of accessibility in practice by stakeholders. The handbook thus not only covers the accessibility measures for vehicles but is also applicable to infrastructure and operation.

The research project had the objective of describing extensive accessibility for all user groups, with not just the interests of wheelchair users and people with reduced mobility being considered but also passengers with sensory, cognitive and movement limitations as well as the elderly and families with children.

The handbook was produced with significant involvement of the decisive stakeholders and shows good examples of accessibility in long-distance bus transport. It offers a guideline for the various users, vehicles manufacturers, transport provides, councils, operators of bus stations and representatives of people with disabilities in order to implement accessibility in long-distance bus transport. For this purpose the viewpoint comprised vehicles, infrastructure and operation. Only the cooperation of all three areas will enable a continuously accessible travel chain in long-distance bus transport.

The handbook "Accessibility in long-distance bus transport" was published in a printed version by the Federal Ministry of Transport and Digital Infrastructure (BMVI) as a seperate publication. The handbook was also made available in an accessible version (PDF) so that the content is available for people who are blind or poorly sighted.

2.1.3. EU project PROSPECT

BASt participated in the EU-funded Horizon 2020 project „PROSPECT“ (PROactive Safety for PEdestrians and CyclisTs). The goal of this project was to increase the overall traffic safety for pedestrians and cyclists by generating a better understanding of relevant critical scenarios and the advancement of active vehicle safety systems, such as autonomous emergency braking and evasive steering applications. On the basis of a detailed analysis of accident data from various countries, the focus for the development of prototype functions and test protocols was set to urban intersection scenarios, which are the most relevant for occurring severe injuries of vulnerable road users (VRU). The developed prototypes within this project feature innovative methods for robust and early VRU detection of pedestrians and bicyclists. The control systems use an increased radial sensor range and high performance actuators to find the optimal combination of quick steering and braking interventions. Advanced sensor interpretation systems allow to better judge the intention of pedestrians and cyclists along the vehicle path with respect to their direction of movement. For the evaluation of these prototypes, new realistic trajectories for cornering maneuvers had to be specified on the test track. Finally, the user acceptance was proved in several simulator studies to verify the high socio-economic benefit of improved future active safety systems. The derived test procedure will expand towards European consumer testing in the next years to achieve a high market penetration as soon as possible.

2.1.4. Intersection assistance (Euro NCAP)

Automatic Emergency Braking (AEB) systems increasingly offer the possibility to address even complex conflict situations, such as found in intersection traffic. Against this background, the development of novel test scenarios with regard to the requirements of consumer information and legislative procedures is of interest. Euro NCAP plans to introduce the assessment of car-to-car junction assist systems from 2020 on. One objective of a project concerning intersections is to provide substantial information on car-to-car accidents in Europe. The Use Cases identified in this context serve as a basis for the definition of representative test scenarios. Based on the official German Road Accident Statistics (Destatis), most relevant accident scenarios were derived by grouping and weighting certain accident types. Subsequently, an investigation of associated crash parameters obtained by the German In-Depth Accident Study (GIDAS) took place, which finally led to the Use Cases. Severe accidents at intersections in Europe occur most frequently at “crossings” and “t- or staggered junctions”. Although pedestrians, cyclists and motorcyclists play a dominant role within these accidents, car-to-car accidents still amount to a share of one-fifth of all severe accidents and of one-quarter of all related fatalities. The Accident Scenarios Straight Crossing Paths (SCP), Left Turn Across Path with an opponent coming from the Opposite Direction (LTAP/OD) and Left Turn Across Path with an opponent coming from the Lateral Direction (LTAP/LD) are of highest relevance. For each of these scenarios, up to six crash parameters (e. g. speed profile, turning radius, collision angle, impact point) could be evaluated. The derived test procedure can expanded towards European consumer testing in the next years to achieve a high market penetration as soon as possible.

2.1.5. Personal Light Electric Vehicles (PLEV)

The aim of this project was to determine whether and under which conditions very small electric vehicles so called Personal Light Electric Vehicles (PLEV) can be operated safely in road traffic, which technical requirements need to be satisfied and which potential conflicts with other road users are to be expected. PLEV are those vehicles without a seat such as electric kick scooters and self-balancing vehicles (e.g. similar to the Segway). They could be approved up to 2016 in accordance with the Framework Directive 2002/24/EC (Type-approval of two or three-wheel motor vehicles / category L vehicles), which is no longer in force. The new Type Approval Regulation (EU) No. 168/2013 for two or threewheel vehicles and quadricycles has been in force since 2016. However, PLEV of this type are out of the scope of this regulation. Instead the approval can be regulated at a national level. An assessment of the traffic safety of such vehicles is required on the one hand to be able to decide on whether they can be approved. On the other hand vehicle dynamics tests are needed to provide information for the classification of these vehicles and to stipulate respective requirements. In this research project, the Federal Highway Research Institute (BASt) prepared suggestions for a classification of this type of specific small electric vehicles and for the technical requirements to be placed on them so that they may be used safely in road traffic. PLEV were investigated in four sub-studies: considerations with regard to active and passive safety, user behaviour and risk assessment as well as traffic area. It emerged that it is possible to propose new categories of PLEV with certain minimum requirements. It is recommended that PLEV should comply with these requirements to be allowed to be driven in traffic. Depending on the proposed vehicle

categories, corresponding traffic areas are recommended for use, based on the analysis of subjective safety and of the potential conflicts with other road users. Recommendations were also derived for (safety-related) technical equipment for the newly proposed PLEV categories. The requirements are based on those for the existing vehicle categories "light moped" and "moped".

2.1.6. Automatic Emergency Braking for Heavy Goods Vehicles

Automatic braking systems for heavy goods vehicles are mandatory across the European Union. While the requirements for pre-accident speed reduction on a moving target with 68 km/h reduction from 80 km/h are quite demanding, the required speed reduction towards a stationary target is not so strict (13 or 28 km/h from 80 km/h, depending on truck type). One major vulnerability of the current technical requirements in the AEBS regulation (UN-Regulation No. 131) is the possibility for drivers to switch the systems off (required for rare conditions where the AEBS sensors cannot interpret the environment and thus might act inappropriately) without requiring a mechanism to re-activate the AEBS at a time when the need to switch off has disappeared. The other aspect that could be optimized is that vehicle deceleration is limited during the mandatory warning phase.

BASt was carrying out a research project to investigate how an automatic re-engagement of those systems could be handled and if an adaption of the speed reduction requirements to the current state of the art might be appropriate. The findings have been delivered to the German Ministry of Transport, which then have been incorporated into a proposal to modify UN-Regulation No. 131 in the following aspects:

- Collisions between heavy vehicles and stationary targets should be avoided up to driving speeds of 70 km/h; the brake strategy should not drastically change for higher driving speeds.
- Driver warnings should not be mandatory anymore in favor of automatic brake intervention for low relative speeds.
- It should not be possible anymore to deactivate AEBS systems at driving speeds above 30 km/h, and systems should automatically reactivate.

Germany's modification proposal is currently in discussion between interested contracting parties and the Industry; delivery of a consensus proposal is aimed for by autumn 2019.

2.1.7. KO-HAF

From 2015 to the end of 2018, a research project concerning cooperative, Level 3 driving (Ko-HAF) was performed. BASt joined a national consortium with automobile and electronics manufacturers, suppliers, communication technology and software companies, research institutes and road administration. The project aimed at the development of cooperative, Level 3 driving on motorways, i.e. for high speed ranges on well constructed road infrastructure. This included a significant improvement of forecasts for environmental detection in addition to the automation of the longitudinal and lateral control of vehicles. Key activities of BASt – in an academic part – was the definition and specification of relevant data on traffic and road conditions to be stored in the backend, the evaluation of usability of external data for the use cases of Level 3 driving, the design of data exchange with third parties and the evaluation of data protection issues. Based on this, BASt supported the development of highly accurate maps acting as an expanded forecast for automated driving. Furthermore, the driver cannot be taken entirely out of the loop during Level 3-driving. Therefore, the resumption of the driving task by the human driver within a certain lead time was also subject to research in Ko-HAF. Several test vehicles were constructed for testing and demonstration of highly automated driving under normal conditions and in case of system failure. The new vehicle operation took place on test tracks and on public roads.

In a practical part, BASt conducted a first driving test to classify the effect of driver’s vigilance and fatigue in a Level 2 drive when permanent monitoring of an automated driving function is necessary over long time intervals. Participants were driven in a 'Wizard of Oz' vehicle, meanwhile fatigue measurements were performed by using psycho-physiological data, e.g. EEG (electroencephalography) as well as behavioral data. The experiment also focused on the influence of small automation failures regarding driver’s vigilance. Typical fatigue patterns influenced by automation failures emerging in fatigue oscillations with strong individual differences were found. In a second step, the effectiveness of possible countermeasures was investigated. At this the driver was free from monitoring and should perform motivating so called “driving unrelated tasks” like

texting on a smartphone or reading a book. In contrast to Level 2 driving, the Level 3 automated period showed a significant decrease in fatigue level.

2.1.8. AFAS

The project “aFAS” (“Driverless Safeguarding Vehicle for Highway Shoulder Roadworks”), was funded by the Federal Ministry of Economic Affairs and Energy. The project focussed on the goal to actually operate a safeguarding vehicle under traffic in driverless mode. As far as known, this was the very first driverless operation of a vehicle in Germany, under traffic and without a safety driver on board. The demonstration was shown alongside the final project event in Frankfurt on the 20th June 2018. The Demonstration took place on the German Motorway “A3” near Frankfurt and under heavy (real) traffic conditions. A video of the driverless demonstration can be accessed under https://youtu.be/8BUWjRs3n_w

Figure 2: MAN Truck & Bus AG, Driverless demonstration of the safeguarding vehicle following on the German Motorway, aFAS press-release, 20th June 2018

The overall focus of the project was on the reduction of risks for workers driving safeguarding vehicles today. During operation the maximum speed of the vehicle was limited to 10 kph (~6 mph) which is the average speed required for roadworks by the vehicle in front (for cleaning, grass cuttings etc.). The safeguarding vehicle is intended to be driven manually up to the place of work where the automation is activated so that no driver is needed within the domain (SAE J3016 Standard version 06/2018; Level 4: driverless within a specific operational design domain, without any expectation that a user will respond to a request to intervene.). The safeguarding vehicle was connected via Wifi to the leading vehicle and relied on a sensor system for safety.

The development of the safety concept required for the driverless application under traffic was the most challenging part. It needed to be ensured that the automated, driverless vehicle would by no means leave the hard shoulder and head into the traffic passing by (being the most critical scenario) to be examined closely. This key aspect was implemented by means of a reliable sensor system able to detect the road marking and activating an immediate emergency stop in this specific case (as minimal risk or safe state on the hard shoulder). This was technically implemented by designing an independent second “safety-path” completely separated from the vehicle control system. Within safety-design the standard ISO 26262 was considered as guideline and reference for the safety-relevant design. BASt was involved in the identification of the legal aspects of driverless implementation and legal inconsistencies in the application of the ISO-Standard 26262 against the background of Road Traffic Regulations and liability.

2.1.9. SENIORS

The efforts put the last years in road safety derived to a reduction of almost 48% of total fatalities in Europe, and the number of elderly fatalities due to road accidents has also decreased. However, among all the road fatalities, the proportion of elderly is steadily increasing. Considering these statistics and the expected demographic

change in our society, the SENIORS project (Safety ENhanced Innovations for Older Road users) funded by the European Commission (GA No. 636136) and coordinated by BASt aimed at providing the needed knowledge and enabling the suitable tools to reduce the number of elderly fatalities and serious injuries suffered in road traffic accidents. The project runtime was from June 2015 to May 2018 (www.seniors-project.eu).

This project primarily investigated and assessed the injury reduction in road traffic crashes that can be achieved through innovative and suitable tools, test and assessment procedures, as well as safety systems in the area of passive vehicle safety. The goal was to reduce the numbers of fatally and seriously injured older road users for both major groups car occupants and external road users (pedestrians, cyclists) by enhancing the introduction of advanced safety systems through the implementation of assessment tools for elderly protection based on PMHS studies, volunteer testing and accident data. The research covered topics such as crash, hospital and behavioural data analysis, biomechanics, the development of test tools, procedures, and assessments. Further, to gain required data, tests with volunteers and with post-mortem human subjects are carried out, sled and impactor tests were conducted and numerical human body model simulations were performed. BASt was deeply involved in nearly all of these technical activities.

Accident data analysis showed that elderly car occupants have a higher risk of injury than younger occupants in particular in the thorax area even in accidents at lower velocities of 30 to 40 kilometers per hour. This issue was addressed within the SENIORS project by various approaches. Improved chest injury criteria for the frontal impact dummy THOR were developed. A new simulation-based approach making use of comparative computer simulations of a human model and a THOR dummy model were applied. The injury criteria for the dummy were thus optimized in the area relevant for older road users. SENIORS proposed the introduction of advanced chest injury criteria and a reduced-impact frontal impact test in new frontal impact test and assessment procedures. Sled tests have shown that these proposals can demonstrate benefits of advanced occupant restraint systems - such as adaptive systems and four-point harnesses - and thus provide improved protection in particular for older occupants.

Based on current injury patterns of pedestrians and cyclists, the vulnerable road user (VRU) safety branch of SENIORS, mainly driven by BASt, proposed modifications to the state-of-the-art pedestrian test and assessment procedures described in legislation and consumer programmes. Human body model (HBM) simulations with MAthematical DYnamic MOdels (MADYMO), replicating the most relevant motor vehicle to cyclist accident scenarios concluded in an extension of the pedestrian head impact zone and modified test parameters towards a combined VRU test procedure. FE simulations with the Total HUman body Model for Safety (THUMS) were used as input for test parameters within the scope of new test and assessment procedures, where a prototyped thorax injury prediction tool (TIPT) was tested against vehicle frontends for the first time. An upper body mass (UBM), representing the pedestrian's torso was applied to the lower legform impactor FlexPLI, improving its injury assessment ability particularly in the femur area and its applicability for high vehicle frontends and against angled surfaces, combing the upper legform to WAD775 and the upper (or lower) legform to bumper test within one single test.

2.1.10. Adoption of UN-GTR9-PH2

With its last meeting in December 2017, the United Nations Informal Working Group on the development of Phase 2 of the Global Technical Regulation on Pedestrian Safety (GTR9-PH2), chaired by Germany, concluded its work related to the introduction of the flexible pedestrian legform impactor (FlexPLI) alongside the definition of injury assessment reference values (IARVs) and the extension of the vehicle bumper test area (BTA); however the modified headform test could not be included. GRSP endorsed the proposal in May 2018 and AC.3 considered and voted for the Amendment 2 to UN-GTR9 during its November 2018 session.

2.1.11. CODECS

Communication of vehicles directly amongst each other and with road infrastructure enables a plethora of information and warning services for a safe, sustainable and comfortable future mobility. These services require new cooperation between private and public sector in order to provide seamless experience for the end user. The issues to be tackles jointly have very different nature ranging from fundamental technical and organisational aspects to legal concerns. Therefore lively exchange between the new collaboration partners is essential. In order to support this and to foster C-ITS deployment in Europe, CODECS (COoperative ITS DEployment Coordination Support) was set up as a nodal point for the various involved stakeholder groups. The Horizon

2020 support action (36 months, 05/2015 – 04/2018) has facilitated the C-ITS deployment coordination activities on European scale.

The CODECS consortium, consisting of road operators, car manufacturers, automotive industry experts as well as user and cities representatives, aimed at pooling the main actors' preferences and requirements for a concerted C-ITS roll-out across Europe. As starting point, in the inventory phase numerous pilots, deployment initiatives and private key stakeholders were brought together and the current plans, concepts and ideas were gathered. Numerous documents were analysed and several workshops organised. The experiences of this knowledge exchange and the constant survey of the C-ITS landscape in Europe were used in the consolidation phase to come up with guidelines and recommendations. The CODECS activities complemented the EC activities like the C-ITS Platform. The harmonisation activities within the project and in the workshops can be seen as precursor of the C-Roads platform which is harmonising specifications and deployment activities within 16 European countries today. CODECS has held its final event at TRA 2018 in Vienna. The heritage of CODECS (Deliverables, workshop documentations etc.) has taken on board of the Amsterdam Group website.

2.2. Ongoing and planned research

2.2.1. Safety potential and testing of reversing assistants for passengers cars (M1) and LGV´s (N1)

To increase the active and passive safety of motor vehicles and also for stylistic reasons, it can be observed that the pillars in vehicle design (A-, B-, C-, D-pillar) were constructed more massive over the years. Next to the advantages in terms of the integrity of the passenger compartment and the torsional stiffness of the vehicle, this measure may also have disadvantages in relation to the driver's field of vision.
Accidents while reversing are often pure material damage accidents when manoeuvring. However, accidents involving personal injury are also reported, e.g. with approaching cyclists while backing out from the driveway or running over children who are behind the vehicle.

Reversing assistance systems (for example radar sensors with acoustic and / or optical display, rear-view cameras, etc.) have been installed in motor vehicles for a number of years and are also frequently retrofitted. These are advertised in particular for the avoidance of property damage accidents or for the ease of manoeuvring. In principle, however, they also have the potential to prevent accidents involving personal injury. At present, however, there are no uniform requirements for such systems that would be necessary in order to generally estimate their safety potential. This is why BASt assigned a study to examine the safety potential and possible test methods for reversing assistance.

When it comes to accidents with reversing vehicles mostly pedestrians and cyclists are injured according to the GIDAS database. These generally move at an angle of approximately 90° to the reversing vehicle.
The analysis of the development of the rearward field of view of various vehicle models confirms the decline of the visual conditions out of the vehicle since the 1970s.
Observations of the view strategies when reversing showed that the available reversing display systems in vehicles are not always used.

In order to configure a test method, the today installed systems were subjected to a benchmark test. For this purpose, ultrasonic sensors were first tested by moving three different test bodies in the direction of the rear end of the vehicle. In doing so the various warning levels were determined and compared. In order to test radar systems, a moving pedestrian dummy was used. In order to test existing camera systems, a standardized dummy was equipped with a scale and placed behind the vehicle. The detection area of the camera was then explored.

Based on an analysis of the systems potential using pre-crash matrix simulations of 200 GIDAS reversing collisions, the quality of the back-up assistance system to avoid accidents with injuries could be evaluated.

2.2.2. Study on winter tires

Winter tire use is mandatory in Germany if there is snow or ice on the road. Commercial vehicles (N1, N2, M2 and M3) are required to have tires with winter characteristics at least fitted to their driven axles due to the current national regulation.

Theoretical considerations suggest that specific winter tires on steering axles might contribute to better braking behavior of commercial vehicles. The steering axle has a large influence on empty truck-and-trailer combinations, while the effect is expected to be lower for fully laden vehicles. The current regulation on tires UN-R 117 specifies requirements for traction tires, but not for steering axle tires. Currently available steering axle winter tires therefore are tested according to these requirements.

Therefore, BASt was asked to compare the performance of winter tires and summer tires that are designed for use on steering axles. Experiments were carried out on prepared snow tracks in northern Europe; the project is expected to finish by Summer 2019.

2.2.3. Automatic Emergency Braking for passenger cars

Automatic braking systems for passenger cars, designed to address car accidents with other cars, pedestrians and / or (to some extent) bicyclists are state of the art and already available in various production vehicles. It is expected that those systems will have a significant effect in improving traffic safety, so the European

Commission has included them in their proposal for the new "General Safety Regulation". The preferred way of setting requirements for technical systems is a broad international discussion on UN ECE level, so the European Commission together with Japan initiated an informal working group with the goal of setting agreed requirements for automatic emergency braking systems for N1/M1 vehicles.

Germany was part of that group and contributed with calculations, simulations as well as experimental data. Finally, the group agreed that AEBS systems should be able to avoid accidents up to a driving speed of 42 km/h on stationary targets and pedestrians and deliver a comparable performance for slow moving targets. These results have been delivered to UN ECE in January 2019 and are expected to be formerly adopted in June this year. The European Commission currently plans to make these systems mandatory in steps and beginning from 2022 (for new types).
Further work is concentrated on developing appropriate requirements for AEB systems also addressing bicycle accidents.

2.2.4. Motorcyclist-friendly safety barriers

Road restraint systems, which offer improved protection for motorcyclists in addition to the protection of vehicle occupants, should comply with the Technical Specification CEN/TS 1317-8:2012 "Motorcycle road restraint systems" published in 2012. In the beginning of 2000 when the systems for motorcyclist protection have been developed and tested in Germany there was no European standard for testing. Since it is now uncertain whether the original systems also meet the requirements of this new specification, this question will be investigated in an ongoing research project. For this purpose, impact tests are carried out on the original and if necessary a modified system (Figure 3). On basis of the results of these impact tests, recommendations for use will then be developed, which will conclude the research project by the end of 2019. The results can be used directly in practice to retrofit existing road restraint systems. This will adapt the systems to the current state of the art and will help to reduce the consequences of an accident of a motorcyclist with a road restraint system.

Figure 3: Impact according CEN/TS 1317-8:2012 (source: DEKRA)

Up to now, the assessment of the sharpness of construction elements in road restraint systems, especially with regard to the impact of motorcyclists, has been rather subjective. In a further research project, therefore, specific indications for the definition of system-neutral sharp-edged construction elements road restraint systems are to be determined. Here, impact tests were carried out with a new type of biofidelic crash test dummy, modeled on humans, on variants of individual construction parts. Initial impact tests (Figure 4) have shown enormous differences in the injury potential of individual construction elements. The impact parameters were derived on basis of an accident analysis and also on CEN/TS 1317-8:2012. Objective criteria for the evaluation of sharp edged construction elements will be developed. In practice, this makes it possible to distinguish between dangerous and less dangerous systems and to achieve a frequent use of good-natured systems. In addition, the results are to be incorporated into national and international regulations or guidelines as well as into European standardization.

Figure 4: Biofidelic crash test dummy at impact point (sigma post covered with a pipe)

2.2.5. Active motorcycle safety

Motorcycle riders are still one of the most endangered groups in modern traffic. Due to the specific driving dynamics of one-track vehicles and the location of the predominantly driven roads, the severity of accidents tends to be considerably above average. Analyses of available accidentology data in the past showed that the cause for a typical accident with a motorcycle on rural roads is loss of control over the vehicle. Prevention of mistakes by the rider in relation to occurring roll angles and braking while cornering are promising starting points for a reduction in motorcycle accidents on rural roads.

To increase the traffic safety for motorcycle riders, BASt conducts own research as well as supervising several external research projects on various topics related to motorcycle safety. Recently, braking in curves is a challenging scenario addressed by the motorcycle industry. Since there are no public studies available evaluating the benefits of the current systems, BASt claims to provide an overview of the potentials for traffic safety including user acceptance. Options for future rider trainings are to be assessed. The comparison of objective and subjective assessment can also serve as a basis for the performance and the limits of future AEB motorcycle safety systems. The currently ongoing research aims to identify boundaries that are set by rider limits (e. g max. longitudinal deceleration or rider acceptance) in which AEB systems could provide a safety benefit. In terms of riding dynamics, it is important that the rider is able to stabilize the vehicle at any time. With the current research roadmap BASt aims to further promote the development of innovative safety systems in motorcycles, which actively support the rider in critical situations.

2.2.6. EU-Project PIONEERS

PIONEERS (Protective Innovations Of New Equipment for Enhanced Rider Safety) updates the current test methods and standards for personal protective equipment for riders and on-board systems.
The main pillars of PIONEERS are to achieve a deep understanding of the injuries sustained by PTW (Powered Two Wheeler) users, improve the performance of safety systems (Personal Protective Equipment, PPEs, and on-board systems), to develop better test and assessment methods and to increase the use rate of PPE.

The improved performance will be achieved by understanding the most safety-critical accident scenarios and impact conditions to reach a higher level of understanding on how the injuries occur and by developing more reliable, realistic and robust test methods. An increased use will be fulfilled by listening to the riders' needs, improving the systems in terms of comfort (without compromising safety) and carrying out active awareness raising and dissemination actions. The main goal of the PIONEERS project is to improve the safety of PTWs by providing an integrated approach to rider protection considering on-rider (PPE) and on-board systems. Therefore, this project will investigate and assess the direct contribution to the reduction of fatalities and the severity of injuries, as well as the number of injured PTW users. The tools for that are developing new PPEs and on-board safety systems, as well as improving the validation and assessment methods and increasing the usage rate of such devices. Developing high-quality products (PPEs and on-board systems) from the European manufacturers and sensitizing the PTW users for the enhanced safety potential of those products will not only increase the safety level for PTW users but will also strengthen European competitiveness.

Finally, the main results of PIONEERS will be: (i) higher understanding of injuries suffered by the riders (ii) better testing methods enabling better performance assessment and (iii) better products (PPEs and on-board systems) achieving an increased safety level for PTW users.

BASt participates in this project by delivering and analysing accident data with the focus on body regions addressed by different elements of PPE. Furthermore BASt will develop test methods to assess helmets and neck protectors. Especially the test method for helmets will consider the current knowledge on head injury mechanisms and will be used to support the update of helmet requirements during the revision of the UNECE-R 22.

2.2.7. Friction prediction

Precise knowledge of the friction potential is of great importance for safe longitudinal and lateral control of a car. This potential is influenced by many parameters like weather conditions, road surface and tyres. While today it is the driver who assesses friction values, it will be necessary for future highly automated vehicles to independently obtain information on environmental conditions. A cause-based estimation procedure for estimating the maximum friction coefficient has been developed which relies solely on information that is available without additional vehicle sensors. This information consists of data which is present in the vehicle itself, such as outside temperature, vehicle speed or rain intensity and on data provided by the surrounding infrastructure. This includes weather data from weather stations or information on road conditions obtained from road weather information systems. By combining and integrating these fields of information, the range of the maximum coefficient of friction is established using the estimation procedure developed in the project. The result of a huge number of test brakes is a comprehensive database with more than 5,000 data sets which includes for each full braking manoeuvre more than 80 parameter information about weather, road state etc. Based on these data the mentioned friction estimation algorithm was developed. Detailed analysis of the data sets of single braking points should help to understand under which circumstances the friction coefficient changes. The evaluation of the estimation algorithm showed, that it provides satisfactory results even if some information are not available.

For the future it is imaginable that numerical weather simulation models, which give detailed weather information and which also consider local effects of the vegetation can improve the friction estimation a lot. Additionally, the use of vehicle dynamic parameters like wheel speed and interventions of ABS and ESP might improve the estimation algorithm.

2.2.8. Bus safety: smoke gas toxicity

Despite that busses are one of the safest means for transport, singular accidents and especially fire events with and without connection to an accidents can become very severe. Vehicle regulations for busses have been adjusted to address various aspects of fire safety, e.g. by introducing fire detection and control systems and burning behavior tests.

One aspect that has not yet been regulated is the smoke gas toxicity. Several standards with specific advantages and disadvantages from other modes of transport exist, but it is unclear which of those standards could best be adopted towards busses.

The focus of an upcoming research project, funded by BASt, will be the investigation of appropriate requirements for bus material smoke gas toxicity and the development of a corresponding, probably more efficient test procedure.

2.2.9. HMI aspects on Camera-Monitor-Systems

Since June 2016 conventional outside and inside rear-view mirrors can be replaced by Camera-Monitor-Systems to present views of the traffic situation behind the vehicle to the driver. At that time the corresponding UN Regulation No. 46 "Uniform provisions concerning the approval of devices for indirect vision and of motor vehicles with regard to the installation of these devices" entered into force.

Based on a previous BASt-study (F112b; Camera-Monitor systems as a replacement for exterior mirrors in cars and trucks) and UN Regulation No. 46 BASt has started a follow-up project which focuses on specific human machine interaction aspects. On the one hand, different display positions (peripheral, central in front of the driver and in the center of the vehicle – according to height variations in accordance with UN-R 46) should be investigated in terms of perceptional speed, discrimination possibilities and human's (direct) view. On the other hand, the effects of merged presentations of backward information on human's perception are explored. Besides that, the project focuses on human's perception of distances and velocities at high differential velocities in a real driving scenario. This project will terminate end of 2019.

2.2.10. Activities with regard to UN R 22 and helmets for S-Pedelecs

Within the frame of the UNECE/GRSP Informal Working Group for Protective Helmets the revision of the UNECE-R 22 has started. The update will include the test methods and test parameters to further extend the protective effects of motorcycle helmets. The new test methods will take tangential impacts and rotational kinematics of head and brain into account to enable an assessment of helmets under more realistic loading conditions. Beside the test method the use of a more advanced headform and the consideration of relevant injury criteria will contribute to helmets with higher protection in the future.
So far, the assessment of motorcycle helmets was mainly focused on linear impacts and excluded the rotational effects of impacts during real accidents associated with brain injuries.
Based on a previous BASt research project to identify the potential optimization of motorcycle helmets BASt will contribute to the working group by promoting and discussing the results.

With the continuing trend towards the electrification of mobility the safety of S-Pedelecs has to be considered. One important aspect is the use of personal protective equipment by the riders of S-Pedelecs. Since these vehicles are classified as motor vehicles (L1e) the use of suitable protective helmets is mandatory in Germany. Current requirements for suitable helmets are defined within the UNECE-R 22 for motorcycle helmets. As motorcycle helmets are made for higher speeds and low physical activity of the rider, the ventilation and mass of current motorcycle helmets are not seen optimal for the use on S-Pedelecs.
BASt compared the protective as well as the comfort related requirements defined in different standards and regulations for helmets. Tests showed that the protective effect of UNECE-R 22 compliant helmets is higher then of helmets for bicycles (EN 1078) and S-Pedelecs (NTA 8776). Since the comfort related characteristics (e.g. ventilation) are not defined or restricted in any of the relevant standards, the optimization of motorcycle helmets is seen as a solution to provide suitable and safe helmets for the use on S-Pedelecs.

2.2.11. Seriously injured road accident casualties

So far, the German Road Traffic Accident Statistics have defined "seriously injured" as those casualties who are treated in a hospital as in-patients and survive for at least 30 days. According to the new common European definition, seriously injured road-users are casualties with an injury severity classified as MAIS3+, i.e. injuries of the maximum abbreviated injury severity of level {3, 4, 5, 6}, and who do not die within 30 days from the effects of the accident. The abbreviated injury scale (AIS) is an anatomical-based coding system that classifies the injury severity by the AIS severity score on a six-point ordinal scale indicating risk for death.

The working group developed methods to determine the number of seriously injured road accident casualties in Germany on the basis of established data sources. The projections were based on the German In-depth Accident Study (GIDAS) and the TraumaRegister of the German Trauma Society® (TraumaRegister DGU®). The applied projection approaches are described in detail and their limitations are discussed. Though GIDAS and the TraumaRegister DGU® have basically different aims (crash analyses versus quality management in hospitals), both databases produce comparable results: the total number of serious injuries in Germany in the year 2015 is 15.442 resp. 14.370 persons. It must be assumed that also in coming years projections are the sole way to determine the number of serious injuries in Germany, as there is no golden standard meaning no nationwide assessment of injured road users according to the new definition.

2.2.12. UNECE IWG on Deployable Pedestrian Protection Systems (Active bonnets)

The UNECE-GRSP Task Force on Deployable Pedestrian Protection Systems (TF-DPPS), chaired by the Republic of Korea, experienced an upgrade to an Informal Working Group in 2018 with the aim to interest a

higher number of contracting parties to the 1998 agreement in the development of an amendment to UN-GTR9, implementing a test procedure for deployable bonnets. BASt emphasized the need for active systems providing at least the same level of protection to vulnerable road users as passive systems, to be ensured by a set of prerequisites prior to impactor testing. Due to very controversial discussions, BASt organized a subgroup of interested parties for developing a common understanding in what needs to be addressed by this IWG. Consensus was found regarding the principal need of DPPS capability to detect pedestrians, to ensure a certain protection level at speeds below the deployment threshold and to provide a correct timing of the system. No agreement was found with respect to the need for pedestrian protection at higher speeds and the actual protection level of active bonnets. The group continues working on further outstanding topics such as an adequate surrogate for the hardest to detect pedestrian and the legitimacy of human body model simulations within UN regulations. The current schedule foresees an adoption of Amendment 4 to UN-GTR9 by AC.3 in June 2020.

2.2.13. GIDAS – new requirements to address new vehicle technology

In summer 1999, a cooperation between FAT (Research Association of Automotive Technology) and BASt (Federal Highway Research Institute) started the German In-Depth Accident Study (GIDAS) which is one of the largest in-depth accident data collections, recording more about 3,500 parameters per crash. Since then vehicles, objectives in road traffic policies and consequently research questions have changed. While the enhancement of passive vehicle safety has been the main objective during the start of GIDAS, requirements to modern field data collections change to gathering crucial information about pre-crash maneuvers and vehicle equipment with respect to crash avoidance technologies.

In modern vehicles, driver assistance functions are increasingly supporting the driver in complex or dangerous situations by applying preventive strategies. These strategies include warnings, enhanced braking assistance, and automatic interventions to increase road safety. A key challenge is to quantitatively assess the safety performance in terms of reduction or mitigation of traffic crashes, as these real-life effects are key considerations for all stakeholders involved in the planning of future mobility. Crash re-simulation and stochastic traffic simulation provide large opportunities to predict these effects. Both approaches require widely recognized models and reliable simulation. Hence, in order to agree on validity and reproducibility, the overall method, from the combined use of heterogeneous data sources in modeling to simulation metrics must be transparent.

Virtual “what-if” re-simulation based on reconstructed crash trajectories may show if a system had affected particular crashes on a case-by-case basis. However, reconstruction relies on limited traces and does not cover the complete traffic situation. But stochastic traffic simulation based on accident data can model how conflicts emerge and how to avoid or mitigate them. The GIDAS consortium supports such activities.
Further, GIDAS will investigate how electronic data recording systems (e.g., EDR) of vehicles which had an accident could be accessed in a larger scale considering the latest data protection laws. By this, the pre-crash and crash phase could be assessed much better than today and in particular in the cases of automatic system interventions. In addition, this forms one basis to be prepared for investigating future accidents involving (highly) automated vehicles.
Note: GIDAS is celebrating its 20th birthday now in 2019.

2.2.14. Human Body Modelling

The relevance of Human Body Models (HBMs) in vehicle safety research is significantly increasing for various reasons. On the hand HBMs are an important research tool for evaluation and improvement of dummies and test experimental tools as well as the respective injury assessment criteria. In the future HBMs might also be directly used for vehicle safety assessment complimentary to experimental based test and assessment procedures. Therefore HBMs are meanwhile used by BASt for various internal and cooperative research studies.

For example within the EU funded project SENIORS HBM simulations were used to develop updated dummy based chest injury criteria to achieve improve injury assessment methods for elderly car occupants. A new simulations based approach was proposed by BASt together with project partners, which makes use of HBM and dummy simulations. To consider age related particularities of elderly car occupant an updated HBM was used for this method taking into account the morphologies differences of an elderly rib cage. The model was developed within the SENIORS project and implemented into the THUMS human model. Based on first

promising results BASt will continue to further improve this HBM simulation based approach to further improve injury assessment criteria.

Another part of SENIORS focused on external road users in which an improved legform impactor with upper body mass (FlexPLI-UBM) and a thorax injury prediction tool (TIPT) were developed mainly based on HBM simulations. Corresponding HBM and impactor simulations were conducted against several actual vehicles and rigs, representing different frontends (Sedan, SUV, Sportscar, MPV). Based on this work impactor prototypes have been developed within SENIORS. Further studies have shown a significantly improved biofidelity of the newly developed FlexPLI-UBM compared to the current FlexPLI. In the next step BASt will extend the biofidelity studies to finalize the development.

In accidents with highly automated vehicles new accident scenarios and new occupant seating positions will be expected. For these new accident conditions current physical test tools like dummies might not be applicable anymore for safety assessment. This will require new simulation based test procedures including human body models. Some of the question related to this will be addressed by BASt in the EU project OSCCAR.

Furthermore, a prerequisite for the potential future use of HBMs in virtual testing procedures will be harmonized HBM validation requirements and application methods. Therefore, BASt continues to support the THUMS User Community (TUC). Within the TUC all project partners are working closely together to archive these goals.

2.2.15. Child Safety at the UNECE with regard to R 129

Within the frame of the UNECE/GRSP Informal Working Group for Child Restraint Systems the work on the third phase for the development of the new regulation on enhanced child restraint systems was finalized. In this third phase, integral child restraint systems, connected to the car by using the vehicle belt system, are included in UN R 129. The proposal was agreed in June 2018 by WP 29, entering into force on the 29. December 2018.

The UN R 129 now includes Integral ISOFIX Enhanced Child Restraint Systems (i-Size and specific vehicle), Non-integral Enhanced Child Restraint Systems (i-Size and specific vehicle booster seat) and Integral Belted Enhanced Child Restraint Systems (universal and specific vehicle). For all Enhanced Child Restraint Systems according to UN R 129 a stature based system depending on the standing height of the child is used. All i-Size CRS will fit on an i-Size labeled vehicle seat.

For the time being only boosters without backrest are not included in UN R 129. A task force of interested experts was asked by GRSP to streamline discussions on draft amendments to the UN R 129, especially with regard to booster cushions. The works of the UNECE/GRSP Informal Group “Child Safety” as well as the task force are supported by BASt.

2.2.16. Development of requirements on automated driving functions for vehicle regulations

Automated driving functions are supposed to be available and to be used in vehicles to a greater extend. The development from the pure driver assistance to higher automation of single driving functions is an evolutionary process with a crucial step to be executed at the moment: The driver can be released in some dedicated parts of the road traffic of his obligation to perform driving task because the vehicle is supposed to be able to take over this task in some defined areas completely. This challenge has to be met both technologically and from the legislator. First changes for technical vehicle regulations on UNECE level were implemented in the UN-Regulation No. 79 for continuously assisted steering functions. The responsible Informal Working Group, chaired by Germany and Japan, which revised UN-Regulation No. 79 regarding automated steering functions (ACSF = Automatically Commanded Steering Functions), now, after requirements for corrective and emergency steering have been established, has the task to develop technical requirements for higher levels of automation (automated lane keeping system (hands-off) for highway applications, e.g. low speed/ traffic jam situations). There are big challenges of the technical requirements on automated steering without the continuous surveillance of the driving task by the driver to be overcome. Reliable safety systems shall be installed and present in the vehicle when automated steering is allowed to be activated and the driver is not any longer obliged to have the hands on the steering wheel and the eyes on the road. In this case the braking system is also of special importance because in case of transferring complete driving task to the vehicle, the longitudinal control with speed and distance control has to be transferred as well. If during the automated driving phase a

sudden and unexpected situation occurs the system shall be able to cope with the situation by itself e.g. by emergency braking. There is a qualitative difference to today's emergency braking systems where normally a warning phase leads to the braking phase and where the systems have to incorporate a possible driver reaction like steering to avoid a crash. In terms of safety a very important issue to decide on is the transition procedure of the driving task from the automated system back to manual driving to ensure at any time a 'driver' is in control of the vehicle.

2.2.17. EU-Project L3-Pilot

In the project "L3Pilot", 34 partners from research, industry and government agencies cooperate in order to test the safety, efficiency and usability of automated cars (SAE levels 3 and 4). BASt participates with a study on user acceptance and trust, and provides input to the safety impact assessment. The project is co-funded by the European Union under the Horizon 2020 programme.

To understand the attitude of drivers towards automated vehicles, it is crucial to examine their trust and acceptance with respect to these technologies. Too much trust can cause misuse, too little trust or acceptance can hinder the use of automated driving functions and thus their positive effects on road safety and efficiency. In L3Pilot, BASt will perform a long-term study with a research vehicle in real motorway traffic in order to investigate participants' trust, acceptance and secondary task engagement and their change over time. The results will show if e.g. gender or age of drivers affects trust and acceptance and if the participants are willing to use the automated riving function for a longer trip.

In the project methods for different fields of evaluation are developed. BASt participates in defining the methods for the impact assessment particularly having a look at implications for safety (accidents with injured casualties) and the scaling up of the results to EU level. The verification of those methods is another important part to make sure plans are feasible to implement. In a top-down approach the proposed methodologies will be checked with respect to the information flow from the intended response to the research questions and also with respect to the outputs and inputs to the processing of indicators and the logging of data.

In contrast to existing projects, the impact assessment in L3Pilot will be based on real world (pilot) data which are complemented with other sources where necessary. GIDAS is a source that will be used to determine the possible effect of the L3Pilot systems.

2.2.18. Development of evaluation methods for driver interaction with assistance and automation (national research and Euro NCAP)

Safety of continuously automated functions strongly depend on and result from successful driver-vehicle-interaction. In short term, this effect is particularly strong in case of already available parallel automation as provided by SAE Level 2 (L2) Systems. Per definition, any L2 system performs both the lateral and longitudinal vehicle motion control with the expectation that the driver completes the Object and Event Detection and Response (OEDR). Nevertheless, every system performs also parts of the OEDR itself, for example providing steering torque if lane markings indicate curvature. This amount of OEDR performed by the system and the expectation that the driver completes the remainder of OEDR varies between different L2 systems. Especially highly reliable L2 systems performing a greater amount of OEDR while at the same time requiring only little driver input over time can make it difficult for drivers to correctly identify their role and responsibility. Based on international standards, literature reviews and expert consultations, a first checklist-based expert-evaluation for currently available vehicles with L2 systems was developed. Assessments are focusing on different sources of user information (e.g. user manual), human-machine-interface design as well as the prevention of unintended use by different driver monitoring techniques. The checklist-tool was developed in cooperation with experts and validated in a common expert workshop to gain high level of standardization and agreement. Besides the assessment of these rather explicit forms of information design criteria, also implicit forms of driver-vehicle-interaction, for example vehicle dynamics or system behavior and reliability within different situations and contexts (e.g. how strong is the steering wheel resisting input of human driver when the system is active), play an important role. Therefore, it is intended that further assessments also include observational and interview measures of user studies. To ensure a holistic assessment, the methodological aim is to take also interaction related processes regarding user´s understanding of roles and responsibilities when applying automated driving functions as well as user´s awareness of automation modes or traffic situations into account. Based on the results

of the development of evaluation methods for assistant functions (L2), further methods and categories for the assessment of higher level automated functions (Level 3 and above) will be developed soon.

2.2.19. EU-Project OSCCAR

The EU project "OSCCAR - Future Occupant Safety for Crashes in Cars" - is dedicated to the improvement and assessment of vehicle safety for car occupants in future accidents involving highly automated vehicles. Highly automated vehicles might enable new, more comfortable seating positions (swivel seats and reclined positions). Furthermore, collisions with highly automated vehicles might also lead to new accident scenarios and thus load condition of vehicle occupants. To continue to protect all passengers in the best possible way, innovative occupant restraint systems (belts, airbags and new seating concepts) will be required.

OSCCAR aims to develop protection principles for these new innovative restraint systems. Furthermore, conventional crash test dummies might not be suitable for the design and evaluation of these new protection systems, especially in new impact scenarios. A possible alternative approach could be the use of human body models. These virtual test tools, which can also represent different road user types in terms of anthropometry and age, could be a possible solution in a process of virtual testing. The further development and improvement of these virtual test and development tools is one main objective of OSCCAR. A new virtual test and assessment method involving human body models will also require a validation procedure for the vehicle environment including new restraint systems. The development of this procedure is one main task of BASt within the OSCCAR project.

2.2.20. PEGASUS

PEGASUS (**p**roject for the **e**stablishment of **g**enerally **a**ccepted quality criteria, tools and methods as well as **s**cenarios and **s**ituations for the release of SAE Level 3 driving functions) develops tools and procedures for the testing and homologation of automated vehicles. The 17 project partners from science and industry fields define a state-of-the-art technology for the safeguarding of Level 3 driving and demonstrate the development in a practical manner, using the example of the ‘highway chauffeur’ until midyear 2019. The objective is to develop a procedure for the testing of automated driving functions, in order to facilitate the rapid implementation of automated driving into practice.

In a practical study BASt focuses on the identification of risks that can arise in the interaction between a highly automated vehicle and the driver. In a field study performed on highways, the influence of traffic density on the driver's takeover capability will first be examined. The driving tests should uncover possible safety risks during transitions and enable an initial assessment of the influence of the traffic situation. In a second study, a test site will be used to investigate effects of a preceding automated drive on the ability to cope with unexpected situations following the successful completion of the takeover request. Both empirical studies use the BASt 'Wizard of Oz' vehicle which is able to simulate the considered automated driving functions.

2.2.21. Development of basic scenarios for the description of control-relevant requirements for continuous automated vehicle guidance

In order to assess and quantify the safety performance of continuously automated vehicles – and thereby assuring their safe deployment into the vehicle fleet - relevant testing procedures have to be developed. Such testing procedures have to be able to reflect realistic traffic scenarios, in particular focusing on critical, accident prone situations. Furthermore they have to provide ways to challenge Level 3 automated vehicle systems with complex situations and environmental conditions which can notably tempt their sensory and decision making abilities. Presently various attempts to establish such testing procedures are primarily based on the selection and appropriate parameterization of traffic scenarios, which are either derived from real world traffic recordings (e.g. NDS, FOTs or In-Depth accident investigations) or generated synthetically.

Testing scenarios can provide a basis for deriving either laboratory track driving tests or can be translated into virtual testing environments for simulation based driving tests. Both techniques will require performance criteria as well; however simple “no crash” criteria might not be sufficient to fully express necessary requirements.
The research project PEGASUS, promoted by the German Ministry of Economic Affairs and Energy, has developed a showcase to demonstrate a complete step-by-step procedure of a scenario based assessment and

validation of Level 3 automated vehicle functions by focusing on the example of the “Highway chauffeur function”. The results of the project can serve as a blueprint for the further development of any scenario based validation approach and shall thereby also enhance associated international co-operation.

2.2.22. EU project HEADSTART

BASt participates in the EU-funded Horizon 2020 project „HEADSTART” (Harmonised European Solutions for Testing Automated Road Transport). The HEADSTART project will define testing and validation procedures of Connected and Automated Driving (CAD) functions including its key enabling technologies (i.e. communications, cyber-security, positioning) by cross-linking of all test instances such as simulation, proving ground and real world field tests to validate safety and security performance according to the needs of key user groups (technology developers, consumer testing groups and type approval authorities).
Five major objectives encompass the HEADSTART project:
Create a dynamic catalogue of existing methodologies, procedures, tools for testing, validation and certification considering multi-stakeholder requirements. Harmonisation of existing testing and validation approaches taking into account other industries and domains. Define and develop test, validation and certification methodologies and procedures for CAD functions building upon existing initiatives. Demonstrate the developed methodologies, procedures and tools through the testing of four CAD use cases (to be defined within the project). Reach consensus by creating and managing an expert network of CAD testing to promote adoption of the project results considering multistakeholder needs.

HEADSTART brings together a large representation of stakeholders across the value chain leveraging the knowledge from European and national activities on CAD testing. The consortium and associated stakeholders will cluster the most relevant initiatives, develop the specific procedures and tools missing and harmonise the whole approach to reach a harmonised European solution for testing, validating and certifying automated road vehicles. This will be achieved by international cooperation with industry, academia and policy makers participating in dedicated working groups of a managed expert network during the whole project duration.

2.2.23. C-Roads Germany

The European Commission has published its C-ITS strategy (COM (2016) 766) in November 2016 which heavily builds on the results of the C-ITS Platform (first phase). C-Roads, as a family of deployment pilots for C-ITS services, is seen from this perspective as the most important, infrastructure related, element of practical pre-deployment throughout the EU. The C-Roads Platform started with eight Member States and doubled this number to 16 in the meantime. Austria, Belgium, Czech Republic, Denmark, Finland, France, Germany, Hungary, Italy, the Netherlands, Norway, Portugal, Slovenia, Spain, Sweden and UK jointly work on harmonising specifications and the necessary measures for a Europe-wide deployment of C-ITS with seamless experience for the end user.

Together they mobilise approx. 199 Mn EUR (thereof 107 Mn EUR co-funded by Connecting Europe Facility) of infrastructure investment in C-ITS services. The investments complements the huge efforts of the automotive industry incl. their suppliers to kick start mass market deployment of C-ITS services in the vehicle fleet by 2019. C-Roads has been officially launched in Brussels in December 2016 (see Figure 8). C-Roads Germany ties together the pilots in Hesse (Rhine Main region) and Lower Saxony (around Braunschweig and Wolfsburg). It is a 10 Mn pilot running until 2020 with the overarching goal of providing interoperable, safety and efficiency targeting C-ITS services. The BASt roles are devoted to the national technical coordination of C-Roads Germany and the provision of coordinated expert input into the various expert groups (addressing issues to be solved for deployment, i.e. organisational issues, security, service harmonisation, infrastructure communication, hybrid communication, validation, evaluation and assessment of the pilots) of the C-Roads Platform. Especially, BASt chairs the task force on security aspects and co-chairs the task forces on hybrid communication and on validation. BASt also supports the Federal Ministry of Transport and Digital Infrastructure in the Steering Committee representation.

As first important results, C-Roads has released the Harmonised C-ITS Specifications for services with infrastructure involvement in Europe which have been included in the Delegated Act on C-ITS (Draft Delegated Act published for Public Consultation on 11.01.2019)). Furthermore, reports on legal and organisational structures as well as on the European security mechanism for C-ITS have been published.

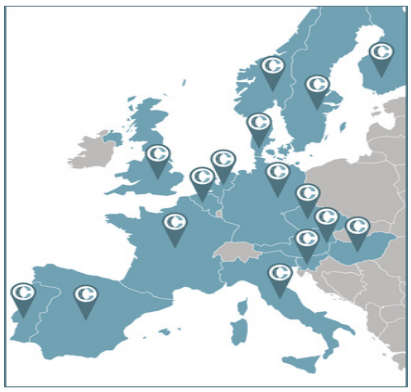

Figure 5: Official launch of C-Roads by EU Commissioner Bulc on 12th December 2016 in Brussels ©EC.

Perspectively, the C-Roads Platform will further grow as a result of projects funded from the CEF Call Transport 2018. This will enlarge the number of cooperating Member States to approximately 20. Even more important is the inclusion of urban C-ITS services into the C-Roads programme. Like several other Member States, Germany has submitted a proposal "C-Roads Germany Urban Nodes" which includes pilots in Hamburg, Kassel and Dresden. The co-funding decision is expected for spring 2019.

2.2.24. Practical Test for the Quality of Congestion-Tail Information

The overall objective of this activity is to reduce the number of end-of-congestion accidents, by providing on-time and accurate warnings on occurring congestion-tails to road travellers. Corresponding information can be nowadays acquired by commercial traffic-data providers, which generate such information from movement patterns of connected road users. Such data seem to offer a good alternative or supplement to conventional detection by road authorities, e.g. via cameras or manual reporting.

However, minimum requirements for such third-party-generated congestion-tail information, as well as framework conditions for their procurement by the public sector, must be defined in advance.

So far, a concept study is available on corresponding minimum requirements and a testing approach (FE 82.0637/2015 "Minimum Requirements for Congestion-Tail Information and Concept for their Practical Testing"). This study suggests an implementation of a practical test to validate the conceptual approaches.
The follow-up project "Concept and Monitoring of a Practical Test for the Quality of Congestion-Tail Information" (FE 03.563/2017)) has been initiated in January 2019. It includes the implementation and evaluation of a test in real-world environment during at least 6 months. During this test, data from different, commercial traffic-data providers will be assessed; and suitable quality assessment criteria will be defined. As a goal, public road authorities will receive guidance in assessing and procuring commercially available congestion-tail information, through e.g. calls for tenders.

The test is planned to start in summer 2019. A final report, including the test evaluation and guidance documents for road authorities, is expected for summer 2020.

2.2.25. Research program road safety

BASt has the task to carry out purposeful planning and coordination of research in the area of road safety and to examine traffic safety improvements.

For this reason BASt elaborates an annual research program, which addresses specific and anticipated safety deficits in road traffic in order to provide scientifically sound information as a base for advice and support of the Federal Ministry of Transport and Digital Infrastructure (BMVI). For example safety of pedestrians in urban areas was the main topic in the 2017 research program road safety, Safety Performance Indicators will be evaluated in the 2019 program.

This document is a place holder for Marion

This document is a place holder for Marion

This document is a place holder for Marion

This document is a place holder for Marion

This document is a place holder for Marion

This document is a place holder for Marion

This document is a place holder for Marion

This document is a place holder for Marion

This document is a place holder for Marion

This document is a place holder for Marion

This document is a place holder for Marion

This document is a place holder for Marion

This document is a place holder for Marion

This document is a place holder for Marion

This document is a place holder for Marion

This document is a place holder for Marion

GOVERNMENT STATUS REPORT OF JAPAN

Hiroyuki INOMATA
Director,
International Affairs Office,
Engineering Policy Division,
Road Transport Bureau,
Ministry of Land, Infrastructure, Transport and Tourism of Japan (MLIT)

1. TRENDS OF THE ROAD TRAFFIC ACCIDENTS IN JAPAN

The number of fatalities (those who died within 24 hours) resulting from traffic accidents in 2018 was 3,532. This represents a great decrease compared to the previous year and is about one-fifth the 16,765 fatalities in 1970, which was the year in which the number reached its peak. In addition, both the number of accidents resulting in injury or death and the number of injured persons decreased for the 14th consecutive year in a row since 2004, when the numbers were at their worst.

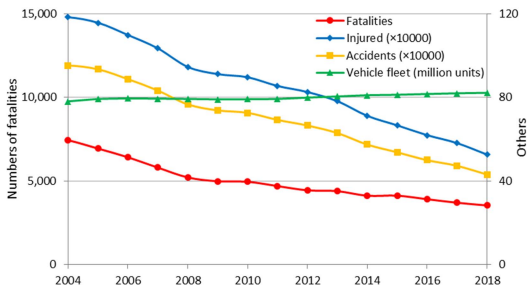

Figure 1. Recent trends of the road traffic accidents in Japan

Japan has had a low rate of road traffic fatalities per 100,000 population, which was 2.8 in 2018, but as a further step, new targets were established in the 10th Fundamental Traffic Safety Program for 2016 - 2020: to reduce the number of fatalities to below 2,500 (those who died within 24 hours) and to below around 3,500(those who died within 30 days) by 2020.

The road transport environment is beginning to change greatly due to the aging society and the introduction of Advanced Safety Technologies. Therefore, on 24th June 2016 the Working Group on Technology and Vehicle Safety of the Council for Transport Policy of the Ministry of Land, Infrastructure, Transport and Tourism (MLIT) reported a target for 2020 to reduce the number of fatalities by 1,000 from the one for 2011 by implementing vehicle safety measures, evaluating their effect, and setting the policy for reaching the new targets.

2. Effective Vehicle Safety Measures

To spread active safety and other safety technologies and to enhance development, it is necessary not only to establish safety regulations, but also to implement various rational measures. These should be considered based on quantitative assessment of the effects and performance as well as the required costs. Therefore, the MLIT is promoting vehicle safety measures through effective linkage between the safety regulations, the Advanced

Safety Vehicle (ASV) project and the New Car Assessment Program (NCAP).

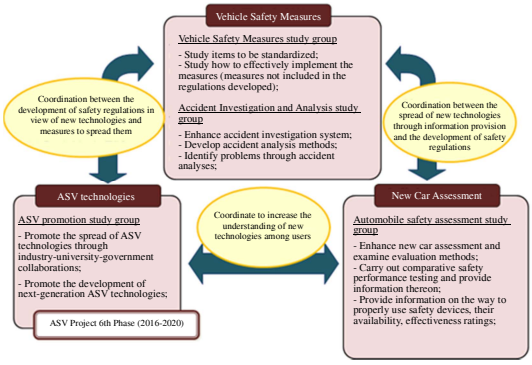

Figure 2. Vehicle safety measures promotion system

2.1. Enhancement of Safety Regulations

With regard to the expansion and enhancement of safety regulations, the MLIT has been considering the introduction of UN regulations and UN GTRs mainly for advanced safety technologies with the harmonization of international regulations in mind.

Recent amendments to safety regulations:

2018 Introduction of amendment to UN R79 on automated lane-change functions; introduction of UN R144 on Accident Emergency Call Systems;

2017 Introduction of amendment to UN R79 on automated lane-keep functions; extension of seats to be covered by seatbelt reminder (UN R16)

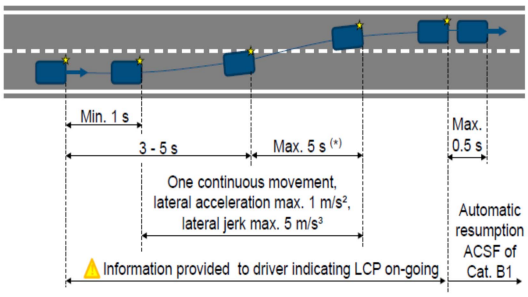

Figure 3. Outline of the international regulation on automated lane-change functions

2.2. Advanced Safety Vehicle (ASV) project

Regarding the ASV Promotion Project which is to promote the development and commercialization of Advanced Safety Vehicles (ASV), the MLIT has been promoting ASV toward automated driving, the theme of the 6th Phase of the project, such as the study of technical requirements of Emergency Driving Stop System, the spread of automated driving technologies including ASV technologies that have already been achieved. Regarding large vehicles such as trucks and buses, we are promoting the introduction of advanced safety technologies such as Advanced Emergency Braking System (AEBS), Emergency Driving Stop System, and Blind Spot Information System through tax incentives and budget distribution.

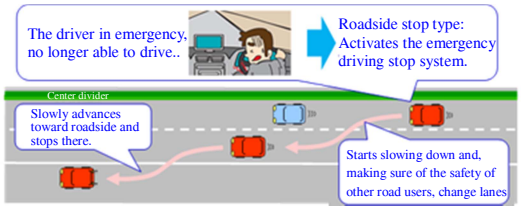

Figure 4. Emergency Driving Stop System in the event that the driver is incapacitated

2.3. New Car Assessment Program (NCAP)

To allow motor vehicle users to select safer

vehicles and promote the development of safer motor vehicles by auto manufacturers, the New Car Assessment Program (NCAP), which assesses and publishes the safety performance of motor vehicles, has been in place since 1995 (Fiscal year; hereinafter the same in this chapter). Since 2011, the collision safety performance assessment has been carried out that assesses each vehicle's performance in both occupant protection and pedestrian protection, and publishes the results with one to five stars. To further improve the collision safety performance, study is now under way to take the safety of elderly occupants into account.

Meanwhile, the preventive safety performance assessment of AEBS or other preventive safety systems has been conducted since 2014, enhancing the assessment by gradually increasing systems to be assessed.

The assessment of acceleration control systems for pedal misapplication was added in 2018 and the assessment will start in 2019 of AEBS to avoid collision with pedestrians under night-time no-streetlight conditions.

From 2020, we will integrate the assessment and publication of the results of collision safety performance and preventive safety performance, which has been conducted separately.

In order to improve the awareness of NCAP among consumers, efforts are being made to spread knowledge and information in cooperation with National Agency for Automotive Safety and Victims' Aid (NASVA) and Regional Transport Bureaus.

Figure 5. Assessment of AEBS to avoid collision with pedestrians (under night-time)

3. Efforts toward the realization of automated driving

Automated driving is expected to have great effects in solving problems such as reducing traffic accidents, relieving traffic jams, ensuring the means of transport for the elderly, etc. As the objectives of the whole government, it aims at realizing highly automated driving on expressways, unmanned autonomous mobility service in specified areas, etc. by around 2020. To this end, the MLIT set up Automated Driving Strategy Headquarters and works to make automated driving a reality, i.e., to (i) develop and improve an environment (regulations and legal systems) for, (ii) promote the development and deployment of, and (iii) carry out field operational testing and social implementation of these technologies.

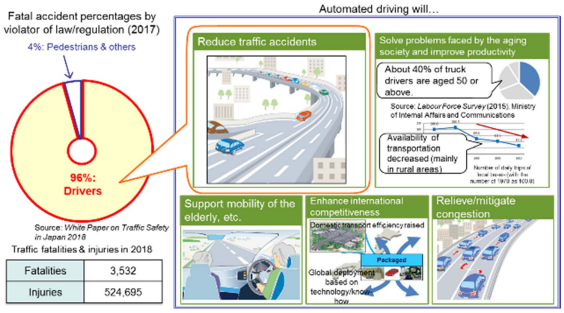

Figure 6. Importance of Automated Driving

3.1. Develop and improve an environment for realizing automated driving

Regarding the development of safety

regulations for automated vehicles, the government, based on the agreement reached at the G7 meeting of ministers in charge of transport held in June 2017 in Italy that the member countries would cooperate at the international level at the United Nations World Forum for Harmonization of Vehicle Regulations (WP.29) to put more highly automated/autonomous driving technology (Level 3 and Level 4) into practical use, contributes to discussions at WP.29 for the development of international regulations on automatically commanded steering function, AEBS, cybersecurity, etc. Domestically, the MLIT developed the Guideline regarding Safety Technology for Automated/Autonomous Vehicles in September 2018 to promote the development and commercialization of safe automated/autonomous vehicles even before the implementation of international regulations on automated/autonomous vehicles of Level 3 and Level 4. This guideline sets the safety goal of "realizing society where traffic accidents caused by automated/autonomous driving systems resulting in injury or death become zero" for the first time in the world and defines ten safety requirements to be satisfied by automated/autonomous vehicles including the safety of the automated/autonomous driving systems, installation of data storage systems, and cybersecurity.

3.2. Promote the development and deployment of automated driving technology

Regarding promoting the development and deployment of automated driving technology, the government set a new numerical target of increasing the rate of newly registered passenger vehicles with AEBS to 90% or more by 2020. To achieve this goal, the MLIT is multiplying efforts both in public and private sectors to promote the development and deployment.

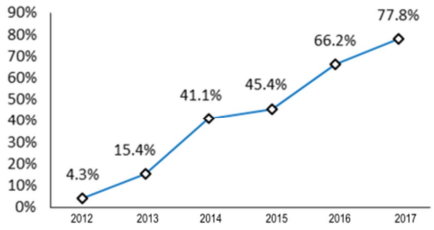

Figure 7. Evolution of the rate of newly registered passenger vehicles with AEBS

3.3. Field operational testing for automated/autonomous driving and its social implementation

The government is working on field operational testing of last mile automated mobility service that connects the nearest stations, etc. and final destinations with automated mini carts, buses, etc. and truck platooning. In the tests of last mile automated mobility service, a two-on-one remote control experiment started in November 2018 in which two vehicles are operated by a single remote monitor/driver.

Regarding truck platooning, a public-road test started in January 2019 on the Shin-Tomei Expressway in which the following vehicles were unmanned.

Figure 8. Field operational testing of last mile automated driving and truck platooning

4. Promote the international harmonization of vehicle regulations in cooperation with various countries

Regarding the promotion of the international harmonization of vehicle regulations, the MLIT makes all-out efforts to work on them as a major task, as mentioned in its growth strategy "Investments for the Future Strategy 2018" (adopted by the Cabinet on June 15, 2018).

Figure 9. Structure of WP.29

4.1. Contribution to international discussion

At the WP.29, in cooperation with other countries, the MLIT contributes to the development of international regulations on automated driving technologies such as automatically commanded steering function and AEBS as well as new technologies such as cybersecurity, detection and warning system for vulnerable road users in close proximity of the vehicle and so on.

4.2. Promote International Whole Vehicle Type Approval (IWVTA)

At the WP.29, an international regulation (UN R0) was adopted in November 2017 and entered into force in July 2018. The MLIT is striving for the smooth operation of IWVTA and promote an active utilization thereof. We are currently studying how we could further enhance IWVTA in the future, including expansion of target devices.

4.3. Promote emerging countries' accession to UN Agreements, etc.

The MLIT actively supports ASEAN and other emerging countries in their accession to UN Agreements, participation in the WP.29 and introducing IWVTA. Moreover, in order to promote the introduction of appropriate traffic safety/environmental preservation measures based on their own traffic and environmental conditions, the MLIT is cooperating with them making good use of its expertise and experience.

CONCLUSION

Measures that are being taken in Japan have been described above. When promoting these measures, the MLIT gathers and analyzes traffic data, and runs a PDCA cycle with the cooperation from various stakeholders.

Furthermore, considering that motor vehicles are globally distributed products, international harmonization should be kept in mind when studying and discussing regulations.

The MLIT would like to continue contributing to international discussions by actively making proposals based on technical grounds.

GOVERNMENT STATUS REPORT OF REPUBLIC OF KOREA

Su-sang KIM
Director General,
Bureau of Motor Vehicles Policy
Ministry of Land, Infrastructure and Transport,
Republic of Korea

Status of Road Traffic Accidents and Policies

Analysis of Road Traffic Accidents Statistics

The fatalities from road traffic accidents steadily decreased due to the Korean government's continuous efforts and the implementation of policies to reduce traffic accidents, while the number of motor vehicle registrations continued to increase over the past 20 years. The number of motor vehicle registrations increased by four folds in 2017 compared to that in 1997, but the fatalities due to traffic accidents decreased by about one third from 1997 to 2017. The fatalities per 100,000 people also declined to below 10 in 2014 for the first time, decreased steadily to 8.1 in 2017.

Table 1. Total fatalities and fatalities per 100,000 (unit: death)

Year	2011	2012	2013	2014	2015	2016	2017
Total Fatalities	5,229	5,392	5,092	4,762	4,621	4,294	4,185
Fatalities per 100,000	10.5	10.8	10.1	9.4	9.1	8.5	8.1
Number of Vehicle Registration (million unit)	18.44	18.87	19.40	20.12	20.99	21.80	22.53

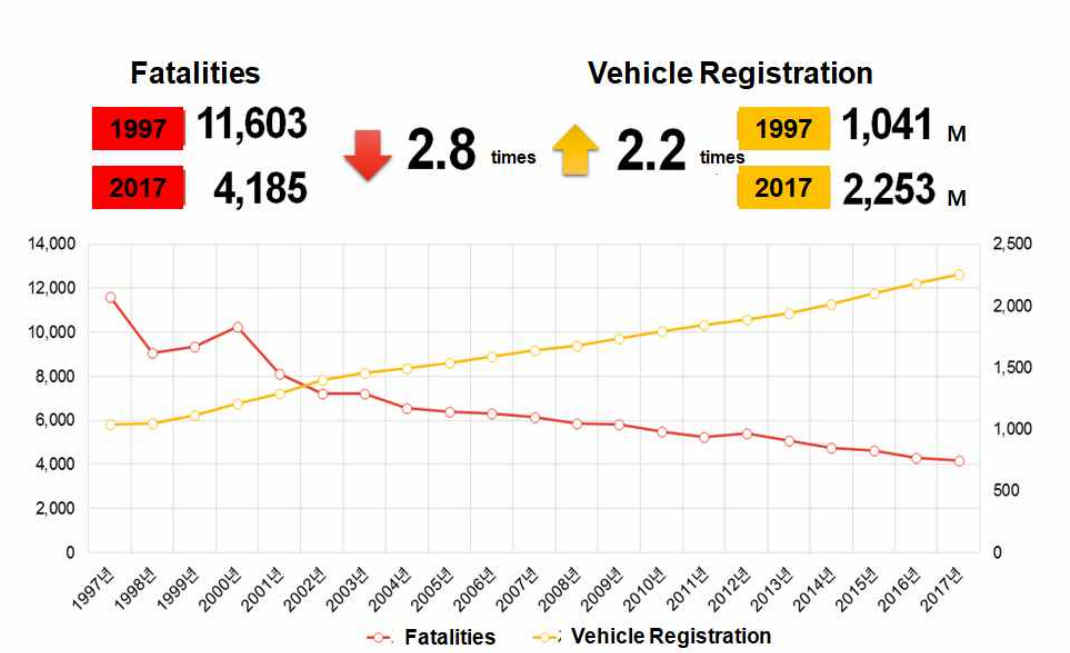

Figure 1. Road traffic fatalities

In order to improve road traffic safety, the Korean government has established a 5-year National Transportation Safety Master Plan every five years. According to the 8th Plan (2017 ~ 2021), the government aims to reduce the fatalities from road traffic accidents to 2,800 or less by 2021 by implementing various measures.

The 2nd Vehicle Policy Framework Plan(2017~2021)

The 2nd Vehicle Policy Framework Plan(2017~2021), established in 2016, sets policy directions for strengthening vehicle safety, strengthening passenger and pedestrian protection from traffic accidents, and implementing vehicle safety and management measures. In particular, regarding the activities for strengthening vehicle safety, the feasibility and implementation studies of international vehicle regulations have been carried out. Regarding international cooperation, Korea has actively participated in the UN ECE WP.29 for the past two years with the aim of strengthening our role in international vehicle regulation legislation.

Activities in International Harmonization of Vehicle Regulations

The Republic Korea is a contracting party to the 1958 Agreement and the 1998 Agreement of UN ECE(United Nations Economic Commission for Europe) WP.29(World Forum for Harmonization of Vehicle Regulations). UN Regulations and UN Global Technical Regulations have been reflected in domestic vehicle regulations.

Researches for International Harmonization of Vehicle Regulations

Since 2006, Korea has introduced international vehicle regulations to domestic vehicle regulations every year based on the feasibility studies to promote international harmonization. From 2017, an annual plan has been established and the feasibility study and implementation of international vehicle regulations have been carried out under the 2nd Vehicle Policy Framework Plan.

In 2019 the studies have been initiated to introduce seven UN Regulations, such as Mechanical coupling(UN Reg 55), the Rollover Stability of Tank Vehicles(UN Reg 111), Superstructure and Seat Strength of a Bus(UN Reg 14, 16, 66, 80, 107).

As of February 2019, about 68% of the domestic vehicle safety regulations were harmonized with international vehicle regulations by introducing 68 UN Regulations and 14 UN Global Technical Regulations. In 2017, 16 items in the domestic vehicle safety regulations were harmonized with UN Regulations including UN Reg 18 and 4 items in the domestic vehicle safety regulations were harmonized with UN Global Technical Regulations including GTR No. 2. Five items in the domestic vehicle safety regulations were harmonized with UN Regulations including UN Reg 77 in 2018.

Table 2 shows the number of items to be revised by year, 16 items of international vehicle regulations to be studied to reflect on domestic vehicle safety regulations, and a total of 43 international vehicle regulations will be reflected on domestic vehicle safety regulations by 2023.

Table 2. Harmonization Rate and Number of Research Items

Category		2019	2020	2021	2022	2023	Total
UN Regulation	to be reflected after study	3	7	4	1	1	16
	to be reflected	10	3	3	2	1	27
UN Global Technical Regulation	to be reflected	4	1	3	-	-	
Number of Items		17	11	10	3	2	43

Activities at UN/ECE WP.29

The Republic of Korea is actively participating in the WP.29 Plenary Meetings and six Expert Meetings(GR) and informal technical group meetings. As of 2019, The Delegate of Korea is serving as Vice-Chairperson of Working Party on Passive Safety(GRSP).

The Delegates of Korea also chair for the informal working group on Panoramic Sunroof Glazing (PSG) to develop an international vehicle regulations to prevent the damage of panorama sunroof and for the informal working group on Deployable Pedestrian Protection System (DPPS) to develop test procedures to mitigate pedestrian injury in pedestrian accidents.
The Delegates of Korea are serving as Vice-Chairperson for the informal working group on 2nd phase Hydrogen and Fuel Cell Vehicles (HFCV) and the informal working group on Vehicle Interior Air Quality (VIAQ) to develop international vehicle regulations in the 2nd phase. The Republic of Korea is actively participating in 13 informal technical working group meetings.
In addition, in order to develop international vehicle regulations for autonomous vehicles, at its February 2018 session, the Inland Transport Committee (ITC) requested WP.29 to consider establishing a dedicated subsidiary Working Party. Following this request, WP.29, at its June 2018 session, decided to convert the Working Party on Brakes and Running Gear (GRRF) into a new Working Party on Automated/Autonomous and Connected Vehicles (GRVA). Five informal technical working group meetings will be operating under GRVA. In response to transition, the Republic of Korea will exercise her full capabilities and participate in the informal technical working group meetings to pursue active roles and activities.

Korean New Car Assessment Program (KNCAP)

The Korean New Car Assessment Program was introduced in 1999 with a full frontal crash test of Hyundai Avante model. Since then, 175 models have been assessed by 2018, and 22 items in the three areas of collision safety, pedestrian safety and accident prevention safety are being evaluated by continuously expanding models and assessment items.
Reflecting technological and social changes such as strengthening the safety of vulnerable road users, cutting-edge automotive technology, and commercialization of autonomous vehicles, the Korean New Car Assessment Program began the evaluation of the collision safety for vulnerable road users such as women drivers and children in 2017. The safety of the accident prevention field was enhanced by including the assessment of ADAS such as AEBS.
To enhance passenger safety in the second row seat the assessment was extended to evaluate the neck injuries of passengers in 2018 and the crash safety of women passengers in 2019. The assessment has been continuously enhanced by evaluating the safety of women and children, whose safety has been somewhat neglected in the program.
In addition, after expanding the number of evaluated ADAS to 13 in 2017 in the accident prevention area, the installation rate of safety devices increased from 57% in 2017 to 66% in 2018 by 9 % points. The Korean New Car Assessment Program played a leading role in enhancing vehicle safety in the accident prevention area.
The second mid to long-term Korean New Car Assessment Program Plan (2019-2023) was established in 2017. The current status of domestic traffic accidents, technological development trends, and overseas NCAP trends were reflected in this Plan according to the 8th National Transportation Safety Master Plan(2017 ~ 2021) and the 2nd Vehicle Policy Framework Plan(2017~2021). In this Plan the following three major strategies and detailed implementations were decided as follows:

A. Strengthening collision protection: Strengthening collision safety of vulnerable occupant such as female passengers in the second row, etc. and strengthening occupant protection in consideration of real world traffic accidents other than typical collision tests.
   1. Safety evaluation of female passengers in the second row seats
   2. Car-to-car collision safety, Far-side passenger safety
   3. Strengthening occupant protection in side impacts
B. Strengthening protection of vulnerable road users: Improving evaluation technology for pedestrian protection with a 40% fatality rate and introducing evaluation for cyclist protection.
   1. Enlargement of pedestrian head impact zone in consideration of vehicle-to-bicycle accidents
   2. A Study on the Improved Pedestrian Leg Model Evaluation Technique
C. Improving accident prevention safety: Encourage the Development and Mandatory Installation of Advanced Emergency Braking System(AEBS), Emergency Steering System (ESF), etc. to cope with

the commercialization of autonomous vehicles in advance.

1. Extending AEBS assessment items to cyclists
2. Research for Evaluation Technology of ESF and Expansion of Evaluation Items
3. Study on the Combined Assessment Scenario of ADAS

Research and Development

Research for the safety assessment technology of autonomous vehicle

The safety assessment technology of autonomous vehicle means a technology for evaluating and verifying the safety of an automobile equipped with autonomous driving technology. As shown in Figure 2, the government's plan to support the commercialization of autonomous driving vehicles focuses on the development of safety assessment technologies and identification of evaluation items that can be applied to level 3 autonomous vehicles safely driven on public highways.

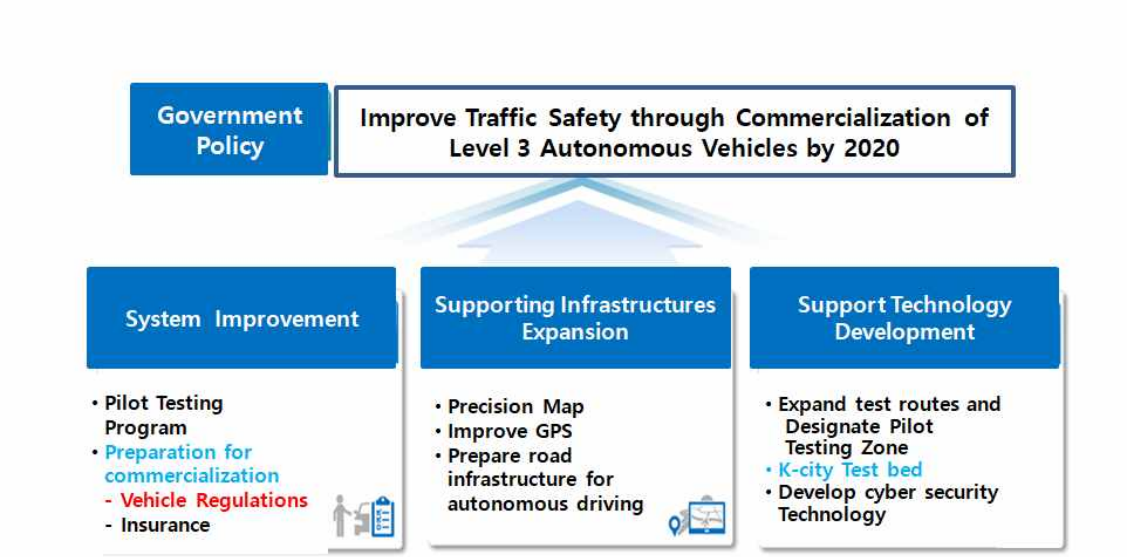

Figure 2. Government Policy for supporting the commercialization of Autonomous Vehicle(5. 2015)

In order to verify and assess the safety of autonomous vehicles the testing environment dedicated to evaluate autonomous driving systems will be established in this study. Also the assessment technology of autonomous driving and fail-safe systems under the normal driving or abnormal situations (including failure conditions) will be developed to assess the safety of the autonomous vehicle. The evaluation technology related to cyber security of autonomous driving systems in the internal and external communication environments will be developed too. Figure 3 shows the overall scope of development processes.

- Establishment of Testing Environment : Establishment of K-City and Evaluation System (e.g. Robo-vehicle) simulating actual roads in order to evaluate autonomous driving systems
- Assessment Technology of Autonomous Driving and Fail-safe Systems: Develop scenario-based evaluation technology to ensure the safe driving of autonomous driving systems in various normal and abnormal conditions such as ODD exit, system failures, emergencies.
- Evaluation Technology of Cyber Security of Autonomous Driving Systems: Conduct a phased study of cyber security of autonomous driving systems in the internal and external communication environments in order to assess the system security against communication disturbances such as jamming radio waves, forgery of communication data and arbitrary collection of operation data.

In order to effectively study and verify these detailed technologies, a consortium of 16 organizations including Hyundai Motors and Seoul National University has been established by the Korea Automobile Testing and Research Institute(KATRI). From June 2016 to June 2019, a total of 21.7 billion wons(roughly 20 million dollars) was funded(including the government fund of 18 billion wons(roughly 16 million dollars)).

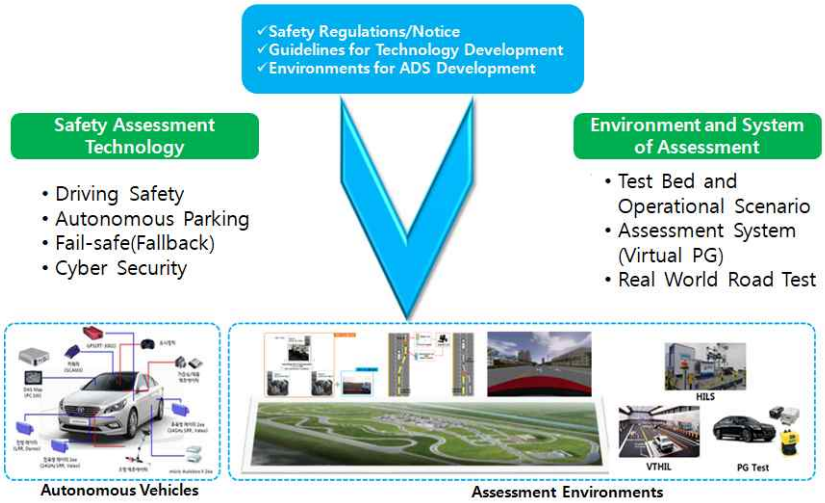

Figure 3. Overview of Assessment Technology Research for Autonomous Vehicle

Based on the research results of this project, the government will amend the existing legal system and present the safety guidelines for of autonomous driving vehicles(motor vehicle safety regulations, NCAP). The government will pave the road for the commercialization of level 3 autonomous driving vehicles on dedicated highways by 2020. Also The government is actively participating in international regulation activities related to autonomous vehicles such as UN/ECE WP29.

Construction of K-City, Test bed for autonomous driving vehicles

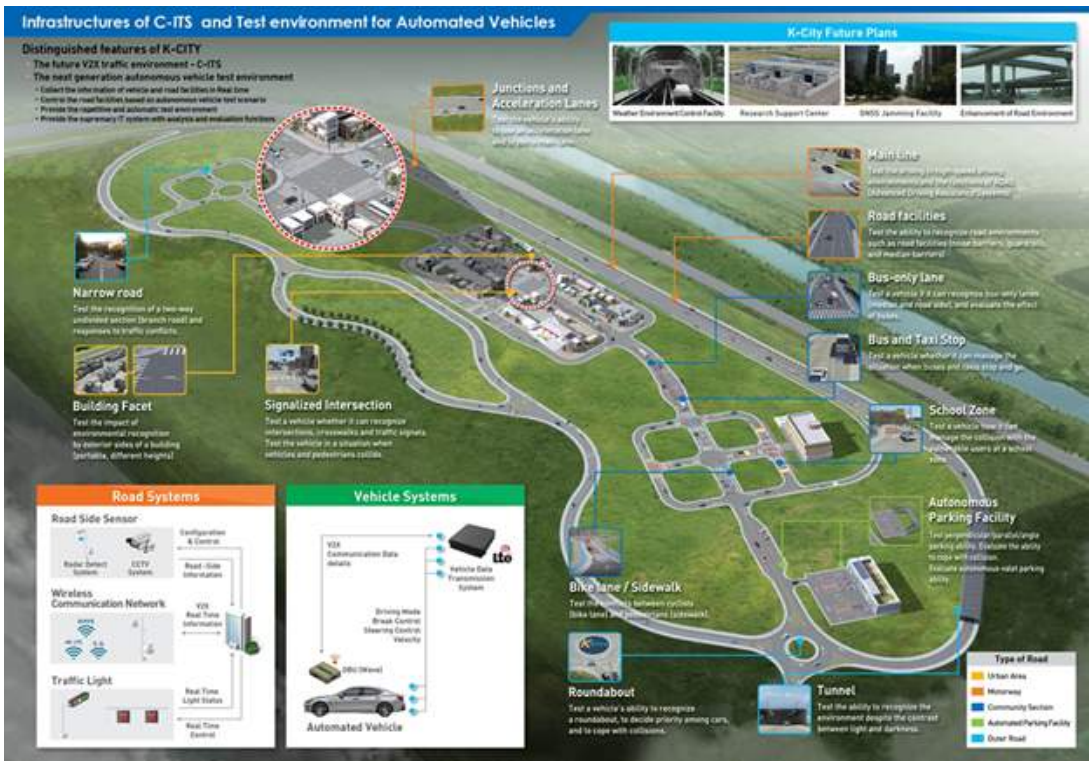

Figure 4. K-City Enhancement Project

- Location : KATRI Proving Ground(Hwaseong city, Gyeonggi-do)
- Composition : motorway, urban area, rural area, residential area(school zone), autonomous parking area
- Size : 3.6 million m2, 5.5km

K-City, a test bed that allows autonomous vehicles to be operated repeatedly and reproducibly in a real world environment, was opened on 10 Dec. 2018. It has been open to small and medium-sized businesses and universities without charges for three months since March to support active development of autonomous driving vehicle technologies.
K-City, shown in Figure 4, provides comprehensive communication environments such as WAVE, LTE and 5G in addition to road infrastructures. It provides 15 virtual service of co-operative Intelligent Transportation Systems (C-ITS) compliant with domestic standards. It is possible to test level 3 or higher autonomous vehicles, too.
In addition, the Ministry of Land, Infrastructure and Transport will build an advanced testing facility that can provide harsh test environments such as weather conditions of rainfall, fog, and communication disturbance like GPS jamming under the K-City Enhancement Project.
It plans to provide an integrated environment for development of autonomous vehicles by adding maintenance centers and data analysis stations in consideration of the characteristics of autonomous vehicles

Autonomous Vehicles DVI

The government aims to establish legal systems to allow the commercialization of level 3 autonomous vehicles(refer to SAE J3016) by 2020 and revise overall systems allow level 5 autonomous vehicles by 2022.
At level 3 of autonomous driving vehicles, the control of the vehicle can be switched between the system and the driver.
In case autonomous driving system experiences a system failure, it needs to develop evaluation technology to verify and ensure the safe transition of vehicle control to a driver.
In addition, this study was conducted to devise measures to promote user acceptance of autonomous vehicles.
DVI research aims to develop elemental technologies to verify the safe transition of vehicle control to a driver and to improve user acceptance in preparation for the commercialization of autonomous driving technology.
In this project there are three main sub-projects as follows; "Development of Evaluation Criteria and Evaluation Platform for Control Transition of Autonomous Driving Vehicles", "In-depth Research and Development of Human Factors and DB in Autonomous Driving Situations", "Improvement of Legal, Ethical, Technical, and Standard Perspectives for Improving Social Acceptance"
KATRI and 21 other agencies are carrying out these projects with a budget of 15.5 billion wons(roughly 13.5 million dollars) from 2017 to 2020. Through this, it is going to ensure the safe transition of vehicle control and present DVI design guidelines. We also expect to resolve distrust and anxiety over autonomous vehicles and protect the lives and property of the people.

Current Status of Amendments to Domestic Safety Regulations

Expansion of Vehicles Categories subject to ESC(14. 11. 2017)

The electronic stability control is a computerized technology that improves a vehicle's stability by detecting and reducing loss of traction. ESC will be applied to all vehicle categories while it was previously applied to passenger vehicles and small trucks with GVW 4.5 tons or less to. Dump trucks and special purpose trucks are exempted.

Safety Regulations for MicroCar(refers to L7 in ECE Regulation) (11. 7. 2018)

Safety regulations for microcars were established on 11. 7. 2018. The criteria for this category are the vehicle weight 600 kg for passenger vehicle, 705 kg for goods, and the maximum speed of 80 km/h. Some Regulations, such as braking, head restraint, esc, seat back, were relaxed. Some Regulations, such as headlamps, braking lamps, etc. were prepared in consideration of vehicle dimensions.

Expansion of Vehicles Categories subject to AEBS and LDWS(11. 7. 2018)

AEBS and LDWS is applied to all buses and trucks and special-purpose trucks with GVW of 3.5 tons or more to prevent vehicle accidents involving heavy vehicles. This requirement was in force from 1. 1. 2019 for buses with a pneumatic service brake, 1. 7. 2021 for other vehicles. Mini-sized buses are exempted.

Relaxation of Ground Clearance and Various Materials for Windows(31. 12. 2018)

The ground clearance regulation was amended from 12 cm to 10 cm to accommodate the dimensions of speed bumps. Various materials are allowed for windows. The direction of an exhaust pipe was relaxed to give more flexibility for vehicle design and performance.

Improvement for Lift Axle and Retro-reflective Markings(31. 12. 2018)

Lift Axles shall be automatically lifted or lowered according to goods weight to prevent serious traffic accidents involving overloaded heavy trucks. Regulations for Retro-reflective Markings was harmonized with UN-R48 and UN-R104 to prevent traffic accidents, such as rear end collision with trucks in the night. Retro-reflective Markings should be fitted on the sides and rear of a truck.

Harmonization of Collision Regulations with International Regulations(31. 12. 2018)

The existing collision regulations similar to US FMVSS were harmonized with UN-R94, UN-R95, UN-R135, UN-R137 in case of off-set frontal collision and pole side impact in consideration of various collision accident types due to changes in the traffic environments.

Conclusion

The Korean government has been making diverse efforts through international cooperation and developing efficient policies to pave the roads in advance for future motor vehicles such as autonomous vehicles and to enhance safety. The Ministry of Land, Infrastructure and Transport has proposed a road map for Korean New Car Assessment Program, which further strengthens vehicle safety even beyond the scope of safety regulations. In addition, the 1st phase of K-City for testing autonomous vehicles was completed so that it provides a place for domestic and overseas vehicle manufacturers to be able to perform the tests of Level 3 autonomous vehicles. Through the K-City Enhancement Project KATRI plans to provide an integrated environment for the development of autonomous vehicles. The Ministry of Land, Infrastructure and Transport strongly promotes the international harmonization of vehicle regulations and will make every effort to build an environment to enhance the safety of future vehicle technology.

REFERENCES

[1] MOLIT, 2017, The 8th Transportation Safety Master Plan
[2] National Police Agency, 2019, "2017 Load Traffic Safety a White Paper
[3] MOLIT, 2016, The 2nd Vehicle Policy Master Plan (2017-2021)
[4] MOLIT, 2018, KNCAP 2023 Roadmap
[5] MOLIT, 2018, Korean Motor Vehicle Safety Standard: KMVSS

This document is a place holder for Marion

This document is a place holder for Marion

This document is a place holder for Marion

This document is a place holder for Marion

This document is a place holder for Marion

This document is a place holder for Marion

This document is a place holder for Marion

This document is a place holder for Marion

This document is a place holder for Marion

This document is a place holder for Marion

This document is a place holder for Marion

This document is a place holder for Marion

This document is a place holder for Marion

This document is a place holder for Marion

This document is a place holder for Marion

This document is a place holder for Marion

This document is a place holder for Marion

This document is a place holder for Marion

This document is a place holder for Marion

This document is a place holder for Marion

This document is a place holder for Marion

This document is a place holder for Marion

This document is a place holder for Marion

This document is a place holder for Marion

This document is a place holder for Marion

This document is a place holder for Marion

This document is a place holder for Marion

This document is a place holder for Marion

This document is a place holder for Marion

This document is a place holder for Marion

This document is a place holder for Marion

This document is a place holder for Marion

European Commission

ROAD SAFETY IN THE EUROPEAN UNION

Trends, statistics and main challenges

April 2018

Mobilty and Transport

Road Safety in the European Union – Trends, statistics and main challenges

European Commission

This report is an internal working document summarising recent road safety statistics reported by the EU Member States.

For more information, contact the European Commission, Directorate-General Mobility and Transport, Unit C2 – Road Safety
move-infos@ec.europa.eu

http://ec.europa.eu/roadsafety

Manuscript completed in April 2018

Neither the European Commission nor any person acting on behalf of the Commission is responsible for the use that might be made of the following information.

Luxembourg: Publications Office of the European Union, 2018

© European Union, 2018

Reuse is authorised provided the source is acknowledged. The reuse policy of European Commission documents is regulated by Decision 2011/833/EU (OJ L 330, 14.12.2011, p. 39).

For any use or reproduction of photos or other material that is not under the EU copyright, permission must be sought directly from the copyright holders.

Print	ISBN 978-92-79-80284-3	ISSN 2363-4375	doi:10.2832/169706	MI-AC-18-001-EN-C
PDF	ISBN 978-92-79-80281-2	ISSN 2363-4383	doi:10.2832/060333	MI-AC-18-001-EN-N

Photographs
Cover image: © European Commission
p. 5: © European Commission;
p. 6: © iStock/ollo;
p. 12: © iStock/Tijana 87;
p. 16: © iStock/cookelma;
p. 19: © iStock/Teo Angelovski;
p. 20: © iStock/wavipicture;
p. 25: ©iStock/Blackzheep.

Table of contents

Foreword 5

1. The EU road safety situation in 2017 6

2. Monthly variation in road fatalities 12

3. Seasonality by modes of transport and type of roads 16

4. Day of the week and time of the day 20

Conclusions 24

COUNTRY ABBREVIATIONS:	
AT	Austria
BE	Belgium
BG	Bulgaria
CY	Cyprus
CZ	Czech Republic
DE	Germany
DK	Denmark
EE	Estonia
EL	Greece
ES	Spain
FI	Finland
FR	France
HR	Croatia
HU	Hungary
IE	Ireland
IT	Italy
LT	Lithuania
LU	Luxembourg
LV	Latvia
MT	Malta
NL	Netherlands
PL	Poland
PT	Portugal
RO	Romania
SI	Slovenia
SK	Slovakia
SE	Sweden
UK	United Kingdom

FOREWORD

People's safety has always been close to my heart. All road users, be it for private or professional reasons, deserve the highest level of safety and care.

The European Union has some of the safest roads in the world. It is leading by example, putting its experience and knowledge at the service of other regions, and is also promoting the highest possible standards on the global stage.

That being said, every year more than 25 000 people still lose their lives on EU roads, while another 135 000 are seriously injured. This is an enormous loss for individuals, families and society as a whole. The socio-economic consequences of this alone are estimated at EUR 120 billion annually for the EU. In light of this, there simply cannot be business as usual when it comes to road safety – I want to see changes urgently.

A year ago, EU transport ministers adopted the 'Valletta Declaration on Road Safety'. This was a major achievement, paving the way for the future, particularly on a new reduction target for serious injuries of 50 % between 2020 and 2030.

On the back of this strong political commitment, we have started work on the road safety policy framework for the period 2020-2030. We intend to reconfirm 'Vision Zero' as our long-term objective and base this framework on the 'Safe System' approach. This is a holistic and inclusive way of ensuring that all key factors are addressed in preventing death and serious injury. The framework will also respond to new challenges, such as the growing number of vulnerable road users, the risk of distraction on the roads, and vehicle automation.

Any action we propose is based on road-safety data that we collect from the 28 EU Member States and beyond. This data allows us to adjust our policies and fine-tune the measures we recommend. There are many factors at play in serious and fatal road crashes, such as the type of roads, the vehicles we use, and the age and gender of road users. In this publication, we give you an in-depth view of monthly, weekly and daily variations in road fatalities.

We strive to further improve road safety in the EU by setting a common agenda for the decade to come and by ensuring road safety actors in the ecosystem come on-board for better results. Let's continue our work today for safer roads tomorrow!

Violeta Bulc
EU Commissioner for Transport

1. The EU road safety situation in 2017

- In 2017, 25 300 people lost their lives on EU roads.
- This means a 2% decrease in the number of road deaths compared to the previous year.
- Between 2010 and 2017, the number of road deaths decreased by 20%, so 6 200 fewer people died on the roads last year than in 2010.
- The EU road fatality rate in 2017 was the lowest ever with 49 dead per million inhabitants.
- In 2017, countries with the lowest number of road deaths per million inhabitants were Sweden (25), the UK (27), the Netherlands (31), Denmark (32), Ireland (33) and Estonia (36).
- Countries with the weakest road safety records were Romania (98), Bulgaria (96) and Croatia (80).
- In 2017, eight EU countries recorded a fatality rate below 40 deaths per million inhabitants and 26 countries below 80 deaths per million inhabitants.

Roads in the EU are the safest in the world. The EU counts on average less than 50 deaths per million inhabitants, against 174 deaths per million globally, 106 deaths per million in the USA and 93 deaths per million in geographical Europe.

FATALITIES BY POPULATION

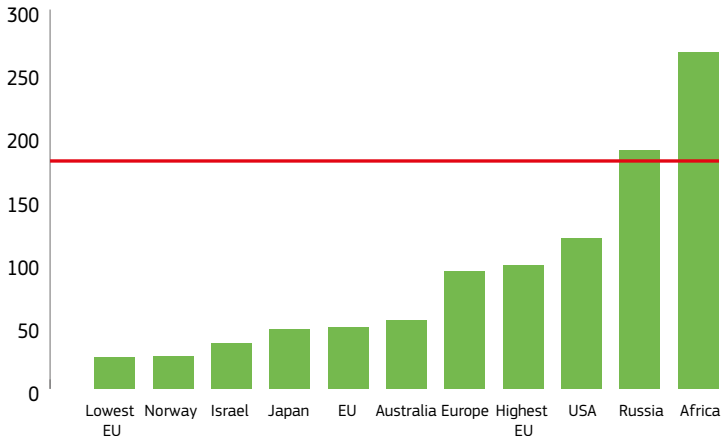

Progress in the last two decades in the EU has been remarkable: the number of fatal crashes fell by 43% from 2001 to 2010, and by another 20% between 2010 and 2017. However, the progress rate has slowed down in recent years. After two years of stagnation, 2016 marked a 2% decrease in the number of road deaths, and 2017 repeated the same pattern.

It is now quite clear that the current rate of reducing fatalities on EU roads will not be enough to reach the 2020 target of halving their number compared to the baseline year of 2010. A reduction rate of 14% would be necessary every year from now on to reach the targeted figures. Nevertheless, the aspirational target remains an important political tool and a powerful driver to achieve better results.

EU FATALITIES AND TARGETS (2010-2020)

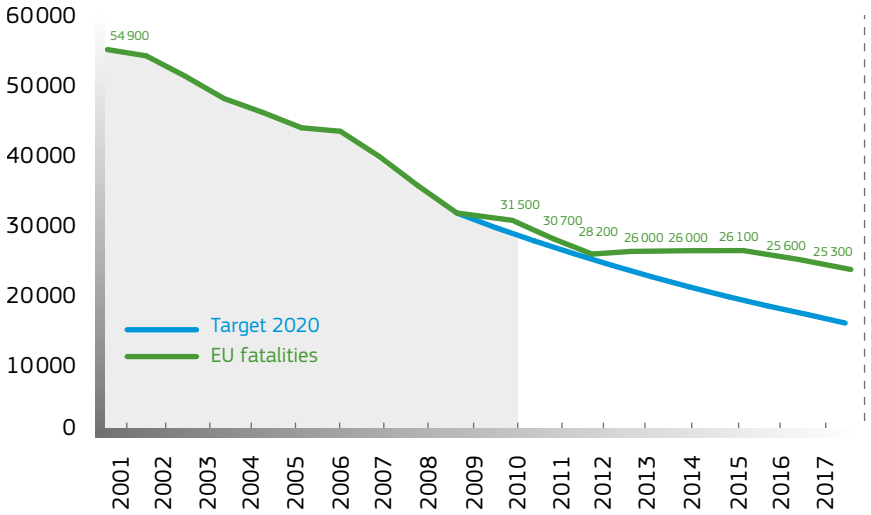

The road safety situation differs widely between Member States. Some of them report substantial progress, while others are still performing significantly below the EU average. However, the gap between the worst- and the best-performing EU Member States has been narrowing year after year. In 2017, none of the Member States registered a fatality rate higher than 100 deaths per million inhabitants, and eight of them recorded a fatality rate lower than 40 deaths per million inhabitants.

In 2017, the EU's best road-safety performers were Sweden (25), the UK (27), the Netherlands (31), Denmark (32), Estonia (36) and Ireland (33). On the other hand, the highest fatality rates were registered in Romania (98) and Bulgaria (96), followed by Croatia (80). From the beginning of the decade, the highest drops in the number of road deaths were recorded in Greece (-41%), Estonia (-39%), Latvia (-38%) and Lithuania (-36%). The EU average decrease was 20%.

In 2017, on average only about 8% of road fatalities occurred on motorways; 37% happened in urban areas and 55% on rural roads.

Car occupants accounted for the largest share of victims (46%). Together, vulnerable road users, including pedestrians, cyclists and motorcyclists accounted for the same proportion and were particularly exposed in urban areas. 21% of all

ROAD FATALITY RATES 2017

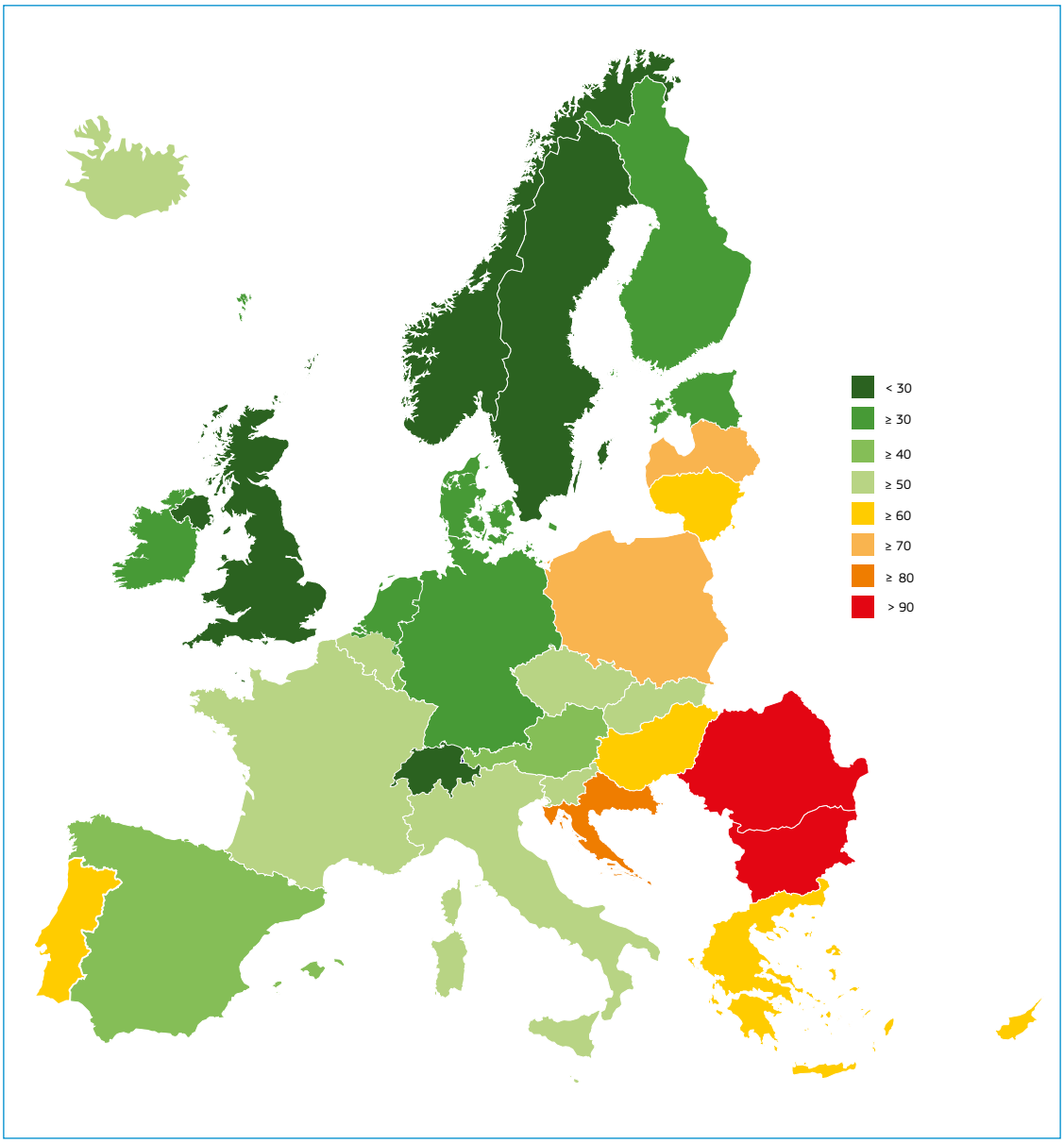

people killed on roads were pedestrians. Cyclists accounted for 8% of all road deaths in the EU. Motorcyclists, who are less protected during a crash, accounted for 14% of road fatalities. In general, fatalities among vulnerable road users have fallen to a much lesser degree in recent decades than among all road users.

In 2017, almost 14% of people killed on EU roads were aged between 18 and 24, although only 8% of the population fell within this age group. Young people are almost twice as likely to be killed in a road crash than the average person. Men were still largely over-represented among young victims: 80% of the young people who died in road crashes were men. This can be explained by different risk-taking behaviour and by the fact that young men statistically tend to take longer trips than young women.

Although older drivers are involved in fewer road crashes, elderly people in general are one of the highest risk groups, due to their fragility and reduced tolerance to injury. Even if the number of elderly road victims has decreased over time, the total number of road deaths has fallen faster, meaning that the proportion of elderly victims tended to rise. While 18% of road fatalities concerned elderly people in 2010, this ratio reached 26% in 2017. Compared to the average population, the risk of being killed on the roads is almost one and a half times higher for an elderly road user.

In general, far more men than women are killed in road crashes: less than one quarter, 24% of all fatalities, concern women, against 76% of male fatalities. The fatality rate of elderly men is over twice the rate of elderly women in most EU countries. Male and female road fatalities also differ by type of road user. Among pedestrians, road fatalities affected almost twice as many women than men.

ROAD FATALITIES IN THE EU BY TYPE OF ROADS (2017)

8 % Motorway

37 % Urban areas

55 % Rural roads

SERIOUS ROAD TRAFFIC INJURIES

According to the European Commission's estimates, about 135 000 people sustain serious road traffic injuries on EU roads per year. This means that for every person killed in traffic crashes, five more suffer serious injuries. Serious injuries are not only more common but also often more costly to society because of long-time rehabilitation and healthcare needs.

As from 2015, Member States started to report data on serious injuries based on a new, commonly agreed definition following medical standards. The international MAIS trauma scale (Maximum Abbreviated Injury Score) has been chosen for the EU definition of serious road traffic injuries. The Scale 3 and more (MAIS3+) applies to the seriously injured.This was a milestone in the work addressing serious road traffic injuries.

With the adoption of the 'Valletta Declaration on Road Safety' in 2017, EU transport ministers made a major step forward with far-reaching joint commitments. Among others, EU Member States agreed to introduce a 50 % reduction target for serious road traffic injuries in the period 2020-2030. The Commission will continue to monitor and benchmark Member States' performance. Member States are encouraged to prioritise actions for the safety of vulnerable road users and safety in urban areas.

2. Monthly variation in road fatalities

- Every year, the least number of road deaths are recorded in February, whilst most fatal accidents happen in July and August.
- The contribution of road fatalities by month varies however from country to country.
- Accident risk also varies seasonally with changing weather conditions.
- Variations throughout the year in the hours of daylight are likely to contribute to seasonal differences too.

The number of fatal road crashes shows a certain monthly variation in the EU. The seasonality or seasonal variations in road fatalities follows a very similar pattern year after year. Although the number of people who die in road accidents in Europe per year has fallen over many years, the monthly distribution of road fatalities has scarcely changed.

Generally speaking, the least number of road fatalities are recorded in February, whilst the most fatal accidents happen during summer holidays, in July and August. Without seasonality, 8.3 % of fatalities would occur every month. Compared to this 'no seasonality' average, there are relatively few fatalities per month from January to April and relatively many more from June to October and in December.

% OF FATALITIES BY MONTH

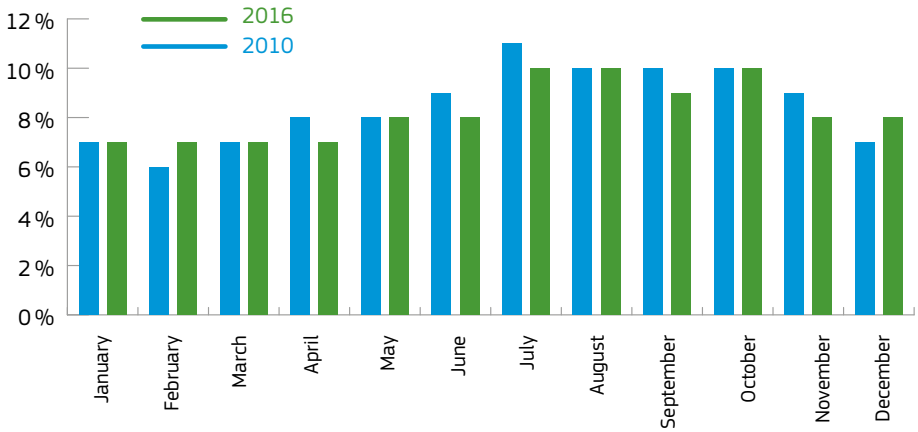

The seasonal variation of road fatalities is the result of several factors. The main cause is probably the change in travel patterns throughout the year. For example, many more trips are made for leisure and recreation during summer than winter.

The monthly variation in road fatalities differs considerably from one country to another. Seasonal variations are below average in most of the Western EU countries, and above average in most Central and Northern EU countries.

SEASONAL VARIATIONS IN ROAD FATALITIES

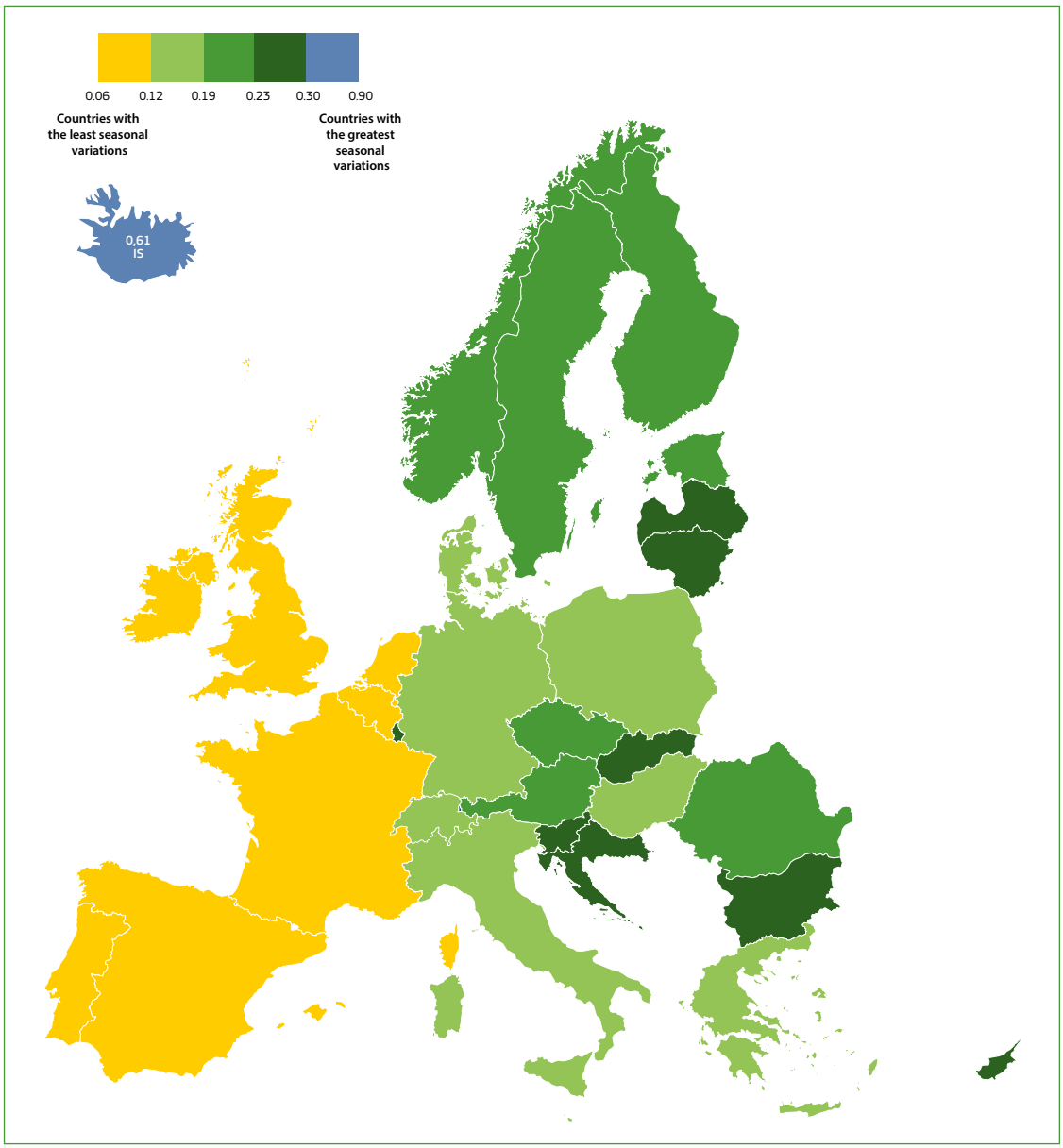

Accident risk also varies seasonally with changing weather conditions. The relative harshness of winters in Northern and Central Europe is likely to contribute to the greater seasonality for several countries in these areas.

Variations throughout the year in the hours of daylight are also likely to contribute to seasonality, as this affects people's mobility patterns, which also vary across Europe. In the EU Member States, over the whole year, 64% of fatalities occurred in daylight (including twilight), but the percentage was below 50% between November and January.

% OF FATALITIES BY MONTH AND LIGHT

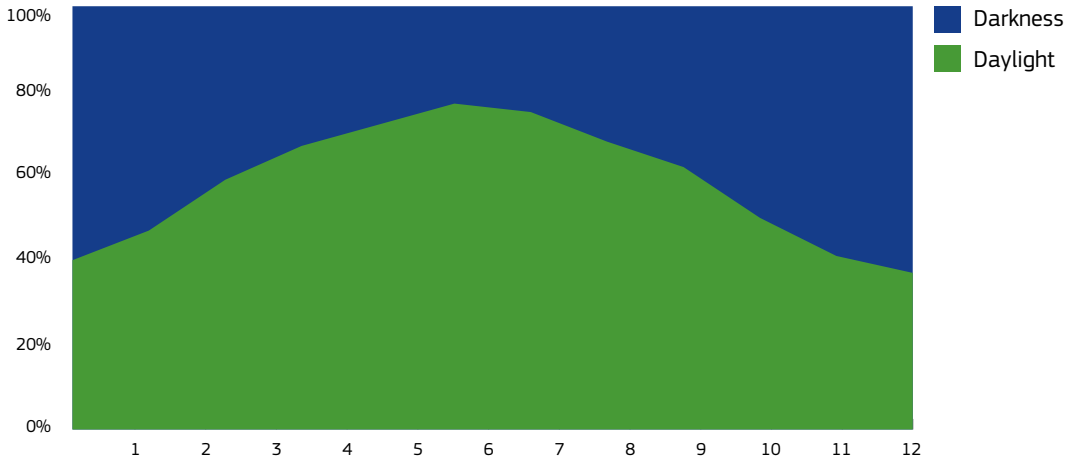

Source: CARE database, data available in April 2018.

3. Seasonality by modes of transport and type of roads

- The monthly distribution of road fatalities varies by modes of transport and type of road.
- The number of pedestrian deaths is highest in the winter, while the number of fatal accidents among motorcyclists is highest in June.
- Motorcycling is the mode of transport with the most seasonal fatality variations.
- There is less seasonal variation on urban roads than on rural roads and motorways.

The seasonal variation in road fatalities also depends on the mode of transport. The seasonality for certain user groups clearly differs from the overall pattern. This is particularly true for vulnerable road users (VRU), such as riders of motorcycles and mopeds (powered two-wheelers), cyclists and pedestrians. For example, more riders of powered two-wheelers (PTW) are killed in summer, and fewer in winter, as a result of there being more users in this group on the roads when the weather is better.

Deviations from the average are similar for cyclists, although to a lesser degree. Their travel habits are certainly affected by weather conditions but less so than PTW riders.

% OF ROAD FATALITIES BY MONTH

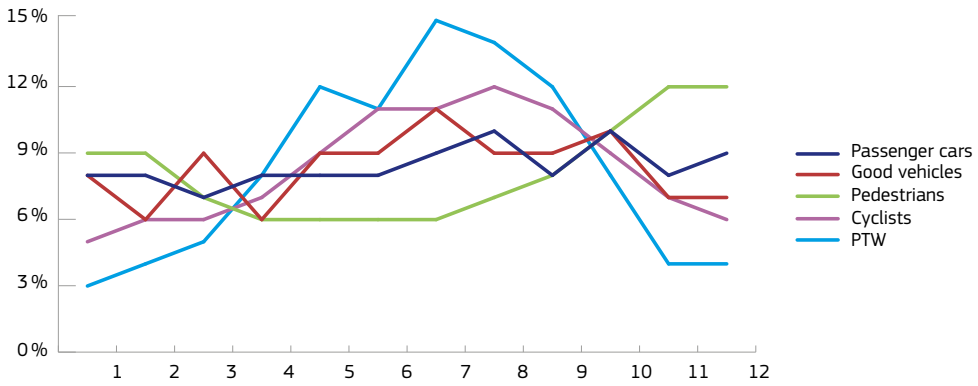

However, there is a category of vulnerable road users for which the monthly distribution of road deaths shows a very different pattern over the year. Most pedestrians are killed in winter, and especially in December, while there are relatively few road fatalities among them in summer.

The reason for the increase in pedestrian fatalities from 6 % of the annual total in April to 13 % in December is probably due to hours of daylight and darkness. The number of pedestrian fatalities in December is almost twice that in June.

PEDESTRIAN FATALITIES

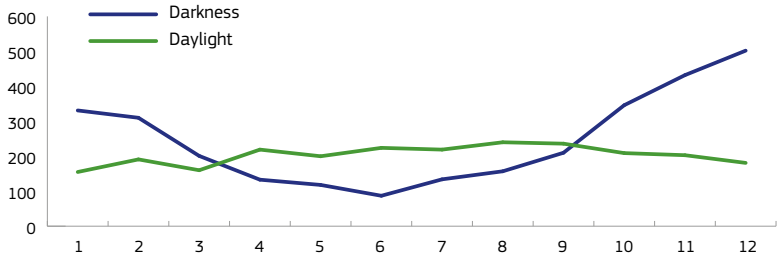

The seasonality of road fatalities also differs by geographical area. In Spain, for example, the proportion of road fatalities shows relatively little change by month, except for cyclists. By contrast, the proportions in the Nordic countries vary considerably by month, especially for pedestrians and motorcyclists. This phenomenon is mostly due to greater changes in weather conditions and hours of daylight in the Northern countries.

The monthly variation in fatal crashes can also be examined by types of road: motorways, rural roads and urban roads. Even if there are no drastic differences, in general, seasonality is in general is lower on urban roads than on rural roads and motorways. This is probably because changes in the hours of daylight and weather conditions have less impact in towns and cities.

4. Day of the week and time of the day

- The distribution of road deaths also varies according to the day of the week and the hour of the day.
- The daily variation in road fatalities is greater on Sundays than on any other day of the week.
- The distribution of road deaths by time of the day is similar from Monday to Thursday.
- Most fatalities happen in the afternoon and relatively few during the night.
- However, there is a peak in fatalities early on Saturday and Sunday mornings.

The distribution of road fatalities also varies by day of the week and time of the day. There are 168 hours in a week so, on average, 0.6 % of fatalities would occur each hour throughout the week, if equally distributed..

FATALITIES BY DAY OF THE WEEK AND HOUR OF THE DAY

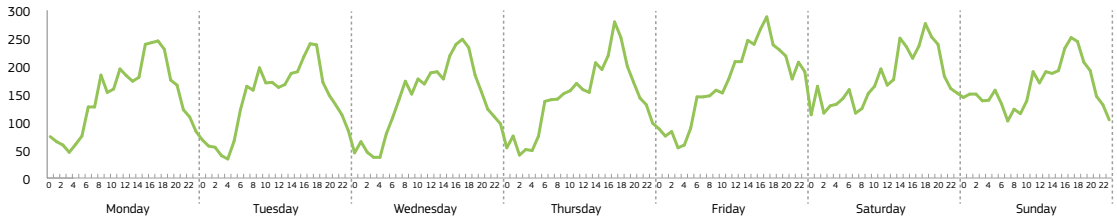

The distribution of road deaths by time of the day is similar from Monday to Thursday. There is an afternoon peak every day and relatively few fatalities during the night. This is in line with changing traffic volumes. A high number of fatalities early on Saturday and Sunday mornings is also notable.

The peak during weekends is particularly pronounced for the age group between 15 and 30, reflecting the social habits of youngsters, and especially young drivers.

FATALITIES OF YOUNG PEOPLE (15-30) BY DAY OF THE WEEK AND HOUR OF THE DAY

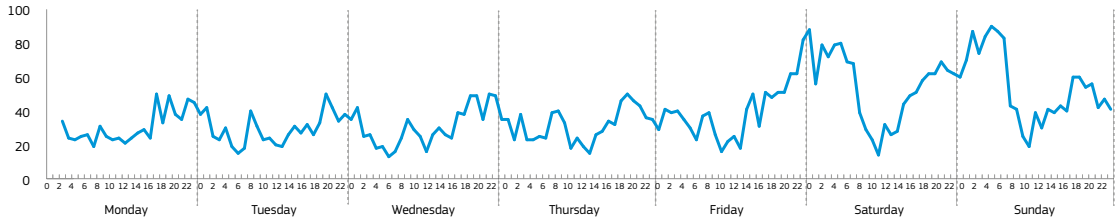

On a daily basis, seasonality is quite similar throughout the year. The main difference concerns Sundays: there are relatively many fatalities on Sundays between June and September, and relatively few between November and February. This can be explained by an increased activity among road users during the summer holidays and a change in the choice of mode of transport, with a preference for riding and cycling.

Comparing different periods of the day, the greatest seasonal variations in the number of road deaths are recorded during the night, between 10pm and 4am. There is a clear peak during the night period in August, reflecting greater mobility during the longer days of the summer holidays.

The variation in road fatalities by time of the day is also affected by geographical factors. The number of fatalities in Spain show a limited variation by month, while much bigger differences can be observed in the EU's Nordic countries. This is certainly due to more significant differences in hours of daylight and weather conditions in the Northern part of Europe over the year.

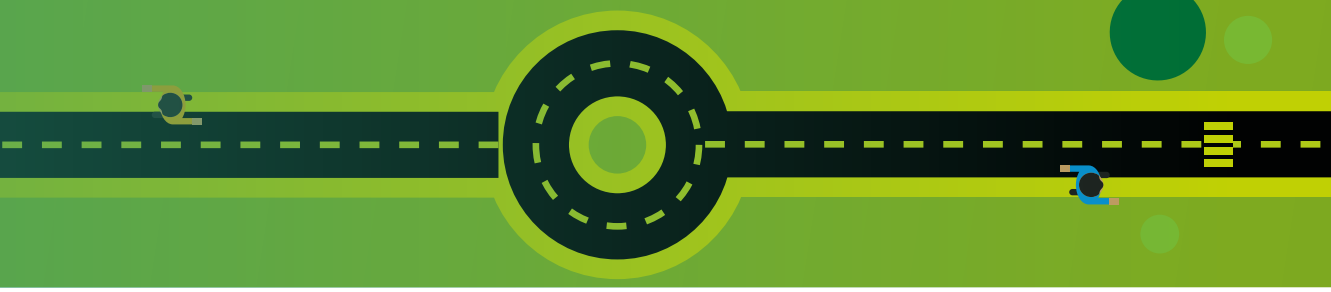

EXAMPLES OF MEASURES REDUCING ROAD-SAFETY RISKS LINKED TO SEASONALITY

EDUCATION

- Raising awareness on road-safety risks in difficult weather conditions;
- Increasing hazard perception in driver training and developing skills to drive in difficult weather conditions;
- Launching targeted communication campaigns for young drivers and passengers travelling in the evening, at night and during the weekend;
- Promoting the use of reflective material by pedestrians, cyclists and motorcyclists.

VEHICLES

- Making daytime running lights compulsory to improve visibility and increase distance and speed perception;
- Promoting the use of winter tyres for adverse weather conditions.

ENFORCEMENT

- Enforcing speed limits adapted to specific weather conditions;
- Enforcing rules on the use of protective equipment for vulnerable road users;
- Intensifying controls for drivers who infringe rules at pedestrian crossings and for pedestrians in breach of traffic regulations.

INFRASTRUCTURE

- Adapting speed limits to weather conditions, i.e introducing winter speed limits;
- Providing safe areas for pedestrian mobility (low-speed zones in residential areas, safe zebra crossings, etc.).

Conclusions

The European Union's progress in making its roads safer has been impressive. The EU cut the number of fatal road crashes by 43% between 2000 and 2010, and reduced them further by 20% from 2011 to 2017. The results are tangible: today, the EU is the world's safest region with 49 deaths per million inhabitants.

However, progress has stalled recently, and has been unequally distributed between different groups of road users. Fatalities among pedestrians, cyclists, motorcyclists and moped riders have not decreased at the same pace as in the overall population. Therefore, these vulnerable groups of road users deserve special attention from policymakers.

Road-safety risks linked to changes in weather conditions as well as risks involved in different mobility patterns depending on the day of the week or the time of day are affecting pedestrians, cyclists and motorcyclists, but also novice drivers much more than other road users. Data on seasonal variations in road fatalities can thus be very useful to fine-tune measures that aim to increase the safety of vulnerable road users. Such measures may encompass a wide range of actions, from education and awareness-raising to infrastructure design and minimum vehicle safety standards through better enforcement of traffic rules.

Today, when fresh efforts are needed to further improve the EU's road-safety records, any progress achieved in the safety of vulnerable road users will have a significant impact. However, this remains a common challenge where decision-makers, road managers and road users share the responsibility of creating a safe mobility system.

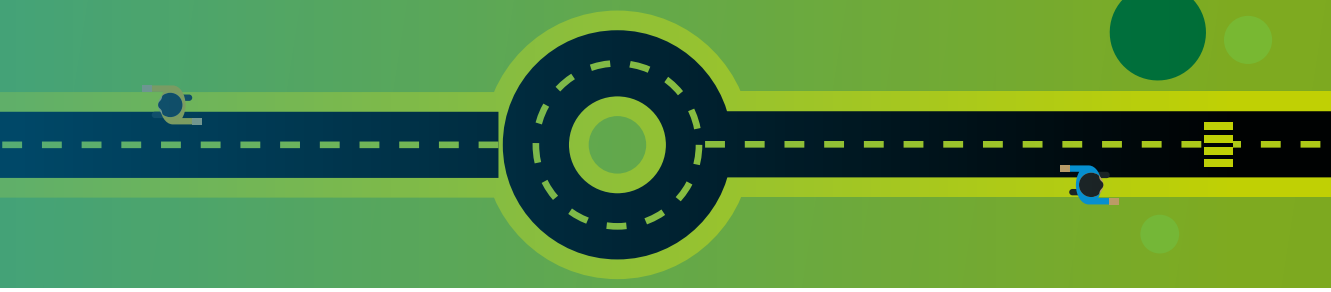

For more information about the European Commission

and road safety, visit our website:

http://ec.europa.eu/roadsafety

MI-AC-18-001-EN-C

Publications Office

ISBN: 978-92-79-80284-3
ISSN: 2363-4375
doi:10.2832/169706

European Commission

European Road Safety Observatory
www.erso.eu

Annual Accident Report

2018

Transport

OVERVIEW-MAJOR ISSUES

Safety performance
High vs Low

Data for **2016** or latest available year

European Road Safety Observatory
www.erso.eu

European Commission

1 Million

Road Accidents per Year - **3.000 per day** (2016) with consequences:

1,4 Million Injured
(3.600 per day)

25.600 Fatalities
(70 per day)

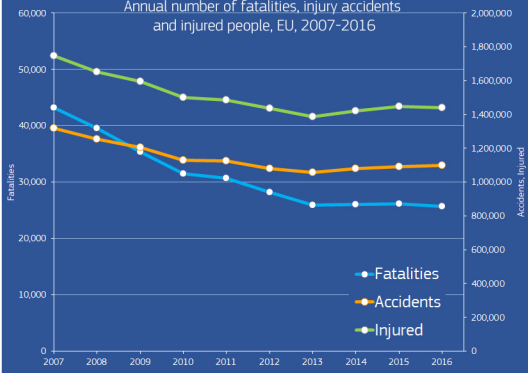

Main progress in **reducing fatalities**

-41%

less in **injury accidents**

-17%

Share of fatalities by area type in the EU, 2016

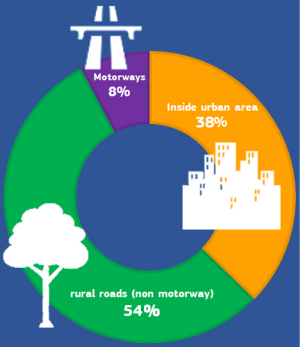

The overall **downward trend** in the number of road fatalities is different for each road user

-44%

-27%

The most significant reduction in the overall number of fatalities between 2007 and 2016 occurred in **Lithuania, Estonia and Latvia**

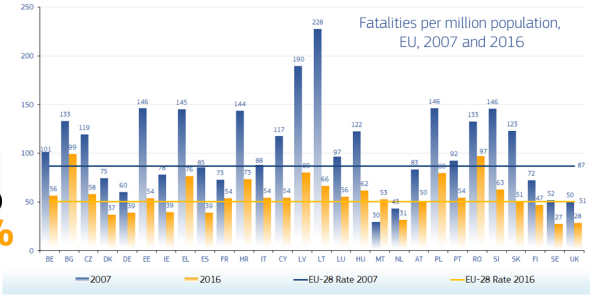

FATALITIES 2016

Safety performance
High vs Low

Data for 2016 or latest available year

European Road Safety Observatory
www.erso.eu

European Commission

Fatalities by type of area and mode of transport in the EU, 2016

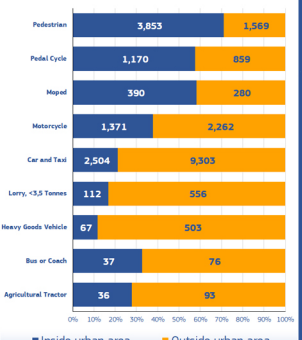

47% of all road fatalities are **car occupants**.

On **motorways** this proportion increases to almost **60%**

Distribution of fatalities by road user type on three types of road, 2016

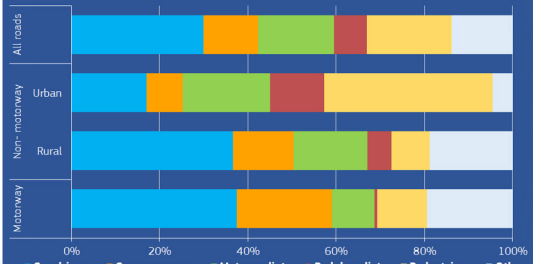

In 2016, **the elderly** (aged >64) represented almost **27%** of deaths in road accidents in the EU

Fatalities on motorways by age and road user type, EU, 2016

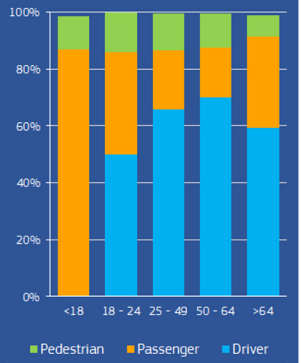

The proportion of fatalities **as passengers or pedestrians** is higher for females than for males

Fatalities by gender and mode of transport in the EU, 2016

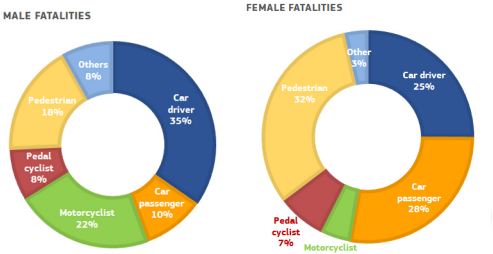

Powered Two Wheelers (PTW) accounted for **17%** of the total number of road accident fatalities in the EU 2016:

Motorcycles

14%

3.644 deaths

Mopeds

3%

663 deaths

TIME SERIES
LAST 10 YEARS IN DETAIL

Safety performance
High vs Low

Data for 2016 or latest available year

European Road Safety Observatory
www.erso.eu

European Commission

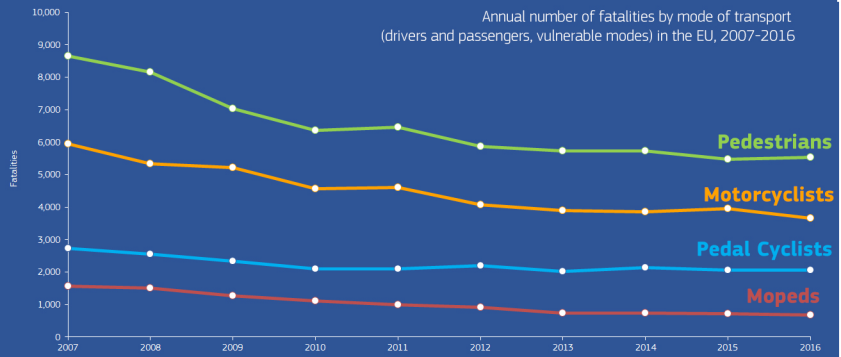

Fatalities on roads outside urban areas were **reduced by 41%** between 2007 and 2016

Over the decade 2006-2015 passenger fatalities in the EU decreased by **48%** driver fatalities by **39%** and pedestrian fatalities by **36%**

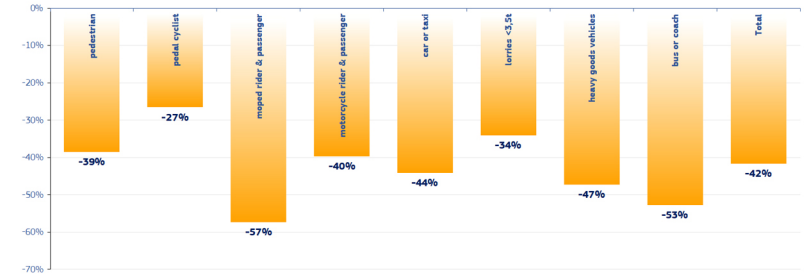

Male fatalities were reduced by **41%** and female fatalities were reduced by **39%** within the decade 2007-2016

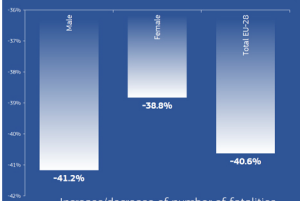

Increase/decrease of number of fatalities by gender in the EU, 2016 and 2007

This is a test document and only a test.

This is a test document and only a test.

This is a test document and only a test.

This is a test document and only a test.

DETECTING POTENTIAL VEHICLE CONCERNS USING NATURAL LANGUAGE PROCESSING APPLIED TO AUTOMOTIVE BIG DATA

Monica G. Eboli
Catherine M. Maberry
Ian A. Gibbs
Ramsi Haddad
Emerging Issues Analytics, Global Vehicle Safety, General Motors
United States of America

Paper Number 19-000000

ABSTRACT

A large volume of unstructured data exists in the automotive industry and needs to be analyzed to detect potential vehicle concerns. Much of this data is textual in nature since customer complaints are made through call center interactions and warranty repairs. Current approaches to detect potential vehicle concerns in text data include various keyword search methods. In this paper, we apply Natural Language Processing (NLP) and shallow machine learning methods on text data to create classifiers to detect the potential vehicle concern of airbag non-deployment. For this potential vehicle concern, we show the performance of multinomial Naïve Bayes (NB), Support Vector Machine (SVM) and Gradient Boosted Trees (GBT) classifiers against keyword search methods. We present challenges of classification model development related to the nature of automotive data and limited training data. Our findings provide insights on robust text classification approaches that can improve identification of potential vehicle concerns.

INTRODUCTION

Automotive corporations and the U.S. federal government [1] are driving improvements in product safety through the collection and analysis of both structured and unstructured (text) data. Despite their efforts, a common problem facing large corporations today is how to extract meaningful insights about product safety from large volumes of unstructured, noisy data that they have accumulated in many disparate systems. These data systems present clear opportunities for analyzing actionable information regarding product complaints and potential defects, but are commonly referred to as "dark data" because they are not easily analyzed due to their unstructured nature [2]. Consider the text data of vehicle warranty claims, call center transactions, and product complaints on social media; these sources all contain valuable information that may describe potential vehicle concerns, but are not represented in a relational structure that can be easily queried. In addition, large corporations, such as General Motors (GM), spend resources maintaining these data systems and encounter challenges efficiently extracting actionable information from them because these systems were not originally created for safety event detection.

At the same time, the U.S. federal government has created several incident reporting and complaint collection systems for a variety of industries: the Food and Drug Administration's (FDA) Adverse Event Reporting System (AERS) [3] for the pharmaceutical industry, the Federal Aviation Administration's (FAA) Aviation Safety Reporting System (ASRS) [4] for the aviation industry, and the National Highway Traffic Safety Administration's (NHTSA) Vehicle Owner Questionnaire (VOQ) [5] and Transportation Recall Enhancement, Accountability and Documentation (TREAD) [6] for the automotive industry. The effort by the U.S. federal government in creating these systems is due to the public interest in ensuring that products created by these industries are safe for consumers. Yet, the fundamental problem still exists; all of these systems contain large volumes of dark data because they all have varying degrees of unstructured data in the form of text.

Ultimately, private industry and the U.S. federal government have a vested interest in developing techniques for the transformation of unstructured data into structured data to facilitate detection and monitoring of potential vehicle concerns within the automotive industry. For both private industry and the government there is a need to produce statistics that provide an overview of how certain types of product failures are reduced in response to their actions

(product recalls, bulletins, etc.), but also to identify trends that should be addressed by those actions in the first place [7].

In this paper we will describe GM's efforts in utilizing Natural Language Processing (NLP) and shallow machine learning methods to transform unstructured text data into structured data that describes potential vehicle concerns [8]. The specific focus will be on the issue of airbag non-deployment, but we have expanded our approach to many other significant potential vehicle concerns. To the best of our knowledge, we believe this publication to be the first instance of NLP and shallow machine learning to be presented in the context of safety monitoring within the automotive industry.

Data for this effort originates from a variety of sources ranging from GM internal data (warranty claims, customer call center transactions) to public data managed by the U.S. government (NHTSA VOQ). For the scope of detecting narratives that involve airbag non-deployment, results presented in this paper will be constrained to NHTSA VOQ and TREAD data. Given their utility for the task of text classification, we present results for multinomial naïve Bayes, support vector machine and gradient boosted trees classifiers compared to traditional keyword-based pattern matching methods. We also discuss fundamental components of developing these classifiers, such as training set development and NLP pipeline development. Through the work described in this paper, it is our hope that we significantly advance the concept of detection and monitoring of potential vehicle concerns within the automotive industry.

BACKGROUND

In order to improve collision outcomes for occupants, front airbags work in concert with seat belts to restrain driver and front passenger seat occupants by inflating when vehicle sensors, measuring acceleration at various vehicle locations, indicate a moderate to severe frontal impact [9]. Airbag deployment is controlled during collision by a complex algorithm that assesses data from multiple vehicle sensors, such as occupant presence, change in velocity (delta V), time to max delta V, principal direction of force (PDOF) and others, to determine whether frontal airbags should deploy [9]. The complexity of the algorithm may contradict the assumption by vehicle occupants that the airbags were faulty in not deploying during a collision.

The value in detecting potential airbag non-deployment events is to enable investigation into these potential vehicle safety concerns by vehicle safety engineers. In the effort to decrease fatalities in frontal collisions related to potential system failure of frontal airbags, reliable, accurate, and robust detection methods in unstructured data are a critical first step.

Data Sources for Classification

Human-labeled datasets required for supervised methods were sourced from two corpora – NHTSA VOQ and TREAD data.

NHTSA VOQ is a publicly available dataset and consists of customer safety complaints about automotive products.

> JULY 20, 2016, WE WERE REAR ENDED BY A HONDA ACCORD DOING 40 MPH WHILE WE WERE STOPPED AT A LIGHT. THE IMPACT SLAMMED US INTO THE CHEVY SILVERADO IN FRONT OF US. NEITHER AIRBAG DEPLOYED.

The customer complaints dataset "contains all safety-related defect complaints received by NHTSA since January 1, 1995" [5]. NHTSA receives complaint documents from various sources including: (1) online submissions from by the general public, (2) vehicle owner questionnaire submitted by the general public, (3) the auto safety hotline submitted by the hotline operator and (4) consumer letters.

Figure 1. Sample NHTSA VOQ document describing a potential airbag non-deployment event.

TREAD is a GM-internal data source that is of interest for potential vehicle concern monitoring because it consolidates data from many disparate systems. The TREAD Act, which describes the requirements for GM's TREAD data system, was created in response to the Ford/Firestone issue and significantly changed the information automotive OEMs must report to the U.S. federal government [6]. The TREAD Act requires manufacturers to submit information related to substantially similar vehicles that may have different names, foreign fatalities, notices of foreign safety recalls and other safety campaign information and Early Warning Reporting (EWR). The EWR component of the TREAD Act results in GM compiling data from many disparate systems. As such, GM's TREAD data provides a broad cross-section of data from many business areas and large volumes of unstructured text data. The centralized nature of this data source is the primary motivating factor for its use in analyzing potential vehicle concerns.

Prior Detection Methods

Prior to the work described in this paper, potential vehicle concerns were monitored in both GM internal and public data sources using IBM Watson Explorer (previously known as IBM Content Analytics). Watson Explorer provides a proprietary version of Apache Lucene that employs an Unstructured Information Management Architecture (UIMA) pipeline for indexing, searching and analyzing text data. Watson Explorer annotators and dictionaries were used as the primary method for transforming unstructured data into structured data [10].

Annotators are compound rule sets for labeling text documents for a specific potential vehicle concern. Each rule within an annotator is designed to match a specific pattern of text. The pattern of text defined by an annotator may be a specific sequence or utilize Boolean logic to detect the presence of one or more words in a sentence, paragraph or document. Dictionaries are used to define the terms used in pattern matching.

An annotator defining airbag non-deployment could be applied to the document in Figure 1. Such an annotator would include a sequence rule matching a pattern of negation ("NEITHER"), followed by the airbag system ("AIRBAG"), followed by a mention of deployment ("DEPLOYED"). This complex rule would require a negation dictionary, an airbag system dictionary, and a deployment dictionary. All dictionaries would be required to include synonyms, misspellings and alternative forms of the base terms. For example, one would need to account for representations of the airbag system as "AIRBAG", "AIRBAGS", "AIR BAG", "SUPPLEMENTAL RESTRAINT SYSTEM", etc. A document stating, "AIRBAGS NEVER DEPLOYED" would not be flagged by the sequence rule because the airbag system is now in the first position of the pattern and negation is in the second position. To mitigate this issue, a Boolean rule would need to be developed that looks for airbag system, negation and deployment in the same sentence while ignoring sequencing. Utilizing Boolean logic loosens the pattern and can lead to tradeoffs between false positives and false negatives.

An IBM Watson Explorer annotator was designed to detect airbag non-deployment in NHTSA VOQ and TREAD. This annotator was developed using subject matter expertise and the same training data was used to develop machine learning methods described in later sections. The airbag non-deployment annotator serves as the baseline for comparing performance of machine learning methods.

METHODS

All document classification models combine supervised machine learning classification with the addition of standard Natural Language Processing (NLP) techniques to effectively transform unstructured text data into structured data. The general process used in this exercise consisted of: (1) training set development, (2) text preprocessing, (3) model development, and (4) and model assessment.

Training Data
Training sets were first developed to facilitate machine learning model development. Vehicle safety experts at GM collaborated to define airbag non-deployment events and related document characteristics. Potentially related document characteristics vary by dataset and consist of inclusion and exclusion criteria focused on terminology, key words, and circumstances described. Resulting definitions were documented and used as the basis for training data sampling and labeling.

The training set was developed for airbag non-deployment using NHTSA VOQ and TREAD data. Training samples from NHTSA VOQ were not restricted to GM manufactured vehicles since airbag non-deployment allegations are found among other automotive manufacturers. Qualitatively, the customer complaints describing airbag non-deployment within NHTSA VOQ were notably homogeneous across automotive manufacturers. The resultant labeled training set contained 2003 documents of which 1000 were sourced from NHTSA VOQ and 1003 were sourced from TREAD data. Within the overall labeled training set, there were 916 positive examples of airbag non-deployment and 1087 negative examples.

Text Preprocessing
Text preprocessing is commonly implemented in text analytics solutions. The goal of text preprocessing is to increase the homogeneity of the corpus through data standardization, aggregation of semantically similar terms and removal of words that contribute little to analysis.

Multiple text preprocessing techniques were used in this exercise including: (1) case standardization, (2) stop word removal, (3) contraction expansion, (4) lemmatization, (5) standardization of dollar values, units of speed and numbers and (6) removal of non-alpha-numeric characters. These techniques were applied to the labeled datasets prior to analysis using a custom developed Python program.

Model Development
NLP and machine learning pipelines were developed to evaluate the use of different machine learning methods to detect airbag non-deployment narratives. In text analytics, it is common that most effort in model development is spent on feature extraction. Features in this context are individual measurable properties extracted from the text that will be used to predict labels on documents (classification) [11]. Furthermore, features extracted in text analytics may include n-grams which are sequences of two or more words (i.e. “red wine” is a bi-gram, “engine control module” is a tri-gram). Pipelines are a collection of processes that can be used to transform data and fit classifiers in a defined sequence. Figure 2 depicts the steps included in the model fitting pipelines. Steps include: (1) feature extraction, (2) feature encoding, (3) feature selection and (4) classifier fitting. Pipeline parameters were tuned using grid search, evaluated using industry standard metrics, tested for generalizability using cross validation, and developed using open source data science technologies.

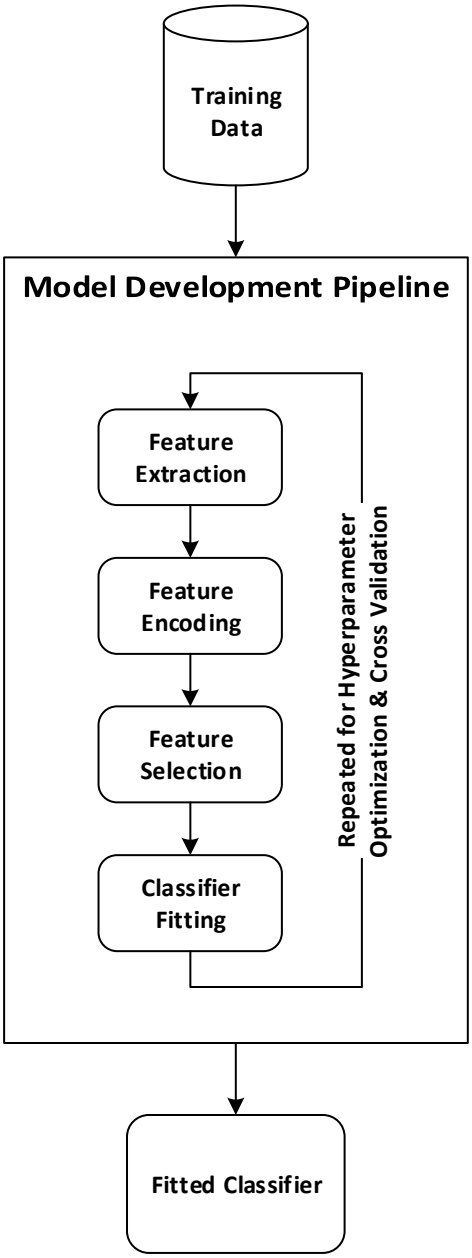

Figure 2. Model development pipeline.

Feature Extraction & Encoding: Features were extracted from the corpus as individual words and also included n-grams, which are a sequence of n adjoining words in a document. For example, if a document read "NEITHER AIRBAG DEPLOYED" bi-gram extraction, where n equals 2, would yield "NEITHER AIRBAG" and "AIRBAG DEPLOYED." Text features were restricted to bag of words (BOW) representations [12].

All features extracted from the labeled data were encoded using Term Frequency-Inverse Document Frequency (TF-IDF, Equation 1). TF-IDF is a feature encoding technique that weights how important a word is in a document within a corpus. Term Frequency ($tf_{t,d}$) describes the frequency of a term or token (t) within a particular document (d) while Inverse Document Frequency (idf_t) describes the inverse of the number of documents in the corpus that contain the term (t)

$$tf\text{-}idf_{t,d} = tf_{t,d} \times idf_t \quad \text{(Equation 1)}$$

Since both TF and IDF are raw frequency measures, it is common to utilize re-scaled and smoothed variants. Sublinear TF ($wf_{t,d}$) is described in Equation 2. A smoothed version of IDF is described in Equation 3 where n_d is the number of documents in the corpus.

$$wf_{t,d} = \begin{cases} 1 + logtf_{t,d} & if\ tf_{t,d} > 0 \\ 0 & otherwise \end{cases} \quad \text{(Equation 2)}$$

$$idf_t = log\,\frac{1+n_d}{1+df_t} + 1 \quad \text{(Equation 3)}$$

In general, frequently occurring terms have low TF-IDF weight and rare terms have a high TF-IDF weight. TF-IDF can be used to devalue words such as "VEHICLE" and "DRIVE" which frequently appear in automotive data but were not filtered out during text preprocessing. Furthermore, "DEPLOY" occurs in a considerable number of documents in the training data and would have a lower TF-IDF weight compared to other words.

Feature Selection: Feature selection is applied prior to classifier training to select the most relevant features for classification. The chi-squared test measures the dependence of the features on the classes being modeled. Features identified as being independent of a class will have a low chi-square test statistic and are not considered useful for classification. Each extracted feature is ranked by the chi-square test statistic from largest to smallest and the top q% of features are used for the model algorithm. The proportion of features selected, dictated by q, is one of the parameters varied in the model fitting pipelines.

Binary Classifiers: Given that detection of airbag non-deployment is a signal detection problem with a binary outcome/class (presence or absence, 1 or 0, yes or no), several binary classification machine learning algorithms were utilized in the model fitting pipelines. The objective in utilizing these algorithms is to fit a model on the extracted and selected features such that the model generates accurate predictions about the binary classes in the training data. These classifiers are discussed below.

Naïve Bayes: Multinomial Naïve Bayes (NB) is a widely used generative classifier in which the conditional probability is used to determine whether a document belongs to a class [12]. The most well-known use of NB in NLP is in sentiment analysis [12].

NB assumes independence for all features and can work well depending on the validity of this assumption. In NLP, NB feature independence would require a word in a document to occur independently of every other word. Since word independence is a false assumption regarding text, we included n-gram word sequences to partially capture word dependence.

Linear Support Vector Machines: Support vector machines (SVM) is a classifier that divides data into two classes using a hyperplane that maximizes the separation of data in each class [13, 14]. SVM has been used in text classification successfully and tests have shown it to be better than naïve Bayes in document classification [15]. SVM is well-suited for high-dimensional data and text feature extraction commonly results in hundreds of thousands of features.

Gradient Boosted Trees: Gradient Boosted Trees (GBT) is an ensemble model that uses several weak learners together to minimize the loss of the model [16]. The composition of the results from the weak learners is performed by gradient descent. New trees are iteratively added to the ensemble to reduce a loss function. Generating a GBT model is computationally expensive because each tree is a sub-classifier that is individually developed and the ensemble classifier is refitted at each iteration.

GBT have been used in sentiment analysis in situations in which there are insufficient data to train other classifiers successfully. For example, it has been used in sentiment analysis with the Greek language where data is not plentiful [17]. Since we are working with a relatively small amount of training data, this method could be optimal for our situation. The largest limitation of this method is the computational cost created by the high-dimensional feature space of NLP problems.

Cross Validation & Hyperparameter Optimization: A critical component of the model development process included the application of a rigorous and systematic method to find the optimal models and their respective parameters. Grid search is an exhaustive hyperparameter optimization technique where model pipelines are fitted using all possible combination of supplied parameters. To find the optimal parameters for the models described in this paper we applied a grid search over relevant parameters in the model pipeline. For example, we varied feature extraction and selection parameters, such as the chi-square proportional cutoff. Each of the models also had specific parameters relevant to those models. For example, the prior probability parameter was varied for the NB model and the slack parameter was varied for the SVM model.

Evaluation and testing is performed using k-fold cross-validation. In k-fold cross validation the data is divided into k groups. Five groups were used in this exercise. Four of the five groups are used to fit the model pipelines and the remaining group is used to evaluate the trained classifier. This process is repeated until each group is used for evaluation of the classifier. The pipeline with the highest average validation F1 score is determined by the grid search.

Model Assessment

The intersections of labeled and classifier predicted classes are depicted in Figure 3. In this case, true positives (TP) are occurrences where the classifier correctly indicated an airbag non-deployment event. True negatives (TN) are occurrences where the classifier correctly did not indicate an airbag non-deployment event. False positives (FP) are occurrences where the classifier incorrectly indicated an airbag non-deployment event. False negatives (FN) are occurrences where the classifier incorrectly did not indicate an airbag non-deployment event. False positives and false negatives are analogous to Type I and Type II errors in statistical hypothesis testing respectively.

		Classifier Predicted Classes	
		1	**0**
Labeled Classes	**1**	**True Positive (TP)**	**False Negative (FN)**
	0	**False Positive (FP)**	**True Negative (TN)**

Figure 3. Confusion matrix used to measure binary classification processes.

Precision, recall, and F1 are commonly used metrics to assess binary classification methods [15]. These metrics build upon test results described within the confusion matrix (Figure 3). Precision is a measure of model performance and is expressed in Equation 4 where precision is calculated by dividing true positive occurrences (TP) by the sum of TP and false positives (FP) occurrences.

$$precision = \frac{TP}{TP+FP} \text{ (Equation 4)}$$

Recall is a measure of completeness and is expressed in Equation 5 where recall is calculated by dividing true positive occurrences (TP) by the sum of TP and false negative (FN) occurrences.

$$recall = \frac{TP}{TP+FN} \text{ (Equation 5)}$$

F1 is the harmonic mean of recall and precision and was used to assess overall model performance in this exercise. Equation 6 states that F1 is two times the product of precision and recall divided by the sum of precision and recall.

$$F1 = 2 \cdot \frac{precision \cdot recall}{precision+recall} \text{ (Equation 6)}$$

RESULTS

Three machine learning classifiers, Multinomial Naïve Bayes (NB), Support Vector Machines (SVM), and Gradient Boosted Trees (GBT) were compared to text annotators to understand which method performed better in identifying potential airbag non-deployment events in text. The primary method of comparison was by F1 score.

Across all data, SVM and GBT showed a similar performance with identical F1 scores of 91.3% (Table 1, graphed in Figure 4). Consistent with identical F1 scores, both SVM and GBT had very similar recall (92.5% and 92.0%) and precision (90.2% and 90.7%) as shown (Table 1). The NB classifier had the poorest performance of the three tested machine learning models (F1 NB 87.8% compared to 93.1% for SVM and GBT, Table 1). Despite its poor performance, the NB classifier performed far better than the annotator across all the data (F1 62.4%, Table 1).

When analyzing by data source (Figure 5), the annotator shows a competitive performance for TREAD (F1 71.2%), which out-performs Naïve-Bayes (F1 64.2%). For VOQ, however, the annotator showed inferior performance (F1 59.1%, Table 2) versus NB (F1 92.3%, Table 2). The profile of TREAD, which is a collection of disparate data sources, is likely to be the reason for the reduced F1 classifier scores relative to the more consistent data exhibited by VOQ. In all cases, however, neither the annotator nor the NB model outperformed the SVM or GBT models (Table 2).

Table 1.
Comparative results of machine learning classifiers across all input data using F1, Recall and Precision.

	F1	Recall	Precision
Annotator	**62.4%**	**54.3%**	**73.5%**
NB	**87.8%**	**89.1%**	**86.6%**
SVM	**91.3%**	**92.5%**	**90.2%**
GBT	**91.3%**	**92.0%**	**90.7%**

Table 2.
Comparative results of machine learning classifiers by data source using F1.

F1	VOQ	TREAD
Annotator	**59.1%**	**71.2%**
NB	**93.4%**	**64.2%**
SVM	**95.0%**	**76.3%**
GBT	**94.6%**	**78.4%**

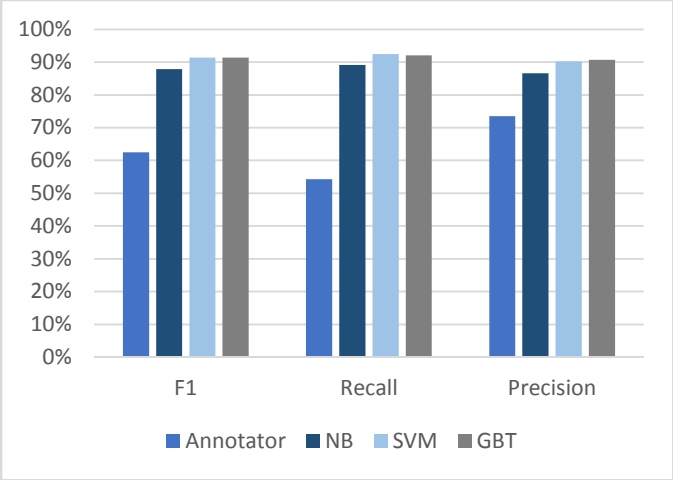

Figure 4. Graph of comparative results of machine learning classifiers across all input data using F1, Recall and Precision. Machine learning is represented by Naïve-Bayes (NB), Support Vector Machine (SVM) and Gradient Boosted Trees (GBT).

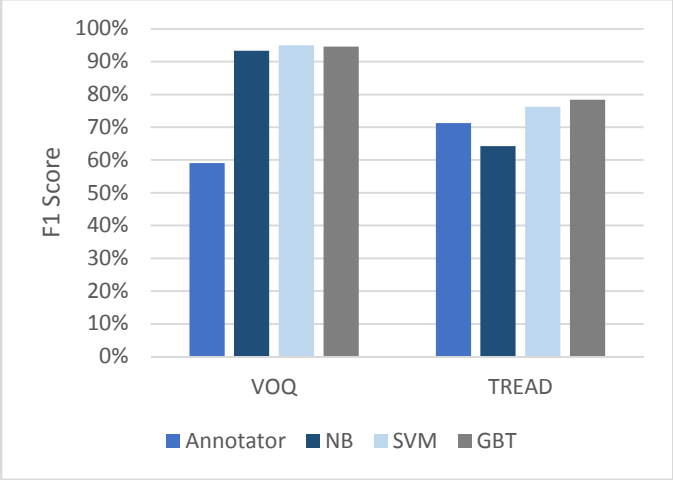

Figure 5. Graph of comparative results of machine learning classifiers by data source using F1. Machine learning is represented by Naïve-Bayes (NB), Support Vector Machine (SVM) and Gradient Boosted Trees (GBT).

CONCLUSIONS

The results shown in this paper illustrate the potential power for machine learning in transforming unstructured "dark data" into meaningful safety event detection. Machine learning methods demonstrated greatly improved classification performance (F1 score, precision, recall) in NHTSA VOQ and TREAD data than IBM Watson Explorer annotators for classification of airbag non-deployment narratives. This was true even in our scope, where training data was scarce and from a variety of data sources. Machine learning models also exhibited better balanced classification solutions compared to annotators which would tend towards having high recall at the cost of precision or vice versa.

The machine learning models yielded the worst classification performance on TREAD data. Indeed, the F1 scores for the three machine learning models tested were 16.2% to 29.2% worse for TREAD data relative to VOQ data. TREAD is the compilation of many disparate data sources at GM. We believe the reduced classification performance of TREAD is consistent with the heterogeneous nature of the data. It is likely that more training data

will be required to increase TREAD classification performance since more TREAD data will include more of each of its constituent data sources.

Despite the improvement in detecting potential airbag non-deployment events, these methods have a number of limitations related to machine learning approaches in general. First, these supervised machine learning approaches require human-labeled data in large quantities to use for training data. Second, machine learning models can only account for features (words) that have been observed in training data. If GM, the U.S. federal government and/or the U.S. public at large were to develop a new term for an airbag, then that term would be unknown to the model described in this paper unless new training data with the new term in it were used to re-fit a new version of the model. Last, our methods ignore the structure of documents and additional information, such as parts of speech (POS), for words. Such grammatical information may improve the robustness and increase the performance of our predictive models.

The application of machine learning methods for detection of potential vehicle concerns presents a robust, reliable and accurate solution. The transformation of unstructured text data into structured data enables subsequent time series analysis of potential airbag non-deployment signals, including comparative trend analysis, anomaly detection, and control charting. Future work will also focus on methods to improve model performance and reduce potential training data bias. Extracting additional features from the text, such as word POS tags, Named Entity Recognition (NER) tagging or tagging text with an ontology, may provide significant performance gains. Additionally, word embeddings could be used as an alternative feature encoding scheme which would capture the semantic meaning of the words being modeled [18]. Utilizing the concept of "data programming" to create large training sets quickly may also enable the transition from shallow learning methods (NB, SVM and GBT) to deep learning methods, such as recurrent neural networks (RNN) utilizing long short-term memory (LSTM) [19].

The data sources used in this paper represent one public and one internal GM data source. Given the robustness of machine learning text classification methods, we intend to expand the application of these models to other publicly available and GM internal data sources. Social media data, such as Twitter, Facebook and automotive forums, contain similarly unstructured data that may describe airbag non-deployment events that are valuable to detect.

We have applied our NLP and machine learning methods to other areas of potential vehicle concern and have been able to increase safety event detection F1 scores by 8 – 24% (Figure 6). In addition, these increases in F1 score for safety event detection have occurred rapidly. While annotator development in IBM Watson Explorer required detailed development of a deterministic ruleset by a human over months, a machine learning algorithm arrives at an optimal solution in minutes. Given that training data is required for both approaches, the transition from annotators to machine learning methods was a natural one.

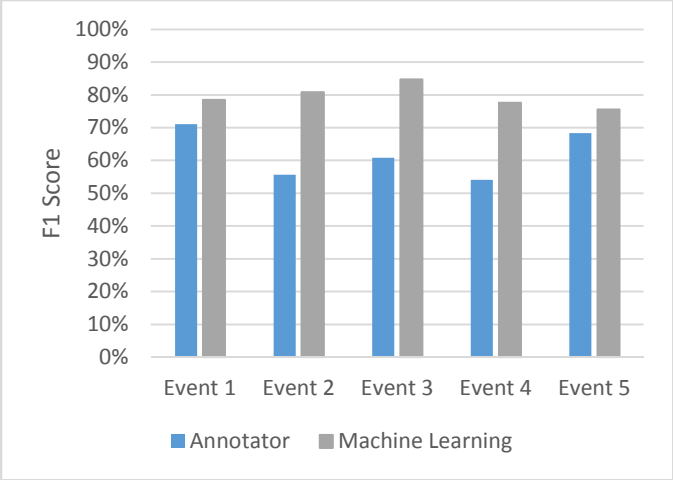

Figure 6. Classification performance improvements for other vehicle safety events. For each event, a specific machine learning model was developed. Each machine learning model is compared to an existing annotator based on F1 score.

REFERENCES

[1] US Department of Transportation, National Highway Traffic Safety Administration. 2015. "NHTSA's Path Forward." June. https://www.nhtsa.gov/staticfiles/communications/pdf/nhtsa-path-forward.pdf.

[2] Zhang, Ce, Jaeho Shin, Christopher Re, Michael Cafarella, and et al. 2016. "Extracting Databases from Dark Data with DeepDive." *Proceedings of the ACM-Sigmod International Conference on Management of Data.* 847-859.

[3] US Food & Drug Administration. 2017. *Questions and Answers on FDA's Adverse Event Reporting System (FAERS).* https://www.fda.gov/drugs/guidancecomplianceregulatoryinformation/surveillance/adversedrugeffects/.

[4] US Federal Aviation Administration. 2017. *Aviation Safety Reporting System.* https://asrs.arc.nasa.gov/.

[5] US Department of Transportation, National Highway Traffic Safety Administration. 2017. *SaferCar.gov.* https://www.safercar.gov/.

[6] US Department of Transportation, National Highway Traffic Safety Administration. 2017. *TREAD Act.* https://one.nhtsa.gov/cars/rules/rulings/index_treadact.html.

[7] Johnson, Chris. 2002. "Software tools to support incident reporting in safety-critical systems." *Safety Science* 40: 765-780.

[8] Tanguy, Lodovic, Nikola Tulechki, Assaf Urieli, Eric Hermann, and et al. 2016. "Natural Language Processing for aviation safety reports: from classification to interactive analysis." *Computers in Industry* (Elsevier) 78: 80-95.

[9] Gabler, Hampton C., and John Hinch. 2008. "Evaluation of Advanced Air Bag Deployment Algorithm Performance using Event Data Recorders." *Annals of Advances in Automotive Medicine / Annual Scientific Conference* 52: 175-184.

[10] Zhu, Wei-Don, Bob Foyle, Daniel Gagne, Vijay Gupta, and et al. 2014. *IBM Watson Content Analytics: Discovering Actionable Insight from Your Content.* 3rd ed. Poughkeepsie, NY: IBM. https://www.redbooks.ibm.com/redbooks/pdfs/sg247877.pdf.

[11] Bishop, Christopher M. 2006. *Pattern Recognition and Machine Learning.* New York, NY: Springer.

[12] Jurafsky, Daniel, and H. James Martin. 2009. Speech and Language Processing: An Introduction to Natural Language Processing, Speech Recognition, and Computational Linguistics. 2nd ed. Upper Saddle River, NJ: Prentice-Hall.

[13] Fan, Rong-En, Kai-Wei Chang, Cho-Jui Hsieh, Xiang-Rui Wang, and Chih-Jen Lin. 2008. "LIBLINEAR: A Library for Large Linear Classification." *Journal of Machine Learning Research* 9: 1871-1874.

[14] Ho, Chia-Hua, and Chih-Jen Lin. 2012. "Large-scale Linear Support Vector Regression." *Journal of Machine Learning Research* 13: 3323-3348.

[15] Joachims, Thorsten. 2002. Learning to Classify Text Using Support Vector Machines. New York, NY: Springer.

[16] Friedman, H. Jerome. 2001. "Greedy Function Approximation: A Gradient Boosting Machine." *The Annals of Statistics* 29 (5): 1189-1232.

[17] Athanasiou, Vasileios, and Manolis Maragoudakis. 2017. "A Novel, Gradient Boosting Framework for Sentiment Analysis in Languages where NLP Resources Are Not Plentiful: A Case Study for Modern Greek." *Algorithms* 10 (1): 34.

[18] Mikolov, Tomas, Ilya Sutskever, Kai Chen, Greg Corrado, and et al. 2013. "Distributed Representations of Words and Phrases and their Compositionality." *NIPS'13 Proceedings of the 26th International Conference on Neural Information Processing Systems.* 3111-3119.

[19] Ratner, Alexander, Christopher De Sa, Sen Wu, Daniel Selsam, and et al. 2017. "Data Programming: Creating Large Training Sets, Quickly." *arXiv:1605.07723 [stat.ML].*

Test

Test

Test

Test

PEER REVIEW PAPER

This paper has been peer-reviewed and published in a special edition of Traffic Injury Prevention 18(S1), by Taylor & Francis Group. The complete paper will be available on the Traffic Injury Prevention and https://www-esv.nhtsa.dot.gov/ websites on June 10, 2019.

To access all Peer-reviewed papers please copy and paste the link below into your browser to access the papers.

https://tandfonline.com/toc/gcpi20/20/sup1?nav=tocList